The Polarization Characteristics and the Thickness of the Catalyst Layers in Fuel Cell Electrodes

Tadao KENJO* and Noriyuki NAKAJIMA†

Department of Applied Science for Energy, Faculty of Engineering, Muroran Institute of Technology, Mizumoto-cho, Muroran 050

(Received January 14, 1982)

The polarization characteristics of poly(tetrafluoroethylene)-bonded Raney nickel hydrogen- and silver oxygen-electrodes have been measured as a function of the thickness of the catalyst layer, and the polarization curves of these electrodes have been analyzed on the basis of the electrolyte film model. The observed polarization curves were divided into several segments and a linear polarization-current equation, derived from the model, has been applied to each segment. The performance of the electrodes approaches asymptotically to an upper limit with the thickening of the catalyst layers. The profiles of the faradayic current density across the electrode wall have been estimated for both electrodes. In contrast with the almost flat profiles of the Raney nickel electrodes, the current densities for the silver electrodes are localized on the liquid side of the electrodes; a thin area of the catalyst layer ranging from the electrode-face/electrolyte interface to 5.3×10^{-3} cm distance sustains most of the load current at a polarization of 220 mV. The catalytic activities of both the silver and Raney nickel catalysts are enhanced with progression of the polarization while the resistivities of the electrolyte film maintained essentially constant. A slight surface oxidation for the Raney nickel and a surface reduction for the silver catalysts have been suggested as probable explanations for the enhanced catalytic activities observed.

The performance of Raney nickel hydrogen-electrodes is markedly improved with increasing catalyst loading[1,2] while that of silver oxygen-electrodes is not so sensitive to the change of the loading as the hydrogen-electrodes.[3,4] The present study involves an attempt to explain this difference on the basis of the electrolyte film model.

The feature of this model is the thin electrolyte film covering the catalyst surface.[1,5,6] Owing to the ionic conductivity of the film the electrode reaction takes place not only on the electrode-face/electrolyte interface but also on the portion of the catalyst located at a distance from the interface. The load current is sustained by the electrode reaction occurring in this zonal area so that the performance of the electrode depends upon the thickness of the catalyst layer as well as on the geometrical working area of the electrode. If the reaction zone extends toward the gas side in a long range, a good performance can be expected when a thick electrode is used. If it is short range, a thin electrode suffices to yield the performance of the upper limit for the catalyst used.

The polarization characteristics and the thickness of the reaction zone are determined by the catalytic activity and the film resistivity. Mund and his coworkers have calculated these parameter values from the polarization data, assuming a linear polarization-faradayic current relation.[1,5] The formula derived from this assumption however cannot be applied to curved polarization characteristics as is observed in the present study. The more rigorous formula that is applicable to curves, is derived from the assumption that the faradayic current is an exponential function of the polarization, but complicated mathematical calculations are required for the derivation of the potential-current relation.[7,8] In the present study, to apply a linear function to curves, the polarization curves observed are divided into several segments that can be regarded as straight lines, and a linear potential-current relation is applied to each segment.

This analytical method for the polarization data is applied to the foregoing hydrogen and oxygen electrodes to estimate the catalytic activities and the film resistivities. These parameter values should explain why the Raney nickel electrodes differ from the silver electrodes in the performance-catalyst loading relationship. Setting desired parameter values that are not yet realized in the experiment, one can calculate polarization curves for unreal electrodes. This may provide us with some hints and orientations for improving the electrode performance.

Experimental

Preparation of the Raney Nickel Catalyst. An ingot containing 40% Ni (99.95% purity) and 60% Al (99.99% purity) was prepared by using an induction furnace. The ingot obtained was crushed and powdered to a particle size of less than 37 μm. The aluminium was leached with a 6 M KOH solution (1 M=1 mol dm^{-3}) at 80 °C for 5 h. The Raney nickel thus obtained was washed with water and methyl alcohol.

Preparation of the Silver Catalyst. Ten grams of silver nitrate (guaranteed reagent, Yoneyama Chemical Co., Ltd.) was dissolved into 5 ml of water with 2.5 ml of formaline (guaranteed reagent, Kanto Chemical Co., Inc.). The solution obtained was added dropwise into 200 ml of 0.6 M KOH solution at 10 °C with stirring. The silver powder thus obtained was washed with water and dried in an oven at 120 °C.

Preparation of the Electrodes. The electrodes were prepared with the same method as in the previous work.[2] Poly(tetrafluoroethylene)(PTFE) (D-1, Daikin Industrial Company) was added to the catalyst powder in an amount proportional to 10% of the weight of the catalyst. The mixture was milled and dried to become a paste. The paste was calender-rolled by hand into sheets. They were used as catalyst layers.

The gas-side layers for the hydrogen-electrodes were prepared by binding nickel black powder with PTFE and by calender-rolling it into sheets.

Those for the oxygen-electrodes were prepared by using a mixture of graphite powder and activated carbon powder

† Present address: Fuji Electric Co., Ltd., Nagasaka, Yokosuka 240-01.

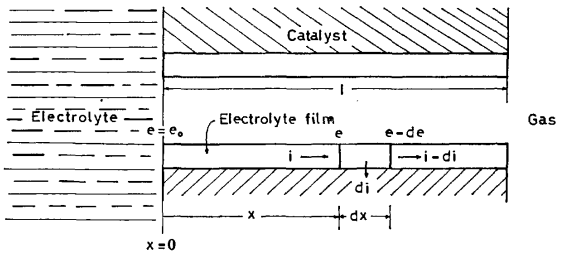

Fig. 1. Schematic cross section of an electrode pore.

instead of nickel black. After the sheets were reinforced with stainless steel screens (60—100 mesh), they were heated at 380 °C for 15 min in a nitrogen atmosphere. The gas-side layers thus obtained were attached to the catalyst layers by pressing at a pressure of 420 kg/cm². The double-layered electrodes obtained were heated in a hydrogen atmosphere at 150 °C for the hydrogen-electrodes and at 380 °C for the oxygen-electrodes.

Measurement of the Polarization. The geometrical working area of the electrodes was 7 cm². The electrolyte was a 6M KOH solution and was circulated at a rate of 5 ml/min. The electrolyte temperature was 60±0.5 °C. The IR voltage drop was eliminated by the current-interruption method.[9]

Theoretical

When the PTFE-bonded electrodes contact with the electrolyte solution, the inner face of the electrode pore is covered with a thin electrolyte film while the electrolyte penetration into the central area of the pore is hindered by the repellency of PTFE. Thus the supplied gas can permeate the porous space to react with the electrolyte on the catalyst surface. This feature can be modeled as a cylindrical electrode pore as shown in Fig. 1. For the potential in the electrolyte film, e, Ohm's law holds:

$$\frac{de}{dx} + i\rho = 0, \tag{1}$$

where x is the distance from the electrode-face/electrolyte interface, i the ionic current density and ρ the resistivity of the electrolyte film. A linear function is assumed for the faradayic current density, di/dx:

$$\frac{di}{dx} + \frac{e}{k} = 0, \tag{2}$$

where k is the impedance for the inner-face/electrolyte interface per unit length of the pore. If ρ and k are independent of both x and e, and the edge effect of the pore can be neglected, Eqs. 1 and 2 can be integrated under the boundary conditions, $e=e_0$ at $x=0$ and $i=0$ at $x=l$:

$$e = e_0 \cdot \frac{\cosh\sqrt{\rho/k}(l-x)}{\cosh\sqrt{\rho/k}\,l} \tag{3}$$

$$i = \frac{e_0}{\sqrt{\rho k}} \cdot \frac{\sinh\sqrt{\rho/k}(l-x)}{\cosh\sqrt{\rho/k}\,l}, \tag{4}$$

where l is the length of the pore. Substituting $x=0$ into Eq. 4 one can obtain a potential-current relation to compare with experimental data:

$$i = \frac{e_0}{\sqrt{\rho k}} \cdot \tanh\sqrt{\rho/k}\,l. \tag{5}$$

Regarding e_0 as the polarization corrected for IR voltage drop, i as the current density per unit working area of the electrode, l as the thickness of the catalyst layer, ρ as the resistivity of the electrolyte film per unit working area of the electrode whose catalyst layer has unit thickness, and k as the impedance per unit thickness of the catalyst layer, one can apply Eq. 5 to the calculation of the polarization curves.

The polarization resistance, ω, is defined as

$$\omega \equiv \left(\frac{e}{i}\right)_{x=0} = \sqrt{\rho k}\coth\sqrt{\rho/k}\,l. \tag{6}$$

The polarization resistance is the slope of the polarization curves and its application is limited to linear polarization characteristics. For application to the curves, they are divided into several segments with polarization values at intervals of 10—20 mV and Eq. 6 is then applied to each segment, regarding it as a straight line. From the polarization curves observed for various catalyst loadings, the reciprocal polarization resistance ω^{-1} can be calculated as a function of the thickness of the catalyst layer l for each of the polarization regions. Thus ρ and k are obtained as values that make curves for Eq. 6 best fit the observed ω^{-1} *vs.* l plots.

The faradayic current density, i_F, can be obtained as a function of x by substituting Eq. 3 into Eq. 2:

$$i_F \equiv \left|\frac{di}{dx}\right| = \frac{e_0}{k} \cdot \frac{\cosh\sqrt{\rho/k}(l-x)}{\cosh\sqrt{\rho/k}\,l}. \tag{7}$$

The ratio of i_F at $x=x$ to that at $x=0$, i_F/i_F°, is given by

$$\frac{i_F}{i_F^\circ} = \frac{\cosh\sqrt{\rho/k}(l-x)}{\cosh\sqrt{\rho/k}\,l}. \tag{8}$$

The above equation gives the profile of the faradayic current density across the electrode wall.

Results

Figure 2 shows plots of the polarization, η, against current density, I, measured for Raney nickel hydrogen-electrodes with variation of the catalyst loading. The ω^{-1} *vs.* l plots obtained from the data above are represented in Fig. 3, where the catalyst loading is given as the scale of the thickness of the catalyst layer; the conversion factor was obtained by measuring the thickness of the catalyst layers with a micrometer as 0.01 cm thickness=30 mg/cm² loading. The solid lines in the figure are the calculated curves of the best fit. The ρ and k values yielding the best fitting curves are shown in Table 1. The solid lines in Fig. 2 are polarization curves calculated from these parameter values using Eq. 5. The agreement with the observed plots is good.

As seen in Fig. 3, the ω^{-1} values reaches 90% of their upper limits when $l=4\times10^{-2}$ cm. Hence one centimeter was used as an l value that gives the upper limit of ω^{-1}. Line 1 in Fig. 2 is a polarization curve calculated for $l=1$ cm holding ρ and k to the values in Table 1. This is the best performance that can be theoretically expected using the Raney nickel catalyst prepared in the present study. If the catalytic activity is improved to yield $k=1.7\times10^{-3}\ \Omega\ \mathrm{cm}^3$, which

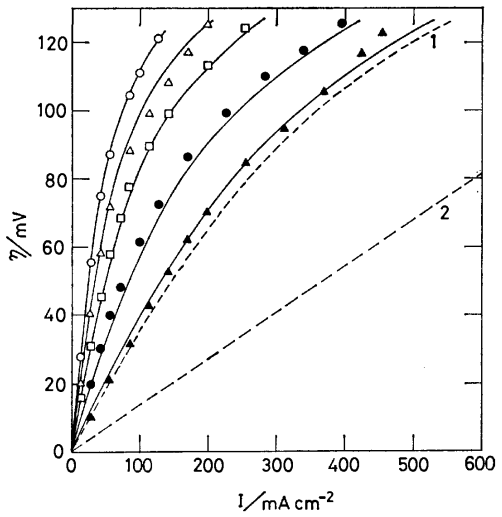

Fig. 2. Polarization curves for PTFE-bonded Raney nickel hydrogen-electrodes, IR drop eliminated.
Electrolyte: 6 M KOH, 60 °C. Catalyst loading: ○; 15.15 mg/cm², △; 21.06 mg/cm², □; 31.74 mg/cm², ●; 61.6 mg/cm², ▲; 130.8 mg/cm². Solid line: Calculated using parameter values for the best fit, Line 1: Calculated for observed ρ and k values and $l=1$ cm, Line 2: Calculated for $k=1.7\times10^{-3}$ Ω cm³, $\rho=$ 11 Ω cm and $l=1$ cm.

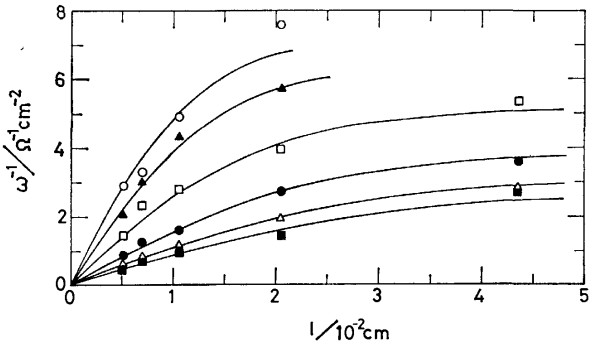

Fig. 3. Reciprocal polarization resistance as a function of thickness of the catalyst layer for PTFE-bonded Raney nickel hydrogen-electrodes.
Polarization region: ■; 0—40 mV, △; 40—60 mV, ●; 60—80 mV, □; 80—100 mV, ▲; 100—110 mV, ○; 110—120 mV. Solid lines: Calculated for the best fit.

is the value for the polarization of 110—120 mV, the polarization curve to be expected is given by Line 2 in the same figure.

Figure 4 shows polarization curves observed for the silver oxygen-electrodes. The ω^{-1} *vs.* l plots are shown in Fig. 5 where the conversion factor 0.01 cm thickness=40 mg/cm² loading (obtained by the thickness measurement) was used for the conversion of the loading to the thickness. The parameter values for the best fit are given in Table 2. The polarization curves calculated from these ρ and k values are shown by solid lines in Fig. 4. The agreement with the observed data is good except in highly polarized regions. The best performance attainable by the silver catalyst prepared in the present study is shown with Curve 1 in Fig. 6 which was calculated for the values

Table 1. The k values for the best fit in the PTFE-bonded Raney nickel hydrogen-electrodes[a)]

η / mV	k / Ω cm³
0—40	1.1×10^{-2}
40—60	8.7×10^{-3}
60—80	6.0×10^{-3}
80—100	3.5×10^{-3}
100—110	2.2×10^{-3}
110—120	1.7×10^{-3}

a) A constant value of 11 Ω cm was used as a ρ value.

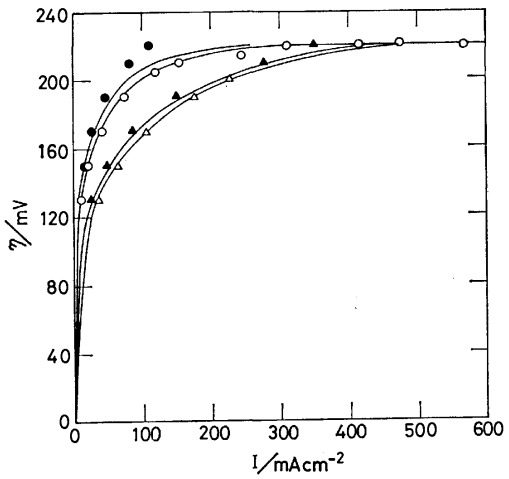

Fig. 4. Polarization curves for PTFE-bonded silver oxygen-electrodes, IR drop eliminated.
Electrolyte: 6 M KOH, 60 °C. Catalyst loading: ●; 22.5 mg/cm², ○; 28 mg/cm², ▲; 109 mg/cm², △; 127 mg/cm². Solid lines: Calculated using parameter values for the best fit.

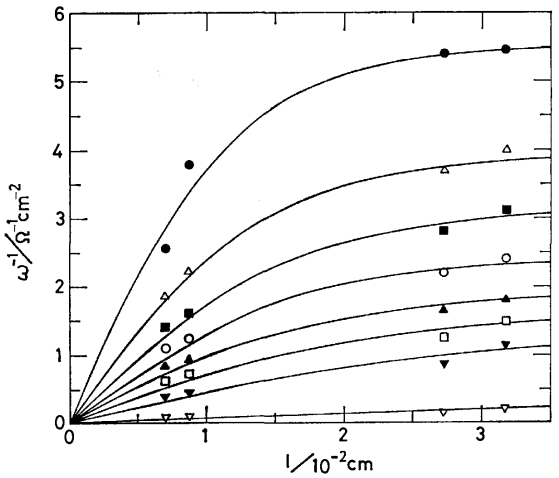

Fig. 5. Reciprocal polarization resistance as a function of thickness of the catalyst layer for PTFE-bonded silver oxygen-electrodes.
Polarization region: ▽; 0—120 mV, ▼; 120—140 mV, □; 140—150 mV, ▲; 150—160 mV, ○; 160—170 mV, ■; 170—180 mV, △; 180—190 mV, ●; 190—200 mV. Solid lines: Calculated for the best fit.

TABLE 2. THE ρ AND k VALUES FOR THE BEST FIT IN THE PTFE-BONDED SILVER OXYGEN-ELECTRODES

η / mV	ρ / Ω cm^3	k / Ω cm^3
0—120	150	1.0×10^{-1}
120—140	30	2.0×10^{-2}
140—150	30	1.3×10^{-2}
150—160	30	9.2×10^{-3}
160—170	25	6.8×10^{-3}
170—180	20	5.1×10^{-3}
180—190	18	3.6×10^{-3}
190—200	15	2.2×10^{-3}
200—210	15	1.2×10^{-3}
210—215	15	5.4×10^{-4}
215—219	15	2.2×10^{-4}
219—220	15	8.0×10^{-5}

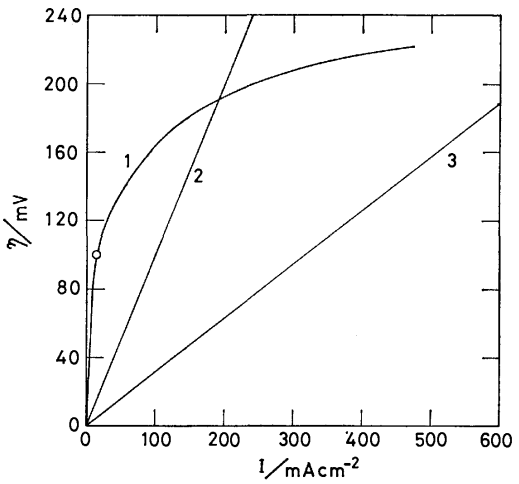

Fig. 6. Calculated polarization curves for silver oxygen-electrodes.
Line 1: Calculated for observed ρ and k values and $l=1$ cm observed datum for $l=0.0318$ cm, Line 2: Calculated for $k=0.1$ Ω cm^3, $\rho=10$ Ω cm and $l=1$ cm, Line 3: Calculated for $k=0.01$ Ω cm^3, $\rho=10$ Ω cm and $l=1$ cm.

of Table 2 and $l=1$ cm. It is very close to the open triangles in Fig. 4 (data for the thickest catalyst layer used in this study). Thus no marked improvement in the performance can be expected from thicker electrodes when the same catalyst is used. If the ρ value can be lowered to 10 Ω cm and $k=0.1$ Ω cm^3, Line 2 can be expected as the best performance. If the k value is lowered to 10^{-2} Ω cm^3 in addition to the above lowering in the ρ value, the best performance attainable is given by Line 3.

Discussion

When the polarization curves are divided into segments, there is a choice of sectionalizing with respect either to polarization or current density. When polarization was chosen, it was assumed implicitly that ρ and k depend upon polarization rather than current density. This assumption was open, but the good agreement found between the calculated and observed plots suggests the validity of the assumption employed.

As seen in Tables 1 and 2, the k values of both the hydrogen- and oxygen-electrodes decrease with progression of the polarization. This is due to an enhancement of the catalytic activity which is probably brought about by polarizing the electrode catalyst. As the hydrogen-electrode is polarized to a noble potential as a result of loading current, the Raney nickel catalyst is apt to accept oxygen onto the surface so that the concentration of the oxygen atom on the surface increases.

It has been recently suggested that the precipitates of oxides or hydroxides dispersed on the metal catalysts not only prevent the catalysts from diminishing the reactive area, but also accelerate the catalytic reaction through unknown metal-oxide interactions.[10-15] Also, in the Raney nickel studied, a slight oxidation of the surface that does not reach the formation of non-conductive oxide film may enhance the catalytic activity for the electrode reaction. Attributing these polarization-induced activating effect for the Raney nickel catalyst to the activating effect of the oxide precipitates, we may identify the decrease in the k values due to polarization with the slightly oxidized surface state as described above. The plots deviate upward from the calculated curves in highly polarized regions, suggesting however that too much oxidation is harmful to the catalytic action.

The silver catalyst is also activated with progression of the polarization (Table 2). Contrary to the case of the hydrogen electrodes, this may be ascribed to surface reduction since the decrease in the k value results from polarizing to a less noble potential. No signs of loss of catalytic activity are observed in the region of high polarization.

In the silver oxygen-electrode studied, a total polarization required to sustain a load of 600 mA/cm^2 is 220 mV, but more than 120 mV out of the total value is expended for an initial 10 mA/cm^2 load. To improve the performance of this electrode, therefore, the reduction of the polarization, particularly in the low load current, is necessary. As expected from Eq. 5, the upper limit of ω^{-1} decreases with increasing ρ for a given k value. The ρ value of the oxygen-electrode studied is as high as 150 Ω cm in the polarization region 0—120 mV (Table 2). This very large value limits ω^{-1} to a very low value and results in only a poor electrode performance. Hence an enhancement in the conductivity of the electrolyte film is needed to improve the polarization characteristics.

Höhne has prepared oxygen-electrodes catalyzed with silver powder coprecipitated with metal hydroxides.[16] His electrode is less polarized than the electrode prepared in the present study: The polarization of his electrode is 60 mV at a load of 40 mA/cm^2 while that of the present electrode is 130 mV at the same load. The same analytical method was applied to his polarization data to estimate the ρ and k values with assuming the same weight of the catalyst layer per 1 cm^3. The parameter values obtained by the analysis are $\rho=15$ Ω cm and $k=4.3\times10^{-3}$ Ω cm^3 in a low load current. These are smaller than the values ob-

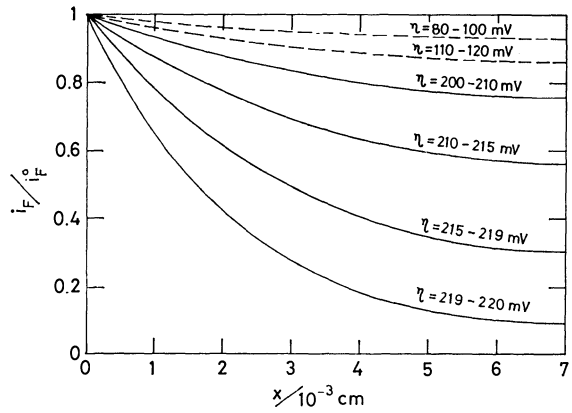

Fig. 7. Profiles of the faradayic current density across the electrode face.
Solid lines: Silver oxygen-electrodes, broken lines: Raney nickel hydrogen-electrodes, $l=7\times10^{-3}$ cm and the ρ and k values in Table 2 used for the calculation.

tained in the present study for the same load current. Höhne's electrodes were dried at 100 °C and no further heat treatment was applied, while the present electrodes were heated at 380 °C to remove the surfactant which had been originally introduced in the PTFE dispersion. The heat treatment at high temperatures deprives the catalyst of wettability and the reactive surface areas. In addition, the co-precipitated hydroxides may enhance the reactive surface area and the wettability of the catalyst. These two factors lower both the ρ and k values, but the lowering in the ρ value is the more important reason for bringing about the better performance.

The profiles for the faradayic current density across the electrode face were calculated for the parameter values in Tables 1 and 2 using Eq. 8. The results are given in Fig. 7. In contrast to the almost flat profiles for the hydrogen electrodes, the current densities for the silver electrodes are localized to the electrode-face/electrolyte interface as the electrodes are polarized; at $\eta=220$ mV, such a thin area of 5.3×10^{-3} cm thickness sustains 90% of the total load. If electrodes thicker than the above value are employed, the portion of the catalyst layer exceeding this thickness makes hardly any contribution to the improvement of the performance. Since the electrode preparation has usually been performed in the thicker region than the above value, the performance of the silver electrodes appears to be less dependent upon the catalyst loading than that of the Raney nickel electrodes. If thinner electrodes can be prepared and their polarizations measured, the dependence of the catalyst loading will be obtained more effectively.

This marked current localization is ascribed to the small k values of silver catalyst (Table 2), as is expected from Eq. 8. The large k values for Raney nickel catalyst, on the other hand, yield almost flat profiles, leading to long-ranging reaction zones. Thus the performance continues to enhance over the long distance in the coordinate of the electrode thickness (Fig. 3). Consequently, in the case of Raney nickel catalyst, thick electrodes yield good performance.

References

1) K. Mund, G. Richter, and F. von Sturm, *J. Electrochem. Soc.*, **124**, 1 (1977).
2) T. Kenjo, *Bull. Chem. Soc. Jpn.*, **54**, 2553 (1981).
3) N. Nakajima, Thesis, Muroran Institute of Technology, Muroran, 1981.
4) K. Koseki, T. Ihara, H. Tajima, and T. Kobayashi, The 22nd Battery Symposium in Japan, Kyoto, November 1981, Abstr. No. A19.
5) K. Mund, *Siemens Forsch.-u. Entwickel.-Ber.*, **4**, 1 (1975).
6) K. Mund, *Siemens Forsch.-u. Entwickel.-Ber.*, **4**, 68 (1975).
7) S. Srinivasan, H. D. Hurwitz, and J. O'M. Bockris, *J. Chem. Phys.*, **46**, 3108 (1967).
8) K. Micka, "Fuel Cell Systems," American Chemical Society, Washington, D. C. (1965), p. 73.
9) K. V. Kordesch and A. Marko, *J. Electrochem. Soc.*, **107**, 480 (1960).
10) F. von Sturm, "Proceeding of the Symposium on Electrode Materials and Processes for Energy Conversion and Storage," ed by J. D. E. Mclntyre, S. Srinivasan, and F. G. Will, The Electrochemical Society, Princeton, New Jersey (1977), pp. 247—264.
11) K. Kinoshita, "Proceedings of the Workshop on the Electrocatalyst of Fuel Cell Reactions," ed by W. E. O'Grady, S. Srinivasan, and R. F. Dudley, The Electrochemical Society, Princeton, New Jersey (1979), pp. 144—164.
12) A. Katayama, *Chem. Lett.*, **1978**, 1263.
13) M. Nakamura, 47th National Meeting of the Electrochemical Society of Japan, Yokohama, April 1980, Abstr. No. C 204.
14) S. J. Tauster, S. C. Fung, and R. L. Garten, *J. Am. Chem. Soc.*, **100**, 170 (1978).
15) R. T. Baker, E. B. Prestridge, and R. L. Garten, *J. Catal.*, **56**, 390 (1979).
16) K. Höhne, *Siemens Forsch-u. Entwickel.-Ber.*, **3**, 31 (1974).

 © 1983 The Chemical Society of Japan Bull. Chem. Soc. Jpn., 56, 6—14 (1983) [Vol. 56, No. 1

Excited-state Reactions of Coumarins in Aqueous Solutions. I. The Phototautomerization of 7-Hydroxycoumarin and Its Derivative

Tetsuo MORIYA

Electrotechnical Laboratory, 1-1-4 Umezono, Sakura-mura, Niihari-gun, Ibaraki, 305

(Received April 12, 1982)

The kinetics and mechanism of the reaction in the photo-excited state of 7-hydroxycoumarin and its derivative have been studied in aqueous solutions by means of measuring the fluorescence spectra and the fluorescence lifetime. The four fluorescence bands have been identified as emissions from the neutral, anionic, tautomeric, and cationic forms of 7-hydroxycoumarins. The quantitative analysis was performed by using the rate equation which included the term for the direct conversion of the excited neutral molecule to its tautomer in addition to the usual reaction term of dissociation. The rate constants of the tautomerization and dissociation were discussed in detail, and it was revealed that the tautomerization in aqueous solutions was mainly caused by the transfer of a proton between two active sites in the molecule. Such an intramolecular proton-transfer of the coumarins, found first in this paper, is considered to be promoted by water molecules with a hydrogen bond surrounding the excited molecule.

In recent years there have appeared many experimental works on the fluorescence behavior of solutions in which there had been dissolved various coumarin derivatives, which are used practically as fluorescennt indicators, and as laser-dye solutions.[1-3] The greater part of the experiments have been performed only on the solutions under particular conditions, and most investigators have used rather qualitative methods for the analysis of fluorescence phenomena. In regard to coumarins with a 7-hydroxyl group as a substituent, complex fluorescence spectra have been observed in a variety of organic solvents and in acidic, neutral, and basic aqueous solutions. It has been revealed that, typically, four fluorescent species exist in the photo-excited state according to the solvent conditions; they have been tentatively identified as neutral, anionic, tautomeric, and protonated species of the excited molecule.

Concerning this 7-hydroxy compound, several authors have studied the reaction kinetics of these molecular species using quantitative or semiquantitative methods;[4-7] they have derived some reaction-rate constants from the fluorescence spectra and the fluorescence lifetime. Although the results obtained by the former workers may be valid under restricted solvent conditions, it will be shown later in this article that an important point is missing in their conclusions and that the total fluorescence data cannot be explained without including a new mechanism in the reaction process to generate a phototautomer. Therefore, we wish to report here the detailed fluorescence data which enabled one to analyze quantitatively the reaction mechanism of the photo-excited 7-hydroxycoumarins in an aqueous solution, and to show a generalized method to treat the reaction kinetics over a very wide range of hydrogen-ion concentrations in solution. The way of analysis performed below should also be applicable to various 7-hydroxycoumarin derivatives and essentially to other types of hydroxy- and amino-substituted coumarins.

Experimental

The 7-hydroxycoumarin (**1**) was obtained from Wako Pure Chemical Ind., and the 7-hydroxy-4-methylcoumarin (**2**), from Tokyo Kasei; they were both recrystallized from ethanol and then washed with diethyl ether. The purity was checked by means of differential thermal analysis (DTA), which could rigorously monitor the melting point of the reagents: **1**, mp 233.5 °C; **2**, mp 186.3 °C. Solutions for the measurement of the absorption and fluorescence spectra were prepared by diluting an aqueous solution of a known concentration with distilled water; their pH (or H_0[8]) value was controlled over wide ranges by the use of $HClO_4$ for the pH (or H_0) —4.3—5 and by utilizing the following buffer solutions for the pH 5—11: pH 5—5.8, succinic acid–borax; pH 5.8—9.2, KH_2PO_4–borax; pH 9.2—11, Na_2CO_3–borax. All the chemicals used for the pH control were analytical or spectrograde reagents. The ionic strength of the buffer solutions was suppressed as much as possible within the limit of effective buffer action in order to avoid the influence of various ions on the excited-state reactions of the molecular species being observed. The absorption spectra were obtained on a Hitachi 323 spectrophotometer, and the fluorescence spectra, on a Hitachi MPF 4 fluorescence spectrophotometer with an S-5 type photomultiplier tube. Usually the output response was not corrected for instrumentaf response, since the correction did not affect the analysis ol the reaction kinetics. The lifetimes of the photo-excited state of each molecular species were measured by using a time-correlated single-photon-counting fluorometer similar to the one described in Ref. 9. When a repetitive short-pulsed light at 337 nm from an air-flash lamp was used as the excitation source, a fluorescence lifetime as short as 1 ns could be measured. In order to observe the steady-state fluorescence, the excitation was effected at the isosbestic point of the absorption spectra, *i.e.*, at 337 nm for 7-hydroxycoumarin and at 334 nm for 7-hydroxy-4-methylcoumarin. The concentrations of the fluorescent molecules in the solution were $\approx 6.1 \times 10^{-5}$ mol dm^{-3} for 7-hydroxycoumarin and $\approx 6.3 \times 10^{-5}$ mol dm^{-3} for 7-hydroxy-4-methylcoumarin; these values are most appropriate for the reliable and stable recording of the fluorescence spectra.[10] The pH value of solutions was measured directly with a Radiometer PHM 64 pH meter equipped with a G2401C combined glass electrode. Much care was taken for each measurement run to set the quartz cell containing the sample solution at exactly the same position, thus ensuring the reproducibility of the recorded fluorescence intensity. The temperature of the solution could be controlled by a cell holder with water circulation. Usual spectral measurements were performed at 20 °C otherwise mentioned.

Results and Discussion

pH Dependence of Absorption and Fluorescence Spectra.

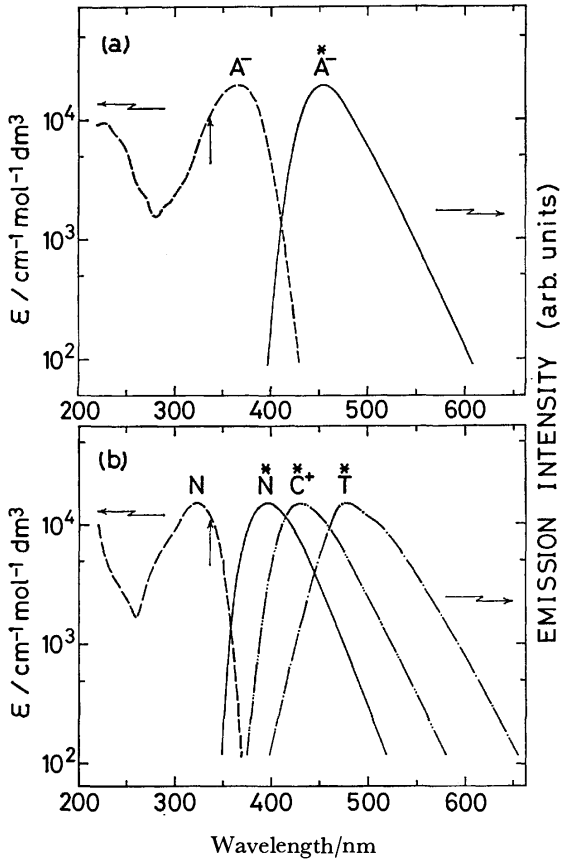

Fig. 1. Absorption and fluorescence spectra of 7-hydroxycoumarin (**1**) in aqueous solutions with various pH values. (a) Spectra at pH$\geqslant$11; (b) spectra at pH$\leqslant$5. A^- and N indicate the absorption spectra, and $\overset{*}{A}^-$, $\overset{*}{N}$, $\overset{*}{T}$, and $\overset{*}{C}^+$ the fluorescence spectra. The fluorescence bands are separated each other by the procedure described in the text and normalized to the same peak intensity. In (b) the fluorescence spectrum of $\overset{*}{A}^-$ is omitted since this is the same as in (a). The little arrow in the figure shows the isosbestic point.

In the electronic ground-state of 7-hydroxycoumarins in aqueous solutions, only two molecular species are spectroscopically detectable. One is a neutral molecule (N), and the other is an ionized molecule (A^-), in which the 7-hydroxyl group is ionized as is shown below:

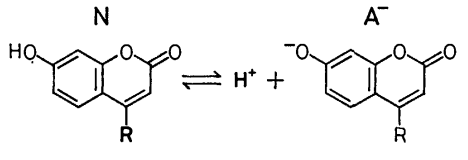

1 : R=H , 2 : R=CH_3

Figures 1 and 2 show the absorption spectra of 7-hydroxycoumarin (**1**) and 7-hydroxy-4-methylcoumarin (**2**) respectively. The absorption maxima of the neutral and anionic forms of **1** and **2** are 324 nm and 366 nm, and 321 nm and 361 nm, respectively. The pK values of the 7-hydroxyl substituent were 7.75 (**1**) and 7.84 (**2**). From these values, it is readily shown that, in the ground state, almost all molecules

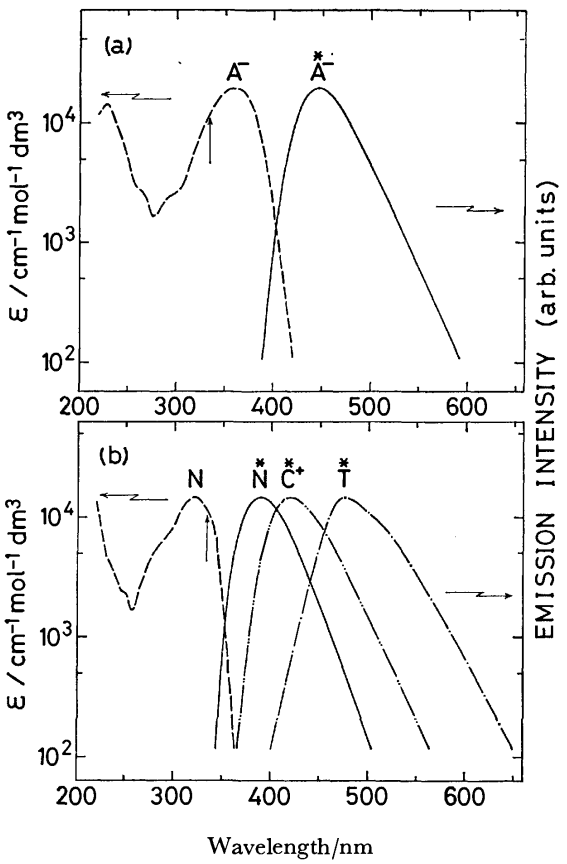

Fig. 2. Absorption and fluorescence spectra of 7-hydroxy-4-methylcoumarin (**2**) in aqueous solutions with various pH values. (a) Spectra at pH$\geqslant$11; (b) spectra at pH$\leqslant$5. The notations are the same as in Fig. 1.

exist as anions at pH$\geqslant$10 and as neutral molecules at pH$\leqslant$6. The isosbestic points of the absorption spectra were 337 nm (**1**) and 334 nm (**2**).

When only the anion was excited at a high pH, the observed fluorescence band was due simply to the anionic form with emission peaks at 453 nm (**1**) and 447 nm (**2**). The interrelation between the corresponding absorption and emission spectra may be read from Figs. 1(a) and 2(a). In contrast to this, when the neutral molecule was excited at a low pH, three kinds of fluorescence bands with emission peaks at about 397 nm, 478 nm, and 431 nm for **1**, and at about 390 nm, 475 nm, and 419 nm for **2**, were observed in addition to the emission from the anion. In many cases, these fluorescence bands overlapped each other to a greater or lesser extent; therefore, we must make an effort to separate each spectral band from the others. In the course of this separation procedure, it is very convenient to plot the emission intensity of the fluorescence spectrum with a logarithmic scale, as is shown in Figs. 1 and 2, because the spectral shape of each band can readily be recognized by shifting the plotted spectral band upward or downward in the graph. At first, each band was roughly separated by the inspection of the graphs obtained for solutions with a variety of pH values; then, the band spectrum was improved by a numerical treat-

ment until a self-consistent relation became realized between every fluorescence band. The emission-band spectra thus separated are shown in Figs. 1 and 2.

From the energy positions of the absorption and emission bands, the fluorescence designated by $\overset{*}{A}^-$ may naturally be thought to originate from an anionic form, and $\overset{*}{N}$, from a neutral form, of the photo-excited molecule. This is supported by the fact that the spectrum of the long-wavelength absorption band of the neutral molecule (N) and the anionic molecule (A^-) coincides very well with a mirror image of their corresponding emission bands, $\overset{*}{N}$ and $\overset{*}{A}^-$, which can easily be read from Figs. 1 and 2. The fluorescence measurement in various solvents also supported this conclusion.[11] When organic solvents without a hydroxyl group, *e.g.*, dioxane, chloroform and acetonitrile, were used, simply an emission band which corresponded to $\overset{*}{N}$ in Figs. 1(b) and 2(b) was observed in the neutral solution; apparently, this originated from the neutral molecule. Further, the luminescence experiment using the method of Beens *et al.*[12] revealed that, on the addition of alkylamines to the solution, a contact ion-pair between –OH and NR_3 as well as an ionized anionic species could exist in the photo-excited state for the solvent without a hydroxyl group, while in basic alcoholic and aqueous solutions only an ionized anionic species was detected because of the higher ionizing ability of such solvents as possessed a hydroxyl group. Therefore, the formerly proposed model of Zinsli,[4] which assumed the existence of a bound ion-pair of the excited molecule in ethanol–water mixtures, is highly improbable.

As for the determination of the origin of the remaining two emission bands, *i.e.*, $\overset{*}{T}$ and $\overset{*}{C}^+$, the case of quinolinols and its analog offers a very similar example which was fully discussed in Refs. 13 and 14. It has been shown that the long-wavelength absorption and fluorescence maxima of quinolinols generally lie at wavelengths, dependent on the ionic species, in the order of: tautomer ($\overset{*}{T}$)>anion ($\overset{*}{A}^-$)>cation ($\overset{*}{C}^+$)>

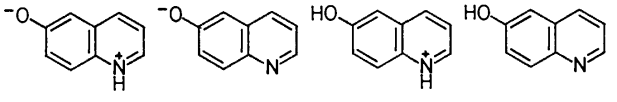

neutral molecule ($\overset{*}{N}$).[14] This conclusion is derived essentially by the use of the general concept that, in MO calculations, the Coulomb integral and the electronegativity of the conjugated atom are roughly proportional to one another, and that the electronegativity is ordered: oxygen>nitrogen>carbon, and positively charged atom>neutral atom>negatively charged atom. By coupling these facts with the one-electron charge densities in the highest-occupied and lowest-unoccupied π-orbitals of the molecule, we are able to account qualitatively for the relative positions of the absorption and emission maxima of the various ionic species formed in the solution. From the similarity of the fluorescent behavior of the 7-hydroxy-

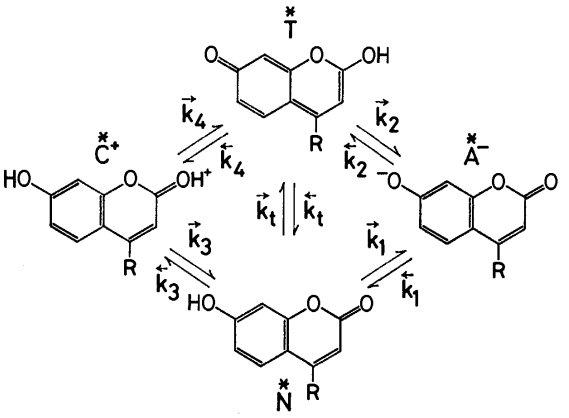

Fig. 3. Reaction scheme of the photo-excited states of 7-hydroxycoumarins. $\overset{*}{N}$, $\overset{*}{A}^-$, $\overset{*}{T}$, and $\overset{*}{C}^+$ represent the excited states of the neutral, anionic, tautomeric and cationic molecular forms, respectively. $\vec{k}$'s and $\overleftarrow{k}$'s are the reaction rate constants between them.

coumarins with that of quinolinols, and also from the MO calculations of the tautomeric form of the molecules,[15,16] $\overset{*}{N}$, $\overset{*}{A}^-$, $\overset{*}{C}^+$, and $\overset{*}{T}$, in Figs. 1 and 2 may naturally be identified as fluorescence from the neutral, anionic, cationic, and tautomeric forms of 7-hydroxycoumarins respectively.

In the most basic solution (pH$\geqslant$11), the anionic form ($\overset{*}{A}^-$) is the only existing species, while in the most acidic solution ($H_0\leqslant -4$), the cationic form ($\overset{*}{C}^+$), probably protonated on the carbonyl oxygen in the molecule, is also generated. For the intermediate pH range, three of the emission bands, *i.e.*, $\overset{*}{N}$, $\overset{*}{A}^-$, and $\overset{*}{T}$, appear simultaneously, and the role of the emission band $\overset{*}{T}$ becomes very important in the reaction kinetics of the excited species, as will be discussed fully below. We concentrated our attention especially on this pH range and took the luminescence data as carefully as possible, because the former workers[4-7] did not notice the coexistence of the $\overset{*}{T}$ band with the $\overset{*}{N}$ and $\overset{*}{A}^-$ bands, which caused much confusion in the interpretation of the phenomenon.

Rate-equation Analysis of Reactions in the Excited State. We have shown in Fig. 3 a generalized total scheme for the excited-state reactions which is different from the previously proposed model in the point that there exist the terms $\vec{k}_t$ and $\overleftarrow{k}_t$ representing a reaction pathway that does not involve a step-by-step protonation or deprotonation process, *i.e.*, a "nondissociative" reaction pathway. $\vec{k}_1$ and $\overleftarrow{k}_1$ are the usual forward and backward reaction rates of the $\overset{*}{N}\rightleftharpoons\overset{*}{A}^-+H^+$ dissociative process respectively; k_2—k_4 have the same meaning. As for the region of pH$\leqslant$6, only the neutral molecule exists in the electronic ground-state, as has been mentioned before, so only the neutral molecule can be excited by light absorption in the first instance. Therefore, this excited molecule in the solution is converted in its lifetime into the anionic or cationic species,

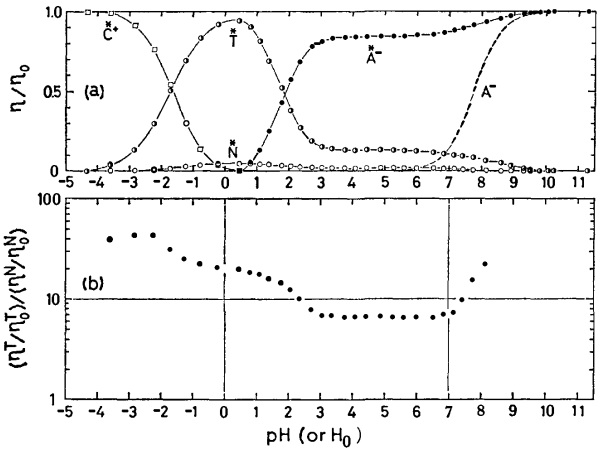

Fig. 4. Relative fluorescence efficiency of the excited species of 7-hydroxycoumarin (**1**) in aqueous solution (6.1×10^{-5} M); $\lambda_{ex}\approx337$ nm; 20 °C. (a) Dependence of the relative efficiency η/η_0 on pH: (○) $\overset{*}{N}$, (●) $\overset{*}{A}^-$, (◑) $\overset{*}{T}$, (□) $\overset{*}{C}^+$. The ground-state equilibration between N and A^- is also indicated by a dashed curve. (b) Dependence of $\overset{*}{K}_t=(\eta^T/\eta_0^T)/(\eta^N/\eta_0^N)$ on pH.

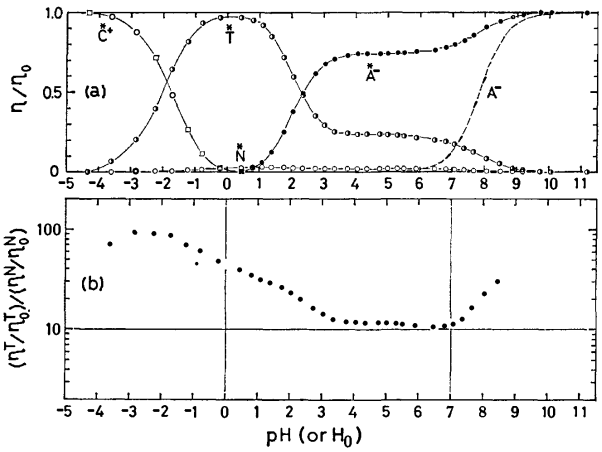

Fig. 5. Relative fluorescence efficiency of the excited species of 7-hydroxy-4-methylcoumarin (**2**) in aqueous solution (6.3×10^{-5} M); $\lambda_{ex}\approx334$ nm; 20 °C. (a) Dependence of the relative efficiency η/η_0 on pH: (○) $\overset{*}{N}$, (●) $\overset{*}{A}^-$, (◑) $\overset{*}{T}$, (□) $\overset{*}{C}^+$. The ground-state equilibration between N and A^- is also indicated by a dashed curve. (b) Dependence of $\overset{*}{K}_t=(\eta^T/\eta_0^T)/(\eta^N/\eta_0^N)$ on pH.

which are the base and acid common to both the neutral molecule and the tautomer. Because of the low concentration of the substrate and the hydroxide ion, and the weak contribution of water as a proton-donating acid, it is inferred, by considering the mechanism of general acid-base catalytic reactions,[17] that, typically, two reaction pathways, *i.e.*, $\overset{*}{N}\rightleftharpoons\overset{*}{A}^-+H^+\rightleftharpoons\overset{*}{T}$ and $\overset{*}{N}+H^+\rightleftharpoons\overset{*}{C}^+\rightleftharpoons\overset{*}{T}+H^+$, are effective for the tautomerization. In the former reaction process, water participates in practice as a proton-accepting base. In addition to the two above-mentioned processes, we have now proposed a direct nondissociative tautomerization process such as $\overset{*}{N}\rightleftharpoons\overset{*}{T}$. Here, the k_t's represent the rate constants for such a nondissociative intramolecular hopping of a hydrogen ion. The mechanism and structural requirements for this type of proton transfer have been studied by Bensaude *et al.*[17] Although their investigation was performed on phenomena in the ground state of molecules, the situation is very similar to our case; the importance of such terms as $\vec{k}_t$ and $\overleftarrow{k}_t$ can be clearly seen by using a rate-equation analysis as will be shown below.

In order to study the reaction kinetics between the ionic species formed in aqueous solutions with various hydrogen-ion concentrations, it was essential to control precisely the pH value over very wide ranges. Each spectrum measured with a given pH value was separated into the respective emission bands, $\overset{*}{N}$, $\overset{*}{A}^-$, $\overset{*}{C}^+$, and $\overset{*}{T}$; then their emission intensity was represented by the relative emission efficiency, η/η_0, in Figs. 4 and 5 rather than by the emission intensity itself, where η is the quantum efficiency of light emission under a given condition and where η_0 is the efficiency when all the molecules are hypothetically of the same species. This relative efficiency is obtainable directly from the ratio of the actual emission intensity, I, and the maximum emission intensity, I_0, the latter being the fluorescence intensity when all the excited molecules are in the single corresponding species. Assuming that the natural lifetime, τ, of the excited molecule and the maximum efficiency, η_0, are independent of the pH value of the solution, the following equation is satisfied under steady-state excitation over the whole pH range:

$$\frac{\eta^N}{\eta_0^N}+\frac{\eta^A}{\eta_0^A}+\frac{\eta^T}{\eta_0^T}+\frac{\eta^C}{\eta_0^C}=1, \qquad (1)$$

where the superscript of η indicates the respective molecular species. Equation 1 is indispensable for the determination of η^N/η_0^N and η^T/η_0^T, because the $\overset{*}{N}$ and $\overset{*}{T}$ bands do not have a pH range in which only the emission from either $\overset{*}{N}$ or $\overset{*}{T}$ is observed, and therefore I_0^N and I_0^T cannot be known directly. The absolute values of η^N/η_0^N and η^T/η_0^T must, then, be consistently determined so as to satisfy Eq. 1 over the whole pH range. The relative emission efficiencies, η/η_0, for the emissimon bands, $\overset{*}{N}$, $\overset{*}{A}^-$, $\overset{*}{T}$, and $\overset{*}{C}^+$, of **1** and **2** are plotted in Figs. 4(a) and 5(a). Excitation was effected at the isosbestic points of **1** and **2**, which are indicated in Figs. 1 and 2 by small arrows. Consequently, the generation rate of the excited molecule was always the same, regardless of species being excited by light absorption, and of course only the neutral molecule could be photo-excited when pH$\leqslant$6. From an inspection of Figs. 4(a) and 5(a), it may be noticed that between pH$\approx$3 and pH$\approx$6 each η/η_0 value is constant. Further, the $\overset{*}{A}^-$ band vanishes if pH$\leqslant$0; instead, the $\overset{*}{C}^+$ band begins to increase, along with the decrease in the pH value. The contribution of the $\overset{*}{T}$ emission to the relative efficiency is larger than that of the $\overset{*}{N}$ emission in the whole pH range. This was first

found by us because we plotted the data not in terms of the emission intensity, but in terms of the relative efficiency. It is noted that the large contribution to the relative efficiency does not always mean a high emission intensity because of the difference in the quantum efficiency of each molecular species.

After all, the fate of the photo-excited 7-hydroxycoumarins can be thoroughly described by the generalized scheme of Fig. 3. In the case of pH$\leqslant$6, where our main concern resides, illuminating light is absorbed solely by neutral molecules, so the generation rates of the molecular species, $\overset{*}{\mathrm{N}}$, $\overset{*}{\mathrm{A}}^-$, $\overset{*}{\mathrm{T}}$, and $\overset{*}{\mathrm{C}}^+$, in the singlet excited-state are expressed as:

$$\frac{\mathrm{d}[\overset{*}{\mathrm{N}}]}{\mathrm{d}t} = G - (n_1+\vec{k}_1+\overleftarrow{k}_3[\mathrm{H}^+]+\vec{k}_t)[\overset{*}{\mathrm{N}}] + \overleftarrow{k}_1[\mathrm{H}^+][\overset{*}{\mathrm{A}}^-] + \vec{k}_3[\overset{*}{\mathrm{C}}^+] + \overleftarrow{k}_t[\overset{*}{\mathrm{T}}], \quad (2)$$

$$\frac{\mathrm{d}[\overset{*}{\mathrm{A}}^-]}{\mathrm{d}t} = -(n_2+\overleftarrow{k}_1[\mathrm{H}^+]+\overleftarrow{k}_2[\mathrm{H}^+])[\overset{*}{\mathrm{A}}^-]+\vec{k}_1[\overset{*}{\mathrm{N}}]+\vec{k}_2[\overset{*}{\mathrm{T}}], \quad (3)$$

$$\frac{\mathrm{d}[\overset{*}{\mathrm{T}}]}{\mathrm{d}t} = -(n_3+\vec{k}_2+\overleftarrow{k}_4[\mathrm{H}^+]+\overleftarrow{k}_t)[\overset{*}{\mathrm{T}}] + \overleftarrow{k}_2[\mathrm{H}^+][\overset{*}{\mathrm{A}}^-] + \vec{k}_4[\overset{*}{\mathrm{C}}^+] + \vec{k}_t[\overset{*}{\mathrm{N}}], \quad (4)$$

$$\frac{\mathrm{d}[\overset{*}{\mathrm{C}}^+]}{\mathrm{d}t} = -(n_4+\vec{k}_3+\vec{k}_4)[\overset{*}{\mathrm{C}}^+]+\overleftarrow{k}_3[\mathrm{H}^+][\overset{*}{\mathrm{N}}]+\overleftarrow{k}_4[\mathrm{H}^+][\overset{*}{\mathrm{T}}], \quad (5)$$

where G is the conversion rate of the neutral molecule to its excited state by the light absorption, and where n_1—n_4, the rates of the deactivation of the excited molecule, are the reciprocals of the lifetimes of $\overset{*}{\mathrm{N}}$, $\overset{*}{\mathrm{A}}^-$, $\overset{*}{\mathrm{T}}$, and $\overset{*}{\mathrm{C}}^+$ respectively. If the steady-state condition is satisfied, we can get the densities of the excited molecules by letting the left-hand side of Eqs. 2—5 be zero, and the relative emission efficiencies are given as:

$$\frac{\eta^{\mathrm{N}}}{\eta_0^{\mathrm{N}}} = \frac{n_1[\overset{*}{\mathrm{N}}]}{G}, \quad \frac{\eta^{\mathrm{A}}}{\eta_0^{\mathrm{A}}} = \frac{n_2[\overset{*}{\mathrm{A}}^-]}{G}, \quad \frac{\eta^{\mathrm{T}}}{\eta_0^{\mathrm{T}}} = \frac{n_3[\overset{*}{\mathrm{T}}]}{G}, \quad \frac{\eta^{\mathrm{C}}}{\eta_0^{\mathrm{C}}} = \frac{n_4[\overset{*}{\mathrm{C}}^+]}{G}. \quad (6)$$

The dependence of η/η_0 on pH predicted by Eq. 6 can be shown to explain extremely well the results in Figs. 4(a) and 5(a). In the relatively high pH region, *i.e.*, pH 4—6, all terms containing $[\mathrm{H}^+]$ become negligible compared with those that do not. This situation can readily be understood by the following consideration. The values of n_1—n_4 are of the order of $10^8\ \mathrm{s}^{-1}$, judging from the fluorescence lifetimes of the excited molecules, which will be discussed later. When the hydrogen-ion concentration $[\mathrm{H}^+]$ is as low as 10^{-4} mol dm^{-3} or less, the terms of $\overleftarrow{k}_{1-4}[\mathrm{H}^+]$ become negligibly small compared with n_{1-4}, because the values of $\overleftarrow{k}_{1-4}$ never exceed the order of the rate constants estimated from diffusion-controlled processes, which are about 10^9—$10^{10}\ \mathrm{mol}^{-1}\ \mathrm{dm}^3\ \mathrm{s}^{-1}$.[18] The appearance of a flat region in the η/η_0 *vs.* pH curves around pH 5 can be consistently explained by these facts. Now, formally letting $[\mathrm{H}^+]\to 0$ in Eqs. 2—5, the limits of the relative efficiencies in the higher pH region are given as:

$$\frac{\eta^{\mathrm{N}}}{\eta_0^{\mathrm{N}}} \to \frac{n_1(n_3+\overleftarrow{k}_t+\vec{k}_2)}{(n_1+\vec{k}_1)(n_3+\overleftarrow{k}_t+\vec{k}_2)+(n_3+\vec{k}_2)\vec{k}_t}, \quad (7)$$

$$\frac{\eta^{\mathrm{A}}}{\eta_0^{\mathrm{A}}} \to \frac{\vec{k}_1(n_3+\overleftarrow{k}_t+\vec{k}_2)+\vec{k}_2\vec{k}_t}{(n_1+\vec{k}_1)(n_3+\overleftarrow{k}_t+\vec{k}_2)+(n_3+\vec{k}_2)\vec{k}_t}, \quad (8)$$

$$\frac{\eta^{\mathrm{T}}}{\eta_0^{\mathrm{T}}} \to \frac{n_3\vec{k}_t}{(n_1+\vec{k}_1)(n_3+\overleftarrow{k}_t+\vec{k}_2)+(n_3+\vec{k}_2)\vec{k}_t}, \quad (9)$$

$$\frac{\eta^{\mathrm{C}}}{\eta_0^{\mathrm{C}}} \to 0. \quad (10)$$

The experimental values obtained from Figs. 4(a) and 5(a), which correspond to Eqs. 7—9 were, at pH 3.5—5.5, $\eta^{\mathrm{N}}/\eta_0^{\mathrm{N}}$:0.020, $\eta^{\mathrm{A}}/\eta_0^{\mathrm{A}}$:0.847, $\eta^{\mathrm{T}}/\eta_0^{\mathrm{T}}$:0.136 for **1**, and $\eta^{\mathrm{N}}/\eta_0^{\mathrm{N}}$:0.021, $\eta^{\mathrm{A}}/\eta_0^{\mathrm{A}}$:0.742, $\eta^{\mathrm{T}}/\eta_0^{\mathrm{T}}$:0.240 for **2**.

It is convenient here to define $\overset{*}{K}_t$ by:

$$\overset{*}{K}_t = \frac{\eta^{\mathrm{T}}/\eta_0^{\mathrm{T}}}{\eta^{\mathrm{N}}/\eta_0^{\mathrm{N}}} = \frac{n_3[\overset{*}{\mathrm{T}}]}{n_1[\overset{*}{\mathrm{N}}]}, \quad (11)$$

which is proportional to the ratio of the concentration of $\overset{*}{\mathrm{T}}$ to the concentration of $\overset{*}{\mathrm{N}}$. Figures 4(b) and 5(b) show the dependence of $\overset{*}{K}_t$ on the pH value. The theoretical expression obtained from Eq. 11 can elucidate fairly well the behavior of $\overset{*}{K}_t$ over a wide pH range. If the hydrogen-ion concentration is so small that the terms containing $[\mathrm{H}^+]$ are negligible in the expression, as before, then Eqs. 7 and 9 give:

$$\overset{*}{K}_t \to \frac{n_3}{n_1}\frac{\vec{k}_t}{n_3+\overleftarrow{k}_t+\vec{k}_2}. \quad (12)$$

The corresponding values of **1** and **2** were, at pH 3.5—5.5, 6 7, and 11.7 respectively.

In the excited state, the protonated carbonyl group of the cation shown in Fig. 3 is a very strong acid comparable with the oxonium ion, $\mathrm{H_3O^+}$ ($\mathrm{p}K_{\mathrm{H_3O^+}} \approx -1.7$), while, in spite of the drastic decrease in the pK of the hydroxyl substituent of the neutral molecule, $\overset{*}{\mathrm{N}}$, with excitation, $\mathrm{p}\overset{*}{K}_{\mathrm{N}}$ remains positive, as will be mentioned later; therefore, the $\mathrm{p}\overset{*}{K}_{\mathrm{C}^+} < \mathrm{p}\overset{*}{K}_{\mathrm{N}}$ relation is satisfied. Combining this inference with the fact that the rate constants for the reaction between charged species with an attractive force, such as $\overleftarrow{k}_1$ and $\overleftarrow{k}_2$, are larger than those without an attractive force, such as $\overleftarrow{k}_3$ and $\overleftarrow{k}_4$,[10] it is naturally assumed that $\overleftarrow{k}_1$ and $\overleftarrow{k}_2$ are much larger than $\overleftarrow{k}_3$ and $\overleftarrow{k}_4$. In the case of Compounds **1** and **2**, as the pH was decreased toward zero, there occurred a pH region around pH 0 where the terms of $\overleftarrow{k}_1[\mathrm{H}^+]$ and $\overleftarrow{k}_2[\mathrm{H}^+]$ become very large, but the terms of $\overleftarrow{k}_3[\mathrm{H}^+]$ and $\overleftarrow{k}_4[\mathrm{H}^+]$ are still negligible compared with the other rate constants. The limiting value of $\overset{*}{K}_t$ calculated from Eq. 11 is written:

$$\overset{*}{K}_t \approx \frac{n_3}{n_1}\frac{\vec{k}_t+\vec{k}_1\overleftarrow{k}_2/(\overleftarrow{k}_1+\overleftarrow{k}_2)}{n_3+\overleftarrow{k}_t+\vec{k}_2\overleftarrow{k}_1/(\overleftarrow{k}_1+\overleftarrow{k}_2)}. \quad (13)$$

The experimental values of $\overset{*}{K}_t$ around pH 0 were $\approx$20 for **1** and $\approx$40 for **2**.

When the solution becomes most acidic, such as when $H_0 \leqslant -3$, the effective concentration of the hydrogen-ion [H^+] is formally taken to be more than 10^3 mol dm^{-3},[8] so the terms of $\overleftarrow{k}_{1-4}[H^+]$ dominate all the other rate constants. Therefore, within such a limit, we have:

$$\overset{*}{K}_t \to \frac{n_3}{n_1}\frac{\overleftarrow{k}_3}{n_4+\vec{k}_3}\frac{\vec{k}_4}{\overleftarrow{k}_4}. \quad (14)$$

The experimental values of **1** and **2** corresponding to this condition were, for $H_0 \leqslant -3$, $\approx$43, and $\approx$92 respectively.

If the reaction pathway represented by $\vec{k}_t$ and $\overleftarrow{k}_t$ does not exist, the limiting value of $\overset{*}{K}_t$ in the high pH region apparently becomes zero, as $\vec{k}_t \to 0$ in Eq. 12. This contradicts the experimental fact that there is in reality no pH region having a zero value of $\overset{*}{K}_t$ as may be seen in Figs. 4(b) and 5(b). Therefore, we must admit the existence of a tautomerization mechanism unrelated to the general acid-base catalyzed scheme. Further, it may be noted that, by comparing Eq. 12 with Eq. 13, the limiting value of $\overset{*}{K}_t$ in the lower pH region can be predicted theoretically to be larger than that in the higher pH region, as is again clearly shown in the results (Figs. 4(b) and 5(b)) between pH 0 and 6. Corresponding to this change in $\overset{*}{K}_t$, η^T/η^T_0 as a function pH has its maximum at about pH 0 and a flat region between pH 3 and 6. Around pH 0, the contribution from η^A/η^A_0, like as that from η^C/η^C_0, becomes nearly zero; on the contrary, the contribution from η^T/η^T_0 becomes nearly unity, although that from η^N/η^N_0 still small. Toward the highest-concentration region of the hydrogen-ion, η^C/η^C_0 increases and reaches unity at the end, since the terms of $\overleftarrow{k}_3[H^+]$ and $\overleftarrow{k}_4[H^+]$ overcome all other terms. Parallel with the change in η^C/η^C_0, $\overset{*}{K}_t$ increases when pH (or H_0) decreases from 0 to -3. This increase is rather accidental, as there is no relation in magnitude between the values of Eqs. 13 and 14. In contrast to these results, the rise in $\overset{*}{K}_t$ and the approach of η^A/η^A_0 to unity toward a pH higher than 6 is caused by another situation, because the amount of the anionic molecule in the ground state becomes large at pH>6; therefore, the assumption used above—that only the neutral molecule is excited from the ground state—must be changed. Although this modification is simple and straightforward, we would not here be concerned with this matter further.

Mechanism for Tautomerization. In earlier studies[4-7] only the dissociative processes such as $\overset{*}{N} \rightleftarrows \overset{*}{A}^- + H^+ \rightleftarrows \overset{*}{T}$ were emphasized for the tautomeric interconversion of the excited molecule; however, this led to erroneous conclusions about the reaction mechanism in the case of 7-hydroxycoumarins. From a careful consideration of $\overset{*}{K}_t$ as a function of the pH, we have come to the conclusion that the direct conversion between the neutral molecule and the tautomeric molecule which proceeds without generating dissociated ionic species as an intermediate, *i.e.*, $\overset{*}{N} \rightleftarrows \overset{*}{T}$, is most essential in the tautomerization reaction. In view of the results of the investigation of Bensaude *et al.*,[17] the most probable model for the origin of the nondissociative process represented by the $\vec{k}_t$ and $\overleftarrow{k}_t$ terms is a concerted bifunctional proton-transfer through water molecules, as is described schematically in Fig. 6. The existence of such a tautomerization process is strongly supported by the following discussion. In general, substituents to aromatic and heteroaromatic compounds can be classified in two types of groups.[18] One is composed of substituents that become more acidic in the excited state than in the ground state, such as hydroxyl and amino groups. The other is composed of substituents that become more basic in the excited state, such as carbonyl and carboxyl groups. In the case of 7-hydroxycoumarins, this tendency makes the transfer of a proton from the hydroxyl group to the carbonyl group very easy in their electronic excited-state. Because of the ability of water to form chains of hydrogen bonds and the Grotthus-type migration of the proton (or proton-hole) along the chain,[19] the proton transfer between the two active sites in a molecule can be promoted cooperatively and the interconversion of the neutral form to the tautomeric form can occur without liberating any proton or ionic species to an outside region of the molecule which is hydrated by participating water molecules. Because this type of proton jump in the molecule is considered to proceed at an extremely high velocity in comparison with other reaction rates, no intermediate species can appear in the rate-equation formulation; instead, the rate constants which represent the direct conversion between the neutral molecule and the tautomeric molecule, *i.e.*, $\vec{k}_t$ and $\overleftarrow{k}_t$, appear.

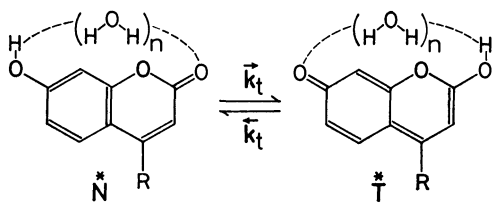

Fig. 6. Concerted mechanism for the tautomerization of 7-hydroxycoumarins in the excited state.

Such a mechanism of tautomerization is also expected for lower alcohols, but the effect will be weaker in that case because the hydrogen bond is much weaker than that of water and the motion of the proton is highly restricted. It has been pointed out by several authors[1-5,7] that the addition of a small amount of water to alcoholic solutions of 7-hydroxycoumarins induced a very large effect on the fluorescent behavior of the excited molecule. As it has become clear that the tautomerization of 7-hydroxycoumarins proceeds through the proton transfer between two sites in the molecule and is accelerated by the participation of water molecules, the reported increase in the ratio of the emission intensity of $\overset{*}{T}$ to that of $\overset{*}{N}$ with an

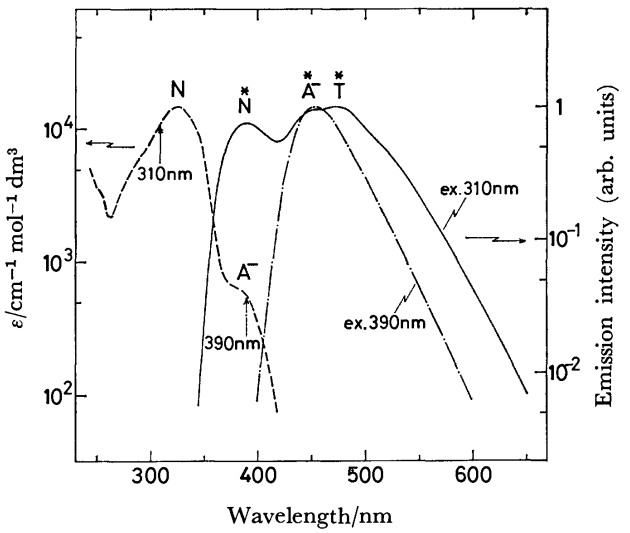

Fig. 7. Absorption and fluorescence spectra of 7-hydroxycoumarin (**1**) in ethanol–water solution (90:10 vol%).
The fluorescence spectra are obtained by using the excitation wavelength at 310 nm (——) and 390 nm (—·—).

increased water content[4,7] is considered to arise from the increase in the value of $\vec{k}_t$, not from the increased rate of the $\overset{*}{N} \rightleftharpoons \overset{*}{A}^- + H \rightleftharpoons \overset{*}{T}$ reaction. This prediction is distinctly proved by the result shown in Fig. 7. From the absorption spectrum of 7-hydroxycoumarin (**1**) it was found, in neutral solutions of ethanol–water mixtures, that both the neutral and the anionic molecule existed in the ground state, as may be seen from Fig. 7. By choosing an appropriate excitation wavelength, it was possible to excite separately either the neutral or the anionic molecule. If the neutral molecule alone was excited by using the wavelength of 310 nm, three of the fluorescence bands, *i.e.*, $\overset{*}{N}$, $\overset{*}{A}^-$, and $\overset{*}{T}$, were obtained simultaneously. On the other hand, only the fluorescence band of $\overset{*}{A}^-$ was detectable if the anionic molecule was excited by using the wavelength of 390 nm. The results are summarized in the following scheme:

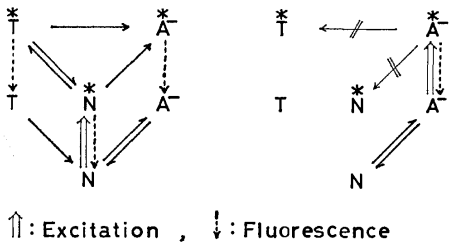

As may easily be recognized from this scheme, the reaction pathway $\overset{*}{N} \rightarrow \overset{*}{A}^- + H^+ \rightarrow \overset{*}{T}$ cannot exist in the ethanol–water solution because the $\overset{*}{A}^- + H^+ \rightarrow \overset{*}{T}$ reaction is forbidden in reality and the $\overset{*}{N} \rightarrow \overset{*}{T}$ pathway alone can generate the tautomeric form of the molecule. The same conclusion was obtained for 7-hydroxy-4-methylcoumarin (**2**).

If the dependence of the rate constants on the water concentration in alcohol–water solutions is approximately written:

$$\vec{k}_t = \vec{k}_t'[H_2O], \quad \overleftarrow{k}_t = \overleftarrow{k}_t'[H_2O],$$
$$\vec{k}_1 = \vec{k}_1'[H_2O], \quad \vec{k}_2 = \vec{k}_2'[H_2O], \tag{15}$$

then, at a low hydrogen-ion concentration (pH 3—6), the ratios of $[\overset{*}{A}^-]$ and $[\overset{*}{T}]$ to $[\overset{*}{N}]$ are given by Eqs. 7—9 as:

$$\frac{n_2[\overset{*}{A}^-]}{n_1[\overset{*}{N}]} \propto \frac{\vec{k}_t'[H_2O](n_3+\overleftarrow{k}_t'[H_2O]+\vec{k}_2'[H_2O])+\vec{k}_2'[H_2O]\vec{k}_t'[H_2O]}{n_1(n_3+\overleftarrow{k}_t'[H_2O]+\vec{k}_2'[H_2O])}, \tag{16}$$

$$\overset{*}{K}_t = \frac{n_3[\overset{*}{T}]}{n_1[\overset{*}{N}]} \propto \frac{n_3\vec{k}_t'[H_2O]}{n_1(n_3+\overleftarrow{k}_t'[H_2O]+\vec{k}_2'[H_2O])}. \tag{17}$$

In the low-concentration region of the water content where $n_3 \gg \overleftarrow{k}_t'[H_2O]$, $\vec{k}_2'[H_2O]$, $[\overset{*}{T}]/[\overset{*}{N}]$ varies linearly with the water concentration, while $[\overset{*}{A}^-]/[\overset{*}{N}]$ increases superlinearly with the increase in the water component, since the numerator of Eq. 16 has a quadratic term of $[H_2O]$. These predictions explain reasonably well the fluorescence behavior of **1** and **2** in alcohol–water solutions, including the results in Refs. 4 and 7. In this manner, the dependence of η/η_0 and $\overset{*}{K}_t$ on the pH was completely described by the formulation of Eqs. 2—5. Above all, it was impossible to explain the behavior of $\overset{*}{K}_t$ if the terms of $\vec{k}_t$ and $\overleftarrow{k}_t$ were not introduced. Further, the dependence of the relative intensity of $\overset{*}{N}$, $\overset{*}{A}^-$, and $\overset{*}{T}$ in aqueous alcoholic solutions on the water content can be understood in terms of Eqs. 16 and 17 if we admit the assumption of Eq. 15.

Fluorescence Lifetimes and Energy-level Considerations. In order to argue about the rate constants that appear in Eqs. 7—14, it is necessary to know the lifetime, τ, which is the reciprocal of the deactivation rate of the excited molecule, n. Table 1 shows the values of the lifetime measured under various solvent conditions at the wavelength of the emission peak of each molecular species. In the case of the anionic and cationic molecular forms, the lifetime measurement was performed when the luminescence from a single molecular species was observable, and so the measured lifetimes τ_A and τ_C naturally correspond to the true lifetimes of the excited state of the anionic and cationic molecular species. On the other hand, $\bar{\tau}_{TN}$ and $\bar{\tau}_{NT}$ indicate the apparent decay times of the fluorescence from $\overset{*}{T}$ and $\overset{*}{N}$ respectively when they coexist at around pH 0. $\bar{\tau}_{NAT}$ is also the apparent decay time of the excited neutral molecule when it coexists with the anionic and tautomeric forms at around pH 4. In the first-order approximation, they are written:

$$\frac{1}{\bar{\tau}_{NT}} = n_1 + \vec{k}_t, \tag{18}$$

Table 1. Lifetimes of the fluorescent molecular species

Substance	τ_C/ns	τ_A/ns	$\bar{\tau}_{TN}$/ns[a]	$\bar{\tau}_{NT}$/ns[a]	$\bar{\tau}_{NAT}$/ns[a]
1	5.8	5.4	4.6	4.5	1.7
2	5.9	5.5	4.9	3.2	1.6

a) The meanings of $\bar{\tau}_{TN}$, $\bar{\tau}_{NT}$, and $\bar{\tau}_{NAT}$ are described in the text.

Table 2. Separations of the energy levels and changes in the thermodynamical functions

Substance	ΔE_N [a] / kcal mol^{-1}	ΔE_A [a] / kcal mol^{-1}	ΔE_T [b] / kcal mol^{-1}	ΔE_C [b] / kcal mol^{-1}	ΔH_{NA} / kcal mol^{-1}	ΔS_{NA} / cal mol^{-1} K^{-1}
1	80.11	70.60	67.61	74.13	4.29	-21.0_4
2	81.17	71.56	67.93	75.97	4.16	-21.8_1

a) Obtained from the absorption and fluorescence data, and accurate within ± 0.1 kcal mol^{-1}. b) Inferred from the fluorescence data, and accurate within ± 0.5 kcal mol^{-1}.

$$\frac{1}{\bar{\tau}_{TN}} = n_3 + \overleftarrow{k}_t, \tag{19}$$

$$\frac{1}{\bar{\tau}_{NAT}} = n_1 + \vec{k}_t + \vec{k}_1. \tag{20}$$

By the use of Eqs. 18 and 20 and the values in Table 1, it can readily be known that $\vec{k}_1$ is 3.7×10^8 s^{-1} for **1** and 3.1×10^8 s^{-1} for **2**. The dissociation constant, $p\overset{*}{K}_{NA}$, corresponding formally to the excited-state equilibrium between $\overset{*}{N}$ and $\overset{*}{A}^-$ can be calculated by the method outlined by Weller as:[18]

$$p\overset{*}{K}_{NA} = pK_{NA} - \frac{\Delta E_N - \Delta E_A}{2.303RT}, \tag{21}$$

where ΔE_N and ΔE_A are the energy-level separations between the singlet ground-state and the singlet excited-state of the neutral and anionic species and are obtainable as the mean of the energies at the absorption-band and emission-band maxima.[20] These values are listed in Table 2, together with ΔE_T and ΔE_C, the energy-level separations for the tautomeric and cationic species, which in this case are inferred from only the emission-band maximum assuming that the Stokes shift is the same for all molecular species. Using the values of ΔE_N and ΔE_A in Table 2, and also pK_{NA}, $p\overset{*}{K}_{NA}$ is calculated to be 0.66 for **1** and 0.68 for **2** at 20 °C. Since the equilibrium constant in the excited state is defined by $\overset{*}{K}_{NA}=\vec{k}_1/\overleftarrow{k}_1$, we get $\overleftarrow{k}_1$ of **1** and **2** as 1.7×10^9 s^{-1} mol^{-1} dm^3 and 1.5×10^9 s^{-1} mol^{-1} dm^3 respectively.

ΔH_{NA} and ΔS_{NA} in Table 2 are the enthalpy and entropy changes in the $N\rightleftharpoons A^-+H^+$ reaction; they were obtained by the measurement of the temperature dependence of pK_{NA} with the aid of the thermodynamical relation: $K=\exp[-(\Delta H-T\Delta S)/RT]$. If we can neglect the change in the PV term of the relation, $H=E+PV$, the enthalpy change, ΔH, is equated to the energy change, ΔE. Considering these facts and the values in Table 2, the energy-level scheme of the reacting molecular species of 7-hydroxycoumarins around pH 3—5 can roughly be drawn as Fig. 8. Since $\Delta E_N+\Delta\overset{*}{H}_{NA}=\Delta E_A+\Delta H_{NA}$, the values of $\Delta\overset{*}{H}_{NA}$ for the $\overset{*}{N}\rightleftharpoons\overset{*}{A}^-+H^+$ reaction are -5.22 kcal mol^{-1} for **1** and -5.45 kcal mol^{-1} for **2**. Putting together

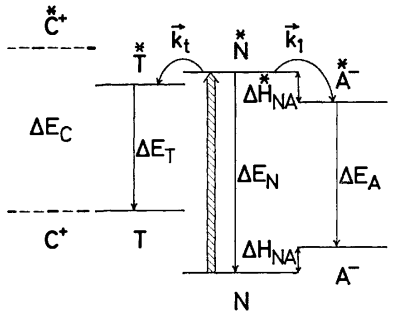

Fig. 8. Energy level diagram of 7-hydroxycoumarins in the weakly acidic solution (pH 3—5). The hatched arrow shows the photo-excitation of N into $\overset{*}{N}$. The levels of C^+ indicated by dashed lines do not take part in the reaction in this pH range.

all the results discussed so far, the interrelation of the energy levels between the neutral and anionic molecules was firmly determined, as is shown in Fig. 8. Although the energy position of the tautomer and the cation relative to that of the neutral molecule could not determined strictly, the energy levels are presumably ordered as $N<A^-\ll C^+$, T in the ground state and as $\overset{*}{A}^-<\overset{*}{T}<\overset{*}{N}<\overset{*}{C}^+$ in the excited state.

Unfortunately, several rate constants defined in Fig. 3 have left unknown because of a lack of information about the reaction process. The main reason for this uncertainty must be sought in the impossibility of transforming the neutral molecule into the tautomeric form in the ground state under any condition of solvents different from the case of the 7-hydroxyquinolines. Therefore, we cannot know about the ground-state equilibration between the neutral and tautomeric molecules, and the direct excitation of the tautomer by light absorption is never possible. In spite of this unfavorable situation, though we are now trying to analyze the decay properties of the excited species over the whole pH range which is controllable. This procedure, which will be described thoroughly in a forthcoming paper, would provide more detailed information about the rate constant and the reaction mechanism.

I wish to thank Dr. Hiroyuki Anzai of this laboratory for his helpful advice and stimulating discussions during the course of this work.

References

1) M. R. Groves, S. C. Haydon, and O. M. Williams, *Opt. Commun.*, **9**, 42 (1973).
2) A. Dienes, C. V. Shank, and R. L. Kohn, *IEEE J. Quantum Electron.*, **QE-9**, 833 (1973).
3) A. Bergman and J. Jortner, *J. Lumin.*, **6**, 390 (1973).
4) P. E. Zinsli, *J. Photochem.*, **3**, 55 (1974/75).
5) G. S. Beddard, S. Carlin, and R. S. Davidson, *J. Chem. Soc., Perkin Trans. 2*, **1977**, 262.
6) S. G. Schulman and L. S. Rosenberg, *J. Phys. Chem.*, **83**, 447 (1979).
7) R. K. Bauer and A. Kowalczyk, *Z. Naturforsch., A*, **35**, 946 (1980).
8) M. A. Paul and F. A. Long, *Chem. Rev.*, **57**, 1 (1957).
9) C. Lewis and W. R. Ware, *Rev. Sci. Instrum.*, **44**, 107 (1973).
10) A. Weller, *Z. Phys. Chem., N.F.*, **3**, 238 (1955).
11) To be published in detail in *Bull. Electrotech. Lab.*
12) H. Beens, K. H. Grellman, M. Gurr, and A. H. Weller, *Discuss. Faraday Soc.*, **39**, 183 (1965).
13) S. F. Mason, *J. Chem. Soc.*, **1959**, 1253.
14) S. F. Mason, J. Philip, and B. E. Smith, *J. Chem. Soc., A*, **1968**, 3051.
15) J. R. Huber, M. Nakashima, and J. A. Sousa, *J. Chem. Phys.*, **77**, 860 (1973).
16) J. Grzywacz, S. Taszner, and J. Kruszewski, *Z. Naturforsch., A*, **33**, 1307 (1978).
17) O. Bensaude, M. Dreyfus, G. Dodin, and J. E. Dubois, *J. Am. Chem. Soc.*, **99**, 4438 (1977).
18) A. Weller, *Prog. React. Kinet.*, **1**, 189 (1961).
19) M. Eigen and L. de Maeyer, "The Structure of Electrolytic Solutions," ed by W. J. Hamer, John Wiley & Sons, London (1959), p. 64.
20) W. Bartok, P. J. Lucchesi, and N. S. Snider, *J. Am. Chem. Soc.*, **84**, 1842 (1962).

Cathodic Reduction of Ubiquinone-10 Dissolved in Carbon-paste Electrode

Tatsuo ERABI* and Masaya TANAKA

Department of Industrial Chemistry, Faculty of Engineering, Tottori University, Koyama, Tottori 680

(Received April 19, 1982)

Carbon-paste electrodes were prepared with use of ubiquinone-10 dissolved in organic liquids, 1-chloronaphthalene, 1-bromonaphthalene, 1-methylnaphthalene and undecane. Ubiquinone-10 shows a well-defined, pH-dependent cathodic reduction wave in each liquid system and its reduction seems to proceed with two electrons and a proton transfer around neutral pH. The experimental results indicate the wave to be diffusion-controlled, and the apparent diffusion coefficient was additionally calculated in each liquid system.

It is generally accepted[1] that ubiquinones and the reduction products take part in the formation of pH gradient across chromatophore membrane, that is indispensable for ATP production, in addition to the role as an electron pool in the photosynthetic electron transport system. Moreover, it has become apparent[2-7] that ubiquinones also function as primary or secondary electron acceptors in the photosynthetic reaction centers. The majority of ubiquinones bound to chromatophores are reduced with two electrons and two protons transfer[8] around neutral pH, but in the case of primary or secondary acceptor, it was suggested that they were reduced with an electron transfer to form corresponding semiquinones,[7,9] similar to a cathodic reduction in an aprotic nonaqueous solvent.[10] Although most of these studies have been carried out by means of analyzing their absorbance[8,9] and/or EPR spectrum,[7] disadvantages of these methods may be that its absorbance and difference spectra are not so distinctive, and the measurements should be carried out at temperature as low as liquid nitrogen in order to sharpen the spectra. On the other hand, electrochemistry provides essentially the knowledge on oxidation-reduction properties of a material of interest. On this viewpoint, we studied electrochemically the reduction of ubiquinone-10 in an aqueous ethanol[11,12] and in a SDS micelle[12] as a model of chromatophore membrane, and all of these reductions seemed to proceed with two electrons transfer. A cyclic voltammetric study of ubiquinone-10 bound to chromatophores was also carried out,[11] but the reaction mechanism is not clear yet because of the difficulty of mass transfer in the suspension. Usually, use of a carbon-paste electrode has been limited to aqueous solutions because of flowing the paste. But, this limitation, as applied to water-insoluble, electroactive organic compounds, can be circumvented by dissolving these organics in electrode itself.[13] In addition, a carbon-paste electrode dissolving ubiquinone-10 is supposed to mimic chromatophore membrane, most of ubiquinones being present at membrane-water interface.[11] So, we report a cathodic behavior of ubiquinone-10 dissolved in a carbon-paste electrode, prior to elucidating the reactivities of ubiquinone-10 bound to chromatophores.

Experimental

Ubiquinone-10 was extracted and purified by the usual method.[14,15] The exactly weighed ubiquinone-10 was dissolved in 1 cm^3 of an organic solvent (1-chloronaphthalene, 1-bromonaphthalene, 1-methylnaphthalene or undecane), 1.7 g of graphite was then added and mixed until the carbon appeared uniformly wetted. The paste was stored in water for a few days at 4 °C. A working electrode was prepared by packing the Teflon cavity (ϕ 2.56 mm × 0.24 mm depth) with the paste, smoothing the surface with a filter paper and removing excess paste from the edge surface of the Teflon with tissue paper. After each measurement, it was necessary to remove all of the paste in which the concentration of ubiquinone-10 had been changed by electrolysis, and the cavity was washed with petroleum ether. Commercially obtained ferrocene was further purified chromatographically on an alumina column with spectroscopic-quality hexane as eluent, and then recrystallized from redistilled methanol. Ferrocene thus purified was used for preparation of a carbon-paste electrode in a similar manner as above, and a peak current for ferrocene oxidation was measured for comparison of specific limiting currents.[16]

A conventional H-type cell was used with the working electrode and a saturated calomel reference electrode located in the main compartment. A platinum disk electrode was served as auxiliary electrode in the other compartment. Buffer solutions of various pH values were prepared with 0.6 mol/dm^3 GTA–HCl or GTA–NaOH.[12] Dissolved oxygen in this solution was removed by bubbling nitrogen for 30 min before electrolysis, and the electrolysis was carried out at 25 °C. A current-potential curve was recorded using a potentiostat PS-1000, a linear potential scanning unit LS-1D (Hokuto Denko Ltd.) and a Hitachi Model 056 recorder. Potential sweep rate was 250 mV/min unless otherwise noted. A coulometric measurement was carried out at a peak potential for ubiquinone-10 reduction controlled by a Hokuto Model HA-104 potentiostat using a working electrode packed with a known weight of carbon-paste containing ubiquinone-10 until the electrolytic current decreased to 1—2% of the initial current. Usually, 100 min of the electrolytic time was required, and the quantity of electricity was measured using a coulometer HF-201 (Hokuto Denko Ltd.).

Results and Discussion

Current-potential curves of ubiquinone-10 dissolved in carbon-paste electrodes always showed typical well-defined, pH-dependent reduction waves. Table 1 shows a comparison of specific limiting currents[16] for ferrocene oxidation and ubiquinone-10 reduction dissolved in 1-chloronaphthalene at pH 7.0. Since the oxidation of ferrocene is known to proceed with one electron transfer,[13] the total number of electrons transferred in ubiquinone-10 reduction can be determined by comparing the both specific limiting currents. The results suggest that the reduction proceeds with two electrons transfer. This presumption is supported by a coulometric measurement summa-

TABLE 1. COMPARISON OF SPECIFIC LIMITING CURRENTS FOR FERROCENE OXIDATION AND UBIQUINONE-10 REDUCTION AT pH 7.0

Exptl No.	$I_{SL}/\mu A\ mmol^{-1}\ dm^3\ cm^{-2}$ a)		Ratio
	Ferrocence oxidation b)	Ubiquinone-10 reduction b)	
1	2.67	−5.34	
2	2.31	−5.58	
3	2.31	−5.44	
	av. 2.43	av. −5.45	2.24

a) I_{SL} is specific limiting current. b) The both concentrations in 1-chloronaphthalene were kept constant at 4.0×10^{-2} mol/dm^3, and potential sweep rate was 250 mV/min. Similar results were obtained in the other liquids.

TABLE 2. COULOMETRIC DATA FOR UBIQUINONE-10 REDUCTION IN 1-CHLORONAPHTHALENE

Exptl No.	Weight of carbon-paste/mg a)	Q/mC		
		Calculated as $n=1$	Measured	Ratio
1	3.8	4.94	8.85	1.79
2	3.6	4.68	7.35	1.57
3	3.3	4.29	6.94	1.62

a) The ubiquinone-10 concentration was kept constant at 4.0×10^{-2} mol/dm^3. Controlled potential electrolyses were carried out for 100 min at −260 mV *vs.* NHE. Similar results were obtained in the other liquids.

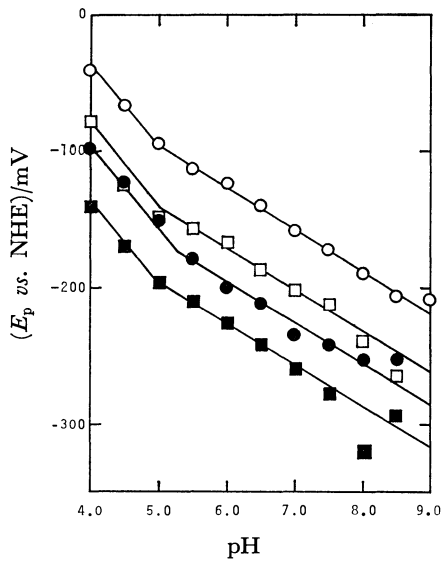

Fig. 1. Plots showing the pH dependence of the peak potentials for ubiquinone-10 reduction.
Symbols in this figure represent the data in each organic liquid as follows: ■; 1-chloronaphthalene, ●; 1-bromonaphthalene, □: 1-methylnaphthalene, or ○; undecane. Potential sweep rate was 250 mV/min. Ubiquinone-10 concentration was 4×10^{-2} mol/dm^3 in each liquid.

rized in Table 2 in which the ratio of measured quantity of electricity to calculated one assuming the number of electrons transferred was 1, could be shown to be about 2. When the plots showing the pH dependence of the peak potentials for ubiquinone-10 reduction were made with each pasting liquid; 1-chloronaphthalene, 1-bromonaphthalene, 1-methylnaphthalene or undecane (Fig. 1), the slope of the straight lines was −60 mV/pH in the more acidic than about pH 5.0 and −30 mV/pH in the more basic region. Therefore, the number of protons transferred is estimated to be 2 in the more acidic than about pH 5.0 and to be 1 in the more basic region because the number of electrons transferred from the electrode is presumed to be 2 from the comparison of the specific limiting currents and the coulometric data. By titrating with mixture of succinate and fumarate, and determining the redox state of ubiquinone-10 spectrophotometrically, Kakuno *et al.*[8] measured a midpoint potential of +23 mV for the endogenous ubiquinone-10 of chromatophore membrane. The reduction was two electrons process, coupled to the uptake of one proton per electron around neutral pH. Our present data indicate the reduction occurs in two electrons transfer, and as expected, ubiquinone-10 dissolved in the carbon-paste seems to be in the similar environment to most of those bound to chromatophore membrane rather than that in an aprotic nonaqueous solvent.[10] However, its reduction potential is quite different from that bound to chromatophores. The peak potentials of ubiquinone-10 reduction at pH 7.0 were −260 mV with 1-chloronaphthalene, −240 mV with 1-bromonaphthalene, −205 mV with 1-methylnaphthalene and −160 mV with undecane, respectively. These potentials in the organic liquids are fairly lower than that in chromatophores even considering that the reaction is totally irreversible electron transfer process, because the transfer coefficient was calculated to be 0.2—0.3 from the slope of Tafel plots. Since Loach[17] reported that the redox potential of ubiquinones became more negative in the more hydrophobic medium, it seems possible that the microenvironment around ubiquinone-10 molecule in chromatophore membrane is more hydrophilic than that in the organic liquids. In any event, the reduction of ubiquinone-10, though that is the reaction in a model system, was first characterized electrochemically in the present study to the best of our knowledge except those in acetonitrile[10] and ethanolic solution.[11,12,18] Studies of the redox properties of the components in photosynthetic and other biological electron transport systems, such as those in nitrogen fixation and oxidative phosphorylation, are very important to the understanding of the reaction mechanism.[19] Especially, the knowledge of the redox potential levels and the number of electrons and protons transferred of the electron carriers in the photosynthetic electron transport system has greatly aided in the assessment of their physiological functions. That is, for instance, determining the phosphorylation sites along the photosynthetic electron transport system because the energy necessary for ATP synthesis must come from the free energy derived from the potential difference and the proton concentration gradient across the biological membrane.[20] So, the development of

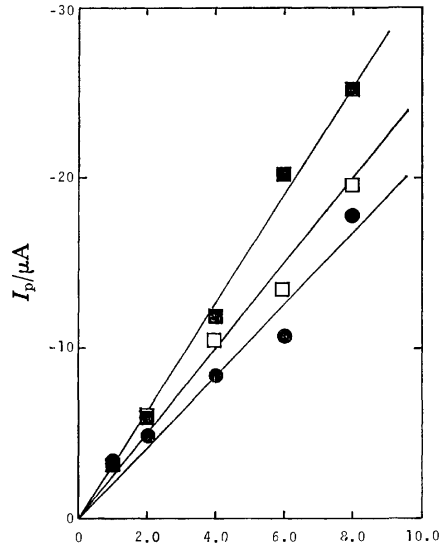

Fig. 2. Relationship of peak current to ubiquinone-10 concentration.
Symbols and experimental conditions are the same as those in Fig. 1, except that ubiquinone-10 concentration is varied and the solution pH is kept constant at 7.0.

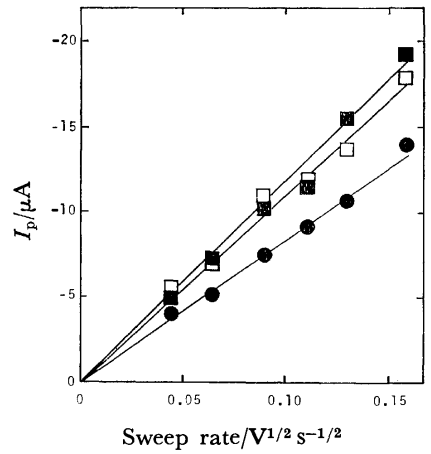

Fig. 3. Relationship of peak current to the square root of potential sweep rate.
Symbols and experimental conditions are the same as those in Fig. 1, except that the potential sweep rate is varied and the solution pH is at 7.0.

other new better model system of chromatophore membrane is still necessary to elucidate clearly the role of ubiquinone-10 in the photosynthetic electron transport system.

In addition, the reduction mechanism of ubiquinone-10 in the organic liquids was briefly examined. The linear relationship of peak current to varying concentration of ubiquinone-10 was observed with each pasting liquid (Fig. 2), and the peak current was proportional to the square root of the potential sweep rate (Fig. 3). It is evident from these results that the observed wave is due to the reduction of ubiquinone-10 itself, and the mass transfer rate is governed by diffusion from the paste. If mass transfer rate is

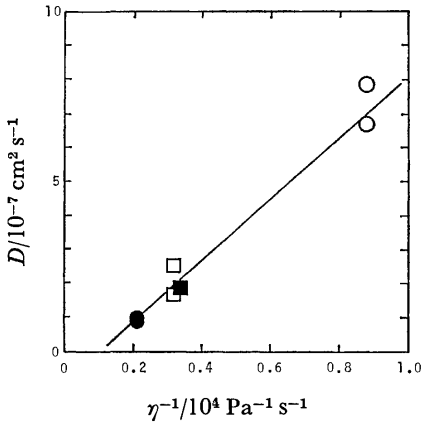

Fig. 4. Relationship of diffusion coefficient to the viscosity of pasting liquids.
Symbols are the same as those in Fig. 1, and values of viscosity are cited from the literture.[13]

governed by diffusion, the viscosity of the pasting liquid should affect this rate and consequently peak current. The Stokes-Einstein relation predicts a linear relationship between the diffusion coefficient and the reciprocal of viscosity. The diffusion coefficient was calculated by an ordinary method,[21,22] and the plots of D *vs.* $1/\eta$, as shown in Fig. 4, are linear but cannot extrapolate to the origin. Since the actual, effective concentration in the pasting liquid is not known, the calculated values of the diffusion coefficient must be considered as apparent values.

This series of studies has been supported by Grants-in-Aid for Scientific Research (No. 511609 and 56112009) from the Ministry of Education, Science and Culture.

References

1) C. A. Wraight, R. J. Cogdell, and B. Chance, "The Photosynthetic Bacteria," ed by R. K. Clayton and W. R. Sistrom, Plenum Press, New York (1978), Chap. 26.
2) P. A. Loach and R. L. Hall, *Proc. Natl. Acad. Sci. U.S.A.*, **69**, 786 (1972).
3) G. Feher, M. Y. Okamura, and J. D. McEroy, *Biochim. Biophys. Acta*, **267**, 222 (1972).
4) R. K. Clayton and S. C. Straley, *Biophys. J.*, **12**, 1221 (1972).
5) L. Slooten, *Biochim. Biophys. Acta*, **272**, 208 (1972).
6) A. Vermeglio, *Biochim. Biophys. Acta*, **459**, 516 (1977).
7) C. A. Wraight, *Biochim. Biophys. Acta*, **459**, 525 (1977).
8) T. Kakuno, K. Hosoi, T. Higuti, and T. Horio, *J. Biochem.*, **74**, 1193 (1973).
9) A. Vermeglio and R. K. Clayton, *Biochim. Biophys. Acta*, **461**, 159 (1977).
10) M. F. Marcus and M. D. Hawley, *Biochim. Biophys. Acta*, **226**, 234 (1971).
11) T. Erabi, T. Higuti, T. Kakuno, J. Yamashita, M. Tanaka, and T. Horio, *J. Biochem.*, **78**, 795 (1975).
12) T. Erabi, H. Hiura, and M. Tanaka, *Bull. Chem. Soc. Jpn.*, **48**, 1354 (1975).
13) F. A. Schltz and T. Kuwana, *J. Electroanal. Chem.*, **10**, 95 (1965).
14) W. W. Parson and H. Rudney, *J. Biol. Chem.*, **240**, 1855 (1965).

15) S. Okayama, N. Yamamoto, K. Nishikawa, and T. Horio, *J. Biol. Chem.*, **243**, 2995 (1968).
16) R. N. Adams, "Electrochemistry at Solid Electrodes," Marcel Dekker, New York (1969), Chap. 2.
17) P. A. Loach, "Progress in Bioorganic Chemistry," Wiley Interscience, New York (1976), Vol. 4, p. 89.
18) V. Moret, S. Pinamonti, and E. Fornasari, *Biochim. Biophys. Acta*, **54**, 381 (1961).
19) M. Hawkridge and B. Ke, *Anal. Biochem.*, **78**, 76 (1977).
20) H. T. Witt, E. Schlodder, and Gräber, *FEBS Lett.*, **69**, 272 (1976).
21) Chap. 5 in Ref. 16.
22) R. S. Nicholson and I. Shain, *Anal. Chem.*, **36**, 706 (1964).

 © 1983 The Chemical Society of Japan Bull. Chem. Soc. Jpn., 56, 19—21 (1983)

Arrhenius Parameters for the Reactions of Hydrogen and Deuterium Atoms with Four Butenes

Takeshi KYOGOKU, Toshifumi WATANABE, Shigeru TSUNASHIMA, and Shin SATO*,†

Department of Applied Physics, Tokyo Institute of Technology, Ookayama, Meguro-ku, Tokyo 152

† *Research Laboratory for Nuclear Reactors, Tokyo Institute of Technology, Ookayama, Meguro-ku, Tokyo 152*

(Received April 27, 1982)

The absolute rate constants of the H and D atom addition to 1-butene, *cis*- and *trans*-2-butenes, and isobutene have been measured over the temperature range 200—500 K at the total pressure of about 600 Torr (1 Torr= 133.3 Pa). The rate constants obtained were well expressed by the Arrhenius equations: $k(\mathrm{H}+1\text{-butene})=(2.48\pm0.43)\exp[-(1492\pm94)/RT]$, $k(\mathrm{H}+cis\text{-2-butene})=(2.67\pm0.39)\exp[-(1918\pm83)/RT]$, $k(\mathrm{H}+trans\text{-2-butene})=(3.96\pm0.27)\exp[-(2096\pm37)/RT]$, $k(\mathrm{H}+\text{isobutene})=(2.08\pm0.16)\exp[-(860\pm49)/RT]$, $k(\mathrm{D}+1\text{-butene})=(2.42\pm0.72)\exp[-(1642\pm169)/RT]$, $k(\mathrm{D}+cis\text{-2-butene})=(2.25\pm0.19)\exp[-(2082\pm48)/RT]$, $k(\mathrm{D}+trans\text{-2-butene})=(2.33\pm0.23)\exp[-(2036\pm55)/RT]$, and $k(\mathrm{D}+\text{isobutene})=(1.54\pm0.19)\exp[-(879\pm81)/RT]$ in units of 10^{-11} cm^3 molecule^{-1} s^{-1}. The isotope effects due to the difference between H and D atoms can simply be explained by the difference in collision frequency. The difference between *cis*- and *trans*-2-butenes in reactivity may be explained in terms of the pre-exponential factors.

The reactions of hydrogen atoms with olefins have long been a subject for chemical kinetics. Twenty years ago, the relative rate constants of addition of hydrogen atoms to a number of simple olefins at room temperature were measured by Jennings and Cvetanović, who used a photochemical competitive technique.[1] Since then, several different experimental approaches were devised for the determination of these relative rate constants, and some disparities in the rate constants were reported.[2,3]

In the last decade, new techniques such as flash photolysis,[4] pulse radiolysis,[5] and a phase shift method[6] were introduced for the determination of the absolute rate constants of simple reactions. Consequently, the absolute rate constants as well as their temperature dependence for a number of simple reactions have been accumulated and are awaiting theoretical analysis. Absolute rate constants of hydrogen atom addition to olefins have also been measured.[7] A few years ago, our laboratory used the pulse radiolysis-resonance absorption technique for the determination of the rate constants of these reactions[8] and confirmed that the relative rate constants reported by Jennings and Cvetanović are the most reliable among earlier measurements.

The temperature dependence for these rate constants, however, has not been reported except for the reaction $\mathrm{H}+\mathrm{C_2H_4}\rightarrow\mathrm{C_2H_5}$. In the preceding paper,[9] we reported the temperature dependence for the reaction $\mathrm{H}+\mathrm{C_3H_6}\rightarrow\mathrm{C_3H_7}$; therefore, we have extended our measurement to the reactions with four butenes: 1-butene, *cis*- and *trans*-2-butenes, and isobutene.

It is well known that among simple mono-olefins at room temperature isobutene is the most reactive to hydrogen atoms. This is probably because the activation energy for this reaction is the smallest; however, the absolute value has not been reported. On the other hand, in many free radical addition reactions, *trans*-2-butene is often found to be about 10% more reactive than *cis*-2-butene;[10] therefore, it may be worthwhile to know whether this difference in the hydrogen atom addition reaction comes from its activation energy or from the pre-exponential factor.

Experimental

The experimental procedure is the same as described in a previous paper.[11] The mixture of about 600 Torr hydrogen or deuterium and a small amount of an olefin (0.01—0.1 Torr) was pulse-irradiated with high energy electrons from a Febetron 706 (Hewlett Packard) and the decay of the concentration of hydrogen or deuterium atoms was followed by the absorption of the Lyman-α radiation.

1-Butene, *cis*- and *trans*-2-butenes, and isobutene were purchased from the Takachiho Shoji Co. and used as supplied. Gas-chromatographic analysis using a 5 m long column packed with dimethyl sulpholane on celite showed that impurities in each butene are less than 1%.

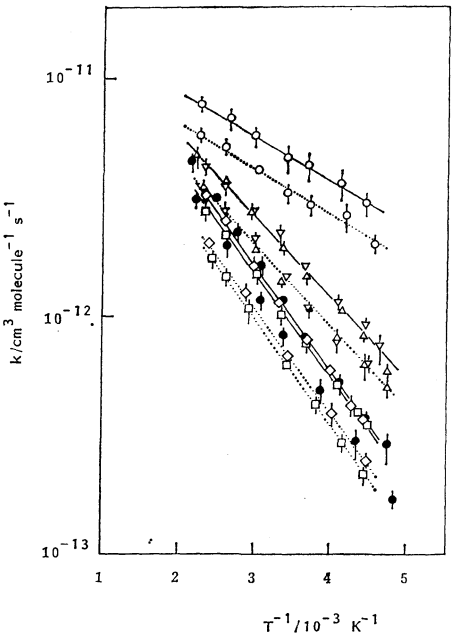

Fig. 1. Arrhenius plots for the reactions of H and D atoms with olefins: (●) ethylene, (△) propylene, (▽) 1-butene, (□) *cis*-2-butene, (◇) *trans*-2-butene, and (○) isobutene.
Solid lines for H atom reactions and dotted lines for D atom reactions.

TABLE 1. RATE CONSTANTS OF H OR D ATOM ADDITION TO C_4 OLEFINS
Uncertainties are 2σ.

Reaction	T/K	$k/10^{-12}$ cm^3 molecule^{-1} s^{-1}	Reaction	T/K	$k/10^{-12}$ cm^3 molecule^{-1} s^{-1}
H+1-Butene	426	4.12±0.32	H+*trans*-2-Butene	423	3.22±0.46
	379	3.56±0.42		379	2.49±0.26
	331	2.66±0.36		333	1.65±0.20
	299	2.19±0.31		299	1.15±0.14
	272	1.60±0.09		269	0.783±0.066
	244	1.10±0.06		249	0.585±0.053
	223	0.914±0.096		233	0.414±0.059
	216	0.730±0.145		225	0.365±0.035
D+1-Butene	428	3.10±0.52	D+*trans*-2-Butene	421	2.03±0.13
	383	2.75±0.41		348	1.26±0.12
	334	2.13±0.12		292	0.679±0.057
	292	1.49±0.17		248	0.394±0.051
	272	1.09±0.08		225	0.244±0.014
	245	0.778±0.070	H+Isobutene	438	7.69±0.44
	222	0.625±0.055		375	6.69±0.61
H+*cis*-2-Butene	423	2.73±0.37		335	5.64±0.43
	380	2.16±0.19		293	4.60±0.88
	330	1.49±0.15		270	4.34±0.46
	297	1.00±0.05		242	3.53±0.60
	270	0.764±0.061		225	2.95±0.33
	243	0.500±0.048	D+Isobutene	447	5.78±0.23
	227	0.390±0.036		390	5.12±0.33
	221	0.356±0.043		333	4.06±0.06
D+*cis*-2-Butene	412	1.74±0.16		295	3.28±0.37
	382	1.47±0.13		270	2.95±0.24
	341	1.05±0.15		240	2.65±0.23
	292	0.612±0.039		221	2.02±0.35
	262	0.423±0.030			
	241	0.288±0.027			
	226	0.215±0.024			

TABLE 2. ARRHENIUS PARAMETERS FOR THE REACTIONS OF H AND D ATOMS WITH C_4 OLEFINS
$A/10^{-11}$ cm^3 molecule^{-1} s^{-1} and E/cal mol^{-1}. Uncertainties are 2σ.

Olefin	H-Atom addition		D-Atom addition	
	A	E	A	E
1-Butene	2.48±0.43	1492±94	2.42±0.72	1642±169
cis-2-Butene	2.67±0.39	1918±83	2.25±0.19	2082±48
trans-2-Butene	3.96±0.27	2096±37	2.33±0.23	2036±55
Isobutene	2.08±0.16	860±49	1.54±0.19	879±81

Results

Table 1 summarizes the rate constants obtained at various temperatures. Each rate constant was estimated as the average of four to five measurements. Figure 1 shows the Arrhenius plots. For comparison, the rate constants obtained with ethylene and propylene are also plotted. All data are well expressed by the Arrhenius equations. The Arrhenius parameters calculated by the least squares method[12] are summarized in Table 2.

Discussion

Isotope Effects Due to the Difference between H and D Atoms and the Tunneling Effect. Figure 1 clearly shows that Arrhenius plots for H and D atom reactions with the same olefin are always parallel and the interval is nearly constant irrespective of the kind of reactant olefin. This fact can simply be explained by the difference in collision frequency as follows:[13]

$$k_H/k_D \approx \left[\frac{m_D m_{olefin}}{m_D + m_{olefin}}\right]^{1/2} \Big/ \left[\frac{m_H m_{olefin}}{m_H + m_{olefin}}\right]^{1/2} \cong \sqrt{2}.$$

Here k_H and k_D are the rate constants of the H and D atom reactions. m_H, m_D, and m_{olefin} are the masses

Table 3. Relative values of pre-exponential factors

Olefin	H-Atom addition	D-Atom addition
Ethylene	(2.0)	(2.0)
Ethylene-d_4	1.94	2.11
cis-2-Butene	1.14	1.34
trans-2-Butene	1.69	1.39
Propylene	1.28	1.18
Propylene-d_6	1.09	1.31
1-Butene	1.05	1.44
Isobutene	0.89	0.92

of H and D atoms and olefin molecules, respectively.

In the hydrogen atom-molecule reaction, $H+H_2 \rightarrow H_2+H$, the Arrhenius plots deviated from linearity at temperatures lower than 300 K and the deviation showed a strong H/D isotope effect.[14] This result has been attributed to the tunneling effect. In the present reaction systems, however, no such deviation from linearity could be observed within experimental error. Although a slightly concave curve can be realized in the Arrhenius plot for the reaction of $H+C_2H_4 \rightarrow C_2H_5$, this is also found in the reaction of $D+C_2D_4 \rightarrow C_2D_5$; therefore, this curvature cannot be attributed to the isotope effect.

The Number of Reaction Site and the Difference in Reactivity between cis- *and* trans-*2-Butenes.* It is now well known that in the reactions of unsymmetric olefins such as propylene, 1-butene, and isobutene, a hydrogen atom adds to the less substituted carbon atom of the double bond. In other words, there is only one reaction site. On the other hand, symmetric olefins such as ethylene and 2-butenes have two identical reaction sites. In the simple collision theory, the difference in the number of reaction sites should appear in the pre-exponential factors. Table 3 compares the relative values for the pre-exponential factors. Although the exact ratio between symmetric and unsymmetric olefins is not clearly determined, the expected trend can be observed.

Another noticeable point in Table 3 is the difference between *cis*- and *trans*-2-butenes. Although the experimental errors prevent us from estimating the quantitative ratio, the difference in reactivity between *cis*- and *trans*-2-butenes may be attributed to the difference in the pre-exponential factors. If methyl radical substitution restricts the reaction zone for an attacking hydrogen atom, unrestricted spaces on two carbons at both sides of the double bond may overlap with each other in the case of *cis*-2-butene, but not in the case of *trans*-2-butene. This difference probably corresponds to the difference in the pre-exponential factors.

Atom Localization Energies. When Jennings and Cvetanović measured the relative rate constants of H atom addition to a series of simple olefins, they compared the logarithms of the rate constants with the atom localization energies of the olefins, which were calculated by the simple Hückel method on the assumption of hyperconjugation, and obtained a linearity.[1] However, it is obvious that the atom localization energies should be compared with the activation energies. Figure 2 shows this comparison. A linear relation has been obtained as expected.

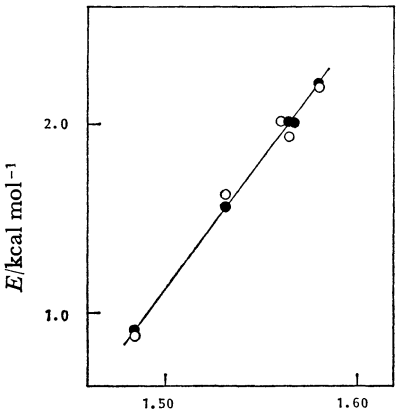

Fig. 2. Correlation between activation energies (○ for H atom reactions and ● for D atom reactions) and atom localization energies of olefins.

The atom localization energy is a very rough concept. A more sophisticated treatment is highly desirable.

References

1) K. R. Jennings and R. J. Cvetanović, *J. Chem. Phys.*, **35**, 1233 (1961).
2) K. Yang, *J. Am. Chem. Soc.*, **84**, 3795 (1962).
3) G. R. Woolley and R. J. Cvetanović, *J. Chem. Phys.*, **50**, 4697 (1969).
4) R. B. Klemm and L. J. Stief, *J. Chem. Phys.*, **61**, 4900 (1974).
5) T. Hikida, J. A. Eyre, and L. M. Dorfman, *J. Chem. Phys.*, **54**, 3422 (1971).
6) R. Atkinson and R. J. Cvetanović, *J. Chem. Phys.*, **55**, 659 (1971).
7) K. Oka and R. J. Cvetanović, *Can. J. Chem.*, **57**, 777 (1979).
8) Y. Ishikawa, M. Yamabe, A. Noda, and S. Sato, *Bull. Chem. Soc. Jpn.*, **51**, 2488 (1978).
9) T. Watanabe, T. Kyogoku, S. Tsunashima, S. Sato, and S. Nagase, *Bull. Chem. Soc. Jpn.*, **55**, 3720 (1982).
10) R. J. Cvetanović and R. S. Irwin, *J. Chem. Phys.*, **46**, 1694 (1967).
11) K. Sugawara, K. Okazaki, and S. Sato, *Bull. Chem. Soc. Jpn.*, **54**, 2872 (1981).
12) R. J. Cvetanović, R. P. Overend, and G. Paraskevopoulos, *Int. J. Chem. Kinet.*, **S1**, 249 (1975).
13) Y. Ishikawa and S. Sato, *Bull. Chem. Soc. Jpn.*, **52**, 984 (1979).
14) A. A. Westenberg and N. deHaas, *J. Chem. Phys.*, **47**, 1393 (1967).

The Corrosion Inhibition of SS 41 Steel by Shoyu Oil

Isao SEKINE* and Masahiro ASAZUMA

Faculty of Science and Technology, Science University of Tokyo, Yamazaki, Noda, Chiba 278

(Received May 6, 1982)

The addition of shoyu (soy sauce) oil to an NaCl solution for use as a corrosion inhibitor of SS 41 steel was investigated by measuring the corrosion weight loss, the polarization curve, the polarization resistance, and the impedance of the metal-solution interface. The value of the weight loss and the double-layer capacitance, C_{dl}, decreased as the shoyu oil was added to NaCl solutions of various concentrations. The value of the corrosion current density, I_{corr}, as calculated from the weight loss, the polarization curve, and the impedance measurement, decreased with an increase in the concentration of shoyu oil. An efficient inhibition of the corrosion of SS 41 steel was observed above an additive concentration of about 0.3%. Thus, the shoyu oil was found to be useful as a corrosion inhibitor of an economical and anti-pollution type. From the results of the IR analysis, the inhibition of the shoyu oil was considered to be caused by the adsorption of fatty acids, especially unsaturated fatty acids involved in the shoyu oil.

It has been reported by Markina and Misler that the sodium soaps of synthetic fatty acids of C_5—C_6, C_{10}—C_{16}, and C_{17}—C_{20} are effective as corrosion inhibitors of 12Khl MF steel, which is a material used for boilers.[1] The corrosion-inhibition effect by the adsorption of amine salts of oleic acid on iron in 0.5 M H_2SO_4 (1 M=1 mol dm^{-3}) has been discussed by Szauer and Brandt.[2,3] According to some articles,[4-6] fatty acid with C_{16}–C_{18} atoms has been considered as exerting the most effective inhibition. Such a corrosion-protection effect is caused by the adsorption of the anion of fatty acid or the cation of amine. The adsorption in this case is known to obey the Frumkin or Temkin isotherm. Further, the adsorption of fatty acid shows a tendency to increase with an increase in the length of the aliphatic chain, while the inhibition effect shows a tendency to decrease with an increase in the number of the double bond of fatty acid.[2,3]

In the present work, we examined the use of shoyu oil added to an NaCl solution as a corrosion inhibitor of metal, for example, SS 41 steel. Since this oil is a by-product of shoyu production and a mixture of five kinds of natural fatty acids with C_{16}—C_{18} atoms, it was expected to be useful and economical as a corrosion inhibitor of an anti-pollution type. Thus, the inhibition effect of the shoyu oil was investigated by measuring the weight loss, the polarization curve, the interfacial impedance, and the polarization resistance in a neutral NaCl solution. From the results obtained, it was found that the shoyu oil inhibits the corrosion of SS 41 steel sufficiently and can be used satisfactorily as an inhibitor of corrosion by cooling water and industrial water. The corrosion inhibition of shoyu oil was considered, from the results of the IR reflection spectrum, to be caused by the adsorption of the anion of fatty acid.

Experimental

Materials. The shoyu oil used as a corrosion inhibitor was from intact soybeans and defatted soybeans. Since these shoyu oils are insoluble in water, soluble sodium salts of them were prepared according to the procedure shown in Fig. 1. The sodium salt of shoyu oil from intact soybeans is abbreviated as SSOI, and the sodium salt of shoyu oil from defatted soybeans, as SSOD. The compositions of these SSOI and SSOD are shown in Table 1. This table shows that the shoyu oils consist of about 80% unsaturated fatty acids and of about 20% saturated fatty acids. The concentrations of the NaCl solutions used as blank solutions were 0.003, 0.03, 0.3, and 3%. The concentrations of these inhibitors were 0.1, 0.3, 0.5, and 1.0% respectively. Before each run, all the solutions were sufficiently aerated and adjusted to pH 7. The specimen used was SS 41 steel.

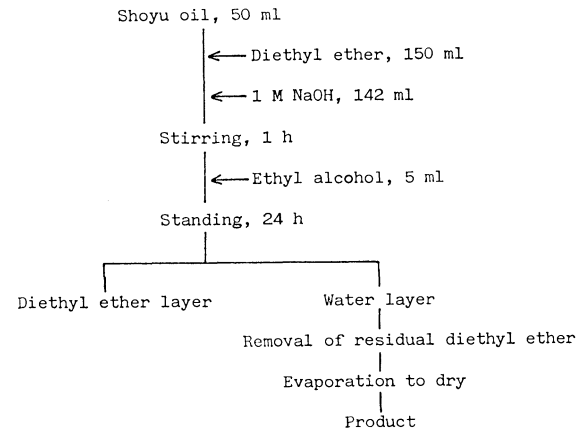

Fig. 1. Preparation of sodium salt of shoyu oil.

TABLE 1. COMPOSITIONS OF SSOI AND SSOD

Sodium salt of fatty acid	SSOI(%)	SSOD(%)
$C_{15}H_{31}COONa$	10.7	16.7
$C_{17}H_{35}COONa$	9.2	6.1
$C_{17}H_{33}COONa$	17.6	27.8
$C_{17}H_{31}COONa$	55.2	45.7
$C_{17}H_{29}COONa$	7.4	3.7

Weight-loss Measurement. The specimen sheet of 25×60×0.5 mm was immersed in the test solution for five weeks at room temperature. Before use, the specimen was abraded with emery papers from No. 240 to No. 1200, and successively washed with distilled water, methanol, and acetone. In the corrosion weight-loss test at high temperature, the weight loss of the specimen was measured after the specimen had been immersed in a test solution maintained at 95 °C for 3 d. The boiling point of the test solution was 95 °C.

Polarization Measurement. A specimen wire 1 mm in diameter was covered with a mixture of paraffin wax and pine resin, and only the cross-section of the specimen was used. The counter electrode was a platinum wire, while the potential was measured with reference to a saturated calomel electrode (SCE). The polarization potentials were scanned from the cathodic region to the anodic region.

Impedance Measurement. The specimen used was the same as that used in the polarization measurement. The corrosion potential, E_{corr}, of the test electrode was stabilized 1—2 h after immersion. Thus, the measurements of the impedance were started when the E_{corr} value was stabilized. In the frequency range of 2 kHz—1 Hz, a lock-in amplifier (NF Circuit Design Block; model LI-574) was used, while in the frequency range of 1 Hz—0.006 Hz, Lissajou's method was used.

Polarization-resistance Measurement. A specimen rod 4 mm in diameter was covered with pine resin except for the bottom 30 mm. The measurement was made by using a corrosion-rate meter (Hokuto Denko; model HK-103). The frequency and time of measurement were 0.1 Hz and 110 h respectively.

IR Analysis. Before the IR analysis, the specimen sheet taken out from the test solution to measure its corrosion weight loss was vacuum-dried for about 30 min. The angle of incidence was 12°, and the number of reflections was one.

Results and Discussion

The weight loss against the concentration of SSOI is shown in Fig. 2. As may be seen in this figure, the value of the weight loss was lowered with an increase in the concentration of SSOI and held constant in concentrations more than 0.3%. Such a tendency was also seen for SSOD. In any concentration of NaCl solution used, the surface of test pieces in the blank solution became dark brown, and then a reddish-brown precipitate in the solution was observed. However, the test pieces immersed in solutions with concentration over 0.3% of SSOI and 0.5% of SSOD kept the same silvery metallic luster as before immersion. Such a surface state may be seen in Photo 1.

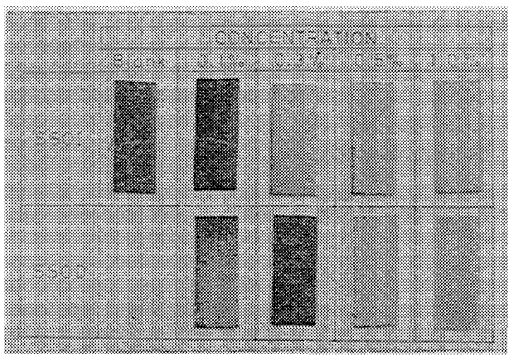

Photo 1. Surface state of specimen after corrosion weight loss for various concentrations of SSOI and SSOD in 3% NaCl solution at room temperature.

Figure 3 shows a comparison between the shoyu oil and other inhibitors. Sodium benzoate (SB) and sodium *p-t*-butylbenzoate (SBB) have been used as corrosion inhibitors for a long time. As can be seen from this figure, the outstanding inhibitive effectiveness at a concentration over 0.3% of SSOI added to a 0.003% NaCl solution was comparable to that of SB and SBB.

Table 2 shows the results of the weight-loss test at 95 °C from the viewpoint of practical utilization. In general, when an inhibitor is used, the adjustment

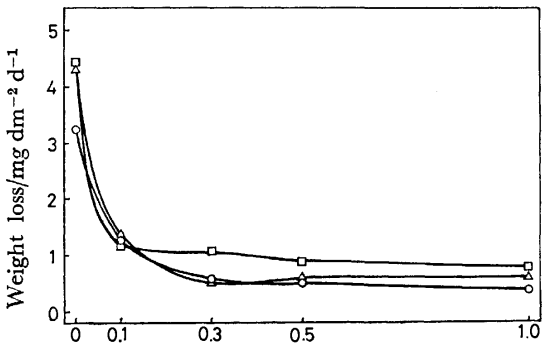

Fig. 2. Corrosion weight loss *vs.* concentration of SSOI curves in various concentrations of NaCl solution. —○—: 0.03%, —△—: 0.3%, —□—: 3%.

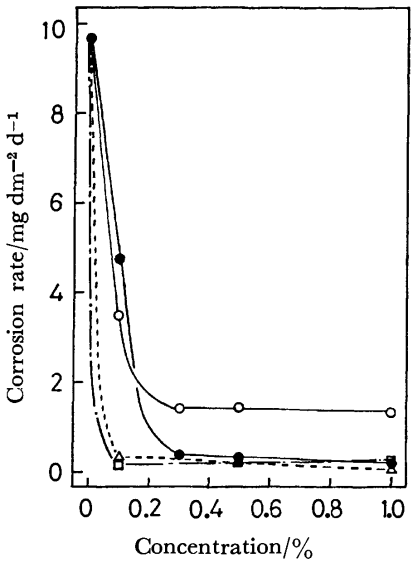

Fig. 3. Corrosion weight loss *vs.* concentration of various inhibitors in 0.003% NaCl solution. —○—: SSOD, —●—: SSOI, --△--: SB, -·-□-·-: SBB.

Table 2. Corrosion weight loss at 95 °C

	Solution	pH	Weight loss / mg dm^{-2} d^{-1}
Blank	0.003% NaCl	7.00	26.5
Natural	0.1% SSOI	10.28	3.67
	0.5% SSOI	10.72	0.87
	1% SSOI	10.90	0.22
	1% SSOD	11.10	2.32
Synthetic	1% SSOI	9.66	8.72
	1% SSOD	9.90	6.65
Comparative	1% $C_{15}H_{31}COONa$	10.03	0.74
	1% $C_{17}H_{35}COONa$	10.15	3.37
	1% $C_{17}H_{33}COONa$	10.30	8.94
	1% $C_{17}H_{31}COONa$	10.15	9.67
	1% $C_{17}H_{29}COONa$	10.55	1.68
	1% C_6H_5COONa	11.00	1.01
	1% $C_5H_{11}COONa$-C_4H_9COONa	6.62	13.4

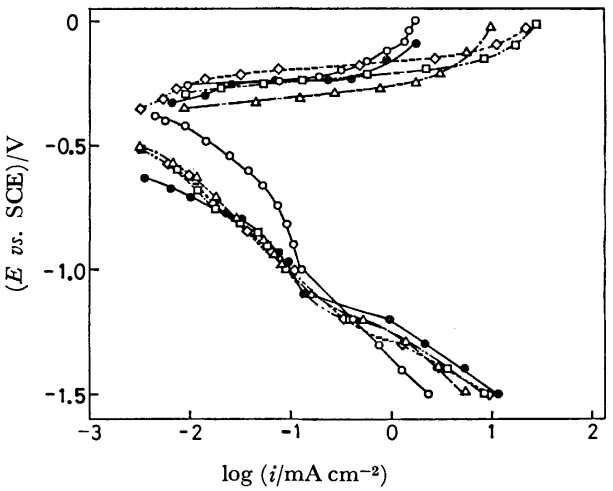

Fig. 4. Polarization curves for SSOD in 0.003% NaCl solution.
—○—: Blank, -·-△-·-: 0.1% SSOD, -·-□-·-: 0.3%, --◇--: 0.5%, —●—: 1.0%.

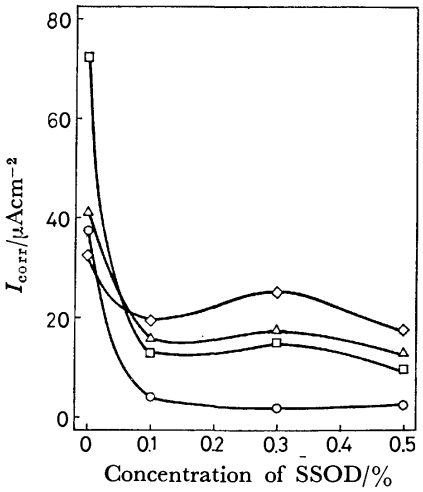

Fig. 5. I_{corr} *vs.* concentrations of SSOD curves in various concentrations of NaCl solution.
—○—: 0.003%, —△—: 0.03%, —□—: 0.3%, —◇—: 3%.

of the pH is very troublesome. Consequently, all runs at 95 °C were carried out without adjusting the pH. This table further compares the natural shoyu oil as a by-product, the synthetic shoyu oil prepared by mixing all the components of Table 1, sodium salt of five fatty acids containing the components of shoyu oil, and the fatty acids with C_5–C_6 atoms reported by Markina *et al.*[1] As can be seen in this table, among all the inhibitors under investigation, natural SSOI is the most efficient. The natural SSOD is less effective than SSOI, as can be seen from Photo 1. However, it seems that both SSOI and SSOD are efficient corrosion inhibitors in view of the utilization of by-products.

The polarization curves for SS 41 steel in a 0.003% NaCl solution containing SSOD are shown in Fig. 4. The current density of the cathodic process decreases with an increase in the concentration of SSOD, and the E_{corr} shifts to the direction of the cathodic

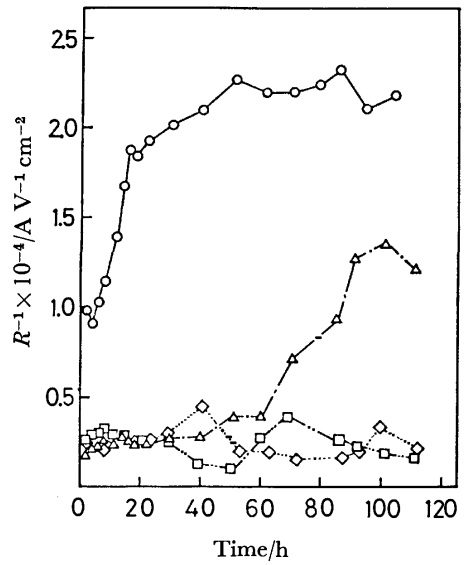

Fig. 6. $1/R$ *vs.* time curves in 0.003% NaCl solution.
—○—: Blank, -·-△-·-: 0.1% SSOI, -·-□-·-: 0.3%, --◇--: 1.0%.

region. In general, when oxygen is dissolved in a neutral solution, the corrosion rate is determined by the limiting current density due to oxygen reduction. The decrease in the cathodic current density with an increase in the concentration of inhibitors indicates a lowering of the corrosion rate.

The relationship between the I_{corr} value and the concentration of SSOD is shown in Fig. 5. At each concentration of NaCl solutions, the I_{corr} value can be seen to decrease with an increase in the concentration of SSOD. Consequently, the SSOD is regarded as a good corrosion inhibitor. However, the I_{corr} value shows something of a tendency to increase at the concentration of 0.3% of SSOD. Since the determination of I_{corr} from the polarization curves is arbitrary, such a tendency may be attributed to the method of drawing the line.

Figure 6 shows the time dependence of $1/R$, which is the quantity corresponding to the corrosion rate ($I_{corr}=K/R$). The value of $1/R$ decreases with an increase in the concentration of SSOI. Especially at a concentration over 0.3% of SSOI, it is seen to be lowered for a long time. A similar result was also obtained for SSOD. From these results, it is considered that both SSOI and SSOD are fairly sufficient inhibitors.

Some typical results of impedance measurements at E_{corr} are shown in Fig. 7. In a high-frequency region, the loci of the circular arcs are seen to be a part of a semicircle whose center is shifted under the real axis. On the other hand, straight lines with a slope of about 45° are obtained in the low-frequency region. The charge-transfer resistance, R_{ct}, obtained by the extraporation of a part of the semicircle to the real axis was about 850 Ω at the blank solution and about 1 kΩ at the solution with 0.3% SSOD added. The straight lines in the low-frequency region seem to be based on the diffusion of oxygen, because all the solutions used are aerated before each run. Consequent-

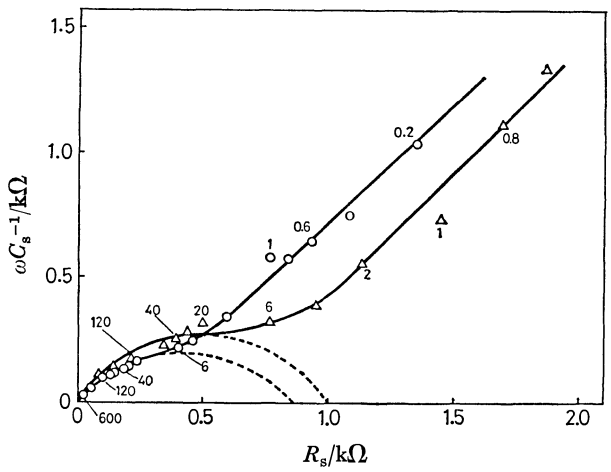

Fig. 7. Complex impedance plane plot at E_{corr} in 3% NaCl solution.
—○—: Blank, —△—: 0.3% SSOD.

Table 3. Comparison of the results obtained in a 3% NaCl solution

SSOD %	Impedance measurement R_{ct} Ω	Impedance measurement C_{dl} μF cm^{-2}	Impedance measurement I_{corr} μA cm^{-2}	Weight loss I_{corr} μA cm^{-2}	$i-E$ curve I_{corr} μA cm^{-2}
0	850	3980	1290	106.0	35
0.1	950	2130	1160	29.1	19
0.3	1000	1010	1100	18.9	26
0.5	1080	470	1020	17.4	17

ly, the diffusion process of oxygen is the rate-determining step. The value of C_{dl} calculated from Fig. 7 was about 4000 μF/cm^2 at the blank solution and about 1000 μF/cm^2 at 0.3% SSOD.

Table 3 shows the values of R_{ct}, C_{dl}, and I_{corr} against each concentration of SSOD. It can be seen that the R_{ct} value increases with an increase in the concentration of SSOD, while the C_{dl} value decreases. When the R_{ct} values, that is, the reaction resistance of corrosion, becomes greater, the SSOD seems to be the better inhibitor. On the other hand, the decrease in C_{dl} can be seen to be based on a reduction of the surface area of the specimen by a corrosion inhibitor. This can be explained by means of a Helmholtz parallel-plate condenser model:[7]

$$C_{dl} = C_H = \varepsilon(S/d),$$

where C_H is the Helmholtz capacity; S, the area of the condenser plates opposite to each other; d, the distance between the condenser plates, and ε, the dielectric constant. These results seem to be evident, for the SSOD leads to an efficient inhibition with an increase in the concentration of SSOD. Further, the values of I_{corr}, as calculated from the polarization curve, correspond very well with those calculated from the weight loss. However, these I_{corr} values differ very much from those calculated from the impedance measurement. This discrepancy can be ascribed to the fact that the determination of R_{ct} is very difficult, because the center of the semicircle obtained is shifted under the real axis. Therefore, the I_{corr} value with respect to R_{ct} may be considered to admit of further argument.

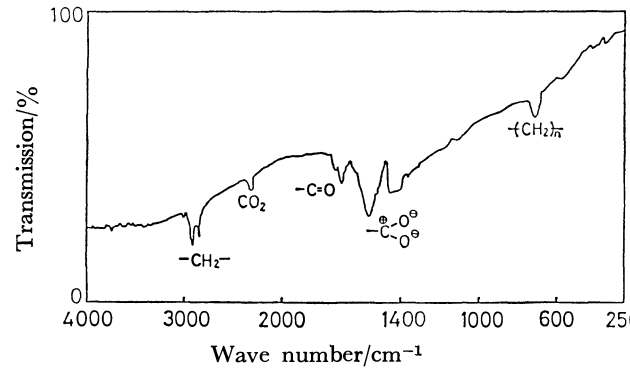

Fig. 8. Result of reflection type IR spectrum in 0.3% NaCl solution with 0.3% SSOD.

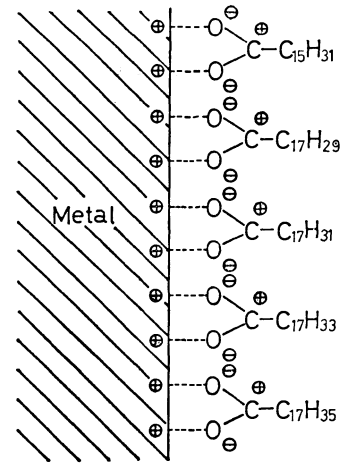

Fig. 9. Adsorption model of SSOI and SSOD.

The inhibition mechanism of SSOI was examined by means of infrared analysis. An example of the spectrum of the IR reflection type is shown in Fig. 8. It shows the spectrum of a specimen immersed for 3 d in a 0.3% NaCl solution containing 0.3% SSOI. In the IR spectrum, the two peaks at 2850 and 2900 cm^{-1} represent the stretching vibration of -C-H of the methylene group; the peak at 1700 cm^{-1}, that of aliphatic carboxylic acid; the two peaks from 1400 to 1600 cm^{-1}, that of the carboxylate ion, and the peak at 700 cm^{-1}, the rocking vibration of the polymethylene chain. Consequently, the adsorption model of SSOI and SSOD is roughly represented in Fig. 9. According to Szauer and Brandt,[2] when the unsaturated fatty acids of C_{18} were used as corrosion inhibitors, the effect of corrosion inhibition is related to the number of the double bond of fatty acid, and the inhibition effect decreases with an increase in the number of the double bond in the order of oleic acid> linoleic acid>linolenic acid. This is considered to be caused by the influence of π electrons in the double bond. In the present study, the adsorption seems to occur in two steps.[8] At first, the hydrophilic carboxylate ions adsorb on the metal surface. Subsequently, the hydrophobic alkyl groups are vertically oriented to the metal surface toward the bulk solution. How-

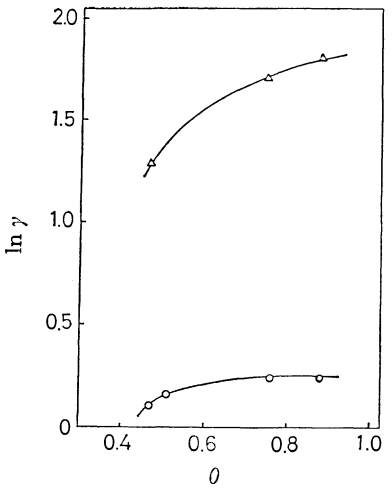

Fig. 10. Dependence of logarithm of inhibition coefficient on surface coverage for iron dissolution.
—○—: Impedance measurement, —△—: weight loss.

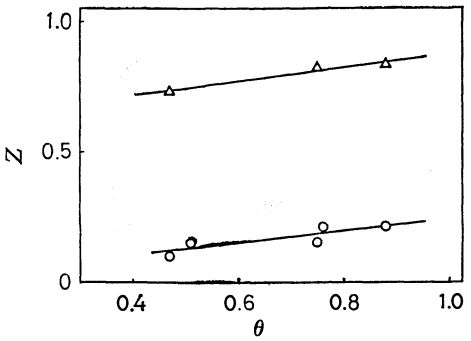

Fig. 11. Inhibition efficiency of iron dissolution *vs.* surface coverage.
—○—: Impedance measurement, —△—: weight loss.

ever, when the double bond is involved in fatty acid, the alkyl groups are bent to the metal surface by the influence of π electrons in the double bond, and then corrosive chemical species (Cl^-, O_2, H_2O, *etc.*) come near to the metal surface. Therefore, it is considered that the inhibition effect decreases with an increase in the number of double bonds. As may be seen in Table 2, linolenic acid exerts the most efficient inhibition compared with the other unsaturated fatty acids. These results differ from those described by Szauer and Brandt.[2] Hence, in order to clarify such a discrepancy, further work would be required from the standpoint of the influence of the double bond.

According to Wolstenholme and Schulman,[9] fatty acid does not simply adsorb on the metal surface, as is represented in Fig. 9, but makes a complex with the iron ion which grows relatively thick. However, the adsorption model in Fig. 9 may be supposed to show not only unsaturated fatty acids, but also saturated ones such as stearic acid, because it is impossible to discriminate the carboxylate ions of both fatty acids by IR analysis. As can be seen from Table 1, since the shoyu oil consists of about 80% unsaturated fatty acids, the adsorption of SSOI and SSOD would be caused chiefly by unsaturated fatty acids. Hence, the adsorption model of shoyu oil shown roughly in Fig. 9 may be considered to be reasonable.

It is generally known that the adsorption of fatty acids on iron obeys Frumkin-Temkin's isotherm. In the present work, the adsorption of shoyu oil is also assumed to obey Frumkin-Temkin's isotherm. Thus, we investigated whether the adsorption is chemisorption or physical adsorption. According to Reshetnikov,[10] when the inhibition takes place by means of physical adsorption, Eq. 1 is valid without chemisorption, and the inhibition by chemisorption satisfies Eq. 2:

$$\ln \gamma = m\theta \tag{1}$$

$$Z = 1 - \frac{1}{\gamma} = \theta, \tag{2}$$

where γ is the inhibition coefficient which is defined by the relation $\gamma = k/k_{inh}$; k and k_{inh}, the rates of iron dissolution in the absence and presence of the inhibitor respectively; Z, the inhibition efficiency; θ, the surface coverage calculated on the basis of the capacitance measurement, and m, the constant. In the present study γ and Z were calculated from I_{corr}, which has itself been obtained from the measurements of the impedance and the weight loss, and θ is the value of C_{dl} at E_{corr} obtained from the impedance measurement.

Figures 10 and 11 show the results plotted for SSOD according to Eqs. 1 and 2. In Fig. 10 the linearity of ln γ *vs.* θ can not be seen, but the plots of Z *vs.* θ in Fig. 11 give a straight line. Consequently, the adsorption in the case of SSOD is regarded as chemisorption.

In order to elucidate more clearly the adsorption state of these inhibitors, there seems to be no alternative but to wait for future work *in situ* by means of optical methods.

The authors are very grateful to Professor Zenjiro Sugizaki of our university for his useful suggestions and to the Kikkoman Co. for the gift of a shoyu oil sample. The authors also wish to thank Messrs. Toshiki Mitsuka, Hiroyuki Mizoguchi, and Hideaki Sako for carrying out a part of the experiments.

References

1) M. V. Markina and Zh. V. Misler, *Zashch. Met.*, **14**, 95 (1978).
2) T. Szauer and A. Brandt, *Electrochim. Acta*, **26**, 1209 (1981).
3) T. Szauer and A. Brandt, *Electrochim. Acta*, **26**, 1219 (1981).
4) H. F. Finley and N. Hackerman, *J. Electrochem. Soc.*, **107**, 259 (1960).
5) R. J. Meakins, *J. Appl. Chem.*, **13**, 399 (1963).
6) M. Smialowski, T. Ostrowska, and Z. Szklarska-Smialowska, *Rocz. Chem.*, **29**, 674 (1955).
7) I. Sekine and H. Ohkawa, *Bull. Chem. Soc. Jpn.*, **52**, 2853 (1979).
8) N. Hackerman and A. C. Makrides, *Ind. Eng. Chem.*, **46**, 523 (1954).
9) G. A. Wolstenholme and J. H. Schulman, *Trans. Faraday Soc.*, **46**, 475 (1950).
10) S. M. Reshetnikov, *Zashch. Met.*, **14**, 597 (1978).

A Solid State Electrochemical Study on the 5,6 : 11,12-Bis(epidithio)-naphthacene–Iodine and Bromine Complexes

Eiji CHINO, Yoshio MATSUNAGA,* and Noboru TANABE
Department of Chemistry, Faculty of Science, Hokkaido University, Sapporo 060
(Received May 8, 1982)

Electromotive force (emf) measurements were made on solid-state galvanic cells, Ag|AgI|TTT-I_n, where TTT-I_n is the 5,6:11,12-bis(epidithio)naphthacene–iodine complex, as functions of the composition, n, and also of the temperature. A continuous increase in the emf at 25 °C from 491 to 593 mV was observed in the range from $n=1.0$ to 1.5, suggesting the occurrence of a nonstoichiometric phase. The upper limit of the existence region agrees with the composition of the well-known metallic phase. The emf changes again continuously up to 628 mV in the range from $n=2.7$ to 2.9, which corresponds with the composition of another highly-conducting complex. Similar measurements were carried out for the cells Ag|AgBr|TTT-Br_n. Distinct phases were found at the following compositions: $n=0.5$—0.8, about 1, about 1.2, about 1.5, and about 2. The Gibbs energy, enthalpy, and entropy of cell reactions as well as complex formation reactions were estimated.

Mixed-valence 5,6:11,12-bis(epidithio)naphthacene–iodine complexes, TTT–I_n,[1] have attracted the interest of many research groups. The complex TTT–$I_{1.5}$ is among the extensively studied organic metals. In addition to this particular complex, Buravov *et al.* have reported the isolation of a complex with $n\simeq 1$ and Kamaras *et al.* have found a complex with the composition range from $n=2.6$ to 2.9.[2,3] Moreover, the preparation of the complex TTT–$I_{0.72}$ has been described by Kathirgamanathan and Rosseinsky.[4] We examined earlier the electrical resistivity and thermoelectric power of TTT–I_n as functions of n using polycrystalline compactions.[5] Our resistivity-composition isotherm at 25 °C showed a minimum of 0.3 Ω cm at the composition of the metallic phase, TTT–$I_{1.5}$, and a shoulder as large as 200 Ω cm at the other phase, TTT–$I_{2.7}$. The presence of the latter phase was also manifested by a drastic increase in the thermoelectric power near $n=2.7$. No singularity due to the other complexes, TTT–$I_{0.72}$ and TTT–I, could be detected by these techniques, however.

The same techniques were employed for the elucidation of the TTT–Br_n complexes.[6] A minimum of about 7 Ω cm found near $n=0.5$ in the resistivity-composition isotherm at 25 °C indicated the formation of a mixed-valence complex, $(TTT)_2{}^+Br^-$. The resistivity increases monotonously up to $n=1.4$ and then abruptly by a factor of forty between $n=1.4$ and 1.5. This change implies the formation of another mixed-valence complex having the ideal composition of $(TTT)_2{}^{3+}(Br^-)_3$. The latter anomaly is accompanied by an increase of the activation energy for semiconduction by a factor of almost two and also by the change of sign in the variation of the thermoelectric power with the temperature from positive to negative. Here again, no indication of a well-established monobromide TTT^+Br^- was found by these techniques.

As our experiments on solid-state galvanic cells involving reactions between silver and the halogen in electronically-conducting thiazine–iodine complexes had provided a powerful tool for elucidating the constitution,[7] we decided to extend the work to the TTT–I_n and TTT–Br_n complexes. The electromotive force (emf) depends on n quite differently from the electrical resistivity and the thermoelectric power studied before. Two-phase mixtures should be identified by a constant emf, a stoichiometric complex by a discontinuous increase and a nonstoichiometric single-phase region by a continuous increase in emf with n.

Experimental

Materials. TTT was synthesized following the method reported by Marschalk and Stumm and recrystallized at least three times from 1,2,4-trichlorobenzene.[8] TTT–I_n samples were prepared by grinding the weighed TTT and iodine in an agate mortar in the presence of a small amount of benzene. The iodine contents were determined by elemental analysis. An additional sample prepared by the reaction between TTT and iodine in boiling nitrobenzene has a composition of $n=1.53$.

$TTT^{2+}(Br^-)_2$ was prepared by the oxidation of powdered TTT suspended in 1,2,4-trichlorobenzene with bromine, as described by Marschalk and Niederhauser.[9] The samples with n values less than two were obtained by grinding the weighed dibromide and TTT. The exact compositions were determined by microanalysis.

Measurements. The galvanic cell, Ag|AgI|TTT-I_n, was assembled. It was found to be necessary to mix intimately the electrolyte and TTT-I_n and to thermostat the cell at 80 °C for several days to attain an initial constant emf. The measurements were carried out in the range from room temperature to 80 °C, only for increasing temperatures. The cell was kept at each temperature for about one hour. The emf was read by means of a high-impedance universal digital meter, Yokogawa 2502. The work on the Ag|AgBr|TTT-Br_n cells was found to be more difficult. Reproducible emf values could be obtained only above 50 °C and only when the cell was kept for several days at each temperature.

Results and Discussion

TTT–I_n Complexes. The compositional variation of the emf at 25 °C is presented in Fig. 1. Below $n=1$, the cell maintains an emf of 491 mV. The samples in this composition range are supposed to be mixtures of the parent organic compound TTT and its iodine complex, TTT–I. The present work failed to provide any evidence supporting the existence of the TTT–$I_{0.72}$ reported by Kathirgamanathan and Rosseinsky. The emf increases continuously between $n=1$ and 1.5, suggesting the formation of a nonstoi-

TABLE 1. THERMODYNAMIC DATA FOR THE COMPLEX FORMATION REACTION, $TTT+n/2\ I_2 \longrightarrow TTT\text{-}I_n$

n	ΔG/kJ mol^{-1}	ΔH/kJ mol^{-1}	ΔS/J K^{-1} mol^{-1}	$(\Delta G/n)$/kJ mol^{-1}
1	−18.8	−21.1±1.1	−7.6±3.7	−18.8
1.5	−26.7	−27.7±1.3	−3.2±4.3	−17.8
2.7	−37.4	−35.8±2.5	5.3±5.2	−13.9
2.9	−38.8	−37.1±3.3	5.7±7.8	−13.6

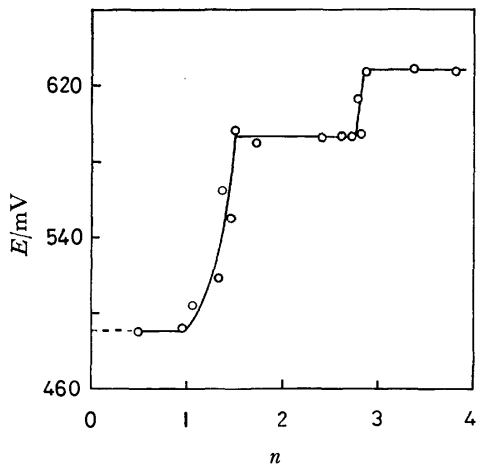

Fig. 1. Electromotive force of the solid-state cell, Ag|AgI|TTT-I_n *versus* n at 25 °C.

chiometric complex covering this range. In addition to the work by Buravov *et al.* mentioned above, Kamaras *et al.* have noted that TTT–I can be produced occasionally together with TTT and TTT-$I_{1.5}$. The compositions of these two complexes are identified as the lower and upper limits of a nonstoichiometric phase. Kaminskii *et al.* have reported that the iodine content in the complex TTT-$I_{1.5}$ may be varied from 1.5 to 1.55.[10] Apparently, the existence region of this nonstoichiometric phase is not limited to such a narrow range.

A plateau indicative of a two-phase region appears between n=1.5 and 2.7, giving an emf of 593 mV. The continuous increase observed between n=2.7 and 2.9 implies that the complex is again homogeneous over this range. In other words, a nonstoichiometric complex is formed. These results are in fair agreement with the observation made by Kamaras *et al.*, namely, the composition of recrystallized samples ranges from n=2.6 to 2.9 and the resistivity value along the needle axis is scattered by a factor of 16.[3] The occurrence of this phase was already confirmed by our resistivity and thermoelectric power measurements. The emf is 628 mV above n=2.9. The upper limit of this two-phase region could not be determined.

Since the current in AgI is exclusively carried by Ag^+ ions, the emf values observed in the two-phase regions below n=1 and between n=1.5 and 2.7 yield the Gibbs energies of the following cell reactions:

$$Ag(s) + TTT\text{-}I(s) \longrightarrow AgI(s) + TTT(s) \quad \text{and}$$

$$Ag(s) + 1/1.2\ TTT\text{-}I_{2.7}(s) \rightarrow AgI(s) + 1/1.2\ TTT\text{-}I_{1.5}(s).$$

Two more cell reactions covering the single phase regions are conceivable. It is convenient to consider the Gibbs energies in terms of the reactions:

$$Ag(s) + TTT\text{-}I(s) \longrightarrow AgI(s) + TTT(s) \quad (1)$$

$$0.5\,Ag(s) + TTT\text{-}I_{1.5}(s) \longrightarrow 0.5\,AgI(s) + TTT\text{-}I(s) \quad (2)$$

$$1.2\,Ag(s) + TTT\text{-}I_{2.7}(s) \longrightarrow 1.2\,AgI(s) + TTT\text{-}I_{1.5}(s) \quad (3)$$

and

$$0.2\,Ag(s) + TTT\text{-}I_{2.9}(s) \longrightarrow 0.2\,AgI(s) + TTT\text{-}I_{2.7}(s). \quad (4)$$

The energies associated with the reactions (1) and (3) are easily calculated to be −47.4 and −68.7 kJ mol^{-1}. As is evident from Fig. 1, these values represent the area under the emf-composition relation between the upper and lower n values defined in each cell reaction. Therefore, the Gibbs energies associated with the reactions (2) and (4), in which the nonstoichiometric complexes participate, may be estimated by a graphic integration to be −25.2 and −11.7 kJ mol^{-1} respectively.

Combining with $\Delta G^\circ_f(AgI) = -66.2$ kJ mol^{-1},[11] the Gibbs energies in terms of the following complex formation reactions:

$$TTT(s) + 1/2\ I_2(s) \longrightarrow TTT\text{-}I(s)$$

$$TTT(s) + 1.5/2\ I_2(s) \longrightarrow TTT\text{-}I_{1.5}(s)$$

$$TTT(s) + 2.7/2\ I_2(s) \longrightarrow TTT\text{-}I_{2.7}(s)$$

$$TTT(s) + 2.9/2\ I_2(s) \longrightarrow TTT\text{-}I_{2.9}(s)$$

are determined as presented in Table 1. The emf of the cell was a linear function of the temperature for all the samples studied. The entropy changes for the cell reactions (1)—(4) are estimated to be 18.5±2.4, 5.6±0.6, 6.8±0.4, and 14.5±1.1 J K^{-1} mol^{-1} on the basis of the temperature coefficients. The application of Gibbs-Helmholtz equation yields enthalpies of −42.0±0.7, −23.5±0.2, −66.7±0.1, and −7.4±0.3 kJ mol^{-1} for these cell reactions. With the aid of $\Delta S^\circ_f(AgI) = 14.6$ J K^{-1} mol^{-1},[11] the entropy changes in terms of the complex formation reactions can be computed, and then with $\Delta H^\circ_f(AgI) = -61.8$ kJ mol^{-1},[11] the enthalpy changes can be estimated. The results are summarized in Table 1. It may be noted that the entropy change is positive above n=2.7, while it is negative below this composition.

The Gibbs energy divided by the number of iodine atoms is in the range from −13.6 to −18.8 kJ mol^{-1}. These values show that the affinity of TTT for iodine is undoubtedly larger than that of the thiazines estimated earlier: *e.g.*, −6.9 kJ mol^{-1} at n=2.8 in the phenothiazine complex and −11.8 kJ mol^{-1} at n=2.7 in the benzo[*a*]phenothiazine complex. The diffusion of iodine in the present complexes appears to be appreciably hindered by strong binding to TTT. As the passage of current results in quick mass-transfer

TABLE 2. THERMODYNAMIC DATA FOR THE CELL REACTION, Δn Ag + TTT-Br_n ⟶ Δn AgBr + TTT-$Br_{n-\Delta n}$

n	Δn	E/mV	ΔG/kJ mol^{-1}	ΔS/J K^{-1} mol^{-1}	ΔH/kJ mol^{-1}
0.5	0.5	281	−13.6	7.5±0.3	−11.4±0.1
0.8	0.3	*	−10.3	4.6±1.3	−8.9±0.4
0.98	0.18	429	−7.5	8.7±1.2	−4.9±0.4
1.04	0.06	*	−2.6	2.9±0.2	−1.9±0.06
1.2	0.16	480	−7.4	8.1±0.1	−5.0±0.03
1.48	0.28	528	−14.3	10.8±0.1	−11.1±0.03
1.54	0.06	*	−3.2	2.3±0.1	−2.5±0.03
1.96	0.42	572	−23.2	15.9±0.4	−18.5±0.1

* One-phase region.

TABLE 3. THERMODYNAMIC DATA FOR THE COMPLEX FORMATION REACTION, TTT + n/2 Br_2 ⟶ TTT-Br_n

n	ΔG/kJ mol^{-1}	ΔH/kJ mol^{-1}	ΔS/J K^{-1} mol^{-1}	$(\Delta G/n)$/kJ mol^{-1}
0.5	−34.9	−38.8±0.1	−13.4±0.3	−69.7
0.8	−53.6	−60.0±0.5	−21.4±1.6	−67.0
0.98	−63.6	−73.2±0.9	−32.3±2.8	−64.9
1.04	−66.8	−77.3±1.0	−35.9±3.0	−64.2
1.2	−74.9	−88.4±1.0	−45.8±3.1	−62.4
1.48	−87.7	−105.4±1.0	−59.9±3.3	−59.3
1.54	−90.3	−108.9±1.0	−62.9±3.4	−58.6
1.96	−107.8	−132.6±1.1	−83.7±3.8	−55.0

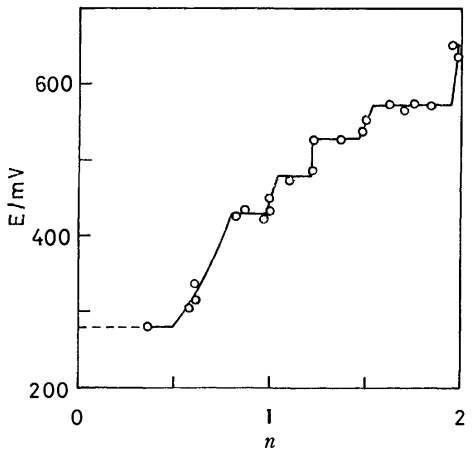

Fig. 2. Electromotive force of the solid-state cell, Ag|AgBr|TTT-Br_n *versus* n at 25 °C.

polarization, the application of a solid-state coulometric titration to the TTT-I_n complexes was found to be impracticable even if AgI is replaced with a highly-conducting AgI-based solid electrolyte.

We concluded that, on the basis of thermoelectric power, the TTT molecule in the iodine complex does not attain a unit positive charge even at n=4.5.[5] By contrast, both TTT^+ and TTT^{2+} bromides have been known by the work of Marschalk and Niederhauser.[9] The existence of these two has been fully supported by the significant differences in their electronic and vibrational spectra.[6,12] Consequently, one might foresee the appearance of many phases in the TTT–Br system in spite of the limitation of the study to the range n<2.

TTT-Br_n Complexes. In Fig. 2, the emf of the TTT-Br_n complexes extrapolated to 25 °C is plotted against n. When n<0.5, the cell exhibits an emf of 281 mV. An increase of the emf seems to be continuous between n=0.5 and 0.8. The lower limit coincides with the composition of the minimum resistivity found in the TTT–Br system. The emf remains at 429 mV until n reaches a little below one, and then increases continuously up to 480 mV in a relatively narrow range. Thus, the monobromide appears to be nonstoichiometric but only to the extent of 0.06. An abrupt increase in the emf at about n=1.2 from 480 to 528 mV suggests that this phase is stoichiometric or nearly so. The third single phase region appearing around n=1.5 corresponds to the mixed-valence compound $(TTT)_2^{3+}(Br^-)_3$ established by the resistivity-composition isotherm approach. The existence region is located from n=1.48 to 1.54; these values are a little higher than those reported before.[6] Then the two-phase region exhibiting an emf of 572 mV appears. Its upper limit is rather arbitrarily located at n=1.96.

The Gibbs energies, enthalpies, and entropies computed for the cell reactions, Δn Ag(s) + TTT-Br_n(s) → Δn AgBr(s) + TTT-$Br_{n-\Delta n}$(s), are summarized in Table 2. With the aid of ΔG_f°(AgBr) = −96.9 kJ mol^{-1}, ΔH_f°(AgBr) = −100.4 kJ mol^{-1}, and ΔS_f°(AgBr) = −11.7 J K^{-1} mol^{-1},[11] the thermodynamic data for the complex formation reactions, TTT(s) + n/2 Br_2(l) → TTT-Br_n(s) were estimated as given in Table 3. The Gibbs energy divided by the number of bromine atoms is in the range from −55.0 to −69.7 kJ mol^{-1}, indicating that bromine forms TTT complexes of greater stability than iodine does. The entropy changes are always negative. The order of magnitude is comparable with that known for the thiazine-iodine complexes. In conclusion, it must be emphasized that not only most of the complexes reported in earlier works but also some new phases have been established for both the iodine and bromine complexes by the present solid-state electrochemical study. The phases

were found to be more or less nonstoichiometric.

This work was partly supported by Grant-in-Aid for Scientific Research No. 434023 from the Ministry of Education, Science and Culture.

References

1) As the trivial name, tetrathiotetracene given by C. Marschalk and C. Stumm (Ref. 8) has been widely used; TTT is the abbreviation in accord with that used in the references.

2) L. I. Buravov, G. I. Zvereva, V. F. Kaminskii, L. P. Rosenberg, M. L. Khidekel, R. P. Shibaeva, I. F. Shchegolev, and E. B. Yagubskii, *J. Chem. Soc., Chem. Commun.*, **1976**, 720.

3) K. Kamaras, K. Ritvay-Emandity, G. Mihaly, and G. Grüner, *Solid State Commun.*, **24**, 93 (1977).

4) P. Kathirgamanathan and D. R. Rosseinsky, *J. Chem. Soc., Chem. Commun.*, **1980**, 356.

5) T. Inabe and Y. Matsunaga, *Bull. Chem. Soc. Jpn.*, **51**, 2813 (1978).

6) Y. Matsunaga and K. Takayanagi, *Bull. Chem. Soc. Jpn.*, **53**, 2796 (1980).

7) T. Matsumoto and Y. Matsunaga, *Bull. Chem. Soc. Jpn.*, **54**, 648 (1981).

8) C. Marschalk and C. Stumm, *Bull. Soc. Chim. Fr.*, **1948**, 418.

9) C. Marschalk and J. P. Niederhauser, *Bull. Soc. Chim. Fr.*, **1952**, 151.

10) V. F. Kaminskii, M. L. Khidekel, R. B. Lyubovskii, I. F. Shchegolev, R. P. Shibaeva, E. B. Yagubskii, A. V. Zvarykina, and G. L. Zvereva, *Phys. Status Solidi A*, **44**, 77 (1977).

11) "Selected Values of Chemical Thermodynamic Properties," National Bureau of Standards, Washington, D. C. (1969), Technical Note 270-4, p. 37.

12) Y. Matsunaga, *Bull. Chem. Soc. Jpn.*, **45**, 770 (1972).

 © 1983 The Chemical Society of Japan Bull. Chem. Soc. Jpn., 56, 31—34 (1983)

Phase Diagrams and Association Structures of Combined Surfactants-Water Systems

Hiromichi SAGITANI† and Stig E. FRIBERG*

Chemistry Department, University of Missouri-Rolla, Rolla, MO., 65401, U.S.A.

(Received May 8, 1982)

Phase regions were determined in systems with water and sodium dodecyl sulfate combined with a series of nonionic surfactants of the structure di-, tetra-, hexa-, and octaoxyethylene dodecyl ethers. The results showed the more hydrophobic members to act as cosurfactants, stabilizing the lamellar structure at high water contents. The more hydrophilic members of the nonionic series acted in a manner similar to ionic surfactants with a slight tendency to stabilization of the lamellar phase for 1:1 combinations of the surfactants.

Modern formulations for use in the laundry process use a combination of nonionic and anionic surfactants, a necessity in order to obtain optimum removal of soil from different kinds of fabric.

The nonionic/ionic surfactant combinations are also of importance for emulsion stability; the well known combination of a long-chain alcohol plus a long-chain ionic surfactant has been extensively discussed.[1-4] Similar surfactant combinations using medium-chain alcohols are well known for their use in microemulsion systems; the literature in that field is as rich as it is varied.[5-11]

These investigations have been confined to essential but limited parts of the total systems, and we found an investigation of the systematic changes in the general features of surfactant combination systems to be desirable in order better to understand their behavior.

The combination chosen was water and sodium dodecyl sulfate with a series of polyoxyethylene dodecyl ethers. The latter were varied from the most hydrophobic one, the alcohol, to a member with distinctly hydrophilic properties, the octaoxyethylene homologue.

Experimental

Materials. Sodium dodecyl sulfate ($C_{12}SO_4Na$), specially pure grade, BDH Chemicals, Ltd., was recrystallized twice from ethanol. Di-, tetra-, hexa-, and octaoxyethylene dodecyl ether ($C_{12}(EO)_n$) were 98% from Nikko Chemical Co.; 1-decanol ($C_{10}H_{21}OH$) was practical grade from Eastman Kodak Co.

Phase Diagrams. The solubility regions were determined by titration of water to a mixture of the other components. The liquid crystalline and crystalline regions were analyzed by visual observation between polarized films and in a microscope with polarized light. The measurements and determinations were made at 30±0.1 °C.

Light Scattering Measurements. The light scattering measurements were done on a Sofica Photo Gonio Diffusometer, Model 42000, at 30 °C and 546 nm. The reported $I_{90°}$ values were scaled to the value of pure benzene, put a 100. The cells were immersed in a chromosulfuric acid solution for 15 h and rinsed several times with twice distilled water. The benzene and the distilled water were filtered through a Millipore filter, 0.22 μm prior to use. Dust particles were finally removed from the solutions by centrifugation at 25000 g for 3 h immediately before the determinations.

X-Ray Measurements. The interlayer spacings of lamellar phases were determined by low angle diffraction X-ray (Siemens Crystalloflex 4) with an X-ray detector (Tennelec, PSD-100) and a multichannel analyzer (Packard, Model 901). The measurements were done at 40 KV, 30 mA, and room temperature (24 °C).

Results

The results have a bearing on both the extension of the phase regions and the structure of the associations. They will be reported in order.

Phase Regions. The combination with 1-decanol, Fig. 1, has the expected phase regions: two isotropic liquid phases, A and B in the figure. A emanating from the pure water corner is an aqueous micellar solution solubilized 1-decanol. B emanating from the 1-decanol is an alcoholic solution solubilized water. This alcoholic solution of water and surfactant will contain inverse micelles.[12] In addition, 2 liquid crystals are found. One has a structure of close-packed cylinders with the amphiphiles radially packed (C), while the other is the well known lamellar structure (D).[13] Observation under polarized light confirmed

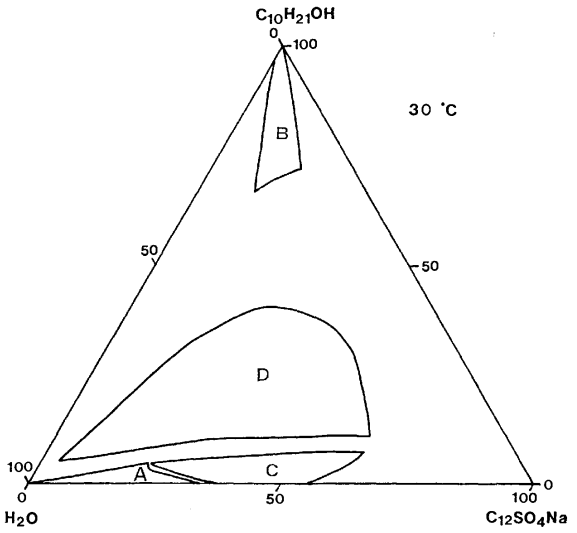

Fig. 1. The phase regions in the system water, sodium dodecyl sulfate ($C_{12}SO_4Na$) and 1-decanol ($C_{10}H_{21}OH$).
The concentrations are given in weight per cent. A: Isotropic aqueous solution, B: isotropic decanol solution, C: liquid crystal with a structure of cylinders in a hexagonal array, D: liquid crystal with lamellar structure.

† Present address: Pola Laboratories, 27-1, Takashimadai, Kanagawa-ku, Yokohama 222.

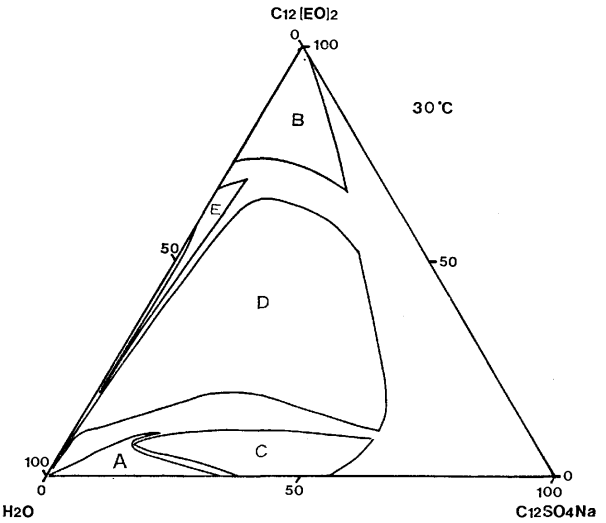

Fig. 2. The phase regions in the system water, sodium dodecyl sulfate ($C_{12}SO_4Na$) and dioxyethylene dodecyl ether ($C_{12}(EO)_2$).
A: Isotropic aqueous solution, B: isotropic ether solution, C: liquid crystal with a structure of cylinders in a hexagonal array, D: liquid crystal with lamellar structure, E: liquid crystal with isotropic structure.

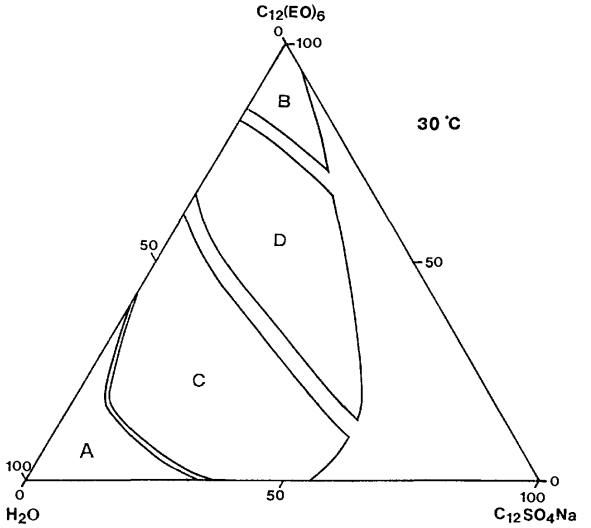

Fig. 4. The phase regions in the system water, sodium dodecyl sulfate ($C_{12}SO_4Na$) and hexaoxyethylene dodecyl ether ($C_{12}(EO)_6$).
A: Isotropic aqueous solution, B: isotropic ether solution, C: liquid crystal with a structure of cylinders in a hexagonal array, D: liquid crystal with lamellar structure.

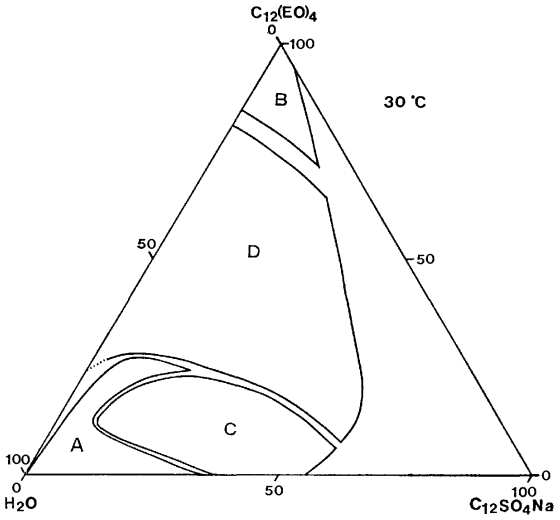

Fig. 3. The phase regions in the system water, sodium dodecyl sulfate ($C_{12}SO_4Na$) and tetraoxyethylene dodecyl ether ($C_{12}(EO)_4$).
A: Isotropic aqueous solution, B: isotropic ether solution, C: liquid crystal with a structure of cylinders in a hexagonal array, D: liquid crystal with lamellar structure.

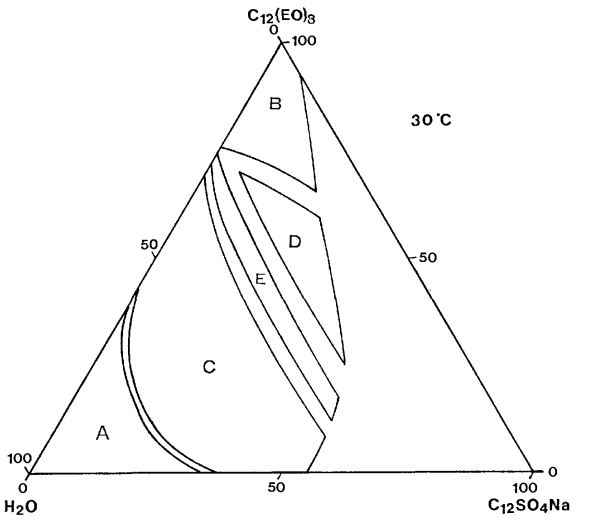

Fig. 5. The phase regions in the system water, sodium dodecyl sulfate ($C_{12}SO_4Na$) and octaoxyethylene dodecyl ether ($C_{12}(EO)_8$).
A: Isotropic aqueous solution, B: isotropic ether solution, C: liquid crystal with a structure of cylinders in a hexagonal array, D: liquid crystal with isotropic structure, E: liquid crystal with isotropic structure.

the structures of C and D phase; the pattern of "Oily streaks" and "Angular texture" for the lamellar and the hexagonal liquid crystals, respectively.[14] The structure and extension of these phases is exactly what would be expected, considering earlier material in this area.[12]

The replacement of 1-decanol with dioxyethylene dodecyl ether led to a series of modifications (Fig. 2). The solubilization of the ether in the aqueous micellar solution was increased, and the lamellar liquid crystalline required a higher content of the nonionic surfactant. The upper limit with a 10:1 weight ratio of the nonionic to anionic surfactant gave a lamellar liquid crystal with a pronounced stability with high contents of water. Its phase region actually reached to 98% water. The third liquid crystalline phase showed a cubic structure (E). The nonionic surfactant solution did not show the typical water solubilization maximum found for alcohols.[12]

With the tetraoxyethylene dodecyl ether (Fig. 3), the cloud point is still below 30 °C, and its lamellar liquid crystal is in equilibrium with pure water. The

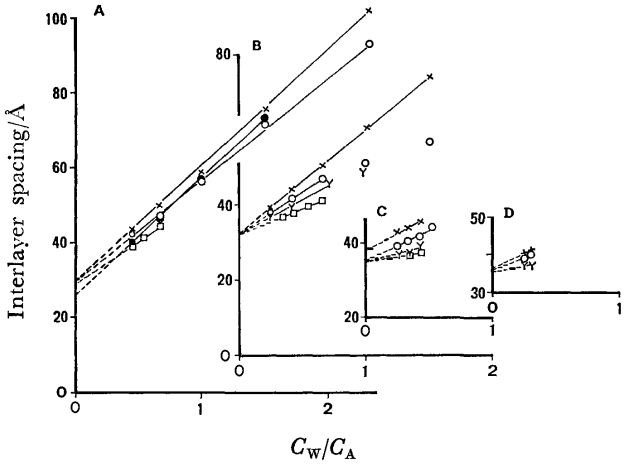

Fig. 6. Interlayer spacing as a function of water/amphiphile mass ratio (C_w/C_a).
From left to right, sodium dodecyl sulfate and:
A. Dioxyethylene dodecyl ether, or 1-decanol: $C_{12}SO_4Na/C_{12}(EO)_2$; x: 0.15/0.85, ○: 0.3/0.7, □: 0.665/0.335, $C_{12}SO_4Na/C_{10}H_{21}OH$; ●: 0.5/0.5.
B. Tetraoxyethylene dodecyl ether: $C_{12}SO_4Na/C_{12}(EO)_4$; x: 0/1, ○: 0.3/0.7, y: 0.5/0.5, □: 0.7/0.3.
C. Hexaoxyethylene dodecyl ether: $C_{12}SO_4Na/C_{12}(EO)_6$; x: 0/1, ○: 0.3/0.7, y: 0.5/0.5, □: 0.7/0.3.
D. Octaoxyethylene dodecyl ether: $C_{12}SO_4Na/C_{12}(EO)_8$; +: 0.2/0.8, ○: 0.3/0.7, y: 0.5/0.5.

changes in the region of the water and continuous phases are a direct continuation and further extension of those found at the shift from 1-decanol to the dioxyethylene ether. The solubilization of the ether in the aqueous micellar solution was very much enchanced, reaching an ether/sulfate weight ratio of 10:1. The extension of the lamellar phase toward the aqueous corner disappeared.

The hexa- and octaoxyethylene ethers both have cloud points in excess of 30 °C, and the diagrams contain only minor details of interest (Figs. 4 and 5). For both compounds the liquid crystal with a hexagonal arrangement showed higher maximum water content for mixtures than for the individual surfactant.[3] Combinations with the octaoxyethylene ether formed an isotropic liquid crystalline between the region of the lamellar and the hexagonal structure.

X-Ray Diffraction Patterns. The X-ray data is plotted in the usual manner as interlayer distance *versus* amphiphilic weight fraction in Fig. 6. The data, with few exceptions, were suited for extrapolation to water content equal to zero. The results show a reduction of interlayer distance with increased content of the ionic surfactant. This is true also for the extrapolated values, although the difference in this case was smaller. The extrapolated value is increased with increased polar chain length of the nonionic surfactant.

Light Scattering. The light scattering of samples in the isotropic liquid of the sample, dioxyethylene dodecyl ether, showed small values (Fig. 7). The values are given as fractions of the scale value for a pure liquid, benzene. The values are approximately unity, showing the scattering to be similar to that from a pure liquid.

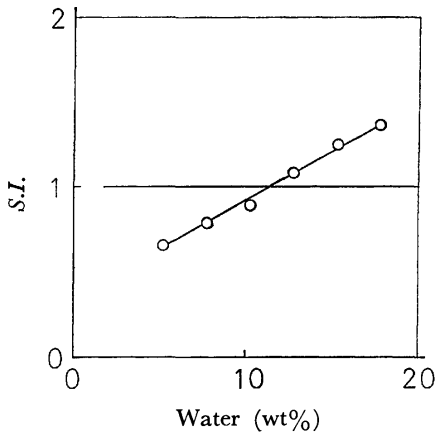

Fig. 7. Light scattering intensity for the dioxyethylene dodecyl ether ($C_{12}(EO)_2$) solution of water and sodium sulfate ($C_{12}SO_4Na$).
$C_{12}(EO)_2/C_{12}SO_4Na$ weight ratio=9:1. The scattering intensity (*S.I.*) is given relative to the value for pure benzene ($S.I._{benzene}=1$).

Discussion

The experiments gave general trends for the phase behavior of the mixed surfactants; the lower homologues performed as hydrophobic cosurfactants enhancing the stability of the liquid crystalline phases. This is most remarkable for the case of the dioxyethylene ether. Its combination gave a liquid crystalline phase with extremely high tolerance toward water. This behavior should indicate this combination to be good as emulsion stabilizers.[15] Subsequent experiments[16] have confirmed this assumption.

The liquid crystalline region C and D in Figs. 4 and 5 do not remarkably change with the ratio of sodium dodecyl sulfate/cosurfactant. This is interpreted that nonionics with long polar chain lengths (hexa- and octaoxyethylene ethers) have hydrophilic properties and behave in a similar manner as the ionic surfactant.

A minimum amount of water was necessary in order to bring the ionic surfactant into solution, which is shown by the right hand solubility limit in Figs. 1—5. The amount of water was identical for all the nonionic surfactants, from the most hydrophilic to the most hydrophobic one. A calculation shows a need of eight water molecules in order to dissolve one molecule of soap. It appears evident that the ether groups do not partake in the polar interactions[17] that lead to the ionic surfactant being dissolved. The ether bridge of the polyoxyethylene compounds obviously do not form sufficiently strong ligands with the metal ion to solubilize the surfactant.

The results also gave information about the structure of the liquid crystalline phase and indirectly about the order of the polar chain of the nonionic surfactant. The extrapolated values (Fig. 6) show a value of 26 Å for the 1-decanol/surfactant combination. A comparison with the corresponding values for the ethers (Fig. 6) shows all values to be larger. The slope of interlayer spacing/(C_w/C_a) for the 1-decanol/surfactant combination is steeper than that for the others. Fur-

thermore, a tendency of lower values with enhanced content of ionic compound is also found. We interpret these results in the form of the following model. The nonionic surfactant allows water to penetrate between the polar layers in accordance with results from NMR spectroscopy.[18,19] The addition of the ionic surfactant causes two changes: the presence of the polar group allows more water to penetrate between the polar chains of the nonionic surfactant and causes an enhanced disorder of its polar part.

This interpretation also accommodates itself to the values for variation of interlayer spacing with water content. The increase of spacing with water content was less for samples which contained also the ionic surfactant, an indication of enhanced disorder and increased water penetration between the molecules.

It is interesting to observe the extremely small values for the light scattering from solutions in the dioxyethylene dodecyl ether solution of water and surfactant. The scattering is similar to the one from a pure liquid. A reasonable interpretation is absence of colloidal aggregates.

References

1) J. T. Davies and G. R. A. Mayers, *Trans. Faraday Soc.*, **56**, 69 (1960).
2) B. C. Blakey and A. C. S. Lawrence, *Discuss. Faraday Soc.*, **18**, 268 (1954).
3) R. D. Vold and K. D. Mittal, *J. Colloid Interface Sci.*, **38**, 541 (1972).
4) S. Friberg, *Kolloid Z. Z. Polym.*, **244**, 333 (1971).
5) D. O. Shah and R. M. Hamlin, *Science*, **171**, 483 (1971).
6) A. W. Adamson, *J. Colloid Interface Sci.*, **29**, 261 (1969).
7) G. Gillberg, H. Lehtinen, and S. Friberg, *J. Colloid Interface Sci.*, **33**, 40 (1970).
8) K. Shinoda and H. Kunieda, *J. Colloid Interface Sci.*, **42**, 381 (1973).
9) H. L. Rosano, *J. Soc. Cosmetic Chem.*, **25**, 609 (1974).
10) H. F. Eicke and H. Christen, *J. Colloid Interface Sci.*, **46**, 417 (1974).
11) E. Ruckenstein and J. C. Chi, *J. Chem. Soc., Faraday Trans. 2*, **71**, 1690 (1975).
12) P. Ekwall, "Advances in Liquid Crystals," ed by G. H. Brown, Academic Press, N.Y. (1975), Vol. 1, p. 1.
13) K. Fontell, "Liquid Crystals and Plastic Crystals," ed by G. W. Gray and W. S. Winsor, Academic Press, N.Y. (1975), p. 80.
14) F. B. Rosevear, *J. Soc. Cosmet. Chem.*, **19**, 581 (1968).
15) S. Friberg, P. O. Jansson, and E. Cederberg, *J. Colloid Interface Sci.*, **55**, 614 (1976).
16) L. Ganzuo and S. Friberg, *J. Am. Oil Chem. Soc.*, in press.
17) B. Bendiksen, S. E. Friberg, and P. L. M. Plummer, *J. Colloid Interface Sci.*, **72**, 495 (1979).
18) H. Christenson and S. E. Friberg, *J. Colloid Interface Sci.*, **75**, 276 (1980).
19) H. Christenson, S. E. Friberg, and D. W. Larsen, *J. Phys. Chem.*, **84**, 3633 (1980).

Infrared ATR Measurements at Low Temperatures. An Apparatus and the Absorption Intensities of Crystalline Benzene and Carbon Disulfide

Haruka YAMADA* and Masao SAHEKI

Department of Chemistry, Kwansei Gakuin University, Nishinomiya 662

(Received May 17, 1982)

An infrared ATR apparatus for use at low temperatures was constructed for the determination of the optical constants and absorption intensities of crystalline samples. The ATR spectra of benzene and carbon disulfide polycrystals were measured with two different incident angles. The optical constants and then the absorption intensities were accurately obtained for the fundamental bands from these ATR spectra. Experiments for transmission spectra were also carried out with an improved absorption cell at low temperatures, confirming the present ATR results. A comparison of the intensities in different phases was made for the ν_{18}, ν_{19}, ν_{20}, and ν_{11} fundamental bands of benzene and the ν_3 band of carbon disulfide.

Studies of infrared intensities have recently attracted revived interest from both theoretical and experimental points of view.[1-4] Infrared intensities on solids had been studied considerably in the 1960s by measuring the absorption spectra of polycrystalline molecular crystals at low temperatures and by comparing their intensities with those of free molecules. They were discussed in connection with the intermolecular interactions and the field effects.[5-13] However, the observed intensities included considerable errors caused by ambiguity in the determination of the sample thickness, because the thicknesses were determined by measuring the interference fringes observed when the samples were sublimed from the gases onto a cold window.

We first applied the ATR method to a naphthalene single crystal[14] in 1971 and succeeded in obtaining the absolute absorption intensities of the fundamental bands. On the basis of the results thus obtained we discussed the deviation from the oriented gas model. Fortunately, naphthalene was a crystal at room temperature and was so soft that good optical contact between naphthalene and an ATR element might be easily made. By the ATR method we could also obtain the infrared intensities for the charge-transfer complexes in a solid.[15] However, molecular crystals consisting of small molecules, which are convenient for theoretical analysis, are usually liquid or gas at room temperature. If the ATR method can be applied at low temperatures, accurate absorption intensities can be obtained for such crystals. In the present study we have tried to construct an ATR apparatus at low temperatures. With the apparatus, the ATR spectra of polycrystalline benzene and carbon disulfide have been measured.

ATR Experiments

Apparatus. *ATR Cell*: A low-temperature cell, with a hemicylinder (ATR element) of KRS-5 (10 mm radius and 30 mm in height), is shown in Fig. 1. A photograph of the sample part is given in Fig. 1-b. It is made of Pyrex glass (except for the sample part A) and consists of two parts: a cooling part for the ATR element and a sample-spraying part. The outer vessel has two windows, attached with Q wax, whose faces make a right angle. The hemicylinder, H, is supported by a copper holder A and can be cooled down to the temperature of the coolant in E through the connection of Kovar and copper. To make good thermal

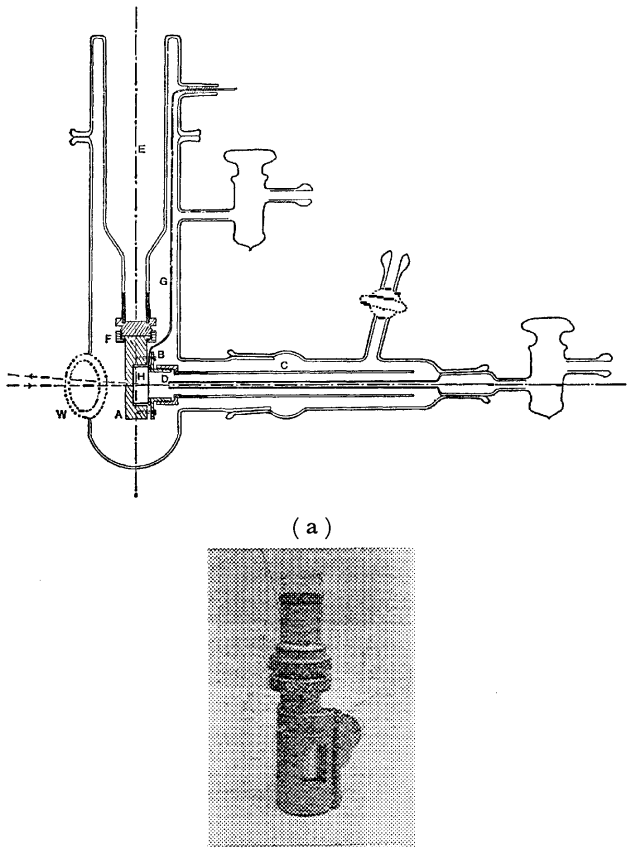

Fig. 1. ATR cell at low temperatures.

contact between A and H, an indium spacer was used. When E was filled with liquid N_2, the center of H (at the reflecting surface) was cooled to *ca.* 100 K. Sample vapor is directly sublimed onto the reflective surface of H (right side) through the nozzle, D, so that good contact between the ATR element and the sample may be attained. The nozzle is covered with a long glass tube (150 mm) to avoid the condensation of the sample on the back side, that is, on the cylindrical surface of H. The connection B is also made of copper and is equipped with screws. The incident light irradiates H (through the hole of A) and reflects at the interface between H and the deposited sample. By connecting the cell to a vacuum line, it can be evacuated to 10^{-4}—10^{-6} Torr (1 Torr = 133.322 Pa).

Optical System: The optical system for the low-temperature ATR apparatus is shown in Fig. 2. A light source

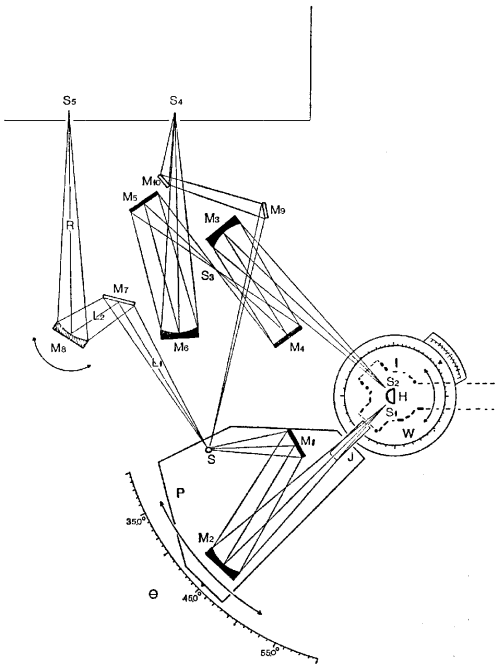

Fig. 2. Optical system.

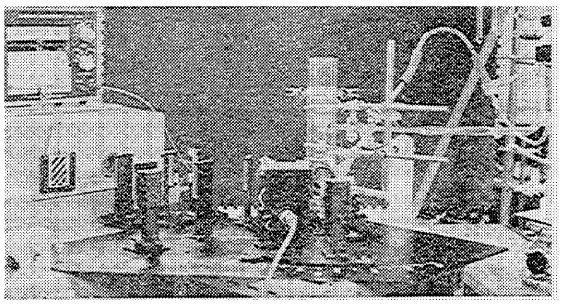

Fig. 3. Uncovered ATR apparatus constructed.

S, a plane mirror M_1, and a concave mirror M_2 ($R=340$ mm) are fixed on a plate P, which can move around the ATR cell as it rotates. The ATR cell described above is fixed by clamps on a circular table, W, so that the rotating axis of W may coincide with the cylindrical axis of H. By rotating the circular table, the ATR cell can be rotated around the vertical axis, that is, the cylindrical axis. Connecting P and W with a bar J, P, and W move simultaneously around the same axis. W has an angle graduation marked in degrees with a vernier, so that the incident angle can be known to an accuracy of one minute. The light beam is first focussed on S_1 in front of the cylindrical surface of H, passes through the hemicylinder H as a parallel beam, and is then refocussed on S_2. Afterwards the light beam is focussed on S_3 and S_4 (the entrance of a monochromator) by concave mirrors, M_3($R=340$ mm) and M_6($R=340$ mm). The mirrors (M_3, M_4, M_5, and M_6) in Fig. 3 are all fixed.

The reference beam from the light source S is focussed on S_5 by M_8 ($R=340$ mm), where $L_1+L_2=R$ (340 mm). A concave mirror M_8 is fixed on its position and can be rotated around the vertical axis; M_7 is approximately placed so as to satisfy: $L_1+L_2=R$ (340 mm).

Two plane mirrors are used for the correction of the zero line (reflectivity zero) so as to introduce extra light (from S) on S_4. M_9 and M_{10} can move and rotate. The angle of incidence can be chosen in the region of 33—59°, making

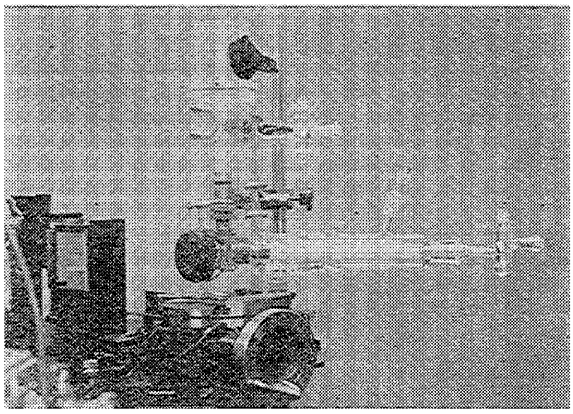

Fig. 4. The ATR cell on the circular table.

a right angle with the cylindrical surface of H.

For the ATR measurements, the optical system can be covered by using plastic sheets and plates; it is blown by dried air to eliminate atmospheric H_2O and CO_2.

Measurements of ATR Spectra. The uncovered apparatus constructed is shown in Fig. 3. It is connected to a JASCO 402-G spectrophotometer by replacing its source and sample parts, while the cell is connected to a vacuum line.

Figure 4 shows the side view of the low-temperature ATR cell on the circular table. The cell can rotate when the handle is operated.

We first set the angle of incidence at 45°, as is shown in Fig. 2; that is, by connecting W with P the cell direction is set so that the mark (incident angle) on P points to 45° on the base. For any other incident angle, we rotate W with P until the mark on P points to the desired angle θ; then we fix P on the base and disconnect P from W. Next, we rotate the cell, only W, in the opposite direction as much as a half of the angle just moved, $|(\theta-45°)|/2$, and then fix the cell at that position.

Sampling. After the apparatus is set as has been described above, the ATR cell is evacuated to 10^{-4}—10^{-6} Torr, and then H is cooled by filling E with a coolant. Sample vapor is sprayed from the nozzle D onto the reflecting surface of H through a needle valve. A uniform film (more than 20 μm in thickness) can be prepared by controlling the speed of sublimation and the vapor pressure. Samples which are solid at room temperature can also be measured with the apparatus when the samples make optical contact with the ATR element, as in the cases of naphthalene[14] and iodoform.[16]

R_s Measurements. The polarized ATR spectra of the samples at about 100 K are measured with an AgCl polarizer placed in front of the thermocouple detector. The reflectivity, R_s(electric vector perpendicular to the incident plane), is measured with two different incident angles, θ_1 and θ_2. The monochromator and the ATR attachment were blown out by dried air passed through molecular sieves.

Background and Zero Line. The background is determined by recording R_s for each incident angle without a sample at that temperature. The zero line of R_s (reflectivity zero) can be recorded when a shutter is placed in front of the ATR cell with the sample. The true zero curve lowers in the region where the sample absorbs.[21] To record such a fluctuation, the level of the sample beam has to be kept a little higher than that of the reference by introducing additive energy using M_9 and M_{10}.

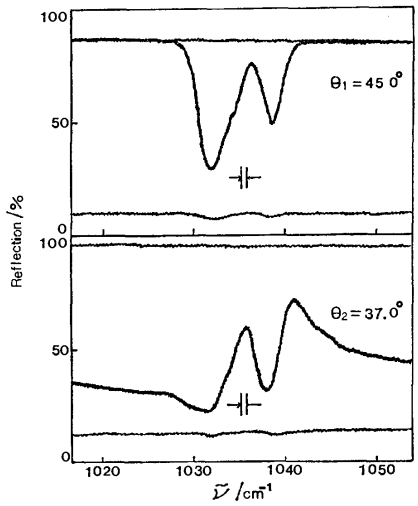

Fig. 5. Apparent R_s curves of the ν_{20} band of polycrystalline benzene with the background and the zero lines at 88 K.
→||← shows spectral slit width.

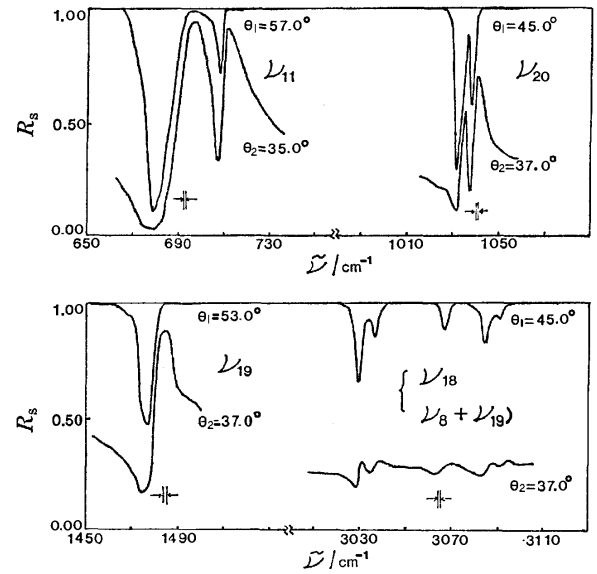

Fig. 6. True R_s curves for the four fundamental bands of benzene at 88 K.

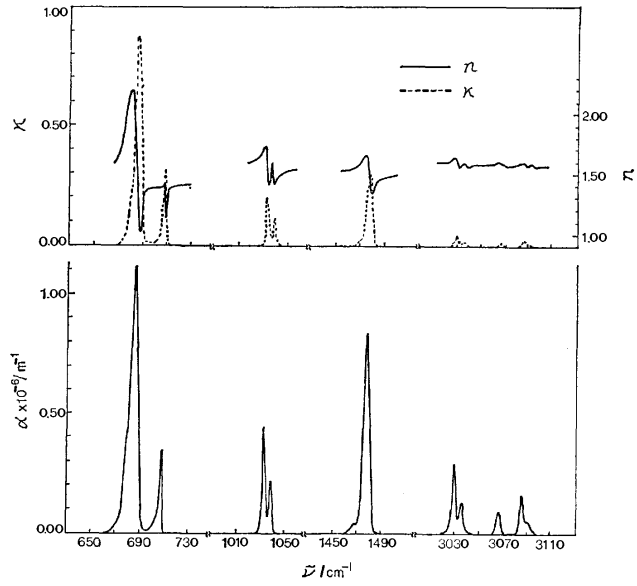

Fig. 7. Optical constants (n, k) and absorption coefficient (α) for polycrystalline benzene at 88 K.

Determination of Optical Constants and Absorption Intensities

The optical constants, refractive index n, and attenuation index k can be obtained from the observed ATR spectra. n and k are calculated from the reflectivities, (R_s)'s measured at two different incident angles, θ_1 and θ_2, by the use of polarized light whose electric vectors vibrate perpendicularly to the incident plane. The method used is essentially the same as that previously reported,[14] namely, the method by Fahrenfort and Visser,[17] with some modifications suggested by Hansen.[18]

The computations were performed on a FACOM 270-38 computer. The refractive indices of KRS-5 at 100 K were obtained by correcting the values[19] for the temperature coefficient. The calculated n, k, and Lambert's $\alpha=4\pi nk/\lambda$ values were plotted *vs.* the wave number with a X-Y plotter.

The absorption intensity, A, is given by:

$$B = \frac{1}{\rho}\int_{\text{band}} \alpha d\tilde{\nu},$$

$$A = \lim_{\Delta s_{1/2}\to 0} B,$$

where ρ is the density of the sample crystal and $\Delta s_{1/2}$, the spectral slit width. The integration was taken over a region three times as wide as the half-width of the band.

Benzene Crystal

ATR Measurements. Crystalline benzene films were prepared at 88 K by subliming the vapor onto the reflecting surface of the ATR element by a technique similar to that used for transmission measurements.[5,7] To obtain uniform films, the vapor was deposited as slowly as possible through a needle valve (Edwards High Vacuum), and the junction part (connection of the ATR cell with the spraying tube) was warmed from the outside to prevent vapor deposition in the vicinity of the top of the nozzle. The ATR spectra were measured for the four fundamental bands of benzene, ν_{18}, ν_{19}, ν_{20}, and ν_{11}.

Figure 5 shows the apparent R_s curves for ν_{20} obtained from the ATR measurements with the background and zero lines. For the four fundamentals bands, R_s curves were obtained as in Fig. 6. The n, k, and α curves calculated are shown in Fig. 7, which were reproducible for several samples. The average refractive index, $\bar{n}$, in the infrared ragion is obtained as 1.57, which agrees well with the value observed from the polycrystalline benzene at 77 K.[5] The α curves obtained coincide well with the transmission curves observed for the stable polycrystalline benzene.[5]

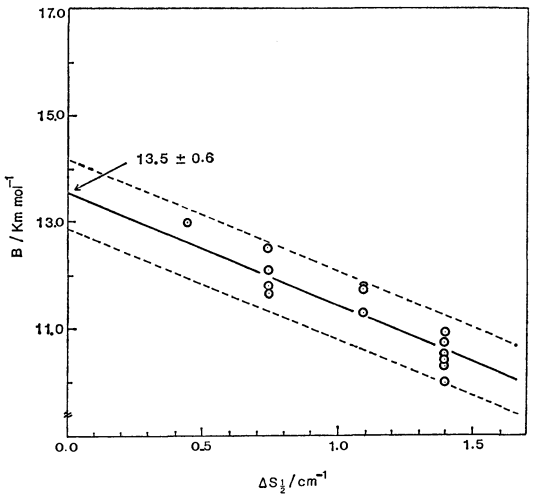

Fig. 8. Plots of B *vs.* spectral slit width for the ν_{20} band of polycrystalline benzene.

TABLE 1. ABSORPTION INTENSITIES OF BENZENE FUNDAMENTALS IN POLYCRYSTALS
(1 km mol^{-1} = 100 cm mmol^{-1})

	$\tilde{\nu}$/cm^{-1}	A_{ATR}	$A_{Transmission}$[a]
$\nu_{18}(e_{1u})$	3060	17.2±2.0	20.0
$\nu_{19}(e_{1u})$	1481	36.1±3.0	37.9
$\nu_{20}(e_{1u})$	1036	13.5±0.6	17.6
$\nu_{11}(a_{2u})$	685	81.5±6.0	92.0(80.0)[b]

a) J. L. Hollenberg and D. A. Dows, *J. Chem. Phys.*, **37**, 1300 (1962). b) D. E. Glover and J. L. Hollenberg, *J. Phys. Chem.*, **73**, 889 (1969).

(R_s)'s could be measured with an error of less than 0.5% for ν_{18}, ν_{19}, ν_{20}, and ν_{11}, resulting in accuracies of ±2% for n, ±(4—13)% for k, and ±(4—12)% for α at the peaks.

The integrated absorption intensities, B, for the four fundamental bands can be obtained from the α curves, using ρ(density) = 1.42×10^4 mol m^{-3}. Since the spectral slit widths, $\Delta S_{1/2}$, used were not so small as the half-widths, $\Delta\tilde{\nu}_{1/2}$, of the respective bands, corrections for a finite spectral slit-width were needed. For ν_{18} and ν_{19}, the condition (1/3) $\Delta\tilde{\nu}_{1/2} > \Delta S_{1/2}$ is satisfied, so $\Delta\tilde{\nu}_{1/2}$ and B are almost constant over the spectral slit-widths used, 1.3—1.8 cm^{-1}; therefore $B \approx A$. On the other hand, the above condition did not hold for ν_{20} and ν_{11}. The absolute absorption intensities for ν_{20} and ν_{11} were then obtained by extrapolating B's to $\Delta S_{1/2} \to 0$. The plots of B *vs.* $\Delta S_{1/2}$ are shown for ν_{20} in Fig. 8.

In Table 1 the absolute absorption intensities, A, obtained from the ATR measurements are given for the fundamental bands, together with the values reported from the transmission measurements. The present ATR values are all smaller than those reported from the transmission measurements. The ratios of the values between ATR and transmission differ from band to band in the 77—95% region. The smaller the intensity value, the smaller the ratio. The values obtained from the ATR measurements are independent of the sample thickness and are certainly more accurate than those reported from the transmission measurements.

Intensity Changes in Different Phases. Now that we have obtained reliable intensities in solid benzene, we can proceed to compare the values in different phases. Going from gas to a solid, the intensity of the ν_{18} band decreases to about 1/3 of the gaseous value, while that of the ν_{19} band increases by three times. The ν_{20} band also increases in intensity a little going from gas to a solid. The intensity changes observed, thus, vary with the bands in both direction and amount, and do not depend on the symmetry species to which the vibrational mode belongs. For the ν_{11} band, the value in the liquid phase is still uncertain, so at present no appropriate comparison can be made for the ν_{11} band.

Transmission Measurements. We have succeeded in obtaining the absorption intensities for the benzene polycrystal from the ATR measurements. The present values are smaller by 5—23% than the intensities reported from the transmission measurements. The inaccuracy in obtaining A from the transmission measurements is mainly caused by the determination of the thickness of the film used. However, it seemes probable to improve the transmission experiments, for during the ATR measurements we noticed that the samples were sublimed easily on the cylindrical (back) surface of the ATR element unless quite a long shielding tube was used. Judging from the structure of the cold cell used previously for the transmission measurements, it is supposed that the samples were sublimed onto both sides of the substrate. Therefore, we tried to modify the old cell in the way shown in Fig. 9.

TABLE 2. COMPARISON OF ABSORPTION INTENSITIES OF FUNDAMENTAL BANDS OF BENZENE IN THREE PHASES (km mol^{-1})

	$\tilde{\nu}$/cm^{-1}	Gas	Liquid		Solid
		Transmission[a]	ATR[b]	Transmission[d]	ATR
$\nu_{18}(e_{1u})$	3060	59.8	(48.0)[c]	44.4	17.2
$\nu_{19}(e_{1u})$	1481	13.0	—	19.1	36.1
$\nu_{20}(e_{1u})$	1036	8.80	12.9	11.5	13.5
$\nu_{11}(a_{2u})$	685	87.8	142	95.4	81.5

a) H. Spedding and D. H. Whiffen, *Proc. R. Soc. London, Ser. A*, **238**, 245 (1956). b) A. C. Gilby, J. Burr, Jr., W. Krueger, and B. Crawford, Jr., *J. Phys. Chem.*, **70**, 1525 (1966). c) G. M. Irons and H. W. Thompson, *Proc. R. Soc. London, Ser. A*, **298**, 160 (1967). d) I. C. Hisatsune and E. S. Jayadevappa, *J. Chem. Phys.*, **32**, 565 (1960).

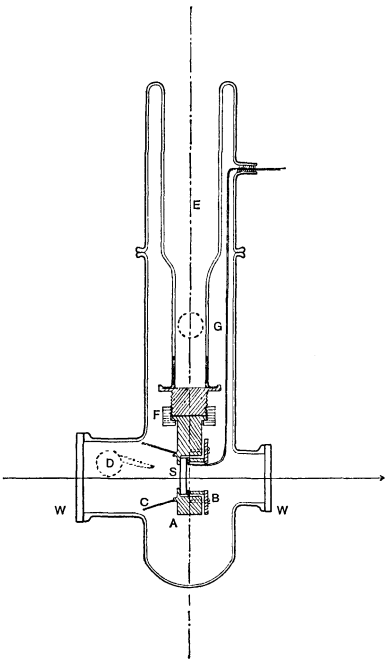

Fig. 9. Improved transmission cell at low temperatures.

A shielding cover, C, made of a thin copper sheet was attached to the copper block, A, with solder around the substrate (KRS-5, 20×10 mm). The top of the nozzle, D, had to be inserted into C, and the separation of D from the substrate surface should be 20 mm, so that the sample vapor can be sublimed uniformly onto the front side (and not onto the back surface) of the substrate.

The transmission spectra of polycrystalline thin films of benzene were measured with a modified cold cell attached to the JASCO DS-402G infrared spectrophotometer. The sampling and spectral measurements were the same as those described earlier.[13,14] The thickness of the sample was estimated by counting the interference fringes which were observed by the Hollenberg-Dows method,[5] when the sample vapor was subliming onto the substrate.

The integrated absorption intensity was calculated by means of:

$$B = \frac{1}{\rho l}\int_{\text{band}} \ln(I_0/I)\mathrm{d}\tilde{\nu},$$

where ρ is the density and l, the thickness of the sample crystal. The intensities, A, corrected for a finite spectral slit width are 16.3 ± 1.0 for ν_{18}, 31.7 for ν_{19}, 14.2 ± 0.6 for ν_{20}, and 74.5 ± 3.5 for ν_{11} in km mol^{-1} units; these are rather close to the values obtained from the ATR measurements and seem to justify the present ATR results.

Carbon Disulfide Crystal

Polycrystalline carbon disulfide was also measured by the ATR method. Because of the high vapor pressure and the low melting point of CS_2, especially careful sublimation was carried out in order to obtain uniform and stable polycrystals. If the holder B was colder than the reflecting surface of H, the CS_2 vapor

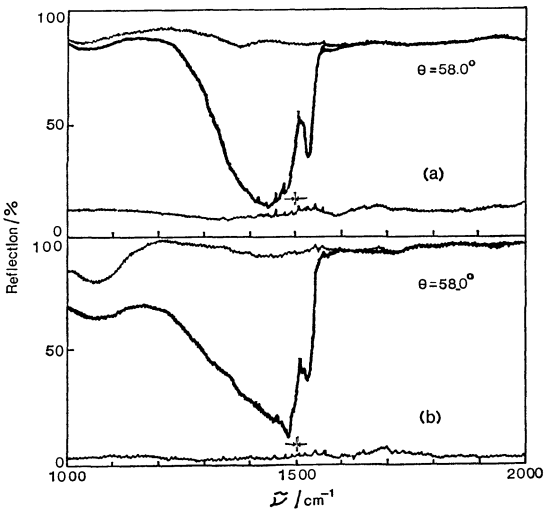

Fig. 10. Apparent R_s curves for sprayed carbon disulfide at 109 K.
(a): Slowly deposited sample, (b): rapidly deposited sample.

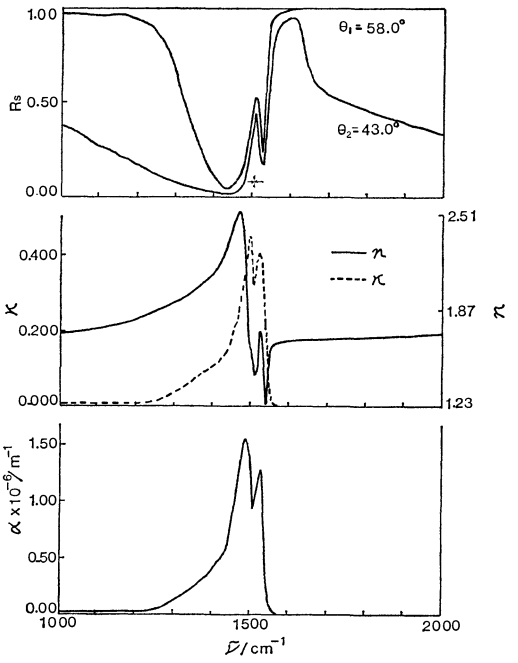

Fig. 11. R_s, n, k, and α curves for polycrystalline carbon disulfide at 109 K.

was first condensed onto B, not on H. We inserted, therefore, a Teflon spacer between B and H, so that the temperature of H was kept higher by 20—30 K than that of H.

The ATR spectra were measured for a fundamental band, ν_3. When the CS_2 vapor was sprayed onto H, two kinds of spectra were observed, depending on the spraying speed. The spectra observed with $\theta=58°$ and at 109 K are shown in Fig. 10; (a) was obtained with the speed of 4.6×10^{-4} mol h^{-1} and (b) with that of 2.8×10^{-2} mol h^{-1}. The (a) spectrum is sharper than the (b) spectrum. Comparing these spectra with those observed for the transmission measurements,[7] the (a) spectrum is, seen to be quite similar to the trans-

TABLE 3. ABSORPTION INTENSITIES OF THE ν_3 BAND OF CS_2 IN THREE PHASES (km mol^{-1})

$\tilde{\nu}$/cm^{-1}	Gas[a)]	Liquid[a)]	Solid	
			ATR	Transmission[a)]
$\approx$1500	567±10	752±20	725±110	800±140

a) H. Yamada and W. B. Person, *J. Chem. Phys.*, **40**, 309 (1964).

mission spectrum observed for the stable thin polycrystalline CS_2, except for a small peak at 1457 cm^{-1} observed for the transmission. The small peak at 1457 cm^{-1}, assigned to the isotopic molecule, $^{13}CS_2$, was also observed during the sample sublimation for the thin film, but was obscured for the present thick sample. The peaks at 1530 and 1485 cm^{-1} are components of ν_3 split by the correlation-field effect.[7)] The (b) or a similar spectrum was observed for a worse (not uniform) or unstable crystal.

The optical constants and absorption intensity were determined for the samples which showed the (a) spectrum. The R_s, n, k, and α curves are shown in Fig. 11. The mean refractive index, $\bar{n}$, is obtained as 1.80, which is close to the value, 1.82±0.05, obtained for the polycrystalline CS_2 at *ca.* 80 K.

The absorption intensity, A, was calculated, to be 725 km mol^{-1}, using $\rho = 2.13 \times 10^4$ mol m^{-3} (109 K), estimated from the X-ray structure;[20)] this value is a little smaller than the value obtained from the transmission measurements.[7)] The ν_3 band is so broad that the correction for the finite spectral slit width is negligible. The A values are tabulated with the values reported from the transmission measurements. The difference in values between ATR and transmission is rather small for the ν_3 band of CS_2. This might be explained as follows: Because of the strength of ν_3, extremely thin films were prepared for the transmission measurements. The sublimation time, therefore, was so short that the back-side deposition of CS_2 might not be so serious as for the benzene crystal. Consequently, it seems that the error included in A was not so serious for the transmission band of ν_3. For the CS_2 crystal, the previous results[7)] are confirmed by the present ATR measurements.

References

1) D. Steele, "Molecular Spectroscopy," ed by R. F. Barrow, D. A. Long, and D. J. Millen, The Chemical Society, London (1978), Vol. 5, p. 106.
2) W. B. Person and D. Steele, "Molecular Spectroscopy," led by R. F. Barrow, D. A. Long, and D. J. Millen, The Chemical Society, London (1974), Vol. 2, p. 357.
3) B. Crawford, Jr., T. G. Goplen, and D. Swanson, "Advances in Infrared and Raman Spectroscopy," ed by R. J. H. Clark and R. E. Hester, Heyden, London (1978), Vol. IV, Chap. 2.
4) R. N. Jones *et al.*, *Appl. Spectrosc.*, **34**, 638, 691 (1980).
5) J. L. Hollenberg and D. A. Dows, *J. Chem. Phys.*, **37**, 1300 (1962).
6) G. M. Wieder and D. A. Dows, *J. Chem. Phys.*, **37**, 2990 (1962).
7) H. Yamada and W. B. Person, *J. Chem. Phys.*, **40**, 309 (1964).
8) H. B. Friedrich and W. B. Person, *J. Chem. Phys.*, **39**, 811 (1963); H. B. Friedrich, H. Yamada, and W. B. Person, *ibid.*, **43**, 418 (1965).
9) H. Yamada and W. B. Person, *J. Chem. Phys.*, **41**, 2478 (1964); **43**, 2519 (1965).
10) T. L. Brown, *J. Chem. Phys.*, **43**, 2780 (1965).
11) D. A. Dows, *Spectrochim. Acta*, **22**, 1479 (1966).
12) C. F. Cook, W. B. Person, and L. C. Hall, *Spectrochim. Acta*, **23A**, 1425 (1967).
13) A. Kimoto and H. Yamada, *Bull. Chem. Soc. Jpn.*, **41**, 1096 (1968).
14) K. Tsuji and H. Yamada, *J. Phys. Chem.*, **76**, 260 (1971).
15) M. Saheki and H. Yamada, *Spectrochim. Acta*, **32A**, 1425 (1976).
16) K. Tsuji and H. Yamada, *Bull. Chem. Soc. Jpn.*, **41**, 1975 (1968).
17) J. Fahrenfort and W. M. Wisser, *Spectrochim. Acta*, **18**, 1103 (1962).
18) W. N. Hansen, *Spectrochim. Acta*, **21**, 209 (1965).
19) W. S. Rodney and I. H. Malitson, *J. Opt. Soc. Am.*, **46**, 956 (1956).
20) N. C. Baenziger and W. L. Duax, *J. Chem. Phys.*, **48**, 2974 (1968).
21) H. Yamada, *Jasco Report*, **2**, No. 12, 7 (1965).

A Rate Equation System Having a Mnemonic Function

Kazutoshi IWAMOTO, Shun-ichi MITOMO, and Manabu SENŌ*
Institute of Industrial Science, The University of Tokyo,
7-22-1 Roppongi, Minato-ku, Tokyo 106
(Received May 31, 1982)

A chemical system having a mnemonic function is constructed and its behavior is analyzed. The system consists of a subsystem having seven steady states and, under suitable conditions, it stays in a stable steady state or in an oscillating state depending on the initial state. Moreover, the system can show an additional oscillating state around the oscillating state and transitions between two different oscillating states occur by a little change in a certain parameter value(input), which is the characteristic point in this system. Therefore, a response behavior of the system to an input differs drastically depending on the states, *i.e.*, oscillating or stationary. This property could be related to appearance of a mnemonic function. Moreover, it is demonstrated that the system could be linked with an excitable subsystem to show more clearly the mnemonic function proposed here.

It has been demonstrated that a chemical system far from an equilibrium state occasionally shows some peculiar behaviors like chemical oscillations,[1,2] periodic pattern formation,[3-5] excitation, [6-8] wave propagation,[9-11] etc. One of the most important points in this field is that these peculiar behaviors are very often observed in a living system,[2] and many articles discussed the behaviors with relation to the activities of the living system.[2,12,13] The chemical oscillation is also criticized in relation to the circadian rhythm,[14] beating of heart,[15] excitation of nerve membrane,[16] and the problem of pattern formation was first discussed in relation to morphogenesis in the living system by Turing.[17]

As one of the various activities of the living system, the functions of the living brain have been treated in various aspects. McCulloch and Pitts[18] analyzed the unidirectional travel of a signal from the output of a neuron to the input of the neurons connected to it. Caianiello developed their model and proposed a mnemonic equation in addition to the neuronic equation which includes absolutely and relatively refractory periods of each neuron.[19] He proposed an idea to treat mathematically the memory function of the brain; that is, the memory gained through experiences is stored in the coupling coefficients a_{ij} by the mechanism that the coupling coefficient a_{ij} increases as increasing number of pulses from neuron j to neuron i, and he led a mnemonic equation describing his idea. He developed his idea for thought-processes and thinking machines.

According to the Caianiello equation, the propagation of signal along the nerve of a living brain was studied by a computer simulation method, and the coexistence of a stably oscillating state and a stationary state was confirmed. Some investigators consider that the oscillating state is of the brain recalling a certain matter.[20] According to this explanation, any system that shows coexistence of a stably oscillating and a stationary states may be a candidate for the system having a mnemonic function. There are some model systems relating to this behavior.[21,22]

In this paper, we intend to analyze the mnemonic function in a chemical system with a different standpoint of views. We refer to the system with a mnemonic function as the system-M and consider that it should respond in quite different ways for an input dependently whether the system-M is storing a memory of not. We consider that there should be another external system-E, which utilize the memory stored in the system-M to attain its own specific purpose. The external system-E changes a given parameter value of the system-M to observe its response in order to draw an information from the system-M.

The essential point of the proposed equations is that there coexist one stable steady state and one stable oscillating state, around which another oscillating state appears by a little change in parameter values, and the system is stationary or oscillating dependently on its career it has experienced. Under this situation, we can say that the system remembers the past events. The phase diagram satisfying the steady state conditions is essential in this treatment and there is not a special meaning in the corresponding model reaction processes. Therefore, our main object in this article is not to construct a model system but to show a possibility of mnemonic function in a chemical reaction system.

In the following sections, the differential equations exhibiting a mnemonic function are proposed and the system behaviors are analyzed, and a little more functional system that an excitable system is linked with the original system is developed. In this system, the response caused by an input is more drastic and our idea about the mnemonic function is clearly shown.

Rate Equations Related to a Mnemonic Function

Let us consider the following rate equations without showing corresponding chemical reaction processes,

$$\frac{dE}{dt} = \alpha(b_1 - b_2EX - b_3X), \tag{1}$$

$$\frac{dX}{dt} = \beta(a_1X^9 - a_2X^8 + a_3X^7 - a_4X^6 - a_5X^5 + a_6X^4 - a_7X^3 + a_8X^2 - a_9X + a_{10} + E), \tag{2}$$

where E and X represent the concentrations of two intermediates E and X. The ninth order equation seems to be essential to display an expected mnemonic function, but it is not necessarily the simplest and the most realizable equation for the mnemonic function. It is considered that the system giving such rate equations is not difficult to be realized as being dis-

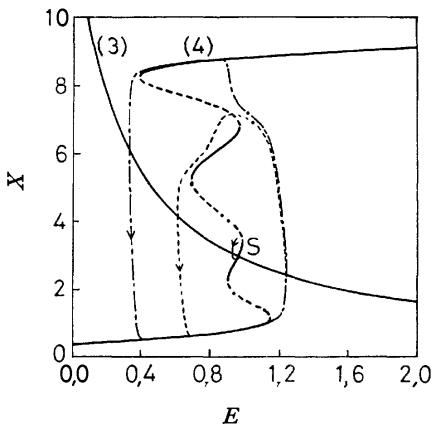

Fig. 1. Relationships between X and E determined by Eqs. 3 and 4.
The numbers in the figure correspond to the equation numbers. The crossing point S of the two curves (3) and (4) is a stable steady state. A thin solid line represents the route into the stable steady state, and a dotted line and a dot and rod line represent the routes of oscillating states of the system-M. Parameter values used for calculations are: $a_1=8.609\times 10^{-6}$, $a_2=3.267\times 10^{-4}$, $a_3=4.609\times 10^{-3}$, $a_4=2.635\times 10^{-2}$, $a_5=7.552\times 10^{-3}$, $a_6=0.8573$, $a_7=4.3985$, $a_8=9.898$, $a_9=10.16$, $a_{10}=2.696$, $b_1=3.65$, $b_2=1.0$, $b_3=0.27$, $\alpha=0.25$, and $\beta=70.0$ for the dotted line and 75.0 for the dot and rod line.

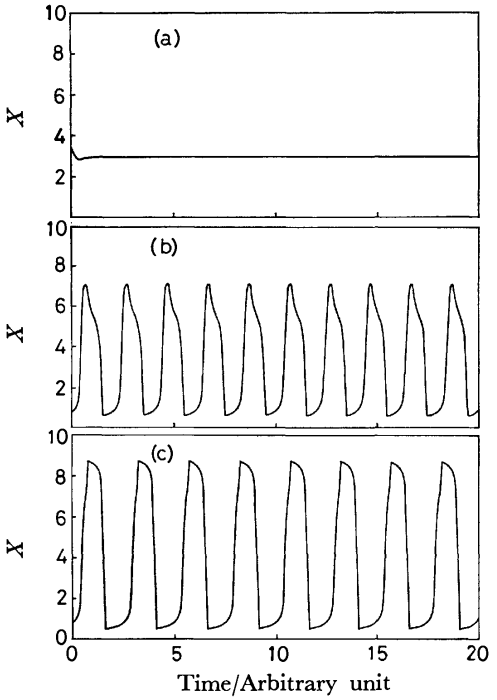

Fig. 2. System behaviors under various conditions.
(a), (b), and (c) show the responses corresponding to the behaviors as shown by solid, dotted, and dot and rod lines, respectively, in Fig. 1.

cussed later. Although the behaviors of the chemical system-M obeying Eqs. 1 and 2 can be determined by direct calculations of these equations with a digital computer, we first discuss the stability of the steady states in order to predict its behaviors. From the steady state conditions, $dE/dt=0$ and $dX/dt=0$, we have

$$b_1 - b_2EX - b_3X = 0, \tag{3}$$

$$a_1X^9 - a_2X^8 + a_3X^7 - a_4X^6 - a_5X^5 + a_6X^4 - a_7X^3 + a_8X^2 - a_9X + a_{10} + E = 0. \tag{4}$$

Equations 3 and 4 determine two relations between X and E at the steady state, which are displayed on the X-E phase plane in Fig. 1. The parameter values used for the calculations are as follows;

$a_1=8.609\times 10^{-6}$, $a_2=3.267\times 10^{-4}$, $a_3=4.609\times 10^{-3}$,
$a_4=2.635\times 10^{-2}$, $a_5=7.552\times 10^{-3}$, $a_6=0.8573$,
$a_7=4.3985$, $a_8=9.898$, $a_9=10.16$, $a_{10}=2.696$,
$b_1=3.65$, $b_2=1.0$, and $b_3=0.27$.

These parameter values are arbitrarily chosen to produce an expected behavior. Of course, this selection is not unique for this purpose. The curve defined by Eq. 4 has six marginal points where dE/dX is equal to zero. The states along the dotted lines are unstable; that is, when the rate equation 2 is solved for an initial state which is deviated a little from the dotted line at a fixed value of E, the value of X develops to another stable state apart from the dotted line.

The steady state is determined by the crossing point of the two curves defined by Eqs. 3 and 4. It is proved from the result by the standard stability analysis[1] that the steady state is stable when the two curves intersect on the solid part of the line (4) in Fig. 1. The present system has a stable steady state S at $E=0.9561$ and $X=2.9770$. In this case, the system, which lies initially in the vicinity of the steady state, goes into and remains stable at this steady state. This behavior is shown with a thin solid line falling into the crossing point S from the initial state, $E=0.95$ and $X=3.5$, in Fig. 1. The values of $\alpha=0.25$ and $\beta=70.0$ are used for calculation. The arrow on the line represents the direction of the temporal change of the system. On the other hand, when the initial state of the system is far from the stable steady state S, say $E=1.0$ and $X=0.8$, the oscillating state shown by a closed cycle with a thin dotted line is realized as a final state for the parameter values, $\alpha=0.25$ and $\beta=70.0$. For the system having the parameter values, $\alpha=0.25$ and $\beta=75.0$, the oscillating state represented by a dot and rod line is realized as a final stable state.

These behaviors discussed above are shown as temporal changes of X in Fig. 2. (a) and (b) are of the steady state and the oscillating state, respectively, for $\alpha=0.25$ and $\beta=70.0$, and (c) is of the oscillating state solved for $\alpha=0.25$ and $\beta=75.0$.

Here, let us investigate how the system behaviors are affected by a change in β value. Initially the value of β is 70.0. Then, the system is stationary or oscillating. When the system lies in the oscillating state shown by a dotted line in Fig. 1, the oscillatory trajectory transfers to the cycle represented by a dot and rod line for an increasing value of β to 75.0. When β is brought back to the original value, the oscillating state regresses reversely to the original state of smaller amplitude. On the contrary, when the system is in

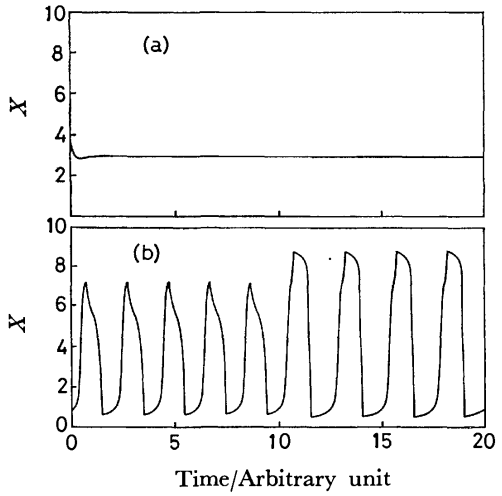

Fig. 3. Response behaviors of the system-M to change in β value.
In both (a) and (b), the value of β is changed from 70.0 to 75.0 at time 10. (a) shows a response of the system-M which is initially in the stable steady state and there is no detectable change. (b) is a response of the system which is initially in the stable oscillatory state and the behavior is suddenly changed in amplitude at time 10. All the parameter values are the same with those of Fig. 1.

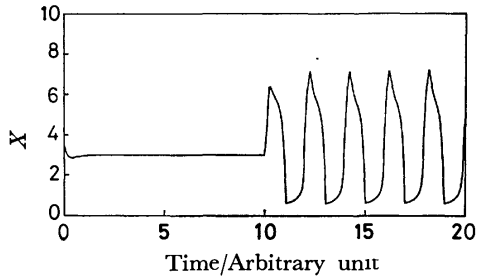

Fig. 4. Response of the system-M initially in the stable steady state to change in E value.
At time 10, the E value is changed into 1.1. The steady state is located at $X=2.9770$ and $E=0.9561$ and other parameter values are the same with those of Fig. 1.

the stable steady state, any changes can not be observed by this change in β value. These responses are demonstrated in Fig. 3. Initially, the system is in the steady state (case a) or in the oscillating state (case b). In both cases (a) and (b), the value of β is changed from 70.0 to 75.0 at time 10. Only the case (b) shows a noticeable response to the change in β value. This is the point on which we have an interest.

Now, let us examine the behavior of the system which is initially in the steady state, being subject to a certain deviation of E value as a result of external stimulus. As an example, when E increases beyond over a threshold value of 1.035, the system falls into the stably oscillating state as shown in Fig. 4. In this example, the E value is increased to 1.1 at time 10, and after that time, the system is in the oscillating state, storing with the memory of this stimulus.

Now, let us introduce another external system-E,

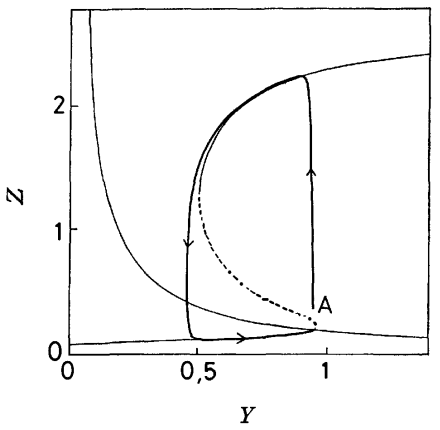

Fig. 5. System behaviors falling into the stable steady state from an initial state A.
Parameter values used for calculations are: $c_1=0.9$, $c_2=4.76$, $d_1=1.332\times10^3$, $d_2=4.864\times10^2$, $d_3=5.02\times10^2$, and $d_4=53.5$.

which may utilize the stored memory in the system-M in order to attain its own specific purpose. In order to draw the memory from the system-M, it should respond to a certain input depending on whether the system-M is storing with a memory or not, because the external system-E can not draw the memory without examining its response to an input. In this meaning, the system-M proposed here can be said that it has a mnemonic function as revealed by the system behaviors shown in Figs. 3 and 4.

System Linked with an Excitable System (System-M')

In the preceding section, we have shown a series of differential equations related to the mnemonic function. Here, we develop a model by combining an excitable subsystem with the system-M in order to demonstrate more drastically the mnemonic function. The newly introduced system is referred hereafter as system-M'.

Let us introduce the following equations[7]

$$\frac{dY}{dt} = c_1 - c_2YZ, \tag{5}$$

$$\frac{dZ}{dt} = d_1YZ^2 - d_2YZ^3 - d_3Z + d_4. \tag{6}$$

For the parameters we choose the following values;
$c_1=0.9$, $c_2=4.76$, $d_1=1.332\times10^3$, $d_2=4.864\times10^2$, $d_3=5.02\times10^2$, and $d_4=53.5$.

As is clear from Fig. 5, the system shows an excitation behavior when the Z value is increased beyond over the critical value on the dotted line.[7] Now, let us construct a system which a large value of X causes an increase in Z. With this device, we could construct a mechanism which generates one pulse by each of the large amplitude oscillation (Fig. 2c) but no pulse by the small amplitude oscillation (Fig. 2b). To this end, Eq. 6 is modified as follows;

$$\frac{dZ}{dt} = d_1YZ^2 - d_2YZ^3 - d_3Z + d_4 + d_5X, \tag{7}$$

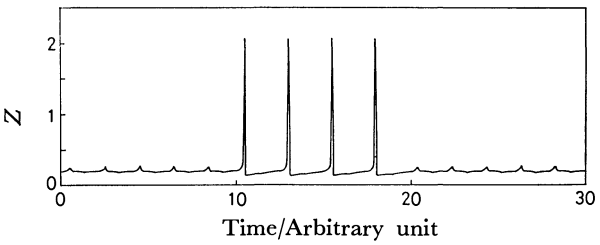

Fig. 6. Effect of change in β value on the behavior of the system-M′.
At time 10, the β value is changed from 70.0 to 75.0, and at time 20, the value is regressed to 70.0. The value of $d_5=0.39$ is used for calculations.

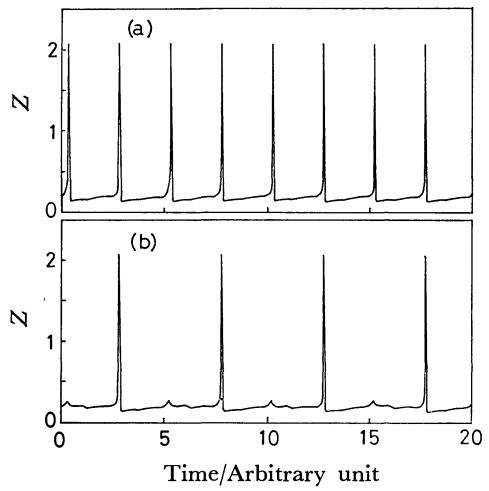

Fig. 7. Behaviors of the system-M′ for the two values of d_5.
(a) $d_5=0.39$ and (b) $d_5=0.38$.

where the last term represents a linkage between the two systems and insures an increase in the Z value owing to an increasing X value.

The behavior of the system-M′ thus constructed is determined by solving Eqs. 1, 2, 5, and 7 with a digital computer. Figure 6 is of an example of the calculated results and shows the response of the system-M′ due to an increase in the parameter β from 70.0 to 75.0 at time 10 and an decrease to its original value at time 20. The input given by the change in β gives large amplitude pulse-like oscillations when the system-M′ stores the memory of the past deviations. Reversely, when the system-M′ does not have any memories, it does not generate any pulses by an input. In this case, the coupling parameter d_5 is assumed to be 0.39

When the value of d_5 is shifted to 0.38, the system-M′ shows a peculiar behavior. Figure 7 shows the behaviors of the system having the d_5 values of 0.39(a) and 0.38(b). In the case of $d_5=0.39$, the excitable subsystem generates pulse-like oscillations as a response to every oscillation of the system-M. On the other hand, in the case of $d_5=0.38$, the excitable subsystem does not respond to every oscillation but responds to every second oscillation. This is because the excitable subsystem has a refractory period after an excitation. In such a situation, a skip of excitation occurs; when a succeeding oscillation of the system-M comes during the refractory period, the excitable subsystem can not respond to this stimulus.

Reaction Processes

In this article, we proposed an artificial rate equation system to show a mnemonic function in a chemical reaction system far from an equilibrium state. The rate equation (2) contains unnatural terms of higher orders than second order. In this section, we show a series of reaction processes to show appearance of a higher order polynomial by a proper selection of bimolecular reaction processes.

For example, let us presume the following consecutive reactions

$$X + X \rightleftharpoons X_2, \quad \text{(R1)}$$

$$X_2 + X \rightleftharpoons X_3, \quad \text{(R2)}$$

$$\cdots\cdots\cdots\cdots$$

$$X_{i-1} + X \rightleftharpoons X_i, \quad \text{(R3)}$$

$$A + X_i \xrightarrow{k} P, \quad \text{(R4)}$$

where we presume that the rate constants of (R1)—(R3) are much larger than k of (R4) and the processes (R1)—(R3) attain nearly equilibria. Then, we get

$$X_i = K \cdot X^i, \quad (8)$$

where K is an overall equilibrium constant which is a product of equilibrium constants of the respective steps (R1)—(R3). Then, the decreasing rate of X in the reaction processes (R1)—(R4) is given by

$$\frac{dX}{dt} = -ikAX_i = -ikKAX^i, \quad (9)$$

this is the i-th order polynomial equation. With a similar procedure, we can deduce the rate equation (2) from a series of bimolecular elementary processes. But the scheme thus constructed is no more than one of the possible schemes and has no essential meaning in this work.

References

1) P. Glansdorff and I. Prigogine, "Thermodynamic Theory of Structure, Stability, and Fluctuations," Wiley, New York (1971).
2) G. Nicolis and I. Prigogine, "Self-Organization in Nonequilibrium Systems," Wiley, New York (1977).
3) A. T. Winfree, *Science*, **175**, 634 (1972).
4) M. Flicker and J. Ross, *J. Chem. Phys.*, **60**, 3458 (1974).
5) C. S. Haase, J. Chadam, D. Feinn, and P. Ortoleva, *Science*, **209**, 272 (1980).
6) H. S. Hahn, A. Nitzan, P. Ortoleva, and J. Ross, *Proc. Natl. Acad. Sci. U.S.A.*, **71**, 4067 (1974).
7) K. Iwamoto and M. Senō, *J. Chem. Phys.*, **70**, 5851 (1979).
8) J. J. Tyson, *J. Chem. Phys.*, **66**, 905 (1977).
9) P. Ortoleva and J. Ross, *J. Chem. Phys.*, **58**, 5673 (1973).
10) E. J. Reusser and R. J. Field, *J. Am. Chem. Soc.*, **101**, 1063 (1979).
11) L. M. Pismen, *J. Chem. Phys.*, **71**, 462 (1979).
12) M. P. Hanson, *J. Chem. Phys.*, **61**, 2081 (1974).
13) A. Boiteux and B. Hess, *Faraday Symp. Chem. Soc.*, **9**, 202 (1974).

14) T. Pavlidis, "Biological Oscillators: Their Mathematical Analysis," Academic, New York (1973).
15) J. Keizer, P. A. Rock, and S. Lin, *J. Am. Chem. Soc.*, **101**, 5637 (1979).
16) A. L. Hodgkin and A. F. Huxley, *J. Physiol.*, **117**, 500 (1952).
17) A. M. Turing, *Philos. Trans. Roy. Soc. (London)*, **B237**, 37 (1952).
18) W. S. McCulloch and W. Pitts, *Bull. Math. Biophys.*, **5**, 115 (1943).
19) E. R. Caianiello, *J. Theor. Biol.*, **2**, 204 (1961).
20) "Seimei No Butsuri," in "Gendai Butsurigaku No Kiso," 2nd ed, ed by H. Yukawa, Iwanami, Tokyo (1978), Vol. 8, pp. 321—330.
21) A. Uppal, W. H. Ray, and A. B. Poore, *Chem. Eng. Sci.*, **29**, 967 (1974).
22) K. Iwamoto and M. Senō, *Bull. Chem. Soc. Jpn.*, **54** 669 (1981).

CIDEP Study of Durosemiquinone Radical in Various Solvents

Akihiko KANEMOTO, Sigeya NIIZUMA,† Siro KONISHI,†† and Hiroshi KOKUBUN*
Department of Chemistry, Faculty of Science, Tohoku University, Aoba, Aramaki, Sendai 980
(Received June 4, 1982)

F-pair polarization and triplet mechanism (TM) polarization of durosemiquinone radical produced by light irradiation of duroquinone–phenol systems were discriminated at 260 K in a simple way based on the analysis of the enhancement factors in the steady-state method with intermittent light irradiation. Both polarizations are not so sensitive to viscosity or polarity of solvents. TM enhancement factor is nearly constant (−0.8) in wide range of viscosity (2.5—25 cP, 1 cP = 0.001 Pa s). F-pair polarization is suppressed in some extent by halogenated solvents while TM polarization is not affected by such solvents.

Semiquinone radicals produced by light irradiation of quinones in the presence of reducing agents show Chemically Induced Dynamic Electron Polarization (CIDEP) arising from both the triplet mechanism (TM) and the radical pair mechanism (RPM).[1,2] The elementary descriptions of these mechanisms are as follows: The TM polarization arises from the anisotropic intersystem crossing from the lowest excited singlet state (S_1) to each spin sublevel of the triplet state (T_n) in a photoexcited molecule, and the RPM polarization comes from the magnetic interaction in radical pairs, which are formed from initial reactions of excited molecules or from random encounters among the radicals in the later stage. Then some fundamental questions arise. Is the magnitude of TM polarization varied by interaction with the external heavy atom because of the change in the anisotropy of the $S_1 \rightarrow T_n$ intersystem crossing as is observed in phosphorescence in solid phase at very low temperatures[3]? And, is the magnitude of RPM polarization influenced by the solvent viscosity, which the interacting period for two radicals is likely to depend upon?

In order to answer such questions, we chose duroquinone–phenol (DQ–PhOH) systems, because durosemiquinone radical produced by light irradiation shows polarizations caused by both mechanisms. Some halogenated solvents were used to see the external heavy atom effect and also used a variety of mixed solvents to change viscosity and polarity.

Experimental

All chemicals were GR grade and used without further purification except 1-bromo-2-propanol, which was distilled under reduced pressure to remove the coloured component. But it remained containing 2-bromo-1-propanol (20%). No effect was observed for the experimental results by the addition of a small amount of water to *i*-PrOH dried over molecular sieves.

In ESR observations, DQ and PhOH concentrations were fixed to 0.1 mol dm^{-3} and 2.2 mol dm^{-3}, respectively, and the temperature was kept at 260 K.

The CIDEP observation system is illustrated in Fig. 1. A JEOL PE-1X type ESR spectrometer using 100 KHz field modulation was improved to have sufficient short responce time (150 μs) to observe the rise and decay of neutral durosemiquinone radical (DQH·). The sample solution was

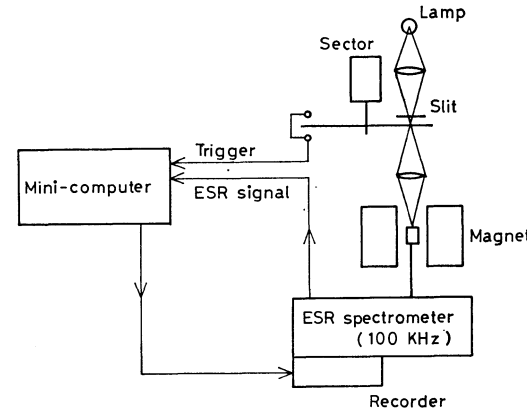

Fig. 1. Block diagram of CIDEP observation.

irradiated intermittently by the sector whose light-ON and light-OFF periods were 13.3 and 26.7 ms, respectively. The light source was a 1 kW Ushio USH-1005D super-high-pressure mercury lamp. The temperature rise of about 1 K during irradiation was observed.

ESR signal was sampled at every 60 μs over 36 ms at a fixed magnetic field corresponding to one of the first derivative peak positions of DQH· spectrum. The time profile of the signal obtained in this way were accumulated 6000—20000 times with a JEOL EC-6 minicomputer (Fig. 2). The time required for accumulation was 5—16 min. Irradiation of this rather long time gave no change in the UV absorption spectra of the samples. The absorption spectra were recorded on a Hitachi EPS-3T spectrophotometer.

Analysis of the Time Profile

The steady-state enhancement factor V_{ss} is defined as:

$$V_{ss} = \frac{I_{ss} - I_{ss.0}}{I_{ss.0}}, \quad (1)$$

where I_{ss} is the intensity of the ESR signal in the presence of CIDEP and $I_{ss.0}$ that in the absence of CIDEP.

It has been known that DQH· produced by light irradiation of DQ–PhOH systems show TM and F-pair polarization.[1,2] The latter is one type of RPM polarization caused by random encounters among DQH· radicals. It is possible that initial (or geminate) pair polarization occurs in the radical pair $\overline{\text{DQH·}\ \text{PhO·}}$ formed by the initial reaction

$$^3\text{DQ}^* + \text{PhOH} \longrightarrow \overline{\text{DQH·, PhO·}}, \quad (\text{I})$$

where ^{3}DQ* is the excited triplet state of DQ and

† Present address: College of Humanities and Social Sciences, Iwate University, Ueda, Morioka 020.

†† Present address: The Institute of Physical and Chemical Research, Wako, Saitama 351.

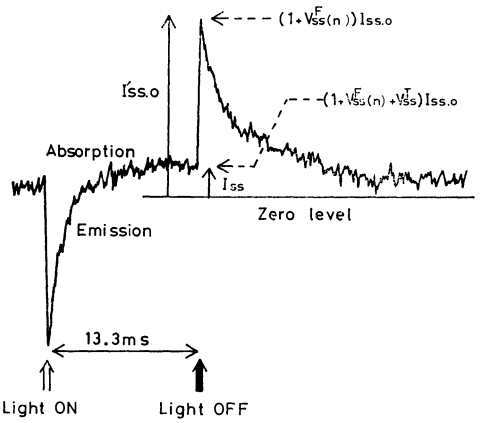

Fig. 2. Time profile of ESR signal intensity.

PhO· phenoxyl radical. As far as photochemically produced geminate radical pairs are concerned, there are few reports about initial pair polarization.[4,5] It is assumed that initial polarization observed in our experiment is due to TM only. We denote the enhancement factor for initial polarization as V_{ss}^{T}, which has no hyperfine dependence. The magnitude of F-pair polarization depends upon the nuclear spin state in DQH·. We denote the enhancement factor of F-pair polarization observed at the nth peak in ESR spectrum as $V_{ss}^{F}(n)$.

In the time profile shown in Fig. 2, the concentration of DQH· immediately after the light-OFF point is equal to the steady-state concentration reached in the light-ON period because of the slow decay of DQH· radical. Therefore the upward spike can be attributed to the rapid disappearance of TM polarization. From the definition (Eq. 1),

$$I_{ss} = (1+V_{ss})I_{ss.0} \tag{2}$$

Signal intensities immediately before and after the light-OFF point (I_{ss} and $I'_{ss.0}$, respectively) can be written as follows:

$$I_{ss} = (1+V_{ss}^{F}(n)+V_{ss}^{T})I_{ss.0} \tag{3}$$

$$I'_{ss.0} = (1+V_{ss}^{F}(n))I_{ss.0}. \tag{4}$$

With our CIDEP observation system, absolute signal intensity can not be measured. Instead, the following dimensionless quantity, which is slightly different from the enhancement factor, is measured.

$$V'(n) = \frac{I_{ss}-I'_{ss.0}}{I'_{ss.0}} \tag{5}$$

From Eqs. 3 and 4, we obtain

$$V'(n) = \frac{V_{ss}^{T}}{1+V_{ss}^{F}(n)}. \tag{6}$$

Since the signal intensity at the center of the ESR spectrum is unaffected by F-pair polarization,[6] there exists the following relation.

$$V'(n)_{center} = V_{ss}^{T} \tag{7}$$

$V_{ss}^{F}(n)$ can be obtained from Eqs. 6 and 7.

Time dependence of signal intensity is written as Eq. 8 following Fessenden's treatment.[7]

$$I(t) = \left(\frac{V_{ss}^{F}(n)}{1+t/t_{1/2}}+1\right)\cdot\frac{I'_{ss.0}}{1+t/t_{1/2}}, \tag{8}$$

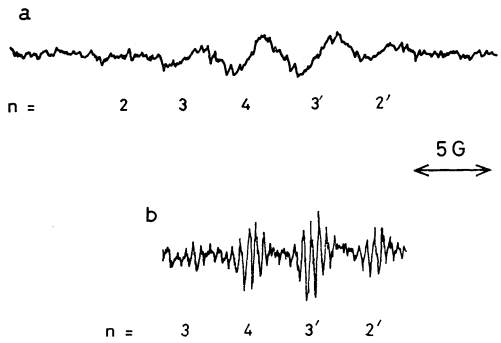

Fig. 3. ESR spectra of durosemiquinone radical DQH· in *i*-PrOH at 260 K.
Concentrations of DQ and PhOH are 0.1 and 2.2 mol dm^{-3}. Modulation width are 2.0 G (a) and 0.2 G (b).

where $t_{1/2}$ is the half-life of a radical. At the center line ($V_{ss}^{F}(n)=0$) Eq. 8 becomes simple second order decay. Signal zero level was so determined that the decay analysis in the light-OFF period gave the best fit to the second order kinetic. Decays of other lines were also well approximated by hyperbolas.

Results and Discussion

On the TM Enhancement Factor. The ESR spectrum of DQH· is shown in Fig. 3. Only neutral radical was detected and durosemiquinone anion radical (DQ^{-}) was not observed. Hyperfine splitting constants of DQH· were 4.8 G (1 G=10^{-4} T, 6H) and 0.6 G (6H). A modulation width of 2.0 G was used to make the spectrum large septet lines.

Light intensity dependence of V_{ss}^{T} was studied to examine the reliability of our apparatus and to find whether the following relation, which had been given for $V_{ss}^{F}(n)$ by Fessenden,[7] could be applied to V_{ss}^{T}.

$$V_{Int} = \frac{V_{ss}t_{1/2}}{T_1}, \tag{9}$$

where V_{int} is the intrinsic enhancement factor independent of the radical concentration, and T_1 is the longitudinal relaxation time. T_1 of DQH· could not be measured because of the long responce time of the spectrometer. It is likely to be constant regardless of the light intensity. If that is the case, $V_{ss}t_{1/2}$ should be independent of the radical concentration, which depends on light intensity. A plot of $V_{ss}^{T}t_{1/2}$ *vs.* the square root of light intensity is shown in Fig. 4. Values of V_{ss}^{T} were measured at the higher and the lower field peaks of the central resonance line (n= 4). The numbering of the septet line is illustrated in Fig. 3. The average of four measurements at each line is taken and listed in Fig. 4.

$V_{ss}^{T}t_{1/2}$ is independent of the light intensity as expected. Therefore the Eq. 9 is valid for V_{ss}^{T} as well as $V_{ss}^{F}(n)$. Fig. 4 also shows the square root dependence of V_{ss}^{T} on the light intensity. This can be attributed to the disproportional radical decay:

$$DQH\cdot + DQH\cdot \longrightarrow DQ + DQH_2. \tag{II}$$

In the neat solvents except *i*-PrOH, DQH· was

TABLE 1. SOLVENT DEPENDENCE OF V_{ss}^{T} AT 270 K[a)]

Added solvent[b)]	Molar fraction[b)]	$-V_{ss}^{T}$	$t_{1/2}$/ms	$-V_{ss}^{T}t_{1/2}$/ms	η/cP	ε[c)]
CH_2Cl_2	0.4	0.75	1.6	1.2	2.5	22
Toluene	0.4	0.83	1.4	1.2	2.5	11
MeOH[d)]	0.6	0.82	1.7	1.4	3.1	22
Cyclohexane	0.4	0.86	1.7	1.5	4.2	11
(*i*-PrOH)	0	0.76	2.0	1.5	8.6	18
1-Bromo-2-propanol	0.2	0.76	2.3	1.8	11.0	
Ethylene glycol	0.2	0.79	2.2	1.8	14.3	20
1-Bromo-2-propanol	0.4	0.74	2.4	1.7	16.9	
1-Bromo-2-propanol	0.6	0.77	2.5	1.9	24.2	
Ethylene glycol	0.4	0.87	2.7	2.3	24.7	23

a) The light intensity was kept constant. b) Added solvents to *i*-PrOH and their content in molar fraction. c) Dielectric constants were calculated from volume ratio of added solvent and PhOH. d) Light intensity change was corrected using the relation (9).

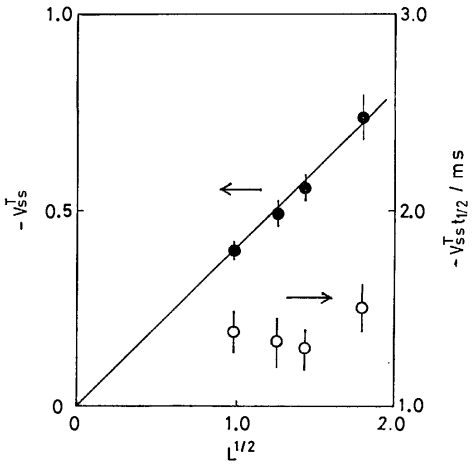

Fig. 4. Light intensity dependence of V_{ss}^{T} and $V_{ss}^{T}t_{1/2}$. L denotes the relative light intensity.

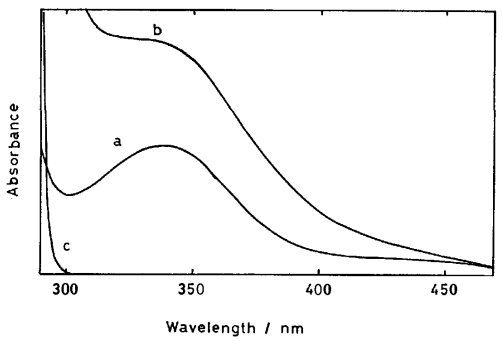

Fig. 5. Absorption spectra of a: DQ (0.07 mol dm^{-3}), b: DQ and PhOH (0.07 and 1.7 mol dm^{-3}) and c: PhOH (1.7 mol dm^{-3}) in *i*-PrOH at room temperature.

not detected. Thus, V_{ss}^{T} was measured in the mixed solvents with *i*-PrOH. Results are listed in Table 1. The light intensity was kept constant.

Only a small change in V_{ss}^{T} was observed with the change of dielectric constants of solvents from 11 to 23. Any simple correlation between V_{ss}^{T} and ε could not be found. Hence $S_1 \rightarrow T_n$ intersystem crossing in DQ* is thought to be unaffected by solvent polarity in spite of the near location of both (n,π^*) and (π,π^*) states with the lowest triplet state.[8)]

It must be noted that the addition of PhOH to the DQ solution gave an obvious change in absorption spectra (Fig. 5). This was referred previously by Elliot and Wan,[1)] and attributed to the change in hydrogen bonding characteristics as the addition of PhOH. However, similar spectral change was observed by the addition of other aromatic compounds such as benzene or toluene, but not with aliphatic additives such as cyclohexane or acetonitrile. Thus, the change of optical spectra is explained in terms of the interaction between aromatic rings of DQ and PhOH rather than the hydrogen bond.

Table 1 also indicates that V_{ss}^{T} is not sensitive to solvent viscosity. V_{int}^{T} was described by Wan and Elliot[1,2)] as follows:

$$\frac{1}{V_{int}^{T}} = \frac{1}{V_{\infty}^{T}}\left(1+\frac{1}{{}^3T_1 \times k_q[\mathrm{PhOH}]}\right), \tag{10}$$

where ${}^3T_1$ is the longitudinal relaxation time of ^{3}DQ*, k_q is the second order rate constant of the reaction (I), and V_{∞}^{T} is the limitting value of V_{int}^{T} at infinite concentration of PhOH. V_{ss}^{T} was expected to be sensitive to solvent viscosity because of the viscosity dependences of T_1, ${}^3T_1$, and k_q. But noticeable dependence of V_{ss}^{T} on solvent viscosity was not observed.

There is a correlation between $V_{ss}^{T}t_{1/2}$ and the viscosity. To discuss this, Eqs. 9 and 10 are combined to give

$$V_{ss}^{T}t_{1/2} = \frac{1}{{}^3T_1^{-1}\cdot k_q^{-1}\times[\mathrm{PhOH}]^{-1}+1}\cdot V_{\infty}^{T}\cdot T_1 \tag{11}$$

If cancellation occures between the effect of ${}^3T_1$ and k_q, the denominator of the right hand side of Eq. 11 is insensitive to the viscosity. This seems to be the case found in the report on $DQ^{\cdot-}$, which was given by Atkins as shown in Table 2.[9)] Values of $k_q \cdot {}^3T_1$ are nearly constant except in methanol. From the same reason, $k_q \cdot {}^3T_1$ is likely to be insensitive to viscosity variation in our systems. Then, if we assume that V_{∞}^{T} is independent of solvent viscosity, from Eq. 11 viscosity dependence of $V_{ss}^{T}t_{1/2}$ is attributed to that of T_1, and from the values of $V_{ss}^{T}t_{1/2}$ it turns out that T_1 increases about twice as the viscosity

Table 2. Rate constant k_q of the reaction $^3DQ^* + (C_2H_5)_3N \rightarrow DQ^{\cdot-} + (C_2H_5)_3N^{+}$ and longitudinal relaxation times in some solvents, by Atkins, *et al.*[9]

Solvent	η / cP	$k_q \times 10^{-8}$ / $mol^{-1}\,dm^3\,s^{-1}$	$^3T_1$ / ns	$^2T_1$ / μs	$^3T_1/{}^2T_1$	$k_q{}^3T_1$ / $mol^{-1}\,dm^3$
CH_3OH	0.61	2.7	2.7	2	1.4×10^{-3}	0.73
$(CH_3)_2CHOH$	2.2	3.6	9.7	8	1.2×10^{-3}	3.5
$(CH_3)_3COH$	4.8	3.9	7.1	9	0.9×10^{-3}	3.0
cyclo-$C_6H_{11}OH$	57	1.9	17	18	0.9×10^{-3}	3.2

Table 3. Solvent dependence of V_{ss}^{F} at 270 K

Added solvent	Molar fraction	$V_{ss}^{F}(3)/\lvert V_{ss}^{T}\rvert$	$V_{ss}^{F}(3')/\lvert V_{ss}^{T}\rvert$	$-V_{ss}^{T}$	$t_{1/2}$ / ms	η / cP
Toluene	0.4	−0.44	0.46	0.79	1.8	2.9
Cyclohexane	0.4	−0.43	0.47	0.82	1.7	4.2
(*i*-PrOH)	0	−0.40	0.43	0.86	1.7	8.6
Ethylene glycol	0.2	−0.36	0.43	0.93	2.0	14.3
Ethylene glycol	0.4	−0.36	0.31	0.70	2.6	24.7
Bromobenzene	0.4	−0.29	0.27	0.75	1.7	4.0
CCl_4	0.4	−0.26	0.34	0.54	2.7	4.7
1-Bromo-2-propanol	0.2	−0.16	0.14	0.93	2.1	11.0
1-Bromo-2-propanol	0.4	−0.10	0.13	0.92	2.3	16.9
1-Bromo-2-propanol	0.6	−0.10	0.15	0.80	2.9	24.2
1,3-Dibromo-2-propanol	0.4	−0.27	0.25	0.64	3.7	36.9

changes from 2.5 to 24.7 cP, and V_{int}^{T} is independent of viscosity.

The above assumption that V_{∞}^{T} is not influenced by solvent viscosity can be rationalized as follows. The enhancement factor V_{int}^{T} can be written as Eq. 12 using the theoretical equation for the magnetization $\langle S_z\rangle$ of a radical polarized due to TM given by Atkins and Evans (Ref. 10, Eq. 5—3).

$$V_{int}^{T} = \frac{\langle S_z\rangle - \langle S_{z.e}\rangle}{\langle S_{z.e}\rangle} \simeq \frac{\langle S_z\rangle}{\langle S_{z.e}\rangle} = \frac{(DK+3EI)}{1+k_T^{-1}\cdot{}^3T_1^{-1}} \cdot \frac{2}{15}\left(\frac{4\omega_0\tau_2^2}{1+4\omega_0^2\tau_2^2} + \frac{\omega_0\tau_2^2}{1+\omega_0^2\tau_2^2}\right) \cdot \frac{1}{\langle S_{z.e}\rangle} \tag{12}$$

where $\langle S_{z.e}\rangle$ is the thermal magnetization of the radical, k_T is the triplet quenching rate which can be substituted by $k_q\cdot$[PhOH] in our case, D and E are zero-field splitting constants, K and I are parameters showing anisotropy of $S_1 \rightarrow T_n$ intersystem crossing rate, ω_0 is angular frequency of the microwave, and τ_2 is the rotational correlation time. In the derivation of $\langle S_z\rangle$, isotropic rotational diffusion and the unity yield of intersystem crossing are assumed. The latter condition is valid for DQ.[11] Then we get Eq. 13 from Eq. 10.

$$V_{\infty}^{T} = \frac{2}{15}\left(\frac{4\omega_0\tau_2^2}{1+4\omega_0^2\tau_2^2} + \frac{\omega_0\tau_2^2}{1+\omega_0^2\tau_2^2}\right)\cdot\frac{DK+3EI}{\langle S_{z.e}\rangle} \tag{13}$$

If we adopt the Debye's relation $\tau = 4\pi\eta r^3/3kT$ for τ_2 (assuming r=4 A), Eq. 13 reduces to Eq. 14 because $\omega_0\tau_2 \gg 1$.

$$V_{\infty}^{T} = \frac{4}{15}\cdot\frac{DK+3EI}{\langle S_{z.e}\rangle}\cdot\frac{1}{\omega_0} \tag{14}$$

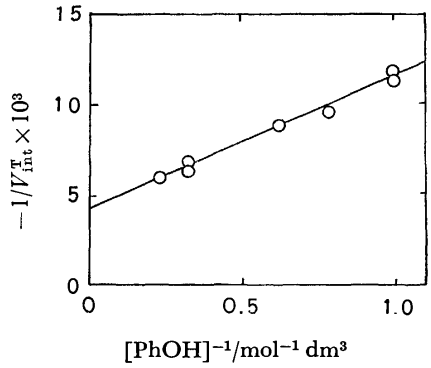

Fig. 6. Effect of phenol concentration on V_{int}^{T} of DQH· in *i*-PrOH at 260 K.

Consequently V_{∞}^{T} does not depend on viscosity.

The value of V_{∞}^{T} can be obtained by extrapolating the plot of $(V_{int}^{T})^{-1}$ *vs.* [PhOH]$^{-1}$ according to Eq. 10 and the value $(DK+3EI)$ of $^3DQ^*$ in liquid phase is calculable from V_{∞}^{T}. This plot was carried out for the PhOH concentration range from 1 to 4 mol dm^{-3} using T_1 values of $DQ^{\cdot-}$ in ethanol reported by Rengan *et al.*[12] The plot was linear and V_{∞}^{T} was obtained to be −240, as shown in Fig. 6. By using Eq. 14, we obtain $(DK+3EI) = -0.1$ cm^{-1}. This is a reasonable value for an aromatic compound. Also $^3T_1$ of $^3DQ^*$ was estimated to be 2.6 ns from the slope of the plot using the value of $k_q = 2\times10^8$ mol^{-1} dm^3 s^{-1}.[1]

With aromatic carbonyls in solid phase, D, E and the rate of intersystem crossing are remarkably influenced by the nature of host and the external heavy atom.[3] On the other hand in liquid phase, the addition of nonpolar or viscous solvents to the $DQ^{\cdot-}$

PhOH system does not affect the TM enhancement factor as discussed above. The addition of halogenated solvents to the system also gives little change in V_{ss}^{T} (see Table 1).

On the RPM Enhancement Factor. In various solvents, $V_{ss}^{F}(3)$ and $V_{ss}^{F}(3')$, together with V_{ss}^{T} were measured. Table 3 lists the ratios of $V_{ss}^{F}(n)/V_{ss}^{T}$ which are intrinsic value independent of the light intensity:

$$V_{ss}^{F}(n)/V_{ss}^{T} = \frac{V_{ss}^{F}(n)t_{1/2}}{T_1} \Big/ \frac{V_{ss}^{T}t_{1/2}}{T_1} = V_{int}^{F}(n)/V_{int}^{T}. \quad (15)$$

This ratio can be regarded as the reflection of the solvent dependence of V_{int}^{F}, because V_{ss}^{T} or V_{int}^{T} is nearly independent of solvents as discussed. The sign of $V_{ss}^{F}(3)$ is negative (emission) and the one of $V_{ss}^{F}(3')$ positive (enhanced absorption). Absolute values of $V_{ss}^{F}(3)$ and $V_{ss}^{F}(3')$ of each sample were equal, which is consistent with the theory of RPM.[6] This fact gives a support to the validity of the simple method of the analysis we adopted.

In the first five lines in Table 3, results on samples without heavy atoms are listed. In spite of the wide change in viscosity ranging from 2.9 to 24.7 cp, the deviation of the ratio is within 25%. As mentioned previously, the change in viscosity is expected to vary the period of magnetic interaction between radicals within the radical pair $\overline{\text{DQH}\cdot\ \text{DQH}\cdot}$, so that the enhancement factor of RPM is likely to be sensitive to solvent viscosity. The result is contrary to this expectation. The value of $V_{ss}^{F}(n)/V_{ss}^{T}$ decreases slightly with increasing viscosity.

$V_{ss}^{F}(n)/V_{ss}^{T}$ is remarkably small when the sample contains 1-bromo-2-propanol, as shown in the lower part of Table 3. Other halogenated solvents have the similar effect to 1-bromo-2-propanol, however the magnitude is small. Two possible causes for this effect are considered. (1) The yield or the rate of the reaction (II), which is the origin of F-pair polarization, decreases for the participation of such solvents. (2) There is the external heavy atom effect on the F-pair polarization, *i.e.*, the reduction of the singlet-triplet mixing in the radical pair $\overline{\text{DQH}\cdot\ \text{DQH}\cdot}$. A possible mechanism for (1) is that a considerable amount of DQH· decays through a process other than (II). This mechanism, however, fails to explain that the half-life of DQH· is unaffected by halogenated solvents. Although the cause (2) cannot explain quantitatively the difference in magnitude of the effect among halogenated solvents, it is likely to exist. A probable mechanism of cause (2) is a suppression of the interaction between radicals by another interaction between radicals and halogenated solvents.

References

1) A. J. Elliot and J. K. S. Wan, *J. Phys. Chem.*, **82**, 444 (1978).
2) J. K. S. Wan and A. J. Elliot, *Acc. Chem. Res.*, **10**, 161 (1977).
3) T. H. Cheng and N. Hirota, *Mol. Phys.*, **27**, 281 (1974).
4) H. Paul, *Chem. Phys.*, **40**, 265 (1979).
5) S. K. Wong, Tak-Ming Chiu, and J. P. Bolton, *J. Phys. Chem.*, **85**, 12 (1981).
6) F. J. Adrian, "Chemically Induced Magnetic Polarization," ed by L. T. Muus, P. W. Atkins, K. A. McLauchlan, and J. B. Pedersen, Reidel, Dordrecht (1977), Chap. 5.
7) R. W. Fessenden, *J. Chem. Phys.*, **58**, 2489 (1973).
8) W. Herre and P. Weis, *Spectrochim. Acta*, **29**, 203 (1973).
9) P. W. Atkins, A. J. Dobbs, and K. A. McLauchlan, *Chem. Phys. Lett.*, **29**, 616 (1974).
10) P. W. Atkins and G. T. Evans, *Mol. Phys.*, **27**, 1633 (1974).
11) E. Amouyal and R. Bensasson, *J. Chem. Soc., Faraday Trans. 1*, **72**, 1247 (1976).
12) S. K. Rengan, H. P. Khakhar, B. S. Prabhananda, and B. Venkataraman, *Pramana*, **3**, 95 (1974).

 © 1983 The Chemical Society of Japan Bull. Chem. Soc. Jpn., 56, 51—54 (1983)

Enthalpies of Combustion of Organic Compounds. IV. Acetanilide and Nicotinic Acid**

Tomoko SATO-TOSHIMA, Akeji KAMAGUCHI, Keiichi NISHIYAMA, Minoru SAKIYAMA,* and Syûzô SEKI†

Chemical Thermodynamics Laboratory and Department of Chemistry, Faculty of Science, Osaka University, Toyonaka 560

(Received June 24, 1982)

Standard energies of combustion at 298.15 K have been determined for crystalline acetanilide and nicotinic acid by static oxygen bomb calorimetry. Derived standard enthalpies of combustion and of formation are $-(4224.8\pm1.0)$ and $-(209.5\pm1.5)$ kJ mol^{-1} for acetanilide, and $-(2730.83\pm0.48)$ and $-(344.81\pm0.92)$ kJ mol^{-1} for nicotinic acid, respectively. Nicotinic acid pellets of 1.2 g in mass showed remarkable tendency to spatter when partially burnt. Factors governing the completeness of combustion of the material have been explored through 28 test combustion experiments.

The role and desired properties of test substances in combustion calorimetry were discussed in detail by Armstrong and Johnson[1] and by Cox.[2] A recommendation was issued from IUPAC on reference materials for enthalpy measurements including combustion calorimetry.[3] Urea,[1-3] acetanilide,[2-4] hippuric acid,[3] and tris(hydroxymethyl)aminomethane[3] were recommended or proposed as test substances and nicotinic acid[1] as a candidate, for oxygen bomb combustion calorimetry of organic compounds containing carbon, hydrogen, oxygen and nitrogen.

For acetanilide and nicotinic acid, Johnson determined standard enthalpies of combustion.[1,4,5] Johnson's value for acetanilide[4] is in good agreement with the value deduced from Wadsö's reaction calorimetric results.[6] However, no other combustion calorimetric results have been reported so far for these compounds.

In this paper, results of combustion calorimetric studies on these compounds are reported. In the course of this study, remarkable tendency of spattering during burning was found for nicotinic acid, so twenty-eight test combustion experiments were carried out on this compound in order to disclose requirements to realize complete combustion. The results of these test experiments are also reported.

Experimental

Materials. Acetanilide used in this study was a commercial standard material for organic microanalysis (Kishida, SMA-SP-1) prepared under the certification of a subcommission of the Japan Society for Analytical Chemistry. The sample as received was pressed into pellets and used in the experiments. The purity was found to be higher than 99.9 mole per cent by the analysis of DSC heating curves in the melting region. Nicotinic acid was a commercial reagent (Nakarai, G. R.), which was purified by recrystallization from aqueous solution and then from ethanol solution, followed by fractional sublimation *in vacuo* and recrystallization from aqueous solution. The last-mentioned step was additionally carried out, since DSC heating curves in the melting region for the sublimed sample gave an indication that it was in a metastable crystalline state. The recrystallized sample was dried *in vacuo* (about 1 Pa) and then subjected to pellet-drying[7-9] to remove a trace of occluded water. Pellets were produced again and stored on anhydrous magnesium perchlorate for one week. The purity of the purified nicotinic acid was found to be higher than 99.9 mole per cent by the method mentioned above. In the test combustion experiments on nicotinic acid, the untreated reagent as well as the purified material was employed. No significant difference was observed between these samples in the tendency of spattering.

Combustion Calorimetry. A constant temperature jacket type rotating bomb calorimeter with a platinum-lined bomb, described elsewhere,[10,11] was used without rotating the bomb. The samples were burnt at 3.04 MPa of oxygen pressure in the presence of 1 g of water. An ordinary platinum crucible with no lid(denoted by **a**; Parr, 43A5, 2.4 cm in diameter, 1.2 cm in depth, and 11 g in mass) was used for acetanilide. For nicotinic acid, a platinum crucible with a small lid[12] (denoted by **b**; 2.4 cm in diameter, 2.5 cm in depth, and 29.5 g in mass) was used to prevent the incomplete combustion. The calorimeter was calibrated by burning thermochemical standard benzoic acid (U.S. National Bureau of Standards, SRM 39i) under certificate conditions. Mean and standard deviation of the mean for the energy equivalent of the empty calorimetric system were (15158.53 ± 0.58) and (15166.91 ± 0.33) J K^{-1} for acetanilide and nicotinic acid experiments, respectively.

Nitric acid was determined by titration with aqueous sodium hydroxide. Carbon monoxide was barely detected in the present combustion calorimetric experiments.

Relative atomic masses were taken from the recommendation of IUPAC Commission on Atomic Weights (1977). Densities, specific heat capacities, and $(\partial U/\partial p)_T$ values at 298.15 K were taken from Refs. 4 and 5. Specific standard enthalpy of combustion at 298.15 K for cotton fuse ($CH_{1.86}O_{0.93}$) was -16507 J g^{-1} and the internal volume of the bomb was 0.3458 dm^3. Uncertainties in this paper are uncertainty intervals defined by Rossini,[13] unless otherwise stated.

Test Combustion Experiments on Nicotinic Acid. Measured amounts of nicotinic acid were pressed into pellets and they were ignited in the same way as in the combustion calorimetric experiments. After every test experiment, the internal surface and the internal fittings of the bomb were visually examined.

Results and Discussion

Combustion Tests on Nicotinic Acid. As was mentioned above briefly, nicotinic acid showed remarkable tendency of spattering to cause incomplete combustion,

** Contribution No. 18 from Chemical Thermodynamics Laboratory, Faculty of Science, Osaka University.

† Present address: School of Science, Kwansei Gakuin University, Nishinomiya 662.

TABLE 1. SUMMARY OF RESULTS OF TEST COMBUSTION ON NICOTINIC ACID

Series	$\frac{m(\text{sample})}{\text{g}}$	Pellet preparation method[a)]	Crucible[b)]	Number of experiments in which combustion was:	
				Complete	Incomplete
I	1.2	A	**a**	1	7
II	1.2	B	**a**	3	3
III	1.2	A	**b**	8	1
IV	0.3	A	**a**	0	2
V	0.3	B	**a**	0	3

a) A: The use of a hand pellet press, B: the use of a high pressure and an evacuable die. b) **a**: An ordinary platinum crucible with no lid, **b**: a deep platinum crucible with a small lid.

when a sample pellet weighing 1.2 g was ignited in an open crucible at 3 MPa of oxygen pressure. Nicotinic acid of 1.2 g mass gives rise to an adiabatic temperature rise of about 1.8 K for our calorimeter, which is of similar magnitude to that for the calibration experiments. In order to evaluate the degree of difficulty of combustion of this material, twenty-eight test combustion experiments were undertaken. If combustion is complete, carbon dioxide, water, nitrogen, and a small amount of nitric acid alone will be produced. The presence of the unburnt material, the carbonized material, or soot, in the bomb after the combustion, is taken to be the evidence of incomplete combustion in this context.

Two methods of pellet preparation were tested. One is the use of a commercial hand pellet press (Parr, 2811), which has been used in most of combustion calorimetric works in this laboratory(method A). The other is the use of a high pressure press with an evacuable die, which has been used for preparing KBr discs for infrared spectrometry (method B). The die, which was charged with powdered nicotinic acid, was evacuated, and then the powder was pressed at 700 MPa to produce a pellet. The die for method A cannot be evacuated. Two kinds of crucibles were examined: crucibles **a** and **b**, described in the experimental section. Pellets of two masses were tested: 1.2 and 0.3 g. Results of the test combustion experiments are given in Table 1.

In series I, pellets weighing 1.2 g were prepared by method A and ignited in crucible **a**. Combustion was complete in one of eight experiments. In the other seven experiments, unburnt nicotinic acid lumps, covered with the carbonized material, were found spattered on the internal bomb wall. This suggests that the fragmentation of the pellets occured in the course of combustion, and the extinction of fire resulted by the collision of the burning fragments with the cold bomb wall.

In series II, pellets weighing 1.2 g were produced by method B, and ignited in crucible **a**. Of six experiments, combustion was complete in three. In the other experiments, the deposition of a small amount of soot was observed on the internal bomb wall, but the spattering of unburnt sample was not experienced. The adoption of the high pressure and the evacuation of the die, both of which would serve to prepare rigid pellets, were considerably effective in suppressing the fragmentation. However, the method used in this series was not sufficient to produce complete combustion.

In series III, pellets weighing 1.2 g were prepared by method A and ignited in crucible **b**. Although spattering was observed in one of nine experiments, combustion was complete in the other eight experiments. The small lid would act as baffle for spattering fragments and at the same time it would serve to form a hot zone in the crucible to prevent the soot formation. This series was the most successful one and the method of this series was adopted in the combustion calorimetric experiments, as described in the experimental section.

In Johnson's experiments,[2)] in which pellets weighing 0.3 g were ignited in a crucible with no baffle plate at 3 MPa of oxygen pressure, incomplete combustion was not experienced.[16)] In order to study the effect of mass decrease on the completeness of combustion, experiments of series IV and V were conducted. Pellets weighing 0.3 g were produced by method A(series IV) or B(series V) and ignited in crucible **a**. In series IV, a small amount of soot was found only in the crucible. In these series, spattering was not experienced. Thus, the decrease of mass was confirmed to be effective in preventing the spattering. The soot formation in these series would probably be caused by insufficient temperature rise around the crucible during combustion, owing to the decrease of mass of the material.

To summarize, the methods other than the use of a crucible with a small lid are more or less insufficient to get complete combustion of a nicotinic acid pellet of the present size. This is the conclusion of the present study on the difficulty of complete combustion of nicotinic acid. The characteristics, disclosed in this study, should be taken into consideration properly, when the material is scrutinized as a candidate test substance.

Standard Enthalpies of Combustion. Each of six combustion calorimetric experiments was carried out for both compounds. Standard energies and enthalpies of combustion reported in this paper refer to the following idealized combustion reactions at 298.15 K:

$$C_aH_bO_cN_d(c) + [(4a+b-2c)/4]O_2(g) = aCO_2(g) + (b/2)H_2O(l) + (d/2)N_2(g), \quad (1)$$

where $a=8$, $b=9$, $c=1$, and $d=1$ for acetanilide and

Table 2. Summary of combustion calorimetric results on acetanilide

Experiment	1	2	3	4	5	6
m'(compd)/g	0.86912	0.86603	0.86086	0.86390	0.86756	0.86490
m'''(fuse)/g	0.00256	0.00308	0.00290	0.00298	0.00278	0.00285
$m^{i}(H_2O)$/g	1.172	1.112	1.219	1.155	1.216	1.188
p^{i}(gas)/MPa	3.040	3.040	3.043	3.043	3.079	3.047
$(T_i-273.15\ K)$/K	23.20757	23.21368	23.19775	23.18550	23.16898	23.17702
$(T_f-273.15\ K)$/K	25.03053	25.02821	25.00493	25.00034	24.98584	24.98874
ΔT_{corr}/K	0.02690	0.02693	0.02849	0.02874	0.02509	0.02446
ΔU_{ign}/J	5.4	5.4	7.1	7.1	5.8	6.0
ΔU_{Σ}/J	14.7	14.4	14.7	14.6	14.9	14.7
$\Delta U_d(HNO_3)$/J	47.5	14.9	47.2	46.1	46.3	45.2
ε^{i}(cont)/J K^{-1}	17.9	20.3	18.1	17.8	24.4	24.2
ε^{f}(cont)/J K^{-1}	19.1	21.6	19.3	19.0	25.6	25.4
$-\Delta U_{IBP}$/J	27252.3	27128.3	26987.8	27099.7	27198.1	27129.2
$-\{\Delta U_c^{\circ}/M\}$/kJ g^{-1}	31.2359	31.2324	31.2223	31.2417	31.2267	31.2431
$-\Delta U_c^{\circ}$/kJ mol^{-1}	4222.01	4221.54	4220.17	4222.80	4220.76	4222.98

Table 3. Summary of combustion calorimetric results on nicotinic acid

Experiment	1	2	3	4	5	6
m'(compd)/g	1.18214	1.24063	1.23510	1.24509	1.24186	1.24401
m'''(fuse)/g	0.00296	0.00290	0.00276	0.00266	0.00260	0.00288
$m^{i}(H_2O)$/g	1.123	1.193	1.123	1.178	1.114	1.137
p^{i}(gas)/MPa	3.049	3.038	3.055	3.076	3.053	3.033
$(T_i-273.15\ K)$/K	23.23376	23.14182	23.15302	23.13627	23.13809	23.14096
$(T_f-273.15\ K)$/K	24.99437	24.99146	24.99010	24.98798	24.98567	24.99136
ΔT_{corr}/K	0.02805	0.03037	0.02634	0.02619	0.02710	0.02717
ΔU_{ign}/J	4.3	4.9	6.1	6.1	2.4	6.1
ΔU_{Σ}/J	20.4	21.6	21.5	21.9	21.6	21.5
$\Delta U_d(HNO_3)$/J	26.7	27.7	29.5	28.0	24.7	22.0
ε^{i}(cont)/J K^{-1}	20.6	20.9	20.7	21.0	20.6	20.7
ε^{f}(cont)/J K^{-1}	21.6	21.9	21.7	22.0	21.7	21.7
$-\Delta U_{IBP}$/J	26308.8	27625.8	27494.8	27720.1	27645.9	27684.1
$-\{\Delta U_c^{\circ}/M\}$/kJ g^{-1}	22.1910	22.1893	22.1830	22.1883	22.1899	22.1808
$-\Delta U_c^{\circ}$/kJ mol^{-1}	2731.93	2731.73	2730.95	2731.60	2731.80	2730.67

a=6, b=5, c=2, and d=1 for nicotinic acid. Combustion calorimetric results on these compounds are presented in Tables 2 and 3. Symbols in these tables are essentially similar to those used by Hubbard *et al.*[14] except for ΔU_{Σ}, the sum of contributions from items 81—85, 87—91, and 93—94 as defined by Hubbard *et al.*[14] Mean and standard deviation of mean of the standard energies of combustion, $\{\Delta U_c^{\circ}/M\}$, are $-(31.2337\pm0.0037)$ and $-(22.1821\pm0.0017)$ kJ g^{-1} for acetanilide and nicotinic acid, respectively.

Derived molar standard thermodynamic quantities are presented and compared with literature values in Table 4. The following CODATA key values for thermodynamics[15] were used to calculate standard enthalpies of formation of both compounds: $\Delta H_f^{\circ}(CO_2, g) = -(393.51 \pm 0.13)$ and $\Delta H_f^{\circ}(H_2O, l) = -(285.830\pm0.042)$ kJ mol^{-1}, where uncertainties are those at the 95 per cent confidence level.

Uncertainties attached to the values of ΔU_c°(c) and ΔH_f°(c) are the uncertainty intervals, defined by Rossini.[13] Uncertainties for the values of ΔH_f°(c) are the square roots of the sum of the squares of weighted uncertainties of ΔH_f°(c), $\Delta H_f^{\circ}(CO_2, g)$, and $\Delta H_f^{\circ}(H_2O, l)$. The weight for ΔH_f°(c) is 1, and those for $\Delta H_f^{\circ}(CO_2, g)$ and $\Delta H_f^{\circ}(H_2O, l)$ are a and $(b/2)$, given in Eq. 1, respectively. Uncertainties of Johnson's standard enthalpies of combustion and of formation[4,5] were recalculated so as to be in accord with the present assignment. The standard enthalpy of formation from Wadsö's experiments on acetanilide was quoted from Ref. 2.

Table 4. Standard thermodynamic quantities at 298.15 K of acetanilide and nicotinic acid and comparison with literature values

	$-\Delta U_c^{\circ}$(c) / kJ mol^{-1}	$-\Delta H_c^{\circ}$(c) / kJ mol^{-1}	$-\Delta H_f^{\circ}$(c) / kJ mol^{-1}
Acetanilide			
Johnson[4]	4221.78±0.75	4224.88±0.75	209.4 ±1.3
Wadsö[6]	——	——	209.37±0.69
This work	4221.7 ±1.0	4224.8 ±1.0	209.5 ±1.5
Nicotinic acid			
Johnson[5]	2731.29±0.38	2730.67±0.38	344.97±0.87
This work	2731.45±0.48	2730.83±0.48	344.81±0.92

The standard enthalpies of combustion for both compounds, obtained in this study, agree with those of Johnson[4,5] within the assigned uncertainties. The present standard enthalpy of formation for acetanilide is in agreement with Wadsö's reaction calorimetric value[6] within the assigned uncertainties. Thus, standard enthalpies of combustion for these compounds have been determined more confirmatively.

References

1) G. T. Armstrong and W. H. Johnson, *Proc. 3rd Int. Conf. Chem. Thermodynamics (Baden, 1973)*, **8**, 55 (1973); G. T. Armstrong and W. H. Johnson, *NBSIR* 73-158 (July, 1973).
2) J. D. Cox, "Experimental Thermodynamics, Vol. 1, Combustion Calorimetry," ed by S. Sunner and M. Månsson, Pergamon, Oxford (1979), p. 57.
3) J. D. Cox, *Pure Appl. Chem.*, **40**, 399 (1974).
4) W. H. Johnson, *J. Res. Natl. Bur. Stds.*, **79A**, 487 (1975).
5) W. H. Johnson, *J. Res. Natl. Bur. Stds.*, **79A**, 425 (1975).
6) I. Wadsö, *Acta Chem. Scand.*, **16**, 471 (1962).
7) M. Beckers, *Bull. Soc. Chim. Belge*, **40**, 518, 571 (1931); **42**, 621 (1933).
8) C. E. Vanderzee and E. F. Westrum, Jr., *J. Chem. Thermodyn.*, **2**, 681 (1970).
9) C. E. Vanderzee and M. Månsson, *J. Chem. Thermodyn.*, **4**, 533 (1972).
10) M. Sakiyama, T. Nakano, and S. Seki, *Bull. Chem. Soc. Jpn.*, **48**, 1705 (1975).
11) K. Nishiyama, M. Sakiyama, S. Seki, H. Horita, T. Otsubo, and S. Misumi, *Bull. Chem. Soc. Jpn.*, **53**, 869 (1980).
12) A. Kamaguchi, T. Sato, M. Sakiyama, and S. Seki, *Bull. Chem. Soc. Jpn.*, **48**, 2203 (1975).
13) F. D. Rossini, "Experimental Thermochemistry," ed by F. D. Rossini, Interscience, New York (1956), Vol. 1, Chap. 12.
14) W. N. Hubbard, D. W. Scott, and G. Waddington, "Experimental Thermochemistry," ed by F. D. Rossini, Interscience, New York (1956), Vol. 1, Chap. 5.
15) CODATA Task Group on Key Values for Thermodynamics, 1977, *CODATA Bull.*, **28**, (1978); *J. Chem. Thermodyn.* **10**, 903 (1978).
16) Private communication from Dr. G. T. Armstrong (July, 1975).

Film Dichroism. VI.[1] Linearly-polarized Absorption Spectra of Neutral and Divalent 3,6-Diaminoacridine Dyes in the Stretched Poly(vinyl alcohol) Film

Kiwamu YAMAOKA* and Mitsuaki SHIMADZU

Faculty of Science, Hiroshima University, Higashisenda-machi, Naka-ku, Hiroshima 730

(Received April 16, 1982)

The linear dichroic spectra of the neutral (uncharged) and divalent (doubly charged) Acridine Orange, Acridine Yellow, and Proflavine were measured at 25 °C in the visible and UV wavelength regions by the film dichroism method. These 3,6-disubstituted symmetric acridine dyes were molecularly dispersed in the heat-treated poly(vinyl alcohol) film by the staining method. The neutral and divalent dye species were prepared by adding a sufficient amount of sodium hydroxide or sulfuric acid to the staining dye solutions. The wavelength dependence of the reduced dichroism, $\Delta A/A$, of the neutral species at a given stretch ratio was very similar to that of the monovalent species previously reported [*Bull. Chem. Soc. Jpn.*, **52**, 3163 (1979)]. Values of $\Delta A/A$ for the divalent species were nearly constant over the entire wavelength region 550—220 nm. The long-axis and short-axis polarized component (A_z and A_y) spectra were computed for the neutral dye species from the observed parallel- and perpendicular-polarized dichroic spectra by using a reduction procedure. The broad, principal band of each dye species in the visible region was deduced to be a composite of two orthogonal (a strong A_z and a weak A_y) electronic transitions.

In previous papers in this series,[2,3] we have shown that the monovalent, symmetrically-substituted acridine dyes can be oriented unidirectionally in the stretched poly(vinyl alcohol) (PVA) film and that the linearly polarized spectra of these dyes can be analyzed into the long-axis and short-axis (A_z and A_y) components whose transition moments are polarized in the molecular plane. For 3,6-disubstituted acridine dyes, such as Acridine Orange and Proflavine, the broad, long-wavelength absorption band in the visible region was resolved, without exception, into composite of a strong A_z-component and a very weak A_y-component.[2,3] Since these dyes are known to bind to various kinds of biopolymers, and since the binding has been studied mostly by the spectrophotometric methods, the optical properties of the individual dyes must be clarified thoroughly to facilitate the correct interpretation of the spectroscopic behavior of the dye–polymer complexes.

The monovalent 3,6-disubstituted acridine dyes are susceptible to deprotonation or further protonation, becoming neutral (uncharged) in alkaline solutions or divalent (doubly charged) in acid solutions. The visible absorption spectra of these neutral and divalent dye species are very different from those of the corresponding monovalent (singly charged) species,[4] but, interestingly, often resemble the metachromatic spectra of the monovalent species in the presence of various kinds of polyelectrolytes.[5] Therefore, the film dichroism study of the neutral and divalent acridine dyes is highly desirable for identifying the electronic transition moments responsible for the visible absorption bands, and, if possible, for confirming the systematic changes of these bands in terms of two overlapping (A_y and A_z) component spectra. For this purpose, painstaking efforts were made in the preparation of the neutral and divalent dye species molecularly dispersed in the PVA film, and in the measurements of the dichroic spectra of the stretched films.

Experimental

Materials. Monovalent dyes in the hydrochloride form have been described elsewhere.[2] Abbreviations used in this work are as follows: Acridine Orange, 3,6-bis(dimethylamino)acridinium chloride (AO); Acridine Yellow, 3,6-diamino-2,7-dimethylacridinium chloride (AY); Proflavine, 3,6-diaminoacridinium chloride (PF). Each of these dyes in the neutral form is denoted as AO°, AY°, and PF°, and the monovalent cations as AO^+, AY^+, and PF^+, whenever so needed. The divalent cations are denoted as AO^{2+}, AY^{2+}, and PF^{2+}. Poly(vinyl alcohol) with a nominal degree of polymerization of 2000 was purchased from Nakarai Chemicals, Ltd. (Kyoto). Other chemicals were of reagent grade.

Preparations of Dye–PVA Films. A stock PVA solution was prepared by dissolving the powdered PVA sample (10 g) in redistilled water (100 ml) under gentle stirring at 80—90 °C. The clear solution was filtered through a G-1 sintered glass filter, cooled to ambient temperature, and then spread onto a glass plate to prepare a clear film (10 cm × 10 cm).[2,6] The well-dried PVA film was cut to rectangular pieces; each piece was subjected to heat-treatment at 80 °C for four hours. The preparation of the dye-containing PVA film from a dye–PVA solution by the standard method[2,6] was unsuccessful because of the following reasons. To retain the respective dye species in the purely neutral or divalent form without being contaminated by the stable monovalent form, a sufficient amount of sodium hydroxide or sulfuric acid must be added to the aqueous dye–PVA solution. Attempts to cast a good-quality film from this mixture failed; the mixture either remained translucent for the neutral dye–PVA system or jellified for the divalent dye–PVA system.

After many trials-and-errors, film-staining was found to be the best method. Two heat-treated PVA films (one for the sample, the other for the reference) were immersed into the aqueous sulfuric acid solution (*ca.* 1.8 M, 1 M = 1 mol dm^{-3}). (If the concentration of the acid is too high, the film tends to dissolve. If it is too low, the film contains both the mono- and divalent dye species.) After sufficient time for swelling, the sample film was stained by the acid dye solution. The reference film was kept immersed in the dye-free acid solution for the same period of time. Both films were then dried on a glass plate. (When hydrochloric acid was used for sulfuric acid, the divalent dye species in the sample film was partly converted back to the monovalent form, probably because of the evaporation of hydrogen chloride from the film.)

The sample and the reference films for the neutral dye species were similarly prepared by immersing two heat-treated PVA films in the aqueous sodium hydroxide solution (*ca.* 2.5 M). The swollen sample film was transferred to the alkaline dye solution which contains ethanol enough for the uncharged dye not to precipitate. On being dried on a glass plate, both sample and reference films formed the white powder of carbonate on the surface. The carbonate was washed off with distilled water and then with ethanol. The transparent films were kept in a desiccator.

Measurements. A large number of dye–PVA films were prepared and the spectra of the nonstretched sample films were carefully compared with the solution spectra of the respective dye species, in order to select the films which were not contaminated by the monovalent species and were suitable for the dichroism measurement. The linear dichroic spectra, which are polarized parallel ($A_\parallel$) and perpendicular ($A_\perp$) to the direction of the film stretch, and the isotropic nonstretched spectrum (A) of the dye–PVA film[6] were measured, together with the visible spectra of dye solutions, at 25 °C as described previously.[2,3] Because of the difficulty in the multiple stretching of a given film, each film was stretched only once to a predetermined macroscopic stretch ratio S, as defined previously.[2,3,6]

Analytical Procedure. The dichroic data were expressed with the reduced dichroism $\Delta A/A$:

$$\frac{\Delta A}{A} = \frac{(A_\parallel - A_\perp)}{1/3(A_\parallel + 2A_\perp)}. \tag{1}$$

For symmetric 3,6-diaminoacridine dyes which belong to the C_{2v} point symmetry group, the reduction procedure[7,8] may be utilized for evaluating the A_y- and A_z-spectra (the short-axis and the long-axis polarized component spectra, respectively) from the observed dichroic $A_\parallel$- and $A_\perp$-spectra as before:[2]

$$\left.\begin{aligned} A_\perp - d_\perp A_\parallel &= \frac{K_z - K_y}{2K_z} A_y \\ A_\parallel - d_\parallel A_\perp &= \frac{K_z - K_y}{1 - k_y} A_z, \end{aligned}\right\} \tag{2}$$

where $d_\parallel$ and $d_\perp$ are the reduction factors, and K_y and K_z are the orientation factors.

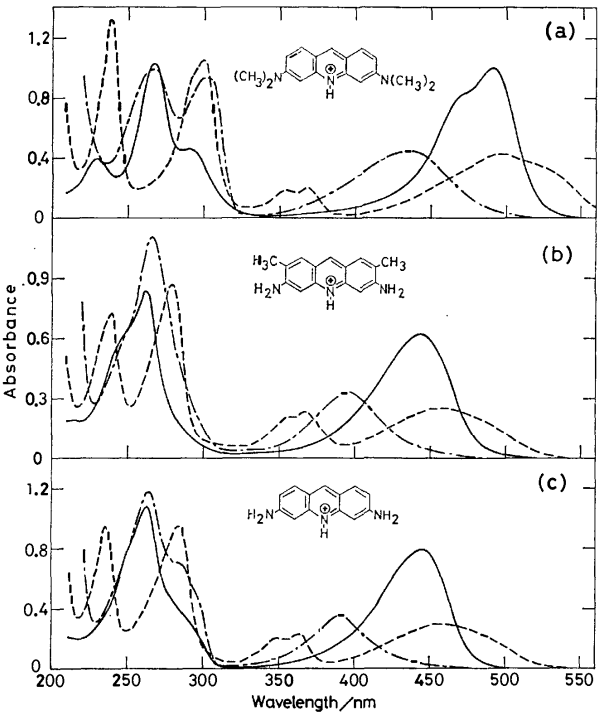

Fig. 1. Absorption spectra of three diaminoacridine dyes in solution at three representative pH regions. The neutral (uncharged) forms in alkaline solution (—·—), the divalent (doubly charged) forms in acid solution (----), and the monovalent (singly charged) forms in aqueous solution (——) for which the structural formulas are given. Conditions are: (a) Acridine Orange, AO° (21 μM) in 0.17 M NaOH solution, AO^+ (25 μM) at a neutral pH, and AO^{2+} (16 μM) in 2.3 M HCl; (b) Acridine Yellow, AY° (16 μM) in 0.17 M NaOH, AY^+ (19 μM) at a neutral pH, and AY^{2+} (14 μM) in 1.7 M HCl; (c) Proflavine, PF° (19 μM) in 0.17 M NaOH, PF^+ (22 μM) at a neutral pH, and PF^{2+} (14 μM) in 2.3 M HCl. The absorption of each solution was measured in a 1-cm cuvette cell.

Results and Discussion

Solution Spectra. Figure 1 shows the solution spectra of three diaminoacridine dyes in the acid, neutral, and alkaline pH regions. In all cases, the neutral (uncharged) dye species give rise to the visible spectra which are hypochromic and hypsochromic relative to those of the monovalent dye cations. The visible spectra of divalent dye cations reveal some remarkable features; the principal band shifts toward the long wavelength and a new twin-peaked band appears in the wavelength region 370—340 nm, where the monovalent and neutral species show only monotonically-decreasing absorption profile. It should be noted that this twin-peaked band, which was earlier observed for AO^{2+} by Zanker,[4] is in fact a feature common to the divalent 3,6-diaminoacridine cations. The purely divalent Trypaflavine, the quaternized homolog of PF^{2+}, was found to show the twin-peaked band at 365—350 nm.[9] It was also confirmed in this work that the divalent cations of the 10-methyl derivatives of AO and AY[3] give rise to the absorption spectra with the twin peak very much similar to those in Fig. 1. Therefore, no further details will be given on the dichroic behavior of the divalent species of those quaternary 3,6-diaminoacridine dyes.

Dichroic Spectra and Reduced Dichroism. Figures 2—4 show the dichroic spectra, *i.e.*, the $A_\parallel$- and $A_\perp$-spectra, and the wavelength dependence of the reduced dichroism $\Delta A/A$ (hereafter denoted as the RD-spectrum) for the neutral species (upper half) and for the divalent species (lower half). The results may be summarized as follows. (1) Regardless of the dye species examined, the $A_\parallel$-spectra are more intense than the $A_\perp$-spectra at a given stretch ratio; hence, the sign of the RD-spectra (filled circles) remains positive throughout the wavelength region. (2) The RD-spectra of the neutral species (AO°, AY°, and PF°) are not constant but decrease on the long and short wavelength sides of the principal band (the error is large for PF° due to the background scattering). This behavior is very similar to that of the corresponding monovalent dye species,[2] immediately indicating that the broad and featureless band of each

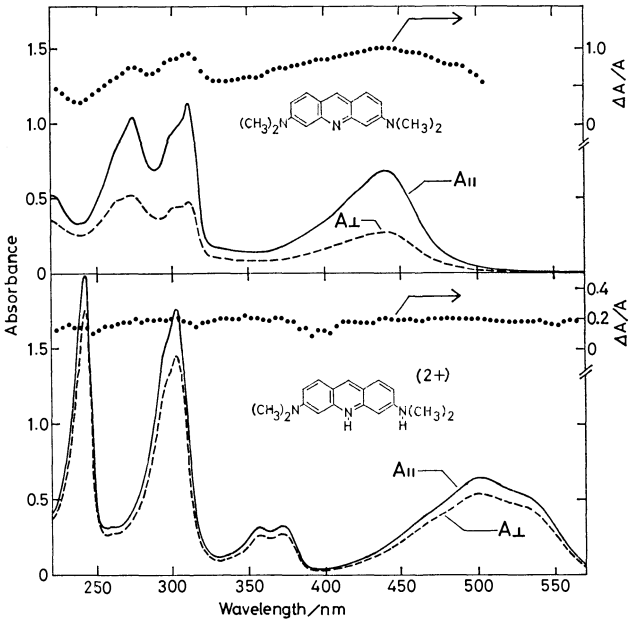

Fig. 2. The dichroic spectra polarized parallel ($A\parallel$) and perpendicular ($A\perp$) to the direction of stretch and the reduced dichroism ($\Delta A/A$) of Acridine Orange in the stretched PVA film. Upper: the neutral form. Lower; the divalent ionic form. The nominal stretch ratio S of the PVA film is 3.8,[2,6] which corresponds to the rotation of the mechanical stretcher of 15 turns.[6] This, in turn, corresponds to the threefold elongation of the PVA sample film along the stretching direction.

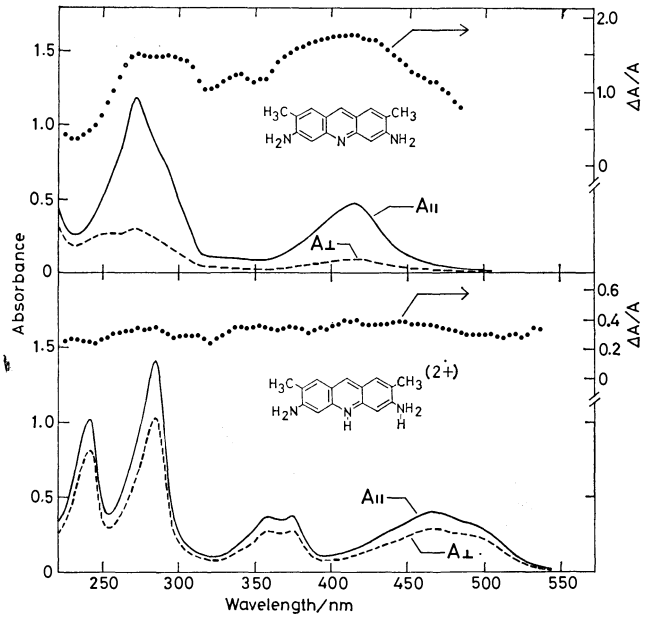

Fig. 3. The dichroic spectra ($A\parallel$ and $A\perp$) and the reduced dichroism ($\Delta A/A$) of Acridine Yellow in the stretched PVA film. The symbols and conditions are the same as in Fig. 2.

neutral species in the visible region (Fig. 1) is only apparent and contains at least two electronic transition moments.[2,3] The close similarity between the monovalent and neutral species may be accounted

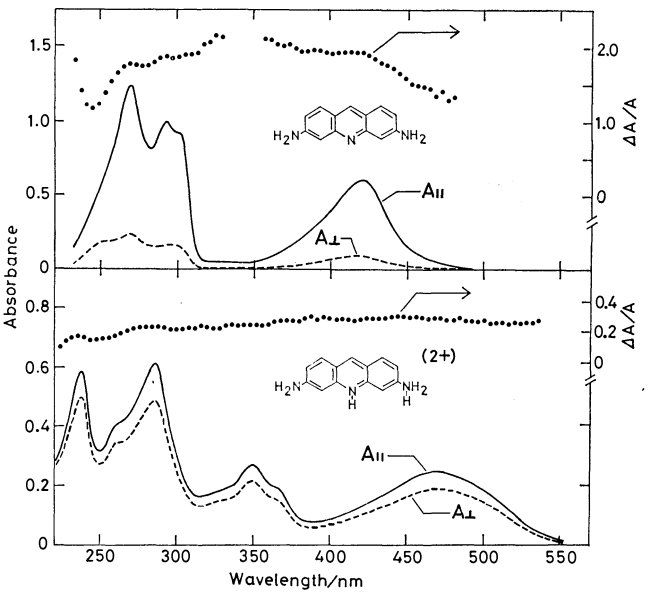

Fig. 4. The dichroic spectra ($A\parallel$ and $A\perp$) and the reduced dichroism ($\Delta A/A$) of Proflavine in the stretched PVA film. The symbols and conditions are the same as in Fig. 2.

for by considering their molecular symmetry and chemical structure: one class is deprotonated and the other is protonated at the ring nitrogen. (3) The RD-spectra of the divalent dye cations (AO^{2+}, AY^{2+}, and PF^{2+}) are nearly constant throughout the visible and UV regions; both the principal band near 450—500 nm and the new twin peak behave similarly on stretching. This is a remarkable contrast with the cases of the neutral and monovalent dye species. (4) The divalent dye cations are less orientable than the uncharged counterparts, *i.e.*, values of $\Delta A/A$ are smaller by a factor of 10—5, at a given stretch ratio; a feasible explanation is that the H_2SO_4-containing PVA film matrix is less rigid than the NaOH-containing one.

Reduction Procedure. Because of the additives (H_2SO_4 and NaOH) in the dye-PVA films, the dichroic measurements for each film could be carried out only at a single stretch. It was not possible to determine the dependence of $\Delta A/A$ on stretch ratio at some selected wavelengths as in previous studies;[2,6,10] hence, the intrinsic value of the dichroism at infinitely high stretch ratio could not be estimated. Nor could the orientational behavior inside the "orientation triangle"[2,10] be established. Since the reduction procedure does not require the exact degree of orientation of the guest molecules,[7,8] this technique will be employed to estimate the short-axis polarized (A_y) and the long-axis polarized (A_z) component spectra. Figure 5 shows an example of the reduction procedure applied to AO°. Both ($A\parallel - d\parallel A\perp$) and ($A\perp - d\perp A\parallel$) were searched for A_y and A_z with a HITAC M-180 computer. While the factor $d\perp$ (hence, the value K_z and an unnormalized A_y-spectrum) could be determined (Fig. 5b), the other factor $d\parallel$ (hence, the value K_y) could not, because none of the trial spectra ($A\parallel - d\parallel A\perp$) falls on (or crosses over) the zero absorbance line. Thus, the normalized A_y- and A_z-spectra are undeterminable. In order to circumvent this prob-

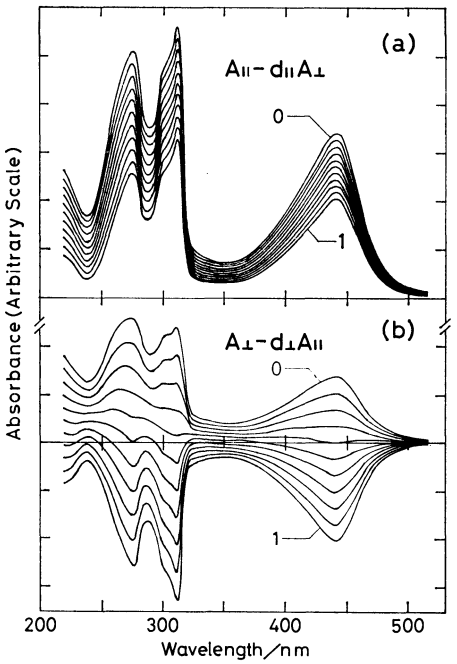

Fig. 5. The reduction procedure applied to the dichroic spectra of Acridine Orange in the neutral form. The $A_{\parallel}$- and $A_{\perp}$-spectra were measured at a nominal stretch ratio of 3.8. The reduction factors $d_{\parallel}$ and $d_{\perp}$ were varied from 0 to 1 at intervals of 0.1.

lem, a plausible assumption is made: the orientation behavior of the neutral form (AO°) is practically the same as that of the monovalent form (AO^+), so that the orientation triangle for AO^+ (Fig. 7 of Ref. 2 or Fig. 4 of Ref. 10) can be utilized to evaluate the orientation factor K_y by using the above K_z. Then, both A_y and A_z may be computed from Eq. 2. The same general techniques apply to other neutral dyes (AY° and PF°). The values of the reduction factors and the orientation factors are given in Table 1.

The Long-axis and Short-axis Polarized Spectra. Figure 6 shows both the long-axis polarized (A_z) and the short-axis polarized (A_y) spectra for three neutral dye species. It is clear that, for each species, the isotropic absorption spectrum in the visible region (Fig. 1) belongs predominantly to the A_z-spectrum, but that the contribution from the A_y-spectrum should not be ignored (dashed lines). The featureless principal band is now concluded to be a composite of two mutually perpendicular transitions (the y- and z-polarizations or the ^1L_a and ^1L_b bands[2-4]). The A_z-spectrum is also predominant in the UV region, but the A_y-spectrum substantially contributes to the observed isotropic band in each case.

The C_{2v} symmetry should be assumed if the reduction procedure is to be applied to the observed $A_{\parallel}$- and $A_{\perp}$-spectra of the divalent dye species on a reliable basis. The C_{2v} symmetry could be preserved for a given divalent species only if an additional proton is attached to the 10-position of the corresponding monovalent acridinium ion. The divalent species probably belong to a class of lower symmetry,[11] since the second protonation is believed to occur at the 3- or 6-position.[4,12] As a consequence, the directions

TABLE 1. THE REDUCTION FACTORS ($d_{\parallel}$ AND $d_{\perp}$) AND THE ORIENTATION FACTORS (K_y AND K_z) AT A CONSTANT STRETCH RATIO S FOR NEUTRAL ACRIDINE DYES

Dyes	$d_{\parallel}$	$d_{\perp}$	K_y	K_z
AO°	0.62	0.38	0.237	0.568
AY°	0.28	0.16	0.123	0.758
PF°	0.37	0.09	0.156	0.847

The nominal value of S is 3.8.[2]

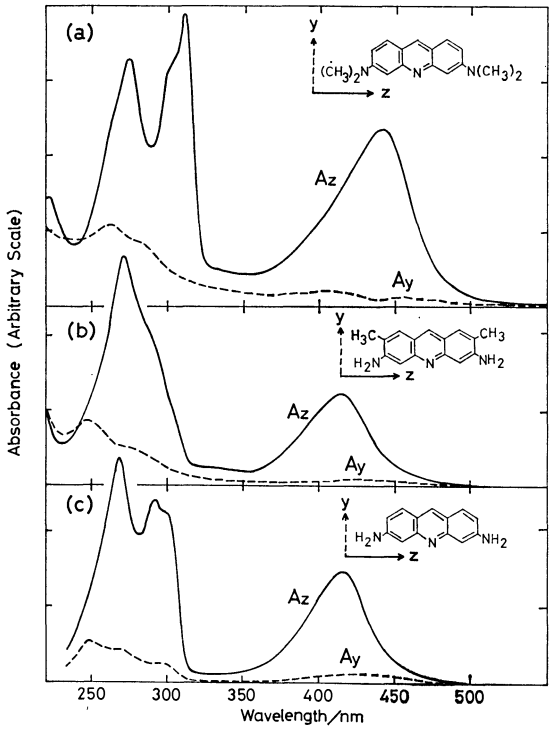

Fig. 6. The short-axis (y) and long-axis (z) polarized component spectra (A_y and A_z) of three 3,6-diaminoacridine dyes in the neutral forms. (a) Acridine Orange, (b) Acridine Yellow, and (c) Proflavine.

of the in-plane transition moments may no longer be mutually perpendicular. We are therefore obliged to postpone the analysis of the dichroic data of the divalent dye species, until an analytical method suitable for the film dichroism of guest molecules of low symmetry is developed.

Closing Remarks. The film dichroism studies on the symmetric 3,6-diaminoacridine dyes in the neutral, monovalent, and divalent forms may be summarized as follows. All dye species in each form clearly show some regular spectral features in the visible absorption spectra. The twin-peaked band appears only in the spectrum of the divalent species. For the neutral and monovalent forms examined so far,[2] the long-axis and the short-axis polarized component spectra overlap each other; the A_z-spectrum is always located on the wavelength side slightly shorter than the A_y-spectrum. We may now conclude that the broad, visible absorption band of the symmetric 3,6-diaminoacridine dyes is a composite of two mutually-polarized, overlapping component spectra regardless of the substituents at the 3,6-nitrogen, at the 2,7-carbon, and at

the 10-nitrogen of the acridine nucleus. These findings should facilitate a new interpretation of the spectral changes of these dyes when bound to various synthetic polyelectrolytes and biopolymers.

We acknowledge with deep gratitude some initial contributions to the present work by Dr. Yukio Matsuoka, who formerly belonged to our research group and was actively engaged in developing film dichroism techniques.

References

1) The preceding paper in this series is Ref. 3.
2) Y. Matsuoka and K. Yamaoka, *Bull. Chem. Soc. Jpn.*, **52**, 3163 (1979).
3) Y. Matsuoka and K. Yamaoka, *Bull. Chem. Soc. Jpn.*, **53**, 2146 (1980). Also references cited therein.
4) V. Zanker, *Z. Phys. Chem. (Frankfurt am Main)*, **199**, 225 (1952).
5) K. Yamaoka and M. Takatsuki, *Bull. Chem. Soc. Jpn.*, **51**, 3182 (1978). Also references cited therein.
6) K. Yamaoka and Y. Matsuoka, *J. Sci. Hiroshima Univ. Ser. A*, **40**, 105 (1976).
7) E. W. Thulstrup, J. Michl, and J. H. Eggers, *J. Phys. Chem.*, **74**, 3868 (1970).
8) J. Michl, E. W. Thulstrup, and J. H. Eggers, *J. Phys. Chem.*, **74**, 3878 (1970).
9) M. Takatsuki and K. Yamaoka, *J. Sci. Hiroshima Univ. Ser. A*, **40**, 387 (1976).
10) Y. Matsuoka, *J. Phys. Chem.*, **84**, 1361 (1980).
11) K. Yamaoka, S. Noji, and M. Yoshida, *Bull. Chem. Soc. Jpn.*, **54**, 31 (1981).
12) A. Albert, "The Acridines," St. Martin's Press, New York (1966), p. 346.

Effect of the Polydispersity of Molecular Length on the Decay Process of Transient Electric Birefringence of Rodlike Macromolecules in Dilute Solution

Kiwamu YAMAOKA* and Kiyohiro FUKUDOME

Faculty of Science, Hiroshima University, Higashisenda-machi, Naka-ku, Hiroshima 730

(Received July 2, 1982)

The effect of polydispersity on transient electric birefringence (EB) was examined for a dilute solution which contains like macromolecules of varying lengths. The molecules were assumed to be rigid rods of cylindrical symmetry, so that the molecular weight is linearly proportional to length. Polydispersity was expressed by the ratio of the weight-average to the number-average lengths l_w/l_n. A logarithmic-normal type continuous length distribution was generally used. Calculations were performed for the birefringence-average relaxation time $\langle\tau\rangle_{EB}$ and initial slope $\langle S\rangle_{EB}$ as a function of the electric field strength E, which is applied prior to the start of the decay process, with the electric parameter $(\beta_w)^2/2\gamma_w$, which is related to the weight-average permanent dipole moment (the β_w-term) and polarizability anisotropy (the γ_w-term). Both $\langle\tau\rangle_{EB}$ and $\langle S\rangle_{EB}$ are very sensitive to E, l_w/l_n, and $(\beta_w)^2/2\gamma_w$. A convenient method was devised for determining the polydispersity parameters (l_w/l_n and l_w) from the weight-averages of relaxation time and initial slope, which are free from the mechanism of field orientation. Examples are given for a polydisperse, rigid rodlike sonicated DNA sample in aqueous solution.

In the preceding paper on the electric birefringence (EB) and electric dichroism (ED) of sonicated DNA in dilute solutions,[1] we have indicated that the measurement of decay processes is promising for determining the overall molecular shape, even if the sample DNA is polydisperse as regards the molecular length. Although the theoretical basis of the transient EB and ED methods is well advanced for monodisperse systems,[2] analyses of the experimental data of a polydisperse system have often been unsatisfactory because of the lack of an appropriate procedure. For a polydisperse system consisting of particles with a continuous length distribution, Yoshioka and Watanabe[3,4] first introduced the area method, by which the electric birefringence-average relaxation time, $\langle\tau\rangle_{EB}$, can be obtained. They have since developed an elegant method for determining the relaxation spectrum from a single decay curve.[5–11] According to our experience, the application of this method to dilute polymer solutions is often difficult due to low signal-to-noise ratio of observed decay signals. Kobayasi has calculated the variation of relaxation time τ with the polydispersity ratio of a continuous weight distribution for rodlike molecules.[12] Schweitzer and Jennings have shown that the initial slope, S, of a decay curve depends not only on the particle-size distribution and electric field strength, but also on the nature of the electric properties of molecules.[13,14] Coles and Weill have discussed the relation between the initial slopes and various averages of rotary diffusion coefficients.[15]

The objective of this paper is to clarify the effect of the molecular length distribution on the electrooptical and hydrodynamic properties of polydisperse samples and to allow the evaluation of the degree of polydispersity, which is defined as the weight-average to the number-average lengths l_w/l_n, and of the weight-average length l_w from the observed decay data. For this purpose, we first calculate the values of $\langle\tau\rangle_{EB}$ and $\langle S\rangle_{EB}$ numerically for an assembly of nonionized and rodlike dipolar macromolecules, showing the dependence of these values on externally applied electric field strength. We secondly discuss the use of a newly devised "mesh method" for evaluating both l_w/l_n and l_w by applying it to the actually observed relaxation data of a polydisperse, rigid rodlike sonicated DNA sample.[1]

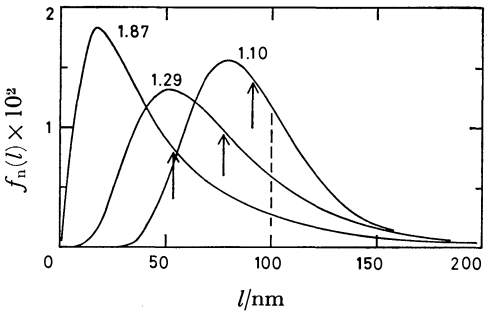

Fig. 1. The logarithmic-normal function $f_n(l)$ for continuous length distribution with various ratios of l_w/l_n. The weight-average length l_w is assumed to be 100 nm in all cases, as indicated by a vertical line. The positions of the number-average length l_n are indicated by arrows. Numerals denote the polydispersity ratio l_w/l_n.

Formalism and Calculations

Continuous Length Distribution. The following assumptions are made. A macromolecular species in a given polydisperse system is a thin, rigid rod of cylindrical symmetry with the longitudinal length l, having the apparent electric permanent dipole moment along the symmetry axis (the 3-axis), μ, and the electric polarizability anisotropy, $\Delta\alpha=(\alpha_{33}-\alpha_{11})$.[16–18] The density and the optical properties of molecules in the system are independent of molecular lengths. Both μ and $\Delta\alpha$ are proportional to l, so that $\mu=\mu_0 l$ and $\Delta\alpha=\Delta\alpha_0 l$, where μ_0 and $\Delta\alpha_0$ are the respective quantities per unit length.[19] The probability density function of l is $f_n(l)$ on the basis of the number of molecules in a solution. For $f_n(l)$, we mostly use a logarithmic-normal distribution, *i.e.*, the Wesslau function (Eq. 1),[20] in order to emphasize the contribution from fewer but longer components. (We have also examined the Schulz-Zimm,[1] the Poisson, and a rectangular distribution function.

The results are qualitatively all the same.)

$$f_n(l) = \frac{l_L}{l^2\omega\sqrt{\pi}\exp\left(\frac{\omega^2}{4}\right)}\exp\left\{-\frac{1}{\omega^2}\left(\ln\frac{l}{l_L}\right)^2\right\}, \quad (1)$$

where l_L is the parameter which determines the absolute position of the distribution and ω is the parameter which determines its breadth. The ratio $l_w/l_n = \exp(\omega^2/2)$, $l_n = l_L\exp(-\omega^2/4)$, and $l_w = l_L\exp(\omega^2/4)$. Figure 1 shows $f_n(l)$ with three different values of l_w/l_n.

Field-strength Dependence of EB Decay Processes. For a polydisperse system, the birefringence-average relaxation time $\langle\tau\rangle_{EB}$ (the same type expressions are also applicable to ED) can be expressed as follows:[3,12,21]

$$\langle\tau\rangle_{EB} = \int_0^\infty \frac{\Delta n(t)}{\Delta n(0)}dt = \frac{\int_a^{a'}\tau(l)\Phi(\beta',\gamma')lf_n(l)dl}{\int_a^{a'}\Phi(\beta',\gamma')lf_n(l)dl}, \quad (2)$$

where $\Delta n(0)$ is the steady-state birefringence at the initial time ($t=0$) when an electric pulse of arbitrary field strength is removed, and $\tau(l)$ is the relaxation time of a component with a length of l. The initial slope is given as[13-15]

$$\langle S\rangle_{EB} = \left[\frac{d\left(\ln\frac{\Delta n(t)}{\Delta n(0)}\right)}{dt}\right]_{t\to 0} = -\left\langle\frac{1}{\tau}\right\rangle_{EB}$$

$$= -\frac{\int_a^{a'}\tau(l)^{-1}\Phi(\beta',\gamma')lf_n(l)dl}{\int_a^{a'}\Phi(\beta',\gamma')lf_n(l)dl}, \quad (3)$$

where $\beta' = \mu_0 lE/kT$ and $\gamma' = \Delta\alpha_0 lE^2/2kT$. Since the orientation function $\Phi(\beta',\gamma')$ approaches unity, as the field strength increases infinitely, both $\langle\tau\rangle_{EB}$ and $\langle S\rangle_{EB}$ at infinitely high field give the weight-average relaxation time $\langle\tau\rangle_w$ and the weight-average initial slope $\langle S\rangle_w$, respectively:

$$\langle\tau\rangle_w = \frac{\int_a^{a'}\tau(l)lf_n(l)dl}{\int_a^{a'}lf_n(l)dl}, \quad (4)$$

and

$$\langle S\rangle_w = -\frac{\int_a^{a'}\tau(l)^{-1}lf_n(l)dl}{\int_a^{a'}lf_n(l)dl}. \quad (5)$$

It should be emphasized that neither $\langle\tau\rangle_w$ nor $\langle S\rangle_w$ depends on the electric properties (β' and γ') and hence, not on the orientation mechanism. The relaxation time $\tau(l)$ for a thin, rodlike molecule of length l may be calculated from several expressions.[2] We employ the Broersma equation[22] (*cf.* Eq. 8 in Ref. 1).

In actual computations for $\Phi(\beta',\gamma')$, $\langle\tau\rangle_{EB}$, and $\langle S\rangle_{EB}$ as a function of electric field strength, the following values were used, unless otherwise specified:

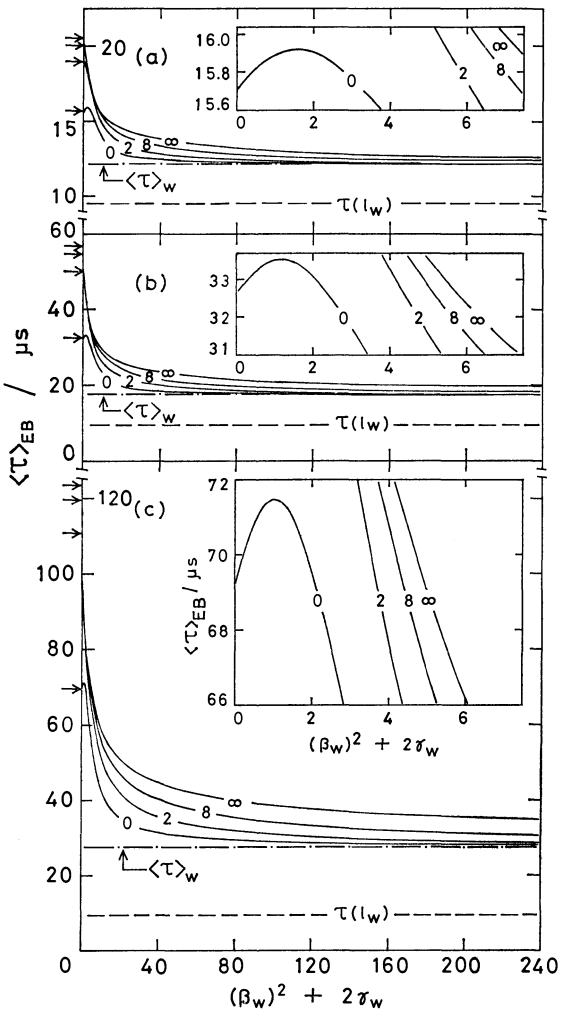

Fig. 2. Electric birefringence-average relaxation time $\langle\tau\rangle_{EB}$ as a function of $[(\beta_w)^2+2\gamma_w]$ for the polydisperse system with the l_w/l_n ratios of (a) 1.10, (b) 1.29, and (c) 1.87. Numerals in each figure correspond to the values of $(\beta_w)^2/2\gamma_w$; polarizability anisotropy only (0), mixed dipole (2 and 8), and permanent dipole only (∞). Lateral arrows on the ordinates indicate values of $\langle\tau\rangle_{EB}$ at limiting low fields. In each figure, the weight-average relaxation time $\langle\tau\rangle_w$ is shown by (—·—), while the field-independent relaxation time $\tau(l_w)$ for a monodisperse system, in which the length $l_w(=l_0)$ is 100 nm, is shown by (----). Inserts are the plots of $\langle\tau\rangle_{EB}$ *vs.* $[(\beta_w)^2+2\gamma_w]$ in the low field region. Note the scale on the ordinate of (a) differs from that of (b) and (c).

$\mu_0 = 3.0\times10^{-19}$ C (or 8.993 D/Å), $\Delta\alpha_0 = 1\times10^{-25}$ F m (or 8.985×10^{-12} cm^2) for the pure anisotropy orientation ($\Delta\alpha$ is variable for the mixed dipole orientation[17,18]), $l_w = 100$ nm, $2b$ (the diameter of a cylinder) $= 1.5$ nm, the viscosity of solvent $\eta_0 = 8.45\times10^{-4}$ Pa s, and $T = 293$ K. The upper and lower integral limits are set as $a = 5$ nm and $a' = 405$ nm, rather than as $a = 0$ and $a' = \infty$, because low molecular-weight-oligomers are often removed from a polymer sample (the upper limit was set for the convenience of completing computations with a sufficient accuracy).

Results and Discussion

Effect of Polydispersity on Relaxation Time. The field-strength dependence of $\langle\tau\rangle_{EB}$, calculated from Eq. 2, is plotted in Fig. 2 against $[(\beta_w)^2+2\gamma_w]$ at several ratios of $(\beta_w)^2/2\gamma_w$, where β_w and γ_w are the weight-averages of β' and γ'. The weight-average relaxation time $\langle\tau\rangle_w$ is drawn in each figure by a dash-dotted line, together with the field-independent single relaxation time $\tau(l_w)$ for the corresponding monodisperse system with the length of $l_o(=l_w)$ (dashed line) for comparison. The results are summarized below. (1) The relaxation time of a given polydisperse system strikingly depends on the electric pulse field applied prior to the start of decay process. This field dependence is quite sensitive to the polydispersity of the sample; hence, it is the best test for a length distribution. (2) The magnitude of $\langle\tau\rangle_{EB}$ is exceedingly large at extremely low electric field, as the ratio l_w/l_n increases. For example, the value of $\langle\tau\rangle_{EB}$ is as high as 123 μs for the most polydisperse sample ($l_w/l_n=1.87$), while it is only 9.62 μs for the corresponding monodisperse system (Fig. 2(c)). This is because $\tau(l)$ is proportional to the cube of l and because the polydisperse sample contains the components whose lengths are much longer than l_w (*cf.* Fig. 1). (3) In each polydisperse system, values of $\langle\tau\rangle_{EB}$ rapidly decrease with increasing field strengths and gradually become level. They should all approach the limiting value, *i.e.*, $\langle\tau\rangle_w$, which depends only on polydispersity and length.[12,17] (4) The field-strength dependence of $\langle\tau\rangle_{EB}$ is characteristic of the orientation mechanism. The pure permanent dipole moment orientation clearly shows a large but monotonous dependence. For pure polarizability orientation, however, the field dependence is not monotonous. In the low field range, there appears a maximum whose magnitude and position depend on polydispersity (see inserts in Figs. 2(a)—(c)). (5) For any polydisperse system, $\langle\tau\rangle_w$ does not coincide with $\tau(l_w)$, unless the length distribution is extremely narrow. This is an important consequence of polydispersity. If an average length of solutes in a polydisperse sample is calculated directly from the Broersma equation by using the experimentally obtained relaxation time $\langle\tau\rangle_w$ or $\langle\tau\rangle_{EB}$, the length would be unreasonably large. (It is $\tau(l_w)$ that is related to the weight-average length l_w.) Hence, an erroneous conclusion may be drawn on the overall solution conformation of the polymer system in which molecular lengths are heterogeneous.

Effect of Polydispersity on Initial Slope. The initial slope $\langle S\rangle_{EB}$ of a decay signal is a measure of polydispersity.[8,9,13,14] The results of the present calculation are illustrated in Fig. 3. Values of $\langle S\rangle_{EB}$ clearly depend on polydispersity ratio and field-orientation mechanism, slowly approaching the weight-average $\langle S\rangle_w$ at limiting high fields, which is, however, independent of the orientation mechanism in a manner similar to the case of relaxation time. It is interesting to note that values of $\langle S\rangle_{EB}$ in the low field range are close to the value of $S(l_w)$ for the monodisperse system (dashed line), if solutes are oriented predominantly by the permanent dipole moment $[(\beta_w)^2/2\gamma_w=\infty—8]$. For pure polarizability orientation, an extremum appears in the low field range, similarly to the case of the corresponding relaxation time.

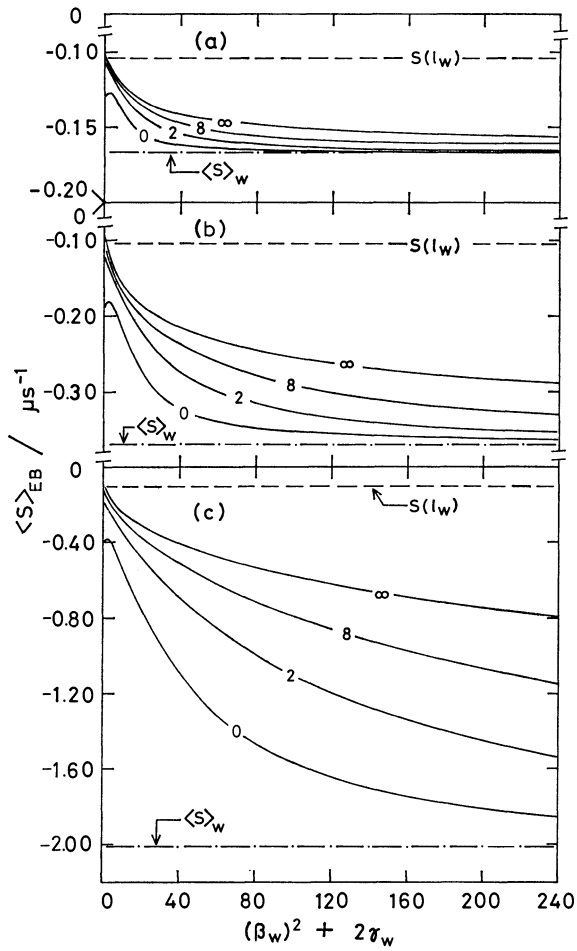

Fig. 3. Electric birefringence-average initial slope $\langle S\rangle_{EB}$ as a function of $[(\beta_w)^2+2\gamma_w]$ for a polydisperse system with three l_w/l_n ratios of (a) 1.10, (b) 1.29, and (c) 1.87. In each figure, the weight-average initial slope $\langle S\rangle_w$ is given by (—·—) and the field-independent initial slope $S(l_w)$ for a monodisperse system by (----), in which the length ($l_w=l_o$) is 100 nm.

Estimation of Weight-average Relaxation Time and Initial Slope. Values of $\langle\tau\rangle_w$ and $\langle S\rangle_w$ can be estimated by extrapolation of those of $\langle\tau\rangle_{EB}$ and $\langle S\rangle_{EB}$ to infinitely high field strength ($E\to\infty$). Figure 4 illustrates this extrapolation procedure with a polydisperse system ($l_w/l_n=1.29$ and $l_w=100$ nm). A problem is associated with the unknown curvature of the plot of $\langle\tau\rangle_{EB}$ or $\langle S\rangle_{EB}$ against the reciprocal of field strength. When $\langle\tau\rangle_{EB}$ is plotted against $[(\beta_w)^2+2\gamma_w]^{-1}$, which is proportional to E^{-2} (Fig. 4(a)), the curvature is convex and quite large for the permanent dipole moment orientation (∞), but it becomes concave with decreasing $(\beta_w)^2/2\gamma_w$ (2 and 0). When $\langle\tau\rangle_{EB}$ is plotted against $[(\beta_w)^2+2\gamma_w]^{-1/2}$, which is proportional to E^{-1} (Fig. 4(b)), the curvature is only slightly concave for all $(\beta_w)^2/2\gamma_w$ (∞—0). The similar results with reversed curvatures are found for $\langle S\rangle_{EB}$ (dashed curves in Figs. 4(a)—(b)). These plots are suggestive of

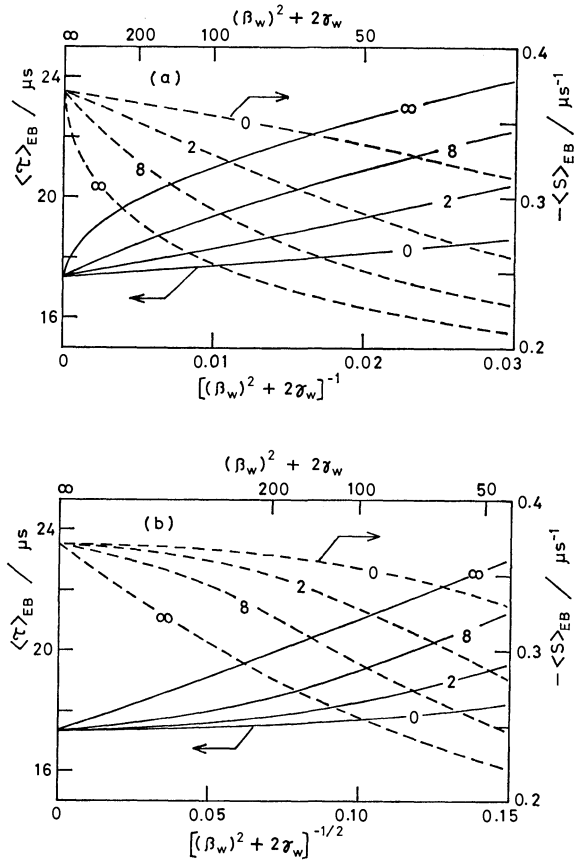

Fig. 4. Extrapolations of the birefringence-average relaxation time $\langle\tau\rangle_{EB}$ and initial slope $\langle S\rangle_{EB}$ to infinitely high electric fields. The birefringence-averages were calculated for a logarithmic-normal distribution with $l_w/l_n=1.29$ and $l_w=100$ nm. Values of $\langle\tau\rangle_{EB}$ (——) and $\langle S\rangle_{EB}$ (----) are plotted against $[(\beta_w)^2+2\gamma_w]^{-1}$ in (a) and against $[(\beta_w)^2+2\gamma_w]^{-1/2}$ in (b). A numeral in each curve is the value of $(\beta_w)^2/2\gamma_w$. Note that all curves intercept the ordinates ($\langle\tau\rangle_w=17.36$ μs and $\langle S\rangle_w=-0.37$ μs^{-1}).

the proper extrapolation procedure for evaluating $\langle\tau\rangle_w$ and $\langle S\rangle_w$. For example, extrapolation of observed values of $\langle\tau\rangle_{EB}$ to the intercept of the ordinate appears to be easier if they are plotted simultaneously against E^{-1} and against E^{-2}.

Application to Measured Decay Signals of sDNA. Figure 5 shows a typical extrapolation to infinitely high field of values of $\langle\tau\rangle_{EB}$ and $\langle S\rangle_{EB}$ which are observed for a sonicated DNA (sDNA) preparation in 0.2 mM NaCl** (the experimental details are found in Ref. 1). In the case of rodlike sDNA in aqueous solutions, the dependence of $\langle\tau\rangle_{EB}$ and $\langle S\rangle_{EB}$ on field strengths has not been fully resolved, since no appropriate counterion-induced orientation function is available as yet. Nevertheless, it has been shown that the "classical" function $\Phi(\beta',\gamma')$ can represent the birefringence and dichroism behavior of sDNA adequately over a wide range of field strength.[1,23,24] The plots in Fig. 4 are based on $\Phi(\beta',\gamma')$; thus, they are instructive as an empirical guide. Observed values of $\langle\tau\rangle_{EB}$ and $\langle S\rangle_{EB}$ for sDNA are plotted both

** 1 M=1 mol dm^{-3}.

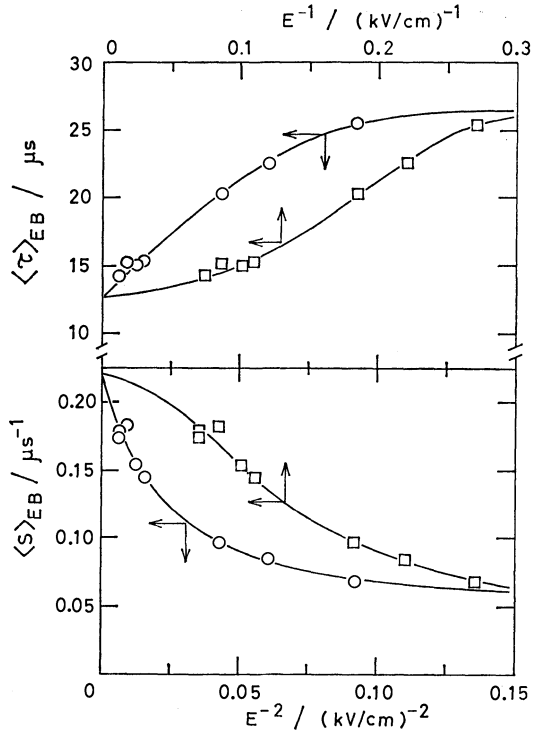

Fig. 5. Extrapolation of values of $\langle\tau\rangle_{EB}$ and $\langle S\rangle_{EB}$ experimentally obtained for a sonicated DNA sample in the 0.2 mM NaCl-containing aqueous solution.

against E^{-2} and against E^{-1} in Fig. 5. Extrapolated values are: $\langle\tau\rangle_w=12.5$ μs and $\langle S\rangle_w=-0.22$ μs^{-1}.

Evaluation of the Degree of Polydispersity and Weight-average Length. With a set of experimental values of $\langle\tau\rangle_w$ and $\langle S\rangle_w$, as obtained in the above section, both the weight-average length l_w and the polydispersity ratio l_w/l_n may be estimated, if the length distribution $f_n(l)$ is known or can be assumed for a given polydisperse system. For this purpose, we devised a new, convenient method, which may be termed the "mesh method," by constructing a theoretical graph of meshes. Examples are shown in Fig. 6, in which theoretical values of $\langle\tau\rangle_w$ (Eq. 4) are plotted against theoretical values of $\langle S\rangle_w$ (Eq. 5) with l_w and l_w/l_n as parameters. The Wesslau function (Fig. 6(a)) and the Schulz-Zimm function (Fig. 6(b))[1] are chosen for the distribution function $f_n(l)$, in order to compare the effect of the distribution curves on the final result. (The latter is said to be an appropriate function for the degradation process of chain length by sonication.[25]) Two values are assigned to 2b to see the effect of the diameter of rodlike molecules on the estimated values of l_w and l_w/l_n. A pair of experimental values ($\langle\tau\rangle_w$ and $\langle S\rangle_w$) defines a point in the $\langle\tau\rangle_w$—$\langle S\rangle_w$ coordinates; hence, the most likely set of l_w and l_w/l_n can be readily evaluated from the network. This mesh method is advantageous in that it can be used for rodlike polymers, whatever the field-orientation mechanism may be, because both $\langle\tau\rangle_w$ and $\langle S\rangle_w$ are independent of the electric parameters β' and γ' or the orientation function $\Phi(\beta',\gamma')$. The optical and electric parameters may be determined separately by the matching method previously mentioned for the steady-state birefringence[23] and dichro-

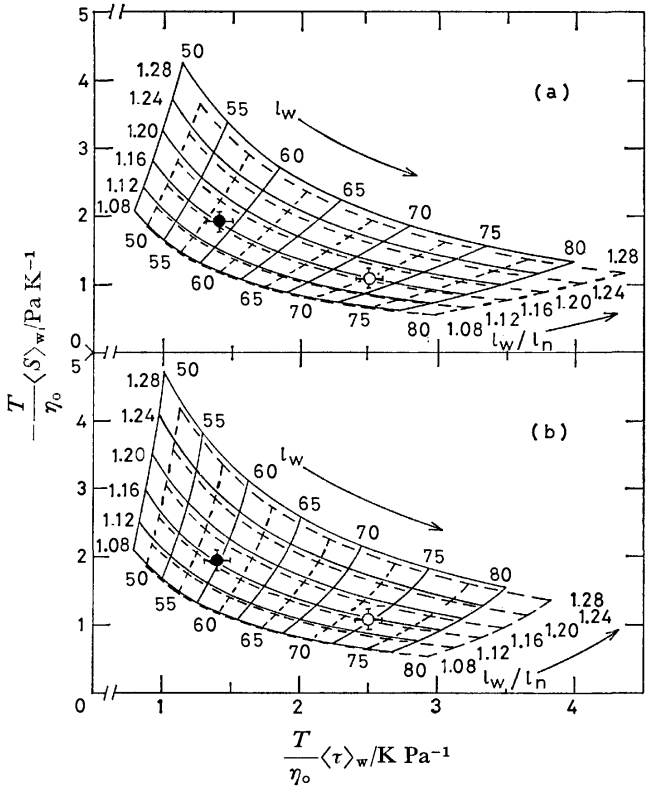

Fig. 6. The relationship between the weight-average relaxation time $\langle\tau\rangle_w$ and initial slope $\langle S\rangle_w$ with the polydispersity ratio l_w/l_n and the weight-average length l_w as the parameters. The distribution functions are the Wesslau type (a) and the Schulz-Zimm type (b). T is the absolute temperature and η_0 is the viscosity of solvent. Two different networks are plotted; one, for which the diameter of cylindrical like molecules, $2b$, is 2 nm (——), and the other with the diameter of 2.6 nm (----). For each set of meshes, values of l_w/l_n are varied between 1.08 and 1.28, while those of l_w between 50 and 80 nm. Experimental values of $\langle\tau\rangle_w$ and $\langle S\rangle_w$ for sDNA are also plotted: (○) in 0.2 mM NaCl and (●) in 0.33 mM $MgCl_2$.

ism,[24] once both l_w and l_w/l_n are available.

Paired-values of $\langle\tau\rangle_w$ and $\langle S\rangle_w$, experimentally obtained for the sDNA sample at different ionic strengths, are also plotted inside the meshes. The most probable values of l_w and l_w/l_n are summarized in Table 1. The effect of the "thickness" of a cylinder on l_w is such that the value of l_w with a diameter of 2.6 nm is smaller than that with 2.0 nm by about 5%. The choice of the distribution function is not too critical, when the range of l_w/l_n is limited to *ca.* 1.2 or less. When values of l_w are divided by the weight-average degree of polymerization or the number of base pairs (=188), the axial translation per base pair can be calculated (*cf.* Table 1 of Ref. 1). The value of l_w/l_n is close to the reported literature values (1.02—1.11),[26-28] which were determined by the sedimentation equilibrium and electron microscopic methods for fractionated sDNA samples. This good agreement, achieved by the utilization of different physical techniques and diverse sonication methods, appears to be a strong support for the present procedure for polydispersity determination.

Table 1. Polydispersity ratio, l_w/l_n, and weight-average length, l_w, of sonicated DNA in aqueous solutions evaluated by use of two distribution functions[a]

		Wesslau function		Schulz-Zimm function[b]	
	$2b$/nm[c]	2.0	2.6	2.0	2.6
A[d]	l_w/l_n	1.16	1.17	1.16	1.17
	l_w/nm	73	70	74	71
B[d]	l_w/l_n	1.16	1.17	1.16	1.17
	l_w/nm	59	56	60	57

a) The number of base pairs of this sDNA is 188.[1] b) The data are cited in Ref. 1. c) The assumed diameter of sDNA. d) sDNA in the 0.2 mM NaCl solution (A) and in the 0.33 mM $MgCl_2$ solution (B).[1]

Conclusion

With numerical calculations we could show how the decay processes of transient EB (and also ED) of a system composed of long, rigid rodlike macromolecules are affected by the polydispersity of continuous length distribution. The dependence of the relaxation time and the initial slope of an EB signal on the electric field strength applied to the system prior to the commencement of the decay is a very sensitive measure of polydispersity and field-orientation mechanism. We could show how incorrect interpretations of experimental data may be avoided. We have also described a new mesh method for determining the degree of polydispersity and the weight-average molecular length. Use of this method in conjunction with well-pursued experimental results will facilitate the EB and ED study of polydisperse, rodlike polymer systems.

References

1) K. Matsuda and K. Yamaoka, *Bull. Chem. Soc. Jpn.*, **55**, 1727 (1982).
2) "Molecular Electro-Optics, Parts 1 and 2," ed by C. T. O'Konski, Marcel Dekker, New York (1976 and 1978).
3) K. Yoshioka and H. Watanabe, *Nippon Kagaku Zasshi*, **84**, 626 (1963).
4) K. Yoshioka and H. Watanabe, "Physical Principles and Techniques of Protein Chemistry, Part A," ed by S. J. Leach, Academic Press, New York (1969), Chap. 7.
5) M. Matsumoto, H. Watanabe, and K. Yoshioka, *Biopolymers*, **6**, 929 (1968).
6) M. Matsumoto, H. Watanabe, and K. Yoshioka, *Biopolymers*, **9**, 1307 (1970).
7) M. Matsumoto, H. Watanabe, and K. Yoshioka, *Kolloid Z. Z. Polym.*, **250**, 298 (1972).
8) M. Matsumoto, H. Watanabe, and K. Yoshioka, *Biopolymers*, **11**, 1711 (1972).
9) M. Matsumoto, H. Watanabe, and K. Yoshioka, *Biopolymers*, **12**, 1729 (1973).
10) K. Tsuji, H. Watanabe, and K. Yoshioka, *Adv. Mol. Relaxation Processes*, **8**, 49 (1976).
11) K. Tsuji and H. Watanabe, *J. Colloid Interface Sci.*, **62**, 101 (1977).
12) S. Kobayashi, *Biopolymers*, **6**, 1491 (1968).
13) J. Schweitzer and B. R. Jennings, *Biopolymers*, **11**, 1077 (1972).

14) J. Schweitzer and B. R. Jennings, *Biopolymers*, **12**, 2439 (1973).
15) H. J. Coles and G. Weill, *Polymer*, **18**, 1235 (1977).
16) C. T. O'Konski and A. J. Haltner, *J. Am. Chem. Soc.*, **78**, 3604 (1956).
17) C. T. O'Konski, K. Yoshioka, and W. H. Orttung, *J. Phys. Chem.*, **63**, 1558 (1959).
18) K. Yamaoka and E. Charney, *J. Am. Chem. Soc.*, **94**, 8963 (1972).
19) P. J. Flory, "Statistical Mechanics of Chain Molecules," John Wiley & Sons, New York (1969), Chap. 9.
20) H. Wesslau, *Makromol. Chem.*, **20**, 111 (1956).
21) K. Yamaoka and K. Ueda, *J. Phys. Chem.*, **86**, 406 (1982).
22) S. Broersma, *J. Chem. Phys.*, **32**, 1626 (1960).
23) K. Yamaoka and K. Matsuda, *Macromolecules*, **14**, 595 (1981).
24) E. Charney and K. Yamaoka, *Biochemistry*, **21**, 834 (1982).
25) A. W. Davis and D. R. Phillips, *Biochem. J.*, **173**, 179 (1978).
26) G. Cohen and H. Eisenberg, *Biopolymers*, **4**, 429 (1966).
27) J. E. Godfrey, *Biophys. Chem.*, **5**, 285 (1976).
28) J. E. Godfrey and H. Eisenberg, *Biophys. Chem.*, **5**, 301 (1976).

Electronic Absorption Spectra and Geometry of Molecular Ions Generated from Stilbene and Related Compounds. III. Radical Ions of (*Z*)-Stilbene and Its α,β-Dialkyl Derivatives

Hiroshi Suzuki,* Keiichiro Ogawa, Tadamasa Shida,† and Akira Kira††

Department of Chemistry, College of General Education, The University of Tokyo, Komaba, Meguro-ku, Tokyo 153

† *Department of Chemistry, Faculty of Science, Kyoto University, Kyoto 606*

†† *The Institute of Physical and Chemical Research, Wako, Saitama 351*

(Received July 10, 1982)

The radical ions of (*Z*)-stilbene and its α,β-dialkyl derivatives were produced by γ-ray irradiation of the parent compounds in frozen matrices at 77 K, and their geometries were investigated by electronic absorption spectroscopy. While the relaxed geometries of the radical ions of (*Z*)-stilbene are probably similar to that of the neutral molecule, those of the radical ions of the α,β-dialkyl derivatives are appreciably different from those of the neutral molecules: The torsion angle of the central ethylenic bond is distinctly larger and that of each C–Ph bond is probably smaller in the radical ions than in the neutral molecules. On illumination the radical ions of (*Z*)-stilbene isomerize to the *E* isomers, but those of the α,β-dialkyl derivatives do not. A mechanism of the photoisomerization is proposed, and an interpretation of the difference in the photochemical behavior between the unsubstituted stilbene radical ions and the α,β-dialkyl derivatives is given.

The present paper reports the result of an electronic spectroscopic study of the geometry of the radical ions of (*Z*)-stilbene (abbreviated as ZS), (*Z*)-α,β-dimethylstilbene (ZαβDMS), and (*Z*)-α,β-diethylstilbene (ZαβDES). The radical ions were produced by γ-ray irradiation of frozen solutions of the respective compounds at 77 K, and their electronic absorption spectra measured before and after illumination or limited warming were examined with respect to the geometry of the radical ions.

This work has three purposes as follows.

(1) Previously, we found that the relaxed geometries of radical ions generated from sterically crowded compounds were appreciably different from those of the parent neutral molecules.[1,2] It is one of the purposes of the present work to examine the geometries of the radical ions of the sterically crowded (*Z*)-stilbenes and to compare them with the geometries of the parent molecules.

(2) The π-bond order of the central ethylenic bond (the α–β bond) of stilbene is smaller in the radical ions than in the neutral molecule.[2] Therefore, the thermal $Z \rightarrow E$ isomerization should occur more readily in the radical ions than in the neutral molecule. As expected, the anion radical produced from ZS by reduction with alkali metals in ethereal solutions readily isomerizes to the anion radical of (*E*)-stilbene (ES).[3] When the anion radical of ZS ($ZS^{-\cdot}$) forms an ion pair with the alkali counterion, its isomerization is comparatively slow.[4,5] When $ZS^{-\cdot}$ is not associated with the counterion, its isomerization occurs especially rapidly.[5,6] Wang *et al.* proposed a mechanism involving a dianion for the isomerization of the counterion-free $ZS^{-\cdot}$ to the counterion-free $ES^{-\cdot}$ in hexamethylphosphoric triamide (HMPT).[7] The radical ions produced by γ-ray irradiation in frozen matrices are counterion-free, and the possibility that the radical ions in the frozen matrices disproportionate to a pair of the diion and the neutral molecule should be extremely small. Therefore, it is of interest to examine whether the radical ions of the (*Z*)-stilbenes in frozen matrices isomerize to the *E* isomers on limited warming. This is the second of the purposes of the present work.

(3) Both the cation and the anion radical of ZS in frozen matrices at 77 K undergo the $Z \rightarrow E$ photoisomerization on visible light illumination.[8,9] It is the third of the purposes to examine whether the photoisomerization occurs also in the radical ions of the crowded α,β-dialkyl derivatives.

Experimental

Materials. (Z)-*Stilbene (ZS)*: A commercial product of Aldrich Chemical Co. was used: UV_{max} (heptane) 278.7 nm (ε 1.031×10^4).

(Z)-*α,β-Dimethylstilbene (ZαβDMS)*: This compound was prepared as described previously:[10] UV_{max} (heptane) 252.0 nm (ε 8.88×10^3).

(Z)-*α,β-Diethylstilbene (ZαβDES)*: This compound was newly prepared as follows. Reductive coupling of propiophenone (4.03 g) with titanium(IV) chloride (8.6 g) and zinc (5.9 g) in dioxane (200 cm^3) was carried out according to the procedure of Mukaiyama *et al.*[11] After work-up, the residue was chromatographed twice on silica gel columns by using hexane as the eluent to give 700 mg of a colorless oil. Kugelrohr distillation of the oil gave an analytically pure sample of ZαβDES, which solidified in the receiver: mp 32.5—34.0 °C, uncorrected; UV_{max} (heptane) 248.8 nm (ε 8.87×10^3); ^1H NMR ($CDCl_3$) δ=7.12 (10H, br s, $2C_6H_5$), 2.62 (4H, q, J=8 Hz, $2CH_2$), 1.00 (6H, t, J=8 Hz, $2CH_3$). Found: C, 91.38; H, 8.73%; M^+, 236. Calcd for $C_{18}H_{20}$: C, 91.47; H, 8.53%; M, 236. Earlier reports[12–14] on this compound are now to be corrected, because the sample prepared previously [an oil: UV_{max} (ethanol) 244 nm (ε 7.74×10^3)] has, in the course of the present work, proved not to be pure.

Spectra of Radical Ions. The radical ions of ZS, ZαβDMS, and ZαβDES were prepared by γ-ray irradiation of frozen solutions of the parent compounds in deaerated 2-methyltetrahydrofuran (MTHF) for anion radicals and in *s*-butyl chloride (BC) or a Freon Mixture (FM: an equivolume mixture of trichlorofluoromethane and 1,2-dibromo-1,1,2,2-tetrafluoroethane) for cation radicals both at 77 K. The electronic absorption spectra of the γ-ray irradiated

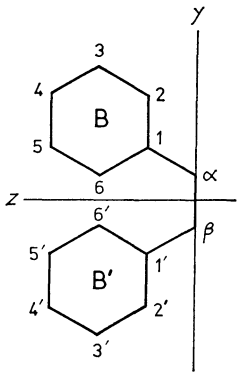

Fig. 1. The carbon skeleton of (Z)-stilbene.

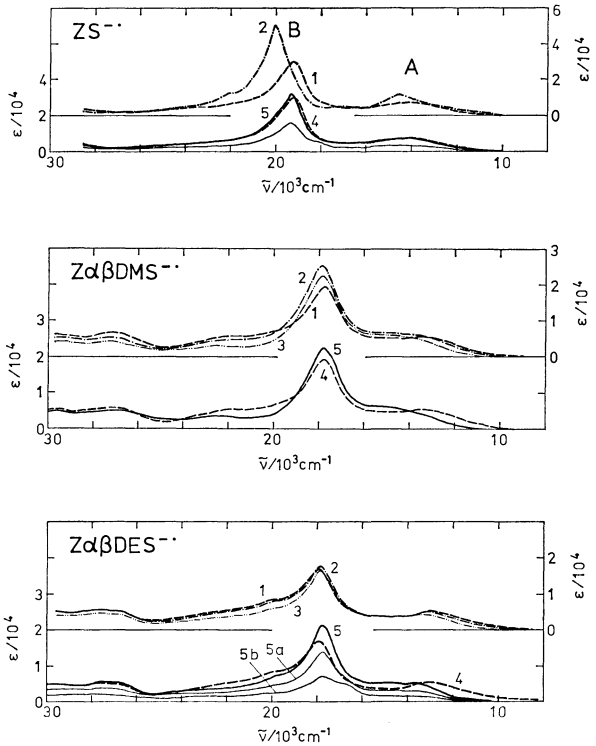

Fig. 2. Electronic absorption spectra of the anion radicals of (Z)-stilbene (ZS), (Z)-α,β-dimethylstilbene (ZαβDMS), and (Z)-α,β-diethylstilbene (ZαβDES). Curves 1 and 4 (----): spectra observed immediately after γ-ray irradiation of frozen solution, designated F in the text. Curve 2 (—·—): spectra observed after illumination of the sample for curve 1 with light of wavelengths corresponding to band A, designated PA in the text. Curve 3 (—··—): spectra observed after illumination of the sample for curve 2 with light of wavelengths corresponding to and longer than band B, designated PB in the text. Curve 5 (——): spectra observed after controlled warming of the sample for curve 4, designated W in the text. Curves 5a and 5b (——): spectra observed after additional controlled warming of the sample for curve 5. The solvent is 2-methyltetrahydrofuran (MTHF) for all the spectra.

samples were measured before and after illumination with visible light or warming for a limited period. The experimental details are the same as described in previous papers.[1,2]

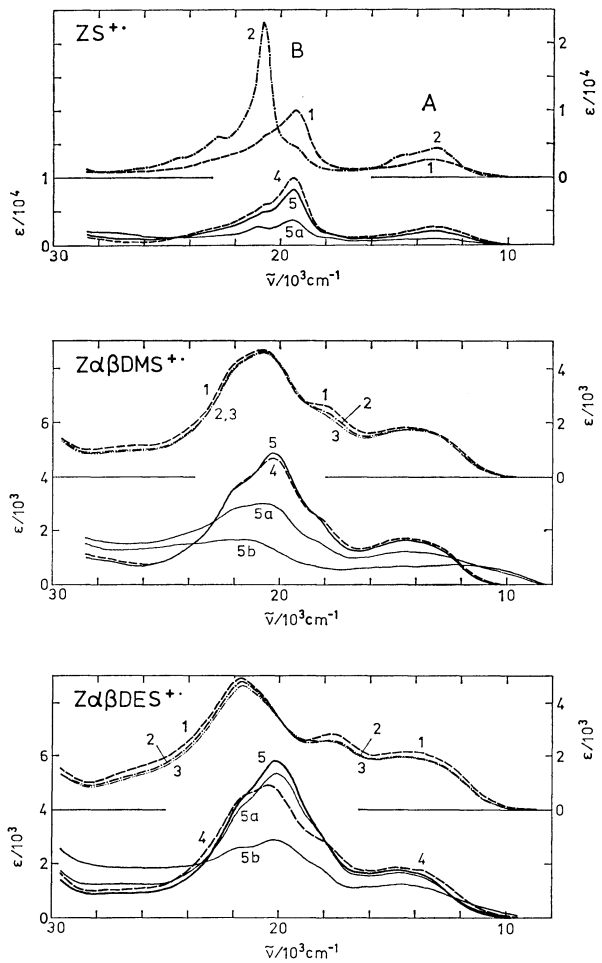

Fig. 3. Electronic absorption spectra of the cation radicals of ZS, ZαβDMS, and ZαβDES. See Caption for Fig. 2. The solvent is s-butyl chloride (BC) for spectra 1, 2, and 3, and is a Freon Mixture (FM) for the other spectra.

Molecular Orbital Calculation

As in the previous work,[1,2] a semiempirical SCF-MO-CI calculation was carried out for the radical ions by the Longuet-Higgins and Pople method.[15]

The numbering of the carbon atoms is illustrated for ZS in Fig. 1. Torsion angles β–α–1–6, α–β–1′–6′, and 1–α–β–1′ are denoted by $\theta_{\alpha 1}$, $\theta_{\beta 1'}$, and $\theta_{\alpha\beta}$, respectively. The value of $\theta_{\alpha\beta}$ is 0° for the planar Z configuration and 180° for the planar E configuration.

Results and Discussion

Designation of Spectra and of Geometries. Representative spectra of the radical ions are shown in Figs. 2 and 3, and relevant data are listed in Tables 1 and 2. As seen in the figures, the radical ions exhibit two major bands in the visible region. The band at the longer wavelength is designated as A, and that at the shorter wavelength as B. For band A, for example, the wavelength (λ) and molar absorption coefficient (ε) at the absorption maximum and the oscillator strength (f) are denoted by λ_A, ε_A, and f_A, re-

Table 1. Data on electronic absorption spectra of anion radicals

Anion radical	Class[a]	No. in Fig. 2	λ_B/nm	$\varepsilon_B/10^4$	f_B	λ_A/nm	$\varepsilon_A/10^4$	f_A	f_A/f_B
ZS$^{-\cdot}$	F(MTHF)	4	520.0	2.975	0.377	707.4	0.714	0.140	0.370
	PA(MTHF)	2	499.4	5.019	0.499	687.5	1.123	0.153	0.306
	W(MTHF)	5	517.8	3.149	0.385	707.4	0.701	0.129	0.335
Z$\alpha\beta$DMS$^{-\cdot}$	F(MTHF)	4	561.8	1.944	0.320	750	0.539	0.080	0.250
	PA(MTHF)	2	559.1	2.521	0.367	690[b]	0.631	0.085	0.231
	W(MTHF)	5	563.2	2.263	0.285	667[b]	0.606	0.072	0.251
Z$\alpha\beta$DES$^{-\cdot}$	F(MTHF)	4	557.2	1.686	0.297	763.2	0.535	0.082	0.277
	PB(MTHF)	3	559.6	1.655	0.250	750.0	0.435	0.061	0.243
	W(MTHF)	5	562.5	2.135	0.302	675.0	0.522	0.062	0.207

a) See the text or caption for Fig. 2. for the notation under the column Class. b) Inflection.

Table 2. Data on electronic absorption spectra of cation radicals

Cation radical	Class[a]	No. in Fig. 3	λ_B/nm	$\varepsilon_B/10^4$	f_B	λ_A/nm	$\varepsilon_A/10^4$	f_A	f_A/f_B
ZS$^{+\cdot}$	F(BC)	1	517.6	1.000	0.152	750.0	0.261	0.041	0.267
	PA(BC)	2	482.5	2.303	0.220	755.0	0.440	0.063	0.286
	F(FM)	4	515.4	1.000	0.141	750.0	0.263	0.044	0.314
	W(FM)	5	515.4	0.819	0.121	750.0	0.199	0.035	0.287
Z$\alpha\beta$DMS$^{+\cdot}$	F(BC)	1	480.4	0.467	0.126	687.5	0.179	0.031	0.246
	F(FM)	4	492.1	0.467	0.104	700.0	0.168	0.030	0.288
	W(FM)	5	492.1	0.487	0.102	700.0	0.161	0.028	0.277
Z$\alpha\beta$DES$^{+\cdot}$	F(BC)	1	460.1	0.490	0.147	714.4	0.212	0.038	0.258
	F(FM)	4	460[b]	0.439					
			485.3	0.490	0.131	675.0	0.184	0.030	0.228
	W(FM)	5	496.5	0.580	0.137	675.0	0.169	0.027	0.195

a) See the text or caption for Fig. 3 for the notation under the column Class. b) Inflection.

Table 3. Results of the MO calculation for the planar (*Z*)-stilbene anion radical with C_{2v} symmetry

Transition[a]	ΔE[b]/eV	f[c]	P[d]	State[e]	Symmetry[f]	Character[g]
1	1.183	0.002	y	D_1	B_1	0.954(−1, −2)
2	1.217	0.001	z	D_2	A_2	0.966(−1, −3)
3	1.498	0.135	y	D_3	B_1	0.956(−1, −4)
4	2.591	0.109	z	D_4	A_2	0.927(−1, −5)
5	3.107	0.202	y	D_5	B_1	0.919(+1, −1)
6	3.676	0.001	y	D_6	B_1	0.759(−1, −6)
7	3.870	0.001	z	D_7	A_2	0.597(−1, −7)
8	4.217	0.037	z	D_8	A_2	0.563(+4, −1)

a) Transitions are numbered in the order of increasing transition energy. b) Transition energy. c) Oscillator strength of the transition. d) Direction of the transition moment (*cf.* Fig. 1). e) The excited state. f) The symmetry species to which the excited state belongs. The ground state (state D_0) belongs to symmetry species A_2. g) The wave function of the excited state. Only the electron configuration whose coefficient in the wave function is the largest is shown, together with the coefficient. Symbol (i, j) denotes the electron configuration arising from the ground configuration by promotion of an electron from π MO ϕ_i to π MO ϕ_j. The orbital index i runs from +7 for the lowest orbital to −7 for the highest one in the order of increasing energy. Orbitals ϕ_{+1} and ϕ_{-1} correspond, respectively, to HOMO and LUMO in the molecule. The coefficient of the ground configuration in the wave function of state D_0 is 0.989.

spectively.

As in Part II of this series,[2] spectra of radical ions measured after different treatments are designated as follows: The spectrum of a radical ion measured immediately after its production by γ-ray irradiation in a frozen matrix is designated as F (*frozen*), that measured after illumination as P (*photobleached*), that measured after controlled warming as W (*warmed*). Sometimes, spectrum P measured after illumination with light of wavelengths corresponding to band A (illumination A) is referred to as spectrum PA, and that measured after illumination with light of wavelengths corresponding to and longer than band B (illumination B) as spectrum PB. If necessary, the solvent is denoted

Table 4. Transition energies (ΔE) and oscillator strengths (f) of the planar (Z)-stilbene anion radical and their variation with geometrical changes[a)]

Symmetry	$\theta_{\alpha 1}$/°	$\theta_{\beta 1'}$/°	$\theta_{\alpha\beta}$/°	ΔE_5/eV	f_5	ΔE_4/eV	f_4	ΔE_3/eV	f_3	f_3/f_5
C_{2v}	0	0	0	3.108	0.202	2.592	0.109	1.498	0.135	0.668
C_2	30	30	0	+0.233	−0.029	−0.256	+0.017	−0.252	+0.007	+0.153
C_s	30	−30	0	+0.230	−0.033	−0.257	+0.018	−0.252	+0.007	+0.172
C_2	0	0	30	−0.312	+0.056	−0.012	−0.013	+0.198	+0.002	−0.137

a) The values for the nonplanar geometries are relative to the planar geometry.

in parentheses: For example, spectrum F of a cation radical in solution in *s*-butyl chloride is referred to as spectrum F(BC).

The same designations are also used to specify the geometries of radical ions after the respective treatments. That is, for example, the geometry of a cation radical immediately after its production in frozen *s*-butyl chloride is referred to as geometry F(BC). The relaxed geometry of a radical ion, that is, the geometry that the radical ion would take in fluid solutions, is referred to as geometry R (*relaxed*), and that of the parent neutral molecule as geometry N (*neutral*). Geometry W is considered to be nearly equal to geometry R.[1,2)]

We should like to emphasize that the spectral changes caused by illumination or controlled warming, shown in Figs. 2 and 3, are definite and reproducible, which should defy possible skepticism about attaching significance to the apparently small spectral changes discussed in the following text. The instrumental reproducibility is within ±0.1% for both the ordinate and the abscissa of these figures.

Assignment of Absorption Bands. The results of the MO calculation for the stilbene anion radical in the planar *Z* form are shown in Table 3. It is notable that the f values of transitions 3 and 5 are considerably smaller than the corresponding values for the anion radical in the planar *E* form (*cf.* Table 3 in Part II), and that the f value of transition 4 is not zero in contrast to the case of the planar *E* form. The results of the MO calculation for the cation radical are similar to those for the anion radical. The character of each state of the radical ions in the *Z* form is analogous to that of the corresponding state of the radical ions in the *E* form.[2)]

As in the case of the *E* isomers,[2)] bands A and B are ascribed to transitions 3 and 5, respectively. The band appearing between bands A and B in spectra of Z$\alpha\beta$DMS$^{+\cdot}$ and Z$\alpha\beta$DES$^{+\cdot}$ is ascribed to transition 4. In the spectra of the other radical ions, the absorption due to transition 4 is probably masked by the tails of bands A and B. The f values in Tables 1 and 2 may be less accurate than the corresponding values for the radical ions of sterically uncrowded or less crowded (*E*)-stilbenes in Part II,[2)] because of the presence of the superposing absorption due to transition 4 and also because of the comparatively small separation of bands A and B.

Expected Effects of Geometrical Changes on the Electronic Transitions. Table 4 lists the calculated values of the transition energy (ΔE) and oscillator strength (f) of transitions 3, 4, and 5 and of the ratio between the f values of transitions 3 and 5 (f_3/f_5) for the stilbene anion radical in the planar *Z* geometry and also the calculated values of the changes in these quantities associated with the changes from the planar *Z* geometry to nonplanar geometries in which $|\theta_{\alpha 1}|$, $|\theta_{\beta 1'}|$, or $|\theta_{\alpha\beta}|$ is 30°. The corresponding values for the cation radical are very close to the values for the anion radical.

The changes in the properties of the transitions of the anion radical associated with the geometrical changes seen in Table 4 and the corresponding ones of the cation radical should represent the effect of the geometrical changes on the absorption bands: It is expected, for example, that an increase in $|\theta_{\alpha 1}|$ and $|\theta_{\beta 1'}|$ will cause a large red shift and a very small increase in intensity of band A, a large blue shift and a small decrease in intensity of band B, and an increase in f_A/f_B, and that an increase in $|\theta_{\alpha\beta}|$ will cause a large blue shift and a very small increase in intensity of band A, a large red shift and a small increase in intensity of band B, and a decrease in f_A/f_B.

Geometry of the Neutral Molecules. Before proceeding to the discussion of the geometries of the radical ions, we briefly mention the geometry of the parent neutral molecules, which is relevant to the later discussion.

According to an electron-diffraction study, the molecule of ZS in the gas phase has a propeller-like geometry with C_2 symmetry, in which $\theta_{\alpha 1}$ and $\theta_{\beta 1'}$ are about 43°.[16)] This value is larger than predicted by most theoretical calculations.[17)] The value for the ZS molecule in solution is probably smaller than that for the molecule in the gas phase. The former is estimated at 29° from the λ_{max} value (278.7 nm) of the main absorption band of ZS in heptane solution.[12,14,20)]

By the method described in Refs. 12—14 and 20, the value of $|\theta_{\alpha 1}|$ and $|\theta_{\beta 1'}|$ is estimated at 52° for Z$\alpha\beta$DMS in solution from its λ_{max} value of 252.0 nm (in heptane) and at 54° for Z$\alpha\beta$DES in solution from its λ_{max} value of 248.8 nm (in heptane). When an allowance for the electronic bathochromic effect of the alkyl substituents is made, these values are revised to 59° and 61°, respectively.[21)]

At any rate, it is evident that the value of $|\theta_{\alpha 1}|$ and $|\theta_{\beta 1'}|$ in the relaxed geometry of the neutral molecule (*i.e.*, geometry N) increases in the order ZS$\ll$ Z$\alpha\beta$DMS$<$Z$\alpha\beta$DES. The value of $\theta_{\alpha\beta}$ in geometries N of these compounds is probably equal or close to 0°.

Broadness of Absorption Bands. Now, let us return to the spectra of the radical ions. The absorption bands of the radical ions of the (*Z*)-stilbenes are structureless and are much broader than those of the radical

ions of sterically uncrowded (*E*)-stilbenes.[24] This seems to indicate the nonplanarity of the geometry of the radical ions of the (*Z*)-stilbenes.

Effect of Warming and Relaxed Geometries. Cation Radicals: In spectra F(BC) of the cation radicals, λ_B/nm decreases in the order $ZS^{+\cdot} > Z\alpha\beta DMS^{+\cdot} > Z\alpha\beta DES^{+\cdot}$. This indicates that $|\theta_{\alpha 1}|$ and $|\theta_{\beta 1'}|$ increase in the order $ZS^{+\cdot} < Z\alpha\beta DMS^{+\cdot} < Z\alpha\beta DES^{+\cdot}$ in geometries F(BC) of the cation radicals as in geometries N. If $\theta_{\alpha\beta}$ were nearly 0° or nearly constant in geometries F(BC) of these cation radicals, λ_A/nm and f_A/f_B would increase in the order $ZS^{+\cdot} < Z\alpha\beta DMS^{+\cdot} < Z\alpha\beta DES^{+\cdot}$. In fact, they increase in the order $Z\alpha\beta DMS^{+\cdot} < Z\alpha\beta DES^{+\cdot} < ZS^{+\cdot}$. This fact suggests that in geometries F(BC) $|\theta_{\alpha\beta}|$ is appreciably larger for $Z\alpha\beta DMS^{+\cdot}$ and $Z\alpha\beta DES^{+\cdot}$ than for $ZS^{+\cdot}$.

Spectrum F(FM) of $ZS^{+\cdot}$ is similar to spectrum F(BC), and remains almost unchanged on limited warming. These facts indicate that geometry F(FM) of this cation radical is similar to geometry F(BC), which is probably similar to geometry N, and that any significant geometrical change does not occur on the warming.

On the other hand, spectra F(FM) of $Z\alpha\beta DMS^{+\cdot}$ and $Z\alpha\beta DES^{+\cdot}$ are significantly different from spectra F(BC), and change appreciably on limited warming. In going from spectra F(BC) to spectra W(FM), λ_B/nm increases for both the cation radicals, and λ_A/nm and f_A/f_B decrease for $Z\alpha\beta DES^{+\cdot}$. These changes indicate an increase in $|\theta_{\alpha\beta}|$ and/or a decrease in $|\theta_{\alpha 1}|$ and $|\theta_{\beta 1'}|$. The geometrical change from F(BC) to W(FM) appears to be larger for $Z\alpha\beta DES^{+\cdot}$ than for $Z\alpha\beta DMS^{+\cdot}$. Spectra W(FM) of these cation radicals are different from spectra W(FM) of the *E* isomers (*cf.* Part II[2]).

In spectra W(FM), λ_B/nm increases in the order $Z\alpha\beta DMS^{+\cdot} < Z\alpha\beta DES^{+\cdot}$, and λ_A/nm and f_A/f_B decrease in the order $Z\alpha\beta DMS^{+\cdot} > Z\alpha\beta DES^{+\cdot}$. These sequences are opposite to the corresponding ones in spectra F(BC). Since it is unlikely that $|\theta_{\alpha 1}|$ and $|\theta_{\beta 1'}|$ are larger in $Z\alpha\beta DMS^{+\cdot}$ than in $Z\alpha\beta DES^{+\cdot}$, the above sequences indicate that in geometries W(FM) and therefore in geometries R (*i.e.*, the relaxed geometries) $|\theta_{\alpha\beta}|$ is considerably larger in $Z\alpha\beta DES^{+\cdot}$ than in $Z\alpha\beta DMS^{+\cdot}$.

Thus, it is concluded that, in geometries W and therefore in geometries R of the cation radicals, $|\theta_{\alpha 1}|$ and $|\theta_{\beta 1'}|$ increase in the order $ZS^{+\cdot} \ll Z\alpha\beta DMS^{+\cdot} \leqq Z\alpha\beta DES^{+\cdot}$ and $|\theta_{\alpha\beta}|$ increases in the order $ZS^{+\cdot} \ll Z\alpha\beta DMS^{+\cdot} \ll Z\alpha\beta DES^{+\cdot}$.

Anion Radicals: In spectra F(MTHF) of the anion radicals, λ_A/nm increases in the order $ZS^{-\cdot} < Z\alpha\beta DMS^{-\cdot} < Z\alpha\beta DES^{-\cdot}$, and λ_B/nm increases and f_A/f_B decreases in the order $ZS^{-\cdot}$, $Z\alpha\beta DES^{-\cdot}$, $Z\alpha\beta DMS^{-\cdot}$. The sequences probably indicate that in geometries F(MTHF) $|\theta_{\alpha 1}|$ and $|\theta_{\beta 1'}|$ increase in the order $ZS^{-\cdot} < Z\alpha\beta DMS^{-\cdot} < Z\alpha\beta DES^{-\cdot}$ and $|\theta_{\alpha\beta}|$ is noticeably larger in $Z\alpha\beta DMS^{-\cdot}$ and $Z\alpha\beta DES^{-\cdot}$ than in $ZS^{-\cdot}$. This means that geometries F(MTHF) of $Z\alpha\beta DMS^{-\cdot}$ and $Z\alpha\beta DES^{-\cdot}$ have already been relaxed to a considerable extent before being warmed, owing to the softness of the MTHF glass at 77 K.[1,2]

On limited warming, the spectrum of $ZS^{-\cdot}$ changes little, indicating that the geometry remains almost unchanged.

On the other hand, for $Z\alpha\beta DMS^{-\cdot}$ and $Z\alpha\beta DES^{-\cdot}$ the limited warming causes a large blue shift of band A and a small red shift and an increase in intensity of band B. The spectral changes indicate an increase in $|\theta_{\alpha\beta}|$ and/or a decrease in $|\theta_{\alpha 1}|$ and $|\theta_{\beta 1'}|$. Spectra W(MTHF) of these anion radicals are different from spectra W(MTHF) of the *E* isomers (*cf.* Part II[2]).

In spectra W(MTHF), the values of λ_A/nm and λ_B/nm of $Z\alpha\beta DMS^{-\cdot}$ are close to those of $Z\alpha\beta DES^{-\cdot}$. This similarity of the band position does not necessarily mean the geometrical similarity of these two anion radicals. Since the value of f_A/f_B is noticeably different between the two anion radicals, and also in view of the above conclusion on geometries W of the corresponding cation radicals, geometries W of these anion radicals seem to be considerably different from each other. Probably both $|\theta_{\alpha\beta}|$ and $|\theta_{\alpha 1}|$ as well as $|\theta_{\beta 1'}|$ increase in the order $Z\alpha\beta DMS^{-\cdot} < Z\alpha\beta DES^{-\cdot}$. The increase in $|\theta_{\alpha\beta}|$ and that in $|\theta_{\alpha 1}|$ and $|\theta_{\beta 1'}|$ should have opposite effects on the band position. The above-mentioned similarity of the band position is probably a result of balancing of the opposite effects.

Thus, it is concluded that, in geometries W and therefore in geometries R of the anion radicals, $|\theta_{\alpha 1}|$ and $|\theta_{\beta 1'}|$ increase in the order $ZS^{-\cdot} < Z\alpha\beta DMS^{-\cdot} < Z\alpha\beta DES^{-\cdot}$ and $|\theta_{\alpha\beta}|$ increases in the order $ZS^{-\cdot} \ll Z\alpha\beta DMS^{-\cdot} < Z\alpha\beta DES^{-\cdot}$.

While the position of band B in spectrum W of $ZS^{-\cdot}$ is close to that in spectrum W of $ZS^{+\cdot}$, band B in spectrum W of $Z\alpha\beta DMS^{-\cdot}$ and that of $Z\alpha\beta DES^{-\cdot}$ are located at much longer wavelength than are those of the corresponding cation radicals. In addition, the magnitude of the blue shift of band A in going from spectrum F to spectrum W is much larger for $Z\alpha\beta DMS^{-\cdot}$ and $Z\alpha\beta DES^{-\cdot}$ than for the corresponding cation radicals. These facts probably indicate that $|\theta_{\alpha\beta}|$ is larger in $Z\alpha\beta DMS^{-\cdot}$ and $Z\alpha\beta DES^{-\cdot}$ in geometry R than in the corresponding cation radicals in geometry R.

Comparison with Other Spectral Data: The value of λ_{max} of the sodium salt of $ZS^{-\cdot}$ in fluid solution in THF was reported to be 500 nm (ε 3.3×10^4).[7] This value is considerably smaller than the values of λ_B of $ZS^{-\cdot}$ in the present work. Since the sodium salt in THF probably exists as a contact ion pair, the difference in the λ_{max} value may be mainly ascribed to the effect of the counterion.

The values of λ_{max} of the anion radicals produced by reduction of 1,2-diphenylcyclopentene (DPCP) and 1,2-diphenylcyclohexene (DPCH) with sodium in HMPT were reported to be 530 nm (ε 3.4×10^4) and 560 nm (ε 2.3×10^4), respectively.[25] In this solvent the anion radicals are probably counterion-free. These anion radicals have a $ZS^{-\cdot}$ π system, and obviously the above data refer to band B of the π system. In $DPCP^{-\cdot}$ $|\theta_{\alpha\beta}|$ should be close to 0°, while in $DPCH^{-\cdot}$ it may deviate to some extent from 0°. The fact that the λ_{max} value of $DPCH^{-\cdot}$ is considerably larger than that of $DPCP^{-\cdot}$ indicates that the value of $|\theta_{\alpha\beta}|$ is considerably larger in $DPCH^{-\cdot}$ than in $DPCP^{-\cdot}$.[26]

The values of λ_{max} and ε_{max} of DPCP$^{-\cdot}$ are close to the values of λ_B and ε_B of spectrum W of ZS$^{-\cdot}$. Since the small difference in the λ value may be largely ascribed to the electronic bathochromic effect of the trimethylene chain in DPCP$^{-\cdot}$, if the difference in $|\theta_{\alpha 1}|$ and $|\theta_{\beta 1'}|$ between these anion radicals is assumed to be small, this spectral similarity is taken as a support to our conclusion that $|\theta_{\alpha\beta}|$ of ZS$^{-\cdot}$ in the relaxed geometry is approximately 0°.

The values of λ_{max} and ε_{max} of DPCH$^{-\cdot}$ are close to the values of λ_B and ε_B of spectra W of Z$\alpha\beta$DMS$^{-\cdot}$ and Z$\alpha\beta$DES$^{-\cdot}$. The electronic effect of the alkyl substituents should be approximately equal in these three anion radicals. Therefore, this spectral similarity indicates the geometrical similarity of the ZS$^{-\cdot}$ π systems in these anion radicals and supports our conclusion that $|\theta_{\alpha\beta}|$ in Z$\alpha\beta$DMS$^{-\cdot}$ and Z$\alpha\beta$DES$^{-\cdot}$ in the relaxed geometry deviates considerably from 0°.

The values of λ_{max} and ε_{max} of spectra F of Z$\alpha\beta$DMS$^{-\cdot}$ and Z$\alpha\beta$DES$^{-\cdot}$ are similar to those of DPCH$^{-\cdot}$, but different from those of DPCP$^{-\cdot}$. This fact seems to support the above inference that geometries F(MTHF) of Z$\alpha\beta$DMS$^{-\cdot}$ and Z$\alpha\beta$DES$^{-\cdot}$ have already been relaxed to a considerable extent.

General Conclusions on the Effect of Warming and on the Relaxed Geometries: From the study of limited warming, the following conclusions are drawn.

(1) Neither the $Z\rightarrow E$ nor the $E\rightarrow Z$ isomerization occurs on limited warming of glassy solutions of the radical ions of ZS, Z$\alpha\beta$DMS, Z$\alpha\beta$DES, or their E isomers (ES, E$\alpha\beta$DMS, E$\alpha\beta$DES).

(2) The relaxed geometries of the radical ions of ZS are almost similar to that of the neutral molecule, in which $|\theta_{\alpha\beta}|$ is approximately 0° and $|\theta_{\alpha 1}|$ and $|\theta_{\beta 1'}|$ are about 30°. It is possible that $|\theta_{\alpha\beta}|$ in the ZS radical ions in the relaxed geometry is slightly larger than that in the neutral molecule and that $|\theta_{\alpha 1}|$ and $|\theta_{\beta 1'}|$ in the former are slightly smaller than those in the latter.

(3) In the radical ions of Z$\alpha\beta$DMS and Z$\alpha\beta$DES in the relaxed geometry $|\theta_{\alpha\beta}|$ deviates considerably from 0°.

(4) $|\theta_{\alpha 1}|$ and $|\theta_{\beta 1'}|$ in the radical ions of Z$\alpha\beta$DMS and Z$\alpha\beta$DES in the relaxed geometry are probably somewhat smaller than those in the corresponding neutral molecules, but they are appreciably larger than those in the radical ions of ZS in the relaxed geometry.

Conclusions 2 and 3 are rationalized as follows. In the radical ions of ZS, the steric interference between the two phenyl groups can be relieved effectively by an increase in $|\theta_{\alpha 1}|$ and $|\theta_{\beta 1'}|$ as in the neutral molecule. There seems to be no need for the increase in $|\theta_{\alpha\beta}|$. On the other hand, in the radical ions of Z$\alpha\beta$DMS and Z$\alpha\beta$DES, the steric interference between the two alkyl groups is relieved only by an increase in $|\theta_{\alpha\beta}|$.

Conclusion 4 also seems to be quite reasonable, since the steric interference between the phenyl group and the alkyl group connected to the same carbon atom in the radical ions of Z$\alpha\beta$DMS and Z$\alpha\beta$DES remains unrelieved even when $|\theta_{\alpha\beta}|$ increases, and can be relieved only by an increase in $|\theta_{\alpha 1}|$ and $|\theta_{\beta 1'}|$.

As mentioned in Part II,[2] the relaxed geometry of a radical ion in its ground state (state D_0) is expected to be intermediate between the geometries of the neutral molecule in its ground state (state S_0) and in its first excited singlet state (state S_1). According to a theoretical calculation by Fischer *et al.*,[19] $\theta_{\alpha\beta}$ is 37° and 49° in ZS and Z$\alpha\beta$DMS, respectively, both in state S_1, while $\theta_{\alpha 1}$ and $\theta_{\beta 1'}$ are 13° in both the molecules in state S_1.[28] The result that $\theta_{\alpha\beta}$ in Z$\alpha\beta$DMS in state S_1 has a considerably large value is consistent with Conclusion 3. However, the other results are inconsistent with Conclusions 2 and 4.

Effect of Illumination. As mentioned above, both the cation and the anion radical of ZS in frozen solutions at 77 K isomerize irreversibly to their E isomers on illumination.

In contrast, the radical ions of Z$\alpha\beta$DMS and Z$\alpha\beta$DES do not isomerize on illumination. The spectra of the cation radicals in frozen BC change only slightly on illumination. In the case of the anion radicals in frozen MTHF, on illumination spectral changes similar to those caused by limited warming occur: Band A shifts to shorter wavelengths, band B increases in intensity, and f_A/f_B decreases. These spectral changes indicate an increase in $|\theta_{\alpha\beta}|$ and a decrease in $|\theta_{\alpha 1}|$ and $|\theta_{\beta 1'}|$ as in the case of warming, but there is no indication of occurrence of the $Z\rightarrow E$ isomerization.

As seen in Part II,[2] the radical ions of E$\alpha\beta$DMS and E$\alpha\beta$DES do not isomerize on illumination. Spectra PB of the radical ions of Z and E isomers of the α,β-dialkylstilbenes ($\alpha\beta$DAS's) appear distinctly different. Thus, it is concluded that in the radical ions of the $\alpha\beta$DAS's in frozen matrices at 77 K neither the photoisomerization between Z and E isomers nor the photoconversion from both Z and E isomers to a common product occurs.

Mechanism of the Z→E *Photoisomerization of the Unsubstituted Stilbene Radical Ions.* We propose here a mechanism of the photoisomerization of the stilbene radical ions and account for the notable difference in the photochemical behavior between the unsubstituted and the α,β-dialkyl-substituted stilbene radical ions.

The photoisomerization process of the stilbene radical ions is explicable by the diagrams in Fig. 4, which show the state energies as functions of $|\theta_{\alpha\beta}|$. The diagrams were drawn in the light of the results of the MO calculation, spectroscopic data, and the fact that the change in $|\theta_{\alpha\beta}|$ should be accompanied by a change in $|\theta_{\alpha 1}|$ and $|\theta_{\beta 1'}|$.

As mentioned above, for both the cation and the anion radical, and for both the Z and the E isomer, state D_5 is approximated as the state arising from state D_0 as a result of promotion of an electron from ψ_{+1} to ψ_{-1}. That is, aside from the closed electron configuration in which the six lowest-energy π orbitals (from ψ_{+7} to ψ_{+2}) are filled, states D_0 and D_5 of the cation radical are approximated by electron configurations $\psi_{+1}{}^1$ and $\psi_{-1}{}^1$, respectively, and states D_0 and D_5 of the anion radical by electron configurations $\psi_{+1}{}^2\psi_{-1}{}^1$ and $\psi_{+1}{}^1\psi_{-1}{}^2$, respectively.

At $|\theta_{\alpha\beta}|=90°$, ψ_{+1} and ψ_{-1} form a degenerate pair of orbitals. When $|\theta_{\alpha\beta}|$ increases from the Z side to the E side across this point, ψ_{+1} and ψ_{-1} are con-

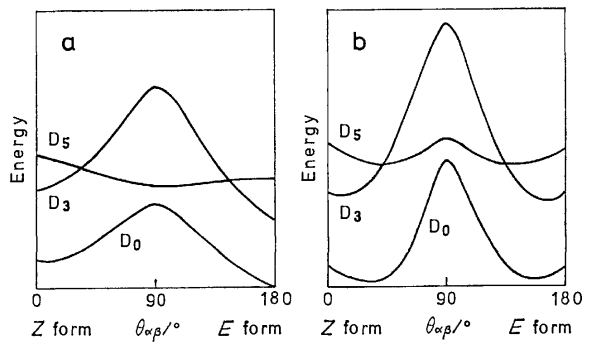

Fig. 4. State energies *vs.* the torsion angle about the central ethylenic bond ($\theta_{\alpha\beta}$).
(a): The unsubstituted stilbene radical ions. (b): The α,β-dialkylstilbene radical ions.

verted into ψ_{-1} and ψ_{+1}, respectively. Therefore, to a first approximation, states D_5 and D_0 are degenerate at $|\theta_{\alpha\beta}|=90°$, and, when $|\theta_{\alpha\beta}|$ increases from the Z side to the E side across this point, states D_5 and D_0 are converted into states D_0 and D_5, respectively. In fact, as a result of configuration interaction, the energy curves for these states must be separated as shown in Fig. 4, but the energy gap between these states at $|\theta_{\alpha\beta}|=90°$ should be small. Therefore, the internal conversion will occur with a high probability from state D_5 to state D_0 near this point.

In the E form of the unsubstituted stilbene radical ions, $|\theta_{\alpha 1}|$ and $|\theta_{\beta 1'}|$ are approximately 0°. In the Z form also they are small. Therefore, the π-bond order of the α–β bond is low. Accordingly, the energy barrier at $|\theta_{\alpha\beta}|=90°$ in state D_0 should be low, and the energy of state D_5 at this point should also be low. Thus, the energy of state D_5 will decrease as $|\theta_{\alpha\beta}|$ increases from 0° to 90°. The possible small decrease in $|\theta_{\alpha 1}|$ and $|\theta_{\beta 1'}|$ associated with the increase in $|\theta_{\alpha\beta}|$ will lower the energies of states D_5 and D_0 to some extent.

After all, the $Z\rightarrow E$ photoisomerization is considered to proceed as follows: $D_0(Z) \longrightarrow D_5(Z) \rightsquigarrow D_5(|\theta_{\alpha\beta}|=90°) \rightsquigarrow D_0(|\theta_{\alpha\beta}|=90°) \rightsquigarrow D_0(E)$. In this scheme, a radiative transition is represented by a straight arrow, and radiationless ones by wavy arrows. The basic assumption in this mechanism is that the photoisomerization proceeds via state D_5, the final state of the electronic transition responsible to band B.

Actually, even illumination A (illumination with light of wavelengths corresponding to band A), that is, the excitation to state D_3, induces the $Z\rightarrow E$ isomerization. In this case, the photoisomerization will proceed as follows. The radical ion passes from state D_3 to state D_5 at the crossing point ($0°<|\theta_{\alpha\beta}|<90°$) of the energy curves of the two states (*cf.* Fig. 4 (a)), and then the isomerization occurs: $D_0(Z) \longrightarrow D_3(Z) \rightsquigarrow D_3$(the crossing point) $\rightsquigarrow D_5$(the crossing point) $\rightsquigarrow D_5(|\theta_{\alpha\beta}|=90°) \rightsquigarrow D_0(|\theta_{\alpha\beta}|=90°) \rightsquigarrow D_0(E)$. Passing from state $D_3(Z)$ to the crossing point involves moving along a rising curve, *i.e.*, overriding a small barrier. The energy necessary to override the barrier must be supplied as vibrational energy.

Recently, Sazhnikov *et al.*[29,30] measured the wavelength dependence of the quantum yield of the $Z\rightarrow E$ photoisomerization of the radical ions of the unsubstituted stilbene in glassy solutions at 77 K, and found the following facts. (1) The quantum yield is very high on illumination with light of wavelengths corresponding to the "second absorption band" (*i.e.*, band B in our designation), 400—600 nm. (2) The maximum value of the quantum yield is extremely high. For the anion radical it is as high as 0.60 at 529 nm (nearly the absorption maximum of band B), a value which is much higher than the corresponding value for the $Z\rightarrow E$ photoisomerization of the neutral stilbene molecule (*ca.* 0.05 at −180 °C). (3) The quantum yield drops sharply to zero when the wavelength of the exciting light is varied from *ca.* 650 nm (for the cation radical) or *ca.* 620 nm (for the anion radical) to 800 nm in the region of the "first absorption band" (*i.e.*, band A in our designation). The 0-0 band of band A is probably located at about 800 nm. Fact 3 means that the illumination at this wavelength cannot cause the isomerization, and that, when the radical ions are excited into higher vibrationally excited levels of state D_3, the quantum yield of the isomerization increases sharply.

The facts found by Sazhnikov *et al.* can be satisfactorily rationalized by the above proposed mechanism. States D_1 and D_2 in their papers should be replaced by states D_3 and D_5, respectively.

Interpretation of Nonoccurrence of the E→Z *Photoisomerization in the Unsubstituted Stilbene Radical Ions.* The $Z\rightarrow E$ photoisomerization of the unsubstituted stilbene radical ions is irreversible. That is, the $E\rightarrow Z$ photoisomerization does not occur. In order to interpret this fact, both intramolecular and intermolecular factors should be taken into consideration.

First, we consider the intramolecular factor. In the case of the radical ions of the unsubstituted stilbene the E isomer should be considerably more stable than the Z isomer, as in the case of the neutral molecule[31,32] and the dianion.[27] Considering the difference in the λ_B value between the E and the Z isomer, we infer that the energy of state D_5 of the E isomer should be comparable to or rather lower than that of the Z isomer. Perhaps, the energy of state D_5 may be lower at $|\theta_{\alpha\beta}|=180°$ than at $|\theta_{\alpha\beta}|=90°$. If it is true, it may be possible that the excitation of the E isomer from state D_0 to state D_5 cannot induce the $E\rightarrow Z$ isomerization. However, this interpretation may not be convincing.

With regard to the intermolecular factor, Gegiou *et al.* found that the quantum yield of the $E\rightarrow Z$ photoisomerization of the unsubstituted stilbene molecule in fluid solutions decreased with increasing viscosity of the medium, while that of the $Z\rightarrow E$ photoisomerization was practically unaffected by the viscosity of the medium.[33] Considering the fact that in solution the nonplanar (Z)-stilbene molecule occupies a larger volume than the planar (E)-stilbene molecule by about 2.5%,[34] these authors ascribed the viscosity effect to an increase in molecular volume somewhere along the path of the $E\rightarrow Z$ photoisomerization. Sazhnikov *et al.* stated that the same interpretation appeared to be true for the radical ions of stilbene.[30] A plausible interpretation for the radical ions may be as follows:

The isomerization of the more bulky nonplanar Z isomer to the less bulky planar E isomer is not resisted by the rigid matrix, but the reverse process (the $E \rightarrow Z$ isomerization), which necessitates an increase in the volume of the radical ion, is inhibited.

It is rather surprising that the $Z \rightarrow E$ isomerization, which is obviously accompanied by a large change in the shape of the radical ion, proceeds easily in the rigid matrix such as frozen *s*-butyl chloride. The thermal energy liberated from the optically excited solute radical ion may locally heat and loosen the matrix around the radical ion.

Interpretation of Nonoccurrence of the Z→E *and the* E→Z *Photoisomerization in the α,β-Dialkylstilbene Radical Ions.* The fact that the radical ions of αβDAS's undergo neither the $Z \rightarrow E$ nor the $E \rightarrow Z$ photoisomerization may not be ascribed to the intermolecular effect, but may be intrinsic to the radical ions: Since both Z and E isomers of the αβDAS radical ions are nonplanar to a comparable extent, the isomerization will not be accompanied by an appreciable increase in the volume of the radical ion. In addition, the differences in the shape of the radical ion among the Z form, the 90° twisted form, and the E form are considered to be rather smaller than those in the unsubstituted stilbene radical ions. In this connection, it may be noted that in sterically hindered stilbene derivatives such as 2,2′,4,4′,6,6′-hexamethylstilbene both the quantum yields of the $Z \rightarrow E$ and the $E \rightarrow Z$ photoisomerization of the molecules in fluid solutions are independent of the viscosity of the medium and that this fact is interpreted on the basis of the inference that the volumes occupied by both the isomers are similar.[33]

We must invoke the intramolecular or intrinsic factor. The reason of the nonoccurrence of the photoisomerization is probably as follows. An state energy diagram schematically drawn for the αβDAS radical ions is shown in Fig. 4 (b). The ground states of the Z and the E isomer of α,β-dimethylstilbene have comparable energies.[10,12,13,32] Accordingly, the energy difference between states $D_0(Z)$ and $D_0(E)$ of the αβDAS radical ions is probably also very small. In these radical ions, $|\theta_{\alpha 1}|$ and $|\theta_{\beta 1'}|$ are always large, and therefore the π-bond order of the α–β bond is high. Therefore, the increase in the energy of state D_0 associated with the deviation of $|\theta_{\alpha\beta}|$ from 0° or 180° should be sharp, and the energy barrier at $|\theta_{\alpha\beta}| = 90°$ in state D_0 should be much higher than in the case of the unsubstituted stilbene radical ions. As a result, the energy of state D_5 should be raised at $|\theta_{\alpha\beta}| = 90°$. Also in this case, the possible small decrease in $|\theta_{\alpha 1}|$ and $|\theta_{\beta 1'}|$ associated with the deviation of $|\theta_{\alpha\beta}|$ from 0° or 180° will lower the energies of states D_5 and D_0 to some extent. Consequently, the energy curve for state D_5 as well as that for state D_0 possibly has a maximum at $|\theta_{\alpha\beta}| = 90°$ and minima between $|\theta_{\alpha\beta}| = 0°$ and 90° and between $|\theta_{\alpha\beta}| = 90°$ and 180°. Therefore, in these radical ions, the excitation to state D_5 does not induce the isomerization in either direction.

References

1) H. Suzuki, K. Koyano, T. Shida, and A. Kira, *Bull. Chem. Soc. Jpn.*, **52**, 2794 (1979).
2) H. Suzuki, K. Koyano, T. Shida, and A. Kira, *Bull. Chem. Soc. Jpn.*, **55**, 3690 (1982).
3) R. Chang and C. S. Johnson, Jr., *J. Chem. Phys.*, **46**, 2314 (1967).
4) G. Levin, T. A. Ward, and M. Szwarc, *J. Am. Chem. Soc.*, **96**, 270 (1974).
5) T. A. Ward, G. Levin, and M. Szwarc, *J. Am. Chem. Soc.*, **97**, 258 (1975).
6) S. Sorensen, G. Levin, and M. Szwarc, *J. Am. Chem. Soc.*, **97**, 2341 (1975).
7) H. C. Wang, G. Levin, and M. Szwarc, *J. Am. Chem. Soc.*, **99**, 2642 (1977).
8) T. Shida and W. H. Hamill, *J. Chem. Phys.*, **44**, 2375 (1966).
9) T. Shida and W. H. Hamill, *J. Chem. Phys.*, **44**, 4372 (1966).
10) O. Simamura and H. Suzuki, *Bull. Chem. Soc. Jpn.*, **27**, 231 (1954).
11) T. Mukaiyama, T. Sato, and J. Hanna, *Chem. Lett.*, **1973**, 1041.
12) H. Suzuki, *Bull. Chem. Soc. Jpn.*, **25**, 145 (1952).
13) H. Suzuki, *Bull. Chem. Soc. Jpn.*, **33**, 396 (1960).
14) H. Suzuki, "Electronic Absorption Spectra and Geometry of Organic Molecules," Academic Press Inc., New York (1967), Chap. 14.
15) H. C. Longuet-Higgins and J. A. Pople, *Proc. Phys. Soc. London, Sect. A*, **68**, 591 (1955).
16) M. Traetteberg and E. B. Frantsen, *J. Mol. Struct.*, **26**, 69 (1975).
17) Papers cited in Ref. 16: H. Suzuki (1952), 29° ($\theta_{\alpha\beta}$ 0°); J. Adrian (1958), 30—40° ($\theta_{\alpha\beta}$ 0°); G. Rasch (1962), 26° ($\theta_{\alpha\beta}$ 13°); A. Bromberg and K. A. Muszkat (1972), 35—40° ($\theta_{\alpha\beta}$ 5°); A. Golebiewski and A. Parczewski (1972), 44° ($\theta_{\alpha\beta}$ 4.5°); T. Beringhelli, A. Gavezzotti, and M. Simonetta (1972), 28°. A. Warshel[18] obtained a value of 35° ($\theta_{\alpha\beta}$ 9°); G. Fischer *et al.*[19] also obtained the same value ($\theta_{\alpha\beta}$ 10°).
18) A. Warshel, *J. Chem. Phys.*, **62**, 214 (1975).
19) G. Fischer, G. Seger, K. A. Muszkat, and E. Fischer, *J. Chem. Soc., Perkin Trans. 2*, **1975**, 1569.
20) H. Suzuki, *Bull. Chem. Soc. Jpn.*, **33**, 379 (1960).
21) The allowance for the electronic bathochromic effect of the substituents was simply made by subtracting 5 nm per substituent from the value of λ_{max}, after Woodward's rule[22] and Fieser and Fieser's rule[23] for conjugated diens, which have the main band in nearly the same wavelength region as those of the α,β-dialkylstilbenes. When the allowance is made, the value of 58° estimated for Eαβ DMS and that of 63° estimated for EαβDES[12–14] are revised to 66° and 71°, respectively.
22) R. B. Woodward, *J. Am. Chem. Soc.*, **64**, 72 (1942).
23) L. F. Fieser and M. Fieser, "Steroids," Reinhold Publishing Corp., New York (1959).
24) The values of $10^4 f_B/\varepsilon_B$ as a measure of broadness of band B for spectra F are as follows: $ZS^{+\cdot}$, 0.15; $Z\alpha\beta DMS^{+\cdot}$, 0.27; $Z\alpha\beta DES^{+\cdot}$, 0.30; $ZS^{-\cdot}$, 0.13; $Z\alpha\beta DMS^{-\cdot}$, 0.17; $Z\alpha\beta DES^{-\cdot}$, 0.18. The values for the radical ions of ZS are larger than those for the radical ions of ES, and the values for the radical ions of ZαβDMS and ZαβDES are much larger and are comparable to those for the radical ions of the E isomers (*cf.* Note 33 in Ref. 2).
25) F. Jachimowicz, G. Levin, and M. Szwarc, *J. Am. Chem. Soc.*, **99**, 5977 (1977).

26) A similar situation is encountered in the corresponding dianions. The values of λ_{max} of the main band of the dianions of the 1,2-diphenylcycloalkenes are as follows: $DPCP^{2-}$, 500 nm (ε 2.9×10^4); $DPCH^{2-}$, 470 nm (ε 2.34×10^4).[25] These bands are attributed to the transition from the ground state (state S_0) to the 3rd excited singlet state (state S_3), a transition which is approximated as a one-electron transition from ϕ_{-1} to ϕ_{-4}.[27] That is, these bands correspond to band A of the anion radicals. According to the result of our MO calculation, the energy of this transition increases as $|\theta_{\alpha\beta}|$ increases from 0°.[27] Therefore, the blue shift of the band of $DPCH^{2-}$ as compared with that of $DPCP^{2-}$ probably reflects the larger value of $|\theta_{\alpha\beta}|$ of $DPCH^{2-}$ as compared with that of $DPCP^{2-}$.

27) H. Suzuki, K. Koyano, and T. L. Kunii, *Bull. Chem. Soc. Jpn.*, **45**, 1979 (1972).

28) According to the study by Fischer *et al.*,[19] on the excitation from state S_0 to state S_1 the calculated value of $\theta_{\alpha\beta}$ increases from 10° to 37° in ZS and from 7° to 49° in Z$\alpha\beta$DMS. That is, the increase ($\Delta\theta_{\alpha\beta}$) is 27° for ZS and 42° for Z$\alpha\beta$DMS. Fischer *et al.* related the observed "Stokes shift" ($\Delta\lambda$) with $\Delta\theta_{\alpha\beta}$. The value of $\Delta\lambda$ is small (26 nm) for ZS and is much larger (76 nm) for Z$\alpha\beta$DMS. The values of $\Delta\lambda_{max}$ and $\Delta\bar{\nu}_{max}$ (*cf.* Note 38 in Ref. 2) are 150 nm and 11.75×10^3 cm^{-1} for ZS, and 200 nm and 16.72×10^3 cm^{-1} for Z$\alpha\beta$DMS.

29) V. A. Sazhnikov, M. Rakhmatov, and M. V. Alfimov, *Dokl. Akad. Nauk SSSR*, **241**, 1378 (1978).

30) V. A. Sazhnikov, M. Rakhmatov, and M. V. Alfimov, *Chem. Phys. Lett.*, **71**, 33 (1980).

31) G. B. Kistiakowsky and W. R. Smith, *J. Am. Chem. Soc.*, **56**, 638 (1934); T. W. J. Taylor and A. R. Murray, *J. Chem. Soc.*, **1938**, 2078.

32) G. Fischer, K. A. Muszkat, and E. Fischer, *J. Chem. Soc., Sect. B*, **1968**, 1156.

33) D. Gegiou, K. A. Muszkat, and E. Fischer, *J. Am. Chem. Soc.*, **90**, 12 (1968).

34) K. von Auwers, *Ber.*, **68B**, 1346 (1935).

 © 1983 The Chemical Society of Japan Bull. Chem. Soc. Jpn., 56, 75—81 (1983)

Kinetic Study of the Oxidation of Formate by Iodine in Micellar Solutions of Alkyltrimethylammonium Chlorides

Katumitu HAYAKAWA,* Mitsuo KANDA, and Iwao SATAKE

Department of Chemistry, Faculty of Science, Kagoshima University, Korimoto, Kagoshima 890

(Received August 23, 1982)

The spectrophotometric study was made of the oxidation of formate by iodine in micellar solutions of decyl- and dodecyltrimethylammonium chlorides. In the presence of the cationic surfactant micelles, the reaction was found to take place only at the micellar surface according to the same mechanism as in water. The experimental second-order rate constant rose steeply to a maximum at the critical micelle concentration and then decreased monotonously with increasing surfactant concentration. A tentative estimation based on a charged-phase separation model led to the true second-order rate constant in micellar phase of 0.03—0.07 mol^{-1} dm^3 s^{-1} at 30 °C, which is comparable with that in water. Thus the observed rate enhancement in cationic surfactant solutions can be interpreted in terms of an increase in surface concentration of the formate ion arising from an electrostatic interaction with the micellar ion. The micellar effects on the formation constant of triiodide ion are also discussed.

In a previous study of the iodine-formate reaction, $I_3^- + HCO_2^- \rightarrow 3I^- + H^+ + CO_2$, in alcohol–water mixed solvents, we confirmed that the reaction proceeds according to the following mechanism.[1]

$$I_2 + I^- \overset{K}{\rightleftharpoons} I_3^-, \quad (1)$$

$$I_2 + HCO_2^- \xrightarrow{k_2} \text{Products}. \quad (2)$$

The second-order rate constant, k_2, was found to depend strongly on the dielectric property of the solvent,[1,2] *e.g.*, it is larger by a factor of about 100 in ethanol than in water at 30 °C.[1] Similar behavior was also observed for the formation constant, K, of triiodide ion.[3]

It is well known that a number of organic reactions involving ionic species such as H^+ or OH^- are catalyzed by oppositely charged micellar ions.[4] One might, therefore, expect that the presence of the cationic surfactant micelle would affect significantly the rate of the iodine-formate reaction through an electrostatic concentration of anionic species to the micellar surface and a possible medium effect of the micellar phase. In this connection, we have determined recently the apparent formation constant, K, of triiodide ion in micellar solution of dodecyltrimethylammonium chloride.[5] It was found that the cationic surfactant micelle solubilizes not only iodine molecule but triiodide ion in its hydrophilic surface region consisting of ionic head groups and results in a remarkable increase in K.

The purpose of the present paper is to study the kinetic aspects of the iodine-formate reaction in micellar solutions of dodecyl- and decyltrimethylammonium chlorides, and to estimate the true rate constant in micellar phase.

Experimental

Materials. Dodecyltrimethylammonium chloride (DTAC) and decyltrimethylammonium chloride (DeTAC), both from Tokyo Kasei Kogyo Co. Ltd., were recrystallized twice from methanol. Other chemicals were of guaranteed grade. Sodium iodide was dried overnight at 100 °C prior to use. Iodine was purified further by sublimation. Sodium formate was purified by recrystallization from water.

Measurements. In the presence of DTAC micelles, the absorption spectrum of the solution of I_2 and NaI is characterized by an absorption band at 360 nm.[5] This is also the case for DeTAC solution. Since in the presence of excess NaI the absorbance at 360 nm is proportional to I_2 concentration, the reaction rate was followed spectrophotometrically as a function of time by measuring the decrease in absorbance at 360 nm. The absorbance was measured with a Hitachi Spectrophotometer model 101 connected to a Valhalla Scientific Digital Multimeter model 4440. The pH and ionic strength of the solution were uncontrolled, because the rate of this reaction in water had been found to be independent of these factors.[1]

The chloride ion activity and the apparent formation constant of triiodide ion in micellar solution of DeTAC were determined by the method described elsewhere.[5]

The measurements were conducted at 21, 30, and 40 °C for DTAC solution and at 21, 30, and 37 °C for DeTAC solution, respectively.

Results and Discussion

Kinetics. In the present system, the micellar effect on the reaction rate is anticipated to arise primarily from an electrostatic interaction between the anionic species and the micellar ion. Therefore, all kinetic measurements were carried out under the conditions of $[\text{Surfactant}] \gg [I^-]$, $[HCO_2^-] \gg [I_2]$, in order to minimize the change in total counterion concentration which is a primary determinant of the electrical potential at the micellar surface. Under these experimental conditions, the reaction rate defined by Eq. 3 was found to be a first-order with respect to triiodide ion.

$$\text{Rate} = -d[I_3^-]_a/dt = k_a[I_3^-]_a \quad (3)$$

Here, the bracket with suffix a refers to the apparent concentration in moles per liter of solution and k_a to the apparent first-order rate constant, respectively. In Fig. 1 is shown the typical change in k_a with surfactant concentration at varying NaI concentrations. Similar results were also obtained at higher temperatures than 21 °C. Unfortunately, we were forced to make the kinetic measurements in the concentration range above the critical micelle concentration (CMC), since at lower surfactant concentrations below CMC the measurements were subject to interference from the precipitate composed presumably of iodine-surfactant complex.[5] However, it is likely that the apparent

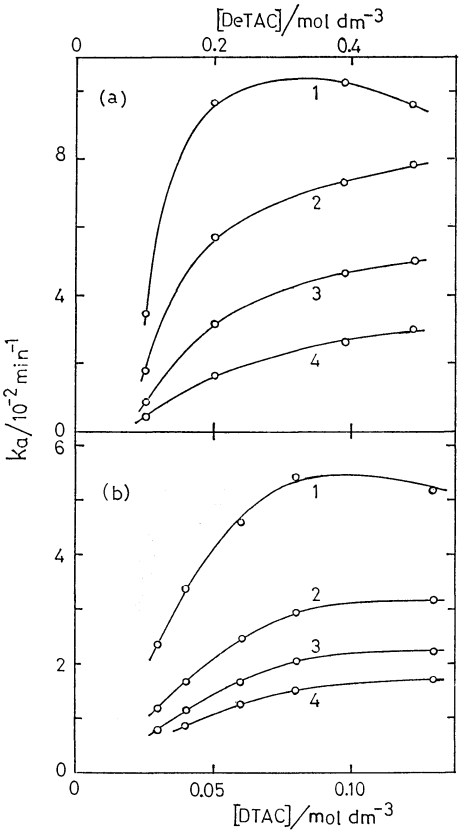

Fig. 1. Plots of the apparent first-order rate constant *vs.* total surfactant concentration at 21 °C.
(a) DeTAC solution containing 0.01 mol dm^{-3} $NaHCO_2$. [NaI]/10^{-3} mol dm^{-3}: 1; 0.188, 2; 0.375, 3; 0.751, 4; 1.50. (b) DTAC solution containing 0.006 mol dm^{-3} $NaHCO_2$. [NaI]/10^{-3} mol dm^{-3}: 1; 0.38, 2; 0.76, 3; 1.14, 4; 1.52.

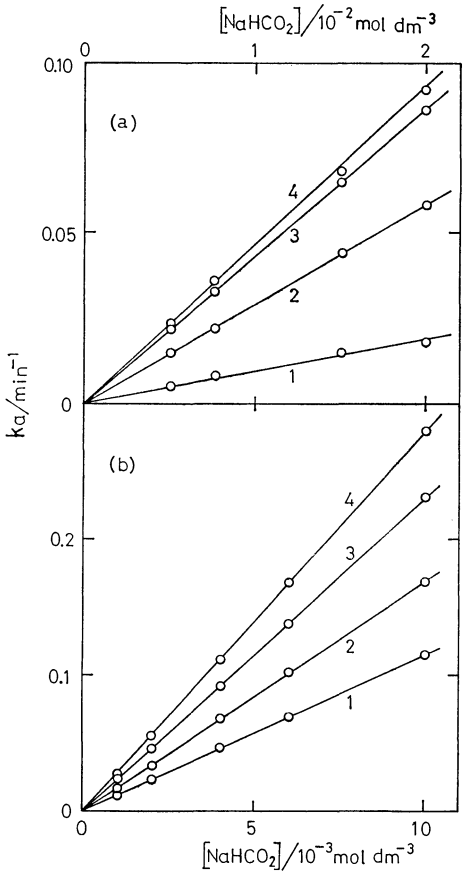

Fig. 2. Plots of the apparent first-order rate constant *vs.* sodium formate concentration at constant concentrations of surfactant and sodium iodide.
(a) DeTAC solution at 21 °C. [DeTAC]/mol dm^{-3} and [NaI]/10^{-3} mol dm^{-3}: 1; 0.10 and 0.75, 2; 0.20 and 0.83, 3; 0.39 and 0.83, 4; 0.49 and 0.85. (b) DTAC solution at 40 °C. [DTAC]/mol dm^{-3} and [NaI]/10^{-3} mol dm^{-3}: 1; 0.03 and 1.29, 2; 0.04 and 1.06, 3; 0.06 and 1.01, 4; 0.13 and 0.93.

first-order rate constant increases abruptly at surfactant concentration around CMC (2.1×10^{-2} mol dm^{-3} for DTAC and 8.7×10^{-2} mol dm^{-3} for DeTAC at 21 °C), though the magnitude of the increase depends regularly on NaI concentration. The k_a *versus* surfactant concentration profile resembles the results observed for micellar catalyzed organic reactions such as alkaline hydrolysis of esters in cationic surfactant solutions[4] in displaying a broad maximum or the leveling-off phenomenon above CMC.

Figure 2 shows the change in k_a with formate concentration at the given concentrations of surfactant and NaI. It can immediately be seen that k_a is directly proportional to the formate concentration, *i.e.*, $k_a=k'[HCO_2^-]_a$. It should be noted here that the value of k' thus determined is still dependent on NaI concentration. In Fig. 3 is plotted the reciprocal of k' against iodide concentration at varying surfactant concentrations. An important feature of Fig. 3 is that the plot of $1/k'$ *vs.* iodide concentration gives a straight line with a small but definite intercept. Based upon these experimental results, the rate equation of the iodine-formate reaction in cationic surfactant solutions can reasonably be written as follows,

$$\text{Rate} = -\frac{d[I_3^-]_a}{dt} = \frac{k''[I_3^-]_a[HCO_2^-]_a}{1+K'[I^-]_a}, \quad (4)$$

$$k_a = \frac{k''[HCO_2^-]_a}{1+K'[I^-]_a}, \quad (5)$$

where k'' denotes the reciprocal of the intercept of the straight line in Fig. 3 and K' the ratio of slope to intercept of the same straight line, respectively. In the determination of these kinetic parameters, however, some inherent errors are unavoidable since the intercepts of the straight lines in Fig. 3 are considerably small. With this reservation in mind, we can estimate the change in k'' and K' with surfactant concentration. The results are summarized in Table 1.

The iodine-formate reaction in methanol–water and ethanol–water mixed solvents proceeds according to Eqs. 1 and 2 as described above.[1] We derived the following rate equation under the assumption that the reaction (1) is in pseudo-equilibrium.

$$\text{Rate} = -\frac{d[I_3^-]_a}{dt} = \frac{k_2[I_3^-]_a[HCO_2^-]_a}{1+K[I^-]_a}. \quad (6)$$

Here, K refers to the formation constant of triiodide ion and k_2 to the rate constant for reaction (2) which is the rate determining step of the overall reaction, respectively. A comparison of Eq. 4 with Eq. 6 leads

Table 1. Kinetic parameters in Eq. 4, and the apparent formation constant of triiodide ion in micellar solutions of DTAC and DeTAC

Temp / °C	[Surfactant] / mol dm^{-3}	K' / 10^4 mol^{-1} dm^3	k'' / mol^{-1} dm^3 s^{-1}	K / 10^4 mol^{-1} dm^3	k_2 / mol^{-1} dm^3 s^{-1}
(a) DTAC solution					
21	0.03	10	2.5	10.4	2.64
	0.04	5.7	2.1	4.97	1.80
	0.06	2.1	1.1	2.05	1.11
	0.08	1.2	0.82	1.20	0.82
	0.13	0.86	0.65	0.67	0.51
30	0.03	4.3	3.8	4.35	3.89
	0.04	2.4	2.8	2.47	2.96
	0.06	1.2	1.8	1.16	1.84
	0.08	0.75	1.4	0.82	1.47
	0.13	0.47	0.90	0.48	0.90
40	0.03	2.4	6.5	—	—
	0.04	1.8	5.7	1.8	5.59
	0.06	0.87	3.7	0.80	3.42
	0.08	0.56	2.9	0.60	3.02
	0.13	0.30	1.7	0.32	1.85
(b) DeTAC solution					
21	0.10	4.7	0.56	6.09	0.726
	0.20	1.0	0.47	1.01	0.457
	0.39	0.38	0.30	0.37	0.287
	0.49	0.26	0.25	0.26	0.250
30	0.10	2.5	1.2	2.56	1.24
	0.20	0.61	0.93	0.74	1.14
	0.39	0.26	0.70	0.28	0.73
	0.49	0.20	0.61	0.22	0.68
37	0.10	1.4	1.4	1.97	1.97
	0.20	0.76	2.0	0.61	1.62
	0.39	0.25	1.2	0.26	1.19
	0.49	0.20	1.1	0.20	1.05

The values of K in DTAC solution are from Ref. 5.

immediately to the prediction that the iodine-formate reaction in surfactant solution will also proceed according to the same mechanism as in water. This, in turn, implies that k'' and K' in Eq. 4 have the same meaning as given hereinabove, *i.e.*, $k''=k_2$ and $K'=K$. It is in fact clearly shown in Table 1 that the values of K' estimated kinetically from Fig. 3 are virtually identical with the apparent formation constants, $K(=[I_3^-]_a/[I^-]_a[I_2]_a)$, of triiodide ion determined independently in solution of surfactant without formate ion. This fact enables us to evaluate more reliable values of k_2 from the relation, $k_2=K/$(the slope of the straight line in Fig. 3). The values of k_2 so determined are summarized in the last column of Table 1 and are plotted in Fig. 4 as a function of surfactant concentration. As would be expected, the agreement between k'' and k_2 is satisfactory. In view of the fact that the second-order rate constant, k_2, is much smaller in water than in surfactant solutions, the value of k_2 is considered to rise steeply to a maximum at CMC. At higher concentrations above CMC, k_2 tends to decrease monotonously with increasing surfactant concentration. It should be noted, however, that even in the highest surfactant concentrations studied, the values of k_2 are still large enough as compared with those in water (*cf.*, $k_2=0.068$ mol^{-1} dm^3 s^{-1} at 30 °C).[1] The qualitative feature of k_2 *versus* surfactant concentration plots in Fig. 4 is in accord with that predicted theoretically by Romsted[6] for second-order reactions between organic molecules and hydrophilic ions in micellar solutions.

Rate Constant in Micellar Phase. In the spectrophotometric determination of the formation constant of the triiodide ion in DTAC solution, we pointed out that both iodine molecule and triiodide ion are solubilized almost completely in the hydrophilic surface region of surfactant micelle and are in equilibrium with the surrounding iodide ions immediately adjacent to the micellar surface.[5] It is therefore highly probable that the iodine-formate reaction in cationic surfactant solutions takes place only at the micellar surface. Thus, if we denote the inside and outside regions of the micellar surface by suffix m and s, the reaction mechanism may be described as

$$I_{2,m} + I_s^- \overset{K_m}{\rightleftharpoons} I_{3,m}^-, \tag{7}$$

$$I_{2,m} + HCO_{2,s}^- \xrightarrow{k_m} 2I_s^- + CO_2 + H^+, \tag{8}$$

where, K_m is the true formation constant of triiodide ion and k_m the true rate constant for reaction (8), both in micellar phase, respectively. The corresponding rate equation can immediately be derived from the analogy to Eq. 6.

$$-\frac{d[I_3^-]_m}{dt} = \frac{k_m[I_3^-]_m[HCO_2^-]_s}{1+K_m[I^-]_s}. \tag{9}$$

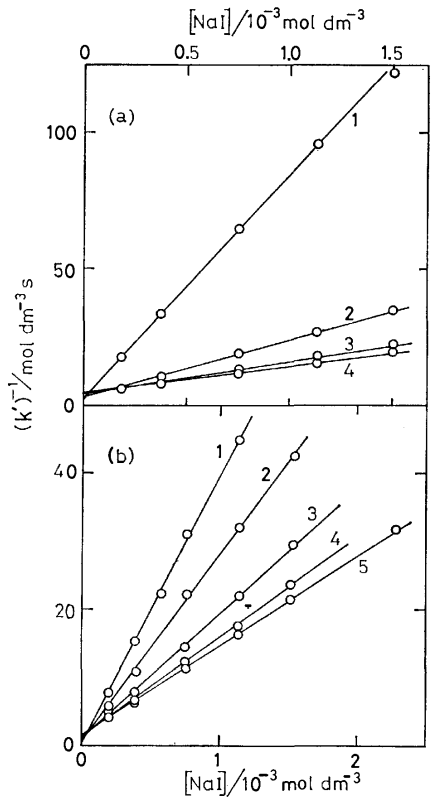

Fig. 3. Plots of $1/k'$ *vs.* sodium iodide concentration at 21 °C.
(a) DeTAC solution. [DeTAC]/mol dm^{-3}: 1; 0.10, 2; 0.20, 3; 0.39, 4; 0.49. (b) DTAC solution. [DTAC]/mol dm^{-3}: 1; 0.03, 2; 0.04, 3; 0.06, 4; 0.08, 5; 0.13.

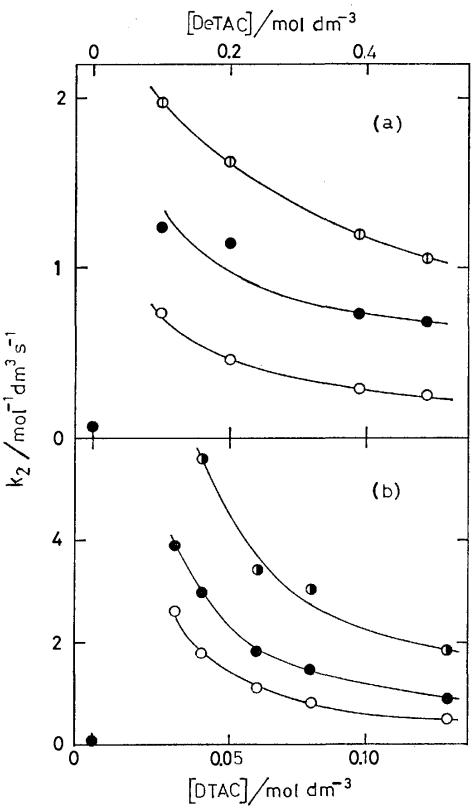

Fig. 4. Effect of the surfactant concentration on the second-order rate constant, k_2.
(a) DeTAC solution. ◑; 37 °C, ●; 30 °C, ○; 21 °C. (b) DTAC solution. ◑; 40 °C, ●; 30 °C, ○; 21 °C.

Here, the bracket with suffix m or s represents the concentration in moles per dm^3 of the respective phase. Since almost all the triiodide ions are solubilized in the surface region of surfactant micelle as noted above, we have

$$\frac{1}{[I_3^-]_a}\frac{d[I_3^-]_a}{dt} = \frac{1}{[I_3^-]_m}\frac{d[I_3^-]_m}{dt}. \quad (10)$$

It follows, therefore, from Eqs. 3 and 9 that

$$k_a = \frac{k_m[HCO_2^-]_s}{1+K_m[I^-]_s}. \quad (11)$$

It is important to note here that both I_s^- and $I_{3,m}^-$ locate at the micellar surface with virtually uniform electrical potential. This means that the activity coefficient ratio of these ions can safely be ignored without loss of accuracy. With this simplification, K_m may be written as follows:

$$K_m = [I_3^-]_m/[I_2]_m[I^-]_s. \quad (12)$$

By taking into account a relationship, $[I_3^-]_m/[I_2]_m = [I_3^-]_a/[I_2]_a$, $K_m[I^-]_s$ in Eq. 11 can be replaced by $K[I^-]_a$. Equation 11 may accordingly be rewritten as

$$k_a = \frac{k_m[HCO_2^-]_s}{1+K[I^-]_a} = \frac{k_m[HCO_2^-]_a}{1+K[I^-]_a}\frac{[HCO_2^-]_s}{[HCO_2^-]_a}. \quad (13)$$

On converting k'' and K' in Eq. 5 to k_2 and K respectively and comparing it with Eq. 13, we have

$$k_2 = k_m[HCO_2^-]_s/[HCO_2^-]_a. \quad (14)$$

According to Eq. 14, the observed second-order rate constant, k_2, should be a decreasing function of surfactant concentration, since an increase in surfactant concentration is necessarily accompanied by a decrease in surface concentration of formate ion by virtue of surface potential depression. Indeed, the foregoing data shown in Fig. 4 are in accord with the prediction based on Eq. 14, reflecting that the coulombic interaction between formate and micellar ions is of primary importance in determining the rate constant, k_2, in surfactant solutions.

Equation 14 allows us to estimate the true rate constant, k_m, in micellar phase provided that an appropriate information is available for $[HCO_2^-]_s/[HCO_2^-]_a$. According to the common practice in theoretical treatment of the micellar catalysis,[4,6,7] it is reasonable to assume that the distribution quilibrium of the formate ion between micellar surface and bulk phase is always established during the course of the reaction. If, therefore, the formate ion has no specific adsorption potential to the micellar surface, the ratio of surface concentration to apparent total concentration of the formate ion may be replaced by that of chloride ion. Thus, noting that $[Cl^-]_a$ is equal to the total surfactant concentration, C, we may write

$$k_2 = k_m C_{1,s}/C, \quad (15)$$

where suffix 1 refers to chloride ion. The usual treatments[6,7] of micellar catalysis suppose that the counterion concentration in surface layer (Stern layer), $C_{1,s}$ is independent of total surfactant concentration

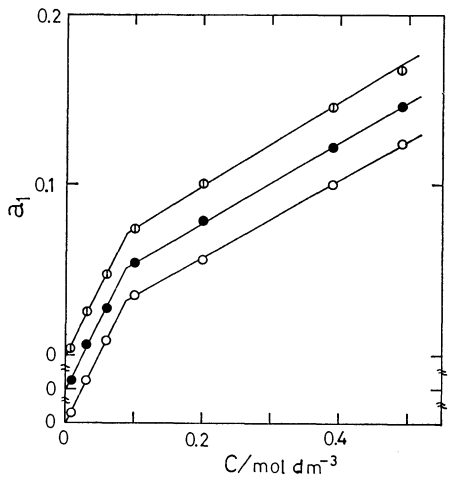

Fig. 5. Change in the chloride ion activity with DeTAC concentration at 37 °C (ⓘ), 30 °C (●), and 21 °C (○).

and is equal to β/LV, where β represents the degree of counterion association to the micelle, V the volume of Stern layer per micelle forming surfactant molecule in dm^3 and L the Avogadro constant, respectively. We can thus estimate the values of k_m by introducing an appropriate value of $C_{1,s}$ into Eq. 15, provided that the product of k_2 and C remains constant throughout whole surfactant concentration range studied. This is in fact the case for the DTAC solution, *i.e.*, the value of k_2C remains virtually constant and lies around 0.12 s^{-1} at 30 °C. However, the situation is somewhat complicated by the fact that in DeTAC solution the value of k_2C increases slightly but regularly with increasing surfactant concentration. In addition, the determination of k_m based on this treatment requires a knowledge of V which is experimentally rather difficult to estimate. For these reasons, we employed the following approach for the estimation of k_m.

Denoting the surfactant ion by suffix 2, the simple thermodynamic consideration leads immediately to the relations

$$kT \ln (C_{1,s}/\text{mol dm}^{-3}) - e\psi = kT \ln a_1, \quad (16)$$

$$\Delta\mu_2^{\circ} + e\psi = kT \ln [a_2/(55.5/\text{mol dm}^{-3})] \quad (17)$$

where, ψ is the surface potential of the micelle, a_i the activity of i-th ion ($C^{\circ}=1$ mol dm^{-3}) and $\Delta\mu_2^{\circ}$ the standard free energy of transfer of surfactant ion from aqueous medium to micellar phase; other symbols have their usual meanings. Combining Eqs. 16 and 17, we have

$$C_{1,s} = (a_1a_2/55.5) \exp(-\Delta\mu_2^{\circ}/kT). \quad (18)$$

Although a_1 and a_2 in Eq. 18 can both be measured potentiometrically as a function of surfactant concentration, the determination of the latter is not necessarily required, because the following relationship based on the phase separation theory[8] has been confirmed to hold in various ionic surfactant solutions.[9]

$$a_2a_1^{\beta} = \text{constant} = K_s \quad (19)$$

It follows, therefore, from Eqs. 15, 18, and 19 that

$$a_1^{1-\beta}/k_2 = (55.5C/k_mK_s) \exp(\Delta\mu_2^{\circ}/kT) \quad (20)$$

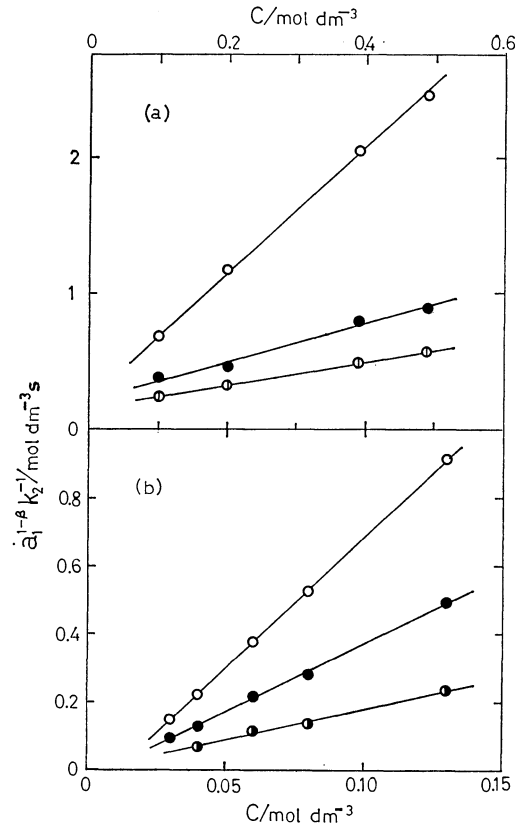

Fig. 6. Plots of the left-hand side of Eq. 20 *vs.* surfactant concentration.
(a) DeTAC solution. ○; 21 °C, ●; 30 °C, ⓘ; 37 °C. (b) DTAC solution. ○; 21 °C, ●; 30 °C, ◑; 40 °C.

This implies that the left-hand side of Eq. 20 should be linearly dependent on total surfactant concentration. Information about β can easily be obtained from the concentration dependence of the chloride ion activity. In Fig. 5 is shown the plots of a_1 *vs.* C for DeTAC solution at varying temperatures. According to Botré *et al.*,[10] the slope of the straight line above CMC divided by the activity coefficient at CMC gives $1-\beta$. Using the values of β so determined for DeTAC and DTAC,[5] the left-hand side of Eq. 20 can now be plotted as a function of surfactant concentration. Figure 6 shows such plots at various temperatures. In accordance with Eq. 20, the plot is found to be linear in all cases studied. Since at CMC the surfactant ion activity is virtually identical with the chloride ion activity, a_1°, the value of K_s can safely be set equal to $(a_1^{\circ})^{1+\beta}$ with reasonable accuracy. In addition, the value of $\Delta\mu_2^{\circ}$ was estimated by Shinoda[11] to be $-1.08\,kT$ per carbon atom in hydrocarbon chain at 25 °C. Introducing these values into Eq. 20 and ignoring the temperature dependence of $\Delta\mu_2^{\circ}$, we can evaluate approximately the true rate constant, k_m, in micellar phase from the slope of the straight line in Fig. 6. The results are summarized in Table 2 together with the rate constants in various solvents.[1] The values of k_m in DTAC solution can also be obtained by estimating an appropriate value of V as described already. On the basis of geometric considerations for various micelle shapes, Tanford[12] has

TABLE 2. A COMPARISON OF THE ESTIMATED VALUES OF THE SECOND-ORDER RATE CONSTANT AND THE FORMATION CONSTANT IN MICELLAR PHASE WITH THOSE IN WATER AND ALCOHOLS

Solvent	Temp °C	β	k_m / mol^{-1} dm^3 s^{-1}	K_m / mol^{-1} dm^3
DTAC solution	21	0.76	0.020	230
	30	0.74	0.033	150
	40	0.73	0.061	90
DeTAC solution	21	0.73	0.023	190
	30	0.72	0.073	150
	37	0.72	0.12	140
Water			0.068(30 °C)[a]	730(25 °C)[b]
Methanol			3.2 (30 °C)[a]	10900(31 °C)[b]
Ethanol			7.8 (30 °C)[a]	20700(28 °C)[c]

a) From Ref. 1. b) From Ref. 3.

derived the relationship between the surface area per polar head group of micelle forming surfactant molecules, S, and the micellar aggregation number. According to his calculation for globular micelles, the micellar aggregation number of DTAC of 57[13] corresponds to S of 0.78 nm^2. With an additional assumption that the thickness of the Stern layer is of the order of the diameter of hydrated chloride ion (0.37 nm),[14] the value of $C_{1,s}$ ($=\beta/LV$) is obtained as 4.3 mol dm^{-3} at 30 °C. Thus the use of Eq. 15 leads immediately to k_m of 0.028 mol^{-1} dm^3 s^{-1} at 30 °C. The result is in good agreement with that given in Table 2, indicating the validity of the present approach.

Apart from the detailed calculation of k_m, it is important to note that the estimated values of k_m are similar in magnitude to those in aqueous medium. This fact is consistent with the foregoing view that the iodine-formate reaction in cationic surfactant solutions will take place at the hydrophilic surface region of the micelle. It may thus be concluded that an increase in surface concentration of the formate ion arising from an electrostatic interaction with polyvalent micellar ion is the principal source of the rate enhancement of the iodine-formate reaction in cationic surfactant solutions. The environmental effect of ionic head groups on k_m seems to be, if any, negligibly small. Unfortunately, the values of k_m given in Table 2 are not of sufficient precision to permit the estimation of the activation parameters in micellar environments, since we ignored the temperature dependence of $\Delta\mu_2^{\ddagger}$ in their computation. At the present stage, therefore, it is rather difficult to give any reasonable account of an appreciable dependence of k_m on surfactant chain length at higher temperatures.

Formation Constant in Micellar Phase. Expressions similar to Eqs. 15 and 20 must also hold for the apparent formation constant, K, of triiodide ion. Since $K_m[I^-]_s$ is equal to $K[I^-]_a$ as described already, the substitution of the ratio of surface concentration to apparent total concentration of iodide ion by that of chloride ion leads immediately to

$$K = K_m C_{1,s}/C \qquad (21)$$

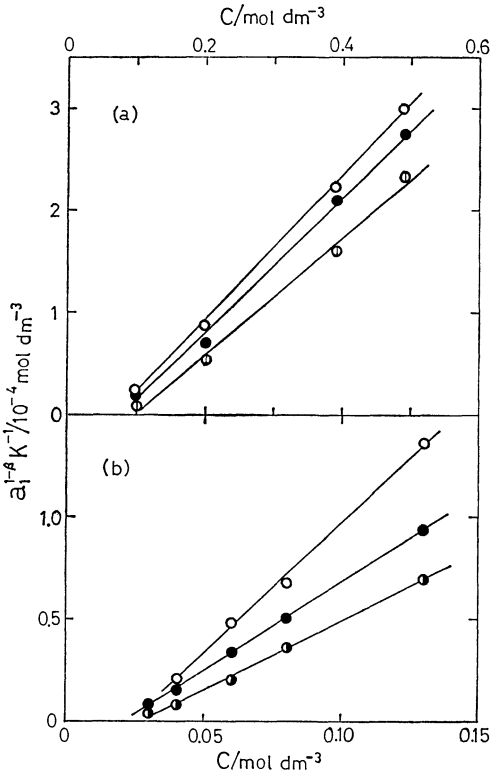

Fig. 7. Plots of the left-hand side of Eq. 22 *vs.* surfactant concentration.
(a) DeTAC solution. ◑; 21 °C, ●; 30 °C, ○; 37 °C. (b) DTAC solution. ◑; 21 °C, ●; 30 °C, ○; 40 °C.

$$a_1^{1-\beta}/K = (55.5C/K_mK_s)\exp(\Delta\mu_2^{\ddagger}/kT). \qquad (22)$$

The resulting expression is noted to be identical with Eq. 20, except that k_2 and k_m are replaced respectively by K and K_m. In Fig. 7 is shown the predicted linear relationship between the left-hand side of Eq. 22 and total surfactant concentration. We can thus estimate the true formation constant, K_m, of triiodide ion in micellar phase from the slope of the straight line in Fig. 7. The results are summarized in the last column of Table 2. For the sake of comparison, the formation constants in various solvents[3] are also included in this table. The fact that the true formation constants are comparable with those in water provides an additional evidence for the occurrence of the iodine-formate reaction at the hydrophilic surface region of the micelle. Thus the marked increase in an apparent formation constant shown in Table 1 is concluded to result predominantly from an increase in surface concentration of the iodide ion due to coulombic interaction with the micellar ion.

In a previous study of K_m in DTAC solution,[5] we applied an expression derived by Shinoda[15] for the surface potential of the lamellar micelle. The only drawback of the treatment was the lack of reliable information about S. For example, a tentative calculation based on S=0.78 nm^2 gave K_m of 650 mol^{-1} dm^3 at 30 °C. On the other hand, the use of S=0.30 nm^2 which corresponds to a lamellar micelle model[12] led to K_m of 190 mol^{-1} dm^3 at 30 °C. It is true that the latter value is in fair agreement with K_m estimated

above from Eq. 22, but we must keep in mind that small errors in the estimation of $\Delta\mu_2^{\ddagger}$ causes an appreciable change in K_m. It is, thus, highly probable that the reliable value of K_m in DTAC solution lies somewhere between 150 and 650 mol^{-1} dm^3 at 30 °C.

References

1) K. Hayakawa and M. Sato, *Bull. Chem. Soc. Jpn.*, **50**, 1767 (1977).
2) F. W. Hiller and J. H. Krueger, *Inorg. Chem.*, **6**, 528 (1967).
3) K. Hayakawa and S. Nakamura, *Bull. Chem. Soc. Jpn.*, **50**, 566 (1977).
4) J. H. Fendler and E. Fendler, "Catalysis in Micellar and Macromolecular Systems," Academic Press, New York (1975), Chaps. 4 and 5.
5) K. Hayakawa, M. Kanda, and I. Satake, *Bull. Chem. Soc. Jpn.*, **52**, 3171 (1979).
6) L. S. Romsted, "A General Kinetic Theory of Rate Enhancements for Reactions between Organic Substrates and Hydrophilic Ions in Micellar Systems," in "Micellization, Solubilization, and Microemulsions," ed by K. L. Mittal, Plenum Press, New York (1977), Vol. 2, p. 509.
7) K. Martinek, A. K. Yatsimirski, A. V. Levashov, and I. V. Berezin, "The Kinetic Theory and Mechanisms of Micellar Effects on Chemical Reactions," in "Micellization, Solubilization and Microemulsions," ed by K. L. Mittal, Plenum Press, New York (1977), Vol. 2, p. 489.
8) K. Shinoda and E. Hutchinson, *J. Phys. Chem.*, **66**, 577 (1962).
9) T. Sasaki, M. Hattori, J. Sasaki, and K. Nukina, *Bull. Chem. Soc. Jpn.*, **48**, 1397 (1975); M. Koshinuma and T. Sasaki, *ibid.*, **48**, 2755 (1975); M. Koshinuma, *ibid.*, **52**, 1790 (1979); **54**, 3128 (1981).
10) C. Botré, V. L. Crescenzi, and A. Male, *J. Phys. Chem.*, **63**, 650 (1959).
11) K. Shinoda, *Bull. Chem. Soc. Jpn.*, **26**, 101 (1953); *J. Phys. Chem.*, **59**, 432 (1955).
12) C. Tanford, *J. Phys. Chem.*, **76**, 3020 (1972).
13) M. F. Emerson and A. Holtzer, *J. Phys. Chem.*, **71**, 1898 (1967).
14) C. B. Monk, "Electrolytic Dissociation," Academic Press, New York (1961), p. 271.
15) K. Shinoda, T. Nakagawa, B. Tamamushi, and T. Isemura, "Colloidal Surfactants," Academic Press, New York (1963), Chap. 1.

The Effect of Temperature on the Formation of Benzyl Radical–Halide Ion Complexes in γ-Irradiated Organic Glassy Matrices

Tatsuo IZUMIDA,† Kuniaki FUJII, Masaaki OGASAWARA, and Hiroshi YOSHIDA*

Faculty of Engineering, Hokkaido University, Kita-ku, Sapporo 060

(Received June 16, 1982)

Broad structureless charge-transfer (CT) bands of benzyl radical-halide ion (Ḃz---X⁻) complexes have been observed in 3-methylhexane (3MHx) and 2-methyltetrahydrofuran (MTHF) matrices containing BzCl and BzBr irradiated with γ-rays at 4.2 K. 3MHx and ethanol matrices containing BzI also showed the CT band when warmed from the irradiation temperature to 77 K. These observations are in marked contrast with previous ones in which the CT band was found to be present only in alkane matrices when irradiated at 77 K. The CT band has been found to shift to the blue with increasing matrix polarity, as expected from a large contribution of the solvation of the ion to the CT transition energy of the radical–anion complex. The observed nature and behavior of the CT bands indicates that the dissociative electron attachment reaction in the matrices is a stepwise process: The formation of a Ḃz---X⁻ complex and its dissociation. These steps proceed readily in more polar environments and for lighter ions. For the electron attachment to BzI at 4.2 K, an even earlier step, an ionic entity prior to the C–I bond dissociation, was indicated.

The dissociative electron attachment to benzyl halide in glassy matrices of nonpolar alkanes γ-irradiated at 77 K was previously found to give benzyl radical–halide ion complexes.[1,2] These complexes provided us with an interesting example of the charge-transfer (CT) interaction between a neutral open-shell free radical and a closed-shell anion. Their CT band, observed by means of the fluorescence spectrophotometric method, shifted depending on both the ionization energy of the electron donors (halide ions)[2] and the electron affinity of the electron acceptors (ring-substituted mono- and dimethylbenzyl radicals[3]). A similar CT band was also observed for the α-methylbenzyl radical formed from (2-chloroethyl)benzene[4] and the diphenylmethyl radical from diphenylmethyl halides[5] in glassy 3-methylhexane (3MHx) at 77 K. It is likely that a complex of this kind is generally formed as a transient intermediate state during the course of dissociative electron attachment reactions. A detailed study on the nature and behavior of this complex is expected to give a mechanistic insight into the reactions occurring in low temperature glassy matrices.

The CT excitation energy should depend significantly on the energy of solvation of the ions (both in the ground and excited states of the complex) for a neutral radical–anion complex. Actually, this has been proved by changing the ionic radius by using the different halide ions.[2] In this respect, it seems worthwhile studying the effect of the matrix polarity on the CT excitation energy. However, so far only the CT band for the benzyl radical–iodide ion complex in semipolar 2-methyltetrahydrofuran (MTHF) at 77 K,[6] apart from alkane matrices, has been observed. The failure in observing the CT band from polar matrices was attributed to ion solvation effects: polar matrix molecules weakening the interaction between the radical and the ion.

The 4.2 K-γ irradiation technique has proven useful in freezing chemical processes so that the early stages in the processes can be followed. This technique has, for example, enabled the spectrophotometric observations of the precursor of the carbon-halogen bond dissociation which resulted from the electron attachment to benzyl chloride[7] and halobenzenes,[8] and of the toluene anion which is the precursor of the methylcyclohexadienyl radical in a glassy toluene matrix.[9]

The present investigation was planned for observing the benzyl radical–halide ion CT band in organic glassy matrices of different polarity using the 4.2 K-γ irradiation technique. Another aim of the investigation was to elucidate the detailed mechanism of the dissociative electron attachment reaction in these matrices.

Experimental

Benzyl chloride (BzCl) of reagent grade was used without further purification. Benzyl bromide (BzBr) of reagent grade was distilled before use. Benzyl iodide (BzI) was synthesized from BrCl and NaI and purified by repeated recrystallization from methanol. 3MHx, MTHF, and ethanol were purified as described elsewhere.[6]

The solutions of the benzyl halides (10^{-2}—10^{-3} mol/dm³) were deaerated by freeze-pump-thaw cycles to 1.4×10^{-3} Pa, sealed in Suprasil quartz tubes of 2 mm outer diameter, and rapidly frozen into the glassy state by immersion in liquid nitrogen. The samples were transferred into a liquid He dewar of quartz (originally for ESR measurement at 4.2 K), irradiated with ^{60}Co γ-rays to a dose of 5×10^{4}—4×10^{5} rad at 4.2 K, after which excitation and emission spectra were measured with a Hitachi Model MPF-2A fluorescence spectrophotometer. The wavelength resolution of the measurements was 2 nm or less. Thermal annealing was carried out by rapidly transferring the irradiated samples into liquid nitrogen and keeping them there for a predetermined period.

Occasionally, optical absorption measurements were made with a Shimadzu MPS-5000 spectrophotometer and sample solutions sealed in an optical absorption cell of quartz (optical path length: 2 mm), as has been described before.[9]

Results

The fluorescence and excitation spectra recorded from the 3MHx containing BzCl or BzBr irradiated at 4.2 K are essentially the same as the spectra ob-

† Present address: Energy Research Laboratory, Hitachi Ltd. Moriyama-cho 1168, Hitachi, Ibaragi 316.

Table 1. The charge-transfer excitation band (energy) of benzyl radical-halide ion complexes

Halide ion	Matrix	λ_{max}/nm (Transition energy/eV) 4.2 K	77 K
Cl^-	3MHx	364 (3.41)	366[a] (3.39)
	MTHF	340 (3.65)	Unobserved
	EtOH	Unobserved	Unobserved
Br^-	3MHx	413 (3.00)	413[a] (3.00)
	MTHF	370 (3.35)	Unobserved
I^-	3MHx	500[b] (2.48)	500[a] (2.48)
	MTHF	No measurement	420[c] (2.95)
	EtOH	345[b] (3.59)	Unobserved

a) Ref. 2. The previously reported 362 nm of Cl^- has been corrected, based on a careful reexamination in this investigation. b) The band appeared when the samples irradiated at 4.2 K were warmed to 77 K. c) Ref. 6.

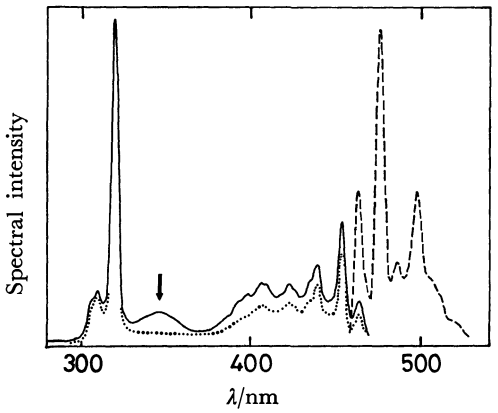

Fig. 1. Fluorescence (dashed curve) and excitation (solid curve) spectra of benzyl radicals generated by irradiating an ethanol matrix containing BzI with γ-rays at 4.2 K and observed immediately after warming to 77 K. Excitation and monitoring were made at 320 nm and 463 nm, respectively. The excitation spectrum changed to that of the dotted curve after 40 min annealing at 77 K. The arrow indicates the CT excitation band of the Ḃz---I^- complex.

served after the irradiation at 77 K.[2] The excitation spectra are comprised of three bands, in the visible (around 460 nm), near-UV (around 320 nm), and far-UV (around 260 nm) regions due respectively to the $1^2A_2 \leftarrow 1^2B_2$, $2^2A_2 \leftarrow 1^2B_2$, and $4^2B_2 \leftarrow 1^2B_2$ electronic transitions in a benzyl radical of C_{2v} symmetry[10] which has been generated by dissociative electron attachment to BzX. In addition, a structureless broad excitation band was observed with a band maximum at 364 nm for BzCl and at 413 nm for BzBr. This band has previously been attributed to the CT band of the Ḃz---X^- complex.[1,2,6] All these excitations induce the fluorescence from the benzyl radical in the wavelength region 460—530 nm.

The main concern of the present investigation was the CT excitation band of the complexes. Upon warming the 3MHx matrices containing BzCl or BzBr to 77 K, no change in the CT band was observed. The CT excitation energy is independent of the irradiation temperature, as can be seen in Table 1. The wavelength difference of 2 nm between 4.2 and 77 K for BzCl/3MHx is within the experimental uncertainty caused by the broad peak of the bands.

The effect of irradiation temperature is significant for the MTHF matrix. CT bands with maximum at 340 nm and 370 nm were observed for BzCl and BzBr after irradiation at 4.2 K. This is in contrast with irradiation at 77 K[2,6] where CT bands were not observed. The CT bands disappeared readily on warming the samples irradiated at 4.2 K to 77 K. The CT band could not be observed for a BzCl/ethanol solution either by irradiation at 77 or at 4.2 K.

The effect of irradiation temperature is more prominent when BzI is the source of benzyl radicals. Immediately after irradiation at 4.2 K, no emission at all was observed from the 3MHx and ethanol matrices. However, the excitation band of the benzyl radical as well as the CT excitation band of the Ḃz---I^- complex could be recorded after warming the samples to 77 K. For BzI/3MHx, the CT band was found to have its maximum at about 500 nm, equal to that observed previously for irradiation at 77 K.[2,6] The CT excited state is lower than the first excited state of the benzyl radical and, therefore, the fluorescent state of the Ḃz---I^- complex, so that a broad structureless CT fluorescence with the maximum at 548 nm was observed. For BzI/ethanol, the CT excitation band was unstable at 77 K: It disappeared within 40 min after its appearance (see Fig. 1).

Table 1 summarizes all the data on the CT excitation band obtained in the present investigation as well as in the previous ones.[2,6]

The absence of a CT band from BzI at 4.2 K raises the question of what the precursor of the Ḃz---I^- complex is. As the precursor does not fluoresce, optical absorption measurements were made for 3MHx, MTHF, and ethanol matrices containing BzI at 4.2 K. Although the shape of the absorption spectra observed varied from sample to sample, typical examples of observed spectra can be seen in Fig. 2. The spectra are generally composed of a sharp line at *ca.* 320 nm (with a satellite line at 310 nm) and a broad component in the longer wavelength region. The latter showed broad peaks whose position is dependent on the matrix. This broad component disappeared upon warming to 77 K. It does not correspond to the CT excitation band. The sharp line has almost the same wavelength position as that of the intense near-UV excitation due to the $2^2A_2 \leftarrow 1^2B_2$ transition of the benzyl radical. The lines seemed to increase in peak intensity and to shift a few nm to the blue side on warming to 77 K. On the whole the observed absorption spectra shows no similarity to the spectrum of the toluene anion generated in the γ-irradiated MTHF matrix.[9] The absorption spectra are very much like the spectrum observed by Higashimura *et al.* from BzCl/ethanol irradiated at 4.2 K.[7] They have attributed the broad component to the precursor of the benzyl radical.

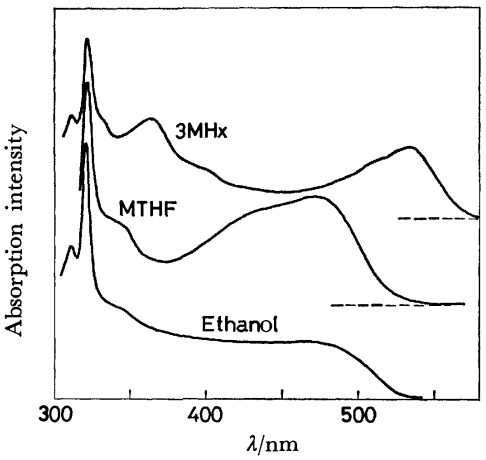

Fig. 2. Optical absorption spectra observed from glassy organic matrices containing BzI irradiated with γ-rays and measured at 4.2 K. Correction has been made for background absorption. The dashed line indicates the zero-absorption level of each spectrum.

Although further studies are evidently needed to attain a definite assignment, the absorption spectra observed here are tentatively assigned to a BzI molecular anion with a partially broken C–I bond (a tightly correlated benzyl radical–iodide ion pair). The absence of fluorescence at 4.2 K seems to indicate that the sharp lines are not due to the (normal) benzyl radicals.

Discussion

The broad structureless excitation band was previously assigned to the CT transition of the transient Ḃz---X$^-$ complexes which are generated by the dissociative electron attachment to BzX in rigid matrices. This assignment was based on the observed dependence of the transition energy on the ionization energy of the electron donors, the halide ions,[2] or on the electron affinity of the electron acceptors, that is benzyl or methyl-substituted benzyl radicals.[2,3]

Following Mulliken's CT resonance model,[11] the CT transition energy, $h\nu_{CT}$, of a weak electron donor-acceptor complex is written as

$$h\nu_{CT} = W_1 - W_0 + \frac{(H_{01}-W_0S_{01})^2+(H_{01}-W_1S_{01})^2}{W_1-W_0}, \quad (1)$$

where W_0 is the eigenvalue of the no-bond wave function ψ_0(A,D) and W_1 the eigenvalue of the dative wave function ψ_1(A$^-$—D$^+$). H_{01} and S_{01} are defined as $\langle\psi_0|H|\psi_1\rangle$ and $\langle\psi_0|\psi_1\rangle$, respectively. The third term on the right hand side cannot be estimated without knowledge of the exact conformation of the complex, but for the Ḃz---X$^-$ case studied here it is small and can be neglected, as will be mentioned below. The main contribution to W_1-W_0 comes from the ionization energy of X$^-$, IP(X$^-$), the electron affinity of Ḃz, EA(Ḃz), and the difference in solvation energy between the excited and ground states of the complex, E_s(Bz$^-$---X)$-E_s$(Ḃz---X$^-$). The solvation energies

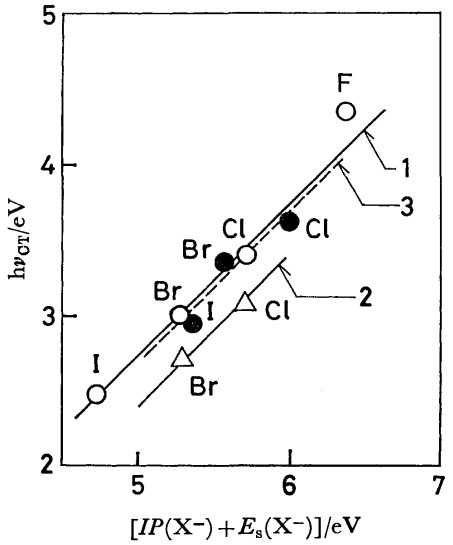

Fig. 3. The dependence of the observed CT transition energy on the calculated sum of the ionization energy and the solvation energy of the halide ion, IP(X$^-$)+E_s(X$^-$). ○: Ḃz---X$^-$ complexes in the 3MHx matrix cited from Ref. 2. Line 1 gives 0.263 nm for the effective radius of Bz$^-$. ●: Ḃz---X$^-$ complexes in the MTHF, for which the dependence expected from an equal effective radius of Bz$^-$ is shown by line 3. △: Dephenylmethyl radical---X$^-$ complex in the 3MHx matrix, cited from Ref. 5, for which a linear dependence with a slope of unity is shown by line 2.

can however be approximated to those of Bz$^-$ and X$^-$ and are then given by Born's formula:

$$E_s = \frac{e^2}{2r}\left(1-\frac{1}{D}\right), \quad (2)$$

where r is the radius of the solvated species. The Franck-Condon principle requires the usage of the static dielectric constant, D_s, and the optical dielectric constant, D_{op}, for the ground and excited states respectively. Thus, Eq. 1 is reduced to

$$h\nu_{CT} = IP(X^-) + E_s(X^-) - \{EA(\dot{B}z)+E_s(Bz^-)\}. \quad (3)$$

A linear relationship between $h\nu_{CT}$ and IP(X$^-$)+E_s(X$^-$) was indeed observed for the Ḃz----X$^-$ complexes in the 3MHx matrix[2] as is shown by the solid line in Fig. 3. From the intercept and the reported EA (Ḃz) value, 0.90 eV,[12] the effective radius of the Bz$^-$ anion can be calculated as 0.263 nm. The linear relationship (3) holds also for diphenylmethyl radical–halide ion complexes.[5]

The present observations of the Ḃz---X$^-$ complex in three different matrices enables us to examine the effect of matrix polarity on the CT excitation energy, as expressed by Eq. 3. Qualitatively speaking, D_{op} is close to 2.0 for all the matrices examined, which means that E_s(Bz$^-$) will be almost constant. The effect of polarity will come mainly from E_s(X$^-$), which is dependent on D_s. For more polar matrices, E_s (X$^-$) will become larger and this will lead to larger $h\nu_{CT}$. Actually, the blue-shift of the CT band was followed by changing the matrix from 3MHx to MTHF,

Table 2. Observed and calculated charge-transfer transition energies of the benzyl radical-halide ion complexes

Matrix	Halide ion	Ionization energy of halide ion[a] $IP(X^-)$	Dielectric const.[b] D_s	Dielectric const.[b] D_{op}	Solvation energy[d] $E_s(X^-)$	Solvation energy[d] $E_s(Bz^-)$	CT excitation energy, $h\nu_{CT}$ Calcd	CT excitation energy, $h\nu_{CT}$ Exptl
MTHF	Cl^-	3.61	2.2[c]	2.0	2.39	1.37	3.73	3.61
	Br^-	3.36	2.2[c]	2.0	2.18	1.37	3.27	3.36
	I^-	3.06	2.88	2.0	2.29	1.37	3.08	2.95
EtOH	I^-	3.06	3.0	1.853	2.34	1.26	3.25	3.59

Energies are given in eV units. a) Ref. 15. b) Ref. 13. c) D_s at 4.2 K is assumed in the present investigation. See text. d) The calculation is based on Born's formula: $E_s=(e^2/2r)(1-1/D)$. $E_s(Bz^-)$ from D_{op} and $r=0.263$ nm, which is assumed to be independent of the solvent. See also Refs. 2 and 6.

for the Cl^- and Br^- series, as shown in Table 1. Combining the new data (the third column) with the previous data (the last column), it can be seen that the CT band for the I^- ion is increasingly blue-shifted in the order 3MHx, MTHF, and ethanol.

The D_s and D_{op} values at 77 and 4.2 K for MTHF and ethanol are needed in order to apply equation (3) for an quantitative examination of the effect of the matrix polarity as observed in the present experiment. From an extrapolation of high temperature data, Kevan has proposed that for MTHF at 77 K, $D_s=2.88$ and $D_{op}=2.0$.[13] Using these values and the reported ionic radii[14] (0.164, 0.180, and 0.205 nm for Cl^-, Br^-, and I^-) and assuming that the Bz^- ion has a constant radius (0.263 nm, irrespective of the matrix), $h\nu_{CT}$ for the $\dot{B}z$---I^- complex in the MTHF matrix has been calculated as 3.08 eV (see Table 2). This is close to the observed value of 2.95 eV at 77 K. The dashed line in Fig. 3 shows the linear relationship between $h\nu_{CT}$ and $IP(X^-)+E_s(X^-)$ calculated for the $\dot{B}z$---X^- complexes in a MTHF matrix with $D_{op}=2.0$. The observed $h\nu_{TC}$ at 4.2 K for the $\dot{B}z$---Cl^- and $\dot{B}z$---Br^- complexes fall on the predicted line, if one assumes that $D_s=2.2$ at 4.2 K. The smaller D_s indicates that the MTHF matrix is similar to nonpolar alkane matrices at 4.2 K. This can be attributed to an inhibition of the rotational relaxation of the polar MTHF molecules surrounding the ions at 4.2 K. Such an inhibition of the rotational relaxation has been verified by observing the evolution of the absorption spectrum of the trapped electrons in a MTHF matrix upon warming from the γ-irradiation temperature 4.2 K to 77 K.[16,17]

By using Kevan's estimates of D_s and D_{op} for ethanol at 77 K,[13] $h\nu_{CT}$ for the $\dot{B}z$---I^- complex can be calculated as 3.24 eV, which is somewhat too small in comparison with the observed value of 3.59 eV (see Table 2). This discrepancy is partly due to the fact that Born's formula, used to calculate the solvation energies, is strictly valid only for the case of continuous matrix media. The main contribution to the solvation, however, will be the rotational relaxation of the polar ethanol molecules in the close vicinity of the I^- ion. In addition, it is possible that the rotational relaxation has not gone to completion after warming the sample to 77 K before the measurement of the CT band. The previous study on the evolution of the spectrum of the trapped electron indicates that the rotational relaxation in the ethanol matrix took about 30 min to be completed at 77 K.[18]

Table 1 shows the general trend in the formation of $\dot{B}z$---X^- complexes. Experimental conditions favor observations of these complexes: (1) When the irradiation temperature is low, (2) when the X^- ion is bulky, and/or (3) when the matrix is nonpolar. Conditions (1) and (2) prevent the ion from escaping from the $\dot{B}z$ radical (cage effect). Condition (3) is somewhat more complex. An increase in matrix polarity will have two effects. The first effect is a solvation effect. The orientational rearrangement of the polar matrix molecules around the X^- ion of the ground state complex increases $E_s(X^-)$ and is the cause of the blue-shift of the CT band. The varying extent of the solvation effect will broaden the band, so that its apparent intensity becomes weaker. The second effect is a separation effect. The molecular reorientation in the immediate vicinity of the X^- ion will push it away from the $\dot{B}z$ radical. A slight increase in the interdistance between X^- and $\dot{B}z$ will significantly reduce the overlap between the electron-donating orbital and the electron-accepting orbital, so that the transition moment of the CT excitation will decrease in magnitude. Neither a blue-shift nor a broadening of the line could be observed during the gradual decay of the $\dot{B}z$---I^- CT band after warming the ethanol matrix to 77 K. This is an indication that the separation effect is more important than the solvation effect in polar matrices.

The absence of both benzyl spectrum or the CT band immediately after 4.2 K irradiation of the matrices containing BzI gives an interesting example of the detailed reaction steps involved in the dissociative electron attachment. A gas phase study has shown that the dissociative attachment of thermal electrons to aromatic halides having low-energy vacant π orbitals occurs according to a mechanism involving an intermediate molecular negative ion as a precursor of the dissociation into a halide ion and a free radical.[19] Although such a precursor is expected to be easily trapped in the solid state, spectroscopic observations of it have been very few.[8,9] In the present case, the precursor was observed at 4.2 K (see Fig. 2). It

unquestionably dissociated into $\dot{B}z$ and I^-, as is evidenced by the excitation spectra after warming BzI/ethanol or 3MHx to 77 K (see, for example, Fig. 1). The cage effect is so prominent at 4.2 K for the most bulky I^- ion that the elongation of the C–I bond distance and/or the change of the $-CH_2$ group from sp^3 to sp^2 conformation is inhibited.

In conclusion, the following reaction steps have been revealed by the present investigation:

$$\mathrm{BzI} \xrightarrow{e^-} \underset{\text{precursor}}{\mathrm{BzI}^-} \longrightarrow \underset{\text{complex}}{(\dot{B}z\text{---}I^-)} \longrightarrow \dot{B}z + I^-.$$

The question whether the precursor observed by the optical absorption measurements is the molecular anion or an intermediate state between the molecular anion and the complex still remains. The precursor dissociates into the complex even at 4.2 K for BzBr and BzCl. The complex is stably trapped at 77 K in the nonpolar 3MHx matrix for all the BzX's examined, but it is unstable in the polar ethanol matrix. The dissociation of the complex could be followed by observing the gradual decay of the CT excitation band for $\dot{B}z\text{---}I^-$ in the ethanol matrix at 77 K. The MTHF matrix is intermediate as concerns the stability of the complex.

References

1) M. Irie, M. Shimizu, and H. Yoshida, *Chem. Phys. Lett.*, **25**, 102 (1974).
2) M. Irie, M. Shimizu, and H. Yoshida, *J. Phys. Chem.*, **80**, 2008 (1976).
3) T. Izumida, T. Ichikawa, and H. Yoshida, *J. Phys. Chem.*, **84**, 60 (1980).
4) T. Saito and H. Yoshida, *Bull. Chem. Soc. Jpn.*, **47**, 3167 (1974).
5) T. Izumida, Y. Tanabe, T. Ichikawa, and H. Yoshida, *Bull. Chem. Soc. Jpn.*, **52**, 235 (1979).
6) T. Izumida, T. Ichikawa, and H. Yoshida, *J. Phys. Chem.*, **83**, 373 (1979).
7) T. Higashimura, A. Namiki, M. Noda, and H. Hase, *J. Phys. Chem.*, **76**, 3744 (1972).
8) A. Namiki, *J. Chem. Phys.*, **62**, 990 (1975).
9) S. Noda, K. Yoshida, M. Ogasawara, and H. Yoshida, *J. Phys. Chem.*, **84**, 57 (1980).
10) V. J. Morrison and J. D. Laposa, *Spectrochim. Acta, Part A*, **32**, 1207 (1976).
11) R. S. Mulliken and W. B. Person, "Molecular Complexes: A Lecture and Preprint Volume," Wiley-Interscience, New York (1969).
12) A. F. Gaines and F. M. Page, *Trans. Faraday Soc.*, **59**, 1266 (1963).
13) L. Kevan, "Advances in Radiation Chemistry," ed by M. Burton and J. L. Magee, Wiley-Interscience, New York (1974), Vol. 4, p. 181.
14) B. S. Gourary and F. J. Adrian, *Solid State Phys.*, **1K**, 127 (1960).
15) E. C. M. Chen and W. E. Wentworth, *J. Chem. Phys.*, **52**, 486 (1975).
16) H. Hase, M. Noda, and T. Higashimura, *J. Chem. Phys.*, **54**, 2975 (1971).
17) M. Yoshizaki, M. Ogasawara, and H. Yoshida, *Bull. Chem. Soc. Jpn.*, **54**, 3143 (1981).
18) M. Ogasawara, K. Shimizu, and H. Yoshida, *Radiation Phys. Chem.*, **17**, 331 (1981).
19) J. C. Steelhammer and W. E. Wentworth, *J. Chem. Phys.*, **51**, 1802 (1969).

Photochemistry of Metal-Metal Bonded Compounds. I. Isolation and X-Ray Molecular Structure Analyses of Orthometalated Triphenyl Phosphite Manganese Carbonyl Derivatives and Reaction Mechanisms of Orthometalation from Photodegradation of Manganese Carbonyl Derivatives with Sn–Mn Bond

Satoru Onaka,* Yoshinori Kondo, Nobuhiro Furuichi,
Koshiro Toriumi,† and Tasuku Ito†

Department of Chemistry, Nagoya Institute of Technology, Gokisocho, Showa-ku, Nagoya 466
† *Division of Applied Molecular Science, Institute for Molecular Science, Myodaiji, Okazaki, 444*

(Received March 5, 1982)

Photochemical degradation of a series of tin-manganese bonded complexes was studied. The apparent reactivity of the tin-manganese bond toward UV irradiation is interpreted on the basis of absorption spectra of relevant complexes and available emissions from the light source. Two kinds of orthometalated products were obtained from photolysis of Me_3Sn–$Mn(CO)_3[P(OPh)_3]_2$ in benzene. Various kinds of experiments suggest that their photochemical reactions proceed through homolytic cleavage of the Sn–Mn bond in the initial stage and the resulting 15-electron intermediates abstract hydrogen from the triphenyl phosphite moiety. Molecular structures of the two kinds of orthometalated products, as clarified by X-ray structure analyses, are described.

There is much current research activity on photochemical reactions of metal-metal bonded complexes.[1,2] The impetus behind these studies is to understand the photochemistry of these complexes in connection with excited states and/or to obtain new intriguing derivatives by exploiting photochemically generated unstable intermediates.[1,2] Although the ultimate goal of these studies is to predict theoretically, and to design or control, photochemical reactions for these complexes, only limited understanding of photochemical reaction mechanisms with regard to the photochemical excitation has been obtained up to the present.[1,2] Those metal carbonyl derivatives which possess transition metal-transition metal bonds and transition metal-group IV metal bonds, have so far been explored intensively.[1–3] We have been studying structures, bondings, and syntheses of manganese carbonyl derivatives which have manganese-group IV metal atom bonds.[4] As part of a systematic investigation on structure, bonding, and reactivity of the aforementioned type of manganese carbonyl derivatives, we were led to investigate photochemical behavior of this series of compounds.

According to Wrighton *et al.*,[5] the photochemistry of group IV metal-transition metal bonds for Ph_3M'–$M(CO)_3L$ (M′=Ge and Sn; M=Mn and Re) is dependent on L, M′, and M, and the initial photochemical process is the charge transfer from the M′–M bond (HOMO) to the π^* of L (LUMO) which leads to labilization of the M′–M bond. Reichel and Wrighton,[6] however, have demonstrated that the main result of photoexcitation of R_3Si–$Co(CO)_4$ (R=Ph and Et) is dissociative loss of CO. These studies suggest that the photochemical behavior of the transition metal-group IV metal bond in R_3M'–$M(CO)_xL_y$ type compounds is very much dependent on the substituent of L on the transition metal atom M, the group IV metal atom M′, and the transition metal atom M itself, and that the photochemical behavior can be interpreted in terms of the molecular orbital diagram. When L has no low-lying empty π^* orbital, the lowest energy excitation for M=Mn or Re is the $d\pi\rightarrow\sigma^*$ or $\sigma_b\rightarrow\sigma^*$(M′–M) transition, which may depends on the sp^3 level of atom M′ (Schemes 1(a) and (b)).[5,6] Scheme 1(a) may hold for M′=Si and Scheme 1(b) for M′=Sn. In the combination of M′=Sn and L which has a low-lying empty π^* orbital, the lowest energy excitation is the $\sigma_b\rightarrow\pi^*$(L) transition (Scheme 1(c)).[5,6] It comes out from Scheme 1 that photochemical cleavage of the M′–M bond becomes efficient, which is otherwise reluctant, when the M′–M bond strength is affected by replacing R or L with another substituent and the $\sigma_b\rightarrow\sigma^*$ (M′–M) transition approaches to available excitation energy. In this regard, the manganese-tin bonds in R_3Sn–$Mn(CO)_xL_y$ and $R_{4-x}Sn[Mn(CO)_5]_x$ are enticing candidates to examine this idea; our previous spectro-

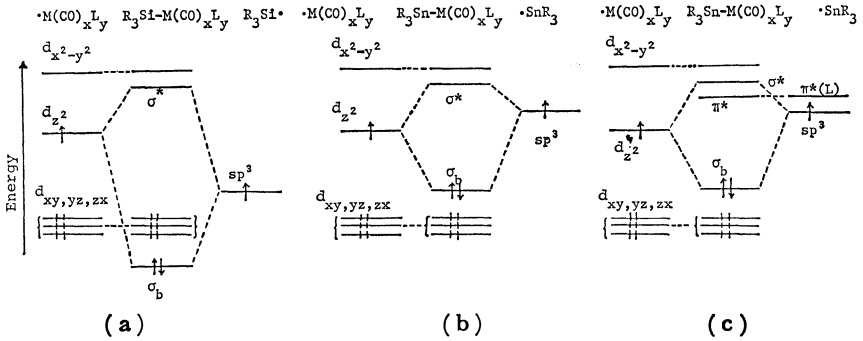

Scheme 1. One-electron energy diagram for R_3M'-$M(CO)_xL_y$.

TABLE 1. ELECTRONIC ABSORPTION SPECTRAL DATA

Complex	λ_{max}/nm (ε/M^{-1} cm^{-1})
Me_3Sn–$Mn(CO)_5$(I)	230 (19000) [a]
$Me_2Sn[Mn(CO)_5]_2$(II)	230 (22200), [a] 320 (17000)
$MeSn[Mn(CO)_5]_3$(III)	230 (38000), [a] 385 (14700)
Me_3Sn–$Mn(CO)_3L_2$(IV)	230 (21900), [a] 270 sh
Me_3Sn–$Mn(CO)_4L$(V)	230 (19600), [a] 270 sh
$Me_2Sn[Mn(CO)_4L]_2$(VI)	230 (18400), [a] 265 sh 320 (14200)
$P(OPh)_3$	265 (1550)

a) Shoulder in hexane solution.

scopic studies have shown that the Sn–Mn bond strength is influenced by replacing the carbonyl in R_3Sn–$Mn(CO)_5$ with triphenylphosphine and its congeners.[4l,4m] The present study was undertaken to demonstrate how the photochemistry of a series of Me_3Sn–$Mn(CO)_{5-x}[P(OPh)_3]_x$ or $Me_{3-x}Sn[Mn(CO)_5]_{x+1}$ (x= 0, 1, and 2) is dependent on change in substituents and to clarify the fate of photochemically generated unstable manganese carbonyl intermediates. A preliminary account appeared elsewhere.[4p]

Experimental

All the syntheses were made under a purified nitrogen atmosphere. Photolyses were performed under a purified argon atmosphere with stirring in a Pyrex reaction vessel in which a Riko 100 W water-cooled high pressure Hg lamp was inserted. No filter was used to isolate particular emission from the Hg lamp. IR spectra were recorded on a JASCO-701G infrared spectrometer with 0.1 mm NaCl windowed liquid cells. Absorption spectra were obtained with a Shimadzu MPS-5000 spectrometer with 1 mm quartz cells. CH_2Cl_2 was employed as a solvent. Absorption data are collated in Table 1.

Materials. Me_3Sn–$Mn(CO)_5$ (I), $Me_2Sn[Mn(CO)_5]_2$ (II), $MeSn[Mn(CO)_5]_3$ (III), and Me_3Sn–$Mn(CO)_3[P(OPh)_3]_2$ (IV) (hereafter L denotes triphenyl phosphite) were prepared as described elsewhere.[4] Me_3Sn–$Mn(CO)_4L$ (V) and $Me_2Sn[Mn(CO)_4L]_2$ (VI) were obtained as follows: 1.4 g (1.5 mmol) of $[Mn(CO)_4L]_2$[7] was dissolved in 30 cm^3 of THF and was reduced to $NaMn(CO)_4L$ by stirring over 1% sodium amalgam. The pale yellow supernatant solution was decanted into a flask and to this was added 0.6 g (3 mmol) of Me_3SnCl or 0.35 g (1.5 mmol) of Me_2SnCl_2 in 25 cm^3 of THF with stirring. The mixture was stirred overnight. The resulting pale yellow solution was filtered by using a fine porosity glass frit and the solvent was vacuum-stripped to leave a pale brown oil. For V, the oil was extracted with hexane and the hexane was almost distilled off at reduced pressure to afford 1.5 g of pale yellow crystals (yield: 78%). For VI, the oil was extracted with hot hexane and the solvent was partially vacuum-stripped to give 1.0 g of pale yellow crystals (Yield: 60%). ν(CO)/cm^{-1} in benzene for V: 2048(w) and 1957(vs); for VI: 2088(vw), 2059(vw), 2036(w), 1990(m,sh), 1970(vs), and 1955(s, sh).

Photolysis of I and V. Each 1.0 g sample was dissolved in 50 cm^3 of dried benzene and was irradiated for more than 15 h, but no appreciable change other than decomposition was detected by IR. More than 95% of I was left intact and about 20% of V was decomposed after 15 h irradiation (based on IR spectra).

Photolysis of II. A 1.0 g sample of II was dissolved in 50 cm^3 of benzene and was photolyzed for 8 h. An IR monitoring showed that II was partially converted into other manganese carbonyl complexes. The solvent was removed under a reduced pressure and the residue was purified by column chromatography over Florisil. An yellow band was eluted with petroleum ether and recrystallization from the same solvent gave a small amount of $Mn_2(CO)_{10}$ (yield: more than 50 mg).

Photolysis of III. A 0.2 g sample of III was dissolved in 40 cm^3 of benzene and the solution was photolyzed for 20 min. An IR monitoring indicated complete digestion of III. Similar work up as in the case of II gave 30 mg of $Mn_2(CO)_{10}$.

Photolysis of IV. A 1.0 g sample of IV was dissolved in 50 cm^3 of benzene and photolysed for 8 h. After the solution was filtered, the solvent was distilled off at reduced pressure to leave a pale brown oil. The oil was dissolved in a minimum amount of benzene and was chromatographed over Florisil (60—100 mesh). Hexane was used as the first eluent. From the first fraction a small amount of V (40 mg) was obtained. Then, a hexane–benzene (1:2) mixture eluted the second, third, and fourth fractions. About 300 mg of the starting material IV was recovered from the second fraction. After the solvents were distilled off from the third and fourth fractions, the pale yellow oil was dissolved in a small amount of benzene and to this was added cyclohexane without agitation. The mixture was stored in a refrigerator for several weeks to yield 30 mg of $(PhO)_2\overline{P(OC_6H_4)}Mn(CO)_2L_2$ (**1**),[4p] 70 mg of *fac-cis*-$(PhO)_2\overline{P(OC_6H_4)}Mn(CO)_3L$ (**2**),[8] and 50 mg of IV. Finally an yellow band was eluted with $CHCl_3$ and recrystallization from benzene gave 15 mg of yellow crystals (**3**). Elemental analyses of **1**. Found: C, 64.24; H, 3.90; P, 8.73%. Calcd for $C_{56}H_{44}MnO_{11}P_3$: C, 64.62; H, 4.26; P, 8.93%.

Photolysis of VI. A 0.6 g sample of VI was dissolved in 50 cm^3 of benzene and the solution was irradiated for 6 h. After similar work up as in the case of IV, the products were separated by column chromatography over Florisil. The first fraction was eluted with hexane to afford a small amount of oil (about 10 mg). The IR spectrum of this oil was consistent with that of authentic $(PhO)_2\overline{P(OC_6H_4)}Mn(CO)_4$ (**4**).[9] An yellow band was then eluted with ethanol. Recrystallization from benzene–petroleum ether gave 15 mg of yellow crystals (**3**).[10]

Yields for photolysis products were averaged for several runs for IV and VI and IR data for photolysis products are given in Table 2.

Photolysis of Orthometalated Products. As a typical example, the photolysis of **2** is described. A 0.27 g sample of **2** was dissolved in 40 cm^3 of benzene and was photolyzed for 3 h. The solvent was removed under a reduced pressure to leave a pale brown oil. The oil was dissolved in a minimum amount of benzene and the solution was loaded on a Florisil column. From the first fraction eluted with petroleum ether, 12 mg of **4** was obtained. The second and third fractions were eluted with hexane–benzene (1:1) and were carefully recrystallized as in the photolysis of IV from benzene–petroleum ether to give 16 mg of **1**, 16 mg of **2** and 38 mg of *mer-trans*-$(PhO)_2\overline{P(OC_6H_4)}Mn(CO)_3L$ (**5**).[11] The fourth fraction was eluted with chloroform and recrystallization from benzene gave a small amount of yellow crystals (**3**).

Photolysis of IV in CCl_4. A 1.0 g sample of IV was dissolved in 50 cm^3 of CCl_4 and the solution was photolyzed for 2 h. After the solvent was vacuum-stripped, the resulting yellow solid was subjected to column chromatography

Table 2. IR data for photolysis products in a Nujol mull

Products	ν(CO)/cm^{-1}	Characteristic peaks of orthometalated $P(OPh)_3$[a] (ν/cm^{-1})
$(PhO)_2\dot{P}(OC_6H_4)\dot{M}n(CO)_2L_2$ (**1**)	1980(vs), 1920(vs)	1103(m), 951(m), 800(m)
$(PhO)_2\dot{P}(OC_6H_4)\dot{M}n(CO)_3L$ (**2**)	2031(vs), 1967(vs), 1943(vs)	1101(m), 952(s), 805(m)
Yellow crystal (**3**)	2068(w), 1987(vs), 1940(vs)	
$(PhO)_2\dot{P}(OC_6H_4)\dot{M}n(CO)_4$ (**4**)	2085(m), 2002(s), 1975(vs), 1962(s)	1101(m), 960(m, sh), 798(m)

a) G. W. Parshall, W. H. Knoth, and R. A. Schunn, *J. Am. Chem. Soc.*, **91**, 4990 (1969); J. L. Levison and S. D. Robinson, *J. Chem. Soc., A*, **1970**, 639; M. Y. Darensbourg, D. J. Darensbourg, and D. Drew, *J. Organomet. Chem.*, **73**, C25 (1974).

Table 3. Atomic positional parameters for **1**[a]

Atom	x	y	z	B_{eq}/Å^2	Atom	x	y	z	B_{eq}/Å^2
Mn	−223(1)	2480(1)	503(1)	3.7	C212	3627(8)	908(3)	2629(9)	5.2
P1	−1111(2)	2503(1)	2115(2)	3.9	C213	4454(9)	422(3)	3104(10)	6.6
P2	343(2)	1635(1)	890(2)	3.9	C214	4171(10)	0(3)	2208(12)	8.0
P3	−260(2)	3331(1)	532(2)	3.7	C215	3080(10)	54(3)	813(11)	7.8
C1	673(8)	2431(3)	−661(8)	4.6	C216	2229(9)	542(3)	301(9)	6.0
C2	−1907(8)	2514(3)	−1007(8)	4.6	C221	−1434(8)	1303(3)	−1648(7)	3.9
O1	1171(6)	2378(2)	−1458(6)	6.3	C222	−2834(8)	1256(3)	−2142(9)	5.2
O2	−2998(6)	2560(2)	−1967(6)	6.8	C223	−3631(9)	1316(3)	−3697(9)	6.0
O11	90(5)	2513(2)	3737(5)	4.7	C224	−3036(9)	1420(3)	−4641(9)	6.1
O12	−2210(5)	3003(2)	1983(5)	4.4	C225	−1646(9)	1464(3)	−4077(8)	5.4
O13	−1801(5)	2031(2)	2457(5)	5.0	C226	−773(9)	1401(3)	−2531(8)	4.7
O21	1748(5)	1440(2)	749(5)	4.8	C231	932(8)	957(3)	3304(8)	4.3
O22	−668(5)	1225(2)	−101(5)	4.2	C232	635(8)	480(3)	2656(9)	5.5
O23	591(6)	1423(2)	2464(5)	5.4	C233	1048(10)	32(3)	3595(10)	6.8
O31	949(5)	3612(2)	454(5)	4.5	C234	1698(11)	73(4)	5120(11)	7.8
O32	−1641(5)	3623(2)	−803(5)	4.6	C235	1946(11)	563(4)	5744(10)	7.8
O33	−244(5)	3615(2)	1963(5)	4.6	C236	1564(9)	1020(3)	4799(8)	6.0
C111	1414(8)	2498(3)	3773(8)	4.6	C311	1534(8)	3562(3)	−551(9)	4.3
C112	1558(7)	2481(3)	2445(7)	4.0	C312	2963(9)	3482(3)	119(9)	5.4
C113	2920(8)	2459(3)	2588(9)	5.3	C313	3676(10)	3450(3)	−756(11)	7.4
C114	4056(8)	2455(3)	4016(11)	7.2	C314	2925(11)	3512(4)	−2304(12)	8.1
C115	3806(9)	2471(3)	5299(10)	7.0	C315	1481(11)	3599(3)	−2954(9)	7.1
C116	2479(9)	2486(3)	5199(9)	6.0	C316	732(10)	3631(3)	−2067(8)	5.8
C121	−2541(8)	3222(3)	3095(8)	4.6	C321	−2259(8)	4145(3)	−912(8)	4.2
C122	−2360(11)	2945(4)	4360(10)	8.0	C322	−3589(9)	4194(3)	−1084(10)	6.5
C123	−2783(12)	3237(5)	5361(10)	9.5	C323	−4277(10)	4705(4)	−1238(12)	8.7
C124	−3287(11)	3759(4)	5090(11)	9.3	C324	−3590(11)	5138(3)	−1193(11)	8.0
C125	−3435(13)	4010(4)	3822(11)	10.1	C325	−2258(10)	5059(3)	−1027(10)	7.4
C126	−3052(11)	3733(3)	2811(11)	7.9	C326	−1548(9)	4545(3)	−925(10)	5.8
C131	−3016(8)	1842(3)	1493(8)	4.8	C331	582(9)	3992(3)	2814(8)	4.9
C132	−4116(8)	2174(3)	438(9)	6.4	C332	−148(12)	4463(3)	2821(11)	8.0
C133	−5319(10)	1956(4)	−462(11)	7.9	C333	630(14)	4842(4)	3722(12)	10.3
C134	−5402(10)	1432(4)	−296(11)	8.1	C334	2041(14)	4705(4)	4481(11)	10.4
C135	−4264(10)	1104(4)	788(10)	7.2	C335	2793(12)	4215(4)	4495(10)	9.2
C136	−3024(10)	1312(3)	1710(9)	5.9	C336	1986(9)	3833(3)	3593(8)	5.8
C211	2557(8)	942(3)	1248(9)	4.7					

a) Positional parameters are multiplied by 10^4 and thermal parameters are given by the equivalent temperature factors.

(Florisil). The first fraction was eluted with hexane–benzene (1:1). Recrystallization from hexane–chloroform gave 220 mg of *mer-trans*-$ClMn(CO)_3L_2$.[12] The second fraction was also eluted with hexane–benzene (1:1) and recrystallization from hexane–chloroform yielded 10 mg of *fac-cis*-$ClMn(CO)_3L_2$.[12]

Photolysis of VI in CCl_4. A 0.5 g sample of **VI** was dissolved in 30 cm^3 of CCl_4 and the solution was photolyzed for 2 h. Similar work up as above gave 10 mg of *cis*-$ClMn(CO)_4L$ and 100 mg of *mer-trans*-$ClMn(CO)_3L_2$.[12]

Table 4. Atomic positional parameters for 2[a)]

Atom	x	y	z	B_{eq}/Å^2	Atom	x	y	z	B_{eq}/Å^2
Mn	2769(1)	585(1)	1243(1)	2.5	C126	1871(2)	2293(2)	3426(6)	3.3
P1	2233(1)	1104(1)	2279(2)	2.4	C131	2456(2)	1026(2)	4678(6)	2.9
P2	2543(1)	−95(1)	2400(2)	2.4	C132	2914(3)	1311(3)	4641(6)	3.6
C1	3107(2)	163(2)	179(6)	3.3	C133	3263(3)	1247(3)	5647(7)	4.4
O1	3322(2)	−106(2)	−525(5)	5.0	C134	3157(3)	917(3)	6634(7)	4.7
C2	3356(2)	744(2)	2094(6)	3.1	C135	2685(3)	642(3)	6641(6)	4.3
O2	3737(2)	848(2)	2591(5)	4.3	C136	2325(3)	692(2)	5655(6)	3.5
C3	2868(3)	1109(2)	145(6)	3.3	C211	1653(2)	−329(2)	3769(6)	2.8
O3	2927(2)	1437(2)	−571(4)	4.7	C212	1135(3)	−319(3)	3389(7)	3.7
O11	1653(1)	1025(2)	1769(4)	2.9	C213	771(3)	−585(3)	4148(8)	4.8
O12	2336(1)	1711(1)	2057(4)	2.9	C214	935(3)	−843(3)	5226(8)	5.1
O13	2087(1)	1072(2)	3726(4)	3.0	C215	1461(3)	−835(3)	5572(7)	4.7
O21	1985(1)	−30(1)	2994(4)	2.9	C216	1832(3)	−575(2)	4841(6)	3.6
O22	2531(2)	−617(1)	1590(4)	2.9	C221	2303(2)	−1087(2)	2020(5)	2.5
O23	2862(1)	−266(2)	3633(4)	2.9	C222	1799(2)	−1182(2)	1681(6)	3.0
C111	1615(2)	679(2)	753(6)	2.7	C223	1564(2)	−1653(2)	2067(6)	3.2
C112	2061(2)	423(2)	358(6)	2.7	C224	1856(2)	−2010(2)	2774(6)	3.2
C113	1988(3)	77(2)	−668(6)	3.6	C225	2372(2)	−1899(2)	3092(6)	3.1
C114	1492(3)	15(3)	−1211(7)	4.1	C226	2607(2)	−1432(2)	2718(6)	2.7
C115	1058(3)	282(3)	−767(7)	4.3	C231	3399(2)	−342(2)	3718(7)	3.4
C116	1118(3)	624(2)	268(6)	3.5	C232	3600(3)	−293(3)	4928(8)	5.3
C121	1940(2)	2088(2)	2246(6)	2.7	C233	4149(3)	−372(3)	5070(9)	6.9
C122	1662(2)	2240(2)	1200(6)	3.4	C234	4445(3)	−486(3)	4042(10)	7.1
C123	1265(3)	2618(3)	1372(7)	4.2	C235	4234(3)	−543(3)	2861(9)	5.9
C124	1185(2)	2834(2)	2546(7)	3.9	C236	3694(3)	−473(3)	2689(8)	4.4
C125	1480(3)	2681(3)	3569(7)	4.0					

a) Positional parameters are multiplied by 10^4 and thermal parameters are given by the equivalent temperature factors.

X-Ray Molecular Structure Analysis of **1**. Colorless crystals were grown up from hexane–benzene. A crystal of approximate dimensions $0.26\times0.19\times0.07$ mm^3 was mounted on a Rigaku AFC-5 automated four circle diffractometer equipped with graphite monochromated Mo $K\alpha$ radiation (λ=0.71073 Å). The crystal belongs to the triclinic system with unit cell dimensions a=10.820(3), b=25.943(3), c=10.061(2) Å, α=90.61(1), β=115.26(1), γ=82.77(1)°, V=2530.8(10) Å^3, and Z=2. A total of 4199 independent reflections with $|F_o|>3\sigma(|F_o|)$ were obtained at room temperature using the θ-2θ scan technique up to 2θ=50°. No absorption correction was applied. The structure was solved by the standard heavy atom method and refined based on P$\bar{1}$ space group by the use of a UNICS-III program package[13] and computers (HITAC M-180 and M-200H) at Institute for Molecular Science. A series of least-squares refinements for 71 nonhydrogen atoms with anisotropic temperature factors reduced R and R_w to 0.069, where anomalous dispersion correction for Mn and P was applied. The final positional parameters are listed in Table 3. The lists of thermal parameters and F_o and F_c are deposited as Document No. 8304 at the Chemical Society of Japan.

X-Ray Molecular Structure Analysis of **2**. Colorless crystals were obtained from cyclohexane–petroleum ether. Weissenberg photographs using Cu K_α indicated 4/m Laue symmetry. A crystal of approximate dimensions $0.24\times0.24\times0.24$ mm^3 was mounted on a Rigaku AFC-5 automated four circle diffractometer. A preliminary reflection data collection revealed systematic absences h00, 0k0, and 00l for h or k or l=2n+1 and hk0 for $h+k$=2n+1, which define the tetragonal space group P4$_2$/n (C_{4h}^4; No 86). The lattice constants, determined by a least-squares fit to 30 high angle ($20°\leq2\theta\leq30°$) reflections are a=b=25.768(3), c=10.720(3) Å, V=7117.9(24) Å^3, and Z=8. Intensity data were collected at −50 °C by using the same scanning technique as with **1** and a total of 3966 unique reflections with $|F_o|>3\sigma(|F_o|)$ were obtained in the region of h, k, l with $0<h$, k, l up to 2θ=55°. No absorption correction was made. The structure was solved by the standard heavy atom method and refined as mentioned above to give R=0.062 and R_w=0.073 for 51 nonhydrogen atoms with anisotropic temperature factors. Anomalous dispersion correction was applied for Mn and P at the final stage of refinement. Final positional parameters are collected in Table 4 and lists of thermal parameters and F_o and F_c are deposited as Document No. 8304 at the Chemical Society of Japan.

Results and Discussion

Absorption Spectra and Photoreactivity. The absorption spectra for the series of $(CH_3)_{3-x}Sn[Mn(CO)_5]_{x+1}$ (x=0, 1, and 2) are very much dependent on the number of manganese carbonyl groups; a strong absorption is observed at 385 nm besides a very strong absorption at 230 nm for III which possesses three tin-manganese bonds and a strong absorption is detected at 320 nm besides a very strong absorption at 230 nm for II which contains two tin-manganese bonds, while only a very strong absorption is observed at 230 nm for I which possesses only one tin-manganese bond. The very strong absorptions at 230 nm are as-

singable to the Mn to π^*(CO) charge transfer band and those strong absorptions at 385 and 320 nm are assignable to the σ_b(Sn–Mn)→σ^*(Sn–Mn) transition.[1,14] This transition may be hidden behind the very strong charge transfer band at 230 nm for I. Those compounds which possess triphenyl phosphite ligand(s) exhibit an extra absorption around 270 nm. This band is assignable to the π→π^* transition due to the phenyl groups in triphenyl phosphite, since free triphenyl phosphite itself shows this absorption. From a comparison of the absorption spectra for two groups of compounds, that is, I, IV, and V, and II and VI, we are led to the conclusion that the replacement of CO by triphenyl phosphite ligand(s) does not afford any obvious influence on the σ_b→σ^*(Sn–Mn) transition. Thus, the σ_b→σ^*(Sn–Mn) transition energy is in the order Sn–Mn > $Sn\langle^{Mn}_{Mn}$ > $Sn\langle^{Mn}_{Mn}$.

In order to understand the photochemical reactivity of the tin-manganese bonded compounds in connection with the excited states (Scheme 1), it is interesting to examine the relation between the reactivity of Sn–Mn bond and the excitation energy of this bond; the Sn–Mn bonds in III are degraded smoothly under UV irradiation to give $Mn_2(CO)_{10}$. III decomposes rapidly even under a fluorescent room light in CH_2Cl_2. II is partially digested by UV irradiation to yield $Mn_2(CO)_{10}$, while I does not react seemingly. The formation of $Mn_2(CO)_{10}$ from II and III is accounted for in terms of homolytic cleavage of the Sn–Mn bond[5,6,15] and coupling of the resulting ·$Mn(CO)_5$ radicals. Thus, the apparent order of the photoreactivity of Sn–Mn bond is inversely proportional to the order of the σ_b→σ^*(Sn–Mn) transition energy. This order also seems to be related to the light intensity of the lamp used; II and III can be excited by the intense emissions at 313 and 366 nm, respectively, but the emissions effective to excite I is weak in intensity and moreover, the solvent, C_6H_6, absorbs this range of light.

For I, IV, and V, it is unlikely that an electron in the σ_b(Sn–Mn) orbital is excited directly to σ^*(Sn–Mn) by emissions from the present Hg lamp as mentioned above. The observation that IV is more photosensitive than I and V tempts us to speculate an alternative photochemical reaction pathway; IV has an absorption at 270 nm which is assignable to the π→π^*(P(OPh)$_3$) transition and thus, it is conceivable that the low-lying empty π^* orbital should have some connection with the photoreactivity of IV. In this regard, two possible mechanisms come out, that is, an electron in σ_b(Sn–Mn) orbital is excited to the π^*(P(OPh)$_3$) orbital (Scheme 1(c)) or the Sn–Mn bond in IV, which should be enfeebled by the introduction of two bulky triphenyl phosphite ligands in cis positions toward the Sn–Mn bond, is readily labilized by an energy transfer mechanisms from the π→π^*(P(OPh)$_3$) transition.[16] At present, we have no evidence to differentiate these two mechanisms and this point must wait for future experiment.

Reaction Mechanisms of Orthometalation. As was described in the Experimental section, photodegradation of IV and VI in benzene gave orthometalated products (shown in Fig. 1), which contain no tin moiety. Therefore, the process of orthometalation should entail cleavage of the Sn–Mn bond in a certain process of the photochemical reaction. The Sn–Mn bond cleavage in the primary photoprocess was suggested by several experiments: Photolysis of IV in CCl_4 gave $ClMn(CO)_3L_2$ and photolysis of IV together with benzyl chloride in C_6H_6 gave bibenzyl. When the photolysis of IV is conducted in air-saturated benzene, only trace amounts of **1**, **2**, and V were obtained. The yields of **1**, **2**, and V were considerably decreased when argon was bubbled into the benzene solution during the photolysis to purge out gaseous products such as CO and H_2. These lines of evidence indicate that (i) the initial process of photolysis is homolytic cleavage[17] of the Sn–Mn bond to yield Me_3Sn· and ·$Mn(CO)_3L_2$ radicals according to

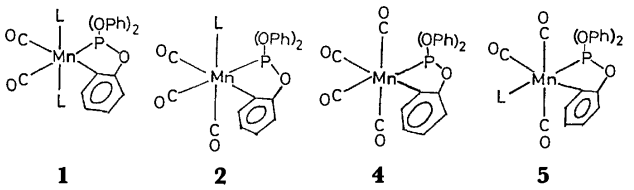

1 **2** **4** **5**

Fig. 1. Schematic pictures of orthometalated manganese carbonyl triphenylphosphite derivatives.

$$Me_3Sn\text{–}Mn(CO)_3L_2 \overset{h\nu}{\rightleftharpoons} Me_3Sn\cdot + \cdot Mn(CO)_3L_2, \quad (1)$$

(ii) the resulting 17-electron manganese carbonyl radical undergoes photochemical or thermal dissociation of the ligand, CO and/or L, according to

$$\cdot Mn(CO)_3L_2 \rightleftharpoons \cdot Mn(CO)_3L + L, \quad (2)$$

$$\cdot Mn(CO)_3L_2 \rightleftharpoons \cdot Mn(CO)_2L_2 + CO, \quad (3)$$

to generate 15-electron intermediates, and (iii) various steps which are likely to account for the formation of orthometalated products **1** and **2** and Me_3Sn–Mn(CO)$_4$L V as are described in Scheme 2 and Scheme 3.

In Scheme 2, the 15-electron intermediates play a key role to abstract hydrogen from a benzene ring in the triphenyl phosphite ligand, while in Scheme 3, the 17-electron radicals which are regenerated from the recombination of the 15-electron intermediates with CO or L abstract hydrogen from a benzene ring in the triphenyl phosphite ligand to form an orthometalated five-membered ring. Although the formations of **4** and Me_3Sn–$Mn(CO)_2L_3$ are expected for both Schemes, we could not isolate these products in spite of our repeated experiments. Me_3Sn–$Mn(CO)_2L_3$ may not be formed, since the steric congestion around the cis positions of the manganese atom toward the Sn–Mn bond, is detrimental to the formation of the Sn–Mn bond or this bond is easily cleaved by UV irradiation. On the other hand, no detection of **4** is enigmatic. Presumably, **4** eluded isolation because of its low yield. In order to differentiate the two schemes, we examined photolyses of orthometalated products, **2** and **5**[11] in benzene. The photolysis of **2** gave **1**, **4**, and **5** and the photolysis of **5** gave **1**, **2**, and **4**. These interconversions should proceed *via* dissociation of the ligand CO or L from the original orthometalated

$$\cdot Mn(CO)_2L_2 \longrightarrow (PhO)_2\overline{P(OC_6H_4)}\overline{Mn(CO)_2L} + 1/2\,H_2, \quad (4)$$

$$\cdot Mn(CO)_3L \longrightarrow (PhO)_2\overline{P(OC_6H_4)}\overline{Mn(CO)_3} + 1/2\,H_2, \quad (5)$$

$$(PhO)_2\overline{P(OC_6H_4)}\overline{Mn(CO)_2L} + L \rightleftharpoons (PhO)_2\overline{P(OC_6H_4)}\overline{Mn(CO)_2L_2}, \quad (6)$$

$$(PhO)_2\overline{P(OC_6H_4)}\overline{Mn(CO)_2L} + CO \rightleftharpoons (PhO)_2\overline{P(OC_6H_4)}\overline{Mn(CO)_3L}, \quad (7)$$

$$(PhO)_2\overline{P(OC_6H_4)}\overline{Mn(CO)_3} + L \rightleftharpoons (PhO)_2\overline{P(OC_6H_4)}\overline{Mn(CO)_3L}, \quad (8)$$

$$(PhO)_2\overline{P(OC_6H_4)}\overline{Mn(CO)_3} + CO \rightleftharpoons (PhO)_2\overline{P(OC_6H_4)}\overline{Mn(CO)_4}, \quad (9)$$

$$\cdot Mn(CO)_2L_2 + \cdot SnMe_3 \rightleftharpoons Me_3Sn\text{-}Mn(CO)_2L_2, \quad (10)$$

$$\cdot Mn(CO)_3L + \cdot SnMe_3 \rightleftharpoons Me_3Sn\text{-}Mn(CO)_3L, \quad (11)$$

$$Me_3Sn\text{-}Mn(CO)_2L_2 + CO \longrightarrow Me_3Sn\text{-}Mn(CO)_3L_2, \quad (12)$$

$$Me_3Sn\text{-}Mn(CO)_3L + CO \longrightarrow Me_3Sn\text{-}Mn(CO)_4L, \quad (13)$$

Scheme 2.

$$\cdot Mn(CO)_2L_2 + L \rightleftharpoons \cdot Mn(CO)_2L_3, \quad (14)$$

$$\cdot Mn(CO)_3L + CO \rightleftharpoons \cdot Mn(CO)_4L, \quad (15)$$

$$\cdot Mn(CO)_3L + L \rightleftharpoons \cdot Mn(CO)_3L_2, \quad (16)$$

$$\cdot Mn(CO)_3L + CO \rightleftharpoons \cdot Mn(CO)_4L, \quad (17)$$

$$\cdot Mn(CO)_2L_3 \longrightarrow (PhO)_2\overline{P(OC_6H_4)}\overline{Mn(CO)_2L_2} + 1/2\,H_2, \quad (18)$$

$$\cdot Mn(CO)_4L \longrightarrow (PhO)_2\overline{P(OC_6H_4)}\overline{Mn(CO)_4} + 1/2\,H_2, \quad (19)$$

$$\cdot Mn(CO)_3L_2 \longrightarrow (PhO)_2\overline{P(OC_6H_4)}\overline{Mn(CO)_3L} + 1/2\,H_2, \quad (20)$$

$$\cdot Mn(CO)_4L + \cdot SnMe_3 \longrightarrow Me_3Sn\text{-}Mn(CO)_4L, \quad (21)$$

$$\cdot Mn(CO)_3L_2 + \cdot SnMe_3 \rightleftharpoons Me_3Sn\text{-}(CO)_3L_2, \quad (22)$$

Scheme 3.

compounds to generate five-coordinate 16-electron intermediates such as those described in Eqs. 4 and 5, and *via* recombination of the intermediates with L or CO to afford six-coordinate products.[18] Thus, it seems reasonable to conclude that five-coordinate orthometalated products can exist with considerable life time. Along the line of this observation together with the reasons described below, we are rather inclined to propose that Scheme 2 represents plausible pathways of the photochemical reaction of Me_3Sn–$Mn(CO)_3L_2$; first, kinetic studies on the photochemical reactions of $Mn_2(CO)_{10}$ with various phosphines and phosphites demonstrated that disubstituted radicals of the type $\cdot Mn(CO)_3L'_2$ are produced during the photolysis, but there is no precedent, to our knowledge,

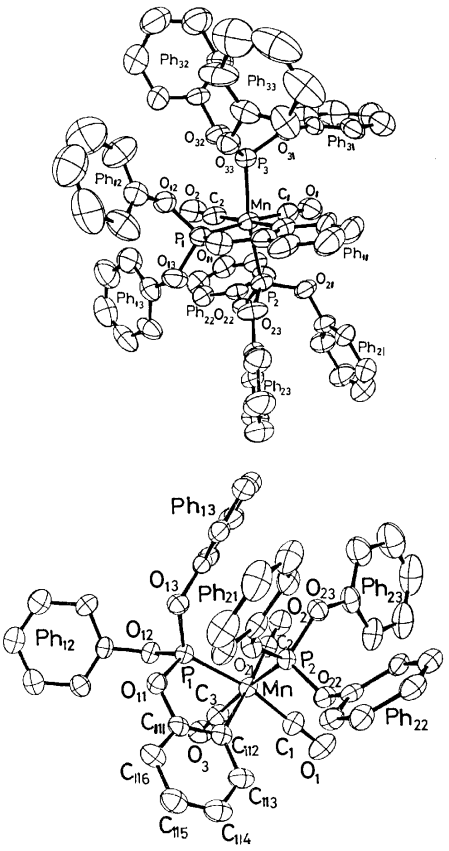

Fig. 2. Molecular structures and atom numbering schemes for **1** (Fig. 2(a)) and for **2** (Fig. 2(b)).

for trisubstituted radicals of the type $\cdot Mn(CO)_2L'_3$, especially for bulky L', the formation of which is mandatory before abstraction of the hydrogen in Scheme 3;[17] second, an ESR study showed that $\cdot Mn(CO)_3L'_2$ radical, which was formed by the photolysis of $Mn_2(CO)_{10}$ with L', possesses a square pyramidal structure where two L' groups occupy basal trans positions. In the present photochemical reaction, it seems certain that the resulting $\cdot Mn(CO)_3L_2$ radical from IV retains its trans geometry as in IV. Therefore, the main product must be **5** even though **5** is partly converted into its isomer **2** if the orthometalated products are formed directly from the 17-electron radical. In spite of this expectation, we could not isolate **5**.

Similar experiments were made for VI as for IV to confirm that the initial photochemical process is homolytic cleavage of the Sn–Mn bond. Photolysis of VI in CCl_4 produced *cis*-$ClMn(CO)_4L$, *mer-trans*-$ClMn(CO)_3L_2$, and a small amount of *fac-cis*-$ClMn(CO)_3L_2$. Photolysis of VI in air-saturated benzene did not afford orthometalated product **4** but gave several unidentified products instead. Photolysis of authentic $ClMn(CO)_4L$ in benzene gave *mer-trans*- and *fac-cis*-$ClMn(CO)_3L_2$. On the basis of these findings, we conclude that the initial photochemical process is homolytic cleavage of one of the Sn–Mn bonds to generate $\cdot Mn(CO)_4L$. Attempts to clarify the fate of the tin moiety have so far been fruitless.

X-Ray Molecular Structure Analyses of ***1*** *and* ***2***. The

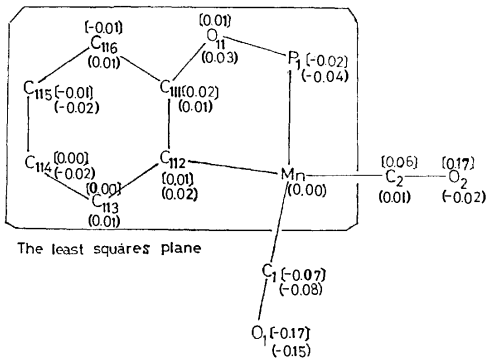

Fig. 3. The least-squares plane and the atom numbering scheme of five-membered orthometalated triphenylphosphite group and the deviations of each atom from the least squares plane; values in [ ] are for **1** and values in ( ) are for **2**.

TABLE 5(a). SELECTED BOND LENGTHS FOR **1**

Bond distance	l/Å	Bond distance	l/Å
Mn-P_1	2.208(3)	O_{11}-C_{111}	1.414(10)
Mn-P_2	2.193(3)	O_{12}-C_{121}	1.408(10)
Mn-P_3	2.204(3)	O_{13}-C_{131}	1.404(10)
Mn-C_{112}(Ph)	2.078(8)	O_{21}-C_{211}	1.429(10)
Mn-C_1	1.805(9)	O_{22}-C_{221}	1.419(10)
Mn-C_2	1.799(9)	O_{23}-C_{231}	1.399(10)
C_1-O_1	1.140(11)	O_{31}-C_{311}	1.401(10)
C_2-O_2	1.155(11)	O_{32}-C_{321}	1.415(10)
P_1-O_{11}	1.597(6)	O_{33}-C_{331}	1.427(10)
P_1-O_{12}	1.611(6)	C_{111}-C_{112}	1.410(12)
P_1-O_{13}	1.623(6)	C_{112}-C_{113}	1.412(12)
P_2-O_{21}	1.604(6)	C_{113}-C_{114}	1.438(14)
P_2-O_{22}	1.631(6)	C_{114}-C_{115}	1.426(15)
P_2-O_{23}	1.581(7)	C_{115}-C_{116}	1.392(14)
P_3-O_{31}	1.605(6)	C_{116}-C_{111}	1.402(13)
P_3-O_{32}	1.623(6)		
P_3-O_{33}	1.604(6)		

TABLE 5(b). SELECTED BOND LENGTHS FOR **2**.

Bond distance	l/Å	Bond distance	l/Å
Mn-P_1	2.220(2)	O_{11}-C_{111}	1.412(7)
Mn-P_2	2.225(2)	O_{12}-C_{121}	1.424(8)
Mn-C_{112}(Ph)	2.099(6)	O_{13}-C_{131}	1.402(7)
Mn-C_1	1.801(7)	O_{21}-C_{211}	1.419(8)
Mn-C_2	1.812(7)	O_{22}-C_{221}	1.423(7)
Mn-C_3	1.809(7)	O_{23}-C_{231}	1.400(8)
C_1-O_1	1.165(8)	C_{111}-C_{112}	1.391(9)
C_2-O_2	1.150(8)	C_{112}-C_{113}	1.428(9)
C_3-O_3	1.152(8)	C_{113}-C_{114}	1.413(10)
P_1-O_{11}	1.605(5)	C_{114}-C_{115}	1.396(10)
P_1-O_{12}	1.605(4)	C_{115}-C_{116}	1.425(10)
P_1-O_{13}	1.598(4)	C_{116}-C_{111}	1.388(9)
P_2-O_{21}	1.582(4)		
P_2-O_{22}	1.601(4)		
P_2-O_{23}	1.618(4)		

molecular structures and atom numbering schemes for **1** and **2** are shown in Fig. 2. The coordination at the manganese atom approximates to a distorted octahedron for both the molecules. The molecular structure of **2** is similar to that of **1** except that the triphenyl phosphite ligand (P_2) has been replaced by a carbonyl group CO(3). The chelating phosphite is coordinated to the manganese atom through both the phosphorus atom and an ortho carbon atom of one of the phenoxyl groups to form a five-membered ring (Fig. 3). The manganese, phosphorus, oxygen, and six carbon atoms in the orthometalated phenyl group are almost coplanar; the greatest deviation of any of these atoms from the least-squares planes is 0.019 Å for **1** and 0.039 Å for **2**. The carbonyl carbon atoms in CO(1)

TABLE 6(a). SELECTED BOND ANGLES FOR **1**

Bond angle	θ/°	Bond angle	θ/°
P_1-Mn-P_2	90.5(1)	Mn-P_2-O_{21}	111.9(2)
P_1-Mn-P_3	90.6(1)	Mn-P_2-O_{22}	122.4(2)
P_2-Mn-P_3	165.7(1)	Mn-P_2-O_{23}	114.7(2)
P_1-Mn-C_{112}	80.0(2)	Mn-P_3-O_{31}	122.5(2)
P_2-Mn-C_{112}	82.2(2)	Mn-P_3-O_{32}	111.3(2)
P_3-Mn-C_{112}	84.0(2)	Mn-P_3-O_{33}	118.0(2)
P_1-Mn-C_1	174.0(3)	Mn-C_{112}-C_{111}	117.5(6)
P_1-Mn-C_2	91.3(3)	Mn-C_{112}-C_{113}	126.9(6)
P_2-Mn-C_1	86.3(3)	P_1-O_{11}-C_{111}	113.5(5)
P_2-Mn-C_2	100.6(3)	P_1-O_{12}-C_{121}	128.2(5)
P_3-Mn-C_1	86.3(3)	P_1-O_{13}-C_{131}	126.9(5)
P_3-Mn-C_2	93.6(3)	O_{11}-C_{111}-C_{112}	119.5(7)
C_1-Mn-C_{112}	94.5(4)	O_{11}-C_{111}-C_{116}	113.7(7)
C_2-Mn-C_{112}	171.0(4)	C_{112}-C_{111}-C_{116}	126.7(8)
Mn-C_1-O_1	175.1(8)	C_{111}-C_{112}-C_{113}	115.6(8)
Mn-C_2-O_2	176.8(8)	C_{112}-C_{113}-C_{114}	120.5(8)
Mn-P_1-O_{11}	109.5(2)	C_{113}-C_{114}-C_{115}	119.7(9)
Mn-P_1-O_{12}	116.4(2)	C_{114}-C_{115}-C_{116}	121.3(9)
Mn-P_1-O_{13}	124.4(2)	C_{115}-C_{116}-C_{111}	116.2(9)

TABLE 6(b). SELECTED BOND ANGLES FOR **2**

Bond angle	θ/°	Bond angle	θ/°
P_1-Mn-P_2	91.9(1)	Mn-P_2-O_{21}	112.2(2)
P_1-Mn-C_{112}	78.7(2)	Mn-P_2-O_{22}	111.4(2)
P_2-Mn-C_{112}	82.4(2)	Mn-P_2-O_{23}	122.5(2)
P_1-Mn-C_1	168.9(2)	Mn-C_{112}-C_{111}	119.1(4)
P_1-Mn-C_2	97.6(2)	Mn-C_{112}-C_{113}	125.9(5)
P_1-Mn-C_3	87.9(2)	P_1-O_{11}-C_{111}	114.1(4)
P_2-Mn-C_1	90.2(2)	P_1-O_{12}-C_{121}	121.7(4)
P_2-Mn-C_2	96.7(2)	P_1-O_{13}-C_{131}	123.5(4)
P_2-Mn-C_3	170.9(2)	O_{11}-C_{111}-C_{112}	118.5(5)
C_1-Mn-C_{112}	90.8(3)	O_{11}-C_{111}-C_{116}	114.7(5)
C_2-Mn-C_{112}	176.1(3)	C_{112}-C_{111}-C_{116}	126.8(6)
C_3-Mn-C_{112}	88.6(3)	C_{111}-C_{112}-C_{113}	114.9(6)
Mn-C_1-O_1	179.0(6)	C_{112}-C_{113}-C_{114}	120.4(6)
Mn-C_2-O_2	177·5(6)	C_{113}-C_{114}-C_{115}	121.9(7)
Mn-C_3-O_3	178.9(6)	C_{114}-C_{115}-C_{116}	118.8(7)
Mn-P_1-O_{11}	109.4(2)	C_{115}-C_{116}-C_{111}	117.1(6)
Mn-P_1-O_{12}	114.2(2)		
Mn-P_1-O_{13}	127.0(2)		

and CO(2) are as much as 0.07 Å away for **1** and 0.08 Å away for **2**, respectively, from the least-squares plane (Fig. 3). Although the coplanarity is believed to suggest possible π-electron delocalization over the relevant ring, the bond lengths associated with this ring do not differ significantly from those in the monodentate triphenyl phosphite groups in the same molecule. The selected bond lengths and bond angles are collated in Tables 5 and 6. A comparison of corresponding bond lengths for **1** and **2** indicates that replacement of the triphenyl phosphite on the manganese atom in **1** with a carbonyl leads to significant elongation of the distances from the manganese atom to the phosphorus, carbonyl carbon, and the ortho carbon atoms of the phenyl ring. The Mn–P distances observed for **1** and **2** are considerably shorter than those in analogous triphenylphosphine manganese complexes, 2.279(3)—2.304(4) Å.[19] The Mn–C(phenyl) distances, 2.078(8)—2.099(6) Å, are similar to the generally found Mn–C distances, 2.001—2.097 Å for analogous manganese triphenylphosphine systems.[19] All bond angles relevant to the chelate ring are smaller than normal bond angles of the related atoms, especially the deviation from the ideal angle of 90° is significant in the P_1–Mn–C(phenyl) angles. This angle for **2** is slightly smaller than that of **1**. The two axial triphenyl phosphite groups (we define the plane containing the orthometalated benzene ring as an equatorial plane) are considerably bent toward the orthometalated benzene ring (the angle P_2–Mn–P_3 is 165.7(1)°). The deviation from 180° is supposed to minimize the steric repulsion of the two axial triphenyl phosphite groups with the benzene rings (Ph_{12} and Ph_{13}) in the equatorial triphenyl phosphite group. This deviation is somewhat relaxed in **2** when one of the axial triphenyl phosphite groups is replaced by CO.

Thanks are due to the Institute for Molecular Science for permission to use the AFC-5 automated X-ray diffractometer (the Instrument Center) and the computer (the Computer Center).

References

1) G. L. Geoffroy and M. S. Wrighton, "Organometallic Photochemistry," Academic Press (1979) and references therein.

2) S. Onaka, "Inorganic Photochemistry," ed by the Chemical Society of Japan (1983), Chap. III and references therein.

3) A. J. Cleland, S. A. Fieldhouse, B. H. Freeland, and R. J. O'Brien, *J. Organomet. Chem.*, **32**, C15 (1971); R. C. Job and M. D. Curtis, *Inorg. Chem.*, **12**, 2514 (1973); K. Triplett and M. D. Curtis, *ibid.*, **15**, 431 (1976); H. C. Clark and J. H. Tsai, *ibid.*, **5**, 1407 (1966); T. Foster, K. S. Chen, and J. K. S. Wan, *J. Organomet. Chem.*, **184**, 113 (1980).

4) a) S. Onaka, Y. Sasaki, and H. Sano, *Bull. Chem. Soc. Jpn.*, **44**, 726 (1971); b) S. Onaka, T. Miyamoto, and Y. Sasaki, *ibid.*, **44**, 1851 (1971); c) S. Onaka, *ibid.*, **44**, 2135 (1971); d) S. Onaka, *Chem. Lett.*, **1972**, 101; e) S. Onaka and H. Sano, *Bull. Chem. Soc. Jpn.*, **45**, 1271 (1972); S. Onaka, *Nippon Kagaku Kaishi*, **1972**, 1978; g) Y. Kume, D. Nakamura, M. Kubo, and S. Onaka, *J. Magn. Reson.*, **10**, 58 (1973); h) S. Onaka, *Bull. Chem. Soc. Jpn.*, **46**, 2444 (1973); i) S. Onaka, *Bull. Nagoya Inst. Tech.*, **1973**, 133; j) S. Onaka, *Nippon Kagaku Kaishi*, **1974**, 255; k) S. Onaka, *J. Inorg. Nucl. Chem.*, **36**, 1721 (1974); l) S. Onaka, *Bull. Chem. Soc. Jpn.*, **48**, 319 (1975); m) S. Onaka and H. Sano, *ibid.*, **48**, 258 (1975); n) S. Onaka, Y. Yoshikawa, and H. Yamatera, *J. Organomet. Chem.*, **157**, 187 (1978); o) S. Onaka, *Chem. Lett.*, **1978**, 1163; p) S. Onaka, Y. Kondo, N. Furuichi, and K. Toriumi, *ibid.*, **1980**, 1343; q) S. Onaka, Y. Kondo, K. Toriumi, and T. Ito, *ibid.*, **1980**, 1605.

5) J. C. Luong, R. A. Faltynek, and M. S. Wrighton, *J. Am. Chem. Soc.*, **102**, 7892 (1980).

6) C. L. Reichel and M. S. Wrighton, *Inorg. Chem.*, **19**, 3858 (1980).

7) D. Drew, D. J. Darensbourg, and M. Y. Darensbourg, *Inorg. Chem.*, **14**, 1579 (1975).

8) M. Y. Darensbourg., D. J. Darensbourg, and D. Drew, *J. Organomet. Chem.*, **73**, C25 (1974).

9) R. J. McKinney, R. Hoxmeier, and H. D. Kaesz, *J. Am. Chem. Soc.*, **97**, 3059 (1975).

10) ν(CO) of **3** in $CHCl_3$ is almost identical with that of authentic *mer-trans*-$XMn(CO)_3L_2$ (X=Cl and Br). We suspected at first that a trace amount of the starting material $BrMn(CO)_3L_2$ to synthesize IV is the origin of **3**. However, this possibility is excluded since it was not employed for the synthesis of VI. All the attempts including X-ray molecular structure analysis has so far been fruitless for characterizing this yellow crystal.

11) This product was obtained from the photolysis of $MeMn(CO)_3L_2$. Details of the photochemical reactions of this compound and related compounds will appear in a subsequent paper.

12) R. A. Angelici, F. Basolo, and A. J. Pöe, *J. Am. Chem. Soc.*, **97**, 6042 (1975).

13) T. Sakurai and K. Kobayashi, *Rikagaku Kenkyusho Hokoku (Rept. Inst. Phys. Chem.)*, **55**, 69 (1979).

14) R. A. Levenson and H. B. Gray, *J. Am. Chem. Soc.*, **97**, 6042 (1975).

15) D. L. Morse and M. S. Wrighton, *J. Am. Chem. Soc.*, **98**, 3931 (1976).

16) It is a reasonable question that why V is inert to photoexcitation despite that V shows a spectrum similar to that of IV. To this question, we propose a rationale that the Sn–Mn bond in V is stronger than that of IV[41,4m] and that the Sn–Mn bond in V is not readily cleaved.

17) M. S. Wrighton and D. Bredensen, *J. Organomet. Chem.*, **50**, C35 (1973); M. S. Wrighton and D. S. Ginley, *J. Am. Chem. Soc.*, **97**, 2065 (1975); D. R. Kidd, C. P. Cheng, and T. L. Brown, *ibid.*, **100**, 4095, 4103 (1978).

18) For an alternative mechanism, one may think of dissociation of the bidentate triphenyl phosphite ligand, which regenerates free triphenyl phosphite ligand, or simple cleavage of the Mn–C(phenyl) bond, which generates "semi-free" triphenyl phosphite and then produces free triphenyl phosphite ligand. However, this mechanism is less likely, because we could not isolate either **1** or **2** or **5** from the prolonged photolysis of **4**. Presumably the five-membered metalation ring is sterically favorable and resists dissociation.[9]

19) R. J. McKinney, C. B. Knobler, B. T. Huie, and H. D. Kaesz, *J. Am. Chem. Soc.*, **99**, 2988 (1977) and references therein.

 © 1983 The Chemical Society of Japan Bull. Chem. Soc. Jpn., 56, 95—98 (1983)

The Preparation and Some Properties of Cobalt(II) Schiff Base Complexes and Their Molecular Oxygen Adducts

Kuninobu KASUGA,* Takeo NAGAHARA, Akira TSUGE,
Kunihisa SOGABE,† and Yasuo YAMAMOTO

Department of Chemistry, Faculty of Science, Shimane University, Matsue 690
† *Department of Chemistry, Faculty of Education, Shimane University, Matsue 690*

(Received April 10, 1982)

Seven new cobalt(II) complexes with a tetradentate Schiff base and their three oxygen adducts were synthesized. The adducts were stable at room temperature for several weeks. The isolated oxygen adducts showed intense new bands in the 1130—1150 cm^{-1} range characteristic of superoxide-like 1:1 oxygenated metal complexes. The ESR spectra of the adducts showed eight-lined, hyperfine structures with a very small splitting (10—20 G)** at 77 K. The adducts obtained were identified as monomeric 1:1 oxygen species, two complexes of which showed a reversible oxygenation in a 1,2-dichloroethane solution at 6 °C.

Cobalt(II) complexes with Schiff base have received considerable attention as biomimic model compounds for oxygen-carrying and storage proteins, such as hemoglobin and myoglobin.[1] Recently, many investigators have devoted their efforts to elucidate the mechanism of the oxygenation of the cobalt(II) complexes.[2-8] For instance, Basolo *et al.* reported that the electron density on a central cobalt(II) ion of the Schiff base complexes is an important factor in determining the oxygen affinity of the complexes.[3] The crystal structures of oxygen adducts of cobalt(II) Schiff base complexes with some peripheral groups in their ligand have also been determined by means of X-ray-diffraction analysis in order to elucidate the influence of the change in the substituents of the in-plane ligand on the cobalt-oxygen geometry.[9,10]

To date, many studies of the adducts of cobalt(II) Schiff base complexes have been published, but only a few monomeric 1:1 oxygen adducts are known to be stable at room temperature.[5,10-12] Therefore, it is of interest to elucidate the factors which determine the stability of the monomeric 1:1 oxygen adduct in the solid state; it is also important to prepare the adduct in order to improve the biomimic model system.

Seven new cobalt(II) complexes with a Schiff base derived from *N,N'*-bis(1-methyl-3-oxobutylidene)ethylenediamine (A-H) and *N,N'*-bis(1-methyl-3-oxo-3-phenylpropylidene)ethylenediamine (B-H) were synthesized; three of these complexes formed stable monomeric 1:1 oxygen adducts in the solid state. We wish to report here that the isolation of the stable oxygen adducts is affected by the kinds of peripheral groups and that the oxygen affinity of the complexes in solution is also dependent on the groups.

Experimental

Syntheses. Schiff Base Ligands: The ligands of A-Cl, A-succ, A-OPh, B-Cl, and B-succ were obtained by the elimination of metal with hydrogen sulfide from their copper(II) complexes, as has been described previously.[13,14] A-CONHPh and B-CONHPh were synthesized according to the method reported by Howells *et al.*[15]

Co(A-Cl): After A-Cl (1.2 g) had been suspended in 25 cm^3 of an ethanol solution saturated with potassium hydroxide, cobalt(II) acetate tetrahydrate (0.6 g) was added to the solution. Then, the solution was refluxed for 20 min under a nitrogen atmosphere, resulting in orange precipitates. The precipitates thus obtained were washed with ethanol and subsequently recrystallized from chloroform and small amounts of hexane. The other complexes were synthesized by a similar method.

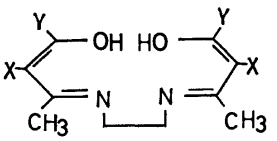

	X =	Y =
A-H,	hydrogen	methyl
A-Cl,	chloro	methyl
A-succ,	succinimido	methyl
A-OPh,	phenoxy	methyl
A-CONHPh,	phenylcarbamoyl	methyl
B-H,	hydrogen	phenyl
B-Cl,	chloro	phenyl
B-succ,	succinimido	phenyl
B-CONHPh,	phenylcarbamoyl	phenyl

Fig. 1. Abbreviation of Schiff base ligands.

Oxygen Adducts of Co(A-Cl): By bubbling air through 10 cm^3 of an acetone solution of Co(A-Cl) (0.2 g) in the presence of small amounts of pyridine at 0 °C for several min, a dark-red oxygenated compound was precipitated. The precipitates were subsequently washed with ether and dried in air. The adducts of Co(A-succ) and Co(B-succ) were also obtained by a similar method. In the case of the other complexes, no oxygenated adducts were isolated.

Measurements. The ^{1}H-NMR spectra were recorded with a JEOL-MH 100 spectrophotometer at a frequency of 100 MHz. The chemical shifts were determined in ppm, using TMS as the internal standard. The electronic spectra in solution and the infrared spectra using Nujol-mull methods were measured on a Hitachi 124 spectrophotometer and a Hitachi 215 spectrophotometer respectively. The ESR spectra (X-band) were measured with a JEOL-1X spectrometer. The reversible oxygenation in a 1,2-dichloroethane solution was observed by means of the method reported by Kubokura *et al.*[5]

Results and Discussion

^{1}H-NMR Spectra of Ligands. The ^{1}H-NMR spectra of the ligands obtained are shown in Table 1.

** 1 G = 10^{-4} T.

TABLE 1. ^{1}H-NHR SPECTRA OF FREE LIGANDS IN 1,2-DICHLOROETHANE-d_4 (ppm)

Ligand	δ_{succ}	δ_{CH_3}	δ_{CH_2}	δ_{CH}	δ_{Ph}	δ_{CHN}
A-H		1.86(d, 12H)	3.30(s, 4H)	4.92(s, 2H)		
A-Cl		2.16(d, 12H)	3.36(s, 4H)			
A-succ	2.84(s, 8H)	1.80(d, 12H)	3.52(br s, 4H)			
A-OPh		1.79(d, 12H)	3.42(m, 4H)		7.17(t, 16H) 7.53(t, 14H)	
A-CONHPh[a]		2.10(s, 12H)	3.63(s, 4H)		7.11—7.77 (m, 10H)	10.20(s, 2H)
B-H		2.13(s, 6H)	3.63(br s, 4H)	5.85(s, 2H)	7.59(s, 6H) 8.04(s, 4H)	
B-Cl		2.34(s, 6H)	3.69(m, 4H)		7.59(m, 6H) 7.74(m, 4H)	
B-succ	1.96(s, 8H)	2.50(m, 6H)	3.68(br s, 4H)		7.24(br s, 10H)	
B-CONHPh[a]		2.25(br s, 6H)	3.78(br s, 4H)		7.32(m, 20H)	10.02(s, 2H)

a) In dimethyl-d_6 sulfoxide. s=Singlet, d=doublet, t=triplet, m=multiplet, and br=broad.

TABLE 2. ELEMENTAL ANALYSES AND YIELDS OF THE COBALT(II) COMPLEXES AND THEIR OXYGEN ADDUCTS

Compound	Found(%)			Calcd(%)			Yield	Absorption λ_{max}/nm (log ε)	
	C	H	N	C	H	N	%		
Co(A-Cl)	40.95	4.44	8.18	40.93	5.15	7.96	24	392(3.30)	475^{sh} (2.41)
Co(A-succ)	49.94	5.22	11.05	50.53	5.09	11.79	88	382(3.58)	455^{sh} (3.02)
Co(A-OPh)	62.17	5.55	6.16	61.94	5.63	6.02	90	396(3.44)	460^{sh} (2.40)
Co(A-CONHPh)	59.85	5.56	10.90	60.11	5.54	10.79	32	390^{sh} (3.32)	450^{sh} (3.01)
Co(B-Cl)	55.73	4.13	6.02	55.72	4.25	5.91	27	411(3.48)	490^{sh} (2.72)
Co(B-succ)	59.36	4.67	9.45	60.10	4.71	9.35	93	394(3.83)	455^{sh} (3.38)
Co(B-CONHPh)	65.50	4.65	8.27	65.15	4.87	8.44	45	360^{sh} (4.04)	450^{sh} (3.20)
Co(A-Cl)pyO_2	44.43	4.50	8.97	44.27	4.59	9.14	26	370	
Co(A-succ)pyO_2	51.09	5.25	11.26	51.21	4.98	11.94	56	355, 525	
Co(B-succ)pyO_2	58.88	5.02	9.25	59.15	4.68	9.86	65	360, 525	

py=Pyridine. Yields are mole percentages. sh=Shoulder.

The ^{1}H-NMR signals arising from the methine protons of the parent ligands, A-H and B-H, disappear in their derivatives, indicating the displacement of the methine protons in the derivatives. The ^{1}H-NMR signals of the succinimido groups in A-succ appear at lower magnetic fields than those of its methyl groups. On the other hand, the signals of the succinimido groups in B-succ are shifted to higher magnetic fields compared with those of its methyl groups. This may result from the effect of a ring current of phenyl groups in B-succ. The inductive effects of chloro and phenylcarbamoyl groups in A-Cl, A-CONHPh, B-Cl, and B-CONHPh shift ^{1}H-NMR signals of their methine and methyl protons to lower magnetic fields compared with their parent ligands.

Cobalt(II) Complexes and Their Oxygen Adducts. While Co(A-Cl) and Co(B-Cl) were dark reddish crystals, the other complexes were yellow or yellowish orange. The yellow Co(A-OPh) complex gradually changed to dark brown in polar-solvent moistures. The molecular oxygen adducts of the cobalt(II) complexes with A-Cl, A-succ, and B-succ were isolated and were stable at room temperature for several weeks (the stability was checked by means of the IR spectra). These adducts are sparingly soluble in common organic solvents. On the other hand, the adducts of the other cobalt(II) complexes could not be isolated, not even below 0 °C. When *N*-methylimidazole was employed instead of pyridine, no adducts were isolated. That is, the acetone solution of the complexes containing small amounts of the bases turned dark red when air bubbled in. Subsequently, reddish, tarry substances were formed by the condensation of the solution under reduced pressure or by the addition of hexane to the solution, but no adducts were isolated. The suitable solubility of a complex into a solution containing small amounts of the base seems to be one of the key factors for isolating the oxygen adduct. The results of elemental analyses, the yields, and the electronic spectra of the cobalt(II) complexes and some of their adducts are listed in Table 2.

The infrared spectra of the isolated adducts are shown in Fig. 2. The adducts show intense new bands arising from O–O stretching vibrations in the 1130—1150 cm^{-1} range characteristic of superoxide-like 1:1 oxygenated metal complexes.[1] The oxygenated complexes with succinimide-substituted, Schiff base complexes, Co(A-succ)pyO_2 and Co(B-succ)pyO_2, each show two ν_{O_2} bands. Such an appearance of the doublet of ν_{O_2} was also found in the oxygen adduct of cobalt(II) picket-fence porphirin with 1-tritylimidazole; it was due to two different conformers of molecular oxygen and to the base orientations.[16] In the case of the succinimide derivatives, the carbonyl groups

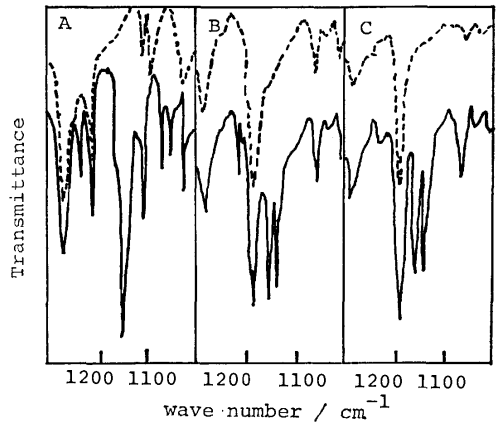

Fig. 2. IR spectra of the complexes and their oxygen adducts.
A: Co(A-Cl), B: Co(A-succ), C: Co(B-succ), ----: complex, ——: oxygen adduct.

vicinal to the imide residues might fix the plane of pyridine with dipole-dipole interactions, resulting in the two conformers.

The ESR data of the adducts were obtained in a 1,2-dichloromethane solution by the use of the X band at 77 K (Table 3). The spectra indicate two signals of $g//$ and $g_\perp$, and each signal consistents of eight lines due to the hyperfine splitting of ^{59}Co nucleus. The eight-lined hyperfine structures with the very small splitting indicate that the 1:1 oxygen adducts are isolated; this is consistent with the results of the IR data.

Reversible Oxygenation. Spectral changes were recorded for a 1,2-dichloroethane solution of Co(A-succ) containing 1% pyridine at different partial pressures of oxygen at 6.0±0.4 °C in order to estimate the oxygen uptake (1):

$$\text{Co(A-succ)py} + \text{O}_2 \overset{K_{\text{O}_2}}{\rightleftharpoons} \text{Co(A-succ)py}\text{O}_2. \quad (1)$$

A new absorption was observed at 525 nm when the complex was oxygenated. The intensity of the band increased with an increase in the partial pressure of oxygen. Subsequently, the original spectrum was recovered by bubbling a nitrogen gas through the solution. The stability constant for oxygenation, K_{O_2} is given by this relation:

$$P_{\text{O}_2} = -1/K_{\text{O}_2} + (\varepsilon_2-\varepsilon_1)[\text{Co(A-succ)}]_t P_{\text{O}_2}/A - A_\text{o}, \quad (2)$$

where A and A_o are the absorbances at 525 nm in the absence of oxygen and at the proper partial pressure of oxygen; ε_1 and ε_2 are the molar absorption coefficients of Co(A-succ)py and Co(A-succ)pyO_2; P_{O_2} is the partial pressure of oxygen; $[\text{Co(A-succ)}]_t$ is the total concentration of the complex. The plot of P_{O_2} against $P_{\text{O}_2}/A-A_\text{o}$ gave a straight line with a slope nearly equal to 1 (Fig. 3). This indicates that the monomeric oxygen adduct is formed in the solution, consistent with the isolation of the monomeric oxygen adduct. The value of $\log K_{\text{O}_2}$ (−2.48±0.01/Torr^{-1}) (1 Torr=133.322 Pa) was also obtained from the intercept of the line. In a similar manner, the value of $\log K_{\text{O}_2}$ (−2.85±0.02/Torr^{-1}) for Co(B-succ) was obtained. In spite of the isolation of the oxygen adduct,

Table 3. The results of IR and ESR spectral data for the oxygen adducts

Adduct	ν_{O_2}/cm^{-1} (Nujol mull)	$g//$	$g_\perp$	$A//$/G	$A_\perp$/G
Co(A-Cl)pyO_2	1141	2.079	1.999	17.5	13.8
Co(A-succ)pyO_2	1136, 1152	2.079	1.999	18.8	13.0
Co(B-succ)pyO_2	1132, 1150	2.079	1.996	17.5	12.5

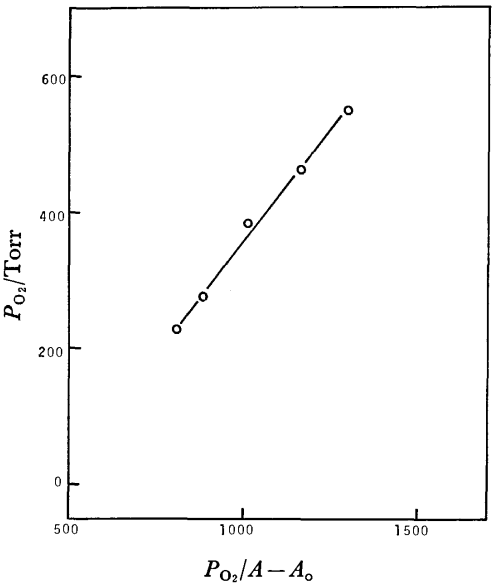

Fig. 3. Plots of P_{O_2} *versus* $P_{\text{O}_2}/A-A_\text{o}$ for the reversible oxygenation of Co(A-succ) (3.4×10^{-4} mol dm^{-3}) in a 1,2-dichloroethane solution containing 1% pyridine at 6.0±0.4 °C.

the reversibility of Co(A-Cl) was not confirmed under the present conditions.

While the phenyl groups in Co(B-succ) withdraw an electron from the chelate ring, resulting in a decrease in the electron density on the cobalt(II) ion, the methyl groups in Co(A-succ) increase the electron density on the cobalt(II) ion and stabilize the binding between the cobalt(II) ion and molecular oxygen. This may stabilize the adduct of Co(A-succ) more strongly than that of Co(B-succ) in solution.

Although the stability of the adduct of Co(A-H) in solution ($\log K_{\text{O}_2}=-2.08\pm0.03$/Torr^{-1} in a toluene solution at 0 °C) is larger than those of Co(A-succ) and Co(B-succ), the adduct of Co(A-H) releases molecular oxygen in the solid state above 0 °C.[17] On the other hand, the adduct of Co(B-H) is relatively stable in the solid state in spite of its low oxygen affinity in solution.[18] This has been explained by means of the coplanarity of the phenyl substituents with the Schiff base cobalt(II) system in the solid state; a π electron donation to the cobalt(II) ion from the π system in the phenyl groups stabilizes the binding between the cobalt(II) ion and molecular oxygen.[19]

However, judging from the fact that the oxygen adducts of Co(A-Cl), Co(A-succ), and Co(B-succ) are stable in the solid state at room temperature, there seem to be predominant factors for stabilizing the adducts in the solid state other than the electronic factor. More detailed studies will be performed in order to

elucidate these factors.

This work was partially supported by a Grant-in-Aid for Scientific Research No. 00547042 from the Ministry of Education, Science and Culture.

References

1) R. D. Jones, D. A. Summerville, and F. Basolo, *Chem. Rev.*, **96**, 139 (1979).
2) B. M. Hoffman, D. L. Diemente, and F. Basolo, *J. Am. Chem. Soc.*, **92**, 61 (1970).
3) M. J. Carter, D. P. Rillema, and F. Basolo, *J. Am. Chem. Soc.*, **96**, 392 (1974).
4) B. S. Torrog, D. J. Kitko, and R. S. Drago, *J. Am. Chem. Soc.*, **98**, 5144 (1976).
5) K. Kubokura, H. Okawa, and S. Kida, *Bull. Chem. Soc. Jpn.*, **51**, 2036 (1978).
6) L. S. Chen, M. K. Koehler, C. P. Pestel, and S. C. Cummings, *J. Am. Chem. Soc.*, **100**, 7243 (1978).
7) K. Miyokawa and I. Matsuda, *J. Inorg. Nucl. Chem.*, **43**, 1495 (1981).
8) M. Suzuki, T. Ishiguro, M. Kozuka, and K. Nakamoto, *Inorg. Chem.*, **20**, 1993 (1981).
9) W. P. Schaefer, B. T. Huie, M. G. Kurilla, and S. E. Ealick, *Inorg. Chem.*, **19**, 340 (1980).
10) B. T. Huie, R. M. Leyden, and W. P. Schaefer, *Inorg. Chem.*, **18**, 125 (1979), and the articles cited therein.
11) C. Floriani and F. Calderazzo, *J. Chem. Soc., A*, **1969**, 946.
12) J. D. Landels and G. A. Rodley, *Synth. Inorg. Metal-Org. Chem.*, **2**, 65 (1972).
13) T. Nagahara, K. Kasuga, and Y. Yamamoto, *Inorg. Chim. Acta*, **47**, 37 (1981).
14) T. Nagahara, K. Kasuga, and Y. Yamamoto, *Inorg. Nucl. Chem. Lett.*, **17**, 235 (1981).
15) P. N. Howells, J. W. Kenny, J. H. Nelson, and R. A. Henry, *Inorg. Chem.*, **15**, 124 (1976).
16) J. P. Collman, J. I. Brauman, T. R. Halbert, and K. S. Suslick, *Proc. Natl. Acad. Sci. U.S.A.*, **73**, 3333 (1976).
17) A. L. Crumbliss and F. Basolo, *J. Am. Chem. Soc.*, **92**, 55 (1970).
18) M. J. Carter, D. P. Rillema, and F. Basolo, *J. Am. Chem. Soc.*, **96**, 392 (1974).
19) G. A. Rodley and W. T. Robinson, *Nature*, **235**, 438 (1972).

 © 1983 The Chemical Society of Japan Bull. Chem. Soc. Jpn., 56, 99—104 (1983)

The Dehydrogenation of Nickel(II) Chelates of *rac*- and *meso*-2,2′-[(1,2-Diphenylethylene)bis(iminomethylene)]diphenol and Related Compounds

Hajime KANATOMI

Laboratory of Chemistry, College of General Education, Kyushu University, Ropponmatsu, Chuo-ku, Fukuoka 810

(Received April 24, 1982)

Nickel(II) acetate tetrahydrate and *rac*- and *meso*-2,2′-[(1,2-diphenylethylene)bis(iminomethylene)]diphenol (*rac*- and *meso*-BzPhen-H_2) formed pale green complexes in methanol. A pyridine solution of these complexes deposited deep red diimine complexes after prolonged heating under aerobic conditions. The saturated ligand system of the initial complexes was dehydrogenated to an unsaturated one by molecular oxygen. From the pyridine solution of the *meso*-isomer, [2,2′-{(*cis*-1,2-diphenylethenylene)bis(nitrilomethylidyne)}diphenolato]nickel(II) ([Ni(SalStil)]) was isolated in addition to the diimine complex ([Ni(*meso*-SalPhen)]). In this case, the –HN–CH–CH–NH– bridge was dehydrogenated to =N–C=C–N= conjugated double bonds; that is, a fully conjugated metal chelate was formed by the dehydrogenation of the coordinated ligand.

The dehydrogenation of coordinated ligands has become of interest in recent years, and several reports have been published concerning the dehydrogenation of macrocyclic polyamines to polyimines,[1,2] of aliphatic 1,2-diamines to 1,2-diimines,[3,4] of primary amines to nitriles,[5,6] and of 3,3′,4,4′-tetrahydro-2,2′-bi-2*H*-benzoxazines to fully conjugated metal chelates.[7]

In these oxidations the net reaction is considered to necessarily involve the prior oxidation of a metal ion to unstable, higher oxidation states, followed by the oxidation of the ligands and the reduction of the metal ion. In practice, iron(III) and ruthenium(III) complexes were isolated as intermediates of the dehydrogenation described below:

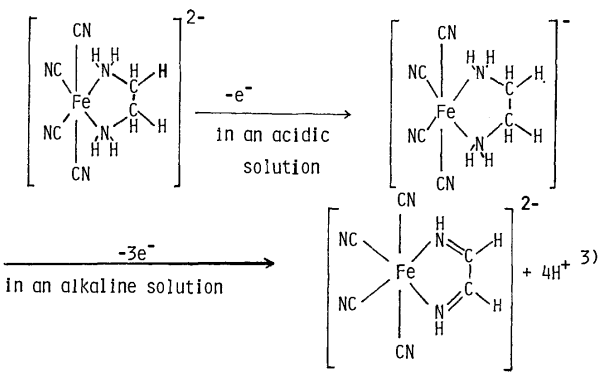

$$[(bipy)_2Ru(en)]^{2+} \xrightarrow{-e^-} [(bipy)_2Ru(en)]^{3+}$$

$$\xrightarrow{-3e^-} [(bipy)_2Ru(diimine)]^{2+} + 4H^+ \ ^{4)}$$

Macrocyclic tetramine complexes were oxidized to imine complexes of varying degrees of unsaturation, depending upon the reaction conditions. Iron(II) complexes were readily dehydrogenated by molecular oxygen,[1,3] while nickel(II) complexes generally required stronger oxidizing reagents such as Br_2 or HNO_3.[3] In the present case, nickel(II) complexes undergo dehydrogenation under mild conditions.

The structures and abbreviations of nickel(II) chelates are given in Fig. 1.

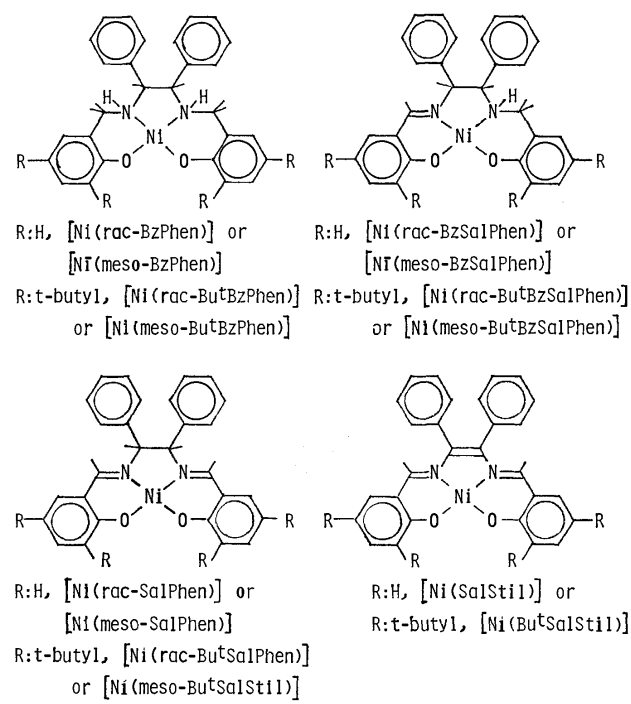

Fig. 1. Structural formulas and abbreviations for starting materials and oxidized products.

Experimental

The analytical data for the free ligands and the nickel(II) chelates are listed in Tables 1 and 2. All the nickel(II) chelates were dried under a vacuum over P_2O_5 at 50 °C.

General Procedure for the Preparation of rac- *and* meso-*BzPhen-H_2, and* rac- *and* meso-*But BzPhen-H_2.* A Schiff base (5 g) was dissolved in pyridine (200 cm³) and to the resulting yellow solution crystals of sodium borohydride were added in small portions on a water bath until the yellow color of the solution disappeared. The reaction mixture was then evaporated to about 50 cm³ under reduced pressure. To the resulting syrup was added dilute acetic acid (300 cm³). The white crystals which separated out were collected by suction and washed with water. The solvents used for recrystallization and the yield of each ligand are listed in Table 1.

N-*(2-Hydroxybenzyl)*-N′-*salicylidene*-meso-*1,2-diphenylethylenedi-*

TABLE 1. ANALYTICAL DATA FOR THE LIGANDS

Compound	Formula	Calcd(%)			Found(%)			Yield	Recryst solvents
		C	H	N	C	H	N	%	
rac-BzPhen-H_2	$C_{28}H_{28}N_2O_2$	79.21	6.65	6.60	79.28	6.77	6.60	80	Pyridine-Water
meso-BzPhen-H_2	$C_{28}H_{28}N_2O_2$	79.21	6.65	6.60	79.12	6.55	6.87	75	Pyridine-Water
meso-BzSalPhen-H_2	$C_{28}H_{26}N_2O_2$	79.60	6.20	6.63	79.31	6.15	6.66		Methanol
rac-Bu^{t}BzPhen-H_2	$C_{44}H_{60}N_2O_2$	81.43	9.37	4.32	81.16	9.24	4.46	60	Chloroform-Methanol
meso-Bu^{t}BzPhen-H_2	$C_{44}H_{60}N_2O_2$	81.43	9.37	4.32	81.37	9.28	4.56	65	Chloroform-Methanol

TABLE 2. ANALYTICAL DATA FOR NICKEL(II) CHELATES

Compound	Formula	Calcd(%)			Found(%)		
		C	H	N	C	H	N
[Ni(*rac*-BzPhen)]	$C_{28}H_{26}N_2O_2Ni\cdot 2H_2O$	65.68	5.91	5.47	65.47	5.66	5.05
[Ni(*meso*-BzPhen)]	$C_{28}H_{26}N_2O_2Ni\cdot 3/2\,H_2O$	66.17	5.57	5.51	66.34	5.64	5.25
[Ni(*rac*-BzSalPhen)]	$C_{28}H_{24}N_2Ni$	70.18	5.05	5.85	69.91	4.99	5.84
[Ni(*meso*-BzSalPhen)(py)]	$C_{28}H_{24}N_2O_2Ni\cdot C_5H_5N$	70.99	5.24	7.53	71.20	5.21	7.51
[Ni(*meso*-Bu^{t}BzSalPhen)]	$C_{44}H_{56}N_2O_2Ni\cdot 3/2\,H_2O$	72.23	8.13	3.83	72.65	8.14	3.98
[Ni(*rac*-Bu^{t}SalPhen)]	$C_{44}H_{54}N_2O_2Ni$	75.32	7.76	3.99	75.10	7.80	3.94
[Ni(*meso*-Bu^{t}SalPhen)]	$C_{44}H_{54}N_2O_2Ni$	75.32	7.76	3.99	75.16	7.82	3.98
[Ni(SalStil)]	$C_{28}H_{20}N_2O_2Ni$	70.77	4.24	5.90	70.90	4.17	6.01
[Ni(Bu^{t}SalStil)]	$C_{44}H_{52}N_2O_2Ni$	75.54	7.49	4.00	75.38	7.49	4.07

*amine (*meso-*BzSalPhen-*H_2*)*. *N*-Benzylidene-*N'*-benzoyl-*meso*-1,2-diphenylethylenediamine[8] (8 g, 0.02 mol) was suspended in concentrated hydrochloric acid (130 cm^3), and the mixture was heated on a water bath for 2 h. After cooling, a colorless precipitate was collected by filtration; from this precipitate *N*-benzoyl-*meso*-1,2-diphenylethylenediamine hydrochloride (1) was extracted by the use of hot methanol (200 cm^3). *N*-Benzoyl-*N'*-salicylidene-*meso*-1,2-diphenylethylenediamine (2) was prepared as colorless crystals from (1) and salicylaldehyde using the ordinary method. (2) was reduced to *N*-benzoyl-*N'*-(2-hydroxybenzyl)-*meso*-1,2-diphenylethylenediamine (3) with sodium borohydride as has been described above. (3) was hydrolyzed by concentrated hydrochloric acid on prolonged heating (24 h) to afford *N*-(2-hydroxybenzyl)-*meso*-1,2-diphenylethylenediamine (4). (4) was then treated with salicylaldehyde to give *N*-(2-hydroxybenzyl)-*N'*-salicylidene-1,2-diphenylethylenediamine (*meso*-BzSalPhen-H_2) as pale yellow crystals, which were subsequently recrystallized from methanol. Yield, 2.5 g.

Preparation of Nickel(II) Complexes. [*Ni(*rac-*BzPhen)*]: *rac*-BzPhen-H_2 (420 mg, 1 mmol) and nickel(II) acetate tetrahydrate (240 mg, 1 mmol) were dissolved in hot methanol (40 cm^3), and the resulting light green solution was allowed to stand overnight at room temperature. The light blue crystals which separated out were collected by filtration and washed with methanol. Yield, 450 mg.

[*Ni(*meso-*BzPhen)*]: *meso*-BzPhen-H_2 (210 mg, 0.5 mmol) and nickel(II) acetate tetrahydrate (120 mg, 0.5 mmol) were dissolved in gently boiling methanol (15 cm^3), after which 4 drops of a 20% sodium hydroxide solution were added to the solution. The pale green crystals which immediately separated out from the pink solution were collected by filtration and washed with methanol. Yield, 200 mg.

[*Ni(*meso-*BzSalPhen)(py)*]: *meso*-BzSalPhen-H_2 (210 mg, 0.5 mmol) and nickel(II) acetate tetrahydrate (120 mg, 0.5 mmol) were dissolved in pyridine (10 cm^3) and water was added to the resulting red solution until it began to become turbid. After the solution had stood several hours, the orange-red crystals which separated out were collected by filtration and washed with pyridine–water. Yield, 180 mg.

[*Ni(*meso-*BzSalPhen)(py)*] *from* [*Ni(*meso-*BzPhen)*]: To a solution of *meso*-BzPhen-H_2 (420 mg, 1 mmol) in acetone (30 cm^3) was added nickel(II) acetate tetrahydrate (240 mg, 1 mmol) in methanol (20 cm^3). To the resulting pale green solution, a 20% sodium hydroxide solution was then added dropwise until the solution turned deep red. After standing overnight at room temperature, the solution was placed in 100-cm^3 flask equipped with a gas inlet tube and a condenser. Air was continuously bubbled through the solution for 5 h at room temperature. After then removing the condenser, the volume of the solution was reduced to 10 cm^3 by air bubbling. The resulting orange-red precipitate was collected by filtration, washed with water, and dissolved in methanol (20 cm^3). The insoluble products were removed by filtration, and the filtrate was evaporated to dryness. The orange-red residue was recrystallized from pyridine–water. Yield, 200 mg (42%).

[*Ni(*meso-*Bu^{t}BzSalPhen)*] *from* [*Ni(*meso-*Bu^{t}BzPhen)*]: *meso*-Bu^{t}BzPhen-H_2 (650 mg, 1 mmol) and nickel(II) acetate tetrahydrate (720 mg, 3 mmol) were dissolved in acetone–methanol (60 cm^3) on a water bath, and 20 drops of a 20% sodium hydroxide solution were added to the solution. The resulting deep red solution was allowed to stand 2 d at room temperature, and the volume of the solution was reduced to about 10 cm^3 by air bubbling. The deep red precipitate was filtered, washed with water, and recrystallized from methanol to give red plates. Yield, 550 mg (75%).

[*Ni(*rac-*BzSalPhen)*] *from* [*Ni(*rac-*BzPhen)*]: *rac*-BzPhen-H_2 (210 mg, 0.5 mmol) and nickel(II) acetate tetrahydrate (120 mg, 0.5 mmol) were dissolved in hot methanol (50 cm^3), after which 12 drops of a 20% sodium hydroxide solution were added to the pale blue solution. The resulting deep red solution was allowed to stand overnight at room temperature, and the orange-red crystals which separated out were collected by filtration and washed with methanol. Yield, 200 mg (84%).

Dehydrogenation in Pyridine Solution. *A)* [*Ni(SalStil)*]

and [*Ni(*meso-*SalPhen)*] *from* [*Ni(*meso-*BzPhen)*]: *meso*-BzPhen-H_2 (420 mg, 1 mmol) and nickel(II) acetate tetrahydrate (240 mg, 1 mmol) were dissolved in pyridine (15 cm^3). The resulting light green solution was heated on a water bath for 30 h. A deep red color formed after heating for 1 h. After cooling, methanol (70 cm^3) was added to the reaction mixture to induce crystallization. The orange-red needles ([Ni(SalStil)]) thus precipitated were filtered and washed with methanol. Yield, 60 mg (13%). After the filtrate had stood overnight at room temperature, [Ni(*meso*-SalPhen)] precipitated from the filtrate as deep red plates. Yield, 200 mg (42%).

B) [*Ni(Bu*^{t}*SalStil)*] *from* [*Ni(*meso-*Bu*^{t}*BzPhen)*]: The procedure was the same as that described for the preparation of [Ni(SalStil)] and [Ni(*meso*-SalPhen)]. *meso*-Bu^{t}BzPhen-H_2 (650 mg, 1 mmol) and nickel(II) acetate tetrahydrate (480 mg, 2 mmol) afforded 430 mg (61%) of [Ni(Bu^{t}SalStil)]. From the filtrate, a trace amount (15 mg) of [Ni(*meso*-Bu^t-SalPhen)] was obtained.

C) [*Ni(*rac-*SalPhen)*] *from* [*Ni(*rac-*BzPhen)*]: *rac*-BzPhen-H_2 (420 mg, 1 mmol) and nickel(II) acetate tetrahydrate (240 mg, 1 mmol) afforded 200 mg (42%) of [Ni(*rac*-SalPhen)].

D) [*Ni(*rac-*Bu*^{t}*SalPhen)*] *from* [*Ni(*rac-*Bu*^{t}*BzPhen)*]: *rac*-Bu^{t}BzPhen-H_2 (650 mg, 1 mmol) and nickel(II) acetate tetrahydrate (240 mg, 1 mmol) afforded 320 mg (46%) of [Ni(*rac*-Bu^{t}SalPhen)].

E) [*Ni(*meso-*SalPhen)*] *from* [*Ni(*meso-*BzSalPhen)*]: *meso*-BzSalPhen-H_2 (210 mg, 0.5 mmol) and nickel(II) acetate tetrahydrate (300 mg, 1.25 mmol) were dissolved in pyridine (10 cm^3), and the resulting red solution was heated on a water bath for 30 h. After cooling, water was added to the reaction mixture until it began to become turbid. The resulting crystals were collected by filtration and washed with methanol. Yield, 150 mg (63%).

F) Formation of [*Ni(*meso-*SalPhen)*] *by* H_2O_2 *oxidation of* [*Ni(*meso-*BzSalPhen)*]: Five drops of a 30% hydrogen peroxide solution were added to a solution of [Ni(*meso*-BzSalPhen)(py)] (110 mg, 0.2 mmol) in pyridine (15 cm^3), after which the mixture was heated on a water bath for 5 h. After cooling, water was added until the mixture began to become turbid. The resulting red crystals were filtered and washed with methanol. Yield, 70 mg (73%).

Measurements. IR spectra and electronic spectra were recorded on a Hitachi EPI S2 spectrometer and a Hitachi EPS 3T spectrometer respectively. NMR spectra were obtained on a Hitachi Model R-24 spectrometer, with Me_4Si as an internal standard.

Results and Discussion

The reaction of *rac*-BzPhen-H_2 or *meso*-BzPhen-H_2 with nickel(II) acetate afforded a pale green nickel(II) chelate, [Ni(*rac*-BzPhen)] or [Ni(*meso*-BzPhen)]. Pyridine solutions of these complexes or a pyridine solution containing an equimolar ligand (*rac*-BzPhen-H_2 or *meso*-BzPhen-H_2) and nickel(II) acetate changed color from light green to deep red on prolonged heating in air. The change was irreversible, and red crystals were deposited from the resulting red-colored solution in each case.

It was found that [Ni(*rac*-BzPhen)] afforded only one deep red product, while [Ni(*meso*-BzPhen)] gave two products, orange-red needles and deep red plates. The deep red products from the *rac*- and *meso*-chelates were identified as [Ni(*rac*-SalPhen)] and [Ni(*meso*-SalPhen)] respectively by a comparison of their IR spectra with those of authentic samples[9] and by elemental analyses.

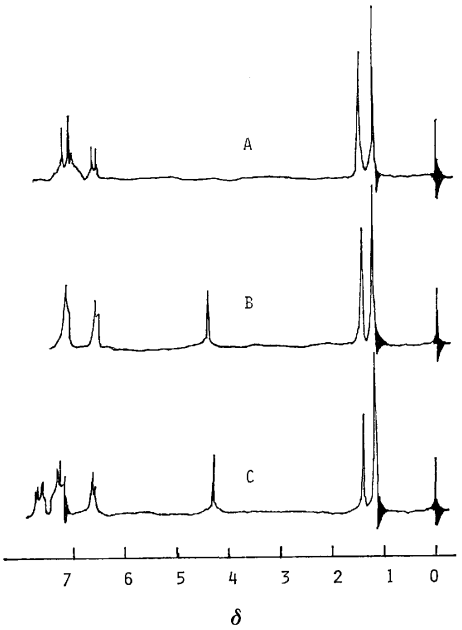

Fig. 2. NMR spectra of [Ni(Bu^{t}SalStil)] (A), [Ni(*meso*-Bu^{t}SalPhen)] (B), and [Ni(*rac*-Bu^{t}SalPhen)] (C).

The IR spectrum of the orange-red product from [Ni(*meso*-BzPhen)] was apparently different from that of [Ni(*meso*-SalPhen)]. It exhibits no absorptions in the region of 2900 cm^{-1}, where the C–H stretching vibrations due to the benzylmethylene and methine on the diamine moiety are expected to appear. The latter was observed at 2900 cm^{-1} in the spectrum of [Ni(*meso*-SalPhen)]. This, together with the analytical data, suggested that this chelate contained a fully conjugated ligand system, namely, [Ni(SalStil)], as is illustrated in Fig. 1.

It was difficult to obtain the precise NMR spectrum of this chelate because of its low solubility in organic solvents. For the purpose of increasing the solubility, *meso*-Bu^{t}BzPhen-H_2 was prepared and allowed to react with nickel(II) acetate. Although the corresponding nickel(II) chelate, [Ni(*meso*-Bu^{t}BzPhen)], could not be isolated as crystals from the methanol solution, a red nickel(II) chelate was obtained successfully from the pyridine solution on prolonged heating. The NMR spectrum of this chelate is compared with those of [Ni(*meso*-Bu^{t}SalPhen)] and [Ni(*rac*-Bu^{t}SalPhen)] in Fig. 2. The spectrum apparently lacks a signal attributable to methine protons on the diamine moiety, which is observed in the spectra of [Ni(*rac*-Bu^{t}SalPhen)] and [Ni(*meso*-Bu^{t}SalPhen)] at δ 4.36 and 4.69 respectively. This indicates that the dehydrogenation took place at the bridged carbon atoms to form the *cis*-stilbene moiety. It can deffinitly be concluded that the reaction of *meso*-Bu^{t}BzPhen-H_2 with the nickel(II) ion in the presence of molecular oxygen proceeds with the dehydrogenation of the ligand and affords predominantly the nickel(II) chelate containing a fully conjugated ligand system, namely, [Ni(Bu^{t}SalStil)], while scarcely [Ni(*meso*-Bu^{t}SalPhen)] was formed in

this reaction.

As has been mentioned above, *meso*-BzPhen-H_2 and nickel(II) acetate in methanol formed a pale pink solution upon the addition of a few drops of an aqueous sodium hydroxide solution, and [Ni(*meso*-BzPhen)] separated out as light green crystals from the solution. Dehydrogenation did not proceed under the present reaction conditions. On the other hand, the addition of more aqueous sodium hydroxide to the pink solution before the precipitation of the chelate produced a deep red color and an orange-red precipitate separated out when the mixture stood overnight at room temperature. Recrystallization from pyridine–water gave brilliant red crystals. It was found that a two-electron oxidation took place in this case; the crystals were identified as [Ni(*meso*-BzSalPhen)(py)], the structure of which is shown in Fig. 1. For the purpose of identification, the ligand, *meso*-BzSalPhen-H_2 was prepared by a different route, and the IR spectrum of its nickel(II) chelate was compared with that of the above sample. Under the same reaction conditions, *rac*-BzPhen-H_2 and *meso*-Bu^{t}BzPhen-H_2 also gave the same types of chelates, [Ni(*rac*-BzSalPhen)], and [Ni(*meso*-Bu^{t}BzSalPhen)], in good yields. Thus, it is clear that this type of dehydrogenation reaction readily occurs for these chelates in a basic solution, even at room temperature. The reaction mechanism can be formulated as in Scheme 1. The addition of alkali causes deprotonation, and the deprotonated species I′ is apparently sensitive to molecular oxygen and is readily oxidized to the mono imine nickel(II) chelates.

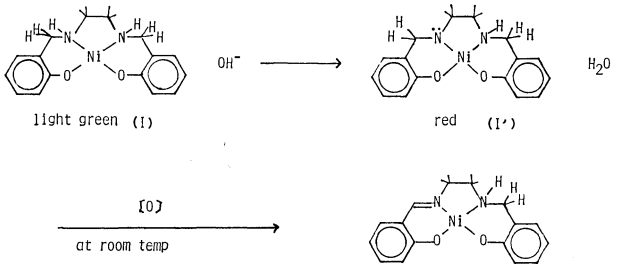

Scheme 1.

The electronic spectra of [Ni(*meso*-Bu^{t}BzSalPhen)], [Ni(*meso*-Bu^{t}SalPhen)], and [Ni(Bu^{t}SalStil)] in pyridine are compared in Fig. 3. The spectra of [Ni(*meso*-Bu^{t}BzSalPhen)] and [Ni(*meso*-Bu^{t}SalPhen)] show d-d transition bands at 580 and 570 nm respectively. The band for [Ni(Bu^{t}SalStil)] is not observed because of the tailing of an intense charge-transfer band. The spectral changes with the time are shown in Fig. 4 for [Ni(*meso*-Bu^{t}BzSalPhen)] in pyridine and for a pyridine solution containing *meso*-Bu^{t}BzPhen-H_2 and nickel(II) acetate in Fig. 5. As may be seen in Fig. 4, the band at 430 nm increases, and the absorption around 500 nm decreases, in intensity with the time. This indicates that [Ni(*meso*-Bu^{t}BzSalPhen)] is formed exclusively from [Ni(*meso*-Bu^{t}BzSalPhen)] and that the formation of [Ni(Bu^{t}SalStil)] does not occur at all under these conditions. On the other hand, as is shown in Fig. 5, the band around 500 nm which is due to the [Ni(Bu^{t}SalStil)] species increases in intensity with the time from the initial stage. This

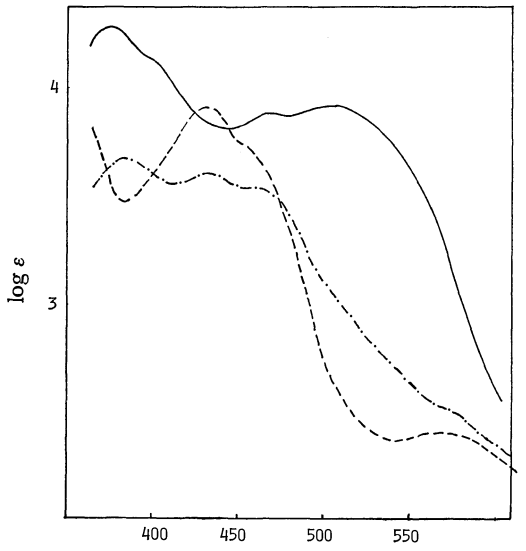

Fig. 3. The electronic spectra of [Ni(Bu^{t}SalStil)] (——), [Ni(*meso*-Bu^{t}SalPhen)] (----), and [Ni(*meso*-Bu^{t}BzSalPhen)] (—·—) in pyridine.

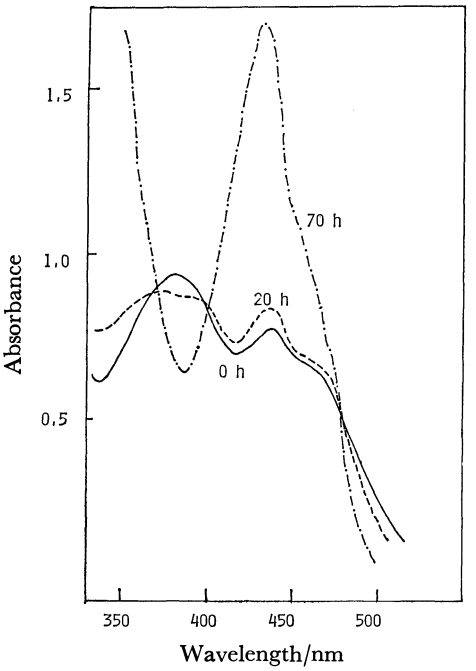

Fig. 4. Spectral changes with the time for the dehydrogenation of [Ni(*meso*-Bu^{t}BzSalPhen)] (1.97×10^{-5} mol) in pyridine (10 cm^3) at 90 °C.

result is consistent with the fact that [Ni(Bu^{t}SalStil)] is exclusively formed in the solution. In other words, the formation of [Ni(Bu^{t}SalStil)] occur even at the initial stage of dehydrogenation. These results give some insight into the formation mechanism of [Ni(Bu^{t}SalStil)] and [Ni(*meso*-Bu^{t}SalPhen)]. The formation of [Ni(*meso*-Bu^{t}SalPhen)] by the dehydrogenation of [Ni(*meso*-Bu^{t}BzPhen)] proceeds in two step by-step processes via the formation of [Ni(*meso*-Bu^{t}BzSalPhen)]. While the formation mechanism of [Ni(Bu^{t}SalStil)] is still unclear, the process via the formation of [Ni(*meso*-

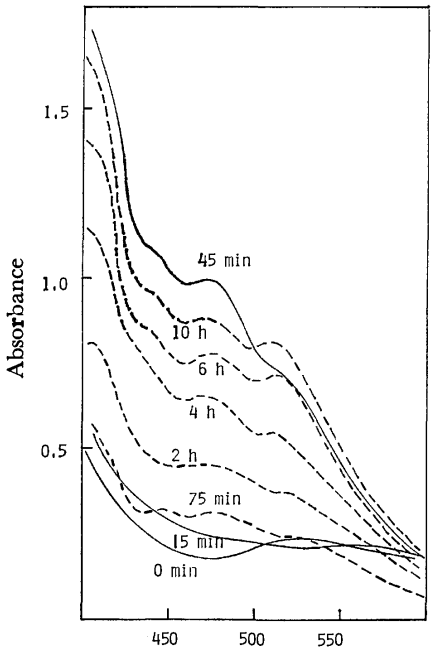

Fig. 5. Spectral changes with the time for the dehydrogenation [Ni(*meso*-Bu^{t}BzPhen)] [*meso*-Bu^{t}BzPhen-H_2 (2.4×10^{-5} mol) and nickel(II) acetate tetrahydrate (3.5×10^{-5} mol) in pyridine (10 cm^3) at 90 °C]; [—— obtained by using 1 cm quartz cell and ---- obtained by using (1 cm quartz cell+9 mm quartz spacer)].

Bu^{t}BzSalPhen)] can be disregarded, as has been described above. Therefore, it is most probable for the formation of [Ni(Bu^{t}SalStil)] to postulate the existence of an intermediate containing an enamine-type ligand system (III). Such intermediates have been isolated in the metal-ion-induced rearrangement of 3,3′,4,4′-tetrahydro-2,2′-bi-2*H*-1,3-benzoxazines and subsequent dehydrogenation reactions,[7] though the isolation of such species was unsuccessful in these cases. The proposed reaction mechanism of the dehydrogenation is summarized in Scheme 2. As has been mentioned before, [Ni(*meso*-BzPhen)] was dehydrogenated to give [Ni(*meso*-SalPhen)], and to give [Ni(SalStil)] as a by-product. This dehydrogenation also proceeds in a manner quite similar to that described in Scheme 2. In practice, the reaction of *meso*-BzSalPhen-H_2 with nickel(II) acetate in pyridine or the dehydrogenation of [Ni(*meso*-BzSalPhen)] with H_2O_2 in pyridine afforded [Ni(*meso*-SalPhen)] as the sole product.

The electron-transfer mechanism in the oxidative dehydrogenation of the nickel(II) chelates is not clear, but probably molecular oxygen combines with the nickel(II) ion at the axial positions and transfers electrons through the nickel(II) ion. If an initial electron loss from the nickel(II) ion is assumed, the transition state of the dehydrogenation may involve the trivalent oxidation state of nickel. The formation of such species has previously been reported in the dehydrogenation of macrocyclic nickel(II) chelates.[10,11] The nickel(III) complexes which were formed by electrochemical or chemical oxidation gave nickel(II) ligand radical species upon treatment with basic solvents such as pyridine according to this scheme;

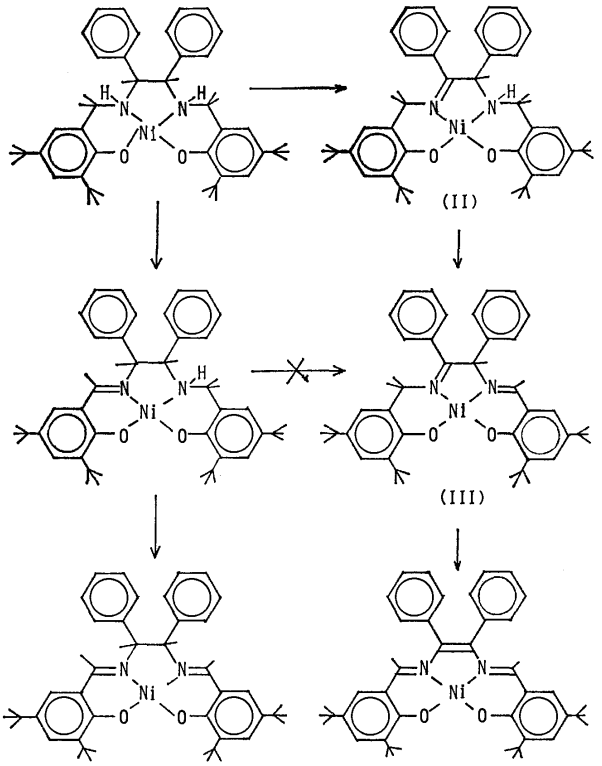

Scheme 2.

$$\text{Ni(III)N-H} + :\text{B} \longrightarrow \text{Ni(II)N}\cdot + \text{HB}^+$$

Further, the free radical species afforded, via several different processes, monoimine nickel(II) chelates.[11] In the present case, similar nickel(III) chelates and free radical species must be involved prior to the ligand oxidation.

It should be noted that the nickel(II) chelates containing a fully conjugated ligand system were formed only when *meso*-chelates were dehydrogenated. In addition, the *t*-butyl groups on the benzene nucleus promoted the formation of fully conjugated chelates. In the dehydrogenation of [Ni(*meso*-BzPhen)], [Ni(SalStil)] was obtained in a low yield as a by-product, while [Ni(Bu^{t}SalStil)] was exclusively obtained from [Ni(*meso*-Bu^{t}BzPhen)]. It is clear that the *t*-butyl groups situated in the *ortho* position of the phenol oxygen atoms exerted such an effect on the dehydrogenation because in the dehydrogenation of a *meso*-chelate having a *t*-butyl group in the position *para* to the OH group of the hydroxybenzyl moiety the situation was quite similar to that of [Ni(*meso*-BzPhen)].

The stereospecific dehydrogenation of *meso*-chelates may be attributable to the conformation of phenyl groups on the diamine moiety; that is, the only possible conformation for the two phenyl groups is axial-equatorial, and they are crowded on one side relative to the metal chelate plane. On the other hand, on the formation of intermediates (II) and (III) from *meso*-chelates, the conformational changes in the two phenyl groups can be assumed to be as is shown in Scheme 3. These conformational changes accompany the partial removal of the unfavourable strain, which

is due to the crowding state of the two phenyl groups in the starting chelate. Thus, this will be the reason why the formation of [Ni(SalStil)] was possible only in the dehydrogenation reaction of the *meso*-chelates.

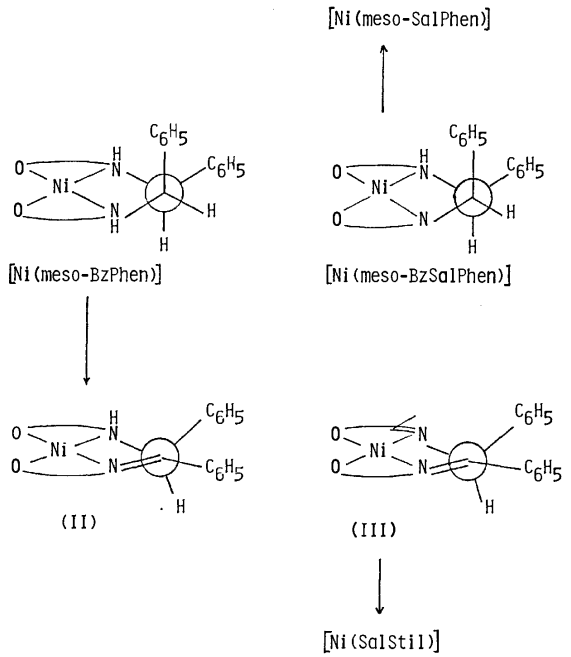

Scheme 3.

In the [Ni(*meso*-Bu^{t}BzPhen)], the steric repulsion due to the two bulky *t*-butyl groups situated in the *ortho* position of the phenol oxygen atoms may produce a considerable distortion, as is depicted below:

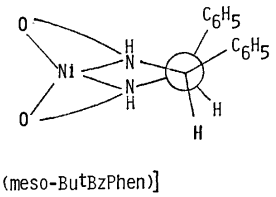

Scheme 4.

In fact, the splitting of the d-d band (540 nm and 630 nm) was observed in the reflectance spectrum of [Cu(*meso*-Bu^{t}SalPhen)], which was considered to be due to a tetrahedral distortion of the chelate ring.[12] Such distortion is common among *meso*-Bu^t-chelates; it may be the reason why the isolation of [Ni(*meso*-Bu^{t}BzPhen)] was difficult. It is apparent that the serious strain in [Ni(*meso*-Bu^{t}BzPhen)] is removed by the formation of the intermediates (II) and (III); this makes it likely to afford [Ni(Bu^{t}SalStil)].

References

1) a) V. L. Goedoken and D. H. Busch, *J. Am. Chem. Soc.*, **94**, 7355 (1972); b) J. C. Dabrowiak and D. H. Busch, *Inorg. Chem.*, **14**, 1881 (1975).
2) a) E. K. Barefield and D. H. Busch, *Inorg. Chem.*, **10**, 108 (1971); b) C. H. Hipp, L. F. Lindoy, and D. H. Busch, *ibid.*, **11**, 1988 (1972).
3) V. L. Goedoken, *J. Chem. Soc., Chem. Commun.*, **1972**, 207.
4) C. M. Brown, T. R. Weaver, F. R. Keene, and T. J. Meyer, *Inorg. Chem.*, **15**, 190 (1976).
5) F. R. Keene, D. H. Salmon, and T. J. Meyer, *J. Am. Chem. Soc.*, **98**, 1884 (1976).
6) S. E. Diamond, G. M. Tom, and T. Taube, *J. Am. Chem. Soc.*, **97**, 2661 (1975).
7) H. Kanatomi and I. Murase, *Inorg. Chem.*, **11**, 1356 (1972).
8) H. A. Staab and F. Vogtle, *Chem. Ber.*, **98**, 2681 (1965).
9) H. Kanatomi, I. Murase, and A. E. Martell, *J. Inorg. Nucl. Chem.*, **38**, 1465 (1976).
10) E. G. Gore and D. H. Busch, *Inorg. Chem.*, **12**, 1 (1973).
11) E. K. Barefield and M. F. Mocella, *J. Am. Chem. Soc.*, **97**, 4238 (1975).
12) M. Honda and G. Schwarzenbach, *Helv. Chim. Acta*, **40**, 27 (1957).

 © 1983 The Chemical Society of Japan Bull. Chem. Soc. Jpn., 56, 105—107 (1983)

Extractive Spectrophotometric Determination of Antimony(III), Bismuth, Indium, and Gallium with Pyrocatechol Violet and Tridodecylethylammonium Bromide

Yoshio Shijo,* Tokuo Shimizu, and Kaoru Sakai

Department of Environmental Chemistry, Faculty of Engineering, University of Utsunomiya, Ishii-machi, Utsunomiya 321

(Received April 28, 1982)

The spectrophotometric method for the determination of trace amounts of antimony(III), bismuth, indium, and gallium based on the solvent extraction of the ion associate formed between anionic metal–Pyrocatechol Violet complexes and tridodecylethylammonium bromide is proposed. The maximum absorbance of the extracted species occur at 530, 564, 600, and 595 nm for antimony(III), bismuth, indium, and gallium. The molar absorptivities for antimony(III), bismuth, indium, and gallium are 3.32×10^4, 3.31×10^4, 8.20×10^4, and 8.00×10^4 $dm^3\ mol^{-1}\ cm^{-1}$. The optimum pH ranges for the extraction of antimony(III), bismuth, indium, and gallium are from 3.7 to 4.8, from 5.8 to 6.7, from 5.3 to 5.4, and from 5.5 to 6.2 respectively. The composition of the extracted complexes (metal:PV:TDEA) are estimated to be 1:2:3 for antimony(III) and 1:2:2 for the other metals. The interference of foreign ions is described.

The extraction of the anionic metal complexes with lipophilic quaternaryammonium salts has been utilized for various analytical purposes, such as the separation of metal ions,[1] and the extractive spectrophotometric,[2] fluorometric,[3] polarographic,[4] and atomic-absorption spectrophotometric[5,6] determination of metals. Trioctylmethylammonium chloride (Aliquat 336 or Capriquat) has been in common use as an extracting reagent in this field. Iodide of antimony and 17 other elements,[6] anionic complexes with EDTA of bismuth and 14 other elements,[7] iodide of bismuth and six other elements,[8] indium in a hydrochloric–sulfuric system,[9] chloride of indium,[10,11] thiocyanate of indium,[12] and chloride of indium and gallium[13] were extracted with the foregoing reagent.

Tridodecylethylammonium bromide (TDEABr), which is more lipophilic than trioctylmethylammonium chloride, is also useful for the extraction of the anionic metal complexes. The Pyrocatechol Violet (abbreviated to PV hereafter) complexes of aluminium,[14] tungsten,[15] vanadium,[16] *etc.* were extracted with TDEABr in organic solvents. The anionic PV complexes of antimony(III), bismuth, indium, and gallium can also be extracted with TDEABr in several nonpolar solvents. The fundamental conditions for the extractive spectrophotometric determination of antimony(III), bismuth, indium, and gallium with PV and TDEABr are studied in this paper.

Experimental

Reagent. A 2.50×10^{-3} mol dm^{-3} antimony(III) solution was prepared by dissolving 0.4174 g of antimony potassium tartrate in 500 cm^3 of 3 mol dm^{-3} hydrochloric acid. A 2.50×10^{-3} mol dm^{-3} bismuth solution was prepared by dissolving 0.2612 g of bismuth metal in 71.4 cm^3 of 7 mol dm^{-3} nitric acid and then diluting the mixture to 500 cm^3. A 2.50×10^{-3} mol dm^{-3} indium solution was prepared by dissolving 0.1435 g of indium metal in 37.2 cm^3 of nitric acid and then diluting the mixture to 500 cm^3. A 2.50×10^{-2} mol dm^{-3} gallium solution was prepared by dissolving 0.1743 g of gallium metal in 53.6 cm^3 of hydrochloric acid and then diluting the mixture to 100 cm^3. Working solutions of the metals were prepared as needed by the dilution of the stock solutions with the corresponding acid. A 1×10^{-3} mol dm^{-3} PV solution was prepared by dissolving 0.0966 g of the Dotite PV in 250 cm^3 of de-ionized water. TDEABr was prepared by the method described in a previous work.[17] The 2×10^{-3} mol dm^{-3} TDEABr solutions were prepared by dissolving 0.3155 g of TDEABr in 250 cm^3 of carbon tetrachloride for antimony(III) and in xylene for bismuth, indium, and gallium. The acetate buffer solutions were used for these metals. All the other chemicals used were of a guaranteed reagent quality.

Apparatus. A Hitachi 101 spectrophotometer, a Hitachi 200-20 UV-vis. recording spectrophotometer, and a Hitachi Horiba F-7 pH meter were employed.

General Procedure. Mix a working solution of a metal, a definite amount of 2 or 0.2 mol dm^{-3} hydrochloric acid, and 1 cm^3 of a 1×10^{-3} mol dm^{-3} PV solution in a 100-cm^3 polypropylene beaker. Adjust the pH of the solution to 4.5, 5.9, 5.3, or 5.6 for antimony(III), bismuth, indium, or gallium respectively by the addition of a 2 mol dm^{-3} sodium acetate solution, and then dilute to 20 cm^3 with de-ionized water. Transfer the solution into a 35-cm^3 test tube and extract with 5 cm^3 of 2×10^{-3} mol dm^{-3} TDEABr in an organic solvent for 5 min. Separate the phases and centrifuge the organic phase for 2 min at 3000 min^{-1}. Measure the absorbance of the extract against the reagent blank.

Results and Discussion

Absorption Spectra. The absorption spectra of the metal–PV–TDEA complexes extracted into the organic phase, and of the anionic metal–PV complexes in the aqueous solutions and also of the respective blank solutions, are shown in Figs. 1 to 4. There is no or only a little bathochromic shift in the absorption spectrum of the metal–PV–TDEA complexes. The absorbance of the extracted complexes for antimony(III) and indium, however, increase remarkably over that in the aqueous phase.

Effect of pH. The effect of the pH on the extraction of the complexes was studied with solutions containing each metal and PV. For the maximum extraction, the optimum pH values for antimony(III), bismuth, indium, and gallium are in the ranges from 3.7 to 4.8, from 5.8 to 6.7, from 5.3 to 5.4, and from 5.5 to 6.2 respectively. The absorbances of extracts are unchanged for indium and gallium, but decrease about 15%, and 20% for antimony(III) and bismuth respectively for 30 min.

Organic Solvents. Several kinds of solvents were

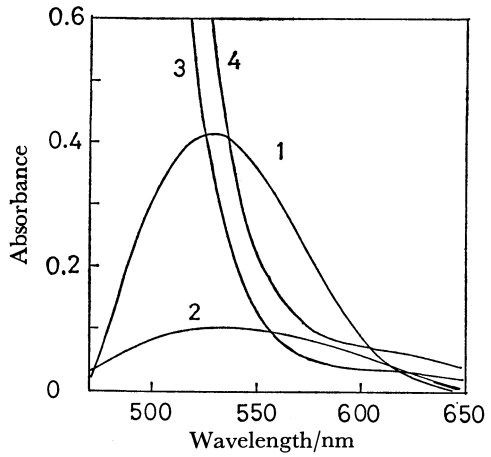

Fig. 1. Absorption spectra of the Sb–PV–TDEA complex in carbon tetrachloride and the Sb–PV complex in aqueous solution.
pH=4.5, V_{aq}=20 cm³, V_o=5 cm³, $[TDEABr]_o=2\times10^{-3}$ mol dm⁻³. 1: Sb–PV–TDEA $[Sb]=3.13\times10^{-6}$ mol dm⁻³, 2: Sb–PV $[Sb]=2.5\times10^{-5}$ mol dm⁻³, 3: PV–TDEA $[PV]=5\times10^{-5}$ mol dm⁻³, 4: PV $[PV]=2\times10^{-4}$ mol dm⁻³.

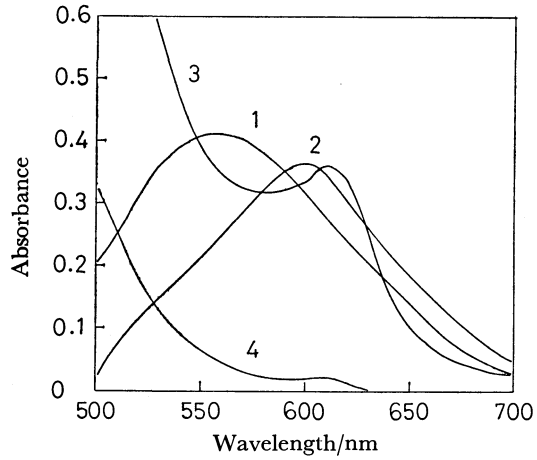

Fig. 2. Absorption spectra of the Bi–PV–TDEA complex in xylene and the Bi–PV complex in aqueous solution.
pH=5.9, V_{aq}=20 cm³, V_o=5 cm³, $[TDEABr]_o=2\times10^{-3}$ mol dm⁻³. 1: Bi–PV–TDEA $[Bi]=3.13\times10^{-6}$ mol dm⁻³, 2: Bi–PV $[Bi]=6.25\times10^{-6}$ mol dm⁻³, 3: PV–TDEA $[PV]=5\times10^{-5}$ mol dm⁻³, 4: PV $[PV]=5\times10^{-5}$ mol dm⁻³.

examined from the standpoints of the absorbance and extractability of the complexes. Spectrophotometric studies indicated carbon tetrachloride to be most efficient for antimony(III), and xylene, for the other metals. The other solvents examined include butyl acetate, chloroform, isobutyl methyl ketone, and 1-butanol. Except for butyl acetate, these vary in performance, causing little or no extraction.

Effect of the Reagent Concentration. The variation in the PV concentration in an aqueous phase containing each metal with the optimum pH gives the constant maximum absorbance of the extracts in the PV concentration ranges from 3×10^{-5} to 1×10^{-4}, from 5×10^{-5} to 2×10^{-4}, 5×10^{-5}, and $>2.5\times10^{-5}$ mol dm⁻³ for antimony(III), bismuth, indium, and

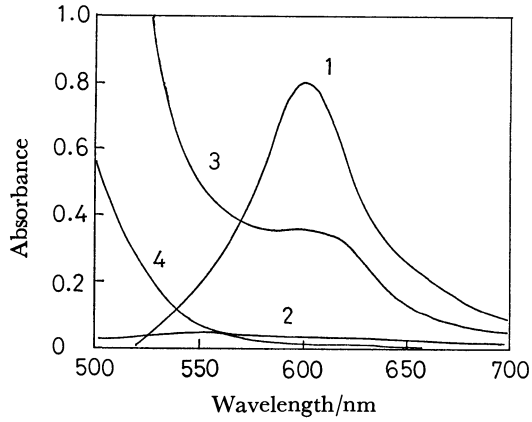

Fig. 3. Absorption spectra of the In–PV–TDEA complex in xylene and the In–PV complex in aqueous solution.
pH=5.3, V_{aq}=20 cm³, V_o=5 cm³, $[TDEABr]_o=2\times10^{-3}$ mol dm⁻³. 1: In–PV–TDEA $[In]=2.5\times10^{-6}$ mol dm⁻³, 2: In–PV $[In]=1\times10^{-5}$ mol dm⁻³, 3: PV–TDEA $[PV]=5\times10^{-5}$ mol dm⁻³, 4: PV $[PV]=8\times10^{-5}$ mol dm⁻³.

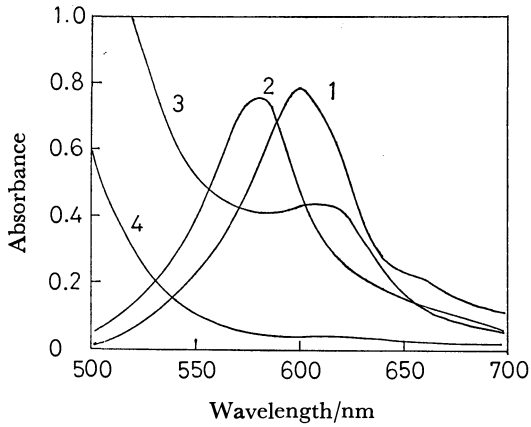

Fig. 4. Absorption spectra of the Ga–PV–TDEA complex in xylene and the Ga–PV complex in aqueous solution.
pH=5.5, V_{aq}=20 cm³, V_o=5 cm³, $[TDEABr]_o=2\times10^{-3}$ mol dm⁻³.
1: Ga–PV–TDEA $[Ga]=2.5\times10^{-6}$ mol dm⁻³, 2: Ga–PV $[Ga]=1\times10^{-5}$ mol dm⁻³, 3: PV–TDEA $[PV]=5\times10^{-5}$ mol dm⁻³, 4: PV $[PV]=8\times10^{-5}$ mol dm⁻³.

gallium respectively. The optimum concentrations of TDEABr in the organic phase are in the ranges from 2×10^{-4} to 5×10^{-3}, $>1\times10^{-3}$, and $>1\times10^{-4}$ mol dm⁻³ for antimony(III), bismuth, and indium or gallium respectively.

Extractability and Molar Absorptivity. An aqueous solution of 20 cm³ containing a definite amount of each metal and PV was shaken with 5 cm³ of 2×10^{-3} mol dm⁻³ TDEABr in organic solvents under the optimum conditions. Extraction was repeated for the remaining aqueous phase after the separation of the extract. The extractability of each metal was calculated from the absorbance of the extracts. It was found that 99.3, 99.0, 97.6, and 98.2% of antimony(III), bismuth, indium, and gallium respectively were extracted by a single extraction. The distribution ratios for antimony(III), bismuth, indium, and gal-

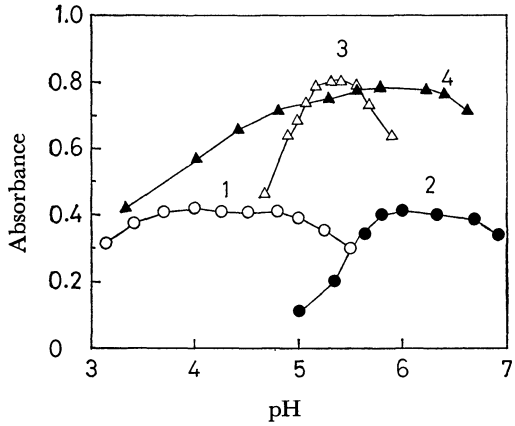

Fig. 5. Effect of pH on the extraction of the metal–PV–TDEA complexes.
[Sb]=[Bi]=3.13×10^{-6} mol dm^{-3}, [In]=[Ga]=2.5×10^{-6} mol dm^{-3}, [TDEABr]$_0$=2×10^{-3} mol dm^{-3}, [PV]=5×10^{-5} mol dm^{-3}. 1: Sb, 2: Bi, 3: In, 4: Ga.

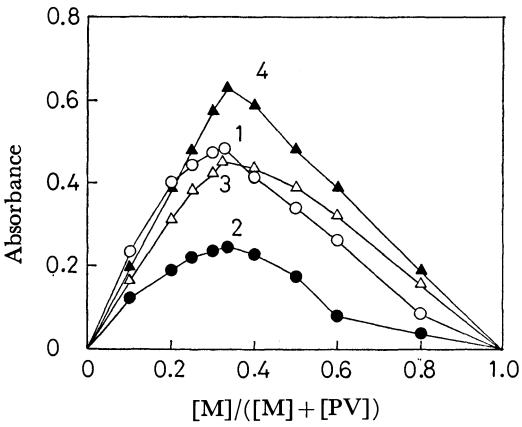

Fig. 6. Continuous variation method applied to the metal–PV–TDEA complexes (metal:PV).
1: Sb–PV–TDEA [Sb]+[PV]=6.25×10^{-5} mol dm^{-3}, 2: Bi–PV–TDEA [Bi]+[PV]=1×10^{-4} mol dm^{-3}, 3: In–PV–TDEA [In]+[PV]=1×10^{-4} mol dm^{-3}, 4:Ga–PV–TDEA [Ga]+[PV]=1×10^{-4} mol dm^{-3}.

lium are 5.59×10^2, 3.96×10^2, 1.63×10^2, and 2.18×10^2 respectively. The molar absorptivity of the complexes are 3.32×10^4, 3.31×10^4, 8.20×10^4, and 8.00×10^4 dm^3 mol^{-1} cm^{-1} for antimony(III), bismuth, indium, and gallium respectively. A calibration curve for the determination of each metal was made under the optimum conditions. A good linear relationship was obtained over the concentration range from 1 to 20, from 2 to 30, from 0.4 to 7.2, and from 0.3 to 4.3 μg of antimony(III), bismuth, indium, and gallium per 5 cm^3 of the organic phase.

The Composition of the Complexes. A continuous-variation method as described in a previous paper[16] was carried out for the metal–PV–TDEA complexes system. The results are shown in Fig. 6 and Fig. 7. The reacting ratios of metal to PV to TDEA balance well at 1:2:3 and 1:2:2 for antimony(III) and for the other metals respectively. Thus, the composition of the complexes are Sb$(PV)_2(R_3R'N)_3$, Bi$(PV)_2(R_3R'N)_2$, In$(PV)_2(R_3R'N)_2$, and Ga$(PV)_2(R_3R'N)_2$ respectively.

Effect of Foreign Ions. The effect of foreign ions

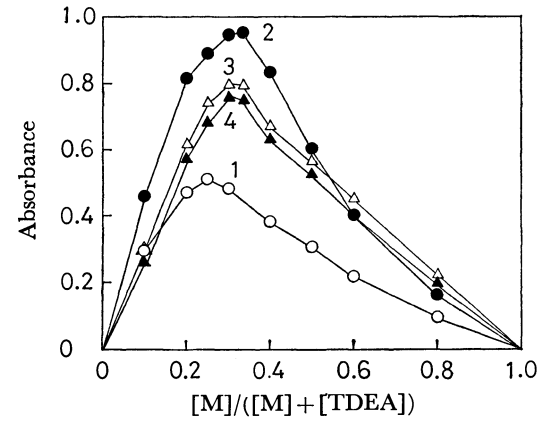

Fig. 7. Continuous variation method applied to the metal–PV–TDEA complexes (metal: TDEA).
1: Sb–PV–TDEA Sb+TDEA=2×10^{-6} mol, 2: Bi–PV–TDEA Bi+TDEA=2×10^{-6} mol, 3: In–PV–TDEA In+TDEA=2×10^{-6} mol, 4: Ga–PV–TDEA Ga+TDEA=1×10^{-6} mol.

on the determination of antimony(III), bismuth, indium, and gallium was examined under optimum conditions. The anionic PV complexes of many metals, such as beryllium, aluminium, titanium(IV), vanadium(V), iron(III), copper, molybdenum(VI), tin(IV), tungsten(VI), thorium, and uranium(VI) can be extracted with TDEABr and interfere with the determination of the foregoing metals. GEDTA for the determination of antimony(III), 1,10-phenanthroline and fluoride for bismuth, and thiourea or hydrogen peroxide for indium and gallium are useful as masking reagents in this system, but the masking power of these reagents is insufficient. Of the anions tested, iodide, thiocyanate, and perchlorate interfere most seriously, giving a negative error.

References

1) T. Sato, H. Watanabe, S. Kotani, M. Yamamoto, and M. Good, *Anal. Chim. Acta*, **84**, 397 (1976).
2) H. Akaiwa, H. Kawamoto, and E. Yoshimatsu, *Nippon Kagaku Kaishi*, **1981**, 79.
3) Y. Kondo, M. Kataoka, and T. Kambara, *Bunseki Kagaku*, **30**, 109 (1981).
4) R. Pribil, Jr., and J. Adam, *Talanta*, **20**, 1338 (1973).
5) I. Tsukahara and M. Tanaka, *Anal. Chim. Acta*, **116**, 383 (1980).
6) J. R. Clark, *Anal. Chem.*, **53**, 61 (1981).
7) H. Irving and R. H. Al-Jarrah, *Anal. Chim. Acta*, **74**, 321 (1975).
8) J. G. Viets, *Anal. Chem.*, **50**, 1097 (1978).
9) N. Souka, F. Abdel-Rehim, and A. Sayed, *Radiochem. Radioanal. Lett.*, **26**, 67 (1976).
10) C. Fischer, H. Wagner, V. V. Bagreev, and E. S. Stojanov, *J. Inorg. Nucl. Chem.*, **39**, 513 (1977).
11) O. V. Singh and S. N. Tandon, *J. Radioanal. Chem.*, **36**, 331 (1977).
12) D. Singh, O. V. Singh, and S. N. Tandon, *Sep. Sci. Technol.*, **13**, 625 (1978).
13) V. V. Bagreev, C. Fischer, L. M. Yudushkina, and Yu. A. Zolotov, *J. Inorg. Nucl. Chem.*, **40**, 553 (1978).
14) Y. Shijo, *Nippon Kagaku Kaishi*, **1974**, 1912.
15) Y. Shijo, T. Shimizu, and K. Sakai, *Bull. Chem. Soc. Jpn.*, **54**, 143 (1981).
16) Y. Shijo, T. Shimizu, and K. Sakai, *Bull. Chem. Soc. Jpn.*, **54**, 700 (1981).
17) Y. Shijo, *Bull. Chem. Soc. Jpn.*, **50**, 1013 (1977).

Magnetic Properties of [μ-(Ethylenediaminetetraacetato)-di-μ-sulfido-bis{oxomolybdate(V)}]$^{2-}$ and [μ-(Ethylenediaminetetraacetato)-di-μ-oxo-bis{oxomolybdate(V)}]$^{2-}$ Ions

Hanako KOBAYASHI,* Ikuji TSUJIKAWA, Takashi SHIBAHARA† and Norikiyo URYÛ††

Department of Chemistry, Faculty of Science, Kyoto University, Sakyo-ku, Kyoto 606

† *Department of Chemistry, Okayama University of Science, Okayama 700*

†† *Department of Applied Science, Faculty of Engineering, Kyushu University, Higashi-ku, Fukuoka 812*

(Received April 30, 1982)

Sodium [μ-(ethylenediaminetetraacetato)-di-μ-sulfido-bis{oxomolybdate(V)}]·n-hydrates, n=2 and 3, are antiferromagnetic dimers with an exchange interaction within a pair of Mo(V) ions of about $-140\,k$ having an averaged g-value of about 2 for each Mo(V) ion. In these salts, magnetic moments of only about 0.5 Bohr magneton are localized at Mo(V) sites, though Mo(V) has one electron in the 4d orbital. Here a π-bonding looped structure is considered to have a contribution to the diamagnetic susceptibilities of about -5.0×10^{-5} (CGSemu). Sodium [μ-(ethylenediaminetetraacetato)-di-μ-oxo-bis{oxomolybdate(V)}]·n-hydrates, n=3, 4, and 6, are the antiferromagnetic dimers with an exchange interaction within a pair of Mo(V) ions of about $-150\,k$ and an averaged g-value of 1.91. The magnetic moments of only about 0.5 Bohr magneton are localized at Mo(V) sites. In these salts, too, a π-bonding structure in each dimer is considered to make a contribution to the diamagnetic susceptibility of about -4.0×10^{-5} (CGSemu). A broad minimum of the molar magnetic susceptibility of [μ-(ethylenediaminetetraacetato)-di-μ-oxo-bis{oxomolybdate(V)}] salts was considered due to the conformation interconversion.

Polynuclear coordination complex compounds of early transition metals with bridges of sulfur between metal ions sometimes show unstable magnetic behaviours. Some compounds among them, for example, Xanthine Oxidase, are well known to have activities as enzymes.[1]

$Na_2[Mo_2O_2S_2(cysteine)_2]\cdot4H_2O$[2] and $Na_2[Mo_2O_2S_2(histidine)_2]\cdot H_2O$,[2] which are Mo(V) dimers with disulfido bridges, and $[Mo_2O\{O_2(C_2H_5OCS_2)_2\}_2]$,[3] which is a Mo(V) dimer with an oxygen bridge, have been reported to be diamagnetic in solid phase.

$(PyH)_4[Mo_2O_4(NCS)_4]$ has been reported to be paramagnetic with Bohr magneton numbers of 0.59 at 293 K and of 0.39 at 120 K. $Na_2[Mo_2O_4(edta)]\cdot4H_2O$ is also known to be paramagnetic at 293 K. Such paramagnetism with small Bohr magneton numbers was observed by Mitchell and Williams.[4]

In the present paper, the magnetic properties of $Na_2[Mo_2O_2S_2(edta)]\cdot nH_2O$($n$=2 and 3) and $Na_2[Mo_2O_4(edta)]\cdot nH_2O$ (n=3, 4, and 6) are investigated as a first step to elucidate the complex activities of Mo(V) dimer structure in the many enzymes.[2] The sexadentate ethylenediaminetetraacetate salts were chosen as the most strongly constructed dimers. The edta ligand coordinates to each molybdenum atom through two carboxylates and with one nitrogen. Mo(V) was chosen because it is in the simplest $4d^1$ state.

Experimental

Chemicals. $Na_2[Mo_2O_2S_2(edta)]\cdot nH_2O$ (n=2 and 3) and $Na_2[Mo_2O_4(edta)]\cdot nH_2O$ (n=3, 4, and 6) were synthesized following Ott *et al.*,[5] Spivack and Dori,[6] and Pecsok and Sawyer.[7] Numbers of crystalline waters were determined from the results of chemical analysis on C, H, and N, as shown in Table 1.

Measurements. The magnetic susceptibilities were measured by the Faraday method balance (Shimadzu MB-2) under about 6000 G** of applied field using the full scale 2 dyn range. An airtight sample cell was made of Teflon. As the measured amount of susceptibility was very small, the measurements of the empty cell were carefully done to assure the calibrations. As a standard of the magnetic susceptibility, $[Cr(NH_3)_6]Cl_3$ or NaCl was used.

Electron paramagnetic resonances were observed on powder samples by a JEOL PE-3X with a microwave oscillator ES-SCXA. Signals were found with 128 min/2000 G scanning under 10 G modulation at amplitude magnified by 1000. When the resonance was observed at low temperatures, DPPH packed in a thin Teflon tubing was put in the sample as reference.

Measurements of X-ray powder patterns and differential scanning calorimetry were made by usual methods.

Results and Discussion

Molar magnetic susceptibilities of $Na_2[Mo_2O_2S_2(edta)]\cdot nH_2O$, n=2 and 3, which were corrected for atomic diamagnetism using Pascal's law and did not need to be corrected for the temperature independent paramagnetism in view of the absence of absorption in the near infrared region, were less than 1.0×10^{-4} cm^3 (CGSemu) or 1.3×10^{-9} m^3 (SI) and showed a very broad maximum between liquid N_2 temperature and room temperature. The atomic diamagnetic susceptibilities of these salts are about -3×10^{-4} cm^3 (CGSemu) or -4×10^{-9} m^3 (SI) as shown in Table 2; therefore the magnetic susceptibilities characteristic of the magnetic dimers with antiferromagnetic mutual exchange interactions are submerged beneath the sea of the diamagnetism. But at room temperature, namely at higher temperature than that showing the broad maximum of the susceptibilities, electron paramagnetic resonances (X-band) were observed in each salt around 3000 G of the applied field: widths were 600—800 G, showing rapid spin lattice relaxations. Figure 1a shows the experimental molar magnetic susceptibility of $Na_2[Mo_2O_2S_2(edta)]\cdot2H_2O$ as a function of temperature. This curve is already corrected for atomic diamagnetic susceptibility of -2.99×10^{-4} cm^3

** 1 G = 10^{-4} T.

TABLE 1. ANALYTICAL DATA

Compound	Found(%)			Calcd(%)		
	C	H	N	C	H	N
$Na_2[Mo_2O_2S_2(edta)]\cdot 2H_2O$	17.95	2.52	4.38	18.2	2.45	4.26
$Na_2[Mo_2O_2S_2(edta)]\cdot 3H_2O$	17.59	2.60	4.19	17.8	2.68	4.14
$Na_2[Mo_2O_4(edta)]\cdot 3H_2O$	18.02	3.28	4.35	18.65	2.82	4.35
$Na_2[Mo_2O_4(edta)]\cdot 4H_2O$	17.71	3.14	4.21	18.14	3.04	4.23
$Ba[Mo_2O_4(edta)]\cdot 6H_2O$	15.79	2.62	3.69	15.86	3.19	3.70

TABLE 2. MOLAR MAGNETIC SUSCEPTIBILITIES, g-VALUES AND LATTICE CONSTANTS

	$Na_2[Mo_2O_2S_2$-(edta)]$\cdot 2H_2O$	$Na_2[Mo_2O_2S_2$-(edta)]$\cdot 3H_2O$	$Na_2[Mo_2O_4$-(edta)]$\cdot 3H_2O$	$Na_2[Mo_2O_4$-(edta)]$\cdot 4H_2O$	$Ba[Mo_2O_4$-(edta)]$\cdot 6H_2O$
χ'_M[a] at 273.15 K/cm³ (CGSemu)	8.4×10^{-5}	9.4×10^{-5}	1.8×10^{-5}	8.6×10^{-5}	6.4×10^{-5}
$\chi_{dia.\ atom.}$/cm³ (CGSemu)	-29.9×10^{-5}	-31.2×10^{-5}	-26.0×10^{-5}	-27.3×10^{-5}	-31.3×10^{-5}
$\chi_{looped\text{-}bonding}$/cm³ (CGSemu)	-5.0×10^{-5}	-5.0×10^{-5}	-4.0×10^{-5}	-4.0×10^{-5}	-4.0×10^{-5}
χ_M[b] at 273.15 K/cm³ (CGSemu)	13.4×10^{-5}	14.4×10^{-5}	5.8×10^{-5}	12.6×10^{-5}	10.4×10^{-5}
χ_M[b] at 273.15 K/m³ (SI)	1.68×10^{-9}	1.81×10^{-9}	7.29×10^{-10}	1.58×10^{-9}	1.31×10^{-9}
g-Values	$g_{av}=2$	$g_{av}=2$	$g_1=1.8700$	$g_1=1.8780$	
			$g_2=1.9184$	$g_2=1.9170$	
			$g_3=1.9328$	$g_3=1.9330$	
Orthorhombic lattice constants/Å	$a=27.838$	$a=27.534$	$a=12.815$	$a=12.834$	$a=14.129$
	$b=6.948$	$b=6.905$	$b=6.130$	$b=6.109$	$b=6.497$
	$c=22.668$	$c=23.264$	$c=19.478$	$c=19.288$	$c=23.860$

a) χ'_M: Experimental molar magnetic susceptibility which is corrected for atomic diamagnetism. b) χ_M: Molar magnetic susceptibility which is corrected for atomic diamagnetism and looped π-bonding diamagnetism.

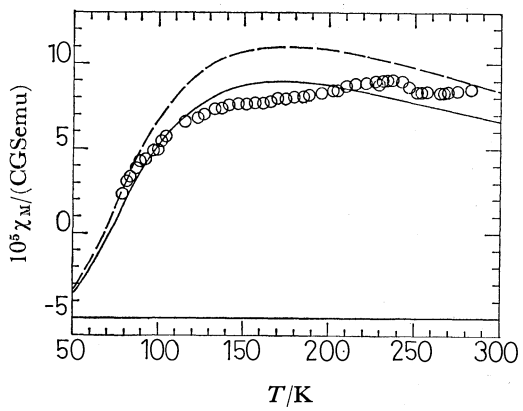

Fig. 1a. The molar magnetic susceptibility of $Na_2[Mo_2O_2S_2(edta)]\cdot 2H_2O$. ○: χ'_M that is the experimental molar magnetic susceptibility corrected for only atomic diamagnetism. ----: The calculated molar magnetic susceptibility of a dimer with $J_{12}=-140k$, $g=2$ and the effective Bohr magneton number $\mu_{eff}=0.56$ at 273.15 K. A base line of this curve is taken at -5.0×10^{-5} (CGSemu). ——: The calculated molar magnetic susceptibility of a dimer with $J_{12}=-140k$, $g=2$, and $\mu_{eff}=0.52$ at 273.15 K. Its base line is at -5.0×10^{-5} (CGSemu).

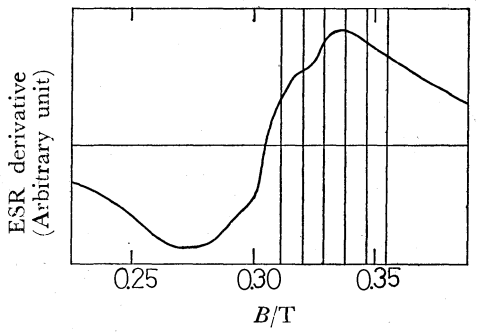

Fig. 1b. The ESR derivative curve of $Na_2[Mo_2O_2S_2$-(edta)]$\cdot 2H_2O$ on powder. The ordinate is in an arbitrary unit. Six lines parallel to the ordinate show the hyperfine splittings of a Mn(II) salt.

(CGSemu) or -3.76×10^{-9} m³ (SI) following Pascal's law. A π-bonding looped structure may have an anisotropic diamagnetic susceptibility because the π-electrons can move along the looped structure when a magnetic field is applied. Lonsdale[8] showed that the aromatic rings give rise to anisotropic diamagnetic susceptibilities. Namely, a looped π-bonding structure with an effective radius r has an anisotropic diamagnetic susceptibility of $\chi_{ring}=(-Ne^2/4mc^2)\sum_p r^2$, where N is the Avogadro number, p is the number of π-electrons in the π-bonding linkage and other symbols have the usual meanings. The unit of e is CGSesu and r is taken in Å. Following her method, the projections of the area of π-bonding looped structure of the Mo(V) dimers on the planes perpendicular to the external magnetic field directions were calculated in order to estimate the anisotropic diamagnetic susceptibilities. The following linkage was considered to be effective in the dimer: 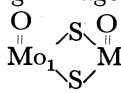 (*cf.* Fig. 6. In the places of the oxygen double bridges in the figure, $[Mo_2O_2S_2(edta)]$ salts have double bridges of sulfur.) with effective area 4.96 Å² [6] and 22 movable π-electrons, that is, three 4p electrons from each Mo(V)

ion whose ligands are a terminal O^{2-} ion, two s^{2-} ions, two O^- ions and a N atom, three 3p electrons from each bridging S^{2-}, and five 2p electrons from terminal O^{2-} ions were accounted for. The diamagnetic susceptibility estimated in this way is about -5.0×10^{-5} cm^3 (CGSemu) or -6.3×10^{-10} m^3 (SI). Setting this value as a new base line, a fit of the experimental magnetic susceptibility to the theoretical susceptibility of the dimer was investigated. If $\vec{S}_1$ and $\vec{S}_2$ denote the spin vectors of the two Mo(V) ions within a dimer and J_{12} the mutual exchange interaction between $\vec{S}_1$ and $\vec{S}_2$, the Hamiltonian $H=-2J_{12}\times(\vec{S}_1\cdot\vec{S}_2)$[9] is taken to calculate the magnetic susceptibility. For the Mo(V) dimer, the molar magnetic susceptibility[1] is

$$\chi_M=\frac{2N\beta^2}{kT}\frac{4}{3+\exp\left(\frac{-2J_{12}}{kT}\right)}, \quad (1)$$

where $g=2$ is used. β is the Bohr magneton, k is Boltzmann's constant and T is absolute temperature. In Fig. 1b an ESR derivative curve of $Na_2[Mo_2O_2S_2$-(edta)]$\cdot2H_2O$ is shown to indicate $g_{av}=2$. The very broad absorption is characteristic of di-μ-sulfido ligands. A tolerable fit of the magnetic susceptibility was obtained if magnetic moments of 0.52 Bohr magneton are assumed to be localized at the Mo sites at 273.15 K, with $J_{12}=-140k$. If one 4d electron of $S=1/2$ is localized at each Mo(V) ion site, the effective Bohr magneton number at 273.15 K is about 0.94.

The molar magnetic susceptibility and ESR of Na_2-$[Mo_2O_2S_2$(edta)]$\cdot3H_2O$ were similar to those of Na_2-$[Mo_2O_2S_2$(edta)]$\cdot2H_2O$ but not completely the same. Therefore X-ray powder patterns were checked for both of $Na_2[Mo_2O_2S_2$(edta)]$\cdot nH_2O$, $n=2$ and 3. These could be assigned to the orthorhombic symmetry, like that of $Cs_2[Mo_2O_2S_2$(edta)]$\cdot2H_2O$ at room temperature. The lattice constants are shown in Table 2, which are near each other but not completely the same, corresponding to the experimental results of the magnetic susceptibilities and ESR.

The experimental molar magnetic susceptibilities of $Na_2[Mo_2O_4$(edta)]$\cdot nH_2O$ ($n=3$, 4, and 6) corrected for the atomic diamagnetism also were smaller than 1.0×10^{-4} cm^3 (CGSemu) or 1.3×10^{-9} m^3 (SI). The atomic diamagnetic susceptibilities are about -3×10^{-4} cm^3 (CGSemu) or -4×10^{-9} m^3 (SI); therefore, Na_2-$[Mo_2O_4$(edta)]$\cdot nH_2O$ salts are seemingly diamagnetic. The molar magnetic susceptibility of $Na_2[Mo_2O_4$-(edta)]$\cdot4H_2O$ is plotted in Fig. 2a. Between liquid N_2 temperature and room temperature, the susceptibility shows two broad maxima accompanied by a very broad minimum centerd about 180 K. As in the case of $Na_2[Mo_2O_2S_2$(edta)]$\cdot nH_2O$ salts, the diamagnetism due to the π-bonding looped structure in the Mo(V) dimer ion was estimated to be about -4.0×10^{-5} cm^3 (CGSemu) or -5.0×10^{-10} m^3 (SI), namely,

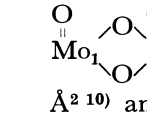

($cf.$ Fig. 5) has an effective area of 3.71 Å^2 [10] and the 22 π-electrons consist of three 4p electrons from each Mo^{5+} ion, three 2p electrons from each bridging O^{2-}, and five 2p electrons from each terminal O^{2-} ion. In Fig. 2b, the ESR of $Na_2[Mo_2O_4$-(edta)]$\cdot4H_2O$ is shown. The signal was obtained by 64 min/1000 G scanning with amplitude magnified 1600 times. The best fit of the g-values to the experimental signals was a set of $g_1=1.8780$, $g_2=1.9170$, and $g_3=1.9330$, with a width of 8 G, neglecting the hyperfine structure which is seen in the ESR but is too weak to analyse by a simulation. It is certain that the spin-lattice relaxation times of di-μ-oxo-bis{oxomolybdate}salts are longer than those of di-μ-sulfido-bis-{oxomolybdate}salts. In Fig. 2a, the dashed line shows the curve of the theoretical magnetic susceptibility with $J_{12}=-150k$, $g_{av}=1.91$ and localized spins of about 0.53 Bohr magneton at 273.15 K and the solid line shows the curve with $J_{12}=-150k$, $g_{av}=1.91$ and localized magnetic moments of 0.51 Bohr magneton at 273.15 K. The base line of the theoretical curve is taken at -4.0×10^{-5} cm^3 (CGSemu) or -5.0×10^{-10} m^3 (SI). To see what is the anomalous temperature dependence of the magnetic susceptibility of this Mo(V) dimer, namely the broad minimum of the susceptibility ceterd at about 180 K, the temperature dependence of ESR was observed. As is shown in Fig. 3, no decrease of the ESR signal between 210 K and 150 K was observed. Therefore this anomalous temperature dependence of the magnetic susceptibility

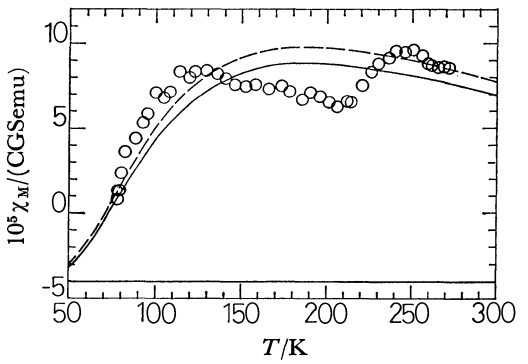

Fig. 2a. The molar magnetic susceptibility of Na_2-$[Mo_2O_4$(edta)]$\cdot4H_2O$. ○: χ'_M, namely, the experimental molar magnetic susceptibility which is corrected for only atomic diamagnetism. ----: The calculated molar magnetic susceptibility of a dimer with $J_{12}=-150k$, $g=1.91$, and $\mu_{eff}=0.53$ at 273.15 K. ——: A dimer with $J_{12}=-150k$, $g=1.91$, and $\mu_{eff}=0.51$ at 273.15 K. The base line of the calculated curves is taken at -4.0×10^{-5} (CGSemu).

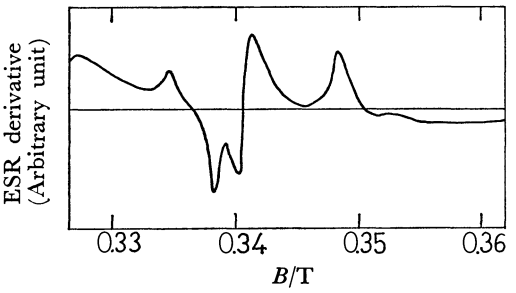

Fig. 2b. The ESR derivative curve of $Na_2[Mo_2O_4$-(edta)]$\cdot4H_2O$ on powder. The ordinate is in an arbitrary unit.

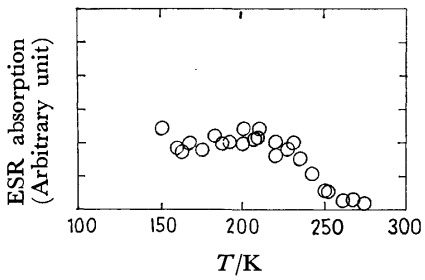

Fig. 3. The temperature dependence of the ESR absorption of $Na_2[Mo_2O_4(edta)]\cdot 4H_2O$ on powder.

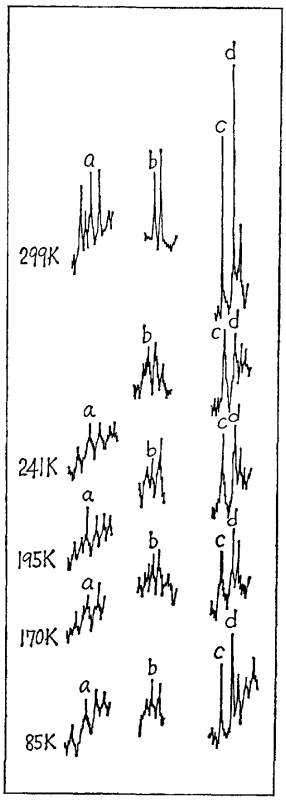

Fig. 4. Temperature dependence of some X-ray diffaction powder patterns. a: Atomic plane distance 3.789 Å, b: 4.822 Å, c: 5.724 Å, and d: 5.946 Å. All the signals were measured by same conditions. In the figure, patterns of each temperature are drawn from the same base line.

is not due to the paramagnetic spins. Then the temperature dependence of the powder X-ray pattern was checked on $Na_2[Mo_2O_4(edta)]\cdot 3H_2O$. When the temperature was changed from 85 K to 299 K, the atomic plane distances did not change but widths and intensities of some lines changed, that is, the widths of the lines of atomic plane distances of 5.946 Å, 5.724 Å, 4.822 Å, and 3.789 Å were broader around 190 K than those of lower and higher temperatures, as shown in Fig. 4. The temperature dependence of the X-ray diffraction intensities was considered due to dynamic vibrations of a conformation, as will be shown below. Differential scanning calorimetries were observed for $Na_2[Mo_2O_4(edta)]\cdot 3H_2O$ and $Na_2[Mo_2O_2S_2(edta)]\cdot 2H_2O$. The former (Fig. 5) showed an exothermic signal at temperatures between 190 K and 230 K in the measurement on cooling from room temperature to 130 K, but the latter showed nothing. It is known from the measurement of ^{13}C NMR[11] that $[Mo_2O_4(edta)]^{2-}$ ion in the aqueous solution has a conformation interconversion. According to Blackmer *et al.*, the ethylene diamine backbone of edta chelate has an interconversion between the two isomeric forms, seen in Fig. 6, which is too rapid at 310 K to split the ^{13}C NMR of about 60 MHz, but at 273 K, the absorption line splits into two, that is, the relaxation time of each conformation becomes long enough to give the line splitting. They assigned a value of 0.5 to the transition coefficient k, since the ethylenediamine backbone of edta complex has an equal probability of returning to its original isomeric conformation or continuing the conversion process to achieve the other isomeric conformational form after reaching a planar intermediate. In the solid state of $[Mo_2O_4(edta)]^{2-}$ complex in a pressed cell, the interconversion has been considered to happen over a broad temperature region from 190 K to 230 K, centerd about 210 K. It is said by X-ray analysis[6] that at room temperature, $[Mo_2O_4(edta)]$ salts have two isomeric conformations with equal probability of the ethylenediamine backbone of edta. The crystal would transform from a higher temperature state to a preferred lower temperature form of the ethylenediamine by the interconversion in the broad temperature region. The interconversion of edta is considered to produce a change of the diamagnetic susceptibility due to the π-bonding

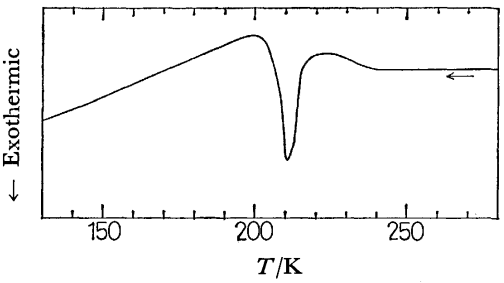

Fig. 5. The differential scanning calorimetry curve of $Na_2[Mo_2O_4(edta)]\cdot 3H_2O$. The graph shows that the sample releases heat in the region between 230 K and 190 K on cooling from room temperature to 130 K.

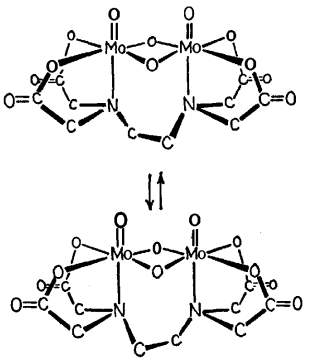

Fig. 6. The interconversion between two isomeric conformations of $[Mo_2O_4(edta)]$ anion.

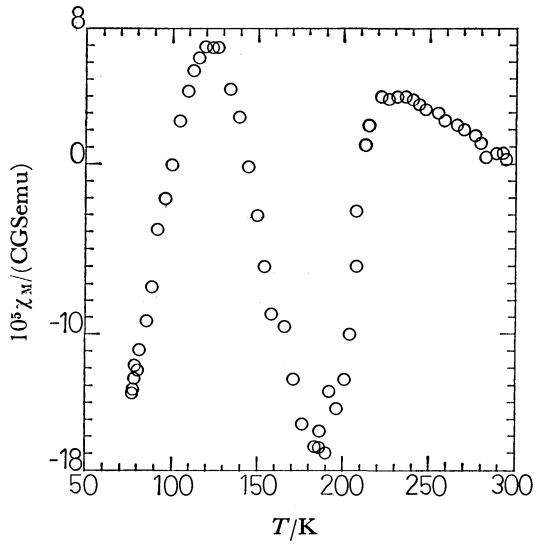

Fig. 7. The molar magnetic susceptibility of $Na_2[Mo_2O_4(edta)]\cdot 3H_2O$ corrected for only atomic diamagnetism as a function of temperature.

looped 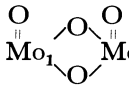 structure, though it is not elucidated yet that the change of the diamagnetic susceptibility is caused by the change of the number of the movable electrons or the change of the effective area of the π-bonding looped structure. Now, though we explained the magnetic susceptibility data of $Na_2[Mo_2O_2S_2(edta)]\cdot nH_2O$ by a simple dimer model, the fit with the theoretical curve was never satisfactory. There may be an interconversion between the two forms of the ethylenediamine of edta in di-μ-sulfido-bis{oxomolybdate(V)} ion and it would make the fit poor. But much less energy would be needed for the interconversion because the distances between two Mo(V) ions and two N atoms in the edta in di-μ-sulfido-bis{oxomolybdate} ion are longer than those of di-μ-oxo-bis{oxomolybdate} ion. Thus the difference of the two forms of the ethylenediamine is so small that the DSC signal could not be observed.

We would like to remark on a datum of the molar magnetic susceptibility of $Na_2[Mo_2O_4(edta)]\cdot 3H_2O$, which showed a much smaller magnetic susceptibility, as shown in Fig. 7, than those of $Na_2[Mo_2O_4(edta)]\cdot 4H_2O$ and $Ba[Mo_2O_4(edta)]\cdot 6H_2O$ though its temperature dependence is similar to them. This phenomenon suggests this salt may be trapping some extra even number of electrons in the π-bonding looped structure.

The experimental results show that the complete determination of the diamagnetic susceptibility on a molecule with π-bonding looped structure is necessary. Of course, the molecular orbitals of many polycyclic aromatic hydrocarbon compounds have been calculated and from their energy under an applied magnetic field anisotropic diamagnetic susceptibilities are obtained. But the molecular orbital calculations at present are possible to molecules with 40 atoms and 127 orbitals, therefore the complete calculation of the diamagnetic susceptibilities for molecules containing 4d transition metals with π-bonding looped structure which have more than 200 orbitals may not be possible in the near future. We are going to elucidate the diamagnetic susceptibilities of 4d transition metal coordination compounds with π-bonding looped structures by the observation of the non-magnetic 4d transition metal coordination compound molecules with π-bonding looped structures.

The authors would like to thank Professor Masayasu Mori, Osaka City University, for the measurements of the magnetic susceptibility and for valuable discussions. They wish to thank Dr. Yukio Sugiura, Kyoto University, for the observations of the ESR and for valuable suggestions. One of the authors (H.K.) thanks the faculty and staff of Osaka City University for their kind hospitality during her stay for the measurements.

References

1) E. I. Stiefel, "Proceedings of the Inorganic Chemistry," An Interscience Publication, John Wiley and Sons, New York (1977), Vol. 22.
2) B. Spivack and Z. Dori, *J. Chem. Soc., D*, **1970**, 1716.
3) A. B. Blake, F. A. Cotton, and J. S. Wood, *J. Am. Chem. Soc.*, **86**, 3024 (1964).
4) P. C. H. Mitchell and R. J. P. Williams, *J. Chem. Soc.*, **1962**, 4570.
5) V. R. Ott, D. S. Swieter, and F. A. Schultz, *Inorg. Chem.*, **16**, 2538 (1977).
6) B. Spivack and Z. Dori, *J. Chem. Soc., Dalton Trans.*, **1973**, 1173.
7) R. L. Pecsok and D. T. Sawyer, *J. Am. Chem. Soc.*, **78**, 5496 (1956)
8) K. Lonsdale, *Proc. R. Soc. London, Ser. A*, **159**, 149 (1936).
9) K. Kambe, *J. Phys. Soc. Jpn.*, **5**, 48 (1950).
10) F. A. Cotton and S. M. Morehouse, *Inorg. Chem.*, **4**, 1377 (1965).
11) G. L. Blackmer, K. J. Johnson, and R. L. Roberts, *Inorg. Chem.*, **15**, 596 (1976).

 © 1983 The Chemical Society of Japan Bull. Chem. Soc. Jpn., 56, 113—121 (1983)

CD Spectra and Absolute Configurations of *fac*(*a*,*b*,*c*)-[Co(a)(b)(c)(1,4,7-Triazacyclononane)]$^{n+}$ Complexes

Shuhei Fujinami,* Takao Hosokawa, and Muraji Shibata

Department of Chemistry, Faculty of Science, Kanazawa University, Kanazawa 920

(Received May 12, 1982)

Seventeen kinds of *fac*(*a*,*b*,NH_3)-[Co(a)(b)(NH_3)(tacn)]$^{n+}$ complexes (a, b=CN^-, NO_2^-, SO_3^{2-}, NCS^-, N_3^-, CH_3COO^-, H_2O, OH^-, Cl^-, or Br^-; tacn=1,4,7-triazacyclononane) have been prepared and optically resolved by column chromatography. The absolute configurations of these complexes have been determined by referring to the CD spectra of the related [Co(a)(gly)(tacn)]$^{n+}$ complexes (a=CN^-, NO_2^-, NCS^-, N_3^-, or Cl^-). It has been found that the signs of the Cotton peaks observed in the first absorption band region are closely related to the ligand field strengths of the unidentate ligands, and that the dominant Cotton peak is associated with the electronic transition which arises in the plane containing no ammonia molecule.

There are some reports on optically active cobalt(III) complexes with a chiral arrangement of donor atoms around a central metal ion. These complexes can be classified into two groups. One includes *cis-cis*-[Co(a)$_2$(b)$_2$(CC)]- and *all-cis*-[Co(a)$_2$(b)$_2$(c)$_2$]-type complexes in which the central metal ions are surrounded with three kinds of donor atoms.[1-4] A typical instance is an *all-cis*-[Co(CN)$_2$(NH_3)$_2$(H_2O)$_2$]$^+$ complex, and Mason[5] has attempted to explain the optical activity of the complex in terms of a dynamic coupling model

The other group represents a *fac*(*D*)-[Co(a)(BC)(DDD)]-type complexes where one octahedral face of the complex is coordinated with a symmetrical terdentate ligand such as 1,4,7-triazacyclononane (=tacn) and the opposite face is occupied by three kinds of donor atoms.[6-9] In spite of the existence of two ring-pairs in this type of complex, the optical activity is considered to be mainly derived from a chiral arrangement of donor atoms.[8,9] However, the bidentate ligand (BC) used is limited to an amino acidate ion, and there is little information on the relation between the CD spectrum and the absolute configuration of the complex.

Recently, we reported the preparations and optical resolutions of [Co(CN)(Br)(NH_3)(tacn)]$^+$ [10] and *fac*-(NH_3)-[Co(NO_2)(gly)(NH_3)$_3$]$^+$.[11] No ring-pair is contained in these complexes, and these types of complexes are adequate to allow a study of the optical activity of the complexes with a chiral arrangement of donor atoms.

This paper will deal with further syntheses and optical resolutions of the complexes with a series of [Co(a)(b)(NH_3)(tacn)]$^{n+}$ (a, b=CN^-, NO_2^-, SO_3^{2-}, NCS^-, N_3^-, H_2O, OH^-, CH_3COO^-, Cl^-, or Br^-). The absolute configurations are determined by referring to the CD spectra of [Co(a)(gly)(tacn)]$^{n+}$ (a=CN^-, NO_2^-, NCS^-, N_3^-, or Cl^-)[8] and by chemical derivations from optically active complexes. The signs of the Cotton peaks in the first absorption band region are discussed on the basis of the absolute configurations of the complexes.

Experimental

Ligand. 1,4,7-Triazacyclononane trihydrochloride (tacn·3HCl) was prepared by the literature method.[12]

Preparation of Complexes. *1) [Co(CN)(Br)(NH_3)(tacn)]Cl*: The preparation of this complex has been described in an earlier paper.[10] The description will be given here again with a few modifications. To an aqueous suspension of the complex, [Co(CN)(SO_3)(NH_3)(tacn)][10] (1 g, 3 mmol in 2 cm^3 H_2O), which had been prepared from [Co(CN)(SO_3)(NH_3)$_4$],[13] was added 10 cm^3 of 47% HBr little by little, and the mixed solution was stirred at 50 °C for 6 h, whereupon the color of the solution turned red. After cooling to room temperature, large amounts of ethanol and ether were successively added to the solution. The precipitated material was filtered and dissolved in water (500 cm^3). The solution was chromatographed on a column of Dowex 50W-X8 (3 cm × 10 cm, Na^+ form). By elution with a 0.3 mol/dm^3 NaCl solution, a red band was discharged from the column. The effluent was concentrated by a rotary evaporator below 35 °C, with simultaneous removal of the precipitated salt used as the eluting agent. After addition of a small amount of ethanol to the final filtrate, reddish crystals deposited on standing the mixture in a refrigerator. This crude product was recrystallized from warm water (*ca.* 40 °C). The yield was *ca.* 0.5 g. Found: C, 24.16; H, 5.35; N, 19.96%. Calcd for [Co(CN)(Br)(NH_3)(tacn)]Cl: C, 24.26; H, 5.25; N, 20.21%.

2) [Co(CN)(H_2O)(NH_3)(tacn)](ClO_4)$_2$·H_2O: An aqueous solution (10 cm^3) of the complex, [Co(CN)(Br)(NH_3)(tacn)]Cl (0.7 g, 2 mmol), was adjusted to pH 9 with 5 mol/dm^3 KOH, and stirred until its color changed from red to orange, whereupon the corresponding hydroxo complex, [Co(CN)(OH)(NH_3)(tacn)]$^+$, formed. After the solution had been acidified with 1 mol/dm^3 $HClO_4$ until pH 5, the resulting solution was once filtered and diluted to 500 cm^3 with water. This solution was poured onto a column of SP-Sephadex C-25 (4.5 cm × 20.0 cm, Na^+ form). By elution with 0.1 mol/dm^3 $HClO_4$, a yellow band was discharged from the column. The eluate was treated in a similar way to that in 1). The yield was *ca.* 0.4 g. Found: C, 18.17; H, 4.60; N, 15.11%. Calcd for [Co(CN)(H_2O)(NH_3)(tacn)](ClO_4)$_2$·H_2O: C, 18.03; H, 4.77; N, 15.03%.

3) [Co(CN)(Cl)(NH_3)(tacn)]Cl: For the preparation of the [Co(CN)(H_2O)(NH_3)(tacn)]$^{2+}$ complex, the elution was carried out with 0.1 mol/dm^3 HCl. When the eluate was concentrated to a small volume, the solution turned red. The solution was stirred at 40 °C for 2 h, and poured onto a column of Dowex 50W-X8 (4 cm × 10 cm, H^+ form). The eluate obtained by the elution with 0.3 mol/dm^3 HCl was concentrated to a small volume by a rotary evaporator at 35 °C, and a small amount of ethanol was added to the concentrate. This solution was kept in a refrigerator until red crystals of the desired complex deposited. The crude product was recrystallized from 6 mol/dm^3 HCl. The yield was *ca.* 0.5 g. Found: C, 27.70; H, 6.13; N, 23.21%

Calcd for $[Co(CN)(Cl)(NH_3)(tacn)]Cl$: C, 27.83; H, 6.01; N, 23.18%.

4) *$[Co(CN)(NO_2)(NH_3)(tacn)]Cl\cdot 1.3H_2O$*: To a solution of $[Co(CN)(H_2O)(NH_3)(tacn)](ClO_4)_2\cdot H_2O$ (1 g, in 50 cm³ H_2O), was added $NaNO_2$ (1 g, 14 mmol). The solution was stirred at room temperature until its color changed from orange to lemon yellow. The reacted solution was diluted to 500 cm³ and charged on a column of Dowex 50W-X8 (3 cm × 5.0 cm, Na^+ form). By elution with a 0.3 mol/dm³ NaCl solution, a lemon yellow band was discharged from the column. The effluent was treated in a similar way to that in 1). The yield was *ca.* 0.7 g. Found: C, 25.29; H, 6.14; N, 24.83%. Calcd for $[Co(CN)(NO_2)(NH_3)(tacn)]Cl\cdot 1.3H_2O$: C, 25.02; H, 6.18; N, 25.01%.

5) *$[Co(CN)(NCS)(NH_3)(tacn)]Cl\cdot 2H_2O$*: An aqueous solution (50 cm³) containing $[Co(CN)(H_2O)(NH_3)(tacn)](ClO_4)_2\cdot H_2O$ (0.5 g) and KSCN (1 g, 10 mmol) was adjusted to pH 3 with $HClO_4$, and then stirred at 50 °C for 4—5 h. The resulting orange solution was chromatographed in the same manner as 1). The yield was *ca.* 0.3 g. Found: C, 26.81; H, 6.05; N, 26.62%. Calcd for $[Co(CN)(NCS)(NH_3)(tacn)]Cl\cdot 2H_2O$: C, 26.64; H, 6.15; N, 23.30%.

6) *$[Co(CN)(N_3)(NH_3)(tacn)]Cl$*: This complex was prepared in the same manner as the isothiocyanato complex, except for the use of NaN_3 (1.0 g, 15 mmol) in place of KSCN. The crystals of the desired complex could not be obtained from the orange effluent, because the desired complex decomposed in the concentrated solution. Therefore, the ε value of the desired complex was determined by atomic absorption analysis with the freshly eluted solution.

7) *$[Co(CN)(SO_3)(NH_3)(tacn)]\cdot 0.5H_2O$*: This complex has been prepared from the reaction of $[Co(CN)(SO_3)(NH_3)_4]$ with tacn·3HCl.[10] In this work, the complex was derived from the $[Co(CN)(H_2O)(NH_3)(tacn)]^{2+}$ complex. To a solution of the aqua complex salt (0.3 g, in 20 cm³ H_2O) was added $NaHSO_3$ (0.5 g, 5 mmol), and the solution was adjusted to pH 4 with $HClO_4$. The solution was then stirred at room temperature until its color changed from orange to lemon yellow. The resulting solution was poured onto a column of Dowex 50W-X8 (3 cm × 30 cm, Na^+ form) and the adsorbed species on the column was eluted with water. Two components of noncharged species were collected. The first eluted species was unknown. The fraction of the second component was concentrated by a rotary evaporator at *ca.* 35 °C. This fraction was identified with the desired complex by absorption spectrum. The yield was *ca.* 0.1 g.

8) *$[Co(CN)(CH_3COO)(NH_3)(tacn)]Cl$*: An aqueous solution (20 cm³) containing the aqua complex salt (0.5 g) and potassium acetate (1 g, 10 mmol) was adjusted to pH 4 with acetic acid, and then stirred at 40 °C for 3 h. The resulting solution was concentrated to a small volume by a rotary evaporator at 40 °C, filtered once, and diluted to 1 dm³ with water. This solution was poured onto a column of Dowex 50W-X8 (3.0 cm × 20 cm, Na^+ form). By elution with a 0.3 mol/dm³ NaCl solution, three components corresponding to univalent cationic species were collected. The optical resolution of each species was attempted by means of column chromatography (Dowex 50W-X8, 200—400 mesh, 2.5 cm × 60 cm) by use of a 0.3 mol/dm³ $Na_2[Sb_2(d\text{-tart})_2]$ solution as eluent. The absorption and CD spectra of the second species agreed with those of the $[Co(CN)(Cl)(NH_3)(tacn)]^+$ complex. The optical resolution of the third species was unsuccessful and this fact indicated that the third species was not the desired complex. On the other hand, the first species could be resolved into the optical antipodes, and by comparison with the spectra of $[Co(CN)(H_2O)(NH_3)(tacn)]^{2+}$ and $[Co(CN)(OH)(NH_3)(tacn)]^+$, it was considered that this species had a $[Co(C)(O)(N)_4]$ chromophore. Therefore, the first species was assigned to the desired complex, $[Co(CN)(CH_3COO)(NH_3)(tacn)]^+$. The fact that the first species was converted to the $[Co(CN)(Cl)(NH_3)(tacn)]^+$ complex by treatment with 6 mol/dm³ HCl at 40 °C also supported the assignment. The ε value of the desired complex was evaluated in the same manner as in 6), because the yield was very poor.

9) *$[Co(NO_2)_2(NH_3)(tacn)]Cl\cdot 2H_2O$*: The ligand, tacn·3HCl (1.0 g, 4.2 mmol), was dissolved in a minimum amount of water and neutralized with aqueous KOH. The resulting solution was added dropwise to a solution containing *cis*-$[Co(NO_2)_2(NH_3)_4]NO_3$[14] (1.5 g, 5.3 mmol in 50 cm³ H_2O). The mixed solution was adjusted to pH 9—10 with a 5 mol/dm³ KOH solution and stirred at 55 °C for 12 h. Then, the color of the solution changed from orange to wine-red. After cooling to room temperature, the solution was diluted to 2 dm³ with water, and poured onto a column of Dowex 50W-X8 (4 cm × 25 cm, Na^+ form). The adsorbed species was washed with water and eluted with a 0.3 mol/dm³ NaCl solution. Three components of univalent cationic species were collected in each fraction. The second and third species were identified with *trans*- and *cis*-$[Co(NO_2)_2(NH_3)_4]^+$ respectively.[14] The first lemon-yellow fraction was treated in a similar way to that in 1). The yield was *ca.* 0.5 g. Found: C, 19.70; H, 6.20; N, 23.14%. Calcd for $[Co(NO_2)_2(NH_3)(tacn)]Cl\cdot 2H_2O$: C, 19.55; H, 6.01; N, 22.80%.

10) *$[Co(Cl)(H_2O)(NH_3)(tacn)]Cl_2\cdot NaCl$*: This complex was prepared by an acid-hydrolysis of $[Co(NO_2)_2(NH_3)(tacn)]Cl\cdot 2H_2O$. The dinitro complex salt (1.0 g) was dissolved in 1 mol/dm³ HCl (20 cm³) and the solution was stirred at 60 °C for 2 h. After cooling to room temperature, the solution was neutralized with 5 mol/dm³ NaOH and concentrated to a small volume by a rotary evaporator with simultaneous removal of deposited NaCl. The concentrate was adjusted to pH 10 with 5 mol/dm³ NaOH and stirred at room temperature for a while. Then, the solution was diluted to 2 dm³ with water and adjusted to pH 5 with 5 mol/dm³ $HClO_4$. The solution was poured onto a column of SP-Sephadex C-25 (4.0 cm × 25 cm, Na^+ form). The adsorbed species were eluted with 0.1 mol/dm³ NaCl, and three bands were discharged from the column. The eluate for each band was collected in a fraction and submitted to the measurement of the absorption spectrum. The first eluted species was identified with the dinitro complex. The second species, which contained a bivalent cation, was assumed to be the mixture of the $[Co(NO_2)(H_2O)(NH_3)(tacn)]^{2+}$ and $[Co(Cl)(H_2O)(NH_3)(tacn)]^{2+}$ complex. The last red species, which contained a tervalent cation, was assumed to be $[Co(H_2O)_2(NH_3)(tacn)]^{3+}$ complex. This last fraction was treated in a similar way to that in 1). The fact that the color changed from red to purple by concentrating the effluent indicated the formation of $[Co(Cl)(H_2O)(NH_3)(tacn)]^{2+}$ species. The yield was *ca.* 0.5 g. Found: C, 19.11; H, 5.21; N, 13.46%. Calcd for $[Co(Cl)(H_2O)(NH_3)(tacn)]Cl_2\cdot NaCl$: C, 18.57; H, 5.20; N, 14.44%.

11) *$[Co(NCS)(H_2O)(NH_3)(tacn)](ClO_4)_2\cdot H_2O$*: An aqueous solution (20 cm³) containing $[Co(Cl)(H_2O)(NH_3)(tacn)]Cl_2\cdot NaCl$ (1.0 g, 3 mmol) and an equimolar amount of KSCN (0.4 g) was adjusted to pH 3 with 5 mol/dm³ $HClO_4$ and stirred at *ca.* 40 °C for 1 h. After cooling to room temperature, the solution was adjusted to pH 10 with 5 mol/dm³ KOH, and stirred for a while. After dilution to 2 dm³ with water, the diluted solution was neutralized with 5 mol/dm³ $HClO_4$ and poured onto a column of SP-Sephadex

C-25 (4 cm × 25 cm, Na^+ form). At first, by elution with 0.03 mol/dm^3 NaCl, a red band corresponding to an univalent cation was discharged. This species was assigned to a $[Co(NCS)_2(NH_3)(tacn)]^+$ complex by elemental analysis. Found: C, 25.34; H, 4.33; N, 21.35%. Calcd for $[Co(NCS)_2(NH_3)(tacn)]Cl\cdot 0.5H_2O$: C, 24.89; H, 4.70; N, 21.27%. A red band corresponding to the bivalent cation of the desired complex was eluted with 0.1 mol/dm^3 $HClO_4$. The solution was treated in a similar way to that in 1). The yield was *ca.* 0.5 g. Found: C, 16.52; H, 4.03; N, 14.37%. Calcd for $[Co(NCS)(H_2O)(NH_3)(tacn)](ClO_4)_2\cdot H_2O$: C, 16.87; H, 4.46; N, 14.06%.

12) *[Co(NCS)(NO$_2$)(NH$_3$)(tacn)]Cl·H$_2$O*: To a solution of $[Co(NCS)(H_2O)(NH_3)(tacn)](ClO_4)_2\cdot H_2O$ (0.5 g in 20 cm^3 H_2O), was added $NaNO_2$ (1.0 g, 14 mmol). The solution was adjusted to pH 3 with $HClO_4$, and stirred at room temperature until the color changed from red to orange. The resulting solution was treated in the same manner as in 4). The yield was *ca.* 0.3 g. Found: C, 23.20; H, 5.33; N, 22.85%. Calcd for $[Co(NCS)(NO_2)(NH_3)(tacn)]Cl\cdot H_2O$: C, 23.18; H, 5.56; N, 23.17%.

13) *[Co(NCS)(N$_3$)(NH$_3$)(tacn)]Cl·0.5H$_2$O*: An aqueous solution (20 cm^3) containing $[Co(NCS)(H_2O)(NH_3)(tacn)](ClO_4)_2\cdot H_2O$ (0.5 g) and NaN_3 (1 g, 15 mmol) was adjusted to pH 3 with $HClO_4$, and then stirred at 50 °C for 4—5 h. The resulting red solution was treated in a way similar to that in 4). The yield was *ca.* 0.3 g. Found: C, 23.63; H, 5.28; N, 32.05%. Calcd for $[Co(NCS)(NO_2)(NH_3)(tacn)]Cl\cdot 0.5H_2O$: C, 24.04; H, 5.48; N, 32.04%.

14) *[Co(N$_3$)(H$_2$O)(NH$_3$)(tacn)](ClO$_4$)$_2$*: This complex was prepared in the same manner as the $[Co(NCS)(H_2O)(NH_3)(tacn)]^{2+}$ complex, except for the use of NaN_3 (0.4 g, 6 mmol) in place of KSCN. Since the yield was very poor, the crystals of the desired complex could not be obtained. The ε value of the complex was evaluated in the same manner as in 6). This complex was also prepared from $[Co(NCS)(N_3)(NH_3)(tacn)]^+$ by treatment of H_2O_2 in an acidic solution.

15) *[Co(NO$_2$)(H$_2$O)(NH$_3$)(tacn)](ClO$_4$)$_2$*: This complex was prepared by the reaction of the $[Co(NCS)(NO_2)(NH_3)(tacn)]^+$ complex with H_2O_2, or by acid-hydrolysis of the $[Co(NO_2)_2(NH_3)(tacn)]^+$ complex.

Method 1: A solution containing $[Co(NCS)(NO_2)(NH_3)(tacn)]Cl\cdot 0.5H_2O$ (0.2 g in 50 cm^3 30% H_2O_2) was adjusted to pH 3 with 5 mol/dm^3 $HClO_4$ and stirred for 5—6 h. The resulting solution was diluted to 3 dm^3 and poured onto a column of Dowex 50W-X8 (2.5 cm × 20 cm, Na^+ form). By elution with 0.3 mol/dm^3 NaCl, a lemon-yellow band corresponding to univalent cation was discharged. This species was identified with $[Co(CN)(NO_2)(NH_3)(tacn)]^+$. After this, two yellow bands corresponding to bivalent cations were eluted with 1 mol/dm^3 $HClO_4$. The earlier eluate was assigned to the desired complex by its absorption spectrum and the later eluate was assumed to be $[Co(NO_2)(NH_3)_2(tacn)]^{2+}$ species. After neutralizing the earlier eluate, the solution was treated in a similar way to that in 14).

Method 2: On the synthesis of $[Co(Cl)(H_2O)(NH_3)(tacn)]^{2+}$, the orange band corresponding to the bivalent cation was rechromatographed on a column of Dowex 50W-X8 (2.5 cm × 20 cm). The orange and red bands were eluted with 1 mol/dm^3 $HClO_4$. The orange band was assigned to $[Co(NO_2)(H_2O)(NH_3)(tacn)]^{2+}$ and the red band to $[Co(Cl)(H_2O)(NH_3)(tacn)]^{2+}$.

Optical Resolution. Except for the $[Co(NO_2)_2(NH_3)(tacn)]^+$ and $[Co(CN)(SO_3)(NH_3)(tacn)]$ complexes all complexes prepared in this study were partially resolved into the optical antipodes by means of column chromatography. In the cases of bivalent cations, the optical resolutions were carried out on a column of SP-Sephadex C-25 (2.5 cm × 120 cm, Na^+ form) using 0.1 mol/dm^3 $K_2[Sb_2(d\text{-tart})_2]$ solution as eluent. On the other hand, since the $[Co(CN)(NO_2)(NH_3)(tacn)]^+$ and $[Co(CN)(NCS)(NH_3)(tacn)]^+$ complexes were yellowish univalent cations, a column of SP-Sephadex C-25 (2.5 cm × 120 cm, Na^+ form) and 0.03 mol/dm^3 $K_2[Sb_2(d\text{-tart})_2]$ solution as eluent were used. For the remaining complexes, the optical resolutions were performed on a column of Dowex 50W-X8 (200—400 mesh, 2.5 cm × 60 cm, Na^+ form) using 0.3 mol/dm^3 $Na_2[Sb_2(d\text{-tart})_2]$ solution as eluent. When the adsorbed band had descended to one tenth of the column height, the band was washed with water and eluted with 0.1 mol/dm^3 $HClO_4$, 0.03 mol/dm^3 NaCl or 0.3 mol/dm^3 NaCl. The eluates thus concentrated were submitted to the measurements of the CD spectra, while the concentrations of the complex species were evaluated from the absorption spectral data. The isomers are stable enough to measure the spectra in a solution.

Derivation from Optically Active Complexes. The $(-)^{CD}_{470}[Co(CN)(H_2O)(NH_3)(tacn)]^{2+}$ complex could be derived from the $(-)^{CD}_{470}[Co(CN)(Br)(NH_3)(tacn)]^+$ complex, according to the procedure described in 2). Furthermore, the $(-)^{CD}_{470}[Co(CN)(H_2O)(NH_3)(tacn)]^{2+}$ complex could be converted to the $(-)^{CD}_{470}[Co(CN)(Cl)(NH_3)(tacn)]^+$, $(-)^{CD}_{470}[Co(CN)(OH)(NH_3)(tacn)]^+$, $(-)^{CD}_{470}[Co(CN)(NCS)(NH_3)(tacn)]^+$, $(-)^{CD}_{470}[Co(CN)(N_3)(NH_3)(tacn)]^+$, $(+)^{CD}_{470}[Co(CN)(NO_2)(NH_3)(tacn)]^+$, and $(+)^{CD}_{460}[Co(CN)(SO_3)(NH_3)(tacn)]$ by the methods described in 3)—7), respectively. The $(-)^{CD}_{470}[Co(CN)(CH_3COO)(NH_3)(tacn)]^+$ complex was converted to the $(-)^{CD}_{470}[Co(CN)(Cl)(NH_3)(tacn)]^+$ complex by the treatment with 6 mol/dm^3 HCl at 40 °C.

The $(-)^{CD}_{470}[Co(NCS)(H_2O)(NH_3)(tacn)]^{2+}$ complex could be converted to the $(+)^{CD}_{470}[Co(NCS)(NO_2)(NH_3)(tacn)]^+$ and $(-)^{CD}_{470}[Co(NCS)(N_3)(NH_3)(tacn)]^+$ complexes according to the procedures described in 12) and 13), respectively. On the other hand, the oxidation of the $(+)^{CD}_{470}[Co(NCS)(NO_2)(NH_3)(tacn)]^+$ complex by aqueous H_2O_2 at *ca.* pH 3 produced the $(+)^{CD}_{470}[Co(CN)(NO_2)(NH_3)(tacn)]^+$ and $(+)^{CD}_{470}[Co(NO_2)(H_2O)(NH_3)(tacn)]^{2+}$ complexes, which were separated chromatographically. The similar oxidation of the $(-)^{CD}_{470}[Co(NCS)(N_3)(NH_3)(tacn)]^+$ complex produced the $(-)^{CD}_{470}[Co(CN)(N_3)(NH_3)(tacn)]^+$ and $(-)^{CD}_{470}[Co(N_3)(H_2O)(NH_3)(tacn)]^{2+}$ complexes. The absorption and CD spectra of the optical isomers obtained by the derivations coincided with those of the isomers obtained by the optical resolutions. Through the above derivations from optically active complexes, the absolute configurations of all complexes prepared in this work could be correlated, except for the $[Co(Cl)(H_2O)(NH_3)(tacn)]^{2+}$ complex.

Measurements. The absorption spectra in aqueous solutions were recorded with a Hitachi 323 recording spectrophotometer. The CD spectra were measured with a JASCO J-40C automatic recording spectropolarimeter equipped with a JASCO Model J-DPZ data processor for CD. The absorption and CD spectra of hydroxo complex species were measured with solutions of the corresponding aqua complexes alkalized with 5 mol/dm^3 NaOH (pH 10). The hydroxo complex species were chromatographically pure, and the absorption and CD spectra of the hydroxo complexes were returned to the original spectra of the parent aqua complexes, when the solutions were again acidified with $HClO_4$. This fact suggests that the base-hydrolysis proceeds with retention of the configuration. To determine the ε values of the complexes which could not be crystallized, a Hitachi 170-150 atomic absorption spectrophotometer was used.

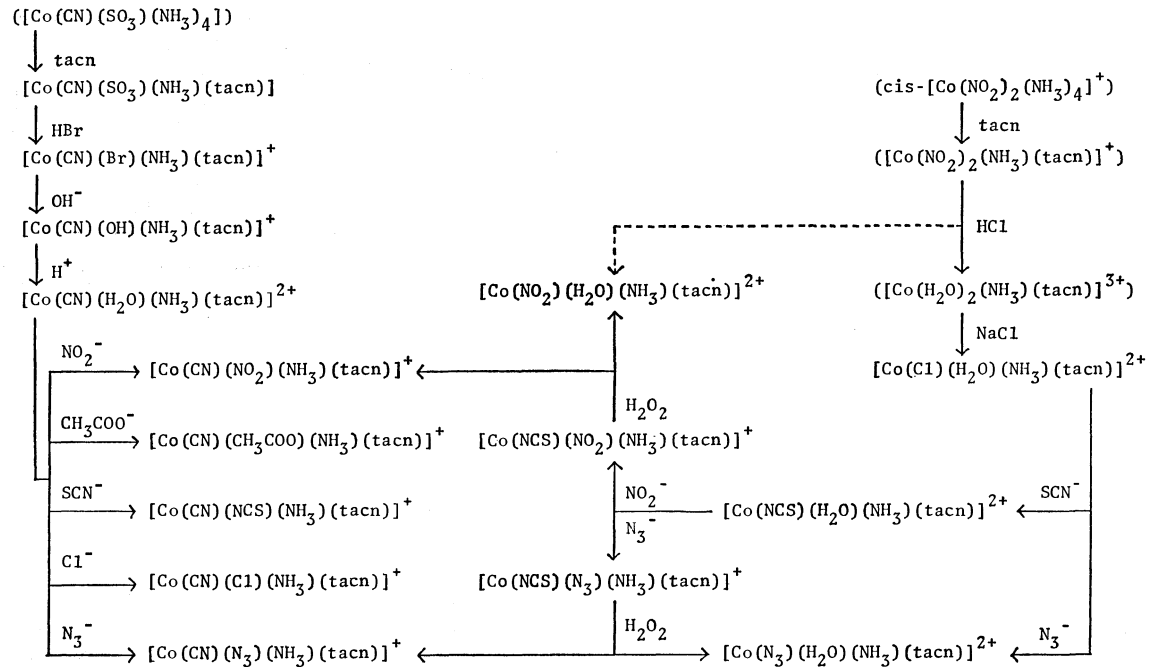

Scheme 1. Pathways of syntheses of $[Co(a)(b)(c)(tacn)]^{n+}$ complexes.

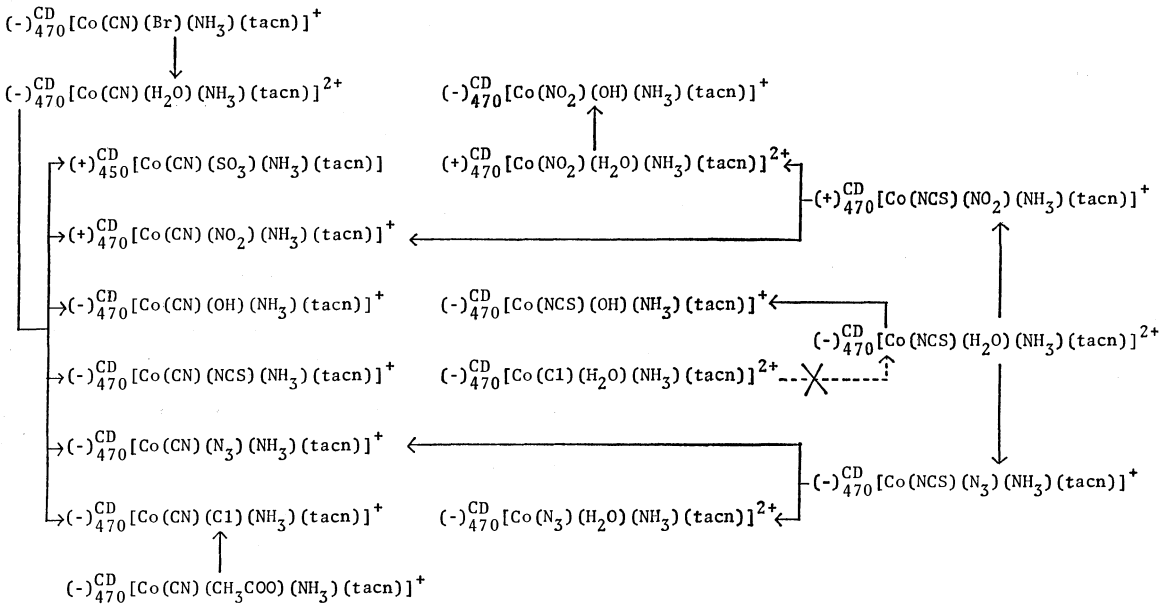

Scheme 2. Derivations of optically active complexes.

Results and Discussion

Preparation and Resolution. Various *fac*(*a*,*b*,*c*)-$[Co(a)(b)(c)(tacn)]^{n+}$-type complexes were prepared by derivations starting from the complexes $[Co(CN)(SO_3)(NH_3)_4]$[13] and *cis*-$[Co(NO_2)_2(NH_3)_4](NO_3)$.[14] Scheme 1 represents the pathways of the present syntheses. We failed to crystallize the $[Co(CN)(N_3)(NH_3)(tacn)]^+$, $[Co(CN)(CH_3COO)(NH_3)(tacn)]^+$, $[Co(NO_2)(H_2O)(NH_3)(tacn)]^{2+}$, and $[Co(N_3)(H_2O)(NH_3)(tacn)]^{2+}$ complexes, but the formations of these complexes were ascertained by absorption spectra, chromatographic behavior, optical resolutions, and chemical reactivities with other unidentate ligands.

All complexes except for $[Co(CN)(SO_3)(NH_3)(tacn)]$ were partially resolved into optical antipodes by a column chromatography using $K_2[Sb_2(d\text{-tart})_2]$ or $Na_2[Sb_2(d\text{-tart})_2]$ as eluting agent. When the $[Co(Cl)(H_2O)(NH_3)(tacn)]^{2+}$ complex was optically resolved, the counter ion was changed into a perchlorate at the last stage of the elution, since a chloride brought about racemization of the complex and the effluent exhibited no optical activity.

Absolute Configuration and CD Spectra. In order to investigate the relation between CD spectra and absolute configurations of the *fac*(*a*,*b*,*c*)-$[Co(a)(b)(c)(tacn)]^{n+}$-type complexes, we tried to derive optically active complexes directly from optically active parent complexes. The conversions were successful in giving

Table 1. Absorption and CD spectral data

	Absorption $\tilde{\nu}/10^3$ cm^{-1} (log ε)	CD $\tilde{\nu}/10^3$ cm^{-1} ($\Delta\varepsilon$)		Absorption $\tilde{\nu}/10^3$ cm^{-1} (log ε)	CD $\tilde{\nu}/10^3$ cm^{-1} ($\Delta\varepsilon$)
$(+)^{CD}_{470}$[Co(CN)(NO_2)-(NH_3)(tacn)]$^+$	23.6 (2.17)	19.6 (−0.01)	$(+)^{CD}_{470}$[Co(NO_2)(H_2O)-(NH_3)(tacn)]$^{2+}$	21.8 (2.13)	19.5 (+0.08)
		21.5 (+0.02)			23.4 (+0.14)
		24.8 (−0.16)		30.6 (3.24)	
	31.4 (3.30)		$(-)^{CD}_{470}$[Co(NO_2)(OH)-(NH_3)(tacn)]$^+$	21.8 (2.32)	19.4 (+0.09)
$(+)^{CD}_{480}$[Co(CN)(SO_3)-(NH_3)(tacn)]	24.1 (2.21)	19.9 (−0.02)			22.8 (−0.04)
		22.9 (+0.26)		31.3 (3.00)	
		25.9 (−0.12)	$(+)^{CD}_{470}$[Co(NCS)(NO_2)-(NH_3)(tacn)]$^+$	21.3 (2.51)	*ca.* 20 (*ca.* +0.03 sh)
	35.5 (4.27)				23.0 (+0.06)
$(-)^{CD}_{470}$[Co(CN)(H_2O)-(NH_3)(tacn)]$^{2+}$	22.1 (1.93)	18.9 (+0.04)		—	27.2 (−0.27)
		21.6 (−0.26)		30.8 (3.51)	30.4 (+0.49)
		24.6 (+0.07)	$(-)^{CD}_{470}$[Co(NCS)(H_2O)-(NH_3)(tacn)]$^{2+}$	20.0 (2.44)	20.4 (−0.20)
	29.9 (1.94)	27.6 (−0.01)		—	25.1 (+0.04)
		30.1 (+0.02)		31.8 (3.86)	
$(-)^{CD}_{470}$[Co(CN)(OH)-(NH_3)(tacn)]$^+$	*ca.* 20 (*ca.* 1.8 sh)	18.8 (+0.13)	$(-)^{CD}_{470}$[Co(NCS)(OH)-(NH_3)(tacn)]$^+$	19.8 (2.32)	18.7 (+0.07)
	22.0 (1.99)	21.8 (−0.29)			20.6 (−0.05)
		25.3 (+0.01)		*ca.* 27 (*ca.* 2.35 sh)	25.0 (+0.07)
	28.7 (2.07)	27.6 (−0.01)	$(-)^{CD}_{470}$[Co(NCS)(N_3)-(NH_3)(tacn)]$^+$	19.7 (2.55)	19.3 (−0.39)
		30.1 (+0.02)			23.0 (+0.01)
$(-)^{CD}_{470}$[Co(CN)(CH_3-COO)(NH_3)(tacn)]$^+$	21.5 (2.05)	19.3 (+0.03)		—	27.9 (−0.35)
		21.9 (−0.28)		31.8 (4.00)	
	29.7 (2.08)	28.1 (+0.03)	$(-)^{CD}_{470}$[Co(N_3)(H_2O)-(NH_3)(tacn)]$^{2+}$	19.5 (2.30)	18.3 (−0.16)
$(-)^{CD}_{470}$[Co(CN)(NCS)-(NH_3)(tacn)]$^+$	21.9 (2.51)	17.7 (+0.01)			19.7 (+0.02)
		20.7 (−0.15)			21.4 (−0.08)
		24.1 (+0.08)		—	24.8 (+0.11)
	33.5 (3.31)				28.1 (+0.10)
$(-)^{CD}_{470}$[Co(CN)(N_3)-(NH_3)(tacn)]$^+$	21.2 (2.50)	21.3 (−0.19)		31.1 (3.75)	
	33.0 (3.86)		$(-)^{CD}_{470}$[Co(Cl)(H_2O)-(NH_3)(tacn)]$^{2+}$	18.6 (1.96)	18.4 (+0.011)
$(-)^{CD}_{470}$[Co(CN)(Cl)-(NH_3)(tacn)]$^+$	19.9 (1.81)	18.0 (+0.01)			20.7 (−0.015)
	ca. 22 (*ca.* 1.6 sh)	20.5 (−0.13)		26.4 (1.89)	24.2 (−0.005)
		23.7 (+0.09)			27.3 (+0.018)
	29.4 (2.00)	28.8 (−0.02)	[Co(NO_2)$_2$(NH_3)(tacn)]$^+$	23.0 (2.36)	
$(-)^{CD}_{470}$[Co(CN)(Br)(NH_3)(tacn)]$^+$	19.4 (1.84)	17.3 (+0.01)		—	
	ca. 22 (*ca.* 1.6 sh)	20.0 (−0.12)		31.0 (3.69)	
		23.4 (+0.07)			
	—	27.4 (+0.06)			
	ca. 32 (*ca.* 3.1 sh)				

the corresponding optically active complexes, except for the [Co(Cl)(H_2O)(NH_3)(tacn)]$^{2+}$ complex. The derivations are shown in Scheme 2. The [Co(CN)-(SO_3)(NH_3)(tacn)] complex could not be resolved by column chromatography, but its active from $(+)^{CD}_{480}$-[Co(CN)(SO_3)(NH_3)(tacn)] was derived from the $(-)^{CD}_{470}$[Co(CN)(H_2O)(NH_3)(tacn)]$^{2+}$ complex.

When the $(+)^{CD}_{470}$[Co(NCS)(NO_2)(NH_3)(tacn)]$^+$ complex was treated with H_2O_2, the $(+)^{CD}_{470}$[Co(CN)-(NO_2)(NH_3)(tacn)]$^+$ and $(-)^{CD}_{470}$[Co(NO_2)(H_2O)(NH_3)-(tacn)]$^+$ complexes were obtained with an optically inactive [Co(CN)(NH_3)$_2$(tacn)]$^{2+}$ complex. The $(-)^{CD}_{470}$[Co(NCS)(N_3)(NH_3)(tacn)]$^+$ complex was also converted to the $(-)^{CD}_{470}$[Co(CN)(N_3)(NH_3)(tacn)]$^+$, $(-)^{CD}_{470}$[Co(N_3)(H_2O)(NH_3)(tacn)]$^{2+}$, and [Co(N_3)-(NH_3)$_2$(tacn)]$^{2+}$ complexes. Similar degradation reaction has been reported for $(-)_{589}$[Co(NCS)-(gly)(tacn)]$^+$; it is considered to proceed with retention of the configuration of the complex.[8] Since optically active isomers are obtained in the substitution or degradation reactions, it is concluded that two complexes which are connected with an arrow in Scheme 2 have the same absolute configuration with respect to the common ligands. Numerical data of absorption and CD spectra of the complexes drawn in Scheme 2 are summarized in Table 1.

For the present chiral complexes, two sources of d-electron optical activity can be considered: 1) A chiral conformation of three chelate rings of tacn and 2) a chiral arrangement of four kinds of donor atoms. However, it is considered that the tacn chelate rings are not fixed to a preferential conformation (λ or δ) and have little effect on the solution CD spectra, since CD spectra of three diastereoisomers of a [Co-(gly)(NH_3)(Metacn)]$^{2+}$ complex are known to be appreciably different from that of an enantiomeric [Co-(gly)(NH_3)(tacn)]$^{2+}$ isomer (Metacn represents (2*R*)-2-methyl-1,4,7-triazacyclononane, the chelate rings of Metacn in the former complex being fixed to λ conformation).[8,9] Therefore, it is considered that the op-

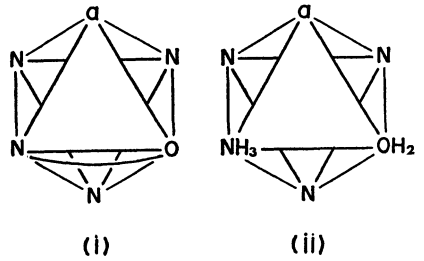

Fig. 1. Absolute configurations of (i) [Co(a)(gly)-(tacn)]$^{n+}$ and (ii) [Co(a)(H_2O)(NH_3)(tacn)]$^{n+}$.

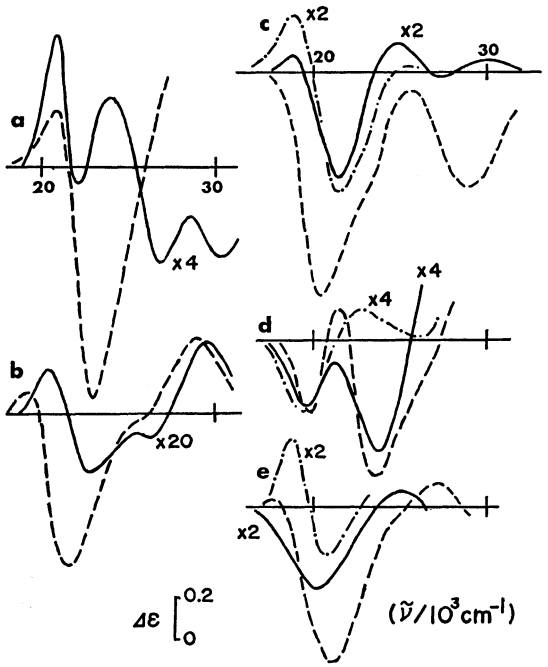

Fig. 2. CD spectra of a) $(+)^{CD}_{470}$[Co(N_3)(H_2O)(NH_3)-(tacn)]$^{2+}$ (——), $(+)_{589}$[Co(N_3)(gly)(tacn)]$^{+}$ (----), b) $(-)^{CD}_{470}$[Co(Cl)(H_2O)(NH_3)(tacn)]$^{2+}$ (——), $(-)_{589}$-[Co(Cl)(gly)(tacn)]$^{+}$ (----), c) $(-)^{CD}_{470}$[Co(CN)(H_2O)-(NH_3)(tacn)]$^{2+}$ (——), $(-)_{589}$[Co(CN)(gly)(tacn)]$^{+}$ (----), $(-)^{CD}_{470}$[Co(CN)(OH)(NH_3)(tacn)]$^{+}$ (—·—), d) $(-)^{CD}_{470}$[Co(NO_2)(H_2O)(NH_3)(tacn)]$^{2+}$ (——), $(-)_{589}$-[Co(NO_2)(gly)(tacn)]$^{+}$ (----), $(+)^{CD}_{470}$[Co(NO_2)(OH)-(NH_3)(tacn)]$^{+}$ (—·—), and e) $(-)^{CD}_{470}$[Co(NCS)(H_2O)-(NH_3)(tacn)]$^{2+}$ (——), $(-)_{589}$[Co(NCS)(gly)(tacn)]$^{+}$ (----), $(-)^{CD}_{470}$[Co(NCS)(OH)(NH_3)(tacn)]$^{+}$ (—·—).

tical source 1) causes little optical activity in the *fac*-(*a*,*b*,*c*)-[Co(a)(b)(c)(tacn)]$^{n+}$ complexes.

A series of [Co(a)(gly)(tacn)]$^{n+}$ complexes (a=CN^-, NO_2^-, NH_3, NCS^-, N_3^-, H_2O, OH^-, or Cl^-) possess the same source of dissymmetry as the present complexes, and the absolute configurations of the glycinato complexes have been determined on the basis of X-ray analysis and chemical derivations.[8,15] The CD spectra of the [Co(a)(gly)(tacn)]$^{n+}$ complexes which have the absolute configuration shown in Fig. 1 (i) are illustrated in Fig. 2 with broken lines. The CD spectra of the [Co(a)(H_2O)(NH_3)(tacn)]$^{2+}$ complexes (a=CN^-, NO_2^-, NCS^-, N_3^-, or Cl^-) are also drawn in Fig. 2 with solid lines. As to the cyano, nitro, isothiocyanato and azido complexes, the enantiomers which exhibit the CD spectra shown in Fig. 2 are

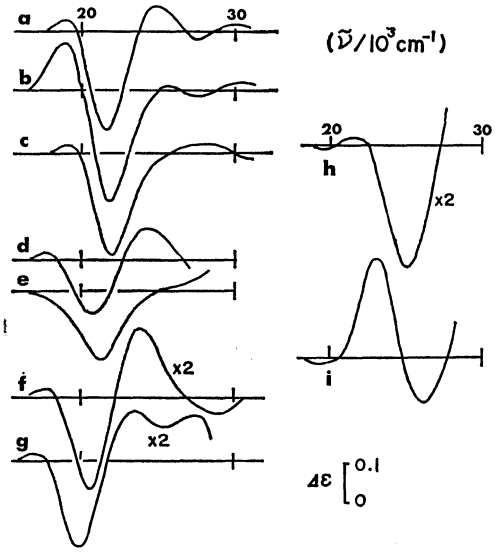

Fig. 3. CD spectra of a) $(-)^{CD}_{470}$[Co(CN)(H_2O)(NH_3)-(tacn)]$^{2+}$, b) $(-)^{CD}_{470}$[Co(CN)(OH)(NH_3)(tacn)]$^{+}$, c) $(-)^{CD}_{470}$[Co(CN)(CH_3COO)(NH_3)(tacn)]$^{+}$, d) $(-)^{CD}_{470}$-[Co(CN)(NCS)(NH_3)(tacn)]$^{+}$, e) $(-)^{CD}_{470}$[Co(CN)(N_3)-(NH_3)(tacn)]$^{+}$, f) $(-)^{CD}_{470}$[Co(CN)(Cl)(NH_3)(tacn)]$^{+}$, g) $(-)^{CD}_{470}$[Co(CN)(Br)(NH_3)(tacn)]$^{+}$, h) $(+)^{CD}_{470}$[Co-(CN)(NO_2)(NH_3)(tacn)]$^{+}$, and i) $(+)^{CD}_{480}$[Co(CN)-(SO_3)(NH_3)(tacn)].

considered to have the same absolute configuration, judging by the chemical derivations drawn in Scheme 2.

When the unidentate, a, is CN^-, NO_2^- or NCS^-, each CD spectrum of the [Co(a)(H_2O)(NH_3)(tacn)]$^{2+}$ complex resembles that of the corresponding [Co(a)-(gly)(tacn)]$^{+}$ complex, although the CD spectra of the azido complexes are somewhat different from each other. Thus, it is concluded that the $(-)^{CD}_{470}$[Co(CN)-(H_2O)(NH_3)(tacn)]$^{2+}$, $(-)^{CD}_{470}$[Co(NO_2)(H_2O)(NH_3)-(tacn)]$^{2+}$, $(-)^{CD}_{470}$[Co(NCS)(H_2O)(NH_3)(tacn)]$^{2+}$, and $(+)^{CD}_{470}$[Co(N_3)(H_2O)(NH_3)(tacn)]$^{2+}$ complexes have the absolute configuration as shown in Fig. 1 (ii).

Though the absolute configuration of $(-)^{CD}_{470}$[Co(Cl)-(H_2O)(NH_3)(tacn)]$^{2+}$ could not be correlated with those of others, it is considered that the $(-)^{CD}_{470}$-isomer has the same absolute configuration as shown in Fig. 1 (ii), since $(-)_{589}$[Co(Cl)(gly)(tacn)]$^{+}$ exhibits a CD spectrum similar to that of the $(-)^{CD}_{470}$-isomer.

The [Co(a)(H_2O)(NH_3)(tacn)]$^{2+}$ complexes are bivalent cations, while the [Co(a)(gly)(tacn)]$^{+}$ complexes are univalent cations. The [Co(CN)(CH_3COO)-(NH_3)(tacn)]$^{+}$ complex is the same univalent cation as [Co(CN)(gly)(tacn)]$^{+}$, and the $(-)^{CD}_{470}$-isomer of the acetato complex exhibits a CD spectrum similar to that of $(-)_{589}$-isomer of the glycinato complex. On this basis, it is predicted that both have the absolute configurations shown in Fig. 1. The absolute configurations of the others can be determined by tracing a pathway in Scheme 2.

a) [Co(a)(CN)(NH_3)(tacn)]$^{n+}$ Complexes. In this series, the unidentate, a, stands for NO_2^-, SO_3^{2-}, NCS^-, H_2O, OH^-, CH_3COO^-, N_3^-, Cl^-, or Br^-. Each of the complexes has a rhombic ligand field, in which there are three electronic transition com-

Table 2. Assignment of Cotton peaks in [Co(a)(CN)(NH_3)(tacn)]$^{n+}$

	Transition component		
[Co(a)(CN)(NH_3)(tacn)]$^{n+}$	($xy\rightarrow x^2-y^2$)	($yz\rightarrow y^2-z^2$)	($zx\rightarrow z^2-x^2$)
a=H_2O	(+)	$(-)_d$	(+)
a=OH^-	(+)	$(-)_d$	(+)
a=CH_3COO^-	(+)	$(-)_d$	
a=NCS^-	(+)	$(-)_d$	(+)
a=N_3^-		$(-)_d$	
a=Cl^-	(+)	$(-)_d$	(+)
a=Br^-	(+)	$(-)_d$	(+)
[Co(a)(CN)(NH_3)(tacn)]$^{n+}$	($xy\rightarrow x^2-y^2$)	($zx\rightarrow z^2-x^2$)	($yz\rightarrow y^2-z^2$)
a=NO_2^-	(−)	(+)	$(-)_d$
a=SO_3^{2-}	(−)	$(+)_d$	(−)

The subscript d shows the peak is dominant.

ponents for the first absorption band. The absorption spectra of the chloro, bromo, and hydroxo complexes exhibit clear splittings of the first absorption bands, while the aqua and acetato complexes show the broad absorption bands.

The CD spectra of [Co(a)(CN)(NH_3)(tacn)]$^{n+}$ with the same absolute configuration are shown in Fig. 3. Our interest is focused on the spectra in the first absorption band region, and the Cotton peaks in the region are described unless otherwise noted. The $(-)^{CD}_{470}$-azido and $(-)^{CD}_{470}$-acetato complexes exhibit one and two Cotton peaks, respectively. The remaining ones exhibit three Cotton peaks with alternating signs; however, the CD spectral pattern on the $(+)^{CD}_{470}$-nitro and $(+)^{CD}_{450}$-sulfito complexes is opposite to that on the $(-)^{CD}_{470}$-aqua, $(-)^{CD}_{470}$-hydroxo, $(-)^{CD}_{470}$-isothiocyanato, $(-)^{CD}_{470}$-chloro, and $(-)^{CD}_{470}$-bromo complexes, the former group exhibits (−), (+), and (−) signs from a lower-frequency side, and the latter group exhibits (+), (−), and (+) signs.

It is predicted by an angular overlap model[16] that three electronic transition components of the first absorption band are well separated with one another in the [Co(a)(CN)(NH_3)(tacn)]$^{n+}$ complexes. The predicted values well coincide with the extrema of the Cotton peaks. When a coordinate system is defined for the [Co(a)(CN)(NH_3)(tacn)]$^{n+}$ complexes as shown in Fig. 4 (i), the transition energy order becomes $E(xy\rightarrow x^2-y^2) < E(yz\rightarrow y^2-z^2) < E(zx\rightarrow z^2-x^2)$ for the aqua, hydroxo, acetato, isothiocyanato, azido, chloro and bromo complexes, and $E(xy\rightarrow x^2-y^2) < E(zx\rightarrow z^2-x^2) < E(yz\rightarrow y^2-z^2)$ for the nitro and sulfito complexes, where the symbols, $E(xy\rightarrow x^2-y^2)$, $E(yz\rightarrow y^2-z^2)$ and $E(zx\rightarrow z^2-x^2)$, designate the transition energies of the electronic transitions in XY, YZ, and ZX plane, respectively. The assignments of the Cotton peaks are listed in Table 2. As to the acetato complex, the two observed Cotton peaks are assigned to the lower-lying two transition components, *i.e.* ($xy\rightarrow x^2-y^2$) and ($yz\rightarrow y^2-z^2$), by comparing with the CD spectra of the aqua and hydroxo complexes. As to the azido complex, the observed Cotton peak is assigned to the ($yz\rightarrow y^2-z^2$) transition, on the basis of the prediction by the angular overlap model.

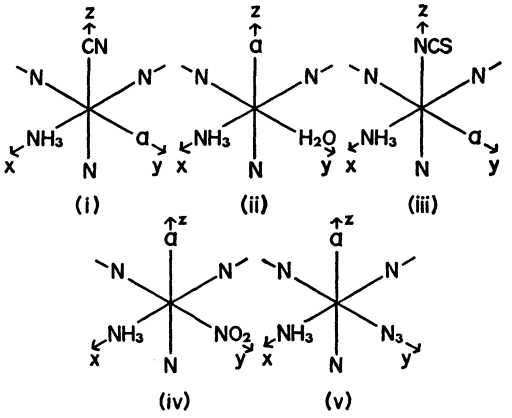

Fig. 4. Absolute configurations and coordinate systems for (i)[Co(a)(CN)(NH_3)(tacn)]$^{n+}$, (ii) [Co(a)(H_2O)(NH_3)(tacn)]$^{n+}$, (iii) [Co(a)(NCS)(NH_3)(tacn)]$^{n+}$, (iv)[Co(a)(NO_2)(NH_3)(tacn)]$^{n+}$, and (v) [Co(a)(N_3)(NH_3)(tacn)]$^{n+}$.

As is seen in Table 2, there are obvious relations between the Cotton signs and the corresponding transition components. The Cotton peaks corresponding to ($zx\rightarrow z^2-x^2$) exhibit positive signs in every complex. As to the peaks corresponding to ($yz\rightarrow y^2-z^2$), negative signs are observed in every complex. On the other hand, the signs of the peaks corresponding to ($xy\rightarrow x^2-y^2$) are variable depending upon the unidentate a. When the unidentate is nitro or sulfito, the sign becomes negative. When the unidentate is aqua, hydroxo, acetato, isothiocyanato, azido, chloro or bromo, the peak has a positive sign. The inversion of the Cotton sign corresponding to the ($xy\rightarrow x^2-y^2$) transition component is considered to relate to the ligand field strengths of the unidentate ligands lying in the XY plane. Nitro and sulfito ligands afford stronger ligand fields than an ammine ligand, and the Cotton peaks corresponding to ($xy\rightarrow x^2-y^2$) exhibit negative signs. On the other hand, the ligand field strengths of H_2O, OH^-, CH_3COO^-, NCS^-, N_3^-, Cl^-, or Br^- are weaker than that of NH_3, and the peaks corresponding to ($xy\rightarrow x^2-y^2$) exhibit positive signs.

As to the YZ plane, the ligand field strength of the unidentate a on the Y axis is weaker than that of the cyano ligand on the Z axis in every complex, and the concerned Cotton peaks exhibit negative signs. The common sign of the peaks corresponding to ($zx \rightarrow z^2-x^2$) associates with the fact that the cyano ligand on the Z axis affords stronger ligand field than the ammine ligand on the X axis. Since the Cotton signs associated with the ($zx \rightarrow z^2-x^2$) transition are independent with the variation of the unidentate a on the Y axis, the sign of the peak corresponding to a given electronic transition is considered to be determined by the ligands ligating in the plane where the electronic transition occurs. It is notable that all negative dominant peaks are assignable to the ($yz \rightarrow y^2-z^2$) transition component, except for the sulfito complex. This electronic transition component is associated with the YZ plane, which contains no ammine ligand.

b) $[Co(a)(H_2O)(NH_3)(tacn)]^{2+}$ Complexes. In these complexes, the unidentate a stands for CN^-, NO_2^-, NCS^-, N_3^-, or Cl^-. The CD spectra of $[Co(a)(H_2O)(NH_3)(tacn)]^{2+}$ are shown in Fig. 2, along with those of the corresponding hydroxo complexes, and the absolute configurations of these enantiomers are illustrated in Fig. 4 (ii). Since the $[Co(CN)(H_2O)(NH_3)(tacn)]^{2+}$ and $[Co(N_3)(H_2O)(NH_3)(tacn)]^{2+}$ complexes exhibit three Cotton peaks, the peaks can be assigned to the electronic transition components in the same manner as in the $[Co(a)(CN)(NH_3)(tacn)]^{n+}$ complexes. In both the complexes, (+), (−), and (+) peaks are observed from a lower frequency side. These peaks are assigned to ($xy \rightarrow x^2-y^2$), ($yz \rightarrow y^2-z^2$), and ($zx \rightarrow z^2-x^2$), respectively, for the cyano complex, and to ($yz \rightarrow y^2-z^2$), ($zx \rightarrow z^2-x^2$), and ($xy \rightarrow x^2-y^2$) for the azido complex. The Cotton peaks corresponding to the ($xy \rightarrow x^2-y^2$) component have (+) signs in these complexes. However, the signs associated with ($yz \rightarrow y^2-x^2$) and ($zx \rightarrow z^2-x^2$) in the cyano complex are opposite to those in the azido complex. These phenomena are also explained in the same manner as in the $[Co(a)(CN)(NH_3)(tacn)]^{n+}$ complexes. The inversions of the Cotton signs are related to the fact that a cyano ligand affords a stronger ligand field than an ammine or aqua ligand, but an azido ligand affords a weaker one than an ammine or aqua ligand. The common Cotton sign associated with ($xy \rightarrow x^2-y^2$) is related to the common ligands in the XY plane. It is also found that the variation of the unidentate on the Z axis does not influence the sign of the peak corresponding to the electronic transition in the XY plane. In both the cyano and azido complexes, the dominant Cotton peaks correspond to the transition component in the plane which contains no ammine ligand (*i.e.*, the YZ plane).

The $[Co(NO_2)(H_2O)(NH_3)(tacn)]^{2+}$ and $[Co(Cl)(H_2O)(NH_3)(tacn)]^{2+}$ complexes exhibit two extrema, and the $[Co(NCS)(H_2O)(NH_3)(tacn)]^{2+}$ complex exhibits one extremum. It is difficult to assign the peaks to the transition components in these complexes. However, if the dominant Cotton peaks can be related to the ($yz \rightarrow y^2-z^2$) component, the negative dominant peaks in the nitro and isothiocyanato complexes support the result in the cyano and azido complexes. A dominant peak with a (−) sign in $[Co(Cl)(H_2O)(NH_3)(tacn)]^{2+}$ may be explained by an overlapping of a peak at 24200 cm^{-1} in the second absorption band region. The chloro complex exhibits a positive Cotton peak at the lowest frequency side like the azido complex.

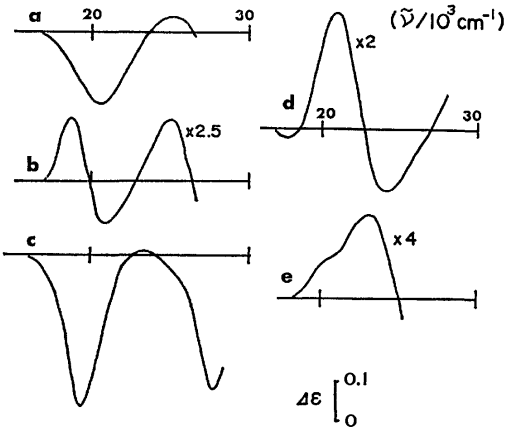

Fig. 5. CD spectra of a) $(-)^{CD}_{470}[Co(NCS)(H_2O)(NH_3)(tacn)]^{2+}$, b) $(-)^{CD}_{470}[Co(NCS)(OH)(NH_3)(tacn)]^{+}$, c) $(-)^{CD}_{470}[Co(NCS)(N_3)(NH_3)(tacn)]^{+}$, d) $(+)^{CD}_{470}[Co(CN)(NCS)(NH_3)(tacn)]^{+}$, and e) $(+)^{CD}_{470}[Co(NO_2)(NCS)(NH_3)(tacn)]^{+}$.

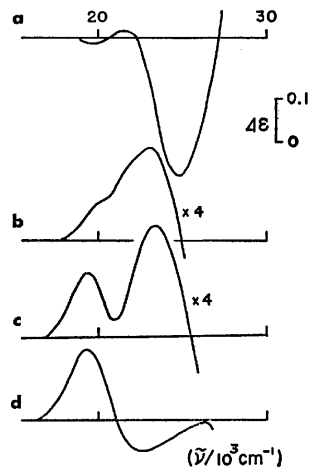

Fig. 6. CD spectra of a) $(+)^{CD}_{470}[Co(CN)(NO_2)(NH_3)(tacn)]^{+}$, b) $(+)^{CD}_{470}[Co(NO_2)(NCS)(NH_3)(tacn)]^{+}$, c) $(+)^{CD}_{470}[Co(NO_2)(H_2O)(NH_3)(tacn)]^{2+}$, and d) $(-)^{CD}_{470}[Co(NO_2)(OH)(NH_3)(tacn)]^{+}$.

The $[Co(CN)(OH)(NH_3)(tacn)]^{+}$ complex exhibits a similar CD spectrum to that of the parent aqua complex, but the spectra of $[Co(NO_2)(OH)(NH_3)(tacn)]^{+}$ and $[Co(NCS)(OH)(NH_3)(tacn)]^{+}$ are different from those of the parent aqua complexes. However, the $[Co(NO_2)(OH)(NH_3)(tacn)]^{+}$ complex also exhibits a (−) dominant peak like the parent aqua complex. It is characteristic that the $[Co(NCS)(OH)(NH_3)(tacn)]^{+}$ complex exhibits an intense peak with positive sign at 25000 cm^{-1} in the second absorption band region.

c) $[Co(a)(NCS)(NH_3)(tacn)]^{n+}$ Complexes. In this series, the unidentate a stands for CN^-, NO_2^-, H_2O, OH^-, or N_3^-. The complexes which have a

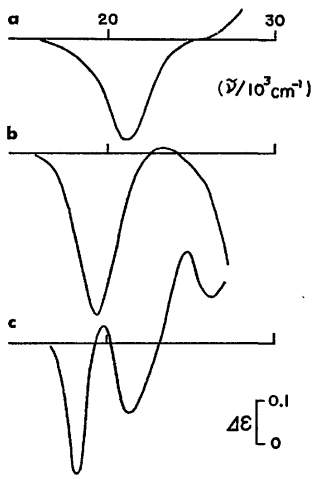

Fig. 7. CD spectra of a) $(-)^{CD}_{470}$[Co(CN)(N_3)(NH_3)-(tacn)]$^+$, b) $(-)^{CD}_{470}$[Co(NCS)(N_3)(NH_3)(tacn)]$^+$, and c) $(-)^{CD}_{470}$[Co(N_3)(H_2O)(NH_3)(tacn)]$^{2+}$.

common absolute configuration drawn in Fig. 4 (iii) exhibit the CD spectra as shown in Fig. 5. Except for the cyano complex, these complexes exhibit one or two Cotton peaks. Positive dominant peaks are observed at the cyano and nitro complexes, and negative ones, at the aqua and azido complexes. This phenomenon is also explained in terms of the ligand field strengths of the unidentates in YZ plane.

d) [Co(a)(NO_2)(NH_3)(tacn)]$^{n+}$ Complexes. In these complexes, the unidentate, a, stands for CN^-, NCS^-, H_2O, or OH^-. The isothiocyanato, aqua and hydroxo complexes exhibit two extrema. As to the complexes with the absolute configuration as shown in Fig. 4 (iv), only the cyano complex exhibits a (−) dominant peak (Fig. 6). This sign is related to the ligand field strength of CN^-, which is stronger than that of NO_2^-.

e) [Co(a)(N_3)(NH_3)(tacn)]$^{n+}$ Complexes. In this series, the unidentate a stands for CN^-, NCS^-, or H_2O. The CD spectra of the enantiomers illustrated in Fig. 4 (v) exhibit (−) dominant peaks (Fig. 7). This observation is also related to the fact that CN^-, NCS^-, and H_2O ligands have stronger ligand field strengths than N_3^-.

As described above, the sign of the Cotton peak of a given electronic transition in the [Co(a)(b)(c)-(tacn)]$^{n+}$ complex is associated with the ligand field strengths of two unidentate ligands contained in the plane where the electronic transition occurs. However, we can not find the obvious participation of two N donors of tacn contained in the same plane. The fact that the Cotton signs are related only with the characters of the unidentates may be concerned with the symmetrical nature of the terdentate ligand. It is notable to point out the followings. The complex, in which the ligand field strengths of three kinds of unidentates decrease clockwise on the octahedral face, exhibits negative, positive, and negative Cotton peaks from the lower frequency side in the first absorption band region, and the complex in which those decrease counterclockwise exhibits positive, negative, and positive Cotton peaks.

References

1) T. Ito and M. Shibata, *Inorg. Chem.*, **16**, 108 (1977).
2) K. Tsuji, S. Fujinami, and M. Shibata, *Bull. Chem. Soc. Jpn.*, **54**, 1531 (1981).
3) S. Fujinami, K. Tsuji, R. Musa, and M. Shibata, *Bull. Chem. Soc. Jpn.*, **55**, 617 (1982).
4) S. Fujinami and M. Shibata, *Bull. Chem. Soc. Jpn.*, **54**, 2939 (1981).
5) S. F. Mason, *Mol. Phys.*, **37**, 843 (1979).
6) K. Yamanari, J. Hidaka, and Y. Shimura, *Bull. Chem. Soc. Jpn.*, **48**, 1653 (1975).
7) Y. Hosokawa, J. Hidaka, and Y. Shimura, *Bull. Chem. Soc. Jpn.*, **48**, 3175 (1975).
8) S. Shimba, S. Fujinami, and M. Shibata, *Bull. Chem. Soc. Jpn.*, **53**, 2523 (1980).
9) S. Fujinami, Y. Matsunami, and M. Shibata, *Bull. Chem. Soc. Jpn.*, **55**, 2101 (1982).
10) S. Shimba, S. Fujinami, and M. Shibata, *Chem. Lett.*, **1979**, 783.
11) S. Fujinami and M. Shibata, *Chem. Lett.*, **1981**, 495.
12) J. E. Richman and T. J. Atkins, *J. Am. Chem. Soc.*, **96**, 2268 (1974).
13) H. Siebert, *Z. Anorg. Chem.*, **327**, 63 (1964).
14) M. Linhard and M. Weigel, *Z. Anorg. Chem.*, **267**, 113 (1951).
15) S. Sato, S. Ohba, S. Shimba, S. Fujinami, M. Shibata, and Y. Saito, *Acta Crystallogr., Sect. B*, **36**, 43 (1980).
16) C. E. Schäffer, *Pure Appl. Chem.*, **24**, 361 (1970).

Effect of Lattice Anions on the Racemization of Optically Active Metal Chelate Salts in the Solid State. 2.[1] $[Co(phen)_3]X_3$, $[Co(phen)_2(en)]X_3$, and $[Co(phen)(en)_2]X_3$, Where $X^-=Cl^-$, Br^-, or I^-

Terufumi FUJIWARA

Department of Chemistry, Faculty of Science, Hiroshima University, Naka-ku, Hiroshima 730

(Received May 24, 1982)

The kinetics of racemization of the anhydrous complexes (−)-$[Co(phen)_3]X_3$, (+)-$[Co(phen)_2(en)]X_3$, and (−)-$[Co(phen)(en)_2]X_3$, where phen=1,10-phenanthroline, en=ethylenediamine, and $X^-=Cl^-$, Br^-, or I^-, have been examined in the solid state. A rapid initial loss of optical activity and a subsequent first-order racemization were observed for the complex salts. Enthalpies and entropies of activation, ΔH^* and ΔS^*, were evaluated for the first-order process of $[Co(phen)_3]X_3$ and $[Co(phen)_2(en)]X_3$. It was found that for $[Co(phen)_3]X_3$ the chloride salt racemizes more rapidly than the bromide salt and that ΔH^* and ΔS^* decrease with the lattice anion in the order $X^-=Br^->Cl^-$. On the other hand, the reverse sequence in ΔH^* and ΔS^*, $X^-=Br^-<Cl^-$, was observed for $[Co(phen)_2(en)]X_3$. Moreover, the rate of racemization of $[Co(phen)(en)_2]X_3$ was found to decrease with the lattice anion in the order $X^-=I^->Br^->Cl^-$. These anion effects for the series were successfully interpreted in terms of the chemical interactions due to donicity and hydrogen bonding ability of anions, but not in terms of the physical factor, lattice energy. Thermal decomposition studies of the complexes lend support to the interpretation of the racemization kinetic data.

In our previous study of the solid-state racemization of halide salts of tris-complexes of 1,10-phenanthroline and 2,2′-bipyridine with iron and nickel ions,[1] a difference in racemization mechanism between the iron and nickel complexes was reported as it is in solution.[2,3] The operation of only a twist process without any nucleophilic interaction of lattice anions is postulated for the iron complexes as in solution.[3,4] On the other hand, ΔH^* and ΔS^* values for the nickel complexes were found to decrease with the lattice anion in the order $X^-=ClO_4^->I^->Br^->Cl^-$. Then, we have pointed out that the trend is attributed to the donicity of the anions[5] to stabilize a 7-coordinate transition state which is generated by attack of the lattice anion on the central metal as proposed for solutions.[6,7] Kutal and Bailar found that the rate of racemization of the complex salt, $[Co(en_3)]X_3\cdot nH_2O$, increases in the order of anions $Cl^-<NCS^-<Br^-<I^-$ for the anhydrous compounds, and it was presumed that hydrogen bonding of the type N–H···X was responsible for the rate differences in the series.[8] On the other hand, activation energies or enthalpies for the dehydration of the series of compounds $[M(NH_3)_5(H_2O)]X_3$ in the solid state[9,10] (where M=Cr, Co, or Ru) were found to decrease with the anion in the order $X^-=I^->Br^->Cl^-$ and an S_N2-type mechanism was proposed for the reaction.

However, a different mechanism from them was proposed recently by House[11] for the solid-state reactions in which the generation of a point defect is considered to be the origin of the transition state. The intramolecular racemization of $[Co(en)_3]X_3$ has been shown to be consistent with the substituted ion type of defect, while the dehydration of $[M(NH_3)_5(H_2O)]X_3$ is consistent with the formation of a Frenkel type of defect. Then, energy of the formation of the transition state is discussed in terms of lattice energy and ionic radii. However, we pointed out in previous paper[12] that the anion effects on the racemization of the iron and nickel complexes cannot be accounted for in terms of House's model or the physical factor alone, lattice energy.

In view of these studies, it is of interest to explore the role of the factors which facilitate or retard the solid-state racemization of the series of homo- and heterochelated tris-complexes of 1,10-phenanthroline and ethylenediamine, $[Co(phen)_3]X_3$, $[Co(phen)_2(en)]X_3$, and $[Co(phen)(en)_2]X_3$. An attempt was made to isolate the optically active complex, (−)-$[Co(phen)_3]^{3+}$, as the halide salts by a conventional method, namely, by addition of an excess of sodium halide solutions to aqueous solutions of the active complex. However, we failed to obtain the active halide salts because the complex racemizes very rapidly in halide-containing solutions.[13] Recently by a freeze-drying method, we successfully isolated the optically active chloride and bromide salts of the complex.[14] In addition to the kinetic data, the results of studies on the thermal decomposition of these complexes were incorporated into the analysis of the effect of lattice anions on the transition state for the solid-state racemization.

Experimental

Materials. The bromide and chloride salts of the optical isomer of $[Co(phen)_3]^{3+}$ isolated in our previous study[14] were employed here. The preparation and resolution of $[Co(phen)_2(en)]^{3+}$ were performed according to the method of Gillard *et al.*[15] The complex, $K_3[(+)_{589}$-$Co(L\text{-}cysu)_3]$ [cysu=cysteinesulfinato(2−)-*SN**], prepared by a previously reported method,[16] was used as the resolving agent. The diastereoisomer with $(+)_{589}$-$[Co(L\text{-}cysu)_3]^{3-}$ was converted to its bromide and chloride salts, $(+)_{436}$-$[Co(phen)_2(en)]Br_3\cdot 6H_2O$ and $(+)_{436}$-$[Co(phen)_2(en)]Cl_3\cdot 6H_2O$, by anion exchange (Dowex 21K resin, Br^- or Cl^- form). Found: C, 36.80; H, 3.68; N, 10.39%. Calcd for $C_{26}H_{36}O_6N_6Br_3Co$: C, 37.75; H, 4.39; N, 10.16%. Found: C, 44.56; H, 4.61; N, 13.03%. Calcd for $C_{26}H_{36}O_6N_6Cl_3Co$: C, 45.00; H, 5.23; N, 12.11%. The complex,

* The ligand, cysu, should read β-sulfinato-L-alaninato: $H_2NCH(CO_2^-)CH_2SO_2^-$.

$[Co(phen)(en)_2]^{3+}$, was prepared and resolved using ammonium $(+)_{589}$-3-bromo-8-camphorsulfonate as previously reported.[17] The optical isomer was isolated as the iodide, bromide, and chloride salts, $(-)_{436}$-$[Co(phen)(en)_2]I_3 \cdot H_2O$, $(-)_{436}$-$[Co(phen)(en)_2]Br_3 \cdot 5H_2O$, and $(-)_{436}$-$[Co(phen)(en)_2]Cl_3 \cdot 6H_2O$. Found: C, 25.76; H, 3.20; N, 10.88%. Calcd for $C_{16}H_{26}ON_6I_3Co$: C, 25.35; H, 3.46; N, 11.09%. Found: C, 27.41; H, 4.50; N, 12.88%. Calcd for $C_{16}H_{34}O_5N_6Br_3Co$: C, 27.89; H, 4.97; N, 12.20%. Found: C, 33.39; H, 4.80; N, 15.37%. Calcd for $C_{16}H_{36}O_6N_6Cl_3Co$: C, 33.49; H, 6.32; N, 14.64%. All the complexes were powdered by grinding with a mortar and pestle to pass a 200-mesh sieve. The preparation of anhydrous samples of the complexes was performed by the method given earlier,[1] except that the operation was performed in the dark since exposure to sunlight affects the optical rotations, especially of $[Co(phen)_3]X_3 \cdot nH_2O$.[14]

Measurements. The racemization rates at different temperatures were measured for each complex by using the same heating apparatus as that used in our previous study.[1] Before the measurements were made, all the solid samples(0.005—0.007 g) of the anhydrous complexes were placed in NMR tubes(5 mm in diameter, 5 cm in length) and preserved in a desiccator over P_2O_5 in the dark. The sample tubes were placed in the heating apparatus where it was possible to prevent the samples from exposure to sunlight. The samples were taken out of the apparatus at timed intervals and cooled rapidly. The optical rotations of the samples were measured in triplicate on aqueous solutions in the conventional manner at 365 nm for $[Co(phen)_3]^{3+}$ and at 436 nm for $[Co(phen)_2(en)]^{3+}$ and $[Co(phen)(en)_2]^{3+}$ by using a Perkin-Elmer Model 141 Polarimeter and a Hg lamp, with a cell of 1-dm length. The concentrations of the solutions were determined spectrophotometrically using a Hitachi Perkin Elmer Model 139 UV-vis spectrophotometer. The wavelengths and molar extinction of absorption maximums employed are as follows: 274 nm and 6.95×10^4 mol^{-1} dm^3 cm^{-1} for $[Co(phen)_3]^{3+}$; 305 nm and 1.255×10^4 mol^{-1} dm^3 cm^{-1} for $[Co(phen)_2(en)]^{3+}$; 273 nm and 3.025×10^4 mol^{-1} dm^3 cm^{-1} for $[Co(phen)(en)_2]^{3+}$. Within experimental uncertainties, the specific rotations of aqueous solutions of the complexes were independent of concentration. These results have a precision of better than 5%. Thermogravimetric analysis (TGA) and differential thermal analysis(DTA) were carried out with a Sinku-Riko Model TGD-3000-RH instrument. Samples(0.01—0.02 g) of the hydrates were used. A heating rate of 5°/min and a static air atmosphere were employed in each run.

Results

Typical plots of $\log(10[\alpha_t]/[\alpha_0])$ *vs.* time for the solid-state racemization of anhydrous salts of $(-)$-$[Co(phen)_3]X_3$, $(+)$-$[Co(phen)_2(en)]X_3$, and $(-)$-$[Co(phen)(en)_2]X_3$ (X=I, Br, or Cl) are given in Figs. 1—3, respectively, where $[\alpha_t]$ is the specific rotation at time t and $[\alpha_0]$ is the specific rotation at time zero. Figures 1 and 2 show that all runs with anhydrous materials of the tris- and bis-phenanthroline complexes have the common characteristic of an initial period during which very rapid loss of optical activity occurs, followed by a first-order racemization process. On the other hand, Fig. 3 shows that the chloride and bromide salts of the mono-phenanthroline complex exhibit decreasing rates of racemization after the initial period

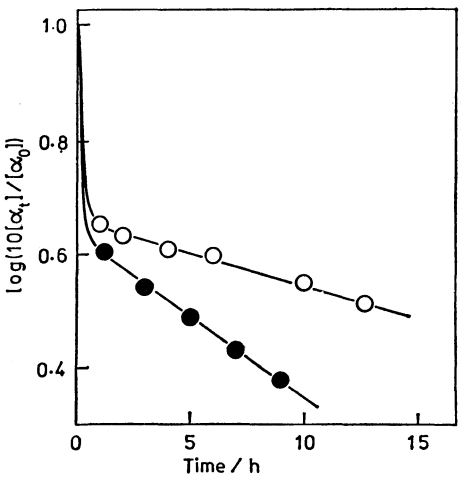

Fig. 1. Racemization of $(-)$-$[Co(phen)_3]Br_3$ at 121 °C (○) and $(-)$-$[Co(phen)_3]Cl_3$ at 119 °C (●).

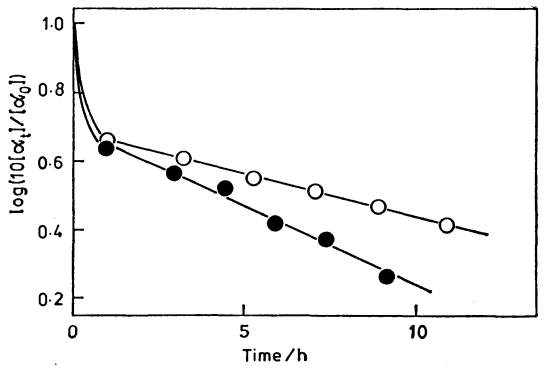

Fig. 2. Racemization of $(+)$-$[Co(phen)_2(en)]Br_3$ (○) and $(+)$-$[Co(phen)_2(en)]Cl_3$ (●) at 148 °C.

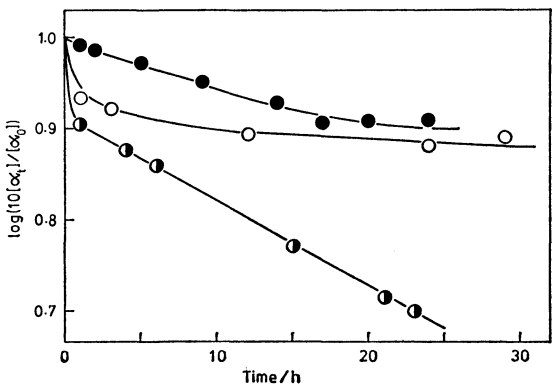

Fig. 3. Racemization of $(-)$-$[Co(phen)(en)_2]Cl_3$ at 145 °C (●), $(-)$-$[Co(phen)(en)_2]Br_3$ at 149 °C (○), and $(-)$-$[Co(phen)(en)_2]I_3$ at 145 °C (◑).

and thus the kinetics depart from simple first-order behavior, although the iodide salt shows a first-order racemization as do the tris- and bis-phenanthroline complexes.

For the first-order racemization, the rate constant, k, is determined by applying the equation used in our previous paper.[1] Table 1 lists the rate constants. The indicated errors are one standard deviation estimated from least-squares fits to the equation. Table 1 shows that the chloride salts racemize faster than

TABLE 1. RATE CONSTANTS OF THE SOLID-STATE RACEMIZATION

Complex	Temp/°C	$k/10^{-6}$ s^{-1}
(−)-$[Co(phen)_3]Br_3$	102	0.169±0.027
	107	0.466±0.083
	114	1.15±0.10
	121	3.17±0.18
(−)-$[Co(phen)_3]Cl_3$	91	0.323±0.045
	100	0.909±0.086
	110	3.92±0.38
	119	9.43±0.69
(+)-$[Co(phen)_2(en)]Br_3$	148	7.53±0.48
	154	11.0±0.6
	158	15.0±1.5
(+)-$[Co(phen)_2(en)]Cl_3$	145	12.3±0.4
	148	17.5±0.6
	150	24.2±1.3

TABLE 2. KINETIC PARAMETERS FOR THE SOLID-STATE RACEMIZATION OF COBALT COMPLEXES WITH THERMAL STABILITY

Complex	ΔH^* / kJ mol^{-1}	ΔS^* / J K^{-1} mol^{-1}	T_d / °C
(−)-$[Co(phen)_3]Br_3$	181±11	108±27	188
(−)-$[Co(phen)_3]Cl_3$	143±7	23±18	170
(+)-$[Co(phen)_2(en)]Br_3$	100±6	−109±14	202
(+)-$[Co(phen)_2(en)]Cl_3$	195±20	124±47	186

the corresponding bromide salts in both series of the complexes. Although attempts were made to fit the racemization data for $[Co(phen)(en)_2]X_3$ to various topochemical rate laws common to solid-state reactions,[18] any fit to such kinetic expressions must be regarded as poor because of the invariably deceleratory plots throughout the course of the racemization.

Activation parameters, ΔH^* and ΔS^*, were determined by least-squares fits to Eyring plots for the first-order racemization as expressed in our previous papers,[1,12] although the first-order process may be the case of random nucleation.[18] These are presented in Table 2. The uncertainties quoted for the activation parameters are the computed standard deviations. Table 2 shows that ΔH^* for $[Co(phen)_3]X_3$ decreases in the order X=Br>Cl, whereas for $[Co(phen)_2(en)]X_3$ the sequence X=Br<Cl lies in the reverse order.

TGA runs on all the hydrated salts of the complexes in static air show that dehydration occurs soon after heating (at 30—35 °C). Then anhydrous weight levels are almost attained at 105—115 °C for $[Co(phen)_3]X_3$ and $[Co(phen)(en)_2]X_3$ and at 115—125 °C for $[Co(phen)_2(en)]X_3$. As the temperature is raised further, thermal decomposition of the complexes occurs in air. The temperatures (T_d) at which weight loss resulting from the decomposition begins are given in Table 2. Under the conditions employed in the racemization rate studies, TGA and DTA confirmed the absence of thermal decomposition, and the lack of color changes offered evidence that there was no change in chemical combination. In addition, when (−)-$[Co(phen)_3]Br_3$ was heated at 114 °C for 38 h in air, no reduction of the complex cation by bromide ion was shown by a conventional potentiometric titration of aqueous solutions of the sample using an Ag/Ag^+ electrode, although the sample lost 70% of its optical activity.

Discussion

A very rapid loss of optical activity in an initial period observed for all the cobalt complexes (Figs. 1—3) is similar to that for $[M(phen)_3]X_2$ and $[M(bpy)_3]X_2$ (M=Fe or Ni and bpy=2,2′-bipyridine).[1] Such an initial phenomenon was also reported for the solid-state racemization of other complexes, $[Co(en)_3]X_3 \cdot nH_2O$[11] and $K_3[Cr(C_2O_4)_3]$[19] and discussed in detail in previous papers.[1,8] Then it was not investigated further in this study and attention is riveted on the racemization process after the initial period as follows.

The cobalt complexes employed here are low-spin d^6 complexes in analogy with the iron complexes[20] and so the operation of the twist mechanism is considered likely. However, $[Co(phen)_3]Cl_3$ was found to racemize more rapidly than $[Co(phen)_3]Br_3$. In addition, the ΔH^* and ΔS^* values for the bromide are larger than those for the chloride. These results indicate that there is interaction of the complex cation with the anions in the transition state. The trend in ΔH^* is the same as observed for $[Ni(phen)_3]X_2$ and $[Ni(bpy)_3]X_2$[1] and then attributed to the donicity of the anions to stabilize the transition state. For the solid-state racemization of tris-chelated metal complexes, an intermolecular mechanism cannot operate owing to the absence of solvents required for dissolution of a released ligand, and for the same reason a mechanism involving one-ended dissociation of a ligand is regarded as improbable.[1,8] Thus it is reasonable to infer that the mechanism of racemization of the cobalt complex would be similar to that of the nickel complexes, that is to say, the mechanism involves expansion of a complex cation to a 7-coordinate transition state with one lattice anion, for example a capped trigonal prism.[21] Moreover, the mechanism is consistent with the decrease in ΔS^* found, as ΔH^* decreases (Table 2) as described for the nickel complexes.[1] Another support for the operation of the mechanism is furnished by thermal decomposition studies of the cobalt complexes. It was pointed out that if the racemization mechanism is operative, the ΔH^* values should be related to T_d values taken as a measure of the strength of metal-anion bonds in thermal decomposition products.[1] This is also corroborated by the present data on ΔH^* and T_d. Table 2 shows that the trend is a decrease in T_d as ΔH^* decreases, indicating that both the mechanisms of racemization and decomposition should be controlled by the donicity of the lattice anion.

It was reported that the rates of thermal decomposition of $[Co(NH_3)_6]X_3$ in the solid state increase with the anion in the order $X^-=Cl^-<Br^-<I^-$, which

agree with that of the electron transfer reaction of the complexes.[22] On the other hand, Kutal and Bailar pointed out in a study of the racemization of $[Co(en)_3]X_3$ that such an electron exchange mechanism is not operative in the solid state.[8] For the racemization of $[Co(phen)_3]X_3$ also, the following results suggest that a process involving reduction of the complex or an electron exchange mechanism is unlikely in the solid state. The order of anion effects on the rate for the complex is opposite to that observed for aqueous solutions ($Cl^- < Br^- < I^-$).[13,23] Moreover, despite the observation that $[Co(phen)_3]Br_3$ lost 70% of its optical activity at 114 °C after 38 h, no reduction of the complex in the solid state was observed.[24] In addition, it was reported that activation energies for the dehydration of the series of compounds $[Co(NH_3)_5(H_2O)]X_3$ in the solid state decrease with the anion in the same order, $X^- = Br^- > Cl^-$, as that observed here for the racemization of $[Co(phen)_3]X_3$.

When one of three phenanthroline ligands in the homochelated tris-complex, $[Co(phen)_3]X_3$, is replaced with an ethylenediamine ligand to yield the heterochelated tris-complex, $[Co(phen)_2(en)]X_3$, it is observed that ΔH^* and ΔS^* values for the bromide of the heterochelated complex are smaller than those for the corresponding chloride. Despite the observation that T_d for $[Co(phen)_2(en)]X_3$ decreases in the order, $X^- = Br^- > Cl^-$, which lies in the order of increasing donor strength of the halide ion as observed for the homochelated complex, the trend in ΔH^* and ΔS^* for the heterochelated complex is opposite to that for the homochelated complex (Table 2). In the racemization studies[1,7] of $[Ni(phen)_3]X_2$ and $[Ni(bpy)_3]X_2$, it was implied that there is no appreciable interaction of the aromatic ligands with the halide ions.[25] Thus, these results reflect some specific effects such as hydrogen bonding, as in $[Co(en)_3]X_3$.[8] If such a twisting motion of all the three chelate rings as in a Bailar twist[26] is performed in the racemization process of the complex, then the hydrogen bonds formed in the ground state are forced to be weakened or broken in the transition state. Thus, the enthalpy of activation for the process should increase with an increase in the strength of hydrogen bonds in the ground state. In conformity with this view, the sequence observed for ΔH^*, $X^- = Br^- < Cl^-$, lies in the order of increasing strength of the hydrogen bonds.[27] The ethylenediamine ligand appears to be frozen more tightly in the lattice owing to the hydrogen bonds for the chloride salt compared with the bromide salt. It is thus reasonable to expect a smaller degree of freedom of the ligand in the ground state for the chloride salt and so a larger increase in the degree of freedom of the ligand on activation. This is reflected in larger ΔS^* for the chloride salt (Table 2).

Table 2 shows that ΔH^* for the bromide of the heterochelated complex is lower than that of the bromide of the homochelated complex in spite of the additional energy required to break the hydrogen bonds on activation, and the entropy of activation is negative. These results may imply that for the racemization of the heterochelated complex such a nucleophilic attack of the halide ions as that for the homochelated complex can occur with the breaking of the hydrogen bonds. Since the ethylenediamine ligand is of lower ligand field strength than the phenanthroline ligand,[28] the replacement of one of three phenanthroline ligands by an ethylenediamine ligand causes a decrease in the enthalpy required to expand Co–N bonds in the transition state. On the other hand, the attack puts restriction on the more flexible ethylenediamine ligands due to removal of any steric hindrance, leading to a decrease in the freedom of movement of the ligand in the transition state. For the chloride salt of the heterochelated complex, however, the effect of the hydrogen bonding interaction in the ground state might be more marked than that of the nucleophilic interaction in the transition state and thus the nucleophilic effect of chloride ion is not appreciable.

Furthermore, for the heterochelated tris-complex, $[Co(phen)(en)_2]X_3$, a more marked retarding effect of the hydrogen bonding was found to be exerted on the racemization as seen in Fig. 3. The rate of racemization of the complex decreases with the lattice anion in the order $X^- = I^- > Br^- > Cl^-$. This sequence lies in the order of increasing strength of the hydrogen bonds of the anions and is the same as that observed for $[Co(en)_3]X_3$,[8] but in the order opposite to that for the homochelated complex, $[Co(phen)_3]X_3$. The iodide salts of the heterochelated complex exhibit a first-order linearity as well as $[Co(phen)_3]X_3$ and $[Co(phen)_2(en)]X_3$. For the chloride and bromide salts, on the other hand, deviations from simple first-order behavior were observed. Similar deviations have been reported for $[Co(en)_3]X_3$.[8]

In the present study, the anion effects for the series cannot be accounted for in terms of House's model as in our previous studies for the nickel complexes.[1,12] House pointed out[11] that the trigonal transition state for the intramolecular racemization process which follows the model is produced only with the expansion of the cation and that the difficulty of the expansion increases with increasing lattice energy according to the Kapustinskii equation;[29] the formation of the transition state would be most difficult in the case of the smallest anion. If the process alone gives rise to anion effects in the racemization of the solid complexes, the rate of racemization is expected to decrease with the lattice anion in the order $X^- = Br^- > Cl^-$ and the expected ΔH^* should increase in the order of anions $Br^- < Cl^-$. However, the opposite orders in the rate and ΔH^*, respectively, were observed for $[Co(phen)_3]X_3$. Moreover, if there is no specific interaction such as hydrogen bonding, the expected order of lattice energy effect for the homochelated complex should be the same as those for the heterochelated complexes and so no change in the order of anion effects on the rate or ΔH^* should be expected for the series. However, the order, in fact, changes as shown above. Therefore, the physical factor alone, lattice energy, is insufficient to explain these anion effects, and thus the chemical factors, donicity and hydrogen bonding ability of lattice anions, as described above, are considered to be responsible for the anion effects or the rate differences. In addition, Kutal and Bailar pointed out that the lattice anions effectively shield the

complex ions from each other.[8)]

The author wishes to thank Prof. Y. Yamamoto for helpful discussions. The author also thanks Mr. S. Sato for his assistance in the experimental work. Grateful acknowledgment is made for the financial support of a Grant-in-Aid for Scientific Research No. 574232 the Ministry of Education, Science and Culture.

References

1) Part 1 of this series; T. Fujiwara and Y. Yamamoto, *Inorg. Chem.*, **19**, 1903 (1980).
2) E. Iwamoto, T. Fujiwara, and Y. Yamamoto, *Inorg. Chim. Acta*, **43**, 95 (1980).
3) F. Basolo and R. G. Pearson, "Mechanisms of Inorganic Reactions," 2nd ed, Wiley, New York (1967), pp 300—334.
4) P. Dowley, K. Garbett, and R. D. Gillard, *Inorg. Chim. Acta*, **1**, 278 (1967).
5) V. Gutmann and R. Schmid, *Coord. Chem. Rev.*, **12**, 236 (1974).
6) T. Fujiwara and Y. Yamamoto, *Inorg. Nucl. Chem. Lett.*, **11**, 635 (1975).
7) M. Yamamoto, T. Fujiwara, and Y. Yamamoto, *Inorg. Nucl. Chem. Lett.*, **15**, 37 (1979).
8) C. Kutal and J. C. Bailar, Jr., *J. Phys. Chem.*, **76**, 119 (1972).
9) R. Tsuchiya, Y. Kaji, A. Uehara, and E. Kyuno, *Bull. Chem. Soc. Jpn.*, **42**, 1881 (1969); K. Nagase and H. Yokobayashi, *ibid.*, **47**, 2036 (1974); A. Ohyoshi, S. Hiraki, T. Odate, S. Kohata, and J. Oda, *ibid.*, **48**, 262 (1975).
10) W. W. Wendlandt and J. L. Bear, *J. Phys. Chem.*, **65**, 1516 (1961); M. Mori, R. Tsuchiya, and Y. Okano, *Bull. Chem. Soc. Jpn.*, **32**, 1029 (1959); M. Mori and R. Tsuchiya, *ibid.*, **33**, 841 (1960).
11) J. E. House, Jr., *Thermochim. Acta*, **38**, 59 (1980).
12) T. Fujiwara and Y. Yamamoto, *J. Chem. Soc., Dalton Trans.*, **1982**, 1174.
13) M. Yamamoto and Y. Yamamoto, *Inorg. Nucl. Chem. Lett.*, **11**, 691 (1975).
14) T. Fujiwara and Y. Yamamoto, *Inorg. Nucl. Chem. Lett.*, **15**, 397 (1979).
15) L. S. Dollimore and R. D. Gillard, *J. Chem. Soc., Dalton Trans.*, **1975**, 369.
16) L. S. Dollimore and R. D. Gillard, *J. Chem. Soc., Dalton Trans.*, **1973**, 933.
17) F. M. Jaeger, *Proc. R. Acad. Sci. Amsterdam*, **29**, 559 (1926).
18) P. W. M. Jacobs and F. C. Tompkins, "Chemistry of the Solid State," ed by W. E. Garner, Butterworths, London (1955), Chap. 7; J. H. Sharp, *Trans. Brit. Ceram. Soc.*, **72**, 21 (1973).
19) D. M. Chowdhury and G. M. Harris, *J. Phys. Chem.*, **73**, 3366 (1969).
20) The feasibility of intersystem crossing along the racemization paths via Bailar twist for low-spin d^6 complexes (*e.g.*, $[Fe(phen)_3]^{2+}$) has been discussed recently: K. F. Purcell, *J. Am. Chem. Soc.*, **101**, 5147 (1979).
21) D. L. Kepert, *Inorg. Chem.*, **13**, 2754, 2758 (1974).
22) N. Tanaka and K. Nagase, *Bull. Chem. Soc. Jpn.*, **40**, 546 (1967).
23) R. J. Mureinik, *Inorg. Nucl. Chem. Lett.*, **12**, 319 (1976).
24) The loss of optical activity of the $[Co(phen)_3]^{3+}$ ion in NaBr or NaCl solutions in the dark has been related to the extent of reduction of the complex, in Ref. 23; R. J. Mureinik and M. Spiro, *J. Chem. Soc., Dalton Trans.*, **1974**, 2493.
25) No direct evidence has been obtained for nucleophilic attack of chloride ion on the phenanthroline ring in the kinetic study of acid solvolysis of $[Fe(phen)_3]^{2+}$ in dimethyl sulfoxide: D. J. Farrihgton, J. G. Jones, and M. V. Twigg, *J. Chem. Soc., Dalton Trans.*, **1979**, 221.
26) J. C. Bailar, Jr., *J. Inorg. Nucl. Chem.*, **8**, 165 (1958).
27) J. Fujita, K. Nakamoto, and M. Kobayashi, *J. Am. Chem. Soc.*, **78**, 3295 (1956).
28) C. K. Jørgensen, "Absorption Spectra and Chemical Bonding in Complexes," Pergamon Press, London (1962), Chap. 7.
29) A. F. Kapustinskii, *Quart. Rev.*, **1956**, 238.

 © 1983 The Chemical Society of Japan Bull. Chem. Soc. Jpn., 56, 127—133 (1983)

Stereochemistry and Properties of *unsym-fac-*, *sym-fac-*, and *mer-* (Iminodiacetato)$_n$(*N*-alkyliminodiacetato)$_{2-n}$cobaltate(III) ($n=0$, 1, or 2) Complexes

Takaji Yasui,* Hiroshi Kawaguchi, Norio Koine,† and Tomoharu Ama

Department of Chemistry, Faculty of Science, Kochi University, Akebono-cho, Kochi 780

† *Department of Industrial Chemistry, Faculty of Engineering, Ehime University, Bunkyo-cho, Matsuyama 790*

(Received June 4, 1982)

Unsymmetrical-facial (*u-fac*) and symmetrical-facial (*s-fac*) isomers of a mixed-ligand type complex, [Co(ida)(Rida)]$^-$ (Rida denotes *N*-methyl- or *N*-ethyliminodiacetate dianion), were prepared and characterized on the basis of their absorption, circular dichroism, ^{1}H NMR, and ^{13}C NMR spectral data. The isomerization and racemization reactions of these isomers were investigated in basic aqueous solution and compared with those of the bis type complexes, [Co(ida)$_2$]$^-$ and [Co(Rida)$_2$]$^-$. The time-course changes in the absorption spectra of [Co(ida)(Rida)]$^-$ and [Co(ida)$_2$]$^-$ indicated that the *mer* isomer exists as a transient labile intermediate in the isomerization reaction of *u-fac* to *s-fac*.

The bis(terdentate) complex of cobalt(III) with *N*-alkyliminodiacetate ion provides three geometrical isomers, as shown in Fig. 1. In a previous paper,[1] we reported the preparation and characterization of the *u-fac* isomers of [Co(mida)$_2$]$^-$ and [Co(eida)$_2$]$^-$, which have large intramolecular steric repulsions. These *u-fac* isomers decomposed in basic aqueous solution; at the same time, the decomposition of the ligands and the reduction of cobalt(III) to cobalt(II) occurred. On the other hand, no such decomposition occurred in the *s-fac* and *mer* isomers of the above two complexes.

In the present paper, the preparation of the mixed-ligand type complexes with both iminodiacetate (ida) and *N*-alkyliminodiacetate (Rida) ions, [Co(ida)(Rida)]$^-$, will be described, and the stereochemistry and the reactivity (isomerization and racemization) in basic aqueous solution will be discussed on the basis of their absorption, circular dichroism (CD), ^{1}H NMR, and ^{13}C NMR spectral data. These results will be compared with those of the bis type complexes, [Co(ida)$_2$]$^-$ and [Co(Rida)$_2$]$^-$.

Experimental

Ligands. Iminodiacetic acid was obtained commercially from Wako Pure Chemical Industries, Ltd. and used without further purification. *N*-Methyl- and *N*-ethyliminodiacetic acids were synthesized by the method in the literature.[2]

Preparation of Complexes. *Potassium Iminodiacetato(N-methyliminodiacetato)cobaltate(III)*, u-fac-*K*[*Co(ida)(mida)*]·2H_2O: This isomer was prepared by a method similar to that used for the *u-fac*-K[Co(mida)$_2$] complex reported in our previous paper.[1]

To a solution containing cobalt(II) chloride hexahydrate (5.95 g, 0.025 mol) in 20 cm^3 of water was added a solution containing a mixture of iminodiacetic acid (3.34 g, 0.025 mol) and *N*-methyliminodiacetic acid (3.68 g, 0.025 mol) in 70 cm^3 of water. Lead dioxide (9.0 g, 0.038 mol) was added gradually to the mixed solution adjusting pH to 4.0—4.5, and then the solution was stirred for 1 h at room temperature. After insoluble materials in the reactant solution were removed by filtration, the filtrate was poured into a QAE-Sephadex column (4.7 cm × 90 cm, Cl$^-$ form). The adsorbed band was separated into a broad red-brown band (containing *s-fac* and *mer* isomers of [Co(mida)$_2$]$^-$, [Co(ida)(mida)]$^-$, and [Co(ida)$_2$]$^-$) and a violet one by elution with an 0.1 mol·dm^{-3} KCl solution. The latter band was separated into three bands of blue (*u-fac*-[Co(mida)$_2$]$^-$), violet (*u-fac*-[Co(ida)(mida)]$^-$), and purple (*u-fac*-[Co(ida)$_2$]$^-$) by repeating developments on the same column. The violet eluate containing *u-fac*-[Co(ida)(mida)]$^-$ was acidified by adding a few drops of acetic acid to it and evaporated by use of a rotary evaporator at 35 °C. The complex obtained from the concentrated solution by addition of methanol and acetone was purified by using a Sephadex G-10 column. Needle crystals of violet color were obtained by recrystallization from water to which a methanol–acetone mixture was added. Found: C, 26.39; H, 3.86; N, 7.06%. Calcd for *u-fac*-K[Co(ida)(mida)]·2H_2O: C, 26.35; H, 3.93; N, 6.83%.

Sodium Iminodiacetato(N-methyliminodiacetato)cobaltate(III), s-fac-*Na*[*Co(ida)(mida)*]·H_2O. This isomer was obtained by the isomerization reaction of *u-fac* to *s-fac*.

An aqueous solution containing *u-fac*-Na[Co(ida)(mida)], which was converted from the corresponding potassium salt using a small SP-Sephadex column of Na$^+$ form, was adjusted to pH 10—10.5 with NaOH aqueous solution and warmed to *ca.* 50 °C. The color of the solution changed immediately from violet to light brown. The solution was evaporated by use of a rotary evaporator. The desired *s-fac* isomer was isolated as flake crystals of light brown by adding methanol to the concentrated solution. Recrystallization was carried out from warm water by addition of methanol. Found: C, 28.60; H, 3.74; N, 7.60%. Calcd for *s-fac*-Na[Co(ida)(mida)]·H_2O: C, 28.74; H, 3.75; N, 7.45%.

An attempt to obtain the *mer* isomer of [Co(ida)(mida)]$^-$ from the red-brown band mentioned above was unsuccessful (*vide post*).

Potassium Iminodiacetato(N-ethyliminodiacetato)cobaltate(III), u-fac-*K*[*Co(ida)(eida)*]·H_2O. This isomer was obtained by the same method as that used for *u-fac*-K[Co(ida)(mida)]·2H_2O. Found: C, 29.25; H, 4.06; N, 6.95%. Calcd for *u-fac*-K[Co(ida)(eida)]·H_2O: C, 29.56; H, 3.97; N, 6.90%.

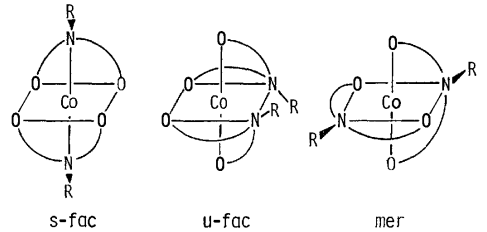

Fig. 1. Three geometrical isomers of [Co(Rida)$_2$]$^-$.

TABLE 1. ABSORPTION DATA OF THE $[Co(ida)_n(Rida)_{2-n}]^-$ TYPE COMPLEXES

Complex	Structure	First band[a]	Second band[a]	Charge-transfer band[a]
$[Co(ida)_2]^-$	*u-fac*	17.83 (2.18)	26.28 (2.14)	45.35 (4.39)
	s-fac	16.47 (1.10)	27.55 (1.78)	42.0 (4.30) sh)
		20.18 (1.76)		46.37 (4.39)
	mer	16.13 (1.39)	26.39 (2.33)	44.64 (4.31)
		19.88 (2.55)		
$[Co(mida)_2]^-$	*u-fac*	17.24 (2.07)	25.32 (1.98)	42.46 (4.36)
	s-fac	16.4 (1.12) sh)	27.25 (1.85)	44.44 (4.41)
		19.76 (1.79)		
	mer	16.0 (1.40) sh)	25.64 (2.39)	44.05 (4.30)
		19.14 (2.52)		
$[Co(eida)_2]^-$	*u-fac*	17.18 (2.13)	25.00 (2.00)	41.84 (4.32)
	s-fac	16.5 (1.10) sh)	27.25 (1.87)	43.86 (4.33)
		19.49 (1.80)		
	mer	16.0 (1.40) sh)	25.45 (2.42)	43.67 (4.26)
		18.83 (2.48)		
[Co(ida)(mida)]$^-$	*u-fac*	17.70 (2.12)	26.04 (2.06)	44.25 (4.37)
	s-fac	16.69 (1.11)	27.40 (1.81)	45.45 (4.39)
		20.04 (1.76)		
[Co(ida)(eida)]$^-$	*u-fac*	17.64 (2.10)	25.97 (2.02)	43.86 (4.34)
	s-fac	16.67 (1.10)	27.32 (1.83)	45.05 (4.40)
		19.88 (1.80)		

a) Wave numbers and $\log \varepsilon$ values (in parentheses) are given in $10^3\,cm^{-1}$ and $mol^{-1}\,dm^3\,cm^{-1}$, respectively. sh) Shoulder bands.

Sodium Iminodiacetato(N-ethyliminodiacetato)cobaltate(III), s-fac-*Na[Co(ida)(eida)]·H₂O*. This isomer was obtained by the same method as that used for *s-fac*-Na[Co(ida)(mida)]·H_2O. Found: C, 30.97; H, 4.17; N, 7.08%. Calcd for *s-fac*-Na[Co(ida)(eida)]·H_2O: C, 30.78; H, 4.13; N, 7.18%.

The preparations of the *u-fac*, *s-fac*, and *mer* isomers of $K[Co(mida)_2]$ and $K[Co(eida)_2]$ are described in our previous paper.[1] The three isomers of $K[Co(ida)_2]$ were prepared by the same method as that used for the isomers of $K[Co(mida)_2]$.[1] The *mer* isomer, which is easily soluble and unstable in water, was obtained as red needle crystals. Recrystallization was carried out from slightly acidic water by adding methanol. Found: C, 25.49; H, 3.02; N, 7.62%. Calcd for *mer*-K[Co(ida)$_2$]·H_2O: C, 25.41; H, 3.20; N, 7.41%.

Optical Resolution. $(+)_{589}$-u-fac-*K[Co(ida)(mida)]*: Resolving agent, $(+)_{589}$-[Co(ox)(en)$_2$]Br·H_2O (1.83 g, 5 mmol) was dissolved in 400 cm^3 of warm water (40 °C) and the bromide ion was converted to the acetate one using a small column containing Dowex 1×8 resin (200—400 mesh, CH_3COO^- form). The solution eluted from the column was concentrated to a volume of *ca.* 30 cm^3. This concentrated solution was mixed with an aqueous solution containing *u-fac*-H[Co(ida)(mida)] (this acidic complex was prepared in solution by loading *u-fac*-K[Co(ida)(mida)]·$2H_2O$ (2.05 g, 5 mmol) on a small column containing Dowex 50W×8 resin of H^+ form). The mixed solution was evaporated to a volume of 20 cm^3 using a rotary evaporator. To the concentrated solution was added 90% methanol until the purple crystals of diastereomer ($(+)_{589}$-[Co(ox)(en)$_2$]-$(+)_{589}$-[Co(ida)(mida)]·$2H_2O$) began to appear. The solution was cooled in a refrigerator for 1—2 h. The crystals which deposited were filtered and washed with water-methanol mixture (1:1), methanol, and then acetone. Yield was 1.40 g. Recrystallization was carried out twice from the concentrated aqueous solution by adding methanol. $[\alpha]_{589}^{15}$ +1274°.

The diastereomer was dissolved in a small amount of water and loaded on a small SP-Sephadex column (K^+ form) to remove $(+)_{589}$-$[Co(ox)(en)_2]^+$. To the solution obtained by elution with water was added a few drops of acetic acid, and the solution was evaporated to a few milliliters. A mixture of methanol–acetone (1:1) was added to the concentrated solution until crystals began to appear, and the solution was allowed to stand in a refrigerator for a few hours. The crystalline powder which deposited was filtered and washed with methanol and then acetone. Recrystallization was carried out from water by adding a methanol-acetone mixture. Found: C, 26.94; H, 3.77; N, 6.98%. Calcd for $(+)_{589}$-*u-fac*-K[Co(ida)(mida)]·$1.5H_2O$: C, 26.75; H, 3.78; N, 7.07%.

The $(-)_{589}$-isomer was obtained from the filtrate of the less soluble diastereomer.

$(+)_{589}$-u-fac-K[Co(ida)(eida)]·2.5H_2O. The diastereomer ($(+)_{589}$-[Co(ox)(en)$_2$]$(+)_{589}$-*u-fac*-[Co(ida)(eida)], $[\alpha]_{589}^{15}$ +1165°) and the $(+)_{589}$-isomer were obtained in the same way as that used for the resolution of *u-fac*-K[Co(ida)-(mida)]·$2H_2O$. Found: C, 27.93; H, 4.17; N, 6.52%. Calcd for $(+)_{589}$-*u-fac*-K[Co(ida)(eida)]·$2.5H_2O$: C, 27.72; H, 4.42; N, 6.47%.

Measurements. The absorption and CD spectra were measured by a Hitachi 557-type spectrometer and a JASCO J-22 spectropolarimeter, respectively. The ^1H NMR spectra were recorded on a JEOL MH-100 NMR spectrometer using DSS as an internal standard. The ^{13}C NMR spectra at 25 MHz were recorded on a JEOL JNM-FX100 spectrometer, in pulsed Fourier transform/proton noise decoupled mode. Peak positions were measured relative to internal dioxane (δ=67.44 ppm).

TABLE 2. OBSERVED CD DATA OF THE $[Co(ida)_n(Rida)_{2-n}]^-$ TYPE COMPLEXES

Complex	First band region[a)]	Second band region[a)]	Charge-transfer band region[a)]
$(+)_{589}$-*u-fac*-$[Co(ida)_2]^-$	17.01 (−2.430)	24.69 (−0.57) sh)	37.45 (−0.70) sh)
	19.65 (+2.541)	26.67 (−0.697)	41.84 (−3.211)
			46.08 (+12.49)
$(+)_{589}$-*u-fac*-$[Co(mida)_2]^-$	16.31 (−2.234)	23.53 (−0.83) sh)	37.31 (−5.034)
	18.32 (+3.155)	25.45 (−0.954)	41.49 (+7.180)
			46.08 (−14.44)
$(+)_{546}$-*mer*-$[Co(mida)_2]^-$	16.3 (−0.17) sh)	25.13 (−0.104)	34.72 (+0.450)
	18.32 (−0.570)	27.55 (+0.112)	43.48 (−2.069)
	20.45 (+0.868)		
$(+)_{589}$-*u-fac*-$[Co(eida)_2]^-$	16.13 (−2.420)	23.26 (−0.802)	36.36 (−4.922)
	18.15 (+3.053)	25.32 (−0.885)	40.65 (+7.981)
			45.05 (−17.39)
$(+)_{589}$-*u-fac*-$[Co(ida)(mida)]^-$	16.89 (−2.521)	24.27 (−0.779)	38.91 (−5.625)
	19.19 (+2.863)	26.11 (−0.829)	44.25 (+10.05)
			48.54 (−13.26)
$(+)_{589}$-*u-fac*-$[Co(ida)(eida)]^-$	16.75 (−3.117)	24.10 (−0.792)	38.91 (−3.513)
	13.98 (+3.101)	26.2 (−0.72) sh)	43.86 (+4.960)
			47.62 (−3.720)

a) Wave numbers and $\Delta\varepsilon$ values (in parentheses) are given in 10^3 cm^{-1} and mol^{-1} dm^3 cm^{-1}, respectively. sh) Shoulder bands.

Results and Discussion

Absorption Spectra. The absorption spectral data of the newly prepared mixed-ligand type complexes are listed in Table 1, together with those of the bis type complexes reported in a previous paper.[1] The comparison of absorption spectra among the three different geometrical isomers of the bis type complexes are shown in Fig. 2. Each isomer exhibits a considerably different spectrum behavior in the d-d transition region. The first ($^1A_1 \rightarrow {}^1T_1$) and second ($^1A_1 \rightarrow {}^1T_2$) bands increase the intensities in the order *s-fac*< *u-fac*<*mer*. This trend is in agreement with that observed in the three geometrical isomers of $[Co(ida)(dien)]^+$.[3] Legg and Cooke have attributed an increment of absorption intensity to the following elements: the removal of the center of the symmetry and the strained structure.[3] If their proposal is applied to the present bis type complexes, the *u-fac* isomer (C_2 symmetry) which lacks the center of symmetry would give a more intense spectrum than the *s-fac* isomer (C_{2h}), which has a plane of symmetry, and the *mer* isomer (C_2), containing both the elements: removal of the center of symmetry and the strained structure would give the most intense spectrum.

In each geometrical isomer, the first and second absorption maxima shift to the lower energy side in the order of $[Co(ida)_2]^-$, $[Co(mida)_2]^-$, and $[Co(eida)_2]^-$ (Fig. 2). This fact indicates that the ligand field strength decreases in the order of ida, mida, and eida, and that the terdentate ligand (ida) containing secondary nitrogen is located at a higher position in the spectrochemical series than the terdentate ligand (mida or eida) containing tertiary nitrogen. This trend agrees with those observed in the *s-fac* and *mer* isomers of $[Co(ida)(dien)]^+$ and $[Co(mida)(dien)]^+$ [3] and in the *s-fac* isomers of the $[Co(dien)_2]^{3+}$ and $[Co(dema)_2]^{3+}$ (dema = 3-methyl-3-azapentane-1,5-diamine) complexes, which contain secondary and tertiary nitrogens, respectively.[4]

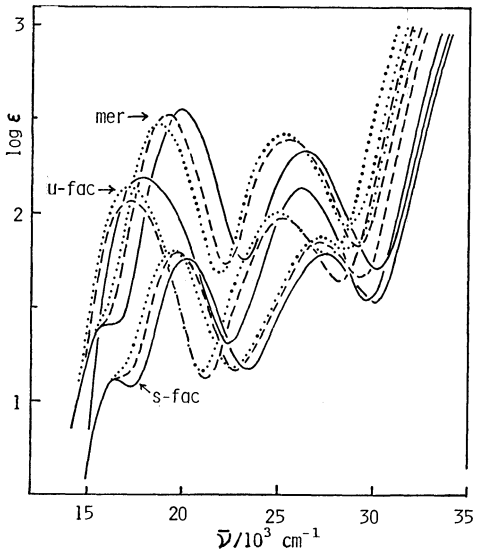

Fig. 2. Absorption spectra of three geometrical isomers of $[Co(ida)_2]^-$ (——), $[Co(mida)_2]^-$ (– – –), and $[Co(eida)_2]^-$ (·····).

As mentioned in the experimental section, for the mixed-ligand type complexes, $[Co(ida)(mida)]^-$ and $[Co(ida)(eida)]^-$, two geometrical isomers with violet and light brown colors were obtained by utilizing the preparative method of acidic conditions. As Fig. 3 shows, the absorption spectra of the violet isomers are identical in band shape and intensity with those of the *u-fac* isomers of the bis type complexes, while the spectra of the light brown isomers are identical with those of the *s-fac* isomers. These facts make it pos-

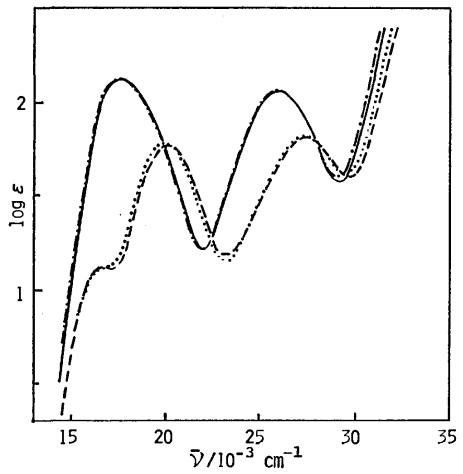

Fig. 3. Absorption spectra of the mixed-ligand complexes: *u-fac* (——) and *s-fac* (----) of [Co(ida)(mida)]⁻; *u-fac* (—·—) and *s-fac* (·····) of [Co(ida)(eida)]⁻.

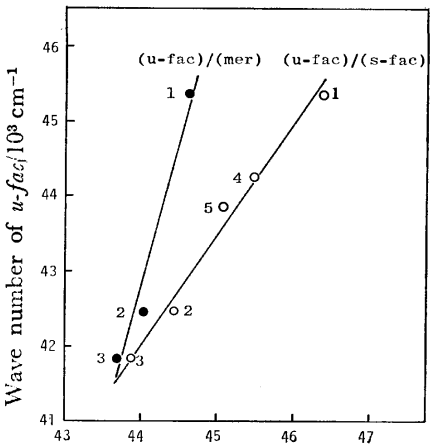

Fig. 4. Correlations of CT band maxima between two geometrical isomers. 1 $[Co(ida)_2]^-$, 2 $[Co(mida)_2]^-$, 3 $[Co(eida)_2]^-$, 4 [Co(ida)(mida)]⁻, and 5 [Co(ida)(eida)]⁻.

sible to assign the structures of the violet and light brown isomers of the mixed complexes to *u-fac* and *s-fac*, respectively.

Both the bis and mixed-ligand complexes exhibit charge transfer (CT) bands with the intensities of log ε=4.26—4.40 in the region 42000—46000 cm^{-1} (Table 1). The maximum positions of these bands vary with the ligands and the geometrical structures. As Fig. 4 shows, all the complexes show linear relationships between the maximum positions of two different isomers. These correlations suggest that the alkyl substituent on the nitrogen atom of coordinated ida brings about a shift of CT band maximum to lower energy in the order *u-fac*>*s-fac*>*mer*.

Circular Dichroism Spectra. The CD data of the *u-fac* isomers of the mixed-ligand type complexes are listed in Table 2, together with those of the bis type complexes. All the $(+)_{589}$-*u-fac* isomers exhibit similar CD patterns in the visible region; that is, these isomers give two component CD bands with (—) and (+) signs at the lower and higher energy sides in

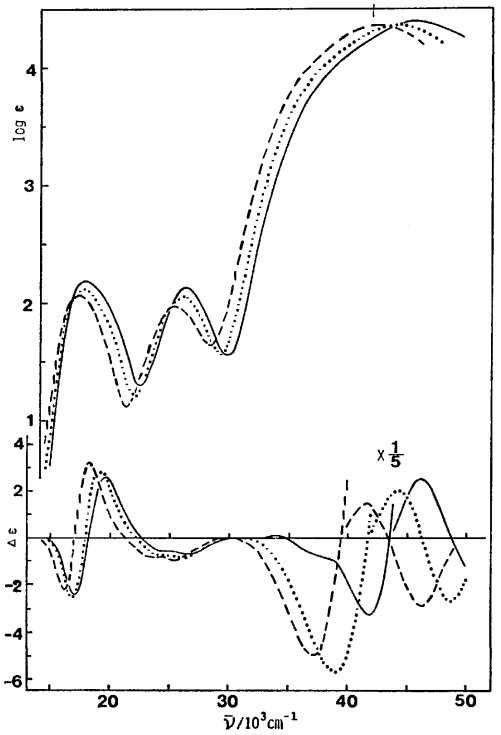

Fig. 5. Absorption and CD spectra of the $(+)_{589}$-*u-fac* isomers: $[Co(ida)_2]^-$ (——), [Co(ida)(mida)]⁻ (·····), and $[Co(mida)_2]^-$ (----).

the first band region, respectively, and with (—) sign in the second band region. Figure 5 shows the comparison of the CD curves among $(+)_{589}$-*u-fac*-[Co(ida)(mida)]⁻, -$[Co(ida)_2]^-$, and -$[Co(mida)_2]^-$. The shift trend of the CD bands is identical with that of the absorption bands.

In a previous study,[1] the absolute configuration of the $(-)_{589}$-isomer in *u-fac*-$[Co(mida)_2]^-$ and -$[Co(eida)_2]^-$ was assigned to $\Lambda\Lambda\Lambda$ (or Λ) from the comparison of CD spectra in the visible region with that of the $(-)_{546}$-isomer of *u-fac*-$[Co(ida)_2]^-$ whose the absolute configuration had been determined as $\Lambda\Lambda\Lambda$.[5,6] Similarly, the absolute configuration of the mixed-ligand complexes can be determined by comparing the CD patterns with those of the bis complexes; that is, the $\Lambda\Lambda\Lambda$ (or Λ) configuration is assigned to the $(+)_{589}$-isomers of *u-fac*-[Co(ida)(mida)]⁻ and -[Co(ida)(eida)]⁻, whose CD spectra give patterns similar to those of $(+)_{589}$-*u-fac*-$[Co(ida)_2]^-$, -$[Co(mida)_2]^-$, and -$[Co(eida)_2]^-$.

Koine *et al.* succeeded in resolving *mer*-$[Co(mida)_2]^-$ into optically active isomers.[7] The optical activity of this isomer arises from a chiral disposition of the two non-coplanar ligands. Therefore, the CD intensity of the *mer* isomer is expected to be lower than that of the *u-fac* isomer, which has the configurational chirality. Actually, the $(+)_{546}$-*mer* isomer give considerably lower CD intensity than those of the $(+)_{589}$-*u-fac* isomers (Table 2). Similar phenomena have been observed for the complexes containing other terdentate ligands, such as dien[7,8] and dema.[4]

^1H NMR Spectra. Cooke measured the ^1H NMR spectra of the *s-fac* and *u-fac* isomers of $[Co(ida)_2]^-$ and the *s-fac* isomer of $[Co(mida)_2]^-$ and as-

Table 3. ^{13}C Chemical shifts (ppm) of the $[Co(ida)_n(Rida)_{2-n}]^-$ type complexes

Complex[a] and free ligand[b]	δ (C_{oxy})	Shift non-equivalence	Δ[c] (C_{oxy})	δ (C_α)	Shift non-equivalence	Δ[c] (C_α)	δ (N-$\underline{C}H_3$)	δ (N-$\underline{C}H_2CH_3$)	δ (N-$CH_2\underline{C}H_3$)
$[Co(ida)_2]^-$									
s-fac	185.66		+16.50	58.32		+10.44			
u-fac	184.93	0.74	+15.77	59.59	1.61	+11.71			
	184.19		+15.03	57.98		+10.10			
mer	184.53	0.19	+15.37	57.05	0.14	+9.17			
	184.34		+15.18	56.91		+9.03			
H_3ida	169.16			47.88					
$[Co(mida)_2]^-$									
s-fac	183.42		+15.20	69.29		+12.28	51.41		
u-fac	183.66	1.60	+15.44	71.39	3.46	+14.38	50.24		
	182.06		+13.84	67.93		+10.92			
mer	183.32	0.58	+15.10	68.42	0.54	+11.41	51.36		
	182.74		+14.52	67.88		+10.87			
H_3mida	168.22			57.01			44.34		
$[Co(eida)_2]^-$									
s-fac	183.86		+15.35	65.35		+10.28		58.28	8.63
u-fac	184.25	1.36	+15.74	67.25	2.78	+12.18		57.55	8.43
	182.89		+14.38	64.47		+9.40			
mer	183.66	0.34	+15.15	65.15	0.88	+10.08		57.06	9.60
	183.32		+14.81	64.27		+9.20			
H_3eida	168.51			55.07				58.80	9.94
$[Co[ida)(mida)]^-$									
s-fac	185.27	(ida)	+16.11	68.81	(mida)	+11.80	51.65		
	183.86	(mida)	+15.64	58.92	(ida)	+11.04			
u-fac	185.22	1.36 (ida)	+16.06	70.02	1.80 (mida)	+13.01	50.14		
	183.86		+14.70	68.22		+11.21			
	183.17	0.72 (mida)	+14.95	59.65	2.20 (ida)	+11.77			
	182.45		+14.23	57.45		+9.57			
$[Co(\bar{i}da)(eida)]^-$									
s-fac	185.27	(ida)	+16.11	65.05	(eida)	+9.98		(58.67)[d]	8.92
	184.25	(eida)	+15.74	(58.82)	(ida)	+10.94			
u-fac	185.27	1.46 (ida)	+16.11	66.03	1.80 (eida)	+10.96		(57.36)[d]	8.43
	183.81		+14.65	64.23		+9.16			
	183.62	0.69 (eida)	+15.11	59.65	2.10 (ida)	+11.77			
	182.92		+14.42	(57.55)[d]		+9.67			

a) Measured in D_2O. b) Measured in 7.5 M DCl. c) $\Delta(C_{oxy})=(\delta(C_{oxy})$ of coordinated ligand$)-(\delta(C_{oxy})$ of free ligand); $\Delta(C_\alpha)=(\delta(C_\alpha)$ of coordinated ligand$)-(\delta(C_\alpha)$ of free ligand). d) Values in parentheses are assigned tentatively.

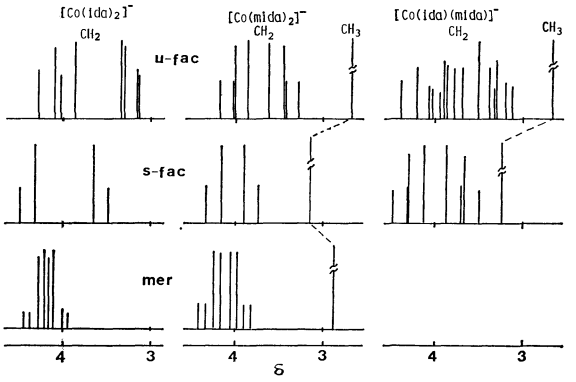

Fig. 6. The ^{1}H NMR spectra of the bis and mixed-ligand complexes in D_2O solution.

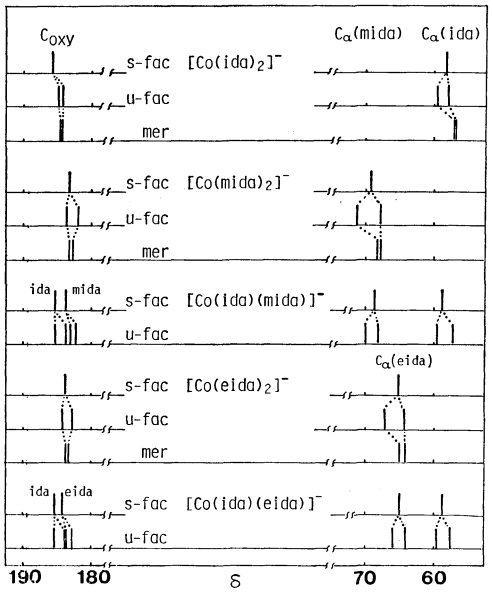

Fig. 7. ^{13}C NMR spectra of bis- and mixed-ligand complexes. The signals of *N*-methyl and -ethyl carbons are omitted.

signed the resonance peaks observed as one or two sets of AB quartets to the acetate-methylene protons.[9] Similar AB patterns (J_{AB}=16.0—18.0 cps) are also observed for the *mer* isomer of $[Co(ida)_2]^-$ and the *u-fac* and *mer* isomers of $[Co(mida)_2]^-$ in the range 3.3—4.3 ppm, as Fig. 6 shows.

The *u-fac* and *s-fac* isomers of $[Co(ida)(mida)]^-$ give the spectra consisting of four and two sets of AB quartets, respectively, in the acetate region (3.1—4.5 ppm), suggesting that the two acetate rings of each ligand are nonequivalent and equivalent in the former and latter isomers, respectively. The spectral patterns of these two isomers are nearly identical with the superimposed spectra of each corresponding isomer in both $[Co(ida)_2]^-$ and $[Co(mida)_2]^-$.

^{13}C NMR Spectra. The ^{13}C NMR chemical shifts of the present complexes are listed in Table 3 and the shift patterns are shown in Fig. 7. In the previous papers,[10,11] we reported that the chelation of α-amino acids to cobalt(III) ion brings about down-field changes (Δ values in Table 3) in the ^{13}C chemical shifts of their carboxyl-carbon (C_{oxy}) and α-carbon (C_α). All the present complexes exhibit down-field shift changes

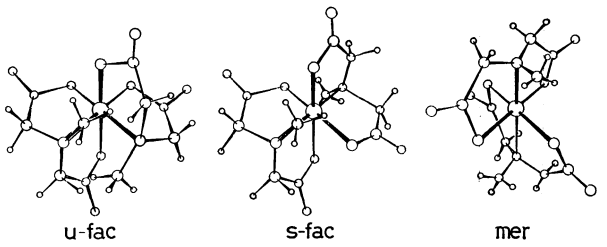

Fig. 8. Molecular models of *u-fac*-, *s-fac*-, and *mer*-$[Co(mida)_2]^-$.

in the range +13.84—+16.50 ppm for carboxyl-carbons, and the values are comparable with those of α-amino acid complexes.[10,11] However, the Δ values (+9.03—+14.38 ppm) of α-carbons for all the present complexes are considerably larger than those (+4.44—+8.29) for the α-amino acid complexes.

It is well-known that ^{13}C resonance patterns reflect the symmetries of the complexes.[12-15] In the cases of $[Co(ida)_2]^-$ and $[Co(Rida)_2]^-$, the ^{13}C signals of the α- and carboxyl-carbons appear as single peaks in the *s-fac* isomer (C_{2h}) and as double peaks in the *u-fac* and *mer* isomers (C_2). The double peaks of the latter isomers indicate that the two acetate rings of each ligand are nonequivalent in chemical environment. As given in Table 3, the shift nonequivalences[13] (resonance separations of the double peaks) are larger in the *u-fac* isomer than in the *mer* one and larger in $[Co(Rida)_2]^-$ than in $[Co(ida)_2]^-$. The difference in shift nonequivalences between these two isomers may be related to the difference in interligand steric repulsions. The molecular model of *u-fac*-$[Co(mida)_2]^-$ (Fig. 8) suggests an existence of large steric repulsions between the *N*-methyl group of one ligand and the methylene and methyl groups of the other ligand. The large steric repulsions can also be related to the fact that the *u-fac*-$[Co(mida)_2]^-$ complex decomposes easily in weakly basic aqueous solution[1] (*vide post*). A similar argument can also be made for the $[Co(eida)_2]^-$ complex.

The assignments of the ^{13}C resonance peaks of $[Co(ida)(Rida)]^-$ were made in comparison with the resonance peaks of $[Co(ida)_2]^-$ and $[Co(Rida)_2]^-$. The α- and carboxyl-carbons of the ida and Rida ligands in *u-fac*-$[Co(ida)(Rida)]^-$ exhibit different behaviors in chemical shift changes from those in *u-fac*-$[Co(ida)_2]^-$ and -$[Co(Rida)_2]^-$ (Fig. 7). For example, the shift nonequivalences of ida (C_α, 2.20 ppm; C_{oxy}, 1.36 ppm) in *u-fac*-$[Co(ida)(mida)]^-$ are larger than those of ida (C_α, 1.61 ppm; C_{oxy}, 0.74 ppm) in *u-fac*-$[Co(ida)_2]^-$. Contrary to this behavior, the shift nonequivalences of mida (C_α, 1.80 ppm; C_{oxy}, 0.72 ppm) in the former complex are smaller than those of mida (C_α, 3.46 ppm; C_{oxy}, 1.60 ppm) in *u-fac*-$[Co(mida)_2]^-$. These observations indicate that the shift nonequivalences of the paired carbons on a ligand are remarkably influenced by the interligand steric repulsions.

Reactions in Basic Aqueous Solution. In a previous paper,[1] we reported that in basic solution the *mer* isomer of $[Co(ida)_2]^-$ isomerizes rapidly to the *u-fac* and/or *s-fac* one and the *u-fac* isomers of $[Co(mida)_2]^-$ and $[Co(eida)_2]^-$ decompose along with

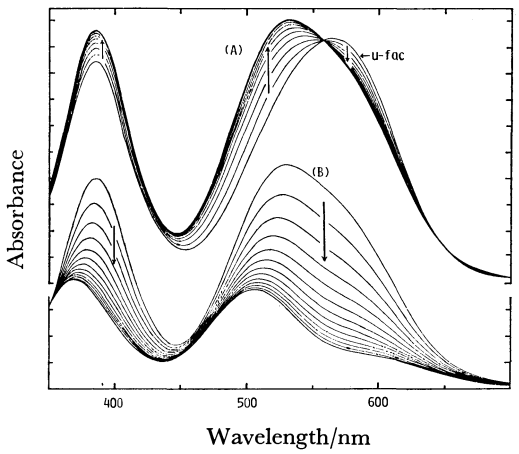

Fig. 9. Time-course changes of absorption spectra of *u-fac*-[Co(ida)(mida)]$^-$ in basic aqueous solutions at 30 °C. Trends of spectral changes with time are shown by arrows. (A): pH, 8.42; record interval, 5 min; time to recording start from pH adjustment, 160 s. (B): pH, 10.10; record interval, 10 min; time to recording start, 40 s.

the decomposition of one ligand per two complex ions and the reduction of cobalt(III) to cobalt(II). Such reactions suggest that the basic conditions are unfavourable to the preparations of the three geometrical isomers of the bis type complexes. Actually, the preparation under basic conditions gave only the *u-fac* and *s-fac* isomers in $[Co(ida)_2]^-$ and only the *s-fac* and *mer* isomers in $[Co(mida)_2]^-$ and $[Co(eida)_2]^-$. The preparation under acidic conditions (pH 4.0—4.5), however, gave all of the three possible isomers in substantial yield; *e.g.* in the case of $[Co(mida)_2]^-$ the formation ratio of the three isomers was *u-fac*:*s-fac*:*mer*=42:34:24. This ratio indicates that the *u-fac* isomer is formed most favourably in an acidic medium, although this isomer is thermodynamically unstable. The preparations of the mixed-ligand complexes have also been performed under the same acidic conditions as used for the bis complexes, but no *mer* isomers were isolated because of the rapid isomerization.

In analogy with the case of *u-fac*-$[Co(ida)_2]^-$ which was described in a previous paper,[1] the *u-fac* isomer of [Co(ida)(mida)]$^-$ also isomerized in basic aqueous solution. Figure 9 shows the spectral changes of *u-fac*-[Co(ida)(mida)]$^-$ in weak and strong basic solutions. In the weak basic solution of pH 8.42, the spectrum changes slowly with the passage of time, giving two isosbestic points at 588 and 647 nm (Fig. 9(A)). A new band peak which is observed near 530 nm is ascribed to the formation of a new complex. However, over about one hour the intensity of the spectrum began to decrease and the prolonged reaction gave a spectrum nearly identical with that of *s-fac*-[Co(ida)(mida)]$^-$. On the other hand, in strong basic solution of pH 10.10, a rapid spectral change is observed (Fig. 9(B)). The pattern of this spectral change is almost identical with that observed in the prolonged reaction of the weak basic solution mentioned above. The spectral changes in these two cases (pH 8.42 and 10.10) suggest that the isomerization of *u-fac* to *s-fac* proceeds in a two-step reaction.

In order to identify the new complex mentioned above, the reactant solution of pH 8.42 was chromatographed by use of a Sephadex G-10 column. The violet band of the unreacted *u-fac* isomer was eluted early and the red band containing the new complex followed as a partially overlapped band. The absorption spectrum of the solution eluted from the red band gave the first and second band maxima at 19490 and 25840 cm^{-1}, respectively. These maximum positions are comparable with those of the *mer* isomers of $[Co(ida)_2]^-$ and $[Co(mida)_2]^-$ (Table 1). This suggests that the new complex takes the *mer* structure. Similar spectral changes were also observed in the basic solutions of *u-fac*-[Co(ida)(eida)]$^-$ and -$[Co(ida)_2]^-$. Therefore, it is expected that the isomerization of these complexes proceeds in a reaction fashion similar to the case of *u-fac*-[Co(ida)(mida)]$^-$.

The preliminary kinetic study of *u-fac*-[Co(ida)(mida)]$^-$ and -$[Co(ida)_2]^-$ in basic aqueous solution give the following results. The rate constants of the racemization and isomerization reactions (*u-fac* to *s-fac*) for [Co(ida)(mida)]$^-$ are 94.8 and 2.03 $M^{-1}\,s^{-1}$ (at 30 °C), respectively; the racemization reaction proceeds more rapid than the isomerization reaction, and these reactions of [Co(ida)(mida)]$^-$ are more rapid than those of $[Co(ida)_2]^-$. These results lead to the following suggestions: the racemization of optically active *u-fac* isomer occurs through the isomerization path of *u-fac* to *mer*; the racemization of *u-fac*-$[Co(ida)_2]^-$ is accelerated by the base catalyzed reaction at the secondary amine nitrogens of coordinated ida,[14] while that of *u-fac*-[Co(ida)(mida)]$^-$ is accelerated by both the base-catalyzed reaction of ida and the steric effect due to *N*-methyl group of mida. A more detailed discussion on the kinetics of the present complexes will be given in the following communication.

Rreferncces

1) T. Ama, H. Kawaguchi, and T. Yasui, *Chem. Lett.*, **1981**, 323.
2) M. Mori, M. Shibata, E. Kyuno, and F. Maruyama, *Bull. Chem. Soc. Jpn.*, **35**, 75 (1962).
3) J. I. Legg and D. W. Cooke, *Inorg. Chem.*, **5**, 594 (1966).
4) M. Kojima, M. Iwagaki, Y. Yoshikawa, and J. Fujita, *Bull. Chem. Soc. Jpn.*, **52**, 3216 (1977).
5) C. W. Van Saun and B. E. Douglas, *Inorg. Chem.*, **8**, 1145 (1969).
6) Y. Yoshikawa, A. Kondo, and K. Yamasaki, *Inorg. Nucl. Chem. Lett.*, **12**, 351 (1976).
7) N. Koine, T. Tanigaki, J. Hidaka, and Y. Shimura, *Chem. Lett.*, **1980**, 871.
8) K. Okamoto, J. Hidaka, and Y. Shimura, *Bull. Chem. Soc. Jpn.*, **48**, 2456 (1975).
9) D. W. Cooke, *Inorg. Chem.*, **5**, 1141 (1966).
10) T. Ama, H. Kawaguchi, and T. Yasui, *Bull. Chem. Soc. Jpn.*, **54**, 3597 (1981).
11) T. Ama, H. Kawaguchi, and T. Yasui, *Mem. Fac. Sci., Kochi Univ., Ser. C*, **3**, 1 (1982).
12) T. Yasui and T. Ama, *Bull. Chem. Soc. Jpn.*, **48**, 3171 (1975).
13) K. D. Gailey, K. Igi, and B. E. Douglas, *J. Coord. Chem.*, **5**, 171 (1976).
14) G. H. Searle, F. Keene, and S. F. Lincoln, *Inorg. Chem.*, **17**, 2362 (1978).
15) K. Sakakibara, Y. Yoshikawa, and H. Yamatera, *Bull. Chem. Soc. Jpn.*, **52**, 2725 (1979).

Crystal and Molecular Structure of [11,13-Dimethyl-12-(*p*-methylbenzoyl)-1,4,7,10-tetraaza-10,12-cyclotridecadienato]nickel(II) Hexafluorophosphate

Naohide MATSUMOTO* and Akira OHYOSHI

Department of Industrial Chemistry, Faculty of Engineering, Kumamoto University, Kurokami 2-39-1, Kumamoto 860

(Received June 7, 1982)

The title complex prepared through an electrophilic substitution of (11,13-diemthyl-1,4,7,10-tetraaza-10,12-cyclotridecadienato)nickel(II) bromide with *p*-methylbenzoyl chloride was subjected to single-crystal X-ray diffraction analysis. The analysis has revealed completion of the substitution reaction, pseudo C_2 symmetry of the macrocyclic complex minus the substituent, and an essentially square planar coordination environment with slight tetrahedral distortion. The substituted *p*-methylbenzoyl group is tilted with respect to the least-squares plane of the conjugated six-membered chelate ring, where the dihedral angle between them is 69.2°.

In our previous paper[1] we reported synthesis and properties of substituted derivatives $[Ni(Me_2E[Z]dienatoN_4)]PF_6$ (E=benzoyl, *p*-methylbenzoyl, and *p*-nitrobenzoyl; Z=13 and 14) (**2**), which are prepared by electrophilic substitution of $[Ni(Me_2[Z]dienatoN_4)]^+$ (**1**) with *p*-substituted benzoyl chlorides, as shown in Fig. 1. Based on electronic spectral tendencies observed for the series of substituted derivatives (**2**) and considerations on the steric hindrance between the benzoyl and two methyl groups in the acetylacetone residue, we predicted that the conjugated six-membered chelate ring would be perpendicular to the benzoyl group.

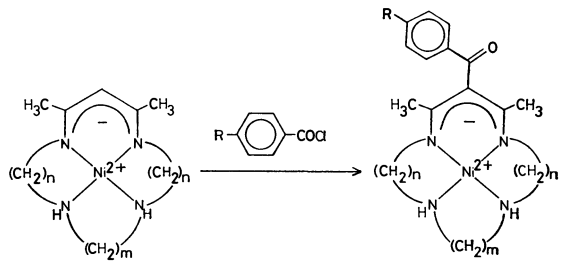

1 **2**

Fig. 1. Electrophilic substitution reaction from the parent complex $[Ni(Me_2[Z]dienatoN_4)]^+$ (**1**) to the substituted complex $[Ni(Me_2E[Z]dienatoN_4)]^+$ (**2**), where E denotes *p*-substituted benzoyl group, and Z=13 ($n=2$, $m=2$) and Z=14 ($n=2$, $m=3$).

In this study, the crystal structure of the title complex has been determined by the single-crystal X-ray diffraction method in order to confirm the completion of the substitution reaction and the above prediction.

Experimental

Physical Measurements. Infrared spectra were recorded with KBr disks on a Shimadzu recording spectrophotometer IR-410. Elemental analysis was performed by Mr. S. Miyazaki at the Technical Service Center of Kumamoto University.

Syntheses. (11,13-Dimethyl-1,4,7,10-tetraaza-10,12-cyclotridecadienato)nickel(II) Bromide Hemihydrate (1) (n=m=2): This parent complex, hereafter abbreviated as $[Ni(Me_2[13]dienatoN_4)]Br\cdot 0.5H_2O$, was prepared by the method of Cummings and Sievers.[2]

[11,13-Dimethyl-12-(p-methylbenzoyl)-1,4,7,10-tetraaza-10,12-cyclotridecadienato]nickel(II) Hexafluorophosphate, [Ni(Me$_2$p-MeBzyl[13]dienatoN$_4$)]PF$_6$ (2) (n=m=2): The previously-described method[1] was slightly modified. *p*-Methylbenzoyl chloride of 0.321 g (1.5 mmol) and triethylamine of 0.152 g (1.5 mmol) were added to a solution of 0.357 g (1 mmol) of $[Ni(Me_2[13]dienatoN_4)]Br\cdot 0.5H_2O$ in 100 cm^3 of dichloromethane. The solution was refluxed for 6 h and then evaporated to dryness under reduced pressure. The resultant viscous oil was dissolved in 30 cm^3 of water and filtered. The pH of the solution was adjusted to 10 with 6 M NaOH (1 M=1 mol dm^{-3}). The solution was added dropwise to 20 cm^3 aqueous solution of excess ammonium hexafluorophosphate to give an orange-red precipitate immediately. The product was collected, recrystallized from a mixture of methanol and dichloromethane and dried *in vacuo*. The yield obtained by this procedure was considerably higher than that obtained by the previously-described method.[1] Found: C, 42.96; H, 5.12; N, 10.54%. Calcd for $NiON_4C_{19}H_{27}PF_6$: C, 42.97; H, 5.29; N, 10.48%. IR: 3250 (ν_{NH}) and 1645 cm^{-1} ($\nu_{C=O}$). The perchlorate and tetrafluoroborate salts (**2**) ($n=m=2$) were prepared in the same way except that NH_4PF_6 was replaced by $NaClO_4$ and $NaBF_4$, respectively. $[Ni(Me_2p\text{-}MeBzyl[13]dienatoN_4)]ClO_4$. Found: C, 46.83; H, 5.75; N, 11.60%. Calcd for $NiON_4C_{19}H_{27}ClO_4$: C, 47.00; H, 5.61; N, 11.54%. IR: 3180 (ν_{NH}) and 1635 cm^{-1} ($\nu_{C=O}$). $[Ni(Me_2p\text{-}MeBzyl[13]dienatoN_4)]BF_4\cdot 0.5H_2O$. Found: C, 47.68; H, 5.93; N, 11.73%. Calcd for $NiON_4C_{19}H_{27}BF_4\cdot 0.5H_2O$. Found: C, 47.35; H, 5.80; N, 11.61%. IR: 3200, 3130 (ν_{NH}), and 1635 cm^{-1} ($\nu_{C=O}$).

X-Ray Analysis. Red prismatic crystals of $[Ni(Me_2p\text{-}MeBzyl[13]dienatoN_4)]PF_6$ were obtained from a mixture of methanol and dichloromethane at room temperature. The unit cell parameters and intensities were measured on a Rigaku AFC-5 automated four-circle diffractometer with a graphite-monochromatized Mo Kα radiation (λ=0.71069 Å). A crystal with approximate dimensions of 0.3×0.3×0.5 mm^3 was used for intensity measurement. The unit cell parameters were deterimined by the least-squares refinement based on 20 reflections in the range of $10°<2\theta<36°$. Crystal data: $NiPF_6ON_4C_{19}H_{27}$, F.W.=531.1, triclinic, space group $P\bar{1}$, a=10.629(5), b=13.424(5), c=9.201(4) Å, α=98.95(4), β=108.11(4), γ=109.85(3)°; V=1122.5(11) Å^3, D_m=1.56 (by the flotation method in a mixture of 1,2-dichloroethane and 1,2-dibromoethane), D_x=1.571 g cm^{-3} (Z=2), and μ(Mo Kα)=10.3 cm^{-1}.

Intensity data were collected by the θ-2θ scan technique with a scan rate of 8° min^{-1}. For weak reflections the peak scan was repeated up to three times depending on their intensities. Three standard reflections were monitored every 100 reflections and their intensities showed a good

TABLE 1. THE FINAL ATOMIC PARAMETERS OF [Ni(Me$_2$*p*-MeBzyl[13]dienatoN$_4$)]PF$_6$[a)]
The anisotropic thermal parameters and the atomic parameters of the hydrogen atoms are deposited as supplementary materials.

Atom	*x*	*y*	*z*	*B*/Å^2	Atom	*x*	*y*	*z*	B_{eq}/Å^2	b)
Ni	1328(1)	3427(1)	3868(1)	3.1	C(17)	3132(8)	9409(5)	2968(9)	4.7	
O	45(5)	6992(4)	3844(6)	5.6	C(18)	2108(7)	8647(5)	3348(8)	4.0	
N(1)	2498(5)	4823(4)	5158(6)	3.1	C(19)	5316(8)	10042(6)	2269(10)	5.9	
N(2)	2449(5)	2920(4)	5373(6)	3.5	P	2606(2)	2083(2)	−294(2)	4.5	
N(3)	370(6)	1952(4)	2492(6)	3.9						
N(4)	−17(5)	3759(4)	2475(6)	3.6	F(1)	313(1)	272(0)	154(1)	6.1(0.1)	0.75
C(1)	3683(7)	4864(5)	6586(8)	4.1	F(2)	206(1)	147(1)	−212(1)	7.1(0.2)	0.65
C(2)	3914(7)	3823(5)	6185(8)	4.1	F(3)	426(1)	252(1)	−8(1)	7.8(0.2)	0.60
C(3)	2276(7)	1823(5)	4576(8)	4.1	F(4)	102(1)	137(1)	−42(1)	7.9(0.3)	0.50
C(4)	720(8)	1222(5)	3456(9)	4.8	F(5)	298(1)	317(1)	−83(2)	8.0(0.3)	0.40
C(5)	−1149(7)	1763(5)	1679(8)	4.8	F(6)	287(1)	105(1)	−2(2)	9.2(0.4)	0.40
C(6)	−1125(7)	2774(6)	1124(8)	4.5	F(7)	134(1)	254(1)	−42(2)	9.5(0.4)	0.40
C(7)	18(6)	4758(5)	2516(7)	3.3	F(8)	160(1)	96(1)	−1(2)	4.9(0.3)	0.28
C(8)	1101(7)	5702(5)	3745(8)	3.3	F(9)	394(1)	174(1)	10(2)	5.2(0.3)	0.28
C(9)	2276(6)	5728(5)	5048(7)	3.2	F(10)	220(2)	306(2)	−82(2)	7.7(0.5)	0.25
C(10)	3247(7)	6774(5)	6341(8)	4.4	F(11)	389(2)	306(1)	−40(2)	6.0(0.4)	0.25
C(11)	−1136(8)	4856(6)	1159(9)	4.9	F(12)	95(2)	190(1)	−65(2)	3.8(0.3)	0.24
C(12)	1025(7)	6790(5)	3693(8)	3.6	F(13)	248(2)	105(2)	−171(3)	6.1(0.5)	0.20
C(13)	2165(6)	7622(5)	3335(7)	3.1	F(14)	281(3)	313(2)	104(3)	7.7(0.6)	0.20
C(14)	3200(6)	7406(6)	2983(7)	3.2	F(15)	328(3)	203(2)	153(3)	7.6(0.6)	0.20
C(15)	4208(7)	8173(5)	2613(8)	3.7	F(16)	186(3)	204(2)	−205(3)	7.7(0.6)	0.20
C(16)	4188(7)	9210(5)	2643(7)	3.8	F(17)	253(2)	113(2)	61(3)	6.4(0.5)	0.20

a) The final atomic coordinates for the nondisordered atoms and the disordered atoms are multiplied by 10^4 and 10^3, respectively. b) Occupancy factors.

stability. A total of 3125 reflections with $2.5°<2\theta<45°$ was collected, of which independent 2768 reflections with $|F_o|>3\sigma(|F_o|)$ were considered as "observed" and used for the structure analysis. The intensity data were corrected for the Lorentz and polarization effects, but not for the absorption.

The structure was solved by the conventional heavy-atom method and refined by the block-diagonal least-squares method. In the least-squares calculation, the function minimized was $\sum w(|F_o|-k|F_c|)^2$ where $w=1/\sigma(|F_o|)^2$ was adopted. The neutral atomic scattering factors for H, C_{cov}, N, O, F, P, and Ni were taken from International Tables for X-Ray Crystallography, Vol. IV.[3] Anomalous dispersion corrections, $\Delta f'$ and $\Delta f''$, for all the component atoms were also taken from Ref. 3. All the calculations were carried out on a FACOM M-200 computer at the Computer Center of Kyushu University by use of the UNICS II Crystallographic Computing System.[4-6]

The coordinates of the nickel atom were obtained from a three-dimensional Patterson synthesis. A Fourier synthesis based on the nickel position revealed all the nonhydrogen atoms except for the fluorine atoms of anion PF_6^-. In the course of structure analysis, it became apparent that the fluorine atoms were subjected to disorder. The occupancy factors were assigned to the possible fluorine positions located in the difference Fourier map according to the peak heights. Hydrogen atom positions were located in the difference Fourier map and included in the final least-squares calculation, where isotropic thermal parameters were used for the disordered fluorine atoms and the hydrogen atoms. The final values for $R=\sum||F_o|-|F_c||/\sum|F_o|$ and $R_w=[\sum w(|F_o|-|F_c|)^2/\sum w|F_o|^2]^{1/2}$ were 6.65 and 6.59%, respectively. The final difference Fourier synthesis showed no significant features except for two peaks (*ca.* 0.8 e Å^{-3}) appearing in the PF_6^- region.

Final positional parameters with their estimated standard deviations are given in Table 1. Lists of structure factors, anisotropic thermal parameters of nonhydrogen atoms, and atomic parameters of hydrogen atoms have been deposited at the Chemical Society of Japan as Document No. 8306.

Results and Discussion

The perspective drawing of [Ni(Me$_2$*p*-MeBzyl[13]-dienatoN$_4$)]$^+$ cation with the atom numbering scheme is shown in Fig. 2. Interatomic bond distances, angles, and torsion angles are given in Table 2.

As shown in Fig. 2, the present X-ray analysis confirmed the completion of the substitution reaction. The macrocyclic cation, minus the substituent *p*-methylbenzoyl group, exhibits nearly exactly a C_2 symmetry, where the twofold axis passes through C(8) and Ni. The nickel ion is coordinated with two iminate and two secondary amine nitrogen atoms in an essentially square planar fashion. However, there is a slight tetrahedral distortion, because the deviations of the constituent atoms from the least-squares plane NiN_4 are in the range from −0.13 to 0.13 Å and because the dihedral angle between the planes Ni–N(1)–N(2) and Ni–N(3)–N(4) is 11.5°. The four Ni–N bond distances fall into two groups, depending on the difference between iminate and secondary amine nitrogen atoms. The average Ni–N (iminate) bond distance of 1.821(6) Å agree with 1.83(1) Å of the parent complex [Ni(Me$_2$[13]dienatoN$_4$)]ClO$_4$[7] within experimental error but is considerably shorter than 1.862-

TABLE 2. BOND DISTANCES, ANGLES, AND TORSION ANGLES OF [Ni(Me$_2$*p*-MeBzyl[13]dienatoN$_4$)]PF$_6$

Bond distance	*l*/Å		*l*/Å
	[Ni(Me$_2$*p*-MeBzyl[13]dienatoN$_4$)]$^+$ cation		
Ni-N (1)	1.810 (5)	C (7) - C (8)	1.402 (10)
Ni-N (2)	1.902 (6)	C (8) - C (9)	1.423 (10)
Ni-N (3)	1.900 (6)	C (7) - C (11)	1.513 (10)
Ni-N (4)	1.832 (6)	C (9) - C (10)	1.479 (10)
N (1) - C (1)	1.489 (9)	C (8) - C (12)	1.497 (10)
N (1) - C (9)	1.326 (9)	C (12) - O	1.203 (9)
N (2) - C (2)	1.472 (9)	C (12) - C (13)	1.507 (10)
N (2) - C (3)	1.462 (10)	C (13) - C (14)	1.344 (9)
N (3) - C (4)	1.482 (10)	C (13) - C (18)	1.396 (10)
N (3) - C (5)	1.464 (10)	C (14) - C (15)	1.383 (10)
N (4) - C (6)	1.484 (10)	C (15) - C (16)	1.395 (10)
N (4) - C (7)	1.323 (9)	C (16) - C (17)	1.344 (11)
C (1) - C (2)	1.509 (10)	C (16) - C (19)	1.507 (12)
C (3) - C (4)	1.491 (11)	C (17) - C (18)	1.395 (11)
C (5) - C (6)	1.517 (11)		
	PF_6^- anion		
P - F (1)	1.588 (7)	P - F (10)	1.604 (22)
P - F (2)	1.573 (8)	P - F (11)	1.577 (19)
P - F (3)	1.586 (10)	P - F (12)	1.605 (16)
P - F (4)	1.582 (11)	P - F (13)	1.688 (24)
P - F (5)	1.576 (14)	P - F (14)	1.612 (27)
P - F (6)	1.548 (16)	P - F (15)	1.631 (28)
P - F (7)	1.631 (16)	P - F (16)	1.543 (27)
P - F (8)	1.639 (15)	P - F (17)	1.621 (25)
P - F (9)	1.588 (16)		
Bond angle	ϕ/°		ϕ/°
N (1) -Ni- N (2)	87.9 (2)	C (5) - C (6) - N (4)	106.9 (6)
N (1) -Ni- N (3)	170.2 (2)	N (4) - C (7) - C (8)	121.6 (6)
N (1) -Ni- N (4)	97.4 (2)	N (4) - C (7) - C (11)	117.6 (6)
N (2) -Ni- N (3)	87.6 (2)	C (8) - C (7) - C (11)	120.6 (6)
N (2) -Ni- N (4)	170.2 (2)	C (7) - C (8) - C (9)	126.1 (6)
N (3) -Ni- N (4)	88.1 (2)	C (7) - C (8) - C (12)	117.3 (6)
Ni-N (1) - C (1)	112.6 (4)	C (9) - C (8) - C (12)	116.5 (6)
Ni-N (1) - C (9)	126.6 (4)	C (8) - C (9) - N (1)	121.4 (6)
C (1) - N (1) - C (9)	120.0 (5)	C (8) - C (9) - C (10)	119.6 (6)
Ni-N (2) - C (2)	106.7 (4)	N (1) - C (9) - C (10)	118.8 (6)
Ni-N (2) - C (3)	109.1 (4)	O - C (12) - C (8)	122.1 (6)
C (2) - N (2) - C (3)	119.4 (5)	O - C (12) - C (13)	119.3 (6)
Ni-N (3) - C (4)	107.7 (4)	C (8) - C (12) - C (13)	118.3 (5)
Ni-N (3) - C (5)	105.9 (4)	C (12) - C (13) - C (14)	122.6 (6)
C (4) - N (3) - C (5)	119.5 (6)	C (12) - C (13) - C (18)	117.5 (6)
Ni-N (4) - C (6)	112.1 (4)	C (14) - C (13) - C (18)	119.7 (6)
Ni-N (4) - C (7)	126.4 (4)	C (13) - C (14) - C (15)	121.5 (6)
C (6) - N (4) - C (7)	121.1 (5)	C (14) - C (15) - C (16)	119.7 (6)
N (1) - C (1) - C (2)	107.4 (5)	C (15) - C (16) - C (17)	118.0 (7)
C (1) - C (2) - N (2)	105.5 (5)	C (15) - C (16) - C (19)	118.9 (6)
N (2) - C (3) - C (4)	106.1 (6)	C (17) - C (16) - C (19)	122.9 (7)
C (3) - C (4) - N (3)	107.3 (6)	C (16) - C (17) - C (18)	122.9 (7)
N (3) - C (5) - C (6)	106.5 (6)	C (13) - C (18) - C (17)	117.8 (6)

Torsion angle	ϕ/°
C (9) - C (8) - C (12) - C (13)	69.4
C (9) - C (8) - C (12) - O	65.4
C (7) - C (8) - C (12) - C (13)	69.5
C (7) - C (8) - C (12) - O	65.4

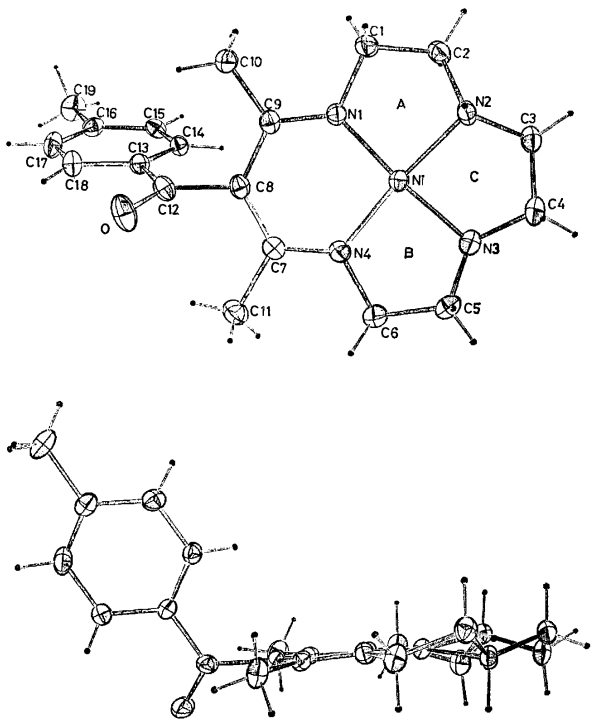

Fig. 2. ORTEP plots of [Ni(Me$_2$*p*-MeBzyl[13]dienatoN$_4$)]$^+$ with the atom numbering scheme.

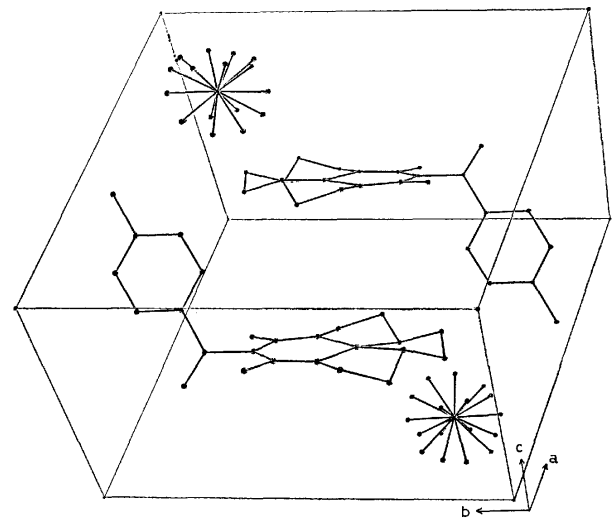

Fig. 3. Perspective view of the contents of the unit cell showing the cation and anion packing. Atoms are represented by points for clarity.

(6) Å of the 14-membered complex [Ni(Me$_2$[14]dienatoN$_4$)]Br·H$_2$O.[1] The average Ni–N (amine) distance of 1.901(6) Å is also compatible with that of the parent complex **1** (n=m=2)[7] and shorter than that of the 14-membered complex **2** (n=2, m=3).[1]

For the unsaturated six-memberd chelate ring, the planarity is preserved, where the deviations of the constituent atoms from the least-squares plane defined by the Ni, N(1), N(4), C(7), C(8), and C(9) are within ±0.03 Å. The C–C and C–N bonds of the unsaturated chelate ring are intermediate between the corresponding single and double bond distances.[8] This result indicates that the chelate ring is a π-electron conjugated system.

The conformation of the triethylene tetramine moiety (trien) is similar to that of the trien in [Cu(trien)SCN]NCS[9] and of the parent complex [Ni(Me$_2$[13]dienatoN$_4$)]ClO$_4$.[7] Two of the three saturated five-membered chelate ring (A and B, Fig. 2) are found to have an asymmetrical gauche conformation and their absolute configurations are $\lambda\lambda$ and/or $\delta\delta$, as indicated by the deviations 0.05 and 0.65 Å for C(1) and C(2), respectively, above the N(1)–Ni–N(2) plane and 0.65 and 0.05 Å for C(5) and C(6), respectively, below the N(3)–Ni–N(4) plane. The remaining five-membered chelate ring (C) has a symmetrical gauche conformation with the deviations 0.33 and −0.34 Å for C(3) and C(4), respectively, from the plane N(2)–Ni–N(3). The two hydrogen atoms bonded to the secondary amine nitrogen atoms are positioned at the different side on the NiN$_4$ plane.

The molecular symmetry and dimensions of the macrocyclic cation, minus the substituent *p*-methylbenzoyl group, are similar to those of the parent complex.[7] This result indicates that the blue shift of the d-d transition band of the substituted complex from the parent complex can be achieved without altering the stereochemistry of the coordination sphere, in which the band maxima are 20.2 and 21.4×10^3 cm^{-1} for [Ni(Me$_2$[13]dienatoN$_4$)]PF$_6$ and [Ni(Me$_2$*p*-MeBzyl[13]dienatoN$_4$)]PF$_6$, respectively.[1]

The most striking feature of the present molecular structure is non-coplanarity between the conjugated six-membered chelate ring and the *p*-methylbenzoyl group, where the dihedral angle between them is 69.2°. The overall molecular symmetry is not C_2, although the ^{1}H NMR spectra gave the methyl proton resonance of the acetylacetone residue as a singlet signal.[1] The methyl proton signal of the substituted complex (1.75 ppm) is shifted to a higher magnetic field than that of the parent complex (1.91 ppm). This can be interpreted in terms of the ring current effect of the benzene ring and the shielding effect of the carbonyl group of the *p*-methylbenzoyl group based on the present X-ray analysis.

Figure 3 shows the packing diagram of complex [Ni(Me$_2$*p*-MeBzyl[13]dienatoN$_4$)]PF$_6$. Anion PF$_6^-$ suffers from disorder. Judging from the occupancy factors of the disordered fluorine atoms and the geometry, anion PF$_6^-$ seems to be rotating randomly about the octahedral axes F(1)–P–F(2) and F(3)–P–F(4). There is no intermolecular bond distance which corresponds to any possible hydrogen bonds between the secondary amine nitrogen atoms and anion PF$_6^-$. The infrared frequency due to the NH vibrational mode in the series of complexes [Ni(Me$_2$*p*-MeBzyl[13]dienatoN$_4$)]X with X=ClO$_4^-$, BF$_4^-$, and PF$_6^-$ moves to higher energy side in the order of counter anions ClO$_4^-$<BF$_4^-$<PF$_6^-$. This can be interpreted in terms of the hydrogen bond between the secondary amine nitrogen atoms and the anion or water molecule. In complex [Ni(Me$_2$*p*-MeBzyl[13]dienatoN$_4$)]BF$_4$·0.5H$_2$O, the NH band splits into two bands (3200 and 3130 cm^{-1}). Such a split has also been observed in complex [Ni(Me$_2$[14]dienatoN$_4$)]Br·H$_2$O, in which the Br and the water molecule are hydrogen bonded to

the secondary amine nitrogen atoms.[1)]

The authors wish to express their thanks to Prof. Sigeo Kida at Faculty of Science, Kyushu University, for allowing them to use the diffractometer. Thanks are also due to Mr. Kenichiro Wakizaka for his valuable assistance.

References

1) N. Matsumoto, K. Wakizaka, and A. Ohyoshi, *Bull. Chem. Soc. Jpn.*, **55**, 3165 (1982).
2) S. C. Cummings and R. E. Sievers, *Inorg. Chem.*, **9**, 1131 (1970).
3) "International Tables for X-Ray Crystallography," Kynoch Press, Birmingham (1974), Vol. IV.
4) S. Kawano, *Rep. Comp. Cent. Kyushu Univ.*, **13**, 39 (1980).
5) T. Sakurai, H. Iwasaki, Y. Watanabe, K. Kobayashi, Y. Bando, and Y. Nakamichi, *Rikagaku Kenkyusho Hokoku*, **50**, 75 (1972).
6) C. K. Johnson, Report No. 3794, Oak Ridge National Laboratory, Oak Ridge, Tennessee (1965).
7) M. F. Richardson and R. E. Sievers, *J. Am. Chem. Soc.*, **94**, 4134 (1972).
8) D. Bruins and D. L. Weaver, *Inorg. Chem.*, **9**, 130 (1970).
9) G. Marongiu, E. C. Lingafelter, and P. Paoletti, *Inorg. Chem.*, **8**, 2763 (1969).

 © 1983 The Chemical Society of Japan Bull. Chem. Soc. Jpn., 56, 139—144 (1983)

Circular Dichroism Spectra and Racemization of Two Geometrical Isomers of the (2-Aminoethanesulfenato-*S*,*N*)[tris(2-aminoethyl)amine]cobalt(III) Ion

Masaaki Kojima and Junnosuke Fujita*

Department of Chemistry, Faculty of Science, Nagoya University, Chikusa-ku, Nagoya 464

(Received June 9, 1982)

Optically active *trans*(*t*-*N*,*S*)(*t*) and *cis*(*t*-*N*,*S*)(*p*) isomers of $[Co\{S(O)CH_2CH_2NH_2\}(tren)]^{2+}$ (tren=tris(2-aminoethyl)amine; *t*-*N*=tertiary amine nitrogen) were prepared, and their circular dichroism spectra were compared with those of *Λ*(*S* or *R*)- and *Λ*(*S* or *R*)-$[Co\{S(O)CH_2CH_2NH_2\}(en)_2]^{2+}$ and two geometrical isomers of $[Co(R\text{-pn})(tren)]^{3+}$ (*R*-pn=(*R*)-1,2-propanediamine) and $[Co(S\text{-dmbn})(tren)]^{3+}$ (*S*-dmbn=(*S*)-3,3-dimethyl-1,2-butanediamine). Racemization or epimerization of these sulfenato complexes was studied in aqueous solutions with ionic strength of 1.0 ($NaClO_4$) in the pH and temperature ranges of 3.65—8.8 and 24.0—40.0 °C, respectively. The rates of *p*- and *t*-isomers of the tren complex are proportional to concentrations of the complex, but independent of pH, the latter isomer accompanying some decomposition during the course of racemization. The first-order rate constants of the *p*- and *t*-isomers are 9.92×10^{-5} and *ca.* 1.2×10^{-6} s^{-1} at 30.0 °C, respectively. No epimerization takes place in the en complexes under the same experimental conditions. The difference in rate of racemization or epimerization of these sulfenato complexes seems to be related closely to the crowding around the S=O group of the complex.

A sulfenate ion becomes chiral upon coordination to a metal ion through the sulfur atom, and a metal–sulfenato complex has a formal analogy with sulfoxides. Sulfoxides are in general optically stable, and typical barriers for the inversion lie in the range of 150 to 180 kJ mol^{-1}.[1] The configurational stability of sulfur atoms in cobalt(III)–sulfenato complexes is also sufficient to support optical activity, and several stable diastereomers involving such chiral sulfur atoms have been obtained.[2–6] However, neither optically active complexes in which a chiral sulfur atom is the sole source of optical activity nor studies on racemization of sulfenato complexes seem to have been reported.

In order to elucidate the optical activity and optical stability of a metal–sulfenato complex, it is desirable to prepare an optically active sulfenato complex whose activity arises only from a chiral sulfur atom. This paper reports resolution, absorption and circular dichroism (CD) spectra, and racemization of two geometrical (*p*- and *t*-)[7] isomers of $[Co\{S(O)CH_2CH_2NH_2\}(tren)]^{2+}$ (Fig. 1; tren=tris(2-aminoethyl)amine) and related complexes, a pair of diastereomers of $[Co\{S(O)CH_2CH_2NH_2\}(en)_2]^{2+}$. Two geometrical isomers of $[Co(R\text{-pn})(tren)]^{3+}$ (*R*-pn=(*R*)-1,2-propanediamine) and $[Co(S\text{-dmbn})(tren)]^{3+}$ (*S*-dmbn=(*S*)-3,3-dimethyl-1,2-butanediamine) were also prepared in order to compare their CD spectra with those of *p*- and *t*-$[Co\{S(O)CH_2CH_2NH_2\}(tren)]^{2+}$.

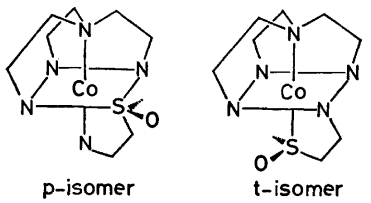

Fig. 1. Two geometrical isomers of $[Co\{S(O)CH_2CH_2NH_2\}(tren)]^{2+}$.

Experimental

The sulfenato complexes in solution were handled in the dark to minimize decomposition.

p- *and* t-[*Co*(*SCH*$_2$*CH*$_2$*NH*$_2$)(*tren*)]*ZnCl*$_4$. These thiolato complexes were prepared by the method of Jackson and Sargeson,[8] and isolated as tetrachlorozincate salts by the same method as that for the corresponding (*R*)-cysteine complex.[8] Found for the *p*-isomer: C, 19.63; H, 4.93; N, 14.34%. Found for the *t*-isomer: C, 19.68; H, 5.08; N, 14.40%. Calcd for $C_8H_{24}N_5Cl_4CoSZn$: C, 19.67; H, 4.95; N, 14.34%.

p-[*Co*{*S*(*O*)*CH*$_2$*CH*$_2$*NH*$_2$}(*tren*)](*ClO*$_4$)$_2$·2*H*$_2$*O and* t-[*Co*{*S*-(*O*)*CH*$_2$*CH*$_2$*NH*$_2$}(*tren*)](*ClO*$_4$)$_2$. These sulfenato complexes were prepared by stoichiometric oxidation of the corresponding thiolato complexes. To a suspension of *p*-$[Co(SCH_2CH_2NH_2)(tren)]ZnCl_4$ (1.95 g, 4 mmol) in a mixture of water (5 cm^3) and 70% $HClO_4$ (1 cm^3) was added an equimolar amount of 35% H_2O_2 (0.39 g, 4 mmol) in 3 cm^3 of water dropwise with stirring. The color of the solution changed immediately from brown to red-orange, and the starting material dissolved completely by reaction with the peroxide. The addition of $NaClO_4$ and cooling led to crystallization of the desired product. It was filtered and recrystallized from water by adding dropwise ethanol saturated with $LiClO_4$. Yield: 1.1 g (52%). Found: C, 18.11; H. 4.94; N, 13.20%. Calcd for $C_8H_{28}N_5Cl_2CoO_{11}S$: C, 18.05; H, 5.30; N, 13.16%.

The *t*-isomer was prepared by a similar procedure, but the complex perchlorate was not precipitated by the addition of $NaClO_4$. The red-orange mixture was diluted with water and passed through a column of SP-Sephadex C-25. After washing the column with water, the product adsorbed was eluted with 1 mol/dm^3 $NaClO_4$, and the effluent was evaporated to a small volume under reduced pressure. The addition of a small amount of ethanol led to crystallization of the desired product. It was filtered and recrystallized by the same method as that for the *p*-isomer. Yield: 30%. Found: C, 19.42; H, 4.94; N, 14.33%. Calcd for $C_8H_{24}N_5Cl_2CoO_9S$: C, 19.36; H, 4.87; N, 14.11%.

Resolution of the p-[*Co*{*S*(*O*)*CH*$_2$*CH*$_2$*NH*$_2$}(*tren*)]$^{2+}$ *Isomer.* To an aqueous solution (15 cm^3) of *p*-$[Co\{S(O)CH_2CH_2NH_2\}(tren)](ClO_4)_2\cdot2H_2O$ (1.16 g, 2 mmol) was added an aqueous solution (10 cm^3) of potassium *d*-tartrate hemihydrate (0.47 g, 2 mmol). The solution was stirred for 30 min and filtered to remove potassium perchlorate precipitated. The filtrate was evaporated to about 5 cm^3 under reduced pressure and filtered again. The filtrate was mixed with 20 cm^3 of methanol and cooled in a refrigerator. After 3 h the orange, crude product was filtered, washed with methanol, and recrystallized twice from water (2 cm^3) by adding 3 cm^3 of

methanol. Yield: 0.35 g. No change in the $\Delta\varepsilon$ value was observed with further recrystallization. Found: C, 29.87; H, 6.86; N, 14.66%. Calcd for $C_{12}H_{32}N_5CoO_9S$=[Co{S-(O)$CH_2CH_2NH_2$}(tren)]($C_4H_4O_6$)·$2H_2O$: C, 29.94; H, 6.70; N, 14.55%.

This diastereomer was converted into perchlorate by use of a DEAE-Sephadex (ClO_4^- form) column. The perchlorate was not isolated and the effluent was used for measurements without delay, because the complex racemizes at a moderate rate (*vide post*). The concentration of the solution was determined by reference to the optical density of the racemate.

Resolution of the t-[*Co*{*S*(*O*)$CH_2CH_2NH_2$}(*tren*)]$^{2+}$ *Isomer.* An aqueous solution of *t*-[Co{S(O)$CH_2CH_2NH_2$}(tren)]-(ClO_4)$_2$ (*ca.* 15 mg) was poured onto a column (ϕ 2.7×50 cm) of SP-Sephadex C-25 and the adsorbed band was eluted with 0.1 mol/dm^3 Na_2[Sb_2(*d*-tartrate)$_2$]. The band was separated into two, the $(+)_{589}$-isomer being eluted faster. Each effluent was diluted with water, passed through an SP-Sephadex column (ϕ 1.5×3 cm), and the complex adsorbed was eluted with 1.0 mol/dm^3 $NaClO_4$. The optically active complex was not isolated because the amount was very small. The $\Delta\varepsilon$ value was determined with the aid of the ε value of the racemate.

Preparation and Resolution of [*Co*{*S*(*O*)$CH_2CH_2NH_2$}(*en*)$_2$]$^{2+}$. The complex was prepared by the method of Adzamli *et al.*[4] The reaction mixture was chromatographed by use of an SP-Sephadex C-25 column. By elution with 0.15 mol/dm^3 Na_2SO_4, the orange band was separated into two, I and II in the order of elution. Bands I and II contain racemates of a pair of diastereomers, $\Lambda(S)$ and $\Lambda(R)$, and $\Delta(R)$ and $\Delta(S)$, respectively. The racemates were isolated as perchlorate by a method similar to that for *t*-[Co{S(O)-$CH_2CH_2NH_2$}(tren)](ClO_4)$_2$. The total yield was about 80%, and the formation ratio, I:II, was *ca.* 2:1. Isomer II is less stable toward decomposition in water. Found for I: C, 15.48; H, 4.84; N, 14.80%. Found for II: C, 15.30; H, 4.71; N, 14.90%. Calcd for $C_6H_{22}N_5Cl_2CoO_9S$: C, 15.33; H, 4.72; N, 14.89%. The racemates were resolved by the same chromatographic method as that for *t*-[Co{S(O)$CH_2CH_2NH_2$}(tren)]$^{2+}$. The faster eluted enantiomers of I and II are $\Lambda(R)$ (I-1) and $\Lambda(S)$ (II-1), respectively. The isomers obtained from the slower eluted bands are thus $\Delta(S)$ (I-2) and $\Delta(R)$ (II-2). The absolute configurations of the isomers were assigned by comparing the CD spectra with that of $\Lambda(S)$-[Co(*R*-cysO)(en)$_2$]$^+$ (*R*-cysO= (*R*)-2-amino-3-sulfenatopropanoate-*N*,*S*),[3] the absolute configuration of which has been determined by the X-ray method.[2] The $\Delta(S)$-isomer (I-2) was isolated as perchlorate by the same method as that for the racemate. Found: C, 15.27; H, 4.59; N, 15.07%. Calcd for $C_6H_{22}N_5Cl_2CoO_9S$: C, 15.33; H, 4.72; N, 14.89%. The enantiomers of isomer II were not isolated because of their instability. Each effluent of the resolved isomer II was loaded on SP-Sephadex C-25, eluted with 1 mol/dm^3 $NaClO_4$, and the effluent was used for measurements.

[*Co*(R-*pn*)(*tren*)](ClO_4)$_3$·*1.5*H_2O *(P-I) and* [*Co*(R-*pn*)-(*tren*]Br_3 *(P-II).* A mixture of (*R*)-1,2-propanediamine dihydrochloride (*R*-pn·2HCl) (0.74 g, 5 mmol) and sodium methoxide (0.54 g, 10 mmol) in methanol (5 cm^3) was stirred for *ca.* 0.5 h. Sodium chloride which deposited was filtered off and washed with a small amount of methanol. The combined filtrate and washings were added to a dimethyl sulfoxide solution (15 cm^3) of [$CoCl_2$(tren)]Cl[9] (1.56 g, 5 mmol), and the mixture was stirred for a day at room temperature. The resulting orange-brown solution was diluted with water and poured onto a column (ϕ2.7×3 cm) of SP-Sephadex C-25. A small portion of the Sephadex charged with the product was placed on the top of a column (ϕ2.7× 120 cm) of SP-Sephadex C-25, and the product was eluted with 0.2 mol/dm^3 Na_2SO_4. The column showed several bands. The effluents of the third (P-I) and fourth (P-II) bands were collected separately. Each effluent was diluted ten times with water and passed again through an SP-Sephadex C-25 column (ϕ1.5×3 cm). Isomer P-II was eluted with 1 mol/dm^3 NaBr, and the effluent was evaporated under reduced pressure to give orange crystals, which were recrystallized from water. Found: C, 20.64; H, 5.68; N, 16.24%. Calcd for $C_9H_{28}N_6Br_3Co$: C, 20.83; H, 5.44; N, 16.19%.

Isomer P-I was isolated as perchlorate, because the bromide was highly soluble. The column charged with isomer P-I was washed with a large amount of 10^{-2} mol/dm^3 HBr, and then the isomer was eluted with 1 mol/dm^3 HBr. The effluent was concentrated to a small volume under reduced pressure. On addition of concd $HClO_4$ the concentrate gave large crystals of the perchlorate, which were filtered and washed with ethanol. Found: C, 17.80; H, 5.08; N, 14.11%. Calcd for $C_9H_{31}N_6Cl_3CoO_{13.5}$: C, 17.88; H, 5.17; N, 13.90%. The formation ratio, P-I:P-II, was *ca.* 1:2, and the total yield was *ca.* 40%.

[*Co*(S-*dmbn*)(*tren*)]Br_3·*2.5*H_2O*(B-I) and* [*Co*(S-*dmbn*)-(*tren*)]Br_3·H_2O *(B-II).* These complexes were prepared by the same method as that for the above *R*-pn complexes, except that (*S*)-3,3-dimethyl-1,2-butanediamine dihydrochloride[10] was used instead of *R*-pn·2HCl. The separation of bands for isomers B-I and B-II was insufficient in chromatography by use of 0.2 mol/dm^3 Na_2SO_4, B-I being eluted faster. The orange effluent containing both isomers B-I and B-II was chromatographed again with 0.15 mol/dm^3 Na_2-[Sb_2(*d*-tartrate)$_2$]. Isomers B-II and B-I were eluted separately in this order, and isolated as bromide by the same method as that for isomer P-II of the *R*-pn complex. The formation ratio, B-I:B-II, was *ca.* 1:1, and the total yield was *ca.* 60%. Found for B-I: C, 23.83; H, 6.42; N, 13.95%. Calcd for $C_{12}H_{39}N_6Br_3CoO_{2.5}$: C, 23.77; H, 6.48; N, 13.86%. Found for B-II: C, 24.88; H, 6.41; N, 14.54%. Calcd for $C_{12}H_{36}N_6Br_3CoO$: C, 24.89; H, 6.27; N, 14.51%.

Measurements. Absorption and CD spectra were recorded on a Hitachi 323 spectrophotometer and a JASCO J-40CS spectropolarimeter, respectively. Optical rotations at 589 nm were measured with a JASCO DIP-4 polarimeter.

Kinetics. All kinetic experiments were carried out in the dark in the pH region of 3.65 (acetate buffer) to 8.8 (phosphate buffer) maintained at constant ionic strength of 1.0 with $NaClO_4$. The complex concentrations were in the range of 1.0×10^{-4} to 2.7×10^{-3} mol/dm^3. The temperatures of the solutions were kept constant in a constant temperature water bath. The racemization or epimerization of the complexes was followed by monitoring CD change as a function of reaction time. Portions of the reacting solution were withdrawn at timed intervals and then their CD spectra were recorded in the range of 400 to 260 nm. CD strengths at two maxima, *ca.* 380 and 280 nm, were used for calculation. Optical densities of bands at *ca.* 370 nm, which are characteristic of the S-bonded sulfenato moiety, were also measured to check the stability of the complexes toward decomposition.

Results and Discussion

Absorption and CD Spectra. Two geometrical isomers of [Co{S(O)$CH_2CH_2NH_2$}(tren)]$^{2+}$ can be prepared easily from the corresponding isomers of [Co-

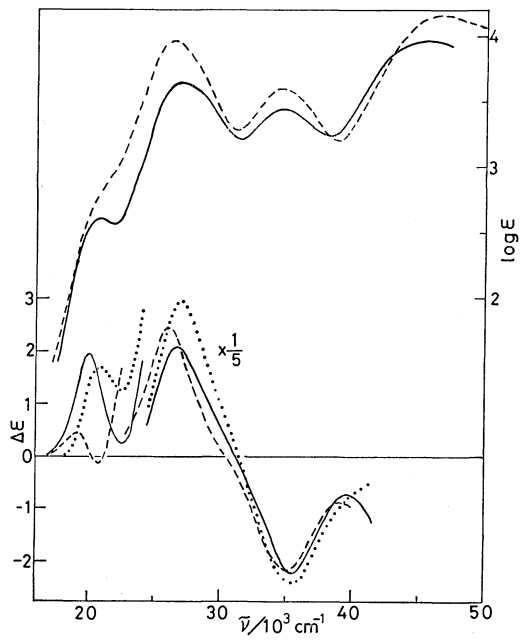

Fig. 2. Absorption and CD spectra of $(+)_{589}$-*p* (——) and $(+)_{589}$-*t* (----) isomers of [Co{S(O)$CH_2CH_2NH_2$}(tren)]$^{2+}$, and calculated CD curve, 1/2{$\Delta\varepsilon$(*Λ*(*S*)-[Co{S(O)$CH_2CH_2NH_2$}$(en)_2$]$^{2+}$)+$\Delta\varepsilon$(*Λ*(*S*)-[Co{S(O)-$CH_2CH_2NH_2$}$(en)_2$]$^{2+}$)} (·····).

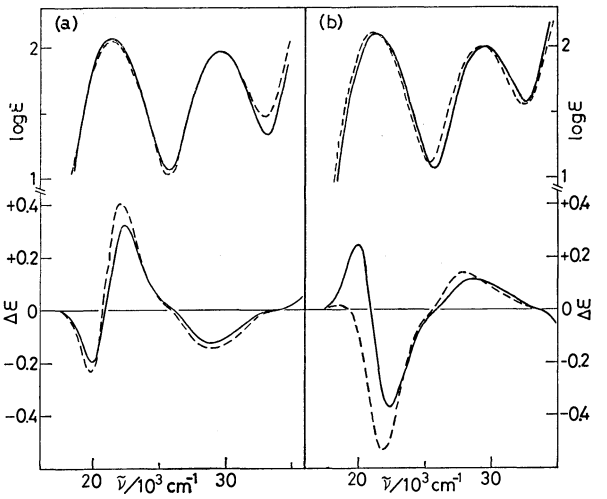

Fig. 3. Absorption and CD spectra of (a) P-I (——) and P-II (----) isomers of [Co(*R*-pn)(tren)]$^{3+}$ and (b) B-I (——) and B-II (----) isomers of [Co(*S*-dmbn)(tren)]$^{3+}$.

$(SCH_2CH_2NH_2)$(tren)]$^{2+}$ [8] by stoichiometric oxidation with hydrogen peroxide. The sulfenato complexes thus obtained should have the same geometrical configuration as those of the respective parent thiolato complexes. The *p*- and *t*-[Co{S(O)$CH_2CH_2NH_2$}(tren)]$^{2+}$ isomers show absorption spectra fairly different from each other as seen in Fig. 2 and Table 1. The *p*-isomer gives a more distinct first d-d band (20830 cm^{-1}) and much weaker Co–S charge transfer bands (27030 and 34600 cm^{-1})[4] than the corresponding bands of the *t*-isomer. The first d-d band of the former appears at the higher energy side than that of the latter. In analogous tren complexes of glycinate[11] and (*S*)-alaninate[12] ions, the *p*-isomer also shows the first d-d band at high energy as compared with that of the *t*-isomer. Such a spectral difference in the d-d band region between the *p*- and *t*-isomers may be attributed to the difference in ligand field strength between the tertiary amine and other primary amine nitrogens. Mitsui *et al.*[11] suggested that in [Co(glycinate)(tren)]$^{2+}$ the tertiary amine nitrogen exerts a weaker ligand field than the primary amine nitrogen.

Figure 2 shows CD spectra of $(+)_{589}$-*p*- and $(+)_{589}$-*t*-[Co{S(O)$CH_2CH_2NH_2$}(tren)]$^{2+}$. In the Co–S charge transfer band region (23000—39000 cm^{-1}), both enantiomers give CD patterns very similar to that of *Λ*(*S*)-[Co(*R*-cysO)$(en)_2$]$^{+}$.[3] Another *Λ*(*R*)-diastereomer of the *R*-cysO complex shows an almost enantiomeric CD pattern in this region. Thus the sulfur atoms in both $(+)_{589}$-enantiomers can be assigned to the *S* configuration. The optical activity of both *p*- and *t*-isomers originates from only the chiral sulfur atom of the sulfenate ligand. Thus these CD spectra represent the vicinal effect of a coordinated chiral sulfur atom in a $[CoSN_5]$-type complex. In Fig. 2 are compared the spectra with the calculated vicinal CD curve for the (*S*)-sulfur atom derived from CD spectra of *Δ*(*S*)- and *Λ*(*S*)-[Co{S(O)$CH_2CH_2NH_2$}$(en)_2$]$^{2+}$. The curve and two spectra are very similar in the Co–S charge transfer region. In the first d-d band region, the CD spectrum of the *p*-isomer resembles the calculated curve, but that of the *t*-isomer is fairly different from it, although all of the main CD bands show the positive sign.

Akamatsu *et al.*[12] reported that each pair of the *p*- and *t*-isomers of [Co{(*S*)-alaninate}(tren)]$^{2+}$ and a similar type complex [Co{(*S*)-alaninate}(nitrilotriacetate)]$^{-}$ give CD spectra almost enantiomeric to each other in the d-d band region. They attributed this remarkable feature to the mutually quasi-enantiomeric configuration in the isomers, and called such optical activity the "quasi-enantiomeric" effect. The *p*- and *t*-isomers of these alaninato complexes seem to be quasi-enantiomeric to each other. However, they are mutually geometrical isomers having the tertiary amine nitrogen and oxygen donor atoms in the cis and trans positions, and exhibit absorption spectra fairly different from each other. Consequently, the isomers would inevitably give CD spectra different from each other. The complexes given by Akamatsu *et al.*[12] would not be suitable for estimating how the quasi-enantiomeric effect contributes to CD spectra.

In order to estimate this effect, we have prepared two isomers of [Co(*R*-pn)(tren)]$^{3+}$ and [Co(*S*-dmbn)(tren)]$^{3+}$ and measured their CD spectra. Each of *R*-pn and *S*-dmbn has two different nitrogen donor atoms, but the difference in ligand field strength between these two nitrogen atoms should be negligibly small as compared with that between the oxygen and nitrogen donor atoms of the (*S*)-alaninate ligand. Molecular models indicate that there is no remarkable difference in strain or non-bonded interaction between the isomers of both *R*-pn and *S*-dmbn complexes. Figure 3 shows absorption and CD spectra of the two isomers of these complexes. The differences in ab-

Table 1. Absorption and CD spectral data

Complex	Absorption $\tilde{\nu}_{max}/cm^{-1}$ (log ε)	CD $\tilde{\nu}_{ext}/cm^{-1}(\Delta\varepsilon)$
$(+)_{589}$-*p*-[Co{S(O)$CH_2CH_2NH_2$}(tren)]$^{2+}$	20830 (2.60)	19960 (+1.99)
	27030 (3.63)	26670 (+10.6)
	34600 (3.46)	35210 (−11.3)
	45660 (3.97)	
$(+)_{589}$-*t*-[Co{S(O)$CH_2CH_2NH_2$}(tren)]$^{2+}$	20000 (2.63)[a]	19160 (+0.437)
		20830 (−0.146)
	26320 (3.94)	26180 (+12.0)
	34600 (3.56)	34970 (−10.6)
	46510 (4.15)	
Δ(*S*)-[Co{S(O)$CH_2CH_2NH_2$}$(en)_2$]$^{2+}$	21100 (2.67)	19120 (−1.39)
		21690 (+2.88)
	27400 (3.83)	27320 (+17.3)
	35030 (3.57)	35590 (−12.2)
	49500 (4.21)	
Λ(*S*)-[Co{S(O)$CH_2CH_2NH_2$}$(en)_2$]$^{2+}$	21190 (2.85)	19800 (+2.76)
	27030 (3.81)	26670 (+12.2)
	35150 (3.60)	35460 (+12.0)
	50000 (4.23)	
(P-I)-[Co(*R*-pn)(tren)]$^{3+}$	21320 (2.07)	19880 (−0.203)
		22270 (+0.329)
	29540 (1.97)	28740 (−0.119)
	45250 (4.29)	44640 (+3.27)
(P-II)-[Co(*R*-pn)(tren)]$^{3+}$	21280 (2.04)	19690 (−0.227)
		22120 (+0.408)
	29540 (1.98)	28570 (−0.139)
	45450 (4.34)	45660 (+3.66)
(B-I)-[Co(*S*-dmbn)(tren)]$^{3+}$	21320 (2.10)	19840 (+0.248)
		22320 (−0.375)
	29590 (2.02)	28490 (+0.118)
	45450 (4.30)	43860 (−4.01)
(B-II)-[Co(*S*-dmbn)(tren)]$^{3+}$	21190 (2.11)	18660 (+0.015)
		21740 (−0.536)
	29330 (1.99)	27930 (+0.137)
	44540 (4.32)	43670 (−5.64)

a) Shoulder.

sorption and CD spectra between the isomers are very small in the *R*-pn complex, while appreciably large in the *S*-dmbn complex. However, the isomers of this *S*-dmbn complex show still the same CD pattern. These observations suggest that the quasi-enantiomeric effect contributes very little to optical activity of metal complexes. The enantiomeric CD spectra reported by Akamatsu *et al.*[12] seem to result from a difference in the order of energies of the d-d transition components between the *p*- and *t*-geometrical isomers. No assignment was made for the geometrical isomers of the *R*-pn and *S*-dmbn complexes.

Racemization at Sulfur Atoms. CD changes of *p*-[Co{S(O)$CH_2CH_2NH_2$}(tren)]$^{2+}$ were recorded over the temperature range of 24.0 to 40.0 °C at $I=1.0$ ($NaClO_4$) in the pH region of 3.65 to 8.8. A representative spectral change is given in Fig. 4. In every kinetic run the plot of $\log(\Delta OD_{376})$ and $\log(\Delta OD_{285})$ against time gave a straight line for at least two half-lives, from which the first-order rate constant k_r/s^{-1} was obtained. No detectable change in the absorption spectrum was observed during the measurements. However, over a longer time period the complex underwent decomposition; the absorbance at 380 nm diminished by 2.3% at 30 °C in 1.0 mol/dm^3 $NaClO_4$ in a day, *i.e.*, 12 half-lives. Eyring treatments of $\log(k_r/T)$ *vs.* T^{-1} yielded an activation enthalpy of 130±3 kJ mol^{-1} and an activation entropy of 109±9 J mol^{-1} K^{-1}. The first-order rate constant is 9.92×10^{-5} s^{-1} at 30.0 °C. The rate was independent of pH. Thus it can be assumed that the racemization takes place intramolecularly. The activation enthalpy of 130 kJ mol^{-1} is smaller by 20—50 kJ mol^{-1} than those reported for sulfoxides.[1] A fairly large difference in activation enthalpy was also observed for the racemization between metal–sulfide complexes (40—60 kJ mol^{-1})[13-19] and sulfonium ions (100—120 kJ mol^{-1}).[1]

The racemization of the *t*-isomer was studied by

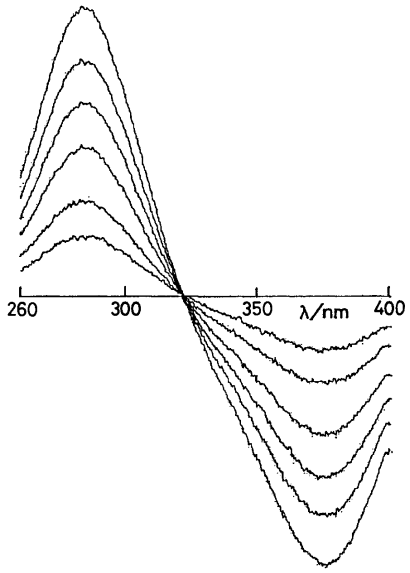

Fig. 4. CD spectral change of *p*-[Co{S(O)CH_2CH_2-NH_2}(tren)]$^{2+}$ in 1.0 mol/dm^3 $NaClO_4$ at 30.0 °C in a period of 264 min.

the same procedure. However, the rate was not determined accurately, because the complex decomposed during the course of racemization. In 1.0 mol/dm^3 $NaClO_4$ at 30.0 °C, the CD strength (382, 286 nm) and absorbance (380 nm) of the complex decreased by 18 and 9.7%, respectively, in a day. When we took the absorbance at 380 nm as a quantitative measure for the concentration of the *t*-isomer, the rate constant of the racemization is approximately 1.2×10^{-6} s^{-1} at 30.0 °C. This value is smaller than that of the *p*-isomer by a factor of *ca.* 80. Thus it is concluded that the *p*-isomer racemizes much faster than the *t*-isomer does, while the former is more stable than the latter toward decomposition. For the analogous [Co($CH_3SeCH_2CH_2NH_2$)(tren)]$^{3+}$ complex, the *t*- and *p*-isomers seem also to have similar relative stability toward racemization; the former was resolved by column chromatography, while the latter was not.[20]

Turley and Haake[21] studied the inversion at sulfur in several platinum(II)–sulfide complexes, and proposed a mechanism involving simultaneous bond making between the metal ion and the other lone-pair on sulfur as the original coordinate bond breaks. This mechanism seems to be a current view on inversion of the sulfur in metal–sulfide complexes. However, Jackson and Sargeson[22] pointed out that the mechanism is the same in principle as the pyramidal inversion mechanism for free sulfoxides and sulfonium ions, which proceeds *via* a trigonal planar intermediate. If we assume that the racemization of [Co{S(O)-$CH_2CH_2NH_2$}(tren)]$^{2+}$ proceeds by the pyramidal inversion at the sulfur atom, the difference in rate of racemization of the *p*- and *t*-isomers seems to stem from a difference in structure around the S=O group between them. According to X-ray analyses on the two [Co(glycinate)(tren)]$^{2+}$ isomers,[11] the cis position to the tertiary amine nitrogen is hindered by atoms H(a) and H(b) as shown in Fig. 5. The trans position is free from such hindrance. Consequently, the

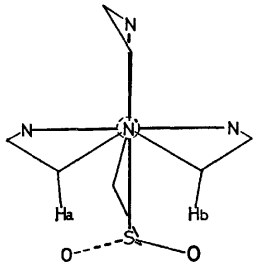

Fig. 5. A schematic structure of *p*-[Co{S(O)CH_2CH_2-NH_2}(tren)]$^{2+}$ viewed from the *t*-N–Co bond axis.

cis ligand is much more labile in substitution reactions than the trans ligand.[23,24] The S=O group in the *p*-isomer of [Co{S(O)$CH_2CH_2NH_2$}(tren)]$^{2+}$ is situated at such a hindered position, and the oxygen atom points close at atom H(a) or H(b). The *t*-isomer seems to have no such hindrance around the S=O group. In the trigonal planar transition state, on the other hand, both *p*- and *t*-isomers seem to have similar structural situation involving no particular steric hindrance around the S=O group. Accordingly, the *p*-isomer will have a lower energy barrier for the inversion than that of the *t*-isomer, and racemizes faster than the *t*-isomer does.

The epimerization at sulfur of a pair of diastereomers, $\Delta(S)$- and $\Lambda(S)$-[Co{S(O)$CH_2CH_2NH_2$}$(en)_2$]$^{2+}$ was examined by the same procedure and the results compared with the racemization of the tren complex. Both en and tren complexes have the same [CoN_5S] type. The structures around the S=O groups of the diastereomers are similar to each other and to that of *t*-[Co{S(O)$CH_2CH_2NH_2$}(tren)]$^{2+}$, and there is no particular steric hindrance among the S=O group and other atoms in these isomers. For the $\Delta(S)$-diastereomer, neither the absorption nor CD spectrum in 1.0 mol/dm^3 $NaClO_4$ showed detectable change in a day at 30.0 °C. On the other hand, the $\Lambda(S)$-diastereomer in 1.0 mol/dm^3 $NaClO_4$ decreased both absorbance (370 nm) and CD strength (375 nm) by the same quantity, 26%, at 30.0 °C in a period of 340 min, being less stable toward decomposition than the $\Delta(S)$-diastereomer. Jackson and Sargeson[22] reported that the Δ-(R) and $\Delta(S)$ diastereomers do not convert into each other over a period of at least 12 h at 25 °C. These results shows that the sulfur atoms in these diastereomers are stable toward racemization like the one in *t*-[Co{S(O)$CH_2CH_2NH_2$}(tren)]$^{2+}$. The *p*-[Co{S(O)-$CH_2CH_2NH_2$}(tren)]$^{2+}$ isomer whose S=O group is hindered by H(a) or H(b) atom racemizes much faster than these isomers do. Thus it is concluded that the rate of racemization of the sulfenate ligand in cobalt(III)–amine complexes is governed by a steric factor, if the racemization proceeds by the pyramidal inversion at the sulfur atom.

References

1) J. B. Lambert, *Topics Stereochem.*, **6**, 19 (1971).
2) W. G. Jackson, A. M. Sargeson, and P. O. Whimp, *J. Chem. Soc., Chem. Commun.*, **1976**, 934.
3) D. L. Harting, C. P. Sloan, A. W. Cabral, and J. H. Krueger, *Inorg. Chem.*, **17**, 1649 (1978).

4) I. K. Adzamli, K. Libson, J. D. Lydon, R. C. Elder, and E. Deutsch, *Inorg. Chem.*, **18**, 303 (1979).
5) M. Kita, K. Yamanari, and Y. Shimura, *Chem. Lett.*, **1980**, 275.
6) M. Kita, K. Yamanari, K. Kitahama, and Y. Shimura, *Bull. Chem. Soc. Jpn.*, **54**, 2995 (1981).
7) The S atoms in the *p*- and *t*-isomers are trans to the primary (*p*) and tertiary (*t*) tren amine nitrogens, respectively.
8) W. G. Jackson and A. M. Sargeson, *Inorg. Chem.*, **17**, 2165 (1978).
9) D. A. Buckingham, P. J. Cresswell, and A. M. Sargeson, *Inorg. Chem.*, **14**, 1485 (1975).
10) C. J. Hawkins and R. M. Peachey, *Aust. J. Chem.*, **28**, 33 (1976).
11) Y. Mitsui, J. Watanabe, Y. Harada, T. Sakamaki, Y. Iitaka, Y. Kushi, and E. Kimura, *J. Chem. Soc., Dalton Trans.*, **1976**, 2095.
12) K. Akamatsu, T. Komorita, and Y. Shimura, *Bull. Chem. Soc. Jpn.*, **54**, 3000 (1981).
13) E. W. Abel, G. W. Farrow, K. G. Orrell, and V. Šik, *J. Chem. Soc., Dalton Trans.*, **1977**, 42.
14) E. W. Abel, A. K. S. Ahmed, G. W. Farrow, K. G. Orrell, and V. Šik, *J. Chem. Soc., Dalton Trans.*, **1977**, 47.
15) G. Hunter and R. C. Massey, *J. Chem. Soc., Dalton Trans.*, **1976**, 2007.
16) G. Hunter and R. C. Massey, *J. Chem. Soc., Chem. Commun.*, **1973**, 797.
17) E. W. Abel, M. Booth, and K. G. Orrell, *J. Chem. Soc., Dalton Trans.*, **1979**, 1994.
18) J. C. Barnes, G. Hunter, and M. W. Lown, *J. Chem. Soc., Dalton Trans.*, **1976**, 1227.
19) E. W. Abel, M. Booth, and K. G. Orrell, *J. Chem. Soc., Dalton Trans.*, **1980**, 1582.
20) K. Nakajima, M. Kojima, and J. Fujita, *Chem. Lett.*, **1982**, 925.
21) P. C. Turley and P. Haake, *J. Am. Chem. Soc.*, **89**, 4617 (1967).
22) W. G. Jackson and A. M. Sargeson, "Rearrangements in Ground and Excited States," ed by P. de Mayo, Academic Press, New York (1980), Vol. 2, p. 273.
23) S. G. Zipp, A. P. Zipp, and S. K. Madan, *Coord. Chem. Rev.*, **14**, 29 (1974).
24) S. K. Madan and J. Peone, Jr., *Inorg. Chem.*, **6**, 229 (1967).

 © 1983 The Chemical Society of Japan Bull. Chem. Soc. Jpn., 56, 145—148 (1983)

The Preparation of $(C_6H_{11})_3Sb(OH)Y$ and Their Infrared Spectra

Yoshikane KAWASAKI,* Yasushi YAMAMOTO, and Masanori WADA

Department of Petroleum Chemistry, Osaka University, Yamadaoka, Suita, Osaka 565

(Received June 14, 1982)

Tris(cyclohexyl)hydroxoantimony(V) compounds, $(C_6H_{11})_3Sb(OH)Y$, Y=Cl, Br, CH_3COO, and NO_3, were prepared by the hydrolysis of μ-oxo-bis[tris(cyclohexyl)haloantimony(V)], $[(C_6H_{11})_3SbX]_2O$, in a mixed solvent of acetone and water(7:3) or by a reaction of silver salts with $[(C_6H_{11})_3SbX]_2O$ in the same solvent. When Y=Cl and Br, the dehydration of the hydroxo compounds, giving the μ-oxo compounds, $[(C_6H_{11})_3SbY]_2O$, occurred readily. However, when Y=CH_3COO and NO_3, the hydroxo form is stable. In the IR spectra of these hydroxo compounds in dichloromethane solution, the ν(O–H) band was observed at *ca.* 3630 cm^{-1} and the ν(Sb–O) band, at 565—513 cm^{-1}. The hydrolysis of several μ-oxo compounds, $[R_3SbY]_2O$, R=CH_3, C_2H_5, *i*-C_3H_7, C_6H_5, and *p*-$CH_3C_6H_4$, Y=Cl, Br, CH_3COO, and NO_3, in a water-saturated dichloromethane solution was studied by using the IR spectra. All the compounds were hydolyzed in this solvent, but only the starting μ-oxo compounds were recovered from this solution.

There has been considerable confusion in the literature regarding the structure of $R_3Sb(OH)Y$ and its dehydrated $[R_3SbY]_2O$ types of compounds. Several workers have reported a number of compounds which were formulated as hydroxo compounds, $R_3Sb(OH)Y$. The hydroxo structure, however, is mainly assigned on the basis of elemental analyses,[1–8] although some workers have obtained the $[R_3SbY]_2O$ type of compounds.[9–12] Therefore, Long and co-workers[13,14] have made a detailed study of these types of compounds. They could not obtain compounds which give elemental analyses corresponding to $R_3Sb(OH)Y$ and which show the hydroxo band in their infrared spectra. The compounds obtained were always $[R_3SbY]_2O$. Accordingly, they concluded that the $R_3Sb(OH)Y$ type of compound probably does not exist in the solid state, although the presence of such species has been assumed in an aqueous solution.[15,16] Recently, however, we have obtained the $R_3Sb(OH)Y$ type of compound when the Y group is a somewhat bulky ligand such as 8-quinolinolate and when R=CH_3, C_6H_5 and *p*-$CH_3C_6H_4$.[8] These compounds show the ν(O–H) band at *ca.* 3610 cm^{-1} and the ν(Sb–O) band at *ca.* 550 cm^{-1}. Therefore, we anticipated that, if the alkyl group is bulky enough, the $R_3Sb(OH)Y$ type of compound may be obtained even if the Y group is halogen. In fact, Hartmann and Kühl have reported the preparation of $(C_6H_{11})_3Sb(OH)Cl$ by the hydrolysis of $(C_6H_{11})_3SbCl_2$.[7] However, they relied only on elemental analysis to elucidate the hydroxo structure of this compound and did not report its infrared spectrum. Actually, there is an error in their calculation, and so their analytical value is much close to that of the μ-oxo compound, $[(C_6H_{11})_3SbCl]_2O$.

In this paper, the preparation of tris(cyclohexyl)-hydroxoantimony(V) compound, $(C_6H_{11})_3Sb(OH)Y$, Y=Cl, Br, CH_3COO, and NO_3, and their infrared spectra in the solid state and in a dichloromethane solution will be reported.

Experimental

*Preparation of μ-Oxo-bis[tris(cyclohexyl)haloantimony(V)], $[(C_6H_{11})_3SbX]_2O$, X=Cl(**1**) and Br(**2**).* To a benzene solution (70 ml) of tris(cyclohexyl)bis(halo)antimony(V) (10 mmol), sodium methoxide (10 mmol) in methanol (10 ml) was added. The mixture was heated at reflux for 1 h, after which the sodium halide thus precipitated was filtered off. The crystalline white compound obtained after distilling off a large portion of the filtrate was purified by recrystallization from dichloromethane.

*Prepartion of Tris(cyclohexyl)halohydroxoantimony(V), $(C_6H_{11})_3Sb(OH)X$, X=Cl(**3**) and Br(**4**).* μ-Oxo-bis[tris(cyclohexyl)haloantimony(V)] (2 mmol) in a mixed solvent of acetone (70 ml) and water (30 ml) was heated at reflux until the solid compound was dissolved (1 h). The crystalline white compound obtained after removing a large portion of the solvent under reduced pressure was recrystallized from a mixed solvent of acetone and water (7:3). The compound was dried in air for a few minutes and then store in a tight-capped bottle. When the compound was stored in a desciccator overnight, air-dried for long time, or recrystallized from acetone, it changed to the dehydrated μ-oxo compound, $[(C_6H_{11})_3SbX]_2O$.

*Preparation of Other Tris(cyclohexyl)hydroxoantimony(V) Compounds, $(C_6H_{11})_3Sb(OH)Y$, Y=CH_3COO (**5**) and NO_3(**6**).* **1** (5 mmol) and the corresponding silver salt (10 mmol) were added to a mixed solvent of acetone (70 ml) and water (10 ml). The mixture was then heated at reflux for 1 h, and the silver chloride thus precipitated was removed by filtration. The crystalline white compounds obtained after removing a large portion of the solvent under reduced pressure was recrystallized from acetone. The compound was then dried in air.

Attempted Preparation of Other $R_3Sb(OH)X$, R=CH_3, C_2H_5, i-C_3H_7, C_6H_5, and p-$CH_3C_6H_4$ and X=Cl and Br. A suspension of μ-oxo-[tris(organo)haloantimony(V)] in a mixed solvent of acetone and water (7:3) was heated at reflux for about 1 h. The hydroxo compound, $R_3Sb(OH)X$, was not obtained by removing the solvent, and only the starting materials were recovered in the case of the phenyl and *p*-tolyl compounds. In the case of the methyl and isopropyl compounds, tris(alkyl)bis(halo)antimony(V) was precipitated from the condensed solution.

*Deuteration of **3**.* **3** (50 mg) was dissolved in a mixture of acetone-d_6 (1 ml) and D_2O (0.3 ml), after which the solution was sealed in a glass ampule. This was heated at about 50 °C for 2 h. After removing the solvent under reduced pressure, the crystalline white compound was obtained. Relevant IR spectral data in Nujol mull; 2520 cm^{-1} (ν(O–D)), 800 cm^{-1} (δ(Sb–O–D)), and 565 cm^{-1} (ν(Sb–O)).

*Reaction of **5** with Picric Acid.* To an acetone solution of **5** (2 mmol), picric acid (2 mmol) was added, after which the mixture was stirred for 30 min at room temperature. A crystalline yellow compound of acetatotris(cyclohexyl)picratoantimony(V) was obtained when the solution had been

TABLE 1. ANALYTICAL DATA OF μ-OXO-BIS[TRIS(CYCLOHEXYL)HALOANTIMONY(V)] AND TRIS(CYCLOHEXYL)HYDROXOANTIMONY(V) COMPOUNDS

	Mp[a] θ_m/°C	Yield %	Found(Calcd) (%) C	H	N
1	198—199	70	51.92 (52.14)	8.19 (8.02)	
2	197—198	88	46.93 (47.09)	7.28 (7.24)	
3	188	61	50.96 (51.03)	8.24 (8.09)	
4	195—196	80	46.29 (46.18)	7.47 (7.32)	
5	135—138	55	53.31 (53.71)	8.40 (8.34)	
6	156—157	25	47.86 (48.02)	7.65 (7.65)	3.10 (3.11)

a) Decomposition occurs gradually before melting.

left to stand at room temperature. This was recrystallized from acetone. Mp 160—171 °C (decomp). Found: C, 47.08; H, 5.93; N, 6.43%. Calcd for $C_{26}H_{38}N_3O_9Sb$: C, 47.43; H, 5.82; N, 6.38%.

Spectral Measurement. The infrared spectra were recorded on a Hitachi 215 spectrometer (4000—650 cm^{-1}) and on a Hitachi EPI-L spectrometer (700—200 cm^{-1}) in Nujol mulls or a dichloromethane solution. The concentration of the solution was 3 wt% or a saturated solution for not very soluble compounds. CaF_2 windows were used for obtaining the solution spectra of the O–H stretching region while KRS-5 plates were used for other region. The cell length used was 0.1 or 0.5 mm.

Conductivity Measurement. The molar conductances of **3**, **5**, and **6** in dichloromethane were measured by using a TOA digital conduct meter, model CM-15A, at 25±0.1 °C. The molar conductances of these compounds at 1×10^{-3} mol dm^{-3} were found to be less than 0.5 Ω^{-1} cm^2 mol^{-1}, indicating that these compounds are non-electrolytes in this solvent.

Solvent. Dichloromethane was dried over P_2O_5 and distilled before use. To dried dichloromethane, water was added and the mixture was shaken vigorously. The amount of water in dichloromethane was determined by referring to the signal strength of the known amount of hexamethylbenzene in the ^1H NMR spectra. The concentration of water was found to be 0.0095 mol dm^{-3}.

Results and Discussion

μ-Oxo-bis[tris(organo)antimony(V)] compound, $[R_3SbY]_2O$, show a characteristic band at around 790—740 cm^{-1} in the IR spectra,[12-14] which is attributed to the presence of the Sb–O–Sb skeleton. Compounds **1** and **2** have given a strong band at 720 cm^{-1}, also indicating the Sb–O–Sb skeleton, this is in accordance with the results of elemental analyses. Such a band, however, was not observed in **3**—**6**, these compounds showed a ν(O–H) band at around 3400—3300 cm^{-1} and ν(Sb–O) band at around 610—560 cm^{-1} in the solid state. Therefore, these compounds were assumed to be hydroxo compounds, $(C_6H_{11})_3Sb(OH)Y$. This is also consistent with the results of elemental analyses.

TABLE 2. RELEVANT IR DATA OF μ-OXO-BIS[TRIS(CYCLOHEXYL)HALOANTIMONY(V)] AND TRIS(CYCLOHEXYL)HYDROXOANTIMONY(V) COMPOUNDS IN THE SOLID STATE AND IN SOLUTION[a]

	ν(O–H) cm^{-1}	ν(Sb–O) cm^{-1}	ν(Sb–O–Sb) cm^{-1}
1	—	—	720
2	—	—	720
3	3420 br (3630 sh)	572 (531)	—
4	3420 br (3628 sh)	569 (538)	—
5	3360 br (3640 sh) (3380 br)	563 (513)	—
6	3340 br (3625 sh) (3400 br)	609 (565)	—

a) Values in parentheses are observed in a dichloromethane solution.

The frequency of the ν(O–H) band is lower than that of the normal one, indicating the presence of an intermolecular hydrogen bond.[17] The frequency of the ν(Sb–O) band in the solid state is a little higher than those reported for $R_3Sb(OH)$(8-quinol) (570—540 cm^{-1}),[8] $(C_6H_5)_4Sb(OH)$ (528 cm^{-1}),[17] and $[F_5Sb(OH)]^-$ (560 cm^{-1}).[18] Upon the deuteration of the hydroxo group of **3**, the ν(O–D) band appeared at 2520 cm^{-1}, and the ν(Sb–O) band, at 565 cm^{-1}. The latter band does not show any large shift upon deuteration. In the dichloromethane solution, the ν(O–H) band of **3**—**6** shifts to a higher frequency and becomes

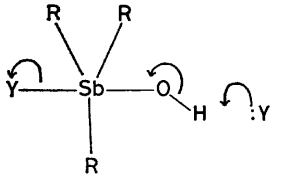

I

sharp. The ν(Sb–O) band, on the other hand, shifts to a lower frequency (see Table 2). One of the reasons for the high-frequency shift of the ν(Sb–O) band in the solid state may be an intermolecular hydrogen bond, as is shown in I. As a result of hydrogen bond, the Sb–O bond gains a partial double-bond character and the Sb–Y bond becomes a little ionic (*vide infra*). In a proton-accepting solvent such as *N*,*N*-dimethylformamide, the ν(Sb–O) band appears at a higher frequency (545 and 607 cm^{-1} for **5** and **6** respectively) than that in dichloromethane. In dichloromethane, this type of hydrogen bond is lost and the partial double-bond character of the Sb–O bond is diminished. The high-frequency shift of the ν(O–H) band in the dichloromethane solution is consistent with the above explanation. Chremos and Zingaro estimated, by using Gordy's formula, the frequencies of the ν(Sb–O) and ν(Sb=O) bands to be 550 and 803 cm^{-1} respectively.[19] In trimethyloxoantimony(V), $(CH_3)_3SbO$, the ν(Sb=O) band was observed at 645 cm^{-1}.[20]

The influence of the Y group on the ν(O–H) and ν(Sb–O) bands of $(C_6H_{11})_3Sb(OH)Y$ observed in the dichloromethane solution is not large. The ν(O–H) band, however, has a tendency to decrease frequency

Table 3. Relevant IR data of CH_3COO group of some trisorganoantimony compounds, $R_3Sb(X)O_2CCH_3$ in the solid state[a)]

R	X	ν_{asym}(O-C-O) / cm^{-1}	ν_{sym}(O-C-O) / cm^{-1}	Δ
c-C_6H_{11}	OH	1600	1380	220
		(1625)	(1375)	250
	O_2CCH_3	1652	1298	354
	pic	1675	1292	383
CH_3	$O_{1/2}$	1622	1374	248

a) Values in parentheses are observed in a dichloromethane solution.

in the following order; NO_3<Cl, Br<CH_3COO. The ν(Sb–O) band, on the other hand, decreases in the reverse order.

The δ(M–O–H) band has been reported to appear in the region of 1200—700 cm^{-1}.[21] In $R_4Sb(OH)$, the band has been reported to be 995 cm^{-1} for R=CH_3[22] and 795 cm^{-1} for R=C_6H_5.[17] Since the IR spectra of **3** and **4** are quite similar to those of **1** and **2** in this region, this band could not be identified, although the deuterated compound of **3** shows the band at 800 cm^{-1}. In **5** and **6**, this band could not be identified unambigously.

In Table 3, some relevant IR data of acetato compounds of tris(cyclohexyl)antimony(V) are shown. In acetato–hydroxo compound, **5**, the frequency of $\nu_{asym}(CO_2)$ is rather low and that of $\nu_{sym}(CO_2)$ is high and the differnce between these frequencies (Δ=$\nu_{asym}(CO_2)-\nu_{sym}(CO_2)$) is the smallest among the compounds shown in Table 3. One of the reasons for small Δ value of **5** in the solid state is the intermolecular hydrogen bond, as is shown in I. The Δ value of **5** in the dichloromethane solution approaches that of $[(CH_3)_3Sb(O_2CCH_3)]_2O$, but it is still smaller than that of diacetate or acetato–picrate. This suggests that, in the acetato–hydroxo compound, **5**, the Sb–$OC(O)CH_3$ bond is more ionic, or the contribution of the Type-III mode to the bond is large, compared with that of diacetate or acetato–picrate, in which the Type-II mode is more predominant.

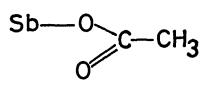

II

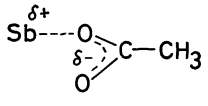

III

The frequencies of the $\nu_{asym}(NO_2)$, $\nu_{sym}(NO_2)$, and ν(N–O) bands of some nitrato compounds of trisorganoantimony(V) are shown in Table 4. The difference (Δ=$\nu_{asym}(NO_2)-\nu_{sym}(NO_2)$) is also shown in this table. These frequencies are characteristic of a nitrato group with essentially a C_{2v} symmetry. Ferraro[23] found that the Δ value is a measure of the covalent character between the metal-nitrato bond of several transition-metal complexes. On the other hand, Gatehouse *et al.*[24] used the frequency of the ν(N–O) band as a criterion of the covalent character of the metal-nitrato bond. As can be seen from Table 4, the Δ value of nitrato–hydroxo compound, **6**, is the smallest, and the frequency of the ν(N–O) band is

Table 4. Relevant IR data of the NO_3 group of trisorganoantimony compounds, $R_3Sb(X)NO_3$, in the solid state[a)]

R	X	$\nu_{asym}(NO_2)$ / cm^{-1}	$\nu_{sym}(NO_2)$ / cm^{-1}	ν(N-O) / cm^{-1}	Δ
c-C_6H_{11}	OH	1420	1305	1037	115
		(1450)	(1295)	(1020)	155
	NO_3	1533	1288	982	245
		1513			
CH_3	$O_{1/2}$	1455	1290	1005	165

a) Values in parentheses are observed in a dichloromethane solution.

Table 5. ν(O–H) and ν(Sb–O) data of $[R_3SbX]_2O$ in dichloromethane saturated with water

R	X	ν(O-H) / cm^{-1}	ν(Sb-O) / cm^{-1}
CH_3	O_2CCH_3	3638, 3420 br	542
	Cl	3625, 3480 br	552
	Br	3620	555
C_2H_5	Br	3632, 3460 br	544
	NO_3	3625, 3500 br	568
i-C_3H_7	Cl	3640, 3460 br	535
	Br	3640, 3475 br	536
c-C_6H_{11}	Cl	3630	531
	Br	3628	538
C_6H_5	O_2CCH_3	3615	535
	Cl	3615	540
	Br	3615	540
	NO_3	3600	568
p-$CH_3C_6H_4$	Br	3610	545

the highest. If the above criterions could be applied to the antimony compounds, the Sb–ONO_2 bond of **6** may have the largest ionic character. The differences in the Δ values and the frequencies of the ν(N–O) bands of **6** in the solid state and in solution may also be explained by the presence of the intermolecular hydrogen bond in the solid state, as in **5**.

Table 5 summarizes the frequencies of the ν(O–H) and ν(Sb–O) bands observed for several μ-oxo compounds, $[R_3SbY]_2O$, in a water-saturated dichloromethane solution, where R=CH_3, C_2H_5, i-C_3H_7, c-C_6H_{11}, C_6H_5, and p-$CH_3C_6H_4$ and Y=Cl, Br, CH_3COO, and NO_3. In isopropyl and cyclohexyl compounds, the two ν(O–H) bands of water disappeared completely, and only one ν(O–H) band due to the hydroxo group bound to the antimony atom was observed at 3640—3630 cm^{-1}. The ν(Sb–O) band appeared at around 535 cm^{-1}. The frequencies of the ν(O–H) and ν(Sb–O) bands of the cyclohexyl compounds in this solvent are similar to those of the hydroxo compounds, **3** and **4**, shown in Table 2. On the other hand, the solubility of the methyl, ethyl, and aryl compounds to this solvent is poor, and so the saturated solutions were used for the spectral measurements. Therefore, the water molecule in dichloromethane was not completely consumed, and the ν(O–H) bands of the water remained. The ν(O–H) band

of the hydroxo group bound to the antimony atom was found at the position of the ν_{sym}(O–H) band of water; *i.e.*, the intensity ratio of $I[\nu_{sym}(O–H)]/I[\nu_{asym}(O–H)]$ becomes large in the $[R_3SbY]_2O$-saturated solution. From the above results, the hydrolysis of the μ-oxo compounds to the hydroxo compounds was found to occur in the dichloromethane. However, the attempted isolation of the hydroxo compounds from this

$$[R_3SbY]_2O + H_2O \overset{CH_2Cl_2}{\rightleftarrows} 2R_3Sb(OH)Y$$

solution failed, and only the starting materials were recovered.

As has been mentioned in the Experimental part, tris(cyclohexyl)halohydroxoantimony(V) is readily dehydrated, giving the μ-oxo compounds in the solid state, although the latter compounds were hydrolyzed easily by a small amound of water in the solvent. In the acetato and nitrato compounds, however, the hydroxo form is stable in air.

References

1) S. Frielander, *J. Prakt. Chem.*, **1**, 70 (1857).
2) G. T. Morgan, F. M. G. Micklethwait, and G. S. Whitby, *J. Chem. Soc.*, **97**, 34 (1910).
3) G. T. Morgan and F. M. G. Micklethwait, *J. Chem. Soc.*, **99**, 2286 (1911).
4) G. T. Morgan and V. E. Yarsley, *Proc. R. Soc. London, Ser. A*, **110**, 534 (1926).
5) K. A. Jensen, *Z. Anorg. Allg. Chem.*, **250**, 268 (1934).
6) G. Wittig and K. Clauss, *Ann. Chem.*, **577**, 26 (1952).
7) H. Hartmann and G. Kühl, *Z. Anorg. All. Chem.*, **312**, 186 (1961).
8) Y. Kawasaki, *Bull. Chem. Soc. Jpn.*, **49**, 817 (1976).
9) A. Hantzsch and H. Hibbert, *Chem. Ber.* **40**, 1508 (1907).
10) D. R. Lyon, F. G. Mann, and G. H. Cookson, *J. Chem. Soc.*, **1947**, 662.
11) L. Kolditz, M. Gitter, and E. Rösel, *Z. Anorg. Allg. Chem.*, **316**, 270 (1962).
12) M. Shindo and R. Okawara, *J. Organomet. Chem.*, **5**, 537 (1966).
13) G. G. Long, G. O. Doak, and L. D. Freedman, *J. Am. Chem. Soc.*, **86**, 209 (1964).
14) G. D. Doak, G. G. Long, and L. D. Freedman, *J. Organomet. Chem.*, **4**, 82 (1965).
15) T. M. Lowry and J. H. Simons, *Chem. Ber.*, **63**, 1595 (1930).
16) P. Nylén, *Z. Anorg. Allg. Chem.*, **246**, 227 (1941).
17) A. L. Beachamp, M. J. Bennett, and F. A. Cotton, *J. Am. Chem. Soc.*, **91**, 297 (1969).
18) L. Kolditz and B. Nussuker, *Z. Anorg. Allg. Chem.*, **337**, 191 (1965).
19) G. N. Chremos and R. A. Zingaro, *J. Organomet. Chem.*, **22**, 637 (1970).
20) W. Morris, R. A. Zingaro, and J. Laane, *J. Organomet. Chem.*, **91**, 295 (1975).
21) K. Nakamoto, "Infrared and Raman Spectra of Inorganic and Coordination Compounds," 3rd ed, John Wiley & Sons, New York (1978).
22) H. Schmidbauer, J. Weidlein, and K. H. Mitschke, *Chem. Ber.*, **102**, 4136 (1969).
23) J. Ferraro, *J. Inorg. Nucl. Chem.*, **10**, 319 (1959).
24) B. M. Gatehouse, S. E. Livingston, and R. S. Nyholm, *J. Inorg. Nucl. Chem.*, **8**, 75 (1958).

Binuclear Metal Complexes. II.[1] Synthesis, ESR, and Electrochemical Properties of Strati-bis Copper(II)-Nickel(II) Complexes

Hisashi Ōkawa,* Miyuki Kakimoto, Tatuo Izumitani, Masaaki Nakamura, and Sigeo Kida

Department of Chemistry, Faculty of Science, Kyushu University 33, Hakozaki, Higashi-ku, Fukuoka 812

(Received June 25, 1982)

Strati-bis copper(II)–nickel(II) complexes, CuNi(R-sata) and CuNi(R-sacta) (R=H, 5-Me, 5-Br), have been prepared, where H_4(R-sata) and H_4(R-sacta) denote 1,2,3,4-tetrakis(R-salicylideneamino)-2,3-dimethylbutane and 1,2-bis(R-salicylideneamino)-1,2-bis(R-salicylideneaminomethyl)cyclohexane, respectively. ESR spectra of the complexes (frozen chloroform solution at liquid nitrogen temperature) showed a tetragonal pattern with a hyperfine coupling constant $A_{//}$ smaller than that of the relevant mononuclear copper(II) complex. Based on cyclic voltammetry and differential pulse polarography, it was shown that the Cu(II)→Cu(I) reduction occurs at a higher potential than that of the mononuclear reference complex. The ESR and electrochemical properties have been interpreted in terms of the stacking of the CuN_2O_2 and NiN_2O_2 planes and hence the electron delocalization over the whole molecule through the ligand π-system.

So far many binucleating ligands have been devised for the studies of magnetic spin-exchange interaction, redox properties and catalytic functions of binuclear metal complexes.[2,3] In almost all of these complexes, metal ions are linked with bridging groups so that two equatorial planes are kept coplanar. On the other hand, there have been obtained few binucleating ligands capable of forming "strati-bis" metal complexes.[4–9]

In the previous paper of this series,[4] we have reported the synthesis and characterization of strati-bis copper(II) complexes of 1,2,3,4-tetrakis(R-salicylideneamino)-2,3-dimethylbutane (H_4(R-sata)) and 1,2-bis(R-salicylideneamino)-1,2-bis(R-salicylideneaminomethyl)cyclohexane (H_4(R-sacta)). By comparing the properties of Cu_2(R-sata) and Cu_2(R-sacta) with Cu(R-salpn) (H_2(R-salpn) = *N*,*N*′-bis(R-salicylideneamino)-1,2-propanediamine) and Cu(R-sacda) (H_2(R-sacda) = 1-(R-salicylideneamino)-1-(R-salicylideneaminomethyl)cyclohexane), respectively, the following characteristics have been recognized for the strati-bis copper(II) complexes: (1) seven-lined hyperfine structure with a small hyperfine coupling constant ($A_{//}\approx 85$ G (1 G=1×10^{-4} T)) in ESR spectrum, (2) red shift of the π-π^* transition band involving azomethine π-character, and (3) one-electron transfer process, Cu(II,II)⇌Cu(II,I), occuring at a high potential compared with the corresponding mononuclear copper(II) complex. These characteristics can be explained in terms of the assumption that the two CuN_2O_2 planes are stacked in a face-to-face manner and interact with each other through the ligand π-system.

As the extension of this study, the strati-bis complexes, CuNi(R-sata) and CuNi(R-sacta), were prepared in the present study and their properties were examined in comparison with those of Cu(R-salpn) and Cu(R-sacda), respectively. Chemical structures of CuNi(R-sata), CuNi(R-sacta), Cu(R-salpn), and Cu(R-sacda) are shown in Fig. 1.

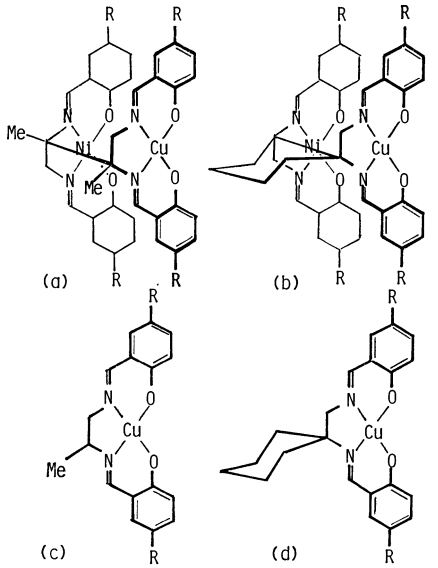

Fig. 1. Chemical structures of (a) CuNi(R-sata), (b) CuNi(R-sacta), (c) Cu(R-salpn), and (d) Cu(R-sacda); R (substituent on the ring)=H, 5-Me, or 5-Br.

Experimental

Syntheses. Synthetic methods for 2,3-dimethyl-1,2,3,4-butanetetramine and 1,2-bis(aminomethyl)-1,2-cyclohexanediamine have been described in the previous paper.[4] Syntheses of Cu(R-salpn)[10] and Cu(R-sacda)[4] were performed by the methods in the literatures.

CuNi(sata). 2,3-Dimethyl-1,2,3,4-butanetetramine (0.30 g) and salicylaldehyde (1.0 g) were dissolved in ethanol (50 cm^3), and the mixture was refluxed with stirring. To this was added an ethanolic solution (30 cm^3) of copper(II) acetate monohydrate (0.41 g) and the mixture was stirred at 60 °C for 10 min. Then, an ethanolic solution (30 cm^3) of nickel(II) acetate tetrahydrate (0.51 g) was added, and the mixture was stirred at 60 °C for 10 min. The reaction mixture was filtered, concentrated to *ca.* 30 cm^3 and allowed to stand in a refrigerator to give brown crystals. They were recrystallized from a chloroform–ethanol mixture.

Found: C, 58.81; H, 4.90; N, 7.91; Cu, 9.37%. Calcd for $C_{34}H_{30}N_4O_4CuNi\cdot H_2O$: C, 58.43; H, 4.62; N, 8.02; Cu, 9.09%.

CuNi(5-Me-sata). This complex was obtained as brown crystals in the same way as that of CuNi(sata), except for using 5-methylsalicylaldehyde instead of salicylaldehyde. It was recrystallized from a chloroform–ethanol mixture.

Found: C, 60.90; H, 5.40; N, 7.34; Cu, 8.26%. Calcd for $C_{38}H_{38}N_4O_4CuNi\cdot 1/2\,H_2O$: C, 61.18; H, 5.27; N, 7.51;

Cu, 8.52%.

CuNi(5-Br-sata). The synthetic method for this complex is the same as that for CuNi(sata), except for using 5-bromosalicylaldehyde instead of salicylaldehyde. It forms brown crystals when crystallized from a chloroform–ethanol mixture.

Found: C, 40.58; H, 3.01; N, 5.33; Cu, 6.52%. Calcd for $C_{34}H_{26}N_4O_4Br_4CuNi \cdot 1/2\,H_2O$: C, 40.61; H, 2.71; N, 5.57; Cu, 6.32%.

CuNi(sacta). An ethanolic solution (50 cm^3) of 1,2-bis(aminomethyl)-1,2-cyclohexanediamine (0.30 g) and salicylaldehyde (0.85 g) was refluxed for 20 min. To this was added copper(II) acetate monohydrate (0.35 g), and the mixture was heated at *ca.* 60 °C for 10 min. To this solution was added nickel(II) acetate tetrahydrate (0.44 g), and the mixture was heated at 60 °C for 10 min. The reaction mixture was filtered and allowed to stand in a refrigerator. A brown precipitate was filtered and recrystallized from a chloroform–ethanol mixture to form brown prisms.

Found: C, 58.44; H, 4.77; N, 7.53; Cu, 8.10%. Calcd for $C_{36}H_{32}N_4O_4CuNi \cdot 2H_2O$: C, 58.20; H, 4.88; N, 7.54; Cu, 8.55%.

CuNi(5-Me-sacta). This complex was obtained as brown prisms in the same way as that of CuNi(sacta), except for using 5-methylsalicylaldehyde in place of salicylaldehyde. It was recrystallized from a chloroform–ethanol mixture.

Found: C, 62.67; H, 5.66; N, 6.80; Cu, 7.74%. Calcd for $C_{40}H_{40}N_4O_4CuNi \cdot C_2H_5OH$: C, 62.35; H, 5.73; N, 6.92; Cu, 7.85%.

CuNi(5-Br-sacta). This complex was obtained as brown prisms in the same way as that of CuNi(sacta), except for using 5-bromosalicylaldehyde instead of salicylaldehyde.

Found: C, 42.73; H, 3.12; N, 5.21; Cu, 6.24%. Calcd for $C_{36}H_{28}N_4O_4Br_4CuNi \cdot C_2H_5OH$: C, 42.71; H, 3.12; N, 5.24; Cu, 5.95%.

Measurements. Electronic spectra were recorded on a Shimadzu MPS-5000 spectrophotometer. Magnetic susceptibilities were measured by the Faraday method at room temperature. Effective magnetic moments were calculated by the equation, $\mu_{eff}=2.828\ (\chi_M \times T)^{1/2}$, where χ_M is the magnetic susceptibility per molecule corrected for diamagnetism by the use of Pascal's constants.[11] ESR spectra were recorded on a JES-FE3X instrument in frozen chloroform solutions near liquid nitrogen temperature. Cyclic voltammograms were recorded on a Yanagimoto P-1000 voltammetric analyzer in dichloromethane containing 0.1 M (1 M = 1 mol dm^{-3}) tetrabutylammonium perchlorate as the supporting electrolyte. The measurements were carried out in a three-electrode cell equipped with a glassy carbon working electrode, a platinum coil auxiliary electrode, and a saturated calomel reference electrode. The potentials were corrected for liquid junction potential by the use of ferrocene as an internal standard.[12,13] Differential pulse polarograms were recorded on the same instrument by the use of dropping mercury electrode instead of glassy carbon electrode.

Results and Discussion

The magnetic moments of CuNi(R-sata) and CuNi(R-sacta) fall in the range 1.80—1.96 BM (Table 1), indicating the presence of one unpaired electron per molecule. Since *N,N'*-disalicylideneethylenediaminatonickel(II) and its congeners are diamagnetic, the magnetic moments in Table 1 clearly indicate that the complexes contain one copper(II) and one nickel(II) ions.

Table 1. Magnetic moments of CuNi(R-sata) and CuNi(R-sacta)

Complex	μ_{eff}/BM
$CuNi(sata) \cdot H_2O$	1.96
$CuNi(5\text{-}Me\text{-}sata) \cdot 1/2\,H_2O$	1.80
$CuNi(5\text{-}Br\text{-}sata) \cdot 1/2\,H_2O$	1.94
$CuNi(sacta) \cdot 2H_2O$	1.80
$CuNi(5\text{-}Me\text{-}sacta) \cdot C_2H_5OH$	1.85
$CuNi(5\text{-}Br\text{-}sacta) \cdot C_2H_5OH$	1.89

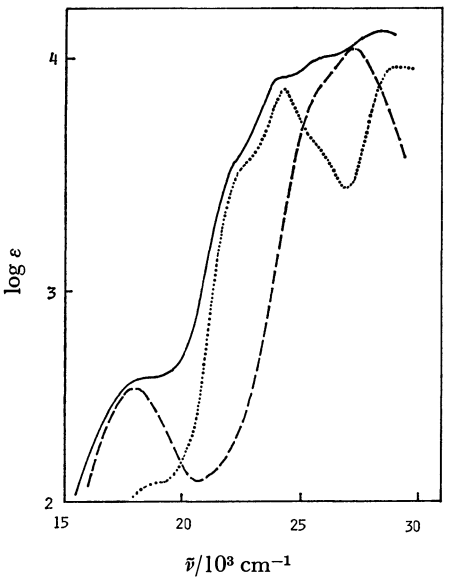

Fig. 2. Electronic spectra of (——) CuNi(sata), (——)-Cu(salpn), and (----)Ni(salpn).

With respect to two asymmetric carbon atoms in the tetramine moieties, two geometrical isomers (*meso-* and *dl-*) are considered for CuNi(R-sata) and CuNi (R-sacta). It has been shown that 1,2-bis(aminomethyl)-1,2-cyclohexanediamine is of the *dl*-form (*trans*-form), since 1,2-dicyano-1,2-cyclohexanediamine (the precursor of 1,2-bis(aminomethyl)-1,2-cyclohexanediamine) forms a *trans*-octahedral nickel(II) complex.[14] The geometrical structure of H_4(R-sacta) has not yet been determined.

Electronic spectra of the CuNi-complexes were well explained by the superposition of the $[CuN_2O_2]$ and $[NiN_2O_2]$ chromophores. The spectrum of CuNi(sata) is shown as an example in Fig. 2, together with the spectra of Cu(salpn) and Ni(salpn) as the references.

ESR spectra of the CuNi-complexes were measured in frozen chloroform solutions (at liquid nitrogen temperature). All the complexes showed a tetragonal pattern. ESR spectrum of CuNi(sata) is shown as an example in Fig. 3. Figure 3 also includes the spectra of Cu_2(sata) and Cu(salpn) for comparison. The spectrum of CuNi(sata) markedly differs from that of Cu_2(sata) and resembles that of Cu(salpn). This clearly indicates that CuNi(sata) is not an equimolar mixture of Cu_2(sata) and Ni_2(sata) but a discrete hetero-metal complex.

The ESR parameters, $A_{//}$ and $g_{//}$, for the CuNi-complexes and their relevant reference complexes are

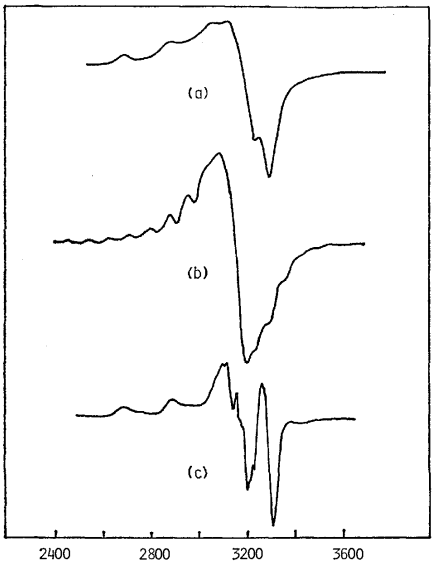

Fig. 3. ESR spectra of (a) CuNi(sata), (b) Cu_2(sata), and (c) Cu(salpn).

TABLE 2. ESR PARAMETERS OF THE CuNi-COMPLEXES AND THEIR REFERENCE COMPLEXES

	$A_{//}$/G	$g_{//}$		$A_{//}$/G	$g_{//}$
CuNi(sata)	183	2.22	Cu(salpn)	193	2.18
CuNi(5-Me-sata)	185	2.22	Cu(5-Me-salpn)	198	2.20
CuNi(sacta)	178	2.24	Cu(sacda)	206	2.18
CuNi(5-Me-sacta)	185	2.25	Cu(5-Me-sacda)	209	2.16

given in Table 2. ESR spectra of CuNi(5-Br-sata) and CuNi(5-Br-sacta) were not well resolved and hence their ESR parameters were not evaluated. Detailed examination of the ESR spectra of the CuNi-complexes revealed that the hyperfine coupling constant $A_{//}$ is smaller than that of the corresponding reference complex. Smaller $A_{//}$ values, compared with the reference complexes, of the CuNi-complexes can be interpreted in terms of the spin-delocalization over the molecule. As was shown for the binuclear copper(II) complexes,[4] it is likely that the CuN_2O_2 and NiN_2O_2 planes are stacked each other and interact through the ligand π-system.

It is to be noted that the $g_{//}$ values for the CuNi-complexes are larger than those of the corresponding reference mononuclear copper(II) complexes. The frequency of the d-d band due to the copper for the CuNi-complexes is practically the same as that of the reference complexes. Therefore, the large $g_{//}$ values of the CuNi-complexes may be attributed to the increase of λ due to the stacked configuration, based on the simple equation $g=2.0-8\lambda/(d_{x^2-y^2}-d_{xy})$.[15]

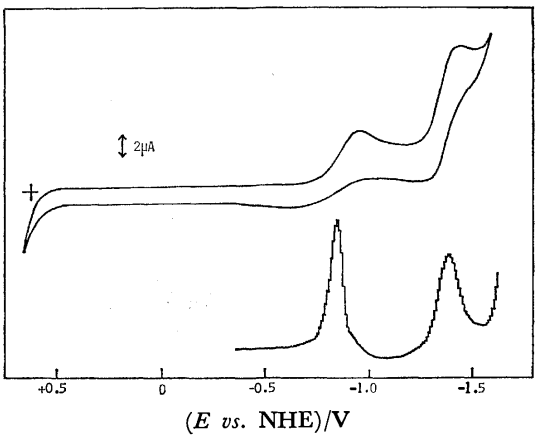

Fig. 4. Cyclic voltammogram and differential pulse polarogram of CuNi(sata).

Both of the cyclic voltammograms and differential pulse polarograms of CuNi(R-sata) and CuNi(R-sacta) showed two reduction waves. Typical examples are given in Fig. 4. The processes are irreversible or quasi-reversible judging from the separation ΔE_p between the cathodic and anodic peaks, E_{pc} and E_{pa}, of the cyclic voltammograms. Electrochemical data for the CuNi-complexes are given in Table 3. Approximate redox potentials $E^f_{1/2}$, which were determined by the arithmetic mean of E_{pa} and E_{pc} of cyclic voltammogram, substantially accord with the half-wave potentials determined from the differential pulse polarogram.

Reduction of Ni(R-salpn) and Ni(R-sacda) did not occur in the accessible range. Thus, all the reduction processes observed for the CuNi-complexes can be attributed to the reduction of copper(II) ion. Appearance of two reduction waves suggests the presence of two species, the stacked and non-stacked species, in solution. Two reduction waves have also been observed for Cu_2(sata), Cu_2(sacta), and Cu_2(5-Me-sacta).[4] For these complexes, the first and second reduction processes can be attributed to the one-electron transfer of the stacked species (Cu(II,II)$\rightleftharpoons$Cu(II,I)) and two electron transfer of the non-stacked species (Cu(II,

TABLE 3. ELECTROCHEMICAL DATA OF THE CuNi-COMPLEXES

	1st				2nd			
	CV			DPP	CV			DPP
	E_{pc}	E_{pa}	$E^f_{1/2}$	$E_{1/2}$	E_{pc}	E_{pa}	$E^f_{1/2}$	$E_{1/2}$
CuNi(sata)	−0.95	−0.77	−0.86	−0.86	−1.44	−1.30	−1.37	−1.38
CuNi(5-Me-sata)	−1.00	−0.83	−0.92	−0.91	−1.49	−1.33	−1.41	−1.45
CuNi(5-Br-sata)	−0.89	−0.69	−0.79	−0.87	−1.32	−1.15	−1.24	−1.27
CuNi(sacta)	−1.06	−0.96	−1.01	−0.89	−1.44	−1.32	−1.38	−1.42
CuNi(5-Me-sacta)	−1.06	−0.81	−0.94	−0.94	−1.47	−1.36	−1.42	−1.41
CuNi(5-Br-sacta)	−0.89	−0.67	−0.78	−0.90	−1.30	−1.14	−1.22	−1.26

$E^f_{1/2}=1/2(E_{pa}+E_{pc})$.

II)⇌Cu(I,I)), respectively, based on the controlled-potential electrolysis.[16] Further, the second reduction potentials of the CuNi-complexes well correspond to the potentials of the reference copper(II) complexes, respectively. Thus, it is natural to assign the first and the second processes to the reductions of copper of the stacked and non-stacked species, respectively.

The redox potential of the stacked species is higher by 0.4—0.5 V than that of the non-stacked species. Therefore, the copper ion of the stacked species must be stabilized by $(3—4)\times10^3$ cm^{-1} (9—12 kcal/mol) compared with that of the non-stacked species or of the reference mononuclear complex. It is likely that such a stabilization is effected by the electron-delocalization over the CuN_2O_2 and NiN_2O_2 coordination units through the ligand π-system. It is also to be noted that the Cu(II)→Cu(I) reduction occurs more easily in the cases of the CuNi-complexes compared with the Cu_2-complexes.[4]

References

1) Part XLVIII: M. Mikuriya, M. Nakamura, H. Ōkawa, and S. Kida, *Inorg. Chim. Acta*, in press.
2) U. Casellato, P. A. Vigato, and M. Vidali, *Coord. Chem. Rev.*, **23**, 31 (1977).
3) H. Ōkawa, *Kagaku No Ryoiki*, **33**, 11 (1979).
4) T. Izumitani, H. Ōkawa, and S. Kida, *Chem. Lett.*, **1981**, 483; T. Izumitani, M. Nakamura, H. Ōkawa, and S. Kida, *Bull. Chem. Soc. Jpn.*, **55**, 2122 (1982).
5) J. P. Collman, C. M. Elliott, T. R. Halbert, and B. S. Tovrog, *Proc. Natl. Acad. Sci. U.S.A.*, **74**, 18 (1977).
6) J. P. Collman, P. Denisevich, Y. Konai, M. Marrocco, C. A. Koval, and F. C. Anson, *J. Am. Chem. Soc.*, **102**, 6027 (1980).
7) M. H. Hatada, A. Tulinsky, and C. K. Chang, *J. Am. Chem. Soc.*, **102**, 7115 (1980).
8) N. E. Kagan, D. Mauzerall, and R. B. Merrifield, *J. Am. Chem. Soc.*, **99**, 5484 (1977).
9) D. A. Buckingham, M. J. Gunter, and L. N. Mander, *J. Am. Chem. Soc.*, **100**, 2899 (1978).
10) R. H. Holm, *J. Am. Chem. Soc.*, **82**, 5632 (1960).
11) F. E. Mabbs and D. J. Machim, "Magnetism and Transition Metal Complexes," Chapman and Hall, London (1973), p. 5.
12) R. R. Gagne, C. A. Koval, and G. C. Lisensky, *Inorg. Chem.*, **19**, 2855 (1980).
13) H. M. Koepp, H. Wendt, and H. Strehlow, *Z. Electrochem.*, **64**, 483 (1960).
14) H. Ōkawa, M. Kakimoto, T. Izumitani, and S. Kida, *Bull. Chem. Soc. Jpn.*, **55** 2671 (1982).
15) J. Owen, *Proc. R. Soc. London, Ser. A*, **227**, 183 (1955).
16) Controlled-potential electrolysis of Cu_2(sacta) (which shows two redox waves at −1.09 and −1.40 V *vs.* SCE) at −1.2 V revealed an electron transfer of *ca.* 0.7. ESR spectrum of the reduced solution showed a tetragonal pattern with the parameters $A_{//}=188$ G and $g_{//}=2.25$. These parameters differ from those ($A_{//}=206$ G and $g_{//}=2.18$) of Cu(sacda) but are similar to those ($A_{//}=178$ G and $g_{//}=2.22$) of CuNi(sacta). Thus, this process can be attributed to a one-electron transfer, Cu(II,II)→Cu(II,I), of the stacked species. Electron number transfered by the further electrolysis at −1.6 V could not be determined because of the concomitant reduction of the ligand with the reduction of the non-stacked species. However, the process at −1.40 V should involve a two-electron transfer, since the controlled-potential electrolysis at −1.60 V of Cu_2(5-Me-sata) (which exists only as the non-stacked species and shows one redox wave at −1.42 V) revealed the transfer of two electrons.

 © 1983 The Chemical Society of Japan Bull. Chem. Soc. Jpn., 56, 153—156 (1983)

The Mode of Stereoselective Association between Complex Cation and Complex Anion[1)]

Ushio Sakaguchi, Ippei Yamamoto, Shinji Izumoto, and Hayami Yoneda*

Department of Chemistry, Faculty of Science, Hiroshima University, Naka-ku, Hiroshima 730

(Received July 7, 1982)

Ion-exchange chromatography on the IEX 220 anion-exchange resin has been used to measure the retention volumes of enantiomers of several complex anions when eluted by an aqueous solution of Δ-$[Co(en)_3]^{3+}$, Δ-$[Co(sep)]^{3+}$, or Δ-$[Co\{(-)\text{-chxn}\}_3]^{3+}$, where en=ethylenediamine, sep=1,3,6,8,10,13,16,19-octaazabicyclo-[6.6.6]eicosane, and chxn=*trans*-1,2-cyclohexanediamine. Comparison of these retention volumes suggests that chiral recognition in solution is effected along the C_2 axis of $[Co(en)_3]^{3+}$, $[Co(mal)_2(en)]^-$, and $[Co(ox)_2(en)]^-$, and along the C_3 (or pseudo C_3) axis of $[Co(chxn)_3]^{3+}$, $[Co(edta)]^-$, $[Co(tdta)]^-$, $[Co(ox)_2(gly)]^{2-}$, $[Cr(mal)_3]^{3-}$, and *fac*-$[Co(\beta\text{-ala})_3]$, where mal=malonate, ox=oxalate, edta=ethylenediaminetetraacetate, tdta=1,4-butanediaminetetraacetate, gly=glycinate, and ala=alaninate. The mode of stereoselective association of these complex ions has been proposed.

Optically active metal complexes have been used more and more frequently as the resolving agent for the optical resolution of complex compounds.[2)] It is now well recognized that an optically active complex cation can discriminate the absolute configuration of an enantiomer of a complex anion in solution. Recently, the mode of stereoselective interaction between optically active complexes in solution has been proposed by several workers.[3–6)] Among these, of particular relevance to the present work is the ion pair $[Co(en)_3]^{3+}\cdots[Co(ox)_2(gly)]^{2-}$,[7)] for which the anion is supposed to face the cation along the C_3 axis of the cation, with its three oxygen atoms of three different chelate rings, thereby forming a triple hydrogen bond with axial N–H hydrogens.[6)] In this work, we have used ion-exchange chromatography to infer the mode of stereoselective ion association between optically active complexes.

Experimental

Materials. The cationic complexes used in this work are the chloride or bromide salts of Δ-$[Co(en)_3]^{3+}$,[8)] Δ-$[Co(sep)]^{3+}$,[9)] and Δ-$[Co\{(-)\text{-chxn}\}_3]^{3+}$,[10)] which were prepared by the literature methods. The preparation and optical resolution of the following anionic complexes were accomplished according to the methods described in the literature; $K_2[Co(ox)_2(gly)]$,[12)] $K[Co(edta)]$,[13)] $Na[Co(ox)_2(en)]$,[14)] and $Na[Co(mal)_2(en)]$.[14)] The complexes $K_3[Cr(mal)_3]$ and *fac*-$[Co(\beta\text{-ala})_3]$ were prepared after Chang[15)] and Celap *et al.*,[16)] respectively.

The preparation of K[Co(tdta)] was reported by Ogino *et al.*[17)] The optical resolution of this complex was effected by Δ-*cis*-$[Co(en)_2(NO_2)_2]^+$ obtained by the method of Dwyer and Garvan.[18)] The Δ enantiomer formed the less-soluble diastereoisomer and the potassium salt of the enantiomer was consistent with the formulation as the monohydrate. Found: C, 33.10; H, 4.25; N, 6.58. Calcd for $KCoC_{12}H_{18}N_2O_9$: C, 33.34; H, 4.20; N, 6.48. The circular dichroism spectrum in water had peaks at 623 ($\Delta\varepsilon=+2.98$), 553 (-4.20), 434 ($+0.752$), and 387 nm ($+1.19$).

The IEX 220 resin was the gift from Dr. S. Yamazaki, Toyo Soda Manufacturing Co., Ltd. (Tokyo).

Chromatographic Experiments. *Type (a) Experiment*: The SP-Sephadex C-25 resin (cation-exchanger) was packed in a column tube with an approximate size of 200 mm × 10 mm (i.d.) and loaded fully with an optically active cationic complex. The column was washed thoroughly with water and a racemic anionic complex was eluted with water. The eluent containing the partially resolved anionic complex was fractionally collected and the circular dichroism spectrum was measured immediately.

Type (b) Experiment: A home-built liquid chromatographic apparatus[19)] was used to measure the retention volume. A column (50 mm × 4 mm) of the IEX 220 resin (anion-exchanger) was equilibrated by an eluent (aqueous solution of an optically active cationic complex). An aqueous solution containing one enantiomer of an anionic complex and bis(glycinato)copper(II), which was used as a marker for void volume measurement, was injected by a syringe on top of the column and eluted by the eluent at an elution rate of 0.3 cm³/min. The adjusted retention volumes were obtained from the elution curves as in the previous studies.[19)] The concentration of the cationic complexes in eluents was varied from 4×10^{-3} to 60×10^{-3} mol dm^{-3}. The retention volumes were found to be reproducible to within 0.002 cm³.

Results and Discussion

In type (a) experiment, an optically active complex cation (Δ cation) was adsorbed on the SP-Sephadex C-25 cation-exchanger and an anionic complex was eluted with water. Thus, the enantiomer that associates more favorably with the Δ cation is eluted later. In some complexes, the degree of optical resolution was very small and unambiguous assertion of later-eluted enantiomers could not be made. Further, it was found that the chirality of the resin matrix itself[20)] contributes to the optical resolution to some extent. Therefore, type (b) experiment was performed to obtain reliable and quantitative data by employing an achiral resin, IEX 220, which is based on the styrene-divinylbenzene-copolymer and carries the tetraalkylammonium functional group. The retention volumes obtained in type (b) experiment are given in Table 1. In type (b) experiment, one enantiomer of an anionic complex was adsorbed on the anion-exchange resin and eluted by an aqueous solution containing a Δ cation. Thus, the enantiomer that associates more favorably with the Δ cation shows a smaller retention volume than its enantiomorph. The results of both types of experiments were consistent with respect to favorable diastereoisomeric combina-

TABLE 1. THE ADJUSTED RETENTION VOLUMES (cm³) OBTAINED IN TYPE (b) EXPERIMENT

		Δ-[Co(en)$_3$]Cl$_3$ 15×10^{-3} mol dm^{-3}	Δ-[Co(sep)]Br$_3$ 4×10^{-3} mol dm^{-3}	Δ-[Co{(−)-chxn}$_3$]Cl$_3$ 4×10^{-3} mol dm^{-3}
K[Co(edta)]	Δ	4.436	9.834	13.890
	Λ	4.380	9.675	14.660
K[Co(tdta)]	Δ	3.879	9.768	8.769
	Λ	3.625	9.711	10.240
Na[Co(ox)$_2$(en)]	Δ	3.213	3.115[a]	6.750[b]
	Λ	3.270	3.120[a]	6.330[b]
Na[Co(mal)$_2$(en)]	Δ	0.903	2.121	3.038
	Λ	0.922	2.143	3.014

a) The eluent concentration was 8.0×10^{-3} mol dm^{-3}. b) The eluent was the aqueous solution of Δ-[Co{(−)-chxn}$_3$]Br$_3$.

TABLE 2. THE ENANTIOMERS WHICH FORM FAVORABLE PAIRS WITH Δ CATIONS

	Δ cation		
	Δ-[Co(en)$_3$]$^{3+}$	Δ-[Co(sep)]$^{3+}$	Δ-[Co{(−)-chxn}$_3$]$^{3+}$
[Co(edta)]$^-$	Λ[a),b),c)]	Λ[a),b)]	Λ[a),b)]
[Co(tdta)]$^-$	Λ[b)]	Λ[b)]	Λ[b)]
[Co(ox)$_2$(en)]$^-$	Δ[b)]	Δ[b)]	Λ[b)]
[Co(mal)$_2$(en)]$^-$	Δ[b)]	Δ[b)]	Λ[b)]
[Co(ox)$_2$(gly)]$^{2-}$	Λ[a),c)]	Λ[a)]	Δ[a)]
[Cr(mal)$_3$]$^{3-}$	Λ[a),c)]	Λ[a)]	Δ[a)]
fac-[Co(β-ala)$_3$]	Λ[a),c)]	Λ[a)]	Δ[a)]

a) From type (a) experiment. b) From type (b) experiment. c) Also reported by A. Tatehata *et al.*; A Tatehara, Y. Ejiri, and K. Kotsuji, Proc. 29th Symposium on Coordination Chemistry, Shizuoka, October 1979, Abstr. No. 1B01, p. 40.

tions. Therefore, both results are incorporated and Table 2 was made to facilitate the following discussion.

Structural Features of Complexes. The cationic complexes chosen for this study were Δ-[Co(en)$_3$]$^{3+}$, Δ-[Co(sep)]$^{3+}$, and Δ-[Co{(−)-chxn}$_3$]$^{3+}$. The chirality of these complexes can be specified by looking at the complexes either along the C_3 axis as P(C_3) or along the C_2 axis as M(C_2). These notations follow those of Mason *et al.*[21] and define the chirality by the handedness of mutual spatial disposition of three or two chelate rings. The chirality of the other complexes used in this work can be specified similarly; a Δ complex has P(C_3) and M(C_2) chiralities. Note here that if an anionic complex approaches a Δ cation from the cation's C_3 axis, the anion will experience the P(C_3) chirality (right-handed propellers), whereas in the case of the C_2 access (the access along the cation's C_2 axis from the side opposite to one ethylenediamine moiety), the anion will experience the reversed chirality, the M(C_2) chirality (left-handed propellers).

The direction of access of anionic complexes that can contribute to chiral discrimination is along either the C_3 or the C_2 axis for Δ-[Co(en)$_3$]$^{3+}$; in other words, Δ-[Co(en)$_3$]$^{3+}$ can "use" its C_3 or C_2 axis in discriminating the chirality of a complex anion. In Δ-[Co(en)$_3$]$^{3+}$, chiral discrimination through the C_3 access has been suggested for the (+)- and (−)-tartrate anions,[22] and that through the C_2 access was proposed for the (+)-tartratoantimonate(III) anion.[23] Therefore, both accesses may potentially contribute to the chiral discrimination by Δ-[Co(en)$_3$]$^{3+}$.

In Δ-[Co(sep)]$^{3+}$, chiral discrimination along its C_3 axis is unlikely owing to the presence of bulky covalent caps along this axis.[9b] This is also supported by the equality of the association constants of Δ-[Co(sep)]$^{3+}$ with (+)- and (−)-tartrate ions (K= 40±2 mol^{-1} dm^3 at 25 °C and μ=0.1 with NaClO$_4$).[24] Thus, the chiral discrimination by this cation along the C_2 axis should be the only possibility, which constitutes the basis for the interpretation of our results.

In Δ-[Co{(−)-chxn}$_3$]$^{3+}$, though it appears that the C_3 access is preferred owing to the presence of bulky cyclohexane rings, the situation is not so clear and we leave both accesses as a possibility.

The reasoning similar to the above can be made for the anionic and electrically neutral complexes. Note here that these complexes contain negatively charged ligands, unlike the cationic complexes which have only electrically neutral ligands. Therefore, significant charge localization is expected for anionic and electrically neutral complexes. Previously, it has been shown[5,25] that in the ion association with complexes with significant charge localization, the site and/or the direction of ion association is dictated by localized electric charges. We here apply this criterion to the direction of ion association of anionic and neutral complexes. Thus, in the case of [Co(ox)$_2$(en)]$^-$ type of complexes, for example, an access of a cation along the C_2 axis and from the side opposite to the ethylenediamine ring is the only likelihood. In [Co(edta)]$^-$ type of complexes, an access of a cation along the anion's pseudo C_3 axis and from the side of three oxygen atoms is conceived. For [Co(ox)$_2$(gly)]$^{2-}$ and [Cr(mal)$_3$]$^{3-}$, we leave the pseudo C_3 and C_3 accesses

as the possibility, respectively. Though other types of accesses can, in principle, lead to chiral discrimination, the above choices for the direction of access will be shown later to be consistent with the experimental results.

Stereoselective Association. The most noteworthy feature in Table 2 is that Δ-$[Co(en)_3]^{3+}$ and Δ-$[Co(sep)]^{3+}$ favor the association with the same enantiomer for all the anionic and electrically neutral complexes investigated here but the opposite enantiomer is preferred by Δ-$[Co\{(-)\text{-chxn}\}_3]^{3+}$. This result indicates clearly that (i) Δ-$[Co(en)_3]^{3+}$ uses its C_2 axis in discriminating the chirality of all the anionic and neutral complexes examined here, because Δ-$[Co(en)_3]^{3+}$ and Δ-$[Co(sep)]^{3+}$ prefer the same enantiomers and the C_2 access is the only effective discriminating interaction in Δ-$[Co(sep)]^{3+}$, (ii) Δ-$[Co\{(-)\text{-chxn}\}_3]^{3+}$ uses its C_3 axis in the chiral discrimination, because this cation has the $P(C_3)$ propellers and prefers the opposite enantiomers to those favored by Δ-$[Co(sep)]^{3+}$ which uses the $M(C_2)$ propellers.

Now that we have identified the directions of the cationic complexes which are used in chiral discrimination and such directions of anionic and neutral complexes are assumed in the above, we can now examine the mode of association between these complexes. Table 2 indicates that Δ-$[Co(en)_3]^{3+}$ favors Δ-$[Co(ox)_2(en)]^-$. Since both ions use their C_2 axes in chiral discrimination, the resulting ion pair should be as illustrated in Fig. 1. Figure 1 depicts schematically the mutual disposition of chelate rings in this Δ-Δ combination, as viewed along the collinear C_2 axes of both ions. The hydrogen atoms are omitted for clarity. As seen from this figure, the handedness of the chelate rings that overlap mutually in association is the same for this pair and this mode of pairing is sterically less hindered. A severe steric hindrance is clearly expected for the Δ-Δ combination, where the first chirality notation refers to the cation and the second one to the anion. The $M(C_2)$–$M(C_2)$ pair depicted in Fig. 1 is also supported by electrostatic considerations; the cation will associate with the anion from the anionic side of the complex anion, namely along the C_2 axis of the anion and from the side opposite to the ethylenediamine chelate ring. Thus, the $M(C_2)$–$M(C_2)$ combination is consistent with both steric and electrostatic considerations. The preference for the pairs Δ-$[Co(en)_3]^{3+}\cdots\Delta$-$[Co(mal)_2(en)]^-$, Δ-$[Co(sep)]^{3+}\cdots\Delta$-$[Co(ox)_2(en)]^-$, and Δ-$[Co(sep)]^{3+}\cdots\Delta$-$[Co(mal)_2(en)]^-$ can be understood similarly.

In the combination of $[Co(ox)_2(en)]^-$ and $[Co(mal)_2(en)]^-$ with Δ-$[Co\{(-)\text{-chxn}\}_3]^{3+}$, the Δ-Δ pair is seen from Table 2 to be preferred. Since the cation uses its C_3 axis and the anions use their C_2 axes in chiral discrimination, this Δ-Δ pair corresponds to the $P(C_3)$–$P(C_2)$ pair. Namely, the propellers of both ions have the same handedness and the preference of this pair can be also understood in terms of a cozy fit of chelate rings of both ions.

Table 2 indicates that Δ-$[Cr(mal)_3]^{3-}$ forms the favorable ion pair with Δ-$[Co(en)_3]^{3+}$ and Δ-$[Co(sep)]^{3+}$. Since this anion uses its C_3 axis and the cations use their C_2 axes in chiral discrimination, these pairs are described as the $M(C_2)$–$M(C_3)$ pairs. Here again we find that the handednesses of chelate rings of cation and anion, as viewed along the direction of the access, coincide. Thus, these Δ-Δ pairs are also explained by the notion that favorable ion pairs are formed between those ions that can fit spatially along the prescribed axes. The fact that the pair Δ-$[Co\{(-)\text{-chxn}\}_3]^{3+}\cdots\Delta$-$[Cr(mal)_3]^{3-}$ is preferred over the Δ-Δ pair is similarly understood by noting that this pair corresponds to the $P(C_3)$-$P(C_3)$ combination. It will be evident from Table 2 that the results for *fac*-$[Co(\beta\text{-ala})_3]$ can be explained in the same way as for $[Cr(mal)_3]^{3-}$.

The Λ-enantiomers of $[Co(edta)]^-$ and $[Co(tdta)]^-$ preferentially associate with Δ-$[Co(en)_3]^{3+}$ and Δ-$[Co(sep)]^{3+}$ (see Table 2). Since these anions use the pseudo C_3 axes and the cations use their C_2 axes in chiral discrimination, the resulting pairs are the $M(C_2)$–M(pseudo C_3) combinations. The mode of ion pairing for the pair Δ-$[Co(edta)]^-\cdots\Delta$-$[Co(en)_3]^{3+}$ is shown schematically in Fig. 2. In Fig. 2, the Δ-$[Co(en)_3]^{3+}$ cation faces the Λ-$[Co(edta)]^-$ anion along the cation's

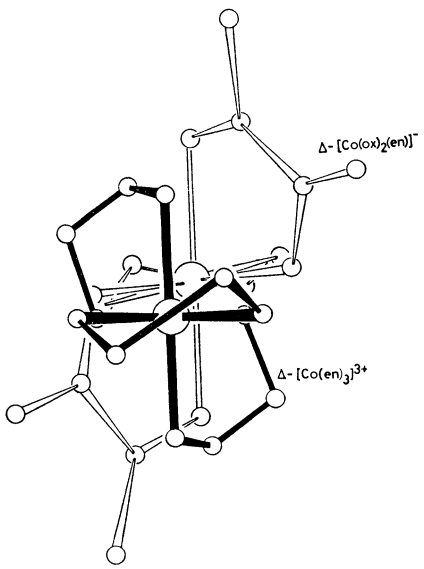

Fig. 1. Proposed structure for the preferred ion pair formed between Δ-$[Co(en)_3]^{3+}$ and Δ-$[Co(ox)_2(en)]^-$.

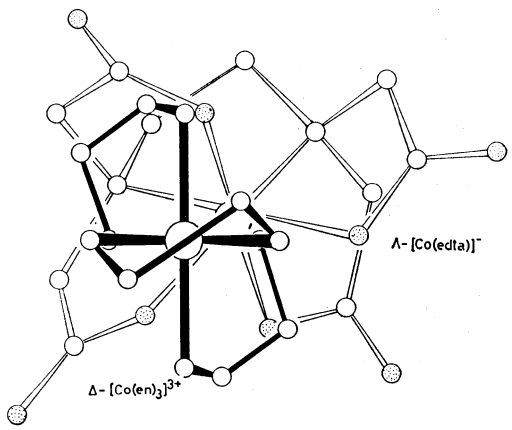

Fig. 2. Proposed structure for the favorable ion pair Δ-$[Co(en)_3]^{3+}\cdots\Lambda$-$[Co(edta)]^-$.

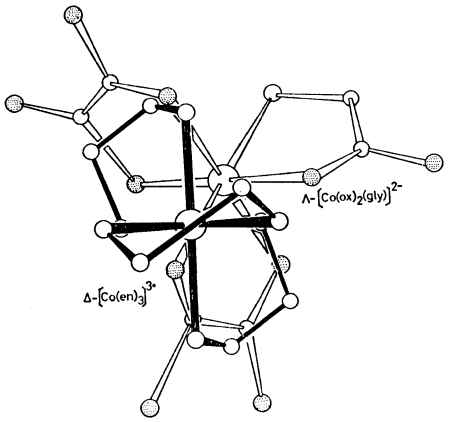

Fig. 3. Proposed mode of ion pairing between *Δ*-[Co(en)$_3$]$^{3+}$ and *Λ*-[Co(ox)$_2$(gly)]$^{2-}$.

C_2 axis and the anion faces the cation along the anion's pseudo C_3 axis with three anionic oxygen atoms. It can be seen from Fig. 2 that the chelate rings of both ions suffer less steric hindrance for the depicted *Δ*-*Λ* combination than for the *Δ*-*Δ* combination. Thus, the *Δ*-*Λ* combinations favored by these ions are again explained by a cozy fit of overlapping chelate rings. The formation of the favorable pair *Δ*-[Co{(−)-chxn}$_3$]$^{3+}$···*Δ*-[Co(edta)]$^-$ or *Δ*-[Co(tdta)]$^-$ can be explained in terms of the P(C_3)-P(pseudo C_3) pair; the propellers of both cation and anion have the same handedness when viewed along the C_3 or the pseudo C_3 axis.

The *Λ*-[Co(ox)$_2$(gly)]$^{2-}$ forms the favorable pairs with *Δ*-[Co(en)$_3$]$^{3+}$ and *Δ*-[Co(sep)]$^{3+}$ (see Table 2). By noting that [Co(ox)$_2$(gly)]$^{2-}$ uses its pseudo C_3 axis and the *Δ*-[Co(en)$_3$]$^{3+}$ cation uses its C_2 axis in chiral discrimination, the structure of the preferred ion pair formed between *Δ*-[Co(en)$_3$]$^{3+}$ and *Λ*-[Co(ox)$_2$(gly)]$^{2-}$ will be as illustrated in Fig. 3. The combination depicted in Fig. 3 is M(C_2)–M(pseudo C_3) and the handednesses of both ions, as viewed along the direction depicted, are the same. The preference of *Δ*-[Co(ox)$_2$(gly)]$^{2-}$ by *Δ*-[Co{(−)-chxn}$_3$]$^{3+}$ is explained in terms of the P(C_3)-P(psedo C_3) combination, namely by the same handedness of overlapping chelate rings.

In conclusion, all the elution orders in Table 2 are consistently explained, if we admit that (i) [Co(en)$_3$]$^{3+}$, [Co(sep)]$^{3+}$, [Co(ox)$_2$(en)]$^-$, and [Co(mal)$_2$(en)]$^-$ use their C_2 axes in chiral discrimination, (ii) [Co(chxn)$_3$]$^{3+}$, [Co(edta)]$^-$, [Co(tdta)]$^-$, [Co(ox)$_2$(gly)]$^{2-}$, and *fac*-[Co(*β*-ala)$_3$] use their C_3 or pseudo C_3 axes in chiral discrimination, and (iii) favorable pairs are formed between those ions that have the same handedness of chelate rings, when viewed along the above axes.

Acknowledgement is made to Dr. S. Yamazaki, Toyo Soda Manufacturing Co., Ltd. (Tokyo), for the gift of the IEX 220 resin.

References

1) Part 2 of "Chiral Recognition in Solution." Part 1; H. Nakazawa, U. Sakaguchi, and H. Yoneda, *J. Am. Chem. Soc.*, in press.

2) F. P. Dwyer and A. M. Sargeson, *J. Phys. Chem.*, **60**, 1331 (1956); S. Fujinami, K. Tsuji, K. Minegishi, and M. Shibata, *Bull. Chem. Soc. Jpn.*, **55**, 1319 (1982); K. Akamatsu, T. Komorita, and Y. Shimura, *ibid.*, **55**, 140 (1982), and references therein.

3) E. Iwamoto, M. Yamamoto, and Y. Yamamoto, *Inorg. Nucl. Chem. Lett.*, **13**, 399 (1977).

4) M. Yamamoto, E. Iwamoto, A. Kozasa, K. Takemoto, Y. Yamamoto, and A. Tatehata, *Inorg. Nucl. Chem. Lett.*, **16**, 71 (1980).

5) K. Miyoshi, Y. Matsumoto, and H. Yoneda, *Inorg. Chem.*, **20**, 1057 (1981).

6) A. Tatehata, M. Iiyoshi, and K. Kotsuji, *J. Am. Chem. Soc.*, **103**, 7391 (1981).

7) Abbreviations; en=ethylenediamine, sep=1,3,6,8,10,13,16,19-octaaza-bicyclo[6.6.6]eicosane, chxn=*trans*-1,2-cyclohexanediamine, ox=oxalate, gly=glycinate, mal=malonate, edta=ethylenediaminetetraacetate, tdta=tetramethylenediaminetetraacetate, ala=alaninate, acac=2,4-pentanedionate, phen=1,10-phenanthroline.

8) J. A. Broomhead, F. P. Dwyer, and J. W. Hogarth, *Inorg. Synth.*, **6**, 183 (1960); M. Iwata, K. Nakatsu, and Y. Saito, *Acta Crystallogr., Sect. B*, **25**, 2562 (1969), and references cited therein.

9) a) J. M. Harrowfield, A. J. Herlt, and A. M. Sargeson, *Inorg. Synth.*, **20**, 85 (1980); b) I. I. Creaser, J. M. Harrowfield, A. J. Herlt, A. M. Sargeson, J. Springborg, R. J. Geue, and M. R. Snow, *J. Am. Chem. Soc.*, **99**, 3181 (1977).

10) F. Galsbøl, P. Steenbøl, and B. S. Sørensen, *Acta Chem. Scand.*, **26**, 3605 (1972); S. E. Harnung, B. S. Sørensen, I. Creaser, H. Maegaard, U. Pfenninger, and C. E. Schäffer, *Inorg. Chem.*, **15**, 2123 (1976); F. Marumo, Y. Utsumi, and Y. Saito, *Acta Crystallogr., Sect. B*, **26**, 1492 (1970).

11) F. P. Dwyer, I. K. Reid, and A. M. Sargeson, *Aust. J. Chem.*, **18**, 1919 (1965).

12) K. Yamasaki, J. Hidaka, and Y. Shimura, *Bull. Chem. Soc. Jpn.*, **42**, 119 (1969).

13) F. P. Dwyer and F. L. Garvan, *Inorg. Synth.*, **6**, 192 (1966); W. T. Jordan, B. J. Brennan, L. R. Froebe, and B. E. Douglas, *Inorg. Chem.*, **12**, 1827 (1973).

14) F. P. Dwyer, I. K. Reid, and F. L. Garvan, *J. Am. Chem. Soc.*, **83**, 1285 (1961). See, also; K. R. Butler and M. R. Snow, *J. Chem. Soc., Dalton Trans.*, **1976**, 259; K. Matsumoto and H. Kuroya, *Bull. Chem. Soc. Jpn.*, **45**, 1755 (1972).

15) J. C. Chang, *Inorg. Synth.*, **16**, 80 (1976).

16) M. B. Celap, S. R. Niketic, T. J. Janjic, and V. N. Nikolic, *Inorg. Chem.*, **6**, 2063 (1967).

17) H. Ogino, S. Kobayashi, and N. Tanaka, *Bull. Chem. Soc. Jpn.*, **43**, 97 (1970).

18) F. P. Dwyer and F. L. Garvan, *Inorg. Synth.*, **6**, 195 (1960).

19) H. Yoneda, S. Wakida, H. Nakazawa, and U. Sakaguchi, *Bull. Chem. Soc. Jpn.*, **55**, 1073 (1982).

20) Y. Yoshikawa and K. Yamasaki, *Coord. Chem. Rev.*, **28**, 205 (1979).

21) A. J. McCaffery, S. F. Mason, and B. J. Norman, *J. Chem. Soc., A*, **1965**, 5094.

22) K. Ogino and U. Saito, *Bull. Chem. Soc. Jpn.*, **40**, 826 (1967); K. Ogino, *ibid.*, **42**, 447 (1969); B. Norden, *Acta Chem. Scand.*, **26**, 111 (1972); M. Fujita and H. Yamatera, *Bull. Chem. Soc. Jpn.*, **49**, 1301 (1976).

23) U. Sakaguchi *et al.*, unpublished; H. Nakazawa and H. Yoneda, *J. Chromatogr.*, **160**, 89 (1978).

24) U. Sakaguchi *et al.*, unpublished results.

25) H. Nakazawa, U. Sakaguchi, and H. Yoneda, *J. Chromatogr.*, **213**, 323 (1981); H. Nakazawa, U. Sakaguchi, H. Yoneda, and Y. Morimoto, *Inorg. Chem.*, **20**, 973 (1981); U. Sakaguchi, H. Nakazawa, and H. Yoneda, *J. Chem. Soc., Chem. Commun.*, **1979**, 356.

 © 1983 The Chemical Society of Japan Bull. Chem. Soc. Jpn., 56, 157—164 (1983)

Preparation and Stereochemistry of *Δ-sym*-[(2*S*,2′*S*)-1,1′-Ethylenedipyrrolidine-2,2′-dicarboxylato]cobalt(III) Complexes with Various Bidentate Ligands

Minahiro Okabayashi,†† Ken-ichi Okamoto,* Hisahiko Einaga,† and Jinsai Hidaka

Department of Chemistry, University of Tsukuba, Ibaraki 305
†*Institute of Materials Science, University of Tsukuba, Ibaraki 305*

(Received June 29, 1982)

Cobalt(III) complexes containing (2*S*,2′*S*)-1,1′-ethylenedipyrrolidine-2,2′-dicarboxylate (*S,S*-epro) and a bidentate ligand were prepared and characterized. The bidentate ligands were ethylenediamine, trimethylenediamine, oxalate, glycinate, (*R*)- or (*S*)-alaninate, (*R*)- or (*S*)-valinate, (*R*)- or (*S*)-prolinate, (*R*)- or (*S*)-pipecolate, sarcosinate, or *N*-ethylglycinate. The *S,S*-epro ligand coordinates stereoselectively to cobalt(III) ion to take only the *Δ-sym* configuration. The stereochemistry was discussed on the basis of the electronic absorption, CD, and ^{1}H and ^{13}C NMR spectra. The rate constants of isomerization and the Gibbs' free energy difference (*ca.* 0.9 kJ mol^{-1}) between the *R*(*N*) and *S*(*N*) isomers of the sarcosinato or *N*-ethylglycinato complex were investigated in relation to the interligand interaction. The thermodynamics and mechanisms of their isomerization process were little influenced by the *N*-alkyl groups.

For most ethylenediamine-*N,N′*-diacetate (edda) complexes, the symmetric (*sym*) isomer is dominantly formed in comparison with the unsymmetric (*unsym*) one.[1-8] The *unsym* isomer isomerizes to the *sym* one in aqueous solution.[9-11] The formation of the *unsym* isomer for the edda complexes depends mainly on the bidentate ligand coordinated in the remaining two coordination sites,[5,9,12] the geometry of the starting complex,[13] and the reaction temperature.[6] However, the stereospecific formation of the complex with this type of ligand has not been clarified yet.[14]

The optically active quadridentate ligand in this work, (2*S*,2′*S*)-1,1′-ethylenedipyrrolidine-2,2′-dicarboxylate (*S,S*-epro), has two asymmetric carbon atoms and two pyrrolidine rings, although the ligand is an O–N–N–O type similar to the edda. Accordingly, the configurations of the *S,S*-epro ligand are regulated to only two, *Δ*-symmetric and *Λ*-unsymmetric, by coordination to cobalt(III) ion. This selective coordination is suitable for investigation of the stereochemical preference of the amino or cyclic imino carboxylate ligands in the remaining two coordination sites.

In the present paper, some aspects of the stereochemistry of the [Co(*S,S*-epro)(L)] type complexes are dealt with; L denotes ethylenediamine, trimethylenediamine, oxalate, glycinate, (*R*)- or (*S*)-alaninate, (*R*)- or (*S*)-valinate, (*R*)- or (*S*)-prolinate, (*R*)- or (*S*)-pipecolate ((*R*)- or (*S*)-2-piperidinecarboxylate, *R*- or *S*-pipec), sarcosinate (sar), or *N*-ethylglycinate (*N*-et-gly). The *S,S*-epro complexes isolated have been characterized from their electronic absorption, CD, and ^{1}H and ^{13}C NMR spectra. The absolute configurations of the coordinated nitrogen atoms of sar, *N*-et-gly, and *R*- or *S*-pipec were assigned by means of their ^{1}H NMR and CD spectra. The rate constants of isomerizations and the Gibbs' free energy differences are considered for the sar and *N*-et-gly complexes.

Experimental

1) Preparation of Ligands. (2*S*,2′*S*)-1,1′-Ethylenedipyrrolidine-2,2′-dicarboxylic acid was prepared from (*S*)-proline and 1,2-dibromoethane according to the method of Schoenberg *et al.*[15] Found: C, 45.80; H, 7.04; N, 8.82%. Calcd for $C_{12}H_{22}N_2O_4 \cdot 0.75NaCl \cdot H_2O$: C, 45.30; H, 6.97; N, 8.80%.

N-Ethylglycine was prepared by the procedure described previously.[16]

2) Δ-sym-*Ba*[*Co*(S,S-*epro*)(*Cl*)(*OH*)]$_2 \cdot C_2H_5OH$. The complex was prepared and separated by a procedure similar to that used for *Λ-unsym*-[Co(*S,S*-tmpro)(Cl)(OH)]$^-$ (where *S,S*-tmpro denotes (2*S*,2′*S*)-1,1′-trimethylenedipyrrolidine-2,2′-dicarboxylate).[16] The CD spectral pattern in the visible region suggested that the violet complex obtained has the *Δ-sym* configuration. Yield; 0.5 g.

3) Δ-sym-[*Co*(S,S-*epro*)(*en*)]$ClO_4 \cdot 2H_2O$. *Method A*: A solution containing 0.3 g of *trans*-[Co(Cl)$_2$(en)$_2$]Cl[17] and 0.33 g of *S,S*-H$_2$epro·0.75NaCl·H$_2$O in 20 cm^3 of water was adjusted to pH 8.0 by addition of 1 mol dm^{-3} NaOH aqueous solution. After addition of *ca.* 0.1 g of activated charcoal, the mixture was stirred at 50 °C for 30 min. The reaction solution was cooled to room temperature and then filtered. The filtrate was concentrated to a small volume and poured onto a column of SP-Sephadex C-25 (Na^+ form, 3 cm × 35 cm). The adsorbed band was separated into two bands, purple-red and yellow in the order of elution, by eluting with 0.05 mol dm^{-3} $NaClO_4$ aqueous solution. The yellow band remained at the top of the column after the purple-red band had been eluted out, and then the band was eluted with a solution saturated with NaCl. It was found, from the absorption and CD spectra, that the purple-red and yellow bands contained *Δ-sym*-[Co(*S,S*-epro)(en)]$^+$ and [Co(en)$_3$]$^{3+}$, respectively. The first eluate was concentrated to a small volume, and to the solution was added ethanol. The resulting crystals were collected and recrystallized from a water–methanol–ethanol (2:1:1) mixture. The needle crystals were collected, washed with ethanol and then ether, and dried in a vacuum desiccator. Yield: 0.24 g.

Method B: The complex was also prepared by the following procedure. A solution containing 0.27 g of $CoCl_2 \cdot 6H_2O$ in 5 cm^3 of water was added to a solution containing 0.06 g of ethylenediamine and 0.32 g of *S,S*-H$_2$epro·0.75-NaCl·H$_2$O in 6 cm^3 of water. To the solution was added 0.24 g of PbO_2 and the mixture was stirred at 50 °C for 3 h. The solution was cooled in an ice bath and then filtered. The filtrate was poured onto a column of Dowex

†† Present address: Tokuyama Soda Co., Ltd., Endo 2051, Fujisawa, Kanagawa 252.

50W-X8 (200—400 mesh, Na^+ form, 2 cm × 15 cm). The adsorbed band was eluted with 0.2 mol dm^{-3} $NaClO_4$ aqueous solution. It was found that the purple-red band contained only the complex, *Δ-sym*-[Co(*S,S*-epro)(en)]$^+$. The needle crystals were collected by filtration. Yield: 0.09 g.

4) Δ-sym-[*Co*(S,S-*epro*)(*tn*)]$ClO_4 \cdot 0.5C_2H_5OH$. The complex was prepared by the same method as in 3), using trimethylenediamine instead of ethylenediamine.

5) Δ-sym-*K*[*Co*(S,S-*epro*)(*ox*)]$\cdot 4H_2O$. This complex was prepared by a procedure similar to that in Method B of 3), using 1.34 g of $CoCl_2 \cdot 6H_2O$, 0.74 g of oxalic acid, and 1.79 g of *S,S*-H_2epro·0.75NaCl·H_2O. The solution obtained was poured onto a column of QAE-Sephadex A-25 (Cl^- form, 5 cm × 30 cm). The adsorbed band was eluted with 0.07 mol dm^{-3} KCl aqueous solution. The two blue-violet bands were eluted. It was found, from the absorption and CD spectra, that the first eluate contained *Δ-sym*-[Co(*S,S*-epro)(Cl)(OH)]$^-$ and the second one *Δ-sym*-[Co(*S,S*-epro)(ox)]$^-$. The second eluate was concentrated to a small volume with a rotary evaporator. To this solution was added ethanol and it was kept in a refrigerator overnight. The resulted needle crystals were collected and recrystallized from ethanol–water (5:1) mixture. Yield: 0.24 g.

6) Δ-sym-[*Co*(S,S-*epro*)(*gly*)]$\cdot 0.5H_2O$. This complex was prepared and separated by a procedure similar to that used for *Δ-unsym*-[Co(*S,S*-tmpro)(gly)].[16] By the column chromatographic separation, only one band was eluted with water and fractionated into six parts. It was found, from their absorption and CD spectra, that all the fractions contained only *Δ-sym*-[Co(*S,S*-epro)(gly)]. The fractions were combined and concentrated to a small volume. To the solution was added a small amount of ethanol and it was kept in a refrigerator overnight. The needle crystals were collected by filtration, and recrystallized from water by addition of ethanol and then acetone. Yield: 0.43 g.

7) Δ-sym-[*Co*(S,S-*epro*)(S-*ala*)]$\cdot H_2O$, -[*Co*(S,S-*epro*)(R-*ala*)]$\cdot H_2O$, -[*Co*(S,S-*epro*)(S-*val*)]$\cdot 1.5H_2O$, -[*Co*(S,S-*epro*)(R-*val*)], *and* -[*Co*(S,S-*epro*)(S-*pro*)]. These complexes were prepared by the same method as that used for *Δ-sym*-[Co(*S,S*-epro)(gly)].

8) Δ-sym-[*Co*(S,S-*epro*)(R(N)-*sar*)]$\cdot H_2O$ *and* -[*Co*(S,S-*epro*)(S(N)-*sar*)]$\cdot 0.5H_2O$. The solution containing *Δ-sym*-[Co(*S,S*-epro)(Cl)(OH)]$^-$ prepared from 2.4 g of $CoCl_2 \cdot 6H_2O$ was evaporated to dryness in a rotary evaporator below 30 °C, and the complex was extracted with 50 cm^3 of methanol. The methanol solution was added to a solution containing 1.2 g of sarcosine in 150 cm^3 of methanol. After addition of a small amount of activated charcoal, the mixture was stirred at 65 °C for 1 h. The solution was cooled to room temperature and then filtered. The filtrate was concentrated to a pasty cake and *ca.* 20 cm^3 of water was added to it. The solution was passed through columns of Dowex 1-X8 and SP-Sephadex C-25 in order to remove the charged compounds. The concentrated eluate was poured onto a column of QAE-Sephadex A-25 ((*R,R*)-tartrate form, 3.5 cm × 85 cm), and eluted with water. The adsorbed band was separated into three bands: violet, violet, and pink, in this order. It was found, from the absorption and CD spectra, that the first eluate contained *Δ-sym*-[Co(*S,S*-epro)(sar)] (the ratio of the *R*(*N*)-sar and *S*(*N*)-sar isomers was *ca.* 2:3), the second violet one contained *mer*-[Co(sar)$_3$], and the third pink one contained cobalt(II) compound. All the fractions of the first eluate were combined and evaporated to dryness below 30 °C. Yield: 1.1 g. This product was dissolved in methanol. After addition of appropriate volume of ether to it, the solution was kept in a refrigerator overnight. The complex consisted of two kinds of crystalline forms, needle and prism, which could be sorted by hand. It was found, from the absorption and ^{1}H NMR spectra, that the needle and prismatic crystals corresponded to the *R*(*N*)-sar and *S*(*N*)-sar isomers, respectively. Each of them was recrystallized repeatedly from methanol by addition of ether until a constant CD spectrum was obtained.

9) Δ-sym-[*Co*(S,S-*epro*)(R(N)-N-*et-gly*)]$\cdot 0.5H_2O$ *and* -[*Co*(S,S-*epro*)(S(N)-N-*et-gly*)]$\cdot 0.25H_2O$. The complex was prepared and separated into two diastereomers by the same procedure as in 8), using *N*-ethylglycine instead of sarcosine. Yield: 0.59 g. From the CD spectra, the reaction solution also contained the *R*(*N*)-*N*-et-gly and *S*(*N*)-*N*-*et-gly* isomers (the ratio: *ca.* 2:3).

10) Δ-sym-[*Co*(S,S-*epro*)(R-*pro*)]$\cdot 0.5H_2O$. The complex was prepared by the same procedure as in 8), using (*RS*)-proline instead of sarcosine. The complex was chromatographed on a column of QAE-Sephadex A-25 ((*R,R*)-tartrate form, 3.5 cm × 85 cm). The adsorbed band was eluted with water. The two bands, which partially overlapped, were fractionated into eight parts. It was found, from their absorption and CD spectra, that the four earlier fractions contained mainly *Δ-sym*-[Co(*S,S*-epro)(*R*-pro)], and the four later ones contained mainly *Δ-sym*-[Co(*S,S*-epro)(*S*-pro)], which was already prepared in 7). The four eariler fractions were combined and concentrated to a small volume and then chromatographed on the column again. This procedure was repeated several times in order to purify the complex. The eluate was concentrated to a small volume. After addition of ethanol and ether to it, the solution was kept in a refrigerator overnight. The crystals obtained were collected and then recrystallized from an ethanol–acetone (2:1) mixture several times. Yield: 0.09 g. The configuration of the α-carbon atom of the coordinated prolinate was confirmed by the DNP method.[16]

11) Δ-sym-[*Co*(S,S-*epro*)(R-*pipec*)]$\cdot H_2O$ *and* -[*Co*(S,S-*epro*)(S-*pipec*)]. These complexes were prepared and separated by a procedure similar to that in 10). The earlier eluate contained *Δ-sym*-[Co(*S,S*-epro)(*R*-pipec)] and the later one *Δ-sym*-[Co(*S,S*-epro)(*S*-pipec)]. The configuration of the asymmetric carbon atoms of the coordinated pipecolate were also determined by the DNP method.[16] Yields: 0.27 g for the *R*-pipec isomer and 0.015 g for the *S*-pipec one.

Analyses. The analytical results for the complexes obtained are summarized in Table 1.

Measurements. The electronic absorption spectra were recorded with JASCO UVIDEC-1 spectrophotometer and the CD spectra with JASCO J-20 spectropolarimeter in an aqueous solution. These spectra changed very little during the measurements. The ^{1}H NMR spectra were recorded on a JEOL FX-100 NMR spectrometer at probe temperature in three kinds of mixtures: $DClO_4$–CD_3OD, D_2O–$DClO_4$, and $(CD_3)_2SO$–DCl. The ^{13}C NMR spectra were recorded on JEOL FX-90Q NMR spectrometer in the D_2O solution. Sodium 2,2-dimethyl-2-silapentane-5-sulfonate (DSS) was used as an internal reference for the ^{1}H and ^{13}C NMR measurements.

The isomerization and the equilibrium and kinetic experiments were carried out using both the *R*(*N*) and *S*(*N*) isomers of *Δ-sym*-[Co(*S,S*-epro)(sar)] or -[Co(*S,S*-epro)(*N*-et-gly)]. The rate of CD change with time was measured for a methanol solution of each isomer (*ca.* 1.5×10^{-3} mol dm^{-3}) with JASCO J-500 spectropolarimeter. The runs were carried out in a quartz cell equipped with the water-jacket thermostated at 23.5 °C. The isomerization was followed until equilibrium was reached. The change in the CD intensity was observed at 300—650 nm.

Table 1. Elemental analyses

Complex	C (%)		H (%)		N (%)	
	Found	Calcd	Found	Calcd	Found	Calcd
Δ-sym-Ba[Co(*S,S*-epro)(Cl)(OH)]$_2$·C_2H_5OH	34.54	34.14	4.52	4.85	5.82	6.12
Δ-sym-K[Co(*S,S*-epro)(ox)]·4H_2O	32.48	32.82	4.98	5.11	5.47	5.47
Δ-sym-[Co(*S,S*-epro)(en)]ClO_4·2H_2O	32.88	33.05	5.93	5.94	11.02	11.01
Δ-sym-[Co(*S,S*-epro)(tn)]ClO_4·0.5C_2H_5OH	37.73	37.69	6.15	6.13	10.45	10.99
Δ-sym-[Co(*S,S*-epro)(gly)]·0.5H_2O	42.34	42.43	5.87	5.60	10.61	10.60
Δ-sym-[Co(*S,S*-epro)(*S*-ala)]·H_2O	43.22	42.97	6.32	6.25	10.43	10.02
Δ-sym-[Co(*S,S*-epro)(*R*-ala)]	44.85	44.89	6.07	6.03	10.71	10.47
Δ-sym-[Co(*S,S*-epro)(*S*-val)]·1.5H_2O	44.97	44.74	6.44	6.85	9.06	9.21
Δ-sym-[Co(*S,S*-epro)(*R*-val)]	48.22	47.56	6.51	6.57	9.97	9.79
Δ-sym-[Co(*S,S*-epro)(*R*(*N*)-sar)]·H_2O	42.69	42.97	6.07	6.25	9.94	10.02
Δ-sym-[Co(*S,S*-epro)(*S*(*N*)-sar)]·0.5H_2O	43.70	43.91	6.28	6.14	10.10	10.24
Δ-sym-[Co(*S,S*-epro)(*R*(*N*)-*N*-et-gly)]·0.5H_2O	45.39	45.29	6.74	6.41	9.75	9.90
Δ-sym-[Co(*S,S*-epro)(*S*(*N*)-*N*-et-gly)]·0.25H_2O	45.88	45.77	6.41	6.30	10.28	10.01
Δ-sym-[Co(*S,S*-epro)(*R*-pipec)]·H_2O	47.37	47.06	6.67	6.58	9.21	9.15
Δ-sym-[Co(*S,S*-epro)(*S*-pipec)]	48.92	48.98	6.52	6.39	9.46	9.52
Δ-sym-[Co(*S,S*-epro)(*R*-pro)]·0.5H_2O	46.99	46.79	6.13	6.24	9.49	9.63
Δ-sym-[Co(*S,S*-epro)(*S*-pro)]	47.41	47.78	6.01	6.13	9.79	9.83

Results and Discussion

Structural Assignments. Only two isomers, *Δ-sym* and *Δ-unsym*, are possible for [Co(*S,S*-epro)(en, tn, or ox)]$^{+\text{ or }-}$, because the *S,S*-epro ligand has two asymmetric carbon atoms, *S*(*C*) and *S*(*C*), and two pyrrolidine rings (Fig. 1). In the ^{13}C NMR spectra of the en and ox complexes, the seven peaks are expected for the *Δ-sym* isomer (C_2 symmetry), whereas fourteen peaks are expected for the *Δ-unsym* one (C_1 symmetry).

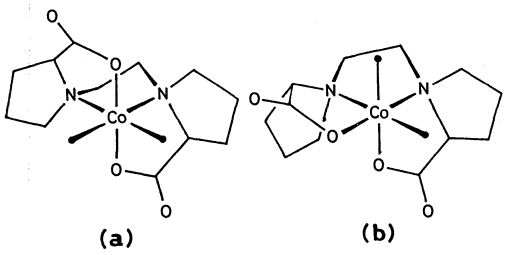

Fig. 1. Two possible configurations of coordinated *S,S*-epro ligand: (a) *Δ-sym* and (b) *Δ-unsym*.

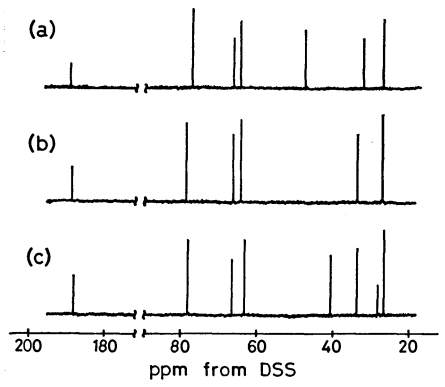

Fig. 2. ^{13}C NMR spectra of *Δ-sym*-[Co(*S,S*-epro)(L)]: L; (a) en, (b) ox, and (c) tn.

As shown in Fig. 2, however, the spectra of the en and ox isomers isolated show seven peaks and indicate that both the isomers are the *Δ-sym*. Similarly, the tn isomer is also the *Δ-sym* type, because it shows eight peaks (C_2 symmetry) (Fig. 2).

The absorption and CD spectra of the en and ox complexes are shown in Fig. 3. The first absorption band of the en and tn complexes have a shoulder at the higher energy side of the major peak (Table 2),

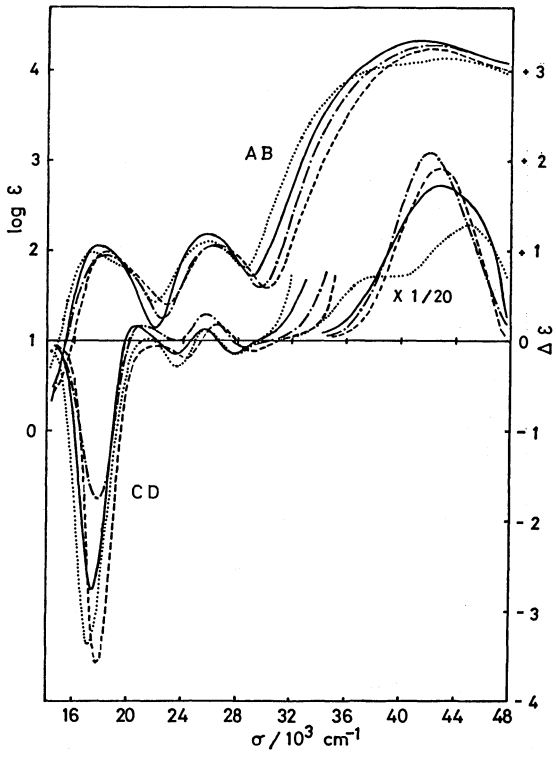

Fig. 3. Absorption and CD spectra of *Δ-sym*-[Co(*S,S*-epro)(L)]: L; ox (——), en (----), (Cl)(OH) (·····), and gly (—·—).

Table 2. Absorption data of *Δ-sym*-[Co(*S,S*-epro)(L)] type complexes

Complex (L)	First band	Second band	Charge transfer band
[Co(*S,S*-epro)(Cl)(OH)]$^-$	17.33(1.98)	25.71(2.11)	40.06(4.1 sh)
	19.42(1.8 sh)		
[Co(*S,S*-epro)(ox)]$^-$	17.78(2.07)	25.74(2.19)	41.67(4.33)
[Co(*S,S*-epro)(en)]$^+$	18.35(1.99)	26.32(2.06)	42.37(4.25)
	20.00(1.8 sh)		
[Co(*S,S*-epro)(tn)]$^+$	18.18(1.92)	26.32(2.07)	41.32(4.43)
	20.00(1.8 sh)		
[Co(*S,S*-epro)(gly)]	18.35(1.95)	26.32(2.05)	42.55(4.29)
[Co(*S,S*-epro)(*R*-ala)]	18.32(1.98)	26.25(2.12)	42.37(4.32)
[Co(*S,S*-epro)(*S*-ala)]	18.25(1.96)	26.32(2.10)	42.55(4.35)
[Co(*S,S*-epro)(*R*-val)]	18.28(1.98)	26.25(2.11)	42.19(4.29)
[Co(*S,S*-epro)(*S*-val)]	18.25(2.00)	26.32(2.11)	42.55(4.31)
[Co(*S,S*-epro)(*R*(*N*)-sar)]	18.08(2.06)	25.91(2.12)	41.67(4.31)
[Co(*S,S*-epro)(*S*(*N*)-sar)]	18.08(2.00)	25.91(2.09)	41.67(4.32)
[Co(*S,S*-epro)(*R*(*N*)-*N*-et-gly)]	18.05(2.09)	25.74(2.13)	41.67(4.28)
[Co(*S,S*-epro)(*S*(*N*)-*N*-et-gly)]	18.05(2.01)	25.97(2.11)	41.49(4.34)
[Co(*S,S*-epro)(*R*-pipec)]	17.86(2.10)	25.61(2.22)	40.65(4.28)
[Co(*S,S*-epro)(*S*-pipec)]	17.95(2.01)	25.84(2.17)	40.65(4.28)
[Co(*S,S*-epro)(*R*-pro)]	18.18(2.05)	26.04(2.15)	41.49(4.26)
[Co(*S,S*-epro)(*S*-pro)]	18.18(1.98)	26.11(2.11)	41.67(4.25)

Wave numbers and log ε values (in parentheses) are given in 10^3 cm^{-1} and mol^{-1} dm^3 cm^{-1}, respectively. sh denotes a shoulder.

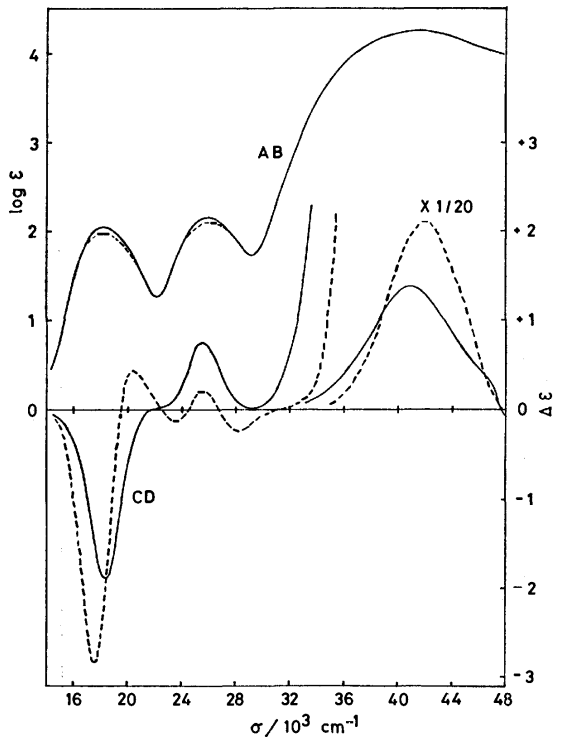

Fig. 4. Absorption and CD spectra of *Δ-sym*-[Co(*S,S*-epro)(L)]: L; R-pro (——) and S-pro (----).

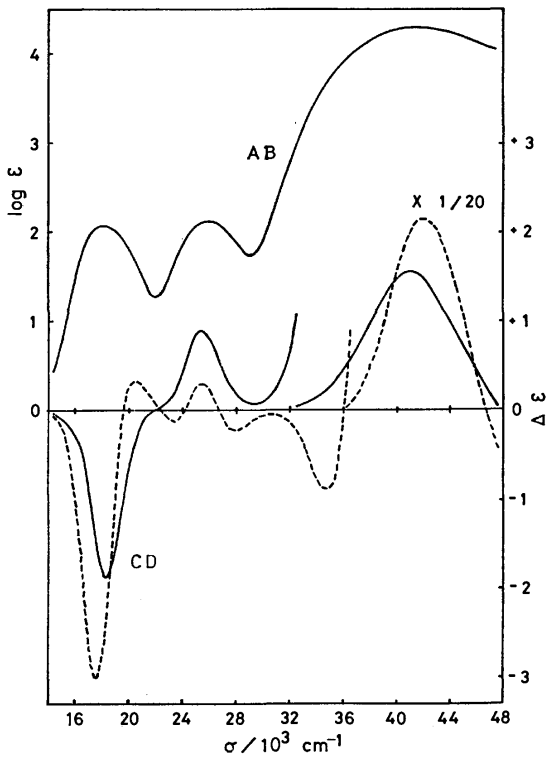

Fig. 5. Absorption and CD spectra of *Δ-sym*-[Co(*S,S*-epro)(L)]: L; *R*(*N*)-sar (——) and *S*(*N*)-sar (----).

indicating the trans(O) structure.[1,6,7,11,18,19] The CD spectra of the en, tn, and ox complexes show the negative major band in the first absorption band region (Table 3). These absorption and CD spectral behaviors suggest that the en, tn and ox complexes commonly take *Δ* configuration.[4,19-21] From these results, the en, tn, and ox complexes isolated can be assigned to the *Δ-sym* configuration.

Of three possible isomers, *Δ-sym*, *Δ-unsym-mer*, and *Δ-unsym-fac*, for [Co(*S,S*-epro)(amino carboxylato)], only one isomer was selectively isolated for each of

TABLE 3. CD DATA OF Δ-*sym*-[Co(*S*,*S*-epro)(L)] TYPE COMPLEXES

Complex (L)	First band region	Second band region	Charge transfer band region
[Co(*S*,*S*-epro)(Cl)(OH)]$^-$	17.06 (−3.38)	23.58 (−0.29)	38.46 (+14.6 sh)
	21.19 (+0.02)	25.64 (+0.13)	45.25 (+24.89)
		27.93 (−0.14)	
[Co(*S*,*S*-epro)(ox)]$^-$	17.48 (−2.76)	23.47 (−0.15)	42.74 (−34.67)
	20.49 (+0.17)	25.64 (+0.15)	
		27.78 (−0.13)	
[Co(*S*,*S*-epro)(en)]$^+$	17.92 (−3.57)	24.27 (−0.19)	42.74 (+38.21)
		26.60 (+0.19)	
		29.07 (−0.12)	
Co(*S*,*S*-epro)(tn)]$^+$	18.41 (−2.12)	26.32 (+0.32)	34.25 (−0.22)
	21.37 (+0.21)		42.19 (+34.89)
[Co(*S*,*S*-epro)(gly)]	17.85 (−1.76)	23.47 (−0.01)	42.19 (+41.67)
	21.01 (+0.18)	25.77 (+0.29)	
		28.74 (−0.07)	
[Co(*S*,*S*-epro)(*R*-ala)]	17.92 (−1.64)	25.77 (+0.33)	42.02 (+36.45)
	20.92 (+0.35)	28.74 (−0.06)	
[Co(*S*,*S*-epro)(*S*-ala)]	17.85 (−2.12)	23.64 (−0.04)	42.37 (+39.03)
	21.74 (+0.02)	26.04 (+0.26)	
		28.74 (−0.10)	
[Co(*S*,*S*-epro)(*R*-val)]	17.85 (−1.30)	25.77 (+0.43)	42.02 (+33.38)
	20.75 (+0.50)	28.90 (−0.04)	
[Co(*S*,*S*-epro)(*S*-val)]	17.85 (−2.52)	23.81 (−0.09)	42.74 (+36.36)
		25.91 (+0.25)	
		28.57 (−0.11)	
[Co(*S*,*S*-epro)(*R*(*N*)-sar)]	18.38 (−1.90)	25.45 (+0.89)	40.98 (+31.45)
[Co(*S*,*S*-epro)(*S*(*N*)-sar)]	17.61 (−3.02)	23.36 (−0.13)	34.97 (−0.88)
	20.49 (+0.34)	25.38 (+0.30)	42.02 (+42.23)
		27.93 (−0.23)	
[Co(*S*,*S*-epro)(*R*(*N*)-*N*-et-gly)]	18.38 (−2.02)	25.32 (+1.06)	40.32 (+28.21)
[Co(*S*,*S*-epro)(*S*(*N*)-*N*-et-gly)]	17.54 (−3.06)	23.26 (−0.12)	34.84 (−0.96)
	20.24 (+0.48)	25.32 (+0.30)	42.02 (+41.00)
		27.78 (−0.26)	
[Co(*S*,*S*-epro)(*R*-pipec)]	18.18 (−3.82)	25.13 (+1.26)	40.00 (+25.33)
[Co(*S*,*S*-epro)(*S*-pipec)]	17.57 (−3.20)	23.09 (−0.01)	41.67 (+38.14)
	20.28 (+0.59)	25.25 (+0.55)	
		27.93 (−0.18)	
[Co(*S*,*S*-epro)(*R*-pro)]	18.25 (−0.89)	25.51 (+0.76)	40.98 (+27.78)
[Co(*S*,*S*-epro)(*S*-pro)]	17.61 (−2.84)	23.47 (−0.13)	42.02 (+42.02)
	20.49 (+0.45)	25.58 (+0.22)	
		28.09 (−0.24)	

Wave numbers and $\Delta\varepsilon$ values (in parentheses) are given in 10^3 cm^{-1} and mol^{-1} dm^3 cm^{-1}, respectively. sh denotes a shoulder.

the seven amino carboxylato complexes (Table 1). These isomers commonly show the broad first absorption band (Figs. 3—5 and Table 2). This absorption spectral pattern points out that the isomers are mer form, namely, Δ-*sym* and Δ-*unsym-mer*.[11,18] Furthermore, all the isomers exhibit a negative major CD band in the first absorption band region (Figs. 3—5 and Table 3). These facts suggest that the complexes isolated are only the Δ-*sym* configuration.[22]

The selective formation for the Δ-*sym* configuration was also observed for the [Co(*S*,*S*-epro)(L)] complexes (L: $(H_2O)_2$, CO_3, and $(Cl)(H_2O)$).[20] Molecular models reveal that the backbone ethylenediamine ring of the *S*,*S*-epro ligand takes a gauche form for the Δ-symmetric coordination, and an envelope form for the Δ-unsymmetric case. These results mean that the Δ-symmetric preference of the *S*,*S*-epro complexes depends mainly on the more stable conformation of the backbone ethylenediamine ring.[23]

^{1}H NMR and CD Spectra. When the *N*-alkyl substituted amino or cyclic imino carboxylate ligand coordinates to the cobalt(III) ion, the nitrogen atom of the ligand becomes chiral, *R*(*N*) or *S*(*N*). Accordingly, two additional isomers, *R*(*N*) or *S*(*N*), are possible for each of the Δ-*sym*-[Co(*S*,*S*-epro)(am)] complexes (am: sar, *N*-et-gly, *R*- or *S*-pro, and *R*- or *S*-pipec).

In the ^{1}H NMR spectra of the Δ-*sym*-[Co(*S*,*S*-epro)-

(am)] complexes, the resonance lines due to the *N*-bonded protons of the needle crystalline isomers appear at lower field than those of the prismatic crystalline ones (Fig. 6). The asymmetric nitrogen atom of the coordinated (*S*)-prolinate ligand is fixed to the *S*(*N*) configuration and that of the (*R*)-prolinate one is fixed to the *R*(*N*) one.[24] The *N*-bonded protons of the *S*(*N*) isomer for the *Δ-sym*-[Co(*S,S*-epro)(*S*-pro)] complex lies above the carbonyl group of the *S,S*-epro ligand (Fig. 7a-2), while that of the *R*(*N*) one lies in the plane involving the other carbonyl group of the ligand (Fig. 7a-1). In the region of the *N*-bonded protons, the resonance line of the *S*-pro complex (at 6.17 ppm) is observed at higher field than that of the *R*-pro one (at 6.40 ppm).[25] The *N*-bonded protons of the *R*(*N*) isomer of the sar, *N*-et-gly, or pipec complex are similar in environment to that of the (*R*)-prolinate, and those of the *S*(*N*) one to that

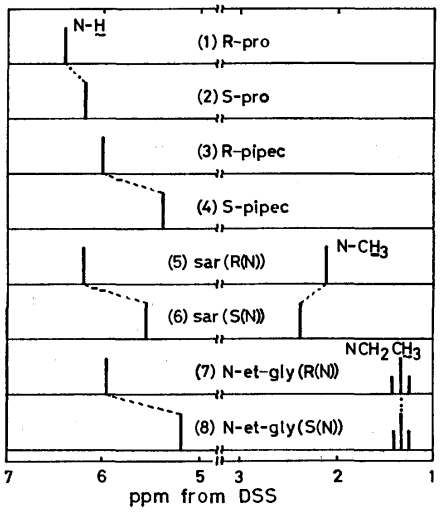

Fig. 6. The distribution of the chemical shifts due to the *N*-bonded and *N*-alkyl protons of *Δ-sym*-[Co(*S,S*-epro)(am)]. (1), (2), (7), and (8) were recorded in $DClO_4$–CD_3OD, (3) and (4) in $(CD_3)_2SO$–DCl, and (5) and (6) in D_2O–$DClO_4$.

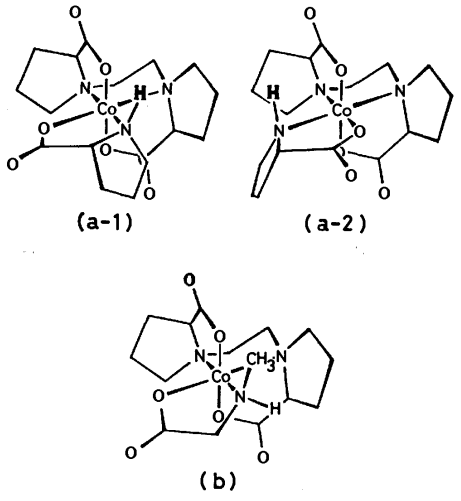

Fig. 7. Probable chiral configurations of the prolinate and sarconsinate ions in *Δ-sym*-[Co(*S,S*-epro)(L)]: L; (a-1) *R*-pro, (a-2) *S*-pro, and (b) *S*(*N*)-sar.

of the (*S*)-prolinate. Accordingly, it is suggested for the *Δ-sym*-[Co(*S,S*-epro)(am)] complexes that the needle crystalline isomers showing the signal at the lower field are the *R*(*N*) configuration and the prismatic crystalline ones at the upper field the *S*(*N*) one. Contrary to the case of the *N*-bonded protons, the resonance lines of the methyl group for the *R*(*N*) isomer of the *Δ-sym*-[Co(*S,S*-epro)(sar)] complex are observed at higher field than that of the *S*(*N*) one. This observation is also explained on the basis of the difference of the magnetic and steric environments of the methyl group.[25] Namely, the methyl group of the *R*(*N*) isomer lies above the carbonyl group of the *S,S*-epro ligand, whereas that of the *S*(*N*) one lies in the plane involving the other carbonyl group of the ligand (Fig. 7b).

In order to estimate the CD contribution of the asymmetric nitrogen atoms in the *Δ-sym*-[Co(*S,S*-epro)-(am)] complexes, the vicinal CD curves are calculated in the same manner as that for the cobalt(III) complexes with the *S,S*-tmpro ligand (Figs. 8 and 9).[16] The vicinal CD curves for the needle crystalline isomers for the sar, *N*-et-gly, and *R*-pipec complexes are similar to that of the *R*-pro complex and the curves of the prismatic ones for the sar, *N*-et-gly, and *S*-pipec complexes are similar to that of the *S*-pro one. Furthermore, the curves for the *R*-pro and *S*-pro complexes show an antipodal relationship in the first absorption band region (Figs. 8 and 9). These results also support the conclusion that the asymmetric nitrogen atoms of the needle and prismatic crystalline isomers take the *R*(*N*) and *S*(*N*) configurations, respectively.

Mutarotation and Equilibrium Distribution. The *R*-(*N*) and *S*(*N*) isomers of the *Δ-sym*-[Co(*S,S*-epro)(sar)] complex show a change of the CD spectra with time in methanol at ambient temperature (23.5 °C), as shown in Fig. 10. When either of the isomers was used as a starting substance, the identical CD curve with two distinct isodichroic points at 512 and 570

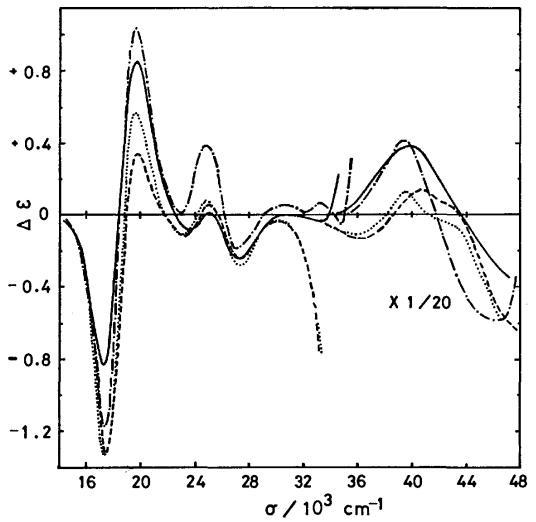

Fig. 8. Calculated vicinal CD curves due to the nitrogen atom of the bidentate ligand in *Δ-sym*-[Co(*S,S*-epro)(am)]: am; *S*(*N*)-sar (----), *S*(*N*)-*N*-et-gly (·····), *S*-pro (——), and *S*-pipec (—·—).

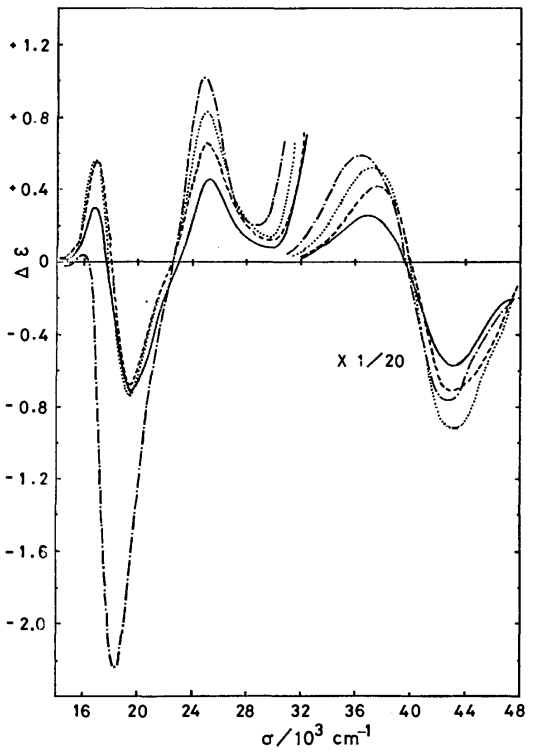

Fig. 9. Calculated vicinal CD curves due to the nitrogen atom of the bidentate ligand in *Δ-sym*-[Co(*S,S*-epro)(am)]: am; *R*(*N*)-sar (----), *R*(*N*)-*N*-et-gly (·····), *R*-pro (——), and *R*-pipec (—·—).

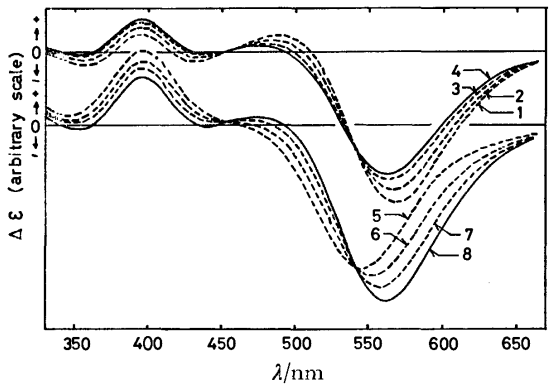

Fig. 10. Change of the CD spectra with time for the *S*(*N*)-sar (upper) and *R*(*N*)-sar (lower) isomers of *Δ-sym*-[Co(*S,S*-epro)(sar)] in methanol at 23.5 °C. The curves 1—4 were measured at 0, 465, 1265, and 3200 min, respectively, and the curves 5—8 at 0, 495, 1295, and 3300 min, respectively.

nm was obtained at equilibrium. No change was noticed with time in the absorption spectra for the two isomers; this fact indicates that mutarotation took place for the two isomers of the sar complex. Similar behavior was also observed for the *R*(*N*) and *S*(*N*) isomers of the *Δ-sym*-[Co(*S,S*-epro)(*N*-et-gly)] complex with two isodichroic points at 516 and 580 nm. These CD spectral characteristics show that epimerization takes place for these isomers at the asymmetric nitrogen atoms as follows:

$$R(N) \underset{k_{SR}}{\overset{k_{RS}}{\rightleftharpoons}} S(N),$$

where k_{RS} and k_{SR} denote the rate constants for the epimerization of the *R*(*N*) isomer to the *S*(*N*) one and of the *S*(*N*) isomer to the *R*(*N*) one, respectively.

The equilibrium constant, K_{eq}, for the epimerization reaction was determined by the CD spectral measurements to be 1.43±0.01 for the sar complex and 1.47±0.01 for the *N*-et-gly one. From these results, the free energy difference, $-\Delta G°$, between the *R*(*N*) and *S*(*N*) isomers could be estimated to be 0.88±0.02 kJ mol^{-1} for the sar complex and 0.95±0.02 kJ mol^{-1} for the *N*-et-gly one, respectively.

The rate constants for the epimerization are calculated from the equilibrium constant and the observed rate constant, k_{obsd}.

$$k_{obsd} = k_{RS} + k_{SR},$$
$$K_{eq} = k_{RS}/k_{SR}.$$

The k_{obsd} was obtained, using each of the two isomers as a starting substance, by the first-order kinetic study:

$$\ln X_e/(X_e - X_t) = k_{obsd} \cdot t,$$

where X_t and X_e stand for concentrations of the isomerized species at any time, *t*, and at equilibrium respectively. The values of k_{RS} and k_{SR}, therefore, were $(1.58\pm0.54)\times10^{-5}$ s^{-1} and $(1.11\pm0.39)\times10^{-5}$ s^{-1} for the sar complex, and $(0.96\pm0.45)\times10^{-5}$ s^{-1} and $(0.65\pm0.31)\times10^{-5}$ s^{-1} for the *N*-et-gly one, respectively.

Both the equilibrium and the kinetic results of the sar complex are in fair agreement with those of the *N*-et-gly one. This fact suggests that the thermodynamics and mechanisms of the isomerization process are little influenced by the size of the *N*-alkyl group on the asymmetric nitrogen atom. The $-\Delta G°$ value of *ca.* 0.9 kJ mol^{-1} for the sar and *N*-et-gly complexes is consistent with that of 1.72 kJ mol^{-1} for the *trans, cis*(*RR*) and *trans,cis*(*SS*) isomers of dichlorobis((*S*)-2-(methylaminomethyl)pyrrolidine)cobalt(III),[26] having two asymmetric nitrogen atoms.

It is interesting to point out from the equilibrium constant value (*ca.* 1.45) that the *N*-alkyl group prefers the *S*(*N*) configuration to the *R*(*N*) one. Inspection of models for the *R*(*N*) and *S*(*N*) isomers of the sar and *N*-et-gly complexes reveal that the *N*-alkyl groups of the *R*(*N*) isomer are in more close proximity to the quadridentate moiety than that of the *S*(*N*) one. It is inferred, therefore, that the preference of the *S*(*N*) configuration over the *R*(*N*) one can be related to an interligand interactions between the *N*-alkyl group and the *S,S*-epro ligand.

Steric Interaction. It was reported that the coordinated *R*- or *S*-pipec have an intrinsic tendency for the stereoselective coordination and take the *S*(*N*), *R*(*C*) and *R*(*N*),*S*(*C*) configurations, respectively.[16,27,28] In the *Δ-sym*-[Co(*S,S*-epro)(pipec)] complex, however, the *R*-pipec takes the *R*(*N*),*R*(*C*) configuration and the, *S*-pipec takes the *S*(*N*),*S*(*C*) one. This selective coordination can be explained in terms of the interligand interaction between the piperidine ring of the pipecolate and the pyrrolidine ring of the *S,S*-epro ligand. Namely, an inspection of the models suggests that the order of the interligand crowd for the possible isomers of the *Δ-sym*-[Co(*S,S*-epro)(*R*- or *S*-pipec)] complex is *S*(*N*),*R*(*C*)>*R*(*N*),*S*(*C*)>*S*(*N*),*S*(*C*)>*R*(*N*),*R*(*C*). This

consideration is supported by X-ray analysis results which show that the *Δ-sym*-[Co(*S*,*S*-epro)(*R*-pipec)], which is the major product, takes the *R*(*N*),*R*(*C*) configuration.[29]

References

1) J. I. Legg and D. W. Cooke, *Inorg. Chem.*, **4**, 1576 (1965).
2) J. I. Legg, D. W. Cooke, and B. E. Douglas, *Inorg. Chem.*, **6**, 700 (1967).
3) J. I. Legg and B. E. Douglas, *Inorg. Chem.*, **7**, 1452 (1968).
4) C. W. Van Saun and B. E. Douglas, *Inorg. Chem.*, **8**, 115 (1969).
5) P. F. Coleman, J. I. Legg, and J. Steele, *Inorg. Chem.*, **9**, 937 (1970).
6) K. Kuroda and K. Watanabe, *Bull. Chem. Soc. Jpn.*, **44**, 1034 (1971).
7) K. Kuroda, *Bull. Chem. Soc. Jpn.*, **45**, 2176 (1972).
8) W. E. Keyes and J. I. Legg, *J. Am. Chem. Soc.*, **98**, 4970 (1976).
9) P. J. Garnett, D. W. Watts, and J. I. Legg, *Inorg. Chem.*, **8**, 2534 (1969).
10) K. Kuroda and F. Mohri, *Chem. Lett.*, **1972**, 719.
11) K. Kuroda, *Chem. Lett.*, **1974**, 17.
12) P. J. Garnett and D. W. Watts, *Inorg. Chim. Acta*, **8**, 293 (1974).
13) L. J. Halloran and J. I. Legg, *Inorg. Chem.*, **13**, 2193 (1974).
14) J. A. Weyh, *Inorg. Chem.*, **16**, 2968 (1977).
15) L. N. Schenberg, D. W. Cooke, and C. F. Liu, *Inorg. Chem.*, **7**, 2386 (1968).
16) M. Okabayashi, K. Okamoto, and J. Hidaka, *Bull. Chem. Soc. Jpn.*, **53**, 2257 (1980).
17) J. C. Bailar, Jr., *Inorg. Synth.*, **2**, 222 (1946).
18) N. Matsuoka, J. Hidaka, and Y. Shimura, *Bull. Chem. Soc. Jpn.*, **40**, 1868 (1967).
19) N. Matsuoka, J. Hidaka, and Y. Shimura, *Bull. Chem. Soc. Jpn.*, **45**, 2491 (1972).
20) a) T. C. Woon and M. J. O'Connor, *Aust. J. Chem.*, **32**, 1661 (1979); b) T. C. Woon, M. F. Mackay, and M. J. O'Connor, *Acta Crystallogr., Sect. B*, **36**, 2033 (1980).
21) N. Matsuoka, J. Hidaka, and Y. Shimura, *Inorg. Chem.*, **9**, 719 (1970).
22) M. Okabayashi, K. Igi, and J. Hidaka, *Bull. Chem. Soc. Jpn.*, **52**, 753 (1979).
23) C. J. Hawkins, "Absolute Configuration of Metal Complexes", Interscience Publishers, Inc., New York (1971).
24) K. Okamoto, J. Hidaka, and Y. Shimura, *Bull. Chem. Soc. Jpn.*, **46**, 475 (1973).
25) L. R. Froebe, S. Yamada, J. Hidaka, and B. E. Douglas, *J. Coord. Chem.*, **1**, 183 (1971).
26) T. Kitamura, Y. Sato, M. Saburi, and S. Yoshikawa, *Bull. Chem. Soc. Jpn.*, **50**, 1780 (1977).
27) M. Saburi and S. Yoshikawa, *Inorg. Chem.*, **7**, 1890 (1968).
28) M. Saburi, M. Homma, and S. Yoshikawa, *Inorg. Chem.*, **8**, 367 (1969).
29) K. Okamoto, M. Okabayashi, M. Ohmasa, H. Einaga, and J. Hidaka, *Chem. Lett.*, **1981**, 725.

 © 1983 The Chemical Society of Japan Bull. Chem. Soc. Jpn., 56, 165—170 (1983)

Preparation and Some Properties of Cobalt(III) Complexes with D-Penicillaminate and Its Derivatives

Ken-ichi Okamoto,* Katsuhiko Wakayama,† Hisahiko Einaga,††
Shoichi Yamada,††† and Jinsai Hidaka
Department of Chemistry, University of Tsukuba, Ibaraki 305
(Received July 15, 1982)

Three kinds of [Co(terdentate-*N,O,S*)$_2$] type complexes were newly prepared; here terdentate-*N,O,S* denotes D-penicillaminate (D-pen), *S*-methyl-D-penicillaminate (D-smp) and *S*-methyl-L-cysteinate (L-smc). Each of the D-smp and L-smc complexes was chromatographically separated into three possible isomers; the D-pen complex was separated into two isomers. These isomers were characterized from their electronic absorption, CD and ^{1}H NMR spectra. Two isomers isolated for [Co(D-pen)$_2$]$^-$ were assigned to *trans(N)* and *trans(O)*, respectively, on the basis of the spectral behavior of the sulfur-to-metal charge transfer band and the reaction with dimethyl sulfate. Three isomers for [Co(D-smp)$_2$]$^+$ were derived from each of two isomers for [Co(D-pen)$_2$]$^-$ by the reaction with dimethyl sulfate. The electronic absorption and CD spectral behaviors are discussed in relation to the comparison of the thioether and thiolato type complexes.

Some cobalt(III) complexes with the thioether type terdentate-*N,O,S* ligands such as L-methionine and *S*-methyl-L-cysteine have been reported,[1-3] and the electronic absorption and CD spectral properties of the thioether type sulfur atom which takes *R* or *S* configuration by coordination have been investigated.[4,5] The contributions of the coordinated thiolato type sulfur atom to the electronic absorption and CD spectra would be interesting in comparison with those of the thioether type sulfur atom; but the electronic absorption and CD spectral behaviors have been little known.[6]

In the present paper, the cobalt(III) complexes with the thioether or thiolato type terdentate-*N,O,S* ligands, [Co(L-smc)$_2$]$^+$, [Co(D-smp)$_2$]$^+$ and [Co(D-pen)$_2$]$^-$, were prepared for the first time and their isomers were chromatographically separated. The three isomers for each of the L-smc and D-smp complexes are characterized from their electronic absorption spectra in comparison with the bis(L-methioninato)cobalt(III) complex, [Co(L-met)$_2$]$^+$.[1] The absolute configurations of the coordinated sulfur atoms for the L-smc and D-smp complexes are suggested on the basis of the ^{1}H NMR spectra. The two isomers for the [Co(D-pen)$_2$]$^-$ complex are assigned on the basis of the spectral behavior of their sulfur-to-metal charge transfer bands and the formation ratios of the D-smp isomers obtained by the reaction with dimethyl sulfate. The electronic absorption and CD spectra are mainly discussed in relation to the comparison of the thioether and thiolato type complexes. A preliminary report has been presented for the [Co(L-smc)$_2$]$^+$ complex.[7]

Experimental

1) Bis(S-methyl-L-cysteinato)cobalt(III) Perchlorate: [*Co(L-smc)$_2$]ClO$_4$*. Three isomers of [Co(L-smc)$_2$]$^+$ were isolated by a procedure similar to that used for those of [Co(L-met)$_2$]$^+$.[1] A solution containing 2.7 g of cobalt(II) chloride hexahydrate in 10 cm^3 of water was added to a hot solution (*ca.* 70 °C) containing *S*-methyl-L-cysteine (3.0 g) in 50 cm^3 of water, and to the mixture 0.5 g of activated charcoal was added. Eight grams of lead dioxide were gradually added to the mixture, which was mechanically stirred at *ca.* 70 °C for 20 min. After cooling to room temperature, the reaction mixture was filtered to remove the activated charcoal and any excess of lead dioxide. A saturated aqueous solution of sodium sulfate (1.5 g) was added to the filtrate and the lead sulfate precipitated was filtered off. The filtrate was poured onto a column of Dowex 50W-X8 (200—400 mesh, H$^+$ form). After the column had been swept with water, two eluates, violet (A-1) and red (A-2), were obtained by eluting with a 0.3 mol dm^{-3} aqueous solution of sodium perchlorate. Another eluate, blue-violet (A-3), was obtained quickly from the remaining adsorbed band by eluting with 0.5 mol dm^{-3} aqueous solution of sodium perchlorate, though the A-3 could be eluted with 0.3 mol dm^{-3} aqueous solution of sodium perchlorate. It was found, from the absorption and CD spectral measurements, that A-1, A-2, and A-3 were *trans(S)*, *trans(O)*, and *trans(N)* isomers, respectively. These eluates were separately concentrated to a small volume with a rotary evaporator at 30 °C and then the deposited sodium perchlorate was filtered off. To each of the filtrates was added a large amount of ethanol. The crude isomers from A-1 and A-3 were recrystallized from as little water as possible by cooling in an ice bath after adding an appropriate amount of ethanol. The isomer from A-2 was less soluble than the other two and was recrystallized from as little warm water (*ca.* 30 °C) as possible by cooling in an ice bath. The pure isomers were washed with ethanol and ether, and then dried in a vacuum desiccator over sulfuric acid. Found for *trans(S)* isomer (A-1): C, 21.70; H, 4.03; N, 6.32%. Found for *trans(O)* isomer (A-2): C, 21.50; H, 4.13; N, 6.08%. Found for *trans(N)* isomer (A-3): C, 21.33; H, 3.99; N, 6.17%. Calcd for [Co(L-smc)$_2$]ClO$_4$·H$_2$O=CoC$_8$H$_{16}$N$_2$O$_8$S$_2$Cl·H$_2$O: C, 21.70; H, 4.09; N, 6.32%.

2) Bis(S-methyl-D-penicillaminato)cobalt(III) Bromide: [*Co(D-smp)$_2$]Br*. This complex was prepared by the reaction of bis(D-penicillaminato)cobalt(III) complex (*vide infra*) with dimethyl sulfate. About 10 cm^3 of dimethyl sulfate was added drop by drop to a solution containing 1 g of the brown isomer of [Co(D-pen)$_2$]$^-$ in 10 cm^3 of water and the mixture was mechanically stirred for a few minutes. When the mixture had been allowed to stand at room temperature for a while, it was separated into two layers, a brown (upper) layer and a cloudy colorless (lower) layer. The former changed gradually to reddish violet. After being allowed

† Present address: TDK Electronic Co., Ltd., 2-14-6, Uchikanda, Chiyoda-ku, Tokyo 101.
†† Present address: Institute of Materials Science, University of Tsukuba, Sakura, Ibaraki 305.
††† Present address: Department of Chemistry, Okayama University of Science, 1-1, Ridai-cho, Okayama 700.

to stand at room temperature for about 6 h, the reddish violet solution was separated and poured onto a column (3.5 cm×30 cm) of Dowex 50W-X8 (200—400 mesh, NH_4^+ form). After the column had been swept with water, the adsorbed reddish violet band was eluted with a 0.05 mol dm^{-3} aqueous solution of ammonium bromide. Three bands, dark red (B-1), reddish violet (B-2), and red (B-3), were progressively eluted in this order. Their absorption spectral measurements showed that B-1, B-2, and B-3 were *trans*-(*O*), *trans*(*N*), and *trans*(*S*) isomers, respectively. The eluates were separately concentrated with a rotary evaporator below 20 °C. The ammonium bromide deposited was filtered off and a small amount of acetone was added to the filtrate. The three isomers obtained were recrystallized from as little water as possible by adding acetone. The isomers were washed with ethanol, acetone and ether, and then dried in a vacuum desiccator over calcium chloride. Found for *trans*(*O*) isomer (B-1): C, 31.11; H, 5.25; N, 6.07%. Found for *trans*(*N*) isomer (B-2): C, 30.25; H, 5.29; N, 6.05%. Calcd for $[Co(D\text{-smp})_2]Br=CoC_{12}H_{24}N_2O_4S_2Br$: C, 31.11; H, 5.25; N, 6.05%. Found for *trans*(*S*) isomer (B-3): C, 28.23; H, 5.66; N, 5.59%. Calcd for $[Co(D\text{-smp})_2]Br\cdot 2H_2O$: C, 28.26; H, 5.61; N, 5.65%.

Similarly, the green isomer of $[Co(D\text{-pen})_2]^-$ gave three isomers of $[Co(D\text{-smp})_2]^+$ by the reaction with dimethyl sulfate. However, the formation ratio of the three D-smp isomers derived from the green isomer of $[Co(D\text{-pen})_2]^-$ differs from that of the three isomers from the brown isomer of $[Co(D\text{-pen})_2]^-$; *trans*(*O*):*trans*(*N*):*trans*(*S*)=20:65:15 for the D-smp isomers derived from the brown isomer and 69:18:13 from the green isomer. It seems that the difference in formation ratio reflects the geometrical configuration of $[Co(D\text{-pen})_2]^-$ which is the starting complex.

3) Potassium Bis(D-penicillaminato)cobaltate(III): *K[Co(D-pen)$_2$]*. *Method A*: To a solution containing 1.6 g of cobalt(II) chloride hexahydrate in 10 cm^3 of water was added 2.0 g of D-penicillamine. After the mixture was stirred for a few minutes, the pH was adjusted to *ca.* 7 by the addition of 3.0 mol dm^{-3} aqueous solution of potassium hydroxide. The color of the solution changed from red to brown. After the reaction mixture had been allowed to stand at room temperature for about 6 h, a small amount of acetone was added to it. Then it was kept in a refrigerator overnight. Brown needle crystals (C-1) deposited. These crystals were collected by filtration, washed with ethanol and ether, and then dried in a vacuum desiccator over calcium chloride. Found for brown isomer (C-1): C, 27.18; H, 5.19; N, 6.48%. Calcd for $K[Co(D\text{-pen})_2]\cdot 2H_2O=KCoC_{10}H_{18}N_2O_4S_2\cdot 2H_2O$: C, 27.99; H, 5.19; N, 6.53%.

The filtrate was poured onto a column (3.5 cm×30 cm) of Dowex 1-X8 (100—200 mesh, Cl^- form) in order to see the formation of the other isomers of $[Co(D\text{-pen})_2]^-$. After the column had been swept with water, the adsorbed brown band was eluted with a 0.07 mol dm^{-3} aqueous solution of potassium chloride. The eluate of a broad band was collected in 10 cm^3 portions in a fraction collector. The absorption and CD spectral measurements indicated that the eluate contained two kinds of complexes. The earlier fractions contained a complex which did not have the sulfur-to-metal charge transfer band (*ca.* 33.0×10^3 cm^{-1})[1,2] and the later fractions showed the same spectra as that of the brown crystalline complex isolated before.

Method B: A hot solution (*ca.* 60 °C) containing 1 g of $[Co(NH_3)_6]Cl_3$[8] in 30 cm^3 of water was adjusted to pH 7 with 3.0 mol dm^{-3} aqueous solution of sodium hydroxide. To this solution were added 2 g of D-penicillamine and 0.5 g of activated charcoal. The mixture was mechanically stirred at 60 °C for 15 min. The reaction mixture was filtered in order to remove activated charcoal after cooling to room temperature. The filtrate was poured onto a column (4 cm×60 cm) of QAE-Sephadex A-25 (Cl^- form). After the column had been swept with water, the adsorbed brown band was eluted with 0.1 mol dm^{-3} aqueous solution of potassium chloride. Five colored bands: brown (C-1), yellow, red brown, dark green, and green (C-2), were eluted in this order. Of these five eluates, the brown (C-1) and green (C-2) eluates produced the thioether type complexes by the reaction with dimethyl sulfate, but the remaining ones did not. These results and the absorption spectral measurements suggest that the brown and green eluates contained the desired complex and the remaining three did not. The brown (C-1) eluate showed the same absorption and CD spectra as the isomer isolated in Method A. The green (C-2) eluate was concentrated to a small volume with a rotary evaporator below 20 °C and the deposited potassium chloride was filtered off. A small amount of acetone was added to the filtrate. The green complex obtained was recrystallized from a small amount of water by adding acetone. The complex was washed with ethanol and ether, and then dried in a vacuum desiccator over calcium chloride. Found for the green isomer (C-2): C, 20.19; H, 4.07; N, 4.85%. Calcd for $K[Co(D\text{-pen})_2]\cdot 3H_2O\cdot 2KCl$: C, 20.19; H, 4.06; N, 4.71%.

4) Potassium (L-Penicillaminato)(D-penicillaminato)cobaltate(III): *K[Co(L-pen)(D-pen)]*. This complex was prepared by the method of Hodgson *et al.*[9] Found: C, 29.12; H, 4.92; N, 6.84%. Calcd for $K[Co(L\text{-pen})(D\text{-pen})]\cdot H_2O=KCoC_{10}H_{18}N_2O_4S_2\cdot H_2O$: C, 29.26; H, 4.91; N, 6.82%.

Measurements. The electronic absorption spectra were recorded with a JASCO UVIDEC-1 spectrophotometer, and the CD spectra with a JASCO J-20 spectropolarimeter. All measurements were carried out in an aqueous solution at room temperature.

The ^1H NMR spectra were recorded in deuterium oxide on a JEOL JNM-MH-100 or FX-100 NMR spectrometer at the probe temperature. Sodium 2,2-dimethyl-2-silapentane-5-sulfonate (DSS) was used as an internal reference.

Results and Discussion

Structural Assignments. Three geometrical isomers are possible for the present [Co(terdentate-*N*,*O*,*S*)$_2$] type complex. The isomers are designated as *trans*(*S*), *trans*(*O*), and *trans*(*N*) with respect to the coordinated atoms, N, O, and S (Fig. 1). The three isomers were chromatographically isolated for each of $[Co(L\text{-smc})_2]^+$ and $[Co(D\text{-smp})_2]^+$, and only two isomers for $[Co(D\text{-pen})_2]^-$. Their absorption and CD spectra are shown in Figs. 2—6 and are summarized in Tables 1 and 2. Of the three isomers for $[Co(L\text{-smc})_2]^+$, the first eluted

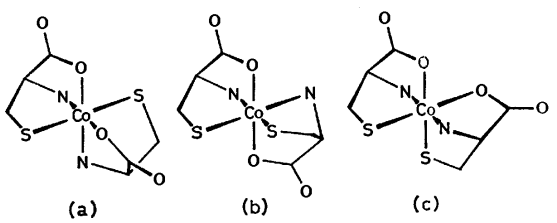

Fig. 1. Three possible isomers of [Co(terdentate-*N*,*O*,*S*)$_2$] type complexes: (a) *trans*(*S*), (b) *trans*(*O*), and (c) *trans*(*N*).

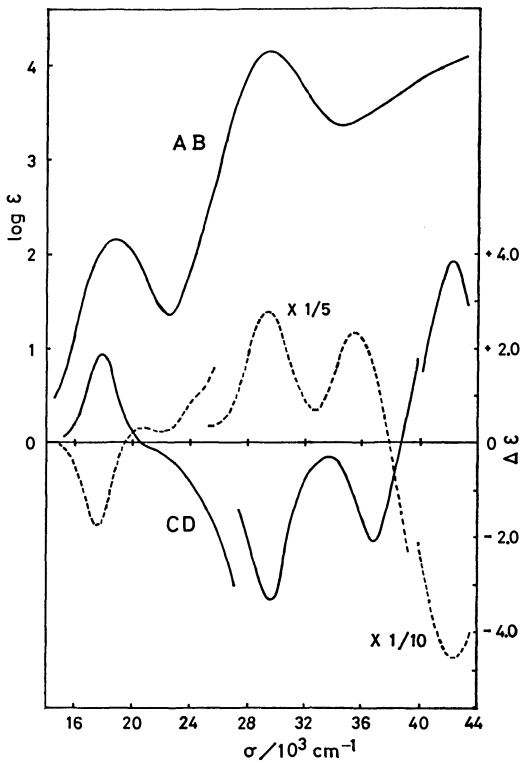

Fig. 2. Absorption and CD spectra of *trans*(*S*)-[Co(L-smc)$_2$]$^+$ (——) and *trans*(*S*)-[Co(D-smp)$_2$]$^+$ (----).

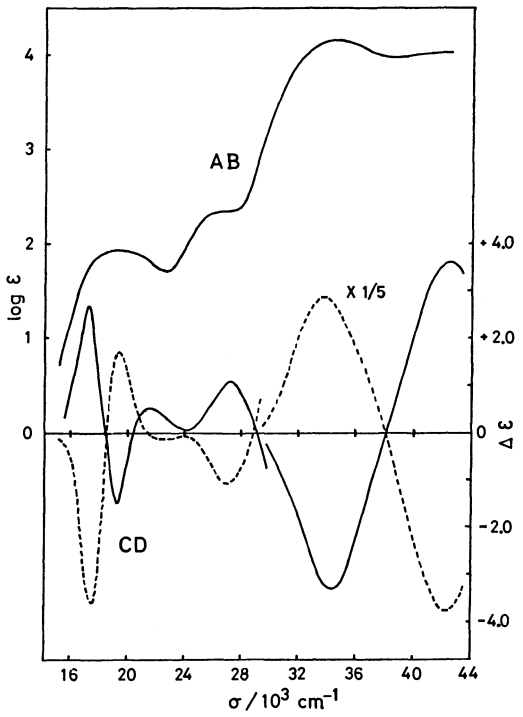

Fig. 3. Absorption and CD spectra of *trans*(*O*)-[Co(L-smc)$_2$]$^+$ (——) and *trans*(*O*)-[Co(D-smp)$_2$]$^+$ (----).

A-1, whose sulfur-to-metal charge transfer band is located at lower energy (29.47×10^3 cm^{-1}) than those of the remaining two isomers (34.47×10^3 cm^{-1} for A-2 and 32.13×10^3 cm^{-1} for A-3),[1,2] was determined to be the *trans*(*S*) isomer by the X-ray crystal structure analysis.[10] The absorption spectra of the isomers for

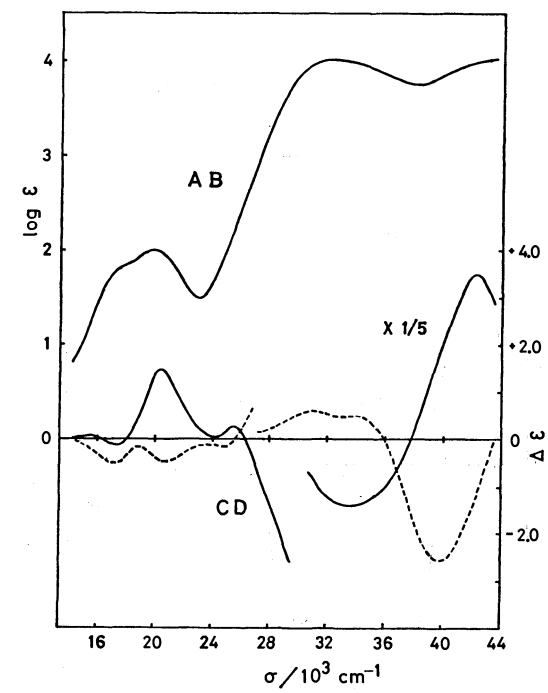

Fig. 4. Absorption and CD spectra of *trans*(*N*)-[Co(L-smc)$_2$]$^+$ (——) and *trans*(*N*)-[Co(D-smp)$_2$]$^+$ (----).

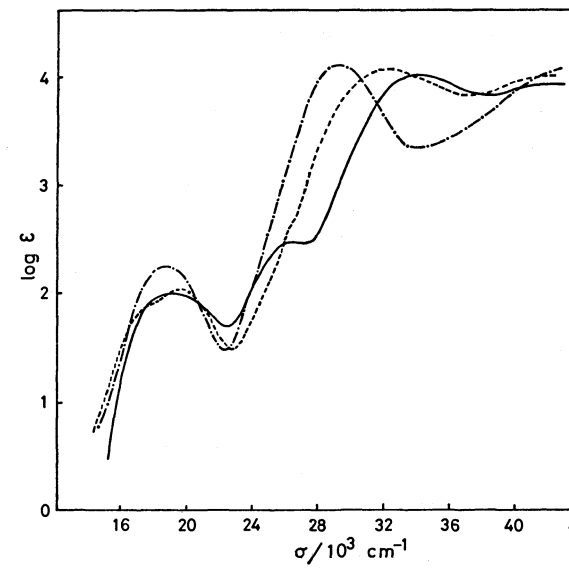

Fig. 5. Absorption spectra for the isomers of [Co(D-smp)$_2$]$^+$: *trans*(*O*) (——), *trans*(*N*) (----), and *trans*(*S*) (—·—).

[Co(L-smc)$_2$]$^+$ correspond quite well with those of the [Co(L-met)$_2$]$^+$ complex,[1] respectively, over the whole region (Figs. 2—4 and Table 1). Accordingly, A-1 can be assigned to *trans*(*S*), A-2 to *trans*(*O*), and A-3 to *trans*(*N*). The same consideration for the absorption spectra of the [Co(L-smc)$_2$]$^+$ isomers is also valid for those of the three isomers, B-1, B-2 and B-3, of [Co(D-smp)$_2$]$^+$ derived from the isomers, C-1 and C-2, of [Co(D-pen)$_2$]$^-$. In the first absorption band region, B-1 shows a broad band with a vague shoulder on the higher energy side, B-2 a band with an explicit shoulder on the lower energy side, and B-3 apparently a sharp band (Fig. 5 and Table 1). These splittings of the first absorp-

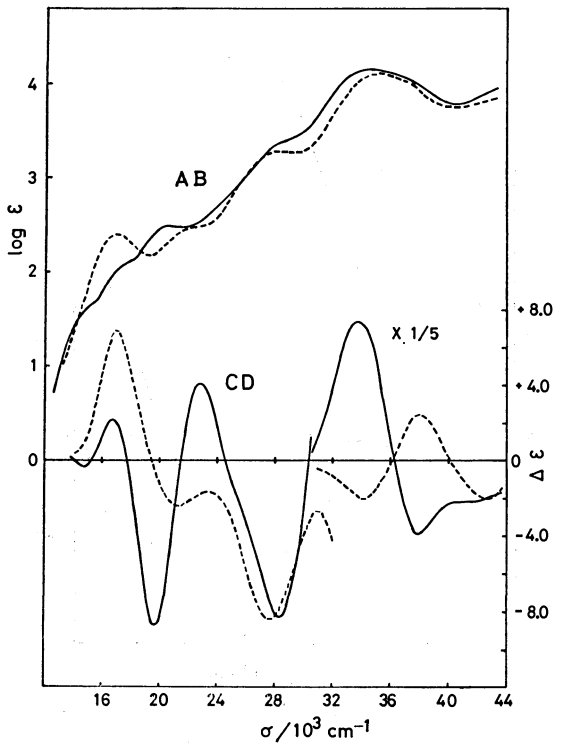

Fig. 6. Absorption and CD spectra of *trans*(*N*)-[Co(D-pen)$_2$]$^-$ (——) and *trans*(*O*)-[Co(D-pen)$_2$]$^-$ (----).

tion bands agree well with those which can be expected from the semiempirical calculation[11] on the basis of the ligand field order $N>S>O$.[2,3] Furthermore, the sulfur-to-metal charge transfer band of B-3 (29.33×10^3 cm^{-1}) locates at lower energy side than those of the remaining two isomers (34.27×10^3 cm^{-1} for B-1 and 32.40×10^3 cm^{-1} for B-2).[1,2] These facts indicate that B-1 is *trans*(*O*), B-2 *trans*(*N*), and B-3 *trans*(*S*).

Of three possible isomers for [Co(D-pen)$_2$]$^-$, only two isomers were obtained, though several preparative methods were attempted. The absorption spectral behavior of [Co(D-pen)$_2$]$^-$, which belongs to [Co(N)$_2$(O)$_2$(S)$_2$] type having two thiolato groups instead of thioether ones, differs from those of [Co(L-smc)$_2$]$^+$ and [Co(D-smp)$_2$]$^+$ (Fig. 6 and Table 1). The notable difference is observed in the region of $(27.0—28.5)\times10^3$ cm^{-1} (*vide infra*).

In the first absorption band region, the splitting for C-1 differs strikingly from that for C-2. Namely, the first absorption band of C-1 is composed of three components (14.1, 17.1 and 20.53×10^3 cm^{-1}) and that of C-2 two components (17.10 and 22.0×10^3 cm^{-1}). However, from the absorption spectral difference in the first absorption band region, it is difficult to distinguish their geometrical structures at present. Recently, it was recognized also for the geometrical isomers having two thiolato donor atoms that the sulfur-to-metal charge transfer band of *trans*(*S*) isomer appears at lower energy than that of *cis*(*S*) one as the case of thioether type complex.[6] The charge transfer bands of the present two isomers are close in maximum position to each other (Fig. 6 and Table 1), specifically, the band of C-1 locates at 33.80×10^3 cm^{-1} and that of C-2 at 34.93×10^3 cm^{-1}. In addition to this fact, *cis*·*cis*·*cis*-[Co(L-pen)(D-pen)]$^-$, which was determined by the X-ray crystal structure analysis,[9] shows the corresponding charge transfer band at 33.77×10^3 cm^{-1}. Taking these facts into consideration, it is probable that the two isomers isolated are *cis*(*S*) rather than *trans*(*S*).

All isomers of the present complexes isomerized in water as was the case of cobalt(III) complexes with terdentate amino carboxylate ligands[12-14] and each isomer generated the mixture of the three isomers after a few days. The isomerization is conspicuous for the isomers of [Co(D-smp)$_2$]$^+$ in comparison with those of [Co(L-smc)$_2$]$^+$ and [Co(L-met)$_2$]$^+$. The three isomers of [Co(D-smp)$_2$]$^+$ were derived from C-1 and from C-2 of [Co(D-pen)$_2$]$^-$. Accordingly, it is probable that the reaction of the coordinated thiolato donor atoms

Table 1. Absorption data of [Co(terdentate-N,O,S)$_2$] type complexes

Complex	First band	Second band	Charge transfer band
trans(*S*)-[Co(L-smc)$_2$]$^+$	18.73 (2.18)		29.47 (4.16)
trans(*O*)-[Co(L-smc)$_2$]$^+$	19.40 (1.93)	26.48 (2.34)	34.47 (4.16)
trans(*N*)-[Co(L-smc)$_2$]$^+$	17.5 (1.81 sh)		32.13 (4.03)
	19.87 (2.01)		
trans(*O*)-[Co(D-smp)$_2$]$^+$	19.20 (1.99)	26.47 (2.46)	34.27 (4.00)
trans(*N*)-[Co(D-smp)$_2$]$^+$	17.5 (1.86 sh)		32.40 (4.06)
	19.73 (2.04)		
trans(*S*)-[Co(D-smp)$_2$]$^+$	18.80 (2.25)		29.33 (4.10)
trans(*N*)-[Co(D-pen)$_2$]$^-$	14.1 (1.44 sh)	28.0 (3.36 sh)	33.80 (4.16)
	17.1 (2.02 sh)		
	20.53 (2.48)		
trans(*O*)-[Co(D-pen)$_2$]$^-$	17.10 (2.38)	28.30 (3.28)	34.93 (4.11)
	22.0 (2.40 sh)		
cis·*cis*·*cis*-[Co(L-pen)(D-pen)]$^-$ [a]	17.27 (2.21)	24.4 (2.85 sh)	33.77 (4.25)
	21.1 (2.41 sh)		

a) Ref. 9. Wave numbers and log ε values (in parentheses) are given in 10^3 cm^{-1} and mol^{-1} dm^3 cm^{-1}, respectively. sh denotes a shoulder.

TABLE 2. CD DATA OF [Co(terdentate-*N*,*O*,*S*)$_2$] TYPE COMPLEXES

Complex	First band region	Second band region	Charge transfer band region
trans(*S*)-[Co(L-smc)$_2$]$^+$	17.87(+1.92)		29.63(−16.5)
			36.80(−11.1)
			42.27(+40.1)
trans(*O*)-[Co(L-smc)$_2$]$^+$	17.23(+2.70)	27.20(+1.08)	34.47(−18.3)
	19.25(−1.44)		42.80(+18.3)
	21.60(+0.57)		
trans(*N*)-[Co(L-smc)$_2$]$^+$	15.47(+0.06)	25.60(+0.23)	33.54(−7.80)
	17.33(−0.11)		42.27(+17.3)
	20.43(+1.44)		
trans(*O*)-[Co(D-smp)$_2$]$^+$	17.40(−3.61)	26.86(−1.07)	33.87(+14.6)
	19.40(+1.71)		42.33(−19.1)
	22.27(−0.12)		
trans(*N*)-[Co(D-smp)$_2$]$^+$	17.17(−0.53)	24.87(−0.14)	31.07(+3.11)
	20.73(−0.48)		33.93(+2.55)
			39.87(−12.9)
trans(*S*)-[Co(D-smp)$_2$]$^+$	17.60(−1.76)		29.47(+14.1)
	20.73(+0.32)		35.60(+11.6)
			42.40(−46.3)
trans(*N*)-[Co(D-pen)$_2$]$^-$	14.83(−0.34)	22.83(+4.17)	33.73(+36.9)
	16.73(+2.24)	28.40(−8.27)	37.93(−19.5)
	19.73(−8.68)		41.00(−10.7)
trans(*O*)-[Co(D-pen)$_2$]$^-$	17.03(+6.96)	27.67(−8.43)	34.13(−10.2)
	21.27(−2.43)		38.03(+12.5)
			42.60(−10.0)

Wave numbers and $\Delta\varepsilon$ values (in parentheses) are given in 10^3 cm^{-1} and mol^{-1} dm^3 cm^{-1}, respectively.

of [Co(D-pen)$_2$]$^-$ with dimethyl sulfate was accompanied by the isomerization. In the preparations, the *trans*(*N*) isomer formed dominantly for the [Co(D-smp)$_2$]$^+$ complex derived from C-1 and the *trans*(*O*) isomer for the complex from C-2, as described in the experimental section. These results suggest that *trans*-(*N*) is preferable for C-1 and *trans*(*O*) for C-2. In addition, considering the fact that the thiolato type ligand prevents the formation of *trans*(*S*) isomer because of the trans effect,[6] it is tentatively assigned that C-1 is *trans*(*N*) and C-2 *trans*(*O*).

^{1}H NMR and CD Spectra. The ^{1}H NMR spectra of *trans*(*S*)-[Co(L-smc)$_2$]$^+$ and -[Co(D-smp)$_2$]$^+$ show a single peak in the *S*-methyl proton region (2.22 ppm for the L-smc isomer and 2.16 ppm for the D-smp one), like that of *trans*(*S*)-[Co(L-met)$_2$]$^+$.[1] In the column chromatographic separation of the *trans*(*S*) isomers, all the fractions of each isomer showed the same CD spectra. The X-ray crystal structure analysis[10] showed that the two coordinated sulfur atoms of *trans*(*S*)-[Co(L-smc)$_2$]$ClO_4 \cdot H_2O$ take the *S*(*S*),*S*(*S*) configuration which has C_2 symmetry. These results suggest that the two sulfur atoms in *trans*(*S*)-[Co(D-smp)$_2$]$^+$ take selectively the *R*(*S*),*R*(*S*) configuration. In contrast with the *trans*(*S*) isomers, the ^{1}H NMR spectra of the *trans*(*N*) and *trans*(*O*) isomers suggest that each of them is a mixture of some configurations of the coordinated sulfur atoms. The *trans*(*N*) isomer shows three signals due to *S*-methyl protons (2.16, 2.09, and 2.00 ppm) for [Co(L-smc)$_2$]$^+$ and two signals (2.12 and 2.04 ppm) for [Co(D-smp)$_2$]$^+$. Inspection of models concerning the crowd of *S*-methyl groups of the ligand coordinated suggests that *trans*(*N*)-[Co(L-smc)$_2$]$^+$ consists of *S*(*S*),-*S*(*S*), and *R*(*S*),*S*(*S*) configurations, and *trans*(*N*)-[Co(D-smp)$_2$]$^+$ of *R*(*S*),*S*(*S*) and *R*(*S*),*R*(*S*) ones. The *trans*(*O*) isomer shows two signals (2.29 and 2.18 ppm) for [Co(L-smc)$_2$]$^+$ and three signals (2.22, 2.18, and 2.12 ppm) for [Co(D-smp)$_2$]$^+$. Similarly, model inspections suggest that *trans*(*O*)-[Co(L-smc)$_2$]$^+$ and -[Co(D-smp)$_2$]$^+$ are a mixture of *S*(*S*),*S*(*S*), *R*(*S*),*S*(*S*), and *R*(*S*),*R*(*S*) configurations, respectively. These ^{1}H NMR spectral behaviors of the *trans*(*N*) and *trans*(*O*) isomers are also similar to that of the corresponding isomers of [Co(L-met)$_2$]$^+$.[1] In the present [Co(terdentate-*N*,*O*,*S*)$_2$] type complex having two thioether groups, it should be noted that only the *trans*(*S*) isomer shows a distinguishable selectivity concerning the orientation of *S*-methyl groups; the reason for this selectivity is unknown at present.

The CD spectra of the [Co(D-smp)$_2$]$^+$ isomers are almost enantiomeric to those of the [Co(L-smc)$_2$]$^+$ ones, respectively, reflecting the similarity of their rigid frameworks (Figs. 2—4 and Table 2). The CD spectral behavior of the [Co(D-pen)$_2$]$^-$ isomers is in contrast to those of the [Co(D-smp)$_2$]$^+$ and [Co(L-smc)$_2$]$^+$ ones (Fig. 6 and Table 2). In the first absorption band region, the *trans*(*O*)-[Co(D-pen)$_2$]$^-$ isomer shows two CD bands corresponding to two absorption components, and the *trans*(*N*) isomer clearly shows three CD bands corresponding to three absorption components. In the sulfur-to-metal charge transfer band region ((33—35) $\times$ 10^3 cm^{-1}), the *trans*(*N*) and *trans*(*O*) iso-

mers show enantiomeric CD patterns. The absorption and CD spectra in the region of $(27—28)\times10^3$ cm^{-1} are noted as a characteristic difference of the thiolato and thioether type complexes. In this region, each of the D-pen isomers shows an extra band (at 28.30×10^3 cm^{-1} for *trans*(*O*) and 28.0×10^3 cm^{-1} for *trans*(*N*)) which does not appear for the spectra of the thioether type complexes, and the CD bands in this region commonly have a negative sign. Similar absorption and CD spectral behaviors were also observed for the three isomers of $[Co(L\text{-pen})(dien)]^+$.[15] These absorption bands seem to be characteristic for the thiol coordination of the pen ligand, and the sign of the CD band in the corresponding region seems to depend on the absolute configuration (*R*(*C*) or *S*(*C*)) of the optically active penicillaminate coordinated.

References

1) J. Hidaka, S. Yamada, and Y. Shimura, *Chem. Lett.*, **1974**, 1487.
2) K. Yamanari, J. Hidaka, and Y. Shimura, *Bull. Chem. Soc. Jpn.*, **50**, 2451, 2643 (1977).
3) T. Isago, K. Igi, and J. Hidaka, *Bull. Chem. Soc. Jpn.*, **52**, 407 (1979).
4) W. G. Jackson and A. M. Sargeson, *Inorg. Chem.*, **17**, 2165 (1978).
5) K. Okamoto, T. Isago, M. Ohmasa, and J. Hidaka, *Bull. Chem. Soc. Jpn.*, **55**, 1077 (1982).
6) K. Yamanari, N. Takeshita, T. Komorita, and Y. Shimura, *Chem. Lett.*, **1981**, 861.
7) J. Hidaka and Y. Shimura, presented at the XVI I.C.C.C., Dublin, Ireland (1974), Paper 1.7a.
8) J. Bjerrum and J. P. McReynolds, *Inorg. Synth.*, **2**, 216 (1946).
9) H. M. Helis, P. de Meester, and D. J. Hodgson, *J. Am. Chem. Soc.*, **99**, 3309 (1977).
10) P. de Meester and D. J. Hodgson, *J. Chem. Soc., Dalton Trans.*, **1976**, 618.
11) H. Yamatera, *Bull. Chem. Soc. Jpn.*, **31**, 95 (1958).
12) M. Watabe, S. Kawaai, and S. Yoshikawa, *Bull. Chem. Soc. Jpn.*, **49**, 1845 (1976).
13) M. Watabe, M. Zama, and S. Yoshikawa, *Bull. Chem. Soc. Jpn.*, **51**, 1354 (1978).
14) M. Watabe, H. Yano, and S. Yoshikawa, *Bull. Chem. Soc. Jpn.*, **52**, 61 (1979).
15) The present authors, to be published.

 © 1983 The Chemical Society of Japan Bull. Chem. Soc. Jpn., 56, 171—174 (1983)

The Reaction of Thio-substituted Cyclopropenium Ions with Sulfonium Methylide

Shinichi INOUE* and Takuya HORI

Department of Applied Chemistry, Aichi Institute of Technology, Yagusa-cho, Toyoda, Aichi 470-03

(Received January 21, 1982)

The reaction between thio-substituted cyclopropenium ions and sulfonium methylides gives unanticipated ketene derivatives. This reaction is supposed to proceed through an intermediate sulfonium salt formed from ylide addition to the cyclopropenyl ring.

Recently, interest has focused on the hetero-atom-substituted three-membered rings because of their highly strained character, and a number of interesting reactions have been reported.[1,2] Among them, a variety of reactions of nitrogen-atom-substituted cyclopropenium compounds were studied.[3] We have recently reported the formation of both cyclopropenimines and *N,N'*-dicyclopropenylidenureas.[4] In reactions of nitrogen-atom-substituted cyclopropenium ions with ylides, ring-opened products were not detected and they were supposed to arise exclusively from the nucleophilic substitution reaction. In this paper, we shall describe the reaction[5] between thio-substituted cyclopropenium ions and sulfonium methylide, and an elucidation of the reaction mechanism.

Results and Discussion

When a mixture of **1a** and **2a** (molar ratio of 1 to 4) in THF was treated at room temperature for 8 h under He atmosphere, bis(ethylthio)ketene (**3a**) was obtained. The structure of **3a** was established from its spectroscopic data as well as its elemental analysis. It was found to be identical with a compound prepared by the reaction of bis(ethylthio)acetyl chloride with triethylamine according to the method[6] for the preparation of bis(alkylthio)ketene. Consequently the structure **3a** is assigned to the product.

While the reaction of **1b** with **2a** in THF give predominantly or exclusively the product **3b**, a small amount of compound **4b** is also produced. The ^{1}H-NMR spectrum of **4b** was found to be identical with that of tetrakis(*t*-butylthio)allene.[7] We, therefore, have investigated the reaction of **1** with **2** under various conditions, because it is known that the allene may arise *via* a cyclopropenylidene intermediate. A compound formed by the reaction between **1e** and **2a** was identified as **4b**. The expected **4a** was not found in the reaction mixture of **1d** and **2c** in THF although ketene **3a** was given. No tetrakis(*p-t*-butylphenylthio)-allene, which would be formed along with the corresponding ketenes from reactions of **1c** and **1f** with **2a**, **2b**, and **2c**, was detected. The equation of the reactions between thio-substituted cyclopropenium ions (**1**) and sulfonium methylide (**2**) can be written as in Scheme 1.

The conditions employed for obtaining **3a** in the preliminary work can be applied to the reactions of other thio-substituted cyclopropenium ions. These results are summarized in Table 1. The generation of **3** from the reaction between thio-substituted cyclopropenium ions and sulfonium methylides showed that the original ylide-carbonyl oxygen remains intact in the ketene. This ketene skeleton seems to be composed of the ylide carbon and the ylide-carbonyl group.

All attempts to produce allenes by the reactions of **1a**, **1e**, **1d**, and **1f** and **2a**—**c** have failed. The ketenes were the only products obtained.

When the reaction of **1a** with **2a** (molar ratio of 1 to 1) was carried out in THF at −5 °C for 8 h under He atmosphere, [[tris(ethylthio)cyclopropenyl](ethoxycarbonyl)methyl]dimethylsulfonium perchlorate (**5a**) was isolated in 7.5% yield, along with **3a**. The structure of **5a** was inferred on the basis of the results of

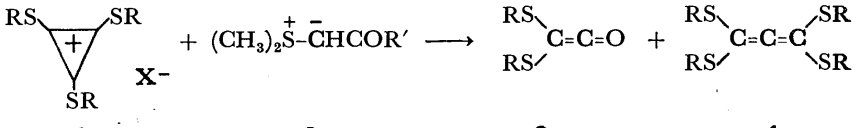

1 **2** **3** **4**

2a: R′=CH_3CH_2O-
2b: R′=C_6H_5-
2c: R′=CH_3CH_2S-

	R	X^-
1a	CH_3CH_2-	ClO_4
1b	$(CH_3)_3C$-	ClO_4
1c	*p*-$(CH_3)_3C$-C_6H_4-	ClO_4
1d	CH_3CH_2-	BF_4
1e	$(CH_3)_3C$-	BF_4
1f	*p*-$(CH_3)_3C$-C_6H_4-	BF_4

3a R=CH_3CH_2-
3b: R=$(CH_3)_3C$-
3c: R=*p*-$(CH_3)_3C$-C_6H_4-

4a: R=CH_3CH_2-
4b: R=$(CH_3)_3C$-
4c: R=*p*-$(CH_3)_3C$-C_6H_4-

Scheme 1. The reaction of thio-substituted cyclopropenium ions with sulfonium methylide.

Table 1. Conditions and yields for reactions of **1a—f** with **2a—c**

Substrate	Reagent	Solvent	Temp	Time/h	Products/%	
1a	**2a**	THF	RT	8	**3a** (61)	
1a	**2b**	THE	RT	8	**3a** (53)	
1b	**2a**	THF	RT	8	**3b** (87)	**4b** (10)
1b	**2b**	THF	RT	8	**3b** (54)	
1c	**2a**	THF	RT	8	**3c** (66)	
1c	**2b**	THF	RT	8	**3c** (61)	
1d	**2a**	THF	RT	6	**3a** (33)	
1d	**2c**	THF	RT	6	**3a** (65)	
1e	**2a**	THF	RT	6	**3b** (40)	**4b** (11)
1e	**2c**	THF	RT	6	**3b** (70)	
1f	**2a**	THF	RT	6	**3c** (56)	
1f	**2c**	THF	RT	6	**3c** (62)	

Table 2. Sulfonium salts

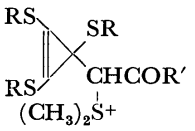

Compd	R	R′	X⁻	Yield %	Mp θ_m/°C	Fomula	Found(%) C	Found(%) H	Calcd(%) C	Calcd(%) H
5a	CH_3CH_2-	CH_3CH_2O-	ClO_4	64	168—170	$C_{15}H_{27}O_6S_4Cl$	38.50	5.82	38.57	5.83
5b	CH_3CH_2-	CH_3CH_2S-	ClO_4	72	190—192	$C_{15}H_{27}O_5S_5Cl$	37.25	5.61	37.29	5.63
5c	$(CH_3)_3C$-	CH_3CH_2O-	ClO_4	45	171—173	$C_{21}H_{39}O_6S_4Cl$	45.68	7.01	45.76	7.13
5d	$(CH_3)_3C$-	CH_3CH_2S-	ClO_4	33	167—169	$C_{21}H_{39}O_5S_5Cl$	44.48	6.89	44.60	6.93
5e	*p*-$(CH_3)_3C$-C_6H_4-	CH_3CH_2O-	ClO_4	57	182—183	$C_{39}H_{51}O_6S_4Cl$	59.98	6.50	60.09	6.60
5g	CH_3CH_2-	CH_3CH_2O-	BF_4	26	163—164	$C_{15}H_{27}O_2S_4BF_4$	39.95	5.94	39.64	5.99
5h	CH_3CH_2-	CH_3CH_2S-	BF_4	59	192—195	$C_{15}H_{27}OS_5BF_4$	38.21	5.75	38.29	5.78
5i	$(CH_3)_3C$-	CH_3CH_2O-	BF_4	27	170—172	$C_{21}H_{39}O_2S_4BF_4$	46.81	7.26	46.83	7.30
5j	$(CH_3)_3C$-	CH_3CH_2S-	BF_4	29	160—162	$C_{21}H_{39}OS_5BF_4$	45.42	6.99	45.47	7.09

the elemental analysis as well as its ^{1}H-NMR spectrum which has a methyl-singlet at δ 3.15 (6H) and ethyl-signals at δ 1.50 (9H, t), 3.05 (4H, q), and 4.18 (2H, q) in addition to signals for ester group at δ 1.35 (3H, t) and 3.40 (2H, q). Under similar conditions, [[tris(*t*-butylthio)cyclopropenyl]-(**5c**) and [[tris(*p*-*t*-butylphenylthio)cyclopropenyl](ethoxycarbonyl)methyl]dimethylsulfonium perchlorates (**5e**) were isolated in 4.8 and 7.3% yields, respectively.

Likewise, **1d** reacts with **2a** and **2c** in THF at 0 °C for 6 h giving [[tris(ethylthio)cyclopropenyl](ethoxycarbonyl)methyl]dimethylsulfonium tetrafluoroborate (**5g**) and [[tris(ethylthio)cyclopropenyl](ethylthiocarbonyl)methyl]dimethylsulfonium tetrafluoroborate (**5h**), respectively.

Thus, an attempt was made to prepare the sulfonium intermediate **5** by the nucleophilic addition reaction. When the reaction of **1a** with **2a** (molar ratio of 1 to 1) was performed in dry THF at −40 °C for 6 h under He atmosphere, the sulfonium salt **5a** was obtained in good yield. Similarly, reactions of **1b—e** with **2a** and **2c** gave the corresponding sulfonium salts, such as [[tris(ethylthio)cyclopropenyl]-(ethylthiocarbonyl)methyl]dimethylsulfonium perchlorate (**5b**), **5c**, [[tris(*t*-butylthio)cyclopropenyl](ethylthiocarbonyl)methyl]dimethylsulfonium perchlorate (**5d**), **5e**, **5g**, **5h**, [[tris(*t*-butylthio)cyclopropenyl](ethoxycarbonyl)methyl]dimethylsulfonium tetrafluoroborate (**5i**), and [[tris(*t*-butylthio)cyclopropenyl](ethylthiocarbonyl)methyl]dimethylsulfonium tetrafluoroborate (**5j**). However, no sulfonium salt, which would be formed from the reaction of **1f**, was detected. Results are summarized in Table 2. The structures of the sulfonium salts **5** were determined by elemental analyses, ^{1}H-NMR spectroscopic data and IR spectra (showing the three-membered ring and >C=O stretching bands). These results strongly suggest that the reaction of cyclopropenium ions with sulfonium ylides proceeds *via* sulfonium salts, nucleophilic addition products.

The structure of **5** permit us to indicate a possible reaction pathway. The reaction should involve, as the first step, nucleophilic attack of ylide carbanion by ring-carbon. Thus the sulfonium salt formation from thio-substituted cyclopropenium ions can occur with sulfonium methylides. Then the sulfonium salts with an appropriate leaving group SR and $(CH_3)_2S^+$ may be subject to elimination of $(CH_3)_2S^+$, intramolecular rearrangement of SR and ring opening to give the ketene **3**. The allene **4** may arise from a cyclopropenylidene intermediate, generated by elimination of a ketene moiety from **5**. Although we do not believe

Table 3. Physical data of sulfonium salts (**5**)

5	^{1}H-NMR: δ ($CDCl_3$)	IR[a] $\tilde{\nu}$/cm^{-1} C=O		UV[b] λ_{max}/nm (ε)
5a	1.35 (3H, t), 1.50 (9H, t), 3.05 (4H, q) 3.15 (6H, s), 3.40 (2H, q), 4.18 (2H, q)	1800	1670	270 (14000), 280 (12000)
5b	1.22 (3H, t), 1.40 (9H, t), 2.90 (2H, q) 3.08 (6H, s), 3.20 (4H, q), 3.45 (2H, q)	1790	1630	244 (8300), 282 (7000) 306 (10000)
5c	1.37 (3H, t), 1.53 (9H, s), 1.68 (18H, s) 3.18 (6H, s), 4.23 (2H, q)	1780	1670	272 (10900), 285*(9100)
5d	1.30 (3H, t), 1.55 (9H, s), 1.68 (18H, s) 2.95 (2H, q), 3.22 (6H, s)	1770	1640	244 (9000), 282*(7000) 306 (11000)
5e	1.29 (27H,s), 1.45 (3H, t), 2.82 (6H, s) 4.25 (2H, q), 7.65 (12H,d)	1800	1680	274 (10000)
5g	1.35 (3H, t), 1.50 (9H, t), 3.05 (4H, q) 3.15 (6H, s), 3.40 (2H, q), 4.18 (2H, q)	1800	1670	270 (33000), 281*(28000)
5h	1.22 (3H, t), 1.40 (9H, t), 2.90 (2H, q) 3.08 (6H, s), 3.20 (4H, q), 3.45 (2H, q)	1780	1630	243 (17000), 281*(14000) 306 (22000)
5i	1.37 (3H, t), 1.53 (9H, s), 1.68 (18H, s) 3.18 (6H, s), 4.23 (2H, q)	1790	1690	274 (35000), 286*(13000)
5j	1.30 (3H, t), 1.55 (9H, s), 1.68 (18H, s) 2.95 (2H, q), 3.22 (6H, s)	1760	1620	248 (15000), 308 (17000)

a) Measured in KBr disk. b) Observed in CH_3CN. * Shoulder.

that the limited data available here can permit us to discuss a further precise mechanism, the present results strongly support the intermediacy of the sulfonium salt such as **5** in reactions between the thio-substituted cyclopropenium ion system and sulfonium methylide.

Experimental

All the melting points are uncorrected. The IR spectra were taken with a Hitachi Model 215 spectrophotometer; the UV spectra with a Hitachi Model EPS-3T spectrometer; and the ^{1}H-NMR spectra with a JEOL Model JNM-C-60H spectrometer. The chemical shifts are expressed in parts per million downfield from internal tetramethylsilane (δ=0). Splitting patterns are indicated as s, singlet; d, doublet; t, triplet; q, quartet; m, multiplet. All the reactions were carried out under He atmosphere unless otherwise noted.

Materials. The sulfonium methylides **2a—c** were synthesized according to reported procedures[8] and identified by elemental analyses and melting points as well as by comparison of IR. The syntheses of thio-substituted cyclopropenium perchlorates (X=ClO_4, **1a—c**) were reported previously.[4,9]

*Tris(ethylthio)cyclopropenium Tetrafluoroborate (**1d**).* To a stirred of tetrachlorocyclopropene (91.6 mmol) in boron trifluoride (abt 49%, 40 g), there was added ethanethiol (36.6 mmol), dropwise, at room temperature. The mixture was stirred under reflux for 3 h. It was then cooled to room temperature, poured into ice–water, and extracted with dichloromethane. The organic layer was dried over $MgSO_4$, stripped of solvent, washed with ether, and dried under reduced pressure to give yellow crystals (**1d**) in 63% yield; mp 107—109 °C; UV_{max} (CH_3OH) 272 nm (ε 3100); IR (KBr) 1250 and 1090 cm^{-1}. Found: C, 35.19; H, 4.82%. Calcd for $C_9H_{15}S_3BF_4$: C, 35.30; H, 4.94%.

*Tris(t-butylthio)- (**1e**) and Tris(p-t-butylphenylthio)cyclopropenium Tetrafluoroborates (**1f**).* In a similar manner to the above, **1e** and **1f** were prepared from the corresponding thiols in 42 and 50% yields, respectively. **1e**: yellow crystals; mp 129—131 °C; UV_{max} (CH_3OH) 272 nm (ε 3570); IR (KBr) 1250 and 1090 cm^{-1}. Found: C, 46.02; H, 7.04%. Calcd for $C_{15}H_{27}S_3BF_4$: C, 46.15; H, 6.97%. **1f**: Colorless needles; mp 149—152 °C; UV max (CH_3OH) 250 (ε 4300) and 275 nm (3600); IR (KBr) 1250 and 1090 cm^{-1}. Found: C, 64.27; H, 6.03%. Calcd for $C_{33}H_{39}S_3BF_4$: C, 64.27; H, 6.35%.

*Reaction of Thio-substituted Cyclopropenium Ions (**1**) with Sulfonium Methylides (**2**). General Procedure*: A mixture of **1** (10 mmol) and **2** (40 mmol) in dry THF (80 or 100 ml) was stirred at room temperature for 6 or 8 h. After which the solvent was removed under reduced pressure. The residue was subjected to column chromatography on silica gel, eluting with carbon tetrachloride to give **3** and **4**. The following ketenes and allene were prepared by this procedure.

Physical Properties: **3a**: Pale yellow oil; UV_{max} (CH_3OH) 288 nm (ε 6000); IR (neat) 2160 (>C=C=O) and 1640 cm^{-1}; ^{1}H-NMR ($CDCl_3$) δ=1.25 (6H, t, J=6.8 Hz, CH_3) and 2.75 (4H, q, J=6.8 Hz, CH_2).

3b: Pale yellow oil; UV_{max} (CH_3OH) 251 nm (ε 6700); IR (neat) 2170 (>C=C=O) and 1640 cm^{-1}; ^{1}H-NMR ($CDCl_3$) δ=1.45 (18H, s, CH_3).

3c: Pale brown oil; UV_{max} (CH_3OH) 251 nm (ε 11000); IR (neat) 2190 (>C=C=O) and 1660 cm^{-1}; ^{1}H-NMR ($CDCl_3$) δ=1.41 (18H, s, CH_3) and 7.15 (8H, m, phenyl).

4b: Colorless needles; mp 140—141 °C; UV_{max} (CH_3OH) 269 nm (ε 6500); IR (KBr) 1910 (>C=C=C<) and 1360 cm^{-1}; ^{1}H-NMR (CCl_4) δ=1.45 (36H, s, CH_3). Found: C, 57.90; H, 9.43%. Calcd for $C_{19}H_{36}S_4$: C, 58.01; H, 9.26%.

*Preparation of Sulfonium Salts (**5**). Preparation of **5e** as a Typical Procedure*: The mixture of **1e** (1.58 mmol) and **2a** (1.58 mmol) in dry THF (80—100 ml) was stirred at −40 °C for 6 h. The reaction mixture was filtered off, and the product was recrystallized from $CHCl_3$–CCl_4 (1:1) to give colorless rod-like crystals, [[tris(*p*-*t*-butylphenylthio)-cyclopropenyl](ethoxycarbonyl)methyl]dimethylsulfonium-perchlorate (**5e**) (57% yield). Other sulfonium salts were prepared by the similar procedure, but **5a**, **5b**, **5c**, **5d**, **5g**, **5h**, **5i**, and **5j** were purified by recrystallization from ethanol. Physical data of **5** are summarized in Tables 2 and 3.

References

1) S. Yoneda, H. Hirai, and Z. Yoshida, *Chem. Lett.*, **1976**, 1051.
2) Z. Yoshida, S. Yoneda, T. Miyamoto, and S. Miki, *Tetrahedron Lett.*, **1974**, 813.
3) Z. Yoshida, *Topics Current Chem.*, **40**, 47 (1973).
4) S. Inoue, G. Yasuda, and T. Hori, *Bull. Chem. Soc. Jpn.*, **51**, 3653 (1978); *Chem. Lett.*, **1976**, 1215.
5) Z. Yoshida, H. Konishi, and H. Ogushi, *Heterocycles*, **5**, 401 (1976).
6) E. Cosserment, R. Biname, and L. Ghosez, *Tetrahedron Lett.*, **1974**, 997.
7) S. Yoneda, H. Hirai, and Z. Yoshida, *Heterocycles*, **15**, 865 (1981).
8) C. B. Payne, *J. Org. Chem.*, **32**, 3351 (1967); T. Wakui, H. Yamaguchi, and S. Motoki, *Bull. Chem. Soc. Jpn.*, **50**, 1645 (1977); K. W. Ratts and A. N. Yao, *J. Org. Chem.*, **31**, 1186 (1965).
9) Z. Yoshida and T. Tawara, *J. Am. Chem. Soc.*, **93**, 2573 (1971).

 © 1983 The Chemical Society of Japan Bull. Chem. Soc. Jpn., 56, 175—179 (1983)

Reactions of Azepine, Diazepine, Tropone, and Cyclopentadienone Derivatives with Some Chlorosilane Derivatives in the Presence of Magnesium

Katsuhiro Saito,* Hisashi Kojima, Tsuguo Okudaira, and Kensuke Takahashi†

Department of Chemistry, Nagoya Institute of Technology, Gokiso-cho, Showa-ku, Nagoya 466

†*Department of Industrial Chemistry, Nagoya Institute of Technology, Gokiso-cho, Showa-ku, Nagoya 466*

(Received February 22, 1982)

The reaction of 1-ethoxycarbonyl-1*H*-azepine with chlorosilane derivatives in HMPA in the presence of magnesium afforded the silanol derivatives, which upon heating gave the corresponding siloxane derivatives. In the same manner, tropone and 2,5-dimethyl-3,4-diphenylcyclopentadienone afforded the reduced dimers of them. However, tetraphenylcyclopentadienone and 2,5-dimethoxy-3,4-diphenylcyclopentadienone were reduced to the corresponding cyclopentenones under the reaction conditions. These reactions are considered to proceed *via* the corresponding radical anions which are formed by electron transfer from magnesium.

Chlorosilane derivatives are known to add to olefins in the presence of magnesium in hexamethylphosphoric triamide (HMPA).[1] However, the reactions to heterocyclic compounds have not been investigated well, although much attention has been paid to the cycloaddition reactions of heterocyclic compounds.[2] Similarly, much effort has been devoted to the study of the Grignard reactions of troponoid compounds, but no report has been published concerning the reactions of chlorosilanes with these types of compounds.[3] We wish to report the results of reactions of some chlorosilanes to azepine, diazepine, tropone, and cyclopentadienone derivatives.

The reaction of 1-ethoxycarbonyl-1*H*-azepine (**1**) with diphenyldichlorosilane in HMPA in the presence of magnesium at room temperature, followed by quenching with water, afforded **7** and **8** in yields of 40 and 23%, respectively. Similarly, **1** was reacted with dimethyldichlorosilane and trimethylchlorosilane to afford **9** and **11** in yields of 35 and 40%, respectively. Upon standing at room temperature as a chloroform solution, **9** was converted to **10** in nearly quantitative yield. On the other hand, **7** afforded **8** almost quantitatively by heating at 120 °C in toluene.

It is clear from the elemental analyses and mass spectrometry that these products are derived from the 1:2 adducts of **1** and the chlorosilanes. The IR spectra indicate that **7** and **9** are silanol derivatives in which the chlorine atoms bonded to the silicon atoms are replaced with hydroxyl groups. The products **8** and **10** were determined to be siloxane derivatives which are derived from the dehydration of **7** and **9**, respectively, on the basis of the spectral data and of the experiments mentioned above. The fact that there are only three signals of the ring protons in their NMR spectra and that each of these three signals corresponds to two ring protons indicate that these adducts have symmetric structures, suggesting that 2,7-addition, 3,6-addition, or 4,5-addition have occurred. The 3,6-addition is rejected by the facts that the NMR spectra showed no three-membered ring proton resonances and that it is impossible for chlorosilanes to add to the 3 and 6 positions without forming an aziridine ring in the azepine nucleus.

In the low temperature NMR spectra (−30 to −50 °C), the signals of H_a and H_b showed no change, but the doublet signal of H_c was split into two doublets at slightly different chemical shifts. Similar behavior was observed with H_α of the compound **12**.[4] The observed splitting at low temperature is a result of a

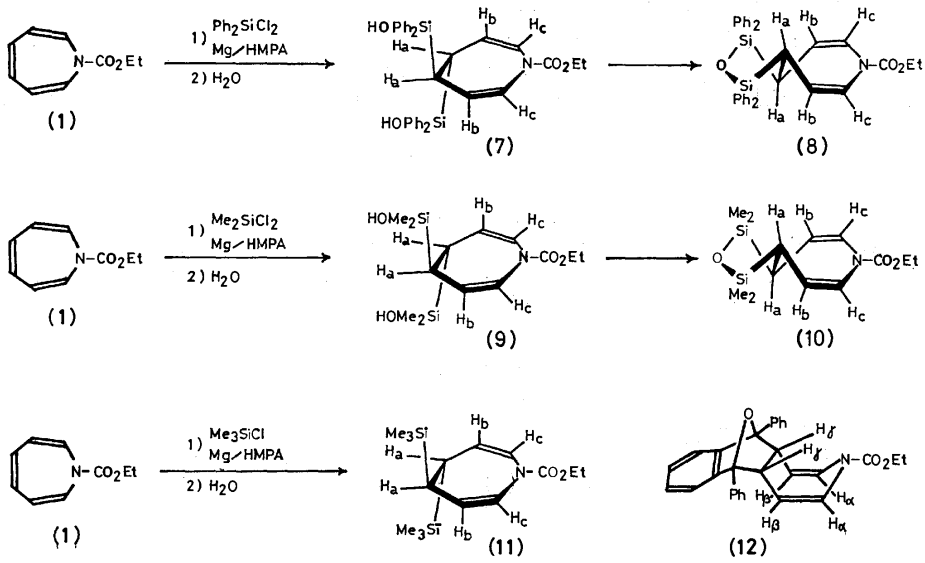

Fig. 1.

different anisotropic effect of the carbonyl group on the two H_e protons, which are revealed to be olefinic protons by the chemical shifts in the NMR spectra. This difference in the anisotropic effect is caused by freezing the free rotation of the ester group.[2b,5] A structure which has olefinic protons adjacent to the nitrogen atom can only be the result of the 4,5-addition. The 4,5-addition is further supported by the similarity of the NMR spectra of the adducts to the spectrum of the structurally analogous compound **12**.

The stereochemistry of the adducts was deduced from the coupling constants between the methine proton H_a and the olefinic proton H_b. The Dreiding models reveal that, for *cis*-addition, the dihedral angle between H_a and H_b is approximately 100°, which corresponds to the coupling constant of about 2 Hz according to the Karplus equation.[6] This value for the coupling constant is in accord with the observed value between H_γ and H_β of the authentic *cis*-adduct **12**. On the other hand, for *trans*-addition, the silyl groups would be expected to be arranged in a diaxial position in order to avoid the steric repulsion between them. In this case, the dihedral angle between the equatorial methine proton H_a and the olefinic proton H_b should be approximately 10°, which corresponds to a coupling constant of approximately 11 Hz. The observed coupling constants of **7**, **9**, and **11** are in accord with the expected value for the *trans*-addition. When the siloxane rings are formed, the silyl groups should be required to approach each other, resulting in the equatorial arrangement of the silyl groups and the axial arrangement of the methine protons. In this conformation, the dihedral angle between the axial methine proton and the olefinic proton is approximately 100°, which corresponds to a coupling constant of about 2 Hz and is in good agreement with the observed values for **8** and **10**. On the basis of these arguments, the structures of these adducts are determined as shown in Fig. 1.

In the same way, tropone (**2**) was reacted with trimethylchlorosilane in HMPA in the presence of magnesium. After quenching with water, **13** was obtained in 27% yield. The similar reactions of **2** with diphenyldichlorosilane or dimethyldichlorosilane resulted in almost the same consequences as above; however, in the absence of chlorosilanes, no reaction occurred.

The elemental analysis and the molecular ion peak in the mass spectrum reveal that **13** is the reduced dimer of **2**. The IR spectrum indicates that the carbonyl group is not conjugated with any double bond.[3b] The NMR spectral data employing the double resonance technique made it clear that **13** contains a 2,4-hexadiene moiety which has geminal protons at one end and a proton at the other end. The coupling constants are reasonably assigned on this carbon arrangement. On the basis of these facts, the structure of **13** is determined as shown in Fig. 2.

The reaction of tetraphenylcyclopentadienone (**3**) with trimethylchlorosilane in HMPA in the presence of magnesium, followed by quenching with water, produced a known cyclopentenone derivative **14**[7] in 74% yield. Similarly, 2,5-bis(methoxycarbonyl)-3,4-

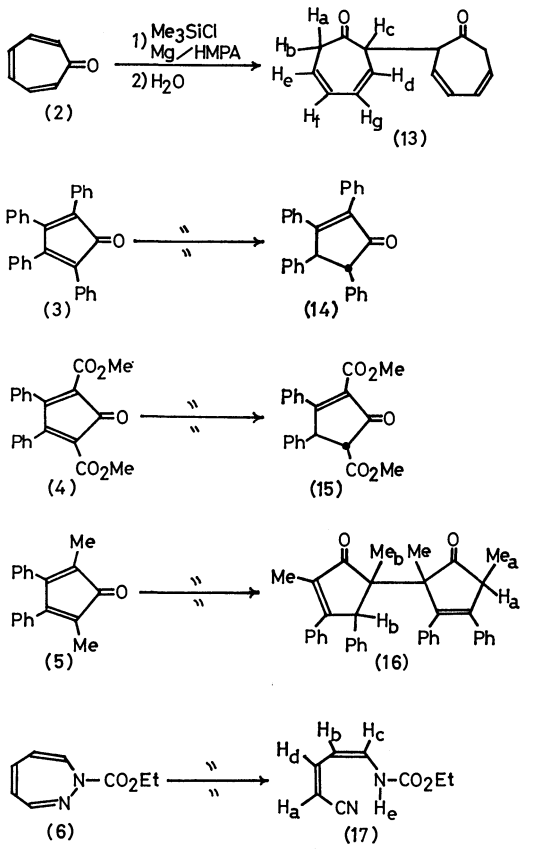

Fig. 2.

diphenylcyclopentadienone (**4**) and 2,5-dimethyl-3,4-diphenylcyclopentadienone (**5**) were reacted with trimethylchlorosilane to yield **15** and **16** in yields of 25 and 18%, respectively. The reactions of **3**, **4**, and **5** with diphenyldichlorosilane or dimethyldichlorosilane gave approximately the same results as above; however, in the absence of chlorosilane derivatives, no reaction proceeded.

The IR spectrum of **15** suggests that this product is a cyclopentenone derivative, which is also supported by the elemental analysis and the molecular ion peak in the mass spectrum. The stereochemistry of **15** was determined on the basis of the coupling constant between the ring protons. The elemental analysis and the molecular ion peak in the mass spectrum reveal that **16** is a reduced dimer of **5**. The IR spectrum indicates the existence of a conjugated and an unconjugated carbonyl group. The NMR spectrum shows that there are two ring protons: one proton (H_a) interacts with a methyl group (Me_a) with a coupling constant of 8 Hz and the other proton (H_b) has a long range coupling of 2 Hz with the other methyl group (Me_b). On the basis of these facts, the structures of **15** and **16** are determined as shown in Fig. 2.

1-Ethoxycarbonyl-1*H*-1,2-diazepine (**6**) was reacted with trimethylchlorosilane in HMPA in the presence of magnesium. After quenching with water, **17** was obtained in 25% yield. However, **17** was also obtained from the reaction of **6** with magnesium in HMPA in the absence of chlorosilanes.

The structure of **17** was determined as shown in

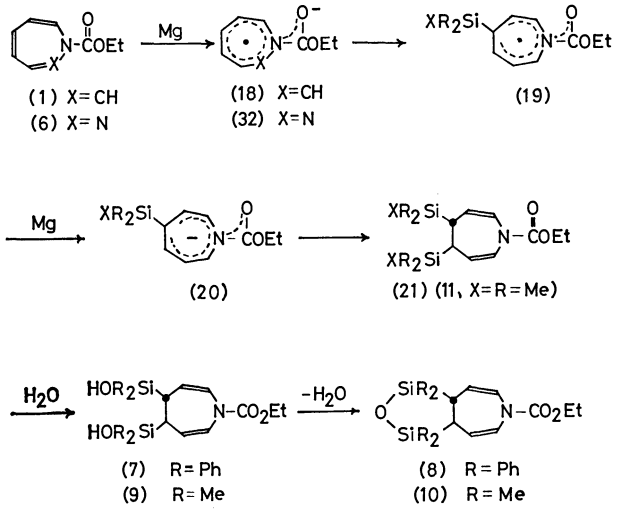

Fig. 3.

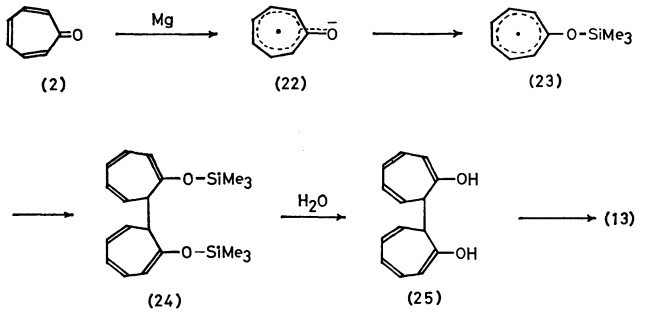

Fig. 4.

Fig. 2 on the basis of its spectral data and the resemblance of its NMR spectrum to that of the analogous compounds.[10]

Discussion

The reaction mechanism of **1** with chlorosilane derivatives can be explained as follows.[1] The first step of the reaction is considered to be one electron transfer from magnesium to **1** in the strongly basic solvent HMPA to form the anion radical **18**, which reacts with chlorosilanes to give the radical **19**, as shown in Fig. 3. One more electron transfer to **19**, followed by the reaction with chlorosilane, gives the disilyl compounds **21** (**11**, X=R=CH_3) *via* the anion **20**. When the reaction mixture is quenched with water, **21** is hydrolyzed to form the silanols. Dehydration of the silanols **7** and **9** to the siloxanes **8** and **10** is a well-documented reaction.[8]

The reaction mechanism of tropone (**2**) is thought to proceed *via* the initial formation of the radical anion **22**, which further reacts with chlorosilanes to yield the silyl ether radical **23**[9] as shown in Fig. 4. Dimerization of **23** affords **24**, which subsequently gives the reduced dimer **13** by the hydrolysis *via* the enol intermediate **25**.

The silyl ether radical **27** is also considered to be formed in the reactions of cyclopentadienones, as shown in Fig. 5. In the case of **5**, which has methyl groups at the 2 and 5 positions, **27** dimerizes to form **28** which

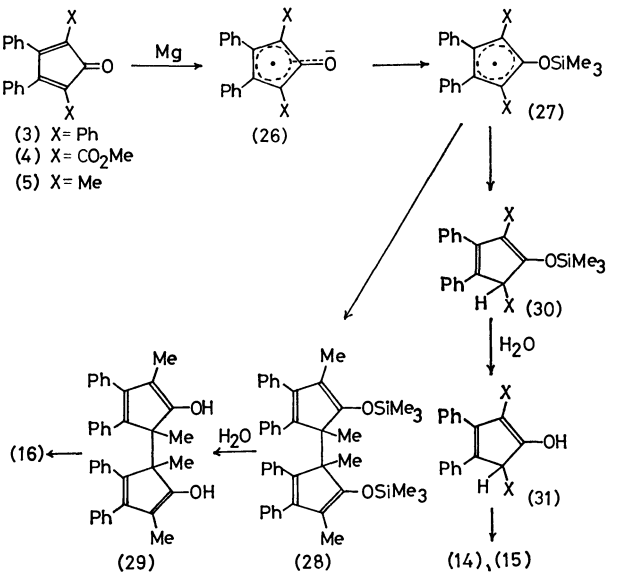

Fig. 5.

affords the reduced dimer **16** by hydrolysis. However, the bulky substituents, phenyl and methoxycarbonyl groups, located at the 2 and 5 positions in **3** and **4**, inhibit the dimerization of **27**. Thus, **27** abstracts a hydrogen from the solvent to yield the silyl ether **30**, which subsequently affords the cyclopentenones **14** and **15** after hydrolysis.

Nitrile compounds similar to **17** are known to be formed in the reaction of diazepine derivatives with strong bases.[10] The reaction products are thought to be formed *via* the N–N bond fission of the radical **32** shown in Fig. 3.

Experimental

All the melting points were uncorrected. IR spectra were measured in carbon tetrachloride solutions or potassium bromide disks and UV spectra in methanol solutions. NMR spectra were measured with Hitachi R-20B or Varian HA-100 spectrometer with deuteriochloroform or carbon tetrachloride as solvent and tetramethylsilane as internal standard. Wakogel C-200 and activated alumina of Wako Pure Chemicals Industries LTD were used for column chromatography.

Reaction of 1 with Diphenyldichlorosilane. A mixture of **1** (1.00 g, 6 mmol), magnesium (0.22 g, 9 mg atom), diphenyldichlorosilane (5.00 g, 20 mmol), and HMPA (30 mL) was stirred at room temperature for 20 h under a nitrogen stream. The reaction mixture was poured into ice water and extracted with ether. The organic layer was washed with water, brine, and dried over anhydrous sodium sulfate. After filtering, the solvent was evaporated on a rotary evaporator to yield a yellow oil (3.7 g). Silica gel chromatography of this oil gave pale yellow crystals **8** (0.85 g) by benzene–ether 50:1, and a pale yellow oil **7** (1.50 g) by benzene–ether 25:1. Recrystallization of **8** from cyclohexane gave colorless crystals (0.73 g, 23%), mp 174—175 °C. The oil **7** was further purified with silica gel chromatography to give a colorless oil (1.30 g, 40%). **7**: Found: C, 70.13; H, 6.11; N, 2.43%. Calcd for $C_{33}H_{33}NO_4Si_2$: C, 70.30; H, 5.90; N, 2.48%. UV_{max} 244 nm (log ε 4.37), 248 (4.39), 254 (4.29), 260 (4.23), 265 (4.01), 272 (3.83). IR (neat) 3420, 1710 cm^{-1}. NMR ($CDCl_3$) δ=1.13 (3H,

t), 2.73 (2H, H_a, d), 3.44 (2H, OH, bs), 4.02 (2H, q), 4.91 (2H, H_b, t), 6.44 (2H, H_c, d), 7.1—7.8 (20H, Ph); coupling constants in Hz $J_{ab}=9.0$, $J_{bc}=11.0$. MS, *m/e* (rel intensity), 545 (M^+-18, 3), 319 (81), 257 (64), 181 (100), 105 (86). **8**: Found: C, 72.88; H, 5.59; N, 2.62%. Calcd for $C_{33}H_{31}NO_3Si_2$: C, 72.62; H, 5.72; N, 2.57%. UV_{max} 244 nm (log ε 4.33), 254 (4.17), 260 (4.11), 265 (4.03), 272 (3.76). IR (KBr) 1720 cm^{-1}. NMR ($CDCl_3$) $\delta=1.22$ (3H, t), 2.73 (2H, H_a, nm), 4.08 (2H, q), 5.20 (2H, H_b, md), 6.62 (2H, H_c, md), 7.1—7.8 (20H, Ph); coupling constants in Hz $J_{ab}=2.0$, $J_{bc}=10.0$. MS, *m/e* (rel intensity) 545 (M^+, 23), 319 (100).

*Reaction of **1** with Dimethyldichlorosilane.* A mixture of **1** (1.65 g, 10 mmol), magnesium (0.36 g, 15 mg atom), dimethyldichlorosilane (4.00 g, 31 mmol), and HMPA (40 mL) was stirred at room temperature for 16 h under a nitrogen stream. The usual workup afforded a pale orange oil (2.55 g), which was chromatographed on silica gel to give pale yellow crystals **9** (1.25 g) by benzene–ether 7:3 and recovered starting material **1** (0.67 g) by benzene–ether 1:1. Recrystallization of **9** from cyclohexane gave colorless crystals (1.10 g, 35%), mp 99—100 °C. Found: C, 49.44; H, 7.96; N, 4.46%. Calcd for $C_{13}H_{25}NO_4Si_2$: C, 49.49; H, 7.99; N, 4.44%. UV_{max} 240 nm (log ε 4.09). IR (KBr) 3400, 1730 cm^{-1}. NMR ($CDCl_3$) $\delta=0.08$ (6H, s), 0.15 (6H, s), 1.41 (3H, t), 2.20 (2H, H_a, d), 3.38 (2H, OH, s), 4.33 (2H, q), 5.24 (2H, H_b, t), 6.68 (2H, H_c, d); coupling constants in Hz $J_{ab}=10.0$, $J_{bc}=10.0$. MS, *m/e* (rel intensity) 315 (M^+, 14), 149 (100).

*Reaction of **1** with Trimethylchlorosilane.* A mixture of **1** (1.00 g, 6 mmol), magnesium (0.22 g, 9 mg atom), trimethylchlorosilane (1.10 g, 10 mmol), and HMPA (20 mL) was stirred under a nitrogen stream for 18 h at room temperature. The usual workup afforded a pale orange oil (1.60 g), which was chromatographed on silica gel to give a colorless oil **11** (0.85 g) by petroleum ether–benzene 3:7 and recovered starting material **1** (0.19 g) by benzene–ether 9:1. The crude oil **11** was purified by chromatography on silica gel to yield a colorless oil (0.76 g, 40%). Found: C, 57.58; H, 9.16; N, 4.52%. Calcd for $C_{15}H_{29}NO_2Si_2$: C, 57.82; H, 9.38; N, 4.50%. UV_{max} 240 nm (log ε 4.16). IR (neat) 1730 cm^{-1}. NMR ($CDCl_3$) $\delta=0.08$ (12H, s), 1.32 (3H, t), 1.79 (2H, H_a, d), 4.11 (2H, q), 4.87 (2H, H_b, t), 6.63 (2H, H_c, d); coupling constants in Hz $J_{ab}=10.0$, $J_{bc}=12.0$. MS, *m/e* (rel intensity) 311 (M^+, 46), 120 (100).

*Reaction of **2** with Trimethylchlorosilane.* A mixture of **2** (2.00 g, 16 mmol), magnesium (0.38 g, 16 mg atom), trimethylchlorosilane (5.43 g, 50 mmol), and HMPA (30 mL) was allowed to react for 2 h at room temperature under a nitrogen stream. The usual workup gave a yellow oil (2.10 g), which was chromatographed on silica gel to give yellow crystals **13** (0.68 g) by benzene. Recrystallization of **13** from methanol gave pale yellow crystals (0.61 g, 27%), mp 91—92 °C. Found: C, 78.25; H, 6.48%. Calcd for $C_{14}H_{14}O_2$: C, 78.48; H, 6.59%. UV_{max} 241 nm (log ε 3.69). IR (KBr) 3010, 2960, 1710 cm^{-1}. NMR ($CDCl_3$) $\delta=3.01$ (2H, H_a, m), 3.53 (2H, H_b, m), 3.90 (2H, H_c, m), 5.65 (2H, H_d, m), 6.04 (2H, H_e, m), 6.35 (4H, H_f, H_g, m); coupling constants $J_{ab}=20.0$, $J_{ac}=1.5$, $J_{ae}=3.5$, $J_{af}=1.5$, $J_{be}=7.0$, $J_{cd}=3.0$, $J_{cg}=0.5$, $J_{dg}=10.5$, $J_{df}=1.5$, $J_{ef}=11.0$, $J_{eg}=1.5$. MS, *m/e* (rel intensity) 214 (M^+, 24), 107 (100).

*Reaction of **3** with Trimethylchlorosilane.* A mixture of **3** (2.50 g, 6.5 mmol), magnesium (0.16 g, 6.6 mg atom), trimethylchlorosilane (2.17 g, 20 mmol), and HMPA (20 mL) was stirred for 20 h at room temperature under a nitrogen stream. The usual workup gave a black mixture of crystalline starting material **3** and a tarry material (3.4 g). After removing the starting material **3** (0.28 g) by filtration, the tarry filtrate was chromatographed on alumina to yield additional starting material **3** (0.22 g) by petroleum ether–benzene 4:6 and colorless crystals **14** (2.03 g) by petroleum ether–benzene 1:9. Recrystallization from cyclohexane gave pure crystals of **14** (1.86 g, 74%), mp 162—163 °C, (lit,[7] 162—163 °C).

*Reaction of **4** with Trimethylchlorosilane.* A mixture of **4** (3.48 g, 10 mmol), magnesium (0.24 g, 10 mg atom), trimethylchlorosilane (4.30 g, 40 mmol), and HMPA (60 mL) was stirred for 2 h under a nitrogen stream at room temperature. The usual workup gave a brown oil (3.33 g) which was chromatographed on silica gel to yield yellow crystals **15** (0.98 g) by benzene–ether 20:1. Recrystallization of **15** from chloroform gave colorless crystals (0.89 g, 25%), mp 113—114 °C. Found: C, 71.92; H, 5.41%. Calcd for $C_{21}H_{18}O_5$: C, 71.99; H, 5.18%. UV_{max} 287 nm (log ε 4.08). IR (KBr) 3030, 2940, 1730 (broad) cm^{-1}. NMR ($CDCl_3$) $\delta=3.58$ (1H, d, $J=3.5$ Hz), 3.80 (6H, s), 5.06 (1H, d, $J=3.5$ Hz), 7.2 (10H, Ph). MS, *m/e* (rel intensity) 350 (M^+, 14), 317 (100).

*Reaction of **5** with Trimethylchlorosilane.* A mixture of **5** (2.03 g, 4 mmol), magnesium (0.19 g, 8 mg atom), trimethylchlorosilane (3.48 g, 32 mmol), and HMPA (20 mL) was stirred at room temperature under a nitrogen stream for 2 h. The usual workup gave a brown oil (2.9 g), which was chromatographed on silica gel to yield yellow crystals **16** (0.41 g) by benzene–ether 20:1. Recrystallization of **16** from ethanol gave colorless crystals (0.36 g, 18%), mp 213—214 °C. Found: C, 87.55; H, 6.39%. Calcd for $C_{38}H_{34}O_2$: C, 87.32; H, 6.56%. UV_{max} 275 nm (log ε 4.26). IR (KBr) 3050, 2970, 1743, 1690 cm^{-1}. NMR ($CDCl_3$) $\delta=$ 0.16 (3H, Me_a, d, $J=8.0$ Hz), 1.30 (3H, Me_b, d, $J=2.0$ Hz), 1.94 (3H, s), 2.08 (3H, s), 3.06 (1H, H_a, q, $J=8.0$ Hz), 4.50 (1H, H_b, q, $J=2.0$ Hz), 7.2 (20H, Ph). MS, *m/e* (rel intensity) 261 ($M^+/2$, 53), 91 (100).

*Reaction of **6** with Trimethylchlorosilane.* A mixture of **6** (0.53 g, 3 mmol), magnesium (0.072 g, 3 mg atom), trimethylchlorosilane (1.08 g, 10 mmol), and HMPA (10 mL) was allowed to react for 2 h at room temperature under a nitrogen stream. The usual workup afforded a red oil (1.5 g), which was chromatographed on silica gel to yield yellow crystals **17** (0.16 g) by benzene–ether 4:1, and recovered starting material **6** (0.086 g) by benzene–ether 3:2. Recrystallization from benzene gave pale yellow crystals **17** (0.13 g, 25%), mp 141—142 °C. Found: C, 57.79; H, 6.23; N, 16.82%. Calcd for $C_8H_{10}N_2O_2$: C, 57.82; H, 6.07; N, 16.86%. UV_{max} 303 nm (log ε 4.43). IR (KBr) 3330, 2210, 1710 cm^{-1}. NMR ($CDCl_3$) $\delta=1.32$ (3H, t), 4.32 (2H, q), 5.09 (1H, H_a, d), 5.73 (1H, H_b, dd), 6.86 (1H, H_c, dd), 7.09 (1H, H_d, dd), 7.75 (1H, H_e, broad); coupling constants in Hz $J_{ad}=10.5$, $J_{bc}=9.0$, $J_{bd}=12.0$, $J_{ce}=12.0$. MS, *m/e* (rel intensity) 166 (M^+, 33), 91 (100).

*Formation of **8** from **7**.* A solution of **7** (1.00 g) in toluene-d_8 (5 mL) was heated at 120 °C under a nitrogen stream for 3 h. The NMR spectrum of this reaction mixture indicated that **7** was converted to **8**. The yield of **8** was found to be nearly quantitative by comparison of the area of the absorption peak of H_c of **8** with the area of the peak of the ethyl group as the standard. The solvent was then evaporated to yield a colorless oil, which was crystallized from cyclohexane to give colorless crystals **8** (0.88 g, 91%).

*Formation of **10** from **9**.* A solution of **9** (0.50 g) in deuteriochloroform (2 mL) was stirred at room temperature under a nitrogen stream for 72 h. The NMR spectrum of this reaction mixture showed that **9** was converted to **10** almost quantitatively, using the absorption signal of H_c of

10 and the signal of the ethyl group as the standard. After evaporation of the solvent, the colorless residue was chromatographed on silica gel to yield a colorless oil **10** (0.14 g, 29%). Compound **10** was unstable and an analytically pure sample could not be obtained. UV_{max} 238 nm (log ε 4.37). IR (neat) 1730 cm^{-1}. NMR ($CDCl_3$) δ=0.16 (6H, s), 0.25 (6H, s), 1.42 (3H, t), 2.06 (2H, H_a, nm), 4.28 (2H, q), 5.13 (2H, H_b, md), 6.68 (2H, H_c, md); coupling constants in Hz J_{ab}=2.0, J_{bc}=10.0. MS, *m/e* (rel intensity) 297 (M^+, 14), 149 (100).

The authors are indebted to Prof. Hideki Sakurai, Prof. Toshio Mukai, and Prof. Takashi Toda of Tohoku University for their kind suggestions. This work was supported by a Scientific Research Grant from Japanese Ministry of Education, Science and Culture.

References

1) J. Dunogues, R. Calas, C. Bilan, and N. Duffaut, *J. Organomet. Chem.*, **23**, C 50 (1970); J. Dunogues, R. Calas, J. Dedier, and F. Pisciotti, *ibid.*, **25**, 51 (1970); T. J. Barton and M. Junet, *Tetrahedron Lett.*, **1975**, 2561.

2) a) K. Saito and K. Takahashi, *Heterocycles*, **12**, 263 (1979); b) S. Iida, T. Mukai, and K. Saito, *ibid.*, **11**, 401 (1978); c) K. Harano, M. Yasuda, T. Ban, and K. Kanematsu, *J. Org. Chem.*, **45**, 4455 (1980); d) J. P. Luttringer and J. Streith, *Tetrahedron Lett.*, **1973**, 4163; e) A. G. Anastassiou, E. Reichmanis, S. J. Girgenti, and R. M. Scaefer, *J. Org. Chem.*, **43**, 315 (1978).

3) a) T. Nozoe, T. Mukai, and J. Minegishi, *Proc. J. Acad.*, **27**, 419 (1951); b) T. Nozoe, T. Mukai, and T. Tezuka, *Bull. Chem. Soc. Jpn.*, **34**, 619 (1961); c) C. A. Cupas and L. Hodakowski, *J. Am. Chem. Soc.*, **96**, 4668 (1974).

4) L. A. Paquette, D. E. Kuhla, J. H. Barret, and M. Leichter, *J. Org. Chem.*, **34**, 2888 (1969).

5) J. P. Luttringer, N. Perol, and J. Streith, *Tetrahedron*, **31**, 2435 (1975).

6) M. Karplus, *J. Am. Chem. Soc.*, **85**, 2870 (1963).

7) N. O. V. Sonntag, S. Linder, E. I. Becker, and P. E. Spoerri, *J. Am. Chem. Soc.*, **75**, 2283 (1953).

8) D. R. Weynberg and L. H. Toporcer, *J. Am. Chem. Soc.*, **84**, 2843 (1962); M. Ishikawa and M. Kumada, *Synth. Inorg. Metal-Org. Chem.*, **1**, 191 (1971).

9) R. Calas, J. Dunogues, J. P. Pillot, C. Brian, and N. Duffaut, *J. Organomet. Chem.*, **25**, 43 (1970); R. Calas, J. Dunogues, and M. Bolourtchian, *ibid.*, **26**, 195 (1971).

10) J. Streith, J. P. Luttringer, and M. Nastasi, *J. Org. Chem.*, **36**, 2962 (1971).

Reaction of Sulfur Dichloride with Nitrile in the Presence of Lewis Acid Forming 1,2,4-Thiadiazole

Mitsuo KOMATSU,* Jun-ichi SHIBATA, Yoshiki OHSHIRO, and Toshio AGAWA

Department of Petroleum Chemistry, Faculty of Engineering, Osaka University, Yamada-oka 2-1, Suita, Osaka 565

(Received March 12, 1982)

Formation of 3,5-disubstituted 1,2,4-thiadiazoles by the reaction of sulfur dichloride with nitriles in the presence of a Lewis acid was found. For example, 3,5-diphenyl-1,2,4-thiadiazole was obtained with its chlorinated products, 3-*o*-chlorophenyl-5-phenyl- and 3-*p*-chlorophenyl-5-phenyl-1,2,4-thiadiazoles, from benzonitrile and sulfur dichloride using aluminium chloride as a catalyst (total yield 80%). The extent of chlorination of the aromatic ring was suppressed by use of iron(III) chloride as the catalyst or of sulfur chloride instead of the dichloride. Some substituted benzonitriles and pivalonitrile also gave thiadiazoles in lower yields.

Sulfur dichloride has long been known as a reactive enophile and its additions to olefinic or diolefinic compounds have been widely applied to syntheses of sulfur-containing heterocyclic compounds.[1] However, only a few addition reactions of sulfur dichloride to carbon-nitrogen multiple bonds have been reported in spite of ready availability of sulfur dichloride and its high reactivity to olefins. While no reports on 1,2-addition of sulfur dichloride to carbon-nitrogen double bonds and to carbon-nitrogen triple bonds of aliphatic nitriles, whose aliphatic moiety was chlorinated[2] or chlorosulfenylated,[3] addition reaction was observed for sulfonyl nitriles.[4] The other examples are also limited to some special cyanides and formations of 3,4-dichloro-1,2,5-thiadiazole from cyanogen,[5] 3,5-dichloro-1,2,4-thiadiazole from phosphorus tricyanide,[6] and 3,4,4,5-tetrachloro-4*H*-1,2,6-thiadiazine from dichloromalononitrile[7,8] are reported.

Here we describe the reaction of nitriles activated by a Lewis acid with sulfur dichloride, which leads to formation of 1,2,4-thiadiazoles.[9] Thiadiazoles have been drawing our considerable attention because many of them are known as potential physiologically active substances[10] and, hence, the present reaction would provide us a new application of sulfur dichloride in this field.

Results and Discussion

To a well-stirred mixture of benzonitrile (6 equiv.) and aluminium chloride (1.2 equiv.) under a nitrogen atmosphere was added dropwise sulfur dichloride (1.0 equiv.) and the mixture was stirred at 90 °C for 20 h to give 3,5-diphenyl-1,2,4-thiadiazole (**3a**), 3-*o*-chlorophenyl-5-phenyl-1,2,4-thiadiazole (**4a**), and 3-*p*-chlorophenyl-5-phenyl-1,2,4-thiadiazole (**5a**). The products were separated by silica-gel chromatography and identified with authentic samples. The formation of

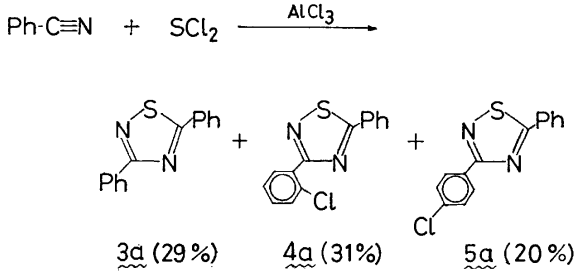

Table 1. Formation of 1,2,4-thiadiazoles from benzonitrile and sulfur dichloride

Conditions[a] Temp/°C	Time/h	Total yield/%[b] **3a**+**4a**+**5a**	Product ratio[b] **3a**/**4a**+**5a**
80	12	15	88/12
120	12	68	43/57
120	12[c]	36	38/62
120	12[d]	24	100/ 0
180	15	49	46/54

a) PhCN (5 equiv.), SCl_2 (1 equiv.), and $AlCl_3$ (1 equiv.) were used. b) Determined by GLC: 1.2 m×3 mmϕ glass column packed with 5% PS-410 on Chromosorb W 60—80 mesh; oven temp 230 °C; carrier gas, He 1.0 kg/cm^2. c) 0.5 equiv. of $AlCl_3$ was used. d) Hydroquinone (0.15 mol%) was added.

the latter two compounds is attributed to chlorination of the phenyl ring during the reaction.

The results of this reaction under several conditions are listed in Table 1. Any of several solvents we examined was not satisfactory and, hence, excessive amount of the nitrile was employed as the solvent. The total yield of the thiadiazoles was cut in half when 0.5 equiv. of aluminium chloride was used (see Table 1), and the reaction did not proceed at all without the Lewis acid. Therefore, an equimolar amount of the Lewis acid is indispensable for the present reaction.

The lower reaction temperature seemed to suppress the chlorination of the phenyl ring but reduced the total yield of the thiadiazoles at the same time. Addition of hydroquinone (0.15 equiv.) also resulted in a decrease in the yield, but completely controlled the chlorination products as shown in Table 1. Smaller amount (0.10 equiv.) of hydroquinone could afford a better yield (47%) but worse selectivity (**3a**/**4a**+**5a**= 81/19). As is already known, substituted phenols react with sulfur dichloride to form thiobis(phenol) derivatives which are useful as antioxidants.[11] Furthermore, Friedel-Crafts reaction of benzene with sulfur dichloride in the presence of aluminium chloride to form diphenyl sulfide is reported.[12] Hence, the decrease in the yield of the thiadiazoles by the addition of hydroquinone might be caused by the reaction of the quinone with sulfur dichloride. However, the decrease in chlorinated products could not be attributed

Table 2. Lewis acids as catalyst for the formation of 1,2,4-thiadiazoles from benzonitrile and sulfur dichloride[a)]

Lewis acid	Total yield/%[b)] **3a**+**4a**+**5a**	Product ratio[b)] **3a**/**4a**+**5a**
$SnCl_4$	71	42/58
$AlCl_3$	68	43/57
$SbCl_5$	66	38/62
$FeCl_3$	62	77/23
$ZnCl_2$	22	64/36
$TiCl_4$	18	28/72
$AlBr_3$	3	(100/ 0)[c)]
$BF_3 \cdot OEt_2$	0	—

a) Mole ratio; PhCN/SCl_2/Lewis acid=5/1/1; reaction conditions; 120 °C, 12 h. b) Determined by GLC. For the conditions, see the footnote b) in Table 1. c) The brominated products corresponding to **4a** and **5a** could not be detected.

Table 3. Formation of 3,5-disubstituted 1,2,4-thiadiazoles from nitriles and sulfur dichloride

Nitrile	Conditions[a)] Temp/°C	Time/h	Product	Yield/%
o-Cl-C_6H_4CN	120	40	**3b**	31
o-Me-C_6H_4CN	120	44	**3c**	—
m-Me-C_6H_4CN	120	25	**3d**	18[b)]
p-Me-C_6H_4CN	120	25	**3e**	45
Me_3CCN	100	45	**3f**	10

a) Mole ratio of the reactants; a nitrile/SCl_2/$AlCl_3$=5/1/1. b) Determined by GLC.

simply to radical trapping ability of the anticipated thiobis(hydroquinone), because other attempts to reduce the extent of chlorination, *e.g.*, the reactions in dark and in the presence of copper(II) chloride or sulfur, were not successful.

As for the catalyst, tin(IV) chloride and antimony (V) chloride were as effective as aluminium chloride. On the other hand, iron(III) chloride depressed the ratio of the chlorinated products. Some effects of Lewis acids as a catalyst are listed in Table 2, and no direct correlation between the yields and acidity was observed.

This reaction could be extended to substituted benzonitriles and pivalonitrile (see Table 3). In these reactions, chlorinated products were isolated in very low yields or not detected at all. *o*-Tolunitrile gave no thiadiazole probably because of steric hindrance. *p*-Chlorobenzonitrile did give the corresponding thiadiazole, but sublimation of the nitrile caused a lower yield. On the contrary, benzyl cyanide and acetonitrile gave no thiadiazoles. Consequently protons α to the cyano group seem to be undesirable for the reaction. In fact small amount of a disulfide derivative was isolated from the reaction mixture of sulfur dichloride and isobutyronitrile which gave no thiadiazole.[2)]

$$Me_2CHCN + SCl_2 \xrightarrow{AlCl_3} Me_2\overset{CN}{\overset{|}{C}}-S-S-\overset{CN}{\overset{|}{C}}Me_2$$

We tentatively assume the reaction path as follows. A complex of aluminium chloride and a nitrile was initially formed and successive addition of sulfur dichloride to the complex gave rise to the intermediate **6**. Formation of the thiadiazole **3** can be interpreted by addition of the nitrile to **6** followed by elimination of aluminium chloride and chlorine. It is likely that aluminium chloride was consumed by complexation with the resulted thiadiazole **3**, since equimolar amount of the chloride was necessary for the reaction. It is not clear whether the aromatic ring was chlorinated by sulfur dichloride or by chlorine liberated during the formation of **3** from **6**. In chlorine atmosphere, the reaction did not give the thiadiazoles, but formation of a large amount of chlorinated benzonitrile was observed.

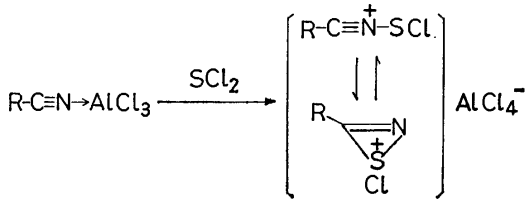

6

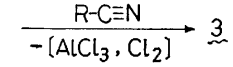

As sulfur dichloride is known to form a complex with aluminium chloride,[13)] an alternative path *via* this type of complex leading to **6** was also conceivable. If this path were valid, the reaction of the isolated sulfur dichloride–aluminium chloride complex with benzonitrile under the same conditions should have given better yields of the thiadiazoles. However, the reaction at 120 °C for 12 h afforded **3a**, **4a**, and **5a** in 42% yield (**3a**/**4a**+**5a**=35/65) which is about two thirds of that obtained by addition of sulfur dichloride to a benzonitrile–aluminium chloride mixture. Therefore the path *via* sulfur dichloride–aluminium chloride complex was less likely and, in this case, the complex was probably converted into the benzonitrile–aluminium chloride complex by exchange of the ligands.

Similarly, exchange of one nitrile with another occurred very easily and, hence, scrambling of nitriles was observed when two nitriles were employed in the reaction. In these cases, a mixture of benzonitrile and sulfur dichloride was added to a well-stirred solution of a nitrile and aluminium chloride and was stirred for 12 h at 120 °C. The product was a mixture of four possible types of thiadiazoles, **3a**, **3b**,**e**,**f**, **7**, and **8**. Reverse addition of the two

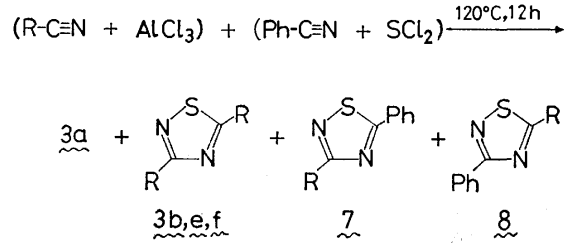

Table 4. Formation of unsymmetrically 3,5-disubstituted thiadiazoles

R-C≡N	Yield/%[a]			
R	**3a**	**3**	**7**	**8**
o-Cl-C_6H_4-	30	**3b** 22	22[b]	9
p-Me-C_6H_4-	6	**3e** 20	20[c]	
Me_3C	9	**3f** 0	29[c]	

a) Yields were determined by GLC. b) Same to the compound **4a**. c) The thiadiazoles **7** and **8** were not separated.

nitriles also resulted in the formation of the above products but caused slight change in the product distribution.

Another ambiguity we should make clear is that sulfur chloride might be the reactive species in this reaction, because the following equilibrium between sulfur dichloride and sulfur chloride is known. However the possibility was excluded out by the fact that

$$2SCl_2 \rightleftharpoons S_2Cl_2 + Cl_2$$

the use of sulfur chloride instead of sulfur dichloride caused a decrease in the yields of the thiadiazoles. A merit of use of sulfur chloride is that no chlorination products were formed under these conditions. The formation of the thiadiazole **3** is explained by genera-

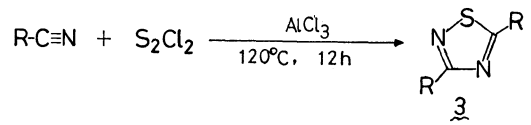

3

3a (R = Ph) 37%
3d (R = p-tolyl) 32%

tion of sulfur dichloride and sulfur from sulfur chloride according to the following equation. Thus the use of sulfur chloride would decrease the extent of free

$$S_2Cl_2 \rightleftharpoons SCl_2 + S$$

chlorine which derives from sulfur dichloride and/or from the thiadiazole formation and this must be the reason for suppression of chlorination products.

Experimental

Melting points were determined on a Yanagimoto micro melting point apparatus MP-21 and melting and boiling points were uncorrected. Infrared spectra were taken on a JASCO IRA-1 spectrometer in Nujol mull unless otherwise noted. ^1H and ^{13}C NMR spectra were obtained with JEOL JNM PMX-60 and JEOL JNM FX 90Q FT spectrometers, respectively, in $CDCl_3$ solutions using TMS as an internal standard. Mass spectrometry was performed with Hitachi RMU-6E spectrometer at an ionizing voltage of 70 eV. GLC analysis was done with Shimadzu model GC-3BT using a glass column (1.2 m × 3 mmϕ) packed with 5% PS-410 on Chromosorb W 60—80 mesh. All the reactions were carried out under a dry nitrogen atmosphere.

Materials. Commercially available SCl_2, S_2Cl_2, and nitirles were distilled prior to use. $AlCl_3$ and the other Lewis acids were used without further purification.

Reaction of SCl_2 with Benzonitrile. To a well-stirred solution of $AlCl_3$ (16.6 g, 124 mmol) in the nitrile (50.6 g, 491 mmol) was added dropwise a mixture of SCl_2 (10.4 g, 100 mmol) and the nitrile (12.9 g, 125 mmol) and the mixture was stirred for 20 h at 90 °C. The resulting mixture was extracted with ether and dilute sodium hydroxide solution and the ethereal extract was dried (Na_2SO_4), and concentrated. Distillation of the residue gave 19.6 g of a mixture of the three thiadiazoles **3a**, **4a**, and **5a** (bp 150—180 °C/267 Pa). A part (2.22 g) of the mixture was chromatographed on a silica-gel column to give 0.79 g (29%) of 3,5-diphenyl-1,2,4-thiadiazole (**3a**, eluted with 1:1 mixture of benzene and hexane), 0.94 g (31%) of 3-*o*-chlorophenyl-5-phenyl-1,2,4-thiadiazole (**4a**, eluted with benzene), and 0.61 g (20%) of 3-*p*-chlorophenyl-5-phenyl-1,2,4-thiadiazole (**5a**, eluted with 1:3 mixture of benzene and hexane).

The thiadiazole **3a** was recrystallized from benzene–hexane as colorless needles: Mp 95.5—96.5 °C; ^1H NMR δ 7.2—7.6(6H, m), 7.8—8.1(2H, m), 8.2—8.5(2H, m); ^{13}C NMR δ (ppm) 188.1(N–C=N), 173.8(S–C=N), and aromatic carbons at 133.0, 131.9, 130.8, 130.3, 129.3, 128.7, 128.4, 127.5; MS *m/e* (rel intensity) 238(43, M^+), 135(100, M^+—PhCN). The infrared and ^1H NMR spectra of the compound were identical with those of an authentic sample prepared by oxidation of thiobenzamide with iodine.[14] Found: C, 70.54; H, 4.09; N, 11.65; S, 13.67%. Calcd for $C_{14}H_{10}N_2S$: C, 70.59; H, 4.20; N, 11.76; S, 13.45%.

The thiadiazole **4a** was isolated as a colorless oil: Bp 140 °C/133 Pa; ^1H NMR δ 7.2—7.6(6H, m), 7.8—8.2(3H, m); ^{13}C NMR δ (ppm) 187.8(N–C=N), 171.9(S–C=N), and aromatic carbons at 133.3, 132.3, 132.0, 130.9, 130.8, 130.5, 129.3, 127.5, 126.7; MS *m/e* (rel intensity) 272(38, M^+), 169(100, M^+—PhCN), 135(30, M^+—ClC_6H_4CN). The infrared and ^1H NMR spectra of the compound were in good agreement with those of an authentic sample prepared from 5-*o*-chlorophenyl-1,3,4-oxathiazol-2-one and benzonitrile.[15] Found: C, 61.82; H, 3.21; N, 10.34; S, 11.57; Cl, 13.33%. Calcd for $C_{14}H_9N_2SCl$: C, 61.65; H, 3.30; N, 10.28; S, 11.74; Cl, 13.03%.

Recrystallization of the compound **5a** from benzene–hexane gave colorless needles: Mp 121.5—122.5 °C; ^1H NMR δ 7.2—7.6(5H, m), 7.8—8.1(2H, m), 8.25(2H, d); ^{13}C NMR δ (ppm) 188.4(N–C=N), 172.7(S–C=N), and aromatic carbons at 136.5, 132.0, 131.4, 130.6, 129.7, 129.3, 128.9, 127.5; MS *m/e* (rel intensity) 272(41, M^+), 169(100, M^+—PhCN), 135(28, M^+—ClC_6H_4CN). The infrared and ^1H NMR spectra of the compound well agreed with those of an authentic sample.[16] Found: C, 61.40; H, 3.07; N, 10.24; S, 11.63; Cl, 13.32%. Calcd for $C_{14}H_9N_2SCl$: C, 61.65; H, 3.30; N, 10.28; S, 11.74; Cl, 13.03%.

Reactions of SCl_2 with the Other Nitriles. Reactions of SCl_2 with *o*-chlorobenzonitirle, *m*-tolunitrile, *p*-tolunitrile, and pivalonitrile were carried out similarly to the reaction with benzonitrile to afford 3,5-bis(*o*-chlorophenyl)-1,2,4-thiadiazole (**3b**), 3,5-di-*m*-tolyl-1,2,4-thiadiazole (**3d**), 3,5-di-*p*-tolyl-1,2,4-thiadiazole (**3e**), and 3,5-di-*t*-butyl-1,2,4-thiadiazole (**3f**), respectively. Reaction conditions and yields are given in Table 3.

*The Thiadiazole **3b**:* Mp 93—96 °C (colorless needles from benzene); ^1H NMR δ 7.2—7.7(6H, m), 7.8—8.2(1H, m), 8.4—8.8(1H, m); ^{13}C NMR δ (ppm) 183.0(N–C=N), 169.7 (S–C=N), and aromatic carbons at 133.8, 133.3, 132.2, 132.1, 132.0, 130.9, 130.7, 130.6, 130.4, 129.5, 127.4, 126.7; MS *m/e* (rel intensity) 306(14, M^+), 169(100, M^+—ClC_6H_4CN). Found: C, 54.28; H, 2.59; N, 9.05%. Calcd for $C_{14}H_8N_2SCl_2$: C, 54.72; H, 2.61; N, 9.12%.

An analytical sample of the thiadiazole **3d** was obtained by preparative GLC as colorless powder: mp 55—56 °C; ^1H NMR δ 2.43(6H, s), 7.2—7.5(4H, m), 7.7—8.0(2H, m),

8.0—8.3(2H, m); MS *m/e* (rel intensity) 266(37, M^+), 149 (100, $M^+-MeC_6H_4CN$).

The Thiadiazole ***3e***: Mp 135—137 °C (colorless powder from benzene); ^1H NMR δ 2.38(6H, s), 7.22(4H, d), 7.84 (2H, d), 8.23(2H, d); MS *m/e* (rel intensity) 266(39, M^+), 149(100, $M^+-MeC_6H_4CN$). Found: C, 72.06; H, 5.13; N, 10.24; S, 12.32%. Calcd for $C_{16}H_{14}N_2S$: C, 72.18; H, 5.26; N, 10.52; S, 12.03%.

The Thiadiazole ***3f***: Bp 70 °C/133 Pa (colorless oil); ^1H NMR δ 1.44(9H, s), 1.46(9H, s); ^{13}C NMR δ (ppm) 201.0 (N–C=N), 184.6(S–C=N), 37.2 and 37.0(tertiary carbons), 30.4 and 29.5(Me carbons); MS *m/e* (rel intensity) 198 (61, M^+), 183(78, M^+-Me), 115(100, M^+-BuCN). Found: C, 60.26; H, 9.13; N, 13.99; S, 15.94%. Calcd for $C_{10}H_{18}N_2S$: C, 60.61; H, 9.09; N, 14.14; S, 16.16%.

Reaction of SCl_2 with Isobutyronitrile. A mixture of SCl_2 (2.10 g, 20.3 mmol), isobutyronitrile (9.84 g, 142 mmol), and $AlCl_3$ (3.33 g, 25 mmol) was heated at reflux for 40 h and worked up as the other runs. From 600 mg of a benzene fraction of chromatographic treatment of the resultant oil on a silica-gel column, 70 mg of crystalline bis(α-cyanopropyl) disulfide was obtained: mp 51—59 °C; IR 2220 cm^{-1} (C≡N); ^1H NMR δ 1.75(s); MS *m/e* (rel intensity) 200(5, M^+), 136(10, M^+-S_2), 69(100, Me_2CHCN^+), 68(72, Me_2CCN^+).

Formation of 3,5-Unsymmetrically Disubstituted Thiadiazoles ***7*** *and* ***8***. To a well-stirred mixture of a nitrile (RCN, 130—150 mmol) and $AlCl_3$ (30 mmol) was added a mixture of SCl_2 (30 mmol) and benzonitrile (100—120 mmol) and the mixture was heated at 120 °C for 20 h. The reaction mixture was worked up as the other runs to give mixtures of the thiadiazoles **3**, **7**, and **8** whose yields were determined by GLC analysis (see Table 4).

In the reaction using *o*-chlorobenzonitrile, the thiadiazole **4a** and 5-*o*-chlorophenyl-3-phenyl-1,2,4-thiadiazole (**8b**) were identified with authentic samples prepared by the Howe's method.[15]

An analytical sample of a mixture of 5-phenyl-3-*p*-tolyl-1,2,4-thiadiazole (**7e**) and 3-phenyl-5-*p*-tolyl-1,2,4-thiadiazole (**8e**) was obtained by preparative GLC. The retention times of the both compounds were in good agreement with those of authentic samples prepared by the method of Howe:[15] ^1H NMR δ 2.41(3H, s), 7.2—8.5(9H, m); MS *m/e* (rel intensity) 252(58, M^+), 149(100, M^+-PhCN), 135 (53, $M^+-MeC_6H_4CN$). The infrared spectrum of the mixture also showed all the absorptions of the both authentic samples.

Similarly a mixture of 3-*t*-butyl-5-phenyl-1,2,4-thiadiazole (**7f**) and 5-*t*-butyl-3-phenyl-1,2,4-thiadiazole (**8f**) was collected from GLC fraction: MS *m/e* (rel intensity) 218(66, M^+), 203(53, M^+-Me), 135(100, M^+-BuCN), 115(47, M^+-PhCN).

Reactions of S_2Cl_2 with Nitriles. The reactions were carried out similarly to the previous runs at 120 °C for 12 h except that S_2Cl_2 was employed in place of SCl_2. Benzonitrile (15.7 g, 152 mmol) and S_2Cl_2 (4.22 g, 31.2 mmol) reacted in the presence of $AlCl_3$ (4.01 g, 30.1 mmol) to give the thiadiazole **3a** (yield 37% by GLC) without formation of the chlorinated products **4a** and **5a**. The yield of the thiadiazole **3d** was determined to be 32% by GLC when the reaction was started with *p*-tolunitrile (17.6 g, 150 mmol), S_2Cl_2 (4.05 g, 30 mmol), and $AlCl_3$ (3.99 g, 30 mmol).

The authors wish to express their hearty thanks to Dr. Robert K. Howe of Monsanto Agricultural Products Co., St. Louis, Missouri, U. S. A. for his giving us spectral data of some of the thiadiazoles. The present work was partially supported by a Grant-in-Aid for scientific research No. 543025 from the Ministry of Education, Science and Culture to which our thanks are due.

References

1) L. Brandsma, J. Meijer, and H. D. Verkruijsse, *J. Chem. Soc., Chem. Commun.*, **1980**, 922; N. M. Morylan, E. L. Abagyan, R. G. Mirzoyan, and Sh. O. Badanyan, *Arm. Khim. Zh.*, **32**, 896 (1979); *Chem. Abstr.*, **93**, 150217 (1980); M. Muehlstaedt and P. Kuhl, *J. Prakt. Chem.*, **320**, 873 (1978); N. M. Morylan, E. L. Abagyan, and L. L. Nikogosyan, *Arm. Khim. Zh.*, **29**, 806 (1976); *Chem. Abstr.*, **86**, 121109 (1977); F. Lautenschlaeger and N. V. Schwartz, *J. Org. Chem.*, **34**, 3990 (1969); F. Lautenschlaeger, *ibid.*, **34**, 3998 (1969); **33**, 2620, 2627 (1968); **31**, 1679 (1966); *Can. J. Chem.*, **44**, 2813 (1966); E. D. Weil, K. J. Smith, and R. J. Gruber, *J. Org. Chem.*, **31**, 1663 (1966); E. J. Corey and E. Block, *ibid.*, **31**, 1663 (1966).

2) D. Martinez, *Z. Chem.*, **20**, 139 (1980); *Chem. Abstr.*, **93**, 167549 (1980).

3) J. Rouchaud and A. Bruylants, *Bull. Soc. Chim. Belg.*, **76**, 50 (1967); *Chem. Abstr.*, **67**, 81634 (1967).

4) M. S. A. Vrijland, *Tetrahedron Lett.*, **1974**, 837.

5) R. D. Vest, U. S. Patent 3115497 (1963); *Chem. Abstr.*, **60**, 5512d (1964).

6) A. E. Barnett, P. Piotis, and B. Tittle, *J. Inorg. Nucl. Chem.*, **38**, 1575 (1976).

7) H. Kristinsson, *Tetrahedron Lett.*, **1973**, 4489.

8) J. Geevers and W. P. Trompen, *Tetrahedron Lett.*, **1974**, 1687.

9) For recent works on synthesis of 1,2,4-thiadiazoles, see: R. K. Howe and B. R. Shelton, *J. Org. Chem.*, **46**, 771 (1981); Y-i. Lin, S. A. Lang, Jr., and S. R. Petty, *ibid.*, **45**, 3750 (1980); R. K. Howe, T. A. Gruner, and J. E. Franz, *ibid.*, **42**, 1813 (1977).

10) L. L. Bambas, "Five Membered Heterocyclic Compounds with Nitrogen and Sulfur or Nitrogen, Sulfur, and Oxygen," Interscience Publishers, New York, N. Y. (1952); F. Kurzer in "Advances in Heterocyclic Chemistry," ed by A. R. Katritzky, Academic Press, New York, N. Y. (1965), Vol. 5, pp. 119—204; L. M. Weinstock and P. I. Pollak, *ibid.*, (1968), Vol. 9, pp. 107—164; J. Sandström, *ibid.*, (1968), Vol. 9, pp. 165—210.

11) G. V. Hutson and M. P. Talbot, Brit. Patent 1511495 (1979); *Chem. Abstr.*, **90**, 87003 (1979); P. Sh. Mamedeva and G. K. Sadykhova, *Chem. Abstr.*, **90**, 137396 (1979); F. Dunning, B. Dunning, Jr., and E. Drake, *J. Am. Chem. Soc.*, **53**, 3466 (1931); R. Lesser and G. Gad, *Ber.*, **56**, 963 (1923).

12) M. J. Böeseken and D. A. W. Koning, *Recl. Trav. Chim. Pays-Bas*, **30**, 116 (1911); M. J. Böeseken, *ibid.*, **24**, 209 (1905).

13) S. N. Nabi and M. A. Khaleque, *J. Chem. Soc.*, **1965**, 3626.

14) A. W. Hofmann, *Ber.*, **2**, 645 (1869).

15) R. K. Howe and J. E. Franz, *J. Org. Chem.*, **39**, 962 (1974).

16) The spectra were kindly offered by Dr. R. K. Howe.

Furan Derivatives. V. The Syntheses of 4,5-Dihydro-3*H*-naphtho[1,8-*bc*]furans Using Strong Bases

Takaaki HORAGUCHI,* Hidetaka NARITA, and Tsuneo SUZUKI†

Department of Chemistry, Faculty of Science, Niigata University, Ikarashi, Niigata 950-21

† *Nippon Dental University, Niigata, 1-8, Hamaura-cho, Niigata 950*

(Received March 15, 1982)

The reaction of ethyl (4-methoxy-8-oxo-5,6,7,8-tetrahydro-1-naphthyloxy)acetate and potassium hydroxide gave a mixture of 6-methoxy-4,5-dihydro-3*H*-naphtho[1,8-*bc*]furan and 6-methoxy-4,5-dihydro-3*H*-naphtho[1,8-*bc*]furan-2-carboxylic acid in total yield above 90%. The mechanisms of formation of two products were examined, and potassium 2a-hydroxy-6-methoxy-2a,3,4,5-tetrahydro-2*H*-naphtho[1,8-*bc*]furan-2-carboxylate was isolated as a precursor of 6-methoxy-4,5-dihydro-3*H*-naphtho[1,8-*bc*]furan. It has become apparent that strong bases such as sodium hydroxide, sodium ethoxide, and sodium hydride were also useful for syntheses of 6-methoxy-4,5-dihydro-3*H*-naphtho[1,8-*bc*]furan derivatives.

4,5-Dihydro-3*H*-naphtho[1,8-*bc*]furans (**4**) are important intermediates to prepare phenanthro[4,5-*bcd*]-furans,[1-4] and unique molecules which have strain[5-8] introduced by condensation of the furan and naphthalene rings at *peri*-positions. Two methods have been employed to synthesize 4,5-dihydro-3*H*-naphtho-[1,8-*bc*]furans (**4**) as shown in Scheme 1. In the first method[9-18] 8-hydroxy-1,2,3,4-tetrahydro-1-naphthalenone (**1**) reacted with ethyl bromoacetate in the presence of potassium carbonate followed by saponification and decarboxylation to give 4,5-dihydro-3*H*-naphtho[1,8-*bc*]furans (**4**).[19] The yields of **2** were below 50% for various kinds of substituents (R^1 and R^2) though decarboxylation reaction of **2** proceeded smoothly in good yields. In the second method[20-28] (8-oxo-5,6,7,8-tetrahydro-1-naphthyloxy)acetic acids (**3**) were treated with acetic anhydride and sodium acetate to give a mixture of 4,5-dihydro-3*H*-naphtho-[1,8-*bc*]furans (**4**) and lactones (**5**).[7,19] The yields of **4** were near 50% because of the formation of lactones (**5**). It seems that these low yields result from the strain[7] in the fused ring system of 4,5-dihydro-3*H*-naphtho[1,8-*bc*]furans. Accordingly, we attempted to improve the yields of 4,5-dihydro-3*H*-naphtho[1,8-*bc*]-furans by using strong bases instead of weak bases. The mechanisms of formation of the furan ring is discussed.

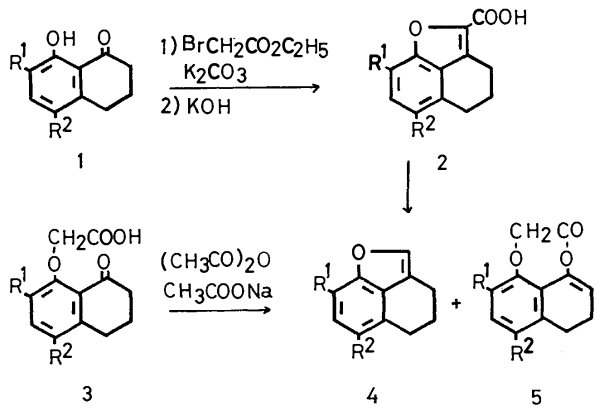

1 2 3 4 5

a) R^1=H; R^2=H
b) R^1=H; R^2=OCH_3
c) R^1=OCH_3; R^2=H
d) R^1=OCH_3; R^2=Cl

Scheme 1.

Results and Discussion

Ethyl (4-methoxy-8-oxo-5,6,7,8-tetrahydro-1-naphthyloxy)acetate (**6**) was obtained in an 88% yield by esterification of (4-methoxy-8-oxo-5,6,7,8-tetrahydro-1-naphthyloxy)acetic acid (**3b**)[19] with diethyl sulfate[39] and potassium carbonate as shown in Scheme 2.

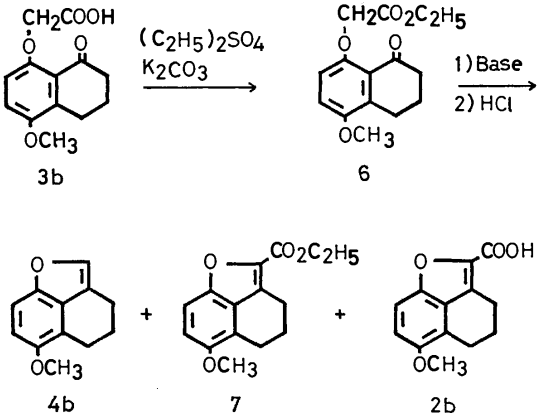

3b 6 4b 7 2b

Scheme 2.

Compound **6** was treated with four kinds of strong bases (potassium hydroxide, sodium hydroxide, sodium ethoxide, and sodium hydride) in anhydrous dioxane. The results are summarized in Table 1.

When **6** was refluxed with five equivalents of potassium hydroxide in dioxane for 1 h followed by acidification with hydrochloric acid, two products, 6-methoxy-4,5-dihydro-3*H*-naphtho[1,8-*bc*]furan (**4b**) and 6-methoxy-4,5-dihydro-3*H*-naphtho[1,8-*bc*]furan-2-car-

Table 1. The reactions of ethyl (4-methoxy-8-oxo-5,6,7,8-tetrahydro-1-naphthyloxy)acetate (**6**) and strong bases in dioxane

Base[a]	Products yield/%			Total yield/%
	4b	**7**	**2b**	
KOH	71	0	22	93
NaOH	47	0	45	92
C_2H_5ONa	44	0	50	94
NaH	24	49	19	92

a) Compound **6** (0.50 g; 1.80 mmol) was treated with 9.00 mmol of each base.

Table 2. The reactions of ethyl (4-methoxy-8-oxo-5,6,7,8-tetrahydro-1-naphthyloxy)acetate (**6**) and strong bases in benzene

Base[a]	Products yield/%				Total yield/%
	4b	**7**	**2b**	**3b**	
KOH	47	0	0	33	80
NaOH	39	0	0	47	86
C_2H_5ONa	42	0	55	0	97
NaH	42	43	10	0	95

a) Compound **6** (0.50 g; 1.80 mmol) was treated with 9.00 mmol of each base.

boxylic acid (**2b**), were obtained in 71 and 22% yields respectively. The total yield of **4b** and **2b** were 93%, and **2b** was smoothly converted to **4b** by decarboxylation.[19] However, the reaction of **6** with one equivalent of potassium hydroxide afforded **4b**, **2b**, and **3b** in 74, 7, and 12% yields respectively. In the presence of one equivalent of potassium hydroxide the yield of **2b** was reduced. The structures of **4b** and **2b** were confirmed by comparing the IR and ^{1}H NMR spectra and melting point with those of authentic samples.[19] Similarly, the reactions of **6** and other three bases gave 6-methoxy-4,5-dihydro-3*H*-naphtho[1,8-*bc*]furans (**4b**, **7**, and **2b**) in total yield above 90%. The structure of **7** was confirmed by comparing the IR and ^{1}H NMR spectra and the melting point with those of an authentic sample.[19]

Nextly, the reactions of **6** with four strong bases were examined in anhydrous benzene. The results are summarized in Table 2.

The reactions of **6** and sodium ethoxide or sodium hydride gave 6-methoxy-4,5-dihydro-3*H*-naphtho[1,8-*bc*]furans (**4b**, **7**, and **2b**) in total yield above 90%. However, the reaction of **6** and potassium hydroxide or sodium hydroxide afforded **4b** in poor yields because of the ready saponification of **6** to the acid **3b**. Though ethanol was used as a solvent, favorable results were not obtained.

From the above results, strong bases are seen to be generally useful for synthesizing 4,5-dihydro-3*H*-naphtho[1,8-*bc*]furan derivatives in good yields. The methods seems to be applicable to syntheses of a variety of 4,5-dihydro-3*H*-naphtho[1,8-*bc*]furans.

We have examined the reaction of **6** and potassium hydroxide in detail in order to explain the mechanisms of formation of 6-methoxy-4,5-dihydro-3*H*-naphtho[1,8-*bc*]furans (**4b**, **7**, and **2b**), since the mechanism of formation of the furan ring had not been explored adequately for benzofuran derivatives.[40–46] When **6** was refluxed with one equivalent of potassium hydroxide in dioxane potassium 2a-hydroxy-6-methoxy-2a,3,4,5-tetrahydro-2*H*-naphtho[1,8-*bc*]furan-2-carboxylate (**8**) was obtained as a precipitate in 76% yield. The structure of **8** was confirmed from the spectral properties. The IR spectrum of **8** showed absorption bands due to the carboxylate ion at 1420 and 1610 cm^{-1}. The ^{1}H NMR spectrum of **8** showed a peak due to a methine proton at 4.60 ppm (1H, s), but a hydroxyl group peak was not found because of an exchange reaction between the hydroxyl group and water. The ^{13}C NMR spectrum of **8** exhibited a peak due to a quaternary carbon (2a-position) at 76.8 ppm and a peak due to a tertiary carbon (2-position) at 96.6 ppm. However, the stereochemical relation between the methine proton and the hydroxyl group was not evident from the spectral properties.

In the reaction of **6** with five equivalents of potassium hydroxide in dioxane, compound **4b** was not present in the reaction mixture before acidification with hydrochloric acid judging from TLC analysis. Therefore, **4b** was produced by acidification of the reaction mixture. The ^{1}H and ^{13}C NMR spectra of the precipitates obtained from the reaction of **6** with five equivalents of potassium hydroxide showed that the precipitates consisted of **8** and potassium 6-methoxy-4,5-dihydro-3*H*-naphtho[1,8-*bc*]furan-2-carboxylate (**9**), that is, potassium salt of **2b** was already present in the reaction mixture before acidification. Compound **8**, once produced, was stable and not converted to **4b** or **9** under the reaction conditions of **6** with potassium hydroxide.

When an aqueous solution of **8** was acidified with hydrochloric acid, **4b** was readily obtained in a 90% yield but the yield of **2b** was only 2%. Therefore, it is clear that **4b** was exclusively produced from the intermediate **8**. The reaction of **8** with diethyl sulfate in dioxane gave **4b** and **7** in 65 and 19% yields respectively. In the presence of potassium hydroxide the reaction of **8** with diethyl sulfate afforded **4b** and **2b** in 3 and 26% yields respectively. The results suggest that the ester **11** was unstable and converted easily to **4b** or **7** by elimination of ethyl hydrogen carbonate or water. In the presence of potassium hydroxide elimination of water was accelerated to give **2b**. Compound **8** was converted to **9** by heating at 240 °C for 2 h under reduced pressure in quantitative yield. From the above results the reaction mechanisms of formation of **4b**, **7**, and **2b** were

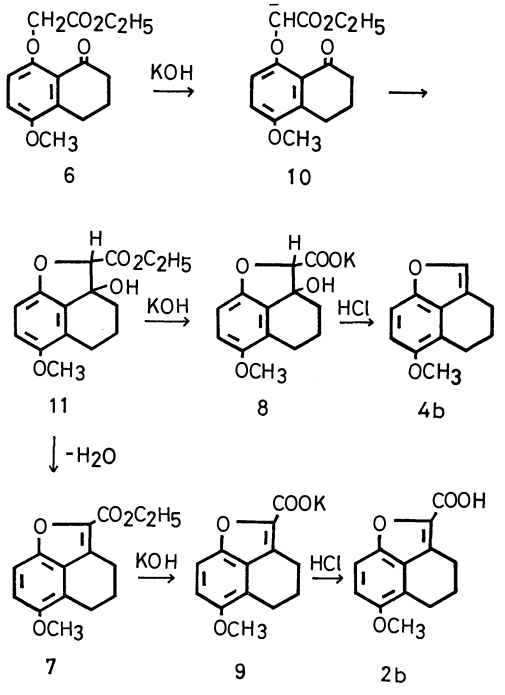

Scheme 3.

elucidated and are summarized in Scheme 3.

A proton of the active methylene group in **6** is removed by potassium hydroxide to give an anion **10**. The anion **10** cyclize to an ester **11** which reacts in two paths. Saponification of the ester **11** gives **8** which is stable under the reaction conditions and is converted to **4b** only by adding hydrochloric acid. Dehydration of the ester **11** affords **7** which can be saponified easily by excess potassium hydroxide to give **9**. Compound **9** is converted to **2b** by adding hydrochloric acid. Therefore, **11** is a precursor of **4b**, **7**, and **2b**, and **8** is a direct precursor of **4b**. The mechanisms of the reaction of **6** with potassium hydroxide will be applicable to the reactions of **6** and other strong bases. The reactivity and stereochemistry of **8** will be further investigated.

Experimental

All the melting points are uncorrected. The column chromatography was performed on silica gel (Wakogel C-200). Unless otherwise stated anhydrous sodium sulfate was employed as the drying agent. The infrared absorption spectra (IR) were determined on a Hitachi EPI-G grating infrared spectrophotometer. The nuclear magnetic resonance spectra (^{1}H and ^{13}C NMR) were determined at 90 MHz on a JEOL JNM-FX 90Q FT NMR spectrometer. Tetramethylsilane (TMS) was used as the internal standard in organic solvents. Methyl groups of sodium 2,2-dimethyl-2-silapentane-5-sulfonate (DSS) were employed as the internal standard in deuterium oxide: The chemical shift of the methyl groups was taken as 0 ppm.

A General Procedure for the Reactions of Ethyl (4-Methoxy-8-oxo-5,6,7,8-tetrahydro-1-naphthyloxy)acetate (6) with Strong Bases. A mixture of **6** (0.50 g; 1.80 mmol), potassium hydroxide (0.50 g; 9.00 mmol), and anhydrous dioxane (10 ml) was refluxed for 1 h. To the mixture water (20 ml) was added, and the solution was poured into 2 M** hydrochloric acid (100 ml). After 15 min the solution was extracted with ether. The ethereal solution was washed three times with a 1 M potassium carbonate solution (30 ml) and then with water, dried, and evaporated. The resulting oil was chromatographed and eluted with benzene to give 0.24 g (71%) of **4b** as colorless oil. The IR and ^{1}H NMR spectra of the oil are identical with those of an authentic sample.[19] Bp 102 °C at 0.7 Torr.*** ^{13}C NMR ($CDCl_3$): δ (TMS) 19.9, 21.7, 23.5, 56.7, 108.0, 109.4, 116.9, 128.8, 138.5, 148.4, 151.2.

The alkaline solution was acidified with 6M hydrochloric acid and the resulting precipitates were extracted with ether. The ethereal solution was washed with water, dried, and evaporated to give 0.09 g (22%) of **2b** as crystals. Recrystallization from dioxane gave colorless needles; mp 229 °C (decomp). The IR spectrum and melting point of the needles are identical with those of an authentic sample.[19] ^{1}H NMR (CD_3COCD_3): δ (TMS) 1.88—2.16 (2H, m, $-CH_2-$), 2.83 (2H, t, J=6 Hz, $-CH_2-$), 3.07 (2H, t, J=6 Hz, $-CH_2-$), 3.88 (3H, s, Ar–OCH_3), 7.13 (1H, d, J=9 Hz, Ar–H), 7.30 (1H, d, J=9 Hz, Ar–H).

Similarly **6** was treated with sodium hydroxide, sodium ethoxide, or sodium hydride in dioxane. Isolation of **4b** and **7** was performed by chromatography using benzene followed by benzene(9)–ether(1) as developing solvents. The reactions of **6** and four kinds of bases in anhydrous benzene were carried out by a method similar to the reaction of **6** with potassium hydroxide in dioxane.

A Reaction of 6 and One Equivalent of Potassium Hydroxide. A mixture of **6** (0.500 g; 1.80 mmol) and potassium hydroxide (0.100 g; 1.80 mmol) was refluxed for 1 h in dioxane (10 ml). The reaction mixture was treated with 2 M hydrochloric acid by the method mentioned above. Thus, **4b** (0.250 g) was obtained in a 74% yield as a neutral product, and a mixture (0.085 g) of **2b** and **3b** was obtained as acidic products. The yields of **2b** and **3b** were determined to be 7 and 12% respectively by NMR analysis.

Ethyl 6-Methoxy-4,5-dihydro-3H-naphtho[1,8-bc]furan-2-carboxylate (7). Colorless needles from ethanol; mp 95—96 °C (lit,[19] 95—96 °C). The IR and ^{1}H NMR spectra of the needles were identical with those of an authentic sample.[19] ^{13}C NMR ($CDCl_3$): δ (TMS) 14.4, 21.4, 21.8, 23.3, 56.7, 60.8, 108.9, 113.3, 120.9, 126.9, 128.6, 139.3, 148.4, 151.5, 160.2.

Ethyl (4-Methoxy-8-oxo-5,6,7,8-tetrahydro-1-naphthyloxy)acetate (6). A mixture of **3b**[19] (10.0 g), diethyl sulfate (20.0 g), potassium carbonate (40.0 g), and acetone (200 ml) was refluxed for 2 h. After removal of the acetone the mixture was extracted with ether. The ethereal solution was washed with water, dried, and evaporated. The resulting oil was chromatographed and eluted with benzene(7)–ether(3) to give 7.60 g (88%) of **6**. Recrystallization from ethanol gave colorless needles; mp 72—73 °C. IR (KBr): ν_{max} 1680 (C=O), 1760 cm^{-1} ($COOC_2H_5$). ^{1}H NMR ($CDCl_3$): δ (TMS) 1.29 (3H, t, J=7 Hz, CH_3), 2.05 (2H, dt, J=6 and 6 Hz, $-CH_2-$), 2.62 (2H, t, J=6 Hz, $-CH_2-$), 2.87 (2H, t, J=6 Hz, $-CH_2-$), 3.81 (3H, s, OCH_3), 4.24 (2H, q, J=7 Hz, $-OCH_2-$), 4.62 (2H, s, $-OCH_2CO-$), 6.81 (1H, d, J=9 Hz, Ar–H), 6.96 (1H, d, J=9 Hz, Ar–H). ^{13}C NMR ($CDCl_3$): δ (TMS) 14.2, 22.2, 23.6, 40.6, 55.9, 61.0, 68.4, 115.0, 115.2, 124.7, 135.1, 151.8, 152.0, 169.2, 197.2. Found: C, 64.63; H, 6.40%. Calcd for $C_{15}H_{18}O_5$: C, 64.74; H, 6.52%.

Potassium 2a-Hydroxy-6-methoxy-2a,3,4,5-tetrahydro-2H-naphtho[1,8-bc]furan-2-carboxylate (8). A mixture of **6** (1.00 g; 3.60 mmol), potassium hydroxide (0.20 g; 3.60 mmol), and anhydrous dioxane (20 ml) was refluxed for 1 h. After cooling the resulting precipitates were collected by filtration to give 0.84 g (76%) of **8**. Recrystallization from water–dioxane gave colorless needles, mp>250 °C. IR (KBr): ν_{max} 1420, 1610 (COO^-), 3250 cm^{-1} (OH). ^{1}H NMR (D_2O): δ (DSS) 1.38—2.98 (6H, m, $-CH_2-$+$-CH_2-$+$-CH_2-$), 3.77 (3H, s, Ar–OCH_3), 4.60 (1H, s, $-CH=$), 6.70 (1H, d, J=8 Hz, Ar–H), 6.75 (1H, d, J=8 Hz, Ar–H). ^{13}C NMR (D_2O): δ (DSS) 20.1, 22.8, 33.6, 59.0 76.8, 96.6, 109.5, 115.1, 127.3, 131.9, 153.8, 154.1, 176.6. Found: C, 51.20; H, 4.89%. Calcd for $C_{13}H_{13}O_5K\cdot H_2O$: C, 50.97; H, 4.94%.

Potassium 6-Methoxy-4,5-dihydro-3H-naphtho[1,8-bc]furan-2-carboxylate (9). Compound **2b** (0.50 g) was dissolved in an alkaline solution (30 ml) containing potassium hydroxide (0.12 g) and the water was removed under the reduced pressure to give 0.58 g (92%) as crystals. Recrystallization from water–dioxane gave colorless plates; mp 103—105 °C. The melting point of the plates after once melting was above 250 °C. IR (KBr): ν_{max} 1405, 1570 cm^{-1} (COO^-). ^{1}H NMR (D_2O): δ (DSS) 1.82 (2H, dt, J=6 Hz, $-CH_2-$), 2.56 (2H, t, J=6 Hz, $-CH_2-$), 2.83 (2H, t, J=6 Hz, $-CH_2-$), 3.80 (3H, s, Ar–OCH_3), 6.89 (1H, d, J=9 Hz, Ar–H), 7.11 (1H, d, J=9 Hz, Ar–H). ^{13}C NMR (D_2O): δ (DSS) 23.5, 24.0, 25.4, 59.6, 111.1, 115.2, 123.1, 125.2, 131.1, 146.7, 149.8, 152.7, 170.2. Found: C, 51.24; H, 4.98%. Calcd for $C_{13}H_{11}O_4K\cdot 2H_2O$: C, 50.97; H, 4.94%.

The Reaction of Potassium 2a-Hydroxy-6-methoxy-2a,3,4,5-tetra-

** 1 M=1 mol dm^{-3}.

*** 1 Torr≈133.322 Pa.

hydro-2H-naphtho[1,8-bc]furan-2-carboxylate (8) and Hydrochloric Acid. Compound **8** (0.100 g) was dissolved in water (10 ml) and the solution was poured into 2 M hydrochloric acid (100 ml). After 15 min the solution was extracted with ether. The ethereal solution was washed three times with a 1 M potassium carbonate solution and then with water, dried, and evaporated to give 0.55 g (90%) of **4b** as colorless oil. The alkaline solution was acidified with 6 M hydrochloric acid and extracted with ether. The ethereal solution was washed with water, dried, and evaporated to give 0.002 g (2%) of **2b** as colorless crystals.

The Reaction of Potassium 2a-Hydroxy-6-methoxy-2a,3,4,5-tetrahydro-2H-naphtho[1,8-bc]furan-2-carboxylate (8) and Diethyl Sulfate. A mixture of **8** (0.100 g), diethyl sulfate (0.110 g), and dioxane (8 ml) was refluxed for 2 h. The mixture was extracted with ether. The ethereal solution was washed with water, dried, and evaporated. The resulting oil was chromatographed and eluted with benzene. The first fraction gave 0.040 g (65%) of **4b** as colorless oil. The second fraction afforded 0.015 g (19%) of **7** as colorless crystals.

Similarly, **8** (0.100 g) was dealt with diethyl sulfate (0.110 g) in the presence of potassium hydroxide (0.100 g) to give **4b** and **2b** in 3 and 26% yields respectively. The total yield of **4b** and **2b** was low because unreacted **8** remained.

The authors wish to thank Mr. Yoshiaki Takahashi for the elemental analyses.

References

1) T. Shimizu and T. Horaguchi, *Bull. Chem. Soc. Jpn.*, **46**, 1722 (1973).
2) T. Horaguchi and T. Shimizu, *Bull. Chem. Soc. Jpn.*, **47**, 485 (1974).
3) T. Horaguchi and T. Shimizu, *Bull. Chem. Soc. Jpn.*, **48**, 488 (1975).
4) T. Horaguchi, *Bull. Chem. Soc. Jpn.*, **50**, 3329 (1977).
5) S. Neidle, D. Rogers, and M. B. Hursthouse, *J. Chem. Soc., Perkin Trans. 2*, **1972**, 760.
6) D. Berry and D. C. C. Smith, *J. Chem. Soc., Perkin Trans. 1*, **1972**, 699.
7) T. Horaguchi, M. Hara, and T. Suzuki, *Bull. Chem. Soc. Jpn.*, **55**, 865 (1982).
8) H. W. W. Ehrlich, *Acta Crystallogr.*, **10**, 699 (1957).
9) S. Tanaka, *Nippon Kagaku Zasshi*, **72**, 307 (1951).
10) S. Tanaka, *J. Am. Chem. Soc.*, **73**, 872 (1951).
11) T. Matsumoto and K. Fukui, *Bull. Chem. Soc. Jpn.*, **30**, 3 (1957).
12) Y. Tanaka, *Bull. Chem. Soc. Jpn.*, **30**, 575 (1957).
13) A. F. Wagner, *Chem. Abstr.*, **54**, 570 (1960).
14) R. Royer, E. Bisagni, and G. Menichi, *Bull. Soc. Chim. Fr.* **1964**, 2112; *Chem. Abstr.*, **62**, 1619d (1965).
15) J. D. Brewer and J. A. Elix, *Tetrahedron Lett.*, **1969**, 4139.
16) M. Ghelardoni, F. Russo, and V. Penstellini, *Bol. Chim. Farm*, **109**, 48 (1970); *Chem. Abstr.*, **73**, 14594 (1970).
17) F. Duro, G. Scapini, and P. Condorelli, *Boll. Sedute Accod. Gioenia Sci. Natur. Catania*, **10**, 332 (1970); *Chem. Abstr.*, **75**, 20065 (1971).
18) P. Spagnolo, M. Tiecco, and A. Tundo, *J. Chem. Soc., Perkin Trans. 1*, **1972**, 556.
19) T. Horaguchi, T. Shimizu, and T. Suzuki, *Bull. Chem. Soc. Jpn.*, **48**, 1249 (1975).
20) A. Rössing, *Ber.*, **17**, 2988 (1884).
21) W. B. Whalley, *J. Chem. Soc.*, **1951**, 3229.
22) G. H. Phillips, A. Robertson, and W. B. Whalley, *J. Chem. Soc.*, **1952**, 4951.
23) F. M. Dean, F. Halewood, S. Mongkolsuk, A. Robertson, and W. B. Whalley, *J. Chem. Soc.*, **1953**, 1250.
24) A. Müller, M. Mészáros, and K. Körmendy, *J. Org. Chem.*, **19**, 472 (1954).
25) G. Lloyd and W. B. Whalley, *J. Chem. Soc.*, **1956**, 3209.
26) S. A. N. N. Bokhari and W. B. Whalley, *J. Chem. Soc.*, **1963**, 5322.
27) A. W. Burgstahler and L. R. Worden, *Org. Synth.*, **46**, 28 (1966).
28) L. R. Worden, K. D. Kaufman, J. A. Weis, and T. K. Schaaf, *J. Org. Chem.*, **34**, 2311 (1969).
29) R. T. Foster, A. Robertson, and A. Bushra, *J. Chem. Soc.*, **1948**, 2254.
30) D. C. Johnson and A. Robertson, *J. Chem. Soc.*, **1950**, 2381.
31) J. S. H. Davies, D. A. McCrea, W. L. Norris, and G. R. Range, *J. Chem. Soc.*, **1950**, 3206.
32) E. D. Elliot, *J. Am. Chem. Soc.*, **73**, 754 (1951).
33) W. B. Whalley and G. Lloyd, *J. Chem. Soc.*, **1956**, 3213.
34) NG. PH. Buu-Hoi, G. Saint-Ruf, T. B. Loc, and NG. D. Xuong, *J. Chem. Soc.*, **1957**, 2593.
35) H. Singh and R. S. Kapil, *J. Org. Chem.*, **24**, 2064 (1959).
36) M. Miyano and M. Matsui, *Chem. Ber.*, **93**, 54 (1960).
37) NG. PH. Buu-Hoi, N. D. Xuong, and N. V. Bac., *J. Chem. Soc.*, **1964**, 173.
38) K. Fukui, M. Nakayama, and S. Tanaka, *Bull. Chem. Soc. Jpn.*, **42**, 1971 (1969).
39) F. H. Stodora, *J. Org. Chem.*, **29**, 2490 (1964).
40) S. Kawai, T. Nakamura, and N. Sugiyama, *Proc. Imp. Acad. (Tokyo)*, **15**, 45 (1939).
41) S. Kawai, T. Nakamura, and N. Sugiyama, *Nippon Kagaku Kaishi*, **60**, 413 (1939).
42) M. M. Bokadia, B. R. Brown, and W. Cummings, *J. Chem. Soc.*, **1960**, 3308.
43) Y. Kawase and S. Nakamoto, *Bull. Chem. Soc. Jpn.*, **35**, 1624 (1962).
44) M. Ghelardoni, V. Pestellini, and C. Musnte, *Gazz. Chim. Ital.*, **99**, 1273 (1969); *Chem. Abstr.*, **73**, 24801v (1970).
45) G. N. Walker and R. T. Smith, *J. Org. Chem.*, **46**, 305 (1971).
46) K. Schofield, R. S. Ward, and A. M. Choudhury, *J. Chem. Soc., C*, **1971**, 2834.

The Stereoselective Dehydrative α-Glucosylation Using 6-*O*-Acetyl- and 6-*O*-*p*-Nitrobenzoyl-2,3,4-tri-*O*-benzyl-D-glucopyranoses

Shinkiti KOTO,* Naohiko MORISHIMA, Yasuhiro KIHARA, Hideko SUZUKI, Shigeharu KOSUGI, and Shonosuke ZEN

School of Pharmaceutical Sciences, Kitasato University, Shirokane, Minato-ku, Tokyo 108

(Received April 5, 1982)

The stereoselective synthesis of α-linked glucobiose derivatives using 6-*O*-acetyl- or 6-*O*-*p*-nitrobenzoyl-2,3,4-tri-*O*-benzyl-D-glucopyranose and a ternary mixture of *p*-nitrobenzenesulfonyl chloride, silver trifluoromethanesulfonate, and triethylamine in dichloromethane is described.

Many methods for systematic oligosaccharide synthesis have been reported.[1] Except for one unique approach,[2] all use the Koenigs-Knorr reaction and relatives[3] to form an interglycosidic linkage. Our objective has been to develop a reagent which will activate the anomeric center of a protected glycose like 2,3,4,6-tetra-*O*-benzyl-α-D-glucopyranose (**1**) in the presence of the alcohol to be glycosylated, in order to simplify the glycosylation procedure as written by Eq. 1[4] (G denotes 2,3,4,6-tetra-*O*-benzyl-D-glucopyranosyl residue and equivalents):[5a,b]

$$\mathrm{GOH} + \mathrm{ROH} \xrightarrow[-\mathrm{H_2O}]{} \mathrm{GOR}. \qquad (1)$$

Until recently, few attempts have been made to simplify the glycosylation procedure.[4,5] This paper will describe the effect of the acyl group of the modified benzylated glucopyranoses, *i.e.*, 6-*O*-acetyl- and 6-*O*-*p*-nitrobenzoyl-2,3,4-tri-*O*-benzyl-D-glucopyranoses (**2** and **3**), on the selectivity of the dehydrative glucosylation using a ternary mixture of *p*-nitrobenzenesulfonyl chloride (NsCl), silver trifluoromethanesulfonate (AgOTf), and triethylamine (Et_3N) (the NST mixture)[4b] in CH_2Cl_2.

Results and Discussion

The NST mixture was found to undergo the stereoselective β-glucosylation of simple alcohols with **1**.[4b] It was later found, however, that such selectivity was retained only for the glucosylation of a primary hydroxyl group and that the glucosylation of a secondary group proceeded with a poor selectivity in the di- and trisaccharide synthesis using **1** and the NST mixture.[6] Therefore, an additional prerequisite is necessary for the dehydrative glucosylation with **1** and the NST mixture to proceed stereoselectively, irrespective of the reactivity of the hydroxyl group of partially benzylated saccharides. This led us to study the dehydrative glucosylation using the NST mixture and such derivatives of D-glucopyranose as **2** and **3**, since the modified benzylated glucopyranosyl bromides with 6-*O*-acetyl- or 6-*O*-*p*-nitrobenzoyl group are good intermediates for the highly stereoselective α-glucosylation.[7,8]

Compound **2** was prepared through the regioselective *O*-deacetylation of 1,6-di-*O*-acetyl-2,3,4-tri-*O*-benzyl-D-glucopyranose (**5**), which is readily available *via* the acetolysis of 1,6-anhydro-2,3,4-tri-*O*-benzyl-β-D-glucopyranose (**6**),[9] by either of three reagents: (i) hot methanolic sodium acetate (NaOAc), (ii) benzylamine ($PhCH_2NH_2$) in $CHCl_3$,[10a] and (iii) N_2H_4 in pyridine.[10b] By the treatment of **6** with acetyl bromide (AcBr),[11] followed by hydrolysis in the presence of Ag_2CO_3, **2** was also prepared. The acylation of 2,3,4-tri-*O*-benzyl-β-D-glucopyranose (**7**)[9] with *N*-acetylimidazole[12] gave **2** with a poor regioselectivity, whereas that with *p*-nitrobenzoyl chloride afforded **3** in a good yield.

As expectedly, **2** was condensed with cyclohexanol by the NST mixture to afford the α-glucoside **8a** predominantly, although a similar glucosylation of the alcohol with **1** showed β-selectivity.[4b] The dehydrative glucosylation of the alcohol with **3** also showed α-selectivity. Judging from the temperature of the precipitation of AgCl, the glucosylation using **2** or **3** appears to proceed at a slightly higher temperature (>−10 °C) than that using **1** (<−20 °C), so that a part of such a simple alcohol as cyclohexanol may be sulfonated concurrently to depress the yield of the glucosides significantly.

The α-glucosylation of the primary hydroxyl group of the protected glucopyranoside **10**[8] with **2** proceeded well: the isomaltose derivative[8] **9a** was synthesized with ease *via* the treatment of a mixture of **2** and **10** with the NST mixture in CH_2Cl_2, followed by *O*-deacetylation, in a 54% yield, while the gentiobiose derivative **9b** was obtained as the by-product in a 21% yield. Compound **3** was similarly condensed with **10** to give the isomaltose derivative,[8] **16a**, and the gentiobiose one, **16b**, in 50 and 29% yields respectively. Thus, it is evident that the α-selectivity was caused by the 6-*O*-acyl group, because a similar glucosylation of benzyl 3-*O*-acetyl-2,4-di-*O*-benzyl-α-D-glucopyranoside with **1** was highly selective to form the gentiobiose derivative.[6] It was found that the glucosylation of the secondary hydroxyl group of the protected glucopyranoside **11**[13] with **2**, followed by *O*-deacetylation, gave the maltose derivative **12** exclusively in a 39% yield; no trace of the cellobiose derivative was found in the reaction mixture.

The present method is more efficient for the α-glucosylation of secondary hydroxyl groups than the method using a mixture of trimethylsilyl bromide (Me_3SiBr), $CoBr_2$, tetrabutylammonium bromide (*n*-Bu_4NBr), and Molecular Sieve (4A) (the TCTM mixture) in CH_2Cl_2,[4d] and may well be balanced with other selective α-glucosylation procedures[14] because of its simplicity and rapidity. For the α-glucosylation of primary hydroxyl groups, the method with the TCTM mixture, which does not need such a modified precursor as **2** or **3**, is more convenient than that with the NST mixture.

The combined use of both methods made it possible to perform the step-by-step synthesis of *O*-α-D-glucopyranosyl-(1→6)-*O*-α-D-glucopyranosyl-(1→4)-D-glucopyranose (panose, **4**),[15] formulated in Fig. 1. The maltose derivative **12**, synthesized through the condensation of **2** and **11** with the NST mixture as has been described above, was glucosylated with **1** using the TCTM mixture to furnish the fully benzylated α-panose (**13a**). The hydrogenolysis of **13a** afforded **4**, which has once been synthesized from maltose.[15c]

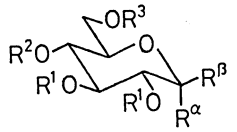

Code	R^{α}	R^{β}	R^1	R^2	R^3
1	OH	H	Bn	Bn	Bn
2	H,	OH	Bn	Bn	Ac
3	H,	OH	Bn	Bn	Pnb
4	OG4	H	H	H	αG
5	H,	OAc	Bn	Bn	Ac
7	H	OH	Bn	Bn	H
8a	OCh	H	Bn	Bn	Ac
8b	H	OCh	Bn	Bn	Ac
9a	OBG6	H	Bn	Bn	H
9b	H	OBG6	Bn	Bn	H
10	SEt	H	Bn	Bn	H
11	OBn	H	Bn	H	Bn
12	OBG4	H	Bn	Bn	H
13a	OBG4	H	Bn	Bn	αBG
13b	OBG4	H	Bn	Bn	βBG
14a	OBG6	H	Bn	Bn	Ac
14b	H	OBG6	Bn	Bn	Ac
15a	OCh	H	Bn	Bn	Pnb
15b	H	OCh	Bn	Bn	Pnb
16a	OBG6	H	Bn	Bn	Pnb
16b	H	OBG6	Bn	Bn	Pnb
17	H,	OAc	Bn	Bn	H
18	H	OPnb	Bn	Bn	H

Ac=Acetyl, Bn=benzyl, Ch=cyclohexyl, Et=ethyl, Pnb=*p*-nitrobenzoyl.

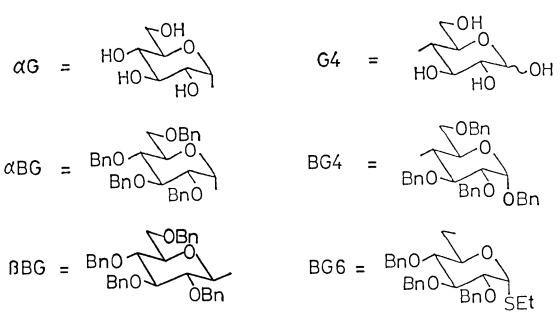

Experimental

General. See Refs. 4b and 6.

6-O-Acetyl-2,3,4-tri-O-benzyl-D-glucopyranose (2). *(1)*: A mixture of **5**[9] (106.4 mg, 0.20 mmol), NaOAc (46 mg), and MeOH (4.6 ml) was refluxed for 5 h. The solution

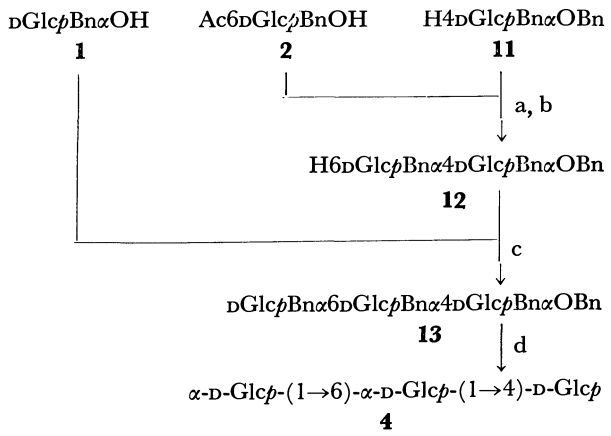

a (NsCl + TfOAg + Et_3N)/CH_2Cl_2
b NaOMe/(MeOH + 1,4-Diox.)
c (Me_3SiBr + $CoBr_2$ + *n*-Bu_4NBr + Mol. Sieve(4Å))/CH_2Cl_2
d Pd-C(10%)/AcOH(+H_2O)

Fig. 1. The scheme for a stepwise synthesis of panose, **4**.

was evaporated at 20 °C and then chromatographed using a mixture of toluene and 2-butanone (10:1). After the elution of **5** (35.2 mg, 33%) and a trace amount of **17**, there appeared **2** (45.2 mg, 69%). ^1H NMR($CDCl_3$, Me_4Si) δ 2.03 (3H, s, Ac), 5.19 (1H, d, J=4.0 Hz, HI), ^{13}C NMR ($CDCl_3$, Me_4Si) δ 20.9 (Ac), 91.1 (Clα), 97.4 (Clβ).

(2): $PhCH_2NH_2$ (Wako, 60 μl) was added to a cooled solution of **5** (94.5 mg, 0.18 mmol) in $(CH_2Cl)_2$ (0.9 ml). The solution was kept standing for 2 d at room temperature. Evaporation and subsequent chromatography gave **2** (71.1 mg, 80%).

(3): $N_2H_4 \cdot H_2O$ (Wako, ≈90%, 6.6 μl) was added to a cooled solution of **5** (96.6 mg, 0.18 mmol) in pyridine (0.9 ml). The solution was kept standing for 4 d at room temperature. Evaporation and subsequent chromatography gave **2** (63.3 mg, 71%).

(4): A mixture of **6**[9] (5.0 g, 11.6 mmol) and AcBr (5 ml) was stirred for 1.5 h at room temperature. The solution was then evaporated, and the residue was stirred into CH_2Cl_2 (5 ml) containing H_2O (2.05 ml) and Ag_2CO_3 (6.4 g). The mixture was chromatographed to give **2** (4.83 g, 75%).

(5): A mixture of **7**[9] (90 mg, 0.20 mmol), *N*-acetylimidazole (Tokyo Kasei, 30.6 mg), and $(CH_2Cl)_2$ (0.4 ml) was stirred for 16 h at room temperature. The mixture was then chromatographed to give **5** (14.5 mg, 14%, R_f 0.70 (toluene–2-butanone, 10:1)), **17** (27.8 mg, 28%, R_f 0.35), **2** (36.4 mg, 37%, R_f 0.30), and then **7** (8.8 mg, 10%, R_f 0.05); ^1H NMR($CDCl_3$, Me_4Si) δ (**17**) 2.02 (Ac-β), 2.13 (Ac-α), 5.62 (d, J=8.0 Hz, HI-β), 6.17 (d, J=3.5 Hz, HI-α).

2,3,4-Tri-O-benzyl-6-O-p-nitrobenzoyl-D-glucopyranose (3). A mixture of **7** (450 mg, 1.0 mmol), *p*-nitrobenzoyl chloride (Tokyo Kasei, 223 mg), and pyridine (10 ml) was stirred for 3 h at −10 °C and then for 16 h at room temperature. Usual processing and subsequent chromatography with benzene–2-butanone (10:1) gave 2,3,4-tri-*O*-benzyl-1,6-bis-*O*-(*p*-nitrobenzoyl)-β-D-glucopyranose (48 mg, 6%, R_f 0.84 (benzene–2-butanone, 10:1), mp 144.5—145.5 °C (lit,[7b] mp 144.5—145.5 °C), **18** (53 mg, 9%, R_f 0.60), **3** (310 mg, 52%, R_f 0.52), and **7** (129 mg, 29%); ^1H NMR($CDCl_3$, Me_4Si) δ (**3**) 5.24 (d, J=3.8 Hz, HI-α), 7.61—8.31 (4H, m, $-C_6H_4-$), (**18**) 5.71 (1H, d, J=8.0 Hz, HI), 8.05—8.33

Table 1. Physical and analytical data of compounds

Compound	Mp θ_m/°C	$[\alpha]_D^{20}$/° (*c*, Solv.)	Molecular formula	Calcd (%)			Found (%)			Lit
				C	H	N	C	H	N	
2	99.5—100	+32(1.0, $CHCl_3$)	$C_{29}H_{32}O_7$	70.71	6.55		70.44	6.50		
3	102.5—103.5	+65(0.4, $CHCl_3$)	$C_{34}H_{33}NO_9$	68.10	5.55	2.34	67.90	5.45	2.28	
4	195—198(decomp)	+147(0.1, H_2O)	$C_{18}H_{32}O_{16}$	42.86	6.39		42.78	6.60		a)
8a	—	+56(0.5, $CHCl_3$)	$C_{35}H_{42}O_7$	73.15	7.37		73.31	7.36		
8b	88—89	+15(0.2, $CHCl_3$)					72.90	7.36		
9b	120—121	+70(0.6, $CHCl_3$)	$C_{56}H_{62}O_{10}S$	72.54	6.74		72.58	6.78		
11	—	+48(2.0, $CHCl_3$)	$C_{34}H_{36}O_6$	75.53	6.71		75.30	6.81		b)
12	—	+64(0.8, $CHCl_3$)	$C_{61}H_{64}O_{11}$	75.29	6.63		74.95	6.60		
13a	—	+75(1.0, $CHCl_3$)	$C_{95}H_{98}O_{16}$	76.28	6.60		76.04	6.75		
13b	—	+57(1.0, $CHCl_3$)					76.17	6.61		
14a	—	+114(0.7, $CHCl_3$)	$C_{58}H_{64}O_{11}S$	71.88	6.60		71.20	6.58		
14b	89—91	+76(0.2, $CHCl_3$)					71.82	6.72		
15a	—	+65(0.9, $CHCl_3$)	$C_{41}H_{45}NO_9$	70.77	6.52	2.01	70.45	6.34	2.08	
15b	91—93	+45(0.2, $CHCl_3$)					70.33	6.34	2.17	
16b	—	+75(0.7, $CHCl_3$)	$C_{63}H_{65}NO_{13}S$	70.31	6.09	1.30	70.27	6.06	1.28	
17	—	+25(1.0, $CHCl_3$)	$C_{29}H_{32}O_7$	70.71	6.55		70.91	6.58		
18	166—167	−44(0.2, $CHCl_3$)	$C_{34}H_{33}NO_9$	68.10	5.55	2.34	68.07	5.49	2.34	
19	148—148.5	+115(0.3, $CHCl_3$)	$C_{42}H_{58}O_{28}$	49.90	5.78		50.27	5.88		c)

a) Ref. 6a; mp 213(decomp), $[\alpha]_D^{25}$ +154° (*c* 2.2, H_2O). b) Ref. 14b; $[\alpha]_D^{20}$ +43° (*c* 1.10, $CHCl_3$). c) Ref. 6b; mp 148.5—150 °C, $[\alpha]_D^{27}$ +120° (*c* 4.0, $CHCl_3$).

(4H, m, $-C_6H_4-$).

*Ethyl 2,3,4-Tri-*O*-benzyl-1-thio-α-*D*-glucopyranoside (**10**)*: A mixture of AcBr (5 ml) and **6** (5.0 g, 11.6 mmol) was stirred for 1.5 h at room temperature and then evaporated. The whole residue was treated with EtSH (Wako, 9.0 ml) in $MeNO_2$ (17 ml) containing 2,6-dimethylpyridine (4.2 ml). After evaporation, the residue was dissolved in MeOH (70 ml) containing methanolic NaOMe (2 M, 10 ml). After 20 h, AcOH (1.5 ml) was added to the mixture, which was evaporated and then chromatographed using benzene–2-butanone (10:1). This gave **10** (4.9 g, 75%), identified with the sample prepared previously through a different route.[8]

*Benzyl 2,3,6-Tri-*O*-benzyl-α-*D*-glucopyranoside (**11**)*: A mixture of benzyl 2,3-di-*O*-benzyl-α-D-glucopyranoside[13a] (0.65 g, 1.44 mmol), $PhCH_2Cl$ (6.5 ml), and NaH (≈50% disp., 70 mg) was vigorously stirred for 40 min at 80 °C. Usual processing and subsequent chromatography with hexane–EtOAc (4:1) gave benzyl 2,3,4,6-tetra-*O*-benzyl-α-D-glucopyranoside (15 mg, 1.7%, R_f 0.75 (hexane–EtOAc, 4:1)), **11** (0.35 g, 45%, R_f 0.52), benzyl 2,3,4-tri-*O*-benzyl-α-D-glucopyranoside[13c] (0.10 g, 13%, R_f 0.30), and the unchanged starting material (0.18 g, 28%, R_f 0.08).

*Cyclohexyl 6-O-Acetyl-2,3,4-tri-*O*-benzyl-α- and -β-*D*-glucopyranoside (**8a** and **8b**)*: Et_3N (31 μl, 0.22 mmol) was added to a mixture of **2** (108 mg, 0.22 mmol), cyclohexanol (21 μl, 0.22 mmol), NsCl (49 mg, 0.22 mmol), and AgOTf (57 mg, 0.22 mmol) in CH_2Cl_2 (1.0 ml) at −35 °C under efficient stirring. The bath temperature was raised to 0 °C at a rate of ≈0.5 °C/min, and then the stirring was continued for 6 h. After the processing described previously,[4b] chromatography with hexane–EtOAc (5:1) gave **8b** (14.6 mg, 12%, R_f 0.66 (hexane–EtOAc, 3:1)), and **8a** (41.4 mg, 33%, R_f 0.60).

*Cyclohexyl 2,3,4-Tri-*O*-benzyl-6-*O*-p-nitrobenzoyl-α- and -β-*D*-glucopyranosides (**15a** and **15b**)*: A similar reaction using **3** (132 mg, 0.22 mmol), cyclohexanol (21 μl), NsCl (49 mg), AgOTf (57 mg), Et_3N (31 μl), and CH_2Cl_2 (1.0 ml) gave **15b** (11.8 mg, 8%, R_f 0.73 (hexane–EtOAc, 3:1)) and **15a** (55.6 mg, 37%, R_f 0.67).

*Ethyl O-(6-O-Acetyl-2,3,4-tri-*O*-benzyl-α- and -β-*D*-glucopyranosyl)-(1→6)-2,3,4-tri-*O*-benzyl-1-thio-α-*D*-glucopyranoside (**14a** and **14b**)*: Et_3N (156 μl, 1.1 mmol) was stirred into a mixture of **2** (492 mg, 1.0 mmol), **10** (494 mg, 1.0 mmol), NsCl (245.5 mg, 1.1 mmol), and AgOTf (283 mg, 1.1 mmol) in CH_2Cl_2 (5.0 ml) at −38 °C, after which the bath temperature was allowed to rise to 0 °C. After having been stirred for 16 h, the mixture was processed[4b] and then chromatographed (benzene–2-butanone, 100:1→3:1, gradient) to give **14a** (543.8 mg, 56%, R_f 0.44, benzene–2-butanone, 20:1)) and **14b** (244.5 mg, 25%, R_f 0.38); ^1H NMR(CCl_4, Me_4Si) δ (**14a**) 1.25 (3H, t, $C\underline{H}_3CH_2S$), 1.94 (3H, s, Ac), 2.57 (2H, m, $CH_3C\underline{H}_2S$), 5.35 (1H, d, J=5.0 Hz, Hl), 7.24 (30H, s, 6Ph); (**14b**) 1.23 (3H, t, $C\underline{H}_3CH_2S$), 1.96 (3H, s, Ac), 2.47 (2H, m, $CH_3C\underline{H}_2S$), 5.30 (1H, d, J=5.0 Hz, Hl), 7.20 (30H, s, 6Ph).

Compound **14a** (530 mg, 0.55 mmol) was treated with methanolic NaOMe (0.05 M, 20 ml) containing 1,4-dioxane (2 ml) to afford **9a** (485 mg, 96%), which was identified with the sample prepared previously.[8]

Compound **14b** (68 mg, 0.07 mmol) was treated with methanolic NaOMe (0.03 M, 3.5 ml) containing Me_2CO (1 ml) to give **9b** (55.2 mg, 85%).

*Ethyl O-(2,3,4-Tri-*O*-benzyl-6-*O*-p-nitrobenzoyl-α- and -β-*D*-glucopyranosyl-(1→6)-2,3,4-tri-*O*-benzyl-1-thio-α-*D*-glucopyranoside (**16a** and **16b**)*: A similar reaction using **3** (100 mg, 0.17 mmol), **10** (84 mg, 0.17 mmol), NsCl (41 mg, 0.19 mmol), AgOTf (48 mg, 0.19 mmol), Et_3N (26 μl, 0.19 mmol), and CH_2Cl_2 (1.0 ml) and subsequent chromatography (benzene–2-butanone, 100:1→5:1, gradient) gave **16a** (90.2 mg, 50%, R_f 0.75 (benzene–2-butanone, 20:1)), identified with the sample synthesized previously[8] and then **16b** (52.0 mg, 29%, R_f 0.65); ^1H NMR(CCl_4, Me_4Si) δ (**16a**) 1.25 (3H, t, $C\underline{H}_3CH_2S$), 2.50 (2H, m, $CH_3C\underline{H}_2S$), 5.28 (1H, d, J= 5.0 Hz, Hl), 7.95—8.17 (4H, m, $-C_6H_4-$); (**16b**) 1.23 (3H, t, $C\underline{H}_3CH_2S$), 2.53 (2H, m, $CH_3C\underline{H}_2S$), 5.27 (1H, d, J=

5.0 Hz, Hl), 8.03—8.12 (4H, m, $-C_6H_4-$).

Benzyl O-(2,3,4-Tri-O-benzyl-α-D-glucopyranosyl)-(1→4)-2,3,6-tri-O-benzyl-α-D-glucopyranoside (12): A similar glucosylation reaction using **2** (180 mg, 0.37 mmol), **11** (197.4 mg, 0.37 mmol), NsCl (97.5 mg, 0.44 mmol), AgOTf (113 mg, 0.44 mmol), Et_3N (61.5 μl, 0.44 mmol), and CH_2Cl_2 (1.8 ml) and subsequent chromatography (benzene–2-butanone) gave a sirup (173.5 mg, R_f 0.60 (benzene–2-butanone, 10:1), this being the sole spot in the region where $R_f > 0.43$). This was then treated with methanolic NaOMe (0.05 M, 11 ml) containing 1,4-dioxane (2 ml) to give a sirup which showed a single spot. ^{13}C NMR of this sirup, composed of **12** (135.6 mg, 39% for **11**), showed no signal of the anomeric carbons corresponding to the β-glucopyranoside; ^{13}C NMR($CDCl_3$, Me_4Si) δ 95.1 (Cl), 96.3 (Cl′).

Benzyl O-(2,3,4,6-Tetra-O-benzyl-α- and -β-D-glucopyranosyl)-(1→6)-O-(2,3,4-tri-O-benzyl-α-D-glucopyranosyl)-(1→4)-2,3,6-tri-O-benzyl-α-D-glucopyranoside (13a and 13b). A mixture of **1** (151 mg, 0.28 mmol), **12** (209 mg, 0.125 mmol), $CoBr_2$ (62 mg, 0.28 mmol), n-Bu_4NBr (90 mg, 0.28 mmol), Molecular Sieve (Linde-4A, 230 mg), and Me_3SiBr (37 μl, 0.28 mmol) in CH_2Cl_2 (0.7 ml) was stirred for 48 h at room temperature. The subsequent chromatography (hexane–2-butanone, 100:1→3:1, gradient) of the reaction mixture gave **13a** (93.2 mg, 29%, R_f 0.58 (hexane–2-butanone, 20:1)) and then **13b** (27.2 mg, 9%, R_f 0.55). ^{13}C NMR ($CDCl_3$, Me_4Si) δ (**13a**) 95.0 (Cl), 96.2 (Cl′), 97.1 (Cl″); (**13b**) 95.1 (Cl), 96.3 (Cl′), 103.7 (Cl″).

O-α-D-Glucopyranosyl-(1→6)-O-α-D-glucopyranosyl-(1→4)-D-glucopyranose (Panose, 4): Two hydrogenations of **13a** (73.8 mg, 0.062 mmol) over Pd–C (10%, 73 mg) in AcOH (7 ml) containing H_2O (0.03 ml) gave a glass, which was then triturated with MeOH to give **4** (19.3 mg, 61%). The ^{13}C NMR (D_2O, Me_4Si (ext.)) of this agreed well with that previously reported;[15d] 61.6 (C6″), 61.8 (C6), 67.0 (C6′), 70.5 (C4″), 70.6 (C4′), 71.1 (C5α), 72.4 (C5′), 72.6 (C2α and C2″), 72.7 (C2′), 72.9 (C5″), 74.2 (C3α, C3′, and C3″). 75.1 (C2β). 75.7 (C3β), 77.2 (C5β), 78.2 (C4β), 78.5 (C4α), 93.0 (C1α), 96.8 (C1β), 99.2 (C1″), 100.8 (C1′).

A sample of **4** (6.8 mg) was treated with aq $NaBH_4$ (0.2%, 4 ml) at room temperature overnight. After the addition of AcOH (1 drop), the mixture was evaporated and coevaporated with MeOH. The residue was stirred in Ac_2O (1 ml)c ontaining NaOAc (14 mg) at 100 °C for 6 h. Subsequent chromatography (benzene–2-butanone) gave a homogeneous glass. This was crystallized with MeOH to give *O*-(2,3,4,6-tetra-*O*-acetyl-α-D-glucopyranosyl)-(1→6)-*O*-(2,3,4-tri-*O*-acetyl-α-D-glucopyranosyl)-(1→4)-1,2,3,5,6-penta-*O*-acetyl-D-glucitol (**19**) (10.0 mg, 74%).

References

1) N. K. Mathur, O. K. Narang, and R. E. Williams, "Polymers as Aids in Organic Chemistry," Academic Press (1981), Chap. 6.

2) S. David, A. Lubineau, and J.-M. Vatèle, *Nouv. J. Chim.*, **4**, 547 (1980).

3) A. F. Bochkov and G. E. Zaikov, "Chemistry of the *O*-Glycosidic Bond, Formation and Cleavage," Engl. ed by C. Schuerch, Pergamon Press, London (1979), Chap. 3.

4) a) S. Koto, N. Morishima, and S. Zen, *Bull. Chem. Soc. Jpn.*, **52**, 784 (1979); b) S. Koto, T. Sato, N. Morishima, and S. Zen, *ibid.*, **53**, 1761 (1980); c) S. Koto, N. Morishima, and S. Zen, *ibid.*, **55**, 1543 (1982); d) N. Morishima, S. Koto, C. Kusuhara, and S. Zen, *Chem. Lett.*, **1981**, 427; S. Koto, N. Morishima, C. Kusuhara, S. Sekido, T. Yoshida, and S. Zen, *Bull. Chem. Soc. Jpn.*, **55**, 2995 (1982); e) S. Koto, N. Morishima, S. Sato, and S. Zen, The 26th International Congress of IUPAC, Tokyo, 1977.

5) a) A. A. Pavia, J.-M. Rocheville, and S. Z. Ung, *Carbohydr. Res.*, **79**, 79 (1980); G. Grynkiewicz, *Pol. J. Chem.*, **53**, 1571 (1979); b) Seemingly, a dehydrative glycosylation has been studied by Russian chemists (*e.g.*, A. M. Gakhokidze, *Zhur. Obsh. Khim.*, **11**, 117 (1941); A. M. Gakhokidze and N. D. Kutidze, *ibid.*, **22**, 247 (1952), *etc.*); c) J. Leroux and A. S. Perlin, *Carbohydr. Res.*, **67**, 163 (1978).

6) S. Koto, S. Inada, T. Yoshida, M. Toyama, and S. Zen, *Can. J. Chem.*, **59**, 255 (1981).

7) a) P. J. Pfaffli, S. H. Hixon, and L. Anderson, *Carbohydr. Res.*, **23**, 195 (1972); b) T. Ishikawa and H. G. Fletcher, Jr., *J. Org. Chem.*, **34**, 563 (1969).

8) S. Koto, T. Uchida, and S. Zen, *Bull. Chem. Soc. Jpn.*, **46**, 2520 (1973).

9) G. Zemplén, Z. Csürös, and S. Angyal, *Chem. Ber.*, **70**, 1848 (1937).

10) a) C. Ferrer Salat, P. Axero Agneseti, and M. Bemporad Caniato, Span. Patent, No. 430636 (*Chem. Abstr.*, **87**, 23683k (1977)); b) Y. Ishido, N. Sakairi, M. Sekiya, and N. Nakazaki, *Carbohydr. Res.*, **97**, 51 (1981).

11) A. R. Jeanes, C. A. Wilham, and G. E. Hilbert, *J. Am. Chem. Soc.*, **75**, 3667 (1953).

12) J. M. McLaren, R. V. Stick, and S. Webb, *Aust. J. Chem.*, **30**, 2689 (1977).

13) a) A. Lubineau, A. Thieffry, and A. Veyriérs, *Carbohydr. Res.*, **46**, 143 (1976); b) S. David, A. Lubineau, and A. Thieffry, *Tetrahedron*, **34**, 299 (1978); c) P. A. Adams, R. Harrison, T. D. Inch, and P. Rich, *Biochem. J.*, **155**, 1 (1976).

14) J. R. Pougny, M. A. A. Nassr, N. Naulet, and P. Sinaÿ, *Nouv. J. Chim.*, **2**, 389 (1978); T. Mukaiyama, T. Nakatsuka, and S. Shoda, *Chem. Lett.*, **1979**, 487; T. Mukaiyama, Y. Murai, and S. Shoda, *ibid.*, **1981**, 431.

15) a) S. C. Pan, L. W. Nicholson, and P. Kolachov, *J. Am. Chem. Soc.*, **73**, 2547 (1951); b) M. L. Wolfrom, A. Thompson, and J. T. Galkowski, *ibid.*, **73**, 4093 (1951); c) M. L. Wolfrom and K. Koizumi, *J. Org. Chem.*, **32**, 656 (1967); d) T. Usui, N. Yamaoka, K. Matsuda, K. Tuzimura, H. Sugiyama, and S. Sato, *J. Chem. Soc., Perkin Trans. 1*, **1973**, 2425.

Synthesis of Biphenyloferrocenophanes

Iwao Shimizu, Yoshio Kamei, Takeshi Tezuka, Taeko Izumi, and Akira Kasahara*

Department of Applied Chemistry, Faculty of Engineering, Yamagata University, Yonezawa 992

(Received April 30, 1982)

Some ferrocenophanes, in which the two cyclopentadienyl rings are linked by biphenyl rings, have been synthesized *via* intramolecular reductive coupling of the corresponding formyl compounds with a low-valent titanium reagent. The structures of these cyclophane compounds were determined by IR, NMR, and UV spectra analyses. Transannular π-electronic interactions between the two biphenyl rings were examined on the basis of electronic spectra.

In contrast to the active interest in cyclophane compounds, the ferrocenophane system having transannular π-electronic interactions has received little attention; the only compounds of this class which have been described are [2.2]ferrocenophane-1,13-diyne,[1] [2.2]-ferrocenophane-1,13-diene,[2] [2]paracyclo[2]paracyclo-[2](1,1′)ferrocenophane,[3] [3.3]- and [5.5](1,1′)ferrocenophane derivatives,[4] and [0]metacyclo[2]metacyclo[0](1,1′)ferrocenophane.[5] We wish to report the synthesis of some ferrocenophanes in which the two cyclopentadienyl rings are linked by biphenyl rings and an ethano or etheno bridge, using the low-valent titanium species.

Results and Discussion

Synthesis. Although a number of synthetic methods have been recently developed for [2.2]cyclophane,[6] a reductive coupling of carbonyl compounds with low-valent titanium reagents[7] is still very convenient and advantageous for the synthesis of cyclophane because of the availability of the intermediary compounds.[2,3,5,8]

In the present work, we applied the same method for the synthesis of [0](4,4′)biphenylo[2](4,4′)biphenylo[0](1,1′)ferrocenophan-13-ene (**1**), [0](4,3′)biphenylo[2](3,4′)biphenylo[0](1,1′)ferrocenophan-13-ene (**3**), and *syn*- and *anti*-[0](4,2′)biphenylo[2](2,4′)biphenylo-[0](1,1′)ferrocenophan-13-ene (**5s** and **5a**). The synthesis of an intermediate, 1,1′-bis(4′-formyl-4-biphenylyl)ferrocene (**13a**), was carried out by the cross coupling reaction[9] of 1,1′-bis(*p*-bromophenyl)ferrocene (**7**) with a Grignard reagent from *p*-bromobenzaldehyde ethylene acetal (**8**) in the presence of phosphino nickel complex. The synthesis of other intermediates, 1,1′-bis(3′-formyl-4-biphenylyl)ferrocene (**13b**) and 1,1′-bis-(2′-formyl-4-biphenylyl)ferrocene (**13c**), were carried out by the Gomberg's arylation of ferrocene with diazonium salt derived from 4′-aminobiphenyl-3-carboxylic acid (**10a**) and 4′-aminobiphenyl-2-carboxylic acid (**10b**), subsequent esterification in methanol, reduction with $LiAlH_4$, and oxidation with active MnO_2 in chloroform.

The reductive coupling reaction of dialdehyde, **13a** and **13b**, with low-valent titanium reagents were carried out according to Mukaiyama's procedure[7a] using a high dilution method. Silica gel column chromatography of the reaction products led to the isolation of **1** and **3**, respectively, accompanied by the formation of the reduction products of **13a** and **13b**. On the other hand, the $TiCl_4$–Zn reductive coupling of **13c** led to the formation of two isomers of **5s** and **5a**.

The catalytic hydrogenation of **1** and **3** with PtO_2 in ethanol–dioxane afforded [0](4,4′)biphenylo[2](4,4′)-biphenylo[0](1,1′)ferrocenophane (**2**) and [0](4,3′)biphenylo[2](3,4′)biphenylo[0](1,1′)ferrocenophane (**4**), respectively. The catalytic hydrogenation of **5s** and **5a** afforded the same product: [0](4,2′)biphenylo[2]-(2,4′)biphenylo[0](1,1′)ferrocenophane (**6**).

Structures. The structures of the cyclophanes, **1**—**6**, were determined on the basis of the IR, NMR, and mass spectra and the elementary analyses. The NMR and IR spectra data of all the cyclophanes and the reference compounds are summarized in Tables 1 and 2, respectively.

In the unsaturated cyclophane **1**, the configuration of –C–C– double bond was confirmed to be *cis*, because the IR spectrum of **1** exhibits a band at 740 cm^{-1} which is characteristic of *cis* vinylene linkage and the characteristic band near 960 cm^{-1} due to *trans* vinylene linkage is absent. In ferrocene, the distance between the two cyclopentadienyl rings is 3.32 Å,[10] while the van der Waals separation between parallel π-system is 3.4 Å.[11] On the other hand, in **1** and **2**, the molecules exist probably in the conformation with the biphenyl rings approximately parallel to one another and approximately coplanar to the plane of the cyclopentadienyl ring. Thus, in **1** and **2**, substantial repulsive interactions must exist between the two biphenyl rings which are bound together by an etheno or ethano bridge at each end. In the NMR spectrum of **1**, as expected, the aromatic protons (δ, 6.85—7.21 ppm) appear at higher fields than the corresponding protons of the reference compounds, 1,1′-bis(4′-methyl-4-biphenylyl)ferrocene (**15a**) (δ, 7.13—7.49 ppm) and (4′-methyl-4-biphenylyl)ferrocene (**16a**) (δ, 7.12—7.56 ppm). In the saturated cyclophane, the protons of biphenyl rings (δ, 6.88—7.21 ppm) are also shifted upfield compared with those of **15a** and **16a**. These phenomena are probably due to diamagnetic shielding effect of the facing biphenyl ring.

In the NMR spectra of **3** and **4**, the aromatic proton signals are observed at nearly the same positions as those of the reference compounds, 1,1′-bis(3′-methyl-4-biphenylyl)ferrocene (**15b**) and (3′-methyl-4-biphenylyl)ferrocene (**16b**). This suggests that the two biphenyl rings in both **3** and **4** are not held a face to face conformation and the *anti*-conformations for **3** and **4** are accommodated.

On the other hand, in two isomers of **5s** and **5a**, the mass spectra show the same pattern, which con-

Table 1. NMR spectra of the cyclophane and reference compounds (δ, in $CDCl_3$)[a)]

Compound	Biphenyl ring protons	Ferrocene ring protons	Other protons
1[a)]	6.85—7.21 (m, 16H)	4.34 (t, 4H, $\underline{H}_\beta$) 4.65 (t, 4H, $\underline{H}_\alpha$)	7.12 (s, 2H, -C$\underline{H}$=C$\underline{H}$-)
2[a)]	6.88—7.21 (m, 16H)	4.32 (t, 4H, $\underline{H}_\beta$) 4.63 (t, 4H, $\underline{H}_\alpha$)	2.67 (s, 4H, -C$\underline{H}_2$-)
15a	7.13—7.49 (m, 16H)	4.27 (t, 2H, $\underline{H}_\beta$) 4.56 (t, 4H, $\underline{H}_\alpha$)	2.39 (s, 6H, -C$\underline{H}_3$)
16a	7.18 (d, 2H, J=8 Hz) 7.33 (d, 2H, J=8 Hz) 7.38 (d, 2H, J=8.5 Hz) 7.55 (d, 2H, J=8.5 Hz)	4.02 (s, 5H, $\underline{H}_\gamma$) 4.33 (t, 2H, $\underline{H}_\beta$) 4.64 (t, 2H, $\underline{H}_\alpha$)	2.33 (s, 3H, -C$\underline{H}_3$)
3	7.07—7.78 (m, 16H)	4.44 (t, 4H, $\underline{H}_\beta$) 4.56 (t, 4H, $\underline{H}_\alpha$)	6.88 (s, 2H, -C$\underline{H}$=C$\underline{H}$-)
4	7.00—7.58 (m, 16H)	4.40 (t, 4H, $\underline{H}_\beta$) 4.56 (t, 4H, $\underline{H}_\alpha$)	2.84 (s, 4H, -C$\underline{H}_2$-)
15b	7.00—7.47 (m, 16H)	4.27 (t, 4H, $\underline{H}_\beta$) 4.54 (t, 4H, $\underline{H}_\alpha$)	2.36 (s, 6H, -C$\underline{H}_3$)
16b	7.08—7.78 (m, 8H)	4.02 (s, 5H, $\underline{H}_\gamma$) 4.30 (t, 2H, $\underline{H}_\beta$) 4.64 (t, 2H, $\underline{H}_\alpha$)	2.38 (s, 3H, -C$\underline{H}_3$)
5s	6.80 (b-s, 12H, $H_a+H_b+H_e+H_f$) 7.09—7.24 (m, 4H, H_c+H_d)	4.33 (t, 4H, $\underline{H}_\beta$) 4.64 (t, 4H, $\underline{H}_\alpha$)	7.22 (s, 2H, -C$\underline{H}$=C$\underline{H}$-)
5a	6.84 (m, 2H, H_a) 7.04—7·58 (m, 14H, $H_{a'}+H_b+H_c+H_d+H_e+H_f$)	4.36 (t, 4H, $\underline{H}_\beta$) 4.56 (t, 4H, $\underline{H}_\alpha$)	7.13 (s, 2H, -C$\underline{H}$=C$\underline{H}$-)
6	6.82 (m, 2H, H_a) 7.06—7.36 (m, 14H, $H_{a'}+H_b+H_c+H_d+H_e+H_f$)	4.31 (t, 4H, $\underline{H}_\beta$) 4.66 (t, 4H, $\underline{H}_\alpha$)	2.74 (s, 4H, -C$\underline{H}_2$-)
15c	7.08—7.34 (m, 16H)	4.24 (t, 4H, $\underline{H}_\beta$) 4.51 (t, 4H, $\underline{H}_\alpha$)	2.24 (s, 6H, -C$\underline{H}_3$)
16c	7·07—7.48 (m, 8H)	4.02 (s, 5H, $\underline{H}_\gamma$) 4.29 (t, 2H, $\underline{H}_\beta$) 4.62 (t, 2H, $\underline{H}_\alpha$)	2.26 (s, 3H, -C$\underline{H}_3$)

a) The spectra of **1** and **2** were observed in pyridine-d_5.

Table 2. IR spectra of the cyclophane and reference compounds (KBr, cm^{-1})

Compound	
1	1600, 1500, 840 (p-disubstituted benzene ring), 1640, 740 (*cis* -CH=CH-, 810 (1,1′-disubstuted ferrocene ring), 720, and 690.
2	1600, 1500, 1450, 830 (p-disubstituted benzene ring), 810 (1,1′-disubstituted ferrocene ring), 725, and 690.
15a	1600, 1500, 840 (p-disubstituted benzene ring), and 805 (1,1′-disubstituted ferrocene ring).
16a	1600, 1500, 840 (p-disubstituted benzene ring), 1100, 1000, and 810 (monosubstituted ferrocene ring).
3	1600, 1500, 780, 750, 695 (aromatic ring), 815 (1,1′-disubstituted ferrocene ring), and 735 (*cis* -CH=CH-).
4	1600, 1500, 1480, 830, 795, 765, 705 (aromatic ring), and 815 (1,1′-disubstituted ferrocene ring).
15b	1605, 1500, 840, 775, 735, 690 (aromatic ring), and 810 (1,1′-disubstituted ferrocene ring).
16b	1600, 1500, 860, 825, 750, 735, 695 (aromatic ring), 1100, 995, and 810 (monosubstituted ferrocene ring).
5s	1600, 1500, 840, 770, 750 (aromatic ring), 800 (1,1′-disubstituted ferrocene ring), and 740 (*cis* -CH=CH-).
5a	1600, 1500, 840, 760, (aromatic ring), 810 (1,1′-disubstituted ferrocene ring), and 975 (*trans* -CH=CH-).
6	1605, 1500, 840, 765, 715 (aromatic ring), and 815 (1,1′-disubstituted ferrocene ring).
15c	1600, 1500, 880, 845, 820, 760, 740, 730 (aromatic ring), and 805 (1,1′-disubstituted ferrocene ring).
16c	1600, 1500, 845, 760, 740 (aromatic ring), 1100, 1000, and 810 (monosubstituted ferrocene ring).

tains the molecular ion peak at *m/e* 514. Thus we call them isomers. The configuration of double bond in **5s** was confirmed to be *cis*, because the IR spectrum of **5s** exhibits a band of 740 cm^{-1} which is characteristic of *cis* vinylene linkage. The configuration of double bond in **5a** exhibits a band of 975 cm^{-1} which is characteristic of *trans* vinylene linkage. The structural difference between **5s** and **5a** is unequivocal in the NMR spectra. In the NMR spectrum of **5s**, it is noteworthy that the vinylene protons of **5s**, which can be easily assigned by relative intensities, appear at lower field than the aromatic protons, in the analogy with the case of [2.2.2](1,3,5)cyclophane-1,9,17-triene.[12] The H_a, H_b, H_e, and H_f protons in **5s** are shifted to higher field than the corresponding protons of the reference compounds, 1,1′-bis(2′-methyl-4-biphenylyl)ferrocene (**15c**) and (2′-methyl-4-biphenylyl)ferrocene (**16c**), showing the strong shielding effect of the proximate aromatic ring. However, the H_c and H_d signals of **5s** were observed at nearly the same positions as those of **15c** and **16c**. These phenomena suggest that the two aromatic A rings in **5s** are approximately parallel and are held face to face with each other; however, the two aromatic B rings are not parallel, and the aromatic A and B rings have a non-planar orientation due to the short length of the side chain which is bridging at the ortho position of B rings. Consequently, the H_a, H_b, H_e, and H_f protons lie closer to the opposed biphenyl ring than do the H_c and H_d protons. The difference of the chemical shifts may be due to the difference in ring current effect of the biphenyl ring on the aromatic protons of **5s**. These data are best accommodated by the *syn*-conformation for **5s**. On the other hand, in **5a**, the shifts of H_a, H_b, H_b', and H_{c-f} protons are negligible, and the upfield shifts (0.24 ppm) of H_a protons are marked and roughly the same as those (0.28 ppm) of H_a protons of **5s**. Small shielding effects on H_a', H_b, H_b', and H_{c-f} protons are also explained by the *anti*-structure for **5a**.

In the NMR spectrum of the saturated cyclophane **6**, the aromatic protons H_a are shifted to higher field by about 0.26 ppm, compared with those of the reference compounds, **15c** and **16c**. However, the signals of H_a' and H_{b-d} were observed at nearly the same positions as those of **15c** and **16c**. These phenomena are also explained by an *anti*-structure for **6**, but not by a *syn*-structure.

The electronic spectra of the cyclophane and the reference compounds are shown in Figs. 1, 2, and 3. Biphenyl itself has no absorption in the long wavelength above 250 nm.[13] The electronic spectra of **1** and **2**, and **5s**, **5a**, and **6** show somewhat bathochromic and hyperchromic shifts and unambiguous broadening in a range 240—310 nm, compared with those of the reference compounds, **15a** and **16a**, and **15c** and **16c**, respectively. This may be due to transannular π-electronic interactions between the two chromopheres in **1**, **2**, **5s**, **5a**, and **6**. The stronger effect in **5s**, relative to that in **5a** or **6**, suggests that the two biphenyl rings in **5s** are closer to being vertically stacked than in the cases of **5a** and **6**. An examination of molecular modela also supports this conclusion.

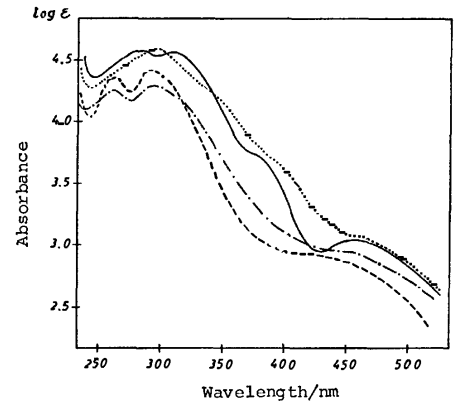

Fig. 1. Electronic spectra of **1**, **2**, **15a**, and **16a** in dioxane.
····· **1**, —— **2**, —·— **15a**, ---- **16a**.

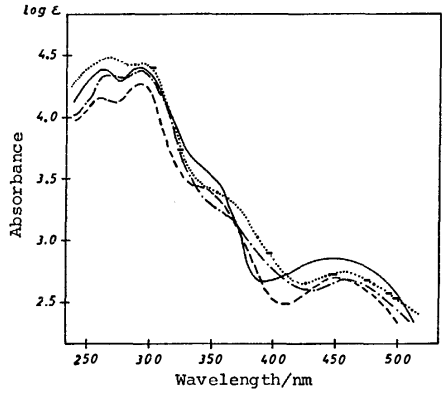

Fig. 2. Electronic spectra of **3**, **4**, **15b**, and **16b** in dioxane.
····· **3**, —— **4**, —·— **15b**, ----**16b**.

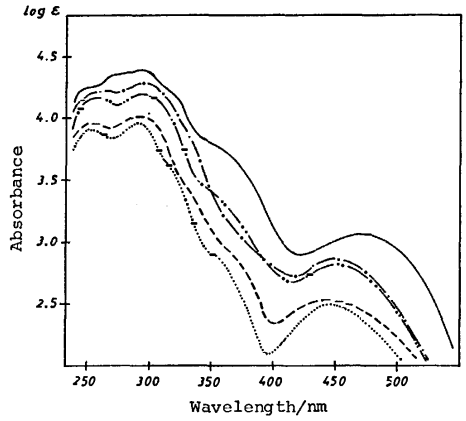

Fig. 3. Electronic spectra of **5s**, **5a**, **6**, **15c**, and **16c** in dioxane.
—— **5s**, —·— **5a**, —··— **6**, ---- **15c**, ····· **16c**.

On the other hand, in the 240—300 nm region, the cyclophanes **3** and **4** exhibit two absorption peaks and the intensity of these bands is somewhat increased; however, the spectra are practically identical with those of the reference compounds, **15b** and **16c**. These phenomena indicate that the interaction between the two biphenyl rings in both **3** and **4** is relatively weak and the *anti*-conformations for **3** and **4** can be accommodated.

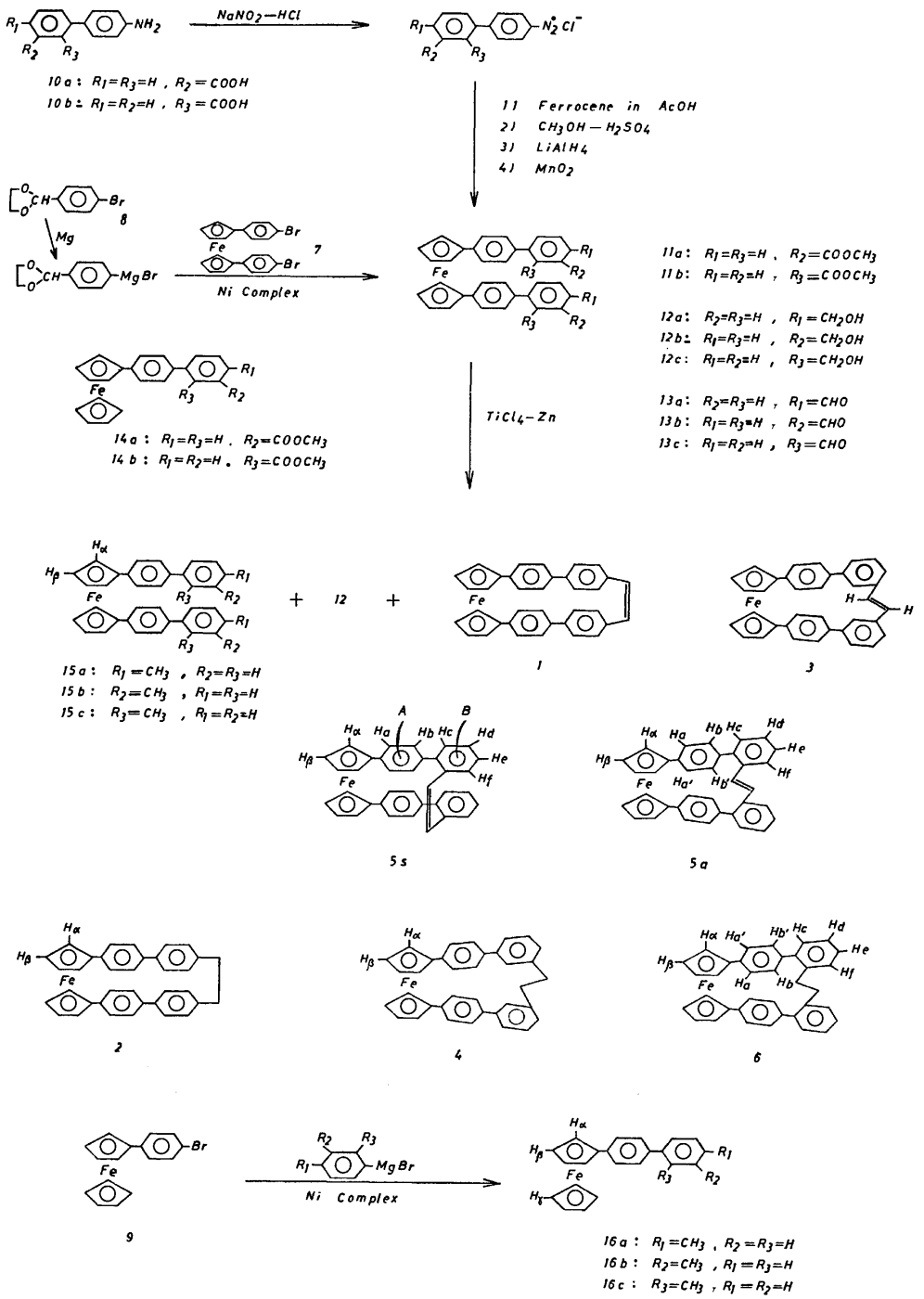

Scheme 1.

The electronic spectra of ferrocene contain two broad absorptions at 325 and 440 nm.[14] It has been shown that both the position and the intensity of the 440 nm band are particularly sensitive to ferrocene ring-tilt distortion.[15] This is also true for [1]-[16] and [2]-ferrocenophanes;[15] the 440 nm band undergoes a bathochromic shift and increases in intensity. In Fig. 1, both **15a** and **16a**, which bear no tilted ferrocene ring, exhibit two weak absorptions near 335 and 450 nm; however, in the electronic spectra of **1** and **2**, both the 325 and 440 nm bands undergo a bathochromic shift and increase in intensity, compared with those of **15a** and **16a**. These phenomena may be due to ferrocene ring-tilt distortion in **1** and **2**.

The IR spectra of the [2.2]paracyclophane system show some obvious features. One is the increase of the intensity of a band in the 1580—1600 cm^{-1} region, which relates to the increased double bond character due to the distortion of the benzene rings.[17] The other is the appearance of a strong new maximum near the 710 cm^{-1} region. Longone and Warren[18] reported that the strong maximum at 725 cm^{-1} in [2.2]-paracyclophane and at 710 cm^{-1} in 4,7,12,15-tetramethyl[2.2]paracyclophane might be characteristic bands associated with the distorted benzene rings in the [2.2]paracyclophane system. Furthermore, Otsubo

et al.[19] reported the same phenomena in the multilayered [2.2]paracyclophane system. The cyclophanes **1** and **2** also exhibit characteristic bands around 700 cm^{-1}, whereas the reference compounds bearing strain-free benzene rings, **15a** and **16a**, exhibit no bands in this region. This phenomenon may be due to the distortion of the benzene rings in **1** and **2**.

In the cyclophane, **3** and **4**, the electronic spectra in the 330—450 nm region are closely similar to those of the reference compounds bearing a no-tilt ferrocene ring: **15b** and **16b**. This indicates that, in **3** and **4**, the ferrocene ring is not tilted. Moreover, near the 710 cm^{-1} region, the IR spectra of **3** and **4** are closely similar to those of the open-chain models, **15b** and **16b**. This may be due to the non-distortion of benzene rings in **3** and **4**.

On the other hand, in the electronic spectra in the 300—400 nm region, **5s**, **5a**, and **6** show an increased intensity and a bathochromic shift at longer wave length, compared with those of **15c**. These phenomena suggest a ferrocene ring-tilt distortion due to the interaction between the two chromophores in **5s**, **5a**, and **6**. However, in the IR spectra near the 720 cm^{-1} region, the cyclophane, **5s**, **5a**, and **6**, and the open-chain models, **15c** and **16c**, have two absorption bands at approximately the same positions. It indicates that **5s**, **5a**, and **6** bear the no-tilt benzene rings.

Experimental

Materials and Measurement. All melting points are uncorrected. IR spectra were measured using a Hitachi 260-10 spectrophotometer. NMR spectra were obtained at 90 MHz with a Hitachi R-22 spectrometer using TMS as the internal standard. Mass spectra were recorded with a Hitachi RMU-6M spectrometer and electronic spectra with a Hitachi 200-10 spectrophotometer.

1,1′-Bis(*p*-bromophenyl)ferrocene (**7**),[20] *p*-bromobenzaldehyde ethylene acetal (**8**),[21] *p*-bromophenylferrocene (**9**),[22] 4′-aminobiphenyl-3-carboxylic acid (**10a**),[23] and 4′-aminobiphenyl-2-carboxylic acid (**10b**)[23] were prepared by the methods described in the literature.

*1,1′-Bis(4′-formyl-4-biphenylyl)ferrocene (**13a**).* Under a nitrogen atmosphere, the Grignard reagent prepared from **8** (9.16 g, 40 mmol) and magnesium turnings (1.19 g, 49 mmol) in dry THF (60 cm^3) was dropwise added to the mixture of **7** (3.52 g, 8 mmol) and dichloro[1,3-bis(diphenylphosphino)propane]nickel(II) (0.9 g, 1.6 mmol) in dry THF (60 cm^3) at 0 °C with stirring over 2 h. The reaction mixture was stirred for 6 h at 0—5 °C and then was allowed to remain overnight at room temperature. The mixture was hydrolyzed with 10% hydrochloric acid under cooling with an ice bath and extracted with ether. The ether extracts were washed successively with 10% hydrochloric acid, water, aqueous sodium hydrogencarbonate, and brine. After drying over $MgSO_4$, the solution was evaporated *in vacuo*. The reddish residue was chromatographed on silica gel, using benzene as the eluent, to give **13a**, which was recrystallized from ethanol, mp 242—244 °C (decomp). IR (KBr): 1690 (–CHO), 1600, 1580, and 820 cm^{-1} (*p*-disubstituted benzene ring). NMR (pyridine-d_5): δ=4.03 (t, 4H, $\underline{H}_\beta$), 4.38 (t, 4H, $\underline{H}_\alpha$), 7.46—7.88 (m, 16H, Ar–$\underline{H}$), and 10.02 (s, 2H, –C$\underline{H}$O). Found: C, 79.04; H, 4.63%; M^+, 546. Calcd for $C_{36}H_{26}FeO_2$: C, 79.13; H, 4.79%; M, 546.

*1,1′-Bis(3′-methoxycarbonyl-4-biphenylyl)ferrocene (**11a**) and (3′-Methoxycarbonyl-4-biphenylyl)ferrocene (**14a**).* The amine **10a** (10.66 g, 50 mmol) was diazotized in 10% sulfuric acid (300 cm^3) at 0—5 °C with sodium nitrite (3.45 g, 50 mmol). After diazotization was complete, the diazotized salt solution was added rapidly to a solution of ferrocene (3.72 g, 20 mmol) in acetic acid (150 cm^3) under a nitrogen atmosphere. The resulting dark brown solution was stirred overnight at room temperature, and was then poured into water. The precipitates which formed were filtered off, washed with water, dried at room temperature, and then were esterified in refluxing methanol (250 cm^3) containing 3 cm^3 of conc H_2SO_4 under a nitrogen atmosphere. After removal of the solvent *in vacuo*, the residue was extracted with $CHCl_3$ and the $CHCl_3$ extracts were washed with 5% sodium hydrogencarbonate solution and brine, dried over $MgSO_4$, filtered, and concentrated. The residue was purified by column chromatography (silica gel–benzene). First elution with benzene gave the starting materials; ferrocene (0.93 g, 25%), mp 173 °C.

Second elution with benzene afforded 0.82 g (10.3%) of **14a**, orange yellow crystals, mp 78—80 °C. IR (KBr): 1715 (ester), 1100, 1000, and 805 cm^{-1} (monosubstituted ferrocene ring). NMR ($CDCl_3$): δ=3.63 (s, 3H, –COOC$\underline{H}_3$), 4.01 (s, 5H, $\underline{H}_\gamma$), 4.18 (b-s, 8H, $\underline{H}_\alpha$+$\underline{H}_\beta$), and 7.18—8.20 (m, 8H, Ar–$\underline{H}$). Found: C, 72.70; H, 4.97%; M^+, 396. Calcd for $C_{24}H_{20}FeO_2$: C, 72.74; H, 5.08%, M, 396.

Third elution with benzene gave 4.24 g (35%) of **11a**, reddish yellow crystals, mp 153—155 °C. IR (KBr): 1720 (ester), 1600, 1580, 880, 835 (*p*- and *m*-disubstituted benzene rings), and 805 cm^{-1} (1,1′-disubstituted ferrocene ring). NMR ($CDCl_3$): δ=3.87 (s, 6H, –COOC$\underline{H}_3$), 4.08 (m, 8H, $\underline{H}_\alpha$+$\underline{H}_\beta$), and 7.21—8.12 (m, 16H, Ar–$\underline{H}$). Found: C, 75.18; H, 4.92%; M^+, 606. Calcd for $C_{38}H_{30}FeO_4$: C, 75.25; H, 4.98%; M, 606.

*1,1′-Bis(2′-methoxycarbonyl-4-biphenylyl)ferrocene (**11b**) and (2′-Methoxycarbonyl-4-biphenylyl)ferrocene (**14b**).* Gomberg's arylation of ferrocene with diazonium salts derived from **10b**, was carried out in the same way as described for **11a**, **11b** (reddish yellow crystals, mp 62—63 °C) and **14b** (reddish yellow crystals, mp 78—80 °C) were obtained in 18 and 22% yields, respectively.

11b: IR (KBr): 1720 (ester), 810 (1,1′-disubstituted ferrocene ring), 1600, 1500, 845, 820, and 730 cm^{-1} (aromatic ring). NMR ($CDCl_3$): δ=3.91 (s, 6H, –COOC$\underline{H}_3$), 4.22 (t, 4H, $\underline{H}_\beta$), 4.51 (t, 4H, $\underline{H}_\alpha$), and 7.11—7.85 (m, 16H, Ar–$\underline{H}$). Found: C, 75.14; H, 4.87%; M^+, 606. Calcd for $C_{38}H_{30}FeO_4$: C, 75.25; H, 4.98%; M, 606.

14b: IR (KBr): 1720 (ester), 1100, 1000, 805 (monosubstituted ferrocene ring), 1600, 1500, 840, 820, and 740 cm^{-1} (aromatic ring). NMR ($CDCl_3$): δ=3.86 (s, 3H, –COOC$\underline{H}_3$), 4.06 (s, 5H, $\underline{H}_\gamma$), 4.22 (t, 2H, $\underline{H}_\beta$), 4.45 (t, 2H, $\underline{H}_\alpha$), and 7.15—8.12 (m, 8H, Ar–$\underline{H}$). Found: C, 72.66; H, 5.01%; M^+, 396. Calcd for $C_{24}H_{20}FeO_2$: C, 72.74; H, 5.08%; M, 396.

*1,1′-Bis(3′-hydroxymethyl-4-biphenylyl)ferrocene (**12b**).* To a solution of $LiAlH_4$ (1.41 g, 37 mmol) in anhydrous ether (200 cm^3) was added dropwise a solution of **11a** (10.90 g, 18 mmol) in dry benzene (100 cm^3) at room temperature during 1 h, and the reaction mixture was then heated under reflux for additional 5 h. After the reaction mixture was decomposed with a small amount of cold water, the organic layer was washed with 5% hydrochloric acid, 5% aqueous sodium hydrogencarbonate, and brine, and dried over anhydrous $MgSO_4$. After removal of the solvents, the residue was purified by column chromatography on silica gel (benzene) to afford **12b** as reddish yellow crystals, which was recrystallized from ethanol, mp 166—168 °C, in 64% yield.

IR (KBr): 3430 (–OH), 1605, 1500, 880, 840 (aromatic ring), and 810 cm^{-1} (1,1′-disubstituted ferrocene ring). NMR ($CDCl_3$): δ=1.50 (s, 2H, –O<u>H</u>), 4.08 (t, 4H, <u>H</u>$_\beta$), 4.29 (t, 4H, <u>H</u>$_\alpha$), 4.57 (s, 4H, –C<u>H</u>$_2$–), and 7.07—7.76 (m, 16H, Ar–<u>H</u>). Found: C, 78.45; H, 5.35%; M^+, 550. Calcd for $C_{36}H_{30}FeO_2$: C, 78.55; H, 5.49%; M, 550.

*1,1′-Bis(2′-hydroxymethyl-4-biphenylyl)ferrocene (**12c**).* A reduction of **11b** with $LiAlH_4$ was carried out in the same way as described for **12b**, and **12c** (reddish yellow crystals, mp 152—153 °C) was obtained in 73% yield. IR (KBr): 3400 (–OH), 1600, 1500, 850, 820, 735 (aromatic ring), and 805 cm^{-1} (1,1′-disubstituted ferrocene ring). NMR ($CDCl_3$): δ=1.58 (s, 2H, –O<u>H</u>), 4.25 (t, 4H, <u>H</u>$_\beta$), 4.48 (t, 4H, <u>H</u>$_\alpha$), 4.56 (s, 4H, –C<u>H</u>$_2$–), and 7.11—7.56 (m, 16H, Ar–<u>H</u>). Found: C, 78.51; H, 5.40%; M^+, 550. Calcd for $C_{36}H_{30}FeO_2$: C, 78.55; H, 5.49%; M, 550.

*1,1′-Bis(3′-formyl-4-biphenylyl)ferrocene (**13b**).* An active manganese dioxide (100 g) was added to a solution of **12b** (6.47 g, 11.7 mmol) in $CHCl_3$ (200 cm^3) at room temperature, and the mixture was stirred in the dark for 20 h. After filtration to remove manganese dioxide and evaporation to dryness *in vacuo*, the residue was chromatographed in benzene on silica gel to afford reddish crystals **13b** (2.81 g, 44%), which were recrystallized from ethanol, mp 162—163 °C. IR (KBr): 2825, 1690 (–CHO), 1610, 1500, 875, 840 (aromatic ring), and 805 cm^{-1} (1,1′-disubstituted ferrocene ring). NMR ($CDCl_3$): δ=3.92 (t, 4H, <u>H</u>$_\beta$), 4.20 (t, 4H, <u>H</u>$_\alpha$), 7.13—7.80 (m, 16H, Ar–<u>H</u>), and 9.98 (s, 2H, –C<u>H</u>O). Found: C, 79.11; H, 4.68%; M^+, 546. Calcd for $C_{36}H_{26}FeO_2$: C, 79.13; H, 4.79%; M, 546.

*1,1′-Bis(2′-formyl-4-biphenylyl)ferrocene (**13c**).* An oxidation of **12c** with active manganese dioxide was carried out in the same way as described for **13b**, and reddish crystals **13c** (mp 175—176 °C) were obtained in 57% yield. IR (KBr): 2820, 1690 (–CHO), 1600, 1500, 845, 820, 740 (aromatic ring), and 800 cm^{-1} (1,1′-disubstituted ferrocene ring). NMR ($CDCl_3$): δ=4.28 (t, 4H, <u>H</u>$_\beta$), 4.56 (t, 4H, <u>H</u>$_\alpha$), 7.15—7.95 (m, 16H, Ar–<u>H</u>), and 9.96 (s, 2H, –CHO). Found: C, 78.96; H, 4.64%; M^+, 546. Calcd for $C_{36}H_{26}FeO_2$: C, 79.13; H, 4.79%; M, 546.

*The Reductive Coupling of **13a** with $TiCl_4$–Zn.* Under a nitrogen atmosphere, Zn dust (1.56 g, 24 mmol) was added in small portions to a stirred solution of $TiCl_4$ (2.27 g, 12 mmol) in dry THF (60 cm^3) at 0—5 °C. After the resulting mixture was refluxed for 2 h, a solution of **13a** (1.31 g, 2.4 mmol) and dry pyridine (0.20 g) in dry THF (80 cm^3) was added to the refluxing solution over 18 h, followed by a further 10 h period of reflux. The reaction mixture was then cooled to room temperature and quenched by addition of 60 cm^3 of saturated aqueous K_2CO_3 solution. The black mixture was stirred for 0.5 h, diluted with $CHCl_3$, and filtered through celite. The filtrate was washed with brine and dried over $MgSO_4$. After removal of the solvents, the residue was dissolved in benzene and chromatographed on silica gel.

The first fraction, eluted with benzene, gave 0.25 g (20%) of compounds **15a**, reddish yellow crystals, mp 137—138 °C. Found: C, 83.26; H, 5.75%; M^+, 518. Calcd for $C_{36}H_{30}Fe$: C, 83.39; H, 5.83%; M, 518.

The second fraction, eluted with chloroform, gave 1,1′-bis(4′-hydroxymethyl-4-biphenylyl)ferrocene (**12a**), orange yellow crystals, mp 250—252 °C (dec), in 2.5% yield. IR (KBr): 3450 (–OH), 1600, 1500, 820 (*p*-disubstituted benzene ring), and 810 cm^{-1} (1,1′-disubstituted ferrocene ring). NMR (pyridine-d_5): δ=1.58 (s, 2H, –O<u>H</u>), 4.23 (t, 4H, <u>H</u>$_\beta$), 4.48 (t, 4H, <u>H</u>$_\alpha$), 4.59 (s, 4H, –C<u>H</u>$_2$–), and 7.18—7.78 (m, 16H, Ar–<u>H</u>). Found: C, 78.52; H, 5.41%; M^+, 550. Calcd for $C_{36}H_{30}FeO_2$: C, 78.55; H, 5.47%; M, 550.

The third fraction, eluted with a mixture of chloroform and ethanol (10:1), gave **1**, reddish crystals, mp 238—240 °C (decomp), in 32% yield. Found: C, 83.87; H, 4.96%; M^+, 514. Calcd for $C_{36}H_{26}Fe$: C, 84.05; H, 5.09%; M, 514.

*The Catalytic Hydrogenation of **1** to **2**.* In the mixture of dioxane (100 cm^3) and ethanol (100 cm^3), compound **1** (0.50 g) was hydrogenated with PtO_2 (0.1 g) at room temperature under ordinary pressure. The reaction mixture was filtered to remove the catalyst and the filtrate was evaporated to dryness *in vacuo*. The residue was chromatographed on silica gel with chloroform to give 0.35 g (70% yield) of **2**, reddish crystals, mp 240—242 °C (decomp). Found: C, 83.61; H, 5.38%; M^+, 516. Calcd for $C_{36}H_{28}Fe$: C, 83.72; H, 5.46%; M, 516.

*The Reductive Coupling of **13b** with $TiCl_4$–Zn.* The reductive coupling of **13b** with $TiCl_4$–Zn was carried out in the same way as described for the reductive coupling of **13a**, and the products were separated by column chromatography on silica gel.

The first fraction, eluted with benzene, gave compound **15b**, reddish yellow crystals, mp 199—200 °C, in 12.5% yield. Found: C, 83.31; H, 5.73%; M^+, 518. Calcd for $C_{36}H_{30}Fe$: C, 83.39; H, 5.83%; M, 518.

The second fraction, eluted with chloroform, gave **12b**, reddish yellow crystals, mp 166—168 °C, in 8.5% yield.

The third fraction, eluted with chloroform, gave **3**, reddish crystals, mp 215—216 °C, in 28% yield. Found: C, 83.92; H, 4.93%; M^+, 514. Calcd for $C_{36}H_{26}Fe$: C, 84.05; H, 5.09%; M, 514.

*The Catalytic Hydrogenation of **3** to **4**.* The catalytic hydrogenation of **3** was carried out in the same way as described for the catalytic hydrogenation of **1**, and the product was purified by column chromatography on silica gel with chloroform to give **4**, orange yellow crystals, mp 239—240 °C, in 80% yield. Found: C, 83.69; H, 5.40%; M^+, 516. Calcd for $C_{36}H_{28}Fe$: C, 83.72; H, 5.46%; M, 516.

*The Reductive Coupling of **13c** with $TiCl_4$–Zn.* The reductive coupling of **13c** was carried out in the same way as described for the reductive coupling of **13a** with $TiCl_4$–Zn, and the products were separated by column chromatography on silica gel.

The first fraction, eluted with benzene, gave compound **15c**, reddish crystals, mp 137—138 °C, in 11% yield. Found: C, 83.30; H, 5.71%; M^+, 518. Calcd for $C_{36}H_{30}Fe$: C, 83.39; H, 5.83%; M, 518.

The second fraction, eluted with chloroform, gave **12c**, reddish yellow crystals, mp 152—153 °C, in 8.5% yield.

The third fraction, eluted with chloroform, gave **5a**, reddish crystals, mp 287—288 °C, in 34% yield. Found: C, 83.91; H, 4.97%; M^+, 514. Calcd for $C_{36}H_{26}Fe$: C, 84.05; H, 5.09%; M, 514.

The fourth fraction, eluted with chloroform, gave **5s**, reddish crystals, mp >280 °C, in 25% yield. Found: C, 83.88; H, 4.91%; M^+, 514. Calcd for $C_{36}H_{26}Fe$: C, 84.05; H, 5.09%; M, 514.

*The Catalytic Hydrogenation of **5s** and **5a** to **6**.* The catalytic hydrogenation of **5s** was carried out in the same way as described for the catalytic hydrogenation of **1**, and the product was purified by column chromatography on silica gel with chloroform to give **6**, reddish crystals, mp 279—280 °C (decomp), in 54% yield. Found: C, 83.70; H, 4.38%; M^+, 514. Calcd for $C_{36}H_{28}Fe$: C, 83.72; H, 5.46%; M, 516.

The catalytic hydrogenation of **5a** also led to the formation of **6**, mp 279—280 °C (decomp), in 65% yield.

*(4'-Methyl-4-biphenylyl)ferrocene (**16a**).* In the presence of nickel complex, the reaction of **9** with the Grignard reagent prepared from *p*-bromotoluene was carried out in the same way as described for **13a**, and the product was purified by column chromatography on silica gel with benzene to give **16a**, reddish orange crystals, mp 174—176 °C, in 57% yield. Found: C, 78.29; H, 5.65%; M^+, 352. Calcd for $C_{23}H_{20}Fe$: C, 78.42; H, 5.72%; M, 352.

*(3'-Methyl-4-biphenylyl)ferrocene (**16b**).* The reaction of **9** with the Grignard reagent derived from *m*-bromotoluene was carried out in the same way as described for **13a**, and the product was purified by column chromatography on silica gel with benzene to give **16b**, reddish orange crystals, mp 106—108 °C, in 44% yield. Found: C, 78.33; H, 5.59%; M^+, 352. Calcd for $C_{23}H_{20}Fe$: C, 78.42; H, 5.72%; M, 352.

*(2'-Methyl-4-biphenylyl)ferrocene (**16c**).* The reaction of **9** with the Grignard reagent derived from *o*-bromotoluene was carried out in the same way as described for **13a**, and the product was purified by column chromatography on silica gel with benzene to give **16c**, reddish orange crystals, mp 137—138 °C, in 48% yield. Found: C, 78.32; H, 5.61%; M^+, 352. Calcd for $C_{23}H_{20}Fe$: C, 78.42; H, 5.72%; M, 352.

The present work was supported by a Grant-in-Aid for Scientific Research No. 554137 from the Ministry of Education, Science and Culture.

References

1) M. Rosenblum, N. M. Brawn, D. Clappenelli, and J. Tancrede, *J. Organomet. Chem.*, **24**, 469 (1970).
2) A. Kasahara and T. Izumi, *Chem. Lett.*, **1978**, 21.
3) A. Kasahara, T. Izumi, and I. Shimizu, *Chem. Lett.*, **1979**, 1119.
4) A. Kasahara, T. Izumi, and I. Shimizu, *Chem. Lett.*, **1979**, 1317; S. Kamiyama, A. Kasahara, T. Izumi, I. Shimizu, and H. Watabe, *Bull. Chem. Soc. Jpn.*, **54**, 2079 (1981).
5) A. Kasahara, T. Izumi, and H. Umezawa, *Chem. Lett.*, **1980**, 1039.
6) S. Misumi, *Kagaku No Ryoiki*, **28**, 927 (1974); **32**, 651 (1978); Y. Sakata, *Yuki Gosei Kyokai Shi*, **38**, 164 (1980).
7) T. Mukaiyama, T. Sato, and J. Hanna, *Chem. Lett.*, **1973**, 1041; J. E. McMurry and M. P. Fleming, *J. Am. Chem. Soc.*, **96**, 4708 (1974); J. E. McMurry and L. R. Krepski, *J. Org. Chem.*, **41**, 3929 (1976); A. Ishida and T. Mukaiyama, *Chem. Lett.*, **1976**, 1127; J. E. McMurry, M. P. Fleming, K. L. Kees, and L. R. Krepski, *J. Org. Chem.*, **43**, 3255 (1978).
8) D. Tanner and O. Wennerstrom, *Tetrahedron Lett.*, **1981**, 2313.
9) K. Tamao, K. Sumitani, Y. Kiso, M. Zembayashi, A. Fujioka, S. Kodama, I. Nakajima, A. Minato, and M. Kumada, *Bull. Chem. Soc. Jpn.*, **49**, 1958 (1976).
10) M. Rosenblum, "Chemistry of The Iron Group Metallocenes," Interscience Publishers, New York (1965), Part 1, p. 31.
11) L. Pauling, "The Nature of The Chemical Bond," 3rd ed, Cornell University Press, Ithaca, New York (1960), p. 262.
12) V. Boeckelheide and R. A. Hollins, *J. Am. Chem. Soc.*, **92**, 3512 (1970).
13) E. S. Stern and C. J. Timmons, "Electronic Absorption Spectroscopy in Organic Chemistry," 3rd ed, Edward Arnold, London (1970), p. 116.
14) Ref. 10, p. 42.
15) T. H. Barr and W. E. Watts, *J. Organomet. Chem.*, **15**, 177 (1968).
16) A. G. Osborn and R. H. Whiteley, *J. Organomet. Chem.*, **193**, 345 (1980).
17) D. J. Cram and H. Steinberg, *J. Am. Chem. Soc.*, **73**, 5691 (1951).
18) D. T. Longone and C. L. Warren, *J. Am. Chem. Soc.*, **84**, 1507 (1962).
19) T. Otsubo, S. Mizogami, I. Ostubo, Z. Tozuka, A. Sakagami, Y. Sakata, and S. Misumi, *Bull. Chem. Soc. Jpn.*, **46**, 3419 (1973).
20) A. N. Nesmeyanov, E. G. Perevalova, R. V. Golovnya, N. A. Simukova, and O. V. Starovskii, *Izv. Akad. Nauk SSSR, Otd. Khim. Nauk*, **1957**, 638.
21) J. A. Landgrebe and R. H. Rynbrandt, *J. Org. Chem.*, **31**, 2585 (1966).
22) J. G. Mason and M. Rosenblum, *J. Am. Chem. Soc.*, **82**, 4206 (1960).
23) P. L. Dannley and M. Sternfeld, *J. Am. Chem. Soc.*, **76**, 4543 (1945).

 © 1983 The Chemical Society of Japan Bull. Chem. Soc. Jpn., 56, 199—202 (1983)

Aryliminodimagnesium Reagents. III. The Deoxygenative Condensation with Nitroso- and Nitroarenes: Electronic Effect of Substituents on Product Distribution

Masao Ōkubo,* Tomoko Takahashi, and Kōji Koga

Department of Chemistry, Faculty of Science and Engineering, Saga University, Honjō-machi, Saga 840

(Received May 12, 1982)

Aryliminodimagnesium reagents ($ArN(MgBr)_2$) condense with nitrosoarenes and nitroarenes giving the corresponding azoarenes and azoxyarenes, respectively. Azoxyarenes were moderately deoxygenated by treatment with excessive amounts of the reagent giving the corresponding azoarenes. The reaction of nitroarenes with differently substituted reagents afforded unsymmetrically substituted azoxy- and azoarenes: Small amounts of symmetrically substituted azoarenes, which originated from the oxidative coupling of the reagent molecules, were also isolated. The distribution of the three types of condensation products are governed by the electronic effect of substituents of both the reagents and the substrates.

It has been reported very recently that aryliminodimagnesium reagents ($ArN(MgBr)_2$, aryl-IDMg), derived from anilines and two molar equivalents of EtMgBr, condense with diaryl ketones giving the corresponding anils[1,2] (Scheme 1). According to the

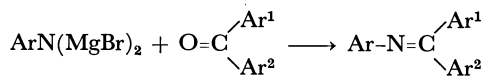

Scheme 1.

manner of deoxygenative condensation, aryl-IDMg are expected to react with a wide variety of substrates. Actually, the treatment of nitroso- and nitroarenes with the reagents afforded the corresponding azo- and azoxyarenes, respectively. In this paper, the electronic effect on the product distribution will be explained in comparison with those reported previously on the reaction of ArMgBr.[3,5,6]

Results and Discussion

The condensation ability of aryl-IDMg towards nitrosoarenes is exemplified by the reaction with highly hindered 2,3,5,6-tetramethylnitrosobenzene(nitrosodurene, Scheme 2 and Table 1). The comparison of the yields of the hindered azoarenes in Expt 1 with that in Expt 2 suggests that the deoxygenative condensation reaction with the nitrosoarene requires two molar equivalents of the reagent: This feature is in contrast with results obtained in the reactions with diaryl ketones which require usually an equimolar amount of the reagent.[1,2] The more strongly electron-donating *p*-methoxyphenyl-IDMg gave an excellent yield of the azo product (Expt 3), though a trace amount of an unidentifiable contaminant was eliminated with difficulty. The less strongly electron-donating *p*-chloro-

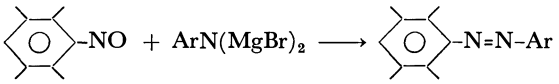

Scheme 2.

phenyl-IDMg reduced the yield (Expt 4), which, however, was improved by heating for more than 3 h and/or by use of three or more molar equivalents of the reagent.

The facts that the formation of a radical species in Expt 1 was detected by ESR and that the more strongly electron-donating reagent is more favorable to the reaction (*p*-MeO > *p*-Me > *p*-Cl) suggest that the condensation reaction is governed by the electron-transfer from the reagent to the substrate: The same order was observed for the formation of the nitroxide radical in the Grignard reaction of the same substrate.[3]

The condensation ability of the IDMg reagents with the nitroso functional group is confirmed. This reaction, however, is of no synthetic importance since the facile condensation of nitrosoarenes with arylamines in acetic acid has been well established.[4] The IDMg reaction with nitrosoarenes was not investigated further.

The reaction of nitrobenzene with more than five molar equivalents of phenyl-IDMg was studied first, the results being given in Table 2. High overall yields of azoxy- and azobenzenes were obtained (Expts 5 and 6). An authentic sample of azoxybenzene was

Table 1. Reaction of nitrosodurene with aryl-IDMg reagents

Expt No.	Nitrosodurene (mmol)	*p*-$RC_6H_4N(MgBr)_2$ R	*p*-$RC_6H_4N(MgBr)_2$ (mmol)	*p*-RC_6H_4-N=N-Dur[a] yield/%
1	4.9	H	4.9	15[b]
2	6.1	Me	12.6	84[c]
3	3.0	MeO	6.1	93[c]
4	3.0	Cl	6.1	31[c]

a) Dur = 2,3,5,6-Me_4C_6H. b, c) Yields, based on the amounts of nitrosodurene used, were obtained after heating at 55 °C b) for 2 h, and c) for 3 h.

Table 2. Reaction of aryl-IDMg for converting nitro- and azoxybenzene into azobenzene

Expt No.	Substates	(mmol)	$ArN(MgBr)_2$ Ar	(mmol)	Molar ratio [IDMg]/[Substr.]	Yields[a]/% Overall	PhN=NAr ↓ O	PhN=NAr
5	$PhNO_2$	(4.1)	C_6H_5	(20.5)	5.0	85.1	53.4	31.7
6	$PhNO_2$	(2.6)	C_6H_5	(20.3)	8.0	82.8	21.5	61.3
7	PhN=NPh ↓ O	(5.5)	p-MeC_6H_4	(11.0)	2.0	97.7	75.0[b,c]	22.7[b]

a) Yields, based on the amount of substrates used, were obtained after heating at 55 °C for 3 h. b) Ar=Ph. c) Recovered amount.

deoxygenated at a moderate rate on treatment with two molar equivalents of p-methylphenyl-IDMg (Expt 7). Thus, the formation of azobenzene *via* the intermediate formation of azoxybenzene followed by its deoxygenation (Scheme 3) is confirmed.

$$Ar^1NO_2 \xrightarrow{ArN(MgBr)_2} Ar^1\overset{\overset{O}{\frown}}{-N=N}-Ar \xrightarrow{ArN(MgBr)_2} Ar^1-N=N-Ar$$

Scheme 3.

Three types of condensation products were obtained in the reaction of a substituted nitroarene with a differently substituted aryl-IDMg (Scheme 4 and

$$Ar^1NO_2 + Ar^2N(MgBr)_2 \longrightarrow Ar^1-N(O)=N-Ar^2 + Ar^1-N=N-Ar^2 + Ar^2-N=N-Ar^2$$

Scheme 4.

Table 3). In the reaction with nitroarenes carried out using a fixed molar ratio of reagent to substrate (Expts 8—11), the distribution of the yields of the unsymmetrically substituted azoxy- and azoarenes varies remarkably with the electronic effect of the substituents of both the substrates and the reagents. The variation can be explained in terms of the electron-accepting and -donating ability of the reactants;[5] the explanation given below is similar to that given previously for the Grignard reaction involving initial electron-transfer process.[6] The process for the Grignard reaction with hindered benzophenones (Scheme 5), as estimat-

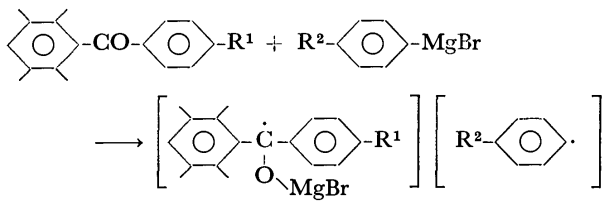

Scheme 5.

ed by ESR, is governed by the effect of the substituents R^1 and R^2 as shown in the following:

faster ← electron-transfer → slower

$R^2 = H$: $R^1 = F$, Cl>H>OMe[6]

(← electron-accepting ability of substrates)

$R^1 = H$: $R^2 = OMe > H > F$[7]

(← electron-donating ability of reagents).

The detection of any radical species by ESR at room temperature in Expts 5—11 was unsuccessful, probably due to the unhindered structure[6,7] of the nitroarenes used.

Symmetrical azoarenes (Expts 8—11), which were not observed in the reaction with diaryl ketones,[1,2] should be formed as the result of oxidative coupling of the reagent molecules due to the much higher electron-accepting ability of nitroarenes than that of ketones.[8,9] Yields of the symmetrical azoarenes increase in the reaction of strongly electron-donating reagent (p-MeO>p-Me>p-Cl) with strongly electron-accepting nitroarene (p-Cl>p-Me>p-MeO).

Typical extremes of the product distribution are demonstrated by the results of Expts 10 and 11. The combination of the highly electron-accepting p-chloronitrobenzene with the highly electron-donating p-methoxyphenyl-IDMg gave a high combined yield of the azo products, but no azoxy product. The other combination of p-methoxynitrobenzene with p-chlorophenyl-IDMg gave the highest yield of the azoxy product together with the lowest combined yield of the azo products.

The effect of the molar ratio of reagent to substrate is another factor governing the distribution of the products especially when the highly electron-donating reagent is used. The highest yield of the azoxyarene in Expt 11 is due to the use of the less electron-donating p-chlorophenyl-IDMg: Even the treatment with ten molar equivalents of the reagent for 10 h reduced the yield only slightly (Expts 12 and 13). In contrast, the use of only two molar equivalents of the more electron-donating p-methoxyphenyl-IDMg reduced the yield of the azoxy product (Expts 14 and 15).

It is important to note that the azoxy products obtained in Expts 14 and 15 are isomeric with those obtained in Expts 9 and 11, respectively. Since any isomerization of an azoxy compound was not detected under the reaction conditions, this method provides a new route for preparing isomeric pairs of azoxyarenes, $Ar^1-N(O)=N-Ar^2$ and $Ar^1-N=N(O)-Ar^2$, independently.[10] A more detailed study on the preparation and the deoxygenation of azoxyarenes will be described in the subsequent paper.

All the aryl-IDMg reagents used in this study are

Table 3. Effect of substituents and molar ratio on product distribution in the reaction of p-$R^1C_6H_4NO_2$ with p-$R^2C_6H_4$-IDMg

Expt No.	Substituents		Molar ratio [IDMg]/[$ArNO_2$]	Yields[a]/%			
	R^1	R^2		Overall	Unsym. azoxy.	Unsym. azo.	Sym. azo.
8	Me	MeO	6.2[b]	90.1	0	73.0	17.1
9	MeO	Me	6.2[b]	89.7	24.3	51.7	13.7
10	Cl	MeO	6.2[b]	84.4	0	57.7	26.7
11	MeO	Cl	6.2[b]	93.1	73.4	14.8	4.9
12	MeO	Cl	5.0[c]	97.7	77	15	5.7
13	MeO	Cl	10.0[d]	89.5	60	22	7.5
14	Me	MeO	2.0[b]	83	39	34	10
15	Cl	MeO	2.0[b]	71.3	50	12	9.3

a) Yields are based on the amount of $ArNO_2$ used. b, c, d) The reaction mixtures were heated at 55 °C for b) 3 h, c) 5 h, and d) 10 h, respectively.

less electron-donating than arylmagnesium bromides since the formers do not affect azoarenes whereas the latters convert azobenzene into hydrazobenzene[11] (Scheme 6). The vigorous reaction of the highly elec-

$$\text{Ph-N=N-Ph} \xrightarrow{\text{ArMgBr}} \text{Ph-N(BrMg)-N(MgBr)-Ph} \xrightarrow{H_2O} \text{Ph-NH-NH-Ph}$$

Scheme 6.

tron-accepting nitrobenzene with the highly electron-donating Grignard reagent (PhMgBr) affords comparable amounts of the products due to the addition-reduction (Ph_2NH), the deoxygenation (PhOH), and the oxidative coupling (Ph–Ph).[12] The reaction has been little studied and attracted no attention until the interesting Grignard reaction of nitrobenzothiazoles was reported.[13] The deoxygenative condensation reaction presented here owes its success to the moderate electron-donating ability of the aryl-IDMg reagents,[1-3] though the detailed structure and the mechanism remain to be investigated.

The overall yield was somewhat lower when the yield of the symmetrical azoarene was higher, and *vice versa* (Table 3): In Expt 10, a recognizable amount of an unidentifiable and poorly soluble black material was formed, probably due to a free radical reaction initiated by the quick electron-transfer from the reagent to the substrate.[14] Some attempts, *i.e.*, the dilution of the reagent and/or the substrate solution, the addition of the reagent solution in the reverse manner, and the addition at −78 °C, were not effective in reducing the formation of the black material as well as the symmetrical azoarene.

The unimportant limitations given are difficult to overcome; nevertheless, the IDMg process provides a general method for preparing unsymmetrical azoxy- and azoarenes.

Experimental

The melting points of azo- and azoxyarenes are uncorrected.

Materials. Nitrosodurene was prepared according to the reported method.[3] All the nitroarenes and the anilines used in this study were commercially available, and were purified by distillation before use.

Procedures. The typical procedure is given as follows. Ethylmagnesium bromide (30.8 mmol) was prepared under N_2 atmosphere as usual in THF (20 ml), and a 2—3% excess amount of the aniline (15.8 mmol) dissolved in THF (15 ml) was added at 0 °C to the Grignard solution. The mixture was stirred gently at 55 °C for 40 min to complete the evolution of ethane.[1] The nitroarene (3.08 mmol) dissolved in THF (15 ml) was added to the IDMg solution at 0 °C; the color of the mixture turned deep reddish brown, The colored mixture was stirred at 55 °C for 3 h, quenched with aqueous NH_4Cl, extracted with diethyl ether followed by washing with dilute HCl (0.5—1.0 mol dm^{-3}) for removing the unreacted aniline. After washing with water, the colored solution was dried on $MgSO_4$ and concentrated under reduced pressure; the product mixture was chromatographed on silica gel (Wako-Gel C-200).

Products. The chromatographic separation of the three types of the products was sometimes incomplete. The yields of the products in individual experiments, however, were estimated easily by ^{1}H-NMR since the signals of the four *ortho*-protons around the –N(O)=N– group appear at lower field than 8.0 ppm while those of the protons around the –N=N– group appear at higher field.

The melting points and ^{1}H-NMR data of azo- and azoxyarenes are given in Tables 4 and 5, respectively. Among the ^{1}H-NMR data, some aromatic proton signals which consist of two AB-quartets are not assigned and the figures are given in parentheses.

The molecular weight of the product was recorded on a Denshi Kagaku EMD-05A Mass Spectrometer. Results of the elemental analyses of the new azo- and azoxyarenes, which are represented by the Expt Nos. as shown in Tables 4 and 5, are given in the following.

(1): Found: C, 81.77; H, 7.51; N, 11.65%. Calcd for $C_{16}H_{18}N_2$: C, 80.67; H, 7.56; N, 11.76%.

(2): Found: C, 81.02; H, 7.85; N, 11.06%. Calcd for $C_{17}H_{20}N_2$: C, 80.95; H, 7.93; N, 11.11%.

(3): Found: C, 76.21; H, 7.40; N, 10.55%. Calcd for $C_{17}H_{22}N_2O$: C, 76.12; H, 7.46; N, 10.44%.

(4): Found: C, 70.31; H, 6.50; N, 10.30%. Calcd for $C_{16}H_{18}ClN_2$: C, 70.20; H, 6.58; N, 10.24%.

(10): Found: C, 63.21; H, 4.52; N, 11.50%. Calcd for $C_{13}H_{11}ClN_2O$: C, 63.28; H, 4.46; N, 11.36%.

(11): Found: C, 60.01; H, 4.09; N, 10.74%. Calcd for $C_{13}H_{11}ClN_2O_2$: C, 59.43; H, 4.19; N, 10.67%.

(14): Found: C, 69.60; H, 5.81; N, 74.30%. Calcd for $C_{14}H_{14}N_2O_2$: C, 69.42; H, 5.78; N, 74.38%.

Table 4. Melting points and NMR data of azoarenes

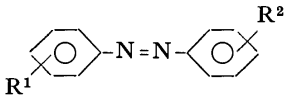

Expt No.	R^1	R^2	Mp θ_m/°C Obsd	Mp θ_m/°C Lit	^{1}H-NMR data δ
5	H	H	68.5	68.5	8.00—7.80(4H, m, Ar); 7.58—7.35(6H, m, Ar).
1	Dur.[a)]	H	90—92	—	7.90—7.70(2H, m, Ar); 7.46—7.00(3H, m, Ar); 6.80 (1H, s, Ar); 2.22(6H, s, Me); 2.05(6H, s, Me).
2	Dur.	*p*-Me	99—101.5	—	7.72 and 7.22(4H, ABq, Ar); 6.84(1H, s, Ar); 2.41 (3H, s, Me); 2.24(6H, s, Me); 2.04(6H, s, Me).
3	Dur.	*p*-MeO	123—125	—	7.80 and 6.92(4H, ABq, Ar); 6.83(1H, s, Ar); 3.83 (3H, s, Me); 2.24(6H, s, Me); 2.04(6H, s, Me),
4	Dur.	*p*-Cl	89.5—91	—	7.84 and 7.44(4H, ABq, Ar); 6.92(1H, s, Ar); 2.24 (6H, s, Me); 2.08 (6H, s, Me).
8	*p*-Me	*p*-MeO	110—113	109—110[15)]	7.98(7.90) and 7.32(4H, ABq, Ar); 7.90(7.98) and 7.00(4H, ABq, Ar); 3.80(3H, s, Me).
10	*p*-Cl	*p*-MeO	123—123.5	—	7.90(7.86) and 7.46(4H, ABq, Ar); 7.86(7.90) and 6.98(4H, ABq, Ar); 3.86(3H, s, Me).
	p-Cl	*p*-Cl	175—178	183—184[16)]	7.90 and 7.52(8H, ABq, Ar).
	p-MeO	*p*-MeO	165—167	163[17)]	7.92 and 7.02(8H, ABq, Ar); 3.86(6H, s, Me).
	p-Me	*p*-Me	139—142	142—143[16)]	7.86 and 7.33(8H, ABq, Ar); 2.43(6H, s, Me).

a) Dur.=2,3,5,6-Me_4C_6H-.

Table 5. Melting points and NMR data of azoxyarenes

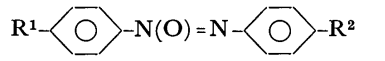

Expt No.	R^1	R^2	Mp θ_m/°C Obsd	Mp θ_m/°C Lit	^{1}H-NMR data δ
6	H	H	35—35.5	35.5	8.40—8.16(4H, m, Ar); 8.52—8.32(6H, m, Ar).
	p-Cl	*p*-MeO	142—146.5	145[18)]	8.56(8.46) and 7.65(4H, ABq, Ar); 8.46(8.56) and 7.17(4H, ABq, Ar); 3.98(3H, s, Me).
11	*p*-MeO	*p*-Cl	105.5—107	—	8.28(8.15) and 7.42(4H, ABq, Ar); 8.15(8.28) and 6.93 (4H, ABq, Ar); 3.87(3H, s, Me).
14	*p*-Me	*p*-MeO	108.5—110	—	8.30(8.20) and 7.24(4H, ABq, Ar); 8.20(8.30) and 6.92 (4H, ABq, Ar); 3.86(3H, s, Me); 2.44(3H, s, Me).
9	*p*-MeO	*p*-Me	77—78.5	—	8.28(8.13) and 7.65(4H, ABq, Ar); 8.13(8.28) and 6.94 (4H, ABq, Ar); 3.84(3H, s, Me); 2.39(3H, s, Me).

(9): Found: C, 69.52; H, 5.69; N, 74.51%. Calcd for $C_{14}H_{14}N_2O_2$: C, 69.42; H, 5.78; N, 74.38%.

The support of this work by research grants from the Ministry of Education, Science and Culture (C-56540307) is gratefully acknowledged.

References

1) Part I: M. Ōkubo and S. Ueda, *Bull. Chem. Soc. Jpn.*, **53**, 281 (1980).
2) Part II: M. Ōkubo, S. Hayashi, M. Matsunaga, and Y. Uematsu, *Bull. Chem. Soc. Jpn.*, **54**, 2337 (1981).
3) M. Ōkubo and T. Takahashi, *Bull. Chem. Soc. Jpn.*, **52**, 3761 (1979).
4) E. Haselbach, *Helv. Chim. Acta*, **53**, 1526 (1970).
5) M. Ōkubo and Y. Uematsu, *Bull. Chem. Soc. Jpn.*, **55**, 1121 (1982).
6) M. Okubo, *Bull. Chem. Soc. Jpn.*, **48**, 2057 (1975); **50**, 2379 (1977), and literatures cited therein.
7) M. Ōkubo, unpublished results.
8) P. Zuman, "Substituent Effects in Organic Polarography," Plenum Press, New York (1967).
9) K. Maruyama and T. Otsuki, *Bull. Chem. Soc. Jpn.*, **41**, 444 (1968).
10) G. M. Badger, R. G. Butterby, and G. E. Lewis, *J. Chem. Soc.*, **1953**, 2143; G. M. Badger and G. E. Lewis, *ibid.*, **1953**, 2147.
11) H. Gilman and J. C. Bailor, *J. Org. Chem.*, **2**, 84 (1937).
12) D. N. Kursanov and P. A. Solodkov, *J. Gen. Chem. USSSR*, **5**, 1487 (1935); *Chem. Abstr.*, **30**, 2181 (1936).
13) G. Bartoli, R. Leardini, M. Lelli, and R. Rosini, *J. Chem. Soc., Perkin Trans. 1*, **1977**, 884.
14) G. A. Russell, E. G. Janzen, and E. T. Strom, *J. Am. Chem. Soc.*, **86**, 1807 (1964).
15) H. Wieland, *Ber.*, **48**, 1098 (1915).
16) F. Meyer and E. Trampedach, *Justus Liebigs Ann. Chem.*, **330**, 125 (1902).
17) K. H. Pausacker, *J. Chem. Soc.*, **1953**, 1989.
18) T. E. Stevens, *J. Org. Chem.*, **29**, 311 (1964).

 © 1983 The Chemical Society of Japan Bull. Chem. Soc. Jpn., 56, 203—207 (1983)

Aryliminodimagnesium Reagents. IV. The Independent Preparation of Unsymmetrically Substituted Azoxyarene Isomers and Their Deoxygenation

Masao Ōkubo* and Kōji Koga

Department of Chemistry, Faculty of Science and Engineering, Saga University, Honjō-machi, Saga 840

(Received May 12, 1982)

By use of the condensation reaction of aryliminodimagnesium reagents ($ArN(MgBr)_2$) with nitroarenes, six symmetrical and eight unsymmetrical azoxyarenes including four pairs of isomers were prepared in 40—80% yields. The deoxygenation reaction of the azoxyarenes by treating with five molar equivalents of p-$MeOC_6H_4N(MgBr)_2$ at 55 °C in tetrahydrofuran was also studied, and the reactivity of deoxygenation was correlated to the shift of the electronic absorption maximum of azoxyarene.

So far, unsymmetrical azoxyarenes have been obtained by oxidation of unsymmetrical azoarenes,[1-3] by condensation of nitrosoarenes with *N*-arylhydroxylamines,[4,5] or by selective substitution on azoxybenzenes.[6] The first method often gives a mixture of isomers, their separation not always being easy.[5] The second method is more selective, but is ultimately limited by the instability of the starting materials. A method involving a Grignard reaction of substituted *N*-nitrosohydroxylamine derivatives[7] has also been reported, depending on the uncommon type of the starting material. These limitations have been an obstacle to the development of azoxyarene chemistry: The electronic effect of substituents on the deoxygenation by use of phosphorus(III) reagents, for instance, has not been studied enough.[8]

In the preceding paper,[9] the condensation of nitroarenes with aryliminodimagnesium reagents ($ArN(MgBr)_2$, aryl-IDMg) was reported. The reaction involves rapid deoxygenative condensation affording the azoxyarenes followed by much slower deoxygenation giving the azoarenes (Scheme 1). Since the intermediately formed azoxyarenes do not isomerize under the reaction conditions,[9] the IDMg method provides a novel route for preparing unsymmetrical azoxyarene isomers independently.

$$Ar^1NO_2 + Ar^2N(MgBr)_2 \longrightarrow Ar^1\text{-}N(O)\text{=}N\text{-}Ar^2 + Ar^1\text{-}N\text{=}N\text{-}Ar^2 + Ar^2\text{-}N\text{=}N\text{-}Ar^2$$

Scheme 1.

The authors first endeavored to find the optimum reaction conditions for preparing typical symmetrical and unsymmetrical azoxyarenes, and second to study their substituent effect on the deoxygenation by the treatment with an aryl-IDMg reagent. The results are reported in this paper.

Results and Discussion

Preparation of Azoxyarenes. On the basis of the reaction profiles given in the preceding paper,[9] the reaction conditions suitable for preparing unsymmetrical azoxyarenes (Scheme 1) are i) a less electron-donating reagent, ii) a less electron-accepting substrate, and iii) a lower molar ratio of reagent to substrate. However, the formation of the final products, unsymmetrical azoarenes, as well as that of the oxidative coupling products, symmetrical azoarenes, are unavoidable.

The molar ratio of the IDMg reagents to the nitroarenes used in Expts 1—6 (Table 1) were chosen in order to convert the substrates completely and also to minimize the subsequent deoxygenation of the primarily produced azoxyarenes. No substrate was recovered except in Expt 3 in which *ca.* 5% of the nitroarene was found in the product mixture. The facts that the most electron-donating *p*-methoxyphenyl-IDMg gave the highest combined yield of the azo products and that the least electron-donating *m*-methoxyphenyl-IDMg gave the lowest yield of the symmetrical azo product accord with the previous results.[9]

In the reactions carried out for preparing symmetrically substituted azoxyarenes (Scheme 2), the amount of the symmetrical azoarenes formed comes partly from the deoxygenation of azoxyarenes and partly from the oxidative coupling of the reagent molecules: The results are given in Table 2 (Expts 7—12).

$$RC_6H_4NO_2 + RC_6H_4N(MgBr)_2 \longrightarrow RC_6H_4\text{-}N(O)\text{=}NC_6H_4R + RC_6H_4\text{-}N\text{=}N\text{-}C_6H_4R$$

Scheme 2.

The remarkable recovery of the substrate in Expt 8 is ascribable to the weakest electron-donating ability of *p*-chlorophenyl-IDMg.

Summarizing the results given in Tables 1 and 2, the optimum molar ratio suitable for preparing azoxyarenes seems to depend mainly on the electron-donating ability of the aryl-IDMg reagents. The most, the medium, and the least electron-donating reagents require the lowest, the medium, and the highest molar ratio respectively (Table 3).

An unusual result was obtained when *p*-dimethylaminophenyl-IDMg, which was expected to be more electron-donating than the *p*-methoxyphenyl reagent, was allowed to react with *N*,*N*-dimethyl-*p*-nitroaniline (molar ratio=1.5). A 35% yield of the final product, the symmetrical azoarene, and a 38% of the unreacted substrate were isolated. The result, which is in conflict with all the preceding ones, is probably to be ascribed to the aggregation of the reagent molecules, due to the coordination ability of the nitrogen atom of the substituent.

The effectiveness of the aryl-IDMg method for pre-

Table 1. Yields of unsymmetrically substituted azoxybenzenes (Scheme 1)

Expt No.	Ar^1	Ar^2	Molar ratio	Yields/% Azoxy	Unsym. azo	Sym. azo
1	C_6H_5	*p*-MeC_6H_4	1.5	(60	: 40)[a]	
2	*p*-MeC_6H_4	C_6H_5	1.5	(70	: 30)[a]	
3	*m*-ClC_6H_4	*p*-$MeOC_6H_4$	1.5	48	21	15
4	*p*-MeC_6H_4	*m*-$MeOC_6H_4$	2.0	62	22	2.8
5	*m*-ClC_6H_4	C_6H_5	2.0	71	17	8.1
6	C_6H_5	*m*-ClC_6H_4	2.0	81	10—12	

a) The product ratio was estimated by NMR.

Table 2. Yields of symmetrically substituted azoxybenzenes (Scheme 2)

Expt No.	R	Molar ratio	Yields/% Azoxy	Azo
7	*p*-MeO	1.2	59	26
8	*p*-Cl	1.5	41[a]	16[a]
9	*p*-Cl	2.0	(71 :	29)[b]
10	*p*-Me	2.0	(64 :	36)[b]
11	*m*-Cl	2.5	78	17
12	*m*eO	2.0	80	15

a) A 27% of *p*-$ClC_6H_4NO_2$ was recovered. b) The product ratio was estimated by NMR.

Table 3. Optimum molar ratio of reagents to substrates based on the electron-donating ability of the reagents

RC_6H_4-IDMg R	Molar ratio	Yields of azoxyarenes/%
p-MeO	1.2—1.5	50—60
p-Me, *m*-MeO, H	1.5—2.0	55—70
p-Cl, *m*-Cl	2.0—2.5	65—80

paring unsymmetrical azoxyarenes is demonstrated by the successful preparation of a new azoxy isomer derived from 1-phenylazonaphthalene (Scheme 3a).

a. 1-$NaphNO_2$ + $PhN(MgBr)_2$ ⟶ 1-Naph-N(O)=N-Ph (α-isomer)

b. $PhNO_2$ + 1-$NaphN(MgBr)_2$ ⟶ 1-Naph-N=N(O)-Ph (β-isomer)

Scheme 3.

The previous study on the peroxy acid oxidation of 1-phenylazonaphthalene[3] showed the exclusive formation of the sterically less hindered "β"-isomer (*cf.* Scheme 3b). By use of two molar equivalents of the respective reagents and the substrates as shown in the scheme, both the "α"- and "β"-isomers were prepared in yields of 43 and 63% respectively.

Deoxygenation of Azoxyarenes by the Aryl-IDMg Procedure. The deoxygenation of the substituted azoxyarenes by the IDMg method was studied. Since the deoxygenation is quite a mild reaction,[9] the azoxyarenes were treated with five molar equivalents of the most electron-donating *p*-methoxyphenyl-IDMg at 55 °C for 3 h (Scheme 4). The percentage of deoxygenation observed is given in Table 4.

Table 4. Deoxygenation of symmetrical and unsymmetrical azoxybenzenes (Scheme 4)
$R^1C_6H_4$-N(O)=N-$C_6H_4R^2$

$R^1=R^2$	Deoxygn. (%)	$R^1 \neq R^2$		Deoxygn. (%)
p-MeO	16	*p*-Cl	*p*-MeO	18
		p-MeO	*p*-Cl	48
p-Me	41	*p*-MeO	*p*-Me	39
		p-Me	*p*-MeO	30
p-Cl	47	*p*-Me	*m*-MeO	59
		p-Me	H	63
H	75	H	*p*-Me	54
		m-Cl	H	80
m-Cl	>100	H	*m*-Cl	>100

$$R^1C_6H_4\text{-}N(O)\text{=}N\text{-}C_6H_5R^2 \xrightarrow[55\,^\circ C,\ 3\,h]{5\ p\text{-}MeOC_6H_4\text{-}IDMg} R^1C_6H_4\text{-}N\text{=}N\text{-}C_6H_4R^2$$

Scheme 4.

Among the results obtained in the deoxygenation of symmetrical azoxyarenes, the strongly retarding effect of the *p*-methoxyl substituent and the accelerating effect of the *m*-chloro substituent of the azoxyarenes should be noted first. The *p*-chloro substituent, which usually shows an electron-attracting character, exhibits a medium retarding effect: Retardation to a comparable extent was also shown by the *p*-methyl substituent which usually acts as a weak electron-donating group. These results suggest a remarkable enhacement of electron-repelling resonance operating in the deoxygenation reaction.

Table 4 also contains the results obtained in the deoxygenation reactions of unsymmetrically substituted azoxyarenes under the same conditions. The effect of the retardation by the *p*-methoxyl substituent as well as the acceleration by the *m*-chloro substituent is evidently enhanced when these groups are attached to the phenyl group opposite to the azoxy nitrogen atom. A qualitative explanation for the retardation by the *p*-methoxyl group opposite to the azoxy nitrogen can be given by the charge-separated resonance structure, A, which reduces the positive charge on the azoxy-nitrogen and prevents the attack of the anionic

Table 5. Physical constants of azoxyarenes
$R^1C_6H_4$-N(O)=N$C_6H_4R^2$

Expt No.[a]	R^1	R^2	Mp θ_m/°C	λ_{max}/nm	NMR data δ
11	*m*-Cl	*m*-Cl	98.5—100[11]	323.0	8.22—7.99(3H, m, ArH), 7.99—7.80(1H, m, ArH), 7.52—7.20(4H, m, ArH).
6	H	*m*-Cl	53.0—53.5	322.0	8.36—8.14(3H, m, ArH), 8.02—7.86(1H, m, ArH), 7.50—7.20(5H, m, ArH).
5	*m*-Cl	H	23.5—24	327.5	8.35—8.02(4H, m, ArH), 7.52—7.10(5H, m, ArH).
P1	H	H	35—35.5[8]	323.5	8.42—8.15(4H, m, ArH), 7.56—7.30(6H, m, ArH).
2	*p*-Me	H	62—64.5[12]	325.5	8.34—8.10(4H, m, ArH), 7.52—7.26(3H, m, ArH), 7.16—6.98(2H, m, ArH), 2.16(3H, s, Me).
4	*p*-Me	*m*-MeO	60—62	325.0	8.06(2H, d, ArH), 7.84—7.60(2H, m, ArH), 7.34—7.02(3H, m, ArH), 6.90—6.86(1H, m, ArH), 3.72(3H, s, Me), 3.22(3H, s, Me).
1	H	*p*-Me	50—51.5[12]	332.5	8.36—8.10(4H, m, ArH), 7.48—7.28(3H, m, ArH), 7.16(2H, d, ArH), 2.30(3H, s, Me).
P1	*p*-MeO	*p*-Cl	105.5—107[1]	340.0	8.27(8.15) and 7.42(4H, ABq, ArH), 8.15 (8.27) and 6.93(4H, ABq, ArH), 3.87(3H, s, Me).
9	*p*-Cl	*p*-Cl	154—156[13]	335.0	8.50—8.24(4H, m, ArH), 7.72—7.50(4H, m, ArH), 7.72—7.50(4H, ArH).
10	*p*-Me	*p*-Me	68—69[14]	333.0	8.24—8.04(4H, m, ArH), 7.18(4H, d, ArH), 2.34(6H, s, Me).
P1	*p*-MeO	*p*-Me	77—79[1]	339.5	8.28(8.13) and 7.28(4H, ABq, ArH), 8.13 (8.28) and 6.94(4H, ABq, ArH), 3.84(3H, s, Me).
P1	*p*-Me	*p*-MeO	108.5—110[1]	349.0	8.30(8.20) and 7.24(4H, ABq, ArH), 8.20 (8.30) and 6.92(4H, ABq, ArH), 3.86(3H, s, Me), 2.44(3H, s, Me).
P1	*p*-Cl	*p*-MeO	144—146.5[1]	359.0	8.56(8.46) and 7.65(4H, ABq, ArH), 8.46 (8.56) and 7.17(4H, ABq, ArH), 3.98(3H, s, Me).
7	*p*-MeO	*p*-MeO	120[15]	353.5	8.40—8.20(4H, m, ArH), 7.10—6.86(4H, m, ArH), 3.84(3H, s, Me), 3.82(3H, s, Me).
12	*m*-MeO	*m*-MeO	51—51.5[11]	325.0	7.96—7.64(4H, m, ArH), 7.44—7.16(2H, m, ArH), 7.04—6.80(2H, m, ArH), 3.78(6H, s, Me).
N	*p*-MeO	H	53—54	331.5	8.38—8.10(4H, m, ArH), 7.54—7.30(3H, m, ArH), 6.98—6.80(2H, m, ArH), 3.78(3H, s, Me).
3	*m*-Cl	*p*-MeO	97—99.5	359.0	8.40—8.10(4H, m, ArH), 7.48—7.38(2H, m, ArH), 6.98—6.80(2H, m, ArH), 3.82(3H, s, Me).
S3	1-Naph.	H	69.5—71	—	8.36—8.16(3H, m, ArH), 7.84—7.64(3H, m, ArH), 7.56(6H, m, ArH).
S3	H	1-Naph.	82.5—84[4]	—	9.10(1H, d, ArH), 8.66—8.56(1H, m, ArH), 8.46—8.30(2H, m, ArH), 7.82—7.72(2H, m, ArH), 7.68—7.36(6H, m, ArH).

a) The number indicates the Expt No. given in Tables 1 and 2. S3 means the products prepared according to Scheme 3, and P1 means the products obtained in the previous work: N indicates that neither the prepative yield nor the deoxygenation reactivity were determined.

part of the reagent molecule. Since the isomeric resonance structure, B, cannot reduce the positive charge, the dramatic retardation is unexpected in this case.

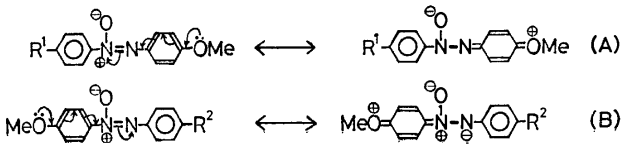

From the given explanation, the reactivity of deoxygenation should be correlated with the shift of the electronic absorption maximum, λ_{max} for $\pi \rightarrow \pi^*$ transition.[10] Since the deoxygenation is generally slow even on treatment with five molar equivalents of the reagent, the percentage of the deoxygenation given in Table 4 can be substituted, as a rough approximation, for the relative reaction rate constant. The λ_{max}'s of

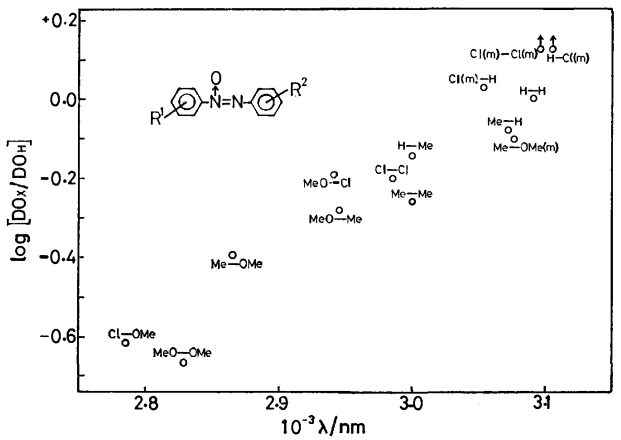

Fig. 1. Correlation between the relative deoxygenation reactivity and $\pi \rightarrow \pi^*$ transition energy.

azoxyarenes are listed in Table 5 together with the other physical constants observed. The expectation is verified as shown in Fig. 1: The logarithm of the relative deoxygenation, $\log[DO_X/DO_H]$ (the value for the unsubstituted substrate was taken as the standard), is less satisfactorily but nevertheless still correlated with the reciprocal of the λ_{max}'s.

Explicit evidence for the attack of the reagent's anionic nitrogen on the substrate's positive nitrogen is provided by the identification of the by-product formed in the reaction. The formation of a trace amount of by-product containing a methoxyl group was detected by NMR in the reaction (Scheme 4) of an azoxyarene which has no methoxyl group; the formation is usually negligible and the structure of the by-product is unidentifiable. The formation, however, becomes notable when a reactive azoxyarene is treated with *p*-methoxyphenyl-IDMg. The most reactive, 3,3'-dichloroazoxybenzene, which was consumed completely under the conditions given in Scheme 4, gave the corresponding azoarene and a 20% yield of 3-chloro-4'-methoxyazobenzene. The same by-product was obtained in a 21% yield in the reaction of 3-chloro-*NNO*-azoxybenzene, m-$ClC_6H_4N(O)=NC_6H_5$. In the reaction of the isomeric 3-chloro-*ONN*-azoxybenzene, m-$ClC_6H_4N=N(O)C_6H_5$, 4-methoxyazobenzene was isolated in a 17% yield. The other possible by-products were not detected. The results show that, in the reaction with $ArN(MgBr)_2$, an unsymmetrical azoxyarene, $Ar^1N(O)=NAr^2$, gives $Ar^1N=NAr$ but not $ArN=NAr^2$ as the by-product.

The mechanism of both the major and minor reaction is still equivocal. Undoubtedly, however, the existence of such an exchange reaction is evidence for the attack of the anionic nitrogen on the positive azoxy nitrogen. In order to reduce the by-product formation in the deoxygenation of the very reactive azoxyarenes, the less electron-donating *p*-methylphenyl-IDMg is recommended.

Experimental

The melting points are uncorrected. All the nitroarenes and the arylamines were commercially available, and were purified by distillation before use.

Procedures. To an aryliminodimagnesium reagent (15.9 mmol) prepared under N_2 atmosphere in THF (35 ml) according to the reported method,[9] a THF solution (15 ml) of nitroarenes was added at once at 0 °C. The deeply colored[9] reaction mixture was stirred gently at 55 °C for 3 h. The mixture was quenched at 0 °C with aqueous ammonium chloride, and worked up as reported previously.[9] The yields of the individual products were obtained by column chromatographic separation as well as estimation by measuring the fractions by NMR.[9]

The experiments for the deoxygenation of azoxyarenes were carried out similarly: The color change of the reaction mixture was slow at 0 °C but a reddish brown color developed on heating.

The electronic spectra of azoxyarenes were recorded on an Hitachi 323 Spectrophotometer using 1.0×10^{-4} mol dm^{-3} solution in 1,4-dioxane (spectrograde).

For convenience, the physical constants of nineteen azoxyarenes prepared in this and the preceding[9] works are summarized in Table 5. The fourteen among the nineteen azoxyarenes are listed in decreasing order of the deoxygenation reactivity (*cf.* Table 4). Among the NMR data, some aromatic proton signals which consist of two AB-quartets are not assigned and the figures are given in parentheses.

Molecular weight of the product was recorded on a Denshi Kagaku EMD-05A Mass Spectrometer. The result of the elemental analyses of the new azoxyarenes, which are represented by the Expt Nos. given in Table 5, are given below.

(6): Found: C, 62.01; H, 3.90; N, 12.00%. Calcd for $C_{12}H_9ClN_2O$: C, 61.93; H, 3.87; N, 12.04%.
(5): Found: C, 62.08; H, 3.82; N, 11.93%. Calcd for $C_{12}H_9ClN_2O$: C, 61.93; H, 3.87; N, 12.04%.
(4): Found: C, 70.01; H, 5.71; N, 11.60%. Calcd for $C_{14}H_{14}N_2O_2$: C, 69.42; H, 5.78; N, 11.57%.
(N): Found: C, 68.50; H, 5.32; N, 12.21%. Calcd for $C_{13}H_{12}N_2O_2$: C, 68.42; H, 5.26; N, 12.28%.
(3): Found: C, 60.01; H, 4.21; N, 10.60%. Calcd for $C_{13}H_{11}ClN_2O_2$: C, 59.43; H, 4.19; N, 10.67%.
(S3): Found: C, 77.49; H, 4.91; N, 11.32%. Calcd for $C_{16}H_{12}N_2O$: C, 77.42; H, 4.83; N, 11.29%.

The support of this work by the research grant from the Ministry of Education, Science and Culture (C-56540307) is gratefully acknowledged. The authors wish to thank Mr. Kōichirō Hirata for the measurement of UV-Vis absorption spectra.

References

1) C. S. Hahn and H. H. Jaffe, *J. Am. Chem. Soc.*, **84**, 949 (1962).
2) B. T. Gillis and K. F. Schimmel, *J. Org. Chem.*, **27**, 413 (1962).
3) G. M. Badger, R. G. Butterby, and G. E. Lewis, *J. Chem. Soc.*, **1953**, 2143; G. M. Badger and G. E. Lewis, *ibid.*, **1953**, 2147, 2151.
4) Y. Ogata, M. Tsuchida, and Y. Takagi, *J. Am. Chem. Soc.*, **79**, 3397 (1957).
5) S. Oae, T. Fukumoto, and M. Yamaguchi, *Bull. Chem. Soc. Jpn.*, **36**, 728 (1963).
6) L. C. Behr, *J. Am. Chem. Soc.*, **76**, 3672 (1954); L. C. Behr, E. G. Alley, and O. Levand, *J. Org. Chem.*, **27**, 65 (1962).
7) T. E. Stevens, *J. Org. Chem.*, **29**, 311 (1964).
8) "Organophosphorus Reagents in Organic Synthesis," ed by J. I. G. Cadogan, Academic Press, London (1979),

Chaps. 6 and 7.
9) Part III: M. Ōkubo, T. Takahashi, and K. Koga, *Bull. Chem. Soc. Jpn.*, **56**, 199 (1983).
10) H. H. Jaffe and M. Orchin, "Theory and Application of Ultraviolet Spectroscopy," John Wiley & Sons Inc., New York (1962), p. 282.
11) N. S. Kozlow and V. A. Soshin, *Uch. Zap. Permsk. Gos. Ped. Inst.*, **32**, 84 (1965); *Chem. Abstr.*, **66**, 2290k (1967).
12) D. Bigiavi and V. Sabatelli, *Gazz. Chim. Ital.*, **57**, 557 (1927).
13) B. T. Newbold and R. P. Leblanc, *J. Org. Chem.*, **27**, 312 (1962).
14) B. T. Newbold and R. P. Leblanc, *J. Chem. Soc.*, **1965**, 1547.
15) M. J. S. Dewar and R. S. Goldberg, *Tetrahedron Lett.*, **1966**, 2717.

Temperature Dependence of Absorption Spectra of Chlorophyll a in Hydrocarbons over the Temperature Range 300—77 K. Enthalpy and Entropy Changes for the Formation of Dimeric Chlorophyll a

Mikio Hoshino,* Kiyoshi Ikehara,† Masashi Imamura, and Yoshimasa Hama†

The Institute of Physical and Chemical Research, Wako, Saitama 351

†*Science and Engineering Research Laboratory, Waseda University, Shinjuku-ku, Tokyo 160*

(Received May 17, 1982)

The absorption spectra of chlorophyll a in isopentane, 3-methylpentane, and methylcyclohexane solutions were studied over the temperature range 300—77 K. In those hydrocarbon solutions which were prepared using methanol treatment, chlorophyll a forms hydrated dimer at low temperatures. The dimer has an absorption peak at 695 nm at 160 K, which gradually shifts to 706 nm with decreasing temperature from 160 K to 77 K. The enthalpy change ($-\Delta H$) for the formation of the dimer was obtained to be 41.0 ± 0.8 kJ mol^{-1}, independent of the solvent used. The entropy changes ($-\Delta S$) were 113 ± 8 J K^{-1} mol^{-1} for isopentane, 118 ± 8 J K^{-1} mol^{-1} for 3-methylpentane and 128 ± 8 J K^{-1} mol^{-1} for methylcyclohexane solutions. Comparative studies carried out of the solutions prepared without the methanol treatment suggest the existence of two kinds of hydrated monomeric chlorophyll a.

Chlorophyll (Chl) a is the best understood of Chl's[1] and has been subject to a variety of studies in connection with the photochemical conversion of solar energy. The optical absorption spectrum of Chl a is known to vary markedly with nature of solvent, temperature, and degree of hydration and aggregation.[2,3]

The absorption spectra of Chl a reported so far are in good agreement with one another as far as polar solvents are used. In nonpolar solvents, on the other hand, the absorption spectrum varies substantially depending on the procedures of preparing the solutions, in particular at low temperatures. Cotton *et al.*[4] reported that the amount of water causes substantial changes in the absorption spectrum of Chl a in hydrocarbon solvents. For instance, the absorption spectrum of Chl a in dry methylcyclohexane+isopentane shows only a slight shift of the peak wavelength from 672 nm at room temperature to 678 nm at 77 K, which is in sharp contrast to the absorption spectral change observed in a toluene solution containing 2 mol H_2O per mol Chl a. For the latter solution, a new absorption band centered at 708 nm was observed to appear with a slight shift of the 667-nm peak to 672 nm at 77 K.

Fong and Koester[5] reported the temperature dependence of the absorption spectrum of Chl a in a 1:1 methylcyclohexane+pentane mixture, in which the absorption peak in the red band region is located at 667 nm at room temperature. The spectrum observed at 121 K indicates that the major Chl a shows the absorption peak at 702.5 nm. This is the first observation that a greater part of Chl a in the hydrocarbon mixture is transformed into a $\approx$700 nm absorbing species at low temperatures.

The formation of 706-nm absorbing species of Chl a (S706) and the optical absorption and ESR studies of its cation radical produced by γ-irradiation, both in glassy 3-methylpentane solutions at 77 K, were reported by Hoshino *et al.*[6] The comparative study on the ESR spectra of the cation radicals of the S706 and monomeric Chl a demonstrates that the S706 is a dimeric Chl a. This result is consistent with the suggestion made by Brody and Broyde[3] that the absorption band centered at around 700 nm appearing at low temperatures is attributed to dimeric Chl a.

The present paper reports the temperature dependence of the absorption spectra of Chl a in isopentane, 3-methylpentane, and methylcyclohexane solutions over the temperature range 300—77 K, and the thermodynamic data for the formation of the dimers.

Experimental

Chl a extracted from spinach leaves with acetone was chromatographed on powdered sugar columns according to standard procedures.[7] Solid Chl a obtained from a Chl a zone of a last column was chromatographed with petroleum ether containing 0.5% 2-propanol as developer. The purified Chl a was dissolved in dry diethyl ether and stored in a freezer at -20 °C. The absorption spectrum of the stock solution had absorption peaks at 428.6 and 660 nm with a ratio of the Soret to red absorption maxima of 1.29 at room temperature.

Isopentane, 3-methylpentane, and methylcyclohexane were distilled and stored on Na–K alloy *in vacuo* in order to remove traces of water.

Absorption spectra were recorded on a Cary 14R spectrophotometer. The temperature was controlled by using an Oxford CF204 cryostat. Optical pathlength of cells were 0.5—1.5 mm.

A suitable volume of the Chl a stock solution was transferred into a cell, and diethyl ether was removed on a vacuum line. After pumped at 10^{-6} Torr (1 Torr=133.322 Pa) at room temperature for 10—20 min, the cell was detached from the vacuum line and freshly distilled methanol was added into the cell. The solid Chl a was completely dissolved in methanol by shaking the cell for a few min. The sample cell was again attached to the vacuum line to remove methanol completely under pumping to 10^{-6} Torr for 10—20 min. This procedure using methanol will be referred to as methanol treatment. The solution was cooled to 77 K and sealed off under pumping.

Comparative studies were also carried out on the Chl a solutions prepared by omission of the methanol treatment described above; unless otherwise specified, the Chl a solutions were prepared using the methanol treatment.

The concentration of Chl a was *ca.* 10^{-4} mol/dm^3 for all the solutions used in the present study.

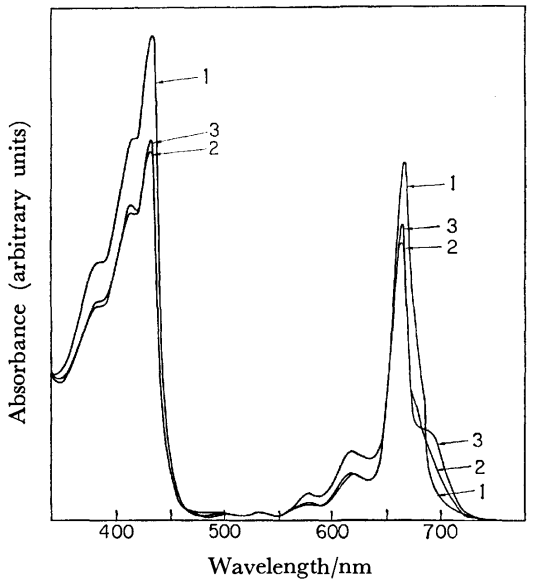

Fig. 1. Temperature-dependent absorption spectra of 3-methylpentane solution of Chl a in the temperature range 300—240 K.
1): 300 K, 2): 270 K, 3): 240 K.

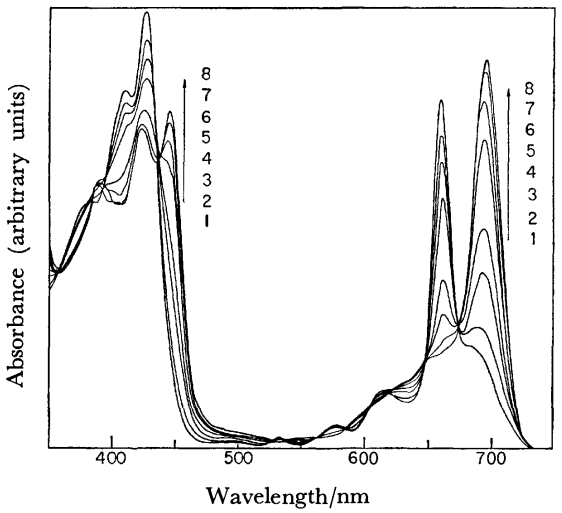

Fig. 2. Temperature-dependent absorption spectra of 3-methylpentane solution of Chl a (the same solution as that in Fig. 1) in the temperature range 240—160 K.
1): 240 K, 2): 219 K, 3): 210 K, 4): 200 K, 5): 190 K, 6): 179 K, 7): 170 K, 8): 161 K.

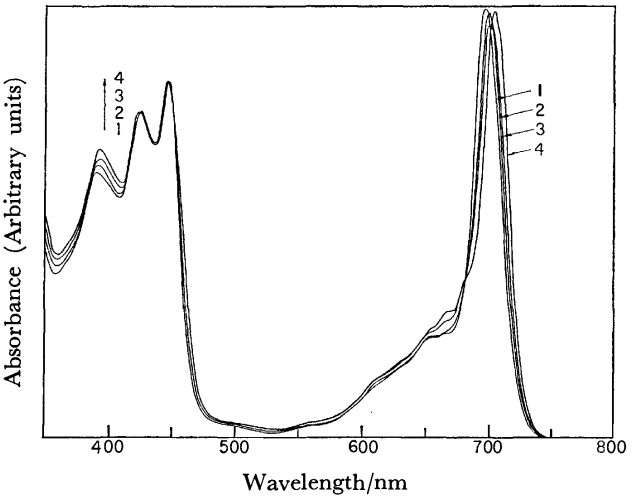

Fig. 3. Temperature-dependent absorption spectra of 3-methylpentane solution of Chl a (the same solution as that in Fig. 1) in the temperature range 150—95 K.
1): 150 K, 2): 130 K, 3): 110 K, 4): 95 K.

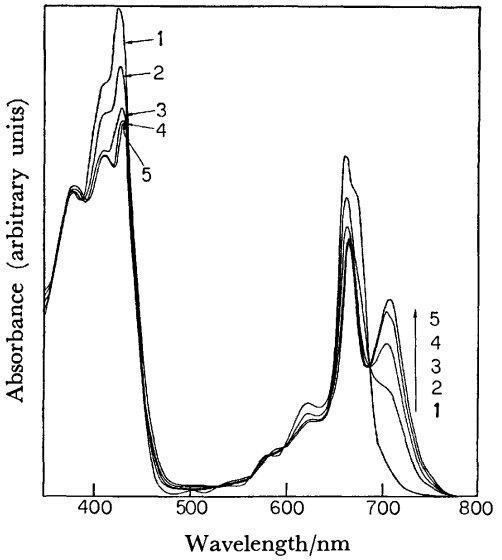

Fig. 4. Temperature-dependent absorption spectra of 3-methylpentane solution of Chl a prepared without methanol treatment (see text) in the temperature range 260—180 K.
1): 260 K, 2): 240 K, 3): 220 K, 4): 200 K, 5): 180 K.

Results

Figure 1 shows the absorption spectra of Chl a in 3-methylpentane in the temperature range 300—240 K. The absorption spectrum at 300 K has an absorption peak at 662 nm with a shoulder at 680 nm in the red-band region. No isosbestic points were observed for the spectral change of the Chl a solution in this temperature range. The complicated features observed for the temperature-dependent absorption spectra are essentially the same as those reported.[5]

Figure 2 shows the temperature-dependent absorption spectra of Chl a in 3-methylpentane in the temperature range 240—160 K. A series of absorption spectra measured in this temperature range evidently shows several isosbestic points, indicating a simple equilibrium between the species absorbing at 663 and 695 nm. The absorbance at 695 nm increases with decreasing intensity of the peak at 663 nm, which ultimately vanishes at 160 K.

The spectral change below 160 K is shown in Fig. 3. The 695 nm peak at 160 K shows only a slight shift toward long wavelengths without showing isosbestic points with decreasing temperature; no equilibrium seems to exist in this temperature range. The peak wavelength ultimately reached 706 nm at 77 K.[6]

The temperature-dependent absorption spectra were also studied on isopentane and methylcyclohexane solutions. The features of the spectral change are essentially the same as those observed for the 3-methyl-

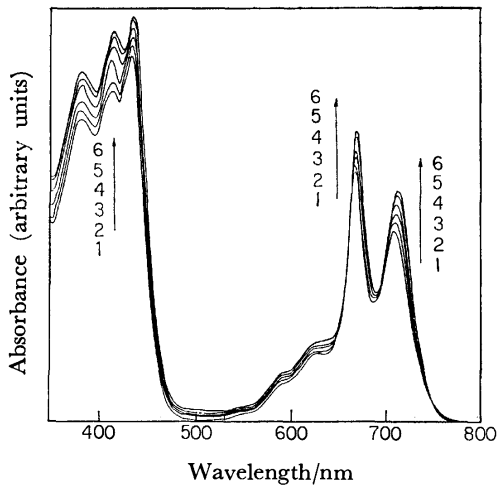

Fig. 5. Temperature-dependent absorption spectra of 3-methylpentane solution of Chl a (the same solution as that in Fig. 4) in the temperature range 180—95 K. 1): 180 K, 2): 160 K, 3): 140 K, 4): 120 K, 5): 100 K, 6): 95 K.

pentane solution; the 663 nm band vanishes at 160 K and a subsequent red shift of the 700 nm band was also observed below 160 K.

Different temperature-dependent absorption spectra were observed for the 3-methylpentane solution of Chl a prepared by omission of the methanol treatment. Typical examples are shown in Figs. 4 and 5. Figure 4 shows the spectral changes in the temperature range 260—180 K. The absorption spectrum at room temperature has an absorption peak at 663 nm with a shoulder at 675 nm. With decreasing temperature, the intensity at 663 nm decreases with a slight shift to 667 nm and a new absorption band appears around 706 nm with an isosbestic point at 678.5 nm. Below 180 K, however, the 667 nm band does not vanish but the intensities of both 667 nm and 706 nm bands increase accompanying slight red shift with decreasing temperature as shown in Fig. 5; their ultimate peak wavelengths reached 668 and 709 nm at 77 K. These results present a striking contrast to those obtained with the Chl a solutions prepared using methanol treatment. These differences will be discussed in the next section.

Discussion

Two Kinds of Hydrated Monomeric Chl a. Fong and Koester[5] reported that Chl a in a hydrocarbon mixture could be transformed into a 702.5 nm absorbing Chl a as a major species at 121 K. Wasielewski *et al.*[8] found that bis(chlorophyllide)ethylene glycol diester in carbon tetrachloride forms a species absorbing at 697 nm at room temperature when the solution was bubbled with wet nitrogen gas. This fact implies that water molecules play an important role in the formation of the ≈700 nm absorbing Chl a. Shipman *et al.*[9] studied the temperature dependence of the absorption spectra of 9.4×10^{-2} mol/dm^3 Chl a solutions in toluene containing 1.5 mol ethanol per mol Chl a and reported the formation of the 702 nm absorbing Chl a as a single species at 175 K. These results indicate that monosolvated Chl a, Chl a·H_2O and Chl a·C_2H_5OH can be converted into the ≈700 nm absorbing species at low temperatures. The structure of the Chl a dimer has been considered to be C_2-symmetrical.[10-12]

The present results show that Chl a in 3-methylpentane has only one absorption peak at 695 nm in the red-band region at 160 K. Since the 695-nm peak grows with decreasing intensity of the absorption at 663 nm from 240 to 160 K, the 663-nm absorbing species is regarded as a precursor of the 695-nm absorbing species. The spectral shift from 695 to 706 nm observed at 160—77 K may be due to some configuration changes of the dimeric Chl a in glassy matrices by cooling. It should be noted that the peak wavelengths reported for the dimeric Chl a are ranged from 695 to 710 nm depending upon the solvent and temperature.

In the present study, we have reasonably concluded that the 695-nm absorbing species at 160 K is a single species from the temperature dependence of the absorption spectra in which clear isosbestic points are observed.

We sometimes observed that Chl a solutions prepared without the methanol treatment show essentially the same temperature dependence as that shown in Figs. 1—3. These observations imply that a trace amount of methanol, which might remain in the samples prepared by using the methanol treatment, is not responsible for the formation of the 695 nm absorbing species at 160 K. The methanol treatment is considered to provide a simple and reproducible procedure for preparing the Chl a solutions which produce 695-nm absorbing species at low temperatures.

The results on the Chl a solutions in 3-methylpentane prepared with and without the methanol treatment seem to indicate that there would be at least two kinds of monomeric Chl a in the hydrocarbon solution: one does form the dimeric Chl a (S706) and other does not. Katz *et al.*[1] examined IR spectra in the OH-stretching region for a nonpolar solution of Chl a containing water, and suggested the presence of two kinds of Chl a species: $Mg\cdots O\langle^{H}_{H}$ and $Mg\cdots O\langle^{H}_{H}\cdots O\langle^{H}_{H}$.

On the basis of their suggested species for the hydrated Chl a, the present results may be interpreted by assuming that the solutions not treated with methanol contain both monohydrated and dihydrated species, the latter of which does not form dimeric Chl a at low temperatures. Supposedly, the methanol treatment used for the preparation of the solutions serves to adjust the water content appropriate for the dimer formation. Since the water content is considered to be not always reproducible for the solutions without the methanol treatment, the complete or nearly complete dimer formation was only sometimes observed for these solutions. In fact, addition of trace amount of water into the methanol treated solutions was found to give similar spectral changes to those shown in Figs. 4 and 5.

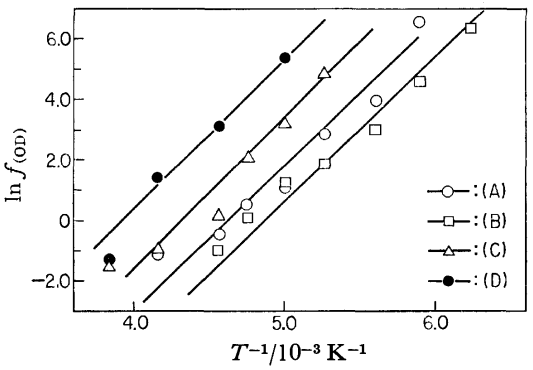

Fig. 6. Plots on $\ln f(A)$ *vs.* T^{-1} for Chl a solutions. (A): 3-Methylpentane, (B): methylcyclohexane, (C): isopentane. A plot (D) was obtained for 3-methylpentane solution of Chl a prepared without methanol treatment.

Enthalpy and Entropy Changes for the Dimer Formation. The spectral changes shown in Figs. 1 and 2 are interpreted in terms of two step equilibria:[5]

$$(\text{Chl a})_2 + 2H_2O \rightleftharpoons 2\text{Chl a}\cdot H_2O \rightleftharpoons (\text{Chl a}\cdot H_2O)_2.$$

The complicated features of the spectral change observed in the temperature range 300—240 K are considered to result from the above two equilibria in the solution. As the temperature decreases below 240 K, the equilibrium shifts toward the right-hand side. The temperature dependence of the spectrum observed between 240 and 160 K is regarded as being due to the equilibrium between Chl a·H_2O (M) and (Chl a·H_2O)$_2$ (D). The equilibrium constant, K, is defined as

$$K = [D]/[M]^2. \quad (1)$$

Below 160 K, M is completely transformed into D, and therefore,

$$2[D] + [M] = 2[D]_0, \quad (2)$$

where $[D]_0$ is the concentration of D at 160 K. From Eqs. 1 and 2,

$$K = [D]/4([D]_0 - [D])^2. \quad (3)$$

Using the molar extinction coefficient of D at 700 nm (ε) and an optical pathlength (l), one obtains

$$K = \varepsilon l A_T/4(A_{160} - A_T) = \varepsilon l \cdot f(A)/4, \quad (4)$$

where A_{160} and A_T are the absorbances at 700 nm at 160 K and T K, respectively.

Equation 4 is transformed into

$$\ln f(A) = [\Delta S/R - \ln(\varepsilon l/4)] - \Delta H/RT. \quad (5)$$

Plots of $\ln f(A)$ *vs.* T^{-1} for the isopentane, 3-methylpentane, and methylcyclohexane solutions are shown in Fig. 6; the data obtained with the 3-methylpentane solutions prepared without the methanol treatment are also plotted for comparison. The enthalpy changes (ΔH) are identical within the experimental errors for these solutions, 41.0 ± 0.8 kJ mol^{-1} (9.8 ± 0.2 kcal mol^{-1}). From the intercept and ε (9.6×10^4 mol^{-1} dm^3 cm^{-1}), the entropy changes (ΔS) are calculated to be 113 ± 8, 118 ± 8, and 128 ± 8 J K^{-1} mol^{-1} for the isopentane, 3-methylpentane, and methylcyclohexane solutions, respectively. The linear plot D in Fig. 6 implies that the monohydrated Chl a existing in the solution forms dimers independently of the coexisting dihydrated species.

The enthalpy change obtained for the dimer formation is double the enthalpy change (4—6 kcal mol^{-1}) estimated for the formation of one hydrogen bond of the type OH···O.[13] This result is in accord with the assumption that a dimeric Chl a has two hydrogen bonds between magnesium atoms and carbonyl groups of two Chl a molecules.

Pheophytins are known to dimerize in hydrocarbon solutions at low temperatures.[14] An estimated enthalpy change of 18 kJ mol^{-1} for the formation of the dimeric pheophytins is about one half that obtained for Chl a. This value also supports the view that two hydrogen bonds serve as principal interaction force between two Chl a molecules in the dimeric Chl a. Slightly different values for the entropy change may be ascribed to somewhat different configurations of the dimer structure in different solvents.

References

1) J. J. Katz, L. L. Shipman, T. M. Cotton, and T. R. Janson, "The Porphyrins, V," ed by D. Dorphin, Academic Press, New York (1978), p. 401.
2) T. M. Cotton, A. D. Trifunac, K. Ballschmiter, and J. J. Katz, *Biochim. Biophys. Acta*, **368**, 181 (1974).
3) S. S. Brody and S. B. Broyde, *Biophys. J.*, **8**, 1511 (1968).
4) T. M. Cotton, P. A. Loach, J. J. Katz, and K. Ballschmiter, *Photochem. Photobiol.*, **27**, 735 (1978).
5) F. K. Fong and V. J. Koester, *Biochim. Biophys. Acta*, **423**, 52 (1976).
6) M. Hoshino, K. Ikehara, M. Imamura, H. Seki, and Y. Hama, *Photochem. Photobiol.*, **34**, 75 (1981).
7) H. H. Strain and W. A. Svec, "The Chloropylls," ed by L. P. Vernon and G. R. Seely, Academic Press, New York (1966), p. 21.
8) M. R. Wasielewski, M. H. Studier, and J. J. Katz, *Proc. Natl. Acad. Sci. U.S.A.*, **73**, 4282 (1976).
9) L. L. Shipman, T. M. Cotton, J. R. Norris, and J. J. Katz, *Proc. Natl. Acad. Sci. U.S.A.*, **73**, 1791 (1976).
10) S. G. Boxer and G. L. Closs, *J. Am. Chem. Soc.*, **98**, 5406 (1976).
11) F. K. Fong, V. J. Koester, and J. S. Polles, *J. Am. Chem. Soc.*, **98**, 6406 (1976).
12) M. R. Wasielewski, U. H. Smith, B. T. Cope, and J. J. Katz, *J. Am. Chem. Soc.*, **99**, 4172 (1977).
13) G. C. Pimentel and A. L. McClellan, "The Hydrogen Bond," Freeman and Co., San Francisco (1960), p. 206.
14) R. P. H. Kooyman, J. J. Schaafsma, G. Jansen, R. H. Clarke, D. R. Hobart, and W. R. Leenstra, *Chem. Phys. Lett.*, **68**, 65 (1979).

Synthesis of Monoaza Crown Ethers from *N,N*-Di[oligo(oxyalkylene)]amines and Oligoethylene Glycol Di(*p*-toluenesulfonates) or Corresponding Dichlorides

Hirokazu MAEDA, Shigeo FURUYOSHI, Yohji NAKATSUJI, and Mitsuo OKAHARA*

Department of Applied Chemistry, Faculty of Engineering, Osaka University, Yamada-oka 2-1, Suita, Osaka 565

(Received May 21, 1982)

Monoaza crown ethers were prepared in satisfactory yields by the one-step reaction between diethanolamine or *N,N*-di[oligo(oxyethylene)]amines and oligoethylene glycol di(*p*-toluenesulfonates) or corresponding dichlorides in *t*-butyl alcohol/dioxane in the presence of sodium or potassium *t*-butoxide. The reaction conditions in the preparation of monoaza 15- and 18-crown ethers were studied. Various monoaza crown ethers having substituents were also prepared and their properties were investigated.

N-Unsubstituted monoaza crown ethers, which are the reactive crown ethers, have complexing ability with metal[1,2] and ammonium cations.[3] Using their reactive amino group, they can be readily transformed to bis-crown compounds,[4-7] lariat ethers,[3,8-10] or *N*-alkyl derivatives useful as surfactants with special properties.[11-13]

The synthetic methods of monoaza crown ethers can be classified into two categories; with or without employing amino protection. In the former, after the preparation of *N*-substituted monoaza crown ethers (*N*-cyano,[14] *N*-(*p*-tolylsulfonyl),[15] *N*-benzyl,[1,4] or *N*-trityl monoaza crown ether[16]), the deprotection of them by proper means gave *N*-unsubstituted crown ethers. However, these methods are more or less laborious, since the introduction and elimination processes of *N*-substituent are necessary.

On the other hand, 1,4,10,13-tetraoxa-7-azacyclohexadecane possessing oxetane ring was prepared by Krespan[17] by the reaction of 3,3-bis(chloromethyl)-oxetane with bis[2-(2-hydroxyethoxy)ethyl]amine without using amino protection. In accordance with the observation in the synthesis of 18-methylene-1,7,10,16-tetraoxa-4,13-diazacyclononadecane by Tomoi *et al.*,[18] and the synthesis of α,ω-diamino-substituted oligo(oxyethylenes) by Böhmer *et al.*,[19] the results substantiate that *O*-alkylation is far more predominant than *N*-alkylation under the basic conditions which generate an alkoxide.

We have previously reported that *N*-unsubstituted monoaza crown ethers can be obtained in satisfactory yields by the reaction of commercially available dialkanolamines with oligoethylene glycol di(*p*-toluenesulfonates) or corresponding dichlorides without protection of the amino group.[20] In the present paper, the detailed results of the synthesis of monoaza crown ethers from diethanolamine or *N,N*-di[oligo(oxyethylene)]amines are described. Monoaza crown ethers bearing various substituents were also prepared and the scope and the limitations of this method were discussed.

Results and Discussion

Diethanolamine (**1a**) was allowed to react with oligoethylene glycol di(*p*-toluenesulfonates) (**2**) or corresponding dichlorides (**3**) in *t*-butyl alcohol/dioxane in the presence of sodium or potassium *t*-butoxide. After

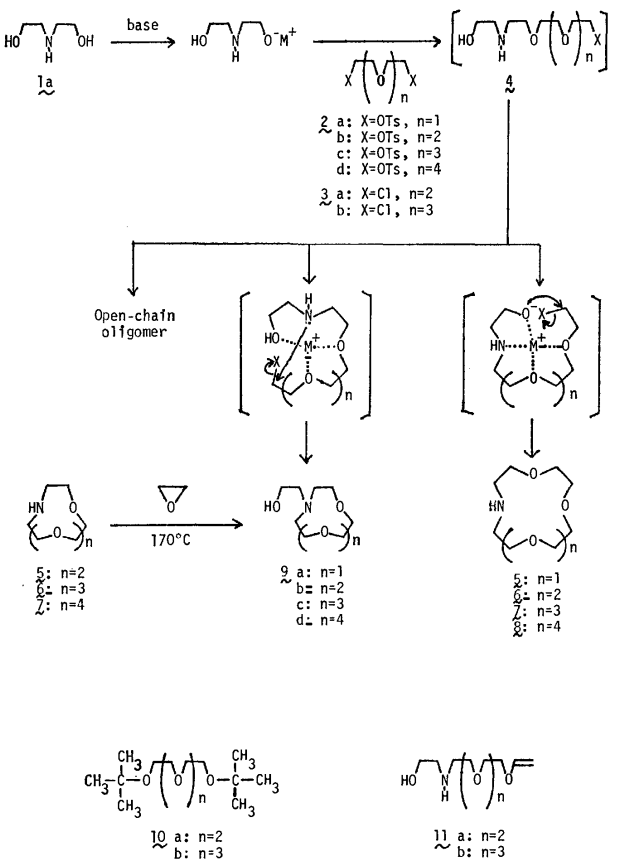

Scheme 1.

the reaction, the crude products of monoaza crown ethers were separated by extraction and the pure compounds were obtained by Kugelrohr distillation.

As shown in Scheme 1, the *in-situ* generated alkoxide anion of one hydroxyl group may react with di(*p*-toluenesulfonate) or its corresponding dichloride to give an intermediate (**4**), which subsequently cyclizes to monoaza crown ether *via* the intramolecular nucleophilic substitution by the aid of a template ion. However, the alternative attack of amino nitrogen may lead to the formation of *N*-(2-hydroxyethyl) monoaza crown ether (**9**).

The synthesis of monoaza-15-crown-5 (**6**) was carried out under the various reaction conditions by changing solvents, bases, temperature and molar ratio of the reactants. The reaction products were carefully

Table 1. Synthesis of monoaza-15-crown-5 (**6**)[a]

Run	Solvent	**2b** or **3a**	**1a**/**2b** or **3a**/Base (Molar ratio)	Base	Reaction temp/°C	Yield/%[b]	
						6	**10a**
1	*t*-BuOH/Dioxane	**2b**	1.0/1.0/2.4	*t*-BuONa	40	53 (43)[c]	4
2	*t*-BuOH/Benzene	**2b**	1.0/1.0/2.4	*t*-BuONa	40	57	3
3	*t*-BuOH/Dioxane	**2b**	2.0/1.0/2.4	*t*-BuONa	40	77 (59)[d]	1
4	*t*-BuOH/Dioxane	**2b**	1.0/1.0/2.4	*t*-BuONa	60	54 (41)	4
5	*t*-BuOH/Dioxane	**2b**	1.0/1.0/6.0	*t*-BuONa	60	43	38
6	*t*-BuOH/Dioxane	**2b**	1.0/1.0/2.4	*t*-BuONa	80	56	6
7	*t*-BuOH/Dioxane	**2b**	1.0/1.0/2.4	*t*-BuOK	40	36	3
8	*t*-BuOH/Dioxane	**2b**	1.0/1.0/2.4	*t*-BuOK	60	38	4
9	*t*-BuOH/Dioxane	**2b**	1.0/1.0/2.4	*t*-BuOK	80	34	4
10	*t*-BuOH/Dioxane	**2b**	1.0/1.0/2.4	NaOH	40	14	0
11	Dioxane	**2b**	1.0/1.0/2.4	NaOH	40	1	0
12	Dioxane	**2b**	1.0/1.0/2.4	*t*-BuOK	40	2	1
13	*t*-BuOH	**3a**	1.0/1.0/2.4	*t*-BuONa	40	30[e]	0
14	*t*-BuOH	**3a**	1.0/1.0/2.4	*t*-BuONa	60	37 (12)[e,f]	0
15	*t*-BuOH	**3a**	1.0/1.0/2.4	*t*-BuONa	80	35[e]	0

a) **2b** or **3a**, 0.01 mol; solvent, 200 ml; reaction time, 4 h. b) Based on **2b** or **3a** and determined by GLC. c) Values in parentheses are isolated yields obtained on larger scale by extraction and distillation. d) The yield obtained in higher concentration; **2b**, 0.12 mol; solvent, 550 ml. e) Reaction time, 40 h. f) Further purified by thermolyzing the complex of **6** with sodium thiocyante.

examined by GLC and NMR to make a survey of the reaction (Table 1).

Triethylene glycol di(*p*-toluenesulfonate) was dissolved in dioxane or benzene because of its insolubility in *t*-butyl alcohol. The reaction proceeded very little in dioxane whichever base, sodium hydroxide or *t*-butoxide, was used, and **2b** was recovered unchanged. This result may be ascribed to the insolubility of the alkoxide. In the range of 40 to 80 °C, the reactions using sodium or potassium *t*-butoxide as a base gave around 55 and 35% yields of monoaza-15-crown-5, respectively. Thus, the reaction temperature does not seem to affect the reaction, but with respect to the effect of the template ion, the sodium cation is superior to the potassium one, as described in the previous investigations.[21-23] Furthermore, when a two molar quantity of diethanolamine was used, the yield of **6** increased to 77%. On the contrary, use of excess base increased the formation of triethylene glycol di-*t*-butyl ether (**10a**) and caused the reduction of the yield of **6**.

Triethylene glycol di-*t*-butyl ether, which was produced by the attack of *t*-butoxide anion to **2b**, was found in the reactions using **2b**.[24]

When sodium hydroxide was used instead of sodium *t*-butoxide, monoaza-15-crown-5 was obtained in a lower yield.

In the reaction using dichloride (**3a**), the reaction was continued for 40 h, because of its low reactivity. The yields of monoaza-15-crown-5 were found to be low compared with those using di(*p*-toluenesulfonate). In these cases, vinyl ether derivative (**11a**), which was supposed to be generated by the elimination of HCl from the intermediate (**4**), was isolated instead of di-*t*-butyl ether (**10a**). As the by-product (**11a**) could not be separated from crude product by extraction, **6** was isolated by thermolyzing monoaza-15-crown-5 complex with sodium thiocyanate in acetone/hexane. Consequently, the difference between isolated yield and GLC yield was larger than that obtained using **2b**.

The products obtained from all reactions showed a single peak in their gas chromatograms using various columns, and were identified unambiguously as monoaza-15-crown-5 by spectral analyses (^{1}H NMR, IR, and MS). However, to make sure that the possible isomer, *N*-(2-hydroxyethyl)monoaza-12-crown-4 (**9b**), is not formed in the reactions, the authentic **9b** was prepared by the ethoxylation of monoaza-12-crown-4. No indication of the presence of **9b** in the reaction products was obtained, despite a precise check by GLC.

Monoaza-18-crown-6 (**7**) was prepared from the reaction between diethanolamine and tetraethylene glycol di(*p*-toluenesulfonate) (**2c**) or corresponding dichloride (**3b**), and yields were determined by GLC (Table 2). In addition, **7** was also prepared from the reactions of the corresponding oligoethylene glycol di(*p*-toluenesulfonate) with *N*-(2-hydroxyethyl)-2-(2-hydroxyethoxy)ethylamine (**1b**) or bis[2-(2-hydroxyethoxy)ethyl]amine (**1c**), which were obtained by the reactions of oligo(oxyethylene)amines with 2-(2-chloroethoxy)ethanol (Scheme 2).

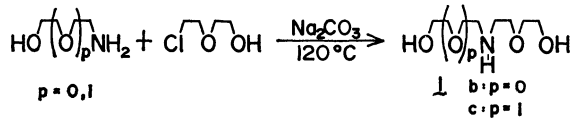

Scheme 2.

In the reactions using **2c**, no remarkable temperature effect was observed. However, unlike the results of monoaza-15-crown-5, use of both sodium and potassium *t*-butoxides gave almost the same yields. Although a small amount of tetraethylene glycol di-*t*-butyl ether was also formed in these cases, improvement of the yield of **7** to about 80% was attained by using excess diethanolamine or by using the amines

with oligo(oxyethylene) units (**1b** and **1c**). This fact may be interpreted by the increased solubilities of alkoxides of these amines in the solvent.

It was confirmed by the comparison with the authentic sample by GLC that the possible isomer (**9c**) by *N,O*-alkylation was not formed in these reactions.

Furthermore, monoaza-21-crown-7 (**8**) was prepared in a 33% yield by the reaction of diethanolamine with pentaethylene glycol di(*p*-toluenesulfonate) (**2d**). In this case, however, presence of a small amount of the isomer, *N*-(2-hydroxyethyl)monoaza-18-crown-6 (**9d**) was observed by GLC analysis, probably because of the ease of 18-crown ring formation. Similarly, treatment of diethanolamine with diethylene glycol di-(*p*-toluenesulfonate) (**2a**) afforded monoaza-12-crown-4 in very low yield (3%).

TABLE 2. SYNTHESIS OF MONOAZA-18-CROWN-6 (**7**)[a]

Run	**1**	**2** or **3**	Base	Reaction temp/°C	Yield of **7**/%[b]
1	**1a**	**2c**	*t*-BuONa	40	62
2	**1a**	**2c**	*t*-BuONa	60	62
3	**1a**	**2c**	*t*-BuONa	80	58
4	**1a**	**2c**	*t*-BuOK	25	61
5	**1a**	**2c**	*t*-BuOK	40	63 (45)[c]
6	**1a**[d]	**2c**	*t*-BuOK	40	78 (65)[c]
7	**1b**	**2b**	*t*-BuOK	40	69
8	**1c**	**2a**	*t*-BuOK	40	84
9	**1a**	**2c**	*t*-BuOK	60	60
10	**1a**	**2c**	*t*-BuOK	80	59
11	**1a**	**3b**	*t*-BuONa	40	27[f]
12	**1a**	**3b**	*t*-BuOK	40	37[f]
13	**1a**	**3b**	*t*-BuOK	60	35 (11)[f,g]

a) **1**, 0.01 mol; **2** or **3**, 0.01 mol; base, 0.024 mol; *t*-BuOH/dioxane, 200 ml; reaction time, 4 h. b) Based on **2** or **3** and determined by GLC. c) Values in parentheses are isolated yields obtained on larger scale by extraction and distillation. d) Excess **1a** was used (0.02 mol). e) The yield in higher concentration; **1a**, 0.24 mol; **2c**, 0.12 mol; base, 0.29 mol; *t*-BuOH/dioxane, 550 ml. f) Solvent, *t*-BuOH; reaction time, 40 h. g) Further purified by recrystallization from hexane.

This method was successfully applied for the preparation of the monoaza crown ethers bearing various substituents. *N*-(2-hydroxyethyl)-2-hydroxyalkylamines (**12**) were prepared by two procedures, as shown in Scheme 3. Equimolar reactions of **12** with oligoethylene glycol di(*p*-toluenesulfonates) were performed in a similar manner to give the substituted monoaza 15- and 18-crown ethers (Table 3).

The yields of crown compounds of which R^1 or R^3 is methyl were observed to be lower than those of crown compounds of which R^2 is ethyl or those of unsubstituted crowns (**6**, **7**). Such results may be attributed to the competitive formation of di-*t*-butyl ethers, because of the lower reactivity of secondary alkoxide than that of normal alkoxide due to a steric effect. The better yields of crown compounds with cyclohexane ring, however, may be explained by the higher solubility of its alkoxide in the solvent. Phenyl monoaza crown ethers (**6e** and **7e**) were also obtained

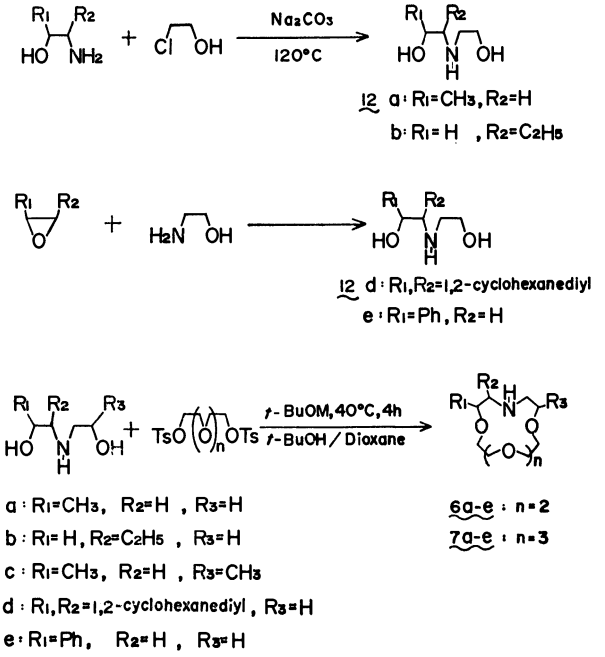

Scheme 3.

TABLE 3. YIELDS AND PROPERTIES OF SUBSTITUTED MONOAZA CROWN ETHERS[a]

Crown ether	**2**	Starting amine (**12**)	R^1	R^2	R^3	Base	Yield %	Refractive index (20 °C)	Amine number (Calcd)
6a	**2b**	**12a**	CH_3	H	H	*t*-BuONa	26	1.4661	237.0(240.5)
6b	**2b**	**12b**	H	C_2H_5	H	*t*-BuONa	46	1.4671	224.2(226.8)
6c	**2b**	**12c**	CH_3	H	CH_3	*t*-BuONa	26	1.4609	218.9(226.8)
6d	**2b**	**12d**	1,2-Cyclohexanediyl		H	*t*-BuONa	52	1.4852[b]	204.7(205.2)
6e	**2b**	**12e**	Ph	H	H	*t*-BuONa	33	1.5171	187.3(189.9)
7a	**2c**	**12a**	CH_3	H	H	*t*-BuOK	39	1.4672	199.8(202.3)
7b	**2c**	**12b**	H	C_2H_5	H	*t*-BuOK	41	1.4689	189.9(192.5)
7c	**2c**	**12c**	CH_3	H	CH_3	*t*-BuOK	28	1.4625[b]	188.8(192.5)
7d	**2c**	**12d**	1,2-Cyclohexanediyl		H	*t*-BuOK	43	1.4837	173.6(176.7)
7e	**2c**	**12e**	Ph	H	H	*t*-BuOK	33	1.5127	159.9(165.3)

a) **2**, 0.02 mol; **12**, 0.02 mol; base, 0.048 mol; *t*-BuOH/dioxane, 360 ml; 40 °C: 4 h. b) Measured at 40 °C: white waxy solid at 20 °C.

in satisfactory yields.

Most of the reactions in this study were run on a rather small scale in dilute solution (0.01 mol of **2**/200 ml of solvent). However, in the practical preparation on a larger scale in higher concentration (0.12 mol of **2**/550 ml of solvent), monoaza crown ethers were obtained in 50 to 70% yields by using the excess dialkanolamines. Thus, together with the high selectivity and ready accessibility of the starting materials, this method is useful for the practical production of monoaza crown ethers.

Experimental

The infrared spectra were taken on a Hitachi 260-10 spectrometer. The ^{1}H NMR spectra were recorded at 100 MHz on a JEOL JNM-PS 100 spectrometer in $CDCl_3$ solution with tetramethylsilane as the internal standard. The mass spectra were measured with a Hitachi RMU-6E mass spectrometer at an ionization potential of 70 eV. The GLC analyses were performed on a Shimadzu gas chromatograph GC-3BF using 1 m×3 mm column packed with 10% Silicone SE-30 on 60—80 mesh Celite 545 or on a Shimadzu gas chromatograph GC-3BT using 0.7 m×3 mm column packed with 10% Carbowax on 60—80 mesh Celite 545. Amine contents were determined by a conventional titration procedure.[25]

Starting Materials. Starting materials were the commercial products of analytical grade. Their purities were checked by GLC and they were purified by distillation when necessary. Oligoethylene glycol di(*p*-toluenesulfonates) were prepared as reported.[26] α-(2-Chloroethyl)-ω-chlorooligo(oxyethylenes) were prepared from the corresponding glycols and thionyl chloride.

*N-(2-Hydroxyethyl)-2-(2-hydroxyethoxy)ethylamine (**1b**).* 2-(2-Chloroethoxy)ethanol (62.3 g, 0.50 mol) was added to a suspension of powdered sodium carbonate (39.8 g, 0.38 mol) in 2-aminoethanol (91.7 g, 1.50 mol) and the mixture was heated at 120 °C with stirring. After 24 h of reaction, it was cooled to room temperature, filtered and excess 2-aminoethanol was recovered from the filtrate. The residue was purified by fractional distillation at 150—152 °C (0.1 Torr) to give 46.1 g (50%) of **1b** as a pale yellow liquid: ^{1}H NMR δ 2.65—2.97 (m, NCH_2, 4H), 3.46—3.89 (m, OCH_2, 8H), 4.38 (s, OH, NH, 3H); IR (neat) 3350, 3300, 2950, 2860, 1460, 1360, 1120, 1070 cm^{-1}.

Found: C, 48.06; H, 10.29; N, 9.52%. Calcd for $C_6H_{15}NO_3$: C, 48.31; H, 10.13; N, 9.39%.

*Bis[2-(2-hydroxyethoxy)ethyl]amine (**1c**).* The above procedure was followed, using 2-(2-aminoethoxy)ethanol and 2-(2-chloroethoxy)ethanol: bp 154—156 °C (0.05 Torr)**; pale yellow liquid; 55% yield; ^{1}H NMR δ 2.79 (t, 4H), 3.44—3.78 (m, 12H), 3.82 (s, 3H); IR (neat) 3320, 3280, 2950, 2850, 1460, 1350, 1120, 1070 cm^{-1}.

Found: C, 49.93; H, 10.04; N, 7.50%. Calcd for $C_8H_{19}NO_4$: C, 49.72; H, 9.91; N, 7.25%.

*N-(2-Hydroxyethyl)-2-hydroxypropylamine (**12a**).* The above procedure was followed with 1-amino-2-propanol and 2-chloroethanol as reactants: bp 96—98 °C (0.015 Torr, Kugelrohr distillation); colorless liquid; 61% yield; ^{1}H NMR δ 1.17 (d, 3H), 2.37—2.68 (m, 2H), 2.77 (t, 2H), 3.56—4.07 (m, 3H), 3.66 (s, 3H); IR (neat) 3300, 2925, 2850, 1460, 1375, 1040 cm^{-1}.

Found: C, 50.20; H, 11.09; N, 11.69%. Calcd for $C_5H_{13}NO_2$: C, 50.40; H, 11.00; N, 11.75%.

** 1 Torr≈133.322 Pa.

*N-(2-Hydroxyethyl)-1-hydroxymethylpropylamine (**12b**).* The above procedure was used with 2-amino-1-butanol and 2-chloroethanol as reactants: bp 90—95 °C (0.015 Torr, Kugelrohr distillation); pale yellow liquid; ^{1}H NMR δ 0.90 (t, 3H), 1.12—1.76 (m, 2H), 2.32—2.98 (m, 3H), 2.99—3.83 (s+m, 7H); IR (neat) 3300, 2930, 2850, 1460, 1370, 1050 cm^{-1}.

Found: C, 53.97; H, 11.46; N, 10.51%. Calcd for $C_6H_{15}NO_2$: C, 54.11; H, 11.35; N, 10.52%.

*N-(2-Hydroxyethyl)-2-hydroxycyclohexylamine (**12d**).* Cyclohexene oxide (4.91 g, 0.05 mol) was added in drops to 2-aminoethanol (15.27 g, 0.25 mol) during 1 h, at 125 °C. After the addition, the reaction was continued for 3 h and excess 2-aminoethanol was removed. The crude product (8.3 g) was purified by Kugelrohr distillation at 115—120 °C (0.05 Torr) to give 7.6 g (95%) of **12d** as a pale yellow liquid: ^{1}H NMR δ 0.88—2.14 (m, CH_2, 8H), 2.15—2.46 (m, NCH, 1H), 2.47—3.02 (m, NCH_2, 2H), 3.14—3.47 (m, OCH, 1H), 3.69 (t, OCH_2, 2H), 4.01 (s, OH, NH, 3H); IR (neat) 3300, 2940, 2860, 1450, 1375, 1130, 1060 cm^{-1}.

Found: C, 60.12; H, 10.74; N, 9.04%. Calcd for $C_8H_{17}NO_2$: C, 60.35; H, 10.76; N, 8.80%.

*N-(2-Hydroxyethyl)-2-hydroxy-2-phenylethylamine (**12e**).* By a procedure similar to that used for **12d**, the reaction between styrene oxide (6.01 g, 0.05 mol) and 2-aminoethanol (15.27 g, 0.05 mol) was performed. The crude product (9.90 g) was purified by recrystallization from benzene to give 7.07 g (78%) of **12e** as a white solid: mp 98.5—100.5 °C; ^{1}H NMR δ 2.58—2.88 (m, 4H), 3.44 (s, 3H), 3.64 (t, 2H), 4.76 (t, 1H), 7.31 (s, 5H); IR (KBr) 3380, 3250, 3050, 2910, 2850, 1460, 1070, 710 cm^{-1}.

Found: C, 65.96; H, 8.24; N, 7.72%. Calcd for $C_{10}H_{15}NO_2$: C, 66.27; H, 8.34; N, 7.73%.

*2,2,13,13-Tetramethyl-3,6,9,12-tetraoxatetradecane (**10a**).* Potassium metal (5.9 g, 0.15 mol) was dissolved in *t*-butyl alcohol (200 ml), and triethylene glycol di(*p*-toluenesulfonate) (**2b**, 22.9 g, 0.05 mol) was added at 60 °C. After 4 h of reaction, the mixture was filtered and the solvent was evaporated off. Water (30 ml) was added to the residue and the solution was extracted several times with hexane. The hexane extracts were combined, the solvent was removed, and the crude product (11.0 g) was distilled by Kugelrohr apparatus at 78—81 °C (0.05 Torr) to give 4.2 g (32%) of **10a** as a colorless liquid: ^{1}H NMR δ 2.18 (s, 18H), 3.45—3.73 (m, 12H); IR (neat) 2990, 2880, 1460, 1365, 1130, 1100 cm^{-1}.

Found: C, 63.62; H, 11.48%. Calcd for $C_{14}H_{30}O_4$: C, 64.09; H, 11.52%.

*Preparation of 1,4,7,10-Tetraoxa-13-azacyclopentadecane (**6**). (i) Reaction of Triethylene Glycol Di(p-toluenesulfonate) (**2b**) with Diethanolamine (**1a**):* Diethanolamine (**1a**, 3.15 g, 0.03 mol) and sodium metal (1.66 g, 0.072 mol) were dissolved in 420 ml of *t*-butyl alcohol, and triethylene glycol di(*p*-toluenesulfonate) (**2b**, 13.8 g, 0.03 mol) in 180 ml of dioxane was slowly added, drop by drop, into the solution over a period of 2 h under stirring at 40 °C. After the addition, the reaction was continued for two more hours and the reaction product was filtered. The precipitate was washed with dichloromethane, and the solvent was removed from the combined solution of filtrate and washings. Water (20 ml) was added to the residue and the solution was extracted two times with hexane to remove hexane-soluble by-products and then extracted several times with dichloromethane. Hexane was recovered from the hexane extracts, and the main by-product was isolated from the residue by preparative GLC and identified as **10a**. The dichloromethane extracts were combined, the solvent was evaporated off, and the

residue (5.21 g) was distilled by Kugelrohr apparatus at 77—81 °C (0.01 Torr) to give **6** (2.83 g, 43%) as a colorless solid: mp 29—32 °C (lit,[20] 30—32 °C); ^{1}H NMR δ 2.78 (t, 4H), 2.96 (s, 1H), 2.55—3.76 (m, 16H); MS, *m/e* (relative intensity) 219 (M^+, 11), 188 (22), 162 (32), 132 (26), 116 (9), 100 (61), 45 (100); IR (neat) 3320, 2940, 2860, 1460, 1350, 1120 cm^{-1}.

Found: C, 54.81; H, 9.71; N, 6.27%. Calcd for $C_{10}H_{21}NO_4$: C, 54.78; H, 9.65; N, 6.39%.

A larger scale experiment in higher concentration was carried out in a similar manner to that described above. Triethylene glycol di(*p*-toluenesulfonate) (55.0 g, 0.12 mol) in dioxane (200 ml) was added to the solution of diethanolamine (25.2 g, 0.24 mol) and sodium metal (6.6 g, 0.29 mol) dissolved in *t*-butyl alcohol (350 ml). The crude product (23.4 g) was distilled by Kugelrohr apparatus to give **6** (15.5 g, 59%).

GLC analyses for the investigation of the reaction conditions were performed using 0.7 m × 3 mm column packed with 10% Carbowax on 60—80 mesh Celite 545. Triethylene glycol di(*p*-toluenesulfonate) (0.01 mol) in a solvent (60 ml) was slowly added to the solution of diethanolamine and base in a solvent (140 ml) during 2 h. After the reaction was continued for 2 h, the mixture was filtered and the precipitate was washed with dichloromethane. The solvent was removed from the combined solution. The GLC analysis was performed on a diluted sample of the residue, and each yield of **6** and **10a** was determined.

*(ii) Reaction of 1,8-Dichloro-3,6-dioxaoctane (**3a**) with Diethanolamine (**1a**)*: Diethanolamine (3.15 g, 0.03 mol) and sodium metal (1.66 g, 0.072 mol) were dissolved in 420 ml of *t*-butyl alcohol. Into the solution, 1,8-dichloro-3,6-dioxaoctane (5.61 g, 0.03 mol) in 180 ml of *t*-butyl alcohol was slowly added over a period of 2 h under stirring at 60 °C. After the addition, the reaction continued for 38 h, and a work-up was performed similarly to the case of di(*p*-toluenesulfonate). The product (2.60 g) obtained by Kugelrohr distillation showed a single peak in the GLC, using Silicone SE-30 on Celite 545. On the more polar column (10% Carbowax on Celite 545), however, it showed two peaks. Then, the by-product was isolated from the distillation product by preparative GLC: ^{1}H NMR δ 2.39 (s, 2H), 2.68—2.94 (m, 4H), 3.53—3.96 (m, 12H), 4.03 (dd, 1H), 4.20 (dd, 1H), 6.52 (dd, 1H); MS, *m/e* (relative intensity) 219 (M^+, 2), 188 (47), 74 (100); IR (neat) 3320, 2940, 2870, 1620, 1460, 1330, 1110, 990 cm^{-1}. From these data this product was identified as **11a**, but the possible isomer, *N*-(2-hydroxyethyl)monoaza-12-crown-4 (**9b**) was not detected in this reaction. The distillation product was further purified by thermolyzing the monoaza-15-crown-5 complex with sodium thiocyanate in acetone/hexane to give the pure product of **6** (0.79 g, 12%).

*1,4,7,10,13-Pentaoxa-16-azacyclooctadecane (**7**).* This compound was prepared, using a method similar to that used for **6**, from diethanolamine (25.2 g, 0.24 mol), tetraethylene glycol di(*p*-toluenesulfonate) (**2c**, 60.3 g, 0.12 mol), and potassium metal (11.3 g, 0.29 mol). The crude product was distilled by Kugelrohr apparatus at 95—99 °C (0.02 Torr) to give 20.5 g (65%) of **7** as a colorless solid: mp 48—51 °C (lit,[15] 49—51 °C); ^{1}H NMR δ 2.70 (s, 1H), 2.79 (t, 4H), 3.56—3.78 (m, 20H); MS *m/e* (relative intensity) 263 (M^+, 6), 233 (20), 220 (18), 204 (19), 188 (9), 176 (35), 100 (60), 45 (100); IR (neat) 3300, 2940, 2850, 1460, 1350, 1120 cm^{-1}.

Found: C, 54.59; H, 9.88; N, 5.60%. Calcd for $C_{12}H_{25}NO_5$: C, 54.73; H, 9.57; N, 5.32%.

In the same manner as in the preparation of **6** using **3a**, the reaction of 1,11-dichloro-3,6,9-trioxaundecane (**3b**, 6.93 g, 0.03 mol) with diethanolamine (3.15 g, 0.03 mol) was carried out. Since the distillation product (3.12 g) was found as a mixture of **7** and **11b**, it was further purified by recrystallization from hexane to give the pure product of **7** (0.87 g, 11%).

Small-scale experiments for the investigation of the reaction conditions were carried out, using oligoethylene glycol di(*p*-toluenesulfonate) or 1,11-dichloro-3,6,9-trioxaundecane (0.01 mol) and corresponding dihydroxy amines (**1a—c**) in the same manner as that used for **6**.

*1,4,7,10,13,16-Hexaoxa-19-azacycloheneicosane (**8**).* Diethanolamine (10.5 g, 0.1 mol) and potassium metal (9.4 g, 0.24 mol) dissolved in 300 ml of *t*-butyl alcohol and pentaethylene glycol di(*p*-toluenesulfonate) (**2d**, 54.7 g, 0.1 mol) in 250 ml of dioxane were allowed to react, using a method similar to **6**. In the GLC analysis of the crude product (27.6 g), a small peak which was ascribed to **9d** was observed. The product was distilled by Kugelrohr apparatus at 111—114 °C (0.001 Torr) to afford 10.0 g (33%) of **8** as a colorless liquid: n_D^{20} 1.4700; ^{1}H NMR δ 2.64 (s, 1H), 2.79 (t, 4H), 3.56—3.80 (m, 24H); MS, *m/e* (relative intensity) 307 (M^+, 4), 276 (7), 232 (10), 220 (17), 204 (19), 176 (15), 100 (35), 45 (100); IR (neat) 3340, 2940, 2860, 1450, 1350, 1120 cm^{-1}.

Found: C, 54.88; H, 9.79; N, 4.50%. Calcd for $C_{14}H_{29}NO_6$: C, 54.70; H, 9.51; N, 4.56%.

*1,4,7-Trioxa-10-azacyclododecane (**5**).* This compound was prepared using a method similar to that for the macrocycle **6**, from diethanolamine (42.1 g, 0.4 mol), sodium metal (11.0 g, 0.48 mol), and diethylene glycol di(*p*-toluenesulfonate) (82.9 g, 0.2 mol). The crude product was purified by Kugelrohr apparatus giving colorless crystals: bp 58—62 °C (0.005 Torr); mp 57—59 °C (lit,[4] 60 °C); 3% yield; ^{1}H NMR δ 2.52 (s, NH, 1H), 2.72 (t, NCH_2, 4H), 3.48—3.89 (m, OCH_2, 12H); MS, *m/e* (relative intensity) 175 (M^+, 10), 144 (15), 118 (35), 100 (33), 86 (61), 74 (21), 72 (21), 57 (100); IR (neat) 3300, 2940, 2870, 1460, 1360, 1130, 1090 cm^{-1}.

Found: C, 54.89; H, 9.91; N, 7.91%. Calcd for $C_8H_{17}NO_3$: C, 54.84; H, 9.78; N, 7.99%.

*11-Methyl-1,4,7,10-tetraoxa-13-azacyclopentadecane (**6a**).* *N*-(2-Hydroxyethyl)-2-hydroxypropylamine (**12a**, 2.38 g, 0.02 mol) and sodium metal (1.10 g, 0.048 mol) were dissolved in 240 ml of *t*-butyl alcohol and triethylene glycol di(*p*-toluenesulfonate) (9.16 g, 0.02 mol) in 120 ml of dioxane was added in drops to the solution over a period of 2 h under stirring at 40 °C. After the addition, the reaction was continued for two more hours, then the reaction mixture was filtered. The precipitate was washed with dichloromethane, and the solvent was removed from the combined solution of filtrate and washings. Water (15 ml) was added to the residue and the solution was extracted two times with hexane to remove hexane-soluble materials and then extracted several times with dichloromethane. The dichloromethane extracts were combined, the solvent was evaporated off, and the residue was distilled by Kugelrohr apparatus at 80—83 °C (0.01 Torr) to give 1.21 g (26%) of **6a** as a pale yellow liquid: ^{1}H NMR δ 1.10 (d, CH_3, 3H), 2.52—2.80 (m, NCH_2, 4H), 2.83 (s, NH, 1H), 2.42—2.92 (m, OCH, OCH_2, 15H); MS, *m/e* (relative intensity) 233 (M^+, 9), 218 (4), 188 (12), 161 (10), 132 (10), 114 (11), 45 (100); IR (neat) 3330, 2930, 2850, 1460, 1360, 1130 cm^{-1}.

Found: C, 56.35; H, 10.00; N, 6.04%. Calcd for $C_{11}H_{23}NO_4$: C, 56.63; H, 9.94; N, 6.00%.

This procedure is typical for the preparation of other *N*-unsubstituted monoaza crown ethers bearing substituents.

Monoaza 15- and 18-crown ethers were prepared from the reaction of dihydroxy amines (**12a—e**) with triethylene and tetraethylene glycol di(*p*-toluenesulfonates), respectively.

*11,15-Dimethyl-1,4,7,10-tetraoxa-13-azacyclopentadecane (**6c**).* Bp 75—80 °C (0.01 Torr, Kugelrohr distillation); colorless liquid; 26% yield; ^{1}H NMR δ 1.05—1.22 (m, 6H), 2.59 (s, 1H), 2.42—2.80 (m, 4H), 3.40—3.84 (m, 14H); MS, *m/e* (relative intensity) 247 (M^+, 6), 232 (5), 202 (37), 174 (7), 158 (6), 146 (6), 114 (18), 101 (49), 45 (100); IR (neat) 3330, 2970, 2870, 1460, 1340, 1110 cm^{-1}.

Found: C, 58.04; H, 10.38; N, 5.60%. Calcd for $C_{12}H_{25}NO_4$: C, 58.27; H, 10.19; N, 5.66%.

*12-Ethyl-1,4,7,10-tetraoxa-13-azacyclopentadecane (**6b**).* Bp 90—93 °C (0.02 Torr, Kugelrohr distillation); colorless liquid; 46% yield; ^{1}H NMR δ 0.89 (t, 3H), 1.28—1.62 (m, 2H), 2.01 (s, 1H), 2.60—2.92 (m, 3H), 3.18—3.80 (m, 16H); MS, *m/e* (relative intensity) 247 (M^+, 23), 218 (95), 188 (57), 172 (21), 159 (42), 128 (29), 69 (100); IR (neat) 3320, 2930, 2860, 1460, 1350, 1120 cm^{-1}.

Found: C, 58.13; H, 10.05; N, 5.63%. Calcd for $C_{12}H_{25}NO_4$: C, 58.27; H, 10.19; N, 5.66%.

*Perhydro-11,12-benzo-1,4,7,10-tetraoxa-13-azacyclopentadecane (**6d**).* Bp 125—128 °C (0.03 Torr, Kugelrohr distillation); white waxy solid at 20 °C; 52% yield; ^{1}H NMR δ 0.88—2.33 (m, 8H), 2.34—2.51 (m, 1H), 2.72 (t, 2H), 2.98 (s, 1H), 2.88—3.09 (m, 1H), 3.30—4.04 (m, 14H); MS, *m/e* (relative intensity) 273 (M^+, 13), 244 (8), 230 (11), 188 (21), 154 (37), 142 (23), 128 (25), 126 (33), 45 (100); IR (neat) 3320, 2940, 2860, 1460, 1355, 1130 cm^{-1}.

Found: C, 61.11; H, 10.33; N, 4.99%. Calcd for $C_{14}H_{27}NO_4$: C, 61.51; H, 9.95; N, 5.12%.

*11-Phenyl-1,4,7,10-tetraoxa-13-azacyclopentadecane (**6e**).* Bp 139—143 °C (0.02 Torr, Kugelrohr distillation); pale yellow liquid; 33% yield; ^{1}H NMR δ 2.47 (s, 1H), 2.72 (t, 2H), 2.74—3.07 (m, 2H), 3.36—4.04 (m, 14H), 4.40—4.64 (m, 1H), 7.12—7.52 (m, 5H); MS, *m/e* (relative intensity) 295 (M^+, 35), 265 (10), 220 (9), 207 (11), 176 (16), 165 (17), 74 (100); IR (neat) 3325, 3050, 2920, 2880, 1460, 1350, 1110, 760, 700 cm^{-1}.

Found: C, 65.02; H, 8.59; N, 4.98%. Calcd for $C_{16}H_{25}NO_4$: C, 65.06; H, 8.53; N, 4.74%.

*14-Methyl-1,4,7,10,13-pentaoxa-16-azacyclooctadecane (**7a**).* By a similar procedure to that used for **6a**, the reaction between *N*-(2-hydroxyethyl)-2-hydroxypropylamine (**12a**, 2.38 g, 0.02 mol) and tetraethylene glycol di(*p*-toluenesulfonate) (**2c**, 10.04 g, 0.02 mol) was performed in the presence of potassium metal (1.87 g, 0.048 mol) dissolved in *t*-butyl alcohol: bp 102—107 °C (0.01 Torr); colorless liquid; 39% yield; ^{1}H NMR δ 1.12 (d, 3H), 2.52—2.84 (m, 4H), 2.65 (s, 1H), 3.40—3.90 (m, 19H); MS, *m/e* (relative intensity) 277 (M^+, 7), 232 (19), 205 (14), 190 (13), 176 (16), 144 (13), 45 (100); IR (neat) 3350, 2930, 2890, 1460, 1350, 1120 cm^{-1}.

Found: C, 55.89; H, 10.00; N, 4.94%. Calcd for $C_{13}H_{27}NO_5$: C, 56.30; H, 9.81; N, 5.05%.

*14,18-Dimethyl-1,4,7,10,13-pentaoxa-16-azacyclooctadecane (**7c**).* Bp 97—101 °C (0.001 Torr, Kugelrohr distillation); white waxy solid at 20 °C; 28% yield; ^{1}H NMR δ 1.06—1.22 (m, 6H), 2.54 (s, 1H), 2.38—2.83 (m, 4H), 3.37—3.89 (m, 18H); MS, *m/e* (relative intensity) 291 (M^+, 3), 276 (4), 246 (20), 190 (10), 146 (7), 133 (8), 116 (14), 101 (24), 45 (100); IR (neat) 3340, 2970, 2870, 1460, 1350, 1120 cm^{-1}.

Found: C, 57.56; H, 10.24; N, 4.39%. Calcd for $C_{14}H_{29}NO_5$: C, 57.71; H, 10.03; N, 4.81%.

*15-Ethyl-1,4,7,10,13-pentaoxa-16-azacyclooctadecane (**7b**).* Bp 120—124 °C (0.04 Torr, Kugelrohr distillation); pale yellow liquid; 41% yield; ^{1}H NMR δ 0.88 (t, 3H), 1.27—1.64 (m, 2H), 2.23 (s, 1H), 2.63—2.86 (m, 3H), 3.23—3.78 (m, 20H); MS, *m/e* (relative intensity) 291 (M^+, 23), 262 (100), 232 (79), 216 (57), 188 (32), 174 (47), 159 (50); IR (neat) 3370, 2920, 2870, 1460, 1360, 1120 cm^{-1}.

Found: C, 57.38; H, 10.15; N, 4.78%. Calcd for $C_{14}H_{29}NO_5$: C, 57.71; H, 10.03; N, 4.81%.

*Perhydro-14,15-benzo-1,4,7,10,13-pentaoxa-16-azacyclooctadecane (**7d**).* Bp 145—150 °C (0.03 Torr, Kugelrohr distillation); pale yellow liquid; 43% yield; ^{1}H NMR δ 0.92—2.23 (m, 8H), 2.24—2.68 (m, 1H), 2.64 (s, 1H), 2.75 (t, 2H), 2.86—3.28 (m, 1H), 3.32—4.04 (m, 18H); MS, *m/e* (relative intensity) 317 (M^+, 8), 288 (9), 274 (9), 242 (14), 205 (15), 154 (36), 143 (27), 45 (100); IR (neat) 3325, 2930, 2860, 1460, 1350, 1120 cm^{-1}.

Found: C, 60.42; H, 9.87; N, 4.50%. Calcd for $C_{16}H_{31}NO_5$: C, 60.54; H, 9.84; N, 4.41%.

*14-Phenyl-1,4,7,10,13-pentaoxa-16-azacyclooctadecane (**7e**).* Bp 153—157 °C (0.02 Torr, Kugelrohr distillation); yellow liquid; 33% yield; ^{1}H NMR δ 2.38 (s, 1H), 2.74 (t, 2H), 2.72—3.08 (m, 2H), 3.38—3.90 (m, 18H), 4.42—4.68 (m, 1H), 7.12—7.45 (m, 5H); MS, *m/e* (relative intensity) 339 (M^+, 14), 309 (9), 280 (7), 264 (8), 205 (11), 176 (19), 74 (100); IR (neat) 3325, 3050, 2930, 2880, 1450, 1350, 1110, 760, 700 cm^{-1}.

Found: C, 63.35; H, 8.77; N, 4.42%. Calcd for $C_{18}H_{29}NO_5$: C, 63.69; H, 8.61; N, 4.13%.

*10-(2-Hydroxyethyl)-1,4,7-trioxa-10-azacyclododecane (**9b**).* After ethylene oxide was passed through 35% NaOH aqueous solution and dried over NaOH and soda lime, it was introduced to 1,4,7-trioxa-10-azacyclododecane (**5**, 0.88 g, 0.005 mol) at 170 °C for 6 h. By distilling the reaction mixture at 80—85 °C (0.03 Torr) using Kugelrohr apparatus, 0.47 g (43%) of **9b** was obtained as a pale yellow liquid. ^{1}H NMR δ 2.67 (t, NCH_2, 2H), 2.72 (t, NCH_2, 4H), 3.39—3.92 (s+m, OH, OCH_2, 15H); MS, *m/e* (relative intensity) 219 (M^+, 6.2), 188 (100); IR (neat) 3300, 2910, 2840, 1640, 1450, 1360, 1130, 1100 cm^{-1}.

Found: C, 54.21; H, 9.85; N, 6.05%. Calcd for $C_{10}H_{21}NO_4$: C, 54.77; H, 9.65; N, 6.39%.

Using a similar procedure, **9c** and **9d** were also obtained.

*13-(2-Hydroxyethyl)-1,4,7,10-tetraoxa-13-azacyclopentadecane (**9c**).* Bp 80—85 °C (0.005 Torr, Kugelrohr distillation); pale yellow liquid; 41% yield; ^{1}H NMR δ 2.65 (t, 2H), 2.75 (t, 4H), 3.48—3.76 (s+m, 19H); MS, *m/e* (relative intensity) 363 (M^+, 2.7), 232 (100); IR (neat) 3300, 2910, 2840, 1640, 1460, 1360, 1110, 1090 cm^{-1}.

Found: C, 54.55; H, 9.69; N, 5.45%. Calcd for $C_{12}H_{25}NO_5$: C, 54.73; H, 9.57; N, 5.32%.

*16-(2-Hydroxyethyl)-1,4,7,10,13-pentaoxa-16-azacyclooctadecane (**9d**).* Bp 138—142 °C (0.005 Torr, Kugelrohr distillation); pale yellow liquid; 52% yield; ^{1}H NMR δ 2.65 (t, 2H), 2.75 (t, 4H), 3.48—3.74 (s+m, 23H), MS, *m/e* (relative intensity) 307 (M^+, 0.6), 276 (100); IR (neat) 3250, 2900, 2840, 1640, 1460, 1360, 1100 cm^{-1}.

Found: C, 54.33; H, 9.65; N, 4.75%. Calcd for $C_{14}H_{29}NO_6$: C, 54.70; H, 9.51; N, 4.56%.

References

1) G. W. Gokel and B. J. Garcia, *Tetrahedron Lett.*, **1977**, 317.

2) H. K. Frensdorff, *J. Am. Chem. Soc.*, **93**, 600 (1971).

3) R. A. Schultz, E. Schlegel, D. M. Dishong, and G. W. Gokel, *J. Chem. Soc., Chem. Commun.*, **1982**, 242.

4) M. J. Calverley and J. Dale, *J. Chem. Soc., Chem. Commun.*, **1981**, 684.

5) M. R. Johnson, I. O. Sutherland, and R. F. Newton, *J. Chem. Soc., Chem. Commun.*, **1979**, 306.

6) M. R. Johnson, I. O. Sutherland, and R. F. Newton, *J. Chem. Soc., Perkin Trans. 1*, **1980**, 586.
7) J. P. Dix and F. Vögtle, *Angew. Chem.*, **90**, 893 (1978).
8) A. Masuyama, Y. Nakatsuji, I. Ikeda, and M. Okahara, *Tetrahedron Lett.*, **22**, 4665 (1981).
9) R. A. Schultz, D. M. Dishong, and G. W. Gokel, *Tetrahedron Lett.*, **22**, 2623 (1981).
10) R. A. Schultz, D. M. Dishong, and G. W. Gokel, *J. Am. Chem. Soc.*, **104**, 625 (1982).
11) M. Okahara, P.-L. Kuo, S. Yamamura, and I. Ikeda, *J. Chem. Soc., Chem. Commun.*, **1980**, 586.
12) P.-L. Kuo, M. Miki, I. Ikeda, and M. Okahara, *J. Am. Oil Chem. Soc.*, **57**, 227 (1980).
13) P.-L. Kuo, I. Ikeda, and M. Okahara, *Tenside Deterg.*, **19**, 4 (1982).
14) H. Maeda, Y. Nakatsuji, and M. Okahara, *Tetrahedron Lett.*, **22**, 4105 (1981).
15) M. R. Johnson, I. O. Sutherland, and R. F. Newton, *J. Chem. Soc., Perkin Trans. 1*, **1979**, 357.
16) R. N. Greene, *Tetrahedron Lett.*, **1972**, 1793.
17) C. G. Krespan, *J. Org. Chem.*, **40**, 1205 (1975).
18) M. Tomoi, O. Abe, M. Ikeda, K. Kihara, and H. Kakiuchi, *Tetrahedron Lett.*, **1978**, 3031.
19) W. Kern, S. Iwabuchi, H. Sato, and V. Böhmer, *Makromol. Chem.*, **180**, 2539 (1979).
20) H. Maeda, Y. Nakatsuji, and M. Okahara, *J. Chem. Soc., Chem. Commun.*, **1981**, 471.
21) P.-L. Kuo, N. Kawamura, M. Miki, and M. Okahara, *Bull. Chem. Soc. Jpn.*, **53**, 1689 (1980).
22) B. R. Bowsher and A. J. Rest, *Inorg. Chim. Acta*, **45**, L5 (1980).
23) B. R. Bowsher and A. J. Rest, *J. Chem. Soc., Dalton Trans.*, **1981**, 1157.
24) P. Veeravagu, R. T. Arnold, and E. W. Eigenmann, *J. Am. Chem. Soc.*, **86**, 3072 (1964).
25) D. E. Terry, K. R. Eilar, and O. A. Moe, *Anal. Chem.*, **24**, 313 (1952).
26) J. Dale and P. O. Kristiansen, *Acta Chem. Scand.*, **26**, 1471 (1972).

Nucleophilic Substitution with Phosphide Anions Prepared by an Action of Sodium Dihydridobis(2-methoxyethanolato)aluminate on Phosphorus Compounds

Mitsuji YAMASHITA,* Nobuyoshi SUZUKI, Manabu YAMADA, Yukio SOEDA. Hiroaki YAMASHITA, Kaname NAKATANI, Tatsuo OSHIKAWA, and Saburo INOKAWA†

Department of Applied Chemistry, Faculty of Engineering, Shizuoka University, Hamamatsu 432

†*Department of Chemistry, Faculty of Science, Okayama University, Okayama 700*

(Received May 31, 1982)

Phosphide anions, prepared by an action of sodium dihydridobis(2-methoxyethanolato)aluminate on derivatives of phosphine, phosphine oxide, or phosphorus esters, react with primary and secondary alkyl halides to produce phosphine derivatives having a newly formed phosphorus-carbon bond. The reactivity increases in the order of chloride<bromide<iodide and of secondary<primary in alkyl halide. Reaction of phosphide anion is also feasible with *p*-toluenesulfonate. Reaction of an anion of diphenylphosphine oxide seems to proceed mainly as an S_N2 type process.

As a chemical modification of sugar derivatives, we[1-3] synthesized compounds having a phosphorus atom instead of oxygen atom in the hemiacetal ring. Paulsen and Greve[4] reported a preparation of sugar derivatives bearing a phosphorus-carbon bond by addition of dialkylphosphonates to glyculoses. The addition of phosphonates to ketoses is a good method to prepare a phosphorus-carbon bond on sugar skeletons,[5] however a fundamental work[6] on the reactivity of α-hydroxyalkylphosphonates with some halogenating reagents failed to afford desired results, *i.e.*, some elimination reactions occurred instead of the substitution reaction.

The addition reaction of phosphorus compounds having a P–H bond to unsaturated double bonds such as C=C, C=N, and C=O always possesses a potential possibility to produce isomeric adducts. Addition of phenylphosphine to 3-*O*-acetyl-5,6-dideoxy-1,2-*O*-isopropylidene-6-*C*-nitro-α-D-*xylo*-hex-5-enofuranose actually gave both compounds of α-D-glucofuranose and β-L-idofuranose derivatives.[7,8]

Preparation and reaction of metal phosphides have widely been investigated.[9] Reactions of alkali phosphides with alkylating reagents are often used for the preparation of tertiary phosphines.[10] Phosphide anions could also be prepared by an action of hydrides on phosphorus compounds in a heterogeneous mixture[9,10] as well as by an action of sodium dihydridobis(2-methoxyethanolato)aluminate (SDMA) in a homogeneous mixture.[11,12] SDMA was sometimes used to prepare a P–H group from P–OR groups of phosphorus esters connected with sugar derivatives such as 5,6-dideoxy-1,2-*O*-isopropylidene-5-*C*-[(methoxy)phenylphosphinyl]-3-*O*-methyl-α-D-*xylo*-hexofuranose;[13] therefore, the reagent seems to be applicable toward sugar derivatives since it does not act on any functional groups other than phosphorus moiety.

To prevent the occurrence of isomeric products at the stage of phosphorus-carbon bond formation, we attempted to adopt a nucleophilic substitution with phosphide anion. This paper deals with a preparation of phosphide anions by an action of SDMA and their reaction with alkyl halides or *p*-toluenesulfonates to produce secondary and tertiary phosphine derivatives.

Results

Reaction with Alkyl Halides. Reaction of diphenylphosphine oxide (**1**) with some alkyl halides was carried out in the presence of SDMA in some solvents under reflux. The reaction proceeded according to

$$\underset{\mathbf{1}}{Ph_2P(O)H} + RX \xrightarrow{NaAlH_2(OCH_2CH_2OMe)_2} \underset{\mathbf{2}}{Ph_2P(O)R}, \quad (1)$$

giving the corresponding alkyldiphenylphosphine oxides in moderate to good yields, results being summarized in Table 1.

The reaction of **1** with SDMA proceeded very fast and predominantly gave the corresponding phosphide anion. The reactivity of the anion with alkyl halides seems to depend largely on the nature of alkyl halides employed. The isolated yield increased in the order of chloride<bromide<iodide in alkyl halides. The reaction with primary alkyl halides proceeded faster than that with secondary alkyl halides which required higher reaction temperature and/or prolonged reaction time. The reaction using SDMA is superior to those using sodium amide or lithium tetrahydridoaluminate, as judged from the product yield. Addition of sodium iodide to the reaction mixture remarkably improved the yield.

Reaction with Alkyl p-*Toluenesulfonates.* Reaction of **1** with alkyl *p*-toluenesulfonates was carried out in the presence of SDMA in tetrahydrofuran under reflux. Yields of products, obtained according to

$$\underset{\mathbf{1}}{Ph_2P(O)H} + R'OTs \xrightarrow{NaAlH_2(OCH_2CH_2OMe)_2} \underset{\mathbf{3}}{Ph_2P(O)R'}, \quad (2)$$

$$R' = i\text{-Pr},\ c\text{-}C_6H_{11},\ C_{10}H_{19}$$

were good and the results were shown in Table 2.

Reaction of Phenylphosphine or Methyl Phosphinates with Alkyl Halides or p-*Toluenesulfonates.* Reaction of methyl phenylphosphinate with isopropyl iodide in tetrahydrofuran in the presence of SDMA under reflux also gave the corresponding phosphine oxide in 46% yield. The reaction of phenylphosphine with alkyl halides or *p*-toluenesulfonates in tetrahydrofuran

Table 1. Reaction of diphenylphosphine oxide with alkyl halides (RX) in the presence of SDMA

RX	Solvent	Reaction temperature/°C	Reaction time/h	Product	Yield/%
EtBr	THF	65	4.5	$Ph_2P(O)Et$	Quant.
EtI	THF	65	8	$Ph_2P(O)Et$	41
$PhCH_2Cl$	THF	65	6	$Ph_2P(O)CH_2Ph$	12 (33)[a]
i-PrBr	THF	65	7	$Ph_2P(O)$*i*-Pr	12 (46)[a]
i-PrI	THF	65	6	$Ph_2P(O)$*i*-Pr	91 (98)[a]
i-PrI	THF	65	4.5	$Ph_2P(O)$*i*-Pr	19[b]
i-PrI	THF	R.T.	5	$Ph_2P(O)$*i*-Pr	0[c]
c-$C_6H_{11}Cl$	Toluene	111	11.5	$Ph_2P(O)$*c*-C_6H_{11}	6
c-$C_6H_{11}Cl$	Toluene	111	110.5	$Ph_2P(O)$*c*-C_6H_{11}	62
c-$C_6H_{11}Cl$	Toluene	111	11	$Ph_2P(O)$*c*-C_6H_{11}	31[d]
c-$C_6H_{11}Cl$	Dioxane	101	10	$Ph_2P(O)$*c*-C_6H_{11}	6
c-$C_6H_{11}Cl$	Diglyme	140	10	$Ph_2P(O)$*c*-C_6H_{11}	55
c-$C_6H_{11}Br$	THF	65	6	$Ph_2P(O)$*c*-C_6H_{11}	21
c-$C_6H_{11}I$	THF	65	6	$Ph_2P(O)$*c*-C_6H_{11}	38
2-$C_8H_{17}Cl$	THF	65	8	$Ph_2P(O)$2-C_8H_{17}	7
$C_{10}H_{19}Cl$[e]	Toluene	111	16	$Ph_2P(O)C_{10}H_{19}$[f]	11
$C_{10}H_{19}Br$[g]	THF	65	5.5	$Ph_2P(O)C_{10}H_{19}$[f]	8

a) Parentheses indicate that the yield was determined from ^1H NMR spectrum. b) Lithium tetrahydridoaluminate was used instead of SDMA. c) Sodium amide was used instead of SDMA. d) Sodium iodide (1 equiv.) was added to the reaction mixture. e) Menthyl chloride. f) Neomenthyl derivative was the major product. g) Menthyl bromide.

Table 2. Reaction of phosphorus compounds with alkyl halides or alkyl *p*-toluenesulfonates (RX) in the presence of SDMA

RX	Phosphorus compound	Solvent	Reaction temperature/°C	Reaction time/h	Product	Yield/%
i-PrOTs[a]	$Ph_2P(O)H$	THF	65	10	$Ph_2P(O)$*i*-Pr	94
$C_{10}H_{19}OTs$[b]	$Ph_2P(O)H$	THF	65	10	$Ph_2P(O)C_{10}H_{19}$[c]	55
c-$C_6H_{11}OTs$[d]	$PhPH_2$	Toluene	75—80	9	PhP(H)*c*-C_6H_{11}	75
i-PrBr	PhP(O)(OMe)Me	THF	65	7	PhP(O)(Me)*i*-Pr	— (6)[e]
i-PrI	PhP(O)(OMe)Me	THF	65	11	PhP(O)(Me)*i*-Pr	15 (46)[e]
$C_{10}H_{19}Cl$[f]	PhP(O)(OMe)H	Diglyme	110	10	PhP(O)(H)$C_{10}H_{19}$[g]	86
i-PrBr	$PhPH_2$	THF	65	6	PhP(H)*i*-Pr	Quant.
c-$C_6H_{11}Cl$	$PhPH_2$	THF	65	12	PhP(H)*c*-C_6H_{11}	77
2-$C_8H_{17}Cl$	$PhPH_2$	THF	65	11	PhP(H)2-C_8H_{17}	95
$C_{10}H_{19}Cl$[f]	$PhPH_2$	THF	65	32.5	PhP(H)$C_{10}H_{19}$[g]	82

a) Isopropyl *p*-toluenesulfonate. b) Menthyl *p*-toluenesulfonate. c) Neomenthyl derivative was the major product. d) Cyclohexyl *p*-toluenesulfonate. e) Parentheses indicate that the yield was determined from ^1H NMR spectrum. f) Menthyl chloride. g) The product was a mixture of neomenthyl and menthyl derivatives.

proceeded according to

$$\underset{\mathbf{4}}{PhPH_2} + R''X \xrightarrow{NaAlH_2(OCH_2CH_2OMe)_2} \underset{\mathbf{5}}{PhP(H)R''}, \quad (3)$$

R″=Secondary alkyl
X=Halogen or *p*-toluenesulfonyloxy

giving the corresponding secondary phosphines in excellent yields. These results are summarized in Table 2.

Discussion

The improvement of the yield of cyclohexyldiphenylphosphine oxide by addition of sodium iodide to the reaction mixture may be attributed to the first attack of iodine on cyclohexyl chloride followed by its replacement with phosphorus. The additivity effect will make valuable the present phosphorus-carbon bond forming reaction.

Ratios of neomenthyldiphenylphosphine oxide to menthyldiphenylphosphine oxide, as determined by optical rotation or HPLC, are 86:14 for the reaction of diphenylphosphine oxide with menthyl chloride, 63:37 for that with menthyl bromide, and 99:1 for that with menthyl *p*-toluenesulfonate. The ratio of neomenthylphenylphosphine to menthylphenylphosphine is 51:49 for the reaction of phenylphosphine with menthyl chloride in the presence of SDMA. The predominant production of the inverted product in the reaction of diphenylphosphine oxide with menthyl derivatives may indicate that the reaction proceeds mainly *via* an S_N2 process.

A comparison of yields of diphenylphosphine oxide

derivatives such as isopropyldiphenylphosphine oxide (48% yield from diphenylphosphinous chloride with propylene oxide)[14] and cyclohexyldiphenylphosphine oxide (30% yield from diphenylphosphine oxide with cyclohexane)[15] with those obtained in the present reaction may suggest that the reaction using SDMA is a good method to prepare a phosphorus-carbon bond. The homogeneous reaction mixture and simple operation and work-up as well as various types of phosphorus compounds being available as the precursor of phosphorus anion will also make the method useful for preparation of various types of derivatives of phosphines and phosphine oxides. The observed good yield for alkyl *p*-toluenesulfonates will make the present method hopeful in the field of carbohydrates.

Experimental

Instruments and Materials. IR spectra were measured on Hitachi-Perkin-Elmer 337 and JASCO (Japan Spectroscopic Co.) A-3 spectrophotometers. ^{1}H NMR spectra were recorded on Hitachi-Perkin-Elmer R-20 (60 MHz) and Hitachi R-24 (60 MHz) spectrometers using tetramethylsilane as the internal standard. Mass spectra were obtained on a Hitachi RMU DMG GC-MS spectrometer. Optical rotations were determined with JASCO DIP-4 digital and Atago Polax photometers.

Isolation of products was performed by high pressure liquid chromatography using JASCO Uniflow-211 and Uvidec-100-II, by liquid chromatography using a UVICON-540 detector and a SF-100G fraction collector from Toyo Scientific Industry, or by thin layer chromatography. Melting and boiling points were uncorrected.

Phenylphosphine (bp 118 °C), methyl phenylphosphinate (bp 94—95 °C/0.5—1.0 mmHg[16]), and methyl methylphenylphosphinate (bp 100 °C/0.5 mmHg) from phenylphosphonous dichloride,[17-20] and diphenylphosphine oxide (mp 49 °C)[21] were used as the phosphide precursors. Commercially available SDMA (benzene or toluene solution) was used. Cyclohexyl chloride (bp 27.2 °C/8 mmHg) and bromide (bp 54 °C/17.5 mmHg) were prepared from cyclohexanol,[22,23] cyclohexyl iodide from cyclohexene,[24] and 2-chlorooctane from 2-octanol.[25] Menthyl chloride (bp 98 °C/18 mmHg) was prepared from L-menthol; $[\alpha]_D^{15}$ −47.7° (*c* 2.4, EtOH).[26] *p*-Toluenesulfonates of 2-propanol (bp 114 °C/3 mmHg), cyclohexanol, and L-menthol were prepared from corresponding alcohols and *p*-toluenesulfonyl chloride.

Synthesis of Menthyl Bromide. To a mixture of L-menthol (3.0 g) and hydrobromic acid (5.0 g) was added 2.5 ml of concentrated sulfuric acid under ice cooling, and then the solution was heated for 5 h at 105 °C. Filtration of the reaction mixture, extraction of the product by petroleum ether, and successive work-up and distillation gave the bromide in 71% yield: bp 113 °C/22 mmHg; ^{1}H NMR ($CDCl_3$) δ=0.73 (d, J=7.1 Hz, 3H, Me), 0.91 (d, J=7.1 Hz, 6H, $CH(C\underline{H}_3)_2$), 0.58—3.00 (m, 9H, $C\underline{H}(CH_3)_2$ and ring protons other than CHBr), and 3.41—4.38 (m, 1H, CHBr); IR ν_{max}^{neat} 692 cm^{-1} (C-Br); $[\alpha]_D^{27.9}$ −29.0° (*c* 1.22, EtOH).

Found: C, 55.20; H, 8.88%. Calcd for $C_{10}H_{19}Br$; C, 54.79; H, 8.75%.

Product Criteria. The following were identified on the basis of spectra for each product purified by liquid or thin layer chromatography: ethyldiphenylphosphine oxide (^{1}H NMR ($CDCl_3$) δ=1.16 (dt, J_{PCCH}=17.4 Hz, J_{HH}=7.5 Hz, 3H, Me), 2.26 (dq, J_{PCH}=11.7 Hz, J_{HH}=7.5 Hz, 2H, CH_2), and 7.10—8.26 (m, 10H, Ph)], benzyldiphenylphosphine oxide [^{1}H NMR ($CDCl_3$) δ=3.64 (d, J_{PCH}=14.0 Hz, 2H, CH_2) and 7.08—8.06 (m, 15H, Ph)], isopropyldiphenylphosphine oxide [^{1}H NMR ($CDCl_3$) δ=1.16 (dd, J_{PCCH}=16.4 Hz, J_{HH}=7.1 Hz, 6H, Me), 1.63—2.04 (m, 1H, P-CH), and 7.05—8.04 (m, 10H, Ph)], cyclohexyldiphenylphosphine oxide [^{1}H NMR ($CDCl_3$) δ=0.74—2.64 (m, 11H, C_6H_{11}) and 7.14—8.18 (m, 10H, Ph); MS m/e=284 (M^+)], neomenthyldiphenylphosphine oxide [^{1}H NMR ($CDCl_3$) δ= 0.25—3.05 (m, 19H, Me, $C\underline{H}(C\underline{H}_3)_2$, and ring protons) and 7.01—8.02 (m, 10H, Ph); MS m/e=340 (M^+)], (1-methylheptyl)diphenylphosphine oxide,[27] isopropylphenylphosphine [^{1}H NMR (CD_3OD) δ=1.01 (pair of dd, J_{PCCH} =18.3 Hz, J_{HH}=6.8 Hz, 6H, $CH(C\underline{H}_3)_2$), 1.8—2.4 (m, 1H, CH), and 6.7—7.9 (m, 5H, Ph)], (1-methylheptyl)phenylphosphine [^{1}H NMR (CD_3OD) δ=0.41—2.63 (m, 17H, C_8H_{17}), and 7.08—8.02 (m, 5H, Ph)], cyclohexylphenylphosphine [^{1}H NMR (CD_3OD) δ=0.7—2.3 (m, 11H, C_6H_{11}) and 7.2—8.1 (m, 5H, Ph)], menthylphenylphosphine [^{1}H NMR (CD_3OD) δ=0.18—2.63 (m, 19H, $C_{10}H_{19}$) and 6.97—8.14 (m, 5H, Ph)], and isopropylmethylphenylphosphine oxide [^{1}H NMR ($CDCl_3$) δ=1.11 (pair of dd, J_{PCCH}=15.8 Hz, J_{HH}=7.5 Hz, 6H, $CH(C\underline{H}_3)_2$), 1.72 (d, J_{PCH}=12.5 Hz, 3H, P-Me), 1.42—1.93 (m, 1H, CH), and 7.21—8.17 (m, 5H, Ph)].

The structure of the produced secondary phosphines was further confirmed by converting them into methyl esters of the phosphinic acids, *e.g.*, methyl isopropylphenylphosphinate [^{1}H NMR ($CDCl_3$) δ=1.11 (pair of dd, J_{PCCH}=17.3 Hz, J_{HH}=7.2 Hz, 6H, $CH(C\underline{H}_3)_2$), 2.01 (dq, J_{PCH}=14.2 Hz, J_{HH}=7.2 Hz, 1H, CH), 3.63 (d, J_{POCH}=10.8 Hz, POMe), and 7.1—8.0 (m, 5H, Ph); IR ν_{max}^{neat} 1203 (P=O) and 1032 cm^{-1} (P-O-Me); MS m/e=198 (M^+)] and methyl cyclohexylphenylphosphinate [^{1}H NMR ($CDCl_3$) δ=0.72—2.42 (m, 11H, C_6H_{11}), 3.65 (d, J_{POCH}=10.8 Hz, 3H, POMe), and 7.29—8.08 (m, 5H, Ph); IR ν_{max}^{neat} 1215 (P=O) and 1033 cm^{-1} (P-O-Me); MS m/e=238 (M^+)] after oxidation by hydrogen peroxide followed by methylation with diazomethane, and/or by converting them into phosphonium salts with methyl iodide, *e.g.*, isopropylmethylphenylphosphonium iodide [^{1}H NMR (CD_3OD) δ=1.06 (pair of dd, J_{PCCH}=14.4 Hz, J_{HH}=7.2 Hz, 6H, $CH(C\underline{H}_3)_2$), 1.06 (d, J_{PCCH}=16.4 Hz, 3H, P-Me), 1.9—2.7 (m, 1H, CH), and 7.2—7.9 (m, 5H, Ph)].

*Reaction of Diphenylphosphine Oxide (**1**) with Isopropyl Iodide in the Presence of SDMA.* To a stirred tetrahydrofuran solution of diphenylphosphine oxide (2.0 g, 10 mmol) was added SDMA (3.0 g, 15 mmol) dropwise under nitrogen flow and then a solution of isopropyl iodide (3.0 g, 18 mmol) in tetrahydrofuran (8 ml) was added. The reaction mixture was refluxed for 6 h. Addition of 1.5 ml of water to the cooled and stirred reaction mixture at room temperature followed by extraction by chloroform and successive evaporation of the solvent gave crude isopropyldiphenylphosphine oxide in 98% yield. Separation by thin layer chromatography gave the pure product in 91% yield: ^{1}H NMR ($CDCl_3$) δ=1.16 (dd, J_{PCCH}=16.4 Hz, J_{HH}=7.1 Hz, 6H, $CH(C\underline{H}_3)_2$), 1.63—2.04 (m, 1H, $C\underline{H}(CH_3)_2$), and 7.05—8.04 (m, 10H, Ph).

*Reaction of Diphenylphosphine Oxide (**1**) with Menthyl Chloride in the Presence of SDMA.* To a toluene (80 ml) solution of **1** (2.0 g, 9.9 mmol) was added SDMA (2 equivalents) in toluene (10 ml), and then menthyl chloride (1.7 g, 9.9 mmol) was successively added under nitrogen atmosphere. Refluxing the mixture for 16 h at 111 °C followed by work-up, separation of the products from the starting materials by liquid chromatography, and crystallization from petroleum ether gave 0.29 g of a mixture of neomenthyldiphenylphosphine oxide (86%) and menthyldiphenylphosphine oxide

(14%) in 11% yield, $[\alpha]_D^{12.4}$ +34.2° (*c* 0.75, EtOH).[28] The structure was confirmed by ^{1}H NMR and mass spectra.

The following product ratios and optical rotation values were obtained: neomenthyldiphenylphosphine oxide: menthyldiphenylphosphine oxide 63:37 from menthyl bromide, $[\alpha]_D^{24}$ +2.1° (*c* 1.6, MeOH); 99:1 from menthyl *p*-toluenesulfonate with diphenylphosphine oxide; neomenthylphenylphosphine: menthylphenylphosphine 51:49 from menthyl chloride with phenylphosphine, $[\alpha]_D^{27}$ −16° (*c* 1.6, EtOH).[26,28]

Reaction of ***1*** *with Isopropyl* p-*Toluenesulfonate in the Presence of SDMA.* To a stirred tetrahydrofuran (20 ml) solution of **1** (0.43 g, 2.1 mmol) and SDMA (2 equivalents) was added isopropyl *p*-toluenesulfonate (0.46 g, 2.1 mmol), and then the reaction mixture was heated for 10 h under reflux in nitrogen flow. Work-up (addition of 1 ml of water and evaporation of volatile materials) of the reaction mixture and separation of the product by liquid chromatography gave isopropyldiphenylphosphine oxide (0.48 g) in 94% yield, whose structure was confirmed by ^{1}H NMR spectrum.

Reaction of ***1*** *with Isopropyl Iodide in the Presence of Lithium Tetrahydridoaluminate.* To a stirred tetrahydrofuran solution of **1** (0.26 g, 2.1 mmol) was added lithium tetrahydridoaluminate (0.11 g, 2.9 mmol), and then isopropyl iodide (0.45 g, 2.6 mmol) was added. The mixture was heated for 4.5 h under reflux in nitrogen flow. Work-up and purification of the product gave isopropyldiphenylphosphine oxide (0.10 g) in 19% yield: mp 143—144 °C;[29] IR $\nu_{max}^{CHCl_3}$ 1165 cm^{-1} (P=O).

*Reaction of Phenylphosphine (****4****) with Isopropyl Bromide.* To a stirred tetrahydrofuran (50 ml) solution of phenylphosphine (1.02 g, 9.3 mmol) was added SDMA (2 equivalents) in 20 ml of tetrahydrofuran dropwise under nitrogen atmosphere, then isopropyl bromide (1.14 g, 9.3 mmol) was added to the solution, and the mixture was heated for 6 h under reflux. Addition of 2 ml of water followed by filtration and evaporation of the solvent under nitrogen atmosphere and removal of volatile material gave isopropylphenylphosphine (1.73 g) in quantitative yield. The ^{1}H NMR spectrum of the product in CD_3OD confirmed the structure. The structure was further reconfirmed by converting the phosphine to methyl isopropylphenylphosphinate.

The authors wish to express their thanks to Dr. Masao Kidokoro of Sankyo Co., Ltd. for elemental analyses and Professor Morio Suzuki's laboratory of Shizuoka University for giving facility for measurement of optical rotation. This work was partially supported by a Grant-in-Aid for Scientific Research No. 475661 from the Ministry of Education, Science and Culture.

References

1) H. Takayanagi, M. Yamashita, K. Seo, H. Yoshida, T. Ogata, and S. Inokawa, *Carbohydr. Res.*, **38**, C19 (1974).
2) M. Yamashita, Y. Nakatsukasa, H. Yoshida, T. Ogata, S. Inokawa, K. Hirotsu, and J. Clardy, *Carbohydr. Res.*, **70**, 247 (1979).
3) M. Yamashita, M. Yoshikane, T. Ogata, and S. Inokawa, *Tetrahedron*, **35**, 741 (1979).
4) H. Paulsen and W. Greve, *Chem. Ber.*, **106**, 2124 (1973).
5) M. Yamashita, P. T. Long, M. Shibata, and S. Inokawa, *Carbohydr. Res.*, **84**, 35 (1980).
6) M. Yamashita, K. Fujita, K. Nakatani, K. Hiramatsu, and S. Inokawa, to be published.
7) H. Takayanagi, K. Seo. M. Yamashita, H. Yoshida, T. Ogata, and S. Inokawa, *Carbohydr. Res.*, **63**, 105 (1978).
8) P. Luger, M. Yamashita, and S. Inokawa, *Carbohydr. Res.*, **84**, 25 (1980).
9) L. Maier, "Organic Phosphorus Compounds," ed by G. M. Kosolapoff, Wiley-Interscience, New York (1972), Vol. 1, Chap. 2.
10) L. Maier, "Organic Phosphorus Compounds," ed by G. M. Kosolapoff, Wiley-Interscience, New York (1972), Vol. 1, Chap. 1.
11) R. B. Wetzel and G. L. Kenyon, *J. Am. Chem. Soc.*, **94**, 1774 (1972).
12) R. B. Wetzel and G. L. Kenyon, *J. Org. Chem.*, **39**, 1531 (1974).
13) M. Yamashita, Y. Nakatsukasa, M. Yoshikane, H. Yoshida, T. Ogata, and S. Inokawa, *Carbohydr. Res.*, **59**, C12 (1977).
14) M. I. Kabachnik, T. Ya Medved, and Yu. M. Polikarpov, *Izv. Akad. Nauk SSSR, Ser. Khim.*, **1966**, 368; *Chem. Abstr.*, **64**, 15917b (1966).
15) E. Müller and H. G. Padeken, *Chem. Ber.*, **100**, 521 (1967).
16) 1 mmHg=133.322 Pa.
17) F. G. Mann and I. T. Millar, *J. Chem. Soc.*, **1952**, 3039.
18) A. N. Pudovik and D. Kh. Yarukhametova, *Izv. Akad. Nauk SSSR, Otdel. Khim. Nauk*, **1952**, 902; *Chem. Abstr.*, **47**, 10469c (1953).
19) H. J. Harwood and D. W. Grisley, Jr., *J. Am. Chem. Soc.*, **82**, 423 (1960).
20) D. M. Coyne, W. E. McEwen, and C. A. V. Werf, *J. Am. Chem. Soc.*, **78**, 3061 (1956).
21) United Kingdom Atomic Energy Authority, Fr. 1 314 704 (1963); *Chem. Abstr.*, **59**, 2860b (1963).
22) J. G. Smith and G. F. Wright, *J. Org. Chem.*, **17**, 1116 (1952).
23) O. Kamm and C. R. Marvel, *Org. Synth.*, Coll. Vol. I, 25 (1956).
24) H. Stone and H. Shechter, *Org. Synth.*, Coll. Vol. IV, 543 (1963).
25) H. R. Hudson, *Synthesis*, **1969**, 112.
26) R. B. King, J. Bakos, C. D. Hoff, and L. Marrkó, *J. Org. Chem.*, **44**, 3095 (1979).
27) D. J. Cram, R. D. Partos, S. H. Pine, and H. Jäger, *J. Am. Chem. Soc.*, **84**, 1742 (1962).
28) J. D. Morrison and W. F. Masler, *J. Org. Chem.*, **39**, 270 (1974).
29) A. Arbuzov, *J. Russ. Phys. Chem. Soc.*, **42**, 395 (1910); *Chem. Abstr.*, **5**, 1397 (1911).

Ozonization of Organic Compounds. VII. Carboxylic Acids, Alcohols, and Carbonyl Compounds

Etsuo NIKI,* Yorihiro YAMAMOTO, Tsuneo SAITO, Keiji NAGANO, Seiichi YOKOI, and Yoshio KAMIYA

Department of Reaction Chemistry, Faculty of Engineering, The University of Tokyo, Hongo, Bunkyo-ku, Tokyo 113

(Received June 1, 1982)

The rate and products of the ozonization of carboxylic acids, alcohols, and ketones have been studied in water at 30 °C. The ozonization of alcohols gave corresponding carbonyl compounds as major product. The ozonization of ketones brought about primarily the carbon-carbon bond cleavage and gave carboxylic acids. Saturated carboxylic acids such as acetic acid, propionic acid, and isobutyric acid were ozonized only slowly in neutral water, but they were ozonized faster in alkaline aqueous solution. On the other hand, α-hydroxy carboxylic acids such as glycolic acid and lactic acid were ozonized even in pure water. The mechanism of ozonization of these compounds and the effect of pH are discussed.

The ozonization of organic compounds has been studied extensively for many years[1–4] and it has been applied for the preparation and identification of organic compounds. Water treatment by ozone has received much attention recently because of its advantages over currently employed methods such as chlorine treatment.[5–7] In order to establish the validity and limit of water treatment by ozone, it is of fundamental importance to know the rate and products of the ozonization of various compounds in water. In the course of our study on the ozonization of organic compounds, we have undertaken the study on the ozonization of carboxylic acids, alcohols, and ketones in water. The ozonization of carboxylic acids is especially important since the ozonization of aromatic hydrocarbons,[8–10] phenol,[11–16] and alkylbenzenesulfonic acids[17,18] gives carboxylic acids and they are known as the typical refractory compounds in water.

Experimental

Materials and Procedures. Commercial alcohols, ketones, and carboxylic acids were used as received. Water was purified by passing through an ion exchange resin followed by distillation. Following buffer solutions were used (1 M = 1 mol dm^{-3}).

pH 1.1 : 0.2 M KCl (50 ml) + 0.2 M HCl (97 ml) + H_2O (53 ml)
pH 5.3 : 1/30 M KH_2PO_4 (32 ml) + 1/30 M Na_2HPO_4 (1 ml)
pH 7.1 : 0.2 M KH_2PO_4 (50 ml) + 0.2 M NaOH (29.6 ml) + H_2O (120.4 ml)
pH 9.9 : 0.1 M Na_2CO_3 (5 ml) + 0.1 M $NaHCO_3$ (5 ml)
pH 12.1: 0.1 M Na_2HPO_4 (50 ml) + 0.1 M NaOH (43.2 ml) + H_2O (6.8 ml)

Ozone was produced by a standard ozone generator, Nippon Ozone Co. Ltd., Model O-3-2, by charging pure oxygen dried beforehand by silica gel.

The ozonization was carried out by bubbling ozone-oxygen gas through the reaction mixture at 30 °C. The gas was introduced at a speed of 100—200 ml/min and the rate of ozone supply was 0.12—0.20 mmol/min.

Analytical Methods. The amounts of substrate reacted and products formed were measured by a gas liquid chromatography (GLC, Shimadzu Model GC-4BPTH, with Porapak Q column and FID detector), a high pressure liquid chromatography (HPLC, JASCO, GP-A30, Shodex Ionpak C-811 column and 0.1% H_3PO_4 eluent), and an isotachophoretic analyzer (IP, Shimadzu Model IP-1B).[9,11] Total amount of peroxides was determined by iodometric titration. Hydrogen peroxide was measured separately from the difference between the titers before and after the treatment with catalase as described previously.[11]

Total yield of carbonyl compounds was measured as follows. Product solution was treated with 2,4-dinitrophenylhydrazine saturated in 2 M aqueous hydrochloric acid, allowed to stand overnight at room temperature, and filtered to remove 2,4-dinitrophenylhydrazone. The filtrate was analyzed spectrometrically to measure the consumption of 2,4-dinitrophenylhydrazine, $\lambda_{max} = 322$ nm and $\varepsilon = 1.1 \times 10^4$ M^{-1} cm^{-1}. In some cases, 2,4-dinitrophenylhydrazone was dried and weighed. Carbon dioxide was analyzed as previously.[11]

Results

Ozonization of Alcohols. The results of ozonization of 2-butanol are shown in Table 1. It was found that appreciable amount of 2-butanol was carried away out of the reaction vessel with ozone-oxygen gas; for example, about 2 mmol of 2-butanol was removed in 2 h when only oxygen was introduced under the similar conditions as in Table 1. Therefore, the amount of disappeared 2-butanol shown in Table 1 is larger than that actually reacted. The poor material balance in Table 1 is apparently due to this disappearance of 2-butanol as well as the formation of carbon dioxide.

However, it is clear that ozonization of 2-butanol in water gave 2-butanone as a major product. For example, ozonization for 30 min gave 2-butanone with 83% selectivity. Small amounts of formic, acetic, and propionic acids and hydrogen peroxide were also found. These products are similar to those in the ozonization of 2-butanol in organic solvent.[19]

The ozonization of 1-butanol gave butanal as a major product with smaller amount of butyric acid.

As shown in Table 1, the rate of ozonization was not much affected by the pH of the solution.

Ozonization of 2-Butanone. The results are shown in Table 2. The major product was acetic acid, and smaller amounts of methylglyoxal, pyruvic acid, formic acid, methanol, and acetaldehyde were also observed. Neither ethyl acetate nor methyl propionate was found.

Ozonization of 3-Pentanone. The results are included in Table 2. Formic, acetic, and propionic acids were observed. At high pH, the amount of formic

Table 1. Ozonization of 2-butanol (BOH) in 100 ml aqueous solution at 30 °C, 2 h

Run No.	1	2	3	4	5	6
Initial pH	1.1	5.3	5.8	6	9.9	12.1
Initial BOH(mmol)	10.90	10.69	10.69	11.91	10.90	10.69
BOH after 1 h[a]	7.3	8.94	9.03		8.23	8.03
BOH after 2 h[a]	6.73	7.63	6.66	9.17	6.85	6.10
BOH reacted in 2 h[a]	4.17	3.06	4.03	2.74	4.05	4.59
Products in mmol						
H_2O_2	0.14	0.14	0.19	0.07	0	0
ROOH	0	0	0	Trace	0	0
HCOOH	0.09	0.06	0.09	0.05	0.09	0.33
CH_3COOH	0.06	0.11	0.14	0.06	0.09	0.96
C_2H_5COOH	0.15	0.20	0.24	0.04	0.55	0.73
$CH_3COCOOH$		Trace	0			0.01
$(COOH)_2$			0			Trace
Carbonyls[b]		1.33				
2-Butanone[c]	0.93[d]	1.13[e]	1.34	1.00	1.61	1.05[f]
Acetaldehyde	0.02	0.03	0.02	0.02		0.06
Methanol	Trace	Trace	0.3			Trace

a) Appreciable amount of 2-butanol was brought away out of the reaction vessel with oxygen-ozone gas, see text. b) Total carbonyls measured from the disappearance of 2,4-dinitrophenylhydrazine, see Experimental. c) By HPLC. d) 0.83 mmol by GLC. e) 1.13 mmol by GLC. f) 1.26 mmol by GLC.

Table 2. Ozonization of 2-butanone (BON), 3-pentanone (PON), and methylglyoxal (MG) in 100 ml water at 30 °C

Run No.	7	8	9	10	11	12	13
Substrate S	BON	BON	BON	PON	PON	PON	MG
Initial S(mmol)	10.32	10.05	1.04	10.2	50.1	50.1	2.94
Final S(mmol)	5.81	6.45	0.54	6	35	30	1.87
S reacted(mmol)	4.51	3.60	0.50	4	15	20	1.07
Time/h	4	2	2	2	3	3	2
Initial pH				6	6	9.9	
Products in mmol							
H_2O_2							0.02
Peroxide	Trace	Trace	Trace	0.04	0.02	0	Trace
Acids[a]				0.11	0.48		
HCOOH[b]	0.11	0.05	Trace	0.02 (0.03)	0.01 (0.01)	0.32	
CH_3COOH[b]	2.17	0.91	0.26	0.07 (0.06)	0.20 (0.22)	0.61	0.18
C_2H_5COOH[b]	Trace	Trace	0	0.08 (0.06)	0.24 (0.25)	0.88	
$(COOH)_2$							0.04
$CH_3COCOOH$	0.09	0.05	0.01				0.55
CH_3OH	0.05	0.09	0.02				Small
CH_3CHO	0.02	0.04	0.01				
CH_3COCHO	0.15	0.08	0.05				
$CH_3COOC_2H_5$			0				
$C_2H_5COOCH_3$			0				

a) By titration. b) By HPLC, numbers in parentheses are by isotachophoretic analysis.

acid increased appreciably. The formation of acetic acid and propionic acid in the ozonization of 3-pentanone has been reported previously.[1]

Some unknown products were observed by HPLC. Although it was not identified conclusively, one of the unknown products may be 2,3-pentanedione. The formation of 2,3-butanedione in the ozonization of 2-butanone has been reported.[20]

Ozonization of Methylglyoxal. The results included in Table 2 show that the major reaction is the oxidation of formyl group to carboxyl group. Smaller amounts of acetic acid and oxalic acid may have been formed through pyruvic acid.

Ozonization of Glycolic Acid and Lactic Acid. The results of ozonization of glycolic acid gave glyoxylic acid as primary and major product, which was further ozonized to oxalic acid (Table 3). Smaller amount of formic acid was also found. The ozonization of

Table 3. Ozonization of glycolic acid (GA) and lactic acid (LA) in water at 30 °C, 2 h

Run No.	14	15	16	17	18	19
Substrate S	GA	GA	LA	LA	LA	LA
Initial S(mmol)	1.17	3.13	1.10	3.31	1.05	1.00
Final S(mmol)	0.40	1.91	0.29	2.44	0.72	0.20
S reacted(mmol)	0.77	1.22	0.81	0.87	0.33	0.80
Initial pH					1.1	9.9
Products in mmol						
H_2O_2	0.01	0.02	0.05	0.04	Trace	0
CO_2		0.78				
HCOOH	0.03	0.09	0.03	0.09	Trace	0
CH_3COOH			0	Trace	0.08	0.07
$CH_3COCOOH$			0.52	0.78	0.22	0.76
OHCCOOH	0.12	0.67				
$(COOH)_2$	0.17	0.31	0.04	0.04	Trace	0.05

Table 4. Ozonization of acetic acid (AA) in water at 30 °C, 1.5 h

Run No.	20	21
Initial AA(mmol)	5.01[a)]	5.07
Final AA(mmol)	4.95	3.02
AA reacted(mmol)	0.06	2.05
Initial pH	7.0	13.0
Final pH	7.0	9.4
Products in mmol		
HCOOH	0	Trace
$HOCH_2COOH$	0	0.00_4
OHCCOOH	0.02	0.03
$(COOH)_2$	0.02	0.50

a) Sodium acetate.

Table 5. Ozonization of propionic acid (PA) in water in 30 °C, 1.5 h

Run No.	22	23	24	25	26
Initial PA(mmol)	4.97	5.07	5.05	2.24	4.97
Final PA(mmol)	4.92	4.99	4.79	1.76	2.44
PA reacted(mmol)	0.05	0.08	0.26	0.48	2.53
Initial pH	1.3	2.8	4.9	8.0	12.6
Final pH	1.3	2.7	4.9	7.6	9.2
Products in mmol					
H_2O_2	0.03	0.01	0.02	0	0
HCOOH	0.03	0.01	0	0	0.02
CH_3COOH	0.02	0.03	0.01	0.10	0.54
$(COOH)_2$	Trace	Trace	0.01	0.03	0.14
$CH_3CH(OH)COOH$				0.01	0.05
$CH_3COCOOH$	0.00_4	Trace	0.05	0.06	0.15

lactic acid gave pyruvic acid as major product with about 90% selectivity. Small amounts of formic acid and oxalic acid were also observed. The formation of hydrogen peroxide was observed from both glycolic acid and lactic acid, but no organic peroxide was found.

Table 3 also shows the effect of pH in the ozonization of lactic acid. The conversion of lactic acid was higher at higher pH. Pyruvic acid was always formed as a major product.

Ozonization of Pyruvic Acid. Acetic and oxalic acids were formed as major products in the ozonization of pyruvic acid.

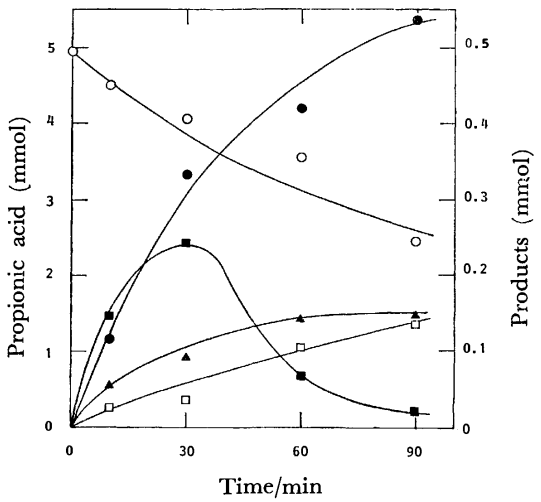

Fig. 1. Ozonization of propionic acid in NaOH-H_2O at 30 °C, initial pH 12.6 (Run 26).
○: Propionic acid; ●: acetic acid; ■: formic acid; ▲: pyruvic acid; □: oxalic acid.

Ozonization of Acetic, Propionic, Isobutyric, and Pivalic Acids. Saturated carboxylic acids such as acetic, propionic, isobutyric, and oxalic acids were stable toward ozone at 30 °C. However, they were ozonized at appreciable rate at higher pH. Table 4 shows the results of ozonization of acetic acid and its sodium salt. Acetic acid has been accepted as an inactive solvent in the ozonization, but it is ozonized in alkaline medium. The products were formic acid, glycolic acid, glyoxylic acid, and oxalic acid. These acids, except oxalic acid, were further ozonized to give eventually oxalic acid and carbon dioxide. Succinic acid was not observed. Sodium acetate was ozonized only slowly at pH 7.

The results of ozonization of propionic acid are shown in Table 5. The change in the product distribution with time is shown in Fig. 1. Again, the rate of ozonization increased with increasing pH of the medium. The products observed were formic acid, acetic acid, lactic acid, pyruvic acid, and oxalic acid. Figure 1 shows that acetic acid and oxalic acid are

Table 6. Ozonization of isobutyric acid (BA) in water at 30 °C, 1.5 h

Run No.	27	28	29	30	31	32
Initial BA(mmol)	4.96	5.05	4.97	5.00	5.03	5.08
Final BA(mmol)	4.91	5.00	4.61	4.34	4.41	3.19
BA reacted(mmol)	0.05	0.05	0.36	0.66	0.62	1.89
Initial pH	1.3	2.7	4.9	7.2	10.1	12.7
Final pH	1.3	2.7	4.9	7.4	8.4	9.4
Products in mmol						
CO_2				0.88	0.51	
Carbonyls				0.19	0.14	
CH_3COCH_3	0.03	0	0.14	0.11	0.15	0.35
HCOOH	0.05	0	0.01	0.02	0.02	0.06
CH_3COOH	0.02		0.13	0.17	0.16	0.58
$(COOH)_2$	0		Trace	0	0	0.03
$CH_3COCOOH$	0.01		0.03	0.07	0.08	0.21
$(CH_3)_2C(OH)COOH$	0.02		0.11	0.03	0.02	0.04

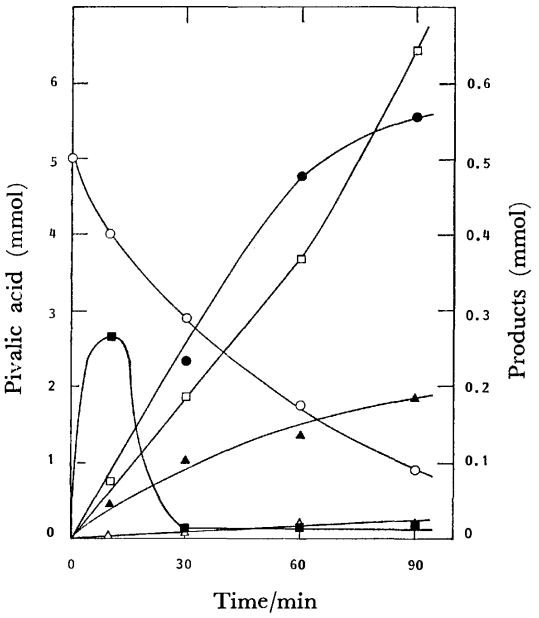

Fig. 2. Ozonization of pivalic acid in water at 30 °C, initial pH 13.0.
○: Pivalic acid; □: acetic acid; ●: acetone ▲: pyruvic acid; ■: formic acid; △: oxalic acid.

stable final products, whereas formic acid is further ozonized to carbon dioxide and water.[11]

The results of ozonization of isobutyric acid are shown in Table 6. Isobutyric acid was virtually resistent toward ozone in water, but the rate of ozonization increased markedly with increasing pH of the solution as observed for propionic acid. The major products were formic acid, acetic acid, pyruvic acid, acetone, and carbon dioxide. Smaller amounts of oxalic acid and α-hydroxyisobutyric acid were also observed. Little peroxide was found.

Pivalic acid was found to be ozonized, although slowly, even in pure water. The rate of ozonization increased similarly at higher pH. Figure 2 shows the results of ozonization of pivalic acid at initial pH 12.97. Acetic acid, acetone, and pyruvic acid were obtained as major products. Acetone and pyruvic acid accounted for 85% of total carbonyls estimated spectrometrically using 2,4-dinitrophenylhydrazine. Formic acid was observed in considerable amount at the initial stage, but it was further ozonized to carbon dioxide and water. Small amount of oxalic acid was also observed.

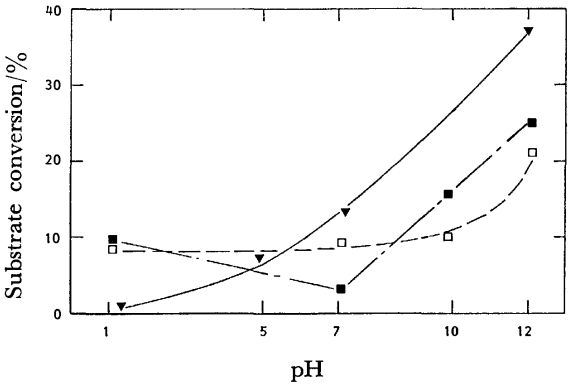

Fig. 3. Effect of pH on the rate of ozonization of isobutyric acid (▼, 5 mmol, 90 min), cyclohexanone (■, 10 mmol, 60 min), and cyclohexanol (□, 10 mmol, 60 min) in 100 ml water at 30 °C.

The effect of pH on the rate of ozonization of isobutyric acid, cyclohexanone, and cyclohexanol is shown in Fig. 3.

Discussion

Ozone can behave as a 1,3-dipole, an electrophile or a nucleophile.[4] It reacts quite rapidly with carbon-carbon double bonds, but its electrophilic attack on carbon-hydrogen bonds is usually slow. This accounts for the well known fact that the rate of removal of carboxylic acids from water by ozone is slow.

In alkaline medium, it has been reported that ozone is unstable and gives hydroxyl radical[21-25] and oxygen atom,[26] both of which are more reactive than ozone toward C–H bond. The pK of the hydroxyl radical is 11.85,[26] and hence at pH above 11.85 the oxygen ion O^- must act as the most important attacking species. Furthermore, since the decomposition of ozone is initiated by OH^- ions and accelerated by a free radical chain reaction, the rate of ozone destruction

and that of active hydroxyl radical formation depend on experimental variables such as pH and solutes present in water. Some solutes accelerate the chain reaction, but some inhibit the chain reaction by scavenging hydroxyl radical.[23] It should be noted, therefore, that the relative importance of various active species also varies with experimental variables.

At pH below 9, ozone molecule must be the sole active species.

The detailed mechanisms of the initial attack of ozone toward carbon-hydrogen bonds has not yet been conclusively established. It appears that the ozonization of carbon-hydrogen bonds can proceed both by radical and ionic processes.[27-30] The formation of 1-chloro- and 1-bromoadamantane in the ozonization of adamantane in the presence of bromotrichloromethane[31] suggests the presence of carbon radical. On the other hand, the high ratio of retention of configuration in the ozonization of saturated hydrocarbons[31,32] implies that this radical is not entirely free. The hydrotrioxide,[30,31] whether it is formed by radical or ionic process, should decompose to give eventually alkoxyl and peroxyl radicals under the present reaction conditions. Murray *et al.*[33] have observed a low temperature NMR that indicated the existence of hydrotrioxide.

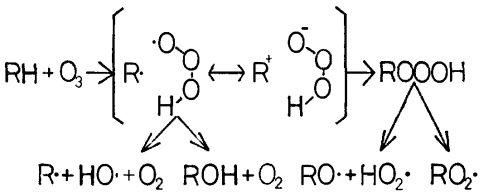

The mechanism of ozonization of alcohols, ketones, and carboxylic acids will be discussed below taking the above discussion into consideration.

A probable reaction pathway for the ozonization of 2-butanol is shown in Fig. 4. The relative importance of these reactions in Fig. 4 depends, as discussed above, on the experimental variables. The compounds in the boxes were found experimentally. Ozone must attack hydrogen α to hydroxyl group to give hydrotrioxide.[31,33] It decomposes to give 2-butanone, the major product observed experimentally. The radical decomposition can yield alkyl, alkoxyl, and peroxyl radicals. The alkoxyl radical must undergo β-scission or hydrogen atom abstraction to give acetic acid, propionic acid, and 2-butanone. The ethyl and methyl radicals formed simultaneously in the β-scission should react with oxygen and give eventually ethanol, acetaldehyde, acetic acid, methanol, and formic acid. Alkyl and peroxyl radicals should give 2-butanone.

As discussed above, the attack on the α-hydrogen by hydroxyl radical and/or oxygen ion formed from ozone becomes more important at higher pH.

In any event, 2-butanone is formed from 2-butanol as a major product. It has been observed that the ozonization of alcohols gives corresponding carbonyl compounds both in water and in organic solvents.[19,31,34,35]

As shown in Table 2, the ozonization of 2-butanone gave acetic acid as a major product and that of 3-

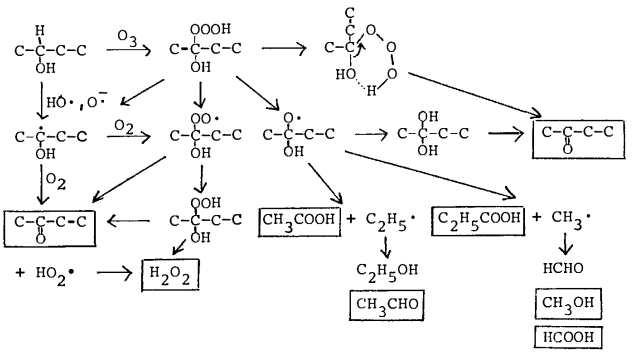

Fig. 4. Major reaction pathway in the ozonization of 2-butanol in water.

pentanone gave acetic acid and propionic acid. Three processes have been considered for the ozonization of ketone;[1] that is, (1) ozonolysis of double bond of the enol form of ketone, (2) nucleophilic attack of ozone to give ester, followed by oxidation of ester, and (3) ozone-initiated oxidation by molecular oxygen. The absence of ethyl acetate and methyl propionate in the ozonization of 2-butanone (Table 2) and also the absence of ethyl propionate in the ozonization of 3-pentanone (Table 2) indicate that the second process does not play an important role under the present reaction conditions. It was found that these esters were not ozonized at appreciable rate.

Thus, the ozonization of ketones must proceed by the processes both (1) and (3), the relative importance depending on pH and the substrate. The rate of ozonization of ketone is accelerated by both acid and alkaline due to a preferred formation of the enol form; for example,

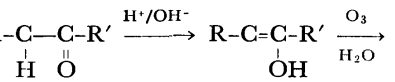

$$\rightarrow RCHO + H_2O_2 + R'COOH.$$

We have previously reported the ozonolysis of unsaturated carboxylic acids.[11,36] Saturated carboxylic acids are in general stable toward ozone. As described above, acetic acid, propionic acid, isobutyric acid, and oxalic acid were not ozonized easily in pure water. However, α-hydroxy carboxylic acids such as glycolic acid and lactic acid were ozonized even in neutral water. The hydroxy group must have some accelerating effect and the ozonization must proceed as that of 2-butanol, giving corresponding carbonyl compounds as the primary and major product.

The probable major reaction pathway in the ozonization of isobutyric acid is shown as an example in Fig. 5. The ozonization of other saturated carboxylic acids should proceed similary. As shown in Fig. 5, the attack of ozone and/or hydroxyl radical on tertiary C–H bond gives 1-carboxy-1-methylethyl radical and its oxygenated radicals, which eventually yield the observed products, *i.e.*, α-hydroxyisobutyric acid, pyruvic acid, acetic acid, formic acid, acetone, and carbon dioxide.

The products formed from the 2-carboxypropyl radical were not found, although small amounts of un-

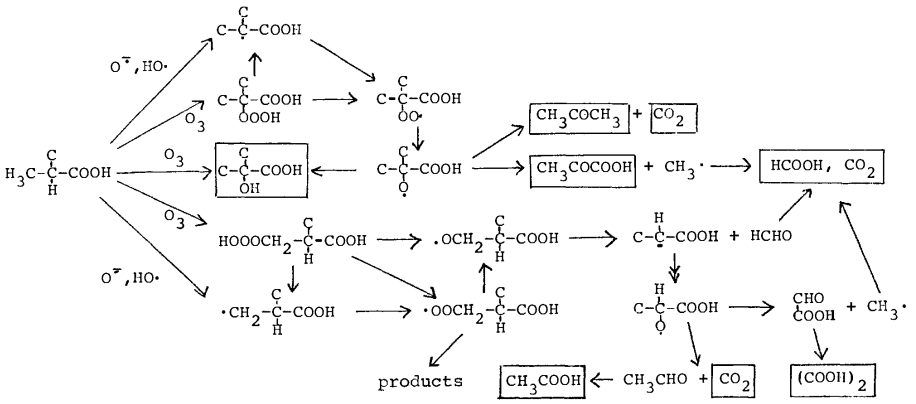

Fig. 5. Probable major reaction pathway in the ozonization of isobutyric acid in water.

identified products were observed.

The increase in the rate of ozonization of carboxylic acids at higher pH must be ascribed to the increase in the reactivities of substrate and to the formation of active attacking species. It has been reported[37] that carboxylate anion has higher reactivity than parent carboxylic acid toward the hydroxyl radical which is also an electron seeking reagent like ozone.

The products observed in the ozonization of carboxylic acids at higher pH are similar with those observed in the oxidation of carboxylic acids induced by hydroxyl radical generated by Fenton reagent and photolysis of hydrogen peroxide.[38]

From the viewpoint of water treatment, it may well be concluded that, as generally accepted, ozone is a powerful oxidizing reagent, especially for aromatic ring, but the complete destruction of saturated carboxylic acids in not practical.

This study was in part supported by The Steel Industry Foundation for the Advancement of Environmental Protection Technology.

References

1) P. S. Bailey, *Chem. Rev.*, **58**, 925 (1958).
2) R. W. Murray, *Acc. Chem. Res.*, **1**, 313 (1968).
3) R. Criegee, *Angew. Chem., Int. Ed. Engl.*, **14**, 745 (1975).
4) P. S. Bailey, "Ozonation in Organic Chemistry. Vol. 1, Olefinic Compounds," Academic Press, New York (1978).
5) "Ozone in Water and Wastewater Treatment," ed by F. L. Evans III, Ann Arbor Sci., Ann Arbor, (1972).
6) G. W. Miller, R. G. Rice, C. M. Robson, R. L. Scullin, W. Kuhn, and H. Wolf, "An Assessment of Ozone and Chlorine Dioxide Technologies for Treatment of Municipal Water Supplies," EPA-600/2-78-147, August 1978.
7) "Ozone/Chlorine Dioxide Oxidation Products of Organic Materials," ed by R. G. Rice and J. A. Cotruvo, Ozone Press International, Ohio (1978).
8) T. Saito, E. Niki, T. Shiono, and Y. Kamiya, *Bull. Chem. Soc. Jpn.*, **51**, 1153 (1978).
9) T. Saito, E. Niki, and Y. Kamiya, *Bull. Chem. Soc. Jpn.*, **54**, 253 (1981).
10) T. W. Nakagawa, L. J. Andrews, and R. M. Keefer, *J. Am. Chem. Soc.*, **82**, 269 (1960).
11) Y. Yamamoto, E. Niki, H. Shiokawa, and Y. Kamiya, *J. Org. Chem.*, **44**, 2137 (1979).
12) J. P. Gould and W. J. Weber, Jr., *J. Water Pollut. Control Fed.*, **48**, 47 (1976).
13) H. R. Eisenhauer, *J. Water Pollut. Control Fed.*, **40**, 1887 (1968).
14) H. Wako, *Nippon Kagaku Kaishi*, **1976**, 1530.
15) E. Bernatek and C. Frengen, *Acta Chem. Scand.*, **15**, 471 (1961).
16) E. Bernatek and C. Frengen, *Acta Chem. Scand.*, **15**, 1454 (1961).
17) P. Joy, E. Gilbert, and S. H. Eberle, *Water Res.*, **14**, 1509 (1980).
18) Y. Yamamoto, M. Iemoto, E. Niki, and Y. Kamiya, unpublished work.
19) W. L. Waters, A. J. Rollin, C. M. Bardwell, J. A. Schneider, and T. W. Aanerud, *J. Org. Chem.*, **41**, 889 (1976).
20) A. Ya. Garehikov, V. D. Komissarov, E. T. Denisov, and C. B. Kochemasova, *Kinet. Katal.*, **13**, 1126 (1972).
21) J. Hoigne, *Science*, **190**, 782 (1975).
22) J. Hoigne and H. Bader, *Water Res.*, **10**, 377 (1976).
23) J. Hoigne and H. Bader, *Environ. Sci. Technol.*, **12**, 79 (1978).
24) J. Hoigne and H. Bader, *Ozone Sci. Eng.*, **1**, 357 (1979).
25) M. Peleg, *Water Res.*, **10**, 361 (1976).
26) S. Nakayama and M. Maeda, *Mizu Shori Gijutsu*, **17**, 157 (1976).
27) S. W. Benson, *Adv. Chem. Ser.*, **77**, 74 (1968).
28) T. M. Hellman and G. A. Hamilton, *J. Am. Chem. Soc.*, **96**, 1530 (1974).
29) H. M. White and P. S. Bailey, *J. Org. Chem.*, **30**, 3037 (1965).
30) P. S. Nangia and S. W. Benson, *J. Am. Chem. Soc.*, **102**, 3105 (1980).
31) M. C. Whiting, A. J. N. Bolt, and J. H. Parish, *Adv. Chem. Ser.*, **77**, 4 (1968).
32) G. A. Hamilton, B. S. Ribner, and T. M. Hellman, *Adv. Chem. Ser.*, **77**, 15 (1968).
33) F. E. Stary, D. E. Emge, and R. W. Murray, *J. Am. Chem. Soc.*, **98**, 1880 (1976).
34) P. P. K. Kuo, E. S. K. Chian, and B. J. Chang, *Environ. Sci. Technol.*, **11**, 1177 (1977).
35) E. Niki, Y. Yamamoto, H. Shiokawa, and Y. Kamiya, *Nippon Kagaku Kaishi*, **1979**, 646.
36) Y. Yamamoto, E. Niki, and Y. Kamiya, *J. Org. Chem.*, **46**, 250 (1981).
37) Y. Ogata, T. Suzuki, and K. Takagi, *J. Chem. Soc., Perkin Trans. 2*, **1979**, 1715.
38) S. Yokoi, E. Niki, and Y. Kamiya, 43rd National Meeting of the Chemical Society of Japan, April 1981.

Oxidation of Lipids. IV. Formation and Reaction of Chromanoxyl Radicals as Studied by Electron Spin Resonance

Jyunichi Tsuchiya, Etsuo Niki,* and Yoshio Kamiya

Department of Reaction Chemistry, Faculty of Engineering, The University of Tokyo, Hongo, Bunkyo-ku, Tokyo 113

(Received June 25, 1982)

In order to study the inhibition of oxidation by vitamin E, the formation and reaction of chromanoxyl radicals and hindered phenoxyl radicals were examined by ESR. *t*-Butoxyl radical abstracted the phenolic hydrogens of α-, β-, γ-, and δ-tocopherols, 2,4,6-tri-*t*-butylphenol (TBP), and 2,6-di-*t*-butyl-4-methylphenol (BMP) to give corresponding phenoxyl radicals which were stable enough to be observed by ESR. 2,2-Diphenyl-1-picrylhydrazyl (DPPH) also induced the formation of chromanoxyl and phenoxyl radicals. The ESR spectra of chromanoxyl radicals were recorded and their hyperfine coupling constants were determined. The phenoxyl radicals from TBP and BMP disappeared quite rapidly when excess *t*-butyl hydroperoxide was added, whereas α-chromanoxyl radical from α-tocopherol remained considerably. α-Chromanoxyl radical and phenoxyl radicals reacted with *p*-*t*-butylbenzenethiol to regenerate α-tocopherol and corresponding phenols respectively. The implications of these results are discussed.

Vitamin E (tocopherols, **1**) is known to contribute in biological systems as a scavenger of peroxyl and alkoxyl radicals, singlet oxygen and superoxide anion radical.[1-3] Among them, the trapping of peroxyl and

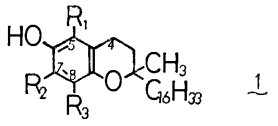

1

α-Tocopherol : 1*a*. $R_1=CH_3$, $R_2=CH_3$, $R_3=CH_3$.
β-Tocopherol : 1*b*. $R_1=CH_3$, $R_2=H$, $R_3=CH_3$.
γ-Tocopherol : 1*c*. $R_1=H$, $R_2=CH_3$, $R_3=CH_3$.
δ-Tocopherol : 1*d*. $R_1=H$, $R_2=H$, $R_3=CH_3$.

alkoxyl radicals, the chain carrying species in peroxidation of lipids, must be the most important role of vitamin E. Although the mechanism of inhibition of autoxidation by synthetic hindered phenols is now well understood,[4,5] it is not fully established how vitamin E suppresses the lipid peroxidation. The objective of the present work is to study by ESR technique the formation and reaction of chromanoxyl radicals[6] from tocopherols and compare them with those from the hindered phenols such as 2,4,6-tri-*t*-butylphenol (TBP) and 2,6-di-*t*-butyl-4-methylphenol (BMP). α-Tocopherol, the major component of vitamin E, was studied most extensively.

Experimental

Materials. Natural α-, β-, γ-, and δ-tocopherols were kindly supplied from Eisai Co. Ltd. Commercial TBP and BMP were recrystallized from methanol. *p*-*t*-Butylbenzenethiol was used after distillation. Di-*t*-butyl diperoxyoxalate (DBPO) used as a *t*-butoxyl radical source was prepared by the method described in the literature.[7] Phenylazotriphenylmethane and 2,2-diphenyl-1-picrylhydrazyl (DPPH) were purchased from Eastman Kodak and used as received. *t*-Butyl hydroperoxide was distilled under reduced pressure prior to use, 42 °C/24 Torr (1 Torr=133.322 Pa). The spin traps, 2-nitroso-2-methylpropane, nitrosobenzene, *N*,*N*′-dioxide-2-methyl-*N*-(4-pyridinylmethylene)-2-propanamine (POBN), and 2,4,6-tri-*t*-butylnitrosobenzene was obtained from Aldrich and used without further purification.

Apparatus and Procedure. ESR spectra were recorded on X-band JEOL FE1X spectrometer at room temperature by the following general procedure. Solid DBPO and TBP or BMP were taken directly into the quartz ESR tube, evacuated and benzene was vacuum transferred into the tube and subjected to ESR analysis. DPPH solution was taken into an ESR tube and the solvent was removed by evacuation. Benzene solution of α-tocopherol and spin trap, when necessary, was taken into a side arm of the ESR tube, frozen, evacuated and then mixed with solution of phenol and DBPO or DPPH. The additives such as *t*-butyl hydroperoxide and *p*-*t*-butylbenzenethiol were introduced into ESR tube by vacuum distillation.

The reaction was carried out at room temperature under vacuum unless otherwise noted. The concentrations of DBPO and DPPH were in the range of 5×10^{-5} to 10^{-2} M (1 M=1 mol dm^{-3}) and excess amount of α-tocopherol, BMP, or TBP was used.

Results and Discussion

It is now understood that hindered phenols such as TBP and BMP inhibit the autoxidation by trapping the chain carrying peroxyl radicals as shown in Eqs. 1 and 2. The rate determining step is Reaction 1, and Reaction 2 proceeds quite rapidly.[4,5] Each TBP or BMP traps two molecules of peroxyl radicals,[4] and peroxyl radical adduct **2** has been isolated and identified.[8]

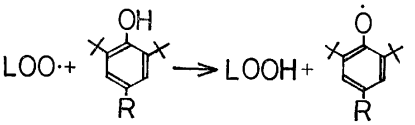

(1)

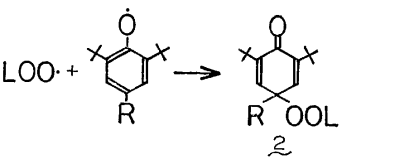

(2)

2

+ : $-C(CH_3)_3$

Upon thermal decomposition, DBPO produces two molecules of *t*-butoxyl radicals. When DBPO was decomposed in benzene solution of tocopherols, TBP or

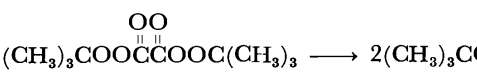

(3)

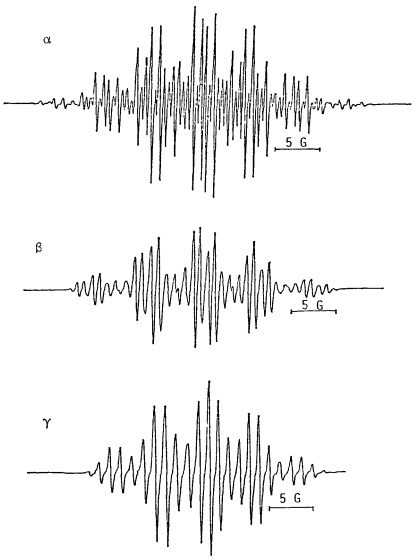

Fig. 1. The ESR spectra of chromanoxyl radicals formed from tocopherols by the reaction with *t*-butoxyl radical.

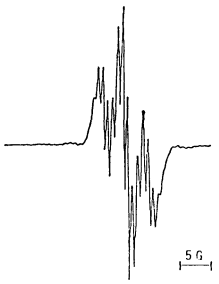

Fig. 2. The ESR spectrum of 2,4,6-tri-*t*-butylphenoxyl radical observed when DBPO was decomposed under vacuum in benzene containing TBP.
[DBPO] = 1×10^{-4} M, [TBP] = 1×10^{-2} M.

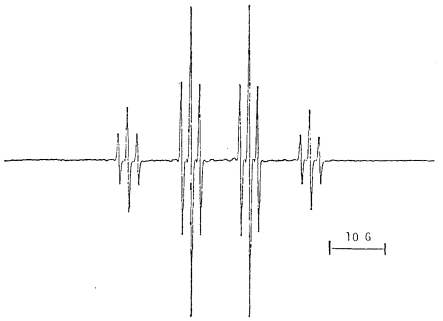

Fig. 3. The ESR spectrum of 2,6-di-*t*-butyl-4-methylphenoxyl radical.
[DBPO] = 1×10^{-4} M, [BMP] = 1×10^{-2} M.

BMP, the corresponding phenoxyl radicals were observed by ESR as shown respectively in Figs. 1, 2, and 3. This shows that *t*-butoxyl radical formed from DBPO abstracts the phenolic hydrogens from tocopherols, TBP, and BMP.

DPPH also gave the same phenoxyl radicals as reported previously,[9-11] that is, when TBP, BMP, or tocopherol was added to the benzene solution of DPPH, the purple color of DPPH, its visible spectrum (λ_{max} = 525 nm), and its ESR spectrum disappeared and new ESR spectra of phenoxyl radicals were observed. On the other hand, when phenylazotriphenylmethane was decomposed instead of DBPO, only triphenylmethyl radical was observed and no phenoxyl radical could be observed.

Table 1. Hyperfine coupling constants of chromanoxyl radicals generated from tocopherols[a]

Radical	5-R_1	7-R_2	8-R_3	4-CH
α-Chromanoxyl	a^{CH_3} 0.602	a^{CH_3} 0.458	a^{CH_3} 0.094	a^{CH_2} 0.148
β-Chromanoxyl	a^{CH_3} 0.625	a^{H} 0.466	a^{CH_3} 0.085	a^{CH_2} 0.168
γ-Chromanoxyl	a^{H} 0.595	a^{CH_3} 0.477	a^{CH_3} 0.116	a^{CH_2} 0.116
δ-Chromanoxyl	a^{H} 0.592	a^{H} 0.460	a^{CH_3} 0.111	a^{CH_2} 0.111

a) In mT, measured in benzene, under vacuum and at room temperature.

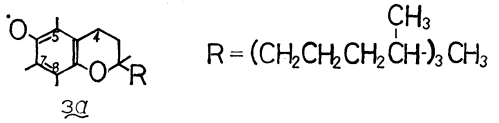

3a

The ESR spectrum of α-chromanoxyl radical **3a** from α-tocopherol shown in Fig. 1 agrees well with those reported previously.[11-13] As assigned previously,[11-13] the ESR spectrum of **3a** shows seven main lines with additional hyperfine structure. The hyperfine splitting constants measured in this work are summarized in Table 1. It is noteworthy that protons at C-5 and C-7 are not equivalent, the spin density being higher at C-5.

The stability of the phenoxyl radicals is dependent on the substituents on the aromatic ring. α-Chromanoxyl radical and 2,4,6-tri-*t*-butylphenoxyl radical were relatively stable at room temperature in the absence of oxygen. On the other hand, 2,6-di-*t*-butyl-4-methylphenoxyl and 2,4,6-trimethylphenoxyl radicals decayed rapidly even in the absence of oxygen. The phenoxyl radicals from α-tocopherol, TBP, and BMP were stable toward spin traps such as 2-methyl-2-nitrosopropane, nitrosobenzene, 2,4,6-tri-*t*-butylnitrosobenzene, and POBN.

Figure 4 shows the rate of disappearance of α-chromanoxyl radical in the absence of oxygen. The second order plot included in Fig. 4 gives the rate constant for the decay of α-chromanoxyl radical as $k = 0.061$ $M^{-1} s^{-1}$. It should be noted that the rate of decay depends on the solvent. The self reaction of α-chromanoxyl radicals is reported to give α-tocopherol and *o*-quinone methide **4a** by disproportionation (Reaction 4).[14-16]

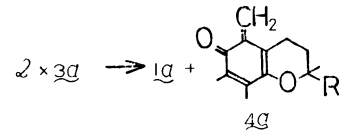

(4)

The effect of addition of hydroperoxide on the sta-

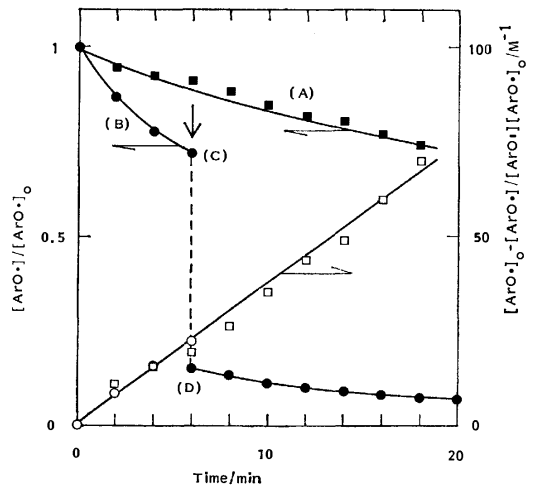

Fig. 4. Decay of α-chromanoxyl radical (ArO·) in benzene at room temperature under vacuum before and after the addition of *t*-butyl hydroperoxide (BOOH).
BOOH was added at the point C indicated by an arrow. There is some time lag (a couple of minutes) between the points C and D due to manipulation.

	ArOH(mM)	DPPH(mM)	BOOH(mM)
(A)	14.9	5.02	0
(B)	24.3	17.7	177

bility of phenoxyl radicals was then studied to know the interaction of α-chromanoxyl radical with peroxyl radical. It was found that, when phenoxyl radical was first generated from TBP or BMP in benzene and then *t*-butyl hydroperoxide was transferred from the side arm of the ESR tube into the above solution, the phenoxyl radicals from TBP and BMP disappeared rapidly and completely. These results suggest that the phenoxyl radicals react with hydroperoxide to give peroxyl radicals, which then react with another phenoxyl radical to give adduct **2** (Reactions 5 and 6).

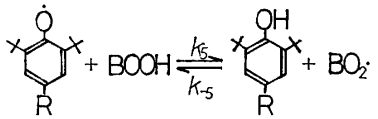

(5)

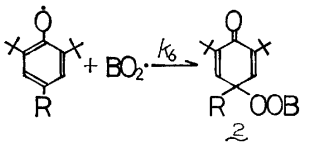

(6)

2

Interestingly, however, it was found that, as shown in Fig. 4, α-chromanoxyl radical from α-tocopherol did not disappear completely when excess *t*-butyl hydroperoxide was added. It was confirmed that this variation of ESR spectrum was due neither to dilution effect nor to solvent induced variation in cavity Q.[17]

The hydroperoxidic hydrogen of *t*-butyl hydroperoxide is readily abstracted by oxygen radicals to generate *t*-butylperoxyl radical.[18-22] The rate constant for the hydrogen atom abstraction from α,α-dimethylbenzyl hydroperoxide by 2,4,6-tri-*t*-butylphenoxyl radical has been reported as $\log k\ (M^{-1}\,s^{-1}) = 7.1 - 10900/2.303RT$,[23] which gives $k_5 = 0.13\ M^{-1}\,s^{-1}$ at 25 °C. The rate of disappearance of phenoxyl radical (ArO·) is given by

$$-\frac{d[ArO\cdot]}{dt} = \frac{2k_5k_6[ArO\cdot]^2[BOOH]}{k_{-5}[ArOH] + k_6[ArO\cdot]} \quad (7)$$

and since $k_6[ArO\cdot][BO_2\cdot] \gg k_5[ArOH][BO_2\cdot]$,

$$-\frac{d[ArO\cdot]}{dt} = 2k_5[ArO\cdot][BOOH]. \quad (8)$$

The amount of *t*-butyl hydroperoxide was 0.1 M and if we assume that *t*-butyl hydroperoxide has the same reactivity as α,α-dimethylbenzyl hydroperoxide toward phenoxyl radical, then, $-d[ArO\cdot]/dt = 0.026\ [ArO\cdot]$, which gives the half life of the phenoxyl radical as about 30 s.

The different behavior of α-chromanoxyl radical from the phenoxyl radicals derived from TBP and BMP observed by the addition of *t*-butyl hydroperoxide may be interpreted by an extraordinary stability of α-chromanoxyl radical; that is, a slower interaction of α-chromanoxyl radical with hydroperoxide and peroxyl radical, higher rate constant for the hydrogen atom abstraction from α-tocopherol by peroxyl radical,[24-26] and/or the instability of the adduct of α-chromanoxyl radical and peroxyl radical. Furthermore, α-tocopherol has much higher equilibrium constant than TBP in the reversible reaction with DPPH and galvinoxyl.

We believe the decrease in α-chromanoxyl radical observed by the addition of *t*-butyl hydroperoxide is not due to oxygen which may possibly be formed from the bimolecular interaction of *t*-butylperoxyl radicals. In one experiment, α-chromanoxyl radical was first generated under vacuum by the reaction with DPPH, analyzed by ESR, and then *t*-butyl hydroperoxide was vacuum transferred into the ESR tube. The amount of α-chromanoxyl radical decreased as observed in Fig. 4. Then the ESR tube was evacuated, but the amount and shape of the ESR spectrum did not change, suggesting that the rapid decrease in α-chromanoxyl radical is not due to oxygen formed from *t*-butylperoxyl radical.[27]

We have previously reported that α-chromanoxyl radical reacted with glutathione and ascorbic acid to regenerate α-tocopherol.[28] Similarly it was found that when *p*-*t*-butylbenzenethiol was added to the mixture of DPPH and phenol in benzene, the phenoxyl radicals from α-tocopherol, TBP, and BMP all disappeared rapidly. When both *p*-*t*-butylbenzenethiol and 2,4,6-tri-*t*-butylnitrosobenzene were added, new ESR spectrum was observed in place of the phenoxyl radical. The observed ESR spectrum shown in Fig. 5 is the same as that observed when DBPO was decomposed in benzene solution of *p*-*t*-butylbenzenethiol and 2,4,6-tri-*t*-butylnitrosobenzene and it is ascribed to spin adduct **5**. The coupling constants obtained, $a_N = 1.630$ mT and $a_H = 0.084$ mT, agree well with those of phenylthiyl radical spin adduct by 2,4,6-tri-*t*-butylnitrosobenzene reported by Terabe and Konaka, $a_N = 1.629$ mT and $a_H = 0.085$ mT.[29]

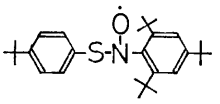

5

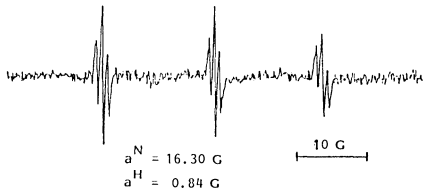

Fig. 5. The ESR spectrum observed when *p*-*t*-butylbenzenethiol was added to the mixture of DPPH, 2,4,6-tri-*t*-butylnitrosobenzene and TBP.

These results suggest that hydrogen atom is quickly transferred from *p*-*t*-butylbenzenethiol to phenoxyl radicals to regenerate the phenols. One of the interesting features of vitamin E in biological systems is the proposed regeneration of vitamin E.[28,30–32] This type of hydrogen transfer from thiol such as glutathione and cysteine to chromanoxyl radicals may contribute in the regeneration and maintenance of vitamin E levels in tissues.

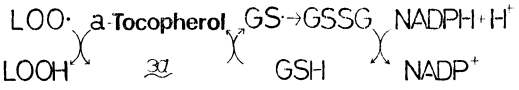

(9)

It must be noted, however, that these observations in vitro in homogeneous solution do not necessarily indicate the contribution of these reactions in heterogeneous systems *in vivo*.

The above results show that *t*-butoxyl radical and DPPH abstract the phenolic hydrogen atom from tocopherols, TBP, and BMP. It has been reported that phenol is more reactive than toluene by a factor of 10^5 to *t*-butylperoxyl radical principally due to a difference in activation energy, even though the heats of these hydrogen atom transfers are comparable.[33] The abstraction of a hydrogen atom by an oxygen radical from oxygen is energetically more favorable than abstraction from carbon. Therefore, the phenolic hydrogen must be abstracted exclusively from α-tocopherol and little benzylic C–H bond should be attacked.

In conclusion, α-tocopherol behaves similarly with TBP and BMP toward alkoxyl radical and DPPH. However, chromanoxyl radical **3** has somewhat different reactivity toward peroxyl radical and/or hydroperoxide.

We wish to express our sincere thanks to Dr. K. U. Ingold for valuable comments and discussion. This work was in part supported by Grant-in-Aid for Developmental Scientific Research of the Ministry of Education, Science and Culture. The financial support by The Toyota Foundation is hereby gratefully acknowledged. A gift of tocopherols from Eisai Co. Ltd. is also acknowledged.

References

1) C. de Duve and O. Hayaishi, "Tocopherol, Oxygen and Biomembranes," Elsevier, Amsterdam (1978).
2) L. J. Machlin, "Vitamin E," Marcel Dekker, New York (1980).
3) L. A. Witting, "Free Radicals in Biology," Academic Press, New York (1980), Vol. IV, Chap. 9.
4) E. C. Horswill, J. A. Howard, and K. U. Ingold, *Can. J. Chem.*, **44**, 985 (1966).
5) L. R. Mahoney, *Angew. Chem., Int. Ed. Engl.*, **8**, 547 (1969).
6) The phenoxyl radicals generated from tocopherols are named in this paper as widely used chromanoxyl radicals for convenience rather than chromanyloxyl radicals that conform with rules of nomenclature.
7) P. D. Bartlett, E. P. Benzing, and R. E. Pincock, *J. Am. Chem. Soc.*, **82**, 1762 (1960).
8) E. R. Altwicker, *Chem. Rev.*, **67**, 475 (1967), and references cited therein.
9) J. S. Hogg, D. H. Lohmann, and K. E. Russell, *Can. J. Chem.*, **39**, 1588 (1961).
10) P. B. Ayscough and K. E. Russell, *Can. J. Chem.*, **43**, 3039 (1965).
11) W. Boguth and H. Niemann, *Biochim. Biophys. Acta*, **248**, 121 (1971).
12) T. Ozawa, A. Hanaki, S. Matsumoto, and M. Matsuo, *Biochim. Biophys. Acta*, **531**, 72 (1978).
13) K. Mukai, N. Tsuzuki, K. Ishizu, S. Ouchi, and K. Fukuzawa, *Chem. Phys. Lipids*, **29**, 129 (1981).
14) D. R. Nelan and C. D. Robeson, *J. Am. Chem. Soc.*, **84**, 2963 (1962).
15) P. Schudel, H. Mayer, J. Metzger, R. Ruegg, and O. Isler, *Helv. Chim. Acta*, **46**, 333 (1963).
16) W. Boguth, *Vitamins Hormones*, **28**, 1 (1970).
17) L. S. Singer, *J. Chem. Phys.*, **30**, 1463 (1959).
18) R. Hiatt, J. Clipsham, and T. Visser, *Can. J. Chem.*, **42**, 2754 (1964).
19) A. Factor, C. A. Russell, and T. G. Traylor, *J. Am. Chem. Soc.*, **87**, 3692 (1965).
20) J. R. Thomas, *J. Am. Chem. Soc.*, **87**, 3935 (1965).
21) J. A. Howard and K. U. Ingold, *Can. J. Chem.*, **47**, 3797 (1969).
22) E. Niki, K. Okayasu, and K. Kamiya, *Int. J. Chem. Kinet.*, **6**, 279 (1974).
23) A. P. Griva and E. T. Denisov, *Int. J. Chem. Kinet.*, **5**, 869 (1973).
24) G. W. Burton, Y. Le Page, E. J. Gabe, and K. U. Ingold, *J. Am. Chem. Soc.*, **102**, 7791 (1980).
25) G. W. Burton and K. U. Ingold, *J. Am. Chem. Soc.*, **103**, 6472 (1981).
26) E. Niki, R. Tanimura, and Y. Kamiya, *Bull. Chem. Soc. Jpn.*, **55**, 1551 (1982).
27) When oxygen was introduced into the ESR tube, the ESR spectrum of the phenoxyl radicals from TBP was broadened, but without appreciable decrease in the height. On the other hand, the introduction of oxygen diminished the ESR spectrum of α-chromanoxyl radical considerably. However, α-chromanoxyl radical was recovered when the ESR tube was evacuated.
28) E. Niki, J. Tsuchiya, R. Tanimura, and Y. Kamiya, *Chem. Lett.*, **1982**, 789.
29) S. Terabe and R. Konaka, *J. Chem. Soc., Perkin Trans. 2*, **1973**, 369.
30) A. L. Tappel, *Geriatrics*, **23**, 97 (1968).
31) T. Nakamura and I. Hishinuma, Ref. 1, pp. 95—108.
32) J. E. Packer, T. F. Slater, and R. L. Willson, *Nature*, **278**, 737 (1979).
33) J. H. B. Chenier, E. Furimsky, and J. A. Howard, *Can. J. Chem.*, **52**, 3682 (1974).

The Effect of Organic Solvents on the Thermal Denaturation of Lysozyme as Measured by Differential Scanning Calorimetry

Yukihisa FUJITA* and Yukinao NODA

Department of Chemistry, Hyogo College of Medicine, Mukogawa, Nishinomiya, Hyogo 663

(Received June 2, 1982)

The thermal denaturation of lysozyme in aqueous solutions of *N,N*-dimethylformamide(DMF), *N,N*-dimethylacetamide(DMA), acetone, and dioxane at pH 3 was investigated by differential scanning calorimetry (DSC). The denaturation temperature, T_d, decreased linearly with an increase in the concentration of organic solvent. The lowering in T_d at identical concentrations of organic solvent increased in the order: acetone< DMF<DMA<dioxane. The calorimetric enthalpy of denaturation, ΔH_d, showed a complex dependence on the solvent composition. For three organic solvents (not dioxane), the ΔH_d first increased slightly with increasing the concentration of organic solvent and then started decreasing at different concentrations of each organic solvent. This behavior is analogous to those observed earlier with monohydric alcohols and with sulfoxides. For dioxane, on the other hand, the ΔH_d decreased gradually with increasing the concentration of dioxane. The effect of these organic solvents on the thermal stability of lysozyme may correlate with their effect on the structure of water, which determines the strength of the hydrophobic interaction of the protein.

Various substances affect the protein–water interactions when added to aqueous protein solution and consequently alter the structural stability of protein. Solvent perturbations have been used extensively as probes of the solution conformation of protein.[1,2] These studies have provided valuable information about the role of the solvent in maintaining the native structure of protein. The conformational changes of lysozyme induced by the addition of organic solvents have been investigated by Hamaguchi and co-workers.[3–5] They have suggested that organic solvents change the conformation of the protein by perturbing the characteristic water structure and by interacting directly with the protein molecule. Izumi and Inoue[6,7] have reported recently the effect of dioxane on the conformation of lysozyme measured by CD, difference spectroscopy, and fluorometry.

Differential scanning calorimetry(DSC) is a useful tool for investigating the thermally induced conformational transition of protein. The thermogram can be used to calculate the van't Hoff enthalpy[8] or an effective enthalpy[9] for comparison to the calorimetric enthalpy to determine the cooperativity of the transition. Application of DSC to the study of protein unfolding has been recently reviewed by Privalov[10] and Biltonen and Freire.[11] A comprehensive thermodynamic investigation of the unfolding of lysozyme has been reported by Pfeil and Privalov.[12]

We have been investigating the effect of various substances on the thermal stability of globular proteins by means of DSC. The thermal denaturation of lysozyme in aqueous solutions of monohydric alcohols and sulfoxides was reported previously.[13,14] These organic solvents lowered the denaturation temperature; this lowering became more pronounced with increasing the concentration and the hydrocarbon content of organic solvent. The calorimetric enthalpy of denaturation passed through a maximum with increasing the concentration of organic solvent. There are many studies of the thermal denaturation of lysozyme in aqueous alcohol solutions by different techniques.[8,15,16] Although various substances may be expected to affect the thermal stability of protein in different ways, the effect of organic solvents other than alcohols on the thermal denaturation of protein has rarely been investigated. So far as we know, Hamaguchi and Sakai[17] have reported the thermal denaturation of lysozyme in aqueous solution of amides and dioxane in a limited concentration of the organic solvent, as determined by spectrophotometry.

In the present paper, the effect of *N,N*-dimethylformamide (DMF), *N,N*-dimethylacetamide (DMA), acetone, and 1,4-dioxane on the thermal denaturation of lysozyme as measured by DSC will be reported.

Experimental

Materials. The hen egg-white lysozyme used was a salt-free, six-times-recrystallized preparation obtained from Seikagaku Kogyo Co. The molecular weight of lysozyme was taken to be 14307. Spectral grade *N,N*-dimethylformamide (DMF), acetone, and 1,4-dioxane were purchased from Wako Pure Chemicals and reagent grade *N,N*-dimethylacetamide (DMA) from Tokyo Kasei Kogyo Co. Solutions were prepared with deionized and distilled water.

Methods. The protein concentration was determined spectrophotometrically on a Hitachi 323 spectrophotometer, using an extinction coefficient of 2.69 dm^3 $(g\ cm)^{-1}$ at 280 nm in glycine buffer at pH 3.0.[17] The organic solvent was added by weight. All the calorimetric experiments were carried out at a protein concentration of 2% in 0.05 mol dm^{-3} glycine buffer adjusted to pH 3.0 as measured by a Horiba model f-7_{ss} pH meter standardized at pH 4.0 in aqueous solution. DSC measurements were performed with a Daini Seikosha SSC-560U differential scanning calorimeter (conduction type). The sample solutions (0.06 cm^3) were hermetically sealed in a silver vessel. An equal amount of solvent was used as reference material. A heating rate of 1 K min^{-1} was typically used, although some measurements were performed at 0.5 to 2.5 K min^{-1} to check the effect of the heating rate. The calorimeter was calibrated with indium, benzophenone, and benzoic acid.

Results and Discussion

Figure 1 presents typical DSC curves for the thermal denaturation of lysozyme in aqueous solutions containing different amounts of DMA at pH 3. In every

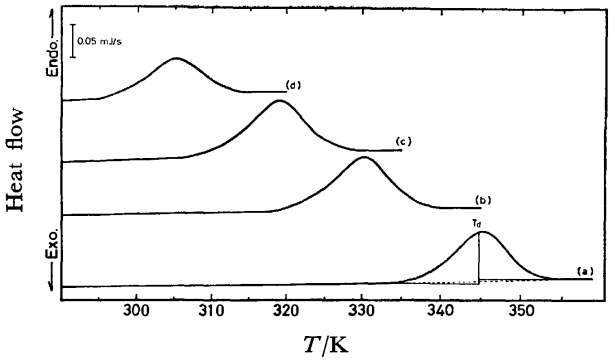

Fig. 1. Typical DSC curves for the thermal denaturation of lysozyme in aqueous DMA solutions at heating rate of 1 K min^{-1}. Protein concentration is 2.0%(w/v).
Curve a is in 0.05 mol dm^{-3} glycine buffer at pH 3.0 with no organic solvent. Curves b, c, and d are with 2, 4, and 6 mol dm^{-3} DMA, respectively.

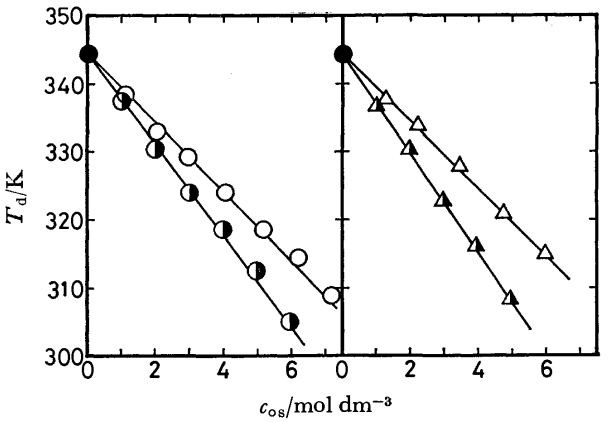

Fig. 2. The denaturation temperature, T_d, of lysozyme as a function of organic solvent concentration.
●: Aqueous, ○: DMF, ◑: DMA, △: acetone, ◭: dioxane.

measurement, a reproducible endothermic peak was observed, occurring over a temperature range of 22—25 K. The endothermic peak shifts to lower temperature with increasing DMA content, while the peak area varies with the solvent composition. The denaturation temperature, T_d, was estimated by assuming that the area under the thermogram was proportional to the amount denatured, and T_d is defined as the temperature at which the protein is half-denatured. According to Velicelebi and Sturtevant,[8] the temperature at which the transition is half complete and the temperature of maximal excess heat flow, T_p, do not coincide, even for a two-state process with no permanent change in heat capacity. They have reported that T_d differs from T_p by 0.75—1.0 K. In the present work, the T_d obtained was lower than the T_p by only 0.3—0.5 K.

There was no significant difference in the T_d obtained at heating rates of 0.5 and 1 K min^{-1}, but the T_d obtained at 2.5 K min^{-1} was higher than those at 0.5 and 1 K min^{-1} by 0.4—0.8 K. This indicates that the denaturation temperature is not much influenced by heating rates lower than 1 K min^{-1}, allowing equilibrium analysis of the data. The denaturation temperature of lysozyme in 0.05 mol dm^{-3} glycine buffer at pH 3.0 was 344.4±0.1 K, which was comparable with previous values obtained from NMR measurements by McDonald *et al.*[18] and from spectrophotometric measurement by Gerlsma and Stuur[15] at similar pH. Parodi *et al.*[16] have reported a slightly lower T_d, 341 K, from ORD measurements, whereas a high T_d value of 347.7 K from calorimetric measurements has been reported by Privalov and Khechinashvili.[19] A number of factors such as protein concentration, ionic strength, and specific buffer effect as well as heating rate could contribute to the difference in T_d values reported from the different laboratories. Variation in the measurement techniques could also contribute to the difference in T_d value.

The calorimetric enthalpy of denaturation, ΔH_d, was estimated by measuring the area between the transition peak and a base line. The ΔH_d obtained was not significantly different from that estimated using the base line based on the heat capacity difference between the native and denatured states. The ΔH_d values have maximum expected errors of ±5%, including errors in calibration constant, sample preparation, and reproducibility. The denaturation enthalpy was almost independent of the heating rate in the range of 0.5 to 2.5 K min^{-1}. The ΔH_d of lysozyme in 0.05 mol dm^{-3} glycine buffer at pH 3.0 was 489 kJ mol^{-1}, the average of nine experiments. Taking into account the difference in measurement conditions, the value of ΔH_d appears to be line with previous values obtained from calorimetric measurements by other investigators, indicating values of 577 kJ mol^{-1} at pH 5[20] and 427[12] and 382 kJ mol^{-1} at pH 2.[8]

There was no significant change in the T_d and ΔH_d on repetitive scans when the sample was rapidly cooled after the preceding scan, indicating that the thermal denaturation of lysozyme in these organic solvent solutions is almost reversible. According to Privalov *et al.*,[9] the effective enthalpy of denaturation, ΔH_{eff}, can be calculated by the half width of the heat absorption peak on the DSC thermogram, if it is assumed that the denaturation is a simple transition between two states without thermodynamically stable intermediate forms. The ratio of the calorimetric to the calculated effective enthalpies of denaturation, $\Delta H_d/\Delta H_{eff}$, showed near-unity value, suggesting that the thermal denaturation of lysozyme in these organic solvent solutions is very nearly a two-state process.

Figure 2 shows the effect of organic solvents on the denaturation temperature. For all the systems investigated, the T_d decreases almost linearly with increasing the concentration of organic solvent. The lowering of T_d at identical concentrations of organic solvent increases in the order: acetone<DMF<DMA<dioxane. The effect of DMF, DMA, and dioxane on the denaturation temperature of lysozyme has been reported earlier from spectrophotometric measurements by Hamaguchi and Sakai.[17] They have observed trends similar to the ones we have observed. The lowering in the T_d of lysozyme by monohydric alcohols and sulfoxides was reported previously.[13,14]

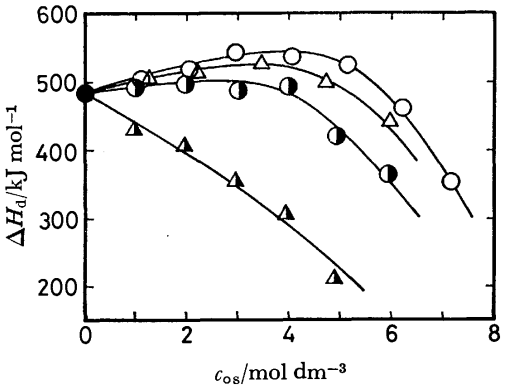

Fig. 3. The denaturation enthalpy, ΔH_d, of lysozyme as a function of organic solvent concentration.
The symbols used are identical with those in Fig. 2.

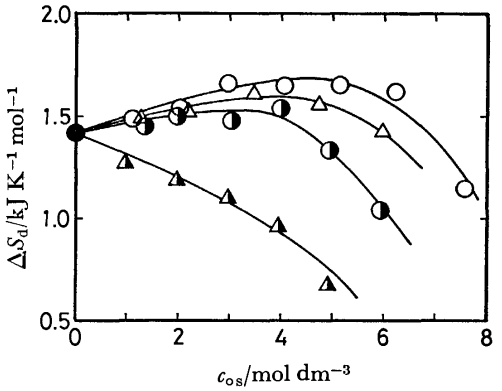

Fig. 4. The denaturation entropy, ΔS_d, calculated at the transition temperature as a function of organic solvent concentration.
The symbols used are identical with those in Fig. 2.

The thermal unstabilization of lysozyme by alcohols has been observed by many investigators through different techniques.[8,15,16] The unstabilizing effect of organic solvents such as alcohols on the thermal stability of protein has been generally interpreted in terms of hydrophobic interactions between the nonpolar groups of protein and the alkyl chain of organic solvent, and thus relatively favoring the denatured state in the mixed solvent. DMA produces a greater decrease in T_d than DMF does, suggesting that the unstabilizing ability of amides is enhanced by an increase in the hydrocarbon content, similarly to those of monohydric alcohols and sulfoxides. This observation also provides the above view with more support.

The dependence of the denaturation enthalpy on the concentration of organic solvent is shown in Fig. 3. For three organic solvents (not dioxane), the ΔH_d shows a maximum, that is, the ΔH_d first increases slightly with increasing the concentration of organic solvent and then starts decreasing at a different concentration of organic solvent. The maximum value of ΔH_d increases in the order: DMA<acetone<DMF. The maximum ΔH_d occurs at approximately 3, 3.5, and 4 mol dm^{-3} for DMA, acetone, and DMF, respectively. The maximum in the ΔH_d of lysozyme has been observed with monohydric alcohols and sulfoxides as well as with the organic solvents used in this experiments.[13,14] A similar trend in ΔH_d with dimethyl sulfoxide has been recently found for ribonuclease A.[21] On the other hand, the ΔH_d with dioxane decreases gradually with an increase in dioxane concentration; this becomes more pronounced at high dioxane contents. It is obvious that the effect of dioxane on the denaturation enthalpy of lysozyme differs from those of other organic solvents.

The entropy of the thermal denaturation, ΔS_d, was calculated for the reversible denaturation by assuming that the free energy change at the midpoint of the transition is zero: $\Delta S_d = \Delta H_d / T_d$. The dependence of ΔS_d on the concentration of organic solvent is shown in Fig. 4. The ΔS_d also shows a behavior similar to ΔH_d. Therefore, the observed decrease in T_d by the addition of organic solvents should result from the complex dependence of ΔH_d and ΔS_d on the solvent composition.

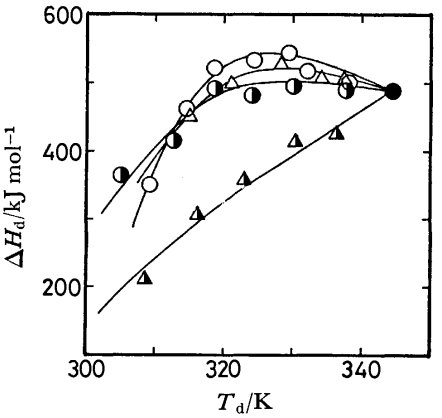

Fig. 5. The variation in the denaturation enthalpy with denaturation temperature.
The symbols used are identical with those in Fig. 2.

Figure 5 represents the dependence of ΔH_d and T_d in the presence of organic solvents. For three organic solvents (not dioxane), the ΔH_d value passes through a maximum with increasing temperature. Such a behavior was also observed with monohydric alcohols and sulfoxides.

For dioxane, on the other hand, the ΔH_d is an increasing function of temperature with slightly downward curvature. There are clear differences in the temperature dependence of ΔH_d for each organic solvent. The dependence of ΔH_d on T_d in the presence of organic solvents thus differs drastically from that reported by Pfeil and Privalov[12] with variations of T_d produced by variation of the pH and addition of guanidine hydrochloride. They found ΔH_d to be a linear function of T_d under all conditions. It is suggested that the nature of the unfolding of lysozyme resulting from the addition of organic solvents is different from that produced by pH changes or by the addition of guanidine hydrochloride.

The conformational changes of lysozyme by the addition of dioxane have been investigated by ORD,[3] CD,[6] and difference spectroscopy.[3,7] These studies show that the tertiary structure of lysozyme is initially disrupted at 20—30% (v/v) dioxane, corresponding to

approximately 3 mol dm^{-3} dioxane, with possible slight disorganization of the ordered secondary structure, and then a pronounced increase in helical structure is induced at very high dioxane concentrations. A similar situation has been observed with DMA and DMF.[3]

These organic solvents have lower dielectric constants than pure water. Thus, electrostatic interaction is stronger in water–organic solvent mixtures than in water, which causes the denaturation enthalpy to increase. However, this contribution appears to be small, as can be seen from decreasing the denaturation enthalpy for the water–dioxane system, because the dielectric constants of aqueous dioxane solutions are relatively lower than those of aqueous solutions of other organic solvents.

The maximum in ΔH_d and ΔS_d for the thermal denaturation of lysozyme has been observed with monohydric alcohols and sulfoxides as well as for the organic solvents examined in the present work. This similarity implies that the effect of organic solvents on the thermal stability of the protein is controlled to a large extent by the common component in the binary mixtures, that is, water. A number of properties of aqueous mixtures of these organic solvents show maxima or minima as a function of composition. This behavior reflects the change in the structure of water by the addition of organic solvents. The complex dependence of ΔH_d and ΔS_d on the solvent composition appears to correlate with the behavior of the water–organic solvent system.

In mixing with water, dioxane[22] shows an exothermic enthalpy of mixing similarly to acetone[23] and both amides,[24] suggesting the strong interactions of dioxane, as well as other organic solvents, with water molecule. The ΔH_d and ΔS_d of lysozyme in water–dioxane mixtures decreased monotonously with increasing concentrations of dioxane, although the maximum in ΔH_d and ΔS_d was predicted. Based on the density data, Oakenfull and Fenwick[25] have suggested that the effect of dioxane on the structure of water differs from those of DMF, ethanol, and dimethyl sulfoxide. The structural contribution to the temperature of maximum density for water–dioxane system shows a negative change, in contrast to a positive change for alcohols and acetone mixing with water.[26,27] Our observation also supports the view that the effect of dioxane on the water structure differs slightly from those of other organic solvents. However, the effects of these organic solvents, including dioxane, on the water structure differ from the so-called structure-making effect of polyhydric alcohols which stabilize the protein strongly against thermal denaturation.[28]

The organic solvents used in the present work, like monohydric alcohols and sulfoxides, unstabilize lysozyme against thermal denaturation. The thermal unstabilization of the protein by organic solvents is enhanced on increasing the concentration and hydrocarbon content of the organic solvent. This observation suggests that organic solvents interact principally with the nonpolar groups of the protein, which causes weakening the hydrophobic interaction of the protein. Bull and Breese[29] have shown from equilibrium dialysis studies that monohydric alcohols are strongly bound to protein. From NMR studies on the solvation of lysozyme in water–dioxane mixtures in the frozen state, Izumi *et al.*[30] have suggested that some water molecules are replaced or expelled by dioxane molecules in the interacting sites due to the more favorable interaction of dioxane with hydrophobic groups lying on the protein surface.

The perturbation of the water structure by the addition of organic solvents also causes the thermal unstabilization of lysozyme. This may contribute more to the thermal unstabilization of the protein than that from the direct interaction of organic solvent with the protein. Since hydrophobic interaction is a result of a rearrangement of the water molecules surrounding hydrophobic groups, the perturbation of the characteristic water structure necessarily causes weakening of the hydrophobic interaction of the protein. Solubility measurements on amino acids in aqueous solutions of ethanol or dioxane have shown favorable free energy of transfer of nonpolar side chains from water to these organic solvent solutions.[31] Thus, the denatured state of protein is stabilized more in the presence of organic solvents than is the native state, since more groups are exposed to solvent in the denatured state than in the native state. It is probable that organic solvents lower the temperature of denaturation as a result of decreased hydrophobic stabilization of the native state.

These results support the hypothesis that the dominant mechanism by which organic solvents unstabilize protein against thermal denaturation is through the perturbation of the characteristic structure of water by organic solvents, which weakens the hydrophobic interaction of the protein.

References

1) C. Tanford, *Adv. Protein Chem.*, **23**, 122 (1968).
2) F. Franks and D. Eagland, *CRC Crit. Rev. Biochem.*, **1975**, 165.
3) K. Hamaguchi and A. Kurono, *J. Biochem. (Tokyo)*, **54**, 497 (1963).
4) K. Hamaguchi, *J. Biochem. (Tokyo)*, **56**, 441 (1964).
5) K. Ikeda and K. Hamaguchi, *J. Biochem. (Tokyo)*, **68**, 785 (1970).
6) T. Izumi and H. Inoue, *J. Biochem. (Tokyo)*, **81**, 1769 (1977).
7) T. Izumi and H. Inoue, *J. Biochem. (Tokyo)*, **83**, 1555 (1978).
8) G. Velicelebi and J. M. Sturtevant, *Biochemistry*, **18**, 1180 (1979).
9) P. L. Privalov, E. I. Tiktopule, and N. N. Khechinashvili, *Int. J. Peptide Protein Res.*, **5**, 229 (1973).
10) P. L. Privalov, *Adv. Protein Chem.*, **33**, 167 (1978).
11) R. L. Biltonen and E. Freire, *CRC Crit. Rev. Biochem.*, **1978**, 85.
12) W. Pfeil and P. L. Privalov, *Biophys. Chem.*, **4**, 23, 33, 41 (1976).
13) Y. Fujita, A. Miyanaga, and Y. Noda, *Bull. Chem. Soc. Jpn.*, **52**, 3659 (1979).
14) Y. Fujita, S. Izumiguchi, and Y. Noda, *Int. J. Peptide Protein Res.*, **19**, 25 (1982).
15) S. Y. Gerlsma and E. R. Stuur, *Int. J. Peptide Protein Res.*, **4**, 377 (1972).
16) R. M. Parodi, E. Bianchi, and A. Ciferri, *J. Biol.*

Chem., **248**, 4047 (1973).
17) K. Hamaguchi and H. Sakai, *J. Biochem. (Tokyo)*, **57**, 721 (1965).
18) C. C. McDonald, W. D. Phillips, and J. D. Glickson, *J. Am. Chem. Soc.*, **93**, 235 (1971).
19) P. L. Privalov and N. N. Khechinashvili, *J. Mol. Biol.*, **86**, 665 (1974).
20) F. Delben and V. Crescenzi, *Biochem. Biophys. Acta*, **194**, 615 (1969).
21) A. L. Jacobson and C. L. Turner, *Biochemistry*, **19**, 4534 (1980).
22) K. W. Morcom and R. W. Smith, *Trans. Faraday Soc.*, **66**, 1073 (1970).
23) D. E. Nicholson, *J. Chem. Eng. Data*, **5**, 309 (1960).
24) J. Burgard and R. Jadot, *J. Chem. Thermodyn.*, **7**, 1185 (1975).
25) D. Oakenfull and D. E. Fenwick, *J. Chem. Soc., Faraday Trans. 1*, **75**, 636 (1979).
26) G. Wada and S. Umeda, *Bull. Chem. Soc. Jpn.*, **35**, 646 (1962).
27) G. Wada and S. Umeda, *Bull. Chem. Soc. Jpn.*, **35**, 1797 (1962).
28) Y. Fujita, Y. Iwasa, and Y. Noda, *Bull. Chem. Soc. Jpn.*, **55**, 1896 (1982).
29) H. B. Bull and K. Breese, *Biopolymers*, **17**, 2121 (1978).
30) T. Izumi, Y. Yoshimura, and H. Inoue, *Arch. Biochem. Biophys.*, **200**, 444 (1980).
31) Y. Nozaki and C. Tanford, *J. Biol. Chem.*, **246**, 2211 (1971)

The Ullmann Condensation Reaction of Haloanthraquinone Derivatives with Amines in Aprotic Solvents. V.[1] The Formation of Active Catalyst by the Partial Oxidation of Copper(I) with Molecular Oxygen

Sadao Arai, Yoshio Hashimoto, Nobuo Takayama, Takamichi Yamagishi, and Mitsuhiko Hida*

Department of Industrial Chemistry, Faculty of Technology, Tokyo Metropolitan University, Fukazawa, Setagaya-ku, Tokyo 158

(Received June 5, 1982)

Although copper(I) is a more effective catalyst than copper(II) in the Ullmann condensation reaction of haloanthraquinones with ethylenediamine in aprotic solvents under a nitrogen atmosphere, the oxidation products of copper(I) by molecular oxygen enhanced the reaction rate compared to copper(I) catalyst. From the studies on the effect of Cu(II) salt addition to Cu(I) salt, solvent effects, and ESR spectra, it was concluded that alkoxycopper(II) species, formed by the oxidation of Cu(I) with molecular oxygen in alcohol–ethylenediamine solution, acted cooperatively with Cu(I) to increase the catalytic activity. The idea was also supported by the fact that the condensation was remarkably accelerated by the combination of Cu(I) and chloromethoxycopper-(II). Reaction pathways including the alkoxo and halogen bridged Cu(I)···Cu(II) mixed valence complex are proposed and discussed.

The Ullmann condensation reaction, a nucleophilic aromatic substitution with the aid of copper catalyst, is used as an important synthetic tool of various aromatic compounds, especially dyestuffs and drugs.[2] The detailed mechanisms, however, remain ambiguous. From our continuing studies on the Ullmann condensation reaction of haloanthraquinones with amines in aprotic solvents, it was clarified that Cu(II) species, formed by an electron transfer from Cu(I) to haloanthraquinone under a nitrogen atmosphere, plays a very interesting role, though Cu(I) salts are more effective catalysts than Cu(II) salts.[3,4] On the basis of the kinetic studies it was concluded that the resulting Cu(II) species acted cooperatively with Cu(I) to increase the catalytic activity of Cu(I) in the condensation with 2-aminoethanol,[5] while in the condensation with ethylenediamine(EN) only Cu(I) was active and the reaction rate decreased with the formation of the Cu(II) species.[1]

We now have found that in the condensation with EN the partial oxidation of Cu(I) catalyst by molecular oxygen unexpectedly enhanced the reaction rate, while the Cu(I) species will be oxidized into inactive Cu(II) by oxygen.

In this paper we will report the unexpected oxygen effect on the condensation with EN and propose that the alkoxycopper(II) species increase the catalytic activity of Cu(I) species.

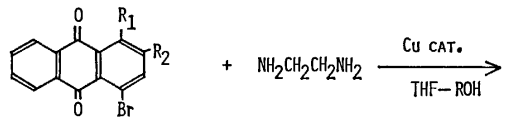

1 : $R_1 = NH_2$, $R_2 = H$

2 : $R_1 = R_2 = H$

3 : $R_1 = NH_2$, $R_2 = Br$

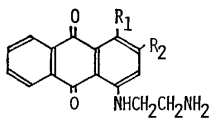

4 : $R_1 = NH_2$, $R_2 = H$

5 : $R_1 = R_2 = H$

6 : $R_1 = NH_2$, $R_2 = Br$

Experimental

Materials. 1-Amino-4-bromoanthraquinone (**1**) and 1-bromoanthraquinone (**2**) were prepared as before.[3] 1-Amino-2,4-dibromoanthraquinone (**3**) was prepared from sodium 1-amino-4-bromoanthraquinone-2-sulfonate by bromination and purified by recrystallization from benzene–ethanol: Found: C, 44.00; H, 1.69; N, 3.63%. Mp 229.4—229.7 °C (cor) (lit,[6] 214 °C). Copper(I) bromide and copper(I) chloride were prepared and purified as described in the literature.[7] Commercially available copper(I) iodide was used without further purification. Copper(II) bromide was purified according to the literature.[8] Copper(II) chloride was dried at 100 °C under vacuum. Chloromethoxycopper-(II) was prepared by the reaction of copper(I) chloride with molecular oxygen in methanol[9] (Found: Cu, 49.0%. Calcd for CH_3OClCu: Cu, 48.87%). All solvents were dried and purified by standard procedure, and stored under a nitrogen atmosphere.

Condensation with Ethylenediamine. Catalyst solution was prepared by the reaction of copper(I) bromide with oxygen in ethanol and EN solution. In a typical experiment, copper(I) bromide (71.7 mg, 5×10^{-4} mol) was weighed into a 40 ml Schlenk type flask equipped with a magnetic stirrer and with a gas inlet connected with a gas buret containing air. After evacuation, N_2 was introduced and the same procedure was repeated several times. Ethanol (5 ml) and EN (8 ml, 1.2×10^{-1} mol) were added into the flask with stirring under a nitrogen atmosphere to give a homogeneous Cu(I) solution. Then oxygen was introduced to the solution with stirring and oxygen consumption was measured by a gas buret. On the other hand, **1** (75.5 mg, 2.5×10^{-4} mol) and the solvent (THF 24 ml, C_2H_5OH 23 ml) were mixed in a 50 ml three necked flask equipped with a reflux condenser, thermometer, and a three-way stopcock. After this solution was brought to the reaction temperature, the reaction was initiated by the addition of the catalyst solution (2.7 ml, Cu content 1.04×10^{-4} mol) with the help of a pipette. The condensation was performed under a dry and oxygen-free nitrogen atmosphere. At regular time intervals, 0.5 ml aliquots of the reaction solution were taken out, diluted in 25 ml of ethanol, and subjected to visible spectral measurements. The yields of **4** based on **1** were determined by use of the absorbance of **4** at 615 nm.[1]

Instruments. UV and visible spectra were measured

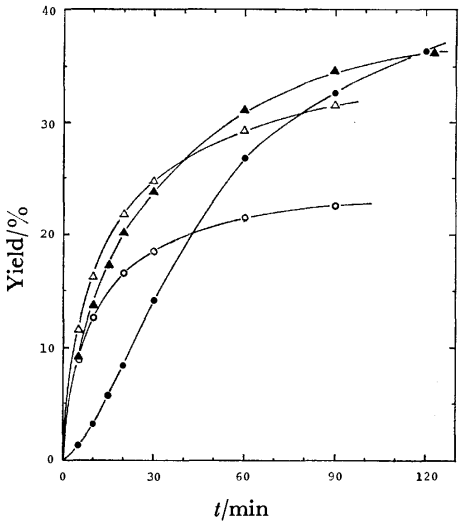

Fig. 1. Time course of the reaction of **1** with EN by Cu catalyst.
$[\mathbf{1}]_0=5.0\times10^{-3}$ mol dm^{-3}, $[EN]_0=0.5$ mol dm^{-3}, $[Cu]_0=2.1\times10^{-3}$ mol dm^{-3}, temp 50 °C, solvent THF–EtOH 1:1. ○: $r([O_2]/[CuBr])=0$, △: $r=0.166$, ▲: $r=0.258$ ●: $r=0.562$.

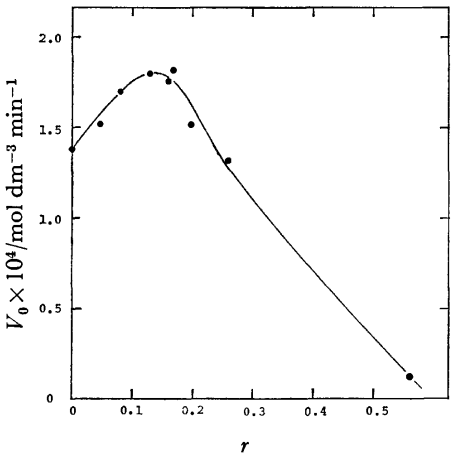

Fig. 2. The dependence of the initial rates (V_0) on the molar ratio $r([O_2]/[CuBr])$ in the reaction of **1** with EN by Cu catalyst.
$[\mathbf{1}]_0=5.0\times10^{-3}$ mol dm^{-3}, $[EN]_0=0.5$ mol dm^{-3}, $[Cu]_0=2.1\times10^{-3}$ mol dm^{-3}, temp 50 °C, solvent THF-EtOH 1:1.

on a Shimadzu UV-210 spectrophotometer. ESR spectra were measured by the use of a JEOL-PE-3X ESR spectrometer, equipped with a 100 KHz field modulation unit.

Results and Discussion

In the condensation with EN using CuBr catalyst under a N_2 atmosphere, the reaction rate decreased with time. The result is interpreted in terms of the formation of ineffective Cu(II) species by an electron transfer from Cu(I) to haloanthraquinone.[1] Upon the introduction of oxygen to the catalyst solution (CuBr–EN–EtOH), the colorless solution turned immediately to deep blue, which indicated the formation of Cu(II) species. By the use of this blue catalyst, the yield of **4** increased unexpectedly, as shown in

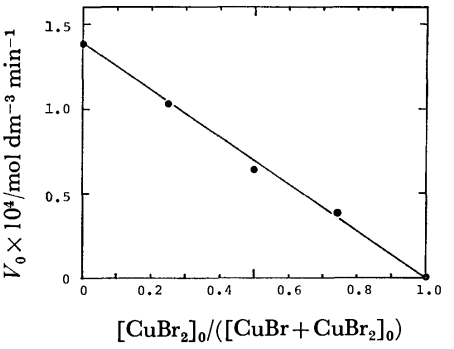

Fig. 3. The effect of the addition of $CuBr_2$ on the initial rates (V_0) in the reaction of **1** with EN by CuBr catalyst.
$[\mathbf{1}]_0=5.0\times10^{-3}$ mol dm^{-3}, $[EN]_0=0.5$ mol dm^{-3}, $[CuBr+CuBr_2]_0=2.1\times10^{-3}$ mol dm^{-3}, temp 50 °C, solvent THF–EtOH 1:1.

Fig. 1. Figure 2 illustrates the plots of the initial rate (V_0) *vs.* the molar ratio(r) of the absorbed oxygen to CuBr. Figures 1 and 2 indicated the following characteristics of the reaction:

i) The initial rate markedly depends on the amount of the oxygen absorbed; the maximum initial rate was observed at the ratio r of about 0.13.

ii) By the catalyst-absorbed small amounts of oxygen, both initial rate and final yield were larger than those obtained by Cu(I) catalyst alone.

iii) In the region of the larger molar ratio(r) the initial rate decreased but the final yield tends to increase. Comparing at 2 h, the catalyst system with a ratio r of 0.56 gave the largest yield, after a clear induction period.

Similar results were observed in other condensation systems such as **1**–EN–CuCl, **2**–EN–CuBr, **2**–EN–CuI, **3**–EN–CuBr, and **3**–EN–CuI. These facts reveal that the oxygen effect is not specific to either haloanthraquinones or copper(I) halides.

Effect of Copper(II) Bromide Addition to Copper(I) Bromide Catalyst System. If copper(II) bromide is used as an alternative to the copper(II) species, formed by the partial oxidation of Cu(I) with molecular oxygen, the reaction rate will increase similarly to the case of the condensation with 2-aminoethanol.[4,5] Figure 3 shows the results of the addition of $CuBr_2$ to CuBr, keeping the total copper amount to be constant, in the condensation with EN under a N_2 atmosphere. Contrary to our expectation, the initial rate decreased linearly with the increase in the molar ratio of $CuBr_2$ to the total copper amount ($CuBr+CuBr_2$). This result shows that $CuBr_2$ does not act as a promoter and only Cu(I) is active in the condensation with EN under N_2. From this result it was concluded that Cu(II) species of the CuBr–EN–EtOH–O_2 catalyst system is different from that of the CuBr–$CuBr_2$–EN–EtOH catalyst system.

Solvent Effects on the Formation of Active Catalyst. The solvent effects on the oxidation of Cu(I) catalyst solution by molecular oxygen were examined as shown in Table 1. These results are compared at the molar ratios(r) ranging from about 0.12 to 0.16: In this region the initial rate revealed a maximum (Fig. 2).

Table 1. Initial rates (V_0) for the reaction of **1** with EN by Cu catalyst[a)]

Entry	Catalyst solution	r[b)]	$V_0\times10^4$/mol dm^{-3} min^{-1}
1	CuBr-EN-EtOH	0.0	1.38
2	CuBr-EN-EtOH-O_2	0.128	1.80
3	CuBr-EN-O_2	0.151	0.91
4	CuBr-EN-O_2+EtOH[c)]	0.130	1.48
5	CuBr-EN-MeOH	0.0	1.32
6	CuBr-EN-MeOH-O_2	0.119	1.74
7	CuBr-EN-py-O_2	0.158	1.53
8	CuBr-EN-*i*-PrOH-O_2	0.135	1.37
9	CuCl-EN-MeOH	0.0	1.45
10	CuCl-EN-MeOH-O_2	0.158	1.58

a) $[\mathbf{1}]_0 = 5.0\times10^{-3}$ mol dm^{-3}, $[EN]_0 = 0.5$ mol dm^{-3}, $[Cu]_0=2.1\times10^{-3}$ mol dm^{-3}, temp 50 °C, solvent THF-EtOH 1:1. b) The molar ratio of the absorbed oxygen to CuX. c) Ethanol was added to CuBr-EN-O_2 system.

The reaction of copper(I) bromide with oxygen in EN-EtOH solution afforded a blue solution containing a blue solid. By this catalyst solution, the yield increased as shown in Fig. 1 (Table 1, Entry 2). The reaction of oxygen with CuBr in EN gave a dark greenish brown solution containing a brown solid. This catalyst solution markedly decreased the initial rate compared with that obtained with CuBr catalyst (Entry 3). However, by the addition of ethanol to the CuBr-EN-O_2 catalyst solution, the color of the solution turned to dark blue and the initial rate increased (Entry 4), though the catalytic activity was smaller than that for the catalyst system CuBr-EN-EtOH-O_2. This result shows that alcohol converted inactive copper(II) species into active ones. The dark greenish brown solution, generated by the reaction of CuBr with O_2 in EN-pyridine solution, also increased the catalytic activity (Entry 7). These results may suggest that ethanol in the condensation solution is related to the formation of active Cu(II) species (see Experimental). The blue catalyst solution formed by the oxidation of CuBr or CuCl with molecular oxygen in EN-MeOH also increased the catalytic activity (Entries 6 and 10). These results indicated that alcohols play a very important role in the formation of active catalyst.

The Role of Alkoxycopper(II) Species. The oxygen uptake by CuBr in methanol was extremely slow without EN, while the reaction of CuCl with oxygen in methanol proceeded moderately and gave a yellowish green solid. The solid is known to be chloromethoxycopper(II) formed by the following stoichiometry:[9)]

$$4CuCl + O_2 \xrightarrow[MeOH]{} 4CuCl(OMe) + 2H_2O. \quad (1)$$

By the addition of CuCl(OMe) the catalytic activity of CuCl increased in spite of the absence of oxygen (Figs. 4 and 5). Further, in the case of CuCl(OMe) alone, an induction period was observed. These results were analogous to the case of oxygen addition.

Figure 6 shows the ESR spectra of the catalyst solution CuCl-EN-MeOH-O_2 (r=0.13), $CuCl_2$-EN-MeOH, and CuCl(OMe)-EN-MeOH at room temperature. The CuCl-EN-MeOH-O_2 system revealed only Cu(II) species as electron paramagnetic species. The coupling constants obtained from the spacing of the third and fourth peaks of the Cu(II) signal are summarized in Table 2. The coupling constant was smaller in the CuX-EN-ROH-O_2 system than in the CuX_2-EN-ROH system. This suggests that the former Cu(II) species has a stronger covalent bond between Cu(II) and the ligand than the latter.[10)] On the other hand, CuCl(OMe) has a more covalent bond character because of strongly electron donating CH_3O ligand than $CuBr_2$ has, and the CuCl(OMe)-EN-MeOH system also indicated a Cu(II) signal with a small coupling constant. These ESR data will also suggest the presence of an alkoxo ligand in the Cu(II)

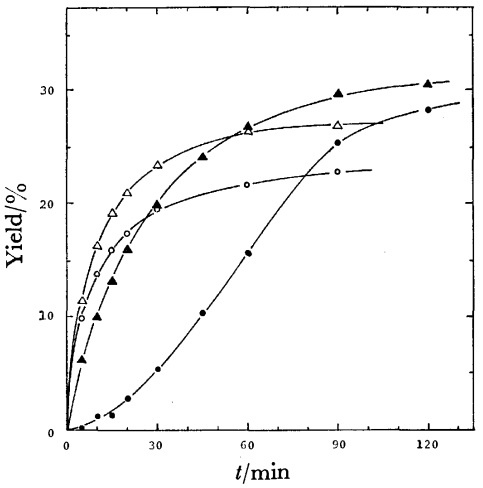

Fig. 4. Time course of the reaction of **1** with EN by CuCl-CuCl(OMe) catalyst.
$[\mathbf{1}]_0=5.0\times10^{-3}$ mol dm^{-3}, $[EN]_0=0.5$ mol dm^{-3}, $[CuCl+CuCl(OMe)]_0=2.1\times10^{-3}$ mol dm^{-3}, temp 50 °C, solvent THF-EtOH 1:1. ○: $r'([CuCl(OMe)]_0/[CuCl+CuCl(OMe)]_0)=0$, △: $r'=0.309$, ▲: $r'=0.751$, ●: $r'=1.0$.

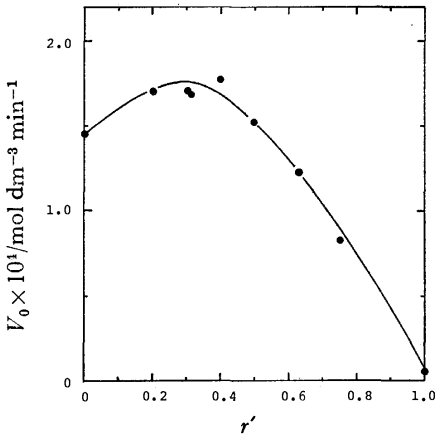

Fig. 5. The dependence of the initial rates (V_0) on the ratio $r'([CuCl(OMe)]_0/[CuCl+CuCl(OMe)]_0)$ in the reaction of **1** with EN.
$[\mathbf{1}]_0=5.0\times10^{-3}$ mol dm^{-3}, $[EN]_0=0.5$ mol dm^{-3}, $[CuCl+CuCl(OMe)]_0=2.1\times10^{-3}$ mol dm^{-3}, temp 50 °C, solvent THF-EtOH 1:1.

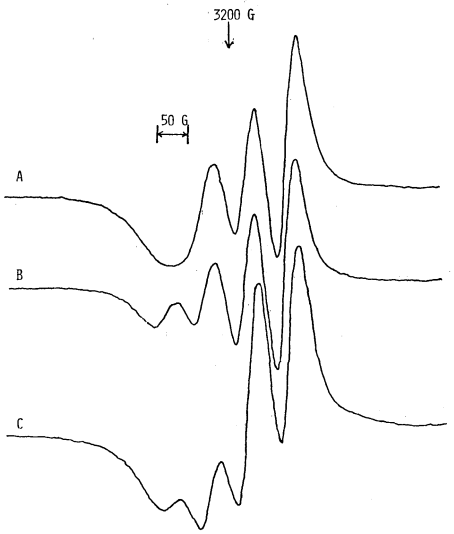

Fig. 6. ESR spectra of Cu catalyst solution at room temperature.
[Cu]$=3.8\times10^{-2}$ mol dm^{-3}, [EN]$=9.2$ mol dm^{-3}. A: CuCl–EN–MeOH–O_2 ($r=0.13$), B: CuCl(OMe)–EN–MeOH, C: $CuCl_2$–EN–MeOH.

Table 2. ESR data of catalyst solution at room temperature[a)]

Catalyst solution	Coupling constants/G[b)]
CuBr–EN–EtOH–O_2[c)]	72.9
CuCl–EN–MeOH–O_2[d)]	71.2
CuCl(OMe)-EN–MeOH	70.9
$CuBr_2$–EN–EtOH	75.8
$CuCl_2$–EN–MeOH	75.4

a) [Cu] $=3.8\times10^{-2}$ mol dm^{-3}, [EN] $=9.2$ mol dm^{-3}. b) 1 G$=10^{-4}$ T. c) $r([O_2]/[CuBr])=0.142$. d) $r=0.205$.

species formed by the oxidation of Cu(I) with molecular oxygen in EN–ROH solution. Consequently, it is concluded that alkoxycopper(II) species is responsible for the activation of Cu(I) catalyst.

In order to clarify the difference between CuX–EN–EtOH–O_2 ($r=0.1$) and CuX–EN–EtOH catalyst system, the apparent activation energy(ΔE^*) was obtained from Arrhenius plots of the initial rate. Partially oxidized catalyst systems have larger activation energies than CuX systems: ΔE^* of **2**–EN–CuI–O_2 and **2**–EN–CuI were 48.5 kJ mol^{-1} and 37.2 kJ mol^{-1} respectively and ΔE^* of **3**–EN–CuI–O_2 and **3**–EN–CuI was 45.2 kJ mol^{-1} and 38.1 kJ mol^{-1}. On the other hand, the preexponential term(A) was increased by the partial oxidation: The ratio of A between **2**–EN–CuI–O_2 and **2**–EN–CuI was 124, and that between **3**–EN–CuI–O_2 and **3**–EN–CuI was 16. These data indicate that the active copper species in the partially oxidized solution differ from the simple Cu(I) species.

In the preparation of the CuBr–$CuBr_2$–EN–EtOH mixture, blue solids were precipitated and these blue precipitates were also observed, though in much smaller amounts, in the CuBr–EN–EtOH–O_2 system. Both of the blue precipitates indicated the same IR spectra and turned to violet (570 nm) when dissolved into THF–MeOH(2:3) solution. It was reported that the colors of $Cu^{II}(EN)$ and $Cu^{II}(EN)_2$ were pale blue and violet respectively, and that the blue $Cu^{II}(EN)_3$ were very unstable and turned to violet $Cu^{II}(EN)_2$ in solution.[11] Consequently, the blue precipitate formed in the presence of large excess EN is considered to be $Cu^{II}(EN)_3$ and it will readily turn to violet $Cu^{II}(EN)_2$ in the reaction mixture(THF–EtOH 1:1).

The blue $Cu^{II}(EN)_3$ or violet $Cu^{II}(EN)_2$ obtained from the CuBr–$CuBr_2$–EN–EtOH system were ineffective to the condensation with EN. Therefore, it was considered that the reaction of CuX and oxygen in EN–ROH generated an inactive copper(II) species and an active alkoxycopper(II) species.

In the CuCl–CuCl(OMe) system, the maximum initial rate appeared when the molar ratio(r') of CuCl(OMe) to total copper was about 0.30 (Fig. 5). On the other hand, in the case of oxygen addition, the maximum rate appeared when the ratio(r) was 0.13 (Fig. 2). If the stoichiometry of the oxidation of Cu(I) by molecular oxygen in EN–ROH solution could be followed by Eq. 2 as done for the oxidation of CuCl in pyridine,[12] these results may be reasonably understood. In Eq. 2, "CuO" and "CuX_2" are active

$$4CuX + O_2 \xrightarrow[EN\text{-}ROH]{} 2\text{“CuO”} + 2\text{“}CuX_2\text{”} \qquad (2)$$

and inactive Cu(II) species, respectively. Thus, in the case of oxygen addition, the maximum initial rate appeared when about a half of the Cu(I) was oxidized. Therefore, the ratio of active Cu(II) to total Cu(II) was 0.25. Thus, the molar ratio of active Cu(II) species to the active copper species was $0.25/(0.5+0.25)=0.33$. This value is in accord with the ratio 0.30 in the CuCl–CuCl(OMe) system under a N_2 atmosphere. The initial rate of CuX–EN–EtOH–O_2 was smaller than that of CuCl–CuCl(OMe). This result can also be understood by the idea that the inactive Cu(II) species was formed along with active Cu(II) species in the CuX–EN–ROH–O_2 system followed by Eq. 2.

Although it has been established that one equivalent of molecular oxygen oxidized 4 molar equivalents of Cu(I),[13–16] Fig. 2 shows that the oxygen consumption in EN–EtOH solution exceeds the molar ratio $r(O_2/CuBr)=0.25$. Davies *et al.* reported that O_2 consumption of more than $r=0.25$ was observed in the reaction of copper(I) chloride with oxygen in pyrrolidine, piperidine, or cyclam, and they described the possibility of the proton removal from N–H groups.[17] In our case, the side reaction such as the oxidation of EN may take place, but the side reaction may occur very slowly and would be negligible at the maximum initial rate, since the oxygen uptake of more than the molar ratio of 0.25 took a very long time.

The Presence of an Induction Period. The induction period is observed when CuBr–EN–EtOH–O_2 ($r=0.56$) or CuCl(OMe) only was used (Figs. 1 and 4). The ESR measurement of these condensation systems showed that the Cu(II) signal height gradually decreased. On the contrary, AQBr–EN–$CuBr_2$ system showed no

decrease of Cu(II) signal height under heating. These facts may indicate that a part of the active alkoxycopper(II) species was reduced to active Cu(I), which accelerates the reaction by the combination with the active Cu(II).

These results will shed light on the cooperative behavior between Cu(I) and Cu(II) in the condensation with 2-aminoethanol(AE). As described in the previous papers,[4,5] the induction period in the condensation system of **1** or **2**–AE–CuBr vanished by the addition of $CuBr_2$, which did not activate the condensation with EN. This fact may be reasonably understood by the idea that 2-aminoethanol itself has a OH group and functions as an alkoxide. Hodgson *et al.* reported the molecular structure of Cu(II) complex, prepared by treating $CuBr_2$ with 2-dibutylaminoethanol, to be an oxygen-bridged dimer:[18]

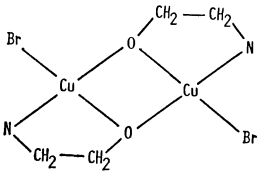

Reaction Pathway. All of the observed results eliminate the possibility of a mechanism as described by Scheme 1,[19] where Cu(I)···O_2 or Cu(II)···superoxide complex functions to activate the condensation reaction:

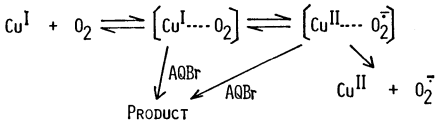

Scheme 1.

The most plausible reaction pathways are shown in Scheme 2.[19] Under a N_2 atmosphere, only Cu(I) is active; the inactive $Cu^{II}(EN)_2$ is formed by an electron transfer from Cu(I) to AQBr and then the reaction rate decreases with the formation of Cu(II) species. In the presence of oxygen there may be several possible reaction pathways. The reaction of Cu(I) with molecular oxygen in EN–ROH solution affords the active alkoxycopper(II) species and inactive $Cu^{II}(EN)_2$. The CuCl(OMe) and $Cu(OMe)_2$ have been known to exist as a polymer.[20] An oxidation of CuCl in methanol containing pyridine generated di-μ-methoxo-bis[chloropyridinecopper(II)], the structure of which was established by X-ray analysis to be the methoxo bridged dimer (Eq. 3):[14]

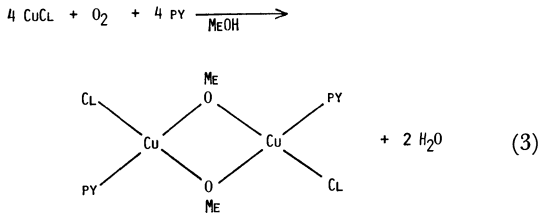

(3)

Therefore, the alkoxycopper(II) species formed by the partial oxidation of Cu(I) in EN–EtOH solution would probably have an ability to form a dimeric structure with Cu(I) or Cu(II) by alkoxo bridge.

One possible pathway is as follows: The Cu^{I}···Cu^{II} mixed valence complex is formed by the reaction between monomeric alkoxycopper(II) species and Cu(I). The cooperative behavior of Cu(I) and Cu(II) may be caused by this dimeric species. The pathway catalyzed by Cu(I) alone also operates independently. On the other hand, in the case of CuCl(OMe) alone the catalytic activity increased gradually with the formation of Cu(I). This result may suggest that alkoxo and/or halogen bridged dimeric species is reduced to give active Cu^{I}···Cu^{II} mixed valence complex.

However, the present data do not exclude another

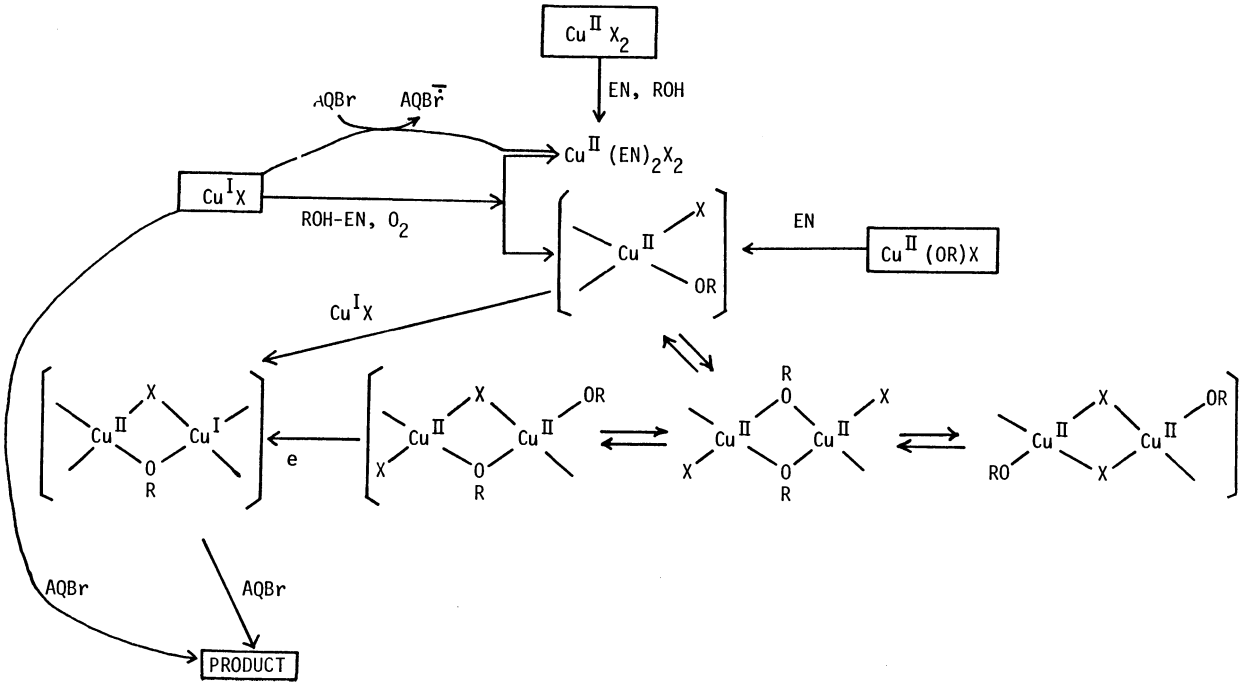

Scheme 2.

pathway on which Cu(I) and Cu(II) do not form any dimeric species but act cooperatively to enhance the catalytic activity.

These results are helpful in exploration of the more active catalyst of the Ullmann condensation reaction.

Further detailed examinations of the cooperative behavior of Cu(I) and Cu(II) are progress and will be reported in the near future.

References

1) Part IV of this series: S. Arai, A. Tanaka, M. Hida, and T. Yamagishi, *Bull. Chem. Soc. Jpn.*, **52**, 1731 (1979).
2) M. Hida, *Yuki Gosei Kagaku Kyokai Shi*, **37**, 207 (1979).
3) S. Arai, T. Yamagishi, S. Ototake, and M. Hida, *Bull. Chem. Soc. Jpn.*, **50**, 547 (1977).
4) S. Arai, M. Hida, T. Yamagishi, and S. Ototake, *Bull. Chem. Soc. Jpn.*, **50**, 2982 (1977).
5) S. Arai, M. Hida, and T. Yamagishi, *Bull. Chem. Soc. Jpn.*, **51**, 277 (1978).
6) F. H. Day, *J. Chem. Soc.*, **1939**, 816.
7) R. N. Keller and H. D. Wycoff, *Inorg. Synth.*, **2**, 1 (1946).
8) S. O. Adeosun and V. O. Nwanze, *J. Inorg. Nucl. Chem.*, **37**, 2091 (1975).
9) H. Finkbeiner, A. S. Hay, H. S. Blanchard, and G. F. Endres, *J. Org. Chem.*, **31**, 549 (1966).
10) B. A. Goodman and J. B. Raynor, "Adv. Inorg. Radiochem," ed by H. J. Emeleus and A. G. Sharpe, Academic Press, New York (1970), Vol. 13, p. 135.
11) Y. Itoh, "Jikken Kagaku Kōza," ed by Nippon Kagaku Kai, Maruzen, Tokyo (1956), Vol. 11, pp. 80—81.
12) a) C. E. Kramer, G. Davies, R. B. Davis and R. W. Slaven, *J. Chem. Soc., Chem. Commun.*, **1975**, 606; b) I. Bodek and G. Davies, *Inorg. Chem.*, **17**, 1814 (1978).
13) H. Praliaud, Y. Kodratoff, G. Coudurier, and M. V. Mathieu, *Spectrochim. Acta, Part A*, **30**, 1389 (1974), and references therein.
14) M. M. Rogic and T. R. Demmin, *J. Am. Chem. Soc.*, **100**, 5472 (1978), and references therein.
15) Y. Ogata and T. Morimoto, *Tetrahedron*, **21**, 2791 (1965).
16) G. Condurier, H. Praliand, and M. V. Mathieu, *Spectrochim. Acta, Part A*, **30**, 1399 (1974).
17) G. Davies, M. F. El-Shazly, D. R. Kozlowski, C. E. Kramer, M. W. Rupich, and R. W. Slaven, *Adv. Chem. Ser.*, **173**, 15 (1979).
18) E. Dixon Estes and D. J. Hodgson, *Inorg. Chem.*, **14**, 334 (1975). Butyl groups are omitted for clarity.
19) Ethylenediamine ligands are omitted from Schemes 1 and 2 for clarity.
20) C. H. Brubaker, Jr., and M. Wicholas, *J. Inorg. Nucl. Chem.*, **27**, 59 (1965).

Crystal Structure of *N*-Benzyl-α-methoxycarbonylmethanimine *N*-Oxide

Yoshinobu INOUYE

Department of Chemistry, University of Tsukuba, Sakura-mura, Niihari-gun, Ibaraki 305

(Received June 5, 1982)

The geometry of *N*-benzyl-α-methoxycarbonylmethanimine *N*-oxide in the crystalline state was established to be *Z* by X-ray crystal analysis. The crystal was monoclinic, space group Pc, $a=11.069(1)$, $b=5.2335(7)$, $c=8.620(1)$ Å, $\beta=105.37(1)°$, $Z=2$. The final *R* value was 0.037 for 1760 reflections.

During the last decade, many approaches have been developed by using a nitrone as a constructive unit to provide various kinds of natural products.[1-4] Most of these nitrones have been cyclic, while acyclic ones have been limited to special cases.[4]

Acyclic nitrones, in contrast to cyclic ones, have the possibility of geometrical isomerism around a C=N bond. However, aldonitrones have generally been shown to exist only in a stable *Z*-configuration (**1a**), both in crystals[5] and in solution.[6]

1a **1b**

In 1974, Bjørgo and his co-workers[7] isolated *E*-aldonitrone (**1b**, R:pentamethylphenyl, R′:methyl) by the oxidation of a corresponding imine with *m*-chloroperbenzoic acid and found that the *E*-isomer isomerized to the more stable *Z*-isomer when heated at 35 °C in the presence of benzoic acid. The final *E*/*Z* ratio was found to be 0.20 in $CDCl_3$.

Recently, we found that *N*-benzyl-α-methoxycarbonylmethanimine *N*-oxide (**2**) and its analogues exist in one configuration in the ctystalline state, but in solution exhibit a facile isomerization to give a mixture of *E*- and *Z*-isomers——the *E*/*Z* ratio being 1.6 in $CDCl_3$ (Fig. 1).[8] The assignment of the configuration was deduced from the difference in the chemical shifts of the benzylic protons in the two isomers.

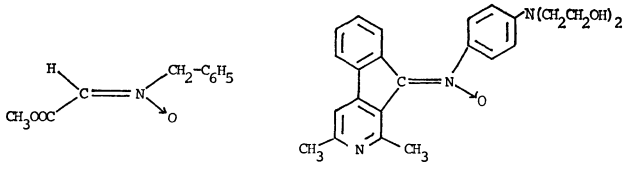

2 **3**

Soon after, a similar time-dependent isomerization of a ketonitrone, **3**, was reported.[9] In both nitrones, **2** and **3**, an *E*-isomer, which is generally thought to be thermodynamically unstable, is predominant in solution.

In this investigation, a single-crystal X-ray analysis of **2** was performed in order to clarify the configuration in the crystalline state.

Experimental

Data Collection. *N*-Benzyl-α-methoxycarbonylmethanimine *N*-oxide (**2**)[4b] was slowly crystallized from benzene. Preliminary oscillation and Weissenberg photographs showed the space group to be either Pc or P2/c. The density was measured by the flotation method in a heptane–carbon tetrachloride mixture. The unit-cell dimensions were refined on a Rigaku automatic four circle diffractometer with graphite-monochromated Mo *Kα* radiation (40 kV, 100 mA). The crystal data are shown in Table 1.

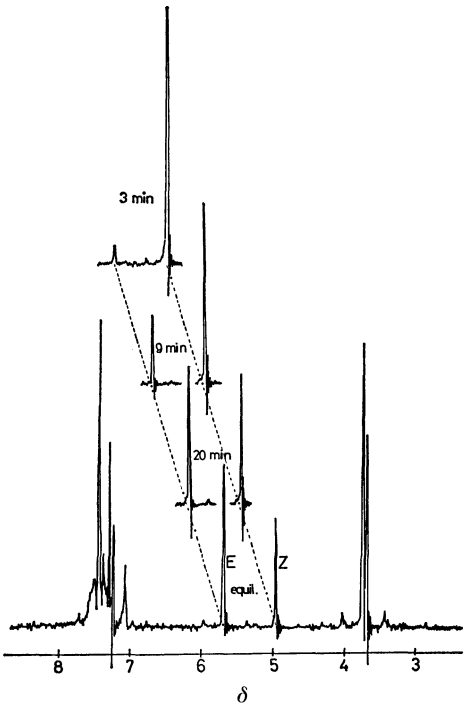

Fig. 1. Time-dependence of the intensities of the benzylic protons in the NMR spectra of **2** in $CDCl_3$.

TABLE 1. CRYSTAL DATA

$C_{10}H_{11}NO_3$	M.W. = 193.2
Monoclinic	Pc
$a=11.069(1)$ Å	
$b=5.2335(7)$ Å	
$c=8.620(1)$ Å	
$\beta=105.37(1)°$	
$D_m=1.32$ g cm^{-3}	
$D_x=1.33$ g cm^{-3}	
$Z=2$	

The intensity data were collected, using a single crystal with dimensions of $0.45\times0.50\times0.53$ mm^3, on a diffractometer by the $\omega/2\theta$ scanning technique within $67°>2\theta$ at room temperature. The intensities of three standard reflections, measured every 50 reflections, were stable within a 2% fluctuation during the course of the data collection.

Of the 1981 unique observed reflections, 1760 reflections with $|F_o|\geq3\sigma(F)$ were used for the structure determinations. The intensities were corrected for Lorentz and polarization effects, but not for absorption. All the computations

Table 2. The final atomic parameters and estimated standard deviations

(1) The non-hydrogen atoms ($\times 10^4$) with the equivalent isotropic temperature factors.[13]

Atom	x	y	z	B_{eq}/Å^2
C(1)	−749(3)	3193(6)	−2040(4)	5.26
O(2)	162(3)	3812(3)	−559(4)	4.64
C(3)	660(3)	1839(3)	388(4)	3.53
O(4)	388(3)	−358(3)	76(4)	4.90
C(5)	1546(3)	2870(3)	1830(4)	3.52
N(6)	2261(3)	1471(2)	2952(3)	3.36
O(7)	2352(3)	−956(2)	2943(4)	4.42
C(8)	3080(3)	2783(3)	4393(4)	3.75
C(9)	4431(3)	2599(3)	4375(4)	3.37
C(10)	4917(3)	4386(4)	3510(4)	4.00
C(11)	6161(3)	4243(4)	3462(4)	4.75
C(12)	6926(3)	2348(5)	4288(4)	4.79
C(13)	6449(3)	567(5)	5150(4)	5.07
C(14)	5213(3)	685(3)	5198(4)	4.39

(2) The hydrogen atoms ($\times 10^3$).

Atom	x	y	z	B/Å^2
H(1)	−99(3)	486(7)	−253(5)	4.6(7)
H(2)	−139(3)	236(6)	−183(4)	4.3(7)
H(3)	−40(3)	212(7)	−261(4)	4.5(7)
H(4)	160(2)	457(5)	196(3)	1.9(4)
H(5)	283(2)	457(5)	440(3)	2.3(4)
H(6)	295(3)	178(5)	535(3)	3.1(5)
H(7)	442(3)	580(4)	297(3)	2.7(5)
H(8)	653(3)	549(5)	292(3)	3.0(5)
H(9)	769(3)	224(6)	426(4)	3.5(6)
H(10)	691(3)	−65(6)	570(4)	3.7(6)
H(11)	487(3)	−55(7)	580(5)	5.0(8)

were carried out on a FACOM M-200 computer in the Science Information Processing Center of the University of Tsukuba.

Structure Determination. Since the number of molecules in the unit cell was 2, the space goup P2/c was certainly excluded. The structure was solved by using Patterson and Fourier methods and was refined by the full-matrix least-squares method with the *RFINE*-2 program.[10] The atomic scattering factors, given by Cromer and Mann[11] for C, N, or O, and listed on the table[12] for H were used.

From the analysis of a three-dimensional Patterson map, the coordinates of a benzene ring were placed on the plane which includes the Y axis and declines 62° from the X-Y plane. The repeated removal-addition of atoms on difference Fourier syntheses revealed the positions of all the non-hydrogen atoms. A nitrone chromophore, instead of a benzene ring, was finally found to be placed on that plane.

The R value at this stage was 0.258 and was reduced to 0.062 when refined with anisotropic temperature factors. Then, the positions of the hydrogens were obtained from a difference Fourier synthesis and were also refined. The final refinement with anisotropic temperature factors for all non-hydrogen atoms and with an isotropic one for hydrogens reduced the R value to 0.037. The residuals in the difference map were within the range of ±0.17 e/Å^3. The final atomic parameters are listed in Table 2 (for the numbering diagram, see Fig. 2). The F_o-F_c table is kept as

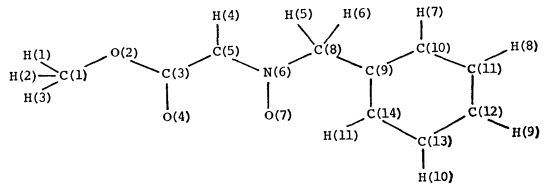

Fig. 2. Numbering diagram for **2**.

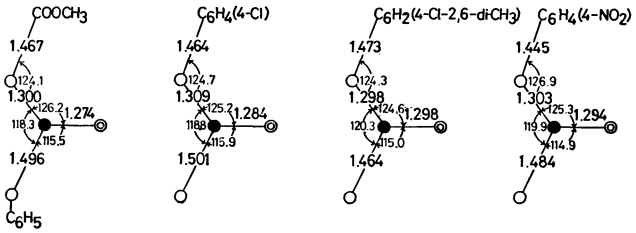

(a) **2** (b) **4**[5a] (c) **5**[5b] (d) **6**[5c]

Fig. 3. Geometries around the nitrone chromophore.
●: Nitrogen, ◎: Oxygen, ○: Carbon

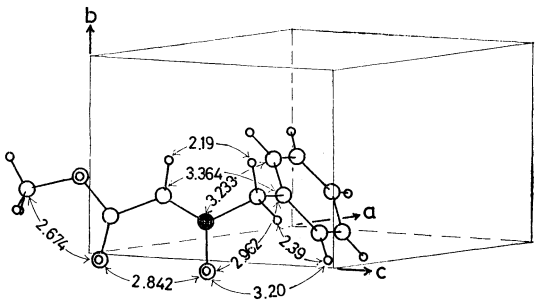

Fig. 4. The conformation of **2** projected on the ester plane.
Small circles show hydrogen atoms.

Document No. 8305 at the Chemical Society of Japan.

Results and Discussion

The configuration around the C=N bond was clearly established to be Z as was previously assumed.[8]

The bond distances and bond angles are listed in Table 3. The geometry around the nitrone chromophor is in good agreement with those of *N*-methyl-α-(4-chlorophenyl)methanimine *N*-oxide (**4**),[5a] *N*-methyl-α-(4-chloro-2,6-dimethylphenyl)methanimine *N*-oxide (**5**),[5b] and *N*-methyl-α-(4-nitrophenyl)methanimine *N*-oxide (**6**),[5c] as is shown in Fig. 3, and no unusual bond distances or angles were observed.

The conformation of the molecule projected on the ester plane [O(2)–C(3)–O(4)] is illustrated in Fig. 4. The figures show some short interatomic distances within a molecule. The ester and the nitrone chromophores exist essentially on the same plane (Table 4). This is due to the conjugation effect of both chromophores. Similar effects had also been observed in **4** and **6** as the coplanarity of the benzene ring with the nitrone chromophore. On the other hand, the benzene ring in **2** is twisted toward the direction of minimizing the van der Waals interaction between O(7)–C(9) and N(6)–C(10).

The crystal structure projected on the (100) plane

Table 3. The bond distances and angles with their standard deviations

Bond distance	l/Å	Bond distance	l/Å
C(1)-O(2)	1.438(4)	C(1)-H(1)	0.97(4)
O(2)-C(3)	1.341(3)	C(1)-H(2)	0.89(4)
C(3)-O(4)	1.201(2)	C(1)-H(3)	0.92(4)
C(3)-C(5)	1.467(4)	C(5)-H(4)	0.90(2)
C(5)-N(6)	1.300(3)	C(8)-H(3)	0.97(3)
N(6)-O(7)	1.274(2)	C(8)-H(6)	1.02(3)
N(6)-C(8)	1.496(3)	C(10)-H(7)	0.97(2)
C(8)-C(9)	1.503(5)	C(11)-H(8)	0.95(3)
C(9)-C(10)	1.390(4)	C(12)-H(9)	0.85(3)
C(9)-C(14)	1.389(3)	C(13)-H(10)	0.87(3)
C(10)-C(11)	1.390(5)	C(14)-H(11)	0.97(4)
C(11)-C(12)	1.374(4)		
C(12)-C(13)	1.381(5)		
C(13)-C(14)	1.381(5)		
Bond angle	ϕ/°	Bond angle	ϕ/°
C(1)-O(2)-C(3)	116.4(2)	C(8)-C(9)-C(10)	119.3(2)
O(2)-C(3)-O(4)	124.3(3)	C(8)-C(9)-C(14)	121.9(3)
O(2)-C(3)-C(5)	107.9(2)	C(10)-C(9)-C(14)	118.8(3)
O(4)-C(3)-C(5)	127.8(2)	C(9)-C(10)-C(11)	120.4(2)
C(3)-C(5)-N(6)	124.1(2)	C(10)-C(11)-C(12)	120.2(3)
C(5)-N(6)-O(7)	126.2(2)	C(11)-C(12)-C(13)	119.6(3)
C(5)-N(6)-C(8)	118.3(1)	C(12)-C(13)-C(14)	120.6(3)
O(7)-N(6)-C(8)	115.5(2)	C(13)-C(14)-C(9)	120.4(3)
N(6)-C(8)-C(9)	110.3(3)		

Table 4. Least-squares planes and dihedral angles
$X=ax+cz\cos\beta$, $Y=by$, $Z=cz\sin\beta$

(1) Equation

I: the ester group [O(2)-C(3)-O(4)]
$-0.8808X+0.0707Y+0.4681Z+0.347=0.0$

II: the nitrone chromophore [C(5)-N(6)-O(7)]
$-0.8889X-0.0744Y+0.4521Z+0.573=0.0$

III: the benzene ring [C(9)-C(10)-C(11)-C(12)-C(13)-C(14)]
$-0.0499X-0.5860Y-0.8088Z+3.933=0.0$

(2) Dihedral angle

between I and II planes (ϕ/°)	8.4
between II and III planes	106.1

is shown in Fig. 5. All the intermolecular atomic contacts are usual van der Waals distances, the shortest ones are O(2) (x, y, z)—O(4) (x, $y+1$, z) (3.10 Å) between non-hydrogen atoms and H(6) (x, y, z)—O(7) (x, $-y$, $z+0.5$) (2.53 Å) involving hydrogen atoms. The value of 2.53 Å is just the sum of the Kitaigorodskii intermolecular radii, R;[14] the C–H···O attraction, initially found in 2-methyl-3-(4-chloro-2,6-dimethylphenyl)oxazolidine (2.30 Å)[15] and followed in **4** (2.15 Å)[5b] and **5** (2.14 Å),[5b] was not recognized in the present nitrone **2**.

The author wishes to express his deep thanks to Dr. Izumi Nakai, University of Tsukuba, for his varied support in the data collections and computations. The *RFINE*-2 program used in this study is that modified by Dr. Hiroyuki Horiuchi, Osaka University, to whom the author is also deeply obliged.

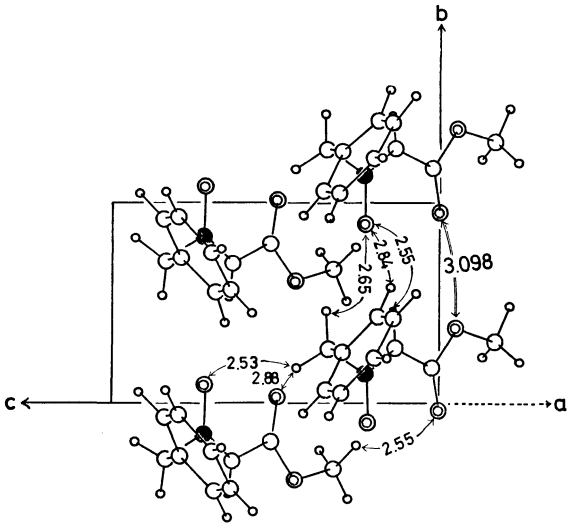

Eig. 5. The crystal structure of **2** projected on (100) plane.

References

1) For a recent review, see J. J. Tufariello, *Acc. Chem. Res.*, **12**, 396 (1979).

2) M. Wovkulich and M. R. Uskoković, *J. Am. Chem. Soc.*, **103**, 3956 (1981).

3) T. Iwashita, T. Kusumi, and H. Kakisawa, *J. Org. Chem.*, **47**, 230 (1982).

4) a) Y. Inouye, Y. Watanabe, S. Takahashi, and H. Kakisawa, *Bull. Chem. Soc. Jpn.*, **52**, 3763 (1979); b) J. Hara, Y. Inouye, and H. Kakisawa, *ibid.*, **54**, 3871 (1981).

5) a) K. Folting, W. N. Lipscomb, and B. Jerslev, *Acta Chem. Scand.*, **17**, 2138 (1963); b) K. G. Jensen and B. Jerslev,

Acta Crystallogr., Sect. B, **25**, 916 (1969); c) F. Bachechi and L. Zambonelli, *ibid.*, **31**, 2499 (1975).

6) a) J. Thesing and W. Sirrenberg, *Chem. Ber.*, **91**, 1978 (1958); b) D. R. Boyd, W. B. Jennings, and R. Spratt, *J. Chem. Soc., D*, **1970**, 745.

7) J. Bjørgo, D. R. Boyd, and D. C. Neill, *J. Chem. Soc., Chem. Commun.*, **1974**, 478.

8) Y. Inouye, J. Hara, and H. Kakisawa, *Chem. Lett.*, **1980**, 1407.

9) D. Tresselt and W. Schulze, *Pharmazie*, **36**, 405 (1981).

10) L. W. Finger and E. Prince, U. S. Nat. Bur. Stand. Tech. Note, 854 (1975).

11) D. T. Cromer and J. Mann, *Acta Crystallogr., Sect. A*, **24**, 321 (1968).

12) "International Tables for X-Ray Crystallography," Kynoch Press, Birmingham (1974), Vol. IV.

13) W. C. Hamilton, *Acta Crystallogr.*, **12**, 609 (1959).

14) A. I. Kitaigorodskii, "Organic Chemical Crystallography," Consultants Bureau, New York (1961).

15) B. Jerslev, *Acta Crystallogr.*, **23**, 645 (1967).

Nucleophilic Substitution on 4-Methylbenzyl Thiocyanate with Nucleophiles

Shigeru OAE,* Norihiro YAMADA, Ken FUJIMORI, and Osamu KIKUCHI
Department of Chemistry, University of Tsukuba, Sakura-mura, Niihari-gun, Ibaraki 305
(Received April 21, 1982)

The reactions of 4-methylbenzyl thiocyanate (**1**) with several nucleophiles have been investigated. Compound **1** possesses three electrophilic sites, *i.e.*, benzylic carbon, sulfur and cyano carbon, to receive nucleophilic attack. PhS^- and CN^- which have HOMO's of high energy levels appear to attack preferentially the sulfur atom. MeO^- was found to attack preferably the cyanide carbon, while amines which have HOMO's of low energy levels prefer benzylic carbon to attack. The nucleophilic substitution on the sulfur or the cyanide carbon generates CN^- or *p*-xylene-α-thiolate anion, strong nucleophiles, as the primary products, which then initiate the complex secondary reactions. The selective reactivities of three attacking sites for nucleophiles in **1** have been rationalized in terms of MO theory.

The reactions between organic thiocyanates and nucleophiles are of interest, because organic thiocyanates possess three reacting sites for the nucleophilic attack, *i.e.*, the carbon linked to thiocyanato group (site a), the sulfur atom (site b), and the cyanide carbon atom (site c), (Fig. 1).[1,2] The reactions of organic thiocyanates with a few nucleophiles have been investigated mainly for synthetic interest to prepare thiols from thiocyanates.[3] Giles and Parker carried out mechanistic studies on the reaction between 2,4-dinitrophenyl thiocyanate and various nucleophiles in DMF.[2] They determined the rate constants for the reactions at the sites a, b, and c with various nucleophiles, and concluded that thiolate anion is the only nucleophile which attacked the sulfur atom (site b) among nucleophiles they used, *i.e.*, RS^-, CN^-, ArS^-, RO^-, ArO^-, SCN^-, N_3^-, amines, halide anions, and NO_2^-.

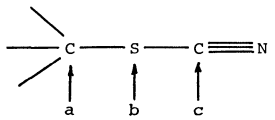

Fig. 1. Three possible sites for the reaction of organic thiocyanate with nucleophiles.

However, no systematic investigation on the reactions between alkyl thiocyanate and various nucleophiles has been reported. Thus, we have initiated the investigation of the reaction between alkyl thiocyanate and various nucleophiles. When the initial attack of nucleophile on 4-methylbenzyl thiocyanate (**1**) took place at the sites b and c, the reactions were found to be very complex because of various secondary reactions initiated by CN^- or $4\text{-}CH_3C_6H_4CH_2S^-$ (**6**) which were generated by the initial nucleophilic displacements at the sites b and c of **1**, respectively. On the other hand, no such secondary reaction was observed, when the initial reaction proceeded at the site a, which produced SCN^-, a relatively weak nucleophile. In order to characterize the leaving ability of thiocyanate upon nucleophilic substitution as a pseudo-halogen, rate constants of the reaction between **1** and 4-methylbenzyl halides and 1,4-diazabicyclo[2.2.2]-octane (DABCO) were measured in an aprotic solvent, *i.e.*, acetonitrile since the nucleophilic attack by DABCO has been found to take place exclusively at the site a.

The nucleophiles used in this work and all possible reaction products with these nucleophiles are listed in Table 1.

Results and Discussion

4-Methylbenzyl thiocyanate (**1**) was chosen as the substrate for this purpose since it has no α-hydrogen atom to initiate the base catalyzed elimination of hydrogen thiocyanate forming olefin and it is convenient to analyze reaction products by the NMR method.

Reaction with Potassium Benzenethiolate in Methanol. The reaction of **1** with potassium benzenethiolate was conducted in methanol at room temperature and followed by GLPC. The starting material **1** was found to disappear immediately, generating 4-methylbenzyl phenyl disulfide (**2**) as the major product along with minor products, *i.e.*, diphenyl disulfide and bis(4-methylbenzyl) disulfide (**4**). Then, three disulfides were gradually converted to 4-methylbenzyl phenyl sulfide (**3**) as shown in Fig. 2. After 2 d at room temperature, **3** was obtained eventually as the sole product (90% isolated yield). This may be rationalized by the mechanism illustrated in Scheme 1. Initial formation of a large amount of the unsymmetrical disulfide **2** as the primary product suggests that the initial

TABLE 1. ALL POSSIBLE REACTION PRODUCTS IN THE REACTIONS OF RSCN WITH NUCLEOPHILES

Nucleophile	Reaction site		
	a	b	c
PhS^-	$R\text{-}SPh + SCN^-$	$RS\text{-}SPh + CN^-$	$PhS\text{-}CN + RS^-$
CN^-	$R\text{-}CN + SCN^-$	$RS\text{-}CN + CN^-$	$NC\text{-}CN + RS^-$
MeO^-	$R\text{-}OMe + SCN^-$	$RS\text{-}OMe + CN^-$	$MeO\text{-}CN + RS^-$
R'_3N	$R\text{-}{}^+NR'_3 + SCN^-$	$RS\text{-}{}^+NR'_3 + CN^-$	$R'_3N^+\text{-}CN + RS^-$
N_3^-	$R\text{-}N_3 + SCN^-$	$RS\text{-}N_3 + CN^-$	$N_3\text{-}CN + RS^-$

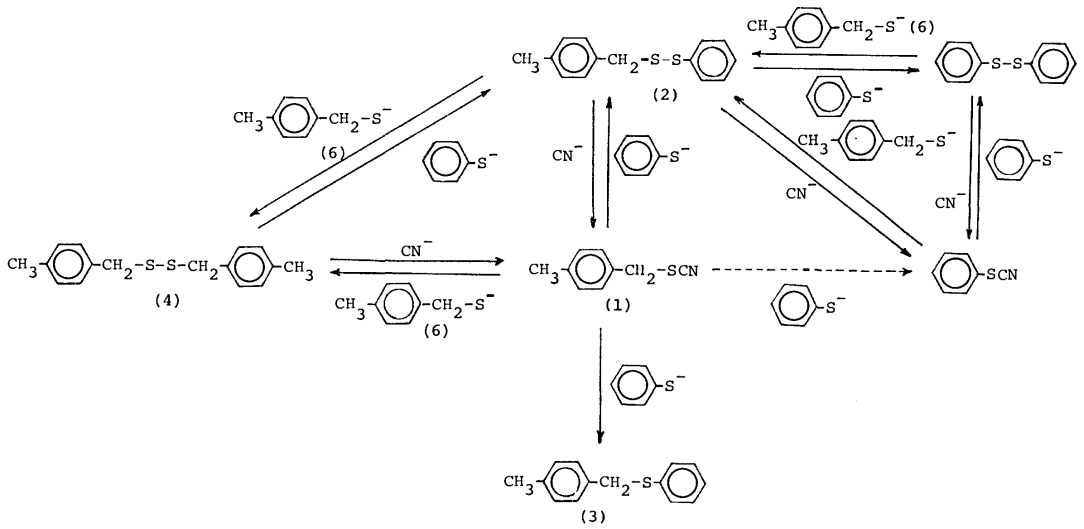

Scheme 1. Possible reaction paths for the reaction of **1** with potassium benzenethiolate.

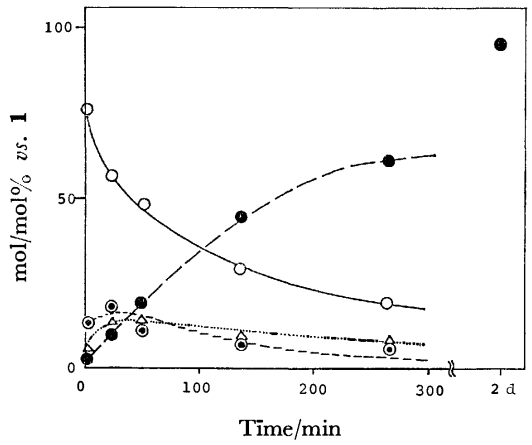

Fig. 2. The reaction of **1** (1.05 mmol) with potassium benzenethiolate (1.24 mmol) in methanol (3 ml) at 25 °C.
○: **2**, ●: **3**, △: **4**, ⊙: diphenyl disulfide.

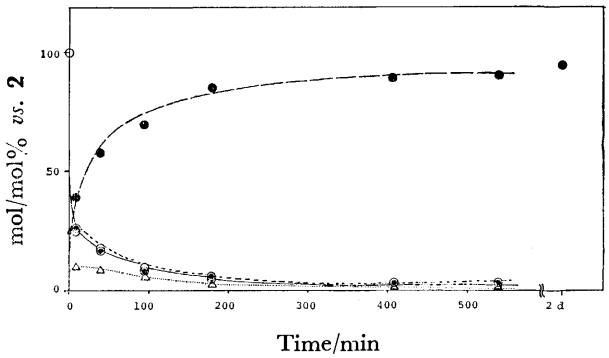

Fig. 3. The reaction of **2** (0.459 mmol) with equimolar amount of sodium cyanide in acetonitrile (5 ml) in the presence of 18-crown-6 (0.114 mmol) at 25 °C.
○: **2**, ●: **3**, △: **4**, ⊙: diphenyl disulfide.

attack of benzenethiolate anion toward **1** takes place mainly on the sulfur atom of **1** (site b) in keeping with the precept that the thiolate anion is an excellent nucleophile toward divalent sulfur,[4] while the reaction at the site a took place very slowly forming **3** irreversibly. However, since cyanide anion, one of the primary product of the reaction at the site b with benzenethiolate anion, has a strong thiophilicity toward divalent sulfur,[4,5] the reaction of the unsymmetrical disulfide **2** with cyanide anion (CN^-) reproduces the staring **1** or generates phenyl thiocyanate depending on the attacking sites of two sulfur atoms of **2**. The unsymmetrical disulfide **2** gives the symmetrical disulfide **4** by the reaction with *p*-xylene-α-thiolate anion (**6**), while the reaction with benzenethiolate anion forms diphenyl disulfide which may react with CN^- to result phenyl thiocyanate. Phenyl thiocyanate reproduces the disulfide **2** and diphenyl disulfide by the reaction with **6** and benzenethiolate anion (PhS^-), respectively.

The control experiment showed, in fact, that the reaction of phenyl thiocyanate with **6** took place immediately to give the same products distribution as the reaction between **1** and PhS^-. The reaction of **1** with **6** (site b) also generates the symmetrical disulfide **4**, which reproduces either **1** upon the reverse reaction with CN^- or **2** by the reaction with PhS^-. In fact, treatment of the symmetrical disulfide **4** with CN^- in a separate experiment gave bis(4-methylbenzyl) sulfide **5** which was produced undoubtedly *via* **1**. Absence of **5** in the final reaction mixture of the reaction of **1** with PhS^- is due to that the steady concentration of the thiolate anion **6** is too small to compare with that of PhS^- during the reaction. Thus, the unsymmetrical sulfide **3** is gradually formed as the final product through the irreversible reaction at the site a of **1** which is regenerated through the reversible reactions, as shown in Scheme 1.

The sequence of the secondary reactions which start from the unsymmetrical disulfide **2** by action of CN^- and thiolate anions have been substantiated by the following control experiment. The reaction between sodium cyanide and the disulfide **2** under the same conditions which have been applied for the reaction of **1** with potassium benzenethiolate, gave the mixture of same products and followed the kinetic course shown in Fig. 3 as the reaction between **1** and potas-

sium benzenethiolate did; *i.e.*, Fig. 3 is roughly identical to Fig. 2.

The consequence of this rapid equilibration among two thiocyanates and two disulfides which are promoted by both CN^- and the thiolate anions is well consistent with the result of Harpp *et al.* who observed that CN^- catalyzed S–S bond fission of unsymmetrical disulfide forms the following equilibrium and eventually affords the symmetrical sulfide (Scheme 2).[5]

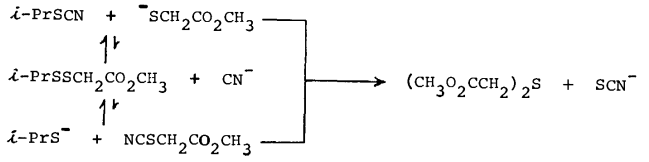

Scheme 2. Cyanide cleavage of unsymmetrical disulfide.

The rate ratio of the reactions at the site a forming **3** *vs.* that at the site c to afford thiocyanate for the reaction of **1** with PhS^- may be greater than that of the reaction at the site a *vs.* that of the site e for the reaction of 2,4-dinitrophenyl thiocyanate with thiolate anion, because the leaving ability of 2,4-dinitrobenzenethiolate must be much better than that of **6**. Therefore, the fact that the reaction at the site a is 10^3 folds faster than that at the site c in the reaction of 2,4-dinitrophenyl thiocyanate with PhS^- may suggest that the reaction at the site c in the reaction of **1** with PhS^- is less important than that at the site a.

Reaction with Sodium Methoxide in Methanol. The reaction between **1** and sodium methoxide in methanol was completed within a minute at room temperature under argon. The symmetrical disulfide **4** was obtained as the major product (89% isolated yield). Any 4-methylbenzyl methyl ether which is expected to be produced by the reaction at the site a was not detected by GLPC analysis of the reaction mixture, however, a small amount of 4-methylbenzyl methyl sulfide (**7**) was found to be formed (3% isolated yield). The possible mechanism is shown in Scheme 3. The initial reaction may be the nucle-

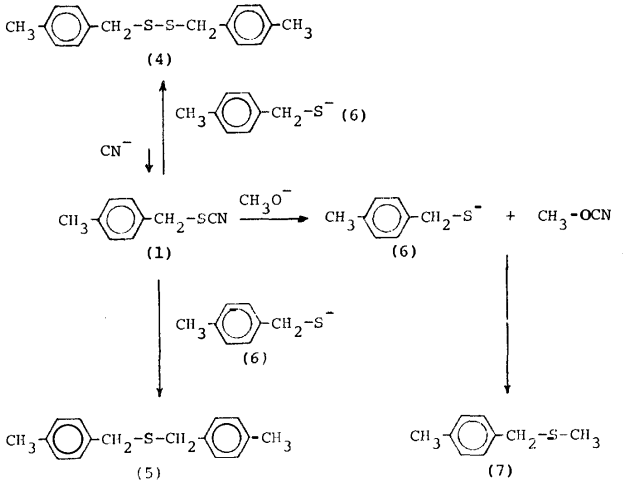

Scheme 3. Possible reaction paths for the reaction of **1** with sodium methoxide.

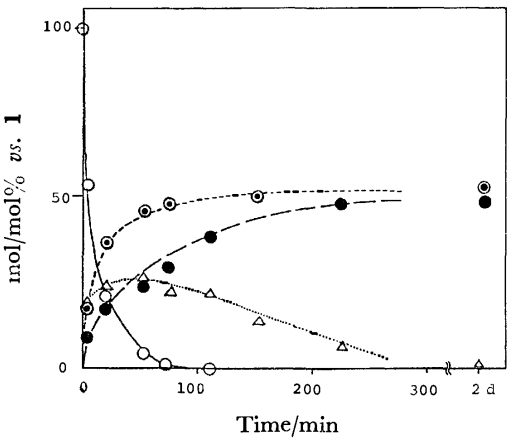

Fig. 4. The reaction of **1** (0.650 mmol) with sodium cyanide (2.5 mmol) in the presence of 18-crown-6 (0.49 mmol) in refluxing acetonitrile (14 ml).
○: **1**, △: **4**, ⊙: **5**, ●: **8**.

ophilic attack of methoxide anion (MeO^-) on the cyanide carbon (site c) of **1** to give the thiolate anion **6** and methyl cyanate. Failure of detection of methyl cyanate may be due to its instability even at room temperature[6] and its easy consumption by the reaction with the thiolate anion **6**. Since a thiolate anion behaves usually as a much stronger nucleophile than MeO^- in protic solvents, the secondary reaction between **1** and **6** proceeded more rapidly than the primary reaction, after once the thiolate anion **6** was formed by the primary reaction between **1** and MeO^-. There are two possible paths to consume **6**, a very strong nucleophile, thus formed. One is the reaction with **1** to afford **4**. The other is the reaction with methyl cyanate to form the sulfide **7**.[7] Product yields suggest that the former path predominates over the latter path. Since the reaction was conducted under argon, the disulfide **4** was undoubtedly formed by the reaction promoted by the thiolate anion **6** formed as a primary reaction product but not formed by the oxidation of thiolate anion **6** with molecular oxygen as assumed by Parker and Giles in their work on aryl thiocyanates.[2] CN^- is also known to be a rather strong nucleophile especially towards a divalent sulfur, however, much weaker nucleophile than the thiolate anion **6**.[4] Therefore, the reaction of **1** with MeO^- was intercepted by **6** before the complex reactions of the disulfide **4** were promoted by CN^-.

Reaction with Sodium Cyanide in Acetonitrile. The reaction of **1** with sodium cyanide was carried out in the presence of 18-crown-6 ether as the phase transfer catalyst in refluxing acetonitrile under argon. The reaction was monitored by GLPC and the result is illustrated in Fig. 4. Inspection of the figure reveals that a substantial amount of the disulfide **4** is produced at the initial stage and then converted to 4-methylbenzyl cyanide (**8**), and bis(4-methylbenzyl) sulfide (**5**) by subsequent reaction with CN^- as shown in Scheme 4 as Harpp observed in the reaction between CN^- and unsymmetrical disulfide (Scheme 2).[5] As illustrated in Scheme 4, CN^- attacks concurrently the benzyl carbon atom (site a) and the cyanide carbon atom

TABLE 2. REACTION SITES OF **1** TOWARD NUCLEOPHILES

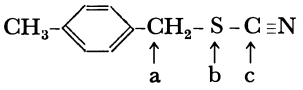

Nucleophile	Solvent	Temp	Time	Attacking site	Initial product	Final product
	MeCN	r. t.	5 h	a	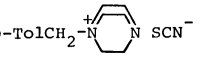	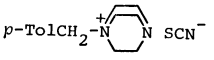
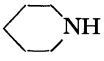	MeCN	r. t.	28 h	a	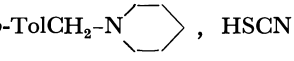	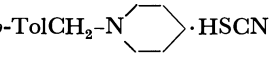
Et_2NH	MeCN	r. t.	48 h	a	*p*-$TolCH_2$-NEt_2·HSCN	*p*-$TolCH_2NEt_2$·HSCN
N_3^- [a]	MeCN	refl.	20 min	a	*p*-$TolCH_2$-N_3	*p*-$TolCH_2$-N_3
PhS^- [b]	MeOH	r. t.	fast	b > a	*p*-$TolCH_2S$-SPh	*p*-$TolCH_2$-SPh
CN^- [c]	MeCN	refl.	3 h	b > c > a	*p*-$TolCH_2S$-*CN *p*-$TolCH_2$-CN, *p*-$TolCH_2S^-$	*p*-$TolCH_2SCH_2$Tol-*p* *p*-$TolCH_2$-CN
MeO^- [d]	MeOH	r. t.	fast	c	*p*-$TolCH_2S^-$, MeO-CN	*p*-$TolCH_2SCH_2$Tol-*p*, *p*-$TolCH_2SMe$

a) NaN_3/18-crown-6. b) PhSK. c) NaCN/18-crown-6. d) MeONa.

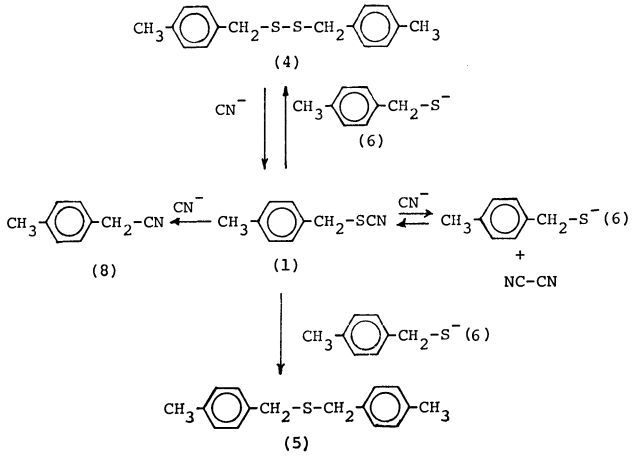

Scheme 4. Possible paths for the reaction of **1** with sodium cyanide.

site C of **1** to generate **8**, and **6** and cyanogen, respectively. The thiolate anion **6** thus formed reacts readily with **1** to give **4** and slowly to give the sulfide **5**. The disulfide **4** may be converted to **5** and **8** *via* forming **1**.

Meanwhile, the nucleophilic displacement of cyano group of alkyl thiocyanates with radioactive cyanide anion ($*CN^-$) was known to proceed even at room temperature.[8] Therefore, in the reaction of **1** with CN^-, the reaction at the site b, *i.e.*, cyanide exchange reaction, is concluded to be the fastest,[8] then the reaction at the site c to form **6** and the reaction at the site a affording **8** is the slowest.

$$RSCN + *CN^- \xrightarrow{25\,^\circ C \text{ in MeOH}} RS*CN + CN^-$$

R = Me, Et, *i*-Pr, *t*-Bu, Benzyl, and Phenyl

Reactions with Amine Nucleophiles in Acetonitrile. Both secondary and tertiary aliphatic amines were found to attack exclusively benzyl carbon of **1** (site a) at room temperature (Menschutkin reaction) as follows.[9] The reaction products were identified by IR and NMR spectroscopic analyses, and elemental analysis.

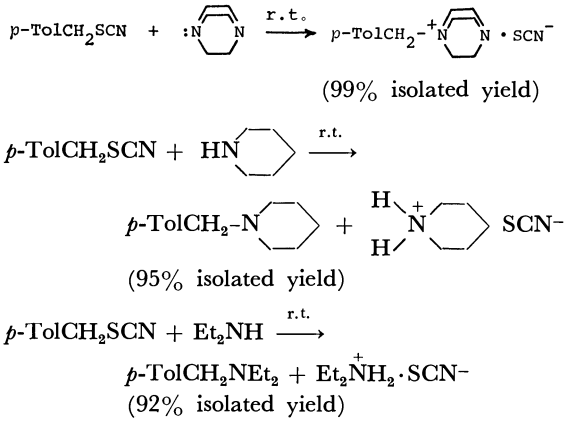

Reaction with Sodium Azide in Acetonitrile. The reaction between **1** and azide anion gave slowly 4-methylbenzyl azide (site a) in 95% isolated yield.

$$p\text{-}TolCH_2SCN + NaN_3 \xrightarrow{\text{reflux}} p\text{-}TolCH_2N_3 + NaSCN$$

*Reaction Site of **1** with Nucleophiles.* As mentioned earlier, the actual reacting site among the three reacting sites of **1** varies with the reacting nucleophile. Table 2 summarizes the preference of the reacting site in the actual reaction of **1** with each nucleophile. Since MeO^- attacks preferentially the site c, the cyanide carbon of **1** is the hardest electrophilic center, while the different reactivities of these nucleophilic reagents toward these three different reacting sites have been explained qualitatively in terms of the HSAB principle.[10] The softest reacting site for the nucleophile is the sulfur atom (site b), while the hardest one is the cyanide carbon atom (site c). In keeping with the HSAB principle, the softest nucleophile, PhS^-, is so thiophilic that it attacks preferentially the site b and even soft CN^- preferentially attacks the site b. Amines and N_3^-, being relatively hard but not very thiophilic, attack the site a. The results of INDO MO calculation are also in a good agreement with those conclusion.

*Theoretical Consideration of Reactivity of **1**.* The

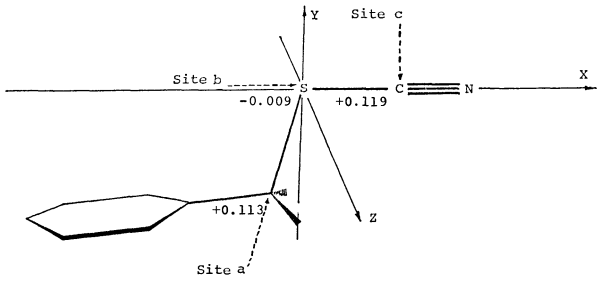

Fig. 5. Geometry of benzyl thiocyanate to be used for the MO calculation, net charge of benzyl thiocyanate and the course of the nucleophilic substitution through the sites a, b, and c.

Table 3. Net-charge on the nucleophilic atom and the HOMO orbital energy of nucleophiles

Nucleophile	Net-charge on the nucleophilic atom	HOMO energy eV
PhS^-	−0.748	−1.84
N_3^-	−0.712	+0.25
MeO^-	−0.694	−1.70
CN^-	−0.576	−0.28
DABCO	−0.184	−10.29

Table 4. Orbital interaction of three reaction sites of benzyl thiocyanate toward various nucleophiles[a)]

Nucleophile	Site a	Site b	Site c
PhS^-	−208	−284	−148
CN^-	−170	−236	−111
N_3^-	−119	−170	−73
MeO^-	−77	−131	−57
DABCO	−16	−30	−15

a) Values are in unit of $10^{-5}\times(\beta_0)^2$, where $\beta_{rs}=S_{rs}\beta_0$. For the calculation procedure, see the experimental part.

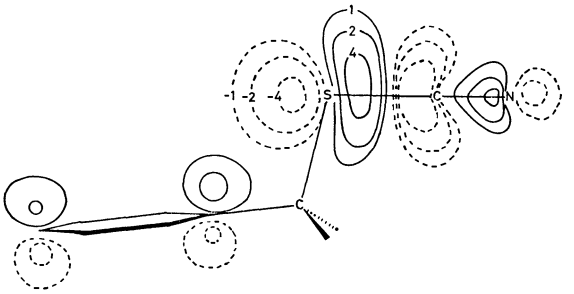

Fig. 6. 28th MO map of benzyl thiocyanate.

observed preferential sites for nucleophilic attack with different nucleophiles (Table 1) can be compared with the results of the INDO MO calculations.[11] The interaction energy between the nucleophile and the electrophile may be divided in the following two terms, *i.e.*, the electrostatic interaction and orbital interaction.[12] The calculated charge distribution of benzyl thiocyanate is shown in Fig. 5†. The net charges on the nucleophilic atoms of the nucleophiles are listed in Table 3. The calculated orbital interaction energies for the three reaction sites of benzyl thiocyanate toward the various nucleophiles are listed in Table 4. The net-charges on the benzyl carbon atom (site a) and the cyanide carbon atom (site c) are positive. On the other hand, the charge density on the sulfur atom (site b) is very small. The orbital interaction is the largest on the sulfur atom. Thus, the calculation suggests that the charge interaction is important in the reactions at the sites a and c, while the orbital interaction is predominant for the reaction at the site b. This prediction is well consistent with the present experimental results, *i.e.*, the PhS^-, which is a typical soft nucleophile[10] and is expected to undergo the orbital-controlled reaction,[12] attacks indeed the sulfur atom, while the MeO^-, which is a typical hard nucleophile[10] and is expected to undergo the charge-controlled reaction,[12] reacts at the positive carbon atom.

As may be seen from Table 4, the orbital interactrons of PhS^- and CN^- are very large. Their largest orbital interactions at the site b are due to the electron transfer from the nucleophiles to the 28th MO of benzyl thiocyanate. As is shown in Fig. 6, the 28th MO of benzyl thiocyanate has a strong anti-bonding character between the S–CN bond, and the electron transfer from a nucleophile (X^-) to this orbital weakens the S–CN bond and causes eventually the bond breaking to give the reaction products, $PhCH_2X$ and CN^- (X=PhS, *CN). The PhS^- and CN^- are thus expected to react at the site b preferentially through the orbital interaction. Since the calculated orbital interaction energies of MeO^- and amines are quite small, they are expected to attack the positive carbon atom of benzyl thiocyanate by the charge interaction. However, the prediction of the preferential reaction sites, a or c, is difficult, because of the following reasons, namely, the mechanism of the reaction at the sites, a and c, are different from each other and any molecular and electronic structural changes during the reaction process were not taken into account in the present calculation. The reaction at the site c may proceed through the following addition-elimination process[13] in which the second step of the reaction can take place only when the nucleophile is MeO^- among several nucleophiles used in this work, since the thiolate anion **6** is a much better leaving group than MeO^-.

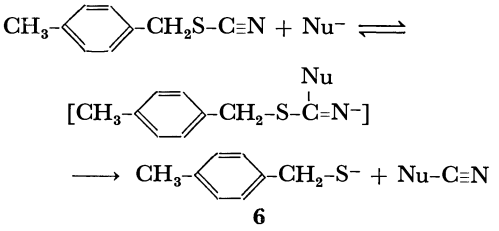

6

Since the reaction at the site a involves the inversion of the sp^3 carbon atom, it requires an appreciable activation energy and hence the reaction of amines at the site a proceeds slowly.

The calculated orbital interaction energies of N_3^-

† MO calculation of benzyl thiocyanate has been carried out instead of **1** to simplify the system.

(Table 3) suggests that N_3^- may react on the sulfur atom of **1** to give *p*-TolCH$_2$–S–N=$\overset{+}{N}$=$\overset{-}{N}$, although the formation of *p*-TolCH$_2$SN$_3$ was not detected in the experiment, and only the product which is produced *via* the reaction at the site a was observed experimentally. Since N_3^- is a very good leaving group, *p*-TolCH$_2$SN$_3$ if formed may undergo very fast reverse reaction with CN^-, a strong nucleophile, to regenerate **1** and N_3^-. However, this was unable to be confirmed in the present experiment.

$$p\text{-TolCH}_2\text{–S–C}\equiv\text{N} + N_3^- \rightleftarrows p\text{-TolCH}_2\text{–S–N=}\overset{+}{N}\text{=}\overset{-}{N} + CN^-$$

1

Leaving Ability of Thiocyanate Anion. Thiocyanate anion has been characterized as a pseudo halogen. It is ranked between iodide and chloride in the nucleophilic order of halide anions: $I^- > SCN^- > Br^- > N_3^- > Cl^- > F^-$ in the reaction in protic solvents.[14,15] Nucleophilic order of halides observed in protic solvents is just opposite to that in aprotic solvents and thiocyanate becomes the worst nucleophile toward methyl tosylate in DMF: $F^- > Cl^- > Br^- > SCN^-$, while the following nucleophilic order $F^- > Cl^- > SCN^- > Br^- > I^-$ was reported in the nucleophilic substitution of SCN group of 2,4-dinitrophenyl thiocyanate in DMF.[2] Meanwhile the leaving ability of thiocyanate in the nucleophilic substitution on sp^3 hybridized carbon has not yet been compared with other halides, while the following leaving abilities in the nucleophilic substitution was reported by Giles and Parker.[2]

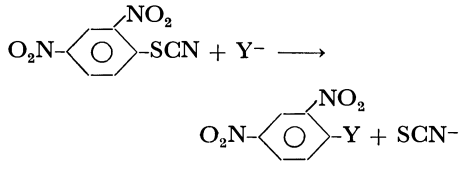

Leaving ability: $Br^- > I^- > SCN^- > Cl^- > F^-$ in DMF

Thus rate constants for the Menschutkin reactions of 4-methylbenzyl thiocyanate, chloride, and bromide have been measured in acetonitrile at 28±0.05 °C using DABCO as the choice nucleophile, since it has been found to attack the site a of **1** exclusively. The kinetic measurement has been carried out by following the increase of conductivity of the reaction mixture due to the formation of quarternary ammonium salt. The reaction was found to be of first order in both **1** and DABCO. The results are shown in Table 5.

Table 5. Second-order rate constants of Menschutkin reaction[a]

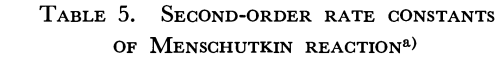

k_{Br}/l mol^{-1} s^{-1}	7.29
k_{Cl}/l mol^{-1} s^{-1}	0.0559
k_{SCN}/l mol^{-1} s^{-1}	0.00328

a) In CH_3CN at 28±0.05 °C.

The rate ratio, $k_{Br}/k_{Cl}=130$, observed in this work is same order as those which have been usually observed in S_N2 reaction on sp^3 carbon (50—180).[16] pK_a Values of the conjugate acid (HX) of the leaving anion (X^-) may be taken as one of criteria for the leaving ability of X. The observed rates, $k_{SCN}:k_{Cl}:k_{Br}=1:17:2200$, is in accordance with pK_a values of HSCN (−1.85), HCl (−6.1), and HBr (−9).[17]

Experimental

All melting points are uncorrected and were taken on Yanaco melting-point apparatus. The IR spectra were obtained on Hitachi 260-50 infrared spectrophotometer and the NMR spectra with Perkin-Elmer Hitachi R-20 (60 MHz) spectrometer. GC-Mass spectra were determined with Hitachi RMU 6MG GC-MS spectrometer equipped with 3 mm×2 m glass column of 15% Silicone OV-1 on Chromosorb W. All the reactions were monitored by the chromatography, namely, TLC (Merck, Kieselgel 60-GF$_{254}$), GLPC (Shimadzu GC-6A or Hitachi 163, using a 7—10% OV-1 on 60—80 mesh Chromosorb W. in 3 mm×2 m glass column), HPLC (Hitachi 638-50).

Materials. Acetonitrile was refluxed over phosphorus pentoxide for 30 h and distilled: bp 82.6 °C/760 mmHg†† Methanol was dehydrated by refluxing with magnesium and distilled: bp 64.0 °C/760 mmHg. Other reagents were obtained from Wako Pure Chemical Industries, Ltd. or Tokyo Kasei Co. Ltd., commercially.

4-Methylbenzyl Thiocyanate (**1**) was prepared by treatment of 4-methylbenzyl chloride with potassium thiocyanate, as follows. A mixture of 5.0 g (0.03 mol) of *p*-methylbenzyl chloride and 5.0 g (0.05 mol) of potassium thiocyanate in 30 ml of 90% ethanol was refluxed for 20 h, diluted with 120 ml of water, extracted three times with 20 ml aliquots of chloroform. The chloroform solution was washed with water, dried over Na_2SO_4 and evaporated to obtain crude 4-methylbenzyl thiocyanate whose GLPC analysis showed the presence of a small amount of 4-methylbenzyl isothiocyanate. 4-Methylbenzyl thiocyanate was separated from the impurities by elution column chlomatography (Merck, Kieselgel 60; eluent: 1:1 benzene–hexane); yield 58%; IR (neat) 2160, 1510, 1250, 820, 720 and 640 cm^{-1}; NMR ($CDCl_3$) δ=2.40 (3H, s, CH_3–), 4.14 (2H, s, –CH_2–) and 7.20 (4H, s, –C_6H_4–).

Found: C, 66.14; H, 5.52; N, 8.79%. Calcd for C_9H_9NS: C, 66.22; H, 5.55; N, 8.58%.

Potassium Benzenethiolate was prepared by dissolving benzenethiol in 2% solution of potassium methoxide in methanol, condensed to dryness under reduced pressure, washed with dry benzene, dried under vacuum and stored in a desiccator.

p-Xylene-α-thiol was prepared by the method reported by Frank and Smith[18] in 63% yield: Colorless oil; bp 110 °C/26.5 mmHg; (lit,[19] 116—118 °C/35 mmHg).

Bis(4-Methylbenzyl) Disulfide (**4**) was prepared by oxidation of *p*-xylene-α-thiol by iodine in 70% yield: Colorless crystals; mp 48.5—50.0 °C (lit,[20] 43 °C); IR (KBr) 1510, 1420, 1205, 820, 720 and 530 cm^{-1}; NMR ($CDCl_3$) δ=2.30 (6H, s, CH_3–), 3.57 (4H, s, –CH_2–) and 7.08 (8H, s, –C_6H_4–).

Bis(4-Methylbenzyl) Sulfide (**5**) was obtained by treating *p*-xylene-α-thiolate with 4-methylbenzyl chloride in ethanol in 90% yield, after recrystallization from ethanol: Colorless crystals; mp 78—79 °C (lit,[21] 76 °C); IR (KBr) 1510, 1420, 1110, 820, 730, and 530 cm^{-1}; NMR ($CDCl_3$) δ=2.36 (6H, s, CH_3–), 3.59 (4H, s, –CH_2–) and 7.12 (8H, s, –C_6H_4–).

4-Methylbenzyl Phenyl Disulfide (**2**). Benzenesulfenyl chloride was prepared by treating diphenyl disulfide with

†† 1 mmHg≈133.3 Pa.

chlorine gas[22] and was purified by vacuum distillation (43.5—44.5 °C/2 mmHg): yield 70%. The disulfide **2** could not be prepared by the method which has been applied for the preparation of other unsymmetrical disulfides by Parker and Kharasch,[4b] but synthesized successfully by the following method. To a solution of benzenesulfenyl chloride 1.05 g (7.25 mmol) dissolved in 10 ml of dry hexane containing dry pyridine was added at −10 °C. Into the mixture, 1.00 g (7.25 mmol) of *p*-xylene-α-thiol was added slowly in dark at −20 °C. The reaction was soon completed and the mixture was washed by water, and then with 5% H_2SO_4 (30 ml). The hexane solution was washed with water again, dried over $MgSO_4$ and evaporated. These must be operated in a dark room to avoid photochemical disproportionation of the unsymmetrical disulfide obtained. The residue was dried with vacuum pump (2 mmHg) for 4 h: Colorless oil; NMR ($CDCl_3$) δ=2.25 (3H, s, CH_3–), 3.82 (2H, s, $-CH_2-$), 6.80—7.60 (9H, m, $-C_6H_4-$ and $-C_6H_5$).

4-Methylbenzyl Phenyl Sulfide (3) was prepared by the same procedure which was applied for the preparation of **5** in 86% yield after recrystallization from ethanol: Colorless crystals; mp 69.0—70.1 °C (lit,[23] 69—70 °C); IR (KBr) 1580, 1510, 1480, 1440, 740, 690, and 480 cm^{-1}; NMR ($CDCl_3$) δ=2.27 (3H, s, CH_3–), 4.00 (2H, s, $-CH_2-$), 7.02 (4H, s, $-C_6H_4-$), and 7.15 (5H, s, C_6H_5–).

1-(4-Methylbenzyl)-4-aza-1-azoniabicyclo[2.2.2]octane Bromide, Chloride and Thiocyanate used for the kinetic study were prepared by the following method. 4-Methylbenzyl halide (0.013 mol) was added into the solution of 0.015 mol of DABCO in 50 ml of dry benzene at room temperature. After 30 min, benzene was evaporated and the residue, a white solid, was recrystallized from acetone–ether.

1-(4-Methylbenzyl)-1,4-Diazoniabicyclo[2.2.2]octane Bromide. 90% yield; Colorless crystals; mp 194.1—196.5 °C; IR (KBr) 2960, 1470, 1060, 820, 600, and 490 cm^{-1}; NMR ($CDCl_3$) δ=2.30 (3H, s, CH_3–), 3.10 (6H, t, J=8 Hz, DABCO), 3.71 (6H, t, J=8 Hz, DABCO), 4.86 (2H, s, $-CH_2-$), 7.01 (2H, d, J=8 Hz, $-C_6H_4-$), and 7.36 (2H, d, J=8 Hz, $-C_6H_4-$).

1-(4-Methylbenzyl)-1,4-Diazoniabicyclo[2.2.2]octane Chloride. 90% yield; Colorless crystals; mp 190.5—193.0 °C; IR (KBr) 2970, 1470, 1060, 820, 600, and 510 cm^{-1}; NMR δ=2.30 (3H, s, CH_3–), 3.07 (6H, t, J=8 Hz, DABCO), 3.69 (6H, t, J=8 Hz, DABCO), 4.86 (2H, s, $-CH_2-$), 6.98 (2H, d, J=8 Hz, $-C_6H_4-$), and 7.35 (2H, d, J=8 Hz, $-C_6H_4-$).

4-Methylbenzyl Cyanide (8) was prepared according to the method reported by Zubrik, Dunbar and Durst[24] in 51% yield after distillation: Colorless oil; bp 84.5 °C/30 mmHg (lit,[25] 220 °C/760 mmHg); IR (neat) 2250, 1515, 1415, 1120, 800, 750, 725, and 480 cm^{-1}; NMR ($CDCl_3$) δ=2.37 (3H, s, CH_3–), 3.67 (2H, s, $-CH_2-$), and 7.18 (4H, s, $-C_6H_4-$).

4-Methylbenzyl Methyl Sulfide (7) was prepared by the alkylation of sodium methoxide with 4-methylbenzyl chloride in 81% yield after distillation: Colorless oil; bp 121 °C/30 mmHg; IR (neat) 1520, 1425, 1240, 1110, 820, 735, 670, 525, and 470 cm^{-1}; NMR ($CDCl_3$) δ=1.94 (3H, s, CH_3–S–), 2.28 (3H, s, CH_3–), 3.56 (2H, s, $-CH_2-$), and 7.02 (4H, s, $-C_6H_4-$).

Reaction of 1 with Potassium Benzenethiolate. 171.0 mg (1.05 mmol) of **1** was added into a 3 ml of dry methanol solution containing 163.4 mg (1.24 mmol) of potassium benzenethiolate. The mixture was allowed to stand in argon atmosphere at room temperature monitoring by GLPC. Products, **2**, **3**, **4**, and diphenyl disulfide were obtained, and were identified by direct comparison with those of authentic samples by GLPC and GC-MS. **2**: (*m/e*) 246 (M^+), 105 ($4\text{-}CH_3C_6H_4CH_2^+$). **3**: (*m/e*) 214 ($M^+$), 105 ($4\text{-}CH_3C_6H_4CH_2^+$). Diphenyl Disulfide: (*m/e*) 218 (M^+), 109 (PhS^+).

Reaction of 4 with Sodium Cyanide. The disulfide **4** (123.1 mg, 0.449 mmol) was added into 5 ml of acetonitrile containing 50.6 mg (1.033 mmol) of sodium cyanide and 297.9 mg (1.128 mmol) of 18-crown-6. The mixture was stirred under reflux in argon atmosphere, the reaction being monitored by GLPC from time to time. The reaction completed in about 20 min. Then **5** and **8** were obtained by GLPC as final products. The same result was obtained when methanol was used as the solvent.

Reaction of Phenyl Thiocyanate with Sodium p-Xylene-α-thiolate. Sodium *p*-xylene-α-thiolate (160 mg, 0.685 mmol) prepared in the same procedure that was applied for the preparation of potassium benzenethiolate, was dissolved in 3 ml of abs. methanol and was added into the solution of phenyl thiocyanate (126.1 mg, 0.933 mmol; prepared by the usual way) at once. The mixture was allowed to stand at room temperature in argon atmosphere, while the reaction was monitored by GLPC at time intervals. Phenyl thiocyanate disappeared within 1 min and the gas liquid chromatogram of the reaction mixture showed the same distribution of products as in the reaction of **1** with potassium benzenethiolate, *i.e.*, initially, **2** was formed, and then disproportionated to **4** and diphenyl disulfide; eventually **3** was obtained as the final product.

Reaction of 2 with Sodium Cyanide. 113.2 mg (0.459 mmol) of **2** was added into a mixture of 24.1 mg (0.492 mmol) of sodium cyanide suspended in 5 ml of acetonitrile containing 30 mg (0.114 mmol) of 18-crown-6 and 56.3 mg (0.366 mmol) of biphenyl which was used as the internal standard on GLPC monitoring. The mixture was stirred in argon atmosphere at room temperature in dark. Figure 3 represents a rough kinetic picture of the reaction.

Reaction of 1 with Sodium Methoxide. Into a solution of sodium methoxide prepared by dissolving 67.8 mg (2.95 mmol) of sodium in 5 ml of absolute methanol, 176.2 mg (1.08 mmol) of **1** was added at once. The mixture was allowed to stand under argon atmosphere at room temperature monitoring by TLC. The reaction completed after 5 min. The remaining sodium methoxide was quenched by adding aqueous acetic acid solution. The mixture was extracted with chloroform twice. The chloroform extracts were combined, washed with water, dried over anhydrous magnesium sulfate and evaporated to afford a mixture of **4** and **7**. The two compounds were separated by silica gel column chlomatography with hexane as eluent. Compound **4** was eluted first (88.9% yield) and then **7** came out (2.2% yield).

Reaction of 1 with Sodium Cyanide. 106.0 mg (0.650 mmol) of **1** was added into a mixture of 121.1 mg (2.50 mmol) of sodium cyanide suspended in 14 ml of acetonitrile which contained 28.9 mg (0.490 mmol) of 18-crown-6. The mixture was refluxed under stirring in argon atmosphere for 300 min while the reaction was monitored by GLPC.

Reaction of 1 with 1,4-Diazabicyclo[2.2.2]octane (DABCO). 461.5 mg (2.80 mmol) of **1** was added into a solution of 272.9 mg (2.40 mmol) of DABCO in 12 ml of acetonitrile in argon atmosphere. The mixture was allowed to stand in argon atmosphere at room temperature, while the reaction was monitored by TLC and GLPC. After 5 h, solvent were distilled off under reduced pressure, the remaining white crystals were washed with hexane and collected, then 1-(4-methylbenzyl)-1,4-diazoniabicyclo[2.2.2]octane thiocyanate was obtained in 99% yield: mp 167.9—169.0 °C; IR (KBr) 2040, 1470, 1380, 1060, 990, 850, 820, and 595 cm^{-1}; NMR ($CDCl_3$) δ=2.41 (3H, s, CH_3–), 3.30 (6H, t, J=6 Hz, $DABCO^+$–), 3.68 (6H, t, J=6 Hz, $DABCO^+$–), 4.77

(2H, s, $-CH_2-$), 7.24 (2H, d, $J=8$ Hz, $-C_6H_4-$), and 7.47 (2H, d, $J=8$ Hz, $-C_6H_4-$).

Found: C, 65.35; H, 7.71; N, 15.04%. Calcd for $C_{15}H_{21}N_3S$: C, 65.42; H, 7.69; N, 15.26%.

Reaction of **1** *with Piperidine.* 338.7 mg (2.08 mmol) of **1** was added into a mixture of 416.2 mg (4.89 mmol) of piperidine and 12 ml of acetonitrile. The reaction mixture was allowed to stand in argon atmosphere at room temperature while the reaction was monitored by TLC and GLPC. After 28 h, the reaction mixture was diluted with 30 ml of water, extracted three times with 10 ml aliquots of ether and the extracts were conbined and washed with 10 ml of water. The solution was dried over anhydrous magnesium sulfate and solvent was evaporated. A colorless oil, obtained, was dissolved in dichloromethane and passed through column of 15 g of Wako activated alumina (200 mesh). The first fraction eluted by dichloromethane gave 30 mg (5%) of **4** which was identified as **4** by comparison with IR and NMR spectra and retention time of GLPC of the authentic sample. Then, the column was washed with ethyl acetate to give 323.2 mg of colorless oil of 1-(4-methylbenzyl)piperidine in 82% yield: IR (neat) 1520, 1440, 1370, 1340, 1300, 1155, 1120, 1100, 1040, 1000, 810, 780, and 490 cm^{-1}; NMR (CCl_4) $\delta=1.25$—1.80 (6H, m, piperidine), 2.04—2.58 (4H, m, piperdine), 2.37 (3H, s, CH_3-), 3.39 (2H, s, $-CH_2-$), 7.01 (2H, d, $J=9$ Hz, $-C_6H_4-$), and 7.12 (2H, d, $J=9$ Hz, $-C_6H_4-$). Colorless crystals of piperidinium thiocyanate 227.9 mg (76%) were obtained from the aqueous layer after evaporation of water and recrystallization of the residue from ethyl acetate: mp 96.5—97.7 °C; IR (KBr) 2960, 2820, 2030, 1435, 1320, 940, and 560 cm^{-1}; NMR (CD_3OD) $\delta=1.50$—2.21 (6H, m, piperidine), 3.06—3.40 (4H, m, piperidine), 4.75 (2H, s, $=N^+H_2$).

Found: C, 49.81; H, 8.39; N, 19.18; S, 21.59%. Calcd for $C_6H_{12}N_2S$; C, 49.96; H, 8.39; N, 19.42; S, 22.23%.

Reaction of **1** *with Diethylamine.* 223.2 mg (1.37 mmol) of **1** was added into a solution of diethylamine 169.1 mg (2.31 mmol) in 7 ml of acetonitrile. The mixture was allowed to stand in argon atmosphere for 15 d at room temperature, while the reaction was monitored by TLC and GLPC. The reaction mixture was diluted with 10 ml of 1% potassium hydroxide aqueous solution, extracted three times each with 10 ml of ether. The combined ether extracts was washed with 10 ml of water, dried over anhydrous magnesium sulfate and upon evaporation of solvent left light yellow oil of *N,N*-diethyl-4-methylbenzylamine (92% yield): IR (neat) 1580, 1515, 1380, 1205, 1170, 820, 800, 755, and 480 cm^{-1}; NMR ($CDCl_3$) $\delta=1.08$ (6H, t, $J=7$ Hz, CH_3CH_2-), 2.37 (3H, s, CH_3-), 2.57 (4H, q, $J=7$ Hz, CH_3CH_2-), 3.56 (2H, s, $-CH_2-$), 7.10 (2H, d, $J=8$ Hz, $-C_6H_4-$), and 7.23 (2H, d, $J=8$ Hz, $-C_6H_4-$).

Reaction of **1** *with Sodium Azide.* 175.7 mg (1.77 mmol) of **1** was added into a mixture of 137.6 mg (2.12 mmol) of sodium azide (containing 10 wt% of methanol and water as stabilizer) suspended in 5 ml of acetonitrile containing 531.3 mg (2.01 mmol) of 18-crown-6 as the phase transfer catalyst. The mixture was refluxed under stirring in argon atmosphere for 20 min, while the reaction was monitored by GLPC. The reaction mixture was diluted with 20 ml of water and extracted three times each with 10 ml of chloroform. Evaporation of the solvent gave a colorless oil of 4-methylbenzyl azide, which was purified through a silica-gel column with 3:1 benzene–hexane: 95% yield; IR (neat) 2080, 1500, 1340, 1250, 800, 750, 530, and 460 cm^{-1}; NMR ($CDCl_3$) $\delta=2.29$ (3H, s, CH_3-), 4.15 (2H, s, $-CH_2-$), and 7.02 (4H, s, $-C_6H_4-$).

Kinetics. A typical run is as follows. To a solution containing the substrate, a solution of DABCO was added at once; the kinetic conditions are shown in Table 5. The temperature was kept at 28 ± 0.05 °C all through the experiment. The conductance of the salt produced in the reaction was measured and recorded automatically, while the concentration of the solution was maintained at constant by comparing with the calibration curve. The rate constants were calculated from the second order rate equation, since the reaction of halides with amine has been known as the Menschutkin reaction which obeyed the second-order rate equation.

Molecular Orbital Calculation. The molecular and electronic structures of benzyl thiocyanate and various nucleophiles were calculated by means of the closed-shell SCF INDO method.[11] All the molecular structures were optimized except the phenyl group in benzyl thiocyanate and benzenethiolate anion. In the calculation of the orbital interaction energies, the resonance integrals were approximated to be proportional to the overlap integrals; $S_{rs}\beta_0$, where S_{rs} is the overal integral between atomic orbitals r and s, and β_0 is a constant. For the donor orbitals, only the HOMO LCAO coefficients on the nucleophilic atom were taken into account. Thus the values listed in Table 3 are:

$$\sum_{m}^{unocc} \frac{(\sum_{r} C_{rm}C_{s,HOMO}S_{rs})^2}{\varepsilon_{HOMO}-\varepsilon_m},$$

where S_{rs} was evaluated between the r AO of benzyl thiocyanate and the s-type AO of the nucleophilic atom in each nucleophile which is placed at 2.0 Å distance along the direction cited in Fig. 5.

References

1) D. E. Giles, "The Chemistry of Cyanates and Their Thio Derivatives," ed by S. Patai, John Wiley & Sons Inc., New York (1977), Part 1, Chap. 12.

2) D. E. Giles and A. J. Parker, *Aust. J. Chem.*, **26**, 273 (1973).

3) D. S. Tarbell and D. P. Harnish, *Chem. Rev.*, **49**, 1 (1951); M. N. Hughes, "Chemistry and Biochemistry of Thiocyanic Acid and Its Derivatives," ed by A. A. Newman, Academic Press Inc., New York (1975), Chap. 1.

4) A. J. Parker and N. Kharasch, *Chem. Rev.*, **59**, 583 (1959); *J. Am. Chem. Soc.*, **82**, 3071 (1960); *J. Org. Chem.*, **24**, 1029 (1959).

5) R. G. Hiskey, W. H. Bowers, and D. N. Harpp, *J. Am. Chem. Soc.*, **86**, 2010 (1964).

6) K. A. Jensen, M. Due, and A. Holm, *Acta Chim. Scand.*, **20**, 2107 (1966).

7) R. K. Olsen and H. R. Snyder, *J. Org. Chem.*, **30**, 187 (1965).

8) G. Bajaro, *Ricerca Sci.*, **25**, 2636 (1955); *Chem. Abstr.*, **50**, 14326 (1956).

9) H. Lecher, *Justus Liebigs Ann. Chem.*, **445**, 77 (1925).

10) R. G. Peason, *J. Am. Chem. Soc.*, **85**, 3533 (1963); R. G. Peason and J. Songstad, *ibid.*, **89**, 1827 (1967); Tse-Lok Ho, "Hard and Soft Acids and Bases Principle in Organic Chemistry," Academic Press Inc., New York (1977).

11) J. A. Pople, D. L. Beveridge, and P. A. Dobosh, *J. Chem. Phys.*, **47**, 2026 (1967).

12) G. Klopman, "Chemical Reactivity and Reaction Paths," ed by G. Klopman, John Wiley & Sons Inc., New York (1974), Chap. 4; *J. Am. Chem. Soc.*, **90**, 223 (1968).

13) K. Brand and H. W. Leyerzapf, *Chem. Ber.*, **70**, 284 (1973); E. Hoggarth and W. A. Sexlon, *J. Chem. Soc.*, **1947**, 815.

14) J. O. Edwards, *J. Am. Chem. Soc.*, **76**, 1540 (1954).
15) R. G. Peason, H. Sobel, and J. Songstad, *J. Am. Chem. Soc.*, **90**, 319 (1968).
16) M. Konrad and C. Bruckner, *Z. Phys. Chem.*, **4**, 631 (1889); P. B. D. de la Mare, *J. Chem. Soc.*, **1955**, 3169.
17) "Lange's Handbook of Chemistry," 12th ed, ed by J. A. Dean, McGraw-Hill Book Company, New York (1979), Chaps. 5—14.
18) T. R. Lewis and S. Archer, *J. Am. Chem. Soc.*, **73**, 2109 (1951).
20) M. Strzelecka, *Komos*, **35**, (Rad.-Festb.) 585; *Chem. Abstr.*, **5**, 1601 (1911).
21) Z. Martynowicz, *Chem. Zentralbl.*, **1910 II**, 1048; *Chem. Abstr.*, **5**, 1600 (1911).
22) G. W. Perold and H. L. F. Snyman, *J. Am. Chem. Soc.*, **73**, 2379 (1951).
23) R. F. Brookes, J. E. Cranham, D. Greenwood, and H. A. Stevenson, *J. Sci. Food Agric.*, **9**, 141 (1958); *Chem. Abstr.* **52**, 11772 (1958).
24) J. W. Zubrik, B. I. Dunber, and H. D. Durst, *Tetrahedron Lett.*, **1975**, 71.
25) A. F. Titly, *J. Chem. Soc.*, **1926**, 508; *Chem. Abstr.*, **20**, 1794 (1926).

Intramolecular Stereospecific Pummerer Reactions of Aryl (Substituted-methyl) Sulfoxides Bearing Electron-withdrawing Groups with Acetic Anhydride

Tatsuo NUMATA, Osamu ITOH, Toshiaki YOSHIMURA, and Shigeru OAE*

Department of Chemistry, University of Tsukuba, Niihari-gun, Sakura-mura, Ibaraki 305

(Received June 7, 1982)

The Pummerer reaction of optically active cyanomethyl aryl sulfoxides with acetic anhydride gave the corresponding α-acetoxy sulfides which were induced with a partial asymmetry nearly 30% at α-carbon, while the ^{18}O-label of the original sulfoxides was retained in more than 85% in the resulting ester, the Pummerer reaction product. Kinetic experiments with cyanomethyl (*p*-substituted phenyl) sulfoxides and α,α-dideuterated cyanomethyl *p*-tolyl sulfoxide in the reaction with acetic anhydride containing a small amount of acetic acid revealed that the rates were correlated with Hammett σ-values and ρ-value of −0.70 was obtained, while the kinetic isotope effect was practically nil, *i.e.*, $k_H/k_D=1.01$. These observations indicate clearly that the rearrangement is intramolecular and proceeds via forming a very intimate ion-pair and the rate-determining step is believed to be the S–O bond cleavage after the initial reversible acylation and deprotonation. Elimination of acetic acid proceeds through the Elcb type process. The uneven distribution of ^{18}O in the two oxygens of the resulted ester, *i.e.*, ether and carbonyl oxygens, suggests the recombination of the α-sulfenyl carbonium ion and acetate ion to be very rapid. The Pummerer reaction of optically active *N,N*-dimethyl-*p*-tolyl-sulfinylacetamide with excess acetic anhydride also gave the corresponding α-acetoxy sulfide in optically active form. In the presence of dicyclohexylcarbodiimide (DCC), the Pummerer reaction was found to be highly stereoselective affording the corresponding α-acetoxy sulfide with 65%e.e. Other optically active α-carbonyl-substituted alkyl sulfoxides, *i.e.*, ethyl *p*-tolylsulfinylacetate and ω-(*p*-tolylsulfinyl)acetophenone also gave the corresponding highly optically active Pummerer rearrangement products in the treatment with acetic anhydride/DCC system. The Pummerer reaction of the ^{18}O-labeled sulfoxides with acetic anhydride/DCC system gave the corresponding α-acetoxy sulfides which retained much of the original ^{18}O-labels of the sulfoxides. These observations reveal clearly that in the Pummerer reaction of these compounds the acetoxyl migration is intramolecular and takes place through intimate ion-pairs.

The reaction of sulfoxides bearing α-methylene protons with acetic anhydride to afford the corresponding α-acetoxy sulfides was named by Horner[2] half a century after the discovery by Pummerer.[1] One earliest investigation of the mechanism of this reaction was our ^{18}O-tracer study using dimethyl sulfoxide and uniformly ^{18}O-labeled acetic anhydride in diethyl ether.[3] On the basis of our finding that all of the oxygen atoms were completely scrambled during the reaction, we suggested the involvement of intermolecular attack of acetate at the α-carbon and also the possible involvement of the acyloxysulfonium ylide. Because of the possible involvement of the Pummerer reaction in the enzymatic demethylation of methionine[4] and the growing potential for versatile organic syntheses,[5] mechanism of this reaction has been investigated quite extensively and well-reviewed.[6,7]

The general scheme of the reaction is believed to be shown in the following four sequential elemental reactions with the rate-determining step varying with changes of both the acylating agent and the sulfoxide. In some cases, the reaction of the steps 2 and 3 became simultaneous, to result in E2 process, as in the Pummerer reaction of *trans*-1- and 2-thiadecalin *S*-oxides with acetic anhydride.[8]

Although there has been no clear-cut example of the Pummerer reaction in which the last recombination step 4 is the rate-determining, we have found all the three examples of the reactions in which each of the three steps is rate-determining.[7c-e]

$$\underset{\underset{O}{\downarrow}}{R\text{-}S\text{-}CH_3} + Ac_2O \overset{\text{step 1}}{\rightleftharpoons} \underset{\underset{OAc}{\downarrow}}{R\text{-}\overset{+}{S}\text{-}CH_3} + AcO^-$$

$$\overset{\text{step 2}}{\underset{-H^+}{\rightleftharpoons}} \left[\underset{\underset{OAc}{\downarrow}}{R\text{-}\overset{+}{S}\text{-}\overset{-}{C}H_2} \longleftrightarrow \underset{\underset{OAc}{\downarrow}}{R\text{-}S\text{=}CH_2} \right] + AcOH$$

$$\overset{\text{step 3}}{\longrightarrow} \left[R\text{-}\overset{+}{S}\text{=}CH_2 \longleftrightarrow R\text{-}S\text{-}\overset{+}{C}H_2 \right]$$
$$\qquad\qquad {}^{-}OAc \qquad\qquad {}^{-}OAc$$

$$\overset{\text{step 4}}{\longrightarrow} R\text{-}S\text{-}CH_2OAc$$

While the first example of the Pummerer reaction which results in a substantial asymmetric induction[9] was the novel cyclization of *o*-carboxyphenyl alkyl sulfoxide with acetic anhydride and dicyclohexylcarbodiimide (DCC)[10] to give cyclized 3*H*-4-thiaisocoumarin in 11.2 and 29.9% e.e., respectively, the rate-determining step of this reaction seems to be the initial acylation (step 1). The second example of the Pummerer reaction which leads to the formation of asymmetrically induced α-acetoxy sulfide was the reaction of open-chain optically active cyanomethyl *p*-tolyl sulfoxide (**1b**) with acetic anhydride.[11] The rate-determining step of this reaction appears to be the heterolysis of the S–O linkage of the sulfonium-ylide-ylene intermediate formed by the initial reversible acylation of the sulfoxide and subsequent reversible deprotonation, while the rearrangement seems to proceed predominantly through intramolecular migration of acetoxyl group when the reaction of the ^{18}O-labeled sulfoxide was carried out.

Other examples of the Pummerer reaction which affords the corresponding asymmetrically induced α-acetoxy sulfides are all with optically active open-chain aryl methyl sulfoxides bearing some electron-

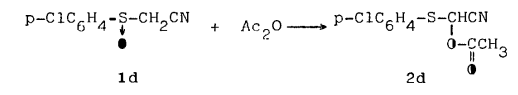

withdrawing groups on methyl group,[12-14] while the reaction of aryl 2-propynyl sulfoxide with acetic anhydride gives not only the Pummerer rearrangement product but also the thio-Claisen type rearrangement product, and hence it will be dealt separately.[14] All these optically active aryl (carbonyl-substituted methyl) sulfoxides **3**, **5**, and **7a** were found to react with acetic anhydride affording the corresponding α-acetoxy sulfides **4**, **6**, and **8a** which are substantially induced with optical activities on the α-carbons. In the presence of DCC, scavenger of acetic acid formed, the amounts of asymmetric induction were markedly increased in the resulting Pummerer products. Meanwhile, the usual ^{18}O-tracer experiments with ^{18}O-labeled sulfoxides **3**, **5**, and **7b** revealed that the rearrangements are predominantly intramolecular in view of the high retentions of ^{18}O-label in the resulted corresponding α-acetoxy sulfides **4**, **6**, and **8b**.

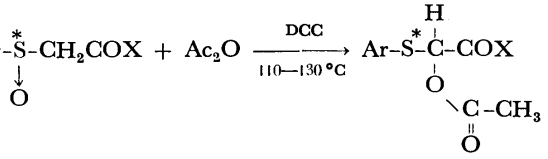

3 Ar=*p*-Tol, X=NMe_2 **4** Ar=*p*-Tol, X=NMe_2
5 Ar=*p*-Tol, X=OEt **6** Ar=*p*-Tol, X=OEt
7a Ar=*p*-Tol, X=Ph **8a** Ar=*p*-Tol, X=Ph
7b Ar=Ph, X=Ph **8b** Ar=Ph, X=Ph

This paper describes detailed accounts of these interesting intramolecular stereoselective Pummerer reactions of aryl (substituted methyl) sulfoxides bearing electron-withdrawing group with acetic anhydride.

Results and Discussion

Reaction of Aryl Cyanomethyl Sulfoxides with Acetic Anhydride. When optically active cyanomethyl *p*-tolyl sulfoxide (**1b**) $[\alpha]_D$ +252°, was allowed to react with a large excess acetic anhydride at 120 °C for 3.5 h, the resulted acetoxycyanomethyl *p*-tolyl sulfide (**2b**) was found to be optically active, $[\alpha]_D$ +26.8°, which corresponds to 29.0±0.8% of e.e. when determined by NMR using the chiral lanthanoide shift reagent, Eu(hfc), tris(heptafluoropropylhydroxymethyl-d-camphorato)europium.

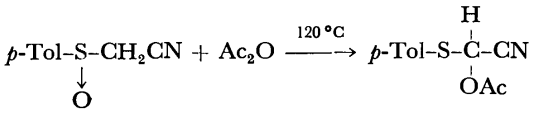

1b $[\alpha]_D$ +252° **2b** $[\alpha]_D$ +26.8°

In the reaction of ^{18}O-labeled cyanomethyl *p*-chlorophenyl sulfoxide (**1d**) (0.680 ex. atom% of ^{18}O) with a large excess of unlabeled acetic anhydride at 50% conversion (120 °C, 1 h) the unreacted sulfoxide recovered and the Pummerer product **2d** separated by column chromatography were found to be incorporated with 0.655 ex. atom% of ^{18}O (for **1d** recovered) and 0.290 ex. atom% (for **2d**), which correspond to the retention of 96.3%(for **1d** recovered) and 85% (for **2**), respectively. Thus, the rearrangement proceeded through an intramolecular 1,2-acetoxyl migration at least 85%. In order to shed further light on the nature of the acetoxyl migration, the distribution of ^{18}O in the resulted ester **2d** was determined by treating the ester **2d** with 3 molar excess of phenylhydrazine to convert acetyl group to 1-acetyl-2-phenylhydrazine which had 0.366 ex. atom% of ^{18}O. Thus the following ^{18}O distribution in the ester **2d** was ob-

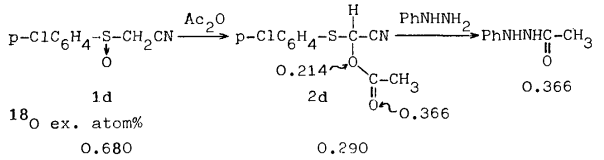

served. This uneven distribution of ^{18}O, rich in favor for carbonyl oxygen, means that the recombination of acetoxyl group to α-carbon after the heterolysis of the S–O linkage is very rapid while the heterolysis of the S–O linkage is partly assisted by the neighboring group effect of carbonyl oxygen at the transition state of the 1,2-acetoxyl migration.

Meanwhile, in the reaction of cyanomethyl-d_2 *p*-tolyl sulfoxide with acetic anhydride containing a small amount of acetic acid, the recovered sulfoxide was found to have lost the D-label completely within a few minutes of the reaction at 120 °C, suggesting strongly that the initial acetylation (step 1) and the deprotonation to form the ylide **9** (step 2) are both fast and reversible, and the rate-determining step is the subsequent S–O bond heterolysis followed by very fast recombination of the resulting α-sulfenyl carbenium ion with acetate within the ion-pair **10a** and **10b**.

Kinetic experiments of the Pummerer reactions of cyanomethyl *p*-substituted phenyl sulfoxides in a large excess acetic anhydride containing a small amount of acetic acid (0—13.8 mmol) were carried out by following the UV absorption spectra of the starting sulfoxides. The rate of the Pummerer reaction was found to increase as the amount of acetic acid increased as shown in Fig. 1 which illustrates the rate change *vs.* the concentration of acetic acid used. When an equimolar amount of DCC was added into the reaction mixture, the Pummerer reaction was extremely slowed down and could have hardly been seen after heating the reaction mixture for a few hours. Acetic acid is undoubtedly acting as a catalyst in the initial acetylation step (step 1). A strong acid such as *p*-toluenesulfonic acid was found to accelerate the Pummerer reaction of these sulfoxides markedly. Meanwhile, the reduction of aryl cyanomethyl sulfoxide with trimethylsilyl chloride in the presence of pyridine is known to be extremely sluggish as compared to other sulfoxides[15] due mainly to the difficulty of the initial trimethylsilylation of the sulfinyl function of which the basicity is very low.

The kinetic data of the Pummerer reactions of a few cyanomethyl (*p*-substituted phenyl) sulfoxides **1a—e** are summarized in Table 1. The rate was found to decrease with the increase of electron-withdrawing effect of substituent and the Hammett plot of the logarithms of rates against σ-values gave ρ-value of

Table 1. Kinetic data for the Pummerer reaction of aryl cyanomethyl sulfoxides (**1a—e**) with acetic anhydride containing acetic acid

p-$YC_6H_4S(O)CH_2CN$ Y		λ[a] nm	[AcOH] M	T °C	10^4k s^{-1}	
CH_3	**1b**	247	0	120	0.31±0.04	
H	**1c**	246	0	120	0.29±0.04	
CH_3O	**1a**	251	6.92	120	11.9 ±0.3	
CH_3	**1b**	247	6.92	120	8.18±0.11	
H	**1c**	246	6.92	120	9.13±0.24	$\rho=-0.70\pm0.1$ (*vs.* σ, $\gamma=0.9803$)
Cl	**1d**	249	6.92	120	5.08±0.18	
NO_2	**1e**	282	6.92	120	2.20±0.06	
CH_3	**1b**	247	3.50	120	4.52±0.22	$k_H/k_D=1.01$
p-$CH_3C_6H_4S(O)CD_2CN$		247	3.50	120	4.47±0.18	
CH_3O	**1a**	251	3.50	120	4.97±0.28	
Cl	**1d**	249	3.50	120	2.42±0.18	
H	**1c**	246	3.50	120	4.73±0.20	$E_a=70.3\pm1.7$ kJ mol^{-1}
H	**1c**	246	3.50	110	2.76±0.13	$\Delta H^*=66.9\pm1.7$ kJ mol^{-1}
H	**1c**	246	3.50	100	1.50±0.10	$\Delta S^*=-141\pm4$ J K^{-1} mol^{-1} (120 °C)

a) Wavelength of UV absorption at which the rate was followed.

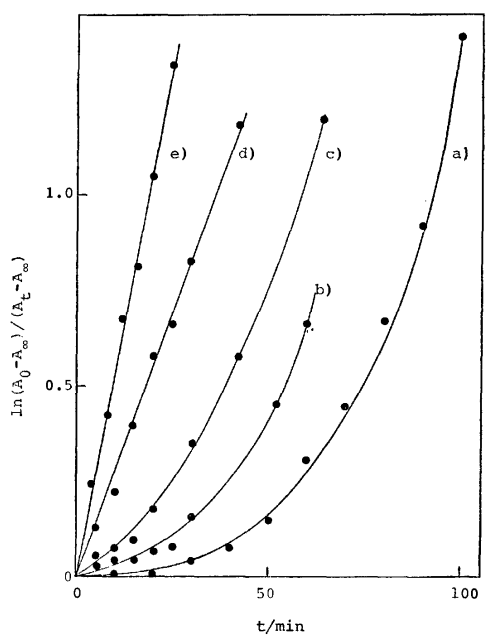

Fig. 1. Time course of the Pummerer reaction of cyanomethyl phenyl sulfoxide (**1c**) with acetic anhydride containing acetic acid.
a): [AcOH]=0 M, b): 0.83 M, c): 1.75 M, d): 3.50 M, e): 6.92 M. A: UV Absorption intensity.

-0.7 ± 0.1 ($\gamma=0.9803$). The negative ρ-value also supports the rate-determining heterolysis of the S–O bond of the ylide intermediate **9**. The values of activation parameters at 120 °C $E_a=(70.3\pm1.7)$ kJ mol^{-1}, $\Delta H^*=(66.9\pm1.7)$ kJ mol^{-1}, $\Delta S^*=(-141\pm4)$ J K^{-1} mol^{-1}, are quite different from those of the intermolecular Pummerer reaction of methyl phenyl sulfoxide at 120 °C ($E_a=88.7$ kJ mol^{-1}, $\Delta S^*=-86.6$ J K^{-1} mol^{-1})[16] and also those of the Pummerer reaction of arylmethylsulfonium bis(methoxycarbonyl)methylide with acetic anhydride ($\Delta H^*=89.5$ kJ mol^{-1}, $\Delta S^*=-92.9$ J K^{-1} mol^{-1}) in which the rate-determining step is believed to be the S–C linkage cleavage.[17] The large negative value of entropy of activation ($\Delta S^*=-141$ J K^{-1} mol^{-1}) seems to suggest the transition state to be very tight, as in a similar intramolecular tosyloxyl migration in the reaction of isoquinoline *N*-oxide with *p*-toluenesulfonyl chloride, *i.e.*, $\Delta H^*=40.2$ kJ mol^{-1}, $\Delta S^*=-168$ J K^{-1} mol^{-1}.[18] Based on all these observations and related data, the scheme of the Pummerer reaction of cyanomethyl aryl sulfoxides leading to the asymmetric induction may be illustrated as shown below. The initial acetylation is an acid-catalyzed equilibrium reaction and the second step of proton-removal is also fast and reversible in view of the lack of kinetic isotope effect, $k_H/k_D=1.01$, and the loss of α-deuterium during the reaction. The rate-determining S–O bond heterolysis is considered to be followed by

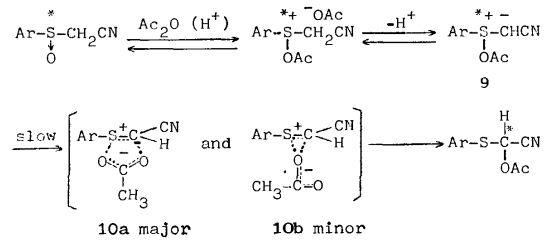

very rapid recombination of acetate with α-carbon atom intramolecularly. The asymmetric induction cannot be caused by the stereoselective proton removal from the acetoxysulfonium salt, as was suggested by Allenmark in their stereoselective Pummerer reaction,[9] since the resulting α-cyano carbanion, the ylide **9**, is known to be a coplaner resonance-stabilized carbanion. The dual pathways for the acetoxyl migration in which the five-membered cyclic path predominates over the three-membered sliding path is not particularly strange. Similar dual paths for acyloxyl migration have been known in several rearrangements of tertiary amine oxides with acylating agents.[18] Then what factor is important in inducing the chirality from the chiral sulfur atom to prochiral α-carbon in this Pummerer reaction? The preferential structural difference between

Table 2. Reaction of optically active sulfoxides with acetic anhydride in the presence of DCC

Sulfoxide	DCC[a]	T °C	t h	Product	Yield %	$[\alpha]_D$ °	e.e.[b] %	Recovered Yield %	Recovered Retention %
1b	—	60	3.5	**2b**	81	+26.8	29	—	—
3	—	120	4	**4**	51	−18.8	(29)[c]	—	—
3	2	110	6	**4**	35	−44.0	65	63	77.7
3	4	120	8	**4**	57	−36.4	57	—	—
5	—	110	4	**6**	26	−24.5	29	68	96
5	2	110	6	**6**	10	−52.5	70	—	—
5	4	120	8	**6**	43	−40.2	(50)[c]	47	87
7a	—	110	1	**8a**	88	−0.5	(0.5)[c]	—	—
7a	2	110	2	**8a**	58	−5.5	(6)[c]	—	—
7a	4	110	1.25	**8a**	32	−35.9	(38)[c]	—	—
7a	4	130	1	**8a**	88	−9.0	10	—	—

a) Equivalent to the sulfoxide. b) e.e. values were determined on the basis of NMR spectra using the chiral shift reagent, $Eu(hfc)_3$. c) e.e. value was calculated on the basis of the other e.e. value determined with the shift reagent.

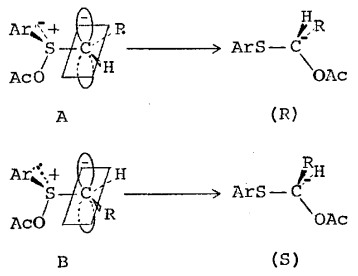

Fig. 2.

the two sulfonium ylides (A) and (B) would reflect on the preferential formation of one enanthiomeric ester to the other. Then which one of the conformers (A) and (B) would be the more favored would be solved when the absolute configuration of the resulted ester is determined. From the X-ray crystallographic analysis of (−)-**4**,[25] which is also product we obtained as optically active form and was recrystallized to optically pure crystals as described in the next section, (−)-**4** was found to have *R*-configuration, suggesting that the sterically more favored structure (A) is predominant among the acetoxysulfonium intermediates (A) and (B).

Reaction of Optically Active Carbonyl-substituted Methyl p-*Tolyl Sulfoxides* ***3***, ***5***, *and* ***7a*** *with Acetic Anhydride.* In the intramolecular Pummerer reactions of optically active sulfoxides to afford the corresponding optically active α-acetoxy sulfides **4**, **6**, and **8a** under the usual conditions, the extent of asymmetric induction has never exceeded 30% e.e. The low percents of e.e. are considered to be due to the formation of acetic acid which assists the dissociation of the intimate ion-pair during the migration of acetoxyl group. Since the Pummerer reaction of optically active carbonyl-substituted methyl *p*-tolyl sulfoxides with acetic anhydride were found to proceed slowly but quite well in the presence of DCC, unlike the cyanomethyl anolog, we have carried out the Pummerer reactions of a few optically active carbonyl-substituted methyl *p*-tolyl sulfoxides **3**, **5**, and **7a** in a large excess of acetic anhydride with two equivalent amounts of DCC in the temperature range of 110—130 °C for a few hours and found a remarkable increase of up to 70% e.e. of asymmetric induction at the α-carbon of the resulted esters.

When optically active *N*,*N*-dimethyl-*p*-tolylsulfinylacetamide (**3**) with $[\alpha]_D$ +188° was heated with a large excess of acetic anhydride in the presence of two equivalent amounts of DCC at 100 °C for 6 h, the recovered sulfoxide and the corresponding α-acetoxy sulfide **4** formed were obtained in 63% and 35% yields, respectively and the Pummerer product **4** was found to be optically active, $[\alpha]_D$ −44.0°, to the extent of 66% e.e. A similar reaction of ethyl *p*-tolylsulfinylacetate (**5**) with $[\alpha]_D$ +188° and ω-(*p*-tolylsulfinyl)-acetophenone (**7a**) with $[\alpha]_D$ +272° under the same conditions gave the corresponding highly optically active α-acetoxy sulfides **6** and **8a** in the early stage of the reaction (before a half completion). The asymmetric induction was found to be rather low, *i.e.*, below 30% e.e., when the Pummerer reaction of these optically active sulfoxides **3**, **5** and **7a** were carried out without DCC, the scavenger of acetic acid. All the stereochemical results of the reactions are tabulated in Table 2. The usual ^{18}O-tracer experiments were carried out using ^{18}O-labeled sulfoxides **3** and **7b** and the esters formed were also allowed to react with 2 equivalent amounts of phenylhydrazine to convert acetyl group to 1-acetyl-2-phenylhydrazine in order to determine the distribution of ^{18}O in the two oxygens of the ester function of the migrated esters **4** and **8b**. The results are summarized in Table 3 and illustrated in the equations shown below. When the Pummerer reaction was carried out with the sulfoxide **3** labeled with 0.607 ex. atom% of ^{18}O in 60 equiv. amounts of acetic acid at 130 °C for 10.5 h without DCC, the corresponding Pummerer reaction product **4**, obtained in 50% yield was found to have 0.198 ex. atom% of ^{18}O while the sulfoxide recovered in 50% yield retained 92% (0.558 ex. atom%) of ^{18}O of the original

Table 3. ^{18}O Experimental data in the Pummerer reaction of ^{18}O-labeled aryl (substituted methyl) sulfoxides with acetic anhydride

$ArSCH_2X$ (^{18}O)	^{18}O-Content (ex. atom%)		Yield %	Pummer product ^{18}O-Content (ex. atom%)	Pummer product Incorporation(%)	^{18}O-Distribution(%) Carbonyl ^{18}O-Content (ex. atom%)	^{18}O-Distribution(%) (Ether)	Recovered sulfoxide Yield %	Recovered sulfoxide ^{18}O-Content (ex. atom%)	Recovered sulfoxide Retention %
1d	0.680	**2d**	35	0.290	85	0.366 63	(37)	55	0.655	96
3	0.607	**4**	50	0.198	49	0.386 65	(35)	50	0.558	92
3[a)]	0.607	**4**	76	0.267	66	0.480 60	(40)	20	0.522	86
7b	0.840	**8b**	74	0.243	43	0.411 56	(44)	—	—	—

a) The reaction was carried out in the presence of 4 equiv. of DCC.

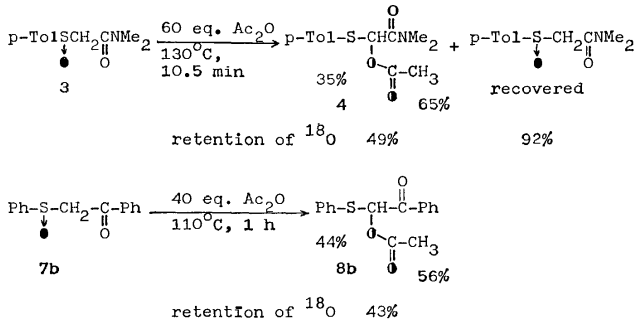

^{18}O-label of the sulfoxide **3**. The uneven distribution of ^{18}O rich in favor for the carbonyl oxygen in the resulting Pummerer product **4** is also in keeping with the result observed in the Pummerer product **2d**. All these observations together with other pertinent data clearly indicate that these stereoselective intramolecular acetoxyl migrations proceed *via* intimate ion-pairs formed by concurrent electron-transfer within the acetoxysulfonium ylide and S–O bond heterolysis, and the subsequent recombination of the sulfenyl carbenium ion and acetate is so rapid that there is not enough time to achieve complete racemization and complete ^{18}O-scrambling in the resulted esters.

Experimental

General. All melting points were uncorrected. IR spectra were taken on a Hitachi 260-50 spectrometer. NMR spectra were recorded with a Hitachi Perkin-Elmer R-20 spectrometer in $CDCl_3$ using TMS as an internal standard. Mass spectra were determined with a Hitachi RMU-6MG mass spectrometer. UV absorptions were measured using a JASCO UNIDEC-1 spectrophotometer. Acetic anhydride was purified by stirring with sodium metal for 7 d followed by a refluxing under reduced pressure below 50 °C for 5 h and then distilled under reduced pressure, bp 47—48 °C/20 mmHg.**

^{18}O-Analysis. ^{18}O-Analysis was carried out by the method developed by Rittenberg and Ponticorvo,[19] with a modification which involves the use of $Pb(OAc)_2$ to remove H_2S gas from the gas produced by the thermolysis of sample: About 20 mg of sample was pyrolyzed with 250 mg each of purified $HgCl_2$ and $Hg(CN)_2$, respectively, in an evacuated sealed pyrex tube at ca 500 °C for 12 h. Then the tube was broken in a vacuum line and CO_2 gas formed was purified by distillation and the mass peaks of *m/e* 44 and 46 which correspond to $C^{16}O_2$ and $C^{16}O^{18}O$, respectively, were recorded on a mass spectrometer.

Materials. *Aryl Cyanomethyl Sulfides*: Chloroacetonitrile was treated with respective sodium arenethiolates in ethanol at room temperature. The sulfides thus obtained in 70—80% yields have the following physical properties. R-S-CH_2CN: R, bp (or mp), NMR ($CDCl_3$) δ; Ph, 107—109 °C/3 mmHg, 3.52 (2H, s), 7.6 (5H, s broad); *p*-tolyl, 114—116 °C/3 mmHg, 2.38 (3H, s), 3.52 (2H, s), 7.1—7.6 (4H, m); *p*-ClC_6H_4, mp 85—87 °C, 3.52 (2H, s), 7.3—7.6 (4H, m); *p*-$MeOC_6H_4$, liquid (bp not determined), 3.46 (2H, s), 3.83 (3H, s), 6.8—7.6 (4H, m).

Cyanomethyl p-Nitrophenyl Sulfide: Chloroacetonitrile was treated with *p*-nitrobenzenethiol in the presence of triethylamine in chloroform at room temperature to give cyanomethyl *p*-nitrophenyl sulfide in 75% yield, mp 84—85 °C, 3.78 (2H, s), 7.5—8.3 (4H, m).

*Aryl Cyanomethyl Sulfoxides (**1a**—**e**)*: The corresponding sulfides were allowed to react with *m*-chloroperbenzoic acid in chloroform at room temperature. The sulfoxides obtained in nearly quantitative yields were recrystallized from either benzene or acetonitrile. Physical properties are the followings. R-S(O)-CH_2CN: R, mp, NMR ($CDCl_3$) δ, anal; *p*-$MeOC_6H_4$, **1a**, 65—66 °C, 3.70 (2H, s), 3.87 (3H, s), 7.0—7.8 (4H, m), Found: C, 55.35; H, 4.72; N, 7.41%. Calcd for $C_9H_9NO_2S$: C, 55.38; H, 4.65; N, 7.18%. *p*-tolyl, **1b**, 72—3 °C, 2.47 (3H, s), 3.70 (2H, s), 7.3—7.8 (4H, m), Found: C, 60.33; H, 5.10; N, 7.66%. Calcd for C_9H_9NOS: C, 60.33; H, 5.06; N, 7.82%. Ph, **1c**, 65—66 °C, 3.70 (2H, s), 7.4—7.8 (5H, m), Found: C, 58.04; H, 4.29; N, 8.68%. Calcd for C_8H_7NOS: C, 58.18; H, 4.27; N, 8.48%. *p*-ClC_6H_4, **1d**, 87—88 °C, 3.73 (2H, s), 7.5—7.8 (4H, m), Found: C, 48.00; H, 3.03; N, 6.86%. Calcd for C_8H_6ClNOS: C, 48.09; H, 3.01; N, 7.01%. *p*-$NO_2C_6H_4$, **1e**, 153—154 °C, (DMSO-d_6) 4.50 (2H, AB quartet), 7.9—8.5 (4H, m), Found: C, 45.73; H, 2.96; N, 13.18%. Calcd for $C_8H_6N_2O_3S$: C, 45.72; H, 2.88; N, 13.33%.

*Optically Active Cyanomethyl p-Tolyl Sulfoxide (**1b**)*: The optically active **1b** was synthesized by either one of the following two procedures.

1): HMPT solution (50 ml) of (+)-bromomethyl *p*-tolyl sulfoxide (2.0 g), synthesized according to the reported procedure,[20] was mixed with aqueous solution (2 ml) of potassium cyanide (1 g), and heated at 50 °C for 1 d. The HMPT sulution was diluted with 100 ml of chloroform, and the whole solution was washed three times with 1000 ml portion of water. Then the resultant chloroform solution was dried and concentrated to afford a dark red oily product which was separated through silica-gel chromatography with chloroform as an eluent, giving crystalline optically active cyanomethyl *p*-tolyl sulfoxide which was recrystallized from benzene-hexane. Thus, (+)-cyanomethyl *p*-tolyl sulfoxide (**1b**) obtained (300 mg, 15% yield) has $[\alpha]_D$ +252° (*c* 1,

** 1 mmHg ≈ 133.3 Pa.

EtOH), mp 72 °C. Upon measurement of NMR contact shift using chiral lanthanoid shift reagent, Eu(hfc)$_3$, the sulfoxide was found to be more than 90% optically pure. (*vide infra*)

2): Optically active bromomethyl *p*-tolyl sulfoxide (220 mg), prepared by usual α-bromination of optically active methyl *p*-tolyl sulfoxide,[20] was treated with 1.2 equiv. amount of KCN (68 mg) in the presence of 18-crown-6 (23 mg) in $CHCl_3$ (10 ml) under reflux for 4 h. The crude optically active cyanomethyl *p*-tolyl sulfoxide (**1b**) (125 mg) obtained in 72% yield was recrystallized from benzene–hexane giving 100 mg of the partially optically active title compound with $[\alpha]_D$ +145° (*c* 1.5, acetone).

Optically Active N,N-*Dimethyl*-p-*tolylsulfinylacetamide (3)*: A solution of 6.4 ml of butyllithium (15 wt% in hexane) was added to a solution containing optically active (+)-(*R*)-methyl *p*-tolyl sulfoxide (1.54 g, 10 mmol) in 20 ml of a freshly distilled THF at −70 °C in an acetone–Dry Ice bath and then the mixture was stirred for 30 min. After dimethylcarbamoyl chloride (537.5 mg, 5 mmol) was added to the THF solution with a syringe at −70 °C, the reaction mixture was allowed to stir at room temperature for 1 h. Into this mixture 20 ml of cold water was added, then the solution was acidified with aqueous solution of ammonium chloride (*ca.* pH 3) and extracted with chloroform. The combined orange layer was washed twice, and then dried over Na_2SO_4. Evaporation of the solvent gave an oily residue which was separated through silica-gel column chromatography with benzene–acetone (4:1) as an eluent. Then the product was distilled to give a colorless oil (584 mg, 40% yield): bp 130 °C/1 mmHg (Kugelrohr), $[\alpha]_D$ +188° (acetone).

Optically Active Ethyl p-*Tolylsulfinylacetate (5)*: Diethyl carbonate (590 mg, 5 mmol) was treated with 2 equivalent molar amount of a *p*-tolylsulfinylmethylide ion dried from the corresponding (+)-methyl *p*-tolyl sulfoxide (1.54 g, 10 mmol) with $[\alpha]_D$ +154° (in acetone) and lithium diethylamide prepared from 6.4 ml of butyllithium solution (0.1 g/ml) in hexane and diethylamine (730 mg, 10 ml) at −70 °C. The reaction mixture was then stirred at 0 °C for 1 h. After addition of 20 ml of water, the solution was acidified with aqueous ammonium chloride solution (*ca.* pH 3) and extracted with 50 ml of chloroform three times, dried over $MgSO_4$, and the solvent was evaporated to give an oily residue which was separated through silica-gel column chromatography with benzene–ethyl acetate (4:1) as an eluent. Then the product was distilled to give a colorless oil (531 mg, 47% yield) with bp 130 °C/1.5 mmHg (Kugelrohr) and $[\alpha]_D$ +188° (*c* 1.0, acetone). IR (KBr) 1730 and 1045 cm^{-1}; NMR ($CDCl_3$) δ=7.36 (4H, ABq), 4.12 (2H, q), 3.67 (2H, ABq), 2.40 (3H, s), 1.21 (3H, s); Found: C, 57.92; H, 6.28%. Calcd for $C_{11}H_{14}O_3S$: C, 58.38; H, 6.28%.

*Optically Active ω-(*p-*Tolylsulfinyl)acetophenone (7a)*: Reaction of ethyl benzoate with *p*-tolylsulfinylmethylide ion prepared by treating (+)-(*R*)-methyl *p*-tolyl sulfoxide ($[\alpha]_D$ +154°, acetone) with butyllithium in diethylamine gave the optically active **7a**: $[\alpha]_D$ +272° (*c* 1, acetone), mp 87—88 °C; lit,[21] $[\alpha]_D$ +264.5° (acetone), mp 74 °C.

^{18}O-*Labeled Cyanomethyl* p-*Chlorophenyl Sulfoxide (1d)*: Cyanomethyl *p*-chlorophenyl sulfide (4.5 g, 24 mmol) was dissolved in a mixture of acetic acid (20 ml), pyridine (6 ml) and ^{18}O-enriched water (1.8 ml) (1.6 atom%). To the cooled sulution was added bromine (3.9 g, 24 mmol) at 0 °C.[22] After keeping the solution for 2 h at 0 °C, the reaction mixture was quenched with 200 ml of water and extracted with chloroform (200 ml). The chloroform solution was washed with aqueous $Na_2S_2O_3$ solution, diluted aqueous HCl solution and water, and then dried ($MgSO_4$). After evaporation of chloroform with a rotary evaporator, an oily substance obtained was separated through silica-gel column chromatography, giving ^{18}O-labeled cyanomethyl *p*-chlorophenyl sulfoxide (**1d**) which was recrystallized from benzene. Thus the ^{18}O-labeled **1d** obtained (600 mg, 12% yield) was found to contain 0.680 ex. ^{18}O atom%.

^{18}O-*Labeled* N,N-*Dimethyl*-p-*tolylsulfinylacetamide (3)*: The ^{18}O-labeled sulfoxide **3** was obtained by the reaction of dimethylcarbamoyl chloride (613 mg, 5.7 mmol) with *p*-tolylsulfinylmethylide ion prepared by treating ^{18}O-labeled methyl *p*-tolyl sulfoxide (1.747 g, 11.3 mmol) with lithium diethylamide (prepared from 0.1 g/ml solution of butyllithium in hexane and diethylamine in THF). Then the usual work-up as mentioned above gave the ^{18}O-labeled **3**: mp 59—60 °C, 0.607 ex. atom% of ^{18}O, IR (KBr) 1640, 1265, and 1045 cm^{-1}, NMR ($CDCl_3$) δ=7.41 (4H, ABq), 3.33 (2H, ABq), 2.93 (3H, s), 2.90 (3H, s) and 2.39 (3H, s); Found: C, 58.77; H, 6.72; N, 6.20%. Calcd for $C_{11}H_{15}NO_2S$: C, 58.64, H. 6.71; N, 6.21%.

^{18}O-*Labeled ω-Phenylsulfinylacetophenone (7b)*: The reaction of ethyl benzoate with the phenylsulfinylmethylide ion prepared by treating ^{18}O-labeled methyl phenyl sulfoxide (1.621 ex. atom%) with butyllithium in diethylamine gave the ^{18}O-labeled **7b**: mp 70—71 °C, (lit,[23] mp 70—71 °C), ^{18}O-content: 0.840 ex. atom%.

Cyanomethyl-d$_2$ *Phenyl and Cyanomethyl*-d$_2$ p-*Tolyl Sulfoxides*: The nonlabeled sulfoxide (370 mg) was dissolved in anhydrous chloroform (10 ml) containing two drops of anhydrous pyridine. The chloroform solution was vigrously shaken with D_2O (1 ml) at room temperature in a separatory unnel, and the aqueous layer was separated out. After the chloroform solution was dried over anhydrous Na_2SO_4 and concentrated under reduced pressure, the solid dideuterated sulfoxide was obtained. Then the partially labeled sulfoxide thus obtained was treated additionally with D_2O for H–D exchange as the same procedure mentioned above. Thus the sulfoxide obtained by the two consecutive H–D exchange was found to be completely labeled by D upon NMR measurement and recrystallized from anhydrous benzene.

Reaction of Aryl Cyanomethyl Sulfoxides (1b—e) with Acetic Anhydride. The sulfoxides **1b—e** (*ca.* 400 mg) were heated with 20 ml of acetic anhydride at 110—115 °C for 4—6 h untill the sulfoxides were found to have disappeared upon monitoring with TLC method. After evaporation of excess acetic anhydride and any volatile product *in vacuo*, the remaining residue was separated by column chromatography through silica gel with benzene as an eluent. The corresponding α-acetoxy sulfides, the Pummerer products, were obtained in 85—90% yields. Physical properties of R–S–CH(OAc)CN (**2b—e**) were the followings: R, mp (or bp), NMR ($CDCl_3$) δ, Anal; *p*-tolyl **2b**: 100 °C/4 mmHg (Kugelrohr), 2.15 (3H, s), 2.39 (3H, s), 6.48 (1H, s), 7.1—7.6 (4H, m). Ph **2c**: 100 °C/4 mmHg (Kugelrohr oven), 2.17 (3H, s), 6.52 (1H, s), 7.4—7.7 (5H, m), Found: C, 57.86; H, 4.50; N, 6.76%. Calcd for $C_{10}H_9NO_2S$: C, 57.97; H, 4.38; N, 6.76%. *p*-ClC_6H_4 **2d**: 53—55 °C, 2.18 (3H, s), 6.49 (1H, s), 7.3—7.7 (4H, m), Found: C, 49.63; H, 3.36; N, 5.80%. Calcd for $C_{10}H_8ClNO_2S$: C, 49.59; H, 3.31; N, 5.79%. *p*-$NO_2C_6H_4$ **2e**: 92—3 °C, 2.21 (3H, s), 6.63 (1H, s), 7.7—8.3 (4H, m).

Reaction of Optically Active Cyanomethyl p-*Tolyl Sulfoxide (1b) with Acetic Anhydride.* *1)*: After heating of the optically active sulfoxide **1b** ($[\alpha]_D$ +252° 50 mg) with 1 ml of acetic anhydride at 120 °C for 3.5 h and then evaporation of an excess acetic anhydride and any volatile product *in vacuo*,

an oily product was purified through column chromatography (silica gel, benzene as an eluent) to afford a colorless oily Pummerer product, acetoxycyanomethyl *p*-tolyl sulfide (**2b**) (50 mg, 81% yield). The oily **2b** was further purified by distillation with micro-distillation apparatus (100 °C/1 mmHg bath temp) giving the pure **2b** with $[\alpha]_D$ +26.8° (*c* 5, EtOH). This optically active α-acetoxy sulfide **2b** was found to be of 29.0±0.8% of enantiomer excess (e.e.) by treatment with the chiral lanthanoids shift reagent, Eu(hfc)$_3$. (*vide infra*). Prolonged heating (120 °C, 7 h) of the sulfoxide **1b** with acetic anhydride also gave the partially optically active Pummerer product **2b** with $[\alpha]_D$ +25.7° (*c* 4.35, EtOH).

2): When the optically active **1b** (50 mg) was heated with 1 ml of acetic anhydride containing 0.2 ml of acetic acid (120 °C, 3 h), the Pummerer product **2b** obtained (52 mg) after the same work-up has only $[\alpha]_D$ +1.2° (*c* 5.2, EtOH).

3): When the optically active **1b** (51 mg) was heated with acetic anhydride (1 ml) at 120 °C for 6 min, the Pummerer reaction was found to have proceeded only to 22% conversion by monitoring with NMR measurement of the reaction mixture of the sulfoxide and the α-acetoxy sulfide **2b** after evaporation of excess of acetic anhydride. The only mixture was separated through column chromatography (silica gel, benzene, and then chloroform as eluents), giving the recovered sulfoxide **1b** (42 mg) with $[\alpha]_D$ +234° (*c* 4.2, EtOH, and with $[\alpha]_D$ +251° (*c* 0.63, EtOH) after recrystallization from benzene-hexane.

Reaction of ^{18}O*-Labeled Cyanomethyl* p*-Chlorophenyl Sulfoxide (**1d**) with Acetic Anhydride. 1)*: When the ^{18}O-labeled title sulfoxide **1d** (600 mg) (0.680 ex. atom%) was heated with 5 ml of acetic anhydride at 120 °C for 1 h, the oily residue obtained after evaporation of excess of acetic anhydride and any volatile product in vacuo was separated by column chromatography through silica gel with benzene and then chloroform as eluents. The sulfoxide recovered and the Pummerer product **2d** were recrystallized from benzene and hexane, respectively, to afford the sulfoxide (332 mg, 55% yield) and the Pummerer product (252 mg, 35% yield). The starting sulfoxide, the recovered sulfoxide and the Pummerer product were subjected to measurement of ^{18}O-content by the routine ^{18}O-analysis technique and the ^{18}O-contents were found to be 0.680, 0.655, and 0.290 ex. atom%, respectively.

2): When the ^{18}O-labeled **1d** (100 mg, 0.680 ex. atom%) was heated with 4 ml of acetic anhydride containing 830 mg of acetic acid at 100 °C for 16 min, the Pummerer reaction proceeded to 10% conversion, and the unreacted starting sulfoxide recovered was found to retain original ^{18}O-label completely (0.680 ex. atom%). While the sulfoxide **1d** (102 mg, 0.680 ex. atom%) was heated with acetic anhydride (2 ml) containing acetic acid (0.4 ml) at 120 °C for 2 h, the Pummerer product **2d** recrystallized from hexane was found to contain 0.154 ex. atom% of ^{18}O.

^{18}O*-Distribution in Ester Function of the Pummerer Product (**2d**).* When the Pummerer product (400 mg, 0.290 ex atom%) was treated with three molar excess of phenylhydrazine (540 mg) in 5 ml of benzene at 60 °C for 0.5 h, 1-acetyl-2-phenylhydrazine precipitated was collected (130 mg) and recrystallized twice from benzene. The pure 1-acetyl-2-phenylhydrazine (80 mg, mp 125—128 °C) was found to contain 0.366 ex atom% of ^{18}O by the routine ^{18}O-analysis.

*Kinetic Procedure for the Pummerer Reaction of Aryl Cyanomethyl Sulfoxide (**1a—e**).* The Pummerer reaction was carried out at 120.0±0.07 °C in sealed tubes, in which each sulfoxide **1a—e** (0.22—0.38 mmol) was dissolved in 2 ml of acetic anhydride solution containing acetic acid (0—13.8 mmol). In this solution, the concentration of acetic anhydride was maintained above 50 molar excess as compared with that of the sulfoxide. A sealed tube containing 200 μl solution of the above mixture was recovered at several time intervals and was cooled in an ice-bath to stop the reaction. The aliquot portion (50—70 μl) was pipetted out and then diluted with ethanol resulting in making of 50 ml of ethanol solution, which was measured by UV spectrometer around 246—282 nm. Thus the rate of the Pummerer reaction was readily obtained by following the decrease of the band of the starting sulfoxide at 246—282 nm, since the starting sulfoxides absorb light at 246—282 nm (ε=7000—7500) and the Pummerer products absorb light at the same range with substantially small absorption coefficient (ε=4000—6000).

Reaction of Aryl Cyanomethyl-d_2 *Sulfoxides with Acetic Anhydride. 1)*: After heating of cyanomethyl-d_2 phenyl sulfoxide (45 mg) with 0.4 ml of acetic anhydride at 120 °C for 40 min, and separation of product mixture through column chromatography, the starting sulfoxide recovered (29 mg, 35% conversion) was found to have lost deuterium substantially (66% H-incorporation) upon determination by NMR measurement.

2): Cyanomethyl-d_2 *p*-tolyl sulfoxide (55 mg) was heated with 2 ml of acetic anhydride solution containing acetic acid (0.416 g, 6.93 mmol) at 120 °C for 16 min, where the Pummerer reaction was found to have proceeded 51% conversion upon determination by monitoring with UV. Then after evaporation of solvent of the reaction solution and measurement of the residue redissolved in $CDCl_3$ with NMR instrument, both the sulfoxide and the Pummerer product were found to retain no deuterium.

Reaction of the Optically Active N,N*-Dimethyl-*p*-tolylsulfinylacetamide with Acetic Anhydride. 1)*: The optically active sulfoxide **3** (74.4 mg, $[\alpha]_D$ +188°) was heated with 2 ml of acetic anhydride at 120 °C for 4 h. Then, after evaporation of excess acetic anhydride and any volatile product *in vacuo*, the remaining residue was separated by column chromatography through silica gel with benzene–ethyl acetate (4:1) as an eluent. The Pummerer product (**4**, 44.7 mg, 51% yield) with $[\alpha]_D$ −18.8° (*c* 2.0, acetone) was obtained.

2): The sulfoxide **3** (55 mg) was heated with 2 ml of acetic anhydride in the presence of 2 equiv. molar amount of DCC to the sulfoxide at 110 °C for 6 h, the Pummerer product **4** (22.7 mg, 35% yield) with $[\alpha]_D$ −44° (acetone) and the recovered sulfoxide (34 mg, 63% yield, $[\alpha]_D$ +146°) were obtained. The product **4** was recrystallized repeatedly from hexane to give optically pure crystals with maximum rotation $[\alpha]_D$ −59.2° (*c* 0.4, acetone). Mp 65—65.5 °C.

3): When the sulfoxide **3** (50 mg) was heated with 2 ml of acetic anhydride in the presence of 4 equiv. of DCC (163 mg) to the sulfoxide at 120 °C for 8 h, the Pummerer product **4** (59.3 mg) with $[\alpha]_D$ −36.4° was obtained.

Reaction of the Optically Active Ethyl p*-Tolylsulfinylacetate (**5**) with Acetic Anhydride. 1)*: The sulfoxide **5** (101 mg, $[\alpha]_D$ +188°) was heated with 2 ml of acetic anhydride at 110 °C for 4 h. Then after evaporation of excess acetic anhydride and any volatile product *in vacuo*, the remaining residue was separated through silica-gel column chromatography with benzene–ethyl acetate (4:1) as the eluent to give the Pummerer product **6** (26 mg, 22% yield) with $[\alpha]_D$ −18.8° (*c* 2.6, acetone) and the sulfoxide recovered retaining nearly the same initial optical purity ($[\alpha]_D$ +180°). The e.e. value of the chiral Pummerer product was found

to be 29% by measurement of the peak splitted on NMR recorder using the chiral lanthanoid shift reagent, Eu(hfc)$_3$. Mp 39.5—41.0 °C; IR (KBr) 1750, 1742, and 1203 cm^{-1}; NMR ($CDCl_3$) δ=7.45 (2H, d, J=8.4 Hz), 7.18 (2H, d, J=8.4 Hz), 6.16 (1H, s), 4.15 (2H, q), 2.35 (3H, s), 2.20 (3H, s), 1.20 (3H, t); Found: C, 58.43; H, 6.02%. Calcd for $C_{13}H_{16}O_4S$: C, 58.19; H, 6.01%.

2): The sulfoxide **5** (100 mg) was heated with 2 ml of acetic anhydride in the presence of 2 equiv. of DCC (182 mg) to the sulfoxide at 110 °C for 6 h. After the work-up as mentioned above, the Pummerer product **6** (11.8 mg, 10%) with $[\alpha]_D$ −52.5° (*c* 1.18, acetone) was obtained. The e.e. value of this Pummerer product induced with optical activity was 69.5% by treatment as mentioned above.

3): The sulfoxide **5** (45.0 mg) was heated with 1 ml of acetic anhydride in the presence of 4 equiv. DCC (165 mg) to the sulfoxide at 120 °C for 8 h. The Pummerer product **6** (22.9 mg, 43% yield with $[\alpha]_D$ +163° was obtained.

*Reaction of the Optically Active ω-(p-Tolylsulfinyl)acetophenone (**7a**) with Acetic Anhydride.* The optically active sulfoxide **7a** (200 mg) was heated with acetic anhydride (5 ml) at 110 °C for 1 h, and after evaporation of excess acetic anhydride and any volatile product an yellow oily residue was separated by column chromatography on silica gel with benzene as an eluent. The Pummerer product **8a** (204 mg, 88% yield) with $[\alpha]_D$ −0.5° (*c* 11, acetone) and a small amount of deoxygenated product (*p*-TolSCH$_2$COPh, 18 mg, 10% yield) were obtained. Both products gave the same IR and NMR spectra of the authentic samples reported.[24]

*Reaction of ^{18}O-Labeled N,N-Dimethyl-p-tolylsulfinylacetamide (**3**) with Acetic Anhydride. 1)*: The ^{18}O-labeled sulfoxide **3** (400 mg, 0.607 ex. atom%) was heated with 60 equiv. acetic anhydride at 130 °C for 10.5 min. Then after work-up as mentioned above the reaction of optically active **3** and chromatography on silica gel gave the Pummerer product **4** (237 mg, 50% yield) and the sulfoxide recovered (200 mg, 50% yield) which were recrystallized from ether–hexane and ethyl acetate–hexane, respectively, were found to have 0.198 and 0.558 ex. atom% of ^{18}O, respectively. **4**: mp 59—60 °C; IR (KBr) 1750, 1653 and 1230 cm^{-1}; NMR ($CDCl_3$) δ=7.5—7.1 (9H, m), 6.20 (1H, s), 2.29 (3H, s), 2.06 (3H, s); Found: C, 58.43; H, 6.42; N, 5.90%. Calcd for $C_{13}H_{17}NO_3S$: C, 58.40; H, 6.40; N, 5.23%.

2) After the sulfoxide **3** (400 mg) was allowed to react with 60 equiv. acetic anhydride at 120 °C for 8 h in the presence of 4 equivalent DCC, the usual work-up and chromatography on silica gel gave the Pummerer product **4** (361 mg, 76% yield). The Pummerer product **4** was found to contain 0.267 ex. atom% of ^{18}O.

*^{18}O-Distribution in Ester Function of the Pummerer Product (**4**).* After the Pummerer products **4** (134 mg, 0.198 ex. atom% of ^{18}O and 143 mg, 0.267 ex. atom% of ^{18}O) in 2 ml of benzene with 2 molar excess of phenylhydrazine were heated at 80 °C for 12 h, the reaction mixture was cooled to precipitate 1-acetyl-2-phenylhydrazine which was filtered off and washed with benzene. Then the product was recrystallized twice from benzene to give pure crystals (48 mg and 50 mg, respectively, mp 130—131 °C) which were found to contain 0.386 and 0.480 ex. atom% of ^{18}O, respectively.

*Reaction of ^{18}O-Labeled ω-Phenylsulfinylacetophenone (**7b**) with Acetic Anhydride.* ^{18}O-Labeled sulfoxide **7b** (310 mg, 0.840 ex. atom%) was heated with acetic anhydride (5 ml) at 110 °C for 1 h. After the usual work-up process, the Pummerer product **8b** obtained was recrystallized from benzene–hexane giving colorless needles (270 mg, 74% yield). The product **8b**: mp 65—67 °C; 0.243 ex. atom% of ^{18}O; IR (KBr) 1730, 1690, and 1220 cm^{-1}; NMR ($CDCl_3$) δ= 2.13 (3H, s), 6.87 (1H, s), 7.2—7.9 (10H, m); MS (20 eV), *m/e* (rel intensity), 286 (M^+, 10), 181 (M−PhCO$^+$, 38), 105 (PhCO$^+$, 72), 43 (Ac$^+$, 100).

*^{18}O-Distribution in the Ester Function of the Pummerer Product (**8b**).* The Pummerer product **8b** (220 mg) with 0.243 ex. atom% of ^{18}O was heated with three equivalent amounts of phenylhydrazine (250 mg) at 120 °C for 1 h. Into this red solution, benzene was added to precipitate 1-acetyl-2-phenylhydrazine which was filtered off and washed with benzene. Then the product was recrystallized from benzene giving colorless crystals (59 mg, 51% yield) with mp 129—131 °C, and 0.411 ex. atom% of ^{18}O.

Authors are grateful to Dr. Fujiko Iwasaki, The University of Electro-Communications, for X-ray crystallographic analysis of **4**, and for Torey Science and Technology Prize and Grants for 1980 and Grant-in-Aid for Scientific Reseach B No. 00547018 of the Ministry of Education, Science and Culture for 1980, which enabled us to continue the research works along this line.

References

1) R. Pummerer, *Ber.*, **42**, 2282 (1909); **43**, 1401 (1910).
2) L. Horner and P. Kaiser, *Justus Liebigs Ann. Chem.*, **626**, 19 (1959); L. Horner, *ibid.*, **631**, 198 (1960).
3) S. Oae, T. Kitao, S. Kawamura, and Y. Kitaoka, *Tetrahedron*, **19**, 817 (1963).
4) S. Oae, T. Kitao, and S. Kawamura, *Tetrahedron*, **19**, 1783 (1963).
5) T. Numata and S. Oae, *Yukī Gosei Kagaku Kyokai Shi*, **35**, 726 (1977); T. Numata, *ibid.*, **36**, 845 (1978).
6) G. A. Russell and G. J. Mikol, "Mechanisms of Molecular Migrations," ed by B. S. Thyagarajan, Interscience, New York (1968), Vol. 1, p. 157; T. Durst, *Adv. Org. Chem.*, **6**, 285 (1969); J. P. Marino, "Topics in Sulfur Chemistry," ed by A. Senning, Georg Thieme Publishers, Stuttgart (1976), Vol. 1, p. 1.
7) a) S. Oae, "Yuki-Io Kagobutsu No Kagaku (Chemistry of Organic Sulfur Compounds)," Kagaku Dojin, Kyoto (1969), Vol. 2, pp. 214—220; b) S. Oae, "Organic Chemistry of Sulfur," ed by S. Oae, Plenum Press, New York (1977), Chap. 8; c) S. Oae, "Topics in Organic Sulfur Chemistry," ed by M. Tišler, University Press, Ljubliana, Yugoslavia (1978), Chap. 11; d) S. Oae and T. Numata, "The Pummerer and Pummerer Type of Reactions," in "Isotopes in Organic Chemistry," ed by E. Buncel and C. C. Lee, Elsevier, New York (1980), Chap. 2; e) S. Oae, T. Numata, and T. Yoshimura, "Heterosulphonium Salts," in "The Chemistry of the Sulphonium Group," ed by C. J. M. Stirling and S. Patai, John Wiley & Sons, New York (1981), Part 2, Chap. 15.
8) S. Oae, O. Itoh, T. Numata, and T. Yoshimura, *Bull. Chem. Soc. Jpn.*, **56**, 270 (1983).
9) B. Stridsberg and S. Allenmark, *Acta. Chem. Scand., Ser. B*, **28**, 591 (1974); **30**, 219 (1976).
10) T. Numata and S. Oae, *Chem. Ind. (London)*, **1972**, 726; *Tetrahedron*, **30**, 2641 (1974).
11) T. Numata and S. Oae, *Tetrahedron Lett.*, **1977**, 1337.
12) T. Numata, O. Itoh and S. Oae, *Chem. Lett.*, **1977**, 909.
13) T. Numata, O. Itoh, and S. Oae, *Tetrahedron Lett.*, **1979**, 1869.
14) O. Itoh, T. Numata, T. Yoshimura, and S. Oae, *Phosphorus and Sulfur*, in contribution.
15) T. Numata, H. Togo, and S. Oae, *Chem. Lett.*, **1979**, 329.

16) M. Kise and S. Oae, *Bull. Chem. Soc. Jpn.*, **43**, 1426 (1970).
17) T. Yagihara and S. Oae, *Tetrahedron*, **28**, 2759 (1972).
18) S. Oae and K. Ogino, "Rearrangements of *t*-Amine Oxides with Acylating Agents," *Heterocycles*, **6**, 583 (1977), and the references are cited therein.
19) D. Rittenberg and L. Ponticorvo, *J. Appl. Rad. Isotopes*, **1**, 208 (1956).
20) M. Cinquini, S. Colona, R. Fornasier, and F. Montanari, *J. Chem. Soc., Perkin Trans. 1*, **1972**, 1886.
21) N. Kunieda, J. Nokami, and M. Kinoshita, *Chem. Lett.*, **1974**, 369.
22) S. Oae, Y. Ohnishi, S. Kozuka, and W. Tagaki, *Bull. Chem. Soc. Jpn.*, **39**, 364 (1964).
23) N. Kunieda, Y. Fujiwara, J. Nokami, and M. Kinoshita, *Bull. Chem. Soc. Jpn.*, **49**, 575 (1976).
24) S. Iriuchijima, K. Maniwa, and G. Tsuchihashi, *J. Am. Chem. Soc.*, **97**, 596 (1975).

Predominant Intramolecular Pummerer Reactions of Substituted Benzyl *p*-Tolyl Sulfoxides with Acetic Anhydride

Osamu Itoh, Tatsuo Numata, Toshiaki Yoshimura, and Shigeru Oae*

Department of Chemistry, University of Tsukuba, Niihari-gun, Sakura-mura, Ibaraki 305

(Received June 7, 1982)

In the Pummerer reactions of ^{18}O-labeled benzyl, and 3,5-dichlorobenzyl *p*-tolyl sulfoxides with a large excess of unlabeled acetic anhydride in the presence of DCC as acid scavenger, the resulted Pummerer reaction products, the α-acetoxy sulfides, were found to have retained substantial amounts of ^{18}O-label of the original sulfoxides, *i.e.*, nearly a half or more. Meanwhile, when optically active benzyl, 3-chlorobenzyl, and 3,5-dichlorobenzyl *p*-tolyl sulfoxides were allowed to react with excess acetic anhydride in the presence of DCC, the α-acetoxy sulfides, the Pummerer reaction products obtained, were found to have no optical activity. These observations suggest that the acetoxyl migration from sulfur atom to α-carbon is predominantly intramolecular, however, the α-(*p*-tolylthio) carbenium acetate ion-pair formed during the reaction prior to racemization is less intimate than those which are formed in the reactions of cyanomethyl and (α-carbonyl-substituted methyl) *p*-tolyl sulfoxides which give the corresponding highly optically active α-acetoxy sulfides.

Most early examples of the Pummerer reaction in the mechanistic studies were found to be intermolecular rearrangements, based mainly on ^{18}O-tracer experiments.[1,2] Sulfoxides are usually dialkyl or aryl alkyl derivatives and the rate-determining setp is generally the α-proton-removal from the acyloxysulfonium salts after the initial acylation of the sulfoxides. Years later, we found a clear-cut case of intramolecular 1,2-rearrangement of acetoxyl group by the aid of ^{18}O-tracer experiments and stereochemistry; namely the Pummerer reaction of optically acetive aryl cyanomethyl sulfoxide with acetic anhydride was stereospecific, inducing a partial asymmetry at α-carbon and most of the ^{18}O-label in the original sulfoxide was retained in the resulted α-acetoxy sulfide.[3] Many more examples of intramolecular Pummerer reaction have been found ever since.[2,4] In these intramolecular rearrangements, the rate-determining step is generally the S–O bond cleavage after the reversible proton removal from the acetoxysulfonium intermediate, and the asymmetric induction from the chiral sulfur atom to the prochiral α-carbon is believed to be due to both the very tight nature of the α-thio carbenium acetate ion-pair, and the very rapid recombination, *i.e.*, ion-pair return.

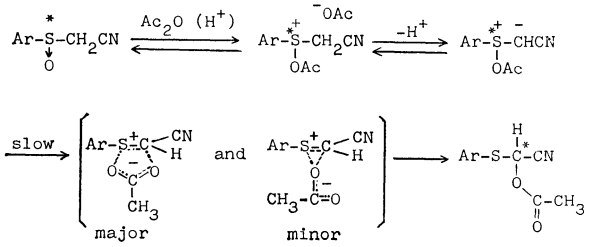

In the solvolytic S_N1 type reactions of optically active alkyl arenesulfonate-^{18}O, stereochemistry and the extent of oxygen scrambling are known to vary with the change of the alkyl derivatives and the reaction medium, and closely related to the tightness of the ion-pair formed by the initial cleavage of C–O bond of the sulfonate.[5] There are cases that the internal return is nearly quantitative with partial oxygen scrambling, however, with nearly complete racemization.[6]

We now have found the Pummerer reaction which proceeds predominantly intramolecularly, however, the original chirality of the sulfoxide is completely lost in the resulted α-acetoxy sulfide, namely, in the Pummerer reactions of benzyl, 3-chlorobenzyl, and 3,5-dichlorobenzyl *p*-tolyl sulfoxides (**1**, **3**, and **5**) with acetic anhydride in the presence of dicyclohexylcarbodiimide (DCC), scavenger of acetic acid. This paper deals with the mechanistic investigation with our usual ^{18}O-tracer and stereochemical experiments and their implication on the understanding of the mechanism.

Results and Discussion

Earlier, when ^{18}O-labeled and optically active aryl benzyl sulfoxides were treated with acetic anhydride at about 100 °C for 1—2 h in polar media, the main reaction was found to be the oxygen exchange which causes racemization and the Pummerer reaction was of rather minor.[7] However, dibenzyl sulfoxide has been known to undergo the Pummerer reaction with acetic anhydride,[8] and when the reaction was carried out at 76 °C, Wilson *et al.* actually obtained the Pummerer rearrangement product, the α-acetoxy sulfide which upon heating further with acetic acid decomposed to afford benzyl disulfide, benzyl sulfide, benzaldehyde and α,α-bis(benzylthio)toluene, as shown below.[9]

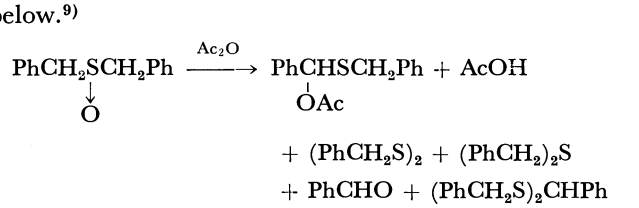

When the reaction of ^{18}O-labeled benzyl *p*-tolyl sulfoxide (**1**) [1.246 ex. atm% of ^{18}O] was allowed to react again, however, this time with a large excess of acetic anhydride in the presence of an equimolar amount of DCC which scavenges acetic acid formed, at 100 °C for 10 h, the corresponding Pummerer reaction product, *i.e.*, α-acetoxy sulfide **2**, was obtained in *ca.* 10% yield while recovering much of the original sulfoxide. The recovered sulfoxide was found to retain 99.6% of original ^{18}O; namely, 1.241 ex. atom% of ^{18}O and the α-acetoxy sulfide was found to be incorporated with 46% of the original ^{18}O-label of the sulfoxide, namely 0.286 ex. atom% of ^{18}O, respectively.

This means, that the oxygen exchange of the sulfoxide with acetic anhydride is catalyzed markedly by acetic acid or any acid formed or present in the reaction mixture, while the overall rearrangement is predominantly intramolecular. However, when optically active benzyl *p*-tolyl sulfoxide (**1**) was allowed to react with excess acetic anhydride in the presence of DCC under the same conditions, the corresponding α-acetoxy sulfide (**2**) was found to have no optical activity while the sulfoxide recovered was found to have retained 90% of the original optical activity. Since α-acetoxybenzyl *p*-tolyl sulfide (**2**) formed in the reaction would be rather unstable, the chirality, once induced in the α-acetoxy sulfide **2** might have lost upon prolonged heating. However, in view of the high retention of

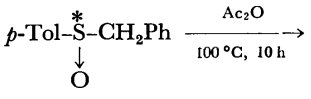

1

$[\alpha]_D$ +251°

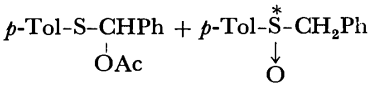

2 recovered

$[\alpha]_D$ 0° $[\alpha]_D$ +243°

^{18}O in the resulting product **2**, the racemization of the α-acetoxy sulfide after its formation is rather inconceivable. Probably the ion-pair between the α-sulfur stabilized carbenium ion and acetate ion-pair is less intimate than those which are formed in the reactions of cyanomethyl aryl sulfoxide and (α-carbonyl-substituted methyl) aryl sulfoxides with acetic anhydride, though the ion-pair would be intimate enough to hold the original ^{18}O. Substitution of an electron-withdrawing group would increase the tightness of the ion-pair so that the corresponding resulting α-acetoxy sulfides can keep more of the original ^{18}O-label of the sulfoxide in the resulted α-acetoxy sulfide **2**, which might also be asymmetrically induced as in the Pummerer reaction of aryl cyanomethyl sulfoxide with acetic anhydride. Thus, the Pummerer reactions of optically active 3-chlorobenzyl *p*-tolyl and 3,5-dichlorobenzyl *p*-tolyl sulfoxides (**3** and **5**) were carried out. When these two optically active sulfoxides were allowed to react with excess acetic anhydride in the presence of 5 equivalent amounts of DCC for 4 h at 120 °C and 130 °C, respectively, the resulting both α-acetoxy sulfides **4** and **6** had no optical activity, while the recovered sulfoxides ($[\alpha]_D$ 290.3° for **3** and $[\alpha]_D$ 164° for **5**) retained the optical activities substantially.

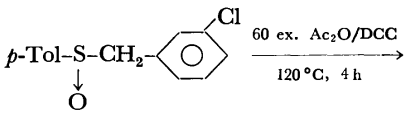

3 $[\alpha]_D$ +295°

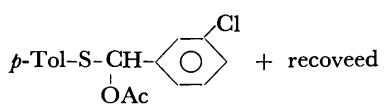

4 $[\alpha]_D$ 0° $[\alpha]_D$ +290.3°

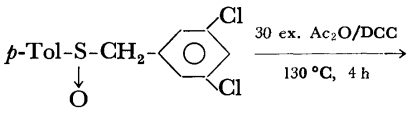

5 $[\alpha]_D$ +288°

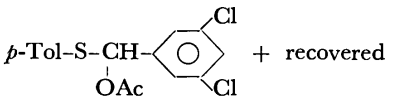

6 $[\alpha]_D$ 0° $[\alpha]_D$ +164°

When ^{18}O-labeled 3,5-dichlorobenzyl *p*-tolyl sulfoxide (**5**) [0.790 ex. atom% of ^{18}O] was heated with a large excess acetic anhydride (60 equiv. amount) in the presence of 5 equiv. amount of DCC under the same conditions for the optically active sulfoxide **5**, the corresponding α-acetoxy sulfide **6** obtained in 9% yield, was found to retain 65% of ^{18}O [0.255 ex. atom% of ^{18}O] of the original ^{18}O-label in the starting sulfoxide **5**. The retention of 65% of ^{18}O in the ester **6** is substantially higher than that, *i.e.*, 46%, found in the ester **2** formed in the reaction of benzyl *p*-tolyl sulfoxide. This means that due to the destabilization of the carbenium ion formed from the acetoxysulfonium ylide derived from benzyl *p*-tolyl sulfoxide bearing two electron-withdrawing chlorines on the aromatic ring of the benzyl group, the ion-pair formed between 3,5-dichlorophenyl(*p*-tolylthio)methylium ion and acetate is considered to be more intimate than that derived from the reaction of unsubstituted benzyl *p*-tolyl sulfoxide and hence the intramolecularity of the migration of acetoxyl group increased. However, this intimate ion-pair is not enough to transfer the chirality on the sulfur atom to α-carbon. The lack of asymmetric induction into the benzylic α-carbon may be partly due to the highly resonance-stabilized nature of benzylic cation.

The Pummerer reaction of aryl benzyl sulfoxides would be at the threshold between a typical intramolecular and an intermolecular rearrangements in the mechanistic stectrum of the 1,2-acetoxyl migration which would reflect on the extent of tightness of the intimate ion-pair formed from the intermediary acetoxysulfonium ylide.

Experimental

General. All melting points were uncorrected. IR spectra were taken on a Hitachi 260-50 spectrometer. NMR spectra were recorded with a Hitachi Perkin-Elmer R-20 spectrometer in $CDCl_3$ using TMS as an internal standard. Mass spectra were determined with a Hitachi RMU-6MG mass spectrometer. Acetic anhydride was purified by stirring with sodium metal for 7 d followed by refluxing under reduced pressure below 50 °C for 5 h under vacuum and then distillation under reduced pressure, bp 47—48 °C/20 mmHg.**

^{18}O-*Analysis.* ^{18}O-Analysis was carried out by the method developed by Rittenberg and Ponticorvo,[10] with a modification which involves the use of $Pb(OAc)_2$ to remove H_2S gas from the gas produced by the thermolysis of sample: About 20 mg of sample was pyrolyzed with

** 1 mmHg≈133.3 Pa.

250 mg each of purified $HgCl_2$ and $Hg(CN)_2$, respectively, in an evacuated sealed Pyrex tube at *ca.* 500 °C for 12 h. Then the tube was broken in a vacuum line and CO_2 gas formed was purified by distillation and the mass peaks of *m/e* 44 and 46 which correspond to $C^{16}O_2$ and $C^{16}O^{18}O$, respectively, were recorded on a mass spectrometer.

Materials. Optically Active Benzyl p-*Tolyl Sulfoxide (1)*:[11] The optically active **1** was prepared by known method[11] from menthyl *p*-toluenesulfinate and benzyl Grignard reagent. $[\alpha]_D$ +251° (acetone).

^{18}O-*Labeled Benzyl* p-*Tolyl Sulfoxide (1)*: The corresponding sulfide (2.16 g, 10 mmol) prepared from benzyl chloride and *p*-toluenethiol was dissolved in a mixture of acetic acid (40 ml), pyridine (2.4 g) and ^{18}O-enriched water (4 ml, 1.5 atom%). To the cooled solution was added bromine (1.60 g, 10 mmol) at 0 °C.[12] When reaction was complete, 100 ml of water was added and extracted with 100 ml portions of chloroform. The chloroform solution was washed with aqueous $Na_2S_2O_3$ solution, diluted aqueous HCl solution and water, and then dried ($MgSO_4$). The solvent was removed and the residue was recrystallized from ethyl acetate–hexane to give the ^{18}O-labeled **1** in 70% yield (1.629 g). The title sulfoxide was found to contain 1.246 ex. atom% of ^{18}O.

Optically Active 3-Chlorobenzyl p-*Tolyl Sulfoxide (3)*: To a stirred solution of 3-chlorobenzylmagnesium chloride prepared from 3-chlorobenzyl chloride (1.23 g, 8 mmol) and magnesium (194 mg, 8 mmol) in 100 ml of dry ether at −15 °C under argon was added diastereomerically pure (−)-menthyl *p*-toluenesulfinate (1.176 g, 4 mmol) at −78 °C. The work-up mentioned above gave the title sulfoxide **3** (972 mg, 92% yield) with $[\alpha]_D$ +295° (acetone). Mp 88—88.5 °C; IR (KBr) 1045 and 820 cm^{-1}; NMR ($CDCl_3$) δ= 7.18—6.73 (8H, m), 3.83 (2H, s), 2.37 (3H, s); Found: C, 63.52; H, 4.90%. Calcd for $C_{14}H_{13}ClOS$: C, 63.50; H, 4.94%.

^{18}O-*Labeled Optically Active 3,5-Dichlorobenzyl* p-*Tolyl Sulfoxide (5)*: To a stirred solution of 3,5-dichlorobenzylmagnesium chloride prepared from 3.128 g (16 mmol) of 3,5-dichlorobenzyl chloride in dry ether at −15 °C under argon was added at −78 °C ^{18}O-labeled diastereomerically pure (−)-menthyl *p*-toluenesulfinate (2.35 g, 8 mmol, $[\alpha]_D$ −199° in acetone) synthesized from the reaction between ^{18}O-labeled *p*-toluenesulfinyl chloride and *l*-methol. The usual work-up gave the title sulfoxide **5** (1.568 g) which have an optical activity $[\alpha]_D$ +288° and ^{18}O-content was found to be 0.790 ex. atom%. Mp 106.5—107 °C; IR (KBr) 1560, 1040, and 800 cm^{-1}; NMR ($CDCl_3$) δ=7.17—6.73 (7H, m), 3.87 (2H, s), and 2.35 (3H, s); Found: C, 56.40; H, 4.04%. Calcd for $C_{14}H_{12}OSCl_2$: C, 56.19; H, 4.40%. Racemic **5** was also prepared by oxidation of the corresponding sulfide with H_2O_2 in acetic acid. Mp 130—130.5 °C.

Reaction of ^{18}O-*Labeled Benzyl* p-*Tolyl Sulfoxide (1) with Acetic Anhydride.* After the ^{18}O-labeled sulfoxide **1** (1.2 g) was heated with 60 equiv. molar amount of acetic anhydride to the sulfoxide in the presence of 5 equiv. DCC at 100 °C for 10 h, a large excess acetic anhydride and any volatile substance were removed under vacuum to afford the residue which was separated through silica gel column chromatography with hexane–ethyl acetate (4:1) and then with chloroform as eluents. The Pummerer product **2** (92 mg) and the sulfoxide (840 mg) which were found to contain 0.288 and 1.241 ex. atom% of ^{18}O, respectively. **2**: mp 66—67 °C; IR (KBr) 1740 and 1220 cm^{-1}; NMR ($CDCl_3$) δ=7.25 (1H, broad s), 7.08 (1H, s) and 1.99 (3H, s). Since **2** is unstable, it was converted to the corresponding sulfone: mp 153—154 °C; IR (KBr) 1755, 1320, 1220, and 1160 cm^{-1}; Found: C, 63.22; H, 5.30%. Calcd for $C_{16}H_{16}O_4S$: C, 63.14; H, 5.29%.

Reaction of Optically Active Benzyl p-*Tolyl Sulfoxide (1) with Acetic Anhydride in the Presence of DCC.* When the optically active sulfoxide **1** (220 mg, $[\alpha]_D$ +251° was heated with 5 ml of acetic anhydride at 100 °C for 10 h in the presence of 5 equiv. DCC to the sulfoxide, the resulting semi-oily residue obtained, after evaporation of excess acetic anhydride and any volatile product *in vacuo*, was separated through silica gel column chromatography with hexane–ethyl acetate (4:1) and then with benzene–ethyl acetate (4:1) as eluents at 0—4 °C in a low-temperature room. The Pummerer product (**2**, $[\alpha]_D$ 0°) was obtained in 10% yield and the sulfoxide recovered was purified through alumina column chromatography with hexane–ethyl acetate (3:1) and then silica-gel column chromatography with chloroform to afford the sulfoxide (158 mg, $[\alpha]_D$ +243°) which retained 97% of optical activity based on the starting sulfoxide.

Reaction of Optically Active 3-Chlorobenzyl p-*Tolyl Sulfoxide (3) with Acetic Anhydride in the Presence of DCC.* After the optically active sulfoxide **3** (397 mg, $[\alpha]_D$ +295°) was heated at 120 °C for 4 h with 7 ml of acetic anhydride in the presence of 5 equiv. DCC, the usual work-up and silica-gel column chromatography with hexane–ethyl acetate (4:1) in a low-temperature room gave the Pummerer product **4** (43.3 mg, 9.4% yield, $[\alpha]_D$ 0°) while the chromatography with benzene–ethyl acetate (4:1) as eluents at room temperature afforded the sulfoxide recovered which was further purified through alumina and then silica-gel column chromatography using hexane–ethyl acetate (3:1) and chloroform, respectively, giving the pure sulfoxide **3** (359 mg, $[\alpha]_D$ +290.3°). **4**: Oil; IR (neat) 1745 and 1217 cm^{-1}; NMR ($CDCl_3$) δ=6.80—7.23 (9H, m), 2.27 (3H, s), 2.00 (3H, s). Sulfone derivative of **4**: mp 113—114 °C; IR (KBr) 1760, 1320, 1205, and 1155 cm^{-1}; NMR ($CDCl_3$ δ=7.08—7.55) (8H, m), 6.55 (1H, s), 2.38 (3H, s); Found: C, 56.81; H, 4.46%. Calcd for $C_{16}H_{15}ClO_4S$: C, 56.72; H, 4.46%.

Reaction of ^{18}O-*Labeled Optically Active 3,5-Dichlorobenzyl* p-*Tolyl Sulfoxide (5) with Acetic Anhydride in the Presence of DCC.* When the title sulfoxide **5** (800 mg) was heated with 60 equiv. acetic anhydride in the presence of 5 equiv. DCC at 130 °C for 4 h, after the usual work-up and chromatography through silica gel with benzene and chloroform as eluents the Pummerer product **6** (64 mg, 7% yield) and the sulfoxide recovered which was purified through alumina column chromatography with hexane–ethyl acetate (4:1) as an eluent giving the pure sulfoxide in 93% yield (716 mg). The Pummerer product had practically no optical rotation but the ^{18}O-content was found to be 0.255 ex. atom% of ^{18}O. No enathiomeric excess of the Pummerer product was observed from a measurement of NMR contact shift using chiral lanthanoids shift reagent, $Eu(hfc)_3$. **6**: Mp 63.5—64 °C; IR (KBr) 1740, 1230, and 800 cm^{-1}; NMR ($CDCl_3$) δ=7.20—6.85 (7H, m), 6.78 (1H, s), 2.30 (3H, s), 2.10 (3H, s); Found: C, 56.43; H, 4.12%. Calcd for $C_{16}H_{14}Cl_2O_2S$: C, 56.31; H, 4.13%.

References

1) S. Oae, T. Kitao, S. Kawamura, and Y. Kitaoka, *Tetrahedron*, **19**, 817 (1963).

2) S. Oae, O. Itoh, T. Numata, and T. Yoshimura, *Bull. Chem. Soc. Jpn.*, **56**, 270 (1983) and references cited therein; S. Oae, T. Numata, and T. Yoshimura, "Heterosulphonium Salts," in "Sulphonium Salts," ed by C. J. M. Stirling and S. Patai, John Wiley & Sons, New York (1981), Chap. 15; S. Oae and T. Numata, "The Pummerer and

Pummerer Type of Reactions," in "Isotopes in Organic Chemistry," ed by E. Buncel and C. C. Lee, Elsevier, New York (1980), Vol. 5, Chap. 2.

3) T. Numata and S. Oae, *Tetrahedron Lett.*, **1977**, 1337.

4) T. Numata, O. Itoh, and S. Oae, *Chemistry Lett.*, **1977**, 909; *Tetrahedron Lett.*, **1979**, 1869; T. Numata, O. Itoh, T. Yoshimura, and S. Oae, *Bull. Chem. Soc. Jpn.*, **56**, 257 (1983) and related references cited therein.

5) H. Weiner and R. A. Sneen, *J. Am. Chem. Soc.*, **87**, 287 (1965); *Tetrahedron Lett.*, **1963**, 1309; R. A. Sneen and J. W. Larsen, *J. Am. Chem. Soc.*, **91**, 362, 6031 (1969); R. A. Sneen, *Acc. Chem. Res.*, **6**, 46 (1973).

6) A. F. Diaz, L. Lazdins, and S. Winstein, *J. Am. Chem. Soc.*, **90**, 1904 (1968) and references cited therein.

7) M. Kise and S. Oae, *Bull. Chem. Soc. Jpn.*, **43**, 1421 (1970).

8) J. A. Smith, *J. Chem. Soc.*, **95**, 349 (1909); L. Horner and P. Kaiser, *Justus Liebigs Ann. Chem.*, **626**, 19 (1959).

9) G. E. Wilson, Jr., and C. J. Strong, *J. Org. Chem.*, **37**, 2376 (1972).

10) D. Rittenberg and L. Ponticorvo, *Int. J. Appl. Radiat. Isot.*, **1**, 208 (1956).

11) K. Mislow, M. M. Green, P. Laur, J. T. Malillo, T. Simmons, and A. L. Ternay, *J. Am. Chem. Soc.*, **87**, 1958 (1965).

12) S. Oae, Y. Ohnishi, S. Kozuka and W. Tagaki, *Bull. Chem. Soc. Jpn.*, **39**, 364 (1964).

Intermolecular Stereoselective Pummerer Reactions of 4-(*p*-Chlorophenyl)thiane 1-Oxides and *trans*-1-Thiadecalin 1-Oxides and 2-Thiadecalin 2-Oxides with Acetic Anhydride

Shigeru Oae,* Osamu Itoh, Tatsuo Numata, and Toshiaki Yoshimura
Department of Chemistry, University of Tsukuba, Niihari-gun, Sakura-mura, Ibaraki 305

(Received June 7, 1982)

The Pummerer reactions of conformationally fixed 4-(*p*-chlorophenyl)thiane 1-oxides and *trans*-1-thiadecalin 1-oxides and *trans*-2-thiadecalin 2-oxides with acetic anhydride are either stereoselective or stereospecific, both in the absence and in the presence of a scavenger of acetic acid formed, such as dicyclohexylcarbodiimide (DCC) or 2,6-lutidine. However, the ^{18}O-tracer experiments with the ^{18}O-labeled sulfoxide revealed the reaction to be an intermolecular rearrangement, while the kinetic experiment with α-deuterated 4-(*p*-chlorophenyl)thiane 1-oxides gave sizable values of kinetic isotope effect, *i.e.*, 2.8 for the *cis* isomer and 3.4 for the *trans* isomer. In the reaction of 4-arylthiane 1-oxides with acetic anhydride, the thermodynamically controlled product is axial 2-acetoxy-4-(*p*-chlorophenyl)thiane while the kinetically controlled product is the equatorial isomer which is formed in the presence of the acid scavenger, DCC. In the Pummerer reaction of the thiadecalins *S*-oxides the equatorial α-acetoxy sulfides are the preferential products, however, the isomer preference is more pronounced in the reaction with DCC. These observations, along with other pertinent data seem to suggest that the rate-determining step in the Pummerer reaction of these simple heterocyclic sulfoxides is E2 elimination of acetic acid from the acetoxysulfonium intermediates.

Since Horner proposed[1] to call the reaction between alkyl sulfoxides with acetic anhydride leading to the formation of corresponding α-acetoxy sulfides as the Pummerer reaction fifty years after the original works of Pummerer,[2] numerous investigations have been carried out to clarify the mechanism of this interesting rearrangement and the mechanistic studies on the Pummerer reaction have been well-documented in many reviews in recent years.[3-10]

The general scheme of the Pummerer reaction is believed to be shown in the following four sequential steps of elemental reactions and the rate-determining step is known to vary with changes of both the acylating agent and the sulfoxide.[8,9] Many of the early examples of the Pummerer reactions of open chain alkyl sulfoxides with acetylating reagents were shown by ^{18}O-tracer studies to be intermolecular rearrangements which have the rate-determining step at step 2 and no stereoselectivity or specificity was observed.[11,12]

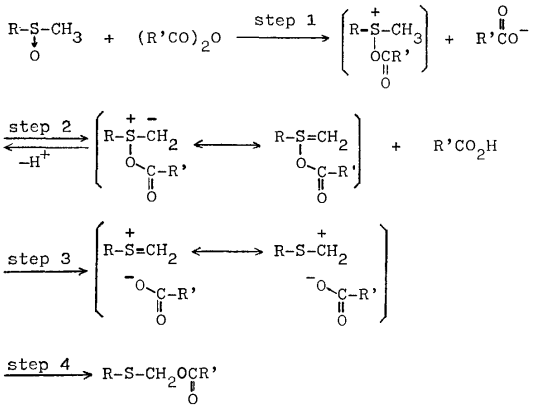

Recently, however, several examples of the Pummerer reactions which proceed through intramolecular migration to afford stereoselective (or stereospecific) products have been reported.[13-17] In most of these intramolecular rearrangements, the slowest step has been shown to be the S–O bond cleavage at step 3 with a few exceptions in which the step 1 is the rate-determining.[18,19] Among several examples of the Pummerer reaction of *S*-oxides of sulfur-heterocycles with acetic anhydride, stereoselectivity was observed in only two cases of five-membered sulfur-heterocycles, *i.e.*, *S*-oxides of thiosugar derivatives[20] and *S*-oxides of 1,3-oxathiolane derivatives.[21] However, no legitimate observation was made as to the nature of acetoxyl migration. Thus, the only example of intermolecular stereoselective Pummerer reaction of the *S*-oxide of a simple sulfur-heterocycle has been that of 4-(*p*-chlorophenyl)thiane 1-oxide (**1**) with acetic anhydride.[22] We now have found that another example of intermolecular stereoselective Pummerer reaction, *i.e.*, the reaction of conformationally rigid *trans*-1-thia- and 2-thiadecalin *S*-oxides (**3** and **5**) with acetic anhydride. This paper gives a full account of our mechanistic investigation on the Pummerer reactions of *cis*- and *trans*-4-(*p*-chlorophenyl)thiane 1-oxides (**1c** and **1t**) and *trans*-1-thiadecalin 1-oxides (axial **3a** and equatorial **3e**) and 2-thiadecalin 2-oxides (axial **5a** and equatorial **5e**) with acetic anhydride.

Results and Discussion

*Reaction of 4-(*p*-Chlorophenyl)thiane 1-Oxides with Acetic Anhydride.* Configurationally fixed *cis*- and *trans*-4-(*p*-chlorophenyl)thiane 1-oxides (**1c** and **1t**) were allowed to react with excess acetic anhydride with or without DCC or 2,6-lutidine, the acetic acid scavenger, both the axial 2-acetoxy-4-(*p*-chlorophenyl)thiane (**2a**), and the equatorial isomer (**2e**), were obtained along with the elimination product, *i.e.*, 4-(*p*-chlorophenyl)-3,4-dihydro-2*H*-thiopyran (**2o**) in the ratios as summarized in Table 1.

When the sulfoxides, **1c** and **1t** were heated with a large excess of acetic anhydride at 100 °C, only the corresponding axial α-acetoxy sulfide **2a** and the olefinic product **2o** were obtained in 72—73% and 20% yields, respectively (runs 1 and 2). The axial α-acetoxy sulfide **2a** was found to be formed stereoselectively (**2e**:**2a**=1:15) from both the *trans*-sulfoxide **1t** and the *cis* isomer **1c**. Whereas, when the sulfoxides (**1t** and **1c**) were allowed to react with excess acetic anhydride in the presence of dicyclohexylcarbodiimide (DCC) or 2,6-lutidine at 100 °C for 4—6 h, the pre-

TABLE 1. THE PUMMERER REACTION OF THE THIANE 1-OXIDES **1t** AND **1c** WITH ACETIC ANHYDRIDE AT 100 °C

Run	Sulfoxide	Acid-scavenger (ratio)[a]	t/h	Products and yields/%	
				2 (**2e**:**2a**)[b]	**2o**
1	**1t**	--	3	70(1:15)	23
2	**1c**	—	3	71(1:15)	21
3	**1t**	—	0.75[c]	40(1:1)	
4	**1c**	—	0.75[c]	40(1:1)	
5	**1t**	DCC(1)	4	78(2:1)	20
6	**1c**	DCC(1)	4	77(2:1)	20
7	**1t**	DCC(3)	4	85(9:1)	11
8	**1t**	DCC(5)	4	83(13:1)	9
9	**1c**	DCC(5)	6	83(14:1)	12
10	**1c**	2,6-Lutidine(5)	4.5	81(5:2)	15
11	**1c**	2,6-Lutidine(10)	4.5	86(5:1)	12

a) Ratio=acid scavenger/sulfoxide. b) The ratio (**2e**:**2a**) was determined by NMR measurement. c) The sulfoxide **1** was recovered in *ca.* 50% yield.

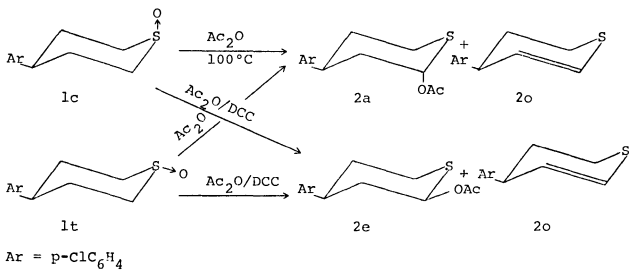

Fig. 1.

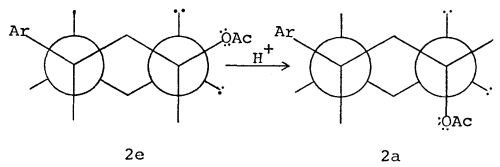

Fig. 2.

ferential product, obtained in 77—80% yield, was the equatorial α-acetoxy sulfide **2e**. Thus, the stereoselectivity of the reaction was found to be changed drastically by addition of DCC or 2,6-lutidine into the reaction mixture (runs 5—11). For example, treatment of the two isomeric sulfoxides with acetic anhydride in the presence of 5 equiv. amounts of DCC gave the corresponding crystalline equatorial α-acetoxy sulfide **2e** as the main product (runs 8 and 9) as shown in Fig. 1.

These interesting stereoselectivities in the Pummerer reaction suggest that the equatorial α-acetoxy sulfide **2e** is the kinetically controlled product and the equatorial α-acetoxy sulfide **2e** is isomerized in the presence of acetic acid formed to the axial isomer **2a** when there is no acid scavenger such as DCC or 2,6-lutidine. Indeed, in the presence of acetic acid, the equatorial α-acetoxy sulfide was found to isomerize readily to the axial isomer **2a** which is considered to be more stable than the equatorial isomer **2e** due mainly to the less electron repulsion between the lone electron pairs of sulfur atom and those of terminal oxygen in **2a** than that in **2e**, as illustrated in Fig. 2.

When one compares runs 1 and 2 with 3 and 4,

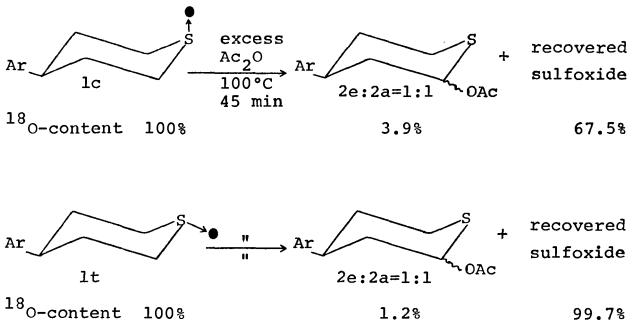

Fig. 3.

the isomerization is found to be multiplied by acetic acid formed in the reaction mixture. Upon treatment of the equatorial isomer **2e** with hot acetic anhydride in the presence of acetic acid at 100 °C for 3 h, the axial isomer **2a** and the olefinic product **2o** were obtained in 70 and 20% yields, respectively. The olefinic sulfide **2o** would obviously be formed by 1,2-elimination of acetic acid from the axial isomer **2a**.

In order to scrutinize the nature of acetoxyl migration, our usual ^{18}O-tracer experiments were carried out using the ^{18}O-labeled sulfoxides and the acetoxyl migration was found to proceed intermolecularly based on the following observations. Namely, when the ^{18}O-labeled *trans*-sulfoxide **1t** [1.092 ex. atom%] was treated with 60 mol equivalents of acetic anhydride at 100 °C for 45 min, during when the reaction was at about half completion, the recovered sulfoxide, [1.089 ex. atom% of ^{18}O], was contaminated with no *cis* sulfoxide **1c**, while the sulfoxide recovered was found to have retained the original ^{18}O-content nearly completely. Whereas, the Pummerer rearrangement product, the α-acetoxy sulfide **2**, was found to retain only 0.013 ex. atom% of ^{18}O which corresponds to 1.2% incorporation of ^{18}O from the starting sulfoxide **1t**-^{18}O. The ^{18}O-labeled *cis* sulfoxide **1c**-^{18}O, [0.495 ex. atom% of ^{18}O] under the same conditions gave the recovered sulfoxide and the Pummerer rearrangement product of which ^{18}O-contents were found to be 0.334 and 0.019 ex. atom% of ^{18}O, which corresponds to 3.9% incorporation of ^{18}O from the starting sulfoxide **1c**-

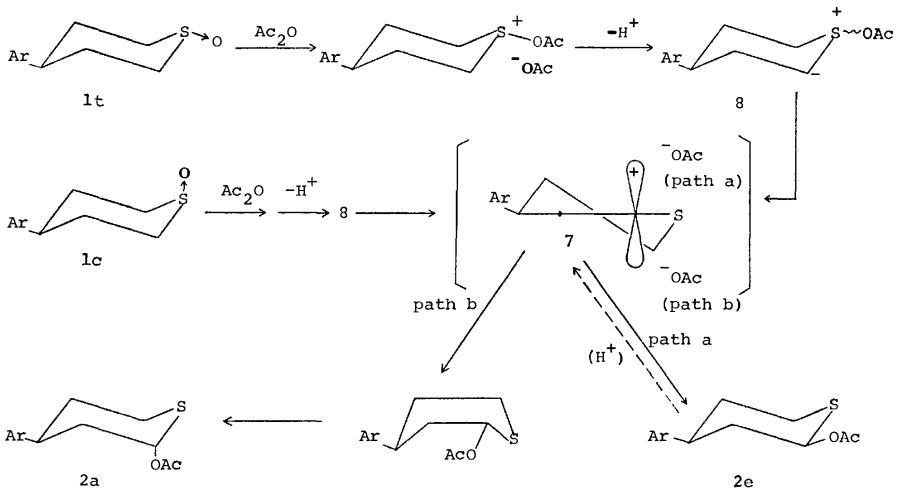

Fig. 4.

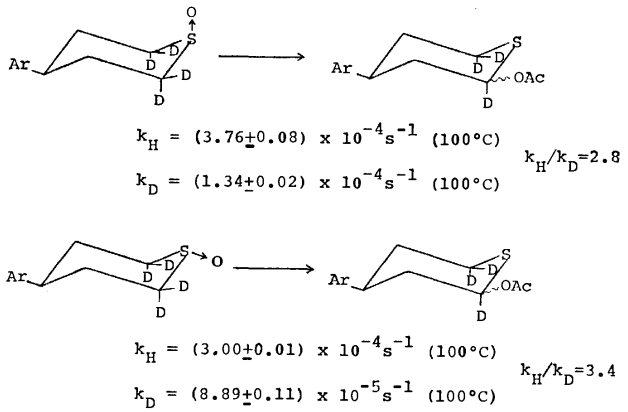

Fig. 5.

^{18}O respectively. The *cis*-sulfoxide **1c**-^{18}O was shown to undergo concurrent oxygen exchange in acetic anhydride[23] to the extent of 35% as illustrated in Fig. 3. All these ^{18}O-tracer data reveal clearly the acetoxyl migration is intermolecular, and the rearrangement is considered to proceed through the formation of the α-sulfenyl carbenium ion intermediate **7** which is then attacked by external acetoxyl group preferentially from the direction (path a) to give the equatorial α-acetoxy sulfide **2e**. The acid-catalyzed isomerization of the α-acetoxy sulfide **2e** to the other isomer **2a** is also considered to proceed via the formation of the carbenium ion intermediate **7** as shown in Fig. 4.

In the Pummerer reaction of most alkyl sulfoxides with acetic anhydride, the rate-determining step seems to be the proton-removal, *i.e.*, step 2, or E2 type elimination of acetic acid in the general scheme of the reaction, as revealed in a few sizable values of kinetic isotope effect, k_H/k_D, found in the rearrangements.[12,24] In order to find out the rate-determining step of the Pummerer reaction of 4-(*p*-chlorophenyl)thiane 1-oxides with acetic anhydride, kinetic experiments with 4-(*p*-chlorophenyl)thiane-2,2,6,6-d_4 1-oxides were carried out, and the values of the kinetic isotope effect (k_H/k_D) were found to be 2.8 for the *cis* isomer and 3.4 for the *trans* isomer. The sizes of the kinetic isotope effects are similar to that in the Pummerer reaction of methyl phenyl sulfoxide with acetic anhydride as illustrated in Fig. 5. Thus the rate-determining step of this reaction is clearly the step 2. If the subsequent S–O bond cleavage is very fast, as was found to be the case, the proton-removal could actually be a part of the E2 reaction, which was found to be the most likely in view of the stereochemistry of the Pummerer reaction of more rigid *trans*-1-thia- and 2-thiadecalin *S*-oxides (**3** and **5**) with acetic anhydride, (*vide infra*).

Reaction of trans-*1-Thiadecalin 1-Oxides (**3**) and* trans-*2-Thiadecalin 2-Oxides (**5**) with Acetic Anhydride.* In the Pummerer reaction of conformationally rigid 4-(*p*-chlorophenyl)-thiane 1-oxides (**1c** and **1t**) with acetic anhydride, the kinetically controlled initial product was the equatorial α-acetoxy thiane **2e**, although the rearrangement was shown to be intermolecular. The stereoselectivity is expected to be more pronounced in the Pummerer reaction of more rigid heterocyclic sulfoxides. Our choice sulfoxides are *trans*-1-thiadecalin 1-oxides (axial **3a** and equatorial **3e**) and *trans*-2-thiadecalin 2-oxides (axial **5a** and equatorial **5e**) which are conformationally more rigid six-membered cyclic sulfoxides than 4-(*p*-chlorophenyl)thiane 1-oxides (**1c** and **1t**). When *trans*-1-thiadecalin 1-oxides (**3a** and **3e**) were allowed to react with excess acetic anhydride at 100 °C for 3—4 h, both in the absence and in the presence of DCC, both the corresponding axial α-acetoxy sulfide **4a** and the equatorial isomer **4e** were obtained, respectively. Similarly, in the reactions between *trans*-2-thiadecalin 2-oxides (**5a** and **5e**) and acetic anhydride at 100 °C for 3 h, both the corresponding axial and equatorial α-acetoxy sulfides [(**6a1**:**6a3**=1:1) and (**6e1**:**6e3**=1:1)] were obtained, respectively both in the absence and in the presence of DCC, as illustrated in Fig. 6.

These data reveal clearly that there is a preferential direction for acetate ion to attack the α-sulfenyl stabilized carbenium ion, *i.e.*, the attack of acetate takes place at the opposite side of γ-axial hydrogen to avoid the steric repulsion of the γ-axial hydrogen. The preferential formation of the equatorial acetoxy sulfides is more pronounced in the Pummerer reactions of these

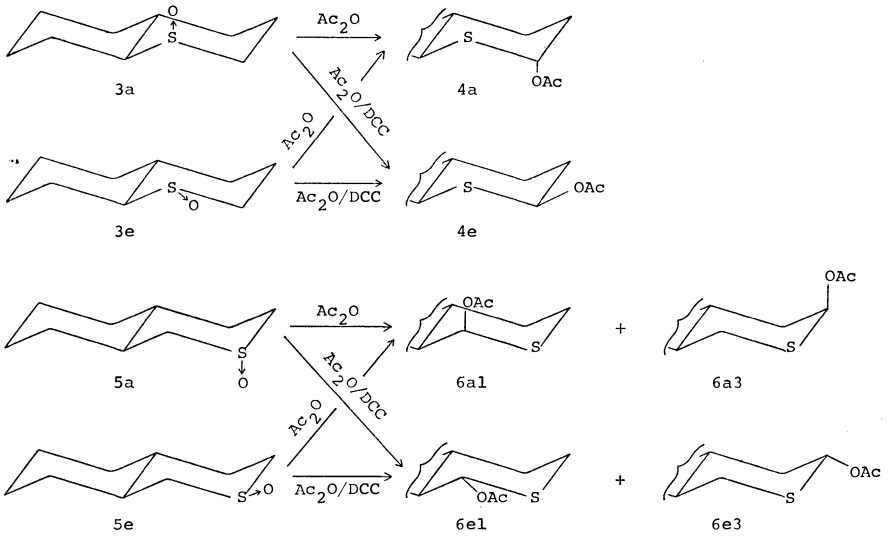

Fig. 6.

Table 2. ^{18}O-Experiments in the reaction of *trans*-1-thiadecalin-1-oxides with acetic anhydride

Sulfoxide (ex. atom% of ^{18}O)	Reaction conditions		Pummerer products			Recovered sulfoxide		
	t/°C	t/min	Yield %	(ex. atom%)	Incorporation %	Yield %	(ex. atom%)	Retention %
3a (0.856)	Ac_2O		28	**4e** (0.057)[a]	13	25	(0.710)	83
	100	45	(**4e**:**4a**=6:1)	**4a** (0.043)[a]	10			
3a (0.856)	Ac_2O/DCC		51	(0.068)[b]	16	30	(0.574)	67
	100	75	(**4e**:**4a**=19:1)					
3e (0.955)	Ac_2O		37	(0)[b]	0	53	(0.774)	81
	100	45	(**4e**:**4a**=8:1)					
3e (0.955)	Ac_2O/DCC		34	(0)[b]	0	59	(0.812)	85
	100	75	(**4e**:**4a**=19:1)					

a) Axial and equatorial acetoxy sulfides were separated through silica-gel column chromatography, and their ^{18}O-contents were analyzed. b) A mixture of axial and equatorial acetoxy sulfides was subjected to ^{18}O-analysis.

highly rigidly fixed *trans*-1- and 2-thiadecalin *S*-oxides. Addition of DCC, the scavenger of acetic acid, was also found to slow down the reaction but the isomeric preference is more remarkable in favor for the equatorial acetoxy sulfides.

The usual ^{18}O-tracer experiments were carried out with ^{18}O-labeled *trans*-1-thiadecalin 1-oxides (**3a**-^{18}O and **3e**-^{18}O) with acetic anhydride both in the absence and in the presence of DCC and the results are shown in Table 2.

The results are quite interesting. The Pummerer reaction of the equatorial sulfoxide **3e** is obviously an intermolecular rearrangement since the acetoxyl group of the resulted ester was found to be completely diluted with oxygen of excess acetic anhydride, while the sulfoxide recovered retained more than 80% of original ^{18}O-label both in the absence and in the presence of DCC. The Pummerer reaction of the axial sulfoxide **3a** is also an intermolecular rearrangement, though the incorporation of 13% or 16% of ^{18}O of the original sulfoxide in the 2-acetoxy-1-thiadecalin (**4**) and the sulfoxide recovered have 83% or 67% of original ^{18}O-label mean that the rearrangement is partially intramolecular. When one looks at the preferential conformations and conformational changes required for the rate-determining elimination of acetic acid and the subsequent rapid recombination for the Pummerer reactions of both isomeric sulfoxides, it is quite evident that both E2 type elimination of acetic acid and recombination with acetate in the reaction of the axial sulfoxide requires less conformational change, and hence the reaction of the axial sulfoxide would be more facile than that of the equatorial sulfoxide which would have to undergo conformational change for E2 elimination and also in the product formation. Perhaps, the facile E2 reaction of acetic acid and recombination would have increased the chance of intramolecular rearrangement for the axial sulfoxide **3a**.

One interesting observation we made was the stereochemistry of proton-removal and cleavage of acetate in this rearrangement. Thus, *trans*-1-thiadecalin-2e-*d* 1a-oxide (D:59%) (**9**), *trans*-1-thiadecalin-2a-*d* 1a-oxide (D:57%) (**10**), and *trans*-1-thiadecalin-2a-*d* 1e-oxide (D:57%) (**11**) were subjected to the Pummerer reaction with excess acetic anhydride in the presence of 5 equivalent amounts of DCC. The deuterium contents of the corresponding 2e-acetoxy sulfides were found to be 59, 13, and 50%, respectively, upon measurement of the NMR spectra using 14% of Eu(dpm)$_3$ shift reagent, to the α-acetoxy sulfides. As

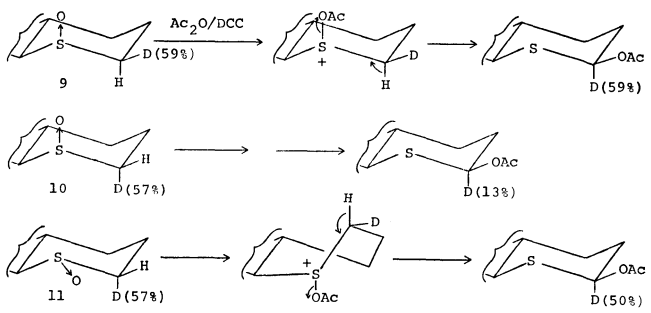

Fig. 7.

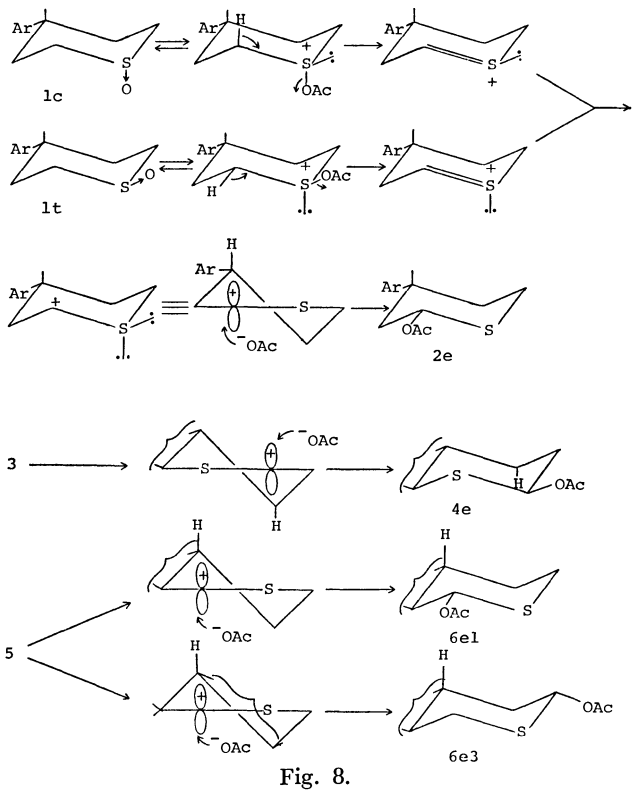

Fig. 8.

the mechanistic scheme indicates, the reaction of each isomer of 2-monodeuterated *trans*-1-thiadecalin 1-oxides gave only the corresponding each one product formed by the E2 elimination of acetic acid from the corresponding acetoxysulfonium intermediate as illustrated in Fig. 7. This is the first clean-cut example of *trans* E2 type elimination of acetic acid from the acetoxysulfonium intermediate in the Pummerer reaction, although E2 elimination was suggested early by us[6,9] and also Wolfe and Kazmeier.[25]

Conclusion

The Pummerer reaction of conformationally rigid six-membered thiane 1-oxides with acetic anhydride is stereoselective and the rearrangement is mainly intermolecular, while the rate-determining step appears to be the E2 1,2-elimination of acetic acid from the acetoxysulfonium intermediates formed in the initial acetylation of the sulfoxides. Meanwhile, the preferential formation of the equatorial α-acetoxy sulfides in the initial rearrangement is considered to be due to the facile sterically access of the acetate to the equatorial position, whereas the isomerization to the more stable axial α-acetoxy sulfide in the case of 4-arylthiane derivatives is catalyzed by acetic acid present in the system. Thus, the overall mechanism of the Pummerer reaction of these conformationally rigid thiane 1-oxides may be illustrated as shown in Fig. 8.

Experimental

General. All melting points were uncorrected. IR spectra were taken on a Hitachi 260-50 spectrometer. NMR spectra were recorded with a Hitachi Perkin-Elmer R-20 spectrometer in $CDCl_3$ using TMS as an internal standard. Mass spectra were determined with a Hitachi RMU-6MG mass spectrometer. Acetic anhydride was purified by stirring with sodium metal for 7 d, followed by a refluxing under reduced pressure below 50 °C for 5 h and then distillation under reduced pressure, bp 47—48 °C/20 mmHg.**

^{18}O-Analysis. ^{18}O-Analysis was carried out by the method developed by Rittenberg and Ponticorvo,[26] with a modification which involves the use of $Pb(OAc)_2$ to remove H_2S gas from the gas produced by the thermolysis of sample: about 20 mg of sample was pyrolyzed with 250 mg each of purified $HgCl_2$ and $Hg(CN)_2$, respectively in an evacuated sealed Pyrex tube at *ca.* 500 °C for 12 h. Then the tube was broken in a vacuum line and CO_2 gas formed was purified by distillation and the mass peaks of *m/e* 44 and 46 which correspond to $C^{16}O_2$ and $C^{16}O^{18}O$, respectively, were recorded on a mass spectrometer.

Materials. The NMR shift reagent $Eu(dpm)_3$ (tris-(dipivaloylmetanato)europium) is Dotite Reagents purchased from Wako Pure Chemical Co.

cis-*4*-(p-*Chlorophenyl)thiane 1-Oxide (**1c**)*: To a stirred solution of 4-(*p*-chlorophenyl)thiane[27] (1.06 g, 5 mmol) in 50 ml of dry methanol cooled to −70 °C in an acetone–Dry Ice bath was added an equimolar amount of *t*-butyl hypochlorite. When the temperature of the bath reached −40 °C, anhydrous sodium carbonate was added. The mixture was allowed to warm up to room temperature and methanol was removed under vacuum. The residue was washed three times with 50 ml portion of chloroform and the chloroform solution was dried. The solvent was evaporated to give a solid product **1c** containing a very small amount of *trans*-4-(*p*-chlorophenyl)thiane 1-oxide (**1t**). The product was recrystallized from ethyl acetate to afford a pure **1c**: mp 171—172 °C (lit,[27] 172.5—173 °C).

trans-*4*-(p-*Chlorophenyl)thiane 1-Oxide (**1t**)*: To a stirred solution of 4-(*p*-chlorophenyl)thiane[27] (1.06 g, 5 mmol) in 50 ml of dichloromethane cooled in an ice bath was added 1.05 equiv. of *m*-chloroperbenzoic acid. The solution was washed with saturated sodium hydrogencarbonate, and the aqueous layer was extracted with 50 ml of chloroform three times. The whole solution was washed with water, dried ($MgSO_4$) and evaporated to afford solid products which were separated through alumina column chromatography with ethyl acetate–chloroform (2:1) as the eluent giving *cis*-4-(*p*-chlorophenyl)thiane 1-oxide from the former solution, *trans*-4-(*p*-chlorophenyl)thiane 1-oxide from the latter solution. Then the solvent was removed to give the *cis* derivative (634 mg, 60%) and the *trans* derivative (372 mg, 35%). The *trans* derivative was recrystallized from ethyl acetate–hexane to afford a colorless crystals: mp 120—120.5 °C (lit,[27] 120—120.5 °C).

** 1 mmHg=133.3 Pa.

trans-*1-Thiadecalin*:[28] *trans*-1-Thiadecalin was prepared by the reported procedure.[28,29] After 4.86 g (30 mmol) of *trans*-2-allylcyclohexanethiol in 200 ml of dry benzene was refluxed in the presence of 1% benzoyl peroxide to the thiol for 10 h, the solvent was removed under reduced pressure. The resultant residue was separated through silica-gel column chromatography with hexane as an eluent to give an oily product (4.05 g, 86%).

trans-*1-Thiadecalin 1-Oxides (**3a** and **3e**)*: The sulfoxides **3a** and **3e** were prepared by the following three methods.

1) To a stirred solution of the corresponding sulfide (156 mg, 1 mmol) in 10 ml of dry methanol cooled to −70 °C with an acetone–Dry Ice bath was added 1 equiv. of *t*-butyl hypochlorite. When the temperature of the bath reached −40 °C, anhydrous sodium carbonate was added. The mixture was allowed to come up to room temperature and then methanol was removed under vacuum. The residue was washed four times with 20 ml portion of chloroform and the chloroform solution was dried and concentrated to afford an oily product which was purified through alumina column chromatography with ethyl acetate as an eluent, giving crystalline *trans*-1-thiadecalin 1-oxide (**3a**) (123 mg, 71% yield).

2) To a stirred solution of the sulfide (2.34 g, 15 mmol) in 150 ml of acetone cooled with an ice bath was added dropwise 1.05 equiv. of sodium periodate dissolved in the least amount of water in which the metaperiodate is soluble. Then the solution was stirred at room temperature for 2 h and poured into 100 ml of water. The solution was extracted with 100 ml of chloroform seven times. The combined solution was dried and concentrated to afford oily substances which were separated through alumina column chromatography with ethyl acetate–benzene as an eluent giving *trans*-1-thiadecalin 1a-oxide (**3a**, 947 mg) from the former solution, *trans*-1-thiadecalin 1e-oxide (**3e**, 374 mg) from the latter solution.

3) To a stirred solution of the sulfide (2.50 g, 6 mmol) and methanesulfonic acid (1.54 g, 8 mmol) in a 30 ml of methanol cooled with ice bath was added 1.1 equiv. of hydrogen peroxide in 30 wt%. The mixture was stirred at room temperature until the sulfide disappeared. The resulting mixture was extracted, dried over K_2CO_3 and then concentrated to give oily products which were separated as in the above-mentioned case. Sulfoxides **3a** and **3e** were obtained in 35% (985 mg) and 38% (1080 mg) yields, respectively. **3a**: mp 87—88 °C (lit,[30,31] 82.5—86.0 °C); IR (KBr) 2930 and 1027 cm^{-1}; Found: C, 62.67; H, 9.45%. **3e**: mp 71—72 °C (lit,[30,31] 72.0—74.0 °C); IR (KBr) 2930 and 1035 cm^{-1}; Found: C, 62.80; H, 9.39%.

trans-*2-Thiadecalin*: *trans*-2-Thiadecalin was synthesized by a similar method as reported by Birch *et al.*[32] from *trans*-1-bromomethyl-2-(2-bromoethyl)cyclohexane prepared by the following procedure which is different from that of Brich *et al.*

1-Ethoxycarbonyl-trans-*hexahydro-2-indanone*. A solution of 32.0 g (0.125 mol) of diethyl *trans*-1,2-cyclohexanediacetate in 840 ml of dry toluene and 3.73 g of sodium ethoxide was heated at 110 °C for 8 h, ethanol formed was removed and then the residue was poured into 200 ml of water. The solution was neutralized with ammonium chloride. The toluene layer was separated and the aqueous layer was extracted with 200 ml of benzene twice. The combined organic solution was dried and the solvent was evaporated to give an oily product which was distilled (14.7 g, 56% yield). Bp 102 °C/12 mmHg; IR (neat) 1753 and 1720 cm^{-1}; NMR (CCl_4) δ=4.14 (2H, q), 2.88—1.00 (13H, m), 1.28 (3H, t).

trans-*2-Oxadecalin-3-one*. A solution of 14.7 g (70.6 mmol) of 1-ethoxycarbonyl-*trans*-hexahydro-2-indanone in 50 ml of 25% sulfuric acid was refluxed for 1.5 h and poured into 50 ml of water. The solution was extracted with 100 ml of ether three times and the ether solution was neutralized with diluted sodium hydroxide, then washed with water and dried. The solvent was evaporated to afford an oily *trans*-hexahydro-2-indanone[33] which was added into 500 ml of dichloromethane. To the dichloromethane solution, 22.5 g of *m*-chloroperbenzoic acid was added gradually under stirring over night. The solution was filtered and the filtrate was neutralized with diluted sodium hydroxide, washed with water and dried. The solvent was evaporated and the residue was distilled to give an oily *trans*-2-oxadecalin-3-one (5.6 g, 52% yield): bp 114—116 °C/4 mmHg (lit,[34] 102—104 °C/0.1 mmHg).

trans-*1-Bromomethyl-2-(2-bromoethyl)cyclohexane*: To a slurry of 1.5 g (40 mmol) of lithium aluminum hydride in 100 ml of dry ether was added dropwise while stirring the solution of 5.6 g (36 mmol) of *trans*-2-oxadecalin-3-one in 50 ml of ether. When the addition was complete, the mixture was refluxed for an additional 1 h and then treated successively with 1.5 ml of water, 1.5 ml of 15% aqueous sodium hydroxide, and 4.1 ml of water under stirring while cooling in an ice bath. The mixture was filtered and the filtrate was dried and concentrated. The residue was dried thoroughly under vacuum to give oily *trans*-2-(hydroxymethyl)-cyclohexaneethanol.[35] A portion of 10.7 g (39 mmol) of phosphorus tribromide was slowly dropped into 30 ml of dichloromethane solution of the oil under cooling in an ice bath. After dichloromethane was removed at 60 °C, the solution was heated at 100 °C for 6 h, cooled in an ice bath, and water was carefully added. Then the solution was extracted with dichloromethane, washed, dried, and concentrated. The residue was distilled with Kugelrohr (6.5 g, 63% yield); bp 115 °C/2 mmHg (lit,[32] 104—106 °C/0.8 mmHg).

trans-*2-Thiadecalin*: To a refluxing solution of sodium sulfide nonahydrate (4.15 g, 17.5 mmol) in 50 ml of 50% aqueous ethanol was added dropwise 6.5 g of the dibromide and an additional 50 ml of the sodium sulfide (4.15 g) solution at such a rate that the addition of both was complete in 1 h. After refluxing for 8 h, the mixture was extracted with ether. The combined organic extract was dried over anhydrous magnesium sulfate, the solvent was removed by evaporation and the residue was purified through silica-gel chromatography with hexane as an eluent (2.135 g, 38% yield).

trans-*2-Thiadecalin 2-Oxides (**5a** and **5e**)*: 1) To a stirred solution of *trans*-2-thiadecalin (156 mg, 1 mmol) in 10 ml of dry methanol cooled to −70 °C with an acetone–Dry Ice bath was added 1 equiv. of *t*-butyl hypochlorite. When the temperature of the bath reached −40 °C, anhydrous sodium carbonate was added. The mixture was allowed to come up to room temperature and then methanol was removed under reduced pressure. The residue was washed three times with 20 ml portion of chloroform and the chloroform solution was dried and concentrated to give an oily product which was separated through alumina column chromatography with ethyl acetate as an eluent, giving crystalline *trans*-2-thiadecalin 2a-oxide (**5a**) (97 mg) in 56% yield.

2) To a stirred solution of the sulfide (80 mg, 5 mmol) in 50 ml of acetone cooled with an ice bath was added dropwise 1.05 equiv. of sodium periodate dissolved in the least amount of water. When the addition was complete, the solution was stirred at room temperature for 2 h and poured into 50 ml of water. The solution was extracted with 100

ml of chloroform four times. The organic solution was dried and concentrated to give oily substance which was separated through alumina column chromatography with ethyl acetate–benzene (1:1) as an eluent giving *trans*-2-thiadecalin 2a-oxide (**5a**, 611 mg) from the former solution and *trans*-2-thiadecalin 2e-oxide (**5e**, 162 mg) from the latter solution.

3) To a stirred solution of the sulfide (5 mmol) in 50 ml of dichloromethane cooled with an ice bath was added 1.05 equiv. of *m*-chloroperbenzoic acid. The solution was washed with saturated sodium hydrogencarbonate, and the aqueous layer was extracted with chloroform three times. The combined organic layer was washed with water, dried and concentrated to afford oily product which was separated as in the above-mentioned case. The sulfoxide **5a** and **5e** were given in 31% (265 mg) and 57% (492 mg) yields, respectively. **5a**: mp 98—99 °C; IR (KBr) 1029 and 2930 cm^{-1}; Found: C, 62.61; H, 9.23%. Calcd for $C_9H_{16}OS$: C, 62.74; H, 9.36%. **5e**: mp 53—54.5 °C; IR (KBr) 1036 cm^{-1}; Found: C, 62.39; H, 9.20%. Calcd for $C_9H_{16}OS$: C, 62.74; H, 9.36%.

^{18}O-*Labeled* trans-*4-(*p-*Chlorophenyl)thiane 1-Oxide (**1t**-^{18}O)*: The title sulfoxide **1t**-^{18}O was prepared by the usual oxidation of the corresponding sulfide with bromine.[36] The sulfide (1 g, 4.7 mmol) was dissolved in a mixture of acetic acid (30 ml), pyridine (5 ml) and ^{18}O-enriched water (3 ml) (1.6 ex. atm%). To the cooled solution was added bromine (753 mg) in 5 ml of acetic acid at 0 °C. After the mixture was kept standing for 2 h at 0 °C, the reaction mixture was quenched with 50 ml of water and extracted with 50 ml of chloroform four times. The chloroform solution was washed with aqueous $Na_2S_2O_3$ solution, diluted aqueous hydrochloric acid, water and then dried ($MgSO_4$). After evaporation of chloroform with a rotary evaporator, a resulting substance was separated through alumina column chromatography with ethyl acetate–chloroform (2:1) as the eluent, giving ^{18}O-labeled corresponding equatorial sulfoxide **1t**-^{18}O (750 mg) and ^{18}O-labeled *cis*-sulfoxide **1c**-^{18}O (108 mg). The ^{18}O-labeled *trans*-4-(*p*-chlorophenyl)thiane 1-oxide was recrystallized from ethyl acetate–hexane and found to contain 1.092 ex. atom% of ^{18}O.

^{18}O-*Labeled* cis-*4-(*p-*Chlorophenyl)thiane 1-Oxide (**1c**-^{18}O)*: To a stirred solution of the *trans*-sulfoxide **1t** (600 mg, 2.63 mmol) in dichloromethane (3 ml) *ca.* 0.9 g (4.73 mmol) of triethyloxonium tetrafluoroborate (Et_3OBF_4) was added. After the mixture was stirred at room temperature for 1 h, 40 ml of anhydrous ether was added at 0 °C to give the oily ethoxysulfonium salt as a precipitate. After the mixture was kept standing for 2 h, the solvent was removed by decantation, and to the residue was added 5 ml of a 2 mol dm^{-3} $Na^{18}OH$ solution which was prepared by treating sodium metal with $H_2{}^{18}O$ (1.5 ex. atm%) under nitrogen atmosphere. The mixture was then extracted with dichloromethane. The solution was dried over $MgSO_4$ and the solvent was evaporated. The residue was then chromatographed on alumina with ethyl acetate–chloroform (2:1) as the eluent. The solvent of the former elution was removed to afford colorless crystals which were recrystallized from ethyl acetate (294 mg, 49%). The title sulfoxide (**1c**-^{18}O) was found to contain 0.4295 ex. atom% of ^{18}O.

^{18}O-*Labeled* trans-*1-Thiadecalin 1e-Oxide (**3e**-^{18}O)*: The *trans*-1-thiadecalin was similarly oxidized with bromine and ^{18}O-enriched water to give an oily substance which was separated through alumina column chromatography with ethyl acetate as the eluent to give the corresponding ^{18}O-labeled equatorial sulfoxide from the latter elution and the corresponding axial sulfoxide from the former one. The ^{18}O-labeled *trans*-1-thiadecalin 1e-oxide (**3e**-^{18}O) (654 mg, 69% yield) was recrystallized from hexane and found to contain 0.955 ex. atom% of ^{18}O.

^{18}O-*Labeled* trans-*1-Thiadecalin 1a-Oxide (**3a**-^{18}O)*: After a solution of 1e-sulfoxide **3e** (900 mg, 5.2 mmol) and Et_3OBF_4 (1.89 g, 9.4 mmol) in dichloromethane (**3** ml) was stirred at room temperature for 1 h, 30 ml of anhydrous ether was added at 0 °C. Then the mixture was kept standing for 2 h, the solvent was removed by decantation, and to the residue was added 3 ml of a 2 mol dm^{-3} $Na^{18}OH$ solution. The usual work-up and alumina chromatography gave the ^{18}O-labeled title sulfoxide **3a** which was recrystallized from hexane, and found to contain 0.856 ex. atom% of ^{18}O.

trans-*1-Thiadecalin-2e*-d *1a-Oxide (**9**)*:[37] After a solution of 1.1 ml of lithium (0.1 g/ml in hexane) was added to a stirred solution of a *trans*-1-thiadecalin 1a-oxide (**3a**) (253 mg, 1.47 mmol) in 5 ml of a freshly distilled THF cooled at −78 °C in an acetone–Dry Ice bath for 1 h, 2 ml of MeOD was added to the cooled solution at −78 °C under stirring for 0.5 h. The reaction mixture was quenched with 20 ml of water and neutralized with 10 ml of aqueous ammonium chloride and extracted with 30 ml of chloroform seven times. The whole solution was dried with $MgSO_4$ and the solvent was evaporated to afford the D-labeled product **9** which was recrystallized from hexane. Thus the title sulfoxide **9** obtained (250 mg, 99% yield) was found to contain 59% of D-atom at α-equatorial position upon treatment with 1 equiv. molar mixture of the lanthanoids shift reagent, Eu(dpm)$_3$ and the sulfoxide.

trans-*1-Thiadecalin-2a*-d *1e-Oxide (**11**)*: The title sulfoxide **11** was synthesized from the equatorial sulfoxide (344 mg) by the work-up as mentioned above (337 mg, 97%). The title sulfoxide **11** was found to contain 57% of D-atom at α-axial position upon treatment with 1 equiv. molar of Eu(dpm)$_3$.

trans-*1-Thiadecalin-2a*-d *1a-Oxide (**10**)*: The title sulfoxide **10** was prepared by the same chemical transformation of *trans*-1-thiadecalin-2a-*d* 1e-oxide (**11**). A solution of **11** (104 mg, 0.6 mmol) and (342 mg, 1.8 mmol) of triethyloxonium tetrafluoroborate in dichloromethane (2 ml) was stirred at room temperature for 1 h and 30 ml of anhydrous ether was added at 0 °C to give the oily ethoxysulfonium salt. After the mixture was kept standing for 2 h, the solvent was removed by decantation twice. Then to the residue was added 10 ml of a 0.5 M NaOH solution. The solution was neutralized with 10 ml of aqueous ammonium chloride solution and extracted with chloroform seven times. The solvent was dried with $MgSO_4$ and evaporated to afford a residue, which was then chromatographed through alumina with ethyl acetate–chloroform (2:1) to give the sulfoxide **10** (12.8 mg, 80%) which was found to contain 57% of D-atom at α-axial position upon treatment with an equimolar amount of Eu(dpm)$_3$.

*Reaction of 4-(*p-*Chlorophenyl)thiane 1-Oxides (**1c** and **1t**) with Acetic Anhydride.* The *trans* **1t** or *cis*-sulfoxide **1c** (45.7 mg, 0.2 mmol) was heated with 1 ml of acetic anhydride at 100 °C for 3 h until the sulfoxide disappeared upon monitoring with TLC. Then after evaporation of excess acetic anhydride and any volatile product *in vacuo*, the remaining residue was separated through silica-gel column chromatography with hexane–ether (4:1) as the eluent, in a low-temperature room at 0—4 °C. The corresponding axial α-acetoxy sulfide **2a** and olefinic product **2o** were obtained in 72—73% and 20% yields, respectively. **2a**: IR (neat) 1740 and 1223 cm^{-1}; NMR ($CDCl_3$) δ=7.15 (4H, aromatic), 5.98 (1H, t-like J=3.0 Hz), 2.12 (3H, s). Oxidation of **2a** gave the corresponding sulfone: mp 204—204.5 °C; IR (KBr) 1755, 1330, 1210, and 1140 cm^{-1}; Found: C, 51.44; H,

4.94%. Calcd for $C_{13}H_{15}ClO_4S$: C, 51.57; H, 4.99%. **2o**: bp 110 °C/5 mmHg (Kugerohr); Found: C, 62.98; H, 5.24%. Calcd for $C_{11}H_{11}ClS$: C, 62.69; H, 5.26%.

*Reaction of 4-(p-Chlorophenyl)thiane 1-Oxides (**1c** and **1t**) with Acetic Anhydride in the Presence of DCC or 2,6-Lutidine. 1)*: The *trans*- or *cis*-sulfoxide **1t** or **1c** (45.7 mg, 0.2 mmol) was heated with 1 ml of acetic anhydride in the presence of 1 equiv. of DCC to the sulfoxide at 100 °C for 4 h. When the reaction mixture was treated according to the above-mentioned procedure, the Pummerer products (the corresponding equatorial α-acetoxy sulfide **2e** and axial α-acetoxy sulfide **2a** in the ratio of 2:1 respectively) and olefinic product **2o** were obtained in 77% and 21% yields, respectively.

2): The *trans*-sulfoxide **1t** was heated with 1 ml of acetic anhydride in the presence of 3 equiv. of DCC at 100 °C for 4 h. The Pummerer products **2e** and **2a** (ratio of 9:1, respectively) and the olefinic product were obtained in 85% and 11% yields, respectively.

3): The *trans*-sulfoxide **1t** was heated with 1 ml of acetic anhydride in the presence of 5 equiv. of DCC at 100 °C for 4 h. The Pummerer products **2e** and **2a** (ratio of 13:1, respectively) and the olefinic product were obtained in 83% and 9% yields, respectively. **2e**: mp 78.5—80 °C; IR (KBr) 1745 and 1225 cm^{-1}; NMR ($CDCl_3$) 7.15 (4H, aromatic) 5.88 (1H, dd, J=9.9 and 3.3 Hz) 2.04 (3H, s); Found: C, 57.75; H, 5.57%. Calcd for $C_{13}H_{15}ClO_2S$: C, 57.66; H, 5.58%.

4): The *cis*-sulfoxide **1c** was heated with 1 ml of acetic anhydride in the presence of 5 equiv. of DCC at 100 °C for 6 h. The Pummerer products (**2e** and **2a** ratio of 14:1, respectively) and the olefinic product were obtained in 83% and 12% yields, respectively.

5): The *cis*-sulfoxide **1c** was heated with acetic anhydride in the presence of 5 or 10 equiv. of 2,6-lutidine at 100 °C for 4.5 h. The Pummerer products (**2e** and **2a** ratio of 5:2 or 5:1, respectively) and the olefinic product were obtained in 81 or 86% and 15 or 12% yields, respectively.

*Isomerization Reaction of 2e-Acetoxy-4-(p-Chlorophenyl)thiane (**2e**) with Acetic Anhydride in the Presence of Acetic Acid.* After the sulfide **2e** (60 mg) was heated with 1 ml of acetic anhydride in the presence of 1 equiv. of acetic acid to the acetoxy sulfide at 100 °C for 3 h and then evaporation of excess acetic anhydride and any volatile substance *in vacuo*, an oily product was purified through silica-gel column chromatography with hexane–ether 4:1 as an eluent at 0—4 °C to afford the corresponding 2a-acetoxy sulfide (**2a** 42 mg, 70% yield) and the olefinic compound **2o** (13 mg, 28%).

Reaction of trans-*1-Thiadecalin 1-Oxides (**3e** and **3a**) with Acetic Anhydride.* The sulfoxide **3e** or **3a** (71.2 mg, 0.4 mmol) was heated with 2 ml of acetic anhydride at 100 °C for 3 or 4 h until the sulfoxide completely disappeared upon monitoring with TLC of alumina. Then after evaporation of excess acetic anhydride and any volatile product *in vacuo*, the remaining residue was separated through silica-gel column chromatography with hexane–ether (5:1) as an eluent in a low temperature room at 0—4 °C. The corresponding equatorial and axial α-acetoxy sulfides **4e** and **4a** (ratio of 1:19, respectively) were obtained in 40—50% yield. To the trapped volatile products in an acetone–Dry Ice bath was added a saturated sodium hydrogencarbonate solution until the solution became alkaline and then the solution were extracted with dichloromethane. The dichloromethane solution was washed with water, dried, and concentrated to afford the olefinic product. **4a**: oil; IR (neat) 2930, 1700, and 1220 cm^{-1}; NMR 5.81 (1H, t, J=3.3 Hz), 2.01 (3H, s). Oxidation of **4a** with *m*-CPBA gave the corresponding sulfone: mp 86—86.5 °C; IR (KBr) 2930, 1760, 1750, and 1215 cm^{-1}; NMR ($CDCl_3$) δ=5.70 (1H, t, J=3 Hz), 2.15 (3H, s); Found: C, 53.63; H, 7.30%. Calcd for $C_{11}H_{18}O_4S$: C, 53.63; H, 7.36%.

Reaction of trans-*1-Thiadecalin 1-Oxides (**3e** and **3a**) with Acetic Anhydride in the Presence of DCC.* The sulfoxide **3a** or **3e** (71.2 mg, 0.4 mmol) was heated with 2 ml of acetic anhydride in the presence of 5 equiv. of DCC to the sulfoxide at 100 °C for 4 h. When the reaction mixture was treated according to the above-mentioned procedure, the corresponding equatorial and axial α-acetoxy sulfides **4e** and **4a** (ratio of 19:1, respectively) were obtained in 45—52% yield. To the trapped volatile products cooled in an acetone–Dry Ice bath was added a saturated sodium hydrogencarbonate solution until the solution became alkaline and then the solution was extracted with dichloromethane. The dichloromethane solution was washed with water, dried $Mg(SO_4)$, and concentrated to give an olefinic product. **4e**: mp 41—42 °C; IR (KBr) 1740 and 1240 cm^{-1}; NMR ($CDCl_3$) δ=5.69 (1H, dd J=9.9 and 3.3 Hz), 2.04 (3H, s); Found: C, 61.75; H, 8.49%. Calcd for $C_{11}H_{18}O_2S$: C, 61.64; H, 8.46%. The olefinic product was converted to the corresponding sulfone: mp 106—7.5 °C; IR (KBr) 2930, 1620, 1300, and 1110 cm^{-1}; Found: C, 57.86; H, 7.53%. Calcd for $C_9H_{14}O_2S$: C, 58.03; H, 7.57%.

Reaction of trans-*2-Thiadecalin 2-Oxides (**5e** and **5a**) with Acetic Anhydride.* The sulfoxide **5e** or **5a** (71.2 mg, 0.4 mmol) was heated with 2 ml of acetic anhydride at 100 °C for 3 h. The usual work-up and silica gel column chromatography with hexane–ether (5:1) as an eluent at 0—4 °C gave 42 mg (48% yield) of a 1:1 mixture of the corresponding 1a- and 3a-acetoxy sulfide **6a1** and **6a3** as main products: oil; IR (neat) 1740, 1230, and 1219 cm^{-1}; NMR ($CDCl_3$) δ=5.67 (t, J=3 Hz, methine proton of **6a1**), 5.88 (d, J=3 Hz, methine protone of **6a3**), 2.13(s). Sulfone: mp 79—80 °C; IR (KBr) 2930, 1760, 1750, and 1215 cm^{-1}; Found: C, 53.75; H, 7.37%. Calcd for $C_{11}H_{18}O_4S$: C, 53.63; H, 7.36%.

Reaction of trans-*2-Thiadecalin 2-Oxides (**5e** and **5a**) with Acetic Anhydride in the Presence of DCC.* The sulfoxide **5e** or **5a** (71.2 mg, 0.4 mmol) was heated with 2 ml of acetic anhydride in the presence of 5 equiv. of DCC to the sulfoxide at 100 °C for 4 h. An about 1:1 mixture of the Pummerer products, the corresponding 1e- and 3e-acetoxy sulfides were obtained as main products (45 mg, 51%): oil; NMR ($CDCl_3$) δ=5.49 (d, J=9.5 Hz, methine proton of **6e1**), 5.82 (dd, J=10.5 and 3.0 Hz, methine proton of **6e3**), and 2.08(s). Sulfone: mp 121—122 °C; IR (KBr) 2970, 1760, 1220, and 1207 cm^{-1}; Found: C, 53.72; H, 7.35%. Calcd for $C_{11}H_{18}O_4S$: C, 53.63; H, 7.36%.

Reaction of ^{18}O-*Labeled* trans-*4-(p-Chlorophenyl)thiane 1-Oxide (**1t**) with Acetic Anhydride.* When the ^{18}O-labeled title sulfoxide **1t** (685.5 mg) was heated with 60 equiv. of acetic anhydride at 100 °C for 0.75 h, the oily residue obtained after evaporation of excess acetic anhydride and any volatile product under vacuum was separated through silica-gel column chromatography with hexane–ether (4:1) as an eluent in a low-temperature room at 0—4 °C and then acetone as eluent to give the Pummerer products **2e** and **2a** (325 mg, 40% yield (e:a/1:1) and the recovered sulfoxide (341 mg, 50% yield), respectively, which was recrystallized from ethyl acetate–hexane. The starting sulfoxide, the Pummerer products and the recovered sulfoxide were subjected to measurement of ^{18}O-content by the routine ^{18}O-analysis technique and the ^{18}O-contents were found to be 1.092, 0.013, and 1.088 ex. atom%, respectively.

Reaction of ^{18}O-*Labeled* cis-*4-(p-Chlorophenyl)thiane 1-Oxide (**1c**-^{18}O) with Acetic Anhydride.* After the ^{18}O-labeled

title sulfoxide (**1c**-^{18}O) (330 mg) was heated with 60 equiv. of acetic anhydride at 100 °C for 0.75 h, the reaction mixture was treated according to the above-mentioned procedure to afford the mixture of Pummerer products **2e** and **2a** (156 mg) in 40% yield (e:a/1:1) and the recovered sulfoxide (155 mg) in 47% yield, which were recrystallized from ethyl acetate. The ^{18}O-contents of the starting sulfoxide, Pummerer products and the recovered sulfoxide were found to be 0.495, 0.019, and 0.334 ex. atom%, respectively.

Reaction of ^{18}O-*Labeled* trans-*1-Thiadecalin 1e-Oxide (**3e**) with Acetic Anhydride.* When the ^{18}O-labeled title sulfoxide **3e** (152.3 mg) thoroughly dried under vacuum was heated with 60 equiv. of acetic anhydride at 100 °C for 0.75 h, the oily residue, obtained after evaporation of excess of acetic anhydride and any volatile product under vacuum, was separated through silica-gel column chromatography with hexane–ether (5:1) as the eluent to give the Pummerer products **4e** and **4a** (52.7 mg, 28% yield, e:a/6:1) and the recovered sulfoxide (81.4 mg, 53% yield) which was recrystallized from hexane. The ^{18}O-contents of starting sulfoxide, the Pummerer products and recovered sulfoxide were found to be 0.955, 0 and 0.812 ex. atom% of ^{18}O, respectively.

Reaction of ^{18}O-*Labeled* trans-*1-Thiadecalin 1a-Oxide (**3a**-*^{18}O*) with Acetic Anhydride.* The ^{18}O-labeled title sulfoxide (**3a**-^{18}O) (152.3 mg) was heated with acetic anhydride (60 equiv.) at 100 °C for 0.75 h. After the work-up procedure as mentioned above, the Pummerer products **4e** and **4a** (80.6 mg, 43% yield, e:a/8:1) and the recovered sulfoxide (43.3 mg, 28% yield) were obtained and the recovered sulfoxide was recrystallized from hexane. The ^{18}O-contents of the starting sulfoxide, the Pummerer products and the sulfoxide recovered were found to be 0.856, 0.057, and 0.710 ex. atom% of ^{18}O, respectively. The Pummerer products (**4e**:**4a**=6:1) incorporated with 13% of ^{18}O, based on the starting sulfoxide, was recrystallized from hexane to give the pure **4e** (mp 43 °C). Then the filtrate was condensed and separated through silica-gel column chromatography with hexane–ether–ethyl acetate (77:2:1) as an eluent. The ^{18}O-contents of the pure **4e** and **4a** were found to be 0.057 and 0.043 ex. atom%.

Reaction of ^{18}O-*Labeled* trans-*1-Thiadecalin 1e-Oxide (**3e**) with Acetic Anhydride in the Presence of DCC.* When the ^{18}O-labeled sulfoxide (**3e**-^{18}O) (152.3 mg) thoroughly dried was heated with 60 equiv. of acetic anhydride in the presence of 5 equiv. DCC to the sulfoxide at 100 °C for 1.25 h, the residue was obtained after evaporation of excess acetic anhydride and any volatile product under vacuum. To the resultant residue was added 5 ml of ether–hexane and the mixture was filtered. The solvent of the filtrate was removed and the oily residue was separated through silica-gel column chromatography with hexane–ether (5:1) as the eluent at 0—4 °C and then with benzene–acetone (1:1) to give the Pummerer products **4e** and **4a** (97.0 mg, 51% yield, e:a/19:1), and the recovered sulfoxide (45.8 mg, 30% yield) which was recrystallized from hexane. The filtered product was recrystallized from ethyl acetate–hexane giving 650 mg of the *N*-acetyl-*N,N'*-dicyclohexylurea (IR 1600 and 1680 cm^{-1}, NMR δ=2.1, 5.0, 1—2). The ^{18}O-contents of the recovered sulfoxide, the Pummerer products and *N*-acetyl-*N,N'*-dicyclohexylurea were found to be 0.812, 0, and 0 ex. atom%, respectively.

Reaction of ^{18}O-*Labeled* trans-*1-Thiadecalin 1a-Oxide (**1a**-*^{18}O*) with Acetic Anhydride in the Presence of DCC.* The ^{18}O-labeled sulfoxide (**3a**-^{18}O) (152.3 mg) was heated with 60 equiv. of acetic anhydride at 100 °C for 1.25 h. After the work-up procedure as mentioned above, the Pummerer products **4e** and **4a** (65.2 mg, 34% e:a/19:1), recovered sulfoxide (89.9 mg, 59% yield) and the *N*-acetyl-*N,N'*-dicyclohexylurea were obtained. The ^{18}O-contents of the recovered sulfoxide, the Pummerer products and the *N*-acetylurea were found to be 0.574, 0.068, and 0 ex. atom%.

*Hydrogen-Deuterium Kinetic Isotope Effect in the Reaction Between 4-(*p*-Chlorophenyl)thiane-2,2,6,6-*d_4 *1-Oxides with Acetic Anhydride.* 4-(*p*-Chlorophenyl)thiane-2,2,6,6-d_4 1-oxides (*cis* and *trans*) were prepared by the treatment with diethyl 3-(*p*-chlorophenyl)glutarate and lithium aluminum deuteride in the ether and the successive procedures mentioned-above.[27]

Each 4-(*p*-chlorophenyl)thiane 1-oxide (*cis* or *trans*) (0.1 mmol) was dissolved in 10 ml of acetic anhydride. The solution was heated at 100 °C. The solution 10 μl picked up with syringe at time intervals was cooled at 0 °C to stop the reaction. The rate of the reaction was followed by measurement of the GLPC peaks of the Pummerer products (OV1 2% on chromosorb 2 m). The rate constants were obtained from the pseudo-first-order kinetic equation.

Reaction of trans-*1-Thiadecalin-2e-*d *1a-Oxide (**9**) with Acetic Anhydride in the Presence of DCC.* The stereoselectively D-labeled sulfoxide **9** (D, 59%, 103 mg at equatorial position) was heated with 2 ml of acetic anhydride in the presence of DCC (617 mg, 5 equiv. molar to the sulfoxide) at 100 °C for 4 h. After the work-up procedure as mentioned, the 2e-acetoxy sulfide, the Pummerer product, obtained in 39% yield (50 mg) was found to retain 59% of D-content upon measurement of NMR using 14% of $Eu(dpm)_3$.

Reaction of trans-*1-Thiadecalin-2a-*d *1a-Oxide (**10**) with Acetic Anhydride in the Presence of DCC.* When the stereoselectively D-labeled axial sulfoxide **10** (49.4 mg, D, 57% at axial position) was heated with 1 ml of acetic anhydride in the presence of DCC (250 mg) at 100 °C for 4 h, the corresponding 2e-acetoxy sulfide given in 45% yield (27.9 mg) was found to contain only 13% of D-content according to the usual procedure.

Reaction of trans-*1-Thiadecalin-2e-*d *1e-Oxide (**11**) with Acetic anhydride in the Presence of DCC.* After the D-labeled title sulfoxide **11** (108 mg, D, 57% at axial position) was heated with 2 ml of acetic anhydride in the presence of DCC (648 mg) at 100 °C for 6 h, the usual work-up was carried out. The corresponding 2e-acetoxy sulfide obtained in 41% yield (55 mg) had 50% of D-content.

References

1) L. Horner, *Justus Liebigs Ann. Chem.*, **631**, 198 (1960).
2) R. Pummerer, *Ber.*, **42**, 2282 (1909); **43**, 1401 (1910).
3) G. A. Russell and G. J. MiKol, "Mechanism of Molecular Migrations," ed by B. S. Thyagarajan, Interscience, New York (1968), Vol. 1, p. 157.
4) T. Durst, *Adv. Org. Chem.*, **6**, 285 (1969).
5) J. P. Marino, "Topics in Sulfur Chemistry," ed by A. Senning, Georg Thieme Publishers, Stuttgart (1976), Vol. 1, p. 1.
6) T. Numata and S. Oae, *Yuki Gosei Kagaku Kyokai Shi*, **35**, 726 (1977).
7) T. Numata, *Yuki Gosei Kagaku Kyokai Shi*, **36**, 845 (1978).
8) a) S. Oae, "Organic Chemistry of Sulfur," ed by S. Oae, Plenum Press, New York (1977), Chap. 8; b) S. Oae "Topics in Organic Sulfur Chemistry," ed by M. Tišler, University Press, Ljubliana, Yugoslavia (1978), Chap. 11.
9) S. Oae and T. Numata, "The Pummerer and Pummerer Type of Reactions," in "Isotopes in Organic Chemistry," ed by E. Buncel and C. C. Lee, Elsevier, New York (1980), Vol. 5, Chap. 2.

10) S. Oae, T. Numata and T. Yoshimura, "Heterosulphonium Salts," in "The Chemistry of the Sulphonium Group," ed by C. J. M. Stirling and S. Patai, John Wiley & Sons, New York (1981), Part 2, Chap. 15.
11) S. Oae, T. Kitao, S. Kawamura, and Y. Kitaoka, *Tetrahedron*, **19**, 817 (1963); S. Oae, T. Kitao, and S. Kawamura, *ibid.*, **19**, 1783 (1963).
12) S. Oae and M. Kise, *Tetrahedron Lett.*, **1968**, 2261; M. Kise and S. Oae, *Bull. Chem. Soc. Jpn.*, **43**, 1426 (1970).
13) T. Numata and S. Oae, *Tetrahedron Lett.*, **1977**, 1337.
14) T. Numata, O. Itoh, and S. Oae, *Chem. Lett.*, **1977**, 909.
15) T. Numata, O. Itoh, and S. Oae, *Tetrahedron Lett.*, **1979**, 1869.
16) M. Mikolajczyk, A. Zatorski, S. Grzejszczak, B. Costisella, and M. Midura, *J. Org. Chem.*, **43**, 2518 (1978).
17) T. Masuda, T. Numata, N. Furukawa, and S. Oae, *Chem. Lett.*, **1977**, 903; *J. Chem. Soc., Perkin Trans. 2*, **1978**, 1302.
18) T. Numata and S. Oae, *Chem. Ind. (London)*, **1972**, 726; S. Oae and T. Numata, *Tetrahedron*, **30**, 2641 (1974); T. Numata and S. Oae, *ibid.*, **32**, 2699 (1976).
19) B. Stridsberg and S. Allenmark, *Acta. Chem. Scand., Ser. B*, **28**, 591 (1974); **30**, 219 (1976).
20) J. E. McCormick and R. S. McElhinney, *J. Chem. Soc., Perkin Trans. 1*, **1976**, 2533.
21) S. Glue, I. T. Kay, and M. R. Kipps, *J. Chem. Soc., D*, **1970**, 1158.
22) T. Numata, O. Itoh, and S. Oae, *Tetrahedron Lett.*, **1979**, 161.
23) S. Oae and M. Kise, *Tetrahedron Lett.*, **1967**, 1409; S. Oae and M. Kise, *Bull. Chem. Soc. Jpn.*, **43**, 1416 (1970); M. Kise and S. Oae, *ibid.*, **43**, 1804 (1970).
24) E. Vilsmeier, 7th International Symposium Org. Sulfur Chem., Hamburg (1976); G. E. Wilson, Jr., and C. J. Strong, *J. Org. Chem.*, **37**, 2376 (1972).
25) S. Wolfe and P. Kazmeier, *Can. J. Chem.*, **57**, 2388 (1979).
26) D. Rittenberg and L. Ponticorvo, *J. Appl. Rad. Isotopes*, **1**, 208 (1956).
27) C. R. Johnson, *J. Am. Chem. Soc.*, **85**, 1020 (1963).
28) V. I. Dronov, V. P. Krivonogov, and V. S. Nikitina, *Khim. Geterotsikl. Soedin.*, **1970**, 335; *Chem. Abstr.*, **73**, 66363j (1970).
29) P. K. Claus, F. W. Vierhapper, and R. L. Willa, *J. Org. Chem.*, **42**, 4016 (1977).
30) P. K. Claus, W. Rieder, and F. W. Vierhapper, *Monatsh. Chem.*, **109**, 609 (1978); *Chem. Abstr.*, **89**, 107851t (1978).
31) R. P. Rooney and S. A. Evans, Jr., *J. Org. Chem.*, **45**, 180 (1980).
32) S. F. Birch, R. A. Dean, and E. V. Whitehead, *J. Org. Chem.*, **19**, 1449 (1954).
33) R. S. Thakur, *J. Chem. Soc.*, **1932**, 2147.
34) E. E. van Tamelen, M. Shamma, and P. Aldrich, *J. Am. Chem. Soc.*, **78**, 4628 (1956).
35) R. Granger, J. Boussinesq, J-P. Girard, and J-C. Rossi, *Bull. Soc. Chim. Fr.*, **1969**, 2801.
36) S. Oae, Y. Ohnishi, S. Kozuka, and W. Tagaki, *Bull. Chem. Soc. Jpn.*, **39**, 364 (1964).
37) G. Chassaing, R. Lett, and A. Marquet, *Tetrahedron Lett.*, **1978**, 471.

N-Alkylation of Pyrrole, Indole, and Several Other Nitrogen Heterocycles Using Potassium Hydroxide as a Base in the Presence of Polyethylene Glycols or Their Dialkyl Ethers

Kazuaki SUKATA

Nihon Tokushu Chemical Ind. Co., Ltd. 3-36, Tohda-cho, Moriguchi, Osaka 570

(Received June 7, 1982)

The alkylation of pyrrole and indole in aqueous potassium hydroxide-organic two-phase systems in the presence of polyethylene glycols (PEG) or their dialkyl ethers (PEG-ether) as phase transfer catalysts (PTC) gave substantial quantities of the *C*-alkylated and *C,N*-polyalkylated products as well as the *N*-alkylated products. This fact is similar to that obtained in the presence of quaternary ammonium salts as PTC. In powdered potassium hydroxide-organic two-phase systems, the yields of the *N*-alkylated products were generally high. Especially, when PEG-ether were employed as solvents, the *N*-alkylated products were obtained in excellent yields under mild conditions. Imidazole, benzimidazole, carbazole, 2-methylindole, and benzotriazole were similarly *N*-alkylated in high yields by this method.

It has been reported that the *N*-alkylation of nitrogen heterocycles such as pyrrole and indole can be achieved by use of various bases such as potassium,[1] sodium amide,[2] sodium hydroxide in hexamethylphosphoric triamide,[3] potassium hydroxide in dimethyl sulfoxide,[4] and thallium(I) ethoxide.[5] Moreover, phase transfer procedures have been recently developed.[6] In many cases, concentrated aqueous sodium hydroxide was employed as a base in the presence of quaternary ammonium salts as phase transfer catalysts (PTC), and substantial quantities of the *C*-alkylated and *C,N*-polyalkylated (*C*- and *C,N*-alkylated) derivatives were obtained as by-products.

On the other hand, Santaniello *et al.*[7] have reported that *N*-alkylpyrrole and indole are obtained in good yields by use of potassium hydroxide as a base in the presence of crown ethers as PTC. Also Guida and Mathre[8] found that the *N*-alkylation of nitrogen heterocycles can be achieved in good yields by use of potassium *t*-butoxide as a base in the presence of crown ethers as PTC.

In this paper, the author reports the *N*-alkylation of nitrogen heterocycles using aqueous or powdered potassium hydroxide as a base in the presence of polyethylene glycols (PEG) or their dialkyl ethers (PEG-ether).

Results and Discussion

N-Alkylation of Pyrrole and Indole in Aqueous Potassium Hydroxide-organic Two-phase Systems in the Presence of PEG or PEG-ether as PTC. Table 1 shows that the results of *N*-alkylation of pyrrole and indole in aqueous potassium hydroxide-organic two-phase systems in the presence of PEG-1000, PEG-1000-diethyl ether (PEG-1000-Et_2) or PEG-600-dibutyl ether (PEG-600-Bu_2) as PTC. The yields of the *N*-alkylation were similar to those of the reported method[6] using quaternary ammonium salts as PTC.

It is well known[9] that the pyrrolyl and indolyl anion exhibit ambident behavior, and thus substantial quantities of the *C*- and *C,N*-alkylated products as well as the *N*-alkylated products are obtained. Under the present experimental conditions, the alkylation of pyrrole also gave many *C*- and *C,N*-alkylated products, which were detected by GLC. In the case of indole, GLC showed the presence of a few components except the *N*-alkylated products. In the cases of both pyrrole and indole, the alkylation with isopropyl bromide gave the *N*-alkylated products in extremely low yields because of the elimination of hydrogen bromide from isopropyl bromide, induced by the pyrrolyl or indolyl anion. This result contrasts with the result in which α-isopropylphenylacetonitrile is obtained in high yields under the same conditions,[10] indicating that the pyrrolyl and indolyl anions are much harder[11] than $PhC\bar{H}CN^{\ominus}$.

N-Alkylation of Pyrrole and Indole in Powdered Potassium Hydroxide-organic Two-phase Systems in the Presence of PEG or PEG-ether as PTC. Table 2 shows the results of the *N*-alkylation of pyrrole and indole using PEG-1000 or PEG-1000-Et_2. On the basis of the results reported by Santaniello *et al.*,[7] equimolar amounts of potassium hydroxide and pyrrole or indole (molar ratio: KOH/heterocycle=1/1) were used. However, the yields of the *N*-alkylation were lower than those reported by them.

Table 3 shows the effects of the relative amount of potassium hydroxide to pyrrole on the *N*-ethylation. For the molar ratio: KOH/pyrrole=1/1, an incomplete conversion of pyrrole to the product was observed. Furthermore, substantial quantities of the *C*- and *C,N*-ethylated products were obtained. For the molar ratio: KOH/pyrrole=2/1—3/1, the yields of the *N*-ethylation came to the constant value (88% by GLC).

On the basis of the data given in Table 3, the *N*-alkylations were carried out under the molar ratio: KOH/heterocycle=3/1, giving *N*-alkylated products in high yields (Table 2). These facts suggest that the water formed is absorbed by the excess potassium hydroxide and fixed in the solid phase, completing the conversion to the product.

N-Alkylation of Pyrrole and Indole Using Powdered Potassium Hydroxide as a Base and PEG-ether as Solvents. Table 4 shows the *N*-alkylation of pyrrole and indole using PEG-400-Et_2 as a solvent (molar ratio: PEG-400-Et_2/heterocycle=1/1 or 2/1). When the alkylating agents except isopropyl bromide and *t*-butyl bromide were employed, the *N*-alkylated products were obtained in extremely high yields. Moreover, the

Table 1. *N*-Alkylation of pyrrole and indole in aqueous-organic two-phase systems in the presence of PEG or PEG-ether as PTC[a]

	Alkyl halide		Catalyst[b] (mmol)	(Product) Yield[c]/% *N*-Alkylation	d)	Starting material
Pyrrole **1**	C_2H_5Br	**a**	A (2.5)	(**1a**) 84[e] (83)	(16)	(1)
	n-C_4H_9Br	**b**	A (2.5)	(**1b**) 65 (69)	(27)	(4)
			B (2.5)	(**1b**) 61[f] (65)	(32)	(3)
			C (2.5)	(**1b**) 66[f] (67)	(28)	(5)
	i-C_3H_7Br	**c**	A (5)	(**1c**) 46[g] (43)	(31)	(26)
	CH_2=$CHCH_2Br$	**e**	A (2.5)	(**1e**) (13)	(73)	(14)
	$PhCH_2Cl$	**f**	A (2.5)	(**1f**) 79 (85)	(10)	(5)
			B (2.5)	(**1f**) 78 (84)	(11)	(5)
			C (2.5)	(**1f**) 79 (84)	(10)	(6)
Indole **2**	C_2H_5Br	**a**	A (2.5)	(**2a**) 90 (94)	(6)	
			B (2.5)	(**2a**) 92 (94)	(6)	
	n-C_4H_9Br	**b**	A (2.5)	(**2b**) 86 (90)	(10)	
	i-C_3H_7Br	**c**	A (5)	(**2c**) (7)	(18)	(75)
	CH_2=$CHCH_2Br$	**e**	A (2.5)	(**2e**) 50 (56)	(44)	
	$PhCH_2Cl$	**f**	A (2.5)	(**2f**) 81 (86)	(14)	
			B (2.5)	(**2f**) 80 (86)	(14)	

a) All reactions were carried out with 0.1 mol of heterocycle, 0.15 mol of alkyl halide, 30 ml of benzene, and 0.5 mol of potassium hydroxide in 14 g of water at 45 °C for 2 h. b) A: PEG-1000-Et_2, B: PEG-1000, C: PEG-600-Bu_2. c) Isolated yields. Values in parentheses are the yields determined by GLC. Unless otherwise noted, the purities of *N*-alkylpyrrole and indole were 98 and 99% by GLC, respectively. d) Total yields of the C- and C, *N*-alkylated products, determined by GLC. However, all the products were not identified. e), f),g) Purities were 93, 97, and 78% by GLC, respectively.

Table 2. *N*-Alkylation of pyrrole and indole in solid-organic two-phase systems in the presence of PEG or PEG-ether as PTC[a]

	Alkyl halide		Catalyst[b] (mmol)	Temp °C	Time h	KOH (mol)	(Product) Yield[c]/% *N*-Alkylation	d)	Starting material
Pyrrole **1**	C_2H_5Br	**a**	A (2.5)	65	4	0.1	(**1a**) (67)	(13)	(20)
	n-C_4H_9Br	**b**	B (2.5)	70	4	0.1	(**1b**) 41[e] (55)	(25)	(21)
			A (2.5)	85	2	0.3	(**1b**) 74 (79)	(21)	
			B (10)	85	2	0.3	(**1b**) 80 (86)	(14)	
	CH_2=$CHCH_2Br$	**e**	A (2.5)	85	2	0.3	(**1e**) (24)	(64)	(12)
	$PhCH_2Cl$	**f**	A (2.5)	70	5	0.1	(**1f**) 65[f] (72)	(15)	(13)
			A (2.5)	85	2	0.3	(**1f**) 88 (90)	(10)	
			A (10)	85	2	0.3	(**1f**) 90 (98)	(2)	
Indole **2**	C_2H_5Br	**a**	A (2.5)	65	4	0.1	(**2a**) 78[g] (85)	(6)	(9)
	n-C_4H_9Br	**b**	B (2.5)	70	4	0.1	(**2b**) 68[h] (80)	(8)	(12)
			A (2.5)	85	2	0.3	(**2b**) 87 (95)	(5)	
			A (10)	85	2	0.3	(**2b**) 94 (98)	(2)	
	CH_2=$CHCH_2Br$	**e**	A (2.5)	85	2	0.3	(**2e**) 56[i] (67)	(33)	
	$PhCH_2Cl$	**f**	A (2.5)	65	3	0.1	(**2f**) 63[j] (68)	(15)	(17)
			A (2.5)	85	2	0.3	(**2f**) 83 (87)	(13)	
			A (10)	85	2	0.3	(**2f**) 88 (95)	(5)	

a) All reactions were carried out with 0.1 mol of heterocycle and 0.15 mol of alkyl halide in 30 ml of benzene. b) A: PEG-1000-Et_2, B: PEG-1000. c),d) see footnotes c), d) in Table 1, respectively. e),f),g),h),i),j) Purities were 92, 97, 92, 91, 97, and 98% by GLC, respectively.

yields of the *C*- and *C*,*N*-alkylated products were generally extremely low. The alkylation of indole with primary alkyl bromide or benzyl chloride gave *N*-alkylated products in almost quantitative yields. Even *N*-allylindole was obtained in 89—91% yields, which were comparable to that of the reported method using sodium hydride as a base in hexamethylphosphoric triamide.[3]

When isopropyl bromide was used as an alkylating agent, the considerable evolution of gas was observed during the reaction, and pyrrole or indole was recovered in 25-8 or 76—80%, respectively. As shown

in Table 1, the reaction of pyrrole or indole with isopropyl bromide using PEG or PEG-ether as PTC also gave pyrrole or indole in 26 or 75% yields, respectively. These facts indicate that the indolyl anion tends to induce the elimination reaction with isopropyl bromide in comparison with the pyrrolyl anion and is much harder[11] than the latter.

When PEG-400 was employed as a solvent in place of PEG-400-Et_2, the yields of *N*-alkylated products were extremely low because of the accompanied alkylation of PEG. For example, the alkylation of pyrrole with ethyl bromide gave pyrrole (49%), *N*-ethylpyrrole (43%), and *C*- and *C,N*-ethylated products (8% by GLC). The alkylation with *n*-butyl bromide gave pyrrole (39%), *N*-butylpyrrole (53%), and *C*- and *C,N*-butylated products (8% by GLC).

Table 3. Influence of the amounts of potassium hydroxide on the ethylation of pyrrole[a]

KOH (mol)	Yield[b]/%		
	1a	c)	Starting material
0.1	67	13	20
0.15	78	14	8
0.2	86	13	1
0.3	88	12	—
0.4	88	12	—
0.5	89	11	—

a) All reactions were carried out with 0.1 mol of pyrrole, 0.15 mol of ethyl bromide, and 30 ml of benzene at 65 °C for 4 h in the presence of 2.5 mmol of PEG-1000-Et_2 as PTC. b) Determined by GLC. c) See footnote d) in Table 1.

Since hydrogen bond is a hard-hard interaction,[11] under the condition containing large amount of water such as the aqueous-organic phase transfer system or in protic solvents such as PEG, water or PEG is capable of forming hydrogen bonding with the harder nitrogen atom of the heterocycle anion, suppressing the *N*-alkylation.[12] Therefore, the *C*-alkylation will increase. However, in PEG-ether, which is aprotic and would greatly increase the degree of dissociation[13] of the heterocycle anion, the exclusive *N*-alkylation could be achieved.

The method using potassium hydroxide as a base and PEG-ether as a solvent was applied to the alkylation of several nitrogen heterocycles. Table 5 shows the results. The alkylation of carbazole, imidazole, and benzimidazole gave 1-alkylated products in extremely high yields. However, in the case of benzotriazole, substantial quantities of 2-alkylbenzotriazole were obtained, in contrast to the alkylation of benzimidazole. This fact indicates that canonical structure of **13** would significantly contribute to the reactivity of the benzotriazolyl anion.

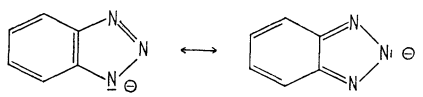

12 13

In contrast to the alkylation of indole, the alkylation of 2-methylindole with ethyl bromide or benzyl chloride gave 1,3-dialkylated products as well as 1-alkylated products in 2 or 16% yields, respectively.

Table 4. *N*-Alkylation of pyrrole and indole in PEG-400-Et_2[a]

	Alkyl halide		PEG-400-Et_2 (mol)	Time h	(Product) Yield[b]/%			
					N-Alkylation		c)	Starting material
Pyrrole **1**	C_2H_5Br	**a**	0.1	2	(**1a**) 88	(97)	(3)	
	n-C_4H_9Br	**b**	0.1	2	(**1b**) 91	(95)	(5)	
			0.2	2	(**1b**) 90	(95)	(5)	
	i-C_3H_7Br	**c**	0.1	3	(**1c**) 50[d]	(67)	(8)	(25)
			0.2	3	(**1c**) 53	(67)	(5)	(28)
	t-C_4H_9Br	**d**	0.1	3				(≈99)
	CH_2=$CHCH_2Br$	**e**	0.1	1	(**1e**) 43[e]	(40)	(53)	(7)
			0.2	1	(**1e**)	(42)	(47)	(11)
	$PhCH_2Cl$	**f**	0.1	2	(**1f**) 94	(99)	(1)	
	n-$C_8H_{17}Br$	**g**	0.1	2	(**1g**) 90	(96)	(4)	
Indole **2**	C_2H_5Br	**a**	0.1	2	(**2a**) 96	(≈100)		
	n-C_4H_9Br	**b**	0.1	2	(**2b**) 96	(≈100)		
	i-C_3H_7Br	**c**	0.1	3	(**2c**)	(21)	(3)	(76)
			0.2	3	(**2c**)	(18)	(2)	(80)
	t-C_4H_9Br	**d**	0.1	3				(≈99)
	CH_2=$CHCH_2Br$	**e**	0.1	1	(**2e**) 89	(92)	(8)	
			0.2	1	(**2e**) 91	(95)	(5)	
	$PhCH_2Cl$	**f**	0.1	2	(**2f**) 97	(≈100)		
	n-$C_8H_{17}Br$	**g**	0.1	2	(**2g**) 96	(≈100)		

a) All reactions were carried out with 0.1 mol of heterocycle, 0.15 mol of alkyl halide, and 0.3 mol of potassium hydroxide in PEG-400-Et_2 at 30 °C. b), c) See footnotes c) and d) in Table 1, respectively. d),e) Purities were 80 and 84% by GLC, respectively.

Table 5. *N*-Alkylation of heterocycles in PEG-400-Et_2[a]

	Alkyl halide[b]		Reaction time/h	(Product) Yield[c]/% 1-Alkylated product		Other product		
2-Methylindole **3**	C_2H_5Br	**a**	2	(**3a**) 95	(98)	d)		(2)
	$PhCH_2Cl$	**f**	2	(**3f**) 80	(84)	1,3-Dibenzyl-2-methylindole (**8**)	14	(16)
Carbazole **4**	C_2H_5Br	**a**	2	(**4a**) 92				
	n-C_4H_9Br	**b**	3	(**4b**) 93				
	CH_2=$CHCH_2Br$	**e**	2	(**4e**) 90				
	$PhCH_2Cl$	**f**	3	(**4f**) 97				
Imidazole **5**	C_2H_5Br	**a**	3	(**5a**) 94	(≈97)			
	CH_2=$CHCH_2Br$	**e**	2	(**5e**) 93	(≈97)			
	$PhCH_2Cl$	**f**	3	(**5f**) 91	(≈97)			
Benzimidazole **6**	C_2H_5Br	**a**	3	(**6a**) 93	(≈100)			
	CH_2=$CHCH_2Br$	**e**	2	(**6e**) 90	(≈97)			
	$PhCH_2Cl$	**f**	3	(**6f**) 97	(≈100)			
Benzotriazole **7**	C_2H_5Br	**a**	3	(**7a**) 35[e]	(40)	2-Ethylbenzotriazole (**9**)	51[f]	(59)
	CH_2=$CHCH_2Br$	**e**	2	(**7e**) 66[g]	(69)	2-Allylbenzotriazole (**10**)	16[h]	(24)
	$PhCH_2Cl$	**f**	3	(**7f**) 70	(78)	2-Benzylbenzotriazole (**11**)		(19)

a) All reactions were carried out with 0.05 mol of heterocycle and 0.15 mol of potassium hydroxide in 0.05 mol of PEG-400-Et_2 at 30 °C. b) In the cases of **3** and **4**, 0.075 mol of alkyl halide was used. In the cases of **5**, **6**, and **7**, 0.0525 mol of alkyl halide was used. c) Isolated yields by distillation or recrystallization. *N*-Ethyl- and *N*-allylimidazole were directly distilled from the reaction mixture. The values in parentheses were the yields determined by GLC. Unless otherwise noted, the purities of the products were >99% by GLC. d) Probably 1,3-diethyl-2-methylindole. e), f), g), and h) Purities were 94, 95, 90, and 91% by GLC, respectively.

This fact suggests that canonical structure of **14** should not be ignored.

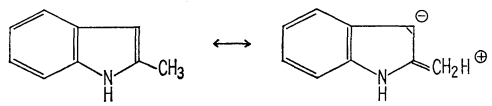

3 14

Experimental

Materials. Pyrrole, indole, carbazole, benzimidazole, imidazole, 2-methylindole, benzotriazole, and alkyl halides (reagent grade, Tokyo Kasei Kogyo Co., Ltd.) were used without further purification. PEG, benzene, and 85% potassium hydroxide (reagent grade, Kishida Kagaku Co., Ltd.) were used also without further purification. PEG-ether were prepared by the method previously reported.[14]

The physical properties of **1a,b,f**,[7] **1c**,[15] **1e**,[16] **1g**,[17] **2a, b,f**,[7] **2e**,[3] **3a**,[7] **3f**,[18] **4a,b,e,f**,[19] **5a**,[20] **5e**,[21] **5f**,[22] **6a**,[23] **6e**,[24] **6f**,[25] **7a**,[26] **7e**,[27] **7f**,[21] **9**,[26] and **10**[27] were in good agreement with those reported in the literatures. *N*-Isopropylindole (**2c**)[12] and 2-benzylbenzotriazole (**11**)[28] were not isolated and were identified by comparing GLC retention times with those of authentic samples prepared by the literature procedures. *N*-Octylindole (**2g**) had bp 131—132 °C/0.3 mmHg (1 mmHg=133.322 Pa). Found: C, 83.60; H, 10.19; N, 6.00%. Calcd for $C_{16}H_{23}N$: C, 83.79; H, 10.11; N, 6.11%. 1,3-Dibenzyl-2-methylindole (**8**) had mp 95 °C (from ethanol). Found: C, 88.98; H, 6.94; N, 4.44%. Calcd for $C_{23}H_{21}N$: C, 88.70; H, 6.80; N, 4.50%.

General Procedure of N-*Alkylation in Aqueous Potassium Hydroxide-organic Two-phase Systems in the Presence of PEG or PEG-ether as PTC.* N-*Butylpyrrole (**1b**)*: *n*-Butyl bromide (20.6 g, 0.15 mol) was added dropwise over a period of 30 min at 45 °C with vigorous stirring to a mixture of 6.7 g (0.1 mol) of pyrrole, 2.7 g (2.5 mmol) of PEG-1000-Et_2, 33.0 g (0.5 mol) of 85% potassium hydroxide, 14 g of water, and 30 ml of benzene. After the mixture had been stirred at 45 °C for further 2 h, it was cooled to room temperature. To the mixture was added 50 ml of water and then the two layers were separated. The aqueous layer was extracted with 10 ml of benzene. The benzene layer was combined with the organic layer, extracted with 3.5% hydrochloric acid (50 ml×2), washed with water (50 ml×3), and then dried. After removal of the benzene, the residue was distilled under reduced pressure, giving *N*-butylpyrrole (**1b**), 8.0 g (65%), bp 75—77 °C/28 mmHg (lit,[7] 171 °C/760 mmHg). The hydrochloric acid extract was treated according to the method previously reported,[10] giving 2.6 g (98%) of PEG-1000-Et_2.

General Procedure of N-*Alkylation in Powdered Potassium Hydroxide-organic Two-phase Systems in the Presence of PEG or PEG-ether as PTC.* N-*Benzylindole (**2f**)*: A mixture of 11.7 g (0.1 mol) of indole, 2.7 g (2.5 mmol) of PEG-1000-Et_2, 19.8 g (0.3 mol) of powdered 85% potassium hydroxide, and 30 ml of benzene was heated under reflux with vigorous stirring for 1 h. Benzyl bromide (19.0 g, 0.15 mol) was added dropwise to the mixture over a period of 30 min at 80—85 °C with vigorous stirring. After the mixture had been heated at 85 °C with vigorous stirring for 2 h, it was cooled to room temperature. To the mixture was added 50 ml of water. The mixture was worked up as described above, giving 17.2 g (83%) of *N*-benzylindole (**2f**), bp 142—144 °C/0.5 mmHg, mp 43 °C (lit,[4] 133—138 °C/0.3 mmHg, mp 42—43 °C).

General Procedure of N-*Alkylation Using Powdered Potassium Hydroxide as a Base and PEG-ether as Solvents.* N-*Allylindole (**2e**)*: A mixture of 11.7 g (0.1 mol) of indole, 46 g (0.1

mol) of PEG-400-Et_2, and 19.8 g (0.3 mol) of powdered 85% potassium hydroxide was vigorously stirred at room temperature for 30 min. Allyl bromide (18.2 g, 0.15 mol) was added dropwise over a period of 30 min at 30 °C with vigorous stirring to the mixture. After the mixture had been vigorously stirred for further 1 h, 50 ml of water was added. The two layers were separated. To the organic layer was added 100 ml of 3.5% hydrochloric acid and extracted with benzene (30 ml × 3). The benzene extract was extracted with 3.5% hydrochloric acid (50 ml × 2), washed with water and then dried. After removal of the benzene, the residue was distilled under reduced pressure, giving 14.0 g (89%) of *N*-allylindole (**2e**), bp 96—98 °C/2 mmHg (lit,[3] bp 114—116 °C/6 mmHg, 72—73 °C/0.12 mmHg). The hydrochloric acid solutions were combined, washed with 10 ml of benzene, added 40 g of sodium hydroxide, and then extracted with benzene (50 ml × 2). The benzene extract was dried and the benzene was removed to recover 45.5 g (99%) of PEG-400-Et_2.

*1-Benzylbenzimidazole (**6f**)*: A mixture of 5.9 g (0.05 mol) of benzimidazole, 23 g (0.05 mol) of PEG-400-Et_2 and 9.9 g (0.15 mol) of powdered 85% potassium hydroxide was vigorously stirred at room temperature for 30 min. Benzyl chloride (6.6 g, 0.0525 mol) was added dropwise over a period of 30 min at 30 °C with vigorous stirring to the mixture. The mixture was vigorously stirred for further 3 h at 30 °C. The reaction mixture was poured into 200 ml of 1.9% hydrochloric acid (0.104 mol). The precipitated solid was collected, washed with water, dried, and recrystallized from ethanol, giving 10.1 g (97%) of 1-benzylbenzimidazole (**6f**), mp 116—117 °C (lit,[25] mp 116—117 °C). The filtrate was washed with 10 ml of benzene and treated according to the manner used for *N*-allylindole (**2e**) to recover 22 g (96%) of PEG-400-Et_2.

The author wishes to thank Nihon Tokushu Chemical Ind. Co., Ltd. for permission to publish this article, and also Dr. Nobuaki Wada for useful suggestions during this work.

References

1) C. F. Hobbs, E. P. Papadopoulos, and C. A. Vanderwerf, *J. Am. Chem. Soc.*, **84**, 43 (1962); E. P. Papadopoulos and K. I. Y. Tabello, *J. Org. Chem.*, **33**, 1299 (1968).
2) K. T. Potts and J. E. Saxton, *Org. Synth.*, **40**, 68 (1960).
3) G. M. Rubotton and J. C. Chabala, *Org. Synth.*, **54**, 60 (1974).
4) H. Heanery and S. V. Ley, *J. Chem. Soc., Perkin Trans. 1*, **1973**, 499; *Org. Synth.*, **54**, 58 (1974).
5) C. F. Candy and R. A. Jones, *J. Org. Chem.*, **36**, 3993 (1971).
6) A. Jonczyle and M. Makosza, *Rocz. Chem.*, **49**, 1203 (1975); *Chem. Abstr.*, **84**, 30793 (1976); A. Barco, S. Benetti, G. P. Pollini, and P. G. Baraldi, *Synthesis*, **1976**, 124; V. Bocchi, G. Casnati, A. Dossena, and F. Villani, *ibid.*, **1976**, 414.
7) E. Santaniello, C. Farachi, and F. Ponti, *Synthesis*, **1979**, 617.
8) W. C. Guida and D. J. Mathre, *J. Org. Chem.*, **45**, 3172 (1980).
9) Ref. 8 and references cited therein.
10) K. Sukata, *Yuki Gosei Kagaku Kyokai Shi*, **39**, 1132 (1981).
11) R. G. Pearson and J. Songstad, *J. Am. Chem. Soc.*, **89**, 1827 (1967); *J. Org. Chem.*, **32**, 2899 (1967); T.-L. Ho, *Chem. Rev.*, **75**, 1 (1975).
12) B. Cardillo, G. Casnati, A. Pochini, and A. Rica, *Tetrahedron*, **23**, 3771 (1967).
13) L. L. Chan, K. H. Wong, and J. Smid, *J. Am. Chem. Soc.*, **92**, 1955 (1970).
14) K. Sukata, *Yuki Gosei Kagaku Kyokai Shi*, **39**, 86 (1981).
15) C. F. Candy, R. A. Jones, and P. H. Wright, *J. Chem. Soc., C*, **1970**, 2563.
16) P. A. Cantor and C. A. Vanderwerf, *J. Am. Chem. Soc.*, **80**, 970 (1958).
17) A. O. Pittet, J. V. Pascale, and D. E. Hruza, U. S. Patent 3980089 (1976).
18) Beil. 20 I, 126.
19) H. Nishi, H. Kohno, and T. Kano, *Bull. Chem. Soc. Jpn.*, **54**, 1897 (1981).
20) H. J. J. Loozen, J. J. M. Drouen, and O. Piepers, *J. Org. Chem.*, **40**, 3279 (1975).
21) R. Gassend, J. C. Maire, and J-C. Pommier, *J. Organomet. Chem.*, **133**, 169 (1977).
22) H. A. Staab and A. Mannschrock, *Chem. Ber.*, **95**, 1284 (1962); *Chem. Abstr.*, **57**, 5848 (1962).
23) Beil. 23 II, 152.
24) E. L. Ringwald and A. B. Craig, U. S. Patent 2623879 (1952); *Chem. Abstr.*, **47**, 9367 (1953).
25) A. M. Simonov, N. O. Vitkevich, and B. K. Martsokha, *Zh. Obshch. Khim.*, **30**, 3062 (1960); *Chem. Abstr.*, **55**, 16520 (1961).
26) F. Krollpfeiffer, A. Rosenberg, and C. Mühlhausen, *Justus Liebigs Ann. Chem.*, **515**, 113 (1935); *Chem. Abstr.*, **29**, 2166[1] (1935).
27) F. Krollpfeiffer, A. Rosenberg, and H. Pötz, *Ber.*, **71B**, 596 (1938); *Chem. Abstr.*, **32**, 4162[1] (1938).
28) R. Beahm, *Pharmazie*, **33**, 83 (1978).

 © 1983 The Chemical Society of Japan Bull. Chem. Soc. Jpn., 56, 285—286 (1983)

Metal-catalyzed Organic Photoreactions. The Photooxidation of Vinylsilanes and Vinyl Sulfides in the Presence of Iron(III) Chloride, and the Regioselective Synthesis of α-Chloro Ketones

Tadashi SATO,* Tamotsu TONEGAWA, Kunio NAOI, and Eigoro MURAYAMA

Department of Applied Chemistry, Waseda University, Ookubo 3, Shinjuku-ku, Tokyo 160

(Received June 26, 1982)

The irradiation of a pyridine solution of vinylsilanes or vinyl sulfides in the presence of iron(III) chloride under oxygen produced α-chloro ketones, with a carbonyl group at the olefinic carbon originally bearing a silicon or sulfur atom.

We have previously reported that the iron(III) chloride-catalyzed photooxidation of mono- or disubstituted olefin gives an α-chloro ketone (Type A), while that of tri- or tetrasubstituted olefin gives a *gem*-dichloro ketone (Type B) or an α,ω-dichloro ketone (Type C), depending upon the substitution pattern of the starting olefins.[1] The selectivity of the reaction type is generally excellent, and no products from the alternative reaction type are observed. In the Type-A reaction of unsymmetrical olefin, however, the regioselectivity is poor, and a 1:1 mixture of 2-chloro-3-octanone (**2**) and 3-chloro-2-octanone (**3**) has been obtained from 2-octene (**1**) in a total yield of 58%. In the present study, we investigated the photooxidation of vinylsilane and vinyl sulfide in order to find a way to control the regioselectivity.

Results and Discussion

Pyridine solutions of vinylsilanes or vinyl sulfides **4**—**12** containing an equivalent amount of iron(III) chloride were irradiated with Pyrex-filtered light for 1 h while oxygen was being bubbled through. The subsequent evaporation of the solvent, followed by extraction, gave α-chloro ketones or aldehyde **13**—**21** as almost exclusive products. The results are summarized in the table. The structures of the products were determined by comparison with authentic samples prepared by known methods. It is evident from the table that the carbonyl group is introduced regioselectively at the olefinic carbon originally bearing a silicon or sulfur atom in every case except the reaction from **4**, which has the trimethylsilyl group at the terminal position. The steric effect caused by the presence of the alkyl group on the ring system is not sufficient to induce the regioselectivity, as exemplified by the reaction of 3-methylcyclohexene. The product was assumed from NMR analysis to be a mixture of *cis*- and *trans*-2-chloro-3-methylcyclohexanone (**18**) and 2-chloro-6-methylcyclohexanone (**21**). The assumption was confirmed by the dehydrochlorination of the mixture with lithium chloride in *N,N*-dimethylformamide to afford a 1:1 mixture of 2- and 3-methyl-2-cyclohexenone. It was confirmed that **21** produced 2-methyl-2-cyclohexenone under dehydrochlorination conditions, presumably because of the isomerization of the primary product, 6-methyl-2-cyclohexenone.

The usefulness of these reactions as a synthetic method is demonstrated by the regioselective preparation of alkyl-substituted 2-chlorocyclohexanones from appropriate vinylsilanes or vinyl sulfides. The requisite vinyl compounds have been conveniently prepared from the appropriate ketones either by an acid-actalyzed reaction with thiols[2] or by a modified Shapiro reaction.[3] These alkyl-substituted 2-chlorocyclohexanones have also been prepared by other methods,[4,5] but the regioselectivity is not as high as that observed in the present study. The diastereoselectivity concerning the alkyl group and chlorine atom was not attained because the α-chloro ketones underwent a *cis-trans* isomerization under the present reaction conditions.

As for the reaction mechanism of the iron(III) chloride-catalyzed photooxidation of olefin, we have proposed a reaction scheme involving a photoinduced interligand electron transfer (long-range electron transfer), followed by a chlorine and oxygen attack on the double bond.[1a] We assumed that the same type of reaction proceeds in the present case and that the chlorine atom produced by the long-range electron transfer attacks the double bond in such a way as to produce a radical stabilized by a silicon or sulfur atom. The succeeding attack by the oxygen-radical anion, followed by protonation, produces a hydroperoxide **23**, which then affords the observed product. The isolated by-product was either *S*-methyl methanethiosulfonate, *S*-ethyl ethanethiosulfonate, or diphenyl disulfide, depending on the substituent (methyl, ethyl, or phenyl respectively) on the sulfur atom of the starting vinyl sulfide. The poor regioselectivity in the case of vinylsilane **4** suggests that the stabilizing effect of the trimethylsilyl group for the α-radical is comparable to that of the alkyl group. However, it seems that the sulfur atom stabilizes the α-radical more effectively than the methyl group, as is indicated by the formation of a single product **17** from vinyl sulfide **8**.

Experimental

Starting Materials. 1-Trimethylsilyl-(*Z*)-1-octene (**4**) was prepared from 1-trimethylsilyl-1-octyne by hydroboration, followed by protonolysis.[6] Vinylsilanes **5**, **6**, **7a**, and **12a** were prepared from the corresponding tosylhydrazones and chlorotrimethylsilane according to the reported method.[7] In a similar way, vinyl sulfide **12b** was prepared from 2-methylcyclohexanone tosylhydrazone and dimethyl disulfide in a 51% yield. **12b**: IR, 3040, 2920, 1620, 1435, 1335, 995, and 790 cm^{-1}; NMR, δ 1.22 (3H, d, J=8 Hz), 1.5—2.0 (4H, m), 2.31 (3H, s), 2.0—2.6 (3H, m), and 5.60 (1H, t, J=4 Hz). Vinyl sulfides **7b**, **7c**, **8**, and **10b** were prepared from the corresponding cyclohexanones and thiols, using *p*-toluenesulfonic acid or titanium(IV) chloride–triethylamine as a catalyst, according to the previously reported method.[2] Vinyl sulfides **9** and **11** were prepared from the

tosylhydrazone of 2-methylcyclohexanone or of 4-methylcyclohexanone respectively by utilizing a modified Shapiro reaction, according to the previously reported method.[3]

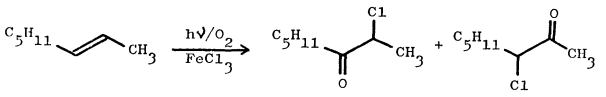

1 **2** **3**

Table 1. Products and yields of the photooxidation of vinyl silanes or vinyl sulfides

Starting material	Product	Yield/%
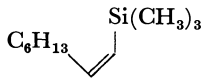 **4**	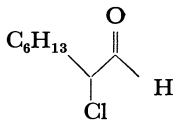 **13**	6
	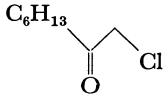 **14**	9
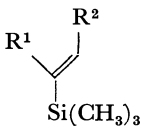 **5** $R^1=C_6H_{13}$, $R^2=H$	**14**	41
6 $R^1=C_3H_7$, $R^2=C_2H_5$	**15**	67
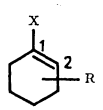 **7** R=H, a: $X=Si(CH_3)_3$; b: $X=SC_6H_5$; c: $X=SC_2H_5$	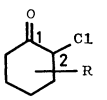 **16**	72; 58; 53
8 $R=2\text{-}CH_3$, $X=SC_6H_5$	**17**	50
9 $R=3\text{-}CH_3$, $X=SCH_3$	**18**	*cis* 32; *trans* 13
10 $R=4\text{-}CH_3$, a: $X=Si(CH_3)_3$; b: $X=SC_2H_5$	**19**	*cis* 28; *trans* 36; *cis* 3; *trans* 31
11 $R=5\text{-}CH_3$, $X=SCH_3$	**20**	*cis* 32; *trans* 8
12 $R=6\text{-}CH_3$, a: $X=Si(CH_3)_3$; b: $X=SCH_3$	**21**	*cis* 38; *trans* 38; *cis* 22; *trans* 22

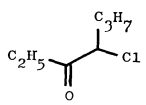

22

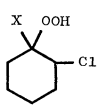

23

X=SR or SiR_3

Photooxidation. The irradiation was carried out on a solution of vinylsilane or vinyl sulfide (10 ml, 0.025 M)† containing an equivalent molar amount of iron(III) chloride; it was done in Pyrex tubes for 30 min or 60 min while oxygen gas was being bubbled through. A high-pressure mercury lamp [Ushio UM 452 (450 W)] was used as the light source. The irradiated solution was worked up by either of the following two ways. Work-up I: The solvent was removed *in vacuo*, and the reaction product was extracted with carbon tetrachloride or dichloromethane from the residue. The extract was passed through a short column of Florisil, and the eluate was concentrated *in vacuo*. The material thus obtained was analyzed directly by GLC or NMR techniques. 1,1,2,2-Tetrachloroethane was used as an internal reference for the NMR analysis. Work-up II: The pyridine solution after the irradiation was neutralized with 4 M hydrochloric acid and shaken with chloroform or dichloromethane. The extract was dried over sodium sulfate, and the solvent was removed *in vacuo*. The residue was analyzed as above.

In all cases except the reaction of **10**, each product was isolated in a pure form on preparative GLC or TLC; the spectroscopic data and retention time on a GLC were compared with those of authentic samples prepared by known methods: **13**,[8] **14**,[1b] **15**,[9] **16**,[1b] **17**,[5b] **18**,[5a] **19**,[4] **20**,[5a] and **21**.[5b] The spectroscopic data of **13** and **15** are as follows: **13**: IR, 2950, 2925, 2855, 2710, 1733, 1470, 1380, and 785 cm^{-1}; NMR δ 0.88 (3H, dist. t), 1.1—1.6 (8H, m), 1.7—2.0 (2H, m), 4.03 (1H, dt, J=6 and 2 Hz), and 9.48 (1H, d, J=2 Hz); **15**: IR, 2960, 2875, 1715, 1460, and 785 cm^{-1}; NMR δ 0.95 (3H, t, J=8 Hz), 1.03 (3H, t, J=8 Hz), 1.4—2.1 (4H, m), 2.62 (2H, t, J=7 Hz), and 3.93 (1H, t, J=7 Hz).

The spectroscopic and GLC analyses of **19** were carried out and the results compared with those of an authentic sample as a mixture of *cis*- and *trans*-isomers.[4]

References

1) a) E. Murayama, A. Kohda, and T. Sato, *J. Chem. Soc., Perkin Trans. 1*, **1980**, 947; b) A. Kohda, K. Ueda, and T. Sato, *J. Org. Chem.*, **46**, 509 (1981); c) A. Kohda and T. Sato, *J. Chem. Soc., Chem., Commun.*, **1981**, 951; d) T. Sato, K. Maemoto, and A. Kohda, *ibid.*, **1981**, 1116.

2) T. Mukaiyama and K. Saigo, *Chem. Lett.*, **1973**, 479.

3) T. Nakai and T. Mimura, *Tetrahedron Lett.*, **1979**, 531.

4) R. MacDonald and T. E. Tabor, *J. Am. Chem. Soc.*, **89**, 6573 (1967).

5) a) F. M. Lasdovics and E. M. Schulman, *J. Am. Chem. Soc.*, **99**, 6672 (1977); b) F. M. Laskovics and E. M. Schulman, *Tetrahedron Lett.*, **1977**, 759.

6) E. C. Ashby and S. R. Noding, *J. Organomet. Chem.*, **177**, 117 (1979).

7) L. A. Paquette, W. E. Fristad, D. S. Dime, and T. R. Bailey, *J. Org. Chem.*, **45**, 3017 (1980).

8) E. Elkik, *Bull. Soc. Chim. Fr.*, **1968**, 283.

9) J. Metzger and B. Koether, *Ann. Univ. Saraviensis I*, **1952**, 151; *Chem. Abstr.*, **47**, 10524 (1953).

† 1 M=1 mol dm^{-3}.

 © 1983 The Chemical Society of Japan Bull. Chem. Soc. Jpn., 56, 295—297 (1983)

Alcoholysis Equilibria of Dialkoxydimethylsilanes Catalyzed by Iodine or Iodine Monobromide

Katsuko Ito and Takeshi Ibaraki*

Department of Natural Science, Osaka Women's University, Daisen-cho, Sakai, Osaka 590

(Received July 29, 1982)

Iodine or iodine monobromide was found to be an especially favorable catalyst for the study of the alcoholysis equilibria of dialkoxydimethylsilanes by gas chromatography. Iodine monobromide was employed to promote the reactions associated with tertiary alcohols, and iodine was used for the other reactions. Eight alcohols were allowed to react with diethoxydimethylsilane, and successive equilibrium constants, K_1 and K_2, were determined at 20 °C. K_1=2.36—2.75 and K_2=0.66—0.69 (by the use of primary alcohols), K_1=1.34—1.38 and K_2=0.28—0.30 (secondary alcohols), and K_1=0.15—0.16 (tertiary alcohols) were observed. These values express precisely the difference of reactivities of the three groups of alcohols with diethoxydimethylsilane. Out of the dialkoxydimethylsilanes used in this study, eight unreported compounds were isolated and characterized.

For alcoholysis or disproportionation of alkoxysilanes, iodine and interhalogen compounds such as iodine monobromide exhibit excellent catalytic action.[1,2] These catalysts lead such reaction systems readily to equilibrium even at ordinary temperature; the reaction mixtures with the catalyst can be satisfactorily analyzed by gas chromatography.

Alcoholysis of diethoxydimethylsilane[3-6] and the other alkoxysilanes has been well studied. However, the equilibrium constants of these reactions can not be found in the literature, although a few quantitative studies of disproportionation equilibria of alkoxysilanes have been reported.[7-9]

Thus, the alcoholysis equilibria of alkylalkoxysilanes catalyzed by iodine or iodine monobromide were investigated, and the equilibrium constants of these reactions were determined. This paper presents the alcoholysis equilibrium data of dialkoxydimethylsilanes at 20 °C, following the previous report on the alcoholyses of alkoxytriethylsilanes.[2]

The reactivities of alcohols to alkoxysilanes are considered in the order of primary>secondary>tertiary,[10,11] and the alcoholysis equilibrium constants of alkoxytriethylsilanes have been found to follow this order.[2] The difference in alcohol reactivities may be revealed more distinctly by the data of dialkoxydimethylsilanes, as the two alkoxyl groups should be exchanged in these cases.

Experimental

General Procedure. Given amounts of dialkoxydimethylsilane and alcohol were placed in a 5-cm^3 reaction vessel. Molar ratios of alcohols to alkoxysilanes in the reaction mixtures were in the range of about 0.7 to 5.1. Iodine or iodine monobromide was added to the reaction mixtures as the solution in each alcohol.

Each reaction associated with primary and secondary alkoxyl groups was promoted by iodine. Three directions were investigated:

A-series: $Me_2Si(OEt)_2$ + ROH ⟶

B-series: $Me_2Si(OEt)(OR)$ + ROH or EtOH ⟶

C-series: $Me_2Si(OR)_2$ + EtOH ⟶

Equilibrium compositions were ascertained by GLPC, from which data K_1 and K_2 values were estimated.

As the pure di-*t*-butoxydimethylsilane and dimethyldi-*t*-pentyloxysilane could not be isolated, the reactions associated with *t*-alkoxyl groups were examined for A- and B-series, and only K_1 values were determined. In this case, iodine monobromide was employed to accelerate the reactions. Each reaction mixture was divided into two or three parts and maintained in a thermostat setting at (20.0± 0.1) °C. One of them was used to monitor the time course of the reaction until the composition became constant, and then the others were used to determine the equilibrium compositions.

Analysis. Analyses were performed by GLPC using a Shimadzu model GC-4B gas chromatograph with a thermal conductivity detector. The packings with the following stationary phases were used. PEG 4000+PEG 6000 (ROH: Bu^nOH), PEG 1000+SPAN 80 (Bu^iOH, Bu^sOH), SPAN 80 (Bu^tOH), PEG 1000 ($C_5H_{11}{}^nOH$, $C_5H_{11}{}^tOH$), PEG 4000 ($MePr^nCHOH$, Et_2CHOH).

Reagents. Diethoxydimethylsilane was prepared by the reaction of octamethylcyclotetrasiloxane with tetraethoxysilane in the presence of potassium hydroxide.[14] The other alkoxysilanes were prepared by iodine or iodine monobromide-catalyzed alcoholysis of diethoxydimethylsilane. After the resulting ethanol and excess alcohol were removed by distillation, each alkoxysilane was obtained by fractional distillation.

Ethoxydimethyl-*t*-pentyloxysilane was purified by means of GLPC fractional elution, employing a Shimadzu model GC-5A gas chromatograph, equipped with a model APP-5 autofraction collector. A stainless column (6 mm ϕ × 4.5 m) containing 25% PEG 1000 on Chromosorb P was used. The other dialkoxydimethylsilanes were purified by repeated fractional distillation.

The fifteen dialkoxydimethylsilanes mentioned below were prepared and characterized by ^{13}C NMR, MS, and elemental analyses. As eight of these were unreported compounds, their boiling points, refractive indices, and analytical data are added. Di-*t*-alkoxydimethylsilanes were detected by GC-MS in the reaction mixtures, but the contents were too small to isolate.

$Me_2Si(OEt)_2$, $Me_2Si(OBu^n)_2$, $Me_2Si(OBu^s)_2$, $Me_2Si(OBu^t)_2$, $Me_2Si(OC_5H_{11}{}^n)_2$, $Me_2Si(OEt)(OBu^n)$, $Me_2Si(OEt)(OBu^s)$.

$Me_2Si(OEt)(OBu^t)$: bp 146.5 °C; n_D^{20} 1.3923; ^{13}C NMR (neat) δ=−3.83(q, 2C), 17.92(q), 18.46(q, 2C), 30.38(d), 57.35(t), 68.58(t). Found: C, 54.49%; H, 11.57%. Calcd for $C_8H_{20}O_2Si$: C, 54.52%; H, 11.44%. $Me_2Si(OEt)(OBu^t)$: 135.0 °C; 1.3905; δ=1.05 (q, 2C), 17.85(q), 31.35(q, 3C), 57.00(t), 71.51(s). Found: C, 54.49%; H, 11.47%. Calcd: C, 54.52%; H, 11.44%. $Me_2Si(OEt)(OC_5H_{11}{}^n)$: 175.2 °C; 1.4016; δ=3.75(q, 2C), 13.58(q), 17.97(q), 22.21(t), 27.82

Table 1. Alcoholysis equilibrium constants of dialkoxydimethylsilanes at 20 °C

$Me_2Si(OEt)_2 + ROH \rightleftharpoons Me_2Si(OEt)(OR) + EtOH$

$K_1 = \{[Me_2Si(OEt)(OR)][EtOH]\}/\{[Me_2Si(OEt)_2][ROH]\}$

$Me_2Si(OEt)(OR) + ROH \rightleftharpoons Me_2Si(OR)_2 + EtOH$

$K_2 = \{[Me_2Si(OR)_2][EtOH]\}/\{[Me_2Si(OEt)(OR][ROH]\}$

ROH		Equilibrium constants K_1 and K_2			
		Reaction system[a]			Mean value of all kinds
		A-series	B-series	C-series	
Bu^nOH	K_1:	2.48±0.05	2.48±0.04	2.51±0.04	2.49±0.04
	K_2:	0.68±0.01	0.68±0.01	0.70±0.02	0.68±0.02
Bu^iOH	K_1:	2.76±0.03	2.75±0.03	2.74±0.02	2.75±0.03
	K_2:	0.69±0.01	0.69±0.01	0.70±0.01	0.69±0.01
Bu^sOH	K_1:	1.34±0.02	1.34±0.03	1.34±0.05	1.34±0.03
	K_2:	0.28±0.01	0.28±0.02	0.29±0.01	0.28±0.01
Bu^tOH	K_1:	0.150±0.008	0.146±0.005		0.148±0.006
$C_5H_{11}{}^nOH$	K_1:	2.34±0.05	2.37±0.02	2.38±0.03	2.36±0.04
	K_2:	0.67±0.02	0.66±0.02	0.66±0.01	0.66±0.02
$MePr^nCHOH$	K_1:	1.43±0.04	1.44±0.04	1.43±0.04	1.43±0.04
	K_2:	0.30±0.01	0.30±0.01	0.30±0.02	0.30±0.01
Et_2CHOH	K_1:	1.37±0.04	1.38±0.02	1.38±0.04	1.38±0.03
	K_2:	0.29±0.01	0.29±0.01	0.29±0.01	0.29±0.01
$C_5H_{11}{}^tOH$	K_1:	0.157±0.008	0.154±0.007		0.156±0.007

a) Equilibrium constants were determined for the reaction systems with one of three different starting dimethyldialkoxysilanes: A: $Me_2Si(OEt)_2$ B: $Me_2Si(OEt)(OR)$ C: $Me_2Si(OR)_2$

(t), 32.11(t), 57.39(t), 61.93(t). Found: C, 56.75%; H, 11.83%. Calcd for $C_9H_{22}O_2Si$: C, 56.79%; H, 11.65%. $Me_2Si(OEt)(OCHMePr^n)$: 166.4 °C; 1.3990; $\delta=-3.02$(q, 2C), 13.63(q), 17.97(q), 18.60(q), 23.31(q), 41.64(t), 57.35 (t), 67.71(d). Found: C, 56.71%; H, 11.85%. Calcd: C, 56.79%; H, 11.65%. $Me_2Si(OEt)(OCHEt_2)$: 165.8 °C; 1.4012; $\delta=3.24$(q, 2C), 9.09(q, 2C), 17.82(q), 28.96(t), 57.22(t), 74.36(d). Found: C, 56.60%; H, 11.80%. Calcd: C, 56.79%; H, 11.65%. $Me_2Si(OEt)(OC_5H_{11}{}^t)$: 156 °C; 1.3998; $\delta=-0.80$(q, 2C), 8.26(q), 18.07(q), 28.84(q, 2C), 37.03(t), 57.32(t), 73.99(s). Found: C, 56.45%; H, 11.85%. Calcd: C, 56.79%; H, 11.65%. $Me_2Si(OCHMePr^n)_2$: 206.5 °C; 1.4092; $\delta=2.19$(q, 2C), 13.73(q, 2C), 18.60(t, 2C), 23.36(q, 2C), 41.69(t, 2C), 67.71(d, 2C). Found: C, 61.62 %; H, 12.33%. Calcd for $C_{12}H_{28}O_2Si$: C, 62.01%; H, 12.14%. $Me_2Si(OCHEt_2)_2$: 205.2 °C; 1.4139; $\delta=-1.97$(q, 2C), 9.36(q, 4C), 29.14(t, 4C), 74.56(d, 2C). Found: C, 61.66%; H, 12.36%. Calcd: C, 62.01%; H, 12.14%.

Alcohols, iodine, and iodine monobromide were purified by methods similar to those previously reported.[1,2]

Results and Discussion

The following successive equilibrium constants were determined at 20 °C.

$Me_2Si(OEt)_2 + ROH \rightleftharpoons Me_2Si(OEt)(OR) + EtOH$

$K_1 = \{[Me_2Si(OEt)(OR)][EtOH]\}/\{[Me_2Si(OEt)_2][ROH]\}$

$Me_2Si(OEt)(OR) + ROH \rightleftharpoons Me_2Si(OR)_2 + EtOH$

$K_2 = \{[Me_2Si(OR)_2][EtOH]\}/\{[Me_2Si(OEt)(OR)][ROH]\}$

The following alcohols were examined in this study:

ROH: Bu^nOH, Bu^iOH, Bu^sOH, Bu^tOH, $C_5H_{11}{}^nOH$, $MePr^nCHOH$, Et_2CHOH, $C_5H_{11}{}^tOH$.

The reactions were well-promoted in the presence of about 0.1 mol% catalyst (iodine or iodine monobromide), and in most cases the reactions attained equilibrium within several hours.

To make sure that the equilibrium compositions can be determined by means of GLPC even in the presence of the catalyst, a test similar to the previous study[1] was attempted. A reaction mixture, $Me_2Si(OEt)_2$–Bu^nOH (I_2), was divided into two parts, one of which was treated with silver powder to remove the catalyst from the reaction system,[15] while the other was left untreated; the compositions of both samples were determined by GLPC at about one hour intervals. In the latter case, the reaction proceeded to equilibrium, and $K_1=2.45$, $K_2=0.69$ were observed. In the former case, $\{[Me_2Si(OEt)(OBu^n)][EtOH]\}/\{[Me_2Si(OEt)_2]-[Bu^nOH]\}=1.27$, 1.33, 1.31, and $\{[Me_2Si(OBu^n)_2]-[EtOH]\}/\{[Me_2Si(OEt)(OBu^n)][Bu^nOH]\}=0.31$, 0.33, 0.30, proving that the reaction practically stopped due to silver-treatment. Moreover, a similar test was undertaken for the equilibrium mixture, and it was confirmed that the equilibrium did not shift during GLPC analysis even in the presence of the catalyst.

Each reaction was carried out from two or three directions as mentioned above, but the resulting equilibrium constants agreed very well with each other; the data are summarized in Table 1.

The K_1 and K_2 values are close to 2 and 0.5, when both alkoxyl groups have about the same binding ability to silicon and both alcohols have similar reactivity.

In case ROH are primary alcohols, *i.e.* Bu^nOH, Bu^iOH, $C_5H_{11}{}^nOH$, $K_1=2.36$—2.75 and $K_2=0.66$—0.69; these values are somewhat larger than those described above.

However, in the case of the reaction systems associated with secondary alkoxyl groups, K_1 and K_2

are smaller than the above values. $K_1=1.34$, $K_2=0.28$ (ROH:Bu^{s}OH); $K_1=1.43$, $K_2=0.30$ (MePr^{n}CHOH); $K_1=1.38$, $K_2=0.29$ (Et_2CHOH). Therefore, secondary alcohols seem to be less reactive to diethoxydimethylsilane than primary alcohols.

Tertiary alcohols are still more inactive than secondary alcohols,[10-13] and so the observed K_1 values of the reactions involving tertiary alcohols are fairly small, *i.e.* 0.148 (ROH:Bu^{t}OH) and 0.156 ($C_5H_{11}{}^tOH$).

As it was impossible to obtain the GLPC calibration curves of the di-*t*-alkoxydimethylsilanes, because of the inaccessibility of the pure sample, the accurate K_2 values could not be evaluated. But these values are estimated to be about 0.005 or below, when the slope of the calibration curves are inferred from analogy with the other alkoxysilanes. Such small values suggest that the di-*t*-alkoxysilanes are especially unstable, based on the steric repulsion between the two *t*-alkoxyl groups.

As described above, the K_1 and K_2 values of the reaction systems associated with primary, secondary, and tertiary alkoxyl groups decrease in this order, and these values reflect clearly the extent of the binding abilities of alkoxyl groups to silicon.

The catalytic function of iodine or iodine monobromide may also be illustrated by a mechanism *via* a four-centered transition state analogous to that previouly proposed.[1,2] Iodine or iodine monobromide forms charge transfer complexes with alcohols, and also with alkoxysilanes, and the dative forms of these complexes, *e.g.* $[ROH\cdots I]^+I^-$ or $[Me_2Si(OR)_2\cdots I]^+I^-$, seem to make up the above transition state.

The authors wish to thank professor Toshiyuki Shono of Osaka University and his co-workers for the elemental analyses and for the NMR and mass spectral data.

References

1) T. Ibaraki and K. Ito, *Bull. Chem. Soc. Jpn.*, **54**, 3235 (1981).
2) K. Ito and T. Ibaraki, *Bull. Chem. Soc. Jpn.*, **55**, 2973 (1982).
3) R. H. Krieble and C. A. Burkhard, *J. Am. Chem. Soc.*, **69**, 2689 (1947).
4) J. L. Speier, *J. Am. Chem. Soc.*, **74**, 1003 (1952).
5) E. Larsson, *Chem. Ber.*, **86**, 1382 (1953).
6) E. Larsson, *Acta Chem. Scand.*, **8**, 898 (1954).
7) K. Moedritzer and J. R. Van Wazer, *Inorg. Chem.*, **3**, 268 (1964).
8) J. R. Van Wazer and K. Moedritzer, *J. Inorg. Nucl. Chem.*, **26**, 737 (1964).
9) D. N. Dolan and G. Nickless, *J. Chromatogr.*, **37**, 1 (1968).
10) M. G. Voronkov and L. A. Zhagata, *J. Gen. Chem. USSR*, **37**, 2630 (1967).
11) B. N. Dolgov, N. P. Kharitonov, and M. G. Voronkov, *J. Gen. Chem. USSR*, **24**, 1169 (1954).
12) D. Ridge and M. Todd, *J. Chem. Soc.*, **1949**, 2637.
13) S. Friedman and M. L. Kaufman, *Anal. Chem.*, **38**, 144 (1966).
14) M. G. Voronkov, *J. Gen. Chem. USSR*, **29**, 890 (1959).
15) W. T. Grubb and R. C. Osthoff, *J. Am. Chem. Soc.*, **77**, 1405 (1955).

Asymmetric Reduction of Chiral Pyruvamide with Sodium Borohydride

Toratane MUNEGUMI and Kaoru HARADA*

Department of Chemistry, University of Tsukuba, Sakura-Mura, Niihari, Ibaraki 305

(Received August 2, 1982)

Several amides of pyruvic acid with (*S*)-amines were reduced with sodium borohydride (NBH) in several alcohols and *N*-[(*R*)-lactoyl]-(*S*)-amines were obtained in excess. When the reductions were carried out in methanol or ethanol in the presence of metallic salt, *N*-[(*S*)-lactoyl]-(*S*)-amines were obtained in asymmetric yields up to 22%.

Many studies[1-4] on the homogeneous reduction of chiral esters of α-keto acids have been performed, while few studies[4] on that of chiral α-keto acid amides have been reported. In the former case, an empirical rule was found between the absolute configuration of the chiral source and that of the product. This rule is called the Prelog's rule[2] and has been applied to the determination of the absolute configuration of chiral alcohols. In the latter, enough data have not been obtained to establish such a rule. The reduction of *N*-[(*S*)-α-methylbenzyl]benzoylformamide with sodium borohydride (NBH) was carried out by Mitsui and Kanai,[4] and (*R*)-mandelic acid was obtained in optical purity of 5.1%. According to the stereochemical consideration using a molecular model of the substrate, it seems unlikely that the benzoyl and the carbamoyl group coexist on the same plane, because of the steric repulsion between the phenyl and the carbamoyl group. In such a case the discussion on the steric course of the NBH reduction is more difficult compared with that of the esters.

In this paper, the NBH reduction of chiral amides of pyruvic acid, in which the above-stated steric repulsion is smaller than that of benzoylformamide, is described. The chiral amines used are (*S*)-α-methylbenzylamine, (*S*)- and (*R*)-α-ethylbenzylamine, and (*S*)- and (*R*)-1-(1-naphthyl)ethylamine. The substrates **2a**—**c** and **2b′**—**c′** were prepared by the condensation of the chiral amines and pyruvic acid with dicyclohexylcarbodiimide and *N*-hydroxysuccinimide (Fig. 1). The solvent used in the NBH reduction were methanol, ethanol, 2-propanol, *t*-butanol. The chemical and asymmetric yields of the products were determined by gas chromatographic analysis. The reduction of the substrate was also carried out in methanol and ethanol in the presence of a metallic salt.

Experimental

All the melting points were uncorrected. Optical rotations were measured with a JASCO DIP-181 Digital Polarimeter. All the GC analyses were carried out with a Hitachi 163 gas chromatograph, and the peaks on the chromatogram were integrated with a Hitachi 834-30 chromatoprocessor.

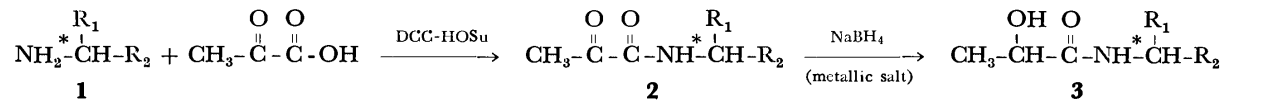

1

1a: $R_1=CH_3$, $R_2=Ph$ (*S*)
1b: $R_1=C_2H_5$, $R_2=Ph$ (*S*)
1b′: $R_1=C_2H_5$, $R_2=Ph$ (*R*)
1c: $R_1=CH_3$, $R_2=Naph$ (*S*)
1c′: $R_1=CH_3$, $R_2=Naph$ (*R*)

2

2a: $R_1=CH_3$, $R_2=Ph$ (*S*)
2b: $R_1=C_2H_5$, $R_2=Ph$ (*S*)
2b′: $R_1=C_2H_5$, $R_2=Ph$ (*R*)
2c: $R_1=CH_3$, $R_2=Naph$ (*S*)
2c′: $R_1=CH_3$, $R_2=Naph$ (*R*)

3

3a: $R_1=CH_3$, $R_2=Ph$ (*S*)
3b: $R_1=C_2H_5$, $R_2=Ph$ (*S*)
3b′: $R_1=C_2H_5$, $R_2=Ph$ (*R*)
3c: $R_1=CH_3$, $R_2=Naph$ (*S*)
3c′: $R_1=CH_3$, $R_2=Naph$ (*R*)

Fig. 1. (*S*) or (*R*): Absolute configuration of chiral amine. **3a**—**c** and **3b′**—**c′**: Diastereomer mixture.

TABLE 1. ELEMENTARY ANALYSES OF THE SUBSTRATES

Substrate	Yield %	Mp θ_m/°C	Optical rotation (ethanol)		Elementary analysis C (%)	H (%)	N (%)
2a	16	76—77	$[\alpha]_D^{16}$ −116° (*c* 1.0)	Found	69.91	6.85	7.31
				Calcd ($C_{11}H_{13}NO_2$)	69.09	6.85	7.32
2b	16	84.5—85.5	$[\alpha]_D^{14}$ −117° (*c* 1.0)	Found	70.31	7.32	6.80
				Calcd ($C_{12}H_{15}NO_2$)	70.22	7.36	6.82
2b′	19	84—85	$[\alpha]_D^{18}$ +122° (*c* 1.1)	Found	70.29	7.40	6.80
				Calcd ($C_{12}H_{15}NO_2$)	70.22	7.36	6.82
2c	33	(Oil)	$[\alpha]_D^{24}$ −3.6° (*c* 1.0)	Found	73.94	6.30	5.88
				Calcd ($C_{15}H_{15}NO_2$)	74.66	6.26	5.80
2c′	29	(Oil)	$[\alpha]_D^{18}$ +3.1° (*c* 1.0)	Found	74.20	6.61	6.09
				Calcd ($C_{15}H_{15}NO_2$)	74.66	6.26	5.80

Table 2. Retention times of O-TFA lactamides

Lactamide	Retention time/min		Separation factor
	First peak	Second peak	
3a	13.2(*R,S*)[a]	13.8(*S,S*)	1.045
3b′	16.8(*R,R*)	17.6(*S,R*)	1.017
3c′	28.8(*R,R*)	29.1(*S,R*)	1.010

a) ( ): Configuration of diastereomeric lactamide.

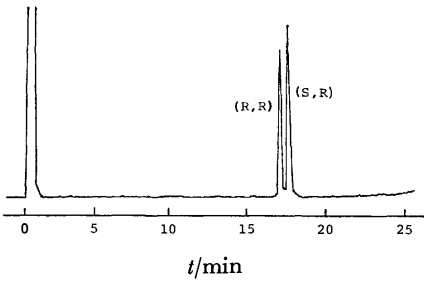

Fig. 2. Typical gas chromatographic peaks of O-TFA derivatives of lactamide **3b′**.

N-[(S)-α-Methylbenzyl]pyruvamide(2a) and Other Substrates 2b—c and 2b′—c′. To a cooled ethyl acetate solution (200 ml), in which pyruvic acid(5.00 g, 0.0567 mol), (*S*)-α-methylbenzylamine(6.87 g, 0.0567 mol), and *N*-hydroxylsuccinimide(7.84 g, 0.0681 mol) were dissolved, dicyclohexylcarbodiimide(12.9 g, 0.0624 mol) was added. The reaction mixture was stirred for 2 h at 0 °C and for 12 h at room temperature and filtered. The filtrate was extracted with three 100 ml portions of 1 mol dm^{-3} HCl, three 100 ml portions of an aquous $NaHCO_3$ solution(10%), and three 100 ml portions of a saturated aquous NaCl solution. The ethyl acetate layer was dried with anhydrous magnesium sulfate. The solvent was removed *in vacuo*, and a crude oily product was obtained. This product was purified by means of silica gel flash chromatography[5] (column: 15 cm×4 cm i.d., eluting solvent: ethyl acetate-hexane(1:5)).

The other four pyruvamide were prepared in a similar method. The optical rotations, elementary analyses, yields and melting points of the products are summarized in Table 1.

NBH Reduction of the Substrates 2a—c and 2b′—c′ without Metallic Salt. Substrates **2a—c** and **2b′—c′** (20 mg, 1×10^{-4} mol) were dissolved in a solvent(methanol, ethanol, isopropanol, and *t*-butanol), and were reduced by NBH (10 mg, 2.6×10^{-4} mol) at 30 °C for 90 min. After the reduction was over, the boron complex was decomposed by addition of 1 mol dm^{-3} HCl (2 ml). An aquous solution (20 ml) of saturated sodium chloride was added in the reaction mixture, and the resulted solution was extracted by three 20 ml portions of ethyl acetate. After drying the ethyl acetate layer, the solvent was removed and an oily product was obtained. Both the reaction yield and the ratio of each diastereomer were determined by gas chromatography.

NBH Reduction of Substrate 2a—c and 2b′ with Metallic Salt. The NBH reduction with a metallic salt(magnesium chloride or zinc chloride) was carried out by addition of NBH (10 mg, 2.6×10^{-4} mol) to 3 ml of a methanol or an ethanol solution of the substrate(20 mg, 1×10^{-4} mol) and the metallic salt(1×10^{-4} mol). The amount of the metallic salt in the reaction mixture of the substrate **2b′** was changed from 10 mg (1×10^{-4} mol) to 100 mg(1×10^{-3} mol). The reaction conditions, the work-up of the reaction mixture, and the analysis of the product was carried out in a similar manner as in the reduction without metallic salt.

Determination of the Reaction Yield. The oily product obtained by reduction was redissolved in chloroform(0.5 ml), and a part of the solution was injected into a gas chromatograph with a stainless column(4 m×3 mm i.d.), which was filled with Chromosorb W AW DMCS coated with 5% SE-52. Column temperature was raised from 100 °C to 250 °C at a rate of 5 °C per minute. The flow rate of carrier gas(nitrogen) was 39 ml/min and the temperature of injection port was 300 °C. The detector was flame-ionization detector.

Determination of the Diastereoisomeric Purity. TMS-Im Method:[6] Ten seconds after the injection of the pyridine solution of *N*-trimethylsilylimidazole, a 3 μl portion of the chloroform solution of the product was applied into the gas chromatograph equipped with the same column(SE-52) as described in the previous section. The column temperature was raised from 100 °C to 250 °C at a rate of 2 °C per minute. The other analytical conditions were same as those of the determination of the chemical yield. The diastereomeric lactamides were separated, and the diastereoisomeric purity was determined from the ratio of the integrated values of the diastereomeric peaks. This TMS-Im method was applied to the analyses of the entries 1—4, 6—9, 12—20, and 26—28.

TFA Method: To the NBH reduction product, trifluoroacetic acid (3 ml) saturated with HCl was added, and the resulting solution was refluxed for 15 min. The residue obtained by the evaporation of trifluoroacetic acid was redissolved in chloroform. The chloroform solution was injected into the gas chromatograph equipped with a glass capillary column(25 m×0.3 mm i.d.) coated with a chiral stationary phase, Chirasil-Val.[7] The O-TFA derivatives of the two diastereomers of each lactamide were separated on the chromatogram. The column temperature was raised from 90 °C to 180 °C at 4 °C per minute. The temperature of the injection port was 250 °C. This method was applied to the analyses of the reactions of entries 5, 10, 11, and 21—25 in Table 3 or 4. The retention times of O-TFA derivatives of the diastereomeric lactamides(**3a**, **3b′**, and **3c′**) are summarized in Table 2, and typical chromatographic peaks of O-TFA derivatives of lactamide **3b′** are shown in Fig. 2. The analyzed asymmetric yields were found to be similar by both TMS-Im and TFA methods.

Results and Discussion

The results of the NBH reduction without and with a metallic salt are shown in Tables 3 and 4, respectively.

In the NBH reduction without metallic salt, *N*-[(*R*)-lactoyl]-(*S*)-amine ((*R,S*)-lactamide) was obtained in excess over *N*-[(*S*)-lactoyl]-(*S*)-amine ((*S,S*)-lactamide) from the pyruvamide in which the chiral source was (*S*)-amine. The asymmetric yields were equal to or less than 11%, and substrate **2a** gave the lowest values. In the NBH reduction with metallic salts, the substrate in which the chiral source was (*S*)-amine gave (*S,S*)-lactamide in excess. Thus, the configuration of the lactoyl moiety of the resulting lactamide was reversed to the opposite structure in the reduction with metallic salts. When magnesium chloride was added to the reaction mixture, the asymmetric yield of (*R,R*)-lactamide increased with the increase of the concen-

TABLE 3. NBH REDUCTION WITHOUT METALLIC SALT

Entry	Substrate	Configuration[a]	Solvent	Yield/%	*Dp*/%[b]	Configuration[c]
1	**2a**	*S*	MeOH	39	0	
2	**2a**	*S*	EtOH	45	1	*R*
3	**2a**	*S*	*i*-PrOH	40	0	
4	**2a**	*S*	*t*-BuOH	40	1	*R*
5	**2a**	*S*	MeOH	58	0	
6	**2b**	*S*	MeOH	39	2	*R*
7	**2b**	*S*	EtOH	48	11	*R*
8	**2b**	*S*	*i*-PrOH	48	7	*R*
9	**2b**	*S*	*t*-BuOH	41	8	*R*
10	**2b′**	*R*	MeOH	58	3	*S*
11	**2b′**	*R*	EtOH	39	9	*S*
12	**2c**	*S*	MeOH	46	2	*R*
13	**2c**	*S*	EtOH	45	10	*R*
14	**2c**	*S*	*i*-PrOH	47	7	*R*
15	**2c**	*S*	*t*-BuOH	54	7	*R*
16	**2c′**	*R*	EtOH	41	10	*S*

a) Configuration of chiral amine. b) Diastereomeric purity. c) Configuration of newly formed asymmetric moiety.

TABLE 4. NBH REDUCTION WITH METALLIC SALT

Entry	Substrate	Configuration[a]	Solvent	Metal(mg)	Yield/%	*Dp*/%[b]	Configuration[c]
17	**2a**	*S*	MeOH	$MgCl_2$(10)	48	7	*S*
18	**2a**	*S*	EtOH	$MgCl_2$(10)	50	15	*S*
19	**2a**	*S*	MeOH	$ZnCl_2$(14)	57	3	*S*
20	**2b**	*S*	MeOH	$MgCl_2$(10)	49	19	*S*
21	**2b′**	*R*	EtOH	$MgCl_2$(10)	51	16	*R*
22	**2b′**	*R*	EtOH	$MgCl_2$(20)	43	18	*R*
23	**2b′**	*R*	EtOH	$MgCl_2$(50)	36	21	*R*
24	**2b′**	*R*	EeOH	$MgCl_2$(100)	27	22	*R*
25	**2b**	*S*	MeOH	$ZnCl_2$(14)	56	22	*S*
26	**2c**	*S*	MeOH	$MgCl_2$(10)	45	18	*S*
27	**2c**	*S*	EtOH	$MgCl_2$(10)	52	19	*S*
28	**2c**	*S*	MeOH	$ZnCl_2$(14)	70	20	*S*

a) Configuration of chiral amine. b) Diastereomeric purity. c) Configuration of newly formed asymmetric moiety.

tration of magnesium chloride in the reaction mixture (entries 21—24 in Table 4).

From these results, the conformation of the substrate in the solution and the steric course of the NBH reduction could be discussed as follows. Because of the electrostatic repulsion between the two carbonyl groups in the molecule, these carbonyl groups and the N–H bond should be on the same plane. Therefore, the asymmetric induction in the reduction without metallic salts could be discussed only by the consideration of the conformation of the chiral amine moiety.

The conformation of the pyruvamide in solution could be a mixture of the two conformers A and B shown in Fig. 3. The (*R,S*)-lactamide is formed in excess from conformer A, and the (*S,S*)-lactamide from conformer B in excess. Therefore, the observed asymmetric yield would be interpreted as the combined asymmetric induction of the reduction of each conformer. Since conformer A is more stable than conformer B, the (*R,S*)-lactamide could be formed in excess over the (*S,S*)-lactamide through the reduction. The X-ray crystallographic study[8,9] and the NMR measurement[10] of similar amides indicate that conformer A is more stable than conformer B. On the other hand, the asymmetric yield of the reduction of substrate **2b** was larger than that of **2a**. This could be explained by the steric repulsion between the ethyl group in the chiral source and the carbonyl group of the amide. Thus, the population of conformer B

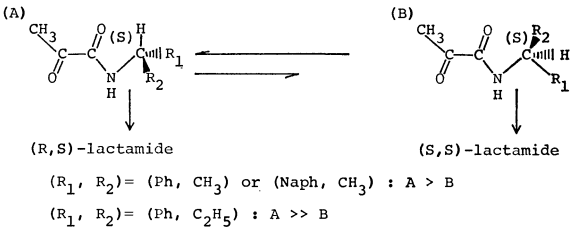

Fig. 3. Steric courses of the reduction without metallic salt.

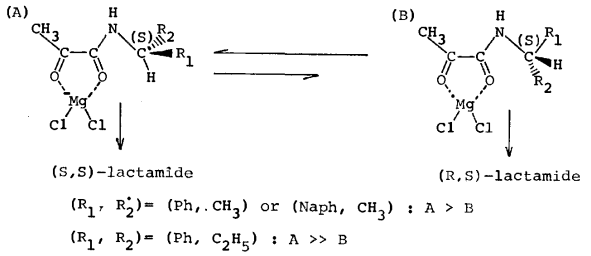

Fig. 4. Steric courses of the reductions with metallic salt.

is much smaller than that of conformer A as shown in Fig. 3, and the reduction of conformer A governs the asymmetric yield of the whole reaction. In the reduction of substrate **2c**, the asymmetric yield would be larger than the reduction of substrate **2a**, because of the difference in the bulkiness between the naphthyl and phenyl groups in substrates **2a** and **2c**.

The reduction with metallic salts may be explained in terms of the formation of a chelated substrate. The two carbonyl groups in the substrate could coordinate to the metallic salt and be fixed weakly in a *s*-cis conformation as shown in Fig. 4. And the asymmetric induction could be determined by the conformation of the asymmetric moiety of the substrate. The most preferred conformation could be that where the C–H bond of the asymmetric moiety is on the same plane with the chelated part of the substrate (Fig. 4). The hydrogenation of the substrate resulted in the formation of the (*S*,*S*)-lactamide. Thus, the configuration of the lactoyl moiety of the product ((*S*,*S*)-lactamide) reversed to the opposite structure from that obtained in the NBH reduction without metallic salt. The asymmetric yields of the NBH reduction with metallic salt were larger than those without metallic salt, possibly because of the fixation of the conformation by the chelation of the two carbonyl groups with the metallic salt.

References

1) V. Prelog, M. Wilhelm, and D. B. Bright, *Helv. Chim. Acta*, **37**, 221 (1954).
2) S. P. Bakshi and E. E. Turner, *J. Chem. Soc.*, **1961**, 168.
3) M. S. Kubitscheck and W. A. Bonner, *J. Org. Chem.*, **26**, 2194 (1961).
4) S. Mitsui and A. Kanai, *Nippon Kagaku Zasshi*, **86**, 627 (1965).
5) W. C. Still, M. Kahn, and A. Mitra, *J. Org. Chem.*, **43**, 2923 (1978).
6) T. Munegumi, S. Nomoto, and K. Harada, *J. Chromatogr.*, **237**, 469 (1982).
7) H. Frank, G. J. Nicolson, and E. Bayer, *J. Chromatogr.*, **146**, 197 (1978).
8) W. H. Pirkle and J. R. Hauske, *J. Org. Chem.*, **41**, 801 (1976).
9) A. T. Hagler, L. Leiseroruitz, and M. Tuval, *J. Am. Chem. Soc.*, **98**, 4600 (1976).
10) G. Helmchen, R. Ott, and K. Sauber, *Tetrahedron Lett.*, **1972**, 3873.

Restricted Rotation Involving the Tetrahedral Carbon. XLIV. Atropisomers of 2,3-Dichloro-9-(1-hydroxy-1-methylethyl)-triptycene and Related Compounds[1]

Michinori Ōki,* Yoshiyuki Tanaka, Gaku Yamamoto, and Nobuo Nakamura
Department of Chemistry, Faculty of Science, The University of Tokyo, Bunkyo-ku, Tokyo 113
(Received August 10, 1982)

Atropisomers of 2,3-dichloro-9-(1-hydroxy-1-methylethyl)triptycene were obtained as stable compounds at room temperature. The barrier to rotation (±*sc*→*ap*) was 34.0 kcal/mol at 153 °C. Other 9-(1-hydroxy-1-methylethyl)triptycenes carrying a substituent in the 1-position of the skeleton gave ±*sc* isomers only. Attempted isomerization of the ±*sc* forms failed because the free energy difference between the ±*sc* and *ap* forms is great due to the steric effect. ±*sc*-9-(1-Methoxy-1-methylethyl)-1,4-dimethyltriptycene was prepared in a hope that increasing the steric size of the hydroxyl group would help to produce an *ap*-isomer on heating. The *ap* isomer was detected but the population ratio *ap*/±*sc* was too small to isolate the *ap*.

Various triptycene derivatives were found to give stable rotational isomers at room temperature provided that the 9-substituent is tertiary and the triptycene skeleton carries a substituent which provides necessary breaking of the symmetry.[2] However, the 9-substituent was confined to those carrying three carbons in the 1-position of the substituent so far. It may be of interest to see how the barriers to rotation and populations of rotamers are affected if one of the substituents in the 1-position of the 9-substituent is changed to a hetero atom. As the first of such investigations, we have undertaken the investigation on the case of a 9-(1-hydroxy-1-methylethyl) substituent. This paper is to report the results and to discuss implications therefrom.

The syntheses of the compounds were rather interesting. Although benzynes are known to react with hydroxylic compounds to give aromatic oxygen derivatives,[3] 9-(1-hydroxy-1-methylethyl)anthracene (**1**) gave the desired triptycenes (**2**) when it was treated

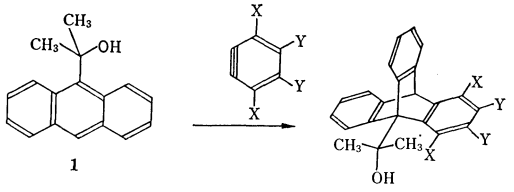

1 2

a: X=Y=H
b: X=H, Y=Cl
c: X=OCH_3, Y=H
d: X=Y=Cl
e: X=CH_3, Y=H

with benzynes. We believe that the result is caused because the anthracene moiety is strongly nucleophilic and the hydroxyl group is protected from the attack by the steric effect. The only exception to the normal cases was the reaction of tetrafluorobenzyne, which gave 9-isopropenylanthracene only as a product of the benzyne reaction. Since tetrafluorobenzyne is very strongly electrophilic, it seems to react with the oxygen of the alcohol (**1**) preferentially. In accordance with this explanation, other benzynes which are strongly electrophilic gave also 9-isopropenylanthracene to some extent.

The reaction, if proceeded as expected, gave ±*sc* conformational isomers of a desired compound as a sole product. This is reasonable in the sense that a methyl group is much larger than an oxygen group: the benzyne addition to 9-substituted anthracene is known to proceed from the less crowded side with great preference.[4] The assignment of the stereostructure of the product is straightforward. The ±*sc* conformation should show two methyl signals in ^{1}H NMR spectra because the environments of the two methyls are different in this conformation, whereas the environments of the methyls in the *ap* conformation are identical.

Table 1. Rates of isomerization (±*sc*→*ap*) and equilibrium constants in 2,3-dichloro-9-(1-hydroxy-1-methylethyl)triptycene (**2b**) in 1-chloronaphthalene

Temperature/°C	k/s^{-1}	K (*ap*/±*sc*)
212	—	0.30
165.6	8.63×10^{-5}	0.27
153.0	3.34×10^{-5}	0.29
144.6	1.69×10^{-5}	0.29
132.5	5.21×10^{-6}	0.31

The rate constants for isomerization of ±*sc*-**2b** are summarized in Table 1. The Eyring plot yielded ΔH^* 29.1±2.5 kcal/mol (1 cal=4.18 J) and ΔS^* −11.5± 6.0 e. u. (1 e. u.=4.18 J K^{-1} mol^{-1}). If these activation parameters are compared with those of 2,3-dichloro-9-(1-methoxycarbonyl-1-methylethyl)triptycene (**3**) (ΔH^* 33.8 kcal/mol and ΔS^* −1.8 e. u.),[5] 2,3-dichloro-9-(1-cyano-1-methylethyl)triptycene (**4**) (ΔH^* 39.4 kcal/mol and ΔS^* 6.5 e. u.),[5] and 2,3-dichloro-9-(1,1-dimethyl-2-phenylethyl)triptycene (**5**) (ΔH^* 35.7

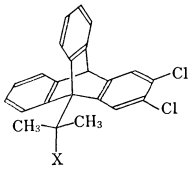

3: X=$COOCH_3$
4: X=CN
5: X=$CH_2C_6H_5$

kcal/mol and ΔS^* −9.3 e. u.),[4] one notices that the enthalpy of activation of **2b** is definitely small. The results may be attributed to the small bulkiness of the oxygen group in **2b** relative to a methoxycarbonyl, cyano, or benzyl group. Namely, the lowering of the transition state energy is more effective than lowering of the ground state energy in determining the barrier

to rotation in **2b**.

The equilibrium constants ($ap/\pm sc$) of **2b** are smaller than the statistical value and are even smaller than those compounds cited above (**3**—**5**). Two possibilities emerge for the explanation. One is that the *ap* conformation of **2b** is destabilized relative to *ap* conformations of other compounds and the other is the special stabilization of the $\pm sc$ conformation of **2b**. The 1-H undoubtedly suffers from the buttressing effect of the 2-Cl group, thus it should be larger in effective size than other *peri*-hydrogens. Then probably the repulsive interaction between the 1-H and the flanking groups (two methyls) in the *ap* conformation is more severe than that between the 8(or 13) -H and two methyl groups in $\pm sc$ conformations. We believe this kind of steric effect is an important factor among others that favor the $\pm sc$ conformation of **2b** in the ground state, since no effect of stabilization of the $\pm sc$ form is apparent. Indeed, 2,3-dichloro-9-(1,1-dimethyl-2-phenylethyl)triptycene (**5**) gives $ap/\pm sc$ of 0.50,[4] which is the statistical value, because the effective sizes of the benzyl and the methyl groups are almost the same.

Other triptycenes (**2**) carrying (a) substituent in 1-position failed to give any sign of the presence of *ap* isomers, although their solutions were heated at 212 °C for a long time. Instead, they afforded compounds of which ^{1}H NMR spectra are compatible with 9-isopropenyltriptycenes (**6**): indeed, 1,4-dimethyl derivative of **6** was characterized. Since this dehydration did not occur at 164 °C after 40 h, the dehydration is caused by heating at >200 °C. The results indicate that the *ap* conformation in these compounds are extremety unstable relative to the $\pm sc$, since the barriers to rotation in other analogous compounds[4,5] suggest that the internal rotation about the C_9–C_{subst} bond must be occurring under the conditions of the heating. It is not clear at the moment at what conformation the dehydration takes place.

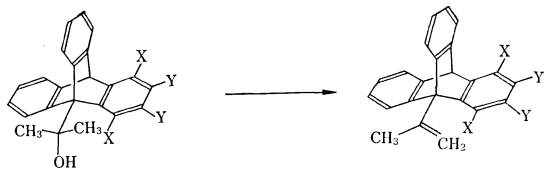

1 6

The ^{1}H NMR spectra of isopropenyltriptycenes (**6**) indicate that the internal rotation about the C_9–C_{ipr} bond in these compounds is fast on the NMR time scale. This is interesting, if one considers a very high barrier to rotation in 9-*t*-alkyltriptycenes. But there is a precedent of this instance: 9-*o*-tolyltriptycenes show rather low barriers to rotation.[6] If a 9-substituent has an sp^2-hybridized carbon in its 1-position, the ground state seems to be raised owing to the interaction of the triptycene skeleton with the trigonal group.

The great stability of the $\pm sc$ forms of **2c**—**e** relative to the *ap* must be attributed to the steric effect. If a 9-substituent in triptycenes contain a small group in its 1-position and the triptycene skeleton carries a *peri*-substituent, there is seen a strong preference of a conformation in which the small group gives the gauche interaction with the *peri*-substituent. If the 9-substituent is a secondary alkyl group, a conformation in which two bulky groups flank the *peri*-substituent is not usually detected.[7] Even in the tertiary alkyl cases, it is true: if a 1-substituent in the 9-substituent of triptycene is either trigonal or linear, the conformation in which the trigonal or linear group is $\pm sc$ to the *peri*-substituent is strongly favored.[5] The case of compound **2** is considered to be in the same line, since the OH group is much smaller than a methyl. The OH-*sc* conformation must be favored relative to the OH-*ap* conformation.

Hydrogen bonding between the OH group and the *peri*-substituent may be playing some role in stabilizing the $\pm sc$ conformation. Indeed, ^{1}H NMR spectra show that the OH proton gives a sharp peak if there is a *peri*-substituent with lone pair electrons, whereas the OH proton signal either was broad or could not be detected in others. However, the effect of the hydrogen bond must be of minor importance, because even the 1,4-dimethyl compound (**2e**) gives only $\pm sc$ conformations.

This consideration suggests that, if the hydroxyl group is modified to make a larger group, there is a possibility that *ap* conformation exists. Thus ester formations and ether formations of both the anthracene–alcohol (**1**) and the triptycene–alcohol (**2**) were tried under various conditions. However, all the attempts failed because of the steric effect except for one case, that is the methylation of **1**.

Treatment of the methyl ether (**7**) with tetrachlorobenzyne did not afford a triptycene derivative but 9-isopropenylanthracene. It is not clear why the methyl ether (**7**) gives 9-isopropenylanthracene, whereas the hydroxy compound (**1**) gives a triptycene to some extent, since the oxygen in the methyl ether seems to be more protected than the hydroxylic oxygen on the steric ground. Probably the electronic effect and/or the steric deceleration of the attack of benzyne toward the anthracene ring, due to introduction of the methyl group to the hydroxyl, is important.

Tetrachlorobenzyne has been known to give an olefin if it reacts with an ether[8] because of its electrophilic nature. If we could lower the electrophilicity of a benzyne, there is a chance of obtaining a triptycene derivative. Thus we treated **7** with 3,6-dimethylbenzyne and indeed obtained *sc*-9-(1-methoxy-1-methylethyl)-1,4-dimethyltriptycene (**8**). Isomerization of **8**, however, gave only a minute amount of the *ap* isomer, of which isolation was not practical. The steric effect of a methoxyl group is indeed greater than a hydroxyl group, because we could detect the presence of the *ap* form of **8**, but is not great enough to give sizable amount of the *ap*.

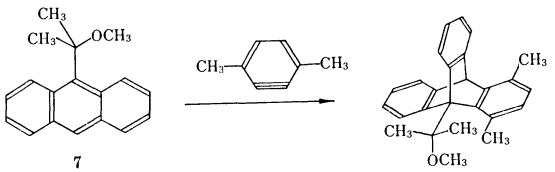

7 8

Experimental

3,6-Dimethoxyanthranilic Acid. To 90 mL of chilled nitric acid (d=1.38) was added portionwise 9.1 g (0.05 mol) of 2,5-dimethoxybenzoic acid[9] during the course of 30 min and the solution was stirred at 0—5 °C for 3 h. The mixture was poured into 300 mL of ice–water and the precipitate was collected by filtration. The product was shown to be a mixture (*ca.* 5:1) of 2,5-dimethoxy-6-nitrobenzoic acid and 2,5-dimethoxy-4(or 3)-nitrobenzoic acid by ^{1}H NMR spectra. The mixture (10.4 g) was hydrogenated over Pd–C in ethyl acetate under normal pressure. Removal of the catalyst, evaporation of the solvent, and recrystallization of the residue from aqueous ethanol gave 3.4 g (38%) of the desired acid as white needles, mp 92—94 °C (lit,[10] mp 97 °C).

*9-(1-Hydroxy-1-methylethyl)anthracene (**1**).* A Grignard reagent was prepared from 1.42 g (60 mmol) of magnesium, 5.0 g (20 mmol) of 9-bromoanthracene[11] and 90 mL of ether. To the solution, 5 mL (68 mmol) of acetone in 20 mL of ether was added and the whole was stirred overnight. The mixture was decomposed with ice and aqueous ammonium chloride and the ether layer was separated. The ether layer was washed thoroughly and dried over magnesium sulfate. After evaporation of the solvent, the residue was recrystallized from benzene. For further purification, the product was submitted to silica gel chromatography (hexane–dichloromethane eluent) to give 1.6 g of the desired product, mp 139.0—140.5 °C (lit,[12] mp 136 °C). ^{1}H NMR ($CDCl_3$, δ): 2.15 (6H, s), 7.1—7.6 (4H, m), 7.7—8.1 (2H, m), 8.28 (1H, s), 8.6—8.9 (2H, m).

*±sc-2,3-Dichloro-9-(1-hydroxy-1-methylethyl)triptycene (**2b**).* To a solution of 473 mg (2.0 mmol) of the alcohol (**1**) and 0.5 mL (3.8 mmol) of isopentyl nitrite in 40 mL of chlorobenzene, was added 828 mg (4.0 mmol) of 4,5-dichloroanthranilic acid[4] in 50 mL of chlorobenzene in *ca.* 2 h with stirring and heating. More isopentyl nitrite was added after *ca.* 1 h during the addition of the anthranilic acid. After heating for another hour, the solvents were evaporated *in vacuo* and the residue was taken up in dichloromethane. The solution was submitted to chromatography on silica gel with hexane–dichloromethane eluents (5:1—2:1) to give *±sc*-**2b**, mp 193.5—195 °C, in 13% yield. Found: C, 72.22; H, 4.62; Cl, 18.47%. Calcd for $C_{23}H_{18}Cl_2O$: C, 72.45; H, 4.76; Cl, 18.60%. ^{1}H NMR ($CDCl_3$, δ): 2.20 (3H, s), 2.24 (3H, s), 5.16 (1H, s), 6.85—7.1 (4H, m), 7.2—7.45 (2H, m), 7.41 (1H, s), 7.55 (1H, m), 8.0 (1H, m), 8.15 (1H, s).

Attempted Synthesis of 1,2,3,4-Tetrafluoro-9-(1-hydroxy-1-methylethyl)triptycene. A similar treatment of the alcohol (**1**) and isopentyl nitrite in dichloromethane with tetrafluoroanthranilic acid[13] in tetrahydrofuran afforded anthraquinone and 9-isopropenylanthracene, mp 84.5—86.0 °C (lit,[14] mp 84.5—86 °C). ^{1}H NMR ($CDCl_3$, δ) of isopropenylanthracene exhibited the following signals: 2.15 (3H, d, J=1 Hz), 5.05 (1H, m), 5.63 (1H, m), 7.2—7.5 (4H, m), 7.7—7.9 (2H, m), 7.9—8.2 (2H, m), 8.18 (1H, s). No tetrafluorotriptycene derivative was detected.

*9-(1-Hydroxy-1-methylethyl)triptycene (**2a**)*, mp 200—202 °C, was prepared similarly from **1** and isopentyl nitrite in dichloromethane and anthranilic acid in acetone in 75% yield. The original product was contaminated with a small amount of 9-isopropenylanthracene. The product was purified by recrystallization from tetrahydrofuran–hexane. Found: C, 88.64; H, 6.39%. Calcd for $C_{23}H_{20}O$: C, 88.43; H, 6.45%. ^{1}H NMR ($CDCl_3$, δ): 2.31 (6H, s), 2.58 (1H, br s), 5.25 (1H, s), 6.8—7.5 (9H, m), 7.5—7.7 (1H, m), 7.9—8.1 (2H, m).

*±sc-1,2,3,4-Tetrachloro-9-(1-hydroxy-1-methylethyl)triptycene (**2d**)*, mp 299—300.5 °C, was similarly prepared from the alcohol (**1**) and isopentyl nitrite in dichloromethane and tetrachloroanthranilic acid[15] in acetone in 11.2% yield. A fair amount of isopropenylanthracene was detected. Found: C, 61.06; H, 3.38; Cl, 31.31%. Calcd for $C_{23}H_{16}Cl_4O$: C, 61.36; H, 3.58; Cl, 31.50%. ^{1}H NMR ($CDCl_3$, δ): 2.12 (3H, s), 2.42 (3H, s), 4.33 (1H, s), 6.03 (1H, s), 6.9—7.25 (4H, m), 7.3—7.6 (2H, m), 7.6—7.8 (1H, m), 8.5—8.7 (1H, m).

*±sc-9-(1-Hydroxy-1-methylethyl)-1,4-dimethoxytriptycene (**2c**)*, mp 272—273 °C, was prepared similarly from the alcohol and isopentyl nitrite in dichloromethane and 3,6-dimethoxyanthranilic acid in tetrahydrofuran in 14% yield. Found: C, 80.72; H, 6.46%. Calcd for $C_{25}H_{24}O_3$: C, 80.62; H, 6.49%. ^{1}H NMR ($CDCl_3$, δ): 2.16 (6H, s), 3.77 (3H, s), 3.82 (3H, s), 5.86 (1H, s), 5.90 (1H, s), 6.55 (2H, s), 6.85—7.1 (4H, m), 7.25—7.55 (2H, m), 7.65 (1H, m), 8.4 (1H, m). On addition of benzene-d_6 to the chloroform-d solution, the methyl proton signal at δ 2.16 was split into two.

*±sc-9-(1-Hydroxy-1-methylethyl)-1,4-dimethyltriptycene (**2e**)*, mp 255—257 °C, was similarly prepared from the alcohol (**1**) and 3,6-dimethylanthranilic acid[16] in 50% yield. Found: C, 88.06; H, 7.01%. Calcd for $C_{25}H_{24}O$: C, 88.20; H, 7.10%. ^{1}H NMR ($CDCl_3$, δ): 2.22 (3H, s), 2.32 (3H, s), 2.46 (3H, s), 2.82 (3H, s), 5.57 (1H, s), 6.71 (2H, s), 6.85—7.1 (4H, m), 7.2—7.45 (2H, m), 7.6 (1H, m), 8.2 (1H, m).

*9-(1-Methoxy-1-methylethyl)anthracene (**7**).* To a solution of 718 mg (3.0 mmol) of the alcohol (**1**) in 100 mL of tetrahydrofuran was added 2 mL of 1.5 M butyllithium in hexane and the whole was stirred for 3 h. Methyl iodide (5 mL) was added and the mixture was stirred for 3 h. The solvent and the excess of methyl iodide were evaporated in vacuo and the residue was taken up in ether. The ethereal solution was washed and dried. Evaporation of the solvent followed by recrystallization of the residue from dichloromethane–hexane afforded 526 mg of the desired product, mp 107—108.5 °C. Found: C, 86.29; H, 7.06%. Calcd for $C_{18}H_{18}O$: C, 86.36; H, 7.25%. ^{1}H NMR ($CDCl_3$, δ): 2.15 (6H, s), 2.80 (3H, s), 7.2—7.45 (4H, m), 7.85—8.05 (2H, m), 8.33 (1H, s), 8.6—8.95 (2H, m).

*±sc-9-(1-Methoxy-1-methylethyl)-1,4-dimethyltriptycene (**8**)*, mp 251—252 °C, was prepared by treating **7** with 3,6-dimethylbenzyne as above. Found: C, 87.95; H, 7.15%. Calcd for $C_{26}H_{26}O$: C, 88.09; H, 7.39%. ^{1}H NMR ($CDCl_3$, δ): 2.09 (3H, s), 2.13 (3H, s), 2.46 (3H, s), 2.64 (3H, s), 3.55 (3H, s), 5.57 (1H, s), 6.69 (2H, s), 6.7—7.2 (4H, m), 7.2—7.4 (2H, m), 7.56 (1H, m), 8.00 (1H, m).

A 1-chloronaphthalene solution of *±sc*-**8** showed the following ^{1}H NMR signals (ppm from internal cyclododecane): 0.52 (6H, s), 1.16 (3H, s), 1.38 (3H, s), 1.87 (3H, s). When the solution was heated in a boiling-nitrobenzene bath, the following ^{1}H NMR signals were observed: 0.72 (6H, s), 0.97 (3H, s), 1.91 (3H, s). Another signal for 1(or 4)-methyl protons is missing: it probably overlaps with one of the signals due to 1- and 4-methyls of the *±sc* form. The equilibrium was reached within 5 h at this temperature and the equilibrium constant (*ap*/*±sc*) was *ca.* 1/30. Prolonged heating of the solution caused decomposition of the solute.

Determination of Barriers to Rotation. A sample (55 mg) of *±sc*-**2b** was dissolved in 1.4 mL of 1-chloronaphthalene and placed in NMR sample tubes, the solution being divided into 4 portions. The NMR sample tube was placed in an appropriate boiling-solvent bath and the isomerization rate was determined by ^{1}H NMR spectroscopy. The temperature was directly read by a thermometer. The integration of the peak area was carried out 5 times and the

average of the middle three was taken for calculation of the rate constant. The conversion rate was treated assuming a reversible first-order reaction. The solvents used for the bath are nitrobenzene (212 °C), mesitylene (165.5 °C), anisole (153.0 °C), *o*-xylene (144.6 °C), and chlorobenzene (132.5 °C). The rate constants were put into the Eyring equation and the activation parameters were obtained.

*ap-2,3-Dichloro-9-(1-hydroxy-1-methylethyl)triptycene (**2b**).* The equilibrium mixture of ±*sc*- and *ap*-**2b**, obtained as a result of the isomerization experiments, was concentrated *in vacuo* and submitted to chromatography on alumina. After the solvent was eluted with hexane, a ±*sc*-*ap* mixture was obtained by elution with dichloromethane. The mixture was separated by TLC on silica gel (2:1 dichloromethane–hexane solvent). The *ap* form, mp 207—209 °C, had a smaller R_f value than the ±*sc* form. High resolution mass spectrum showed molecular ion peaks at *m/e* 380.0775, 382.0759, and 384.0707, whereas $C_{23}H_{18}Cl_2O$ requires those at 380.0735, 382.0706, and 384.0676. The intensities of these peaks agreed well with those calculated from the natural abundance of ^{35}Cl and ^{37}Cl. ^1H NMR ($CDCl_3$, δ): 2.26 (6H, s), 5.17 (1H, s), 6.85—7.1 (4H, m), 7.2—7.45 (2H, m), 7.46 (1H, s), 7.59 (1H, s), 8.0 (2H, m).

*9-Isopropenyl-1,4-dimethyltriptycene (**6**: X=CH_3, Y=H).* A solution of ±*sc*-**2e** (20 mg) in 0.4 mL of 1-chloronaphthalene was heated in a boiling-nitrobenzene bath for 40 h. The solution was submitted to chromatography on alumina (hexane eluent) and the product was recrystallized from pentane to give 14 mg of the product, mp 149—150 °C. Found: C, 92.99; H, 6.84%. Calcd for $C_{25}H_{22}$: C, 93.12; H, 6.88%. ^1H NMR ($CDCl_3$, δ): 2.27 (3H, s), 2.44 (6H, s), 5.48 (1H, s), 5.79 (1H, br s), 5.93 (1H, br s), 6.63 (2H, s), 6.85—7.1 (4H, m), 7.2—7.6 (2H, m), 7.6—7.9 (2H, m).

Determination of Spectra. ^1H NMR spectra were obtained on a Varian EM 390 spectrometer.

References

1) For Part XLIII, see M. Aoki, M. Nakamura, and M. Ōki, *Bull. Chem. Soc. Jpn.*, **55**, 2512 (1982).
2) M. Ōki, *Angew. Chem., Int. Ed. Engl.*, **15**, 87 (1976).
3) M. Stiles and R. G. Miller, *J. Am. Chem. Soc.*, **82**, 3802 (1960); G. Wittig and R. W. Hoffmann, *Chem. Ber.*, **95**, 2718 (1962).
4) G. Yamamoto and M. Ōki, *J. Chem. Soc., Chem. Commun.*, **1974**, 713; *Bull. Chem. Soc. Jpn.*, **48**, 3686 (1975).
5) S. Otsuka, G. Yamamoto, T. Mitsuhashi, and M. Ōki, *Bull. Chem. Soc. Jpn.*, **53**, 2095 (1980).
6) M. Nakamura and M. Ōki, *Bull. Chem. Soc. Jpn.*, **48**, 2106 (1975).
7) F. Suzuki, M. Ōki, and H. Nakanishi, *Bull. Chem. Soc. Jpn.*, **47**, 3114 (1974); M. Suzuki, G. Yamamoto, H. Kikuchi, and M. Ōki, *ibid.*, **54**, 2383 (1981); H. Kikuchi, S. Hatakeyama, G. Yamamoto, and M. Ōki, *ibid.*, **54**, 3832 (1981).
8) Reaction of diethyl ether with tetrachlorobenzyne to give ethyl tetrachlorophenyl ether and ethene is known: J. P. N. Brewer, H. Heaney, and J. M. Jablonski, *Tetrahedron Lett.*, **1968**, 4455.
9) P. K. Banerjee and D. N. Chandhbury, *J. Indian Chem. Soc.*, **36**, 257 (1959).
10) F. J. Villani and J. Laug, *J. Am. Chem. Soc.*, **72**, 2301 (1950).
11) D. C. Nonhebel, *Org. Synth.*, Coll. Vol. V, 206 (1973).
12) C. Jean and M. Ernest, *C. R. Hebd. Seances Acad. Sci., Ser. C*, **286**, 169 (1978).
13) S. Hayashi and N. Ishikawa, *Nippon Kagaku Zasshi*, **91**, 1000, (1970).
14) E. G. E. Hawkins, *J. Chem. Soc.*, **1957**, 3858.
15) V. Villiger and L. Blangey, *Ber.*, **42**, 3549 (1909).
16) S. Gronowitz and G. Hansen, *Ark. Kemi*, **27**, 145 (1967).

Restricted Rotation Involving the Tetrahedral Carbon. XLV. Appearance of a Maximum in the Rotational Barriers of 9-(1,1-Dimethyl-2-phenylethyl)triptycenes at a Medium-sized *peri*-Substituent[1]

Gaku YAMAMOTO, Masahiko SUZUKI, and Michinori ŌKI*

Department of Chemistry, Faculty of Science, The University of Tokyo, Bunkyo-ku, Tokyo 113

(Received August 10, 1982)

Rotational isomers of seven *peri*-substituted 9-(1,1-dimethyl-2-phenylethyl)triptycene derivatives were stereoselectively synthesized and classical kinetics on rotational isomerization were studied. While compounds with relatively small *peri*-substituents (F and OCH_3) showed higher barriers than the *peri*-unsubstituted one, the *peri*-chloro compound had almost the same barrier with and those carrying bulkier *peri*-substituents (Br, CH_3, and CF_3) showed lower barriers than the *peri*-unsubstituted one. These apparently anomalous phenomena may be explained in terms of large molecular deformation of these highly congested compounds.

We have shown by NMR spectroscopy that 9-substituted triptycene derivatives constitute an excellent model system in the investigation of rotational isomerism about a single bond.[2] The compounds have high barriers to rotation about the bridgehead-to-substituent bond because of the rigidity of the triptycene skeleton. Thus, even a methyl group shows restricted rotation on the NMR time scale in some 9-methyltriptycene derivatives.[3]

Bulkiness of the 9-substituent is the largest factor governing the height of the barrier. Thus, 9-*t*-alkyltriptycenes have high rotational barriers enough to give rise to rotational isomers isolable at room temperature (atropisomers).[4]

Substitution at *peri*-positions (1-, 8-, and 13-positions) also has a large influence on the barrier. While 9-benzyltriptycenes carrying one *peri*-substituent showed the rotational barrier of *ca.* 12 kcal mol^{-1} (1 cal=4.184 J),[5] a triply *peri*-substituted 9-benzyltriptycene could give rise to stable atropisomers with the barrier of 25.3 kcal mol^{-1}.[6] Influence of the nature (mainly steric) of *peri*-substituents on the rotational barrier has been studied in some of singly *peri*-substituted 9-alkyl(or aralkyl)triptycenes. When the 9-substituent is a primary or a secondary alkyl group, the barrier increases with the bulkiness of the *peri*-substituent.[3,7,8] This tendency can be easily understood if one accepts that the effect of steric crowding due to the *peri*-substitution should be larger in the transition state than in the ground state.

In the case of 9-(1-cyano or 1-methoxycarbonyl-1-methylethyl)triptycene, however, introduction of a chloro or a methyl group into a *peri*-position was found to decrease the rotational barrier, the clear explanation remaining to be solved.[9]

In order to see if this phenomenon is generally observed in 9-*t*-alkyltriptycene derivatives, and also to get a deeper insight into the origin of the phenomena by investigating the effects of some other *peri*-substituents, we studied the rotational barriers of a variety of *peri*-substituted 9-(1,1-dimethyl-2-phenylethyl)triptycene derivatives **2**—**8**.[10] The results are presented in this paper. The choice of this particular system is based on the following reasons. Firstly, the 9-substituent has no polar bond which might have special interaction with *peri*-substituents. Secondly, similarity in bulkiness between methyl and benzyl groups might not cause a large shift of the rotational equilibrium from the statistical value, which would make kinetic measurements easy. Thirdly, we previously reported on the synthesis of and the rotational barrier in the *peri*-unsubstituted derivative **1**.[4]

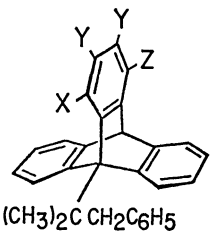

	X	Y	Z
1	H	Cl	H
2	F	H	H
3	OCH_3	H	OCH_3
4	Cl	H	H
5	Cl	H	Cl
6	Br	H	H
7	CH_3	H	CH_3
8	CF_3	H	H

Results

Syntheses. Triptycenes investigated were synthesized by the reactions of 9-(1,1-dimethyl-2-phenylethyl)-anthracene (**9**) with benzynes **10** and **11**. The benzyne (**11a**) was generated by decomposition of 2,6-difluorophenyllithium prepared from *m*-difluorobenzene and butyllithium.[11] The other benzynes were generated by decomposition of 3- or 3,6-substituted 2-diazoniobenzoates prepared from the corresponding anthranilic acids and isopentyl nitrite. The triptycenes formed existed exclusively in the *ap* atropisomer in accordance with the stereoselectivity previously found in the case of **1**. Thus, the atropisomer is selectively formed in which the bulkier group in the 9-substituent assumes the antiperiplanar position to the benzeno bridge derived from the benzyne.[4] In the reactions of **9** with benzynes **11**, the regioisomeric 4-substituted triptycenes were formed in addition to the desired 1-substituted ones. Identification of the regioisomers was made by the chemical shifts of the bridgehead protons: those of 1-substituted derivatives appeared at δ 5.20—5.27, while those of 4-substituted ones appeared at a lower field because of the anisotropic and/or steric compression effects of the 4-substituent. The ratio of formation of 1- *vs.* 4-substituted compounds were as follows: 5.0 for **2**/**2**′, 1.3 for **4**/**4**′, 1.0 for **6**/**6**′ and **8**/**8**′. Preferred formation of the more crowded regioisomers may be apparently anomalous, but is not unprecedented.[12] Separation of the two regioisomers was successfully made by chromatography for **4**/**4**′, **6**/**6**′, and **8**/**8**′pairs. In the case of the fluoro derivatives (**2**/**2**′), the separation was extremely difficult, and the pure sample of

2 was obtained only in a minute amount. Therefore, synthesis of **2** by another route was explored. 9-(1,1-Dimethyl-2-phenylethyl)-1-fluoroanthracene (**14**) was prepared by the reaction of 1,1-dimethyl-2-phenylethylmagnesium chloride with 1-fluoroanthrone (**12**) followed by dehydration, and was treated with benzyne. In this reaction, the ±*sc* rotamer of **2** was stereoselectively obtained.

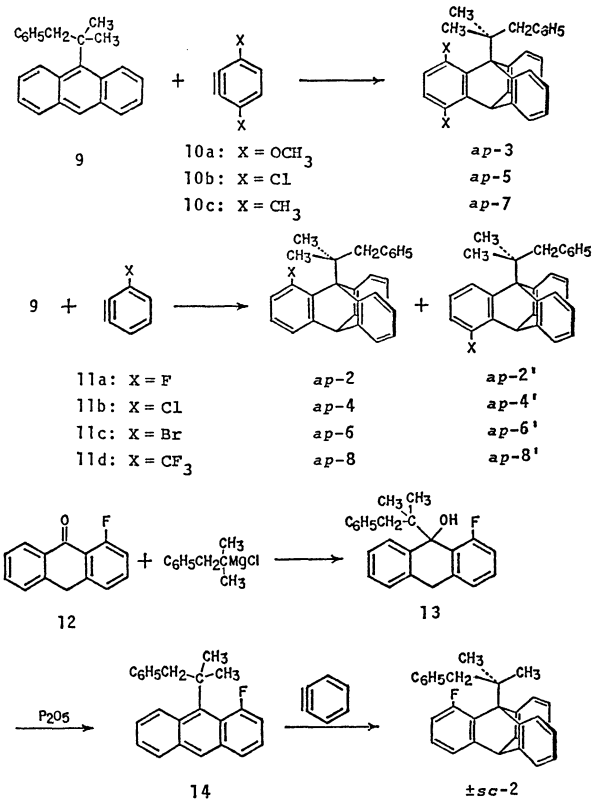

First choice for the isolation of the ±*sc* rotamers of compounds **3**—**8** was chromatography of the equilibrated rotamer mixture on alumina or silica-gel columns. In all cases the *ap* rotamers eluted slightly faster than the ±*sc*. The intrinsically small differences of the chromatographic properties between the rotamers as well as the unavolidable tailing of the bands of *ap* rotamers made isolation of the pure ±*sc* rotamers highly difficult, and the isolation in pure state was successful only for **3**. Secondly, separation by fractional recrystallization was tried but here again the situation was similar because the *ap* rotamers generally had better crystallizability than the ±*sc* rotamer and complete purification of the ±*sc* rotamer was made only for **7**. For compounds **4**, **5**, and **6**, the ±*sc*-enriched mixtures with the content of the *ap* rotamers of 20, 15, and 8%, respectively, were finally obtained. As for **8**, the ±*sc* rotamer was enriched only to 25%.

NMR Spectra. ^{1}H NMR spectral data for both rotamers of the triptycenes (**1**—**8**) are given in Table 1. As for the ±*sc* rotamers of **4**, **5**, **6**, and **8**, the data were obtained from the most enriched samples mentioned above by subtracting the signals due to the *ap* rotamers. Rotameric assignment was explicitly made from the NMR data. The *gem*-dimethyl groups of the *ap* rotamers are enantiotopic and appear as a singlet except for those of **2** and **8**, in which they appear as a doublet and a quartet, respectively, because of the long-range couplings with ^{19}F.[13] The methylene protons are singlets in all of the *ap* rotamers.

In the ±*sc* rotamers, the *gem*-dimethyl groups are *a priori* diastereotopic and actually are anisochronous. Positional assignment of the methyl signals was made as follows. In fluorine-containing compounds **2** and **8**, the signal exhibiting a large coupling with ^{19}F was assigned to the ±*sc*-methyl group, because the coupling should operate through-space under these circumstances and thus the protons located proximate to the ^{19}F nuclei show the coupling.[13]

Nuclear Overhauser effect (NOE) experiments allowed the definite assignment of the methyl signals for **3**—**6**. In any of the compounds, irradiation of the higher-field methyl signal enhanced the intensity of both of the *peri*-proton (8-H and 13-H) signals which appeared as two isolated multiplets at the lowest field region (δ 7.7—8.1). On the other hand, only the

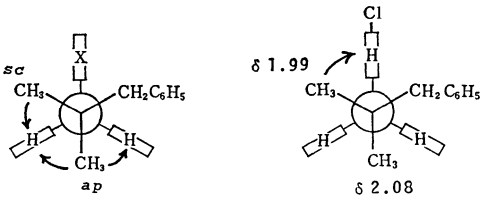

lower-field *peri*-proton signal showed enhancement of the intensity upon irradiation of the lower-field methyl signal. Therefore, the higher-field methyl signal is assigned to the *ap*-methyl group as shown in Table 1. In the ±*sc* rotamer of **1**, the 1-H signal appeared as a singlet at the lowest field (δ 8.03) together with two multiplets for 8-H and 13-H, and its intensity increased only when the higher-field methyl signal at δ 1.99 was irradiated, indicating that the signal should be assigned to the ±*sc*-methyl group. In ±*sc*-**7**, NOE experiments did not afford any information on the assignment because of the small chemical shift difference between the *gem*-dimethyl signals, and tentative assignment is given in Table 1.

It is noticed that the *ap*-methyl signal appears at a lower field than that for the ±*sc*-methyl in **1** and **2**, but the reverse is observed in the other compounds. Roughly speaking, the ±*sc*-methyl signal shifts downfield and the *ap*-methyl upfield as the bulkiness of the *peri*-substituent increases. Large downfield shifts of the ±*sc*-methyl signals in **4**, **5**, **6**, and **8** must be due to the anisotropy and/or steric compression effects exerted by the *peri*-substituents. Upfield shift of the *ap*-methyl signals in these compounds may partly be ascribed to the molecular deformation, which is discussed in the later section.

The methylene protons of the ±*sc* rotamers are diastereotopic and appear as an AB-quartet except for those of ±*sc*-**8**, which give an apparent singlet in $CDCl_3$ because of the small chemical shift difference but show an AB-quartet signal (δ 4.11 and 4.24, J= 15.3 Hz) in a benzene solution.

Kinetics of Isomerization. A solution of a pure rotamer (±*sc* for **2**, *ap* for the others) in 1-chloronaphthalene was heated at a given temperature using

TABLE 1. ^{1}H NMR SPECTRAL DATA IN $CDCl_3$ AT 35 °C[a]

Compound	Atropisomer	*ap*-CH_3	$\pm sc$-CH_3	CH_2	10-H	1,4-Substituents
1[b]	*ap*		2.03	3.86	5.17	
	$\pm sc$	2.08	1.99	3.75 d, 3.89 d (14.6)	5.17	
2	*ap*		2.06 d (8.4[c])	3.90	5.27 d (1.8[a])	
	$\pm sc$	2.10	1.97 d (7.9[c])	3.77 d, 3.96 dd (14.4) (14.4 and 2.1[c])	5.27 d (1.7[c])	
3	*ap*		2.10	3.86	5.92	3.65, 3.79
	$\pm sc$	2.04	2.10	3.95 d, 4.22 d (14.4)	5.92	3.71, 3.81
4	*ap*		2.33	3.85	5.23	
	$\pm sc$	2.05	2.35	4.08 d, 4.57 d (15.0)	5.23	
5	*ap*		2.33	3.85	6.05	
	$\pm sc$	2.07	2.35	4.09 d, 4.50 d (15.3)	6.04	
6	*ap*		2.44	3.82	5.20	
	$\pm sc$	1.98	2.51	4.06 d, 4.86 d (15.2)	5.21	
7	*ap*		2.28	3.90	5.62	2.51, 2.61
	$\pm sc$	2.21[d]	2.25[d]	3.95 d, 4.27 d (16.0)	5.61	2.50, 2.75
8	*ap*		2.27 q (4.2[c])	3.75	5.25	
	$\pm sc$	1.85	2.40 q (4.6[c])	4.04[e]	5.25	

a) Chemieal shifts are shown in ppm downfield from internal tetramethylsilane. Signals are singlets unless otherwise stated; d: doublet, dd: doublet of doublets, q: quartet. In parentheses are coupling constants in Hz. b) Ref. 4. c) Long-range coupings with ^{19}F. d) Tentatively assigned. See text. e) Apparent singlet. An AB-quartet in benzene.

TABLE 2. THERMODYNAMIC PARAMETERS FOR ROTAMER EQUILIBRIUM[a]

Compound	ΔH kcal mol^{-1}	ΔS° [b] e.u.	ΔG°_{500} [b] kcal mol^{-1}	K_{500}	r_P[c] Å	r_C[d] Å
1[e]	0±0	0±0	0	2.0	1.2	1.20
2	0.20±0.62	−0.2±1.2	0.3	1.52	1.35	1.47
3	0.59±0.27	0.1±0.5	0.5	1.18	1.40	1.52
4	1.31±0.11	0.2±0.2	1.2	0.60	1.80	1.75
5	1.15±0.04	−0.2±0.1	1.3	0.57	1.80	1.75
6	1.35±0.03	−0.1±0.1	1.4	0.52	1.95	1.85
7	1.54±0.18	−0.2±0.4	1.6	0.39	2.0	1.97[f]
8	1.99±0.14	0.4±0.4	1.8	0.32		2.43[f]

a) Obtained from the data in Table 4. b) Degeneracy of $\pm sc$ rotamers is taken into account. c) Van der Waals radius according to Pauling: L. Pauling, "The Nature of the Chemical Bond," 3rd ed, Cornell University Press, New York (1960), p. 260. d) Van der Waals radius according to Charton: M. Charton, *J. Am. Chem. Soc.*, **91**, 615 (1969). e) Ref. 4. f) $(r_{v,min}+r_{v,max})/2$.

a boiling solvent bath. At appropriate intervals the sample was taken out of the bath and cooled to room temperature. NMR spectrum was taken to obtain the rotamer population. The ^{19}F signals were used for compounds **2** and **8**, and the *gem*-dimethyl proton signals for the others. Change in the rotamer population upon time obeyed the rate law for a first-order reversible reaction and the rate constant for the isomerization was obtained. The measurements were made at three to four temperatures over the range of 32—50 °C, and the Eyring kinetic parameters were calculated using least square analysis. In Table 4 are given the rate constants for the $ap \rightarrow \pm sc$ conversion by taking into account the degeneracy of the $\pm sc$ rotamers and the free energies of activation therefrom. Eyring parameters as well as free energies of activation and rate constants at 500 K are given in Table 3. The thermodynamic parameters were calculated from the equilibrium constants using the van't Hoff equation and are given in Table 2. Here also the degeneracy of the $\pm sc$ rotamers was taken into account.

Table 3. Kinetic parameters for rotamer isomerization[a)]

Compound	ΔH^* / kcal mol^{-1}	ΔS^* / e.u.	ΔG^*_{500} / kcal mol^{-1}	k_{500} / s^{-1}	k_{rel}
1[b)]	35.5±2.2	−9.8±4.4	40.4	2.4×10^{-5}	20
2	41.2±1.3	−4.1±2.5	43.2	1.2×10^{-6}	1
3	42.6±0.2	0.2±0.3	42.5	2.8×10^{-6}	2
4	36.4±0.9	−8.0±1.9	40.4	2.1×10^{-5}	18
5	35.3±0.9	−9.2±1.9	39.9	3.6×10^{-5}	30
6	34.9±0.9	−8.7±1.9	39.2	7.2×10^{-5}	60
7	34.0±0.6	−8.7±1.2	38.4	1.8×10^{-4}	150
8	29.7±1.8	−8.0±4.5	33.8	1.9×10^{-2}	16000

a) Obtained from the data in Table 4. b) Ref. 4.

Discussion

General Consideration. Inspection of molecular models reveals that even in the simplest 9-*t*-alkyltriptycene, 9-*t*-butyltriptycene, the distance between a *peri*-hydrogen and the nearest methyl-hydrogen in the staggered conformation is only 1.5 Å, far shorter than the sum of the van der Waals radii, indicating that the compound itself is a highly crowded molecule. This suggests that introduction of a substituent into one of the *peri*-positions of the triptycyl skeleton should heavily affect the geometry and energy of the molecule.

As an energy barrier to internal rotation is the difference between the ground and the transition states, the influence of the *peri*-substitution on the energy barrier should be understood in terms of perturbation to the both states by the *peri*-substitution. Although the geometry and energy of the transition state can not be directly obtained experimentally, information about those of the ground state may be obtained from several sources.

X-Ray structural analysis of 9-*t*-butyl-1,2,3,4-tetrachlorotriptycene (**15**) revealed the presence of considerable molecular deformation.[14] The most prominent features are the tiltings of the *t*-butyl and the *peri*-chloro groups away from each other (*t*-Bu–C_9–C_{1a}: 118.9°, C_{1a}–C_1–Cl: 125.4°) and the elongation of the C_9–C_{arom} bonds (especially C_9–C_{1a}: 1.603 Å) owing to steric compression.

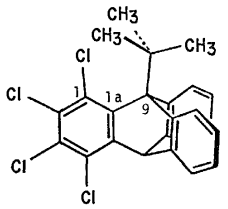

15

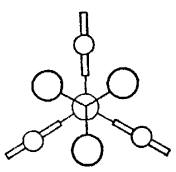

16

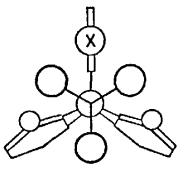

17

We now concentrate our attention to the tilting of the *t*-butyl–C_9 bond from the axis of the triptycene skeleton. The Newman projection of a *peri*-unsubsti-

Table 4. Thermodynamic and kinetic data

$ap \underset{k_{-1}}{\overset{2k_1}{\rightleftharpoons}} \pm sc \qquad K=2k_1/k_{-1}$

Compound	Temp / °C	K	k_1 / s^{-1}	ΔG^* / kcal mol^{-1}
2	258	1.55	1.61×10^{-5}	43.3_4
	246	1.50	5.99×10^{-6}	43.3_6
	238	1.54	3.39×10^{-6}	43.2_5
	226.5	1.27	1.27×10^{-6}	43.2_3
3	259	1.22	3.90×10^{-5}	42.4_9
	246	1.21	1.38×10^{-5}	42.5_0
	239	1.18	8.03×10^{-6}	42.4_6
	220	1.17	1.49×10^{-6}	42.5_0
4	258[a)]	0.66		
	246[a)]	0.63		
	224	0.60	1.72×10^{-5}	40.4_4
	212	0.57	7.15×10^{-6}	40.2_8
	196.5	0.56	1.97×10^{-6}	40.1_7
	175	0.52	2.83×10^{-7}	40.0_2
5	225	0.57	3.16×10^{-5}	39.9_2
	212	0.55	1.21×10^{-5}	39.7_8
	189	0.52	1.71×10^{-6}	39.6_4
	175	0.50	5.54×10^{-7}	39.4_2
6	240[a)]	0.52		
	224.5	0.50	6.10×10^{-5}	39.2_3
	212	0.48	2.49×10^{-5}	39.0_8
	189	0.45	4.09×10^{-6}	38.8_4
	175	0.43	1.10×10^{-6}	38.8_1
7	219	0.38	1.02×10^{-4}	38.3_8
	212.5	0.37	6.55×10^{-5}	38.2_9
	187	0.34	8.61×10^{-6}	37.9_4
8	170[a)]	0.25		
	155[a)]	0.23		
	139.5	0.21	2.92×10^{-5}	32.9_9
	125.5	0.20	6.74×10^{-6}	33.0_0
	111.5	0.18	1.67×10^{-6}	32.8_8
	99.5	0.16	5.37×10^{-7}	32.6_7

a) Only the equilibrium constants are measured.

tuted 9-*t*-butyltriptycene along the *t*-butyl–C_9 bond is shown by **16**. If a substituent is introduced into one of the *peri*-positions, the steric repulsion between the *peri*-substituent and the *t*-butyl group should cause the tilting of the axis bond away from the *peri*-substituent. This feature can be represented by the Newman projection **17**. The degree of the tilting of the axis bond should become larger as the bulkiness of the *peri*-substituent increases. Similar molecular deformation should occur in 9-(1,1-dimethyl-2-phenylethyl)triptycenes.

^{1}H NMR spectral data in Table 1 indicate the tendency that the *ap*-methyl signal of the $\pm sc$ rotamer shifts upfield as the *peri*-substituent becomes bulkier. It is especially remarkable in the *peri*-trifluoromethyl derivative **8**, which shows the *ap*-methyl signal at δ 1.85. This trend seems compatible with the hypothesis that the molecular deformation becomes larger as the *peri*-substituent becomes bulkier. Thus, the larger tilting of the axis bond is rendering the *ap*-methyl group more susceptible to the shielding effect of the flanking benzene rings. Although less remarkable, similar trend is also observed in the methylene signals of the *ap* rotamers.

These features suggest that the ground state of a 9-(1,1-dimethyl-2-phenylethyl)triptycene becomes less and less stable as the *peri*-substituent becomes bulkier.

Rotational Equilibrium. Table 2 shows that the equilibrium is mainly governed by the enthalpy term ($\Delta H°$), the entropy term ($\Delta S°$) being very small. The equilibrium constant K for the *peri*-unsubstituted derivative **1** is a statistical value of 2.0, and this is thought reasonable if one admits that the 2,3-dichloro groups exert no appreciable effects as the first approximation. The $\Delta H°$ value gradually increases and the equilibrium constant at 500 K, K_{500}, monotonously decreases as the *peri*-substituent becomes bulkier. The bulkiness of the substituents is evaluated from the van der Waals radii of the groups. As for a methoxyl group, the radius of an oxygen atom may be used because the steric interaction of the *peri*-methoxyl group with the 9-substituent occurs primarily at the oxygen atom.

If one admits that a benzyl group is bulkier than a methyl, and that the degree of the tilting of the axis bond is similar between the rotamers, it is understood that the $\pm sc$ rotamer is more destabilized than the *ap* rotamer with the increasing bulkiness of the *peri*-substituent, in accordance with the observed tendency.

Rotational Barriers. Table 3 reveals a very interesting dependence of the rotational barrier on the *peri*-substituent. Introduction of a relatively small substituent, such as fluoro and methoxyl, raises the rotational barrier relative to the *peri*-unsubstituted compound **1**, which seems natural according to the normal chemical intuition. However, further increase in the bulkiness of the *peri*-substituent decreases the barrier. Thus, the *peri*-chloro derivatives **4** and **5** have almost the same barrier as **1**, and the *peri*-bromo (**6**) and the *peri*-methyl (**7**) compounds show lower barriers than **1**. Compound **8**, with the bulkiest *peri*-substituent examined, has a barrier 6.6 kcal mol^{-1} lower than that of **1**. Difference in free energies of activation between **2** and **8** amounts to 9.4 kcal mol^{-1}, which corresponds to the rate ratio of 16000 at 500 K. Drop in the barrier height upon introduction of a chloro or a methyl group into a *peri*-position is in accordance with our earlier observation in 9-(1-cyano or methoxycarbonyl-1-methylethyl)triptycenes,[9] and these phenomena seem to be general in 9-*t*-alkyltriptycenes.

As discussed above, the ground state should become less and less stable with the increasing bulkiness of the *peri*-substituent. The trend of the observed barrier heights implies that in the compounds with a bulky *peri*-substituent such as bromo, methyl, and trifluoromethyl, the transition state for rotation is destabilized to a lesser extent than the ground state and that this tendency becomes more remarkable as the *peri*-substituent becomes bulkier. In compounds **2** and **3** with a small *peri*-substituent the destabilization of the transition state exceeds that of the ground state.

It is noteworthy that in the compounds carrying a bulky *peri*-substituent the transition state is not destabilized to such an extent that is expected from the bulkiness of the *peri*-substituent. Consideration on the deformed model with the tilted axis bond mentioned above affords a transition state model which may partly explain the lesser stabilization of the transition state relative to the ground state, as described in the following sections.

For the sake of simplicity, we will discuss on the 9-*t*-butyl compounds, but the similar argument should apply to the 9-(1,1-dimethyl-2-phenylethyl) system. We now consider to rotate the *t*-butyl group around the tilted axis. Here we assume that both the triptycyl skeleton and the *t*-butyl group can be regarded as rigid rotors. The rotational itinerary can be shown by the Newman projections in Scheme 1. We notice

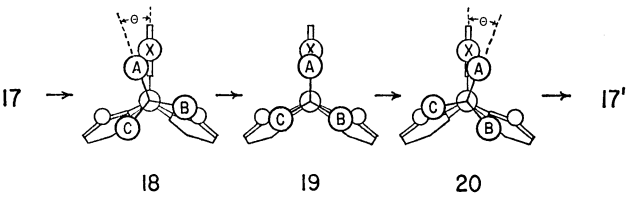

Scheme 1.

that the eclipsing of a methyl in the *t*-butyl group with the *peri*-substituent or a *peri*-hydrogen does not occur simultaneously but sequentially at the three sites. Thus, while eclipsing of methyl A with the *peri*-substituent X occurs in the conformation **19**, that of methyls B and C with nearby *peri*-hydrogens is attained before and after **19**, in conformations **18** and **20** with the torsion angle of $\pm\theta$. Intervals of the maximal eclipsing at the three sites as expressed by the torsion angle θ should become larger as the bulkiness of the *peri*-substituent increases.

Figure 1 schematically illustrates how these situations affect the energy barrier to rotation. We assume that the potential energy profile for rotation (solid lines) can be divided into three mutually independent potential curves (broken lines), each of

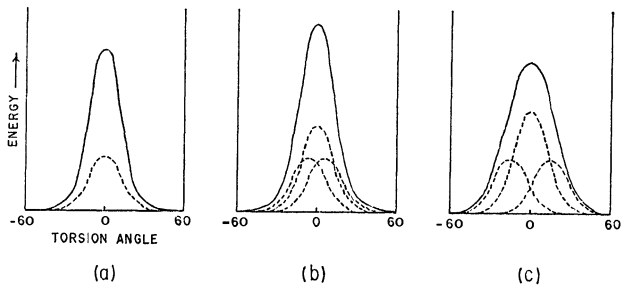

Fig. 1. Schematical illustration of the dependence of the rotational barrier on the molecular deformation. Increase of the tilting of the axis bond causes the increase of separation of the maximal points of the component curves (broken lines) on the abscissa. (a) *peri*-Unsubstituted derivative. (b) Derivatives with a small *peri*-substituent. (c) Derivatives with a bulky *peri*-substituent.

which represents the steric interaction between a methyl of the *t*-butyl group and a nearby *peri*-substituent or a *peri*-hydrogen. Figure 1a shows the energy profile for a *peri*-unsubstituted compound; steric interaction between a methyl and a *peri*-hydrogen has the same potential curve at the three sites and reaches the maximum simultaneously, and thus the solid curve is just three times of the broken line. Figure 1b represents the energy profile for the derivatives with a small *peri*-substituent such as fluoro and methoxyl. Intervals between the maximal interactions at the three sites is small because the tilting of the axis bond is not large, and the rotational barrier (solid line) is higher than that for the *peri*-unsubstituted compound, reflecting that the eclipsing interaction of a methyl with a *peri*-substituent is larger than that with a *peri*-hydrogen. Figure 1c represents the energy profile for the derivatives with a bulky *peri*-substituent. Steric repulsion due to the bulky *peri*-substituent causes a large tilting of the axis bond and thus large separation of the maximal points of the component curves. This results in an energy barrier as high as or even lower than that for the *peri*-unsubstituted compound, in spite of the large increase of the eclipsing interaction between a methyl and the *peri*-substituent.

It has thus been shown that the rough model of two connected rigid rotors with a tilted axis bond can partly explain the observed dependence of the rotational barriers on the bulkiness of the *peri*-substituents. We have assumed that the factors other than the degree of tilting of the axis bond are common among all the derivatives. Quite naturally in actual molecules, each derivative has its own relaxed structure and the triptycene skeleton itself should have different geometry depending on the substitution pattern. Therefore, a substituent remote from the axis bond could affect the rotational equilbrium and the energy barrier. An example is shown by comparison of the data for compounds **4** and **5** which differ only in the presence of the 4-chloro substituent. Although no meaningful difference is observed in the thermodynamic data, the rate data show a small but significant differnce between the two. Compound **5** isomerizes 1.7 times faster than **4** at 500 K with the $\Delta\Delta G^*$ of 0.5 kcal mol^{-1}. This should come from the subtle difference in the structural deformation which is neglected in our rough model.

Experimental

Melting points are not corrected. ^{1}H NMR spectra were recorded on a Hitachi R-20B (60 MHz) or a Varian EM-390 (90 MHz) spectrometer at *ca.* 35 °C with tetramethylsilane as an internal standard. ^{19}F NMR spectra were obtained on a Varian EM-390 spectrometer at 84.67 MHz and the chemical shifts are given in ppm downfield from internal hexafluorobenzene.

1-Fluoroanthraquinone. A mixture of 36.4 g (0.15 mol) of well-dried 1-chloroanthraquinone and 31 g (0.20 mol) of completely anhydrous caesium fluoride in 100 mL of anhydrous dimethyl sulfoxide was heated at 140 °C for 6 h with magnetic stirring. After being cooled to room temperature, the mixture was poured into water. The solid formed was collected by filtration, washed with water and dried in air. The solid was taken up in dichloromethane and then was chromatographed through an alumina column with dichloromethane–hexane (1:4) as eluent, affording 25.1 g (74%) of 1-fluoroanthraquinone as yellow crystals, mp 228—230 °C (lit,[15] 220 °C). ^{19}F NMR ($CDCl_3$): 51.1 ppm (dd, J=4.8 and 10.5 Hz).

*9-(1,1-Dimethyl-2-phenylethyl)-1-fluoro-9,10-dihydro-9-anthrol (**13**).* A mixture of 4.52 g (20 mmol) of 1-fluoroanthraquinone and 1.8 g of aluminium powder in 50 mL of concentrated sulfuric acid was stirred at room temperature for 6 h and poured onto ice–water. The solid formed was collected by filtration, washed with water and dried in air. The crude product was shown to be a 10:1 mixture of 1-fluoroanthrone (^{19}F NMR in $CDCl_3$: 50.0 ppm) and 4-fluoroanthrone (43.9 ppm). Recrystallization from benzene–hexane gave 2.86 g (67%) of a crystalline solid, which was still a 10:1 mixture of the two anthrones. The mixture was used in the subsequent reaction without further purification.

To an ethereal Grignard solution prepared from 16.9 g (100 mmol) of 1,1-dimethyl-2-phenylethyl chloride,[16] was added portionwise 11.0 g (51.3 mmol) of 1-fluoroanthrone and the mixture was decomposed with aqueous ammonium chloride after stirring at room temperature for 1 h. Column chromatography on alumina gave 2.67 g (15%) of **13** as colorless crystals, mp 128—130 °C. Found: C, 83.14; H, 6.60%. Calcd for $C_{24}H_{23}FO$: C, 83.21; H, 6.69%. ^{1}H NMR ($CDCl_3$, δ): 0.75 (3H, d, J_{HF}=1.5 Hz), 0.80 (3H, d, J_{HF}=2.1 Hz), 2.59 and 2.74 (2H, AB-q, J=12.3 Hz), 3.71 (1H, d, J_{HF}=16.3 Hz), 3.90 and 4.18 (2H, AB-q, J=20.0 Hz), 6.6—7.5 (11H, m), 7.92 (1H, m). ^{19}F NMR ($CDCl_3$): 52.21 ppm (br t; br d upon addition of D_2O, J=13 Hz).

*±sc-9-(1,1-Dimethyl-2-phenylethyl)-1-fluorotriptycene (±sc-**2**).* To a solution of 1.445 g (4.17 mmol) of the alcohol (**13**) in 60 mL of carbon tetrachloride was added *ca.* 10 g of phosphorus pentaoxide. The mixture was heated under reflux for 2 min with continuous shaking, and filtered while hot. The solid was washed with hot carbon tetrachloride. The combined solutions were found to contain almost equal amount of 9-(1,1-dimethyl-2-phenylethyl)-1-fluoroanthracene (**14**) and 1-fluoroanthracene, indicating that the dealkylation of **14** under the reaction conditions was considerably fast. The anthracene mixture was immediately treated with 2.0 g of anthranilic acid and 1 mL of isopentyl nitrite in boiling dichloromethane. Column chromatography of the reaction mixture on alumina with hexane as eluent afforded 546 mg (32% based on **13**) of ±*sc*-**2**, mp 193—195 °C. Found: C, 89.20; H, 6.20%. Calcd for $C_{30}H_{25}F$: C, 89.07;

6.23%. ^{19}F NMR ($CDCl_3$): 67.64 ppm (br s).

ap-*9-(1,1-Dimethyl-2-phenylethyl)-1-fluorotriptycene* (ap-**2**). To a solution of 621 mg (2.0 mmol) of 9-(1,1-dimethyl-2-phenylethyl)anthracene (**9**)[17] and 0.4 mL (*ca.* 4 mmol) of *m*-difluorobenzene in 50 mL of anhydrous diethyl ether was added 3.0 mmol of butyllithium in hexane at −78 °C. The mixture was stirred at −78 °C for 1 h, allowed to gradually warm up to room temperature with stirring overnight, and then heated under reflux for 1 h. The ethereal solution was washed with water, dried over magnesium sulfate and evaporated to afford 544 mg (67%) of a 5:1 mixture of *ap*-**2** (^{19}F NMR in $CDCl_3$: 65.07 ppm) and *ap*-**2′** (37.19 ppm). Repeated fractional recrystallizations from hexane gave a pure sample of *ap*-**2**, mp 189—190 °C. Found: C, 88.96; H, 6.25%. Calcd for $C_{30}H_{25}F$: C, 89.07; H, 6.23%. ^{19}F NMR ($CDCl_3$): 65.07 ppm (br s).

General Procedure for the Synthesis of Triptycenes Using Anthranilic Acids. A solution of 2—3 fold excess of an appropriate anthranilic acid in tetrahydrofuran or acetone was added dropwise to a boiling solution of 9-(1,1-dimethyl-2-phenylethyl)anthracene (**9**)[17] and 3-fold excess of isopentyl nitrite in dichloromethane (1,2-dimethoxyethane in the case of **8**) during the course of 1 h and the mixture was heated under reflux for 1 h. After evaporation of the solvent, the residual mixture was chromatographed through an alumina column unless otherwise stated. The desired fractions were evaporated and recrystallized from tetrahydrofuran–hexane.

ap-*9-(1,1-Dimethyl-2-phenylethyl)-1,4-dimethoxytriptycene* (ap-**3**), mp 285—288 °C, was obtained from **9** and 3,6-dimethoxyanthranilic acid[1] in 27% yield. Found: C, 86.04; H, 6.71%. Calcd for $C_{32}H_{30}O_2$: C, 86.06; H, 6.77%.

ap-*1-Chloro-9-(1,1-dimethyl-2-phenylethyl)triptycene* (ap-**4**). Reaction of **9** with 3-chloroanthranilic acid[18] and isopentyl nitrite gave a mixture of *ap*-**4** and *ap*-**4′** in 4:3 ratio. The mixture was chromatographed on a Lobar LiChroprep Si 60 column with hexane as eluent. *ap*-**4′** eluted faster: mp 264—266 °C. Found: C, 85.72; H, 5.72; Cl, 8.40%. Calcd for $C_{30}H_{25}Cl$: C, 85.59; H, 5.99; Cl, 8.42%. ^{1}H NMR ($CDCl_3$, δ): 2.06 (6H, s), 3.92 (2H, s), 5.91 (1H, s), 6.7—8.1 (16H, m). *ap*-**4** followed *ap*-**4′** and was obtained in 16% yield: mp 214—216 °C. Found: C, 85.88; H, 5.75; Cl, 8.50%. Calcd for $C_{30}H_{25}Cl$: C, 85.59; H, 5.99; Cl, 8.42%.

ap-*1,4-Dichloro-9-(1,1-dimethyl-2-phenylethyl)triptycene* (ap-**5**), mp 297—299 °C, was obtained from **9** and 3,6-dichloroanthranilic acid[19] in 48% yield. Found: C, 79.03; H, 5.03; Cl, 15.37%. Calcd for $C_{30}H_{24}Cl_2$: C, 79.12; H, 5.31; Cl, 15.57%.

ap-*1-Bromo-9-(1,1-dimethyl-2-phenylethyl)triptycene* (ap-**6**). Reaction of **9** with 3-bromoanthranilic acid[18] and isopentyl nitrite gave a mixture of *ap*-**6** and *ap*-**6′** in 1:1 ratio. The mixture was chromatographed on a silica-gel column with hexane as eluent. *ap*-**6′** eluted faster: mp 282—284 °C. Found: C, 77.60; H, 5.61; Br, 17.51%. Calcd for $C_{30}H_{25}Br$: C, 77.42; H, 5.41; Br, 17.17%. ^{1}H NMR ($CDCl_3$, δ): 2.07 (6H, s), 3.92 (2H, s), 5.91 (1H, s), 6.6—8.1 (16H, m). Following *ap*-**6′**, *ap*-**6** was obtained in *ca.* 15% yield: mp 226—227 °C. Found: C, 77.63; H, 5.20; Br, 17.46%. Calcd for $C_{30}H_{25}Br$: C, 77.42; H, 5.41; Br, 17.17%.

ap-*9-(1,1-Dimethyl-2-phenylethyl)-1,4-dimethyltriptycene* (ap-**7**), mp 306—308 °C, was obtained from **9** and 3,6-dimethylanthranilic acid[20] in 26% yield. Found: C, 92.99; H, 7.48%. Calcd for $C_{32}H_{30}$: C, 92.71; H, 7.29%.

ap-*9-(1,1-Dimethyl-2-phenylethyl)-1-(trifluoromethyl)triptycene* (ap-**8**). Reaction of **9** with 3-(trifluoromethyl)anthranilic acid[18] and isopentyl nitrite in boiling 1,2-dimethoxyethane gave a 1:1 mixture of *ap*-**8** and *ap*-**8′** in 12% yield. The mixture was separated by chromatography on a Lobar LiChroprep Si 60 column with hexane as eluent. *ap*-**8′** eluted faster mp 249—250 °C. Found: C, 81.74; H, 5.54%. Calcd for $C_{31}H_{25}F_3$: C, 81.92; H, 5.54%. ^{1}H NMR ($CDCl_3$, δ): 2.07 (6H, s), 3.95 (2H, s), 5.83 (1H, s), 6.8—8.2 (16H, m). ^{19}F NMR ($CDCl_3$): 102.90 ppm (s). *ap*-**8** eluted following *ap*-**8′**: mp 210—211 °C. Found: C, 81.67; H, 5.54%. Calcd for $C_{31}H_{25}F_3$: C, 81.92; H, 5.54%. ^{19}F NMR ($CDCl_3$): 115.05 ppm (septet, J=4 Hz).

±sc-*9-(1,1-Dimethyl-2-phenylethyl)-1,4-dimethoxytriptycene* (±sc-**3**) was eluted following the *ap* rotamer in the column chromatography on alumina of the equilibrated mixture of rotamers: mp 218—219 °C. Found: C, 85.78; H, 6.81%. Calcd for $C_{32}H_{30}O_2$: C, 86.06; H, 6.77%.

±sc-*9-(1,1-Dimethyl-2-phenylethyl)-1,4-dimethyltriptycene* (±sc-**7**). The equilibrated mixture of rotamers (±*sc*/*ap*= 0.4) was recrystallized from dichloromethane. Almost pure *ap*-**7** crystallized, leaving a ±*sc*-enriched mixture (±*sc*/*ap*= 5) in the mother liquor, which was evaporated and recrystallized from tetrahydrofuran–hexane affording pure ±*sc*-**7**: mp 209—211 °C. Found: C, 92.48; H, 7.18%. Calcd for $C_{32}H_{30}$: C, 92.71: H, 7.29%.

Kinetic Measurements. Pure rotamers of the compounds examined (±*sc* for **2** and *ap* for the others) were dissolved in 1-chloronaphthalene to make up *ca.* 5—7 wt% solutions. To solutions of **2** and **8** were added *ca.* 3% of 1,4-dibromo-2,3,5,6-tetrafluorobenzene and *p*-chlorobenzylidyne trifluoride, respectively, as lock substances for ^{19}F NMR measurements. An aliquot of *ca.* 0.4 mL of the solutions was put in an NMR sample tube and was heated at a given temperature using a bath of an appropriate boiling liquid. The liquids used are as follows: diphenyl ether (258 °C), diethylene glycol (246 °C), quinoline (238—239 °C), hexylbenzene (226.5 °C), *o*-nitrotoluene (224—225 °C), naphthalene (219—220 °C), nitrobenzene (212—212.5 °C), *trans*-decalin (187—189 °C), decane (175 °C), *p*-xylene (139.5 °C), 2-methoxyethanol (125.5 °C), toluene (111.5 °C), and heptane (99.5 °C). Boiling points were constant within ±0.5 °C. The sample was taken out of the bath at appropriate intervals and the rotamer ratio was obtained by integration of the NMR signals (^{19}F for **2** and **8**, the *gem*-dimethylprotons for the others). Time dependence of the rotamer ratio was analyzed in terms of a first-order reversible reaction and the rate constant was calculated. This procedure was performed at three to four temperatures over 32—50 °C range for each compound, and the Eyring parameters were obtained.

References

1) Part XLIV: M. Ōki, Y. Tanaka, G. Yamamoto, and N. Nakamura, *Bull. Chem. Soc. Jpn.*, **56**, 302 (1983).

2) M. Ōki, *Angew. Chem., Int. Ed. Engl.*, **15**, 87 (1976).

3) M. Nakamura, M. Ōki, and H. Nakanishi, *J. Am. Chem. Soc.*, **95**, 7169 (1973); M. Nakamura, M. Ōki, H. Nakanishi, and O. Yamamoto, *Bull. Chem. Soc. Jpn.*, **47**, 2415 (1974).

4) G. Yamamoto and M. Ōki, *J. Chem. Soc., Chem. Commun.*, **1974**, 713; *Bull. Chem. Soc. Jpn.*, **48**, 3686 (1975).

5) M. Kono, H. Kihara, N. Nakamura, F. Suzuki, and M. Ōki, *Bull. Chem. Soc. Jpn.*, **52**, 1682 (1979); M. Ōki, M. Kono, H. Kihara, and N. Nakamura, *ibid.*, **52**, 1686 (1979).

6) G. Yamamoto and M. Ōki, *Angew. Chem., Int. Ed. Engl.*, **17**, 518 (1978); *Bull. Chem. Soc. Jpn.*, **54**, 473 (1981).

7) F. Suzuki, M. Ōki, and H. Nakanishi, *Bull. Chem. Soc. Jpn.*, **47**, 3114 (1974).

8) Strictly speaking, complete parallelness between the

barriers and the bulkiness of the *peri*-substituents is not obtained. Explanation for these phenomena is still controversial. See: W. D. Hounshell, L. D. Iroff, D. J. Iverson, R. J. Wroczynski, and K. Mislow, *Isr. J. Chem.*, **20**, 65 (1980).

9) S. Otsuka, T. Mitsuhashi, and M. Ōki, *Bull. Chem. Soc. Jpn.*, **52**, 3663 (1979); S. Otsuka, G. Yamamoto, T. Mitsuhashi, and M. Ōki, *ibid.*, **53**, 2095 (1980).

10) A preliminary report has been published: G. Yamamoto, M. Suzuki, and M. Ōki, *Angew. Chem., Int. Ed. Engl.*, **20**, 607 (1981).

11) G. W. Gribble and W. J. Kelly, *Tetrahedron Lett.*, **22**, 2475 (1981).

12) R. W. Franck and E. G. Leser, *J. Org. Chem.*, **35**, 3932 (1970); J. E. Anderson, R. W. Franck, and W. L. Mandella, *J. Am. Chem. Soc.*, **94**, 4608 (1972).

13) Details of the long-range ^{1}H–^{19}F couplings in triptycene derivatives will be discussed elsewhere: G. Yamamoto and M. Ōki, in preparation. See also: J. P. N. Brewer, I. F. Eckhard, H. Heaney, and B. A. Marples, *J. Chem. Soc., C*, **1968**, 664.

14) M. Mikami, K. Toriumi, M. Konno, and Y. Saito, *Acta Crystallogr., Sect. B*, **31**, 2474 (1975).

15) A. Y. Meyer and A. Goldblum, *Isr. J. Chem.*, **11**, 791 (1973).

16) W. G. Brown, C. J. Mighton, and M. Senkus, *J. Org. Chem.*, **3**, 62 (1938).

17) G. Yamamoto, M. Nakamura, and M. Ōki, *Bull. Chem. Soc. Jpn.*, **48**, 2592 (1975).

18) S. J. Holt and P. W. Sadler, *Proc. R. Soc. London, Ser. B*, **148**, 481 (1958).

19) B. R. Baker, R. E. Schaub, J. P. Joseph, F. J. McEvoy, and J. H. Williams, *J. Org. Chem.*, **17**, 149 (1952).

20) S. Gronowitz and G. Hansen, *Ark. Kemi*, **27**, 145 (1967).

Kinetics and Mechanism of the Addition of Iodine Monochloride to Alkenes in Acetic Acid

Nagarajan AMIRTHA, Seshaiyer VISWANATHAN,* and Ramachandran GANESAN

Department of Physical Chemistry, University of Madras, Madras 600025, India

(Received April 16, 1982)

A kinetic investigation of the addition of iodine monochloride (ICl) to some allyl and vinyl compounds in dry acetic acid medium has been carried out at 20,30,40, and 50 °C. In all the cases, the reaction obeys a total third order kinetics, second order in ICl and first order in the substrate. The product formed has been analysed by ^{1}H NMR technique. The reaction stoichiometry was found to be 1:1. The formation of a 1:1 complex between an alkene and ICl has been established for the first time spectrophotometrically and the equilibrium constant evaluated. The effect of the addition of the chloride ion on the reaction rate has been studied. The kinetic and thermodynamic parameters evaluated strongly suggest a mechanism involving dipole-dipole interaction with a bridged iodonium ion intermediate.

This paper deals with the kinetics and mechanism of iodine monochloride addition to some alkenes in acetic acid solvent. Investigations carried out so far on the addition of ICl to unsaturated compounds show that ICl has been mainly used as a reagent to estimate unsaturation. The kinetic aspect of the problem has not received sufficient attention. Only the relative rates of Cl_2–, ICl–, and BrCl– addition to alkenes[1] and the kinetics and mechanism of ICl addition to allyl alcohol,[2] stilbene,[3] and α-eleostearic acid[4] have been reported. This paper reports the first systematic study of the kinetics of ICl addition to allyl and vinyl compounds in dry acetic acid. In this article we report and discuss the kinetic and thermodynamic parameters obtained in the present investigation.

Experimental

Materials. Iodine monochloride,[5] 1-hexene,[6] and methyl crotonate[7] were prepared by the procedures given in the literature. Allyl chloride from BDH (LR) and allyl acetate from Fluka AG (Pract.) were purified by distillation. Methyl acrylate and methyl methacrylate both from Koch Light Co., England,[8] acrylamide from American Cyanamide Co., New York,[9] methacrylamide from Rohm and Haas, Philadelphia,[10] allyl bromide from Riedel,[11] and acetic acid from BDH (LR, 99.5% assay)[12] were all purified according to the methods given in the literature. Potassium iodide, sodium thiosulfate and potassium dichromate used were all BDH analytical grade samples.

Kinetic Measurements. Required volumes of the ICl and the substrate solutions in dry acetic acid of required concentration were thermostated and then mixed in a 500 cm^3 iodine flask with a B-19 standard ground-glass stopper. Known volumes of aliquots were withdrawn after various intervals of time and estimated iodometrically. From the observations made in several experiments, it has been concluded that, unlike in any other halogenation reaction, the loss of ICl from its solution due to volatility is practically nil. It is worth noting that the reproducibility of kinetic runs throughout this study was therefore excellent. Moreover, the reaction was found to be unaffected by light.

Stoichiometry. The stoichiometry of the reaction was investigated by employing the well-known method[13] using a mixture of $KBrO_3$ and KBr.

Product Analysis. The solutions of the substrate and ICl in dry acetic acid of required concentration were mixed and the reaction was allowed to go to completion at 30 °C (24 h). Then the solvent acetic ac l was completely neutralized by the addition of a required quantity of sodium hydrogencarbonate solution. The organic material was then ether extracted, dried with sodium sulfate, the ether was distilled off, and it was subjected to TLC and ^{1}H NMR analyses. TLC analysis showed a single spot indicating the formation of one product only. Further analyses of the products of iodochlorination of allylic and vinylic compounds were carried out in Varian T60 NMR spectrometer using carbon tetrachloride as the solvent and TMS as the internal standard.

UV Absorption Studies. During the course of this work, the existence of an alkene–ICl complex has been proved for the first time spectrophotometrically.[14] The measurements were made on a Specord UV-VIS recording spectrophotometer. The nature of the complex and its formation constant were also determined experimentally.

Results and Discussion

The overall order of the reaction and the individual orders in the reactants were determined by the integration and the differential methods, respectively.[15] The total order was found to be three for allyl and vinyl substrates (Fig. 1). The orders in ICl and in substrate were found to be two and one, respectively (Fig. 2).

With equal initial molar concentrations (in the range 1.0×10^{-3}—4.0×10^{-2} mol dm^{-3}) of the reactants, the reactions were carried out at 20, 30, 40, and 50 °C. The experimental data fitted well into the integrated third order equation which was used in the form $1/(a-x)^2=2k_3t+1/a^2$. The values of $1/(a-x)^2$ were plotted against the time (t) and the rate constant (k_3) values were calculated from the slope of the straight line obtained. Figure 3 shows the integration plots for the methyl acrylate–ICl reaction at different temperatures. Plots were made with $\log k_3$ *versus* $1/T$ (Figs. 4 and 5) for the determination of Arrhenius activation energies (E_a) for the ICl addition to various alkenes studied. The data were analyzed by a least-squares procedure (computer programmed) to get the E_a values together with their standard deviations. The activation entropies (ΔS^*) and the free energies of activation (ΔG^*) were evaluated at 30 °C.

The stoichiometry of the reaction was established

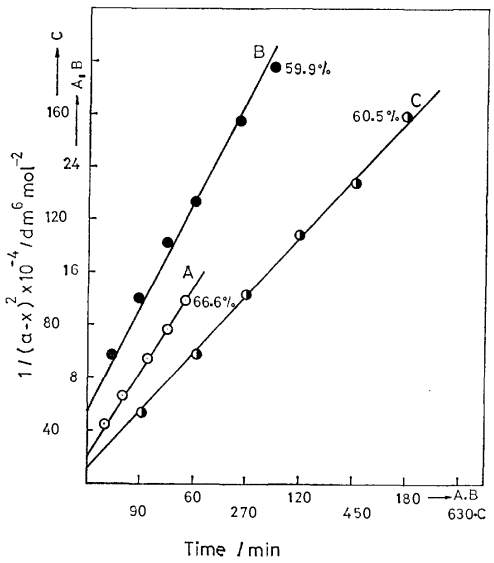

Fig. 1. Plots of $1/(a-x)^2$ against time for allyl chloride-ICl reaction with various equal initial molar concentrations at 50 °C.
A: 8.00×10^{-3} mol dm^{-3}, B: 4.45×10^{-3} mol dm^{-3}, C: 2.00×10^{-3} mol dm^{-3}.

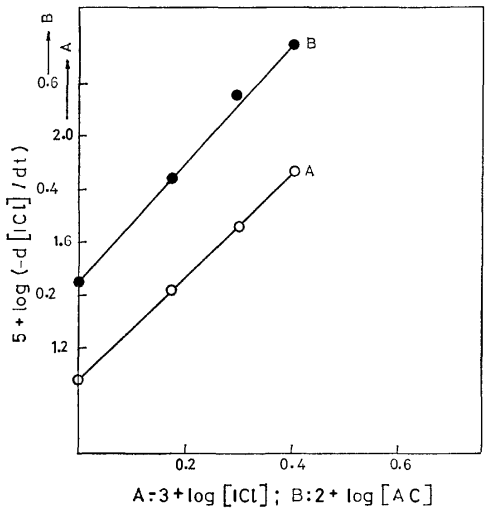

Fig. 2. Plots of log (initial rate) against
A: log [ICl], B: log [AC] for allyl chloride-ICl reaction at 30 °C.

as 1:1. ^{1}H NMR analysis showed $CH_2ICHClCH_2X$ (X=Cl, Br, $COOCH_3$, and $CH_2CH_2CH_3$) to be the product of the allyl substrate–ICl reactions. For the methyl acrylate–ICl reaction, the product was found to be $CH_2ClCHICOOCH_3$. The mode of addition of I and Cl is very similar to this in the case of the other vinyl compounds also. The complex between an alkene and ICl had a characteristic absorption in the region 290—310 nm. Applying Benesi-Hildebrand equation[16] to the methyl methacrylate–ICl reaction, as an example, the formation of a 1:1 complex was proved (ε_c=769.3 dm^3 mol^{-1} cm^{-1}; $K=2.42\times10^{-1}$ dm^3 mol^{-1}).[14]

Based on the above results, the following mechanism, involving a dipole-dipole interaction, may be proposed: Therefore, based on the above mechanism, the rate

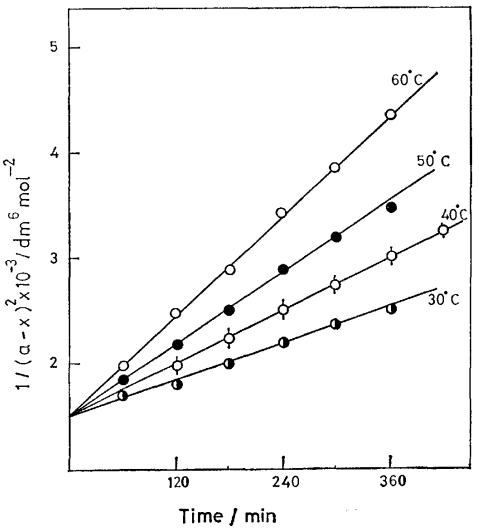

Fig. 3. Plots of $1/(a-x)^2$ against time for methyl acrylate-ICl reaction at different temperatures. [MA]=[ICl]=2.6×10^{-2} mol dm^{-3}.

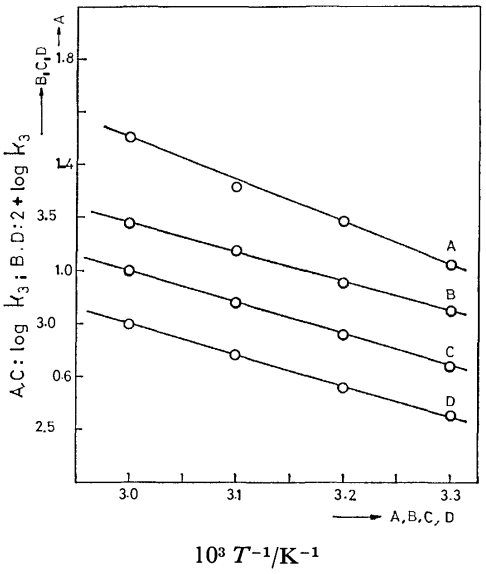

$10^3\,T^{-1}/K^{-1}$

Fig. 4. Plots of log k_3 against $1/T$ for allyl compounds.
A: Allyl chloride, B: allyl bromide, C: allyl acetate, D: 1-hexene.

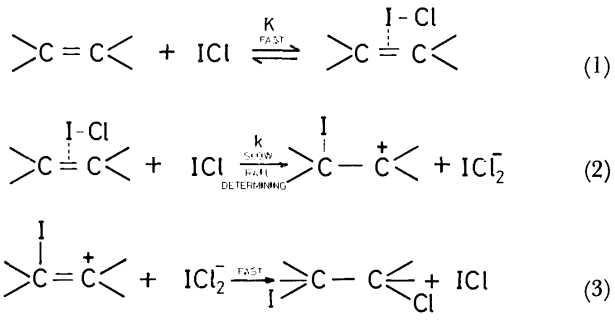

(1)

(2)

(3)

equation can be written as

$$\frac{-d[ICl]}{dt} = k[\pi\text{-complex}][ICl]. \quad (4)$$

The formation of the π-complex is a fast equilibrium process and substituting the expression for [π-complex]

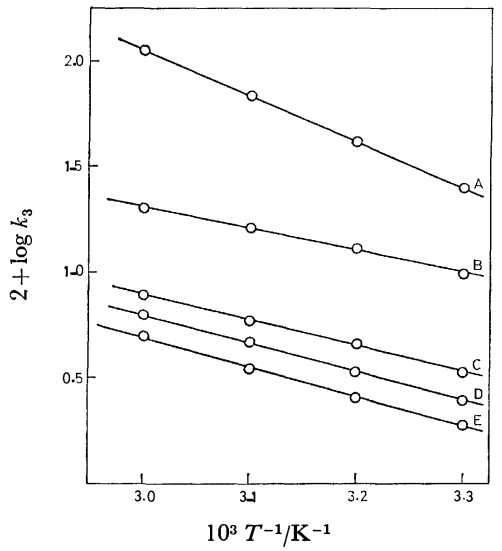

Fig. 5. Plots of log k_3 against $1/T$ for vinyl compounds. A: Acrylamide, B: methacrylamide, C: methyl methacrylate, D: methyl acrylate, E: methyl crotonate.

from Eq. 1 in Eq. 4, the rate equation becomes

$$\frac{-\mathrm{d[ICl]}}{\mathrm{d}t} = kK[\text{alkene}][\text{ICl}]^2, \qquad (5)$$

where $kK=k_3$, (unit $\mathrm{dm^6\,mol^{-2}\,s^{-1}}$). This mechanism, in which a dipolar ICl molecule is the attacking species, is thus consistent with the observed overall third order kinetics with first order in alkene and second order in ICl.

The formation of the π-complex was identified experimentally as mentioned earlier. The second molecule of ICl which attacks the π-complex seems to facilitate the heterolysis of the I–Cl bond in the π-complex by forming ICl_2^- and the carbonium ion. The open carbonium ion formed in Eq. 2 can rearrange itself, in a very fast step, into a more stable cyclic iodonium ion by the interaction of the unshared electrons of iodine with the carbonium ionic centre, as shown below.

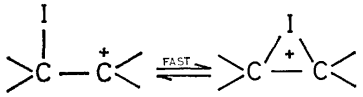

(6)

The existence of the bridged iodonium ion intermediate has been well established by Olah and Bollinger[17] by NMR studies. The activated complex and the measured activation energy correspond to the step (2).

Contrary to the structure **1** proposed in the literature[1] for the π-complex, structure **2** is proposed by

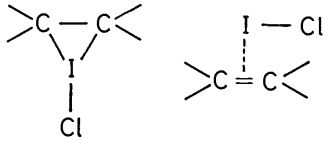

1 **2**

us. As structure **1** is somewhat rigid, free rotation of the I–Cl bond can be only about the I–Cl axis, thus preventing other types of rotations. Moreover, the structure **1** being rigid, the chances of attack by the second molecule of ICl with it will be very remote. If we assume that the C=C bond be in one plane, the I–Cl bond almost parallel to and above or below this plane and the dotted line to be only a loose molecular binding, then the ICl molecule, as depicted in structure **2**, can freely rotate about the dotted line. The second molecule of ICl can, of course, attack the loosely-bound and freely-rotating ICl molecule from any direction. A carbonium ion intermediate is thus formed from the interaction of neutral but slightly dipolar reactant molecules. The activated complex for such a reaction may therefore be expected to be more polar than the reactants and it should closely resemble the ionic intermediate.

The products formed need some explanation. The allyl chloride–ICl and the methyl acrylate–ICl reactions may be considered as representative examples. In the case of allyl chloride, the iodonium ion formed can be opened in two ways (structures **3** and **4**) by

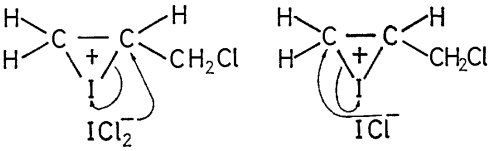

3 **4**

the attack of the nucleophile, ICl_2^-. The opening as in III leads to a secondary carbonium ion and that in IV, a primary carbonium ion. Since the former is more stable than the latter, the iodine atom should attach to the primary carbon and the chlorine atom to the secondary carbon and hence the product, $CH_2ICHClCH_2Cl$. The reverse was, however, found to be the case with methyl acrylate, that is, iodine goes to the secondary carbon and chlorine to the primary carbon. Due to the electron-withdrawing ability of '$COOCH_3$' group and the extensive conjugation, the primary carbon becomes more positive

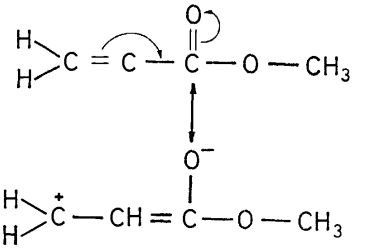

than the secondary. Therefore, in the case of methyl acrylate, iodine atom attaches itself to the secondary carbon and chlorine atom to the primary carbon. Ingold and Smith[18] also obtained a similar product for the reaction between CH_2=CH–SO_3H and ICl. By analogy with the reactions involving the addition of iodine azide[19] and iodine isocyanate,[20] it may be suggested that the ring opening of the iodonium ion intermediate would be expected to occur in a trans manner leading to trans addition products. The iodonium ion proposed in this investigation is strongly supported by these evidences.

Table 1 shows that as the concentration of added chloride ion increases, the rate of the reaction between

Table 1. Effect of added chloride ion on allyl chloride-ICl reaction at 30 °C
[Allyl chloride] = [ICl] = 4.0×10^{-3} mol dm^{-3}.

[Chloride ion] $\times 10^4$/mol dm^{-3}	$(-d[ICl]/dt) \times 10^3$/mol dm^{-3} s^{-1}
5.6	22.05
6.7	19.45
8.7	15.09
10.5	13.03
12.3	9.56

allyl chloride and ICl decreases. This may be due to the equilibrium process

$$ICl + Cl^- \rightleftharpoons ICl_2^-, \quad (7)$$

which results in a decrease of [ICl] available for the reaction. Since ICl is the attacking species, the reaction rate decreases as more and more chloride ion is added to the system. The formation of ICl_2^- is well established and its existence has been reported.[21]

Another possible mechanism to explain the third order kinetics is to postulate the existence of the dimeric species $(ICl)_2$, which can simply react with the alkene to give the products. No evidence could be obtained for the existence of such a dimer, however. From spectrophotometric measurements, it was found that the solutions of ICl in acetic acid obeyed Beer's law over a range in which the concentration of ICl was increased twenty times.

From Table 2, it is seen that the ΔS^* values are negative showing loss in entropy during the formation of the activated complex. The large negative values for ΔS^* are consistent with the fact that the overall reaction is of the third order. The E_a values for the compounds allyl chloride, allyl bromide and allyl acetate are more or less constant. It may be said that the substituents, which are far away from the double bond, do not have any significant effect on the electron density at the reaction site. This is true because the unsubstituted simple alkene, 1-hexene, also has the same E_a value. The subtle changes in the rate constants are due to variations in ΔS^*. In the case of methyl acrylate, methyl methacrylate, methyl crotonate, acrylamide and methacrylamide, the E_a value for a methyl substituted alkene is always lower than that of the corresponding unsubstituted one. It is evident that the electron density at the double bond of the former is greater due to both inductive (+I) and hyperconjugative effects of a methyl group. The same reason can be attributed to the difference in the E_a and k_3 values observed between methyl methacrylate and methyl crotonate.

The rate constants are reversed in the case of the pair, acrylamide and methacrylamide because of the very high and negative ΔS^* value for methacrylamide compared to that for acrylamide. That is, the gain in energy is lost in entropy, in the case of methacrylamide.

The ΔG^* values remain more or less the same for the allyl substrates studied, showing that E_a and ΔS^* compensate each other. The same is found to be the case with the vinyl substrates too.

References

1) E. P. White and P. W. Robertson, *J. Chem. Soc.*, **1939**, 1509.
2) P. B. D. de la Mare, P. G. Naylor, and D. L. H. Williams, *J. Chem. Soc.*, **1963**, 3429.
3) G. Heublein, *Z. Chem.*, **6**, 186 (1966).
4) DjiBin Hu and Sheng-WnWan, *J. Chinese Chem. Soc.*, **10**, 83 (1943).
5) A. I. Vogel, "A Text-book of Practical Organic Chemistry," 3rd ed, (1956), p. 974.
6) J. Von Braun and E. Anton, *Chem. Ber.*, **64**, 2865 (1931).
7) Ref. 5, p. 927.
8) Rohm and Haas, "Technical Bulletin for Monomeric Acrylic Esters," 3rd ed, (1951), p. 8.
9) F. S. Dainton and M. Tordoff, *Trans. Faraday Soc.*, **53**, 499 (1957).
10) F. S. Dainton and W. D. Sisley, *Trans. Faraday Soc.*, **59**, 1369 (1963).
11) Ref. 5, p. 280.
12) K. J. P. Orton and A. E. Bradfield, *J. Chem. Soc.*, **1927**, 983.
13) G. Mino and S. Kaizermann, *J. Polym. Sci.*, **38**, 393 (1959).
14) N. Amirtha and R. Ganesan, *Indian J. Chem.*, **19**, 1119 (1980).
15) K. J. Laidler, "Chemical Kinetics," 2nd ed, McGraw Hill, New York (1965), pp. 5 and 15.
16) J. G. Traynham and J. R. Olechowski, *J. Am. Chem. Soc.*, **81**, 571 (1959).
17) G. A. Olah and J. M. Bollinger, *J. Am. Chem. Soc.*, **89**, 4744 (1967); **90**, 947 (1968).
18) C. K. Ingold and H. G. Smith, *J. Chem. Soc.*, **1931**, 2742.
19) A. Hassner, F. W. Fowler, and L. A. Levy, *J. Am. Chem. Soc.*, **89**, 2077 (1967).
20) A. Hassner and C. H. Heathcock, *Tetrahedron Lett.*, **19**, 1125 (1964).
21) R. B. Heslop and P. L. Robinson, "Inorganic Chemistry," Elsevier, Amsterdam (1960), pp. 245 and 371.

Table 2. Kinetic and thermodynamic parameters for allylic and vinylic compounds

Compound	k_3 (at 30 °C) dm^6 mol^{-2} s^{-1}	E_a kJ mol^{-1}	ΔS^* (at 30 °C) J K^{-1} mol^{-1}	ΔG^* (at 30 °C) kJ mol^{-1}
Allyl chloride	10.49	30.6±1.1	−133.1	68.3
Allyl bromide	11.11	27.2±0.4	−143.6	68.3
Allyl acetate	6.25×10^2	30.1±0.4	−100.5	58.2
1-Hexene	3.67	28.1±0.7	−150.3	71.2
Methyl acrylate	2.43×10^{-2}	28.1±0.3	−191.8	83.7
Methyl methacrylate	3.33×10^{-2}	20.9±1.2	−212.7	82.9
Methyl crotonate	1.95×10^{-2}	24.7±0.3	−190.9	84.2
Acrylamide	25.00×10^{-2}	43.1±0.4	−122.7	77.9
Methacrylamide	9.72×10^{-2}	20.9±1.4	−203.9	80.4

Metal Catalyzed Aquation of Tris(malonato)chromate(III)ion. Kinetics and Mechanistic Study†

Arup Kumar BASAK*,†† and Chinmoy CHATTERJEE**,†††

Inorganic Chemistry Laboratories, University College of Science, Calcutta 700009, India

***Department of Chemistry, Indian Institute of Technology, Powaii, Bombay 400076, India*

(Received February 16, 1982)

Metal ion catalyzed aquation of tris(malonato)chromate(III) ion has been followed spectrophotometrically in perchloric acid solution ($[H^+]=0.05$ M) over a temperature range at an ionic strength of 2.0 M. Under these conditions $k_{obsd}=k_H[H^+]+k_M[M^{2+}]$ where k_{obsd} is the observed first order rate constants for the protons and the metal ion catalyzed pathways. Metal ions exert appreciable catalytic effect on the aquation of the complex with k_M following the sequence Cu(II)>Ni(II)>Co(II)>Zn(II)>Mn(II), which runs parallel to the metal monomalonato complex formation constants. A plausible mechanism for the metal promoted reactions is proposed.

Electrophillic catalysis by metal ions on the coordinated ligands receives much attention in recent years because of the vital role played by Lewis acids in biological processes. It is well known that the phosphate, carboxylate, amino and imidazolyl groups are important metal ion binding sites in biological systems.[1] Metal ions promoted hydrolysis of such coordinated ligands in metal complexes serves as a model for a better understanding of the mechanistic aspects of the biological processes. Bivalent metal ions are required by most enzymes which catalyze phosphate transfer reactions.[2] However the role of Zn(II) and Cu(II) in promoting the biologically important decarboxylation reactions of various acids,[3-5] amino acids and their esters[6] have recently been reviewed and in all cases promotions of hydrolytic reactions requires at least in aqueous solvents the involvement of the catalyzing metal ions and the potentially coordinating sites of the respective acids or esters.

The results of many investigations[7] have already been reported on various reactions of oxalato complexes of Cr(III), but much less informations is available on the analogous Cr(III)–malonato complex because of the inherent instability (kinetic and thermodynamic) of the six membered ring of the malonato system in comparison to the more stable (kinetic and thermodynamic) five membered ring of the oxalato complexes.

Some aquation;[8,9] anation,[10] and isomerization[7,11-13] reactions have been studied and the behavior of the malonato complex appears to be somewhat intriguing from that of the corresponding oxalato complex. In the acid assisted aquation of several carboxylato complexes of Cr(III) it was reported[8,14a-d] that aquation proceeds by a rapid preequilibrium protonation followed by cleavage of the Cr(III)–O bond. In continuation to our earlier studies[15,16] on the metal ion catalyzed aquation of Cr(III) complexes[15-18] it appears worthy of investigation to study the aquation of the title complex into cisdiaquabis(malonato)chromate(III) ion by bivalent metal ions of first transition series.

Here we are reporting the results of investigations on Mn(II), Co(II), Ni(II), Cu(II), and Zn(II) ion catalyzed aquation of $Cr(mal)_3^{3-}$ and the probable mechanism of the Lewis acid catalyzed aquations have been discussed.

The present investigation was undertaken with a view to examine the i) complexing ability of the chelated ligand towards the incoming metal ions and ii) effectiveness of various metal ions in promoting the hydrolysis of the coordinated malonato ligand to chromium(III).

Experimental

Materials and Method. Pure samples of potassium salt of tris and bis complex anions, $K_3[Cr(C_3H_2O_4)_3]\cdot 3H_2O$[19] and *cis*-$K[Cr(C_3H_2O_4)_2(OH_2)_2]$[10] were prepared by methods described in the literature. The purity of the compounds was checked by elemental analysis. Metal(II) perchlorate solutions were prepared by dissolving the corresponding carbonates with A.R. grade perchloric acid and after complete ceasession of the effervesence a slight excess of perchloric acid was added to check any possibility of hydrolysis. The metal ions and the free acid concentrations were determined by standard methods.[20] Other chemicals used were of reagent quality.

Complex		Cr(%)	C(%)	H(%)
$K_3[Cr(C_3H_2O_4)_3]\cdot 3H_2O$	Calcd	9.82	20.42	2.27
	Found	9.90	20.31	2.40
cis-$K[Cr(C_3H_2O_4)_2(OH_2)_2]$	Calcd	15.71	21.76	2.42
	Found	15.66	21.60	2.51

Experimental procedures are the same as described elsewhere.[16] Plots of $\log\{(A_0-A_t)/(A_t-A_\infty)\}$ *versus* time (t) were linear for at least three to four half lives and passing through the origin, where A_∞ is the absorbance of diaqua species and A_t are that at different time interval. The preliminary spectral observations of the reacting solutions after digesting for at least ten half lives agrees well with spectra of the corresponding cis-diaqua product which further indicates that the reaction is free of any undue complication, which may arise from the subsequent aquation of diaqua to tetraaqua products.

Results and Discussion

At a constant hydrogen ion concentration the pseudo first order rate constant, k_{obsd}, is found to increase

† Presented at the XXIst ICCC at Toulouse, France 1980.

†† Present address: Institut für Anorganische Chemie, Universitat Basel, Spitalstrasse 51, CH 4056, Basel, Switzerland.

††† Present address: Chemistry Department, University College, London, England.

with increasing metal ion concentration and at a fixed metal ion concentration, k_{obsd}, also increases with increase in the acidity of the medium.

Detailed analysis of the results indicates that the dissociation of the title complex follows a two term rate law:

$$k_{obsd} = k_1[H^+] + k_2[M^{2+}], \quad (1)$$

where k_1 represents the specific rate constants for the acid catalyzed pathway and k_2 is the catalytic rate constant for the metal-ion-catalyzed process. Using the least squares method, values of $k_1[H^+]$ and k_2 have been evaluated from the linear plot of k_{obsd} *versus* $[M^{2+}]$ (*cf.* Fig. 1). The present k_1 values agree well with that reported earlier.[14b] Values of k_{obsd} at 40 °C for all the metal ions are given in Table 1. Values of k_1 and k_2 corresponding to H^+ ion and different metal ions catalyzed path and the corresponding activation parameters are given in Table 2.

The metal ions exert a substantial catalytic effect and a possible mechanism for the metal ion catalyzed pathway is summarized in Fig. 2.

The mechanistic feature of the above mentioned process is thought to involve a rapid pre-equilibrium step to form an ion pair or a binuclear bridged complex followed by the cleavage of the first Cr(III)–O malonate bond in a slow rate determining step. Very

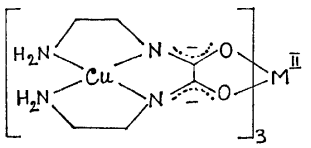

1

recently Kida *et al.*[21] isolated and characterised some tetranuclear bridged complexes of **1** where M^{II}=Co(II),Ni(II). From this it appears that the electron rich carbonyl oxygen can form bonds with catalyzing aquo metal ion centre in the transition state which enhances the ring opening of the malonate ligand as shown in Fig. 2. In view of the above findings the

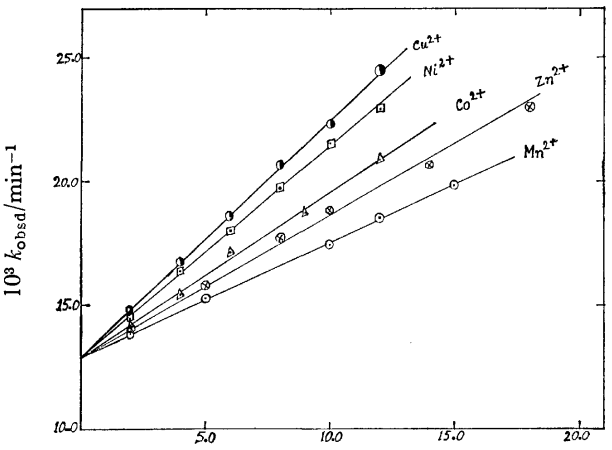

Fig. 1. Dependence of k_{obsd} on the metal ion concentrations at 40 °C, I=2.0 M ($NaClO_4$).

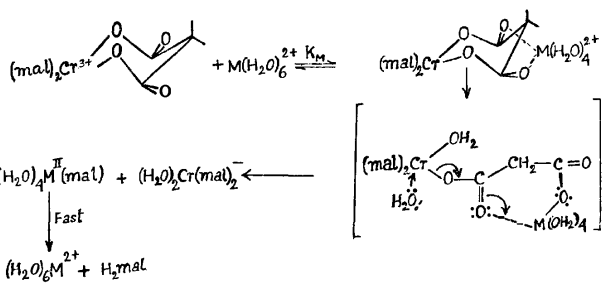

Fig. 2. Probable mechanism for the metal ion catalyzed aquation of $[Cr(mal)_3]^{3-}$ ion.

Table 1. Metal(II) catalyzed aquation of tris(malonato)chromate(III) ion at 40 °C and at ionic strength 2.0 M

[Complex]: 2×10^{-3} M; $[HClO_4]$: 5×10^{-2} M

$10^2[M^{2+}]$ / mol dm^{-3}	$10^3\,k_{obsd}$/min^{-1}				
	Mn(II)	Co(II)	Ni(II)	Cu(II)	Zn(II)
2.0	13.94	14.21	14.43	14.84	14.06
4.0	—	15.42	16.42	16.78	—
5.0	15.35	—	—	—	15.81
6.0	—	17.18	18.02	18.61	—
8.0	—	—	19.76	20.64	17.73
9.0	—	18.72	—	—	—
10.0	17.46	—	21.56	22.26	18.87
12.0	18.55	20.84	22.87	24.42	—
14.0	—	—	—	—	20.63
15.0	19.83	—	—	—	—
18.0	—	—	—	—	22.97

Table 2. Values of k_{cat} for proton and different metal ion catalyzed paths at different temperatures and the corresponding activation parameters at μ=2.0 M

Acid: 5×10^{-2} M; Complex 2×10^{-3} M

Temperature / K	$10^3\,k_{cat}$[a]/s^{-1} M^{-1}					
Ions	H^+	Mn^{2+}	Co^{2+}	Ni^{2+}	Cu^{2+}	Zn^{2+}
303	1.06	0.17	0.47	0.54	0.67	0.35
308	2.15	0.42	0.75	0.94	1.08	0.63
313	4.28	0.79	1.12	1.43	1.63	0.99
ΔH^*/kJ mol^{-1} [b]	109.2	118.9	67.2	73.5	67.6	80.2
ΔS^*/J K mol^{-1} [c]	+55.0	+72.7	−89.5	−67.6	−86.1	−50.0

a) $\sigma(k_{cat})=\pm5\%$. b) $\sigma(\Delta H^*)=\pm2.5$ kJ mol^{-1}. c) $\sigma(\Delta S^*)=\pm5.5$ J K mol^{-1}. N.B. For H^+, k_{cat} stands for k_1 and for other metal ions it represents k_2.

formation of a bridged complex is quite probable in the transition state of the metal catalyzed pathway for the present system.

The kinetic scheme for the aquation of the title complex are as follows.

a) Acid catalyzed pathway was discussed earlier.[14b]

b) Metal ion assisted pathway:

$$Cr(mal)_3^{3-} + M^{2+} \overset{K_2}{\rightleftharpoons} [Cr(mal)_3^{3-} \cdot M^{2+}]$$

$$mal = CH_2(COO^-)_2 \qquad k_2' \downarrow \text{slow}$$

$$(k_2 = k_2' \cdot K_2) \qquad \text{Products.}$$

The catalytic rate constants k_2 is related to K_2 and k'_2 by the relation

$$k_2 = \frac{k_2' \cdot K_2}{1 + K_2[M^{2+}]}. \qquad (2)$$

Under the present experimental conditions $K_2[M^{2+}] \ll 1$ as evident from the linearity of the plot of k_{obsd} *vs.* $[M^{2+}]$ even at highest metal ion concentrations. Hence Eq. 2 reduces to

$$k_2 = k_2' \cdot K_2.$$

The activation parameters corresponding to k_2 values involve both rate constants and equilibrium constants. The overall rate constants for the metal catalyzed process follows the sequence $Cu^{2+} > Ni^{2+} > Co^{2+} > Zn^{2+} > Mn^{2+}$, which follows the Irving-Williams natural order of stability,[22] of the catalyzing metal monomalonato complex. The activation parameters clearly reveal that the metal ion catalyzed aquations with lowest activation enthalpies have more negative entropies of activation whereas for reactions of high enthalpy of activation have positive entropy of activation. The parrallel increase of both ΔH^* and ΔS^* clearly suggests the applicability of kinetic compensation law.[23] Further a linear correlation between $\log k_2$ and $\log K_M$ (K_M=the formation constants of the monomalonato complexes) clearly reflects the dominating effect of K_2 on the metal catalyzed pathway.

We thankfully acknowledge the assistance offered by Professor D. Banerjea, Calcutta University, India regarding laboratory facilities and other critical suggestions in writting the paper.

References

1) H. Sigel and D. B. McCormick, *Acc. Chem. Res.*, **3**, 201 (1970).
2) R. M. Bock, "The Enzymes," ed by P. D. Beyer, M. Lardy, and K. Myrback, 2nd ed, Academic Press, N.Y. (1960), Vol. 2, p. 22.
3) W. D. Covey and D. L. Leussing, *J. Am. Chem. Soc.*, **96**, 3360 (1960).
4) D. L. Leussing and N. V. Raghavan, *J. Am. Chem. Soc.*, **96**, 7147 (1974).
5) N. V. Raghavan and D. L. Leussing, *J. Am. Chem. Soc.*, **99**, 2188 (1977).
6) R. W. Hay, "Metal Ions in Biological Systems," ed by H. Sigel, Marcel Dekker, Basle (1977), Vol. 5.
7) K. Uchita and Y. Takinami, *Bull. Chem. Soc. Jpn.*, **53**, 3522 (1980).
8) D. Banerjea and C. Chatterjee, *J. Inorg. Nucl. Chem.*, **29**, 2387 (1967).
9) C. Furlani and E. Mantovani, *J. Inorg. Nucl. Chem.*, **31**, 1213 (1969).
10) R. E. Hamm and R. H. Perkins, *J. Am. Chem. Soc.*, **77**, 2083 (1955).
11) M. Casula, G. Illuminati, and G. Ortaggi, *Inorg. Chem.*, **11**, 1062 (1972).
12) K. R. Ashley and K. Lane, *Inorg. Chem.*, **9**, 1795 (1970).
13) M. J. Frank and D. H. Huchital, *Inorg. Chem.*, **11**, 776 (1972).
14) a) D. Banerjea and M. S. Mohan, *J. Inorg. Nucl. Chem.*, **27**, 1643 (1965); b) D. Banerjea and C. Chatterjee, *ibid.*, **30**, 3354 (1968); c) D. Banerjea and M. S. Mohan, *ibid.*, **26**, 613 (1964); d) J. C. Chang, *ibid.*, **30**, 945 (1968).
15) R. N. Banerjee and D. Banerjea, *J. Ind. Chem. Soc.*, **55**, 969 (1978).
16) A. K. Basak, D. Banerjea, R. W. Hay, and C. Chatterjee, *J. Coord. Chem.*, **11**, 195 (1981).
17) D. Banerjea, *J. Ind. Chem. Soc.*, **54**, 44 (1977).
18) L. Goswami, S. Sarkar, and D. Banerjea, *Z. Anorg. Allg. Chem.*, **435**, 301 (1977).
19) H. T. S. Britton and M. E. D. Jarrett, *J. Chem. Soc.*, **1935**, 1728.
20) A. I. Vogel, "Text Book of Quantitative Analysis," 4th ed, Longmans, London (1978).
21) H. Okawa, Y. Kawahara, M. Mikuriya, and S. Kida, *Bull. Chem. Soc. Jpn.*, **53**, 549 (1980).
22) H. Irving and R. J. P. Williams, *Nature*, **162**, 746 (1948).
23) R. Romeo, M. L. Tobe, and M. Trozzi, *Inorg. Chim. Acta*, **11**, 231 (1974).

Spectrofluorimetric Determination of Zirconium in Hafnium Metal with Salicylic Acid and Rhodamine B after Its Separation Using Chloroacetic Acid and Salicylic Acid

T. V. RAMAKRISHNA* and M. S. SUBRAMANIAN

Department of Chemistry, Indian Institute of Technology, Madras-600 036, India

(Received April 12, 1982)

A spectrofluorimetric method is described for the determination of 2 to 16 μg of zirconium based on the formation of an ion-association complex with salicylic acid and Rhodamine B. Hafnium behaved similarly to zirconium, but the interference can be overcome by selective extraction of zirconium at pH 1.4—1.6 from 1 mol dm^{-3} chloroacetic acid medium into 0.3 mol dm^{-3} solution of salicylic acid in 2:3 mixture of isobutyl methyl ketone (IBMK) and chloroform. The spectrofluorimetric method in conjunction with the separation procedure has been used for the determination of 4.4 to 14.5% of zirconium in hafnium metal.

Methods have been described for the spectrophotometric determination of zirconium based on the ion-association between its anionic chelates with cationic dyes.[1,2] These complexes were not fluorescent and were extracted into organic solvents prior to determination. In the present work it was found that the ion-association complex involving zirconium(IV), salicylic acid and Rhodamine B can form the basis of an extractive spectrofluorimetric procedure as the presence of traces of zirconium with salicylic acid caused the nonfluorescent Rhodamine B in benzene to intensely fluoresce. However, hafnium behaved very similarly to zirconium and therefore necessitated their separation to be realised beforehand.

Methods have been described for the extractive separation of zirconium from various carboxylic acid solutions. Zirconium was shown to be preferentially extracted in the presence of H_2O_2 at pH 3.2 to 3.6 into organic phase containing 0.5 mol dm^{-3} solution of mixed C_7 to C_9 fatty acids.[3] Cole and Brown[4] achieved a separation factor of 22 for zirconium by using a saturated solution of salicylic acid (1.115 mol dm^{-3}) in furfural. Quantitative extraction of zirconium from 33% trichloroacetic acid solution into 1-butanol[5] and from 0.01 mol dm^{-3} malonic acid at pH 3.0 into a 4% solution of Amberlite LA-1 or LA-2 in xylene[6] have been reported, but the use of these methods for the separation of zirconium from hafnium has not been demonstrated. The preferential extraction of zirconium to the extent of 80% from solutions at pH 1.4± 0.1 into a chloroform solution containing 0.05 mol dm^{-3} salicylic acid and 0.37 mol dm^{-3} collidine has also been described.[7] In the course of our study, it was found that zirconium can be selectively extracted from hafnium, rapidly and quantitatively, from 1 mol dm^{-3} chloroacetic acid at pH 1.4—1.6 into IBMK and chloroform mixture containing salicylic acid. The organic phase upon equilibration with dilute hydrochloric acid returned the zirconium quantitatively into the aqueous phase thus making it available for fluorimetric determination. In conjunction with the extractionprocedure the fluorimetric method developed was found useful for application to samples containing high concentration of hafnium.

Experimental

Reagents. *Standard Zirconium Solution*: Dissolve 0.3532 g of $ZrOCl_2 \cdot 8H_2O$ in 20 cm^3 of 1:1 perchloric acid and dilute to 100 cm^3 with distilled water to provide a 1000 ppm Zr stock solution. Dilute appropriate volume of the stock solution with water, just before use, to obtain 100 ppm and 4 ppm solution.

Salicylic Acid Extraction Solution (0.3 mol dm^{-3}): Dissolve 4.14 g of salicylic acid in 1000 cm^3 of 2:3 mixture of IBMK and chloroform.

Chloroacetic Acid (3 mol dm^{-3}):

Hydrochloric Acid (2.5 mol dm^{-3}):

Salicylic Acid Solution (2%): Dissolve 2 g of salicylic acid in 100 cm^3 methanol and store in a stoppered bottle.

Rhodamine B Solution (0.03%):

Acetate Buffer (pH 4.0):

Apparatus. A Carl Zeiss PMQ II spectrophotometer with a ZFM fluorescent attachment provided with a 250 VA mercury vapour lamp was used. Slit widths of 5 mm for excitation filter and 0.03 mm for emission monochromator were employed for the fluorescence measurements with 10 mm × 10 mm × 45 mm quartz cells with polished bottoms. The instrument was standardised using standard glass fluorescer F53 supplied by the manufacturer.

Procedure. To an aliquot of the sample containing not more than 1000 μg of zirconium, add 5 cm^3 of 3 mol dm^{-3} chloroacetic acid and adjust the pH of the solution to 1.4 to 1.6 using dilute sodium hydroxide and hydrochloric acid. Transfer the solution to 60 cm^3 separatory funnel and dilute to 15 cm^3 with water. Equilibrate the solution for 1 min with 10 cm^3 of salicylic acid extraction solution. Drain the organic phase into another separatory funnel and strip twice with 5 cm^3 portions of 2.5 mol dm^{-3} hydrochloric acid. Boil the solution over a hot plate for 5 min, cool and make up to a suitable volume with water.

Determination of Zirconium: Transfer an aliquot of the stripped phase containing not more than 16 μg of zirconium into a 25 cm^3 beaker. Add 1 cm^3 each of salicylic acid and Rhodamine B solution followed by 5 cm^3 of 0.5 mol dm^{-3} solution of sodium acetate. Adjust the pH to 4.0 and transfer to a 60 cm^3 separatory funnel. Dilute the solution to about 15 cm^3 with water and shake for 1 min with 5 cm^3 benzene. After separating the benzene phase and centrifuging off the water droplets measure the fluorescence intensity of the extracts at 575 nm using 546 nm excitation filter. Subtract the blank reading and establish the concentration of zirconium by reference to a calibration graph prepared by applying the procedure to 0.5 cm^3 to 4 cm^3 of 4 ppm zirconium solution in place of sample solution.

Results and Discussion

The fluorimetric method resulted from an investiga-

TABLE 1. EFFECT OF DIFFERENT PARAMETERS ON THE EXTRACTION OF THE COMPLEX
(Salicylic acid (2.0%) and Rhodamine B (0.03%) solutions 1 cm^3 each at pH 4.0 except when varied as shown) (Zr : 10 μg).

pH	3.4	3.6	3.7	3.9	4.1	4.3	4.4
Fluorescence intensity	19	32	40	40	40	30	25
Salicylic acid solution (%)	0.25	0.5	1.0	2.0	3.0	4.0	5.0
Fluorescence intensity	20	30	40	40	40	37	20
Rhodamine B solution 0.01% (cm^3)	0.5	1.0	2.0	3.0	4.0	4.5	5.0
Fluorescence intensity	20	28	40	41	40	37	35
Extraction time/min	0.5	1	2	3	4	5	
Fluorescence intensity	40	41	41	39	40	40	
Aqueous phase volume (cm^3)	10	12	15	17	20	25	30
Fluorescence intensity	41	40	41	40	40	30	26

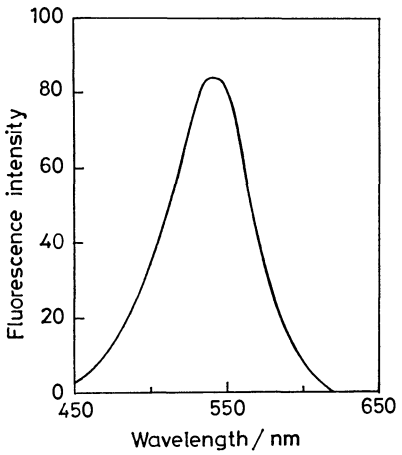

Fig. 1. Excitation spectra (uncorrected) 10 μg of zirconium treated as in determination.

tion of the interaction of Rhodamine B with zirconium after the addition of various carboxylic acids over the pH range 1 to 5. The carboxylic acids examined included mandelic acid, cinnamic acid, anthranilic acid, salicylic acid, and *N*-phenylanthranilic acid. Amongst these, salicylic acid was found to be the best as in its presence the benzene extract was found to be strongly fluorescent with excitation and emission maximum at 546 nm and 575 nm respectively (Figs. 1 and 2). The blank was found to fluoresce only feebly under similar conditions. Using 5 cm^3 benzene for extraction purposes and maintaining an equeous phase volume of 15 cm^3, optimum analytical conditions were established and the results are summarised in Table 1.

The fluorescent intensity of the benzene extract remained stable for at least 4 h and the calibration graph was linear in the range 2 to 16 μg of zirconium.

Ten replicate standard solution containing 10 μg of zirconium gave an average recovery of 101% with a relative standard deviation of 3.9%.

Composition of the Complex. The ratio of zirconium to Rhodamine B in the complex was found to be 1:1 by both mole ratio and continuous variation methods. However the ratio of zirconium to salicylic acid in the complex could not be found out since the extraction of the ion-association complex into benzene was found to be negligible when the salicylic acid

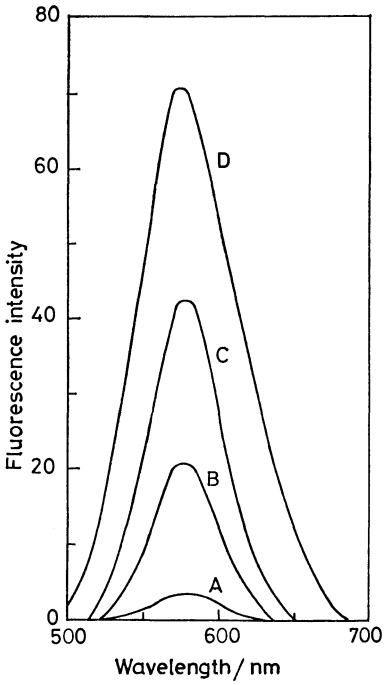

Fig. 2. Emission spectra. (A) 0 μg, (B) 5 μg, (C) 10 μg, and (D) 15 μg of zirconium treated as in determination.

concentration was present in molar proportions.

Interference Studies. Besides hafnium many ions were found to interfere in the determination of 10 μg of zirconium when present in excess of the amounts shown in parantheses. The ions that caused enhancement of fluorescent intensity included UO_2^{2+} (10 μg), Th^{4+} (50 μg) and Sb^{5+} (50 μg), while the presence of Al^{3+} (200 μg), Fe^{3+} or Fe^{2+} (50 μg), Cr^{3+} (50 μg), Ce^{4+} (50 μg), VO_3^- (500 μg), Ti^{4+} (100 μg), MoO_4^{2-} (500 μg), WO_4^{2-} (500 μg), Pd^{2-} (500 μg), Pt^{4+} (500 μg), Bi^{3+} (200 μg), and Sn^{2+} (100 μg) caused a decrease in fluorescent intensity. No interference was encountered from one milligram amounts of Ag^+, Mg^{2+}, Sr^{2+}, Ba^{2+}, Co^{2+}, Ni^{2+}, Cu^{2+}, Mn^{2+}, Zn^{2+}, Hg^{2+}, Cd^{2+}, rare earths, CrO_4^{2-}, AsO_4^{3-}, $S_2O_3^{2-}$, SO_4^{2-}, and SCN^-.

Extractive Separation of Zirconium. Initial studies were made using 1 mol dm^{-3} solution of chloroacetic acid and trichloroacetic acid and 100 μg of zirconium or hafnium. Extractions were made from 15 cm^3 aque-

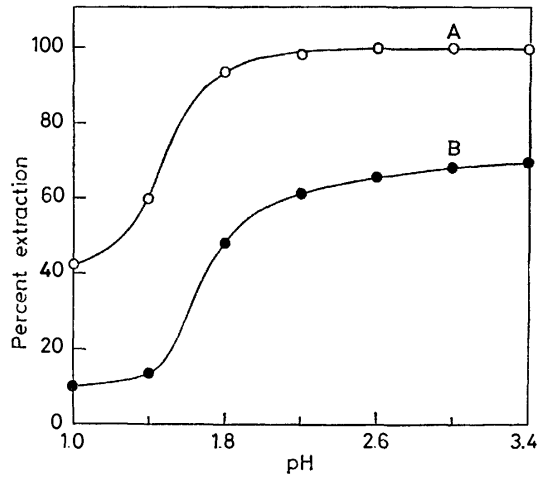

Fig. 3. Percentage extraction of (A) 100 μg of zirconium (B) 100 μg of hafnium as a function of pH. Chloroacetic acid: 1 mol dm^{-3}, IBMK solvent.

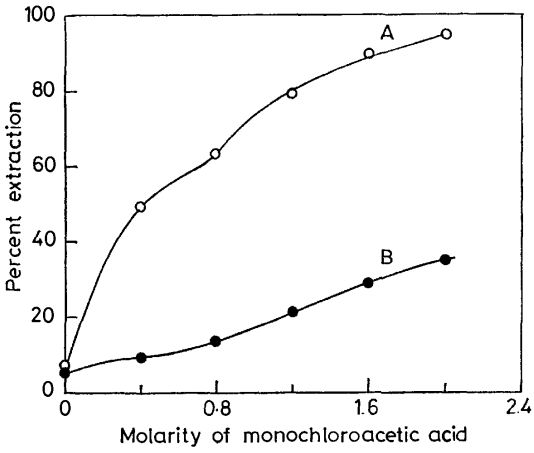

Fig. 4. Percentage extraction of (A) 100 μg of zirconium and (B) 100 μg of hafnium as a function of chloroacetic acid concentration. pH: 1.5, IBMK solvent.

ous phase maintained at pH 0.5, 1.5, and 2.5 into 10 cm^3 IBMK for 5 min. The percentage of zirconium or hafnium extracted was established after stripping the organic phase twice with 5 cm^3 of 2.5 mol dm^{-3} of hydrochloric acid and applying the quercetin procedure.[8] The results showed that zirconium and hafnium extract to varying extent from each of these aqueous systems. Chloroacetic acid at pH 2.5 was found to quantitatively extract zirconium and 60% of hafnium while under similar conditions trichloroacetic acid extracted 82% of zirconium and 40% of hafnium. At other pH conditions, zirconium and hafnium were found to extract to a lesser extent from both systems. Extraction from chloroacetic acid was therefore chosen for further study.

The extraction of zirconium or hafnium as a function of pH is shown in Fig. 3. It is evident that the extraction of zirconium (curve A) is quantitative at pH's greater than 2.5. Hafnium (curve B), though did not extract quantitatively, showed a trend which was very similar to zirconium. The separation factor

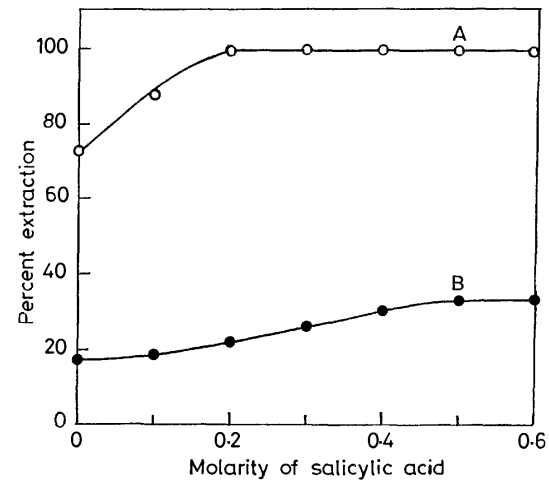

Fig. 5. Effect of salicylic acid concentration on the extraction of (A) 100 μg of zirconium and (B) 100 μg of hafnium into IBMK from 1 mol dm^{-3} chloroacetic acid at pH 1.5.

for zirconium was maximum (13.8) at pH 1.5, where zirconium extraction was incomplete (75%) and hafnium coextracted to a significant extent (18%).

Figure 4 shows the effect of chloroacetic acid concentration maintained at pH 1.5 on the extraction of zirconium (curve A) and hafnium (curve B) into IBMK. It is clear that zirconium extraction does not reach a quantitative value even upon raising the concentration of chloroacetic acid to 2 mol dm^{-3}. In addition, as evident from curve B, the presence of higher concentration of chloroacetic acid also increased the coextraction of hafnium and therefore it was decided to confine the investigation using 1 mol dm^{-3} solution.

Other solvents examined included chloroform butyl acetate, cyclohexanone, benzene, cyclohexane, 1-butanol, and carbon tetrachloride to ascertain the most suitable solvent for the quantitative extraction of zirconium from hafnium. Amongst these chloroform and carbon tetrachloride did not extract either zirconium or hafnium. Cyclohexanone, 1-butanol, cyclohexane, and benzene gave very low separation factor for zirconium. Butyl acetate behaved almost similar to IBMK, but the extraction of hafnium into this solvent was slightly more (22%) than into IBMK (18%).

Studies to improve the extraction of zirconium revealed that the addition of salicylic acid to be effective, as its presence in IBMK was found to quantitatively extract zirconium from 1 mol dm^{-3} chloroacetic acid at pH 1.5. Figure 5 shows the effect of variation of salicylic acid concentration on the extraction of these elements. It is evident that the salicyclic acid concentration should be at least 0.2 mol dm^{-3} for the quantitative extraction of zirconium and that its presence in excess of this amount also increases the extraction of hafnium. To ensure quantitative extraction of zirconium, it was decided to use a 0.3 mol dm^{-3} solution of salicyclic acid in IBMK, though this resulted in the coextraction of hafnium to an extent of 25%.

Attempts to render the organic extract free from hafnium revealed that retrograde extraction with a

fresh aqueous phase of 1 mol dm^{-3} chloroacetic acid at pH 1.5 is ineffective as it caused 5% decrease in the recovery of zirconium. As chloroform did not extract zirconium or hafnium the use of 0.3 mol dm^{-3} salicyclic acid in IBMK–chloroform mixture for extraction was considered. Detailed examination showed that the presence of 5.5 to 6.5 cm^3 of chloroform in 10 cm^3 of the solvent mixture was sufficient for the quantitative extraction of zirconium without the coextraction of hafnium. The presence of chloroform in excess of the volume indicated, resulted in the lower recovery of zirconium.

A shaking time of 1 min was found to be sufficient for the quantitative extraction of zirconium and the extraction remained unaffected up to an aqueous to organic phase volume ratio of 3:2. After extraction, equilibration for 1 min with 10 cm^3 of hydrochloric acid of acidity 1.25 mol dm^{-3} was found to be sufficient for stripping the zirconium quantitatively from the organic phase. However, the use of 2.5 mol dm^{-3} hydrochloric acid was preferred for back-extraction as polymerization of zirconium in this medium has been shown to be minimum.[9]

The results of extraction and back-extraction of 5 to 1000 μg of zirconium showed quantitative recovery over the concentration range examined. In the presence of hafnium there was no evidence of its extraction up to 500 μg. However, when hafnium was present at 1 mg level a slight enhancement in the recovery of zirconium (to the extent of 4%) was noticed.

Nature of the Extracted Species. The plots of log *D* *vs.* log[chloroacetic acid] when extractions were carried out using IBMK containing 0.3 mol dm^{-3} salicyclic acid at pH 1.5 gave straight lines for both zirconium and hafnium with slopes of 0.80 and 0.98 respectively indicating that chloroacetic acid forms 1:1 species with both zirconium and hafnium. Similarly plot of log *D* *vs.* log[salicylic acid] when extractions were carried in the presence of 1 mol dm^{-3} chloroacetic acid, gave slopes of 1.2 and 0.84 for zirconium and hafnium, thus showing that both zirconium and hafnium form 1:1 complexes with both chloroacetic acid and salicylic acid.

Attempts to establish the molar ratio of solvent to metal using benzene as diluent were unsuccessful probably due to the existence of many species with varying number of solvent molecules occupying the coordination positions.

Under the optimal conditions for zirconium, the behaviour of aluminium, titanium, iron(III), thorium, uranium(VI), and vanadium(V) were ascertained using 1 mg amounts of the respective metal ions. After the organic phase was stripped twice with 5 cm^3 portions of 2.5 mol dm^{-3} hydrochloric acid, the concentration of the metal ion in the strippings and in the aqueous phase first subjected to extraction were spectrophotometrically determined using arsenazo III for thorium and uranium,[10] hydrogen peroxide for titanium,[11] 1,10-phenanthroline for iron,[12] Eriochrome cyanine R for aluminium[13] and tungstophosphoric acid for vanadium.[14] The results showed that uranium was not detected in the strippings but 5% of titanium, aluminium, and vanadium, 2.5% of iron and 2% of thorium were found to accompany zirconium.

TABLE 2. RECOVERY OF ZIRCONIUM IN SYNTHETIC MIXTURE

Mixture compositions (μg)	Amount of Zr found (μg)
Zr(100)+Hf(100)+Ti(1000)+SO_4^{2-}(1000)	101
Zr(500)+Hf(5)+La(1000)+Fe(III)(1000)	495
Zr(5)+Hf(500)+U(VI)(1000)+Al(1000)	5.0
Zr(10)+Hf(10)+Th(1000)+U(VI)(1000)	10.2
Zr(20)+Hf(200)+La(1000)+Ti(1000)	19.8

TABLE 3. DETERMINATION OF ZIRCONIUM IN HAFNIUM METAL[a]

Weight of the sample taken (mg/100 cm^3)	Zr added (wt%)	Zr found (wt%)	Average concentration %
50	—	4.40	
50	—	4.60	
50	2.5	7.20	4.60
50	5.0	9.75	
50	10.0	14.50	

a) The sample containing 4.55% zirconium was supplied by Bhabha Atomic Research Centre, Bombay.

The results of the study of the anions revealed that the presence of one milligram amounts of fluoride and phosphate caused a low recovery and sulfate up to 2 mg does not affect the extraction of zirconium.

The method developed was applied in conjunction with the fluorimetric procedure for the determination of 2 to 16 μg of zirconium. After back-extraction into two 5 cm^3 portions of 2.5 mol dm^{-3} hydrochloric acid, the combined strippings in each instance was heated on a hot plate to reduce the volume to 5 cm^3. The solutions were then subjected to determination as described under experimental. A linear relationship was obtained over the whole range and the slope was identical to that obtained for aliquots of standard zirconium solutions that were not subjected to extraction and back-extraction step.

Recovery Studies. The method developed was applied in conjunction with spectrofluorimetry for the determination of zirconium in synthetic mixtures. After back-extraction, the strippings were subjected to the determination as described under determination. The results shown in Table 2 indicate satisfactory recovery in all instances.

Analysis of Hafnium Metal. The zirconium content of a hafnium metal sample was determined by the method developed. 50 mg of the impure hafnium metal was initially brought into solution by dissolving in 3 to 4 drops of hydrofluoric acid in a platinum crucible. Then 10 cm^3 of perchloric acid was added and the solution was evaporated to fumes of perchloric acid. The solution was cooled and made up to 100 cm^3 with water. A suitable aliquot of the solution was pipetted out and the zirconium content was determined by the method described under procedure. Samples to which known amounts of zirconium were added prior to dissolution were also analysed. The

results are shown in Table 3. The close agreement of the results obtained with the reported value suggests that the method developed is useful for the determination of zirconium in hafnium-containing samples.

References

1) S. V. Bel'tyukova, N. S. Poluektov, and S. B. Meshkova, *Zh. Anal. Khim.*, **27**, 191 (1972).
2) Yu. M. Dedkov and T. I. Podvigina, *Zh. Anal. Khim.*, **32**, 437 (1977).
3) Ts. B. Konunova, M. S. Popov, and L. P. Chernega, *Izv. Vyssh. Uchebn. Zaved., Khim. Khim. Tekhnol.*, **19**, 69 (1976); *Anal. Abstr.*, **31**, 2B141 (1976).
4) F. K. Cole and L. H. Brown, *Ind. Eng. Chem.*, **51**, 58 (1959).
5) C. Dragulescu, T. Simenescu, and G. Nemes, *Rev. Roum. Chim.*, **13**, 1469 (1968); *Anal. Abstr.*, **18**, 2337 (1970).
6) M. A. Sawent and S. M. Khopkar, *Talanta*, **27**, 451 (1980).
7) S. K. Kochetkova, V. I. Fadeeva, and V. P. Kalistratova, *Zh. Anal. Khim.*, **31**, 44 (1976).
8) F. S. Grimaldi and C. E. White, *Anal. Chem.*, **25**, 1886 (1953).
9) P. Pakalns, *Anal. Chim. Acta*, **44**, 73 (1969).
10) S. B. Savvin, *Talanta*, **8**, 673 (1961).
11) A. Weissler, *Ind. Eng. Chem., Anal. Ed.*, **17**, 695 (1945).
12) A. I. Vogel, "A Text Book of Quantitative Inorganic Analysis," 3rd ed, The English Language Book Society and Longmans, London (1968), p. 787.
13) A. Bacon, *Analyst*, **77**, 90 (1952).
14) E. B. Sandell, "Colorimetric Determination of Traces of Metals," 3rd ed, Interscience Publishers, New York (1959), p. 926.

Reaction of Quinoxaline Derivatives with Nucleophilic Reagents

Mahmoud Zarif Amin BADR,* Galal Mohamed EL-NAGGAR, Hassan Ahmad Hassan EL-SHERIEF, Abdou El-Sayed ABDEL-RAHMAN, and Moustafa Fouzy ALY

Chemistry Department, Faculty of Science, Assiut University, Assiut, Egypt

(Received February 3, 1982)

2-Chloro-3-methylquinoxaline reacts with aromatic amines in basic medium forming 2-arylamino-3-methylquinoxalines, also it reacts with mercaptoacetic acid. The 3-methyl-2(1*H*)-quinoxalinone condenses with aromatic aldehydes forming the corresponding 3-(substituted styryl)-2(1*H*)-quinoxalinones which add bromine in acetic acid to yield the corresponding dibromo derivatives which react with morpholine, sodium methoxide, and piperidine to give the corresponding compounds. 3-Methyl-2(1*H*)-quinoxalinone undergoes side-chain bromination to yield 3-bromomethyl-2(1*H*)-quinoxalinone, which reacts with aromatic amines, sodium salt of saccharine, potassium phthalimide··· 3-Methyl-2(1*H*)-quinoxalinone with P_2S_5 gave 3-methyl-2(1*H*)-quinoxalinethione which reacts with 2-aminoethanol, dimethyl sulfate, and halo acids.

2- and 3-Substituted quinoxalines were prepared by direct condensation of *o*-phenylenediamines with the proper reagents.[1] However many of such substituents could be prepared by direct substitution on the nucleus[2] or on the side chain.[3]

The present study deals with the synthesis and study of the reactivity of different 2- and 3-substituted quinoxalines and quinoxalinones towards nucleophilic substitution and condensation reactions.

3-Methyl-2(1*H*)-quinoxalinone (**1**) was prepared by condensation of *o*-phenylenediamine and sodium pyruvate.[4] The 3-methyl-2(1*H*)-quinoxalinone reacts with phosphoryl chloride[5] to yield 2-chloro-3-methylquinoxaline (**2**), whose NMR spectra showed a singlet at δ 2.85 (3H, $-CH_3$) and a multiplet centered at δ 7.85 (4H, aromatic ring).

2-Chloro-3-methylquinoxaline reacts with aromatic amines as nucleophilic reagents in dry benzene in presence of anhydrous potassium carbonate and potassium iodide forming the corresponding 2-arylamino-3-methylquinoxalines (**3a—c**).

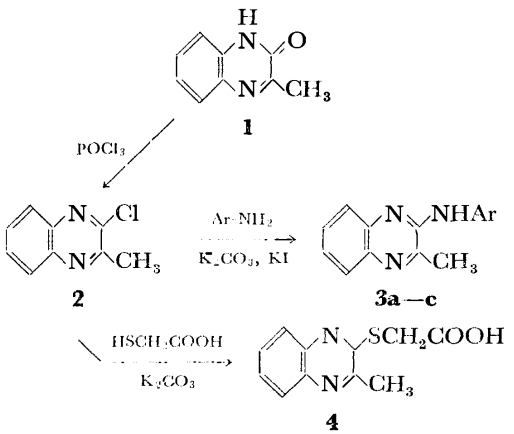

The NMR of the compounds (**3a—c**) were in agreement with the given structures as shown in Table 1. Their IR spectra showed NH band at 3350—3200 cm^{-1}.

Similarly, 2-chloro-3-methylquinoxaline reacts with mercaptoacetic acid in presence of potassium carbonate in dry benzene to yield 2-(carboxymethylthio)-3-methylquinoxaline (**4**) whose IR spectrum showed absorption band at 1710 cm^{-1} (C=O of COOH) and a broad band between 3000—2500 cm^{-1} (associated –OH of COOH). The NMR spectrum shows a singlet at δ 2.75 (3H, $-CH_3$), a singlet at δ 4.1 (2H, $-CH_2-$), a multiplet at δ 7.85 (4H, aromatic ring) and a singlet at δ 11 (1H, –COOH).

3-Methyl-2(1*H*)-quinoxalinone undergoes condensation on fusion with aromatic aldehydes in presence of piperidine forming the corresponding 3-(substituted styryl)-2(1*H*)-quinoxalinones (**5a—k**). The IR spectra showed absorption band at 1620 cm^{-1} of the conjugated C=C. In UV spectra (Table 2) a bathochromic shift (red shift) of the K-band observed in 3-styryl-2(1*H*)-quinoxalinones (**5a—k**) as compared with the parent compound (**1**) (λ_{max} 340 nm) which was attributed to the difference in auxochromic character of the quinoxalinone ring in conjugation with –C=N– group.

o-Hydroxystyryl derivative (λ_{max} 400 nm) showed less bathochromic shift than its *p*-isomer (λ_{max} 406 nm) and this may be attributed to the steric hindrance of the bulky group at the ortho-position, thus distorting the coplanarity of the conjugated system.

The coupling constant of the styryl protons is 15—16 Hz indicating its trans configuration (Table 3).

3-(Substituted styryl)-2(1*H*)-quinoxalinones (**5a—k**) undergo reactions characteristic for α,β-unsaturated compounds. Bromine adds on such compounds in acetic acid to yield the corresponding dibromo derivatives **6a—d**. In the UV spectra of these dibromo compounds, peak near 390—396 nm corresponding to the parent styryl group **5** disappears and only absorbs in the region 346—350 nm which is closely similar to the absorption of the parent quinoxalone nucleus, confirming the absence of the sidechain conjugation at position-2. The NMR spectrum of the dibromide **6b** showed the following characteristic signals: two doublets at δ 2.42 (1H, –CH–C=N) and δ 3.23 (1H, –CH–ph); singlet at δ 6.1 (1H, NH) and symmetrical multiplet centered at 7.52 (8H, aromatic).

The effect of *p*-substituents of the phenethyl moiety of **6a**, **6b** on the halogen susceptibility towards some nucleophilic displacement reactions have been examined. The presence of an electron-donating group such as the *p*-methoxyl group in compound **6a** facilitates the removal of the bromine atoms when refluxed with ethanol to give the corresponding styryl compound. However when refluxed with morpholine in dry benzene it gave a product which contains no bromine

Table 1. NMR spectra of 2-arylamino-3-methylquinoxalines

Compd No.	Ar-	δ			
		CH_3	Aromatic	-NH-	Substituent
3a	C_6H_5	2.6(s)	7.4 —7.8(m)	8.15(s)	—
3b	p-$CH_3C_6H_4$-	2.5(s)	7.35—7.75(m)	8.00(s)	2.5(s, p-CH_3-)
3c	p-ClC_6H_4-	2.7(s)	7.35—7.8(m)	6.65(s)	—

Table 2. UV spectra of 3-(substituted styryl)-2(1*H*)-quinoxalinones

Compd No.	Ar-	λ_{max}/nm	$\varepsilon \times 10^5$
1	—	340	0.09
5a	C_6H_5	390	0.155
5c	p-$CH_3C_6H_4$-	394	0.293
5d	p-$(CH_3)_2NC_6H_4$-	450	0.60
5e	p-ClC_6H_4-	390	0.438
5g	o-HOC_6H_4-	400	0.17
5h	p-HOC_6H_4-	406	0.375
5j	α-$C_{10}H_7$-	396	0.280
5k	p-$NO_2C_6H_4$-	396	0.226

Table 3. NMR spectra of 3-(substituted styryl)-2(1*H*)-quinoxalinones (**5b, d**)

Compd No.	Substituent	NH	-CH=CH-Ar		Aromatic
5b	4.0 (s) (3H, $-OCH_3$)	6.7	7.15	8.2	7.65
5d	3.15(s) (6H, $-N(CH_3)_2$	6.8	7.4	8.25	7.7

and is identified as 3-[1,2-dimorpholino-2-(p-methoxyphenyl)ethyl]-2(1*H*)-quinoxalinone (**7**).

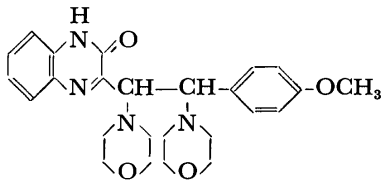

7

On the other hand, the presence of an electron-withdrawing group such as the p-nitro group **6d** gives an additional stability to the halogen atoms to such an extent that they are displaced by sodium methoxide in methanol to give 3-[1,2-dimethoxy-2-(p-nitrophenyl)ethyl]-2(1*H*)-quinoxalinone (**8**).

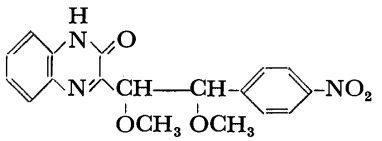

8

When the dibromide **6d** was refluxed with piperidine in dry dioxane, dehydrobromination of the β-bromine occurs followed by substitution of the α-bromine to give the corresponding (α-piperidinostyryl)quinoxalinone (**9**) where the IR spectrum showed absorption band at 1610 cm^{-1} of conjugated C=C. The UV spectra showed λ_{max} at 380 nm confirming the presence of conjugating styryl residue at position-3 with the quinoxalinone ring system.

3-Methyl-2(1*H*)-quinoxalinone dissolved in acetic acid undergoes side-chain bromination in the presence of sodium acetate[6] yielding 3-bromomethyl-2(1*H*)-quinoxalinone (**10**). The latter compound reacts with p-bromoaniline and 1-naphthylamine forming the corresponding 3-arylaminomethyl-2(1*H*)-quinoxalinones (**11a, 11b**). Also it reacts with phenylhydrazine to give 3-(2-phenylhydrazinomethyl)-2(1*H*)-quinoxalinone (**12**) whose IR spectrum showed side-chain -NH- absorption band at 3380 cm^{-1}. The NMR spectrum of compound **12** showed a singlet at δ 2.4 (1H, $-CH_2-NH-$), a singlet at δ 3.3 (2H, $-CH_2-$), a singlet at δ 6.8 (1H, -NH- of quinoxalinone nucleus), a multiplet centered at δ 7.3 (9H, aromatic rings) and a singlet at δ 8.2 (1H, -NH-ph).

3-Bromomethyl-2(1*H*)-quinoxalinone reacts with the sodium salt of saccharin, potassium phthalimide, sodium p-nitrophenolate, thiophenol, silver acetate and thiourea in ethanol as a solvent to give the corresponding substituted compounds **13**, **14**, **15**, **16**, **17**, and **18** respectively.

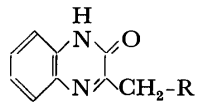

R		R	
11a	p-BrC_6H_4NH-	**15**	$O_2N-C_6H_4-O-$
11b	α-$C_{10}H_7NH$-	**16**	C_6H_4-S-
12	C_6H_5NHNH-	**17**	CH_3COO-
13	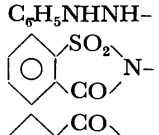	**18**	$HN=C(NH_2\cdot HBr)-S-$
14	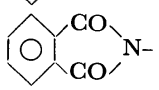		

3-Methyl-2(1*H*)-quinoxalinone (**1**) when refluxed with phosphorus pentasulfide in dry pyridine gave 3-methyl-2(1*H*)-quinoxalinethione (**19**), where IR spectrum showed bands at 3350 cm^{-1} (NH) and 1550 cm^{-1} (C=S).

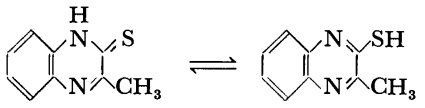

19

The NMR spectrum is in agreement with the thione form and showed a singlet at δ 2.8 (3H, $-CH_3$), a singlet at δ 7.25 (1H, NH) and a multiplet at δ 7.35—7.95 (4H, aromatic).

3-Methyl-2(1*H*)-quinoxalinethione (**19**) reacts with 2-aminoethanol to yield 2-(2-hydroxyethylamino)-3-methylquinoxaline (**20**).

Table 4. 3-(Substituted styryl)-2(1*H*)-quinoxalinones (**5a**—**k**)

Compd No.	Ar–	Yield %	Cryst. solvent	Mp θ_m/°C	Formula	Found (%) C	H	N	Calcd (%) C	H	N
5a	C_6H_5–	53	Dioxane	252	$C_{16}H_{12}N_2O$	—	—	11.30	—	—	11.29
5b	*p*-$CH_3OC_6H_4$–	54	Benzene	249	$C_{17}H_{14}N_2O_2$	—	—	9.98	—	—	10.07
5c	*p*-$CH_3C_6H_4$–	58	Ethanol	250	$C_{17}H_{14}N_2O$	—	—	10.71	—	—	10.68
5d	*p*-$(CH_3)_2NC_6H_4$–	83	Benzene	256	$C_{18}H_{17}N_3O$	74.23	5.71	—	74.23	5.84	—
5e	*p*-ClC_6H_4–	71	1-Butanol	276	$C_{16}H_{11}ClN_2O$	67.93	3.91	9.93	67.96	3.89	9.91
5f	C_6H_5CH=CH–	37	Ethanol	230	$C_{18}H_{14}N_2O$	78.89	5.14	—	78.83	5.11	—
5g	*o*-HOC_6H_4–	38	Ethanol	240	$C_{16}H_{12}N_2O_2$	72.69	4.69	—	72.73	4.55	—
5h	*p*-HOC_6H_4–	76	Benzene	285	$C_{16}H_{12}N_2O_2$	72.80	4.44	—	72.73	4.55	—
5i	2,4-$(OH)_2C_6H_3$–	50	Ethanol	250	$C_{16}H_{12}N_2O_3$	68.50	4.31	—	68.57	4.29	—
5j	α-$C_{10}H_7$–	17	Benzene	230	$C_{20}H_{14}N_2O$	80.50	4.3	—	80.54	4.7	—
5k	*p*-$NO_2C_6H_4$–	52	Acetic acid	310	$C_{16}H_{11}N_3O_3$	—	—	14.55	—	—	14.33

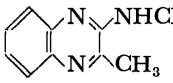

20

The NMR spectrum showed a singlet at δ 2.55 (3H, CH_3), triplet at δ 3.85 (4H, $-CH_2-CH_2-$), singlet at 4.85 (1H, –OH), singlet at δ 5.42 (1H, NH) and multiplet at δ 7.65 (4H, aromatic).

The thione derivative **19** undergo *S*-alkylation, where it reacts with dimethyl sulfate in alkaline medium to give 2-methyl-3-(methylthio)quinoxaline (**21**), with chloroacetic acid to give 3-(carboxymethylthio)-2-methylquinoxaline (**4**) and with 3-bromopropionic acid to give 3-(2-carboxyethylthio)-2-methylquinoxaline (**22**). The NMR spectra of **21** showed a singlet at δ 2.65 (6H, $-CH_3$, S–CH_3) and a symmetrical multiplet centered at δ 7.75 (4H, aromatic).

2-Methyl-3-(methylthio)quinoxaline (**21**) dissolved in acetic acid undergoes side-chain bromination in presence of anhydrous sodium acetate to yield 2-bromomethyl-3-(methylthio)quinoxaline (**23**), whose NMR spectrum showed a singlet at δ 2.75 (3H, S–CH_3), a singlet at δ 4.75 (2H, $-CH_2Br$) and symmetrical multiplet centered at δ 7.85 (4H, aromatic ring).

Experimental

Melting points reported are uncorrected. Elemental analysis was carried out at the microanalytical unit of the National Research Center, El-Doky, Cairo. IR spectra were recorded on a Beckman 20 infrared spectrophotometer using KBr Wafer technique. UV spectra in ethanol were recorded on a Pye-Unicam SP 8000 spectrophotometer and NMR spectra on 90 MHz Bruker spectrospin and Varian EM-390 90 MHz.

*3-Methyl-2(1H)-quinoxalinone (**1**).*[4] White needles from benzene, mp 245 °C.

*2-Chloro-3-methylquinoxaline (**2**).*[5] Colourless needles from light petroleum, mp 86 °C.

Reaction of 2-Chloro-3-methylquinoxaline with Aromatic Amines. A mixture of 2-chloro-3-methylquinoxaline (0.01 mol) and an aromatic amine (0.012 mol) was refluxed for 10 h in dry benzene (20 ml) in presence of anhydrous potassium carbonate and potassium iodide. The reaction mixture was filtered while hot, concentrated and cooled. The separated product was recrystallized from the proper solvent.

*2-(Anilino)-3-methylquinoxaline (**3a**),* colourless needles from ethanol, mp 126—27 °C. Found: N, 17.83%. Calcd for $C_{15}H_{13}N_3$: N, 17.87%. The IR spectrum showed (NH) band at 3350 cm^{-1}.

*2-(p-Toluidino)-3-methylquinoxaline (**3b**),* gray crystals from benzene, mp 172—73 °C. Found: C, 77.08; H, 6.03%. Calcd for $C_{16}H_{15}N_3$: C, 77.11; H, 6.02%. The IR spectrum showed bands, (NH) at 3200 cm^{-1}, (C=N) at 1620 cm^{-1}.

*2-(p-Chloroanilino)-3-methylquinoxaline (**3c**),* yellow crystals from benzene, mp 124 °C. Found: N, 15.53%. Calcd for $C_{15}H_{12}ClN_3$: N, 15.58%. The IR spectrum showed bands, at 3270 cm^{-1} (NH), 1620 cm^{-1} (C=N).

*2-(Carboxymethylthio)-3-methylquinoxaline (**4**).* A mixture of 2-chloro-3-methylquinoxaline (0.01 mol) and mercaptoacetic acid (0.012 mol) was refluxed for 4 h in dry benzene (20 ml) in presence of anhydrous potassium carbonate. Solvent was evaporated and the residue was treated with dil hydrochloric acid and extracted with ether. The ethereal layer was dried and evaporated. The solid product was recrystallized from benzene as yellow crystals, mp 150 °C. Found: C, 56.46; H, 4.26; N, 11.9%. Calcd for $C_{11}H_{10}N_2O_2S$: C, 56.41; H, 4.27; N, 11.97%.

Reaction of 3-Methyl-2(1H)-quinoxalinone with Aromatic Aldehydes. 3-Methyl-2(1*H*)-quinoxalinone (**1**) (0.1 mol) and the aldehyde (0.12 mol) were fused together in presence of few drops of piperidine. The reaction product washed with petroleum ether (60—80 °C) and recrystallized from the proper solvent (Table 4).

Addition of Bromine on 3-(Substituted styryl)-2(1H)-quinoxalinone. To a cold solution of the styryl compound (0.01 mol) in glacial acetic acid (30 ml), bromine (0.01 mol) in glacial acetic acid was added gradually while stirring and the reaction mixture stirred for 1 h. The product was precipitated, filtered off, washed with glacial acetic acid and recrystallized from xylene, yield 65—75%.

*3-[1,2-Dibromo-2-(p-methoxyphenyl)ethyl]-2(1H)-quinoxalinone (**6a**),* white crystals, mp 180 °C. Found: N, 6.45; Br, 36.4%. Calcd for $C_{17}H_{11}Br_2N_2O_2$: N, 6.39; Br, 36.2%.

*3-[1,2-Dibromo-2-(p-chlorophenyl)ethyl]-2(1H)-quinoxalinone (**6b**),* white crystals, mp 255—56 °C. Found: C, 43.36; H, 2.50; N, 6.39%. Calcd for $C_{16}H_{11}Br_2ClN_2O$: C, 43.29; H, 2.48; N, 6.31%.

*3-[1,2-Dibromo-2-(m-nitrophenyl)ethyl]-2(1H)-quinoxalinone (**6c**),* white crystals, mp 275 °C. Found: C, 42.30; H, 2.58; N, 9.23%. Calcd for $C_{16}H_{11}Br_2N_3O_3$: C, 42.38; H, 2.42; N, 9.27%.

*Reaction of Nucleophiles with the Dibromides **6** to Produce the α,β-Disubstituted Products. General Procedure:* A mixture of **6** (0.01 mol) and nucleophile (0.024 mol) in solvent (40 ml) was refluxed together. The hot solution filtered, evap-

orated and the solid separated crystallized from the proper solvent.

3-[1,2-Dimorpholino-2-(p-methoxyphenyl)ethyl]-2(1H)-quinoxalinone (7). From morpholine in dry benzene; 4 h reflux, recrystallized from dioxane as yellow crystals, mp 245 °C, yield 23%. Found: N, 12.37%. Calcd for $C_{25}H_{30}N_4O_4$: N, 12.44%.

3-[1,2-Dimethoxy-2-(p-nitrophenyl)ethyl]-2(1H)-quinoxalinone (8). From sodium methoxide in methanol, 3 h reflux, recrystallized from aqueous methanol as yellow crystals, mp 265 °C, yield 29%. Found: N, 11.90%. Calcd for $C_{18}H_{17}N_3O_5$: N, 11.83%.

3-(α-Piperidino-p-nitrostyryl)-2(1H)-quinoxalinone (9). A mixture of **6d** (0.01 mol) and piperidine (0.024 mol) in dry dioxane (50 ml) was refluxed for 1 h. The hot solution was filtered and concentrated and diluted with drops of water. The separated solid was recrystallized from petroleum ether (60—80) as orange crystals, mp 232—33 °C, yield 49%. Found: N, 14.86%. Calcd for $C_{21}H_{20}N_4O_3$: N, 14.89%.

3-Bromomethyl-2(1H)-quinoxalinone (10),[6] white crystals by sublimation, mp 225 °C (decomp).

Reaction of 3-Bromomethyl-2(1H)-quinoxalinone with Aromatic Amines. A mixture of 3-bromomethyl-2(1*H*)-quinoxalinone (**10**) (0.01 mol), the aromatic amine (0.012 mol) and sodium carbonate was refluxed in ethanol (40 ml) for 3 h. The hot solution was filtered and concentrated, then diluted with few drops of water and the separated solid was recrystallized from the proper solvent.

3-(p-Bromoanilinomethyl)-2(1H)-quinoxalinone (11a), crystallized from ethanol, mp 250 °C (decomp), yield 61%. Found: C, 54.63; H, 3.62; N, 12.75%. Calcd for $C_{15}H_{12}BrN_3O$: C, 54.54; H, 3.63; N, 12.72%.

3-(1-Naphthylaminomethyl)-2(1H)-quinoxalinone (11b), crystallized from ethanol, mp 335 °C, yield 50%. Found: N, 14.04%. Calcd for $C_{19}H_{15}N_3O$: N, 14.00%.

3-(2-Phenylhydrazinomethyl)-2(1H)-quinoxalinone (12), red needles from dioxane, mp 305 °C, yield 83%. Found: C, 67.6; H, 5.22%. Calcd for $C_{15}H_{14}N_4O$: C, 67.66; H, 5.26%.

Reaction of 3-Bromomethyl-2(1H)-quinoxalinone with Organic Acid and Base Compounds. A mixture of 3-bromomethyl-2(1*H*)-quinoxalinone (**10**) (0.01 mol) and (0.012 mol) of each one of the following compounds; sodium salt of saccharin, potassium phthalimide, sodium *p*-nitrophenolate, thiophenol, silver acetate, thiourea, was refluxed for 4 h in ethanol (30 ml). The hot solution was filtered and concentrated, then diluted with few drops of water, the separated solid was recrystallized from aqueous ethanol.

N-(3-Oxo-3,4-Dihydro-2-Quinoxalinylmethyl)saccharin (13), pale brownish crystals, mp 265 °C, yield 59%. Found: N, 12.33%. Calcd for $C_{16}H_{11}N_3O_4S$: N, 12.30%. The IR spectrum showed bands at 3450 cm^{-1} (NH), 1740 cm^{-1} (C=O of saccharin), 1670 cm^{-1} (C=O of quinoxalinone).

3-(Phthalimidomethyl)-2(1H)-quinoxalinone (14), reddish crystals, mp 188 °C, yield 50%. Found: N, 13.74%. Calcd for $C_{17}H_{11}N_3O_3$: N, 13.77%. The IR spectrum showed bands at 3120 cm^{-1} (NH), 1780, 1730 cm^{-1} (2 C=O of phthalimide), 1675 cm^{-1} (C=O of quinoxalinone nucleus).

3-(p-Nitrophenoxymethyl)-2(1H)-quinoxalinone (15), yellowish crystals, mp 190 °C, yield 51%. Found: C, 60.53; H, 3.74%. Calcd for $C_{15}H_{11}N_3O_4$: C, 60.60; H, 3.70%. The IR spectrum showed bands at 3450 cm^{-1} (NH), 1670 cm^{-1} (C=O), 1610 cm^{-1} (C=N), 1520 and 1350 cm^{-1} (NO_2).

3-(Phenylthiomethyl)-2(1H)-quinoxalinone (16), pale brownish needles, mp 178 °C, yield 75%. Found: C, 67.09; H, 4.55%. Calcd for $C_{15}H_{12}N_2OS$: C, 67.16; H, 4.47%. The IR spectrum showed bands at 3150 cm^{-1} (NH), 1675 cm^{-1} (C=O), 1610 cm^{-1} (C=N).

3-(Acetyloxymethyl)-2(1H)-quinoxalinone (17), red crystals, mp 180 °C (decomp), yield 46%. Found: N, 12.82%. Calcd for $C_{11}H_{10}N_2O_3$: N, 12.84%. The IR spectrum showed bands at 3450 cm^{-1} (NH), 1740 cm^{-1} (C=O of ester), 1670 cm^{-1} (C=O of quinoxalinone).

S-(3-Oxo-3,4-dihydro-2-quinoxalinylmethyl)thiouronium Bromide (18), pale brownish needles, mp 232 °C (decomp), yield 64%. Found: C, 38.12; H, 3.54; N, 17.69; Br, 25.42%. Calcd for $C_{10}H_{11}BrN_4OS$: C, 38.09; H, 3.49; N, 17.78; Br, 25.39%. The IR spectrum showed bands at 3300 cm^{-1} (C=NH), 3200 cm^{-1} (NH of quinoxalinone nucleus), 3100—3080 cm^{-1} ($-\overset{+}{N}H_3$), 1655 cm^{-1} (C=O), 1620 cm^{-1} (C=N) and 1280 cm^{-1} (S–R).

3-Methyl-2(1H)-quinoxalinethione (19), 3-Methyl-2(1*H*)-quinoxalinone (**1**) (0.1 mol) and phosphorus pentasulfide (0.1 mol) were refluxed for 4 h in dry pyridine (100 ml). The solvent was evaporated, the residue washed with dil acetic acid, then with water and crystallized from ethanol as yellowish needles, mp 250 °C (sublm.), yield 86%. Found: C, 61.39; H, 4.71; N, 15.79%. Calcd for $C_9H_8N_2S$: C, 61.36; H, 4.54; N, 15.90%. The IR spectrum showed bands at 3350 cm^{-1} (NH), 1620 cm^{-1} (C=N), and 1500 cm^{-1} (C=S).

2-(2-Hydroxyethylamino)-3-methylquinoxaline (20), A mixture of 3-methyl-2(1*H*)-quinoxalinethione (0.01 mol) and 2-aminoethanol (0.012 mol) was refluxed in absolute ethanol (20 ml) for 2 h. The hot solution was filtered and evaporated. The product was recrystallized from ethanol as reddish crystals, mp 105—107 °C, yield 15%. Found: N, 20.76%. Calcd for $C_{11}H_{13}N_3O$: N, 20.69%. The IR spectrum showed bands at 3400 cm^{-1} (OH), 3300 cm^{-1} (NH).

2-Methyl-3-(methylthio)quinoxaline (21), Dimethyl sulfate (0.01 mol) was stirred with 3-methyl-2(1*H*)-quinoxalinethione (0.01 mol) in sodium hydroxide solution (0.01 mol in 10 ml H_2O). The reaction mixture was kept overnight. Ammonium hydroxide was added and the solid product was filtered, washed with water, recrystallized from petroleum ether (60—80) as pale brown crystals, mp 53—54 °C, yield 79%. Found: C, 63.06; H, 5.32; N, 14.47%. Calcd for $C_{10}H_{10}N_2S$: C, 63.15; H, 5.26; N, 14.74%. The IR spectrum showed bands at 1620 cm^{-1} (C=N) and 1250 cm^{-1} (S–CH_3).

Reaction of 3-Methyl-2(1H)-quinoxalonethione with Chloroacetic Acid and 3-Bromopropionic Acid. A mixture of 3-methyl-2(1*H*)-quinoxalinethione (0.01 mol), chloroacetic acid or 3-bromopropionic acid (0.01 mol) and potassium carbonate in ethanol (20 ml) was heated for 15 min. The hot solution filtered and acidified with drops of acetic acid. The product was separated after cooling and recrystallized from the proper solvent.

2-(Carboxymethylthio)-3-methylquinoxaline (4), yellowish crystals from benzene, mp 150 °C, yield 55%. Found: S, 13.62 %. Calcd for $C_{11}H_{10}N_2O_2S$: S, 13.68%. The IR spectrum was coincident with that of reference sample.

2-(2-Carboxyethylthio)-3-methylquinoxaline (22), brownish needles from methanol, mp 194—95 °C, yield 80%. Found: S, 12.82%. Calcd for $C_{12}H_{12}N_2O_2S$: S, 12.90%. The IR spectrum showed bands at 3000—2500 cm^{-1} (associated OH of –COOH), 1730 cm^{-1} (C=O of acid).

3-Bromomethyl-2-(methylthio)quinoxaline (23), a solution of bromine (0.01 mol in 5 ml acetic acid) was added gradually while stirring to a mixture of 2-methyl-3-(methylthio)quinoxaline (0.01 mol) and anhydrous sodium acetate (0.01 mol) in acetic acid (30 ml). The reaction mixture was heated for 15 min. The reaction product was collected by filtration and recrystallized from ethanol as white needles,

mp 136 °C, yield 19%. Found: C, 44.74; H, 3.42; N, 10.12; Br, 29.45%. Calcd for $C_{10}H_9BrN_2S$: C, 44.60; H, 3.35; N, 10.40; Br, 29.74%. The IR spectrum showed bands at 1620 cm^{-1} (C=N) and 1220 cm^{-1} (S–CH_3).

References

1) H. Ohle and W. Gross, *Ber.*, **68**, 2262 (1935); R. B. Barlow, H. R. Ing, and I. M. Lewis, *J. Chem. Soc.*, **1951**, 3242; F. E. King and J. W. Clark-Lewis, *ibid.*, **1951**, 3379; F. D. Chattaway and W. G. Hunphrey, *ibid.*, **1929**, 645; O. Westphall and K. Javn, *Ann.*, **605**, 8 (1957); S. Bodforss, *ibid.*, **609**, 103 (1957).

2) R. K. Anderson and G. W. H. Cheeseman, *J. Chem. Soc., Perkin Trans. 1*, **1974**, 192; R. M. Acheson, *J. Chem. Soc.*, **1956**, 4731; F. J. Wolf, R. M. Welson, Jr., and M. Tishler, *J. Am. Chem. Soc.*, **76**, 2266 (1954); D. C. Morrison and A. Furst, *J. Org. Chem.*, **21**, 470 (1956); H. Saikachi and S. Tagami, *Chem. Pharm. Bull.*, **9**, 941 (1961); *Chem. Abstr.*, **57**, 16614f (1962); C. O. Okafor, *J. Heterocycl. Chem.*, **16**, 1025 (1979).

3) A. H. Cook, J. Garner, and C. A. Perry, *J. Chem. Soc.*, **1942** 710; A. H. Cook and C. A. Perry, *ibid.*, **1943**, 394; W. Borsche and W. Doeller, *Ann.*, **537**, 39 (1938); F. W. Bergstrom and A. Moffat, *J. Am. Chem. Soc.*, **59**, 1494 (1937).

4) D. C. Morrison, *J. Am. Chem. Soc.*, **76**, 4483 (1954), C. Hinsberg, *Ann.*, **292**, 249 (1896).

5) G. T. Newbold and F. S. Spring, *J. Chem. Soc.*, **1948**, 519.

6) C. L. Loso and H. N. Rydon, *J. Chem. Soc.*, **1955**, 303.

© 1983 The Chemical Society of Japan

NOTES

Bull. Chem. Soc. Jpn., 56, 331—332 (1983)

Zeta Potentials of Metal Oxide Surfaces Modified with Silane Coupling Agents

Kunio Esumi* and Kenjiro Meguro

Department of Applied Chemistry, Faculty of Science, Science University of Tokyo, Kagurazaka, Shinjuku-ku, Tokyo 162

(Received June 22, 1982)

Synopsis. The zeta potentials of metal oxide surfaces modified with silane coupling agents were measured as a function of pH in the suspensions. The methylations of the samples by methyltrimethoxysilane showed lower zeta potential values than those of the samples untreated. On the other hand, the treatment of the samples by two different amino silanes rendered the surfaces more cationic. The stability of the deposited silane layers was low; such a layer was easily removed from alumina and anatase-type titanium dioxide.

Coupling agents for modifying many oxide surfaces have been used to improve the bonding between reinforcements and polymer matrix. To elucidate the modified metal oxide surfaces, Fourier transform infrared spectroscopy and Auger electron spectroscopy have been employed. Chiang and Koenig[1] used Fourier transform infrared spectroscopy to study the orientation of silane coupling agents on glass surfaces. However, when surface treatments are applied to a dispersion system containing porous material in solution, the above techniques become inapplicable. In this case, electrokinetic measurements such as zeta potential could be a useful method to detect changes in surface properties. Indeed, Koh[2] reported the change in surface charge density of alumina coated with (3-aminopropyl)triethoxysilane from streaming potential measurements. However, no systematic study has been made on the electrokinetic effects of metal oxides modified with silane coupling agents.

In this work surface properties of several metal oxides modified with silane coupling agents were investigated by measuring the zeta potentials as a function of pH in aqueous solution.

Three silane coupling agents, (3-aminopropyl)tri-

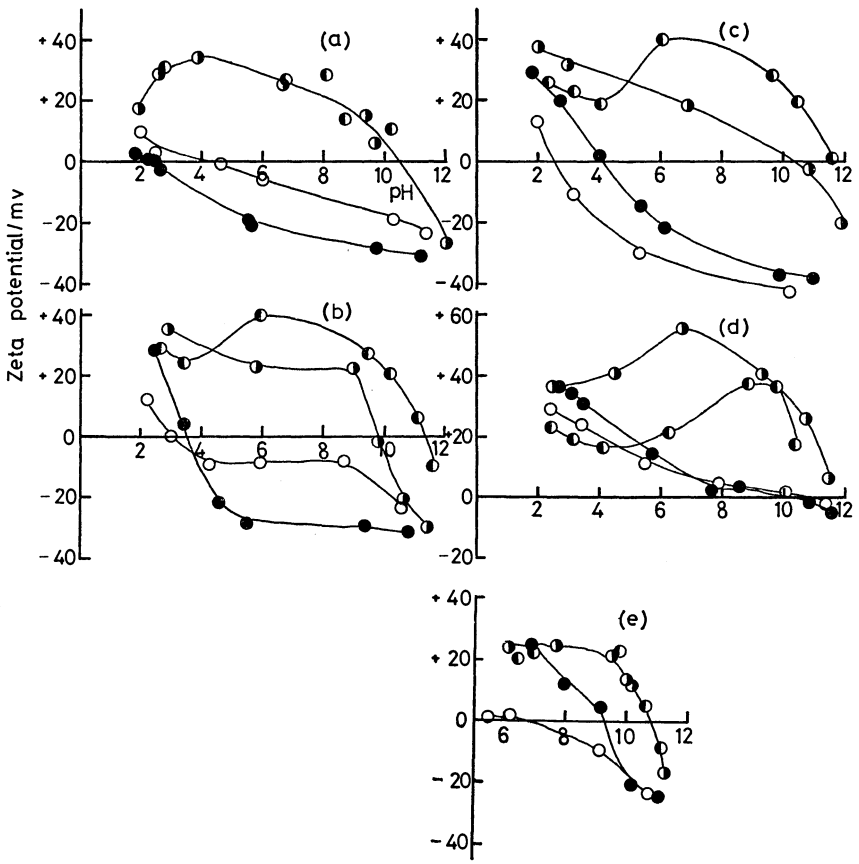

Fig. 1. Zeta potentials of untreated and silane coupling agents treated metal oxides as a function of pH in suspensions: (a) silica, (b) iron oxide, (c) rutile-type titanium dioxide, (d) anatase-type titanium dioxide, (e) alumina; (●) untreated, (○) methyltrimethoxysilane, (◑) (3-aminopropyl)triethoxysilane, (◐) [3-(2-aminoethylamino)propyl]trimethoxysilane.

ethoxysilane, [3-(2-aminoethylamino) propyl] trimethoxysilane, and methyltrimethoxysilane were kindly supplied by Tisso Chemicals, and were used without further purification. Metal oxides employed were titanium dioxide(anatase-type, rutile-type), alumina, iron oxide, and silica supplied by Teikoku Chemicals, Kokusan Chemicals, Titan Chemicals, and Nippon Aerosil Co., respectively.

Coating of silane coupling agents on metal oxide surfaces was carried out with about 3 wt% solution of silane coupling agents in methanol–water mixture (4:1 by volume). Two drops of glacial acetic acid were added to catalyze the hydrolysis. The metal oxide was added and stirred into the silane coupling agent solution for 20 min at room temperature. Then the metal oxide coated with the silane coupling agent was collected and dried in an oven at 80 °C for 10 min.

Measurements of zeta potential for the metal oxides before and after their silane coupling treatments were made using a Pen Kem Laser 500 Zeta Potential. The pH of the suspension containing the metal oxide treated with a silane coupling agent was adjusted with HCl or NaOH.

The stability of untreated and silane coupling agent treated metal oxide suspensions was compared visually in small beakers. The untreated metal oxides were readily dispersible by gentle shaking, whereas the treated metal oxides were initially aggregated. However, they dispersed when the suspensions were treated in an ultrasonic cleaning bath.

Figure 1 depicts zeta potentials of untreated and silane coupling agents treated metal oxides as a function of pH in the suspensions. As can be seen from Fig. 1, the magnitude of zeta potentials for most of the samples treated with methyltrimethoxysilane was smaller over the entire pH range(pH 2—12) than that of untreated samples. This suggests that methylation for the metal oxides affects the electrical double layers to some extent. Further, it was found that the zero point of charge(zpc) for all the samples was not changed significantly after the methyltrimethoxysilane treatment. On the other hand, the zeta potentials of all the samples treated with (3-aminopropyl)-triethoxysilane and [3-(2-aminoethylamino)propyl]trimethoxysilane were positively over a wide pH range. In the case of silica and alumina, no differences of the zeta potentials treated with two kinds of amino silane coupling agents were observed. It is noteworthy

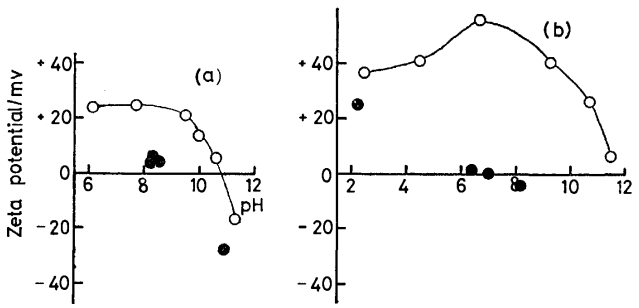

Fig. 2. Change in zeta potential of metal oxide treated with (3-aminopropyl)triethoxysilane: (a) alumina, (b) anatase-type titanium dioxide; (○) immediately, (●) after 1 d.

that the zpc of all the samples treated with two kinds of amino silane coupling agents is shifted to pH 10—12, in spite of the different acid-base character for the metal oxides. These results support the assertion that the polyaminosiloxanes films formed from the hydrolysis of the amino silane coupling agents are coated completely on the metal oxides.

It is also important to study the stability of deposited silane layers on the metal oxides. For this purpose, the samples treated with two kinds of amino silane coupling agents were allowed to stand for one day in aqueous solution a some pH value and then the zeta potential was measured. The results are shown in Fig. 2. The zeta potential after one day became near the original value due to detachment of the silane layers from the metal oxide surface. Especially, as shown in Fig. 2, the changes in the zeta potential after one day were remarkably significant for alumina and anatase-type titanium dioxide coated with the amino silane. Chiang and Koenig[1] studied the hydrothermal stability of silica treated with diamino silane coupling agent; they found that the coupling agent was rapidly removed from the silica surface after it was immersed in boiling water.

Accordingly, zeta potential measurement is a useful method to analyze surface properties of metal oxides treated with silane coupling agents.

References

1) C. H. Chiang and J. L. Koenig, *J. Colloid Interface Sci.*, **83**, 361 (1981).
2) W. H. Koh, *J. Colloid Interface Sci.*, **71**, 613 (1979).

Fluorescence as a Means for Kinetic Studies. II. Preparation and Reactions of Bifunctional Fluorescent Reagents as Kinetic Probes

Akio Okamoto,* Kumiko Toyoshima, and Itaru Mita

Institute of Interdisciplinary Research, Faculty of Engineering, The University of Tokyo, 4-6-1, Komaba, Meguro-ku, Tokyo 153

(Received August 12, 1982)

Synopsis. 1,5-Naphthalenedisulfonyl dichloride was found to be useful as a bifunctional fluorescent probe for kinetic studies. Its reaction with butylamine in chloroform proceeds stepwise. The first reaction produces a nonfluorescent monosulfonamide and the second slow process forms a fluorescent disulfamide. Their rate constants were obtained. Another bifonunctional fluorescent probe was also examined briefly.

Bifunctional reagents have been used extensively in coupling reactions for the network formation of polymers *etc.* The coupling reactions of a bifunctional reagent, X-X, with functional groups in polymers, Y-Ⓟ, consist of two elementary steps, *viz.*, X-X+Y-Ⓟ→X-Ⓟ (k_2^1) and Ⓟ-X+Y-Ⓟ→Ⓟ-Ⓟ (k_2^2). The latter step is a polymer-polymer reaction and may differ from a corresponding polymer-small molecule reaction. However, kinetic studies on the latter step, separately from the former, have been rarely reported because of its experimental difficulties.[1,2] When appropriate bifunctional fluorescent reagents are prepared, they will become useful "kinetic probes" to analyse the coupling reactions for following reasons: (i) The coupling reaction can be traced by fluorometry in very dilute concentration region (10^{-5} to 10^{-7} M) and (ii) if only the final reaction product is fluorescent, the reaction of the second functional group could be traced independently. Fluorescent reagents used widely in biochemistry are usually effective only in aqueous media.[3] But in our previous paper,[4] some monofunctional fluorescent reagents for amine were shown to react with substrates quantitatively by simple bimolecular reaction in organic solvents.

In this note, the reaction of some bifunctional fluorescent reagents with butylamine are investigated in chloroform as a simple model reaction and it will be shown that the reagents meet the requirments stated above and they are useful as bifunctional reagents for the coupling reaction of amino groups.

Experimental

Materials. 1,5-Naphthalenedisulfonyl dichloride (NDSCl) was prepared by the reaction of disodium 1,5-naphthalenedisulfonate with phosphorus pentachloride (72% yield).[5] 7-Dimethylamino-2,4-naphthalenedisulfonyl dichloride (DNDSCl) was prepared from 7-amino-2,4-naphthalenedisulfonic acid *via* trimethylammonium formation (the method of Cope *et al.*:[6] 76% yield), and dimethylamination (a similar method to that of Hünig *et al.*:[7] 83% yield), followed by chlorination (60% yield). The orange extract by chloroform was recrystallized from diethyl ether to give red needles which melted at 124—125 °C (68% yield). The structure was ascertained by NMR and IR. NMR ($CDCl_3$): δ 3.2 (N-C<u>H</u>$_3$), δ 7.6—9.2 (Ar<u>H</u>). IR: 1170 and 1370 cm^{-1} (<u>S</u>O$_2$Cl), 2900 cm^{-1} (N-<u>C</u>H$_3$). Butylamine (*n*-BuNH_2) and 5-dimethylamino-1-naphthalenesulfonyl chloride (DNSCl), both from Tokyo Kasei, and chloroform of "Dotite Spectrosol" grade were used as received.

Apparatus. NMR and infrared spectra were obtained with a 100-MHz JEOL MH-100 and a JASCO IR-G spectrometer, respectively. A Toyo Soda GPC chromatograph (HCL-802UR; G2000H8×2) was used with THF at 40 °C. The fluorometry for kinetic studies was performed without degassing with a JASCO FP-550 spectrofluorometer. Fluorescence was excited at 290 nm (350 nm) and observed in the range of 320—350 nm (475—500 mn) for NDSCl(DNSCl and DNDSCl).

Results and Discussion

As we have reported already,[4] DNSCl is unstable and converted to fluorescent products at room temperature in polar solvents such as methanol, pyridine, and DMF, while it is stable in less polar solvents such as THF, ethyl acetate, and chloroform. In organic solvents, hydrogen chloride formed reacts imediately with amine. The total reaction of NDSCl with amines is expressed as

$$ClO_2S\text{-}R\text{-}SO_2Cl + 2H_2NR' \xrightarrow{k_2^1} ClO_2S\text{-}R\text{-}SO_2NHR' + H_3N^+R'Cl^- \quad (1)$$

and

$$ClO_2S\text{-}R\text{-}SO_2NHR' + 2H_2NR' \xrightarrow{k_2^2} R'NHO_2S\text{-}R\text{-}SO_2NHR' + H_3N^+R'Cl^-. \quad (2)$$

As a bifunctional fluorescent kinetic probe, NDSCl has to satisfy the following requirements: (i) Only the disulfonamide is fluorescent and (ii) the reaction of the second sulfonyl chloride with amine is the rate determining step.

Fluorescence of each of the GPC fraction of the mixture of NDSCl, the monosulfonamide, and the disulfonamide was checked and it was confirmed that only the disulfonamide is fluorescent. Its fluorescence spectrum is shown in Fig. 1 together with its absorption spectrum.

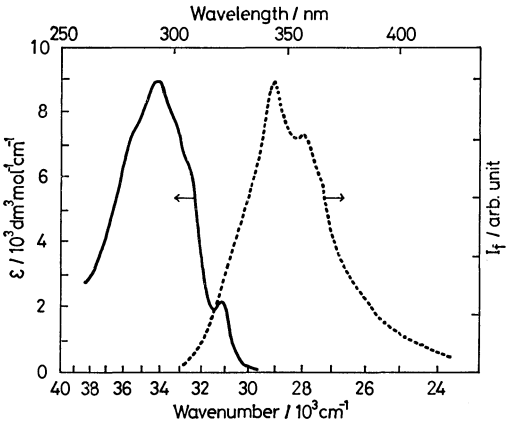

Fig. 1. Absorption and fluorescence spectra of the final reaction product of NDSCl with *n*-BuNH_2 in chloroform.

Table 1. Reaction conditions and k_2^1 for competitive reactions of NDSCl and DNSCl with n-$BuNH_2$

$[n\text{-BuNH}_2]_0$ / 10^{-5} M	$[\text{DNSCl}]_0$ / 10^{-5} M	$[\text{NDSCl}]_0$ / 10^{-5} M	t_1		t_2	
			$\frac{[\text{DNSCl}]}{[\text{DNSCl}]_0}\times 100$	k_2^1 / $M^{-1}\,s^{-1}$	$\frac{[\text{DNSCl}]}{[\text{DNSCl}]_0}\times 100$	k_2^1 / $M^{-1}\,s^{-1}$
1.01	0.99	1.00	9.32	0.56	9.83	0.53
0.99	0.98	—	28.2		30.3	
0.20	0.99	0.20	3.78	0.59	3.90	0.59
0.20	0.99	—	5.66		5.90	

While the chloroform solution of NDSCl (*ca.* 10^{-5} M) and n-$BuNH_2$ in equimolar amount or excess to the sulfonyl group becomes highly fluorescent in a few hours at room temperature, the reaction mixture with n-$BuNH_2$ in half equimolar amount to the sulfonyl chloride group or less is almost nonfluorescent even after a few days. This preliminary test clearly shows that the reaction of the first sulfonyl chloride group is much faster than that of the second one.

The second-order rate constants, k_2^1 and k_2^2, were estimated from the pseudo first-order rate constants for the reaction of NDSCl with large excess of n-$BuNH_2$ $k_1=k_2^1[n\text{-BuNH}_2]$ and $k_2=k_2^2[n\text{-BuNH}_2]$. The concentration of the final product, [$BuNHO_2S$-R-SO_2NHBu], at a certain time t can be obtained as,

$$\frac{[\text{BuNHO}_2\text{S-R-SO}_2\text{NHBu}]}{[\text{ClO}_2\text{S-R-SO}_2\text{Cl}]_0} = 1 - \frac{k_2}{k_2-k_1}\cdot\exp(-k_1t) - \frac{k_1}{k_1-k_2}\cdot\exp(-k_2t). \quad (3)$$

For $k_1>k_2$ and large t, the last term can be disregarded and Eq. 3 is converted to

$$\ln\left(1-\frac{[\text{BuNHO}_2\text{S-R-SO}_2\text{NHBu}]}{[\text{ClO}_2\text{S-R-SO}_2\text{Cl}]_0}\right) = \ln\left(\frac{k_1}{k_1-k_2}\right) - k_2t. \quad (4)$$

Figure 2 shows the pseudo first-order plot of the reaction of NDSCl with large excess of n-$BuNH_2$ in chloroform at 40 °C. The slope and the intercept of the extraporation of the linear line at the later stage of the reaction give k_2 (hence k_2^2) and the ratio k_1/k_2 (hence k_2^1). They are: $k_2^1=5.0\times10^{-1}\,M^{-1}\,s^{-1}$ and $k_2^2=4.8\times10^{-2}\,M^{-1}\,s^{-1}$.

The values of k_2^2 of the reaction was obtained also by the analysis of the three competitive reactions, *i.e.*, the reactions (1), (2), and the reaction of DNSCl with n-$BuNH_2$,

$$\text{DN-SO}_2\text{Cl} + 2\text{H}_2\text{N-Bu} \xrightarrow{k_2^3} \text{DN-SO}_2\text{NHBu} + \text{H}_3\text{N}^+\text{BuCl}^-. \quad (5)$$

For the reactions between DNSCl and n-$BuNH_2$ with and without NDSCl in chloroform at 40 °C, the concentration of the reaction product from DNSCl at a certain time was obtained by fluorometry. With the values of k_2^2 and k_2^3 (4.8×10^{-2} and 3.3×10^{-2}[5] $M^{-1}\,s^{-1}$ respectively), computer simulations of the competitive and non competitive reactions were performed to obtain the optimum value of k_2^1 which satisfies a couple of values of $[\text{DNSCl}]/[\text{DNSCl}]_0$ at a certain time. Table 1 shows that four values of k_2^1, obtained independently for two different concentrations of NDSCl and two different moments, are in fair agreement with each other. The mean value of k_2^1, 0.57 $M^{-1}\,s^{-1}$, is in accord with the value from the pseudo first-order reaction described above. These results confirm that the reactivity of the first sulfonyl chloride group in NDSCl is about 10 times higher than that of the second one and the rate determining step is the reaction of the second sulfonyl chloride group.

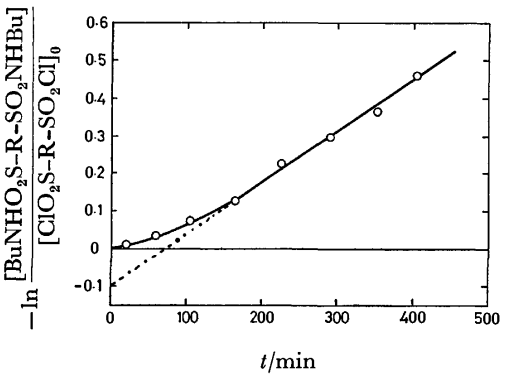

Fig. 2. Pseudo first-order plot of the reaction of NDSCl with n-$BuNH_2$ in chloroform at 40 °C: $[\text{NDSCl}]_0=1.13\times10^{-5}$ M and $[n\text{-BuNH}_2]_0/[\text{NDSCl}]_0=42$.

As another bifunctional fluorescent amine reagent, DNDSCl was synthesized and its reaction with n-$BuNH_2$ was studied briefly. The preliminary test similar to NDSCl indicates that the second reaction of DNDSCl with amine can be detected by the fluorometry which is characterized by an excitation wavelength reached at visible region (absorption maxima: 280 and 390 nm). DNDSCl may, therefore, be more useful than NDSCl as a general fluorescent probe for studies in many fields, because even the presence of most chromophores (benzene derivatives, indole rings, *etc.*) does not interfere the fluorescence measurements with the excitation wavelength.

In conclusion, NDSCl and probably DNDSCl as well are proved to be useful as bifunctional fluorescent probes to analyse the coupling reaction of amino groups kinetically. Its application will be published in near future.[8]

References

1) V. B. Vollmert and H. Stutz, *Angew. Makromol. Chem.*, **35**, 75 (1974).
2) A. Okamoto, Y. Shimanuki, and I. Mita, *Eur. Polym. J.*, **18**, 545 (1982).
3) Y. Kanaoka, *Angew. Chem.*, **89**, 142 (1977).
4) A. Okamoto, K. Uchiyama, and I. Mita, *Bull. Chem. Soc. Jpn.*, **55**, 3068 (1982).
5) P. D. Caesar, *Org. Synth.*, Coll. Vol. IV, 693 (1963).
6) A. C. Cope, E. Ciganek, L. J. Fieckenstein, and M. A. P. Meisinger, *J. Am. Chem. Soc.*, **82**, 4651 (1960).
7) S. Hunig, H. Quast, W. Brenninger, and E. Frankenfeld, *Org. Synth.*, Coll. Vol. V, 1018 (1973).
8) A. Okamoto, K. Toyoshima, and I. Mita, *Eur. Polym. J.*, in press

Relative Stabilities of 2*n* Framework Electron Clusters. Perhalogenated Neutral *closo*-Boranes

Jun-ichi AIHARA

Department of Chemistry, Faculty of Science, Shizuoka University, Oya, Shizuoka 422

(Received January 8, 1982)

Synopsis. As in the case of the *closo*-borane dianions, relative stabilities of the title compounds can be elucidated by means of the graph theory of aromaticity.

The perhalogenated neutral *closo*-boranes are of special interest because so little is known about their bonding character.[1,2] In many cluster compounds the geometric shape of the framework is determined by the number of electrons delocalized within the framework molecular orbitals.[3,4] Polyhedral species with $(2n+2)$ framework electrons usually have deltahedral geometries while those with only 2n framework electrons are often found to be capped deltahedra.[3,4] The perhalogenated *closo*-boranes of the general formula B_nX_n (X=Cl, Br), however, appear to be quite a different class of molecules which do not adopt the structures predicted by the framework electron counting rules.[1,2] Each of these boranes has only $2n$ framework electrons, but the structures observed for them are mostly the ones associated with the frameworks containing two additional electrons.[1,2,4,5]

We have been developing the graph theory of aromaticity.[6] I previously applied it to the *closo*-borane dianions,[7] and correctly predicted high stabilities of $B_{12}H_{12}^{2-}$ and $B_{10}H_{10}^{2-}$. Therefore, we can fully expect that the same theory might be useful for estimating stabilities of the neutral *closo*-boranes, and that the results might give an important clue to predicting stabilities of the perhalogenated derivatives. In order for this to be seen, the theory was applied to nine neutral *closo*-boranes. All the frameworks were assumed to be deltahedral in shape.[5] The Kettle-Tomlinson bonding model[8] was adopted to describe the framework molecular orbitals. This model uses three-center BBB bonding orbitals, localized at the individual faces of deltahedral borane, as basis functions for the molecular orbital calculation. Resonance energies thus calculated for the neutral *closo*-boranes, *i.e.*, the stabilization energies due to aromaticity, are listed in Table 1. Reference polynomials needed to evaluate the resonance energies can easily be obtained by the use of the computer program reported by Mohar and Trinajstić.[11] The quntity 'resonance energy per face (REPF)' was defined as the resonance energy divided by the number of faces of the deltahedral framework.[7] This can be regarded as a resonance energy normalized with respect to the size of the framework. The REPF values are also listed in Table 1. All the energies are given in units of β or the absolute value of the resonance integral between three-center BBB bonding orbitals which correspond to polyhedron faces with an edge in common.

First, the resonance energies of all B_nH_n species are found to be much smaller than the resonance energy of any *closo*-borane dianion. This implies that the neutral *closo*-boranes are not highly aromatic, and tend to undergo reductions to the dianions. These species should be much less stable. Incidentally none has been observed to date.

TABLE 1. RESONANCE ENERGIES OF NEUTRAL *closo*-BORANES

Species	$RE^{a)}/\beta$	$REPF^{b)}/\beta$
B_4H_4	0.0000	0.0000
B_5H_5	−0.9806	−0.1634
B_6H_6	−1.0196	−0.1274
B_7H_7	−0.9125	−0.0913
B_8H_8	0.1523	0.0127
B_9H_9	0.4596	0.0328
$B_{10}H_{10}$	0.0723	0.0045
$B_{11}H_{11}$	0.2517	0.0140
$B_{12}H_{12}$	0.1829	0.0091

a) Resonance energy. b) Resonance energy per face.

In sharp contrast, perhalogenated derivatives of these neutral boranes, B_4Cl_4, B_8Cl_8, B_9Cl_9, and B_9Br_9, have been prepared and isolated.[12,13] Massey's group confirmed the formation of the compounds B_nCl_n (n=8—12) in the mass spectra.[13,14] Kutz and Morrison recently prepared B_7Br_7, B_8Br_8, and $B_{10}Br_{10}$ by the thermal decomposition of B_2Br_4.[1] Although these compounds lack the number $(2n+2)$ of framework electrons, they are considered to be deltahedral in shape.[1,2,5] They are not air stable, but thermally stable. The most stable of the compounds, B_9Br_9, survives temperatures of 300 °C for days and 200 °C for weeks.[1] One of the most distinct features of the perhalogenated borane series is that the nine-atom cluster is much more stable than the ten-atom cluster,[1,2,13,14] which is the opposite of the results reported for carboranes and *closo*-borane dianions.[15] The existence and isolation of the neutral B_nX_n species have been postulated as owing to extensive halogen back-donation into the polyhedra.[1,2,4] This explanation may be supported by the limited structural data of some compounds,[2] but it cannot justify the highest stability of B_9X_9. The details of the back-bonding are as yet unknown.

The present REPF values may be only approximations for the perhalogenated species since they do not take the substituents into account. It is, however, noteworthy that these values are quite consistent with the chemistry of perhalogenated *closo*-boranes. The most familiar species B_nCl_n (n=8—12)[13,14] are all derivatives of weakly aromatic neutral *closo*-boranes. The REPF value of B_9H_9 is larger than that of any other *closo*-borane. This compound alone may be classified as aromatic in comparison with the dianions.[7] In harmony with this, B_9X_9 is the most stable perhalogenated species and naturally much more stable than $B_{10}X_{10}$. B_5H_5 and B_6H_6 are predicted to be

the most antiaromatic *closo*-boranes with the largest negative REPF values. Their halogenated derivatives have been neither prepared nor observed in the mass spectra. As mentioned above, B_4Cl_4 and B_7Br_7 have also been isolated.[1,12] B_7Br_7 is the only antiaromatic species so far prepared and identified.[1] $B_{11}H_{11}$ and $B_{12}H_{12}$ are predicted to be as stable as B_8H_8 and $B_{10}H_{10}$. Although $B_{11}X_{11}$ and $B_{12}X_{12}$ have not been isolated yet, the formation of these species has often been observed in the mass spectra.[13,14] These will be isolated in the near future.

The present comparative study showed that although the effect on cluster stabilities of the back bonding between the boron cluster and the halogen substituents may not be negligible, the relative stabilities of perhalogenated *closo*-boranes are primarily determined by the aromatic character of the clusters. This implies that the halogen substituents uniformly modify the Coulomb and resonance integrals in the cluster. Furthermore, bulky halogen substituents and large B–X bond energies possibly enhance the kinetic stability of the B_nX_n series. These all are quite likely to constitute the reason why the B_nX_n species are more stable than the B_nH_n species. Finally, it should be stressed that by means of our graph theory of aromaticity[6,7] stabilities of the neutral *closo*-boranes and their dianions can be explained consistently.

References

1) N. A. Kutz and J. A. Morrison, *Inorg. Chem.*, **19**, 3295 (1980).

2) E. H. Wong and R. M. Kabbani, *Inorg. Chem.*, **19**, 451 (1980).

3) K. Wade, *Chem. Commun.*, **1971**, 792; *Adv. Inorg. Radiochem.*, **18**, 1 (1976); D. M. P. Mingos, *Nature (London), Phys. Sci.*, **236**, 99 (1972); R. E. Williams, *Adv. Inorg. Radiochem.*, **18**, 67 (1976); R. B. King and D. H. Rouvray, *J. Am. Chem. Soc.*, **99**, 7834 (1977); A. J. Stone, *Inorg. Chem.*, **20**, 563 (1981).

4) R. W. Rudolph, *Acc. Chem. Res.*, **9**, 446 (1976).

5) M. Atoji and W. N. Lipscomb, *Acta Crystallogr.*, **6**, 547 (1953); R. A. Jacobson and W. N. Lipscomb, *J. Chem. Phys.*, **31**, 605 (1959); M. B. Hursthouse, J. Kane, and A. G. Massey, *Nature (London)*, **228**, 659 (1970).

6) J. Aihara, *J. Am. Chem. Soc.*, **98**, 2750 (1976); *Pure Appl. Chem.*, **54**, 1115 (1982); M. Milun, I. Gutman, and N. Trinajstić, *J. Am. Chem. Soc.*, **99**, 1692 (1977).

7) J. Aihara, *J. Am. Chem. Soc.*, **101**, 3339 (1978).

8) The electronic structure of boranes has in general been rationalized in terms of central three-center BBB bonds,[9] in each of which all three boron atoms are pairwise neighbors and topologically equivalent. Kettle and Tomlinson demonstrated that the localized three-center BBB bonds may be used as basis functions for molecular orbital calculations on *closo*-boranes.[10] They located a localized three-center BBB bonding orbital at every face of a deltahedral borane, and took the individual such orbitals to be non-orthogonal to each other. The framework electrons can then be treated in a Hückel manner, each localized three-center orbital being assigned a Coulomb integral α and all resonance integrals being set equal to zero, except those between orbitals which correspond to polyhedron faces with an edge in common, which are given the value β. This bonding model leads to a delocalized molecular orbital energy level scheme similar to those obtained from more elaborate molecular orbital calculations.[10]

9) W. N. Lipscomb, "Boron Hydrides," W. A. Benjamin, New York (1963).

10) S. F. A. Kettle and V. Tomlison, *J. Chem. Soc., A*, **1969**, 2002, 2007.

11) B. Mohar and N. Trinajstić, *J. Comput. Chem.*, **3**, 28 (1982).

12) G. Urry, T. Wartik, and H. I. Schlesinger, *J. Am. Chem. Soc.*, **74**, 5809 (1952).

13) G. F. Lanthier and A. G. Massey, *J. Inorg. Nucl. Chem.*, **32**, 1807 (1970); G. F. Lanthier, J. Kane, and A. G. Massey, *ibid.*, **33**, 1569 (1971); M. S. Reason and A. G. Massey, *ibid.*, **37**, 1593 (1975).

14) M. S. Reason and A. G. Massey, *J. Inorg. Nucl. Chem.*, **38**, 1789 (1976); S. A. Awad, D. W. Prest, and A. G. Massey, *ibid.*, **40**, 395 (1978).

15) E. L. Muetterties and W. H. Knoth, "Polyhedral Boranes," Marcel Dekker, New York (1968).

Determination of Fe-O Bond Energy in Water-gas Shift Catalyst

G. SENGUPTA,* Keshav PRASAD, and S. P. SEN
Projects and Development India Limited, Sindri, Bihar, India
(Received November 27, 1981)

Synopsis. Oxygen catalyst bond energy may play an important role in determining the catalytic activity in water-gas shift reaction. In the present investigation a method for determining this parameter from electrical conductivity has been suggested.

In view of the fact that water-gas shift reaction in iron(III) oxide catalysts is a typical oxidation-reduction reaction, it is quite obvious that there should exist some correlation between the oxygen catalyst bond energy and shift reaction activity. In case of redox reaction in presence of oxygen this bond energy has been measured by various techniques.[1,2] But in case of reactions taking place under reducing conditions *e.g.*, water-gas shift reactions, the only reported method is that of Rachkovsky and Yurjeva[3] who studied the isotope exchange between hydrogen and deuterium oxide on spinels to estimate the oxygen-catalyst bond energy under reducing conditions. In the present investigation a simple method has been suggested to measure this bond energy from electrical conductivity of iron oxide catalyst.

Experimental

The samples A to E were all shift catalysts of commercial variety containing different type of iron(III) oxides promoted with 7—10% chromium(III) oxide. Sample F is pure iron oxide prepared by precipitation from iron(II) sulfate solution with ammonium carbonate followed by curing in air at 500 °C.

The conductivity cell and the circuit used for measurement have been described in detail in an earlier communication.[4] Prior to measurement the catalyst was heated to 200 °C in a flow of N_2+steam in the ratio of 1:5. At 200 °C nitrogen was replaced by hydrogen and the temperature was slowly raised to 350±10 °C. The catalyst was finally stabilized at 460±10 °C. The stabilization was indicated by a constant value of the potential drop. The temperature was slowly brought down to 250 °C and the potential drop was measured at different temperatures after stabilization. Both heating and cooling cycles gave good reproducibility of conductivity values.

Results and Discussion

On reduction with H_2+H_2O mixture the iron oxide catalysts are all reduced to Fe_3O_4. In the present investigation it has been observed that all catalysts show good conductivity which means conduction takes place through Fe_3O_4 phase only irrespective of the presence of chromium(III) oxide. Following Suenaga[5] and Parravano[6] the Fe_3O_4 phase can be assumed to be in oxygen excess nonstoichiometric form which can be represented as:

$$Fe^{3+}[\square_{\delta}Fe^{2+}_{1-3\delta}\ Fe^{3+}_{1+2\delta}]O_4, \qquad (1)$$

where $\square$ is the cation vacancy and δ is the mole fraction of cation vacancies and is a measure of the degree of nonstoichiometry. The conductivity (σ) at any temperature T (in K) can then be written as[7]

$$\sigma = C[1-3\delta][1+2\delta]\exp(-E/RT), \qquad (2)$$

where C is constant and E is activation energy of conduction. Since δ is very small,

$$\sigma = C[1-\delta]\exp(-E/RT). \qquad (3)$$

Therefore,

$$\log\sigma = \log C + \log(1-\delta) - \frac{E}{2.303RT}. \qquad (4)$$

Let δ_i, δ, and σ_i, σ are the degree of nonstoichiometry and conductivities at temperature T_i and T respectively,
Then

$$\log\frac{\sigma_i}{\sigma} = \log\frac{(1-\delta_i)}{(1-\delta)} + \frac{E}{2.303R}\left(\frac{1}{T}-\frac{1}{T_i}\right). \qquad (5)$$

If the catalyst is stoichiometric ($\delta=0$) at the temperature T,

$$\log\frac{\sigma_i}{\sigma} = \log(1-\delta_i) + \frac{E}{2.303R}\left(\frac{1}{T}-\frac{1}{T_i}\right). \qquad (6)$$

From Fig. 1 it can be seen that the plot of $\log(\sigma_i/\sigma)$ *vs.* $(1/T-1/T_i)$ where T_i is the maximum temperature of measurement *i.e.*, 460±10 °C consists of two parts-linear at lower temperature and nonlinear at higher temperature for all catalysts. The general nature of the conductivity temperature plot obtained for different catalysts is presented in Fig. 2. This shows that the catalyst exhibits variable nonstoichiometry only when $T>T_s$. Thus Eq. 5 is obeyed for $T>T_s$ and Eq. 6 for $T\leqslant T_s$. If the catalyst does not show any variation in stoichiometry throughout the temperature range studied the conductivity temperature relationship can be represented by extrapolating the linear portion corresponding to lower temperature part

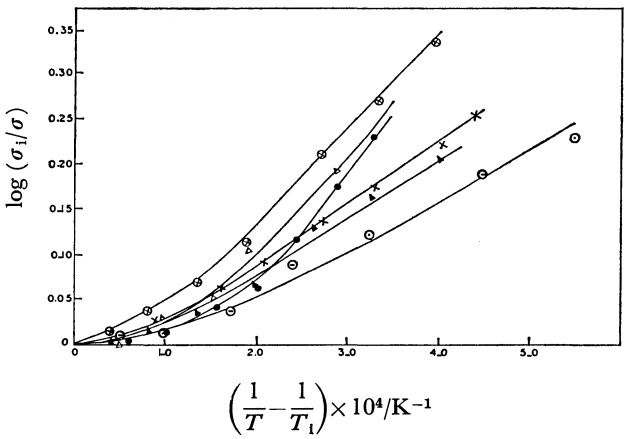

Fig. 1. Variation of resistance of the catalyst with temperature.
Sample A: —△—△—, Sample B: —⊗—⊗—, Sample C: —×—×—, Sample D: —●—●—, Sample E: —▲—▲—, Sample F: —⊙—⊙—.

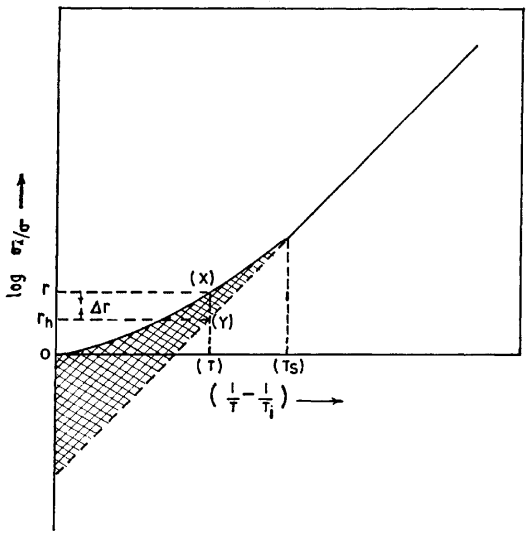

Fig. 2. Change in log (conductivity) *vs.* (temperature)$^{-1}$ plot due to variation in degree of nonstoichiometry.

to higher temperature as shown by the dotted line in Fig. 2. Let σ and σ_h be the conductivities at temperature T corresponding to points X and Y on the actual curve and on the hypothetical extrapolated line respectively. Since Eq. 5 holds for point X and Eq. 6 for point Y respectively then combining both Eqs. 5 and 6,

$$\log\frac{\sigma_h}{\sigma} = \log\frac{\sigma_i}{\sigma} - \log\frac{\sigma_i}{\sigma_h} = r - r_h = \Delta r$$
$$= -\log(1-\delta), \qquad (7)$$

if E is assumed to be independent of the degree of nonstoichiometry. Such an assumption can be justified on the basis of the reported value of E for Fe_3O_4 and γ-Fe_2O_3.[8,9]

The degree of nonstoichiometry (δ) of an oxide catalyst can be expressed by the following empirical equation.

$$1-\delta = \left[\exp\left\{-\frac{\Delta H}{R}\left(\frac{1}{T_s}-\frac{1}{T}\right)\right\}\right]\left(\frac{p^s_{O_2}}{p_{O_2}}\right)^{1/2}, \qquad (8)$$

where ΔH is enthalpy of vacancy formation/mol, $p^s_{O_2}$, p_{O_2} are the equilibrium partial pressure of oxygen at temperatures T_s and T respectively. When $T=T_s$, $p_{O_2}=p^s_{O_2}$, and $\delta=0$. Since in the present case the partial pressure of oxygen at different temperatures is determined by the dissociation of steam ($H_2O \rightleftharpoons H_2+\frac{1}{2}O_2$) we can write

$$\frac{1}{2}\log\left(\frac{p^s_{O_2}}{p_{O_2}}\right) = -\frac{\Delta H_w}{2.303R}\left(\frac{1}{T_s}-\frac{1}{T}\right), \qquad (9)$$

where ΔH_w is the enthalpy of dissociation of steam. Combining Eqs. 7, 8, and 9 and putting $T=T_r$

$$\Delta r = \frac{1}{2.303R}\left(\frac{1}{T_s}-\frac{1}{T_i}\right)(\Delta H+\Delta H_w). \qquad (10)$$

ΔH for different catalysts has been calculated from Eq .10 utilizing the values of Δr and $(1/T_s-1/T_i)$ from Fig. 1 and are presented in Table 1. The average value of oxygen catalyst bond energy is 61.6±2.4 kcal/mol. Since the adsorption/desorption of each oxygen atom results in formation/rupture of two Fe–O bond, average energy per bond is 30.8±1.2 kcal which is good agreement with that calculated by Vijh.[10]

Table 1. Calculation of oxygen catalyst bond energy(ΔH)

ΔH_w=59.3 kcal/mol, T_i=460±10 °C.

	Sample					
	A	B	C	D	E	F
Δr	0.157	0.077	0.053	0.205	0.050	0.100
$\frac{(1/T_s-1/T_i)}{10^{-4}\,K}$	2.9	1.675	1.675	2.475	1.75	4.25
ΔH/kcal mol^{-1}	61.7	61.0	60.7	63.0	60.5	60.3

References

1) G. K. Boreskov, V. V. Popovskii, and V. A. Sazanov, *Proc. 4th Int. Cong. Catal.*, **1**, 439 (1968).
2) A. M. H. Sachtler, G. J. H. Dorgels, J. Fahrenfort, and R. J. H. Voorhoeve, *Proc. 4th Int. Cong. Catal.*, **1**, 454 (1968).
3) Quoted by G. K. Boreskov, "Fundamentals of Gas Surface Interactions," ed by H. S. Saltsburg, Academic Press, New York (1967), p. 240.
4) D. Kumar, G. Sengupta, K. Prasad, and S. P. Sen, *Technology*, **12**, 204 (1975).
5) A. Suenaga, *Kogyo Kagaku Zasshi*, **64**, 518 (1963).
6) G. Parravano, *J. Catal*, **8**, 29 (1967).
7) D. S. Tannhauser, *J. Phys. Chem. Solids*, **23**, 25 (1962).
8) J. Martinet, *C. R. Acad. Sci., Paris*, **234**, 2167 (1952).
9) E. J. W. Verwey, P. W. Hayman, and F. C. Romeijn, *J. Chem. Phys.*, **15**, 181 (1947).
10) A. K. Vijh, *J. Catal.*, **38**, 525 (1975).

Synthesis and Properties of Novel Type Binuclear Copper(II) Complexes Whose Coordination Units Are Linked by a Flexible Polyatomic Chain

Kazuhiro TAKAHASHI, Yuzo NISHIDA,* and Sigeo KIDA

Department of Chemistry, Faculty of Science Kyushu University 33, Higashi-ku, Fukuoka 812

(Received May 4, 1982)

Synopsis. Binuclear copper(II) complexes with two bis(2-benzimidazolylmethyl)amine moieties linked by a flexible polyatomic chain were prepared. Their ESR spectral properties were highly dependent on the bridging chains linking two coordination units.

In the preceding paper,[1] we reported that the reactivities of binuclear copper(I) complexes with (L-px), (L-mx), and (L-cy) (for the abbreviations of the ligands, see Fig. 1) towards molecular oxygen are highly dependent on the bridging chains (R in Fig. 1) linking two coordination units. The above facts are suggesting that the steric arrangements of the two copper ions in these binuclear complexes are controlled by the bridging chain, making the reactivity of the copper(I) complexes towards O_2 molecule different from each other. In order to obtain additional support for the above view, in this study, we have investigated the ESR spectra of the copper(II) complexes with the binucleating ligands shown in Fig. 1.

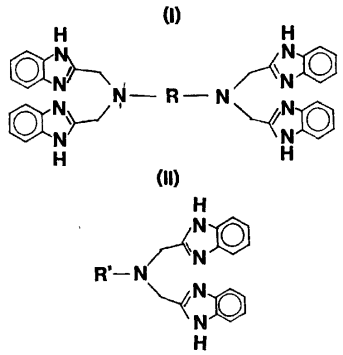

Fig. 1. Chemical structures of the ligands cited in this study and their abbreviations.
(I) Binucleating ligands, R=$-CH_2CH_2-$, (L-2); R=$-(CH_2)_3-$, (L-3); R=$-(CH_2)_4-$, (L-4); R=$-(CH_2)_6-$, (L-6); R=$-CH_2-C_6H_4-CH_2-$, (L-px); R=$C_6H_4(CH_2-)_2$ (L-mx); R=$C_6H_{10}(CH_2-)_2$, (L-cy) (II) mononucleating ligand, R'=H, (ibz); R'=$-CH_2-C_6H_5$, (babz).

Experimental

The ligands cited in Fig. 1 were prepared according to the method described in the literature.[1] The analytical data of the new compounds are summarized in the Table 1. The copper(II) complexes were obtained as blue or bluish-green crystals by mixing the methanol solution of the ligand and the stoichiometric amount of $Cu(NO_3)_2 \cdot 3H_2O$, and recrystallized from a *N,N*-dimethylformamide–methanol solution. The analytical data of the copper(II) complexes are listed in the Table 1.

ESR spectra of the complexes ($[Cu^{2+}]=1\times10^{-3}$ mol dm^{-3}) were obtained with a JEOL ESR apparatus model JES FE3X by the use of an X-band at 77 and 291 K.

Results and Discussion

ESR spectra of Cu_2(L-2)$(NO_3)_4$[2] and Cu_2(L-3)$(NO_3)_4$ in *N,N*-dimethylforamide, obtained at 291 K are shown in Fig. 2. The spectrum of mononuclear complex, Cu(babz)$(NO_3)_2$ is similar to that of Cu_2(L-2)$(NO_3)_4$, showing four hyperfine splittings due to the nuclear spin($I=3/2$) of copper atom. In the spectrum of other binuclear copper(II) complexes, only a broad peak was observed, as exemplified by Cu_2(L-3)$(NO_3)_4$ in Fig. 2.

ESR spectra of the binuclear copper(II) complexes obtained at 77 K are shown in Fig. 3. Mononuclear complex, Cu(babz)$(NO_3)_2$ exhibits the spectrum characteristic of the tetragonal copper(II) complexes[3] ($g_{//}=2.27$, $g_\perp=2.05$, $|A_{//}|=145$ G, 1 G$=1\times10^{-4}$ T). In the spectrum of Cu_2(L-4)$(NO_3)_4$, six hyperfine peaks (the seventh peak may be overlapped with the $g_\perp$

Table 1. Analytical data of the new compounds

Compound	C (%) Found(Calcd)	H (%) Found(Calcd)	N (%) Found(Calcd)	Cu(%) Found(Calcd)
(L-3)	70.17(70.69)	5.75(5.76)	23.36(23.55)	
(L-4)·H_2O	69.24(68.99)	6.08(6.11)	22.23(22.35)	
(L-6)·H_2O	70.20(69.70)	6.42(6.47)	21.56(21.39)	
(L-mx)·H_2O	70.89(71.19)	5.75(5.68)	20.43(20.76)	
(L-px)·1/2 H_2O	72.43(72.16)	5.63(5.60)	20.99(21.04)	
Cu_2(L-3)$(NO_3)_4\cdot3H_2O$	40.97(41.06)	3.87(3.94)	18.98(19.15)	12.4(11.9)
Cu_2(L-4)$(NO_3)_4\cdot2H_2O$	42.12(42.40)	3.84(3.95)	18.97(19.23)	12.7(12.5)
Cu_2(L-6)$(NO_3)_4\cdot H_2O$	44.35(44.32)	4.02(4.11)	18.94(19.04)	12.5(12.3)
Cu_2(L-mx)$(NO_3)_4\cdot H_2O$	45.72(45.70)	3.58(3.64)	18.36(18.65)	12.4(12.1)
Cu_2(L-px)$(NO_3)_4\cdot H_2O\cdot CH_3OH$	45.51(45.70)	3.94(3.64)	18.65(18.12)	11.7(11.7)
Cu_2(L-cy)$(NO_3)_4\cdot4H_2O$	43.37(43.28)	4.37(4.54)	17.67(17.67)	11.5(11.4)

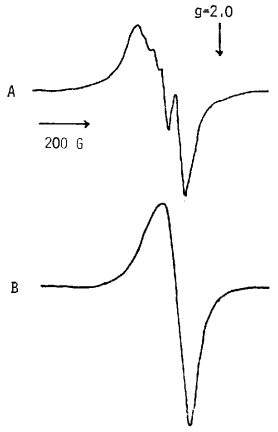

Fig. 2. ESR spectra of A: $Cu_2(L\text{-}2)(NO_3)_4$ and B: $Cu_2(L\text{-}3)(NO_3)_4$ (dmf, 291 K).

peak) are observed; hyperfine splitting ($|A|=71$ G) is as half as that of $Cu(babz)(NO_3)_2$. The spectra of $Cu_2(L\text{-}px)(NO_3)_4$ and $Cu_2(L\text{-}cy)(NO_3)_4$ were similar to that of $Cu_2(L\text{-}4)(NO_3)_4$.

The spectrum of $Cu_2(L\text{-}6)(NO_3)_4$ (and also $Cu_2(L\text{-}mx)(NO_3)_4$) is different from that of $Cu_2(L\text{-}4)(NO_3)_4$, and similar to those of $Cu_2(L\text{-}2)(NO_3)_4$ and $Cu(babz)(NO_3)_2$. The spectrum of $Cu_2(L\text{-}3)(NO_3)_4$ is rather complicated, different from either of $Cu_2(L\text{-}4)(NO_3)_4$ and also $Cu_2(L\text{-}6)(NO_3)_4$. In the case of $Cu_2(L\text{-}2)(NO_3)_4$, the ESR spectra at 291 and 77 K closely resemble those of mononuclear complex, $Cu(babz)(NO_3)_2$. Thus, it has became apparant that the ESR spectral properties of the binuclear copper(II) complexes obtained in this study are dependent on

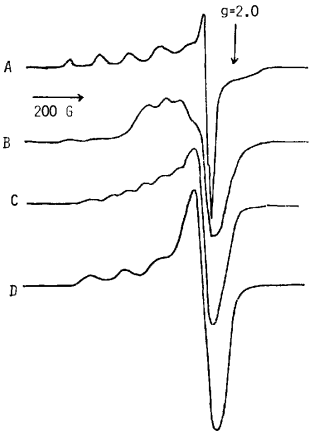

Fig. 3. ESR spectra of binuclear copper(II) complexes (dmf, 77 K).
A: $Cu_2(L\text{-}2)(NO_3)_4$, B: $Cu_2(L\text{-}3)(NO_3)_4$, C: $Cu_2(L\text{-}4)(NO_3)_4$, D: $Cu_2(L\text{-}6)(NO_3)_4$.

the bridging chains linking two coordination units. These facts may be due to the difference in the weak interaction between two copper(II) ions, controlled by the flexible polyatomic chain used.

References

1) Y. Nishida, K. Takahashi, H. Kuramoto, and S. Kida, *Inorg. Chim. Acta*, **54**, L103 (1981).
2) H. M. J. Hendricks, W. O. B. Huinink, and J. Reedijk, *Recl. Trav. Chim. Pays-Bas.*, **98**, 499 (1979).
3) B. J. Hathaway, *Coord. Chem. Rev.*, **5**, 143 (1970).

Alizarin Red-S, an Amperometric Reagent for Ultramicro and Microgram Estimation of Sm^{3+} and Gd^{3+}

S. C. LAVALE* and K. S. PITRE

Department of Chemistry, University of Saugar, Sagar (M. P.) 470003, India

(Received January 5, 1982)

Synopsis. Alizarin Red-S has been employed successfully as an amperometric reagent for the precise determination of Sm^{3+} and Gd^{3+} in aqueous and partially non aqueous media. Amperometric titrations have been performed at −0.7 V *vs.* Hg-pool, pH=4.5 and μ=0.1. The current-volume titration curves obtained were well defined, indicating 1:2 stoichiometric ratio of metal:ARS complexation in each case. The absorptiometric studies made on the equilibrium of above complexation also confirm the said ratio. Many ions do not interfere the titration procedure.

Alizarin Red-S (Abbr. as ARS) has been employed in analytical chemistry since Atack[1] discovered that Al^{3+} could be detected with this reagent. The use of ARS as an complexometric, spectrophotometric and pH-metric reagent is described in the literature.[2-5] Larson and Hirozawa[6] have studied the complexation of Zr^{2+} and Hf^{2+} with ARS in aqueous and alcoholic media using amperometric titrations. In continuation of our work[7-10] on trace estimation of rare earths, the present paper deals with the results of amperometric estimation of Sm^{3+} and Gd^{3+} with ARS using a d.m.e. -Hg pool electrode system. The amperometric estimations have been supplemented by absorption studies to establish the metal-ligand equilibria.

Experimental

The chemicals used were of AnalaR or Extra pure quality. Sm^{3+} and Gd^{3+} solutions were prepared and standardized.[10] The solution of ARS was prepared by dissolving requisite quantity of this reagent in conductivity water and standardized by the analytical procedure developed by Larson and Hirozawa.[6]

Amperometric titrations were done on mannually operated polarograph with multiflex galvanometer (sens. 8.10×10^{-9} A/div.) using d.m.e. as indicator and Hg-pool as reference electrode. An Elico digital pH meter (model LI.120) was used for measuring pH of the test solutions. A Beckman DU-2 spectrophotometer was used to study the equilibrium of metal-ligand complexation.

For titrations a number of solutions, containing calculated amounts of Sm^{3+} or Gd^{3+} in 0.1 mol/dm^3 KCl as supporting electrolyte were prepared and pH of these test solutions was fixed at 4.5 using acetate buffer.

Results and Discussion

The current voltage behaviour of ARS has been studied in 0.1 M (1 M=1 mol dm^{-3}) KCl and acetate buffer at pH 4.5. ARS gives a well defined cathodic wave[11] (Fig. 1-A). The height of diffusion current is proportional to the concentration of ARS. The test solution of Sm^{3+} or Gd^{3+} was taken in a titration cell. The plateau potential of the polarogram for ARS *i.e.* −0.7 V *vs.* Hg pool (at which Sm^{3+} or Gd^{3+} do not give any diffusion current Fig. 1-M) was applied.

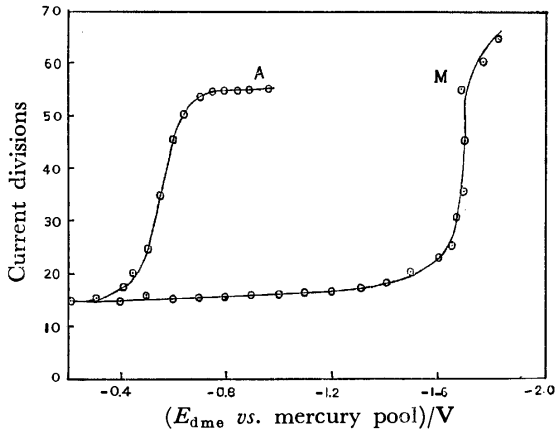

Fig. 1. A: Polarogram of 1 mM Alizarin Red-S in 0.1 M KCl at pH=4.5. M: Polarogram of 2 mM metal(Sm^{3+} or Gd^{3+}) in 0.1 M KCl at pH=4.5.

The standard solution of ARS (pH=4.5) was added drop by drop from 1 cm^3 semi-micro burette, a pinkish red coloration was observed. The current was noted with multiflex galvanometer. On plotting galvanometer reading after necessary volume correction[12] against titrant volume a reversed L shaped curve was obtained. The end point indicated a metal: ARS ratio of 1:2, which is in good agreement with the results reported in the literature[13,14] and that observed by the authors with absorbtiometric studies discussed in this paper. Moreover, it is also observed that each of these titrations can be performed in 25% ethanol medium which may be fruitful for the estimation of Sm^{3+} and Gd^{3+} in a compound or ore soluble in partially ethanol medium.

Study of the Effect of Diverse Ions. For interference studies, known amout of foreign ions were added to a definite amount of metal ion (Sm^{3+} or Gd^{3+}) and the metal was titrated following the procedure described above. The maximum amount of diverse ions reported in Table 1. do not hamper the titrations. It is also observed that 100 folds of concentrations of the ions NH_4^+, Cl^-, ClO_4^-, SO_4^{2-}, NO_3^-, and CH_3COO^- do not interfere in this titrimetric procedure. However, small amounts of Ag^+, Pb^{2+}, Bi^{3+}, Ca^{2+}, Al^{3+}, Fe^{3+}, VO_3^{2-}, $Cr_2O_7^{2-}$, MoO_4^{2-}, and CO_3^{2-} ions interfere the titration procedure appreciably.

Absorbtion Studies on Complexation. Vosburgh and Cooper's[15] method was used to study the nature of complex formed. The visible absorbtion spectra of 1×10^{-4} M ARS at pH 4.5 consists a single maximum at 420 nm and ARS complexes with Sm^{3+} or Gd^{3+} at 530 nm. The shift in λ_{max} is attributed to the formation of complex. Under varying ratio of mixing and varying pHs only one absorption maximum was obtained, supports to the formation of complex. To determine the stoichiometry of the complexes job's

Table 1. An amperometric determination of Sm^{3+} and Gd^{3+} with ARS in presence of diverse ions

Metal taken: Sm^{3+}=1.504 mg (0.01 mM), Gd^{3+}=1.592 mg (0.01 mM).

Diverse ion added	Sm^{+3} found (mg)	% error	Gd^{3+} found (mg)	% error
K^+ (195 mg)	1.49	−0.97	1.599	+0.43
Na (115 mg)	1.499	−0.32	1.587	−0.31
Mg^{2+} (48.6 mg)	1.51	+0.39	1.584	−0.50
Zn^{2+} (24.3 mg)	1.518	+0.93	1.60	+0.50
Tl^{+1} (15.3 mg)	1.501	−0.19	1.601	+0.56
Sn^{2+} (11.86 mg)	1.51	+0.39	1.588	−0.25
Cd^{2+} (11.24 mg)	1.495	−0.59	1.583	−0.56
Hg^{2+} (10 mg)	1.491	−0.86	1.607	+0.94
Se^{4+} (3.94 mg)	1.507	+0.19	1.59	−0.12
Te^{4+} (3.19 mg)	1.498	+0.39	1.583	−0.56

a) The figure within parenthesis shows the amount of foregn ion added under the prescribed experimental conditions.

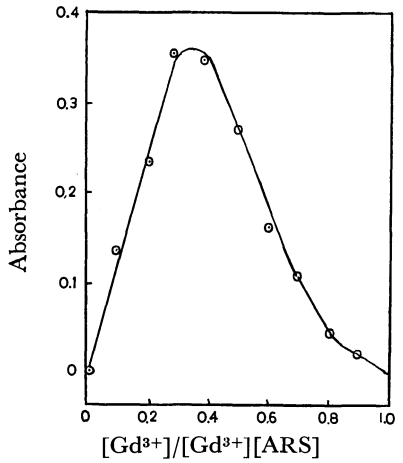

Fig. 2. Job's plot for composition at 530 nm.

method of continuous variations[16] (Fig. 2) has been successfully applied. The measurements were carried out at pH 4.5 and wavelength 530 nm. The fresh solution of ARS was prepared before use and the experimental sets were made. The color development of complex is instanteneous. Absorbtion studies were made within 1 h, as it is found that a gelatineous precipitation takes place on standing for nearly three hours. Stoichiometric ratio of Sm^{3+} and Gd^{3+} complexes with ARS were found to be 1:2 in both the cases, which confirms the ratio observed by authors in amperometric titration technique. The equilibrium constants were evaluated by mole ratio method and nonlinear method of job. The log conditional formation constants are found to be 10.94 and 11.51 for Sm^{3+}–ARS and Gd^{3+}–ARS complexes in solution. The molar ratio and numerical values of stability constants obtained using absorption studies supplemented the authors view on amperometric estimations of Sm^{3+} and Gd^{3+} with ARS.

Accuracy and Precision. The ultramicro and microgram quantities of Sm^{3+} and Gd^{3+} have been estimated amperometrically with an error of less than ±0.8%. For each set replicate titrations were done and statistical methods have been applied to interpret the data obtained. A more accurate measure of precision known as coefficient of variation never exceeded 0.55.

One of the authors (SCL) is grateful to the UGC, New Delhi, for awarding him Teacher Fellowship.

References

1) Atack, *J. Soc. Chem. Ind.*, **34**, 936 (1915).
2) H. A. Liebhafsky and E. H. Winslov, *J. Am. Chem. Soc.*, **60**, 1776 (1938).
3) A. K. Mukerji and A. K. Dey, *Bull. Chem. Soc. Jpn.*, **31**, 521 (1958).
4) R. W. Renehant, *Anal. Chem.*, **26**, 1820 (1954).
5) A. Varadarajulu and U. V. Seshaiah, *J. Indian Chem. Soc.*, **48**, 11 (1971).
6) E. M. Larson and S. T. Hirozawa, *J. Inorg. Nucl. Chem.*, **3**, 198 (1956).
7) S. C. Lavale and K. S. Pitre, *J. Electrochem. Soc. India.*, **30**, 328 (1981).
8) S. C. Lavale and K. S. Pitre, *Rev. Roum. Chim.*, in press.
9) K. S. Pitre and S. C. Lavale, *J. Inst. Chem. (India)*, **53**, 211 (1981).
10) S. C. Lavale and K. S. Pitre, *Proc. Natl. Acad. Sci. India*, in press.
11) N. H. Furman and K. G. Stone, *J. Am. Chem. Soc.*, **71**, 3055 (1948).
12) J. T. Stock, "Amperometric Titrations," R. E. Krieger Pub. Com. Huntington, New York (1975), p. 7.
13) A. E. Harvey and D. L. Manning, *J. Am. Chem. Soc.*, **74**, 4744 (1952).
14) L. L. Soni and G. Vishwanath, *J. Indian Chem. Soc.*, **48**, 799 (1971).
15) W. C. Vasburgh and G. R. Cooper, *J. Am. Chem. Soc.*, **63**, 437 (1941); **64**, 1630 (1942).
16) P. Job, *Ann. Chim.*, **9**, 113 (1928); **6**, 97 (1936).

Intermolecular Pummerer Rearrangement Reactions of Alkyl Phenyl and Dialkyl Sulfoxides with Acetic Anhydride

Osamu Itoh, Tatsuo Numata, Toshiaki Yoshimura, and Shigeru Oae*

Department of Chemistry, The University of Tsukuba, Niihari-gun Sakura-mura, Ibaraki 305

(Received June 7, 1982)

Synopsis. The Pummerer reactions of alkyl phenyl sulfoxides, PhS(O)R (R: methyl and isobutyl), and benzyl methyl sulfoxide with acetic anhydride were found to proceed through the intermolecular acetoxyl migration, based on the ^{18}O-tracer experiments with ^{18}O-labeled sulfoxides and unlabeled acetic anhydride.

In our earliest ^{18}O-tracer experiment on the Pummerer reaction of dimethyl sulfoxide with 3 equiv. molar amount of uniformly ^{18}O-labeled acetic anhydride in ether solution, the amount of ^{18}O-label in the resulting ester was 9/10 of that of the acetic anhydride used.[1] Namely, all the oxygen atoms of the starting materials were found to be completely scrambled in the resulting ester as shown below. Thus,

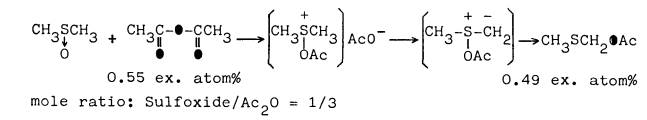

the intermolecular migration of acetate from the acetoxysulfonium ion to the α-carbon was postulated for this Pummerer reaction. Years later, we found that sulfoxides undergo oxygen exchange with acetic anhydride[2] and various other acids.[3,4] However, the rate of oxygen exchange of methyl *p*-tolyl sulfoxide with acetic anhydride at 120 °C was found by us to be only 1/6 of that of the Pummerer reaction, revealing clearly that the earlier postulate of the predominant intermolecular nucleophilic attack of acetoxyl group at the α-carbon terminal is still valid.[5,6] However, our recent findings of several intramolecular Pummerer reactions with the aid of ^{18}O-tracer experiments[7–9] and others[7d,8d] have led us to reinvestigate the Pummerer reactions of a few other alkyl aryl sulfoxides and dialkyl sulfoxides, using this time ^{18}O-labeled sulfoxides so that the ^{18}O-distribution in the resulting ester can be determined in order to estimate the extent of the intermolecular acetoxyl migration and also the extent of ^{18}O-exchange in the recovered sulfoxides. As the results of this new investigation, our earlier observation and conclusion have been found to be quite acceptable.

Results and Discussion

The Pummerer reactions of two alkyl aryl sulfoxides with a large excess of unlabeled acetic anhydride have been carried out using ^{18}O-labeled methyl phenyl sulfoxide (**1**) and isobutyl phenyl sulfoxide (**3**) to examine the fate of ^{18}O-label in the resulting ester, **2** and **4**, along with the sulfoxide recovered at partial completion of the reaction. ^{18}O-Labeled benzyl methyl sulfoxide **5** was treated similarly. These ^{18}O-tracer experimental results are illustrated in the following equations.

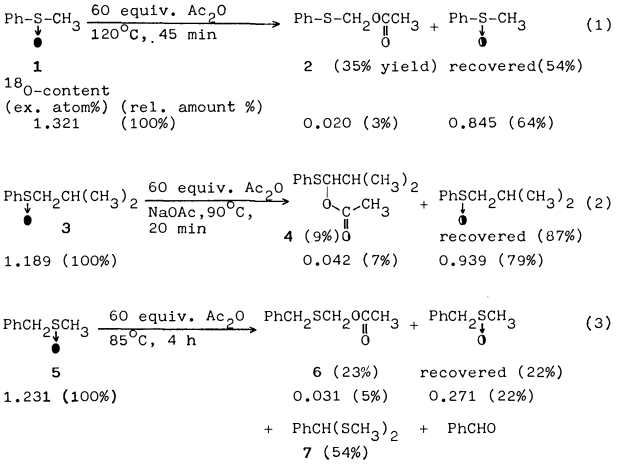

When the Pummerer reaction product (**2**-^{18}O) [0.760 ex. atom% of ^{18}O] was allowed to react with 60 equiv. amount of acetic anhydride in the presence of ether 0.4 or 2 equiv. amount of acetic acid at 120 °C for 45 min, the ^{18}O-content of the α-acetoxy sulfide, the Pummerer reaction product (**2**-^{18}O) recovered were found to retain 0.755 or 0.708 ex. atom% of ^{18}O, respectively. This implies explicitly that acetoxymethyl phenyl sulfide (**2**) once formed does not seem to exchange acetoxyl group readily with acetic acid present under the Pummerer reaction conditions. The sulfoxides recovered, **1** and **3** after 40 and 10% conversions respectively were found to have retained the ^{18}O-label of the original sulfoxides in 64 and 79%, respectively. Thus the large loss of ^{18}O-label in the Pummerer reaction products is not due to the concurrent oxygen exchange of the ^{18}O-labeled sulfoxides with acetic anhydride.[5] All these observations suggest clearly that the Pummerer reaction of these sulfoxides proceeds through the intermolecular acetoxyl migration, after the rate-determining α-proton-removal.[3] Earlier, acetoxyl group was reported to migrate preferentially to the benzylic carbon in the reaction of sulfoxide **5** with acetic anhydride.[10] However, we found that the migration of acetoxyl group occurs to both benzylic and methyl carbon in the ratio of 2:1. α,α-Bis(methylthio)toluene (**7**) is the secondary product formed by the migration of acetoxyl group to the benzylic carbon. The Pummerer reactions of dibenzyl and benzyl phenyl sulfoxides are not facile and require relatively higher temperatures than would be expected from the acidity of benzylic protons.[11–14] The relatively low basicity of the sulfinyl oxygen in **5** and steric shielding by phenyl group may be partly responsible for the somewhat low reactivity of the Pummerer reaction, however, the oxygen exchange reaction of this sulfoxide **5** with acetic anhydride is as facile as that of benzyl phenyl sulfoxide with acetic anhydride.[13]

The large kinetic isotope effect k_H/k_D=5—9 in the

Pummerer reaction of dibenzyl sulfoxide with acetic anhydride,[11,12] seems to indicate that the rate-determining step of this intermolecular rearrangement of benzyl methyl sulfoxide is the α-proton removal.

Experimental

^{18}O-Analysis. ^{18}O-Analysis was carried out by the method developed by Rittenberg and Ponticorvo.[15]

^{18}O-Labeled Sulfoxides. ^{18}O-Labeled methyl phenyl sulfoxide (**1**), isobutyl phenyl sulfoxide (**3**), and benzyl methyl sulfoxide (**5**) were synthesized according to our usual method by oxidation of the corresponding sulfides with bromine in the presence of ^{18}O-enriched water.[16] Thus methyl phenyl sulfoxide, isobutyl phenyl sulfoxide, and benzyl methyl sulfoxide containing 1.321, 1.189, and 1.231 ex. atom% of ^{18}O, respectively, were obtained in 65, 61, and 57% yields.

Reaction of ^{18}O-Labeled Methyl Phenyl Sulfoxide (1), Isobutyl Phenyl Sulfoxide (3), and Benzyl Methyl Sulfoxide (5) with Acetic Anhydride. When the ^{18}O-labeled title sulfoxides **1**, **3**, and **5** (a few hundred mg) were heated separately with a large excess (*ca.* 60 fold) of acetic anhydride at a set temperature for some length of time, the oily residue, obtained after evaporation of excess acetic anhydride and any volatile product in vacuo, was separated through column chromatography with benzene and then $CHCl_3$ as eluents or Kugelrohr distillation. The Pummerer product **2** (120 °C/20 mmHg** (Kugelrohr)), **4** (130 °C/20 mmHg (Kugelrohr)), and **6** (126 °C/20 mmHg (Kugelrohr)) and the recovered sulfoxides were obtained along with some minor by-products as shown in Eqs. 1, 2, and 3.

Preparation of ^{18}O-Labeled Acetoxymethyl Phenyl Sulfide (2-^{18}O). When methyl phenyl sulfoxide (**1**) (500 mg) was allowed to react with 2 equiv. molar amount of ^{18}O-labeled acetic anhydride at 120 °C for 3 h. The ^{18}O-labeled Pummerer product **2** (0.760 ex. atm% of ^{18}O) was obtained in 90% yield (585 mg), upon distillation with Kugelrohr (120 °C/20 mmHg).

Acetate Exchange Reaction of ^{18}O-Labeled Acetoxymethyl Phenyl Sulfide (2-^{18}O) with Acetic Anhydride in the Presence of Acetic Acid. After the ^{18}O-labeled title compound **2**-^{18}O [0.760 ex. atom% of ^{18}O] was heated with 60 equiv. acetic anhydride in the presence of ether 0.4 or 2 equiv. amount of acetic acid to the ester (**2**-^{18}O) at 120 °C for 45 min. Upon removal of the solvent *in vacuo*, chromatography and final distillation, the pure acetoxymethyl phenyl sulfide recovered was found to remain either 0.755 or 0 708 ex. atom% of ^{18}O, respectively.

** 1 mmHg≈133.3 Pa.

References

1) S. Oae, T. Kitao, S. Kawamura, and Y. Kitaoka, *Tetrahedron*, **19**, 817 (1963).

2) S. Oae and M. Kise, *Tetrahedron Lett.*, **1967**, 1409.

3) S. Oae and M. Kise, *Bull. Chem. Soc. Jpn.*, **43**, 1416 (1970); M. Kise and S. Oae, *ibid.*, **43**, 1804 (1970).

4) N. Kunieda and S. Oae, *Bull. Chem. Soc. Jpn.*, **46**, 1745 (1973); **41**, 1025 (1968); S. Oae, M. Yokoyama, and M. Kise, *ibid.*, **41**, 1221 (1968); W. Tagaki, K. Kikukawa, N. Kunieda, and S. Oae, *ibid.*, **39**, 614 (1966); K. Mislow, T. Simons, J. T. Melillo, and L. Terney, Jr., *J. Am. Chem. Soc.*, **86**, 1452 (1964); H. Yoshida, T. Numata, and S. Oae, *Bull. Chem. Soc. Jpn.*, **44**, 2875 (1971); H. Kwart and H. Omura, *J. Am. Chem. Soc.*, **93**, 7250 (1971); N. Kunieda, T. Numata, and S. Oae, *Phosphorus and Sulfur*, **3**, 1 (1977); and references cited therein.

5) S. Oae and M. Kise, *Tetrahedron Lett.*, **1968**, 2261.

6) M. Kise and S. Oae, *Bull. Chem. Soc. Jpn.*, **43**, 1426 (1970).

7) a) T. Numata and S. Oae, *Chem. Ind. (London)*, **1972**, 726; b) S. Oae and T. Numata, *Tetrahedron*, **30**, 2641 (1974); c) T. Numata and S. Oae, *ibid.*, **32**, 2699 (1976); d) H. Stridsberg and S. Allenmark, *Acta Chem. Scand., Ser. B*, **28**, 591 (1974); **30**, 219 (1976).

8) a) T. Numata and S. Oae, *Tetrahedron Lett.*, **1977**, 1337; b) T. Numata, O. Itoh, and S. Oae, *Chem. Lett.*, **1977**, 909; c) T. Numata, O. Itoh, and S. Oae, *Tetrahedron Lett.*, **1979**, 1869; d) M. Mikolajczyk, A. Zatorski, S. Grzejsczak, B. Costisella, and M. Midura, *J. Org. Chem.*, **43**, 25 (1978).

9) T. Masuda, T. Numata, N. Furukawa, and S. Oae, *Chem. Lett.*, **1977**, 903; *J. Chem. Soc., Perkin Trans. 2*, **1978**, 1302.

10) W. E. Parham and L. D. Edwards, *J. Org. Chem.*, **33**, 4150 (1968).

11) G. E. Wilson, Jr., and C. J. Strong, *J. Org. Chem.*, **37**, 2376 (1972).

12) Wilson and Strong[11] found $k_H/k_D \approx 5$—9 in the Pummerer reaction of benzyl benzyl-α,α-d_2 sulfoxide with acetic anhydride at 76 °C for 1200 h in chloroform, and observed that the value of k_H/k_D decreases from initial 9 to final 4.5. We also obtained $k_H/k_D = 5.0$ in the same reaction at 100 °C for 10 h (10% conversion) in acetic anhydride but in the presence of 5 equiv. DCC to the sulfoxide.

13) M. Kise and S. Oae, *Bull. Chem. Soc. Jpn.*, **43**, 1421 (1970).

14) T. D. Harris and V. Baekelheide, *J. Org. Chem.*, **41**, 2770 (1976).

15) D. Rittenberg and L. Ponticorvo, *Int. J. Appl. Radiat. Isot.*, **1**, 208 (1956).

16) S. Oae, Y. Ohnishi, S. Kozuka, and W. Tagaki, *Bull. Chem. Soc. Jpn.*, **39**, 364 (1964).

One-step Synthesis of Long-chain Aliphatic α,ω-Dicarboxylic Acids Utilizing the Copper-catalyzed Reaction of β-Propiolactone with α,ω-Di-Grignard Reagents

Tamotsu FUJISAWA,* Toshio SATO, Tatsuo KAWARA, and Hideyuki TAGO
Chemistry Department of Resources, Mie University, Tsu, Mie 514

(Received June 28, 1982)

Synopsis. Copper-catalyzed reaction of β-propiolactone with α,ω-di-Grignard reagents, followed by esterification gave six-carbon homologated α,ω-dicarboxylic acid esters in good yields.

Long-chain aliphatic α,ω-dicarboxylic acids or esters are useful synthetic intermediates for many-membered carbon rings. Especially, α,ω-dicarboxylic acids of C_{14}—C_{18} have been used for the syntheses of alicyclic ketones which possess a musk or civet odor.[1] Although a number of synthetic methods for these acids have been reported,[2-4] the most direct ones are the Kolbe electrolytic synthesis from half esters of α,ω-dicarboxylic acids[3] or α-alkylation of carboxylic acids or esters with α,ω-dibromoalkanes.[4] However, such methods are generally not satisfactory with respect to yield or to availability of starting materials.

Recently the regioselective ring-opening reaction of β-propiolactones with Grignard reagents in the presence of a copper(I) catalyst has been found to give three-carbon homologated carboxylic acids in high yields.[5] We wish to describe here a novel one-step synthesis of six-carbon homologated α,ω-dicarboxylic acids (**1**) by the reaction of two equivalents of β-propiolactone (**3**) with α,ω-di-Grignard reagents (**4**) in the presence of a copper catalyst.[6]

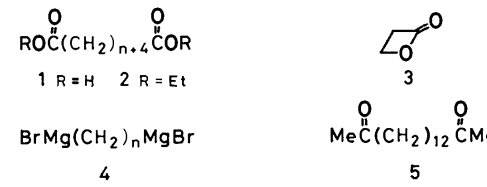

Scheme 1.

Grignard reagent **4**, easily prepared from α,ω-dibromoalkane,[7] was added to a solution of two equivalents of **3** and a copper catalvst (2—3 mol%) at −10 °C. After the reaction mixture was allowed to warm to 0 °C and stirred for 3 h, **1** was obtained. As a catalyst, lithium tetrachlorocuprate was slightly superior to copper(I) iodide. Esterification of **1** with ethanol gave diester **2**, which was isolated by distillation. The yields of **2** of C_{14}—C_{18} are listed in Table 1.

Tetradecanedioic acid (**2**, n=8), prepared by the reaction of **3** with 1,8-octanediyldimagnesium dibromide, was easily converted into hexadecane-2,15-dione (**5**), which is a useful precursor for 3-methylcyclopentadecanone (muscone).[8] The acid was treated with thionyl chloride and then bromomagnesium dimethylcuprate to give **5** in an overall yield of 57% from the Grignard reagent.

Diethyl (*Z*)-9-octadecene-1,18-dioate (**6**), an important precursor for (*Z*)-9-cycloheptadecenone (civetone)[9] was easily obtained in 53% yield by the reaction

Table 1. Yields of α,ω-dicarboxylic acid diesters **2**

Grignard reagent	**2**	Yield/%
$BrMg(CH_2)_8MgBr$	$EtO_2C(CH_2)_{12}CO_2Et$	68
$BrMg(CH_2)_9MgBr$	$EtO_2C(CH_2)_{13}CO_2Et$	63
$BrMg(CH_2)_{10}MgBr$	$EtO_2C(CH_2)_{14}CO_2Et$	60
$BrMg(CH_2)_{11}MgBr$	$EtO_2C(CH_2)_{15}CO_2Et$	68
$BrMg(CH_2)_{12}MgBr$	$EtO_2C(CH_2)_{16}CO_2Et$	62

of **3** with di-Grignard reagents **7**. According to the modified procedure of Normant *et al.*,[10] alkylation of dialkenylcuprate **9**, prepared from Grignard reagent **8**,[11] copper(I) iodide and acetylene, with 1-chloro-5-iodopentane and deprotection gave chloro alcohol **10** which was converted to **7** *via* α,ω-dichloride **11**.

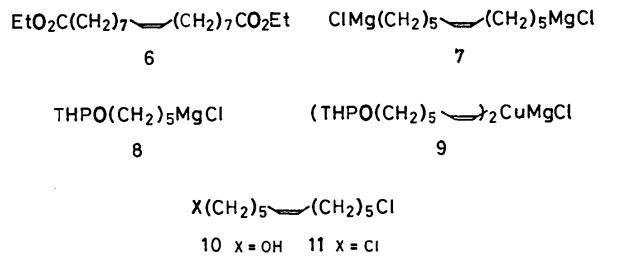

Scheme 1.

Experimental

The IR spectra were recorded on a Hitachi EPI-G2 spectrometer. The NMR spectra were taken with a Varian A-60 spectrometer in CCl_4 using TMS as an internal standard. Di-Grignard reagent was prepared from α,ω-dibromoalkane in THF.[7]

General Procedure for the Reaction of β-Propiolactone (3) with α,ω-Di-Grignard Reagents 4. To a solution of Li_2CuCl_4 (3 mmol) and **3** (5.62 g, 78 mmol) in THF (250 ml) was slowly added **4** (30 mmol) at −10 °C and stirred at 0 °C for 3 h. After addition of 3 M† HCl (100 ml), the mixture was extracted with ether and concentrated. The residue was solved in methanol (20 ml) and 3 M KOH (100 ml) was added. After removal of methanol, the solution was washed with ether and acidified with 6 M HCl (100 ml). Extraction with ether and concentration gave crude **1**. Esterification of **1** with ethanol by an azeotropic method and distillation gave pure **2**. Yields and physical data of **2** are as follows: Diethyl tetradecanedioate (yield 68%); bp 144—151 °C/0.4 Torr (lit,[12] 135—136 °C/0.15 Torr); mp 28.0—29.0 °C (lit,[12] 27 °C). Diethyl pentadecanedioate (yield 63%); bp 160—161 °C/0.35 Torr (lit,[3b] 152 °C/0.23 Torr); mp 29.5—30.0 °C (lit,[1a] 30 °C). Diethyl hexadecanedioate (yield 60%); bp 146—148 °C/0.1 Torr (lit,[3a] 165 °C/1 Torr); mp 38.0—39.0 °C (lit,[3c] 39.0 °C). Diethyl heptadecanedioate (yield 68%); bp 153—155 °C/0.15 Torr (lit,[3b] 162 °C/0.02 Torr); mp 40.0—40.5 °C (lit,[1a] 40—41 °C). Diethyl octadecanedioate (yield 62%); bp 165—170 °C/0.45

† 1 M=1 mol dm^{-3}.

Torr (lit,[3a] 180—190 °C/0.35 Torr; mp 46.0—47.0 °C (lit,[3c] 47.8—48.4 °C).

Hexadecane-2,15-dione (5). The crude tetradecanedioic acid (11.43 g), obtained by the reaction of **3** (2.39 g, 33 mmol) with 1,8-octanediyldimagnesium dibromide (10.7 mmol), was added into thionyl chloride (9.84 g, 82 mmol) and stirred at room temp overnight and at 40 °C for 2 h. Excess thionyl chloride was evaporated and the residue was dissolved in 10 ml of THF. To a suspension of bromomagnesium dimethylcuprate, prepared from copper(I) iodide (8.55 g, 45 mmol) and methylmagnesium bromide (90 mmol) in THF (150 ml) and Me_2S (15 ml) at −30 °C for 1.5 h, was added the solution of the acid chloride at −78 °C. After stirring at −78 °C for 30 min, cold sat. NH_4Cl solution was added. Extraction with ether and distillation gave **5** (1.55 g, 57%); bp 152—154 °C/0.25 Torr; mp 82—83 °C (lit,[13] 83.5—84.5 °C).

(Z)-12-Chloro-6-dodecen-1-ol (10). To a solution of copper(I) iodide (1.90 g, 10 mmol) in THF (30 ml) and Me_2S (3 ml) was added Grignard reagent **8**[11] (20 mmol) at −30 °C and stirred for 1 h. After allowing the mixture to warm to −25 °C, acetylene (560 ml) was introduced over a period of 30 min, and stirring was continued at −25—−20 °C for 30 min. Hexamethylphosphoric triamide (4 ml), 1-chloro-5-iodopentane (4.66 g, 20 mmol), and trimethyl phosphite (3.5 ml) were added successively and stirred at room temp overnight. After cooling to 0 °C, 3 M HCl (20 ml) was added. The mixture was extracted with hexane and concentrated. After the residue was heated in methanol (100 ml) in the presence of *p*-toluenesulfonic acid monohydrate (0.2 g) at 50 °C for 3 h, sat. $NaHCO_3$ solution (50 ml) was added. Extraction with hexane and distillation gave **10** (2.7 g, 63%); bp 116—120 °C/0.35 Torr; NMR δ 1.1—2.3 (16H), 3.13 (1H, s), 3.48 (2H, t, J=7 Hz), 3.52 (2H, t, J=7 Hz), 5.29 (2H, t, J=5 Hz); IR (neat) 3400 (OH) and 720 cm^{-1} (*cis*-CH=CH). Found: C, 65.90; H, 10.45; Cl, 16.06%. Calcd for $C_{12}H_{23}ClO$: C, 65.88; H, 10.60; Cl, 16.21%.

(Z)-1,12-Dichloro-6-dodecene (11). Chloro alcohol **10** (2.99 g, 13.7 mmol) and triphenylphosphine (9.40 g, 40 mmol) were refluxed in CCl_4 (28 ml) for 1 h. After addition of dry hexane (14 ml), the white precipitate was filtered off. Concentration and distillation gave **11** (2.13 g, 66%); bp 106—108 °C/0.3 Torr; NMR δ 1.5—2.2 (16H), 3.51 (4H, t, J=6 Hz), 5.30 (2H, t, J=4 Hz); IR (neat) 720 cm^{-1} (*cis*-CH=CH). Found: C, 60.56; H, 9.54; Cl, 29.61%. Calcd for $C_{12}H_{22}Cl_2$: C, 60.76; H, 9.35; Cl, 29.89%.

Diethyl (Z)-9-Octadecene-1,18-dioate (6). Grignard reagent **7** was prepared in 79% yield from **11** (2.11 g, 8.91 mmol) and magnesium in THF (23 ml) under reflux for 2 h. Diester **6** was prepared from **3** and **7**. Purification by TLC on silica gel (R_f 0.4, hexane:ether=5:1) gave **6** (1.19 g, 50%); bp 156—160 °C/0.3 Torr; NMR δ 1.23 (6H, t, J=7 Hz), 1.30—2.1 (24H), 2.20 (4H, t, J=7 Hz), 4.05 (4H, q, J=7 Hz), 5.33 (2H, t, J=4 Hz); IR (neat) 1725 (C=O) and 720 cm^{-1} (*cis*-CH=CH). Found: C, 71.80; H, 10.76%. Calcd for $C_{22}H_{40}O_4$: C, 71.69; H, 10.94%.

References

1) a) M. Stoll and A. Rouvé, *Helv. Chim. Acta*, **30**, 1822 (1947); b) M. Stoll, *ibid.*, **30**, 1837 (1947).

2) For example, V. V. Dhekne, B. B. Ghatge, U. G. Nayak, K. K. Chakravarti, and S. C. Bhattacharyya, *Indian J. Chem.*, **4**, 524 (1966); E. Seoane, M. Arnó, J. R. P. Llinares, and J. S. Parareda, *Chem. Ind. (London)*, **1978**, 165; S. Hünig and W. Lendle, *Chem. Ber.*, **93**, 909 (1960).

3) a) Y. Iwakura and K. Uno, *Nippon Kagaku Zasshi*, **78**, 1507 (1957); b) Y. Iwakura and K. Uno, *ibid.*, **78**, 1511 (1957); c) R. Goto, A. Ishizawa, and M. Yamamura, *ibid.*, **88**, 678 (1967).

4) K. Sisido, Y. Kazama, H. Kodama, and H. Nozaki, *J. Am. Chem. Soc.*, **81**, 5817 (1959); B. Angelo, *C. R. Acad. Sci., Ser. C*, **273**, 1767 (1971).

5) T. Sato, T. Kawara, M. Kawashima, and T. Fujisawa, *Chem. Lett.*, **1980**, 571.

6) Without a copper catalyst the reaction of β-propiolactone with 1,4-butanediyl- and 1,5-pentanediyldimagnesium dibromide gave 1-(2-hydroxyethyl)cyclopentanol and 1-(2-hydroxyethyl)cyclohexanol, respectively: P. Canonne, G. B. Foscolos, and D. Bélanger, *J. Org. Chem.*, **45**, 1828 (1980).

7) K. Diemert, P. Haas, and W. Kuchen, *Chem. Ber.*, **111**, 629 (1978).

8) J. Tsuji, T. Yamada, M. Kaito, and T. Mandai, *Tetrahedron Lett.*, **1979**, 2257.

9) J. Tsuji and S. Hashiguchi, *Tetrahedron Lett.*, **21**, 2955 (1980).

10) A. Alexakis, G. Cahiez, and J. F. Normant, *Synthesis*, **1979**, 826.

11) J. Buendia, *Bull. Soc. Chim. Fr.*, **1966**, 2778.

12) V. Hněvsová, V. Smělý, and I. Ernest, *Chem. Listy*, **50**, 573 (1956).

13) J. Tsuji, M. Kaito, and T. Takahashi, *Bull. Chem. Soc. Jpn.*, **51**, 547 (1978).

Sweetness of Hesperetin Dihydrochalcone Derivatives Linked to ω-Amino Acid or Its Oligomer

Masao KAWAI,* Kyoko KUWABARA, Ritsuko KIMURA, and Sachiko SEKIDO
Mitsubishi-Kasei Institute of Life Sciences, Minamiooya 11, Machida, Tokyo 194
(Received May 15, 1982)

Synopsis. Derivatives of hesperetin dihydrochalcone having ω-amino acid, oligoglycine, or oligo-(γ-aminobutyric acid) were synthesized and tasted. The hydrophobicity of the introduced group is important for understanding the structure-sweet taste relationship of these compounds, though other factors than hydrophobicity also must be taken into account.

Neohesperedin dihydrochalcone (**1**) is an intensely sweet substance derived from a rind-constituent of citrus fruits.[1] The aglycone of **1**, namely hesperetin dihydrochalcone (**2**) (DHC–OH), and its ω-carboxyalkyl derivatives DHC–O$(CH_2)_mCO_2H$ (**3**) (m=1, 3) and ω-sulfoalkyl derivatives DHC–O$(CH_2)_mSO_3H$ (**4**) (m=1—4) are also known to elicit sweet sensation.[2] We have attempted to prepare derivatives of **2** having an amino acid or peptide in group R in Fig. 1 for the purpose of investigating the structure-sweet taste relationship of these compounds.

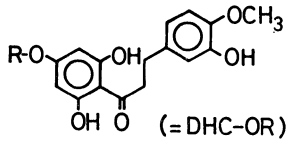

Fig. 1. Structure of hesperetin dihydrochalcone derivatives (DHC–OR).
1: R=$C_{12}H_{21}O_9$ (β-neohespesperidosyl), **2**: R=H, **3**—**8**: see text and Tables 1 and 2.

Results and Discussion

Oligomers of glycine were introduced to **3** (m=3)[3] affording DHC–O$(CH_2)_3CO(NHCH_2CO)_nOH$ (**5**). Results of semiquantitative taste evaluation are given in Table 1. The compound having one glycyl residue, **5** (n=1), is sweeter than the parent compound **3** (m=3), but further addition of glycyl residue results in decrease in sweetness. Another series of derivatives prepared includes those having ω-amino acid residue in the side chain, namely DHC–O$(CH_2)_3CONH(CH_2)_nCO_2H$ (**6**), the sweetness of which is summarized in Table 2. Successive addition of a methylene group causes marked decrease in sweet potency, finally giving tasteless derivative **6** (n=5).

Since the sweetness of aglycone **2** is of the same order of magnitude as that of the parent glycoside **1**,[2a] group R in Fig. 1 is considered not to be directly involved in the interaction of these sweetener molecules with the taste receptors. DuBois *et al.*[4] recently reported zwitterionic amino acid derivatives of **2**, relating their relative sweetness to a chromatographic parameter which quantitates the hydrophobic-hydrophilic balance of molecule. We assumed that the change in hydrophobicity caused by the introduction of group R would mainly affect the sweet potency. Thus the structure-sweet taste relationship found here for the **5** and **6** series can be explained in terms of increase and decrease in hydrophobicity of molecule,

Table 1. Relative sweetness, melting points, and analytical data of DHC–O$(CH_2)_3CO(NHCH_2CO)_nOH$ (**5**)

n	Relative sweetness[5]	Mp θ_m/°C (crystallized from)	Found(%)			Calcd(%)		
			C	H	N	C	H	N
0[a]	300	190—192[b] (EtOH)						
1	500	126—130 (MeOH)	58.18	5.65	3.14	57.89	5.74	3.07[c]
2	400	175—176 (MeOH)	56.61	5.67	5.24	56.63	5.64	5.50[d]
3	300	110—118 (MeOH–AcOEt)	53.20	5.57	7.25	53.06	5.82	7.14[e]
4	200	200—205 (MeOH)	51.72	5.88	8.94	52.09	5.78	8.68[e]

a) Compound **3** (m=3). b) Ref. 3, 193—195 decomp. c) $\frac{1}{2}H_2O$. d) $\frac{1}{4}H_2O$. e) $\frac{3}{2}H_2O$.

Table 2. Relative sweetness, melting points, and analytical data of DHC–O$(CH_2)_3CONH(CH_2)_nCO_2H$ (**6**)

n	Relative sweetness[5]	Mp θ_m/°C (crystallized from)	Found(%)			Calcd(%)		
			C	H	N	C	H	N
1[a]	500	see Table 1						
2	200	66—68 (lyophilized)	60.13	5.66	3.07	59.86	5.90	3.04
3	200	178—183 (MeOH)	60.20	6.14	3.03	60.62	6.15	2.95
4	100	166—167 (MeOH)	60.03	6.33	2.74	59.87	6.76	2.69[b]
5	0	204—208 decomp (MeOH–AcOEt)	61.63	6.51	2.60	62.01	6.61	2.78

a) Compound **5** (n=1). b) $C_{25}H_{31}O_9N\cdot CH_3OH$.

respectively, suggesting that group R be required to possess optimal hydrophobicity for showing sweet taste. Indeed, maximal sweetness is developed for the compounds of the **4** series when the number of methylenes is 2.[2b] In the case of DHC–$OCH_2CONH(CH_2)_n$-CO_2H (**7**), relative sweetness[5] is as follows: 200 (n=1), 200—300 (n=2), 200 (n=3), and 100—200 (n=5), *i.e.*, the compound (n=2) is the sweetest in this series, though its sweetness is less than that of **5** (n=1). In view of substituent constants of hydrophobic parameters[6] it is expected that the hydrophobicity of a molecule will not be much affected by the introduction of a γ-aminobutyric acid residue $NH(CH_2)_3CO$. The sweetness of DHC–$O(CH_2)_3CO[NH(CH_2)_3CO]_nOH$ (**8**) (100, n=2; 0, n=4)[5] is, however, less than those of the corresponding oligoglycine derivatives **5**, indicating that not only the hydrophobicity but also other factors must be considered for better understanding of the structure-sweet taste relationship of these compounds.

Experimental

Melting points were uncorrected. Compounds **3** (m=1 and 3) were prepared from hesperetin as described in Ref. 3.

N-Hydroxysuccinimide Ester of **3** *(m=3).* To an ice-cooled solution of 4 mmol of **3** (m=3) and 6 mmol of *N*-hydroxysuccinimide in tetrahydrofuran (10 cm^3) was added 4.4 mmol of 1-ethyl-3-(3-dimethylaminopropyl)carbodiimide hydrochloride and the mixture was stirred at room temperature. After 42 h the solution was evaporated and the residue dissolved in AcOEt was washed successively with aqueous solutions of 10% citric acid, 4% $NaHCO_3$, and saturated NaCl. The *N*-hydroxysuccinimide ester was crystallized from AcOEt–hexane, mp 137—142 °C (Found: C, 58.55; H, 5.29; N, 2.93%. $C_{24}H_{25}O_{10}\cdot\frac{1}{4}H_2O$).

General Procedures. *Method A*: Amino acid or peptide (0.6—0.7 mmol) was dissolved in H_2O containing Et_3N (0.6—0.7 mmol) and added to a solution of 0.5 mmole of *N*-hydroxysuccinimide ester of **3** (m=3) in tetrahydrofuran. After stirring at room temperature the reaction mixture was acidified and evaporated and the residue was subjected to Sephadex LH-20 column chromatography using MeOH as eluent. Crystallization from MeOH or MeOH–AcOEt afforded the desired product **5** or **6**.

Method B: To a solution of hydrochloride of methyl or ethyl ester of amino acid or peptide (1.5 mmol) in $CHCl_3$ or H_2O were added Et_3N (1.5 mmol) and a solution of 1 mmol of *N*-hydroxysuccinimide ester of **3** (m=3) in tetrahydrofuran and stirred at room temperature. Usual workup and SiO_2 column chromatography (if necessary) gave the methyl or ethyl ester of the dihydrochalcone derivative. Without further purification the ester was dissolved in 0.5 M NaOH (1 M=1 mol dm^{-3}) and stirred for 20 min at room temperature. The solution was acidified by addition of HCl aq and the precipitate was purified by Sephadex LH-20 column chromatography.

Method C: To an ice-cooled solution of 1 mmol of **3** (m=1), amino acid methyl or ethyl ester hydrochloride (1.5 mmol), Et_3N (1.5 mmol), and 1-hydroxybenzotriazole (0.5 mmol) in a mixture of tetrahydrofuran and *N,N*-dimethylformamide was added 1.5 mmol of 1-ethyl-3-(3-dimethylaminopropyl)carbodiimide hydrochloride. After stirring for 24—48 h at room temperature the reaction mixture was worked up as usual and the product was subjected to alkaline hydrolysis as described in Method B.

Mp's and results of elemental analyses of **5** and **6** are given in Tables 1 and 2. Compounds **5** (n=2 and 3) and **6** (n=2—4) were synthesized with Method A. The following derivatives were prepared by using method B *via* ethyl ester: **5** (n=1 and 4); **8** (n=2), mp 166—167 °C (Found: C, 59.44; H, 6.32; N, 4.92%. $C_{28}H_{36}O_{10}N_2\cdot\frac{1}{4}H_2O$); **8** ($n$=4), mp 131—134 °C. Compound **6** (n=5) was prepared with method B *via* methyl ester. Method C afforded the following compounds: **7** (n=1) *via* ethyl ester, mp 198—210 °C decomp (Found: C, 55.92; H, 5.21; N, 2.97%. $C_{20}H_{21}O_9N\cdot\frac{1}{2}H_2O$); **7** ($n$=2) *via* methyl ester, mp 173—180 °C (Found: C, 57.10; H, 5.34; N, 2.91%. $C_{21}H_{23}O_9N\cdot\frac{1}{2}H_2O$); **7** ($n$=3) *via* ethyl ester, mp 240—256 °C decomp (Found: C, 58.08; H, 5.63; N, 3.08%. $C_{22}H_{25}O_9N\cdot\frac{1}{2}H_2O$); **7** ($n$=5) *via* methyl ester, mp 211—212 °C (Found: C, 50.65; H, 6.39; N, 3.01%).

The authors are grateful to Dr. Ukon Nagai of our Institute for helpful discussions and to the members of the Analytical Department of System Engineering Laboratory, Mitsubishi-Kasei Industries, Ltd. for elemental analyses.

References

1) R. M. Horowitz and B. Gentili, *J. Agric. Food Chem.*, **17**, 696 (1969).

2) a) G. E. DuBois, G. A. Crosby, and P. Saffron, *Science*, **195**, 397 (1977); b) G. E. DuBois, G. A. Crosby, R. A. Stephenson, and R. E. Wingard, Jr., *J. Agric. Food Chem.*, **25**, 763 (1977).

3) G. E. DuBois, G. A. Crosby, and P. Saffron, *Synth. Commun.*, **7**, 49 (1977).

4) G. E. DuBois, G. A. Crosby, J. F. Lee, R. A. Stephenson, and P. C. Wang, *J. Agric. Food Chem.*, **29**, 1269 (1981).

5) Relative sweetness is given on a molar basis taking sucrose as standard. One-mM solutions containing equimolar amount of NaOH were tested by a taste panel. Each solution was compared with 0.1—0.6 M sucrose solutions.

6) A. Leo, C. Hansch, and D. Elkins, *Chem. Rev.*, **71**, 525 (1971).

C-Sulfinylation of Grignard Reagents and Enamines with Sulfinic Acid

Yoshihide NOGUCHI, Kenkichi KUROGI, Minako SEKIOKA, and Mitsuru FURUKAWA*

Faculty of Pharmaceutical Sciences, Kumamoto University, 5-1 Oe-hon-machi, Kumamoto 862

(Received May 19, 1982)

Synopsis. Direct *C*-sulfinylation of Grignard reagents with sulfinic acid (**4**) in the presence of activating reagents, such as phenyl phosphorodichloridate (**1**), diphenyl phosphorochloridate (**2**), and 3-phthalimidooxy-1,2-benzisothiazole 1,1-dioxide, were investigated. β-Keto sulfoxides were also formed by the reaction of enamines with **4** using **1** and **2** under similar conditions.

We have recently developed a series of new one-pot *O*- and *N*-sulfinylations with sulfinic acid in the presence of an activating reagent,[1] and more recently found that some reagents were sufficiently effective for *S*-sulfinylation of thiols, giving thiosulfinates in comparatively good yields.[2]

We newly tried to extend these methods to *C*-sulfinylations of Grignard reagents and enamines. The employed activating reagents are as follows: Phenyl phosphorodichloridate (**1**), diphenyl phosphorochloridate (**2**), and 3-phthalimidooxy-1,2-benzisothiazole 1,1-dioxide (**3**). The methods differ from each other only in the reagents employed for activation of sulfinic acid. In one case, **1** or **2** and pyridine (or triethylamine) are used, and in the other, **3** and 1,8-diazabicyclo-[5,4,0]undec-7-ene (DBU).

The reagent **1** has been reported to be sufficiently effective as an activating reagent for transformation of carboxylic acids to the esters[3] under virtually neutral and mild conditions. In the present study, p-toluenesulfinic acid (**4**) was treated with an equivalent of **1** and an excess pyridine in THF at −15—0 °C; when this mixture was then allowed to react with Grignard reagents (**5**) at room temperature, the corresponding sulfoxides (**6**) were obtained in low yields.

A comparable activating effect was observed by using **2**, which possesses a similar structural moiety; this gave somewhat lower yields of **6**. The reaction probably proceeds *via* a mixed anhydride intermediate, as well as by *O*-sulfinylation.[2]

Better results for sulfinylation of **5** were obtained by using **3** and DBU in some cases. The reaction was achieved by adding a solution of two equivalents of **5** in ether to a mixture of equivalents of **4**, **3**, and DBU in THF below −5 °C under a nitrogen stream and by stirring the reaction mixture at room temperature. Purification was carried out by silica gel column chromatography. The yields of sulfoxides obtained by these methods are shown in Table 1.

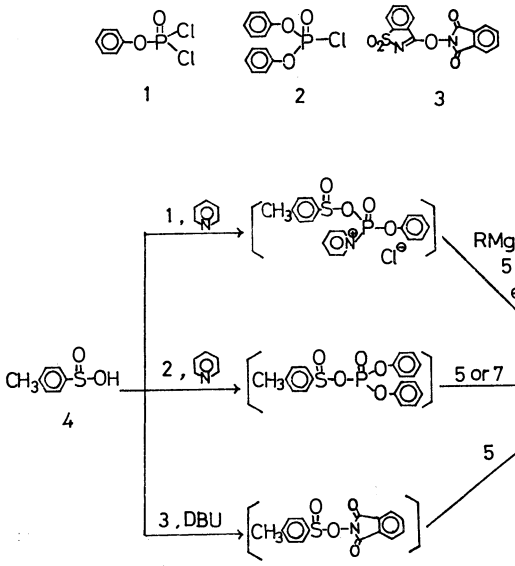

Scheme 1.

We also tried to extend these methods to sulfinylation of enamines (**7**). An example of β-sulfinylation of **7** has not been reported in the literature. The reaction was carried out by treating **7** with an equivalent of **4** in dichloromethane in the presence of equivalent of **1** and an excess of triethylamine to afford the corresponding β-keto sulfoxides (**6**, R=α-keto alkyl) in 10—43% yields, along with small amounts of several

Table 1. Yields of sulfoxides and β-keto sulfoxides $CH_3C_6H_4S(O)R$

R	Yield/%			Mp θ_m/°C	IR $\tilde{\nu}_{max}$/cm^{-1}		Calcd (Found) (%)	
	Method A	Method B	Method C		S=O	C=O	C	H
C_2H_5	40	26	18	Oil	1045			
i-C_3H_7	25	16	19	Oil	1045			
C_6H_5	31	14	53	64—15	1050			
$C_6H_5CH_2$	35	15	37	141—142	1038			
$C_6H_5COCH_2$	10	34		75—78	1048	1680	69.77(69.77)	5.43(5.39)
$C_6H_5COCHCH_3$	12	36		98—99	1045	1660	70.56(70.22)	5.92(5.90)
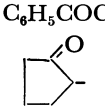	11	41		92—93	1040	1738	64.84(64.72)	6.35(6.38)
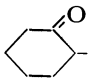	43	50		99—101	1042	1710	66.10(66.05)	6.78(6.84)

by-products such as disulfide and thiosulfonate.

Better results were obtained by using **2** instead of **1** to give **6** (R=α-keto alkyl) in 34—50% yields. In this case, a small amount of diphenyl *N,N*-pentamethylenephosphoramidate was isolated as the by-product, no formation of disulfide and thiosulfonate being observed. In both cases, purification was carried out by column chromatography on silica gel. The results are summarized in Table 1. Unfortunately, **3** was inaffective as the activating reagent.

β-Keto sulfoxides are known to be useful starting materials and versatile synthetic intermediates in organic synthesis.[4] These vicinally difunctionalized compounds have previously been prepared by oxidation of α-substituted thioketone,[5] acylation of sulfinyl stabilized carbanions with esters,[6] or sulfinylation of ketone enolate anions with sulfinates.[7] An especially notable feature of our methods is the application of mild and nearly neutral conditions throughout the reactions; therefore the acid or base sensitive functional groups will be expected to remain unaffected.

Experimental

All the melting points are uncorrected. IR and NMR spectra were measured on a JASCO IRA-1 grating infrared spectrometer and JEOL high resolution NMR instrument C-60 at 60 MHz, respectively. Mass spectra were determined at 75 eV on a JEOL-01SG mass spectrometer.

Preparation of Sulfoxides (6). *Method A*: A solution of **1** (2.11 g, 10 mmol) in anhyd THF (5 ml) was added dropwise with stirring into a solution of **4** (1.56 g, 10 mmol) and pyridine (2.37 g, 30 mmol) in anhyd THF (30 ml) at −15 °C under a nitrogen atmosphere; then the mixture was stirred for 1 h. A Grignard reagent (**5**) (20 mmol) prepared in the usual way in ether was added slowly to the mixture below −5 °C under a nitrogen atmosphere. The mixture was stirred for 3 h from 0 °C up to room temperature. After the solvents were evaporated under reduced pressure, the residue was dissolved in $CHCl_3$ (60 ml), and the solution was washed with 1 M HCl (1 M = 1 mol dm^{-3}), 5% aq $NaHCO_3$, and finally with H_2O, dried over anhyd Na_2SO_4 and evaporated. The residue was chromatographed on silica gel by using benzene–ethyl acetate (4:1) as an eluent to give **6** and by-products, di-*p*-tolyl disulfide and *S*-*p*-tolyl *p*-toluenethiosulfonate.

Method B: A solution of pyridine (0.9 g, 12 mmol) in anhyd THF (5 ml) was added dropwise with stirring into a solution of **4** (1.56 g, 10 mmol) and **2** (2.7 g, 10 mmol) in anhyd THF (30 ml) at −10 °C under a nitrogen atmosphere, and the mixture was stirred for 1 h. A solution of **5** (20 mmol) prepared in the usual way in ether was added slowly to the mixture below −5 °C. After stirring for 3 h, the mixture was quenched with H_2O and extracted with ether (50 ml × 3), and the extracts were worked up and chromatographed as in Method A to give **6**, along with di-*p*-tolyl disulfide and *S*-*p*-tolyl *p*-toluenethiosulfonate.

Method C: To a solution of **4** (0.78 g, 5 mmol) and **3** (1.64 g, 5 mmol) in anhyd THF (30 ml) was added dropwise with stirring a solution of DBU (0.76 g, 5 mmol) in anhyd THF (5 ml) at room temperature under a nitrogen atmosphere. Grignard reagent **5** (15 mmol) prepared in the usual way in ether was added slowly to the mixture below −5 °C under a nitrogen stream. After stirring at −15 °C for 30 min, the mixture was stirred at room temperature for 1.5 h and evaporated. The residue was dissolved in $CHCl_3$ (60 ml), and the solution was treated and chromatographed as in Method A to give **6** along with di-*p*-tolyl disulfide and *S*-*p*-tolyl *p*-toluenethiosulfonate as by-products.

Preparation of β-Keto Sulfoxides (6, R=α-Keto Alkyl). *Method A*: A solution of triethylamine (1.1 g, 11 mmol) in anhyd CH_2Cl_2 (10 ml) was added dropwise with stirring into a solution of **4** (1.56 g, 10 mmol) and **1** (2.3 g, 11 mmol) in anhyd CH_2Cl_2 (30 ml) at −10 °C under a nitrogen atmosphere, and the mixture was stirred for 1 h below −10 °C. A solution of **7** (12 mmol) and triethylamine (2.2 g, 22 mmol) in anhyd CH_2Cl_2 (10 ml) was added gradually to the mixture. After stirring for 3 h, the mixture was washed with 0.1 M HCl, 1% aq $NaHCO_3$, and H_2O, dried over anhyd Na_2SO_4, and evaporated. The residue was purified by silica gel column chromatography using benzene–ethyl acetate (4:1 100 ml, 2:1 50 ml, 1:1 150 ml) to give β-keto sulfoxide along with di-*p*-tolyl disulfide and *S*-*p*-tolyl *p*-toluenethiosulfonate as by-products.

Method B: A solution of triethylamine (1.2 g, 12 mmol) in anhyd CH_2Cl_2 (10 ml) was added dropwise with stirring into a solution of **4** (1.56 g, 10 mmol) and **2** (2.7 g, 10 mmol) in anhyd CH_2Cl_2 (40 ml) at −10 °C under a nitrogen atmosphere. After the mixture was stirred for 1 h, a solution of **7** (12 mmol) and triethylamine (1.2 g, 12 mmol) in anhyd CH_2Cl_2 (15 ml) was gradually added. The mixture was stirred for 2 h at room temperature, and washed with 0.1 M HCl, 1% aq $NaHCO_3$, and with H_2O, dried over anhyd Na_2SO_4, and evaporated. The residue was purified by silica-gel column chromatography using benzene–ethyl acetate (4:1 100 ml, 2:1 50 ml, 1:1 100 ml) to give β-keto sulfoxide along with diphenyl *N,N*-pentamethylenephosphoramidate.

Preparation of 3-Phthalimidooxy-1,2-benzisothiazole 1,1-Dioxide (3). A solution of triethylamine (3.8 g, 28 mmol) in acetonitrile (10 ml) was added dropwise into a suspension of 3-chloro-1,2-benzisothiazole 1,1-dioxide (5.6 g, 28 mmol) and *N*-hydroxyphthalimide (4.8 g, 30 mmol) in acetonitrile (60 ml) with stirring at 0—5 °C, and the mixture was stirred overnight. After removal of the precipitates, the filtrate was concentrated. The residue was recrystallized from $CHCl_3$–CH_2Cl_2. Yield 66%. Mp 238—241 °C. Found: C, 54.85; H, 2.25; N, 8.53%. Calcd for $C_{15}H_8N_2O_5S$: C, 54.87; H, 2.45; N, 8.53%. IR (KBr): 1760, 1625, 1570, 1470, 1350, 1190, and 800 cm^{-1}. MS *m/e*: 328 (M^+), 166, 162, 104, 76.

References

1) M. Furukawa, T. Ohkawara, Y. Noguchi, M. Nishikawa, and T. Tomimatsu, *Chem. Pharm. Bull. (Tokyo)*, **28**, 134 (1980); M. Furukawa, T. Ohkawara, Y. Noguchi, M. Isoda, and T. Hitoshi, *Synthesis*, **1981**, 937.

2) Y. Noguchi, M. Isoda, K. Kuroki, and M. Furukawa, *Chem. Pharm. Bull. (Tokyo)*, **30**, 1646 (1982).

3) H. J. Liu, W. H. Chan, and S. P. Lee, *Tetrahedron Lett.*, **1978**, 4461.

4) L. Field, *Synthesis*, **1972**, 101; **1978**, 713.

5) B. M. Trost and T. N. Salzmann, *J. Am. Chem. Soc.*, **95**, 6840 (1973); N. J. Leonard and C. R. Johnson, *J. Org. Chem.*, **27**, 282 (1962).

6) H. D. Becker, G. J. Mikol, and G. A. Russel, *J. Am. Chem. Soc.*, **85**, 3410 (1963); E. J. Corey and M. J. Chaykovsky, *ibid.*, **86**, 1639 (1964); **87**, 1345 (1965); P. G. Gassman and G. D. Rickmond, *J. Org. Chem.*, **31**, 2335 (1966); T. L. Moore, *ibid.*, **32**, 2786 (1967).

7) R. M. Coates and H. D. Pigott, *Synthesis*, **1975**, 319.

The Reactivity of Radical Anions Generated by Electron-transfer Reaction of Allyl Acetates

Kazuo TSUJIMOTO,* Yojiro KAMIYAMA, Yuji FURUKAWA, and Mamoru OHASHI
Department of Materials Science, The University of Electro-Communications, Chofu, Tokyo 182
(Received May 21, 1982)

Synopsis. Photoinduced electron-transfer reactions of 3-(2-naphthyl)-2-butenyl acetate gave the reduced products, while the electrochemical and Birch reduction of the acetate furnished (*E*)-2-(2-naphthyl)-2-butene as the sole product. One-electron reduction was suggested by mechanistic studies of the photoreaction on the basis of deuterium incorporation into the products. A similar mechanism can operate in the photoreduction of cinnamyl acetate.

For ten years many photochemists have focused[1] their interest on photoinduced electron-transfer reactions. The reactions involving a system which consists of a pair of donor and acceptor molecules are triggered by irradiation. Now we report the reactivity of the anion radical produced by electron-transfer in the photoinduced reaction of an allyl acetate.[2]

Results and Discussion

Irradiation upon acetonitrile solution of 3-(2-naphthyl)-2-butenyl acetate (**1**) in the presence of triethylamine[3] gave 3-(2-naphthyl)-1-butene (**2**), (*Z*)- and (*E*)-2-(2-naphthyl)-2-butene (**3** and **4** respectively), and 2-(2-naphthyl)-1,3-butadiene (**5**) as hydrocarbon fractions in 14, 2.6, 7.0, and 3.0% yields respectively. When diethylamine and butylamine, which have higher ionization potentials than that of triethylamine, were used as an electron donor, the yields of **2**, **3**, and **4** decreased. The formation of **5**, however, is independent of the ionization potential of the donor, as shown in Table 1. Results which suggest that the photoreaction is proceeding *via* charge transfer in the excited state were also observed in fluorescence quenching of **1** with aliphatic amines, as shown in Table 2.

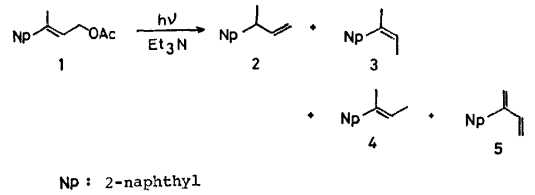

Scheme 1.

When a mixture of methanol–acetonitrile (1:1) was used instead of acetonitrile as a solvent, a photosolvolytic reaction took place to give 3-methoxy-3-(2-naphthyl)-1-butene (**6**) in 44% yield as a major product.[4] The hydrocarbon products were also isolated. Deuterium incorporation by use of methanol-*d* in place of methanol was observed in the formation of **3** and **4**, while the use of methan-d_3-ol contributed little to the incorporation, as shown in Table 3.

The Birch reduction of **1** in liquid ammonia gave **4** in 49% yield, together with a small amount of dihydro- and tetrahydronaphthalenes. In a reduction similar to the Birch reaction, **1** was reduced on the anode. When an acetonitrile solution of **1** with tetrabutylammonium iodide was electrolyzed in 2.1 F/mol, the product **4** was isolated in 73% yield.

Among three kinds of reactions, the photochemical, the Birch, and the electrochemical reduction,[5] the products for the anion radical generated photochemically are different from that of the others. In the photoinduced electron-transfer reaction, the radical which results from the ionic dissociation of the anion radical can hydrogen-abstract from triethylamine to furnish reduction products. On the other hand, the radical generated from the ionic dissociation of the anion radical can be reduced further in the Birch or the electrochemical reaction, resulting in the formation of an anion intermediate which subsequently reacts with the proton added.

In conclusion, the following schematic mechanism is proposed to elucidate the reactivity of the intermediate, as shown in Scheme 2.

According to the reactivity of the radical generated from a photochemical electron-transfer reaction, it is understandable that the photoreaction of cinnamyl acetate with aliphatic amines gave not only 1-phenylpropene (16%) but also allylbenzene (22%).

TABLE 1. PRODUCT YIELDS[a]

Amines	2	3	4	5
Triethylamine	14	2.6	7.0	3.0
Diethylamine	3.3	0.2	1.7	8.6
Butylamine	—	—	—	4.6

a) Yields were measured by GC analyses based on the amount of **1** used.

TABLE 2. FLUORESCENCE QUENCHING ($k_q\tau$/mol^{-1} dm^3) OF **1** WITH ALIPHATIC AMINES

Solvents	Amines		
	Triethylamine	Diethylamine	Butylamine
Acetonitrile	103	29	3
Cyclohexane	57	22	0

TABLE 3. DEUTERIUM INCORPORATION FOR THE PHOTOREDUCTION OF **1**[a]

Deuterated solvents	Photoproducts (% of the deuterated)			
	2	3	4	5
CH_3OD	11	24	24	—
CD_3OH	—	—	—	—

a) Experimental errors are within ±3%.

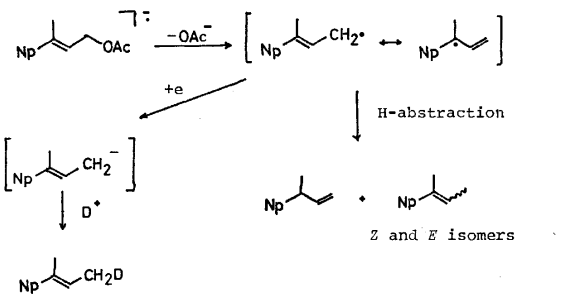

Scheme 2.

Experimental

Melting points were obtained with a hot-stage apparatus and are uncorrected. IR spectra were determined on a JASCO IRA-1 spectrometer. NMR spectra were detected by using a Hitachi R-20B 60-MHz instrument. GC-MS analyses were carried out on a Hitachi RMU-6MG instrument. A Pyrex column (0.3 cm i.d.×1.2 m) packed with Diasolid ZF 80—100 mesh (Nippon Chromato Kogyo Co.) was used for separation. Quantitative and preparative GC were performed on a Shimadzu GC-3BF and on a Varian 90 P-3 instrument, respectively. Fluorescence spectra were recorded on a Hitachi 204 spectrometer.

*Preparation of 3-(2-Naphthyl)-2-butenyl Acetate (**1**).* To a suspension of NaH (5.5 g, 50% oil dispersion) in dry 1,2-dimethoxyethane (70 cm³, DME) was added a solution of triethyl phosphonoacetate (17.8 g) in dry DME (50 cm³) at 0 °C under N_2 gas. Then a solution of 2-acetylnaphthlene (10.3 g) in anhydrous DME (70 cm³) was added dropwise at 0 °C under stirring and the mixture was stirred continuously at room temp for 8 h. After extraction with diethyl ether, the obtained material was chromatographed on a short-column (PF_{254} Merck/10% ether in hexane), and the pure *E*-isomer (7.0 g) was obtained in 48% yield. Mp 45.3—45.7 °C. MS *m/z* 240(M^+), ^{1}H-NMR (CCl_4) δ=1.26 (3H, t, J=8 Hz), 2.63(3H, d, J=1.5 Hz), 4.17(2H, q, J=8 Hz), 6.17(1H, q, J=1.5 Hz), and 7.2—7.8(7H, m). The *Z*-isomer was also isolated by the chromatography, of which NMR spectrum showed peaks at δ=0.93(3H, t, J=8 Hz), 2.16(3H, d, J=1.5 Hz), 3.88(2H, q, J=8 Hz), 5.86 (1H, q, J=1.5 Hz), and 7.1—7.8(7H, m).

To a suspension of $LiAlH_4$ (3.1 g) in anhydrous ether (70 cm³) was added an etheral solution of the *E*-isomer (7.0 g in 90 cm³) at room temp under N_2 atmosphere. After stirring for 5 h, the ether extraction afforded crude crystals which were recrystallized from benzene–hexane (1:1). The recrystallized alcohol weighed 4.3 g (74%), mp 85.8—86.5 °C. MS *m/z* 198(100, M^+), 180(66, $M-H_2O$), 179(48), 178(21), 165(62). ^{1}H-NMR δ=1.74(1H, s, OH), 2.13(3H, d, J=1.5 Hz), 4.40(2H, d, J=7 Hz), 6.11(1H, tq, J=7 and 1.5 Hz), and 7.3—7.9(7H, m).

To a solution of the alcohol (2.0 g) in anhydrous ether (60 cm³) was added acetyl chloride (3.0 cm³) and then triethylamine (6.0 cm³) at 0 °C. After 90 min, the ether extracted fraction was chromatographed on silica gel (PF_{254}/20% ether in hexane). The obtained crystals weighed 2.3 g(95%); their mp was in the range of 47.8—48.5 °C. MS 241(18), 240(100, M^+), 198(38), 197(41), 183(45), 180(55), 179(34), 169(25), and 165(53). Found: *m/z* 240.1152. Calcd for $C_{16}H_{16}O_2$: M, 240.1150. ^{1}H-NMR δ=2.0(3H, s), 2.18 (3H, s), 4.75(2H, d, J=8 Hz), 5.96(1H, t, J=8 Hz), and 7.2—7.8(7H, m). IR(KBr) 1740 cm^{-1}. UV(CH_3CN) 243 (44000), 274(10000), 284(12000), 295(8900) nm.

*Preparative Photoreaction of **1** with Triethylamine.* A 0.02 M acetonitrile solution (200 cm³) of **1** with triethylamine (6.0 cm³) was irradiated with a high-pressure mercury arc for 1.5 h at room temp under N_2 bubbling. After removal of low-boiling point materials, the residue was chromatographed on a precolumn of silica gel (Wako gel Q-50/10% ether in hexane) and rechromatographed on silica gel PF_{254}/hexane). The developed fraction was collected and injected in a GC. Four products showed the following chromatograms: retention time: **2**, 14′; **3**, 12′; **4**, 25′ and **5**, 18′. **2**: MS *m/z* 183(12), 182(69, M^+), 181(15), 168(14), 167(100), 166(13), 165(15), and 152(11). Found: *m/z* 182.1071. Calcd for $C_{14}H_{14}$: M, 182.1094. IR 1640 cm^{-1}. ^{1}H-NMR δ=1.40(3H, d, J=7 Hz, CH_3), 3.57(1H, qdt, J=7, 6, and 2 Hz), 5.05(2H, dd, J=17 and 2 Hz and dd, J=10 and 2 Hz), 6.05(1H, ddd, J=17, 10 and 6 Hz), and 7.4(7H, m). **3**: MS *m/z* 183(22), 182(100, M^+), 181(26), 168(17) 167(70), 166(13), and 165(17). ^{1}H-NMR δ=1.65(3H, d, J=7 Hz), 2.09(3H, s), 5.75(1H, q, J=7 Hz), and 7.5(7H, m). **4**: MS *m/z* 183(20), 182(100, M^+), 181(26), 168(16), 167(84), 166(16) and 165(20). Found: *m/z* 182.1079. Calcd for $C_{14}H_{14}$: M, 182.1094. ^{1}H-NMR 1.82(3H, d, J=7 Hz), 2.09(3H, s), 5.92(1H, q, J=7 Hz), and 7.5(7H, m). **5**: MS *m/z* 181(18) 180(100, M^+), 179(77), 178(32), and 165 (41). Found: *m/z* 180.0943. Calcd for $C_{14}H_{12}$: M, 180.0939. ^{1}H-NMR δ=5.2(2H, dd, J=17 and 9 Hz), 5.3 (2H, s), 6.7(1H, dd, J=17 and 9 Hz), and 7.5(7H, m).

*Photoreaction of **1** with Methanol.* A mixture of methanol–acetonitrile (1:1) was used (80 cm³) as a solvent for irradiation of **1** (400 mg) in the presence of triethylamine (2.4 cm³) with a 6 W-low pressure mercury arc for 1.5 h. TLC separation (PF_{254}/10% ether in hexane) gave **2**, **3**, **4**, **5**, and **6** in 20, 1.6, 14, 10, and 44% yields respectively. **6**: MS *m/z* 212(52), 197(43), 182(7), 181(45), 180(100), 179(73), 178(16), 166(18), and 165(59). Found: *m/z* 212.1212. Calcd for $C_{15}H_{16}O$: 212.1200. ^{1}H-NMR δ= 1.60(3H, s), 3.12(3H, s), 5.15(1H, dd, J=10 and 2 Hz), 5.20(1H, dd, J=18 and 2 Hz), 6.00(1H, dd, J=18 and 10 Hz), and 7.5(7H, m).

*Electrolytic Reduction of **1**.* An acetonitrile solution (40 cm³) of **1** (114 mg) with tetrabutylammonium iodide (1.48 g) as a supporting electrolyte was electrolyzed (3.3 V, Pt) under N_2 gas for 1 h. The etheral extraction and TLC separation gave **4** (63 mg).

*Birch Reduction of **1** in Liquid Ammonia.* At −78 °C, an acetonitrile solution (2.0 cm³) of **1** (105 mg) was dropwise added to a liquid ammonia solution (100 cm³) of sodium (762 mg). After adding methanol (0.5 cm³) the mixture was allowed to warm up. The etheral extraction and then TLC separation gave **4** in 49% yield.

Photochemical Reaction of Cinnamyl Acetate with Triethylamine. An acetonitrile solution (350 cm³) of cinnamyl acetate (1.89 g) with triethylamine (10.9 g) was irradiated with a 12-W low pressure mercury arc under N_2 gas for 2.5 h. The reaction mixture was short-path chromatographed on silica gel with ether. The obtained mixture (190 mg) showed two peaks in GC (10% DEGS on Diasolid 80—100 mesh). Each fraction was preparatively isolated. The first fraction was identified with allylbenzene and the last was 1-phenylpropene by comparison with the spectral data (^{1}H-NMR, IR, and UV). Quantum yields for the formation of the products were 0.22 (allylbenzene) and 0.17 (1-phenylpropene).

References

1) For reviews: H. Sakurai, C. Pac, M. Ohashi, and I. Saito, "Yūki-kōkagaku No Shintenkai," ed by the Chemical Society of Japan, Japan Scientific Societies Press, Tokyo (1982), Vol. 33, Chaps. 4, 5, 6, and 8.

2) Reports on photolysis of benzyl acetate: D. C. Appleton, B. Brocklehurst, J. McKenna, J. M. McKenna, S. Thackeray, and A. R. Walley, *J. Chem. Soc., Perkin Trans. 2*, **1980**, 87.

3) In the absence of triethylamine, **5** was obtained in 4.5% yield.

4) The reaction mechanism can be interpreted as the photosolvolytic reaction with the cation rearrangement. H. E. Zimmerman and V. R. Sandel, *J. Am. Chem. Soc.*, **85**, 915 (1963).

5) Reports on electroorganic reactions of benzyl acetates: J. P. Coleman, N-ud-din, H. G. Gilde, J. H. P. Utley, B. C. L. Weedon, and L. Eberson, *J. Chem. Soc., Perkin Trans. 2*, **1973**, 1903.

Hydrogenation of Diphenylethyne Catalyzed by $PdCl_2$ in CH_2Cl_2 and Polyethylene Glycol

Nobutaka SUZUKI,* Yasuo AYAGUCHI, Tsuneaki TSUKANAKA, and Yasuji IZAWA

Department of Industrial Chemistry, Faculty of Engineering, Mie University, Tsu, Mie 514

(Received June 3, 1982)

Synopsis. A practically homogeneous system of $PdCl_2$ in CH_2Cl_2 in the presence of polyethylene glycol catalyzed hydrogenation reactions of diphenylethyne (**1**) and *cis*-1,2-diphenylethene (**2**) to **2** and/or 1,2-diphenylethane (**4**). Under the conditions, the selectivity of the hydrogenation of **1** to **2** against that of **1** to **4** was excellent, compared to that using the Pd/C system.

Polyethylene glycol (PEG) is an excellent substitute of crown ether because of its low-price, low-toxicity, non-volatility, and solubility in both organic solvents and water (easily removable). It has been used as a co-solvent as described in our previous reports[1] and in others.[2]

Much data have been accumulated for the heterogeneous[3] and homogeneous[4] catalysts of hydrogenation. However, there has been no report on the hydrogenation catalyzed by $PdCl_2$ which is made soluble in organic solvents by means of some co-solvent(s). Although a few nucleophilic additions to alkenes and alkynes proceeding by initial formation of a double or triple bond-$PdCl_2$ complex were known,[5] there have been no reports on the hydrogenation of them catalyzed by $PdCl_2$. We describe here a novel homogeneous catalyst for the hydrogenation of diphenylethyne (**1**) and 1,2-diphenylethene (**2**) to the corresponding *cis*-olefin (**2**) and the saturated hydrocarbon (**4**), respectively. Good selectivity for the partial reduction of **1** to **2** was achieved. The reactions can be interrupted simply by washing with water. This makes it easy to maximize the selectivity. This is the first example of a homogeneous catalyst using a host-guest complex between PEG and palladium for the hydrogenation of alkynes and olefins.

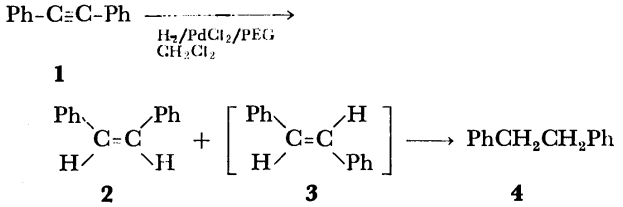

Palladium chloride[6] placed in a round-bottomed flask was covered with H_2 gas. Into the flask was added a solution of diphenylethyne[6] (**1**) in CH_2Cl_2 or some other solvent(s) with or without PEG[7] through an injection needle. The resulting clear solution was stirred at 10 °C. The hydrogenation reactions were monitored by GLC by comparing with the authentic *cis*- and *trans*-1,2-diphenylethenes[6] (**2** and **3**) and 1,2-diphenylethane[7] (**4**). Palladium/C (10%) was employed for comparisons. The results are shown in Table 1. In the case of using PEG, the aliquots were washed with water to remove the PEG and the other water soluble components before the application on GLC. Conversion yields for **2** and **4** were calculated on the basis of the conversion of **1**, ignoring a trace of **3** (less than few %). Selectivity is represented by the ratio of [**2**]/[**4**]. Palladium black seemed not to be formed during the reaction.

Table 1 shows that $PdCl_2$ worked in EtOH similarly to the Pd/C, but the selectivity is lower than for the latter (runs No. 1 and 2 in Table 1). In CH_2Cl_2, Pd/C did not catalyze the reaction well and the conversion of **1** was low, while $PdCl_2$ worked well (runs No. 4—5).

Employment of PEG as a co-solvent in CH_2Cl_2 accelerated the reaction and gave higher selectivity (runs No. 3 and 7). A higher concentration of PEG #200, however, seems to lower the reaction rate and the selectivity (runs No. 3 and 6). The viscosity of the medium may affect these values.

Molecular weight of PEG affected both the rates and the selectivity: PEG #400 gave the highest selectivity (runs No. 6—9). This may be explained by the ease of the formation of complex between the PEG molecule and Pd^{2+} cation.[8] If the cation forms a complex bound with PEG too tightly, the complex formation might also cause the difficulty of contact between the catalyst and the substrate: Consequently, the reaction rates decreased when PEG of higher molecular weight was used.

The other solvents used gave less effective results (runs No. 10—13). PEG #200 did not give higher selectivity in $CHCl_3$.

Ethylene oxide-condensed pentaerythritols (PEO-8.3EO and PEO-15.8EO)[9] worked well as co-solvents as PEG (runs No. 14—15).

Similar catalytic hydrogenation occurred when *cis*-1,2-diphenylethene (**2**) was used as a substrate (see Table 2) under similar conditions to those used above. The conversion yields were quantitative, but the reaction rates were not satisfactory for the preparation of **4**.

Experimental

Diphenylethyne[6] (**1**), *cis*- and *trans*-1,2-diphenylethenes[6] (**2** and **3**), 1,2-diphenylethane[6] (**4**), $PdCl_2$,[6] and 10% Pd/C were purchased. Polyethylene glycols #200, #400, #600, and #1000 were purchased[7] and dried azeotropically (benzene) before use. EtOH (Mg) and CH_2Cl_2 (CaH_2) were dried over and distilled from the desiccant shown in the parentheses. GLC tests were performed on a Yanagimoto Yanaco G-80F (FID): 5% PEG-20 M on Gasport (60—80 mesh) in a stainless steel column (ϕ 2 mm×2.0 m); col. temp 160 °C, inj. temp 180 °C, carrier gas (N_2), 20.9 ml/min.

Catalytic Hydrogenation of Diphenylethyne (1) or cis*-1,2-Diphenylethene (2).* Palladium chloride or 10% Pd/C (final concentration: 0.94 mM) (1 M=1 mol dm^{-3}) was placed in a 50 ml-round-bottomed flask which was kept in a thermostated bath (10±0.5 °C) with a serum cap. The flask

Table 1. Hydrogenation of diphenylethyne (**1**) at 10 °C

Run No.	Solvent	Catalyst[a]	Co-solvent (M)	Conversion of 1 / %	Time / min	Conversion yield[b]/% 2	4	[2]/[4]
1	EtOH	Pd/C[c]	—[g]	60	8.5	75	25	3.00
				90	17	65	35	1.86
2		$PdCl_2$	—	60	9	55	45	1.22
				90	20	46	64	0.72
3	CH_2Cl_2		PEG #200[d] 1.0	60	50	71	29	2.45
				90	90	57	43	1.33
4		Pd/C	—	54	300	83	17	4.88
5		$PdCl_2$	—	60	83	67	33	2.03
				90	180	58	42	1.38
6			PEG #200 0.5	60	23	78	22	3.55
				90	45	62	38	1.63
7			PEG #400 0.5	60	31	80	20	4.00
				90	79	72	28	2.57
8			PEG #600 0.5	60	51	74	26	2.85
				90	120	57	43	1.33
9			PEG #1000 0.5	60	89	72	28	2.57
				81	180	57	43	1.33
10	Et_2		—	60	23	59	41	1.44
				90	54	40	60	0.67
11	Me_2CO		—	60	15	59	41	1.44
				90	64	25	75	0.33
12	$CHCl_3$		—	60	188	62	38	1.63
				66	240	62	38	1.63
13			PEG #200 1.0	60	225	50	50	1.00
				84	420	42	58	0.72
14	CH_2Cl_2		PEO-8.3EO[e] 1.0	60	28.5	69	31	2.23
				90	53	55	45	1.22
15			PEO-15.8EO[f] 1.0	60	31	68	32	2.13
				90	82	59	41	1·44

a) [**1**]: 10 mM; [cat.]: 0.94 mM. b) Trace amounts of **3** were also detected. c) Pd/C: 10% Palladium charcoal. d) PEG with mean mol. wt. of 200; others as written (Nakarai Chem. Co.). e) PEO-8.3EO: Pentaerythritol-8.3 ethylene oxide (Ref. 9). f) PEO-15.8EO: Pentaerythritol-15.8 ethylene oxide (Ref. 9). g) Not employed.

Table 2. Hydrogenation of *cis*-1,2-diphenylethene (**2**)

Run	Solvent	Catalyst[a]	PEG (M)	Conversion / %	Time / min	Conversion yield of **4**/%
1	CH_2Cl_2	Pd/C[b]	—	80	300	100
2	CH_2Cl_2	Pd/C	#200[c] 1.0	18	480	100
3	EtOH	Pd/C	—	90	100	82
4	CH_2Cl_2	$PdCl_2$	—	80	480	100
5	CH_2Cl_2	$PdCl_2$	#200 1.0	90	400	100
6	EtOH	$PdCl_2$	—	90	80	90
7	CH_2Cl_2	—	#200 1.0	0	120	—

a) [**1**]: 10 mM; [cat.]: 0.94 mM. b) Pd/C: 10% Palladium charcoal. c) PEG with mean mol. wt. of 200.

was evacuated with an aspirator through an injection needle which pierced the serum cap. A balloon containing H_2 gas was attached through another injection needle. The evacuation and the filling with H_2 gas were repeated three times. Finally, the needle with the aspirator was disconnected, while the needle with the balloon of H_2 gas was kept in place. A solution (25 ml) of diphenylethyne (**1**: 10 mM) or *cis*-1,2-diphenylethene (**2**: 40 mM) in CH_2Cl_2 or the other solvent(s) with/without PEG (1 M) was added into the flask through an injection needle. The resulting clear solution was stirred at 10 °C. The hydrogenation reactions were monitored by GLC, comparing with the authentic samples, *cis*- and *trans*-1,2-diphenylethenes (**2** and **3**) and/or 1,2-diphenylethane (**4**). Recovery of **1** and generation of **2**, **3**, and **4** were observed. Conversion yields for **2** and **4** were calculated on the basis of the conversion of **1**, ignoring the trace amounts of **3** (less than a few %). Selectivity of the hydrogenation is represented by the ratio of [**2**]/[**4**]. The results are summarized in Tables 1 and 2.

We thank Yokkaichi Chem. Ind., Yokkaichi, Japan for providing PEO-mEO's.

References

1) Part 1: N. Suzuki, K. Shimazu, T. Ito, and Y. Izawa, *J. Chem. Soc., Chem. Commun.*, **1980**, 1253; N. Suzuki, Y. Ayaguchi, K. Shimazu, T. Ito, and Y. Izawa, *Polymer Preprints*, **23**, 188 (1982) and references cited therein.

2) For dark reactions using PEG: W. P. Weber and G. W. Gokel, in "Phase Transfer Catalysis in Org. Synth.," Springer-Verlag, Berlin (1978), p. 3; E. Santaniello, A. Manzocchi, and P. Sozzani, *Tetrahedron Lett.*, **1979**, 4581; V. N. R. Pillai, M. Mutter, E. Baeyer, and I. Gatfield, *J. Org. Chem.*, **45**, 5364 (1980); K. Sukata, *J. Synth. Org. Chem. Jpn.*, **39**, 86, 443, 1131 (1981).

3) M. Freifelder, "Practical Catalytic Hydrogenation," Wiley-Interscience, New York, N. Y. (1971); H. O. House, "Modern Synth. Reactions," 2nd ed, Benjamin, Menlo Park, CA. (1972), pp. 1—34.

4) B. R. James, "Homogeneous Hydrogenation," Wiley-Interscience, New York, N. Y. (1973).

5) R. P. Houghton, "Metal Complexes in Org. Chem.," Cambridge Univ. Press, Cambridge (1979), pp. 186—194.

6) Purchased from Wako Chem. Ind. (Kyoto).

7) Purchased from Nakarai Chem. Co. (Kyoto).

8) S. Yanagida and M. Okahara, "Chemistry of Crown Ethers," ed by R. Oda, T. Shono, and I. Tabushi, as "Kagaku Zokan," Kagaku Dojin, Kyoto (1978), Vol. 74, pp. 149—166.

9) PEO-*m*EO: Pentaerythritols condensed with *m* mol of ethylene oxide units (Prepared by Yokkaichi Synth. Ind.).

Steroids. III.[1] New Synthesis of Ring-D Seco Steroids

Tomoyoshi TAKAHASHI* and Yasuo SATOH†

Department of Chemistry, The Jikei University School of Medicine, Kokuryo Chofu, Tokyo 182

† *Department of Chemistry, Faculty of Science, Rikkyo University, Nishi-Ikebukuro, Toshima-ku, Tokyo 171*

(Received June 3, 1982)

Synopsis. 16β-Azido-5α-androstan-17-one derivatives were cleaved with bromine in acetic acid at room temperature, to furnish 16-cyano and 16-carbamoyl-16,17-seco-5α-androstan-17-oic acids. 17-Aza-D-homo-5α-androstan-16,17a-dione derivatives were also synthesized.

Recently, we described a novel single step C–C bond cleavage of various α-azido steroidal ketones.[1,2] Our preliminary studies concerning the cleavage of a cyclopentane ring having an α-azido ketone group and the fact that certain ring D seco derivatives show hypocholesterolemic activity[3]prompted us to investigate the cleavage reaction in ring D of a steroid.

Treatment of α-azido steroidal ketones **1a** and **1b** with bromine (1 equiv.) in acetic acid for 10 h gave seco-carboxylic acids **2a** and **2b**, respectively. The IR spectra of **2a** and **2b** confirmed the presence of the cyano and carboxyl groups. The ^{1}H NMR spectra displayed a three-proton singlet at δ 2.00 (**2a**), 1.95 (**2b**) assigned to the 3-CH_3CO, and a broad one-proton peak at δ 10.19 (**2a**), 9.23 (**2b**) assigned to the carboxylic proton. 18-Angular methyl group appeared as a singlet at lower field, δ 1.25, suggesting that ring D was no longer intact but had undergone a cleavage with formation of a carboxyl group.

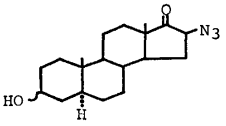

1a: 3α-OH
1b: 3β-OH

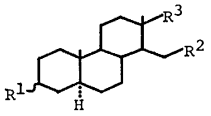

	R^1	R^2	R^3
2a:	α-OAc	CN	COOH
2b:	β-OAc	CN	COOH
3a:	α-OAc	$CONH_2$	COOH
3b:	β-OAc	$CONH_2$	COOH
4a:	α-OAc	$CONH_2$	$COOCH_3$
4b:	β-OAc	$CONH_2$	$COOCH_3$

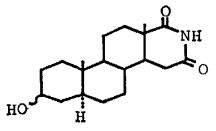

5a: 3α-OH
5b: 3β-OH

When **1a** and **1b** were allowed to react under the above conditions for a long period of time, the seco-amides **3a**[1] and **3b** were formed by hydrolysis. The IR spectra showed absorption bands at 2600—2700 cm^{-1} and 1706 cm^{-1} indicative of a carboxyl group. The ^{1}H NMR spectra of **3b** showed two peaks for the amide protons at δ 6.54 and δ 6.98, which disappeared on addition of deuterium oxide.

The cleavage reaction was also useful for introduction of a nitrogen atom into the steroid D ring. Treatment of the seco-amides **3a** and **3b** with diazomethane in ether gave the methyl esters **4a** and **4b**. The ^{1}H NMR spectra showed a characteristic three-proton singlet for the methyl ester at δ 3.66, and the broad peaks centered at δ 6.63 and 7.18 (**4a**), and 6.30 (**4b**), assigned to the amide protons.

The esters were cyclized with sodium methoxide in methanol to give the imides **5a** and **5b**. The imides were characterized by their IR spectra which showed the signals for the carbonyl groups at 1690, 1726 (**5a**) and at 1690, 1721 cm^{-1} (**5b**).

Experimental

General. All the melting points are uncorrected. The IR spectra were measured with a Hitachi model 215 infrared spectrophotometer. The ^{1}H NMR spectra were obtained in a CCl_4 solution, with TMS as the internal standard, using a Hitachi-Perkin Elmer R-20A. The MS spectra were measured by means of a Hitachi M-80 instrument with direct inlet at 70 eV.

*16β-Azido-3β-hydroxy-5α-androstan-17-one (**1b**).* This compound was synthesized from 3β-hydroxy-16α-bromo-5α-androstan-17-one[4] by Ponsold's method[5] as prisms, mp 113—116 °C; Found: C, 68.85; H, 8.6; N, 12.8%. Calcd for $C_{19}H_{29}N_3O_2$: C, 68.85; H, 8.82; N, 12.68%; IR (KBr): 3300, 2100 (N_3), and 1749 cm^{-1}; ^{1}H NMR (CCl_4) δ=3.67 (2H, m, 3α-H and 16-H).

*3α-Acetoxy-16-cyano-16,17-seco-5α-androstan-17-oic Acid (**2a**) and 3β-Acetoxy-16-cyano-16,17-seco-5α-androstan-17-oic Acid (**2b**).* To a solution of **1a**[1] (200 mg) in acetic acid (10 ml) was added bromine (97 mg) in acetic acid (5 ml) with stirring for 10 h at room temperature. After the usual work-up, the resulting oil was chromatographed on a silica-gel column. Elution with 20% ether in benzene afforded an oil (**2a**) (152 mg, 70%), which resisted crystallization from various solvents. IR (NaCl): 3150, 2700—2600 (bonded COOH), 2250 (CN), 1730, and 1698 cm^{-1}; ^{1}H NMR (CCl_4) δ=1.25 (3H, s, 18-CH_3), 2.00 (3H, s, MeCO), 2.27 (2H, m, 15-CH_2), 4.92 (1H, m, 3β-H), and 10.19 (1H, br, COOH).

A similar cleavage reaction of **1b** (200 mg) gave **2b** (144 mg, 66%) as a colorless oil. IR (NaCl): 3100, 2700—2600 (bonded COOH), 2250 (CN), 1730, and 1697 cm^{-1}; ^{1}H NMR (CCl_4) δ=1.25 (3H, s, 18-CH_3), 1.95 (3H, s, MeCO), 2.25 (2H, m, 15-CH_2), 4.56 (1H, m, 3α-H), and 9.23 (1H, br, COOH).

*3β-Acetoxy-16-carbamoyl-16,17-seco-5α-androstan-17-oic Acid (**3b**).* To a solution of the α-azido ketone (**1b**) (2 g) in acetic acid (100 ml) saturated with hydrogen chloride gas was added bromine (1 g) in acetic acid (50 ml), and the reaction mixture was stirred for one week at room temperature. After work-up, crystallization of the resulting oil from hexane–ether gave compound **3b** (1.261 g, 55%), mp 185—192 °C; Found: *m/e* 379.2372. Calcd for $C_{21}H_{33}NO_5$: M, 379.2359; IR (KBr): 3450, 3350, 3200, 2700—2600 (bonded COOH), 1728, 1706, 1694, 1655 (sh), 1592, and 1241 cm^{-1}; ^{1}H NMR (DMSO) δ=1.97 (3H, s, MeCO), 4.53 (1H, br, 3α-H), 6.54 (1H, br, NH), and 6.98 (1H, br, NH); MS (70 eV), *m/e* (rel intensity), 379 (100%, M^+), 301 (66), 216 (75), and 201 (93).

Methyl 3α-Acetoxy-16-carbamoyl-16,17-seco-5α-androstan-17-oate

(4a) and Methyl 3β-Acetoxy-16-carbamoyl-16,17-seco-5α-androstan-17-oate (4b). An excess of diazomethane in ether was added dropwise to a stirred solution of the amido-acid (**3a**) (500 mg) in ether (50 ml) at room temperature until the yellow color persisted. Evaporation and crystallization of the residue from carbon tetrachloride gave compound **4a** (320 mg, 62%), mp 149—151 °C; Found: *m/e* 393.2521. Calcd for $C_{22}H_{35}NO_5$: M, 393.2515; IR (KBr): 3425, 3350, 3200, 1724, 1713, 1660, 1608, and 1247 cm^{-1}; ^1H NMR (CCl_4) $\delta=1.98$ (3H, s, MeCO), 3.66 (3H, s, MeO), 4.93 (1H, br, 3β-H), 6.63 (1H, br, NH), and 7.18 (1H, br, NH); MS (70 eV), *m/e* (rel intensity), 393 (100%, M^+), 376 (10), 361 (20), 348 (16), 333 (25), and 274 (40).

The compound **4b** was obtained in a similar way. After the usual work-up, the resulting oil was chromatographed on silica-gel column. Elution with 40% benzene in ethyl acetate afforded compound **4b** (40%), mp 75—82 °C; Found: *m/e* 393.2572. Calcd for $C_{22}H_{35}NO_5$: M, 393.2515; IR (KBr): 3430, 3350, 3200, 1723, 1608, and 1239 cm^{-1}; ^1H NMR (CCl_4) $\delta=1.93$ (3H, s, MeCO), 3.66 (3H, s, MeO), and 6.30 (2H, br, NH_2); MS (70 eV), *m/e* (rel intensity), 393 (100%, M^+), 376 (9), 361 (15), 348 (22), 333 (17), and 274 (25).

3α-Hydroxy-17-aza-D-homo-5α-androstan-16,17a-dione (5a) and 3β-Hydroxy-17-aza-D-homo-5α-androstan-16,17a-dione (5b). The synthesis was carried out following the procedure of Meakins.[6] The amic-ester (**4a**) (500 mg) was dissolved in a solution of sodium (35 mg) in methanol (7 ml), and the solution was refluxed for 10 min. After the usual work-up, crystallization of the resulting oil from ether–methanol gave **5a** (170 mg, 42%), mp 223—226 °C; Found: *m/e* 319.2149. Calcd for $C_{19}H_{29}NO_3$: M, 319.2147; IR (KBr): 3420, 3260, 3100, 1726, 1690, 1675, and 1275 cm^{-1}; ^1H NMR ($CDCl_3$) $\delta=4.03$ (1H, br, 3β-H) and 8.16 (1H, br, NH); MS (70 eV), *m/e* (rel intensity), 319 (27%, M^+), 304 (51), 301 (100), 286 (100), and (12).

Compound **5b** was obtained in a similar way. The reaction mixture was refluxed for 20 min. After the usual work-up, crystallization of the resulting oil from ethyl acetate gave **5b** (46%), mp 216—219 °C; Found: *m/e* 319.2152. Calcd for $C_{19}H_{29}NO_3$: M, 319.2147; IR (KBr): 3370, 3200, 3070, 1721 (sh), 1705 (sh), 1690, and 1270 cm^{-1}; ^1H NMR ($CDCl_3$) $\delta=3.60$ (1H, br, 3α-H), and 8.50 (1H, br, NH); MS (70 eV), *m/e* (rel intensity), 319 (54%, M^+), 304 (35), 301 (100), 286 (52), and 261 (24).

References

1) Part II: T. T. Takahashi and J. Y. Satoh, *J. Chem. Soc., Perkin Trans. 1*, **1980**, 1916.
2) T. T. Takahashi and J. Y. Satoh, *J. Chem. Soc., Chem. Commun.*, **1978**, 409.
3) J. S. Baran, *J. Med. Chem.*, **10**, 1039 (1967).
4) E. R. Glazier, *J. Org. Chem.*, **27**, 4397 (1962).
5) Von B. Schonecker and K. Ponsold, *J. Pract. Chem.*, **313**, 817 (1971).
6) R. T. Aplin, G. D. Meakins, K. T. Tuba, and P. D. Woodage, *J. Chem. Soc., C*, **1969**, 1602.

Photochromic Behavior of Schiff Base-Metal Complexes. I. Photoinduced Hydrolysis of Pyridoxal 5′-Phosphate- and Salicylaldehyde-α-amino Acid-Zinc(II) Complexes

Yoshiaki KURAUCHI, Kazuya OHGA,* Akihiko YOKOYAMA, and Shigeru MORITA
Department of Environmental Chemistry and Engineering, Oita University, Dannoharu, Oita 870-11

(Received June 16, 1982)

Synopsis. Pyridoxal 5′-phosphate-α-amino acid-Zn(II) complexes and their salicylaldehyde analogues showed photochromic behavior in borate buffer at pH 9.5. A detailed comparison of UV spectral changes during the thermal back reaction with those for the complex formation indicates that the photoexcitation of the complexes induces the hydrolysis of the Schiff base ligands and that the back reaction corresponds to regeneration of the complexes.

Pyridoxal 5′-phosphate (PLP) is an essential cofactor for many amino acid transformations in biological systems. PLP or pyridoxal (PL) itself also non-enzymically catalyzes some of these reactions, which proceed *via* the Schiff bases with amino acids.[1] We have found that the photoexcitation of the PLP Schiff bases causes a half-reaction of decarboxylation-dependent transamination.[2] This type of decarboxylation has not been observed in thermal model systems for α-amino acids having an α-hydrogen. This difference between the photochemical and thermal reactions led us to investigate the photochemical behavior of the Schiff base-metal ion complexes which have been used much more frequently in the non-enzymic model systems.

The Zn(II) complex of PL–Val (Val=valine) Schiff base has been reported by Metzler *et al.*[3] to be exceedingly photolabile in aqueous solutions. We here report that the Zn(II) complexes of PLP–α-amino acid Schiff bases and their salicylaldehyde (SAL) analogues are photochemically hydrolyzed in an aqueous solution.

Experimental

PLP (Sigma), α-amino acids (Wako),[4] and zinc perchlorates (Kishida) were of reagent grade or better and were used without further purification. SAL (Wako) was distilled under reduced pressure and stored in the dark at about −20 °C. UV absorption spectra were taken with a Shimadzu UV 202 spectrophotometer. All kinetic runs were carried out spectrophotometrically in 0.05 mol dm^{-3} borate buffer (pH 9.5) at an ionic strength of 0.5 (KCl) with a Shimadzu MPS-5000 spectrophotometer. The cell compartments were thermostated (±0.1 °C) at desired temperatures.

Complex Formation and Rate Determination. α-Amino acid, zinc perchlorate, and PLP or SAL were simultaneously mixed. The Zn(II) complex solutions equilibrated within 30 min or less showed absorption maxima at 378 nm (0 in Fig. 1, ε 5620) for PLP-Ala (Ala=alanine), 375 nm (ε 5820) for PLP-AIB (AIB=α-aminoisobutyric acid), 351 nm (ε 5880) for SAL-Ala, and 350 nm (ε 5920) for SAL-AIB complexes. The molar absorption coefficients in parentheses were based on the initial concentration (1.00×10^{-4} mol dm^{-3}) of PLP or SAL, and were obtained under the conditions of the relative concentrations of three components given in the footnote of Table 1. These concentration conditions gave the greatest absorbances at the absorption maxima of the complexes. The molar absorption coefficient for the SAL-Ala-Zn(II) complex is in good agreement with that reported by Leussing and Bai.[5] The first-order rate constants (k_c) of the complex formations were determined by recording the increases in absorbances (A) at the wavelengths of the absorption maxima with respect to time, and by plotting $-\ln(A_\infty-A)$ *vs.* time. A_∞ is the absorbance at $t=\infty$. The activation energies ($E_{a,c}$) were calculated from the Arrhenius plot of the rate constants obtained.

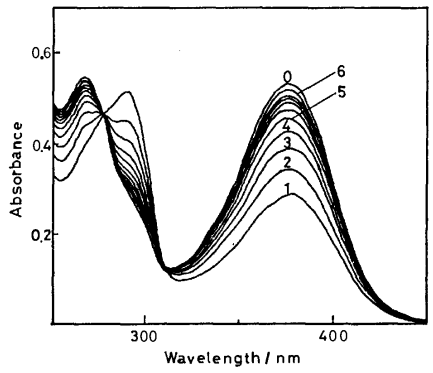

Fig. 1. Spectral changes of the PLP-Ala-Zn(II) complex in 0.05 mol dm^{-3} borate buffer at 25 °C after UV irradiation.
0: Before irradiation, 1: immediately after irradiation of 3 min, 2—5: thermal UV spectral changes at intervals of 1.5 min, 6: 30 min after irradiation. Other conditions: see the footnote in Table 1.

UV Irradiation and Thermal Back Reaction. The equilibrated solutions of the Zn(II) complexes were deaerated by repeated evacuation and flushing with argon gas seven or more times. The solutions were then placed in a 1-cm quartz spectrophotometric cell, thermostated at desired temperatures, and irradiated with a 500-W super high-pressure Hg lamp (Ushio USH-500D) through glass filters (Toshiba UV-39 transmitting less than 10% light below 380 nm, for PLP complexes; UV-D36A transmitting less than 10% light below 330 nm, for SAL complexes). The progress of a thermal back reaction was followed by determining the absorption spectra. The kinetic data (k_b and $E_{a,b}$) of this process were obtained by the method described above.

Results and Discussion

The irradiation of a buffered solution of the PLP–Ala–Zn(II) complex in an argon atmosphere caused the immediate decrease of the complex absorption band at 378 nm (Fig. 1, 0→1). When the photolysate was kept in the dark, a thermal reaction occurred; the UV spectrum of the photolysate returned more than 98% to its initial figure within 30 min at 25 °C (Fig. 1, 1→6), and showed two isosbestic points at 278 and 311 nm. The spectral changes during the thermal reaction were the same in shape as those during the complex formation. In addition, more than 95% of the original absorbance at 378 nm was restored even after the photochemical and thermal processes were repeated three times. These results suggest that the

Table 1. Kinetic data of the Schiff base–Zn(II) complex formation and the thermal back reaction[a)]

Schiff base	Temp/°C	$10^3\,k_c/s^{-1}$ [b)]	$E_{a,c}$/kJ mol^{-1} [b)]	$10^3\,k_b/s^{-1}$ [b)]	$E_{a,b}$/kJ mol^{-1} [b)]
PLP-Ala	10.0	1.12±0.03	61.5±2.0	—[c)]	64.5±2.6
	15.0	1.70±0.01		1.68±0.04	
	20.0	2.62±0.01		2.60±0.04	
	25.0	4.00±0.03		3.95±0.07	
PLP-AIB	25.0	1.48±0.01		1.44±0.02	
SAL-Ala	15.0	1.95±0.02	34.6±0.6	1.93±0.02	35.6±3.0
	20.0	2.47±0.02		2.37±0.04	
	25.0	3.05±0.03		2.88±0.02	
	30.0	3.95±0.05		4.02±0.08	
SAL-AIB	20.0	1.80±0.01		1.80±0.02	

a) All the experiments were carried out in 0.05 mol dm^{-3} borate buffer, pH 9.5 (0.5 mol dm^{-3} KCl). The initial concentration of PLP or SAL was 1.00×10^{-4} mol dm^{-3}. The initial concentrations of amino acid and Zn^{2+} were 1.0×10^{-2} and 7.0×10^{-4} for PLP-Ala, 5.0×10^{-2} and 5.0×10^{-3} for PLP-AIB, 1.0×10^{-2} and 1.5×10^{-3} for SAL-Ala, and 5.0×10^{-2} and 5.0×10^{-3} mol dm^{-3} for SAL-AIB systems, respectively. b) Errors given are standard deviations. c) Not determined.

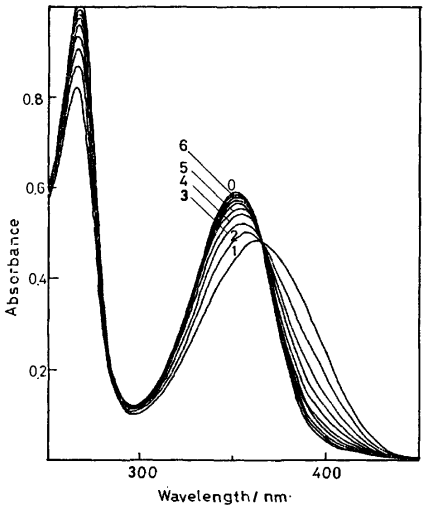

Fig. 2. Spectral changes of the SAL–Ala–Zn(II) complex in 0.05 mol dm^{-3} borate buffer at 25 °C after UV irradiation.
The numbers represent the order of the spectral changes at the same intervals as those in Fig. 1. Other conditions: see the footnote in Table 1.

photoexcitation of the complex caused the hydrolysis of the Schiff base ligand followed by the thermal regeneration of the complex (Scheme 1), and that a very minor side reaction took place only during irradiation. When other amino acids, Val and AIB were used, almost the same spectral changes were observed. The Zn(II) complex of SAL–Ala or SAL–AIB Schiff base also showed the same photochromic behavior (Fig. 2 for SAL–Ala–Zn(II) complex). The photochemical hydrolysis of these Zn(II)–Schiff base complexes was confirmed by the excellent agreement between the observed kinetic data (k_b and $E_{a,b}$) of the thermal back reaction and those of the complex formation (k_c and $E_{a,c}$), as shown in Table 1.

It has been proposed on the basis of kinetics of SAL–amino acid–divalent metal systems by Leussing *et al.*[6)] that rapid preequilibrium just after mixing the three components gives a mixed complex such as **2**, which is slowly transformed into the Schiff base

Scheme 1

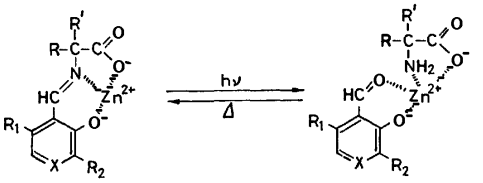

1 **2**

PLP systems: X=N, $R_1=CH_2OPO_3^{2-}$, $R_2=CH_3$
SAL systems: X=CH, $R_1=R_2=H$

complex (**1**) *via* an α-hydroxy amine complex. Under the conditions of excess Zn^{2+} and amino acid concentrations and at pH 9.5 employed in this work, the *o*-hydroxy aromatic aldehydes of UV-absorbing species are considered to exist in the mixed complex form after the photochemical hydrolysis. The first-order rate constants observed are probably those for the proton-independent formation path of the Schiff base complexes from the mixed complexes.

Metal-free PLP–α-amino acid Schiff bases underwent photochemically decarboxylation.[2)] Evidently the coordination of the carboxylato group to Zn(II) depresses this photo-decarboxylation.

An irreversible absorption band due to a by-product appeared around 330 nm on irradiation of the PLP–Ala–Zn(II) complex in air. It seems to us that the by-product, probably an oxidation product, corresponds to a photoproduct from PL–Val–Zn(II) complex[3)] having a similar absorption at 330 nm.

References

1) H. C. Dunathan, *Adv. Enzymol.*, **35**, 79 (1971) and references therein.
2) Y. Kurauchi, K. Ohga, M. Moriguchi, and S. Morita, *Agric. Biol. Chem.*, **44**, 2499 (1980).
3) L. Davis, F. Roddy, and D. E. Metzler, *J. Am. Chem. Soc.*, **83**, 127 (1961).
4) Amino acids except for α-aminoisobutyric acid are of L configuration.
5) D. L. Leussing and K. S. Bai, *Anal. Chem.*, **40**, 575 (1968).
6) B. E. Leach and D. L. Leussing, *J. Am. Chem. Soc.*, **93**, 3377 (1971); D. Hopgood and D. L. Leussing, *ibid.*, **91**, 3740 (1969); K. S. Bai and D. L. Leussing, *ibid.*, **89**, 6126 (1967).

The Preparation of Tri-*t*-butoxysiloxy-substituted 1,3,5-Triazines

Yoshimoto ABE,* Yukinori NAGAO, Kenji SATO, and Takahisa MISONO

Department of Industrial Chemistry, Faculty of Science and Technology, Science University of Tokyo, Noda, Chiba 278

(Received June 17, 1982)

Synopsis. The title derivatives were prepared to obtain 1,3,5-triazines with a better solubility than chloro- and amino-1,3,5-triazine, which are not very soluble in common organic solvents.

Several reports have been published on the preparation and reaction of 1,3,5-triazines substituted with trimethylsilyl groups.[1-6] These silicon-containing derivatives are prepared by the reaction of cyanurate, ammeline, and melamine with hexamethyldisilazane, which are purified by distillation *in vacuo*. This implies that the substitution with trimethylsilyl group affords a high volatility and/or a good solubility to the starting materials by prevention of interactions among molecules. However, these derivatives are sensitive to hydrolysis.

In this work, therefore, the chloro- and amino-substituted 1,3,5-triazines with tri-*t*-butoxysiloxy group were prepared. Our hope was that derivatives with a good solubility in organic solvents together with hydrolytic stability may be obtained by the prevention of interactions among molecules through introducing this group into the 1,3,5-triazine ring. Earlier results showed that condensations of functional groups such as amino and hydroxyl group are effectively protected.[7]

The experimental results showed that the reaction of cyanuric chloride with sodium tri-*t*-butoxysilanolate gave the compound **1**, but further replacement of the chlorine atom of **1** by this group did not take place. Compound **1** was allowed to react with ammonia, diethylamine and butylamine to give the derivatives **2,3**, and **4**, respectively. The reaction of **2** with ammonia did not occur under the conditions. Amines such as diethylamine and butylamine, however, were reacted with **2** to form the products **5** and **6**, which indicates that a low reactivity of the last chlorine atom is not due to the steric factor of tri-*t*-butoxysiloxy group but to the low electrophilicity of the carbon of carbon–chlorine bond. An attempt to isolate **7** from the reaction product of **2** with sodium amide in liquid ammonia was not successful, but it was obtained as the hydrochloride.

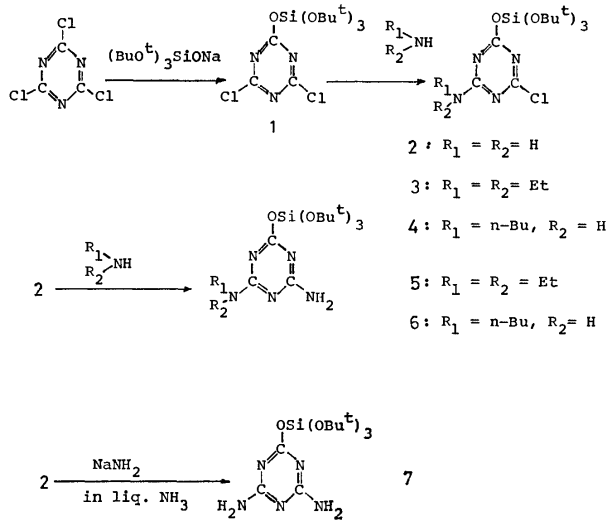

All these compounds were very soluble in organic solvents such as methanol, ethanol, acetone, ether, tetrahydrofuran, chloroform, and benzene and were stable to hydrolysis; most of **2** was recovered without hydrolysis after it was heated at 50 °C for about thirty minutes in a mixed solvent of water and dioxane. The hydrochloride of **7** was also soluble in methanol, ethanol, and acetone. These results indicate that introduction of tri-*t*-butoxysiloxy group affords an appreciable solubility and hydrolytic stability to the derivatives.

Experimental

Materials. All the melting points and boiling points were uncorrected. The solvents and reagents were dehydrated and purified by distillation or recrystallization. Tri-*t*-butoxysilanol was prepared by the method already mentioned.[7] Sodium tri-*t*-butoxysilanolate was prepared by the reaction of tri-*t*-butoxysilanol and sodium in benzene and was used without isolation.

2,4-Dichloro-6-(tri-t-butoxysiloxy)-1,3,5-triazine (1). Sodium silanolate prepared by the reaction of tri-*t*-butoxysilanol (14.0 g) with sodium (1.1 g) in benzene (80 ml) was reacted with cyanuric chloride (9.2 g) in benzene (100 ml) under reflux for 3 h to give **1**, 12.9 g (62.8%); bp 139 °C—/2 Torr†; IR 1533, 1501, 1475, 1393, 1377, 1085, 1038, 855, 818 cm^{-1}. Found: C, 43.59; H, 10.07; N, 6.81; Si, 6.52%. Calcd for $C_{15}H_{17}N_3Cl_2O_4Si$: C, 43.69; H, 10.19; N, 6.60; Si, 6.81 %.

2-Amino-4-chloro-6-(tri-t-butoxysiloxy)-1,3,5-triazine (2). The reaction of **1** (30.0 g) in benzene (300 ml) with dry ammonia gas at 5—10 °C for 2 h gave **2**; 23.3 g (recrystallized from hexane 73.3%); mp 105 °C; IR: 3350, 3225, 1608, 1557, 1517, 1393, 1370, 1082, 1030, 820 cm^{-1}. Found: C, 45.42; H, 7.35; N, 13.79; Si, 7.13%. Calcd for $C_{15}H_{19}N_4ClO_4Si$: C, 45.85; H, 7.44; N, 14.26; Si, 7.15%.

Compound **2** was also obtained by introducing ammonia into the reaction mixture of sodium tri-*t*-butoxysilanolate with cyanuric chloride without isolation of **1** (44% yield).

2-Chloro-4-diethylamino-6-(tri-t-butoxysiloxy)-1,3,5-triazine (3) and 2-Chloro-4-butylamino-6-(tri-t-butoxysiloxy)-1,3,5-triazine (4). To the reaction mixture of tri-*t*-butoxysilanol (28.0 g) with sodium (2.3 g) in benzene (150 ml), followed by addition of cyanuric chloride (18.4 g) in benzene (200 ml), diethylamine or butylamine (15.0 g) in benzene (100 ml) was added. Recrystallization of a residue from the reaction mixtures with hexane gave the compounds: **3**, 21.5 g (47.8%); mp 58.0—58.5 °C; IR 1595, 1514, 1430, 1405, 1378, 1080, 1060, 810 cm^{-1}; NMR (CCl_4): δ 1.2 (t, 6H), 1.35 (s, 27H), 3.62 (q, 4H); MS: *m/e* 448 (M^+). Compound **4**, 28.3 g (63%); mp 94.3—94.5 °C; IR 1585, 1550, 1405, 1380, 1080, 1055, 1030, 813 cm^{-1}; NMR (CCl_4): δ 0.95 (m, 7H),

† 1 Torr ≈ 133.322 Pa.

1.35 (s, 27H), 3.50 (q, 2H), 8.08 (t, 1H); MS: *m/e* 448 (M^+). Found for **3**: C, 51.36; H, 8.64; N, 12.16%. Found for **4**: C, 50.30; H, 8.45; N, 12.57%. Calcd for $C_{19}H_{27}N_4ClO_4Si$; C, 50.82; H, 8.30; N, 12.48%.

*2-Amino-4-diethylamino-6-(tri-t-butoxysiloxy)-1,3,5-triazine (**5**) and 2-amino-4-butylamino-6-(tri-t-butoxysiloxy)-1,3,5-triazine (**6**).* Compound **2** (5.0 g) in benzene (100 ml) was reacted with diethyamine or butylamine (2.0 g) in benzene (50 ml) under reflux for 2 h. Removal of the solvent and subsequent recrystallization of a residue with ether (**5**) or petroleum ether (**6**) gave the compounds: **5**, 5.9 g (56.8%); mp 89.0—90.0 °C; IR: 3390, 3220, 3070, 1640, 1540, 1520, 1404, 1380, 1045, 1028, 830 cm^{-1}; NMR (CCl_4): δ 1.14 (t, 6H), 1.34 (s, 27H), 3.53 (q, 4H); MS: *m/e* 429 (M^+). Compound **6**, 2.3 g (44.5%); mp 110.0 °C (decomp); IR: 3510, 3050, 3000, 1646, 1547, 1503, 1403, 1378, 1050, 1025, 830 cm^{-1}; MS: *m/e* 429 (M^+). Found for **5**: C, 53.17, H, 9.39; N, 16.30%. Found for **6**: C, 53.28; H, 9.42; N, 16.18%. Calcd for $C_{19}H_{38}N_4O_4Si$: C, 53.12; H, 9.15; N, 16.30%.

*2,4-Diamino-6-(tri-t-butoxysiloxy)-1,3,5-triazine (**7**).* Into a flask containing dry liquid ammonia (about 100 ml) trapped under cooling with Dry Ice–acetone was added with stirring first a catalytic amount of iron (III) nitrate hydrate (0.05 g) and then 0.55 g of sodium divided into several pieces over several times. After the completion of disappearance of a blue color, 10.1 g of **2** was added, and the mixture was stirred for 2 h. The ammonia was evaporated while the reaction mixture was allowed to rise to room temperature after addition of hexane. The mixture was refluxed, and the solid was filtered by hot filtration. After drying in vacuo and dissolving into methanol, it was reacted with a dilute hydrochloric acid solution. The precipitate was filtered, washed with water, and dried. It was recrystallized with methanol to give crystals (2.7 g, 30% yield) of the hydrochloride of **7**. Mp 178 °C (decomp); IR: 3160, 3080, 2985, 1710, 1590, 1430, 1396, 1379, 1080, 843 cm^{-1}; NMR ($(CD_3)_2SO$): δ 1.25 (s, 28H), 8.70 (s, 4H). Found for hydrochloride of **7**: C, 44.38; H, 7.41; N, 17.07; Si, 6.87%. Calcd for $C_{15}H_{32}N_5O_4ClSi$: C, 43.93; H, 7.86; N, 17.08; Si, 6.85%.

References

1) E. H. Amonoo-Neizer, R. C. Golesworthy, R. A. Shaw, and B. C. Smith, *J. Chem. Soc.*, **1965**, 5452.

2) E. Nachbaur, W. Kosmus, H. J. Krannich, and W. Sundermeyer, *Monatsh. Chem.*, **109**, 1211 (1978).

3) A. S. Gordetsov, I. A. Vosmokov, V. A. Galprin, and U. I. Dergunov, *Zh. Obshch. Khim.*, **46**, 1654 (1976).

4) A. S. Gordetsov, I. A. Vosmokov, V. A. Galprin, and U. I. Dergunov, *Zh. Obshch. Khim.*, **46**, 1573 (1976).

5) V. P. Kozukov, Y. K. Dobrovinskaya, and U. F. Muronov, *Zh. Obshch. Khim.*, **46**, 1531 (1976).

6) U. I. Gorbamenko, M. P. Gertsky, and L. I. Samarai, *Zh. Org. Khim.*, **13**, 899 (1977).

7) Y. Abe and I. Kijima, *Bull. Chem. Soc. Jpn.*, **42**, 1118, 2570 (1969).

Convenient Methods for the Preparation of *p*-Dialkylaminophenylacetylenes

Shuzo AKIYAMA,* Shin'ichi NAKATSUJI, Keiko YOSHIDA, Kenichiro NAKASHIMA, Toshimitsu HAGIWARA,† Haruki TSURUTA,† and Toshio YOSHIDA†

Faculty of Pharmaceutical Sciences, Nagasaki University, 1-14 Bunkyo-machi, Nagasaki 852

†*Central Research Laboratory, Takasago Perfumery Co., Ltd., 5-36-31 Kamata, Ohta-ku, Tokyo 144*

(Received June 24, 1982)

Synopsis. Two convenient methods for the preparation of *p*-dialkylaminophenylacetylenes are reported: a) Dehydrobromination of the brominated compounds obtained easily from the dialkylamino substituted cinnamic acids in acetic acid instead of chloroform; b) dehydrochlorination of the 2-chlorostyrene derivative obtained from the reaction of *p*-dimethylaminobenzaldehyde with chloromethylenetriphenylphosphorane.

In our study on ethynologs of triphenylmethane dyes,[1] *p*-dialkylaminophenylacetylenes (**6**) are important starting materials. However, no convenient method is known for easy and large-scale production. The synthesis of *p*-dimethylaminophenylacetylene (**6**, R=CH_3) has been reported by Barbieri[2] and by Oliver and Walton.[3] Barbieri's method is depicted by the path (**2**→**3**→**4**→**6**) in Scheme 1. The yield of **6** based on **2** was only 18%. On the other hand, Oliver and Walton's method is made up by the reaction of *p*-dimethylaminophenylcopper with (iodoethynyl)trimethylsilane, from which **6** as trimethylsilyl derivative is obtained in 52% yield.

p-Diethylaminophenylacetylene (**6**, R=C_2H_5) has been prepared as a mixture of *p*- and *m*-isomers by the reaction of *p*-bromophenylacetylene with diethylamine in the presence of sodium amide.[4]

Now, we wish to report here the convenient synthesis of *p*-dialkylaminophenylacetylenes and their derives, as outlined in Scheme 1.

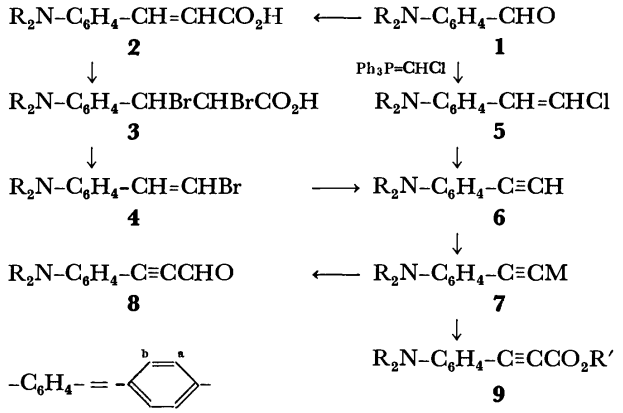

Scheme 1.

The bromination of **2** to obtain **3** according to the literature[2] has been reinvestigated unsatisfactorily in chloroform. The reaction seemed to proceed very little because **2** is almost insoluble in chloroform. However, we have found that the reaction proceeds dramatically under homogeneous conditions to give the brominated acid **3** if we use acetic acid instead of chloroform as a solvent. The bromide **4** obtained by the treatment of **3** with aq Na_2CO_3 was dehydrobrominated with several bases (*e.g.*, *n*-BuLi, $NaNH_2$, and *t*-BuOK) yielding the acetylene **6** in moderate yields. The above method seems to be easy and suitable for larger scale production. Contrary to this, Oliver and Walton's method appears to be fairly troublesome because of tedious reagents' preparation. Furthermore, we have developed an alternative route (**1**→**5**→**6**). The reaction of *p*-dimethylaminobenzaldehyde (**1**) with easily accessible chloromethylenetriphenylphosphorane[5] generated from the corresponding phosphonium salt by the treatment with the base (*t*-BuOK or *n*-BuLi) at low temperature gave 2-chlorovinyl compound (**5**, R=CH_3), which could be easily isolated and interestingly was composed mostly of *cis*-isomers.[6] The action of one mol of *n*-BuLi, *t*-BuOK, or $NaNH_2$ against **5** (R=CH_3) provided **6** (R=CH_3) in a high yield. Two mol of *n*-BuLi or *t*-BuOK gave the metalated compound (**7**, R=CH_3, M=Li or K), which reacted succeedingly with ethyl chloroformate to yield the ester (**9**, R=CH_3, R'=C_2H_5) and with *N*,*N*-dimethylformamide to give the aldehyde (**8**, R=CH_3).

It was clear that the general procedure for preparing ethylnyl compounds from acetyl derivatives was not applied here, since the attempted chlorination of *p*-dimethylaminoacetophenone (**10**)[7] with PCl_5 in benzene under reflux to obtain the corresponding chloride was unsuccessful due to decomposition under several reaction conditions.[8]

In conclusion, the preparation of **6** became easy along the route (**2**→**3**→**4**→**6**) including the modified bromination method. The alternative route (**1**→**5**→**6**) had also an advantage of being able to isolate **5** easily.

Experimental

The melting points were uncorrected. The IR spectra were obtained on a JASCO IRA-2 spectrophotometer. The ^1H NMR spectra were measured on a JEOL FX 90Q and the parameters were given in δ-values with respect to TMS used as an internal standard. The UV spectra were obtained in EtOH on a Shimadzu UV 300.

p-*Dimethylaminophenylacetylene* (**6**, *R*=CH_3). *From* p-*Dimethylaminocinnamic Acid* (**2**, *R*=CH_3): *Bromination of* **2**: To a solution of **2** (R=CH_3, 9.50 g, 0.05 mol) in acetic acid (300 ml) was added over 10 min bromine (8.0 g, 0.05 mol) in the same solvent (10 ml) at 16—20 °C. After the mixture had been stirred for 30 min, the solvent was evaporated. The residue was stirred with Na_2CO_3 (40 g, 0.38 mol) in water (200 ml) at room temperature for 30 min and extracted with hexane (400 ml). The extract, after being washed with brine and dried ($MgSO_4$), was concentrated to give a light brown oily substance (10.20 g); this was **4** and was used without purification in the next reaction.

Dehydrobromination. a) By Potassium t-*Butoxide*: To the above bromide (10.20 g) in THF (60 ml) was added *t*-BuOK (12.0 g, 0.11 mol) in THF (100 ml) over 1 h at room temperature. After stirring overnight the mixture was evaporated, worked up in the usual way, and then extracted with hexane (250 ml). The extract was washed with brine and dried ($MgSO_4$). Orange yellow crystals obtained on evaporating the solvent were dissolved in cyclohexane–benzene and passed through a short column of alumina (10

g). The filtrate was concentrated to give light yellow crystals (**6**, 2.01 g, 28% from **2**), mp 52—53 °C, lit,[2] 52—53 °C, ^{1}H NMR ($CDCl_3$) δ=2.73 (1H, s, ≡CH), 2.93 (6H, s, NMe_2), 6.49 (2H, d, J=8 Hz, H^b), and 7.25 (2H, d, J=8 Hz, H^a). (Found: C, 82.56; H, 7.68; N, 9.39%; M^+, 145).

b) By Sodium Amide: To a suspension of $NaNH_2$ (prepared from Na, 3.0 g, 0.13 mol in NH_3 (l) (150 ml)) was added **4** (10.45 g) which was prepared from **2** (R=CH_3, 9.50 g, 0.05 mol) in THF (50 ml) over 15 min at −60 °C. After being stirred overnight at −50——30 °C, the mixture was worked up in the usual way. The residue was extracted with benzene (250 ml). The extract was washed with water and dried ($MgSO_4$). The orange-brown material obtained on evaporating the solvent was dissolved in hexane–benzene and passed through a short column of alumina (20 g). The eluate was concentrated to afford **6** (2.67 g, 37%), mp 52—53 °C.

c) By Butyllithium: To a solution of **4** (8.54 g, derived from **2**, 7.60 g, 0.04 mol) in THF (50 ml) was added *n*-BuLi in hexane (1.5 M 40.0 ml, 60 mmol) with stirring under nitrogen atmosphere at −60 °C for 1 h. From the reaction mixture worked up in the usual way, **6** (2.23 g, 38%, mp 52—53 °C) was obtained.

*From p-Dimethylaminobenzaldehyde: p-Dimethylamino-β-chlorostyrene (**5**, R=CH_3)*: To a suspension of chloromethyltriphenylphosphonium chloride[5] (3.57 g, 0.01 mol) in THF (20 ml) was added a hexane solution of *n*-BuLi (1.5 M 6.7 ml, 0.01 mol) in an ice–salt bath. After the mixture being stirred for 30 min, powdered *p*-dimethylaminobenzaldehyde (1.04 g, 7 mmol) was added to the resulting orange red solution of chloromethylenetriphenylphosphorane. The mixture was stirred overnight at room temperature. The residue obtained by evaporating the solvent was extracted with heptane (300 ml). The extract was percolated through a short column of silica gel (5 g) and concentrated to give light yellow crystals (**5**, 0.96 g, 76% based on **1**), which were recrystallized from ether and exclusively composed of *cis*-isomer of **5**, as shown by ^{1}H NMR; mp 42—44 °C, IR (KBr) 1610 cm^{-1} (C=C), ^{1}H NMR ($CDCl_3$) δ=2.95 (6H, s, NMe_2), 6.00 (1H, d, J=8 Hz, olefinic H), 6.48 (1H, d, J=8 Hz, olefinic H), 6.66 (2H, d, J=9 Hz, H^b), and 7.61 (2H, d, J=9 Hz, H^a).

Found: C, 66.13; H, 6.70; N, 7.78%; M^+, 183. Calcd for $C_{10}H_{12}NCl$: C, 66.11; H, 6.66; N, 7.71%; M, 183.

*Dehydrochlorination of **5** (R=CH_3)*: To a solution of **5** (0.20 g, 1.1 mmol) in THF was added *n*-BuLi in hexane (1.5 M 2.0 ml, 3 mmol) for 30 min in an ice–salt bath under nitrogen atmosphere. After being stirred for 1 h, the mixture was quenched by adding water (50 ml). The aq layer was extracted with benzene (50 ml). The combined organic layer was dried ($MgSO_4$) and evaporated to give **6** (R=CH_3) as light yellow crystals (0.15 g, 94%, mp 52—53 °C). The use of *t*-BuOK instead of *n*-BuLi gave nearly the same result. The yield by $NaNH_2$ in NH_3(l) was 61%.

*p-Diethylaminophenylacetylene (**6**, R=C_2H_5)*: According to the same procedure as used for the dimethyl derivative, the bromination of **2** (R=C_2H_5)[9] was done. The successive dehydrobromination of **4** by *n*-BuLi, $NaNH_2$, and *t*-BuOK gave **6** in 42,[10] 28,[11] and 27%[12] based on **2**, respectively: bp 116 °C (4 mmHg); IR (Neat) 3290 (≡CH) and 2090 cm^{-1} (C≡C); MS M^+, 173, M, 173; ^{1}H NMR ($CDCl_3$) δ=1.16 (6H, t, J=7 Hz, $CH_2C\underline{H}_3$), 3.34 (4H, q, J=7 Hz, $C\underline{H}_2CH_3$), 2.94 (1H, s, ≡CH), 6.56 (2H, d, J=9 Hz, H^b), and 7.32 (2H, d, J=9 Hz, H^a).

*Ethyl p-Dimethylaminophenylpropiolate (**9**, R=CH_3, R'=C_2H_5)*: To a solution of **5** (R=CH_3, 2.00 g, 11 mmol) in THF (20 ml) was added *n*-BuLi in hexane (1.5 M 8.00 ml, 12 mmol) with stirring under nitrogen atmosphere in an ice–salt bath. After the mixture was stirred for 1 h, an excess of ethyl chloroformate (3.3 g, 30 mmol) was added; the resulting mixture was stirred overnight, and extracted with benzene (200 ml). The extract was passed through a short column of alumina (10 g) and concentrated to give yellow crystals (0.96 g, 40%), mp 36—38 °C. UV: 335 (ε 36000); IR (KBr) 2200 (C≡C) and 1700 cm^{-1} (C=O); ^{1}H NMR ($CDCl_3$) δ=1.65 (3H, t, J=7 Hz, $CH_2C\underline{H}_3$), 3.35 (6H, s, NMe_2) 4.50 (2H, q, J=7 Hz, $C\underline{H}_2CH_3$), 6.49 (2H, J=9 Hz, H^b), and 7.15 (2H, J=9 Hz, H^a). Found: C, 71.70; H, 6.99; N, 6.52%; M^+, 217. Calcd for $C_{13}H_{15}NO_2$: C, 71.86; H, 6.96; N, 6.45%; M, 217.

*p-Dimethylaminophenylpropynal (**8**, R=CH_3)*: To a solution of **5** (R=CH_3, 1.02 g, 5.6 mmol) in THF (40 ml) was added *n*-BuLi in hexane (1.5 M 5.0 ml, 7.5 mmol) with stirring under nitrogen atmosphere in an ice–salt bath. After 1 h, an excess of DMF (1 ml) was added and stirred for 1 h. The reaction mixture was worked up with 1% H_2SO_4 and extracted with benzene (200 ml). Crude crystals obtained here by concentrating the extract were dissolved in benzene (3 ml). The solution was passed through a short column of alumina (10 g) and concentrated to give **8** as light yellow crystals (0.39 g, 40%), mp 86—88 °C, IR (KBr) 2200 (C≡C) and 1660 cm^{-1} (C=O); ^{1}H NMR ($CDCl_3$) δ=3.18 (6H, s, NMe_2), 6.60 (2H, d, J=8 Hz, H^b), 7.41 (2H, d, J=8 Hz, H^a), and 9.32 (1H, s, CHO); UV: 365 (ε 15200). Found: C, 76.05; H, 6.39; N, 7.66%; M^+, 174. Calcd for $C_{10}H_{11}NO$: C, 76.27; H, 6.40; N, 8.09%; M, 174.

We thank Misses Rika Doi, Sanae Nishiyama, and Mie Kawano for their assistance in the experimental work. The present work was partly supported by a Grant-in-Aid for Scientific Research (No. 56470022). The authors (S. A., S. N., and K. N.) are grateful to the Ministry of Education, Science and Culture.

References

1) S. Akiyama, K. Yoshida, M. Hayashida, K. Nakashima, S. Nakatsuji, and M. Iyoda, *Chem.Lett.*, **1981**, 311.
2) P. Barbieri, *C. R. Acad. Sci., Ser. C*, **231**, 57 (1950).
3) R. Oliver and D. R. M. Walton, *Tetrahedron Lett.*, **1972**, 5209.
4) M. P. Terpugova and I. L. Kotryarevskii, *Dokl. Vses. Konf. Khim. Atsetilena, 4th* **1972**, **1**, 379: *Chem. Abstr.*, **79**, 18247b (1973); M. P. Terpugova, I. L. Kotryyarevskii, Y. I. Amosov, and R. N. Nyasnikova, *Izv. Akad. Nauk SSSR, Ser. Khim.*, **1975**, 2808; *Chem. Abstr.*, **84**, 73786e (1976); Physical data on **6** (R=C_2H_5) are not described.
5) G. Köblich, H. Trapp, K. Flory, and W. Drischel, *Chem. Ber.*, **89**, 689 (1966).
6) *Cf.* M. Matsumoto and K. Kuroda, *Tetrahedron Lett.*, **1980**, 4021.
7) We have found that **10** is prepared easily by Oppenauer oxidation of 2-(*p*-dimethylaminophenyl)ethanol in a 76% yield.
8) *Cf.* C. M. Wong and T. L. Ho, *Synth. Commun.*, **4**, 25 (1974).
9) A. Furst, H. A. Harper, R. J. Seiward, M. D. Morris, and R. A. Neve, *Arch. Biochem. Biophys.*, **31**, 190 (1951); *Chem. Abstr.*, **45**, 7572i (1951); C. W. Shoppee, *J. Chem. Soc.*, **1930**, 968.
10) The yield by GLPC analysis (5% FFAP, 200 °C) of the distillate containing *p*-diethylaminostyrene (18%).
11) The yield by GLPC analysis (5% FFAP, 200 °C) of the distillate containing *N,N,p*-triethylaniline (18%).
12) Isolated yield by distillation.

Asymmetric Cross-coupling of Organozinc Reagents with Alkenyl Bromides Catalyzed by a Chiral Ferrocenylphosphine–Palladium Complex

Tamio HAYASHI, Toshiya HAGIHARA, Yoshio KATSURO, and Makoto KUMADA*

Department of Synthetic Chemistry, Faculty of Engineering, Kyoto University, Kyoto 606

(Received July 12, 1982)

Synopsis. Organozinc reagents, prepared from secondary alkyl Grignard reagents (ArRCHMgCl: Ar=Ph, *p*-Tol; R=Me, Et) and excess zinc halides, were allowed to react with vinyl bromide and (*E*)-*β*-bromostyrene in the presence of dichloro[(*R*)-*N*,*N*-dimethyl-1-[(*S*)-2-(diphenylphosphino)ferrocenyl]ethylamine]palladium(II) as a catalyst to give the corresponding coupling products of up to 86% enantiomeric excess.

It has been well recognized that asymmetric synthesis catalyzed by chiral phosphine-transition metal complexes is one of the most useful methods for preparation of optically active compounds, and intense interest is now aroused by asymmetric carbon-carbon bond forming reactions with chiral transition metal catalysts.[1] Nickel- or palladium-catalyzed asymmetric Grignard cross-coupling has been reported by us and other research groups to afford optically active olefins of moderate to high enantiomeric excess: 3-Phenyl-1-butene obtained from reaction of 1-phenylethylmagnesium chloride has 68, 81, 67, and 15% ee with nickel catalysts for phosphine ligands, PPFA, Valphos, Norphos, and DIOP, respectively.[2-5] We report here that coupling products of higher enantiomeric purities can be obtained by use of organozinc reagents instead of Grignard reagents.

Results and Discussion

The secondary alkyl zinc reagents **1** were prepared *in situ* by mixing corresponding Grignard reagents with excess zinc halides. Preparation from alkyl halides and zinc metal was less convenient due to low yield and poor reproducibility. For the reaction of 1-phenylethylzinc halide (**1a**) with vinyl bromide, several nickel and palladium complexes with chiral phosphine ligands have been examined. Dichloro[(*R*)-*N*,*N*-dimethyl-1-[(*S*)-2-(diphenylphosphino)ferrocenyl]ethylamine]palladium(II) ($PdCl_2$[(*R*)-(*S*)-PPFA])[2,6] was found to be the most effective catalyst giving rise to high yield of optically active 3-phenyl-1-butene (**2a**) in THF at 0 °C for 20—40 h. It is noteworthy that the coupling reaction of the zinc reagents proceeded successfully only in THF,[7] although ether is usually the best solvent for the reaction of Grignard reagents.[2] Palladium complexes with other phosphine ligands were less catalytically active. Nickel complexes were almost inactive under the reaction conditions.

Results obtained for the asymmetric cross-coupling of **1** in the presence of $PdCl_2$[(*R*)-(*S*)-PPFA] catalyst are summarized in Table 1, which also contains data obtained for the reaction of organomagnesium and -aluminium reagents for comparison. The organozinc reagent **1a** prepared from 1-phenylethylmagnesium chloride and zinc chloride or iodide gave the olefin **2a** of 85—86% ee (*S*) in quantitative yield (entries 1 and

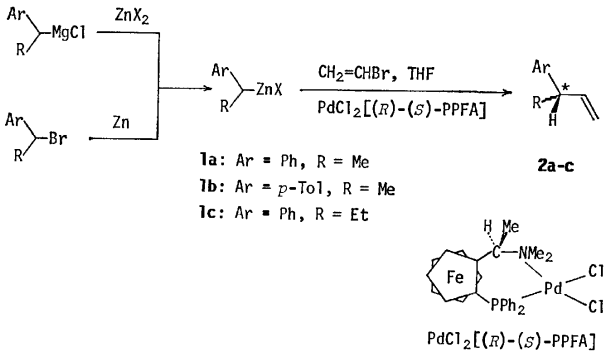

TABLE 1. ASYMMETRIC CROSS-COUPLING OF ORGANOZINC REAGENTS WITH VINYL BROMIDE CATALYZED BY $PdCl_2$[(*R*)-(*S*)-PPFA]

Entry		Organometallics	Solvent	Reaction condition		Yield[a]	$[\alpha]_D^{22}$/° (neat)	% ee (Confign.)
				Temp/°C	Time/h	%		
1	**1a**	PhMeCHMgCl/$ZnCl_2$ (1/2)	THF/Et_2O	0	40	>95	+5.05	85[b] (*S*)
2	**1a**	PhMeCHMgCl/ZnI_2 (1/2)	THF/Et_2O	0	21	>95	+5.08	86[b] (*S*)
3	**1a**	PhMeCHZnBr	THF	10	70	51	+5.10	86[b] (*S*)
4		PhMeCHMgCl	Et_2O	0	21	>95	+3.86	65[b] (*S*)
5		PhMeCHMgCl/$AlCl_3$ (1/2)	Et_2O	5	22	>95	+2.52	43[b] (*S*)
6	**1b**	*p*-TolMeCHMgCl/ZnI_2 (1/2)	THF/Et_2O	0	44	>95	+6.97	86[c] (*S*)
7	**1c**	PhEtCHMgCl/ZnI_2 (1/2)	THF/Et_2O	0	22	57	+35.0[d]	61[e] (*S*)
8[f]	**1a**	PhMeCHMgCl/$ZnCl_2$ (1/2)	THF/Et_2O	0	22	88	−31.7[g]	60[h] (*S*)

a) Yields based on vinyl bromide were determined by GLC analysis using an internal standard. Isolated yields were usually over 70%. b) (*R*)-3-Phenyl-1-butene (**2a**) has $[\alpha]_D^{22}$ −5.91±0.04° (neat), d_4^{22} 0.8809 (Ref. 2). c) (*R*)-3-*p*-Tolyl-1-butene (**2b**) has $[\alpha]_D^{23}$ −8.15° (neat), d_4^{23} 0.885 (Ref. 8). d) $[\alpha]_D^{20}$ (*c* 6, benzene). e) The olefin **2c** was oxidized into the known (*R*)-(−)-2-phenylbutyric acid; $[\alpha]_D^{21}$ −60.0° (*c* 3, benzene) (Ref. 9). f) Reaction with (*E*)-*β*-bromostyrene. g) $[\alpha]_D^{20}$ (*c* 3, benzene). h) (*R*)-(*E*)-1,3-Diphenyl-1-butene has $[\alpha]_D^{20}$ +52.9° (*c* 3, benzene) (Ref. 2).

2). The reagent **1a** from 1-phenylethyl bromide and zinc metal also gave (*S*)-**2a** of 86% ee, though the reaction was slower (entry 3). The stereoselectivity attained here is the highest for the asymmetric cross-coupling. The olefin **2a** of lower enantiomeric purity was obtained in a similar reaction of 1-phenylethylmagnesium chloride or organoaluminium reagent prepared *in situ* from the Grignard reagent and aluminium chloride (entries 4 and 5). The palladium complex $PdCl_2$[(*R*)-(*S*)-PPFA] also catalyzed effectively the reaction of other zinc reagents, (*S*)-3-*p*-tolyl-1-butene (**2b**) (86% ee) and (*S*)-3-phenyl-1-pentene (**2c**) (61% ee) being produced from the corresponding *in situ* organozinc reagents **1b** and **1c** (entries 6 and 7).

Experimental

Asymmetric Cross-coupling. The results are summarized in Table 1. The following experimental procedure for entry 2 is typical. To a mixture of 31 mg (0.05 mmol) of $PdCl_2$-[(*R*)-(*S*)-PPFA] and 19.2 g (60 mmol) of ZnI_2 were added successively 70 ml of THF, 42 ml (30 mmol) of 0.7 M 1-phenylethylmagnesium chloride in ether (1 M=1 mol dm^{-3}), and 1.07 g (10 mmol) of vinyl bromide under argon at −78 °C. The mixture was stirred at 0 °C for 21 h and hydrolyzed with 10% hydrochloric acid. GLC analysis of the organic layer indicated the formation of quantitative yield of 3-phenyl-1-butene (**2a**). The organic layer and ether extracts from the aqueous layer were combined, washed with saturated $NaHCO_3$ and then 10% $Na_2S_2O_3$, and dried over anhydrous Na_2SO_4. Distillation under reduced pressure (65 °C/20 mmHg) (1 mmHg=133.322 Pa) and purification by preparative GLC (Silicone DC550) gave 1.05 g (80%) of pure **2a**: $[\alpha]_D^{22}$ +5.08° (neat).

Oxidation of **2c** into 2-phenylbutyric acid was effected with sodium periodate and potassium permanganate in *t*-butyl alcohol according to a reported procedure.[10]

We thank the Ministry of Education, Science and Culture Japan for the Grant-in-Aid for Scientific Research No. 00547080 serving as a partial financial support for this work.

References

1) Reviews: a) H. B. Kagan and J. C. Fiaud, *Top. Stereochem.*, **10**, 175 (1978); b) B. Bosnich and M. D. Fryzuk, *ibid.*, **12**, 119 (1981).

2) a) T. Hayashi, M. Konishi, M. Fukushima, T. Mise, M. Kagotani, M. Tajika, and M. Kumada, *J. Am. Chem. Soc.*, **104**, 180 (1982); b) T. Hayashi, M. Tajika, K. Tamao, and M. Kumada, *ibid.*, **98**, 3718 (1976).

3) T. Hayashi, M. Fukushima, M. Konishi, and M. Kumada, *Tetrahedron Lett.*, **21**, 79 (1980).

4) H. Brunner and M. Prōbster, *J. Organomet. Chem.*, **209**, C1 (1981).

5) a) G. Consiglio and C. Botteghi, *Helv. Chīm. Acta*, **56**, 460 (1973); b) Y. Kiso, K. Tamao, N. Miyake, K. Yamamoto, and M. Kumada, *Tetrahedron Lett.*, **1974**, 3.

6) T. Hayashi, K. Tamao, Y. Katsuro, I. Nakae, and M. Kumada, *Tetrahedron Lett.*, **21**, 1871 (1980).

7) E. Negishi, A. O. King, and N. Okukado, *J. Org. Chem.*, **42**, 1821 (1977).

8) K. Tamao, T. Hayashi, H. Matsumoto, H. Yamamoto, and M. Kumada, *Tetrahedron Lett.*, **1979**, 2155.

9) R. Weidmann and A. Horeau, *Bull. Soc. Chim. Fr.*, **1967**, 117.

10) L. F. Fieser and M. Fieser, "Reagents for Organic Synthesis," Wiley, New York (1967), p. 810.

One-step Synthesis of (2-Amino-2-carboxyethylthio)dopas (Cys-dopas) from Dopa and Cysteine by Hydrogen Peroxide in the Presence of Iron-EDTA Complex

Shosuke Ito

Institute for Comprehensive Medical Science, School of Medicine, Fujita-Gakuen University, Toyoake, Aichi 470-11

(Received July 22, 1982)

Synopsis. 5-(2-Amino-2-carboxyethylthio)dopa, 2-(2-amino-2-carboxyethylthio)dopa, and 2,5-bis(2-amino-2-carboxyethylthio)dopa were synthesized from dopa and cysteine by oxidation in a neutral buffer with H_2O_2 in the presence of iron-EDTA complex. H_2O_2, iron salt, and EDTA were essential for the reaction. Ultimate oxidizing species seem to be hydroxyl and superoxide radicals.

(2-Amino-2-carboxyethylthio)dopas (represented as Cys-dopas in the following; **2**—**5**) arise in melanocytes by the addition of cysteine to dopaquinone formed by tyrosinase oxidation of dopa (3,4-dihydroxyphenylalanine; **1**).[1] They are precursors of pheomelanin, yellow to reddish-brown pigment of feathers and hair. Increased amounts of these catechols, especially **2**, have been found in the urine of melanoma patients.[2] We have recently shown that **2** is selectively toxic to a variety of human tumor cells *in vitro* and possesses antitumor activity against murine L1210 leukemia and B16 melanoma.[3]

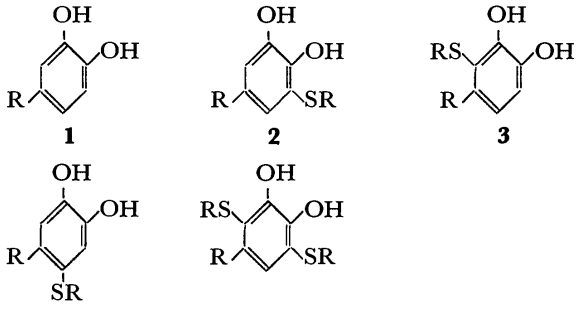

R=$CH_2CH(NH_2)COOH$

Three methods have been reported for the preparation of Cys-dopas (**2**—**5**). 1) Tyrosinase-catalyzed oxidation of dopa in the presence of cysteine gives Cys-dopas (**2**—**5**) in a high total yield;[4] however, this method is not suitable for a large-scale preparation. 2) Multi-step chemical synthesis of **2** and **3** involving nucleophilic addition of cysteine to *N*-acetyldopaquinone ethyl ester requires expensive silver oxide as oxidant.[5,6] 3) Reaction of dopa with cystine in boiling aqueous HBr yields Cys-dopas (**2**—**4**) with the 6-isomer (**4**) being the major product (6—7% yield).[6] This paper presents a more convenient method for a large-scale preparation of **2**, **3**, and **5** by oxidation of a mixture of dopa and cysteine with H_2O_2 and Fe^{2+}–EDTA complex.

The oxidation, performed on an analytical scale, was followed by TLC on cellulose (in 1-propanol–1 M HCl,† 3:2) and the increase of absorbance at 300 nm where Cys-dopas (**2**—**5**) show strong absorption[6] while **1** does not. In some instances the products were also analyzed by column chromatography. Under the standard conditions (Expt 1 in Table 1), **2**, **3**, and **5** were obtained in 13.9, 3.1, and 4.2%, respectively, while **4** was found only in a trace amount (much less than 1%). The relative yields of the Cys-dopa isomers (**2**—**4**) paralleled those obtained with the tyrosinase oxidation,[4] suggesting that the present reaction also proceeds *via* dopaquinone. Most of the cysteine was consumed as cystine in addition to Cys-dopas. Sum of the yields of **1**—**5** approached nearly 100%, indicating that the reaction did not give pigments or ill-defined products.

Effects of pH, concentrations of H_2O_2, iron salts, and EDTA, and addition of radical scavengers were summarized in Table 1. The optimum pH of the reaction was around pH 7 (Expts 2—4). Omitting any one of H_2O_2, iron salts, and EDTA resulted in no formation Cys-dopas (Expts 5, 8, 15). Almost identical yields of Cys-dopas were obtained when $FeCl_3$ was used in place of $FeSO_4$ (Expt 13), while $CuSO_4$ had no catalytic activity (Expt 14). Doubling the amount of H_2O_2 (and cysteine) did not improve the yield of **2**, but it led to a great increase in the yield of **5** (Expts 21, 22).

Reaction of H_2O_2 with Fe^{2+}–EDTA complex produces hydroxyl radical (·OH) (Reaction 1) which is a powerful oxidizing agent.[7] The resulting Fe^{3+}–EDTA complex may be reduced back by H_2O_2 with the formation of superoxide radical ($O_2^{\cdot-}$) (Reaction 2).[7]

$$Fe^{2+}\text{-EDTA} + H_2O_2 \longrightarrow Fe^{3+}\text{-EDTA} + \cdot OH + OH^- \quad (1)$$

$$Fe^{3+}\text{-EDTA} + H_2O_2 \longrightarrow Fe^{3+}\text{-EDTA} + O_2^{\cdot-} + 2H^+ \quad (2)$$

Scavengers of hydroxyl radical, D-mannitol and formate,[8] inhibited the formation of Cys-dopas by 20 and 17%, respectively (Expts 18, 19). Addition of superoxide dismutase also caused a 21% inhibition of the reaction (Expt 20). These results suggest that not only ·OH (Reaction 1) but also $O_2^{\cdot-}$ (Reaction 2) participated in the iron–EDTA-catalyzed oxidation of dopa with H_2O_2. We have recently shown that superoxide radical generated in hypoxanthine–xanthine oxidase system can mediate the formation of Cys-dopas from dopa and cysteine.[9]

When **2** was used in place of **1**, a 6.3% yield of **5** was obtained with a 93.6% recovery of **2**.

Based on these results, the following conditions were established for the preparation of **2**, **3**, and **5** on a preparative scale. The reaction mixture consisted of dopa, cysteine (added in 5 portions), $FeSO_4$, EDTA·2Na, and H_2O_2 (added in 5 portions) at a molar ratio

† 1 M=1 mol dm^{-3}.

Table 1. Effects of pH, concentrations of H_2O_2, iron salts, and EDTA, and radical scavengers on the formation of Cys-dopas from DOPA and cysteine[a)]

Expt No.	Conditions	$A_{300}-A_{340}$[b)]	Yield/%			
			1	2	3	5
1	Complete system (pH 7.0)[a)]	0.117	77.0	13.9	3.1	4.2
2	pH 5.0	0.036				
3	pH 6.0	0.096				
4	pH 8.0	0.064				
5	H_2O_2 omitted (Fe^{2+} or Fe^{3+})	0.000				
6	H_2O_2 (1 mmol; in 50 portions)	0.054				
7	H_2O_2 (1 mmol; in one portion)	0.091				
8	Fe^{2+} omitted	0.000				
9	Fe^{2+} (0.01 mmol)	0.048				
10	Fe^{2+} (0.05 mmol)	0.083				
11	Fe^{2+} (0.2 mmol)[c)]	0.162	68.4	16.5	3.5	4.1
12	Fe^{2+} (1.0 mmol)	0.109				
13	Fe^{3+} (0.1 mmol)	0.127	74.8	13.9	3.0	4.0
14	Cu^{2+} (0.1 mmol)[d)]	0.000				
15	EDTA omitted	0.000				
16	EDTA (0.2 mmol)	0.116	76.0	16.0	3.0	2.8
17	EDTA (5.0 mmol)	0.069				
18	L-Mannitol (10 mmol) added	0.079	ND[e)]	12.4	2.2	2.3
19	HCOONa (10 mmol) added	0.092	ND	11.7	2.2	3.7
20	SOD (5 mg) added	0.083	82.3	12.3	2.1	2.3
21	Complete system[f)]	0.144	70.5	18.6	3.4	7.4
22	Complete system[g)]	0.265	54.6	17.9	5.5	13.1

a) L-Dopa (1 mmol), L-cysteine (2 mmol), and $FeSO_4$ (0.1 mmol) were dissolved in water (100 ml), pH being adjusted to 7.0 with Na_2HPO_4. Then, H_2O_2 (1 mmol) was added in 5 portions every 10 min and the mixture was vigorously stirred at room temperature (23—26 °C). The reaction was terminated 10 min after the final addition of H_2O_2 by adding 1 ml of 6 M HCl. The mixture was applied on a column (1.0 cm×7 cm) of Dowex 50W-X2 and the products eluted with 3 M HCl after washing with 0.5 M HCl (100 ml). The products were separated by rechromatography on Dowex 50W-X2 (2.0 cm×24 cm; equilibrated with 2 M HCl) as described in Ref. 4. b) Difference in absorbances at 300 and 340 nm. Cys-dopas (2—5) show strong absorptions at 300 nm where 1 shows no absorption. Aliquots of the reaction mixture were diluted 50-fold with 1 M HCl and the UV spectra recorded. c) Some formation of purple pigment was noted. d) The formation of cystine was greatly accelerated. e) Not determined. f) L-Cysteine (2 mmol) was added in 5 portions 1 min prior to the additions of H_2O_2. g) L-Cysteine (4 mmol) and H_2O_2 (2 mmol) were added in 10 portions every 10 min.

of 1:2:0.1:0.2:1. Starting from 9.9 g of dopa and 12.1 g of cysteine, the reaction gave, in addition to 7.5 g (76%) of dopa recovered, 2.4 g (14%) of **2**, 0.5 g (3%) of **3**, and 0.9 g (4%) of **5** after chromatographic separation and crystallization. Thus, the present method appears to be the most convenient one for the large-scale preparation of **2**, **3**, and **5**.

Udenfriend and co-workers[10)] have described a system, consisting of L-ascorbic acid, iron-EDTA complex, and either O_2 or H_2O_2, and a buffer around neutral pH, which can hydroxylate various aromatic compounds. Our present system offered another example of chemical oxidation using H_2O_2 and iron–EDTA complex which mimics enzymic oxidation.

Experimental

Synthesis of Cys-dopas on a Preparative Scale. A solution of 9.86 g (50 mmol) of L-dopa, 3.72 g (10 mmol) of EDTA·2Na, and 1.39 g (5 mmol) of $FeSO_4 \cdot 7H_2O$ in 5 l of water was adjusted to pH 7.0 with crystals of $Na_2HPO_4 \cdot 12H_2O$. To the vigorously stirred solution were added at 23 °C 2.42 g (20 mmol) of L-cysteine and 1 min later 860 μl (10 mmol) of 11.6 M H_2O_2. The additions of the same amounts of L-cysteine and H_2O_2 were repeated 5 times at 10-min intervals. The reaction was terminated 10 min after the final addition of H_2O_2 by adding 50 ml of 6 M HCl and 5 ml of mercaptoacetic acid. The mixture was evaporated *in vacuo* at 60 °C to *ca.* 300 ml and stored overnight in a refrigerator. The resulting precipitate of cystine and EDTA was filtered off and the filtrate was applied on a column (3.6 cm×25 cm) of Dowex 50W-X2 (H^+ form, 200—400 mesh; equilibrated with water). Elution with 0.5 M HCl gave dopa (frs. 48—144; 20 ml per fraction) which was recovered as 7.48 g (75.9%) of crystals after evaporation and neutralization. Further elution with 3 M HCl afforded a mixture of **2**—**5** (frs. 20—140; 20 ml per fraction). The mixture was rechromatographed on a column (3.6 cm×25 cm) of Dowex 50W-X2 (equilibrated and eluted with 3 M HCl) and fractions of 20 ml were collected and analyzed by UV. Fractions 104—128, 132—220, and 229—325 contained **3**, **2**, and **5**, respectively, which were evaporated to give HCl salts of the amino acids. They were crystallized from aqueous 1% $Na_2S_2O_5$ adjusted to pH 6 with CH_3COONa to afford 2420 mg (14.4%) of **2**, 520 mg (2.8%) of **3**, and 932 mg (4.0%) of **5**. These catechols were identified with the authentic samples[6)] by comparison of chromatographic behaviors and UV spectra.

The author wishes to thank Prof. Keisuke Fujita for his continuous support and encouragement for this study.

References

1) G. Prota, *J. Invest. Dermatol.*, **75**, 122 (1980).
2) G. Agrup, P. Agrup, T. Andersson, L. Hafström, C. Hansson, S. Jacobsson, P.-E. Jönsson, H. Rorsman, A.-M. Rosengren, and E. Rosengren, *Acta Dermatovener. (Stockholm)*, **59**, 381 (1979).
3) K. Fujita, S. Ito, S. Inoue, Y. Yamamoto, J. Takeuchi, M. Shamoto, and T. Nagatsu, *Cancer Res.*, **40**, 2543 (1980).
4) S. Ito and G. Prota, *Experientia*, **33**, 1118 (1977).
5) G. Prota, G. Scherillo, and R. A. Nicolaus, *Gazz. Chim. Ital.*, **98**, 495 (1968).
6) S. Ito, S. Inoue, Y. Yamamoto, and K. Fujita, *J. Med. Chem.*, **24**, 673 (1981).
7) C. Walling, *Acc. Chem. Res.*, **8**, 125 (1975).
8) B. Halliwell, *FEBS Lett.*, **92**, 321 (1978).
9) S. Ito and K. Fujita, *Biochem. Pharmacol.*, **31**, 2887 (1982).
10) S. Udenfriend, C. T. Clark, J. Axelrod, and B. B. Brodie, *J. Biol. Chem.*, **208**, 731 (1954); B. B. Brodie, J. Axelrod, P. A. Shore, and S. Udenfriend, *ibid.*, **208**, 741 (1954).

Synthesis of Lactone-opened Derivatives of *anti* and *syn* Head-to-Head Coumarin Dimers

Noriyuki YONEZAWA and Masaki HASEGAWA*

Department of Synthetic Chemistry, Faculty of Engineering, The University of Tokyo, Hongo, Bunkyo-ku, Tokyo 113

(Received July 29, 1982)

Synopsis. *anti* and *syn* Head-to-head coumarin dimers reacted readily with amines and alcohols to give the corresponding diamides, diesters, imides, or the monoactone derivatives.

Little work has been reported on the lactone-opening reaction of coumarin dimers except for the synthesis of 3,4-bis(2-hydroxyphenyl)-1,2-cyclobutanedicarboxylic acids.[1-3] It prompted us to study the lactone-opening reactions of coumarin dimers with amines or alcohols, as reported briefly in the preceding communications.[4-6] The configuration of two strained lactone rings is sterically so tight that these rings are readily opened by nucleophiles. In this paper we wish to report a preparative study on several lactone-opened derivatives of *anti* and *syn* head-to-head coumarin dimers.

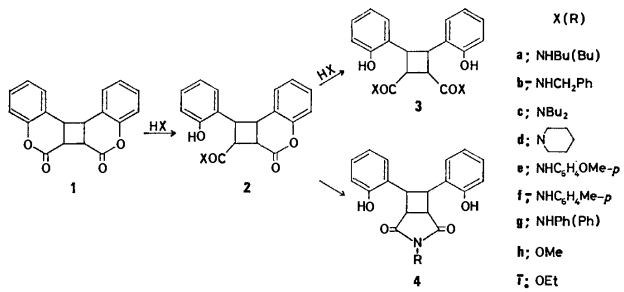

anti Head-to-head coumarin dimer (*anti* **1**) reacted smoothly with aliphatic amines such as butylamine, benzylamine, dibutylamine, and piperidine in dioxane at 60 °C within 2 h to give *N,N'*-dibutyl-, *N,N'*-dibenzyl-, and *N,N,N',N'*-tetrabutyl-*t*-3,*c*-4-bis(2-hydroxyphenyl)-*r*-1,*t*-2-cyclobutanedicarboxamides, and *N,N'*-[*t*-3,*c*-4-bis(2-hydroxyphenyl)-*r*-1,*t*-2-cyclobutanedicarbonyl]dipiperidine (*anti* **3a**—**d**) in high yields. When weaker amines such as *p*-anisidine, *p*-toluidine, and aniline were employed as nucleophiles, a longer reaction time (4 h) was required for high conversions to the corresponding diamides (*anti* **3e**—**g**).

By treatment with methanol or ethanol at refluxing temperature, *anti* **1** was also converted to the corresponding dimethyl or diethyl dicarboxylate (*anti* **3h,i**) in a quantitative yield. In the early stage of the esterification with ethanol, the heterogeneous mixture became clear. At this stage, the monolactone/monoester, 2-ethoxy-1-(2-hydroxyphenyl)-1α,2α,2aβ,8bβ-tetrahydro-3*H*-cyclobuta[*c*]chromen-3-one (*anti* **2i**), was isolated as the sole product in a high yield. The structure of *anti* **2i** was confirmed by comparing its ^{1}H-NMR, ^{13}C-NMR, and IR spectra with those of *anti* **1** and *anti* **3i**. Similarly, the monolactone/monoamide derivatives (*anti* **2a,g**) were obtained in moderate yields by the reaction of *anti* **1** with an equimolar amount of amines in dioxane. The reaction produced the diamide as a minor product, and the amount of the diamide decreased with decreasing the nucleophilicity of the amine used. The attainable isolation of the monolactone derivatives implies that the lactone ring in the monolactone derivatives is less reactive than that in *anti* **1**. The higher stability of the monolactone derivatives would be attributed to the release of strain by the first lactone-opening in *anti* **1**.

Contrarily, *N*-butyl- and *N*-phenyl-*c*-3,*c*-4-bis(2-hydroxyphenyl)-*r*-1,*c*-2-cyclobutanedicarboximide (*syn* **4a, g**) were produced exclusively by the reaction of *syn* **1** with butylamine and aniline, respectively. The diamide, *syn* **3a**, was obtained in a high yield only when the reaction was carried out under specified conditions, whereas the dianilide, *syn* **3g**, was undetectable under any reaction conditions examined. In all cases, *syn* monolactone derivatives could not be isolated. These results show that in *syn* **1**, contrary to *anti* **1**, the second lactone-opening reaction is faster than the first one, since in the monolactone derivatives of *syn* **1** the newly introduced steric repulsion between *o*-hydroxyphenyl group, carbonyl group, and 2-chromanone moiety is considered to overcome the released strain through the first lactone-opening reaction. Further, in the second lactone-opening there are two types of reactions, namely, inter- and intramolecular nucleophilic attacks. At low temperature the intermolecular attack of an amine occurred preferentially to the intramolecular attack of the carbamoyl group in *syn* monolactone/monoamide. With raising the reaction temperature and with decreasing the amount of the amine, intramolecular attack becomes advantageous and gives the imide preferentially. A relatively weak primary amine such as aniline requires rather drastic conditions for the first lactone-opening; this in turn results in the formation of the imide by the successive intramolecular second lactone-opening. The imide was also obtained by the intramolecular substitution of *syn* **3a** at higher temperature (>144 °C)[6] with the release of the repulsion.

Similar intramolecular substitution was observed in the attempts to isolate *syn* diester. The quantitative formation of *syn* **3i** *in situ* was confirmed by spectroscopy, but, *syn* **3i** was always contaminated with *syn* **1** by re-lactonization on recrystallization.

The lactone-opening reaction of *syn* **1** with dibutylamine did not proceed at temperatures below 130 °C, whereas the reaction took place at 150 °C to give *N,N,N',N'*-tetrabutyl-*c*-3,*c*-4-bis(2-hydroxyphenyl)-*r*-1,*t*-2-cyclobutanedicarboxamide (*syn'* **3c**) in a high yield with quantitative epimerization, which is similar to Anet's observation in the synthesis of dimethyl *c*-3,*c*-4-bis(2-methoxyphenyl)-*r*-1,*t*-2-cyclobutanedicarboxylate.[1] In the case of secondary amine, the epimerization would occur instead of the imide formation to dissolve the large repulsion between the four substituents situated on the same side of the cyclobutane ring.

Table 1. Yields, elemental analyses, and physical data for lactone-opened derivatives of *anti* **1** and *syn* **1**

	Yield/%[a]	Mp(decomp) θ_m/°C	Found (Calcd)/(%) C	H	N	IR(KBr) $\bar{\nu}$/cm^{-1}		^{1}H-NMR(Me_2SO-d_6,δ) Cyclobutane Ring protons[b]	
anti **3a**	95(56)	223—225	71.16 (71.20	7.96 7.81	6.26 6.39)	1640	1540	3.47	4.57
anti **3b**	100(78)	227.5—229	—	—	—	1640	1530	3.69	4.81
anti **3c**	100(84)	(237.5)	74.00 (74.14	9.13 9.15	5.15 5.09)	1610		3.96	4.62
anti **3d**	98(36)	271—271.5	—	—	—	1590		4.01	4.58
anti **3e**	76(64)	233—235	71.10 (71.36	5.64 5.61	5.18 5.20)	1645	1515	3.80	4.73
anti **3f**	97(35)	244.5—248	—	—	—	1645	1520	3.83	4.73
anti **3g**	73(46)	217—218	75.33 (75.30	5.14 5.48	6.07 5.85)	1650	1530	3.88	4.77
anti **3h**	100(73)	(164)	67.34 (67.41	5.72 5.66)		1715		3.64	4.67
anti **3i**	100(50)	(183.5)	68.71 (68.73	6.20 6.29)		1690		3.61	4.66
anti **2a**	65(14)	(199)	—	—	—	1760 1545	1640	3.5—4.5[c]	
anti **2g**	64(27)	(207.5)	75.01 (74.79	4.95 4.97	3.60 3.63)	1735 1555	1660	3.7—4.6[c]	
anti **2i**	100(90)	(165)	71.21 (71.00	5.53 5.36)		1760	1720	3.5—4.5[c,d]	
syn **3a**	100(48)	141—143	71.24 (71.20	7.92 7.81	6.35 6.39)	1630	1550	3.70	4.49
syn **4a**	100(47)	217.5—218.5	72.59 (72.31	6.43 6.34	3.87 3.83)	1755	1670	3.70	4.74
syn **4g**	93(70)	(216)	75.01 (74.79	5.01 4.97	3.82 3.63)	1770	1695	3.87	4.80
syn' **3c**	100(32)	181—185	74.45 (74.14	9.48 9.15	5.08 5.09)	1615		3.1—4.9[c,e]	

a) Yields are listed for the crude substances which are spectrometrically identical with recrystallized ones. Yields in parentheses are those of substances purified by recrystallization. b) The cyclobutane ring protons appeared as two pseudo doublets of A,A',B,B' systems. The peaks of aromatic protons and hydroxy protons of *o*-hydroxyphenyl groups appeared at δ=6.0—7.6(m) and at δ=8.83—9.44(s), respectively. All other peaks appeared at reasonable positions. c) 4H(m) of ABCD system. d) Two methylene protons of ethyl group were overlapped. e) Six methylene protons of butyl groups were overlapped.

Experimental

^{1}H-NMR spectra were recorded on a HITACHI R-40 spectrometer (90 MHz). IR spectra were measured on JASCO IRA-1 spectrophotometer. Both *anti* and *syn* **1** were synthesized by the method of Krauch *et al.*[2]

Synthesis of the anti *Diamides (*anti ***3a—g***).* A solution of *anti* **1** (1.00 g, 3.42 mmol) and 4 equimolar amounts of aliphatic amine in dioxane (10 ml) was heated at 60 °C for 2 h, followed by cooling to room temperature. The white precipitates were collected by filtration, washed with dioxane, and dried *in vacuo* (recrystallized from acetone). When aromatic amine was employed, the reaction time was prolonged to 4 h.

Synthesis of the anti *Esters (*anti ***3h, i***; ***2i***).* A suspension of *anti* **1** (5.0 g, 17.1 mmol) in an alcohol (160 ml) was heated at refluxing temperature for 12 h. The solution was concentrated and dried *in vacuo* (recrystallized from corresponding alcohol). In the reaction of *anti* **1** with ethanol, evaporation of the solvent just after the solution became clear (about 10 min) resulted in the isolation of *anti* **2i** (recrystallized from benzene).

Synthesis of the anti *Monolactone/Monoamides (*anti ***2a,g***).* A solution of *anti* **1** (1.00 g, 3.42 mmol) and an equimolar amount of an amine in dioxane (150 ml) was heated at 60 °C for 2—4 h. After filtration of powdery white precipitates, the filtrate was evaporated and dried *in vacuo*. The crude product of monolactone/monoamide, containing a small amount of *anti* **1**, was recrystallized from acetone.

Synthesis of syn ***3a***. To butylamine (16.4 g, 0.22 mol), cooled at −25 °C, was added *syn* **1** (2.20 g, 7.53 mmol) with vigorous stirring. Then the reaction temperature was gradually raised to room temperature over a period of 2 h and the solution was stirred for additional 40 min. The solution was poured into petroleum ether (1000 ml) to yield white precipitates. The precipitates were collected by filtration, washed with petroleum ether, and dried *in vacuo* (recrystallized from acetone).

Synthesis of syn ***4a***. A suspension of *syn* **1** (5.9 g, 20 mmol) in methanol (200 ml) containing butylamine (10.0 g, 0.14 mol) was heated at refluxing temperature for 2 h. After evaporation of the solution, the residue was dissolved into 1 M aqueous KOH (50 ml), then the solution was acidified with 2 M HCl (30 ml) to yield white precipitates, which were collected by filtration, washed thoroughly with water, and dried *in vacuo* (recrystallized from acetone).

Synthesis of syn ***4g***. A mixture of *syn* **1** (2.0 g, 6.8 mmol) and aniline (20.4 g, 0.22 mol) was stirred at room temperature for 24 h. The solution was poured into ice-cooled 1 M HCl (200 ml). The resulting precipitates were collected by filtration, washed thoroughly with water, and dried *in vacuo* (recrystallized from acetone).

Synthesis of syn' ***3c***. A mixture of *syn* **1** (1.00 g, 3.42 mmol) and dibutylamine (77.0 g, 0.60 mol) was heated at 150 °C for 3.5 h. The solution was evaporated and dried *in vacuo* (recrystallized from acetone).

References

1) R. Anet, *Can. J. Chem.*, **40**, 1249 (1962).
2) C. H. Krauch, S. Farid, and G. O. Schenck, *Chem. Ber.*, **99**, 625 (1966).
3) M. Hasegawa, Y. Suzuki, and N. Kita, *Chem. Lett.*, **1972**, 317.
4) Y. Suzuki, M. Hasegawa, and N. Nishikawa, *J. Polym. Sci., Polym. Lett. Ed.*, **11**, 173 (1973).
5) M. Hasegawa, N. Yonezawa, T. Kanoe, and Y. Ikebe, *J. Polym. Sci., Polym. Lett. Ed.*, **20**, 309 (1982).
6) M. Hasegawa, H. Katsuki, N. Yonezawa, T. Yoshida, and Y. Ikebe, *Chem. Lett.*, **1982**, 1325.

 © 1983 The Chemical Society of Japan Bull. Chem. Soc. Jpn., 56, 369—374 (1983)

Vibrational Spectra of Organic Conductors. Charge Transfer Salts of TTF with Substituted *p*-Benzoquinones

Susumu MATSUZAKI, Toshiharu MORIYAMA, Mitsukazu ONOMICHI,† and Koichi TOYODA*
Department of Chemistry, Faculty of Science, Kumamoto University, Kumamoto 860
†*College of Medical Technology, Kumamoto University, Kumamoto 860*
(Received May 17, 1982)

Charge transfer salts of tetrathiafulvalen (TTF) with five substituted *p*-benzoquinones (fluoranil, chloranil, bromanil, iodanil, and 2,3-dichloro-5,6-dicyano-*p*-benzoquinone) were prepared by diffusion and cooling methods. IR, Raman, and electronic spectra of these salts measured at room temperature showed that all except fluoranil salt formed two crystal phases, *i.e.*, the diffusion and the cooling methods gave a mixed-valent and a monovalent ionic phases respectively. The degrees of charge transfer (ρ) of the mixed-valent salts were estimated from the Raman frequencies of a_g ν_3 of TTF, and nearly equal values (*ca.* 0.7) were obtained for all of them.

Since the discovery of the unusual electrical properties of TTF-TCNQ,[1] a vast amount of research has been carried out to understand the properties of the organic conductors. The research has shown that the organic charge transfer salts must satisfy two essential requirements in order to exhibit high electrical conductivity:[2] (1) The component molecules form segregated stacks of donors and acceptors; (2) charge transfer from the donor to the acceptor is incomplete, *i.e.*, $\rho<1$. At present, it is difficult to control the first requirement, whereas conditions for the satisfaction of the second requirement have been discussed considerably;[3] *i.e.*, incomplete charge transfer occurs when the difference between the ionization potential of the donor and the electron affinity of the acceptor is comparable to the crystal Madelung energy.

Determination of ρ is important to understand the conduction mechanism in organic conductors and various methods have been used to estimate the value.[4] Recently we found that the plot of Raman frequencies *vs.* ρ is linear in the case of TCNQ salts[5] and TTF salts,[6] and demonstrated that Raman spectroscopy is a useful and reliable means to estimate ρ of organic conductors.

In this work, many charge transfer salts of TTF with substituted *p*-benzoquinones are prepared by use of two different methods. The vibrational and electronic spectra of the salts are compared with each other, and the degrees of charge transfer of the mixed-valent salts are estimated from the Raman frequencies.

Experimental

TTF was synthesized by the method of Wudl *et al.*,[7] and recrystallized from hexane–cyclohexane, and sublimed twice *in vacuo*. The product was identified by spectral methods (IR and Raman) and elemental analysis. Fluoranil (tetrafluoro-*p*-benzoquinone), chloranil (tetrachloro-*p*-benzoquinone), bromanil (tetrabromo-*p*-benzoquinone), and 2,3-dichloro-5,6-dicyano-*p*-benzoquinone were all obtained commercially, and recrystallized twice from benzene and sublimed *in vacuo*: These acceptors are abbreviated to FA, CA, BA, and DDQ respectively. Iodanil (tetraiodo-*p*-benzoquinone) was synthesized by the method of Torrey and Hunter,[8] and recrystallized several times from ethyl acetate: This acceptor is abbreviated to IA.

Charge transfer salts of TTF with the substituted *p*-benzoquinones were prepared by the following two methods: (1) Diffusion method in acetonitrile (same as reported in the literature)[9] and (2) cooling method (mixing of the stoichiometric amounts of the components in hot acetonitrile and cooling of the solution). Preparation by the diffusion method was performed at 34 ± 1 °C in evacuated H-tubes which were placed in a thermostated air bath of our own making and the periods of preparation were typically *ca.* 3 months. The composition of the salts was determined by elemental analysis.

Raman spectra of the powder samples were recorded (in the back scattering geometry) on a JASCO R-800 spectrometer equipped with NEC GLG-3200 Ar^+ and GLG-108 He–Ne lasers as exciting light sources. In order to avoid thermal decomposition of the sample, exciting laser light was focused by a cylindrical lens and sample-rotating technique was used. IR and electronic absorption spectra of the powder samples dispersed in KBr were recorded on a JASCO DS-403G IR spectrometer and a Hitachi 200-20 or a(EPS-3T) spectrophotometer, respectively. Electrical conductivity was measured bythe two probe method in an evacuated bell jar by use of a Takeda Riken TR-8561 electrometer.

Results and Discussion

TTF–FA, TTF–CA, and TTF–BA. Recently, Torrance *et al.*[10] reported that TTF formed mixed-valent crystals of good conductivity with fluoranil, whereas it formed monovalent poor conductors with chloranil and bromanil. In this work, we also have obtained a mixed-valent salt for TTF–FA by both methods, and the IR and Raman spectra are shown in Fig. 1. This salt was fairly unstable and the reproducibility of the spectra was not so good; nevertheless, the

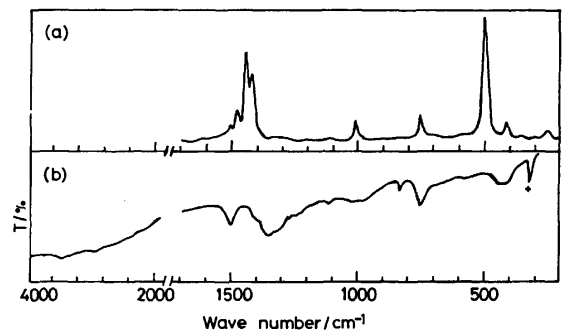

Fig. 1. Vibrational spectra of TTF-FA. (a) Raman and (b) IR; +, fault signal which is due to the exchange of gratings of the instrument.

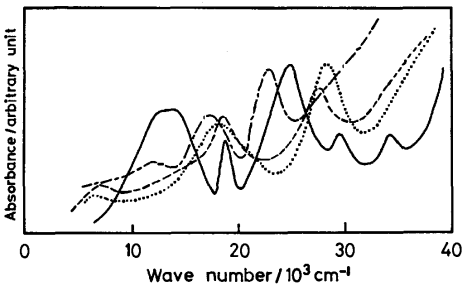

Fig. 2. Electronic spectra of TTF–CA and TTF–BA. TTF-CA(I), ------; TTF-CA(II), ——; TTF-BA(I), ·····; TTF-BA(II), —·—.

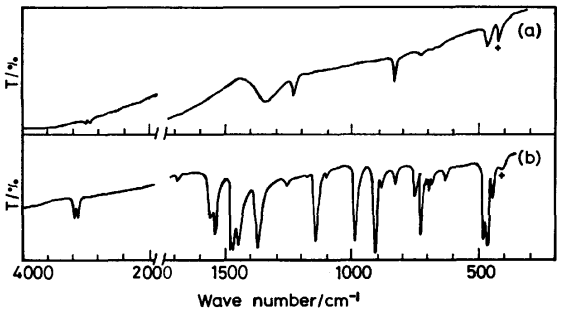

Fig. 3. IR spectra of TTF–CA. (a) TTF-CA(I) and (b) TTF-CA(II); +, fault signal which is due to the exchange of gratings of the instrument.

IR spectrum clearly shows the mixed-valency (see the discussion for TTF–CA). The Raman lines at 1443 cm^{-1} and 1418 cm^{-1} will be assigned to a_g ν_3 modes of mixed-valent and monovalent TTF cations respectively.[11] The result shows that the sample is a mixture of two salts.[12]

On the other hand, for TTF-CA and TTF-BA, we have found that the salts give a monovalent or a mixed-valent phase depending on the method of preparation.[13] The salts prepared by the diffusion method and the cooling method are represented by the symbols (I) and (II), respectively, throughout this section. Both TTF–CA(I) and TTF-CA(II) were obtained as black needles. Electronic spectra of the two salts are shown in Fig. 2. Absorption bands in the higher frequency region are assigned to LE transitions of TTF^+, which are 18500 and 27500 cm^{-1} for the salt (I), and 18700, 24700, and 29000 cm^{-1} for the salt (II).[14] Thus the result shows that both the salts contain TTF^+. In the spectrum of the salt (I), an absorption band appears at *ca.* 6700 cm^{-1} tailing to the middle infrared region (Fig. 3). It is known that mixed-valent TTF salts exhibit a low frequency band around 5000 cm^{-1} which is assigned to the mixed-valent CT transition between the neutral molecule (TTF^0) and the cation radical (TTF^+).[14,15] The band at 6700 cm^{-1} will be assigned to this CT transition, and appearance of the band strongly suggests that TTF–CA(I) is a mixed-valent salt. On the other hand, the salt (II) shows no such a low frequency band but a broad absorption band of an unusual profile at 13500 cm^{-1}. This feature will be attributed to an overlap of the two dimer-type CT bands of $(TTF^+)_2$ and $(CA^-)_2$.[15,16] The result suggests that TTF–CA(II) is a monovalent salt of dimeric structure. The salt probably corresponds to the monovalent salt reported in the literature.[10]

In the IR spectrum of TTF–CA(I), a characteristic broad band appears at 1347 cm^{-1}, whereas the corresponding band is fairly sharp in the salt (II) (Fig. 3). The component molecules have no IR-active modes in this region, and the band will be attributed to the IR-activation of a_g modes by the electron-vibration mechanism. Bozio *et al.*[11] reported that $(TTF^+)_2$ exhibits a strong IR band at 1360 cm^{-1} in DMSO solution, and assigned it to a_g ν_3 of TTF^+. Normal vibrations of the component molecules couple to each other in the dimer unit, and new normal vibrations of the dimer are produced. In the case of a_g modes, in-phase coupling modes are totally symmetric and Raman-active, whereas out-of-phase coupling modes are ungerade and IR-active. The latter promotes electron oscillation between the component radicals of the dimer, and has strong IR intensity and a lowered frequency; on the other hand the former causes no vibronic effect and the frequency is almost equal to that of the component radical.[17] Therefore, IR frequency of the out-of-phase coupling mode is usually several tens of wave numbers lower than the corresponding Raman frequency of the in-phase coupling mode. Vibronically allowed a_g modes of CA^- are also expected to be observed in the spectrum of the salt (II) because the dimerization of CA^- is suggested from the electronic spectrum as mentioned above. A strong band at 987 cm^{-1} probably arises from such an activation mechanism and will be assigned to the out-of-phase coupling mode of a_g ν_3 of CA^- because the component molecules have no IR-active fundamentals in this region and $(CA^-)_2$ was reported to show a strong IR band at 1008 cm^{-1} in potassium salt of chloranil which was assigned to this mode.[18,19]

Electronic spectra (Fig. 2) and IR spectra of TTF–BA showed characteristic features similar to those of TTF–CA. Thus it is concluded also in this case that TTF–BA(I) and TTF–BA(II) are a mixed-valent and a monovalent salts respectively. Observed IR frequencies and the tentative assignment of TTF–BA are given in Table 1 together with those of TTF–CA.

Raman spectra of TTF–CA are shown in Fig. 4. Almost all the Raman lines observed are attributable to a_g modes of TTF^+ (Table 2). This result probably arises from stronger resonance enhancement of the

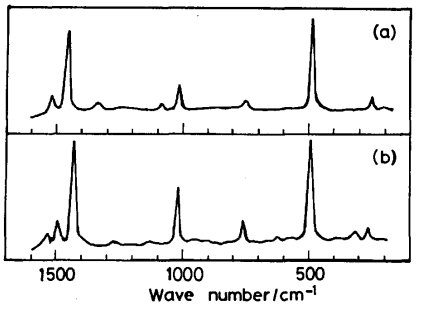

Fig. 4. Raman spectra of TTF–CA. (a) TTF-CA(I) and (b) TTF–CA(II); 514.5 nm excitation.

Table 1. Infrared frequencies of TTF-CA and TTF-BA

TTF-CA(I) $\tilde{\nu}$/cm^{-1}	TTF-CA(II) $\tilde{\nu}$/cm^{-1}	Assignment[a]	TTF-BA(I) $\tilde{\nu}$/cm^{-1}	TTF-BA(II) $\tilde{\nu}$/cm^{-1}	Assignment[a]
459 m	457 m	b_{1u} ν_{18} (TTF^+)	462 w	461 m	b_{1u} ν_{18} (TTF^+)
476 vw	476 vs	b_{1u} ν_{13} (CA^-)		616 m	b_{2u} ν_{20} (BA^-)
	484 m		639 w		
	628 w			686 s	b_{3u} ν_{28} (BA^-)
	686 w		700 w		
	696 w	b_{3u} ν_{28} (CA^-)	737 w		
731 w	725 s	b_{2u} ν_{20} (CA^-)		746 w	b_{1u} ν_{17} (TTF^+)
	750 m	b_{1u} ν_{17} (TTF^+)		821 w	
824 m	828 m	b_{1u} ν_{16} (TTF^+)	830 m	832 s	b_{1u} ν_{16} (TTF^+)
	886 w			873 vs	b_{1u} ν_{12} (BA^-)
	910 vs	b_{1u} ν_{12} (CA^-)		910 w	
	987 vs	a_g ν_3 (CA^-)	1054 m		
1072 vw		b_{1u} ν_{15} (TTF^+)	1065 m		b_{1u} ν_{15} (TTF^+)
	1171 vw			1133 w	
1236 m		b_{2u} ν_{23} (TTF^+)	1215 w	1215 vw	
	1261 w		1237 m	1246 s	b_{2u} ν_{23} (TTF^+)
1347 s, br	1370 s	a_g ν_3 (TTF^+)		1250 sh	
	1447 s		1349 s, br	1367 s	a_g ν_3 (TTF^+)
	1462 s	b_{1u} ν_{14} (TTF^+)		1482 s	b_{1u} ν_{14} (TTF^+)
	1471 sh		1500 w		
1500 w				1516 vs	b_{1u} ν_{10} (BA^-)
	1534 s	b_{1u} ν_{10} (CA^-)	1675 m		
	1545 sh	b_{2u} ν_{18} (CA^-)	3057 w	3076 w	b_{1u} ν_{13} (TTF^+)
3044 w	3044 m	b_{2u} ν_{22} (TTF^+)			
	3065 m	b_{1u} ν_{13} (TTF^+)			

a) The assginment follows Bozio *et al.* (Ref. 11) and Girlando *et al.* (Ref. 19).

Table 2. Raman frequncies[a] of TTF-CA and TTF-BA

TTF-CA(I) $\tilde{\nu}$/cm^{-1}	TTF-CA(II) $\tilde{\nu}$/cm^{-1}	Assignment[b]	TTF-BA(I) $\tilde{\nu}$/cm^{-1}	TTF-BA(II) $\tilde{\nu}$/cm^{-1}	Assignment[b]
258 w	264 m	a_g ν_7 (TTF^+)	214 m	216 m	a_g ν_5 (BA^-)
	311 m		264 m	266 m	a_g ν_7 (TTF^+)
497 vs	509 vs	a_g ν_6 (TTF^+)	391 w		
	623 m			447 w	
753 w	758 m	a_g ν_5 (TTF^+)		475 w	
	818 w		498 vs	504 s	a_g ν_6 (TTF^+)
	911 w		756 w	759 w	a_g ν_5 (TTF^+)
1013 w	1016 s	a_g ν_3 (CA^-)		905 w	
1086 w		a_g ν_4 (TTF^+)		942 w	a_g ν_3 (BA^-)
	1103 w		996 m		
	1131 w			1025 w	
	1266 w		1083 w	1090 w	a_g ν_4 (TTF^+)
1448 vs	1421 vs	a_g ν_3 (TTF^+)		1158 w	
	1481 m		1236 w	1237 w	
1524 m	1506 w	a_g ν_2 (TTF^+)	1342 w		
	1525 m	a_g ν_1 (CA^-)	1447 vs	1420 vs	a_g ν_3 (TTF^+)
			1515 m	1503 m	a_g ν_2 (TTF^+)
			1586 m	1570 m	a_g ν_2 (BA^-)
				1590 m	

a) 514.5 nm excitation. b) The assignment follows Bozio *et al.* (Ref. 11) and Girlando *et al.* (Ref. 19).

Raman lines of TTF^+ than those of CA^- with 514.5 nm excitation. We have already reported[6] that the frequency of TTF a_g ν_3 is very sensitive to the formal charge and can be a suitable measure of ρ.. This mode is observed at 1448 cm^{-1} in TTF-CA(I). The frequency is located between TTF^0 (1518 cm^{-1}) and the monovalent salt (1421 cm^{-1}), and clearly shows the mixed-valency of the salt. The salt (I) was unstable under strong laser-irradiation even by use of the cylindrical lens and the sample-rotating technique, and showed a time-dependence of the spectrum similar to that of mixed-valent TTF halides reported previously.[6] The spectrum shown in Fig. 4 was, therefore, measured under the minimized laser power (<20 mW). Kinetic study on the dependence will be reported elsewhere.[20] TTF-BA(I) and TTF-BA(II) gave the Raman spectra

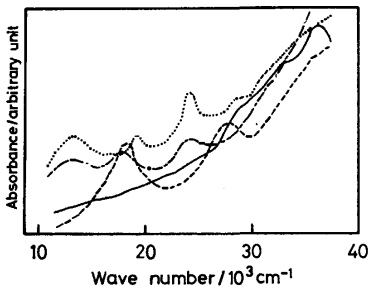

Fig. 5. Electronic spectra of TTF–IA and TTF–DDQ. TTF-IA(I), ------; TTF-IA(II), ——; TTF-DDQ(I), ·····; TTF-DDQ(II), —·—.

similar to those of TTF–CA(I) and TTF-CA(II) respectively. The frequencies and tentative assignment of the salts are given in Table 2 together with those of TTF–CA.

Electrical conductivity of TTF–CA(I) was measured to be $1\times10^{-2}\ \Omega^{-1}\ cm^{-1}$. The shape of the crystals was not so good and the maximum values were taken for the dimensions, so that the conductivity corresponds to the minimum value. This value is two to three orders of magnitude lower than those of the mixed-valent TMTTF–CA and TMTTF–BA reported by Torrance, *et al.*,[10] probably due to imperfections of the crystals in this work. Nevertheless, the value is large enough to demonstrate the mixed-valency of TTF–CA(I).

Stoichiometries of TTF-CA(II) and TTF–BA(II) were found to be 1 : 1 by the elemental analyses, but the values of the salts (I) varied from 2 : 1 to 1 : 2. This variation probably arises from mixing of the component molecules with the crystals of the salts, because it was observed by an optical microscope that yellow areas scattered on the black surface of the crystals. Thus the compositions of the salt (I) are unknown at present. It has been reported that TMTTF forms the mixed-valent salts of 1 : 1 stoichiometry with chloranil and bromanil,[10] and it seems natural to consider the 1 : 1 stoichiometry also in the present case.

TTF–IA. TTF–IA(I) and TTF–IA(II) were obtained as black powder and black needles respectively. Electronic spectra of the two salts are much different from one another (Fig. 5). TTF-IA(II) shows no absorption bands around 18000 cm^{-1}, so that it contains no TTF^+ species; furthermore, IR and Raman spectra (Figs. 6 and 7) of the salt are reasonably explained as an overlapp of those of TTF^0 and IA^0 (Tables 3 and 4). The result shows that the salt (II) is a non-ionic CT complex and will be an analog of the neutral mixed-stack crystals of TTF–CA and TTF–BA reported by Mayerle *et al.*[21] On the other hand, the absorption bands of TTF^+ appear in the electronic spectrum of TTF-IA(I) (Fig. 5); furthermore, the IR spectrum shows apparent similarity to that of the mixed-valent TTF–CA(I) (Figs. 6 and 3). The Raman spectrum also shows the mixed-valent TTF $a_g\ \nu_3$ line at 1448 cm^{-1} (Fig. 7). It is, therefore, evident that TTF–IA(I) is a mixed-valent salt.[22]

No vibrational assignment has been reported for the Raman-active fundamentals, and we have assigned them by referring to the assignment for chloranil and bromanil by Girlando *et al.*[19] As given in Table 4, main Raman lines are reasonably assigned on the basis of the rule that the frequency must be lowered because of the larger atomic weight of iodine than chlorine and bromine. Assignment of the IR-active vibrations has been reported by Iida,[23] and we use the result in this study.

Several vibrational features show fairly large frequency shifts (20—40 cm^{-1}) by the complex formation, *e.g.*, ν_1 and ν_{10} of iodanil, and ν_3 of TTF (the frequency of TTF^0 is 1518 cm^{-1}). The result shows the fairly strong CT interaction operating between TTF and iodanil in this non-ionic CT complex. The degree of charge transfer is estimated to be 0.3 from the ν_3 frequency of TTF assuming that the linear relation between the frequency and ρ is valid for mixed-stack complexes.

IR spectrum of this non-ionic CT complex is influenced by the vibronic effect as in the radical salts. A

Table 3. Infrared frequencies of TTF–IA

TTF–IA(I) $\tilde{\nu}/cm^{-1}$	TTF–IA(II) $\tilde{\nu}/cm^{-1}$	Iodanil $\tilde{\nu}/cm^{-1}$	Assignment[a]
460 w	439 s		$b_{1u}\ \nu_{18}$ (TTF)
	491 w		
		535 vw	
568 vw	565 m	570 s	$b_{2u}\ \nu_{20}$ (IA)
	576 vw	580 w	
	615 w		
		628 vw	
	646 s		$b_{3u}\ \nu_{34}$ (TTF)
	664 s		
	686 s	694 s	$b_{3u}\ \nu_{28}$ (IA)
	733 m		$b_{1u}\ \nu_{17}$ (TTF)
	780 m		$b_{1u}\ \nu_{16}$ (TTF)
	793 s		$b_{1u}\ \nu_{25}$ (TTF)
818 sh	806 vw		
824 w		825 vw	
	843 m	842 w	$b_{1u}\ \nu_{12}$ (IA)
	866 vw		
1015 m	1017 vs	1019 vs	$b_{1u}\ \nu_{11}$ (IA)
	1031 w	1029 w	
	1087 vw		
	1095 m		$b_{1u}\ \nu_{15}$ (TTF)
	1158 w	1150 sh	
1171 w	1172 s	1177 vs	$b_{2u}\ \nu_{19}$ (IA)
	1187 sh	1194 w	
1240 m	1255 s		$b_{2u}\ \nu_{23}$ (TTF)
		1269 w	
1344 s,br			$a_g\ \nu_3$ (TTF^+)
		1362 m	
		1500 sh	
	1487 vs		$a_g\ \nu_3$ (TTF)
1518 w		1520 vs	$b_{2u}\ \nu_{18}$ (IA)
	1540 m		
		1554 w	
	1562 w		
1663 m	1633 vs	1659 vs	$b_{1u}\ \nu_{10}$ (IA)
3044 w	3061 m		$b_{2u}\ \nu_{22}$ (TTF)
	3082 w		

a) The assignment of IR-active fundamentals follows Iida (Ref. 23).

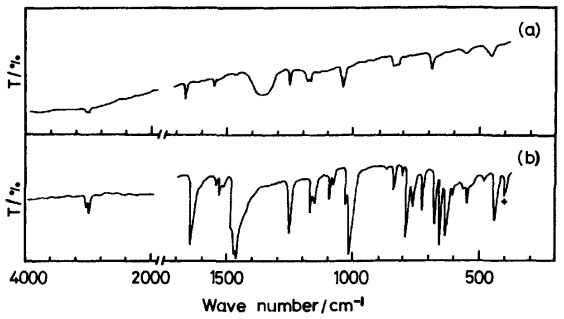

Fig. 6. IR spectra of TTF–IA. (a) TTF–IA(I) and (b) TTF–IA(II); +, fault signal which is due to the exchange of gratings of the instrument.

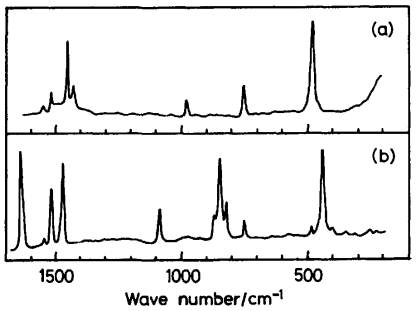

Fig. 7. Raman spectra of TTF–IA. (a) TTF–IA(I) and (b) TTF–IA(II); 514.5 nm excitation.

strong IR band at 1487 cm^{-1} has the same frequency as the Raman line of TTF a_g ν_3 (Tables 3 and 4) and will be assigned to this mode. In the case of mixed-stack CT complexes, the normal vibration of totally symmetric modes itself promotes the electron oscillation between the donor and the acceptor. Therefore, the IR frequency is equal to the Raman frequency, in contrast to the case of the segregated-stack radical salts of dimeric structure where the Raman and IR intensities are induced by the in-phase and out-of-phase coupling modes respectively. It may also be possible to assign the band at 1487 cm^{-1} to b_{2u} ν_{18} of iodanil. However, it is hard to accept from the standpoint of the frequency shift. Ion radical of iodanil has not yet been prepared and the frequency shift by full charge transfer ($\rho=1$) is unknown, but the shifts in chloranil and bromanil were reported to be 27 and 20 cm^{-1} respectively.[19] Therefore, it is not reasonable to expect that the shift of 33 cm^{-1} occurs in the present case of the partial charge transfer ($\rho=0.3$).

TTF–DDQ. Electron affinities of all the tetrahalo-*p*-benzoquinones are practically equal to each other; on the other hand, DDQ has the fairly larger value than the others.[24] Therefore, formation of the mixed-valent phase was considered to be difficult. The cooling method gave the monovalent salt, TTF–DDQ(II), as evident from the spectra (Figs. 5, 8, and 9). Mayerle and Torrance[25] reported the formation of single crystals of the monovalent salt by the diffusion method. The samples obtained by this method were mostly the monovalent salt also in this work; nevertheless, a few samples, TTF–DDQ(I),[26] showed the characteristic IR

Table 4. Raman frequencies[a] of TTF–IA

TTF–IA(I) $\tilde{\nu}$/cm^{-1}	TTF–IA(II) $\tilde{\nu}$/cm^{-1}	Iodanil $\tilde{\nu}$/cm^{-1}	Assignment
	452 vs	472 vs	a_g ν_4 (IA)
493 vs	490 w		a_g ν_6 (TTF)
753 m	732 w		a_g ν_5 (TTF)
	844 s	846 m	
	869 vs	872 s	a_g ν_3 (IA)
989 w			
	1095 m		a_g ν_4 (TTF)
		1200 w	
1417 m			a_g ν_3 (TTF^+)[b]
1448 s	1486 vs		a_g ν_3 (TTF)
	1529 vs	1543 vs	a_g ν_2 (IA)
1512 m	1543 m		a_g ν_2 (TTF)
	1615 vs	1654 vs	a_g ν_1 (IA)

a) 514.5 nm excitation. b) This line is probably attributable to a monovalent TTF^+ contained as an impurity.

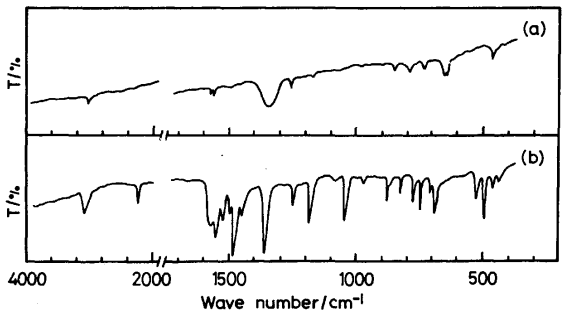

Fig. 8. IR spectra of TTF–DDQ. (a) TTF–DDQ(I) and (b) TTF–DDQ(II).

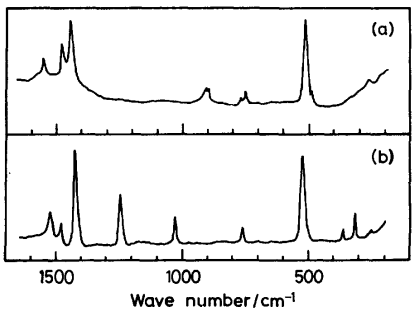

Fig. 9. Raman spectra of TTF–DDQ. (a) TTF–DDQ(I) and (b) TTF–DDQ(II); 514.5 nm excitation.

and Raman spectra of the mixed-valent salt (Figs. 8 and 9). Raman lines at 1423 and 1453 cm^{-1} are assigned to a_g ν_3 modes of the monovalent and the mixed-valent TTF cations respectively. Relative intensity of the two lines shows that the fraction of the mixed-valent salt is small, *i.e.*, the salt is not so easy to be formed. The result is consistent with the large electron affinity of DDQ.

Estimation of ρ. In the case of TTF salts, it has been shown that the ν_3 mode gives the best result for the estimation of the degree of charge transfer (ρ).[6] In this investigation, therefore, the values of ρ of the mixed-valent salts were estimated from the ν_3 frequencies by use of the calibration curve obtained previously. The

values of ρ thus obtained are: 0.75 (TTF–FA); 0.71 (TTF–CA); 0.72 (TTF–BA); 0.71 (TTF–IA); and 0.66 (TTF–DDQ). These values inherently contain uncertainty because of the crystal field effect on the frequency.[5] The uncertainty is estimated to be 0.1 for TTF ν_3 from the frequency variation of many monovalent salts of TTF. Therefore, it should be considered that the mixed-valent salts in this work have the values of ρ which are practically equal to each other.[27] The degree of charge transfer is determined by the two quantities, $(I-A)$ and E_M, in the mixed-valent salt of the segregated structure,[2,3] where $(I-A)$ is the difference between the ionization potential (I) of the donor and the electron affinity (A) of the acceptor, and E_M is the crystal Madelung energy. If $(I-A)>E_M$, neutral ground state is more stable in energy and, on the contrary, ionic ground state is favorable if $(I-A)<E_M$. The mixed-valent state will be realized when $(I-A)\simeq E_M$. The tetrahalo-*p*-benzoquinones have the electron affinities which are almost equal to each other, and $(I-A)$ is practically constant in all the mixed-valent salts except the DDQ salt. The result of the practically equal values of ρ, therefore, suggests that E_M is almost constant in all the salts, *i.e.*, the crystal structures are similar to each other. On the other hand, the electron affinity of DDQ is fairly large;[24] therefore, it may be difficult to explain the value of ρ from this standpoint. X-ray structural analyses of these salts are necessary for further discussion.

The present work was partially supported by a Grant-in-Aid for Scientific Research No. 56470009 from the Ministry of Education, Science and Culture.

References

1) M. J. Cohen, L. B. Coleman, A. F. Garito, and A. J. Heeger, *Phys. Rev. B*, **10**, 1298 (1974).
2) J. B. Torrance, "Synthesis and Properties of Low-Dimensional Materials," Ann. N. Y. Acad. Sci. (1978), p. 210.
3) J. B. Torrance and B. D. Silverman, *Phys. Rev. B*, **15**, 788 (1977); J. B. Torrance, *Acc. Chem. Res.*, **12**, 79 (1979).
4) S. Megtert, J. P. Pouget, and R. Comes, in Ref. 2, p. 234; P. Coppens and T. N. Guru Row, in Ref. 2, p. 244; F. Devreux and M. Nechtshein, "Quasi One-Dimensional Conductors. I," ed by S. Barisic, A. Bjelis, J. R. Cooper, and B. Leontic, Springer-Verlag, Berlin (1979), p. 153.
5) S. Matsuzaki, R. Kuwata, and K. Toyoda, *Solid State Commun.*, **33**, 403 (1980).
6) S. Matsuzaki, T. Moriyama, and K. Toyoda, *Solid State Commun.*, **34**, 857 (1980).
7) F. Wudl, M. L. Kaplan, E. J. Hufnagel, and E. W. Southwick, Jr., *J. Org. Chem.*, **39**, 3608 (1974).
8) H. A. Torrey and W. H. Hunter, *J. Am. Chem. Soc.*, **34**, 702 (1912).
9) J. R. Andersen, E. M. Engler, and K. Bechgaard, in Ref. 2, p. 293.
10) J. B. Torrance, J. J. Mayerle, V. Y. Lee, and K. Bechgaad, *J. Am. Chem. Soc.*, **101**, 4747 (1979).
11) R. Bozio, I. Zanon, A. Girlando, and C. Pecile, *J. Chem. Phys.*, **71**, 2282 (1979).
12) Spectra of the pure sample of mixed-valent TTF–FA have not yet been obtained because the salt was fairly unstable and decomposed rapidly to a monovalent salt by laser-irradiation.
13) Neutral mixed-stack crystals of TTF–CA and TTF–BA reported in Ref. 21 have not been obtained in this work.
14) T. Sugano, K. Yakushi, and H. Kuroda, *Bull. Chem. Soc. Jpn.*, **51**, 1041 (1978).
15) J. B. Torrance, B. A. Scott, B. Welber, F. B. Kaufman, and P. E. Seiden, *Phys. Rev. B*, **19**, 730 (1979).
16) S. Hiroma and H. Kuroda, *Bull. Chem. Soc. Jpn.*, **46**, 3645 (1973).
17) M. J. Rice, *Solid State Commun.*, **31**, 93 (1979).
18) R. Bozio, A. Girlando, and C. Pecile, *Chem. Phys.*, **21**, 257 (1977).
19) A. Girlando, I. Zanon, R. Bozio, and C. Pecile, *J. Chem. Phys.*, **68**, 22 (1978).
20) T. Moriyama, S. Matsuzaki, and K. Toyoda, to be published.
21) J. J. Mayerle, J. B. Torrance, and J. I. Crowley, *Acta Crystallogr., Sect. B*, **35**, 2988 (1979).
22) A Raman line at 1417 cm^{-1} is assigned to a_g ν_3 of TTF^+. Appearance of this line shows that TTF–IA(I) was contaminated by a monovalent salt. The amount is probably very small because the intensity of the Raman line is weak: The line has very large intensity in monovalent salts (Fig. 4).
23) Y. Iida, *Bull. Chem. Soc. Jpn.*, **50**, 1337 (1977).
24) E. C. M. Chen and W. E. Wentworth, *J. Chem. Phys.*, **63**, 3183 (1975).
25) J. J. Mayerle and J. B. Torrance, *Bull. Chem. Soc. Jpn.*, **54**, 3170 (1981).
26) Amount of the salt (I) obtained was so small that the elemental analysis was not feasible.
27) TTF–FA and TTF–DDQ seem to have a larger and a smaller values than the others respectively; however, taking into account the uncertainty, the differences should not be regarded as significant at present.

 © 1983 The Chemical Society of Japan Bull. Chem. Soc. Jpn., 56, 375—378 (1983)

NMR Lanthanoid-probe Analyses of Conformational Properties of 8,2′-*S*-Cycloadenosine 3′-Monophosphate in Aqueous Solution

Shigeyuki Yokoyama, Tetsuya Oida, Seiichi Uesugi,† Morio Ikehara,† and Tatsuo Miyazawa*

Department of Biophysics and Biochemistry, Faculty of Science, The University of Tokyo, Hongo, Bunkyo-ku, Tokyo 113

†*Faculty of Pharmaceutical Sciences, Osaka University, Suita, Osaka 565*

(Received May 21, 1982)

The advanced method of NMR lanthanoid-probe analyses was used for studying the molecular conformations of 8,2′-anhydro-8-thio-9-β-D-arabinofuranosyladenine (8,2′-*S*-cycloadenosine) 3′-monophosphate in aqueous solution. From the observed ratios of Pr(III)-induced shifts, Gd(III)-enhanced relaxation rates as well as vicinal spin-coupling constants, the most probable values (and standard deviations) of the fractional populations of the local conformations for the C5′–C4′ bond, sugar ring, C3′–O3′ bond, and O3′–P bond and the internal rotation angles of the two forms about the C3′–O3′ bond were determined by the program COFLEM. The internal rotation equilibrium about the C3′–O3′ bond was found to be interrelated with the puckering of the sugar ring. The advanced lanthanoid probe method is thus useful for the analyses of the conformational characteristics of cyclonucleotides as well as of unmodified nucleotides in aqueous solution.

The conformational properties of modified nucleotide units have been found to be related with the biological functions of transfer ribonucleic acids. For example, 2-thiouridine derivatives contribute to the correct codon recognition,[1] and to the thermostability[2] through the conformational characteristics that the C3′-endo form is much more stable than the C2′-endo form. Previously, NMR chemical shifts, spin-coupling constants, nuclear relaxation rates, and nuclear Overhauser effect have been used for elucidating local conformations.[3] However, these NMR data are not sufficient for studying overall conformations of nucleotide molecules. For such studies on flexible molecules, the lanthanoid probe analyses have been successfully utilized.[4] Recently, we have developed an advanced computer program (COFLEM) for the lanthanoid probe analysis;[5] the overall conformer mixture of flexible molecule is now treated as a combination of local conformational equilibria.

8,2′-Anhydro-8-thio-9-β-D-arabinofuranosyladenine (8,2′-*S*-cycloadenosine, to be abbreviated as A^s) (Fig. 1) is a cyclic nucleoside with the fixed internal rotation angle ($\chi \approx 120°$) about the glycosidic bond.[6] This χ value of A^s is in the high-anti region, as compared with the anti χ value ($\approx 0°$) of adenosine (A). By the analyses of the UV and CD spectra, the molecules of dinucleoside monophosphate (A^spA^s) and oligonucleotides $(pA^s)_n$ [$n=2$—10] have been found to take left-handed helical conformations with stacked bases.[6] For A^spA^s in aqueous solution, the proton NMR spectra have been analyzed.[7] However, as an aid for studying the conformation of A^spA^s in solution, it is important to analyze the conformational feature of the modified nucleoside A^s, which will be different from that of A. Accordingly, in the present study, the advanced lanthanoid probe analysis has been made for elucidating the conformational characteristics of the sugar-phosphate moiety of 8,2′-*S*-cycloadenosine 3′-monophosphate (A^sp) in aqueous solution.

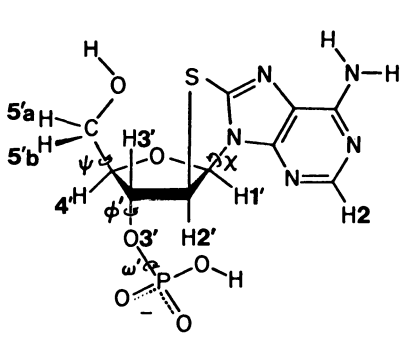

Fig. 1. Structure of A^sp.

Experimental

Materials. The sample of A^sp was synthesized as reported previously.[8] The nitrates of Pr(III) and Gd(III) of higher than 99.9% purity were obtained from Nakarai Chemical Co. Lanthanum oxide of higher than 99.99% purity was purchased from Nakarai Chemical Co. and was dissolved in nitric acid to obtain lanthanum nitrate.

Sample Solutions. For the measurements of lanthanoid-induced proton shift-ratios of A^sp, the successive dilution method[9,10] was used. The initial concentrations of A^sp and Pr(III) ion were 50 mM and 45 mM, respectively, in ^2H_2O solution at pH 1.7 (direct pH meter reading). Diamagnetic La(III) ion was used for the correction for the complex formation shifts. The initial solution was diluted stepwise with ^2H_2O, so that the sample solution was lowered from 50 mM to 5 mM without changing the molar ratio of A^sp/Pr(III) or A^sp/La(III). For the measurements of Gd(III)-enhanced proton relaxation rates of A^sp in ^2H_2O solution (A^sp 60 mM, pH 1.7), the concentration of Gd(III) ion was raised stepwise, by 5 μM, from 0 to 20 μM. The ^{13}C NMR spectrum of A^sp was measured in ^2H_2O solution (85 mM) at pH 2.0.

NMR Measurements. NMR spectra were measured with a Bruker WH270 spectrometer operating at 270 MHz for ^1H and 67.9 MHz for ^{13}C. The probe temperature was kept at 23 °C. Spin-lattice relaxation rates were obtained by a standard 180°-τ-90° pulse sequence.

Data Analyses. The computer program COFLEM developed previously[5] was used on the M-200H system at the Computer Center of the University of Tokyo.

Conformational Analysis

Observed NMR Data. The observed ratios of Pr(III)-induced shifts and Gd(III)-enhanced relaxation

TABLE 1. RATIOS OF Pr(III)-INDUCED SHIFTS AND Gd(III)-ENHANCED RELAXATION RATES, AND VICINAL COUPLING CONSTANTS OF A^sp

	Shift ratio		Relax. ratio	
	Obsd	Calcd	Obsd	Calcd
H1′	0.39	0.44	0.30	0.21
H2′	1.20	1.29	1.58	1.60
H3′	2.17	1.82	2.50	2.56
H4′	1.00	1.00	1.00	1.00
H5′a	0.28	0.38	0.60	0.59
H5′b	0.35	0.42	0.70	0.70
H2	0.04	0.08	0.10	0.01

	Spin-coupling constant/Hz	
	Obsd	Calcd
H1′–H2′	7.0	9.2
H2′–H3′	2.6	4.2
H3′–H4′	4.0	3.8
H4′–H5′a	3.7	3.7
H4′–H5′b	5.5	5.5
H3′–P	7.4	7.7
C2′–P	3.0	2.5
C4′–P	6.7	6.6

rates of A^sp are listed in Table 1. The ^1H resonances of A^sp in ^2H_2O solution (pH 2) are broadened on addition of a large excess of $LaCl_3$ but the ^1H–^1H and ^1H–^{31}P vicinal coupling constants are unaffected within the experimental uncertainty of 0.3 Hz. Therefore, the ^1H–^1H, ^1H–^{31}P, and ^{13}C–^{31}P coupling constants of free A^sp (Table 1) may be used for conformation analyses.

Local Conformations. The ribose ring and deoxyribose ring of unmodified nucleosides have been known to take two puckering forms, namely the N (C3′-endo) form or the S (C2′-endo) form. However, for 8,2′-*S*-cyclonucleosides, the N and S forms of the sugar ring are probably distorted from those of unmodified nucleosides, because the C2′ atom of 8,2′-*S*-cyclonucleosides is covalently linked, through a sulfur atom, to the C8 atom of the purine base. In fact, in the crystal of 8,2′-*S*-cycloinosinyl-(3′,5′)-8,2′-*S*-cycloadenosine (I^spA^s) hexahydrate,[11] the sugar ring of I^s nucleoside is slightly distorted from the C2′-endo form to the C4′-endo form. On the other hand, the sugar-ring conformation of A^s nucleoside in I^spA^s is nearly the same as the C3′-endo form. Accordingly, in the present conformation analysis of A^sp in aqueous solution, the C3′-endo (N) form and C4′-endo (S) form were used as the two types of sugar-ring conformations of A^sp. For this sugar ring, there is only one population parameter since the sum of the fractional populations of N and S forms is equal to unity. As for the internal rotation about the C3′–O3′ bond of A^sp, the two rotamers (G^+ and G^-)[5] were used (Fig. 2), and accordingly there is only one population parameter for this flexible site. The ϕ' [C4′–C3′–O3′–P] angles of these two rotamers of A^sp were taken as adjustable structure parameters in the present study. The three-rotamer equilibria were adopted for the internal rotation about the C5′–C4′ bond (gg, gt, and tg) and the O3′–P bond (g^+, t, and g^-) (see Fig. 2 of Ref. 5).

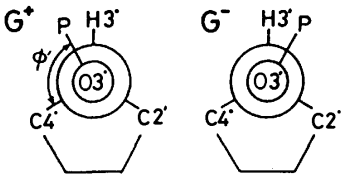

Fig. 2. Two rotamers about the C3′–O3′ bond of A^sp.

For each of these bonds, there are two population parameters since the sum of the fractional populations of three rotamers is equal to unity. The lanthanoid ion was set on the bisector of monoanionic OPO angle, 0.3 nm away from the phosphorus atom as in the case of uridine 3′-monophosphate.[5]

Interrelations among Local Conformational Equilibria. As a prominent feature of the advanced lanthanoid probe method of conformation analyses,[5] the interrelations among local conformational equilibria of flexible sites may be elucidated quantitatively. For the example of uridine 3′-monophosphate, the fractional populations of the G^+ and G^- forms have been determined for each of the C3′-endo form and C2′-endo form.[5]

In the present conformation analysis on A^sp in aqueous solution, four schemes of interdependency were examined among local conformational equilibria of three flexible sites, namely C5′–C4′ bond, sugar ring, and C3′–O3′ bond. The rotamer equilibrium about the O3′–P bond was set to be independent of the conformational equilibria of the other three flexible sites, as found previously for uridine 3′-monophosphate.[5]

Conformation of A^sp in Solution. By the use of the program COFLEM,[5] the most probable values (and standard deviations) of population parameters and structure parameters were obtained, so that the calculated values of the ratios of lanthanoid-induced shifts and relaxation rates as well as spin-coupling constants agreed best with the observed data (Table 1). There are six shift ratios, six relaxation-rate ratios and eight coupling constants and thus are a total of twenty observed data for the conformation analysis of A^sp in aqueous solution. The quality of the fit between the calculated values and observed data was judged by the agreement factor (R), as described previously.[5]

In Scheme 1, the local conformation equilibria are all independent of one another, and there are eight adjustable parameters, including six population parameters and two structure parameters. Even with this small number of parameters, the total of twenty observed data were reproduced with the agreement factor of R= 9.2%. On the introduction of the interdependency between the puckering of sugar ring and the internal rotation about the C5′–C4′ bond (Scheme 2), the number of adjustable parameters was increased from eight to ten and the agreement factor was slightly improved to 8.6%. On the other hand, the introduction of the interdependency between the ring-puckering and the internal rotation about the C3′–O3′ bond (Scheme 3) increased the number of parameters only by one but significantly improved the agreement factor to 8.3%. With this scheme, the calculated values of shifts ratios, relaxation-rate ratios and coupling con-

stants agreed quite well with the observed data (Table 1). However, when the internal-rotation equilibria about the C5′–C4′ bond and the C3′–O3′ bond were both assumed to depend upon the ring puckering (Scheme 4 with eleven parameters), the agreement factor (R=8.2%) was nearly the same as that of Scheme 3 and the standard deviations of adjustable parameters were much larger than those for Scheme 2. This indicates that, in Scheme 4, there are actually too many parameters as compared with the available set of observed data even though the number of parameters is much smaller than the nominal number of observed data. Thus, in the present study, Scheme 3 was adopted as the most reliable model and the most probable values (and standard deviations) of the population parameters and structure parameters are shown in Fig. 3.

It may be remarked here that the structure of the C1′–C2′–C3′ moiety of A^{s}p is different from that of ribonucleotides. Because of 8,2′-*S*-cyclization, the N–C1′–C2′ bond angle of A^{s}p is decreased by about 10° and the spin-coupling constants of the C1′–C2′–C3′ moiety are possibly affected. In fact, for the H1′–H2′ and H2′–H3′ coupling constants, the deviations of the calculated values from the experimental ones are larger than those for other coupling constants (Table 1). Nevertheless, the conformational analysis of the A^{s}p has been successfully carried out by the use of lanthanoid-induced shifts and relaxations as well as various spin coupling constants.

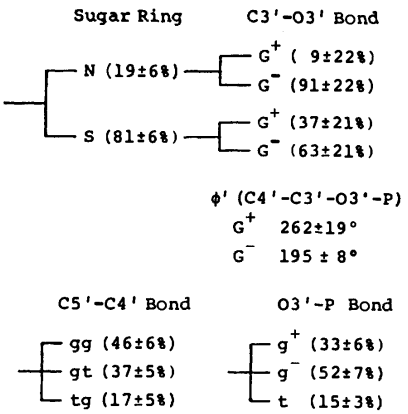

Fig. 3. Molecular conformation and conformational equilibrium of A^{s}p in aqueous solution (Scheme 3).

Discussion

Recently, the crystal structure of A^{s}p was analyzed, and crystallographically independent two molecules of A^{s}p were both found to take the S (C4′-endo) form of the sugar ring.[12] However, in the present study, the conformational equilibria of A^{s}p in aqueous solution were quantitatively analyzed by the advanced lanthanoid probe method.[5] Thus, the fractional populations of the S (C4′-endo) form and N (C3′-endo) form of the sugar ring were determined to be 81±6% and 19±6%, respectively, in solution (Fig. 3). This is consistent with the observation that the molecules of 8,2′-cyclonucleotides mostly take the S form in crystal.[12]

The interdependency of the sugar-ring puckering and the internal rotation about the C3′–O3′ bond of A^{s}p was experimentally established, in the present study, by the lanthanoid probe method. For the sugar ring in the N (C3′-endo) form, the fractional populations of the G$^+$ and G$^-$ forms are found to be 9±22% and 91±22%, respectively (Fig. 3); in other words, the sugar ring of the N form exclusively takes the G$^-$ form. This is probably because of strong steric repulsion between the 5′-CH_2OH group and the 3′-phosphate group in the N-G$^+$ form of the sugar-phosphate moiety. The molecular conformation of the gg-N-G$^-$-g$^-$ form is shown in Fig. 4.

For the sugar ring in the S (C4′-endo) form, the fractional populations of the G$^+$ and G$^-$ forms are found to be 37±21% and 63±21%, respectively (Fig. 3). In this case, the 5′-CH_2OH group is nearly oriented to the axial direction and there is no serious steric repulsion between the 5′-CH_2OH group and the 3′-phosphate group even in the S-G$^+$ form. By the combination of local conformational equilibria of the sugar ring and C3′–O3′ bond, the fractional populations of the S-G$^+$ form and S-G$^-$ form of A^{s}p are obtained to be about 30% and 50%, respectively, in aqueous solution. This again is consistent with the result of the X-ray

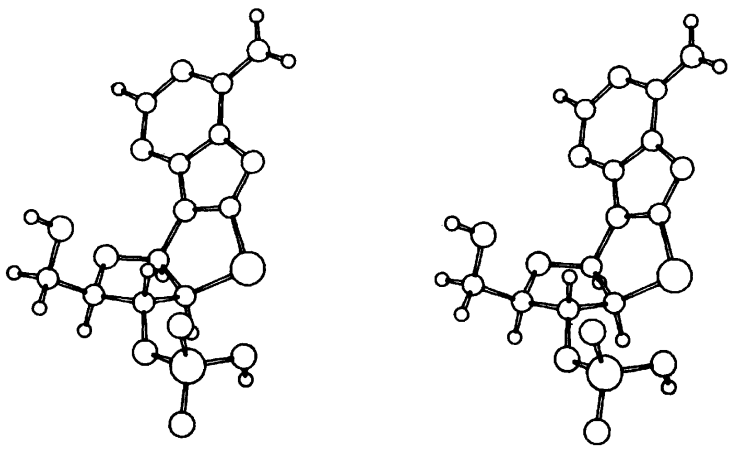

Fig. 4. The stereoscopic view of the gg-N-G$^-$-g$^-$ form drawn by the ORTEP program (Ref. 13).

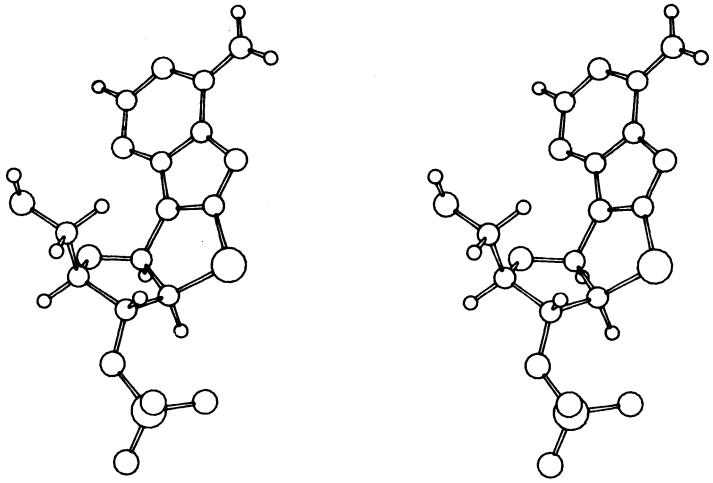

Fig. 5. The stereoscopic view of the gt-S-G$^-$-g$^-$ form drawn by the ORTEP program (Ref. 13).

analysis[12] that, in the crystal of A^{s}p, one molecule takes the S-G$^+$ form and the other takes the S-G$^-$ form. Furthermore, in the present study, the internal rotation angles (ϕ') about the C3′–O3′ bond were determined to be $262\pm19°$ and $195\pm8°$ for the G$^+$ and G$^-$ forms, respectively, in aqueous solution. Surprisingly, these values for A^{s}p in solution closely agree with the ϕ' values found in the crystal (G$^+$: 255° and G$^-$: 192°),[12] indicating the potentiality of the advanced lanthanoid probe method of conformation analyses.[5]

As for the local conformations about the C5′–C4′ bond, both of the two A^{s}p molecules in the crystal were found to take the gt form. However, in aqueous solution, the gt and gg forms are both the major conformations about the C5′–C4′ bond (Fig. 3). Previously, for the molecule of uridine 3′-monophosphate, the local conformational equilibrium about the C5′–C4′ bond was found to be interrelated with the ribose ring puckering.[5] However, in the present study on the 8,2′-cycloadenosine moiety, the conformational equilibrium about the C5′–C4′ bond was not found to depend significantly on the puckering of sugar ring. The molecular conformation of a major form (gt-S-G$^-$-g$^-$) of A^{s}p in solution is shown in Fig. 5.

Thus, the advanced lanthanoid-probe method[5] is further found to be useful for the quantitative elucidation of the molecular conformations and conformational equilibria of modified cyclonucleotides as well as of unmodified nucleotides (such as uridine 3′-monophosphate[5]). The conformational characteristics of the A^{s}p molecule in aqueous solution, as elucidated in the present study, may be utilized in the model-building analyses on the left-handed helical conformations of A^{s}p containing polynucleotides.

The authors are grateful to Professor K. Tomita of Osaka University for the atomic coordinates of I^{s}pA^s and for helpful discussions.

References

1) S. Yokoyama, Z. Yamaizumi, S. Nishimura, and T. Miyazawa, *Nucleic Acids Res.*, **6**, 2611 (1979).
2) K. Watanabe, S. Yokoyama, F. Hansske, H. Kasai, and T. Miyazawa, *Biochem. Biophys. Res. Commun.*, **91**, 671 (1979).
3) D. B. Davies, *Prog. Nucl. Magn. Reson. Spectrosc.*, **12**, 135 (1978).
4) F. Inagaki and T. Miyazawa, *Prog. Nucl. Magn. Reson. Spectrosc.*, **14**, 67 (1981).
5) S. Yokoyama, F. Inagaki, and T. Miyazawa, *Biochemistry*, **20**, 2981 (1981).
6) S. Uesugi, J. Yano, E. Yano, and M. Ikehara, *J. Am. Chem. Soc.*, **99**, 2313 (1977).
7) M. M. Dhingra, R. H. Sarma, S. Uesugi, and M. Ikehara, *J. Am. Chem. Soc.*, **100**, 4669 (1978).
8) M. Ikehara, T. Nagura, and E. Ohtsuka, *Nuclic Acids Res.*, **2**, 1345 (1975).
9) F. Inagaki, S. Takahashi, M. Tasumi, and T.Miyazawa, *Bull. Chem. Soc. Jpn.*, **48**, 853 (1975).
10) F. Inagaki, M. Tasumi, and T. Miyazawa, *Bull. Chem. Soc. Jpn.*, **48**, 1427 (1975).
11) K. Hamada, Y. Matsuo, A. Miyamae, S. Fujii, and K. Tomita, *Acta Crystallogr., Sect. B*, **38**, 2528 (1982).
12) A. Miyamae, K. Tanaka, K. Hamada, S. Fujii, and K. Tomita, *Acta Crystallogr., Sect. B*, **38**, 1937 (1982).
13) C. K. Johnson, ORTEP. Report ORNL-3794, Oak Ridge National Laboratory (1965).

 © 1983 The Chemical Society of Japan Bull. Chem. Soc. Jpn., 56, 379—385 (1983)

A Study of Local Structure Formation in Binary Solutions of 2-Butoxyethanol and Water by Rayleigh Scatterring and Raman Spectra

Nobuyuki Ito,† (the late)Tsunetake Fujiyama, and Yasuo Udagawa*

Institute for Molecular Science, Myodaiji, Okazaki 444

†*Department of Chemistry, Faculty of Science, Tokyo Metropolitan University, Setagaya-ku, Tokyo 158*

(Received June 22, 1982)

The concentration dependence of concentration fluctuations at 21, 32, and 42 °C and of Raman spectra at 21 °C were measured for binary solutions of 2-butoxyethanol (BE) and water. The existence of the two kinds of local structures is inferred; clathrate hydrate-like structure $g[(H_2O)_{50}BE]$ and aggregate $h[(H_2O)_4BE]$. The compositions of these two structures are the same as those of the two phases into which the solution separates above the critical solution temperature. The phase separation is understood to be the end of the growth of the local structures, which already exist well below the critical solution temperature.

Molecules such as acetone and *t*-butyl alcohol (TBA) are known to form solid clathrate hydrates at low temperature.[1] The existence of clathrate hydrate-like structure of these molecules has been reported in aqueous solutions also.[2-5] In the binary solution of TBA and water, an increase in the mean-square concentration fluctuations with temperature has been observed and interpreted to be due to the growth of clathrate hydrate-like structure. This has lead us to conjecture that the growth of the aggregates with temperature eventually causes phase separation.[2] Since the TBA–water mixture does not show phase separation at atmospheric pressure, however, the relationship between the local structure formation and the phase separation has not been proved.

The binary solution of 2-butoxyethanol (BE) and water is known to show phase separation and has a lower critical solution temperature (LCST) at atmospheric pressure. In the previous work the concentration fluctuation and mutual diffusion coefficients at 21 °C were reported and the formation of clathrate hydrate-like structure was concluded.[4] In the present work, concentration fluctuations are measured at various temperatures below the LCST in order to make clear the relationship between the local structure formation and the phase separation.

The formation of local structures in BE–water mixture has been postulated because of thermodynamic studies[9] and light scattering measurements,[4] but it seems that no one has studied it in terms of molecular structure. In the formation of clathrate hydrate-like structure, flexible molecules such as BE with many internal rotational axes are expected to show conformational changes. In other words, observation of conformational changes would be evidence for such a structure. Vibrational spectroscopy is known to be sensitive to such changes. In this paper Raman spectra of BE at various concentration are investigated in relation to the conformational changes by local structure formation.

Experimental

Measurements of Concentration Fluctuations. The light scattering spectra were observed with a spectrometer designed and constructed in our laboratory.[5] The refractive indices of the sample solution were measured by means of an Abbe refractometer (Atago). All the measurements were performed at 21, 32, and 42 °C (±0.5 °C).

Measurements of Raman Spectra. The Raman spectra were obtained at 21 °C by the use of a Spex 1403 spectrometer with a Spectra Physics 165-09 argon ion laser.

Measurement of Miscibility Curve. The miscibility curve was measured by the following procedures. The samples in sealed tubes were set in a water bath and irradiated with a He–Ne laser light. By the visual observation of scattered light with raising the temperature, the phase-separation temperatures were determined. Each point recorded is the average of at least two readings. The temperature was measured by the use of a Hewlett Packard quartz thermometer (model 2804A).

Materials. 2-Butoxyethanol (BE) purchased from Tokyo Kasei Co. Ltd. was used without further purification for the measurements of light scattering and Raman spectra. BE used for the measurement of the miscibility curve was, distilled with a spinning band distiller. The purity was ascertained to be better than 99.99% by gas chromatography. Water was passed through the Mili-Q Purification System (Millipore) after distillation. The relative electric resistance of water was more than 15 MΩ cm^{-1}. Deuterium oxide purchased from E. Merck AG. was used for the measurement of Raman Spectra without further purification.

Normal Coordinate Calculations. For the assignments of Raman bands, a normal coordinate treatment was carried out with a computer program NCTB (IMS program library) and HITAC M 200Hcomputer system at the Computer Center of Institute for Molecular Science (IMS).

Results

Concentration Fluctuations and the Miscibility Curve. Figure 1 shows the miscibility curve obtained in this work along with those reported in the literatures.[6,7] It was noticed that the miscibility curve is strongly affected by the existence of impurities. This is the reason for the wide discrepancies in the literature. Accordingly special care was taken to purify the material and the curve reported here is believed to be better than those previously reported. BE and water mix at all temperatures in the concentration range of $x_{BE}<0.02$ and $x_{BE}>0.2$, but the solution separates into two phases upon raising the temperature when $0.02<x_{BE}<0.2$. The steep edges of the miscibility curve at both ends suggest that the concentrations of the two phases have tendencies to be close to 0.2 or 0.02. This implies that the solution have particularly stable structures when $x_{BE}=0.02$ an 0.2. It is found that the LCST is 49.4 °C

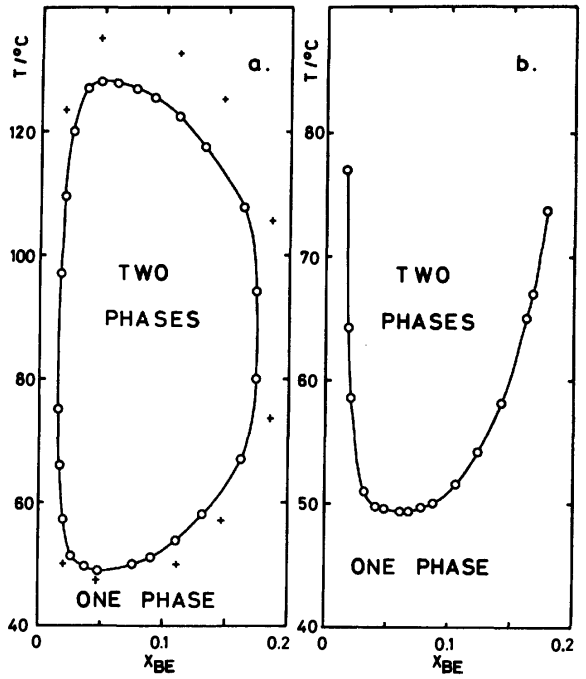

Fig. 1. Miscibility curves of 2-butoxyethanol and water mixture.
(a): ○ is from Ref. 6 and + is from Ref. 7, (b): present results.

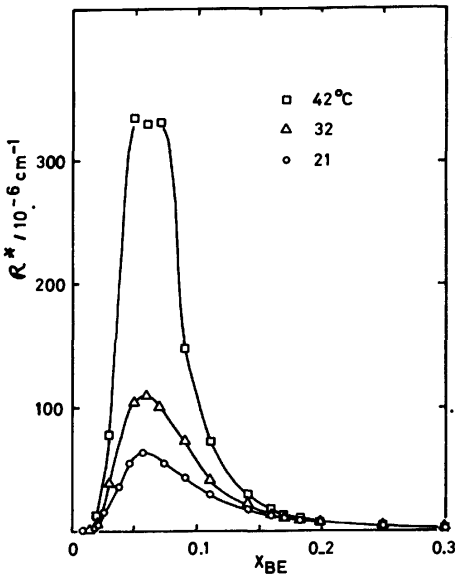

Fig. 2. Concentration dependence of Rayleigh intensities for BE–water mixtures.

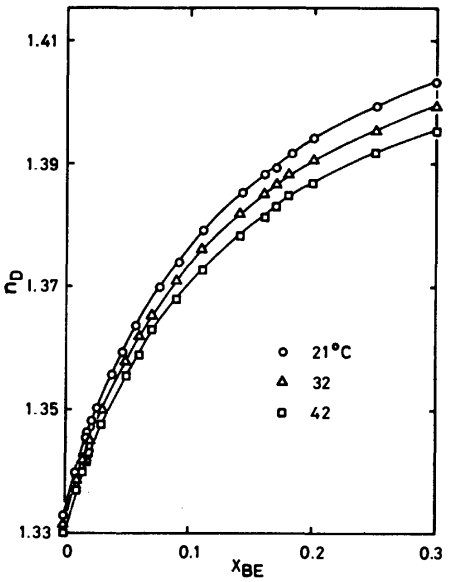

Fig. 3. Concentration dependence of the refractive index of BE–water mixtures.

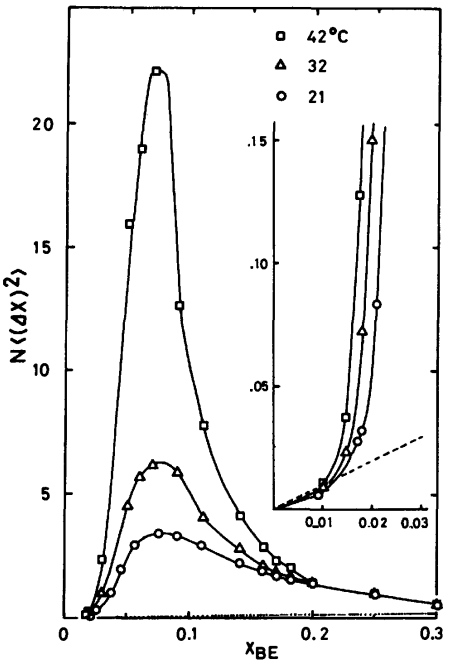

Fig. 4. Concentration dependence of the concentration fluctuation observed for BE–water mixtures. The dashed line corresponds to the concentration fluctuation expected for a n ideal binary solution.

at $x_{BE}=0.07$. As will be shown below the concentration fluctuations $N\langle(\Delta x)^2\rangle$ take its maximum value at the same concentration as the LCST. This indicates that local structure formation is closely related to the phase separation.

The concentration fluctuations can be derived from the light scattering intensity and the refractive indices which are shown in Figs. 2 and 3, respectively. The procedure is the same as described in the previous paper.[8] The isobaric heat capacity and the density necessary for the calculation were obtained from the literature.[9] In Fig. 4 the mean-square concentration fluctuations, $N\langle(\Delta x)^2\rangle$, at various temperatures are plotted against the mole fraction of BE, x_{BE}, where N is the total number of molecules in the observation volume. The dashed line in the figure corresponds to the $N\langle(\Delta x)^2\rangle$ expected for an ideal binary solution. It is seen from the figure that the observed concentration fluctuations are close to those of an ideal binary solution in the concentration range $0<x_{BE}<0.02$. However, it increases abruptly near $x_{BE}=0.02$, attains a maximum

at about $x_{BE}=0.07$, the value of which is about two orders of magnitude larger than that of the ideal solution, and decreases gradually with the increase of concentration of BE, and especially above 0.2 it varies little in magnitude. Also it is noticed from the figure that the $N\langle(\Delta x)^2\rangle$ increases rapidly with temperature in the concentration range $0.02<x_{BE}<0.2$. On the other hand, it is almost independent of the temperature if x_{BE} is above 0.2 and below 0.02.

Analysis of $N\langle(\Delta x)^2\rangle$. In the previous papers we have reported that the local structures existing in the solution can be determined from the analysis of the concentration dependence of $N\langle(\Delta x)^2\rangle$.[8] In the case of the ideal solution the concentration fluctuation is expressed as $x_B(1-x_B)$ for the binary solution of A and B, where x_B is the mole fraction of B. In the case where the same species gather together, the concentration fluctuation is greater than that of the ideal solution. In the case in which the different species gather together, the concentration fluctuation is smaller than that of the ideal solution. The observed concentration fluctuation indicates that BE-water mixture belongs to the former case.

From a comparison of the concentration dependence of $N\langle(\Delta x)^2\rangle$ with the miscibility curve, we can make a picture of the local structure formed in the solution. It is seen from Fig. 1 and Fig. 4 that the concentration where the concentration fluctuations increase/decrease corresponds to that where the miscibillity curve rises/falls. As mentioned above, this suggests the fact that stable local structures are formed at these concentrations. Their compositions must be $A_{50}B$ and A_4B, where A means water and B means BE, because the concentrations at issue are 0.02 and 0.2.

In order to understand the mixing state of BE–water mixture in all the concentration range, the following model is assumed; (1) local structures of types A_l and $A_lB(l=50)$ in the concentration range $0<x_B<0.02$, (2) simultaneous existence of A_lB and $A_mB(l=50, m=4)$ in the concentration range $0.02<x_B<0.2$, and (3) a local structure of type $A_mB(m=4)$ and molecules B in the concentration range $0.2<x_B$. The distribution of the two types of local structure calculated from the model above is shown in Fig. 5a. The concentration fluctuation for this model can be calculated for the following concentration range as:

$[0<x_B<0\ 02]$

$$N\langle(\Delta x_B)^2\rangle = x_B(1-x_B)[1-(l+1)x_B] \tag{2a}$$

$[0\ 02<x_B<0\ 2]$

$$N\langle(\Delta x_B)^2\rangle = x_B[(l+1)x_B-1][1-(m+1)x_B] \tag{2b}$$

$[0\ 2<x_B<0\ 3]$

$$N\langle(\Delta x_B)^2\rangle = x_B(1-x_B)[1-(m+1)x_B] \tag{2c}$$

Figure 5b demonstrates the concentration dependence of concentration fluctuations calculated from Eq. 2 for $l=50$ and $m=4$. The calculated concentration fluctuations coincide well with the observed ones in the following ways: (1) The calculated concentration fluctuation is small and close to that expected for the ideal solution for $0<x_B<0.02$, and (2) it has a minimum at near $x_{BE}=0.02$ and 0.2 where the slope of observed ones change abruptly, and (3) it reaches a maximum in the concentration rage of $0.02<x_B<0.2$.

However, the observed concentration fluctuation is much greater than the calculated one by an order of magnitude, as is noticed from the ordinate of Fig. 4 and Fig. 5b. In order to overcome this, we have to modify the model in the following manner. In the concentration range of $0.02<x_B<0.2$, the local structures of types A_lB and A_mB gather together and form $g(A_lB)$ and $h(A_mB)$, respectively. In this case the concentration fluctuation is given by the following equation:

$$N\langle(\Delta x_B)^2\rangle=(l-m)^{-1}[(l+1)x_B-1][1-(m+1)x_B] \times\{g[(l+1)x_B-1]+h[1-(m+1)x_B]\} \tag{2b'}$$

The concentration fluctuations increase with both g and h, but these two can not be determined independently.

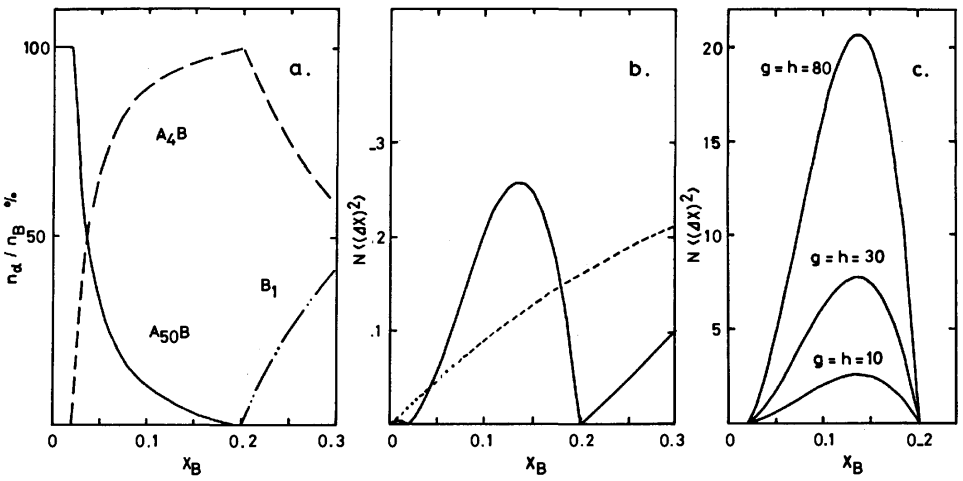

Fig. 5. (a) Distribution of B molecules among several local structures α; $A_{50}B$, A_4B, and B_1. In the figure n_B means the total number of B molecule and n_α means the number of α species. All the B molecules are in $A_{50}B$ for $0<x_{BE}<0.02$, in $A_{50}B$ and A_4B for $0.02<x_{BE}<0.2$, and in A_4B and B_1 for $0.2<x_{BE}<0.3$. (b) The theoretical value of concentration fluctuation calculated from Eq. 2. (c) The theoretical value calculated from Eq. 2b′ in the concentration range $0.02<x_{BE}<0.2$ for $g=h=10$, 30, and 80.

By arbitrarily assuming $g=h$, the calculated concentration fluctuations are shown in Fig. 5c. The maximum values of observed ones at 21 and 42 °C are close to calculated ones when $g=h$ are about ten and one hundred, respectively. Also it takes maximum at about $x_B=0.1$ in both the observed and calculated ones.

While the calculated concentration fluctuation become zero at $x_B=0.02$ and 0.2, the observed one does not. In the above model, all the local structure is assumed to be $A_{50}B$ and A_4B at 0.02 and 0.2, respectively. This is improved by taking the following association equilibrium Eq. 3 into consideration. Although the association of A_{50} may proceed stepwise in real solution, Eq. 3 is assumed since this is the simplest form in order to examine the contribution of the equilibrium. If more equilibrium were taken into account, the calculation should be tedious and meaningless for the understanding of the mixing state of binary solution.

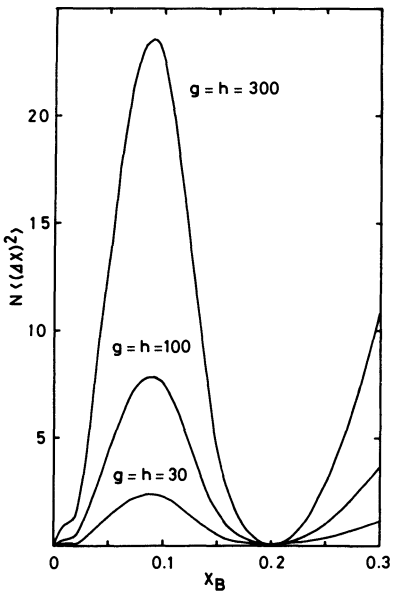

Fig. 6. Theoretical value of concentration fluctuation calculated by equillibrium of Eq. 3 for $g=h=30$, 100, 300, $K_1=10^3$, $K_2=10$, and $K_3=1$.

$$A_{50} + B \rightleftharpoons K_1 \rightleftharpoons A_{50}B \longrightarrow g(A_{50}B) \quad (3a)$$

$$A_4 + B \rightleftharpoons K_2 \rightleftharpoons A_4B \longrightarrow h(A_4B) \quad (3b)$$

$$4A_{50} \rightleftharpoons K_3 \rightleftharpoons 50A_4 \quad (3c)$$

Figure 6 shows the concentration dependence of concentration fluctuation numerically calculated assuming the above equilibrium for $K_1=10^3$, $K_2=10$, $K_3=1$, and various $g=h$. The calculated concentration fluctuations correspond more closely with the observed ones. Figure 7 shows the aggregation schematically. In principle it is possible to search for the best set of parameters (K_1, K_2, K_3, l, m, g, h) that gives the best fit to the observed concentration fluctuation. This was not attempted because none of them can be determined uniquely.

From the analysis of concentration fluctuation given above the following conclusions are obtained. (1) For $0<x_{BE}<0.02$ local structures of types $A_{50}B$ and A_{50} are formed. (2) For $0.02<x_{BE}<0.2$ local structures of types $g(A_{50}B)$ and $h(A_4B)$ exist simultaneously. The values of g and h depend on temperature, and vary between ten and several hundreds. (3) For $0.2<x_{BE}$ the local structures of types $h'(A_4B)$ and B_1 are formed, where the value of h' is independent of temperature. The conclusions are consistent with the Raman Spectra described in the following section.

Raman Spectra. Raman spectra of aqueous BE solution at various concentrations were obtained in order to ascertain whether a conformational change of BE occurs through the formation of clathrate hydrate-like structure. Shimanouchi *et al.* studied the Raman and IR spectra of many long chain ethers and have reached the following conclusions.[10] (1) Various rotational isomers due to many internal rotation axes exist in the liquid state. (2) The spectra of the various isomers are different, especially in the 200—600 cm^{-1} region of the skeletal deformation and torsional vibration modes and in the 800—1200 cm^{-1} region of the skeletal stretching and methyl and methylene rocking vibrations. Since the conformation of BE molecule is supposed to alter when it is within a clathrate hydrate structure, the change of the Raman spectra in these two regions are expected. Since water has a strong and broad Raman signal in the low frequency region, however, only the high frequency region gave positive results.

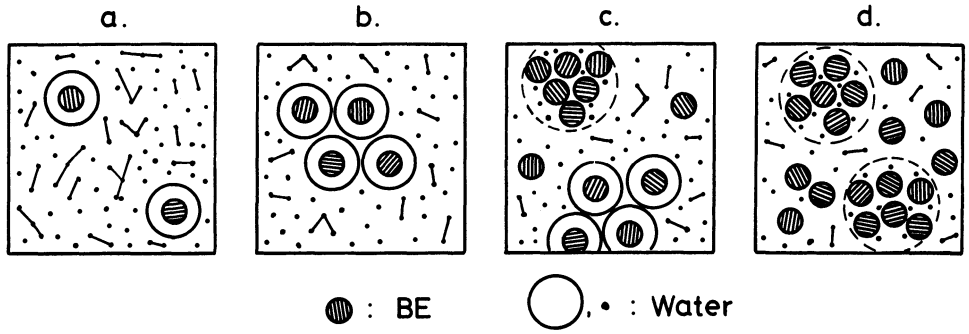

Fig. 7. Mixing state of BE–water mixtures drawn schematically. (a); for $0.02>x_{BE}$, (b); for $0.02<x_{BE}<0.05$, (c); for $0.05<x_{BE}0.2$, and (d); for $0.2<x_{BE}$. (○, ●) and ◍ correspond to the water molecule and the BE molecule, respectively. ◎ and ❁ mean clathrate hydrate-like structure $g(A_{50}B)$ and aggregate $h(A_4B)$, respectively.

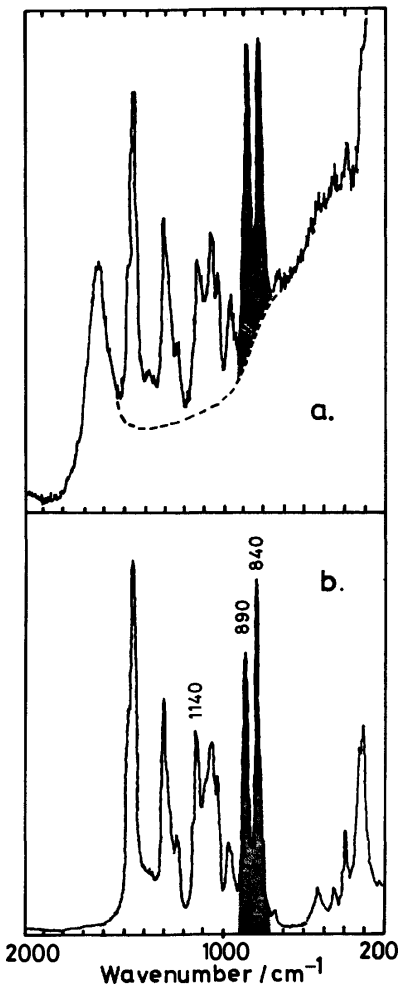

Fig. 8. Observed Raman spectra of aqueous BE solution of x_{BE}=0.009 (a) and neat liquid of BE (b) in the 200—2000 cm^{-1} region. Dashed line in (a) is the scattering from solvent water.

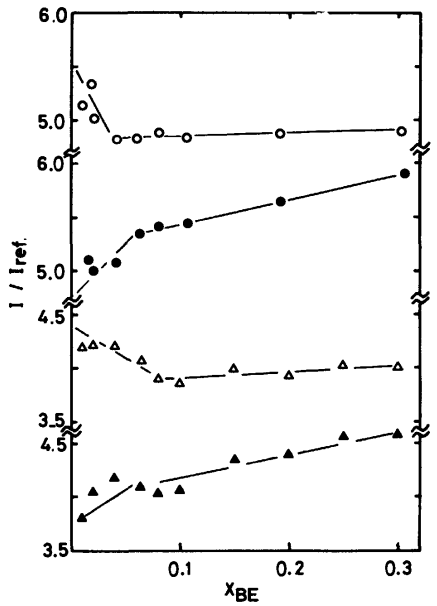

Fig. 9. Intensities of 840 and 890 cm^{-1} peaks relative to the intensity of 970 cm^{-1} peak in the Raman spectra of BE as functions of the concentration in aqueous solution at 21 °C. ●; $I(\approx840)/I(\approx970)$, ○;$(\approx890)/I(\approx970)$. For BE–deuterium oxide mixture, ▲; $I(840)/I(\approx970)$, △; $I(\approx890)/I(\approx970)$.

In Fig. 8 the Raman spectra of neat liquid and aqueous (x_{BE}=0.009) solution of BE are shown. From the comparison of Fig. 8a and b, it is evident that the peak intensities of bands at 840, 890, and 1140 cm^{-1} change with the concentration of BE. Out of the above three bands the one at 1140 cm^{-1} shifts in the BE–deuterium oxide solution, and is due to alcoholic OH groups. By comparison with Shimanouchi *et al.*'s results, the other two can be assigned to C–O stretching vibrations of ether bond. Since the bandwidths scarcely alter with concentration, peak heights can be taken as intensities if background from the solvent is properly subtracted. Figure 9 shows the intensity ratios of the 840 and 890 cm^{-1} bands to the 970 cm^{-1} band as a function of concentration.[11] As is seen from the dotted line in Fig. 8, a broad Raman signal from the solvent water overlaps the BE Raman signal and may lead to error. Since the use of deuterium oxide reduces the overlap, the data with deuterium oxide are also obtained and shown in Fig. 9. Both water and deuterium oxide give similar results. It can be seen from Fig. 9 that the intensity of 840 cm^{-1} band decreases and that of 890 cm^{-1} band increases with concentration. However, the changes are not monotonic but rather there are bends around x_{BE}=0.05, where the change in concentration fluctuation is the largest.

These observations as well as the results of Shimanouchi *et al.* lead to the following conclusions; a clathrate hydrate-like structure is formed at low concentration and the BE molecule changes its conformation when freed from clathrate above x_{BE}=0.05. At higher concentration where x_{BE}>0.05, the conformation of BE molecules is the same as that in neat liquid. The BE molecule in clathrate must prefer a compact form to an elongated one, and must assume the gauche form around some internal rotation axes. In order to make this conclusion clearer, a normal coordinate calculation was carried out with general force constants given by Shimanouchi *et al.*[12] Unfortunately the force constants for the alcohol were not available, so the calculation was done for butyl ethyl ether. The Raman spectrum of this molecule is similar to that of BE, reflecting that the skeleton of these two are the same.

Since butyl ether has four internal rotation axes, there are thirty four rotational isomers. Shimanouchi *et al.* have reported that ethyl propyl ether (CH_3CH_2–CH_2–O–CH_2CH_3) assumes the forms of GTT and TTT, and butyl methyl ether (CH_3CH_2–CH_2–CH_2–OCH_3) takes the forms of TTT and TGT in the liquid state.[13] That is, the trans conformation about CO–CC axis is much more stable than the gauche, but gauche conformation is also as stable as the trans about C–C axis. From these results the forms of TTTT, TGTT, GGTT, and GTTT are most likely for butyl ethyl ether (CH_3CH_2–CH_2–CH_2–O–CH_2CH_3) in the liquid state. As mentioned above, the COC symmetric vibration dominates in the 800—1000 cm^{-1} region of the Raman

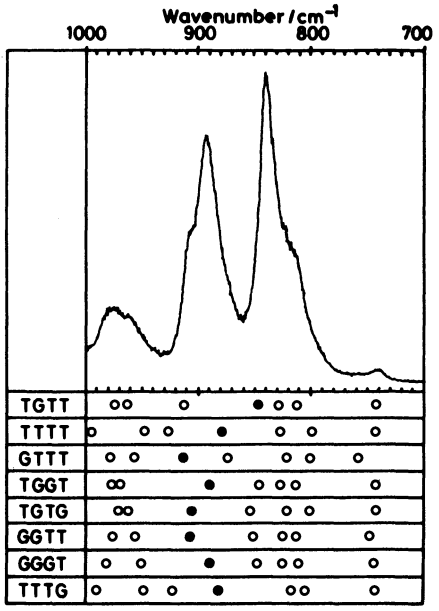

Fig. 10. Observed Raman spectra of BE and the calculated frequencies of butyl ethyl ether in the 700—1000 cm^{-1} region. Solid circles indicate C–O stretching vibrations, which are expected to dominate in this region.

spectrum of ethers,[14] and the bands at 840 and 890 cm^{-1} in Fig. 9 are assigned to this vibration of several rotational isomers. Calculations show that only TGTT has COC stretching frequency smaller than 850 cm^{-1}, and frequencies of other conformers all fall between 880 and 910 cm^{-1}, as is shown in Fig. 10. Since the intensity of 840 cm^{-1} vibration is higher than that of 890 cm^{-1}, the major form of BE is TGTT in the neat liquid. In higher concentrations of water, the intensity of 890 cm^{-1} band increases and that of the 840 cm^{-1} band decreases. This means that proportion of TGTT gets smaller with dilution and conformers such as GTTT and GGTT increase in number. By the formation of clathrate hydrate-like structure, BE is surrounded by water. Since the gauche conformation about CO–CC axis is more advantageous for the ether –O– in contact with water molecule, the conformers such as TGGT and TGTG must also increase. Nevertheless the frequency differences are too small to distinguish those rotational isomers.

Discussion

In the previous papers,[2] it was shown that in a binary solution of TBA and water the local structures of types $g[(H_2O)_{20}TBA]$ and $(H_2O)_{20}$ are formed for $0<x_{TBA}<0.04$ and local structures of types $g[(H_2O)_{20}TBA]$ and $(TBA)_s$ are formed for $0.04<x_{TBA}$. The local structure of $g[(H_2O)_{20}TBA]$ has been postulated to be a clathrate hydrate-like structure. From the analysis of mutual diffusion coefficients the clathrate hydrate-like structure has been considered to be an "aggregated polyhedron" (that is, one in which the polyhedra gather together to form an aggregate without sharing faces with each other), not an "associated polyhedron" (that is, one in which water molecules form polyhedra, each of which encages a guest molecule and that the several polyhedra share one of their faces).

In the binary solution of BE and water, the local structure of type $g[(H_2O)_{50}BE]$ is also considered to be "aggregated polyhedron." Below the concentration $x_{BE}=0.05$ more BE molecules whose conformation is close to spherical one are expected to exist from the analysis of Raman spectra. The conformation change of BE must be due to the formation of polyhedra of water molecules. The difference in size between the polyhedra formed in TBA–water and those in the BE–water mixture arises from the difference in bulk of the hydrophobic group of the two molecules. Above the concentration $x_{BE}=0.05$, the local structure of type $g[(H_2O)_{50}BE]$ is destroyed and the amount of local structures of type $h[(H_2O)_4BE]$ increases due to the increase of BE molecules, as shown in Fig. 8a, where the distribution of two types of local structures is expressed as $A_{50}B$ and A_4B, respectively. Formation of the local structure of type $h[(H_2O)_4BE]$ is reminiscent of micelles in an aqueous solution of surfactants. BE molecule is a member of polyethylene glycol monoalkyl ether $C_nH_{2n+1}O(CH_2CH_2O)_mH$ family where $n=4$ and $m=1$. Micelle formation is known in this class of molecules where $n\geqq 8$ in the case of $m=1$. The critical micelle concentration (CMC) for $n=8$ and $m=1$ is 4.9 mmol/l (that is, about 1×10^{-4} in the mole fraction of solute) which is about five hundred times lower than the concentration at which BE takes the form $h[(H_2O)_4BE]$. Since BE has a relatively strong affinity for water, the hydrophobic interaction between BE molecules is weaker than that between its longer chain homologs. It does not have distinct CMC.

The phase transition is understood from the idea of the local structure in the following manner. The increase of concentration fluctuation with temperature is caused by the increase of either g and h of local structures of types $g[(H_2O)_{50}BE]$ and $h[(H_2O)_4BE]$. That is, by raising the temperature the "aggregated polyhedron" and the aggregates of BE molecules gather together and become larger, and finally the solution separates into two phases at critical solution temperature. Therefore the phase separation is the result of the growth of local structures which already exist about thirty degrees below the LCST. In TBA–water mixture the aggregate of TBA does not seem to become large enough with the increase of temperature. This can be attributed to the small size of hydrophobic part of TBA.

The existence of local structure has been postulated by a thermodynamic study of G. Roux, G. Perron, and J. E. Desnoyers. They have reported the apparent molal heat capacity ϕ_c and volume ϕ_v.[9] They indicate that the change in mixing states occurs near the concentration $x_{BE}=0.02$ where ϕ_c has maximum, and the microphase which is constructed from aggregate of BE is made beyond the concentration. They have also pointed out that the clathrate hydrate-like structures may be formed in the concentration region where ϕ_c has a maximum. The present results support their explanation from another viewpoint.

Concluding Remark. The phase separation phe-

nomenon has been treated as one of the critical phenomena which occur at near critical solution temperature. The present results indicate that the phase separation occurs in microscopic regions even thirty degrees below the critical solution temperature. It is well-known that there is an LCST in many nonelectrolyte aqueous solutions. The formation of local structures with clathrate hydrate-like structure and the aggregates of solutes will be common in those systems and essential factors for phase separation.

The authors wish to express their thanks to Dr. Yoko Sugawara of the Institute for Physical and Chemical Research for her help in the normal coordinate calculation with a computer program LCTB. We also would like to thank Prof. J. E. Desnoyers of Univ. de Sherbrooke for suggesting to us this interesting system, Prof. Hidemasa Takaya of IMS for his helpful advices for preparing high quality BE, and Prof. P. G. Wolynes of Univ. of Illinois for a critical reading of manuscript.

References

1) D. W. Davidson, "Water," ed by F. Franks, Plenum Press, New York-London (1973), Vol. 2, Chap. 3.

2) K. Iwasaki and T. Fujiyama, *J. Phys. Chem.*, **83**, 463 (1979); **81**, 1908 (1977).

3) N. Ito, T. Kato, and T. Fujiyama, *Bull. Chem. Soc. Jpn.*, **54**, 2573 (1981).

4) N. Ito, K. Saito, and T. Fujiyama, *Bull. Chem. Soc. Jpn.*, **54**, 991 (1981).

5) T. Kato, M. Yudasaka, and T. Fujiyama, *Bull. Chem. Soc. Jpn.*, **54**, 1632 (1981).

6) H. L. Cox and L. H. Cretcher, *J. Am. Chem. Soc.*, **48**, 451 (1926).

7) G. Poppe, *Bull. Soc. Chim. Belg.*, **44**, 640 (1935).

8) K. Iwasaki, Y. Katayanagi, and T. Fujiyama, *Bull. Chem. Soc. Jpn.*, **49**, 2988 (1976): T. Kato, and T. Fujiyama, *J. Phys. Chem.*, **80**, 2771 (1976).

9) G. Roux, G. Perron, and J. E. Desnoyers, *J. Solution Chem.*, **7**, 639 (1978).

10) T. Shimanouchi, Y. Ogawa, M. Ohta, H. Matsuura, and I. Harada, *Bull. Chem. Soc. Jpn.*, **49**, 2999 (1976).

11) It is seen from Raman spectra that the peak intensity of 970 cm^{-1} scarcely change with the concentration. By the calculation, this band is assinged as CH_2 rocking vibration.

12) T. Shimanouchi, H. Matsuura, Y. Ogawa, and I. Harada, *J. Phys. Chem. Ref. Data*, **7**, 1323 (1978).

13) The generic symbols T and G which represent the conformation of rotational isomers is described in Ref. 10.

14) F. R. Dollish, W. G. Fateley, and F. F. Bentley, "Characteristic Raman Frequencies of Organic Compounds," John Wiley and Sons, Inc., New York (1974), Chap. 3. It has been known that the CCO symmetric vibration of alcohol is also strong in the 800—1000 cm^{-1} region. The intensity of the Raman band of ethanol at 890 cm^{-1}, however, dose not show concentration dependence. Therefore the concentration dependence of 890 cm^{-1} in BE–water mixture is due to the conformational change of butoxy group.

Study of the Behavior of "Uptake and Release" of Oxygen into Perfluorocarbon-Water Emulsions

Kenjiro MEGURO,* Hiroshi WATANABE, Hiromu KATO, Kimihiko OGIHARA, and Kunio ESUMI
Department of Applied Chemistry, Faculty of Science, Science University of Tokyo, Kagurazaka, Shinjuku-ku, Tokyo 162
(Received June 30, 1982)

Stable O/W type emulsions of perfluorocarbon such as perfluorodecalin (FDC) and perfluorotributylamine (FTBA) were prepared by using poly(oxyethylene)-poly(oxypropylene) block copolymer (Pluronic F-68) and sorbitan monolaurate (SL-10) as emulsifiers. The relationships between the behavior of "uptake and release" of oxygen into the emulsions and the factors responsible for a stable emulsion were studied. The initial rates of "uptake and release" of oxygen into the emulsions decreased with increasing the mean particle size, the concentration of emulsifiers, and the viscosities of the emulsions. On the other hand, the saturated amount of oxygen in the emulsions was independent on the mean particle size, but depended on the total amount of the perfluorocarbons in the emulsion.

Perfluorocarbon compounds have a characteristic property of dissolving a relatively large amounts of gases such as oxygen and carbon dioxide.[1,2] This property can be applied to the preparation of an artificial blood. Indeed, many researches on the use of perfluorochemical emulsions in artificial blood have been proceeding.[3-12] To use perfluorochemicals effectively for this purpose, it is necessary to prepare them as stable O/W type emulsion. Such emulsions should exhibit suitable behavior of "uptake and release" of oxygen, but there have been few reports about fundamental studies of these emulsions from the view point of colloid science.

In this work, the relationship between "uptake and release" of oxygen into perfluorocarbon emulsions and the factors associated with stable emulsions will be discussed.

Experimental

Materials. Perfluorocarbon compounds used for preparing an artificial blood substitute must be nontoxic and have the ability to dissolve oxygen. From this standpoint, perfluorodecalin (FDC) and perfluorobutylamine (FTBA) were employed. They were supplied by Dainippon Ink Chemical Co., Ltd.

For the preparation of O/W type emulsion of these compounds, poly(oxyethylene)-poly(oxypropylene) block copolymer (Pluronic F-68) and sorbitan monolaurate (SL-10) were used as emulsifiers. They were supplied by Nikko Chemical Co.

Emulsification. For the preparation of the emulsion in a small scale, a homogenizer was used. While in a large scale, FDC and FTBA were preemulsified by use of the homogenizer for several minutes, followed by passing through a Manton Gaulin Homogenizer under about 500 kg/cm^2.

Measurements. The particle size distribution of the emulsion was determined by using a centrifugal particle size analyzer (Shimadzu Seisakusho Ltd.). The viscosity of the emulsion was measured by using a corn plate type rotation viscometer (Tokyo Keiki Co., Ltd.). The amount of oxygen dissolved in the emulsion was measured by an oxygen meter (Central Kagaku Co., Ltd.) at 25±0.1 °C. The procedure was as follows; after setting 100 ml of the emulsion into a beaker, nitrogen gas was blown into it to displace the oxygen initially dissolved in the emulsion. Oxygen was then blown into this emulsion until saturation was achieved. This process is named "uptake" of oxygen. Next, the oxygen was replaced with nitrogen, which process is called "release" of oxygen. These processes are shown in Fig. 1. Here, the concentration of oxygen in the emulsion is estimated by subtracting the concentration of oxygen in water phase from that in the total system.

Results and Discussion

For the application of a perfluorochemical emulsion to an artificial blood, the emulsion must have fine particles and exhibit a high stability for a long period. Thus, it is necessary to prepare a stable emulsion of perfluorocarbon compound. Since it is important to select suitable emulsifiers for the preparation of stable emulsions of FDC and FTBA, the emulsification tests were carried out by using several different emulsifiers. As a result, it was found that the combination of Pluronic F-68 and SL-10 provided relatively stable emulsions for both FDC and FTBA. Accordingly, these two emulsifiers were used for preparing the emulsions in this experiment.

In order to estimate optimum conditions for emulsifying FDC and FTBA, the emulsification stability tests were conducted using various ratios of Pluronic F-68 and SL-10. Figure 2 shows the photographs of emulsions of FDC with different HLB values. From Fig. 2, it can be seen that the required HLB value of FDC is located at 9.5. Also, Figure 3 illustrates the photographs of emulsions prepared with different concentra-

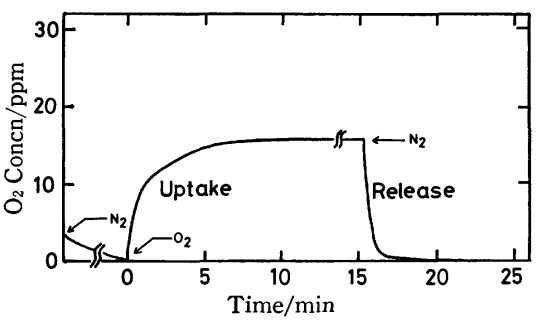

Fig. 1. The processes of "uptake and release" of oxygen into emulsion.

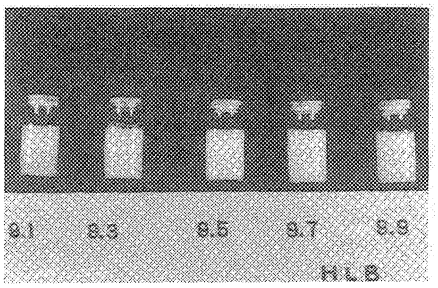

Fig. 2. Photographs of FDC emulsions with different HLB values.

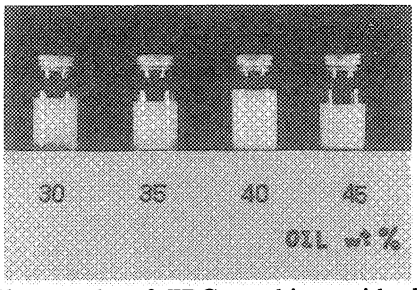

Fig. 3. Photographs of FDC emulsions with different concentration of FDC.

tion of FDC. The emulsion became stable when the concentration of FDC was above 40 wt%. Further, it was found that the stable emulsion was obtained when the concentration of the emulsifiers was above 30 wt% of FDC concentration. In the case of FTBA, similar results were obtained. That is, the required HLB value of FTBA was found to be 10.3 and the stable FTBA emulsion was prepared at the conditions which the concentration of FTBA was above 40 wt% and the concentration of the emulsifiers was above 30 wt% of FTBA concentration. The mean particle size of FDC and FTBA emulsions prepared in the above conditions was below 0.2 μm and further the separation of FDC and FTBA from the continuous phase was not observed for period exceeding 60 d, respectively.

The relationships between the rates of "uptake and release" of oxygen into the emulsion and the factors which affect the emulsion stability of FDC and FTBA were examined. At first, in order to study the effect of particle size distributions of the emulsions, three kinds of FDC and FTBA emulsions with different particle size distributions were prepared. The rates of "uptake and release" of oxygen into these emulsions were measured. The proportions in weight of the emulsion particles below 0.2 μm were 96.5% in A, 58.7% in B, and 17.5% in C, respectively. The results are shown in Table 1. In the process of "uptake and release" of oxygen, the concentration of oxygen in the emulsion was changed most rapidly in A, but most slowly in C for FDC and ETBA. These results can be correlated with the interfacial area between the emulsion particles and the continuous phase. That is, the initial rates of "uptake and release" of oxygen decreased with decreasing interfacial area. Furthermore, it is noteworty

Table 1. The initial rates of "uptake and release" of oxygen into the fluorocarbon emulsions

Sample	Initial rate of uptake/ppm min^{-1}	Initial rate of release/ppm min^{-1}
FDC-A	12.4	6.8
FDC-B	4.4	1.8
FDC-C	2.4	0.9
FTBA-A	8.0	6.9
FTBA-B	4.4	4.9
FTBA-C	—	—
FDC-10%	10.8	8.9
FDC-20%	3.0	4.9
FDC-30%	0.4	1.7
FDC-0 d	18.4	8.9
FDC-30 d	1.0	4.9

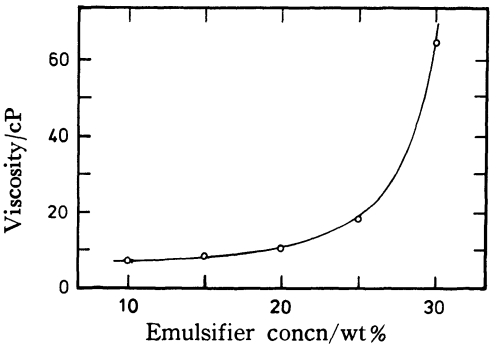

Fig. 4. The changes of the viscosity of FDC emulsion against the concentration of emulsifier.

that the saturated amounts of oxygen in the emulsions were constant for three samples in spite of different mean particle sizes. This indicates that the amount of oxygen dissolved in the emulsion is dependent on the total amount of perfluorocarbon, but is independent on the interfacial properties between perfluorocarbon and the continuous phase.

Figure 4 depicts how the concentrations of the emulsifiers affect the viscosity of FDC emulsions. The viscosity of the emulsion increased with increasing concentration of the emulsifiers, rapidly at above 30 wt% of them. As a next step, the effect of the viscosity of the emulsions on the rates of "uptake and release" of oxygen into them was studied. This result is given in Table 1. The concentrations of the emulsifier against FDC were 10, 20, and 30 wt%, respectively. In this case, from the measurement of particle size distribution, it was confirmed that the mean particle sizes of the three emulsions were almost the same. When the concentration of the emulsifier was 10 wt%, the concentration of oxygen dissolved in the emulsion was changed most rapidly, while at 30 wt%, it was changed most slowly. Thus, the initial rates of "uptake and release" of oxygen decreased with increasing the concentration of the emulsifier from 10 to 30 wt%. This suggests that the interfacial film of the emulsion particles would become thicker on increasing the concentration of the emulsifier.

Further, the relationship between the aging of the emulsions and the rates of "uptake and release" of

oxygen into them was studied. In this study, two FDC emulsions were used. One was the emulsion freshly prepared, and the other was that aged for 30 d. The initial rates of the two emulsion are given in Table 1. The increases of the mean particle size and the viscosity were observed for the emulsion aged for 30 d compared with that freshly prepared. In addition, the initial rate of "uptake and release" of oxygen for the emulsion aged for 30 d was slower than that freshly prepared.

The results obtained in this study are summarized as follows:

(1) The initial rate of "uptake and release" of oxygen into the emulsion decreased with increasing the mean particle size of the emulsion.

(2) The saturated amount of oxygen in the emusion was independent of the mean particle size of the emulsion, but was dependent on the total amount of fluorocarbon in the emulsion.

(3) The initial rate of "uptake and release" of oxygen into the emulsion decreased with increasing the concentration of the emulsifiers and the viscosity of the emulsion.

We thank Dr. S. Yoshikawa and Mr. N. Yanagi for their suggestion and assistance in this work.

References

1) K. Yokoyama, *Hyomen*, **15**, 147 (1977).
2) J. W. Sargent and R. J. Seffl, *Fed. Proc.*, **29**, 1699 (1970).
3) Y. Kobatake and J. H. Hildebrand, *J. Phys. Chem.*, **65**, 331 (1961).
4) H. Ohyanagi and T. Mitsuno, *Igaku No Ayumi*, **93**, 569 (1975).
5) J. O. Osburn, *Fed. Proc.*, **29**, 1704 (1970).
6) D. D. Dixon and D. G. Holland, *Fed. Proc.*, **34**, 1444 (1975).
7) T. Mitsuno and H. Ohyanagi, *Kagaku Kogyo*, **26**, 181 (1975).
8) H. A. Sloviter and T. Kamimito, *Nature*, **216**, 458 (1967).
9) L. C. Clark and F. Gollan, *Science*, **152**, 1755 (1966).
10) R. P. Geyer, *Fed. Proc.*, **32**, 927 (1973).
11) T. H. Maugh, *Science*, **179**, 669 (1973).
12) K. Yokoyama, A. Suzuki, I. Utsumi, and R. Naito, *Chem. Pharm. Bull.*, **22**, 2966 (1974).

 © 1983 The Chemical Society of Japan Bull. Chem. Soc. Jpn., 56, 389—391 (1983)

Laser Flash Photolysis of Benzene. VI.[1] Photolysis in Aqueous Solution

Nobuo SHIMO,† Nobuaki NAKASHIMA, and Keitaro YOSHIHARA*
Institute for Molecular Science, Myodaiji, Okazaki 444
(Received July 21, 1982)

Three transient absorption spectra in aqueous solution were observed by irradiation of benzene with an excimer laser (KrF, 248 nm or ArF, 193 nm). A short-lived absorption with a peak at 275 nm is assigned to the $S_n \leftarrow S_1$ absorption. A long-lived absorption, which appears as a clear shoulder at 230 nm, stays longer than 500 ns and is not shortened by oxygen. This species is tentatively assigned to benzvalene, and the quantum yield is determined to be *ca.* 0.1. Solvated electron with a peak at 720 nm was formed *via* multiphoton processes at a power level of 60 mJ/cm² of an ArF laser. The $T_n \leftarrow T_1$ absorption was lower than our detection limit ($\Phi_T < 0.1$).

Nanosecond laser photolysis has been successfully applied to benzene in cyclohexane and in the gas phase, and $S_n \leftarrow S_1$ absorptions, a $T_n \leftarrow T_1$ absorption, a vibrationally highly excited state, and mist formation were observed.[2-5] The first three observations brought detailed information on the properties of excited states and the last observations gave an interesting phenomenon of multiphoton photochemistry in the gas phase. Phenol was observed at quantum yield of 0.01 in the presence of O_2. Most recently we observed with gaseous benzene that the major deactivation process at 248 nm excitation was formation of highly excited vibrational states in the ground electronic manifold.[1] In order to investigate photochemistry of benzene in solution, we chose aqueous solution in this report because of the following reasons.

(1) The photochemistry of benzene in aqueous solution was investigated by Kaplan[6] and Stein[7,8] with steady-state irradiation and the conventional flash photolysis technique in the microsecond timescale. They reported that excitation of benzene to the $^1B_{2u}$ or $^1B_{1u}$ state in aerated aqueous solution gave the final photoproduct **1**. Benzvalene has been postulated as an intermediate, which reacts with H_2O or O_2 to produce **1**. The quantum yield of total process is 0.07[6] or 0.18.[7] (Eqs. 1 and 2)

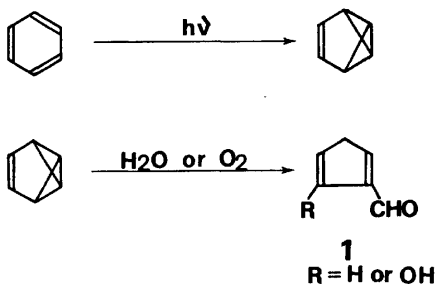

(1)

(2)

(2) Since the quantum yields of fluorescence and triplet formation are only 0.006[7] and 0.07,[9] respectively, the major process (0.75) is unknown in aqueous solution. Thus photochemical reaction leading to benzvalene as an unstable photoproduct is expected to occur. Internal conversion to the ground state must also be an important process. (3) Because of the low yield of triplet formation, some transient species other than the triplet benzene could be observed in aqueous solution. It is essential to confirm Eq. 1 and to know the nature of the unknown processes.[10]

† On leave from Idemitsu Kosan Co., Ltd., Central Research Laboratory, Kamiizumi, Sodegaura, Kimitsu, Chiba 292-01.

Experimental

Benzene in aerated aqueous solution (10^{-3} M, 1 M = 1 mol dm^{-3}) in a $1 \times 1 \times 2.5$ cm³ quartz cell was excited by an excimer laser (KrF, 248 nm or ArF, 193 nm). The laser beam was not focused and had a cross section of 2.5×0.2 cm². The details of the flash photolysis apparatus have been described elsewhere.[2,3] Sample was renewed at every laser excitation because of an efficient formation of photoproducts. The absorbance of each wavelength at each laser shot was normalized at 230 nm by dual beam observation, one at 230 nm and the other at different wavelengths. Benzene (Merck, 99.9%), acetonitrile (Merck, Uvasol), methyl alcohol (Katayama Chemical, absorption spectrum grade), and oxygen (Nippon Sanso) were used without further purification. Water was distilled and passed through ion exchange resin (Toyo Aquarius GS-100T).

Results and Discussion

Figures 1 and 2 show three transient absorption spectra (A,B,C) of benzene in aqueous solution. The spectra of components A and C are taken immediately after excitation and the spectrum of component B is taken

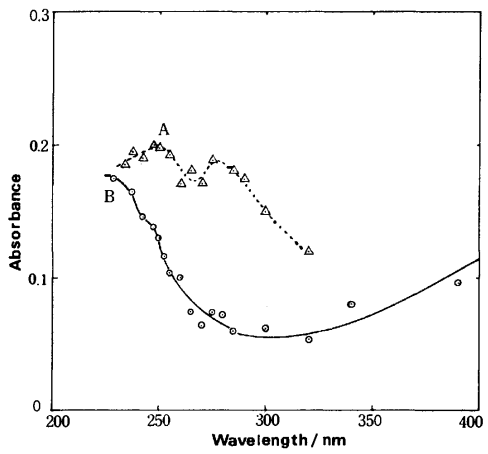

Fig. 1. Transient absorption spectra of benzene in aqueous solution by excitation at 193 nm (ArF). The spectrum A is taken immediately after excitation and the spectrum B is taken at 100 ns after excitation. Absorbance is normalized at 230 nm.

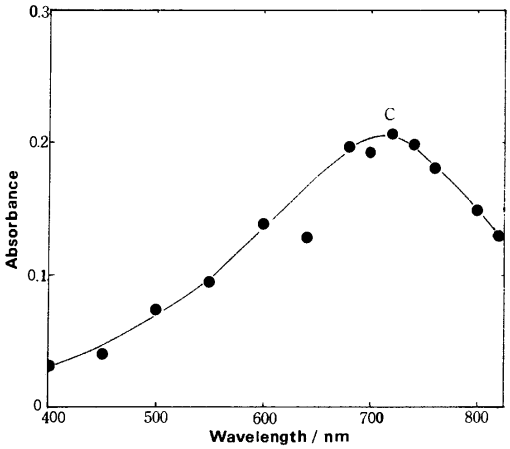

Fig. 2. Transient absorption spectrum of benzene in aqueous solution by excitation at 248 nm (KrF). The spectrum is taken immediately after excitation. Absorbance is normalized at 230 nm.

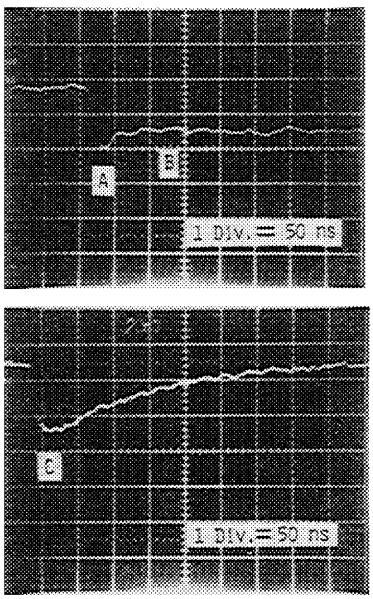

Fig. 3. Photolysis of benzene in water by excimer laser. (1) Excitation by ArF laser (193 nm), monitoring at 260 nm. (2) Excitation by KrF laser (248 nm), monitoring at 800 nm. The spectra of A (Fig. 1) and C (Fig. 2) are taken immediately after excitation, and the spectrum of B (Fig 1) is taken at 100 ns after laser excitation.

at 100 ns after laser excitation (Fig. 3). The spectra obtained by excitation at 248 nm (KrF) and at 193 nm (ArF) are similar to each other.

The broad absorption spectrum (C), between 400 nm and 850 nm, has a maximum absorbance at 720 nm. Both absorption peak position and the long-tailing character of the spectrum are in good agreement with that of solvated electron in water (hydrated electron).[11] The lifetime ($\approx$150 ns) of this transient absorption is reasonably explained by quenching of solvated electron by oxygen (Eq. 3).[12]

$$e^-_{aq} + O_2 \longrightarrow O_2^- \qquad (3)$$

In acetonitrile, methyl alcohol, or cyclohexane solutions, no absorption corresponding to the spectrum C is observed in the present power level. Because the laser power dependence of the formation of C is not linear even with 193 nm (6.4 eV) excitation, solvated electron is formed *via* ionization of benzene by multiphoton process. Integrated concentration of excited species is 4.2×10^{-4} M at a laser power of 60 mJ, while the concentration of solvated electron is estimated to be 1.5×10^{-5} M. About 7% of absorbed laser energy was utilized for formation of solvated electron. It should be noted that solvated electron is rather efficiently formed only in aqueous solution among the solvents we used.

The other transient absorptions, A and B, are obtained between 220 nm and 350 nm. The spectrum of component A, with a peak at 275 nm, is quite similar to that of the $S_n \leftarrow S_1$ absorption observed previously.[4] This component decays just after excitation and is not quenched by oxygen, because the fluorescence lifetime in water is too short (2 ns) to interact with oxygen.[13] These observations indicate that this spectrum is due to the $S_n \leftarrow S_1$ absorption. The absorbance at the 248 nm excitation is stronger than at the 193 nm excitation to some extent. This is reasonable because the fluorescence quantum yield decreases by excitation to the S_2 and/or S_3 electronic states.[8]

The component B, with a clear shoulder at 230 nm has a slightly weaker absorbance than the $S_n \leftarrow S_1$ absorption. This component does not decay during the period of observation ($\approx$500 ns) and is not quenched by oxygen saturated in water. These observations indicate that the absorption is not due to the $T_n \leftarrow T_1$ absorption. The latter should have an absorption peak at 235 nm and should be quenched by oxygen with a bimolecular rate constant of $\approx 6 \times 10^9$ M^{-1} s^{-1}.[2] The saturated concentration of oxygen in water is 0.3×10^{-3} M.[12] Thus, if the absorption were due to the triplet state, it should have decayed with a lifetime of $\approx$600 ns. It is reasonable that no $T_n \leftarrow T_1$ absorption is observed in our experiment, because the quantum yield of triplet formation is known to be only 0.07.[10]

The component B has a linear dependence on laser power at the 248 nm excitation, while the solvated electron is produced with a hyper-linear dependence. The situation is almost the same at the 193 nm excitation. The component B is suggested to be formed by one photon process. The absorption spectrum of benzvalene shows a shoulder at 230 nm in isohexane.[14] The component B has a similar absorption spectrum to benzvalene. Thus, we tentatively assign this transient to benzvalene.

If the component B is benzvalene, the quantum yield is estimated to be about 0.1 by calculating the concentration of excited species and the extinction coefficient of benzvalene. This value is close to the previous data.[6,7] The spectral shape, dynamic behavior, and other discussions on component B suggest that benzvalene is formed as an intermediate of product **1** in Eq. 2. We irradiated aqueous benzene solution with a KrF excimer laser and actually confirmed the final product **1** by UV absorption spectroscopy.

Judging from production of solvated electron, benzene

cation or dimer cation must also be formed. However we were unable to observe these species, which should appear at ≈550 nm or ≈900 nm. Benzene cation is known to react efficiently with water,[8,15] thus the transient concentration must be very low. The absorption of the product from benzene cation also seems to be too weak to be observed. It is less than our detection limit. Very recently Irion *et al.* photolized an aqueous benzene solution by excimer lasers. Phenol was observed with low quantum yield of 10^{-3} *via* multiphoton absorption.[16]

Photolysis of benzene in cyclohexane solution gave ring opening products, trienes.[2] As these compounds are postulated to be formed *via* triplet state,[2] it is reasonable that the absorption spectra of the ring opening products are not observed in aqueous solution because of low triplet yield.

In aqueous solution, high yield of solvated electron is observed, but in cyclohexane the yield of electron transfer process seems to be very small. We were not able to observe the dimer cation.

The quantum yield of processes other than fluorescence and triplet formation in aqueous solution is known to be about 0.92. In our present investigation with laser photolysis, we observed formation of a photoproduct, which is most likely to be benzvalene, with a quantum yield of *ca.* 0.1. We do not observe the high yield of other photoproducts or transients. The major process is suggested to be a nonradiative transition to the ground state.[1]

References

1) Part V of this series. N. Nakashima and K. Yoshihara, *J. Chem. Phys.*, **77**, 6040 (1982).
2) N. Nakashima, M. Sumitani, I. Ohmine, and K. Yoshihara, *J. Chem. Phys.*, **72**, 2226 (1980).
3) N. Nakashima, H. Inoue, M. Sumitani, and K. Yoshihara, *J. Chem. Phys.*, **73**, 4693 (1980).
4) N. Nakashima, H. Inoue, M. Sumitani, and K. Yoshihara, *J. Chem. Phys.*, **73**, 5976 (1980).
5) N. Nakashima, and K. Yoshihara, *Bull. Chem. Soc. Jpn.*, **55**, 2783 (1982).
6) L. Kaplan, L. A. Wemdling, and K. E. Wilzbach, *J. Am. Chem. Soc.*, **93**, 3819, 3821 (1971).
7) M. Luria and G. Stein, *J. Phys. Chem.*, **76**, 165 (1972).
8) Y. Ilan, M. Luria, and G. Stein, *J. Phys. Chem.*, **80**, 584 (1976).
9) R. B. Cundall, and L. C. Pereira, *Chem. Phys. Lett.*, **18**, 371 (1973).
10) N. Shimo, N. Nakashima, and K. Yoshihara, Proceedings of Symposium on Photochemistry 1981, Sapporo, 135 (1981).
11) E. J. Hart and J. W. Boag, *J. Am. Chem. Soc.*, **84**, 4090 (1962); S. Tagawa, private communication.
12) J. P. Keene, *Nature*, **197**, 47 (1963).
13) M. Luria, M. Ofran, and G. Stein, *J. Phys. Chem.*, **78**, 1904 (1974).
14) I. E. D. Besten L. Kaplan, and K. E. Wilzbach, *J. Am. Chem. Soc.*, **90**, 5868 (1968).
15) M. K. Eberhardt, *J. Am. Chem. Soc.*, **103**, 3876 (1981).
16) M. P. Irion, W. Fuss, and K.-L. Kompa, *Appl. Phys.*, **B27**, 191 (1982).

Molecular Force Fields of *s-trans*-1,3-Butadiene and the Second Stable Conformer

Yukio FURUKAWA,† Hideo TAKEUCHI,† Issei HARADA,† and Mitsuo TASUMI*
Department of Chemistry, Faculty of Science, The University of Tokyo, Bunkyo-ku, Tokyo 113
(Received July 23, 1982)

Normal-coordinate analyses of *s-trans*-1,3-butadiene and its various deuterated and ^{13}C-substituted analogs were performed using the group-coordinate force field, and a set of force constants was determined. The infrared spectra of the second stable conformer of 1,3-butadiene-d_0, -1,1,4,4-d_4, and -d_6 were analyzed on the basis of normal-coordinate calculations of the planar *s-cis* form and a nonplanar *gauche* form. Such an analysis suggests that the second stable conformer takes a *gauche* form rather than the *s-cis*. To increase the number of reliable data to be used in this study, the infrared and Raman spectra of the d_0, 1,1,4,4-d_4, and d_6 species were observed in low-temperature Ar matrices. The infrared spectra of the second stable conformer were also observed using a combination of the high-temperature nozzle and low-temperature matrix techniques.

1,3-Butadiene has been a target molecule of numerous structural, spectroscopic, and theoretical studies. Part of these studies has treated the structure of the most stable *s-trans* form of this molecule[1-5] and the assignments of the vibrational spectra arising from this form.[6-15] On the other hand, various efforts have been made toward the elucidation of the internal-rotation potential and the second stable conformer around the central C–C bond.[16-23] This subject has been studied also by various methods of quantum-chemical calculations.[24-33] Interest in this direction of study has been renewed by the recent observation of the infrared bands associated with the second stable conformer trapped in low-temperature Ar matrices.[34-36] The in-plane vibrational frequencies as well as the in-plane force constants of the *s-trans* and *s-cis* forms were calculated by an *ab initio* method[37] and the normal-coordinate analyses based on the observed data for deuterated and ^{13}C-substituted species were also performed.[36]

The purpose of the present study is twofold. (1) One is to obtain reliable force constants which can be conveniently used (at least as initial values) in the normal-coordinate analyses of longer molecules with conjugated double bonds, for example, isomers of 1,3,5-hexatriene, poly(acetylene), various isomers of retinal and β-carotene, *etc.* Although many authors have already reported various sets of force constants of *s-trans*- and *s-cis*-1,3-butadiene,[13-15,36,37] those force constants do not seem satisfactory for such a purpose. (2) The other is to examine if it is possible to obtain information on the internal-rotation angle of the second stable conformer through the normal-coordinate analyses. Whether the second stable conformer is in the planar *s-cis* form or in the nonplanar (*gauche*) form is a long-standing problem which still remains to be solved.

Reliable experimental data are absolutely necessary for this kind of study. Therefore, we have observed the infrared and Raman spectra of 1,3-butadiene and its 1,1,4,4-d_4 and d_6 analogs in low-temperature Ar matrices. Also, we have observed the infrared spectra of these compounds using a combination of the high-temperature nozzle and the low-temperature Ar matrix techniques, in order to obtain the bands due to the second stable conformer. In this way we have confirmed the results of other authors for the d_0 and d_6-samples[34-36] and have obtained the data for the 1,1,4,4-d_4 analog for the first time.

Method

Infrared and Raman Measurements. Infrared and Raman spectra were observed for 1,3-butadiene-d_0 and two deuterated analogs (1,1,4,4-d_4 and d_6) in low-temperature Ar matrices. The d_0 sample was obtained from Takachiho Kagaku Kogyo Co., Ltd. (purity 99%) and the d_4 and d_6 samples from Merck Sharp and Dohme Canada Ltd. (98 atom% D). No further purification was undertaken.

Infrared spectra were recorded on a Hitachi 260-50 infrared spectrophotometer. Raman spectra were observed on a Raman spectrometer consisting of a Spex 1401 double monochromator, an NEC GLG 3300 Ar-ion laser, an HTV 649 photomultiplier and a home-made photon counter.

The low-temperature apparatus for the low-temperature matrix infrared measurements consisted of a CTI Model 21 Cryocooler and a sample chamber equipped with a CsI plate, KBr windows, and a fine Pyrex nozzle through which the Ar/sample mixture was passed. The temperature of the nozzle could be raised to about 770 K with a surrounding tungsten heater. The temperature of the Ar/sample mixture was monitored with an alumel-chromel thermocouple placed inside the nozzle. For low-temperature Raman measurements an Osaka Oxygen Co. Cryo Mini D equipped with a cold head of silver-coated copper and a sample chamber with quartz windows was used.

TABLE 1. INTERNAL COORDINATES

Symbol	Description
Δr_{ij}	Stretching of the bond linking the atoms i and j
$\Delta\phi_{ijk}$	Bending of the angle between the two bonds r_{ij} and r_{jk}
$\Delta\theta_{i-jkl}$	Out-of-plane bending of the plane formed by the atoms i(apex), j, k, and l.
Δt_{ij}	Torsion around the bond r_{ij}

† Present address: Pharmaceutical Institute, Tohoku University, Aobayama, Sendai 980.

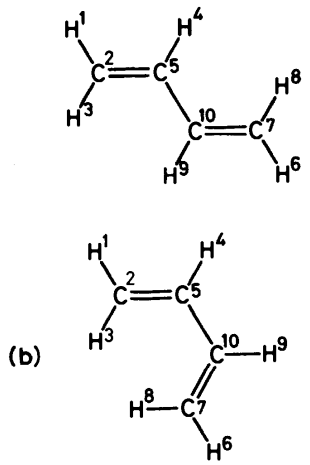

Fig. 1. Numbering of the atoms of (a) *s-trans-* and (b) *s-cis*-1,3-butadiene.

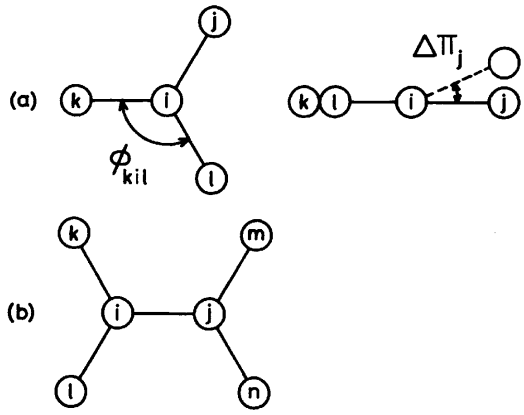

Fig. 2. Numbering of the atoms and the angles relating to the definitions of (a) out-of-plane bending and (b) torsion.

Normal Coordinate Analysis. The normal coordinate analyses of 1,3-butadiene-d_0 and its deuterated and ^{13}C-substituted analogs were performed using the program NCTB[38] on a FACOM M190 computer system at the Laboratory of International Collaboration on Elementary Particle Physics, Faculty of Science, the University of Tokyo.

The structure and numbering of atoms of *s-trans-* and *s-cis*-1,3-butadiene are shown in Fig. 1. The notations for the internal coordinates are given in Table 1. The out-of-plane bending coordinate ($\Delta\theta_{i-jkl}$) and the torsional coordinate (Δt_{ij}) are defined according to the IUPAC recommendations.[39] Therefore, $\Delta\theta_{i-jkl}$ is defined as

$$\Delta\theta_{i-jkl} = \Delta\pi_j \sin\phi_{kil}$$

where $\Delta\pi_j$ and ϕ_{kil} are given in Fig. 2(a). The sign of $\Delta\theta_{i-jkl}$ is defined in such a way that $\Delta\pi_j$ is plus when the atom j moves above the plane defined by the atoms k, i, and l. The torsional coordinate Δt_{ij} is defined as

$$\Delta t_{ij} = (\Delta\tau_{kijm} + \Delta\tau_{kijn} + \Delta\tau_{lijm} + \Delta\tau_{lijn})/4,$$

where $\Delta\tau_{xijy}$ denotes the change in the individual torsional angle between the bonds xi and yj [see Fig. 2(b)].

Group coordinates were defined on the basis of the internal coordinates as given in Table 2. (Previously the group coordinates were called the local-symmetry coordinates.[40])

In the first step of the normal coordinate analysis the

Table 2. Group coordinates[a]

Group coordinate	Mode [Abbreviation]
$S_a^1=(\Delta r_{12}+\Delta r_{23})/\sqrt{2}$	CH_2^1 symmetric stretching [$\nu_s(CH_2^1)$]
$S_a^2=(\Delta r_{67}+\Delta r_{78})/\sqrt{2}$	CH_2^2 symmetric stretching [$\nu_s(CH_2^2)$]
$S_b^1=(\Delta r_{12}-\Delta r_{23})/\sqrt{2}$	CH_2^1 antisymmetric stretching [$\nu_a(CH_2^1)$]
$S_b^2=(\Delta r_{67}-\Delta r_{78})/\sqrt{2}$	CH_2^2 antisymmetric stretching [$\nu_a(CH_2^2)$]
$S_c^1=\Delta r_{45}$	CH^1 stretching [$\nu(CH^1)$]
$S_c^2=\Delta r_{90}$	CH^2 stretching [$\nu(CH^2)$]
$S_d^1=\Delta r_{25}$	$C{=}C^1$ stretching [$\nu(C{-}C^1)$]
$S_d^2=\Delta r_{70}$	$C{=}C^2$ stretching [$\nu(C{=}C^2)$]
$S_e^1=(2\Delta\phi_{123}-\Delta\phi_{325}-\Delta\phi_{521})/\sqrt{6}$	CH_2^1 scissors [$\delta(CH_2^1)$]
$S_e^2=(2\Delta\phi_{678}-\Delta\phi_{870}-\Delta\phi_{076})/\sqrt{6}$	CH_2^2 scissors [$\delta(CH_2^2)$]
$S_f^1=(\Delta\phi_{325}-\Delta\phi_{521})/\sqrt{2}$	CH_2^1 rocking [$\gamma_r(CH_2^1)$]
$S_f^2=(\Delta\phi_{870}-\Delta\phi_{076})/\sqrt{2}$	CH_2^2 rocking [$\gamma_r(CH_2^2)$]
$S_g^1=(2\Delta\phi_{250}-\Delta\phi_{054}-\Delta\phi_{452})/\sqrt{6}$	$C{=}C{-}C^1$ deformation [$\delta(CCC^1)$]
$S_g^2=(2\Delta\phi_{705}-\Delta\phi_{509}-\Delta\phi_{907})/\sqrt{6}$	$C{=}C{-}C^2$ deformation [$\delta(CCC^2)$]
$S_h^1=(\Delta\phi_{452}-\Delta\phi_{054})/\sqrt{2}$	CH^1 in-plane bending [$\delta(CH^1)$]
$S_h^2=(\Delta\phi_{907}-\Delta\phi_{509})/\sqrt{2}$	CH^2 in-plane bending [$\delta(CH^2)$]
$S_i=\Delta r_{50}$	C–C stretching [ν(C–C)]
$S_j^1=\Delta\theta_{2-135}$	CH_2^1 wagging [$\gamma_w(CH_2^1)$]
$S_j^2=\Delta\theta_{7-680}$	CH_2^2 wagging [$\gamma_w(CH_2^2)$]
$S_k^1=\Delta\theta_{5-420}$	CH^1 out-of-plane bending [$\gamma_w(CH^1)$]
$S_k^2=\Delta\theta_{0-975}$	CH^2 out-of-plane bending [$\gamma_w(CH^2)$]
$S_l^1=\Delta t_{25}$	CH_2^1 twisting [$\gamma_t(CH_2^1)$]
$S_l^2=\Delta t_{70}$	CH_2^2 twisting [$\gamma_t(CH_2^2)$]
$S_m=\Delta t_{50}$	C–C torsion [τ(C–C)]

a) The index zero in the subscripts corresponds to the atom 10.

Table 3. Definition of group-coordinate force constants

Symbol	Description
(1) In-plane force constants	
(i) Diagonal force constants	
F_a	CH_2 symmetric stretching
F'_a	CD_2 symmetric stretching
F''_a	CHD symmetric stretching
F_b	CH_2 antisymmetric stretching
F'_b	CD_2 antisymmetric stretching
F''_b	CHD antisymmetric stretching
F_c	CH stretching
F'_c	CD stretching
F_d	C=C stretching
F_e	CH_2 scissors
F_f	CH_2 rocking
F_g	C=C–C deformation
F_h	CH in-plane bending
F_i	C–C stretching
(ii) Off-diagonal force constants	
F_{dd}	C=C stretching/C=C stretching
F_{de}	C=C stretching/CH_2 scissors
F_{dg}	C=C stretching/C=C–C deformation
F_{dh}	C=C stretching/CH in-plane bending
F_{di}	C=C stretching/C–C stretching
F_{eh}	CH_2 scissors/CH in-plane bending
F_{fh}	CH_2 rocking/CH in-plane bending
F_{gi}	C=C–C deformation/C–C stretching
F_{hi}	CH in-plane bending/C–C stretching
F_{gg}	C=C–C deformation/C=C–C deformation
F_{hh}	CH in-plane bending/CH in-plane bending
(2) Out-of-plane force constants	
(i) Diagonal force constants	
F_j	CH_2 wagging
F_k	CH out-of-plane bending
F_l	CH_2 twisting
F_m	C–C torsion
(ii) Off-diagonal force constants	
F_{jk}	CH_2 wagging/CH out-of-plane bending
F_{kl}	CH out-of-plane bending/CH_2 twisting ($\underline{CH_2}$=$\underline{CH}$–)
F_{kk}	CH out-of-plane bending/CH out-of-plane bending
F'_{kl}	CH out-of-plane bending/CH_2 twisting ($\underline{CH_2}$–CH–$\underline{CH}$=CH_2)
F_{ll}	CH_2 twisting/CH_2 twisting

modified Urey-Bradley-Shimanouchi force field[40] based on the work of Abe[13] was assumed. However, it became clear that some force constants were strongly correlated and accordingly had large uncertainties. Then, we employed the group-coordinate force field (GCFF),[41] which was previously called the local-symmetry force field (LSFF).[40] The definition of the GC force constants used are given in Table 3.

s-trans-*1,3-Butadiene*: The planar C_{2h} structure[4] with $r_{C=C}$=1.342 Å, r_{C-C}=1.463 Å, r_{C-H}=1.093 Å, $\phi_{C=C-C}$=123.6°, and $\phi_{C=C-H}$ (three kinds)=120.9° was used in the present calculation. The least-squares adjustments of the in-plane GC force constants were made against 96 observed frequencies in total (11 for d_0, 11 for 1,1,4,4-d_4, 11 for d_6, 9 for 1,1,2-d_3, 9 for *trans,trans*-1,4-d_2, 8 for *cis,cis*-1,4-d_2, 7 for 2,3-d_2, 10 for *trans*-1-d_1, 4 for *cis*-1-d_1, 7 for 1,4-$^{13}C_2$, and 9 for 1-$^{13}C_1$). The observed frequencies of the d_0, 1,1,4,4-d_4, and d_6 samples were obtained from the present low-temperature matrix infrared and Raman measurements. The observed frequencies of the other deuterated and ^{13}C-substituted analogs were selected from Refs. 13—15 and 36. The following assumptions were made to obtain a good fit between the calculated and observed frequencies using a relatively small number of force constants (9 diagonal and 11 off-diagonal). (a) The CH_2 and CH stretching frequencies (CD_2, CD, and CHD stretching as well) were not included in the least-squares adjustments because of their uncertainties due to possible Fermi resonances. The diagonal force constants (F_a and F_b for CH_2 and F_c for CH) were fixed to the values given in Table 4 and no off-diagonal constants were taken into account. Slightly different values were used for the diagonal force constants of CD_2 (F'_a and F'_b), CD (F'_c), and CHD (F''_a and F''_b). (b) The off-diagonal force constants F_{di}(C=C/C–C) and F_{dd}(C=C/C=C) had large uncertainties when they were included in the least-squares adjustments. Therefore, these force constants were fixed to the values which were obtained from an *ab initio* calculation.[37]

For the out-of-plane vibrations nine force constants listed in Tables 3 and 4 were determined by the least-squares method against 74 observed frequencies in total (7 for d_0, 7 for 1,1,4,4-d_4, 7 for d_6, 6 for 1,1,2-d_3, 5 for *trans,trans*-1,4-d_2, 5 for *cis,cis*-1,4-d_2, 5 for *cis,trans*-1,4-d_2, 4 for 2,3-d_2, 6 for *trans*-1-d_1, 5 for *cis*-1-d_1, 6 for 2-d_1, 6 for 1,4-$^{13}C_2$, and 5 for 1-$^{13}C_1$). Here again, the observed data of the d_0, 1,1,4,4-d_4, and d_6 samples were from the present measurements, while those of the other deuterated and ^{13}C-substituted analogs were taken from Refs. 13—15 and 36. Choice of the kinds of force constants used was somewhat arbitrary, but the agreement between the calculated and observed frequencies was quite satisfactory.

Second Stable Conformer of 1,3-Butadiene: Since the structure of the second stable conformer of 1,3-butadiene has not been experimentally determined, two model structures, *s-cis* and *gauche*, were chosen for normal coordinate analysis. For the *s-cis* form all the bond lengths and bond angles were set equal to those of the *s-trans* form and the internal-rotation angle around the central C_5–C_{10} bond was rotated by 180° from *s-trans* as shown in Fig. 1(b). The same kinds of force constants as used for *s-trans* were taken into account. Normal-coordinate calculations were carried out in two steps. At first the force constants of *s-trans* were transferred to *s-cis* and the observed infrared bands of the latter were assigned with reference to the results of this calculation. The force constants of *s-cis* were then adjusted in order to obtain the best fit between the calculated and observed frequencies. In this procedure the force constants associated with the in-plane vibrations of the terminal CH_2 group were fixed to the values of *s-trans*. The off-diagonal force constants, F_{dd} and F_{di}, were again fixed to the values obtained from an *ab initio* calculation.[37] The other six force constants, F_d, F_g, F_h, F_i, F_{gg}, and

TABLE 4. GROUP-COORDINATE FORCE CONSTANTS OF *s-trans*, *s-cis*, AND *gauche* 1,3-BUTADIENE AND THEIR UNCERTAINTIES (IN PARENTHESES). UNITS ARE mdyn Å^{-1} ($=10^2$ N m^{-1}) FOR STRETCHING AND STRETCH-STRETCH INTERACTION FORCE CONSTANTS, mdyn ($=10^{-8}$ N) FOR STRETCH-BEND INTERACTION FORCE CONSTANTS, AND mdyn Å ($=10^{-18}$ N m) FOR BENDING, BEND-BEND INTERACTION, AND TORSIONAL FORCE CONSTANTS.

Force constant	*s-trans*	*s-cis*	*gauche*
In-plane			
F_a	5.068	5.068	5.068
F'_a	5.214	5.214	5.214
F''_a	5.570	—	—
F_b	5.057	5.057	5.057
F'_b	5.123	5.123	5.123
F''_b	4.724	—	—
F_c	4.995	4.995	4.995
F'_c	4.981	4.981	4.981
F_d	8.886 (0.105)	8.976 (0.122)	9.003 (0.075)
F_e	0.455 (0.003)	0.455	0.455
F_f	0.577 (0.007)	0.577	0.577
F_g	0.691 (0.011)	0.699 (0.193)	0.546 (0.070)
F_h	0.519 (0.006)	0.532 (0.011)	0.531 (0.007)
F_i	5.428 (0.164)	4.964 (0.286)	4.914 (0.155)
F_{dd}	−0.1	−0.1	−0.1
F_{de}	−0.197 (0.012)	−0.197	−0.197
F_{dg}	0.257 (0.095)	0.257	0.257
F_{dh}	0.232 (0.030)	0.232	0.232
F_{di}	0.4	0.4	0.4
F_{eh}	−0.013 (0.004)	−0.013	−0.013
F_{fh}	0.056 (0.005)	0.056	0.056
F_{gi}	0.082 (0.049)	0.082	0.082
F_{hi}	−0.225 (0.023)	−0.225	−0.225
F_{gg}	0.073 (0.010)	0.008 (0.193)	−0.026 (0.071)
F_{hh}	0.037 (0.004)	0.024 (0.011)	0.021 (0.007)
Out-of-plane			
F_j	0.297 (0.001)	0.297	0.297
F_k	0.409 (0.005)	0.352 (0.006)	0.387 (0.015)
F_l	0.511 (0.005)	0.533 (0.009)	0.550 (0.018)
F_m	0.109 (0.005)	0.046 (0.003)	0.055 (0.009)
F_{jk}	0.055 (0.002)	0.045 (0.003)	0.038 (0.008)
F_{kl}	−0.027 (0.002)	−0.010 (0.003)	−0.028 (0.009)
F_{kk}	−0.005 (0.004)	0.024 (0.005)	0.013 (0.015)
F'_{kl}	0.023 (0.002)	−0.026 (0.003)	−0.014 (0.009)
F_{ll}	−0.017 (0.005)	0.011 (0.008)	−0.003 (0.017)

F_{hh}, were adjusted freely by the least-squares method using 30 observed frequencies in total (6 for d_0, 7 for 1,1,4,4-d_4, 7 for d_6, 5 for 1,4-$^{13}C_2$, 5 for 1-$^{13}C_1$). The observed data for the 1,4-$^{13}C_2$ and 1-$^{13}C_1$ analogs were taken from Ref. 36. As for the out-of-plane vibrations, the eight force constants, F_k, F_l, F_m, F_{jk}, F_{kl}, F_{kk}, F'_{kl}, and F_{ll} were adjusted freely by the least-squares method using 28 observed frequencies (7 for d_0, 6 for 1,1,4,4-d_4, 4 for d_6, 5 for 1,4-$^{13}C_2$, 6 for 1-$^{13}C_1$). Only the CH_2 wagging force constant, F_j, was fixed to the value of *s-trans*.

As the structural parameters of the *gauche* form the values calculated by Skaarup *et al.*[30] were slightly modified with reference to the deviations between the *ab initio* and experimental results for the *s-trans* form. The parameters used were as follows: $r_{C=C}=1.341$ Å, $r_{C-C}=1.474$ Å, $r_{C-H}=1.092$ Å, $\phi_{C=C-C}=119.3°$, $\phi_{C=C-H}(2\text{-}5\text{-}4)=119.3°$, $\phi_{C=C-H}(5\text{-}2\text{-}3)=121.5°$, $\phi_{C=C-H}(5\text{-}2\text{-}1)=121.8°$, and t(internal-rotation angle around C_5–C_{10})=40° from *s-cis*. In the normal-coordinate analysis of the *gauche* form no interaction force constants between the "in-plane" and "out-of-plane" coordinates were taken into account. Under the same assumptions as made for the *s-cis* case the 14 force constants were determined from 58 observed frequencies by the least-squares method.

Results

The infrared and Raman spectra of 1,3-butadiene and its 1,1,4,4-d_4 and d_6 analogs observed in low-temperature Ar matrices are shown in Figs. 3 and 4. Since the Ar/sample ratio was not high, the sample molecules might not be completely isolated in the Ar matrix. However, the sharpness of individual bands inherent to the low-temperature matrix measurements made it possible to detect many weak bands. The Raman spectra of these compounds in low-temperature

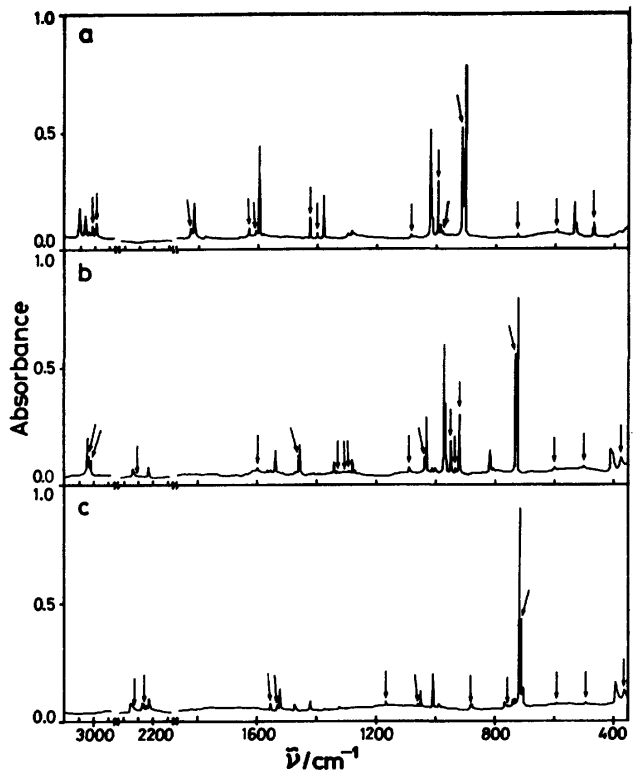

Fig. 3. Infrared spectra of (a) 1,3-butadiene-d_0, (b) -1,1,4,4-d_4, and (c) -d_6 observed in Ar matrices at 20 K. Mixtures of Ar and the samples (Ar/sample ratio 250) were heated to about 770 K in the nozzle and then deposited onto the cold CsI plate. The arrows indicate the bands due to the second stable conformer.

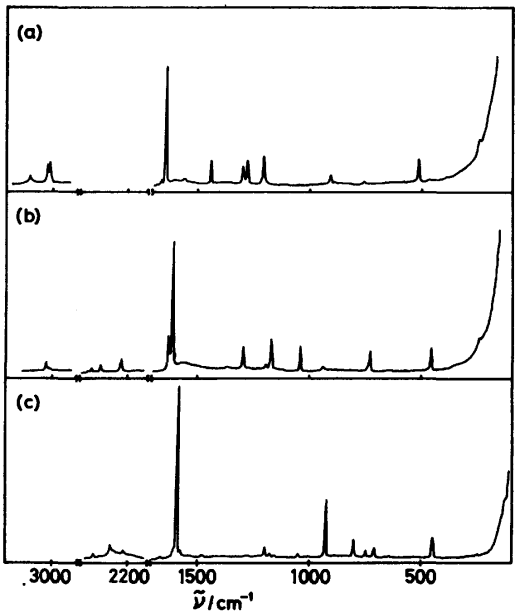

Fig. 4. Raman spectra of (a) 1,3-butadiene-d_0, (b) -1,1,4,4-d_4, and (c) -d_6 observed in Ar matrices (Ar/sample ratio 50) at 15 K. Excitation wavelength, 514.5 nm.

Ar matrices were observed in this study for the first time. The infrared spectra in Fig. 3 were observed from the low-temperature Ar matrices obtained by depositing a mixture of Ar and the sample which had been heated to about 770 K. Therefore, the intensities of the bands due to the second stable conformer are enhanced in Fig. 3 and they are indicated with arrows. The bands without arrows are associated with the most stable *s-trans* form. The bands with arrows were found to decrease in intensity on irradiation of light from a Xe-lamp, indicating that these bands were due to the second stable conformer.[35] Our present results for the d_0 and d_6 samples (Figs. 3a and 3c) agreed with the findings of previous authors,[34-36] except for some minor features. Huber-Wälchli and Günthard[36] observed more bands than we did; for example, we could not observe the medium-intensity band at 1740 cm^{-1} of the d_0 species which they assigned to a combination tone of the second stable conformer. The infrared spectrum of the second stable conformer of the 1,1,4,4-d_4 species (Fig. 3b) was obtained for the first time.

The results of normal-coordinate analyses will be described below.

Discussion

Band Assignments and Force Constants of the s-trans *Form.* As described earlier, we started the normal-coordinate analyses of 1,3-butadiene and its deuterated and ^{13}C-

Table 5. Observed and calculated vibrational frequencies of *s-trans*-1,3-butadiene-d_0 and mode assignments

Species	No.	Obsd $\tilde{\nu}$/cm^{-1}	Calcd $\tilde{\nu}$/cm^{-1}	Mode and PED[a]
a_g	ν_1	3105	3102	$\nu_a(CH_2^*)$ 49
	ν_2	3025	3039	$\nu(CH^*)$ 47
	ν_3	3014	2997	$\nu_s(CH_2^*)$ 46
	ν_4	1644	1645	$\nu(C{=}C^*)$ 36, $\nu(C{-}C)$ 21
	ν_5	1441	1446	$\delta(CH_2^*)$ 38, $\nu(C{-}C)$ 11
	ν_6	1279	1296	$\delta(CH^*)$ 18, $\nu(C{=}C^*)$ 10
	ν_7	1206	1203	$\nu(C{-}C)$ 27, $\delta(CH^*)$ 14, $\gamma_r(CH_2^*)$ 11
	ν_8	887	901	$\nu(C{-}C)$ 37, $\gamma_r(CH_2^*)$ 29
	ν_9	513	510	$\delta(CCC^*)$ 33
a_u	ν_{10}	1022	1019	$\gamma_t(CH_2^*)$ 31, $\gamma_w(CH^*)$ 18
	ν_{11}	905	908	$\gamma_w(CH_2^*)$ 51
	ν_{12}	535	527	$\gamma_w(CH^*)$ 28, $\gamma_t(CH_2^*)$ 21
	ν_{13}	163[b]	162	$\tau(C{-}C)$ 89
b_g	ν_{14}	974	969	$\gamma_w(CH^*)$ 30, $\gamma_t(CH_2^*)$ 25
	ν_{15}	908	910	$\gamma_w(CH_2^*)$ 50
	ν_{16}	754	751	$\gamma_t(CH_2^*)$ 24, $\gamma_w(CH^*)$ 18
b_u	ν_{17}	3103	3101	$\nu_a(CH_2^*)$ 50
	ν_{18}	3062	3029	$\nu(CH^*)$ 46
	ν_{19}	2986	2997	$\nu_s(C{=}H_2^*)$ 48
	ν_{20}	1597	1601	$\nu(C{=}C^*)$ 37, $\delta(CH_2^*)$ 17
	ν_{21}	1381	1387	$\delta(CH_2^*)$ 33, $\nu(C{=}C^*)$ 10
	ν_{22}	1297	1293	$\delta(CH^*)$ 33
	ν_{23}	988	995	$\gamma_r(CH_2^*)$ 40, $\delta(CH^*)$ 16
	ν_{24}	301[b]	300	$\delta(CCC^*)$ 55

a) The asterisk in the mode notation indicates that the two group coordinates of the same mode (having superscript 1 and 2) have equal PED's; for example, $\nu_a(CH_2^*)$ 49 represents $\nu_a(CH_2^1)$ 49 and $\nu_a(CH_2^2)$ 49. In this Table PED's are not normalized to a total of 100. b) Ref. 18.

Table 6. Observed and calculated vibrational frequencies of *s-trans*-1,3-butadiene-1,1,4,4-d_4 and mode assignments

Species	No.	Obsd $\tilde{\nu}$/cm^{-1}	Calcd $\tilde{\nu}$/cm^{-1}	Mode and PED[a)]
a_g	ν_1	3026	3038	ν(CH*) 49
	ν_2	2316	2340	ν_a(CD$_2^*$) 49
	ν_3	2225	2233	ν_s(CD$_2^*$) 46
	ν_4	1612	1602	ν(C=C*) 34, ν(C–C) 26
	ν_5	1298	1296	δ(CH*) 30
	ν_6	1170	1183	ν(C–C) 46
	ν_7	1040	1036	δ(CD$_2^*$) 40
	ν_8	740	726	γ_r(CD$_2^*$) 34
	ν_9	454	462	δ(CCC*) 31
a_u	ν_{10}	968	957	γ_w(CH*) 25, (CD$_2^*$) 23
	ν_{11}	722	724	γ_w(CD$_2^*$) 51
	ν_{12}	404	399	γ_t(CD$_2^*$) 29, γ_w(CH*) 21
	ν_{13}	149[b)]	148	τ(C–C) 89
b_g	ν_{14}	940	934	γ_w(CH*) 43
	ν_{15}	728	732	γ_w(CD$_2^*$) 44
	ν_{16}	610[c)]	602	γ_t(CD$_2^*$) 31
b_u	ν_{17}	3037	3027	ν(CH*) 50
	ν_{18}	2337	2339	ν_a(CD$_2^*$) 49
	ν_{19}	2228	2236	ν_s(CD$_2^*$) 46
	ν_{20}	1533	1525	ν(C=C*) 44
	ν_{21}	1274	1263	δ(CH*) 45
	ν_{22}	1028	1022	δ(CD$_2^*$) 46
	ν_{23}	811	811	γ_r(CD$_2^*$) 44
	ν_{24}	258[c)]	262	δ(CCC*) 52

a) See the footnote a) of Table 5. b) Ref. 18. c) Ref. 13.

Table 7. Observed and calculated vibrational frequencies of *s-trans*-1,3-butadiene-d_6 and mode assignments

Species	No.	Obsd $\tilde{\nu}$/cm^{-1}	Calcd $\tilde{\nu}$/cm^{-1}	Mode and PED[a)]
a_g	ν_1	2349	2342	ν_a(CD$_2^*$) 47
	ν_2	2275	2275	ν(CD*) 34, ν_s(CD$_2^*$) 10
	ν_3	2218	2220	ν_s(CD$_2^*$) 37, ν(CD*) 11
	ν_4	1592	1586	ν(C=C*) 36, ν(C–C) 29
	ν_5	1199	1190	ν(C–C) 37, δ(CD$_2^*$) 11
	ν_6	1050	1030	δ(CD$_2^*$) 33
	ν_7	925	918	δ(CD*) 35
	ν_8	743	723	γ_r(CD$_2^*$) 32, ν(C–C) 24
	ν_9	445	451	δ(CCC*) 31
a_u	ν_{10}	766	759	γ_w(CD*) 23, γ_t(CD$_2^*$) 22
	ν_{11}	715	717	γ_w(CD$_2^*$) 41
	ν_{12}	391	389	γ_w(CD*) 25, γ_t(CD$_2^*$) 24
	ν_{13}	142[b)]	139	τ(C–C) 92
b_g	ν_{14}	800	796	γ_w(CD*) 43, γ_w(CD$_2^*$) 14
	ν_{15}	705	702	γ_w(CD$_2^*$) 33
	ν_{16}	603[c)]	592	γ_t(CD$_2^*$) 39
b_u	ν_{17}	2350	2339	ν_a(CD$_2^*$) 49
	ν_{18}	2269	2263	ν(CD) 23, ν_s(CD$_2^*$) 22
	ν_{19}	2222	2209	ν(CD) 25, ν_s(CD$_2^*$) 25
	ν_{20}	1521	1511	ν(C=C*) 43
	ν_{21}	1046	1043	δ(CD$_2^*$) 30, δ(CD*) 14
	ν_{22}	1006	989	δ(CD$_2^*$) 16, δ(CD*) 15, γ_r(CD$_2^*$) 10
	ν_{23}	738	738	γ_r(CD$_2^*$) 32, δ(CD*) 24
	ν_{24}	250	255	δ(CCC*) 53

a) See the footnote a) of Table 5. b) Ref. 18. c) Ref. 13.

Table 8. Observed and calculated vibrational frequencies of *s-cis*-1,3-butadiene-d_0 and mode assignments

Species	No.	Obsd $\tilde{\nu}$/cm^{-1}	Calcd $\tilde{\nu}$/cm^{-1}	Mode and PED[a)]
a_1	ν_1	3103	3101	ν_a(CH$_2^*$) 49
	ν_2	3014	3033	ν(CH*) 47
	ν_3	2986	2997	ν_s(CH$_2^*$) 47
	ν_4	1633	1627	ν(C=C*) 38, ν(C–C) 17
	ν_5	1425	1432	δ(CH$_2^*$) 34, ν(C–C) 15
	ν_6		1338	δ(CH*) 27
	ν_7	1087	1075	γ_r(CH$_2^*$) 22, ν(C–C) 16, δ(CH*) 13
	ν_8		878	ν(C–C) 54, γ_r(CH$_2^*$) 20
	ν_9		256	δ(CCC*) 47
a_2	ν_{10}	983[b)]	980	γ_t(CH$_2^*$) 29, γ_w(CH*) 22
	ν_{11}	915[c)]	914	ν_w(CH$_2^*$) 50
	ν_{12}	727[b)]	729	γ_w(CH*) 23, γ_t(CH$_2^*$) 19
	ν_{13}	136[d)]	135	τ(C–C) 97
b_1	ν_{14}	3103	3101	ν_a(CH$_2^*$) 49
	ν_{15}	3014	3034	ν(CH*) 47
	ν_{16}	2986	2998	ν_s(CH$_2^*$) 47
	ν_{17}	1612	1623	ν(C=C*) 37, δ(CH$_2^*$) 12
	ν_{18}	1403	1415	δ(CH$_2^*$) 35, δ(CH*) 11
	ν_{19}		1278	δ(CH*) 23
	ν_{20}		1043	γ_r(CH$_2^*$) 35, δ(CH*) 13
	ν_{21}	596	591	δ(CCC*) 42
b_2	ν_{22}	996	997	γ_t(CH$_2^*$) 36, γ_w(CH*) 14
	ν_{23}	914	909	γ_w(CH$_2^*$) 51
	ν_{24}	470	470	γ_w(CH*) 40, γ_t(CH$_2^*$) 15

a) See the footnote a) of Table 5. b) See the text as for the assignment of these bands. c) Estimated from $\nu_{11}+\nu_{23}=1829$ cm^{-1}. d) Ref. 21.

substituted analogs using the modified Urey-Bradley-Shimanouchi force constants obtained by Abe.[13] Since the band assignments by Abe and other authors[36] mostly seemed reasonable, we refined the GC* force constants on the basis of their assignments. By fixing the force constants relating to the carbon-hydrogen stretching (F_a, F_b, and F_c) and the interaction force constants between the skeletal stretchings (F_{dd} and F_{di}) to reasonable values (see the section of Method), a convergent set of force constants was obtained with satisfactorily small uncertainties as given in Table 4. The results of calculation for the d_0, 1,1,4,4-d_4, and d_6 species in the *s-trans* form are shown in Tables 5—7, together with the observed frequencies. The results of calculation for the other deuterated and ^{13}C-substituted analogs are available on request.

Internal-rotation Angle of the Second Stable Conformer. The normal frequencies of the planar *s-cis* and nonplanar *gauche* forms were calculated in the same manner as is described in the section on Method. The results of calculations for the d_0 species are given in Tables 8 and 9. Similar tables for the 1,1,4,4-d_4 and d_6 species are available from the authors on request. The force constants obtained for the *s-cis* and *gauche* forms are also listed in Table 4. Although most of the observed frequencies can be interpreted on the basis of either the *s-cis* or *gauche* form, the presence of a very weak band at

Table 9. Observed and calculated vibrational frequencies of *gauche*-1,3-butadiene-d_0 and mode assignments

Species	No.	Obsd $\tilde{\nu}$/cm^{-1}	Calcd $\tilde{\nu}$/cm^{-1}	Mode and PED[a]
a	ν_1	3103	3098	$\nu_a(CH_2^*)$ 50
	ν_2	3014	3032	$\nu(CH^*)$ 46
	ν_3	2986	3000	$\nu_s(CH_2^*)$ 47
	ν_4	1633	1629	$\nu(C{=}C^*)$ 38, (C–C) 18
	ν_5	1425	1432	$\delta(CH_2^*)$ 36, ν(C–C) 13
	ν_6		1328	$\delta(CH^*)$ 29
	ν_7	1087	1081	$\gamma_r(CH_2^*)$ 24, ν(C–C) 16, $\delta(CH^*)$ 12
	ν_8	983	982	$\gamma_t(CH_2^*)$ 29, $\gamma_w(CH^*)$ 23
	ν_9	915[b]	915	$\gamma_w(CH_2^*)$ 47
	ν_{10}		872	ν(C–C) 55, $\gamma_r(CH_2^*)$ 18
	ν_{11}	727	731	$\gamma_w(CH^*)$ 21, $\gamma_t(CH_2^*)$ 18
	ν_{12}		256	$\delta(CCC^*)$ 46
	ν_{13}	136[c]	137	τ(C–C) 89
b	ν_{14}	3103	3098	$\nu_a(CH_2^*)$ 50
	ν_{15}	3014	3032	$\nu(CH^*)$ 46
	ν_{16}	2986	3001	$\nu_s(CH_2^*)$ 47
	ν_{17}	1612	1619	$\nu(C{=}C^*)$ 37, $\delta(CH_2^*)$ 13
	ν_{18}	1403	1413	$\delta(CH_2^*)$ 34, $\delta(CH^*)$ 11
	ν_{19}		1278	$\delta(CH^*)$ 24
	ν_{20}		1040	$\gamma_r(CH_2^*)$ 36, $\delta(CH^*)$ 11
	ν_{21}	996	996	$\gamma_t(CH_2^*)$ 35, $\gamma_w(CH^*)$ 15
	ν_{22}	914	907	$\gamma_w(CH_2^*)$ 50
	ν_{23}	596	597	$\delta(CCC^*)$ 20, $\gamma_w(CH^*)$ 17
	ν_{24}	470	465	$\delta(CCC^*)$ 23, $\gamma_w(CH^*)$ 19

a) See the footnote a) of Table 5. b) Estimated from $\nu_9+\nu_{22}=1829$ cm^{-1}. c) Ref. 21.

983 cm^{-1} and a weak band at 727 cm^{-1} is better acounted for by assuming the *gauche* form. When the *s-cis* form is assumed, both of these bands must be assigned to the infrared-inactive a_2 modes, ν_{10} and ν_{12}, in which the CH_2 twisting and CH out-of-plane bending are almost equally coupled. The corresponding bands are found at 927 cm^{-1} (ν_{10}) and 594 cm^{-1} (ν_{12}) for the 1,1,4,4-d_4 species and at 587 cm^{-1} (ν_{12}) for the d_6 species. It is likely that the a_2 modes of the *s-cis* form (C_{2v}) are made infrared-active due to the lowering of molecular symmetry from C_{2v} (*s-cis*) to C_2 (*gauche*).

As described above, the second stable conformer probably exists in the *gauche* form rather than in the *s-cis* form. However, it is interesting to note that most of the infrared bands due to the second stable conformer can be reasonably assigned on assuming the planar *s-cis* form. Therefore, as far as the vibrational assignment for a less stable conformer of a compound with conjugated double bonds is concerned, it seems justifiable to use the *s-cis* form as a practical model instead of paying too much attention to the problem of internal-rotation angle which is inherently difficult to determine.

Assignments of Infrared and Raman Bands. Most of the infrared and Raman bands shown in Figs. 3 and 4 could be assigned. The tables which list the observed infrared and Raman frequencies together with their assignments are available from the authors on request.

References

1) A. Almenningen, O. Bastiansen, and M. Traetteberg, *Acta Chem. Scand.*, **12**, 1221 (1958).
2) D. J. Marais, N. Sheppard, and B. P. Stoicheff, *Tetrahedron*, **17**, 163 (1962).
3) A. R. H. Cole, G. M. Mohay, and G. A. Osborne, *Spectrochim. Acta, Part A*, **23**, 909 (1967).
4) K. Kuchitsu, T. Fukuyama, and Y. Morino, *J. Mol. Struct.*, **1**, 463 (1967—1968).
5) K. Kuchitsu, T. Fukuyama, and Y. Morino, *J. Mol. Struct.*, **4**, 41 (1969).
6) R. S. Rasmussen and R. R. Brattain, *J. Chem. Phys.*, **15**, 131 (1947).
7) C. M. Richards and J. R. Nielsen, *J. Opt. Soc. Am.*, **40**, 438 (1950).
8) L. M. Sverdlov and N. V. Tarasova, *Opt. Spectrosc.*, **9**, 159 (1960).
9) R. K. Harris, *Spectrochim. Acta*, **20**, 1129 (1964).
10) E. M. Popov and G. A. Kogan, *Opt. Spectrosc.*, **17**, 362 (1964).
11) Yu. N. Panchenko, Yu. A. Pentin, V. I. Tyulin, and V. M. Tatevskii, *Opt. Spectrosc.*, **16**, 536 (1964).
12) I. S. Borshagovskaya, Yu. N. Panchenko, and Yu. A. Pentin, *Opt. Spectrosc.*, **22**, 194 (1967).
13) K. Abe, Ph. D. Thesis, The University of Tokyo, Tokyo, Japan, 1970.
14) Yu. N. Panchenko, *Spectrochim. Acta, Part A*, **31**, 1201 (1975).
15) E. Benedetti, M. Aglietto, S. Pucci, Yu. N. Panchenko, Yu. A. Pentin, and O. T. Nikitin, *J. Mol. Struct.*, **49**, 293 (1978).
16) J. G. Aston, G. Szasz, H. W. Woolley, and F. G. Brickwedde, *J. Chem. Phys.*, **14**, 67 (1946).
17) W. G. Fateley, R. K. Harris, F. A. Miller, and R. E. Witkowski, *Spectrochim. Acta*, **21**, 231 (1965).
18) A. R. H. Cole, A. A. Green, and G. A. Osborne, *J. Mol. Spectrosc.*, **48**, 212 (1973).
19) R. L. Lipnick and E. W. Garbisch, Jr., *J. Am. Chem. Soc.*, **95**, 6370 (1973).
20) J. R. Durig, W. E. Bucy, and A. R. H. Cole, *Can. J. Phys.*, **53**, 1832 (1975).
21) L. A. Carreira, *J. Chem. Phys.*, **62**, 3851 (1975).
22) D. A. C. Compton, W. O. George, and W. F. Maddams, *J. Chem. Soc., Perkin Trans. 2*, **1976**, 1666.
23) K. Kveseth, R. Seip, and D. A. Kohl, *Acta Chem. Scand., Ser. A*, **34**, 31 (1980).
24) R. J. Buenker and J. L. Whitten, *J. Chem. Phys.*, **49**, 5381 (1968).
25) L. Radom and J. A. Pople, *J. Am. Chem. Soc.*, **92**, 4786 (1970).
26) B. Dumbacher, *Theor. Chim. Acta*, **23**, 346 (1972).
27) U. Pincelli, B. Cadioli, and B. Lévy, *Chem. Phys. Lett.*, **13**, 249 (1972).
28) P. N. Skancke and J. E. Boggs, *J. Mol. Struct.*, **16**, 179 (1973).
29) Yu. N. Panchenko, P. Pulay, and F. Török, *J. Mol. Struct.*, **34**, 283 (1976).
30) S. Skaarup, J. E. Boggs, and P. N. Skancke, *Tetrahedron*, **32**, 1179 (1976).
31) J. A. Altman and W. F. Reynolds, *J. Mol. Struct.*, **36**, 149 (1977).
32) C. W. Bock, P. George, M. Trachtman, and M. Zanger, *J. Chem. Soc., Perkin Trans. 2*, **1979**, 26.
33) P. George, C. W. Bock, and M. Trachtman, *J. Mol. Struct.*, **69**, 183 (1980).

34) P. Huber-Wälchli, *Ber. Bunsenges. Phys. Chem.*, **82**, 10 (1978).
35) M. E. Squillacote, R. S. Sheridan, O. L. Chapman, and F. A. L. Anet, *J. Am. Chem. Soc.*, **101**, 3657 (1979).
36) P. Huber-Wälchli and Hs. H. Günthard, *Spectrochim. Acta, Part A*, **37**, 285 (1981).
37) C. W. Bock, M. Trachtman, and P. George, *J. Mol. Spectrosc.*, **84**, 243 (1980).
38) T. Shimanouchi, "Computer Program for Normal Coordinate Treatment of Molecules," The University of Tokyo, Tokyo (1968).
39) IUPAC Commission on Molecular Structure and Spectroscopy, *Pure Appl. Chem.*, **50**, 1707 (1978).
40) T. Shimanouchi, "The Molecular Force Field," in "Physical Chemistry. An Advanced Treatise," ed by H. Eyring, D. Henderson, and W. Jost, Academic Press, New York (1970), Vol. IV, Chap. 6, pp. 233—306.
41) H. Matsuura and M. Tasumi, "Force Fields for Large Molecules," in "Vibrational Spectra and Structure," ed by J. R. Durig, Elsevier, Amsterdam, Vol. 12, in press.

A Model of Nematic Liquid Crystals for Viscosity and Self-diffusion

Seiichi MIYAJIMA,*,† Nobuo NAKAMURA, and Hideaki CHIHARA
Department of Chemistry, Faculty of Science, Osaka University, Toyonaka 560
(Received August 2, 1982)

A Geometrical model is presented which rationalizes the viscosity and self-diffusion coefficients and their anisotrcpies in nematic liquid crystals. The model is an extension of Eyring's theory of the liquid state to the anisotropic fluid, based on the geometry of the constituent molecule. A novel concept, effective anisotropy factor of a molecule, is introduced which is determined from the viscosity coefficients. An empirical law on the principal viscosity coefficients by Kneppe *et al.* is given its molecular basis by this model. Self-diffusion coefficient tensor calculated from the available viscosity data of PAA, MBBA, and HBAB agree well with experiment.

General understanding of cohesion of organic molecules shows that the nature of mesophases which appear between the rigid molecular crystal and the isotropic liquid is essentially determined by the geometrical characteristics of the constituent molecules: The liquid crystalline mesophase is formed by a rodlike molecule having a certain degree of internal rigidity,[1] whereas the special kinds of mesophases such as discotic or columnar ones are formed by a disk-like molecule[2] and the plastic crystal consists of a globular molecule.[3] One is thus tempted to develop a model theory of such mesophases, which will help to understand their features at least qualitatively like the one presented here for viscosity and self-diffusion in the nematic liquid crystal, the most typical mesophase formed by rodlike molecules.

Since Miesowicz[4] pointed out that external magnetic field has an effect on the viscosity of 4,4′-dimethoxyazoxybenzene (PAA) in 1935, the flow properties of nematic liquid crystals have been one of the interesting problems in rheology[5] and molecular dynamics.[6] Continuum theory of the viscoelastic properties of nematic liquid crystal was developed by Ericksen and Leslie.[7] On the basis of their theory, Lubensky[8] proposed relations between Franck's elastic constants and the nematic order parameter, $\langle p_2 \rangle$, and later, Imura and Okano[9] derived phenomenological relations between $\langle p_2 \rangle$ and viscosity coefficients. These theories could, however, interpret the experimental data with only partial success.[10] Recently, a comparative experimental study of the viscosity coefficients of some nematic liquid crystals were carried out by Kneppe *et al.*[11] and some rules concerning relationship among the principal viscosity coefficients were found in a purely empirical manner.

Our standpoint is very different from the models of the former authors; it is not an elastic continuum theory but a very simple model theory based on the geometrical characteristic of the constituent molecule. Our treatment has its origin in Eyring's theory of the rate processes[12] and of significant liquid structure,[13] and is an extension of Eyring's theory of the liquid state to the system of uniaxial symmetry. We will describe in this paper how the anisotropic shape of the molecule is reflected on anisotropies of the diffusion coefficient tensor and of the viscosity coefficients and will derive phenomenological relations between diffusion and viscosity coefficients. Finally, comparisons with the experiments will be given. An empirical law recently found by Kneppe *et al.*[11] will find its molecular basis in our simple model.

Theory

The essential points of Eyring's idea are: (1) the liquid state consists of solid-like molecules and gas-like mobile molecules adjacent to the holes, (2) viscous flow and diffusion can be treated on a common physical basis by supposing that the two phenomena are the results of molecular friction when a molecule jumps into a hole. Eyring *et al.* developed their theory for isotropic liquids, and we will now treat the case of anisotropic fluid.

Diffusion coefficient tensor in a three-dimensional system is defined by the Fick's first law,

$$\boldsymbol{J} + \boldsymbol{D}\nabla c = 0. \tag{1}$$

Here, c and $\boldsymbol{J}$ denote the concentration of the diffusing solute and the flow density, respectively. If we take a coordinate system in which the z-axis is parallel to $\boldsymbol{n}$, the nematic director, the tensor $\boldsymbol{D}$ can be diagonalized according to the axial symmetry of the system,

$$\boldsymbol{D} = \begin{bmatrix} D_\perp & 0 & 0 \\ 0 & D_\perp & 0 \\ 0 & 0 & D_{//} \end{bmatrix}, \tag{2}$$

and Eq. 1 consists of two independent differential equations. If the velocity of flow is represented by $\boldsymbol{u}$, the following set of equations hold by virtue of the relation, $\boldsymbol{J}=c\boldsymbol{u}$ for the flow along the axis q_j (q denotes the generalized coordinate and j indicates a specific direction, x, y, or z):

$$c\,u_j + D_{jj}\frac{\partial c}{\partial q_j} = 0. \tag{3}$$

On the other hand, the viscosity of the nematic liquid crystal can be defined by the Newton's law.†† When the shear stress is applied along j on the plane perpendicular to i, the viscosity coefficient η_{ji} is represented by

$$\eta_{ji} = \frac{(F_{ji}/A_i)}{\left[\dfrac{\partial u_j(q_i)}{\partial q_i}\right]}, \tag{4}$$

† Present address: Department of Chemistry, College of Humanities and Sciences, Nihon University, Sakurajosui, Setagaya-ku, Tokyo 156.

†† In fact, Newtonian property of nematic liquid crystals was confirmed experimentally (in Ref. 18) under ordinary rate of shear.

where F_{ji} denotes the shear force, and A_i is the area on which the shear force acts. If we consider a gas–like mobile molecule jumping into the nearby hole by overcoming the friction arising from interactions with solid-like molecules, the denominator in Eq. 4 is replaced by u_j/σ_i (σ_i is the nearest neighbor distance along i), and Eq. 4 is replaced by

$$\eta_{ji} = \frac{\sigma_i}{A_i} \cdot \frac{F_{ji}}{u_j}. \tag{5}$$

Let us now relate the viscosity coefficient to the diffusion coefficient by thermodynamic considerations. Generalized force $\boldsymbol{f}$ which is brought about by the spatial gradient of chemical potential is represented by

$$f_j = -kT \frac{\partial \ln \lambda}{\partial q_j}, \tag{6}$$

where λ is the absolute activity. Suppose that some fraction, κ_j, of this phenomenological force acts as the shear force along j on the plane perpendicular to i, *i.e.*,

$$F_{ji} = \kappa_j f_j. \tag{7}$$

The information about the local structure of the fluid system is included in the phenomenological parameter κ_j. Combinig Eqs. 3 and 5—7, one gets

$$\eta_{ji} = kT \frac{\sigma_i}{A_i} \cdot \frac{\kappa_j}{D_{jj}} \cdot \frac{\partial \ln \lambda}{\partial \ln c}, \tag{8}$$

which is an extended equation of Eyring and Ree[13] and can be applied to an anisotropic system. We will treat in this paper the high concentration limit, $\lambda = c$, which corresponds to the case of self-diffusion.

We now derive specific expressions of viscosity in nematic liquid crystals. In such an anisotropic fluid, viscosity depends on the direction of flow (j) and of the velocity gradient (i) with respect to the orientation of the director, $\boldsymbol{n}$. Miesowicz[14] first gave definitions of the three principal viscosity coefficients corresponding to the cases in which $\boldsymbol{n}$ is (1) parallel to the velocity gradient, (2) parallel to the flow, and (3) perpendicular to both the flow and the velocity gradient. The orientations are drawn in Fig. 1, in which η_1, η_2, and η_3 are defined by

$$\eta_1 \equiv \eta_{yx},\ \eta_2 \equiv \eta_{zy},\ \text{and}\ \eta_3 \equiv \eta_{yz},$$

corresponding to the definition by Helfrich,[15] Gähwiller,[16] and Kneppe and Schneider.[17] Note, however, the difference (η_1 and η_2 have been interchanged) from the definition by Miesowicz,[14] and Porter and Johnson.[18] An appropriate set of the geometrical factors, A_i and σ_i, are necessary to describe

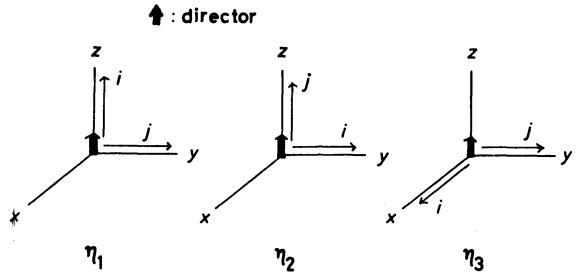

Fig. 1. Geometries for the three principal viscosity coefficients in a wall-aligned nematic liquid crystal system.

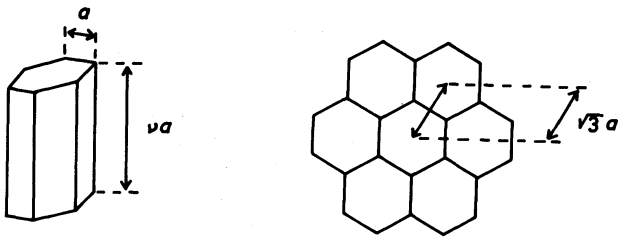

Fig. 2. Model of packing of molecules in the nematic liquid crystal.

these viscosity coefficients through Eq. 8. We will thus introduce a very simple model treatment for these factors. The nematic liquid crystal system is regarded as an assembly of closely packed molecules having a shape of elongated regular hexagonal prism as shown in Fig. 2. We assume according to Eyring's significant structure theory that some of the molecular sites are vacant, the concentration of the holes being dependent on temperature. The symbols, a and νa, represent the dimensions of individual molecules, with ν the effective anisotropy factor of the molecular shape. This model may be called the "pencil model," by use of which A_i and σ_i can be determined from purely geometrical considerations for each of the three principal viscosity coefficients, *i.e.*, in the case of η_2, all of the six side-planes undergo a shear stress, whereas in the case of η_1, the two base hexagons, and in the case of η_3 two side-planes do, respectively. The quantity σ_i is equal to νa for η_1 whereas $\sqrt{3}\ a$ for η_2 and η_3. It will be noticed that steric hindrance is rather strong when a molecule jumps perpendicularly to $\boldsymbol{n}$ but when it jumps parallel to $\boldsymbol{n}$, the steric hindrance will be weaker and the effective forces between molecules are mainly shear forces. Therefore, we put $\kappa_z = 1$ and $\kappa_y = \kappa$, where κ remains to be determined empirically.

The following set of equations are thus obtained from Eq. 8:

$$\eta_1 = \frac{\sqrt{3}\nu}{9a} \cdot \frac{\kappa kT}{D_\perp}, \tag{9}$$

$$\eta_2 = \frac{\sqrt{3}}{6\nu a} \cdot \frac{kT}{D_{//}}, \tag{10}$$

and

$$\eta_3 = \frac{\sqrt{3}}{2\nu a} \cdot \frac{\kappa kT}{D_\perp}, \tag{11}$$

which provide phenomenological relations between the viscosity and the diffusion coefficients.

A simple relation

$$\nu = 3\left(\frac{\eta_1}{2\eta_3}\right)^{1/2} \tag{12}$$

is obtained from Eqs. 9 and 11, which enables us to determine ν when the experimental data of the viscosity coefficients are available. Anisotropy of the diffusion coefficient tensor may be predicted from Eqs. 9—11 to be

$$\frac{D_{//}}{D_\perp} = \frac{\eta_3}{3\kappa\eta_2} = \frac{3\eta_1}{2\kappa\nu^2\eta_2}. \tag{13}$$

Comparison with Experiment

Now, comparisons of our model with experiments will be made on three typical nematic liquid crystals, 4,4'-dimethoxyazoxybenzene, *N*-(4-methoxybenzylidene)-4-butylaniline, and 4-(4-hexyloxybenzylideneamino)benzonitrile, which will be called in this paper PAA, MBBA, and HBAB according to their usual acronyms.

Table 1 lists the principal viscosity coefficients of PAA measured by Miesowicz,[14] those of MBBA by Kneppe and Schneider,[17] and those of HBAB by Gähwiller.[16] Anisotropic self-diffusion coefficients of nematic liquid crystals were first measured by Yun and Frederickson[19] for PAA by means of ^{14}C radioactive tracer technique, and later by Zupančič *et al.*[20] for MBBA by means of NMR pulsed field gradient technique coupled with multiple-pulse line-narrowing technique. The diffusion coefficients of HBAB were estimated from NMR relaxation measurements by the present authors.[21] These data are tabulated in Table 2.

Effective Anisotropy Factor of a Molecule in the Nematic State. This factor, ν, can be calculated from the data of η_1 and η_3 (Table 1) by using Eq. 12, and is shown in Table 2 for each of the three compounds. Temperature-dependences of ν in MBBA and in HBAB are also calculated††† and shown in Figs. 3 and 4, where temperatures are reduced by T_c, the clearing temperature. In these figures the temperature-dependences of the nematic orientational order parameter, $\langle p_2 \rangle$, are also shown.

Table 1. Experimental data of principal viscosity coefficients[a]

	Temperature	Principal viscosity coefficients		
	T/K	η_1	η_2	η_3/Pa s
PAA[a]	395.15	0.0092	0.0024	0.0034
MBBA[b]	298.15	0.1361	0.0240	0.0413
HBAB[c]	333.15	0.0960	0.0175	0.0290

a) Ref. 14. b) Ref. 17. c) Ref. 16.

Table 2. Comparison of theoretical prediction with experiment[a]

	T/K	ν_{theory}	$D_{//theory}$ / $D_{//expt}$	$D_{\perp theory}$ / $D_{\perp expt}$	$(D_{//}/D_{\perp})_{theory}$ / $(D_{//}/D_{\perp})_{expt}$
PAA	395.15	3.49	6.5×10^{-10}	5.5×10^{-10}	1.2
			4.1×10^{-10}	3.2×10^{-10}	1.3
MBBA	298.15	3.85	4.4×10^{-11}	3.1×10^{-11}	1.4
			1.2×10^{-10}	9.0×10^{-11}	1.3
HBAB	333.15	3.86	3.9×10^{-11}	2.9×10^{-11}	1.4
			(2.7×10^{-10})	1.7×10^{-10}	(1.6)

a) Diffusion coefficients are given in units of $m^2\ s^{-1}$. Experimental data of the diffusion coefficients are quoted from Ref. 19 (^{14}C-tracer) for PAA, from Ref. 20 (NMR pulsed field gradient) for MBBA, and from Ref. 21 (NMR relaxation) for HBAB. The data $D_{//}$ and $D_{//}/D_{\perp}$ of HBAB are less reliable because $D_{//}/D_{\perp} \to 2.0$ in the low temperature limit was assumed to derive them.

††† The data on the temperature-dependences of η_1 and η_3 of PAA are not available to the authors.

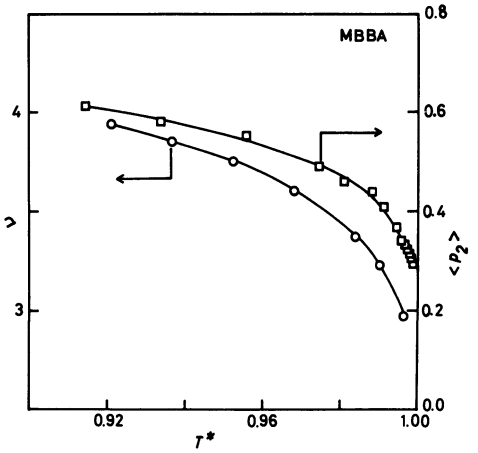

Fig. 3. Effective anisotropy factor ν of a molecule (○), and orientational order parameter $\langle p_2 \rangle$ (□) in MBBA as a function of reduced temperature, $T^* = T/T_c$. The ν was calculated from the data of Ref. 17 by using Eq. 12; the $\langle p_2 \rangle$ was taken from Ref. 22.

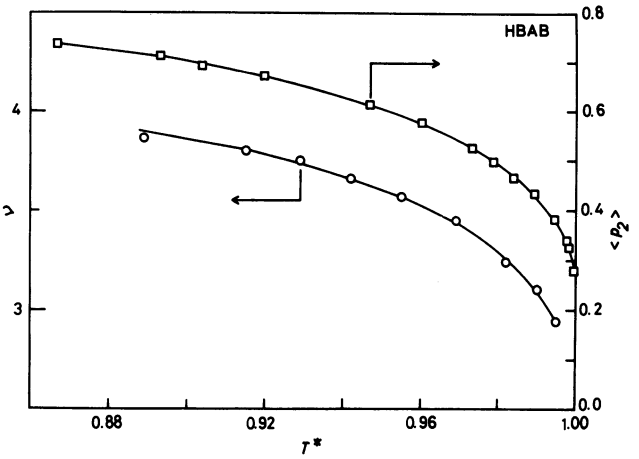

Fig. 4. Effective anisotropy factor ν of a molecule (○), and orientational order parameter $\langle p_2 \rangle$ (□) in HBAB as a function of reduced temperature, $T^* = T/T_c$. The ν was calculated from the data of Ref. 16 by using Eq. 12; the $\langle p_2 \rangle$ was taken from Ref. 21.

According to our model, ν calculated from η_1 and η_3 is a measure of the effective geometrical anisotropy of a molecule at each temperature, and should exhibit the temperature-dependence that resembles that of $\langle p_2 \rangle$ because $\langle p_2 \rangle$ is defined as the ensemble average of the second rank Legendre polynomial

$$\langle p_2 \rangle = \langle p_2(\cos\Theta) \rangle = \frac{1}{2}\langle 3\cos^2\Theta - 1 \rangle,$$

where Θ is the angle between $\boldsymbol{n}$ and the instantaneous molecular axis. In other words, both ν and $\langle p_2 \rangle$ are some motional average of the shape of molecular volume. The asymptotic value of ν in the low temperature limit, *i.e.*, on the condition $\langle p_2 \rangle = 1$ will be identical with ν derived on the basis of static molecular structure. The results of calculation given in Figs. 3 and 4 and Table 2 show that these are in fact the case: The ν_0, asymptotic value of ν in the low temperature limit, are

$$\nu_0 = 4.2 \pm 0.1 \text{ for MBBA,}$$

and

$$\nu_0 = 4\ 1 \pm 0\ 1 \text{ for HBAB.}$$

The ν of PAA is smaller than the ν of the other two compounds, corresponding to the fact that only PAA does not have an end chain. Thus, the calculated value of ν for the three compounds reflect their static molecular structure well in their relative as well as the absolute magnitude. The temperature dependence of ν in the two compounds has good parallelism to that of $\langle p_2 \rangle$.

We can thus conclude that the quantity ν derived from the "pencil model" has a clear physical significance as an effective anisotropy factor of a molecule in the nematic liquid crystalline state.

Self-diffusion Coefficient Tensor. Experimental data on self-diffusion coefficient tensor known until now[19,20] has revealed that its anisotropy, $D_{//}/D_{\perp}$, is not strongly dependent on material, and that $D_{//}/D_{\perp} \approx 1.4 \pm 0.2$ holds except in the close vicinity of T_c. The value κ, the only adjustable parameter in our theory is estimated to be $\kappa \approx 0.4$ by utilizing Eq. 13 and the viscosity data.

The principal values of the tensor $\boldsymbol{D}$ can now be calculated by using Eqs. 9—11 and the viscosity data (Table 1), and by assuming $\kappa = 0.4$. The value of a was taken from the X-ray work[23] ($\sqrt{3}\,a = 0.50$ nm, for all materials). The results of the calculation are tabulated and compared with the experimental data in Table 2. The agreements are satisfactory.

Kneppe-Schneider-Sharma's Empirical Law on η_3/η_2. Kneppe, *et al.*[11] pointed out recently that the quantity η_3/η_2 is almost independent of temperature, and has a relatively constant value irrespective of the material. The η_3/η_2 for MBBA and HBAB are shown in Fig. 5, which confirms that empirical law. The law is interesting as the quantity η_3/η_1, on the contrary, exhibits strong dependence on temperature as discussed above.

This law can be rationalized by our model. By rewriting Eqs. 12 and 13, the relations

$$\frac{\eta_3}{\eta_1} = \frac{9}{2\nu^2} \tag{14}$$

and

$$\frac{\eta_3}{\eta_2} = 3\kappa \frac{D_{//}}{D_{\perp}} \tag{15}$$

follow. Strongly temperature-dependent factor ν does not appear in Eq. 15. One can see that the empirical law by Kneppe *et al.* is consistent with the well-accepted knowledge[6] that the diffusion anisotropy $D_{//}/D_{\perp}$ is not strongly dependent on either material or temperature. If we take a rough approximation that diffusion anisotropy is independent of temperature, *i.e.*, $D_{//}/D_{\perp} = 1.40$ and taking $\kappa = 0.40$, Eq. 15 gives

$$\frac{\eta_3}{\eta_2} = 1.68, \tag{16}$$

which is in fair agreement with experiment as is seen in Fig. 5. The residual small dependence of η_3/η_2 on temperature will be attributed to the temperature-dependence of $D_{//}/D_{\perp}$.

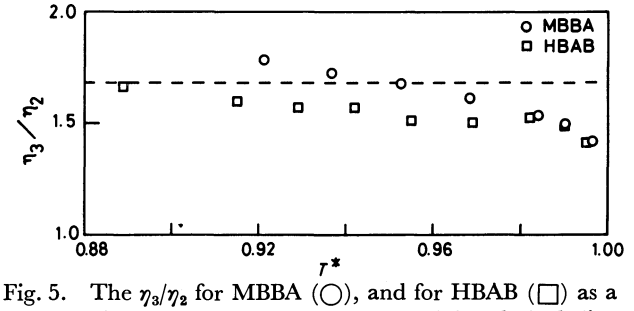

Fig. 5. The η_3/η_2 for MBBA (○), and for HBAB (□) as a function of reduced temperature. The dashed line represents Eq. 16.

In conclusion, it has been demonstrated that the properties of viscosity and self-diffusion in the nematic liquid crystals can be explained fairly well by using the "pencil model," a simple model which is based on the geometrical characteristic of the constituent molecule and which involves only one adjustable parameter κ ($\kappa = 0.4$ is universally adopted in this paper).

We thank Dr. Ch. Gähwiller for kindly providing us with the numerical data of the viscosity coefficients of HBAB. One of the authors (S. M.) is grateful to the fellowship of Yukawa Memorial Fund.

References

1) G. W. Gray, "The Molecular Physics of Liquid Crystals," ed by G. R. Luckhurst and G. W. Gray, Academic Press, New York and London (1979), Chap. 1.
2) S. Chandrasekhar, *Mol. Cryst. Liq. Cryst.*, **63**, 171 (1981).
3) W. J. Dunning, "The Plastically Crystalline State," ed by J. N. Sherwood, John Wiley and Sons, New York (1979), Chap. 1.
4) M. Miesowicz, *Nature*, **136**, 261 (1935).
5) R. S. Porter and J. F. Johnson, "Rheology," ed by F. Eirich, Academic Press, New York and London (1967), Vol. 4, p. 317; J. T. Jenkins, *Ann. Rev. Fluid Mech.*, **10**, 197 (1978).
6) S. Zumer and M. Vilfan, *Phys. Rev. A*, **17**, 424 (1978).
7) For a review on the continuum theory of viscoelastic properties of nematic liquid crystal, see Ref. 5 and P. G. de Gennes, "The Physics of Liquid Crystals," Clarendon Press, Oxford (1974), Chap. 5.
8) T. C. Lubensky, *Phys. Rev. A*, **2**, 2497 (1970).
9) H. Imura and K. Okano, *Jpn. J. Appl. Phys.*, **11**, 1440 (1972).
10) B. C. Benicewicz, J. F. Johnson, and M. T. Shaw, *Mol. Cryst. Liq. Cryst.*, **65**, 111 (1981).
11) H. Kneppe, F. Schneider, and N. K. Sharma, *Ber. Bunsenges. Phys. Chem.*, **85**, 784 (1981).
12) H. Eyring, *J. Chem. Phys.*, **4**, 283 (1936); S. Glasstone, K. J. Laidler, and H. Eyring, "The Theory of Rate Processes," McGraw-Hill, New York and London (1941).
13) H. Eyring and T. Ree, *Proc. Natl. Acad. Sci. U. S. A.*, **47**, 526 (1961); H. Eyring and M. S. John, "Significant Liquid Structures," John-Wiley and Sons, New York (1969), Chap. 5.
14) M. Miesowicz, *Nature*, **158**, 27 (1946).
15) W. Helfrich, *J. Chem. Phys.*, **50**, 100 (1969); **53**, 2267 (1970).
16) Ch. Gähwiller, *Mol. Cryst. Liq. Cryst.*, **20**, 301 (1973); Ch. Gähwiller, private communication.
17) H. Kneppe and F. Schneider, *Mol. Cryst. Liq. Cryst.*, **65**, 23 (1981).
18) R. S. Porter and J. F. Johnson, *J. Phys. Chem.*, **66**, 1826

(1962).
19) C. K. Yun and A. G. Frederickson, *Mol. Cryst. Liq. Cryst.*, **12**, 73 (1970).
20) I. Zupancic, J. Pirs, M. Luzar, and R. Blinc, *Solid State Commun.*, **15**, 227 (1974).
21) S. Miyajima, Ph. D. Thesis, Osaka University, Toyonaka (1981); S. Miyajima, N. Nakamura, and H. Chihara, *Mol. Cryst. Liq. Cryst.*, in press.
22) R. Cheng, *Mol. Cryst. Liq. Cryst.*, **30**, 155 (1975).
23) A. J. Leadbetter, P. M. Richardson, and N. Colling, *J. Phys.* (*Paris*), *Colloq.*, **36**, Cl-37 (1975).

 © 1983 The Chemical Society of Japan Bull. Chem. Soc. Jpn., 56, 405—411 (1983)

Electronic Spectra and Crystal Structure of Organic Radical Salt: Dimethyldibenzotetrathiafulvalenium Tetrafluoroborate

Chizuko TANAKA,* Jiro TANAKA, Karlheinz DIETZ,†† Chuji KATAYAMA, and Masashi TANAKA†

Department of Chemistry, Faculty of Science, Nagoya University, Chikusa-ku, Nagoya 464

†*College of General Education, Nagoya University, Chikusa-ku, Nagoya 464*

(Received August 16, 1982)

The single crystal of dimethyldibenzotetrathiafulvalenium tetrafluoroborate (1 : 1) has been prepared by electrocrystallization. The crystal structure has been determined by X-ray crystal analysis. The salt crystallizes in Ibam with $a=14.637(3)$, $b=17.625(6)$, $c=13.614(3)$ Å. The radical cations align along the c axis at nearly equal spacing forming eclipsed dimers and the dimeric units are stacked with a staggered mode. The electronic spectra of the radical cation and the dimer have been measured in solution and the assignment has been presented with an aid of the MO calculation by Pariser-Parr-Pople method. A charge transfer (CT) band observed in the dimer has been correlated with the charge resonance of unpaired electron between the HOMOs of the radical cations. Polarized reflection spectra of single crystal have been measured with three different crystal planes and the assignment of both the CT and molecular type bands have been confirmed with polarization measurement. The energy and the intensity of the CT band indicate that the unpaired electron is localized on each radical, but the CT configuration is involved significantly. The crystal is an insulator as is expected from the electronic structure; the large U, which is evidenced by the energy of the CT band, and the staggered packing hinders electronic conduction. It implies that a monovalent radical salt is difficult to be metallic unless a mixed valence state is involved.

Tetrathiafulvalene (TTF) and its family are good electron donors[1] which form donor-acceptor complex[2,3] and mixed valence salts as well as monovalence salts depending on the oxidation conditions. The oxidation is carried out either by the chemical method with suitable oxidants[4] or electron acceptor, or by electrochemical method.[5,6] A structural characteristic of organic metal is that the crystal has segregated columns of mixed valence donor or/acceptor stacks.[7] Torrance[8] discussed the relation between the redox-potentials of the donor and acceptor and the degree of charge transfer. The examination of the crystal structures and properties of ion-radical salts and charge transfer compounds is of theoretical and experimental importance to develop new organic metal.

The title compound is a 1 : 1 salt of cation radical of 5,5′-dimethyl-2,2′-bi-1,3-benzodithiol-2-ylidene, which is a dimethyl derivative of dibenzotetrathiafulvalene (DBTTF) and is abbreviated as DMDBTTF in the present paper. Hünig *et al.*[9] reported the oxidation potentials and the electronic spectra of TTF, DBTTF, DMDBTTF, and their cation radicals. The oxidation potential of DMDBTTF is slightly lower than that of DBTTF and the comparison of the structures of these complexes will be interesting. Both DMDBTTF–TCNQ[10] and DBTTF–TCNQ are insulators with alternating donor acceptor stacking.[11–13] DBTTF–$TCNQCl_2$ shows high electrical conductivity because it crystallizes in the segregated stacks of the donor and acceptor.[14,15] DBTTF–DDQ also shows high electrical conductivity and is considered as a mixed valence crystal with a segregated stack of acceptor.[16] DBTTF–$(BF_4)_{0.8}$ has been reported to be a mixed valence and conducting material,[17] but its crystal structure has not been reported yet.

In this paper we report the preparation, the crystal structure and the electronic spectra of DMDBTTF·BF_4 (1 : 1) crystal. We also discuss the electronic structure of the radical monomer and dimer as well as the crystal. The crystal structure found is an unique dimeric type and it is an insulator because the dimer is so stable that the delocalization of unpaired electron is limited within the dimer, and the CT state has fairly large energy characterized by U.

Preparation

DMDBTTF was prepared by the following reaction route using commercial GR. grade toluene-3,4-dithiol.

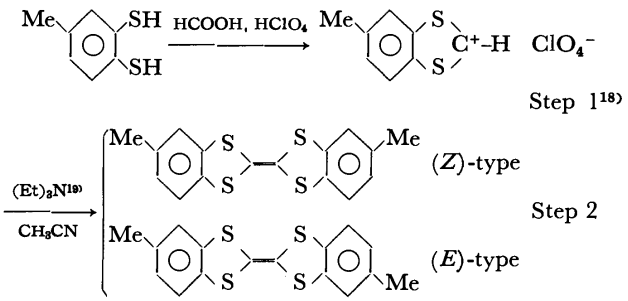

5-Methyl-1,3-benzodithiol-2-ylium perchlorate (4.2 g) obtained in Step 1 was dissolved in 180 ml of acetonitrile. Stirring the solution at 0 °C, acetonitrile solution of triethylamine (2.8 g/10 ml) was added dropwise. Yellow precipitate of DMDBTTF formed immediately. The stirring was continued for 15 min after the addition was completed. The precipitate was collected, washed with acetonitrile and dried. The yields of Steps 1 and 2 were 82 and 93% respectively. The product was purified by column chromatography and recrystallized with benzene and acetonitrile. As shown in above scheme two isomers, (*Z*) and (*E*), are considered for 5,5′-dimethyl-2,2′-bi-1,3-benzodithiol-2-ylidene. But it is not certain whether our product consists of only one isomer or a mixture of isomers.[10]

The electrocrystallization was carried out in the H shaped glass tube with Pt wire electrodes (same results were obtained with Ni electrodes) using dry CH_2Cl_2 solution of DMDBTTF and $(n\text{-Bu})_4N\cdot BF_4$ in inert atmosphere. The yellow color of

†† Permanent address: Institüt für Anorganische Chemie, Universität Heidelberg, West Germany. JSPS post-doctoral fellow 1981—1982 at Nagoya University.

neutral DMDBTTF changed to dark green by electrolysis. Within a few days dark violet prisms covered the (+) electrode, and these crystals were used for X-ray and spectral investigations.

Structural Determination

The crystal shape is shown in Fig. 1. The reflection color of the crystal is dark violet on the (010), silvery purple on the (110) and (1$\bar{1}$0), and brilliant pink on the (001) plane. The Weissenberg photographs showed the space group either Ibam or Iba2 from systematic absences. The reflection data for X-ray structural determination were collected with a Rigaku four-circle diffractometer AFC-5 using graphite-monochromatized Cu $K\alpha$ radiation. Intensities of 1617 reflections were measured up to $\theta=63°$ with the crystal of the size $0.2\times0.08\times0.08$ mm^3. The intensity statistics indicated the structure to be centrosymmetric, therefore the space group was determined as Ibam. The lattice parameters determined using 13 selected reflections are given in Table 1. The structure was solved by Patterson function method. The refinement of the structure was performed by the block-diagonal least-squares method with 1058 independent reflections of $|F_o|\geqq3\sigma$ with anisotropic thermal parameters. The final R index converged to 0.082.** The atomic parameters are shown in Table 2,

TABLE 1. CRYSTAL DATA OF DMDBTTF·BF_4

$C_{16}H_{12}S_4BF_4$	F.W.=419.33
Orthorhombic	Space group: Ibam
$a=14.637(3)$Å, $b=17.625(6)$Å, $c=13.614(3)$ Å	
$V=3512.1$ Å^3	
$D_m=1.584$ Mg m^{-3}, $D_c=1.586$ Mg m^{-3} ($Z=8$)	
μ(Cu $K\alpha$)$=51.2$ cm^{-1}	

TABLE 2. FRACTIONAL COORDINATES AND THEIR STANDARD DEVIATIONS[a)]

	x	y	z	B_{eq}/Å^2 [b)]
S(1)	0.0603(1)	0.1125(1)	0.1240(2)	3.8
S(3)	0.1404(1)	−0.0393(1)	0.1215(1)	3.8
C(2)	0.0414(4)	0.0157(4)	0.1234(5)	3.5
C(3a)	0.2158(4)	0.0347(4)	0.1272(5)	3.5
C(4)	0.3127(6)	0.0266(5)	0.1311(6)	5.4
C(5)	0.3667(6)	0.0903(5)	0.1365(7)	5.4
C(6)	0.3264(5)	0.1634(5)	0.1394(6)	4.8
C(7)	0.2367(6)	0.1735(5)	0.1365(6)	5.2
C(7a)	0.1778(5)	0.1063(4)	0.1296(5)	3.8
C(m)	0.3916(8)	0.2356(7)	0.1459(10)	9.7
B	0.1240(10)	0.3388(10)	0.0	5.4
F(1)	0.0980(6)	0.2672(4)	0.0	8.2
F(2)	0.0694(6)	0.3948(5)	0.0	10.9
F(3)	0.1933(6)	0.3477(4)	0.0640(9)	15.9

a) The estimated standard deviations are given in parentheses and refer to the last decimal position of respective values. b) $B_{eq}=8\pi^2(U_1^2U_2^2U_3^2)^{1/3}$, where U_i is the root-mean-square deviation in the ith principal axis of the thermal ellipsoid.

** The anisotropic thermal factors and the complete F_o-F_c data are deposited as Document No. 8311 at the Office of the Editor of Bull. Chem. Soc. Jpn.

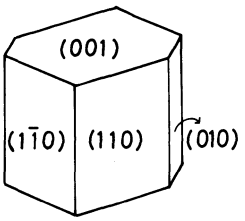

Fig. 1. Crystal shape.

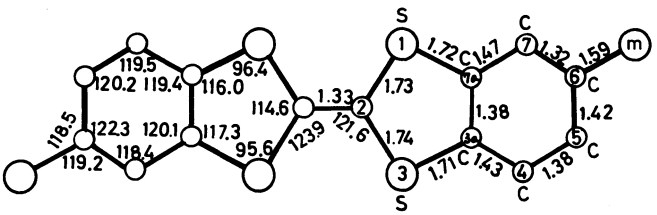

Fig. 2. Bond length (Å) and angles (°) of DMDBTTF$^+$.

and the molecular structure is illustrated in Fig. 2.

The DMDBTTF radical cation is approximately planar, but it is slightly bent towards both ends. The crystallographic two-fold axis coincides with the two-fold axis of the molecule. The least-squares plane for the half of the molecule, the 1,3-benzodithiole ring, is represented as $-0.0348x-0.0371y+0.9987z=1.6100$ (x, y, and z are coordinates in Å referred to the a, b, and c crystal axses, respectively). The deviation of the atoms from the plane is less than 0.04 Å. The dihedral angle between this and the other corresponding plane is 5.8°. The boron atom and two of the four fluorine atoms, F(1) and F(2), of the tetrafluoroborate ion are on the mirror plane and the remaining two fluorine atoms, F(3), are above and below the plane keeping the mirror symmetry. Three residual peaks, which could not be explained by hydrogen atoms, were found in the difference Fourier map. Two of them were around the anion site indicating disordered arrangement of anions. The other one was found in the region to which the methyl group attached to C(5) could be assigned. This suggests the stack includes some molecules whose methyl groups occupy the site on C(5) instead of C(6). However the distance between the methyl group on C(5) and the fluorine atom, F(2), is considerably shorter than normal contact. This may be related to the unusually short bond length of B–F(2), 1.27 Å, and the large anisotropy of thermal ellipsoid of boron atom. Hence, it is considered that the disordered arrangement of the anion is closely connected with that of the cation radical.

The projection of the cations onto three different planes are illustrated in Figs. 3, 4, and 5. Two adjacent cations form an eclipsed dimer whose interplanar spacing at the central bond region is 3.36 Å. The S···S contacts in the dimer are 3.31 and 3.37 Å. These values are comparable with the values found in the eclipsed dimer in TTF·I_3[20] and other integral oxidation state salts.[21,22] The dimers align along the c axis in a staggered mode.

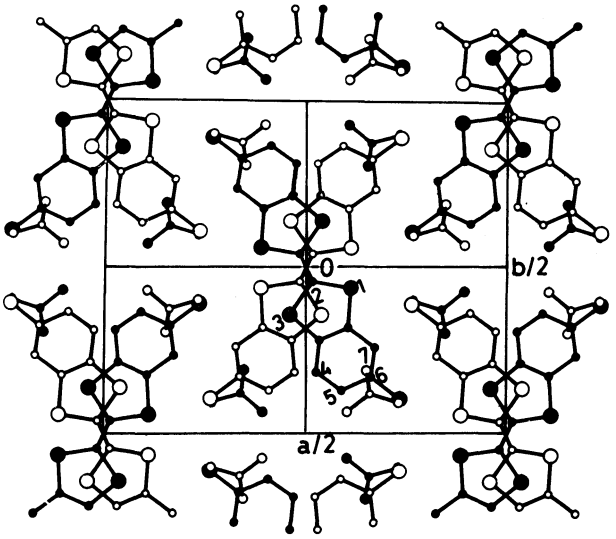

Fig. 3. Projection of the structure onto the (001) plane. The molecules shown with black circles locate above and below the mirror plane at $z=0$. The molecules shown with white circles locate above and below the mirror plane at $z=1/2$. Boron atoms are on the mirror planes.

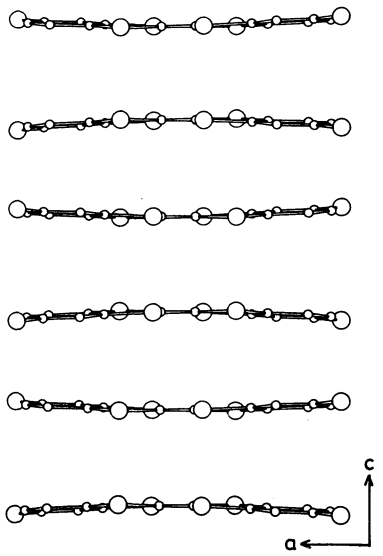

Fig. 4. Projection of the structure onto the (010) plane.

The interplanar spacing between the centers of molecules in the staggered overlapping is 3.45 Å which is almost equal to the interplanar spacing in the dimer. Such a pattern of cation stacking is rather unique as a monocation salt. The structural characteristic will be reflected on the optical and other electronic properties of the crystal.

Electrical Conductivity

The powder conductivity of the crystal is measured with a compressed pellet (diameter=5 mm) under the pressure of 20 kg/cm^2 at room temperature. The conductivity was $\sigma=5\times10^{-8}\ \Omega^{-1}\,cm^{-1}$. It indicates that the crystal is an insulator. This is reasonable since the crystal is not a mixed valence having an odd electron

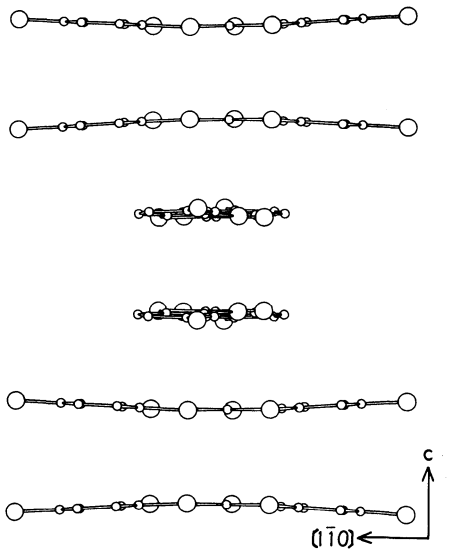

Fig. 5. Projection of the structure onto the (110) plane.

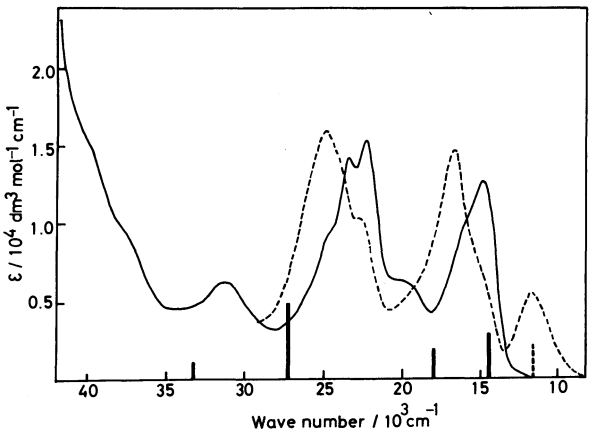

Fig. 6. Absorption spectra of DMDTTF$^+$ in solution (——, 0.26×10^{-5} mol dm^{-3} in CH_2Cl_2 at room temp; ------, 0.67×10^{-3} mol dm^{-3} in CH_3CN at *ca.* −40 °C) and calculated values (——, L1, M1, L2, and M2 for the monomer, from right to left; ------, CT for the dimer).

on each site as is shown by structural analysis and stoichiometry. The electrostatic repulsive energy is big enough to prevent electrons moving freely in the crystal. This point will be discussed below from optical evidence and its theoretical analysis.

Electronic Spectra of the Cation Radical in Solution

Electronic absorption spectra of the cation radical salt in monomeric and dimeric states measured in dichloromethane and in acetonitrile solutions, respectively, are shown in Fig. 6. As reported by Hünig *et al.*,[9] the neutral molecule has only a weak absorption band in the region below 25000 cm^{-1}, therefore the strong bands observed at 14600 and 22000—24000 cm^{-1} region are attributed to the radical monomer. The monomer has no absorption band in the region between 5000—11000 cm^{-1}. The electronic spectra of the dimer

was already reported by Hünig *et al.*,[9] and we confirmed their result more clearly by measuring the spectra at lower temperature as is shown in Fig. 6. In the dimeric state, the CT band between the radicals is observed at 11600 cm^{-1}. The bands at 14600 and 22000—24000 cm^{-1} in the monomeric state are shifted by 2000—2600 cm^{-1} to higher energy upon dimerization. Similar spectral change was reported in TTF^+ dimer.[23]

Calculation of the Excited States of the Monomer

In order to give an assignment of radical monomer spectra, Pariser-Parr-Pople type calculation for the open shell system was performed. The computer program developed in our laboratory based on the scheme of Lowitz[24] was used for the calculation. The value of the valence state orbital energies and the one-center Coulomb integrals used in our calculation were as follows; $U_{cc}=-11.22$ eV, $(CC|CC)=10.60$ eV, $U_{ss}=-9.16$ eV, $(SS|SS)=10.01$ eV. The values for U_{cc} and $(CC|CC)$ are the standard values. The value of $(SS|SS)$ has been evaluated from the data of Hinze and Jaffe[25] by the use of Pariser-Parr approximation. The value of U_{ss} was selected in order that the result of the calculation might be in reasonable agreement with the observed data. The core resonance integral β was calculated by the use of Wolfsberg and Helmholz formula,[26] where the proportional constant was set as $K=0.39$. All calculations were carried out using the single exponent Slater AO. The results of the calculation on energies, intensities and polarizations are shown in Table 3 and illustrated in Fig. 6. The bands at 14600 and 22000—24000 cm^{-1} are found to be polarized in the direction of the molecular long axis (L1 and L2), while the 19500 and 31500 cm^{-1} bands are polarized in the direction of the molecular short axis (M1 and M2). The agreement of the calculated and observed values was satisfactory particularly on sequence of transition energies and intensities, and on polarizations. The polarization characteristics were all confirmed by the polarized spectral measurement of the single crystal as is discussed below.

Table 3. ELECTRONIC EXCITED STATES OF RADICAL CATION

	Monomer spectra in solution		Open sheell P-P-P caluculation		
State	Energy/10^3 cm^{-1}	f	Energy/10^3 cm^{-1}	Pol.	f
L1	14.6	0.19	14.5	L	0.28
	16.0				
M1	19.5	0.05	17.9	M	0.18
L2	22.1	0.22	27.3	L	0.52
	23.4				
	24.8				
M2	31.1	0.13	33.3	M	0.11
	Dimer spectra in solution		Calculated excited states of dimer		
CT	11.6	0.12	11.6	N	0.17
L1	16.6	0.40	16.7	L	0.38
M1	19.6	0.09			
L2	25.0	0.68	24.2	L	0.44

Theoretical Treatment of the Dimer Spectra

Before going to the discussion of the crystalline spectra, we will consider the electronic structure of the dimer, since molecules are paired tightly in the crystal forming the eclipsed dimer. The molecular overlap integral between the molecules in the eclipsed pair is 0.0260, while that between the molecules in the staggered pair is 0.0015, therefore the molecular interaction is much larger in the eclipsed pair than in the staggered pair. Under this condition the crystalline electronic states can be described as an assembly of the eclipsed dimer.

The electronic structure of the cation radical dimer can be described by Hubbard Hamiltonian as was shown in our earlier paper on TCNQ complexes.[7] The electronic states are factored into a symmetric and an antisymmetric states under the inversion symmetry of the dimer. Matrix elements of the secular equations are given as follows.

$$\begin{vmatrix} 0 & 2t_{mm} & 0 \\ & U & \sqrt{2}\,t_{mm-1} \\ & & \Delta-\delta \end{vmatrix} \begin{matrix} \text{G} \\ \text{CT}^{(+)} \\ \text{LE}^{(+)} \end{matrix} \qquad \begin{vmatrix} U & \sqrt{2}\,(t_{mm-1}+2\text{D}) \\ & \Delta+\delta \end{vmatrix} \begin{matrix} \text{CT}^{(-)} \\ \text{LE}^{(-)} \end{matrix}$$

Symmetric state Antisymmetric state

The dipole transition from the G to the $CT^{(-)}$ and $LE^{(-)}$ states are allowed by the selection rule. The diagonal energy of the CT state is given as $U=\eta(U^{pp}_{mm}-U^{pq}_{mm})$, where U^{pp}_{mm} is the Coulomb repulsion energy between two electrons on the (mth) MO (HOMO) of the same molecule (p), and U^{pq}_{mm} is the one between two electrons on the HOMOs of the adjacent molecule (p and q). The numerical values of U^{pp}_{mm} and U^{pq}_{mm} were calculated as 4.12 and 2.44 eV respectively, by the use of Nishimoto-Mataga potential. The difference between these two terms was 1.68 eV. Δ is the energy of the LE state in the monomer (1.81 eV for the L1 state and 2.74 eV for the L2 state). η is the screening constant due to the electronic polarization. t_{mm} in the off-diagonal matrix element is a transfer integral, the numerical value of which is estimated by the relation $t_{mm}=-kS_{mm}$ where S_{mm} is the overlap integral between the HOMOs m, and k is an empirical parameter. t_{mm-1} and D (the dipole interaction energy between the $CT^{(-)}$ and $LE^{(-)}$ states) can be ignored because the symmetries of the states are different and the transition moments are orthogonal to each other. The diagonal energy for the $LE^{(-)}$ states, Δ, are lifted by the amount δ, the exiton type dipole-dipole interaction, which was not explicitly described in the earlier paper.[7] The numerical value of δ was evaluated as 0.07 eV, by a dipole calculation based on a weak coupling model scaled by the transition density method[27] for the L1 and the L2 bands. When the set of parameters $\eta=0.74$ and $k=10.0$ eV were chosen to estimate U and t, the calculated transition energies from the G state to the $CT^{(-)}$, $L1^{(-)}$, and $L2^{(-)}$ states are in good agreement

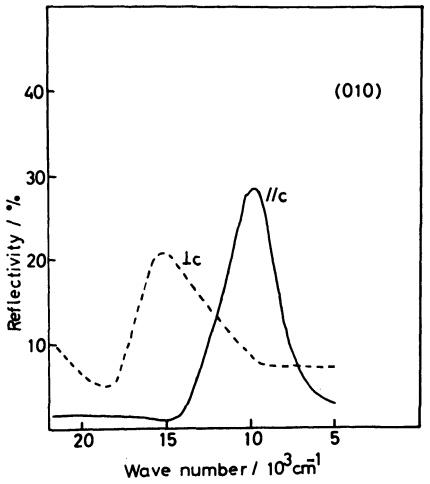

Fig. 7a. Polarized reflection spectra on the (010) plane.

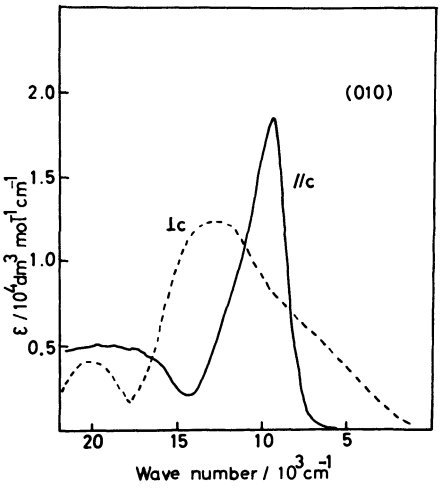

Fig. 7b. Polarized absorption spectra (K-K transformed) on the (010) plane.

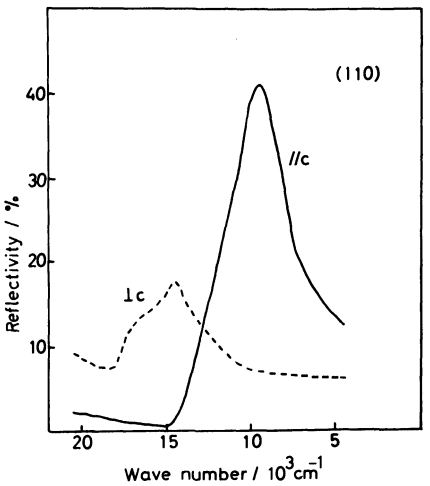

Fig. 8a. Polarized reflection spectra on the (110) plane.

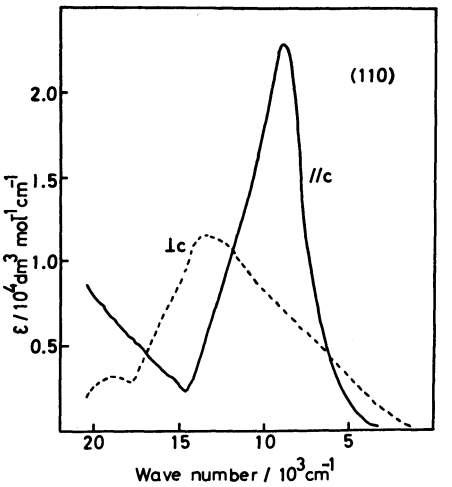

Fig. 8b. Polarized absorption spectra (K-K transformed) on the (110) plane.

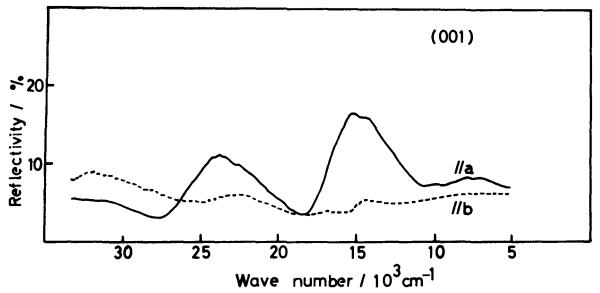

Fig. 9a. Polarized reflection spectra on the (001) plane.

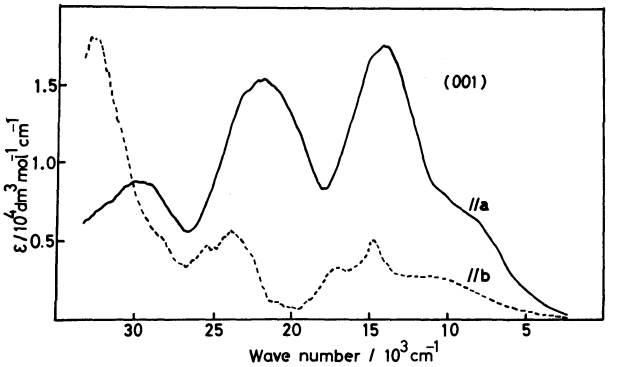

Fig. 9b. Polarized absorption spectra (K-K transformed) on the (001) plane.

with the observed energies of the dimer in solution (Table 3). The assignment of the dimer spectra is confirmed by this calculation.

Electronic Spectra of Crystals

The crystalline reflection spectra were measured with the crystals of the size about $0.3\times0.3\times0.6$ mm^3 for the (010) and (110) faces and $0.5\times0.3\times0.2$ mm^3 for the (001) face by the use of a polarized microspectrophotometer. The results are shown in Figs. 7—9. The calculation of the excited states were carried out for these planes by summing up the dipole-dipole interaction over molecules within 200 Å radius and 30 Å depth in order to consider the directional dispersion of the exciton states.[28,29] The transition energies of the dimer

in solution were used for the diagonal energies of the CT, L1, M1, and L2 bands. However, we made the correction for the standard of the state energies by $-1000\ cm^{-1}$ for the CT level and $-2000\ cm^{-1}$ for other levels by taking into account the crystalline polarization effect. For the calculation of the off-diagonal energies of the dipole-dipole interaction, the length of transition moment estimated from the solution spectra of the dimer for each bands were used. All calculations were based on the dimer unit and the transition moments are placed in the center of the dimer. By this procedure the second order mixing and the exaggeration of the band shift were avoided. The results of calculation are tabulated in Table 4 and the calculated transition energies are compared with the observed crystalline spectra in the following.

In Figs. 4 and 5 the projection of molecules onto the (010) and (110) planes are illustrated. On these planes, the CT band is expected along the c axis. In Figs. 7 and 8 the reflectivities, Kramers-Kronig transformed spectra are illustrated. Although the absolute magnitude of reflectance is different between the planes, the CT band is found with a great intensity only along the c axis. The intensity is enhanced in the crystal by a factor of 2—4 as compared with that of the dimer in solution. This gives an evidence of an increase of the intermolecular CT interaction in the crystal. The observed CT energies were at 9000—9400 cm^{-1}, while the calculated values were 9000—9100 cm^{-1}, hence the agreement between the calculated and observed values was quite satisfactory. The result shows that the electron electron repulsion U is predominant in determining the energy level of the CT band in the monovalence radical salt. A similar spectral characteristic was reported by Kuroda *et al.*[30] and by Torrance *et al.*[23] on several TTF salts.

For the (001) plane the projection of molecules is shown in Fig. 3 and the reflection spectra and Kramers-Kronig transformation to molar absorption coefficent are shown in Fig. 9. The long-axis of the molecule is at the angle of 24.5° with the a axis, therefore the L type bands should be stronger along the a axis than the b axis, while that of the M type bands are stronger along the b axis. The Kramers-Kronig transformed spectra are in perfect agreement with this expectation that the L1 band appearing at 15000 cm^{-1} region and the L2 band at 22000 cm^{-1} range are stronger along the a axis than the b axis, while the M1 and M2 bands found at 17000 and 31000 cm^{-1}, which are correlated with the solution bands at 19500 cm^{-1} and 31500 cm^{-1}, are stronger along the b axis than along the a axis. The observed band position for the (001) plane are well explained by the calculation of the exciton splitting, however, the Davydov splitting for the L1 band is reversed in order. The calculated intensities shown in Table 4 are larger by a factor of 2, but the order of its size is in agreement with the observed ones. Although the intermolecular CT transition is not expected with the (001) plane since it is polarized along the c axis, but the absorption tail is found around at 10000 cm^{-1} region, and it may be due to the admixture of the c axis transition in this measurement because the incident beam has a glazing angle of 4—11°, hence it may have a slight component along the c axis.

Table 4. Polarized crystalline spectra

Plane	State	Pol. axis	Energy/$10^3\ cm^{-1}$		f	
			Obsd	Calcd	Obsd	Calcd
(001)	L1	a	14.2	14.8	0.50	0.91
		b	14.7	13.3	0.09	0.22
	M1	a		17.4		0.07
		b	17.0	17.6	0.05	0.24
	L2	a	22.5	23.2	0.33	1.81
		b	22.0	22.0	0.17	0.28
	M2	a	31.0		0.14	
		b	29.5		0.48	
	CT	c	—	10.3	—	0.35
(110)	CT	c	9.0	9.0	0.50	0.31
	L1	[1$\bar{1}$0]	13.5	16.2	0.36	0.23
				14.2		0.11
(010)	CT	c	9.4	9.1	0.23	0.32
	L1	a	13.0	14.8	0.43	0.91

Thus the assignment of electronic transitions is confirmed by the polarized spectral measurement and the calculation of exciton band shift for each planes.

Conclusion

$(DMDBTTF)^+$ radical obtained by electrochemical oxidation of neutral molecule crystallizes with BF_4^- forming a pseudo-one-dimensional crystal with unpaired electrons on each site. The radicals form eclipsed dimers in the crystal, and the dimers are aligned along the crystalline c axis with a staggered mode. This type of molecular packing may be occurred through a steric hindrance of the methyl groups at both ends. In this structure the transfer integral for the eclipsed pair (t_1) is much larger than that of the staggered pair (t_2), therefore the electronic structure of the dimer is conserved in the crystal. Namely the electronic spectra of the crystal is almost same with that of the dimer in solution, except that the molecular bands are red shifted and the CT band is enhanced. It reflects that the molecular character of the dimer is reserved in the crystal in spite of the CT interaction is conceivable between the dimer. It is reasonable since t_2 is negligibly small as compared to t_1.

The energy of the CT band gives an estimate of U for the dimer interaction, where the value of U is the change of repulsive energy of electrons accompanied with the charge transfer. It is significantly large as $U=1.24$ eV ($\simeq 5t_1$). The CT configuration in the ground state is estimated as 12% from the normalized wavefunction. A fairly large oscillator strength of the CT band is accounted for by this contribution. The crystal is an insulator in spite of apparent one-dimensional stacking of radicals, because U is large as usually found in monovalence salts. Moreover, the one-dimensional equality of the electronic structure is not realized since $t_1 \gg t_2$. Anyway the mixed valence state is most important to find organic metal.

All computations were carried out at the Nagoya University Computation Center; NUNICS program was used for crystal structure analysis.

The authors thank to JSPS for the fellowship to K. Dietz.

References

1) F. Wudl, G. M. Smith, and E. J. Hufnagel, *Chem. Commun.*, **1970**, 1453.
2) J. Ferraris, D. O. Cowan, V. Walatka, Jr., and J. H. Perlstein, *J. Am. Chem. Soc.*, **95**, 948 (1973).
3) A. J. Heeger, "Highly Conducting One-Dimensional Solids," ed by J. T. Devreese, R. P. Evrard, and V. E. van Doren, Plenum Press, New York (1979), p. 69.
4) F. Wudl, D. E. Schafer, W. M. Walsh, Jr., L. W. Rupp, F. J. DiSalvo, J. V. Waszczak, M. L. Kaplan, and G. A. Thomas, *J. Chem. Phys.*, **66**, 377 (1977).
5) F. B. Kaufman, E. M. Engler, D. C. Green, and J. Q. Chambers, *J. Am. Chem. Soc.*, **98**, 1596 (1976).
6) K. Bechgaard, C. S. Jacobsen, K. Mortensen, H. J. Pedersen, and N. Thorup, *Solid State Commun.*, **33**, 1119 (1980).
7) J. Tanaka, M. Tanaka, T. Kawai, T. Takabe, and O. Maki, *Bull. Chem. Soc. Jpn.*, **49**, 2358 (1976).
8) J. B. Torrance, *Acc. Chem. Res.*, **12**, 79 (1979).
9) S. Hünig, G. Kiesslich, H. Quast, and D. Scheutzow, *Justus Liebigs Ann. Chem.*, **1973**, 310.
10) G. S. Bajwa, K. D. Berlin, and H. A. Pohl, *J. Org. Chem.*, **41**, 145 (1976).
11) R. P. Shibaeva and O. V. Yarochkina, *Dokl. Akad. Nauk SSSR*, **222**, 91 (1975).
12) H. Kobayashi and J. Nakayama, *Bull. Chem. Soc. Jpn.*, **54**, 2408 (1981).
13) T. J. Kistenmacher, T. J. Emge, F. M. Wiygul, W. A. Bryden, J. S. Chappell, J. P. Stokes, L-Y. Chiang, D. O. Cowan, and A. N. Bloch, *Solid State Commun.*, **39**, 415 (1981).
14) C. S. Jacobsen, H. J. Pedersen, K. Mortensen, and K. Bechgaard, *J. Phys. C*, **13**, 3411 (1980).
15) H. Soling, G. Rindorf, and N. Thorup, *Acta Crystallogr., Sect. B*, **37**, 1716 (1981).
16) J. J. Mayerle and J. B. Torrance, *Bull. Chem. Soc. Jpn.*, **54**, 3170 (1981).
17) I. V. Krivoshei, V. P. Babiyczuk, I. M. Guella, I. F. Golovkina, N. V. Mansia, V. A. Starodub, and S. A. Chueva, *Phys. Status Solidi A*, **50**, K197 (1978).
18) L. Soder and R. Wizinger, *Helv. Chim. Acta*, **42**, 1733 (1959).
19) F. Wudl, M. L. Kaplan, E. J. Hufnagel, and E. W. Southwick, Jr., *J. Org. Chem.*, **39**, 3608 (1974).
20) R. C. Teitelbaum, T. J. Marks, and C. K. Johnson, *J. Am. Chem. Soc.*, **102**, 2986 (1980).
21) B. A. Scott, S. J. La Placa, J. B. Torrance, B. D. Silverman, and B. Welber, *J. Am. Chem. Soc.*, **99**, 6631 (1977).
22) K. Yakushi, S. Nishimura, T. Sugano, H. Kuroda, and I. Ikemoto, *Acta Crystallogr., Sect. B*, **36**, 358 (1980).
23) J. B. Torrance, B. A. Scott, B. Welber, F. B. Kaufman, and P. E. Seiden, *Phys. Rev. B*, **19**, 730 (1979).
24) D. A. Lowitz, *J. Chem. Phys.*, **46**, 4698 (1967).
25) J. Hinze and H. H. Jaffé, *J. Am. Chem. Soc.*, **84**, 540 (1962).
26) M. Wolfsberg and L. Helmholtz, *J. Chem. Phys.*, **20**, 837 (1952).
27) J. N. Murrell and J. Tanaka, *Mol. Phys.*, **7**, 363 (1964).
28) M. R. Philpott, *J. Chem. Phys.*, **58**, 588 (1973).
29) J. Tanaka, M. Tanaka, and M. Hayakawa, *Bull. Chem. Soc. Jpn.*, **53**, 3109 (1980).
30) T. Sugano, K. Yakushi, and H. Kuroda, *Bull. Chem. Soc. Jpn.*, **51**, 1041 (1978).

A Simple Pressurized High-temperature Proton NMR Apparatus for the Thermal Degradation of Polymers†

Shigezo SHIMOKAWA,* Eiji YAMADA, and Kazuo MAKINO††
NMR Laboratory, Faculty of Engineering, Hokkaido University, Sapporo 060
††*Department of Applied Chemistry, Faculty of Engineering, Hokkaido University, Sapporo 060*
(Received August 17, 1982)

A simple pressurized, externally heated, high-temperature proton NMR apparatus for the temperature range from 293 to 823 K and pressure range from 0.1 to 40 MPa is reported. The sample cell has a capillary opening and the vessel is pressurized by inert gas. An application of this apparatus to the thermal degradation of poly(vinyl chloride) is presented.

Some of polymers in the molten state at high temperature are in an equilibrium where competitive reactions such as the decomposition, polymerization and polycondensation are balanced. And there are some ordered states such as liquid crystalline phases (mesophase) in the molten state under growing temperature.[1] Previously we showed[2] that the thermal decomposition of poly(vinyl chloride) (TD-PVC) is a good model to study such a molten state at high temperatures. It was found[3] that high-temperature high resolution proton NMR provided a useful tool to detect the dynamic structure of molten polymers at high temperature.

However, such an atmospheric pressure experiment gives sometimes insufficient information, because the escape of gaseous products causes much loss of the liquid residue product. It is well known that a pressure vessel for thermal reaction is almost black box which is used only for the detection of thermal change.[4]

There is dangerous and difficult procedure for us to increase the pressure, keeping high temperature in the static magnetic field. Several studies[5-11] of high-temperature and high-pressure NMR only focused on pure liquid materials, for example, water or molten metals. As far as we know, there is no example of application of NMR under pressure to the process of thermal reaction at high temperature. Recently we developed an internally heated high-temperature and high-pressure C-13 NMR apparatus for direct measurements of pyrolysis of polymers.[12] In this report, the design of an externally heated high-temperature and high-pressure proton NMR apparatus and its application to thermal degradation process of TD-PVC have been presented.

Design of Apparatus

We constructed a heat and pressure resisting vessel for NMR study at high temperature of 823 K under high pressure of 40 MPa. Figure 1 shows the block-diagram of the homemade apparatus used in this study. The apparatus consists of a high resolution magnet, an externally heated high pressure vessel, a pressurizing system with inert gas, and an external field frequency lock system. A wide gap (6 cm) electromagnet of modified JEOL 3H type was used. The electromagnet was equipped with homogeneity current shim coils, a flux stabilizer and an external ^1H field frequency lock system in order to keep the good homogeneity and stability of the magnetic field. The basic spectrometer

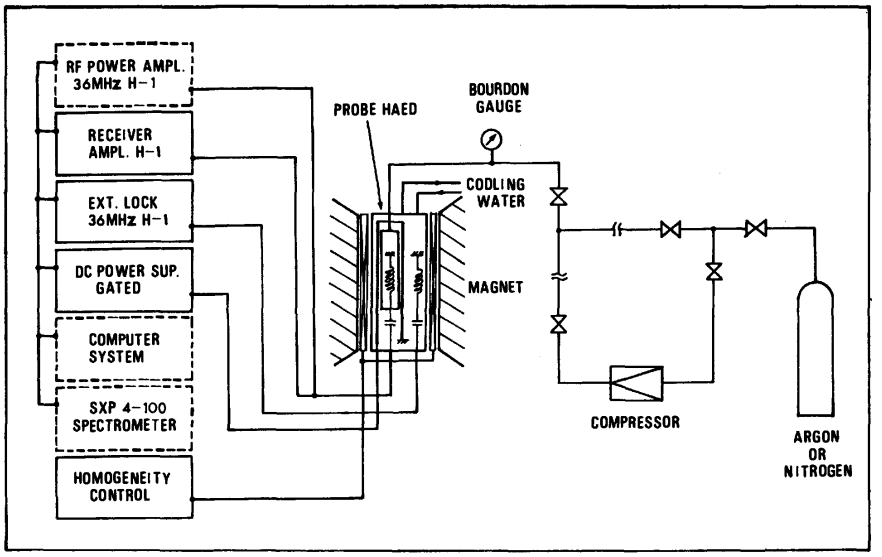

Fig. 1. Block-diagram of a simple pressurized high-temperature proton NMR apparatus, ------ denotes Bruker spectrometer units.

† Presented at the 19th Symposium on NMR, Sapporo, September, 1980.

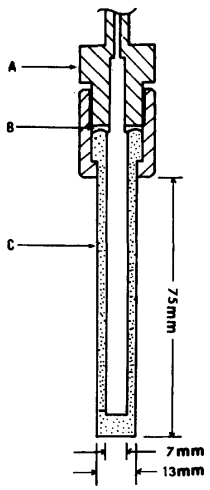

Fig. 2. High-pressure vessel of titanium alloy.
A; SUS 316 stainless steel, B; copper sealing washer, C; titanium alloy vessel.

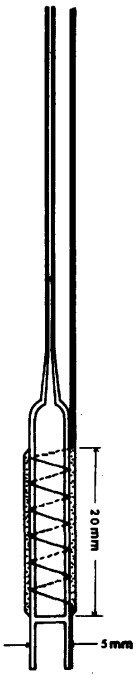

Fig. 3. Sample cell with a capillary opening.

used was a Bruker SXP 4-100 high power pulse spectrometer with Nicolet BNC-12 computer system.

Figure 2 shows the high pressure vessel made of titanium alloy (KS-130A, supplied by Kobe Steel Co. Ltd.). The vessel was externally heated. The tensile strength of the titanium alloy was 11600 kg cm^{-2} over extended periods (10000 h) at 673 K. The maximum working pressure of the vessel was reached over 40 MPa, but in this study the working pressure was restricted to 30 MPa, because of the limiting pressure of the Bourdon gauge and valves. Figure 3 shows a simple sample cell. The cell was made of heat resisting glass and it consists of three parts, *i.e.*, the bottom of the cell, the body of coil and the capillary. The bottom of the cell, which was needed for homogeneity of H_1 field for relaxation measurement. The sample cell was simply inserted into the vessel. 0.2 g of powder sample can be put into the cell. After introduction of the sample, the top of the cell was made in the form of capillary. Resonance coil for each sample cell was wound and fixed on the cell by heat resisting cement (Sauereisen cement No. 8). Rf lead wire was insulated by 1 mm ceramic tube. The sample cell was always renewed after each experimental run and tuning for probe balance was readjusted easily. The top of the vessel which contained the closure plug and nuts with rf terminals was cooled by a water jacket: The sealing was made by copper washer and an rf lead wire was insulated by ceramic tubes. The outlet of the rf lead wire was sealed and insulated by Teflon cone, which was located away from the vessel. One of the terminals of the lead wire was grounded to the vessel. The escape of the sample from the sample cell as gaseous products at high temperature was much reduced by use of capillary. Very small amount of eluted gas caused slight contamination of the inner wall of the vessel as well as outer surface of the sample cell. This did not, however, give any trouble to get a good signal from the sample.

A high temperature probe assembly was made of aluminum block. A pure Nichrome wire noninductively wound on a quartz tube (25 mm o.d.). The temperature on the surface of the bottom of the titanium vessel was monitored by a YEW 2575 digital thermometer using an Alumel/Chromel thermocouple. Cooling water of controlled temperature was flown through the aluminum jacket. There was no dissipation of heat to the magnet and to external lock probe even at temperature above 823 K. 150 W of the electric power was used to elevate temperature up to 823 K. Readjustment of the field homogeneity control was necessary for each setting of the power supply. The resolution of signal for water proton of 5 mm sample cell in this vessel was about 10 Hz at 293 K, 1 MPa without sample spinning. Line width of 10 Hz is considered to be good enough for measurements of the thermal decomposition process of polymers in the molten state, because at high temperature proton spectra of molten polymer are usually complicated by superposition of various signals and line widths become much broader due to thermally produced radicals.

Results and Discussion

Figure 4 shows the proton spectra of TD-PVC at various temperatures and pressures. Assignment of the two peaks was made by comparing them with the peaks of pure ethylbenzene. The chemical shift difference of the two peaks was 5.5 ppm (200 Hz). Because TD-PVC was thermally pretreated to liberate HCl at 623 K under atmospheric pressure, only hydrocarbons were considered in the residue of the thermal degradation PVC. It is known[2] that the TD-PVC melts at about 673 K. Then, liquid crystalline phases were formed in the TD-PVC under growing temperature.[3] This formation of liquid crystalline phases depended on heating rate. The heating rate was 2 K min^{-1} in further experiments. From the temperature and pressure dependence of the spectra given in Fig. 4, it is

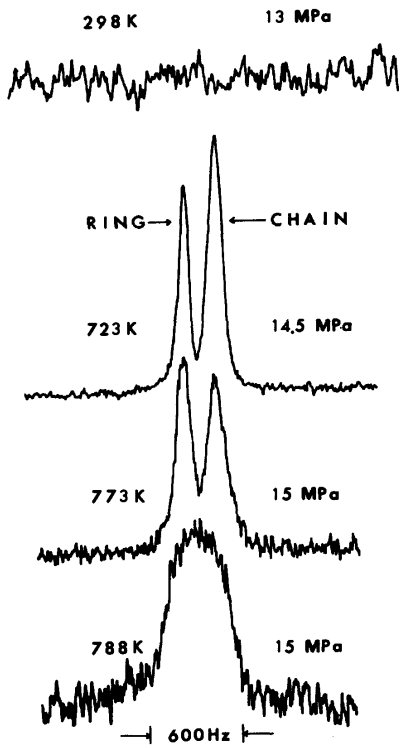

Fig. 4. Temperature and pressure dependence of proton spectra for TD-PVC.

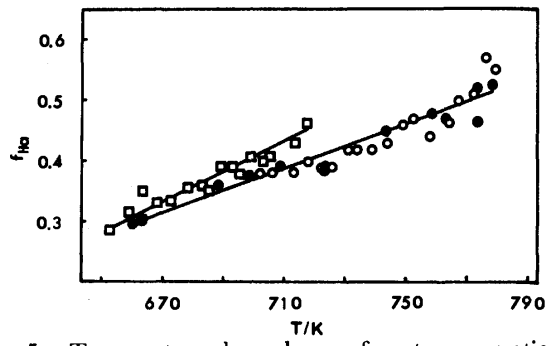

Fig. 5. Temperature dependence of proton aromaticity of TD-PVC.
□: Atmospheric pressure; pressurized condition. ●: (13 to 15 MPa), ○: (23 to 31 MPa).

found that the ring formation already occurs in the residue of TD-PVC at 723 K. At this temperature, aromatic protons are 30% of total protons. On further heating, the line width of the two peaks is broadened. At 815 K and 15 MPa, the spectrum shows an early stage of growing of liquid crystalline phases. The formation of the liquid crystalline structure was confirmed by the observation of polarized light-microscopy of quenched samples from this temperature.

It is very important to compare the present results with the data on the same material under atmospheric pressure. We define the hydrogen aromaticity as

$$f_{Ha} = H_{aroma}/(H_{alipha}+H_{aroma}), \quad (1)$$

where H_{aroma} and H_{alipha} are the integral intensities of signals for aromatic and aliphatic protons, respectively. At atmospheric pressure the hydrogen aromaticity (f_{Ha}) became 0.5 at 723 K but the same aromaticity was attained at 773 K under the pressurized condition, as shown in Fig. 5. The difference in the observed aromaticity for the atmospheric and pressurized conditions can be explained by the fact that the data at atmospheric pressure did not give a correct aromaticity, because the experiment at atmospheric pressure was made allowing an elusion of hydrocarbon gases from degradated TD-PVC residue. It was found that the pressure dependence of the aromaticity was not detected in the pressure range from 15 to 30 MPa.

It is known that free radicals are generated in the dehydrochlorinated PVC at high temperature.[2] The concentration of the unpaired electrons in the TD-PVC residue quenched from 673 K was found to $\approx 10^{18}$ spins·g^{-1} from ESR measurements. The TD-PVC melt at 683 K takes a polyene-like structure and the unpaired electrons are delocalized in the aromatic ring and polyene chains. Although there are two possible mechanisms for proton spin-lattice relaxation, *i.e.*, proton-proton dipolar interaction and proton-electron interaction, the latter is reasonably assumed to be predominant. We examined the spin-lattice relaxation time, T_1, of two kinds of protons. The values of T_1 measured by partially relaxed Fourier transform method at 733 K and 17 MPa were 151 and 153 ms for the ring and chain protons, respectively. These values of T_1 are larger by a factor of about 1.5 than those obtained at atmospheric pressure and 693 K.[3] We suppose that the existence of free radicals is suppressed in the pressurized condition by the remaining lower molecular weight fraction. This corresponds to the observed longer relaxation times in the pressurized condition at 733 K.

Conclusion

A simple pressurized high-temperature proton NMR apparatus was constructed and applied to the study of thermal degradation process of TD-PVC up to 823 K and 30 MPa. From the temperature and pressure dependence of the observed proton spectra, correct values of hydrogen aromaticity were obtained as a function of temperature. This result was also supported by spin-lattice relaxation measurements. This apparatus can also be used for investigation of thermal reaction processes of various organic compounds at high pressures, which are ordinarily carried out in autoclaves.

We greatly appreciate the encouragement of the work by Mr. Yuichi Kanda, Dr. Toshio Sato, and Professor J. Sohma and the financial support of Nishin Soft Science Foundation.

References

1) J. D. Brooks and G. H. Taylor, *Carbon*, **3**, 185 (1965).
2) S. Shimokawa, Y. Ohno, J. Sohma, H. Hirano, and K. Endoh, *Nippon Kagaku Kaishi*, **1973**, 2016.
3) S. Shimokawa and E. Yamada, *Am. Chem. Soc., Div. Polym. Chem. Prepr.*, **20**, 685 (1979); T. Yokono, K. Miyazawa, Y. Sanada, E. Yamada, and S. Shimokawa, *Fuel* **58**, 237 (1979); K. Miyazawa, T. Yokono, Y. Sanada, T. Chiba, E. Yamada, and S. Shimokawa, "Advances in Chemi-

stry Series 192, Coal Structure," ed by M. L. Gorbaty and K. Ouchi, Am. Chem. Soc., Washington (1981), pp. 59—71; S. Shimokawa and E. Yamada *Bull. Facul. Eng. Hokkaido University*, **102**, 155 (1981).

4) A. Sawaoka and S. Saito, "Shin Jikken Kagaku Koza," ed by the Chemical Society of Japan, Maruzen, Tokyo (1977), Chap. 10, pp. 536—539.

5) G. B. Benedek, "Magnetic Resonance at High Pressure," Interscience publishers, New York (1963).

6) D. W. G. Smith and J. G. Powles, *Mol. Phys.*, **10**, 451 (1966).

7) J. G. Powles and M. C. Gouch, *Mol. Phys.*, **16**, 349 (1969).

8) J. Jonas, *Rev. Sci. Instr.*, **43**, 643 (1972).

9) T. H. DeFries and J. Jonas, *J. Magn. Reson.*, **35**, 111 (1979).

10) W. J. Lamb and J. Jonas, *J. Chem. Phys.*, **74**, 913 (1981).

11) U. El-Hanay and W. W. Warren, Jr., *Phys. Rev. Lett.*, **34**, 1276 (1975).

12) S. Shimokawa and E. Yamada, *J. Magn. Reson.*, **51**, Jan. (1983), in press.

Infrared Intensities in Methyl Chloride. I. The Fundamental Bands

Shigeo KONDO,* Yoshinori KOGA, Taisuke NAKANAGA, and Shinnosuke SAËKI
National Chemical Laboratory for Industry, Tsukuba Research Center, Yatabe, Ibaraki 305
(Received August 20, 1982)

The integrated intensities of the fundamental bands of CH_3Cl and CD_3Cl molecules have been measured by the pressure broadening technique. The Coriolis intensity perturbation between ν_3 and ν_6 bands of CD_3Cl has been analysed to determine the sign to be negative. The intensity analysis has been carried out to determine the correct signs of $(\partial p/\partial Q_i)$. The resulting signs are $(-++)$ for A_1 and $(-+-)$ for E species. The $(\partial p/\partial S_J^R)$ values as well as the atomic polar tensors have been obtained.

Recently, several investigations have been carried out on the infrared intensities of a series of methyl halide molecules.[1-4] This is not only because these molecules are fundamental ones from a spectroscopic viewpoint, but because there has been a well known sign ambiguity problem which was described in a very clearcut manner by Abbate and Gussoni.[3]

A first study on the subject made by Barrow and McKean[5] did not give any definite answer to this question, for they only measured intensities of the parent molecules, and had nothing but chemical intuition to determine the correct sign combination for $(\partial p/\partial Q_i)$, which can not be enough to solve this tough problem in the infrared intensity studies. On the other hand, Dickson *et al.*[6] have measured the fundamental band intensities for both CH_3X and CD_3X molecules, where X=Cl, Br, and I. Their measurements were carried out very carefully, and reasonably accurate intensity values have been obtained except those which are badly overlapped with each other. In fact, they have almost succeeded in determining the signs of $(\partial p/\partial Q_i)$ simply by comparing the values of the intensity parameters obtained for the two isotopic molecules for various sign combinations. Their best sign choice was $(-++)$ for A_1 and $(-+-)$ for E species.[6] However, Russell *et al.*[1] have pointed out that a number of other sign combinations become possible when the intensity errors due to overlappings and also the force field errors are taken into account.

On the other hand, Newton and Person[2] have selected a sign combination of $(\partial p/\partial Q_i)$ of methyl fluoride on the basis of the CNDO/2 method, and extended that particular choice to the methyl chloride molecule. Their signs are $(-++)$ both for A_1 and E species.[2] Later, however, Abbate and Gussoni[3] have pointed out that the choice for methyl fluoride made by Newton and Person[2] is definitely against the isotopic invariance rule.

In a previous paper,[4] we have shown that this confusion on the sign problem of methyl fluoride was completely due to an erroneous intensity value of ν_6 band of CD_3F molecule. The final answer was found to be $(-++)$ both for A_1 and E species of this molecule. Then, a question arises whether we can still extend the same sign combination to the methyl chloride molecule.

Considering the experimental results reported thus far, there seems little doubt that the signs for A_1 species are $(-++)$. However, the signs for E species are still debatable. Therefore, the current question is whether the recently improved technique for the infrared intensity measurement and analysis can give a definite answer for the E species signs. For that purpose, we have carefully remeasured all the fundamental band intensities of CH_3Cl and CD_3Cl molecules. We have also determined the sign of the Coriolis interaction between ν_3 and ν_6 of CD_3Cl molecule. Then, a least squares calculation has been carried out to determine definitely the correct signs of $(\partial p/\partial Q_i)$.

Experimental

The CH_3Cl gas was purchased from Takachiho Chemical Co. and CD_3Cl gas from Merck Sharp and Dohme Co. Canada. The purity of CH_3Cl was stated as 99.5% and that of CD_3Cl was 99 atom%. Inspection of full region of the infrared spectra of these gases well guaranteed the stated sample purities.[7]

Spectra were all observed with a resolution of 0.25 cm^{-1} (optical path length of 4 cm, with Happ-Genzel apodization). A Nicolet model 7199 FT-IR spectrophotometer was used with a mercury-cadmium telluride detector. For intensity measurements, a 6 cm high pressure cell accommodated with KBr windows was used under a total pressure of 1.11×10^6 Pa. In order to investigate rotational fine structure of the bands, a conventional 10 cm glass body cell was also used. The sample pressure was measured with an MKS baratron type 220, which covers a pressure range of 1.333×10^5 to 1.333×10^2 Pa with a stated accuracy of 0.25%. Integration of the "isolated" band area were carried out in a manner similar to the one described in Ref. 8. Separation of the overlapping bands was done by the simulation technique as usual.[4,9]

Results

Fundamental Band Intensities. In the CH stretching region of CH_3Cl molecule, ν_1 and ν_4 overlap with each other. Also $2\nu_5$ band appears with a fairly high intensity presumably due to the Fermi resonance with the ν_1 band. Separation of the ν_1 and ν_4 bands was made by a simulation calculation taking account of the Fermi resonance between ν_4 and $3\nu_6$ bands, by using the molecular parameters in Refs. 10 and 11. The result is shown in Fig. 1. The $2\nu_5$ intensity was obtained simply by integrating the absorption area from 2920 through 2820 cm^{-1}. The integrated band intensity is defined by

$$B_i = (1/nl)\int_{\text{band}} \ln(T_0/T)\mathrm{d}\nu, \qquad (1)$$

where n is the sample concentration (mol/m^3), l is the optical path length (m), T and T_0 are the transmittance

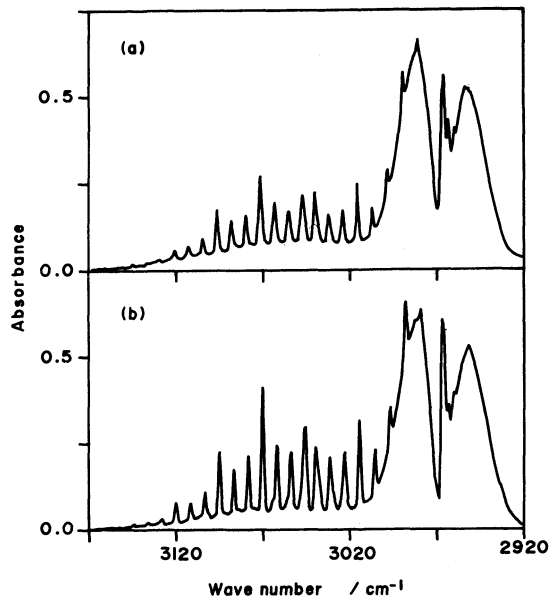

Fig. 1. Observed and calculated spectra of ν_1 and ν_4 region of CH_3Cl. (a) Observed spectrum with a sample pressure of 1.245×10^4 Pa in a 6 cm cell under a total presure of 1.11×10^6 Pa of nitrogen. Resolution of 0.25 cm^{-1} was used. (b) Calculated spectrum with the molecular parameters in Refs. 10 and 11.

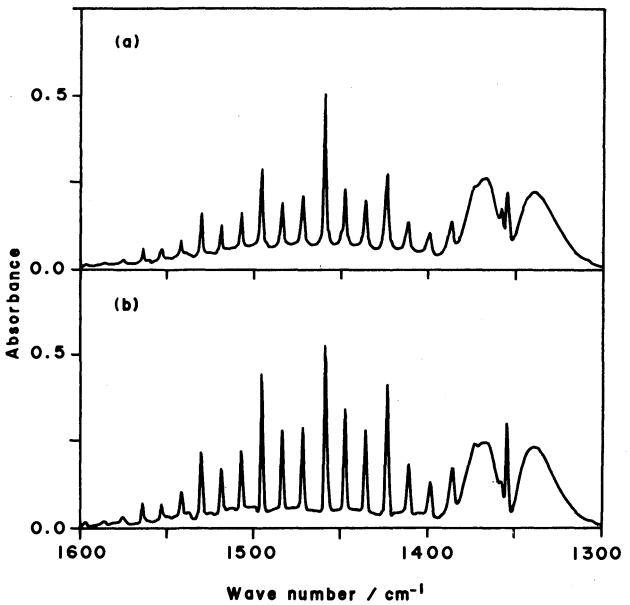

Fig. 2. Observed and calculated spectra of ν_2 and ν_5 region of CH_3Cl. (a) Observed spectrum with a sample pressure of 1.245×10^4 Pa in a 6 cm cell under a total pressure of 1.11×10^6 Pa of nitrogen. Resolution of 0.25 cm^{-1} was used. (b) Calculated spectrum for a negative Coriolis perturbation between ν_2 and ν_5. The molecular constants in Ref. 14 were utilized.

values of the cell with and without the sample gas, respectively. The band intensity is given by units of km/mol. In the CH deformation region, ν_2 and ν_5 bands overlap with each other. Band separation was made by using the molecular parameters reported in the literature,[12–14] taking into account the Coriolis

Table 1. Observed band intensities of methyl chloride (km/mol)

Band		ν_i[a]/cm^{-1}	This work[b]	Ref. 2	Ref. 1
CH_3Cl	ν_4	3038.91[c]	10.77(120)	9.69	9.70
	ν_1	2967.76[d]	19.15(144)	17.56	20.17
	$2\nu_5(a_1)$	2879	4.16(34)	3.86	7.46
	ν_5	1452.12[e]	11.38(78)	12.31	9.72
	ν_2	1354.95[e]	8.41(68)	6.80	8.97
	ν_6	1017.26[e]	3.85(42)	4.02	4.19
	ν_3	732.88[e]	23.69(94)	23.19	20.94
CD_3Cl	ν_4	2283.29[e]	5.42(12)	5.12	
	ν_1	2160.24[e]	11.96(24)	11.39	
	$2\nu_5(a_1)$	2104	2.56(13)	3.34	
	$2\nu_2$	2034.39[e]	1.29(10)	...	
	ν_5	1059.970[f]	5.76(46)	6.91	
	ν_2	1028.673[f]	12.37(37)	10.76	
	ν_6	767.61[e]	0.57(10)	1.11	
	ν_3	701.36[e]	17.70(35)	15.36	

a) Frequencies for ^{35}Cl molecules. b) Numbers in parentheses are the uncertainties to be used in the intensity calculation, which are the largest of 0.10 km/mol, 2 % of the band intensity and the estimated error for the band. The estimated error is twice the standard error from the Beer's law plot plus something due to the overlappings, where necessary. c) Ref. 10. d) Ref. 11. e) Ref. 12. f) Ref. 14.

interaction between ν_2 and ν_5. The result is shown in Fig. 2. On the other hand, the ν_3 and ν_6 bands are well isolated from other bands, and their intensities were obtained by simply integrating the respective band area. The result is summarized in Table 1.

In the CD stretching region of CD_3Cl, ν_4 band is well isolated from other bands. As for the ν_1 band, which is the symmetric CD_3 stretching mode, there are two neighboring overtone bands, $2\nu_5$ and $2\nu_2$. However, since their band contours are all similar (parallel bands), and overlappings are not so serious, separation of these bands is by no means difficult.

On the other hand, in the CD deformation region ν_2 and ν_5 bands are mutually heavily overlapped, and furthermore, they are in strong Coriolis resonance as well. Their separation was carried out by simulation method by using the parameters reported in Ref. 14, and is shown in Fig. 3.

ν_3 band is the strongest fundamental band of the CD_3Cl molecule, near which a weak perpendicular band of ν_6 is observed. Since the ν_6 band is very much weaker than the ν_3 band, it is quite possible that the former suffers a considerable intensity perturbation from the latter. By using the molecular parameters in Refs. 12 and 14, together with the calculated value for the zeta constant $\zeta_{3,6a}^{y}$ (+0.276), simulation calculations have been carried out for different signs of the perturbation. If the sign is negative, the higher frequency region of ν_6 band is such that partly obscured Q branch peaks are distributed over a rather thick back ground which is composed of the degraded R and P branches, and in the lower frequency region rather sharp Q branches are located against a relatively thin back ground. On the other hand, if the sign is positive,

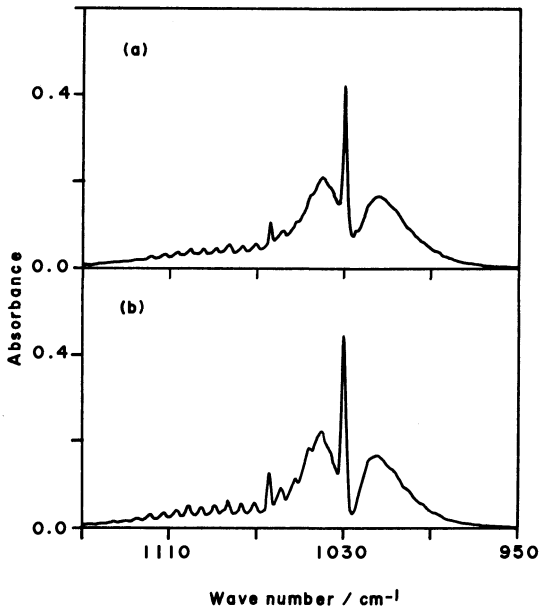

Fig. 3. Observed and calculated spectra of ν_2 and ν_5 region of CD_3Cl. (a) Observed spectrum with a sample pressure of 6.64×10^3 Pa in a 6 cm cell under a total presure of 1.11×10^6 Pa of nitrogen. Resolution of 0.25 cm^{-1} was used. (b) Calculated spectrum for a negative Coriolis perturbation between ν_2 and ν_5. The molecular constants in Ref. 14 were employed.

TABLE 2. SYMMETRY COORDINATES OF METHYL CHLORIDE

A_1:	$S_1=(\Delta r_1+\Delta r_2+\Delta r_3)/\sqrt{3}$
	$S_2=[K(\Delta\alpha_1+\Delta\alpha_2+\Delta\alpha_3)-(\Delta\beta_1+\Delta\beta_2+\Delta\beta_3)]/\sqrt{3(1+K^2)}$ [a]
	$S_3=\Delta R$
E:	$S_{4a}=(2\Delta r_1-\Delta r_2-\Delta r_3)/\sqrt{6}$
	$S_{5a}=(2\Delta\alpha_1-\Delta\alpha_2-\Delta\alpha_3)/\sqrt{6}$
	$S_{6a}=(2\Delta\beta_1-\Delta\beta_2-\Delta\beta_3)/\sqrt{6}$
	$S_{4b}=(\Delta r_2-\Delta r_3)/\sqrt{2}$
	$S_{5b}=(\Delta\alpha_2-\Delta\alpha_3)/\sqrt{2}$
	$S_{6b}=(\Delta\beta_2-\Delta\beta_3)/\sqrt{2}$

a) $K=-3\sin\beta\cos\beta/\sin\alpha$.

completely the reverse is true. These features are exactly what are expected from the theory by DiLauro and Mills.[15] The observed spectrum definitely agrees better with the one calculated for a negative sign, as shown in Fig. 4. Thus, the sign of the ν_3-ν_6 interaction in CD_3Cl molecule has been determined as negative. The ν_6 band intensity was obtained through simulation calculation for a pressurized spectrum of this region.

Intensity Calculation. If the pressure broadening effect is sufficiently large compared with the employed spectral resolving power,[16] the integrated band intensity B_i can be taken as the absolute intensity A_i which is expressed by,[17]

$$A_i = (N\pi/3c^2)(\partial p/\partial Q_i)^2, \quad (2)$$

where N is Avogadro's number, c is the light velocity, p is the molecular dipole moment, and Q_i is the ith normal coordinate. Further, $(\partial p/\partial Q_i)$ is expressed by a linear combination of $(\partial p/\partial S_j)$, where S_j is the jth symmetry

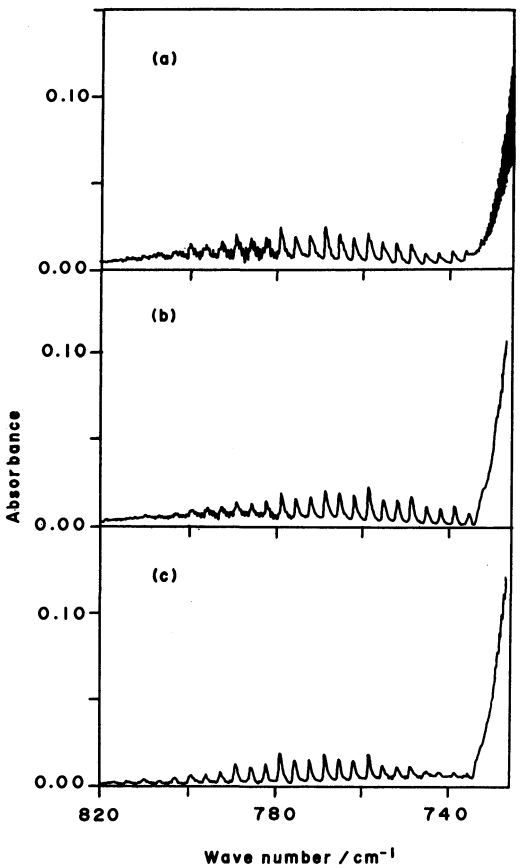

Fig. 4. Observed and calculated spectra of ν_6 region of CD_3Cl. (a) Observed spectrum with sample pressure of 4.95×10^3 Pa in a 10 cm cell.Resolution of 0.25 cm^{-1} was used, and calculated spectra (b) with a negative Coriolis perturbation between ν_6 and ν_3, and (c) with a positive interaction. The molecular constants reported in Ref. 14 were used.

coordinate, namely,

$$(\partial p/\partial Q_i) = \Sigma(\partial p/\partial S_j)L_{ji}, \quad (3)$$

where L_{ji} is the L matrix element.

As usual, the intensity parameter is defined by the following equation,[18]

$$p_j = (\partial p/\partial S_j^R) = (\partial p/\partial S_j) + p^0K_j, \quad (4)$$

where p^0 is the permanent dipole moment and K_j is the rotational correction coefficient. The symmetry coordinates were defined the same as in Ref. 4, and are shown in Table 2. The molecular coordinate system and the internal coordinates are shown in Fig. 5. As usual, we have preferred to set up the whole molecular system so that we may have a positive permanent dipole moment. (The positive dipole moment is defined to be directed from the negative to the positive end of the molecule. There may be little doubt that the chlorine atom is the negative end of the methyl chloride molecule.) The absolute value of p^0 has been determined as 1.869(10) D by Shulman *et al.*[19]

Table 3 shows the L matrices for CH_3Cl and CD_3Cl molecules, which are obtained by using the harmonic force field reported by Duncan *et al.*[20] Definition of the symmetry coordinates in reference molecule S_j^R

Table 3. L matrices of methyl chloride[a)]

CH_3Cl	A_1:	1.008	−0.012	0.001	E:	1.051	0.021	−0.001
		−0.075	1.376	0.168		0.112	1.499	−0.222
		−0 044	0.084	0 321		−0.101	0.315	0.906
CD_3Cl	A_1:	0.722	0 003	0.009	E:	0.781	0.000	0.010
		−0.133	1.060	0.022		0.192	1.100	−0.085
		−0.066	0.148	0.292		−0.137	0.135	0.693

a) Calculated for the ^{35}Cl species from the force field and molecular geometry in Ref. 19. Units are either $u^{-1/2}$ or rad $u^{-1/2}$Å^{-1} depending on whether S_j is the bond stretching or angle bending coordinate.

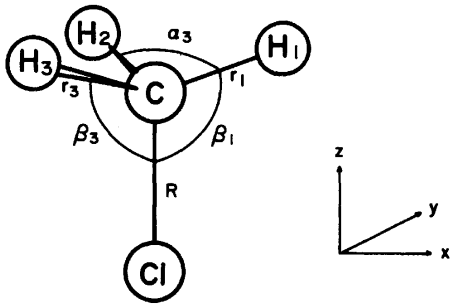

Fig. 5. The methyl chloride molecule, molecular axis, and the internal coordinates.

Table 4. Symmetry coordinates of reference molecule S_j^R and the rotational correction coefficients K_j in methyl chloride[a)]

S_j^R	Fixed atoms	CH_3Cl	CD_3Cl
4a	C, Cl	+0.038	+0 057
5a	C, Cl	+0.037	+0 056
6a	C, Cl	−0 070	−0.111

a) Units are Å^{-1} for S_{4a} and rad^{-1} for S_{5a} and S_{6a}.

and the values of the rotational correction coefficients are listed in Table 4.

Intensity calculations were carried out by a least squares method varying the signs of $(\partial p/\partial Q_i)$ for A_1 and E species separately. For the calculation, the residual value was defined as,

$$\text{Res.} = \Sigma(X_i^{obsd} - X_i^{calcd})^2/(\Delta X_i^{obsd})^2, \quad (5)$$

where X_i denotes the dipole moment derivatives $(\partial p/\partial Q_i)$ for the parent molecule and the band intensity A_i for the isotopic species. The signs of $(\partial p/\partial Q_i)$ for the parent molecule are actually examined in that calculation. The residual value was used to examine the propriety of the sign combination postulated in the calculation.[18)] Since there are three normal vibrations both for A_1 and E species, eight sign combinations are possible for each of them. In Table 5, residual values have been obtained from the least squares calculations for eight sign combinations of both symmetry species.

In A_1 species, considering that the number of the intensity data is six, possibility is limited either to $(-++)$ or to $(+--)$ set, for these are only sets whose residuals are less than the data number of six, while those of other sets are by far larger than that. Similarly, in E species, the residual values for $(++-)$ and $(-+-)$ sets are much smaller than the others. Therefore, we may pick up these two sets as possible ones. But for the sake of security, we also included $(+--)$ and $(---)$ sets together to go to further checking.

Table 5. Residual values from the least squares calculations for the intensities varying the signs of $(\partial p/\partial Q_i)$[a)]

A_1 species $(123)^H(123)^D$	Res.	E species $(456)^H(456)^D$	Res.
(+++)(+++)	91	(+++)(+++)	236
(−++)(−++)	2.0	(−++)(−++)	220
(+−+)(+−+)	689	(+−+)(+−+)	159
(−−+)(−−+)	608	(−−+)(−−+)	156
(++−)(++−)	608	(++−)(++−)	0.8
(−+−)(−+−)	689	(−+−)(−+−)	1.5
(+−−)(+−−)	2.0	(+−−)(+−−)	20
(−−−)(−−−)	91	(−−−)(−−−)	34

a) The residual is defined in the text; Eq. 5.

Table 6. Comparison of the observed values of the intensity parameters with the *ab initio* values

Parameter	Obsd[a)] $(-++)(-+-)^H$	Obsd[a)] $(-++)(++-)^H$	*ab initio*[b)]
p_1/D Å^{-1}	−0.610(12)[c)]	−0.610	−0.78
p_2/D rad^{-1}	0.197(13)	0.197	0.40
p_3/D Å^{-1}	2.224(29)	2.224	2.97
p_4/D Å^{-1}	−0.294(6)	0.356	−0.43
p_5/D rad^{-1}	0.353(9)	0.348	0.34
p_6/D rad^{-1}	−0.293(12)	−0.299	−0.38

a) The preferred combination is $(-++)(-+-)^H$. b) Calculated with the 6-31G* basis set; Ref. 20. c) Numbers in parentheses are the standard errors from least squares calculations.

Now, we can further restrict possibility by the Coriolis sign information. According to DiLauro and Mills,[15)] the sign of ν_2-ν_5 Coriolis interaction in CD_3Cl molecule is negative. Since the zeta constant $\zeta_{2,5a}^y$ is calculated as negative (−0.596) from the present L matrices, which are shown in Table 3, the sign of the product $(\partial p/\partial Q_2)(\partial p/\partial Q_5)$ must be positive, *i.e.* $(\partial p/\partial Q_2)^D$ and $(\partial p/\partial Q_5)^D$ are of the same sign. Further, as described in a previous section, the sign of the ν_3-ν_6 Coriolis perturbation of CD_3Cl has been found to be negative. Since the zeta constant $\zeta_{3,6a}^y$ is calculated to be +0.276 from the L matrix, the sign of $(\partial p/\partial Q_3)(\partial p/\partial Q_6)^D$ must be negative. Therefore, inspection of the $(-++)$ and $(+--)$ sets of A_1 species together with the $(++-)$, $(-+-)$, $(+--)$, and $(---)$ sets of E species reveals that only possible combinations are $(-++)$ set from A_1 together with either $(++-)$ or $(-+-)$ set

from E species.

Finally, of the two sets preferred in E species, there is at present no experimental preference of one to the other. We need additional information to determine the final choice. For that purpose, the CNDO/2 method[2] or ab initio calculation[21] may be helpful. Table 6 shows a comparison of the resulting parameter values for the $(-++)(-+-)^{H}$ and $(-++)(++-)^{H}$ sets with the *ab initio* values. As is seen in the table, the obtained values of the parameters other than p_4 agree well with the *ab initio* result. As for the parameter p_4, the sign is different in the two sets while the magnitude is obtained almost the same. The *ab initio* calculation predicts it to be negative. Therefore, the $(-++)(-+-)$ set may be the correct signs of $(\partial p/\partial Q_i)$ for methyl chloride. Table 7 shows a comparison of the observed band intensities with the calculated. The polar tensor[22] calculated from these parameter values is shown in Table 8.

TABLE 7. OBSERVED AND CALCULATED INTENSITIES OF THE FUNDAMENTAL BANDS OF METHYL CHLORIDE(km/mol)

Band		Obsd[a]	Calcd[b]
CH_3Cl	ν_1	23.31(148)[c]	22.40
	ν_2	8.41(68)	9.13
	ν_3	23.69(94)	23.55
	ν_4	10.77(120)	9.50
	ν_5	11.38(78)	11.46
	ν_6	3.85(42)	3.71
CD_3Cl	ν_1	15.82(32)[d]	15.92
	ν_2	12.37(37)	12.13
	ν_3	17.70(35)	17.77
	ν_4	5.42(12)	5.44
	ν_5	5.76(46)	5.76
	ν_6	0.57(10)	0.60

a) Numbers in parentheses are the uncertainty indicators, reciprocal squares of which were utilized as the weighting factors in the least squares calculation. See Table 1. b) Calculated with the parameter values obtained for the $(-++)(-+-)^{H}$ signs. c) Sum of the intensities for ν_1 and $2\nu_5$ in Table 1. d) Sum of the intensities for ν_1, $2\nu_5$, and $2\nu_2$ in Table 1.

Discussion

As was discussed by Russell *et al.*,[1] major contributions to the errors in the resulting intensity parameters are from the uncertainties in the intensity data and force constants. For the experimental data utilized in Ref. 1, the latter was shown to be much smaller than the former. Furthermore, the errors in the force field utilized in the present study have been reduced much (on the average, a factor of ten for A_1 and of about three for E species[20]). Therefore, in the present case, contribution from the force error should be negligible and the intensity factor only remains effective, which has also been reduced much, indeed. Besides that, we have been able to use two pieces of definite information on the relative signs of $(\partial p/\partial Q_i)$. These were obtained from the Coriolis intensity analyses in Ref. 15 (for ν_2-ν_5) and in the present study (for ν_3-ν_6) for the CD_3Cl molecule. Considering these conditions, it is a natural consequence that the correct sign combination has definitely been determined in this study.

It has become widely known that *ab initio* calculations can be critically checked by use of the experimentally determined values and signs of the molecular dipole moment and its derivatives. Wiberg[21] has carried out *ab initio* calculations to predict that the correct signs of $(\partial p/\partial Q_i)$ for methyl fluoride is $(-++)(-++)$, which perfectly agreed with the result in Ref. 4. He has also calculated the dipole derivatives of methyl chloride, and expected that the signs may be $(-++)$ for A_1 and $(-+-)$ for E species. In the present study this prediction has certainly been confirmed to be correct. Moreover, the sign of $(\partial p/\partial Q_4)$ was so determined that the resulting sign of p_4 agrees with the *ab initio* result.

We are planning in a subsequent paper[7] to analyze the intensities of the overtones and combinations of this molecule, utilizing the result obtained here for the fundamentals.

References

1) J. W. Russell, C. D. Needham, and J. Overend, *J. Chem. Phys.*, **45**, 3383 (1966).
2) J. H. Newton and W. B. Person, *J. Chem. Phys.*, **64**, 3036 (1976).
3) S. Abbate and M. Gussoni, *Chem. Phys.*, **40**, 385 (1979).
4) S. Kondo and S. Saëki, *J. Chem. Phys.*, **76**, 809 (1982).
5) G. M. Barrow and D. C. McKean, *Proc. R. Soc. London, Ser. A*, **213**, 27 (1952).
6) A. D. Dickson, I. M. Mills, and B. Crawford, Jr., *J. Chem. Phys.*, **27**, 445 (1957).
7) S. Kondo, Y. Koga, T. Nakanaga, and S. Saëki, to be published.
8) S. Kondo and S. Saëki, *J. Chem. Phys.*, **74**, 6603 (1981).
9) S. Kondo and W. B. Person, *J. Mol. Spectrosc.*, **52**, 287 (1974).
10) A. G. Maki and R. Thibault, *J. Chem. Phys.*, **48**, 2163 (1968).

TABLE 8. ATOMIC POLAR TENSORS P_x IN METHYL CHLORIDE[a] (in D/Å)

			$H_1(D_1)^{b}$			C			Cl		
CH_3Cl	e_a	$-+-$	−0.215	0	−0.171	0.565	0	0	−0.847	0	0
	e_b	$-+-$	0	0.402	0	0	0.565	0	0	−0.847	0
	a_1	$-++$	−0.302	0	−0.238	0	0	2.955	0	0	−2.242
CD_3Cl	e_a	$-+-$	−0.198	0	−0.161	0.547	0	0	−0.851	0	0
	e_b	$-+-$	0	0.401	0	0	0.547	0	0	−0.851	0
	a_1	$-++$	−0.288	0	−0.248	0	0	2.960	0	0	−2.216

a) For the coordinate system in Fig. 5. b) H_1 atom in Fig. 5.

11) M. Morillon-Chapey and G. Graner, *J. Mol. Spectrosc.*, **31** 155 (1969).
12) E. W. Jones, R. J. L. Popplewell, and H. W. Thompson, *Spectrochim. Acta*, **22**, 659, 669 (1966).
13) J. L. Duncan, *J. Mol. Struct.*, **6**, 447 (1970).
14) M. Imachi, T. Tanaka, and E. Hirota, *J. Mol. Spectrosc.*, **63**, 265 (1976); C. Yamada and E. Hirota, *ibid.*, **64**, 31 (1977).
15) C. DiLauro and I. M. Mills, *J. Mol. Spectrosc.*, **21**, 386 (1966).
16) In the present study, the measurement was carried out under the pressure of 1.11×10^6 Pa, which means that the true width of individual vibration-rotation lines is expected to be about 2 cm^{-1}. On the other hand, the resolution used was 0.25 cm^{-1}. Considering the fact that the absorption bands are composed of many overlapping vibration-rotation lines, the present combination of line width and resolution should indeed be sufficient to obtain the absolute band intensities.
17) E. B. Wilson, J. C. Decius, and P. C. Cross, "Molecular Vibration," McGraw-Hill, New York (1955).
18) S. Kondo and Y. Koga, *J. Chem. Phys.*, **69**, 4022 (1978).
19) R. G. Shulman, B. P. Dailey, and C. H. Towns, *Phys. Rev.*, **78**, 145 (1950).
20) J. L. Duncan, A. Allan, and D. C. McKean, *Mol. Phys.*, **18**, 289 (1970).
21) K. B. Wiberg, *J. Am. Chem. Soc.*, **101**, 1718 (1979).
22) W. B. Person and J. H. Newton, *J. Chem. Phys.*, **61**, 1040 (1974).

The Crystal and Molecular Structure of Bis(methanol)-α,β,γ,δ-tetraphenylporphinatomanganese(III) Perchlorate-Methanol. A Molecular Structure Relevant to the Intermediate-spin Six Coordinate Iron(III) Porphyrin

Keiichiro HATANO,* Kazunori ANZAI, and Yoichi IITAKA†
Department of Pharmaceutical Sciences, Nagoya City University, Mizuho-ku, Nagoya 467
†*Faculty of Pharmaceutical Sciences, The University of Tokyo, Bunkyo-ku, Tokyo 113*
(Received September 28, 1981)

Bis(methanol)-α,β,γ,δ-tetraphenylporphinatomanganese(III) perchlorate crystallizes as the methanol solvate in the triclinic system, space group $P\bar{1}$, $a=16.225(8)$, $b=13.167(7)$, $c=10.793(5)$ Å, $\alpha=106.51(5)°$, $\beta=100.36(5)°$, $\gamma=101.60(5)°$, and $Z=2$. The structure was determined by the heavy-atom method and the block-diagonal least-squares refinement using a total of 9992 reflections. The final R and R_w values are 6.3 and 7.1%, respectively. Two slightly different but substantially identical coordination spheres of high-spin Mn(III) porphyrin were revealed. The long axial Mn–O(methanol) bond distance and medium-sized porphyrin core were emphasized as structural characteristics in relation to the intermediate-spin iron(III) porphyrin.

Althoug there is no support for the idea that manganese chlorophyll or porphyrin is involved in photosynthesis, the photochemistry of manganese[1,2] and other metal porphyrins[3–5] is interesting to explore the possibility of the solar energy conversion imitating biological systems. In a previous paper,[3] we reported the photochemical reduction of the central metal ions of some metal-TPPS[6] by alcohols ligating the axial positions. The coordination of weakly ligating substances, *e.g.*, water, alcohol, and DMSO, to metalloporphyrins has only recently been established by the definitive X-ray studies.[7–9,22] Thus, this work aims, at first, to establish the explicit occupation of methanols on the axial positions of $MnTPP^+$ as a basis of our interpretation of the photochemical reaction mechanism of Mn-porphyrins in alcoholic solution.

On the other hand, the extensive studies of the spin state/stereochemistry relationship in metalloporphyrins conducted by Scheidt and co-workers have proposed two structural types of intermediate-spin iron(III) porphyrins,[10–12] namely five coordination[10,11,13] and six-coordination.[12] The high-spin state of Mn(III) porphyrins has an electron configuration analogous to the intermediate-spin iron(III) porphyrins, *i.e.*, unoccupied $d_{x^2-y^2}$ and singly occupied d_{z^2}. The crystal structure of the high-spin six-coordinate $MnTPP^+$ is a proper example for supporting the assignment of structural characteristics of the six-coordinate intermediate-spin iron(III) porphyrin.

Experimental

Preparation. The starting manganese porphyrin, MnTPP(OH), which has not yet been characterized definitively, was prepared as described previously.[14] All other chemicals and solvents were reagent grade and used without further purification.

A chloroform solution of MnTPP(OH) (200 mg/100 ml) was shaken with an aqueous $HClO_4$ solution (*ca.* 10%) in a separatory funnel. The chloroform layer was separated and evaporated to dryness under reduced pressure. The resulting solid was extracted with methanol. Single crystals of $MnTPP(CH_3OH)_2ClO_4\cdot CH_3OH$ were obtained by slow evaporation of solvent from the solution (yield: 100 mg as crystals). The crystals appear to lose easily the methanol molecule of solvation; hence freshly prepared crystals were sealed into thin-walled glass capillaries.

The infrared spectrum of the crystalline material was obtained as a KBr pellet on a JASCO IRA-2 spectrometer. The intence and broad absorption centered at 1090 cm^{-1} and the strong, sharp band at 620 cm^{-1} were consistent with the assignment of free perchlorate ion.[15]

Found: C, 65.69; H, 3.88; N, 6.72%. Calcd for $MnC_{47}H_{40}N_4ClO_7$: C, 65.40; H, 4.68; N, 6.50%. The low value found for hydrogen may be due to loss of methanol. UV (CH_3OH) λ_{max} (log ε): 597 (3.66), 564 (3.80), 514 (3.54), 467 (4.74), 439 (4.14), 399 (4.50), and 378 nm (4.50).

Magnetic Measurement in Solution. The Evans NMR method[16] was applied to measure the magnetic susceptibility of this Mn(III) porphyrin, using a coaxial NMR double tube (4 mm o.d.) purchased from Nippon Seimitsukagaku Co., Ltd. TMS in $CDCl_3$ (*ca.* 2 vol%) was used as the tracer signals in the reference and sample in the tube, since TMS would not coordinate to the metalloporphyrin. A 0.166 ppm splitting of the TMS ptotons in 7.8 mmol dm^{-3} $MnTPP^+$ solution from the reference was observed in the spectrum recorded on a JEOL FX-100 spectrometer operating at 99.5 MHz radiowave frequency and at 20 °C. The magnetic moment was calculated with diamagnetic corrections according to the reported equation.[16] The μ_{eff} was 5.3 μ_B.

Crystal Structure Determination. A crystal of $MnTPP(CH_3OH)_2ClO_4\cdot CH_3OH$ with approximate dimensions of $0.5\times0.7\times0.9$ mm was mounted in a thin-walled capillary. Lattice constants were determined by the angular settings for 18 carefully centered reflections on a Philips PW-1100 four-circle X-ray diffractometer. Crystallographic data at 20 ± 1 °C ($\lambda=0.71069$ Å): triclinic, $a=16.225(8)$, $b=13.167(7)$, $c=10.793(5)$ Å, $\alpha=106.51(5)°$, $\beta=100.36(5)°$, $\gamma=101.60(5)°$, the unit cell volume (U)=2095.6 Å^3, $Z=2$, the calculated density (D_x)=1.368 g/cm^3, and the experimentally determined density (D_m)=1.373 g/cm^3.

Intensity data were collected using graphite-monochromated Mo $K\alpha$ radiation and θ-2θ scanning. All independent reflections for which $(\sin\theta)/\lambda<0.704$ Å^{-1} were measured. A total of 9992 reflections (81% of the theoretical number possible) having F_o greater than $2\sigma(F_o)$ were used in the solution and refinement of structure. No absorption or extinction correction was made. Data collection and reduction were carried out at the Unversity of Tokyo.

A Patterson map revealed that the manganese atoms are

TABLE 1. FRACTIONAL COORDINATES AND ISOTROPIC TEMPERATURE FACTORS FOR MnTPP $(CH_3OH)_2ClO_4CH_3OH$[a,c]

Atom	x	y	z	B_{eq}[b]/Å^2	Atom	x	y	z	B_{eq}[b]/Å^2
Mn_1	0.0	0.0	0.0	2.6	C_{a8}	0.51354(14)	0.74458(17)	0.0599(2)	3.2
N_1	0.10089(11)	0.11137(14)	−0.01103(17)	2.9	C_{b5}	0.31083(15)	0.26378(19)	−0.3361(2)	3.9
N_2	0.07536(11)	−0.01895(15)	0.15607(17)	3.1	C_{b6}	0.29217(14)	0.35580(19)	−0.3499(2)	3.5
C_{a1}	0.10233(14)	0.16325(18)	−0.1058(2)	3.3	C_{b7}	0.41506(16)	0.75826(19)	−0.1049(2)	3.7
C_{a2}	0.18504(13)	0.14401(18)	0.0674(2)	3.1	C_{b8}	0.47534(17)	0.81815(18)	0.0094(3)	4.0
C_{a3}	0.16356(13)	0.03050(19)	0.2105(2)	3.3	C_{m3}	0.35628(13)	0.55717(17)	−0.2310(2)	3.1
C_{a4}	0.05089(14)	−0.08458(19)	0.2301(2)	3.4	C_{m4}	0.42146(14)	0.22398(17)	−0.1766(2)	3.0
C_{b1}	0.18776(15)	0.2305(2)	−0.0835(3)	4.1	C_{13}	0.29271(14)	0.57882(17)	−0.3330(2)	3.2
C_{b2}	0.23885(14)	0.2186(2)	0.0224(2)	3.9	C_{14}	0.22190(16)	0.6141(2)	−0.3027(2)	4.0
C_{b3}	0.19362(15)	−0.0050(2)	0.3198(3)	4.3	C_{15}	0.16184(17)	0.6289(2)	−0.4005(3)	4.7
C_{b4}	0.12497(15)	−0.0748(2)	0.3325(3)	4.3	C_{16}	0.17323(17)	0.6109(2)	−0.5279(3)	4.7
C_{m1}	0.03202(14)	0.15089(19)	−0.2094(2)	3.4	C_{17}	0.24271(19)	0.5757(3)	−0.5582(3)	5.3
C_{m2}	0.21461(13)	0.10578(19)	0.1701(2)	3.3	C_{18}	0.30299(16)	0.5599(2)	−0.4610(3)	4.4
C_1	0.04592(14)	0.2100(2)	−0.3071(2)	3.8	C_{19}	0.39020(14)	0.10479(17)	−0.2637(2)	3.3
C_2	0.0614(2)	0.1570(3)	−0.4258(3)	5.2	C_{20}	0.41239(18)	0.0737(2)	−0.3846(3)	4.3
C_3	0.0698(2)	0.2086(3)	−0.5207(3)	6.5	C_{21}	0.38048(19)	−0.0342(2)	−0.4711(3)	5.0
C_4	0.06461(18)	0.3129(3)	−0.4946(3)	6.9	C_{22}	0.32638(18)	−0.1095(2)	−0.4368(3)	5.2
C_5	0.0510(2)	0.3687(3)	−0.3753(4)	7.5	C_{23}	0.30589(18)	−0.0808(2)	−0.3178(4)	5.7
C_6	0.0409(2)	0.3159(3)	−0.2820(3)	6.1	C_{24}	0.33817(18)	0.0270(2)	−0.2283(3)	4.8
C_7	0.30995(14)	0.1468(2)	0.2408(2)	3.6	O_1	0.03894(12)	−0.13380(15)	−0.13905(18)	4.7
C_8	0.36433(16)	0.0783(2)	0.2173(3)	4.7	C_{25}	0.1158(2)	−0.1178(3)	−0.1854(4)	8.2
C_9	0.45196(17)	0.1158(3)	0.2844(3)	5.7	O_2	0.39428(11)	0.49369(16)	0.11212(17)	4.7
C_{10}	0.48426(16)	0.2203(3)	0.3739(3)	5.8	C_{26}	0.4099(3)	0.5113(4)	0.2488(4)	8.7
C_{11}	0.43135(19)	0.2884(3)	0.3978(3)	5.6	O_3	0.0316(3)	−0.3186(3)	−0.0896(6)	18.1
C_{12}	0.34371(17)	0.2515(2)	0.3311(3)	4.8	C_{27}	−0.0420(8)	−0.4021(5)	−0.1214(7)	21.4
Mn_2	0.5	0.5	0	2.5	Cl	0.23990(9)	0.68149(11)	0.11689(11)	10.3
N_3	0.40851(11)	0.40986(14)	−0.16794(16)	2.8	O_4	0.2584(3)	0.5857(4)	0.0459(4)	14.5
N_4	0.47576(11)	0.63783(14)	−0.02561(17)	2.8	O_5	0.2343(3)	0.7510(4)	0.0415(4)	16.6
C_{a5}	0.38351(13)	0.29652(17)	−0.2233(2)	2.9	O_6	0.1680(3)	0.6638(4)	0.1668(6)	19.1
C_{a6}	0.35356(13)	0.44739(17)	−0.2468(2)	3.0	O_7	0.3105(4)	0.7325(5)	0.2312(5)	19.4
C_{a7}	0.41363(14)	0.64541(17)	−0.1263(2)	3.2					

a) The estimated standard deviations of the least significant digits are given in parentheses. b) Parameters as calculated from $B_{eq}=4/3(\beta_{11}a^2+\beta_{22}b^2+\beta_{33}c^2+1/2(\beta_{12}\ ab\ \cos\gamma+\beta_{13}\ ac\cos\beta+\beta_{23}\ bc\cos\alpha))$, where β_{ij} are dimensionless thermal values employed during computation as $\exp(-\sum_{j\geq i}\beta_{ji}h_ih_j)$. c) The atoms labeled Mn_2 to C_{24} and O_2 to C_{26} in this Table belong to the second molecule shown in Fig. 4.[30]

TABLE 2. SELECTED INTERATOMIC DISTANCES FOR $MnTPP(CH_3OH)_2\ ClO_4CH_3OH$[a]

Bond distance	l/Å		l/Å	Bond distance	l/Å		l/Å
Mn_1–N_1	2.011(2)	C_{a7}–C_{b7}	1.434(4)	C_1–C_2	1.369(4)	C_{18}–C_{13}	1.378(4)
Mn_1–N_2	1.998(2)	C_{a8}–C_{b8}	1.425(4)	C_2–C_3	1.386(5)	C_{19}–C_{20}	1.386(4)
Mn_2–N_3	2.004(2)	C_{a1}–C_{m1}	1.392(3)	C_3–C_4	1.347(6)	C_{20}–C_{21}	1.397(4)
Mn_2–N_4	2.012(2)	C_{a2}–C_{m2}	1.386(3)	C_4–C_5	1.372(6)	C_{21}–C_{22}	1.363(5)
N_1–C_{a1}	1.376(3)	C_{a3}–C_{m2}	1.377(4)	C_5–C_6	1.386(6)	C_{22}–C_{23}	1.353(5)
N_1–C_{a2}	1.382(3)	C_{a4}–C'_{m1}	1.390(3)	C_6–C_1	1.367(4)	C_{23}–C_{24}	1.407(5)
N_2–C_{a3}	1.388(3)	C_{a6}–C_{m3}	1.399(3)	C_7–C_8	1.390(4)	C_{24}–C_{19}	1.375(4)
N_2–C_{a4}	1.377(3)	C_{a7}–C_{m3}	1.396(3)	C_8–C_9	1.392(5)	Mn_1–O_1	2.252(2)
N_3–C_{a5}	1.387(3)	C_{a5}–C_{m4}	1.391(3)	C_9–C_{10}	1.375(5)	Mn_2–O_2	2.270(2)
N_3–C_{a6}	1.377(3)	C_{a8}–C'_{m4}	1.386(3)	C_{10}–C_{11}	1.367(5)	O_1–C_{25}	1.424(5)
N_4–C_{a7}	1.381(3)	C_{b1}–C_{b2}	1.349(4)	C_{11}–C_{12}	1.391(5)	O_2–C_{26}	1.391(6)
N_4–C_{a8}	1.390(3)	C_{b3}–C_{b4}	1.348(4)	C_{12}–C_7	1.381(4)	O_3–C_{27}	1.366(15)
C_{a1}–C_{b1}	1.426(4)	C_{b5}–C_{b6}	1.346(4)	C_{13}–C_{14}	1.381(4)	Cl–O_4	1.402(5)
C_{a2}–C_{b2}	1.426(4)	C_{b7}–C_{b8}	1.345(4)	C_{14}–C_{15}	1.385(4)	Cl–O_5	1.386(6)
C_{a3}–C_{b3}	1.424(4)	C_{m1}–C_1	1.493(4)	C_{15}–C_{16}	1.378(4)	Cl–O_6	1.375(6)
C_{a4}–C_{b4}	1.434(4)	C_{m2}–C_7	1.508(4)	C_{16}–C_{17}	1.360(5)	Cl–O_7	1.415(7)
C_{a5}–C_{b5}	1.429(3)	C_{m3}–C_{13}	1.494(3)	C_{17}–C_{18}	1.388(5)		
C_{a6}–C_{b6}	1.434(3)	C_{m4}–C_{19}	1.514(3)				

a) Primed (′) atoms are related to unprimed atoms by the symmetric transformation.

TABLE 3. SELECTED INTERATOMIC ANGLES FOR $MnTPP(CH_3OH)_2\ ClO_4CH_3OH$[a)]

Bond angle	ϕ/°		ϕ/°	Bond angle	ϕ/°		ϕ/°
N_1–Mn_1–N_2	90.3(2)	C_{a3}–C_{b3}–C_{b4}	107.4(3)	C_1–C_{m1}–C'_{a4}	117.3(2)	C_{10}–C_{11}–C_{12}	119.7(3)
N_1–Mn_1–N'_2	89.7(2)	C_{a4}–C_{b4}–C_{b3}	107.7(3)	C_1–C_{m1}–C_{a1}	118.7(2)	C_{11}–C_{12}–C_7	120.5(3)
N_3–Mn_2–N_4	89.8(2)	C_{a5}–C_{b5}–C_{b6}	107.2(2)	C_7–C_{m2}–C_{a2}	118.0(2)	C_{18}–C_{13}–C_{14}	119.1(2)
N_3–Mn_2–N'_4	90.3(2)	C_{a6}–C_{b6}–C_{b5}	107.8(2)	C_7–C_{m2}–C_{a3}	117.3(2)	C_{13}–C_{14}–C_{15}	120.2(3)
Mn_1–N_1–C_{a1}	127.2(2)	C_{a7}–C_{b7}–C_{b8}	107.5(2)	C_{13}–C_{m3}–C_{a6}	116.8(2)	C_{14}–C_{15}–C_{16}	120.3(3)
Mn_1–N_1–C_{a2}	126.8(2)	C_{a8}–C_{b8}–C_{b7}	107.7(2)	C_{13}–C_{m3}–C_{a7}	119.3(2)	C_{15}–C_{16}–C_{17}	119.7(3)
Mn_1–N_2–C_{a3}	126.7(2)	N_1–C_{a1}–C_{m1}	125.7(2)	C_{19}–C_{m4}–C_{a5}	116.3(2)	C_{16}–C_{17}–C_{18}	120.4(3)
Mn_1–N_2–C_{a4}	127.2(2)	N_1–C_{a2}–C_{m2}	125.4(2)	C_{19}–C_{m4}–C'_{a8}	119.5(2)	C_{17}–C_{18}–C_{13}	120.4(3)
Mn_2–N_3–C_{a5}	126.7(2)	N_2–C_{a3}–C_{m2}	126.0(2)	C_{m1}–C_1–C_2	119.9(3)	C_{24}–C_{19}–C_{20}	119.0(3)
Mn_2–N_3–C_{a6}	127.1(2)	N_2–C_{a4}–C'_{m1}	125.9(2)	C_{m1}–C_1–C_6	121.1(3)	C_{19}–C_{20}–C_{21}	120.8(3)
Mn_2–N_4–C_{a7}	127.4(2)	N_3–C_{a5}–C_{m4}	126.1(2)	C_{m2}–C_7–C_8	120.0(2)	C_{20}–C_{21}–C_{22}	119.6(3)
Mn_2–N_4–C_{a8}	126.9(2)	N_3–C_{a6}–C_{m3}	126.2(2)	C_{m2}–C_7–C_{12}	120.7(2)	C_{21}–C_{22}–C_{23}	120.2(3)
C_{a1}–N_1–C_{a2}	105.7(2)	N_4–C_{a7}–C_{m3}	125.6(2)	C_{m3}–C_{13}–C_{14}	121.3(2)	C_{22}–C_{23}–C_{24}	121.1(3)
C_{a3}–N_2–C_{a4}	106.1(2)	N_4–C_{a8}–C'_{m4}	125.6(2)	C_{m3}–C_{13}–C_{18}	119.6(2)	C_{23}–C_{24}–C_{19}	119.3(3)
C_{a5}–N_3–C_{a6}	105.9(2)	C_{m1}–C_{a1}–C_{b1}	124.8(2)	C_{m4}–C_{19}–C_{20}	119.2(2)	N_1–Mn_1–O_1	89.4(2)
C_{a7}–N_4–C_{a8}	105.7(2)	C_{m2}–C_{a2}–C_{b2}	124.5(2)	C_{m4}–C_{19}–C_{24}	121.8(2)	N_2–Mn_1–O_1	89.7(2)
N_1–C_{a1}–C_{b1}	109.6(2)	C_{m2}–C_{a3}–C_{b3}	124.3(2)	C_6–C_1–C_2	119.0(3)	N_3–Mn_2–O_2	88.2(2)
N_1–C_{a2}–C_{b2}	110.0(2)	C_{m1}–C_{a4}–C_{b4}	124.6(2)	C_1–C_2–C_3	120.8(3)	N_4–Mn_2–O_2	87.8(2)
N_2–C_{a3}–C_{b3}	109.6(2)	C'_{m4}–C_{a5}–C_{b5}	124.2(2)	C_2–C_3–C_4	119.6(4)	Mn_1–O_1–C_{25}	124.6(3)
N_2–C_{a4}–C_{b4}	109.2(2)	C_{m3}–C_{a6}–C_{b6}	124.5(2)	C_3–C_4–C_5	120.9(4)	Mn_2–O_2–C_{26}	124.0(3)
N_3–C_{a5}–C_{b5}	109.7(2)	C_{m3}–C_{a7}–C_{b7}	124.8(2)	C_4–C_5–C_6	119.2(4)	O_4–Cl–O_5	111.1(3)
N_3–C_{a6}–C_{b6}	109.4(2)	C'_{m4}–C_{a8}–C_{b8}	124.9(2)	C_5–C_6–C_1	120.6(3)	O_4–Cl–O_6	114.5(3)
N_4–C_{a7}–C_{b7}	109.5(2)	C_{a1}–C_{m1}–C'_{a4}	123.8(2)	C_{12}–C_7–C_8	119.4(3)	O_4–Cl–O_7	105.6(4)
N_4–C_{a8}–C_{b8}	109.6(2)	C_{a2}–C_{m2}–C_{a3}	124.7(2)	C_7–C_8–C_9	119.8(3)	O_5–Cl–O_6	110.0(4)
C_{a1}–C_{b1}–C_{b2}	107.9(2)	C_{a6}–C_{m3}–C_{a7}	123.9(2)	C_8–C_9–C_{10}	119.9(3)	O_5–Cl–O_7	109.6(4)
C_{a2}–C_{b2}–C_{b1}	106.8(2)	C_{a5}–C_{m4}–C'_{a7}	124.3(2)	C_9–C_{10}–C_{11}	120.8(3)	O_6–Cl–O_7	104.7(4)

a) Primed (') atoms are related to unprimed atoms by the symmetric transformation. The estimated standard deviations of the least significant digits are given in parentheses.

located at 0,0,0 and 1/2, 1/2, 0. A series of difference Fourier calculations phased with two Mn and several atoms of the porphyrin skeleton revealed the positions of all non-hydrogen atoms. Atomic scattering factors were taken from Table 2.2B of Ref. 17. After several cycles of block-diagonal least-squares refinement with anisotropic temperature factors for all non-hydrogen atoms, difference Fourier maps revealed all hydrogen atom positions except those of the solvated methanol. These invisible hydrogens were ignored in this work. The 36 hydrogen atoms refined two cycles, then, placed on the positions as the fixed contributors with their isotropic thermal parameters.

The refinement was carried to convergence using anisotropic temperature factors for all non-hydrogen atoms. The final values of the discrepancy indexes were $R=\sum||F_o|-|F_c||/\sum|F_o|=0.063$ and $R_w=[\sum(w(|F_o|-|F_c|)^2)/\sum w(F_o)^2]^{1/2}=0.071$, $w=1/\sigma^2(F_o)$. The highest residual in the difference map, 1.1 e/Å^3, was found near one oxygen atom (O_4) of the perchlorate ion and others (less than 0.6 e/Å^3) were featureless. All calculations were carried out at the Computing Center of Nagoya City University using locally modified versions of the X-ray programs.[18)]

Tables of the anisotropic thermal factors of 61 non-hydrogen atoms, the coordinates and isotropic thermal factors of hydrogen atoms, the observed and calculated structure factors (29 pages), and Fig. 4[30)] are available as supplementary materials on request (kept at the Editorial Office of the Chemical Society of Japan as a Document No. 8301).

Results and Discussion

Atomic coordinates and the associated isotropic equivalent temperature factors of the final non-hydrogen atoms are listed in Table 1. Figures 1 and 4[30)] are computer-drawn models of the two unique $MnTPP(CH_3OH)_2^+$ ions. The two Mn ions, the hydrogen bonds formed by the coordinated methanols with perchlorate ion and solvated methanol, and the nearest contacts to them are collectively illustrated in Fig. 2. Individual bond lengths and angles are summarized in Tables 2 and 3.

The requirement of the inversion symmetry with respect to both manganese positions leads to square bipyramidal coordination spheres made of the porphinato core and axial methanols with rigorous centering of the Mn(III) ions. The symbols and displacements of the atoms from the least-squares mean plane of the porphyrin core for both ions are given by means of the usual diagram expression[19)] in Fig. 3. This shows planar porphyrin core normally seen in the six-coordinate Mn(III)[20)] and iron(III) porphyrins.[19)]

The conformation of two independent $MnTPP(CH_3OH)_2^+$ ions is apparently identical. The dihedral angles between the least-squares mean planes of porphyrin core (24 atoms) and peripheral phenyl rings are 84.4° and 75.2° for the molecule shown in Fig. 1 and 70.8° and 72.7° for the second molecule.[30)] These are normal dihedral angles observed in ordinary TPP conformation.[21)] The most crucial structural difference distinguishing the complexes is the geometry of ions, ligands, and solvated molecules linked by the hydrogen bonds. As seen in Fig. 2, one oxygen atom (O_4) of the

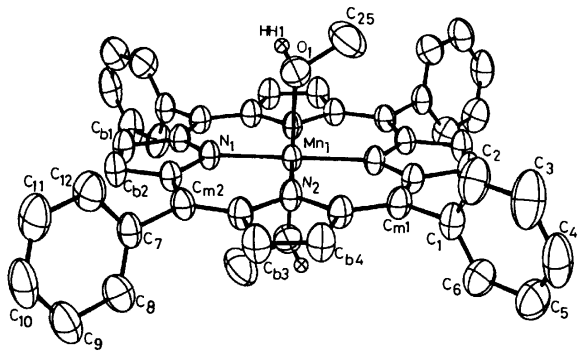

Fig. 1. Computer-drawn model of the first MnTPP$(CH_3OH)_2^+$ species. The thermal ellipsoids are contoured at the 50% probability level except for the hydrogen atom HH1.

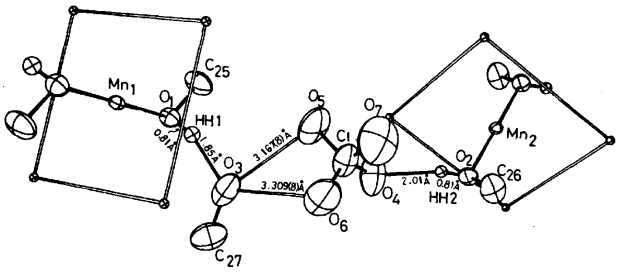

Fig. 2. An ORTEP plot of a pair of Mn(III)porphyrin ions and a perchlorate ion. The porphyrin planes are shown by simple squares linking the *meso*-carbons of the skeleton. Interatomic distances between perchlorate and solvated methanol oxygens and tentative distances between hydrogen and oxygen atoms forming hydrogen bonds are entered on the diagram.

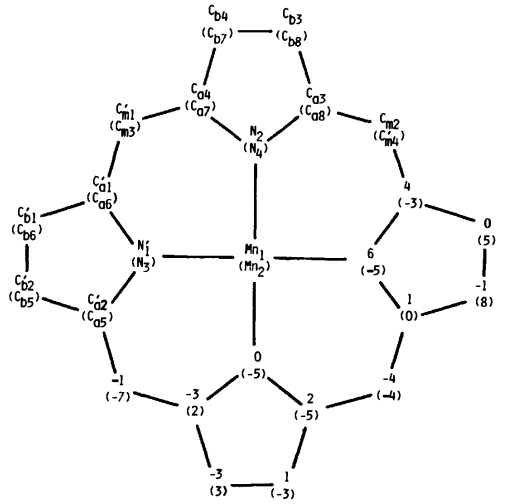

Fig. 3. A formal diagram of the porphinato core of the two unique Mn(III)porphyrins correspondings to Figs. 1 and 4[30] (in parentheses), respectively. On the upper left, the numbering scheme used for the atoms is displayed. The number on the atom positions in the centrosymmetric diagram, on the lower right, is the perpendicular displacement from the mean plane of the porphyrin core in units of 0.01 Å.

perchlorate ion interacts directly with the oxygen (O_2) of methanol coordinated to Mn_2 through a hydrogen bond (O_4–O_2 distance 2.798(5) Å). On the other side, the perchlorate ion has a close contact only with the solvated methanol at 3.16 Å that is too far for significant hydrogen bonding. The solvated methanol makes a dimeric interaction with the methanol coordinated to Mn_1 through an apparent hydrogen bond (O_1–O_3 distance 2.618(7) Å). Therefore, the crystal structure suggests a better description of the molecules in the solid state as $[MnTPP((CH_3OH)_2)_2]^+$ and $[MnTPP(CH_3OH\cdot ClO_4)_2]^-$ forming an ion pair. However, the description is not necessarily or strictly adapted to the present system because of the possible disorder suggested by the large thermal parameters and the high residual electron densities around the perchlorate and solvated methanol.

The ion pair makes a quasi-linear arrangement parallel to the (a—b) vector on the (0,0,1) plane; hence two manganese atoms sitting at 0,1,0 and 1/2,1/2,0 can be linked as shown in Fig. 2. The closest distance between two manganese atoms sitting on the quasi-chain is 9.3 Å. The dihedral angle between the two independent porphyrin planes is 51.8°.

The axial bond length of Mn_1–O_1 and Mn_2–O_2 are 2.252(2) Å (in the cationic species) and 2.270(2) Å (in the anionic species), respectively. These distances are considerably longer than the 2.11—2.16 Å values found in $[FeOEP(C_2H_5OH)_2]^+$ [8] and $[FeTPP(C_2H_5OH)_2]^+$[22] in which both Fe(III) ions are assigned to be high-spin, but fairly shorter than 2.329(7) Å in $MnTPP(N_3)(CH_3OH)$.[20] The distances are comparable rather to the longer pair of Mn–N (imidazolate) bond lengths (2.280(4) Å) in $(MnTPP(Im))_n$[23] or the value 2.308(3) Å found in the high-spin $MnTPP(1\text{-}MeIm)_2ClO_4$[24] in spite of the weak ligating nature of alcohol to metals. Axial bond lengths of high-spin Mn(III) porphyrin complexes are unexceptionally long (>2.2 Å) compared with normal equatorial Mn–N (porphyrin) bond lengths (*vide infra*). The difference between the axial bond lengths in the two independent species is statistically significant but substantially not distinct, since the 0.018 Å difference is small and considered to be due to the subtle electrostatic or crystal packing effect.

The average equatorial bond length (Mn–N(porphyrin)) in these ions is 2.006(2) Å, which is at the short limit of those found in four six-coordinate Mn(III) porphyrins; 2.009(9) Å in MnTPP(Cl)(Py),[25] 2.015(4) Å in $MnTPP(1\text{-}MeIm)_2ClO_4$,[24] 2.019(4) Å in $(MnTPP(Im))_n$,[23] and 2.031(12) Å in $MnTPP(N_3)(CH_3OH)$.[20] The present average length of Mn–N is located at the middle of the extent of the equatorial bond lengths (1.93—2.09 Å) observed for a series of the first row transition metal-porphyrins.[29] Thus, the long axial bonds to methanol and medium size porphyrin core surround the high-spin Mn(III) ions. These structural characteristics in the six-coordinate high-spin Mn(III) porphyrins have already been pointed out as the tetragonal distortion found in those complexes.[20,23,25]

We are interested in the spin state/structure relationship of metalloporphyrins, especially biologically important iron porphyrins. Spin states of the central metal

TABLE 4. THE STRUCTURE-ELECTRONIC CONFIGURATION IN SELECTED SIX-COORDINATE METALLOPORPHYRINS HAVING ONE ELECTRON IN THE e_g ORBITAL

Number of electrons in 3d-orbital	Electronic configuration and spin state	Metalloporphyrins	Bond length of metal to axial ligand l/Å	Average bond length of metal to porphyrin l/Å	Ref.
4	$(t_{2g})^3(e_g)^1$	$MnTPP(CH_3OH)_2^+$	2.250(2) 2.272(2)	2.006(2)	This work
	$S=4/2$	$MnTPP(1\text{-}MeIm)_2^+$	2.308(3)	2.009(9)	24
		$(MnTPP(Im))_n$[a]	2.280(4)	2.019(4)	23
5	$(t_{2g})^4(e_g)^1$ $S=3/2$	$(FeTPP(C(CN)_3))_n$	2.317(3)	1.995(3)	12
6	$(t_{2g})^5(e_g)^1$ $S=2/2$	Unknown			
7	$(t_{2g})^6(e_g)^1$	CoTPP(Pip)$_2$[b]	2.436(2)	1.987(2)	27
	$S=1/2$	CoOEP(β-Pic)$_2$[b]	2.386(2)	1.992(1)	28

a) The high-spin form. b) Abbreviations: Pip=piperidine, OEP=octaethylporphinato, and β-Pic=3-methylpyridine.

ions define the distribution of electrons in the 3d-orbitals. The high-spin manganese(III) has an electron population in the 3d-orbitals of $(d_{xy},d_{yz},d_{zx})^3(d_{z^2})^1(d_{x^2-y^2})^0$ or $(t_{2g})^3(e_g)^1$ in the expression of cubic symmetry. The structures of the metalloporphyrins with similar electron configuration and six-coordinate geometry are compared and summarized in Table 4. The presence of a single electron in the e_g orbitals leads to a structural similarity, *i.e.*, tetragonal distortion. The addition of electrons into half-occupied t_{2g} orbitals -spin-pairing- appears to give only minor changes in the structural prameters of the porphyrin core, *i.e.*, metal to porphyrin bond lengths.

For the six-coordinate intermediate-spin iron(III) porphyrin, a true 3/2 spin-state has been suggested[12] as distinguished from a quantum mechanically admixed $S=3/2$, 5/2 state postulated for the five-coordinate iron(III) complexes.[11,13] The comparison of the structural parameters in Table 4 including the present Mn(III) porphyrins gives a stereochemical support for the assignment of the $S=3/2$ ground state electron configuration of the six-coordinate $FeTPP(C(CN)_3)$ in the solid state, despite of the higher than expected value of the observed magnetic moment. The magnetic properties may be elucidated by various experimental and theoretical ascriptions such as the thermal "spin-equilibrium" or the admixture of the excited state with the ground state configuration as has been adapted to the low-spin hemes.[26] We wish to remark conclusively that the present structure will contribute not only to the coordination chemistry of methanol to Mn(III) porphyrins but also to the electronic state consideration of related metalloporphyrins.

We are grateful to Prof. W. R. Scheidt of the University of Notre Dame for helpful discussions and editorial assistance. The aid of Ayako Ohta, Kuniko Uchiyama, and Kyoko Kawasaki in computing work is also acknowledged. K. H. thanks Prof. Noritake Yasuoka for the access to the source programs for the X-ray analysis filed at the Computing Center of the Osaka University.

References

1) G. Engelsma, A. Yamamoto, E. Markham, and M. Calvin, *J. Phys. Chem.*, **66**, 2517 (1962).
2) A. Harriman and G. Porter, *J. Chem. Soc., Faraday Trans. 2*, **75**, 1543 (1979); **76**, 1429 (1980).
3) K. Hatano, K. Usui, and Y. Ishida, *Bull. Chem. Soc. Jpn.*, **54**, 413 (1981).
4) C. Bartocci, F. Scandola, A. Ferri, and V. Carassiti, *J. Am. Chem. Soc.*, **102**, 7067 (1980).
5) C. J. Boreham, J-M. Latour, J-C. Marchon, B. B. Cocolios, and R. Guilard, *Inorg. Chim. Acta*, **45**, L69 (1980).
6) Abbreviations: TPPS = *meso*-tetra (*p*-sulfophenyl) porphinato; TPP=*meso*-tetraphenylporphinato; DMSO=dimethyl sulfoxide; TMS=tetramethylsilane; Im=imidazolate; 1-MeIm=1-methylimidazole; Py=pyridine.
7) W. R. Scheidt, I. A. Cohon, and M. E. Kastner, *Biochemistry*, **18**, 3546 (1979).
8) F. W. B. Einstein and A. C. Willis, *Inorg. Chem.*, **17**, 3040 (1978).
9) T. Mashiko, M. E. Kastner, K. Spartalian, W. R. Scheidt, and C. A. Reed, *J. Am. Chem. Soc.*, **100**, 6354 (1978).
10) M. E. Kastner, W. R. Scheidt, T. Mashiko, and C. A. Reed, *J. Am. Chem. Soc.*, **100**, 666 (1978).
11) C. A. Reed, T. Mashiko, S. P. Bently, M. E. Kastner, W. R. Scheidt, K. Spartalian, and G. Lang, *J. Am. Chem. Soc.*, **101**, 2948 (1979).
12) D. A. Summerville, I. A. Cohon, K. Hatano, and W. R. Scheidt, *Inorg. Chem.*, **17**, 2906 (1978).
13) H. Masuda, T. Taga, K. Osaki, H. Sugimoto, Z-I. Yoshida, and H. Ogoshi, *Inorg. Chem.*, **19**, 950 (1980).
14) J. T. Landrum, C. A. Reed, K. Hatano, and W. R. Scheidt, *J. Am. Chem. Soc.*, **100**, 3232 (1978).
15) K. Nakamoto, "Infrared Spectra of Inorganic and Coordination Compounds," Wiley-interscience, New York (1970); D. Dolphin, J. R. Sams, and T. B. Tsin, *Inorg. Chem.*, **16**, 711 (1977).
16) D. F. Evans, *J. Chem. Soc.*, **1959**, 2003.
17) D. T. Cromer and J. T. Waber, "International Tables for X-ray Crystallography," ed by J. A. Ibers and W. C. Hamilton, The Kynoch Press, Birmingham (1974), Vol. IV.
18) The local versions are based on Johnson's ORTEP II, Okaya and Ashida's XNBLS, and Sakurai's KFR-5. The authors of the latter two programs are representative.
19) W. R. Scheidt, K. J. Haller, and K. Hatano, *J. Am. Chem. Soc.*, **102**, 3017 (1980).
20) V. W. Day, B. R. Stults, E. L. Tasset, R. O. Day, and R. S. Marianelli, *J. Am. Chem. Soc.*, **96**, 3650 (1974).
21) To our knowledge, the smallest angle is 54.0° which appears in W. R. Scheidt, D. A. Summerville, and I. A. Cohon, *J. Am. Chem. Soc.*, **98**, 6623 (1976).

22) P. Gans, G. Buisson, E. Duee, J.-R. Regnard, and J.-C, Marchon, *J. Chem. Soc., Chem. Commun.*, **1979**, 393 (1979).
23) J. T. Landrum, K. Hatano, W. R. Scheidt, and C. A. Reed, *J. Am. Chem. Soc.*, **102**, 6729.
24) This is cited in Ref. 23.
25) J. F. Kirner and W. R. Scheidt, *Inorg. Chem.*, **14**, 2081 (1975).
26) M. Sato, T. Ohya, and I. Morishima, *Mol. Phys.*, **42**, 475 (1981).
27) W. R. Scheidt, *J. Am. Chem. Soc.*, **96**, 84 (1974).
28) R. G. Little and J. A. Ibers, *J. Am. Chem. Soc.*, **96**, 84 (1974).
29) W. R. Scheidt, "The Porphyrin," ed by D. Dolphin, Academic Press, N. Y. (1978), Vol. III; W. R. Scheidt, M. E. Kastner, and K. Hatano, *Inorg. Chem.*, **17**, 706 (1978).
30) Figure 4 displays the same information about the second molecule as in Fig. 1. The computer-drawn model is kept at the office of the Chemical Society of Japan as a supplementary material according to the editors' suggestion.

The Reaction of Sodium Nitrite with Silica

Osami Abe, Taizo Utsunomiya, and Yoshio Hoshino*
Research Laboratory of Engineering Materials, Tokyo Institute of Technology, Nagatsuta, Midori-ku, Yokohama 227
(Received September 28, 1981)

The reaction of sodium nitrite with silica has been investigated over the relatively wide composition range (Na/Si=0 to 10.0) below 800 °C. In an argon atmosphere, sodium nitrite reacts with oxygen to form sodium nitrate above 400 °C and decomposes to sodium oxide *via* other oxide species above 500 °C, irrespective of the coexistence of silica. The reaction of sodium nitrite with silica in an argon atmosphere consists of two stages. In the early stage (<600 °C), the main gaseous product is NO, while in the later stage nearly equimolar amounts of NO and O_2 are formed. The early stage is further divided into two reaction processes: Process I, in which peroxide is considered to be formed in the melt by generating NO, and Process II, in which nitrate and silicates are formed by generating NO and a trace amount of O_2. Peroxide is supposed to be stabilized at the solid-liquid interface, even if no silicates have been formed at relatively low temperatures. In the later stage, the reaction process or mechanism can be regarded as similar to that of sodium nitrate with silica, as the concentration of nitrite in the melt is very low.

The high-temperature behavior of alkali-metal nitrates, especially sodium nitrate, accompanying thermal decomposition is of interest in the manufacture of multicomponent glass fibers for optical wave guides, the vitrification of radioactive wastes from nuclear reactors, the surface treatment of metals and alloys, *etc.* In the previous papers,[1,2] it has been revealed that several wt% of sodium nitrite is formed as an intermediate during the decomposition of sodium nitrate, irrespective of the coexistence of silica. The investigation of the thermal decomposition of sodium nitrite should give some useful information on the high-temperature behavior of the nitrates.

With respect to the thermal decomposition of sodium nitrite, only a few studies have been made. Reactions 1 and 2 have been investigated by Freeman[3] and Bond *et al.*[4] respectively:

$$NaNO_2 + 1/2\ O_2 \rightleftarrows NaNO_3 \quad (1)$$

$$NaNO_2 = 1/2\ Na_2O + \text{Gaseous Products (in Ar)} \quad (2)$$

Freeman[3] has calculated the changes in the free energy of Reaction 1 to be −14.8, −7.4, and −2.8 kJ mol^{-1} at 600, 650, and 700 °C respectively, and the apparent activation energy to be 86.6 kJ mol^{-1} for the forward reaction and 187 kJ mol^{-1} for the backward reaction. The apparent activation energy of 179 kJ mol^{-1} has been obtained for Reaction 2 by analyzing the thermograms with the Avrami-Erofe'ef equation.[4] There is, however, not enough data with respect to the gaseous and solid reaction products in the paper by Bond *et al.*[4]

According to the acid-base theory by Lux and Flood, both sodium nitrate and nitrite behave as bases, namely oxide-ion donors, during the decomposition process. Therefore, in the binary system containing an acidic oxide, the reaction process to form oxide species, such as O^{2-}, O_2^{2-}, and O_2^-, is supposed to be predominant. This may be a clue to the clarification of the reaction mechanism. In the present study, the reaction of sodium nitrite with silica has been mainly investigated by a simultaneous measurement of thermogravimetry (TG), differential thermal analysis (DTA), differential thermogravimetry (DTG), and gas chromatography (GC), and the analysis of the solid reaction products. The decomposition mechanism of sodium nitrite is also discussed.

Experimental

Materials. Reagent-grade sodium nitrite (Wako Pure Chemical Industries, Ltd.) was ground under 100 mesh in an agate mortar and dried in an oven at 100 °C. Commercially available α-quartz was ground by means of a ball mill, washed with nitric acid and distilled water, and dried in the oven. The sodium nitrite and silica were mixed by dry-blending for each run. The compositions of the sample mixtures will be represented by the atomic ratio of silicon to sodium (Si/Na=Y_{Si}).

Apparatus and Procedure. For the TG-DTA measurement, a high-temperature thermobalance (Rigaku Denki Co., Ltd.) was used. DTG was carried out with a differentiator (Rikadenki Kogyo Co., Ltd.) in order to differentiate thermograms. A GC-2C-type gas chromatograph (Simadzu Seisakusyo, Ltd.) was used for quantitative gas analysis, in which silica gel and molecular sieve 5A were used as column-packing reagents after treatment by the method described by Sakaida *et al.*[5]

A weighed sample mixture (6.9—66.9 mg) containing 0.1 or 0.2 mmol of sodium nitrite in a platinum vessel was placed on a sample holder in the thermobalance; the ambient gas (Ar or O_2) was then introduced and adjusted to the desired flow rate (50 $cm^3\ min^{-1}$). Then the sample was heated at the rate of 5.0 or 20 °C min^{-1} after holding it at 250 °C for an hour to remove a trace amount of adsorbed water. The gas formed from the sample was introduced into the gas chromatograph every two minutes by using Ar as the carrier gas.

On the other hand, the solid reaction products were identified by means of X-ray diffractometry with Cu $K\alpha$ radiation, followed by chemical analysis. The heat-treated samples were kept in a desiccator with magnesium perchlorate as a desiccant. For the quantitative analysis, 100 mg portions of the reaction products were dissolved in water and then filtered with a membrane filter. Unreacted silica was determined by gravimetry. The amounts of sodium and silicon in the filtrate were determined by means of flame spectrophotometry and atomic absorption spectrometry respectively. The sodium nitrate and nitrite were determined by means of ion-exchange chromatography (with Dionex model 10).

The details of the experimental procedures and various factors which seem to affect the reaction have been discussed in the previous papers.[1,2]

Results and Discussion

Reaction Products. Figures 1 and 2 show the gaseous and solid reaction products respectively. The gases formed up to 720 °C were O_2 and NO on the thermal decomposition of sodium nitrite, irrespective of the presence of silica. A trace amount of N_2 was generated above 680 °C. The final solid reaction product was sodium metasilicate and/or disodium disilicate. It is evident from Figs. 1 and 2 that sodium nitrite decomposes above 400 °C generating only NO, and above 500 °C generating NO and O_2 to form sodium nitrate, sodium metasilicate, and disodium disilicate. It is also evident from Fig. 1 that the sample weight scarcely affects the reaction.

Figure 3 show the distribution of the sodium ion among the solid reaction products. In Fig. 3 (A) and (B), analytical values can be obtained below 600 °C, for sodium nitrite reacts with the platinum vessel above 600 °C, in the absence of silica.[6] In an argon atmosphere, sodium nitrite decomposed above 450 °C to form almost equimolar sodium nitrate and sodium oxide by generating NO [Fig. 3 (A)]. In an oxygen atmosphere, sodium nitrite reacted with O_2 above 400 °C to form nitrate, while above 500 °C it decomposed to form oxide [Fig. 3 (B)]. Under a high partial pressure of atmospheric oxygen, such highly oxidized compounds as peroxide might be formed. The reactions are expressed by the following equations:

$$3\,NaNO_2 = NaNO_3 + Na_2O + 2\,NO(\text{in Ar}) \quad (3)$$

$$2\,NaNO_2 + O_2 = 2\,NaNO_3(\text{in } O_2) \quad (4)$$

The reaction of sodium nitrite with silica in an argon

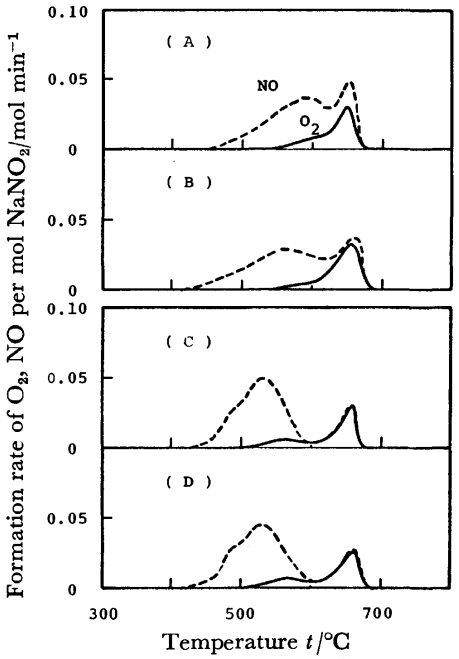

Fig. 1. Behavior of gas formation in the reaction of sodium nitrite with silica.
Atmosphere : Ar, heating rate : 5.0 °C min^{-1}. (A): $Y_{Si}=1.0$ (0.1 mmol $NaNO_2$), (B): $Y_{Si}=1.0$ (0.2 mmol $NaNO_2$), (C): $Y_{Si}=2.0$ (0.1 mmol $NaNO_2$), (D): $Y_{Si}=2.0$ (0.2 mmol $NaNO_2$).

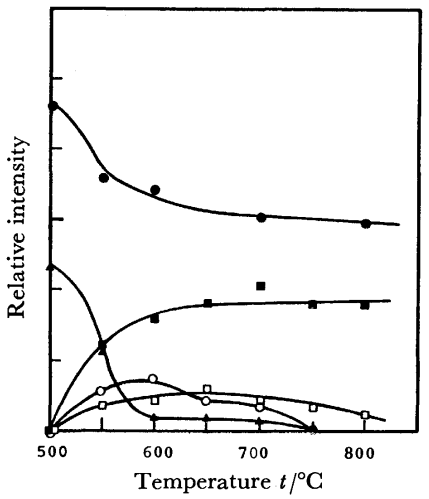

Fig. 2. Solid reaction products in sodium nitrite–silica system ($Y_{Si}=1.0$).
Atmosphere: Ar, heating rate: 5.0 °C min^{-1}. ●: SiO_2 (20.8°), ▲: $NaNO_2$ (44.5°), ○: $NaNO_3$ (47.9°), □: α-$Na_2Si_2O_5$ (23.6°), ■: Na_2SiO_3 (16.8° in 2θ).

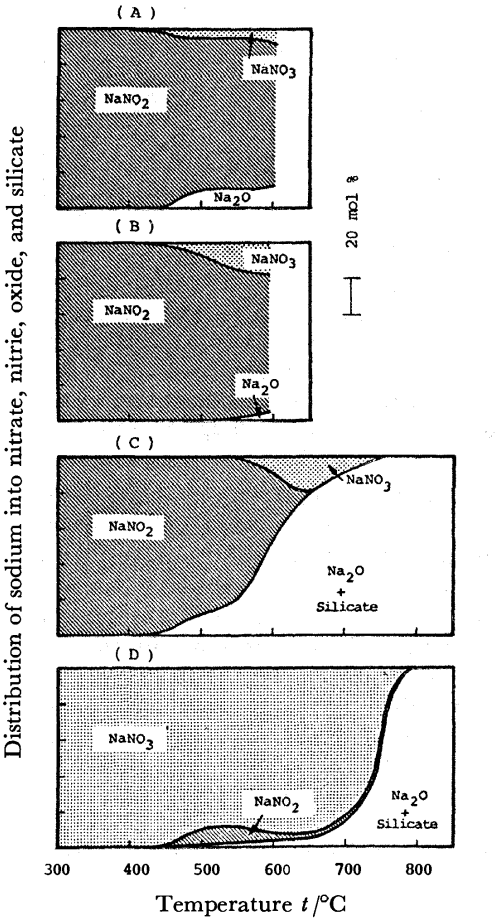

Fig. 3. Fraction of sodium compounds in reaction products.
Heating rate: 5.0 °C min^{-1}. (A): $NaNO_2$ in argon atmosphere, (B): $NaNO_2$ in oxygen atmosphere, (C): $NaNO_2$–SiO_2 in argon atmosphere ($Y_{Si}=1.0$), (D): $NaNO_3$–SiO_2 in argon atmosphere ($Y_{Si}=1.0$).

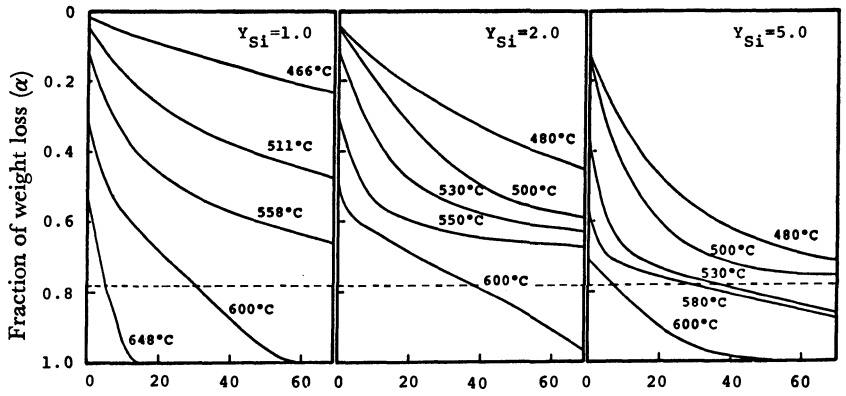

Fig. 4. Isothermal thermograms of sodium nitrite–silica system in argon atmosphere. The dashed line at $\alpha=0.789$ indicates the fraction of weight loss when all of sodium nitrite in sample decomposed to form peroxide according to Eq. 5.

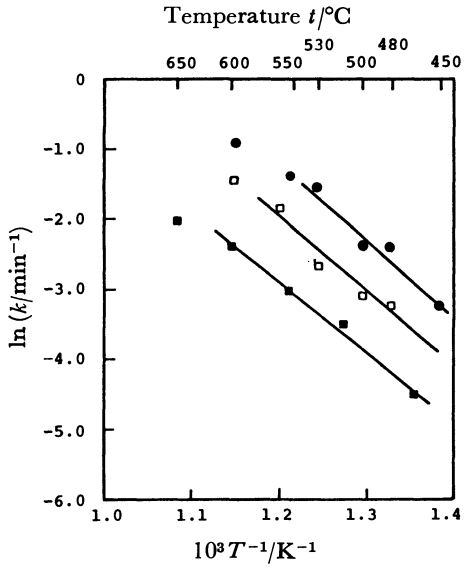

Fig. 5. Arrhenius plots for NO formation reaction.
■: Y_{Si}=1.0, □: Y_{Si}=2.0, ●: Y_{Si}=5.0.

atmosphere can be roughly classified into two stages. In the early stage (<600 °C), especially below 530 °C, the main anion species in the melt is nitrite. In Fig. 3 (C), the mol percent of sodium compounds other than nitrate and nitrite is about 20% at 530 °C. However, it was found by chemical analysis that silicates are scarcely formed below 530 °C. This indicates that some oxide species, probably including peroxide,[7] can exist stably in an argon atmosphere. The reaction below 530 °C is expressed by Eq. 5:

$$2\,NaNO_2 = Na_2O_2 + 2\,NO \qquad (5)$$

Sodium nitrate and silicates were formed in the temperature range from 530 to 600 °C. In the later stage (>600 °C), the reaction is almost identical with that of sodium nitrate with silica, as the main anion species in the melt is nitrate. In the present paper, the early stage of the reaction is mainly discussed.

Isothermal Reaction of Sodium Nitrite with Silica. Figure 4 shows thermograms obtained when samples containing 0.1 mmol of sodium nitrite were heated at various temperatures in an argon atmosphere. Thermograms have a trend to approach gradually the dashed line below 550 °C at 1.0 and 2.0 in Y_{Si}, or below 500 °C at 5.0 in Y_{Si}. After a reaction time of 3 h, α indicates a value from 0.789 to 1.000 in all cases. This suggests that the reaction of sodium nitrite with silica consists of two stages: the rapid formation of sodium peroxide, and the sluggish reaction of peroxide with silica. These two reaction stages correspond to the early and later stages described above. The apparent activation energy (ΔE) and the frequency factor ($\ln k^\circ$) for the rapid reaction were obtained by extrapolating DTG curves to 0 in the fraction of weight loss (α) and by plotting the $(d\alpha/dt)_{\alpha=0}$ values versus the reciprocal temperatures. The plot is shown in Fig. 5. The values of ΔE and $\ln k^\circ$ are listed in Table 1. The fact that the apparent activation energies at both 2.0 and 5.0 in Y_{Si} are almost the same, irrespective of the composition, strongly indicates that the early-stage reaction is characteristic of the decomposition of sodium nitrite to form peroxide in the melt. In the later stage, the thermograms for the sample with 1.0 in Y_{Si} were analyzed by the Avrami-Erofe'ef equation as was described in a previous paper.[2] The Arrhenius plot showed a good linearity, and the value of 181 kJ mol^{-1} was obtained for the apparent activation enrgy. This value is quite close to that obtained for the final stage of the reaction of sodium nitrate with silica, 179 kJ mol^{-1}, and to that obtained by Bond *et al.*[4]

Table 1. Activation energy and frequency factor for the NO-formation reaction obtained from Fig. 5

Composition Y_{Si}	Apparent activation energy, ΔE/kJ mol^{-1}	Frequency factor, $\ln(k^\circ/\text{min}^{-1})$
1.0	81.2	8.8
2.0	98.3	12.3
5.0	97.1	12.9

Reaction of Sodium Nitrite with Silica at a Constant Heating Rate. It is difficult to obtain data to discuss the elementary reactions in the early stage isothermally, because the nitrite considerably decomposes before reaching the desired temperatures. Therefore, the

reaction of sodium nitrite with silica was investigated at a constant heating rate.

Zambonin *et al.*[8–10] reported that oxide species such as O_2^-, O_2^{2-}, O^-, and O^{2-} act as bases in the nirate melt. For the early reaction stage of sodium nitrite with silica, the following assumptions are appropriate judging from the results of various analyses of reaction products, *etc*:

(i) The formation and the dissociation of O_2 are neglected.

(ii) The formed nitrate does not decompose.

(iii) Approximately spherical ions with an identical charge, for example O_2^- and O_2^{2-}, do not react with each other.

(iv) The gas formed (NO) is carried away from the system by the carrier gas.

If these assumptions are valid, the following equations may be considered for the reaction mechanism:

$$NO_2^- \xrightarrow{k_1} NO + O^- \quad (6)$$

$$NO_2^- + O^- \xrightarrow{k_2} NO + O_2^{2-} \quad (7)$$

$$O_2^{2-} \underset{k_4}{\overset{k_3}{\rightleftharpoons}} O^{2-} + O \quad (8)$$

$$O_2^{2-} \xrightarrow{k_5} O^- + O^- \quad (9)$$

$$O_2^- \underset{k_7}{\overset{k_6}{\rightleftharpoons}} O^- + O \quad (10)$$

$$NO_2^- + O \xrightarrow{k_8} NO_3^- \quad (11)$$

$$NO_2^- + O \xrightarrow{k_9} NO + O_2^- \quad (12)$$

For the thermal decomposition of sodium nitrite, the concentration of O, O^-, O_2^-, and O_2^{2-} is supposed to be very low.[8–10] If the stationary state is assumed to the formation of these species, Eq, 13 is obtained:

$$-\frac{d[NO_2^-]}{dt} = 3k_8[O][NO_2^-] \quad (13)$$

As [O] is considered to be almost constant in a relatively narrow temperature range, Eq. 13 can be rearranged, thus:

$$-\ln[NO_2^-] = 3k_8[O]t \quad (14)$$

The concentration of nitrite, the reaction time (t), and the kinetic constant (k_8) are expressed by Eqs. 15 to 17:

$$[NO_2^-] = \frac{3(1-1.9\alpha)}{3-1.9\alpha} \quad (15)$$

$$t = \frac{T-T_0}{v} \quad (16)$$

$$k_8 = k_8^\circ \exp\left(-\frac{\Delta E_8}{RT}\right) \quad (17)$$

where the constant value of 1.9 in Eq. 17 is the ratio of the final weight loss of Reaction 18 to that of Reaction 3 per mol of sodium nitrite:

$$4\,NaNO_2 = 2\,Na_2O + 4\,NO + O_2 \quad (18)$$

T, T_0, and v are the sample temperature, the temperature when the reaction starts, and the heating rate respectively. By substituting Eqs. 15, 16, and 17 into Eq. 14, Eq. 19 can be obtained:

$$y = \ln\left[-\ln\frac{3(1-1.9\alpha)}{3-1.9\alpha}\right] - \ln\frac{3(T-T_0)}{v} = \ln k_8^\circ[O] - \frac{\Delta E_8}{RT} \quad (19)$$

For the reaction of sodium nitrite with silica, Reaction 5 consists of the elementary reactions of (6) and (7). Assuming the stationary state with respect to the formation rate of O^-, Eqs. 20 and 21 are obtained:

$$-\frac{d[NO_2^-]}{dt} = 2k_1[NO_2^-] \quad (20)$$

$$y = \ln\left[-\ln\frac{2(1-1.27\alpha)}{2-1.27\alpha}\right] - \ln\frac{2(T-T_0)}{v} = \ln k_1^\circ - \frac{\Delta E_1}{RT} \quad (21)$$

where the constant value of 1.27 in Eq. 21 is the ratio of the final weight loss of Reaction 18 to that of Reaction 5 per mol of sodium nitrite.

Thermograms obtained for the samples heated at a constant rate of 5 °C min^{-1} are analyzed by means of Eq. 19 for the decomposition of sodium nitrite and by means of Eq. 21 for the reaction of sodium nitrite with silica. The heating rate from 1.25 to 10.0 °C min^{-1} scarcely affected the y *versus* T^{-1} plot.

Figures 6 and 7 show the thermograms and the DTG curves for the samples containing 0.1 mmol of sodium nitrite. The DTG curve with 1.0 in Y_{Si} has three peaks (550, 600, and 640 °C). The two peaks at lower temperatures belong to the early stage of the reaction.

Figures 8 and 9 show the y *versus* T^{-1} plots for the thermal decomposition of sodium nitrite and for the reaction of sodium nitrite with silica respectively. In Figs. 8 and 9, the y *versus* T^{-1} plots consist of two straight lines, irrespective of the coexistence of silica, and the early stage of the reaction is further divided into two reaction processes; Process I at lower temperatures and Process II at higher temperatures.

In Process I, the value of ΔE_8 for the thermal decomposition of sodium nitrite was 111 kJ mol^{-1}. The value of ΔE_1 in Process I for the reaction of sodium nitrite with silica were almost constant; their average value was 69

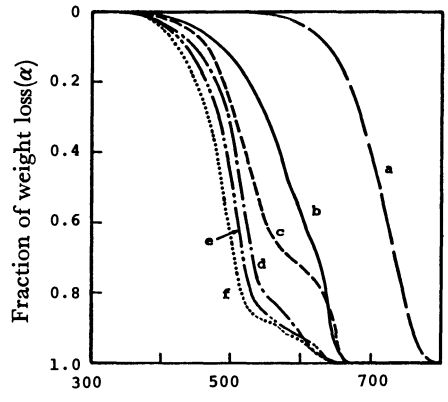

Fig. 6. Thermograms in sodium nitrite–silica system at constant heating rate in argon atmosphere.
a: $Y_{Si}=0$, b: $Y_{Si}=1.0$, c: $Y_{Si}=2.0$, d: $Y_{Si}=5.0$, e: $Y_{Si}=7.5$, f: $Y_{Si}=10.0$.

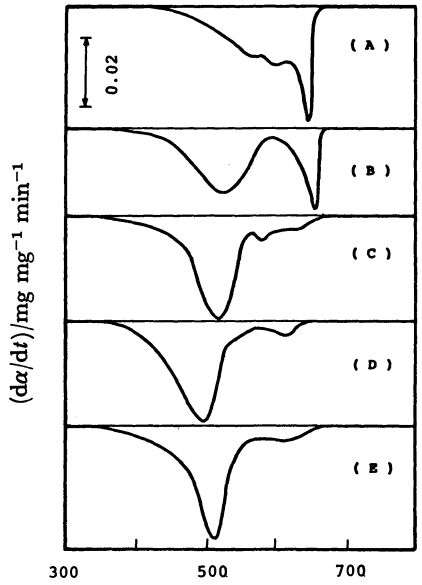

Fig. 7. DTG curves in sodium nitrite–silica system at constant heating rate in argon atmosphere.
(A): $Y_{Si}=1.0$, (B): $Y_{Si}=2.0$, (C): $Y_{Si}=5.0$, (D): $Y_{Si}=7.5$, (E): $Y_{Si}=10.0$.

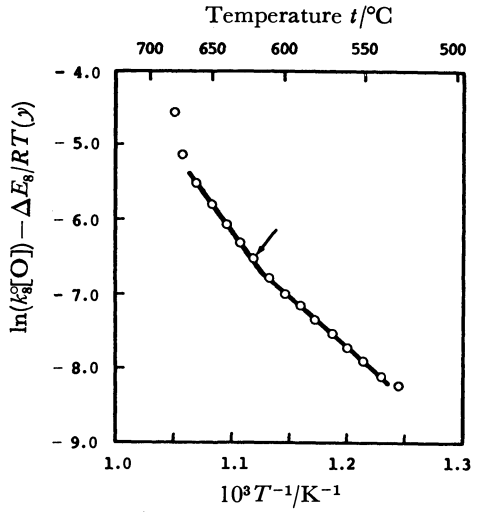

Fig. 8. $[\ln(k_8^\circ[O])-\Delta E_8/RT)]$ *vs.* T^{-1} plot for the thermal decomposition of sodium nitrite in argon atmosphere.
$T_0=278$ °C, $v=5.0$ °C min^{-1}. The arrow indicates the point where oxygen was detected by gas chromatography.

kJ mol^{-1} (S. D.: 8 kJ mol^{-1}), which was considerably smaller than the value of 111 kJ mol^{-1} for ΔE_8. It is clear from this result that silica acts an acid and lowers the activation energy of the formation of peroxide by stabilizing the peroxide at the solid-liquid interface on the melt and silica.

In Process II, the value of 187 kJ mol^{-1} was obtained for the activation energy of the thermal decomposition of sodium nitrite. For the system of sodium nitrite and silica, the activation energies in Process II are listed in Table 2. These values depend upon the composition and tend to increase with an increase in Y_{Si} below 5.0. Above 5.0 in Y_{Si}, however, they are almost constant, and the average value is 211 kJ mol^{-1} (S. D.: 10 kJ mol^{-1}). This large value of activation energy compared to that for Process I may be caused by the formation of disilicate on the solid-liquid interface because of the existence of a considerable quantity of silica compared to that of the melt above 5.0 in Y_{Si}.

In Process II, the reactions accompanying a trace amount of O_2 generation might be caused by the increase in the amount of atomic oxygen in the melt. These

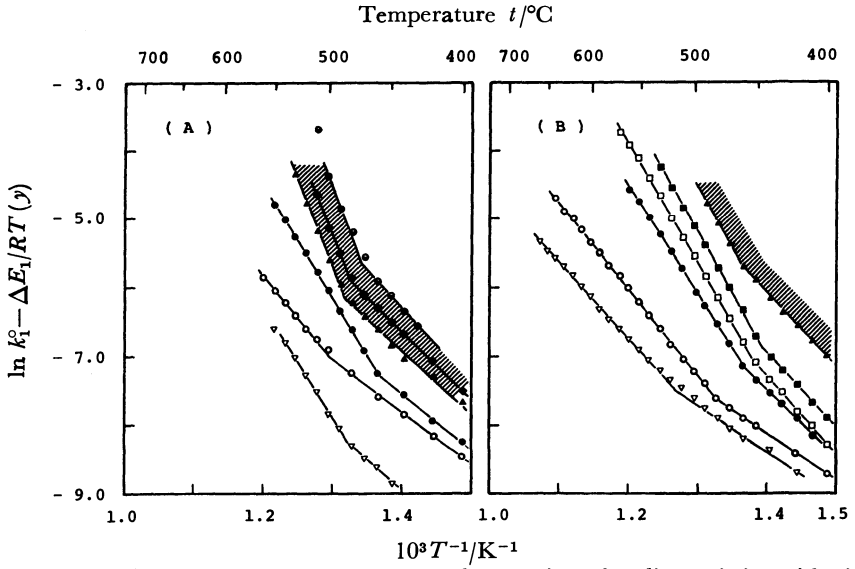

Fig. 9. $[\ln k_1^\circ-\Delta E_1/RT]$ *vs.* T^{-1} plots for the reaction of sodium nitrite with silica in argon atmosphere.
$T_0=278$ °C, $v=5.0$ °C min^{-1}. (A): 0.1 mmol $NaNO_2$, (B): 0.2 mmol $NaNO_2$, ▽: $Y_{Si}=0.5$, ○: $Y_{Si}=1.0$, ●: $Y_{Si}=2.0$, □: $Y_{Si}=3.0$, ■: $Y_{Si}=4.0$, ▲: $Y_{Si}=5.0$, ◒: $Y_{Si}=7.5$, ◆: $Y_{Si}=10.0$.
Above 5.0 in Y_{Si} (Shadows), the effect of silica addition on the reaction is not evident.

Table 2. Activation energy for process II obtained by the use of the y *vs.* T^{-1} plot

Composition Y_{Si}	Apparent activation energy/kJ mol^{-1}	
	0.1 mmol $NaNO_2$	0.2 mmol $NaNO_2$
0.25	97.7	—
0.50	127	89.4
1.00	94.2	103
2.00	137	131
3.00	—	148
4.00	—	159
5.00	209	213
7.50	203	—
10.00	217	—

reactions are expressed by Eqs. 22 and 23:

$$O + O_2^{2-} \longrightarrow O_2 + O^{2-} \quad (22)$$

$$O + O \longrightarrow O_2 \quad (23)$$

Atomic oxygen would be supplied by the following reactions:

$$NO_3^- \longrightarrow NO_2^- + O \quad (24)$$

$$2\,SiO_2 + O_2^{2-} \longrightarrow Si_2O_5^{2-} + O \quad (25)$$

$$Si_2O_5^{2-} + O_2^{2-} \longrightarrow 2\,SiO_3^{2-} + O \quad (26)$$

$$O_2^{2-} \longrightarrow O^{2-} + O \quad (8)$$

$$O_2^- \longrightarrow O^- + O \quad (9)$$

Below 1.0 in Y_{Si}, the activation energy in Process II is quite close to that for the decomposition of sodium nitrite in Process I, and the rate-determining step of these processes seems to be Reaction 11. This is supported by the facts that the amount of oxygen generated in these processes is quite small and that both processes are nitrate-formation reactions. The apparent activation energy obtained by analyzing the thermograms at 1.0 in Y_{Si} with Eq. 19 agrees with the activation energy for the decomposition of sodium nitrite in Process I better than the average value of the activation energies for the system of sodium nitrite and silica below 1.0 in Y_{Si}, 102 kJ mol^{-1}.

The authors wish to thank the Kato Kagaku Shinkokai foundation for its helpfull support. They also wish to thank Mr. Akinori Ohba for carrying out a part of the experiments. This work was partly supported by a Grant-in-Aid for Scientific Research No. 56550544 from the Ministry of Education, Science and Culture.

References

1) Y. Hoshino, T. Utsunomiya, T. Utsugi, and O. Abe, *Nippon Kagaku Kaishi*, **1980**, 690.
2) Y. Hoshino, T. Utsunomiya, and O. Abe, *Bull. Chem. Soc. Jpn.*, **54**, 1385 (1981).
3) E. S. Freeman, *J. Phys. Chem.*, **60**, 1487 (1956).
4) B. D. Bond and W. M. Jacobs, *J. Chem. Soc.*, **1966**, 1265.
5) R. R. Sakaida, R. G. Rinker, R. F. Cuffel, and W. H. Corcoran, *Anal. Chem.*, **33**, 32 (1961).
6) S. S. Al Omer and D. H. Kerridge, *J. Inorg. Nucl. Chem.*, **40**, 975 (1978).
7) F. Paniccia and P. G. Zambonin, *J. Phys. Chem.*, **78**, 1693 (1974).
8) P. G. Zambonin and J. Jordan, *J. Am. Chem. Soc.*, **91**, 2225 (1969).
9) P. G. Zambonin, *J. Electroanal. Chem.*, **33**, 245 (1971).
10) F. Paniccia and P. G. Zambonin, *Electrochim. Acta*, **21**, 605 (1976).

Mineralogical Characterization of the Reference Material of "Pond Sediment"

Yasuo IWATA, Hiroki HARAGUCHI,* Jon C. VAN LOON,† and Keiichiro FUWA
Department of Chemistry, Faculty of Science, The University of Tokyo, Hongo, Bunkyo-ku, Tokyo 113
†*Department of Geology and Chemistry, The Institute for Environmental Studies, University of Toronto, Toronto, Ontario, Canada*

(Received January 13, 1982)

The identification of rock-forming and clay minerals contained in the reference material of "Pond Sediment" (Reference Material NIES No. 2 from the National Institute for Environmental Studies, Japan) has been made with X-ray diffraction method. It was found that the sediment contained α-quartz and feldspars as the principal components along with small quantity of pyroxenes, amphiboles, and some clay minerals. The sediment sample was treated chemically for extraction, and also separated with density and with grain sizes. Elemental compositions of such extracted or separated fractions of the sediment were determined by inductively coupled argon plasma emission and atomic absorption spectrometry. The identified minerals and the elemental distributions in the separated fractions helped to characterize the pond sediment.

In recent years, much attention has been paid to environmental and biological reference materials because of the importance of pollution control. Recently NBS issued a standard reference material of "River Sediment."[1] We have also prepared independently a reference material of "Pond Sediment,"[2] which was collected from the Sanshiro-ike (Pond at the University of Tokyo), and issued as Reference Material No. 2 from the National Institute for Environmental Studies, Japan. The Sanshiro-ike pond sediment consists basically of volcanic ash called Kanto loam, atmospheric dust, and organic matters originating from plants, animals, and microorganisms. There have been no significant flows of freshwater, and industrial or sewage waste into the pond. Therefore, the composition of the sediment sample should mainly reflect air pollution from a big city environment (*i.e.*, imports of pollutants arisen from traffic and industrial discharges into the air). Goldberg reported that the history of the environmental pollution in Tokyo was recorded in the Palace Moat Sediment.[3]

The procedure for preparing reference materials, homogeneity test, and its elemental composition have been reported in the previous communication.[2] In order to understand the significance of the "Pond Sediment," it may be further desirable to investigate the elemental distributions in a variety of partial extractions of the sedimant. Hence, in this study, extraction tests and mineralogical characterization of the "Pond Sediment" have been performed, and the origins and the chemical forms of elements are described.

Experimental

Chemicals. All the chemicals used were of analytical reagent grade. Standard solutions were prepared by dissolving pure metals, metallic oxides and their salts in acidic or deionized distilled water. Final acidity of each working standard solution was adjusted at 1 M (1 M=1 mol dm^{-3}) with nitric acid and/or hydrochloric acid. In addition, standard rock sample JB-1 (basalt) from the Geological Survey of Japan[4] was also analysed to examine the accuracy and precision of the analytical method for elemental compositions.

Instruments. X-Ray diffraction measurements were performed using an X-ray diffractometer, Model JEOL-GOS. The diffraction patterns were measured in the range of the diffraction angle (2θ) from 4° to 70°. An inductively coupled plasma (ICP) emission spectrophotometer (Model Jarrell-Ash Plasma AtomComp Mark II), and an atomic absorption spectrophotometer (Model Shimadzu AA-640-13) was used for the determination of the elemental distributions in separated fractions. Total carbon and nitrogen were determined using a C. H. N. Coder (Model Yanagimoto MT-2).

Separation of the Sediment for Mineral Identification. The "Pond Sediment" was separated into 4 groups, *i.e.*, organic matters and carbonates, iron oxides, primary and secondary minerals, and heavy and light minerals. The separation procedure which is a modified method of those reported in the literature,[5,6] is summarized as follows:

(1) Organic Matter and Carbonates: Ten ml of 30% H_2O_2 was added to 5 g of the sediment sample, and the mixture was heated until the vigorous reaction was over. After cooling, 50 ml of 0.2 M HCl was added with stirring for 1 h at room temperature. Then, the suspension was filtered by means of suction with a No. 5C filter paper (Toyo Co., Ltd.). The filtrate was diluted to 100 ml with water (F-1).

(2) Iron Oxides: The air-dried residue of (1) was suspended in 50 ml of 0.3 M sodium citrate solution, and 5 g of sodium dithionite was added into suspension. The suspension was heated at 80 °C with occasional agitation for about 30 min, and then filtered by means of suction with a No. 5C filter paper. The filtrate was diluted to 100 ml (F-2).

(3) Primary and Secondary Minerals: The residue of (2) was transferred into water. Then, the secondary minerals (diameters less than 20 μm) was separated from the primary minerals (diameters larger than 20 μm) by the elutriation as follows: After stirring the suspension vigorously, the mixture was allowed to stand for 4 min and 48 s. Then the supernatant down to 10 cm depth was removed with a siphon. This siphoning was repeated several times. In this procedure, the particles of diameter larger than 20 μm remain in the lower part of the solution, which was difined as the primary minerals. Most of these particles may be classified as fine sand, and consist mainly of the primary minerals. The siphoned materials, which is the mixture of silt and clay, consists mainly of secondary minerals.

(4) Heavy and Light Minerals: The air-dried primary minerals of (3) was treated with heavy organic liquids such as dibromomethane (d=2.5), tribromomethane (d=2.9), and diiodomethane (d=3.3) for further separation. Each fraction of heavy organic liquids was separated by centrifugation, and each separated sample was washed well with acetone, and then

dried under an IR lamp.

In addition to the above treatments, magnetic minerals were separated independently using a magnet, although they were found in very small quantities. In order to determine the elemental distributions, the sample was boiled with 12 M HCl.[6] The residue in 12 M HCl solution was dried at 500 °C to examine on the primary minerals.

Elemental Analysis of Separated Fractions. Each separated fraction was treated for elemental analysis according to the following procedure, which was modified from the one reported by Yoshida.[7] The sample was digested with a mixture of 10 ml concd HNO_3 and 10 ml concd $HClO_4$ for 30 min on a hot plate at 200 °C. After cooling, 20 ml of HF was added and the mixture was kept standing at room temperature for 30 min. Then it was evaporated until fuming, and 5 ml HNO_3 and 5 ml $HClO_4$ were again added, and the mixture was heated. After dissolution the mixture was heated to incipient dryness. The residue was dissolved with 10 ml of 6 M HCl and then diluted to 100 ml with water.

Results and Discussion

The amount of each separated fraction in weight % is shown in Table 1. Organic matter, oxides, and minerals were approximately 20, 15, and 60%, respectively. Fine sand (>20 μm), silt (2—20 μm), and clay (<2 μm), separated by the siphoning procedure, were found to be 20, 30, and 10%, respectively.

Mineral Composition. Minerals identified by the X-ray diffraction are summarized in Tables 2 and 3. For identification the ASTM (American Society for Testing Materials) cards were used.

Table 2 shows good agreement between the densities of separated primary minerals and their reported values.[8] These results are substantiated by the data of the elemental analyses mentioned later. It can then be stated that this "Pond Sediment" contains quartz and feldspars as the principal components, together with a small quantity of pyroxenes, amphiboles, micas, and iron ores.

Besides these rock-forming minerals, the sediment contains montmorillonite, halloysite, vermiculite, and many other clay minerals, as shown in Table 3. Since the separation of clay minerals was difficult and their X-ray peaks were not sharp, the identification of secondary minerals was not so easy. However, a few clay minerals could be identified, and these are summarized in Table 3. In addition to the above clay minerals, the sediment contains likely gibbsite and hematite, because much Al and Fe were found in the extractable fractions of the "Pond Sediment." However, X-ray peaks of these minerals were not identified because of the interferences of other large peaks. Further separation of the secondary minerals were tried based on sinking velocity using mixtures of bromoform and acetone as heavy liquids. Separation of secondary minerals could not, however, be made because of co-adsorption of fine particles.

It is known that allophane is present in high concentration in the Tachikawa loam in the upper stratum of the Kanto loam.[8] Although the "Pond Sediment" may contain such a non-crystalline clay mineral, allophane could not be identified by X-ray diffraction.

Table 1. Amount of each fraction separated with various treatments

Fraction	Amount weight %
H_2O_2–HCl soluble (organic matter and carbonates, F-1)	20
Citrate–dithionite soluble 15 (free iron oxides, F-2)	15
Minerals	60
Primary minerals (ϕ>20 μm)	20
Magnet	<1
H-1(d>3.3)	1
H-2(3.3>d>2.9)	2
H-3(2.9>d>2.5)	13
H-4(2.5>d)	4
Secondary minerals (ϕ<20 μm)	40
Silt	30
Clay	10

Table 2. Identification of rock-forming minerals in the primary minerals of the "Pond Sediment"

Fraction No.	Identified minerals (density[a])
Magnet	magnetite (5.174)
H-1 (d>3.3)	hypersthene (3.37), augite (3.34), ilmenite ? (4.2)
H-2 (3.3>d>2.9)	hornblende (3.2)
H-3 (2.9>d>2.5)	α-quartz (2.65), feldspars (orthoclase (2.57), albite (2 61), anorthite (2.76), etc.)
H-4 (2.5>d)	α-quartz (2.65), feldspars, clay minerals
R.M.[b]	hypersthene (3.37), α-quartz (2.65), feldspars, muscovite (2.76—3.0)

a) Cited from Ref. 8. b) Residual minerals after hot HCl treatment.

Table 3. Identification of clay minerals in the secondary minerals of the "Pond Sediment"[a]

Mineral	Treatment		
	None[b]	H_2O_2[c]	$Na_2S_2O_4$[d]
Montmorillonite	+	(+)	(+)
Chlorite	+	+	+
Vermiculite	(+)	(+)	−
Illite	+	(+)	(+)
Halloysite	+	+	(+)
Metahalloysite	(+)	−	+

a) Symbols: + positive, (+) not conclusive, − not identified. b) Separated by the siphoning method without any chemical treatment. c) Separated by the siphoning method after H_2O_2 treatment. d) Separated by the siphoning method after H_2O_2 and $Na_2S_2O_4$ treatments.

Elemental Compositions of Fractions Separated with Density. The elemental compositions concerned with major constituents in primary minerals are shown in Fig. 1 for each fraction separated with heavy liquids. The separated fractions are represented as H-1 (d>3.3), H-2 (3.3>d>2.9), H-3 (2.9>d>2.5), and H-4 (d<2.5).

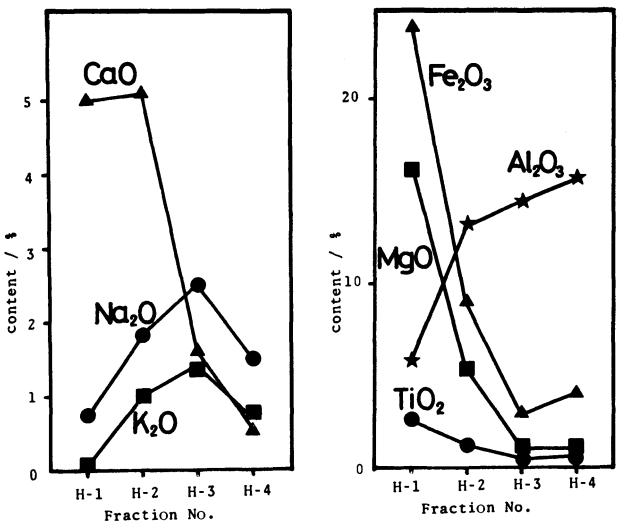

Fig. 1. Elemental compositions of primary minerals in the "Pond Sediment" separated with heavy liquids.
Fraction No. H-1: $d>3.3$, H-2: $3.3>d>2.9$, H-3: $2.9>d>2.5$, H-4: $d>2.5$.

Fraction H-1 contains Ca, Mg, and Fe as the principal constituents. This result may be related to the fact that pyroxenes have Ca, Mg, and Fe end-members of the solid solution $[(Ca, Mg, Fe)_2Si_2O_6]$.[10] As can be seen in Fig. 1, the contents of Fe, Mg and Ca are high, while that of Al is less. These elemental compositions also suggest that fraction H-1 contains much hypersthene $[(Mg, Fe)SiO_3]$ and a little augite $[Ca(Mg, Fe, Al)(Si, Al)O_6]$.[10] In addition Fe and Ti are richer in fraction H-1 than in other fractions. This may indicate that magnetite $[Fe_3O_4]$ and ilmenite $[FeTiO_3]$ are contained in fraction H-1,[11] although they could not be identified clearly. Consequently, the large contents of Fe, Ca, Mg, and Ti in fraction H-1 may be interpreted by the existence of minerals such as pyroxenes, hypersthene, and augite as well as magnetite and ilmenite.

Fraction H-2 ($3.3>d>2.9$) contains much Al, Ca, Mg, and Fe (see Fig. 1). Since the densities of amphiboles are in the range from 2.9 to 3.3, it is likely that fraction H-2 mainly contains amphiboles. In many cases, hornblende $[Ca_2Na_{0-1}(Mg, Fe, Al)_5[(Al, Si)_4O_{11}]_2]$[10] can be identified by X-ray diffraction. The elemental composition of fraction H-2 supports the presence of hornblende, and it likely consists of hornblende as the principal component, as well as of small quantities of other amphiboles.

As can be seen in Fig. 1 the contents of Na and K were largest in fraction H-3 ($2.9>d>2.5$), although Na, K, and Ca were contained at almost equal levels in this fraction. Fraction H-3 appears to contain much feldspar in a mixture of solid solutions which consist of three end-members such as $NaAlSi_3O_8$, $KAlSi_3O_8$, and $CaAlSi_2O_8$.[10]

There were more clay minerals in fraction H-4 ($d<2.5$), although the elemental composition was almost similar to fraction H-3. Fraction H-4 contains clay minerals, quartz, and feldspars which are not separated by the siphoning treatment and/or by heavy liquid separation because of co-adsorption and fineness of the materials.

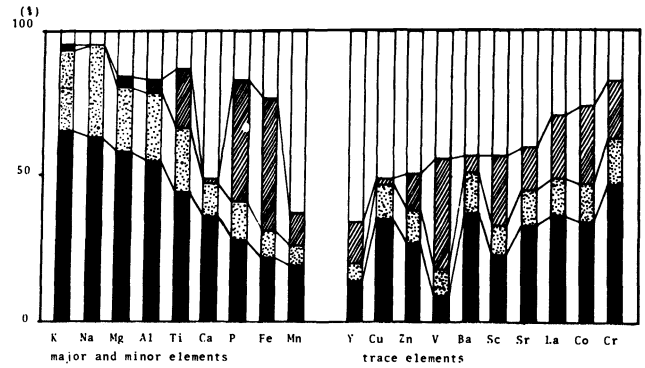

Fig. 2. Distributions of major, minor, and trace elements in the fractions separated with various treatments.
□: "H_2O_2" treatment, ▨: "$Na_2S_2O_4$" treatment, ▩: secondary minerals, ■: primary minerals.

Distribution of Major, Minor, and Trace Elements in the Fractions. The distribution of major, minor and trace elements in each separated fraction was determined, and the calculated percentage of each element is illustrated in Fig. 2. The separated fractions of "H_2O_2" and "$Na_2S_2O_4$" in Fig. 2 correspond to solutions F-1 and F-2, respectively, as described previously in the separation procedure. The "primary" and "secondary" in Fig. 2 indicate primary and secondary minerals, respectively, which were separated and digested with HNO_3, $HClO_4$, and HF, as described previously. From these results, it is evident that Fe, P, and Ti are mostly leached with the dithionite-citrate treatment. This suggests that these elements may be present mainly in the chemical form of easily reducible oxides. It is known that hydrous iron oxides have great scavenging efficiency, and so many trace elements may be caught by the concretion or coatings around the second particles.

The fraction treated with hydrogen peroxide and hydrochloric acid contains much Mn and Ca. Calcium may be in the form of carbonate minerals such as dolomite or in the form of exchangeable cations. Manganese is considered to be in two modes: the one is related to the organic matter which is decomposed by hydrogen peroxide, and the other is hydrous manganese oxides which are decomposed by the mixture of hydrogen peroxide and hydrochloric acid. Na, K, Mg, and Al exist mostly in primary and secondary minerals, and more than half of them appear in the fractions containing the rock-forming minerals.

Most of trace elements were leached in the fraction treated with hydrogen peroxide–hydrochloric acid. Therefore, they may be present as species adsorbed on the minerals or as the constituents in the organic matter.

Variation of Major and Minor Components in Minerals. Figure 3 shows the variations of elemental compositions in primary minerals with and without various chemical treatments. The amount of Fe and Al decrease after each treatment step, suggesting that various oxides and organic matter exist as coatings around mineral particles which were separated only by the siphoning method. Therefore, the primary fractions after the hydrogen peroxide–hydrochloric acid and dithionite–citrate treat-

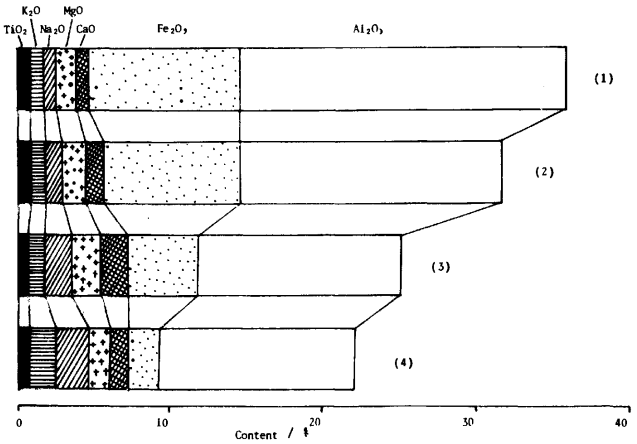

Fig. 3. Major and minor constituents of primary minerals in the "Pond Sediment" with and without various chemical treatments.
(1): Original sample, (2): primary minerals without chemical treatment, (3): primary minerals with H_2O_2 and $Na_2S_2O_4$ treatments, (4): residual minerals with hot HCl treatment.

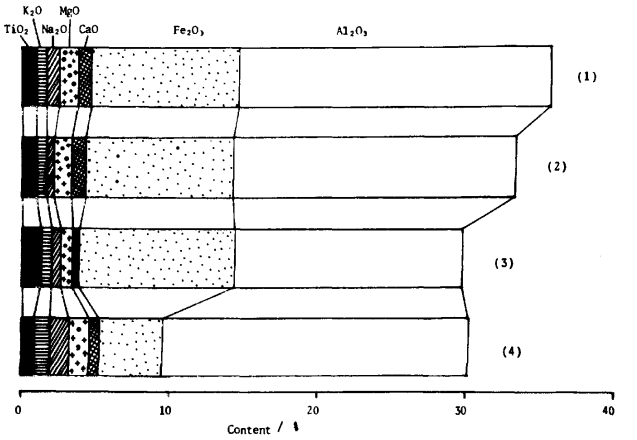

Fig. 4. Major and minor constituents of secondary minerals in the "Pond Sediment" with and without various chemical treatments.
(1): Original sample, (2): secondary minerals without chemical treatment, (3): secondary minerals with H_2O_2 treatment, (4): secondary minerals with H_2O_2 and $Na_2S_2O_4$ treatments.

Table 4. The contents of carbon, nitrogen, and phosphorus in the "Pond Sediment"

Element	Content/%
C	5.5
N	0.27
P	0.12

Ignition loss was 15.5%.

ments contain only rock-forming minerals.

The variation of major and minor components in secondary minerals are also shown in Fig. 4. Without the dithionite–citrate treatment the content (%) of most elements slightly decreased. This decrease may be caused by the loss of the principal elements of rock-forming minerals. In the last bar which corresponds to the dithionite–citrate treatment Fe decreases significantly, and the percentages of other elements increase slightly. Most of the removed Fe is considered to be iron oxides and some clay minerals (*e.g.*, goethite) which are easily degradable.

The elemental composition of secondary minerals treated with dithionite–citrate is almost identical to that of primary minerals with the same treatment, which their X-ray diffraction patterns showed some differences.

Evaluation of Non-metallic Elements. The analytical results of carbon and nitrogen are summarized in Table 4 along with the content of phosphorus. The results show that the "Pond Sediment" contains much carbon. Most of carbon exists as organic matter, and the remainder appears to be carbonate minerals such as dolomite [$(Ca, Mg)CO_3$] and calcite [$CaCO_3$].[10] The content of Ca in the hydrogen peroxide–hydrochloric acid soluble fraction is large, suggesting the presence of calcite in the "Pond Sediment." Carbonate minerals, however, were not positively identified probably because all the carbonate minerals were degraded by the chemical treatments using acids.

Half of phosphorus content occurs in the mineral fractions, but the phosphorus-rich minerals like apatite were not identified by the X-ray diffraction method, and the petrographic microscopic method is required for positive identification.

The content of nitrogen in the "Pond Sediment" (2700 $\mu g\ g^{-1}$) is close to the average value of the general soils, which contain nitrogen in the range of 200—5000 $\mu g\ g^{-1}$.[11]

Conclusion

It has been found that the principal components of the pond sediment are quartz and feldspars. Other identified minerals present at lower levels were pyroxenes, amphiboles, and clays. Olivines were not found in the sample. These results indicate that this sediment has not undergone extensive weathering because of the existence of many rock-forming minerals along with quartz. The results obtained by the extraction with citrate–dithionite suggest a scavenging action of trace metals by iron oxides.

Besides the identification of minerals the fractionation including chemical extraction has been found to be useful for environmental and geochemical characterization of sediments, because some elements are partitioned into specific fractions separated with appropriate chemicals.

The authors thank Dr. T. Yamanaka in the Department of Mineralogy, Faculty of Science, The University of Tokyo, for his assistance and discussion in mineral identifications. They also thank Dr. K. Okamoto in the National Institute for Environmental Studies for providing the sediment samples and carrying out the determination of carbon and nitrogen by a C. H. N. Corder. One of the authors (J.C.V.L.) expresses his sincere thanks to the Japan Society for Promotion of Science for supporting the fellowship to stay in the University of Tokyo as the visiting professor (1981).

This research has been supported by Grant-in-Aid for Environmental Science No. 56030019 from the Ministry of Education, Science and Culture.

References

1) *Certificate for Analysis, River Sediment SRM* **1645**, U. S. Department of Commerce, National Bureau of Standards, Washington D. C. (1978).
2) Y. Iwata, K. Matsumoto, H. Haraguchi, K. Fuwa, and K. Okamoto, *Anal. Chem.*, **53**, 1136 (1981).
3) E. D. Goldberg, V. Hodge, M. Koide, and J. J. Griffin, *Geochem. J.*, **10**, 163 (1976).
4) A. Ando, *Geochem. J.*, **1**, 155 (1967).
5) T. Sudo, "Nendo-Kobutsu Gaku," Iwanami, Tokyo (1974).
6) "Bunseki Kagaku Binran," 3rd ed, ed by the Japan Society for Analytical Chemistry, Maruzen, Tokyo (1981).
7) M. Yoshida, *Kankyo To Sokutei Gijutsu*, **5**, 55 (1978).
8) N. Konuma, "Uchu-Chikyu Kagaku," in "Shin Jikken Kagaku Koza," ed by the Chemical Society of Japan, Maruzen, Tokyo (1976), Vol. 10, p. 233.
9) S. Sugawara (Kaneko), *Nendo Kagaku No Shinpo*, **2**, 360, (1960).
10) N. Morimoto, I. Sugawara, and A. Miyashiro,"Kobutsu Gaku," Iwanami, Tokyo (1975).
11) H. J. M. Bowen, "Environmental Chemistry of the Elements," Academic Press, New York and London (1979), p. 60.

 © 1983 The Chemical Society of Japan Bull. Chem. Soc. Jpn., 56, 439—442 (1983)

Mössbauer and ESR Studies of Potassium Borophosphate Glasses

Tetsuaki NISHIDA,* Yoshiaki MIYAMOTO, and Yoshimasa TAKASHIMA
Department of Chemistry, Faculty of Science, Kyushu University 33, Hakozaki, Higashi-ku, Fukuoka 812
(Received January 20, 1982)

A linear decrease in isomer shifts of Fe^{3+} and Fe^{2+} was observed with an increase in alkali content of borophosphate glasses. The decrease is attributed to a change in the role of iron from a network modifier to a network former, or a decrease in the interatomic distance between iron and oxygen atoms. A linear decrease in quadrupole splitting and linewidth was also observed with increasing alkali content, and the decrease is attributed to the increased symmetry around iron nucleus. A linear decrease in relative absorption area of Fe^{2+} in Mössbauer spectra was also observed with increasing alkali content of the glasses. This result is attributed to an increased oxidation atmosphere brought about by alkali oxide into BPO_4 units. Gamma-ray irradiation (1×10^8 R) experiments resulted in no change in these Mössbauer parameters, indicating that the glasses are less sensitive to γ-rays than borate or phosphate glasses. ESR absorption intensity of PO_4^{2-} observed in γ-ray irradiated, iron-free borophosphate glasses increased linearly with an increase in the alkali content in the lower alkali region, and the increase is attributed to a linear increase in the fraction of non-bridging oxygen in PO_4 tetrahedra constituting BPO_4 (and PO_4) units.

Mössbauer studies of borate glasses[1-6] suggested formation of non-bridging oxygen (NBO) to start at an alkali content of 20 mol%. The fraction of NBO constituting BO_4 or FeO_4 tetrahedra was obtained from the Mössbauer absorption area of Fe^{2+} produced by γ-ray irradiation of borate glasses[5] containing a small amount of iron, and also from the absorption area of a hyperfine structure in partially relaxed spectra observed at low temperature.[6] These two results are well consistent with each other, within the experimental error, and the fraction of NBO proved to increase linearly with increasing alkali content of the borate glasses in the alkali region$\geqslant$20 mol%. Gamma-ray irradiation experiments of borate glasses containing 7 mol% of Fe_2O_3 resulted in an increase in s-electron density at the iron nucleus,[3] and this was confirmed from the reduction of Fe^{3+} to Fe^{2+} in γ-ray irradiated borate glasses[3,5] containing a small amount of Fe_2O_3. Mössbauer and ESR studies of potassium phosphate glasses[7,8] were also performed to investigate the formation of NBO in these glasses, and a continuous increase in relative absorption area of Fe^{2+} in the Mössbauer spectra was attributed to an increase in the fraction of NBO. This was also confirmed from a linear increase in ESR absorption intensity of PO_4^{2-} radicals in γ-ray irradiated, iron-free phosphate glasses.[7] The γ-ray irradiation experiments also resulted in a decrease in the Mössbauer absorption area of Fe^{2+} ions.[8] As for borophosphate glasses, it is well known that the glasses are essentially composed of BPO_4 units[9] in which individual boron and phosphorus atoms are tetrahedrally bonded with oxygen atoms to form BO_4 and PO_4 tetrahedra.

The present study was carried out to investigate the formation of NBO and γ-ray irradiation effects in borophosphate glasses.

Experimental

All the glass samples denoted by a formula $x\mathrm{K_2O}\cdot(100-x)(\mathrm{B_2O_3},\mathrm{P_2O_5})\cdot7\mathrm{Fe_2O_3}$ were prepared by fusing the individual mixture of weighed quantitities of K_2CO_3, H_3BO_3, $NH_4H_2PO_4$, and Fe_2O_3 of guaranteed reagent grade at 1200 °C for 3 h in an electric muffle furnace. Prior to this fusion, the mixture in a platinum crucible was calcined at 800 °C for 30 min. The value of x was changed from 10 to 50, and the molar ratio of P_2O_5 to B_2O_3 was so chosen as to be 1.0 and 2.0. Transparent and dark brown glasses were prepared by quenching the platinum crucible with cold water in a beaker. All the glass sample prepared in this way were confirmed to be amorphous by X-ray diffractometry, and they were preserved in a desiccator filled with dry nitrogen gas to protect them from the atmospheric moisture.

These glasses were exposed to γ-rays of 1×10^6 R and 1×10^8 R with a dose rate of 1×10^6 R/h at the ambient temperature in the ^{60}Co-γ ray irradiation facilities of Kyushu University and Japan Atomic Energy Research Institute. During the irradiation each glass sample was kept in a polyethylene bag filled with dry nitrogen gas, and the bag was placed in a glass tube filled with nitrogen gas and silica gel.

Mössbauer measurements were performed by the constant acceleration method at room temperature, with a source of cobalt-57 diffused into a palladium foil. A pure iron foil enriched with iron-57 was used to calibrate the velocity of spectrometer and for the reference of isomer shift. All the Mössbauer spectra were fitted to Lorenzian lineshapes by computer calculations. ESR measurements (X-band) of γ-ray irradiated borophosphate glasses were performed at room temperature in the National Universities' Laboratory for the Common Use of the JAERI Facilities, and also in Kyushu University. The magnetic field was calibrated by using JEOL standard material of MgO : Mn^{2+}.

Results and Discussion

Each of the Mössbauer spectra for potassium borophosphate glasses consists of two quadrupole doublets due to Fe^{3+} and Fe^{2+} ions. Isomer shifts for both the iron species are shown in Fig. 1 as a function of the alkali content of the borophosphate glasses having a P_2O_5/B_2O_3 ratio of 1.0. It is seen from Fig. 1 that both the Fe^{3+} and Fe^{2+} ions are primarily surrounded by six oxygen atoms just like in phosphate glasses.[7,8,10-12] Iron will therefore be present at the interstitial site of the three dimensional network structure of BPO_4 units constituted by BO_4 and PO_4 tetrahedra, facing to two or three NBOs. A linear decrease in isomer shift (Fig. 1) is attributed to an increase in covalency of both iron species, probably because the coordination number of some parts of iron changes from 6 to 4 with the

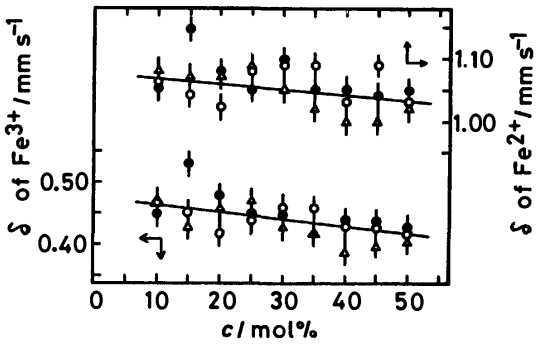

Fig. 1. Isomer shift of Fe^{2+} (above) and Fe^{3+} (below) plotted against the alkali content (c) of potassium borophosphate ($P_2O_5/B_2O_3=1.0$) glasses.
○: Non-irrad., ●: 1×10^6 R irrad., △: 1×10^8 R irrad.

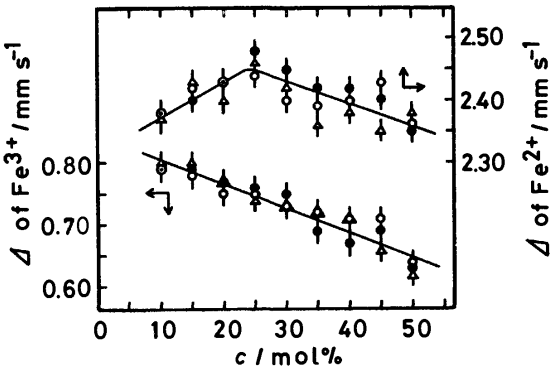

Fig. 2. Quadrupole splitting of Fe^{2+} (above) and Fe^{3+} (below) plotted against the alkali content of potassium borophosphate ($P_2O_5/B_2O_3=1.0$) glasses.
○: Non-irrad., ●: 1×10^6 R irrad., △: 1×10^8 R irrad.

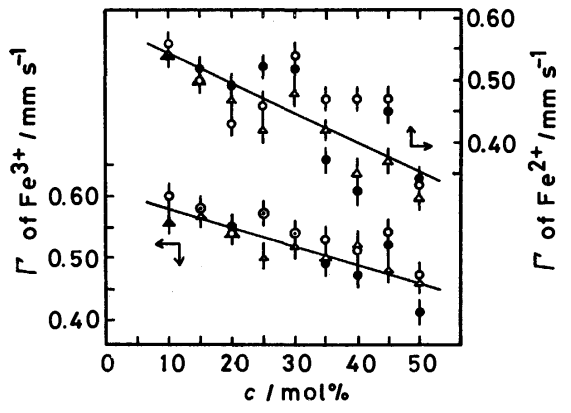

Fig. 3. Linewidths of Fe^{2+} (above) and Fe^{3+} (below) plotted against the alkali content of potassium borophosphate ($P_2O_5/B_2O_3=1.0$) glasses.
○: Non-irrad., ●: 1×10^6 R irrad., △: 1×10^8 R irrad.

increase in the alkali content of the glasses.[10-12] This change in the coordination number means the formation of FeO_4 tetrahedra in which iron plays a role of network former, instead of a network modifier at the interstitial site. Another possible reason for the increase in the covalency is a decrease in the interatomic distance between iron and oxygen, produced by the introduction

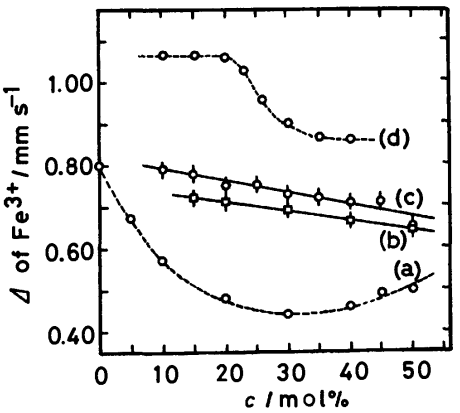

Fig. 4. Quadrupole splitting of Fe^{3+} in glasses.
(a): Potassium phosphate, (b): potassium borophosphate ($P_2O_5/B_2O_3=2.0$), (c): potassium borophosphate ($P_2O_5/B_2O_3=1.0$), (d): potassium borate.

of alkali oxide into BPO_4 units.

Quadrupole splitting values for both the iron species are plotted against the alkali content of the borophosphate glasses ($P_2O_5/B_2O_3=1.0$) in Fig. 2, where the values decrease linearly with increasing alkali content. The decrease in quadrupole splitting of Fe^{3+} (high spin) means the increase in the symmetry around the iron nucleus because each d-orbital of Fe^{3+} ion is occupied by one electron and therefore the effect of valence electrons on the electric field gradient can be negligible. Quadrupole splitting for Fe^{2+} ion also decreased in the alkali region $\geqslant$25 mol%, and the decrease is attributed to the increase in the symmetry around the iron nucleus. An increase in the quadrupole splitting of Fe^{2+} ion in the lower alkali region is difficult to explain, but the alkali content at which quadrupole splitting shows a distinct maximum, *i.e.*, 25 mol%, is well consistent with that in the composition dependence of ESR intensity of PO_4^{2-} to be discussed later.

Linewidth (FWHM) values for Fe^{3+} and Fe^{2+} ions also show a linear decrease when the alkali content of the glasses increases (Fig. 3). The broad linewidth for iron in glasses is attributed to the non-uniformity of the steric configuration around the individual iron nucleus.[12-14] The decrease in linewidth therefore suggests that the steric configuration around iron nucleus becomes more uniform as the fraction of alkali oxide increases in these borophosphate glasses. It is seen from the Mössbauer results Figs. (1—3) for the γ-ray irradiated borophosphate glasses that iron atoms in these glasses are not affected by γ-ray irradiation up to 1×10^8 R. This is inconsistent with the results of borate[3] or phosphate[8] glasses where a decrease in isomer shift of Fe^{3+} or a linear decrease in the absorption area of Fe^{2+} ions was observed by γ-ray irradiation. These results lead to a conclusion that the borophosphate glasses are less sensitive to γ-rays than the parent borate or phosphate glasses.

Mössbauer studies of potassium borophosphate glasses with a P_2O_5/B_2O_3 ratio of 2.0 were also performed. These results are summarized in Table 1. Isomer shifts and linewidths are well consistent with the corresponding values of the borophosphate glasses with a P_2O_5/B_2O_3

Table 1. Mössbauer parameters for the potassium borophosphate (P_2O_5/B_2O_3=2.0) glasses

$X^{a)}$ mol%	Species	$\delta^{b)}$ mm s^{-1}	$\Delta^{c)}$ mm s^{-1}	$\Gamma^{d)}$ mm s^{-1}	$A^{e)}$ %
15	Fe^{3+}	0.45	0.72	0.56	74.2
15	Fe^{2+}	1.09	2.42	0.54	25.8
20	Fe^{3+}	0.45	0.71	0.53	74.1
20	Fe^{2+}	1.10	2.49	0.53	25.9
30	Fe^{3+}	0.45	0.69	0.55	76.4
30	Fe^{2+}	1.09	2.44	0.52	23.6
40	Fe^{3+}	0.44	0.66	0.48	78.7
40	Fe^{2+}	1.04	2.37	0.41	21.3
50	Fe^{3+}	0.42	0.65	0.48	86.7
50	Fe^{2+}	1.01	2.26	0.41	13.3

a) Alkali content of the glasses. b) Isomer shift. c) Quadrupole splitting. d) Linewidth. e) Absorption area.

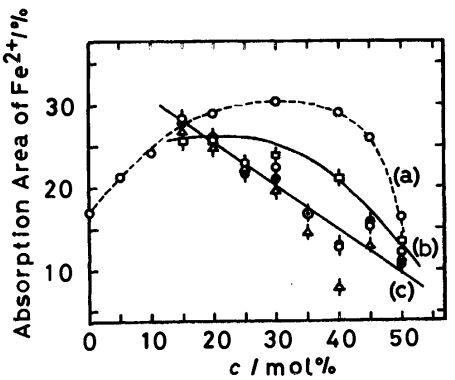

Fig. 5. Mössbauer absorption area of Fe^{2+} in glasses.
(a): Potassium phosphate, (b): potassium borophosphate (P_2O_5/B_2O_3=2.0), (c): potassium borophosphate (P_2O_5/B_2O_3=1.0).
○: Non-irrad., ●: 1×10^6 R irrad., △: 1×10^8 R irrad.

ratio of 1.0. Quadrupole splitting values of Fe^{3+} ions in these borophosphate glasses are also shown in Fig. 4, where the previous results on borate and phosphate glasses are shown for comparison. It is obvious from Fig. 4 that the quadrupole splitting values for the borophosphate glasses are intermediate between those for the borate and phosphate glasses, and that the values increase when the concentration of B_2O_3 increases. These results suggest that the symmetry around iron nucleus decreases with the introduction of B_2O_3 into phosphate glasses of which network comprises only PO_4 units, probably because the network structure becomes more complicated as a result of the formation of BPO_4 units in which equal numbers of BO_4 and PO_4 tetrahedra are arranged alternately. The network structure is considered to be more complicated for the borophosphate glasses with an P_2O_5/B_2O_3 ratio higher than 1.0 because the network is composed of both PO_4 and BPO_4 units.

Absorption areas of Fe^{2+} ions in these glasses are shown in Fig. 5, in which a linear decrease in the absorption area is observed with increasing alkali content for the borophosphate glasses having a P_2O_5/B_2O_3 ratio of 1.0. This is quite different from the

Table 2. ESR parameters for thf PO_4^{2-} radical in the potassium borophosphate (P_2O_5/B_2O_3=1.0) glasses

$X^{a)}$ mol%	$g^{b)}$	$A^{c)}$ G	$I^{d)}$
15	2.01	41	1.1
18	2.01	41	1.2
20	2.01	41	1.3
25	2.01	40	1.6
30	2.01	38	1.2
40	2.01	34	0.9
45	2.01	33	0.8

a) Alkali content of the glasses. b) g-value. c) Coupling constant. d) Peak intensity.

Table 3. ESR parameters for thf PO_4^{2-} radical in thf potassium borophosphate (P_2O_5/B_2O_3=2.0) glasses

$X^{a)}$ mol%	$g^{b)}$	$A^{c)}$ G	$I^{d)}$
18	2.01	41	1.7
20	2.01	41	1.9
30	2.01	39	2.7
40	2.01	35	2.2
50	2.01	32	1.7

a) Alkali content of the glasses. b) g-value. c) Coupling constant. d) Peak intensity.

results for phosphate glasses, in which formation of NBO was speculated.[7,8] The decrease in the absorption area is attributed to an increased oxidation atmosphere brought about by the introduction of alkali oxide into BPO_4 units in which all the boron and phosphorus atoms are singly bonded with oxygen atoms to form BO_4 and PO_4 tetrahedra.[9] It is seen from the results for the borophosphate glasses with a P_2O_5/B_2O_3 ratio of 2.0 (Fig. 5; curve 5b is intermediate between 5a and 5c) that some parts of iron are in the environment similar to that of phosphate glasses. This is explained by the presence of PO_4 units as well as BPO_4 units because one half of phosphorus atoms can be assumed to be present as PO_4 units having P=O double bonds when the P_2O_5/B_2O_3 ratio is 2.0.

The ESR spectrum of γ-ray (1×10^8 R) irradiated, iron-free borophosphate glasses consists of an almost isotropic doublet. The g value and hyperfine coupling constant of ^{31}P were found to be 2.01 and 41-32 G (1 G=10^{-4} T), respectively. The doublet has been attributed to PO_4^{2-} radical[7,15-20] produced by X-ray or γ-ray irradiation. As is shown in our previous paper,[7] the absorption intensity of PO_4^{2-} can be correlated with the fraction of NBO in PO_4 units because the energy level for the electrons on NBO is known to be higher than that on bridging oxygen[21] and therefore more electrons will be scattered by γ-ray irradiation in the former. The ESR results are summarized in Tables 2 and 3, from which a decrease in coupling constant of PO_4^{2-} doublet is seen when the alkali content of borophosphate glasses exceeds 25 or 30 mol%. This is identical with the decrease in the absorption intensity of the PO_4^{2-}

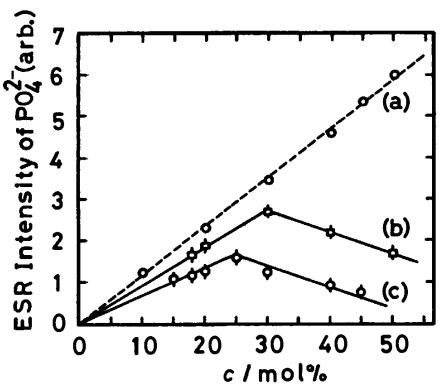

Fig. 6. ESR absorption intensity of PO_4^{2-} in glasses.
(a): Potassium phosphate, (b): potassium borophosphate ($P_2O_5/B_2O_3=2.0$), (c): potassium borophosphate ($P_2O_5/B_2O_3=1.0$).

radical, *i.e.*, the intensity shows a distinct maximum at 25 or 30 mol% when the P_2O_5/B_2O_3 ratio is 1.0 or 2.0, respectively. This is shown in Fig. 6, where the result of phosphate glasses[7] which are free from iron is also shown for comparison. Figure 6 demonstrates that the concentration of PO_4^{2-} radical in borophosphate glasses increases with increasing alkali content in the lower ($x \leq 25$ or 30 mol%) alkali region. This is the same as the result of phosphate glasses (Fig. 6a). The increase in the absorption intensity of the PO_4^{2-} radical is therefore attributed to a linear increase in the fraction of NBO in PO_4 tetrahedra constituting BPO_4 units for the borophosphate glasses with a P_2O_5/B_2O_3 ratio of 1.0, of which composition is expressed as $xK_2O\cdot(100-x)BPO_4\cdot 7Fe_2O_3$. It is very noteworthy that the absorption intensity shows a maximum at an alkali content of 25 mol%, which is not observed in the study of phosphate glasses. The decrease in the absorption intensity in the alkali region higher than 25 mol% will be attributed to the formation of NBO in BO_4 tetrahedra which are the other component of BPO_4 units, although the formation could not be confirmed in the present study. It is therefore considered that the formation reaction of NBO in borophosphate glasses is competitive between PO_4 and BO_4 tetrahedra, and that the formation in PO_4 tetrahedra is predominant in the alkali region lower than 25 mol%, *i.e.*, in such an alkali region that the K_2O/BPO_4 ratio is less than one third. This is also the case for the borophosphate glasses with a P_2O_5/B_2O_3 ratio of 2.0 of which composition is expressed as $xK_2O\cdot 2/3(100-x)BPO_4\cdot 1/3(100-x)P_2O_5\cdot 7Fe_2O_3$. That is to say, formation of NBO at PO_4 tetrahedra in BPO_4 units is predominant until 18 mol% ($K_2O/BPO_4=1/3$) and then the formation in PO_4 units of which environment is essentially the same as that of phosphate glasses will be predominant in the alkali region of 18—30 mol%. It is then considered in borophosphate glasses that the fraction of NBO bonded with phosphorus atoms is increased with increasing fraction of P_2O_5.

The authors are grateful to Dr. Toshiyuki Isobe of Kyushu University for his kind help in the ESR measurements of the glass samples. They are also grateful to Dr. Hisao Yamamoto and Mr. Kiyoshi Matsumoto of Kyushu University for the kind help in the γ-ray irradiation experiments.

References

1) S. S. Sekhon and R. Kamal, *J. Non-Cryst. Solids*, **33**, 169 (1979).
2) T. Nishida and Y. Takashima, *J. Non-Cryst. Solids*, **37**, 37 (1980).
3) T. Nishida, Y. Takashima, and Y. Nakayama, *J. Solid State Chem.*, **33**, 141 (1980).
4) T. Nishida, T. Hirai, and Y. Takashima, *Radiochem. Radioanal. Lett.*, **42**, 189 (1980).
5) T. Nishida, T. Shiotsuki, and Y. Takashima, *J. Non-Cryst. Solids*, **41**, 161 (1980).
6) T. Nishida, T. Hirai, and Y. Takashima, *J. Non-Cryst. Solids*, **43**, 221 (1981).
7) T. Nishida, T. Shiotsuki, and Y. Takashima, *J. Non-Cryst. Solids*, **43**, 115 (1981).
8) T. Nishida, T. Shiotsuki, and Y. Takashima, *J. Non-Cryst. Solids*, **43**, 123 (1981).
9) T. Hanada, Y. Yoshioka, N. Soga, and M. Kunugi, *Yogyo Kyokai Shi*, **87**, 395 (1979).
10) C. Hirayama, J. G. Castle, Jr., and M. Kuriyama, *Phys. Chem. Glasses*, **9**, 109 (1968).
11) M. F. Taragin, J. C. Eisenstein, and W. Haller, *Phys. Chem. Glasses*, **13**, 149 (1972).
12) C. R. Kurkjian and E. A. Sigety, *Phys. Chem. Glasses*, **9**, 73 (1968).
13) M. F. Taragin and J. C. Eisenstein, *J. Non-Cryst. Solids*, **3**, 311 (1970).
14) Ch. Labar and P. Gielen, *J. Non-Cryst. Solids*, **13**, 107 (1973/74).
15) G. O. Karapetyan and D. M. Yudin, *Fiz. Tverd. Tela*, **3**, 2827 (1961).
16) Y. Kobayashi and N. Matsuura, *Bull. Chem. Soc. Jpn.*, **46**, 1346 (1973).
17) Y. Nakai, *Bull. Chem. Soc. Jpn.*, **38**, 1308 (1965).
18) M. Miura and A. Hasegawa, *Bull. Chem. Soc. Jpn.*, **39**, 1432 (1966).
19) A. Hasegawa and M. Miura, *Bull. Chem. Soc. Jpn.*, **40**, 2553 (1967).
20) T. Nishida, Y. Takashima, and Y. Nakayama, *Mem. Fac. Sci., Kyushu Univ., Ser. C*, **12**, 65 (1979).
21) D. L. Griscom, *J. Non-Cryst. Solids*, **13**, 107 (1973/1974).

 © 1983 The Chemical Society of Japan Bull. Chem. Soc. Jpn., 56, 443—448 (1983)

X-Ray Diffraction Studies on the Structures of Hydrated Oxonium Ion, and the Chlorocobalt(II) and Tetrachlorocobaltate(II) Complexes in Aqueous Solutions

Hyo-Gwang Lee, Yukiei Matsumoto, Toshio Yamaguchi, and Hitoshi Ohtaki*

Department of Electronic Chemistry, Tokyo Institute of Technology at Nagatsuta, Nagatsuta-cho, Midori-ku, Yokohama 227

(Received March 1, 1982)

The structure of hydrated oxonium ion has been determined in a concentrated hydrochloric acid solution by the X-ray diffraction method. The oxonium ion H_3O^+ combines with four water molecules to form a trigonal pyramid structure in which three water molecules have an H_3O^+–H_2O distance of 2.44 Å, while the water molecule at the apex of the pyramid is separated by 2.90 Å from the central oxygen atom of the oxonium ion. The structure of the $CoCl^+$ determined in a relatively dilute lithium chloride solution (the Cl/Co mole ratio is 3.38) shows that the cobalt(II) ion is coordinated with five water molecules, the Co–OH_2 distance being 2.14 Å. The Co–Cl distance within the complex is 2.35 Å. The $CoCl_4^{2-}$ complex has a regular tetrahedral structure both in a concentrated lithium chloride (Cl/Co=22.1) and a hydrochloric acid (Cl/Co=21.1) solutions with the Co–Cl bond length of 2.29 Å.

Proton is present as H_3O^+ in water. The H_3O^+ ion is further hydrated with some water molecules through hydrogen bonds to form hydrated oxonium ion $H_3O(H_2O)_n^+$. The hydration number of oxonium ion has been determined by various methods, but the results are not well consistent with each other. For instance, the hydration number n is estimated to be 3—4 from X-ray and neutron diffraction measurements,[1-3] but the number is zero (*i.e.* H_3O^+) or one according to compressibility studies.[4] Most thermodynamic investigations give the hydration number of 3, *i.e.*, $H_9O_4^+$.[5,6]

Oxonium ion H_3O^+ can probably combine with four water molecules through hydrogen bonds. In crystal, however, an oxonium ion has three hydrogen bonds to combine with other oxonium ions or anions.[7-9] A theoretical calculation by a molecular orbital method[10] suggests that an oxonium ion has an almost planar structure in which each hydrogen atom binds to a water molecule through the hydrogen bond, the bond energy being about 190 kJ mol^{-1}. One water molecule situates above the oxonium ion, but the interaction between the oxonium ion and the water molecule is so weak that the bond energy is about 0 kJ mol^{-1}.[10]

The structure of oxonium ion so far estimated by diffraction methods[1-3] was regular tetrahedral, which was not in a satisfactory agreement with the structure expected from the crystallographic analysis[7-9] and the quantum mechanical calculation.[10] Moreover, the hydration number of an oxonium ion determined by the diffraction methods does not coincide with the numbers obtained by other methods. One of the aim of the present study is to establish the structure of hydrated oxonium ion in solution.

Cobalt(II) chloride complexes are formed in an alkali chloride or in a hydrochloric acid solution. It is a well known fact that cobalt(II) chloride solutions show dichromism with temperature and concentrations of chloride ions originating from a change of the octahedral structure to the tetrahedral one with varying numbers of chloride ions and water molecules coordinated.

A number of equilibrium studies have been carried out for cobalt(II) chloride complexes in aqueous solutions with various techniques. According to stability constants determined by Bjerrum *et al.*[11,12] and Smithson and Williams,[13] the mono- and tetrachloro complexes are present as dominant species in solutions of relatively low and high concentrations, respectively, of chloride ions, while the dichloro and trichloro complexes have a narrow concentration range of the existence.

X-Ray diffraction measurements of aqueous and alcoholic solutions of cobalt(II) chloride have been made by Wertz *et al.*,[14] and they have determined the structures of the $Co(OH_2)_6^{2+}$ and $CoCl_4^{2-}$ complexes in the solutions. The structure of hexahydrated cobalt(II) ion has also been determined by Ohtaki *et al.*[15] who obtained the Co–OH_2 bond length of 2.08 Å.

In the present investigation the structures of hydrated oxonium ion, and the $CoCl^+$ and $CoCl_4^{2-}$ complexes have been determined in aqueous solutions of lithium chloride and hydrochloric acid by the X-ray diffraction method.

Experimental

Preparation and Analysis of Sample Solutions. Cobalt(II) chloride and lithium chloride (Wako Pure Chemical Co., reagent grade) were recrystallized twice from water. Three sample solutions (A, B, and C) were prepared for the X-ray diffraction measurements. Solutions A and B contained lithium chloride and solution C was a concentrated hydrochloric acid solution, in all the solutions cobalt chloride was dissolved. The former two solutions were prepared by mixing a cobalt(II) chloride solution with a lithium chloride solution. Suitable Cl/Co mole ratios of the solutions for the present study were estimated from the stability constants given by Bjerrum *et al.*[11,12] In solution A the $CoCl^+$ complex existed as the main species, besides the hydrated cobalt(II) ion. On the other hand, the $CoCl_4^{2-}$ complex was formed in solutions B and C. A small amounts of hydrochloric acid was added to solutions A and B in order to prevent the hydrolysis of Co(II) ion.

The concentration of cobalt(II) ions was determined both by EDTA titration using a Cu–PAN indicator and electrogravimetry. The results obtained by the two methods agreed each other within the error of $\pm 0.2\%$. The concentration of chloride ions was determined gravimetrically as AgCl. Con-

Table 1. The composition (g-atoms dm^{-3}) and stoichiometric volume V per cobalt atom in the solutions

	A	B	C
Co	2.133	0.6129	0.5235
Cl	7.200	13.57	11.02
Li	2.902	12.28	—
O	49.38	39.35	42.92
H	98.79	78.76	95.81
V/Å^3	778.4	2709	3172
Cl/Co	3.38	22.1	21.1

centrations of hydrogen ions in the lithium chloride–cobalt chloride systems were determined coulometrically. The concentration of lithium ions was estimated from the material balance of ions in the solutions. The density of the solutions was measured with a pycnometer. The composition of the solutions is given in Table 1.

X-Ray Scattering Measurements. X-Ray scattering measurements were carried out with a JEOL θ-θ diffractometer in a room thermostated at (25±1) °C. Mo $K\alpha$ radiation (λ= 0.7107 Å) was used as an X-ray source. The scattering intensities were measured at discrete points of θ values from 1° to 70°, where 2θ is the scattering angle. Times required to accumulate 80000 counts were measured at each angle. Details of the measurements and treatments of X-ray scattering data were described in previous papers.[15–17]

All calculations were carried out by using programs KURVLR[18] and NLPLSQ.[15]

Results and Discussion

When several complexes coexist in a solution, it is usually necessary to know the formation constants of the complexes for analyzing X-ray scattering data. Since the formation constants determined in high ionic media are available in the literature for cobalt(II) chloride complexes,[11,12] the distribution of the complexes can be estimated for the sample solutions used in the present study.

Solution A contained two kinds of complexes, about 60 mol% of $CoCl^+$ and 40 mol% of Co^{2+}. In solutions B and C, the only $CoCl_4^{2-}$ complex should be formed, since the solutions contained a large excess of chloride ions. In solution C, H_3O^+ ions are present in contrast to hydrated lithium ions which are contained in solution B. The observed $s \cdot i(s)$ and $D(r)$ curves are shown in Figs. 1 and 2, respectively.

Solution A. The solution A is magenta. In the $D(r)$ (Fig. 2A) and $D(r)-4\pi r^2\rho_0$ (Fig. 3) curves we see four peaks around 1.0, 2.2, 3.3, and 4.5 Å. The small and broad peak at 1.0 Å is due to the O–H bond distance in water molecules. The second peak is attributed to the interactions between the central Co(II) and ligand atoms of its first neighbor. The Li–O distance of hydrated Li^+ ions also partly contributes to this peak. The third peak can be attributed to the Cl–O contact of hydrated Cl^- ions. The fourth peak contains contributions from several kinds of atom pairs; for instance, O–O interactions due to the tetrahedral network of bulk water and interactions between the Co(II) atom and solvent molecules in the second coordination shell. In order to estimate the structural parameters of the

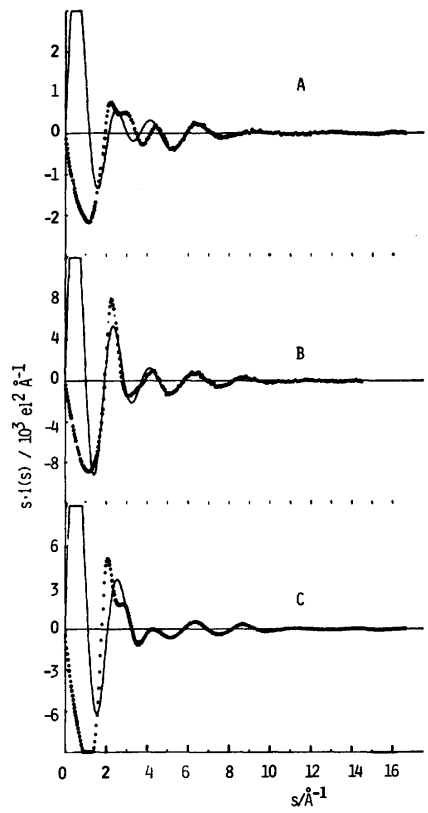

Fig. 1. The reduced intensities multiplied by s for solutions A, B, and C. The observed $s \cdot i(s)$ curves are shown by circles and the calculated ones by solid lines.

$CoCl^+$ complex, the appropriate interactions within hydrated cobalt, lithium and chloride ions should be subtracted from the observed radial distribution curve. The structural parameters used for the subtraction were quoted from the result reported for aqueous solutions of cobalt(II) perchlorate by Ohtaki *et al.*,[15] ($Co(OH_2)_6^{2+}$, Co–OH_2: 2.08 Å) and lithium chloride by Licheri *et al.*,[20] ($Li(OH_2)_4^+$, Li–OH_2: 2.10 Å; $Cl(H_2O)_6^-$, Cl–H_2O: 3.20 Å). The residual curve (chain line) in Fig. 3 shows two peaks which locate around 2.2 Å and 3.0 Å. The peak around 2.2 Å should be due to the Co–Cl and Co–O bonds within the $CoCl^+$ complex. The structure of the $CoCl^+$ complex was thus determined from the residual curve by a trial-and-error method. From the analysis, we found that the Co(II) ion within $CoCl^+$ complex combines with one chloride ion and five water molecules at the distance of 2.35 Å and 2.14 Å, respectively. Subtraction of peaks due to the Co–Cl, Co–O, O–O, and Cl–O interactions within the $CoCl(OH_2)_5^+$ complex from the residual curve led to a smooth background curve (broken line) having no appreciable peak over the range $r<4$ Å, except for the peak at about 2.9 Å which was ascribed to the O–O bonds within the bulk water. The parameter values thus estimated from the analysis of the radial distribution curve were finally refined by the least-squares method for the $s \cdot i(s)$ curve over the range $s>5$ Å^{-1}. The low-angle scattering data, which were dominated by contributions from long-range intermolecular interactions, were not included in the refinements. The results are summerized in Table 2. In the A-1 calculation, all

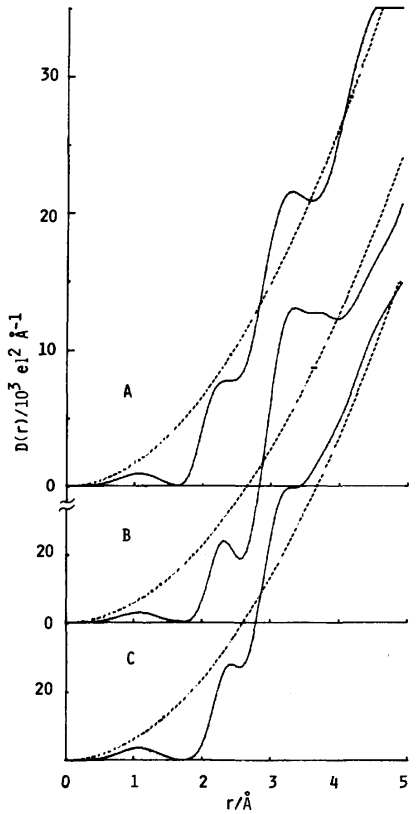

Fig. 2. Radial distribution functions $D(r)$ (solid lines) and $4\pi r^2\rho_0$ curves (broken lines) for solutions A, B, and C.

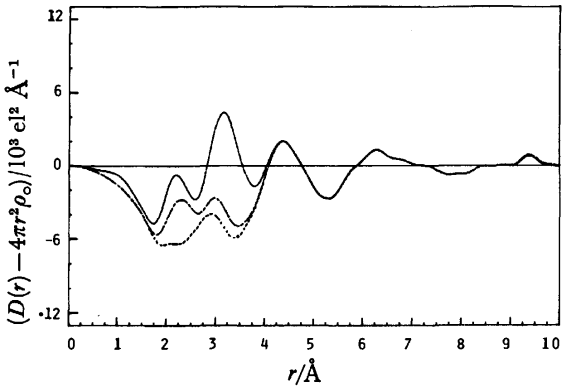

Fig. 3. The $D(r)-4\pi r^2\rho_0$ curve for solution A.
The chain line shows the residual curve obtained by subtracting the contributions of the hexaaquacobalt(II) ion, the hydrated chloride and the hydrated lithium ions from the original curve (solid line). The broken line gives the curve after subtraction of the peak shape due to the monochlorocobalt(II) ions from the chain-curve.

parameters given in the table were floated, the values being first guessed from the analysis of the radial distribution curve of solution A. On the other hand, the frequency factors of the atom-pairs in the table were fixed at the given values in the A-2 treatment. No significant difference was found in the bond lengths in the both calculations. The Co–OH_2 bond within the $CoCl(OH_2)_5^+$ complex is longer by 0.06 Å than that within the $Co(OH_2)_6^{2+}$ complex. This result suggests

Table 2. Results of the least-squares refinements for solution A

Standard deviations are given in parentheses. r: Bond distance, b: temperature factor, n: frequency factor.

Interaction	Parameter	A-1	A-2
$CoCl(OH_2)_5^+$			
Co–Cl	r/Å	2.353(9)	2.348(12)
	b/Å²	0.0063(6)	0.0057(7)
	n	1.03(3)	1.0[a]
Co–O	r/Å	2.135(5)	2.138(7)
	b/Å²	0.0058(3)	0.0056(4)
	n	5.0(1)	5.0[a]
Cl–O	r/Å	3.09(3)	3.08(4)
	n	4.1(3)	4.0[a]
O–O	r/Å	2.99(4)	2.99(5)
	n	8.7(8)	8.0[a]
$Cl(H_2O)_6^-$			
Cl–O	r/Å	3.193(7)	3.190(9)
	n	5.98(8)	6.0[a]

a) The values were kept constant during the calculations.

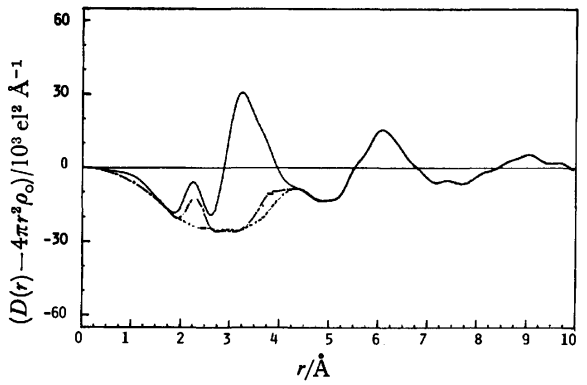

Fig. 4. The $D(r)-4\pi r^2\rho_0$ curve for solution B.
The chain line shows the residual curve obtained by subtracting the contributions of the hydrated lithium and hydrated chloride ions from the original curve (solid line). The broken line gives the curve after subtraction of the peak shape due to the tetrachlorocobaltate(II) ions from the chain-curve.

that a stronger electron-donation from the Cl^- ion compared with that from a water molecule weakens the Co–OH_2 bond within the former complex. The Li–O distance was not definitely determinable by the least-squares method, because of the low concentration and low scattering power of lithium ion.

Solution B. The solution B is blue and the $D(r)$ and $D(r)-4\pi r^2\rho_0$ curves in Figs. 2B and 4 show three peaks and a shoulder at about 1.0, 2.3, 3.2, and 3.7 Å, respectively, in the range of $r<4$ Å. The peaks at 1.0 and 3.2 Å are ascribed to the O–H and Cl–O interactions, respectively, as previously observed in the case of solution A. The second peak centered around 2.3 Å may correspond to the interatomic distance between Co(II) and Cl^- ions, which has been found in the $CoCl_4^{2-}$ complex in alcoholic solutions.[14] A part of the peak is also due to the Li–O distance within hydrated lithium ions.

In the analysis of the radial distribution curve, the

Table 3. Results of the least-squares refinements for solution B

Standard deviations are given in parentheses. r: Bond distance, b: temperature factor, n: frequency factor.

Interaction	Parameter	B-1	B-2
$CoCl_4^{2-}$			
Co-Cl	r/Å	2.29(1)	2.29(1)
	b/Å^2	0.0019(5)	0.0018(5)
	n	4.1(1)	4.0[a]
Cl-Cl	r/Å	3.74(7)	3.74(6)
	n	4.9(6)	6.0[a]
$Li(OH_2)_4^+$			
Li-O	r/Å	2.18(2)	2.18(2)
	n	4.3(3)	4.4(2)
$Cl(H_2O)_6^-$			
Cl-O	r/Å	3.19(1)	3.19(1)
	n	6.1(1)	6.2(1)

a) The values were kept constant during the calculations.

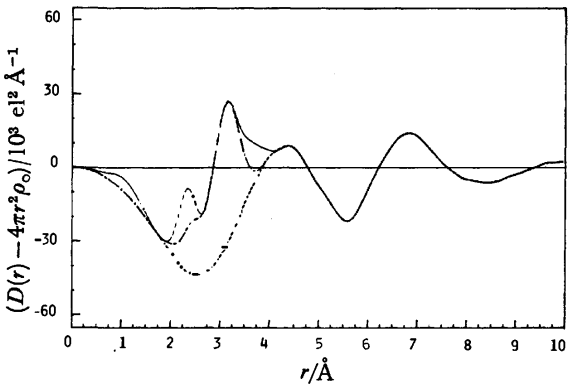

Fig. 5. The $D(r)-4\pi r^2\rho_0$ curve for solution C.
The chain line shows the residual curve obtained by subtracting the contribution of the tetrachlorocobaltate(II) ion from the original curve (solid line). The broken line gives the curve after subtraction of the peak shape calculated from model c of the hydrated oxonium and the hydrated chloride ions.

essentially same procedure as that used for solution A was employed. After subtraction of theoretical peaks due to the interatomic interactions within $Li(OH_2)_4^+$ and $Cl(H_2O)_6^-$, the chain line was obtained as the residual curve as seen in Fig. 4, from which we estimated the parameter values of interatomic interactions within the $CoCl_4^{2-}$ complex. The Co–Cl and Cl–Cl distances within the $CoCl_4^{2-}$ complex were estimated to be 2.30 Å and 3.75 Å, respectively. The ratio of the distances of Co–Cl to Cl–Cl is close to the value expected from a tetrahedral structure. The results of least-squares refinements are given in Table 3. In the course of the least-squares refinement of the structural parameters of the atom-pairs given in the table, all parameter values were allowed to change to search the best-fit result in the B-1 calculation, while the frequency factors of the Co–Cl and Cl–Cl atom-pairs were fixed at 4.0 and 6.0, respectively, in the B-2 calculation. The essentially same results were obtained in the both treatments. No evidence has been found for the existence of the hexacoordinated tetrachlorocobaltate(II) ion, $CoCl_4(OH_2)_2^{2-}$, in the present system and, therefore, no information has been obtained for the equilibrium between the hexa- and tetracoordinated $CoCl_4^{2-}$ ions.

In the $CoCl^+$ and $CoCl_4^{2-}$ complexes the Co-Cl bond distance of the former is slightly longer than that of the latter. According to Shannon,[21] the crystal radius of Co^{2+} ion having the coordination number 6 is 0.79 Å, but the radius of the Co^{2+} ion becomes 0.72 Å when the coordination number of the Co^{2+} ion decreases to 4. The change in the Co–Cl distance with changing number of chloride ion within $CoCl_n^{(2-n)+}$ complexes observed in the present investigation is consistent with Shannon's estimation for the ionic radius of cobalt(II) ion.

Solution C. The Cl/Co mole ratios of solutions B and C are almost the same. Therefore, we can reasonably assume that the $CoCl_4^{2-}$ complex in solution C has the same structure with that in solution B, and then, calculated the theoretical $s\cdot i(s)$ curve for the interactions due to Co–Cl and Cl–Cl pairs within the $CoCl_4^{2-}$ complex and the Cl–O contact within hydrated Cl^- ions. However, a comparison between the theoretical and experimental $s\cdot i(s)$ curve gave no satisfactory agreement. This might arise from the structure of hydrated oxonium ions which was not taken into consideration in the calculation in spite of a very high concentration of hydrochloric acid in the solution. Therefore, at the next step of the analysis of the $D(r)$ curve, the structure of $H_3O(H_2O)_n^+$ was taken into account. At first, peak shapes due to the Co–Cl and Cl–Cl interactions within $CoCl_4^{2-}$ were subtracted from the radial distribution curve, as seen in Fig. 5. The residual curve (chain line) shows a peak centered at 2.45 Å. The peak has not been observed in the $D(r)$ curve of the lithium chloride systems. Triolo and Narten[2] observed that the peak characteristic of the O–O hydrogen bond in hydrochloric acid solutions shifts toward a shorter distance with increasing HCl concentration from 2.85 Å in $HCl{-}95.7H_2O$ to 2.52 Å in $HCl{-}3.99H_2O$. The peak found at about 2.45 Å should be ascribed to the O–O bond within hydrated oxonium ion.

In order to determine the structure of the hydrated oxonium ion, a least-squares method was applied to the following three models.

(a) $H_3O^+(OH_2)_4$ (regular tetrahedron)
(b) $H_3O^+(OH_2)_3$ (planar triangle)
(c) $H_3O^+(OH_2)_3\cdots(H_2O)$ (trigonal pyramid)

for searching the optimum distance for the H_3O^+–H_2O interactions.

Defining an R-factor as a measure of propriety of models

$$R=\frac{\Sigma\{s\cdot i(s)_{\mathrm{calcd}}-s\cdot i(s)_{\mathrm{obsd}}\}^2}{\Sigma\{s\cdot i(s)_{\mathrm{obsd}}\}^2},$$

we calculated the R-values for the three models over the ranges $5\ \text{Å}^{-1}<s<16\ \text{Å}^{-1}$ and found the R-factor to be 0.110, 0.100, and 0.065 at the best values of the H_3O^+–H_2O bond distances for models a, b, and c, respectively. The results are summarized in Table 4. The $s\cdot i(s)$ curves of model c gave the best fit result

Table 4. Results of the least-squares refinements for models a, b, and c (solution C)
Standard deviations are given in parentheses. r: Bond distance, b: temperature factor, n: frequency factor.

Interaction	Parameter	a	b	c
$CoCl_4^{2-}$				
Co–Cl	r/Å	2.28(1)	2.292(2)	2.290(2)
	b/Å^2	0.0035(2)	0.0031(1)	0.0030(1)
	n	4.0[a]	4.0[a]	4.0[a]
Cl–Cl	r/Å	3.70(3)	3.72(3)	3.69(3)
	n	6.0[a]	6.0[a]	6.0[a]
$H_3O(H_2O)_n^+$				
O–O	r/Å	2.46(2)	2.45(2)	2.44(1), 2.90(2)
	n	4.0[a]	3.0[a]	3.0[a], 1.0[a]
$Cl(H_2O)_n^-$				
Cl–O	r/Å	3.110(2)	3.121(2)	3.130(2)
	n	5.17(2)	5.03(2)	4.98(1)

a) The values were kept constant during the calculations.

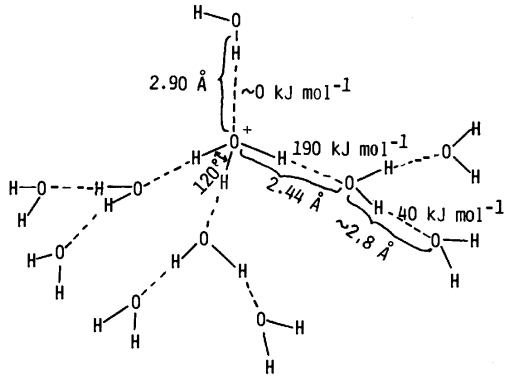

Fig. 6. The structure of the hydrated oxonium ion.

to the experimental data. The structure of model c well explains the picture of hydrated oxonium ion proposed by Grahn[10] from a molecular orbital calculation. The calculations of the total energy of the hydrated H_3O^+ ion by Grahn as a function of the H–O–H bond angle led to the minimum value when the bond angle to be 120°, *i.e.*, a planar configuration for the $H_3O^+(H_2O)_3$ moiety. The H–O–H bond angle of the hydrated H_3O^+ ion has been estimated to be 115—119° from NMR measurements for crystalline hydrates of strong acids.[22,23] From these results the structure of the $H_3O^+(OH_2)_3$ unit of the hydrated oxonium ion is anticipated to be an almost planar triangle, and one water molecule combines with the central oxygen atom of the $H_3O^+(H_2O)_3$ moiety of the hydrated oxonium ion through a weak interaction. The structure of the hydrated oxonium ion is depicted in Fig. 6, together with the bond energies calculated by Grahn.[10]

The picture shown in Fig. 6 well explains structural models of oxonium ion so far proposed by various authors by using different methods. Thus, a method which can detect water molecules most strongly combined with a proton (H^+) (*e.g.*, the compressibility method) reveals the structure of the H_3O^+ ion. When we use a method by which water molecules having relatively strong interactions compared with those between water molecules in the bulk, we might determine the hydration number of the oxonium ion to be 3. Most thermodynamic methods may be included in this category. On the other hand, diffraction methods detect water molecules at the nearest neighbor of the central oxonium ion independent of the strength of the interactions, and therefore, the methods give the hydration number four for each oxonium ion, if the oxonium ion has the structure shown in Fig. 6. The result obtained by the neutron diffraction method[3] perhaps gave an average value of the two different H_3O^+–H_2O distances, which were observed in the present investigation. The water molecule at the apex of the pyramidal structure of the hydrated oxonium ion, which interacts very weakly with the central oxygen atom of the oxonium ion, may be removed by crystallization.

Thus, the structure of oxonium ion determined in the present study gives a satisfactory interpretation for different models previously proposed by various methods, and moreover, it agrees well with the result of the theoretical calculation.[10]

The hydration number of 5.0 was obtained for a chloride ion in the hydrochloric acid system (solution C). The value is significantly smaller than that found in the lithium chloride systems, *i.e.*, n=6 (solutions A and B). The decrease in the hydration number of the chloride ion in the concentrated hydrochloric acid solution may be explained by assuming the formation of a contact ion pair between H_3O^+ and Cl^- ions. In the concentrated hydrochloric acid solution the distance between an oxonium ion and a chloride ion may simply be estimated to be about 3.1 Å, and there is practically no free water molecule in the solution. Therefore, some oxonium ions may exist in the first solvation shell of chloride ions, and the ion-dipole repulsion between the oxonium ion and water molecules in the nearest neighbor of the chloride ion becomes so large that some water molecules may be expelled from the solvation shell of the chloride ion. If a part of the total chloride ions pairing with oxonium ions has a much lower coordination number ($n \ll 6$) compared with the free chloride ion (n=6), the average coordination number of the total chloride ions in the concentrated hydrochloric acid solution may become small even if the concentration of the $H_3O^+ \cdot Cl^-$ pair is relatively low.

The present study has been partially supported by the Grant-in-Aid for Special Project Research No. 510806 from the Ministry of Education, Science and Culture.

References

1) D. S. Terekhova, *Zh. Strukt. Khim.*, **11**, 530 (1970).
2) R. Triolo and A. H. Narten, *J. Chem. Phys.*, **63**, 3624 (1975).
3) N. Ohtomo, K. Arakawa, M. Takeuchi, T. Yamaguchi, and H. Ohtaki, *Bull. Chem. Soc. Jpn.*, **54**, 1314 (1981).
4) A. Passynskii, *Acta Physicochim. URSS*, **8**, 835 (1938).
5) R. P. Bell and K. N. Bascombe, *Discuss. Faraday Soc.*, **24**, 158 (1957).
6) E. Wicke, M. Eigen, and T. Ackermann, *Z. Phys. Chem. (Frankfurt)*, **1**, 342 (1954).
7) J. O. Lundgren and I. Olovsson, "The Hydrated

Proton in Solids," in "The Hydrogen Bond," ed by P. Schuster, G. Zundel, and C. Scandorfy, North-Holland Publ., Amsterdam (1976), Vol. II, Chap. 10.

8) I. Olovsson, *J. Chem. Phys.*, **49**, 1063 (1968).

9) R. Attig and J. M. Williams, *Angew. Chem.*, **88**, 507 (1976).

10) R. Grahn, *Arkiv Fysik*, **1**, 13 (1962).

11) J. Bjerrum, A. S. Holonin, and L. H. Skibsted, *Acta Chem. Scand., Ser. A*, **29**, 326 (1975).

12) L. H. Skibsted and J. Bjerrum, *Acta Chem. Scand., Ser. A*, **32**, 429 (1978).

13) J. M. Smithson and R. J. P. Williams, *J. Chem. Soc.*, **1958**, 457.

14) D. L. Wertz and R. F. Kruh, *J. Chem. Phys.*, **50**, 4313 (1969).

15) H. Ohtaki, T. Yamaguchi, and M. Maeda, *Bull. Chem. Soc. Jpn.*, **49**, 701 (1976). "Analytical Chemistry—Essays in Memory of Anders Ringbom" ed by E. Wänninen, Pergamon, Oxford (1977), pp. 163—168.

16) H. Ohtaki and M. Maeda, *Bull. Chem. Soc. Jpn.*, **47**, 2194 (1974).

17) H. Ohtaki, M. Maeda, and S. Ito, *Bull. Chem. Soc. Jpn.*, **47**, 2217 (1974).

18) G. Johansson and M. Sandström, *Chem. Scripta*, **4**, 195 (1973).

19) T. Yamaguchi, Doctoral Thesis, Tokyo Institute of Technology, March (1978).

20) G. Licheri, G. Piccaluga, and G. Pinna, *J. Appl. Crystallogr.*, **6**, 392 (1973).

21) R. D. Shannon, *Acta Crystallogr., Sect. A*, **32**, 751 (1976).

22) R. E. Richards and J. A. S. Smith, *Trans. Faraday Soc.*, **47**, 1261 (1951).

23) D. E. O' Reilly, E. M. Peterson, and J. M. Williams, *J. Chem. Phys.*, **54**, 96 (1971).

Studies of the Metal Complexes of Cyclohexane Derivatives. VII.[1] Preparation and Properties of Platinum(II) and Cobalt(III) Complexes of (1*R*,2*S*)-1-Aminomethyl-2-methylcyclohexylamine

Reiko SAITO* and Yoshinori KIDANI†

Aichi Junior College of Nursing, Kamishidanmi, Moriyama-ku, Nagoya, 463

†*Faculty of Pharmaceutical Sciences, Nagoya City University, Tanabe-dori, Mizuho-ku, Nagoya 467*

(Received May 17, 1982)

Optically active (1*R*,2*S*)-1-aminomethyl-2-methylcyclohexylamine (*R*,*S*-2m-amcha) was synthesized and two Pt(II) and two types of Co(III) complexes containing this ligand were prepared. ^{1}H-NMR and ^{13}C-NMR spectra of the Pt(II) complexes and CD spectrum of *trans*-$[CoCl_2(R,S\text{-2m-amcha})_2]^+$ indicated that the chelate ring takes predominantly the λ conformation with the equatorial C_1–C_2 bond of the cyclohexane ring. The absolute configuration of the ligand has been assigned on the basis of the conformation of the complexes. All possible isomers of the tris Co(III) complex, *fac*-$\Delta(lel_3)$, *mer*-$\Delta(lel_3)$, *mer*-$\Lambda(ob_3)$, and *fac*-$\Lambda(ob_3)$, were isolated and characterized.

It is widely known that a chelated 1,2-diamine having mono- or disubstitution at the carbon atom of the chelate ring, such as 1,2-propanediamine or racemic 2,3-butanediamine, preferentially adopts the conformation with the substituent disposed equatorially.[2-4] However, there have been few reports on complex formation with 1,2-diamines which have two different substituents at the same carbon atom. (1*R*,2*S*)- or (1*S*,2*R*)-1-Aminomethyl-2-methylcyclohexylamine (abbreviated as 2m-amcha) is regarded as a *C*,*C*-unsymmetrically disubstituted 1,2-ethanediamine. These compounds are considered to take a fixed chair conformation with the methyl group equatorial. By virture of this group, the 2m-amcha chelate ring prefers a conformation in which C_1–C_2 bond of the cyclohexane ring lies in the equatorial position with regard to the chelate ring. In this paper we describe the preparation of (1*R*,2*S*)-1-aminomethyl-2-methylcyclohexylamine (*R*,*S*-2m-amcha), the four isomers of $[Co(R,S\text{-2m-amcha})_3]^{3+}$, *trans*-$[CoCl_2(R,S\text{-2m-amcha})_2]^+$, as well as $[Pt(NH_3)_2(R,S\text{-2m-amcha})]^{2+}$ and $[Pt(bpy)(R,S\text{-2m-amcha})]^{2+}$ (bpy=2,2′-bipyridine). Characterization of the ligand and the complexes was made by means of CD and NMR spectral analysis.

Experimental

Preparation and Resolution of the Ligand. 1-Amino-2-methylcyclohexanecarbonitrile was obtained by a slight modification of the method of Steiger.[5] To a mixture containing NaCN (50 g) and NH_4Cl (59 g) in water (240 cm^3) was added aqueous ammonia (70 cm^3, 25—28%). The resulting solution was stirred at 10—20 °C, and to this was added 2-methylcyclohexanone (112 g) in methanol (160 cm^3) dropwise. After the addition ,the mixture was stirred vigorously at 50—55 °C for 5 h. The reaction mixture was cooled, diluted with water (200 cm^3), and then extracted with ether. The ether extract was evaporated to a smalll volume. The concentrate was diluted with ethanol (100 cm^3) and cooled. Then 4 mol/dm^3 HCl (300 cm^3) was added to this ice chilled solution with stirring. The resulting amino nitrile hydrochloride was filtered by suction and washed with a small amount of cold 4 mol/dm^3 HCl.

To a cold aqueous suspension of the amino nitrile hydrochloride so obtained, was added 7 mol/dm^3 NaOH solution (200 cm^3). The oil which separated was extracted with ether. After removal of the ether, the amino nitrile was dried over K_2CO_3. The amino nitrile was reduced with $LiAlH_4$ by the usual manner.[6] In a typical reduction, 36.2 g of amino nitrile yielded 30.7 g of crude *trans*-diamine which contained small amounts of unreduced amino nitrile and *cis*-diamine.

The reaction product was purified as follows. To a solution of the crude diamine (25 g in 30 cm^3 of ethanol), a solution of (2*R*, 3*R*)-tartaric acid (52 g in 40 cm^3 of H_2O) was added. The solution was kept standing at about 60 °C for 5 min and then cooled. The product which deposited was collected by filtration and washed with ethanol. It was recrystallized from ethanol to give 33 g of colorless powder. Found: C, 41.02; H, 7.32; N, 6.04%. Calcd for $C_{16}H_{30}O_{12}\cdot 3/2\ H_2O$: C, 40.94; H, 7.09; N, 5.97%. Free racemic *trans*-2m-amcha was obtained from the diamine-hydrogentartrate as described in the literature.[7] To a solution of this salt (30 g in 70 cm^3 H_2O) was added a solution of KCl (12 g in 30 cm^3 H_2O). After heating for a while and succesive ice-cooling, the precipitated potassium hydrogentartrate was filtered off. To the filtrate, KOH (60 g) was added . The oil thus separated was extracted with ether. Racemic *trans*-diamine (9 g) was obtained by evaporationg the extract.

To a solution of (2*R*, 3*R*)-di-*O*-benzoyltartaric acid monohydrate (30.4 g in 200 cm^3 of 2-propanol), a solution of racemic 2m-diamine (11.2 g in 60 cm^3 H_2O) was added. The mixed solution was boiled for a few minutes, then cooled to afford 31.9 g of crystals (mp: 156—163 °C). Twice recrystallization of this salt from water gave 12.0 g of the less soluble (2*R*, 3*R*)-di-*O*-benzoyltartarate, mp: 156 °C, $[\alpha]_D=-74.0°$ (1.0 g in 100 cm^3 of methanol). Found: C, 51.87; H, 7.38; N, 4.72%. Calcd for $C_{26}H_{32}N_2O_8\cdot 6H_2O$: C, 51.31; H, 7.38; N, 4.60%. Treatment of this salt (12 g) with 70 cm^3 of 3 mol/dm^3 HCl gave the dihydrochloride of *R*,*S*-2m-amcha (4.5 g) whose absolute configuration was assigned by the CD spectrum of *trans*-$[CoCl_2(R,S\text{-2m-amcha})_2]^+$ as described later. Found: C, 41.57; H, 9.91; H, 11.62%. Calcd for $C_8H_{18}N_2\cdot 2HCl\cdot H_2O$: C, 41.21, H, 9.51; H, 12.01%. $[\alpha]_D=-6.2°$ (2.7 g in 100 cm^3 of H_2O). The optically active free diamine was obtained from this dihydrochloride by adding a stoichiometric quantity of sodium methoxide. It was used for the preparation of the complexes without further purification.

Preparation of Complexes. *[Pt(NH$_3$)$_2$(R,S-2m-amcha)]Cl$_2$ and [Pt(bpy)(R,S-2m-amcha)]Cl$_2$*: $[Pt(NH_3)_2(R,S\text{-2m-amcha})]Cl_2$ was synthesized by a method similar to that described in the literature.[8] $[Pt(bpy)(R,S\text{-2m-amcha})]Cl_2$ was prepared from $[PtCl_2(bpy)]$ and the ligand, according to the literature method.[9]

trans-*[CoCl$_2$(R,S-2m-amcha)$_2$]Cl*: This complex was prepared by the usual method. To a methanol solution of

TABLE 1. ANALYTICAL DATA OF COMPLEXES PREPARED

Complex	Found (Calcd) (%)		
	C	H	N
$[Pt(NH_3)_2(R,S\text{-2m-amcha})]Cl_2 \cdot 3/2\ H_2O$	20.58(20.47)	5.84(5.80)	11.73(11.94)
$[Pt(bpy)(R,S\text{-2m-amcha})]Cl_2 \cdot 4\ H_2O$	33.73(33.97)	5.04(5.38)	8.61(8.80)
trans-$[CoCl_2(R,S\text{-2m-amcha})_2]Cl \cdot H_2O \cdot CH_3OH \cdot 3/2$ HCl	39.41(39.49)	8.07(8.09)	10.90(10.84)
B-1: $[Co(R,S\text{-2m-amcha})_3]Cl_3 \cdot 2H_2O \cdot 3/2$ HCl	42.08(42.22)	8.97(8.79)	12.21(12.31)
B-2: $[Co(R,S\text{-2m-amcha})_3]Cl_3 \cdot 5/2\ H_2O$	45.33(45.25)	9.77(9.34)	13.25(13.19)
B-3: $[Co(R,S\text{-2m-amcha})_3]Cl_3 \cdot 5/2\ H_2O \cdot 1/2$ HCl	44.02(43.99)	9.13(9.15)	12.95(12.82)
B-4: $[Co(R,S\text{-2m-amcha})_3]Cl_3 \cdot 3\ H_2O$	44.33(44.62)	9.67(9.36)	13.10(13.01)

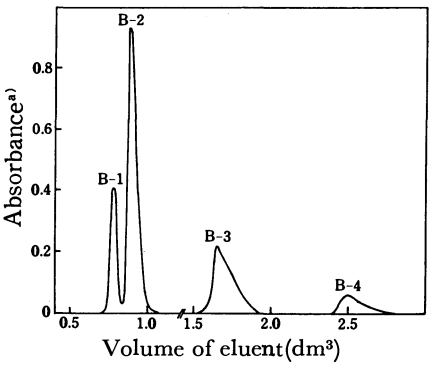

Fig. 1. Elution curve of the isomers of $[Co(R,S\text{-2m-amcha})_3]^{3+}$.
Eluent: 0.20 mol/dm³ Na_2SO_4, a) at 20.8×10^3 cm^{-1}.

$CoCl_2 \cdot 6H_2O$ was added a methanol solution of twice the amount of *R,S*-2m-amcha. The mixture was air-oxidized for 4—5 h and then evaporated. An excess amount of concentrated hydrochloric acid was added to the resulting brown residue. The green powder which formed was collected and washed thoroughly with acetone. The crude complex thus obtained was recrystallized from methanol.

Four Isomers of $[Co(R,S\text{-2m-amcha})_3]Cl_3$: Four isomers of the tris-complex were prepared by the published method[10] with slight modification. To a dimethyl sulfoxide solution (6 cm³) of *trans*-$[CoCl_2py_4]Cl_2 \cdot 6H_2O$(2 mmol) was added *R,S*-2m-amcha (8.4 mmol) dropwise. The resulting solution was stirred for 30 min, diluted with water to 2 dm³ and the pH adjusted to about 3 with hydrochloric acid. The product was adsorbed on SP-Sephadex C-25. A small portion of the adsorbed product was charged on the top of an SP-Sephadex C-25 column (2.7 cm × 65 cm) and the product was eluted with a 0.2 mol/dm³ Na_2SO_4 solution. The four bands which descended were called B-1, B-2, B-3, and B-4 (Fig. 1). Each fraction was adsorbed again on SP-Sephadex and the complex was eluted with 1 mol/dm³ hydrochloric acid solution. The eluent was concentrated on a water bath and then evaporated in a vacuum desiccator over NaOH and P_2O_5. The four complexes named B-1, B-2, B-3, and B-4 were obtained as orange powders. The B-1, B-3, and B-4 complexes were recrystallized from dilute hydrochloric acid. Recrystallization of B-2 in the chloride form was unsuccessfull. It was used without further purification. The analytical data for the complexes are given in Table 1.

Measurements: ^{1}H-NMR spectra were recorded on a JEOL JNM-MH-100 spectrometer with D_2O as a solvent and DSS as an internal reference. ^{13}C-NMR spectra were recorded on a JEOL-FX-100 spectrometer with D_2O as a solvent and TMS as an external reference. CD spectra were measured with a JASCO-J-40 spectropolarimeter, and the absorption spectra with a Shimadzu UV-210-A spectrophotometer. Optical rotations at 589 nm were measured with a JASCO-DIP-4 polarimeter.

Results and Discussion

Conformation of the Ligand. The 2m-amcha ligand has two geometrical isomers, *cis* and *trans*. Chart 1 shows the conformational pairs of the two isomers. Munday[11] reported that 1-amino-2-methylcyclohexanecarboxylic acid obtained by hydrolysis of amino nitrile by Strecker synthesis has an axial carboxyl group. However, Cremlyn[12,13] claimed that the carboxyl group of the same compound is in the equatorial position. As mentioned in the literature,[11] 1-amino-2-methylcyclohexanecarbonitrile resists hydrolysis by an ordinary method. We also obtained a similar experimental result; that hydrolysis of this compound had to be carried out in a sealed vessel at high temperature. This seems to indicate that the cyano group lies in an equatorial position close to the equatorial 2-methyl group. The 2m-amcha obtained *via* Strecker synthesis is considered to have a configuration similar to that of the corresponding amino carboxylic acid. Accordingly, the *trans*-configuration shown in Chart 1, **2a** is a dopted for this diamine.

The 100 MHz ^{1}H-NMR spectrum of amcha·2HCl is shown in Fig. 2. Two multiplet peaks around 1.4 and 1.7 ppm are attributable to the axial and equatorial methylene protons in the cyclohexane ring, respectively, although they were overlapped by one another. The signal around 2.1 ppm was assigned to the methin proton bonded axially to C_2 carbon of the cyclohexane ring, because an equatorial methin proton signal is expected to appear at a lower field. The two doublets (3.36 and 3.61 ppm) regarded as an AB pattern were assigned to the methylene protons of the aminomethyl

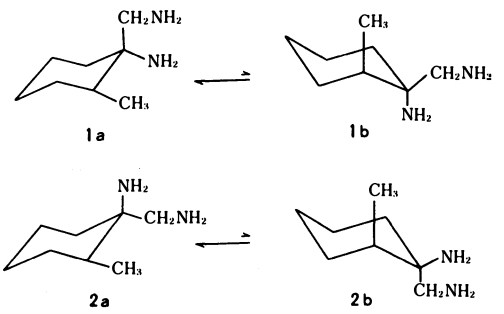

Chart 1. The possible structures of *cis*-2m-amcha (**1a**, **1b**) and *trans*-2m-amcha (**2a**, **2b**).

TABLE 2. ^{13}C-NMR AND ^{1}H-NMR CHEMICAL SHIFTS[a] AND COUPLING CONSTANTS($J_{^{195}Pt-^{13}C}$ and $J_{^{195}Pt-^{1}H}$)[b]

Complex	^{13}C resonance				^{1}H resonance	
	Cyclohexane ring			CH_2NH_2	CH_2NH_2	
	C_1	C_2	C_6		H_{eq}	H_{ax}
R,S-2m-amcha·2HCl	59.86	39.42	32.06	40.96	3.61[c]	3.36[c]
$[Pt(NH_3)_2(R,S\text{-2m-amcha})]^{2+}$	66.90[d]	37.91 (31.74)	32.11[d]	50.34 (12.20)	2.80[e] (56)	2.70[e,f]
$[Pt(bpy)(R,S\text{-2m-amcha})]^{2+}$	67.54[d]	39.18 (34.18)	34.01[d]	47.61[d]	3.06[g] (62)	2.91[f,g]

a) In ppm. b) In Hz. c) $J_{H-H}=-15$ Hz. d) Platinum satellite were not clearly observed. e) $J_{H-H}=-13$ Hz. f) One of platinum satellite peak was observed, but other was overlapping with H resonance. g) $J_{H-H}=-13$ Hz.

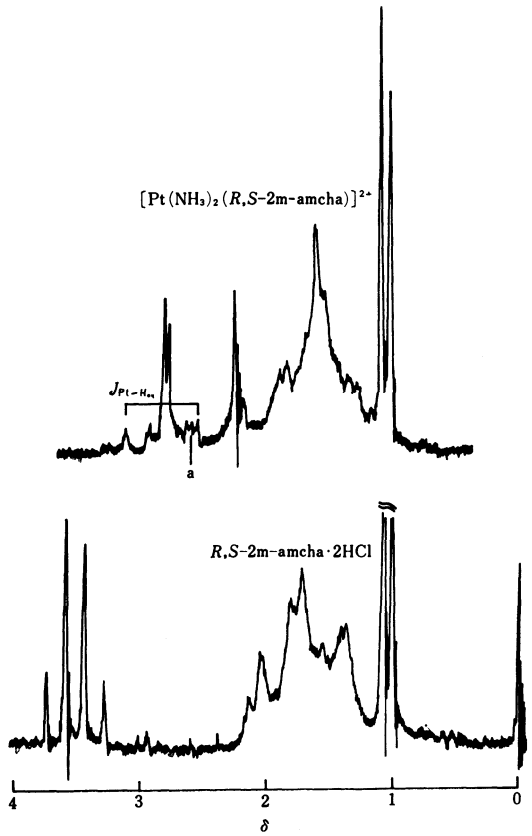

Fig. 2. ^{1}H-NMR spectra of *R,S*-2m-amcha·2HCl and $[Pt(NH_3)_2(R,S\text{-2m-amcha})]^{2+}$.
a: One of platinum satellite peaks based on the Pt–H_{ax} coupling.

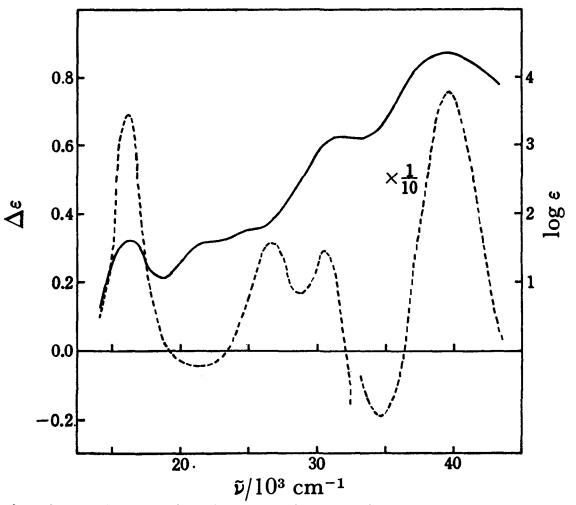

Fig. 3. Electronic (—) and CD (----) spectra of *trans*-$[CoCl_2\text{-}(R,S\text{-2m-amcha})_2]^{+}$.

group. This spectral pattern suggests that *trans*-2m-amcha has the rigid structure shown in Chart 1, **2a**.

Resolution of the racemic *trans*-diamine was accomplished by recrystallization of its less soluble (2*R*,3*R*)-di-*O*-benzoyltartrate. The absolute configuration of (−)-*trans*-2m-amcha was assigned to (1*R*,2*S*) as described below.

Conformation of the Chelate Ring of the Pt(II) Complexes. In $[Pt(NH_3)_2(R,S\text{-2m-amcha})]^{2+}$ and $[Pt(bpy)(R,S\text{-2m-amcha})]^{2+}$, the equatorial proton of the aminomethyl group showed the $^{3}J_{Pt-H}$ values of 56 and 62 Hz, respectively, while the C_2 carbon of the cyclohexane ring exhibited $^{3}J_{Pt-C}$ 31.7 and 34.2 Hz, respectively (Table 2). These values were somewhat smaller than those of $[Pt(NH_3)_2(pn\text{-}d_1)]^{2+}$ [14] and $[Pt(bpy)(pn)]^{2+}$ [9] (pn-d_1= 1,2-propane-2-*d*-diamine). They were fairly small compared to those of $[Pt(NH_3)_2(R,R\text{-bn})]^{2+}$ [15] and $[Pt(bpy)(chxn)]^{2+}$ [9] having a strongly prefered conformation (*R,R*-bn=*R,R*-2,3-butanediamine, chxn=*trans*-1,2-cyclohexanediamine). We observed that the $^{3}J_{Pt-C}$ value for $[Pt(NH_3)_2(amcha)]^{2+}$ whose chelate ring is considered to interconvert between two conformations was 22.6 Hz (amcha=1-aminomethylcyclohexylamine).[16] This value is also relatively lower than that of $[Pt(bpy)(ms\text{-bn})]^{2+}$ with two conformational forms by rapid ring inversion (*ms*-bn=*meso*-2,3-butanediamine).[9] Erickson *et al.* estimated the relative contribution for the λ conformer of $[Pt(bpy)(pn)]^{2+}$ to be 72%.[9] On the other hand, Yano *et al.* reported that the $^{3}J_{Pt-C}$ values of unsymmetrical diamine complexes are smaller than those of symmetrical ones.[14] As shown in Chart 2 (b), the methyl group of 2m-amcha locates above the chelate ring, if the complex adopts a conformation with axial C_1–C_2 bond. The conformational preference of

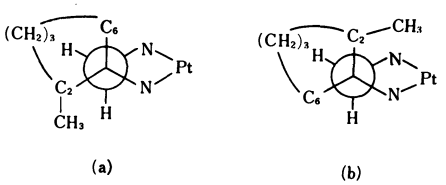

Chart 2. The chelate ring viewed down on C_1–CH_2NH_2 bond.
(a): λ conformaiton of *R,S*-2m-amcha complex, (b): λ conformaiton of *S,R*-2m-amcha complex.

Table 3. Electronic and CD spectral data

Complex	Electronic		CD	
	$\tilde{\nu}/10^3$ cm^{-1}	(log ε)	$\tilde{\nu}/10^3$ cm^{-1}	($\Delta\varepsilon$)
trans-[$CoCl_2$(*R*,*S*-2m-amcha)$_2$]$^+$	16.3	(1.61)	16.2	(+0.69)
	22.2	(1.59)	21.6	(−0.05)
	25.0	(1.78)	26.7	(+0.31)
	31.6	(3.14)	30.6	(+0.30)
			34.6	(−1.90)
	39.4	(4.38)	39.7	(+7.60)
fac-Λ(lel_3)-[Co(*R*,*S*-2m-amcha)$_3$]$^{3+}$	20.8	(2.11)	20.1	(−3.54)
			23.4	(+0.06)
	28.7	(2.10)	27.6	(−0.15)
			30 sh	(−0.11)
	46.7	(4.28)	42.6	(+23.9)
mer-Λ(lel_3)-[Co(*R*,*S*-2m-amcha)$_3$]$^{3+}$	20.8	(2.09)	19.9	(−3.48)
			23.1	(+0.13)
	29.0	(2.07)	27.4	(−0.20)
			29—31 sh	(−0.11)
	46.7	(4.28)	42.4	(+24.2)
mer-Λ(ob_3)-[Co(*R*,*S*-2m-amcha)$_3$]$^{3+}$	20.9	(2.09)	20.6	(+4.47)
	29.0	(2.07)	28.4	(−0.13)
			31.0	(+0.06)
	46.7	(4.28)	41.7	(−11.3)
fac-Λ(ob_3)-[Co(*R*,*S*-2m-amcha)$_3$]$^{3+}$	21.1	(2.04)	20.6	(+3.91)
	29.0	(2.03)	26.7	(+0.09)
			28.9	(−0.09)
			31.3	(+0.04)
	46.3	(4.26)	41.7	(−14.7)

sh: Shoulder.

2m-amcha complex is considered to be strong owing to the steric hindrance by this methyl group. Therefore, the smaller $^3J_{Pt-C}$ values for the present complexes are probably due to the unsymmetrical conformation, as claimed by Yano *et al.*,[14] rather than relative population for the $\lambda \rightleftarrows \delta$ equilibrium.

Absolute Configuration of the Ligand. It has been recognized that the conformation of a chelate ring can be assigned on the basis of the signs of the Cotton effect of *trans*-[$CoCl_2$(1,2-diamine)$_2$]$^+$ complexes in the first absorption region.[17,18] To decide the configuration (1*R*,2*S*) or (1*S*,2*R*) of (−)-*trans*-2m-amcha, we prepared *trans*-[$CoCl_2$((−)-2m-amcha)$_2$]$^+$ and examined its electronic and CD spectra. The absorption spectrum of this complex was quite similar to those of *trans*-[$CoCl_2$(*R*-pn)$_2$]$^+$[17,18] and *trans*-[$CoCl_2$(*R*-chxn)$_2$]$^+$[18,19] (Fig. 3 and Table 3). The CD sign of the (−)-2m-amcha complex was positive in the I_a (16200 cm^{-1}) and negative in the I_b (21600 cm^{-1}) regions similar to those of the *R*-pn and *R*-chxn complexes with a λ conformation. In addition, the CD spectral pattern of the (−)-2m-amcha complex in the charge-transfer region resembled those of the corresponding *R*-pn and *R*-chxn complexes, although the intensity of the CD peak was weaker for the present complex. These results indicate that the (−)-2m-amcha complex has a λ conformation. Chart 2 illustrates the λ conformation of (1*R*,2*S*)-2m-amcha and (1*S*,2*R*)-2m-amcha chelate rings. Assuming the (1*S*,2*R*)-configuration of the ligand, the considerably larger steric hindrance between the hydrogen attached

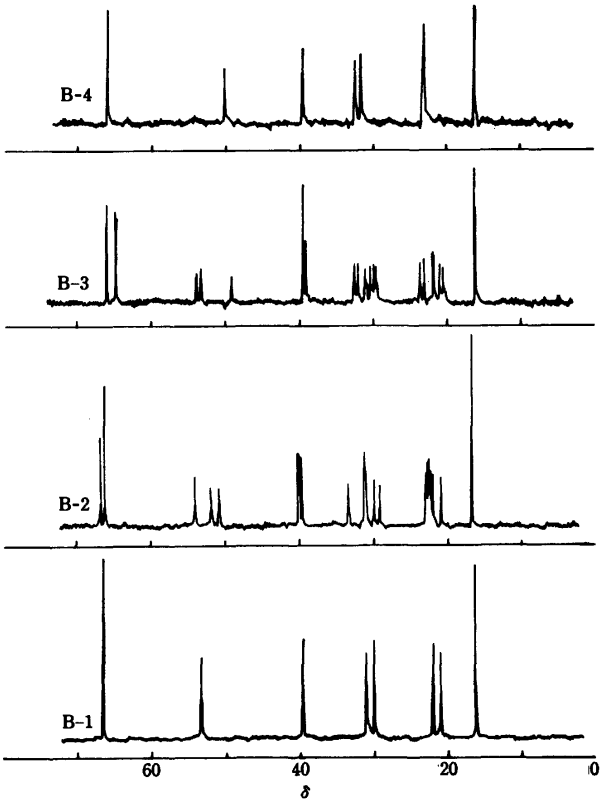

Fig. 4. ^{13}C-NMR spectra of the B-1, B-2, B-3, and B-4 isomers of [Co(*R*,*S*-2m-amcha)$_3$]$^{3+}$.

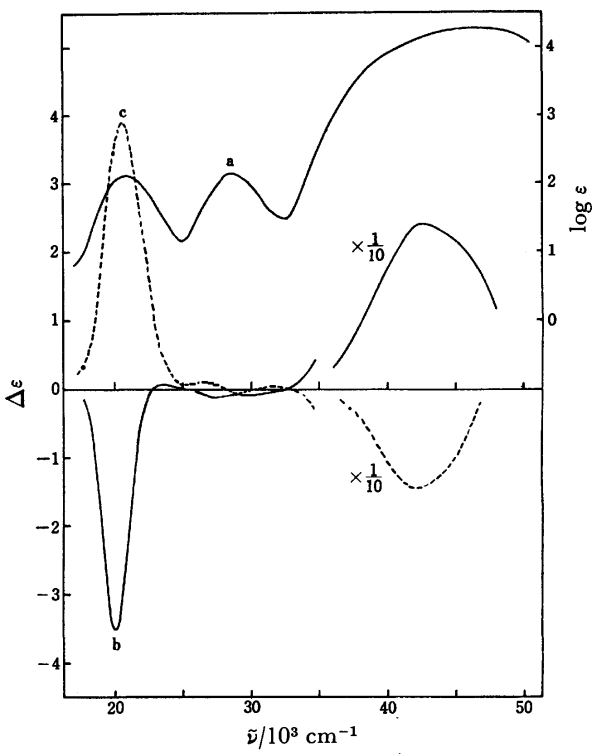

Fig. 5. Electronic (a) and CD (b, c) spectra.
—: *fac*-Λ(*lel*$_3$)-[Co(*R*,*S*-2m-amcha)$_3$]$^{3+}$ (B-1),
---: *fac*-Λ (*ob*$_3$)-[Co(*R*,*S*-2m-amcha)$_3$]$^{3+}$ (B-4).

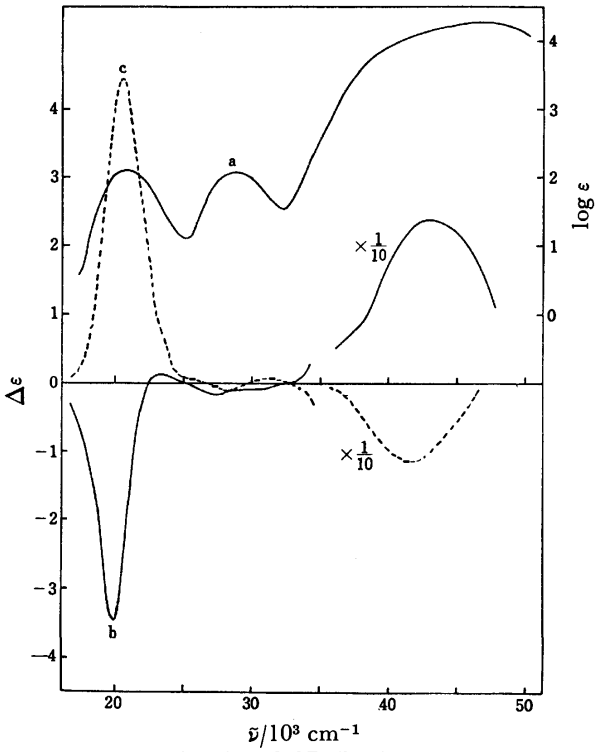

Fig. 6. Electronic (a) and CD (b, c) spectra.
—: *mer*-Λ(*lel*$_3$)-[Co(*R*,*S*-2m-amcha)$_3$]$^{3+}$ (B-2),
---: *mer*-Λ(*ob*$_3$)-[Co(*R*,*S*-2m-amcha)$_3$]$^{3+}$ (B-3).

to the nitrogen of the aminomethyl group and the hydrogen of the methyl group would be explained. Therefore the absolute configuration of the (—)-2m-amcha has been deduced to be (1*R*,2*S*).

The Isomers of [*Co*(R,S-*2m-amcha*)$_3$]$^{3+}$. Four isomers named B-1, B-2, B-3, and B-4 were isolated by an SP-Sephadex C-25 chromatography (Fig. 1). The relative ratio, B-1 : B-2 : B-3 : B-4 was approximately 1 : 6 : 1.5 : 0.3. Figure 4 shows their ^{13}C-NMR spectra. Eight and seven signals were observed for the B-1 and B-4 complex, respectively. Therefore, both complexes were assigned to *fac*-isomers (C_3 symmetry). The B-2 and B-3 complexes were assigned to *mer*-isomers (C_1 symmetry) because nonequivalences for each carbon chemical shift were observed. The same assignments were also obtained from ^{1}H-NMR spectra. The B-1 and B-4 isomers showed one doublet in the methyl region, whereas complicated signals appeared for the B-2 and B-3 isomers. The resonances for methin carbons in the *lel* ring of [Co(*R*-pn)$_3$]$^{3+}$ [20] and [Co(en)$_x$-(*R*,*R*-bn)$_y$]$^{3+}$ [21] were shown to be downfield compared with those in the *ob* ring. Almost all of the signals in ^{13}C-NMR spectrum for the B-1 complex were observed in a region downfield to those of the corresponding B-4 complex. Similar downfiled shifts were also observed in the spectrum of the B-2 isomer compared with the B-3 isomer. This spectral behavior, together with relative formation ratio, suggests that the B-1, B-2, B-3, and B-4 are *fac*-(*lel*$_3$), *mer*-(*lel*$_3$), *mer*-(*ob*$_3$), and *fac*-(*ob*$_3$), respectively.

The electronic and CD spectra of these isomers are shown in Figs. 5 and 6. The numerical data are listed

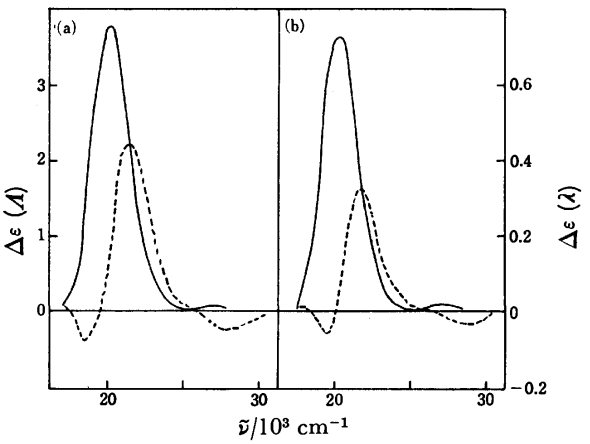

Fig. 7. Configurational effect of CD ($\Delta\varepsilon(\Lambda)$) (—) and vicinal effect of CD ($\Delta\varepsilon(\lambda)$) (---) of [Co(*R*,*S*-2m-amcha)$_3$]$^{3+}$.
(a) —: Calculated $\Delta\varepsilon(\Lambda)=1/2\{mer\text{-}\Lambda(ob_3)-mer\text{-}\Lambda(lel_3)\}$, ---: calculated $\Delta\varepsilon(\lambda)=1/6\{mer\text{-}\Lambda(ob_3)+mer\text{-}\Lambda(lel_3\}$. (b) —: Calculated $\Delta\varepsilon(\Lambda)=1/2\{fac\text{-}\Lambda(ob_3)-fac\text{-}\Lambda(lel_3)\}$, : --- calculated $\Delta\varepsilon(\lambda)=1/6\{fac\text{-}\Lambda(ob_3)+fac\text{-}\Lambda(lel_3)\}$.

in Table 3. The electronic spectral patterns of the four complexes closely resembled each other. In the CD spectra, the B-1 and B-2 isomers showed a negative band in the first absorption region and the B-3 and B-4 isomers a strong positive band in the same region. Accordingly, the former B-1 and B-2 isomers can be assigned to Λ configuration and the latter two isomers to Λ configuration, respectively. These assignments

were also supported by the CD signs and the relative intensities of the ultraviolet band, refering to the published reports.[4,22] It is known that the CD spectra of the *fac* and *mer* isomers of tris complexes having the same configuration are almost identical.[23-25] It was clearly observed that the CD spectrum of B-1(*fac*) isomer closely resembled that of B-2(*mer*) isomer. Therefore, these isomers have the same configuration. Similarly, B-3(*mer*) and B-4(*fac*) isomers have also the same configuration because they showed a similar CD patterns. In conclusion, we have assigned B-1, B-2, B-3, and B-4 isomers to *fac*-$\Delta(lel_3)$, *mer*-$\Delta(lel_3)$, *mer*-$\Lambda(ob_3)$, and *fac*-$\Lambda(ob_3)$, respectively.

Figure 7 shows the configurational and the vicinal CD curves derived from each pair ((B-2 and B-3) and (B-1 and B-4)). The calculated vicinal and configurational CD curves derived from the *fac* isomers were essentially equal to those from the *mer* isomers, respectively. This results suggest that the above assignments for the isomers were reasonable.

The authors would like to thank Misses Setsuko Kato, Shizuko Iwauchi, and Toshiko Naito of the Analytical Center of the Nagoya City University for their measurements of the NMR spectra and elemental analyses.

References

1) Part VI of this series: R. Saito and Y. Kidani, *Bull. Chem. Soc. Jpn.*, **52**, 2320 (1979).
2) E. F. Corey and J. C. Bailar, *J. Am. Chem. Soc.*, **81**, 2620 (1959).
3) H. Iwasaki and Y. Saito, *Bull. Chem. Soc. Jpn.*, **39**, 92 (1966).
4) S. E. Harnung, W. Kallesoe, A.M. Sargeson, and C. E. Schäffer, *Acta Chem. Scand.*, **28**, 385 (1974),
5) R. E. Steiger, *Org. Synth.*, Coll. Vol, III, 66 (1955).
6) R. F. Nystrom. W. G. Brown, *J. Am. Chem. Soc.*, **70**, 3738 (1948).
7) H. Toftlund and E. Pederson, *Acta Chem. Scand.*, **26**, 4019 (1972).
8) T. G. Appleton and J. R. Hall, *Inorg. Chem.*, **9**, 1800 (1970).
9) L. E. Erickson, J. E. Sarneski, and N. Reilley, *Inorg. Chem.*, **14**, 3007 (1975).
10) M. Kunimatsu, H. Kanno, M. Kojima, K. Kashiwabara, and J. Fujita, *Bull. Chem. Soc. Jpn.*, **53**, 1571 (1980).
11) L. Munday, *J. Chem. Soc.*, **1961**, 4372.
12) R. J. W. Cremlyn, *J. Chem. Soc.*, **1962**, 3977.
13) R. J. W. Cremlyn, *J. Chem. Soc.*, **1967**, 2269.
14) S. Yano, T. Tukada, M. Saburi, and S. Yoshikawa *Inorg. Chem.*, **17**, 2520 (1978).
15) S. Bagger, *Acta Chem. Scand.*, **28** 467 (1974).
16) R. Saito and Y. Kidani, presented at the 30th Symposium on Coordination Chemistry (Japan), 3P2g (1980).
17) C. J. Hawkins, D. Larsen, and I. Olsen, *Acta Chem. Scand.*, **19**, 1915 (1965).
18) S. Yano, M. Saburi, S. Yoshikawa, and J. Fujita, *Bull. Chem. Soc. Jpn.*, **49**, 101 (1976).
19) R. S. Treptow, *Inorg. Chem.*, **5**, 1593 (1966).
20) M. Kojima and K. Yamasaki, *Bull. Chem. Soc. Jpn.*, **48**, 1093 (1975).
21) S. Bagger and O. Bang, *Acta Chem. Scand.*, **30**, 765 (1976).
22) S. E. Harnung, B. S. Sörensen, I. Creaser, J. Maegaard, U. Pfenninger, and C. E. Schäffer, *Inorg. Chem.*, **15**, 2123 (1976).
23) T. E. Macdermott, *Inorg. Chem. Acta*, **2**, 81 (1968).
24) M. Kojima, Y. Yoshikawa, and K. Yamasaki, *Inorg. Nucl. Chem. Lett.*, **9**, 689 (1973).
25) M. Kojima and J. Fujita, *Bull. Chem. Soc. Jpn.*, **54**, 2691(1981).

 © 1983 The Chemical Society of Japan Bull. Chem. Soc. Jpn., 56, 455—457 (1983)

The Preparation of Poly(dicarbon monofluoride) *via* the Graphite Intercalation Compound

Nobuatsu WATANABE,* Tsuyoshi NAKAJIMA, Masayuki KAWAGUCHI, and Akira IZUMI
Department of Industrial Chemistry, Faculty of Engineering, Kyoto University, Sakyo-ku, Kyoto 606
(Received May 26, 1982)

Poly(dicarbon monofluoride), $(C_2F)_n$ is prepared with a higher reaction rate *via* the graphite interca lation compound formed through a reaction with F_2 and AlF_3 than from exfoliated graphite itself. The former process also has the advantage of including the formation of exfoliated graphite by the decomposition of an intercalation compound and its fluorination. The graphite fluoride thus prepared contained $(C_2F)_n$ by 60—78%. The reaction time required for completing the reaction did not give a linear relationship, but a minimum point around 267×10^2 Pa against the fluorine pressure and there was almost no increase above 667×10^2 Pa of fluorine. However, the F/C ratios of graphite fluoride had, inversely, a maximum point against the fluorine pressure, indicating that the $(C_2F)_n$ content in graphite fluoride was approximately proportional to the reaction time.

There are two kinds of graphite fluorides, poly(carbon monofluoride), $(CF)_n$ and poly(dicarbon monofluoride), $(C_2F)_n$.[1] The former is now commercially available and is used as a cathode material of lithium batteries and as a solid lubricant. $(C_2F)_n$ also has great possibilities as a new active mass for lithium batteries because it shows a higher discharge potential than $(CF)_n$,[2] however, compared with $(CF)_n$, it takes a significantly longer time to prepare $(C_2F)_n$ due to the low formation temperature, 350—400 °C. In order to facilitate the reaction rate of carbon with fluorine, exfoliated graphite[3] has been employed as a starting material; the results indicate that $(C_2F)_n$ in prepared at lower temperatures, 335—374 °C, with a higher reaction rate than in the case of flaky natural graphite.[4] It has been found that metal fluorides, such as AlF_3 and MgF_2, with a high sublimation or boiling point are intercalated into graphite layers with fluorine and that $(C_2F)_n$ is formed through the decomposition and subsequent fluorination of the graphite intercalation compound.[5,6] In this paper, the preparation of $(C_2F)_n$ *via* the graphite intercalation compound is reported.

Experimental

The starting materials are Madagascar natural graphite (149—279 μm, purity 99.4%), petroleum coke heat-treated at 2700 °C, commercial aluminum fluoride (purity 98%), and high-purity fluorine gas (purity 99.7%) supplied by the Daikin Kogyo Company, Ltd. The fluorination reaction was carried out using an automatic thermobalance.[7] Aluminum fluoride (50 mg) and graphite (50 mg) were placed in a nickel vessel hung by a nickel spring. After fluorine gas had been introduced into the nickel reaction vessel, the reaction system was kept at room temperature for 1 or 2 h; the temperature was then increased to 357—393 °C at a rate of 16 °C/min, followed by a reaction at that temperature until no weight increase was observed. The graphite fluoride thus prepared was analyzed by means of X-ray diffractometry and elemental analysis. The reaction was stopped prior to the complete fluorination of graphite, and the reaction rate was compared with that in the fluorination of exfoliated graphite by analysing the intermediate products.

Results and Discussion

Formation Process of Graphite Fluoride via *Graphite Intercalation Compound.* A typical thermogravimetric curve is shown in Fig. 1. Almost no weight charge was detected in the AlF_3–F_2 system at temperatures between room temperature and 400 °C; however, in the ternary system of natural graphite, AlF_3, and F_2, a weight increase due to the formation of a graphite intercalation compound was observed. The increase in temperature to 350—400 °C caused the decomposition of the intercalation compound, with an accompanying weight decrease, when natural graphite was expanded along the c-axis by release of the intercalant. A large weight increase was observed due to the subsequent fluorination of exfoliated graphite at temperatures between 350 and 400 °C:

$$\text{Graphite} + AlF_3 + F_2 \xrightarrow[\text{Room temperature}]{} C_xF(AlF_3)_y$$

$$\xrightarrow[350\text{—}400\ ^\circ C]{F_2} \text{Formation of exfoliated graphite} \xrightarrow[350\text{—}400\ ^\circ C]{F_2}$$

$$\text{Graphite fluoride} + AlF_3$$

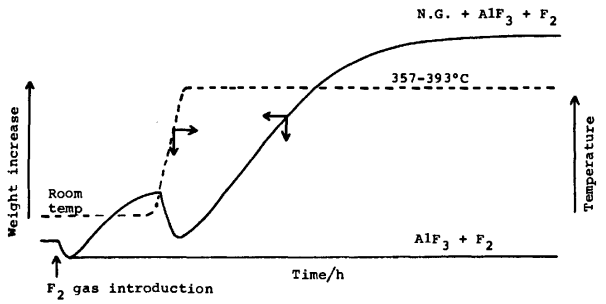

Fig. 1. Thermogravimetry for the reactions of AlF_3 with F_2 and of natural graphite (N.G.)+AlF_3 with F_2.

Table 1. Composition of intermediate products prepared from natural graphite + AlF_3 and from exfoliated graphite at 357 °C

Reaction time/h	Natural graphite + AlF_3 F/C ratio	Exfoliated graphite F/C ratio
0.3	0.06	0.03
1	0.17	0.05
2	0.15	0.07
4.5	0.40	0.16

TABLE 2. REACTION TIME AND STRUCTURAL PARAMETERS OF GRAPHITE FLUORIDE PREPARED FROM NATURAL GRAPHITE–AlF_3 SYSTEM (F_2: 267×10^2 Pa)

Reaction temp/°C	Reaction time at room temp / h	Reaction time at 357—393 °C / h	d_{001}/nm	β_{001}/°	F/C ratio
357	1	49	0.86	3.4	0.55
357	2	22	0.81	3.5	0.69
376	2	16	0.84	3.8	0.64
393	2	9	0.83	3.9	0.71
357[a)]	—	32	0.89	2.9	0.57

a) Prepared from exfoliated graphite.

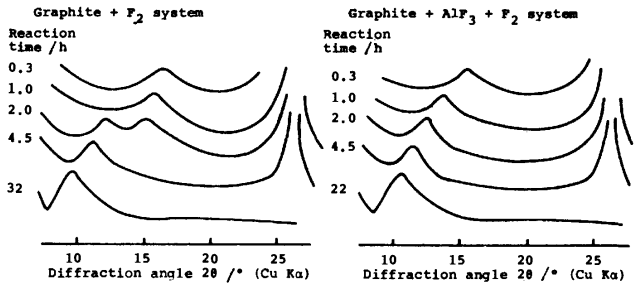

Fig. 2. Variation of (001) diffraction patterns of graphite fluoride prepared at 357 °C as a function of reaction time.

Comparison of Reaction Rates between Exfoliated Graphite and Graphite with AlF_3 Systems. In order to compare the reaction rate of exfoliated graphite with that of flaky natural graphite with an AlF_3 system, the fluorination was stopped at the initial stages of the reaction and the intermediate products were analysed. The reaction times for graphite with an AlF_3 system were those when the reaction system was above 335 °C, while for the reaction of exfoliated graphite, fluorine gas was introduced into the thermobalance maintained at a reaction temperature and the elapsed time after fluorine introduction was adopted as the reaction time. The results of elemental analyses of the products are shown in Table 1. The products obtained from graphite with an AlF_3 system contained more fluorine than those from exfoliated graphite, though the complete combustion of the products was difficult in analysis by the conventional oxygen-flask method.[8)] Figure 2 shows the X-ray diffraction patterns of these products. The small peaks between 10° and 15° in 2θ (by Cu $K\alpha$) are due to graphite fluoride, while the strong ones around 26° are due to the unreacted graphite. Since much unreacted graphite remains at the initial stage of the reaction, the intensity of the X-ray diffraction peaks for graphite fluoride was much weaker than those of unreacted graphite, though they gradually increased with the progress in the fluorination reaction. With an increase in the reaction time, the diffraction peak shifted from a higher angle due to $(CF)_n$ to a lower one due to $(C_2F)_n$ for both exfoliated graphite and graphite with AlF_3 systems, which means that $(CF)_n$ is first formed around the surface with disordered structure, followed by the formation of $(C_2F)_n$. The movement of the diffraction peak to a lower angle is faster in graphite with an AlF_3 system than for exfoliated graphite. Table 2 gives the analytical data of the products as a function of the reaction time at room temperature and also the reaction temperatures after the temperature-increase to 350—400 °C. The time required for completing the reaction was 22 h for graphite with an AlF_3 system, while it was 32 h for exfoliated graphite at 357 °C. The fluorination of graphite proceeds faster *via* the graphite intercalation compound than that of exfoliated graphite. Another advantage is that the former process includes the formation of exfoliated graphite and its fluorination.

The amount of F_2 and AlF_3 intercalated into graphite depends on the reaction time at room temperature. When the reaction time is short, only a small amount of F_2 and AlF_3 is intercalated into graphite. As a result, graphite is not fully expanded in the temperature-increase process and it takes a longer time to finish the fluorination of graphite. However, the product contains larger amount of $(C_2F)_n$ because of the lower expansion of graphite. The reaction time decreased with an increase in the reaction temperature between 357—393 °C. Compared with graphite fluoride prepared from exfoliated graphite at 357 °C, the interlayer spacing, d_{001}, of that prepared from graphite with an AlF_3 system decreased by 0.05—0.08 nm, while the half-width and the F/C ratio increased by 0.6—1° and 0.07—0.14 respectively, which means that the latter graphite fluoride contains a smaller amount of $(C_2F)_n$ than the former. These results are attributed to the larger expansion of the graphite formed by the decomposition of the intercalation compound than that of the exfoliated graphite used for comparison; this attribution was confirmed by the analytical data (Table 2) of the expanded products.

Effect of Fluorine Pressure on the Reaction Rate. The time required for completing the reaction did not give a linear relationship, but a minimum point around 267×10^2 Pa against the fluorine pressure. The reaction times were almost the same above 667×10^2 Pa of fluorine, whereas under 133×10^2 Pa it was about twice that under 267×10^2 Pa (Fig. 3). On the contrary, the F/C ratio of the products had a maximum value under 267×10^2 Pa of fluorine (Fig. 4). As was reported in a previous paper,[3)] the $(C_2F)_n$ contained in graphite fluoride can be related to the F/C ratio by representing the amounts of $(C_2F)_n$ and $(CF)_n$ as x and $1-x$ respectively: $F/C=1-1/2\times x$. The values calculated by the above equation are as follows: $(C_2F)_n$, 76—78% (F_2: 800×10^2—1013×10^2 Pa); $(C_2F)_n$, 70% (F_2: 133×10^2,

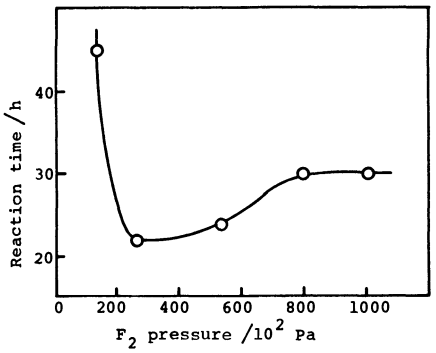

Fig. 3. Variation of reaction time of graphite fluoride as a function of F_2 pressure. Reaction temperature: 357 °C.

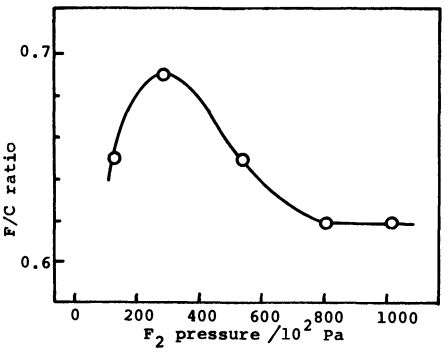

Fig. 4. Variation of F/C ratio of graphite fluuoride as a function of F_2 pressure. Reaction temperature: 357 °C.

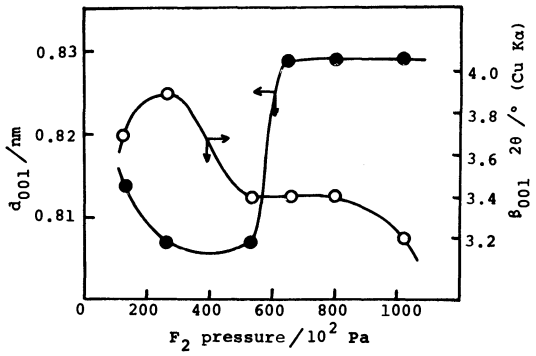

Fig. 5. Variation of d_{001} and β_{001} of graphite fluoride as a function of F_2 pressure. Reaction temperature: 357 °C.

533×10^2 Pa); $(C_2F)_n$, 62% (F_2: 267×10^2 Pa). With a decrease in the content of $(C_2F)_n$ in graphite fluoride, the interlayer spacing d_{001}, decreases, while the half-width, β_{001}, increases much as in graphite fluoride with a low crystallinity. These results show that the highest reaction rate observed under 267×10^2 Pa of fluorine is attributable to the rapid decomposition of the intercalation compound, accompanied by the large expansion of graphite. The fluorine uptake by graphite was almost the same at room temperature even under fluorine pressures of higher than 267×10^2 Pa; however, in the same range of fluorine pressure, a smaller expansion of graphite was observed, probably because the release of fluorine by the decomposition of the intercalation compound was restrained by the higher atmospheric pressure in the temperature-increase process. As a result, the reaction rate of graphite with fluorine is slower under fluorine pressure above 267×10^2 Pa. On the other hand, under a fluorine pressure of 133×10^2 Pa, the amount of fluorine absorbed by graphite at room temperature was much smaller than in other cases and the graphite was not largely expanded on the temperature-increase, which would lead to a slow reaction rate under a low fluorine pressure.

Table 3. Preparation of $(C_2F)_n$ from petroleum coke (PC)

Reaction system	Reaction temp/°C	Reaction time/h	F/C ratio	d_{001}/nm	β_{001}/°
PC–AlF_3	385	7	0.71	0.76	4.4
PC–MgF_2	383	9	0.73	0.81	4.4
PC	380	33	0.71	0.87	4.3
PC	380	13	0.67	0.86	4.3

F_2 pressure: 1013×10^2 Pa.

Preparation of $(C_2F)_n$ from Petroleum Coke (PC). Table 3 shows the data for graphite fluoride prepared from petroleum coke. As in the case of natural graphite, the reaction time decreased in the presence of AlF_3. The addition of MgF_2 also gave a similar result. The F/C ratios and half-widths of the (001) diffraction lines were slightly larger than those for graphite fluorides prepared by the direct fluorination of petroleum coke whereas the interlayer spacings, d_{001}, had an opposite relation.

As is shown in Fig. 4, graphite fluoride prepared under a fluorine pressure of 267×10^2 Pa contains the maximum amount of $(CF)_n$ in the case of natural graphite. A comparison of this graphite fluoride with that prepared from petroleum coke in the presence of AlF_3 or MgF_2 reveals that $(C_2F)_n$ is preferentially formed from natural graphite with larger crystallites. The $(C_2F)_n$ content is estimated to be 54—58% for PC with an AlF_3 or MgF_2 system and 59—66% for a PC system.

References

1) Y. Kita, N. Watanabe, and Y. Fujii, *J. Am. Chem. Soc.*, **101**, 3832 (1979).
2) N. Watanabe and K. Morigaki, *Denki Kagaku*, **47**,169 (1977).
3) "Exfoliated graphite" is prepared by the thremal decomposition of an intercalation compound of flaky natural graphite. Graphite is expanded largely in the direction of the c-axis when the thermal decomposition occurs, so that exfoliated graphite has a larger surface area and volume than flaky natural graphite. *Cf.* N. Watanabe, Y. Kita, and T. Kawaguchi, *Nippon Kagaku Kaishi*, **1977**, 191.
4) N. Watanabe, A. Izumi, and T. Nakajima, *J. Fluorine Chem.*, **18**, 475 (1981).
5) T. Nakajima, M. Kawaguchi, and N. Watanabe, *Z. Naturforsch., Teil B*, **36**, 1419 (1981).
6) T. Nakajima, M. Kawaguchi, and N. Watanabe, *Carbon*, **20**, 287 (1982).
7) M. Takashima and N. Watanabe, *Nippon Kagaku Kaishi*, **1976**, 1222.
8) K. Hozumi and N. Akimoto, *Bunseki Kagaku*, **20**, 467 (1971).

The Synthesis and Decomposition of Calcium Bis(hydrogenphosphoramidate)

Makoto WATANABE,* Toshihiko INAGAKI, and Shoji SATO

Department of Industrial Chemistry, Chubu Institute of Technology, Matsumoto-cho, Kasugai, Aichi 487

(Received June 16, 1982)

Calcium bis(hydrogenphosphoramidate)–water (2/3) was made by adding an aqueous calcium chloride solution to an aqueous potassium hydrogenphosphoramidate solution. The product decomposed slowly to diammonium calcium diphosphate monohydrate in air at room temperature. When the product was heated above 600 °C, the decomposition product was β-type calcium metaphosphate. According to the result of the isothermal decomposition of the product at 150 °C in air, no formation of P–NH–P linkages by the elimination of NH_3 from P–NH_2 linkages was observed, and it was concluded that the phosphoramidate thermally decomposed to form only polyphosphates in air.

Phosphoramidates have P–N covalent bonds and have potential of new chemical fertilizers containing phosphorus and nitrogen. Several papers concerning synthesis, decomposition, or hydrolysis of ammonium and alkali-metal salts of phosphoramidic or phosphorodiamidic acid have been published, but other salts of these phosphoramidic and phosphorodiamidic acids have not been studied. This paper describes the synthesis and decomposition of calcium bis(hydrogenphosphoramidate).

Experimental

Materials and Procedure. Ethanol was purified by distillation. Other chemicals used were of reagent grade and used without further purification. Potassium hydrogenphosphoramidate was prepared by the method described in a previous paper,[1] and 0.08 mol of the phosphoramidate was dissolved in 85 cm^{-3} of water. Calcium chloride was dissolved in 40 cm^3 of water by 0.04 mol. The calcium chloride solution was added slowly to the phosphoramidate solution below 5 °C to prevent the hydrolysis of the latter. The resulting mixture was stirred for several minutes. The pH of the solution was 6.5—6.3 during the treatment. A white precipitate was formed and was filtered off, washed with cooled water, ethanol, and then acetone. The product was dried under 5330 Pa at 25 °C for 2 d.

Elemental Analysis. Phosphorus in the product was determined by the gravimetric technique. About 0.2 g of the product was dissolved in 20 cm^3 of 6-mol nitric acid and the solution was heated on a water bath for 1 h. A few drops of concentrated hydrochloric acid was added to the solution and the solution was heated for several hours on a water bath. The orthophosphate in the solution was determined as $Mg_2P_2O_7$ by the gravimetric method.[2] Nitrogen and calcium in the product were determined by the Kjeldahl method and the EDTA (disodium dihydrogen ethylenediaminetetraacetate dihydrate) back-titration method with a calcein indicator respectively.

Paper Chromatography. One-dimensional paper chromatography was used for the separation of the phosphate species in a sample by using acidic (for the separation of chain phosphates) and basic (for the separation of ring phosphates) solvents.[3] About 0.1 g of a sample was dissolved in 10 cm^3 of a 2% EDTA aqueous solution. The pH value of the solution was adjusted to about 7 with a 0.5-mol dm^{-3} aqueous sodium hydroxide solution. About 8 mm^3 of the solution was spotted on Toyo No. 51A filter paper (2 by 50 cm). The development was run at 5 °C for 2 d.

Colorimetric Measurement of Phosphates. Every individual spot on the chromatogram was cut at the demarcation line and placed in a 100-cm^3 beaker containing 10 cm^3 of a 0.1-mol dm^{-3} ammonia solution. After 1 h, the solution was transferred to a 25-cm^3 volumetric flask, together with 10 cm^3 of wash water, and a 1-cm^3 portion of Lucena-Conde and Prat's reagent[4] was added to the flask. The flask was heated in a boiling-water bath for 1 h, subsequently cooled by placing it in a both of cold water, and diluted to the mark with water. The absorbance of the blue solution was measured with a Shimadzu Spectronic 88 spectrophotometer at 830 nm. The phosphate content (P%) was calculated from the absorbance data.

X-Ray Diffractometry. An X-ray diffraction diagram of a testing material was taken with nickel-filtered Cu *Kα* radiation by using a Toshiba X-ray diffractometer, ADG-102.

IR Measurement. IR spectra of samples were measured with a JASCO IR spectrophotometer, model A-3, using a KBr disk method.

DTA and TG. A sample was heated at the heating rate of 5 °C min^{-1} in air by using a Cho Balance $TRDA_1$-H-type apparatus.

^{31}P NMR. About 50 mg of a sample was put in 1.2 cm^3 of a 6% EDTA deuterated-water solution and stirred for several minutes. The ^{31}P NMR spectrum of the solution was recorded on a JEOL JNM-FX-60-FT-NMR instrument.

Determination of Bound Water. The amount of bound water in a sample was determined by the Karl Fisher method with an MK-AII apparatus made by Kyoto Denshi.

Decomposition in Air. The decomposition of the product at room temperature and 150 °C in air was studied by paper chromatography, X-ray diffractometry, IR spectrophotometry, and ^{31}P NMR as described above.

Results and Discussion

Composition of the Product. The yield of the product thus obtained was about 10 g. Found: P, 23.1; N, 10.4; Ca, 16.5; H_2O, 11.0%. Calcd for $Ca(HPO_3NH_2)_2 \cdot 1.5H_2O$: P, 23.9; N, 10.8; Ca, 15.5; H_2O, 10.4%. So the product is calcium bis(hydrogenphosphoramidate)–water (2/3). The product was only slightly soluble in water but soluble in an aqueous solution of EDTA.

Decomposition at Room Temperature. The stability of the product was checked at room temperature in air. The distribution of phosphate species in the decomposition product at several reaction times are listed in Table 1. The phosphoramidate decomposed to form polyphosphates. The main decomposition product was diphosphate. The IR spectra of the decomposition products

Table 1. Distribution of phosphate species in the decomposition product of $Ca(HPO_3NH_2)_2 \cdot 1.5H_2O$ at room temperature in air

Reaction time/d	Phosphate/P(%)			
	Amide and Ortho	Di	Tri	Higher
0	100	—	—	—
15	85	15	—	—
55	66	26	5	3
176	18	70	10	2
220	14	75	9	2

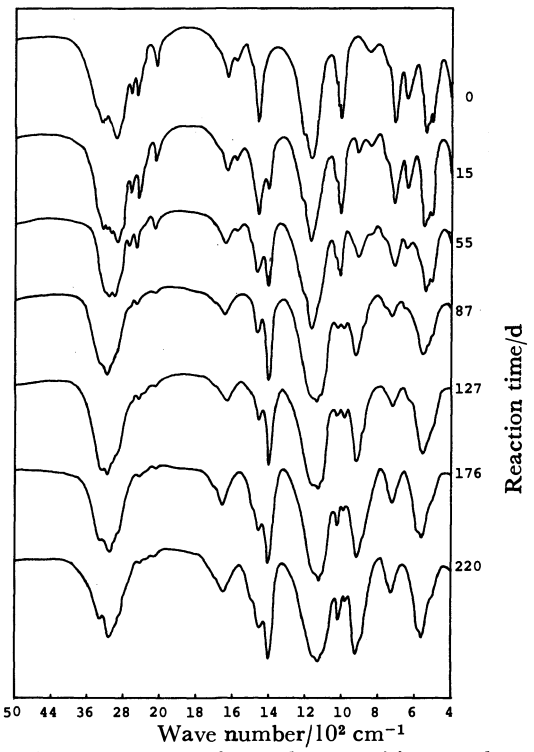

Fig. 1. IR spectra of the decomposition products of $Ca(HPO_3NH_2)_2 \cdot 1.5H_2O$ at room temperature.

are shown in Fig. 1. The assignment of the absorptions is listed in Table 2. The absorption due to a P–O–P linkage appeared and the intensity of the absorption increased with the elapse of the reaction time. The peaks of a $(PO_3)^{2-}$ group were strong even at 220 d. So the degree of polymerization of phosphates seemed to be very low. This means that most of the phosphates contained in the decomposition products are di- and triphosphates. This conclusion agrees well with that shown in Table 1. The absorption due to an ammonium ion appeared and grew with the passage of time, while the height of the absorptions associated with P–O–H and P–N–H linkages decreased with an increase in the reaction time. As Table 3 shows, the total nitrogen content in the decomposition product decreased and that of nitrogen as an ammonium ion increased with tiem. This means that an amido group is converted to an ammonium ion and the ammonia escapes gradually into the air. The discussion explains well the change in the IR spectra. Phosphoramidate having an OH-group is considered to be connected with zwitterion formation as follows:[7]

Table 2. Assignment of thf spectra of thf products

Position of absorption maxima $\tilde{\nu}/cm^{-1}$	Assignment[a]
3450	νO–H of bound water
3300—2950	ν(P)–N–H and N–H of NH_4^+
2630—2100	ν(P)–O–H
1635	δ(P)–N–H and/or δH–O–H of bound water
1580	δ(P)–N–H
1460	δ(P)–O–H
1400	δNH_4^+
1280	$\nu_{as}(PO_2)^-$
1150	$\nu_{as}(PO_3)^{2-}$
1100	$\nu_s(PO_2)^-$
1020—980	νP–O–(H) and/or $\nu_s(PO_3)^{2-}$
910	ν_{as}P–O–P
840[b]	(P–N–H or P–O–H)
780—730	νP–O–P
720—640	νP–N–(H)
580—560	$\delta(PO_2)^-$ and/or $\delta(PO_3)^{2-}$
530—500	δP–O–(H)

a) The assignment was made on the basis of Refs. 5 and 6. b) The absorption could not be assigned, but seemed to be associated with a P–N–H or a P–O–H linkage since the absorption decreased with the passage of reaction time and finally disappeared.

Table 3. Content of nitrogen in the decomposition products of $Ca(HPO_3NH_2)_2 \cdot 1.5H_2O$ at room temperature in air

Reaction time/d	Total N(%)	N(%) as NH_4^+
0	10.4	0
15	10.2	1.2
55	9.9	3.0
176	8.3	7.5
220	8.2	7.6

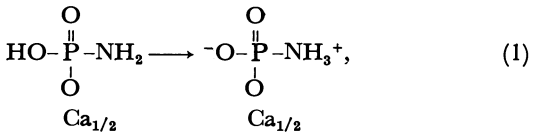

$$HO\text{-}P(=O)(O)\text{-}NH_2 \longrightarrow {}^{-}O\text{-}P(=O)(O)\text{-}NH_3^{+}, \quad (1)$$

$Ca_{1/2}$ $Ca_{1/2}$

The zwitterion seems to be unstable and to decompose to diphosphate with water,

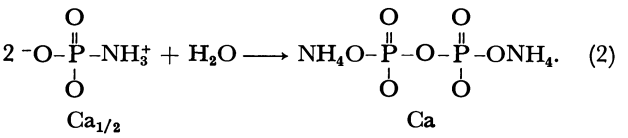

$$2\ {}^{-}O\text{-}P(=O)(O)\text{-}NH_3^{+} + H_2O \longrightarrow NH_4O\text{-}P(=O)(O)\text{-}O\text{-}P(=O)(O)\text{-}ONH_4. \quad (2)$$

$Ca_{1/2}$ Ca

The formation of polyphosphates higher than diphosphate can be represented as follows:

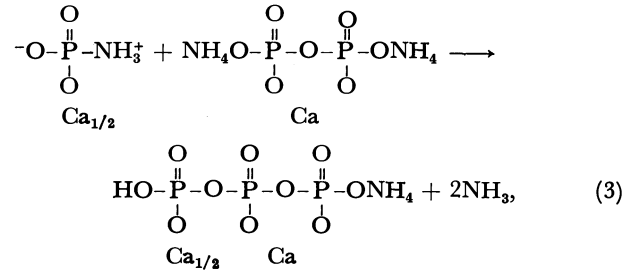

$$^{-}O\text{-}P(=O)(O)\text{-}NH_3^{+} + NH_4O\text{-}P(=O)(O)\text{-}O\text{-}P(=O)(O)\text{-}ONH_4 \longrightarrow$$

$Ca_{1/2}$ Ca

$$HO\text{-}P(=O)(O)\text{-}O\text{-}P(=O)(O)\text{-}O\text{-}P(=O)(O)\text{-}ONH_4 + 2NH_3, \quad (3)$$

$Ca_{1/2}$ Ca

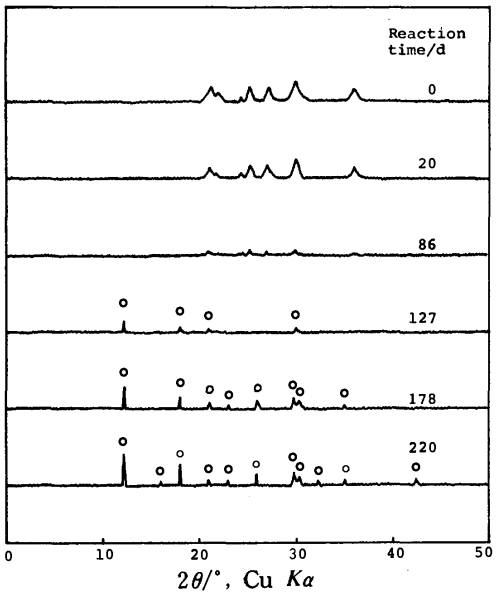

Fig. 2. X-Ray diffraction diagrams of the decomposition products of $Ca(HPO_3NH_2)_2 \cdot 1.5H_2O$ at room temperature.
○: Peaks due to $(NH_4)_2CaP_2O_7 \cdot H_2O$ (ASTM card, No. 22-38).

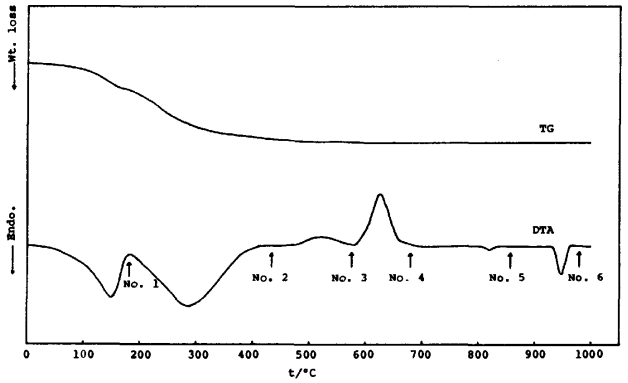

Fig. 3. DTA and TG curves of $Ca(HPO_3NH_2)_2 \cdot 1.5H_2O$.

TABLE 4. WEIGHT LOSS OF THE PRODUCT AND NITROGEN AND WATER CONTENT OF THE THERMAL DECOMPOSITION PRODUCTS

Sample	Total N(%)	Water(%)	Wt. loss/%
Product	10.4	11.0	0
No. 1	7.5	1.2	10.8
No. 2	0.8	—	23.0
No. 3	0.3	—	23.4
No. 4	—	—	23.7

and so on. The X-ray diffraction patterns of the decomposition products are shown in Fig. 2. The intensity of the diffraction peaks decreased with the passage of reaction time and the decomposition product gave very weak peaks at 86 d. Then new peaks appeared and the intensity of the peaks increased with the elapse of time. These new peaks were assigned to diammonium calcium diphosphate monohydrate, $(NH_4)_2CaP_2O_7 \cdot H_2O$ (ASTM card, No. 22-38). The result

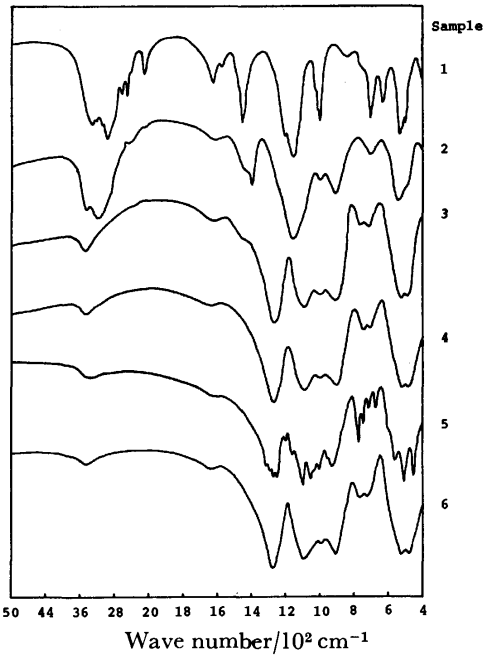

Fig. 4. IR spectra of the thermal decomposition products of $Ca(HPO_3NH_2)_2 \cdot 1.5H_2O$.
1: $Ca(HPO_3NH_2)_2 \cdot 1.5H_2O$, 2: No. 1, 3: No. 2, 4: No. 3, 5: Nos. 4 and 5, 6: No. 6.

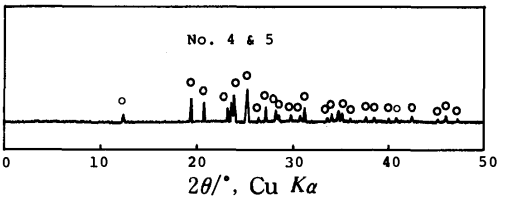

Fig. 5. X-Ray diffraction diagrams of the thermal decomposition products of $Ca(HPO_3NH_2)_2 \cdot 1.5H_2O$.
○: Peaks due to β-$Ca(PO_3)_2$ (ASTM card, No. 17-500).

agrees with that of Table 1. According to the above results, one can write a decomposition process for calcium bis(hydrogenphosphoramidate)–water (2/3) to diammonium calcium diphosphate monohydrate as follows:

$$Ca(HPO_3NH_2)_2 \cdot 1.5H_2O + 0.5H_2O \longrightarrow (NH_4)_2CaP_2O_7 \cdot H_2O. \quad (4)$$

DTA and TG. To study the thermal decomposition of the product, DTA and TG measurements of the product were made with the result shown in Fig. 3. The product decomposes at room temperature, as described above. So the product was used for the analysis immediately after synthesis to prevent the contamination by the decomposition products. The samples as numbered on Fig. 3 were removed from a furnace, cooled in a silica-gel desiccator, and subjected to further analysis. The results are presented in Table 4, and Figs. 4 and 5. As Table 4 shows, the endothermic reaction accompanying weight loss below 170 °C seemed mainly to be due to loss of bound water; the elimination of ammonia from the product was also observed in this

reaction. The sample No. 1 was amorphous and exhibited an IR absorption due to an ammonium ion and a P–O–P linkage. Polyphosphates seemed to be formed in the sample No. 1, but the strong absorption of the antisymmetric stretching of a $(PO_3)^{2-}$ group was also observed at about 1150 cm^{-1} and the absorptions of a $(PO_2)^-$ group (ν_{as}; about 1280 cm^{-1}, ν_s; about 1100 cm^{-1}) were not observed. Accordingly, the main decomposition product at this point may be diphosphate and the paper-chromatographic data concerning the distribution of phosphates in the decomposition product supported the conclusion. There appeared a broad endothermic peak and a corresponding weight loss between 170 and 430 °C. According to Table 4, the elimination of ammonia caused the weight loss. A broad exothermic peak accompanying a slight amount of weight loss was observed between 470 and 570 °C. IR spectra of Nos. 2 and 3 were very similar to each other and they involved a very small amount of nitrogen. The strong absorptions due to a $(PO_2)^-$ group and a P–O–P linkage appeared, while no obvious absorption of a $(PO_3)^{2-}$ group was observed for these samples. So the decomposition products could be highly polymerized phosphates. The samples of Nos. 2 and 3 were X-ray diffractometrically amorphous. A large exothermic peak was observed between 580 and 660 °C. The sample No. 4 gave X-ray diffraction peaks and these were all assigned to those of β-calcium metaphosphate (ASTM card, No. 17-500). Each IR peak of No. 3 split into a few peaks in the spectra of Nos. 4 and 5. According to Table 4, small difference of chemical composition was observed between the samples of Nos. 3 and 4. Therefore, the exothermic reaction may be due to the crystallization of amorphous calcium metaphosphate to the β-form. A small endothermic peak at around 820 °C may be caused by the melting of a small part of the sample because the sample after the thermal reaction was sintered. The melting of the β-form of calcium metaphosphate gave the last endothermic peak at around 950 °C. According to the above results, the following equation can be written for the overall-thermal decomposition reaction of calcium bis(hydrogenphosphoramidate)–water (2/3):

$$Ca(HPO_3NH_2)_2 \cdot 1.5H_2O \xrightarrow{(heat)} Ca(PO_3)_2 + 2NH_3 + 1.5H_2O. \quad (5)$$

The final weight loss of the product was also very close to the calculated value for the above condensation reaction.

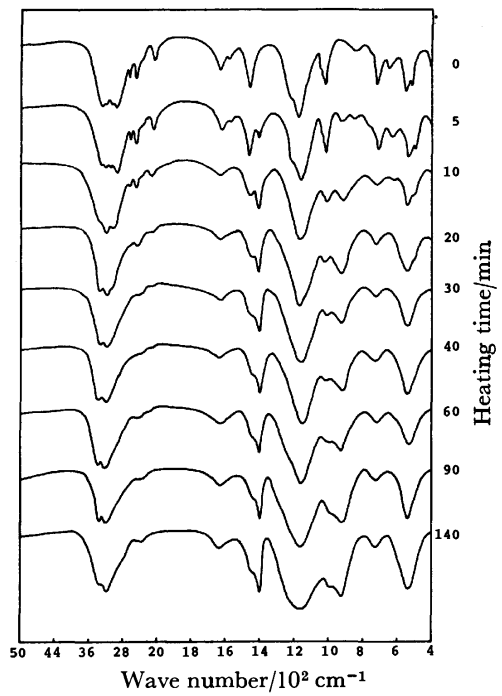

Fig. 6. IR spectra of the thermal decomposition products of $Ca(HPO_3NH_2)_2 \cdot 1.5H_2O$ at 150 °C.

Table 5. Weight loss of the product and nitrogen and water content of the thermal decomposition products at 150 °C in air

Reaction time/min	Total N(%)	N(%) as NH_4^+	Water (%)	Wt. loss/%
0	10.4	—	11.0	—
10	8.7	4.5	3.0	7.4
20	7.2	4.5	1.5	9.6
30	6.7	4.8	1.5	10.1
60	5.8	4.8	1.5	11.2
140	5.0	4.4	1.5	12.6

Table 6. Distribution of phosphate species in the decomposition products at 150 °C in air

Reaction time/min	Phosphate/P(%)			
	Amido and Ortho	Di	Tri	Higher
0	100	—	—	—
5	80.1	12.8	4.4	2.7
10	56.6	29.5	9.3	4.6
20	34.3	41.9	15.4	8.3
30	27.1	41.4	17.8	13.7
60	19.9	44.6	23.0	12.5
140	18.3	42.4	24.7	14.6

Decomposition at 150 °C. To gain further detailed data about the thermal decomposition of the product, an isothermal decomposition at 150 °C was run. As Table 5 shows, an amido group was converted rapidly to an ammonium ion and elimination of the ammonia from the product also took place rapidly. Bound water in the product could not be removed completely at this temperature. The IR spectra of the decomposition products are shown in Fig. 6. The peaks of P–N–H and P–O–H linkages disappeared gradually, and those due to an ammonium ion and a P–O–P linkage appeared with the elapse of reaction time. The absorptions due to a $(PO_2)^-$ group were equivocal, so the amount of phosphates having a P–O–P linkage longer than triphosphate seemed to be small in the decomposition product. As Table 6 shows, the determination of the phosphates contained in the decomposition products supported this conclusion. The main decomposition product was diphosphate. The decomposition products associated with a heating time longer than 20 min were X-ray diffractometrically amorphous. According to the above results, it is not apparent if the formation of a

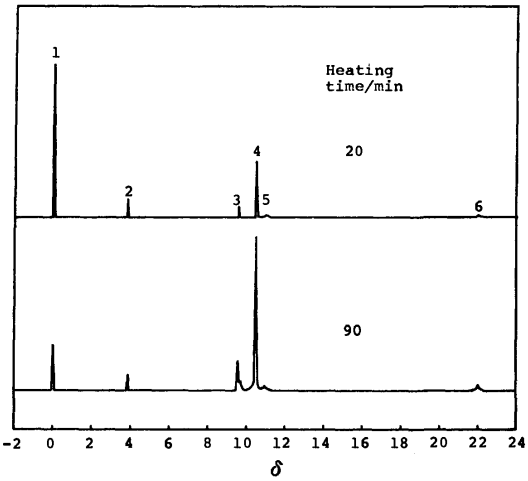

Fig. 7. ^{31}P NMR spectra of the decomposition products at 150°C.
1: Orthophosphate, 2: phosphoramidate, 3 and 4: diphosphate, 5: end PO_4 group of triphosphate, 6: middle PO_4 group of triphosphate.

P–NH–P linkage is proceeded by the elimination of ammonia between P–NH_2 linkages as follows:

$$-\overset{|}{\underset{|}{P}}-NH_2 + NH_2-\overset{|}{\underset{|}{P}}- \longrightarrow -\overset{|}{\underset{|}{P}}-NH-\overset{|}{\underset{|}{P}}- + NH_3 \quad (6)$$

The ^{31}P NMR spectra of the decomposition products at 20 and 90 min are shown in Fig. 7. No peak of any phosphorus compounds having a P–NH–P linkage was observed in the spectra. It was concluded that calcium bis(hydrogenphosphoramidate)–water (2/3) did not decompose thermally to form imidophosphates. The same decomposition processes as Reactions 1, 2, and 3 may be responsible for the thermal decomposition of the product.

References

1) "Shin Gitsuken Kagaku Koza," ed by the Chemical Society of Japan, Maruzen, Tokyo (1976), Vol. 8, p. 354.
2) "Bunseki Kagaku Binran," ed by the Japan Society for Analitical Chemistry, Maruzen, Tokyo (1971), pp. 205 and 1492.
3) S. Ohashi, *Kagaku To Kogyo*, **21**, 878 (1968). The A_2 and B_2 solvents in Table 3 were used.
4) F. Lucena-Conde and L. Prat, *Anal. Chim. Acta*, **16**, 473 (1957).
5) M. Grayson and E. J. Griffith, "Topics in Phosphorus Chemistry," John Wiley and Sons, New York (1969), Vol. 6, p. 235.
6) K. Nakanishi, "Sekigai Kyushu Supekutoru," Nankodo, Tokyo (1960).
7) D. E. C. Corbridge, "Phosphorus," Elsevier, Amsterdam (1980), p. 222.

 © 1983 The Chemical Society of Japan Bull. Chem. Soc. Jpn., 56, 463—466 (1983)

Preparation and Chelation Properties of Polystyrene-Divinylbenzene Copolymer Resins Containing Pyridylamines, Salicylamine, and 2-Thenylamine

Toshiro YOKOYAMA, Atsushi KIKUCHI, Tetsuo KIMURA, and Toshishige M. SUZUKI*
Government Industrial Research Institute, Tohoku, Nigatake, Haranomachi, Sendai 983

(Received February 8, 1982)

Bidentate and tridentate ligands, 2-pyridylmethylamine, *N*-[2-(2-pyridyl)ethyl]ethylenediamine, salicylamine, and 2-thenylamine are incorporated into polystyrene–2%-divinylbenzene copolymer beads. These chelating resins are evaluated for their chelation capacity toward transition metal ions (Co^{2+}, Ni^{2+}, Cu^{2+}, and Zn^{2+}) at various pH. The chelating resins containing pyridine derivatives show a high capacity and selectivity. The selectivity of the resins for the metal ions is in the order, $Cu^{2+} \gg Ni^{2+} > Co^{2+} \geq Zn^{2+}$ which is in accord with the order of the formation constants of the introduced ligands. Separation of a metal ion mixture (Cu^{2+}, Ni^{2+}, Zn^{2+}) into its components is undertaken by a column containing the chelating resin derived from *N*-[2-(2-pyridyl)ethyl]ethylenediamine. The present resins can also be used for the elimination of trace amount of harmful heavy metal ions such as Hg^{2+} and CrO_4^{2-}.

Much attention has been drawn to the chelating polymers having the function to recover metal ions from mine tailings[1] and to eliminate trace amount of harmful metal ions from industrial effluents.[2] A large number of chelating polymers have been developed,[3] and some of them are commercially available.[4] Polystyrene–divinylbenzene copolymer is an extensively used matrix for chelating polymers because it is readily available and sufficiently durable. For the chelating polymers used in an aqueous solution, it is essential to introduce a hydrophilic character into the hydrophobic polymer matrix. Multidentate polyamines are such ligands and many polyamine-type chelating polymers based on polystyrene–divinylbenzene copolymer have been synthesized.[5] However, the introduction of multidentate polyamine tends to be accompanied by intra- and inter-strand bridging reactions which create an ambigous structure around the ligand moiety and steric restrictions for the chelate formation.[5a]

In the present work, bidentate and tridentate amines containing an aromatic side arm (Fig. 1) are introduced into insoluble polymer beads by reaction with chloromethylated polystyrene–2%-divinylbenzene copolymer. The ligands must preferentially be linked to the polymer by *N*-alkylation of the primary amine and not from the aromatic ring side. Thus, the undesirable bridging reactions can be greatly diminished. We also took into consideration Pearson's "hard and soft acid and base" concept[6] for the design of the ligands.

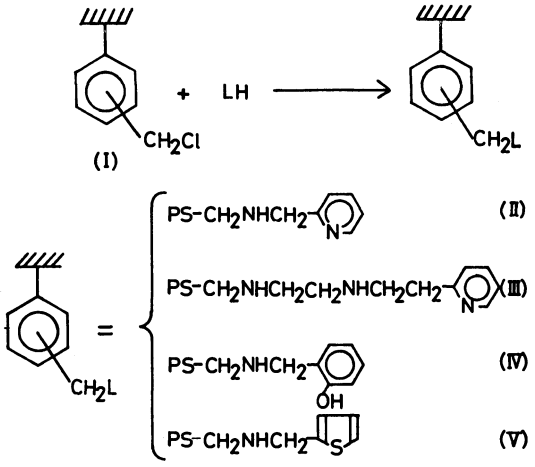

Fig. 1. Proposed structures of polymer chelating resins.

This paper deals with the preparation of the chelating resins, the examination of their capacity and selectivity toward some transition metal ions. Applications for the separation of mixed metal ions into their components and the elimination of harmful metal ions (Hg^{2+}, CrO_4^{2-}) using these resins are also investigated.

Experimental

General Procedures. All the melting and boiling points are uncorrected. The pH from 3.0 to 7.0 was adjusted with acetate buffer and below pH 3.0 with hydrochloric acid. Infrared spectra were recorded with a Hitachi 285 grating infrared spectrophotometer. ^1H NMR spectra were measured with a JEOL FX-100 spectrometer in chloroform-*d* with TMS as the internal standard. Metal ion concentration was determined with a Shimadzu atomic absorption/flame photometer Model AA-610S. Hg^{2+} was analyzed as follows: Solution containing Hg^{2+} was extracted with dithizone–chloroform solution and the solvent was evaporated on a porcelain boat. The dried sample was heated and the evaporized Hg was analyzed with an atomic absorption photometer.

Ligands. 2-Pyridylmethylamine was supplied from Aldrich Chemical Co. and purified by distillation before use. *N*-[2-(2-Pyridyl)ethyl]ethylenediamine, and salicylamine were prepared according to the method described in the literature.[7,8] 2-Thenylamine was prepared by a method similar to that for 2-pyridylmethylamine[9] using thiophene-2-aldehyde instead of pyridine-2-aldehyde. This method gave a better yield than the published one.[10] All the ligands were purified by distillation or recrystallization and identified by ^1H NMR.

Chloromethylated Polystyrene. Polystyrene-2%-divinylbenzene copolymer beads (200—400 mesh, Kanto Chemical Co.) were chloromethylated with chloromethyl methyl ether and tin(IV) chloride according to a published method.[11] The chloromethylated resin was thoroughly extracted with dioxane and dried *in vacuo* at 50 °C.

Preparation of Polymer Chelating Resins. The present ligands were incorporated into polystyrene beads using the following procedure.

TABLE 1. ANALYTICAL DATA AND CAPACITY OF LIGANDS INCORPORATED IN POLYSTYRENE

Resin	Analytical data (%)		Ligand capacity	Conversion
	Cl	N	mequiv. g^{-1} a)	% b)
I	20.82	—	5.86	86.0
II	1.29	8.03	2.87	69.4
III	3.07	9.51	2.26	67.7
IV	8.44	3.20	2.29	58.7
V	0.70	4.07	2.91	71.8

a) Calculated from the actual chlorine content (I), and nitrogen content (II, III, IV, and V).[1b] Ligand capacity (mequiv. g^{-1}) $= \frac{\%\,N}{14\,n} \times 10$, where % N = % nitrogen in product, and n = number of nitrogen atoms in the ligand. b) Based on the ratio of the actual ligand content to the theoretical value calculated from the total displacement of chlorine by the ligand.[1b] % Conversion $= \frac{\%\,N}{14\,n} \times \frac{(L-35.5)\%Cl/100+35.5}{\%Cl/100}$, where % Cl = % chlorine in the original chloromethylated polystyrene, L = ligand molecular weight minus 1.

A mixture of chlorolmethylated polystyrene beads (17.3 g, 0.1 mol) and ligand (0.4 mol) in dioxane (250 cm^3) was refluxed for 48 h with stirring. The resin was filtered off, washed first with water, and then with dioxane and transfered into a Soxhlet extractor. After extraction with dioxane for 48 h, the resin was collected, washed thoroughly with diethyl ether and dried *in vacuo* at 50 °C. The dried resins thus obtained were pale yellow or slightly brown. The analytical results (Cl, N) are summerized in Table 1.

Determination of Capacity for Metal Ion Uptake. Complexation capacities of the resins were determined as a function of pH by treating with buffered solution of Co^{2+}, Ni^{2+}, Cu^{2+}, and Zn^{2+}. Experiments were typically undertaken as follows.

One gram of dry resin was added to 100 cm^3 of buffered metal ion solution (0.2 mol/dm^3). After 20 h stirring at room temperature, the resin was loaded on a glass column (ϕ 1.0 cm × 20 cm) and washed with water. The chelated ion was stripped from the resin by elution with 2 M hydrochloric acid.† The eluate was collected in a volumetric flask and finally diluted to the mark with water. The amount of matal ion in the eluate was determined with and atomic absorption spectrometer. In most cases the resins can be regenerated by treating successively with 0.2 M hydrochloric acid, 0.2 M ammonia, and water. No significant change in capacity was detected after several times recycling the resins except for the treatment with Co^{2+}.

Chromatographic Separation of Metal Ion Mixture. One milliliter of metal salt mixture ($NiCl_2 \cdot 6H_2O$, $CuCl_2 \cdot 2H_2O$, $ZnCl_2 \cdot 2H_2O$; 1 g of each salt was dissolved in 100 cm^3 of water) was poured onto a column (ϕ1.0 cm × 13 cm) containing resin III in Table 1 (5.0 g, dry weight) which was treated with 0.1 M acetate buffer (pH 5.5) in advance. The adsorbed band was eluted at a rate of 0.27 cm^3 min^{-1} with the desired eluent: 0.1 M acetate buffer (pH 5.2) for Zn^{2+}; 0.1 M acetic acid for Ni^{2+}; and 0.5 M hydrochloric acid for Cu^{2+}. The eluate was fractionated into 4 cm^3 portions and the amount of metal ion was determined.

Elimination of Harmful Metal Ions. *Hg^{2+}*: One hundred millgram of dry resin was stirred with a buffered solution (50 cm^3) containing Hg^{2+} (1×10^{-3} g dm^{-3}) at various pH. The resin was removed by filtration after an appropriate time, and the residual Hg^{2+} in the filtrate was analyzed. The time-course of the Hg^{2+} uptake was followed by occasional extraction of samples from the mother liquor without removing the resin. The effect of ionic strength on the elimination of Hg^{2+} was examined using sodium chloride as a co-existing salt.

Cr(VI) (CrO_4^{2-}): The procedure of the elimination experiment was essentially the same as that for Hg^{2+} except that the initial concentration of Cr(VI) was 2.0×10^{-2} g dm^{-3}.

† 1 M = 1 mol dm^{-3}.

Results and Discussion

Preparation of Polymer Chelating Resins. Polystyrene–divinylbenzene copolymer is a convenient substrate for studies of polymer-support ligands because it is readily available and chemically durable. It has been pointed out that the increase in the degree of cross-linking brings about an increase in steric hindrances due to the bulky benzene nuclei, but the reduction of the cross-linking diminishes the mechanical strength of the polymer particles.[2b,5b] The polystyrene–2%-divinylbenzene beads which were used in the present study are low in divinylbenzene content, but have mechanical strength sufficient for the usual experiments. Four-fold excess of ligand to the chloromethylated polystyrene was used throughout this work, since the reaction conversion did not improve on addition of a further amount of ligand. A part of the ligand is quenched as the acid acceptor. The capacity of the incorporated ligand and the reaction conversion derived from the analytical data are summerized in Table 1. The reaction conversion was in the range of 60 to 70% with respect to the available chloromethyl groups. Although the structure of the chloromethylated polystyrene remains ambigous,[12] the ligand must be linked to the polymer matrix by the reaction of the chloromethyl group with the nucleophilic amine. The chlorine contents of the resins II and V are relatively lower than those expected from the reaction conversions. This must be due to the intra- and inter-strand bridging reactions with further alkylation of the hetero atoms. A rough estimation based on the elemental analysis of the resins II and V revealed that 65—70% of the introduced ligands have the structure depicted in Fig. 1. The undesirable side reactions are not significant for the resins III and IV and more than 80% of the ligands incorporated take up a non-bridged structure.

Complexation Capacity of Chelating Resins with Co^{2+}, Ni^{2+}, Cu^{2+}, and Zn^{2+}. The capacity of the polymer chelating resins were evaluated for the uptake of Co^{2+}, Ni^{2+}, Cu^{2+}, and Zn^{2+} as a function of pH. The maximum

TABLE 2. MAXIMUM CHELATION CAPACITY OF POLYMER RESINS FOR TRANSITION METAL IONS

Resin	Co^{2+}	Ni^{2+}	Cu^{2+}	Zn^{2+} (mequiv. g^{-1})
II	0.64	0.98	2.02	1.19
III	0.29	0.77	1.61	0.98
IV	0.01	0.00	0.17	0.08
V	0.03	0.00	0.05	0.10

capacity of the present resins are given in Table 2. The resins containing pyridine derivatives (II, III) reveal high capacities comparable to those of commercial resins[13] for the uptake of the ions. However, resins IV and V which contain relatively "softer" ligating atoms than nitrogen show little or no affinity towards these metal ions. Such a result is in accord with the fact that metal chelates of salicylamine with Cu^{2+}, Ni^{2+}, and Zn^{2+} were not formed in methanol.[14] All the chelating resins revealed a reproducible capacity on repeated adsorption and desorption cycling for most of the metal ions except for III with Co^{2+}. When Co^{2+} was adsorbed on resin III, a considerable amount of the metal ion was strongly retained on the resin, so that it could not be stripped off even by treatment with conc. hydrochloric acid. This is presumably because Co^{2+} is partially oxidized on the resin giving an inert Co^{3+} complex.

The chelating capacity *vs.* pH curves for the resins II and III are given in Figs. 2 and 3, respectively. Copper(II) was most strongly retained on these resins giving a characteristic blue color and the chelation capacity is larger than for other ions. Nickel(II) ion was retained at lower pH region than Co^{2+} and Zn^{2+}. Considerable overlapping of curves is seen for the Co^{2+} and Zn^{2+} indicating that the difference in affinity of the two ions is very small. The pH dependence curves clearly imply that the order of affinity for the resins II and III is $Cu^{2+} \gg Ni^{2+} > Co^{2+} \geq Zn^{2+}$, which is in good accordance with the order of formation constants of introduced ligands, *i.e.*, 2-pyridylmethylamine[15] and *N*-[2-(2-pyridyl)ethyl]ethylenediamine.[7] This observation prompted us to separate a metal ion mixture into its components by column chromatography. A solution containing Cu^{2+}, Ni^{2+}, and Zn^{2+} was adsorbed on a column loaded with resin III and the adsorbed band was eluted with a solution of decreasing pH. Figure 4 shows the elution curve in which the three metal ion components are well separated. This order is in agreement with the results of Storch and Manecke.[16]

Elimination of Harmful Metal Ions. *Hg^{2+}*: Elimination of trace amount of Hg^{2+} was examined under batch process using these chelating resins. Figure 5 shows the plot of residual Hg^{2+} against the pH of the solution. All the resins examined are found to be effective for the removal of nearly 99% of the initial Hg^{2+} at their optimum conditions. Resins II and III can adsorb the ion over a relatively wide pH range, while resins IV and V are effective below pH 3.0 and 2.0, respectively. It is noted that the latter two resins remove Hg^{2+} nearly quantitatively in spite of their low affinity towards the first transition metal ions. This selectivity may be understood by considering that Hg^{2+} is a "soft" acid which prefers to associate with "soft" ligand atoms.[6] Hence the resins IV and V can be used for the selective elimination of Hg^{2+} in the presence of "hard" metal ions. The time-course of Hg^{2+} uptake by the resins IV and V was followed by extraction of samples from the mother solution at appropriate

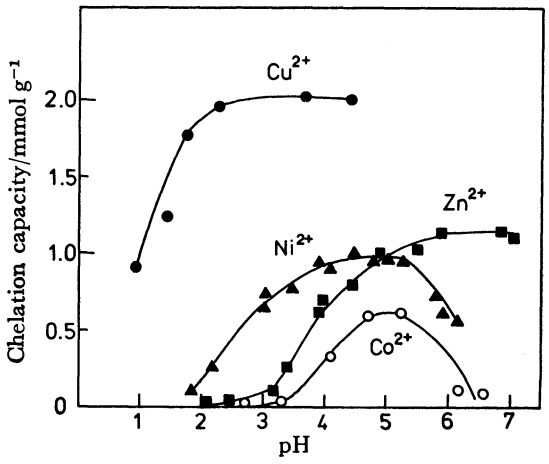

Fig. 2. Chelation capacity of resin II as a function of pH.
-●-: Cu^{2+}, -▲-: Ni^{2+}, -■-: Zn^{2+}, -○-: Co^{2+}.

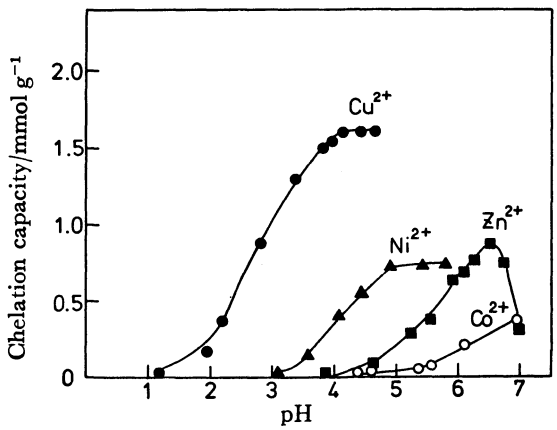

Fig. 3. Chelation capacity of resin III as a function of pH.
-●-: Cu^{2+}, -▲-: Ni^{2+}, -■-: Zn^{2+}, -○-: Co^{2+}.

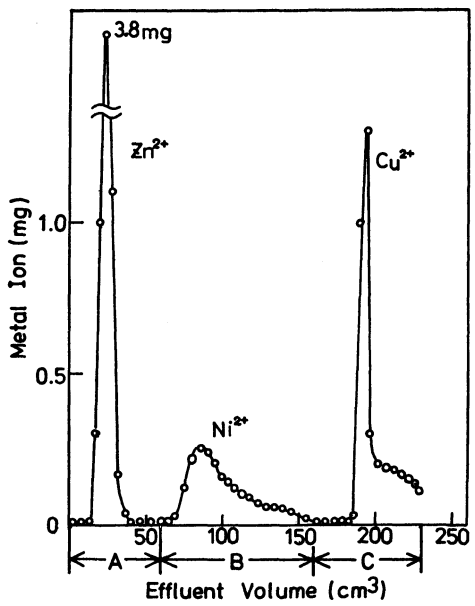

Fig. 4. Chromatographic separation of a three-components metal ion mixture.
A: 0.1 M acetate buffer(pH 5.2),B: 0.1 M acetic acid (pH 3.02), C: 0.5 M HCl.

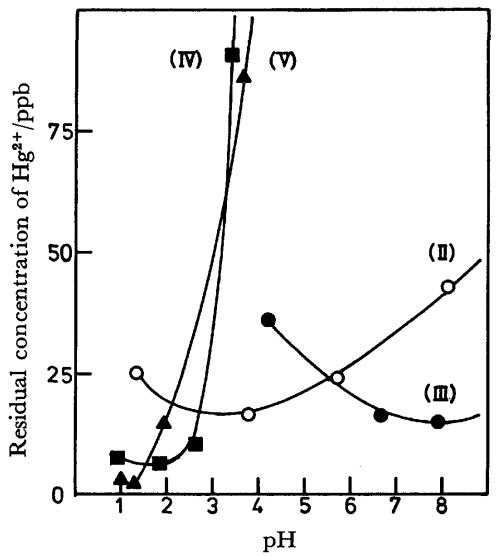

Fig. 5. Elimination of Hg^{2+} by resin II, III, IV, and V.
Conditions: amount of resin; 100 mg in 50 cm^3, concentration of Hg^{2+}; 1×10^{-3} g dm^{-3}, treating time; 15 h.

intervals. In both cases, the rapid decrease in Hg^{2+} concentration was observed and the equilibrium was attained after *ca.* 1 h. The effect of sodium chloride on the removal of Hg^{2+} was also examined for these resins. The activities of both resins do not change significantly in the presence of 0.1 M NaCl and only slightly decreases when the concentration reached 1 M. Thus these resins would be promising materials for the removal of Hg^{2+} in an effluent from soda/chlorine industry in which high concentrations of NaCl are encountered.

CrO_4^{2-}: The removal of CrO_4^{2-} was examined under batch-wise process. Resins II, III, and IV can remove CrO_4^{2-} nearly quantitatively at pH ranging 3 to 6, while the resin V reveals little affinity towards this ion. Thus it seems that "hard" ligating atoms are preferable to "soft" ones towards CrO_4^{2-}. The rate of adsorption of CrO_4^{2-} was examined at the optimum pH of each resin. Resins II and III which contain pyridine derivatives adsorbed 99% of CrO_4^{2-} in less than 10 min and the equilibrium was attained within 30 min, whereas resin IV required *ca.* 3 h for equilibriation. In all cases, CrO_4^{2-} was captured very strongly on the resin and hence quantitative recovery of the ion from the resin was difficult. Resin-CrO_4^{2-} complexes turned dark brown on standing in an aqueous solution for several hours due to oxidation of the ligand moiety. Thus the reduction in activity of the resins is inevitable on repeated cycling. Decrease in activity of the resins was also observed when sodium sulfate (>0.1 M) co-existed in the solution. This may suggest that the resins act as anion exchanger in some extent rather than a chelating agent. The details of the structure of the resin-CrO_4^{2-} complexes are under investigation.

The authors wish to thank Dr. Yoichi Sasaki of Tohoku University for his helpful suggestions and discussions.

References

1) a) D. S. Flett, *Chem. Ind.* (*London*), **1977**, 706; b) L. R. Melby, *J. Am. Chem. Soc.*, **97**. 4044 (1975).
2) a) A. K. Coleman, *Chem. Ind. (London)*, **1975**, 534; b) F. Vernon, *ibid.*, **1977**, 634; c) H. F. Walton, *Anal. Chem.*, **50**, 36R (1978); d) J. H. Hodgkin, *Chem. Ind.* (*London*), **1979**, 153.
3) A. Akalah and D. C. Sherrington, *Chem. Rev.*, **81**, 557 (1981).
4) Polystyrene beads containing iminodiacetate or alkylpolyamine group are commercially available.
5) a) E. Blasius and I. Bock, *J. Chromatogr.*, **14**, 244 (1964); b) H. Egawa and H. Saeki, *Kogyo Kagaku Zasshi*, **74**, 772 (1971); c) H. Egawa and K. Sugawara, *ibid.*, **74**, 1026 (1971).
6) R. G. Pearson, *J. Am. Chem. Soc.*, **85**, 3533 (1963).
7) R. G. Lacoste and A. E. Martell, *Inorg. Chem.*, **3**, 881 (1964).
8) H. Kanatomi and I. Murase, *Bull. Chem. Soc. Jpn.*, **43**, 226 (1970).
9) L. C. Craig and R. M. Hixon, *J. Am. Chem. Soc.*, **53**, 4367 (1931).
10) H. D. Hartough and S. L. Meisel, *J. Am. Chem. Soc.*, **70**, 4018 (1948).
11) K. W. Pepper, H. M. Paisiey, and M. A. Young, *J. Chem. Soc.*, **1953**, 4097.
12) Chloromethylation of polystyrene can lead to a mixture of isomers due to various substitutions on the aromatic ring.
13) For example, Dowex A-1 (chelate resin containing iminodiacetate ligand) has a maximum capacity *ca.* 1.8 mmol g^{-1} of dry resin toward Cu^{2+}.
14) S. Matsumoto and Y. Matsushima, *Chem. Pharm. Bull.* (*Tokyo*), **23**, 106 (1975).
15) D. E. Goldberg and W. C. Fernelius, *J. Am. Chem. Soc.*, **63**, 1246 (1959).
16) W. Storch and G. Manecke, *Makromol. Chem.*, **121**, 129 (1969).

The Autoxidation of 2,3-Dihydroxy-2-propenal (Triose Reductone). The Effects of the pH on the Rate Constants

Yasuo ABE,* Hideo HORII, Setsuo TANIGUCHI, Kazuo KAMAI,† and Masanosuke TAKAGI†
Radiation Center of Osaka Prefecture, Shinke-cho, Sakai 593
†*College of Agriculture, University of Osaka Prefecture, Mozu-umemachi, Sakai 591*
(Received March 8, 1982)

The autoxidation of 2,3-dihydroxy-2-propenal (triose reductone) was investigated between pH 2.83 and 13.91 in the presence of disodium dihydrogen ethylenediaminetetraacetate (EDTA 2NA). The reaction obeyed the first-order rate law with respect to the triose reductone and the zeroth-order rate law with respect to oxygen when the oxygen concentration was higher than 0.246 mM (1 mM = 10^{-3} mol dm^{-3}) at 30 °C. The pH dependence of the reaction rates showed that the reaction rates are governed by the acid-base equilibrium of triose reductone. The rate constants for neutral and singly- and doubly-charged anions of triose reductone at 30 °C were $(3.6\pm0.1)\times10^{-6}$, $(7\pm1)\times10^{-5}$, and $(1.8\pm0.1)\times10^{-2}$ s^{-1} respectively. The hydrogen peroxide produced as a result of the triose reductone oxidation was also found to oxidize triose reductone.

The 2,3-dihydroxy-2-propenal produced from dextrose by alkaline hydrolysis is called triose reductone because of its strong reducing ability. The stoichiometry of the oxidation of triose reductone with hydrogen peroxide,[1] periodic acid,[2] sodium periodate,[3] iodine,[4] iron(III) chloride,[4] 2,6-dichlorophenolindophenol (DCIP),[4] and selenium oxide[5] has been studied by only a few workers. The first kinetic study of the oxidation was attempted by Arndt *et al.*,[4] but they did not determine the rate constants. Recently, Obata *et al.*[6] studied the reduction of DCIP with triose reductone in the pH range between 2 and 11; they obtained the second-order rate constants. The enzymatic autoxidation of the reductone using oxidase and peroxidase was studied in detail.[7] Although the nonenzymatic autoxidation of triose reductone was well known,[8,9] no one has studied it kinetically. Since triose reductone is an endiol compound whose redox behavior quite resembles that of the physiologically important L-ascorbic acid, we were interested in studying the autoxidation of the reductone.

Experimental

The triose reductone was prepared and purified by the method of Euler and Martius.[10] The formic acid,[11] glyoxylic acid,[12] glycolic acid,[12] glyoxal,[13] and hydrogen peroxide[14] were determined colorimetrically according to the procedures described in the literature.

Kinetic Method. The triose reductone was dissolved in a given volume of a solution, containing 4 mM each of acetic acid, phosphoric acid, and boric acid, and 1 mM of EDTA. The concentrations of the dissolved oxygen were controlled by saturating with argon, air, or oxygen gas so as to be 0.246, and 1.23 mM respectively, based on the known oxygen solubility at a given temperature. An aliquot of an aqueous solution of sodium hydroxide was added to 3 cm^3 of the triose reductone solution in a capped quartz cell, with precaution taken to avoid any change in the oxygen concentration. The oxidation time courses were followed spectrophotometrically with a Hitachi 323 Recording Spectrophotometer by measuring the decreasing absorption at 267 or 293 nm. The temperature was controlled at 30±0.1 °C. The pseudo first-order rate contant, k_{obsd}, was determined from the slope of the linear plots of log OD against time in the usual manner. The pH values of the reaction solutions were measured with a digital pH meter (Toyo Model PT-3D) before and after the reaction; we thus confirmed no appreciable pH change during the reaction. The hydrogen peroxide solution was added to the solution of triose reductone before the injection of the sodium hydroxide solution.

Results and Discussion

Dissociation Constants of Triose Reductone. Though the pK_a value for the first dissociation of triose reductone has been reported to be 5.00,[10] 4.93,[15] or 5.12,[16] the value for the second dissociation has not been available in the literature. The UV absorption spectra of triose reductone at pH 3.80, 8.00, and 13.5 under an argon atmosphere are shown in Fig. 1. An acidic solution (pH 1.5—4.1) of triose reductone showed an absorption maximum at 268 nm (ε=16300), neutral and slightly basic solutions (pH 6.8—10.0), at 293 nm (ε=24600), and a strongly basic solution (pH>13.5), at 323 nm

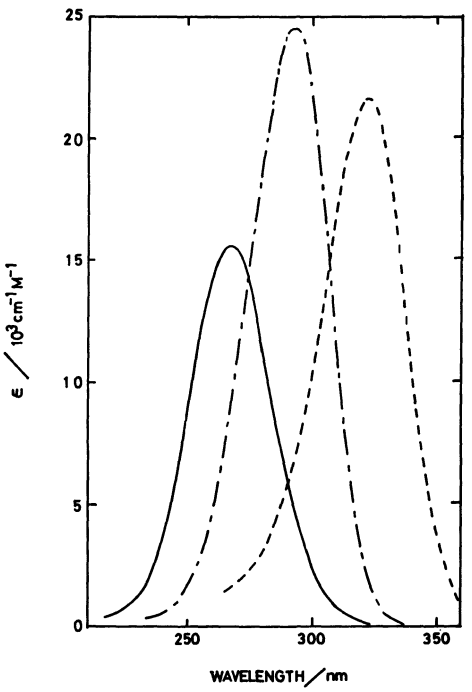

Fig. 1. Absorption spectra of triose reductone.
——: pH 3.80, —·—: pH 8.00, ------: pH 13.5.

(ε=23300). Triose reductone has two dissociable hydrogen atoms according to the following acid-base equilibria:

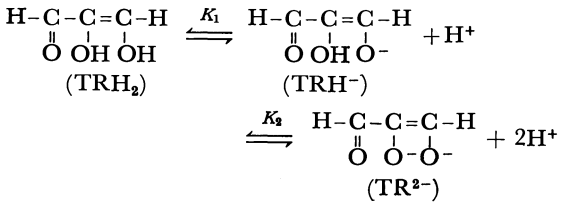

the three absorption spectra corresponding to the neutral molecule (TRH_2), the monoanion (TRH^-), and the dianion (TR^{2-}). The values of pK_{a1} and pK_{a2} can be calculated by means of Eqs. 1 and 2. The concentrations of TRH_2 and TRH^- in Eq. 1 were

$$pK_{a1} = pH + \log \frac{[TRH_2]}{[TRH^-]} \quad (1)$$

$$pK_{a2} = pH + \log \frac{[TRH^-]}{[TR^{2-}]} \quad (2)$$

computed from the spectra at pH 5—6, and those of TRH^- and TR^{2-} in Eq. 2, from the spectra at pH 12—13. The values of pK_{a1} and pK_{a2} obtained were 5.03 and 13.0 respectively at 30 °C.

Stoichiometry of the Oxidation. In the case of the autoxidation of a concentrated triose reductone solution without buffer capacity and EDTA, hydrogen peroxide was detected in the course of the reaction. However, the hydrogen peroxide disappeared after the triose reductone had been completely consumed. Table 1 shows the yields of the oxidation products from triose reductone. It has been reported that the oxidation of triose reductone with an excess of hydrogen peroxide gave carbon dioxide and formic acid.[1] In a similar way, periodic acid gave formic acid and glyoxylic acid,[2] and selenium oxide gave 2,2-dihydroxypropanedial (dehydroreductone hydrate).[5] Sodium periodate gave formic acid and glyoxylic acid in the first step, and then glyoxylic acid was oxidized to formic acid and carbon dioxide.[3] Formic acid and glyoxylic acid were detected in the present work; further, the total concentration of the two acids was found to amount to twice the triose reductone consumed (Table 1). It may be reasonable to consider that the oxidation of triose reductone with oxygen proceeds *via* a step-by-step oxidation as has been described above. The oxidation also proceeds in a similar way with the hydrogen peroxide produced by the reduction of oxygen.

Table 1. Autoxidation of aqueous solution of triose reductone

Product	Yield/%[a]
Hydrogen peroxide	0 (12)[b]
Glyoxylic acid	30
Glycolic acid	0
Formic acid	167
Glyoxal	0

a) The yield presented is based on the assumption that 1 mol of triose reductone yields 1 mol of each of the products. b) The yield in parentheses is a value observed in the course of the reaction.

Effect of pH on Rate of Autoxidation. The UV spectra of a triose reductone solution saturated with oxygen or air were identical with those shown in Fig. 1 below pH 10. However, above pH 10 it was not clear whether or not these spectra were identical due to the fast degradation of the reductone.

The first-order rate constants (k_{obsd}/s^{-1}) were obtained from the slopes of the linear $\log[TR]_t$ *vs.* time plots, where t denotes the total analytical concentration. The pH-rate profile for the autoxidation of triose reductone at 30 °C is sigmoid (Fig. 2). For the effect of the oxygen concentration on the rate, no difference in k_{obsd} was observed in the oxygen concentration range between 0.246 and 1.23 mM. Since no oxidant other than oxygen was involved in the reaction system, the reaction rates should depend on the oxygen concentration. However, the rates were practically constant and independent of the oxygen concentration when it was over 0.246 mM. The pH-rate profile clearly reflects the involvement of various triose reductone species. We may envisage the reaction scheme shown in Scheme 1.

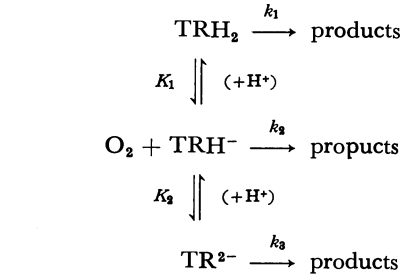

TRH_2 = H–C(=O)–C(OH)=C(OH)–H, $K_1 = 9.3\times10^{-6}$, and $K_2 = 1.0\times10^{-13}$.

Scheme 1.

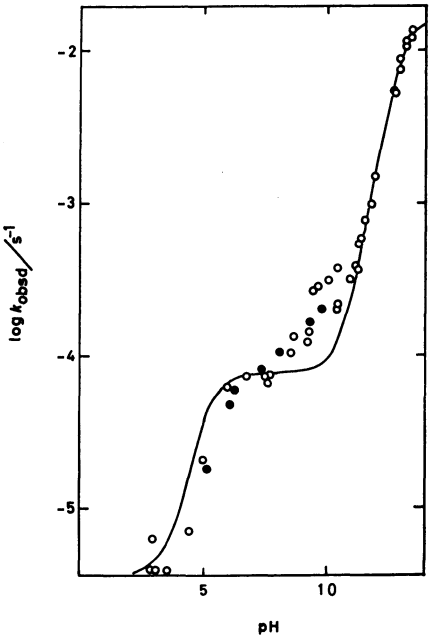

Fig. 2. Relation between log k_{obsd} and pH for the autoxidation of triose reductone at 30 °C.
○: Oxygen saturated, ●: air saturated. The solid line reflects log k_{calcd} according to Eq. 10.

Thus, at a constant acidity, the simplest rate expression is given by Eq. 3:

$$\text{rate} = k[\text{TR}]_t. \quad (3)$$

At various pH values:

$$[\text{TR}]_t = [\text{TRH}_2] + [\text{TRH}^-] + [\text{TR}^{2-}] \quad (4)$$

$$[\text{TRH}_2] = \frac{[\text{H}^+]^2}{[\text{H}^+]^2 + [\text{H}^+]K_1 + K_1K_2}[\text{TR}]_t$$

$$[\text{TRH}^-] = \frac{[\text{H}^+]K_1}{[\text{H}^+]^2 + [\text{H}^+]K_1 + K_1K_2}[\text{TR}]_t, \text{ and}$$

$$[\text{TR}^{2-}] = \frac{K_1K_2}{[\text{H}^+]^2 + [\text{H}^+]K_1 + K_1K_2}[\text{TR}]_t. \quad (5)$$

Hence, the rate equation becomes:

$$-\frac{\text{d}[\text{TR}]_t}{\text{d}t} = \frac{k_1[\text{H}^+]^2 + k_2[\text{H}^+]K_1 + k_3K_1K_2}{[\text{H}^+]^2 + [\text{H}^+]K_1 + K_1K_2}[\text{TR}]_t. \quad (6)$$

Hence, from Eq. 3 we obtain:

$$k = \frac{k_1[\text{H}^+]^2 + k_2[\text{H}^+]K_1 + k_3K_1K_2}{[\text{H}^+]^2 + [\text{H}^+]K_1 + K_1K_2}. \quad (7)$$

In the pH range of 2.8—7.7, Eq. 7 can be simplified to Eq. 8, since there is triose reductone in TRH_2 and TRH^-:

$$k = \frac{k_1[\text{H}^+]^2 + k_2[\text{H}^+]K_1}{[\text{H}^+]^2 + [\text{H}^+]K_1 + K_1K_2}. \quad (8)$$

By substituting the observed values for k and $[\text{H}^+]$ in Eq. 8, k_1 and k_2 were obtained as $(3.6\pm0.1)\times10^{-6}$ and $(7\pm1)\times10^{-5}\,\text{s}^{-1}$ respectively. Similarly, Eq. 7 can be simplified to Eq. 9 in the pH range of 10.4—13.4:

$$k = \frac{k_2[\text{H}^+]K_1 + k_3K_1K_2}{[\text{H}^+]^2 + [\text{H}^+]K_1 + K_1K_2}. \quad (9)$$

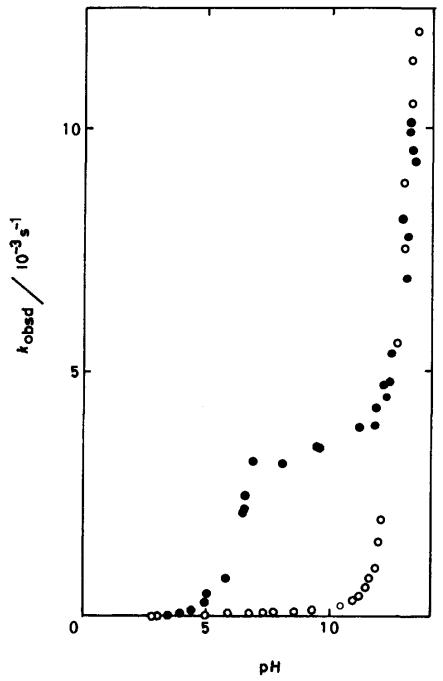

Fig. 3. Relation between k_{obsd} and pH for the autoxidation of triose reductone in the presence and absence of EDTA at 30 °C.
○: In the presence of EDTA, ●: in the absence of EDTA.

The k_3 value thus obtained was $(1.8\pm0.1)\times10^{-2}\,\text{s}^{-1}$, while k_2 was not constant. This fact suggests that the monoanion of triose reductone might be consumed by side reactions at these pHs. Considering the detection of hydrogen peroxide in the course of the autoxidation, the side reaction must be the oxidation of triose reductone with the hydrogen peroxide produced (see below). The solid line in Fig. 2 represents the theoretical plot of log k, calculated using Eq. 7, against the pH. The calculated values of k agree well with the observed k values below pH 8 and above pH 11.

The autoxidation rate constants of L-ascorbic acid at 20 °C have been reported as $8.3\times10^{-7}\,\text{s}^{-1}$ for the monoanion and $8.3\times10^{-2}\,\text{s}^{-1}$ for the dianion; furthter

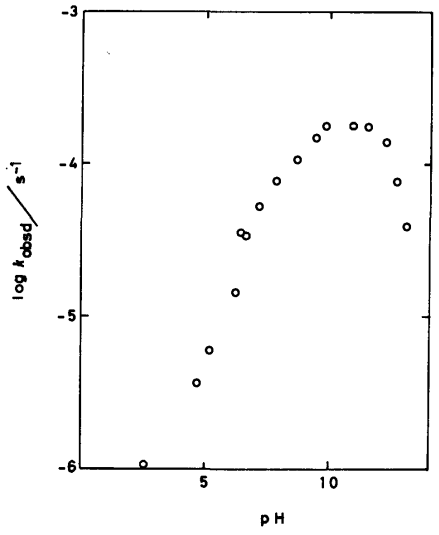

Fig. 4. Relation between log k_{obsd} and pH for the oxidation of triose reductone with hydrogen peroxide in the absence of oxygen at 30 °C.

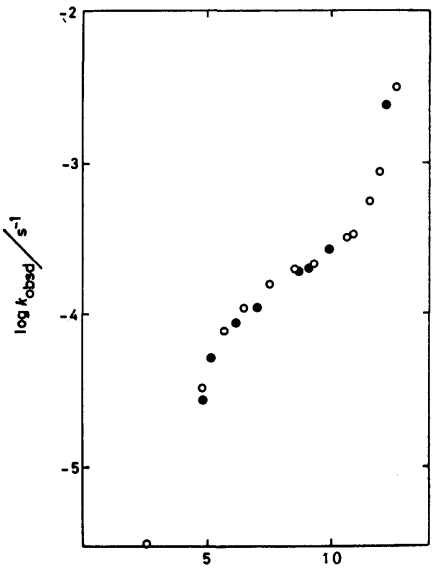

Fig. 5. Relation between log k and pH for the oxidation of triose reductone with hydrogen peroxide in the presence of oxygen at 30 °C.
○: Observed, ●: calculated.

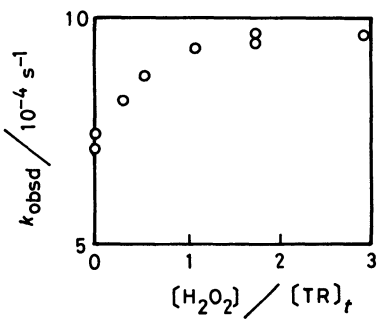

Fig. 6. Relation between k_{obsd} and ratio of hydrogen peroxide to triose reductone in the presence of oxygen at pH 6.6±0.2 and 30 °C.

the reaction rates of the monoanion are independent of the oxygen concentration.[17] Although the reaction rates of triose reductone with DCIP are slower than those of L-ascorbic acid with DCIP throughout the pH range,[6] the autoxidation rate constants are faster than those of L-ascorbic acid in the acidic and neutral pH ranges, but slower in the alkaline range.

Effect of EDTA. The autoxidation of a triose reductone solution without EDTA also obeyed the first-order rate law. Figure 3 shows the pH-rate profile of the autoxidation of triose reductone with and without EDTA. Although the effect of EDTA on rate constants was not appreciable below pH 4 or above pH 12.5, the rate constants for the autoxidation without EDTA were fifty times larger than those with EDTA at pH 7—10. The study of the inhibition of a copper catalyst on the autoxidation of L-ascorbic acid with EDTA[18] suggests that a trace amount of a metal cation may also have a catalytic effect on the autoxidation of triose reductone.

Reaction of Triose Reductone with Hydrogen Peroxide. A triose reductone solution prepared in a manner similar to the solution for the oxygen autoxidation was deoxygenated with argon. This solution was treated with a 2—3-times excess of hydrogen peroxide at 30 °C. The reaction obeyed the first-order rate law with respect to triose reductone. A plot of log k_{obsd} *vs.* pH (Fig. 4) resulted in a bell-shaped curve with a rate maximum at pH 11. On the other hand, when the solution was saturated with air instead of argon, a plot of log k_{obsd} *vs.* pH resulted in a broadly sigmoid curve (Fig. 5) resembling that in Fig. 2. For the effect of the hydrogen peroxide concentration on the rates for the system saturated with air at pH 6.48—6.80, $k_{obsd}-7.4\times10^{-4}$ was proportional to the hydrogen peroxide concentration until the latter reached the mole of triose reductone. However, k_{obsd} was constant, independently of the hydrogen peroxide concentration, when the concentration was larger than that of triose reductone (Fig. 6).

If the oxidation rate constant also depends on the dissociation of both triose reductone and hydrogen peroxide, the relationship of log k_{obsd} and pH (3—13) should be a sigmoid curve and not a bell-shaped curve. Therefore, some reactions to consume hydrogen peroxide in a higher pH range other than reduction with triose reductone might occur in the reaction system. Although the oxidation of triose reductone with hydrogen peroxide has not been explained kinetically, the reaction-rate constants for the oxidation of triose reductone with hydrogen peroxide in the presence of an oxygen molecule agreed with the sum of the reaction-rate constants for the oxygen molecule and those for hydrogen peroxide in the absence of oxygen at the same pH (Fig. 5).

References

1) H. v. Euler and H. Hasselquist, *Z. Naturforsch., B*, **11**, 176 (1956).
2) G. Hesse and K. Mix, *Chem. Ber.*, **92**, 2427 (1959).
3) P. Szabo and L. Szabo, *C. R. Acad. Sci., Ser. C*, **262**, 513; *Chem. Abstr.*, **64**, 17913 (1966).
4) F. Arndt, L. Loewe, and E. Ayca, *Chem. Ber.*, **84**, 333 (1951).
5) J. R. Holker, *J. Chem Soc.*, **1955**, 579.
6) H. Obata, M. Tatsuno, T. Tokuyama, Y. Nitta, M. Takagi, and K. Hiromi, *Agric. Biol. Chem.*, **43**, 1021 (1979).
7) I. Yamazaki and L. H. Piette, *Biochim. Biophys. Acta*, **77**, 47 (1963).
8) J. de Clerk, *Chem. Zentralbl.*, **1942, II**, 1637.
9) H. Omura, A. Fujita, M. Sato, M. Otsuki, and M. Iio, *Kyushu Daigaku Nogakubu Gakugei Zasshi*, **28**, 79 (1974); *Chem. Abstr.*, **80**, 146422 (1974).
10) H. v. Euler and C. Martius, *Justus Liebigs Ann. Chem.*, **505**, 73 (1933).
11) M. Grant, *Anal. Chem.*, **20**, 267 (1948).
12) S. R. Sarfati and P. Szabo, *Carbohydr. Res.*, **12**, 290 (1970).
13) E. Sawicki, T. R. Hauser, and R. Wilson, *Anal. Chem.*, **34**, 505 (1962).
14) G. M. Eisenberg, *Anal. Chem.*, **15**, 327 (1943).
15) G. Carpeni, *C. R. Acad. Sci.*, **202**, 1065 (1936).
16) R. P. Bell and R. R. Robinson, *Trans. Faraday Soc.*, **57**, 965 (1961).
17) A. Weissberger, J. E. LuValle, and D. S. Thomas, Jr., *J. Am. Chem. Soc.*, **65**, 1934 (1943).
18) S. Ito, T. Yamamoto, and Y. Tokushige, *Chem. Lett.*, **1980**, 1411.

 © 1983 The Chemical Society of Japan Bull. Chem. Soc. Jpn., 56, 471—473 (1983)

Photooxidation of Some Aromatic Sulfonic Acids with Alkaline Hypochlorite[1)]

Makoto KIMURA and Yoshiro OGATA*

Department of Applied Chemistry, Faculty of Engineering, Nagoya University, Chikusa-ku, Nagoya 464

(Received April 3, 1982)

Photochemical oxidation of aromatic sulfonic acids such as *p*-cumenesulfonic, 2-mesitylenesulfonic, 1- and 2-naphthalenesulfonic acids with aqueous sodium hypochlorite has been studied. Addition of a large excess of alkali enhances the decomposition of sulfonic acids remarkably. *p*-Cumenesulfonic and 2-mesitylenesulfonic acids are oxidized faster than 1- and 2-naphthalenesulfonic acids. The photooxidation of sulfonic acids with an equimolar amount of hypochlorite gives intermediary oxidation products involving desulfonation to parent hydrocarbons, aromatic hydroxylation, side-chain oxidation, and ring cleavage; *e.g.*, *p*-cumenesulfonic acid gives cumene, 2- and 4-isopropylphenol and 2-phenyl-2-propanol; 1- and 2-naphthalenesulfonic acids give phthalic anhydride. Light-absorbing aromatic sulfonic acids sensitize the decomposition of hypochlorite ion leading to hydroxyl radical, which reacts mainly with ground state sulfonic acid to give radical intermediates. The photooxidation may also involve direct C–S bond fission of sulfonic acids.

Alkyl-substituted aromatic sulfonic acids which are important for surfactants and dyestuffs are often present in waste water causing environmental pollution, being difficultly decomposed by the biochemical method involving microbes. UV-irradiation decomposes aromatic sulfonic acids to their parent hydrocarbons as exemplified by benzenesulfonic acid,[2)] 1-napthalenesulfonic acid, *etc.*[3)] Suitable oxidizing agents are further needed to decompose sulfonic acids into harmless substances such as carbon dioxide and water.

Sodium hypochlorite which oxidizes various organic compounds in the dark[4)] exhibits much higher oxidation power under UV-irradiation because of the formation of atomic oxygen.[5)] Thus, alkylbenzenesulfonic acids,[6)] some ethers[7)] and carboxylic acids[8)] are effectively oxidized by irradiation in the presence of a large excess of hypochlorite to carbon dioxide and water, *etc.*

We wish to report here the photochemical hypochlorite oxidation of other aromatic sulfonic acids such as *p*-cumene-, 2-mesitylene-, 1- and 2-naphthalenesulfonic acids to clarify their intermediary oxidation products and mechanism. Effects of alkali added on sulfonic acid decomposition and relative reactivity of the above sulfonic acids are also examined to elucidate the oxidation pathways.

Results and Discussion

Photodecomposition of Sodium Hypochlorite and Aromatic Sulfonic Acids. Aqueous *p*-cumene-, 2-mesitylene-, 1- and 2-naphthalenesulfonic acids were stable toward alkaline sodium hypochlorite (NaClO) in the dark at room temperature for several days. Short time irradiation of the sulfonic acids and NaClO with UV-light (λ>290 nm) brought about rapid decomposition of NaClO (iodometry) and partial decomposition of sulfonic acids (HPLC analysis). Though the extent of decomposition of sulfonic acid increased with increasing amount of NaClO added, the time for >90% decomposition of NaClO was unaffected (40—60 min) in spite of 1—20 fold change in relative amount of NaClO added. When NaClO equimolar to sulfonic acid was used, the decomposition time of NaClO was apparently independent of the kind of sulfonic acid (the decompostion extent of each sulfonic acid was *ca.* 5%). The above results indicate that the decomposition of NaClO is sensitized by excited sulfonic acids. The excitation energy of aromatic sulfonic acids (>400 kJ/mol), which is much higher than the bond-breaking energy of ClO^- (*ca.* 200 kJ/mol), would cause the effective sensitized decomposition of ClO^- irrespective of the kind of sulfonic acids.

The decomposition of sulfonic acid was found to be increased by addition of a large amount of alkali. Table 1 exemplifies the effect of alkali on the decomposition of *p*-cumenesulfonic acid. Likewise, other sulfonic acids were much more effectively decomposed by the addition of a mixture of NaOH and NaClO than by independent addition of NaOH or NaClO alone.

In order to compare the relative reactivities of sulfonic acids, a mixture of sulfonic acid, an equimolar amount of NaClO and 10-fold mol of NaOH was irradiated for 30 min by an external irradiation to measure the decomposition extents of NaClO and sulfonic acid (Table 2). The consumption of NaClO relates to the total reactivity of sulfonic acid including subsequent reactions between initial products and NaClO, while the consumption of sulfonic acid expresses the disappearance of sulfonic acid itself. The difference in two consumptions may be a measure of the subsequent reactions. Based on the consumption of NaClO, the relative reactivity of sulfonic acid is in the order of *p*-cumene- > 2-mesitylene- > 1-naphthalene- $\gtrsim$ 2-naphthalenesulfonic acid (though the former three sulfonic acids shows a similar initial reactivity on the basis of the consumption of sulfonic acid). Hence, aromatic sulfonic acids possesing side-chain alkyl substituents are relatively more susceptible to the photooxidation leading to carbon dioxide.

Intermediary Products. As observed previously with alkylbenzenesulfonic acids,[8)] the present sulfonic acids can be oxidized to carbon dioxide and water by a large excess of NaClO under irradiation. The necessary amount of NaClO for the complete oxidation was several times as much as the theoretical (25 fold mol). Use of an equimolar amount of NaClO in the photooxidation results in the formation of various intermediates. The photolysis products from a mixture of aqueous sulfonic acid, equimolar NaClO and 10 fold mol of NaOH were analyzed by GLC and GC-MS

TABLE 1. EFFECT OF ALKALI ON THE PHOTO-DECOMPOSITION OF AQUEOUS SODIUM *p*-CUMENESULFONATE[a)]

Additive (rel mol)	Decomposition (%)
None	7.5
NaClO (1)	6.8
NaClO (1) + NaOH (10)	38.0
NaOH (10)	6.4

a) Initial concentration of the sulfonate was 33.3 mM. Internal irradiation (λ>290 nm) was carried out for 45 min at room temperature.

TABLE 2. RELATIVE REACTIVITY IN THE PHOTOOXIDATION OF SODIUM ARENESULFONATE WITH AQUEOUS ALKALINE NaClO[a)]

Sulfonic acid	Consumption (%)	
	NaClO	$ArSO_3^-$
p-Cumene-	74	23
2-Mesitylene-	58	20
1-Naphthalene-	50	23
2-Naphthalene-	49	14

a) Initial concentration of each sulfonic acid was 33.3 mM. The mol ratio of $ArSO_3^-$: NaClO: NaOH was 1 : 1 : 10. External irradiation was conducted for 30 min at room temperature.

techniques, being identified by comparison with the corresponding authentic samples (Table 3).

Alkyl-substituted sulfonic acids such as *p*-cumene- and 2-mesitylenesulfonic acids gave their parent hydrocarbons (*i.e.*, cumene and mesitylene, respectively) in accord with our previous report on *p*-toluene- and *p*-ethylbenzenesulfonic acids.[6)] Though naphthalene was obtained in the simple photolysis of aqueous sodium 1-naphthalenesulfonate alone,[3)] no naphthalene was detectable in the photooxidation of 1- and 2-naphthalenesulfonic acids. Also no benzene was formed in the photooxidation of benzenesulfonic acid with NaClO, while it was formed in 16% yield in the photolysis of benzenesulfonic acid alone. Hence, alkyl substituents in sulfonic acids are hydrogen sources for the conversion of aromatic radicals to aromatic hydrocarbons.

Since the NaClO decomposition is sensitized by aromatic sulfonic acid as noted above, the present photooxidation seems to proceed *via* excited hypochlorite ion ClO^-* (Eq. 1) with less probability of the direct reaction between excited sulfonate ion $ArSO_3^-$* and ground-state hypochlorite ClO^-. Excited hypochlorite ion is known to give oxygen atoms such as O· and O$^{\tau}$,[5)] which react with water to give hydroxyl radical HO· (Eq. 2).[9)]

$$ArSO \xrightarrow{h\nu} ArSO_3^-* \xrightarrow{ClO^-} ArSO_3^- + ClO^-* \quad (1)$$

$$ClO^-* \xrightarrow[-Cl^-(\text{or } Cl\cdot)]{} O\cdot(\text{or } O^{\tau}) \xrightarrow{H_2O} HO\cdot \quad (2)$$

Some products in Table 3 can be explained in terms of an attack of HO·. Phenols such as 4-isopropylphenol and 2,4,6-trimethylphenol were obtained, indicative of aromatic hydroxylation by HO·. Though neither 1- nor 2-naphthol was detectable, 2-naphthalenesulfonic acid gave 1-chloro-2-naphthol which is readily formed even in the dark from 2-naphthol and NaClO. These phenols may be formed by the coupling of HO· with aryl radical precidently cleaved from aromatic sulfonic acid by UV-light (Eq. 3).

$$R\text{-}Ar\text{-}SO_3^- \xrightarrow[-SO_3^{\tau}]{h\nu} R\text{-}Ar\cdot \xrightarrow{HO\cdot} R\text{-}Ar\text{-}OH \quad (3)$$

As to 2-isopropylphenol which was formed in *ca.* 5 time amounts of the 4-isomer, initial hydroxylation of *p*-cumenesulfonic acid followed by Ar–SO_3^- cleavage might occur.

Products oxidized at alkyl side-chain are 2-phenyl-2-propanol from *p*-cumenesulfonic acid, and 3,5-dimethylbenzyl alcohol and 3,5-dimethylbenzoic acid from 2-mesitylenesulfonic acid. Their product ratios in Table 3 suggest that alkylbenzenesulfonic acid undergoes predominantly side-chain oxidation rather than aromatic hydroxylation, in accord with the cases of *p*-toluene- and *p*-ethylbenzenesulfonic acids.[6)] This may be reflected to the reactivities of *p*-cumene- and 2-mesitylenesulfonic acids toward NaClO, which are higher than those of 1- and 2-naphthalenesulfonic acids. The pathway for the side-chain oxidation is explained assuming radical isomerization of aromatic type to benzylic one (Eq. 4), leading successively to alcohol, aldehyde and carboxylic acid (Eq. 5).

TABLE 3. PRODUCTS AND MASS SPECTRA DATA IN THE PHOTOOXIDATION OF SOME AQUEOUS SODIUM ARENESULFONATES WITH ALKALINE NaClO[a)]

Sulfonic acid	Products (rel mol)	*m/e* (rel intensity)[b)]
p-Cumene-	Cumene (1.0)	120(57, P), 105(100)
	2-Isopropylphenol (1.6)	136(67, P), 121(100)
	4-Isopropylphenol (0.3)	136(62, P), 121(100)
	2-Phenyl-2-propanol (6.8)	118(100, P-18), 94(62)
2-Mesitylene-	Mesitylene (1.0)	120(100, P), 105(48)
	2,4,6-Trimethylphenol (2.1)	136(100, P), 121(54)
	3,5-Dimethylbenzyl alcohol (0.9)	136(100, P), 134(26), 121(50)
	3,5-Dimethylbenzoic acid (0.6)	150(100, P), 105(39), 91(31)
1-Naphthalene-	Phthalic anhydride	148(20, P), 104 (100)
2-Naphthalene-	Phthalic anhydride (1.0)	148(20, P), 104(100)
	1-Chloro-2-naphthol (0.1)	180(33, P+2), 178(100, P)

a) Aqueous solutions (300 ml) of sodium sulfonate (10 mmol), NaClO (10 mmol), and NaOH (0.1 mol) were irradiated at room temperature for 45—60 min. b) GC-MS spectra were measured at 20 eV.

$$Me_3C_6H_2\cdot \longrightarrow \cdot CH_2Me_2C_6H_3 \xrightarrow{HO\cdot} Me_2C_6H_3CH_2OH \quad (4)$$

$$Me_2C_6H_3CH_2OH \xrightarrow{[O]} Me_2C_6H_3CHO \xrightarrow{[O]} Me_2C_6H_3CO_2H \quad (5)$$

Formation of phthalic anhydride from both 1- and 2-naphthalenesulfonic acids may involve aromatic hydroxylation by HO·, ring clevage and oxidation to carboxylic acid.

Experimental

Materials. An aqueous NaClO solution was prepared by introducing chlorine gas to 4.0 M (1 M = 1 mol dm^{-3}) NaOH until the iodometry showed 1.85 M NaClO.

Arenesulfonic acids were used as their sodium salts. *p*-Cumenesulfonic acid[10] and 2-mesitylenesulfonic acid[11] were obtained from sulfonation of cumene and mesitylene, respectively. Sodium 1- and 2-naphthalenesulfonates were of commercial reagnts. Since these salts were often contaminated with NaCl, Na_2SO_4 and water, the salts were purified as follows. Crude sodium sulfonate was converted to its anilinium salt with aniline and hydrochloric acid as precipitate from aqueous solution. After repetition of crystallization from water, the resulting pure anilinium sulfonate was again converted to precipitate of sodium salt with an equivalent amount of sodium methoxide in methanol–ether. UV absorption maxima (molar extinction coefficient) of pure sodium sulfonate: *p*-cumesulfonate, 222 nm (1.22×10^4), 260 (400); 2-mesitylenesulfonate 222 (9.3×10^3), 271 (890), 280 (920); 1-naphthalenesulfonate, 222 (5.2×10^4), 283 (5.3×10^3), 317 (600); 2-naphthalenesulfonate, 227 (1.0×10^5), 274 (5.0×10^3), 320(700).

Authetic 2-phenyl-2-propanol was prepared by the Grignard reaction of methylmagnesium iodide with acetophenone.[12] Authentic 3,5-dimethylbenzoic acid was prepared by the oxidation of mesitylene with dilute HNO_3;[13] mp 165—166 °C (lit,[13] 165.5—166.5 °C). 3,5-Dimethylbenzyl alcohol was prepared by $LiAlH_4$ reduction of 3,5-dimethylbenzoic acid;[14] bp 102—103 °C/2 mm (lit,[14] 115—117.5 °C/10 mm). 1-Chloro-2-naphthol was prepared by the NaClO chlorination of sodium 2-naphtholate (80%); mp 70—71 °C (aq EtOH) (lit,[15] 71 °C). The other authentic samples were of commercial guaranteed grade.

Instruments. HPLC analyses for sulfonic acid determination[16] were carried out on a JEOL-Twincle model equipped with an ODS column using H_2O (0.01 M NaCl)/MeOH = 8/1 as the eluent. GC-MS spectra were recorded on a JMS-RD 300 model with the ionization potential set at 20 eV. GLC analyses were carried ont on a Yanaco G-180 using Silicone DC 550 or PEG 20M column.

Irradiation experiments were generally carried out in a 300 ml vessel equippped with a Halos 100 W high-pressure mercury lamp. Controlled irradiation (Table 2) was conducted on a merry-go-round apparatus equipped with a Halos 300 w high-pressure mercury lamp.

Photodecomposition of Sulfonic Acid with NaClO. An aqueous solution (300 ml) of sulfonic acid (10 mmol) and an appropriate amount of NaClO was irradiated internally at ambient temperature. The change in concentration of NaClO was followed by iodometry. When consumption of NaClO reached over 90%, sulfonic acid left was determined by HPLC. Runs in Table 1 were similarly carried out by the addition of 0.10 mol of NaOH.

In the experiments for the relative reactivity of sulfonic acids (Table 2), mixtures of each 10 ml of 0.10 M aqueous sulfonic acid, 0.1 M NaOH and 0.101 M NaClO were irradiated externally for 30 min.

Products in the Photooxidation of Sulfonic Acids with NaClO. An aqueous solution (300 ml) of a sulfonic acid (10 mmol), NaClO (10 mmol), and NaOH (0.1 mol) was irradiated internally until NaClO was consumed over 90% (45—60 min). The resulting solution was acidified with dil. HCl and extracted with ether (100 ml × 2). The ethereal layer was dried over anhydrous sodium sulfate, concentrated by distillation and analyzed by GLC aod GC-MS. Products in Table 3 were identified on the basis of accordance with the authentic samples in their GLC retention times and mass fragment patterns. All products were in low yields. In the case of 2-mesitylenesulfonic acid, formation of 2- and 4-chloro-3,5-dimethylbenzoic acids was indicated by GC-MS (rel mol *ca.* 1.0). Attempts to separate two isomers failed.

We wish to thank Professor T. Tsuda of Nagoya Institute of Technology for his kind advice on the HPLC analysis of sulfonic acids.

References

1) Contribution No. 304.
2) Y. Ogata, K. Takagi, and S. Yamada, *Bull. Chem. Soc. Jpn.*, **50**, 2205 (1977).
3) Y. Izawa, N. Suzuki, A. Inoue, K. Ito, and T. Ito, *J. Org. Chem.*, **44**, 4581 (1979) and references cited therein.
4) S. K. Chakrabartty, "Oxidation in Organic Chemistry," ed by W. S. Trahanovsky, Academic Press, New York and London (1978), Part C, Chap. V; Y. Ogata and M. Kimura, *Yuki Gosei Kagaku*, **37**, 581 (1979).
5) G. V; Buxton and M. S. Subhani, *J. Chem. Soc., Faraday Trans. 1*, **1972**, 947, 958, 970.
6) M. Nakamura and Y. Ogata, *Bull. Chem. Soc. Jpn.*, **50**, 2396 (1972).
7) Y. Ogata, K. Takagi, and T. Suzuki, *J. Chem. Soc., Perkin Trans. 2*, **1978**, 562.
8) Y. Ogata, T. Suzuki, and K. Takagi, *J. Chem. Soc., Perkin Trans. 2*, **1979**, 1715.
9) B. L. Gall and L. M. Dorfman, *J. Am. Chem. Soc.*, **91**, 2199 (1969); D. Zehani and J. Rabani, *J. Phys. Chem.*, **75**, 1738 (1971).
10) R. L. Frank, R. E. Berry, and L. Shotwell, *J. Am. Chem. Soc.*, **71**, 3891 (1949).
11) C. M. Suter and A. W. Weston, *Org. React.*, **3**, 141, (1946).
12) T. Suzuki, *Nippon Kagaku Zasshi*, **63**, 124 (1942).
13) H. R. Snyder, R. B. Adams, and A. V. McIntosh, Jr., *J. Am. Chem. Soc.*, **63**, 3281 (1941).
14) W. Q. Beard, Jr., D. N. van Eenam, and C, R. Hauser, *J. Org. Chem.*, **26**, 2310 (1961).
15) O. Ginsberg, *J. Am. Chem. Soc.*, **73**, 2723 (1951).
16) R. H. Stehl, *Anal. Chem.*, **42**, 1802 (1970); P. Jandera and J. Churacek, *J. Chromatogr.*, **197**, 181 (1980).

Regioselective Carboxylation of 9-Xanthenones with Manganese(III) Acetate

Hiroshi NISHINO* and Kazu KUROSAWA
Department of Chemistry, Faculty of Science, Kumamoto University, Kurokami 2-39-1, Kumamoto 860
(Received April 8, 1982)

Seven 9-xanthenones were oxidized with manganese(III) acetate to give carboxy-, dicarboxy-, (acetoxymethyl)-(carboxy)-, (carboxy)(hydroxymethyl)-, and acetoxymethyl-9-xanthenones, and to yield small amounts of (carboxymethyl)(carboxy)-, carboxymethyl-, (acetoxymethyl)(carboxymethyl)-, bis(acetoxymethyl)-, and diacetoxymethyl-9-xanthenones. The carboxyl group was preferentially introduced into the peri positions and the acetoxymethyl groups were located at positions ortho to the methoxyl or methyl group. The regioselectivity and mechanism of the carboxylation reaction is discussed briefly.

We have previously reported that the oxidation of 2-hydroxybenzophenones with manganese(III) acetate gave the corresponding 9-xanthenones and trace amounts of acetoxymethylated 9-xanthenones as by-products.[1] The acetoxymethylated products were considered to be formed by further oxidation of 9-xanthenones. This prompted us to study the reaction of 9-xanthenones with manganese(III) acetate.

The reaction of several aromatic compounds with manganese(III) acetate was first investigated by S. A. Zonis.[2] This oxidation reaction mainly yielded acetoxylated compounds and ketones, and was kinetically studied by Dewar *et al.*[3] However, on oxidation under vigorous reaction conditions acetoxymethylation occurred.[4,5] This reaction specifically takes place in the manganese(III) acetate oxidation and to some extent in lead(IV) acetate oxidation.[6] Heiba and his coworkers oxidized toluene with manganese(III) acetate and obtained acetoxymethyl derivatives.[4] They studied the reaction mechanism kinetically and concluded that a carboxymethyl radical, $\cdot CH_2COOH$, formed directly from manganese(III) acetate, is involved in this reaction. We carried out the oxidation of 9-xanthenones, and obtained carboxy and acetoxymethyl derivatives. In this paper we will discuss the regioselectivity and the mechanisms of these carboxylation reactions of substituted 9-xanthenones.

Results and Discussion

The compounds studied were 9-xanthenone (**1a**), 3-methoxy-9-xanthenone (**1b**), 3,6-dimethoxy-9-xanthenone (**1c**), 2,3,6-trimethoxy-9-xanthenone (**1d**), 3-methoxy-4-methyl-9-xanthenone (**1e**), 3-methoxy-5-methyl-9-xanthenone (**1f**), and 1-methoxy-3-methyl-9-xanthenone (**1g**).

9-Xanthenones were oxidized with manganese(III) acetate dihydrate in boiling acetic acid containing acetic anhydride and the products were separated by TLC. The results are shown in Table 1 and Fig. 1.

When 9-xanthenone (**1a**) was oxidized with manganese(III) acetate, it was found that a significant amount

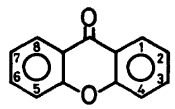

1a
1b: 3-CH_3O
1c: 3,6-$(CH_3O)_2$
1d: 2,3,6-$(CH_3O)_3$
1e: 3-CH_3O-4-CH_3
1f: 3-CH_3O-5-CH_3
1g: 1-CH_3O-3-CH_3
12b: 2-HO_2CCH_2-3-CH_3O
16g: 1-CH_3O-3-$AcOCH_2$
19a: 1-$(AcO)_2CH$

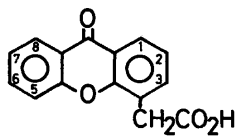

11b: 3-CH_3O
11c: 3,6-$(CH_3O)_2$
11d: 2,3,6-$(CH_3O)_3$
11g: 6-CH_3-8-CH_3O
13g: 5-$AcOCH_2$-6-CH_3-8-CH_3O

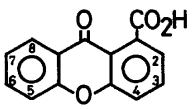

2a
2b: 6-CH_3O
2c: 3,6-$(CH_3O)_2$
2d: 2,3,6-$(CH_3O)_3$
2e: 5-CH_3-6-CH_3O
2f: 4-CH_3-6-CH_3O
2g: 6-CH_3-8-CH_3O
3d: 3,6,7-$(CH_3O)_3$
3e: 3-CH_3O-4-CH_3
4a: 8-HO_2C
4e: 3-CH_3O-4-CH_3-8-HO_2C
5e: 3-CH_3O-4-CH_3-5-HO_2CCH_2
6b: 5-$AcOCH_2$-6-CH_3O
6f: 4-CH_3-5-$AcOCH_2$-6-CH_3O
6g: 5-$AcOCH_2$-6-CH_3-8-CH_3O
7a: 4-$AcOCH_2$
7b: 3-CH_3O-4-$AcOCH_2$
7c: 3,6-$(CH_3O)_2$-4-$AcOCH_2$
7d: 3,6,7-$(CH_3O)_3$-4-$AcOCH_2$
8c: 3,6-$(CH_3O)_2$-4,5-$(AcOCH_2)_2$
9a: 4-$HOCH_2$
9b: 3-CH_3O-4-$HOCH_2$
9c: 3,6-$(CH_3O)_2$-4-$HOCH_2$
9d: 3,6,7-$(CH_3O)_3$-4-$HOCH_2$
10b: 5-$HOCH_2$-6-CH_3O

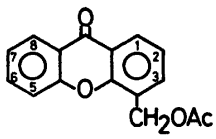

14a
14b: 3-CH_3O
14c: 3,6-$(CH_3O)_2$
14d: 3,6,7-$(CH_3O)_3$
14f: 3-CH_3O-5-CH_3
14g: 1-CH_3O-3-CH_3
17c: 3,6-$(CH_3O)_2$-5-$AcOCH_2$
17g: 1-CH_3O-3-CH_3-5-$AcOCH_2$
18c: 3,6-$(CH_3O)_2$-7-$AcOCH_2$

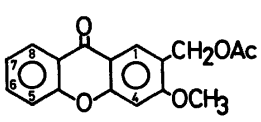

15b
15c: 6-CH_3O
15d: 6,7-$(CH_3O)_2$
15f: 5-CH_3

Fig. 1. 9-Xanthenones (**1a—g**) and the oxidation products **2—19**.

Table 1. Oxidation of 9-xanthenones (**1a—g**) with manganese(III) acetate in acetic acid containing acetic anhydride at reflux temperature

Entry	Substrate	Reaction conditions: Molar ratio of substrate: oxidant	Reaction conditions: Time / min	Recovered substrate (%)	Product (yield/%)[a,b]
1	**1a**	1 : 10	40	20	**2a**(30), **4a**(12), **9a**(6), **14a**(2), **19a**(1)
2	**1b**	1 : 12	43	13	**2b**(11), **9b**(4), **10b**(3), **14b**(10), **15b**(4)
3[c]	**1b**	1 : 12	24	26	**2b**(10), **9b**(4), **10b** (4), **11b** (10), **12b**(3), **14b**(6), **15b**(3)
4	**1c**	1 : 12	29	10	**2c**(7), **9c**(14), **11c**(4), **14c**(13), **15c**(6), **17c**(4), **18c**(3)
5[d]	**1c**	1 : 12	50	11	**2c**(5), **7c**(5), **8c**(5), **9c**(6), **11c**(3), **14c**(16), **15c**(7), **17c**(7), **18c**(3)
6	**1d**	1 : 10	27	23	**2d**(7), **3d**(3), **9d**(5), **11d**(3), **14d**(16), **15d**(5)
7	**1e**	1 : 10	30	17	**2e**(11), **3e**(28), **4e**(11), **5e**(4), **9b**(7), **14b**(3)
8	**1f**	1 : 10	26	15	**2f**(20), **6f**(7), **14f**(8), **15f**(3)
9	**1g**	1 : 10	30	12	**2g**(10), **6g**(12), **11g**(3), **13g**(5), **14g**(25), **16g**(1), **17g**(4)

a) The yields are based on the amount of the substrate consumed. b) The yields of the acidic products are calculated as their methyl esters. c) Potassium acetate (60 mmol) was added to the reaction mixture. d) This oxidation was carried out under an atmosphere of nitrogen.

of acidic compounds were present in the product mixture, from which five compounds (**2a**, **4a**, **9a**, **14a**, and **19a**) were isolated (Entry 1). The IR spectrum of **2a** indicated absorptions at 1720 and 2500—3200 cm^{-1} due to carboxyl group. Its NMR spectrum showed a broad singlet at $\delta=13.0$ for a carboxylic acid and a multiplet at $\delta=7.4$—8.3 for seven aromatic protons, one of which is deshielded. Therefore, the structure of **2a** was determined to be 1-carboxy-9-xanthenone the melting point of which was close to the literature value.[10] **4a** was identified as 1,8-dicarboxy-9-xanthenone by methylation. The NMR spectrum of the methyl ester of **9a** indicated the presence of a hydroxymethyl group, $-CH_2OH$, $\delta=3.5$ (1H, broad s) and 4.99 (2H, s), and an AB quartet due to two aromatic protons $\delta=7.19$ (1H, d, $J=7.8$ Hz, $H_{(2)}$) and 7.80 (1H, d, $J=7.8$ Hz, $H_{(3)}$). In its IR spectrum two carbonyl and a hydroxyl absorptions appeared at 1645, 1745, and 3300—3500 cm^{-1}, respectively. When the corresponding methyl ester was treated with acetic anhydride in pyridine–acetic acid, the NMR spectrum of the product (**7a**) showed an acetoxymethyl group at $\delta=2.16$ (3H, s) and $\delta=5.46$ (2H, s). Accordingly, these spectral data supported the 1-carboxy-4-hydroxymethyl-9-xanthenone (**9a**) structure. Other acidic products were also formed in this oxidation reaction, but they could not be purified by TLC. **14a** was identified as 4-acetoxymethyl-9-xanthenone by comparison of its NMR spectrum with those of other 4-acetoxymethylated derivatives. The NMR spectrum of **19a** indicated the presence of a diacetoxymethyl group, $-CH(OAc)_2$, $\delta=2.16$ (6H, s) and 8.86 (1H, s), and the disappearance of one of the deshielded aromatic protons in **1a**. The IR spectrum showed carbonyl absorptions at 1686, 1755, and 1768 cm^{-1}. These spectroscopic properties are consistent with the 1-diacetoxymethyl-9-xanthenone (**19a**) structure.

The reaction of 3-methoxy-9-xanthenone (**1b**) with manganese(III) acetate gave 1-carboxy-6-methoxy- (**2b**), 1-carboxy-4-hydroxymethyl-3-methoxy- (**9b**), 1-carboxy-5-hydroxymethyl-6-methoxy- (**10b**), 4-acetoxymethyl-3-methoxy- (**14b**), and 2-acetoxymethyl-3-methoxy-9-xanthenone (**15b**) (Entry 2). The structures were confirmed by examining their IR, mass, and NMR spectra, and by elemental analyses. The NMR spectrum of **14b** showed the methylene proton of the acetoxymethyl group at $\delta=5.47$, while the methylene proton of **15b** appeared at $\delta=5.18$.

3,6-Dimethoxy-9-xanthenone (**1c**) gave 1-carboxy-3,6-dimethoxy- (**2c**), 1-carboxy-4-hydroxymethyl-3,6-dimethoxy- (**9c**), 4-carboxymethyl-3,6-dimethoxy- (**11c**), 4-acetoxymethyl-3,6-dimethoxy- (**14c**), 2-acetoxymethyl-3,6-dimethoxy- (**15c**), 4,5-bis(acetoxymethyl)-3,6-dimethoxy- (**17c**), and 2,5-bis(acetoxymethyl)-3,6-dimethoxy-9-xanthenone (**18c**) (Entry 4). The structure of the methyl ester of **11c** was elucidated from the spectroscopic evidence showing the presence of a methoxycarbonylmethyl group $\delta=3.72$ (3H, s) and 3.90 (2H, s), an AB quartet due to two aromatic protons $\delta=7.02$ (1H, d, $J=10.2$ Hz, $H_{(2)}$) and 8.29 (1H, d, $J=10.2$ Hz, $H_{(1)}$), and *m/e* 328.0939 (M^+). **18c** was not separated from **17c** because both have the same R_f values on TLC. However, the NMR spectrum of the mixture could be explained by assuming that it consists of two compounds, **17c** and **18c**. Elemental analysis also agreed with the calculated values for the molecular formula of $C_{21}H_{20}O_8$ that is the same for both compounds.

2,3,6-Trimethoxy-9-xanthenone (**1d**) yielded **2d**, **3d**, **9d**, **11d**, **14d**, and **15d** (Entry 6).

3-Methoxy-4-methyl-9-xanthenone (**1e**) gave five acidic and one neutral product. The acidic products were found to be **2e**, **3e**, **4e**, **5e**, and **9b** which is identical with the product obtained from the reaction of **1b**. The neutral product was found to be **14b**, identical with the sample obtained from the oxidation of **1b** (Entry 7).

3-Methoxy-5-methyl-9-xanthenone (**1f**) yielded two carboxylated products, the structures of which were determined as **2f** and **6f**, being characterized as their methyl esters, and two acetoxymethyl-3-methoxy-5-methyl-9-xanthenones (**14f** and **15f**) substituted at the positions ortho to the methoxyl group (Entry 8).

Oxidation of 1-methoxy-3-methyl-9-xanthenone (**1g**) gave four acidic products (**2g**, **6g**, **11g**, and **13g**) and three neutral products (**14g**, **16g**, and **17g**) (Entry 9).

Carboxy derivatives were obtained in 3—30% yields and acetoxymethylated products in 2—25% yields. However, when **1g** was oxidized with eight equivalents of manganese(III) acetate, the yield of **14g** increased to 38% based on the **1g** consumed, while the other products were obtained only in small amounts.

It is known that the addition of potassium acetate to manganese(III) acetate oxidation increases the yield of the $-CH_2OAc$ product.[4] We studied the effect of added potassium acetate on the oxidation of **1b** (Entry 3). Contrary to our expectation the yields of the acetoxymethyl products did not increase, but two new carboxymethyl derivatives (**11b** and **12b**)were produced.

The reaction mechanism of acetoxymethylation of aromatic compounds has been established by the work of Heiba and his co-workers.[4] The carboxymethyl radical, $\cdot CH_2COOH$, which is somewhat electrophilic, attacks the positions of highest electron density. The CH_2COOH group is then converted, by oxidative decarboxylation, into the CH_2OAc group and hence these acetoxymethyl groups are situated at positions ortho to methoxyl or methyl groups. The reaction mechanism of the carboxylation, however, was not straightforward.

It is well known that the introduction of a carboxymethyl groups is the first step in the manganese(III) acetate oxidation of aromatic substrate of a higher ionization potential.[4] However, the introduction of a carboxyl group has been mentioned only by Dewar *et al.*[3] We wondered why carboxyl groups were introduced preferentially at the peri position. In the case of 9-xanthenones it is thought that the electron density of the peri position is lower because of the electron attraction by the carbonyl group, accordingly the rate of the attack at this position by the carboxymethyl radical should be slower. When a $\cdot CH_2COOH$ radical attacked at the position ortho to the methoxyl group, the oxidation reaction stopped at the stage of the $-CH_2OAc$ product. But when the $\cdot CH_2COOH$ radical attacked the peri position the oxidation did not stop at this stage, and further oxidation occurred to give a carboxyl product *via* a $-CH(OAc)_2$ compound.

To explain the fact mentioned above, we suggest that manganese(III) acetate forms a complex with the carbonyl function of 9-xanthenone and the complex subsequently decomposes to form a $\cdot CH_2COOH$ radical near the peri position. Then this position is attacked by the $\cdot CH_2COOH$ radical to form the $-CH_2COOH$ product, which is further oxidized to an acetoxymethyl compound. Another manganese(III) acetate complexes with the carbonyl group of 1-acetoxymethyl-9-xanthenones, and the second complex is decomposed again in acetic acid to yield another $\cdot CH_2COOH$ radical near the acetoxymethyl group. Consequently, the $-CH_2OAc$ compound is attacked by this radical and is then oxidized to give 1-diacetoxymethyl-9-xanthenone, which forms a third complex with manganese(III) acetate and is finally converted into the corresponding carboxy derivative *via* a similar oxidation sequence (Scheme 2). Aerial oxidation was not involved in the carboxylation, because the yields of carboxy derivatives scarcely changed as shown in

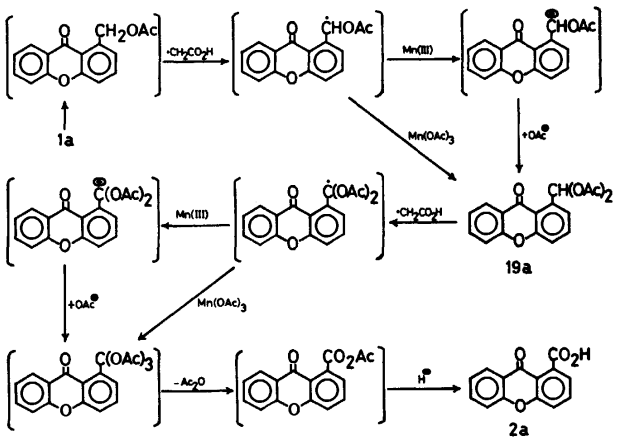

Scheme 1. Reaction mechanism of carboxylation of 9-xanthenone (**1a**) by manganese(III) acetate.

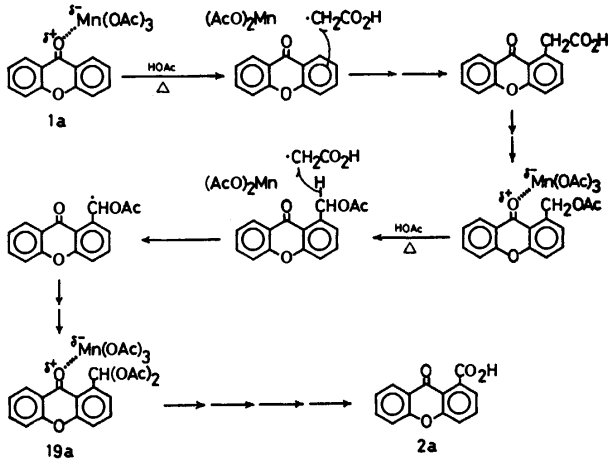

Scheme 2. Complexation between 9-xanthenone (**1a**) and manganese(III) acetate.

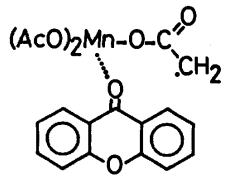

Fig. 2

the oxidation of **1c** under an atmosphere of nitrogen (Entry 5). It is also possible that the $\cdot CH_2COO-$ radical is formed on the manganese(III) acetate which is coordinated with 9-xanthenone as shown in Fig. 2, and then attacks the peri position intramolecularly.

The idea that a substrate will be oxidized *via* a complex with manganese(III) acetate has not been proposed previously. We can explain the regioselectivity of the carboxylation of the 9-xanthenone system only by assuming the complexation.

In order to investigate the carboxylation for other aromatic compounds, we carried out the oxidation of anthraquinone and benzophenone under the same reaction conditions. However, these compounds gave carboxymethyl, acetoxymethyl, and diacetoxymethy derivatives, and an aldehyde, but carboxylated products

were not detected.

It is known that **2a** is synthesized from 3-chlorophthalic acid and phenol in three steps and that it needs a long reaction time (yield: 25%).[14] On the other hand the reaction of **1a** with manganese(III) acetate gave **2a** (yield: 30%) in one step for a short reaction time. Therefore, it may be a convenient synthetic method for **2a** in some cases. The other carboxylated 9-xanthenones are new compounds and their synthetic methods are not known.

A small amount of 4- or 5-hydroxymethyl-9-xanthenones was also obtained. It seems that the corresponding acetoxymethyl-9-xanthenones were hydrolyzed to give the hydroxymethyl derivatives during the work-up.

Experimental

Measurements. ^{1}H-NMR spectra were recorded on a Hitachi Perkin-Elmer R-24 spectrometer with TMS as an internal standard. IR spectra were taken on a JASCO IRA-1 grating spectrometer. Mass spectra were measured on a Hitachi M-80 high resolution, and a JEOL JMS-01 SG-2 mass spectrometer, and a JMS-01 SG-2 instrument with direct inlet at 75 eV. HPLC analyses were performed on an Altex model 330/110A/153 isocratic liquid chromatograph equipped with a HY- ODS-5U column. Melting points were determined with a Yanagimoto micromelting point apparatus and were not corrected.

*Preparation of 9-Xanthenones (**1a—g**).* 9-Xanthenone (**1a**) was commercially available. The general proedure for the preparation of 9-xanthenones (**1b**, **c**, **f**, and **g**) was as follows.[8] A mixture of a benzoic acid (0.15 mol), a resorcinol (0.23 mol), fused zinc chloride (80 g), and phosphoryl chloride (100 ml) was heated for 3 h at 65 °C. The reaction mixture was poured into ice water (1.2 l) containing concd HCl (100 ml). The red gum which formed was decanted and triturated with an aqueous sodium hydrogencarbonate solution (800 ml). A benzophenone was formed and collected by filtration. The benzophenone (0.04 mol) and water (100 ml) were heated for 2.5 h at 210 °C in an autoclave, and the corresponding 9-xanthenone which was obtained was then methylated. **1e** was prepared from 2,4-dihydroxy-2′-methoxy-3-methylbenzophenone, which was heated with potassium hydroxide in ethanol followed by methylation.[9] **1d** was synthesized by the oxidation of 2-hydroxy-3′,4,4′-trimethoxybenzophenone with manganese(III) acetate.[11]

*Oxidation of 9-Xanthenones (**1a—g**).* The typical procedure for the oxidation of 9-xanthenones was as follows. To a mixture of the substrate (1 mmol) and acetic acid (25 ml) containing acetic anhydride (4 ml), the excess amount of manganese (III) acetate dihydrate[3] as shown in Table 1 was added. The mixture was then heated under reflux until the brown color of Mn(III) ion disappeared. After the removal of solvent *in vacuo*, the residue was triturated with 1 M (1 M=1 mol dm^{-3}) sulfuric acid (25 ml) and extracted with chloroform. The chloroform solution was washed with an aqueous sodium hydrogencarbonate solution (100 ml) and concentrated. The aqueous solution was acidified with concd hydrochloric acid and subsequently extracted with ethyl acetate. The ethyl acetate was removed and the acidic products were methylated with diazomethane in methanol. The neutral and esterified products, respectively, were separated on TLC (Wakogel B-10) with chloroform as the developing solvent, and recrystallized. The yields are summarized in Table 1.

*Oxidation Products of **1a**.* 1-*Carboxy-9-xanthenone* (**2a**): Mp 226—228 °C (EtOH) (lit,[10] mp 229—230 °C); IR (KBr) 1680 and 1720 (C=O), and 2500—3200 cm^{-1} (OH); NMR ($(CD_3)_2SO$) δ=7.39−8.26(7H, m, aromatic), and 13.0(1H, br. s, COOH).

*The Methyl Ester of **2a***: Mp 117 °C (MeOH); IR ($CHCl_3$) 1680 (C=O) and 1752 cm^{-1} ($COOCH_3$); NMR ($CDCl_3$) δ=4.03 (3H, s, $COOCH_3$), and 7.04—8.16 (7H, m, aromatic). Found: C, 71.00; H, 4.12%. Calcd for $C_{15}H_{10}O_4$: C, 70.86; H, 3.96%.

*Dimethyl Ester of 1,8-Dicarboxy-9-xanthenone (**4a**)*: Mp 183—184 °C (MeOH); IR ($CHCl_3$) 1685 (C=O) and 1750 cm^{-1} ($COOCH_3$); NMR ($CDCl_3$) δ=3.99 (6H, s, 2×$COOCH_3$), and 7.27—7.92 (6H, m, aromatic). Found: C, 65.12; H, 3.97%. Calcd for $C_{17}H_{12}O_6$: C, 65.38; H, 3.87%.

*Methyl Ester of 1-Carboxy-4-hydroxymethyl-9-xanthenone (**9a**)*: Mp 185—186 °C (MeOH); IR(KBr) 1645 (C=O), and 1745 ($COOCH_3$), and 3300—3500 cm^{-1} (OH); NMR ($CDCl_3$) δ=3.5 (1H, br. s, OH), 4.05 (3H, s, $COOCH_3$), 4.99 (2H, s, $-CH_2-$), 7.04—8.35 (4H, m, aromatic), 7.19 (1H, d, J=7.8 Hz, $H_{(2)}$), and 7.80 (1H, d, J=7.8 Hz, $H_{(3)}$). Found: *m/e* 284.0685 (M^+). Calcd for $C_{16}H_{12}O_5$: M, 284.0685.

*Acetylation of the Methyl Ester of **9a***: The methyl ester of **9a** was treated with acetic anhydride in pyridine–acetic acid at room temperatrure overnight to afford the methyl ester of 4-acetoxymethyl-1-carboxy-9-xanthenone (**7a**); mp 84—85 °C (EtOH); IR ($CHCl_3$) 1675 and 1745 cm^{-1} (C=O); NMR ($CDCl_3$) δ=2.16 (3H, s, OAc), 4.02 (3H, s, $COOCH_3$), 5.46 (2H, s, $-CH_2-$), 7.2—8.3 (4H, m, aromatic), 7.28 (1H, d, J=7.8 Hz, $H_{(2)}$), and 7.76 (1H, d, J=7, 8 Hz, $H_{(3)}$).

*4-Acetoxymethyl-9-xanthenone (**14a**)*: Mp 118—119 °C (EtOH); IR ($CHCl_3$) 1673 (C=O) and 1745 cm^{-1} (OAc); NMR ($CDCl_3$) δ=2.14 (3H, s, OAc), 5.50 (2H, s, $-CH_2-$), and 7.25—8.39 (7H, m, aromatic). Found: *m/e* 268.0736 (M^+). Calcd for $C_{16}H_{12}O_4$: M, 268.0736.

*1-Diacetoxymethyl-9-xanthenone (**19a**)*: Mp 181—182 °C (EtOH); IR (KBr) 1686 (C=O), 1755 and 1768 cm^{-1} (OAc); NMR($CDCl_3$) δ=2.18(6H, s, 2×OAc), 7.24—8.43 (7H, m, aromatic), and 8.86 (1H, s, >CH−). Found: C, 66.25; H, 4.54%. Calcd for $C_{18}H_{14}O_6$: C, 66.25; H, 4.32%.

*Oxidation Products of **1b**. Methyl Ester of 1-Carboxy-6-methoxy-9-xanthenone (**2b**)*: Mp 132—133 °C (MeOH); IR ($CHCl_3$) 1673 (C=O) and 1746 cm^{-1} ($COOCH_3$); NMR ($CDCl_3$) δ=3.82 (3H, s, OCH_3), 4.03 (3H, s, $COOCH_3$), and 6.6—8.2 (6H, m, aromatic). Found: C, 67.48; H, 4.34%. Calcd for $C_{16}H_{12}O_5$: C, 67.60; H, 4.26%.

*Methyl Ester of 1-Carboxy-4-hydroxymethyl-3-methoxy-9-xanthenone (**9b**)*: Mp 212—213 °C (MeOH); IR ($CHCl_3$) 1675 (C=O), 1750 ($COOCH_3$), and 3300—3600 cm^{-1} (OH); NMR ($CDCl_3$) δ=2.5 (1H, br. s, OH), 4.00 (3H, s, OCH_3), 4.05 (3H, s, $COOCH_3$), 5.08 (2H, s, $-CH_2-$), 6.97 (1H, s, $H_{(2)}$), and 7.2—8.3 (4H, m, aromatic); MS *m/e* 314 (M^+).

*Acetylation Product (Methyl Ester of **7b**) of the Methyl Ester of **9b***: Mp 174—175 °C (MeOH); IR ($CHCl_3$) 1670 and 1745 cm^{-1} (C=O); NMR ($CDCl_3$) δ=2.06 (3H, s, OAc), 3.97 (3H, s, OCH_3), 4.03 (3H, s, $COOCH_3$), 5.46 (2H, s, $-CH_2-$), 6.95 (1H, s, $H_{(2)}$), and 7.2—8.3 (4H, m, aromatic). Found: *m/e* 356.0895 (M^+). Calcd for $C_{19}H_{16}O_7$: M, 356.0896.

*Methyl Ester of 1-Carboxy-5-hydroxymethyl-6-methoxy-9-xanthenone (**10b**)*: Mp 198—199 °C (MeOH); IR ($CHCl_3$) 1675 (C=O), 1748 ($COOCH_3$), and 3300—3600 cm^{-1} (OH); NMR ($CDCl_3$) δ=2.4 (1H, br. s, OH), 3.98 (3H, s, OCH_3), 4.03 (3H, s, $COOCH_3$), 4.99 (2H, s, $-CH_2-$), 6.93 (1H, d, J=9.0 Hz, $H_{(7)}$), 7.15—7.65 (3H, m, aromatic), and 8.18 (1H, d, J=9.0 Hz, $H_{(8)}$); MS *m/e* 314 (M^+).

Acetylation Product (Methyl Ester of ***6b****) of the Methyl Ester of* ***10b***: Mp 199—200 °C (MeOH); IR ($CHCl_3$) 1675 and 1745 cm^{-1} (C=O); NMR ($CDCl_3$) δ=2.06 (3H, s, OAc), 3.96 (3H, s, OCH_3), 4.02 (3H, s, $COOCH_3$), 5.47 (2H, s, $-CH_2-$), 7.02 (1H, d, J=9.0 Hz, $H_{(7)}$), 7.23—7.87 (3H, m, aromatic), and 8.26 (1H, d, J=9.0 Hz, $H_{(8)}$). Found: *m/e* 356.0887 (M^+). Calcd for $C_{19}H_{16}O_7$: M. 356.0896.

4-Acetoxymethyl-3-methoxy-9-xanthenone (***14b***): Mp 185—186 °C (EtOH); IR ($CHCl_3$) 1670 (C=O) and 1748 cm^{-1} (OAc); NMR ($CDCl_3$) δ=2.07 (3H, s, OAc), 3.97 (3H, s, OCH_3), 5.47 (2H, s, $-CH_2-$), 6.99 (1H, d, J=9.0 Hz, $H_{(2)}$), 7.20—8.35 (4H, m, aromatic), and 8.30 (1H, d, J=9.0 Hz, $H_{(1)}$). Found: C, 68.14; H, 4.90%. Calcd for $C_{17}H_{14}O_5$: C, 68.45; H, 4.73%.

2-Acetoxymethyl-3-methoxy-9-xanthenone (***15b***): Mp 186—187 °C (EtOH); IR ($CHCl_3$) 1675 (C=O) and 1755 cm^{-1} (OAc); NMR ($CDCl_3$) δ=2.16 (3H, s, OAc), 3.95 (3H, s, OCH_3), 5.18 (2H, s, $-CH_2-$), 6.86 (1H, s, $H_{(4)}$), 7.24—8.36 (4H, m, aromatic), and 8.23 (1H, s, $H_{(1)}$). Found: C, 68.43; H, 4.77%. Calcd for $C_{17}H_{14}O_5$: C, 68.45; H, 4.73%.

Oxidation Products of ***1c***. *Methyl Ester of 1-Carboxy-3,6-dimethoxy-9-xanthenone* (***2c***): Mp 181 °C (MeOH); IR ($CHCl_3$) 1660 (C=O) and 1745 cm^{-1} ($COOCH_3$); NMR ($CDCl_3$) δ=3.89 (6H, s, 2×OCH_3), 4.02 (3H, s, $COOCH_3$), 6.80 (1H, dd, J=10.2 and 2.4 Hz, $H_{(7)}$), 6.84 (2H, br. s, $H_{(2)}$ and $H_{(4)}$), 6.97 (1H, d, J=2.4 Hz, $H_{(5)}$), and 8.12 (1H, d, J=10.2 Hz, $H_{(8)}$). Found: C, 65.06; H, 4.77%. Calcd for $C_{17}H_{14}O_6$: C, 64.96; H, 4.49%.

Methyl Ester of 1-Carboxy-3,6-dimethoxy-4-hydroxymethyl-9-xanthenone (***9c***): IR ($CHCl_3$) 1665 (C=O), 1750 ($COOCH_3$), and 3300—3600 cm^{-1} (OH); NMR ($CDCl_3$) δ=2.5 (1H, br. s, OH), 3.82 (3H, s, OCH_3), 3.91 (3H, s, OCH_3), 3.97 (3H, s, $COOCH_3$), 4.90 (2H, s, $-CH_2-$), 6.74 (1H, s, $H_{(2)}$), and 6.7—8.1 (3H, m, aromatic).

Acetylation Product (Methyl Ester of ***7c****) of the Methyl Ester of* ***9c***: Mp 178—180 °C (MeOH); IR ($CHCl_3$) 1670 and 1745 cm^{-1} (C=O); NMR ($CDCl_3$) δ=2.06 (3H, s, OAc), 3.90 (3H, s, OCH_3), 3.96 (3H, s, OCH_3), 4.01 (3H, s, $COOCH_3$), 5.43 (2H, s, $-CH_2-$), 6.85 (1H, s, $H_{(2)}$), and 6.8—8.2 (3H, m, aromatic). Found: *m/e* 386.0984 (M^+). Calcd for $C_{20}H_{18}O_8$: M, 386.1002.

Methyl Ester of 4-Cardoxymethyl-3,6-dimethoxy-9-xanthenone (***11c***): Mp 196—197 °C (MeOH); IR ($CHCl_3$) 1660 (C=O), and 1750 cm^{-1} ($COOCH_3$); NMR ($CDCl_3$) δ=3.72 (3H, s, $COOCH_3$), 3.90 (2H, s, $-CH_2-$), 3.95 (6H, s, 2×OCH_3), 6.92 (1H, dd, J=8.7 and 2.4 Hz, $H_{(7)}$), 7.02 (1H, d, J=10.2 Hz, $H_{(2)}$), 7.07 (1H, d, J=2.4 Hz, $H_{(5)}$), 8.25 (1H, d, J=8.7 Hz, $H_{(8)}$), and 8.29 (1H, d, J=10.2 Hz, $H_{(1)}$). Found: C, 65.78; H, 5.01%; *m/e* 328.0939 (M^+). Calcd for $C_{18}H_{16}O_6$: C, 65.85; H, 4.91%; M, 328.0947.

4-Acetoxymethyl-3,6-dimethoxy-9-xanthenone (***14c***): Mp 203 °C (EtOH); IR ($CHCl_3$) 1660 (C=O) and 1745 cm^{-1} (OAc); NMR ($CDCl_3$) δ=2.09 (3H, s, OAc), 3.90 (3H, s, OCH_3), 3.96 (3H, s, OCH_3), 5.44 (2H, s, $-CH_2-$), 6.90 (1H, dd, J=8.4 and 2.4 Hz, $H_{(7)}$), 6.96 (1H, d, J=9.0 Hz, $H_{(2)}$), 6.97 (1H, d, J=2.4 Hz, $H_{(5)}$), 8.14 (1H, d, J=8.4 Hz, $H_{(8)}$), and 8.30 (1H, d, J=9.0 Hz, $H_{(1)}$). Found: C, 65.88; H, 4.94%. Calcd for $C_{18}H_{16}O_6$: C, 65.85; H, 4.91%.

2-Acetoxymethyl-3,6-dimethoxy-9-xanthenone (***15c***): Mp 188 °C (EtOH); IR ($CHCl_3$) 1670 (C=O) and 1755 cm^{-1} (OAc); NMR ($CDCl_3$) δ=2.16 (3H, s, OAc), 3.90 (3H, s, OCH_3), 3.93 (3H, s, OCH_3), 5.14 (2H, s, $-CH_2-$), 6.79 (1H, s, $H_{(4)}$), 6.87 (1H, dd, J=9.0 and 2.4 Hz, $H_{(7)}$), 6.96 (1H, d, J=2.4 Hz, $H_{(5)}$), 8.20 (1H, d, J=9.0 Hz, $H_{(8)}$), and 8.21 (1H, s, $H_{(1)}$). Found: C, 65.54; H, 4.98%. Calcd for $C_{18}H_{16}O_6$: C, 65.85; H, 4.91%.

4,5-Bis(acetoxymethyl)-3,6-dimethoxy-9-xanthenone (***17c***) *and 2,5-Bis(acetoxymethyl)-3,6-dimethoxy-9-xanthenone* (***18c***): The mixture of **17c** and **18c** could not be completely separated. However, the NMR spectrum and HPLC study, and the result of elemental analysis supported the structures. Mp 234—235 °C (EtOH); IR ($CHCl_3$) 1665 (C=O) and 1750 cm^{-1} (OAc). NMR spectrum of **17c**; ($CDCl_3$) δ=2.07 (6H, s, 2×OAc), 3.98 (6H, s, 2×OCH_3), 5.47 (4H, s, 2×$-CH_2-$) 6.99 (2H, d, J=9.0 Hz, $H_{(2)}$ and $H_{(7)}$), and 8.27 (2H, d, J=9.0 Hz, $H_{(1)}$ and $H_{(8)}$). NMR spectrum of **18c**; ($CDCl_3$) δ=2.08 (3H, s, OAc), 2.14 (3H, s, OAc), 3.98 (6H, s, 2×OCH_3), 5.19 (2H, s, $-CH_2-$), 5.47 (2H, s, $-CH_2-$), 6.85 (1H, s, $H_{(4)}$), 6.99 (1H, d, J=9.0 Hz, $H_{(7)}$), 8.19 (1H, br. s, $H_{(1)}$) and 8.29 (1H, d, J=9.0 Hz, $H_{(8)}$). Found: C, 62.70; H, 5.15%. Calcd for $C_{21}H_{20}O_8$: C, 62.99; H, 5.04%.

Oxidation Products of ***1d***. *Methyl Ester of 1-Carboxy-2,3,6-trimethoxy-9-xanthenone* (***2d***): Mp 197—198 °C (MeOH); IR ($CHCl_3$) 1665 (C=O) and 1755 cm^{-1} ($COOCH_3$); NMR ($CDCl_3$) δ=3.87 (3H, s, OCH_3), 3.89 (3H, s, OCH_3), 3.98 (3H, s, OCH_3), 4.04 (3H, s, $COOCH_3$), 6.79 (1H, d, J=2.4 Hz, $H_{(5)}$), 6.86 (1H, dd, J=9.0 and 2.4 Hz, $H_{(7)}$), 6.86 (1H, s, $H_{(4)}$), and 8.14 (1H, d. J=9.0 Hz, $H_{(8)}$). Found: *m/e* 344.0892 (M^+). Calcd for $C_{18}H_{16}O_7$: M, 344.0896.

Methyl Ester of 1-Carboxy-3,6,7-trimethoxy-9-xanthenone (***3d***): **12d** could not be completely separated from **11d**, but the NMR spectrum, high resolution mass spectrum, and HPLC study supported the structure. Mp 171—172 °C (MeOH); IR ($CHCl_3$) 1660 (C=O) and 1745 cm^{-1} ($COOCH_3$); NMR ($CDCl_3$) δ=3.84 (3H, s, OCH_3), 3.90 (3H, s, OCH_3), 3.94 (3H, s, OCH_3), 4.02 (3H, s, $COOCH_3$), 6.77 (1H, s, $H_{(5)}$), 6.80 (2H, br. s, $H_{(2)}$ and $H_{(4)}$), and 7.50 (1H, s, $H_{(8)}$). Found: *m/e* 344.0884 (M^+). Calcd for $C_{18}H_{16}O_7$: 344.0896.

Methyl Ester of 1-Carboxy-4-hydroxymethyl-3,6,7-trimethoxy-9-xanthenone (***9d***): IR ($CHCl_3$) 1650 (C=O), 1745 ($COOCH_3$), and 3300—3600 cm^{-1} (OH); NMR ($CDCl_3$) δ=2.5 (1H, br. s, OH), 3.93 (3H, s, OCH_3), 3.97 (3H, s, OCH_3), 3.98 (3H, s, OCH_3), 4.03 (3H, s, $COOCH_3$), 4.89 (2H, s, $-CH_3-$), 6.82 (1H, s, $H_{(5)}$), 6.85 (1H, s, $H_{(2)}$), and 7.51 (1H, s, $H_{(8)}$); MS *m/e* 374 (M^+).

Acetylation Product (Methyl Ester of ***7d****) of the Methyl Ester of* ***9d***: Mp 262—263 °C (MeOH); IR ($CHCl_3$) 1660 and 1745 cm^{-1} (C=O); NMR ($CDCl_3$) δ=2.07 (3H, s, OAc), 3.92 (3H, s, OCH_3), 3.96 (3H, s, OCH_3), 3.99 (3H, s, OCH_3), 4.02 (3H, s, $COOCH_3$), 5.42 (2H, s, $-CH_2-$), 6.90 (2H, s, $H_{(2)}$ and $H_{(5)}$), and 7.54 (1H, s, $H_{(8)}$). Found: *m/e* 416.1115 (M^+). Calcd for $C_{21}H_{20}O_9$: M, 416.1107.

Methyl Ester of 4-Carboxymethyl-2,3,6-trimethoxy-9-xanthenone (***11d***): Mp 198—200 °C (MeOH); IR ($CHCl_3$) 1660 (C=O) and 1755 cm^{-1} ($COOCH_3$); NMR ($CDCl_3$) δ=3.69 (3H, s, $COOCH_3$), 3.92 (2H, s, $-CH_2-$), 3,93 (3H, s, OCH_3), 3.97 (3H, s, OCH_3), 3.99 (3H, s, OCH_3), 6.87 (1H, d, J=2.4 Hz, $H_{(5)}$), 6.87 (1H, dd, J=9.0 and 2.4 Hz, $H_{(7)}$), 7.61 (1H, s, $H_{(1)}$), and 8.23 (1H, d, J=9.0 Hz, $H_{(8)}$). Found: *m/e* 358.1059 (M^+). Calcd for $C_{19}H_{18}O_7$: M, 358.1053.

5-Acetoxymethyl-2,3,6-trimethoxy-9-xanthenone (***14d***): Mp 233 °C (EtOH); IR ($CHCl_3$) 1655 (C=O) and 1745 cm^{-1} (OAc); NMR ($CDCl_3$) δ=2.08 (3H, s, OAc), 3.95 (6H, s, 2×OCH_3), 3.97 (3H, s, OCH_3), 5.40 (2H, s, $-CH_2-$), 6.85 (1H, s, $H_{(4)}$), 6.97 (1H, d, J=9.0 Hz, $H_{(7)}$), 7.54 (1H, s, $H_{(1)}$), and 8.26 (1H, d, J=9.0 Hz, $H_{(8)}$). Found: C, 63.54; H, 5.28%. Calcd for $C_{19}H_{18}O_7$:C, 63.68; H, 5.06%.

2-Acetoxymethyl-3,6,7-trimethoxy-9-xanthenone (***15d***): Mp 208—209 °C (EtOH); IR ($CHCl_3$) 1660 (C=O) and 1750 cm^{-1} (OAc); NMR ($CDCl_3$) δ=2.12 (3H, s, OAc), 3.91 (3H, s, OCH_3), 3.94 (6H, s, 2×OCH_3), 5.12 (2H, s, $-CH_2-$), 6.74 (1H, s, $H_{(5)}$), 6.79 (1H, s, $H_{(4)}$), 7.53 (1H, s, $H_{(1)}$), and 8.16 (1H, s, $H_{(8)}$). Found: *m/e* 358.1043 (M^+). Calcd for $C_{19}H_{18}O_7$: M, 358.1053.

Oxidation Products of ***1e***. *Methyl Ester of 1-Carboxy-6-methoxy-5-methyl-9-xanthenone* (***2e***): Mp 184—185 °C (MeOH); IR ($CHCl_3$) 1665 (C=O) and 1748 cm^{-1} ($COOCH_3$); NMR ($CDCl_3$) δ=2.31 (3H, s, CH_3), 3.92 (3H, s, OCH_3), 4.03 (3H, s, $COOCH_3$), 6.89 (1H, d, J=9.0 Hz, $H_{(7)}$), 7.15—7.82 (3H, m, aromatic), and 8.11 (1H, d, J=9.0 $H_{(8)}$). Found: C, 68.20; H, 4.92%. Calcd for $C_{17}H_{14}O_5$: C, 68.45; H, 4.73%.

1-Carboxy-3-methoxy-4-methyl-9-xanthenone (***3e***): Mp 250 °C (EtOH); IR (KBr) 1610 and 1720 (C=O), and 2800—3100 cm^{-1} (OH); NMR ($(CD_3)_2SO$) δ=2.32 (3H, s, CH_3), 4.00 (3H, s, OCH_3), 7.17 (1H, s, $H_{(2)}$), 7.34—8.23 (4H, m, aromatic), and 13.0 (1H, br. s, COOH): MS *m/e* 284 (M^+). Found: C, 67.48; H, 4.40%. Calcd for $C_{16}H_{12}O_5$: C, 67.60; H, 4.26%.

Methyl Ester of ***3e***: Mp 211—212 °C (MeOH); IR ($CHCl_3$) 1670 (C=O) and 1748 cm^{-1} ($COOCH_3$); NMR ($CDCl_3$) δ=2.33 (3H, s, CH_3), 3.93 (3H, s, OCH_3), 4.02 (3H, s, $COOCH_3$), 6.86 (1H, s, $H_{(2)}$), and 7.15—8.29 (4H, m, aromatic). Found: C, 68.21; H, 4.77%. Calcd for $C_{17}H_{14}O_5$: C, 68.45; H, 4.73%.

Dimethyl Ester of 1,8-Dicarboxy-3-methoxy-4-methyl-9-xanthenone (***4e***): Mp 200—201 °C (MeOH); IR ($CHCl_3$) 1680 (C=O) and 1750 cm^{-1} ($COOCH_3$); NMR ($CDCl_3$) δ=2.34 (3H, s, CH_3), 3.94 (3H, s, OCH_3), 3.96 (6H, s, 2×$COOCH_3$), 6.91 (1H, s, $H_{(2)}$), and 7.18—7.68 (3H, m, aromatic). Found: C, 64.01, H, 4.70%. Calcd for $C_{19}H_{16}O_7$: C, 64.04; H, 4.53%.

Dimethyl Ester of 5-Carboxymethyl-1-carboxy-3-methoxy-4-methyl-9-xanthenone (***5e***): Mp 179—180 °C (MeOH); IR ($CHCl_3$) 1675 (C=O) and 1750 cm^{-1} ($COOCH_3$); NMR ($CDCl_3$) δ=2.37 (3H, s, CH_3), 3.68 (3H, s, $COOCH_3$), 3.93 (5H, s, $-CH_2-$ and OCH_3), 4.01 (3H, s, $COOCH_3$), 6.88 (1H, s, $H_{(2)}$), and 7.00—8.24 (3H, m, aromatic). Found: *m/e* 370.1051 (M^+). Calcd for $C_{20}H_{18}O_7$: M, 370.1053.

Oxidation Products of ***1f***. *Methyl Ester of 1-Carboxy-6-methoxy-4-methyl-9-xanthenone* (***2f***): Mp 193—194 °C (MeOH); IR ($CHCl_3$) 1670 (C=O) and 1755 cm^{-1} ($COOCH_3$); NMR ($CDCl_3$) δ=2.45 (3H, s, CH_3), 3.81 (3H, s, OCH_3), 3.99 (3H, s, $COOCH_3$), 6.78 (1H, d, J=2.4 Hz, $H_{(5)}$), 6.83 (1H, dd, J=9.0 and 2.4 Hz, $H_{(7)}$), 7.11 (1H, s, J=7.8 Hz, $H_{(2)}$), 7.24 (1H, d, J=7.8 Hz, H $_{(3)}$),and 8.05 (1H, d, J=9.0 Hz, $H_{(8)}$). Found: C, 68.50; H, 4.82%. Calcd for $C_{17}H_{14}O_5$: C, 68.45; H, 4.73%.

Methyl Ester of 5-Acetoxymethyl-1-carboxy-6-methoxy-4-methyl-9-xanthenone (***6f***): Mp 152—153 °C (MeOH); IR ($CHCl_3$) 1675 (C=O) and 1747 cm^{-1} ($COOCH_3$ and OAc); NMR ($CDCl_3$) δ=2.06 (3H, s, OAc), 2.54 (3H, s, CH_3), 3.96 (3H, s, OCH_3), 3.99 (3H, s, $COOCH_3$), 5.44 (2H, s, $-CH_2-$), 6.98 (1H, d, J=9.0 Hz, $H_{(7)}$), 7.16 (1H, d, J=7.8 Hz, $H_{(2)}$), 7.48 (1H, d, J=7.8 Hz, $H_{(3)}$), and 8.22 (1H, d, J=9.0 Hz, $H_{(8)}$), Found: *m/e* 370.1043 (M^+). Calcd for $C_{20}H_{18}O_7$: M, 370.1053.

4-Acetoxymethyl-3-methoxy-5-methyl-9-xanthenone (***14f***): Mp 212 °C (EtOH); IR ($CHCl_3$) 1665 (C=O) and 1750 cm^{-1} (OAc); NMR ($CDCl_3$) δ=2.08 (3H, s, OAc), 2.49 (3H, s, CH_3), 3.99 (3H, s, OCH_3), 5.48 (2H, s, $-CH_2-$), 6.96 (1H, d, J=9.0 Hz, $H_{(2)}$), 6.84—8.20 (3H, m, aromatic), and 8.31 (1H, d, J=9.0 Hz, $H_{(1)}$). Found: C, 68.98; H, 5.24%. Calcd for $C_{18}H_{16}O_5$: C, 69.22; H, 5.16%.

2-Acetoxymethyl-3-methoxy-5-methyl-9-xanthenone (***15f***): Mp 187—188 °C (EtOH); IR ($CHCl_3$) 1670 (C=O) and 1755 cm^{-1} (OAc); NMR ($CDCl_3$), δ=2.16 (3H, s, OAc), 2.57 (3H, s, CH_3), 3.98 (3H, s, OCH_3), 5.24 (2H, s, $-CH_2-$), 6.96 (1H, s, $H_{(4)}$), 6.97—8.27 (3H, m, aromatic), and 8.28 (1H, s, $H_{(1)}$). Found: *m/e* 312.0993 (M^+). Calcd for $C_{18}H_{16}O_5$: M, 312.0998.

Oxidation Products of ***1g***. *Methyl Ester of 8-Carboxy-1-methoxy-3-methyl-9-xanthenone* (***2g***): Mp 186—187 °C (Benzene); IR ($CHCl_3$) 1670 (C=O) and 1750 cm^{-1} ($COOCH_3$); NMR ($CDCl_3$) δ=2.39 (3H, s, CH_3), 3.96 (3H, s, OCH_3), 4.04 (3H, s, $COOCH_3$), 6.57 (1H, d, J=2.4 Hz, $H_{(2)}$), 6.79 (1H, d, J=2.4 Hz, $H_{(4)}$), and 7.14—7.80 (3H, m, aromatic). Found: C, 68.37; H, 4.91%. Calcd for $C_{17}H_{14}O_5$: C, 68.45, H, 4.73%.

Methyl Ester of 4-Acetoxymethyl-8-carboxy-1-methoxy-3-methyl-9-xanthenone (***6g***): Mp 197—198 °C (MeOH); IR ($CHCl_3$) 1675 (C=O) and 1750 cm^{-1} ($COOCH_3$ and OAc); NMR ($CDCl_3$) δ= 2.06 (3H, s, OAc), 2.44 (3H, s. CH_3), 3.97 (3H, s, OCH_3), 4.03 (3H, s, $COOCH_3$), 5.41 (2H, s, $-CH_2-$), 6.64 (1H, br. s, $H_{(2)}$), and 7.19—7.83 (3H, m, aromatic), Found: C, 64.60; H, 4.95%. Calcd for $C_{20}H_{18}O_7$: C, 64.86; H, 4.90%.

Methyl Ester of 5-Carboxymethyl-1-methoxy-3-methyl-9-xanthenone (***11g***): Mp 158—159 °C (EtOH); IR ($CHCl_3$) 1670 (C=O) and 1755 cm^{-1} ($COOCH_3$); NMR ($CDCl_3$) δ=2.41 (3H, s. CH_3), 3.68 (3H, s, $COOCH_3$), 3.90 (2H, s, $-CH_2-$), 3.97 (3H, s, OCH_3), 6.58 (1H, d, J=2.4 Hz, $H_{(2)}$), 6.83 (1H, d, J=2.4 Hz, $H_{(4)}$), and 7.08—8.29 (3H, m, aromatic). Found: *m/e* 312.0994 (M^+). Calcd for $C_{18}H_{16}O_5$: M, 312.0998.

Methyl Ester of 4-Acetoxymethyl-5-carboxymethyl-1-methoxy-3-methyl-9-xanthenone (***13g***): Mp 184—185 °C (EtOH); IR ($CHCl_3$) 1670 (C=O) and 1755 cm^{-1} ($COOCH_3$ and OAc); NMR ($CDCl_3$) δ=2.08 (3H, s, OAc), 2.51 (3H, s, CH_3), 3.70 (3H, s, $COOCH_3$), 3.95 (2H, s, $-CH_2-$), 4.00 (3H, s, OCH_3), 5.38 (2H, s, $-CH_2-$), 6.67 (1H, br. s, $H_{(2)}$), and 7.15—8.32 (3H, m, aromatic). Found: *m/e* 384.1196 (M^+). Calcd for $C_{21}H_{20}O_7$: M, 384.1209.

4-Acetoxymethyl-1-methoxy-3-methyl-9-xanthenone (***14g***): Mp 149 °C (EtOH); IR ($CHCl_3$) 1660 (C=O) and 1745 cm^{-1} (OAc); NMR ($CDCl_3$) δ=2.07 (3H, s, OAc), 2.43 (3H, s, CH_3), 3.99 (3H, s, OCH_3), 5.41 (2H, s, $-CH_2-$), 6.59 (1H, s, $H_{(2)}$), and 7.2—8.3 (4H, m, aromatic). Found: C, 69,29; H, 5.28%. Calcd for $C_{18}H_{16}O_5$: C, 69.22; H, 5.16%.

3-Acetoxymethyl-1-methoxy-9-xanthenone (***16g***): Mp 174—175 °C (EtOH); IR ($CHCl)_3$ 1670 (C=O) and 1760 cm^{-1} (OAc); NMR ($CDCl_3$) δ=2.17 (3H, s, OAc), 3.99 (3H, s, OCH_3), 5.11 (2H, s, $-CH_2-$), 6.70 (1H, d, J=1.8 Hz, $H_{(2)}$), 6.98 (1H, d, J=1.8 Hz, $H_{(4)}$), and 7.20—8.35 (4H, m, aromatic), Found: *m/e* 298.0807 (M^+). Calcd for $C_{17}H_{14}O_5$: M, 298.0841.

4,5-Bis(acetoxymethyl)-1-methoxy-3-methyl-9-xanthenone (***17g***): Mp 174—175 °C (EtOH); IR ($CHCl_3$) 1675 (C=O) and 1755 cm^{-1} (OAc); NMR ($CDCl_3$) δ=2.06 (3H, s, OAc), 2,13 (3H, s, OAc), 2.54 (3H, s, CH_3), 4.00 (3H, s, OCH_3), 5.43 (4H, s, 2×$-CH_2-$), 6.69 (1H, s, $H_{(2)}$), and 7.19—8.34 (3H, m, aromatic). Found: *m/e* 384.1221 (M^+). Calcd for $C_{21}H_{20}O_7$: M, 384.1209.

Oxidation of ***1b*** *with Manganese(III) Acetate in the Presence of Potassium Acetate.* Potassium acetate (60 mmol) was dissolved in hot acetic acid (25 ml) containing acetic anhydride (4 ml). **1b** (1 mmol) and manganese(III) acetate dihydrate (12 mmol)were added to this mixture, which was heated under reflux until the brown color of Mn(III) ions disappeared. The resulting liquid was treated in a manner similar to that described above, giving **2b**, **9b**, **10b**, 4-carboxymethyl-3-methoxy-9-xanthenone (**11b**), 2-carboxymethyl-3-methoxy-9-xanthenone (**12b**), **14b**, and **15b**.

Methyl Ester of ***11b***: Mp 181 °C (MeOH); IR ($CHCl_3$) 1675 (C=O) and 1749 cm^{-1} ($COOCH_3$); NMR ($CDCl_3$) δ=3.81 (3H, s, $COOCH_3$), 3.95 (2H, s, $-CH_2-$), 3.95 (3H, s, OCH_3), 6.96 (1H, d, J=9.0 Hz, $H_{(2)}$), 6.81—8.35 (4H, m, aromatic), and 8.29 (1H, d, J=9.0 Hz, $H_{(1)}$). Found: *m/e* 298.0863 (M^+). Calcd for $C_{17}H_{14}O_5$: M, 298.0841.

Methyl Ester of ***12b***: Mp 217—218 °C (MeOH); IR ($CHCl_3$) 1670 (C=O) and 1752 cm^{-1} ($COOCH_3$); NMR ($CDCl_3$)

δ=3.71 (3H, s, $COOCH_3$), 3.71 (2H, s, $-CH_2-$), 3.93 (3H, s, OCH_3), 6.90 (1H, s, $H_{(4)}$), 7.22—8.38 (4H, m, aromatic), and 8.12 (1H, s, $H_{(1)}$). Found: *m/e* 298.0824 (M^+). Calcd for $C_{17}H_{14}O_5$: M, 298.0841.

Oxidation of ***1c*** *with Manganese(III) Acetate under an Atmosphere of Nitrogen.* **1c** (1 mmol) was oxidized with manganese(III) acetate dihydrate (12 mmol) under an atmosphere of nitrogen to give **2c** (mp 181 °C), **7c** (mp 178—180 °C), 1-carboxy-4,5-bis(acetoxymethyl)-3,6-dimethoxy-9-xanthenone (**8c**), **9c**, **11c** (mp 196—197 °C), **14c** (mp 203 °C), **15c** (mp 188 °C), **17c** and **18c** (mp 234—235 °C).

Methyl Ester of ***8c***: Mp 233—234 °C (MeOH); IR ($CHCl_3$) 1675 (C=O) and 1748 cm^{-1} ($COOCH_3$ and OAc); NMR ($CDCl_3$) δ=2.06 (6H, s, 2×OAc), 3.97 (6H, s, 2×OCH_3), 4.01 (3H, s, $COOCH_3$), 5.41 (4H, s, 2×$-CH_2-$), 6.87 (1H, s, $H_{(2)}$), 6.93 (1H, d, J=8.4 Hz, $H_{(7)}$), and 8.24 (1H, d, J=8.4 Hz, $H_{(8)}$). Found: *m/e* 458.1232 (M^+). Calcd for $C_{23}H_{22}O_{10}$: M, 458.1213.

Oxidation of Anthraquinone. Anthraquinone (2 mmol), manganese(III) acetate dihydrate (20 mmol), acetic acid (50 ml), and acetic anhydride (8 ml) were heated under reflux for 40 min under an atmosphere of nitrogen. The reaction mixture was treated in the manner described before to give 2-diacetoxymethylanthraquinone (2%): Mp 144—146 °C (EtOH); IR ($CHCl_3$) 1700 and 1775 cm^{-1} (C=O); NMR ($CDCl_3$) δ=2.15 (6H, s, 2×OAc), 7.27 (1H, s, >CH–), and 7.2—8.4 (7H, m, aromatic); MS *m/e* (rel intensity), 296 (14) ($M^+-CH_2=C=O$), 278 (26) (M^+-AcOH), 254 (24), 237 (100) ($R-\overset{+}{C}HOH$), 236 (74) ($R-CHO^+$), 235 (91) ($R-C=O^+$), and 208 (19) ($M^+-C_5H_6O_4$), 2-formylanthraquinone (3%): Mp 287—290 °C (EtOH); IR ($CHCl_3$) 1700 and 1725 cm^{-1} (C=O); NMR ($CDCl_3$) δ=7.2—8.5 (6H, m, aromatic), 8.77 (1H, br. s, $H_{(1)}$), and 10.16 (1H, s, CHO); Found: *m/e* 236.0493 (M^+), Calcd for $C_{15}H_8O_3$: M, 236.0474, and 1-carboxymethylanthraquinone (5%) characterized as its methyl ester: Mp 179—181 °C (MeOH); IR ($CHCl_3$) 1690 and 1745 cm^{-1} (C=O); NMR ($CDCl_3$) δ=3.74 (3H, s, $COOCH_3$), 4.22 (2H, s, $-CH_2-$), and 7.56—8.44 (7H, m, aromatic); Found: *m/e* 280.0738 (M^+), Calcd for $C_{17}H_{12}O_4$: M, 280.0736.

Oxidation of Benzophenone. Benzopenone (1 mmol) and manganese(III) acetate dihydrate (10 mmol) were heated under reflux for 39 min in acetic acid (25 ml) containing acetic anhydride (4 ml) to yield diacetoxymethylbenzophenone (The position of the substituent group could not be determined.) (4%): IR ($CHCl_3$) 1675 and 1770 cm^{-1} (C=O); NMR ($CDCl_3$) δ=2.14 (6H, s, 2×OAc), 7.61 (1H, s, >CH–), and 7.2—7.9 (9H, m, aromatic); Found: *m/e* 312.1014 (M^+), Calcd for $C_{18}H_{16}O_5$: M, 312.0998. Although some acetoxymethyl and carboxymethyl products were also formed, they could not be purified on TLC.

The authors wish to thank Professor Hitoshi Takeshita, of Kyushu University, Mr. Shuichi Ueda of the Taiho Pharmaceutical Co. Ltd., Tokushima, and Dr. Shinzaburo Hishida, of the Hitachi Co. Ltd., Katsuda, for their measurement of the mass spectra.

The authors also wish to thank Dr. John F. W. McOmie of Bristol University, England, for his helpful discussion and for reading the manuscript.

References

1) S. Ueda and K. Kurosawa, *Bull. Chem. Soc. Jpn.*, **50**, 193 (1977).
2) S. A. Zonis, *Sbornik Statei Obshchei Khim.*, **2**, 1091 (1953); *Chem. Abstr.*, **49**, 5414 g (1955).
3) P. J. Andrulis, Jr., M. J. S. Dewar, R. Dietz, and R. L. Hunt, *J. Am. Chem. Soc.*, **88**, 5473 (1966).
4) E. I. Heiba, R. M. Dessau, and W. J. Koehi, Jr., *J. Am. Chem. Soc.*, **91**, 138 (1969).
5) K. Kurosawa and H. Harada, *Bull. Chem. Soc. Jpn.*, **52**, 2386 (1979).
6) E. I. Heiba, R. M. Dessau, and W. J. Koehl, Jr., *J. Am. Chem. Soc.*, **90**, 1082 (1968).
7) R. Van Helden, A. F. Bickel, and E. C. Kooyman, *Recl. Trav. Chim. Pays-Bas*, **80**, 1237, 1257 (1961).
8) P. K. Grover, G. D. Shah, and R. C. Shah, *J. Chem. Soc.*, **1955**, 3982.
9) W. J. McMaster, A. I. Scott, and S. Trippett, *J. Chem. Soc.*, **1960**, 4628.
10) O. Kruber, *Chem. Ber.*, **70B**, 1556 (1937); *Chem. Abstr.*, **31**, 6656 (1937).
11) K. Kurosawa, Y. Sasaki, and M. Ikeda, *Bull. Chem. Soc. Jpn.*, **46**, 1498 (1973).
12) A. Kasahara, T. Jzumi, A. Suzuki, and T. Takeda, *Bull. Chem. Soc. Jpn.*, **49**, 3711 (1976).
13) K. Oishi and K. Kuroaswa, *Bull. Chem. Soc. Jpn.*, **53**, 179 (1980).
14) A. A. Goldberg and A. H. Wragg, *J. Chem. Soc.*, **1958**, 4227.

Synthesis of Octachlorobicyclo[3.3.0]octa-1,4,6-triene and Lewis Acid Catalyzed Isomerization of Hexachlorobicyclo[3.3.0]octa-3,5,8-trien-2-one*

Kousuke KUSUDA

Research Institute for Atomic Energy, Osaka City University, Sugimoto-cho, Sumiyoshi-ku, Osaka 558

(Received April 23, 1982)

Treatment of decachloro(4-allylidenecyclopentene) with enneacarbonyldiiron(0) gave octachlorobicyclo-[3.3.0]octa-1,3,7-triene (δ-C_8Cl_8) in 40% yield. Dechlorination of decachlorobicyclo[3.3.0]octa-2,6-diene with powdered selenium, sulfur, phosphorus, or titanium in the presence of anhydrous aluminium chloride without any adde d solvent at 90—100 °C afforded octachlorobicyclo[3.3.0]octa-1,4,6-triene (**2**) (ε-C_8Cl_8) in good yield. Hexa-chlorobicyclo[3.3.0]octa-3,5,8-trien-2-one obtained from **2** was chlorinated by a concentrated solution of antimony-(V) chloride in refluxing dichloromethane to give octachlorobicyclo[3.3.0]octa-3,6(or 7)-dien-2-one, but in a dilute solution (less than 0.1 g of antimony(V) chloride/cm^3 of dichloromethane) hexachlorobicyclo[3.3.0]octa-4,6,8-trien-2-one (**14**) was obtained. Mechanism of the isomerization is discussed in terms of antiaromaticity of cyclo-pentadienyl cation. Reaction of **14** with methanol afforded pentachloro-4-methoxybicyclo[3.3.0]octa-3,5,7-trien-2-one. Ethanol or 2-propanol reacted with **14** similarly giving pentachloro-4-ethoxybicyclo[3.3.0]octa-3,5,7-trien-2 -one or pentachloro-4-isopropoxybicyclo[3.3.0]octa-3,5,7-trien-2-one, respectively.

In a series of continuing studies on the chemistry of cyclic conjugated chlorocarbons,[1] the author reported on reactions of δ-C_8Cl_8 (**1**) and ε-C_8Cl_8 (**2**) with antimony(V) chloride or anhydrous aluminium chloride to give dicationic complexes.[2] In the report, octachloro-bicyclo[3.3.0]octa-1,3,7-triene and octachlorobicyclo-[3.3.0]octa-1,4,6-triene were assigned to the structure of **1** and **2**, respectively, which were confirmed later by X-ray crystallographic analyses.[3]

The objective of the present work was to extend the investigation on these chlorocarbons toward develop-ment of a new synthetic method for **2** and elucidation of Lewis acid-catalyzed isomerization of a per-chlorinated ketone obtained from **2**. Since the reported syntheses of **1** and **2**[4] seemed to be unsuitable for a large-scale preparation, it has been desired to develop a convenient synthetic method for **1** or **2**.

Treatment of decachlorobicyclo[3.3.0]octa-2,6-diene (**3**)[5] with tributylstannane[6] at around 50 °C gave a mixture, from which a small amount of 1,2,3,4,4,5,6,7,8-nonachlorobicyclo[3.3.0]octa-2,6-diene (**4**), C_8HCl_9, mp 134 °C, was separated by column chromatography on silica gel eluted by petroleum ether. Dehydrochlorina-tion of **4** with methanolic sodium hydroxide at room temperature gave yellow crystals of **1**. Dechlorination of decachloro(4-allylidenecyclopentene) (**5**)[7] with ennea-carbonyldiiron(0) at room temperature afforded **1** in 37% yield. A reasonable pathway for the formation of **1** could involve transformation of **5** to reactive octa-chlorovinylfulvene (**A**) followed by cyclization, as is similar to the mechanism postulated for the formation of dihydropentalene derivatives.[8] Attempted isolations of intermediate **A** and its iron carbonyl complex[9] were unsuccessful.

As the foregoing preparations of **1** were unsatisfactory for a large-scale preparation, synthesis of **2** was inves-tigated. When a mixture of **3** and anhydrous aluminium chloride was heated at 220—240 °C for 2.5 h, the reaction mixture changed into a reddish brown mass and sublimed white crystals, from which octachloro-

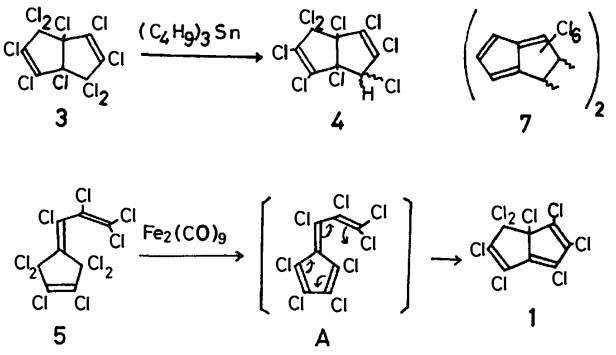

cyclopentene and hexachlorobenzene were separated by making use of solubility in methanol. Treatment of the dark solid on the bottom of flask with a mixture of water and carbon tetrachloride afforded **2** and hexachlorobicyclo[3.3.0]octa-3,5,8-trien-2-one (**6**), C_8Cl_6O, mp 82 °C, in yields of 35 and 28%, respectively. Structural assignment of **6** rested on its IR, UV, and ^{13}C NMR spectra. Dechlorinations of **3** with powdered copper in petroleum benzine, tin(II) chloride in aq acetone, or aluminium amalgam in diethyl ether[10] gave a dimer of hexachloropentalene (**7**).[4a] It seemed difficult to obtain an octachlorodihydropentalene from **3** by regulating conditions of the usual dechlorination. However, it was expected that Lewis acid metal halide in the reaction mixture should react with an octachloro-dihydropentalene produced by dechlorination of **3**, thus preventing further dechlorination, since known per-chlorinated dihydropentalenes, **1** and **2**, easily react with Lewis acid metal halide affording stable complexes. Most of the popular dehalogenating reagents[11] are inadequate because they react with anhyd aluminium chloride and/or because they are usually used in some solvent which is reactive to anhyd aluminium chloride. With these restrictions taken into account, powdered selenium was chosen for the dechlorination. A mixture of **3**, selenium, and two equivalents of anhyd aluminium chloride was heated at 90 °C for 1 h and then quenched with 2 M (1 M=1 mol dm^{-3}) hydrochloric acid. The crude product was purified by the conventional isolation procedure including chromatography on silica gel to

* Dedicated to Emeritus Professor Takeo Sakan on his 70th Anniversary.

give **2** in 98% yield. Under similar conditions, sulfur, red phosphorus, or titanium gave **2** in yield of 91, 52, or 64%, respectively, but powdered aluminium, tin, silicon, and zinc were ineffective for the dechlorination. A mixture of selenium or sulfur and antimony(V) chloride did not react with **3** at 100 °C. When a mixture of **3** and sulfur was heated at 180 °C, **7** was the only product identified. These findings indicate that anhyd aluminium chloride activates selenium and sulfur in the dechlorination of **3**. Dechlorinations of hexachlorocyclopropane,[12] octachloro(4-methylenecyclopentene),[13] and octachloro(1,2-dimethylenecyclobutane)[14] with selenium–anhyd aluminium chloride were unsuccessful. Treatment of 1,2,3,4,5,6,7,8,8-nonachlorobicyclo[3.3.0]octa-2,6-diene (**8**)[15] with two equivalents of anhyd aluminium chloride at 150 °C gave a black solid, which gave **2** in 69% yield upon quenching with concd hydrochloric acid. The reaction probably proceeds similarly to the rearrangement of homonorbornadienyl cation:[16]

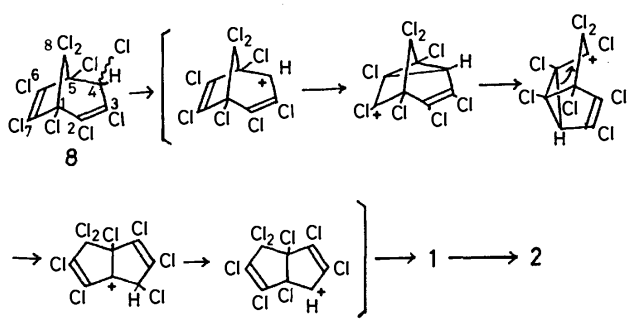

^{35}Cl nuclear quadrupole resonance (NQR) spectra of **2** (Table 1) furnish useful information on the chemical structure. There are six resonance lines indicating the presence of six kinds of chlorine atoms, hence the planarity of the molecule. Each signal in MHz at 78 K shifts downward at higher temperatures. Four lines between 37.056 and 37.372 MHz are in the proper region for vinylic chlorines, whereas two lines at 38.898 and 39.053 MHz suggest two equivalent chlorine atoms on a carbon.[17]

Treatment of **2** with formic acid or sulfuric acid afforded **6** in 65—72% yield.[4d] In order to hydrolyze a dichloromethylene group of **2**, excess fuming nitric acid was added to powdered **2** at room temperature, causing an exothermic reaction immediately. From the reaction mixture **6** and tetrachloro-2,5-cyclopentadiene-1,2-dicarboxylic acid (**9**), $C_7H_2Cl_4O_4$, mp 208 °C, were isolated. The structure of **9** was speculated on the basis of the elemental analysis and IR and UV spectra. Refluxing a mixture of **6** and powdered potassium carbonate in abs methanol afforded pentachloro-4-methoxybicyclo[3.3.0]octa-3,5,8-trien-2-one (**10**), $C_9H_3Cl_5O_2$, mp 96 °C. The transformation is similar to that of **2** with secondary amines.[4d]

Table 1. NQR signals of **2** (MHz)[a]

Temp/K	78	200	296
	39.053	38.722	38.392
	38.898	38.577	38.245
	37.372	37.089	36.826
	37.348	37.074	36.785
	37.268	36.976	36.637
	37.056	36.809	36.493

a) Accuracy: ±0.003 MHz.

When a mixture of **6** and excess antimony(V) chloride in dichloromethane was refluxed for 5 h, a deep red color developed during the reaction, but a colorless oily material, octachlorobicyclo[3.3.0]octa-3,6(or 7)-dien-2-one (**11**), C_8Cl_8O, was the product, which was obtained also by chlorination of hexachlorobicyclo[3.3.0]octa-3,7-diene-2,6-dione (**12**) or hexachlorobicyclo[3.3.0]-octa-3,6-diene-2,8-dione (**13**)[5] with phosphorous(V) chloride. The complete structure of **11** remains to be determined. However, diluted antimony(V) chloride (less than 0.1 g/cm^3 of dichloromethane) does not chlorinate **6** but catalyzes a rearrangement, affording quantitatively deep red crystals of hexachlorobicyclo-[3.3.0]octa-4,6,8-trien-2-one (**14**), C_8Cl_6O, mp 70 °C. Treatment of **6** with anhyd aluminium chloride under similar conditions yielded a mixture of **6** and **14** in approximately 1 : 1 ratio (*vide infra*). Reaction of **14** with concd antimony(V) chloride in the same solvent furnished **11**.[18]

The ^{13}C NMR spectrum of **14** shows a peak due to a chlorinated sp^3 carbon at 85.1 ppm and no alkenic carbon peak characteristic of α,β-unsaturated ketone.[19] It can be assumed that the UV spectrum of **14** (Fig. 1) consists of two groups of higher intensities, one between 220 and 300 nm and the other between 300 and 350 nm, and one broad peak of lower intensity. The maxima in the region 300—450 nm are similar to that of hexachlorofulvene (**15**)[20] and quite different from that of cyclopentadienone derivative.[21] These spectral data were all compatible with the assigned structure, which was further confirmed by the following chemical reaction indicating absence of cyclopentadienone moiety. Neither maleic anhydride nor furan reacted with **14** in refluxing benzene. Chlorination of **14** with liquid chlorine in a sealed tube at room temperature afforded white crystals of decachlorobicyclo[3.3.0]oct-6(or 7)-en-2-one (**16**), $C_8Cl_{10}O$, mp 130 °C, which was stable to treatment with anhyd aluminium chloride in boiling dichloromethane. The structure of **16** was assigned on the basis of elemental analysis and IR and UV spectra. Ethereal diazomethane apparently reacted with **14** with evolution of nitrogen gas and with its red color fading, but isolation of a pure product was unsuccessful.

When methanol was added to **14**, a moderate exothermic reaction furnished yellow crystals of pentachloro-4-methoxybicyclo[3.3.0]octa-3,5,7-trien-2-one (**17a**), $C_9H_3Cl_5O_2$, mp 152 °C. Similarly, ethoxy derivative (**17b**), $C_{10}H_5Cl_5O_2$, mp 186 °C, or 2-propoxy derivative (**17c**), $C_{11}H_7Cl_5O_2$, mp 149 °C, was obtained by the reaction with ethanol or 2-propanol, respectively, but 2-methyl-2-propanol did not react with **14** under similar conditions. Methanolic solution of **14a** yielded 1,3,6,7,8-pentachlorobicyclo[3.3.0]octa-5,7-diene-2,4-dione(**18**)[4d] on standing at room temperature for 2 d. Comparison of the UV spectra of **1** and **17a—d** makes it clear that these chlorocarbons have a similar double bond

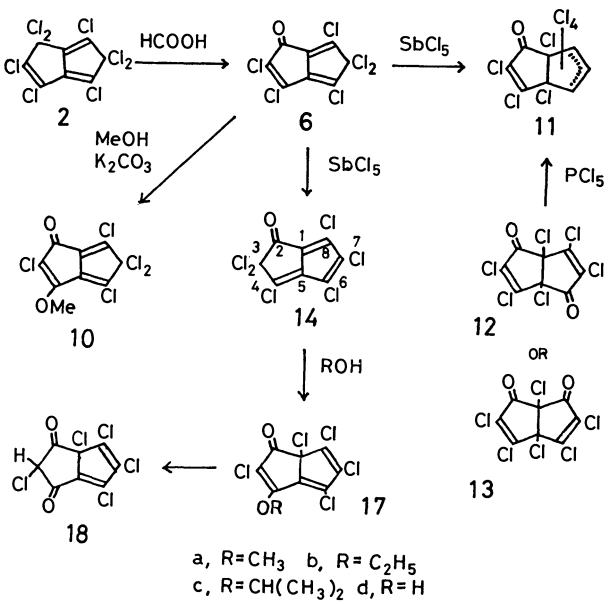

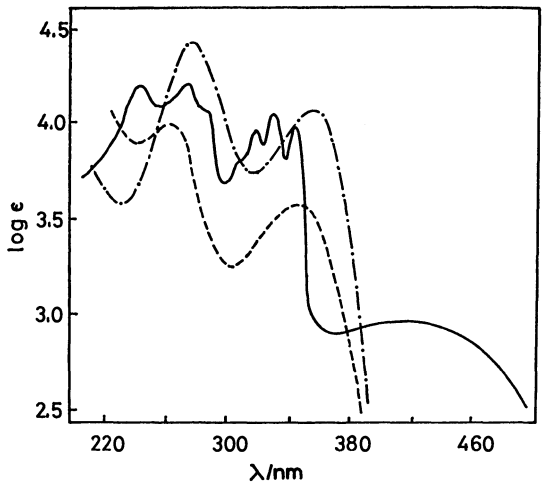

Fig. 1. Ultraviolet and visible absorption spectra of **1**, **14** and **17a**.
------: **1** (in dichloromethane), ——: **14** (in hexane), -·-·-: **17a** (in hexane).

system (Fig. 1 and Experimental section). ^{13}C NMR and IR spectra as well as these findings support the proposed structures **17a—d**.

In view of the generalization that nucleophilic substitution on a polychlorinated double bond proceeds through the addition-elimination mechanism,[22] the formation of **17a—c** seemed to be abnormal. Although a mechanism composed of catalyzed isomerization of the double bonds of **14** followed by substitution of an alkoxyl group can be written, isomerization of the double bonds is probably not the initial step since **14** cannot be isomerized by hydrochloric acid or acetic acid. On the other hand, it has been known that nucleophiles will initially attack on C(6) of **15**, then allowing the addition-elimination reaction to occur.[23] It is considered that the reactions of alcohols with **14** take place on C(4) similarly with **15**, then allowing the isomerization of the double bonds and 1,7-rearrangement of a chlorine atom to proceed.

Addition of excess antimony(V) chloride to a concd solution of **6** in dichloromethane immediately precipitated a yellow complex (**19**), IR spectrum of which is quite similar to that of **6** in the region 1500—500 cm^{-1}. On the other hand, a large difference was found in the carbonyl and C=C double bond regions, indicating that the complex was formed by coordination of antimony(V) chloride to the carbonyl group. Quenching **19** with 6 M hydrochloric acid afforded **6** quantitatively. The isomerization of **6** to **14** presumably takes place through cationic species (B—E) produced by the attack of antimony(V) chloride on **19**. Monocationic B—D are considered unstable because of the contribution of antiaromatic cyclopentadienylium cation,[24] whereas E is free from such destabilization and contains stable polychlorinated fulvene moiety and hence contribution of E seems to be predominant.[25] Recombination of chloride anion with E completes the rearrangement.

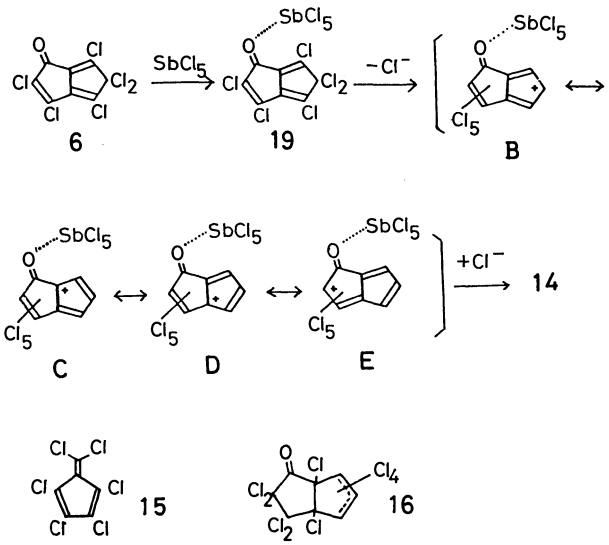

Experimental

General. The melting points were determined on a Yanagimoto micro melting point apparatus and were uncorrected. Elemental analyses of carbon and hydrogen were performed by Mr. J. Goda of Osaka City University. Chlorine analyses, when required, were carried out according to the combustion method by use of a modified flask.[26] IR spectra were recorded on a Perkin-Elemer Model 337 spectrophotometer as mulls in Nujol between KBr disks unless otherwise mentioned. Significant absorptions are reported. UV spectra werer ecorded on a Hitachi Model 200-10 spectrophotometer in solution. Nuclear quadrupole resonance spectra were recorded on a Decca Radar NQR spectrometer and summarized in Table 1. Both ^{1}H and ^{13}C NMR spectra were recorded on a JEOL FX-60 F-T NMR spectrometer. Mass spectra were recorded on a JEOL JMS-01SG-2 double focus mass spectrometer at 80 eV ionizing potential. Petroleum ether and petroleum benzine used are hydrocarbon mixtures boiling in the ranges 48—66 and 68—69 °C, respectively.

1,2,3,4,4,5,6,7,8-Nonachlorobicyclo[3.3.0]octa-2,6-diene (4). A mixture of 4.5 g (10 mmol) of **3** and 5.8 g (20 mmol) of tributylstannane in 30 cm^3 of benzene was heated at around

50 °C under a nitrogen atmosphere with stirring for 33 h. After removal of the solvent under reduced pressure, the reaction mixture was chromatographed on silica gel (3 cm × 60 cm) with petroleum ether as eluent. The crude product obtained from a slightly yellow band was washed with ethanol and crystallized from ethanol to give 48 mg of **4**: mp 133—134 °C; IR 1630, 1610, 1235, 1205, 1175, 1030, 1022, 832, and 755 cm^{-1}; ^1H NMR (CCl_4) δ=5.07. Found: C, 23.29; H, 0.45; Cl, 76.58%. Calcd for C_8HCl_7: C, 23.09; H, 0.24; Cl, 76.67%.

*Octachlorobicyclo[3.3.0]octa-1,3,7-triene (**1**) (δ-C_8Cl_8).* *a) From **4***: To an ethereal solution (1 cm^3) of **4** (35 mg, 0.048 mmol) was added 5 drops of 20% methanolic potassium hydroxide solution and the mixture was stirred for 30 min at room temperature, whereupon the solution turned light yellow. Water was added and the organic materials were extracted with diethyl ether. The combined ethereal solution was washed with water and dried over sodium sulfate. The solvent was evaporated under vacuum to give 30 mg of yellow crystals of **1**. Identification was made by comparison of the IR and UV spectra with those of authentic sample synthesized by the reported method: IR 1615, 1545, 1535, 1267, 1215, 1130, and 765 cm^{-1}; UV λ_{max}^{hexane} 260 (3.99) and 352 (3.67).

*b) From **5***: A mixture of 1.73 g (3.84 mmol) of **5** and 1.40 g (3.84 mmol) of enneacarbonyldiiron(0) in 15 cm^3 of petroleum benzine was stirred for 3 h at 35 °C and was kept at room temperature overnight. The reaction mixture was filtered and the solvent was evaporated to dryness to give 0.546 g (37%) of crude **1**. Column chromatography on silica gel eluted by petroleum benzine gave a pure sample.

*A Dimer of Hexachloropentalene (**7**).* Powdered sulfur (0.50 g) was mixed with 1.32 g (2.93 mmol) of **3** and the mixture was heated at 150—180 °C for 1.5 h. The organic products were extracted with carbon tetrachloride by use of a Soxhlet extractor. The crystals obtained by evaporation of the solvent were sublimed at 135 °C/3 mmHg (1 mmHg= 133.3 Pa) to remove a volatile yellow solid. The residue was 244 mg (27%) of bright deep red crystals of the dimer of hexachloropentalene: mp 315 °C; IR 1638, 1604, 1500, 1232, and 1155 cm^{-1}; UV $\lambda_{max}^{dichloromethane}$ 250 (3.57), 290 sh (3.86), 300 (3.96), 390—460 (2.64). Found: C, 31.15; H, 0.14; Cl, 68.34%. Calcd for $C_{16}Cl_{12}$: C, 31.12; Cl, 68.88%. Identification was made by comparison of mp and IR and UV spectra with those of the authentic sample.

*Octachlorobicyclo[3.3.0]octa-1,4,6-triene (**2**). (ε-C_8Cl_8) a)*: A mixture of 5.00 g (11.1 mmol) of **3**, 1.05 g (13.29 mg atom) of selenium, and 2.96 g (22.17 mmol) of powdered anhyd aluminium chloride was heated in an oil bath at around 90 °C with stirring for 1 h. The reaction mixture melted and turned dark brown. After being cooled to room temperature, the reaction mixture was quenched with a mixture of 2 M hydrochloric acid and chloroform under ice cooling. A small amount of insoluble materials was removed by filtration and the chloroform solution was separated. The water layer was extracted twice with a small amount of chloroform. The combined solution was dried over sodium sulfate. The crude product obtained by evaporation of the solvent was chromatographed on silica gel (12 mm × 7 cm) with petroleum benzine as eluent. Evaporation of the solvent gave 4.14 g (98.2%) of pure **2**: mp 111—112 °C; IR 1685, 1640, 1530, and 800 cm^{-1}; UV λ_{max}^{hexane} 262 (4.01) and 325 (3.38); MS *m/e* (%) 376 (3.1), 341 (33.8), 306 (100), 271 (30.8), 236 (24.6), 201 (13.8), and 153 (29.2).

Dechlorinations of **3** by use of sulfur, red phosphorus and titanium are summarized in Table 2.

e): A mixture of powdered anhyd aluminium chloride (0.60 g, 4.5 mmol) and 0.82 g (2.2 mmol) of **8** was heated at 150 °C for 1.25 h. A dark brown reaction mixture was solidified on standing at room temperature. The reaction mixture was quenched by a mixture of ice and concd hydrochloric acid. Extraction with carbon tetrachloride, drying over sodium sulfate, and evaporation of the solvent gave 0.56 g (69%) of **2**.

Table 2. Dechlorinations of **3**

Dechlorinating reagent(g)	**3**(g)	$AlCl_3$ (g)	Temp/°C	Time/h	Yield of **2**/g(%)
b) S: 0.33	4.60	6.90	80—85	3	3.25(91)
c) Red P: 0.10	1.80	1.21	100	2	0.79(52)
d) Ti: 0.12	1.80	1.21	98—100	2	0.98(64)

f): A mixture of 5.0 g (11.1 mmol) of **3** and 5.0 g (37.5 mmol) of powdered anhyd aluminium chloride in a 50 cm^3 flask was heated at 220—240 °C in an oil bath for 2.5 h. White powders sublimed were collected and treated with water. The mixture was separated by making use of solubility in methanol. The white crystal (20 mg) insoluble in methanol was hexachlorobenzene and the crystal (700 mg) obtained by evaporation of the methanol was octachlorocyclopentene. The reddish-brown reaction mixture on the bottom of the flask was decomposed with a mixture of water and carbon tetrachloride and the organic layer was separated. Evaporation of the solvent gave 3.98 g of mixture. Column chromatography on silica gel (2.2 cm × 13 cm) eluted with petroleum benzine gave 1.48 g (35%) of **2** and 1.02 g (28%) of **6** successively. Both the oily material (0.14 g) from the third and the yellow crystals (0.26 g) from the fourth fraction were not identified.

*Hexachlorobicyclo[3.3.0]octa-3,5,8-trien-2-one (**6**) and Tetrachloro-2,5-cyclopentadiene-1,2-dicarboxylic Acid (**9**).* Fuming nitric acid (d=1.535) was added to 15.0 g (39.5 mmol) of powdered **2**, whereupon a moderate exothermic reaction took place. After having been stirred for 15 min at room temperature, the reaction mixture was diluted with water and the organic materials were extracted with chloroform. Concentration of the organic solution and addition of petroleum benzine afforded 3.46 g of **6**. Recrystallization from petroleum benzine gave an analytical sample of **6**, mp 80—82 °C. Identification was made by comparison of mp and IR spectrum with reported data:[4d] IR (hexane) 1730, 1665, 1630, and 1505 cm^{-1}; UV λ_{max}^{hexane} 260 (4.32) and 270 (4.34); ^{13}C NMR ($CHCl_3$) δ=171.2, 146.1, 142.4, 134.0, 128.9, 127.6, 125.6, and 89.8. Evaporation of the mother solution afforded 11.1 g of an oily product, which was chromatographed on silica gel (18 mm × 14 cm) with petroleum benzine as eluent. The first light yellow band and the second light brown band gave 4.27 g of **6** and the third brown band gave 2.01 g of an oily mixture of **6** and nitro compounds. The upper black part of column was separated and extracted with ethyl acetate. Evaporation of the solvent gave 1.46 g of crude **9**, which was crystallized from a mixed solvent of chloroform and ethyl acetate (4 : 1) to give an analytical sample: mp 204—208 °C; IR 1710 and 1575 cm^{-1}; UV λ_{max}^{hexane} 328 (3.30). Found: C, 28.88; H, 0.69; Cl, 48.69%. Calcd for $C_6H_2Cl_4O_4$: C, 28.80; H, 0.68; Cl, 48.58%.

*Pentachloro-4-methoxybicyclo[3.3.0]octa-3,5,8-trien-2-one (**10**).* A mixture of 1.00 g (3.08 mmol) of **6**, half of 0.426 g (3.08 mmol) of potassium carbonate, and 10 cm^3 of abs methanol was stirred at room temperature for 30 min, then the rest of the potassium carbonate was added and heated to reflux for 1 h. The reaction mixture was diluted with water and the organic materials were extracted with chloroform. Drying over sodium sulfate and evaporation of the solvent afforded 0.84 g of crystals. Recrystallization from petroleum ether gave an

analytical sample of **10**: mp 92—96 °C; IR 1700, 1660, 1630, 1550, 1350, and 800 cm^{-1}. Found: C, 33.49; H, 0.93%. Calcd for $C_9H_3Cl_5O_2$: C, 33.53; H, 0.99%.

*Hexachlorobicyclo[3.3.0]octa-4,6,8-trien-2-one (**14**).* To a suspension of 1.5 g (4.6 mmol) of **6** in 5 cm^3 of dichloromethane was added a solution of 4.10 g (13.7 mmol) of antimony(V) chloride in 40 cm^3 of dichloromethane and the solution was heated to reflux for 3 h. Chloroform (20 cm^3) was added to the deep red reaction mixture and the antimony(V) chloride was decomposed with concd hydrochloric acid. The organic phase was separated and washed twice with water. The solution was dried over sodium sulfate and the solvent was evaporated to dryness. Chromatography of silica gel with petroleum ether gave **14** quantitatively: mp 68—70 °C; IR 1750, 1615, 1560, 1455, 830, and 765 cm^{-1}; UV λ_{max}^{hexane} 245 (4.17), 274 (4.21), 285 sh (4.11), 318 (3.94), 331 (4.06), 346 (3.97), and 410—420 (2.97); ^{13}C NMR ($CHCl_3$) δ=171.6, 144.2, 142.5, 136.8, 130.8, 120.7, 119.8, and 85.1. Found: C, 29.86; H, 0.15%. Calcd for C_8Cl_6O: C, 29.58%.

*Reaction of **6** with Anhydrous Aluminium Chloride.* To 0.92 g (2.83 mmol) of **6** dissolved in 15 cm^3 of dried dichloromethane was added 1.0 g (7.5 mmol) of anhyd aluminium chloride and the mixture was heated under reflux for 7 h and quenched by hydrochloric acid. The organic solution was separated and dried over sodium sulfate and the solvent was evaporated under reduced pressure to give 0.91 g of brown solid, whose IR spectrum showed it was an approximately 1 : 1 mixture of **6** and **14**.

*Decachlorobicyclo[3.3.0]oct-6(or 7)-en-2-one (**16**).* *a) Chlorination of **14** in Liquid Chlorine*: A mixture of 0.377 g (1.16 mmol) of **14** dissolved in 10 cm^3 of carbon tetrachloride and about 10 cm^3 of liquid chlorine was sealed in a thick wall glass tube and kept under sunlight for one week. The tube was chilled in a Dry Ice-acetone bath and opened. Excess chlorine was removed by evaporation and the residue was chromatographed on silica gel (13 mm × 10 cm) with petroleum ether as eluent. The product was eluted as a light brown band. Evaporation of the solvent and recrystallization from a mixture of methanol and ethanol afforded white crystals of **16**: mp 126—130 °C; IR 1795, 1760, 1620, and 1585 cm^{-1}; UV λ_{max}^{hexane} 230 (3.98). Foun d: C, 20.85; H, 0.10; Cl, 75.97%. Calcd for $C_8Cl_{10}O$: C, 20.59; Cl, 75.98%.

b) Chlorination with Phosphorus(V) Chloride: Phosphorus(V) chloride (0.55 g) was mixed with 0.566 g (1.74 mmol) of **14** in a sealed tube and the mixture was heated at 170—200 °C for 4 h. The crude product was purified by column chromatography on silica gel eluted with petroleum benzine. Yield: 0.208 g (26.0%).

*Pentachloro-4-methoxybicyclo[3.3.0]octa-3,5,7-trien-2-one (**17a**).* Abs methanol (5 cm^3) was mixed with with 1.821 g (5.61 mmol) of **14** at room temperature and stirred for 5 min to precipitate yellow crystals. Then, 2 cm^3 of petroleum ether was added and the crystals were separated by filtration. Recrystallization three times from petroleum ether gave 0.365 g of an analytical sample of **17a**: mp 152 °C; IR 1740, 1730, 1595, 1550, and 1290 cm^{-1}; UV λ_{max}^{hexane} 220 (3.70), 277 (4.44), and 355 (4.13); ^{13}C NMR ($CHCl_3$) δ=174.4, 165.4, 140.7, 125.3, 124.6, 117.1 (d),[27] 81.6, and 65.1. Found: C, 33.67; H, 0.92; Cl, 55.60%. Calcd for $C_9H_3Cl_5O_2$: C, 33.74; H, 0.94; Cl, 55.34%.

*Pentachloro-4-ethoxybicyclo[3.3.0]octa-3,5,7-trien-2-one (**17b**).* Into a mixture of ethanol (4.7 cm^3) and chloroform (9.3 cm^3) was dissolved 1.624 g of **14** and the solution was stirred for 5 h at room temperature to precipitate yellow crystals. The solvent was evaporated under reduced pressure to give yellow crystal sludge. The crystals were separated by filtration and washed with a small amount of acetic acid. Crystallization from 7 cm^3 of chloroform afforded 0.67 g of **17b**: mp 186 °C; IR 1740, 1730, 1600, and 1550 cm^{-1}; UV λ_{max}^{hexane} 220 (3.65), 276 (4.50), and 357 (4.19); ^{13}C NMR ($CHCl_3$) δ=174.4, 165.0, 140.6, 125.0, 116.0, 117.1, 82.1, 74.9, and 14.7.[28] Found: C, 35.77; H, 1.50; Cl, 53.25%. Calcd for $C_{10}H_5Cl_5O_2$: C, 35.92; H, 1.50; Cl, 53.01%.

*Pentachloro-4-isopropoxybicyclo[3.3.0]octa-3,5,7-trien-2-one(**17b**).* A mixture of 2-propanol (10 cm^3), chloroform (5 cm^3) and 0.913 g of **14** was stirred for 1 h and kept at room temperature overnight. The yellow crystals obtained by evaporation of the solvent under reduced pressure were separated by filtration and crystallized from carbon tetrachloride: mp 149 °C dec; IR 1740, 1730, 1590, and 1540 cm^{-1}; UV λ_{max}^{hexane} 220 (3.68), 277 (4.27), and 355 (4.16); ^{13}C NMR ($CHCl_3$) δ=174.5, 164.5, 140.1, 124.9, 124.4, 116.6, 115.9, 83.0, and 22.0. Found: C, 37.51; H, 1.97; Cl, 50.88%. Calcd for $C_{11}H_7Cl_5O_2$: C, 37.92; H, 2.02; Cl, 50.88%.

*Pentachloro-4-hydroxybicyclo[3.3.0]octa-3,5,7-trien-2-one (**17d**).* Methanol (10 cm^3) was added to 1.038 g of **14** and refluxed gently for 10 min. The solution turned strongly acidic and dark greenish brown. Evaporation of the solvent left greenish yellow crystals, which were crystallized from a mixture of benzene (5 cm^3) and petroleum ether (3 cm^3) to give 0.837 g of yellow crystals of **17d**: mp 178 °C decomp; IR 3600, 3375, 1715, 1645, 1265, and 1130 cm^{-1}; UV λ_{max}^{hexane} 220 (3.62), 276 (4.56), and 357 (4.23). Found: C, 30.69; H, 0.67%. Calcd for $C_8HCl_5O_2 \cdot 1/2\ H_2O$: C, 30.43; H, 0.64%.[29]

*Chlorination of **6** with Antimony(V) Chloride. Formation of **11**:* A mixture of 5.5 g (16.9 mmol) of **6**, 6.13 g (20.5 mmol) of antimony(V) chloride, and 40 cm^3 of dry dichloromethane was refluxed for 4 h. After quenching the red reaction mixture with 50 cm^3 of concd hydrochloric acid, organic products were extracted with carbon tetrachloride. The organic solution was washed with water and dried over sodium sulfate. Evaporation of the solvent left 3.30 g of crude product. Distillation at 180—190 °C/2 mmHg gave a pure sample which showed single peak on gas chromatography (Nikki Model G-77) column: 20% SE-30 on Celite 545, mesh 60—80, and 2 m, He flow: 16.4 cm^3/min; column temperature: 250 °C: IR 1757, 1616, and 1590 cm^{-1}; UV λ_{max}^{hexane} 248 (3.90). Found: C, 24.80; H, 0.06%. Calcd for C_8Cl_8O: C, 24.28%.

*Chlorination of **12** with Phosphorus(V) Chloride.* In a thick wall glass tube, 1.126 g (3.3 mmol) of **12** and 0.894 g (4.3 mmol) of phosphorus(V) chloride was sealed and heated at 140—150 °C in an oil bath for 8 h, and allowed to cool to room temperature. The reaction mixture was treated with water and the products were taken up in carbon tetrachloride. The crude product was chromatographed on silica gel with petroleum benzine as eluent. A fraction eluted as a light yellow band was collected and evaporation of the solvent afforded 479 mg of **11**. Found: C, 24.38; H, 0.16; Cl, 71.83%. Calcd for C_8Cl_8O: C, 24.28; Cl, 71.68%.

*Chlorination of **13** with Phosphorus(V) Chloride.* Phosphorus(V) chloride (896 mg) was allowed to react with 467 mg of **13** under the same conditions as mentioned for the preceding reaction and 560 mg of **11** was obtained by the conventional isolation procedure.

*3,6,7,7,8-Pentachlorobicyclo[3.3.0]octa-5,8-diene-2,4-dione (**18**).* A methanolic solution of 1.325 g of **17a** was kept at room temperature for 2 d. Evaporation of the solvent afforded a brown oily product, which crystallized on trituration with petroleum ether. The product was chromatographed on silica gel (13 mm × 11 cm) with chloroform as eluent. The first yellowish brown band yield, after being stripped of the solvent, 0.3 g of **18**. Recrystallization from petroleum ether gave an analytical sample, mp 118—119 °C. Identification

was made by comparison of the IR spectrum with that of authentic sample prepared from **1** by the reported method.[4d]

*A Complex of **6** with Antimony(V) Chloride. Formation of **19**:* To a saturated solution of 0.488 g of **6** in dry dichloromethane (2.0 cm^3) were added 4 drops of antimony(V) chloride to precipitate an orange-brown crystalline material immediately, which was washed with a small amount of dichloromethane: IR (suspension in dichloromethane) 1690, 1640, 1500, 1305, 1245, 1195, 1100, 1033, 860, 805, 765, 745, and 580 cm^{-1}.

*Quantitative Analysis of **19**.* To a solution of **6** (0.40 g) in 1 cm^3 of carbon tetrachloride in a dry centrifuge tube (20 mm×9 cm) sealed with a rubber cup was added 0.75 g of antimony(V) chloride in 1 cm^3 carbon tetrachloride. Precipitated yellow crystals were washed with two portions of carbon tetrachloride (2 cm^3) and the residual solvent was evaporated under reduced pressure on phophorus pentaoxide to give 0.595 g of **19**. The complex was decomposed with 40 cm^3 of 6 M hydrochloric acid to give yellow crystals, which were separated by filtration and washed with a small amount of distilled water. Yield: 0.298 g (96.2%) of **6**. To the aq mother solution was added 0.90 g sodium sulfite and the solution was kept at room temperature for 17 h and then refluxed gently for 1.5 h to remove excess sulfite ion (potassium periodate–starch test paper). The filtrate (50.479 g) was divided into three portions and 20 cm^3 of distilled water was added to each portion, which was titrated with 0.02 M potassium permanganate solution. The average volume of permanganate solution corresponding to the whole filtrate was 19.52±0.29 cm^3 (1.1% in excess of the value calcd for $C_8Cl_6O \cdot SbCl_5$).

The author wishes to express his thanks to Professor Toshio Miwa of Osaka City University for useful discussion. He would like also to thank Dr. Takashi Tokuyama of Osaka City University and Dr. Shoji Imakoto of Suntory Co., Ltd. for measuring the mass spectra, and Dr. Koichi Mano of our institute for measuring the NQR spectra.

References

1) R. West, *Acc. Chem. Res.*, **3**, 130 (1969); *Pure Appl. Chem.*, **28**, 379 (1971).
2) K. Kusuda and N. Osaka, *J. Chem. Soc., Chem. Commun.*, **1972**, 508.
3) a) G. Mandel and J. Donohue, *Acta Crystallogr., Sect. B*, **1973**, 710; b) J. Haase and P. Widmann, *Z. Naturforsch., A*, **1973**, 1573; c) J. Haase and P. Widmann, *ibid.*, **1973**, 1737.
4) a) A. Roedig, *Angew. Chem.*, **81**, 157 (1969); b) A. Roedig, R. Helm, R. West, and R. M. Smith, *Tetrahedron Lett.*, **1969**, 2137; c) R. Criegee and R. Huber, *Chem. Ber.*, **103**, 1862 (1970); d) A. Roedig, G. Bonse, and R. Helm, *ibid.*, **106**, 2156 (1973); e) A. Roedig and M. Foersch, *Justus Liebigs Ann. Chem.*, **1978**, 1775.
5) K. Kusuda, M. Endo, R. West, and V. N. M. Rao, *J. Org. Chem.*, **39**, 1641 (1974).
6) H. G. Kuivila, *Acc. Chem. Res.*, **1**, 288 (1968); H. G. Kuivila, *Synthesis*, **1970**, 499 and the literature cited therein.
7) K. Kusuda and A. Roedig, *Bull. Chem. Soc. Jpn.*, **52**, 811 (1979).
8) J. J. Gajewski and C. J. Cavender, *Tetrahedron Lett.*, **1971**, 1075; R. Kaiser and K. Hafner, *Angew. Chem.*, **82**, 877 (1970).
9) T. Matsukura, K. Mano, and A. Fujino, *Bull. Chem. Soc. Jpn.*, **48**, 2464 (1975).
10) K. Kusuda, H. Maeda, H. Wachi, and A. Fujino, *Synthesis*, **1975**, 631.
11) C A. Buehler and D. E. Pearson, "Survey of Organic Synthesis," Wiley-Interscience, New York (1970), p. 80.
12) S. W. Tobey and R. West, *Tetrahedron Lett.*, **1963**, 1179.
13) H. J. Prins, *Recl. Trav. Chim. Pays-Bas*, **65**, 455 (1946).
14) A. Roedig and F. Bischoff, *Naturwissenschaften*, **49**, 448 (1962).
15) K. Kusuda, unpublished work.
16) H. Hart and M. Kuzuya, *J. Am. Chem. Soc.*, **98**, 1551 (1976).
17) Examples of structural determination by NQR: R. M. Smith and R. West, *Tetrahedron Lett.*, **1969**, 2141; K. Kusuda, R. West, and V. N. M. Rao, *J. Am. Chem. Soc.*, **93**, 3627 (1971).
18) For other examples of chlorination with antimony(V) chloride see S. Uemura, O. Sasaki, and M. Okano, *J. Chem. Soc., Chem. Commun.*, **1971**, 1064; D. M. Gale and S. C. Cherkofsky, *J. Org. Chem.*, **38**, 475 (1975).
19) Hexachlorobicyclo[3.3.0]octa-1(5),3,5,6-trien-2-one or hexachlorobicyclo[3.3.0]octa-1(5),3,7-trien-2-one was assigned to the structure of a chlorocarbon on the basis of ^{13}C NMR spectra. G. E. Hawkes, R. A. Smith, and J. D. Roberts, *J. Org. Chem.*, **39**, 1276 (1974).
20) A. Roedig, *Justus Liebigs Ann. Chem.*, **569**, 161 (1950), E. T. McBee, J. D. Idol, Jr., and C. W. Roberts, *J. Am. Chem. Soc.*, **77**, 4375 (1955). Hexachlorofulvene: λ_{max}^{hexane} 288 (4.20), 297 (4.33), 308 (4.32), 322 (4.03), and 450 (2.4).
21) M. A. Ogliaruso, M. G. Romanelli, and I. I. Becker, *Chem. Rev.*, **65**, 261 (1965); E. W. Garbish, Jr., and R. G. Sprecher, *J. Am. Chem. Soc.*, **91**, 6785 (1969).
22) P. C. Billot, R. G. Barker, K. Mackenzie, and P. R. Young, *Tetrahedron Lett.*, **1973**, 3059; E. T. McBee, D. L. Crain, L. R. Belohlar, and H. P. Braendlin, *J. Am. Chem. Soc.*, **84**, 3557 (1962).
23) E. T. McBee, E. P. Wesseler, R. Hurnaus, and T. Hodgins, *J. Org. Chem.*, **37**, 1100 (1972).
24) R. Breslow, *Acc. Chem. Res.*, **6**, 393 (1973).
25) R. W. Johnson, *J. Am. Chem. Soc.*, **99**, 1461 (1977).
26) S. Oota, *Bunseki Kagaku*, **15**, 689 (1966); **17**, 1322 (1968); **18**, 1257 (1969).
27) The fact that a peak at 117.1 ppm is a doublet was revealed by the x-axis expansion technique. Corresponding peaks of **17b** and **17c** are clearly separated.
28) By the comparison of ^{13}C NMR spectra of **17a—c**, it can be speculated that the peak at 125.0 ppm is a result of overlapping of two peaks.
29) Measurement of ^{13}C NMR spectrum of **17d** was unsuccessful because of its instability in chloroform.
30) K. Ueno, "Kireitotekitei (Chelate Titration)," Nankodo, Tokyo (1972), p. 375; I. M. Kolthoff, R. Belcher, V. A. Strenger, and G. Matsuyama, "Volumetric Analysis," (Oxidation Reduction Reactions), Interscience, New York (1975), Vol. 3, p. 73.

Studies on the Polymerization of Acrolein Oxime. XVII.† The Structure of the β-Form of the Bicyclic Trimer from Methacrylaldehyde Oxime

Tadatoshi Ota,* Seizo Masuda, Hitoshi Tanaka, Yasuo Inazawa, and Masaru Kido††

Department of Applied Chemistry, Faculty of Engineering, Tokushima University, Minamijosanjima-cho, Tokushima 770

††*Tokushima Research Institute, Ōtsuka Pharmaceutical Co. Ltd., Kawauchi-cho, Tokushima 771-01*

(Received April 30, 1982)

The thermal oligomerization of methacrylaldehyde oxime leads to 2,4,7-trimethylperhydroisoxazolo[2,3-*a*]-pyridine-2,7-dicarbaldehyde dioxime (**1**). The β-form of **1** was separated, and its crystal structure was determined by X-ray analysis. It is monoclinic with space group $P2_1/c$, $a=13.274(11)$, $b=8.652(7)$, $c=11.618(14)$ Å, $\beta=96.73(8)°$, and $Z=4$. The molecules are linked by two N···O hydrogen bonds, with the N(13)···O(14) and N(8)···O(18) distance of 2.824(5) and 2.897(5) Å respectively.

In the course of a study of the thermal polymerization of α,β-unsaturated aldehyde and ketone oximes, which have a vinylic double-bond conjugated with a hydroxyiminomethyl group, it has been found that methacrylaldehyde oxime (MAOM) and 3-methyl-3-buten-2-one oxime preferentially give a bicyclic trimer and a dimer respectively.[1,2] The bicyclic trimer from MAOM, 2,4,7-trimethylperhydroisoxazolo[2,3-*a*]pyridine-2,7-dicarbaldehyde dioxime (**1**), is isomeric. In our previous paper,[3] the crystal structure of the α-form of **1** was determined by means of X-ray diffraction; the chemical structure of the β-form was assumed on the basis of the spectrometrical data because of the very low yield and the failure to crystallize.

The present paper will describe the separation of the β-form and its X-ray structure analysis.

Experimental

Oligomerization of MAOM. Methacrylaldehyde was prepared by the Mannich reaction of propionaldehyde and formaldehyde,[4] and then oximated with hydroxylamine hydrochloride according to the procedure of Mowry.[5] The oligomerization of MAOM was carried out at 80 °C for 100 h in an ampoule. After the unreacted MAOM had been removed under reduced pressure, the residue was poured into a large amount of ether to precipitate the α-form of **1**. The precipitates were filtered off, and then the ether solution was concentrated and subjected to a large amount of hexane so that a yellow powder containing seven or more compounds was precipitated. The β-form was separated from the yellow powder by preparative TLC on silica gel in chloroform-ethyl acetate (7: 1) and recrystallized form its methanol solution. Colorless columnar crystals with the melting point of 192 °C (decomp). IR: 3325 (ν_{OH}), 1640 ($\nu_{C=N}$), 1380 (δ_{CH3}), and 930 cm^{-1} (ν_{NO}). MS *m/e* (relative intensity): 225 (M^+, 15), 240 (100), and 211 (38). ^{1}H-NMR (DMSO-d_6): $\delta=$ 10.67 (1H, s, OH), 10.55 (1H, s, OH), 7.31 (1H, s, CH=N), 7.21 1H, s, CH=N), 3.00 (1H, broad m, H(9), $J_{9.4}=4$ Hz), 2.25 (1H, t, H(3), $J_{3.3}=11$, $J_{3.9}=11$ Hz), 2.08 (1H, broad m, H(4)), 1.89 (1H, q, H(3), $J_{3.9}=7$ Hz), 1,75 (2H, broad d, H(6)), 1.39 (2H, broad m, H(5)), 1.29 (3H, s. CH_3), 1.20 (3H, s, CH_3), and 0.94 (3H, d, CH_3, $J_{10.4}=7$ Hz).

X-Ray Measurements. A crystal $0.4\times0.4\times0.1$ mm^3 in size was used for the X-ray measurements. The unit-cell dimensions were determined precisely by the least-squares fit of 2θ values of 16 reflections measured on a Syntex R-3 automated four-circle diffractometer with graphite-monochromated Mo $K\alpha$ radiation. The crystal data are as follows;** $C_{12}H_{21}N_3O_3$, M. W.=255.32, monoclinic, space group $P2_1/c$, $a=13.274(11)$, $b=8.652(7)$, $c=11.618(14)$ Å, $\beta=96.73(8)°$, $U=1325$ Å^3, $Z=4$, $D_x=1.28$ g cm^{-3}, μ(Mo $K\alpha$)=1.0 cm^{-1}.

The reflections within the range of $2\theta<45°$ were collected by the use of an ω-scan mode. The intensities of three reference reflections were measured periodically; they showed no significant fluctuation during the data collection. A total of 1743 independent reflections were collected, among which 1214 reflections with $I\geqq1.96\sigma(I)$ were used for structure refinement. The intensities were corrected for Lorentz and polarization effects, but not for absorption.

Structure Determination and Refinement. The structure was solved by the direct method using the MULTAN program.[6] The atomic parameters were refined by the block-diagonal least-suqares method. The function minimized was $\Sigma w(|F_o|-|F_c|)^2$, where w was fixed as unity for non-zero reflections. The final value of R was 0.063. All the calculations were carried out on a NOVA 3 computer connected to the diffractometer, using the Syntex XTL programs. The atomic scattering factors were taken from the "International Tables for X-Ray Crystallography."[7]

Other Measurements. The ^{1}H-NMR spectra were recorded on a JEOL JNM-FX200 spectrometer (200 MHz), and the ^{13}C-NMR spectra, on a Hitachi R-42 spectrometer (22.6 MHz). The mass spectra were taken on a Shimadzu LKB-9000 mass spectrometer.

Results and Discussion

The atomic parameters, bond distances, and bond angles are listed in Tables 1—3 respectively.[8] Figure 1 shows a perspective drawing of the β-form of **1** and numbering scheme of the atoms. The six-membered ring has a chair form, while the five-membered ring, which is in a half-chair form, is fused to the six-membered ring through two equatorial-type bonds. The two rings are approximately coplanar to each other. The methyl group at the C(4) carbon is axial, while the methyl and hydroxyiminomethyl groups at the C(7) carbon are axial and equatorial respectively. In addition, the

† Part XVI: T. Ota, S. Masuda, H. Tanaka, and M. Kido, *Bull. Chem. Soc. Jpn.*, **55**, 171 (1982).

** There is a printing error in one of our published papers, *Bull. Chem. Soc. Jpn.*, **53**, 3240 (1980). The correct space group of the α-form of **1** is $P2_1/c$.

TABLE 1. ATOMIC COORDINATES, MULTIPLIED BY 10^4 FOR NON-HYDROGEN ATOMS AND BY 10^3 FOR HYDROGEN ATOMS, WITH ESTIMATED STANDARD DEVIATIONS IN PARENTHESES

Atom	x	y	z	B_{eq}/Å^2 a)	Atom	x	y	z	B/Å^2
O(1)	7912(2)	2646(4)	2844(3)	3.6	H(31)	925(3)	178(5)	470(3)	10(9)
O(14)	6136(3)	−580(5)	−58(3)	5.0	H(32)	890(3)	329(5)	546(3)	52(11)
O(18)	11032(2)	3784(4)	2233(3)	4.4	H(4)	750(3)	83(5)	620(3)	44(11)
N(8)	7644(3)	1221(5)	3405(3)	2.5	H(51)	628(3)	−147(6)	546(4)	84(15)
N(13)	5914(3)	162(5)	967(3)	3.8	H(52)	599(3)	64(5)	509(3)	40(11)
N(17)	10217(3)	4294(5)	2827(3)	3.5	H(61)	562(3)	−88(5)	328(4)	66(13)
C(2)	8745(4)	3372(6)	3625(4)	3.1	H(62)	678(3)	−174(5)	356(3)	52(12)
C(3)	8772(3)	2465(6)	4746(4)	3.5	H(9)	721(3)	276(5)	477(3)	55(11)
C(4)	7521(4)	303(6)	5398(4)	3.3	H(101)	891(3)	−73(5)	582(3)	72(13)
C(5)	6458(4)	−266(7)	4968(5)	4.2	H(102)	838(3)	−169(5)	470(3)	52(11)
C(6)	6336(4)	−605(6)	3654(4)	4.0	H(103)	808(3)	−196(5)	608(3)	98(14)
C(7)	6600(3)	788(6)	2912(4)	2.7	H(111)	603(3)	302(4)	258(3)	42(10)
C(9)	7737(3)	1691(6)	4630(4)	2.7	H(112)	572(3)	253(5)	365(3)	69(13)
C(10)	8291(4)	−1009(7)	5467(5)	4.4	H(113)	514(3)	166(5)	250(3)	41(10)
C(11)	5826(4)	2091(7)	2912(5)	4.3	H(12)	733(3)	−4(5)	146(4)	49(12)
C(12)	6672(3)	165(6)	1711(4)	3.4	H(151)	782(3)	510(5)	423(3)	52(11)
C(15)	8468(4)	5038(6)	3785(5)	4.0	H(152)	901(3)	561(5)	433(4)	62(13)
C(16)	9677(3)	3144(6)	3024(4)	3.0	H(153)	838(3)	571(4)	319(3)	36(10)
					H(16)	981(3)	201(5)	268(3)	38(10)
					HO(14)	549(3)	−59(5)	−52(4)	82(15)
					HO(18)	1137(3)	464(5)	222(4)	45(12)

a) Equivalent isotropic thermal parameters were calculated from the refined anisotropic thermal parameters.[9]

TABLE 2. BOND DISTANCES, WITH ESTIMATED STANDARD DEVIATIONS IN PARENTHESES

Bond distance	l/Å	Bond distance	l/Å
O(1)-N(8)	1.461(5)	O(1)-C(2)	1.478(6)
O(14)-N(13)	1.414(5)	O(18)-N(17)	1.419(5)
N(8)-C(9)	1.471(6)	N(8)-C(7)	1.484(6)
N(13)-C(12)	1.248(6)	N(17)-C(16)	1.263(6)
C(2)-C(3)	1.517(7)	C(2)-C(15)	1.505(7)
C(2)-C(16)	1.504(7)	C(3)-C(9)	1.520(7)
C(4)-C(5)	1.523(7)	C(4)-C(9)	1.543(7)
C(4)-C(10)	1.522(8)	C(5)-C(6)	1.544(8)
C(6)-C(7)	1.545(7)	C(7)-C(11)	1.525(7)
C(7)-C(12)	1.509(7)		

methyl and hydroxyiminomethyl groups at the C(2) carbon are on the same side of the average coplane of the rings, and on the opposite side, respectively, with the methyl group at the C(7) carbon.

In the previous paper,[3] the chemical structure of the β-form has been spectrometrically assumed. However. the results of X-ray analysis show that the crystal structure of the β-form differs from the estimated one and is the same as that of the α-form, except that the methyl groups at the C(4) and C(7) carbons are axial. This finding is also supported by the ^{1}H-NMR spectra. The C(4) proton resonates at 2.08 ppm with the coupling constant $J_{4,9}$=4 Hz; *i.e.*, the H(4) hydrogen is equatorial, and the C(4) carbon is thus axial. On the basis of these results, a schematic drawing of **1** is shown in Fig. 2.

The mass spectra of both α- and β-forms have a molecular ion peak at m/e 255, and they give similar fragmentation patterns except for the base ion peaks,

TABLE 3. BOND ANGLES, WITH ESTIMATED STANDARD DEVIATIONS IN PARENTHESES

Bond angle	ϕ/°	Bond angle	ϕ/°
N(8)-O(1)-C(2)	106.9(3)	O(1)-N(8)-C(9)	101.6(3)
O(1)-N(8)-C(7)	108.1(3)	C(9)-N(8)-C(7)	114.3(4)
O(14)-N(13)-C(12)	110.7(4)	O(18)-N(17)-C(16)	108.9(4)
O(1)-C(2)-C(3)	104.4(4)	O(1)-C(2)-C(15)	108.0(4)
O(1)-C(2)-C(16)	104.6(4)	C(3)-C(2)-C(15)	111.7(4)
C(3)-C(2)-C(16)	113.1(4)	C(15)-C(2)-C(16)	114.2(4)
C(2)-C(3)-C(9)	102.8(4)	C(5)-C(4)-C(9)	106.8(4)
C(9)-C(4)-C(10)	116.2(4)	C(5)-C(4)-C(10)	111.5(4)
C(4)-C(5)-C(6)	111.8(4)	C(5)-C(6)-C(7)	113.5(4)
N(8)-C(7)-C(6)	104.1(4)	N(8)-C(7)-C(11)	114.3(4)
N(8)-C(7)-C(12)	106.8(4)	C(6)-C(7)-C(11)	112.3(4)
C(6)-C(7)-C(12)	106.3(4)	C(11)-C(7)-C(12)	112.3(4)
N(8)-C(9)-C(3)	100.4(4)	N(8)-C(9)-C(4)	110.1(4)
C(3)-C(9)-C(4)	121.2(4)	N(13)-C(12)-C(7)	120.5(4)
N(17)-C(16)-C(2)	119.8(4)		

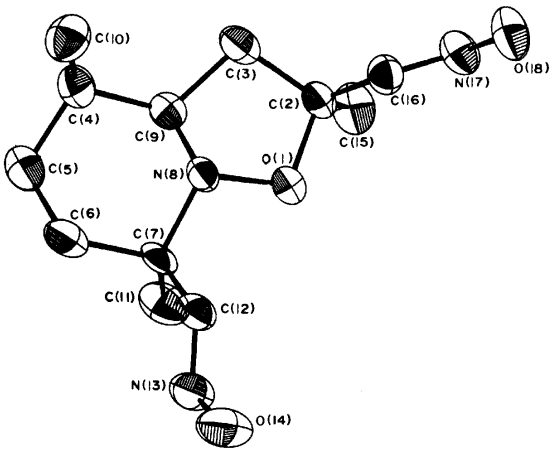

Fig. 1. A perspective drawing of the β-form molecule and the numbering scheme. Thermal ellipsoids of non-hydrogen atoms were drawn by ORTEP.[10]

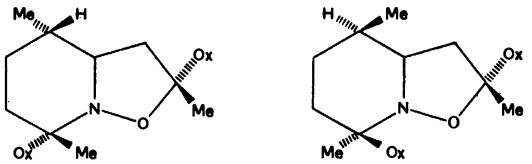

Fig. 2. Schematic drawing of isomeric **1**.

which appear at *m/e* 211 (the lost of the hydroxyiminomethyl radical) for the former and at *m/e* 240 (the lost of the methyl radical) for the latter. These observations show that the axial substituent at the C(7) carbon is more liable to be eliminated than the equatorial one because of steric hindrance.

There are characteristic bond angles which are common to the α- and β-forms. The axial conformation of the substituents at the C(4) and C(7) atoms always gives larger substituent-related interbond angles than do the equatorial ones; *i.e.*, the C(5)–C(4)–C(10), C(9)–C(4)–C(10), C(5)–C(4)–H(4), C(9)–C(4)–H(4), N(8)–C(7)–C(11), C(6)–C(7)–C(11), N(8)–C(9)–C(12), and C(6)–C(7)–C(12) angles are larger in the axial position of C(10), C(11), C(12), and H(4) atoms than those in the equatorial ones.

Figure 3 shows the crystal structure of the β-form viewed along the b axis. There are two intermolecular hydrogen bonds; the N(13)···H(14)–O(14) ($1-x$, $-y$, $-z$) and N(8)···H(18)–O(18) ($2-x$, $0.5+y$, $0.5-z$), with angles of 158(4) and 156(4)° respectively. The bond distances of N(13)···O(14), N(13)···H(14), O(14)–H(14), N(8)···O(18), N(8)···H(18), and O(18)–H(18) are 2.824(5), 1.91(5), 0.96(5), 2.897(5), 2.08(4), and 0.87(4) Å respectively.

The ^{13}C-NMR peak assignments are shown in Table 4, together with those of the α-form. These peak position were assigned by using the off-resonance technique and on the basis of the molecular structure determined by X-ray analysis. The signals assignable to the C(10) and C(11) carbons in the β-form and the C(12) carbon in the α-form are shifted to higher magnetic fields due

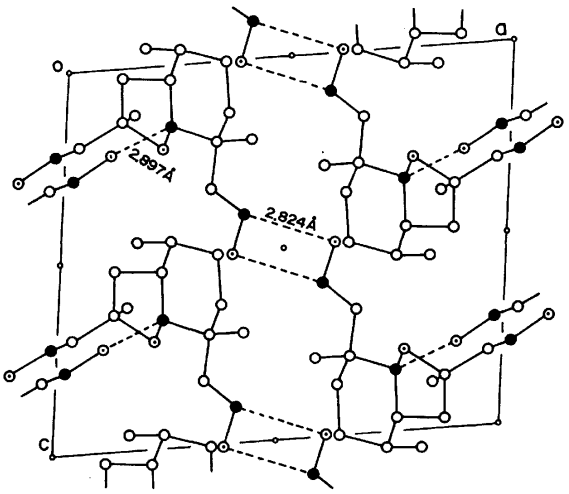

Fig. 3. Orthogonal projection of the crystal structure viewed along the b axis.
○: Carbon ●: nitrogen, ⊙: oxygen.

Table 4. Assignment of ^{13}C-NMR peaks of **1**

Carbon	Multiplicity	Peak position/ppm from TMS	
		α-Form	β-Form
-C(10)H_3	q	27.42	12.59
-C(11)H_3	q	18.79	10.86
-C(15)H_3	q	24.42	24.38
>C(3)H_2	t	30.16	30.78
>C(5)H_2	t	35.28	27.15
>C(6)H_2	t	44.41	41.75
>C(4)H	d	36.44	30.47
>C(9)H	d	65.99	59.13
>C(2)–O	s	77.62	77.16
>C(7)–N	s	60.75	61.41
-C(12)H=N	d	150.40	156.54
-C(16)H=N	d	154.44	154.41

s: Singlet, d: doublet, t: triplet, q: quartet.

to the axial position of the methyl and hydroxyiminomethyl groups. Since the carbon at the 4-position in a piperidine ring is known to resonate in a higher field than that at the 3-position,[11] the peak assignment of three methylene carbons seems to be reasonable.

Reference

1) T. Ota, E. Matsushima, and S. Masuda, *Polym. J.*, **11**, 909 (1979).
2) T. Ota, S. Masuda, and H. Tanaka, *Chem. Lett.*, **1981**, 411.
3) T. Ota, S. Masuda, and M. Kido, *Bull. Chem. Soc. Jpn.*, **53**, 3240 (1980).
4) A. F. Maclean and B. G. Frenz, U. S. Patent, 2848499 (1958); *Chem. Abstr.*, **53**, 3062a (1959).
5) D. J. Mowry and R. R. Morner, *J. Am. Chem. Soc.*, **69**, 1831 (1949).
6) G. Germain, P. Main, and M. M. Woolfson, *Acta Crystallogr., Sect. A*, **27**, 368 (1971).
7) "International Tables for X-Ray Crystallography,"

Kynoch Press, Birmingham (1974), Vol. IV, p. 71.
8) The F_o-F_c table, thermal parameters, bond distances, and bond angles related to hydrogen atoms are kept as Document No. 8302 at the Chemical Society of Japan.
9) A. Ouchi, M. Shimol, T. Takeuchi, and H. Saito, *Bull. Chem. Soc. Jpn.*, **54**, 2290 (1981).
10) C. K. Johnson, *ORTEP*, ORNL-3794, Oak Ridge National Laboratory, Tennessee (1965).
11) I. Morishima, K. Okada, T. Yonezawa, and K. Goto, *J. Am. Chem. Soc.*, **93**, 3922 (1971).

 © 1983 The Chemical Society of Japan Bull. Chem. Soc. Jpn., 56, 491—493 (1983)

Furanosesquiterpenoids: Total Synthesis of Pallescensins 2, F, and G

Takashi MATSUMOTO* and Shuji USUI

Department of Chemistry, Faculty of Science, Hiroshima University, Higashisenda-machi, Naka-ku, Hiroshima 730

(Received June 7, 1982)

Oxidation of the synthetic pallescensin 1 with *m*-chloroperbenzoic acid, followed by treatment of the resulting epoxide with lithium diethylamide, afforded 3-[2-(2-furyl)ethyl]-4,4-dimethyl-2-methylenecyclohexanol (**6**). The alcohol **6** was dehydrated with refluxing hexamethylphosphoric triamide to give pallescensin 2. Oxidation of **6** with pyridinium chlorochromate, followed by intramolecular cyclization with 85% phosphoric acid, afforded 5,5a,6,7,8,9,9a,10-octahydro-6,6-dimethyl-4*H*-benzo[5,6]cyclohepta[1,2-*b*]furan-9-one. This was converted into the corresponding α,β-unsaturated ketone (**10**) *via* an α-phenylseleno ketone. Reduction of **10** with lithium aluminium hydride, followed by dehydration with hexamethylphosphoric triamide at 200—210 °C, afforded pallescensin G, which was further isomerized to pallescensin F.

Pallescensins 2, F, and G, have recently been isolated from the marine sponge *Disidea pallescens* by Cimino *et al.*[1] On the basis of spectroscopic studies, they deduced the structures of pallescensins 2, F, and G, to be **1**, **2**, and **3**, respectively. To confirm the validity of these unique structures, we have attempted the total syntheses of **1**, **2**, and **3**, starting from pallescensin 1 (**4**)[2] which was prepared from α-cyclocitral in our laboratory.

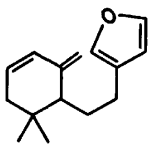

1

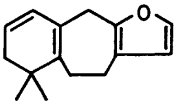

2

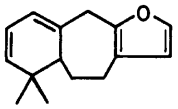

3

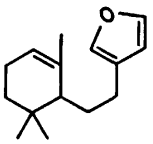

4

Oxidation of **4** with *m*-chloroperbenzoic acid in dichloromethane at 0—5 °C afforded the corresponding epoxide (**5**) which, without purification, was treated with lithium diethylamide[3] in refluxing tetrahydrofuran to give 3-[2-(2-furyl)ethyl]-4,4-dimethyl-2-methylenecyclohexanol (**6**) in 49% yield from **4**. The structure of **6** was supported by its ^{1}H NMR spectrum, which showed broad singlet signals at δ 2.66 (1H) due to a hydroxyl group and at δ 4.71 (1H) and 5.22 (1H) due to an *exo*-methylene group. Dehydration of **6** with refluxing hexamethylphosphoric triamide[4] under a stream of nitrogen afforded the desired 3-[2-(6,6-dimethyl-2-methylene-3-cyclohexenyl)ethyl]furan (**1**) in 89% yield. The ^{1}H NMR spectrum of the synthetic **1** was identical with that of natural pallescensin 2.

Our next effort was directed toward the syntheses of **2** and **3**. Oxidation of **6** with pyridinium chlorochromate in dichloromethane at room temperature afforded the corresponding α,β-unsaturated ketone (**7**) in 80% yield. The IR spectrum of **7** showed a conjugated carbonyl absorption band at 1690 cm^{-1} and its ^{1}H NMR spectrum showed two doublet signals at δ 4.91 (1H, J=2 Hz) and 5.69 (1H, J=2 Hz) due to an *exo*-methylene group. These spectral data suggested the structure of **7** to be 3-[2-(2-furyl)ethyl]-4,4-dimethyl-2-methylenecyclohexanone. Intramolecular cyclization of **7** with 85% phosphoric acid in tetrahydrofuran at room temperature afforded a single tricyclic ketone[5] (**8**) in 79% yield. The ^{1}H NMR spectrum of **8** showed a *gem*-dimethyl group at δ 1.01 (3H, s) and 1.03 (3H, s) and a furan moiety at δ 5.92 (1H, d, J=2 Hz) and 6.97 (1H, d, J=2 Hz). The presence of a non-conjugated carbonyl group (IR: 1705 cm^{-1}) and the chemical shifts of two furan protons suggested the structure of **8** to be 5,5a,6,7,8,9,9a,10-octahydro-6,6-dimethyl-4*H*-benzo-[5,6]cyclohepta[1,2-*b*]furan-9-one. In the present study, the stereochemistry of the ring juncture in **8** has remained unsettled. Treatment of **8** with benzeneselenenyl bromide[6] in tetrahydrofuran at −70 °C in the presence of lithium diisopropylamide under a stream of nitrogen afforded the corresponding α-phenylseleno ketone (**9**) in 80% yield. The ketone **9** in tetrahydrofuran was then treated with 30% hydrogen peroxide at room temperature to give an α,β-unsaturated ketone (IR: 1670 cm^{-1}), 5,5a,6,9,9a,10-hexahydro-6,6-dimethyl-4*H*-benzo[5,6]cyclohepta[1,2-*b*]furan-9-one (**10**), in 69% yield. The ^{1}H NMR spectrum of **10** showed two doublet signals at δ 5.79 (1H, J=10 Hz) and 6.50 (1H, J=10 Hz) due to two olefinic protons, supporting the presence of a disubstituted olefinic moiety. Reduction of **10** with lithium aluminium hydride in ether at 0—5 °C, followed by heating of the resulting alcohol (**11**) with hexamethylphosphoric triamide at 200—210 °C under a stream of nitrogen, afforded the desired 5,5a,6,10-tetrahydro-6,6-dimethyl-4*H*-benzo[5,6]cyclohepta[1,2-*b*]-furan (**3**) in 51% yield from **10**. The structure of **3** was supported by its ^{1}H NMR spectrum, which showed signals at δ 0.99 (3H) and 1.06 (3H) due to a *gem*-dimethyl group, at δ 5.4 (1H) and 5.73 (2H) due to three olefinic protons, and at δ 6.12 (1H) and 7.18 (1H) due to two furan protons. Isomerization of **3** with refluxing hexamethylphosphoric triamide under a stream of nitrogen afforded an isomer (**2**) in 75% yield. The ^{1}H NMR spectrum of **2** showed a *gem*-dimethyl group at δ 1.03 (6H), four methylene groups at δ 2.03 (2H), 2.47 (4H), and 3.37 (2H), two olefinic protons at δ 5.52 (1H) and 5.74 (1H), and two furan protons at δ 5.97 (1H) and 7.02 (1H). These spectral data,

especially the presence of signals due to four methylene groups and two olefinic protons, suggested the structure of **2** to be the desired 5,6,7,10-tetrahydro-6,6-dimethyl-4*H*-benzo[5,6]cyclohepta[1,2-*b*]furan. The ^{1}H NMR spectra of the synthetic **2** and **3** were also in good agreement with those[1] of natural pallescensins F and G.

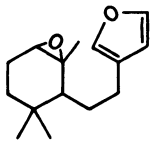

5

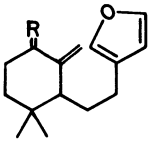

6 R = H,OH
7 R = O

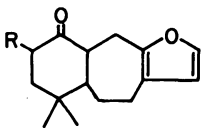

8 R = H
9 R = SePh

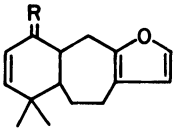

10 R = O
11 R = H,OH

Experimental

The melting point is uncorrected. The IR spectra were measured in chloroform and the ^{1}H NMR spectra in carbon tetrachloride at 90 MHz, with tetramethylsilane as an internal standard, unless otherwise stated. The chemical shifts are presented in terms of δ values; s: singlet, bs: broad singlet, d: doublet, bd: broad doublet, dd: double doublet, t: triplet, dt: double triplet, m: multiplet, dm: doublet of multiplet. Column chromatography was performed using Merck silica gel (0.063—0.200 mm).

3-[2-(2,6,6-Trimethyl-2-cyclohexenyl)ethyl]furan (Pallescensin 1) (**4**). Pallescensin 1 was prepared from (±)-α-cyclocitral by the known procedure.[2]

3-[2-(2-Furyl)ethyl]-4,4-dimethyl-2-methylenecyclohexanol (**6**). A solution of **4** (412 mg) and 85% *m*-chloroperbenzoic acid (420 mg) in dichloromethane (6.0 ml) was stirred at 0—5 °C for 1 h and then diluted with ether. The solution was washed successively with 10% aqueous potassium iodide, aqueous sodium thiosulfate, aqueous sodium hydrogencarbonate, and brine. The dried solution was evaporated *in vacuo* to give a crude epoxide (**5**); ^{1}H NMR (60 MHz): 0.83 (3H, s) and 0.90 (3H, s) (–C(CH$_3$)$_2$), 1.30 (3H, s, –OCCH$_3$), 6.23 (1H, bs), 7.18 (1H, bs), and 7.26 (1H, t, J=2 Hz) (furan protons).

A solution of the crude **5** in dry tetrahydrofuran (2.0 ml) was added to a solution of lithium diethylamide which was prepared from butyl lithium in hexane [1.6 M (1 M=1 mol dm^{-3}): 6.0 ml] and diethylamine (1.0 ml) in dry tetrahydrofuran (4.0 ml) at room temperature for 30 min. The mixture was refluxed for 3 h, cooled, and diluted with ether. The solution was washed successively with aqueous ammonium chloride and brine, dried over sodium sulfate, and evaporated *in vacuo*. The crude product was purified by column chromatography on silica gel (Merck, 0.063 mm: 40 g), usingether–benzene (1: 9) as the eluent, to give **6** (215 mg: 49% from **4**); IR: 3610, 3450 br cm^{-1}; ^{1}H NMR (60 MHz): 0.73 (3H, s) and 0.96 (3H, s) (–C(CH$_3$)$_2$), 2.66 (1H, bs, –OH), 3.88 (1H, m, $W_{1/2}$=16 Hz, –CHOH), 4.71 (1H, bs) and 5.22 (1H, bs) (–C=CH$_2$), 6.18 (1H, bs), 7.12 (1H, bs), and 7.27(1H, t, J=2 Hz) (furan protons). Found: C, 76.75; H, 9.73%. Calcd for $C_{15}H_{22}O_2$: C, 76.88; H, 9.46%.

3-[2-(6,6-Dimethyl-2-methylene-3-cyclohexenyl)ethyl]furan (Pallescensin 2) (**1**). A solution of **6** (200 mg) in hexamethylphosphoric triamide (2.0 ml) was refluxed for 1.5 h under a stream of nitrogen. The solution was cooled, poured into dilute hydrochloric acid, and extracted with ether. The ether extract was washed with brine, dried over sodium sulfate, and evaporated *in vacuo*. The crude product was purified by column chromatography on silica gel (20 g), using hexane as the eluent, to give **1** (164 mg: 89%); ^{1}H NMR: 0.84 (3H, s) and 0.97 (3H, s) (–C(CH$_3$)$_2$), 4.71 (1H, bs) and 4.87 (1H, bs) (–C=CH$_2$), 5.57 (1H, dm, J=10 Hz, –CH=CH–C=), 5.99 (1H, bd, J=10 Hz, –CH=CH–C=), 6.14 (1H, bs), 7.10 (1H, bs), and 7.23 (1H, t, J=2 Hz) (furan protons). Found: C, 83.00; H, 9.35%. Calcd for $C_{15}H_{20}O$: C, 83.28; H, 9.32%. The ^{1}H NMR spectrum of the synthetic **1** was identical with that of natural pallescensin 2.

3-[2-(2-Furyl)ethyl]-4,4-dimethyl-2-methylenecyclohexanone (**7**). A mixture of **6** (165 mg) and pyridinium chlorochromate (230 mg) in dichloromethane (4.0 ml) was stirred at room temperature for 3 h, poured into aqueous sodium carbonate, and extracted with ether. The ether extract was washed with brine, dried over sodium sulfate, and evaporated *in vacuo*. The crude product was chromatographed on silica gel (15 g), using ether–benzene (2: 98) as the eluent, to give **7** (132 mg: 80%); IR: 1690 cm^{-1}; ^{1}H NMR: 1.01 (3H, s) and 1.08 (3H, s) (–C(CH$_3$)$_2$), 4.91 (1H, d, J=2 Hz) and 5.69 (1H, d, J=2 Hz) (–C=CH$_2$), 6.17 (1H, bs), 7.12 (1H, bs), and 7.26 (1H, t, J=2 Hz) (furan protons). Found: C, 77.27; H, 8.79%. Calcd for $C_{15}H_{20}O_2$: C, 77.55; H, 8.68%.

5,5a,6,7,8,9,9a,10-Octahydro-6,6-dimethyl-4H-benzo-[5,6]cyclohepta[1,2-b]furan-9-one (**8**). A solution of **7** (368 mg) in tetrahydrofuran (2.0 ml) was added to a mixture of 85% phosphoric acid (16 ml) and tetrahydrofuran (30 ml). The mixture was stirred at room temperature for 10 h, diluted with ice-water, and extracted with ether. The ether extract was washed with brine, dried over sodium sulfate, and evaporared *in vacuo*. The crude product was purified by column chromatography on silica gel (40 g), using ether–benzene (2 : 98) as the eluent, to give **8** (292 mg: 79%); IR: 1705 cm^{-1}; ^{1}H NMR: 1.01 (3H, s) and 1.03 (3H, s) (–C(CH$_3$)$_2$), 5.92 (1H, d, J=2 Hz) and 6.97 (1H, d, J=2 Hz) (furan protons). Found: C, 77.48; H, 8.78%. Calcd for $C_{15}H_{20}O_2$: C, 77.55; H, 8.68%.

5,5a,6,7,8,9,9a,10-Octahydro-6,6-dimethyl-8-phenylseleno-4H-benzo[5,6]cyclohepta[1,2-b]furan-9-one (**9**). A solution of **8** (67 mg) in dry tetrahydrofuran (1.0 ml) was added at −70 °C to a solution of lithium diisopropylamide [prepared from butyl lithium in hexane (1.6 M: 0.450 ml) and diisopropylamine (0.100 ml) in dry tetrahydrofuran (2.0 ml) at −70 °C] under a stream of nitrogen. The solution was stirred at the same temperature for 10 min and then a solution of benzeneselenenyl bromide (170 mg) in dry tetrahydrofuran (1.0 ml) was added. The mixture was stirred at −70 °C for 10 min more, poured into ice–dilute hydrochloric acid, and extracted with ether. The ether extract was washed with brine, dried over sodium sulfate, and evaporated *in vacuo*. The crude product was purified by column chromatography on silica gel (10 g), using benzene as the eluent, to give **9** (89 mg: 80%). This was recrystallized from methanol; mp 115- 117 °C; IR: 1700 cm^{-1}; ^{1}H NMR: 0.99 (6H, s, –C(CH$_3$)$_2$), 4.18 (1H, dd, J=8 and 12 Hz, C_6H_5SeCH–), 5.98 (1H, d, J=2 Hz) and 7.01 (1H,d, J=2 Hz) (furan protons), 7.0—7.6 (5H, m, C_6H_5Se–). Found:

C, 65.27; H, 6.40%. Calcd for $C_{21}H_{24}O_2Se$: C, 65.11; H, 6.24%.

*5,5a,6,9,9a,10-Hexahydro-6,6-dimethyl-4*H*-benzo[5,6]cyclohepta-[1,2-*b*]furan-9-one (**10**).* A solution of **9** (165 mg) and 30% hydrogen peroxide (0.09 ml) in tetrahydrofuran (4.0 ml) was stirred at room temperature for 1.5 h and then diluted with aqueous sodium hydrogencarbonate. The mixture was extracted with ether. The ether extract was washed with brine, dried over sodium sulfate, and evaporated *in vacuo*. The crude product was chromatographed on silica gel (5 g), using ether–benzene (1:99) as the eluent, to give **10** (68 mg: 69%); IR: 1670 cm^{-1}; ^1H NMR: 1.09 (3H, s) and 1.19 (3H, s) ($-\dot{C}(CH_3)_2$), 5.79 (1H, d, $J=10$ Hz) and 6.50 (1H, d, $J=10$ Hz) ($-CH=CHCO-$), 5.98 (1H, d, $J=2$ Hz) and 7.03 (1H, d, $J=2$ Hz) (furan protons); MS (*m/e*): 230 (M^+).

*5,5a,6,10-Tetrahydro-6,6-dimethyl-4*H*-benzo[5,6]cyclohepta[1,2-*b*]furan (Pallescencin G) (**3**).* A mixture of **10** (68 mg) and lithium aluminium hydride (15 mg) in dry ether (2.0 ml) was stirred at 0—5 °C for 30 min. The mixture was poured into ice–dilute hydrochloric acid and extracted with ether. The ether extract was washed with brine, dried over sodium sulfate, and evaporated *in vacuo* to give a crude alcohol (**11**); IR: 3590, 3430br cm^{-1}; ^1H NMR: 0.93 (3H, s) and 0.98 (3H, s, $-\dot{C}(CH_3)_2$), 2.40 (1H, bs, –OH), 3.72 (1H, bd, $J=10$ Hz, $-\dot{C}\underline{H}OH$) 5.28 (1H, d, $J=10$ Hz) and 5.42 (1H, d, $J=10$ Hz) ($-CH=CH-$), 5.99 (1H, d, $J=2$ Hz) and 7.03 (1H, d, $J=2$ Hz) (furan protons).

The crude alcohol **11** was heated with hexamethylphosphoric triamide (2.0 ml) at 200—210 °C for 1 h under a stream of nitrogen. The mixture was cooled, poured into ice–dilute hydrochloric acid, and extracted with ether. The ether extract was washed successively with dilute hydrochloric acid and brine, dried over sodium sulfate, and evaporated *in vacuo*. The crude product was purified by column chromatography on silica gel (10 g), using hexane–benzene (1 : 1) as the eluent, to give **3** (32 mg: 51% from **10**); ^1H NMR ($CDCl_3$): 0.99 (3H, s) and 1.06 (3H, s) ($-\dot{C}(CH_3)_2$), 3.41 (1H, d, $J=17$ Hz) and 3.67 (1H, d, $J=17$ Hz) ($=\dot{C}CH_2\dot{C}=$), 5.4 (1H, m) and 5.73 (2H, m) (olefinic protons), 6.12 (1H, d, $J=2$ Hz) and 7.18 (1H, d, $J=2$ Hz) (furan protons); MS (*m/e*): 214 (M^+). The ^1H NMR spectrum of the synthetic **3** was in good agreement with that of natural pallescensin G.

*5,6,7,10-Tetrahydro-6,6-dimethyl-4*H*-benzo[5,6]cyclohepta[1,2-*b*]furan (Pallescensin F) (**2**).* A solution of **3** (22.0 mg) in hexamethylphosphoric triamide (2.0 ml) was refluxed for 1 h under a stream of nitrogen. After the same work-up as described for the preparation of **3**, the crude product was chromatographed on silica gel (5 g), using hexane–benzene (1 : 1) as the eluent, to give **2** (16.4 mg: 75%); ^1H NMR: 1.03 (6H, s, $-\dot{C}(CH_3)_2$), 2.03 (2H, dd, $J=4$ and 2 Hz, $=CHC\underline{H}_2\dot{C}-$), 2.47 (4H, s, $-CH_2CH_2-$), 3.37 (2H, bs, $=\dot{C}CH_2\dot{C}=$), 5.52 (1H, dt, $J=10$ and 4 Hz) and 5.74 (1H, dt, $J=10$ and 2 Hz) ($-CH=CH\dot{C}=$), 5.97 (1H, d $J=2$ Hz) and 7.02 (1H, d, $J=2$ Hz) (furan protons); MS (*m/e*): 214 (M^+). The ^1H NMR spectrum of the synthetic **2** was in good agreement with that of natural pallescensin F.

The authors are grateful to Dr. G. Cimino for kindly supplying the spectral data of natural pallescensins.

References

1) G. Cimino, S. De Stefano, A. Guerriero, and L. Minale, *Tetrahedron Lett.*, **1975**, 1417, 1421.

2) T. Matsumoto and S. Usui, *Chem. Lett.*, **1978**, 105.

3) J. K. Crandall and L. C. Lin, *J. Org. Chem.*, **33**, 2375 (1968).

4) R. S. Monson, *Tetrahedron Lett.*, **1971**, 567; R. S. Monson and D. N. Priest, *J. Org. Chem.*, **36**, 3826 (1971).

5) When the cyclization was carried out with 85% phosphoric acid in dichloromethane at room temperature, a mixture of **8** and its other isomer (**8a**) (*ca.* 3 : 7) was obtained in 33% yield. The ^1H NMR spectrum of **8a** showed a *gem*-dimethyl group at δ 1.04 (3H, s) and 1.25 (3H, s) and a furan moiety at δ 5.96 (1H, d, $J=2$ Hz) and 7.04 (1H, d, $J=2$ Hz).

Synthetic Studies on the Validamycins. I. Synthesis of β-D-Glucopyranosylvalidamine: 1L-2-O-(β-D-Glucopyranosyl)-(1,3,4/2,6)-4-amino-6-hydroxymethyl-1,2,3-cyclohexanetriol[1]

Seiichiro OGAWA, Yasuhito SHIBATA, Noritaka CHIDA, and Tetsuo SUAMI*
Department of Applied Chemistry, Faculty of Science and Technology, Keio University, Hiyoshi, Kohoku-ku, Yokohama 223
(Received June 10, 1982)

β-D-Glucopyranosylvalidamine, the structure of which had first been assigned to a degradation product of validamycin A, was synthesized by condensation of a protected validamine with 2,3,4,6-tetra-O-acetyl-α-D-glucopyranosyl bromide, followed by removal of protecting groups. The synthesized β-D-glucopyranoside was not identical with an authentic sample derived from the antibiotic.

Validamycin A is a main component of the validamycin complex which is used to control sheath blight of rice plants and produced by *Streptomyces hygroscopicus* var. *limoneus*. It was isolated by Iwasa *et al.*[2] in 1970 and the structure was first assigned by Horii and Kameda[3] in 1972 on the basis of degradative studies. The unique structural feature of the validamycins prompted us to study the synthesis and structure-activity relationship of this class of antibiotics.

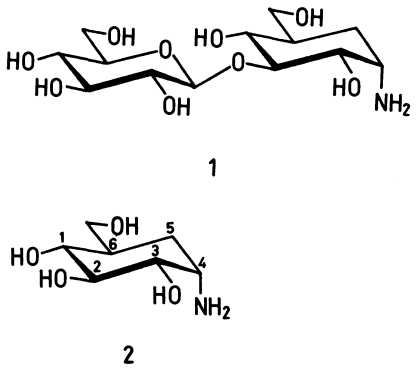

1

2

Scheme 1.

The hydrogenolitic cleavage of validamycin A yields β-D-glucopyranosylvalidamine (**1**), validatol, and deoxyvalidatol.[4] Compound **1** was hydrolyzed to afford validamine (**2**) and D-glucose, and its structure was formulated as shown in Scheme 1 based on results of the periodate oxidation of its *N*-acetyl derivative.[4] The present paper, as part of studies directed toward total synthesis of validamycin A and related substances, describes the synthesis of the original structure of **1**, 1L-2-O-(β-D-glucopyranosyl)-(1,3,4/2,6)-4-amino-6-hydroxymethyl-1,2,3-cyclohexanetriol, by condensation of a properly protected DL-validamine with 2,3,4,6-tetra-O-acetyl-α-D-glucopyranosyl bromide. In addition, two diastereomeric β-D-glucopyranosides thus obtained were hydrolyzed to generate enantiomeric validamines, which constituted an optical resolution of racemic validamine.

Acid hydrolysis of DL-penta-*N*,*O*-acetyl-(1,3,4/2,6)-4-amino-6-hydroxymethyl-1,2,3-cyclohexanetriol (peracetyl-DL-validamine) (**3**)[5] with 4 M hydrochloric acid (1 M=1 mol dm^{-3}) at reflux temperature gave the amine hydrochloride (**4**) as an amorphous solid in quantitative yield. Treatment of **4** with benzyloxycarbonyl chloride in an alkaline solution gave a crystalline *N*-benzyloxycarbonyl derivative (**5**), which was further characterized as the tetra-O-acetyl derivative (**6**). Compound **5** was then converted into the *N*,*O*-carbonyl derivative (**7**) in 75% yield by treatment with 10% aqueous sodium hydroxide, whose IR spectrum revealed an absorption at 1730 cm^{-1}, indicative of the cyclic carbamate function. The structure of **7** was confirmed by the ^{1}H NMR spectrum of the corresponding tri-O-acetyl derivative (**8**). Thus, the signals for H-1, H-2, and H-3 protons appeared as a triplet (J=9 Hz), a doublet of doublets (J=6.5 and 9 Hz), and a doublet of doublets (J=6.2 and 6.5 Hz) at δ 4.99, 5.26, and 4.60, respectively, being consistent with the chair conformation slightly distorted by the introduction of the cyclic carbamate portion. Isopropylidenation of **7** with 2,2-dimethoxypropane in *N*,*N*-dimethylformamide (DMF) in the presence of *p*-toluenesulfonic acid gave the 1,7-O-isopropylidene derivative (**9**) in 97% yield. The assigned structure was supported by the ^{1}H NMR spectra of the corresponding O-acetyl (**10**), di-*N*,*O*-

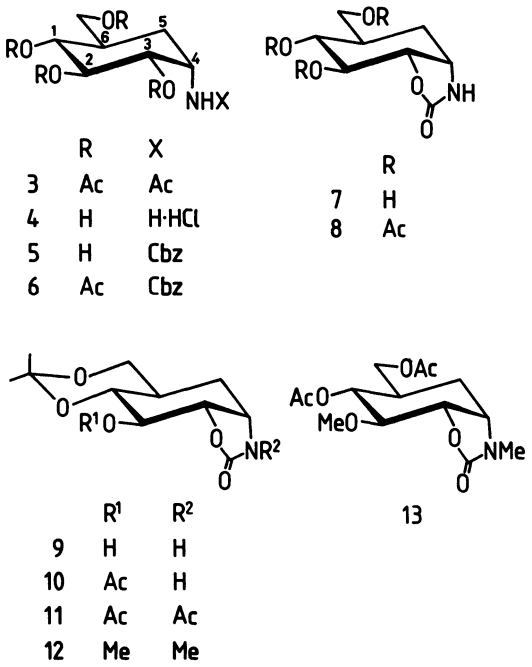

	R	X
3	Ac	Ac
4	H	H·HCl
5	H	Cbz
6	Ac	Cbz

	R
7	H
8	Ac

	R^1	R^2
9	H	H
10	Ac	H
11	Ac	Ac
12	Me	Me

13

Scheme 2. Synthesis of protected DL-validamine. All compounds are racemic. The formulas depict one of the respective enantiomers.

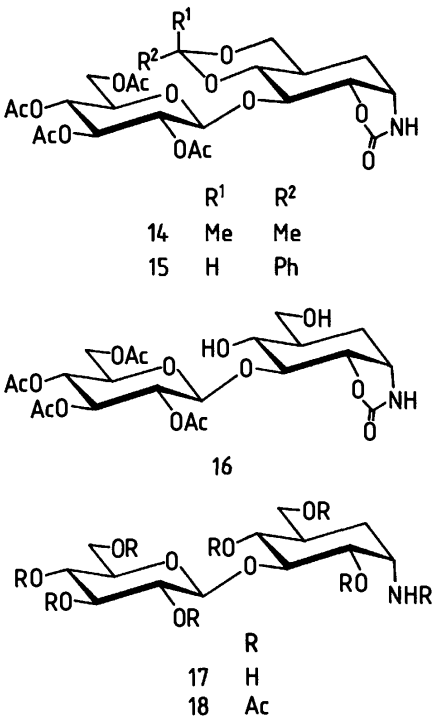

Scheme 3. Synthesis of β-D-glucopyranosylvalidamine. The formulas depict one of the respective diastereomers.

acetyl (**11**), and di-*N*,*O*-methyl derivatives (**12**). For further confirmation, **9** was transformed into DL-1,7-di-*O*-acetyl-3,4-*N*,*O*-carbonyl-2,4-di-*N*,*O*-methyl-(1,3,4/2,6)-4-amino-6-hydroxymethyl-1,2,3-cyclohexanetriol (**13**), whose ^{1}H NMR spectrum was fully consistent with the assigned structure. Thus, there appeared two coupled doublets of doublets (J=6 and 8 Hz) attributable to H-2 and H-3 at δ 3.36 and 4.50, respectively. Therefore, **9** was shown to possess a free hydroxyl group at C-2, being a suitable intermediate for the synthesis of **1**.

Condensation of **9** with 2,3,4,6-tetra-*O*-acetyl-α-D-glucopyranosyl bromide was carried out in a mixture of benzene and dioxane (2 : 1, v/v) in the presence of mercury(II) cyanide and anhydrous calcium sulfate at 65 °C for 6 d. Formation of two components was observed and they were clearly separated by chromatography on silica gel with 2-butanone–toluene (1 : 1, v/v) as an eluent, giving the protected β-D-glucopyranosides [**14**(+)], $[\alpha]_D$+77.8°, and [**14**(−)], $[\alpha]_D$−30.4°, as a syrup in 47 and 50% yields, respectively. They were shown to have four acetoxyl, one carbonyl, and one isopropylidene groups by the IR and ^{1}H NMR spectra, and their analytical data supported the assigned structures. The β-configurations were proposed both by the optical rotations and by the reaction conditions employed for the condensation reaction. Treatment of **14**(+) and **14**(−) with 80% aqueous acetic acid at ambient temperature afforded the corresponding dihydroxy compounds [**16**(+)] and [**16**(−)] in 44 and 76% yields, respectively. The presence of two hydroxyl groups at C-1 and C-7 was evidenced by the exclusive transformation into the 1,7-*O*-benzylidene derivatives [**15**(+) and **15**(−)] in 74 and 66% yields, respectively, by treatment with 1,1-dimethoxy-1-phenylmethane in DMF in the presence of acid catalyst. The ^{1}H NMR spectra of **15**(+) and **15**(−) exhibited one-proton sharp singlets at δ 5.56 and 5.55, respectively, due to the benzylic protons. Removal of the protecting groups of **16**(+) and **16**(−) was effected by treatment with refluxing 10% aqueous barium hydroxide. The free bases [**17**(+) and **17**(−)] thus obtained as a homogeneous syrup were further characterized as the corresponding octa-*N*,*O*-acetyl derivatives [**18**(+) and **18**(−)]. Acid hydrolysis of **17**(+) with 6 M hydrochloric acid gave D-glucose and validamine hydrochloride, which were detected by TLC on cellulose. They were acetylated in the usual way to give, after chromatography, penta-*O*-acetyl-α-D-glucopyranose and penta-*N*,*O*-acetyl-(+)-validamine [**3**(+)], $[\alpha]_D$ +60.2°, mp 146—148 °C. The latter compound was identified with an authentic sample, $[\alpha]_D$ +61.6°, mp 147—149 °C, prepared from (+)-validamine hydrochloride,[6,7] by the mixed melting point method and by comparison of their IR (in chloroform) and ^{1}H NMR spectra, and behavior on TLC. The enantiomer **3**(−), $[\alpha]_D$ −59.8°, mp 147—149 °C, similarly obtained from **17**(−), was shown to be identical with an authentic sample except for the optical rotations being opposite in sign. Therefore, the optical resolution of racemic validamine was accomplished by the above experiments.

Attempts were then made to compare **18**(+) with an authentic sample[6] derived from validamycin A, and they were found to be completely different from each other, on the basis of ^{1}H and ^{13}C NMR spectra, and chromatographic behavior. Consequently, we concluded that the original structure of β-D-glucopyranosylvalidamine must be reinvestigated and revised. We will report an unequivocal synthesis of β-D-glucopyranoside identical with an authentic sample in all respects in the succeeding paper.

Experimental

Unless otherwise noted, melting points were determined on a Mitamura Riken micro hot stage and uncorrected. The ^{1}H NMR spectra were taken on a Varian EM-360 (60 MHz) in chloroform-*d* ($CDCl_3$) or dimethyl-d_6 sulfoxide (DMSO-d_6) with reference to tetramethylsilane as an internal standard and the peak positions are given in terms of δ-values. Values given for coupling constants are of first-order. The IR spectra were measured on a Hitachi 225 spectrometer in potassium bromide pellets or in chloroform. Optical rotations were measured on a Japan Spectroscopic DIP-4 polarimeter in a 10 mm cell. TLC was performed on a precoated silica gel 60 F-254 plate or cellulose F-254 plate (Merck, Darmstadt). The silica gel used for column chromatography was Wakogel C-300.

DL-*(1,3,4/2,6)-4-Amino-6-hydroxymethyl-1,2,3-cyclohexanetriol Hydrochloride (DL-Validamine Hydrochloride) (**4**).* A solution of DL-tetra-*O*-acetyl-(1,3,4/2,6)-4-acetamido-6-hydroxymethyl-1,2,3-cyclohexanetriol (**3**)[5] (3.8 g) in 4 M hydrochloric acid (240 ml) was refluxed for 2 h. The reaction mixture was concentrated to give a pale yellow syrup, which was dissolved in water and decolorized with active carbon. Evaporation of the solvent gave **4** (2.1 g, 100%) as a chromatographically homogeneous glass, which showed a single spot at R_f 0.41 on TLC [cellulose, 1-butanol–ethanol–water–17% aqueous ammonia (4 : 5 : 2 : 4)].

Found: C, 39.07; H, 7.74; N, 6.39; Cl, 16.33%, Calcd for $C_7H_{15}NO_4 \cdot HCl$: C, 39.35; H, 7.55; N, 6.56; Cl, 16.59%.

DL-*(1,3,4/2,6)-4-Benzyloxycarbonylamino-6-hydroxymethyl-1,2,3-cyclohexanetriol (5).* To a stirred solution of **4** (2.1 g) in a mixture of acetone–water (2 : 1) (220 ml) containing 1 M aqueous sodium hydroxide (30 ml) was added dropwise 30% benzyloxycarbonyl chloride in toluene (11 ml) at ambient temperature. The reaction mixture was agitated for 17 h at ambient temperature, and then neutralized with 1 M hydrochloric acid and concentrated. The residue was extracted with acetone and the extracts were concentrated to give a white solid, which was crystallized from ethyl acetate to give **5** (1.51 g, 52.3%) as prisms: mp 148—150 °C; IR (KBr disk) 1710 cm^{-1} (C=O).

Found: C, 57.69; H, 6.72; N, 4.35%. Calcd for $C_{15}H_{21}NO_6$: C, 57.86; H, 6.80; N, 4.50%.

DL-*Tetra*-O-*acetyl-(1,3,4/2,6)-4-benzyloxycarbonylamino-6-hydroxymethyl-1,2,3-cyclohexanetriol (6).* Compound **5** (0.1 g) was treated with acetic anhydride (1 ml) in pyridine (2 ml) at ambient temperature overnight. The reaction mixture was poured into ice–water and the resulting gum was collected by decantation. The product was dried over phosphorus pentaoxide under vacuum to give **6** (0.1 g, 69%) as a homogeneous syrup: ^1H NMR ($CDCl_3$) δ=1.91 (3H, s), 1.99 (3H, s), 2.00 (3H, s), and 2.05 (3H, s) (OAc), 4.32 (1H, m, H-4), 5.06 (2H, s, $C\underline{H}_2Ph$), and 7.29 (5H, broad s, phenyl).

Found: C, 57.58; H, 6.12; N, 2.82%. Calcd for $C_{23}H_{29}NO_{10}$: C, 57.61; H, 6.10; N, 2.92%.

DL-*3,4*-N,O-*Carbonyl-(1,3,4/2,6)-4-amino-6-hydroxymethyl-1,2,3-cyclohexanetriol (7).* To a solution of **5** (0.8 g) in acetone–water (3 : 1) (30 ml) was added 1 M aqueous sodium hydroxide, the pH of the solution being adjusted to 11. After having been stood at ambient temperature for 4 h, the reaction mixture was neutralized with 1 M hydrochloric acid, concentrated, and dried by coevaporation with ethanol. The residue was extracted with hot 1,4-dioxane (5 ml × 3) and, after being cooled, the extracts gave **7** (0.39 g, 75%) as prisms: mp 164—165 °C; IR (KBr disk) 3500—3200 (OH) and 1730 cm^{-1} (cyclic carbamate).

Found: C, 47.29; H, 6.52; N, 6.71%. Calcd for $C_8H_{13}NO_5$: C, 47.29; H, 6.45; N, 6.89%.

Compound **7** (1.2 g) was directly obtained in 77% yield from **3** (2.9 g) without isolation of the intermediates.

DL-*Tri*-O-*acetyl-3,4*-N,O-*carbonyl-(1,3,4/2,6)-4-amino-6-hydroxymethyl-1,2,3-cyclohexanetriol (8).* Compound **7** (0.1 g) was acetylated in the conventional manner and the product was crystallized from ethanol to give **8** (0.14 g, 85%) as needles: mp 133—134 °C; ^1H NMR ($CDCl_3$) δ=2.04 (6H, s) and 2.06 (3H, s) (OAc), 3.90 (2H, q) and 4.22 (2H, q) ($J_{6,7}$=3 Hz, $J_{6,7'}$=5 Hz, J_{7gem}=11.5 Hz, H-7 and H-7'), 4.60 (1H, dd, $J_{2,3}$=6.2 Hz, $J_{3,4}$=6.5 Hz, H-3), 4.99 (1H, t, $J_{1,2}$=$J_{1,6}$=9 Hz, H-1), 5.26 (1H, dd, H-2), and 6.40 (1H, s, NH).

Found: C, 50.80; H, 5.67; N, 4.11%. Calcd for $C_{14}H_{19}NO_8$: C, 51.06; H, 5.82; N, 4.25%.

DL-*3,4*-N,O-*Carbonyl-1,7*-O-*isopropylidene-(1,3,4/2,6)-4-amino-6-hydroxymethyl-1,2,3-cyclohexanetriol (9).* To a solution of **7** (1.2 g) in dry *N,N*-dimethylformamide (8 ml) was added 2,2-dimethoxypropane (3.5 ml) and *p*-toluenesulfonic acid (20 mg), and the mixture was heated at 80 °C for 2 h. The mixture was treated with Amberlite IRA 400 (OH^-) (2.5 ml) and then concentrated to give a crystalline product. Recrystallization from ethanol gave **9** (1.1 g, 79%) as crystals: mp 243—244 °C (decomp); IR (KBr disk) 3400—3300 (OH and NH) and 1740 cm^{-1} (cyclic carbamate); ^1H NMR (DMSO-d_6) δ=1.27 (3H, s) and 1.37 (3H, s) (isopropylidene), 4.16 (1H, t, $J_{2,3}$=$J_{3,4}$=6.5 Hz, H-3), 5.28 (1H, d, $J_{2,OH}$=5 Hz, OH), and 7.29 (1H, broad s, NH).

Found: C, 54.05; H, 6.89; N, 5.89%. Calcd for $C_{11}H_{17}NO_5$: C, 54.31; H, 7.04; N, 5.76%.

DL-*2*-O-*Acetyl-3,4*-N,O-*carbonyl-1,7*-O-*isopropylidene-(1,3,4/2,6)-4-acetamido-6-hydroxymethyl-1,2,3-cyclohexanetriol (11).* Compound **9** (0.1 g) was treated with acetic anhydride (2 ml) in pyridine (3 ml) at 50 °C for 3 d. The reaction mixture was poured into saturated aqueous sodium hydrogencarbonate and the precipitates were collected by decantation. The product was dissolved in ethyl acetate, and the solution was washed with water and dried. Evaporation of the solvent gave a syrup (0.12 g), which was crystallized from ethanol to give **11** (30 mg, 22%) as needles: mp 142—144 °C; ^1H NMR ($CDCl_3$) δ=1.34 (3H, s) and 1.41 (3H, s) (isopropylidene), 2.10 (3H, s, OAc), 2.51 (3H, s, NAc), 3.58 (1H, t, $J_{1,2}$=$J_{1,6}$=10 Hz, H-1), 4.52 (2H, d, H-3 and H-4), and 5.03 (1H, m, H-2).

Found: C, 54.77; H, 6.40; N, 4.10%. Calcd for $C_{15}H_{21}NO_7$: C, 55.04; H, 6.47; N, 4.28%.

DL-*2*-O-*Acetyl-3,4*-N,O-*carbonyl-1,7*-O-*isopropylidene-(1,3,4/2,6)-4-amino-6-hydroxymethyl-1,2,3-cyclohexanetriol (10).* Compound **9** (61 mg) was treated with acetic anhydride (1 ml) in pyridine (2 ml) at ambient temperature for 25 h. TLC indicated the formation of one major component (R_f 0.28) and one minor component (R_f 0.77) [silica gel, 2-butanone–toluene (1 : 1)]. The reaction mixture was concentrated and the crude product, without further purification, was subjected to measurement of ^1H NMR spectrum. The product was shown to be contaminated with **11**: ^1H NMR ($CDCl_3$) δ=1.34 (3H, s) and 1.41 (3H, s) (isopropylidene), 2.06 (3H, OAc), 3.50 (1H, t, $J_{1,2}$=$J_{1,6}$=10 Hz, H-1), 4.48 (1H, t, $J_{2,3}$=$J_{3,4}$=7 Hz, H-3), 5.14 (1H, dd, H-2), and 6.37 (1H, s, NH).

DL-*1,7-Di*-O-*acetyl-3,4*-N,O-*carbonyl-2,4-di*-N,O-*methyl-(1,3,4/2,6)-4-amino-6-hydroxymethyl-1,2,3-cyclohexanetriol (13).* To a solution of **9** (0.22 g) in dry *N,N*-dimethylformamide (10 ml) was added silver oxide (1 g) and methyl iodide (1 ml), and the mixture was vigorously stirred at ambient temperature in the dark for 14 h. An insoluble material was removed by filtration and washed thoroughly with ethyl acetate. The filtrate and washings were combined and concentrated. The residue was dissolved in ethyl acetate and filtered through a short column of alumina. The filtrate was concentrated to give DL-3,4-*N,O*-carbonyl-1,7-*O*-isopropylidene-2,4-di-*N,O*-methyl-(1,3,4/2,6)-4-amino-6-hydroxymethyl-1,2,3-cyclohexanetriol (**12**) as a homogeneous syrup: ^1H NMR δ=1.40 (3H, s) and 1.47 (3H, s) (isopropylidene), 2.75 (3H, s, NCH_3), 3.55 (3H, s, OCH_3), and 4.37 (1H, t, $J_{2,3}$=$J_{3,4}$=7 Hz, H-3).

Crude **12** was treated with 80% aqueous acetic acid (10 ml) at 65 °C for 3 h. The reaction mixture was concentrated and dried by coevaporation with toluene. The product was acetylated in the conventional manner to give a syrup, which was crystallized from ethanol to give **13** (90 mg, 31% yield based on **7** used) as needles: mp 108—110 °C; ^1H NMR ($CDCl_3$) δ=2.02 (3H, s) and 2.05 (3H, s) (OAc), 2.78 (3H, s, NCH_3), 3.36 (1H, dd, $J_{1,2}$=8 Hz, $J_{2,3}$=6 Hz, H-2), 3.48 (3H, s, OCH_3), 4.50 (1H, dd, $J_{3,4}$=8 Hz, H-3), and 4.85 (1H, t, $J_{1,6}$=8 Hz, H-1).

Found: C, 53.00; H, 6.65; N, 4.34%. Calcd for $C_{14}H_{21}NO_7$: C, 53.33; H, 6.71; N, 4.44%.

Koenigs-Knorr Reaction of **9** *and 2,3,4,6-Tetra*-O-*acetyl-α-*D-*glucopyranosyl Bromide.* A mixture of **9** (1.0 g), 2,3,4,6-tetra-*O*-acetyl-α-D-glucopyranosyl bromide (6 g, 3.6 molar equiv.), and benzene–1,4-dioxane (2 : 1) (120 ml) was heated at 65 °C in the presence of mercury(II) cyanide (7 g) and anhydrous calcium sulfate (Drierite) (7.2 g) for 140 h. During the course of reaction, additional bromide (3 g) was added at an interval of 50 h. TLC indicated the disappearance of **9** and the formation of two new components in an approximately equal proportion, together with several side

products. An insoluble material was removed by filtration through a bed of caoline and washed thoroughly with chloroform (50 ml×4). The filtrate and washings were combined and concentrated. The residue was dissolved in ethyl acetate (200 ml) and the solution was washed successively with saturated aqueous sodium hydrogencarbonate and water, dried over anhydrous sodium sulfate, and then concentrated to give a pale yellow syrup (11 g). The product was chromatographed on a silica-gel column (100 g, 35 mm×300 mm) packed with 2-butanone–toluene (3 : 8). The first fractions obtained by elution with the same solvent (1 l) were discarded. Succeeding elution with methanol (500 ml) gave a homogeneous mixture of two β-D-glucopyranosides, which was again chromatographed on a silica-gel column (150 g, 30 mm×500 mm) with 2-butanone–toluene (1 : 1) as an eluent. The first fraction [R_f 0.38, silica gel, 2-butanone–toluene (2 : 1)] gave 1L-3,4-*N,O*-carbonyl-2-*O*-(2,3,4,6-tetra-*O*-acetyl-β-D-glucopyranosyl)-1,7-*O*-isopropylidene-(1,3,4/2,6)-4-amino-6-hydroxymethyl-1,2,3-cyclohexanetriol[**14**(+), 1.09 g, 47%] as a homogeneous glass: $[\alpha]_D^{20}$ +77.8° (*c* 1.02, chloroform); ^{1}H NMR ($CDCl_3$) δ=1.33 (3H, s) and 1.44 (3H, s) (isopropylidene), 1.99 (6H, s), 2.00 (3H, s), and 2.09 (3H, s) (OAc), 6.22 (1H, s, NH).

Found: C, 52.56; H, 6.20; N, 2.46%. Calcd for $C_{25}H_{35}NO_{14}$: C, 52.35; H, 6.15; N, 2.44%.

The second fraction (R_f 0.31) gave the diastereomer [**14**(−), 1.16 g, 50%] as a homogeneous glass: $[\alpha]_D^{20}$ −30.4° (*c* 1.02, chloroform); ^{1}H NMR ($CDCl_3$) δ=1.42 (6H, broad s, isopropylidene), 2.01 (9H, s) and 2.08 (3H, s) (OAc), and 6.18 (1H, broad s, NH).

Found: C, 52.48; H, 6.32; N, 2.49%. Calcd for $C_{25}H_{35}NO_{14}$: C, 52.35; H, 6.15; N, 2.44%.

1L-*3,4*-N,O-*Carbonyl-2*-O-*(2,3,4,6-tetra*-O-*acetyl-β-D-glucopyranosyl)-(1,3,4/2,6)-4-amino-6-hydroxymethyl-1,2,3-cyclohexanetriol* [***16***(+)]. A solution of **14**(+) (0.45 g) in 80% aqueous acetic acid (10 ml) was allowed to stand at ambient temperature for 18 h. The reaction mixture was concentrated to give a crystalline residue (0.36 g), which was recrystallized from ethanol to give **16**(+) (0.18 g, 44%): mp 180—182 °C; $[\alpha]_D^{20}$ +73.4° (*c* 1.01, chloroform); ^{1}H NMR ($CDCl_3$) δ=1.99 (3H, s), 2.02 (3H, s), 2.07 (3H, s), and 2.12 (3H, s) (OAc), and 6.31 (1H, s, NH).

Found: C, 49.29; H, 5.80; N, 2.49%. Calcd for $C_{22}H_{31}NO_{14}$: C, 49.53; H, 5.86; N, 2.63%.

1D-*3,4*-N,O-*Carbonyl-2*-O-*(2,3,4,6-tetra*-O-*acetyl-β-D-glucopyranosyl-(1,3,4/2,6)-4-amino-6-hydroxymethyl-1,2,3-cyclohexanetriol* [***16***(−)]. Compound **14**(−) (0.39 g) was treated with 80% aqueous acetic acid (10 ml) as in the preparation of **14**(+). The product (0.35 g) was recrystallized from ethanol to give **16**(−) (0.27 g, 76%) as needles: mp 216—219 °C; $[\alpha]_D^{20}$ −62.8° (*c* 0.85, methanol); ^{1}H NMR (DMSO-d_6) δ=1.98 (3H, s), 2.00 (3H, s), 2.03 (3H, s), and 2.12 (3H, s) (OAc), and 7.47 (1H, s, NH).

Found: C, 49.75; H, 5.83; N, 2.45%. Calcd for $C_{22}H_{31}NO_{14}$: C, 49.53; H, 5.86; N, 2.63%.

Compounds **16**(+) and **16**(−) showed single spots at R_f 0.43 and 0.38, respectively, on TLC [silica gel, chloroform–methanol (5 : 1)], and were clearly differentiated from each other.

1L-*1,7*-O-*Benzylidene-3,4*-N,O-*carbonyl-2*-O-*(2,3,4,6-tetra*-O-*acetyl-β-D-glucopyranosyl)-(1,3,4/2,6)-4-amino-6-hydroxymethyl-1,2,3-cyclohexanetriol* [***15***(+)]. To a solution of **16**(+) (63 mg) in dry *N,N*-dimethylformamide (3 ml) were added 1,1-dimethoxy-1-phenylmethane (0.06 ml) and a catalytic amount of *p*-toluenesulfonic acid, and the mixture was heated at 60 °C for 1.5 h. TLC indicated the formation of a single product [R_f 0.40, silica gel, 2-butanone–toluene (2 : 1)]. The reaction mixture was neutralized with Amberlite IRA-400 (OH^-) (1.2 ml), and then concentrated to give a colorless glass, which was crystallized from ethanol to give **15**(+) (54 mg, 74%) as needles: mp 240—243 °C; $[\alpha]_D^{20}$ +56° (*c* 0.80, chloroform); ^{1}H NMR ($CDCl_3$) δ=1.97 (9H, s) and 2.14 (3H, s) (OAc), 5.56 (1H, s, benzylic), 5.91 (1H, s, NH), and 7.39 (5H, broad s, phenyl).

Found: C, 56.08; H, 5.67; N, 2.25%. Calcd for $C_{29}H_{35}NO_{14}$: C, 56.04; H, 5.68; N, 2.25%.

1D-*1,7*-O-*Benzylidene-3,4*-N,O-*carbonyl-2*-O-*(2,3,4,6-tetra*-O-*acetyl-β-D-glucopyranosyl)-(1,3,4/2,6)-4-amino-6-hydroxymethyl-1,2,3-cyclohexanetriol* [***15***(−)]. Compound **16**(−) (70 mg was treated with 1,1-dimethoxy-1-phenylmethane (0.1 ml) and *p*-toluenesulfonic acid in DMF (3 ml) as in the preparation of **15**(+). The crude product was recrystallized from ethanol to give **15**(−) (54 mg, 66%) as prisms: mp 192—194 °C; $[\alpha]_D^{20}$ −74° (*c* 0.60, chloroform); ^{1}H NMR ($CDCl_3$) δ=1.52 (3H, s), 1.98 (3H, s), 2.02 (3H, s), and 2.09 (3H, s) (OAc), 5.55 (1H, s, benzylic), and 6.16 (1H, s, NH).

Found: C, 56.01; H, 5.59; N, 2.26%. Calcd for $C_{29}H_{35}NO_{14}$: C, 56.04; H, 5.68; N, 2.25%.

Compounds **15**(+) and **15**(−) showed single spots at R_f 0.40 and 0.36, respectively, on TLC [silica gel, 2-butanone–toluene (2 : 1)] and were clearly differentiated from each other.

1L-*2*-O-*β-D-Glucopyranosyl-(1,3,4/2,6)-4-amino-6-hydroxymethyl-1,2,3-cyclohexanetriol* [***17***(+)] *and Its Peracetate* [***18***(+)]. A mixture of **16**(+) (0.142 g), barium hydroxide (0.5 g), and 1,4-dioxane–water (1 : 1) (50 ml) was heated under reflux for 24 h. The reaction mixture was neutralized by addition of solid carbon dioxide and the precipitates were removed by filtration The filtrate was concentrated to give **17** (+) as a syrup, which was shown to be homogeneous on TLC [R_f 0.18, cellulose, 1-butanol–pyridine–water–acetic acid (6 : 4 : 3 : 1)]. The syrup was treated with acetic anhydride (4 ml) in pyridine (4 ml) at ambient temperature for 18 h. The reaction mixture was concentrated and the residue was dissolved in chloroform and the solution was passed through a short column of alumina. The eluate was concentrated to give **18**(+) (0.11 g, 59%) as a homogeneous syrup: $[\alpha]_D^{20}$ −9.5° (*c* 0.89, chloroform): ^{1}H NMR ($CDCl_3$) δ=1.92, 1.96, 2.00, 2.03, and 2.05 (24H, NAc and OAc), and 5.77 (1H, d, $J_{4,NH}$=7.5 Hz, NH); IR (KBr disk) 3400 (NH), 1755 (ester), 1660, and 1535 cm^{-1} (amide).

Found: C, 51.79; H, 6.33; N, 1.93%. Calcd for $C_{29}H_{41}NO_{17}$: C, 51.56; H, 6.12; N, 2.07%.

1D-*2*-O-*β-D-Glucopyranosyl-(1,3,4/2,6)-4-amino-6-hydroxymethyl-1,2,3-cyclohexanetriol* [***17***(−)] *and Its Peracetate* [***18***(−)]. Compound **16**(−) (0.264 g) was hydrolyzed with aqueous barium hydroxide as in the preparation of **17**(+). The free base **17**(−) showed a single spot on TLC [R_f 0.18, cellulose, 1-butanol–pyridine–water–acetic acid (6 : 4 : 3 : 1)]. It was acetylated in the conventional way to give **18**(−) (0.31 g, 92%) as a homogenous syrup: $[\alpha]_D^{20}$ −41.7° (*c* 1.07, chloroform); ^{1}H NMR ($CDCl_3$) δ=1.93, 1.99, 2.04, and 2.09 (total 24H, s, NAc and OAc), and 6.02 (1H, d, $J_{4,NH}$=7 Hz, NH); IR (KBr disk) 3400 (NH), 1755 (ester), 1660, and 1535 cm^{-1} (amide).

Found: C, 51.60; N, 6.21; N, 2.10%. Calcd for $C_{29}H_{41}NO_{17}$: C, 51.56; H, 6.12; N, 2.07%.

Attempts were made to identify **17**(+) and **18**(+) with authentic samples derived from validamycin A. The IR and ^{1}H NMR spectra of **17**(+) and **18**(+) were both shown to be different from those of authentic samples. Compound **17**(+) revealed a single spot at R_f 0.18, while the corresponding authentic sample showed a single spot at R_f 0.12 on TLC [cellulose, 1-butanol–pyridine–water–acetic acid (6 : 4 : 3 : 1)]. Compound **18**(+) revealed a single spot at R_f 0.32 and the authentic sample at R_f 0.51 [silica gel, chloroform–methanol

(10: 1)].

Acid Hydrolysis of **17**(+) *and* **17**(−). *Preparation of Enantiomeric Validamines.* A mixture of **17**(+) (0.13 g) and 4 M hydrochloric acid (6 ml) was heated under reflux for 1 h. The reaction mixture was concentrated and the residue was dried by coevaporation successively with water, ethanol, and toluene. A partly crystalline product was acetylated in the conventional way and the product was chromatographed on a silica-gel column (20 g) with 2-butanone–toluene (1 : 4). The fractions first eluted gave penta-*O*-acetyl-D-glucopyranose (68 mg) as a pale yellow syrup, homogeneous on TLC [R_f 0.52, 2-butanone–toluene (1 : 2)], identical with an authentic sample. The second fractions gave tetra-*O*-acetyl-1L-(1,3,4/2,6)-4-acetamido-6-hydroxymethyl-1,2,3-cyclohexanetriol [(+)-validamine] (73 mg, 40%) as a syrup: $[\alpha]_D^{20}$ +42.6° (*c* 1.08, chloroform). The syrupy product gradually crystallized from ethanol to give prisms or plates: mp 197—202 °C. On the other hand, crystallization from ether gave needles: mp 146—148 °C; $[\alpha]_D^{20}$ +60.2° (*c* 0.60, chloroform). These two crystals were shown to be dimorphic crystals by spectroscopic methods. The compound (needles) was identified with an authentic sample by comparison of IR (in chloroform) and ^{1}H NMR (in $CDCl_3$) spectra and TLC behavior.

Found: C, 52.92; H, 6.41; N, 3.70%. Calcd for $C_{17}H_{25}NO_9$: C, 52.71; H, 6.51; N, 3.62%.

A reference compound was prepared by the conventional acetylation of validamine hydrochloride kindly provided by Dr. Satoshi Horii. The peracetate slowly crystallized from a small amount of chloroform to give needles, which were again recrystallized from ether: mp 147—149 °C; $[\alpha]_D^{20}$ +61.6° (*c* 0.71, chloroform). Found: C, 52.46; H, 6.39; N, 3.57%.

A crude **17**(−) (0.15 g) was treated with 4 M hydrochloric acid as described above. TLC indicated the formation of D-glucose (R_f 0.45) and (−)-validamine hydrochloride (R_f 0.25) [cellulose, 1-butanol–pyridine–water–acetic acid (6: 4: 3: 1)]. The mixture was acetylated in the conventional way and the products were fractionated on a silica-gel column to give penta-*O*-acetyl-D-glucopyranose (57 mg) as a syrup and tetra-*O*-acetyl-1D-(1,3,4/2,6)-4-acetamido-6-hydroxymethyl-1,2,3-cyclohexanetriol [(−)-validamine] (0.13 g, 76%) as a syrup: $[\alpha]_D^{20}$ −54.1° (*c* 0.98, chloroform). This compound crystallized from ethanol to give plates, mp 197—199.5 °C, and from ether to give needles: mp 147—149 °C; $[\alpha]_D^{20}$ −59.8° (*c* 1.3, chloroform). Its IR (in chloroform) and ^{1}H NMR (in $CDCl_3$) spectra were superimposable on those of an authentic sample.

Found: C, 52.95; H, 6.41; N, 3.66%. Calcd for $C_{17}H_{25}NO_9$: C, 52.71; H, 6.51; N, 3.62%.

The present work was partially supported by a Grand-in-Aid for Scientific Research No. 355376 from the Ministry of Education, Science and Culture. The authors wish to express their thanks to Mr. Saburo Nakada for elemental analyses.

References

1) A preliminary account of portions of this article was previously presented: S. Ogawa, Y. Shibata, N. Chida, and T. Suami, *Chem. Lett.*, **1980**, 135.

2) T. Iwasa, H. Yamamoto, and M. Shibata, *J. Antibiot.*, **23**, 595 (1970).

3) S. Horii and Y. Kameda, *J. Chem. Soc., Chem. Commun.*, **1972**, 747.

4) S. Horii, T. Iwasa, and Y. Kameda, *J. Antibiot.*, **24**, 57 (1971).

5) S. Ogawa, K. Nakamoto, M. Takahara, Y. Tanno, N. Chida, and T. Suami, *Bull. Chem. Soc. Jpn.*, **52**, 1174 (1979). The nomenclature and numbering of cyclitols used in this paper follow IUPAC and IUB Tentative Rules for Cyclitol Nomenclature [*J. Biol. Chem.*, **243**, 5809 (1968)].

6) An authentic sample was kindly provided by Dr. Satoshi Horii (Takeda Chemical Industires, Ltd., Osaka).

7) The absolute configuration of (+)-validamine was established as depicted in Scheme 1 by X-ray spectroscopic analysis of its hydrobromide [K. Kamiya, Y. Wada, S. Horii, and M. Nishikawa, *J. Antibiot.*, **24**, 317 (1971)].

 © 1983 The Chemical Society of Japan Bull. Chem. Soc. Jpn., 56, 499—504 (1983)

Synthetic Studies on the Validamycins. II. Synthesis of 1L-1-*O*-(β-D-Glucopyranosyl)-(1,3,4/2,6)-4-amino-6-hydroxymethyl-1,2,3-cyclohexanetriol[1)]

Seiichiro OGAWA, Noritaka CHIDA, Hiroyuki ITO, and Tetsuo SUAMI*

Department of Applied Chemistry, Faculty of Science and Technology, Keio University, Hiyoshi, Kohoku-ku, Yokohama 223

(Received June 10, 1982)

The title β-D-glucopyranoside was synthesized *via* an unequivocal route and found to be identical with β-D-glucopyranosylvalidamine derived from antibiotic validamycin A. The position at which the validamine moiety is substituted with D-glucopyranose in validamycin A is revised to C-1 on the basis of the present synthesis.

In the preceding paper,[2)] we described an unequivocal synthesis of the original structure of β-D-glucopyranosyl-validamine (**1**) and found that it was not identical with an authentic sample derived from validamycin A. These results suggested that, contrary to the previous assignment by Horii and Kameda,[3)] D-glucopyranose should be attached to the C-1 or C-3 hydroxyl group rather than to the C-2 hydroxyl group of 1L-(1,3,4/2,6)-4-amino-6-hydroxymethyl-1,2,3-cyclohexanetriol [(+)-validamine] (**2**). Therefore, in order to elucidate the position of the β-glucosidic linkage, attempts were initially made to prepare the 1-*O*-β-D-glucopyranoside (**3**) *via* an unambiguous route. In the present paper, we wish to describe the detail of the successful synthesis of **3**, identical with an authentic sample, and to discuss on the revised structure of validamycin A along with ^{13}C NMR spectral data.

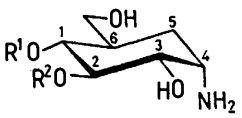

	R^1	R^2
1	H	β-D-glucopyranosyl
2	H	H
3	β-D-glucopyranosyl	H

Scheme 1.

DL-7-*O*-Benzoyl-2,3-*O*-isopropylidene-(1,3,4/2,6)-4-azido-6-hydroxymethyl-1,2,3-cyclohexanetriol (**8b**) was chosen as a protected precursor of the aglycone moiety for a condensation with 2,3,4,6-tetra-*O*-acetyl-α-D-glucopyranosyl bromide, and was prepared by starting from readily available DL-tri-*O*-acetyl-(1,3/2,4,6)-4-bromo-6-bromomethyl-1,2,3-cyclohexanetriol (**4**)[4)] in the following sequence.

Treatment of **4** with refluxing aqueous ethanol containing 5% hydrobromic acid gave the trihydroxy compound (**5**) in 95% yield. Isopropylidenation of **5** with 2,2-dimethoxypropane in *N,N*-dimethylformamide (DMF) in the presence of *p*-toluenesulfonic acid at 60 °C for 2 h yielded a crystalline mixture of the 1,2-*O*- (**6a**) and 2,3-*O*-isopropylidene derivatives (**6b**) in 86% yield. Without separation, the mixture was directly treated with 2 molar equiv. of sodium benzoate in 90% aqueous DMF at 70 °C for 6 h to give through a preferential displacement of the 7-bromine atom a mixture of the benzoates (**7a** and **7b**). They were clearly separated, by chromatography on silica gel and later

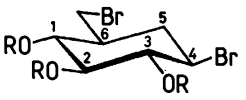

	R
4	Ac
5	H

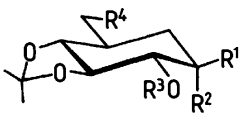

a

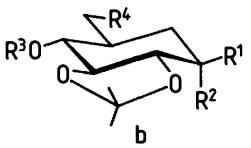

b

	R^1	R^2	R^3	R^4
6a,b	Br	H	H	Br
7a,b	Br	H	H	OBz
8a,b	H	N_3	H	OBz
9a,b	H	N_3	Ac	OBz
10a,b	H	N_3	Me	OBz

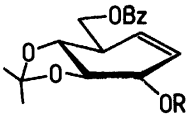

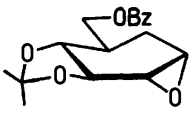

13

	R
11	H
12	Ac

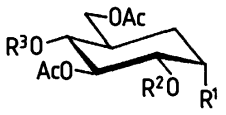

	R^1	R^2	R^3
14	NHAc	Me	Ac
15	N_3	Ac	Me
16	NHAc	Ac	Me
17	NHAc	Ac	Ac

Scheme 2. Synthesis of protected precursors of DL-validamine. All compounds are racemic. The formulas depict one of the respective enantiomers.

by fractional crystallization, to **7a** and **7b** in 8 and 35% yields, respectively. As one of side products, the olefin (**11**) was isolated in pure form, which was further characterized as the acetate (**12**). Compound **11** was also obtained from **7a** in 12% yield by treatment with 1,8-diazabicyclo[5.4.0]undec-7-ene in toluene, together with the epoxide (**13**, 33%). Azidolysis of **7a** with sodium azide in dimethyl sulfoxide (DMSO) at 110 °C for 20 h afforded the azide (**8a**) and **11** in 64 and 4% yields, respectively. On the other hand, a similar treatment of **7b** with an azide ion gave the azide (**8b**) selectively in 73% yield. No formation of any olefinic compound was observed in this case. The structures of **8a** and **8b** were confirmed by converting them into the corresponding *O*-acetyl (**9a** and **9b**), and *O*-methyl derivatives (**10a** and **10b**). Thus, in the ^{1}H NMR spectra, **9a** and **9b** showed a one-proton doublet of doublets (δ=5.05, J=4 and 10.5 Hz) and a one-proton triplet (δ=5.19, J=9 Hz) attributable to a proton attached to the carbon atom bearing the acetoxyl group, respectively, which indicated the location of the acetoxyl groups at C-3 in **9a** and at C-1 in **9b**. For further confirmation, both **8a** and **8b** were converted into penta-*N*,*O*-acetyl-DL-validamine (**17**) by the following sequence: *O*-deisopropylidenation, *O*-deacylation, catalytic reduction, and acetylation. Therefore, **8b** was expected to be a suitable intermediate for the synthesis of the desired β-D-glucopyranoside (**3**). In addition, in order to furnish several reference compounds for assignment of the ^{13}C NMR spectral data of the validamine derivatives, **10a** and **10b** were transformed into the peracetates of 4-*O*-methyl (**16**) and 2-*O*-methyl-validamine (**14**),[5] respectively.

Condensation of **8b** with 2,3,4,6-tetra-*O*-acetyl-α-D-glucopyranosyl bromide was conducted in dry benzene in the presence of mercury(II) cyanide and anhydrous calcium sulfate at 70 °C for 50 h. Under these conditions, only β-D-glucopyranosides were expected to be obtainable. The mixture of products was roughly separated by chromatography on silica gel with 1 : 10 2-butanone–toluene as an eluent to give a syrupy mixture of condesation products [**18**(+) and **18**(−)], showing a single spot in several solvent systems. Without further separation, it was *O*-deisopropylidenated by treatment with Amberlite IR-120B (H^+) in ethanol at ambient temperature overnight. The dihydroxy compounds thus obtained could be fractionated by a silica-gel column with 2: 5 2-butanone–toluene to afford **19**(+), $[\alpha]_D$ +27°, and **19**(−), $[\alpha]_D$ −16°, in 18 and 13% yields, respectively, based on **8b** used. Isopropylidenation of **19**(+) and **19**(−) in the usual way could regenerate crystalline **18**(+) and **18**(−) in pure forms, respectively. Judging from the optical rotations, **19**(+)

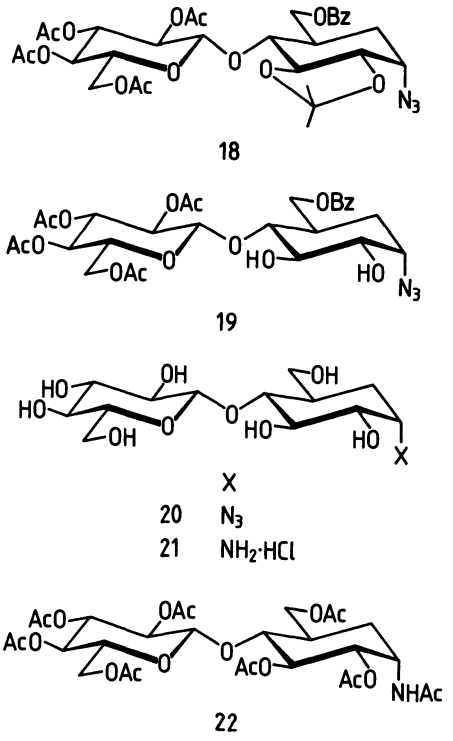

Scheme 3. Synthesis of 4-*O*-(β-D-glucopyranosyl)validamine. The formulas depict one of the respective diastereomers.

was tentatively assigned as the β-D-glucopyranoside that contained the precursor of (+)-validamine as the aglycone moiety. *O*-Deacylation of **19**(+) with methanolic sodium methoxide in methanol gave the hydroxy azide [**20**(+)], which was successively hydrogenated with 5% palladium on carbon in ethanol containing an excess of hydrochloric acid to give the amine hydrochloride [**21**(+)], $[\alpha]_D$ +22° (H_2O), as a homogeneous syrup in 94% overall yield. This compound was shown to be identical with an authentic sample of β-D-glucopyranosylvalidamine hydrochloride by comparison of chromatographic behavior (TLC on cellulose and silica gel) in several solvent systems. It was further characterized by conversion into the octa-*N*,*O*-acetyl derivative [**22**(+)], $[\alpha]_D$ +16° (lit,[3] $[\alpha]_D$ +17.6°), whose IR (in chloroform) and ^{1}H NMR spectra were superimposable on those of an authentic sample.[6]

On the other hand, the diastereomeric amine hydrochloride **21**(−) obtained similarly from **19**(−) *via* the hydroxy azide [**20**(−)] showed spectral properties similar to those of **21**(+); however, they were clearly differentiated from each other by TLC. Its octa-*N*,*O*-acetyl derivative [**22**(−)] has $[\alpha]_D$ −49°.

Table 1. ^{13}C NMR chemical shifts of peracetates of validamine derivatives in $CDCl_3$

Compound	C-1	C-2	C-3	C-4	C-5	C-6	C-7	OMe
3-*O*-Me (**14**)	71.33	72.83	79.24	45.37	27.90	34.65	63.13	57.21
1-*O*-Me (**16**)	80.24	73.15	71.60	46.32	28.42	36.13	63.64	60.16
17	←———	71.41, 71.63	———→	46.78	28.43	35.21	63.16	
22(+)	—	—	—	45.99	27.92	37.17	62.93	
2-*O*-β-D-Glc[2]	—	—	—	46.15	28.16	35.02	63.51	

A part of the ^{13}C NMR spectral data of validamine derivatives were shown in Table 1. Assignment of the resonances was carried out by comparing the spectrum of the peracetyl derivative with those of the *O*-methyl derivatives. Substitution of the acetoxyl group by methoxyl group causes a downfield shift of the signals for α-carbon atom (8—9 ppm) and β-carbon atom (1—1.5 ppm).[7] The signal for C-6 of octa-*O*-acetyl-2-*O*-β-D-glucopyranosylvalidamine[2] appears at 35.02 ppm, indicative of the location of the acetoxyl group at C-1, whereas the C-6 of **22**(+) resonates downfield at 37.02 ppm, suggesting that D-glucopyranose attaches to the C-1 hydroxyl group by way of β-glucosidic linkage. These assumptions may be compatible with the result of the present synthesis.

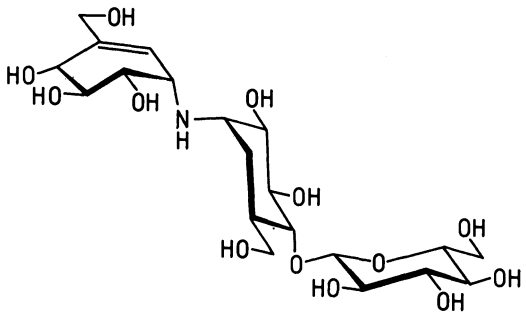

Scheme 4. The revised structure of validamycin A.

On the basis of the synthetic studies and the ^{13}C NMR spectral data, the structure of β-D-glucopyranosylvalidamine should be revised to 1L-1-*O*-(β-D-glucopyranosyl)-(1,3,4/2,6)-4-amino-6-hydroxymethyl-1,2,3-cyclohexanetriol. Accordingly, the structure of validamycin A was convincingly formulated as shown in Scheme 4.

Experimental

General Methods. The same method was used as described in the preceding paper.[2] ^{13}C NMR spectra were determined on a Varian FT-80 spectrometer at 20 MHz. The resonance signals are expressed in ppm downfield from the signal of tetramethylsilane.

DL-*(1,3/2,4,6)-4-Bromo-6-bromomethyl-1,2,3-cyclohexanetriol (**5**).* A mixture of DL-1,2,3-tri-*O*-acetyl-(1,3/2,4,6)-4-bromo-6-bromomethyl-1,2,3-cyclohexanetriol (**4**)[4] (4 g) in ethanol (160 ml) containing 48% hydrobromic acid (20 ml) was refluxed for 4 h. The reaction mixture was concentrated, and the crystallized residue was triturated with water and filtered to give a practically pure **5** (2.7 g, 95%). Recrystallization from ethanol and water gave an analytically pure sample (2 g, 71%) as prisms: mp 153.5—154 °C.

Found: C, 27.76; H, 3.92; Br, 52.48%. Calcd for $C_7H_{12}Br_2O_3$: C, 27.66; H, 3.98; Br, 52.57%.

DL-*1,2*-O- *(**6a**) and* DL-*2,3*-O-*Isopropylidene-(1,3/2,4,6)-4-bromo-6-bromomethyl-1,2,3-cyclohexanetriol (**6b**).* A mixture of **5** (2 g), *N,N*-dimethylformamide (DMF) (20 ml), and 2,2-dimethoxypropane (9 ml) was heated in the presence of *p*-toluenesulfonic acid (5 mg) at 70 °C for 2 h. After being cooled to room temperature, the reaction mixture was treated with Amberlite IRA-400 (OH^-) (1.5 ml) and then concentrated. Recrystallization of the residue gave **6a** and **6b** (2 g, 88%) as a homogeneous crystalline mixture: mp 122—125 °C; they showed similar mobilities on TLC in several solvent systems; ^1H NMR ($CDCl_3$) δ=1.42 (6H, s) and 1.48 (6H, s) (isopropylidene).

Found: C, 34.77; H, 4.60; Br, 46.69%. Calcd for $C_{10}H_{16}Br_2O_3$: C, 34.91; H, 4.69; Br, 46.45%.

DL-*1,2*-O- *(**7a**) and* DL-*2,3*-O-*Isopropylidene-(1,3/2,4,6)-6-benzoyloxymethyl-4-bromo-1,2,3-cyclohexanetriol (**7b**).* A crystalline mixture of **6a** and **6b** (2 g) was treated with sodium benzoate (1.7 g) in 90% aqueous DMF (40 ml) at 70—80 °C for 6 h. TLC showed the formation of two main components (R_f 0.38 and 0.32, developed twice in 1 : 8 2-butanone–toluene), together with several minor ones. The reaction mixture was then cooled to room temperature and diluted with ethyl acetate (50 ml), and an insoluble material was removed by filtration. The filtrate was concentrated, the residue was dissolved in chloroform, and the solution was passed through a short column of alumina. Evaporation of the solvent gave a syrupy residue, a small portion of which was fractionated on a silica-gel column with 1 : 8 2-butanone–toluene as an eluent to give pure crystals of **7a** and **7b**. The remaining syrup was dissolved in a small amount of ethanol and crystallization was induced by seeding in turn crystals of **7a** and **7b**. Compound **7b** was first obtained as needles (0.78 g, 35%): mp 130—132 °C; ^1H NMR ($CDCl_3$) δ=1.48 (6H, s, isopropylidene), 4.34 (1H, dd, J_{gem}=11 Hz, $J_{6,7}$=2 Hz, H-7), 4.68 (1H, dd, $J_{6,7'}$=4 Hz, H-7′), and 7.33—8.15 (5H, m, phenyl). The second crop of crystals was **7a** (0.29 g, 13%) obtained as prisms: mp 125—127 °C; ^1H NMR ($CDCl_3$) δ= 1.44 (6H, s, isopropylidene), 4.21 (1H, dd, J_{gem}=11 Hz, $J_{6,7}$= 6 Hz, H-7), 4.58 (1H, dd, $J_{6,7'}$=4 Hz, H-7′), and 7.35—8.15 (5H, m, phenyl).

Found for **7a**: C, 52.78; H, 5.60; Br, 20.88%, and for **7b**: C, 53.12; H, 5.44; Br, 20.59%. Calcd for $C_{17}H_{21}BrO_5$: C, 53.00; H, 5.49; Br, 20.74%.

The mother liquor from **7a** and **7b** was concentrated and the residue was chromatographed on a silica-gel column with 1 : 10 2-butanone–toluene as an eluent. DL-2,3-*O*-Isopropylidene-(1,3/2,4)-4-benzoyloxymethyl-5-cyclohexene-1,2,3-triol (**11**) was purely obtained out of four minor products and recrystallized from ethanol to give prisms (20 mg): mp 105—107 °C; ^1H NMR ($CDCl_3$, 90 MHz) δ=1.43 (6H, s, isopropylidene), 2.43 (1H, broad d, OH), 2.58—3.01 (1H, m, H-4), 3.51 (1H dd) and 3.60 (1H, dd) (J=10 and 11 Hz, H-2 and H-3), 4.27 (1H, dd, J_{gem}=11 Hz, $J_{4,7}$=6 Hz, H-7), 4.53 (1H, dd, $J_{4,7'}$=5 Hz, H-7′), 5.67 (2H, s, H-5 and H-6), and 7.28—8.08 (5H, m, phenyl).

Found: C, 66.82; H, 6.53%. Calcd for $C_{17}H_{20}O_5$: C, 67.09; H, 6.62%.

Compound **11** (41 mg) was treated with acetic anhydride (1 ml) and pyridine (1 ml) at room temperature overnight. Concentration of the reaction mixture gave a crude product, which was crystallized from ethanol to give the acetate (**12**, 20 mg, 43%) as thin needles: mp 99.5—102.5 °C; ^1H NMR ($CDCl_3$, 90 MHz) δ=1.47 (6H, s, isopropylidene), 2.13 (3H, s, OAc), 2.77—3.06 (1H, m, H-4), 3.64 (1H, t, $J_{2,3}$=$J_{3,4}$=9 Hz, H-3), 3.82 (1H, t, $J_{1,2}$=9 Hz, H-2), 4.33 (1H, dd, J_{gem}=11 Hz, $J_{4,7}$=6 Hz, H-7), 4.59 (1H, dd, $J_{4,7'}$=5 Hz, H-7′), 5.56 (1H, broad d, H-1), 5.73, (2H, broad d, H-5 and H-6), and 7.33—8.23 (5H, m, phenyl).

Found: C, 66.08; H, 6.53%. Calcd for $C_{19}H_{22}O_6$: C, 65.88; H, 6.40%.

DL-*1,2*-O-*Isopropylidene-(1,3,4/2,6)-4-azido-6-benzoyloxymethyl-1,2,3-cyclohexanetriol (**8a**) and **11**.* A mixture of **7a** (1.5 g), sodium azide (1 g), and dry dimethyl sulfoxide (30 ml) and heated at 110 °C for 20 h. TLC indicated the formation of two components (R_f 0.40 and 0.33, 1 : 5 2-butanone–toluene). Ethyl acetate (45 ml) was added to the reaction mixture and an insoluble material was removed by filtration. The filtrate

was successively washed with aqueous sodium chloride and water, and passed through a short column of alumina. The eluate was concentrated and the residue was chromatographed on a silica-gel column (75 g) with 1 : 10 2-butanone–toluene. The first fraction was concentrated to give crystals which were recrystallized from ethanol to give **8a** (0.89 g, 64%) as prisms: mp 118.5—121 °C; IR 3460 (OH), 2150 (N_3), and 1715 cm^{-1} (C=O); ^1H NMR ($CDCl_3$) δ=1.45 (6H, s, isopropylidene), 2.92 (1H, broad s, OH), 3.24 (1H, dd, $J_{1,2}$=10 Hz, $J_{1,6}$=8 Hz, H-1), 3.75 (1H, t, $J_{2,3}$=10 Hz, H-2), 4.26—4.70 (2H, m, H-7 and H-7′), and 7.33—8.16 (5H, m, phenyl).

Found: C, 58.54; H, 6.10; N, 11.85%. Calcd for $C_{17}H_{21}N_3O_5$: C, 58.78; H, 6.09; N, 12.10%.

Compound **8a** (35 mg) was acetylated as described for the preparation of **12**. The crude product was recrystallized from ethanol to give the acetate (**9a**, 25 mg, 64%) as prisms: mp 150—153 °C; ^1H NMR ($CDCl_3$) δ=1.43 (3H, s) and 1.47 (3H, s) (isopropylidene), 2.19 (3H, s, OAc), 3.34 (1H, dd, $J_{1,2}$=8.5 Hz, $J_{1,6}$=10.5 Hz, H-1), 3.95 (1H, dd, $J_{2,3}$=10.5 Hz, H-2), 5.05 (1H, dd, $J_{3,4}$=4 Hz, H-3), and 7.35—8.16 (5H, m, phenyl).

Found: C, 58.34; H, 6.02; N, 10.67%. Calcd for $C_{19}H_{23}N_3O_6$: C, 58.60; H, 5.95; N, 10.79%.

The second fraction gave a syrup which crystallized from ethanol to give **11** (52 mg, 4.4%) as prisms, mp 103—105 °C, identical with the compound derived from **6a**.

Reaction of ***7a*** *with 1,8-Diazabicyclo[5.4.0]undec-7-ene (DBU).* A mixture of **7a** (0.2 g), DBU (0.39 ml), and toluene (6 ml) was stirred at 120 °C for 7 h. TLC showed the formation of two major components (R_f 0.58 and 0.21) together with a trace of **7a** (R_f 0.35, 1 : 5 2-butanone–toluene). The reaction mixture was concentrated and the products were fractionated on a silica-gel column (8 g) with 1 : 5 2-butanone–toluene as an eluent. The first fraction gave crystals, which were recrystallized from ethanol to give 1,2-anhydro-3,4-*O*-isopropylidene-(1,2,4/3,5)-5-benzoyloxymethyl-1,2,3,4-cyclohexanetetrol (**13**, 26 mg, 33%) as prisms: mp 87—89.5 °C; IR 1715 (C=O) and 1610 cm^{-1} (phenyl); ^1H NMR ($CDCl_3$) δ=1.45 (6H, s, isopropylidene), 4.26 (1H, dd, J_{gem}=11 Hz, $J_{5,7}$=5 Hz, H-7), 4.53 (1H, dd, $J_{5,7'}$=4 Hz, H-7′), and 7.40—8.18 (5H, m, phenyl).

Found: C, 66.81; H, 6.56%. Calcd for $C_{17}H_{20}O_5$: C, 67.09; H, 6.62%.

The second fraction gave **11** (19 mg, 12%) mp 103—105 °C, identical with the compound obtained from **6a**.

DL-*2,3-O-Isopropylidene-(1,3,4/2,6)-4-azido-6-benzoyloxymethyl-1,2,3-cyclohexanetriol (**8a**).* A mixture of **7b** (1.1 g), sodium azide (0.75 g), and dimethyl sulfoxide (10 ml) was stirred at 120 °C for 18 h. The reaction mixture was processed as described for the preparation of **8a**. The syrupy product was crystallized from ethanol to give **8b** (0.72 g, 73%) as needles: mp 105—108 °C; IR 3480 (OH), 2170 (N_3), 1730 (C=O), and 1610 cm^{-1} (phenyl); ^1H NMR ($CDCl_3$) δ=1.45 (3H, s) and 1.50 (3H, s) (isopropylidene), 3.31 (1H, m, OH), 3.52 (1H, dd, $J_{2,3}$=9 Hz, $J_{3,4}$=3 Hz, H-3), 3.67 (1H, dd, $J_{1,2}$=9 Hz, $J_{1,6}$=8 Hz, H-1), 4.03 (1H, t, H-2), 4.30 (1H, dd, J_{gem}=11 Hz, $J_{6,7}$=2 Hz, H-7), 4.77 (1H, dd, $J_{6,7'}$=4 Hz-H-7′), and 7.35—8.15 (5H, m, phenyl).

Found: C, 58.63; H, 6.11; N, 11.88%. Calcd for $C_{17}H_{21}N_3O_5$: C, 58.78; H, 6.09; N, 12.10%.

Compound **8b** (50 mg) was acetylated in the usual way and the product was recrystallized from ethanol to give the acetate (**9b**, 30 mg, 54%) as needles: mp 116—119 °C; ^1H NMR ($CDCl_3$) δ=1.49 (6H, s, isopropylidene), 2.13 (3H, s, OAc), 3.63 (1H, dd, $J_{2,3}$=9 Hz, $J_{3,4}$=3 Hz, H-3), 4.09 (1H, t, $J_{1,2}$=9 Hz, H-2), 5.19 (1H, t, $J_{1,6}$=9 Hz, H-1), and 7.35—8.20 (5H, m, phenyl).

Found: C, 58.72; H, 5.98; N, 10.84%. Calcd for $C_{19}H_{23}N_3O_6$: C, 58.60; H, 5.95; N, 10.79%.

DL-*1,2-O-Isopropylidene-3-O-methyl-(1,3,4/2,6)-4-azido-6-benzoyloxymethyl-1,2,3-cyclohexanetriol (**10a**).* A mixture of **8a** (0.3 g), methyl iodide (0.54 ml), and silver oxide (0.4 g) in dry DMF (3 ml) was stirred at room temperature for 20 h in the dark. Acetone (10 ml) was added to the reaction mixture and an insoluble material was removed by filtration. The filtrate was concentrated and the residue was coevaporated with 1-butanol several times. The product was dissolved in ethyl acetate and the solution was passed through a short column of alumina. The eluate was concentrated and the residue was crystallized from ethanol to give **10a** (0.13 g, 40%) as prisms: mp 82—85 °C; IR 2150 (N_3), 1720 (C=O), and 1610 cm^{-1} (phenyl); ^1H NMR ($CDCl_3$) δ=1.42 (6H, s, isopropylidene), 3.20 (1H, dd, $J_{1,2}$=9 Hz, $J_{1,6}$=10 Hz, H-1), 3.49 (1H, dd, $J_{2,3}$=10 Hz, $J_{3,4}$=3 Hz, H-3), 3.52 (3H, s, methoxyl), 3.84 (1H, dd, H-2), 4.18 (1H, q, $J_{4,5\,ax}$=$J_{4,5\,eq}$=3 Hz, H-4), 4.22 (1H, dd, J_{gem}=11.5 Hz, $J_{6,7}$=5.5 Hz, H-7), 4.50 (1H, dd, $J_{6,7'}$=4.5 Hz, H-7′), and 7.34—8.13 (5H, m, phenyl).

Found: C, 59.54; H, 6.33; N, 11.85%. Calcd for $C_{18}H_{23}N_3O_5$: C, 59.80; H, 6.42; N, 11.63%.

DL-*2,3-O-Isopropylidene-1-O-methyl-(1,3,4/2,6)-4-azido-6-benzoyloxymethyl-1,2,3-cyclohexanetriol (**10b**).* A mixture of **8b** (1 g), methyl iodide (1.8 ml), and silver oxide (1.3 g) in dry DMF (10 ml) was stirred at room temperature for 20 h in the dark. At this stage, TLC showed the presence of **9b**. Then an additional amount of methyl iodide (0.9 ml) was added to the mixture and the stirring was continued for 23 h. The reaction mixture was processed as described for the preparation of **10a**. The crude product was recrystallized from ethanol to give **10b** (0.33 g, 32%) as needles: mp 105—107 °C; IR 2140 (N_3), 1730 (C=O), and 1610 cm^{-1} (phenyl); ^1H NMR ($CDCl_3$) δ 1.48 (3H, s) and 1.51 (3H, s) (isopropylidene), 3.32 (1H, t, $J_{1,2}$=$J_{1,6}$=9 Hz, H-1), 3.52 (1H, dd, $J_{2,3}$=9 Hz, $J_{3,4}$=3 Hz, H-3), 3.55 (3H, s, methoxyl), 4.03 (1H, t, H-2), 4.21 (1H,q, $J_{4.5ax}$=$J_{4,5eq}$=3 Hz, H-4), 4.47 (2H, d, J=3 Hz, H-7 and H-7′), and 7.35—8.13 (5H, m, phenyl).

Found: C, 59.82; H, 6.36; N, 11.39%. Calcd for $C_{18}H_{23}N_3O_5$: C, 59.80; H, 6.42; N, 11.63%.

DL-*1,2,7-Tri-O-acetyl-3-O-methyl-(1,3,4/2,6)-4-acetamido-6-hydroxymethyl-1,2,3-cyclohexanetriol (**14**).* Compound **10a** (0.1 g) was treated with Amberlite IR-120 (H^+) (1.5 ml) in ethanol (8 ml) at room temperature for 3 h. TLC indicated the formation of a single product (R_f 0.15, 1:2 2-butanone–toluene, **10a**: R_f 0.77). The resin was removed and the solution was concentrated to give a syrup which was treated with 0.3 M methanolic sodium methoxide(3 ml)(1 M=1 mol dm^{-3}) at room temperature for 0.5 h. TLC showed the presence of a single product (R_f 0.46, 5 : 1 chloroform–methanol, the starting compound: R_f 0.78). The reaction mixture was neutralized with Amberlite IR-120 (H^+) (1.5 ml) and then concentrated to give crystals (62 mg). A solution of it in methanol containing 1 M hydrochloric acid (3 ml) was hydrogenated in the presence of 5% palladium on carbon (15 mg) at room temperature for 16 h. The product showed a single spot (R_f 0.27) on TLC (4 : 1 : 1 1-propanol–acetic acid–water). The catalyst was removed by filtration and the filtrate was concentrated to give a crystalline 2-*O*-methyl-DL-validamine hydrochloride (46 mg, 78%). An aqueous solution of the hydrochloride was treated with Amberlite IRA-400 (OH^-) (1.5 ml) and then concentrated to a syrup, which was treated with acetic anhydride and pyridine in the usual way to give the total acetate. Recrystallization from ethanol gave **14** (22 mg, 22%) as prisms: mp 205.5—208 °C; IR 3350, 1645, and 1545 (amide), 1750 cm^{-1} (ester); ^1H NMR ($CDCl_3$, 90 MHz) δ=2.00 (3H, s), 2.03 (6H, s), and 2.04 (3H, s) (NAc and OAc), 3.34 (3H, s, methoxyl), 3.35 (1H, dd, $J_{2,3}$=9 Hz,

$J_{3,4}$=5 Hz, H-7), 3.86 (1H, dd, J_{gem}=11 Hz, $J_{6,7}$=4 Hz, H-7), 4.14 (1H, dd, $J_{6,7'}$=5 Hz, H-7'), 4.42 (1H, m, H-4), 4.88 (1H, t, $J_{1,2}=J_{1,6}$=9 Hz, H-1), 5.10 (1H, t, $J_{2,3}$=9 Hz, H-2), and 5.87 (1H, broad d, J=6 Hz, NH).

Found: C, 53.21; H, 6.87; N, 3.72%. Calcd for $C_{16}H_{25}NO_8$: C, 53.47; H, 7.01; N, 3.90%.

DL-*2,3,7-Tri*-O-*acetyl-1*-O-*methyl-(1,3,4/2,6)-4-azido-6-hydroxymethyl-1,2,3-cyclohexanetriol* (**15**). Compound **10b** (0.1 g) was treated with Amberlite IR-120 (H^+) (1 ml) in ethanol, and the product was successively treated with 0.3 M methanolic sodium methoxide to give a crystalline hydroxy azide (56 mg, 93%). This compounds was acetylated in the usual way and the acetate was recrystallized from ethanol to give **15** (47 mg, 50%) as needles: mp 71—73 °C; IR 2130 (N_3) and 1740 cm^{-1} (C=O); ^1H NMR ($CDCl_3$) δ=2.08 (9H, s, OAc), 3.15 (1H, dd, $J_{1,2}$=9 Hz, $J_{1,6}$=10.5 Hz, H-1), 3.38 (3H, s, methoxyl), 4.05 (1H, q, $J_{3,4}=J=_{4.5ax}=J_{4.5eq}$=3 Hz, H-4), 4.13 (2H, d, J=4 Hz, H-7 and H-7'), 4.86 (1H, dd, $J_{2,3}$=10 Hz, H-3), and 5.38 (1H, dd, H-2).

Found: C, 49.08; H, 6.13; N, 12.32%. Calcd for $C_{14}H_{21}N_3O_7$: C, 48.95; H, 6.17; N, 12.24%.

DL-*2,3,7-Tri*-O-*acetyl-1*-O-*methyl-(1,3,4/2,6)-4-acetamido-6-hydroxymethyl-1,2,3-cyclohexanetriol* (**16**). Compound **15** (75 mg) was hydrogenated and then acetylated as described for the preparation of **14**. The crude product was purified on a silica-gel column (5 g) with 1 : 1 2-butanone–toluene as an eluent to give **16** (60 mg, 76%) as a homogeneous solid: IR 3290, 1655, and 1550 (amide), and 1750 cm^{-1} (ester); ^1H NMR ($CDCl_3$, 90 MHz) δ=2.00 (3H, s), 2.02 (3H, s), and 2.08 (6H, s) (NAc and OAc), 3.11 (1H, t, $J_{1,2}=J_{1,6}$=9 Hz, H-1), 3.41 (3H, s, methoxyl), 4.15 (2H, d, J=4 Hz, H-7 and H-7'), 4.48 (1H, m, H-4), 4.86 (1H, dd, $J_{2,3}$=10 Hz, $J_{3,4}$= 5 Hz, H-3), 5.18 (1H, dd, $J_{1,2}$=9 Hz, H-2), and 6.03 (1H, broad d, J=8 Hz, NH).

Found: C, 53.18; H, 6.85; N, 3.76%. Calcd for $C_{16}H_{25}NO_8$; C, 53.47; H, 7.01; N, 3.90%.

L-[*19*(+)] *and* D-*1*-O-*(2,3,4,6-Tetra*-O-*acetyl-β-D-glucopyranosyl-1,3,4/2,6-4-azido-6-benzoyloxymethyl1,-2,3-cyclohexanetriol* [*19*(−)]. A mixture of **8b** (1.1 g), mercury(II) cyanide (7 g), anhydrous calcium sulfate (Drierite) (7 g), and dry benzene (300 ml) was refluxed at 90 °C with stirring, and 140 ml of benzene was removed by distillation. Then freshly prepared 2,3,4,6-tetra-*O*-acetyl-α-D-glucopyranosyl bromide (5.2 g) was added to the mixture and it was stirred vigorously at 65—70 °C for 50 h. After being cooled to room temperature, the reaction mixture was treated with triethylamine (3 ml) and an insoluble material was removed by filtration through a caoline bed and washed thoroughly with chloroform. The filtrate and washings were combined and concentrated to give a brown syrup, which was dissolved in ethyl acetate (180 ml), washed successively with aqueous sodium hydrogencarbonate (3×200 ml) and water (2×200 ml), and dried. Evaporation of the solvent gave a syrup (9.3 g) which was chromatographed on a silica-gel column (130 g) with 1 : 10 2-butanone–toluene as an eluent. Fractions having R_f 0.24 in the same solvent system (irrigated twice) were concentrated to give a pale yellow syrup (1.3 g), whose ^1H NMR spectrum showed the presence of one isopropylidene, four acetoxyl, and one benzoyloxyl groups, and a contamination of traces of unidentified side-products. A 1.3 g-portion of the syrup was dissolved in ethanol (10 ml) and treated with Amberlite IR-120B (H^+) (20 ml) at room temperature for 21 h. The resin was filtered off and the filtrate was concentrated to a syrup (1.3 g), which was chromatographed on a silica-gel column (60 g) with 2 : 5 2-butanone–toluene as an eluent. The main fraction (R_f 0.41, 1 : 1 2-butanone–toluene) gave crystals 0.363 g (18%), which were recrystallized from ethanol to give **19**(+) (0.262 g, 13%) as needles: mp 182—183.5 °C; $[\alpha]_D^{24}$ +27° (*c* 1.0, chloroform); IR 3540 (OH), 2150 (N_3), 1750 (C=O), and 1610 cm^{-1} (phenyl); ^1H NMR ($CDCl_3$) δ=2.00 (3H, s), 2.04 (3H, s), 2.07 (3H, s), and 2.16 (3H, s) (OAc), and 7.35—8.13 (5H, m, phenyl).

The second fractions (R_f 0.34) were concentrated to give an amorphous solid (0.262 g, 13%), which was recrystallized from ethanol and ether to give **19**(−) (0.162 g, 8%) as needles: mp 158—161 °C; $[\alpha]_D^{23}$ −16° (*c* 1.5, chloroform); IR 3500 (OH), 2150 (N_3), 1750 (C=O), and 1610 cm^{-1} (phenyl); ^1H NMR ($CDCl_3$) δ=1.99 (3H, s), 2.0 2(3H, s), 2.10 (3H, s), and 2.17 (3H, s) (OAc), and 7.36—8.13 (5H, m, phenyl).

Found for **19**(+): C, 52.84; H, 5.47; N, 6.32%, and for **19**(−): C, 52.50; H, 5.51; N, 6.45%. Calcd for $C_{28}H_{35}NO_{14}$: C, 52.72; H, 5.54; N, 6.59%.

Preparation of the Isopropylidene Derivative ***18***(+) *of* ***19***(+). A mixture of **19**(+) (50 mg), 2,2-dimethoxypropane (0.1 ml), DMF (2 ml), and *p*-toluenesulfonic acid (2 mg) was heated at 65—70 °C for 11 h. During this reaction time, 0.2 ml portions of 2,2-dimethoxypropane were added to the reaction mixture at intervals of 3 h. TLC showed one major spot (R_f 0.44) and one minor spot (R_f 0.09) due to **19**(+) in 1 : 3 2-butanone–toluene. The mixture was treated with Amberlite IRA-400 (OH^-) (1 ml) and then concentrated to a syrup ,which was chromatographed on a silica gel (2 g) with 1 : 3 2-butanone–toluene as an eluent. The main fraction gave a syrup, which crystallized from ethanol to give **18**(+) (20 mg, 38%) as plates: mp 166—170 °C $[\alpha]_D^{23}$ +21° (*c* 0.5, chloroform); ^1H NMR ($CDCl_3$) δ=1.48 (6H, broad s, isopropylidene), 1.92 (3H, s), 1.99 (3H, s), 2.02 (3H, s), and 2.06 (3H, s) (OAc), and 7.34—8.12 (5H, m, phenyl).

Found: C, 55.00; H, 5.90; N, 6.07%. Calcd for $C_{31}H_{39}N_3O_{14}$: C, 54.94; H, 5.80; N, 6.20%.

Preparation of the Isopropylidene Derivative ***18***(−) *of* ***19***(−). Compound **19**(−) (50 mg) was *O*-isopropylidenated as described for the preparation of **18**(+) to give **18**(−) (49 mg, 92%) as a homogeneous solid, which crystallized from ethanol to give needles (29 mg, 56%): mp 174—174.5 °C; $[\alpha]_D^{23}$ −26° (*c* 0.58, chloroform): ^1H NMR ($CDCl_3$) δ=1.48 (6H, broad s, isopropylidene), 1.99 (6H, s), 2.01 (3H, s), and 2.08 (3H, s) (OAc), and 7.32—8.12 (5H, m, phenyl).

Found: C, 55.16; H, 5.91; N, 6.10%. Calcd for $C_{31}H_{39}N_3O_{14}$: C, 54.94; H, 5.80; N, 6.20%.

Both **18**(+) and **18**(−) had similar mobilities on TLC (R_f 0.44, 1 : 3 2-butanone–toluene).

L-*1*-O-*(β-D-Glucopyranosyl)-(1,3,4/2,6)-4-amino-6-hydroxymethyl-1,2,3-cyclohexanetriol Hydrochloride* [*21*(+)]. To a solution of **19**(+) (100 mg) in methanol (5 ml) was added 1 M methanolic sodium methoxide (8 ml) and the mixture was kept at room temperature for 24 h. The reaction mixture was treated with Amberlite IR-120B (H^+) (12 ml) and then concentrated to give the hydroxy azide **20**(+) (61 mg) as a homogeneous syrup (R_f 0.61, 4 : 1 : 1 1-propanol–acetic acid–water). This compound was directly hydrogenated in a mixture of methanol (4 ml) and water (4 ml) containing 0.5 M hydrochloric acid (0.38 ml) in the presence of 5% palladium on carbon (10 mg) at room temperature overnight. The catalyst was removed by filtration and the filtrate was concentrated to give **21**(+) [56 mg, 94% yield based on **19**(+)] as a syrup, $[\alpha]_D^{23}$ +22° (*c* 1.9, water). This compound was identical with an authentic sample derived from validamycin A, as found from comparison of the mobilities on TLC: silica gel, R_f 0.24 in 4 : 1 : 1 1-propanol–acetic acid–water and R_f 0.35 in 4 : 5 : 2 : 4 1-butanol–ethanol–acetic acid–water; cellulose, R_f 0.15 in 6 : 4 : 3 : 1 1-butanol–pyridine–water–acetic acid (ref. validamine hydrochloride, R_f 0.17).

D-O-*(β-D-Glucopyranosyl)-(1,3,4/2,6)-4-amino-6-hydroxy-*

methyl-1,2,3-cyclohexanetriol Hydrochloride [**21**(−)]. Compound **19**(−) (100 mg) was *O*-deacylated with methanolic sodium methoxide as described for the preparation of **20**(+). The hydroxy azide **20**(−) (64 mg) thus obtained was hydrogenated similarly to give **21**(−) [53 mg, 88% yield based on **19**(−)] as a syrup, which was clearly differentiated from **21**(+) on TLC, showing mobilities slightly higher than those of **21**(+) in all the solvent systems examined; silica gel, R_f 0.28 in 4 : 1 : 1 1-propanol–acetic acid–water and R_f 0.40 in 4 : 5 : 2 : 4 1-butanol–ethanol–acetic acid–water; cellulose, R_f 1.18 in 6 : 4 : 3 : 1 1-butanol–pyridine–water–acetic acid when **21**(+) was used as an reference (R_f 1.0).

1L-1,2,3,6-Tetra-O-acetyl-1-O-(2,3,4,6-tetra-O-acetyl-β-D-glucopyranosyl)-(1,3,4/2,6)-4-acetamido-6-hydroxymethyl-1,2,3-cyclohexanetriol [**22**(+)]. Compound **21**(+) (50 mg) was dissolved in water (5 ml) and treated with Amberlite IRA-400 (OH^-) (1.5 ml) at room temperature for 30 min. The resin was removed by filtration and the filtrate was dried by azeotropic distillation with ethanol and toluene. The residual free base was treated with acetic anhydride (2 ml) and pyridine (2 ml) at 50 °C for 20 h. The reaction mixture was concentrated and the residue was chromatographed on a silica-gel column (4 g) with 1 : 1 2-butanone–toluene as an eluent. The fraction having R_f 0.43 in 20 : 1 chloroform–methanol was concentrated to give **22**(+) (50 mg, 57%) as an amorphous solid: $[\alpha]_D^{23}$ +16° (*c* 0.75, chloroform) [lit,[3] $[\alpha]_D^{23}$+17.6° (chloroform)]; IR ($CHCl_3$) 3440 (NH), 1770—1740 (C=O), 1680, and 1520 cm^{-1} (amide); ^1H NMR ($CDCl_3$) δ=1.98 (3H, s), 2.00 (6H, s), 2.02 (9H, s), 2.07 (3H, s), and 2.10 (3H, s) (NAc and OAc), and 6.30 (1H, d, J=7 Hz, NH). The spectrum was superimposable on that of an authentic sample.[6]

Found: C, 51.30; H, 6.19; N, 2.20%. Calcd for $C_{29}H_{41}NO_{17}$: C, 51.56; H, 6.12; N, 2.07%.

Compound **22**(+) showed a double melting point. Thus, the amorphous solid melted at 114—118 °C (lit,[3] 117—119 °C) and the melt, on continuous heating on a hot stage, crystallized at 150—160 °C to give needles, which melted sharply at 187—189 °C. The same melting and crystallization behavior was observed for an authentic sample (mp 112—119 and 183—185 °C).

1D-1,2,3,6-Tetra-O-acetyl-1-O-(2,3,4,6-tetra-O-acetyl-β-D-glucopyranosyl)-(1,3,4/2,6)-4-acetamido-6-hydroxymethyl-1,2,3-cyclohexanetriol [**22**(−)]. Amine hydrochloride **21**(−) (53 mg) was acetylated as described for the preparation of **22** (+) to give **22**(−) (41 mg,44%) as a homogeneous syrup (R_f 0.51, 20 : 1 chloroform–methanol): $[\alpha]_D^{24}$ −49° (*c* 0.75, chloroform); IR ($CHCl_3$) 3440 (NH), 1740—1765 (C=O), 1680, and 1505 cm^{-1} (amide); ^1H NMR ($CDCl_3$) δ=1.99 (3H, s), 2.01 (6H, s), 2.02 (6H, s), 2.11 (3H, s), and 2.17 (6H, s) (NAc and OAc), and 6.06 (1H, broad d, J=7 Hz, NH).

Found: C, 51.48; H, 6.15; N, 1.93%. Calcd for $C_{29}H_{41}NO_{17}$: C, 51.56; H, 6.12; N, 2.07%.

The present work was partially supported by a Grant-in-Aid for Scientific Research No. 355376 from the Ministry of Education, Science and Culture. The authors wish to express their sincere thanks to Mr. Saburo Nakada for his elemental analyses.

References

1) A preliminary account of portions of this article was previously presented: S. Ogawa, N. Chida, and T. Suami, *Chem. Lett.*, **1980**, 139.

2) S. Ogawa, Y. Shibata, N. Chida, and T. Suami, *Bull. Chem. Soc. Jpn.*, **56**, 494 (1983).

3) S. Horii and Y. Kameda, *J. Chem. Soc., Chem. Commun.*, **1972**, 747.

4) S. Ogawa, K. Nakamoto, M. Takahara, Y. Tanno, N. Chida, and T. Suami, *Bull. Chem. Soc. Jpn.*, **52**, 1174 (1979). The nomenclature and numbering of cyclitols used in this paper follow IUPAC and IUB Tentative Rules for Cyclitol Nomenclature [*J. Biol. Chem.*, **243**, 5809 (1968)].

5) The absolute configuration of (+)-validamine was established by X-ray spectroscopic analysis of its hydrobromide and it was named 1*S*-(1,2,4/3,5)-1-amino-5-hydroxymethyl-2,3,4-cyclohexanetriol in the original paper [K. Kamiya, Y. Wada, S. Horii, and M. Nishikawa, *J. Antibiot.*, **22**, 317 (1971)]

6) An authentic sample of **22**(+) was kindly provided by Dr. Satoshi Horii (Takeda Chemical Industries, Ltd., Osaka).

7) J. B. Stothers, "Carbon-13 NMR Spectroscopy," Academic Press, New York and London (1972), pp 458—462.

 © 1983 The Chemical Society of Japan Bull. Chem. Soc. Jpn., 56, 505—513 (1983)

Synthetic Studies on the Validamycins. III. Bromination of DL-Tri-*O*-acetyl-(1,3/2)-4-methylene-5-cyclohexene-1,2,3-triol. Preparation of Several Branched-chain Unsaturated Cyclitols Related to Valienamine[1)]

Tatsushi Toyokuni, Yasuo Abe, Seiichiro Ogawa, and Tetsuo Suami*

Department of Applied Chemistry, Faculty of Science and Technology, Keio University, Hiyoshi, Kohoku-ku, Yokohama 223

(Received June 10, 1982)

Bromination of DL-tri-*O*-acetyl-(1,3/2)-4-methylene-5-cyclohexene-1,2,3-triol with bromine in an appropriate solvent yielded mainly two 1,4-addition products, from which several branched-chain unsaturated cyclitols, related to biologically interesting valienamine, were selectively prepared. Reaction courses are discussed for the bromination of the diene and the debromination of the bromo(bromomethyl)cyclohexenetriol triacetates obtained under various conditions.

Validamycin A (**1**)[2)] is the major and most active component of the antibiotic validamycins, produced by *Streptomyces hygroscopicus* var. *limoneus* and widely used in order to control sheath blight in rice plants. Microbial degradation of validamycin A with a cell suspension of *Pseudomonas denitrificans* gave, besides validamine,[3)] a branched-chain unsaturated aminocyclitol, valienamine (**2**), which is a common building block of validamycins and the structure of which was assigned to 1D-(1,3,6/2)-6-amino-4-hydroxymethyl-4-cyclohexene-1,2,3-triol on the basis of ^{1}H NMR spectroscopy.[4)]

In recent years, some biologically active branched-chain unsaturated cyclitols such as glyoxalase I inhibitor[5)] and rancinamycins I—IV[5)] have been discovered. Very recently, the valienamine moiety linked to D-glucose or 6-deoxy-D-glucose *via* an imino linkage has been found as an essential unit in a homologous series of pseudo-oligosaccharides such as acarboses,[7)] trestatins,[8)] and adiposins,[9)] all of which show a marked inhibitory effect against α-glucosidases in mammals.[10)] Furthermore, valienamine itself has been found to show both the α-glucosidase inhibition and the antibiotic activity against *Bacillus* species.[11)]

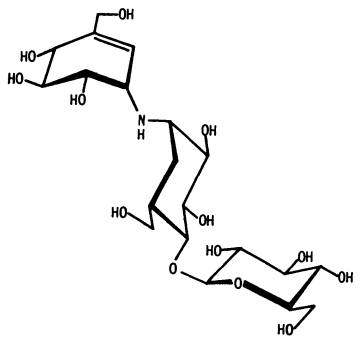

Validamycin A (1)

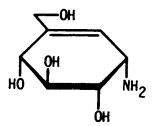

Valienamine (2)

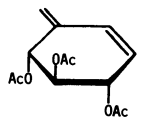

3

In connection with our synthetic studies on the validamycins,[12)] we now report the synthesis of several branched-chain unsaturated cyclitols related to valienamine. The synthetic route involved the preferential 1,4-addition of bromine to the conjugated diene, DL-tri-*O*-acetyl-(1,3/2)-4-methylene-5-cyclohexene-1,2,3-triol (**3**),[13)] assembling all the carbon atoms present in valienamine, and the stereocontrolled syntheses of the branched-chain unsaturated cyclitols by utilization of the different reactivities of the allylic primary and secondary bromine atoms and the neighboring group participation of acetoxyl groups in the replacement process. This synthetic approach may be extended to the synthesis of other analogs of this kind as well. Some intermediates obtained in this study are also important precursors of amino analogs including valienamine.

By consideration of the transition state analogous theory,[14)] the synthetic branched-chain unsaturated cyclitols are expected to display some glucosidase inhibitory activity similarly to valienamine.

Results and Discussion

*Bromination of Conjugated Diene **3** with Bromine. Synthesis of Bromo(bromomethyl)cyclohexenetriol Triacetates **5** and **6**:* Since electrophilic addition to conjugated diene often gives 1,4-addition product in much larger amount than 1,2-addition product, we have undertaken the bromination of readily available **3** with bromine in order to construct the carbon skelton of valienamine.

Treatment of **3** with a molar equiv. of bromine produced preferentially the 1,4-addition products **5** and **6**. In the ^{1}H NMR spectrum, the signal due to the olefinic proton (H-5) of **5** appeared as a doublet (J=5.5 Hz) at δ 6.19, indicating that the C-6 bromine atom is situated at a pseudoaxial position in a favored half-chair conformation,[15)] whereas that of **6** appeared as a broad singlet at δ 6.13, supporting that **6** is the C-6 epimer of **5**. Therefore, the structures of **5** and **6** were assigned to DL-(1,3,6/2)- and DL-(1,3/2,6)-6-bromo-4-bromomethyl-4-cyclohexene-1,2,3-triol triacetates, respectively.

Of interest here is the fact that the product-distribution was affected by the polarity of the solvent used and by reaction temperature. Table 1 gives a summary of the results of the bromination of **3**. When the reaction was carried out in carbon tetrachloride, **6** was produced predominantly over **5** at −15 °C, whereas at room temperature the reverse was the case. On the other hand, the reaction in acetic acid at room temperature resulted in preferential formation of **6**. Both **5** and **6** were found to be interconvertible in the presence of a trace of bromine, but the interconversion took place so slowly that it would be negligible during the following work-up.

The above results can be interpreted by assuming the

Table 1. Bromination of 3 with an equimolar amount of bromine

Solvent	Temp/°C	Isolated yield/%[a] 5	6	Total yield/%	Product ratio[b] 5/6
	−15	18	40	79	1.6
CCl_4	−4	33	29	90	0.7
	r.t.	48	17	89	0.4
AcOH	r.t.	10	43	72	3.4
50%aq AcOH[c]	r.t.	7	18	49[d]	2.1

a) After silica-gel column chromatography. b) Determined by ^{1}H NMR analysis of the mixture. c) The resulting product was successively acetylated with acetic anhydride containing a trace of sulfuric acid. d) In addition to **5** and **6**, bromo tetraacetate **7** was obtained in 22% yield.

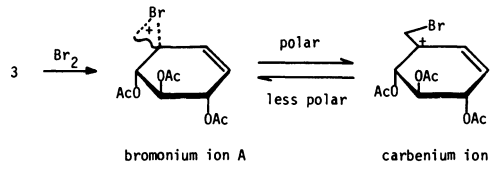

reaction course, which involves the equilibrium between bromonium ion **A** and carbenium ion **B**.[16] The observed solvent dependence of the bromination may be the result of differential solvation requirement of the bromonium ion **A** and carbenium ion **B** in their equilibrium, leading to more bromonium ion character in nonpolar solvent. Therefore, in carbon tetrachloride at room temperature the equilibrium lies to the bromonium ion **A**. The 1,4-addition product is known to be formed by opening of a bromonium ion by an S_N2' attack by at bromide ion.[17] Although a most theoretical analysis of S_N2' reactions has indicated a preference for syn attack by nucleophile, Toromanoff[18] has recently reported that, if the leaving group departs from an axial position in a half-chair conformation, S_N2' reaction is of syn stereochemistry, and that, if the leaving group is of an axial orientation in a boat form, anti stereochemistry is important. Thus, if bromine approaches from below, the reaction will proceed *via* the transition state **C** (half-chair), resulting in S_N2' attack by a bromide ion in syn stereochemistry, whereas if bromine approaches from above, the reaction will proceed *via* the transition state **D** (boat), resulting in S_N2' attack in anti stereochemistry. Both pathways give **5**.

On the other hand, in acetic acid carbenium ion **B** can be stabilized by allylic rearrangement with an assistance of the C-1 acetoxyl group, producing the 1,6-cyclic acetoxonium ion **E**, which is then opened by attack by a bromide ion from the back side at C-6 to give **6**. Carbenium ion **B** may also be stabilized by an assistance of the C-3 acetoxyl group, resulting in the formation of the 3,4-cyclic acetoxonium ion **F**, but this participation must be unfavorable because of the steric hindrance at C-4. Bromo triacetates **13**, **14**, and **20** were obtained as side-products in trace amounts. Compounds **13** and **14** could result from the opening of the cyclic acetoxonium **E** by attack by a trace of water present, and **20** from a similar opening of **F**. Furthermore, when the reaction was run in 50% aqueous acetic acid, bromotetraacetate **7** was obtained in 22% yield, after acetylation with acetic anhydride containing a trace of sulfuric acid. These findings substantiated the proposed mechanism for the bromination in acetic acid.[19]

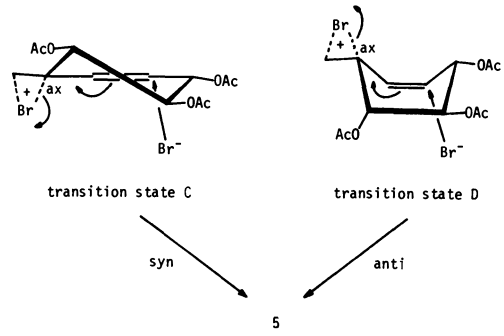

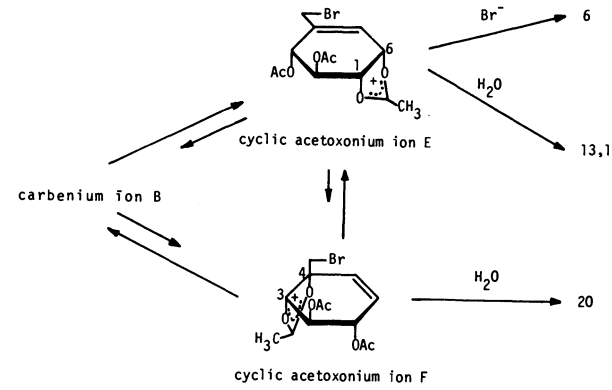

Compound **6** could be readily available by crystallization of the bromination products in acetic acid–acetic anhydride[20] from ethanol. From the mother liquor, an inseparable mixture of **7** and **8** was obtained by fractionation by a silica-gel column. These were considered to be formed, respectively, by subsequent acetylation of **13** and **14** under the reaction conditions and by the opening of the acetoxonium ion **E** by an acetate ion from the back side at C-6.

When an excess bromine was used for the bromination in carbon tetrachloride at 0—5 °C, tetrabromides, presumably consisting of two isomers **4a** and **4b**, were obtained as crystals in 91% yield. Recrystallization from ethanol gave one of the isomers **4a** in a pure form in 59% yield. Monitoring of the reaction by TLC indicated the reaction to proceed *via* **5** and **6**, but the structures of the tetrabromides could not definitively be determined by analysis of the ^{1}H NMR spectral data. Hydrogenolysis of **4a** in ethyl acetate with Raney nickel T-4[21] in the presence of Amberlite IR-45 (OH^-) gave a mixture of tri-*O*-acetyl-DL-deoxyvalidatol and its 4-epimer, identical with authentic samples.[13]

Debromination of **5** and **6** was attempted with tributyltin(IV) hydride or with lithium aluminium hydride but, instead of desired debrominated product, **3** was regenerated in a good yield. Compounds **5** and **6** were expected to be potential intermediates for the present synthetic study.

Hydrobromination of Conjugated Diene 3. Hydro-

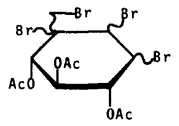

4a,b

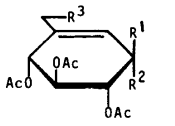

	R^1	R^2	R^3
5	H	Br	Br
6	Br	H	Br
7	H	OAc	Br
8	OAc	H	Br
9	H	Br	OAc
10	Br	H	OAc
11	H	OAc	OAc
12	OAc	H	OAc

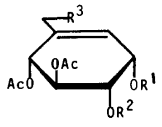

	R^1	R^2	R^3
13	Ac	H	Br
14	H	Ac	Br
15	Ac	H	OAc
16	H	Ac	OAc

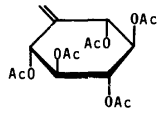

17

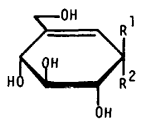

	R^1	R^2
18	H	OH
19	OH	H

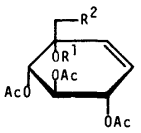

	R^1	R^2
20	H	Br
21	H	OMe
22	Ac	OMe
23	H	OAc
24	Ac	OAc

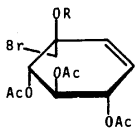

	R
25	H
26	Ac

bromination of **3** using *N*-bromoacetamide (NBA) or *N*-bromosuccinimide (NBS) resulted in the preferential formation of 1,2-addition products in contrast to the bromination of **3** with a molar equiv. of bromine.

Treatment of **3** with a molar equiv. of NBA in aqueous acetone buffered with sodium acetate at room temperature for 5 d, followed by acetylation, gave a mixture of products from which 1,2-addition products **20** (9%), **23** (21%), and **26** (trace), and 1,4-addition product **11** (10%) were isolated by a silica-gel column chromatography. On the other hand, when **3** was treated with 1.5 molar equiv. of NBS in aqueous dimethyl sulfoxide for 5 h below 10 °C, 1,2-addition products **20** (36%) and **25** (12%), and 1,4-addition products **13** and **14** (5%) were obtained after chromatography.

The structures of **11**, **13**, **14**, and **20** were confirmed by comparison of their ^{1}H NMR spectra with those of authentic samples prepared later *via* unambiguous routes. In the ^{1}H NMR spectrum of **23**, the signals due to the olefinic protons (H-5 and H-6) appeared as a two-proton singlet at δ 5.37. The facts that acetoxymethyl protons of **23** appeared as AB-quartet (J=12 Hz) at δ 3.84 and 4.02 and that no signal changed upon deuteration except the disappearance of the signal at δ 2.57 due to the hydroxyl proton, indicated that **23** has a tertiary hydroxyl group. Further acetylation of **23** with acetic anhydride and pyridine for 7 d yielded pentaacetate **24** quantitatively. In the ^{1}H NMR spectrum of **24** the H-3 signal appeared as a doublet of doublets (J=9 Hz, 10.5 Hz) at δ 5.19, whereas in that of **23** it appeared in the vicinity of δ 5.33—5.62, partly overlapping with the H-4 signal. This observation suggested that the C-1 hydroxyl group of **23** would occupy a 1,3-diaxial position with respect to H-3, and hence the orientation of the acetoxymethyl group of **23** was assumed to be pseudoequatorial in a favored half-chair conformation. The structure of **25** was tentatively assigned by the elemental analysis and by comparing its ^{1}H NMR spectrum with that of **20**. The spectrum of **25** exhibited two olefinic protons as two doublets (J=10 Hz) at δ 6.00 and 6.09. The ^{1}H NMR spectrum of **26** resembled that of **25** in the region for the ring protons (H-2, H-3, and H-4), except that signals for the bromomethyl protons appearing as a AB-quartet (J=11 Hz) shifted down-field by *ca.* 0.13 ppm, supporting the assigned structure of **26**.

The reaction products suggested that the hydrobromination of **3** using NBA in aqueous conditions would not differ fundamentally from the aforementioned bromination of **3** with bromine in acetic acid. Therefore, the reaction is thought to proceed *via* the carbenium ion **B**. Since solvents such as dimethyl sulfoxide[22] and water are known to serve as nucleophiles, the carbenium ion **B** might be attacked by solvents to give the 1,2-addition products preferentially.

Compounds **11** and **23** were probably derived from the corresponding intermediate spiro-epoxides formed by the dehydrobromination of **20** and **25**, respectively, during subsequent acetylation. Compound **11** seemed to be yielded by the replacement of the remaining allylic bromine atom in **13** and **14** with an acetate ion present followed by acetylation. When the mixture of **13**, **14**, **20**, and **25**, obtained by the hydrobromination of **3** with NBS in aqueous dimethyl sulfoxide, was acetylated, the formation of **7**, **11**, **20**, **23**, and **26** was observed by TLC, supporting partly the above assumption.

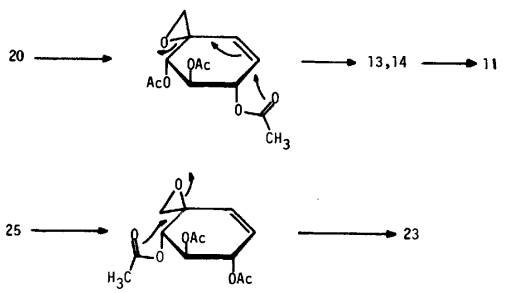

Reaction of Dibromocyclohexenes **5** *and* **6**: *Synthesis of Branched-chain Unsaturated Cyclitols.* With **5** and **6** in hand in which two kinds of allylic bromine atoms are present at C-6, we initiated a stereocontrolled synthesis of branched-chain unsaturated cyclitols by taking advantage of different reactivities of the bromine atoms.

With Sodium Acetate: Preferential replacement of the primary allylic bromine atoms in both **5** and **6** by an acetate ion was effected by the reaction with a molar equiv. of sodium acetate in *N*,*N*-dimethylformamide (DMF) at room temperature for 24 h, and a *ca.* 3.5 : 1 mixture of the bromo tetraacetates **9** and **10** was obtained in both cases, from which **9** was easily isolated in 47—49% yield by crystallization from ethanol. The structure of **9** was confirmed by the ^{1}H NMR spectrum

which revealed a down-field shift of the signal due to the C-7 methylene group, resulting from the replacement of the bromine atom by an acetoxyl group, and an olefinic proton (H-5) present as a broad doublet (J=*ca.* 5 Hz) at δ 6.07. A comparison of the ^{1}H NMR spectrum of the mixture of **9** and **10** with that of **9** showed that **10** is the C-6 epimer of **9**. The H-5 signal of **10** appeared as a singlet at δ 5.99.

Interestingly, the product-distribution was almost independent of starting from either **5** or **6**. The C-6 bromine atom seems to be readily exchangeable upon an S_N2 attack of a bromide ion generated in course of the reaction.

When both **5** and **6** reacted with an excess of sodium acetate in DMF at room temperature for 2 d, a 2—3 : 1 mixture of pentaacetates **11** and **12** was obtained.

With Silver Acetate: In the presence of silver ion, alkyl halides, even primary, react *via* and S_N1-like mechanism, and the participation of neighboring acetoxyl group in replacement reactions has been extensively studied by Winstein and Buckles.[23]

According to their results, some branched-chain unsaturated cyclitols were expected to be selectively prepared by the following reaction sequences. Treatment of **6** with a molar equiv. of silver acetate in 90% aqueous acetic acid at room temperature for 2 h gave a 3 : 1 mixture of **13** and **14** as crystals in 73% yield, together with a 3 : 1 mixture of tetraacetates **15** and **16** in 13% yield. The latter was readily obtainable from **6** in 56% yield by using 4 molar equiv. of silver acetate in a similar condition at 90 °C for 1 h. On the other hand, treatment of **6** with 1 or 4 molar equiv. of silver acetate in acetic acid–acetic anhydride[20] at 80 °C gave **8** (63%) or **12** (73%). The *exo*-olefin **17**[24] was produced concomitantly by the reaction when 4 molar equiv. of silver acetate was used. Compound **12** was also obtained selectively by the reaction of **8** with sodium acetate at room temperature for 24 h.

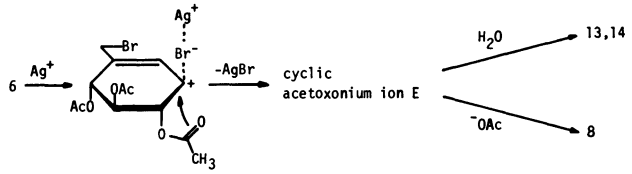

In both conditions, acetoxonium ion **E** is considered to be formed as an intermediate by the participation of the neighboring C-1 acetoxyl group either simultaneously with or very short after the removal of the C-6 bromine atom by a silver ion. The cyclic intermediate is then opened by attack of water in the case of the former condition to give a mixture of **13** and **14**, which is further converted into a mixture of **15** and **16**, whereas under the latter condition it is opened by a back-side attack of an acetate ion at C-6 to give **8**, which is then converted into **12**. Compound **17** seemed to be formed from **8** *via* the intermediate **G**. Isolations of **13** and **14** and of **15** and **16** were unsuccessful because of their similar chromatographic mobilities on silica gel.

The structures of **13** and **14** were tentatively assigned by the elemental analysis and ^{1}H NMR spectral data.

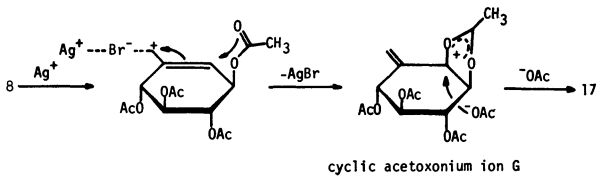

The fact that the signal due to the H-2 proton appeared as a doublet of doublets (J=5 Hz, 11 Hz) at δ 3.91 for **13** and as a doublet of doublets (J=3 Hz, 10 Hz) at δ 4.93 for **14**, indicated that the hydroxyl group of **13** was located at C-2, whereas that of **14** is at C-1. Similarly, the H-2 signals of **15** and **16** appeared as a doublet of doublets (J=4 Hz, 11 Hz) at δ 3.87 and a doublet of doublets (J=5 Hz, 11 Hz) at δ 4.91, respectively, being consistent with the assigned structures.

Acetylation of a mixture of **13** and **14** gave the bromotetraacetate **7**, which was convertible into the pentaacetate **11** by the reaction with sodium acetate in aqueous DMF. Compound **11** was also obtainable either by acetylation of a mixture of **15** and **16** or by treatment of a mixture of **13** and **14** with sodium acetate followed by acetylation.

The structures of **11** and **12** were assigned by the ^{1}H NMR spectra in which the olefinic protons (H-6) of **11** and **12** appeared as a doublet of doublets (J=2 Hz, 6 Hz) at δ 5.94 and a broad singlet at δ 5.82 partly overlapping with the H-4 signal, respectively.

O-Deacetylation of **11** and **12** with methanolic sodium methoxide gave crystalline pentols **18** and **19**, respectively.

When **5** reacted with 1.1 molar equiv. of silver acetate in 90% aqueous acetic acid at room temperature for 24 h, **20** was obtained in 52% yield. Since in the case of **5** the C-1 acetoxyl group and C-6 bromine atom are cis to each other, any neighboring group participation of the C-6 acetoxyl group is unfavorable. Therefore, the reaction is presumed to involve successively an allylic rearrangement (S_N1') with an assistance of the C-3 acetoxyl group, the formation of the 3,4-cyclic acetoxonium ion **F**, and its cleavage by water.

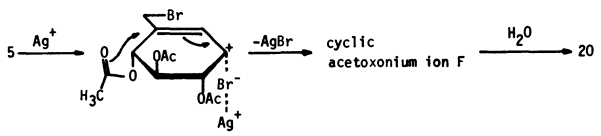

The structure of **20** was assigned on the basis of the appearance of the two-proton singlet at δ 5.83 attributable to two olefinic protons.

An attempt failed to remove the remaining bromine atom in **20** by further treatment with excess silver acetate at 90 °C, presumably because of the low reactivity of C-7 bromine atom under the S_N1-like conditions. On the other hand, reaction of **20** with sodium methoxide in methanol gave a crystalline methyl ether **21**, which was converted into the tetraacetate **22** by acetylation with acetic anhydride in pyridine at room temperature for 9 d. The reaction is considered to proceed *via* a spiro-epoxide, which is subsequently opened by a methoxide ion. The ^{1}H NMR spectrum of **22** showed

the presence of four acetoxyl groups and two olefinic protons (H-5 and H-6); for H-5, a doublet of doublets (J=2 Hz, 10 Hz) at δ 5.76 and for H-6, a doublet of doublets (J=1 Hz, 10 Hz) at δ 6.33.

Reaction of Bromo Tetraacetate ***9*** *with Alcohol.* Nucleophilic substitution of **9** with an alcohol such as methanol, ethanol, or 2-propanol in the presence of silver perchlorate proceeded predominantly with inversion at C-6 leading to the corresponding alkyl ether derivative **28**, **30**, or **32**, respectively (Table 2). This result can be derived as a consequence of either S_N2 attack by alcohol at C-6 or heterolysis of C-6 bromine atom leading to an allyl cation that is stabilized by neighboring group participation of C-1 acetoxyl group, followed by opening of the 1,6-cyclic acetoxonium ion by back-side attack of alcohol. In each case **15**, **16**, and **23** as a mixture were separated in 15% yield as side-products. This fact indicated that both 1,6- and 3,4-cyclic intermediate acetoxonium ions are formed during the course of reaction.

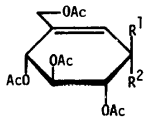

	R^1	R^2
27	H	OCH_3
28	OCH_3	H
29	H	OC_2H_5
30	OC_2H_5	H
31	H	$OC(CH_3)_2$
32	$OC(CH_3)_2$	H

TABLE 2. REACTION OF **9** WITH ALCOHOL CATALYZED BY SILVER ION

Alcohol	Time/min	Yield/%[a]	Product ratio[b]
Methanol	60	25	Only **28**
Ethanol	70	21	**29**/**30**=1/4
2-Propanol	50	17	**31**/**32**=1/4

a) After silica-gel column chromatography. b) Determined by ^{1}H NMR analysis of the mixture.

When **9** was treated with methanolic sodium methoxide at room temperature or with ethanol containing a trace of hydrogen bromide, a 1 : 1 mixture of **27** and **28** in 71% yield or a 1 : 1 mixture of **29** and **30** in 64% yield was obtained, respectively, after acetylation with acetic anhydride and pyridine.

Though each pair of C-1 epimers, **27** and **28**, **29** and **30**, and **31** and **32**, could not be separated because of their similar chromatographic mobilties, **28** was selectively formed by the reaction of **9** with methanol in the presence of silver perchlorate. Their structures were easily assigned by the ^{1}H NMR spectral data, which showed olefinic protons at δ 6.02 (broad d, J=6 Hz), 5.99 (broad d, J=6 Hz), and 5.90 (broad d, J=5 Hz) for **27**, **29**, and **30** and δ 5.82 (broad s), 5.82 (broad s), and 5.75 (broad s) for **28**, **30**, and **32**.

Experimental

General. Melting points were determined on a Büchi 510 capillary melting point apparatus and uncorrected. Unless otherwise noted, ^{1}H NMR spectra were taken on a Varian EM-390 (90 MHz) in chloroform-*d* ($CDCl_3$) with reference to tetramethylsilane as an internal standard. The peak positions were given in terms of δ-values and values given for coupling constants were of first-order. TLC was performed on a precoated silica gel 60 F-254 plaques (Merck, Darmstadt; 0.25 mm thickness), and the spots were visualized by heating above 150 °C after spraying concd sulfuric acid. The silica gel used for the column chromatography was Wakogel C-300 (Wako Pure Chemical Industries, Ltd.). Solutions were dried over anhydrous sodium sulfate and evaporated under reduced pressure at 40—50 °C. Acetylation was conventionally carried out with acetic anhydride in anhydrous pyridine at room temperature overnight and the reaction mixture was evaporated to remove the excess of reagents. Crude syrupy products (acetates) were usually purified preliminarily by rapid passage through a short column of active alumina with chloroform. Catalytic hydrogenations were carried out in a Parr shaker type apparatus at initial hydrogen pressure of 3.2 kg/cm^2.

Bromination of Conjugated Diene ***3*** *with Bromine. With Excess Bromine: Tetrabromides* **4a**,**b**. To a stirred solution of **3** (0.5 g) in carbon tetrachloride (8 ml) was added dropwise bromine (0.35 ml, *ca.* 3.5 molar equiv.) at 0—5 °C, and the mixture was stirred at the same temperature overnight. After removal of the solvent, the residual solid was crystallized from ethanol to give a mixture of **4a**, **b** (1g, 91%) as crystals, (Found: C, 26.32; H, 2.73; Br, 54.65%). Recrystallization from ethanol gave **4a** (0.65 g, 59%), one of the isomers, in a pure forms: mp 147—148 °C; ^{1}H NMR δ=1.96 (3H, s), 2.04 (3H, s), and 2.07 (3H, s) (OAc), 3.58 and 4.02 (AB-quartet, J=11.7 Hz, CH_2Br), 4.68—5.03 (2H, m, H-5 and H-6), and 5.36—5.59 (3H, m, H-1, H-2, and H-3).

Found: C, 26.47; H, 2.85; Br, 54.52%. Calcd for $C_{13}H_{16}Br_4O_6$: C, 26.56; H, 2.74; Br, 54.37%.

From the mother liquor, a mixture of **4a**,**b** was obtained. The other isomer **4b** could not be isolated because of their similar chromatographic mobilities on silica gel. The ^{1}H NMR spectrum of the mixture showed the signal for the bromomethyl protons of **4b** at δ 3.95 and 4.34 as an AB-quartet (J=7.5 Hz).

With an Equimolar Amount of Bromine: Synthesis of DL-*(1,3,6/2)-(5) and* DL-*(1,3/2,6)-6-Bromo-4-bromomethyl-4-cyclohexene-1,2,3-triol Triacetate (****6****):* The results are summarized in Table 1.

General Procedure. a) In Carbon Tetrachloride: To a stirred solution of **3** (0.3 g) in carbon tetrachloride (15 ml) was added dropwise over a period of 15 min 5% bromine solution in the same solvent (1.5 ml, a molar equiv.) at various temperatures, and stirring was continued at the same temperature for 30 min. The mixture was then diluted with carbon tetrachloride (15 ml), washed thoroughly with aqueous sodium hydrogencarbonate solution and water, dried, and evaporated to give a syrup, which was shown by TLC (1: 5 2-butanone-toluene) to contain two major components (R_f 0.65 and 0.62). Chromatography of the products on a silica-gel column (30 g) with 1 : 20 2-butanone-toluene as an eluent gave **5** (R_f 0.65) as a syrup and **6** (R_f 0.62) as crystals (mp 109—110 °C): ^{1}H NMR (60 MHz)[25] for **5**, δ=2.04 (3H, s), 2.09 (3H, s), and 2.11 (3H, s) (OAc), 3.75 and 3.97 (AB-quartet, J=11 Hz, $C\underline{H}_2Br$), 4.75—5.06 (2H, m, H-1 and H-6), 5.62 (1H, dd, J=7 and 10 Hz, H-2), 6.00 (1H, d, J=7 Hz, H-3), and 6.19 (1H, broad d, J=5.5 Hz, H-5), and for **6**, δ=2.04 (3H, s) and 2.11 (6H, s) (OAc), 3.81 and 4.09 (AB-quartet, J=11 Hz, $C\underline{H}_2Br$), 4.67 (1H, m, H-6), 5.10 (1H, dd, J=7 and 10 Hz, H-1), 5.55 (1H, dd, J=8 and 10 Hz, H-2),) 5.85—6.08 (1H, m, H-3), and 6.13 (1H, broad s, H-5).

Found: for **5**, C, 36.64; H, 3.83; Br, 37.47%, and for **6**, C, 36.29; H, 3.75; Br, 37.42%. Calcd for $C_{13}H_{16}Br_2O_6$: C, 36.48; H, 3.77; Br, 37.33%.

When the reactions were carried out at −4 °C and at

−15 °C, trace amounts of **13**, **14**, and **20** were produced as side-products. *b) In Acetic Acids*: The reaction was carried out in the same way as in *a*), except that the reaction mixture was diluted with ethyl acetate (30 ml). Similar to the reaction in carbon tetrachloride at low temperature, **13**, **14**, and **20** were obtained in trace amounts as side-products.

c) In 50% Aqueous Acetic Acid. After the reaction had been carried out in a similar way as described above, the reaction mixture was evaporated below 30 °C, without dilution or washing of the mixture, because TLC analysis (1: 5 2-butanone-toluene) revealed the presence of a large amount of slower-moving components in addition to a small amount of the desired products **5** and **6**. The yellow syrupy residue was treated with acetic anhydride (2 ml) in the presence of a trace of concd sulfuric acid at room temperature overnight and then neutralized with saturated aqueous sodium hydrogencarbonate solution. The mixture was diluted with ethyl acetate (30 ml), and the organic layer was washed with water and dried. Evaporation of the solvent left a syrup which was chromatographed similarly on a silica-gel column. After **5** and **6** had been eluted, tetraacetate **7** was obtained in 22% yield: mp 109—111 °C. The ^{1}H NMR spectrum of **7** is described later. In all cases, tetrabromides **4a**,**b** were detected by TLC analysis.

Interconversion of 5 and 6: When **6** was treated with carbon tetrachloride containing a trace of bromine at room temperature overnight, formation of an equilibrium mixture of **5** and **6** was detected by TLC analysis. Without bromine no interconversion occurs.

Practical Synthesis of 6: To a stirred solution of **3** (1 g) in 3 : 1 acetic acid–acetic anhydride (40 ml)[20] was added dropwise over a period of 50 min 5% bromine solution in the same solvent (3.86 ml, a molar equiv.), and stirring was continued for 50 min. The reaction mixture was processed according to the general procedure and the product was directly crystallized from ethanol (8 ml) to give **6** (0.71 g, 45%): mp 108.5—109.5 °C.

From the mother liquor, an inseparable mixture (0.23 g, 15%) of **7** and **8** was obtained by chromatography on silica gel. The ^{1}H NMR spectrum showed it to be a *ca.* 1 : 1 mixture of **7** and **8**.

Reduction of Tetrabromide 4a with Raney Nickel. A solution of **4a** (0.25 g) in ethyl acetate (10 ml) was hydrogenolyzed with Raney nickel T-4[21] (5 ml) and Amberlite IR-45 (OH^-) (7 ml) at room temperature overnight. After removal of the catalyst and resin by filtration, the filtrate was evaporated to a syrup, which was purified by passage through a short column of alumina with chloroform to give an inseparable syrupy mixture (114 mg, 99%) of tri-*O*-acetyl-DL-deoxyvalidatol and its 4-epimer[13] (*ca.* 1 : 1).

Reduction of 5 and 6. With Tributyltin(IV) Hydride: A solution of **5** (0.17 g) in dry toluene (10 ml) was treated with tributyltin(IV) hydride (0.22 ml) at room temperature overnight under a nitrogen atmosphere. Evaporation of the mixture left an oil, which was purified by passage through a silica-gel column with 1 : 10 2-butanone-toluene to give **3** (87 mg, 80%) as needles: mp 66.5—68 °C.

Similar treatment of **5** with tributyltin(IV) hydride gave **3** in 89% yield: mp 66—67 °C.

With Lithium Aluminium Hydride: A suspension of **5** (0.26 g) and lithium aluminium hydride (0.14 g) in tetrahydrofuran (10 ml) was refluxed gently for 7 h. The mixture was then diluted with water carefully, and the precipitates were removed by filtration. Evaporation of the filtrate left a syrup, which was acetylated in the ususl way. The mixture was evaporated and the residue was purified by an alumina column and crystallized from ethanol to give **3** (0.11 g, 63%) as needles: mp 67—68.5 °C.

Similar treatment of **6** with lithium aluminium hydride gave **3** in 60% yield: mp 67—68 °C.

Hydrobromination of Conjugated Diene 3. With N-Bromoacetamide (NBA): To a stirred solution of NBA (0.25 g, a molar equiv.) and sodium acetate (0.23 g) in water (10 ml) was added dropwise over a period of 10 min a solution of **3** (0.5 g) in acetone (20 ml), and stirring was continued at room temperature for 5 d. The aqueous mixture was then extracted with ether (40 ml + 30 ml × 2) and the organic layer was dried and evaporated. The residue was acetylated in the usual way, during which time the mixture became orange. Evaporation of the mixture left a yellow syrup, which was chromatographed on a silica-gel column 1 : 8 2-butanone-toluene as an eluent. The first and second fractions gave **11** (0.10 g, 10%) and **20** (61 mg, 9%), respectively. They were identical with the samples of which preparations *via* unequivocal routes are to be described later.

The third fraction gave DL-2,3,4,7-tetra-*O*-acetyl-(1,2,-4/3)-1-*C*-hydroxymethyl-5-cyclohexene-1,2,3,4-tetrol (**23**) (0.14 g, 21%) as a homogeneous syrup: ^{1}H NMR δ=2.00 (3H, s), 2.04 (6H, s), and 2.08 (3H, s) (OAc), 2.57 (1H, s, OH, caused to disappear on deuteration), 3.84 and 4.02 (AB-quartet, J=12 Hz, C$\underline{H}_2$OAc), 5.13 (1H, broad d, J=*ca.* 10 Hz, H-2), 5.33—5.62 (2H, relatively sharp m, H-3 and H-4), and 5.37 (2H, s, H-5 and H-6).

Found: C, 52.43; H, 5.85%. Calcd for $C_{15}H_{20}O_9$: C, 52.32; H, 5.85%.

Acetylation of **23** in the usual way for 7 d gave DL-penta-*O*-acetyl-(1,2,4/3)-1-*C*-hydroxymethyl-5-cyclohexene-1,2,3,4-tetrol (**24**) as a syrup quantitatively: ^{1}H NMR δ=2.00 (3H, s), 2.02 (3H, s), 2.05 (3H, s), and 2.07 (6H, s) (OAc), 4.15 and 4.51 (AB-quartet, J=11 Hz, C$\underline{H}_2$OAc), 5.19 (1H, dd, J=9 and 10.5 Hz, H-3), 5.29—5.64 (2H, m, H-2 and H-4), 5.73 (1H, dd, J=2 and 10 Hz, H-5), and 6.33 (1H, dd, J=1 and 10 Hz, H-6).

Found: C, 53,12; H, 5.72%. Calcd for $C_{17}H_{22}O_{10}$: C, 52.85; H, 5.74%.

A trace amount of the other product was isolated from the faster moving component. The structure was tentatively assigned as DL-tetra-*O*-acetyl-(1,3/2,4)-1-*C*-bromomethyl-5-cyclohexene-1,2,3,4-tetrol (**26**): ^{1}H NMR (60 MHz)[25] δ=2.04 (6H, s), 2.06 (3H, s), and 2.10 (3H, s) (OAc), 3.58 and 3.82 (AB-quartet, J=11 Hz, C$\underline{H}_2$Br), 5.20—5.84 (3H, m, H-1, H-2, and H-3), and 6.00 (1H, d, J=10 Hz) and 6.09 (1H, d, J=10 Hz) (olefinic proton).

Found: C, 43.98; H, 4.52; Br, 19.98%. Calcd for $C_{15}H_{19}BrO_8$: C, 44.24; H, 4.70; Br, 19.62%.

With N-Bromosuccinimide (NBS): To a stirred mixture of **3** (0.5 g), dimethyl sulfoxide (10 ml), and water (0.1 ml) was added NBS (0.5 g, 1.5 molar equiv.) as one portion, and then stirring was continued for 5 h below 10 °C. The reaction mixture was then quenched by addition of water (40 ml) and extracted with ether (20 ml × 4). The extracts were dried and evaporated to give a yellow syrup, which was chromatographed on a silica-gel column (50 g) with 1 : 4 2-butanone-toluene. The first fraction gave a syrup (78 mg, 12%), of which structure was tentatively assigned as DL-2,3,4-tri-*O*-acetyl-(1,3/2,4)-1-*C*-bromomethyl-5-cyclohexene-1,2,3,4-tetrol (**25**): ^{1}H NMR (60 MHz)[24] δ=2.04 (6H,s) and 2.11 (3H, s) (OAc), 3.30—3.72 (1H, broad m, O$\underline{H}$, caused to disappear on deuteration), 3.46 and 3.68 (AB-quartet, J=11 Hz, C$\underline{H}_2$Br), 5.10—5.55 (3H, m, H-2, H-3, and H-4), and 5.60 (1H, dd, J=1 and 11 Hz) and 5.87 (1H, dd, J=0.8 and 11 Hz) (olefinic proton).

Found: C, 42.84; H, 4.59; Br, 21.73%. Calcd for

$C_{13}H_{17}BrO_7$: C, 42.76; H, 4.69; Br, 21.88%.

The second fraction gave **20** (0.25 g, 36%) as a syrup.

The third fraction gave an inseparable mixture (33 mg, 5%) of **13** and **14**, whose ^1H NMR spectrum indicated it to be a 3 : 1 mixture of **13** and **14**. The spectrum was superimposable on that of an authentic sample prepared later *via* an unequivocal route.

When the reaction products, without fractionation, were acetylated in the usual way, formation of **7**, **11**, **20**, **23**, and **26** was detected by TLC analysis.

DL-*Tetra*-O-*acetyl*-(*1,2,4/3*)-*5-bromomethyl-5-cyclohexene-1,2,3,-4-tetrol* (**7**). A mixture of **6** (0.11 g), silver acetate (41 mg, a molar equiv.), and 90% aqueous acetic acid (10 ml) was vigorously stirred with protection from light at room temperature for 2 h. The precipitates were then removed by filtration and the filtrate was evaporated to give a syrup, which was chromatographed on a silica-gel column (3 g) with 1 : 3 2-butanone–toluene. Crystallization from ethanol gave an inseparable crystalline mixture (66 mg, 73%) of DL-1,3,4-(**13**) and DL-2,3,4-tri-*O*-acetyl-(1,2,4/3)-5-cyclohexene 1,2,3,4-tetrol (**14**): mp 110.5—111 °C; the ^1H NMR spectrum showed it to be a 3 : 1 mixture of **13** and **14**; ^1H NMR for **13**, δ=2.12 (6H, s) and 2.14 (3H, s) (OAc), 2.42—2.72 (1H, broad s, O<u>H</u>), 3.78 and 3.99 (AB-quartet, J=11 Hz, C<u>H</u>$_2$Br), 3.91 (1H, dd, J=5 and 11 Hz, H-2), 5.32 (1H, dd, J=7.5 and 11 Hz, H-3), 5.35—5.49 (1H,m, H-1), 5.82 (1H, broad d, J=8 Hz, H-4), and 6.15 (1H, J=5 Hz, H-6), and for **14**, δ=4.93 (1H, dd, J=3 and 10 Hz, H-2), and 5.42 (1H, dd, J=7 and 10 Hz, H-3).

Found: C, 42.48; H, 4.69; Br, 21.54%. Calcd for $C_{13}H_{17}BrO_7$: C, 42.76; H, 4.69; Br, 21.88%.

From the mother liquor a mixture of **15** and **16** was separated in 13% yield by chromatography.

The mixture of **13** and **14** (50 mg) was acetylated with acetic anhydride (5 ml) in the presence of a trace of concd sulfuric acid at room temperature overnight and then neutralized with saturated aqueous sodium hydrogencarbonate solution. The mixture was diluted with ethyl acetate, and the organic layer was washed with water and dried. Evaporation of the solvent gave crystals, which were recrystallized from ethanol to give **7** (55 mg, 98%): mp 134—135 °C; ^1H NMR (60 MHz)[25] δ=2.02 (3H, s), 2.04 (3H, s), and 2.08 (6H, s) (OAc), 3.80 and 4.01 (AB-quartet, J=11 Hz, C<u>H</u>$_2$Br), 5.11 (1H, dd, J=3.5 and 10 Hz, H-2), 5.32—5.68 (2H, m, H-1 and H-3), 5.83 (1H, broad d, J=*ca.* 6.5 Hz, H-4), and 6.02 (1H, broad d, J=*ca.* 6 Hz, H-6).

Found: C, 44.04; H, 4.73; Br, 19.86%. Calcd for $C_{15}H_{19}BrO_8$: C, 44.24; H, 4.70; Br, 19.62%.

DL-*Tetra*-O-*acetyl*-(*1,3/2,4*)-*5-bromomethyl-5-cyclohexene-1,2,-3,4-tetrol* (**8**). A mixture of **6** (0.42 g), silver acetate (0.17 g, a molar equiv.), and acetic acid–acetic anhydride (20 ml)[20] was heated to 80 °C with protection from light for 40 min. After cooling, the precipitates were removed by filtration and the filtrate was evaporated to give a syrup, which was purified by a short column of silica gel to give crystals. Recrystallization from ethanol gave **8** (0.25 g, 63%) as columns: mp 133.5—134 °C; ^1H NMR δ=2.01 (6H, s), 2.06 (3H, s), and 2.08 (3H, s) (OAc), 3.79 and 3.99 (AB-quartet, J=11 Hz, C<u>H</u>$_2$Br), 5.25—5.68 (3H, m, H-1, H-2, and H-3), and 5.77—6.01 (2H, m, H-4 and H-6).

Found: C, 44.14; H, 4.65; Br, 19.87%. Calcd for $C_{15}H_{19}BrO_8$: C, 44.24; H, 4.70; Br, 19.62%.

DL-*Penta*-O-*acetyl*-(*1,2,4/3*)-*5-hydroxymethyl-5-cyclohexene-1,2,-3,4-tetrol* (**11**). *a*): A mixture of **6** (0.14 g), silver acetate (0.21 g, 4 molar equiv.), and 90% aqueous acetic acid (10 ml) was heated to 90 °C with protection from light for 1 h. The precipitates were removed by filtration and the filtrate was evaporated to give a syrup, which was chromatographed on a silica-gel column (5 g) with 1 : 3 2-butanone–toluene to give an inseparable mixture (61 mg, 56%) of DL-1,3,4,7- (**15**) and DL-2,3,4,7-tetra-*O*-acetyl-(1,2,4/3)-5-hydroxymethyl-5-cyclohexene-1,2,3,4-tetrol (**16**). The ^1H NMR spectrum indicated it to be a 3 : 1 mixture of **15** and **16**: ^1H NMR for **15**, δ=2.02 (3H, s), 2.04 (3H, s), 2.09 (3H, s), and 2.10 (3H, s) (OAc), 3.71—4.00 (1H, m, H-2, caused to change to dd with J=4 and 11 Hz at δ 3.87 on deuteration), 4.31 and 4.68 (AB-quartet, J=13 Hz, C<u>H</u>$_2$OAc), 5.29 (1H, dd, J=8 and 11 Hz, H-3), 5.38 (1H, dd, J=4 and 6 Hz, H-1), and 5.65 (1H, broad d, J=8 Hz, H-4), 6.02 (1H, broad d, J=6 Hz, H-6), and for **16**, δ=4.91 (1H, dd, J=5 and 11 Hz, H-2).

Found: C, 52.56; H, 5.95%. Calcd for $C_{15}H_{20}O_9$: C, 52.32; H, 5.85%.

A trace of mixture of **13** and **14** was separated from the fast migrating component.

The mixture of **15** and **16** (76 mg) was acetylated in the usual way to give **11** (81 mg, 95%) as a homogeneous syrup: ^1H NMR (60 MHz)[25] δ=2.00 (3H, s), 2.03 (3H, s), 2.04 (6H, s), and 2.09 (3H, s) (OAc), 4.32 and 4.70 (AB-quartet, J=13 Hz, C<u>H</u>$_2$OAc), 5.10 (1H, ddd, J=2, 4, and 10 Hz, H-2), 5.47 (1H, dd, J=7 and 10 Hz, H-3), 5.57 (1H, dd, J=4 and 6 Hz, H-1), 5.66 (1H, broad d, J=7 Hz, H-4), and 5.94 (1H, dd, J=2 and 6 Hz, H-6).

Found: C, 52.63; H, 5.69%. Calcd for $C_{17}H_{22}O_{10}$: C, 52.85; H, 5.74%.

b): The mixture of **13** and **14** (0.1 g) was treated with sodium acetate (24 mg, 1.1 molar equiv.) in 10% aqueous DMF (10 ml) at room temperature for 7 h. Evaporation of the mixture left a residue, which was purified by an alumina column to give a homogeneous syrup. The syrup was acetylated and the product was chromatographed on a silica-gel column (2 g) with 1 : 5 2-butanone–toluene to give **11** (0.9 g, 86%) as a homogeneous syrup.

c): A mixture of **7** (50 mg), sodium acetate (20 mg, 2 molar equiv.), and DMF (1 ml) was stirred at room temperature for 2 d. The mixture was then evaporated and the residue was purified by an alumina column to give **11** (33 mg, 70%) as a homogeneous syrup.

DL-*Penta*-O-*acetyl*-(*1,3/2,4*)-*5-hydroxymethyl-5-cyclohexene-1,2,3,-4-tetrol* (**12**). *a*) A mixture of **6** (1 g), silver acetate (1.56 g, 4 molar equiv.), and acetic acid–acetic anhydride (60 ml)[20] was treated similarly as described in the preparation of **8** for 3 h. The crystalline product was recrystallized from ethanol to give DL-penta-*O*-acetyl-(1,3,5/2,4)-6-methylene-1,2,3,4,5-cyclohexanepentol (**17**) (0.1 g, 12%): mp 188.5—189 °C (lit,[24] 189—190 °C); ^1H NMR δ=1.93 (9H, s) and 2.03 (6H, s) (OAc) and 4.72—5.67 (7H, m, H-1, H-2, H-3, H-4, H-5, and exocyclic methylene).

Found: C, 52.63; H, 5.62%. Calcd for $C_{17}H_{22}O_{10}$: C, 52.85; H, 5.74%.

Evaporation of the mother liquor and crystallization from ethanol gave **12** (0.59 g, 73%): mp 81.5—82.5 °C; ^1H NMR δ=2.03 (3H, s), 2.04 (3H, s), 2.05 (3H, s), 2.06 (3H, s), and 2.08 (3H, s) (OAc), 4.41 and 4.76 (AB-quartet, J=14 Hz, C<u>H</u>$_2$Br), 5.16—5.72 (3H, m, H-1, H-2, and H-3), and 5.82 (2H, broad s, H-4 and H-6).

Found: C, 53.05; H, 5.76%. Calcd for $C_{17}H_{22}O_{10}$: C, 52.85; H, 5.74%.

b): A mixture of **8** (0.26 g), sodium acetate (79 mg, 1.5 molar equiv.), and DMF (5 ml) was stirred at room temperature for 24 h. The mixture was then evaporated and the residue was purified by an alumina column to give crystals. Recrystallization from ethanol gave **12** (0.26 g, 91%): mp 81—82 °C.

DL-(*1,2,4/3*)-*5-Hydroxymehthtyl-5-cyclohexene-1,2,3,4-tetrol*

*(**18**).* A solution of **11** (0.1 g) in methanol (10 ml) was treated with 1 M† methanolic sodium methoxide (0.2 ml) and allowed to stand at 0—5 °C overnight. The mixture was then neutralized with Amberlite IR-120 (H^+) and evaporated to give a syrup, which was crystallized from ethanol to give **18** (40 mg, 87%): mp 139.5—141 °C; ^{1}H NMR (90 MHz, D_2O)[26] δ=3.46—3.86 (2H, m, H-2 and H-3), 4.00—4.42 (4H, m, H-1, H-4, and C$\underline{H}_2$OH), and 5.88 (1H, dd, J=1.5 and 5 Hz).

Found: C, 47.65; H, 6.77%. Calcd for $C_7H_{12}O_5$: C, 47.72; H, 6.87%.

DL-*(1,3/2,4)-5-Hydroxymethyl-5-cyclohexene-1,2,3,4-tetrol (**19**).* Compound **12** (0.1 g) was treated with 1 M methanolic sodium methoxide in the same way as in the preparation of **18**. The crude product was recrystallized from aqueous ethanol to give **19** (45 mg, 98%): mp 150.5—151.5 °C; ^{1}H NMR (90 MHz, D_2O)[25] δ=3.26—3.70 (2H, m, H-2 and H-3), 4.05—4.36 (4H, m, H-1, H-4, and C$\underline{H}_2$OH), and 5.62 (1H, d, J=1.5 Hz).

Found: C, 47.66; H, 6.72%. Calcd for $C_7H_{12}O_5$: C, 47.72; H, 6.87%.

*Reaction of **5** and **6** with Sodium Acetate. With an Equimolar Amount of Sodium Acetate: Synthesis of* DL-*Tetra-O-acetyl-(1,3,6/2)-4-hydroxymethyl-6-bromo-4-cyclohexene-1,2,3-triol (**9**):* A mixture of **5** (0.2 g), sodium acetate (37 mg, a molar equiv.), and DMF (10 ml) was stirred at room temperature for 24 h. The mixture was then diluted with ethyl acetate (20 ml), and the organic layer was washed with water and dried. Evaporation of the solvent left a syrup, which was crystallized from ethanol to give **9** (86 mg, 47%) as needles: mp 66—67.5 °C; ^{1}H NMR δ=2.02 (6H, s), 2.05 (6H, s), and 2.11 (3H, s) (OAc), 4.32 and 4.66 (AB-quartet, J=14 Hz, C$\underline{H}_2$OAc), 4.82 (1H, dd, J=4.5 and 10 Hz, H-1), 4.82—5.00 (1H, m, H-6), 5.58 (1H, dd, J=9 and 10 Hz, H-2), 5.81 (1H, d, J=9 Hz, H-3), and 6.07 (1H, broad d, J=*ca.* 5 Hz, H-5).

Found: C, 44.18; H, 4.69; Br, 19.73%. Calcd for $C_{15}H_{19}BrO_8$: C, 44.24; H, 4.70; Br, 19.62%.

From the mother liquor an inseparable 1.5 : 1 mixture (63 mg, 35%) of **9** and its C-6 epimer **10** was obtained. (Found: C, 43.97; H, 4.60; Br, 19.31%.) The ^{1}H NMR spectrum of **10** could be read in that of the mixture by elimination of the spectrum of **9**: ^{1}H NMR δ=4.32 and 4.66 (AB-quartet, J=14 Hz, C$\underline{H}_2$OAc), 5.11 (1H, dd, J=7.5 and 10 Hz, H-1), 5.46 (1H, dd, J=8 and 10 Hz, H-2), 5.79 (1H, broad d, J=8 Hz, H-3), and 5.99 (1H, broad s, H-5).

When **6** was used instead of **5**, **9** was similarly obtained in 49% yield.

With Excess Sodium Acetate: A mixture of **5** (90 mg), sodium acetate (0.7 g, 4 molar equiv.), and DMF (10 ml) was stirred at room temperature for 2 d. The mixture was worked up in a similar manner as above and the crude product was chromatographed on a silica-gel column (3 g) with 1 : 5 2-butanone–toluene to give an inseparable syrupy mixture (0.5 g, 60%) of **11** and **12**. Found: C, 52.60; H, 5.53%. From a comparison of the ^{1}H NMR spectrum with those of the authentic samples of **11** and **12**, it was found to be a 1 : 2—3 mixture of **11** and **12**.

When **6** was used instead of **5**, a similar result was obtained; a 1 : 2—3 mixture of **11** and **12** in 57% yield.

DL-*2,3,4-Tri-O-acetyl-(1,2,4/3)-1-C-bromomethyl-5-cyclohexene-1,2,3,4-tetrol (**20**).* A mixture of **5** (0.63 g), silver acetate (0.27 g, 1.1 molar equiv.), and 90% aqueous acetic acid (20 ml) was stirred with protection from light at room temperature for 24 h. The precipitates were then removed by filtration and the filtrate was evaporated to give a syrup, which was chromatographed on a silica-gel column (15 g) with 1 : 3 2-butanone–toluene to give **20** (0.28 g, 52%) as a homogeneous syrup: ^{1}H NMR (60 MHz)[25] δ=2.03 (3H, s), 2.06 (3H, s), and 2.13 (3H, s) (OAc), 2.78 (1H, s, O$\underline{H}$), 3.39 (2H, s, C$\underline{H}_2$Br), 5.21—5.66 (3H, m, H-2, H-3, and H-4), and 5.83 (2H, broad s, H-5 and H-6).

Found: C, 42.51; H, 4.72; Br, 21.60%. Calcd for $C_{13}H_{17}BrO_7$: C, 42.76; H, 4.69; Br, 21.88%.

When **20** was treated with an excess of silver acetate at 90 °C for a prolonged period, no further substitution reaction occurred.

DL-*Tetra-O-acetyl-(1,2,4/3)-1-C-methoxymethyl-5-cyclohexene-1,2,3,4-tetrol (**22**).* To a solution of **20** (0.11 g) in methanol (5 ml) was added 1 M methanolic sodium methoxide (1.3 ml, 4 molar equiv.), and the mixture was allowed to stand at room temperature overnight. After the mixture was neutralized by treatment with Amberlite IR 120 (H^+), it was evaporated and the residue was acetylated in the usual way. The product was chromatographed on a silica-gel column (5 g) with 1 : 3 2-butanone–toluene. The first fraction gave, after recrystallization from ethanol, **22** (7 mg, 6%): mp 130—130.5 °C; ^{1}H NMR (60 MHz)[25] δ=2.02 (3H, s), 2.04 (3H, s), and 2.09 (6H, s) (OAc), 3.29 (3H, s, OC$\underline{H}_3$), 3.39 and 3.83 (AB-quartet, J=5 Hz, C$\underline{H}_2$OCH$_3$), 5.17—5.61 (3H, m, H-2, H-3, and H-4), 5.76 (1H, dd, J=2 and 10 Hz, H-5), and 6.33 (1H, dd, J=1 and 10 Hz, H-6).

Found: C, 53.42; H, 6.08%. Calcd for $C_{16}H_{22}O_9$: C, 53.63; H, 6.19%.

The second fraction gave DL-2,3,4-tri-*O*-acetyl-(1,2,4/3)-1-*C*-methoxymethyl-5-cyclohexene-1,2,3,4-tetrol (**21**) (70 mg, 71%) as a homogeneous syrup: ^{1}H NMR (60 MHz)[25] δ=2.00 (3H, s), 2.03 (3H, s), and 2.06 (3H, s) (OAc), 3.02 (1H, s, O$\underline{H}$), 3.30 (5H, s, OC$\underline{H}_3$ and C$\underline{H}_2$OCH$_3$), 5.03—5.69 (3H, m, H-2, H-3, and H-4), and 5.81 (2H, s, H-5 and H-6).

Found: C, 53.29; H, 6.36%. Calcd for $C_{14}H_{20}O_8$: C, 53.16; H, 6.47%.

Further acetylation of **21** for 9 d gave **22** quantitatively.

*Reaction of **9** with Alcohols in the Presence of Silver Ion.* The results are summarized in Table 2.

General Procedure: To a vigorously stirred solution of **9** (0.3 g), alcohol (5 ml), and Drierite (0.5 g) in dry ether (8 ml) was added silver perchlorate (0.2 g) with ice-cooling under a nitrogen atmosphere, and stirring was continued with protection from light for an appropriate time. After the precipitates had been removed by filtration, the filtrate was washed with saturated aqueous sodium hydrogencarbonate solution and water, and then dried. Evaporation of the solvent left a yellow syrup, which was chromatographed on a silica-gel column (6 g) with 1 : 10 2-butanone–toluene to give the corresponding alkyl ether.

After the alkyl ether had been eluted from the column, a mixture of **15**, **16**, and **23** was separated in 13—15% yield. The ratio of (**15**, **16**) and **23** was estimated to be *ca.* 1 : 1.3 from the ^{1}H NMR spectrum.

With Methanol: DL-2,3,4,7-Tetra-*O*-acetyl-1-*O*-methyl-(1,3/2,4)-5-hydroxymethyl-5-cyclohexene-1,2,3,4-tetrol (**28**) only was formed as a syrup: ^{1}H NMR δ=1.96 (3H, s), 1.98 (3H, s), 2.01 (3H, s), and 2.02 (3H, s) (OAc), 3.34 (3H, s C$\underline{H}_3$), 3.92—4.14 (1H, m, H-1), 4.28 and 4.60 (AB-quartet, J=13 Hz, C$\underline{H}_2$OAc), 5.03—5.35 (2H, m, H-2 and H-3), 5.57—5.76 (1H, m, H-4), and 5.82 (1H, broad s, H-6).

Found: C, 53.48; H, 6.20%. Calcd for $C_{16}H_{22}O_9$: C, 53.63; H, 6.19%.

With Ethanol: A 1 : 4 mixture of DL-2,3,4,7-tetra-*O*-acetyl-1-*O*-ethyl-(1,2,4/3)-5-hydroxymethyl-5-cyclohexene-1,2,3,4-tetrol (**29**) and its C-1 epimer (**30**) was formed as a syrup: ^{1}H NMR for **29**, δ=1.17 (3H, t, J=7.5 Hz, C$\underline{H}_3$CH$_2$), 5.48 (1H,

† 1 M=1 mol dm^{-3}.

t, J=8 Hz, H-3), 5.99 (1H, broad d, J=6 Hz, H-6), and for **30**, δ=1.16 (3H, t, J=7.5 Hz, $C\underline{H}_3CH_2$), 1.97 (3H, s), 2.01 (3H, s), and 2.04 (6H, s) (OAc), 3.57 (2H, q, J=7.5 Hz, $CH_3C\underline{H}_2$), 4.01—4.20 (1H, m, H-1), 4.31 and 4.65 (AB-quartet, J=14 Hz, $C\underline{H}_2OAc$), 5.13—5.33 (2H, m, H-2 and H-3), 5.65—5.78 (1H, m, H-4), and 5.82 (1H, broad s, H-6).

Found: C, 54.90; H, 6.41%. Calcd for $C_{17}H_{24}O_9$: C, 54.83; H, 6.50%.

With 2-Propanol: A 1 : 4 mixture of DL-2,3,4,7-tetra-*O*-acetyl-1-*O*-isopropyl-(1,2,4/3)-5-hydroxymethyl-5-cyclohexene-1,2,3,4-tetrol (**31**) and its C-1 epimer (**32**) was obtained as a syrup: ^{1}H NMR for **31**, δ=5.90 (1H, broad d, J=5 Hz, H-6), and for **32**, δ=1.10 (3H, d, J=6 Hz) and 1.15 (3H, d, J=6 Hz) (CMe_2), 1.97 (3H, s), 1.99 (3H, s), and 2.01 (6H, s) (OAc), 3.65 (1H, heptet, J=6 Hz, $\underline{H}CMe_2$), 3.95—4.15 (1H, m, H-1), 4.25 (1H, d) and 4.59 (1H, broad d) (AB-quartet, J=12 Hz, $C\underline{H}_2OAc$), 5.00—5.31 (2H, m, H-2 and H-3), 5.59—5.72 (1H, m, H-4), and 5.75 (1H, broad s, H-6).

Found: C, 56.25; H, 6.73%. Calcd for $C_{18}H_{25}O_9$: C, 56.10; H, 6.54%.

*Treatment of **9** with Methanolic 1 M Sodium Methoxide.* To a solution of **9** (0.2 g) in methanol (5 ml) was added 1 M sodium methoxide (two drops with a syringe) with vigorous stirring at 0 °C, and the mixture was allowed to stand at room temperature for 3 d. At this time the pH of the mixture was 1. After neutralization with IRA 400 (OH^-), the filtrate was evaporated to give a colorless syrup (79 mg), which showed a negative Beilstein test. The syrup was acetylated and the product was purified by an alumina column, giving a 1 : 1 syrupy mixture (125 mg, 71%) of **27** and **28**. Found: C, 53.43; H, 6.21%. The ^{1}H NMR spectrum of **27** could be read partly in that of the mixture by elimination of the spectrum of **28**: ^{1}H NMR δ=3.39 (3H, s, $OC\underline{H}_3$), 5.45 (1H, t, J=9 Hz, H-3), and 6.02 (1H, broad d, J=6 Hz, H-6).

*Treatment of **9** with Ethanol Containing a Trace of Hydrogen Bromide.* To a stirred solution of **9** (0.27 g) in ethanol (5 ml) was added 30% hydrogen bromide in acetic acid (0.06 ml) at 0 °C, and the mixture was allowed to stand at the same temperature for 5 d. After neutralization with IRA 400 (OH^-), the filtrate was evaporated to give a colorless syrup (83 mg), which had a negative Beilstein test. The syrup was acetylated and the product was purified by an alumina column, giving a 1 : 1 syrupy mixture (155 mg, 64%) of **29** and **30**.

Found: C, 54.93; H, 6.31%. Calcd for $C_{17}H_{24}O_9$: C, 54.83; H, 6.50%.

The authors express their sincere thanks to Mr. Saburo Nakada for his elementally analyses, and to Mr. Masaji Omata and Mr. Yoshikazu Iwasawa for assistance in preparative experiments. The present work was partially supported by a Grant-in-Aid for Scientific Research No. 56550617 from the Ministry of Education, Science and Culture.

References

1) A preliminary account of portions of this articles was previously presented: S. Ogawa, T. Toyokuni, and T. Suami, *Chem. Lett.*, **1980**, 713.

2) T. Iwasa, H. Yamamoto, and M. Shibata, *J. Antibiot.*, **23**, 595 (1970); S. Horii and Y. Kameda, *J. Chem. Soc., Chem. Commun.*, **1972**, 747. The proposed structure of validamycin A has recently been revised: T. Suami, S. Ogawa, and N. Chida, *J. Antibiot.*, **33**, 98 (1980).

3) See S. Ogawa, Y. Shibata, N. Chida, and T. Suami, *Chem. Lett.*, **1980**, 135 and the references cited therein.

4) S. Horii and Y. Kameda, *J. Chem. Soc., Chem. Commun.*, **1972**, 746.

5) T. Takeuchi, H. Chimura, M. Hamada, H. Umezawa, O. Yoshioka, N. Oguchi, Y. Takahashi, and A. Matsuda, *J. Antibiot.*, **28**, 737 (1975); H. Chimura, H. Nakamura, T. Takita, S. Saito, T. Tomisawa, and Y. Iitake, *ibid.*, **28**, 743 (1975).

6) A. D. Argoudelis, R. W. Spvague, and S. A. Mizsak, *J. Antibiot.*, **29**, 387 (1976).

7) D. D. Schmidt, W. Frommer, B. Junge, L. Müller, W. Wingender, E. Truscheit, and D, Schafer, *Naturwissenschaften*, **64**, 535 (1977); W. Frommer, B. Junge, L. Müller, D. D. Schmidt, and E. Truscheit, *J. Med. Plant Res.*, **35**, 195 (1979).

8) K. Yokose, K. Ogawa, Y. Suzuki, M. Suhara, and P. Buchschacher, 23rd Symposium of the Chemistry of Natural Products, Nagoya, October 1980, Abstr. No. 82.

9) S. Namiki, T. Nagate, K. Kamigori, H. Hara, K. Sugita, S. Omura, and M. Ozeki, 223rd Scientific Meeting JARA, Tokyo, March 1981.

10) Review: E. Truscheit, W. Frommer, B. Junge, L. Müller, D. D. Schmidt, and W. Wingender, *Angew. Chem., Int. Ed. Engl.*, **20**, 744 (1981).

11) Y. Kameda, N. Asano, M. Yoshikawa, and K. Matsui, *J. Antibiot.*, **33**, 1575 (1980).

12) Part II: S. Ogawa, N. Chida, H. Ito, and T. Suami, *Bull. Chem. Soc. Jpn.*, **56**, 499 (1983).

13) S. Ogawa, T. Toyokuni, M. Omata, N. Chida, and T. Suami, *Bull. Chem. Soc. Jpn.*, **53**, 455 (1980). The nomenclature is based on the IUPAC-IUB Tentative Cyclitol Nomenclature Rule [*J. Biol. Chem.*, **22**, 5809 (1968)]. For convenience, the formulas depict only one of the respective enantiomers.

14) N. R. Lindquist, "Medicinal Chemistry," ed by E. J. Ariens, Academic Press, New York-San Francisco-London (1975), Vol. 11 (V), p. 24.

15) R. J. Abraham, H. Gottschalck, H. Paulsen, and W. A. Thomas, *J. Chem. Soc.*, **1965**, 6268; A. A. Chalmers and R. H. Hall, *J. Chem. Soc., Perkin Trans. 2*, **1974**, 728.

16) S. P. McManus and P. E. Peterson, *Tetrahedron Lett.*, **1976**, 2753; S. P. McManus and S. D. Worley, *ibid.*, **1977**, 555.

17) C. W. Jefford, A. Sweeney, D. T. Hill, and F. Delay, *Helv. Chim. Acta*, **54**, 1961 (1971); C. W. Jofford, A. Sweeney, and F. Delay, *ibid.*, **55**, 2214 (1972).

18) M. E. Toromanoff, *C. R. Hebd Séances Acad. Sci., Ser. C*, **284**, 113 (1977).

19) For the reaction in carbon tetrachloride at low temperature, it is thought that the preferential production of **6** may be due to the slightly increasing polarity of the medium by condensation of water vapor; that is to say, the reaction would follow a similar reaction mechanism with the reaction in acetic acid. This speculation was supported by the production of **13**, **14**, and **20** as side-products. Several attempts to make anhydrous conditions were unsuccessful.

20) For the sake of removal of the trace of water present, acetic acid–acetic anhydride was refluxed for 3 h before use.

21) S. Nishimura, *Bull. Chem. Soc. Jpn.*, **32**, 61 (1959).

22) D. R. Dalton, V. P. Dutta, and D. C. Jones, *J. Am. Chem. Soc.*, **90**, 5498 (1968).

23) S. Winstein and R. E. Buckles, *J. Am. Chem. Soc.*, **64**, 2780 (1942); **64**, 2787 (1942).

24) Th. Posternak and D. Reymond, *Helv. Chim. Acta*, **36**, 1370 (1953).

25) Taken on a Varian EM-360A (60 MHz) spectrometer.

26) Sodium 2,2-dimethyl-2-silapentane-5-sulfonate was used as an internal standard.

Electrophilic Additions of Rigid Methylenecyclohexane. A Correlation of the Stereochemical Course of the Methoxymercuration-demercuration and the 1,3-Dipolar Cycloaddition[1]

Makoto NITTA,* Akihiko OMATA, Setsuko HIRAYAMA, and Yuji YAJIMA
Department of Chemistry, School of Science and Engineering, Waseda University, Shinjuku-ku, Tokyo 160
(Received June 10, 1982)

The stereochemical course of the methoxymercuration-demercurations and the 1,3-dipolar cycloadditions of mesitonitrile oxide on the exocyclic double bonds of 2,4-dimethyl-7-methylenetetracyclo[3.3.0.0.^{2,8}0^{4,6}]octan-3-one (**4a**), its corresponding *exo*-3-ol (**4b**), *endo*-3-ol (**4c**), and 2,3,4-trimethyl-7-methylenetetracyclo[3.3.0.0.^{2,8}0^{4,6}]octan-3-*exo*-ol (**4d**) were investigated. In the methoxymercurations of **4a** and **4b**, the methoxyl group was incorporated in the *exo* and *endo* positions, with *endo* preferred over *exo*. On the other hand, **4c** and **4d** underwent the stereospecific incorporation of the methoxyl group in the *endo* position. In the 1,3-dipolar cycloadditions, **4a** or **4b** afforded *exo*- and *endo*-adducts, with the *exo*-adduct preferred. These results seem to imply similar stereochemical course of the formation of the mercurinium-ion intermediates and the 1,3-dipolar cycloadditions. The results are discussed on the basis of the steric hindrance of the molecular framework and the substituents which are located at the C-3 position.

Recently, stereoselectivities of electrophilic additions of molecules containing proximal π-bonds have been explored.[2-5] Previously, we have also shown that the solvomercuration-demercuration and its related reactions on the exocyclic double bond of 1,5-dimethyl-6-methylenetricyclo[3.2.1.0^{2,7}]oct-3-en-8-one and its related compounds, such as **1**, exhibit a remarkable stereoselectivity to give **2**.[6] This stereoselectivity is explained by the steric hindrance and/or electronic factor[7] of the mercurinium-ion formation and the stereoelectronic control of the subsequent incorporation of the nucleophile. The initial addition of +Hg(OAc) to **1** was supposed to give the mercurinium ions, M-*exo* and M-*endo*, which may exist in equilibrium with each other. The *trans* addition of the nucleophile to M-*exo* is hindered by the repelling interaction of the nucleophile with the π-electron lobe of the endocyclic double bond. Therefore, the nucleophile is incorporated into M-*endo* to give **2**. A similar stereoselectivity is also obtained in the 1,3-dipolar cycloaddition of mesitonitrile oxide (2,4,6-trimethylbenzonitrile oxide) with **1** to lead **3**.[8]

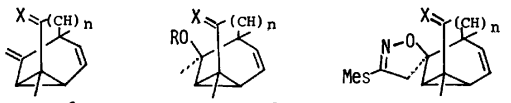

1 2 3

n = 0 or 1 ; X = O or H, OH

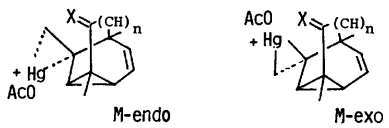

M-endo M-exo

Regarding the mechanistic aspect of the solvomercuration-demercuration of olefins, it has been of further interest to explore the various controlling factor of the stereoselectivities.[9] In this connection, methoxymercuration and 1,3-dipolar cycloadditions, using mesitonitrile oxide, with 2,4-dimethyl-7-methylenetetracyclo[3.3.0.0.^{2,8}0^{4,6}]octan-3-one (**4a**), its corresponding *exo*-3-ol (**4b**), *endo*-3-ol (**4c**), and 2,3,4-trimethyl-7-methylenetetracyclo[3.3.0.0.^{2,8}0^{4,6}]octan-3-*exo*-ol (**4d**) were investigated. The compounds, **4a—d**, contain a boat methylenecyclohexane ring and various degrees of steric hindrance at C-3. Furthermore, **4a—d** also contain a bishomofulvene moiety. Therefore, the methoxymercuration-demercuration sequences should proceed *via* a mercurinium ion intermediate (**A**), because of the bishomoantiaromatic nature of the opened cation (**B**).[10] Consequently, it might be possible to assess how the steric hindrance affects the stereochemical courses of the methoxymercuration and 1,3-dipolar cycloadditions. We wish to discuss here the stereochemical correlation between the solvomercuration reactions and the concerted 1,3-dipolar cycloadditions of mesitonitrile oxide.

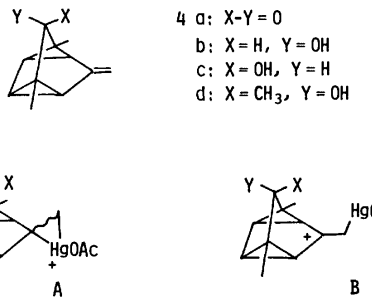

A B

Results and Discussion

Methoxymercuration-demercuration Reactions. The preparation of **4a** and **4b** was previously reported.[11] The preparation of **4d** was also achieved by the photoirradiation of 1,5,8-trimethyl-6-methylenetricyclo[3.2.1.0^{2,7}]oct-3-en-8-*endo*-ol[12] (see Experimental section). The *endo* alcohol derivative **4c** was prepared by the reduction of **4a** with lithium aluminium hydride (LAH), along with *exo* alcohol **4b**. The ratio of **4c**/**4b** (4.5) would indicate the stereochemical preference of the *exo*-attack of the hydride ion.

A solution of **4a** in anhydrous methanol was allowed to react with 1.2 molar equivalent of mercury(II) acetate. The reaction proceeded very slowly, and, after a total reaction time of 6 h, *in situ* reduction[13] by sodium

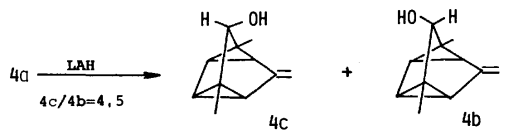

borohydride gave a 58% overall yield of two products, along with a recovery of **4a** in a 26% yield. The methoxyl group was incorporated preferentially at the more hindered site (see the ratio of **4c**/**4b** in the reduction of **4a** with LAH), giving the *endo* and *exo* isomer, **5**-en and **5**-ex, in a ratio of 1.8/1.0. The structural assignment to **5**-en and **5**-ex follows convincingly from their spectral properties. The carbonyl absorption band at 1710 cm^{-1} of **4a** was shifted to 1721 cm^{-1} and 1713 cm^{-1} for **5**-en and **5**-ex respectively. The NMR spectra of **5**-en and

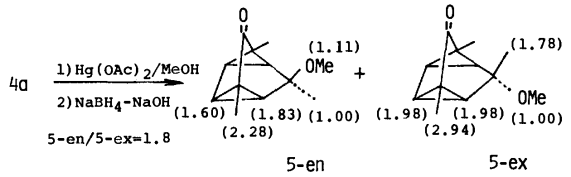

5-ex exhibited five signals, suggesting the symmetric structures (see Experimental section). These facts clearly indicate that the methoxymercuration-demercuration occurred on the exocyclic double bond. The protons of the methoxyl group and the methyl group at C-7 of **5**-en appear as singlets at δ 3.16 and δ 1.46 respectively. For **5**-ex, these signals appear at δ 3.34 and δ 1.23. These characteristics suggest that the methoxyl group of **5**-en and the methyl group of **5**-ex are much shielded by the σ-bond in the molecular framework. Therefore, the orientations of the methoxyl group of **5**-en and **5**-ex were determined as depicted. Furthermore, supportive evidence for the stereochemistries of the methoxyl group was also obtained from the pseudo-contact NMR spectra obtained by using Eu(fod)$_3$.[14] The relative downfield shifts of δ's are given in parentheses in the structural formulae **5**-en and **5**-ex. The relatively small shifts of the methoxyl groups of **5**-en and **5**-ex suggest that the coordination of Eu(fod)$_3$ does not occur on methoxyl oxygen, but on the carbonyl oxygen. The small shift (1.00) of the methyl group of **5**-en as compared to that (1.78) of **5**-ex suggests that the methyl group of **5**-ex is located syn to the carbonyl group. Consequently, the stereochemistry of **5**-en and **5**-ex was clarified.

The reaction of **4b** with mercury(II) acetate and subsequent reduction afforded two products, **6**-en and **6**-ex, in a ratio of 5.0/1.0 and in a 73% yield, along

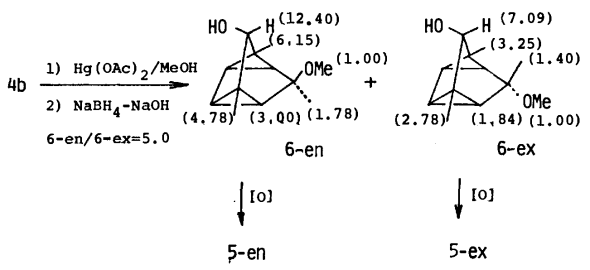

with the starting material, **4b**, in a 25% yield. The structures of **6**-en and **6**-ex were deduced from the spectral data (see Experimental section). The pseudo-contact NMR spectra obtained by using Eu(fod)$_3$,[14] however, could not reveal the stereochemistry of the methoxyl group.

On the oxidation of **6**-en or **6**-ex with pyridinium chlorochromate,[15] **5**-en or **5**-ex was obtained in a fairly good yield. Therefore, the stereochemistry of **6**-en and **6**-ex was confirmed. In this case, the methoxyl group is also incorporated preferentially at the more hindered site.

On the other hand, the reaction of **4c** or **4d** with 1.2 molar equivalents of mercury(II) acetate and the subsequent reduction afforded a single product, **7**-en or **8**-en, in a 70% or in a 60% yield respectively, along with the starting material, **4c** (21%) or **4d** (20%). The structures of **7**-en and **8**-en were deduced from the spectral data (see Experimental section). The large coupling constant (J=12.0 Hz) between the protons at C-3 and the hydroxyl proton for **7**-en indicates the intramolecular hydrogen bonding of the hydroxyl hydrogen with methoxyl oxygen. Furthermore, on oxidation with pyridinium chlorochromate, **7**-en was

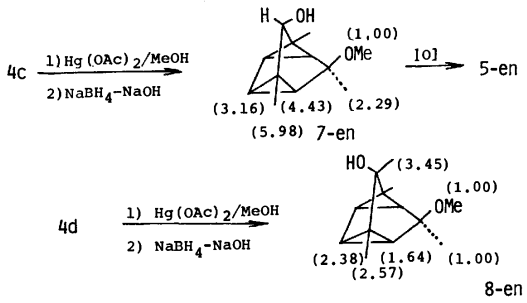

converted to **5**-en in a fairly good yield. Consequently, the stereochemistry of the methoxyl group was assessed. In this case, the methoxyl group was also introduced at the more hindered site. The stereochemistry of the methoxyl group in **8**-en is not clear from its pseudo-contact NMR spectra obtained by using Eu(fod)$_3$,[14] however, the orientation can tentatively be assigned as *endo* on the basis of the similarities of the preferential *endo* orientation in the reactions of **4a**—**c**.

In all of the presented reactions, methanol was incorporated preferentially from the much-hindered site on the exocyclic double bond (see the ratio of **4c**/**4b** in the reduction of **4a** with LAH), and the original tetracyclic skeleton did not undergo rearrangement. These results seems to suggest the formation of such mercurinium ions as **9** and **10**, as is shown in the scheme.[16-19] Such cationic species[20-22] as **12** should be energetically unfavorable because of an antiaromatic nature of the bishomocyclopentadienyl cation,[10] which would be expected to undergo rearrangement.[23] Recently it has been shown that 3-methyltetracyclo[3.3.0.0.^{2,8}0^{4,6}]-octan-3-yl cation rearranges to another compound at −95 °C.[24] Previously, we have shown that the stabilization of the cationic center of the cyclopropylmethyl cation by the mercury moiety adjacent to the cationic center is preferable over the resonance-electron donation

of the cyclopropane ring.[6] Therefore the cationic center would be stabilized by making such mercurinium ions as **9** and **10**. In the initial addition of $+Hg(OAc)$[25] to the exocyclic double bond, the formation of **9** seems to be faster than the formation of **10** because of the steric hindrance of the molecular framework and the substituent at C-3. Furthermore, **9** should also be thermodynamically more stable than **10**, because of the

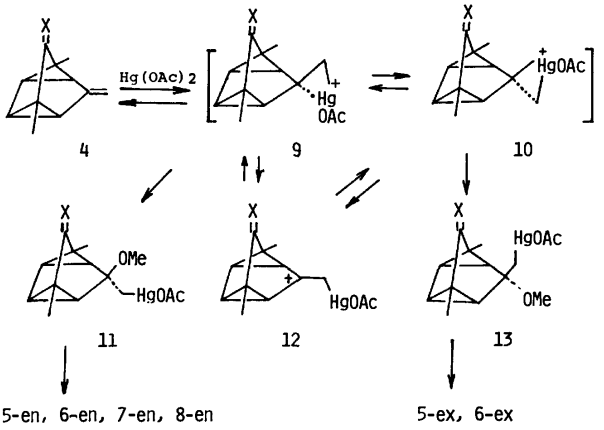

nonbonded interaction of the substituent with the mercury moiety. If the rapid equilibrium between **9** and **10** *via* the possible short-lived intermediate **12** or *via* the mercuration-demercuration sequence is thought to participate in the present reaction, the equilibrium between **9** and **10** should be shifted to **9** as well. Consequently, the *trans* addition of methanol, affording **11** or **13**, and the subsequent reaction should give **5**-en, **6**-en, **7**-en, and **8**-en or **5**-ex and **6**-ex.

The *endo-exo* ratio in the case of **4a** is 1.8, while that in the case of **4b** is 5.0. These values probably reflect the large steric hindrance of the hydrogen at C-3 with the mercury moiety, as compared to that of the carbonyl group in **4a**. Furthermore, in the case of **4c** and **4d**, the hydroxyl group and the methyl group are larger than hydrogen, so such mercurinium ion as **10** should be absent, and only **7**-en or **8**-en could be obtained *via* **9**.

The stereocontrol by a neighboring hydroxyl group in oxymercuration has been demonstrated to proceed *via* an intermediate such as **14**, which includes a favorable interaction of the hydroxyl group with the mercury moiety.[26] In the reaction of **4c**, however, no expected product, such as **7**-ex *via* **15**, could be obtained. In **14**, the hydroxyl group, which is located close to the bisected plane including the mercurinium ion, should coordinate to the mercury moiety in such a way as to make a tetrahedral arrangement. In **15**, however, the hydroxyl group is located on the plane including the postulated mercurinium ion. Therefore, it can be suggested that the interaction of hydroxyl oxygen with the mercurinium ion is not possible in a planar arrangement such as **15**. Also indicated is a favorable interaction of the mercury moiety with the hydroxyl oxygen, which is located on the bisected plane of a postulated mercurinium ion such as **16**.[8]

1,3-Dipolar Cycloaddition of Mesitonitrile Oxide. As has been described above, the solvomercuration of

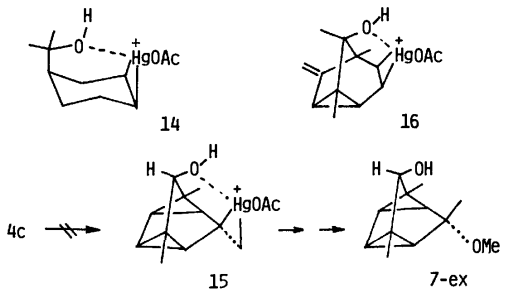

4a—d seemed to be much affected by the steric hindrance of various substituents at C-3 in the step of mercurinium-ion formation. A study dealing with the steric hindrance is of interest in order to gain insight into the correlation between the mercurinium-ion formation and the 1,3-dipolar cycloaddition, in which two bonds are formed in a concerted manner. For this reason, the steric effect of substituents located at C-3 was investigated. Less is known about the influence of the steric hindrance in concerted 1,3-dipolar cycloadditions. However, it has been shown that the relative rates of the cycloaddition of aromatic nitrile oxide with substituted ethylenes are influenced by the steric factor.[27]

The cycloaddition of **4a** with mesitonitrile oxide (MNO) in dichloromethane gave **17**-ex and **17**-en in 42 and 11% yields respectively. The structural assignment of **17**-ex and **17**-en follows convincingly from their physical properties and the chemical transformations. The carbonyl absorption bands at 1711 cm^{-1} for **17**-ex and, at 1706 cm^{-1} for **17**-en suggest the existence of the tetracyclic skeleton. The mass spectral data, as well as the analytical data, suggest that **17**-ex and **17**-en are one-to-one adducts of **4a** and MNO. The NMR

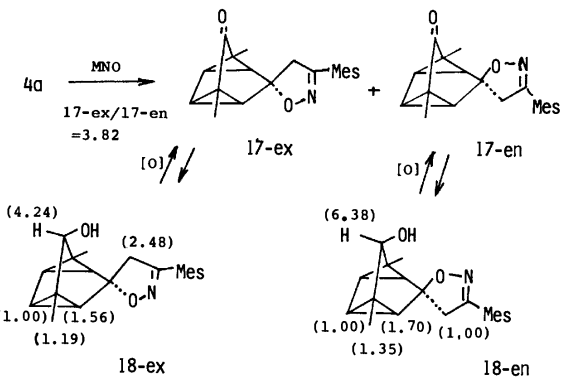

spectra suggested the symmetric structures (see Experimental section), and the addition occurred on the exocyclic double bond of **4a**. The chemical shifts of the protons of the isoxazoline moiety of **17**-ex (δ 3.09) and of **17**-en (δ 3.27) are suggestive of the regiochemistry of the C=N–O moiety, as is depicted.[28] On the reduction of **17**-ex or **17**-en with sodium borohydride, **18**-ex and **18**-en were obtained in good yields. On the oxidation of **18**-ex and **18**-en with pyridinium chlorochromate, **17**-ex and **17**-en were regenerated. The skeletons of **17**-ex and **17**-en are not changed in these chemical

transformations.

The stereochemical arrangements of the C=N–O moiety in **18**-ex and **18**-en were obtained from pseudo-contact NMR spectra obtained by using $Eu(fod)_3$.[14] The relative downfield shifts of δ's of hydrogens for the isoxazoline moiety are 2.48 for **18**-ex and 1.00 for **18**-en. Therefore, it is clarified that the coordination of $Eu(fod)_3$ occurs on the hydroxyl oxygens and that the C=N–O moieties are exo for **18**-ex and endo for **18**-ex. Consequently, the stereochemical arrangements of **17**-ex and **17**-en are assessed.

Similarly, **4b** and MNO gave two adducts, **19**-ex and **19**-en, in 63 and 20% yields respectively. On oxidation with pyridinium chlorochromate, **19**-ex and **19**-en were converted to **17**-ex and **17**-en respectively.

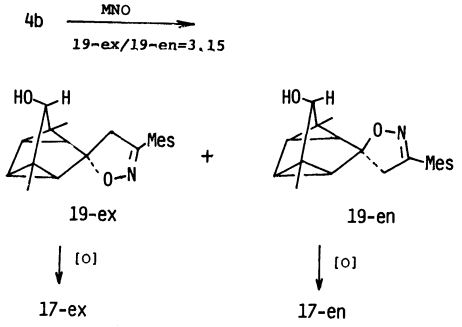

This chemical transformation and the results of a comparison of the spectral data with those of **17**-ex, **17**-en, **18**-ex, and **18**-en revealed the structures of **19**-ex and **19**-en convincingly.

On the other hand, **4d** and MNO gave a single adduct, **20**-ex, in an 80% yield, along with 10% of the starting material, **4d**. The structure was deduced from the spectral data. The stereochemical arrangement of the C=N–O moiety is not clarified from the pseudo-contact NMR spectra, however, it should be *exo* because of the large steric effect of the methyl group on C-3.

The regiochemistry of the present cycloadditions seems to suggest the electrophilic nature of MNO, since the unsubstituted terminus of dicyclopropylethylene (large

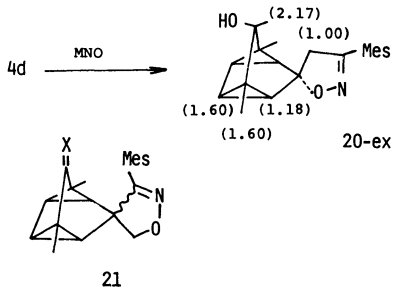

HOMO coefficient) was bound to the carbon terminus of MNO (larger LUMO coefficient).[29] The regiochemistry observed here is also favorable for a steric reason: the van der Waals non-bonded interaction energies should be very large in such material as **21** as compared to the above products. Recently, theoretical as well as experimental studies of the 1,3-dipolar cycloadditions of nitrile oxide with methyleneadamantane have been shown to exhibit a regiochemistry similar to that of the present reactions.[28]

In the case of the reaction of **4a**, **17**-ex/**17**-en is 3.82, while in that of **4b**, **19**-ex/**19**-en is 3.5. The reaction of **4d**, which has the methyl group at C-3 position, gave only **20**-ex. Previously, the degree of polarization of the exocyclic double bonds of **4a** and **4b** has been ascertained from the ^{13}C-NMR values, in which the electron-withdrawing carbonyl group seems to reduce the polarization through two cyclopropane rings.[30] Therefore, the possible π-orbital distortion of the exocyclic double bond may also conceivably affect the exo, endo-selectivity.[31] However, the increase in the *exo*-adduct **20**-ex upon the introduction of the bulky group on C-3, like the decrease in the *endo* products observed for mercuration reactions of **4a**—**d**, can be classified as a steric effect. The value of **5**-en/**5**-ex (1.8), which could correspond to the ratio of the mercurinium-ion formation of **9**/**10** for the ketone **4a**, is smaller than that of **17**-ex/**17**-en (3.82). The much suppressed **17**-en formation, as compared to that of **17**-ex, may be attributable to the coulombic repulsion of mesitonitrile oxide with the π-electron of the carbonyl function at C-3. Since similar trends for the *exo-endo* ratios of the postulated mercurinium ion formation and the 1,3-dipolar cycloaddition are obtained here, the steric effect seems to affect the reaction pathways in a similar manner. The stereochemical courses of the mercuration reactions of various kinds of compounds may be clarified in comparison with the reaction such as 1,3-dipolar cycloadditions, which involve a two-bond-forming process in the reaction sequences.

Experimental

The IR spectra were recorded on a Shimadzu IR-400 spectrometer. The mass spectral studies were conducted using a Hitachi RMU-60 spectrometer. All NMR spectra were recorded on a JEOL PS-100 high resolution spectrometer, using tetramethylsilane as the internal standard. The shift data were obtained by adding small increments of $Eu(fod)_3$ to the sample and by the n noting the extent to which each peak was shifted. The relative shift-slopes were obtained by dividing each slope by the slope of the least-shifted signal. VPC separations were performed on a Varian model-920 chromatograph, using a column packed with 5% FFAP on Chromosorb W at 110 °C. The analyses were performed by the Science and Engineering Research Laboratory, Waseda University.

Methoxymercuration-demercuration of ***4a***. A solution of **4a** (400 mg, 2.5 mmol) and mercury(II) acetate (960 mg, 3.0 mmol) in 8 cm^3 of anhydrous methanol was stirred for 6 h at room temperature. To this reaction mixture, was added 2.6 cm^3 of 3 mol dm^{-3} aqueous sodium hydroxide. After stirring for 15 min, 10 cm^3 of brine was added to the reaction mixture and mercury precipitated was filtered through Celite. The filtrate was extracted with ether, and the ether extract was dried over sodium sulfate. The removal of the ether *in vacuo* gave an oily material, which was separated by TLC on silica gel, using dichloromethane as the eluent, to give 99 mg (25%) of **4a** and a mixture of **5**-en and **5**-ex in a ratio of 177 mg (37%)/99 mg (21%). This mixture was separated by VPC to give pure **5**-en and **5**-ex. For **5**-en: IR (CCl_4), 2974, 2930, 1721, 1138, 873 cm^{-1}; NMR (CCl_4), δ 1.05 (6H, s), 1.46 (3H, s), 1.53 (2H, d, J=6.0 Hz), 2.10 (2H, d, J=6.0 Hz), 3.16 (3H,

s); MS, *m/e* (rel intensity), 192 (M^+, 63), 161 (100). Found: C, 74.78; H, 8.17%. Calcd for $C_{12}H_{16}O_2$: C, 74.97; H, 8.39% For **5**-ex: IR (CCl_4), 2983, 2939, 1713, 1068, 869 cm^{-1}; NMR ($CDCl_3$), δ 1.05 (6H, s), 1.23 (3H, s), 1.52 (2H, d, J=6.0 Hz), 2.24 (2H, d, J=6.0 Hz), 3.34 (3H, s); MS, *m/e* (rel intensity), 192 (M^+, 63), 161 (100). Found: C, 74.99; H, 8.70%. Calcd for $C_{12}H_{16}O_2$: C, 74.97; H, 8.39%.

Methoxymercuration-demercuration of ***4b***. A solution of **4b** (452 mg, 2.79 mmol) and mercury(II) acetate (1.069 g, 3.35 mmol) in 10 cm^3 of anhydrous methanol was stirred at room temperature for 8 h, followed by the addition of 5 cm^3 of 3 mol dm^{-3} aqueous sodium hydroxide and then sodium borohydride (127 mg, 3.35 mmol) in 5 cm^3 of aqueous sodium hydroxide. A workup similar to that described above gave 502 mg of an oil, which was revealed by VPC analysis and NMR spectroscopy to contain **4b** (112 mg, 25%), **6**-en (328 mg, 61%), and **6**-ex (63 mg, 12%). For **6**-en: IR (CCl_4), 3515—3294 (broad band), 2939, 1136, 1059, 1024 cm^{-1}; NMR (CCl_4), δ 1.11 (6H, s), 1.28 (3H, s), 1.28 (2H, d, J=5.7 Hz, overlapping with methyl signal), 1.59 (2H, d, J=5.7 Hz), 2.75 (1H, s), 3.15 (3H, s), 3.93 (1H, s). For **6**-ex: IR (CCl_4), 3561—3393 (broad band), 2939, 1076, 1061, 1023 cm^{-1}; NMR (CCl_4), δ 1.11 (6H, s), 1.18 (3H, s), 1.18 (2H, d, J=5.7 Hz, overlapping with methyl signal), 1.71 (2H, d, J=5.7 Hz), 1.8—2.0 (1H, broad s), 3.26 (3H, s), 3.56 (1H, s).

Oxidation of ***6****-en*. A suspension of pyridinium chlorochromate (141 mg, 0.65 mmol), anhydrous sodium acetate (11 mg, 0.14 mmol), and **6**-en (70 mg, 0.36 mmol) in 5 cm^3 of dichloromethane was stirred for 6 h under a nitrogen atmosphere. The reaction mixture was then chromatographed on Florisil, using dichloromethane as the eluent, to give a quantitative yield of **5**-en, which was identical with the authentic specimen.

Oxidation of ***6****-ex*. A suspension of pyridinium chlorochromate (50 mg, 0.22 mmol), anhydrous sodium acetate (4 mg, 0.04 mmol), and **6**-ex (24 mg, 0.12 mmol) in 2 cm^3 of dichloromethane was stirred for 6 h under a nitrogen atmosphere. The reaction mixture was then chromatographed on Florisil, using dichloromethane as the eluent, to give 18 mg (76%) of **5**-ex, which was identical with the authentic specimen.

Methoxymercuration-demercuration of ***4c***. A solution of **4c** (300 mg, 1.85 mmol) and mercury(II) acetate (709 mg, 2.23 mmol) in 5 cm^3 of anhydrous methanol was stirred for 11 h at room temperature, followed by the addition of 2 cm^3 of 3 mol dm^{-3} aqueous sodium hydroxide and sodium borohydride (85 mg, 2.23 mmol) in 2 cm^3 of 3 mol dm^{-3} aqueous sodium hydroxide. A workup similar to that described above gave 312 mg of an oil, which was revealed by VPC and NMR spectroscopy to contain **4c** (63 mg, 21%) and **7**-en (251 mg, 70%). This mixture was separated by VPC to afford pure **4c** and **7**-en. For **7**-en: IR (CCl_4), 3422, 2956, 1461, 1128, 1045 cm^{-1}; NMR (CCl_4), δ 1.06 (6H, s), 1.12 (2H, d, J=6.0 Hz), 1.38(3H, s), 1.46 (2H, d, J=6.0 Hz), 3.02 (3H, d, J=12.0 Hz) ,3.28 (3H, s), 3.83 (1H, d, J=12.0 Hz).

Oxidation of ***7****-en*. A mixture of pyridinium chlorochromate (141 mg, 0.65 mmol), anhydrous sodium acetate (11 mg, 0.14 mmol), and **7**-en (69 mg, 0.36 mmol) in 5 cm^3 of dichloromethane was stirred for 5 h at room temperature under a nitrogen atmosphere. The reaction mixture was then chromatographed on Florisil, using dichloromethane as the eluent, to give 53 mg (78%) of **5**-en, which was identified with the authentic specimen.

Methoxymercuration-demercuration of ***4d***. A solution of **4d** (500 mg, 2.84 mmol) and mercury(II) acetate (1.008 g, 3.42 mmol) in 10 cm^3 of anhydrous methanol was stirred for 11 h at 40 °C, followed by the addition of 5 cm^3 of 3 mol dm^{-3} aqueous sodium hydroxide and sodium borohydride (130 mg, 3.42 mmol) in 5 cm^3 of 3 mol dm^{-3} aqueous sodium hydroxide. A workup similar to that described above gave 424 mg of an oil, which was revealed to contain **4d** (102 mg, 20%) and **8**-en (321 mg, 64%). This oil was separated by VPC to afford pure **8**-en: IR (CCl_4), 3586, 3451, 2965, 2939, 1383, 1130, 1065, 919 cm^{-1}; NMR (CCl_4), δ 1.00 (6H, s), 1.24 (3H, s), 1.29 (3H, s), 1.08 (2H, d, J=6.0 Hz), 1.43 (2H, d, J=6.0 Hz). Found: C, 74.86; H, 9.29%. Calcd for $C_{13}H_{20}O_2$: C, 74.96; H, 9.68%.

Reduction of ***4a*** *with Lithium Aluminium Hydride (LAH)*. A solution of **4a** (875 mg, 5.47 mmol) and LAH (208 mg, 5.47 mmol) in 10 cm^3 of anhydrous tetrahydrofuran was refluxed for 5 h. The usual workup afforded 735 mg (83%) of a mixture of **4b** (133 mg, 15%) and **4c** (602 mg, 68%). This mixture was separated by VPC to afford pure **4b** and **4c**. For **4c**: NMR (CCl_4), δ 1.10 (6H, s), 1.58 (2H, d, J=6.0 Hz), 1.82 (2H, d, J=6.0 Hz), 3.97 (1H, broad s), 4.83 (2H, s); MS, *m/e* (rel intensity), 162 (M^+, 23), 58 (100).

Irradiation of 1,5,8-Trimethyl-6-methylenetricyclo[3.2.1.0^{2,7}*]oct-3-en-8-*endo*-ol*. A solution of the tricyclic alcohol (1.0 g, 5.68 mmol) in 200 cm^3 of anhydrous acetonitrile was irradiated using RPR-254 nm lamps for 48 h under a nitrogen atmosphere. After the removal of the solvent, the residue was chromatographed on alumina (30 g), using benzene as the eluent, to give **4d**, which was then recrystallized from hexane to give 582 mg (58%) of pure **4b**: IR (CCl_4), 3595, 3437, 2974, 1653, 1443, 1379, 1342, 1131, 925, 862 cm^{-1}; NMR (CCl_4), δ 1.02 (3H, s), 1.05 (6H. s), 1.45 (2H, d, J=6.0 Hz), 1.77 (2H, d, J=6.0 Hz), 4.76 (2H, s). Found: C, 81.57; H, 9.17%. Calcd for $C_{12}H_{16}O_2$: C, 81.77; H, 9.15%.

Cycloaddition of ***4a*** *with Mesitonitrile Oxide (2,2,6-Trimethylbenzonitrile Oxide)*. A solution of **4a** (160 mg, 1 mmol) and mesitonitrile oxide (161 mg, 1 mmol) in 4 cm^3 of dichloromethane was refluxed for 4 d. After solvent removal *in vacuo*, the resulting residue was separated by TLC on silica gel, using dichloromethane as the eluent. The first band from the TLC plates gave 12 mg (8%) of **4a**. The second band from the TLC plates gave 134 mg (42%) of colorless crystals of **17**-ex: mp 164—165 °C (from ethanol); IR (KBr) 1711, 1609, 1333, cm^{-1}; NMR ($CDCl_3$), δ 1.12 (6H, s), 1.97 (2H, d, J=6.0 Hz) 2.20 (9H, s), 2.48 (2H, d, J=6.0 Hz), 3.09 (2H, s), 6.80 (2H broad s); MS, *m/e* (rel intensity), 321 (M^+, 61), 159 (100). Found: C, 78.62; H, 7.14; N, 4.28%. Calcd for $C_{21}H_{23}O_2N$: C, 78.47; H, 7.21; N, 4.36%. The third band from the TLC plates gave 34 mg (11%) of **17**-en: mp 288—289 °C (from ethanol); IR (KBr), 1706, 1610, 1332 cm^{-1}; NMR ($CDCl_3$), δ 1.15 (6H, s), 1.75 (2H, d, J=6.0 Hz), 2.23 (9H, s), 2.26 (2H, d, J=6.0 Hz), 3.27 (2H, s), 6.83 (2H, s); MS, *m/e* (rel intensity), 321 (M^+, 27), 159 (100). Found: C, 78.41; H, 7.21; N, 4.18%. Calcd for $C_{21}H_{23}O_2N$: C, 78.47; H, 7.21; N, 4.36%.

Reduction of ***17****-ex*. A solution of **17**-ex (70 mg, 0.22 mmol) and sodium borohydride (9 mg, 0.22 mmol) in 11 cm^3 of benzene–ethanol (10/1) was stirred overnight. This reaction mixture was concentrated and extracted with dichloromethane, and then the extract was dried over sodium sulfate. After solvent removal *in vacuo*, the residue was recrystallized from ethanol to give 56 mg (80%) of **18**-ex: mp 230—231 °C; IR (KBr), 3309, 1601, 1333, 1067 cm^{-1}; NMR ($CDCl_3$), δ 1.13 (6H, s), 1.63 (2H, d, J=6.0 Hz), 1.82 (2H, d, J=6.0 Hz), 2.27 (9H, s), 3.37 (2H, s), 4.17 (1H, d, J=3.7 Hz), 6.85 (2H, s).

Oxidation of ***18****-ex*. To a suspension of pyridinium chlorochromate (20 mg, 0.093 mmol) and anhydrous sodium acetate (2 mg), was added **18**-ex (17 mg, 0.052 mmol) in 0.5 cm^3 of dichloromethane under a nitrogen atmosphere. This mixture was stirred for 3 h. Reaction mixture was then chromatographed on Florisil, using dichloromethane as the eluent, to give 14 mg (84%) of **17**-ex.

Reduction of ***17****-en.* The reduction was carried out as has been described above using 48 mg (0.3 mmol) of **17**-en and 6 mg (0.15 mmol) of sodium borohydride. The product was recrystallized from ethanol to give 39 mg (80%) of **18**-en: mp 193—194 °C; IR (KBr), 3468, 1609, 1321, 1043 cm^{-1}; NMR ($CDCl_3$), δ 1.17 (6H, s), 1.35 (2H, d, J=6.0 Hz), 1.68 (2H, d, J=6.0 Hz), 2.26 (9H, s), 3.02 (1H, d, J=11.6 Hz), 3.17 (2H, s), 4.15 (1H, d, J=11.6 Hz), 6.90 (2H, s).

Oxidation of ***18****-en.* The reaction was carried out using **18**-en (30 mg, 0.09 mmol), pyridinium chlorochromate (30 mg, 0.14 mmol), and anhydrous sodium acetate (3 mg). A workup similar to that described above afforded **17**-en (26 mg, 82%).

Cycloaddition of ***4b*** *with Mesitonitrile Oxide.* A solution of **4b** (324 mg, 2 mmol) and mesitonitrile oxide (322 mg, 2 mmol) in 6 cm^3 of dichloromethane was refluxed for 56 h. The reaction was monitored by TLC (silica gel, dichloromethane). After solvent removal *in vacuo*, the resulting residue was separated by TLC on silica gel, using dichloromethane as the eluent. The first band from the TLC plates afforded 404 mg (63%) of **19**-ex: mp 158—159 °C (from ethanol); IR (KBr), 3307, 1609, 1062 cm^{-1}; NMR ($CDCl_3$), δ 1.13 (6H, s), 1.65 (2H, d, J=6.0 Hz), 1.95 (2H, d, J=6.0 Hz), 2.21 (9H, s), 3.00 (2H, s), 3.50 (1H, d, J=8.0 Hz), 6.86 (2H, s). Found: C, 77.80; H, 7.82; N, 4.24%. Calcd for $C_{21}H_{25}O_2N$: C, 77.98; H, 7.79; N, 4.33%. The second band from the TLC plates gave 127 mg (20%) of **19**-en: mp 205—206 °C (from ethanol); IR (KBr), 3386, 1604, 1331 cm^{-1}; NMR ($CDCl_3$), δ 1.23 (6H, s), 1.38 (2H, d, J=6.0 Hz), 1.84 (2H, d, J=6.0 Hz), 2.27 (9H, s), 3.15 (2H, s), 4.26 (1H, d, J=7.8 Hz), 6.09 (2H, s). Found: C, 77.82; H, 7.78; N, 4.66%. Calcd for $C_{21}H_{25}O_2N$: C, 77.98; H, 7.79; N, 4.38%.

Oxidation of ***19****-ex.* The reaction was carried out using **19**-ex (100 mg, 0.31 mmol), pyridinium chlorochromate (100 mg, 0.31 mmol), and anhydrous sodium acetate (20 mg, 0.24 mmol). A workup similar to that described above afforded 83 mg (83%) of **17**-ex, which was characterized by the spectral data.

Oxidation of ***19****-en.* The oxidation was carried out as has been described above, using 50 mg (0.15 mmol) of **19**-en, pyridinium chlorochromate (60 mg, 0.08 mmol), and anhydrous sodium acetate (6 mg, 0.08 mmol). Exactly the same workup as has been described above afforded 28 mg (57%) of **17**-en, which was identified by a mixed-melting-point determination and by a comparison of the spectral data.

Cycloaddition of ***4d*** *with Mesitonitrile Oxide.* A solution of **4d** (176 mg, 1 mmol) and mesitonitrile oxide (161 mg, 1 mmol) in 3 cm^3 of benzene was refluxed for 7 h. After solvent removal *in vacuo*, the resulting residue was separated by TLC on silica gel, using dichloromethane as the eluent. The first band from the TLC plates contained 17 mg (10%) of **4d**. The second band from the TLC plates afforded 279 mg (82%) of the adduct, **20**-ex: mp 163—164 °C; IR ($CHCl_3$), 3340—3210, 1611 cm^{-1}; NMR ($CDCl_3$), δ 1.11 (6H, s), 1.16 (3H, s), 1.62 (2H, d, J=6.0 Hz), 1.86 (2H, d, J=6.0 Hz), 2.24 (6H, s), 2.25 (3H, s), 3.15 (2H, s), 6.84 (2H, s); MS, *m/e* (rel intensity), 337 (M^+, 21), 294 (100). Found: C, 78.07; H, 7.83; N, 3.95%. Calcd for $C_{22}H_{27}O_2N$: C, 78.30; H, 8.07; N, 4.15%.

References

1) This paper was presented at the National Meeting of Chemical Society of Japan, October 1981.

2) K. Okada and T. Mukai, *J. Am. Chem. Soc.*, **100**, 6509 (1978).

3) L. A. Paquette, L. W. Hartel, R. Gleiter, and M. C. Bohm, *J. Am. Chem. Soc.*, **100**, 6510 (1978).

4) L. W. Hartel and L. A. Paquette, *J. Am. Chem. Soc.*, **101**, 7620 (1979).

5) L. A. Paquette, L. W. Hartel, R. Gleiter, M. C. Bohm, M. A. Beno, and G. G. Christoph, *J. Am. Chem. Soc.*, **103**, 7106 (1981).

6) M. Nitta, A. Omata, and H. Sugiyama, *Chem. Lett.*, **1980**, 1615; *Bull. Chem. Soc. Jpn.*, **55**, 569 (1982).

7) M. Nitta, A. Omata, and H. Nakatani, in submission to *Bull. Chem. Soc. Jpn.*

8) M. Nitta, A. Omata, and S. Okada, to be published.

9) Y. Senda, S. Kamiyama, and S. Imaizumi, *J. Chem. Soc., Perkin Trans. 1*, **1978**, 530; H, C, Brown and W. J. Hammer, *Tetrahedron*, **34**, 3405 (1978), and the references cited therein.

10) A. F. Diaz, M. Makai, and S. Winstein, *J. Am. Chem. Soc.*, **92**, 7477 (1970).

11) M. Nitta, O. Inoue, and M. Tada, *Chem. Lett.*, **1977**, 59.

12) G. Muherjee-Müller, P. Gilgen, J. Zsindely, and H. Schmid, *Helv. Chim. Acta*, **60**, 1758 (1977).

13) H. C. Brown and P. Geoghegan, Jr., *J. Am. Chem. Soc.*, **89**, 1522 (1967).

14) The numerical values presented in the parentheses in the structural formulae in this paper are the relative downfield shifts of δ's obtained by using Eu $(fod)_3$.

15) E. J. Corey and A. S. Suggs, *Tetrahedron Lett.*, **1975**, 2647.

16) M. C. Cabaleiro, A. D. Araya, and M. D. Johnson, *J. Chem. Soc., Perkin Trans. 2*, **1973**, 1207; D. Dodd and M. D. Johnson, *J. Chem. Soc., B*, **1971**, 662.

17) R. D. Bach and R. F. Richter, *Tetrahedron Lett.*, **1973**, 4099; *J. Org. Chem.*, **38**, 3442 (1976).

18) S. J. Christol, J. S. Perry, Jr., and R. S. Beckley, *J. Org. Chem.*, **41**, 1912 (1976).

19) H. C. Brown and J. H. Kawakami, *J. Am. Chem. Soc.*, **95**, 8665 (1973).

20) T. J Taylor and A. W. Baker, *J. Am. Chem. Soc.*, **85**, 2746 (1963).

21) F. T. Bond, *J. Am. Chem. Soc.*, **90**, 5326 (1968).

22) J. F. Galle and A. Hassner, *J. Am. Chem. Soc.*, **94**, 3930 (1972).

23) W. Lotsh and A. S. Kende, *Angew. Chem.*, **83**, 581 (1971).

24) H. Volz, J-H. Shin, and H. Hettel, *Liebigs Ann. Chem.*, **1982**, 480.

25) H. C. Brown and P. Geoghegan, Jr., *J. Org. Chem.*, **37**, 9937 (1972).

26) H. B. Henbest and R. S. McElhinney, *J. Chem. Soc.*, **1959**, 1834.

27) K. Bast, M. Christl, R. Huisgen, and W. Mack, *Chem. Ber.*, **106**, 3313 (1973); A. Battaglia, S. M. Shaw, C-S. Hsue, and K. N. Houk, *J. Org. Chem.*, **44**, 2800 (1979).

28) T. Sasaki, S. Eguchi, T. Esaki, and T. Suzuki, *Tetrahedron*, **35**, 1073 (1979).

29) K. N. Houk, *Acc. Chem. Res.*, **8**, 361 (1975).

30) M. Nitta and T. Kuroki, *Bull. Chem. Soc. Jpn.*, **55**, 1323 (1982).

31) J. Klein, *Tetrahedron Lett.*, **1973**, 4307.

Studies on 2-Aziridinecarboxylic Acid. IX.[1] Convenient Synthesis of Optically Active *S*-Alkylcysteine, *threo*-*S*-Alkyl-β-methylcysteine, and Lanthionine Derivatives *via* the Ring-opening Reaction of Aziridine by Several Thiols

Kiichiro NAKAJIMA,* Hitomi ODA, and Kenji OKAWA
Department of Chemistry, Faculty of Science, Kwansei Gakuin University, Nishinomiya 662

(Received June 11, 1982)

A convenient synthesis of optically active *S*-alkylcysteine, *threo*-*S*-alkyl-β-methylcysteine, and lanthionine derivatives has been investigated. Benzyl 1-benzyloxycarbonyl-(2*S*)-2-aziridinecarboxylate and benzyl (2*S*,3*S*)-1-benzyloxycarbonyl-3-methyl-2-aziridinecarboxylate, and their enantiomers were treated with several thiols, and the corresponding *S*-alkylcysteine, *threo*-*S*-alkyl-β-methylcysteine, and lanthionine derivatives were prepared *via* the ring-opening reaction of aziridine in the presence of a catalytic amount of boron trifluoride etherate in good yields.

Our previous paper[2] reported on the reaction of 1-aminoacyl-2-aziridinecarboxylic acid peptide, namely Z-Gly-L-Azy-Gly-OBzl, with thiophenol, and preparation of the corresponding *S*-phenylcysteine-containing peptide *via* the ring-opening reaction of the aziridine. Bernstein and Ben-Ishai[3] also reported that the 1-substituted 2-aziridinecarboxylate was transformed into the corresponding DL-*S*-methylcysteine derivative *via* a similar ring-opening reaction of the aziridine.

This study reports the synthesis of several optically active *S*-alkylcysteines, *threo*-*S*-alkyl-β-methylcysteines, and lanthionines *via* the ring-opening reaction of (2*S*)-Z-Azy-OBzl (**1**), (2*S*,3*S*)-Z-3-MeAzy-OBzl (**2**), and their enantiomers (**3**, **4**); these were prepared from the corresponding optically active serine and threonine as described in our previous papers.[4] The reactions were carried out with the appropriate thiols. The reaction procedure is shown in Scheme 1.

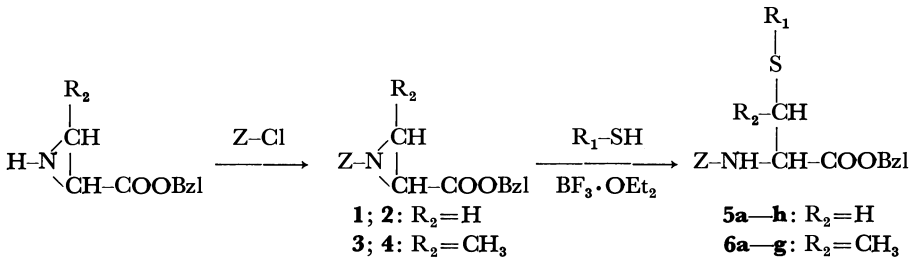

Scheme 1.

TABLE 1. PROPERTIES AND YIELDS OF L-*S*-ALKYLCYSTEINE (**5**) AND L-*threo*-*S*-ALKYL-β-METHYLCYSTEINE (**6**) DERIVATIVES

Product[a]	R_1	Product yield/%	Mp θ_m/°C	$[\alpha]_D^{23}$/°(MeOH)	Reaction time/d
5a	$-CH_3$	86.0	Syrup	−20.7(*c* 1.2)	2
5b	$-CH(CH_3)_2$	81.9	Syrup	−7.0(*c* 0.9)	3
5c	$-CH(CH_3)CH_2CH_3$	74.2	Syrup	−16.2(*c* 1.0)	3
5d	$-C(CH_3)_3$	90.0	Syrup	−14.2(*c* 1.1)	4
5e	$-C_6H_{11}$	80.9	42—44	−16.2(*c* 1.2)	2
5f	$-C_6H_5$	77.8	53—55	−13.6(*c* 1.0)	2
5g	$-CH_2C_6H_5$	72.0	68—70	−45.3(*c* 1.1)	3
5h[b]	$-CH_2C_6H_5$	67.5	65—68	+45.9(*c* 0.9)	3
6a	$-CH_3$	92.3	Syrup	−15.9(*c* 1.1)	2
6b	$-CH(CH_3)_2$	73.4	Syrup	+1.0(*c* 1.0)	3
6c	$-CH(CH_3)CH_2CH_3$	69.5	Syrup	+4.2(*c* 1.0)	3
6d	$-C(CH_3)_3$	53.5	76.5—79.0	−5.8(*c* 1.1)	4
6e	$-C_6H_{11}$	52.5	99—100.5	−1.2(*c* 1.1)	4
6f	$-C_6H_5$	81.7	52—53	+41.3(*c* 1.0)	2
6g	$-CH_2C_6H_5$	68.3	115—118.5	−16.6(*c* 1.0)	5

a) The result of (2*S*)-Z-Azy-OBzl(**1**) and (2*S*, 3*S*)-Z-3-MeAzy-OBzl(**3**) with R_1SH. b) The result of (2*R*)-Z-Azy-OBzl(**2**) with $C_6H_5CH_2SH$.

We carried out the reaction of **1**, **2**, or **3** (1 mmol) with a large excess of thiol in a solution of dichloromethane (3 ml) containing a catalytic amount of boron trifluoride etherate at room temperature. The Azy derivatives were very stable in the thiol solution and the ring-opening reaction did not occur at all, but when boron trifluoride etherate was added, the expected ring-opening reaction easily occurred.

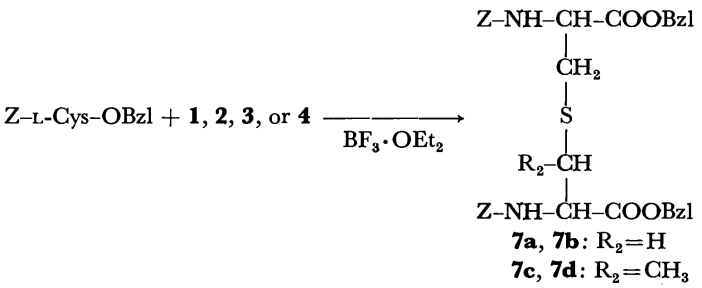

Scheme 2.

Table 2. Properties and yields of lanthionine derivatives (**7a—d**)

Product[a]		Yield/%	Mp θ_m/°C	$[\alpha]_D^{23}$/°(MeOH)
Z-L-Ala-OBzl S Z-L-Ala-OBzl	(**7a**)	37	94.5—95.0	−31.5(*c* 1.1)
Z-L-Ala-OBzl S Z-D-Ala-OBzl	(**7b**)	21	86—87	—
Z-L-Ala-OBzl S Z-L-Aba-OBzl	(**7c**)[b]	22	Syrup	−11.6(*c* 1.0)
Z-L-Ala-OBzl S Z-D-Aba-OBzl	(**7d**)[b]	12	104.5—107	−32.0(*c* 1.1)

a) The reaction was carried out in a CH_2Cl_2 solution at 20 °C for 5 d, and Z-L-Cys-OBzl used was 1 equimolar against the Azy derivatives (**1**, **2**, **3**, and **4**). b) Aba: *threo*-2-aminobutylic acid residue.

The reaction results summarized in Table 1 show that this ring-opening reaction of aziridine is very convenient for synthesizing the optically active *S*-substituted cysteine (**5**) and β-methylcysteine (**6**) derivatives. In paticular, the optically active *threo*-β-methylcysteine derivatives (**6**) retained the original configuration of the starting threonine *via* two stereospecific procedures. That is, the aziridine ring-formation and the ring-opening procedures. Thus, the *allo*-threonine derivative is not needed as the starting material to prepare *S*-alkyl-*threo*-β-methylcysteine derivatives (**6**).

We also synthesized lanthionine derivatives from the reaction of **1**, **2**, **3**, and **4** (1 mmol) with benzyl *N*-benzyloxycarbonyl-L-cysteinate (1 mmol) as a thiol component under the same reaction conditions, except for the thiol amount, as shown in Scheme 2. Although the reaction results summarized in Table 2 show that the synthetic yield of each lanthionine derivative was not very good, this procedure is useful for synthesizing optically active lanthionines.

Experimental

Melting points are uncorrected. Optical rotations were determined at the D line on a Perkin-Elmer 141 polarimeter. NMR spectra were obtained with a Hitachi R-20 B high-resolution NMR spectrometer using TMS as the internal reference. The homogeneity of the products was checked by thin-layer chromatography on silica-gel plates.

*Benzyl (2S)-1-Benzyloxycarbonyl-2-aziridinecarboxylate (**1**).* To a solution of (2*S*)-H-Azy-OBzl[4] (2.4 g, 13.4 mmol) and Et_3N (1.52 ml, 10.8 mmol) in $CHCl_3$ was added Z-Cl[1] (1.72 ml, 10.8 mmol) at 0 °C with stirring. After being stirred overnight, the solution was washed with 10% citric acid, 1 M $NaHCO_3$, and water, then dried over Na_2SO_4 and concentrated *in vacuo*. The residue was purified by silica gel column chromatography ($CHCl_3$) and the pure product was isolated as a syrup, 3.2 g (95% from Z-Cl), $[\alpha]_D^{23}$ −19.0° (*c* 1.0, MeOH). NMR ($CDCl_3$) δ: 2.37 (1H q, *J*=1.5, 5.0 Hz), 2.54 (1H q, *J*=1.5, 3.0 Hz), 3.08 (1H q, *J*=3.0, 5.0 Hz), 5.05, 5.07 (4H 2s), 7.26 (10H s).

Found: C, 69.15; H, 5.53; N, 4.42%. Calcd for $C_{18}H_{17}O_4N$: C, 69.44; H, 5.50; N, 4.50%.

*Benzyl (2R)-1-Benzyloxycarbonyl-2-aziridinecarboxylate (**2**).* This compound was prepared by the same procedure from (2*R*)-H-Azy-OBzl[4] and Z-Cl. Compound **2** was obtained as a syrup, $[\alpha]_D^{23}$ +20.0° (*c* 0.9, MeOH). NMR ($CDCl_3$) spectra of **2** was identified with that of **1**.

Found: C, 69.52; H, 5.60; N, 4.39%. Calcd for $C_{18}H_{17}O_4N$: C, 69.44; H, 5.50; N, 4.50%.

*Benzyl (2S, 3S)-1-Benzyloxycarbonyl-3-methyl-2-aziridinecarboxylate (**3**).* To a solution of (2*S*, 3*S*)-H-3-MeAzy-OBzl[4] (4.57 g, 24 mmol) and Et_3N (3.36 ml, 24 mmol) in THF (30 ml) was added Z-Cl (3.84 ml, 24 mmol) at 0 °C with stirring. After being stirred for 4 h, the solution was concentrated *in vacuo*. The residue was dissolved in ethyl acetate and washed with 10% citric acid, 1 M $NaHCO_3$, and water, then dried over Na_2SO_4 and concentrated *in vacuo*. The residue was purified by silica gel column chromatography ($CHCl_3$). Compound **3** was obtained as a syrup, 7.62 g (98%), $[\alpha]_D^{23}$ −66.2° (*c* 1.0, MeOH). NMR ($CDCl_3$) δ: 1.26 (3H d, *J*=6.0 Hz), 2.75 (1H m), 3.18 (1H d, *J*=6.5 Hz), 5.06, 5.12 (4H 2s), 7.27 (10H s).

Found: C, 69.95; H, 5.92; N, 4.28%. Calcd for $C_{19}H_{19}O_4N$: C, 70.14; H, 5.89; N, 4.31%.

*Benzyl (2R, 3R)-1-Benzyloxycarbonyl-3-methyl-2-aziridinecarboxylate (**4**).* This compound was prepared by the same procedure from (2*R*, 3*R*)-H-3-MeAzy-OBzl[4] and Z-Cl. Compound **4** was obtained as a syrup, $[\alpha]_D^{23}$ +66.4° (*c* 1.2, MeOH). NMR ($CDCl_3$) spectra of **4** was identified with that of **3**.

Found: C, 70.26; H, 5.95; N, 4.21%. Calcd for $C_{19}H_{19}O_4N$: C, 70.14; H, 5.89; N, 4.31%.

*N-Benzyloxycarbonyl-S-methyl-L-cysteine Benzyl Ester (**5a**).* *General Procedure for The Reaction of Azy with Thiol*: To a solution of **1** (200 mg, 0.64 mmol) in $CHCl_3$ (3 ml) was added a solution of MeSH (1 g, excess) in $CHCl_3$ (15 ml) and BF_3·OEt_2 (3 drops). After being left for 2 d at room temperature, the solution was concentrated *in vacuo*. The residue was dis-

solved in ethyl acetate, washed with 1 M $NaHCO_3$, dried over Na_2SO_4, and concentrated *in vacuo*. The crude product was purified by silica-gel column chromatography ($CHCl_3$–hexane, 2 : 1 v/v). Compound **5a** was obtained as a syrup, 199 mg (86%), $[\alpha]_D^{23}$ −20.7° (*c* 1.2, MeOH). NMR ($CDCl_3$) δ: 1.96 (3H s), 2.86 (2H d, J=5.9 Hz), 4.59 (1H m), 5.08, 5.12 (4H 2s), 5.80 (1H bd), 7.28 (10H s).

Found: C, 63.41; H, 5.96; N, 3.99; S, 8.86%. Calcd for. $C_{19}H_{21}O_4NS$: C, 63.49; H, 5.89; N, 3.90; S, 8.92%.

N-Benzyloxycarbonyl-S-benzyl-L-cysteine Benzyl Ester (5g). To a solution of **1** (200 mg, 0.64 mmol) in $CHCl_3$ (3 ml) was added α-toluenethiol (3 ml, excess) and $BF_3 \cdot OEt_2$ (3 drops) at room temperature. After being left for 3 d, the solvent was removed *in vacuo*. The residue was dissolved in ethyl acetate, washed with 1 M $NaHCO_3$, dried over Na_2SO_4, and concentrated *in vacuo*. The crude product was purified by silica gel column chromatography ($CHCl_3$). Compound **5g** was obtained as crystals from $CHCl_3$–hexane, 196 mg (72%), mp 68—70 °C, $[\alpha]_D^{23}$ −45.3° (*c* 1.1, MeOH). [Standard sample prepared from L-Cys(Bzl): mp 68—70 °C, $[\alpha]_D^{23}$ −45.1° (*c* 1.0, MeOH)].

Found: C, 68.76; H, 5.82; N, 3.16; S, 7.42%. Calcd for $C_{25}H_{25}O_4NS$: C, 68.94; H, 5.79; N, 3.22; S, 7.36%.

N,N′-Dibenzyloxycarbonyl-L-lanthionine Dibenzyl Ester (7a). To a solution of **1** (427 mg, 1.37 mmol) in CH_2Cl_2 (5 ml) was added Z-L-Cys-OBzl (473 mg, 1.37 mmol) and $BF_3 \cdot OEt_2$ (3 drops) at room temperature. After 5 d, the solvent was removed *in vacuo*. The residue was dissolved in ethyl acetate and was worked up as described above. The crude product was purified by silica-gel column chromatography (hexane–ethyl acetate, 3 : 1 v/v). Compound **7a** was obtained as crystals from ethyl acetate–hexane, 335.5 mg (37.3%), mp 94.5—96.0 °C, $[\alpha]_D^{23}$ −31.5° (*c* 1.1, MeOH).

Found: C, 65.46; H, 5.48; N, 4.24; S, 4.99%. Calcd for $C_{36}H_{36}O_8N_2S$: C, 65.84; H, 5.53; N, 4.27; S, 4.88%.

N,N′-Dibenzyloxycarbonyl-meso-lanthionine Dibenzyl Ester (7b). To a solution of **2** (311 mg, 1 mmol) in CH_2Cl_2 (5 ml) was added Z-L-Cys-OBzl (345 mg, 1 mmol) and $BF_3 \cdot OEt_2$ (3 drops) at room temperature. After 5 d, the reaction mixture was worked up as described above. Compound **7b** was obtained as crystals from ethyl acetate–ether–hexane, 149 mg (21%), mp 86—87 °C.

Found: C, 65.33, H, 5.34; N, 4.29; S, 4.90%. Calcd for $C_{36}H_{36}O_8N_2S$: C, 65.84; H, 5.53; H, 4.27; S, 4.88%.

N,N′-Dibenzyloxycarbonyl-threo-β-methyl-L-lanthionine Dibenzyl Ester (7c). To a solution of **3** (325 mg, 1 mmol) in CH_2Cl_2 (5 ml) was added Z-L-Cys-OBzl (345 mg, 1 mmol) and $BF_3 \cdot OEt_2$ (3 drops) at room temperature. After 5 d, the reaction mixture was worked up as described above. Compound **7c** was obtained as a syrup, 145 mg (22%), $[\alpha]_D^{23}$ −11.6° (*c* 1.0, MeOH).

Found: C, 66.32; H, 5.86; N, 4.06; S, 4.74%. Calcd for $C_{37}H_{38}O_8N_2S$: C, 66.25; H, 5.71; N, 4.18; S, 4.78%.

N,N′-Dibenzyloxycarbonyl-threo-β-methyl-meso-lanthionine Dibenzyl Ester (7d). To a solution of **4** (325 mg, 1 mmol) in CH_2Cl_2 (5 ml) was added Z-L-Cys-OBzl (345 mg, 1 mmol) and $BF_3 \cdot OEt_2$ (3 drops) at room temperature. After 5 d, the reaction mixture was worked up as described above. Compound **7c** was obtained as crystals from ethyl acetate–ether–hexane, 81.4 mg (12%), mp 104.5—107.0 °C, $[\alpha]_D^{23}$ −32.0° (*c* 1.1, MeOH).

Found: C, 66.24; H, 5.81; N, 4.04; S, 4.71%. Calcd for $C_{37}H_{38}O_8N_2S$: C, 66.25; H, 5.71; N, 4.18; S, 4.78%.

References

1) Part VIII: K. Nakajima, T. Tanaka, M. Neya, and K. Okawa, *Bull. Chem. Soc. Jpn.*, **55**, 3237 (1982). The abbreviations of the IUPAC-IUB commision (*J. Biol. Chem.*, **247**, 977 (1972)) are used. Z: benzyloxycarbonyl; Bzl: benzyl; Z-Cl: benzyloxycarbonyl chloride; "Azyline" is used as the name of 2-aziridinecarboxylic acid, "Azy" being its abbreviation. 3-MeAzy: 3-methyl-2-aziridinecarboxylic acid.

2) K. Okawa, K. Nakajima, T. Tanaka, and T. Maeda, "Peptide Chemistry 1976," ed by T. Nakajima, Protein Research Foundation, Osaka (1977), p. 13.

3) Z. Bernstein and D. Ben-Ishai, *Tetrahedron*, **33**, 881 (1976).

4) N^{α}-free Azy-OBzl, N^{α}-free 3-MeAzy-OBzl, and their enantiomers were prepared from 1-Trt-Azy-OBzl and 1-Trt-3-MeAzy-OBzl by the treatment of TFA or HCOOH in MeOH as described in our papers: K. Okawa, K. Nakajima, T. Tanaka, and Y. Kawana, *Chem. Lett.*, **1975**, 591; K. Okawa and K. Nakajima, *Biopolymers*, **20**, 1811 (1981). (2*S*)-Azy-OBzl: syrup, $[\alpha]_D^{23}$ −27.7 (*c* 0.97, MeOH), +11.8 (*c* 0.99, THF). (2*R*)-Azy-OBzl: syrup, $[\alpha]_D^{23}$ +26.5 (*c* 1.0, MeOH), −10.9 (c 1.0, THF). (2*S*, 3*S*)-3-MeAzy-OBzl: mp 52.5—3.5 °C, $[\alpha]_D^{23}$ −38.6 (*c* 0.9, MeOH), +5.6 (*c* 1.0, THF). (2*R*, 3*R*)-3-MeAzy-OBzl: $[\alpha]_D^{23}$ +40.0 (*c* 1.1, MeOH), −5.6 (*c* 0.96, THF), mp 51—52 °C.

Effects of Divalent Metal Cations on Circular Dichroism and ^1H Nuclear Magnetic Resonance Spectra of Linear and Cyclic Peptides Having Side-chain Imidazolyl and Acetamido Groups

Masato KODAKA,*,† Toru SHIMIZU, and Masahiro HATANO
Chemical Research Institute of Non-aqueous Solutions, Tohoku University, Sendai 980
†*National Chemical Laboratory for Industry, Tsukuba 305*
(Received June 16, 1982)

A linear peptide, *N-t*-butoxycarbonyl-*S*-acetamidomethyl-L-cysteinyl-D-leucyl-L-histidyl-*S*-acetamidomethyl-L-cysteinyl-D-leucyl-L-histidine methyl ester (**1**) was synthesized by the solid phase method. Subsequent cyclization by the azide method offered a cyclic peptide, *cyclo*-*S*-acetamidomethyl-L-cysteinyl-D-leucyl-L-histidyl-*S*-acetamidomethyl-L-cysteinyl-D-leucyl-L-histidyl (**2**). The circular dichroism (CD) and ^1H NMR were observed for these peptides **1** and **2**, in the absence and presence of metal cations, Zn(II), Ca(II), Mg(II). Spectral results for Zn(II) complexes indicated striking contrasts to those of Ca(II) and Mg(II) complexes. Thus, in H_2O, the addition of Zn(II) caused CD spectral changes for both peptides, while Ca(II) and Mg(II) did not cause changes in any CD spectral region. In methanol, the additions of Zn(II) and Ca(II) caused CD changes, while the addition of Mg(II) did not cause any CD changes. The changes caused by adding Zn(II) were quite different from those by Ca(II), suggesting that Zn(II) is coordinated with the peptides in a mode different from that of Ca(II). ^1H NMR data also suggested the different coordination mode between these two metal complexes in methanol.

A number of studies have been undertaken about the complexation between metal cations and cyclic or linear oligopeptides in order to simulate the natural ionophores such as valinomycin[1] or the natural metalloproteins such as blue copper proteins.[2-4] In the former cases, the peptides studied are cyclic and the most cations used belong to alkali or alkaline earth metals, which are coordinated with the carbonyl oxygens of the main-chain peptide bonds.[5-8] In the latter cases, however, the peptides thus far investigated are primarily linear and metal cations belong to transition metals such as Cu(II), Ni(II), Pd(II), *etc.*, which are coordinated with imidazole, thiol, *etc.*, or deprotonated peptide-bond nitrogen anions.[9-11] There are in nature certain enzymes which contain Zn(II) at their active sites, such as carboxypeptidase A.[12] Since the properties of Zn(II) are intermediate between those of the diamagnetic metal ions and those of the paramagnetic transition metal ions, it seems to be interesting to investigate the interaction between Zn(II) and peptides. However, relatively few studies about Zn(II)–peptide complexes have been carried out. In the present study, therefore, the linear and the cyclic peptides having imidazolyl and acetamido groups at the side chains were synthesized, and circular dichroism (CD) spectra and ^1H NMR spectra of these peptides were measured in the presence or absence of Zn(II). Zn(II) is expected to be coordinated with the imidazolyl and the acetamido groups of the side chains in these complexes. Interactions with divalent diamagnetic metal ions, Ca(II) and Mg(II), were also investigated as well for comparison.

Experimental

Materials. The linear peptide, *N-t*-butoxycarbonyl-*S*-acetamidomethyl-L-cysteinyl-D-leucyl-L-histidyl-*S*-acetamidomethyl-L-cysteinyl-D-leucyl-L-histidine methyl ester (**1**) (Boc-L-Cys(*S*-Acm)-D-Leu-L-His-L-Cys(*S*-Acm)-D-Leu-L-His-OCH_3), and the cyclic peptide, *cyclo*-*S*-acetamidomethyl-L-cysteinyl-D-leucyl-L-histidyl-*S*-acetamidomethyl-L-cysteinyl-D-leucyl-L-histidyl (**2**) (*cyclo*(-L-Cys(*S*-Acm)-D-Leu-L-His-L-Cys(*S*-Acm)-D-Leu-L-His-)), used in this study were synthesized by the solid phase method and subsequent cyclization as follows. *N-t*-Butoxycarbonyl-*S*-acetamidomethyl-L-cysteinyl-D-leucyl-N^{Im}-tosyl-L-histidyl-*S*-acetamidomethyl-L-cysteinyl-D-leucyl-N^{Im}-tosyl-L-histidine-resin was synthesized from *N-t*-butoxycarbonyl-N^{Im}-tosyl-L-histidine-resin (0.27 mmol His/g-resin) on 1 mmol scale by the solid phase procedure in a Beckman model 990B Peptide Synthesizer according to the schedule shown in Table 1. The tosyl group was removed by suspending the obtained resin (*ca.* 4 g) in a solution of 1-hydroxybenzotriazole (1 g) in DMF (30 ml) at room temperature for 8 h.[13] The peptide was then removed from the resin by treatment with 1 M (1 M = 1 mol dm^{-3}) triethylamine in methanol (300 ml) at room temperature for 20 h.[14] The peptide was purified by preparative thin-layer chromatography (preparative TLC) on silica gel in *n*-BuOH–AcOH–H_2O (10 : 1 : 3 in vol.) and by gel filtration on Sephadex LH-20 in methanol. The purified peptide (**1**) showed a single spot (Pauly test, positive; ninhydrin test, negative) at R_f 0.29 on TLC in *n*-BuOH–AcOH–H_2O (10 : 1 : 3 in vol.). ^1H NMR

TABLE 1. SCHEDULE FOR THE SOLID PHASE SYNTHESIS

Step	Operation and reagent	Mixing time / min
1	$CHCl_3$, 45 ml (3 times)	1.5
2	25% trifluoroacetic acid/$CHCl_3$, 45 ml (once)	1.5
3	25% trifluoroacetic acid/$CHCl_3$, 45 ml (once)	30
4	$CHCl_3$, 45 ml (6 times)	1.5
5	10% triethylamine/$CHCl_3$, 45 ml (3 times)	1.5
6	$CHCl_3$, 45 ml (3 times)	1.5
7	CH_2Cl_2, 45 ml (3 times)	1.5
8	Boc-amino acid (3 equivalents) in CH_2Cl_2,[a] 22 ml, and 0.25 M DCC in CH_2Cl_2, 10 ml (once)	120
9	CH_2Cl_2, 45 ml (3 times)	1.5
10	$CHCl_3$, 45 ml (3 times)	1.5

a) The solvent of Boc-L-Cys(*S*-Acm)-OH was the mixture of CH_2Cl_2 (20 ml) and DMF (2 ml).

(D_2O, DMSO-d_6) and field desorption mass spectrometry (FDMS) spectral data were in good agreement with those of the expected structure. Amino acid analysis: Leu : His= 1.00 : 0.93, Cys was not determined correctly. Found: C, 51.20; H, 7.23; N, 16.22; S, 6.13%. Calcd for $C_{42}H_{68}N_{12}O_{11}S_2 \cdot 1/2C_2H_4O_2$: C, 51.09; H, 6.93; N, 16.63; S, 6.34%. The cyclization procedure was as follows. Boc-L-Cys(*S*-Acm)-D-Leu-L-His-L-Cys(*S*-Acm)-D-Leu-L-His-$NHNH_2$ was prepared from **1** (100 mg) by treatment with hydrazine hydrate (0.7 ml) in methanol (2 ml) for 12 h, followed by the removal of *t*-butoxycarbonyl (Boc) group with trifluoroacetic acid (1 ml) in the presence of dimethyl sulfide (0.2 ml) for 10 min. To a solution of H-L-Cys(*S*-Acm)-D-Leu-L-His-L-Cys(*S*-Acm)-D-Leu-L-His-$NHNH_2 \cdot 4CF_3COOH$ (*ca.* 100 mg) in DMF (1 ml) were added 6 M HCl in dioxane (0.07 ml) and isopentyl nitrite (0.02 ml) at −50 °C, and the mixture was stirred in an ice–salt bath until hydrazine test became negative (*ca.* 10 min).[15] The reaction mixture was then added drop by drop into cold pyridine (*ca.* 500 ml) in an ice–salt bath with vigorous stirring.[16] After stirring for an additional 30 min, it was allowed to stand at 4 °C for 48 h and then at room temperature for 12 h. After the solvent was evaporated under reduced pressure at 30—40 °C, the residue was purified by preparative TLC on silica gel in *n*-BuOH–AcOH–H_2O (10 : 1 : 3 in vol.) and by gel filtration on Sephadex LH-20 in methanol. The purified cyclic peptide (**2**) showed a single spot (Pauly test, positive; ninhydrin test, negative) at R_f 0.40 on TLC in *n*-BuOH–AcOH–H_2O (4 : 1 : 2 in vol.). ^1H NMR (D_2O, DMSO-d_6) and FDMS (*m/e*; 848) spectral data agreed well with those of the expected structure. Found: C, 47.68; H, 6.41; N, 17.50; S, 7.50%. Calcd for $C_{36}H_{56}N_{12}O_8S_2 \cdot 1/2\ C_2H_4O_2 \cdot 3H_2O$: C, 47.64; H, 6.87; N, 18.03; S, 6.87%.

Methods. CD spectra were measured on a JASCO J-20 or J-500 spectropolarimeter using 0.1 or 1 mm cells at room temperature. In the case of aqueous solutions, 0.1 M NaCl was contained. Proton NMR spectra were recorded on a Bruker CXP-300 FT NMR spectrometer operating in the pulsed Fourier transform mode at 300.07 MHz in a spinning 5 mm tube at room temperature. Sodium 2,2-dimethyl-2-silapentane-5-sulfonate (DSS) (0.00 ppm) was used as an internal reference in D_2O solution. In the case of methanol-d_4 solution, the solvent (4.78 ppm from DSS) was used as a reference.

Results

Figure 1 shows CD spectra of the linear peptide at

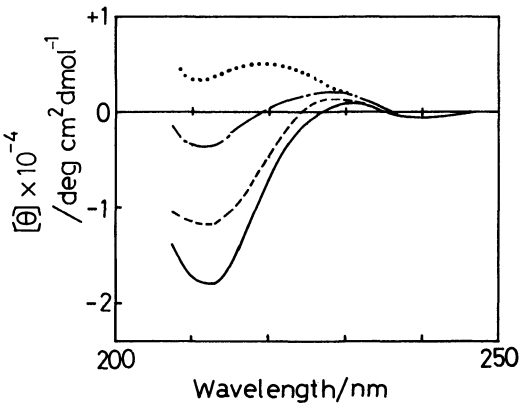

Fig. 1. CD spectra of Boc-(L-Cys(*S*-Acm)-D-Leu-L-His)$_2$-CCH_3 in H_2O: peptide concentration, 2.8×10^{-4} M; pH, 3.57 (——), 5.52 (------), 6.40 (—·—), 7.55 (……).

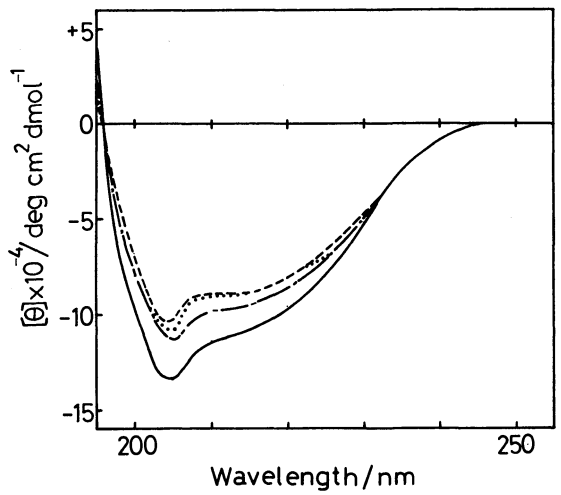

Fig. 2. CD spectra of *cyclo*-(L-Cys(*S*-Acm-D-Leu-L-His)$_2$ in H_2O: peptide concentration, 4.0×10^{-4} M; pH, 3.06 (——), 6.25 (—·—), 8.59 (----); in the presence of $ZnCl_2$ (4.0×10^{-3} M) at pH 6.25 (……).

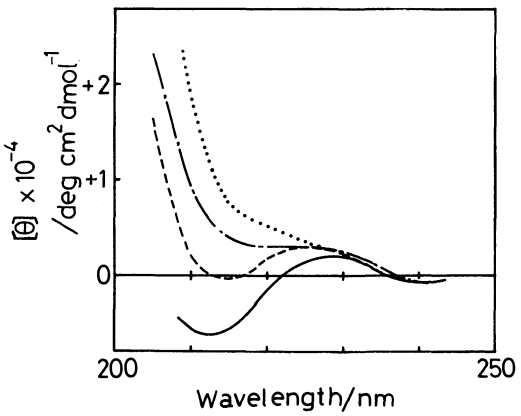

Fig. 3. CD spectra of Boc-L-(Cys(*S*-Acm)-D-Leu-L-His)$_2$-OCH_3 in H_2O: peptide concentration, 2.8×10^{-4} M; pH 6.25; $ZnCl_2$ concentration, 0 M (——), 2.8×10^{-4} M; (------), 5.6×10^{-4} M (—·—), 1.1×10^{-3} M (……).

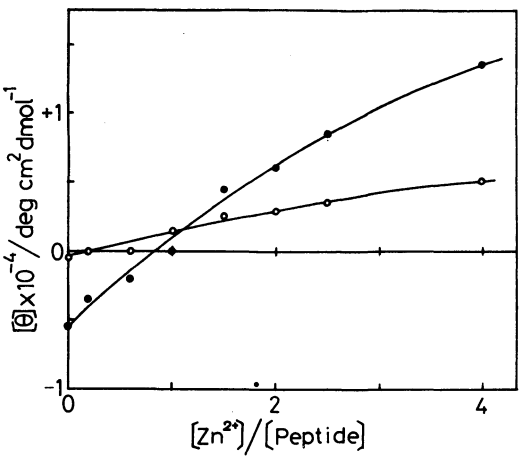

Fig. 4. Relation between molar ellipticity [θ] (deg cm^2 dmol^{-1}) and $[Zn^{2+}]$/[peptide] in H_2O: concentration of Boc-(L-Cys(*S*-Acm)-D-Leu-L-His)$_2$-OCH_3, 2.8×10^{-4} M; at 212 nm (—●—) and 220 nm (—○—).

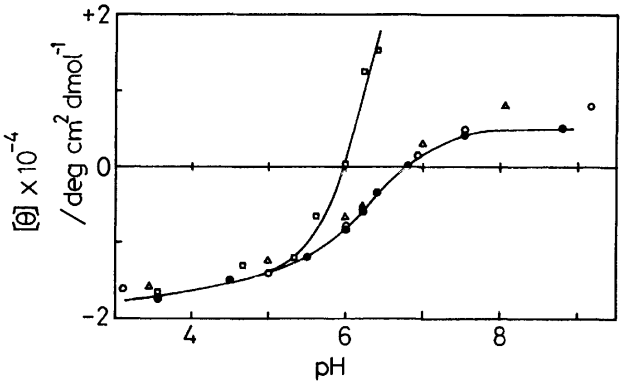

Fig. 5. Titration curves of molar ellipticity [θ] (deg cm^2 dmol^{-1}) at 212 nm of Boc-(L-Cys(*S*-Acm)-D-Leu-L-His)$_2$-OCH_3 in H_2O: peptide concentration, 2.8 $\times 10^{-4}$ M; metal salt free (-●-), 5.6×10^{-3} M $MgCl_2$ (-○-), 5.6×10^{-3} M $CaCl_2$ (-△-), 1.1×10^{-3} M $ZnCl_2$ (-□-).

Table 2. Chemical shift (ppm) of imidazolyl C-2 and C-5 protons of linear or cyclic peptides in D_2O at pD 6.22[a]

[Zn^{2+}]/[Peptide]	Linear peptide		Cyclic peptide	
	C-2	C-5	C-2	C-5
0	8.22	7.11	8.28	7.20
	8.15			
3	8.08	7.14	—	—
		6.98		
10	8.05	7.11	8.22	7.17
		6.95		

a) Peptide concentration, 1.0×10^{-3} M; sodium 2,2-dimethyl-2-silapentane-5-sulfonate (DSS) was used as an internal reference (0.00 ppm); C-2 and C-5 are numbered as in the following figure:

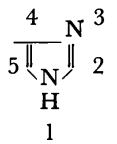

neutral and acidic pH regions. Remarkable CD changes dependent upon the pH values are noted. Thus, the CD peak around 218 nm observed at pH 7.55 is decreased when the pH value is decreased. Instead, a CD trough at 212 nm is to be seen at acidic pH regions.

In contrast to the pH-dependent CD spectra of the linear peptide, the CD trough observed from 205 nm to 230 nm of the cyclic peptide is much less pH-dependent as can be seen in Fig. 2. The CD magnitude of the cyclic peptide at pH 8.59 is increased by 20—30% when the pH is decreased to pH 3.06.

Effects of metal salts added to the peptide solutions were investigated at pH 6.25. Typical CD spectrum in the presence of Zn(II) is shown in Fig. 2 (dotted line) for the cyclic peptide. As can be seen, no remarkable CD spectral change is observed by adding Zn(II) to the cyclic peptide solution. Figure 3 shows the effects of Zn(II) on the CD spectra of the linear peptide. CD spectra of the linear peptide are markedly changed by adding Zn(II). The CD magnitudes of the linear peptide are correlated with the Zn(II) concentrations as is shown in Fig. 4 where the molar ellipticity [θ] at ordinate is the values at 212 and 220 nm. Additions of Ca(II) and Mg(II) to the linear peptide solution did not cause any marked change in the CD spectra. In Fig. 5 are shown the pH-titration curves of [θ] at 212 nm of the linear peptide in the presence or absence of the metal salts ($ZnCl_2$, $CaCl_2$, $MgCl_2$). In this case, $ZnCl_2$ brings about a characteristic titration curve in contrast with that of free form, while $CaCl_2$ and $MgCl_2$ essentially do not cause change in the titration curve.

Table 2 summarizes ^{1}H NMR signals of imidazole C-2 and C-5 protons of the linear and the cyclic peptides in D_2O at pD 6.22 (not corrected for isotope effects). The C-2 and C-5 signals of the both peptides as a whole move to high field by adding Zn(II). However, the C-5 signal at 7.11 ppm of the linear peptide splits to two signals at 7.11 and 6.95 ppm when the Zn(II) concentration is large excess against that of the linear

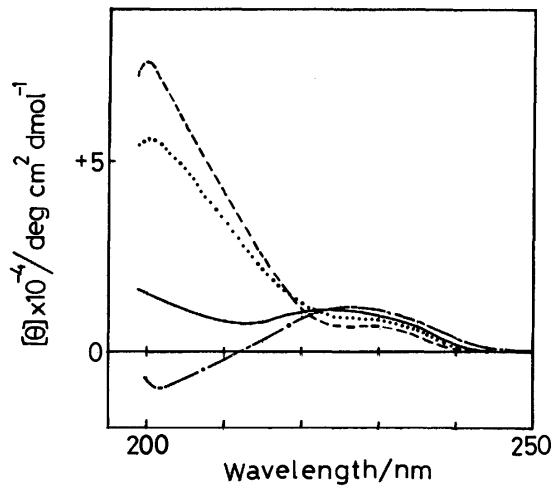

Fig. 6. CD spectra of Boc-(L-Cys(*S*-Acm)-D-Leu-L-His)$_2$-OCH_3 in MeOH: peptide concentration, 2.8×10^{-3} M ;metal salt free or 5.6×10^{-2} M $MgCl_2$ (——), 2.0×10^{-3} M $ZnCl_2$ (----), 2.8×10^{-2} M $ZnCl_2$ (……), 5.6×10^{-2} M $CaCl_2$ (—•—).

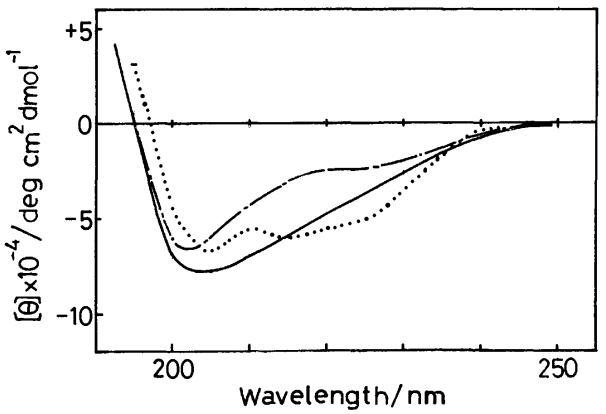

Fig. 7. CD spectra of *cyclo*-(L-Cys(*S*-Acm)-D-Leu-L-His)$_2$ in MeOH: peptide concentration, 4.0×10^{-4} M; metal salt free or 8.0×10^{-3} M $MgCl_2$ (——), 8.0×10^{-3} M $CaCl_2$ (……), 8.0×10^{-3} M $ZnCl_2$ (—•—).

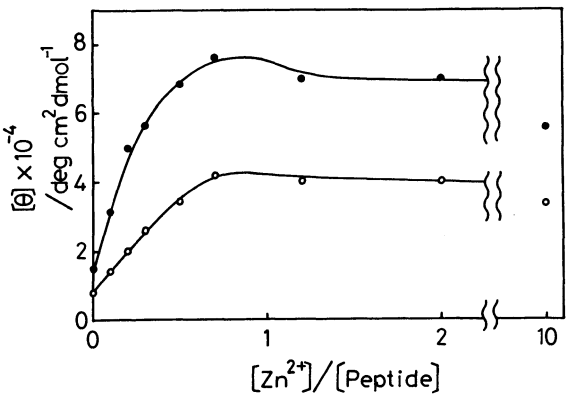

Fig. 8. Relation between molar ellipticity [θ] (deg cm^2 dmol^{-1}) and [Zn^{2+}]/[peptide] in MeOH: concentration of Boc-(L-Cys(*S*-Acm)-D-Leu-L-His)$_2$-OCH_3, 2.8×10^{-3} M; at 200 nm (—●—) and 210 nm (—○—).

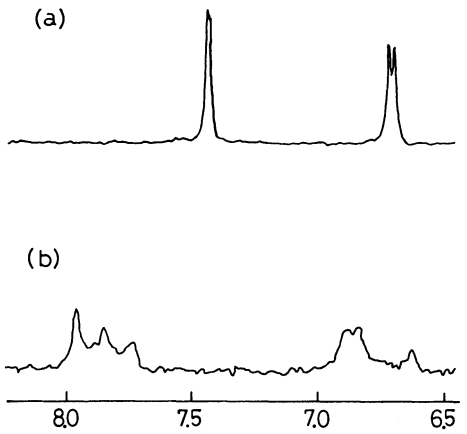

Fig. 9. ^{1}H NMR spectra of Boc-(L-Cys(*S*-Acm)-D-Leu-L-His)$_2$-OCH_3 in methanol-d_4: peptide concentration, 2.0×10^{-3} M; (a) in the absence of $ZnCl_2$, (b) in the presence of 2.0×10^{-3} M $ZnCl_2$.

peptide. In addition, the C-2 signals at 8.22 and 8.15 ppm of the linear peptide coalesce into a signal at 8.05 ppm by the Zn(II) addition.

In less polar solvent, such as methanol, Ca(II) or Mg(II) seems to coordinate with the linear and the cyclic peptides. Figures 6 and 7 show effects of metal cations on the CD spectra of those peptides in methanol. For the linear peptide, Ca(II) as well as Zn(II) brought about the spectral changes, while Mg(II) did not. However, the changes caused by Ca(II) are different from those by Zn(II), possibly because of the differences of the coordination structures between these two metal complexes. For the cyclic peptide, no remarkable CD spectral changes are noted by adding Mg(II), Ca(II) or Zn(II) (Fig. 7). The molar ellipticities [θ] at 200 and 210 nm are plotted against Zn(II)-linear peptide concentration ratios as shown in Fig. 8. One can see that [θ] increases rapidly until [Zn^{2+}]/[peptide] is *ca.* 0.7 and then decreases gradually.

Proton NMR spectra were measured in methanol-d_4, too. As Fig. 9 shows, Zn(II) causes the splitting and the broadening of the imidazolyl resonances of the linear peptide. For the cyclic peptide, the imidazolyl resonances are shifted to lower magnetic field without any significant signal broadenings (Table 3). Effects of Mg(II) and Ca(II) on the peptide NMR signals in methanol-d_4 are summarized in Table 3 for comparison.

TABLE 3. CHEMICAL SHIFT (ppm) OF LINEAR OR CYCLIC PEPTIDES IN METHANOL-d_4 IN THE PRESENCE OR ABSENCE OF METAL SALT[a]

Linear peptide[b]

Metal salt	His C-2	His C-5	OCH_3	Acm-CH_3	Boc-CH_3
Free	7.46	6.74	3.57	1.85	1.29
	7.45	6.71		1.83	
$MgCl_2$ 20 mM	7.52	6.75	3.57	1.85	1.29
	7.49			1.83	
$CaCl_2$ 20 mM	7.54	6.78	3.58	1.86	1.30
	7.51	6.76		1.85	
$ZnCl_2$ 2 mM[c]	7.96	6.89	3.64	1.84	1.30
	7.85	6.85	3.59		
	7.74	6.64			

Cyclic peptide[d]

Metal salt	His C-2	His C-5	Acm-CH_2		Leu[e] α-CH	Acm-CH_3
Free	7.45	6.72	4.31	4.11	3.92	1.84
			4.26	4.06		
$MgCl_2$ 24 mM	7.54	6.77	4.32	4.11	3.92	1.85
			4.28	4.07		
$CaCl_2$ 24 mM	7.57	6.81	4.30	4.17	3.99	1.87
			4.26	4.12		
$ZnCl_2$ 2.4 mM	7.79	7.42	4.35	4.27	4.08	1.85
			4.30	4.22		

a) Methanol-d_4 was used as a reference (4.78 ppm). b) Concentration, 2.0×10^{-3} M. c) Histidyl C-2 and C-5 proton resonances were broadened and split, so the chemical shift values described here are those of the representative resonances. d) Concentration, 2.4×10^{-3} M. e) Triplet resonances apparently.

Discussion

The CD spectra of both the cyclic and the linear peptides in aqueous solution shown in Figs. 1 and 2 can tell us conformational and/or electronic differences between the two types of peptides we studied. It is generally known that β-turn conformation can be seen in certain cyclic hexapeptides.[17,18] Therefore, there is a possibility that the cyclic peptide studied here may take a β-turn. However, the absorptions due to the low-energy band of the split amide π-π^* and the amide n-π^* transitions of the main chain seem to overlap with those due to the imidazolyl π-π^* and the Acm-amide π-π^* or n-π^* transitions of the side chains, and thus the detailed conformational analysis is difficult in the present study. It is shown that the CD spectra of the linear peptide vary remarkably with pH while those of the cyclic one change a little. This indicates that the conformation of the cyclic peptide is fairly rigid, while that of the linear peptide is flexible. For the linear peptide, the spectra at lower pH value might be ascribed to relatively extended conformations caused by electro-

static repulsion force between the charged imidazolyl groups, while those at high pH value might be attributed to less perturbated conformations. From Figs. 3—5, it is concluded that in aqueous solution Zn(II) is much more liable to be coordinated with the linear peptide compared with Ca(II) or Mg(II). On the other hand, the CD spectrum of the cyclic peptide is affected very little by $ZnCl_2$ as shown in Fig. 2, which also suggests the rigid conformation of the cyclic peptide. Since Zn(II) is a medium soft acid, it seems likely that Zn(II) is bound to histidyl imidazoles.

The binding of Zn(II) to histidyl imidazole is supported by the results of ^1H NMR spectra in deuterium oxide (D_2O) at pD 6.22 in that the imidazolyl C-2 and C-5 proton resonances in both the cyclic and the linear peptides were split or shifted on addition of Zn(II) as Table 2 shows. These resonances are shifted to higher magnetic field in general. The splitting in the linear peptide must be due to the environmental difference between the two imidazoles in the molecule.

The CD spectral changes of the linear peptide observed by adding Zn(II) in methanol are correlated with the Zn(II)/peptide concentration ratios as shown in Fig. 8. The first increasing stage of the titration trace observed at 200 or 210 nm is considered to be due to the formation of 1 : 2 ($[Zn^{2+}]$/[peptide]) complex and the next decreasing stage due to that of 1 : 1 or other complexes.

The NMR spectra changes of the linear peptide by adding Zn(II) (Fig. 9) will suggest that there are various populations of conformational isomers interconverting at or near the coalescence state on the NMR time scale. In contrast to this, the corresponding resonances of the cyclic peptide are shifted to lower magnetic field without significant broadening. This will suggest that the population of a certain isomer is predominant or that the interconversion between isomers is sufficiently rapid on the NMR time scale. In view of the conformational rigidity of the cyclic peptide, the former interpretation seems to be more reasonable. For both of the peptides, the magnitude of the induced shifts is as a whole in the order: Zn(II)> Ca(II)>Mg(II), except for the Acm-CH_3. From the Acm-CH_3 chemical shift, an appreciable effect of Ca(II) ion addition is noted. From these results, it seems likely that Ca(II) is bound to the Acm–amide carbonyl, but Zn(II) does not interact with the Acm–CONH group. These NMR findings suggest the structural differences between Zn(II) and Ca(II) peptide complexes, which have been implied by the CD findings.

In concluding remarks, CD and NMR findings offered convincing evidences that the cyclization of the peptide we studied makes the peptide conformation rigid, and the coordination ability of the peptide to metal cations markedly changes. It seems very likely, in addition, that the cyclization of the peptide reduces the differences in the coordination abilities among metal cations to the peptide. As has been shown in the present study, it seems to be very helpful to use the techniques of both CD and NMR, since CD offers the information about the overall structure of a molecule, while NMR offers that about the local structure of a molecule. Although ^1H NMR of the peptides was investigated in the present study, the NMR of the metal cations, such as ^{67}Zn(II),[19,20] ^{43}Ca(II),[19] or ^{25}Mg(II),[21] would be also very useful for the present study.

References

1) Y. A. Ovchinnikov, *Eur. J. Biochem.*, **94**, 321 (1979).
2) E. I. Solomon, J. W. Hare, D. M. Dooley, J. H. Dawson, P. J. Stephens, and H. B. Gray, *J. Am. Chem. Soc.*, **102**, 168 (1980).
3) J. E. Roberts, T. G. Brown, B. M. Hoffman, and J. Peisach, *J. Am. Chem. Soc.*, **102**, 825 (1980).
4) K. W. Penfield, R. R. Gay, R. S. Himmelwright, N. C. Eickman, V. A. Norris, H. C. Freeman, and E. I. Solomon, *J. Am. Chem. Soc.*, **103**, 4283 (1981).
5) D. W. Hughes and C. M. Deber, *Biopolymers*, **21**, 169 (1982).
6) V. Madison, C. M. Deber, and E. R. Blout, *J. Am. Chem. Soc.*, **99**, 4788 (1977).
7) T. Sugihara, Y. Imanishi, and T. Higashimura, *Biopolymers*, **15**, 1529 (1976).
8) D. G. Davis, B. F. Gisin, and D. C. Tosteson, *Biochemistry* **15**, 768 (1976).
9) Y. Sugiura and Y. Hirayama, *J. Am. Chem. Soc.*, **99**, 1581 (1977).
10) N. Ueyama, M. Nakata, and A. Nakamura, *Inorg. Chim. Acta*, **55**, L61 (1981).
11) G. F. Bryce, R. W. Roeske, and F. R. N. Gurd, *J. Biol. Chem.*, **241**, 1072 (1966).
12) W. N. Lipscomb, *Acc. Chem. Res.*, **3**, 81 (1970).
13) T. Fujii and S. Sakakibara, *Bull. Chem. Soc. Jpn.*, **47**, 3146 (1974).
14) H. C. Beyerman, H. Hindriks, and E. W. S. DeLeer, *Chem. Commun.*, **1968**, 1668.
15) J. Honzl and J. Rudinger, *Collect. Czech. Chem. Commun.*, **26**, 2333 (1961).
16) M. Ohno, K. Kuromizu, H. Ogawa, and N. Izumiya, *J. Am. Chem. Soc.*, **93**, 5251 (1971).
17) L. G. Pease, C. M. Deber, and E. R. Blout, *J. Am. Chem. Soc.*, **95**, 258 (1973).
18) K. D. Kopple, T. J. Schamper, and A. Go, *J. Am. Chem. Soc.*, **96**, 2597 (1974).
19) T. Shimizu and M. Hatano, *Biochem. Biophys. Res. Commun.*, **104**, 1356 (1982).
20) T. Shimizu, M. Kodaka, and M. Hatano, *Biochem. Biophys. Res. Commun.*, **106**, 988 (1982).
21) T. Shimizu and M. Hatano, *Biochem. Biophys. Res. Commun.*, **104**, 720 (1982).

Lewis Acid Mediated Synthesis of 2-Alkenenitriles Using *C,N*-Bis(trimethylsilyl)ketenimine and Carbonyl Compounds

Isamu MATSUDA,* Hisashi OKADA, and Yusuke IZUMI
Department of Synthetic Chemistry, Faculty of Engineering, Nagoya University, Furo-cho, Chikusa-ku, Nagoya 464
(Received June 23, 1982)

2-Substituted 2-alkenenitriles are obtained in the condensation reaction of carbonyl compounds with *C,N*-bis(trimethylsilyl)ketenimine in the presence of Lewis acid. The combination of tris(trimethylsilyl)ketenimine and aldehydes results in the high *E*-selective formation of 2-trimethylsilyl-2-alkenenitriles. Among some Lewis acids, magnesium bromide gives the best *E*-selectivity in the formation of 2-trimethylsilyl-2-undecenenitrile. Stereospecific protodesilylation of 2-trimethylsilyl-2-alkenenitriles in an aqueous methanol solution of potassium fluoride accomplishes a new route to (*Z*)-2-alkenenitriles from aldehydes.

2-Alkenenitriles have been prepared by the carbonyl olefination with various cyanated reagents under the basic conditions.[1–15] Of these reactions, the silicon methods suffers from the lack of the stereoselectivity in spite of the higher reactivity.[13,14] Introduction of bulky substituents on the silicon atom and exchange of counter cation, lithium to magnesium, are reported in order to circumvent the deficiency.[15] On the other hand, we reported a stereoselective synthesis of methyl 2-alkenoate in the reaction of *C,O*-bis(trimethylsilyl)ketene acetal with aldehydes under the acidic conditions.[16] The bulky trimethylsilyl group on the carbon atom plays an important role to control the stereochemical course in that reaction.

Although it is widely accepted that trimethylsilyl enol ethers behave as an effective C nucleophile in the presence of Lewis acid,[17] there are very few examples[18] of *N*-trimethylsilylketenimine derivatives as an equivalent of α-cyano carbanions. Therefore, it is interesting to reveal a C nucleophilic character of *N*-trimethylsilylketenimine derivatives and to explore the stereoselective route to **3** by use of the trimethylsilyl group as a key stereocontrolling factor. A recent report[18] prompts us to publish our results of the carbonyl olefination using *C,N*-bis(trimethylsilyl)ketenimine (**1**) and Lewis acid, in which 2-substituted 2-alkenenitriles (**4**, **5**, and **6**) are produced in one-pot reactions and 2-alkenenitriles (**3**) are formed *Z*-selectively by the subsequent protodesilylation of **4**.

Results and Discussion

Tris(trimethylsilyl)ketenimine (**1a**) reacted with an equivalent of aldehydes, acetals, and 2-octanone in the presence of an equivalent of $BF_3 \cdot Et_2O$ to give 2-trimethylsilyl-2-alkenenitriles (**4**) in good yields as shown in Table 1. The discrimination of both geometrical isomers in **4** was based on the chemical shift of the vinyl proton in the ^1H NMR spectra[19] and the ratio of the both isomers was determined by HPLC analyses. The reaction is susceptible to the steric environment around the electrophilic carbon, because **1a** is relatively hindered as a nucleophile. Acetal showed lower *E*-selectivity than the corresponding aldehydes (entries 5 and 6 in Table 1) and 2-octanone gave poor result in the yield and the stereoselectivity (entry 7 in Table 1). On the contrary, bis(trimethylsilyl)acetonitrile anion (**7**) derived from bis(trimethylsilyl)acetonitrile could not react with benzaldehyde to give **4c**. Therefore, **1a** is important as a synthon of **7**.

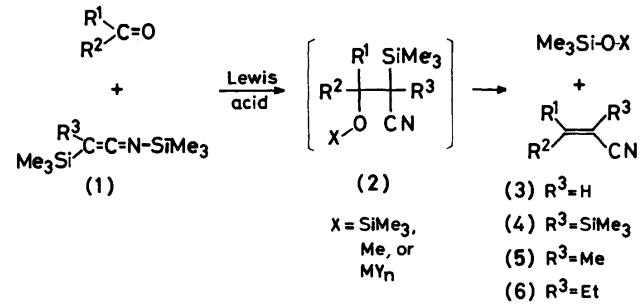

Scheme. 1

TABLE 1. CARBONYL OLEFINATION OF **1a** BY THE ASSIST OF $BF_3 \cdot Et_2O$

Entry	Carbonyl compound	4 Yield/% [a]	4 *E*/*Z* [b]
1	Nonanal	79	96/4
2	Heptanal	67	96/4
3	PhCHO	99	100/0[c]
4		64	95/5
5	$CH_3(CH_2)_7CH(OMe)_2$	90	81/19
6	$PhCH(OMe)_2$	89	98/2[c]
7	2-Octanone	45	66/34

a) Isolated yields. b) Determined by HPLC (UV 233 nm, porous silica, hexane/*i*-PrOH=150/1). c) Determined by HPLC (UV 254 nm, porous silica, hexane/*i*-PrOH=150/1).

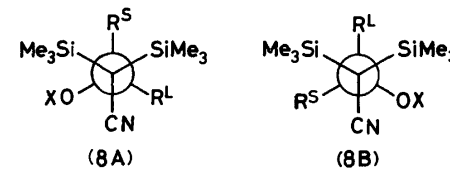

The present condensation proceeds through an intermediate such as aldol type adduct **2**, which is transformed to product **4** by the subsequent β-elimination of Me_3SiOX. The formation of both isomers (*E*)- and (*Z*)-**4** should be attributed to staggered conformers **8A** and **8B** because the *anti* elimination of β-hydroxy trimethylsilyl derivatives is well established[16,20] and the interconversion between *E* and *Z* isomers is not observed under the reaction conditions. Conformer **8A** would

Table 2. The effect of lewis acid in the condensation of **1a** with nonanal

Lewis acid	Solvent	Condition	**4a** Yield/%[a]	**4a** E/Z[b]
$BF_3 \cdot Et_2O$	CH_2Cl_2	−78 °C, 0.5 h ⟶ r.t. 3 h	79	96/4
$ZnCl_2$	C_6H_6/Et_2O = 5/8	r.t. 14 h	73	98/2
$MgBr_2$	C_6H_6/Et_2O = 5/12	r.t. 2 h ⟶ reflux 2.5 h	83	99/1
$TiCl_4$	CH_2Cl_2	−78 °C, 1 h ⟶ r.t. 2 h	47	99/1
$SnCl_4$	CH_2Cl_2	−78 °C, 2 h ⟶ r.t. 24 h	0	—
$MgCl_2$	C_6H_6/Et_2O = 5/12	r.t. 24 h	0	—

a) Isolated yields. b) Determined by HPLC (UV 233 nm, porous silica, hexane/*i*-PrOH=150/1).

be rather stabilized than **8B** because of the presence of two bulky trimethylsilyl groups on the same carbon atom. Therefore, the observed stereoselectivity can be attributed to the predominant presence of **8A** or much faster β-elimination in **8A** than in **8B**. Regardless of the manner (*syn* or *anti*) of Me_3SiOX elimination, respective conformer **8A** and **8B** corresponds specifically to (*E*)-**4** and (*Z*)-**4**. The thermodynamically controlled process would result in the greater stereochemical selectivity. Thus, several kinds of Lewis acid were compared in order to improve the stereoselectivity in the condensation of **1a** with nonanal. The results are summarized in Table 2. Excellent *E*-selectivity (*E*/*Z*= 99/1) was attained by the assist of magnesium bromide. The fruitful result obtained by magnesium bromide makes possible the application of this type condensation to more unstable aldehydes. For example, a reaction of 2-acetoxydecanal with **1a** gives **9** in 60% yield by the assist of magnesium bromide (Eq. 1). The structure of **9** might be convertible to furan and 2-buten-4-olide derivatives.

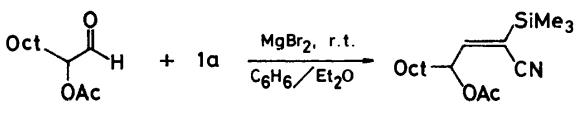

(9)

Protodesilylation of (*E*)-**4** in an aqueous methanol solution of potassium fluoride gave (*Z*)-**3** selectively. Interconversion of (*Z*)-**3** to (*E*)-**3** was not detected at all in the reaction conditions. The stereospecificity of the reaction is well explained by Koenig and Webers' mechanism.[21] Although a similar protodesilylation of vinylsilane was carried out by hydroiodic acid,[22] iodine and water,[22] or dry hydrogen chloride,[23] potassium fluoride is suitable for stereospecific protodesilylation of **4**. Since it is difficult to form (*Z*)-**3** selectively by Peterson type olefination of aldehydes with trimethylsilylacetonitrile anion,[14,15] the present two-steps method composed of **1a** and aldehydes provides a facile *Z*-selective route to 2-alkenenitriles (**3**).

A similar C-nucleophilicity of **1b** (R^3=Me) and **1c** (R^3=Et) was observed in the condensation with aldehydes. The reaction proceeded smoothly to give trisubstituted olefins **5** or **6** as a mixture of two geometrical isomers at room temperature in the presence of magnesium bromide. Even enolizable aldehydes such as nonanal and cyclohexanecarbaldehyde gave good results under the present conditions. Since *C,N*-bis(trimethylsilyl)ketenimines are easily prepared from α-unsubstituted nitriles,[24] this method could exploit a new general route to 2-substituted alkenenitriles. Experimental simplicity and mildness of conditions make the present method highly advantageous for the direct synthesis of 2-alkenenitriles **5** and **6** from aldehydes. In contrast, the reported methods include the reactions under strong basic conditions.[1-15] Although the stereochemistry could not be controlled in the formation of **5** and **6**, this problem might be solved by the kinetic control in the formation of the posturated intermediate **2**.

Experimental

All reactions were carried out under an atmosphere of argon. The IR spectra in carbon tetrachloride were recorded on a JASCO IR-403G. A JEOL C-60HL instrument was used to record the ^1H NMR spectra in carbon tetrachloride using tetramethylsilane as the internal standard. HPLC analyses were done on a JASCO TWINKLE equipped with a Model VL-611 injector and UVIDEC-100-II spectrophotometer. GLC analyses were performed on a Shimadzu GC-4BPT with TCD and a 2 m×3 mm i.d. column of 10% PEG-2M on Uniport B. Preparative TLC was carried out on precoated silica gel F-254 plates. Ketenimines, **1a**,[25] **1b**,[24] and **1c**[24] were prepared according to the literature. Magnesium bromide was prepared from 1,2-dibromoethane and magnesium in ether.

Condensation of ***1a*** *with Carbonyl Compounds in the Presence of* $BF_3 \cdot Et_2O$. *2-Trimethylsilyl-2-undecenenitrile (****4a****)*: A solution of **1a** (1.92 g, 7.47 mmol) in 15 ml of CH_2Cl_2 was added to a solution of nonanal (0.59 g, 4.16 mmol) and $BF_3 \cdot Et_2O$ (0.87 g, 6.20 mmol) in 20 ml of dry CH_2Cl_2 at −78 °C. The mixture was stirred for 30 min at −78 °C, gradually warmed to 20 °C, and stirred at the same temperature for 3 h. After quenching the mixture with saturated aqueous Na_2CO_3 (10 ml), the phases were separated and the aqueous layer was extracted with ethyl acetate (20 ml×4). The combined organic portions were washed with saturated brine (20 ml× 2), dried over anhydrous $MgSO_4$, and concentrated under reduced pressure. The residual oil was purified by column chromatography on silica gel using a mixed solvent (hexane/ethyl acetate=7/1) as an eluent and Kugelrohr distillation (65—70 °C/0.2 mmHg) [1 mmHg=133.322 Pa] to give 0.79 g (79%) of **4a** (*E*/*Z*=96/4) as a colorless liquid. Found: C, 70.58; H, 11.66; N, 5.95%. Calcd for $C_{14}H_{27}NSi$: C, 70.80; H, 11.46; N, 5.90%. Both isomers of **4a** were isolated, respectively, by a preparative TLC with hexane/etyl acetate (15/1).

(*E*)-**4a**: IR 2200 ($\nu_{C\equiv N}$), 1595 ($\nu_{C=C}$), and 1252 cm^{-1}

($\delta_{S\ Si-C}$). ^{1}H NMR δ 0.20 (s, 9H, Si-C$\underline{H}_3$), 0.85 (t, J=4.7 Hz, 3H, $CH_2C\underline{H}_3$), 1.1—1.5 (broad m, 12H), 2.39 (q, J=7.0 Hz, 2H, C=C-C$\underline{H}_2$), and 6.35 (t, J=6.8 Hz, 1H, C=C$\underline{H}$).

(*Z*)-**4a**: IR 2200 ($\nu_{C\equiv N}$), 1592 ($\nu_{C=C}$), and 1253 cm^{-1} ($\delta_{S\ Si-C}$). ^{1}H NMR δ 0.30 (s, 9H, Si-C$\underline{H}_3$), 0.90 (t, J=4.7 Hz, 3H, $CH_2C\underline{H}_3$), 1.1—1.7 (broad m, 12H), 2.26 (q, J=7.3 Hz, 2H, C=C-C$\underline{H}_2$), and 6.99 (t, J=7.8 Hz, 1H, C=C$\underline{H}$).

4a: An analogous treatment of **1a** (0.502 g, 1.95 mmol) with 1,1-dimethoxynonane (0.198 g, 1.05 mmol) and $BF_3\cdot Et_2O$ (0.220 g, 1.55 mmol) in CH_2Cl_2 (10 ml) gave **4a** (0.225 g, 90%, E/Z=81/19).

*2-Trimethylsilyl-2-nonenenitrile (**4b**)*: An analogous treatment of **1a** (0.932 g, 3.61 mmol) with heptanal (0.182 g, 1.60 mmol) and $BF_3\cdot Et_2O$ (0.34 g, 2.40 mmol) in CH_2Cl_2 (15 ml) gave **4b** as a colorless liquid (bp 53 °C/0.15 mmHg, 0.224 g, 67%, E/Z =96/4). Found: C, 68.70; H, 10.96; N, 6.70% Calcd for $C_{12}H_{23}NSi$: C, 68.83; H, 11.07; N, 6.69%.

(*E*)-**4b**: IR 2200 ($\nu_{C\equiv N}$), 1595 ($\nu_{C=C}$), and 1253 cm^{-1} ($\delta_{S\ Si-C}$). ^{1}H NMR δ 0.23 (s, 9H, Si-C$\underline{H}_3$), 0.91 (t, J=5.3 Hz, 3H, $CH_2C\underline{H}_3$), 1.1—1.4 (broad m, 8H), 2.44 (q, J=7.5 Hz, 2H, C=C-C$\underline{H}_2$), and 6.45 (t, J=7.5 Hz, 1H, C=C$\underline{H}$).

(*Z*)-**4b**: IR 2200 ($\nu_{C\equiv N}$), 1592 ($\nu_{C=C}$), and 1252 cm^{-1} ($\delta_{S\ Si-C}$). ^{1}H NMR δ 0.29 (s, 9H, Si-C$\underline{H}_3$), 0.92 (t, J=5.3 Hz, 3H, $CH_2C\underline{H}_3$), 1.1—1.6 (broad m, 8H), 2.31 (q, J=7.4 Hz, 2H, C=C-C$\underline{H}_2$), and 7.09 (t, J=7.4 Hz, 1H, C=C$\underline{H}$).

*3-Phenyl-2-trimethylsilylpropenenitrile (**4c**)*: An analogous treatment of **1a** (0.981 g, 3.80 mmol) with benzaldehyde (0.209 g, 1.97 mmol) and $BF_3\cdot Et_2O$ (0.400 g, 2.83 mmol) in CH_2Cl_2 (15 ml) gave **4c** as a colorless liquid (bp 88 °C/0.5 mmHg, 0.398 g, 99%, E/Z=100/0). Found: C, 71.64; H, 7.72; N, 7.05%. Calcd for $C_{12}H_{15}NSi$: C, 71.58; H, 7.51; N. 6.96%.

(*E*)-**4c**: IR 2200 ($\nu_{C\equiv N}$), 1590 ($\nu_{C=C}$), and 1254 cm^{-1} ($\delta_{S\ Si-C}$). ^{1}H NMR δ 0.32 (s, 9H, Si-C$\underline{H}_3$), 7.02 (s, 1H, C=C$\underline{H}$), and 7.2—8.0 (m, 5H, $C_6\underline{H}_5$).

4c: An analogous treatment of **1a** (0.861 g, 3.34 mmol) with dimethoxyphenylmethane (0.326 g, 2.14 mmol) and $BF_3\cdot Et_2O$ (0.390 g, 2.75 mmol) in CH_2Cl_2 (17 ml) gave **4c** (0.382 g, 89%, E/Z=98/2).

*3-Cyclohexyl-2-trimethylsilylpropenenitrile (**4d**)*: An analogous treatment of **1a** (0.987 g, 3.80 mmol) with cyclohexanecarbaldehyde (0.204 g, 1.82 mmol) and $BF_3\cdot Et_2O$ (0.390 g, 2.80 mmol) in CH_2Cl_2 (14 ml) gave **4d** as a colorless liquid (bp 57 °C/0.2 mmHg, 0.241 g, 64%, E/Z=95/5). Found: C, 69.48; H, 10.26; N, 6.78%. Calcd for $C_{12}H_{21}NSi$: C, 69.50; H, 10.21; N, 6.75%.

(*E*)-**4d**: mp 42—42.5 °C. IR 2200 ($\nu_{C\equiv N}$), 1595 ($\nu_{C=C}$), and 1250 cm^{-1} ($\delta_{S\ Si-C}$). ^{1}H NMR δ 0.21 (s, 9H, Si-C$\underline{H}_3$), 0.7—2.0 (m, 10H), 2.3—3.0 (m, 1H, C=C-C$\underline{H}$), and 6.24 (d, J=9.1 Hz, 1H, C=C$\underline{H}$).

(*Z*)-**4d**: IR 2200 ($\nu_{C\equiv N}$), 1588 ($\nu_{C=C}$), and 1252 cm^{-1} ($\delta_{S\ Si-C}$). ^{1}H NMR δ 0.30 (s, 9H, Si-C$\underline{H}_3$), 0.7—2.0 (m, 10H), 2.0—2.6 (m, 1H, C=C-C$\underline{H}$), and 6.80 (d, J=10.5 Hz, 1H, C=C$\underline{H}$).

*3-Methyl-2-trimethylsilyl-2-nonenenitrile (**4e**)*: An analogous treatment of **1a** (0.977 g, 3.79 mmol) with 2-octanone (0.251 g, 1.96 mmol) and $BF_3\cdot Et_2O$ (0.390 g, 2.75 mmol) in CH_2Cl_2 (12 ml) gave **4e** as a colorless liquid (bp 80 °C/0.4 mmHg, 0.197 g, 45%, E/Z=66/34). Found: C, 69.72; H, 11.19; N, 6.10%. Calcd for $C_{13}H_{25}NSi$: C, 69.88; H, 11.28; N, 6.27%.

(*E*)-**4e**: IR 2200 ($\nu_{C\equiv N}$), 1595 ($\nu_{C=C}$), and 1252 cm^{-1} ($\delta_{S\ Si-C}$). ^{1}H NMR δ 0.28 (s, 9H, Si-C$\underline{H}_3$), 0.90 (t, J=4.5 Hz, 3H, $CH_2C\underline{H}_3$), 1.1—1.6 (broad m, 8H), 1.93 (s, 3H, C=C-C$\underline{H}_3$), and 2.44 (broad t, J=6.9 Hz, 2H, C=C-C$\underline{H}_2$).

(*Z*)-**4e**: IR 2200 ($\nu_{C\equiv N}$), 1595 ($\nu_{C=C}$), and 1252 cm^{-1} ($\delta_{S\ Si-C}$). ^{1}H NMR δ 0.28 (s, 9H, Si-C$\underline{H}_3$), 0.91 (t, J=4.5 Hz, 3H, $CH_2C\underline{H}_3$), 1.1—1.6 (broad m, 8H), 2.13 (s, 3H, C=C-C$\underline{H}_3$), and 2.24 (broad t, J=7 Hz, 2H, C=C-C$\underline{H}_2$).

*Condensation of **1a** with Nonanal in the Presence of Various Lewis Acids.* Analogous reactions of **1a** with nonanal were carried out on a 3 mmol scale in the presence of $ZnCl_2$, $MgBr_2$, $TiCl_4$, $SnCl_4$, and $MgCl_2$, respectively. Reaction conditions, yields of **4a**, and ratios of *E* and *Z* isomers are summarized in Table 2.

*Protodesilylation of **4** with Potassium Fluoride. 2-Undecenenitrile (**3a**)*: To a solution of (*E*)-**4a** (0.263 g, 1.11 mmol) in methanol (8 ml) was added potassium fluoride (0.460 g, 7.92 mmol) and water (0.7 ml). The clear homogenized solution was stirred for 12 h at room temperature and concentrated under reduced pressure. The residue contained water was diluted with ethyl acetate (70 ml). The solution was washed with water (20 ml×2), dried ($MgSO_4$), and concentrated under reduced pressure. The residual oil was purified by Kugelrohr distillation to give **3a** as a colorless liquid (bp 70 °C/0.2 mmHg,[26] 0.178 g, 97%, E/Z=0/100). Found: C, 79.86; H, 11.71; N, 8.31%. Calcd for $C_{11}H_{19}N$: C, 79.94; H, 11.59; N, 8.48%. IR 2240 ($\nu_{C\equiv N}$) and 1622 cm^{-1} ($\nu_{C=C}$). ^{1}H NMR δ 0.89 (t, J=4.5 Hz, 3H, $CH_2C\underline{H}_3$), 1.1—1.6 (broad m, 12H), 2.42 (d of t, J=7.5 and 7.5 Hz, 2H, C=C-C$\underline{H}_2$), 5.21 (t of d, J=1.5 and 10.8 Hz, 1H, C=C$\langle^{\underline{H}}_{CN}$), and 6.36 (t of d, J=7.5 and 10.8 Hz, 1H, $NC\rangle C=C\langle^{\underline{H}}$).

A crude product obtained by a condensation reaction of **1a** (0.969 g, 3.76 mmol), nonanal (0.452 g, 3.18 mmol), and $MgBr_2$ (0.759 g, 4.12 mmol) in a mixed solvent of benzene (15 ml) and diethyl ether (5 ml) was treated with potassium fluoride (1.865 g, 32.1 mmol) in methanol (20 ml) and water (1.5 ml). After an analogous treatment to (*E*)-**4a**, pure **3a** (0.457 g, 87% based on nonanal, E/Z=1/99) was obtained.

*Cinnamonitrile (**3c**)*: An analogous protodesilylation of (*E*)-**4c** (0.260 g, 1.29 mmol) gave **3c**[14] (0.159 g, 95%, E/Z= 0/100).

*3-Cyclohexylpropenenitrile(**3d**)*: An analogous protodesilylation of (*E*)-**4d** (0.138 g, 0.665 mmol) gave **3d** as a colorless liquid (bp 110 °C/7 mmHg, 0.086 g, 96%, E/Z=0/100). Found: C, 79.82; H, 9.51; N, 10.42%. Calcd for $C_9H_{13}N$: C, 79.95; H, 9.69; N, 10.36%. IR 2230 ($\nu_{C\equiv N}$) and 1622 cm^{-1} ($\nu_{C=C}$). ^{1}H NMR δ 0.9—2.0 (m, 10H), 2.4—2.8 (broad m, 1H, C=C-C$\underline{H}$), 5.12 (d, J=11.3 Hz, 1H, C=C$\langle^{\underline{H}}_{CN}$), and 6.18 (d of d, J=9.5 and 11.3 Hz, 1H, $NC\rangle C=C\langle^{\underline{H}}$).

*Condensation of **1a** with 2-Acetoxydecanal in the Presence of $MgBr_2$.* To a solution of $MgBr_2$ prepared from Mg (0.035 g, 1.44 mgatm) and 1,2-dibromoethane (0.336 g, 1.79 mmol) in benzene (3.5 ml) and diethyl ether (3.5 ml) were added 2-acetoxydecanal (0.200 g, 0.93 mmol) and **1a** (0.467 g, 1.81 mmol) successively at room temperature. The mixture was stirred for 3 h at room temperature, refluxed for 1 h, and poured into ethyl acetate (80 ml). The solution was washed with water (20 ml×2), dried ($MgSO_4$), and concentrated under reduced pressure. The residual oil was treated analogously to the case of **4a** to give pure (*E*)-**9** as a colorless liquid (bp 100 °C/0.9 mmHg, 0.172 g, 60%). Found: C, 65.93; H, 10.35; N, 4.52%. Calcd for $C_{17}H_{31}NO_2Si$: C, 65.97; H, 10.10; N, 4.53%. IR 2200 ($\nu_{C\equiv N}$), 1750 ($\nu_{C=O}$), and 1254 cm^{-1} ($\delta_{S\ Si-C}$). ^{1}H NMR δ 0.26 (s, 9H, Si-C$\underline{H}_3$), 0.90 (t, J=5.1 Hz, 3H, $CH_2C\underline{H}_3$), 1.1—1.8 (m, 17H), 2.07 (s, 3H, C(=O)-C$\underline{H}_3$), 5.46 (q, J=6.6 Hz, 1H, O-C$\underline{H}$), and 6.31 (d, J=6.6 Hz, 1H, C=C$\underline{H}$).

*Condensation of **1b** with Aldehydes in the Presence of $MgBr_2$. 2-Methyl-2-undecenenitrile (**5a**)*:[27] Nonanal (0.159 g, 1.12 mmol) and **1b** (0.549 g, 2.76 mmol) were added successively

into a solution of $MgBr_2$ (0.315 g, 1.70 mmol) in benzene (4 ml) and diethyl ether (9 ml) at room temperature. The mixture was stirred for 4h at the same temperature and poured into ethyl acetate (70 ml). The solution was washed with water (20 ml×2), dried ($MgSO_4$), and concentrated under reduced pressure. The residual oil was dissolved in methanol (7 ml). Acidic ammonium fluoride (0.223 g, 5.87 mmol) was added into the solution. The homogeneous solution obtained by the addition of water (0.8 ml) was stirred for 10 min at room temperature and concentrated under reduced pressure. The residue was poured into ethyl acetate (80 ml). The solution was washed with water (15 ml×2), dried ($MgSO_4$), and concentrated under reduced pressure. The residual oil was purified by column chromatography through short pad of silica gel (eluent; hexane/ethyl acetate, 5/1) and Kugelrohr distillation to give **5a** as a colorless liquid (bp 85 °C/2 mmHg, 0.196 g, 98%, E/Z=69/31).

(*E*)-**5a**: IR 2210 ($\nu_{C\equiv N}$) and 1640 cm^{-1} ($\nu_{C=C}$). ^1H NMR δ 0.88 (t, J=5.1 Hz, 3H, $CH_2C\underline{H}_3$), 1.0—1.5 (m, 12H), 1.83 (d, J=1.8 Hz, 3H, C=C–C$\underline{H}_3$), 1.9—2.4 (m, 2H, C=C–C$\underline{H}_2$), and 6.15 (q of t, J=1.8 and 7.5 Hz, 1H, C=C$\underline{H}$).

(*Z*)-**5a**: IR 2210 ($\nu_{C\equiv N}$) and 1640 cm^{-1} ($\nu_{C=C}$). ^1H NMR δ 0.88 (t, J=5.1 Hz, 3H, $CH_2C\underline{H}_3$), 1.0—1.5 (m, 12H), 1.91 (d, J=1.8 Hz, 3H, C=C–C$\underline{H}_3$), 2.0—2.6 (m, 2H, C=C–C$\underline{H}_2$), and 5.93 (q of t, J=1.8 and 7.8 Hz, 1H, C=C$\underline{H}$).

*2-Methyl-3-phenylpropenenitrile (**5c**)*:[6,28,29] An analogous treatment of **1b** (0.861 g, 4.33 mmol) with benzaldehyde (0.136 g, 1.28 mmol) gave **5c** as a colorless liquid (0.150 g, 82%, E/Z =38/62).

*3-Cyclohexyl-2-methylpropenenitrile (**5d**)*:[27] An analogous treatment of **1b** (0.517 g, 2.60 mmol) with cyclohexanecarbaldehyde (0.165 g, 1.47 mmol) gave **5d** as a colorless liquid (bp 135 °C/22 mmHg, 0.187 g, 86%, E/Z=55/45).

(*E*)-**5d**: IR 2210 ($\nu_{C\equiv N}$) and 1640 cm^{-1} ($\nu_{C=C}$). ^1H NMR δ 0.8—1.9 (m, 10H), 1.86 (d, J=1.8 Hz, 3H, C=C–C$\underline{H}_3$), 2.1—2.8 (m, 1H, C=C–C$\underline{H}$), and 6.02 (q of d, J=1.8 and 11.2 Hz, 1H, C=C$\underline{H}$).

(*Z*)-**5d**: IR 2210 ($\nu_{C\equiv N}$) and 1640 cm^{-1} ($\nu_{C=C}$). ^1H NMR δ 0.8—1.9 (m, 10H), 1.90 (d, J=1.8 Hz, 3H, C=C–C$\underline{H}_3$), 2.1—2.8 (m, 1H, C=C–C$\underline{H}$), and 5.83 (q of d, J=1.8 and 9.9 Hz, 1H, C=C$\underline{H}$).

*Condensation of **1c** with Aldehydes in the Presence of $MgBr_2$. 2-Ethyl-2-undecenenitrile(**6a**)*: A reaction of **1c** (0.736 g, 3.45 mmol) with nonanal (0.429 g, 3.01 mmol) in the presence of $MgBr_2$ (0.642 g, 3.39 mmol) gave **6a** as a colorless liquid analogously to the case of **5a** (bp 90 °C/0.75 mmHg, 0.358 g, 62%, E/Z=43/57). Found: C, 80.54; H, 12.13; N, 7.05%. Calcd for $C_{13}H_{23}N$: C, 80.76; H, 11.99; N, 7.24%. IR 2215 ($\nu_{C\equiv N}$) and 1630 cm^{-1} ($\nu_{C=C}$). ^1H NMR δ 0.91 (t, J=6.0 Hz, 3H, $CH_2C\underline{H}_3$), 1.16 (t, J=7.5 Hz, 3H, $CH_2C\underline{H}_3$), 1.0—1.5 (broad m, 12H), 2.23 (q, J=7.5 Hz, 4H, 2×C$\underline{H}_2$$CH_3$), 6.06 (t, J=7.5 Hz, $\underline{H}\rangle C=C\langle_{CN}$), and 6.21 (t, J=7.5 Hz, $\underline{H}\rangle C=C\langle_{CN}$).

*2-Ethyl-3-phenylpropenenitrile (**6c**)*: An analogous treatment of **1c** (0.361 g, 1.69 mmol) with benzaldehyde (0.162 g, 1.53 mmol) gave **6c** as a pale yellow liquid (bp 90 °C/0.2 mmHg, 0.156 g, 65%, E/Z=65/35). Found: C, 83.86; H, 7.14; N, 8.69%. Calcd for $C_{11}H_{11}N$: C, 84.04; H, 7.05; N, 8.91%. IR 2220 ($\nu_{C\equiv N}$) and 1620 cm^{-1} ($\nu_{C=C}$). ^1H NMR δ 1.26 (t, J=7.8 Hz, 3H, $CH_2C\underline{H}_3$), 2.41 (q, J=7.8 Hz, 2H, $C\underline{H}_2CH_3$), 6.79 (s, $\underline{H}\rangle C=C\langle_{CN}$), 7.02 ($\underline{H}\rangle C=C\langle_{CN}$), and 7.2—7.6 (m, $C_6\underline{H}_5$).

*3-Cyclohexyl-2-ethylpropenenitrile (**6d**)*: An analogous treatment of **1c** (0.739 g, 3.46 mmol) with cyclohexanecarbaldehyde (0.326 g, 2.91 mmol) gave **6d** as a colorless liquid (bp 85 °C/0.2 mmHg, 0.276 g, 58%, E/Z=32/68). Found: C, 80.67; H, 10.62; N, 8.64%. Calcd for $C_{11}H_{17}N$: C, 80.92; H, 10.50; N, 8.58%. IR 2210 ($\nu_{C\equiv N}$) and 1630 cm^{-1} ($\nu_{C=C}$). ^1H NMR δ 1.15 (t, J=7.2 Hz, 3H, $CH_2C\underline{H}_3$), 1.0—1.9 (m, 10H), 2.0—2.7 (m, 3H, C=C–C$\underline{H}_2$ and C=C–C$\underline{H}$), 5.84 (t of d, J=1.2 and 9.3 Hz, $\underline{H}\rangle C=C\langle_{CN}$) and 6.01 (t of d, J=0.9 and 9.0 Hz, $\underline{H}\rangle C=C\langle_{CN}$).

The authors thank Mr. Yoshimi Fukutani for an experimental assistance, Shinetsu Chemical Co. for the supply of chlorotrimethylsilane, and Sumitomo Electric Industries Co. for the supply of fluoropore.

References

1) G. P. Schiemenz and H. Engelhard, *Chem. Ber.*, **94**, 578 (1961).
2) S. Trippett and D. M. Walker, *J. Chem. Soc.*, **1961**, 1266.
3) W. S. Wadsworth, Jr. and W. D. Emmons, *J. Am. Chem. Soc.*, **83**, 1733 (1961).
4) G. Jones and R. F. Maisey, *Chem. Commun.*, **1968**, 543.
5) J. H. Babler and T. R. Mortell, *Tetrahedron Lett.*, **1972**, 669.
6) B. Deschamps, G. Lefebvre, and J. Seyden-Penne, *Tetrahedron*, **28**, 4209 (1972).
7) A. Redjal and J. Seyden-Penne, *Tetrahedron Lett.*, **1974**, 1733.
8) C. Piechucki, *Synthesis*, **1974**, 869.
9) A. Loupy, K. Sogadji, and J. Seyden-Penne, *Synthesis*, **1977**, 126.
10) B. Deschamps, J. P. Lampin, F. Mathey, and J. Seyden-Penne, *Tetrahedron Lett.*, **1977**, 1137.
11) S. A. DiBiase and G. W. Gokel, *Synthesis*, **1977**, 629.
12) F. Texier-Boullet and A. Foucaud, *Synthesis*, **1979**, 884.
13) I. Ojima, M. Kumagai, and Y. Nagai, *Tetrahedron Lett.*, **1974**, 4005.
14) I. Matsuda, S. Murata, and Y. Ishii, *J. Chem. Soc., Perkin Trans. I*, **1979**, 26.
15) Y. Yamakado, M. Ishiguro, N. Ikeda, and H. Yamamoto, *J. Am. Chem. Soc.*, **103**, 5568 (1981).
16) I. Matsuda and Y. Izumi, *Tetrahedron Lett.*, **22**, 1805 (1981).
17) T. Mukaiyama, *Angew. Chem., Int. Ed. Engl.*, **16**, 817 (1977).
18) Y. Sato and Y. Niinomi, *J. Chem. Soc., Chem. Commun.*, **1982**, 56.
19) L. H. Jackman and S. Sternhell, "Application of Nuclear Magnetic Resonance Spectroscopy in Organic Chemistry," 2nd ed, Pergamon Press, Oxford (1969), p. 185.
20) P. F. Hudrlik and D. Peterson, *J. Am. Chem. Soc.*, **97**, 1464 (1975).
21) K. E. Koenig and W. P. Weber, *J. Am. Chem. Soc.*, **95**, 3416 (1973).
22) K. Utimoto, M. Kitai, and H. Nozaki, *Tetrahedron Lett.*, **1975**, 2825.
23) T. H. Chan, W. Mychajlowskij, B. S. Ong, and D. N. Happ, *J. Organomet. Chem.*, **107**, C1 (1976).
24) D. S. Watt, *Synth. Commun.*, **4**, 127 (1974).
25) C. R. Krueger and E. G. Rochow, *Angew. Chem., Int. Ed. Engl.*, **2**, 617 (1963); G. A. Gornowicz and R. West, *J. Am. Chem. Soc.*, **93**, 1714 (1971).

26) Y. Okamoto, T. Nitta, and H. Sakurai, *Bull. Chem. Soc. Jpn.*, **42**, 543 (1969).
27) K. Tanaka, N. Ono, Y. Kubo, and A. Kaji, *Synthesis* **1979**, 890.
28) E. J. Moriconi and C. C. Jabandoni, *J. Org. Chem.*, **35**, 3796 (1970).
29) T. Funabiki, H. Hosomi, S. Yoshida, and K. Tarama, *J. Am. Chem. Soc.*, **104**, 1560 (1982).

Photochemical Nitrogen Extrusion of 5-Amino-1-vinyl-4,5-dihydro-1*H*-1,2,3-triazoles. Formation of Unusual Pyrroles[1)]

Masato M. Ito, Yujiro Nomura,* Yoshito Takeuchi, and Shuji Tomoda
Department of Chemistry, College of General Education, The University of Tokyo, Komaba, Meguro-ku, Tokyo 153
(Received June 23, 1982)

Photolysis of 4-alkyl-5-amino-1-vinyl-4,5-dihydro-1*H*-1,2,3-triazoles gave not 3-alkylpyrroles, but unexpected 2-alkylpyrroles in 80—83% yields. 1-Vinylaziridines were assumed as a possible intermediate of this unusual pyrrole formation. In the photolysis of 7a-morpholino-1-styryl-3a,4,5,6,7,7a-hexahydro-1*H*-1,2,3-benzotriazole, however, nitrogen extrusion did not occur, but *trans-cis* isomerization took place.

Three reaction paths are expected in decomposition of 1-vinyl-4,5-dihydro-1*H*-1,2,3-triazoles (**1**) after elimination of nitrogen as shown in Scheme 1: The first is a 1,2-alkyl (or hydrogen) shift to N^2-vinylamidines (**2**) (path a), the second is a direct ring closure to form 1-vinylaziridines (**3**) (path b), and the third is formation of a C–C bond between C-4 of the dihydrotriazole and β-position of the vinyl group to give 1-pyrrolines (**4**) (path c). The N^2-vinylamidines have a 2-aza-1,3-butadiene skeleton, of which no general synthetic method has yet been developed, although its reactivity as a heterodiene has recently attracted attentions,[2-5)] and 1-vinylaziridines are only sparsely reported class of compounds.[6,7)]

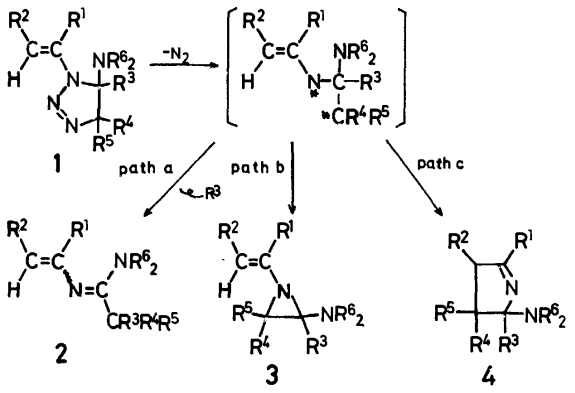

Scheme 1. Expected paths for N_2 extrusion reactions of 1-vinyldihydrotriazoles (**1**).

Recently we reported that thermolysis[4)] or acid decomposition[8)] of **1** gave the corresponding N^2-vinylamidines (**2**) *via* path a, in accord with the general trends of 5-aminotriazolines.[9)] In order to elucidate the different reactivity of **1** in different conditions as well as the possibility of controlling reaction paths, we have examined the photo decomposition of the dihydrotriazoles (**1**).

Results and Discussion

Formation of Unusual Pyrroles. The dihydrotriazoles (**1**) were irradiated in methanol at 0 °C with a 100 W high-pressure mercury lamp through a Pyrex filter. The results were shown in Table 1. In 45—140 min **1** was completely consumed, and chromatographic separation of the products gave the 1*H*-pyrroles (**5**) or 2*H*-pyrroles (**6**) in 19—83% yields (Runs 5—8). The pyrroles (**5** or **6**) were not detected among the initial products just after irradiation. This suggests that the pyrroles were formed by deamination during the chromatographic separation from certain initial products, possibly 1-pyrrolines (**7**).

Irradiation of **1a** was carried out in various solvents, but no significant difference was observed either in time required for complete consumption of **1a** or in yields of the pyrrole (**5a**) (Runs 1—5).

Table 1. Photolysis of 5-amino-1-vinyl-4,5-dihydro-1*H*-1,2,3-triazoles (**1**)

Run	Reactant	R^1	R^2	R^3	R^4	R^5	NR^6_2	Solvent	Irradiation time / min	Product (Yield/%)
1	**1a**	Ph	H	H	CH_3	H	N⟨ ⟩	*cyclo*-C_6H_{12}	60	**5a** (73)
2	**1a**							CH_2Cl_2	75	**5a** (83)
3	**1a**							Et_2O	75	**5a** (56)
4	**1a**							CH_3CN	60	**5a** (81)
5	**1a**							CH_3OH	45	**5a** (83)
6	**1b**	Ph	H	$(CH_2)_4$		H	N⟨ ⟩	CH_3OH	140	**5b** (73)
7	**1c**	Ph	H	H	C_2H_5	H	N⟨ ⟩	CH_3OH	45	**5c** (80)
8	**1d**	H	Ph	Ph	H	H	N⟨ ⟩O	CH_3OH	60	**5d** (19)
9	**1e**	Ph	H	H	CH_3	CH_3	N⟨ ⟩	CH_3OH	60	**6e** (70)
10	**1f**	H	Ph	H	CH_3	CH_3	N⟨ ⟩	CH_3OH	45	**6f** (74)

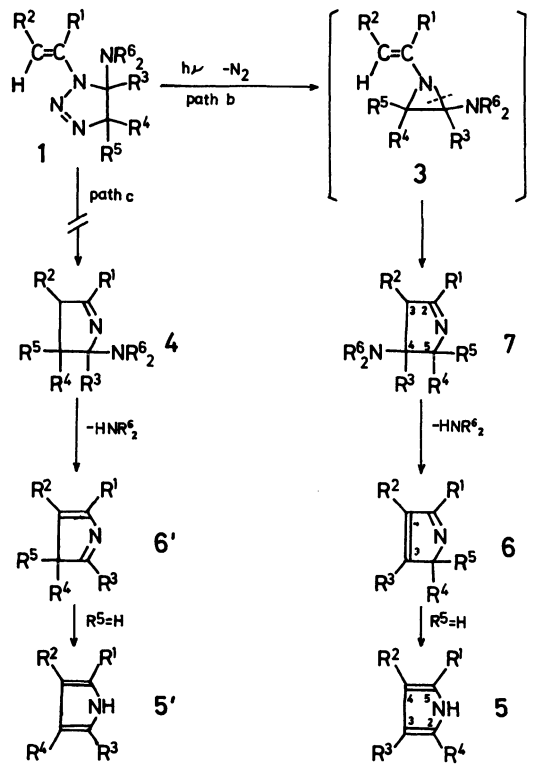

Scheme 2. A tentative route for the photolysis of 1-vinyldihydrotriazoles (**1**).

Table 2. ^{13}C NMR data of pyrroles (**5**) and 1-pyrrolines (**7**) (δ in $CDCl_3$)

	C-2[a]	C-3[a]	C-4[a]	C-5[a]
5a	128.0 s	(106.2 d	108.0 d)[b]	130.7 s
5b	128.4 s	118.8 s	105.2 d	130.1 s
5c	136.1 s	(106.5 d	106.6 d)[b]	131.0 s
5d	117.6 d	123.3 s	123.3 s	117.6 d
7a	170.1 s	40.2 t	69.5 d	72.2 d
7b	171.5 s	38.5 t	65.6 s	72.8 d
7e	167.8 s	40.7 t	73.1 d	73.5 s

a) Numbers referred to Scheme 2. b) Or may be reversed.

The 2*H*-pyrroles (**6e**, **f**) formed from **1** (**e**, **f**) (Runs 9, 10) were the same as those formed by thermolysis of **1** (**e**, **f**).[4] Structure of 1*H*-pyrroles (**5**) was determined by spectral and analytical results. In the case of **5a**, for instance, existence of an N–H bonds was indicated by the absorption at 3290 cm^{-1} in its IR spectrum. In ^1H NMR, the singlet at δ 2.28 (3H) and the signals at δ 7.3—7.8 (5H) indicated the existence of methyl and phenyl groups, and it was unequivocally demonstrated by ^{13}C NMR that the product was a 2,5-disubstituted pyrrole (Table 2). The signals at δ 106.2 and 108.0 (both are doublet in off-resonance decoupling) are assigned to the methine carbons of the pyrrole ring by two reasons: a) The signal of 3- or 4-methine carbon of pyrrole appears at δ 108,[10] and b) alkyl and aryl substituents on a pyrrole ring have little influence upon chemical shift of its ring carbons which are not connected with these substituents.[11] Thus, it was demonstrated that the product was 2-methyl-5-phenylpyrrole (**5a**). ^{13}C NMR data pertinent to structural confirmation of other pyrroles (**5b—d**) were also listed in Table 2.

In the case of **1e**, 5,5-dimethyl-2-phenyl-4-(1-pyrrolidinyl)-1-pyrroline (**7e**) was isolated among the irradiation products. Mixtures of the 1-pyrrolines (**7a**, **b**) and the corresponding pyrroles (**5a**, **b**) could be afforded from the irradiation products of **1a**, **b**.

^{13}C NMR data corresponding to the pyrrolines (**7a**, **b**, **e**) were collected in Table 2. Both of two signals corresponding to C-4 and C-5 of the 1-pyrroline ring appeared at about δ 70, thus supporting the structure of 1-pyrrolines (**7**) in which C-4 and C-5 are connected with a pyrrolidine and a pyrroline nitrogen atoms, respectively. The 1-pyrrolines (**7**) were gradually deaminated into the corresponding 1*H*-pyrroles (**5**) or the 2*H*-pyrrole (**6e**) by repeated chromatographic separation or simply on standing at ambient temperature.

These results, together with the fact that no pyrroles were detected among the initial irradiation products, indicate that it was 1-pyrrolines (**7**) that were directly formed by photolysis of **1**.

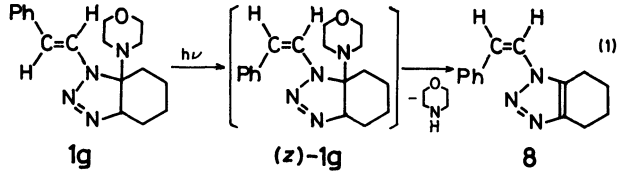

trans-cis *Isomerization by Irradiation of 7a-Morpholino-1-styryl-3a,4,5,6,7,7a-hexahydro-1*H*-1,2,3-benzotriazole (**1g**).* Irradiation of 7a-morpholino-1-[(*E*)-styryl]-3a,4,5,6,7,7a-hexahydro-1*H*-1,2,3-benzotriazole (**1g**) took relatively long time (4.5 h) until **1g** was completely consumed, compared with other dihydrotriazoles (**1a**—**f**). Chromatographic separation of the products gave, accompanied by considerable amount of polymeric substances, 1-[(*Z*)-styryl]-4,5,6,7-tetrahydro-1*H*-1,2,3-benzotriazole (**8**) in 13% yield.

It is likely to consider that irradiation caused C=C bon isomerization into 1-(*Z*)-styryldihydrotriazole ((*Z*)-**1g**) and subsequent chromatographic separation resulted in deamination to give **8**. Although *trans-cis* photoisomerization of C=C bond is quite usual,[12] this is the only case, so far as examined, in which C=C bond isomerization of 1-vinyldihydrotriazole derivatives (**1**) actually occurred (and pyrrole ring (**5**) was not formed).

Mechanistic Consideration. It is unusual that photolysis of **1** gave 1-pyrrolines (**7**), 1*H*-pyrroles (**5**) or 2*H*-pyrroles (**6**) and that no pyrrolines (**4**), 1*H*-pyrroles (**5'**) or 3*H*-pyrroles (**6'**), which were expected from a direct 1,5-ring closure after loss of nitrogen from **1** (path c), were isolated from the irradiation products. The path including the 1-vinylaziridines (**3**) as an intermediate was tentatively assumed to rationalize most simply the formation of 1-pyrrolines (**7**) by photolysis of **1**: After removal of nitrogen, the 1-vinylaziridines (**3**) would be formed *via* path b. Then, selective ring cleavage of **3** at one of the C–N bonds under the reaction conditions followed by ring closure would give **7** as

depicted in Scheme 2. The amino group on the aziridine ring would play a crucial role for the selective C–N bond cleavage.

Photolysis of 4,5-dihydro-1*H*-1,2,3-triazoles is known to give aziridines.[13] Scheiner claims that this reaction proceeds *via* a singlet biradical intermediate.[14] Absence of solvent effect on consumption of **1** (Table 1, Runs 1—5) may indicate a similar radical path in the first stage of the present reaction.

De Poortere and De Schryver reported the formation of 2-dialkylamino-1-phenylaziridines by photolysis of 5-dialkylamino-1-phenyl-4,5-dihydro-1*H*-1,2,3-triazoles.[15] Some 1-vinylaziridines have been prepared from vinyl azides by thermal reactions.[7] Comparing the present results with the stability of 2-amino- and 1-vinylaziridines, if the present reaction really proceeds *via* the 1-vinylaziridines (**3**), the aziridines (**3**) must be unexpectedly unstable.

Both C–C and C–N bond fissions were reported for photolysis of aziridine derivatives, but C–C fission predominantly occurs.[16] The present reaction may add an example of photochemical selective C–N bond fission of an aziridine ring.

Experimental

General. Melting points were determined on a Mitamura Riken hot-stage melting point apparatus and were uncorrected. Infrared spectra were determined on JASCO DS-403G and A-202 grating infrared spectrophotometers. Nuclear magnetic resonance spectra were determined on JEOL MH-100, FX-90Q, Varian EM-390, and FT-80A spectrometers (splitting patterns in ^{13}C NMR data were obtained by off-resonance decoupling). Mass spectra were determined on a Hitachi RMU-6MG mass spectrometer.

4,5-Dihydro-1*H*-1,2,3-triazoles (**1**) were prepared according to the previously reported method.[17] Solvents were distilled under anhydrous conditions before use.

Photolysis of 5-Amino-1-vinyl-4,5-dihydro-1H-1,2,3-triazoles (1). General Procedure: The solution (150 ml) of **1** (3—3.7 mmol) in an appropriate solvent was irradiated with a high pressure mercury lamp (100 W) through a Pyrex filter at 0 °C under nitrogen atmosphere until **1** was completely consumed, as detected by high pressure liquid chromatography (through a Waters 7.8 mm × 30 mm μ-Bondapak C_{18} column eluting with methanol–water (7 : 3)). The solvent was removed *in vacuo* and the residue was separated with column chromatography.

When the neutral alumina (Akt. II) column eluting with hexane–ethyl acetate (2 : 1) was used, 5,5-dimethyl-4-(1-pyrrolidinyl)-1-pyrroline (**7e**) was isolated from the product from **1e**. Separation of the products from **1a**, **b** in a similar manner also gave the pyrrolines (**7a**, **b**), which were accompanied by the pyrroles (**5a**. **b**).

Photolysis of 1-(1-Phenylvinyl)-7a-(1-pyrrolidinyl)-3a,4,5,6,7,7a-hexahydro-1H-1,2,3-benzotriazole (1b): Photolysis of **1b** (1.30 g, 4.39 mmol) in methanol (150 ml) at 0 °C followed by chromatographic purification with neutral alumina (Woelm, Akt. II) eluting with diethyl ether gave 1.10 g of 80 : 20 mixture of 2-phenyl-3a-(1-pyrrolidinyl)-3a,4,5,6,7,7a-hexahydro-3*H*-indole (**7b**) and 2-phenyl-4,5,6,7-tetrahydroindole (**5b**). Elution of the mixture through a neutral alumina (Akt. I) column eluting with dichloromethane gave 480 mg (73% yield) of **5b** as colorless crystals.

2-Phenyl-4,5,6,7-tetrahydroindole (5b): Analytically pure sample was obtained by recrystallization from methanol: mp 105—106.5 °C; MS *m/e* 197 (M^+); IR (KBr) 3405 cm^{-1} (N–H); ^{1}H NMR ($CDCl_3$) δ 1.6—1.9 (4H, m), 2.3—2.7 (4H, m), 6.21 (1H, d, J=3 Hz), 7.0—7.4 (5H, m), and 7.75 (1H, br, NH); ^{13}C NMR ($CDCl_3$) δ 22.8 (2C, t), 23.4 (t), 23.7 (t), 105.2 (d), 118.8 (s), 123.3 (*m*-2C, d), 125.4 (*p*-C, d), 128.4 (s), 128.7 (*o*-2C, d), 130.1 (s), and 133.2 (*ipso*-C, s).

Found: C, 85.08; H, 7.83; N, 7.12%. Calcd for $C_{14}H_{15}N$: C, 85.24; H, 7.66; N, 7.10%.

2-Phenyl-3a-(1-pyrrolidinyl)-3a,4,5,6,7,7a-hexahydro-3H-indole (7b): MS *m/e* 268 (M^+); IR (neat) 1600 cm^{-1} (C=N); ^{1}H NMR ($CDCl_3$) δ 1.1—2.1 (12H, m), 2.4—2.8 (4H, m), 2.64 (1H, dd, J=17 and 1 Hz), 2.95 (1H, dd, J=17 and 1 Hz), 4.15 (1H, m), 7.3—7.7 (3H, m), and 7.8—8.1 (2H, m); ^{13}C NMR ($CDCl_3$) δ 20.8 (2C, t), 23.6 (2C, t), 28.4 (t), 31.6 (t), 38.5 (t), 47.1 (2C, t), 65.6 (s), 72.8 (d), 127.3 (*m*-2C, d), 128.3 (*o*-2C, d), 130.2 (*p*-C, d), 135.0 (*ipso*-C, s), and 171.5 (s, C=N).

2-Methyl-5-phenylpyrrole (5a): Sublimed at 80—90 °C/13 Pa; mp 92.5—94 °C; MS *m/e* 157 (M^+); IR (KBr) 3290 cm^{-1} (NH); ^{1}H NMR ($CDCl_3$) δ 2.28 (3H, s), 5.95 (1H, m), 6.41 (1H, m), 7.3—7.8 (5H, m), and 8.4 (1H, br, NH); ^{13}C NMR ($CDCl_3$) δ 13.2 (q), 106.2 (d), 108.0 (d), 123.4 (*m*-2C, d), 125.6 (*p*-C, d), 128.0 (s), 128.8 (*o*-2C, d), 130.7 (s), and 133.0 (*ipso*-C, s).

Found: C, 84.33; H, 7.05; N, 9.19%. Calcd for $C_{11}H_{11}N$: C, 84.04; H, 7.05; N, 8.91%.

5-Methyl-2-phenyl-4-(1-pyrrolidinyl)-1-pyrroline (7a): Obtained by elution of the photolysis product from **1a** (220 mg, 0.86 mmol) through neutral alumina (Woelm Akt. II) with hexane–ethyl acetate (2 : 1) as a 65 : 35 mixture (150 mg) with **5a**. ^{13}C NMR ($CDCl_3$) δ 21.4 (q), 23.3 (2C, t), 40.2 (t), 52.0 (2C, t), 69.5 (d), 72.2 (d), 127.5 (*m*-2C, d), 128.4 (*o*-2C, d), 130.4 (*p*-C, d), 134.5 (*ipso*-C, s), and 170.1 (s, C=N).

5,5-Dimethyl-2-phenyl-4-(1-pyrrolidinyl)-1-pyrroline (7e): MS *m/e* 242 (M^+); IR (KBr) 1615 cm^{-1} (C=N); ^{1}H NMR ($CDCl_3$) δ 1.22 (3H, s), 1.49 (3H, s), 1.8 (4H, m), 2.6 (5H, m), 3.0 (2H, d, J=8 Hz), 7.4 (3H, m), and 7.8 (2H, m); ^{13}C NMR ($CDCl_3$) δ 21.3 (q), 23.3 (2C, t), 29.4 (q), 40.7 (t), 54.2 (2C, t), 73.1 (s), 73.6 (d), 127.3 (*m*-2C, d), 128.2 (*o*-2C, d), 130.1 (*p*-C, d), 134.8 (*ipso*-C, s), 167.8 (s, C=N).

2-Ethyl-5-phenylpyrrole (5c): Sublimed at 45 °C/130 Pa; mp 47—48.5 °C; MS *m/e* 171 (M^+); IR (KBr) 3390 cm^{-1} (N–H); ^{1}H NMR ($CDCl_3$) δ 1.17 (3H, t, J=7.5 Hz), 2.42 (2H, q, J=7.5 Hz), 5.95 (1H, m), 6.40 (1H, m), 7.1—7.6 (5H, m), 7.9—8.3 (1H, br, NH); ^{13}C NMR ($CDCl_3$) δ 14.1 (q), 21.4 (t), 106.5 (d), 106.6 (d), 123.8 (*m*-2C, d), 126.0 (*p*-C, d), 129.2 (*o*-2C, d), 131.0 (s), 133.4 (*ipso*-C, s), 136.1 (s).

Found: C, 84.46; H, 7.78; N, 8.04%. Calcd for $C_{12}H_{13}N$: C, 84.17; H, 7.65; N, 8.18%.

3,4-Diphenylpyrrole (5d): Distilled with the Kugelrohr apparatus at 115 °C/13 Pa; mp 94.5—95.5 °C (lit, 99 °C[18]); MS *m/e* 219 (M^+); IR (KBr) 3420 cm^{-1} (N–H); ^{1}H NMR ($CDCl_3$) δ 6.79 (2H, d, J=3 Hz), 7.2—7.4 (10H, m), 8.18 (1H, br, NH); ^{13}C NMR ($CDCl_3$) δ 117.6 (2C, d), 123.3 (2C, s), 125.7 (*p*-2C, d), 128.2 (*m*-4C, d), 128.5 (*o*-4C, d), and 136.0 (*ipso*-2C, s).

Found: C, 87.81; H, 5.75; N, 6.35%. Calcd for $C_{16}H_{13}N$: C, 87.64; H, 5.98; N, 6.39%.

Photolysis of 7a-Morpholino-1-[(E)-styryl]-3a,4,5,6,7,7a-hexahydro-1H-1,2,3-benzotriazole (1g): Methanol (150 ml) solution of **1g** (824 mg, 2.64 mmol) was irradiated with a high pressure mercury lamp (100 W) through a Pyrex filter at 0 °C for 4.5 h, until **1g** was completely consumed. The methanol was removed *in vacuo* and the residue was separated with alumina column chromatography to give 1-[(*Z*)-styryl]-4,5,6,7-tetrahydro-1*H*-1,2,3-benzotriazole (**8**) in 13% yield (73 mg). Recrystallized from methanol: mp 91.5—92.5 °C; MS *m/e*

225 (M^+); IR (KBr) 1650 (C=C) and 940 cm^{-1} ($^{H}\!>\!C=C\!<^{H}$); ^1H NMR ($CDCl_3$) δ 1.5—1.8 (4H, m), 2.0—2.2 (2H, m), 2.6—2.8 (2H, m), 6.63 (1H, d, J=9.5 Hz), 6.85 (1H, d, J=9.5 Hz), 6.8—7.0 (2H, m), and 7.1—7.3 (3H, m); ^{13}C NMR ($CDCl_3$) δ 20.3 (t), 21.8 (t), 22.3 (t), 22.5 (t), 121.5 (d, PhCH=) 128.6 (d, *o* and *m*), 128.8 (d), 129.6 (d), 132.7 (s), 133.1 (s), 143.4 (s).

Found: C, 74.17; H, 6.60; N, 18.36%. Calcd for $C_{14}H_{15}N_3$; C, 74.64; H, 6.71; N, 18.65%.

References

1) For preliminary communication, see: M. M. Ito, Y. Nomura, Y. Takeuchi, and S. Tomoda, *Chem. Lett.*, **1981**, 1519.

2) A. Demoulin, H. Gorissen, A.-M. Hesbain-Frisque, and L. Ghosez, *J. Am. Chem. Soc.*, **97**, 4409 (1975).

3) S. D. Worley, K. G. Taylor, B. Venugopalan, and M. S. Clark, Jr., *Tetrahedron*, **34**, 833 (1978).

4) Y. Nomura, Y. Takeuchi, S. Tomoda, and M. M. Ito, *Bull. Chem. Soc. Jpn.*, **54**, 2779 (1981).

5) Some synthetically useful methods appeared recently; T. Kauffmann, U. Koch, F. Sternseifer, and A. Vahrenhorst, *Tetrahedron Lett.*, **1977**, 3341; A. K. Dehnel, J. P. Finet, and G. Lavielle, *Synthesis*, **1977**, 474; H. Böhme and A. Ingendoh, *Chem. Ber.*, **112**, 1297 (1979); R. Gompper and U. Heinemann, *Angew. Chem., Int. Ed. Engl.*, **19**, 217 (1980); **20**, 296 (1981).

6) W. E. Truce and D. G. Brady, *J. Org. Chem.*, **31**, 3543 (1966); W. E. Truce and L. D. Markley, *ibid.*, **35**, 3275 (1970); T. Sasaki, T. Yoshida, and K. Shoji, *J. Chem. Soc., C*, **1969**, 1086; E. L. Stogryn and S. J. Brois, *J. Am. Chem. Soc.*, **89**, 605 (1967); M. A. Calgagno and E. E. Schweizer, *J. Org. Chem.*, **43**, 4207 (1978).

7) Y. Nomura, N. Hatanaka, and Y. Takeuchi, *Chem. Lett.*, **1976**, 901; A. Hassner, B. A. Belinka, Jr., M. Haber, and P. Munger, *Tetrahedron Lett.*, **22**, 1863 (1981).

8) M. M. Ito, Y. Nomura, Y. Takeuchi, and S. Tomoda, *Bull. Chem. Soc. Jpn.*, **56**, 641(1983).

9) R. Fusco, G. Bianchetti, and D. Pocar, *Gazz. Chim. Ital.*, **91**, 933 (1961); R. Huisgen, L. Mobius, and G. Szeimies, *Chem. Ber.*, **98**, 1138 (1965).

10) F. J. Weigert and J. D. Roberts, *J. Am. Chem. Soc.*, **90**, 3543 (1968); R. J. Pugmire and D. M. Grant, *ibid.*, **90**, 4232 (1968).

11) J. B. Stothers, "Carbon-13 NMR Spectroscopy," Academic Press, New York (1972), Chaps. 6 and 7.

12) N. J. Turro, "Modern Molecular Photochemistry," Benjamin/Cummings Co., (1978), Chap. 12, p. 473.

13) G. L'abbé, *Chem. Rev.*, **68**, 345 (1968), and references cited therein.

14) P. Scheiner, *J. Am. Chem. Soc.*, **88**, 4759 (1966).

15) M. De Poortere and F. C. De Schryver, *Tetrahedron Lett.*, **1970**, 3949.

16) R. Huisgen, W. Scheer, and H. Huber, *J. Am. Chem. Soc.*, **89**, 1753 (1967); H. Nozaki, S. Fujita, and R. Noyori, *Tetrahedron*, **24**, 2193 (1968); A. Padwa and L. Hamilton, *J. Am. Chem. Soc.*, **87**, 1821 (1965); **89**, 1761 (1967); A. Padwa and W. Eisenhardt, *ibid.*, **90**, 2442 (1968).

17) Y. Nomura, Y. Takeuchi, S. Tomoda, and M. M. Ito, *Bull. Chem. Soc. Jpn.*, **54**, 261 (1981).

18) M. Friedman, *J. Org. Chem.*, **30**, 859 (1965).

 © 1983 The Chemical Society of Japan Bull. Chem. Soc. Jpn., 56, 537—541 (1983)

Simple Synthesis and Chemicophysical Properties of Polyoxa[*n*]-ferrocenophanes and Its Alkali Metal Complexes

Sadatoshi AKABORI,* Yoichi HABATA, Yhoko SAKAMOTO, Masaru SATO,† and Seiji EBINE††

Department of Chemistry, Toho University, Funabashi, Chiba 274

†*Chemical Analysis Center, Saitama University, Urawa, Saitama 338*

††*Department of Chemistry, Saitama University, Urawa, Saitama 338*

(Received July 3, 1982)

Polyoxaferrocenophanes were synthesized by a one-pot reaction of 1,1′-diacetoxyferrocene with dichloride. Crystalline 1 : 1 complexes of **3a** with LiSCN, NaSCN, and KSCN were isolated. The ^{1}H-NMR and Mössbauer spectra of these complexes suggest the possibility of a certain interaction between the iron atom of the ferrocene nuclei and complexed cation. The new type of ferrocenophane **3a** extracts a thallium ion most effectively, the extractability of several metal ions being in this order; $Tl^+ > Rb^+ > K^+ > Cs^+ > Na^+$.

Although a number of crown ethers and benzo crown ethers have already been reported,[1] polyoxa[*n*]ferrocenophane and its homologs are rare.[2] Polyoxa[*n*]-ferrocenophane (**3**) is a crown ether-like compound including ferrocene subunit as a ring member; in it, the iron atom may act as a coordinatable heteroatom. Therefore, it is of interest to know what kind of interaction can be expected between the iron atom and the complexed cation. With regard to this expectation, several groups of workers[2] have synthesized this type of compounds. Biernat *et al.*[3] have recently reported the preparation of **3** and concluded, on the basis of their electronic spectral data, that there is no interaction between **3b** and the rubidium cation in methanol. On the other hand, we ourselves previously observed a certain interaction between the iron atom of oxathia-ferrocenophane and the complexed silver ion.[4] We now wish to report on a facile modified Williamson synthesis and some chemicophysical properties of **3** and alkali metal complexes of **3a** and **3b**.

Synthesis of 3a—e. The hydrolysis of **1** was carried out under a nitrogen atmosphere by the usual method. A mixture of the potassium salt of 1,1′-dihydroxyferrocene with the dihalide (**2**) in 60% ethanol was refluxed for 5 h. In every case, cyclization proceeded smoothly to afford the desired product, **3**, in a 25—60% yield. Many other products were also observed, but not confirmed because of their tiny amounts. The yields and physical properties of **3** are summarized in Table 1. The results suggest that the yields of **3** remarkably are dependent on the size of the rings, decreasing in this order: $n=4>3>2>1>0$. It is considered that the potassium cation acts as a template in the cyclization, as has been mentioned by Green.[5] It is noteworthy that this new method for preparing **3** directly starting from **1** avoids the isolation of very unstable 1,1′-dihydroxyferrocene[6] and that the yield of **3** is much higher than that in the Biernat method.[3] The structures of these compounds have been assigned on the basis of the following evidence. The IR spectrum of **3** indicates ether-linkage absorption near 1125 cm^{-1} and ferrocene-ring CH absorption near 1440 cm^{-1}, but no absorption attributable to hydroxyl or carbonyl groups. The UV spectra of **3** (λ_{max} (MeOH) 438 nm) suggest the presence of ferrocene nucleus. The mass spectra show the corresponding molecular ion. The electronic, ^{1}H-NMR, and ^{13}C-NMR spectral data are listed in Table 2. However, our ^{1}H-NMR spectra of **3a—d** are completely different from the data in the literature.[3] For example, Biernat *et al.*[3] reported that the ^{1}H-NMR spectrum of **3a** in $CDCl_3$ showed the ferrocene-ring protons at δ 3.35—3.45 as two doublets (J=6.25 Hz), together with methylene protons at δ 3.50—3.60 as multiplet. In the ^{1}H-NMR spectrum of **3a** (Table 2), the signals at δ 4.14 and 3.86 as triplets (J=2.0 Hz) are attributable to α- and β-protons of cyclopentadienyl rings,[7] while the two singlets at δ 3.70 and 3.78 and the two triplets at δ 3.86 and 4.05 (J=4.6 Hz) are attributable to the methylene protons of macrocycle. Furthermore, the ^{13}C-NMR, electronic and mass spectra and microanalysis data also support the idea that the structures of **3a—c** assigned by us are

TABLE 1. YIELDS, MASS-SPECTRAL DATA, AND PHYSICOCHEMICAL PROPERTIES OF COMPOUNDS **3a—e**

Compound	Mp θ_m/°C (lit)	Yield %	Molecular formula MW	Mass spectra M^+	Found(%) C	Found(%) H	Calcd(%) C	Calcd(%) H
3a	40—41 (oil)	60	$C_{20}H_{28}O_6Fe$ 420.3	420	57.08	6.81	57.14	6.67
3b	60—61 (59—60.5)	58	$C_{18}H_{24}O_5Fe$ 376.2	376	57.50	6.40	57.45	6.38
3c	58—59 (oil)	50	$C_{16}H_{20}O_4Fe$ 332.2	332	57.75	6.13	57.83	6.02
3d	120—121 (119—120)	32	$C_{14}H_{16}O_3Fe$ 288.1	288	58.38	5.78	58.33	5.56
3e	129—131	26	$C_{12}H_{12}O_2Fe$ 244.1	244	59.08	5.12	59.02	4.92

Table 2. ^{1}H-, ^{13}C-NMR, and electronic spectral data of compounds **3a—e**

Compound	^{1}H-NMR (200 MHz, $CDCl_3$)	^{13}C-NMR (22.5 MHz, $CDCl_3$)	λ_{max}/nm(ε)
3a	4.14 (4H, t, J=2.0 Hz, H_α), 3.86 (4H, t, J=2.0 Hz, H_β), 3.70 (4H, s, OCH_2CH_2), 3.78 (8H, s, OCH_2CH_2O), 3.86 (4H, *t*, J=4.6 Hz) and 4.05 (4H, t, J=4.6 Hz, OCH_2CH_2)[b]	127.1 (C_b),[a] 56.2 (C_α), 61.9 (C_β), 71.2, 70.6, 70.1 (methylene)	438 (127)
3b	4.15 (4H, t, J=2.0 Hz, H_α), 3.86 (4H, t, J=2.0 Hz, H_β), 3.71 (8H, s, OCH_2CH_2), 3.83 and 4.06 (4H, t, J=5 Hz, OCH_2CH_2)[b]	126.9 (c_b), 56.4(C_α), 61.9 (C_β), 71.3, 70.7, 70.3, 70.0 (methylene)	438 (126)
3c	4.17 (4H, t, J=2.0 Hz, H_α), 3.85 (4H, t, J=2.0 Hz, H_β), 3.76 and 3.85 (4H, t, J=5.2 Hz, OCH_2CH_2)	127.2 (C_b), 56.5 (C_α), 61.8 (C_β), 71.8 and 70.2 (methylene)	438 (119)
3d	4.22 (4H, t, J=2.0 Hz, H_α), 3.81 (4H, t, J=2.0 Hz, H_β), 3.85—3.94 and 4.06—4.15 (8H, A_2B_2 pattern, OCH_2CH_2)	126.1 (C_b), 56.0 (C_α), 61.5 (C_β), 70.6 and 70.1 (methylene)	438 (132)
3e	4.38 (4H, t, J=2.0Hz, H_α), 3.89 (4H, t, J=2.0 Hz, H_β), 4.32 (4H, s, OCH_2CH_2)	122.5(C_b), 58.9(C_α), 63.6(C_β), 71.8 (methylene)	428 (120)

a) C_b indicates bridge-head carbon. b) Measured at 40 °C.

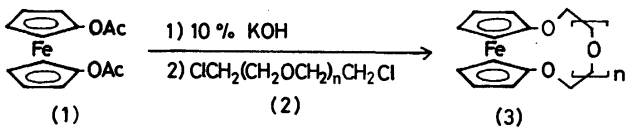

2a, 3a : n = 4
2b, 3b : n = 3
2c, 3c : n = 2
2d, 3d : n = 1
2e, 3e : n = 0

correct, although the ^{1}H-NMR spectral data of **3a—d** and the melting points of **3a** and **3c** are different from the results in the literature.

It is noteworthy in Table 2 that **3e** showed a singlet assignable to bridge methylene protons appearing at δ 4.32, in addition to two triplet absorptions of the α- and β-cyclopentadienyl ring protons at δ 4.38 and 3.89 respectively. The downfield shift of about 0.25 ppm of the methylene protons in **3e**, compared with that of the corresponding methylene protons in **3a—d**, may be explained by using the deshielding effect of the ferrocene nucleus proposed by Mulay and Fox,[8] although other possibilities can not be ruled out. The ^{1}H-NMR spectral comparison of **3e** with **3a—d** revealed that the chemical shifts of the β-ring protons of **3a—d** (δ 3.81—3.86) are almost equal to that of **3e** (δ 3.89), whereas in the case of **3e** the α-ring protons appeared considerably downfield (δ 4.38) relative to that of **3a—d** (δ 4.14—4.22) (Table 2). Similar abnormalities are observed in the ^{13}C-NMR and electronic spectra. The ^{13}C-NMR spectra showed that the bridge head carbon of **3e** shifted upfield by about 4.5 ppm compared with that of strain-free **3a—d**, while the α- and β-carbon shifted downfield compared with the corresponding carbon atoms of **3a—d**. The Dreiding ferrocene stereo-model suggests that the ferrocene nucleus can be readily spanned by a four-atom bridge without any distortion of its preferred geometry. Therefore, in the present case, although details are not known at present, the above results may be interpreted in terms of the steric compression[9] or, more probably, in terms of anisotropy effects[10] associated with the OCH_2 bonds. The absorption band of **3e** showed a hypsochromic shift of about 10 nm, although in the case of the ring tilting alkyl bridged [2]- and [3]ferrocenophanes,[9] bridged with two and three methylene groups respectively, the absorption band near 440 nm characteristic of the ferrocene nucleus shifted to 466 nm. The hypsochromic shift may be due to the tilt-deformation of two cyclopentadienyl rings by the bridging, but its real reason is not known at present.

The Additive Effect of Alkali Metal Thiocyanate on the Electronic Spectra of Compounds 3 in Methanol. As is shown in Table 3, all the polyoxaferrocenophanes showed the characteristic peak near 440 nm associated with the d-d transition. On the addition of potassium or sodium thiocyanates to **3a** and **3b** in methanol, a small shift in the absorption peak at 438 nm and a change in the intensity of the absorption band occurred on complexing with cations. Furthermore, the absorption band of the complex of **3c** with KCN and NaCN did not shift, although the absorbance is slightly increased. A similar relationship was observed in the absorption band of **3a—c** when lithium thiocyanate was added. This suggests that the lithium complexes are unstable, probably because lithium ion is too strongly solvated by the solvent. From the above results, it can be concluded that compounds **3a** and **3b** were complexed with sodium and potassium thiocyanate

Table 3. Electronic absorption spectra data and their metal complexes in methanol (λ/nm (ε))[a]

Compound	Additive Salt			
	None	LiSCN	NaSCN	KSCN
3a	438(127)	438(139)	435(129)	434(121)
3b	438(125)	438(127)	434(117)	435(123)
3c	438(117)	438(125)	438(125)	438(125)
3d	438(132)	438(134)	438(132)	438(134)
3e	428(120)	428(122)	428(122)	428(122)

a) Measured in the presence of about a 50-fold molar excess of alkali metal thiocyanate at 20 °C.

Table 4. Extraction of metal picrates from the aqueous to the organic phase (%)

Compound	Li^+ (1.20)	Na^+ (1.90)	K^+ (2.66)	Rb^+ (2.96)	Cs^+ (3.34)	Ag^+ (2.52)	Tl^+ (2.88)	Ba^+ (2.70)
3a	—	1.62	22.7	29.1	18.4	Dec.	79.7	—
3b	—	1.49	4.5	4.6	5.6	Dec.	25.2	—
3c	—	—	—	—	—	Dec.	4.4	—
3d	—	—	—	—	—	Dec.	3.4	—
3e	—	—	—	—	—	Dec.	0.6	—
B18C6		22.3	94.7			84.3	97.3	
B15C5		23.9	50.1			33.6	56.0	

Solvent: water and dichloromethane (1 : 1). Concentration of polyether: 7×10^{-4} M (1 M=1 mol dm^{-3}). Concentration of picric acid: 7×10^{-5} M. Concentration of metal nitrates: 0.1 M.

in methanol, although the changes in the absorption band at 438 nm were very complicated.

Extractability. The complexing ability of polyoxaferrocenophanes with alkali, alkaline earth, and transition-metal cations was measured by Pedersen's extraction method.[15] The data are summarized in Table 4, along with that of benzo crown ethers. Unlike from the data obtained by the TLC method,[3] the polyoxaferrocenophanes **3** showed little or no extractability toward alkali and alkaline earth metal cations, the extractability, if any, was much smaller than that of benzo crown ether. This seems reasonable considering that the incorporation of the iron atom of the ferrocene nucleus (a soft atom) or, more likely, the ferrocene nucleus itself into the macrocyclic polyether ring has an influence on the complexing ability with alkali and alkaline earth metal cation (a hard atom). The extractability of these cations is dependent on the size of the crown ether-ring part in polyoxaferrocenophanes. Thus, hexaoxa[16]ferrocenophane (**3a**) and pentaoxa[13]ferrocenophane (**3b**) extract 23 and 4% of the potassium ion respectively, but the ferrocenophanes, with a smaller polyether ring part, showed no extractability toward the potassium ion. Significantly, the selectivity of **3a** and **3b** toward the thallium ion should be noted. Thus, the extractability of **3a** and **3b** toward the thallium ion is remarkably higher than that toward other alkali and alkaline earth metal ions, while benzo crown ether showed a similar extractability toward any of the cations described above. The extractability of several metal ions was in this order: $Tl^+>Rb^+>K^+>Cs^+>Na^+$. No extraction of the silver ion by the polyoxaferrocenophanes was observed because of the oxidative decomposition of the ferrocenophanes.

Isolation of the Complex of Polyoxaferrocenophanes with Alkali Thiocyanates. The uptake of alkali metal cations with **3a** or **3b** containing six or five oxygen atoms was attempted. To an acetonitrile solution of equimolar amounts of **3a** or **3b** and alkali thiocyanate, we added hexane until a yellow or red precipitate appeared. After the precipitate has been completed in a refigerator, the complexes were obtained. These complexes (**4a—c**, **5a**, and **5b**) showed higher melting point than metal-free ligand and were confirmed by microanalysis to be 1 : 1 complexes. Their ^{1}H-NMR spectra gave much information about the character of the complexes **5a** and **5b**. The proton signals of the complexes **5a** and **5b** showed some downfield shift

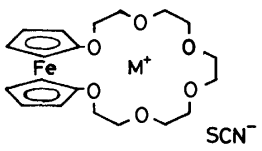

4a : M = Li
4b : M = Na
4c : M = K

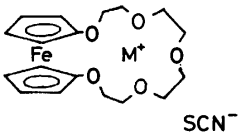

5a : M = Li
5b : M = Na

compared with those of the free ligands **3a** and **3b**. Ferrocene ring protons of the complexes remained in the A_2B_2 pattern, suggesting that the alkali metal cation is strongly incorporated into the center of the cavity of the macrocyclic polyether, because the coordination to one of the sides of the ligand leads to the ABCD pattern of the ring protons. The shifts of the ferrocene ring protons ($\Delta\delta=0.22(H_\alpha)$ and $0.05(H_\beta)$ in **5b**) were larger than those of the methylene protons of the oxyethylene chain ($\Delta\delta=0.03$ in **5b**). The Mössbauer spectra of **3b**, **5a**, and **5b** were measured at room temperature.[12] It was found in this study that both of the complexes (**5a** and **5b**) give larger values (2.55 mm s^{-1}) of quadrupole splitting (qs) than that (2.50 mm s^{-1}) of metal-free ferrocenophane **3b**, although the chemical isomer shifts have the same value as that (0.44 mm s^{-1}) of **3b**. It has been reported that the electron-attracting substituents[13] decrease the qs of ferrocene and that some ferrocene derivatives with electron-donating substituents[14] give larger values of qs than that of ferrocene. Therefore, if the alkali metal cation exerts an electron-attracting effect through the $Na^+\cdots O\cdots C_b$ on the cyclopentadienyl ring, compounds **4a** and **4b** can be expected to give smaller values of qs than that of metal-free ferrocenophane (**3b**). However, as has been described above, the complexes which incorporated sodium and lithium cations into the macrocyclic ether of ferrocenophane gave larger values of qs than that of **3b**. The results obtained suggest that the larger values of qs estimated for these complexes may be ascribed to some interaction between the alkali metal cation incorporated and the iron atom of ferrocene nucleus, although the possibility of the effect of the counter anion ($^-$SCN) on the e_{2g} (or a_{1g}) d-orbital of the ferrocene nucleus can not be ruled out.[16]

Experimental

The melting point are uncorrected. The IR spectra were

measured on a JASCO IRA-2 Diffraction Grating Infrared Spectrometer. The mass spectra were taken by using a JEOL-JMS-OlSG-2 Spectrometer. The ^{1}H-NMR spectra were measured on Varian XL-200 and a Hitachi R24B Spectrometer, TMS being chosen as the internal standard. The ^{13}C-NMR spectra were obtained on a Hitachi R-900 Spectrometer. The electronic spectra were measured on a Hitachi Model 200-10 spectrometer.

Material. The silica gel used for thin-layer chromatography was Wakogel B-5F. 1,2-Dichloroethane (**2e**), bis(2-chloroethyl) ether (**2d**), and 1,8-dichloro-3,6-dioxaoctane (**2c**) were commercially available and were used without further purification. 1,11-Dichloro-3,6,9-trioxaundecane (**2b**) and 1,14-dichloro-3,6,9,12-tetraoxatetradecane (**2a**) were prepared according to the procedures described in the literature.[17] The solvent were purified by distillation. Lithium thiocyanate, sodium thiocyanate, and potassium thiocyanate of Tokyo Kasei Kogyo (first grade) were used without further purification.

*Preparation of 1,1′-Diacetoxyferrocene (**1**).* **1** was prepared by the reaction of 1,1′-dibromoferrocene with copper(I) acetate according to the following modified procedure: 1,1′-Dibromoferrocene (4.5 g, 0.013 mol) and copper(I) acetate (15 g, 0.075 mol) in 50% aqueous ethanol (500 ml) were refluxed for 40 min at the reflux temperature under nitrogen. After the mixture had been cooled to room temperature, the solid was filtered off and the filtrate was added to water (600 ml). The aqueous solution was extracted with ether, washed with water, and dried over anhydrous $MgSO_4$. The residue obtained on the evaporation of the solvent was solidified to give a dark orange solid. Recrystallization from benzene–hexane gave a pure sample (2.2 g, 56% yield) as yellow needles; mp 46—48 °C (lit,[6] 55—56 °C).

*Preparation of Polyoxa[n]ferrocenophanes. General Procedure: 1,4,7,10,13,16-Hexaoxa[16]ferrocenophane (**3a**).* **1** (0.670 g, 2.20 mmol) was added to a 10% aqueous potassium hydroxide solution (10 ml) under nitrogen, and the mixture was stirred under reflux. After 30 min, a solution of 1,14-dichloro-3,6,9,12-tetraoxatetradecane (**2a**) (0.920 g, 3.30 mmol) in 60% ethanol (50 ml) was added all at once, the mixture was then stirred for 5 h at reflux temperature. After the solution had been cooled to room temperature, 100 ml of water was added to the reaction mixture. The aqueous solution was extracted with three 25 ml portions of ether. The ether extracts were combined, washed with water, and concentrated *in vacuo*. The residual oil was chromatographed by silica gel TLC (using benzene–ethyl acetate 5 : 1 as the eluent). The main band was eluted with acetone at room temperature, followed by filtration. The evaporation of the solvent gave yellow oil which solidified on standing, The pure product was obtained as yellow needles by recrystallization from hexane.

General Procedure for the Preparation of the Alkali Metal Thiocyanate Complex. Alkali metal thiocyanate (0.14 mmol) and **3a—b** were dissolved in anhydrous acetonitrile. To the mixture, hexane was added until precipitation occurred. The reaction mixture was then cooled in a refrigerator. After the precipitation was complete, the crystalline product was filtered off and washed with small amounts of acetonitrile and hexane. An almost quantitative yield of these complexes was obtained.

*Lithium Thiocyanate Complex of **3a** (**4a**).* The complex, (yellow needles), exhibited the following physical and spectral properties; mp 123—128 °C. Found: C, 52.19; H, 5.89; N, 2.68%. Calcd for $C_{21}H_{28}O_6NSLiFe$: C, 51.96; H, 5.77; N, 2.89%. ^{1}H-NMR (60 MHz, in $CDCl_3$): δ 4.19 (4H, t, J=2.0 Hz, H_α), 3.93 (4H, t, J=2.0 Hz, H_β), 3.77 (4H, s, OCH_2CH_2O), 3.75 (8H, s, OCH_2CH_2O), 4.00—3.78 (8H, m, OCH_2CH_2O).

*Sodium Thiocyanate Complex of **3a** (**4a**).* Mp 135—137 °C. Found: C, 50.50; H, 5.87; N, 2.53%. Calcd for $C_{21}H_{28}O_6NSNaFe$: C, 50.30; H, 5.59; N, 2.79%. ^{1}H-NMR ($CDCl_3$): δ 4.14 (4H, t, J=2.0 Hz, H_α), 3.87 (4H, t, J=2.0 Hz, H_α), 3.69 (4H, s, OCH_2CH_2O), 3.78 (4H, s, OCH_2CH_2O), and 4.02—3.80 (8H, m, OCH_2CH_2O).

*Potassium Thiocyanate Complex of **3a** (**4c**).* Mp 164—167 °C. Found: C, 49.05; H, 5.72; N, 2.88%. Calcd for $C_{21}H_{28}O_6SNKFe$: C, 48.74; H, 5.42; N, 2.71%. ^{1}H-NMR ($CDCl_3$): δ 4.16 (4H, t, J=2.0 Hz, H_α), 3.91 (4H, t, J=2.0 Hz, H_β), 3.76 (8H, s, OCH_2CH_2O), 3.75 (4H, s, OCH_2CH_2O), and 4.00—3.78 (8H, m, OCH_2CH_2O).

*Lithium Thiocyanate Complex of **3b** (**5a**).* Mp 147—149 °C. Found: C, 51.53; H, 5.74; N, 3.12%. Calcd for $C_{19}H_{24}O_5SNLiFe$: C, 51.70; H, 5.44; N, 3.17%. ^{1}H-NMR ($CDCl_3$): δ 4.32 (4H, t, J=2.0 Hz, H_α), 3.98 (4H, t, J=2.0 Hz, H_β), 3.79 (8H, s, OCH_2CH_2O), and 4.12—3.80 (8H, m, OCH_2CH_2O).

*Sodium Thiocyanate Complex of **3b** (**5b**).* Mp 165.5—167 °C. Found: C, 50.19; H, 5.78; N, 3.01. Calcd for $C_{19}H_{24}O_5SNNaFe$: C, 49.89; H, 5.44; N, 3.17%. ^{1}H-NMR ($CDCl_3$): δ 4.37 (4H, t, J=2.0 Hz, H_α), 3.91 (4H, t, J=2.0 Hz, H_β), 3.74 (8H, s, OCH_2CH_2O), and 4.02—3.80 (8H, m, OCH_2CH_2O).

The Method of Solvent Extraction. Extractability of polyoxaferrocenophanes with the alkali metal cation was examined by the extraction method described by Pedersen.[15] Equal volumes (5 ml) of dichloromethane containing 7×10^{-4} M of polyoxaferrocenophane and an aqueous solution containing 1×10^{-1} M MNO_3 (M; alkali metal cation) and 7×10^{-5} M picric acid were agitated thoroughly at 25 °C. The solution was then equilibrated at 25 °C, the aliquot of the upper aqueous solution was withdrawn, and the electronic spectrum was recorded. A similar extraction was performed with pure dichloromethane. The extractability was determined by reading the difference between the two absorbances of picrate in the aqueous solution. The extractability was calculated by means of the following equation:

$$\text{Extractability} = \frac{A_0 - A}{A_0} \times 100.$$

A_0 is the absorbance in the absence of MNO_3 and A is the absorbance in the presence of MNO_3.

The authors wish to thank Professor Masuo Takeda, Department of Chemistry, Toho University, for the measurement of the Mössbauer spectra.

References

1) R. E. Izatt and J. J. Christensen, "Synthetic Multidentate Macrocyclic Compounds," Academic Press, New York (1978).

2) a) G. Oepen and F. Vögtle, *Justus Liebigs Ann. Chem.*, **1976**, 1094; b) A. P. Bell and C. D. Hall, *J. Chem. Soc., Chem. Commum.*, **1980**, 163; B. Czech and A. Ratajczak, *Polish J. Chem.*, **54**, 767 (1980).

3) J. F. Biernat and T. Wilczewski, *Tetrahedron*, **36**, 2521 (1980).

4) M. Sato. M. Kubo, S. Ebine, and S. Akabori, *Tetrahedron Lett.*, **1982**, 185.

5) R. N. Greene, *Tetrahedron Lett.*, **1972**, 1973.

6) A. N. Nesmeyanov, V. A. Sazonova, and V. N. Drozd, *Chem. Ber.*, **93**, 2117 (1960).

7) D. W. Slocum and C. R. Ernest, *Tetrahedron Lett.*, **1972**, 5217.

8) L. N. Mulay and M. E. Fox, *J. Chem. Phys.*, **38**, 760 (1963).

9) S. Winstein, P. Carter, F. A. L. Anet, and A. J. R. Bourn, *J. Am. Chem. Soc.*, **87**, 5247 (1965).
10) J. A. Pople, W. G. Schneider, and H. J. Bernstein, "High-resolution Nuclear Magnetic Resonance," McGraw-Hill Book Company, New York (1959), p. 176.
11) T. H. Barr and W. E. Watts, *Tetrahedron*, **24**, 6111 (1968).
12) The isomer shift data are reported with respect to metalic iron foil.
13) A. V. Lesikar, *J. Chem. Phys.*, **40**, 2746 (1964).
14) S. Iijima, I. Motoyama, and H. Sano, *Bull. Chem. Soc. Jpn.*, **53**, 3180 (1980).
15) C. J. Pedersen, *Federation Proceedings*, **27**, 1305 (1968).
16) Although no details were reported, an earlier study showed a small difference between the Mössbauer spectra of the ferrocenophanes prepared from ferrocene-1,1′-dicarboxylic acid and those of the corresponding metal complexes.[28]
17) C. J. Pedersen, *J. Am. Chem. Soc.*, **89**, 7017 (1967).

Chemical Studies on the Mistletoe. V.[1] The Structure of Taxillusin, a New Flavonoid Glycoside Isolated from *Taxillus kaempferi*[2]

Atsushi SAKURAI* and Yasuaki OKUMURA
Department of Chemistry, Faculty of Science, Shizuoka University, Ohya, Shizuoka 422
(Received July 7, 1982)

A new flavonoid glycoside, taxillusin was isolated from *Taxillus kaempferi* (DC.) Danser and (2*R*,3*R*)-taxifolin 3-β-D-glucopyranoside 6″-gallate was assigned to this substance from studies on the hydrolysis products and from analyses of the ^{1}H-NMR and carbon-13 NMR spectra.

Japanese mistletoe, *Taxillus kaempferi* (DC.) Danser (Matsugumi in Japanese) is a perennial shrub of *Viscaceae*. In our previous paper[1] we reported the isolation and structure of isoglucodistylin (**1**), a flavonoid constituent of this plant, which was assigned to be (2*R*,3*S*)-taxifolin 3-β-D-glucopyranoside. During the course of the isolation of **1** by Sephadex LH-20 column chromatography, we isolated another new flavonoid glycoside and named it taxillusin (**2**). We now wish, to report the isolation and the results which lead to the structure of taxillusin (**2**).

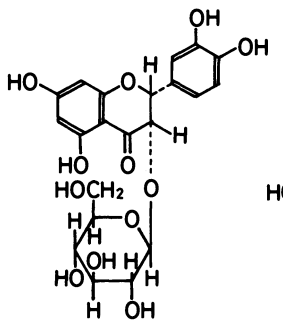

1

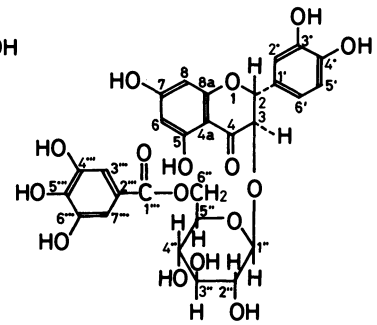

2

Compound **2** is hygroscopic faintly yellowish crystals, mp 198—203 °C and optically active, $[\alpha]_D$ +5.2°. Elemental analyses show that **2** has a composition of $C_{28}H_{26}O_{16}$. The UV spectrum of **2** in ethanol shows the absorption maximum at 292 nm, and this absorption maximum and its pattern were similar to those reported for a number of flavonoids of taxifolin type.[3] The IR spectrum of **2** shows absorption bands characteristic of flavonoid glycosides and indicative of the existence of a conjugated ester group at 1690 and 1250 cm^{-1} besides them.

Acetylation of **2** with acetic anhydride and pyridine gave a decaacetate of **2** as colorless fine crystals, mp 125—129 °C.

Acid hydrolysis of **2** with 5% sulfuric acid in 50% aqueous ethanol[4] gave taxifolin (**3**), gallic acid (**4**), and D-glucose as the components. Since the optical rotation value of **3** ($[\alpha]_D$ +12°) is identical with that of (+)-taxifolin,[5,6] the absolute configuration of **3** is 2*R* and 3*R*.[7] Methylation of **2** with dimethyl sulfate and potassium carbonate in acetone followed by acid hydrolysis in the same manner as described above and then air oxidation[3c] gave 3′,4′,5,7-tetra-*O*-methylquercetin (**5**),[3c,8] which was identified with the authentic sample prepared by methylation and acid hydrolysis of rutin in the same manner. This result indicates that either D-glucose or gallic acid might be linked at the 3-position of **3**.

Treatment of **2** with hydrogen chloride in methanol gave **3**, methyl gallate (**6**), methyl α-D-glucopyranoside (**7**), and a substance **8**. The IR spectrum of **8** shows absorption bands indicative of the existence of a conjugated ester group at 1700 and 1240 cm^{-1}. Since **8** gives **6** and **7** by further treatment with hydrogen chloride in methanol, D-glucose and gallic acid should be linked by an ester bond. The ^{1}H-NMR spectrum of a trimethylsilyl derivative of **8** in $CDCl_3$ shows a sharp singlet ascribed to the methoxyl group at δ 3.37 ppm, a doublet corresponding to the 1-proton of glucose at δ 4.62 ppm (J=3 Hz, axial/equatorial coupling indicative of α-D-glucoside), and a sharp singlet attributed to the 3′- and 7′-protons of galloyl group at δ 7.23 ppm. This result indicates **8** to be a gallate of methyl α-D-

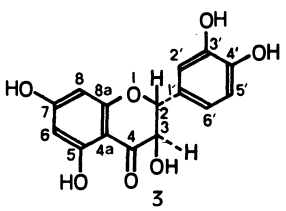

3

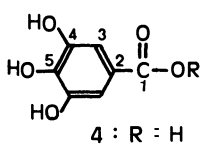

4 : R = H
6 : R = CH_3

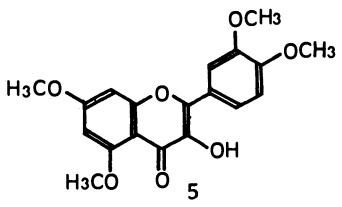

5

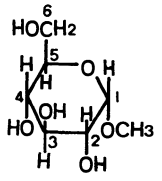

7

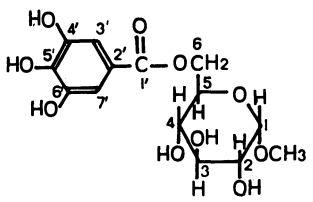

8

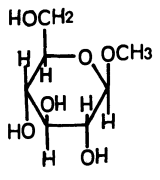

9

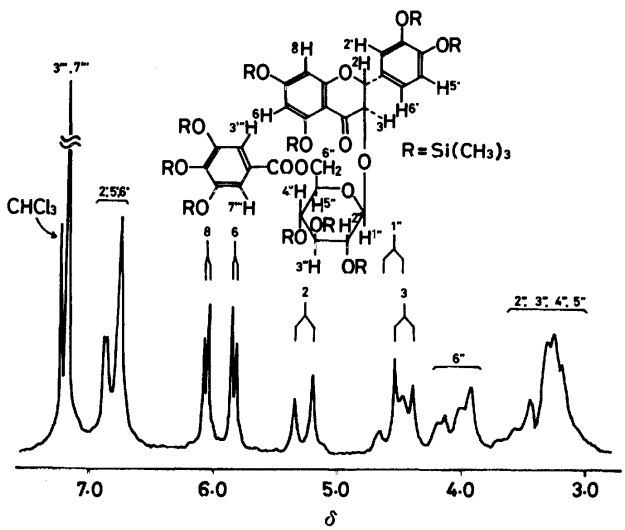

Fig. 1. The ^{1}H-NMR spectrum of trimethylsilyl derivative of taxillusin (**2**) in $CDCl_3$.

glucoside.

The position of linkage between the D-glucose and gallic acid in **8** was confirmed by comparison of the carbon-13 NMR spectra of **6**, **7**, **8**, and their trimethylsilyl derivatives as shown in Table 1. The 6-carbon of the glucose in **8** appears at a field lower by 2.7 ppm and the 5-carbon of the glucose in **8** appears at a field higher by 2.0 ppm than those of **7**. The 5- and 6-carbons of the glucose in a trimethylsilyl derivative of **8** also appear at fields higher by 2.4 ppm and lower by 1.6 ppm respectively than those of a trimethylsilyl derivative of **7**. These results indicate that the gallic acid in **8** should be linked by an ester bond at the 6-position of **7**.

Beisdes the signals characteristic of **3** as shown in Fig. 1, the ^{1}H-NMR spectrum of a trimethylsilyl derivative of **2** in $CDCl_3$ shows a sharp singlet of 3‴- and 7‴-protons of galloyl group at δ 7.20 ppm, signals of the protons in 2′-, 3′-, 4′-, and 5′-positions of glucose between δ 3.0 and 3.8 ppm, a broad doublet of 1″-proton of glucose at δ 5.24 ppm (J= *ca.* 11 Hz, axial/axial coupling indicative of β-D-glucoside), and a two proton AB-type multiplet of 6″-protons of glucose at δ 4.04 ppm (down-field shift by galloyl group). This result indicates that **2** might be (2*R*,3*R*)-taxifolin 3-β-D-glucopyranoside 6″-gallate.

The structure of **2** is supported also by the carbon-13 NMR spectra of **1**, **2**, **3**, **6**, and methyl β-D-glucopyranoside (**9**) in DMSO-d_6 as shown in Table 1. The 1-carbon of the glucose in **2** appears at a field higher by 2.7 ppm than that of **9** and the 4-carbonyl carbon in **2** also appears at a field higher by 5.6 ppm than that of **3**. This fact is the consequence of steric compression between the C-1 of glucose and the C-4 of taxifolin. The 3- and 4-carbons of the taxifolin in **1** appear at fields higher by 1.1 ppm and lower by 0.7 ppm respectively

Table 1. Carbon-13 NMR chemical shifts[a] of **1**, **2**, **3**, **6**, **7**, **8**, **9**, and trimethylsilyl derivatives of **7** and **8**

Compound		**6**	**7**	TMS[b] of **7**	**9**	**8**	TMS of **8**	**3**	**1**	**2**
Solvent		DMSO-d_6	DMSO-d_6	$CDCl_3$	DMSO-d_6	DMSO-d_6	$CDCl_3$	DMSO-d_6	DMSO-d_6	DMSO-d_6
Taxifolin	2	—	—	—	—	—	—	82.9	80.6	80.5
	3	—	—	—	—	—	—	71.3	75.2	76.3
	4	—	—	—	—	—	—	197.5	192.6	191.9
	4a	—	—	—	—	—	—	100.2	101.0	101.0
	5	—	—	—	—	—	—	163.1	163.3	163.3
	6	—	—	—	—	—	—	95.8*	95.9*	95.9*
	7	—	—	—	—	—	—	166.5	167.0	167.0
	8	—	—	—	—	—	—	94.8*	95.0*	95.0*
	8a	—	—	—	—	—	—	162.3	161.6	161.3
	1′	—	—	—	—	—	—	127.8	126.5	126.3
	2′	—	—	—	—	—	—	115.1**	114.6**	114.4**
	3′	—	—	—	—	—	—	145.5***	145.5***	145.4***
	4′	—	—	—	—	—	—	144.7***	145.0***	145.0***
	5′	—	—	—	—	—	—	115.1**	115.4**	115.5**
	6′	—	—	—	—	—	—	119.2	118.7	118.3
Glucose	1	—	99.5	99.9	103.7	99.7	100.0	—	101.0	101.0
	2	—	72.4	74.2	73.2	71.9	74.1	—	73.4	73.5
	3	—	73.2	75.6	76.6	73.3	75.2	—	77.1	76.3
	4	—	70.2	72.3	69.9	70.5	72.9	—	69.8	69.3
	5	—	71.8	72.3	76.5	69.8	69.9	—	76.5	74.0
	6	—	60.9	62.5	60.9	63.6	64.1	—	61.0	63.2
Gallic acid	1	166.2	—	—	—	165.8	166.2	—	—	165.7
	2	119.2	—	—	—	119.2	122.6	—	—	119.4
	3	108.4	—	—	—	108.7	115.7	—	—	108.7
	4	145.4	—	—	—	145.5	148.0	—	—	145.4
	5	138.2	—	—	—	138.4	143.8	—	—	138.3
	CH_3	51.5	54.2	54.8	55.9	54.5	55.1	—	—	—

a) In parts per million down-field from tetramethylsilane. b) TMS: trimethylsilyl derivative. c) Asterisks indicate that assignments are not unambiguous.

than those of **2**. This fact is the consequence of the difference in the configuration at the 3-position of taxifolin between **1** and **2**. The 5- and 6-carbons of the glucose in **2** appear at fields higher by 2.5 ppm and lower by 2.3 ppm respectively than those of **9** and also appear at fields higher by 2.5 ppm and lower by 2.2 ppm respectively than those of **1**, which indicates that gallic acid is linked by an ester bond at the 6-position of D-glucose.

These ^{1}H-NMR and carbon-13 NMR spectroscopic data and all experimental results described above support the structure of taxillusin (**2**) to be (2*R*,3*R*)-taxifolin 3-β-D-glucopyranoside 6″-gallate.

Experimental

All melting points are uncorrected. The proton and carbon nuclear magnetic resonance spectra were measured with a JEOL JNM-PFT-60 NMR spectrometer, and the latter spectra were obtained on sampling interval of 2.0 s. Chemical shifts were obtained by δ value (ppm) from tetramethylsilane as internal standard at 15.04 MHz for carbon and 59.8 MHz for proton. The UV spectra were measured with a Hitachi EPS-3 recording spectrophotometer. The optical rotations were measured with a Union PM-101 polarimeter.

Extraction and Isolation of Taxillusin (2). The fresh leaves and twigs of the mistletoe (2 kg)[9] were extracted with ethanol (6 l) in the usual way, and the extract was condensed to a syrup under reduced pressure. The syrup was triturated with water (2 l) and chloroform (2 l), and the undissolved material which accumulated between both layers was collected and washed with water. After being dried in a desiccator over calcium chloride, the faintly yellowish powder (11.5 g) was dissolved in ethanol (50 ml), and the solution was subjected to chromatography on a column of Sephadex LH-20 (7×40 cm) eluting with ethanol.[10] The last effluent was rechromatographed with a column of Sephadex LH-20 (3.5×120 cm) in the same manner as described above. After removal of the solvent, recrystallization from aqueous ethanol gave taxillusin (**2**) as hygroscopic faintly yellowish crystals: mp 198—203 °C (decomp); yield, 9.2 g (0.46% from wet plant); $[\alpha]_D^{25}$ +5.2° (*c* 1.0, EtOH); UV (EtOH): λ_{max} 292 nm (ε 23300); IR (KBr disk): ν_{max} 3400—3200, 1690, 1653, 1620, 1610, 1550, 1531, 1516, and 1250 cm^{-1}. Found: C, 51.31; H, 4.78%. Calcd for $C_{28}H_{26}O_{16}\cdot 2H_2O$: C, 51.38; H, 4.62%.

Acetylation of 2. Acetylation of **2** with acetic anhydride and pyridine in the usual way gave a decaacetate of **2** as colorless fine crystals: mp 125—129 °C; UV (EtOH): λ_{max} 241 (ε 31900, inflexion), 263 (ε 17900), and 312 nm (ε 6490). Found: C, 55.16; H, 4.42%. Calcd for $C_{48}H_{46}O_{26}$: C, 55.49; H, 4.46%.

Acid Catalyzed Hydrolysis of 2. **2** (100 mg) was dissolved in 50% aqueous ethanol (20 ml) containing concd sulfuric acid (1 ml) and the mixture was refluxed for 3 h. After removal of ethanol by evaporation under reduced pressure, the solution was extracted with ethyl acetate. The extract was subjected to chromatography on a column of Sephadex LH-20 (2×75 cm) eluting with ethanol and gave **3** (mp 240—242 °C; yield, 32 mg; $[\alpha]_D^{25}$ +12° (*c* 0.75, EtOH)) and **6** (mp 233—237 °C (decomp); yield, 12 mg).

Hydrolyzate free from **3** and **6** was neutralized with barium carbonate and was concentrated under reduced pressure, which was subjected to thin layer chromatography for detection of the sugar component. The sugar was proved to be identical with D-glucose.

Methylation of 2. According to Fukui, Nakadome, and Ariyoshi's method,[3c] **2** was methylated with dimethyl sulfate and potassium carbonate in acetone followed by acid hydrolysis and then by air oxidation. The product was identical with authentic 3′,4′,5,7,-tetra-*O*-methylquercetin (**5**) which was prepared by methylation and acid hydrolysis of rutin in the same manner. **5**: mp 194—196 °C[3c]; UV(EtOH): λ_{max} 253 and 362 nm;[8] ^{1}H-NMR ($CDCl_3$): δ 3.92 (3H, s, CH_3O), 3.98 (9H, s, CH_3O), 6.37 (1H, d, J=2 Hz, H-6), 6.54 (1H, d, J=2 Hz, H-8), 6.99 (1H, d, J=9 Hz, H-5′), 7.38 (1H, broad s, 3-OH), 7.78 (1H, dd, J=2 and 9 Hz, H-6′), and 7.81 ppm (1H, d, J=2 Hz, H-2′).

Methanolysis of 2. **2** (620 mg) was dissolved in dry methanol (15 ml), and 30% methanolic hydrogen chloride (5 ml) was added to this solution. After having been allowed to stand for 12 h at room temperature, the reaction mixture was evaporated to dryness under reduced pressure. The residue was subjected to chromatography on a column of Sephadex LH-20 (3×120 cm) eluting with methanol in the same manner as described above and gave **3** (yield, 105 mg), **6** (mp 198—200 °C; yield, 55 mg), **7** (mp 169—170 °C; yield, 60 mg; $[\alpha]_D^{20}$ +159° (*c* 0.5, H_2O)), and **8** (colorless powder from methanol and ether; mp 120—124 °C; yield, 110 mg; $[\alpha]_D^{22}$ +37° (*c* 0.2, EtOH); IR (KBr disk): ν_{max} 3350, 1700, 1614, 1535, 1240, 1150, 1045, 878, 770, and 745 cm^{-1}; Found: C, 48.83; H, 5.23%. Calcd for $C_{14}H_{18}O_{10}$: C, 48.56; H, 5.24%).

Further treatment of **8** with methanolic hydrogen chloride in the same manner as described above gave **6** and **7**.

Acetylation of **8** with acetic anhydride and pyridine in the usual way gave a hexaacetate of **8** as colorless crystals: mp 77—79 °C. Found: C, 51.97; H, 5.01%. Calcd for $C_{26}H_{30}O_{16}$: C, 52.18; H, 5.05%.

Trimethylsilylation. Flavonoid or sugar (50 mg) was treated with anhydrous pyridine (5 ml), trimethylchlorosilane (0.5 ml), and hexamethyldisilazane (1 ml). The mixture was allowed to stand overnight at room temperature. After being evaporated to dryness under reduced pressure, the residue was dissolved in chloroform, and the undissolved materials which separated were filtered off and washed with chloroform. The filtrate and washings were evaporated to dryness under reduced pressure. No further attempt was made to purify the trimethylsilyl derivative before measurement of the NMR spectra.

References

1) Part IV: A. Sakurai, K. Okada, and Y. Okumura, *Bull. Chem. Soc. Jpn.*, **55**, 3051 (1982).

2) A preliminary communication of this work has been reported: A. Sakurai and Y. Okumura, *Chem. Lett.*, **1978**, 259.

3) a) H. L. Hergert and O. Goldschmid, *J. Org. Chem.*, **23**, 700 (1958); b) H. Aft, *ibid.*, **26**, 1958 (1961); c) Y. Fukui, K. Nakadome, and H. Ariyoshi, *Yakugaku Zasshi*, **86**, 184 (1960).

4) N. Ohta and K. Yagishita, *Agric. Biol. Chem.*, **34**, 900 (1970).

5) J. C. Pew, *J. Am. Chem. Soc.*, **70**, 3031 (1948).

6) H. Shimada, T. Sawada, and S. Fukuda, *Yakugaku Zasshi*, **72**, 578 (1952).

7) J. W. Clark-Lewis and W. Korytnyk, *J. Chem. Soc.*, **1958**, 2367.

8) T. Sasaki, *Yakugaku Zasshi*, **84**, 47 (1964).

9) The mistletoe which occurred on a Japanese red pine (*Pinus densiflora*) was collected at Mt. Udo of Shizuoka City in the spring of 1977.

10) From this effluent, quercetin, (+)-taxifolin, avicularin quercitrin, hyperin, and guaijaverin were isolated besides taxillusin and isoglucodistylin.

N-Methyl-*N*-(phenylsulfonyl)benzohydrazonoyl Chloride as a Potential Intermediate for Nitrogen-heterocycles. Preparation of 1-Methyl-3-phenyl-1*H*-1,2,4-triazoles and -pyrazoles

Suketaka Ito,* Yumo Tanaka, Akikazu Kakehi, Toshihiko Fukuyama,† Nobuo Osawa,†† and Noboru Sayo†††
Department of Industrial Chemistry, Faculty of Engineering, Shinshu University, Wakasato, Nagano 380

(Received July 7, 1982)

3,5-Disubstituted 1-methyl-1*H*-1,2,4-triazoles and -pyrazoles were obtained in good to moderate yields by the reaction of *N*-methyl-*N*-(phenylsulfonyl)benzohydrazonoyl chloride with nitriles and with acetylenes in the presence of aluminum chloride. The triazoles were also formed by the reaction of acid chlorides with *N*-methyl-*N*-(phenylsulfonyl)benzamidrazone which was generated from the hydrazonoyl chloride and ammonia.

N-Phenylbenzohydrazonoyl chloride (**1**) gives 1-phenyl-1*H*-1,2,4-triazoles by the reaction with nitriles *via* a nitrilium ion (generated from **1** and aluminum chloride)[1] as well as *via* diphenylnitrilimine generated from **1** and triethylamine.[2] *N,N*-Disubstituted hydrazonoyl halides such as *N*-methyl-*N*-phenylbenzohydrazonoyl chloride[3] cannot afford 1,2,4-triazoles as a matter of course. As has been shown in the reaction of *N*-(phenylsulfonyl)benzohydrazonoyl chloride (**2**) with *N,N'*-disubstituted benzamidines and *N*-substituted benzimidates,[4] however, such an arylsulfonyl group attached to the amino nitrogen of hydrazonoyl chlorides as that of **2** can be eliminated as an arenesulfonyl cation. Thus, the title hydrazonoyl chloride carrying an *N*-phenylsulfonyl group can be expected as a potential source for 1-methyl-1*H*-1,2,4-triazoles and -pyrazoles. The present paper deals with the Lewis acid-catalyzed reaction of *N*-methyl-*N*-(phenylsulfonyl)benzohydrazonoyl chloride (**3**) with nitriles and with acetylenes and, in addition, the reaction of *N*-methyl-*N*-(phenylsulfonyl)benzamidrazone (**4**) derived from **3**.

Results and Discussion

The Lewis Acid-catalyzed Reactions of N-*Methy*-N-*(phenylsulfonyl)benzohydrazonoyl Chloride (3) with Nitriles and Acetylenes. Preparation of 3*: Hydrazonoyl chloride **3** was obtained in an almost quantitative yield by the *N*-methylation of *N*-(phenylsulfonyl)benzohydrazonoyl chloride (**2**) with diazomethane. The thionyl chloride treatment of 1-benzoyl-2-methyl-2-phenylsulfonylhydrazine (**5**) obtained from 1-benzoyl-2-phenylsulfonylhydrazine (**6**) by the *N*-alkylation with methyl iodide was also available for preparing **3** (Scheme 1). Except for the trouble and hazard in the preparation of diazomethane, the former method may be convenient. Hydrazonoyl chloride **3** is a stable crystalline compound, but was observed to undergo hydrolysis more appreciably than **2** when allowed to stand in contact with the atmosphere for a long time.

Reactions of 3: A mixture of **3** and small excess amounts of benzonitrile and aluminum chloride was heated at 115—125 °C (oil bath) in a solvent for 30 min. Work-up gave 1-methyl-3,5-diphenyl-1*H*-1,2,4-triazole (**7a**) in a 77% (maximum) yield: in the case of low reaction temperature, unaltered **3** was recovered (Table 1). When the reaction was carried out in the presence of titanium(IV) chloride or boron trifluoride etherate as a catalyst, **7a** was obtained in a diminished yield (at 115—125 °C in *o*-dichlorobenzene). The results are summarized in Table 2 along with those obtained in the reaction with acetonitriles. The reaction of the *N*-unalkylated hydrazonoyl chloride, **2**, with benzonitrile as a control experiment gave 3,5-diphenyl-1*H*(or 4*H*)-1,2,4-triazole (49%), which should be generated by the hydrolysis of 1-phenylsulfonyl-3,5-diphenyl-1*H*-1,2,4-triazole. Under the same reaction conditions, phenylacetylene and diphenylacetylene gave 1-methyl-3,5-diphenyl (**8a**) and 1-methyl-3,4,5-triphenyl-1*H*-pyrazole

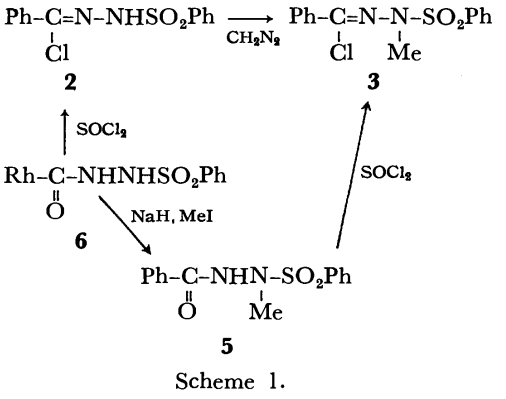

Scheme 1.

Table 1. 1-Methyl-3,5-diphenyl-1*H*-1,2,4-triazole (**7a**) by the aluminum chloride-catalyzed reaction of **3** with benzonitrile

Reaction temp[a] °C	Solvent	Yield/%[b] **7a**	Yield/%[b] **3**[c]
Reflux	CH_2Cl_2	0	≈100
Reflux	CS_2	0	≈100
75—85	*o*-$C_6H_4Cl_2$	15	55
95—105	*o*-$C_6H_4Cl_2$	47	16
115—125	*o*-$C_6H_4Cl_2$	77	0
135—145	*o*-$C_6H_4Cl_2$	63	0
115—125	*sym*-$C_2H_2Cl_4$	72	0
Reflux (146)	*sym*-$C_2H_2Cl_4$	74	0

a) Reaction time: 30 min. b) Isolated yield. c) Unaltered hydrazonoyl chloride.

† Present address: Fujitsu Co. Ltd., Kami-odanaka, Kawasaki 211.

†† Present address: Mochida Research Laboratories, Mochida and Co., Ltd., Gotemba 412.

††† Present address: Department of Chemical Technology, Tokyo Institute of Technology, Meguro-ku, Tokyo 152.

Table 2. Some 1-methyl-1*H*-1,2,4-triazoles (**7**), 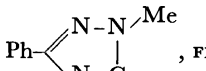 , from RC≡N and -pyrazoles (**8**), 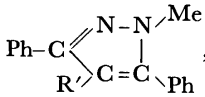 , from R′C≡CPh

Azoles **7** or **8**	Mp θ_m/°C	Catalyst	Reaction conditions[a]	Yield %[b]
7a (R=Ph)	79—81[c]	$TiCl_4$	A	55
		BF_3·Et_2O	A	7
7b (R=$PhCH_2$)	70—71	$AlCl_3$	A	77
		$TiCl_4$	A	49
7c (R=Me)	119—120[d]	$AlCl_3$	A	63
		$TiCl_4$	A	49
8a (R′=Ph)	187—188[e]	$AlCl_3$	A	26
		$AlCl_3$	B	20
		$AlCl_3$	C	18
		$TiCl_4$	A	7
8b (R′=H)	71—72[f]	$AlCl_3$	A	14
		$TiCl_4$	A	16

a) A: Heating at 115—125 °C in *o*-$C_6H_4Cl_2$ for 30 min. B: Heating at 135—145 °C in *o*-$C_6H_4Cl_2$ for 30 min. C: Heating at 115—125 °C in *sym*-$C_2H_2Cl_4$ for 30 min. b) Isolated yield. c) Lit, mp 84 °C: Ref. 12. d) Lit, mp 117 °C: Ref. 12. e) Lit, mp 189—190 °C: A. M. Comrie, *J. Chem. Soc., C*, **1971**, 2807. f) Lit, mp 69 °C: A. R. McCarthy, W. D. Ollis, and C. A. Ramsden, *J. Chem. Soc., Perkin Trans. 1*, **1974**, 624.

(**8b**) in moderate yields, respectively (Table 2).

The triazoles and pyrazoles obtained were identified by their analytical and spectral data, and the confirmation of the known compounds was made also by direct comparison with authentic specimens. To the present reactions, the following nitrilium ion mechanism[1] may be applicable most reasonably (Scheme 2).

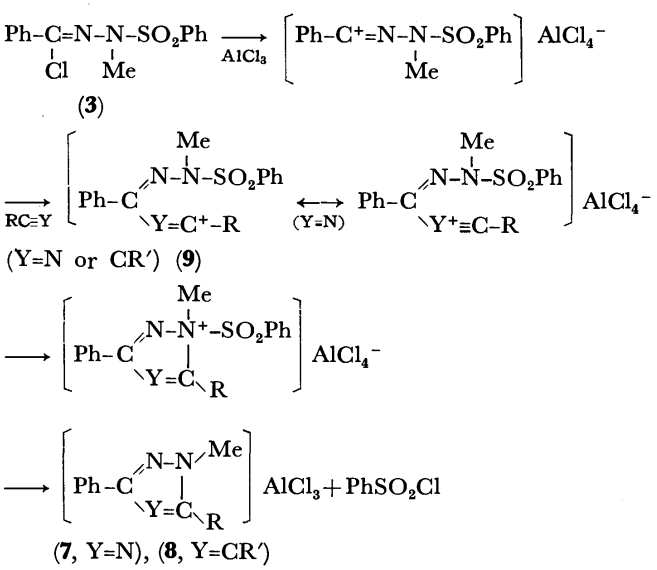

Scheme 2.

The lower yields in the pyrazole formation should be ascribed to the relative instability of the secondarily formed nitrilium ion(**9**,Y=CR′) and/or the weak nucleophilicity of acetylenes. In contrast to the reaction of **1**,[1] no dihydrotetrazine formation from two molecules of **3** could be observed, which may be due to the potential crowdedness of the intermediate ammonium ion required for the dihydrotetrazine formation.

Attempted Reactions with Olefins. Attempts to prepare pyrazolines by the aluminum chloride-catalyzed reaction of **3** with olefins such as cyclohexene, acenaphtylene, and norbornene were unsuccessful. However, small amounts (3%) of (3a*RS*,7a*SR*)-3-phenyl-1-phenylsulfonyl-4,7-methano-3a,4,5,6,7,7a-hexahydro-1*H*-indazole was obtained by the reaction of **2** with norbornene in the presence of aluminum chloride at room temperature.[5]

In this case, the reaction may proceed alternatively *via* the 1,3-dipolar cycloaddition of *N*-(phenylsulfonyl)-benzonitrilimine.[6]

Preparation of Triazoles (7) via N-Methyl-N-(phenylsulfonyl)benzamidrazone (4) (an Indirect Method for Preparing 7 from 3). Amidrazone **4** may fall under one of the simplest classes of derivatives from **3** and its –N–C(Ph)=N–N– part of molecule should be available for constructing a 1,2,4-triazole ring. Compound **4** was obtained in a good yield by the treatment of **3** in DMF with gaseous ammonia.[7]

When amidrazone **4** was allowed to react with benzoyl chloride under reflux in THF, *N*-methyl-*N*-phenylsulfonyl-*N*″-benzoylamidrazone was obtained along with the hydrochloride of **4**. However, fusion of **4** with an aroyl or acyl chlorides at an elevated temperature (145—155 °C) gave 3,5-disubstituted 1-methyl-1*H*-1,2,4-triazoles (**7**) in good yields. The results are summarized in Table 3. A similar treatment with acetic anhydride resulted in no formation of **7c**.

The reaction of hydrazonoyl chloride **3** with benz-

Table 3. Triazoles from amidrazone **4**

Reactant	Triazole	Yield/%[a]
PhCOCl	**7a**	77
$PhCH_2COCl$	**7b**	54
MeCOCl	**7c**	64
EtCOCl	**7d**[b]	70

a) Isolated yield. b) 1-Methyl-5-ethyl-3-phenyl-1*H*-1,2,4-triazole, mp 51—52 °C.

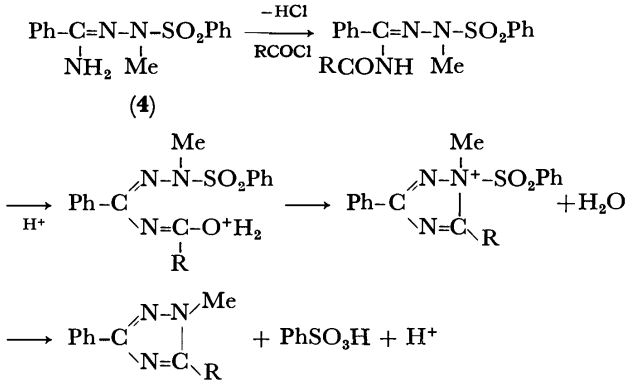

Scheme 3.

amide and with acetamide under the conditions of fusion afforded triazoles **7a** and **7c** in poor yields (18 and 10%, respectively) together with hydrazide **5**. The inferiority in yields should be due to the weak nucleophilicity of amides and also to the hydrolysis of **3** by water generated *in situ*.

The reaction of amidrazone **4** with acid chlorides can be formulated as follows (Scheme 3).

The formation of five-membered heteroaromatics *via* condensation or related reactions is well known to proceed smoothly in general. This specific tendency may be ascribed to the probable aromatic or quasi-aromatic character of the activated complex in reactions. Such situation has been partly discussed elsewhere,[8] and can be postulated in the present reactions including the Lewis acid-catalyzed reaction described above. The attempted pyrazoline-forming reaction is lacking in this type of stabilization.

Evaluation as a Preparative Method. Because of the inferiority in yields, the present Lewis acid-catalyzed reaction may be almost useless for obtaining pyrazoles. For preparing 1-alkyl-1*H*-1,2,4-triazoles, the following four procedures are available as general methods:[9,10,11] the condensation of diacylamines with alkylhydrazines (Einhorn-Brunner reaction), the condensation of amides with 2-alkylhydrazides (Pellizzari reaction), the reaction of *N*-alkylamidrazones with acid derivatives,[12] and the *N*-alkylation of *N*-unsubstituted 1,2,4-triazoles.[13] The former three methods require alkylhydrazines which are expensive or hardly available. In the fourth method, the *N*-alkylation proceeds usually at a specific position when the *C*-substituents are unlike each other. However, this specificity should be reduced in the case that the starting *N*-unsubstituted triazoles bear similar C_3- and C_5-substituents. On the other hand, the present method using *N*-methyl-*N*-sulfonylhydrazonoyl chloride or *N*-methyl-*N*-sulfonylamidrazone does not have such disadvantages as described above, and may be applicable to the preparation of *N*-higher alkyl homologs, since their precursor 1-benzoyl-2-alkyl-2-phenylsulfonylhydrazines can be easily obtained by the alkylation of **6**. Thus, in view of the good to comparable yields of products, the present method is useful for preparing 1-alkyl-1*H*-1,2,4-triazoles.

Experimental

Melting poins were determined with a Yanagimoto MP-S3 micromelting point apparatus, and are uncorrected. Molecular weights were determined with a Hitachi-Perkin-Elmer molecular weight apparatus Model 115. The microanalysis was performed on a Perkin-Elmer 240 elemental analyzer. The IR and NMR spectra were recorded with a Hitachi 260-10 and a Varian EM-360A spectrometer, respectively.

Preparation of N-*Methyl*-N-*(phenylsulfonyl)benzohydrazonoyl Chloride (3). Method A*: To a solution of *N*-(phenylsulfonyl)benzohydrazonoyl chloride[14] (**2**, 2.95 g, 10 mmol) in THF (30 ml), slightly excess amounts of an ethereal solution of diazomethane was added by portions. The reaction came to an end almost immediately with the evolution of nitrogen. The removal of solvent gave almost pure **3** (3.12 g), which was recrystallized from benzene or methanol. Mp 112—113 °C; IR (KBr, cm^{-1}): 1589 (C=N), 1355, 1164 (SO_2); NMR ($CDCl_3$, δ): 3.05 ppm (3H s, N-CH_3), 7.23—8.15 ppm (10H m, 2Ph). Found: MW, 305; C, 54.44; H, 4.25; N, 9.12%. Calcd for $C_{14}H_{13}N_2O_2SCl$: MW, 309; C, 54.46; H, 4.24; N, 9.07%.

Method B: To a solution of 1-benzoyl-2-phenylsulfonylhydrazine (**6**, 5.52 g, 20 mmol) in DMF (50 ml), a 0.58 g-portion (net 24 mmol) of sodium hydride dispersion (70% in liquid paraffin) was added under external cooling. After the ceasing of gas evolution (a few minutes), methyl iodide (3.12 g, 22 mmol) was added to the mixture. After stirring for 1 h at room temperature, the DMF solution was poured into water to separate 1-benzoyl-2-methyl-2-phenylsufonylhydrazine (**5**, 5.50 g), which was purified by crystallization from methanol. Mp 186—187 °C; IR (KBr, cm^{-1}): 3217 (NH), 1667 (C=O), 1352, 1154 (SO_2). Found: MW, 294; C, 57.76; H, 4.83; N, 9.57%. Calcd for $C_{14}H_{14}N_2O_3S$: MW, 290; C, 57.92; H, 4.86; N, 9.65%. A mixture of **5** (4.35 g, 15 mmol) and 30 ml of thionyl chloride was refluxed for 3 h. Removal of excess thionyl chloride *in vacuo* and washing the resulting yellowish residue with small amounts of methanol gave cryatalline **3** (4.40 g), which was recrystallized from methanol or benzene. Mp 112—113 °C.

Reaction of 3 with Nitriles in the Presence of a Lewis Acid. Typical Procedure: A mixture of benzonitrile (0.57 g, 5.5 mmol), freshly sublimed aluminum chloride (0.47 g, 5.5 mmol), **3** (1.55 g, 5.0 mmol), and *o*-dichlorobenzene (5 ml) was heated at 115—125 °C for 30 min in an oil bath. After being cooled. the reaction mixture was basified with a dilute aqueous sodium hydroxide solution and extracted with chloroform. The chloroform layer was washed with dilute hydrochloric acid and then water. After removal of the solvent, the chloroform extract was chromatographed on a silica-gel column (2.0 cm-d, 20 cm-h; eluents: hexane, benzene, and benzene–diethyl ether) to give **7a** (0.91 g, 77%), which was purified by recrystallization from benzene. The results are listed in Table 1 and 2.

*1-Methyl-3-phenyl-5-benzyl-1*H*-1,2,4-triazole (7b)*: Mp 70—71 °C (ethanol); IR (KBr, cm^{-1}): 1600, 1069, 1024 (1,2,4-triazole ring vibrations);[15] NMR ($CDCl_3$, δ): 3.73 ppm (3H s, N-CH_3), 4.23 ppm (2H s, -CH_2-), 7.10—7.60 ppm (8H m, *m,m'*- and *p*-protons of 3-Ph and Ph-CH_2-), 7.97—8.26 ppm (2H m, *o,o'*-protons of 3-Ph). Found: C, 77.00; H, 6.09; N, 17.06%. Calcd for $C_{16}H_{15}N_3$: C, 77.08; H, 6.06; N, 16.85%.

Aluminum Chloride-catalyzed Reaction of 2 with Benzonitrile (A Control Experiment). The reaction and the work-up in a similar way gave 3,5-diphenyl-1*H*(or 4*H*)-1,2,4-triazole. Yield: 49%; mp 191—192 °C (lit,[16] mp 189—190 °C). Found: C, 75.72; H, 5.34; N, 18.93%.

Reaction of 3 with Acetylenes. The reaction was carried out in a manner similar to above except the use of diphenylacetylene or phenylacetylene in the place of nitriles. The results are summarized in Table 2.

Preparation of N-*Methyl*-N-*(phenylsulfonyl)benzamidrazone (4).* Into a solution of **3** (15.5 g, 50 mmol) in DMF (60 ml) which was externally heated at approximately 80 °C in an oil bath, anhydrous ammonia was bubbled. After the completion of precipitation of ammonium chloride (about 30 min), the reaction mixture was cooled and then poured into water to separate *N*-methyl-*N*-(phenylsulfonyl)benzamidrazone (**4**, 13.0 g, 45 mmol), which was purified by crystallization from ethanol. Mp 156—158 °C; IR (KBr, cm^{-1}): 3479, 3373 (NH), 1625 (C=N), 1326, 1155 (SO_2); NMR ($CDCl_3$, δ): 2.83 ppm (3H s, N-CH_3), 5.75 ppm (2H brs, N-H), 7.23—8.12 ppm (10H m, 2Ph). Found: C, 58.07; H, 5.20; N, 14.50%. Calcd for $C_{14}H_{15}N_3O_2S$: C, 58.11; H, 5.23; N, 14.52%.

Reaction of 4 with Benzoyl Chloride in THF under Reflux. A solution of **4** (0.87 g, 3 mmol) and benzoyl chloride (0.42 g,

3 mmol) in THF (20 ml) was refluxed for 7 h. From the reaction mixture, *N*-methyl-*N*-(phenylsulfonyl)benzamidrazone hydrochloride was separated as precipitates. Yield: 0.56 g (1.7 mmol, 57%); mp 186—188 °C; IR (KBr, cm^{-1}): 3370—2600 (broad peaks, $[H_2N\cdots C\cdots N-]^+H$), 1673 (C=N), 1355, 1162 (SO_2). Found: C, 51.36; H, 4.85; N, 12.96%. Calcd for $C_{14}H_{16}N_3O_2SCl$: C, 51.61; H, 4.95; N, 12.90%. After the removal of solvent from the THF layer, the residue was crystallized from ethanol to give *N*-methyl-*N*-phenylsulfonyl-*N''*-benzoylbenzamidrazone (0.37 g, 0.94 mmol, 31%). Mp 179—181 °C; IR (KBr, cm^{-1}): 3330 (NH), 1697 (C=O), 1605 (C=N), 1340, 1162 (SO_2); NMR ($CDCl_3$, δ): 2.94 ppm (3H s, N–CH_3), 7.29—8.30 ppm (10H m, 2Ph), 9.93 ppm (1H brs, N–H). Found: C, 63.91; H, 4.90; N, 10.72%. Calcd for $C_{21}H_{19}N_3O_3S$: C, 64.11, H, 4.87; N, 10.68%.

Reaction of ***4*** *with Acid Chlorides under the Conditions of Fusion. General Procedure*: A mixture of **4** (3 mmol) and an acid chloride (3 mmol) was heated at 145—155 °C in an oil bath for 3.5 h (under the reflux of the acid chloride). After being cooled, the reaction mixture was extracted with chloroform and a portion of dilute sodium hydroxide solution. The chloroform extract was concentrated and chromatographed on a silica-gel column (2.0 cm-d, 15 cm-h) to give the corresponding triazole, which was crystallized from benzene, hexane, or ethanol. The results are summarized in Table 3.

*1-Methyl-5-ethyl-3-phenyl-1*H*-1,2,4-triazole (****7d****)*: Yield: 70 %; mp 51—52 °C (*picrate*: mp 166—167 °C); IR(KBr, cm^{-1}): 1603, 1066, 1024 (1,2,4-triazole ring vibrations);[15] NMR ($CDCl_3$, δ): 1.39 ppm (3H t, J=7.6 Hz, $C\underline{H}_3CH_2$–), 2.84 ppm (2H q, J=7.6 Hz, $CH_3C\underline{H}_2$–), 3.87 ppm (3H s, N–CH_3), 7.23 7.59 ppm (3H m, *m,m'*- and *p*-protons of Ph), 7.94—8.23 ppm (2H m, *o,o'*-protons of Ph). Found: C, 70.64; H, 7.07; N, 22.18%. Calcd for $C_{11}H_{13}N_3$: C, 70.56; H, 7.00; N, 22.44%. (*Picrate*: Found: C, 49.00; H, 3.87; N, 20.33%. Calcd for $C_{17}H_{16}N_6O_7$: C, 49.04; H, 3.87; N, 20.19%).

References

1) S. Conde, C. Corral, and R. Madronero, *Synthesis*, **1974**, 28.

2) a) R. Huisgen, M. Seidel, J. Sauer, J. W. McFarland, and G. Wallbillich, *J. Org. Chem.*, **24**, 892 (1959); b) R. Huisgen M, Seidel, G. Wallbillich, and H. Knupfer, *Tetrahedron*, **17**, 3 (1962); c) R. Huisgen, R. Grashey, M. Seidel, G. Wallbillich, H. Knupfer, and R. Schmidt, *Justus Liebigs Ann. Chem.*, **653**, 105 (1962).

3) P. Wolkoff, *Can. J. Chem.*, **53**, 1333 (1975).

4) S. Ito, Y. Tanaka, A. Kakehi, and H. Miyazawa, *Bull. Chem. Soc. Jpn.*, **50**, 2969 (1977).

5) The major products from reactions of **2** with norbornene and the other olefins were 3,6-diphenyl-1,4-bis(phenylsulfonyl)-1,4-dihydro-1,2,4,5-tetrazine, 3,6-diphenyl-1,2,4,5-tetrazine, *N*-(phenylsulfonyl)-*N*-[*N*-(phenylsulfonyl)benzohydrazonoyl]-benzohydrazonoyl chloride, and 1-benzoyl-2-phenylsulfonylhydrazine. As for these compounds, see S. Ito, Y. Tanaka, A. Kakehi, and T. Matsuno, *Bull. Chem. Soc. Jpn.*, **51**, 327 (1978).

6) S. Ito, A. Kakehi, T. Matsuno, and T. Sasaki, *Chem. Lett.*, **1979**, 733; T. Sasaki, S. Eguchi, and Y. Tanaka, *Tetrahedron*, **36**, 1565 (1980).

7) On treatment with ammonia, hydrazonoyl chloride **2** underwent dehydrochlorodimerization to give exclusively 3,6-diphenyl-1,4-bis(phenylsulfonyl)-1,4-dihydro-1,2,4,5-tetrazine.

8) S. Ito, Y. Tanaka, A. Kakehi, and K. Kondo, *Bull. Chem. Soc. Jpn.*, **49**, 1920 (1976).

9) Concerning the synthesis of 1,2,4-triazoles, see J. H. Boyer, "Heterocyclic Compounds," ed by R. C. Elderfield, John Wiley and Sons, Inc., New York (1961), Vol. 7. Chap. 5.

10) The 1,3-dipolar cycloaddition of *N*-methylbenzonitrilimine (generated *in situ* from 2-methyl-5-phenyltetrazole by thermolysis) to nitriles[2a] may be unavailable as a general route for preparing 3,5-disubstituted 1-methyl-1*H*-1,2,4-triazoles, because the precursor tetrazole yields on heating not only the 1,3-dipole but also methyl azide and benzonitrile,[2c] which should complicate the reaction.

11) For references concerned with other routes to 1-alkyl-1*H*-1,2,4-triazoles, see C. Grundmann and R. Ratz, *J. Org. Chem.*, **21**, 1037 (1956); G. Pifferi and P. Consonni, *J. Heterocycl. Chem.*, **9**, 581 (1972); H. J. Timpe, *Z. Chem.* **12**, 333 (1972) [*Chem. Abstr.*, **78**, 43384f (1973)]; T. Tadeusz and M. Dobosz, *Ann. Univ. Mariae Curie-Sklodowska, Sect. AA*, **26/27**, 17 (1971) [*Chem. Abstr.*, **79**, 18620t (1973)]; B. V. Ioffe and V. A. Chernyshev, *Khim. Geterotsikl. Soedin.*, **1976**, 563 [*Chem. Abstr.*, **85**, 46523f (1976)]; F. Risitano, G. Grassi, and F. Foti, *J. Chem. Res. (S)*, **1981**, 65; *ibid. (M)*, **1981**, 0831.

12) M. R. Atkinson and J. B. Polya, *J. Chem. Soc.*, **1954**, 3319.

13) *E.g.*, M. R. Atkinson and J. B. Polya, *J. Chem. Soc.*, **1954**, 141.

14) S. Ito, Y. Tanaka, and A. Kakehi, *Bull. Chem. Soc. Jpn.*, **49** 762 (1976).

15) For a reference to IR spectra of 1,2,4-triazoles, see E. Lieber, D. R. Levering, and L. J. Patterson, *Anal. Chem.*, **23**, 1594 (1951).

16) M. Fujimori, E. Haruki, and E. Imoto, *Bull. Chem. Soc. Jpn.*, **41**, 1372 (1968).

 © 1983 The Chemical Society of Japan Bull. Chem. Soc. Jpn., 56, 549—553 (1983)

Hydrolysis of Some Chromogenic Substrates and Adenosine Triphoshate Catalyzed by Phosphodiesterase-phosphomonoesterase from *Fusarium moniliforme*

Hiroshi Yoshida,* Masayuki Kawai, Chiseko Okimura, Nobuyuki Hirama, and Osamu Konno
Department of Chemistry, Faculty of Science, Tohoku University, Aobayama, Sendai 980
(Received July 16, 1982)

For comparison with known phosphodiesterases, the mode of action of phosphodiesterase-phosphomonoesterase from *Fusarium moniliforme* toward some key substrates was examined. The enzyme catalyzed the hydrolysis of either thymidine 3′-(4-nitrophenylphosphate) or thymidine 5′-(4-nitrophenylphosphate). The former substrate was hydrolyzed processively into thymidine, inorganic phosphate and 4-nitrophenol, whereas the latter was split into 4-nitrophenol and thymidine 5′-phosphate. The kinetic constants determined on the basis of 4-nitrophenol liberation were: $K_m = 4.6$ mmol dm^{-3} and $k_{cat} = 115$ s^{-1} for thymidine 3′-(4-nitrophenylphosphate); $K_m = 0.46$ mmol dm^{-3} and $k_{cat} = 19.7$ s^{-1} for thymidine 5′-(4-nitrophenylphosphate) at pH 5.3 and 37 °C. 4-Nitrophenyl phenylphosphonate was a good substrate for the enzyme showing kinetic constants $K_m = 1.4$ mmol dm^{-3} and $k_{cat} = 360$ s^{-1} at pH 5.3 and 37 °C. However, its chiral thio analogue, *O*-(4-nitrophenyl) phenylphosphonothioate, was hydrolyzed by the enzyme only very slowly in a stereo-nonspecific manner. The three phosphoryl groups in adenosine triphosphate was removed by the enzyme sequentially from the terminal position. These findings have made the uniqueness of *Fusarium* phosphodiesterase-phosphomonoesterase clearer.

Snake venom phosphodiesterase and spleen phosphodiesterase are representatives of many phosphodiesterases so far known. Although the classification of these two enzymes is based on the mode of hydrolysis of polynucleotides, they can easily be distinguished by the use of artificial chromogenic substrates; thymidine 3′-(4-nitrophenylphosphate) (TpONph) and thymidine 5′-(4-nitrophenylphosphate) (NphOpT). Snake venom phosphodiesterase is active only with the latter, whereas spleen phosphodiesterase is active only with the former.[1]

Kelly *et al.*[2] introduced a new chromogenic substrate, 4-nitrophenyl phenylphosphonate (PhPONph) for distinguishing these two phosphodiesterases. They showed that PhPONph is hydrolyzed only by phosphodiesterases of snake venom type (5′-nucleotide phosphodiesterases according to their terminology). Dudman and Benkovic[3] showed that the thio analogue of PhPONph, *O*-(4-nitrophenyl) phenylphosphonothioate (PhP(S)-ONph), is hydrolyzed by phosphodiesterases of the same type. PhP(S)ONph has a chiral phosphorus center. Snake venom phosphodiesterase hydrolyzes specifically the S_p diastereomer.[4]

Phosphodiesterase-phosphomonoesterase (PDMase) of the phytopathogenic fungus, *Fusarium moniliforme*, is a unique phosphohydrolase active with either phosphoric diesters or phosphoric monoesters. Yoshida *et al.*[5] pointed out that PDMase resembles snake venom phosphodiesterase, because a diribonucleoside monophosphate is first split by PDMase into a nucleoside and a 5′-nucleotide. Thus it is of interest to compare PDMase with snake venom phosphodiesterase more precisely using the above chromogenic substrates. This paper describes the action of PDMase on these substrates along with adenosine triphosphate (ATP).

Experimental

Materials. TpONph and NphOpT were purchased from Sigma and Calbiochem, respectively. Snake venom phosphodiesterase of *Crotalus adamanteus* was the product of Sigma (Type II), the activity of which was assayed at 37 °C with 1 mmol dm^{-3} bis(4-nitrophenyl) phosphate as a substrate in 50 mmol dm^{-3} Tris–HCl buffer (pH 8. 8) containing 1 mmol dm^{-3} $MgCl_2$. One unit (U) of activity was defined as that amount which liberates 1 μmol of 4-nitr ophenol per min under the above conditions. PDMase was purified from dried powder of the culture filtrate of *F. moniliforme* (commercial name, Toyocelase A, Toyo Brewery Co.) as described previously.[6] An isozyme mixture was used, because no difference in enzymic properties had so far been found among the isozymes.[7] PDMase was determined on the basis of activity toward 4-nitrophenyl phosphate. The assay was performed as described previously.[8] One unit (U) of activity which hydrolyzes 1 μmol of the substrate per min at pH 5.3 and 37 °C was assumed to correspond to 86 pmol of PDMase.[7]

Determination of Kinetic Constants. The kinetic constants of PDMase for TpONph, NphOpT, and PhPONph were determined by the measurements of the initial velocity of 4-nitrophenol liberation at various substrate concentrations. The reaction mixture contained, in a total volume of 2.0 cm^3, various amount of a substrate, sodium acetate buffer, pH 5.3 (100 μmol) and an appropriate amount of PDMase. The mixture was incubated at 37 °C for 10 min, then 0.5 mol dm^{-3}, Na_2CO_3 (1.0 cm^3) was added to stop the reaction. The liberated 4-nitrophenol was determined by measurement of the absorbance at 400 nm of the resulting solution using molar absorbance 18500. At least five different amounts of the substrate were used to cover a substrate concentration range involving K_m for the substrate. A computer-aided determination of K_m and k_{cat} was carried out basically according to the method of Wilkinson.[9]

High Performance Liquid Chromatography (HPLC). A high-speed liquid chromatograph HLC-803A (Toyo Soda) equipped with a variable wavelength UV monitor was used. The column was IEX-540 DEAE (4×150 mm) from the same company. The conditions for elution and detection varied depending on the experiment and will be described each time. The flow rate was fixed at 1.0 cm^3 min^{-1}.

Chemical Syntheses. *4-Nitrophenyl Phenylphosphonate*: The method described by Kelly *et al.*[2] was modified as follows. The solutions of phenylphosphonic dichloride and 4-nitrophenol in dry pyridine, each 16 cm^3 containing 41 mmol of either reagent, were added dropwise at approximately equal rates into 10 cm^3 of dry pyridine under stirring over 2 h. The temperature of the reaction mixture was maintained at 22—

30 °C by cooling in an ice bath. After the complete addition of the reagents, the mixture was stirred overnight at room temperature, then poured onto ice (100 g). After the ice thawed, the solution was adjusted to pH 1 with concd HCl (about 30 cm^3) and extracted three times with chloroform (each 70 cm^3). The combined chloroform layer was washed three times with 1 mol dm^{-3} HCl and twice with half-saturated aqueous NaCl. The chloroform solution was dehydrated with anhydrous Na_2SO_4, filtered and evaporated *in vacuo*. The residue was dissolved in acetone (15 cm^3). Concd aqueous ammonia was added to the solution until pH 7, then the solution was cooled in an ice bath for 1 h. The resulting precipitate of the ammonium salt of PhPONph was collected by centrifugation, washed extensively with cold acetone until no 4-nitrophenol was detected in the supernatant, and dried *in vacuo*. Yield 54%. Found: C, 48.79; H, 4.36; N, 9.27%. Calcd for $C_{12}H_{13}O_5N_2P$: C, 48.68; H, 4.43; N, 9.46%. UV_{max} (H_2O) 292 nm (ε 9800). ^1H NMR (D_2O) δ=8.67 (2H, d, J=9.0 Hz), 8.06—8.54 (5H, m), and 7.73 (2H, d, J=9.0 Hz).

O-(4-Nitrophenyl) Phenylphosphonothioate. Although Dudman and Benkovic[3] obtained the title compound by partial hydrolysis of the corresponding diester, we developed a new method for direct synthesis of the monoester. To phenylphosphonothioic dichloride (24 mmol) in 15 cm^3 of dry pyridine, 4-nitrophenol (24 mmol) in 12 cm^3 of dry pyridine was added dropwise under stirring over 2 h. The temperature of the reaction mixture was maintained at 2—10 °C by cooling in an ice bath. After the complete addition, the mixture was stirred overnight at room temperature, then poured onto ice (65 g). The product was extracted with chloroform (total 60 cm^3) as described in the synthesis of PhPONph. The extract was evaporated up and water (20 cm^3) was added to the residue. The mixture solidified on cooling. The resulting mass of the diester was triturated after addition of ethanol (20 cm^3) and filtered off. The filtrate was evaporated up and the residue was redissolved in water (20 cm^3). After a small amount of insoluble material was filtered off, 1 mol dm^{-3} cyclohexylammonium chloride (25 cm^3) was added to the solution. The precipitate formed on cooling was filtered, dried *in vacuo*, and recrystalized from hot acetonitrile. Yield 41%. Found: C, 54.52; H, 6.16; N, 7.40%. Calcd for $C_{18}H_{23}O_4N_2PS$: C, 54.81; H, 5.88; N, 7.10%. UV and ^1H NMR data agreed with those reported by Dudman and Benkovic.[3] The preparation, however, turned out to contain about 2% of PhPONph as described later.

Isolation of R_p Diastereomer of PhP(S)ONph. One of the diastereomers of chiral PhP(S)ONph was obtained by treatment of the synthetic racemate with snake venom phosphodiesterase. The reaction mixture contained, in a total volume of 12.1 cm^3, PhP(S)ONph (100 μmol), Tris-HCl buffer, pH 8.8 (500 μmol), $MgCl_2$ (10 μmol) and snake venom phosphodiesterase (0.28 U). The mixture was incubated at 37 °C for 25 h, then adjusted to pH 1 with concd HCl and extracted twice with chloroform (each 6 cm^3). The extract was charged on a column (2.2 cm × 14 cm) of silica gel preequilibrated with chloroform. After 4-nitrophenol was washed away with ethyl acetate (150 cm^3), the diastereomeric PhP(S)ONph was eluted with 1 : 1 mixture (50 cm^3) of ethyl acetate and methanol. The eluate was evaporated to dryness, taken up in water (2.0 cm^3), and adjusted to pH 7 with a dilute NaOH solution. The diastereomer thus obtained was not hydrolyzed by snake venom phosphodiesterase and showed CD ($[\theta]_{290\ nm}$ +630° $cm^2\ dmol^{-1}$).

Results

Hydrolysis of TpONph and NphOpT. PDMase hydrolyzed both TpONph and NphOpT, but in different ways. TpONph was degraded into thymidine, inorganic phosphate and 4-nitrophenol (Fig. 1A). A small amount of thymidine 3′-phosphate was detected, whereas 4-nitrophenyl phosphate was not. These results demonstrate that the two ester bonds in TpONph are hydrolyzed processively at the active site of PDMase. Presumably, 4-nitrophenol is the first leaving group, because thymidine 3′-phosphate, though little, was detected during the hydrolysis. On the contrary, NphOpT was cleaved first into 4-nitrophenol and

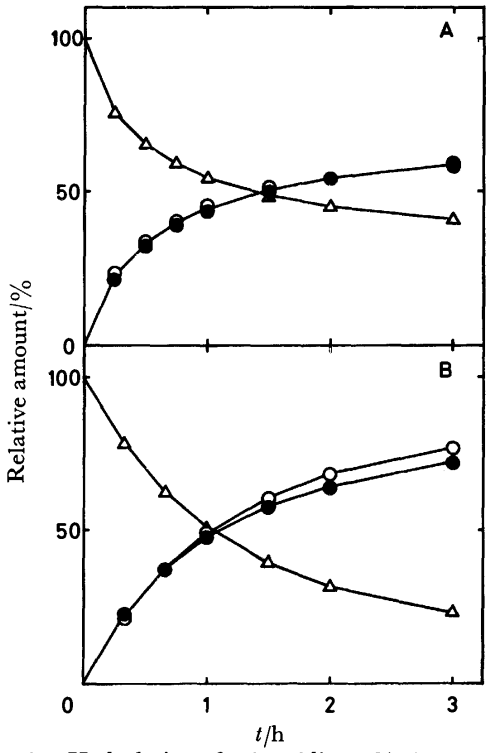

Fig. 1. Hydrolysis of thymidine 3′-(4-nitrophenylphosphate) (A) and thymidine 5′-(4-nitrophenylphosphate) (B) by PDMase.
The reaction mixture contained, in a total volume of 0.12 cm^3, TpONph (340 nmol) or NphOpT (220 nmol), sodium acetate buffer, pH 5.3 (15 μmol) and PDMase (116 mU). Incubation was at 37 °C. At the indicated times, portions (0.01 cm^3) of the mixture were withdrawn and analyzed by HPLC. The eluents were 0.25 and 0.125 mol dm^{-3} KH_2PO_4 for experiments A and B, respectively. Each compound was detected by absorbance at 290 nm and determined on the basis of peak height. Other conditions of HPLC were described in Experimental. The amount of each conpound is expressed in per cent to the sum of 4-nitrophenol and the remaining substrate. The retention times of the compounds were: (A) thymidine (●) 5.3 min, 4-nitrophenol (○) 11.2 min, TpONph (△) 13.1 min; (B) thymidine 5′-phosphate (●) 9.8 min, 4-nitrophenol (○) 11.3 min, NphOpT (△) 14.4 min. Besides the compounds described above, a small and nearly constant amount (less than 1%) of thymidine 3′-phosphate (retention time, 7.7 min) was detected in experiment A. A small and increasing amount (1.8% at 3 h) of thymidine (retention time, 5.3 min) was observed also in experiment B.

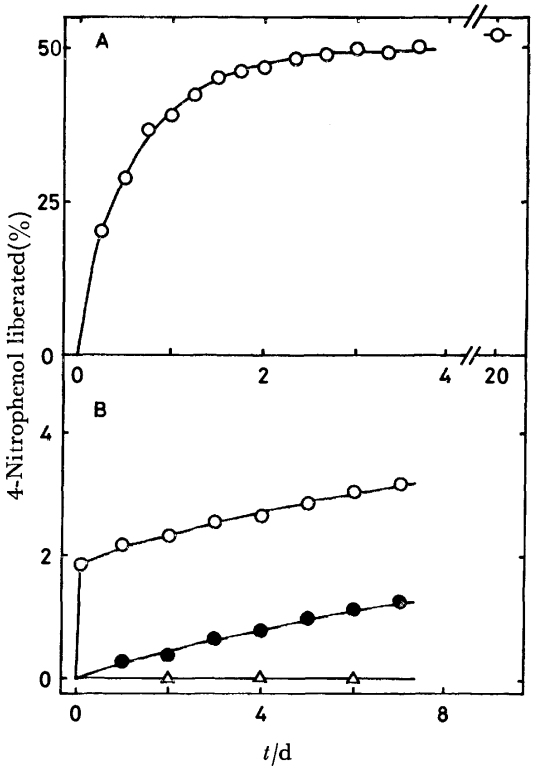

Fig. 2. Hydrolysis of *O*-(4-nitrophenyl) phenylphosphonothioate by snake venom phosphodiesterase (A) and PDMase (B). (A) The reaction mixture contained, in a total volume of 2.0 cm^3, PhP(S)ONph, racemate (2 μmol), Tris-HCl buffer, pH 8.8 (100 μmol), $MgCl_2$ (2 μmol) and snake venom phosphodiesterase (28 mU). Incubation was at 37 °C. At the indicated times, portions (0.05 cm^3) of the mixture were withdrawn and analyzed for 4-nitrophenol. (B) The reaction mixture contained, in a total volume of 1.0 cm^3, PhP(S)ONph, racemate (○) or R_p diastereomer (●) (3.5 μmol), sodium acetate buffer, pH 5.3 (50 μmol) and PDMase (3.9 U). Incubation was at 37 °C. At 1 h intervals, portions (0.1 cm^3) of the mixture were withdrawn and assayed for 4-nitrophenol. A control experiment (△) with the racemate was run in the absence of the enzyme under otherwise the same conditions.

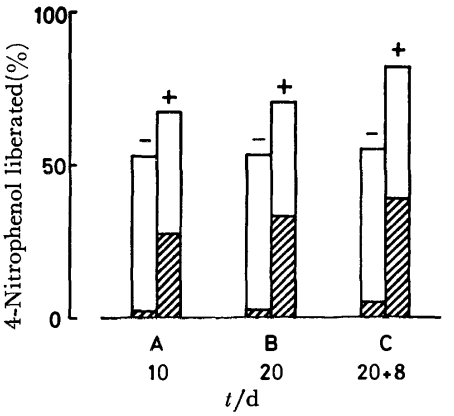

Fig. 3 Examination of the stereochemical course of hydrolysis of *O*-(4-nitrophenyl) phenylphosphonothioate by PDMase using snake venom phosphodiesterase. PhP(S)ONph, racemate (2.2 μmol) was incubated with sodium acetate buffer, pH 5.3 (50 μmol), NaN_3 as an antiseptic (1 mg) and PDMase (19 U) in a total volume of 1.0 cm^3 at 37 °C (first incubation). After 10 d (A) or 20 d (B) of the incubation, a portion (0.05 cm^3) of the mixture was withdrawn and assayed for 4-nitrophenol. Another portion (0.2 cm^3) of the mixture was taken and incubated with Tris-HCl buffer, pH 8.8 (40 μmol), $MgCl_2$ (0.4 μmol) and snake venom phosphodiesterase (12 mU) in a total volume of 0.4 cm^3 at 37°C (second incubation). After 3 h, a portion (0.1 cm^3) of the mixture was analyzed for 4-nitrophenol. The first incubation was renewed after 20 d: 0.2 cm^3 of the reaction mixture was mixed with 0.2 cm^3 of PDMase (7.5 U) solution in 10 mmol dm^{-3} sodium acetate buffer (pH 5.3), incubated at 37 °C for 8 more days (C), and analyzed as described above. The plus and minus signs on the histograms show the presence and absence, respectively, of PDMase during the first incubation. Hatched and blank areas in the histograms represent the percentage of 4-nitrophenol liberated by the first and second incubations, respectively.

thymidine 5′-phosphate, which was dephosphorylated very slowly (Fig. 1B). The kinetic constants for these substrates were determined to be: $K_m=(4.6\pm0.2)$ mmol dm^{-3} and $k_{cat}=(115\pm3)s^{-1}$ for TpONph; $K_m=(0.46\pm0.01)$ mmol dm^{-3} and $k_{cat}=(19.7\pm0.1)s^{-1}$ for NphOpT at pH 5.3 and 37 °C.

Hydrolysis of PhPONph and PhP(S)ONph. PhPONph was a good substrate for PDMase. The kinetic constants were $K_m=(1.4\pm0.3)$mmol dm^{-3} and $k_{cat}=(360\pm40)s^{-1}$ at pH 5.3 and 37 °C. The chiral thio analogue PhP(S)ONph synthesized by us was hydrolyzed by snake venom phosphodiesterase to an extent of 52.1% (Fig. 2A), confirming the observation of Dudman and Benkovic.[3] When this preparation was subjected to PDMase action, a portion (1.8%) was hydrolyzed rapidly but the rest was cleaved only very slowly (Fig. 2B). The R_p diastereomer was hydrolyzed by PDMase at almost the same rate as the racemate. The initial burst of 4-nitrophenol observed with the racemate but not with the R_p diastereomer may be due to contaminating PhPONph, which had resulted from desulfurylation of PhP(S)ONph probably during the isolation procedure in the synthesis.

The rate of 4-nitrophenol liberation from PhP(S)-ONph shown in Fig. 2B (25 pmol min^{-1} U^{-1}) corresponds to only 2×10^{-3}% of the rate which would be observed with PhPONph as the substrate under the same conditions. The low rate of hydrolysis is not due to an extremely high K_m, because the reduction of substrate concentration by a factor of 1/2 did not affect the rate appreciably (data not shown).

Although PhP(S)ONph (racemate) was hydrolyzed very slowly by PDMase, a considerable portion of the substrate could be hydrolyzed by a prolonged incubation with a large amount of the enzyme. When the remaining substrate was treated with snake venom phosphodiesterase, half its amount was always susceptible to the enzyme action (Fig. 3). These results indicate that neither diastereomer was concentrated in the remaining substrate. Therefore, PDMase hydrolyzed both dia-

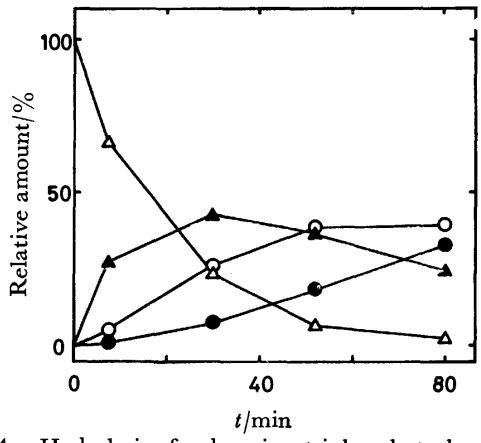

Fig. 4. Hydrolysis of adenosine triphosphate by PDMase. The reaction mixture contained, in a total volume of 0.21 cm^3, ATP (1.1 μmol), sodium acetate buffer, pH 5.3 (10 μmol) and PDMase (350 mU). Incubation was at 37°C. At the indicated times, portions (4 mm^3) of the mixture were withdrawn and analyzed by HPLC. The eluent was 0.5 mol dm^{-3} KH_2PO_4. Each compound was detected by absorbance at 260 nm and determined on the basis of peak area. Other conditions of HPLC were described in Experimental. The retention times of the compounds were: adenosine (●) 5.5 min, AMP (○) 8.9 min, ADP (▲) 13.9 min and ATP (△) 21.6 min.

stereomers at the same rate.

Hydrolysis of ATP. Figure 4 shows that ATP yielded adenosine diphosphate (ADP), adenosine monophosphate (AMP) and adenosine successively on incubation with PDMase. This indicates that the three phosphoryl groups in ATP is removed by PDMase in a sequential way from the terminal position.

Discussion

4-Nitrophenyl esters of thymidine 3′-phosphate and 5′-phosphate are currently used as key substrates for distinguishing phosphodiesterases between snake venom type and spleen type. Snake venom phosphodiesterase is active with NphOpT, whereas spleen phosphodiesterase is active with TpONph. The present study has shown that *Fusarium* PDMase acts on either of these substrates. Recently, Matsuzaki and Hashimoto[10] also reported that the acid phosphodiesterase of cultured tobacco cells was capable of hydrolyzing both NphOpT and TpONph. The dual activity may therefore be a feature common to acid phosphodiesterases of fungal or plant origin.

PDMase hydrolyzed the two chromogenic substrates in different ways. Processive hydrolysis occurred with TpONph as a substrate, whereas hydrolysis of NphOpT proceeded in a stepwise manner. The processive hydrolysis of a phosphodiester is the most prominent feature of PDMase. For example, bis(4-nitrophenyl) phosphate has been shown to be hydrolyzed into two moles of 4-nitrophenol and one mole of inorganic phosphate without appreciable release of the intermediary phosphomonoester, 4-nitrophenyl phosphate.[8] The same phenomenon was observed with TpONph. Presumably, stepwise hydrolysis of NphOpT resulted from the resistance of thymidine 5′-phosphate to PDMase action. The kinetic constants for these substrates were also different by an order of magnitude. Although the reason for such a big difference is not clear at present, it is worth noting that the k_{cat}/K_m value, a measure for goodness of a substrate, is of the same magnitude for these two substrates.

Kelly *et al.*[2] showed that phenylphosphonate esters are hydrolyzed by phosphodiesterase of snake venom type (5′-nucleotide phosphodiesterase according to their terminology), but not by spleen phosphodiesterase. Thus they proposed that phosphonate esters could serve as key substrates for distinguishing between the two types of phosphodiesterases. We have shown that PhPONph is a good substrate of PDMase. In fact, this compound has the highest k_{cat} (360 s^{-1}) among the substrates so far examined.

Dudman and Benkovic[3] demonstrated that the chiral thio analogue of PhPONph, PhP(S)ONph, is hydrolyzed by snake venom phosphodiesterase in a stereospecific manner. They claimed that the thio analogue is hydrolyzed by the same pattern of enzymes which catalyze hydrolysis of PhPONph. Further studies on the stereochemical course of snake venom phosphodiesterase strongly suggest that the S_p diastereomer of PhP(S)ONph is hydrolyzed specifically by the enzyme.[4,11,12] We have shown that the thio analogue is a poor substrate of PDMase, although the parent phosphonate ester is readily hydrolyzed by the enzyme. The rate of hydrolysis of PhP(S)ONph by PDMase was only 2×10^{-3}% of that of PhPONph. Both diastereomers of PhP(S)ONph seems to be hydrolyzed by the enzyme at almost equal rates. These results are in sharp contrast to the observation made with snake venom phosphodiesterase.

As for the mode of hydrolysis of ATP, PDMase also differs from snake venom phosphodiesterase. PDMase removes the three phosphoryl groups in ATP sequentially from the terminal position, whereas snake venom phosphodiesterase splits ATP into AMP and inorganic pyrophosphate.[4]

Precise comparison is now feasible between *Fusarium* PDMase and snake venom phosphodiesterase on the basis of our present and previous studies. PDMase, though unique in its wide substrate specificity, has certain resemblances to snake venom phosphodiesterase. (1) It yields 5′-nucleotide on acting diribonucleoside monophosphate.[5] (2) It hydrolyzes PhPONph. However, PDMase clearly differs from snake venom phosphodiesterase, to say nothing of pH optima and metal ion requirements, in the following points. (1) It hydrolyzes TpONph in addition to NphOpT. (2) It hydrolyzes chiral PhP(S)ONph only very slowly in a stereo-nonspecific manner. (3) It removes the three phosphoryl groups in ATP sequentially from the terminal position.

As a conclusion, the present study has made the uniqueness of *Fusarium* PDMase clearer. It does not seem to fit any entry of the current phosphohydrolase classification. We propose that a new entry be necessary for this unique enzyme, most appropriately among

EC 3.1.4 phosphoric diester hydrolases.

We thank Professor Nobuo Tamiya for valuable discussions, Dr. Yasuo Kikuchi for advice in the chemical syntheses, Dr. Masafumi Yasunami for NMR measurements, and Mr. Kunio Matsumoto of Toyo Brewery Co. for the generous gift of the enzyme source "Toyocelase A." This work was supported in part by a Grant-in-Aid for Scientific Research No. 56580094 from the Ministry of Education, Science and Culture.

References

1) W. E. Razzel, "Phosphodiesterase," in "Methods in Enzymology," ed by S. P. Colowick, N. O. Kaplan, Academic Press, London (1963), Vol. 6, pp. 236—258.
2) S. J. Kelly, D. E. Dardinger, and L. G. Butler, *Biochemistry*, **14**, 4983 (1975).
3) N. P. Dudman and S. J. Benkovic, *J. Am. Chem. Soc.*, **99**, 6113 (1977).
4) F. R. Bryant and S. J. Benkovic, *Biochemistry*, **18**, 2825 (1979).
5) H. Yoshida, K. Ishimaru, and O. Tsuchikura, *J. Biochem.*, **89**, 791 (1981).
6) K. Kakii and H. Yoshida, *J. Biochem.*, **81**, 1691 (1977).
7) S. Kanaya and H. Yoshida, *J. Biochem.*, **85**, 791 (1979).
8) H. Yoshida, *J. Biochem.*, **73**, 23 (1973).
9) G. N. Wilkinson, *Biochem. J.*, **80**, 324 (1962).
10) H. Matsuzaki and Y. Hashimoto, *Agric. Biol. Chem.*, **45**, 1317 (1981).
11) P. M. J. Burgers, B. K. Sathyanarayana, M. Saegner, and F. Eckstein, *Eur. J. Biochem.*, **100**, 585 (1979).
12) P. M. J. Burgers, F. Eckstein, and D. H. Hunneman, *J. Biol. Chem.*, **254**, 7476 (1979).

Highly Stereoselective Isomerization of Monosubstituted 1-Alkenes to (*E*)-2-Alkenes by Catalysis of $(C_5Me_5)_2TiCl_2/NaC_{10}H_8$

Munetaka AKITA, Hajime YASUDA, Kinya NAGASUNA, and Akira NAKAMURA*
Department of Macromolecular Science, Faculty of Science, Osaka University, Toyonaka, Osaka 560
(Received July 19, 1982)

The catalyst systems which consist of $MCl_2(C_5R_5)_2$(M=Ti, Zr; R=H, CH_3)/$NaC_{10}H_8$, *i*-C_3H_7MgBr, *n*-C_4H_9Li or $LiAlH_4$ in 1 : 2 ratio were highly effective for the stereoselective isomerization of monosubstituted 1-alkenes to (*E*)-2-alkenes. Unconjugated dienes were converted to (*E*)- or (*E,E*)-dienes. The catalysis of (C_5Me_5)-$TiCl_2/NaC_{10}H_8$ was extremely high and resulted in the complete isomerization of 1-alkenes in >99% stereoselectivity within a short period. The use of the bulky C_5Me_5 ligand is essential to find out the excellent stereoselectivity. Systems, $(C_5H_5)_2TiCl_2/NaC_{10}H_8$ and $(C_5H_5)_2TiCl_2$/*i*-C_3H_7MgBr showed less selectivity and the catalysis of the corresponding zirconium systems was very poor irrespective of the reducing agents and substrates.

Transition metal catalyzed isomerization of terminal olefins into internal olefins has been extensively studied with metal hydrides,[1] metal carbonyls[2] and others.[3] In general, these catalysts require relatively high temperatures (>50 °C) and result in a mixture of 1-alkenes, (*E*)- and (*Z*)-2-alkenes reflecting the thermodynamic equilibrium. The *Z*/*E* ratio varies in a wide range from 0.1 to 3.5. The reactions in some cases involve the carbon skeletal change[4] and the multiple double bond movement.[2a] Exceptional is [Ir(cyclooctadiene)$(PMePh_2)_2$]PF_6 which catalyzes isomerization of allyl ethers to (*E*)-1-propenyl ethers in extreme stereoselectivity at room temperature.[5a] Enantioselective isomerization of allylamines with a Rh(I) complex has also been reported recently.[5b]

We wish to report here the excellent catalysis of low valent titanocene species, "$(C_5Me_5)_2Ti$" and "$(C_5H_5)_2$-Ti", for highly stereoselective isomerization of 1-alkenes to (*E*)-2-alkenes under the mild conditions. Though titanocene species are generally accepted as efficient catalysts for hydrogenation[6] and hydrometalation of olefins,[7] the catalysis for isomerization of olefins has not yet been extensively studied except some works using $(C_5H_5)_2Ti$ species.[8] We found now that these species, especially $(C_5Me_5)_2Ti$, have a good catalysis toward the isomerization of 1-alkenes, allylamines and unconjugated dienes which lead to (*E*)-2-internal alkenes or (*E,E*)-dienes. The use of permethylcyclopentadienyl ligand was crucial to observe the high stereoselectivity.

Results and Discussion

*Catalytic Isomerization of 1-Hexene to (*E*)-2-Hexene.* The catalysts used in this work were generated by reduction of $(C_5Me_5)_2TiCl_2$ (**1**), $(C_5H_5)_2TiCl_2$ (**2**), or $(C_5H_5)_2ZrCl_2$ (**3**) with two equivalents of sodium naphthalene ($NaC_{10}H_8$), *i*-C_3H_7MgBr, butyllithium, or $LiAlH_4$. Photolysis of $(C_5Me_5)_2Ti(p\text{-tolyl})_2$ (**4**), $(C_2H_5)_2Ti(p\text{-tolyl})_2$ (**5**), and $(C_5H_5)_2Zr(p\text{-tolyl})_2$ (**6**) were also examined since ultraviolet ray irradiation to these complexes is known to generate low valent metallocene species.[9]

Catalyst systems	Catalyst systems
Ia $(C_5Me_5)_2TiCl_2/NaC_{10}H_8$	IIa $(C_5H_5)_2TiCl_2/NaC_{10}H_8$
Ib $(C_5Me_5)_2TiCl_2$/*i*-C_3H_7MgBr	IIb $(C_5H_5)_2TiCl_2$/*i*-C_3H_7-MgBr
Ic $(C_5Me_5)_2TiCl_2$/*n*-C_4H_9Li	IIc $(C_5H_5)_2TiCl_2$/*n*-C_4H_9Li
Id $(C_5Me_5)_2TiCl_2/LiAlH_4$	IId $(C_5H_5)_2TiCl_2/LiAlH_4$
IIIa $(C_5H_5)_2ZrCl_2/NaC_{10}H_8$	Ie $(C_5Me_5)_2Ti(p\text{-tolyl})_2/h\nu$
IIIb $(C_5H_5)_2ZrCl_2$/*i*-C_3H_7MgBr	IIe $(C_5H_5)_2Ti(p\text{-tolyl})_2/h\nu$
IIIc $(C_5H_5)_2ZrCl_2$/*n*-C_4H_9Li	IIIe $(C_5H_5)_2Zr(p\text{-tolyl})_2/h\nu$
IIId $(C_5H_5)_2ZrCl_2/LiAlH_4$	

The result of isomerization of 1-hexene at 20 °C was listed in Table 1 as a typical example. The distribution of the products was determined by gas chromatographic analysis with authentic samples and the structure of the respective isomers was determined from the chemical shift values of the ^{13}C-NMR spectra. The rate of isomerization was expressed as turnover max (mol/mol min) since these catalyst systems in many cases have an

TABLE 1. DISTRIBUTION OF THE PRODUCTS OBTAINED BY ISOMERIZATION OF 1-HEXENE WITH CATALYST SYSTEMS Ia—e, IIa—e, AND IIIa—e AND THEIR RATE OF ISOMERIZATION[a]

Reducing agent	Solvent	Distribution of (*E*)-2-hexene/(*Z*)-2-hexene/(*E*)-3-hexene(%) and turnover max (parentheses, mol/mol min)					
		$(C_5Me_5)_2Ti$ System(I)		$(C_5H_5)_2Ti$ System(II)		$(C_5H_5)_2Zr$ System(III)	
(a) $NaC_{10}H_8$	THF	100/0/0	(128)	83/17/0	(>4)	97/3/0	(8×10^{-3})
(b) *i*-C_3H_7MgBr	Ether	100/0/0	(0.2)	51/29/20	(54)	100/0/0	(4×10^{-2})
(c) *n*-C_4H_9Li	Ether	100/0/0	(0.4)	73/18/9	(77)	99/1/0	(1×10^{-2})
(d) $LiAlH_4$	Ether	100/0/0	(0.1)	66/17/17	(1.3)	No isomerization[b]	
(e) $(C_5R_5)_2M(p\text{-tolyl})_2$	Benzene	No isomerization		85/15/0	(>7)[c]	100/0/0	(2×10^{-2})[c]

a) Molar ratio of $(C_5R_5)_2MCl_2$(R: H, CH_3; M: Ti, Zr)/reducing agent/1-hexene was 1.0/2.0/200. Reaction was carried out at 20 °C for 1 h when Ia—e or IIa—e was used while the reaction with IIIa—e was done for 10 h. The ratio of 1-hexene to a solvent was 1.2/1.0 (v/v). b) Hydroalumination occurred. c) The reproducibility was invariably poor.

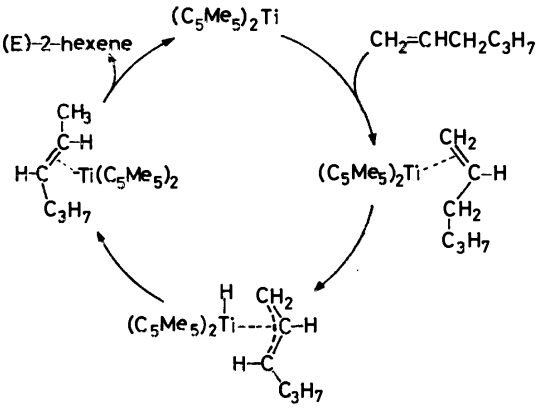

Scheme 1.

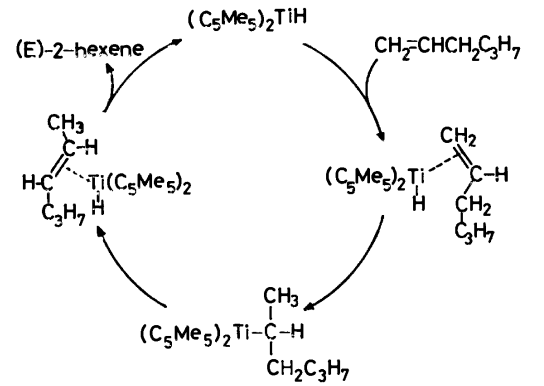

Scheme 2.

induction period (2—30 min).

1-Hexene was converted to (*E*)-2-hexene quantitatively when 1 mol-% of the catalyst system Ia—d which consists of **1** and $NaC_{10}H_8$(a), *i*-C_3H_7MgBr(b), *n*-C_4H_9Li(c) or $LiAlH_4$(d) in 1 : 2 ratio was added at 20 °C under atmospheric pressure. Catalysis of Ia was especially high in comparison to others and >98% of the substrate was converted to (*E*)-2-hexene within 5 min after the addition of the catalyst. The reaction of $(C_5Me_5)_2TiCl_2$ with $NaC_{10}H_8$ is reported to give "$(C_5Me_5)_2Ti$" which equilibrates with $(C_5Me_5)[(C_5(CH_3)_4(CH_2)]TiH$.[10] Therefore, it seems most likely that the isomerization proceeds following the cycle given in Scheme 1. The coordination of 1-hexene to $(C_5Me_5)_2$-Ti occurs in the initial step and "(η^3-allyl)TiH" species is produced by the successive β-hydride elimination. Liberation of 2-hexene results in the regeneration of $(C_5Me_5)_2Ti$. A similar $^3\eta$-allyltitanium hydride has been postulated as an intermediate in olefin hydrogenation[8a] and, actually, η^3-allylhafnium hydride was recently isolated.[11]

A similar catalytic cycle (1,3-hydrogen shift mechanism) has already been proposed for the isomerization of olefins catalyzed by a Pd(II) complex (though the selectivity was rather poor).[2a] The coordination of liberated (*E*)-2-hexene to the metal is hindered by the steric effect of permethylcyclopentadienyl ligand. The selective formation of (*E*)-2-hexene may be ascribed to the preferential formation of *syn*-η^3-allylic titanium hydride species. The X-ray structure of $(C_5H_5)_2Ti$(*syn*-η^3-butenyl) supports this assumption.[12]

In contrast to Ia, the turnover max for Ib, Ic and Id was remarkably small. Since the system IIb is known to afford $(C_5H_5)_2TiR$ which readily decomposes at ambient temperature to $(C_5H_5)_2TiH$ by β-hydride elimination,[13] the isomerization with Ib—c is best interpreted by the conventional addition-elimination mechanism as shown in Scheme 2.[1c] Actually, these systems have an induction period (5—30 min) before the largest turnover appears while the catalyst system Ia can initiate the isomerization immediately. Raising the reaction temperature to 60 °C (1—3 min) in the initial stage resulted in the shortening of the induction period which was observed for Ib—d.

Stereocontrol of the product will come from the predominant elimination of *threo*-hydrogen at the β-carbon. Two intermediates (A) and (B) are conceivable for the adduct, $(C_5Me_5)_2TiH$/1-hexene. However, the placement of (A) will favor over (B) from the steric reasons. If the intermediate assumes the geometry (B), steric repulsion among the C_5Me_5 ring, C_3H_7 and CH_3 group will prevent access of β-hydrogen to metal while the placement of (A) can diminish the steric repulsion. Hence, β-hydride abstraction from (A) was estimated to occur preferentially.

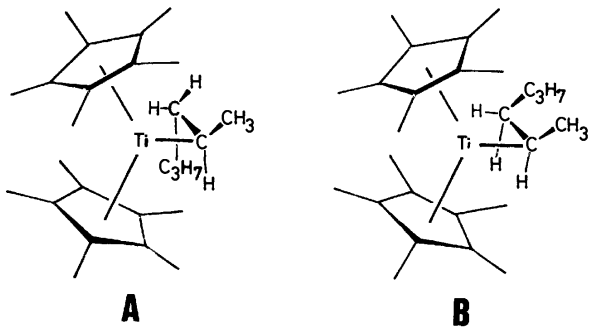

The catalysis of "$(C_5H_5)_2Ti$" or "$(C_5H_5)_2TiH$" was examined to evaluate the importance of the methyl groups of C_5Me_5 in stereoregulation. The catalysis of $(C_5H_5)_2TiCl_2/NaC_{10}H_8$ (IIa) was characterized by the low stereoselectivity (83%) and the diminished activity (turnover max). Isomerization to 3-hexene was not observed. The well-known spontaneous dimerization of $(C_5H_5)_2Ti$ to catalytically inactive $Ti_2H_2(\eta^5\text{-}C_5H_5)_2(\eta^{10}\text{-}C_{10}H_8)$ may be invoked for the lower activity.[14] When $(C_5H_5)_2Ti$ species were immobilized on a polystyrene matrix to inhibit the dimerization, a significant increase in activity was observed as reported by Bergbreiter *et al.*, though the stereoselectivity remained unchanged (72—85%).[8a]

Catalysts IIb—d showed a moderate activity. However, the stereoselection was insufficient and, further, these systems caused the isomerization to 3-hexene. The formation of 3-hexene implies that the isomerization takes place following the addition-elimination mechanism shown below.

Photolysis of $(C_5H_5)_2Ti(p\text{-tolyl})_2$ is also utilized for generation of a catalyst[9] but both activity and stereocontrol are insufficient. In addition, the reproducibility was poor with respect to the rate of isomerization. All

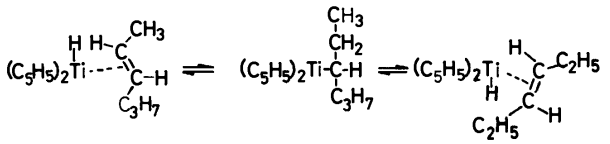

of the above results indicate that coordination of bulky ligand such as C_5Me_5 to metal is crucial to realize this highly stereoselective isomerization. The thermal-stability of Ia gave us an additional advantage in handling the catalyst; no decrease in activity was observed when Ia was kept at 20 °C for 6 h.

We have also examined the catalysis of the corresponding zirconium systems IIa—e and found very poor results irrespective of the reducing agents and substrates. The observed catalysis may be caused by a minute quantities of certain Zr(III) or Zr(II) species formed in the reaction system. Zr(IV) species are generally less readily reduced to Zr(II) or Zr(III) species in comparison to the Ti(IV) species.[15] The poor activity of IIIa—d will be ascribed to such natures existing in zirconium complexes. Photolysis of **6** did not give catalytically active species because **6** is highly resistant to ultraviolet rays under the normal conditions.

Though titanacyclopentane has been proposed as an intermediate in the dimerization of 1-alkenes,[16] any dimerization of alkenes was not observed in the present work.

Characteristics and the Limitation of Titanocene Species as Catalysts. Isomerization of a wide range of terminal olefins was examined with Ia to find broad applications. The results are given in Table 2. C_4–C_8 1-alkenes were readily converted to (*E*)-2-alkenes within a short time even in the absence of a solvent. Thus, the present system provides a very convenient method for preparation of (*E*)-2-alkenes. Treatment of the products with aq HCl followed by one flash distillation or even one filtration is sufficient to obtain the pure sample. In the similar manner, (*E*)-1-phenyl-1-propene and (*E*)-*N*,*N*-diethyl-1-propenylamine were prepared in good yield from 3-phenyl-1-propene and *N*,*N*-diethyl-2-propenylamine, respectively.

Table 2. Isomerization of mono- and disubstituted alkenes with catalyst system Ia at 20 °C[a]

Substrate	Product	*E*/*Z* ratio %	Conversion %
1-Butene	2-Butene	99/1	100
1-Pentene	2-Pentene	100/0	99
1-Octene	2-Octene	100/0	99
3-Phenyl-1-propene	1-Phenyl-2-propene	99/1	100
N,*N*-Diethyl-2-propenylamine	*N*,*N*-Diethyl-1-propenylamine	99/1	98
2-Methyl-1-pentene	Recovered	—	0
3-Methyl-1-pentene	Recovered	—	0
4-Methyl-1-pentene	4-Methyl-2-pentene	99/1	25
Allyl phenyl ether	Recovered	—	0
Allyl acetate	Recovered	—	0

a) Reaction conditions: reaction time, 1 h; ratio of Ia/alkenes, 1/100 (mol/mol); solvent was not used.

In contrast to the results obtained with terminal olefins, internal olefins such as (*E*)- or (*Z*)-isomers of 2-butene, 2-pentene and 3-hexene were completely inert toward the catalyst Ia at 20—50 °C. No isomerization from (*Z*)- to (*E*)- or (*E*)- to (*Z*)-isomer occurred under these reaction conditions. It should be noted, however, that conversion of (*E*)-2-hexene to (*Z*)-2-hexene was observed when the mixture of (*E*)-2-hexene and Ia (100 : 1 molar ratio) was heated to 120 °C for 48 h in a sealed tube. The ratio of (*E*)-, (*Z*)-2-hexene and (*E*)-3-hexene was 94 : 5 : 1. The mechanism may involve (η^3-allyl)TiH species followed by elimination.

Isomerization of 1-alkenes with an alkyl substituent varying in size was examined using Ia as catalyst. Thus, 2-methyl- and 3-methyl-1-pentene were not isomerized but 4-methyl-1-pentene could be converted to (*E*)-4-methyl-2-pentene in low yield (25% at 20 °C for 12 h). The catalyst IIa has higher catalysis for these olefins; *i.e.*, 3- and 4-methyl-1-pentene were converted quantitatively (>98%) to 3-methyl-2-pentene and 4-methyl-2-pentene, respectively, when the reaction was carried out for 12 h at 20 °C. Catalyst Ia was also inert to 1,3-hexadiene, 5-trimethylsilyl-1,3-pentadiene and 1,5-cyclooctadiene. Addition of a stoichiometric amount (3 mol equivalents to Ia) of alkyl allyl ether, allyl alcohol or allyl acetate resulted in the complete deactivation of the catalyst. This will be due to the cleavage of alkyl allyl ether, allyl ester or vinyl ether which was formed by double bond migration. Further studies are required to clarify the stoichiometric reaction.

Catalytic Isomerization of Unconjugated Dienes. The result of isomerization of unconjugated dienes was given in Table 3. The catalyst Ia showed a sufficiently high selectivity for 1,5-hexadiene and 1,7-octadiene, whereas IIa and IIb showed a rather poor selectivity and induced an undesired skeletal isomerization leading to 1-methylcyclopentene. The pathway for formation of 1-methylcyclopentene is interpreted by the catalytic cycle given in Scheme 3. Since $(C_5H_5)_2TiCl_2$ is known to catalyze the hydromagnesiation of olefins,[7b] the formation of 5-hexenylmagnesium compound is most probable in the initial stage. The resulting magnesium compound is readily converted into 5-hexenyltitanium

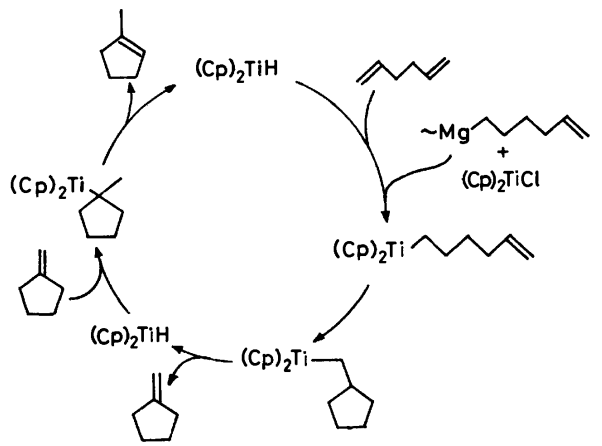

Scheme 3.

Table 3. Distribution of the products obtained by isomerization of 1,5-hexadiene and 1,7-octadiene with catalysts Ia, IIa and IIb[a)]

Catalyst system	Isomerization of 1,5-hexadiene Products/%				Isomerization of 1,7-octadiene Products/%			
	2,4-Hexadiene			1-Methylcyclopentene	2,6-Octadiene			(*E*)-1,6-Octadiene
	(*E*, *E*)	(*E*, *Z*)	(*Z*, *Z*)		(*E*, *E*)	(*E*, *Z*)	(*Z*, *Z*)	
Ia	99.6	0.4	0.0	0.0	96.4	0.0	0.0	3.6
IIa	78.3	15.1	0.3	6.3	41.9	43.2	10.1	4.8
IIb	56.3	15.2	0.7	27.8	35.6	45.6	13.7	5.2

a) Reaction conditions: reaction time, 20 °C for 1 h; ratio of Ia to dienes, 1/100(mol/mol). Solvent was not used.

Table 4. Stereocontrolled regioselective isomerization of monosubstituted unconjugated dienes with Ia at 20 °C[a)]

Substrate	Product	Stereoselectivity/%[b)]	Conversion/%[b)]
1,4-Pentadiene	(*E*)-1,3-Pentadiene	>99	99
(*E*)-1,4-Hexadiene	(*E*, *E*)-2,4-Hexadiene	>99	100
2-Methyl-1,4-pentadiene	(*E*)-2-Methyl-1,3-pentadiene	>99	97
2-Methyl-1,5-hexadiene	(*E*)-2-Methyl-1,4-hexadiene	>99	97

a) Reaction conditions: reaction time, 20 °C for 2 h; ratio of Ia to dienes, 1/100; solvent was not used. b) Determined by gas chromatographic analysis.

derivative by the metal exchange reaction. Ring closure gives (cyclopentylmethyl)titanium species which releases methylenecyclopentane by the β-elimination. The isomerization of methylenecyclopentane to 1-methylcyclopentene will follow the addition-elimination mechanism similar to that reported by Lehmkuhl.[17)]

Stereocontrolled Regioselective Isomerization of Substituted Dienes. The substrate selectivity observed in the above-mentioned olefin isomerization prompted us to try the regioselective (chemoselective) isomerization of substituted dienes. As shown in Table 4, vinyl groups were shifted to internal (*E*)-type olefins while vinylidene moiety was unaffected. Thus, regio- and stereoselective isomerization of a series of methylpentadienes was established with the catalyst Ia. 4-Vinylcyclohexene was isomerized with the catalyst IIa but not with Ia. A mixture of 4-ethylidenecyclohexene (69%) and 3-ethylidenecyclohexene (31%) were obtained in 91% yield by catalysis of IIa (1 mol%) at 20 °C for 12 h. Recently, quantitative isomerization of

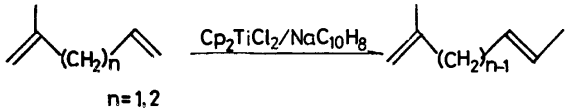

vinylcycloalkanes to ethylidenecycloalkanes was accomplished under rather vigorous conditions (180 °C) with the catalyst IId.[8b)] In these reaction conditions, the catalyst IId was also capable of converting 2,5-dimethyl-1,5-hexadiene or bicyclo[4.3.0]-3,7-nonadiene to conjugated 1,3-dienes.[8b-c)]

The extremely good selectivity and chemoselectivity observed in this work utilizing $(C_5Me_5)_2Ti$ species will be valuable for organic syntheses since the isomerization took place under the mild conditions in a short period.

Experimental

All operations were conducted by Schlenk techniques under an argon atmosphere. ^1H- and ^{13}C-NMR spectra were recorded at 100 and 25.05 MHz on a Varian XL-100 and a JEOL FX-90Q spectrometer, respectively. The infrared pectra were recorded on a Hitachi EPI-2 spectrometer. The structure of the products was determined from the chemical shift values of ^{13}C-NMR spectra referring to the reported data.[18)] The product distribution was determined with a Hitachi Model 163 gas chromatograph. $(C_5Me_5)_2TiCl_2$,[10)] $(C_5H_5)_2TiCl_2$,[19)] and $(C_5H_5)_2ZrCl_2$[19)] were prepared according to the method previously reported. Tetrahydrofuran, diethyl ether and benzene were dried over sodium-potassium alloy and were distilled. All olefins and dienes (Aldrich Chem.) were dried over calcium hydride and purified by distillation.

Isomerization of 1-Hexene with Ia. To a stirred suspension of $(C_5Me_5)_2TiCl_2$ (39.0 mg, 0.10 mmol) in 0.8 ml THF was added a solution of $NaC_{10}H_8$ (30 mg, 0.2 mmol) in THF (1 ml) at room temperature. The color of the solution changed into dark yellow green. After stirring for 10 min, mixture was evaporated to dryness and was extracted with pentane (10 ml) at 20 °C. After the removal of the salt with a centrifuge, flash distillation of the pentane extract was performed *in vacuo* to give the species Ia as a green solid (32 mg). To the resulting catalyst species was added 1-hexene (1.25 ml, 10 mmol) at −70 °C and the mixture was immediately warmed to 20 °C to induce the isomerization. A small portion of the reaction mixture was taken out and hydrolyzed to monitor the reaction with a gas chromatograph. After stirring the mixture for 30 min at 20 °C, 6 mol dm^{-3} aq HCl was added and organic layer was distilled to give (*E*)-2-hexene (1.1 ml, 9 mmol). The removal of the salts or solvent was not neccessarily required because the presence of these materials did not affect on catalysis.

Preparation of Ib—d and IIa—d. To a mixture of $(C_5Me_5)_2TiCl_2$ (19 mg, 0.05 mmol) and ether (0.5 ml) was added $i\text{-}C_3H_7MgBr\cdot(OEt_2)_2$ (26 mg, 0.1 mmol) in ether (1.5 ml). The mixture was stirred at 20 °C for 10 mix the and precipitates was separated by centrifugation using a specially designed two-necked tube fitted with septum caps. The ether solution was evaporated to dryness to give Ib as a green solid and 1-hexene was added to the solid at 20 °C to induce the isomerization. In essentially the same way for Ia, diethyl ether solution (1.5 ml) of butyllithium (6 mg, 0.1 mmol) or $LiAlH_4$ (4 mg, 0.05 mmol) was allowed to react with $(C_5Me_5)_2TiCl_2$ (0.1 mmol) for 10 min and 60 min, respectively, to generate the catalyst Ic

and Id. The ether soluble green solid was used as catalysts. The systems IIa—d were prepared in the similar manner.

Photolysis of $(C_5Me_5)_2Ti$(p-tolyl)$_2$ and $(C_5H_5)_2Ti$(p-tolyl)$_2$. $(C_5Me_5)_2Ti(p\text{-tolyl})_2$ **4** and $(C_5H_5)_2Ti(p\text{-toyl})_2$ **5** were prepared according to the reported procedures.[9] After the addition of **4** or **5** (1 mmol) to 1-hexene (100 mmol) in benzene (10 ml), ultraviolet ray irradiation was carried out with stirring for 2 h using a high pressure (250 W) mercury lamp.

Characterization of the Products. ^{13}C-NMR assignment of a series of (*E*)- or (*Z*)-olefins and dienes including the products obtained in this paper is already established by Haan *et al.*[18] Therefore, the structure was determined with reference to the reported data. The distribution of the products was analyzed using authentic samples (Aldrich Chem.) with a gas chromatograph fitted with a capillary column, HB-2000 or CW (45 m, Gaschro Kogyo, Co.). When the product was contaminated with isomers, characterization was done after the separation into the respective isomers by a preparative gas chromatograph fitted with a Benton-34 or SiDC-560 column. The geometry of *N,N*-diethyl-1-propenylamine was determined by the ^{1}H-NMR spectrum referring with the data reported by Sauer.[20] The IR and ^{1}H-NMR spectra of 1-methylcyclopentene agreed with the data reported by Becker.[21]

References

1) a) C. A. Tolman, *J. Am. Chem. Soc.*, **94**, 2994 (1972); b) D. Bingham, D. E. Webster, and P. B. Wells, *J. Chem. Soc., Dalton Trans.*, **1974**, 1519; c) W. T. Hendrix and J. L. von Rosenberg, *J. Am. Chem. Soc.*, **98**, 4850 (1976).

2) a) D. Bingham, B. Hudson, B. D. E. Webster, and P. B. Wells, *J. Chem. Soc., Dalton Trans.*, **1974**, 1521; b) M. Orchin, *Adv. Catal.*, **16**, 1 (1966).

3) a) D. Bingham, D. E. Webster, and P. B. Wells, *J. Chem. Soc., Dalton Trans.*, **1974**, 1514; b) J. Andrieux, D. H. R. Barton, and H. Patin, *J. Chem. Soc., Perkin Trans. 1*, **1977**, 359.

4) R. G. Miller, P. A. Pinke, R. D. Stauffer, H. J. Golden, and D. J. Baker, *J. Am. Chem. Soc.*, **96**, 4211 (1974).

5) a) D. Baudry, M. Ephritikhine, and H. Ferkin, *J. Chem. Soc., Chem. Commun.*, **1978**, 694; b) K. Tani, T. Yamagata, S. Otsuka, S. Akutagawa, H. Kumobayashi, T. Taketomi, H. Takaya, A. Miyashita, and R. Noyori, *ibid.*, **1982**, 600.

6) a) G. W. Watt, L. J. Baye, and F. O. Drummond, Jr., *J. Am. Chem. Soc.*, **88**, 1138 (1966); b) E. S. Chandrasekaran, R. H. Grubbs, and C. H. Brubaker, Jr., *J. Organomet. Chem.*, **120**, 49 (1976); c) C-P. Lau, B-H. Chang, R. H. Grubbs, and C. H. Brubaker, Jr., *ibid.*, **214**, 325 (1981).

7) a) K. Isagawa, K. Tatsumi, and Y. Ohtsuji, *Chem. Lett.*, **1976**, 1145; b) F. Sato, H. Ishikawa, and M. Sato, *Tetrahedron Lett.*, **21**, 365 (1980); **22**, 85 (1981); c) F. Sato, H. Ishikawa, Y. Takahashi, M. Miura, and M. Sato, *ibid.*, **1979**, 3745; d) F. Sato, S. Sato, and M. Sato, *J. Organomet. Chem.*, **131**, C26 (1977); e) F. Sato, Y. Tomuro, H. Ishikawa, T. Oikawa, and M. Sato, *Chem. Lett.*, **1980**, 103.

8) a) D. E. Bergbreiter and G. L. Parsons, *J. Organomet. Chem.*, **208**, 47 (1981); b) F. Turecek, H. Antropiusova, K. Mach, V. Hanus, and P. Sedmera, *Tetrahedron Lett.*, **21**, 637 (1980); c) K. Mach, F. Turecek, H. Antropiusova, L. Petrusova and V. Hanus, *Synthesis*, **1982**, 53.

9) a) M. D. Rausch, W. H. Boon, and E. A. Mintz, *J. Organomet. Chem.*, **160**, 81 (1978); b) E. Samuel, *ibid.*, **198**, C65 (1980); c) H. S. Tung and C. H. Brubaker, Jr., *Inorg. Chim. Acta*, **52**, 197 (1981).

10) J. E. Bercaw, *J. Am. Chem. Soc.*, **96**, 5087 (1974).

11) R. H. Grubbs, private communication.

12) H. J. L. Meijer and F. Jellinek, *Inorg. Chim. Acta*, **4**, 651 (1970).

13) H. A. Martin and F. Jellinek, *J. Organomet. Chem.*, **12**, 149 (1968).

14) H. H. Brintzinger and J. E. Bercaw, *J. Am. Chem. Soc.*, **92**, 6182 (1970).

15) For example, D. B. Carr and J. Schwartz, *J. Am. Chem. Soc.*, **101**, 3521 (1979).

16) a) J. X. McDermott, M. E. Willson, and G. M.. Whitesides, *J. Am. Chem. Soc.*, **98**, 6529 (1976); b) G. Erker and K. Kropp, *ibid.*, **101**, 3659 (1979).

17) H. Lehmkuhl and S. Fustero, *Liebigs Ann. Chem.*, **1980**, 1361.

18) J. W. Haan and L. J. M. van de Ven, *Org. Magn. Reson.*, **5**, 147 (1973); P. A. Couperus, A. D. H. Clague, and J. P. C. M. van Dongen, *ibid.*, **8**, 426 (1976).

19) G. Wilkinson and J. M. Birmingham, *J. Am. Chem. Soc.*, **76**, 4281 (1954).

20) J. Sauer and H. Prahl, *Tetrahedron Lett.*, **1966**, 2863.

21) K. B. Becker, *Helv. Chim. Acta*, **60**, 68 (1977).

Proton-driven Ion Transport and Metal-assisted Amino Acid Transport with an Anion-capped Azacrown Ether[1)]

Seiji SHINKAI,* Hidefumi KINDA, Yoshikazu ARARAGI, and Osamu MANABE*
Department of Industrial Chemistry, Faculty of Engineering, Nagasaki University, Nagasaki 852
(Received August 9, 1982)

We have found that 1,10-diaza-4,7,13,16-tetraoxa-18-crown-6 with a carboxylate cap and a hydrophobic dodecanoyl group (**1**) acts as a new class of ion carrier for membrane transport. The rate of K^+ transport across a chloroform liquid membrane was significantly affected by pH of the OUT aqueous phase: The rate decreased with increasing or decreasing pH, providing a maximum at around pH 5. The main species of **1** in the neutral pH region should be zwitterionic $\mathbf{1}^{\pm}$, so that one may rationalize the pH-rate profile in terms of (i) "enforced ion release" due to protonation of the ring nitrogen and (ii) high lipophilic nature of zwitterionic $\mathbf{1}^{\pm}$. The efficiency of **1** was further demonstrated by active K^+ transport from the basic IN aqueous phase to the neutral OUT aqueous phase. Also, **1** was capable of carrying amino acids in the presence of alkaline earth metal cations. These results suggest that, being different from conventional anion-capped crown ethers, the aza crown ethers carrying the *N*-substituted carboxylate cap exhibit a new class of ionophore functions.

Cations are known to be transported through biological membranes with the aid of antibiotics.[2,3)] In particular, polyether antibiotics such as nigericin and monension feature "enforced ion-release" and coupled counter-transport of cations and protons due to interconversion between cyclic and acyclic forms.[2-5)] Although coupled counter-transport can be mimicked in an artificial system using anion-capped crown ethers,[6-8)] acyclic polyethers,[9-13)] and metal complexes,[14-16)] few of them permit as ready an enforced ion release as do the polyether antibiotics.[17,18)] As show in Scheme 1, for example, the conventional anion-capped crown ethers mediate the ion-transport, the basic functions of these carriers being related only to the ion-binding ability due to charge neutralization by an intramolecular anionic cap.

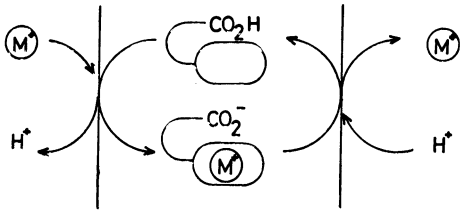

Scheme 1.

Recently, several new ionophores have been synthesized from 1,10-diaza-4,7,13,16-tetraoxa-18-crown-6 which is commercially available.[19-24)] In order to attain the "facile enforced ion-release" like natural ionophores, we sythesized an ionophore **1** for which the following novel behaviors are expected (Scheme 2): (i) Ion-release is enforced by protonation of the ring nitrogen, (ii) the main species in the neutral pH region, $\mathbf{1}^{\pm}$, should be highly lipophilic owing to its zwitterionic structure, and (iii) the counter-current of protons should be mediated by the ring nitrogen but not by the carboxylato group and should occur from the neutral OUT aqueous phase. With these expectations in view, we carried out the proton-driven ion-transport and the metal-assisted amino acid transport through a liquid membrane.

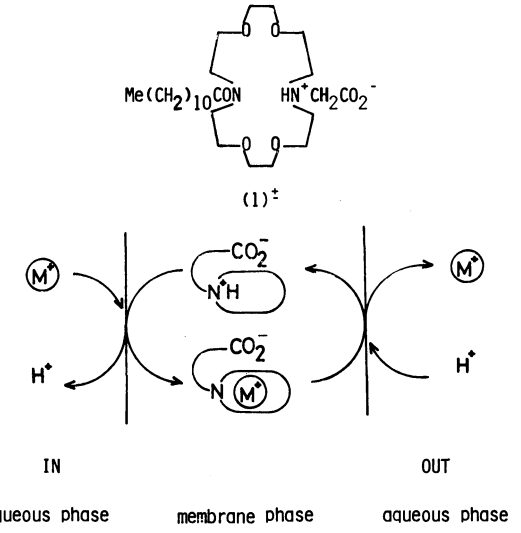

Scheme 2.

Experimental

Materials. 1-Dodecanoyl-10-carboxymethyl-1,10-diaza-4,7,13,16-tetraoxa-18-crown-6 (**1**) was prepared by mono-*N*-alkylation of 1,10-diaza-4,7,13,16-tetraoxa-18-crown-6 with chloroacetic acid, followed by acylation of the remaining amine with dodecanoyl chloride. The aqueous solution (20 ml) containing 1.19 g (12.5 mmol) of chloroacetic acid was adjusted to pH 9.0 with sodium carbonate. After the addition of 3.00 g (11.4 mmol) of 1,10-diaza-4,7,13,16-tetraoxa-18-crown-6, the reaction mixture was heated at 90—100 °C with stirring. The progress of the reaction was followed by the potentiometric titration of the aliquot withdrawn from the solution with silver nitrate. The titration showed that the stoichiometric amount of Cl^- was produced after 8 h. The reaction mixture was diluted to 100 ml with water and adjusted to pH 11 with sodium carbonate. The aqueous solution was extracted with chloroform to remove the unreacted diaza crown ether. The aqueous layer was concentrated *in vacuo*, the residue being taken with absolute ethanol. Thus, 3.47 g of the oily product (monocarboxymethylated diaza crown ether) was obtained. The HPLC analysis showed that the product contained a

small amount of bis(carboxymethylated) diaza crown ether, but we used the oil without further purification. 3.47 g of the oil was dissolved 34 ml of *N,N*-dimethylformamide (DMF) containing 4 ml of triethylamine. While stirring the DMF solution at room temperature, 2.50 g (11.4 mmol) of dodecanoyl chloride in 10 ml of DMF was added dropwise. After the addition, the reaction mixture was heated at 60 °C for 1 h. The solution was diluted with 50 ml of water, extracted with chloroform, and the chloroform solvent was evaporated to dryness. The oily residue was dissolved in water adjusted to pH 6.5 and extracted with chloroform. The chloroform solution was concentrated *in vacuo*. Finally, the product (**1**) was isolated by the TLC separation (silica gel, chloroform: ethanol=4 : 1 in volume); oil, yield 16.7%. NMR ($CDCl_3$): CH_3, 0.88 ppm (3H); $(CH_2)_9$, 1.28 ppm (18H); NCO-CH_2, 2.30 ppm (2H); C-N-CH_2 (ring proton), 2.76 ppm (4H); N-CH_2-CO, 3.12 ppm (2H); OCH_2, 3.64 ppm (16H); CO-N-CH_2, 3.80 ppm (4H). IR (KBr disk) of the sodium salt; $\nu_{C=O}$ 1630 and 1600 cm^{-1}, ν_{C-O-C} 1100 cm^{-1}. Found: C, 59.42; H, 10.04; N, 4.95%. Calcd for $C_{26}H_{49}N_2O_7Na$: C, 59.21; H, 9.77; N, 5.31%.

Method of Ion-transport. The ion-transport was carried out using a U-tube apparatus immersed in a thermostated water bath (30 °C). The transport system consists of 50 ml of a liquid membrane phase (chloroform) and 25 ml of IN and OUT aqueous phases in a U-tube with 2.5 cm diameter. The membrane phase was stirred slowly at a constant speed (180 rpm). The concentrations of alkali and alkaline earth metal cations were determined by an atomic absorption spectrophotometer (Shimadzu AA-640), while those of amino acids were determined by the treatment with fluorescamine.[25] Usually, the sampling was continued for 12 h at intervals of 1 h. After an induction period (about 1 h) a linear increase in metal (or amino acid) was observed, from which we determined the transport rates across a chloroform membrane barrier.

Results and Discussion

Transport of Alkali and Alkaline Earth Metal Cations. Potentiometric titration of **1** (30 °C) gave two pK_a values: $pK_{a1}=3.45$ and $pK_{a2}=6.99$. The fraction of zwitterionic $\mathbf{1}^{\pm}$ thus becomes maximum at pH 5.22 $(=(pK_{a1}+pK_{a2})/2)$. As a preliminary step to ion-transport, we estimated the partition of **1** between chloroform and aqueous solution by its absorbance at 270—300 nm which is on the lower slope of the absorption band of **1**. The partitions of **1** to the chloroform layer after agitation with equal volumes of following aqueous solutions were: 90% with 0.01 M HCl,† 96% with pH 5.23 (0.05 M Tris–AcOH), 73% with 0.01 M Et_4NOH, and 99% with 0.01 M KOH. The result indicates that the solubility of **1** in chloroform is in the order, $\mathbf{1}^-$–K^+ complex$>\mathbf{1}^{\pm}>\mathbf{1}^+>\mathbf{1}^-$.

The transport of alkali and alkaline earth metal cations across a chloroform membrane was studied using a U-tube apparatus immersed in a thermostated water-bath (30 °C). The typical experimental results are summarized in Table 1. In passive transport of K^+ (Runs No. 1—5), the rate of K^+ transport gave a maximum when the OUT aqueous phase was maintained in the neutral pH region. When the OUT aqueous phase was strongly basic or acidic, the rates of K^+ transport were significantly suppressed. The plot of K^+ transport rate *vs.* pH of the OUT aqueous phase is well correlated with the pH-dependence of the fraction of zwitterionic $\mathbf{1}^{\pm}$ (Fig. 1). These results establish that the best K^+ transport system consists of the coupled counter-transport of K^+ and protons by interconversion between the $\mathbf{1}^-$–K^+ complex (IN→OUT) and $\mathbf{1}^{\pm}$ (OUT→IN) (see Scheme 2).

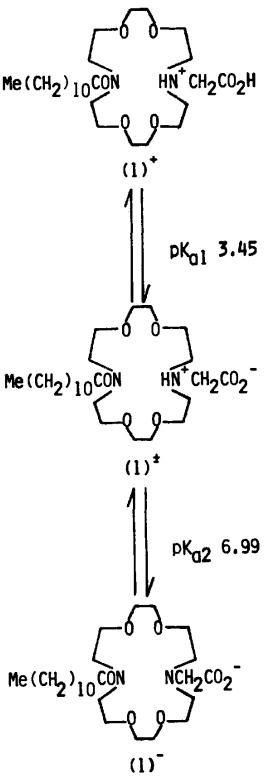

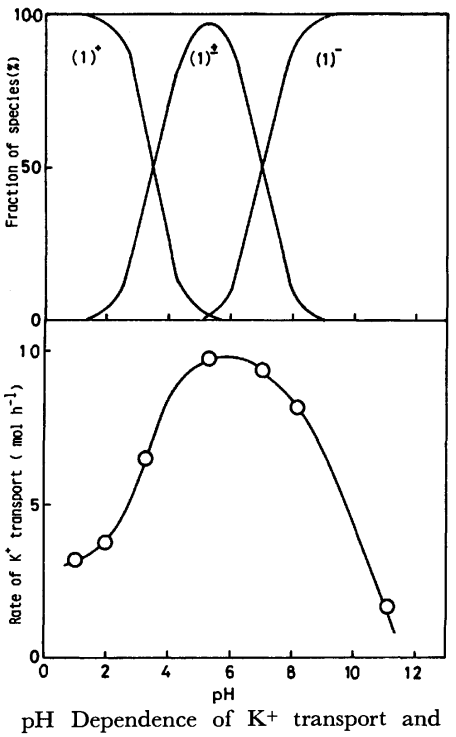

Fig. 1. pH Dependence of K^+ transport and carrier species.

† 1 M=1 mol dm^{-3}.

Table 1. Ion transport of alkali and alkaline earth metal cations with carrier **1**

Run No.	IN Aqueous phase (c/mM)	[**1**]	pH or additive in OUT aqueous phase (c/mM)	Rate of ion-transport (μmol h^{-1})	Relative rate
1	KOH(10)	1.0	HCl(100)	3.25	1.9
2	KOH(10)	1.0	HCl(10.0)	3.80	2.2
3	KOH(10)	1.0	pH 5.24[a]	9.80	5.8
4	KOH(10)	1.0	pH 6.99[b]	9.40	5.5
5	KOH(10)	1.0	Et_4NOH(10.0)	1.70	1.0
6	NaOH(10)	1.0	pH 6.99[b]	2.51	1.5
7	KOH(10)	0.50	KCl(10)+HCl(50.0)	$\approx$0	0
8	KOH(10)	0.50	KCl(10), pH 5.24[c]	0.97	0.57
9	$CaCl_2$(8.9)[d] $Ca(OH)_2$(2.0)	1.0	HCl(10.0)	2.33	1.4
10	$CaCl_2$(8.9)[d] $Ca(OH)_2$(2.0)	1.0	pH 5.25[c]	0.95	0.56
11	$CaCl_2$(8.9)[d] $Ca(OH)_2$(2.0)	1.0	Et_4NOH(10.0)	$\approx$0	0
12	$Ba(OH)_2$(12.5)	1.0	pH 5.25[c]	22.6	13.3

a) Buffer: tartarate (50 mM) and Tris. b) Buffer: Tris (50 mM) and HCl. c) Buffer: AcOH (50 mM) and Tris. d) Picric acid (3.8 mM) was added. e) Picric acid (4.3 mM) was added.

Being different from the conventional ion transport with anioncapped carriers (Scheme 1), the transport with (**1**) features that (i) the ion release is enforced by protonation of the ring nitrogen and (ii) proton flux in the counter-current is carried by the ring nitrogen but not by the carboxylate cap. The fact that the rate of the ion-transport is dependent upon the pH of the OUT aqueous phase supports the involvement of the ion-release step in the rate-limiting step. Conceivably, the ion-release is a slow, rate-limiting step when the OUT aqueous phase is basic, whereas the ion-release is facilitated by the "enforced" ion-release due to protonation of the ring nitrogen when the OUT aqueous phase is neutral. A similar enforced ion-release may be expected for the acidic OUT aqueous phase. However, $\mathbf{1}^+$, the main species in acidic pH region, is less soluble in the membrane phase, so that overall transport efficiency is inferior to that of $\mathbf{1}^\pm$.

The proton-driven active transport of K^+ demonstrates the high transport efficiency of $\mathbf{1}^\pm$ more clearly. As recorded in Table 1 (Runs No. 7, 8), the net active transport from the basic IN aqueous phase to the neutral OUT aqueous phase took place (0.97 μmol h^{-1}), whereas that to the acidic OUT aqueous phase was not observed at all. The result implies that only $\mathbf{1}^\pm$ is capable of serving as a recycle ion carrier and carring K^+ against its concentration gradient. As described in introduction, the $\mathbf{1}^-$–K^+ complex is converted to $\mathbf{1}^\pm$ when it contacts with the neutral OUT aqueous phase. Since $\mathbf{1}^\pm$ is highly lipophilic, the species is easily carried back to the side in contact with the IN aqueous plase (see Scheme 2). In case the OUT aqueous phase is strongly acidic, $\mathbf{1}^+$ is the main species after the ion-release. In order to stay in the membrane phase, $\mathbf{1}^+$ must extract some anion, X^-(probably Cl^-) from the OUT aqueous phase. Although we did not estimate the extraction of anion from the acidic aqueous phase, the result in Run No. 7 suggests that the counter-current of $\mathbf{1}^+X^-$ is not sufficient enough to mediate the active transport.

In passive transport, Na^+ was carried less effectively than K^+. This is attributed to the higher affinity of the diaza crown ring toward K^+ in preference to Na^+. Similarly, Ca^{2+} was carried less effectively than Ba^{2+}. Interestingly, Ca^{2+} was transported to the acidic OUT aqueous phase more efficiently than to the neutral OUT aqueous phase. This implies that the enforced Ca^{2+} release occurs only from $\mathbf{1}^+$ and the protonation of the ring nitrogen is not enough to eject the bound Ca^{2+} ion. The trend is quite different from that of K^+ transport. The difference probably stems from the high affinity of Ca^{2+} with the carboxylato group.[2,6]

Amino Acid Transport with ***1****–Metal Complexes.* The transport of amino acids across biological membranes is assumed nowadays to be coupled with Na^+ transport.[26] The transport of amino acids has been investigated by several groups,[27–31] but they mostly employed protected amino acids instead of biologically relevant "free" amino acids. An efficient transport system of free amino acids was reported by Behr and Lehn,[27] who demonstrated that a cationic surfactant is useful for the transport from the basic IN aqueous phase to the acidic OUT aqueous phase, while an anionic surfactant is useful for the transport from the acidic IN aqueous phase to the basic OUT aqueous phase.

It occurred to us that zwitterionic $\mathbf{1}^\pm$ may carry zwitterionic amino acids from the neutral IN aqueous phase to the basic OUT aqueous phase, while alkali metal cations may be carried back from the OUT to the IN aqueous phase. If it occurs, the system has characteristic, like the biological system, of the amino acid transport coupled with the counter-current of alkali metal cations. We thus measured the rate of the transport of phenylalanine from the neutral IN aqueous phase to the basic OUT aqueous phase containing KOH.[32] However, phenylalanine was not transported in an appreciable velocity. This implicates the difficulty

TABLE 2. TRANSPORT OF AMINO ACIDS WITH CARRIER **1**[a]

Run No.	IN Aqueous phase (*c*/mM)		OUT Aqueous phase (*c*/mM)	IN → OUT (mol h^{-1})		OUT → IN (μmol h^{-1})
	Amino acid	Metal		Amino acid	Ca^{2+}	Li^+
13	Phe(20)	$CaCl_2$(190), $Ca(OH)_2$(10)	pH 2.6[b]	0.12	1.67	0
14	Phe(20)	$CaCl_2$(190), $Ca(OH)_2$(10)	pH 8.0[b]	0.84	0.81	0.038
15	Phe(20)	$CaCl_2$(190), $Ca(OH)_2$(10)	pH 8.0[c,d]	0.90	1.13	0.054
16	Phe(20)	$CaCl_2$(190), $Ca(OH)_2$(10)	LiOH(6.25)	1.33	0	2.08[e]
17	Phe(20)	$BaCl_2$(150), $Ba(OH)_2$(50)	pH 8.0[c]	0.86	1.08[g]	0.050
18	Phe(20)	KOH(200)	pH 8.0[c]	0.031	2.14[f]	0.052
19	Phe(20)	$CaCl_2$(190), $Ca(OH)_2$(10)	KOH(6.25)	0.060	0	0.625[f]
20	Leu(20)	$CaCl_2$(190), $Ca(OH)_2$(10)	pH 8.0[c]	0.079	1.70	0.047
21	Ala(20)	$CaCl_2$(190), $Ca(OH)_2$(10)	pH 8.0[c]	0	1.30	0.035

a) Chloroform membrane phase: $[\mathbf{1}]=1.0\times10^{-3}$ M. b) Buffer: H_3PO_4 (50 mM) and LiOH (6.25 mM). c) Buffer: H_3BO_3 (50 mM) and LiOH (6.25 mM). d) $[LiClO_4]=1.0$ mM in the OUT aqueous phase. e) The rate of Li^+ transport decreased with time and became undected after 5 h. 2.08 μmol h^{-1} is the initial rate of Li^+ transport. f) Rate of K^+ transport. g) Rate of Ba^{2+} transport.

to extract zwitterionic amino acids to the membrane phase.

Here, a new idea arises that the $\mathbf{1}^-$–Ca^{2+} complex may be capable of extracting free amino acids from the basic IN aqueous phase and carrying them to the slightly basic OUT aqueous phase, because Ca^{2+} is scarcely ejected to the basic OUT aqueous phase (Table 1) and the extremely low solubility of zwitterionic amino acids in the membrane phase is rather favorable in the ion-release process. We thus constructed an amino acid transport system with the OUT aqueous phase adjusted mainly to pH 8.0, expecting the $\mathbf{1}^-$–Ca^{2+} complex to extract an anionic amino acid from the basic IN aqueous phase as a counteranion and to release it to the slightly basic OUT aqueous phase as a zwitterionic amino acid (Scheme 3). The pH of the OUT aqueous phase was adjusted with boric acid and LiOH. LiOH was selected because of its low affinity for **1**. The results are summerized in Table 2.

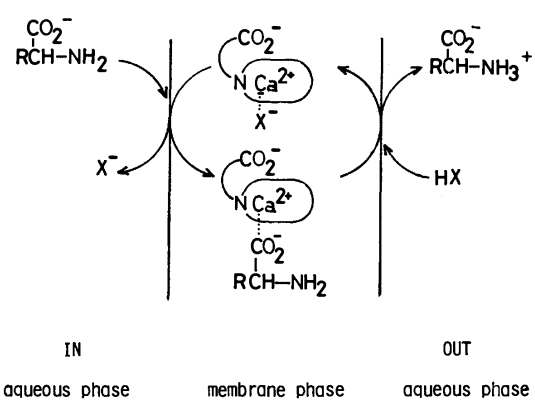

Scheme 3.

Experimental Runs No. 13—16 show the effect of pH in the OUT aqueous phase on the rate of phenylalanine transport. The maximum rate was observed for the strongly basic OUT aqueous phase where Ca^{2+} is not released at all (Run No. 16). Usually, the Li^+ concentration in the IN aqueous phase increased linearly with time. In Run No. 16, however, the counter-current of Li^+ was very fast in the initial stage but became undetected after 5 h. This implies that all the carrier molecules are occupied by Ca^{2+} after 5 h. When the OUT aqueous phase was adjusted to pH 8.0, the rate of phenylalanine transport was somewaht slower than that observed for the basic OUT aqueous phase and Ca^{2+} was released in a speed comparable with phenylalanine. These results show that the release of phenylalanine is not necessarily facilitated in its zwitterionic structure. We added $LiClO_4$ to the OUT aqueous in order to estimate the influence of the X^- concentration. Run No. 15 shows, however, that the effect is almost negligible. In case K^+ was used instead of Li^+ (compare Run No. 19 with Run No. 16), the rate of phenylalanine transport was reduced by 14 fold. Since K^+ is efficiently bound to $\mathbf{1}^-$ in the counter-current path, the rate suppression is attributed to the exchange between K^+ and Ca^{2+} at the interface between the membrane and the IN aqueous phase.

Runs No. 17 and 18 demonstrate that the phenylalanine transport is mediated by Ba^{2+} but not by K^+. In other words, only the $\mathbf{1}^-$–alkaline earth metal complexes are capable of extracting phenylalanine. The comparison of Runs No. 10 and 20 with Run No. 14 reveals that the transport rate is associated with the hydrophobicity of amino acids: The rate of leucine transport is smaller by one order of magnitude than that of phenylalanine transport, and the rate of alanine

transport is undetected in the present experimental precision.

Concluding Remark. The present paper has demonstrated a new class of ion transport involving the rate acceleration due to the enforced ion release and an amino acid transport system with the $\mathbf{1}^-$–metal complexes. The former system well mimicks the basic functions of the natural antibiotics, while the latter system seems still incomplete to call a biomimetic amino acid transport system. We believe, however, that the crown–metal complexes would have greater possibilities as amino acid carriers than simple phase transfer catalysts. Further study is now continued in this laboratory.

References

1) Preliminary communication: S. Shinkai, H. Kinda, T. Sone, and O. Manabe, *J. Chem. Soc., Chem. Commun.*, **1982**, 125.
2) E. M. Choy, D. F. Evans, and E. M. Cussler, *J. Am. Chem. Soc.*, **96**, 7085 (1974).
3) E. L. Cussler, *Am. Inst. Chem. Eng. J.*, **17**, 1300 (1971).
4) B. C. Pressman, *Ann. Rev. Biochem.*, **45**, 501 (1976).
5) J. W. Westly, *Ann. Rep. Med. Chem.*, **10**, 246 (1975).
6) W. Wierenga, B. F. Evans, and J. A. Woltersom, *J. Am. Chem. Soc.*, **101**, 1334 (1979).
7) L. A. Federick, T. M. Fyles, V. A. Malik-Diemer, and D. M. Whitfield, *J. Chem. Soc., Chem. Commun.*, **1980**, 1211.
8) S. Shinkai, T. Minami, Y. Kusano, and O. Manabe, *J. Am. Chem. Soc.*, **104**, 1967 (1982).
9) M. J. Umen and A. Scarpa, *J. Med. Chem.*, **21**, 505 (1978).
10) J. O. Cardner and C. C. Beard, *J. Med. Chem.*, **21**, 357 (1978).
11) H. Tsukube, *Tetrahedron Lett.*, **23**, 2109 (1982).
12) K. Hiratani, *Chem. Lett.*, **1981**, 21.
13) N. Yamazaki, A. Hirao, and S. Nakahama, *J. Macromol. Sci. Chem.*, **A13**, 321 (1979).
14) S. Matsuno, A. Ohki, M. Tagaki, and K. Ueno, *Chem. Lett.*, **1981**, 1543.
15) J. J. Grimaldi and J.-M. Lehn, *J. Am. Chem. Soc.*, **101**, 1333 (1979).
16) K. Maruyama, H. Tsukube, and T. Araki, *J. Chem. Soc., Chem. Commun.*, **1980**, 966.
17) S. Shinkai, T. Nakaji, T. Ogawa, K. Shigematsu, and, O. Manabe, *J. Am. Chem. Soc.*, **103**, 111 (1981).
18) J. Rebek, Jr., and R. V. Wattley, *J. Am. Chem. Soc.*, **102**, 4853 (1980).
19) M. Takagi, M. Tazaki, and K. Ueno, *Chem. Lett.*, **1978**, 1179.
20) I. Cho and S. Chang, *Chem. Lett.*, **1981**, 515.
21) Ph. Gramain and Y. Frere, *Macromolecules*, **12**, 1038 (1979).
22) S. Shinkai, T. Ogawa, T. Nakaji, Y. Kusano, and O. Manabe, *Tetrahedron Lett.*, **1979**, 4569.
23) S. Shinkai, T. Minami, T. Kouno, Y. Kusano, and O. Manabe, *Chem. Lett.*, **1982**, 499.
24) S. Shinkai, Y. Honda, Y. Kusano, and O. Manabe, *J. Chem. Soc., Chem. Commun.*, **1982**, 848.
25) S. D. Bernardo, M. Weigele, V. Toome, K. Manhart. W. Leimgruber, P. Bohlen, S. Stein, and S. Udenfriend, *Arch. Biochem. Biophys.*, **163**, 390 (1974).
26) K. Ring, *Angew. Chem., Int. Ed. Engl.*, **9**, 345 (1970).
27) J.-P. Behr and J.-M. Lehn, *J. Am. Chem. Soc.*, **95**, 6108 (1973).
28) M. Newcomb, J. L. Toner, R. C. Helgeson, and D. J. Cram, *J. Am. Chem. Soc.*, **101**, 4941 (1979).
29) K. Maruyama, H. Tsukube, and T. Araki, *Tetrahedron Lett.*, **22**, 2001 (1981).
30) H. Tsukube, *Tetrahedron Lett.*, **22**, 3981 (1981).
31) Recently, Sunamoto *et al.* have found that spiropyrans carry free amino acid under photoirradiation.
32) Membrane phase: $[\mathbf{1}]=1.0\times10^{-3}$ M. OUT aqueous phase: $[KOH]=1.0\times10^{-2}$ M. IN aqueous phase: [phenylalanine] $=1.0\times10^{-1}$ M, pH 5.26 with tartrate (5.0×10^{-2} M)–triethanolamine. The significant increase in the concentration of phenylalanine was not detected in the OUT aqueous phase.

NAD(P)$^+$-NAD(P)H Model. 39. Asymmetric Reduction by 1,4-Dihydronicotinamide Derivative Bound to Protein

Atsuyoshi Ohno,* Satoshi Ushida, and Shinzaburo Oka
Institute for Chemical Research, Kyoto University, Uji, Kyoto 611
(Received August 18, 1982)

1,4-Dihydronicotinamide derivatives covalently bound to NH_2 or SH group of proteins such as reduced keratin (RK), egg white albumin (EWA), and bovine serum albumin (BSA) have been synthesized and subjected to the reductions of α,α,α-trifluoroacetophenone derivatives. Chiral alcohol is obtained in the reaction with 1,4-dihydronicotinamide modified by the SH group of BSA.

Since our first report on an asymmetric reduction by a model compound of NAD(P)H,[1] many 1,4-dihydronicotinamide derivatives that have chiralities in the molecules have been synthesized.[2,3] Among asymmetric reductions with these model compounds some can compete, in terms of stereospecificity, with enzymic reactions.[3] However, the enzymic reaction is still much more superior to the model reactions in versatility and in reaction rate. Moreover, the stereospecificity in enzymic reactions that require NAD(P)H as a cofactor does not stem from the chirality in NAD(P)H, but from the chiral environment constructed by the enzymes. In fact, NAD(P)H-dependent dehydrogenases are classified into two categories depending on which of hydrogens on the 4-position of 1,4-dihydronicotinamide they utilize during the reduction.[4] The apoenzyme thus plays an important role for the formation of reaction field.

It is interesting to study how far the field effect, exerted by enzymes can be mimicked by organic chemistry, that is, by model compounds. At the same time, it is worthy for organic chemists to study the scope of asymmetric reaction by the use of abundant natural products.

Previously, we reported the syntheses and reactions of 1,4-dihydronicotinamide derivatives covalently bound to protein.[5] In the present work we attempted asymmetric reductions by the use of models covalently linked to proteins. Baba and his coworkers already reported the production of chiral alcohol in the reduction of α,α,α-trifluoroacetophenone (**1**) by 1-propyl-1,4-dihydronicotinamide (PNAH) in aqueous solution of bovine serum albumin (BSA).[6] Kaiser and his coworkers synthesized flavopapain[7] where the active site of the hydrolytic enzyme was utilized for the reaction site of flavin and the modified enzyme was found to exert a dehydrogenase-like property.[8]

Results

Modification of NH_2 Group in Proteins. The NH_2 groups in certain proteins were modified by 1,4-dihydronicotinamide. *N*-Hydroxysuccinimide ester of *N*-propylnicotinic acid (**2**) was employed for the modification as shown in Scheme 1. Thus obtained protein has an absorption maximum at 360 nm which is virtually identical with those of other 1,4-dihydronicotinamide derivatives.[4] This 1,4-dihydronicotinamide derivative of protein can reduce several substrates such as Malachite Green, chloranil, and *N*-methylacridinium iodide in buffered aqueous solution.

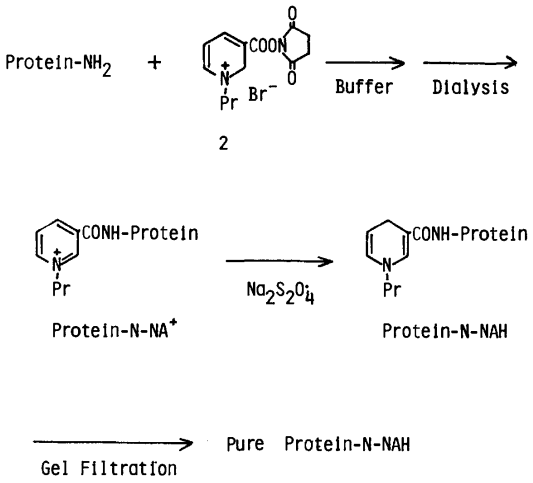

Scheme 1.

Table 1. Reductions of α,α,α-trifluoroacetophenone derivatives by BSA-N-NAH

pH[a]	Substrate	[BSA] / mmol dm^{-3}	Molar ratio A[b]	Molar ratio B[c]	Yield/%[d]
8.0	**3**	0.34	3.0	11	19
8.0	**3**	0.31	1.9	23	26
6.5	**3**	0.69	0.82	15	27
6.0	**3**	0.37	0.65	12	15
6.0	**1**	0.41	0.66	3	6

a) For modification reaction. b) [dihydropyridine]/[BSA] determined from the absorbance at 360 nm (ε=5900). c) [Substrate]/[BSA]. d) Based on 1,4-dihydropyridine moiety.

The NH_2 groups of *S*-carboxymethylated reduced keratin from human hair (CMRK), *S*-(2-ammonioethyl)ated reduced keratin from wool (AERK), and egg white albumin (EWA) were similarly modified with 1,4-dihydronicotinamide and the proteins were subjected to the reductions of **1** and *m*-trifluoromethyl-α,α,α-trifluoroacetophenone (**3**). The reduction was carried out in an aqueous solution of 0.05 mol dm^{-3} $Na_2B_4O_7$ containing about 2×10^{-4} mol dm^{-3} of 1,4-dihydronicotinamide moiety and $(4—8)\times10^{-3}$ mol dm^{-3} of the substrate. The produced alcohol was converted into the ester of (*R*)-(+)-α-methoxy-α-trifluoromethylphenylacetic acid ((*R*)-(+)-MTPA)[9] and the ratio of two diastereoisomers was determined on GLC. Unfortunate-

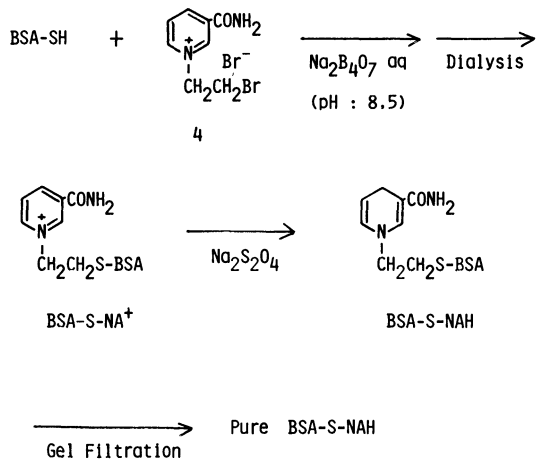

Scheme 2.

ly, thus obtained alcohols were racemic in all cases.

Modification of NH_2 Group in BSA. BSA, a carrier protein, is known to act as a chiral environment for certain reactions.[10] On this basis we synthesized 1,4-dihydronicotinamide derivative covalently bound to the NH_2 groups in BSA (BSA-N-NAH). As shown in Table 1, modification was carried out under different pH's to change the number of dihydronicotinamide moiety in a molecule of BSA ([dihydronicotinamide]/[BSA]). The alcohols obtained from the reductions of **1** and **3** were, however, again racemic.

Modification of SH Group in BSA. It has been accepted that BSA contains one SH group in one of three hydrophobic domains.[11] We attempted to modify the SH group with 1,4-dihydronicotinamide by using 1-(2-bromoethyl)-3-carbamoylpyridinium bromide (**4**) according to Scheme 2[12] and obtained BSA-S-NAH with a UV-absorption maximum at 355 nm. That only the SH group was modified and that no other residues of BSA such as $-NH_2$ and $-OH$ were influenced under the reaction conditions employed were confirmed by the following three results: 1) The concentration of modified 1,4-dihydropyridine moiety was comparable to that of original SH group in BSA. 2) When a same procedure was applied to BSA whose SH group had been protected by a carboxymethyl group, no product with an absorption maximum at 355 nm was obtained. 3) L-Cystein reacts with **4** under similar conditions to afford the corresponding sulfide, 1-[2-[(2-amino-2-carboxyethyl)thio]ethyl]-3-carbamoylpyridinium salt. After gel filtration BSA-S-NAH was subjected to the reductions of **1** and **3** at pH 9.4. As shown in Table 2, it was found that thus modified BSA induces chirality in the reduction products and that stereoselectivity increases as the molar ratio of the substrate to BSA decreases.

Table 2. Reaction of α,α,α-Trifluoroacetophenone derivatives with BSA-S-NAH[a]

Substrate	[BSA] mmol dm^{-3}	Molar ratio A[b]	Molar ratio B[c]	e.e./%	Config.
1	0.69	0.52	13	5	*R*
3	0.67	0.48	13	5	*R*
1	1.0	0.32	3.1	10	*R*
1	1.1	0.29	3.0	11	*R*
3	1.1	0.32	2.9	17	*R*
3	1.0	0.32	3.1	15	*R*

a) Reaction was run in 0.05 mol dm^{-3} $Na_2B_4O_7$ (pH: 9.4) at room temperature. The yield of alcohol was about 5% based on 1,4-dihydropyridine moiety. b) [Dihydropyridine]/[BSA] determined from the absorbance at 355 nm (ε=5500). c) [Substrate]/[BSA].

Discussion

The basic idea underlying the present study is to use chiral environment around 1,4-dihydronicotinamide moiety for biomimetic reductions by means of chemical modification on protein, as enzymes do.

When simple proteins, such as RK and EWA, are subjected to modification no chiral products were obtained. In the case of BSA, which is presumed to have much higher degree of functionality than the others, modification of its SH group by 1,4-dihydronicotinamide affords chiral products but modification of its NH_2 group does not. It has been established that BSA contains one SH group in one of three hydrophobic domains. Therefore, by SH modification it must be possible to set a 1,4-dihydronicotinamide moiety into a single chiral circumstance. On the other hand, since BSA and other proteins that we used contain various kinds of NH_2 groups, it seems difficult to carry out the modification selectively. Even if each of modified 1,4-dihydronicotinamide moiety sits itself in a chiral field, the chiralities may be neutralized totally because of a variety of types in modifications. Since NH_2 groups in different environment have different basicities, it is expected that the modification of NH_2 groups under different pH might result in selectively modified protein. However, the attempt was not successful as seen in Table 1.

Alternatively, it is also possible that chiral fields supplied by the protein locate far from the 1,4-dihydronicotinamide moiety, because most of free NH_2 groups stick out of the main domain of the protein.

The present result with BSA-S-NAH is the first example of biomimetic reduction where the chirality in the protein-1,4-dihydronicotinamide complex is transferred, as is observed in enzymic reactions, into a substrate during the reaction in water. Results shown in Table 2 reveal that the reaction between BSA-S-NAH and free substrate does not exert stereoselectivity. On the other hand, the reaction of a substrate trapped on BSA and free reductant ($NaBH_4$ or PNAH) exerts stereoselectivity of about 40% e.e.[6,10] Thus, it seems likely that protein-protein interaction between BSA which binds a substrate and BSA which binds 1,4-dihydronicotinamide is important in the present reaction to determine the stereoselectivity.

There is another possibility; for a bimolecular reaction in micellar system, it is assumed that when one reagent is incorporated into one micelle and the other reagent into another micelle, no reaction takes place because each reagent has no chance to collide each other.[13] Similarly, a substrate incorporated into BSA

might not be able to find a chance to react with 1,4-dihydronicotinamide which is bound to BSA. If this is the case, the substrate which is trapped into a 1,4-dihydronicotinamide-containing crevice of BSA is the only substrate that can undergo the asymmetric reaction. The situation is quite similar to that of ternary complex in an enzymic reaction.

In any case, there is no doubt that the reduction proceeds in a chiral field offerred by such a protein as that which is quite different from dehydrogenases. Although the present result is not satisfactory, it promises further success by appropriate use of crevice in a protein. It should be noted, however, that in the asymmetric reduction with a chiral 1,4-dihydronicotinamide derivative, the interaction between reduced and oxidized forms of the model compound is important in order to exert high stereospecificity.[14,3] If similar situation operates in the present system, high stereoselectivity cannot be expected with BSA-S-NAH because extraordinarily bulky substituent prevents the model compound from the formation of aggregates and more sophisticated design will be necessary for the model compound.

Experimental

Melting and boiling points were not corrected.

Instruments. UV, NMR, and mass spectra were obtained on Union Giken SM-401, JEOL JNMFX-100, and Hewlett Packard 5992B GC/MS spectrometers, respectively. A Yanaco G-1800F was used for GLC analyses. Preparative-scale GLC separations were carried out by using Varian Aerograph Model 920.

Materials. BSA was Fraction V grade from Armour. α,α,α-Trifluoroacetophenone (**1**) (bp 423 K) was prepared according to the literature procedure.[15] *m*-Trifluoromethyl-α,α,α-trifluoroacetophenone (**3**) was prepared from *m*-trifluoromethylphenylmagnesium bromide and trifluoroacetic acid.[16] (*R*)-(+)-α-methoxy-α-trifluoromethylphenylacetic acid was purchased from Aldrich Chem. Co. and was converted into the corresponding chloride (MTPACl) by the use of thionyl chloride.[9]

S-Carboxymethylated Reduced Keratin from Human Hair (CMRK). Human hair (5.0 g) was reductively solubilized by sodium mercaptoacetate (5.0 g) in aqueous sodium sulfide (200 cm^3, pH: 12.0). After being kept for 5 d at room temperature under nitrogen atmosphere, 3.15 g of sodium borohydride was added and the solution was allowed to stand for a day. Carboxymethylation of free SH groups was effected by the addition of iodoacetic acid (8.2 g) at pH 8.5. Thus obtained CMRK was subjected to the modification after dialysis against 2 dm^3 of borate buffer for several times.

Reduced Keratin from Wool Whose SH Group Was Protected with (2-Bromoethyl)trimethylammonium Bromide (AERK).[17] Wool (1.7 g) was reductively solubilized using 2-mercaptoethanol (1.2 g) in 100 cm^3 of 8 mol dm^{-3} urea–0.01 mol dm^{-3} Tris in the presence of 0.001 mol dm^{-3} EDTA. The solution was stirred for 3—5 h at room temperature under nitrogen atmosphere. To the solution 3 g of (2-bromoethyl)trimethylammonium bromide was added. After being kept for a day the solution was dialyzed against 2 dm^3 of borate buffer for several times. Thus obtained solution of AERK was subjected to further modification.

N-Hydroxysuccinimide Ester of N-*Propylnicotinic Acid (2).* Dicyclohexylcarbodiimide (10.3 g) was added to a suspension of nicotinic acid (6.15 g) and *N*-hydroxysuccinimide (5.75 g) in 150 cm^3 of dioxane. The precipitate was separated by filtration. The dioxane was removed from the filtrate under reduced pressure to give *N*-hydroxysuccinimide ester of nicotinic acid quantitatively. Thus obtained ester (10 g) was dissolved in propyl bromide. The mixture was refluxed for a day. The precipitate was separated, washed with anhydrous acetone, and kept *in vacuo* to constant weight (9.4 g, 60% yield).

1-(2-Bromoethyl)-3-carbamoylpyridinium Bromide (4). A mixture of nicotinamide (0.60 g) and 1,2-dibromoethane (7 cm^3) was stirred at 313—323 K for 5 d. The solid was collected and extracted with hot methanol. After the removal of the solvent, the crude product was washed with acetone. Twice recrystalization from methanol gave 0.40 g of **4** (mp 465—467 K).

Found: C, 31.13; H, 3.28; N, 8.95%. Calcd for $Br_2C_8H_{10}N_2O$: C, 31.00; H, 3.25; N, 9.04%.

^1H NMR (D_2O, δ from TSP): 4.09 (2H, t, J=6 Hz), 5.22 (2H, t, J=6 Hz), 8.27 (1H, m), 8.80—9.10 (2H, m), 9.28 (1H, bs).

Modification of NH_2 Group in CMRK, AERK, and EWA. To a buffered solution of a protein (20 cm^3) about 100 mg of **2** was added. After the dialysis against 2 dm^3 of 0.05 mol dm^{-3} $Na_2B_4O_7$ for a day modified pyridinium ion was reduced with sodium dithionite (*ca.* 20 mg). Excess dithionite was removed by gel filtration on a column of Bio-gel P-6.

Modification of NH_2 Group in BSA. The same procedure as described above was employed for a 0.05 mol dm^{-3} $Na_2B_4O_7$ solution of BSA (0.5 mmol dm^{-3}). The amount of **2** and pH of the buffered solution were changed in compliance of the cases.

Modification of SH Group in BSA. To a solution of BSA (1.5 mmol dm^{-3}) in 0.05 mol dm^{-3} $Na_2B_4O_7$ (50 cm^3, pH: 8.5), 50 mg of **4** was added. The BSA contained 0.45—0.55 free SH groups in a molecule. The solution was kept at room temperature under nitrogen atmosphere for about 3 d until no SH group could be detected by DTNB-method. After the dialysis against 2 dm^3 of 0.05 mol dm^{-3} $Na_2B_4O_7$ for several times, 50 mg of sodium dithionite was added to the solution of BSA-S-NA$^+$. Excess dithionite was removed by gel filtration on a column of Bio-gel P-6 to afford pure BSA-S-NAH.

UV-Absorption of Modified Protein. Thus obtained modified protein exerts an absorption maximum at around 360 nm due to 1,4-dihydronicotinamide moiety. The amount of 1,4-dihydronicotinamide moiety in the protein was determined by titration with *N*-methylacridinium iodide on monitoring the absorption at around 360 nm.

Reactions of α,α,α-Trifluoroacetophenone Derivatives. To a solution of modified protein **1** or **3** was added. The solution was stirred for 1—2 weeks until UV-absorption at around 360 nm disappeared. The mixture of the products and starting material was extracted with ether.

Determination of Enantiomer Excess. The ether solution of extracted reaction mixture was concentrated to 0.1 cm^3 under atmospheric pressure and the enantiomeric alcohols were separated by preparative GLC on a PEG column and collected as a solution of carbon tetrachloride (0.1—0.2 cm^3). The alcohol was subjected to esterification by (*S*)-(+)-MTPACl[9] and the mixture of diastereomeric esters was submitted to the GLC analysis. Since the esterification is diastereotopic reaction, it should be confirmed that all the starting alcohol is esterified. Otherwise, GLC analysis does not give correct result.

Diastereomeric esters of **5** and **6** (**7** and **8**, respectively) were separated on GLC (10% DEGS, 1 m). The peaks were identified by comparison with those of authentic **7** and **8**. The

structures of **7** and **8** were also identified by GC/MS analyses. The value of enantiomer excess was determined from the ratio of peak areas for the diastereomeric esters. The ratio for racemic **7** and **8** were 50 : 50, respectively.

References

1) Y. Ohnishi, M. Kagami, and A.Ohno, *J. Am. Chem. Soc.*, **97**, 4766 (1975).

2) J. W. ApSimon and R. P. Seguin, *Tetrahedron*, **35**, 2797 (1979); T. Endo, H. Kawasaki, and M. Okawara, *Tetrahedron Lett.*, **1979**, 23; N. Baba, J. Oda, and Y. Inouye, *Bull. Inst. Chem. Res., Kyoto Univ.*, **58**, 379 (1980).

3) A. Ohno, M. Ikeguchi, T. Kimura, and S. Oka, *J. Am. Chem. Soc.*, **101**, 7036 (1979); b) M. Seki, N. Baba, J. Oda, and Y. Inouye, *ibid.*, **103**, 4613 (1981).

4) T. C. Bruice and S. J. Benkovic, "Bioorganic Mechanisms," W. A. Benjamin Inc., New York, N. Y. (1966), Vol. 2, p. 301.

5) A. Ohno, S. Ushida, and S. Oka, *Tetrahedron Lett.*, **21**, 2969 (1980).

6) N. Baba, Y. Matsumura, and T. Sugimoto, *Tetrahedron Lett.*, **1978**, 4281.

7) H. L. Levine and E. T. Kaiser, *J. Am. Chem. Soc.*, **100**, 7670 (1978).

8) H. L. Levine and E. T. Kaiser, *J. Am. Chem. Soc.*, **102**, 343 (1980).

9) J. A. Dale, D. L. Dull, and H. A. Mosher, *J. Org. Chem.*, **34**, 2543 (1969).

10) T. Sugimoto, T. Kokubo, Y. Matsumura, J. Miyazaki, S. Tanimoto, and M. Okano, *Bioorg. Chem.*, **10**, 104, 311(1981).

11) H. H. Hull, R. Chang, and L. J. Kaplan, *Biochim. Biophys. Acta*, **400**, 132 (1975); J. R. Brown, *Fed. Proc.*, **35**, 2141 (1976).

12) Similar reagent is reported for the modification of SH group: H. A. Itano and E. A. Robinson, *J. Biol. Chem.*, **247**, 4819 (1972).

13) C. A. Bunton, "Applications of Biochemical Systems in Organic Chemistry," ed by J. B. Jones, C. J. Sih, and D. Perlman, John Wiley and Sons, Inc., New York, N. Y. (1976), Part 2, Chap. 4, pp. 731—814.

14) A. Ohno, T. Kimura, S. Oka, and Y. Ohnishi, *Tetrahedron Lett.*, **1978**, 757.

15) J. D. Park, H. A. Brown, and J. R. Lacher, *J. Am. Chem. Soc.*, **73**, 709 (1951).

16) R. Stewart and R. van der Linden, *Can J. Chem.*, **38**, 399 (1960).

17) J. H. Bradbury, *Adv. Protein Chem.*, **27**, 111 (1973).

Facile Synthesis of Cyclic Dipeptides and Detection of Racemization

Toshihisa UEDA,* Morinobu SAITO,† Tetsuo KATO, and Nobuo IZUMIYA
Laboratory of Biochemistry, Faculty of Science, Kyushu University 33, Higashi-ku, Fukuoka 812
(Received September 10, 1982)

Several cyclic dipeptides were synthesized by refluxing methanolic solution of dipeptide methyl esters in high yield and purity. Cyclic dipeptides prepared by the Fischer method, the Nitecki method, and the present methanol-reflux method were compared with respect to yield and optical purity. The methanol-reflux method usually gave good results. High-performance liquid chromatography was effectively applied to detect racemization.

Various natural cyclic dipeptides (2,5-piperazinedione derivatives) are known by their diverse biological activities such as antibiotic,[1] bitter taste,[2] plant growth retardation,[3,4] and inhibition of hormone secretion.[5] With regard to synthetic cyclic dipeptides, Izumiya *et al.* observed highly asymmetric induction on hydrogenation of cyclic dehydrodipeptides.[6] Shiba *et al.* studied structure-activity relationships of bitter cyclic dipeptides.[7] Kopple *et al.* utilized cyclic dipeptides as a model for studying peptide conformation.[8,9]

Cyclic dipeptides have been prepared by the Fischer method: Aminolysis of dipeptide ester in methanolic ammonia.[10] This method is simple to apply and usually gives high yield. Nitecki *et al.*, however, pointed out appreciable racemization derived from this procedure and proposed another method:[11] Deprotection of Boc-dipeptide methyl ester by formic acid and subsequent reflux of the deprotected ester formate with a mixture of *s*-butyl alcohol and toluene.[12] This Nitecki method was reported to be less prone to racemization. Lee *et al.*[13] reported that a side reaction occurred at the side chain of a serine residue in the course of the Nitecki method. Thus, both synthetic methods seemed to envisage undesired side reactions.

It is well-known that dipeptide esters spontaneously cyclize to form cyclic dipeptides upon hydrogenolysis of a benzyloxycarbonyl protecting group. As a modification of this reaction, reflux of methanolic solution of dipeptide esters has been tried in the present study to facilitate cyclization, and experimental conditions have been examined to improve yield and optical purity of products.

For detection of diastereomers of cyclic dipeptides, Nitecki *et al.*[11] and Westley *et al.*[14] used NMR, TLC, and gas liquid partition chromatography. These methods are easy to operate but precision and sensitivity are insufficient to detect a small amount of racemates. Lee *et al.*[13] and Kanmera *et al.*[15] reported detection of racemization by the Manning-Shimohigashi method.[6,16,17] This method using an amino acid analyzer can be applied with high precision, but the procedure is so complicated that an unexpected error might be possible. Recently, high-performance liquid chromatography has come into use in peptide chemistry.[18,19] This technique is expected to give a simple and convenient method for racemization test.

We report here convenient synthesis of cyclic dipeptides by refluxing methanolic solution of dipeptide methyl esters. Rapid and highly sensitive detection of racemization by HPLC[12] is also described.

TABLE 1. YIELDS AND PHYSICAL CONSTANTS OF CYCLIC DIPEPTIDES

Compound	Yield %	Mp θ_m/°C, decomp	$[\alpha]_D^{20}$ a)/°	Formula	Found(%) (Calcd(%)) C	H	N
cyclo(-L-Val-L-Val-)	64	272—273	−62.0 (*c* 0.5, AcOH)	$C_{10}H_{18}O_2N_2$	60.37 (60.58	9.31 9.15	14.13 14.13)
cyclo(-L-Val-D-Val-)	45	>300		$C_{10}H_{18}O_2N_2$	60.43 (60.58	9.24 9.15	14.14 14.13)
cyclo(-L-Ala-L-Ala-)	80	276—280	−22.8 (*c* 0.5, AcOH)	$C_6H_{10}O_2N_2$	50.78 (50.70	7.17 7.09	19.49 19.71)
cyclo(-L-Ala-D-Ala-)	88	256—259		$C_6H_{10}O_2N_2$	50.84 (50.70	7.14 7.09	19.51 19.71)
cyclo(-L-Ser-L-Ser-)	77	231—233	−54.0 (*c* 0.1, DMF)	$C_6H_{10}O_4N_2$	41.32 (41.38	5.93 5.79	15.97 16.08)
cyclo(-L-Ser-D-Ser-)	74	261—264		$C_6H_{10}O_4N_2$	41.33 (41.38	5.88 5.79	15.99 16.08)
cyclo(-L-Pro-L-Pro-)	64	141—142	−148 (*c* 1, AcOH)	$C_{10}H_{14}O_2N_2$	61.54 (61.84	7.35 7.27	14.20 14.42)
cyclo(-L-Pro-D-Pro-)	83	176—177		$C_{10}H_{14}O_2N_2$	61.53 (61.84	7.34 7.27	14.24 14.42)

a) $[\alpha]_D$ of all *cyclo*(-L-AA-D-AA-) should be 0°, therefore measurement was not carried out.

† Present address: Teikoku Hormone Mfg. Co., Takatsu-ku, Kawasaki 213.

Table 2. Separation conditions by HPLC[a)]

Compound	Filler; LiChrosorb	Eluent (ratio)	Column (cm)	Pressure kg cm^{-2}	Retention time/min LL	Retention time/min DL	Absorption intensity ratio (LL/DL)
cyclo(-L-Leu-(L and D)-Leu-)	PR-18	H_2O–CH_3CN (8 : 2)	0.26×15	300	7.5	5.4	1.06
cyclo(-L-Val-(L and D)-Val-)	RP-18	H_2O–CH_3CN (9 : 1)	0.26×15	300	4.0	2.3	0.98
cyclo(-L-Ala-(L and D)-Ala-)	RP-8	H_2O	0.4 ×25	150	10.3	7.8	1.05
cyclo(-L-Ser-(L and D)-Ser-)	RP-18	KH_2PO_4–Na_2HPO_4[b)]	0.26×50	450	31.7	27.4	1.03

a) Other conditions are as follows: Hitachi 635A liquid chromatograph; flow rate, 1 ml/min; wavelength, 210 nm; temperature, 20 °C. b) 3 M (1 M=1 mol dm^{-3}) at pH 6.6.

Results and Discussion

Separation Conditions of Diastereomers by HPLC. Table 1 shows cyclic dipeptides prepared in this study as model peptides. *cyclo*(-L-Leu-L-Leu-), *cyclo*(-L-Leu-D-Leu-), *cyclo*(-L-Phe-L-Phe-), and *cyclo*(-L-Phe-D-Phe-) were also prepared according to the literature.[11)] Separation conditions by HPLC were examined. Satisfactory separation was obtained by reversed-phase chromatography with LiChrosorb RP-8 and RP-18 as filler, experimental conditions being shown in Table 2. Diastereomers of *cyclo*(-L-Ser-(L and D)-Ser-) were separated by phosphate buffer better than by water. Generally, LiChrosorb RP-18 shows longer retention time than LiChrosorb RP-8 does. On the other hand, unsatisfactory results were obtained for adsorption chromatography with Hitachi gel #3040 and reversed-phase chromatography with gels of large particle size. *cyclo*(-L-Pro-(L and D)-Pro-) could not be satisfactorily separated.

Experimental Conditions for the MeOH-reflux Method. Reaction conditions for the MeOH-reflux method were studied by the use of *cyclo*(-L-Leu-(L and D)-Leu-) as a model. Degree of racemization is given by racemization (%)=[LD%/(LL%+LD%)]×100. A rough estimate of reaction was given in terms of the reaction time elapsed until a TLC spot of the starting ester had disappeared.

Effect of Methyl and Ethyl Ester Groups. Cyclization of H-L-Leu-L-Leu-OMe and H-L-Leu-L-Leu-OEt in MeOH was compared in order to study the effect of methyl and ethyl groups on reaction rate, racemization, and yield of *cyclo*(-L-Leu-L-Leu-). The reaction time, racemization, and yield were 80 h, 1.2%, and 76% for methyl, and 160 h, 1.9%, and 65% for ethyl ester, respectively. Therefore, methyl ester was used hereafter.

Table 3. Effect of reflux solvent on cyclization of H-L-LEU-L-LEU-OME

Solvent	Bp θ_b/°C	Reaction rate h	Racemization (%)	Yield to produce cyclic dipeptide %
MeOH	64	80	1.2	76
EtOH	79	70	0.8	66
s-BuOH	100	48	>26	15
Toluene	110	50	1.9	75

Effect of Reflux Solvent. Table 3 shows the effect of reflux solvent. The reaction rate and racemization increased with the raise of the boiling point of a solvent. Severe racemization was detected in the case of *s*-BuOH and a side reaction was suggested by TLC. Racemization was negligible for MeOH and EtOH, and MeOH gave higher yield. Based on these results, reflux of methanolic solution of dipeptide methyl ester is recommended for facile synthesis of cyclic dipeptides.

Effect of Salt on Racemization. Boc-L-Leu-L-Leu-OMe was deprotected with HCOOH, subsequently neutralized with NEt_3, and the methanolic solution of the mixture was refluxed. The same procedure was repeated without salt, and the degree of racemization was compared. When 1.2, 1.0, and 0 equivalent of $HCOOH \cdot NEt_3$ were present, 2.3, 1.8, and 1.2% racemizations were observed respectively. Clearly, excess of acid and base should be avoided.

Effect of Side Chain of Amino Acid Residues on Cyclization Rate. The effect of the size of a side chain in H-dipeptide-OMe on reaction rate was studied. When H-Gly-L-Ala-OMe, H-L-Ala-L-Ala-OMe, and H-L-Leu-L-Ala-OMe were used as starting compounds, the reaction times to give a cyclic dipeptide were 10, 20, and 24 h, respectively. For H-Gly-L-Leu-OMe and H-L-Leu-L-Leu-OMe, 24 and 80 h, respectively. As expected, cyclization rate decreased with the increase of the size of a side chain.

Effect of Diastereomers in a Dipeptide Ester. Cyclization of H-L-Leu-L-Leu-OMe and H-L-Leu-D-Leu-OMe was compared to examine diastereomeric difference. Reaction time, racemization, and yield of cyclization were 80 h, 1.2%, and 76% for H-L-Leu-L-Leu-OMe, and 70 h, 1.1%, and 67% for H-L-Leu-D-Leu-OMe. The effect of diastereomeric difference is only slight if any.

Comparison of Synthetic Methods. Cyclic dipeptides shown in Table 4 were prepaed by the three methods, and racemization of these peptides except for *cyclo*(-L-Phe-L-Phe-) was detected by HPLC. Racemization of *cyclo*(-L-Phe-L-Phe-) was detected by the Manning-Shimohigashi method.[16)] The Fischer method occasionally gave low yield possibly because of the formation of dipeptide amide. The Fischer method caused appreciable racemization for *cyclo*(-L-Ser-L-Ser-), al-

TABLE 4. COMPARISON OF THE THREE METHODS

Compound obtained	Fischer method		Nitecki method		MeOH-reflux method	
	Yield %	Racemization (%)	Yield %	Racemization (%)	Yield %	Racemization (%)
cyclo(-L-Leu-L-Leu-)	70	1.5	71	5.5	76	1.2
cyclo(-L-Val-L-Val-)	20	0.9	58	0.4	64	0.6
cyclo(-L-Ala-L-Ala-)	72	0.4	85	0.3	81	0.3
cyclo(-L-Ser-L-Ser-)	53	2.7	40	1.5	63	1.4
cyclo(-L-Phe-L-Phe-)	86	0.6	89	0.6	93	0.1

though detected racemization was much lower than reported by Nitecki *et al.* (5—40%).[11] It should be noted that H-dipeptide-OMe was treated with methanolic ammonia in the shortest reaction time in this study, whereas reported reaction time was 1 d to 5 d.[11]

The Nitecki method caused comparatively less racemization. In the case of *cyclo*(-L-Leu-L-Leu-), however, 5.5% racemization was observed. We can not explain this result at present. A side reaction was observed also in the case of *cyclo*(-L-Ser-L-Ser-) producing a mixture of three components. Each component separated by silica gel chromatography was found to be HCO-L-Ser-L-Ser-OMe (**1**), a formylated derivative (**2**) of **1**, and desired *cyclo*(-L-Ser-L-Ser-). This side reaction was observed only in the case of dipeptides containing serine.

Nitecki *et al.* presumed that racemization took place only on cyclization step.[11] However, Fig. 1 shows that racemization proceeds mainly after cyclization. Cyclic dipeptide is found to be susceptible to racemization in the presence of excess base. Possible reason of racemization is keto-enol tautomerism resulted from deprotonation from α-carbon.

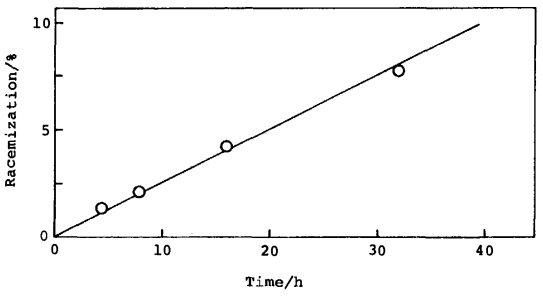

Fig. 1. Time-course of racemization of *cyclo*(-L-Leu-L-Leu-) in methanolic ammonia.

Although the MeOH-reflux method is recommendable compared to the Fischer method and the Nitecki method, it should be noted that Suzuki *et al.*[20] have recently proposed a similar method, AcOH-catalyzed aminolysis of dipeptide esters, *s*-BuOH being used as a solvent. Additionally, Takahashi *et al.* described synthesis of cyclic dipeptides using *N*-carboxy amino acid and amino acid esters.[21]

Experimental

The melting points are uncorrected. TLC was carried out on silica gel G (Merck) with the following solvent systems: R_f^1, $CHCl_3$-MeOH (5 : 1); R_f^2, $CHCl_3$-MeOH-AcOH (50 : 10 : 2). The ratio in parentheses after a solvent system is indicated by volume. HPLC was carried out with a Hitachi 635A liquid chromatograph equipped with multi-wavelength UV monitor 635-0900. Solvents for HPLC were filtered and degassed before use. A Hitachi amino acid analyzer KLA-5 was used for the determination of amino acids and diastereomeric dipeptides under the following conditions: column, 0.6×55 cm; jacket temperature, 55 °C; flow rate, 30 ml/h. ^1H NMR spectra were obtained on a JEOL FX-90Q spectrometer with tetramethylsilane as an internal standard.

Z-Dipeptide Esters. *Z-L-Val-L-Val-OMe*: Preparation of this compound is described as an example of the preparation of Z-dipeptide esters. To a chilled solution of Z-L-Val-OH (1.51 g, 6 mmol), H-L-Val-OMe·HCl (1.01 g, 6 mmol) and NEt_3 (0.84 ml, 6 mmol) in CH_2Cl_2 (18 ml), was added DCC (1.30 g, 6.3 mmol) at 0 °C. The reaction mixture was stirred at 0 °C for 4 h and allowed to stand at room temperature overnight. After removal of *N,N'*-dicyclohexylurea, the filtrate was evaporated *in vacuo* and the residue was dissolved in EtOAc. The solution was washed successively with 2% HCl, 4% $NaHCO_3$, and water, dried (Na_2SO_4), and evaporated. The residue was recrystallized from EtOAc–ether–petroleum ether; yield, 1.68 g (77%); mp 145—147 °C; $[\alpha]_D^{20}$ −28.0° (*c* 1, MeOH); R_f^1 0.88.

Found: C, 62.78; H, 8.00; N, 7.60%. Calcd for $C_{19}H_{28}O_5N_2$: C, 62.62; H, 7.74; N, 7.69%.

Several Z-Dipeptide Esters: Other compounds were prepared in a similar manner. New compounds prepared were as follows: Z-L-Leu-D-Leu-OMe, Z-L-Leu-D-Leu-OEt, Z-L-Ala-D-Ala-OEt, Z-L-Ser-D-Ser-OEt, Z-L-Pro-D-Pro-OMe, and Z-L-Phe-D-Phe-OMe.

Boc-Dipeptide Esters. *Boc-L-Ala-L-Ala-OMe*: Coupling of Boc-L-Ala-OH (0.95 g, 5 mmol) and H-L-Ala-OMe·HCl (0.70 g, 5 mmol) by DCC (1.03 g, 5 mmol) was carried out as described above. The product was recrystallized from EtOAc–ether–petroleum ether; yield, 1.03 g (75%); mp 108—109 °C; $[\alpha]_D^{20}$ −57.8° (*c* 1, MeOH); R_f^2 0.79.

Found: C, 52.55; H, 8.18; N, 10.25%. Calcd for $C_{12}H_{22}O_5N_2$: C, 52.54; H, 8.08; N, 10.21%.

Several Boc-Dipeptide Esters: Known Boc-dipeptide esters such as Boc-L-Leu-L-Leu-OMe were prepared similarly. New compound prepared was Boc-L-Val-D-Val-OMe.

Authentic Cyclic Dipeptides. cyclo(-L-Val-L-Val-): Z-L-Val-L-Val-OMe (182 mg, 0.5 mmol) was dissolved in MeOH (5 ml) and hydrogenolyzed in the presence of Pd black. After the catalyst was filtered off, the filtrate was evaporated *in vacuo* and the residue was dissolved in MeOH (10 ml). The solution was refluxed for 110 h and evaporated *in vacuo*. The residue was recrystallized from MeOH–ether; yield, 63 mg (64%); physical constants being shown in Table 1.

Several Cyclic Dipeptides: Other compounds were prepared by the same procedure. Yields and physical constants are shown in Table 1.

Separation of Cyclic Dipeptide Diastereomers by HPLC.

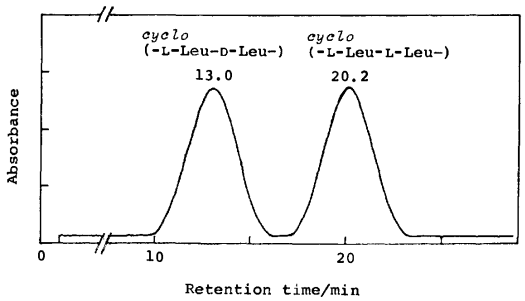

Fig. 2. Separation of cyclic dipeptide diastereomers by adsorption HPLC. Column, Hitachi gel #3040, 0.26×50 cm; eluent, hexane–EtOH (9:1); flow rate, 1 ml/min; wavelength, 210 nm.

a) Reversed-phase HPLC: Hitachi Gel #3050 (particle size, 20—25 μm), #3053 (10 μm), LiChrosorb RP-8 (5 μm), and LiChrosorb RP-18 (5 μm) were used as filler, and aqueous mixtures such as water–MeOH, water–MeOH–*i*-PrOH, water–CH_3CN, and water–CH_3CN–*i*-PrOH were tested as solvent systems. Optimal conditions are shown in Table 2. In the case of *cyclo*(-L-Ser-L,D-Ser-), phosphate buffer was used, which was tested over the wide range of concentrations at pH 6.6. The filler was filled by slurry method.

b) Adsorption HPLC: Solvent systems were tested by TLC using various two or three component systems with MeOH, EtOH, *i*-PrOH, hexane, and CH_3CN. The solvent system, hexane–EtOH, gave good results for the separation of *cyclo*(-L-Leu-L-Leu-) as shown in Fig. 2. However, the separation of other cyclic dipeptides were unsuccessful.

c) Determination of Racemization: Separation conditions for four cyclic dipeptides were shown in Table 2. Ten μl of a sample solution, concentration of which was about 1 mg/ml, was applied to HPLC and analyzed. All values of racemization were corrected with the ratio of absorption intensity.

Effects of Factors on Formation of Cyclic Dipeptide by the MeOH-reflux Method. a) Effect of Ester Groups: Z-L-Leu-L-Leu-OMe or Z-L-Leu-L-Leu-OEt (0.5 mmol each) dissolved in MeOH (5 ml) was treated with H_2/Pd and the solution was refluxed as described in the section of Authentic Cyclic Dipeptides.

b) Effect of Salt on Racemization: After deprotection of Boc-L-Leu-L-Leu-OMe with HCOOH, the solution was evaporated and dried *in vacuo* overnight. After neutralization with NEt_3, the residue was dissolved in MeOH and the solution was refluxed for 72 h. After the solution was evaporated, the residue was dissolved in MeOH and applied to HPLC in order to detect racemization.

c) Effect of Reflux Solvent: H-L-Leu-L-Leu-OMe (0.5 mmol), which was prepared by hydrogenolysis of Z-L-Leu-L-Leu-OMe, was dissolved in 5 ml each of MeOH, EtOH, *s*-BuOH, or toluene, and each solution was refluxed. Effect of each solvent on racemization and yield were compared, the results being shown in Table 3.

Determination of Racemization during the Formation of Cyclic Dipeptides. a) Fischer Method: Z-L-Leu-L-Leu-OMe (0.5 mmol) was dissolved in MeOH (5 ml) and hydrogenolyzed. The filtrate was evaporated, the residue was dissolved in methanolic ammonia (5 ml) and allowed to stand for 12 h, and the solution was evaporated. The residue was dissolved in MeOH (20 ml), a portion of which was applied to HPLC. The rest of the solution was evaporated and the residue was recrystallized from MeOH–ether; yield, 79 mg (70%). Other cyclic dipeptides were prepared by the same procedure, and the yield and racemization are shown in Table 4.

b) Nitecki Method: Boc-L-Leu-L-Leu-OMe (0.5 mmol) was dissolved in HCOOH (2.5 ml) and the solution was allowed to stand for 24 h at room temperature. After evaporation of the solution, the residue was dried *in vacuo* overnight and dissolved in a mixture of *s*-BuOH (5 ml) and toluene (3 ml). After the solution was refluxed for 6 h and evaporated, the residue was dissolved in MeOH (20 ml). A portion of the methanolic solution was evaporated and the residue was recrystallized from MeOH–ether; yield, 71%. Other cyclic dipeptides were prepared by the same procedure, and yields and racemization are shown in Table 4.

c) MeOH-reflux Method: Cyclic dipeptides were prepared by the same procedure as described in the section of Authentic Cyclic Dipeptides. Yields and racemization are shown in Table 4.

Side Reaction in the Nitecki Method. Boc-L-Ser-L-Ser-OMe (168 mg, 0.5 mmol) was dissolved in HCOOH (3 ml) and the solution was allowed to stand for 6 h. After evaporation of the solution, the residue was dried, and dissolved in a mixture of *s*-BuOH (5 ml) and toluene (3 ml). The solution was refluxed for 5 h, evaporated, and the residue (65 mg) was obtained as a mixture of three components, which were separated to component HCO-Ser-Ser-OMe (**1**), a *O*-formylated derivative (**2**) of **1**, and *cyclo*(-L-Ser-L-Ser-) by silica gel chromatography under the following conditions: column size, 1.1×50 cm; eluent, $CHCl_3$–MeOH (9 : 1); fraction volume, 0.7 ml, flow rate, 7 ml/h. Separated compounds were recrystallized from MeOH–ether and afforded **1** and **2**. Yield of **1**, 17 mg (13%); mp 153 °C; ^{1}H NMR (DMSO-d_6) δ=8.02 (s, CHO). Yield of **2**, 7 mg, (5%); mp 138—142 °C; ^{1}H NMR (DMSO-d_6) δ=8.02 (s, CHO), 8.20 (s, CHO). Yield of *cyclo*(-L-Ser-L-Ser-), 38 mg (40%); mp 231—233 °C (dec). The structures of **1** and **2** were assessed by the results of ^{1}H NMR as HCO-Ser-Ser-OMe and its *O*-formylated derivative. However, the formylated hydroxyl group was not identified.

In the case of H-L-Ser-L-Ser-OEt also, ethyl esters **1′** (mp 153—155 °C) and **2′** (mp 116—118 °C) corresponding to **1** and **2** were obtained by the same procedure. *N*-formyl and *N*,*O*-diformyl nature of **1′** and **2′** were ascertained by elemental analyses and ^{1}H NMR.

Degree of Racemization in the Fischer Method. *cyclo*(-L-Leu-L-Leu-) (10 mg) was dissolved in methanolic ammonia (2 ml), and the solution was allowed to stand at room temperature. After 4, 8, 16, and 32 h, an aliquot of the solution was taken and evaporated. The residue was dissolved in MeOH (5 ml), and the solution was applied to HPLC, the results being shown in Fig. 1.

We thank Dr. H. Aoyagi and Dr. M. Waki, Kyushu University, for their helpful discussions during this work.

References

1) T. Kamiya, S. Maeno, M. Hashimoto, and Y. Mine, *J. Antibiot.*, **25**, 576 (1972).
2) K. Nunami and T. Shiba, *Proc. 11th Symposium on Peptide Chem.*, p. 97 (1973).
3) Y. S. Chen, *Bull. Agric. Chem. Soc. Jpn.*, **24**, 379 (1960).
4) Y. Kodaira, *Agric. Biol. Chem.*, **25**, 261 (1961).
5) K. Bauer, K. K. Graf, A. F. Bauman, S. Beier, A. T. Vidal, and H. Kleinkauf, *Nature*, **274**, 174 (1978).
6) N. Izumiya, S. Lee, T. Kanmera, and H. Aoyagi, *J. Am. Chem. Soc.*, **99**, 8346 (1977).
7) T. Shiba, *Farumashia*, **12**, 313 (1976).
8) K. D. Kopple and D. H. Marr, *J. Am. Chem. Soc.*, **89**, 6193 (1967).

9) K. D. Kopple and M. Ohnishi, *J. Am. Chem. Soc.*, **91**, 962 (1969).
10) E. Fischer, *Ber.*, **39**, 2893 (1906).
11) D. E. Nitecki, B. Halpern, and J. W. Westley, *J. Org. Chem.*, **33**, 864 (1968).
12) Abbreviations according to IUPAC-IUB Commission, *J. Biol. Chem.*, **247**, 977 (1972), are used throughout. Additional abbreviations: DCC, dicyclohexylcarbodiimide; DMF, *N,N*-dimethylformamide; HPLC, high-performance liquid chromatography.
13) S. Lee, T. Kanmera, H. Aoyagi, and N. Izumiya, *Int. J. Pept. Protein Res.*, **13**, 207 (1979).
14) J. W. Westley, V. A. Close, D. E. Nitecki, and B. Halpern, *Anal. Chem.*, **40**, 1888 (1968).
15) T. Kanmera, S. Lee, H. Aoyagi, and N. Izumiya, *Int. J. Pept. Protein Res.*, **16**, 280 (1980).
16) Y. Shimohigashi, S. Lee, and N. Izumiya, *Bull. Chem. Soc. Jpn.*, **49**, 3280 (1976).
17) J. M. Manning and S. Moore, *J. Biol. Chem.*, **243**, 5591 (1968).
18) E. P. Kroeff and D. J. Pietrzyk, *Anal. Chem.*, **50**, 1353 (1978).
19) S. Terabe, R. Konaka, and K. Inoue, *J. Chromatogr.*, **172**, 163 (1979).
20) K. Suzuki, Y. Sasaki, N. Endo, and Y. Mihara,"Peptide Chemistry," ed by K. Okawa, Protein Research Foundation, Osaka (1980), p. 11.
21) T. Takahashi, M. Kaneko, and M. Oya, *Nippon Nogei Kagaku Kaishi*, **56**, 277 (1982).

 © 1983 The Chemical Society of Japan Bull. Chem. Soc. Jpn., 56, 573—576 (1983)

The Mechanism of the Reaction of (Aryloxy)trimethylstannane with Methanesulfonyl Chloride. Solvent and Substituent Effects on the Rate of the Reaction

Seizi KOZUKA,* Shigeru YAMAGUCHI, and Waichiro TAGAKI
Department of Applied Chemistry, Faculty of Engineering, Osaka City University, Sugimoto 3-chome, Sumiyoshi-ku, Osaka 558
(Received September 10, 1982)

A kinetic study has been conducted on the reactions of (aryloxy)trimethylstannanes with methanesulfonyl chloride giving chlorotrimethylstannane and aryl methanesulfonates. The reaction was found to obey a second order kinetic equation. The solvent effect on the rate of the reaction appeared obscure although a small rate enhancement was observed in a polar solvent. Substituent effect of the aryloxyl group was found to be dependent on the solvent used while a clear isokinetic relationship was observed. A charge separated four-center transition state has been suggested for the reaction.

The mechanism of the bimolecular IVb–VIb bond cleavage reactions may be classified into three different types. The first one is a nucleophilic attack of the VIb atom (I). The reaction of (arylthio)trimethylstannane

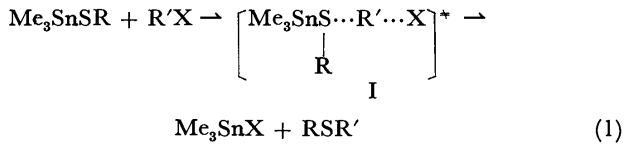

$$Me_3SnSR + R'X \rightarrow [Me_3SnS\cdots R'\cdots X]^{*} \rightarrow \underset{\text{I}}{\begin{bmatrix} Me_3SnS\cdots R'\cdots X \\ | \\ R \end{bmatrix}^{*}} \rightarrow Me_3SnX + RSR' \quad (1)$$

R = alkyl, aryl; R′ = alkyl; X = halogen.

with haloalkanes has been considered to be the nucleophilic reaction based on the kinetic results (Eq. 1). Namely, the reaction obeyed a second order kinetic equation with apparently negative substituent effect of the arylthio moiety ($\rho = -1.4$). Other evidence observed in support of the mechanism were: the solvent effect on the rate of the reaction ($k_{PhCN}/k_{C_6H_6} = ca.$ 100), relative reactivity of the haloalkanes which appeared in comparable to that of common S_N2 reactions, and inversion of configuration of the alkyl group of the haloalkane.[1] The reactions of (aryloxy)trimethylstannane with benzyl bromide[2] and (arylthio)trimethylstannane with benzoyl chloride[3] have also been suggested to proceed in similar manners.

The second is the reaction involving five-coordinated intermediate (II) as has been suggested for the reaction of (arylthio)trimethylsilane with phenacyl bromide based on the kinetic results. A large positive ρ value due to the arylthio moiety (+2.2) was observed with a large negative entropy of activation (-156 J K^{-1} mol^{-1}). As a result, five-coordinated silicon intermediate was suggested to be involved prior to the rate-determining heterolysis of the Si–S bond (Eq. 2).[4] Five-coordinated silicon intermediates have also been suggested for acyloxyl exchange reaction of acyloxysilane with carboxylic acid[5] and the reaction of arylthiosilane with carboxylic acid.[6]

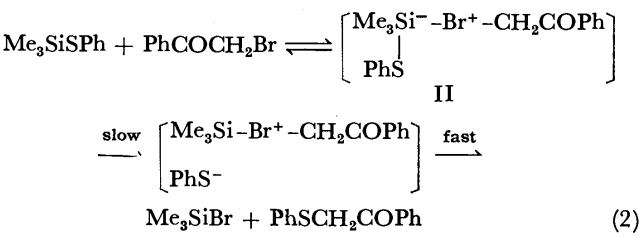

$$Me_3SiSPh + PhCOCH_2Br \rightleftharpoons \underset{\text{II}}{\begin{bmatrix} Me_3Si^{-}\text{-}Br^{+}\text{-}CH_2COPh \\ | \\ PhS \end{bmatrix}} \xrightarrow{\text{slow}} \begin{bmatrix} Me_3Si\text{-}Br^{+}\text{-}CH_2COPh \\ PhS^{-} \end{bmatrix} \xrightarrow{\text{fast}} Me_3SiBr + PhSCH_2COPh \quad (2)$$

The third possibility is a four-centered mechanism. The reaction of alkoxytrimethylsilanes with benzenesulfinyl chloride had once been suggested to involve nonionic four-centered transition state (III) based on the kinetic resuls that the rate of the reaction was little influenced by the solvent polarity but sensitive to the steric effect of the alkoxyl group.[7] This was the only one bimolecular IVb–VIb bond cleavage reaction involving this mechanism supported by kinetic evidences. The mechanism, however, was suspected and a nucleophilic attack of the oxygen atom (IV) has been suggested since the rate of the reaction was clearly accelerated in a more polar solvent and a negative ρ value (-1.44) was observed by the reaction of arylthiosilanes (Eq. 3).[8] Thus, the four-center mechanism

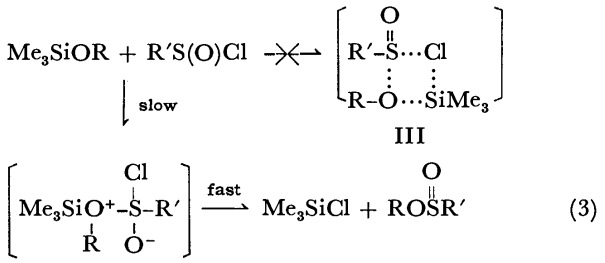

$$Me_3SiOR + R'S(O)Cl \rightleftarrows \underset{\text{III}}{\begin{bmatrix} O \\ \| \\ R'\text{-}S\cdots Cl \\ \vdots \quad \vdots \\ R\text{-}O\cdots SiMe_3 \end{bmatrix}} \quad \text{(slow)}$$

$$\begin{bmatrix} Cl \\ | \\ Me_3SiO^{+}\text{-}S\text{-}R' \\ | \quad | \\ R \quad O^{-} \end{bmatrix}_{\text{IV}} \xrightarrow{\text{fast}} Me_3SiCl + ROSR' \quad (3)$$

R = Me, Et, R′ = Ph; R = Aryl, R′ = Me.

had once been ruled out for the bimolecular IVb–VIb bond cleavage reaction. Our recent preliminary results of the reaction of (aryloxy)trimethylstannane with methanesulfonyl chloride, however, could only be rationalized by the four-center mechanism.[9] A detailed account of this reaction will be described.

Results and Discussion

Product Analysis. Trimethylphenoxystannane was refluxed with an equimolar amount of methanesulfonyl chloride in carbon tetrachloride. The reaction was found to give chlorotrimethylstannane and phenyl methanesulfonate in nearly quantitative yield (Eq. 4).

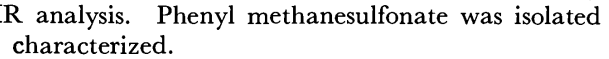

$$Me_3SnOPh + MeSO_2Cl \xrightarrow[CCl_4]{\text{reflux 5 h}} Me_3SnCl + MeSO_2OPh \quad (4)$$

No other product was found in the reaction solution by NMR analysis. Phenyl methanesulfonate was isolated and characterized.

Table 1. Rate constants for the reaction of $Me_3SnOC_6H_5$ (0.242 mol dm^{-3}) with $MeSO_2Cl$ (0.175 mol dm^{-3}) in various solvents

Solvent	$(\varepsilon)^{a)}$	Temp °C	$k_2\times10^4$ dm^3 mol^{-1} s^{-1}	k_{rel}	$\Delta H^{\ddagger}_{400}$ kJ mol^{-1}	$\Delta S^{\ddagger}_{400}$ J K^{-1} mol^{-1}
CCl_4	(2.23)	120	2.50 ± 0.21		44.5	−204
CCl_4		130	3.74 ± 0.12	1.00	γ=0.998$^{b)}$	
CCl_4		150	6.94 ± 0.50			
CH_2Br_2	(6.7)	120	1.04 ± 0.037		41.2	−221
CH_2Br_2		130	1.41 ± 0.06	0.38	γ=0.999	
CH_2Br_2		140	1.98 ± 0.11			
CH_2Cl_2	(8.9)	130	1.20 ± 0.06	0.32	38.6	−228
CH_2Cl_2		150	2.39 ± 0.16		γ=0.997	
CH_2Cl_2		160	2.82 ± 0.23			
C_6H_5CN	(25.2)	120	5.11 ± 0.17		47.0	−192
C_6H_5CN		130	7.56 ± 0.91	2.0	γ=0.999	
C_6H_5CN		140	10.7 ± 1.1			
CH_3CN	(36.2)	100	8.58 ± 0.79		59.2	−148
CH_3CN		110	13.0 ± 1.1		γ=0.997	
CH_3CN		130	37.8 ± 2.3	10		

a) Dielectric constant. b) Correlation coefficiency of the Arrhenius plot.

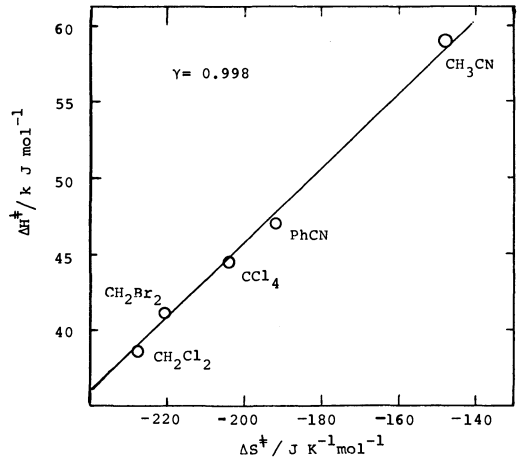

Fig. 1. Plot of $\Delta H^{\ddagger}$ *vs.* $\Delta S^{\ddagger}$ in various solvents.

Kinetics and Mechanism. The rate of the reaction of trimethylphenoxystannane (0.242 mol dm^{-3}) with methanesulfonyl chloride (0.175 mol dm^{-3}) was measured by following the decrease and rise of the ^{1}H NMR methyl signal of the starting chloride ($MeSO_2Cl$, δ 3.58 ppm) and of the sulfonate (δ 3.03 ppm). A good second order kinetic plot (γ=0.998) was obtained for more than 80% completion with tolerable reproducibility (±8%). The rates of the reactions at various temperatures were measured in five different solvents including carbon tetrachloride as a nonpolar solvent and acetonitrile as the most polar one. The results are summerized in Table 1.

The solvent effect shown in Table 1 is quite smaller than that observed for the nucleophilic reaction of arylthiostannane with haloalkane[1] and abnormal. No dependency of the rates on the solvent polarities was observed although it was slightly accelerated in polar solvents except for that in carbon tetrachloride. The result may suggest different mechanism for the reaction in carbon tetrachloride from that in polar solvents.

Table 2. Rate constants for the reactions of $Me_3SnOC_6H_4X$-*p* (0.242 mol dm^{-3}) with $MeSO_2Cl$ (0.175 mol dm^{-3})

Solvent	Temp/°C	Substituent X	k_2/dm^3 mol^{-1} s^{-1}
CCl_4	130	OCH_3	$5.37\pm0.51\times10^{-4}$
CCl_4	130	CH_3	$3.99\pm0\ 29\times10^{-4}$
CCl_4	130	H	$3.74\pm0.12\times10^{-4}$
CCl_4	130	Cl	$2.81\pm0.15\times10^{-4}$
CCl_4	130	NO_2	$4.17\pm0.90\times10^{-5}$
CH_2Cl_2	130	OCH_3	$5.13\pm0.20\times10^{-4}$
CH_2Cl_2	130	CH_3	$3.23\pm0.19\times10^{-4}$
CH_2Cl_2	130	H	$1.20\pm0.06\times10^{-4}$
CH_2Cl_2	130	Cl	$4.66\pm0.37\times10^{-5}$
CH_2Cl_2	130	NO_2	$1.74\pm0.29\times10^{-5}$
C_6H_5CN	130	OCH_3	$1.73\pm0.29\times10^{-3}$
C_6H_5CN	130	CH_3	$9.67\pm0.59\times10^{-4}$
C_6H_5CN	130	H	$7.56\pm0.91\times10^{-4}$
C_6H_5CN	130	Cl	$6.18\pm0.23\times10^{-4}$
C_6H_5CN	130	NO_2	$7.58\pm0.91\times10^{-4}$
CH_3CN	100	OCH_3	$5.04\pm0.51\times10^{-4}$
CH_3CN	100	CH_3	$6.28\pm0\ 38\times10^{-4}$
CH_3CN	100	H	$8.58\pm0.79\times10^{-4}$
CH_3CN	100	Cl	$1.34\pm0.29\times10^{-3}$
CH_3CN	100	NO_2	$5.68\pm0.52\times10^{-3}$

The hypothesis, however, conflicts with the isokinetic relationship. Plots of the activation parameters observed in all the solvents examined, gave a clear straight line as shown in Fig. 1, which strongly rules out the possibility of the different mechanism in polar and nonpolar solvents.

Substituent effects of the aryloxyl groups were examined in these solvents in order to obtain more evidence about the reaction mechanism. The reactions were carried out at 130 °C except for the reactions in acetonitrile which were conducted at 100 °C since some reactions in this solvent were too fast to be measured at the higher temperatures. The results are given in Table 2 and Hammett plots are shown in Figs. 2—5.

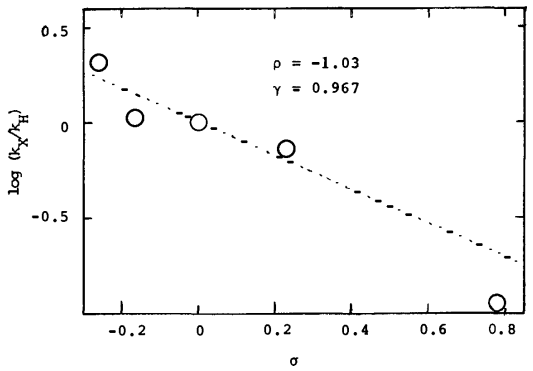

Fig. 2. Hammett plot of the rates in CCl_4 at 130 °C.

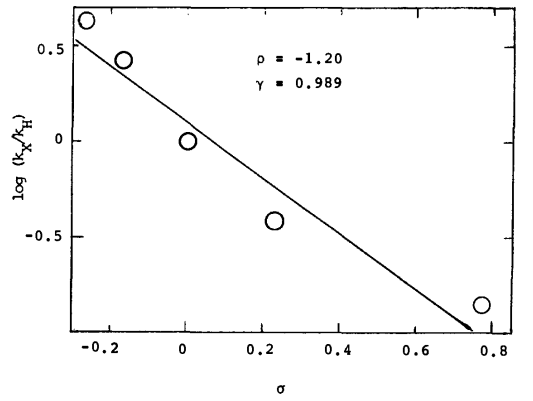

Fig. 3. Hammett plot of the rates in CH_2Cl_2 at 130 °C.

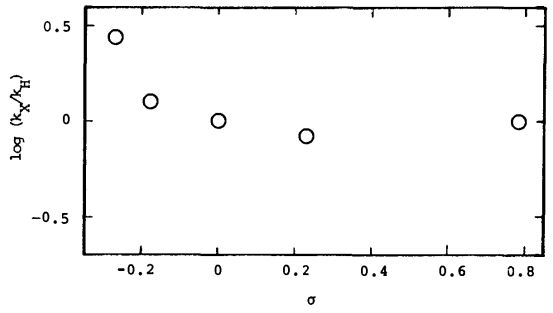

Fig. 4. Hammett plot of the rates in C_6H_5CN at 130 °C.

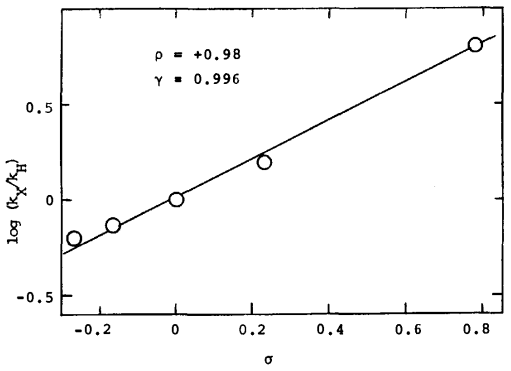

Fig. 5. Hammett plot of the rates in CH_3CN at 100 °C.

As shown in Figs. 2—5, the substituent effects are markedly dependent on the solvent used. Negative ρ values were observed for the reactions in carbon tetrachloride and dichloromethane though the magnitudes are somewhat smaller than most of that of the IVb-VIb bond cleavage reactions involving nucleophilic attacks of the VIb atom.[1-3] On the contrary, almost no substituent effect and a small positive ρ value were observed in benzonitrile and in acetonitrile, respectively.

The negative ρ values observed in carbon tetrachloride and in dichloromethane may postulate an ionic process for the reaction *i.e.*, a nucleophilic attack of the oxygen atom on the sulfonyl sulfur. The mechanism, however, is inconsistent with the substituent effects observed in benzonitrile and in acetonitrile and also conflicts with the small and obscure solvent effect. If such ionic process was operative even in the nonpolar solvent, it should be facilitated more in the polar solvents. The ρ values observed in the polar solvents have to appear clearly negative and more enhanced solvent effect would be expected as were observed for the analogous reactions.[1,3,8] The ρ values presently observed in the polar solvents together with the solvent effect are inconsistent with these considerations. Furthermore, the positive ρ value observed in acetonitrile could not be explained by postulation of a five-coordination process in the solvent. Different mechanisms in individual solvents are hardly acceptable for the reaction in view of the isokinetic relationship as discussed above.

Large negative entropy of activations were observed for the present reaction in all the solvents as shown in Table 1. These paramters would be an evidence in support of a four-centered mechanism although they could not be a definite evidence. Namely, large negative entropy of activation values were observed for the nucleophilic[1,8] and five-coordination[4] reactions involving cleavages of IVb-VIb bonds, regardless of their mechanisms. Most of the values presently observed, however, are substantially more negative than those observed previously. Consequently, the activation parameters could be considered to be an evidence suggesting a four-center process for the reaction and this is the only remaining possible mechanism.

It is difficult, however, to rationalize the solvent and the substituent effects by a fully concerted nonionic four-center transition state like III. An alternative four-center transition state is a charge separated one, similar to the associative mechanism which has been suggested for the unimolecular rearrangement of β-keto silanes.[10] In the rearrangement of β-keto silanes, little[11] or noticeable solvent effect was observed[10] although a wide variety of solvents has not yet been examined for the rearrangement. Moreover, small substituent effects were also observed for the rearrangements.[11,12] These observations quite resemble to those of the present study although the effect of the solvent on the substituent effect has not been reported yet for the rearrangement. As an analogy, a charge separated associative four-center transition state (V) would be the most suitable process for the present reaction.

Some modifications of the transition state, as shown in Va—d, may profit to account for the present observa-

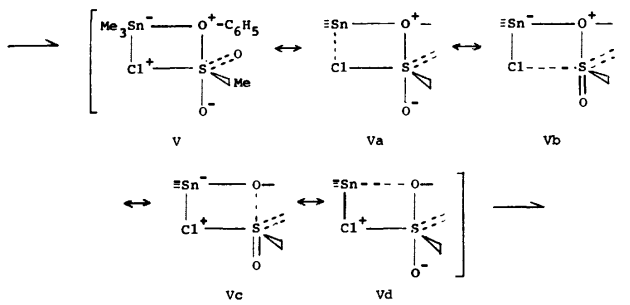

V Va Vb

Vc Vd

tions. In the nonpolar solvents, the transition state is characterized by the O–S bond forming. The nucleophilic character of the oxygen atom, as depicted in Va as an extreme, would account for the negative substituent effect. Another way to rationalize the negative ρ value in nonpolar solvent is considering the Cl–S bond cleavage at the transition state (Vb). On the other hand, the positive substituent effect observed in acetonitrile may due to the Sn–Cl bond formation (Vc) or to the Sn–O bond fission (Vd) at the transition state. The reaction in benzonitrile may involve nearly ideal four-center transition state, V. All these transition states involve charge separations despite of the small deviations in their characters dependent on the solvents used. Thus, the small but noticeable solvent effect would be expected as was observed except for that in carbon tetrachloride. The small rate enhancement in carbon tetrachloride than in dibromo- and dichloro-methanes is difficult to explain, however, a similar slight rate enhancement in carbon tetrachloride was also observed for the reaction of ketenimine with thioketone.[13] The solvent may be too poor to solvate and to stabilize the reactants and may allow them to cohere and facilitate the bimolecular reactions in some extents.

Experimental

Materials. Preparations of (aryloxy)trimethylstannanes were carried out according to the literature.[2] Solvents for the kinetic runs were dried and distilled before use.

Product Analysis. Trimethylphenoxystannane (0.92 g) was refluxed for 5 h with methanesulfonyl chloride (0.40 g) in carbon tetrachloride (20 ml). The reaction solution was subjected to NMR analysis before work up. Only chlorotrimethylstannane and phenyl methanesulfonate were detected in the solution. The mixture was washed with water and extracted with chloroform. Phenyl methanesulfonate was isolated from the extract by evaporation of the solvent followed by recrystallization from hexane–chloroform (0.55 g, 91%) and identified by comparing with an authentic sample.

Kinetics. A typical procedure is described. (Aryloxy)-trimethylstannane (0.242 mol dm^{-3}) and methanesulfonyl chloride (0.175 mol dm^{-3}) were dissolved in a solvent using 5 ml volumetric flask. The sotution was devided into 10 portions and sealed in glass tubes of *ca.* 0.7 ml volume. The tubes were heated in a constant temperature bath (130 °C) and samples were taken out at time intervals. Each solutions were subjected to ^{1}H NMR analysis with 7—8 repeated recording of methyl signals of methanesulfonyl chloride (δ 3.58 ppm) and of the sulfonate (δ 3.03 ppm). The second order rate constant, k_2 was obtained by least square calculation of the averaged peak intensities of the methyl signals at time t.

References

1) S. Kozuka and S. Ohya, *Bull. Chem. Soc. Jpn.*, **51**, 2651 (1978).
2) S. Kozuka, A. Kikuchi, and S. Yamaguchi, *Bull. Chem. Soc. Jpn.*, **54**, 307 (1981).
3) S. Kozuka and I. Naribayashi, *Bull. Chem. Soc. Jpn.*, **52**, 3639 (1979).
4) S. Kozuka, T. Higashino, and T. Kitamura, *Bull. Chem. Soc. Jpn.*, **54**, 1420 (1981).
5) S. Kozuka, T. Kitamura, N. Kobayashi, and K. Ogino, *Bull. Chem. Soc. Jpn.*, **52**, 1950 (1979).
6) S. Kozuka and T. Kitamura, *Bull. Chem. Soc. Jpn.*, **52**, 3384 (1979).
7) D. N. Harpp, B. T. Friedlander, C. Larsen, K. Steliou, and A. Stockton, *J. Org. Chem.*, **43**, 3481 (1979).
8) S. Kozuka and T. Higashino, *Bull. Chem. Soc. Jpn.*, **54**, 1184 (1981).
9) S. Kozuka, S. Yamaguchi, and W. Tagaki, *Chem. Lett.*, **1981**, 1299.
10) H. Kwart and W. E. Barnett, *J. Am. Chem. Soc.*, **99**, 614 (1977).
11) A. G. Brook, D. M. MacRae, and A, R. Bassindale, *J. Organomet. Chem.*, **86**, 185 (1975).
12) G. L. Larsou and Y. V. Fernandez, *J. Organomet. Chem.*, **86**, 193 (1975).
13) A. Dondoni, A. Battaglia, F. Bernardi, and P. Giorgianni, *J. Org. Chem.*, **45**, 3773 (1980).

 © 1983 The Chemical Society of Japan Bull. Chem. Soc. Jpn., 56, 577—582 (1983)

Crystal Structure and Related Properties of Phenothiazine Cation Radical-Hexachloroantimonate. Monoclinic(I) Form

Tokiko Uchida,* Masanori Ito, and Kozo Kozawa
Department of Industrial Chemistry, Faculty of Science and Technology, Science University of Tokyo, Noda, Chiba 278

(Received March 15, 1982)

Three forms of crystals were obtained from mixed solutions of phenothiazine and $SbCl_5$; the crystal structure of the monoclinic(I) modification was determined using 2827 reflections at room temperature. Crystal data: $(C_{12}H_9NS)^{+\cdot}SbCl_6^-$, $F.W.=533.7$, monoclinic, $a=16.253(3)$, $b=14.334(1)$, $c=15.786(3)$ Å, $\beta=104.07(1)°$, space group C2/c, $D_m=2.00$, $D_x=1.99$ g cm^{-3}, $Z=8$, $\mu=25.73$ cm^{-1} (Mo $K\alpha$). The structure was solved by the heavy-atom method and refined by block-diagonal least-squares method to $R=0.072$. The crystal consists of phenothiazine cation radicals($PT^{+\cdot}$) and hexachloroantimonate anions($SbCl_6^-$), and every ion exists as a monomer in the crystal. Each $SbCl_6^-$ forms a distorted octahedron. The two C–S distances of $PT^{+\cdot}$ are 1.705 and 1.711 Å, and the C–S–C angle is 103.9°. The dihedral angle between the two outer phenyl rings of $PT^{+\cdot}$ is 176.5°. From the ESR measurements of a single crystal, three principal g-values were determined: $g_1=2.003$, $g_2=2.007$ and $g_3=2.008$. The direction of g_1 is normal to the molecular plane of $PT^{+\cdot}$. These facts suggest some π-delocalization in the central ring of $PT^{+\cdot}$. Absorption spectra polarized parallel to the molecular plane of $PT^{+\cdot}$ are very similar to the polycrystalline reflection spectra of $PT^{+\cdot}$ salts obtained by other authors, and there are no intense bands in the spectra polarized perpendicular to $PT^{+\cdot}$ molecular plane over the wave number range 10 to 27×10^3 cm^{-1}.

Phenothiazine (PT) is a very characteristic electron donor possessing several stepwise oxidation states[1–3] and a variety of folding angles of the molecular plane.[4] On the other hand, antimony chlorides have been known as electron acceptors or Lewis acids strong enough to provide cation radicals of some aromatic molecules easily.[5] Many works have been published about the solid state behavior of electron donor-acceptor complexes[5–8] or graphite intercalation compounds[9] including antimony chlorides. However, few of them discussed their results on the basis of the strictly determined crystal structures, since the samples were usually obtained in very fine polycrystals. Magnetic and optical properties of polycrystalline "PT–$SbCl_5$" were described by Sato *et al.* more than ten years ago.[7,8] Recently, we have been able to distinguish at least three kinds of crystals in the precipitates of a mixture of PT and $SbCl_5$. They are different from each other in both color and crystal system.

In this paper, we wish to report the crystal structure, paramagnetic resonance and electronic absorption spectra for a brown monoclinic single crystal of phenothiazine cation radical-hexachloroantimonate.

Experimental

Preparation of Single Crystals. Both PT and $SbCl_5$ dissolved in 1,2-dichloroethane (concentration of about 3.5×10^{-3} mol dm^{-3}) were mixed in approximately 1 : 1 mol ratio in a dry box at room temperature. By slow evaporation of solvent in a dry atmosphere, three types of crystals were distinguishable in the precipitates: monoclinic(I), monoclinic(II), and triclinic modifications. The monoclinic(I) crystals are brown rectangular platelets with (010) plane developed and [20$\bar{1}$] direction elongated. The monoclinic(II) and triclinic crystals were hexagonal prisms and black parallelepiped columns, respectively.[10] The crystals were fairly stable in the air for a month, if they were completely dried up in a nitrogen atmosphere.

This report concerns the monoclinic(I) modification that consists of the ionic salt of phenothiazine cation radical($PT^{+\cdot}$) and hexachloroantimonate anion($SbCl_6^-$).[11] Triclinic crystals, which will be reported elsewhere, are (3,7-dichlorophenothiazine)$^{+\cdot}$ $SbCl_6^-$, but the components of monoclinic(II) crystals still remain unknown.

X-Ray Data Collection. After determining preliminary cell constants and space group from Weissenberg photographs, a crystal of $0.3\times0.2\times0.08$ mm^3 was mounted on a Hilger & Watts diffractometer with Mo $K\alpha$ radiation at room temperature. From the 12 setting angles, θ's of which were greater than 10.7°, the lattice constants were calculated by a least-squares method. Intensity data were collected by the θ-2θ scan technique at every 0.01° of θ step up to $2\theta\leq55°$. The scan width of θ was 0.8° for all the reflections. Counting time was 1 s per step for peak measurements, and each background was measured for 10 s at the beginning and the end of the scan range. Three standard reflections were monitored every 50 measurements to check both crystal and apparatus. No systematic changes in intensities of the standard reflections were observed throughout the data collection. Lorentz and polarization effects were corrected, but no absorption correction was made. Of the 4345 independent reflections measured, 2827 with $F_o\geq3\sigma(F)$ were used in the subsequent analysis. Density was observed by the flotation method. Crystal data are shown in Table 1. The systematic absences indicated the space group to be either Cc or C2/c, but the further study showed it to be C2/c.

Electronic Absorption Spectra. The solution spectra and

Table 1. Crystal data

$(C_{12}H_9NS)^{+\cdot}$ $SbCl_6^-$
$F.W.=533.7$
Monoclinic
C2/c
$a=16.253(3)$ Å
$b=14.334(1)$ Å
$c=15.786(3)$ Å
$\beta=104.07(1)°$
$V=3567$ Å^3
$Z=8$
$D_m=2.00$ g cm^{-3}
$D_x=1.99$ g cm^{-3}
μ(Mo $K\alpha$)$=25.73$ cm^{-1}

polycrystalline reflection spectra were recorded on a Hitachi spectrophotometer, Model 323, at room temperature. Solution spectra were measured with 1,2-dichloroethane as solvent. Polarized absorption spectra with single crystals were observed with Olympus MSP-A-IV microspectrophotometer over the wave number range 10 to 27×10^3 cm^{-1} at room temperature.

Electron Spin Resonance. Measurements of electron spin resonance(ESR) were carried out with a JES-FE3X spectrometer operating at 9.4 GHz microwave and 100 KHz magnetic field modulation. The polycrystalline sample was measured both at room temperature and at 77 K. Angular dependence of resonance field about a single crystal was observed at room temperature. New orthogonal coordinates. a′, b′, and c′, were defined to rotate a specimen: a′ was parallel to the developing [20$\bar{1}$] axis, b′ agreed with the crystal b axis, and the c′ was perpendicular to the a′b′ plane. The resonance field was recorded at every 15° rotation around the a′, b′, and c′ axes. The *g*-values were calculated from spectra in which the resonance fields of both specimen and Mn^{2+}/MgO (a_{Mn}= 8.69 mT) were recorded simultaneously. The spin concentrations were not measured.

Solution and Refinement of the Structure

The structure was solved by the heavy-atom method. From the Patterson synthesis, two Sb atoms were found to occupy two different special equivalent positions (b and e of Wyckoff positions), one on the center of symmetry and the other on the two-fold rotation axis. A Fourier map, computed using the phases from two Sb atoms, revealed the positions of all the non-hydrogen atoms. After five cycles of the isotropic block-diagonal least-squares refinements, the discrepancy index *R* converged at 0.112. Then, five additional cycles of the anisotropic refinement gave the *R* to be 0.075. At this stage of the refinements, the difference Fourier map clearly revealed all the hydrogen atoms. The final cycle was calculated including hydrogen atom parameters with a fixed isotropic thermal parameters, *B*= 4.0 Å^2, and converged to *R*=0.072. The quantity minimized was $\sum w(|F_o|-k|F_c|)^2$, where the weighting scheme $w=(F_{max}/F_o)^2$ for $F_o>F_{max}$, and $w=1$ for $F_o\leq F_{max}$. F_{max}=32.5 after scaling F_o to F_c.[12] In the final cycle, the parameter shifts almost converged to zero except for those of hydrogen atoms which were less than the corresponding standard deviations. A final difference Fourier map showed no extra peaks. The neutral atomic scattering factors and anomalous dispersion factors of Sb were taken from the "International Tables for X-Ray Crystallography."[13] All the computations were carried out at the Computer Centre of the University of Tokyo with the UNICS program system.[14]

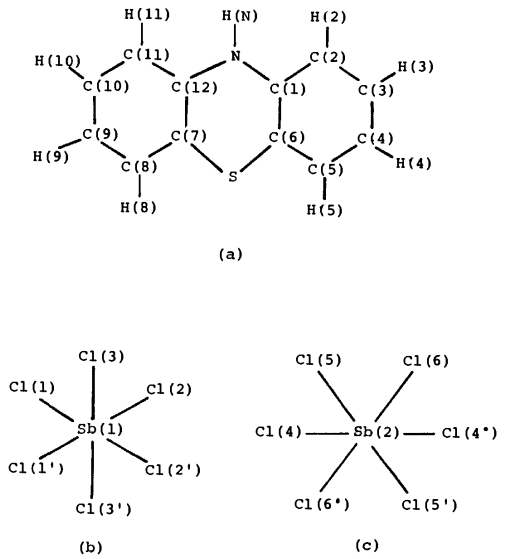

Fig. 1. The numbering of atoms.
(a): $PT^{+\bullet}$. (b): $SbCl_6^-$ with 2 symmetry. (c): $SbCl_6^-$ with $\bar{1}$ symmetry.

Results and Discussion

Crystal Structure. The atomic positional parameters with their estimated standard deviations are

Table 2. The final positional parameters ($\times10^4$; for H, $\times10^3$) and equivalent isotropic thermal parameters

Estimated standard deviations are given in parentheses. The equivalent isotropic thermal paramers for non-hydrogen atoms are calculated using the expression: $B_{eq}=\frac{4}{3}\Sigma_i\Sigma_j a_i a_j \beta_{ij}$, where the a_i's are the unit cell edges in direct space. The isotropic thermal parameter of hydrogen atoms is fixed, *B*=4 0 Å^2.

	x	*y*	*z*	B_{eq}/Å^2
Sb(1)	0000	727(1)	2500	3.0(0)
Sb(2)	0000	5000	0000	3.0(0)
Cl(1)	1(2)	−438(2)	1435(2)	3.9(1)
Cl(2)	40(3)	1898(3)	1463(3)	5.1(1)
Cl(3)	1509(2)	673(3)	2911(3)	4.4(1)
Cl(4)	−327(3)	6507(3)	429(3)	5.2(1)
Cl(5)	−44(3)	5569(3)	−1425(2)	4.6(1)
Cl(6)	1462(2)	5343(4)	462(3)	5.1(1)
S	1717(2)	851(3)	521(3)	4.3(1)
N	3241(7)	209(10)	1964(8)	4.2(4)
C(1)	3136(8)	1143(11)	1839(9)	4.0(4)
C(2)	3774(10)	1757(14)	2379(10)	5.2(6)
C(3)	3684(15)	2677(15)	2229(15)	7.3(11)
C(4)	3012(13)	3077(12)	1606(13)	5.8(7)
C(5)	2405(10)	2497(12)	1100(11)	4.9(5)
C(6)	2478(8)	1505(10)	1197(9)	3.9(6)
C(7)	2020(8)	−274(10)	793(9)	3.5(4)
C(8)	1556(9)	−997(12)	358(11)	4.6(6)
C(9)	1785(10)	−1893(11)	552(11)	4.5(5)
C(10)	2472(11)	−2126(11)	1188(12)	5.2(6)
C(11)	2974(11)	−1433(13)	1683(11)	5.2(6)
C(12)	2746(8)	−500(11)	1485(8)	3.6(4)
H(N)	361(11)	8(13)	229(12)	
H(2)	438(11)	142(13)	282(13)	
H(3)	389(11)	308(13)	250(12)	
H(4)	290(12)	387(13)	157(12)	
H(5)	198(11)	272(13)	69(12)	
H(8)	114(11)	−80(13)	−1(13)	
H(9)	139(11)	−235(13)	14(12)	
H(10)	282(12)	−278(13)	132(12)	
H(11)	358(11)	−153(13)	218(12)	

Table 3. Bond distances and angles of $SbCl_6^-$ anions

Bond distance	l/Å	Bond angle	ϕ/°
Sb(1)–Cl(1)	2.369(4)	Cl(1)–Sb(1)–Cl(2)	90.3(2)
Sb(1)–Cl(2)	2.357(5)	Cl(1)–Sb(1)–Cl(3)	89.6(1)
Sb(1)–Cl(3)	2.381(4)	Cl(1)–Sb(1)–Cl(1′)	90.4(1)
		Cl(1)–Sb(1)–Cl(2′)	178.4(2)
		Cl(1)–Sb(1)–Cl(3′)	87.8(1)
		Cl(2)–Sb(1)–Cl(3)	90.7(2)
		Cl(2)–Sb(1)–Cl(2′)	89.2(2)
		Cl(2)–Sb(1)–Cl(3′)	92.0(2)
		Cl(3)–Sb(1)–Cl(3′)	176.3(2)
Sb(2)–Cl(4)	2.362(5)	Cl(4)–Sb(2)–Cl(5)	90.0(2)
Sb(2)–Cl(5)	2.377(4)	Cl(4)–Sb(2)–Cl(6)	90.1(2)
Sb(2)–Cl(6)	2.361(5)	Cl(5)–Sb(2)–Cl(6)	91.0(2)

Table 4. Bond distances and angles of $PT^{+\cdot}$ cation radical

Bond distance	l/Å	Bond angle	ϕ/°
N–C(1)	1.36(2)	C(1)–N–C(12)	127(1)
C(1)–C(2)	1.47(3)	N–C(1)–C(2)	117(1)
C(2)–C(3)	1.34(3)	N–C(1)–C(6)	122(1)
C(3)–C(4)	1.40(3)	C(2)–C(1)–C(6)	121(1)
C(4)–C(5)	1.39(3)	C(1)–C(2)–C(3)	117(2)
C(5)–C(6)	1.43(2)	C(2)–C(3)–C(4)	124(2)
C(6)–C(1)	1.38(2)	C(3)–C(4)–C(5)	119(2)
S–C(6)	1.71(2)	C(4)–C(5)–C(6)	120(2)
S–C(7)	1.71(2)	C(1)–C(6)–C(5)	119(1)
C(7)–C(8)	1.37(2)	S–C(6)–C(1)	125(1)
C(8)–C(9)	1.35(2)	C(6)–S–C(7)	103.9(7)
C(9)–C(10)	1.35(3)	S–C(6)–C(5)	117(1)
C(10)–C(11)	1.40(3)	S–C(7)–C(8)	120(1)
C(11)–C(12)	1.40(2)	S–C(7)–C(12)	122(1)
C(7)–C(12)	1.44(2)	C(8)–C(7)–C(12)	118(1)
N–C(12)	1.40(2)	C(7)–C(8)–C(9)	121(2)
		C(8)–C(9)–C(10)	122(2)
		C(9)–C(10)–C(11)	120(2)
		C(10)–C(11)–C(12)	118(2)
		N–C(12)–C(7)	120(1)
		N–C(12)–C(11)	119(1)
		C(7)–C(12)–C(11)	119(1)

presented in Table 2. The atomic numbering is given in Fig. 1.

There are two crystallographically different halves of ($SbCl_6^-$)'s and a $PT^{+\cdot}$ in an asymmetrical unit. Each $SbCl_6^-$ anion forms a slightly distorted octahedron. The bond lengths and angles, given in Table 3, are consistent with those found in other $SbCl_6^-$.[15] Of the six independent Sb–Cl distances, Sb(1)–Cl(3) and Sb(2)–Cl(5) are slightly longer than the other four.

In Table 4, the bond distances and angles of $PT^{+\cdot}$ are presented. The C–S bond distances are significantly shorter than those of neutral PT (1.762 Å for orthorhombic form[16] and 1.770 Å for monoclinic form[17]). The sum of the covalent radii is 1.81 Å for C–S single bond, and is 1.61 Å for C–S double bond.[18] The observed C–S bond length of 1.71(2) Å is just an average of these values. It suggests the π-delocalization is spread over the whole molecule of $PT^{+\cdot}$ including the central ring. Similar C–S distances, around 1.71 Å, were found in many compounds,[19] in which the shortening of the C–S bonds and the planarity of the systems characterized a π-delocalization including S atoms.

Much attention has been paid to the planarity of $PT^{+\cdot}$, namely, the dihedral angle between the external two benzene rings of PT molecule (these two planes are denoted as Bz1 and Bz2 in this paper. See Table 5). For substituted phenothiazines, this angle ranges from 134.4° to 173.6°, depending on the kinds and the positions of the substituents at the external benzene rings.[4] Andreetti *et al.* discussed the dihedral angle (so-called butterfly angle) of PT derivatives related to the degree of delocalization in the central ring, which was estimated from the shortening of the C–S bond lengths.[4] Table 5 lists the dihedral angles and related value of PT moieties in complex compounds[20–24] as well as the two modifications of PT itself.[16,17] The top two compounds in Table 5 are $PT^{+\cdot}$ ion radical salts and the next four compounds are charge-transfer (CT) complexes of weak π-π type. Every dihedral angle between Bz1 and Bz2 of PT moiety is close to 180° except for PT–DNB,[24] and the flattened PT moiety

Table 5. Comparison of some parameters of PT species

Compound	Dihedral angle θ/° [a]				Bond distance l/Å		Bond angle ϕ/°		Ref.
	Bz1-Bz2	P1-P2	Bz1-P1	Bz2-P2	C–S (average)	CN (average)	C–S–C	C–N–C	
$PT^{+\cdot}$–$SbCl_6^-$	175.8	177.1	178.5	179.5	1.71	1.38	104	127	This work
$PT^{+\cdot}$–$Ni(tfd)_2^-$	172.2[b]	177.44	179.09	179.56	1.73	1.41	102.8	121	20
PT–PMDA	176.4	173.8	178.6	178.6	1.758	1.403	103.2	125.3	21
PT–TCNQ	Planar[c]				1.73	1.36	104	134	22
PT–TNB	Planar within the accuracy				1.76	1.40	102	126	23
PT–DNBA	156[d]	—	—	—	1.76	1.39	101	123	24
PT(orthorh)	158.5	—	—	—	1.762	1.399	100.9	124.4	16
PT(monocl)	153.3	—	—	—	1.770	1.406	99.6	121.5	17

a) Least squares planes are defined as follows. A maximum deviation of constituent atom of each plane is presented in parenthesis. Bz1: C(1), C(2), C(3), C(4), C(5), and C(6) (0.009 Å); Bz2: C(7), C(8), C(9) C(10), C(11), and C(12) (0.01 Å); P1: S, N, C(1) and C(6) (0.009 Å); P2: S, N, C(7) and C(12) (0.001 Å). b) Folding angle of two halves being approximated planar. c) Fundamental structure in disordered crystal. d) Dihedral angle between two planar halves folded along the N–S axis. Nomenclature: tfd=(z)-1,2-bis(trifluoromethyl)-1,2-ethylenedithiolate, PMDA=1,2:4,5-benzenetetracarboxylic dianhydride(pyromellitic dianhydride), TCNQ=7,7,8,8-tetracyanoquinodimethan, TNB=1,3,5-trinitrobenzene, DNBA=3,5-dinitrobenzoic acid.

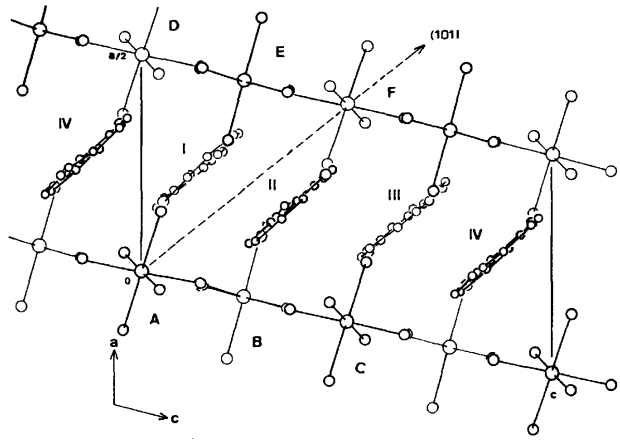

Fig. 2. The packing arrangements in the crystal lattice projected along the b axis. The numbering from I to IV correspond to $PT^{+\cdot}$'s, and those from A to F correspond to $(SbCl_6^-)$'s. The same notations are employed in Figs. 3 and 4. The broken line indicates the direction of [101] together with the intersection of (010) and $(10\bar{1})$ planes.

Symmetry code

$PT^{+\cdot}$: I x, y, z
II $1/2-x, 1/2+y, 1/2-z$
III $x, -y, 1/2+z$
IV $1/2-x, 1/2-y, 1-z$
IV' $1/2-x, 1/2-y, -z$

$Sb(1)Cl_6^-$:
B x, y, z; $-x, y, 1/2-z$
E $1/2-x, 1/2+y, 1/2+z$; $1/2+x, 1/2+y, z$

$Sb(2)Cl_6^-$:
A x, y, z; $-x, 1/2-y, -z$
C $x, -y, 1/2+z$; $-x, y, 1/2-z$
D $1/2+x, 1/2+y, z$; $1/2-x, 1/2-y, -z$
F $1/2+x, 1/2-y, 1/2+z$; $1/2-x, -1/2+y, 1/2-z$

does not always accompany the shortened C–S bond, namely the delocalization of the central ring.

Anthonj *et al.*[21] cited some disorder of PT in the PT–PMDA CT complex: approximately one in fifty molecules has the positions of the S and N atoms reversed. Their basis for disorder was an asymmetrical peak around the N atom, which they interpreted as a twin peak of the H(N) and the disordered S atoms. In the case of the present crystal, however, all the S, N, and H(N) atom peaks were symmetric within the errors. So, the positional disorder was not considered for the $PT^{+\cdot}$ moiety in $PT^{+\cdot}SbCl_6^-$.

Figures 2 and 3 give the packing arrangement in the crystal projected along the b axis and onto the $(10\bar{1})$ plane, respectively. Figure 2 shows that all the Sb atoms exist on (200) planes, and that the $PT^{+\cdot}$ cation radicals put their molecular planes almost parallel to $(10\bar{1})$. However, the four $PT^{+\cdot}$ cation radicals, numbered from I to IV in Fig. 2, do not have any overlap, as illustrated in Fig. 3. In other words, a strong CT interaction is not expected between the $PT^{+\cdot}$ cation radicals in this crystal.

Figure 4 illustrates the relation between the nearest neighbor species viewed down the [101] direction, which is horizontal in Fig. 3. In the figure, the shortest distances between neighboring species are also exhibited.

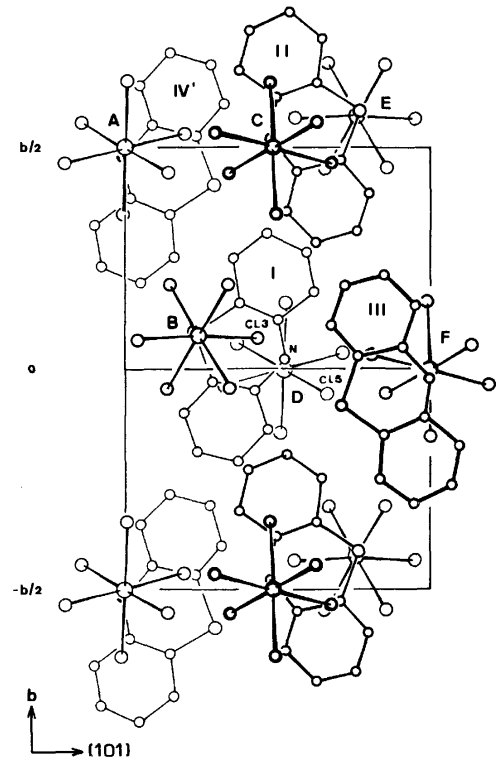

Fig. 3. The packing arrangements in the crystal lattice projected onto the $(10\bar{1})$ plane.

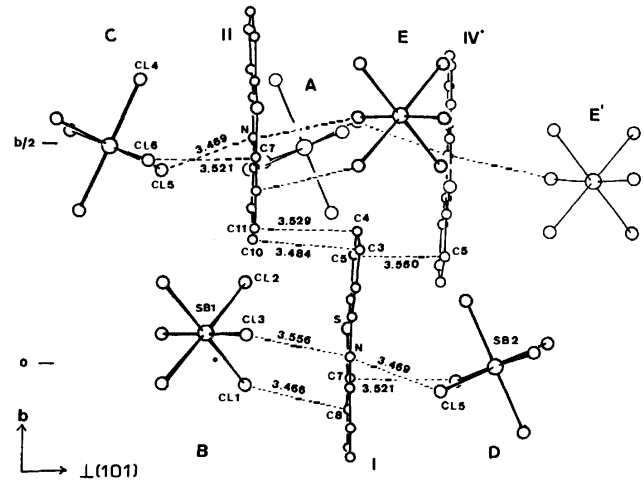

Fig. 4. Perspective relation between the cations and the anions viewed down the [101] direction. Intermolecular atomic distances (Å), less than 3.6 Å, are shown.

It is interesting that the slightly elongated two Sb–Cl bonds, namely Sb(1)–Cl(3) and Sb(2)–Cl(5), are pointed at the N atom of $PT^{+\cdot}$ from both sides of the cation, though the N···Cl intermolecular distances do not suggest considerable shortened contacts of them. Nevertheless the structure implies an appropriate charge deviation in each ion.

Polarized Absorption Spectra. Figure 5(a) shows polarized absorption spectra for the cases parallel to and perpendicular to [101] on the (010) face of a single

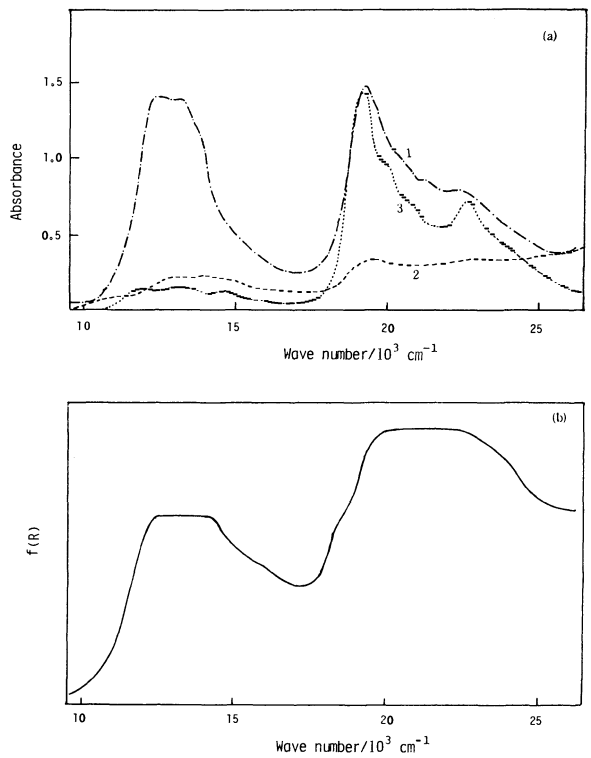

Fig. 5. (a) Polarized absorption spectrum of a single crystal, 1 (—·—·—): //[101], 2(------): ⊥[101], and 3 (·····): solution spectrum in 1,2-dichloroethane. (b) Polycrystalline reflection spectrum.

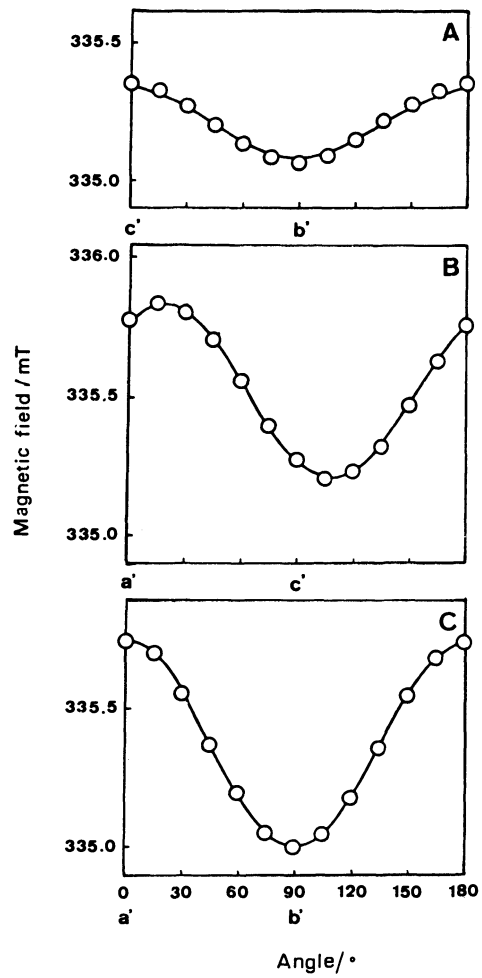

Fig. 6. Angular dependence of the resonance field for rotation about the A: a′ axis, B: b′(=b) axis, and C: c′ axis, where the orthogonal axes a′, b′, and c′ are defined in the text. Circles are experimental, and solid lines are calculated ones.

crystal of $PT^{+\cdot}SbCl_6^-$, as well as its solution spectrum. As mentioned in the previous section and shown in Fig. 3, [101] direction is very close to the short axis in the $PT^{+\cdot}$ molecular plane. The polycrystalline reflection spectrum of monoclinic(I) crystals is shown in Fig. 5(b). They lack the absorption band at 10×10^3 cm^{-1} (1000 nm) that was found in "$PT^+(SbCl_5)^-$" polycrystalline spectra and assigned as the CT band between $PT^{+\cdot}$ radicals by Sato *et al.*[8] Since the monoclinic(I) crystal is a simple salt, as mentioned in the previous section, it is reasonable that the CT band between cation radicals does not appear in the absorption spectra. However, crystals of other forms still have the possibility of being "$PT^+(SbCl_5)^-$" described by Sato *et al.*[8]

Curve 1 in Fig. 5(a), //[101] spectrum, is essentially similar to the polycrystalline reflection spectra of monoclinic(I) (Fig. 5(b)), $PT^{+\cdot}Br^-$,[3,25] $PT^{+\cdot}HSO_4^-\cdot H_2O$ and $PT^{+\cdot}$ picrate;[3] it consists of two intense bands around $(12—14)\times10^3$ cm^{-1} and $(19—23)\times10^3$ cm^{-1}. The latter band well agrees with the solution spectrum (Curve 3), in which the absorption maxima at 19.2 and 22.6×10^3 cm^{-1} are characteristic to $PT^{+\cdot}$.[2,3] On the other hand, the former band at $(12—14)\times10^3$ cm^{-1} is intense only in the solid state. If this band is attributed to cation-anion interaction, it should be weaker in the [101] direction than the other direction according to the structural consideration. Since Curve 2 has no intense band, the lower frequency band at $(12—14)\times10^3$ cm^{-1} is possibly assigned to the $PT^{+\cdot}$ intramolecular electronic transition, the intensity of which is enhansed in the solid state. As a result, in the range of wave numbers measured, there exist only local excitation bands of $PT^{+\cdot}$ cation radical.

Electron Spin Resonance. The ESR spectra of polycrystalline samples at room temperature showed anisotropy of *g*-factor without hyperfine structure. At 77 K, neither the line-splitting nor any large change of line-shape occurred.

The single crystal spectra consisted of a line corresponding to a unique arrangement of $PT^{+\cdot}$ radicals in the crystal lattice. Namely, all the eight $PT^{+\cdot}$ radicals in a unit cell are geometrically parallel and magnetically equivalent to each other. The line width, ΔH_{msl}, was slightly changed from 0.09 to 0.17 mT with the orientation of the crystal to the magnetic field. The observed angular dependencies of the spectra, as shown in A and C of Fig. 6, are symmetrical around the b axis, which is also the crystallographically unique axis. The calculated direction cosines of the magnetic field with respect to the a′, b′, and c′ axes are presented in Table 6, together with the three principal *g*-values. The g_1 value is close to that of free electron, and is directed normal to the molecular plane of the $PT^{+\cdot}$ within the experimental error($\pm3°$). The direction of g_2 is in accord

Table 6. Principal g values and their direction consines with respect to the a′, b′, and c′ axes

	g	Direction cosine		
		a'	b'	c'
g_1	2.003(1)	±0.96(2)	0.00(5)	∓0.29(5)
g_2	2.008(1)	0.00(5)	±1.00	0.00(5)
g_3	2.007(1)	±0.29(5)	0.00(5)	±0.96(2)

with the crystal b axis, and the g_3 approximately coincides with the [101] direction (see Fig. 3). Both g_2 and g_3 are in the molecular plane of $PT^{+\cdot}$. The anisotropic difference between the principal values of g_1 and g_2 is not so large as in the case of the unpaired electron localized at S atom.

Many authors have observed the hyperfine structures of $PT^{+\cdot}$ in solution.[26-29] Malrieu and Pullman calculated the spin density distribution in the ring system of $PT^{+\cdot}$ with a simple MO method, and estimated the same order of the spin density for both N and S atoms (0.244 and 0.217, respectively), provided the radical was assumed to be planar.[27] Chiu *et al.* obtained values similar to those of Malrieu and Pullman by the observation of hyperfine splitting from H, N, and ^{33}S atoms of $PT^{+\cdot}$ in solution.[28] Their experimentally estimated spin density distributions are 0.234 and 0.218 for N and S atoms, respectively. Since the orbital states occupied by unpaired electron of $PT^{+\cdot}$ in solid state should not be much different from that in solution, it is reasonable to conclude for the present crystal that the unpaired electron of $PT^{+\cdot}$ is delocalized in the ring system including hetero-atoms.

The authors express their hearty thanks to Professor Hiroshi Takahashi and Mr. Minoru Suzuki of Tokyo University for the ESR measurements. The authors are also indebted to Professor Haruo Kuroda and Dr. Kyuya Yakushi of Tokyo University for the use of the microspectrophotometer.

References

1) J.-P. Billon, *Ann. Chim.(Paris)*, **1962**, 183; J.-P. Billon, *Bull. Soc. Chim. Fr.*, **1961**, 1923.
2) H. J. Shine and E. Mach, *J. Org. Chem.*, **30**, 2130 (1965).
3) Y. Iida, *Bull. Chem. Soc. Jpn.*, **44**, 663 (1971).
4) G. D. Andreetti, G. Bocelli, and P. Sgarabotto, *Acta Crystallogr., Sect. B*, **36**, 1839 (1980), and references cited therein.
5) A. C. Buchanan, R. Livingston, A. S. Dworkin, and G. P. Smith, *J. Phys. Chem.*, **84**, 423 (1980); D. J. Sandman, A. Troup, and G. T. Fekete, *Mol. Cryst. Liq. Cryst.*, **64**, 57 (1980); T. Yoshioka, *Bull. Chem. Soc. Jpn.*, **52**, 375 (1979); T. Yoshioka, K. Watanabe, and H. Ohya-Nishiguchi, *ibid.*, **48**, 2533 (1975); A. Zweig and W. G. Hodgson, *Proc. Chem. Soc.*, **1964**, 417.
6) F. P. Chen and P. N. Prasad, *Solid State Commun.*, **21**, 871 (1977); S. N. Bhat and C. N. R. Rao, *Can. J. Chem.*, **47**, 3899 (1969); M. S. Frant and R. Eiss, *J. Electrochem. Soc.*, **110**, 769 (1963); G. E. Blomgren and J. Kommandeur, *J. Chem. Phys.*, **35**, 1636 (1961).
7) Y. Sato, M. Kinoshita, M. Sano, and H. Akamatu, *Bull. Chem. Soc. Jpn.*, **40**, 2539 (1967).
8) Y. Sato, M. Kinoshita, M. Sano, and H. Akamatu, *Bull. Chem. Soc. Jpn.*, **42**, 548 (1969).
9) P. C. Eklund, D. S. Smith, and V. R. K. Murthy, *Syn. Met.*, **3**, 111 (1981); P. C. Eklund, D. S. Smith, V. R. K. Murthy, and S. Y. Leung, *ibid.*, **2**, 99 (1980); E. R. Falardeau and J. E. Fischer, *Solid State Commun.*, **32**, 631 (1979); H. Fuzellier, J. Melin, and A. Herold, *Carbon*, **15**, 45 (1977).
10) We confirmed the crystal systems of the three modifications with the Weissenberg photographs. We also observed microscopically three different types of crystals: brown platelets, black columns, and green hexagonal platelets. The former two crystals completely agreed with those determined by X-ray photographs as the monoclinic(I) and triclinic modifications in both color and appearance. The latter green platelet, however, has still not been identified as the monoclinic(II) crystal.
11) It is not clear what kind of reaction occurred in the mixture solution, since $SbCl_5$ is a very active reagent not only for phenothiazine but also for solvent molecules or traces of water.
12) Tables of structure factors, anisotropic temperature parameters, and least-squares planes, have been deposited in the office of the Chemical Society of Japan (Document No. 8308).
13) "International Tables for X-Ray Crystallography," The Kynoch Press, Birmingham (1974), Vol. IV, pp. 72—102.
14) "Universal Crystallographic Computation Program System," ed by T. Sakurai, Crystallographic Society of Japan, Tokyo (1967).
15) A. Lipka, *Z. Anorg. Allg. Chem.*, **469**, 229 (1980); R. Faggiani, R. J. Gillespie, C. J. L. Lock, and J. D. Tyrer, *Inorg. Chem.*, **17**, 2975 (1978); S. Gorter and G. C. Verschoor, *Acta Crystallogr., Sect. B*, **32**, 1704 (1976); B. Chevrier, J.-M. Carpentier, and R. Weiss, *J. Am. Chem. Soc.*, **94**, 5718 (1973); *Acta Crystallogr., Sect. B*, **28**, 2673 (1972); J.-M. Carpentier and R. Weiss, *ibid.*, **28**, 1430 (1972).
16) J. J. H. McDowell, *Acta Crystallogr., Sect. B*, **32**, 5 (1976); B. W. van de Waal and D. Feil, *ibid.*, **33**, 314 (1977).
17) J. D. Bell, J. F. Blount, O. V. Briscoe, and H. C. Freeman, *J. Chem. Soc., Chem. Commun.*, **1968**, 1656.
18) L. Pauling, "The Nature of the Chemical Bond," Cornell Univ. Press, Ithaca, New York (1960).
19) D.Zobel and G. Ruban, *Acta Crystallogr., Sect. B*, **37**,1867 (1981); E. S. Raper, R. E. Oughtred, I. W. Nowell, and L. A. March, *ibid.*, **37**, 928 (1981); J.-E. Andersson, *ibid.*, **37**, 401 (1981); M. D. Glick and R. E. Cook, *ibid.*, **28**, 1336 (1972); J. L. Derissen, J. W. M. Kocken, and R. H. Weelden, *ibid.*, **27**, 1692 (1971); W. R. Harshbarger and S. H. Bauer, *ibid.*, **26**, 1010 (1970); W. Furey, F. Jordan, Y. H. Mariam, and R. A. Lalancette, *ibid.*, **37**, 1147 (1981).
20) A. Singhabhandhu, D. P. Robinson, J. H. Fang, and W. E. Geiger, Jr., *Inorg. Chem.*, **14**, 318 (1975).
21) R. Anthonj, N. Karl, B. E. Robertson, and J. J. Stezowski, *J. Chem. Phys.*, **72**, 1244 (1980); B. E. Robertson and J. J. Stezowski, *Mol. Cryst. Liq. Cryst.*, **52**, 319 (1979).
22) H. Kobayashi, *Acta Crystallogr., Sect. B*, **30**, 1010 (1974).
23) C. J. Fritchie, Jr., *J. Chem. Soc., A*, **1969**, 1328.
24) C. J. Fritchie, Jr., and B. L. Trus, *J. Chem. Soc., Chem. Commun.*, **1968**, 833.
25) S. Doi and Y. Matsunaga, *Bull. Chem. Soc. Jpn.*, **48**, 3747 (1975); Y. Matsunaga and K. Shono, *ibid.*, **43**, 2007 (1970).
26) B. S. Gilbert, P. Hanson, R. O. C. Norman, and B. T. Sutcliffe, *J. Chem. Soc., Chem. Commun.*, **1966**, 161; P.D. Sullivan and J. R. Bolton, *J. Magn. Reson.*, **1**, 356 (1969).
27) J.-P. Malrieu and B. Pullman, *Theor. Chim. Acta*, **2**, 293 (1964).
28) M. F. Chiu, B. C. Gilbert, and P. Hanson, *J. Chem. Soc., B*, **1970**, 1700.
29) D. Clarke, B. C. Gilbert, and P. Hanson, *J. Chem. Soc., Perkin Trans. 2*, **1978**, 1103; **1977**, 517; **1976**, 114; **1975**, 1078.

The Formation of Electronically Excited Fragments by the Electron Impact of Furan and Related Five-membered Heterocycles

Ikuo TOKUE,* Masami IKARASHI, Sadachika TAKIZAWA, and Yoshio ITO
Department of Chemistry, Faculty of Science, Niigata University, Ikarashi, Niigata 950-21
(Received June 19, 1982)

In the wavelength region of 200—600 nm, photoemissions from electronically excited H, CH, C_2, and CS (only from thiophene and tetrahydrothiophene) were observed when furan, tetrahydrofuran, thiophene, and tetrahydrothiophene were excited by electron impact (0—70 eV). Hydrogen atoms ($n=4$) and CH($A^2\Delta$) radicals were produced from these five-membered heterocycles *via* single collision excitations, while CS($A^1\Pi$) radicals from thiophene and tetrahydrothiophene were partly formed in secondary processes. The appearance potentials for the hydrogen Balmer β and the CH($A^2\Delta$-$X^2\Pi$) bands from these five-membered heterocycles are determined, and the dissociation processes forming H($n=4$) and CH(A) are discussed.

The excited electronic states of furan, tetrahydrofuran, thiophene, and tetrahydrothiophene have been investigated by means of their ultraviolet absorption spectra for more than sixty years. Recently, the excited electronic states of these heterocycles have also been studied by means of ultraviolet photoelectron spectroscopy.[1,2] Several decay processes from the electronically excited states of these five-membered heterocycles have been investigated by means of photolysis,[3] flash photolysis,[4] and electron-impact mass spectroscopy.[5-7] However, we have only a little information about electronically excited fragments from five-membered heterocycles and their fragmentation mechanisms. There seem to be only a few papers[8,9] on this subject.

In a previous paper, we have reported on the emission spectra of the fragment species from pyrrole and pyrrolidine.[10] The appearance potentials for the hydrogen Balmer β (H_β), CH($A^2\Delta$-$X^2\Pi$), and NH($A^3\Pi$-$X^3\Sigma$) bands from pyrrole and pyrrolidine are 18—23 eV about twice as large as the first ionization potentials of the parent heterocycles. In these cases, it appears that an ionic fragment is a by-product of the formation of neutral fragments.[10]

This paper will present the emission spectra of the fragments produced by the electron-impact dissociation of furan, tetrahydrofuran, thiophene, and tetrahydrothiophene. Further, the appearance potentials for the H_β and CH(A-X) emissions from these heterocycles are determined and possible dissociation processes forming H($n=4$) and CH(A) are discussed.

Experimental

The apparatus consists of a collision chamber, a photon-detection system, and a control system. The collision chamber and the photon-detection system have been described in detail previously.[9] The sample pressures in the collision chamber during the emission measurements, as measured by means of an ionization gauge, were 5—40 mPa. An HTV R585 photomultiplier and an HTV C1230 photon-counter were used with the spectral resolution of 0.6 nm (FWHM). Electron-beam currents of 10 μA near the threshold and 40—50 μA at higher energies were used for the measurement of the excitation function.

A schematic electronic block diagram of the automatic control system used for the measurement of the excitation function is shown in Fig. 1. An AD converter (ICL 7109) is interfaced to a microcomputer (MZ-80K). After a preset

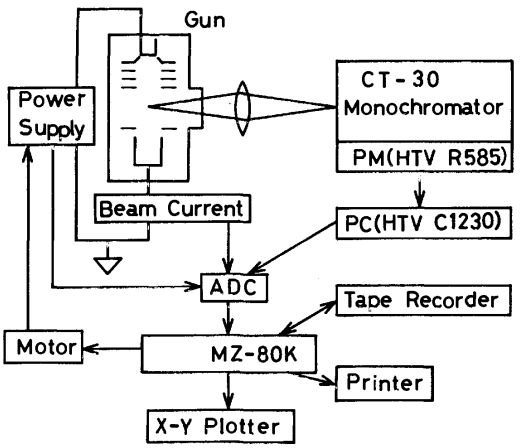

Fig. 1. The schematic electronic block diagram for the automatic control system.

counting time, the current electron-accelerating potential, the electron-beam current, and the photo-electron current are measured. These measurements are repeated several times at the same electron-accelerating potential. At the end of a counting cycle, the microcomputer sends a signal to a motor to advance the voltage regulator to the next voltage, thus setting a new counting cycle. After the experiment, the three values are recorded with a cassette tape recorder. These data, as well as the calculated excitation function, can be printed with a dot printer, while this excitation function can be plotted with as MIPLOT WX4671.

The energy scale for the impinging electron was calibrated on the basis of both the peak of the excitation function for the (0, 0) band of the N_2($C^3\Pi$-$B^3\Pi$) emission reported by Finn *et al.*[11] and the appearance potential for the (0,0) band of the N_2^+($B^2\Sigma$-$X^2\Sigma$) emission reported by Borst and Zipf.[12] Nitrogen was mixed with the sample vapor, and their excitation functions were measured alternately.

The furan, thiophene, and tetrahydrothiophene (Nakarai guaranteed grade), and tetrahydrofuran (Wako guaranteed grade) were dried over sodium for several days. All the samples were subjected to several freeze-pump-thaw cycles just before use.

Results

Emission Spectra and Emission Intensities of Excited Fragment. Figure 2 shows the emission spectra produced by the electron impact of furan and tetrahydrofuran at an electron energy of 70 eV. Many

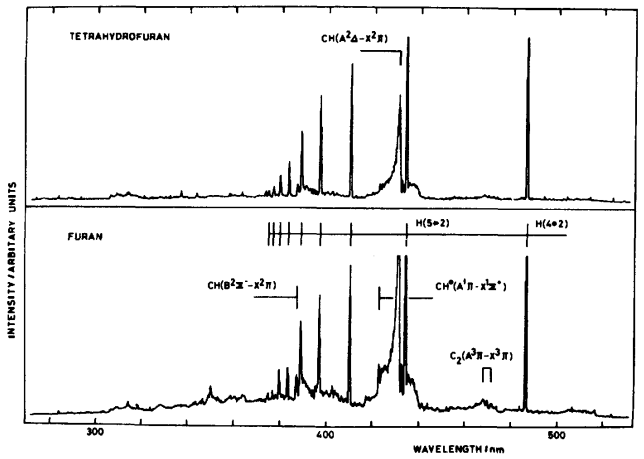

Fig. 2. Emission spectra by electron impact (70 eV, 0.5 mA) of tetrahydrofuran at 26 mPa and furan at 27 mPa.

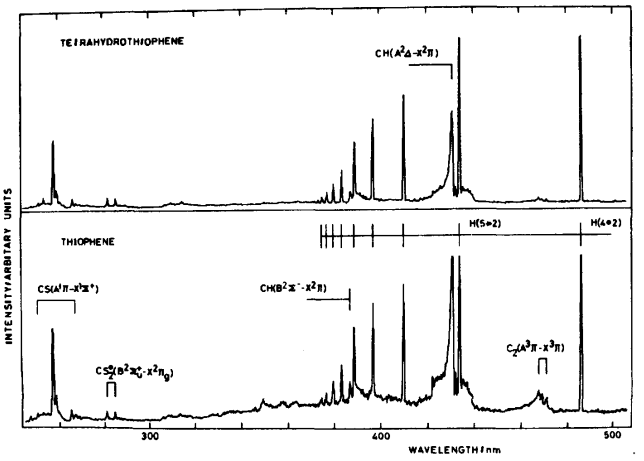

Fig. 3. Emission spectra by electron impact (70 eV, 0.5 mA) of tetrahydrothiophene at 27 mPa and thiophene at 27 mPa.

sharp bands were assigned to the hydrogen Balmer series (n=4—10→2), the CH($A^2\Delta$-$X^2\Pi$) band around 431 nm, the CH($B^2\Sigma$-$X^2\Pi$) band around 388 nm, the CH^+($A^1\Pi$-$X^1\Sigma$) band around 423 nm, and the C_2($A^3\Pi$-$X^3\Pi$) band around 470 nm. Further, weak emissions from CO and CO^+ were observed in the region of 240—470 nm. Figure 3 shows the emission spectra obtained from thiophene and tetrahydrothiophene. Besides the emission spectra for the hydrogen Balmer series and the CH(A-X) and CH(B-X) bands, the CS($A^1\Pi$-$X^1\Sigma$) band around 258 nm and the CS_2^+($B^2\Sigma$-$X^2\Pi$) band around 282 nm were observed.

The photoemission intensities of the H_β and CH(A-X) bands from furan, tetrahydrofuran, thiophene, and tetrahydrothiophene were proportional to the electron-beam current up to 0.5 mA and to the sample pressure up to 35 mPa in the collision chamber.

The emissions of the CS(A-X) band from thiophene and tetrahydrothiophene were weak. The intensities of the CS(A-X) band measured at a sample pressure of 30 mPa were found to deviate significantly from the proportional increase with the electron-beam current. If we assume that the emission intensity of the CS(A-X)

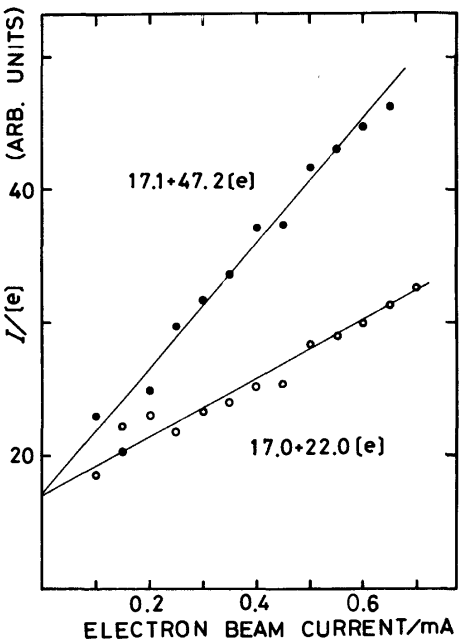

Fig. 4. Dependence of the photoemission intensity divided by the electron-beam current, $[I]/[e]$, on the electronbeam current. CS(A-X) emissionf rom thiophene (○), and from tetrahydrothiophene (●).

band, $[I]$, includes the quadratic term on the electron-beam current, $[e]$, the emission intensity divided by the electron-beam current, $[I]/[e]$, can be represented by the following formula,[13] where A and B are adjustable constants:

$$[I]/[e] = A + B[e]. \quad (1)$$

Figure 4 shows the plot of $[I]/[e]$ as a function of $[e]$ for the CS(A-X) bands from thiophene and tetrahydro-

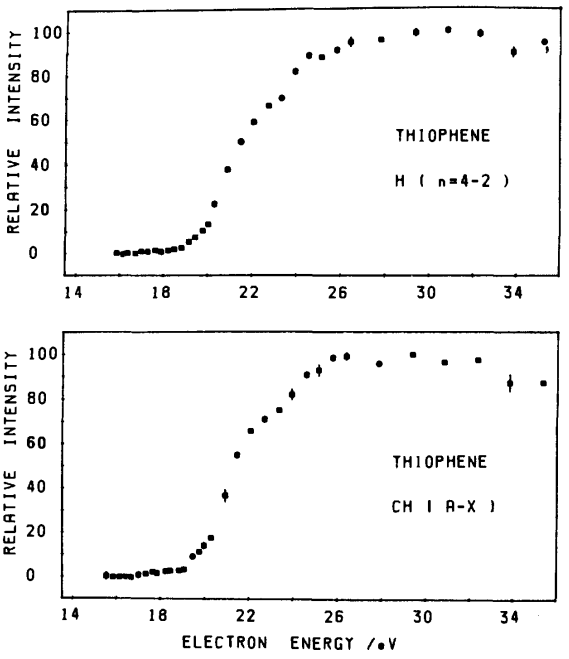

Fig. 5. The excitation functions for the H_β and CH(A-X) bands from thiophene. The error bar represents ± one standard deviation.

Table 1. Dissociation processes for the formation of H(n=4)

Dissociation process	Threshold/eV Estd	Obsd
$(CH)_4O \longrightarrow C_4H_3O\cdot + H(n=4)$	17.6[a]	20.5±0.8
$(CH_2)_4O \longrightarrow C_4H_7O\cdot + H(n=4)$	17.1[b]	18.7±0.8
$(CH)_4S \longrightarrow C_4H_3S\cdot + H(n=4)$	17.6[a]	18.9±0.8
$(CH_2)_4S \longrightarrow C_4H_7S\cdot + H(n=4)$	17.1[b]	19.7±0.8

a) Estimated from the bond-dissociation energy of the C–H bond for benzene.[14] b) Estimated from the bond-dissociation energy of C–H for saturated hydrocarbon.[15]

thiophene. The reasonable fit to a straight line in each plot indicates that the emission intensities of the CS(A-X) band fairly well include the quadratic term on the electron-beam current. On the other hand, the emission intensities of the CS(A-X) band from thiophene and tetrahydrothiophene were found to be proportional to the sample pressure up to 35 mPa. This is probably because the number density of target molecules in the column of the electron beam is about two orders of magnitude lower than the electron density.

Appearance Potentials for the H_β and CH(A-X) Bands. Figure 5 shows the excitation functions for the H_β and CH(A-X) emissions from thiophene from their thresholds to 35 eV. The appearance potentials thus obtained for H(n=4) are listed in the third column of Table 1, while those for CH(A) are listed in the third column of Table 2.

Discussion

Photoemissions from Electronically Excited Fragments. The intensities of the hydrogen Balmer line and the CH(A-X) band from furan, tetrahydrofuran, thiophene, and tetrahydrothiophene were proportional to the electron-beam current and the sample pressure in the collision chamber. The excitation functions for the H_β and CH(A-X) band from these heterocycles were measured at sample pressures of 5—11 mPa; the appearance potentials were found to be independent of the sample pressure. Therefore, the H atoms and CH radicals from these heterocycles seem to be formed by fragmentation *via* a single-collision excitation. The two-step collision with another electron seems to be negligible.

On the other hand, the photoemission intensities of the CS(A-X) band from thiophene and tetrahydrothiophene fairly well include the quadratic term on the electron-beam current. Unknown secondary processes seem to participate in the formation of CS(A) to an appreciable extent; that is, the formation of CS(A) by way of a two-step excitation *via* an unidentified intermediate species is comparable to that by single-collision excitation at a beam current of more than 0.2 mA. The formation rates of CS(A) *via* single-collision excitations from thiophene and tetrahydrothiophene are of the same order of magnitude, for the A values for thiophene and tetrahydrothiophene, which were measured under similar experimental conditions, are nearly equal (see Fig. 4). The relative contributions of the two-electron excitation process to the single-electron excitation process, B/A, for thiophene and tetrahydrothiophene are estimated to be 1.3 and 2.8 respectively from the slope of $[I]/[e]$ and its extrapolation with beam-current to zero. That is, secondary processes in the formation of CS(A) from tetrahydrothiophene are twice

Table 2. Dissociation processes for the formation of $CH(A^2\Delta)$ and heat of formation for radicals and ions

Dissociation process	Threshold/eV Estd	Obsd
$(CH)_4O \longrightarrow C_2H_2(X) + CHO(X) + CH(A)$	11.4[a]	19.6±0.8
$\longrightarrow C_3H_3^+(X) + O + CH(A)$	16.3—25.1[b]	
$\longrightarrow C_3H_2^+(X) + OH(X) + CH(A)$	17.7—25.4[b]	
$(CH_2)_4O \longrightarrow CH_3OH(X) + C_2H_3(X) + CH(A)$	10.3[a]	18.8±1.0
$\longrightarrow C_2H_3^+(X) + CH_3OH(X) + CH(A)$	20.4[a]	
$\longrightarrow C_3H_6^+(X) + OH(X) + CH(A)$	21.2[a]	
$(CH)_4S \longrightarrow C_2H_2S^+(X) + CH(X) + CH(A)$	15.5—25.4[b]	18.7±1.0
$\longrightarrow CHS^+(X) + C_2H_2(X) + CH(A)$	>17.0[b]	
$(CH_2)_4S \longrightarrow C_2H_4S^+(X) + CH_3(X) + CH(A)$	19.8[a]	20.1±1.1
$\longrightarrow C_2H_3S^+(X) + CH_4(X) + CH(A)$	19.4[a]	

Species	ΔH_f°/kJ mol^{-1}	Ref.
CH	500.78 ± 0.4	16
OH	38.9 ± 1.2	16
CH_3	149.03 ± 0.84	16
C_2H_3	274—282	Estimated
CHO	−19.6	17
$C_2H_3^+$	1125	18
$C_3H_6^+$	960	18
$C_2H_4S^+$	866	6
$C_2H_3S^+$	1037.6	6

a) Estimated from the heat of formation. b) Estimated from the appearance potential of the by-product ion.[5]

as abundant as those from thiophene.

Ogawa *et al.*[13,19] have reported several similar results and have classified the excited species the emission intensities of which show non-linear relationships with the electron-beam current into the following two groups: (a) Fragments which have at least two heavy atoms and which are produced through the scission of two skeletal bonds, and (b) fragments with a new chemical bond. The CS(A) from thiophene and tetrahydrothiophene can be classified in Group (a). This result is consistent with the fact that the CS_2^+(B-X) band from thiophene and tetrahydrothiophene appears upon electron impact. The formation of the CS_2^+ ion can be classified in Group (b).

Formation of H(n=4). The onsets for the H_β emissions from furan, tetrahydrofuran, thiophene, and tetrahydrothiophene are found at 20.5±0.8, 18.7±0.8, 18.9±0.8, and 19.7±0.8 eV respectively. The dissociation processes which are expected to play an important role in the formation of H(n=4) and CH(A) near their thresholds are shown in the first column of Tables 1 and 2. The threshold energies of the dissociation processes listed in the second column of Table 1 are calculated by using the excitation energy of H(n=4), 12.75 eV,[20] and the bond dissociation energy of the C–H bond, 4.86 eV from benzene[14] or 4.31 eV from saturated hydrocarbons.[15] The excess energy of 1.3—2.9 eV for the difference between the observed and estimated thresholds in these processes is probably dissipated as the kinetic energy of the leaving hydrogen atom. These dissociation processes for the formation of excited H atoms following neither the cleavage of skeletal bonds nor new bond formation are similar to those with benzene,[9,21] pyridine and pyrazine[69] and pyrrolidine.[10]

Derrick *et al.*[22,23] have reported the structure of the Rydberg series in the photoelectron spectra of furan and thiophene and the associated ionization potentials. They have assigned the vertical ionization potentials of 17.5, 19.0, and 19.5 eV in furan to the $7a_1$, $6a_1$, and $4b_2$ orbitals respectively. This energy region is close to the onset of H(n=4). The approximate descriptions of the bonding orbitals have shown[22] that the r-type orbital, $7a_1$, is C–H bonding; the s-type orbital, $6a_1$, is C–C bonding, and the s-type orbital, $4b_2$, is strongly C–H bonding. On the basis of the character of the molecular orbitals and the comparison between the onset of H(n=4) and the ionization potentials, H(n=4) from furan seems to be produced *via* the Rydberg state, converging to the $4b_2$ ionization potential. The vertical ionization potentials of 16.16, 17.6, and 18.3 eV in thiophene have been assigned to the $7a_1$, $4b_2$ and $6a_1$ orbitals respectively by Derrick *et al.*[23] According to the approximate descriptions of the bonding orbitals,[23] the r-type orbital, $7a_1$, is characterized as C–H bonding, and the s-type orbitals, $4b_2$ and $6a_1$, as strongly C–H bonding. In similar considerations of the characters of the molecular orbitals and the ionization potentials, it is concluded that H(n=4) from thiophene is produced *via* the Rydberg state, converging to the $4b_2$ or the $6a_1$ ionization potential.

Formation of CH(A). The onsets for the CH(A-X) band from furan, tetrahydrofuran, thiophene, and tetrahydrothiophene are found at 19.6±0.8, 18.8±1.0, 18.7±1.0, and 20.1±1.1 eV respectively. The dissociation processes leading to the formation of CH(A) from these heterocycles are still uncertain because the available data of the heat of formation of ionic products are insufficient. Nevertheless, if one assumes that the threshold energy consists of the electron-excitation energy of CH(A) and the heat of formation, the main dissociation processes leading to the formation of CH(A) seem to include an ionic by-product. The appearance potentials observed for CH(A) are much higher than the first ionization potentials for furan, 9.06 eV;[24] for tetrahydrofuran, 9.57 eV;[25] for thiophene, 8.87 eV,[26] and for tetrahydrothiophene, 8.57 eV.[6] Accordingly, it is possible that an ionic fragment is a by-product in the formation of CH(A). The threshold energies of the dissociation processes leading to the formation of CH(A) from tetrahydrofuran and tetrahydrothiophene, listed in the second column of Table 2, are calculated from the excitation energy of CH(A) and the heat of formation. The threshold energies for these processes from furan and thiophene are calculated from the excitation energy of CH(A) and the appearance potential for a by-product ion reported by Hissel.[5] The heat of formation and the appearance potentials used for the calculation of the thresholds are summarized in Table 2. The by-product ions in the dissociation processes forming CH(A) (see Table 2) are abundant in mass-spectroscopy measurements.[5,6]

Another possibility for the formation of CH(A) is that by-products are formed in their electronically excited states. It is not possible to derive the processes which may be involved, because the relevant dissociation energies and the electronic energies are not known.

The onsets for the CH(A-X) band resulting from the formation of only neutral fragments are estimated to be 10—16 eV.[9,20] On the basis of the electron-impact energy-loss spectra of furan and thiophene[27] and the photoelectron spectra of furan[22] and thiophene,[23] we may expect the excitation cross-sections for the collision of electrons with furan and thiophene in these energy regions to be relatively large; these excitations seem to be spin-forbidden transitions, mainly in the 11—13 eV region. However, no onset for the CH(A-X) band from any five-membered heterocycles were observed in the 10—16 eV region; competing processes, such as ionization or radiationless decay, may be abundant.

References

1) D. W. Turner, C. Baker, A. D. Baker, and C. R. Brundle, "Molecular Photoelectron Spectroscopy," John Wiley & Sons, London (1970).

2) K. Kimura, S. Katsumata, Y. Achiba, T. Yamazaki, and S. Iwata, "Handbook of HeI Photoelectron Spectra of Fundamental Organic Molecules," Japan Sci. Soc. Press, Tokyo (1981).

3) B. C. Roquitte, *J. Am. Chem. Soc.*, **91**, 7664 (1969).

4) S. L. N. G. Krishnamachari and T. V. Venkitachalam, *Chem. Phys. Lett.*, **55**, 116 (1978).

5) J. Hissel, *Bull. Soc. Roy. Sci. Liege*, **21**, 457 (1952).

6) E. J. Gallegos and R. W. Kiser, *J. Phys. Chem.*, **66**, 136

(1962).
7) A. S. Siegel, *Tetrahedron Lett.*, **1970**, 4113.
8) T. Ogawa, M. Toyoda, and N. Ishibashi, *Eng. Sci. Repts. Kyushu Univ.*, **2**, 17 (1980).
9) I. Tokue and M. Ikarashi, *Bull. Chem. Soc. Jpn.*, **54**, 2565 (1981).
10) I. Tokue, M. Ikarashi, and Y. Ito, *Bull. Chem. Soc. Jpn.*, **55**, 1250 (1982).
11) T. G. Finn, J. F. M. Aarts, and J. P. Doering, *J. Chem. Phys.*, **56**, 5632 (1972).
12) W. L. Borst and E. C. Zipf, *Phys. Rev. A*, **1**, 834 (1970).
13) M. Tsuji, T. Ogawa, Y. Nishimura, and N. Ishibashi, *Bull. Chem. Soc. Jpn.*, **50**, 2432 (1977).
14) A. S. Rodgers, D. M. Golden, and S. W. Benson, *J. Am. Chem. Soc.*, **89**, 4578 (1967).
15) J. D. Coxon and G. Pilcher, "Thermochemistry of Organic and Organometallic Compounds," Academic Press, New York (1970).
16) D. R. Stull and H. Prophet, "JANAF Thermochemical Tables," 2nd ed, Nt. Stand. Ref. Data Ser., Nat. Bur. Stand., **37**, 1141 (1971).
17) R. I. Reed and J. C. D. Brand, *Trans. Faraday Soc.*, **54**, 478 (1958).
18) H. M. Rosenstock, K. Draxl, B. W. Steiner, and J. T. Herron, *J. Phys. Chem. Ref. Data*, **6**, Suppl. No. 1 (1977).
19) T. Ogawa, T. Iwasaka, M. Toyoda, M. Tsuji, and N. Ishibashi, *Bull. Chem. Soc. Jpn.*, **48**, 645 (1975).
20) S. Bashkin and J. O. Stoner, Jr., "Atomic Energy Levels and Grotrian Diagrams," North-Holland, Amsterdam (1975), Vol. 1.
21) C. I. M. Beenakker and F. J. de Heer, *Chem. Phys. Lett.*, **29**, 89 (1974).
22) P. J. Derrick, L. Asbrink, O. Edqvist, B.-O. Jonsson, and E. Lindholm, *Int. J. Mass Spectrom. Ion Phys.*, **6**, 161 (1971).
23) P. J. Derrick, L. Asbrink, O. Edqvist, B.-O. Jonsson, and E. Lindholm, *Int. J. Mass Spectrom. Ion Phys.*, **6**, 177 (1971).
24) K. Watanabe, *J. Chem. Phys.*, **26**, 542 (1957).
25) A. D. Bain, J. C. Bunzli, D. C. Frost, and L. Weiler, *J. Am. Chem. Soc.*, **95**, 291 (1973).
26) R. A. W. Johnstone and F. A. Mellon, *J. Chem. Soc., Faraday Trans. 2*, **69**, 1155 (1973).
27) W. M. Flicker, O. A. Mosher, and A. Kuppermann, *J. Chem. Phys.*, **64**, 1315 (1976).

Chemiluminescence from Reactions of $N_2^*(A^3\Sigma_u^+)$ with Solid Organic Compounds at 77 K

Kenichi Mitsumori and Kenzo Hiraoka*
Faculty of Engineering, Yamanashi University, Takeda-4, Kofu 400
(Received July 5, 1982)

The luminescence from reactions of $N_2(A^3\Sigma_u^+)$ with solid benzene, toluene, hexane, cyclohexane and those doped with biacetyl at 77 K has been investigated. For benzene, a broad band appeared in the range of 350—550 nm whose radiative lifetime was determined to be 2.5 s. This band was largely eliminated by addition of a small amount of biacetyl, indicating the participation of an intermediate excited state in solid benzene, *i.e.* triplet excitons. The emitter of the broad band was tentatively assigned to reaction products, possibly benzene isomers. For toluene, a strong appearance of benzyl radical emission was observed. With an addition of biacetyl, the elimination of benzyl emission and a strong growth of biacetyl phosphorescence were observed as for the benzene/biacetyl system. With an increase of biacetyl concentration, a remarkable red shift were observed for biacetyl phosphorescence, while no shift was observed for benzyl emission, indicating the difference of the solvent effect for these electronic transitions. No luminescence was observed for solid hexane and cyclohexane.

The major difficulty in elucidating the reaction mechanisms of reactions of active nitrogen with organic compounds was mainly due to the existence of several active species in active nitrogen which were produced by electrical discharge. The major active species in active nitrogen are long-lived $N(^4S)$ and $N_2(A^3\Sigma_u^+)$.[1] The rate constants for the reactions of $N(^4S)$ with organic compounds have been measured,[2,3] but the reported data are not in good agreement with each other, possibly owing to the contamination of $N(^4S)$ with $N_2(A)$. In order to elucidate the reaction mechanisms of active nitrogen unequivocally, it is indispensable to isolate the active species and study its reactions with organic compounds.

So far only a few investigations have been performed which dealt with $N_2(A)$.[4-6] Dessaux[4,5] reported a simple method for producing "pure" $N_2(A)$ by passing active nitrogen (discharged N_2) through a liquid nitrogen cooled trap. By this method, $N_2(A)$ in the absence of N atoms can be made available owing to the favorable recombination of nitrogen atoms on the cold surface of the trap. Devolder[6] observed the disappearance of ESR signals of nitrogen atoms after passing the active nitrogen through the cold trap at 77 K. Dessaux[4] observed the phosphorescence from the reaction of $N_2(A)$ with solid benzene and he concluded that the emitter of the phosphorescence is the charge transfer complex of $N_2(A)$ and C_6H_6, *i.e.* $N_2(A)^{\pm}\cdots C_6H_6^{\mp}$. We think that Dessaux's conclusion is less likely because the phosphorescence spectrum is very similar to those observed for solid benzene induced by electron impact.[7,8] In this work, the emission spectra from the reactions of $N_2(A)$ with various solid oragnic compounds were measured in order to obtain information on the reaction of $N_2(A)$ with organic compounds at 77 K.

Experimental

The nitrogen gas (0.5 Torr†, Nippon Sanso ultra pure, 99.99999%) was passed through a trap at 77 K and led to a microwave cavity. The active nitrogen generated was passed through a second trap at 77 K and then flowed to the cold finger at 77 K on which organic compounds were deposited. The vacuum system was made of greese-free Pyrex glass. In the presence of nitrogen atoms, a characteristic yellow afterglow (first positive band, $B^3\Pi_g\rightarrow A^3\Sigma_u^+$) was observed which is due to the reaction $2N+M=N_2^*+M$. The yellow afterglow disappeared completely on passing the active nitrogen through the trap at 77 K. The flow speed of N_2 was 4 m/s.

For luminescence measurements, a quartz window was placed on the port of the vacuum system opposite the side face of the cold finger. An Optech GM-N-250 monochromator with a Hamamatsu TV-R585 photomultiplier was positioned in front of the window. A synchronous motor was used to scan the grating and the output from the monochromator was detected by a Hamamatsu TV-C1230 photon counter, and displayed on an x-y recorder. The resolution of the monochromator was 7 nm.

All samples except benzene were Tokyo-Kasei extra pure. Benzene for fluorometry was purchased from Merck. Samples were vacuum degassed prior to inletting by multiple freeze-pump-thaw cycles.

Results and Discussion

Benzene. In Fig. 1(a) is shown the emission spectrum from a reaction of $N_2(A)$ with solid benzene at 77 K. A broad band with a maximum at 400 nm (hereafter, cited as band A) was observed. The decay of the luminescence was recorded by setting the monochromator at the maximum wavelength, following the manual shutting off of the excitation power over a period of time. The lifetime of the luminescence was determined to be 2.5 s, in good agreement with the value obtained by Dessaux.[4] Dessaux suggested that the emitter of the long-lived phosphorescence is the charge transfer complex of $N_2(A)$ with C_6H_6, *i.e.* $N_2(A)^{\pm}\cdots C_6H_6^{\mp}$. If the charge transfer complex $N_2(A)^{\pm}\cdots C_6H_6^{\mp}$ was really formed on the surface of solid benzene, the quenching of this state by the energy transfer to the impurity molecules should be inefficient because of the localization of the charge transfer complex in the benzene matrix. In order to investigate the energy transfer processes in solid benzene, the luminescence spectra of solid benzene doped with biacetyl were measured as a function of the concentration of biacetyl. As shown in Fig. 1, by doping biacetyl in solid benzene,

† 1 Torr = 133.322 Pa.

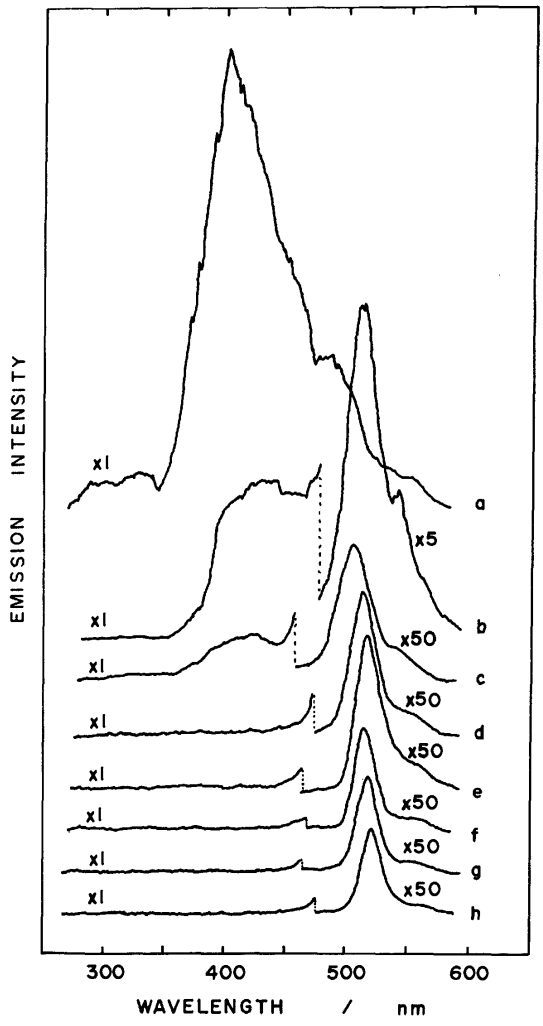

Fig. 1. The luminescence spectra from the reaction of $N_2(A^3\Sigma_u^+)$ with solid benzene doped with biacetyl at 77 K. The mol% of biacetyl in biacetyl-benzene solid solution are: (a) 0, (b) 0.1, (c) 1.0, (d) 5.1, (e) 10.2, (f) 20.4, (g) 50.6, (h) 100.

a remarkable suppression of the band A and an appearance of a characteristic phosphorescence of biacetyl are observed. This result indicates the importance of energy migration in the benzene matrix after the triplet electronic energy transfer from $N_2(A)$ to the benzene molecule. Apparently, the emission of the band A is induced by the long-range energy transfer of triplet excitation in solid benzene. The possibility that the emitter of the band A is the charge transfer complex is, therefore, unlikely. The experimental results described above led us to conclude that the luminescence from the reaction of $N_2(A)$ with solid benzene is due to the emission of some reaction products produced in the benzene matrix.

It is worthwhile noting that the emission spectrum shown in Fig. 1(a) is very similar to that observed for solid benzene induced by electron impact.[9,10] When an ultrathin film of benzene deposited under vacuum at 77 K was bombarded by low-energy electrons ($<\approx$10 eV), only a benzene fluorescence ($^1B_{2u}\rightarrow{}^1A_{1g}$) was observed.[9] With the increase of the incident electron energy ($\geq\approx$20 eV), new bands with maxima at 295 and 400 nm appeared. These bands could still be observed when the incident electron energy was decreased below 10 eV. This result strongly suggests that the emitters of these bands are the radiation products formed in the solid benzene film.

Phillips and Schug[10] also observed the broad band appearing at 400 nm under the stimulation of solid benzene by 1 MeV electrons. They assigned this band to the triplet and triplet excimer emission. We think that their assignment is dubious because the observation of emission from the triplet state in pure organic crystals has been unsuccessful due to the triplet excitation migration and the rapid triplet-triplet annihilation. The large exchange resonance interaction is no doubt a general phenomenon for π-electron system and it corresponds to a transition time for excitation transfer between nearest neighbors of less than 10^{-12} s.[11]

As described previously, the luminescence of benzene induced by electron impact consists of 295 and 400 nm bands as well as the benzene monomer fluorescence at 270 nm. In Fig. 1, a weak band at 290 nm is observed as well as the strong band A at 400 nm. The emitters of these bands seem to be the same for both of these experiments. Quite a few studies have been made of the vacuum-ultraviolet photochemistry of benzene.[12] Benzene irradiated by ultraviolet radiation in the gas and liquid phase is known to undergo isomerization to yield benzene isomers, *i.e.*, mainly benzvalene and fulvene.[13] Although no luminescence of these benzene isomers has been reported, we would like to propose that the 290 nm band and the 400 nm band are fluorescence and phosphorescence of a benzene isomer produced in the benzene matrix. The weak fluorescence of the benzene isomer at 290 nm would be induced by the energy transfer from the singlet excitons which are formed by the homofusion of triplet excitons in the benzene matrix. The formation of benzene isomers from triplet states' benzene has not been reported before,†† but the temperature-dependent radiationless transitions from T_1 are attributed to transitions to an isomeric singlet state.[14] The identification of the benzene isomer could not be done at the present stage. The emitter of the 325 nm band in Fig. 1 could not be specified either. A more detailed investigation is apparently needed in these respects.

With decreasing concentration of biacetyl from 100 to 10 mol%, the phosphorescence intensity of biacetyl shows a gradual increase. This suggests that the efficiency of the energy transfer from $N_2(A)$ to biacetyl is smaller than that from triplet benzene to biacetyl. This seems reasonable because the energy difference between triplet states of $N_2(A)$ and biacetyl is appreciably larger than that between benzene and biacetyl and the energy transfer efficiency for the former pair is considered to be smaller than that for the latter pair (Dexter's theory[15]).

With increase of the concentration of biacetyl, the phosphorescence spectrum of biacetyl shows a red shift as shown in Fig. 1. This indicates that the degree

†† Energetically, $N_2(A^3\Sigma_u^+)$ could excite benzene molecules up to T_3.

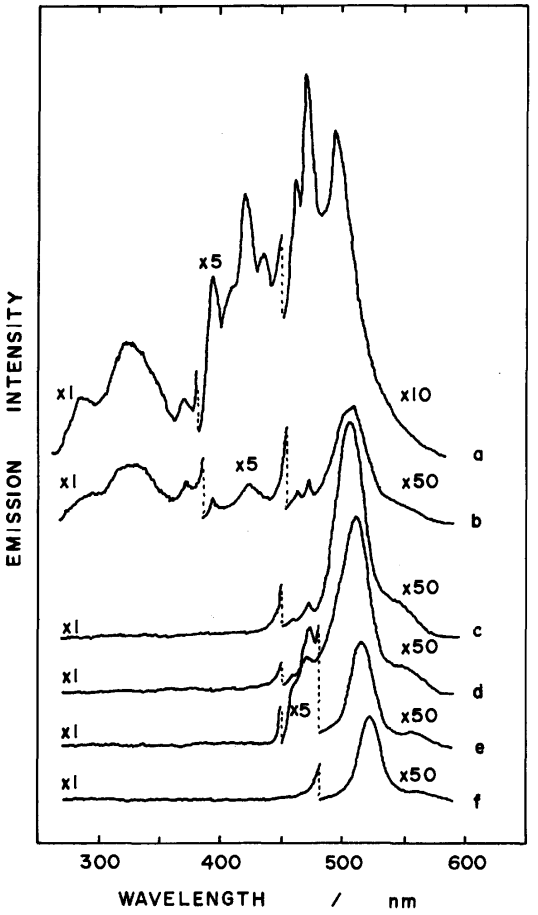

Fig. 2. The luminescence spectra from the reaction of $N_2(A^3\Sigma_u^+)$ with solid toluene doped with biacetyl at 77 K. The mol% of biacetyl in biacetyl-toluene solution are: (a) 0, (b) 0.1, (c) 5.9, (d) 23.0, (e) 54.4, (f) 100.

of solvation of triplet biacetyl by benzene molecules is different from that by biacetyl molecules. Because the polarizability of benzene (10.3 Å^3) is larger than that of biacetyl (9.2 Å^3), the larger solvation energy of biacetyl would be due to its intramolecularly dipolar property. The observation of the red shift of biacetyl phosphorescence indicates that a considerable degree of solvation of the triplet state of biacetyl (*i.e.* rotation of solvent molecules) takes place in rigid solid at 77 K during the lifetime of this state ($\approx 2.25 \times 10^{-3}$ s[16]).

After the measurements of luminescence, the benzene sample was analysed by gas chromatography. No gaseous or liquid products were deteced. The formation of solid products was not observed either on the wall of the cold finger after the evaporation of the benzene sample.

Toluene. The luminescence spectrum from reactions of $N_2(A)$ with solid toluene at 77 K is shown in Fig. 2(a). The three longest-wavelength lines beginning at about 460 nm are easily identified as the fluorescence of the benzyl radical.[17] By doping with 0.1 mol% of biacetyl, a strong emission of biacetyl phosphorescence appeared, clearly indicating the migration of triplet energy in solid toluene. The benzyl emission showed a rather gradual suppression when the biacetyl concentration was increased. In contrast to the case of benzene/biacetyl system the benzyl emission was still observed with a biacetyl concentration of 54 mol%. Because the emission of the benzyl radical by a single collision of $N_2(A)$ with toluene is endoergic, the persistence of benzyl emission must be due to the high concentration of benzyl radicals formed in the toluene matrix.

In addition to the benzyl emission, sharp emission lines are observed in the range of 380—440 nm (Fig. 2(a)). Phillips and Schug[10] also observed similar emission lines from solid toluene induced by 1 MeV electrons. They proposed the benzyl ion to be the most probable candidate for this emission. Although the ionization energy of benzyl radical (7.27 eV[18]) is about 1 eV higher than the available energy of $N_2(A)$ (6.17 and 6.30 eV for $v'=0$ and $v'=1$, respectively), the ionization of benzyl radicals in the solid toluene by $N_2(A)$ could be energetically possible because the polarization energies of ions in solid organic compounds are generally higher than 1 eV.[19-21] For $N_2(A)$, the favored Franck-Condon factors tend to reduce the available energy from 6.17 eV to $\approx$4.7 eV, and this might explain the relatively weak emission of these lines compared to the results obtained by Phillips and Schug.[10] Almost a complete elimination of these emission lines is observed with the addition of 5 mol% of biacetyl, indicating that the concentration of the emitter of these bands is much lower than that of benzyl radical.

Two short-wavelength lines appearing weakly at 290 and 325 nm are observed. These bands could be assigned to monomer and excimer fluorescences of these compounds. The excited singlet states can be formed by a homofusion of triplet excitons (triplet-triplet annihilation) in the solid matrix. The assignment of the band at 325 nm as an excimer emission may not be conclusive because solid thin films of benzene and toluene bombarded by electrons gave only the monomer fluorescence and the excimer emission was not observed.[9,22] These results indicate that solid benzene and toluene deposited at 77 K were crystalline. Thus the band at 325 nm may not be due to the excimer but to some other reaction products.

As in the benzene/biacetyl system, phosphorescence spectra of biacetyl show a red shift with an increase of the concentration of biacetyl as shown in Fig. 2. On the contrary, the emission spectra of the benzyl radical appearing at 465 and 475 nm do not show any noticeable shift with an increase of biacetyl concentration. This indicates that the ground and excited benzyl radical are almost equally solvated by solvent toluene or biacetyl. This seems reasonable because the distributions of a nonbonding electron for the ground and excited states of benzyl radical are highly delocalized owing to the π-electron character of the nonbonding electron.

Alkanes. No chemiluminescence was observed for the reactions of $N_2(A)$ with solid hexane or cyclohexane at 77 K. With an addition of 0.1 mol% of biacetyl in solid hexane or cyclohexane, only a very weak phosphorescence of biacetyl was observed. Its intensity was about 0.1% of the phosphorescence of solid benzene doped with the same amount of biacetyl. The weakness of the phosphorescence suggests that the

phosphorescence was induced by the direct energy transfer from $N_2(A)$ to biacetyl. Apparently an efficient triplet energy migration does not occur in solid alkanes. The absence of the energy migration suggests either that the energy transfer from $N_2(A)$ to alkanes does not occur or that the triplet energy transfered to alkanes does not migrate in the solid matrix. From the results obtained by the ultraviolet absorption spectroscopy and the low-energy electron impact spectroscopy,[23] it is known that a characteristic feature of alkanes is the absence of observable excitation below about 7 eV. This lower limit of energy for the excitation is about 1 eV higher than the available energy of $N_2(A)$ and the energy transfer from $N_2(A)$ to alkanes is endoergic. Actually neither gaseous nor solid products were detected by GC or FT-IR after the reaction of $N_2(A)$ with solid alkanes at 77 K for more than 10 h.

References

1) A. N. Wright and C. A. Winkler, "Active Nitrogen," Academic Press, New York (1968).
2) S. Sato, K. Sugawara, and Y. Ishikawa, *Chem. Phys. Lett.*, **68**, 557 (1979).
3) J. V. Michael, *Chem. Phys. Lett.*, **76**, 129 (1980).
4) O. Dessaux, *J. Chim. Phys.*, **67**, 1137 (1970).
5) R. Demary and O. Dessaux, *J. Chim. Phys.*, **71**, 555 (1974).
6) M. P. Devolder, *C. R. Acad. Sci., Ser. C*, **282**, 791 (1976).
7) P. M. Johnson and A. C. Albrecht, *J. Chem. Phys.*, **48**, 851 (1968).
8) K. Hiraoka and W. H. Hamill, *J. Phys. Chem.*, **77**, 1616 (1973).
9) Y. Iijima, M. Nara, and K. Hiraoka, 45th National Meeting of the Chemical Society of Japan, 1982, to be published.
10) D. H. Phillips and J. C. Schug, *J. Chem. Phys.*, **50**, 3297 (1969).
11) G. C. Nieman and G. W. Robinson, *J. Chem. Phys.*, **39**, 1298 (1963).
12) N. J. Turro, "Modern Molecular Photochemistry," Benjamin, London (1978), p. 499.
13) L. Kaplan and K. E. Wilzbach, *J. Am. Chem. Soc.*, **90**, 3291 (1968).
14) J. B. Birks, "Organic Molecular Photophysics," John Wiley and Sons, London (1973), Vol. I, p. 48.
15) D. L. Dexter, *J. Chem. Phys.*, **21**, 836 (1953).
16) D. S. McClure, *J. Chem. Phys.*, **17**, 905 (1949).
17) P. M. Johnson and A. C. Albrecht, *J. Chem. Phys.*, **48**, 851 (1968).
18) F. P. Lossing, *Can. J. Chem.*, **49**, 357 (1971).
19) L. E. Lyons, *J. Chem. Soc.*, **1957**, 5001.
20) K. Hiraoka, *J. Phys. Chem.*, **85**, 4008 (1981).
21) K. Hiraoka and M. Nara, *Bull. Chem. Soc. Jpn.*, **54**, 3317 (1981).
22) P. B. Merkel and W. H. Hamill, *J. Chem. Phys.*, **54**, 1695 (1971).
23) M. B. Robin, "Higher Excited States of Polyatomic Molecules," Academic Press, New York (1975), Vol. 1.

Electronic Structures and Spectra of a Novel Diquinone; 1,4 : 5,8-Anthracenediquinone

Masahiko FUKUDA, Akio TAJIRI, Masaji ODA,† and Masahiro HATANO*
Chemical Research Institute of Non-aqueous Solutions, Tohoku University, Katahira, Sendai 980
†Department of Chemistry, Faculty of Science, Osaka University, Toyonaka, Osaka 560
(Received June 28, 1982)

Assignment of the electronic absorption spectrum of 1,4 : 5,8-anthracenediquinone (1,4 : 5,8-ADQ) has been carried out with the aid of magnetic circular dichroism and LCAO MO SCF CI calculations including all valence electrons. The lowest energy absorption region of 1,4 : 5,8-ADQ has been revealed to be composed of the n-π^* transition or transitions. The higher energy absorption region has been concluded to consist of four π-π^* transitions, which are regarded as L_b, L_a, B_a, and B_b in the Platt's notation for anthracene. The above assignment of 1,4 : 5,8-ADQ has been experimentally confirmed with its linear dichroism spectra in stretched polyethylene sheets and its circular dichroism spectra in the β-cyclodextrin solution. The relationship between the absorption spectra of 1,4 : 5,8-ADQ and 1,4-naphthoquinone has been discussed from the experimental and theoretical points of view.

In spite of the extensive studies on the electronic structures, spectra and reactivities of quinones, those on the chemical and physical properties of diquinones have been little known. They are a potential subject of synthetic and theoretical research.

Anthracenediquinone (ADQ) is considered to be a representative of this interesting quinonoid system. Two isomers of para-ADQ illustrated below are **1** for 1,4 : 9,10-ADQ and **2** for 1,4 : 5,8-ADQ. The electronic

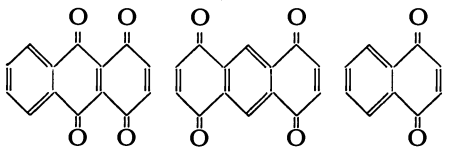

1 **2** **3**

absorption spectrum of **1** in solution has been interpreted in terms of the n-π^* transition and four π-π^* transitions.[1] The π-π^* electronic absorption occurring in **1** has been theoretically confirmed on the basis of an LCAO MO SCF CI calculation.[2] The synthesis of **2** was reported along with its spectroscopic data,[3] where **2** in *N*,*N*-dimethylformamide is described to exhibit absorption at 353 nm. The diquinone **2** was also obtained by selenium dioxide oxidation of a photochemical addition product of 2-cyclohexene-1,4-dione with acetylene.[4] A theoretical calculation based on the simple HMO method was given to elucidate the redox potential of **2**.[5]

In this paper, the electronic absorption, magnetic circular dichroism (MCD) spectra[6,7] in solution, and linear dichroism (LD) spectra[8] in stretched polyethylene sheets of **2** are reported in addition to its circular dichroism (CD) spectrum in the β-cyclodextrin (β-CDx) solution, where the observed CD is known as induced circular dichroism (ICD).[9-11] The experimental spectra of **2** are compared with those of 1,4-naphthoquinone, **3**, and discussed in conjunction with LCAO MO SCF CI calculations including all valence electrons (CNDO/S), so as to give a spectroscopic assignment of the characteristic electronic absorption of **2**.

Experimental and Theoretical

The diquinone **2** and **3** were purified by sublimation under reduced pressure after several recrystallizations from dioxane and petroleum ether. Inclusion complexes of quinones with commercially available β-CDx were prepared in the aqueous solutions. The electronic absorption spectra were recorded on a JASCO UVIDEC 510 recording spectrophotometer. The MCD spectra were measured with a JASCO J500C recording circular-dichrometer equipped with a 1.14T electromagnet. All measurements were carried out at room temperature using spectrograde solvents without further purification.

The experimental oscillator strengths, f, and Faraday parameters, B, were evaluated from the observed spectra after resolving the spectrum into its components according to the curve-fitting procedure assuming a Gaussian function, where B was expressed in units of (Debye)^2 μ_B/cm^{-1}.**

Polyethylene sheets including quinones were prepared by the usual method[8] and stretched five times. Absorption of the set stretched sheets was recorded both for the electric vectors parallel and perpendicular to the stretching direction. The LD spectra in the wavenumber region higher than 25000 cm^{-1} were obtained from the observed dichroic spectra according to the procedure proposed by Thulstrup *et al.*,[8] neglecting out-of-plane polarized absorption.

The electronic transition energies, oscillator strengths and Faraday B terms of **2** and **3** were calculated within the framework of the CNDO/S method,[12,13] including CI among singly excited configurations below 10 eV. The values of the bonding parameters for the carbon and the hydrogen atoms were adjusted so that the ionization potentials and the transition energies of benzene and hydrogen molecules are well reproduced.[14] The values of bonding parameter for the oxygen atom and the empirical σ-π separation parameter, κ, were determined so as to reproduce the n-π^* and the first π-π^* transition energies of *p*-benzoquinone. The quinone ring in **2** was assumed to be identical with that in **3**, while the central six-membered ring was assumed to be a regular hexagon with bond lengths of 1.40 Å. The geometry of **3** was taken from the X-ray diffraction data.[15]

For a molecule possessing non-degenerate states, the theoretical MCD for the transition, a←0, is usually discussed in terms of the Faraday B term. All the atomic integrals in the calcula-

** B-terms in SI units of 10^{-60} C^2 m^2 T^{-1} can be obtained by multiplying by 5.19.

tion of the B terms were evaluated using the Slater AOs, with which the orthogonalized CNDO basis set was expanded by the inverse Löwdin transformation.[16]

Results and Discussion

The electronic absorption spectrum of **2** in dichloromethane is reproduced in Fig. 1. It is characterized by three absorption regions; the first (20000—25000 cm^{-1}) the second (25000—35000 cm^{-1}), and the third (35000—42000 cm^{-1}).

The MCD spectrum of **2** in Fig. 1 reveals a distinct negative extreme at 22200 cm^{-1} in contrast to a discernible shoulder in its electronic absorption spectrum. The first region in the absorption and MCD spectra is considered to arise from an electronic transition or transitions which is or are n-π^* in nature. The n-π^* assignment is partially supported by the solvent effect on the lowest energy absorption and MCD bands. As is clear from Fig. 2, the blue-shift takes place on changing solvents from nonpolar to polar.

The phosphorescence spectrum of **2** was measured in an ether-isopentane-ethanol (EPA) mixture (volume ratio, 5 : 5 : 2) at 77 K, and it is reproduced in Fig. 3. The spectrum exhibits the vibrational structure with spacing of *ca.* 1600 cm^{-1}, which is considered to be due to the carbonyl stretching progression. From the 0-0 band position, which was assumed to be the most intense peak of the spectrum, the lowest triplet level of **2** is estimated to be at 2.45 eV. Provided that the 0-0 band position is at 21350 cm^{-1}, which was assumed to be the lowest wavenumber extreme of the MCD spectrum of **2** in benzene, the energy difference between the lowest singlet and the lowest triplet states is estimated to be 1590 cm^{-1}. The small energy difference and the carbonyl stretching progression suggest that the lowest

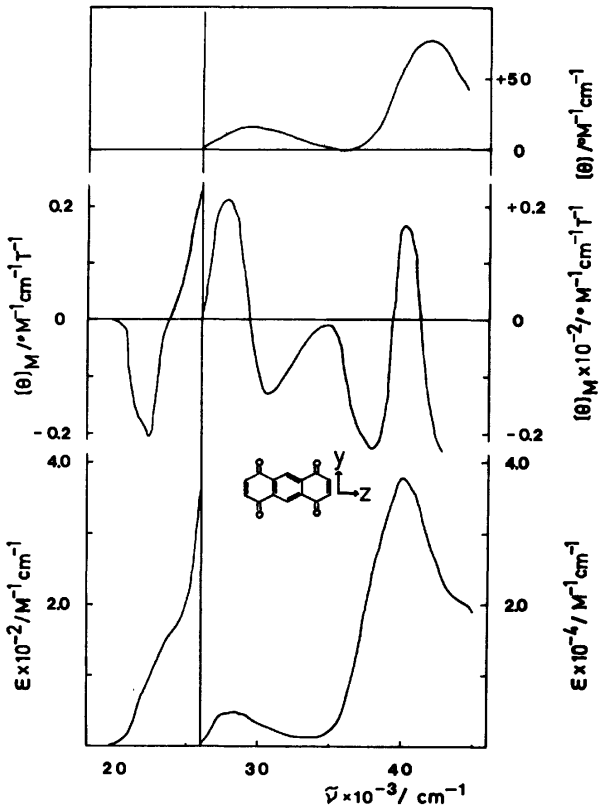

Fig. 1. The magnetic circular dichroism (center) and electronic absorption (bottom) spectra of 1,4 : 5,8-anthracenediquinone in dichloromethane and the circular dichroism (top) spectrum of the β-cyclodextrin complex with 1,4:5,8-anthracenediquinone in water at room temperature.

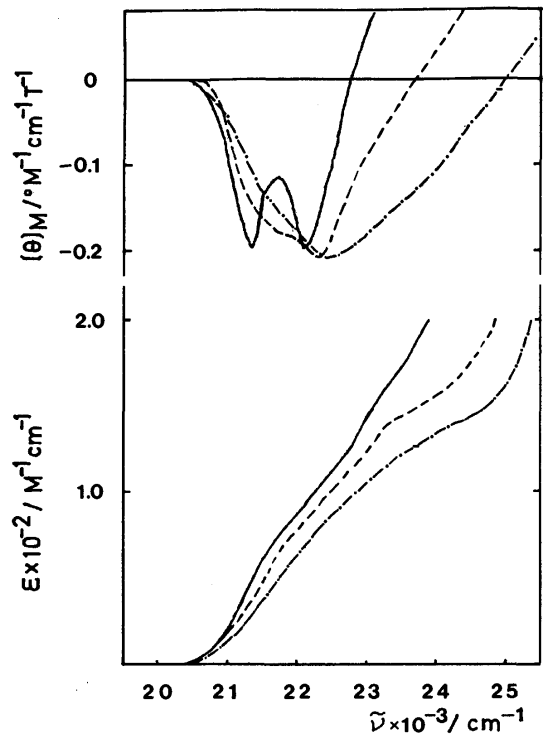

Fig. 2. The magnetic circular dichroism (top) and electronic absorption (bottom) spectra of 1,4:5,8-anthracenediquinone in benzene (——), dichloromethane (-----), and acetonitrile (·—·—) at room temtemperature.

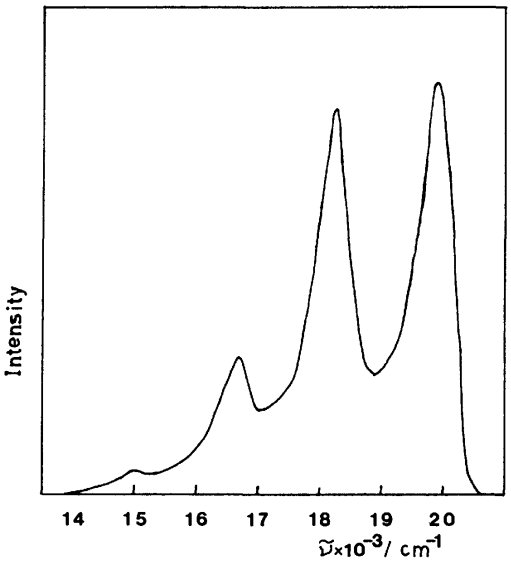

Fig. 3. The phosphorescence spectrum of 1,4:5,8-anthracenediquinone in EPA at 77 K.

TABLE 1. THE CALCULATED AND EXPERIMENTAL TRANSITION ENERGIES, ΔE, OSCILLATOR STRENGTHS, f, AND FARADAY B TERMS, B, FOR 1,4 : 5,8-ANTHRACENEDIQUINONE.

Symmetry	Calculated (CNDO/S)		Experimental (MCD)	
	$\frac{\Delta E\times 10^{-3}}{\text{cm}^{-1}}(f)$	$\frac{B\times 10^{4}}{\mu_B\,\text{D}^2\,\text{cm}}$	$\frac{\Delta E\times 10^{-3}}{\text{cm}^{-1}}(f)$	$\frac{B\times 10^{4}}{\mu_B\,\text{D}^2\,\text{cm}}$
B_{2g} $(\pi^*\leftarrow n)$	20.6 (Forb)	0		
B_{3u} $(\pi^*\leftarrow n)$	20.7 (6×10^{-5})	3.99	22.2 (0.002)	0.05
B_{1g} $(\pi^*\leftarrow n)$	20.8 (Forb)	0		
A_u $(\pi^*\leftarrow n)$	21.0 (Forb)	0		
B_{2u} $(\pi^*\leftarrow \pi)$	30.2 (0.055)	−10.57	27.8 (0.067)	−5.28
B_{1u} $(\pi^*\leftarrow \pi)$	32.9 (0.043)	6.84	30.3 (0.031)	3.73
B_{1u} $(\pi^*\leftarrow \pi)$	40.0 (0.217)	1058.69	37.8 (0.274)	5.19
B_{2u} $(\pi^*\leftarrow \pi)$	40.2 (0.383)	−356.75	40.2 (0.527)	−1.77

phosphorescence state is n-π^* in origin, and in turn that the lowest singlet state is also n-π^* in nature.

In the present work, a symmetry allowed $B_{3u}\leftarrow A_g$ transition is assigned to the observed lowest energy absorption and MCD bands. This seems to require a further confirmation, however.

The MCD spectrum exhibits a positive extreme at 27800 cm^{-1} and a negative extreme at 30300 cm^{-1} in the second absorption region, suggesting that two electronic origins are included in the corresponding spectral region. Both bands are roughly equal in magnitude, but opposite in sign. In the third region, the MCD spectrum manifests two electronic transitions which have never been resolved in the absorption spectrum due to overlapping.

The CD spectrum of the inclusion complex of **2** with β-CDx is shown in Fig. 1. No ICD for the first absorption region has been observed, due to the low solubility of **2** in water. The inclusion complex exhibits only two positive CD extrema, corresponding to the second and third absorption regions. If the long axis of the guest molecule is parallel to the seven-fold symmetry axis of β-CDx (an axial inclusion), the transition polarized along the z-axis gives positive CD and the transition polarized along the y-axis gives negative CD.[9-11] Therefore, the observed positive extreme in the CD spectrum originates from the transition polarized along the z-axis. In general, the positive CD band in inclusion complexes tends to appear larger than the negative one.[17] The negative CD component expected to come from the transition polarized along the y-axis seems to be compensated by the larger positive CD component.

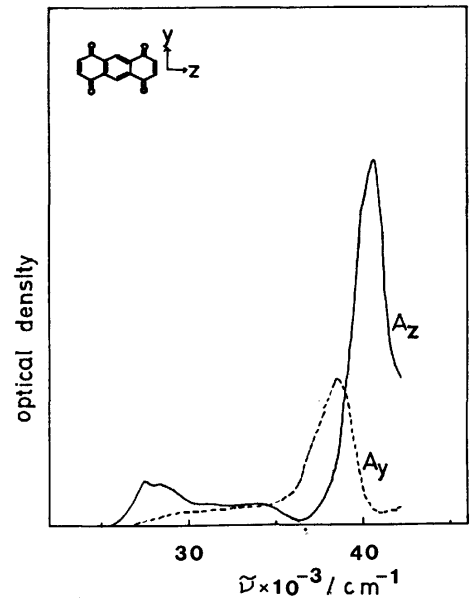

Fig. 4. The linear dichroism spectra of 1,4:5,8-anthracenediquinone in stretched polyethylene sheets at room temperature (redution factors $d^0_{\parallel}=1.02$, $d^0_{\perp}=0.77$). The solid and broken lines stand for the absortion components polarized along the z- and y-axis respectively.

The LD spectra of **2** in the y-direction, A_y, and z-direction, A_z, are illustrated in Fig. 4, which were obtained from the experimental dichroic spectra using the reduction factors of $d^0_{\perp}=0.77$ and $d^0_{\parallel}=1.02$ respectively. The reduction factors, $d^0_{\perp}$ and $d^0_{\parallel}$, were estimated on the assumption that the z- and y-polarized absorption bands have their maxima at 40800 and 35700 cm^{-1} respectively.

According to the present calculation, the lowest two π-π^* transitions take place at 30200 and 32900 cm^{-1} with their directions of polarization along the z- and y-axis respectively. Theoretical B values associated with these transitions are negative for the lower energy transition and positive for the higher, in agreement with the experiment. Therefore, the positive and negative bands are considered to be assigned to the predicted B_{2u} and B_{1u} states respectively. The assignment is further supported by the LD spectra which show the two components polarized along the z-axis in the lower energy region and along the y-axis in the higher. Thus, in the second region there are two π-π^* transitions, where the lower energy transition is polarized along the z-axis and the higher energy one along the y-axis.

The negative and positive MCD bands in the third absorption region are assigned to the $B_{1u}\leftarrow A_g$ and $B_{2u}\leftarrow A_g$ transitions predicted at 40000 and 40200 cm^{-1} respectively. The calculated B values for the both transitions are too large to reproduce experimental values, however. This arises from the small energy difference between two states predicted in the present calculation. The assignment is supported by the LD spectra (Fig. 4) which exhibit the y-component at the lower energy region and the z-component at the higher.

Table 2. The calculated and experimental transition energies, ΔE, oscillator strengths, f, and Faraday B terms, B, for 1,4-naphthoquinone

Symmetry	Calculated (CNDO/S)		Experimental (MCD)	
	$\frac{\Delta E\times 10^{-3}}{\text{cm}^{-1}}(f)$	$\frac{B\times 10^{4}}{\mu_B\ \text{D}^2\ \text{cm}}$	$\frac{\Delta E\times 10^{-3}}{\text{cm}^{-1}}(f)$	$\frac{B\times 10^{4}}{\mu_B\ \text{D}^2\ \text{cm}}$
B_1 ($\pi^*\leftarrow$n)	19.1 (1×10^{-6})	4×10^{-3}	22.8 (3×10^{-4})	0.01
A_2 ($\pi^*\leftarrow$n)	19.7 (Forb)	0		
A_1 ($\pi^*\leftarrow\pi$)	32.9 (0.028)	−4.77	28.8 (0.026)	−4.49
B_2 ($\pi^*\leftarrow\pi$)	36.0 (0.030)	3.17	32.0 (0.046)	2.36
A_1 ($\pi^*\leftarrow\pi$)	41.1 (0.110)	18.88	40.0 (0.261)	−4.66
B_2 ($\pi^*\leftarrow\pi$)	41.9 (0.171)	−13.31	− −	+

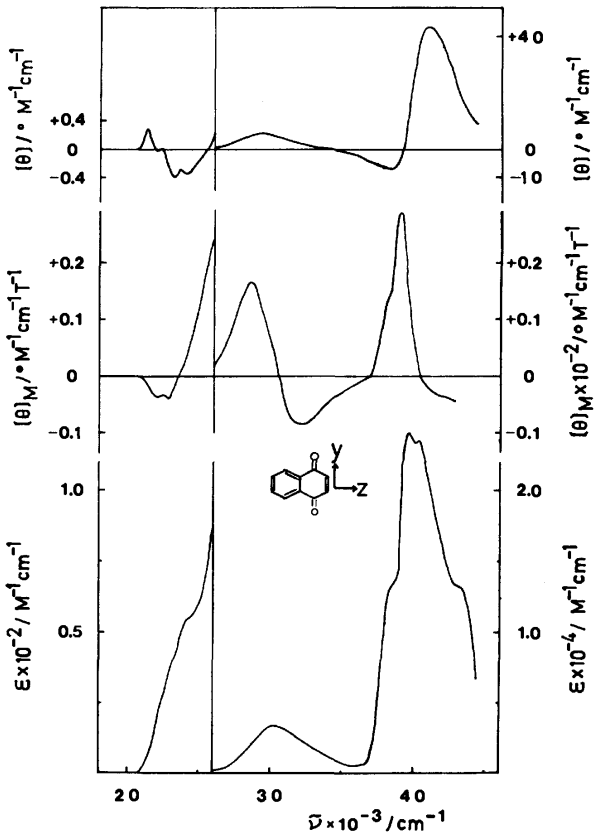

Fig. 5. The magnetic circular dichroism (center) and electronic absorption (bottom) spectra of 1,4-naphthoquinone in dichloromethane and the circular dichroism (top) spectrum of β-cyclodextrin complex with 1,4-naphthoquinone in water at room temperature.

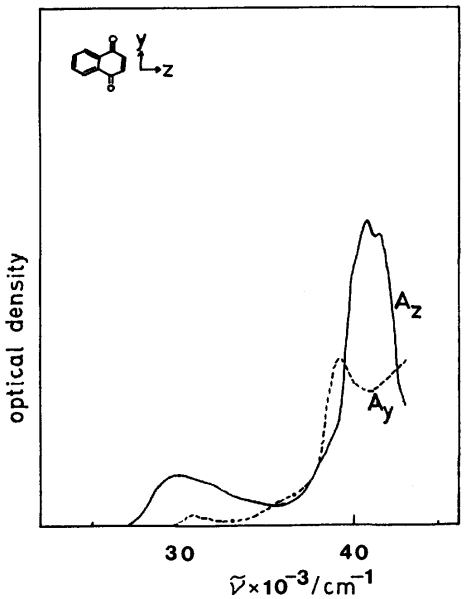

Fig. 6. The linear dichroism spectra of 1,4-naphthoquinone in stretched polyethylene sheets at room temperature (redution factors $d_{\parallel}^{0}=1.07$, $d_{\perp}^{0}=0.69$). The solid and broken lines stand for the absorption components polarized along z- and y-axis respectively.

Taking the theoretical and experimental results into consideration, the third absorption region is concluded to consist of two π-π^* transitions: One is polarized along the y-axis and the other along the z-axis.

The electronic absorption spectrum of **3** in Fig. 5 is divided into three characteristic spectral regions. The first region of the absorption and MCD spectra is considered to come from the n-π^* transitions, which are predicted to take place at the lowest energy region (see Table 2). The ICD spectrum in this region exhibits two extrema at 21280 and 23260 cm^{-1}, which are considered to be either electronic or vibrational in origin.

The positive and negative MCD bands in the second region are considered to be assigned to the theoretically predicted A_1 and B_2 states respectively. The assignment is supported by the LD spectra in Fig. 6, where the lower energy transition is polarized along the z-axis and the higher energy one along the y-axis.

The LD and ICD spectra show that the third absorption region consists of two π-π^* transitions, where the lower energy transition is polarized along the y-axis and the higher energy one along the z-axis. On the contrary, the present CNDO/S calculation predicts the $A_1\leftarrow A_1$ (41100 cm^{-1}) and $B_2\leftarrow A_1$ (41900 cm^{-1}) transitions with the transition moments directed along the z- and y-axis respectively. The theoretical result is in disagreement with the experimental result. The latter, however, is consistent with that of Kuboyama and his coworkers.[18]

The spectral profile of **2** and **3** in the wavenumber region higher than 26000 cm^{-1} seems to be related to the skeletal π-π^* transitions in the annelated aromatics. The singly excited configurations contributing dominantly to the lowest $B_{2u}\leftarrow A_g$ and $B_{1u}\leftarrow A_g$ transitions in the second region of **2** are respectively due to the

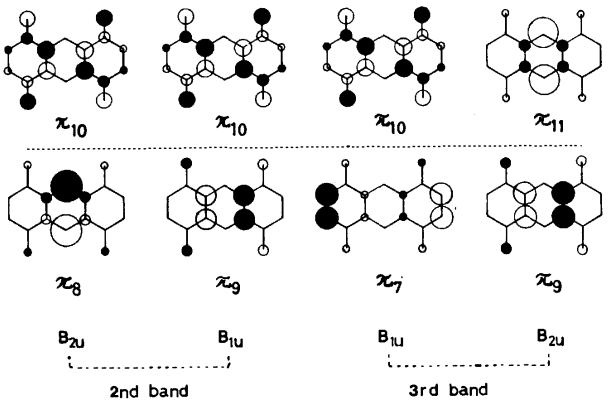

Fig. 7. The bonding π-MOs (bottom) and anti-bonding π-MOs (top) associated with the π-π^* electronic transitions in 1,4: 5,8-anthracenediquinone.

$\pi_8 \rightarrow \pi_{10}$ and $\pi_9 \rightarrow \pi_{10}$, and illustrated in Fig. 7. The two configurations are correlated to the L_b and L_a bands in anthracene. Further, the B_{1u} and B_{2u} states included in the third absorption region of **2** are B_b and B_a respectively, in nature.

Concluding Remarks

The assignment of the electronic absorption spectra of **2** has been carried out. The first absorption region is considered to arise from the n-π^* electronic transition or transitions. The absorption region higher than 25000 cm^{-1} is concluded to consist of four π-π^* transitions.

The present CNDO/S calculation seems to reproduce the absorption and MCD spectra of **2** and **3** fairly well. As has been seen above, however, the agreement between the theoretical and experimental is considered to be less satisfactory in the higher energy region than in the lower energy region.

The authors wish to thank Professor Kokubun of Tohoku University for his kindness in putting a phosphorescence spectrophotometer at their disposal.

References

1) A. Kuboyama and K. Wada, *Bull. Chem. Soc. Jpn.*, **38**, 569 (1965).
2) T. Kunii and H. Kuroda, *Rep. Comput. Cent. Univ. Tokyo*, **1**, 119 (1968).
3) P. Boldt and F. Vandakis, *Angew. Chem.*, **77**, 1137 (1965).
4) M. Oda, unpublished work.
5) A. K. Kar, A. B. Sannigrahi, and S. Patai, *Indian J. Chem.*, **6**, 353 (1968).
6) A. D. Buckingham and P. J. Stephens, *Ann. Rev. Phys. Chem.*, **17**, 399 (1966).
7) J. Michl, *J. Am. Chem. Soc.*, **100**, 6801 (1978).
8) E. W. Thulstrup, J. Michl, and J. H. Eggers, *J. Phys. Chem.*, **74**, 3868 (1970); J. Michl, E. W. Thulstrup, and J. H. Eggers, *ibid.*, **74**, 3878 (1970).
9) K. Harata and H. Uedaira, *Bull. Chem. Soc. Jpn.*, **48**, 375 (1975).
10) N. Ikeda and H. Yamaguchi, *Chem. Phys. Lett.*, **56**, 167 (1978).
11) H. Shimizu, A. Kaito, and M. Hatano, *Bull. Chem. Soc. Jpn.*, **52**, 2678 (1979); **54**, 513 (1981).
12) J. A. Pople, D. P. Santry, and G. A. Segal, *J. Chem. Phys.*, **43**, S129 (1965); J. A. Pople and G. A. Segal, *ibid.*, **43**, S136 (1965); **44**, 3289 (1966).
13) J. Del. Bene and H. H. Jaffé, *J. Chem. Phys.*, **48**, 1807 (1968); G. Kuehnlenz and H. H. Jaffé, *ibid.*, **58**, 2238 (1973).
14) A. Kaito, A. Tajiri, and M. Hatano, *J. Am. Chem. Soc.*, **97**, 5060 (1975); **98**, 384 (1976); **99**, 5241 (1977).
15) J. Gaultier and C. Hauw, *Acta Crystallogr.*, **18**, 179 (1965).
16) P. O. Löwdin, *J. Chem. Phys.*, **18**, 365 (1950).
17) H. Shimizu, Ph. D. Thesis, Tohoku University 1980.
18) A. Kuboyama, S. Matsuzaki, H. Takagi, and H. Arano, *Bull. Chem. Soc. Jpn.*, **47**, 1604 (1974).

 © 1983 The Chemical Society of Japan Bull. Chem. Soc. Jpn., 56, 597—601 (1983)

Pure Spectra of Actinomycin D Bound to DNA at Various Ionic Strengths Extracted by the Principal-component-analysis Method[1)]

Takumi MATSUDA, Saburo KASHIRAMOTO, and Kiwamu YAMAOKA*
Faculty of Science, Hiroshima University, Higashisenda-machi, Naka-ku, Hiroshima 730
(Received July 6, 1982)

The interaction between actinomycin D (AMD) and native and heat-denatured DNA was studied spectrophotometrically at 25 °C. By applying the principal-component-analysis (PCA) method to the series of observed spectra, the number of light-absorbing components was determined. Two spectroscopically different species of bound AMD, *i.e.*, AMD–DNA complexes, were formed when an aqueous AMD solution was titrated with either the native or the denatured DNA solution over a wide range of the nucleotide residue-to-AMD mixing ratios (P/D) between 0 and 30. The pure spectra of AMD bound to DNA were extracted in the P/D range 0—4 by the extended PCA method with an appropriate binding scheme. These bound-AMD spectra were affected by the DNA conformation but not by the addition of NaCl (1—500 mmol dm^{-3}). The fractions of bound AMD were calculated as a function of P/D.

Actinomycin D (AMD)[2-4)] is an antibiotic that inhibits DNA-dependent RNA synthesis by binding to DNA;[5,6)] the interactions between AMD and DNA and other related compounds have been studied by many physicochemical methods.[5-22)] For example, two classes of AMD–DNA complexes with different binding constants have been reported;[5-7)] the first class is the "strongly" binding complex and the second is the "weakly" binding complex. Although the strongly binding complex has been studied extensively, few attempts have been made to clarify the weakly binding complex. In particular, the absorption spectrum of the AMD–DNA complex, free from the spectrum of unbound AMD, has not been unmasked because of the strong overlap between the two spectra in the visible wavelength region.

The pure spectrum of the AMD–DNA complex or the *bound*-AMD spectrum is important in interpreting the optical behavior and the binding mode of AMD in the AMD–DNA complex. In this paper, therefore, the interaction between AMD and DNA was studied spectrophotometrically, and the results were analyzed with a new technique—the principal-component-analysis (PCA) method.[1,23-27)] This method is useful, because no additional measurement such as equilibrium dialysis is required. By applying the PCA method to a series of observed spectra of AMD–DNA solutions, the number and the pure spectra of light-absorbing components in the system can be determined. The binding curve of AMD can also be evaluated by using an appropriate equilibrium equation.

Experimental

Materials. Actinomycin D was a gift of Merck Sharp and Dohme, Inc. (USA) and used without further purification. The aqueous solution of AMD was filtered through a sintered glass filter and stored in the refrigerator under dark. The concentration of AMD was determined to be 1.81×10^{-5} M (1 M = 1 mol dm^{-3}) with the molar absorption coefficient ε_{441} of 24800 cm^{-1} M^{-1}.[7)] Calf thymus DNA was purchased from Worthington Biochemical Corp.[1)] The concentration of the stock native DNA (nDNA) solution was 9.35×10^{-4} M, which was determined by using the absorption coefficient ε_{260} of 6400 cm^{-1} M^{-1}.[8)] Heat-denatured DNA (dDNA) in 1 mM NaCl was prepared as before.[1,8)] The hyperchromicity of the DNA solution was *ca.* 34% in 1 mM NaCl. Spectrophotometric titration was carried out at 25 °C in a 1 or 2 cm long cuvette cell by the successive addition of the stock DNA solution in the same manner as before.[1)]

Analysis. The absorption spectra of the AMD–DNA solution were analyzed by the PCA procedure, for which the following equilibrium equation was used (Eq. 2 of Ref. 1):

$$K_a = \frac{[DP^*]}{[D][P]}\left(\frac{[P]}{[D]_0}\right)^{1-\alpha}, \quad (1)$$

where K_a is the apparent equilibrium (binding) constant, the brackets denote the equilibrium concentration, DP* is the bound AMD or the AMD–DNA residue complex, D is the free AMD, P is the unoccupied DNA residue (in the nucleotide unit), and $[D]_0$ is the initial AMD concentration. The adjustable parameter α has been introduced to reproduce the sigmoidal change of optical titration curves for various dye-polymer combinations.[1,24,26,27)] When $\alpha=1$, Eq. 1 reduces to the commonly postulated equilibrium scheme, $K'=[DP^*]/[D]\cdot[P]$. When $\alpha>1$, Eq. 1 represents a sigmoidal change in the titration curve.

Results and Discussion

Observed Spectra of AMD–DNA Systems and Number of Light-absorbing Components. Figure 1 shows representative absorption spectra of AMD solutions obtained from the successive titration with (a) nDNA and (b) dDNA in the presence of 1 mM NaCl. The molar absorption coefficients, ε, of the spectra of AMD–DNA solutions are almost the same at 461 nm for nDNA and at 457 nm for dDNA (the isosbestic points) in the low P/D range. The spectral change near 380 nm at higher P/D values, together with the gradual deviation from the isosbestic points, indicates that more than two independent, light-absorbing components are present in each system. (The absorbance of the DNA component is negligibly small above 370 nm.) The exact number of these components may be determined by comparing the relative magnitudes of the eigenvalues, which are obtained from a family of the observed AMD–DNA spectra by the PCA method.[1,23-27)]

The eigenvalues calculated for the AMD–nDNA system at 1 mM NaCl are shown in Fig. 2(a). According to the previously set criteria,[1,23-27)] the significant number of light-absorbing components is determined

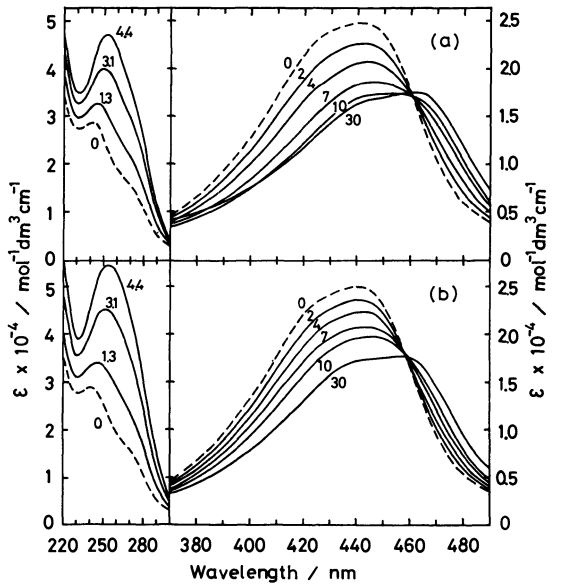

Fig. 1. Representative solution spectra of AMD observed in the presence of nDNA (a) and dDNA (b) at 1 mM NaCl. The dashed curves ($P/D=0$) are the spectra of AMD in the absence of DNA. The numerals denote values of P/D. The apparent molar absorption coefficient, ε, is expressed with the concentration of AMD in aqueous solution which is 1.81×10^{-5} M throughout this work.

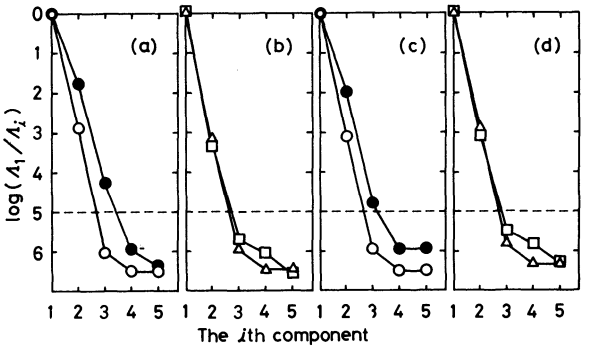

Fig. 2. Variations in eigenvalue Λ_i ($i=1$, 5) with the ith light-absorbing component for the AMD–nDNA solutions (a) and (b) and for the AMD–dDNA solutions (c) and (d). The concentrations of NaCl in those solutions are 1 mM (○), 100 mM (△), and 500 mM (□). The ordinate is expressed in terms of the ratios of the eigenvalue of the first component, which is the largest, to that of the ith component. The dashed lines indicate the criteria set for the significant component. Open symbols are used for the observed spectra which are limited to the low P/D range between 0 and 4, and the closed circle is used for the observed spectra whose P/D values range between 0 and 30.

to be three in a wide P/D range of 0—30. One of these species must be the free AMD and, hence, two differently bound AMD species may exist in agreement with previous reports that calf thymus DNA possesses two classes of binding sites for AMD (strong and weak binding sites).[6,7] The number of absorbing components reduces to two, if the P/D region is limited between 0

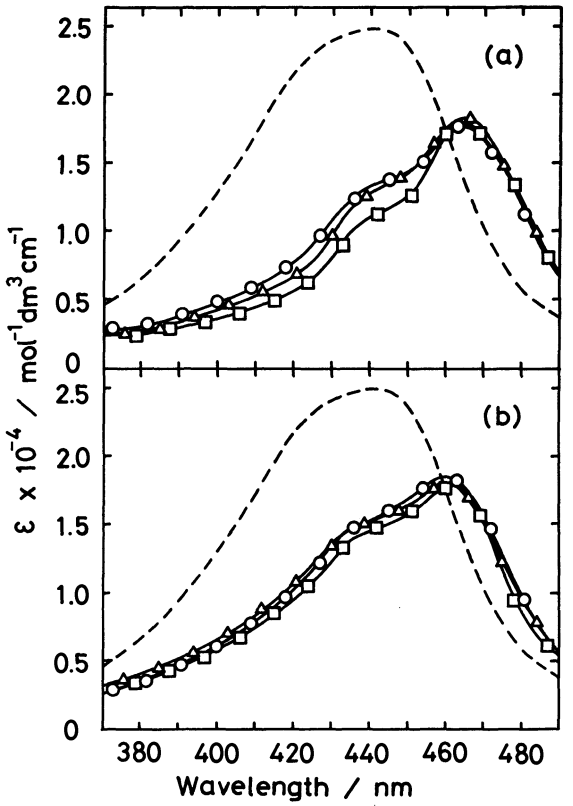

Fig. 3. The pure spectra of AMD bound to nDNA (a) and to dDNA (b). Concentrations of NaCl are 1 mM (○), 100 mM (△), and 500 mM (□). The spectrum of free AMD is shown by the dashed curve for comparison.

and 4; therefore, it may be concluded that the strongly bound AMD almost disappears in the low P/D region and that the dominant species are the weakly bound AMD and the free AMD. The eigenvalues for the AMD–nDNA system at higher ionic strengths (100 and 500 mM NaCl) are shown in Fig. 2(b). The result is the same as in the case of 1 mM NaCl; namely, free AMD and weakly bound AMD are present in the low P/D region.

The eigenvalues for the AMD–dDNA system are shown in Figs. 2(c)—(d). The results are similar to those of the AMD–nDNA system; three light-absorbing components, free AMD and two differently bound AMD, in the wide P/D range 0—30 and two components in the low P/D range 0—4. It is clearly shown that the number of light-absorbing components can be estimated in a straightforward manner by the PCA method without relying on the delicate isosbestic points.

Pure Spectra of AMD Bound to nDNA and dDNA at Various Ionic Strengths. Figure 3(a) shows the pure absorption spectra of AMD, which is weakly bound to nDNA, at three different concentrations of added NaCl. Each bound-AMD spectrum could be extracted by the extended PCA method from a family of observed (five to eight) spectra in the low P/D region 0—4. The binding constant K_a and the parameter a were also determined and are listed in Table 1. Three pure bound-AMD spectra of AMD–nDNA complexes in Fig. 3(a) are nearly identical regardless of the NaCl concen-

Table 1. The apparent binding constants, K_a and K', and the parameter α evaluated by the PCA method

[NaCl] mM	AMD–nDNA			AMD–dDNA		
	α	$K_a\times10^{-3}$	$K'\times10^{-3}$	α	$K_a\times10^{-3}$	$K'\times10^{-3}$
1	1.2	6.0	7.7	1.0	5.3	5.3
100	1.0	4.4	4.4	1.2	6.3	8.2
500	1.1	2.7	3.0	1.1	5.7	6.3

The dimension of K_a is in $(\text{mol/dm}^3)^{-1}$. $K'=K_a([P]/[D]_0)^{\alpha-1}$ and was calculated at $P/D=4$.

trations. This result is surprising in that a five hundred-fold change in ionic strength does not affect the bound-AMD spectrum and, hence, the binding mode. The three bound-AMD spectra all show the absorption maximum at 465 nm and a distinct shoulder at 440—430 nm, being bathochromic and hypochromic relative to the free-AMD spectrum. In addition, the spectral profile is similar to that of the free AMD observed in less polar organic solvents such as benzene and ethanol.[2]

Figure 3(b) shows the pure absorption spectra of AMD, which is weakly bound to dDNA, in the low P/D region at different concentrations of NaCl. Values of K_a and α are given in Table 1. Three bound-AMD spectra at different NaCl concentrations are again almost identical with each other, indicating that nearly the same AMD–dDNA complexes are formed as in the case of the AMD–nDNA system. The bound-AMD spectra of the AMD–dDNA system show both bathochromism and hypochromism relative to the free-AMD spectrum, but the spectral characteristics are less prominent than those of the AMD–nDNA system. Since a bound-AMD molecule would occupy several nucleotide base pairs,[7,9] the difference could be attributed to the presence or absence of the stable double-helical conformation over several base pairs, where the AMD molecule is bound, and also to the extent of the exposure of the AMD-bound site to the environmental water.

The usefulness of the PCA method is clear; a well-defined bound-AMD spectrum (Fig. 3) could be extracted from the broad, nearly featureless experimental spectra of AMD–DNA solutions (Fig. 1). The bound-AMD spectra in Fig. 3 are in excellent accord with the ORD[2] or circular dichroism (CD)[2,12] data previously reported for the AMD–nDNA complex. The CD spectra show three negative bands at 465 nm, 440 nm, and 385 nm in the visible region. The locations of the first two CD bands correspond exactly to the peak and the pronounced shoulder of the bound-AMD absorption spectrum [Fig. 3(a)]. Since the latter reveals a slight hump in the 400—370-nm region, a third, weak-intensity band probably exists there. This absorption band may be related to a large negative CD band at 385 nm. Auer *et al.*[12] have assigned the 465-nm CD band to the quinoid and the 385-nm band to the benzenoid portion of the phenoxazone ring of AMD. We may assign the 440-nm shoulder to a vibrational component of the 465-nm electronic transition on the basis of the spectral profile of the bound-AMD spectrum.

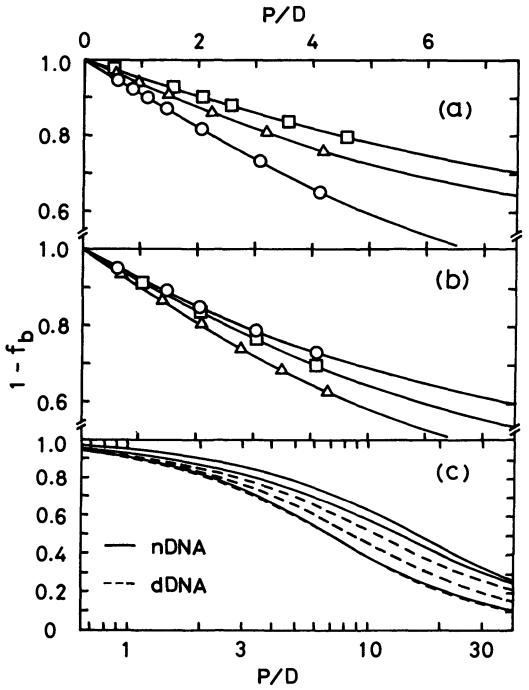

Fig. 4. Fractions of AMD, f_b, bound to nDNA (a) and to dDNA (b) as a function of P/D. Concentrations of NaCl are 1 mM (○), 100 mM (△), and 500 mM (□). Binding curves (solid lines) are expressed in terms of the fraction of the free AMD, $(1-f_b)$. In (c) shown are the curves which are calculated with values of K_a and α over a wider P/D range.

Binding Curves of AMD toward Native and Denatured DNA. Figure 4 shows plots of the mole fraction of free AMD, $(1-f_b)$, against P/D (solid lines).[1] Values of $(1-f_b)$ were calculated with values of K_a and α given in Table 1, and also directly from the **C** matrix by the PCA procedure (symbols).[24-27] Less than 50% of AMD are probably bound to DNA at P/D values 6—15, but more than 90% of AMD may become bound at P/D values >50 for dDNA and >200 for nDNA [Fig. 4(c)], provided that the binding scheme can be described by Eq. 1 throughout the P/D range 0—200. The values of K_a show a trend to decrease with increasing salt concentrations for AMD–nDNA, while they are nearly constant for AMD–dDNA. The small effects of added sodium chloride on K_a and on the bound-AMD spectra (Fig. 3) suggest that the binding mode of AMD toward the DNA site is nonelectrostatic. In the low P/D range, the apparent binding constants, K_a, are in the order of 10^3 for both AMD–nDNA and –dDNA systems (Table 1). In the high P/D range, the values of K_a for the strong binding mode have been reported to be in the order of 10^6 for AMD–DNA.[7,9,10] Thus, it is now clear that the weak binding between AMD and DNA is less by an order of three.

In a number of dye-synthetic polyelectrolyte systems, optical titration curves change sigmoidally in the very low P/D region.[1,24-27] This sigmoidal change has been reproduced well with the adjustable parameter α, if its value is larger than unity.[24,26,27] In the AMD–DNA systems, the fraction of free AMD decreases almost linearly with respect to P/D, as reflected by the values

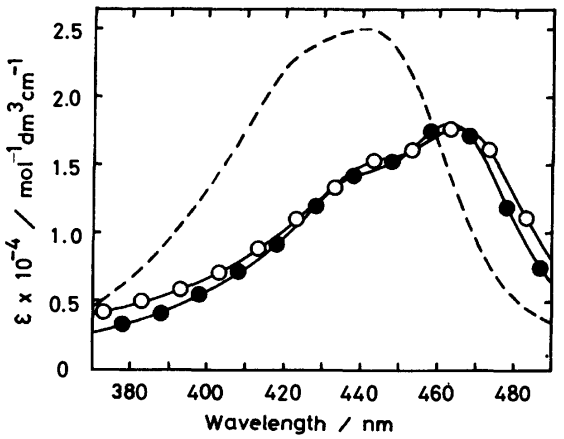

Fig. 5. Mixed-bound spectra of AMD at $P/D=31$ in the presence of 1 mM NaCl. AMD–nDNA (○) and AMD–dDNA (●). The spectrum of free AMD is shown by the dashed curve.

of α which are close to unity (Table 1). It is worth notice that the values of α are also close to unity in other dye–DNA complexes such as crystal violet, trypaflavine, and ethidium bromide.[1,24] This fact supports the use of the commonly postulated binding scheme, *i.e.*, $K'=[DP^*]/[D]\cdot[P]$ $[=K_a([P]/[D]_o)^{\alpha-1}]$, for the binding equilibrium between DNA and small ligands.

Mixed Bound-AMD Spectra in AMD–DNA Systems. At P/D about 30, where both strongly and weakly bound AMD species may coexist (*cf.* Fig. 2), the absorption spectrum of bound AMD results from the mixture of these two bound AMD species. Such a spectrum has been termed the mixed bound-spectrum, expressed with ε_{mix} at a given wavelength,[25] which can be obtained if the equilibrium scheme (Eq. 1) holds for AMD–DNA systems at $P/D \fallingdotseq 30$:

$$\varepsilon_{mix} = \varepsilon_f + (\varepsilon_{obsd}-\varepsilon_f)/f_b, \qquad (2)$$

where ε_f and ε_{obsd} are the molar absorption coefficients of AMD in the free-AMD solution and the AMD–DNA mixture, respectively, and f_b is the mole fraction of bound AMD at a given P/D (*cf.* Fig. 4). Figure 5 shows the mixed bound-AMD spectra for AMD–nDNA and –dDNA complexes at a P/D of 31. These mixed bound-AMD spectra possess the absorption peak and the prominent shoulder almost at the same wavelengths as those of the pure bound-AMD spectra in Fig. 3. Hence, the pure spectrum of the strongly bound AMD in a high P/D range may not differ too markedly from that of the weakly bound AMD in the low P/D range.

Bound-AMD Spectra in the UV Region. Since both AMD and DNA have absorption bands in the ultraviolet region,[2] the AMD–DNA solution also shows a resultant spectrum (Fig. 1). The pure ultraviolet absorption spectrum of weakly bound AMD species, ε_b, can be calculated as

$$\varepsilon_b = \varepsilon_f + (\varepsilon_c-\varepsilon_f)/f_b. \qquad (3)$$

The sum total of the molar absorption coefficients of free and bound AMD, ε_c, is given as

$$\varepsilon_c = (A_{obsd}-A_{DNA})/[D]_o l, \qquad (4)$$

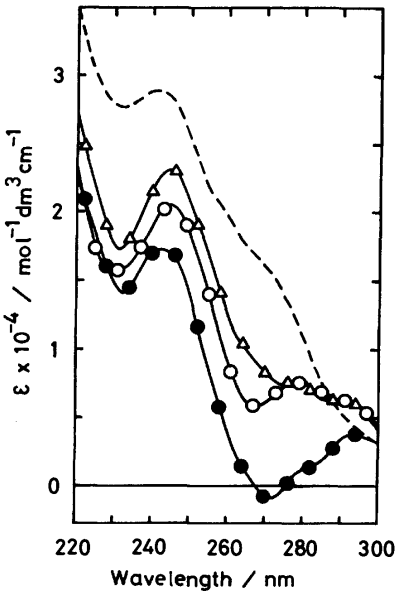

Fig. 6. Pure UV spectra of AMD bound to DNA at 1 mM NaCl calculated from the observed spectra of AMD ($P/D=0$) and of AMD–DNA solutions ($P/D=4.4$), which are shown in Fig. 1. AMD–nDNA (○) and AMD–dDNA (●), both of which were calculated with Eqs. 3 and 4. AMD–dDNA (△) is calculated with Eqs. 3 and 5. The spectrum of free AMD is shown by a dashed curve for comparison.

where l is the optical path length, A_{obsd} is the observed absorbance of the AMD–DNA solution, and A_{DNA} is the absorbance of the DNA component in this solution. For the A_{DNA} of AMD–nDNA solution, the absorbance of nDNA in an AMD-free solution may be assumed (the concentrations of DNA should be the same in the two solutions), considering that the possible conformational change of nDNA by binding of AMD would be small, if any. The procedure, which was utilized for nDNA, was likewise adopted for dDNA of the AMD–dDNA system.

Figure 6 shows the bound-AMD spectra in the ultraviolet region which were calculated on the above assumption. The pure spectrum of AMD bound to nDNA (open circles) seems reasonable, but the pure spectrum of AMD bound to dDNA (closed circles) is unrealistic, because a part of the spectrum has a negative absorbance near 270 nm. This may indicate that the conformation of dDNA in the AMD–dDNA complex (hence, the absorbance of dDNA in Eq. 4) differs from the disordered, single-stranded coil without AMD. Recovery of some kind of partially ordered structure in the AMD–dDNA complex is possible as reported before.[7] If the binding of AMD to dDNA induces an ordered structure, Eq. 4 may be modified as

$$\varepsilon_c = \frac{1}{[D]_o l}\{A_{obsd}-[f_{ord}\cdot A_{ord}+(1-f_{ord})A_{dDNA}]\}, \qquad (5)$$

where f_{ord} and A_{ord} are the fraction and the absorbance of the ordered portion of the dDNA in the AMD–dDNA complex, and A_{dDNA} is the absorbance of dDNA in the absence of AMD.

The pure spectrum of AMD bound to dDNA can be calculated from Eqs. 3 and 5 with appropriate values for f_{ord} and A_{ord}. The ordered structure of dDNA in the AMD-dDNA complex may be approximated as the same as, or close to, the double-helical structure of nDNA. The molar absorption coefficient of the ordered portion of dDNA, ε_{ord}, is then equal to that of nDNA, ε_{nDNA}. The fraction of the ordered structure, f_{ord}, may range between 0 and 1, a unique value being difficult to assign. On the assumption that four nucleotide bases per bound AMD molecule are needed to induce the ordered structure in the AMD–dDNA complex, the following relation may be written as $f_{ord}=4f_b(P/D)^{-1}$; then, $f_{ord}=0.26$ at $P/D=4.4$ ($f_b=0.29$, read from the binding curve in Fig. 4). With these A_{ord} and f_{ord}, the absorbance of the bound AMD in the AMD–dDNA complex was calculated. It now becomes reasonably positive in the 290—260-nm region, as shown in Fig. 6 (open triangles). Although these pure UV spectra of AMD bound to nDNA and dDNA were calculated for the purpose of illustration and can never be claimed unique, they appear to be different from the free-AMD spectrum and hypochromic relative to it.

Conclusion

By using the PCA method, the number of bound AMD species in each of the AMD–nDNA and –dDNA complexes was determined to be one in a low P/D range (0—4) and two in a wide P/D range (0—30). The pure visible absorption spectra of bound AMD were extracted, for the first time, in the weak-binding region. They show a distinct absorption peak at 465 nm (bound to nDNA) and at 460 nm (bound to dDNA) together with a pronounced shoulder near 440 nm. These spectral features are in excellent accord with the measured CD spectra. The variation of the fraction of bound AMD with P/D was calculated from the apparent binding constant K_a which was determined by the extended PCA method. The effect of added sodium chloride on K_a is modest; hence, the binding of AMD to DNA is probably nonelectrostatic. The pure ultraviolet spectrum of AMD bound to dDNA indicates the partial recovery of "nativeness" to the AMD–dDNA conformation. The PCA method is a very useful technique to extract the pure spectra of light-absorbing components from a series of experimentally measured absorption spectra.

References

1) This is Part XI of *Metachromasy*. For the preceding paper of this series, see K. Yamaoka, T. Matsuda, D. Shiba, and M. Takatsuki, *Bull. Chem. Soc. Jpn.*, **55**, 1300 (1982).
2) H. Ziffer, K. Yamaoka, and A. B. Mauger, *Biochemistry*, **7**, 996 (1968).
3) D. M. Crothers, S. L. Sabol, D. I. Ratner, and W. Müller, *Biochemistry*, **7**, 1817 (1968).
4) U. Hollstein, *Chem. Rev.*, **74**, 625 (1974).
5) E. Kahan, F. M. Kahan, and J. Hurwitz, *J. Biol. Chem.*, **238**, 2491 (1963).
6) L. Cavalieri and R. Nemchin, *Biochim. Biophys. Acta*, **87** 641 (1964).
7) M. Gellert, C. E. Smith, D. Neville, and G. Felsenfeld, *J. Mol. Biol.*, **11**, 445 (1965).
8) K. Yamaoka and H. Ziffer, *Biochemistry*, **7**, 1001 (1968).
9) W. Müller and D. M. Crothers, *J. Mol. Biol.*, **35**, 251 (1968).
10) R. D. Wells and J. E. Larson, *J. Mol. Biol.*, **49**, 319 (1970).
11) P. Davanloo and D. M. Crothers, *Biochemistry*, **15**, 5299 (1976).
12) H. E. Auer, B. E. Pawlowski-Konopnicki, and T. R. Krugh, *Biopolymers*, **17**, 1891 (1978).
13) S. C. Jain and H. M. Sobell, *J. Mol. Biol.*, **68**, 1 (1972).
14) H. M. Sobell and S. C. Jain, *J. Mol. Biol.*, **68**, 21 (1972).
15) T. R. Krugh and J. W. Neely, *Biochemistry*, **12**, 1775, (1973).
16) T. R. Krugh and J. W. Neely, *Biochemistry*, **12**, 4418 (1973).
17) D. J. Patel, *Biochemistry*, **13**, 2388 (1974).
18) D. J. Patel, *Biochemistry*, **13**, 2396 (1974).
19) T. R. Krugh and Y.-C. Chen, *Biochemistry*, **14**, 4912 (1975).
20) T. A. Early, D. R. Kearns, J. F. Burd, J. E. Larson, and R. D. Wells, *Biochemistry*, **16**, 541 (1977).
21) T. R. Krugh, E. S. Mooberry, and Y.-C. C. Chiao, *Biochemistry*, **16**, 740 (1977).
22) C. G. Reinhardt and T. R. Krugh, *Biochemistry*, **16**, 2890 (1977).
23) M. Takatsuki and K. Yamaoka, *J. Sci. Hiroshima Univ. Ser. A*, **40**, 387 (1976).
24) K. Yamaoka and M. Takatsuki, *Bull. Chem. Soc. Jpn.*, **51**, 3182 (1978).
25) M. Takatsuki and K. Yamaoka, *Bull. Chem. Soc. Jpn.*, **52**, 1003 (1979).
26) K. Yamaoka and T. Matsuda, *Biophys. Chem.*, **12**, 235 (1980).
27) K. Yamaoka, T. Matsuda, and T. Murakami, *Bull. Chem. Soc. Jpn.*, **54**, 3859 (1981).

Concentration Dependence of the Conversion between the Intermolecular β-Structure and the Disordered State of Poly(*S*-carboxymethyl-L-cysteine) in Aqueous Solutions

Hiroshi MAEDA,* Kaoru SAITO, and Shoichi IKEDA
Department of Chemistry, Faculty of Science, Nagoya University, Chikusa-ku, Nagoya 464
(Received August 21, 1982)

The effects of polymer concentration on the reversible conversion between the intermolecular β-structure and the disordered state of poly(*S*-carboxymethyl-L-cysteine) were examined by means of circular dichroism at constant pHs in 20 mM $NaClO_4$ solutions. The data were tentatively analyzed based on an assumed all-or-none model. A value of −1.1 kJ (−250 cal) per mole of residues was obtained for the standard free energy of association. It was suggested that the obtained results depended significantly on the molecular weight distribution of the used samples.

An important aspect of the β-structure of polypeptides in solution is the problem of whether it is formed by intermolecular association or by chain folding of a single polymer molecule. It is likely that these two types coexist in proportion to their relative stabilities and that other mixed types are also present. Accordingly, assignment of either of the two types can be done only under favorable conditions. Recently, we have shown that fractionated low molecular weight samples of poly(*S*-carboxymethyl-L-cysteine) form the β-structure only by association.[1,2] Further, the conditions for a reversible β-disorder conversion were explored.[2] The stability of the β-structure relative to the disordered state can be thus estimated based on the free energy of association using low molecular weight samples which form the β-structure entirely by association.

In the present study, the concentration dependence of the β-disorder conversion was examined on the same sample as used in the previous study[2] by circular dichroism (CD) in 20 mM $NaClO_4$ solutions at constant pHs: the condition prerequisite to a quantitative analysis.[2] The stability of the intermolecular β-structure was estimated from the concentration dependence based on an assumed type of association.

Another sample of similar molecular weight but significantly different extent of polydispersity was also used to examine the effects of polydispersity on the β-disorder conversion.

Experimental

Two samples (sample code SMA and SMA-2) were prepared from polydisperse low molecular weight samples (A/I=8, 12, and 16) of poly(*S*-carboxymethyl-L-cysteine) by ion-exchange chromatography. The fractionation procedure will be given elsewhere.[3] A sample SMA, used in a previous study,[2] was obtained as a pooled fraction originating from samples A/I=8 and 12, eluted at an ionic strength range 0.59—0.67 M. Another sample SMA-2 was obtained as a fraction originating from sample A/I=16, eluted at an ionic strength range 0.61—0.71 M.

Circular dichroism (CD) was recorded on a Jasco circular dichrograph J-40 A at 25±1 °C using cells of path lengths, 10, 5, 2, 1, 0.5 and 0.2 mm. Measurements of pH were carried out with a Hitachi-Horiba pH meter Model F-7 SS. Light scattering was measured on a Chromatix low angle light-scattering photometer KMX-6 using a 6—7° annulus which collected the scattered light about 4—5° from the cell. The whole assembly was as follows. A Hamilton syringe (5 ml) containing a 3—4 ml solution was connected to a filter holder (Millipore XX30-012-00) by a teflon tubing (ϕ=2 mm). The filter holder equipped with a membrane filter (0.1 μm pore size) (VC WP 01300) was mounted onto the scattering cell. The weight average molecular weight $\overline{M}_w$ was calculated according to the formula

$$\frac{Kc_p}{\Delta R_o} = \overline{M}_w^{-1} + B_2 c_p, \quad (1)$$

here ΔR_o represents the reduced scattering intensity at zero scattering angle (solvent contribution is subtracted), which was approximated by the value at scattering angle of 4—5°. K denotes the optical constant including the refractive index increment $(\partial n/\partial c_p)$. The refractive index increment at a constant salt concentration of 0.2 M NaCl was determined as 0.191 (ml/g) (unpublished results). The concentration c_p was expressed in g/ml referred to sodium salt of the polymer.

Ion-exchange chromatography was carried out on a DEAE-Sephacel (Pharmacia, particle size 40—150 μm) column (ϕ=1.6 cm, l=90 cm) at 25±0.5 °C. Gel permeation chromatography was carried out on a Sephadex G-75 column (ϕ=1.5 cm, l=85 cm) at 25±2 °C. In both chromatographic runs, the effluent was monitored by ultraviolet absorption at 220—235 nm (depending on the applied amount) on a Shimadzu UV-200 S spectrophotometer using a flow cell of 1 cm light path.

Polymer concentration is expressed in residue molarity C_p(N) and 20 mM (1 M=1 mol dm^{-3}) $NaClO_4$ solutions were used as a solvent throughout, unless otherwise stated. Solutions were mostly prepared from the solutions of neutral pH by the addition of HCl. Sometimes, solutions were prepared by dilution. In this case pH changed on dilution and the pH was readjusted to the same value as that before dilution.

Results

Molecular Weight Distributions of Samples. The results of the light scattering measurements on two samples SMA and SMA-2 in their fully charged state in 0.2 M NaCl solutions are given in Fig. 1. Molecular weights and the degrees of polymerization (DP) (in parentheses) were calculated as $(3.1\pm0.2)\times10^3$ (17 ± 1) and $(3.7\pm0.2)\times10^3$ (20 ± 1) for sample SMA and SMA-2, respectively. These values will be increased slightly if the effect of dialysis on the value of the refractive index increment is taken into consideration. Ion-exchange chromatography on DEAE-cellulose and

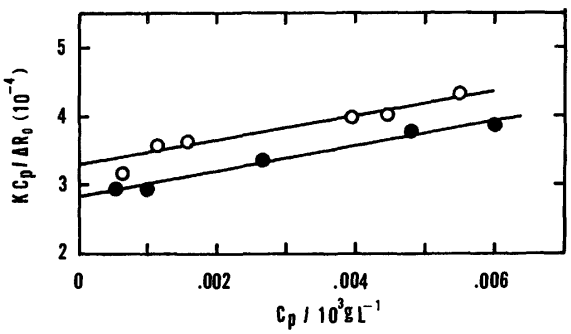

Fig. 1. Light scattering data for sample SMA(○) and SMA-2(●) at pH 7 in 0.2 M NaCl solutions.

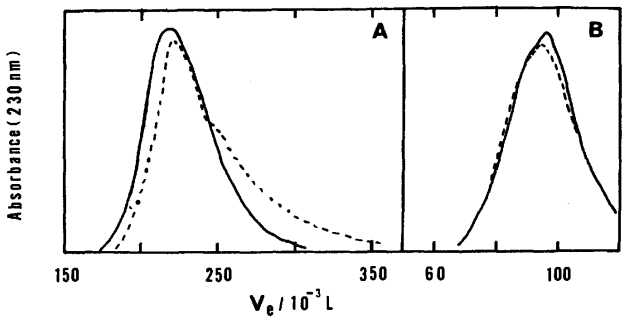

Fig. 2. Elution patterns on a DEAE-cellulose column (A) and sephadex G-75 (B) at pH 7.4. Samples: SMA (——), SMA-2(·····). Ionic strengths: (A) 0.56 M, (B) 0.20 M.

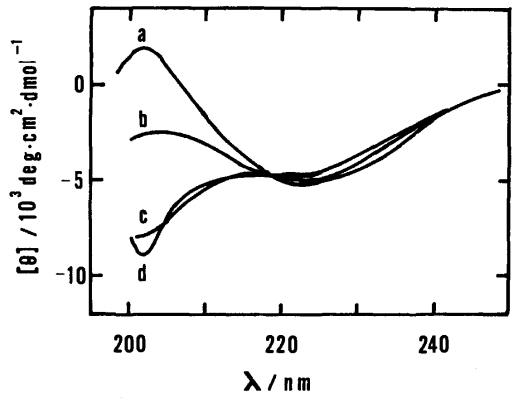

Fig. 3. CD spectra at pH 3.45 in 20 mM $NaClO_4$ solutions. Sample SMA. Concentrations (10^{-4} N): (a) 20, (b) 6.0, (c) 1.5, and (d) 0.50.

gel permeation chromatography on Sephadex G-75 were carried out on these two samples to examine the difference in their molecular weights more closely, although these measurements provide rather qualitative information. In Fig. 2(A), the elution patterns on a DEAE-cellulose column at an ionic strength of 0.56 M (0.55 M NaCl+phosphate buffer pH 7.4) are shown for the two samples. The peak position of sample SMA-2 is slightly shifted toward higher molecular weights as compared with that of sample SMA. A shoulder near V_e=250 ml is significant in the case of sample SMA-2.

As shown in Fig. 2(A), the main components constituting these two samples have nearly identical molecular weights but a considerable fraction of longer chains is

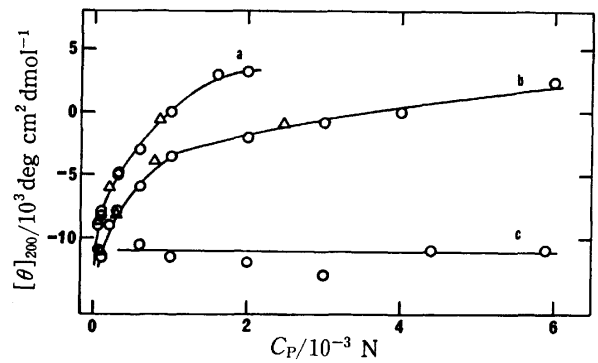

Fig.4. Concentration dependence of the residue ellipticity at 200 nm $[\theta]_{200}$ at constant pH. Sample SMA. pH: (a) 3.30±0.05 (●) and 3.45±0.05 (open symbols) in 20 mM $NaClO_4$, (b) 3.60 in 20 mM $NaClO_4$, and (c) 4.00±0.08 in 10 mM acetate buffer. Triangles refer to the solutions prepared by dilution from the solution of the highest concentration at a given pH.

contained in sample SMA-2. In Fig. 2(B) the elution patterns of the two samples in 0.2 M NaCl solutions on a Sephadex G-75 column are given. The peak positions are V_e=95.4 ml and 94.3 ml for samples SMA and SMA-2, respectively. The distribution shifts only slightly toward higher molecular weights for sample SMA-2 compared to sample SMA. All these three independent measurements, light scattering, ion-exchange chromatography, and gel permeation chromatofraphy, gave consistent results.

Concentration Dependent Conversion at Constant pHs.

In Fig. 3, selected CD spectra of sample SMA at a constant pH of 3.45 in 20 mM $NaClO_4$ solutions are shown for different concentrations. An isodichroic point near 218 nm exists at all concentrations examined at pH 3.45 as well as at pH 3.30 and 3.60 (not shown). The presence of an isodichroic point suggests that charges of each polymeric species are kept constant irrespective of the polymer concentration. This result contrasts with that obtained in the previous study where dilution at a constant degree of neutralization caused enhanced ionization at extremely low concentrations.[2] Further, the p.esence of an isodichroic point shows that the stacking of the pleated sheets does not occur appreciably.[4]

In Fig. 4, the residue ellipticities at 200 nm, $[\theta]_{200}$, are shown at three different pHs, 3.30, 3.45, and 3.60, as functions of the polymer concentration. The variation of pH was within 0.05 in every case. In Fig. 4 the data obtained in 10 mM acetate buffer (pH=4.00±0.08) are also shown. Reversible conversion is shown both at pH 3.45 and 3.60, as expected from the results of the previous study.[2] Further, in 20 mM $NaClO_4$ solutions it was shown that electrostatic interaction among polyion species was negligible due to shielding effect.[2] Accordingly, the concentration dependent conversion shown in Fig. 4 deserves quantitative analyses to estimate the free energy of association, which in turn can be related to the stability of the intermolecular β-structure.

As seen in Fig. 4, the β-structure is favored at lower pHs if compared at a constant concentration. At the

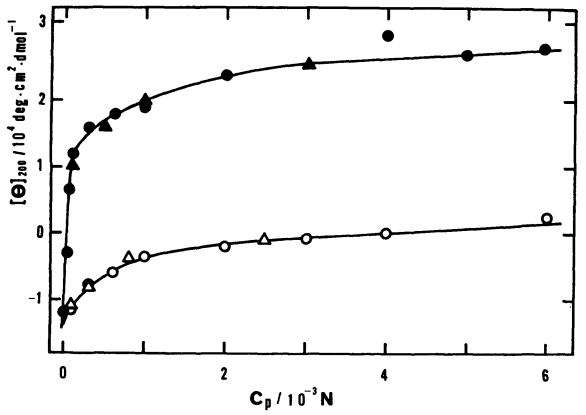

Fig. 5. Concentration dependence of the residue ellipticity at 200 nm at pH 3.60 for two samples. Samples: SMA (open symbols) and SMA-2 (filled symbols). Triangles have the same mening as in Fig. 4.

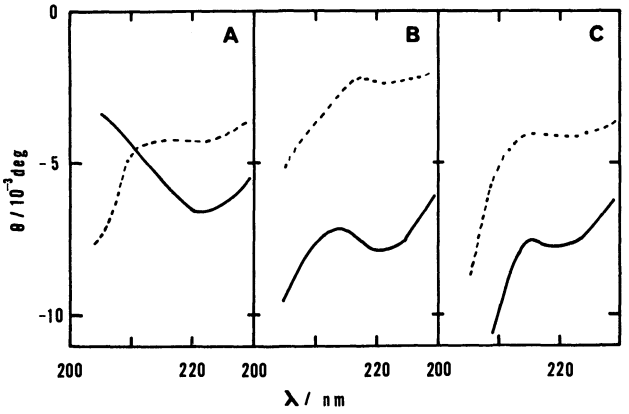

Fig. 6. CD spectra of the solutions at low pHs in 20 mM $NaClO_4$ before and after filtration by membrane filter. Sample: SMA. Solid curves: solutions before filtration Dotted curves: solutions after filtration. Ordinate gives the ellipticity. (A) Initial concentration 5.0×10^{-4} N, pH 3.45, cell length 5 mm. (B) Initial concentration 1.5×10^{-4} N, pH 3.45, cell length 1 cm. (C) Initial concentration 1.5×10^{-4} N, pH 3.60. cell length 1 cm.

same time, solubility decreases from about 6×10^{-3} N at pH 3.60 to about 2×10^{-3} N at pH 3.45 and 3—5×10^{-4} N at pH 3.30. It is to be noted that in Fig. 4 the data obtained at pH 3.30 and at 3.45 are identical within experimental error. This coincidence indicates that the effects of electrostatic interactions on the conversion can be approximately neglected at these pHs, although solubility still depends on the value of pH. On the other hand, it is necessary to separate the electrostatic contribution from the data at pH 3.60 in order to obtain the nonelectric interactions responsible for the β-formation.

The concentration dependent conversion at pH 3.60 was examined for two samples of slightly different molecular weights, SMA and SMA-2. A large difference was found between these two samples as is shown in Fig. 5. As shown in Fig. 2(A), sample SMA-2 contains longer chains much more than sample SMA. These components can form the intermolecular β-structure not only with themselves but also with shorter chains. In other words, the association occurs among chains of different lengths and long chain components act as nuclei for short chain components. This result suggests that the conversion is sensitive to the molecular weight distribution of used samples. From these results, we have to conclude that the extent of the polydispersity of sample SMA-2 is too broad to allow an evaluation of the type of assocation as well as an exact free energy change. It is also uncertain whether the molecular weight distribution of sample SMA is narrow enough for these evaluations.

The light scattering measurements were also carried out on the solutions of sample SMA at low pHs, 3.60 and 3.45, in order to evaluate the aggregation numbers However, a considerable decrease of the polymer concentration was found after solutions were passed through the measuring assembly.

In Fig. 6(A) results obtained for the solution (pH= 3.45, $C_p=5.0\times10^{-4}$ N) are shown. After filtration, the CD spectra (a dashed curve) show a disordered state. while the CD spectra of the solution before filtration show the presence of the β-structure. This kind of change was thought due to the presence of large aggreates which were filtered off. Such an interpretation has been widely accepted since the report of Li and Spector on poly(L-lysine).[5] However, in the present samples, we can prepare non-charged polymer in disordered state and hence we can examine the effects of charge density independently of the aggregation. Such examination cannot be carried out for long chain polymers. At the polymer concentration of 1.5×10^{-4} N most of the polymers are in disordered state at pH 3.45, as easily confirmed from Fig. 4. The decrease of concentration was even pronounced for this solution (pH= 3.45, $C_p=1.5\times10^{-4}$ N) as shown in Fig. 6(B). It is now clear that the decrease of polymer concentration in the present case is a direct consequence of low charge densities rather than due to the presence of large aggregates. From the data of Figs. 6(A) and (B), we calculated the final concentrations as 3.6×10^{-4} N and 4.4×10^{-5} N, respectively. Accordingly, the extent of the concentration decrease became relatively small as the initial concentration increased. In Fig. 6(c), the results on the solution (pH=3.60, $C_p=1.5\times10^{-4}$ N) are shown. The final concentration was 8.1×10^{-5} N. When the results in Figs. 6(B) and (C) are compared, the concentration decrease becomes considerably small as pH increases from 3.45 to 3.60. At neutral pH, the light scattering measurements can be performed without trouble as revealed in Fig. 1.

A Simple Analysis of the Concentration Dependence of the CD Data. A simple analysis of the CD data given in Fig. 4 is considered in the present section. These data give the first example for the conversion between the intermolecular β-structure and the disordered state in aqueous solutions.

We consider mainly the data of sample SMA at pH 3.30 and 3.45, which can be approximated to the conversion of noncharged polymers. For the growth of the pleated sheets consisted of noncharged polypeptides, it is a reasonable assumption that the association takes place with a single association constant K

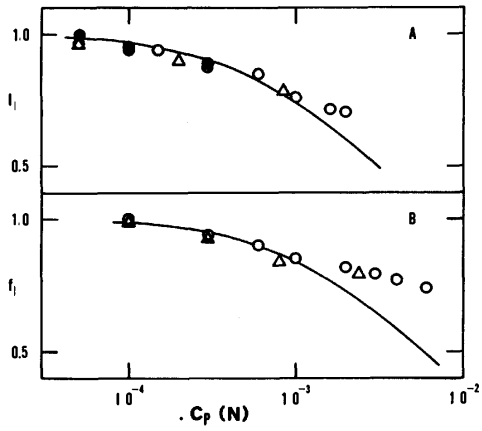

Fig. 7. Fraction of unassociated polymer f_1 as functions of polypeptide concentration C_p at constant pHs in $NaClO_4$ solutions. Sampe: SMA. pH: (A) 3.30(●) and 3.45 (open symbols) and (B) 3.60. Triangles have the same meaning as in Fig. 4. Solid curves are drawn according to Eq. 3 for $K=1.82\times10^2$ N^{-1} (A) and 1.00×10^2 N^{-1} (B).

for any successive addition except dimerization.

$$A_{i-1} + A \overset{K}{=} A_i \qquad (i \geqq 3)$$
$$2A \overset{K^2}{=} A_2 \qquad (i = 2) \qquad (2)$$

The dimerization constant is here approximated as K^2, neglecting the additional contribution for dimerization Then, the fraction f_1 of unassociated polymer is given as follows.[6]

$$KC_p = KC_pf_1 + (KC_p)^2f_1^2(2-KC_pf_1)(1-KC_pf_1)^{-2} \qquad (3)$$

Accordingly, if f_1 is observed as a function of C_p, then we can find a value of K from the concentration C_p^* which satisfies a relation $KC_p^*=1$. At $C_p=C_p^*$, $f_1=(3-5^{1/2})/2$.

With the assumption that all aggregates are in register, we can put $f_1=f_c$, where f_c denotes the fraction of residues in the disordered state. This all-or-none model represents one of the simplest pictures of the pleated sheet proposed by Pauling and Corey.[7] The fraction f_c can be calculated as follows from the CD data.

$$f_1 = f_c = \frac{3.8\times10^4 - [\theta]_{200}}{4.9\times10^4} \qquad (4)$$

Here 3.8×10^4 stands for the residue ellipticity of the β-structure at 200 nm. This value was chosen when available data on the β-structure of the pesent polypeptide were taken into consideration.[1,2,4,8] The residue ellipticity for the disordered state at 200 nm for this pH range (3.30—3.45) was chosen as -1.1×10^4, as shown in Figs. 4 and 5. Accordingly, the figure 4.9×10^4 represents the difference in the residue ellipticity at 200 nm between the β-structure and the disordered state.

In Fig. 7(A), f_1 is plotted against log C_p for the data at pH 3.45, (open symbols) and pH 3.30 (closed symbols). The solid line is drawn assuming that K is 1.82×10^2 N^{-1}. The fit is rather satisfactory. If we take the degree of polymerizationas 20, then K is 3.6×10^3 M^{-1}. The corresponding standard free energy change per polymer ΔG° and that per residue ΔG°(res) are:

$$\Delta G^\circ = -RT\ln K = -20.5 \text{ kJ/mol}$$
$$(-4.9\times10^3 \text{ cal/mol})$$
$$\Delta G^\circ(\text{res}) = \Delta G^\circ/20 = -1.05 \text{ kJ/mol}$$
$$(-2.5\times10^2 \text{ cal/mol}).$$

It is to be noted that the value of ΔG° depends on the concentration unit employed.

In Fig. 7(B) the data at pH 3.60 are analyzed similarly. Deviation from the assumed model is pronounced. This is reasonable, since electrostatic energy of the aggregate cannot be expected to increase linearly with its aggregation number. In other words, the "isodesmic" model is a poor approximation for the aggregation of charged particles.

In the previous study,[2] the converion was examined at a constant degree of neutralization α' rather than at a constant pH. When these data were analysed in the same way, they gave a good fit as shown in Fig. 8. At present, it is not certain whether the good fit is only incidental or not. For the assumed degree of polymerization of 20, the obtained values of $K(10^3$ $M^{-1})$ were 3.8, 3.2, and 2.2 for $\alpha'=0$, 0.15 and 0.25, respectively.

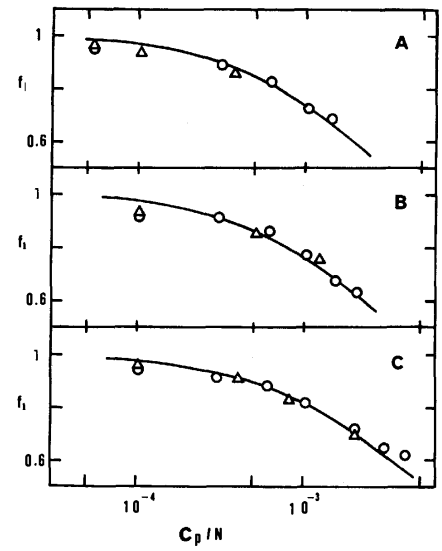

Fig. 8. Fraction of unassociated polymer f_1 as functions of polypeptide concentration C_p at constant degrees of neutralization in 20 mM $NaClO_4$ solutions. Sample SMA. Degrees of neutralization: (A) 0, (B) 0.15, and (C) 0.25. Triangles have the same meaning as in Fig. 4. Solid curves are drawn according to Eq. 3 for $K=1.92\times10^2$ N^{-1} (A), 1.67×10^2 N^{-1} (B), and 1.11×10^2 N^{-1} (C).

Discussion

The non-electrostatic free energy difference between the β-structure and random coils has been estimated from potentiometric titrations of ionizable polypeptides.[9-11] Reported values (per mole of residue) are: −1.25 kJ (−300 cal) for poly(L-tyrosine),[9] −590 J (−140 cal) for poly(L-lysine),[10] and −3.09 kJ (−740 cal) and −4.10 kJ (−980 cal) for poly(*S*-carboxymeth-

yl-L-cysteine) and poly(*S*-carboxyethyl-L-cysteine).[11] In most cases, however, the free energy change evaluated from the potentiometric titrations includes the contributions from various processes; chain folding and aggregation occur often simultaneously and stacking of the pleated sheets occurs as the amount of the β-structure increases. Accordingly, the free energy change cannot be identified with the standard free energy change of any single process, unless the conversion is confirmed to occur as the chain folding process in the absence of aggregation or as the intermolecular association without chain folding process. Plausible but indirect arguments for the absence of aggregation have been provided only for the case of poly(L-tyrosine)[9,12] and poly(*S*-carboxymethyl-L-cysteine).[1]

The stability of the β-structure can be best evaluated if the equilibrium constant for a unimolecular transconformation is obtained in the absence of aggregation. However, this has not been done until now.

In the present study, a value of about -1.1 kJ (-350 cal) was obtained as the standard free energy of association. With this value alone, it is difficult to separate the contribution of a propagation step (or equivalently the formation of a number of hydrogen bonds between peptide groups) from that of an association step. However, when the standard free energies of association are obtained with other samples of different chain lengths, the contributions from the two steps can be separated.

In the case of the intermolecular β-structure, the type of association has to be determined in order to define proper equilibrium constants. It is necessary, therefore to measure average aggregation number in addition to the weight fraction of the residues in the β-structure. Nevertheless, the study of the intermolecular β-structure seems promising for the evaluation of the stability of the β-structure, in contrast to the difficulties to avoid aggregation in the study of the intramolecular β-structure.

References

1) H. Maeda, K. Kadono, and S. Ikeda, *Macromolecules*, **15**, 822 (1982).
2) K. Saito, H. Maeda, and S. Ikeda, *Biophys. Chem.*, **16**, 67 (1982).
3) H. Maeda, T. Ito, H. Suzuki, S. Hirata, I. Kako, M. Yoshino, and S. Ikeda, *Biopolymers*, submitted; *Polym. Prepr. Jpn.*, **31**, 2217 (1982).
4) K. Ooi and H. Maeda, *Biopolymers*, **20**, 1549 (1981).
5) L.-K. Li and A. Spector, *J. Am. Chem. Soc.* **91**, 220 (1969).
6) J. Engel and D. Winklmair, "Protein-Protein Interactions," Springer, Berlin-Heidelberg (1972), pp. 159—181.
7) L. Pauling and R. B. Corey, *Proc. Natl. Acad. Sci. U. S. A.*, **37**, 729 (1951); **39**, 253 (1953).
8) S. Ikeda, A. Fukutome, T. Imae, and T. Yoshida, *Biopolymers*, **18**, 335 (1979).
9) R. P. McKnight and H. E. Auer, *Macromolecules*, **9**, 939 (1976).
10) D. Pederson, D. Gabriel, and J. Hermans, Jr., *Biopolymers*, **10**, 2133 (1971).
11) H. Maeda and S. Ikeda, *Biopolymers*, **14**, 1623 (1975).
12) E. Patton and H. E. Auer, *Biopolymers*, **14**, 849 (1975).

 © 1983 The Chemical Society of Japan Bull. Chem. Soc. Jpn., 56, 607—613 (1983)

Magnetic-superexchange Interactions of Uranium(IV) Chloride-addition Complexes with Amides. I

Chie Miyake,* Yukio Hinatsu, and Shosuke Imoto
Department of Nuclear Engineering, Faculty of Engineering, Osaka University, Suita, Osaka 565
(Received December 7, 1981)

Studies of magnetic susceptibility, χ, from 300 to 2 K on seventeen UCl_4–amide complexes showed that six complexes had maxima in χ between 155 and 82 K. This unusual magnetic behavior occurred only with *N*-methyl or ethyl-substituted amide complexes. Infrared and chemical evidence indicates that these six complexes probably have dimeric structure, in which two U(IV) ions are bridged by the amide ligands. Assuming a dimer structure and a two-spin Heisenberg model with $-2J_{ex}$ of about 90 cm^{-1} for the dimer, the magnetic susceptibilities for the six complexes were calculated in good agreement with the experimental results in the temperature region of the maxima in χ.

Magnetic-exchange interactions at low temperatures in polynuclear complexes of transition metals, especially of dimeric copper(II) complexes, have been extensively studied for thirty years.[1] Similar magnetic behavior of complexes of actinoid ions has been reported previously. Tetrakis(diethylamido)uranium(IV)[2] and tris[bis-(*N*,*N*′-dimethylethylenediamido)]uranium(IV)[3] have dimer and trimer structures respectively, as determined by X-ray-diffraction analysis. In these complexes, magnetic-exchange interactions might be expected to occur, but their magnetic susceptibility increases down to the temperature of liquid helium without showing any magnetic susceptibility maxima. Recently, the superexchange phenomena have been first observed by us on uranium(IV) chloride-addition complexes with amides.[4]

This paper will report on the temperature-dependent magnetic susceptibilities of uranium(IV) chloride-addition complexes with seventeen amide molecules, among which six complexes showed a maximum in their magnetic susceptibility-*versus*-temperature curves that indicates intradimer superexchange interaction. Some results of the infrared-absorption measurements are reported.

Experimental

Table 1 lists the full names of the complexes studied, the abbreviated formula, and the substituents on the carbon and nitrogen atoms of each amide.

Materials. Reagent-grade amides were used as purchased without any further purification. The anhydrous uranium tetrachloride was synthesized by the solid-vapor-phase reaction of uranium dioxide and carbon tetrachloride at 500 °C.[5] The cesium hexachlorouranate was obtained as a crystalline powder by dissolving cesium chloride in a hydrochloric acid solution of uranium tetrachloride and by then slowly evaporating the water.[6]

Preparation of Complexes. *UCl_4·2.5DEA*: A five-fold excess of diethylacetamide was added to a hot acetone solution of Cs_2UCl_6, thus precipitating cesium chloride. After filtering the precipitates, the oily product was obtained by adding isopentane to the filtrate. The oil was dissolved in hot acetone and then precipitated again with isopentane. After several repetitions of this procedure, a green solid was obtained: it was

Table 1. Formulae for uranium (IV) chloride–amide complexes

Complex	Abbreviation of complex	Substituents[a]		
		R_I	R_{II}	R_{III}
Uranium(IV)chloride–*N*,*N*-Dimethylacetamide (1/2.5)	UCl_4·2.5 DMA	CH_3	CH_3	CH_3
Uranium(IV)chloride–*N*,*N*-Diethylacetamide (1/2.5)	UCl_4·2.5 DEA	CH_3	C_2H_5	C_2H_5
Uranium(IV)chloride–*N*,*N*-dimethylformamide (1/2.5)	UCl_4·2.5 DMF	H	CH_3	CH_3
Uranium(IV)chloride–*N*,*N*-Dimethylbenzamide (1/3)	UCl_4·3 DMBA	Ph	CH_3	CH_3
Uranium(IV)chloride–*N*-Methylacetanilide (1/3)	UCl_4·3 MAA	CH_3	CH_3	Ph
Uranium(IV)chloride–*N*,*N*-Diphenylacetamide (1/3)	UCl_4·3 DPA	CH_3	Ph	Ph
Uranium(IV)chloride–*N*-Methylformanilide (1/3)	UCl_4·3 MFA	H	CH_3	Ph
Uranium(IV)chloride–Benzamide (1/4)	UCl_4·4 BAM	Ph	H	H
Uranium(IV)chloride–Benzanilide (1/4)	UCl_4·4 BAN	Ph	Ph	H
Uranium(IV)chloride–Acetanilide (1/4)	UCl_4·4 AAN	CH_3	Ph	H
Uranium(IV)chloride–*N*,*N*-Diphenylformamide (1/4)	UCl_4·4 DPF	H	Ph	Ph
Uranium(IV)chloride–*N*-Methylacetamide (1/4)	UCl_4·4 MA	CH_3	CH_3	H
Uranium(IV)chloride–*N*-Ethylacetamide (1/4)	UCl_4·4 EA	CH_3	C_2H_5	H
Uranium(IV)chloride–*N*-Methylformamide (1/4)	UCl_4·4 MF	H	CH_3	H
Uranium(IV)chloride–Acetamide (1/6)	UCl_4·6 AA	CH_3	H	H
Uranium(IV)chloride–Acrylamide (1/6)	UCl_4·6 AcA	CH_2CH	H	H
Uranium(IV)iodidedichloride–*N*,*N*-Dimethylacetamide (1/5)	UI_2Cl_2·5 DMA	CH_3	CH_3	CH_3

a) $R_I-C(=O)-N<^{R_{II}}_{R_{III}}$

TABLE 2. ELEMENTAL ANALYSES

Complex	C(%)		H(%)		N(%)		Cl(%)		U(%)	
	Found	Calcd	Found	Calcd	Found	Calcd	Found	Calcd	Found	Calcd
UCl_4·2.5DMA	20.04	20.09	4.11	3.77	5.76	5.86	23.18	23.74	40 01	39 85
UCl_4·2.5DEA	26.32	26.97	4.72	4.87	5.50	5.25	20.98	21.25	36.67	35.67
UCl_4·2.5DMF	16.50	16.01	3.23	3.11	6.36	6.22	25.02	25.22	40 62	42 33
UCl_4·3DMBA	37.21	39.19	3.86	3.99	4.98	5.08	18.55	17.15	28.59	28.79
UCl_4·3MAA	38.51	39.18	4.14	3.99	4.48	5.08	17 60	17.17	30 00	28.78
UCl_4·3DPA	50.06	49.76	3.79	3.85	3.81	4.15	14 07	14 00	24 37	23 50
UCl_4·3MFA	35.93	37.00	3.42	3.44	5.44	5.35	18.31	18 07	30 96	30.33
UCl_4·4BAM	37.61	38.90	3.37	3.24	6.61	6.48	17.72	16 42	28 02	27 55
UCl_4·4BAN	53.79	53.43	3.61	3.77	4.69	4.80	13.01	12.14	18.90	20.38
UCl_4·4AAN	41.41	41.75	3.80	3.91	6.11	6.09	15.71	15.42	25.60	25.88
UCl_4·4DPF	53.08	53.43	3.65	3.77	4.69	4.80	12.06	12.14	18.92	20.38
UCl_4·4MA	21.30	21.43	4.11	4.17	8.30	8.34	20.79	21.11	35.04	35.43
UCl_4·4EA	25.26	26.38	4.60	4.95	7.44	7.69	19.00	19.48	33.75	32.70
UCl_4·4MF	15.47	15.59	3.11	3.25	8.88	9.09	22.88	23.03	40.19	38.65
UCl_4·6AA	19.96	19.62	3.82	4.09	11.33	11.45	19.03	19.32	32.61	32.43
UCl_4·6AcA	27.64	26.81	3.72	3.73	10.57	10.42	17.74	17.60	28.54	29.54
UI_2Cl_2·5DMA	23.72	24.06	4.38	4.51	6.89	7.02	32.15 (Cl+I)	32.55	23.05	23.85

dried over P_2O_5.

UCl_4·3DPA: Oily solids were obtained from an acetone solution of anhydrous uranium tetrachloride by adding, successively, a dichloromethane solution of the ligand and then petroleum ether. The precipitates were dried under a vacuum.

UCl_4·3MFA and UCl_4·4BAN: Oily solids were obtained from acetone solutions of anhydrous uranium tetrachloride by adding an acetone solution of the ligand. Then the precipitates were dried under a vacuum.

UCl_4·4BAM: Oily solids were precipitated from an acetone solution of anhydrous uranium tetrachloride by adding, successively, a small excess of benzamide in the acetone solution and then petroleum ether. The product was dried under a vacuum and stored in a vessel with P_2O_5.

UCl_4·4AAN: An excess of an acetone solution of acetanilide was added to the acetone solution of uranium tetrachloride, and the product was precipitated by adding isopentane. The precipitates were dried under a vacuum.

UCl_4·4MF: Precipitates were obtained from an ethyl acetate solution of anhydrous uranium tetrachloride by adding an ethyl acetate solution of the ligand. After washing with ethyl acetate, the precipitates were dried in a vacuum.

UCl_4·6AcA: An acetone solution of the ligand and then isopentane was added to an acetone solution of anhydrous uranium tetrachloride to precipitate the product. The precipitates were dried in a vacuum.

UCl_4·2.5DMA,[7] UCl_4·2.5DMF,[8] UCl_4·3DMBA,[9] UCl_4·3MAA,[9] UCl_4·4DPF,[9] UCl_4·4MA,[10] UCl_4·4EA,[11] UCl_4·6AA,[7] and UI_2Cl_2·5DMA[12] were synthesized according to the methods previously reported.

Chemical Analysis. The uranium content was determined gravimetrically by the ammonium method,[13] while the chlorine content was determined by potentiometric titration with a standard $AgNO_3$ solution. The carbon, hydrogen, and nitrogen contents were determined with the Yanagimoto CHN coder, MT-2. The results of elemental analyses are listed in Table 2.

Magnetic Measurement. The magnetic susceptibilities were measured with a torsion balance from room temperature down to 2 K, using powdered $Co[Hg(SCN)_4]$ as a standard[14] and with $\chi_g = 16.44 \times 10^{-6}$ emu g^{-1} (emu $g^{-1} \times 4\pi 10^{-3} \rightarrow m^3$ kg^{-1}) at 20 °C. The temperature was measured with a Au-Co/Cu thermocouple for the range from room termperature to 20 K and with a carbon resistor below 32 K. To test for ferromagnetic impurities in the samples, the dependence of the magnetic susceptibility on the magnetic field was measured at 400, 1470, 3320, 5400, and 7200 Oersted at room temperature, 77 and 4.2 K.

TABLE 3. DIAMAGNETIC SUSCEPTIBILITY CORRECTIONS

Complex	$\chi_{dia} \times 10^6$/emu
UCl_4·2.5DMA	−275.0
UCl_4·2.5DEA	−334.3
UCl_4·2.5DMF	−245.3
UCl_4·3DBMA	−416.8
UCl_4·3MAA	−416.8
UCl_4·3DPA	−530.6
UCl_4·3MFA	−372.7
UCl_4·4BAM	−421.6
UCl_4·4BAN	−618.3
UCl_4·4AAN	−469.1
UCl_4·4DPF	−639.8
UCl_4·4MA	−303.6
UCl_4·4EA	−353.5
UCl_4·4MF	−258.6
UCl_4·6AA	−325.3
UCl_4·6AcA	−349.1
UI_2Cl_2·5DMA	−479.2

(emu $mol^{-1} \times 4\pi \times 10^{-6} \rightarrow m^3 \times mol^{-1}$)

Table 3 lists the values of the diamagnetic-susceptibility correction used in calculating the paramagnetic susceptibility of complexes from the experimentally measured values.[15]

Infrared Absorption. The infrared-absorption spectra were recorded on HITACHI-225 Spectrophotometer using a prism disk of KRS-5 (TlBr-TlI), either as neat compounds or as Nujol mulls. The spectra were also measured in 0.1% CCl_4 solution, if required.

Results and Discussion

Figure 1 shows the magnetic susceptibility *versus*

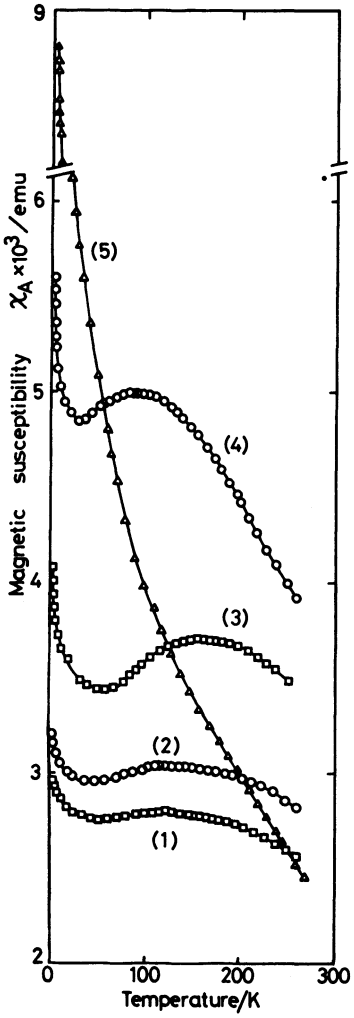

Fig. 1. Temperature dependence of magnetic susceptibility per gram atom.
(1): $UCl_4 \cdot 2.5DMA$, (2): $UCl_4 \cdot 2.5DEA$, (3): $UCl_4 \cdot 4MA$, (4): $UCl_4 \cdot 4EA$, (5): $UCl_4 \cdot 3DPA$. (emu $mol^{-1} \times 4\pi \times 10^{-6} \rightarrow m^3\ mol^{-1}$).

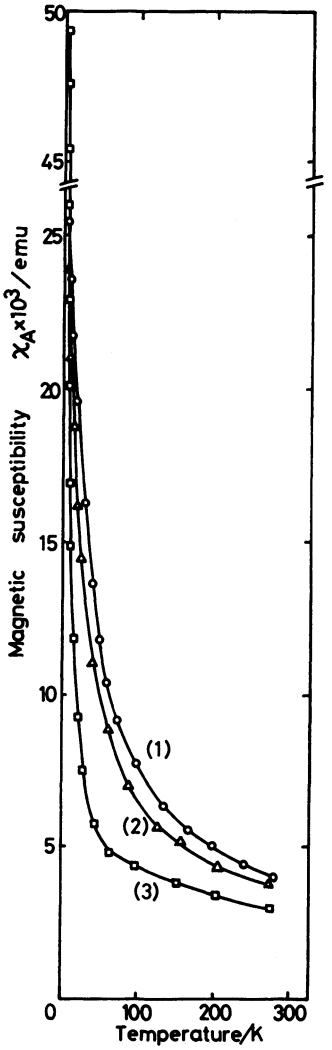

Fig. 2. Temperature dependence of magnetic susceptibility per gram atom.
(1): $UCl_4 \cdot 6AcA$, (2): $UCl_4 \cdot 6AA$, (3): $UI_2Cl_2 \cdot 5DMA$.

temperature curves for $UCl_4 \cdot 2.5DMA$, $UCl_4 \cdot 2.5DEA$, $UCl_4 \cdot 4MA$, $UCl_4 \cdot 4EA$, and $UCl_4 \cdot 3DPA$. Figure 2 also shows the magnetic susceptibility *versus* temperature curves for $UCl_4 \cdot 6AcA$, $UCl_4 \cdot 6AA$, and $UI_2Cl_2 \cdot 5DMA$. Figure 3 presents the magnetic susceptibility *versus* temperature curves for $UCl_4 \cdot 3DMBA$, $UCl_4 \cdot 3MAA$, $UCl_4 \cdot 4BAN$, $UCl_4 \cdot 4BAM$, and $UCl_4 \cdot 4AAN$. As may be seen from Fig. 1, broad but clearly distinguishable maxima appear at 121.8, 112.0, 155.1, and 81.8 K for $UCl_4 \cdot 2.5DMA$, $UCl_4 \cdot 2.5DEA$, $UCl_4 \cdot 4MA$, and $UCl_4 \cdot 4EA$ respectively, while for $UCl_4 \cdot 3DMBA$ and $UCl_4 \cdot 3MAA$ of Fig. 3, the maxima appear at 134.2 and 142.0 K respectively. For the other eleven complexes, the magnetic susceptibilities monotonically ncrease down to the temperature of liquid helium (see also Fig. 6). The magnetic-susceptibility maxima shown in Figs. 1 and 3 have not previously been observed for uranium(IV) complexes and can not be explained by the usual concept of paramagnetic susceptibility. As has previously been reported,[4] magnetic-exchange interaction is believed to occur between uranium ions in these complexes. The additional maximum at a temperature lower than the 134.2 K of the curve of $UCl_4 \cdot 3DMBA$ in Fig. 3 might be due to the existence of another kind of magnetic-exchange interaction between uranium ions. According to Bagnall *et al.*, the series of *N,N*-dimethylacetamide addition complexes of uranium(IV) are probably dimers, judging from their behavior in preparation and the measurements of their electric conductivities.[7,12,16] Bagnall proposed that $UCl_4 \cdot 2.5DMA$ is a dimer with one ligand bridge and two chlorine ion bridges,[12] while Gans proposed that it had three ligand bridges.[17] Uranium(IV) chloride-*N,N*-dimethyl-*α,α*-diphenylacetamide (1/2.5) shows temperature-independent paramagnetism; this result can be explained by considering a dimeric structure with one ligand bridge and two chlorine-ion bridges per dimer.[9] Although the crystal structure of UCl_4-addition complexes of amides has not yet been determined by X-ray diffraction, $UCl_4 \cdot 2.5DMA$ and $UCl_4 \cdot 2.5DEA$ should have polynuclear structures, probably a dimer structure, judging from their molecular formula. On the other hand, $UCl_4 \cdot 3Me_2SO$ is known

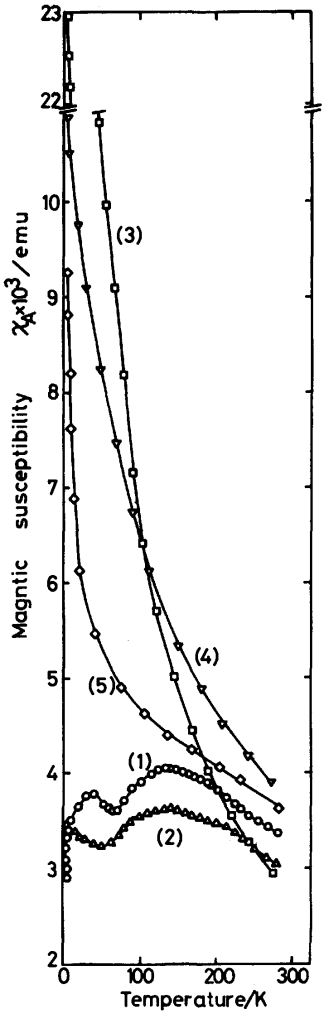

Fig. 3. Temperature dependence of magnetic susceptibility pre gram atom.
(1): UCl_4·3DMBA, (2): UCl_4·3MAA, (3): UCl_4·4BAN, (4): UCl_4·4BAM, (5): UCl_4·4AAN.

by X-ray diffraction to have an ionic-pair structure, $[UCl_2(Me_2SO)_6]^{2+}[UCl_6]^{2-}$.[18] We have recently observed its magnetic susceptibility to increase monotonically down to 4.2 K and explained its magnetic susceptibility as a sum of those of the individual ions on the basis of the crystalline-field theory.[19]

Assuming that the complexes with maxima have dimer structures, and that magnetic-superexchange interaction operates between the central uranium ions, we can propose an explanation for the anomalous magnetic behavior. According to the Heisenberg model, the exchange-interaction Hamiltonian for a two-spin system is expressed by Eq. 1;

$$H = -2J_{ex}\vec{S}_1\cdot\vec{S}_2, \quad (1)$$

where J_{ex} is the exchange integral for the intradimer interaction between uranium ions with spin angular momenta, $\vec{S}_1$ and $\vec{S}_2$. When the uranium(IV) ion has

Table 4. Temperatures with magnetic-susceptibility maximum and magnetic-exchange parameters for complexes

Complex	$T\chi_{max}$/K	$2J_{ex}$/cm^{-1}
UCl_4·3DMBA	134.2	−91.0
UCl_4·3MAA	142.0	−96.6
UCl_4·2.5DMA	121.8	−82.6
UCl_4·2.5DEA	112.0	−77.0
UCl_4·4MA	155.1	−106.4
UCl_4·4EA	81.8	−56.6

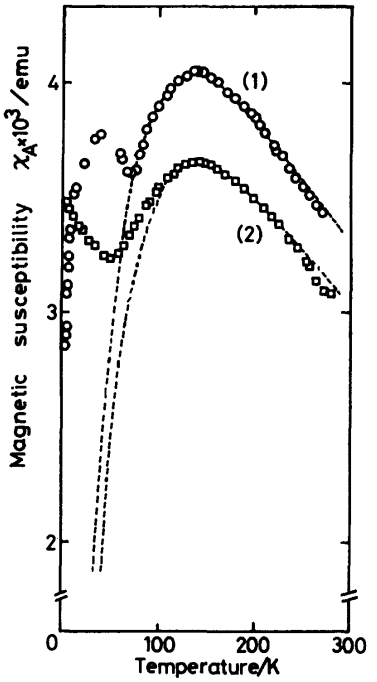

Fig. 4. Magnetic susceptibility *versus* temperature curve.
(1): UCl_4·3DMBA, (2): UCl_4·3MAA. ○, □: Experimental, ------: calculated.

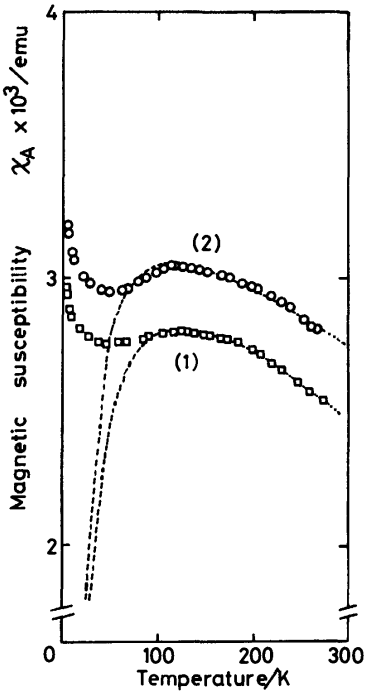

Fig. 5. Magnetic susceptibility *versus* temperature curve.
(1): UCl_4·2.5DMA, (2): UCl_4·2.5DEA. ○, □: Experimental, ------: calculated.

a non-degenerate ground state, $S_1=S_2=1$. From the well-known van Vleck equation[20] and Eq. 1, the magnetic susceptibility per gram of the atom is given as:

$$\chi_A = \frac{Ng^2\mu_B{}^2}{kT}\frac{5+\exp(-4J_{ex}/kT)}{5+3\exp(-4J_{ex}/kT)+\exp(-6J_{ex}/kT)}+N\alpha. \quad (2)$$

The value of J_{ex} can be obtained by the relation to the temperature of maximum susceptibility. $N\alpha$ is estimated by extrapolating the magnetic-susceptibility curve to the higher-temperature region (Table 4). Putting values of J_{ex} and $N\alpha$ and $g=2$ in Eq. 2, the magnetic susceptibilities per gram of the atom were calculated: they are shown in Figs. 4 and 5. The calculated curves of Fig. 5 include the effect of the molecular field; they will be discussed in a paper (Part II) to be published later. The discrepancy in the lower-temperature region might be partly due to paramagnetic impurities, such as a monomer, and partly due to the neglect of the orbital contribution. For the temperature region where the data fit the Curie-Weiss law, the Weiss constant and the effective Bohr magneton number are listed in Table 5.

As is shown in Table 6(a), the complexes with the maxima in their magnetic susceptibility versus temperature curves have at least one methyl or ethyl substituent on the amide nitrogen. (See the complexes combined by arrows.) Figure 6 shows the dependence of the magnetic susceptibility on the temperature for four complexes having no substituent on the carbon of amide. None of the four complexes exhibits a maximum similar to those shown in Figs. 1 and 3. Substitution on the carbon of amide is apparently necessary for the complexes to exhibit a maximum in the magnetic susceptibility *versus* temperature curve. (Note the relation in Table 6(b) and recall the experimental susceptibility.) The facts that the kind of substituent on the amide ligand is responsible for the magnetic-exchange interaction and that the value of J_{ex} of the amide complexes has some significance in the comparison of the strength of exchange interaction among the complexes suggest that the amide ligand is involved

Table 5. Curie-Weiss constants and effective Bohr magnetons

Complex	Temperature range/K	θ/K	μ_{eff}/μ_B
UCl_4·2.5DMA	210 —r.t.	−869	2.35
UCl_4·2.5DEA	240 —r.t.	−625	2.46
UCl_4·2.5DMF	150 —r.t.	−460	2.48
UCl_4·3DMBA	190 —r.t.	−418	2.72
UCl_4·3MAA	235 —r.t.	−265	2.59
UCl_4·3DPA	70 —r.t.	−175	2.32
UCl_4·3MFA	115 —r.t.	−179	2.42
UCl_4·4BAM	4.2 —r.t.	−143	2.88
UCl_4·4BAN	4.2 —r.t.	−38	2.55
UCl_4·4AAN	35 —r.t.	−455	2.83
UCl_4·4DPF	30 —r.t.	−85	3.08
UCl_4·4MA	195 —r.t.	−875	2.73
UCl_4·4EA	195 —r.t.	−276	2.88
UCl_4·4MF	115 —r.t.	−120	3.13
UCl_4·6AA	95 —r.t.	−90	2.75
UCl_4·6AcA	110 —r.t.	−87	2.96
UI_2Cl_2·5DMA	70 —r.t.	−273	2.56

a) Curie-Weiss law as $\chi_A = \frac{C}{T-\theta}$.

Table 6. Effect of the substituent of the amide molecule on the magnetic behavior

Complexes with no maximum susceptibility[a]		Complexes with maximum susceptibility[a]
(a) Substituents on the amide nitrogen		
UCl_4·6AA (H, H)	⟷	UCl_4·2.5DMA (CH_3, CH_3)
UCl_4·4AAN (Ph, H)	⟷	UCl_4·2.5DEA (C_2H_5,C_2H_5)
$UCl_4$3DPA (Ph, Ph)	⟷	UCl_4·4MA (CH_3, H)
	⟷	UCl_4·4EA (C_2H_5, H)
UCl_4·4BAM (H, H)	⟷	UCl_4·3DMBA (CH_3, CH_3)
UCl_4·4BAN (Ph, H)	⟷	
UCl_4·4AAN (H, Ph)	⟷	UCl_4·3MAA (CH_3, Ph)
UCl_4·3DPA (Ph, Ph)	⟷	
(b) Substituents on the carbon of amide		
UCl_4·2.5DMF (H)	⟷	UCl_4·2.5DMA (CH_3)
	⟷	UCl_4·3DMBA (Ph)
UCl_4·4MF (H)	⟷	UCl_4·4MA (CH_3)
UCl_4·3MFA (H)	⟷	UCl_4·3MAA (CH_3)

a) The groups in parentheses are the substituent.

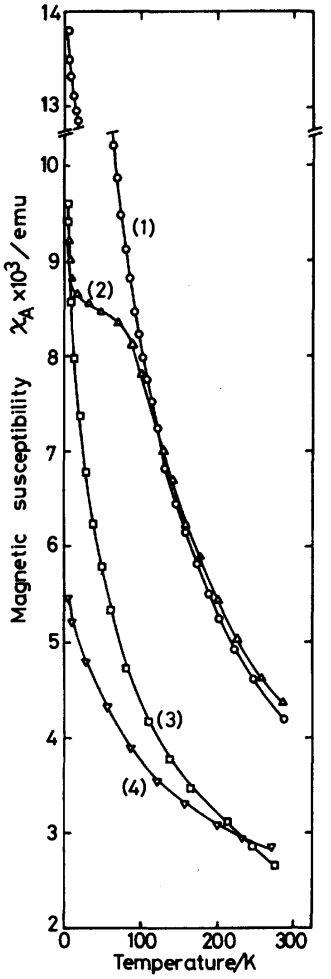

Fig. 6. Temperature dependence of magnetic susceptibility per gram atom.
(1): UCl_4·4DPF, (2): UCl_4·4MF, (3): UCl_4·3MFA, (4): UCl_4·2.5DMF.

Table 7. Amide-band frequencies

Complex	Amide I		Amide II		Amide III	
	ν/cm^{-1}	Δ	ν/cm^{-1}	Δ	ν/cm^{-1}	Δ
N-Methylacetamide	1660		1567		1298	
UCl_4·4MA	1600	−60	1564	−3	1251	−47
N-Ethylacetamide	1656		1562		1298	
UCl_4·4EA	1605	−51	1461	−101	1296	−2
N-Methylformamide	1664		1530		1244	
UCl_4·4MF	1625	−39	1536	6	1251	7

Table 8. N–H stretching frequencies

Complex	State	ν(N–H) / cm^{-1}	$\Delta\nu$/cm^{-1}
N-Methylacetamide	Gas phase	3473	
	Hydrogen-bonded	3290	−253
UCl_4·4MA		3220	−70
N-Ethylacetamide	Gas phase	3459	
	Hydrogen-bonded	3298	−182
UCl_4·4EA		3277	−21
N-Methylformamide	Gas phase	3468	
	Hydrogen-bonded	3299	−143
UCl_4·4MF		3325	26

in the magnetic-exchange interaction pathway between uranium(IV) ions.

The coordination of the amide molecule was further examined on the basis of the infrared spectra. The amide with the skeleton of RCONHR′ has the characteristic vibration of a peptide, constituted of six amide bands, *i.e.*, amide-band frequencies I—VI. Table 7 shows the results of the measurements of three amide bands, I, II, and III, of free amides and complexes. Amide I absorption is assigned 80% to the C=O stretching vibration; Amide II, 60% to the bending vibration in the plane of N–H and 40% to the C–N stretching vibration, and Amide III, 40% to the C–N stretching vibration and 30% to the bending vibration in the plane of N–H.[21] If the nitrogen of the amide molecule coordinates directly to the uranium ion, the absorptions of Amides II and III are expected to shift toward a lower frequency. In UCl_4·4MA and UCl_4·4EA (with the magnetic susceptibility maxima), and UCl_4·4MF (without the maximum), the directions of the shifts are opposite one another. This indicates a difference in the coordination of amides, suggesting the possibility of coordination through nitrogen in the former case. The N–H absorption for the ligand is known to shift to about 200 cm^{-1} lower than that in the free ligand due to the strong hydrogen bonding. In all three complexes, this absorption shifts to a lower frequency (Table 8). Furthermore, in UCl_4·4MA and UCl_4·4EA, the absorption shifts to a lower frequency, even compared with the N–H stretching frequency in the hydrogen-bonding state, but in UCl_4·4MF the shift is to a higher frequency. Accordingly, in the former two complexes the N–H bonding becomes weaker with complex formation than the strength of N–H bonding, which contributes to the hydrogen bonding. These data also support the possibility of nitrogen coordination. On the other hand, the frequencies of Amide I all shift to lower frequencies, indicating that oxygen

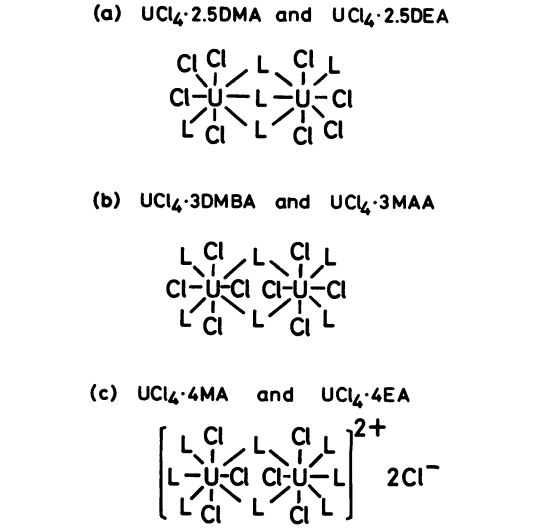

Fig. 7. Structural formulas suggested for dimers which are considered to be octa-coordinated, according to the references 7, 12, 17) for (a) and 9, 12) for (c). Amide molecules are represented as L.

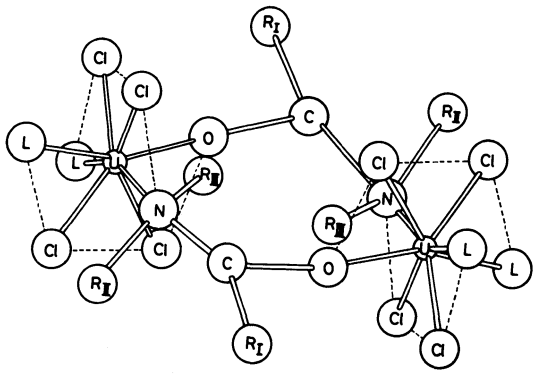

Fig. 8. A coordination diagram for UCl_4·3L type complexes by both oxygen and nitrogen atoms. Amide molecules which do not bridge are represented as L. Broken line shows dodecahedral coordination.

coordinates to the uranium ion. In $Co(DMA)_4(ClO_4)_2$, both oxygen and nitrogen of *N*,*N*-dimethylacetamide are reported to coordinate to the central metal ion.[22] Taking the results of magnetic behavior and infrared absorption into account, both oxygen and nitrogen are considered to coordinate to the uranium ion in UCl_4·4MA and UCl_4·4EA.

It is noteworthy that, in two pairs of a methyl derivative and an ethyl derivative of a given amide, UCl_4·2.5DMA and UCl_4·2.5DEA, and UCl_4·4MA and UCl_4·

4EA, the temperatures of the χ_{max} of the methyl derivatives are higher than those of the corresponding ethyl derivatives. This is consistent with the facts that an amide ligand contributes to the pathway between uranium ions and that the effect of the methyl substituent is predominant over the ethyl substituent in electron-releasing property. Concerning the origin of bridging, these facts indicate that, as the electron dinsity on the nitrogen atom is enhanced by the methyl (ethyl) group, in the case of a large metal ion such as uranium, both oxygen and nitrogen can coordinate to the metal ion; this amide molecule then acts as a bridging molecule. The values of the magnetic susceptibility of methyl derivatives are thus smaller than those of the corresponding ethyl derivatives. Furthermore, the value of the magnetic susceptibility of $UCl_4 \cdot 3MAA$ is smaller than that of $UCl_4 \cdot 3DMBA$, and the temperature of χ_{max} is higher in the former than in the latter. This fact can be explained by the existence of an antiferromagnetic interaction in the dimer.

In conclusion, the complexes which have the maximum of magnetic susceptibility *versus* temperatur curve are considered to be dimers (see Fig. 7), and the pathway for the magnetic-superexchange interaction is considered to be a polyatomic bridging of the amide molecule, probably by coordinating in the manner of U–N–C–O–U, as is shown in Fig. 8.

References

1) W. E. Hatfield, "Properties of Magnetically Condensed Compounds," in "Theory and Applications of Molecular Paramagnetism," ed by E. A. Boudreaux and L. N. Mulay, John Wiley and Sons, N. Y. (1976).

2) J. G. Reynolds, A. Zalkin, D. H. Templeton, N. M. Edelstein, and L. K. Templeton, *Inorg. Chem.*, **15**, 2498 (1976).

3) J. G. Reynolds, A. Zalkin, D. H. Templeton, and N. M. Edelstein, *Inorg. Chem.*, **16**, 599 (1977).

4) C. Miyake, Y. Hinatsu, and S. Imoto, *Chem. Phys. Lett.*, **63**, 529 (1979).

5) T. Yoshimura, C. Miyake, and S. Imoto, *J. Nucl. Sci. Technol.*, **8**, 498 (1971).

6) J. Kooi, E. Weisskopt, and D. M. Gruen, *J. Inorg. Nucl. Chem.*, **13**, 310 (1960).

7) K. W. Bagnall, A. M. Deane, T. L. Markin, P. S. Robinson, and M. A. A. Stewart, *J. Chem. Soc.*, **1961**, 1611.

8) P. Gans and B. C. Smith, *J. Chem. Soc.* **1964**, 4177.

9) J. G. H. du Preez, M. L. Gibson, and C. P. J. can Vuuren, *J. South African Chem. Inst.*, **24**, 135 (1971).

10) K. W. Bagnall, D. Brown, P. J. Jones, and P. S. Robinson, *J. Chem. Soc.*, **1964**, 2531.

11) K. W. Bagnall, D. Brown, J. G. H. du Preez, J. Bajorek, L. Bonner, H. Cooper, and G. Segel, *J. Chem. Soc., Dalton Trans.*, **1973**, 2682.

12) K. W. Bagnall, D. Brown, P. J. Jones, and J. G. H. du Preez, *J. Chem. Soc.*, **1965**, 3594.

13) T. Nakai, "Muki Kagaku Zensho XII-I Uranium," Maruzen, Tokyo (1960), p. 69.

14) H. St. Rade, *J. Phys. Chem.*, **77**, 424 (1973).

15) L. N. Mulay, "Definitions and Units for Magnetic Terms," in "Theory and Applications of Molecular Paramagnetism," ed by E. A. Boudreaux and L. N. Mulay, John Wiley and Sons, N. Y. (1976).

16) K. W. Bagnall, D. Brown, and R. Colton, *J. Chem. Soc.*, **1965**, 3594.

17) P. Gans, Ph. D. Thesis, London University (1964).

18) G. Bombieri and K. W. Bagnall, *J. Chem. Soc., Chem. Commum.*, **1975**, 188.

19) H. Sakurai, C. Miyake, and S. Imoto, *J. Inorg. Nucl. Chem.*, **42**, 69 (1980).

20) J. H. van Vleck, "The Theory of Electric and Magnetic Susceptibilities," Oxford Univ. Press, London (1932).

21) T. Miyazawa, T. Shimanouchi, and S. Mizushima, *J. Chem. Phys.*, **29**, 611 (1958).

22) B. B. Wayland, R. J. Fitzgerald, and R. S. Drago, *J. Am. Chem. Soc.*, **88**, 4600 (1966).

Magnetic-superexchange Interactions of Uranium(IV) Chloride-addition Complexes with Amides. II. Complexes with Lactams

Chie MIYAKE,* Yukio HINATSU, and Shosuke IMOTO
Department of Nuclear Engineering, Faculty of Engineering, Osaka University, Suita, Osaka 565
(Received December 14, 1981)

The magnetic susceptibilities of five cyclic amide (lactam)-addition complexes of uranium(IV) chloride were measured between room temperature and 2 K. Magnetic-exchange interaction was found only for *N*-methyl-substituted amide complexes, and a dimer structure was assumed for them on the basis of their chemical properties. Treating interdimer interaction with a molecular-field approximation, the magnetic susceptibilities were calculated to be in good agreement with the experimental results in the temperature region of the maxima in χ_A. The transmission of antiparallel spin coupling *via* the π orbitals of the bridging amide ligands is proposed to explain the strong intradimer superexchange interaction for the uranium(IV) chloride–amide complexes with the magnetic-susceptibility maximum.

In the preceding paper,[1] a series of amide-addition complexes of uranium(IV) chloride, $UCl_4 \cdot nL$ (L= $R_1CONR_2R_3$), were prepared, and their magnetic susceptibilities measured. Among the complexes studied, six showed a magnetic-exchange interaction and their magnetic-exchange parameters were calculated, assuming a dimer structure from their chemical properties. The effects of substituents on the bridging amide ligands were discussed.

To elucidate further the effects of the substituents, five uranium(IV) chloride-addition complexes were prepared with lactam (cyclic amide) ligands. Magnetic-exchange interactions were found only for complexes with a methyl group substituted with hydrogen on the amide nitrogen. This paper will report on the magnetic-susceptibility results, and a mechanism for the transmission of spin-exchange coupling in the complexes with *N*-methyl substituents is proposed.

Experimental

Reagents. Reagent-grade 5-, 6-, and 7-membered lactams and *N*-methyl-substituted 5- and 7-membered lactams were purchased from the Nakarai Chemical Industry Co., Ltd., and were used without further purification. Uranium(IV) chloride was prepared by passing carbon tetrachloride vapor over uranium dioxide at 500 °C in a vacuum.[2]

Preparations. Uranium(IV) chloride-*γ*-butyrolactam (1/4), $UCl_4 \cdot 4BuL$, and uranium(IV) chloride-*N*-methyl-*γ*-butyrolactam (1/2.5), $UCl_4 \cdot 2.5MBuL$: An oily product was obtained from an acetone solution of anhydrous uranium(IV) chloride by adding, successively, an excess acetone solution of the ligand and isopentane. After washing with ethyl acetate, the precipitates were rapidly dried in a vacuum and then kept over P_2O_5 for about a week.

Uranium(IV) chloride–*δ*-valerolactam (1/4), $UCl_4 \cdot 4Val$,[3] uranium(IV) chloride–*ε*-caprolactam (1/4), $UCl_4 \cdot 4CaL$,[4] and uranium(IV) chloride–*N*-methyl-*ε*-caprolactam (1/2.5), $UCl_4 \cdot 2.5MCaL$,[4] were synthesized according to the methods previously reported.

Analytical. The uranium content was determined gravimetrically as U_3O_8.[5] The chlorine content was determined by potentiometric titration with a standard $AgNO_3$ solution. The carbon, hydrogen, and nitrogen contents were determined with a Yanagimoto CHN coder MT-2. The analytical results are shown in Table 1.

Magnetic Measurements. The magnetic susceptibilities were measured by the Faraday method from 2 to 300 K on powder samples sealed in quartz tubes. The apparatus was calibrated with $Co[Hg(SCN)_4]$ as a standard.[6] The temperature was measured with a Au-Co/Cu thermocouple for temperature above 20 K and with a carbon resistor below 32 K. The dependence of the magnetic susceptibility on the mangetic-field strength was measured at field strengths of 400, 1470, 3320, 5400, and 7200×10^{-4} T at room temperature, the temperature of liquid nitrogen, and the temperature of liquid helium. No dependence of the susceptibilities on the magnetic field was found. The experimental values for magnetic susceptibilities were corrected for the diamagnetism of the sample using the values reported by Dawson,[7] Pascal's constants, and their constitutive correction.[8] The values of the diamagnetic corrections are listed in Table 2.

Rusults and Discussion

Unsubstituted lactams form $UCl_4 \cdot 4L$ complexes (L= BuL, VaL, and CaL), and the U(IV) ion probably has a coordination number of eight, the most common coordination number for U(IV) complexes. *N*-methyl-substituted lactams coordinate to form $UCl_4 \cdot 2.5L$ complexes (L=MBuL and MCaL), in which the lactam ligands probably bridge between U(IV) ions.

Figure 1 shows the magnetic susceptibility *vs.* temperatue curves for the five lactam complexes. $UCl_4 \cdot$

Table 1. Elemental analyses

Complex	C(%)		H(%)		N(%)		Cl(%)		U(%)	
	Found	Calcd	Found	Calcd	Found	Calcd	Found	Calcd	Found	Calcd
$UCl_4 \cdot 4BuL$	25.25	26.67	2.81	3.89	7.42	7.78	21.68	19.70	33.60	33.06
$UCl_4 \cdot 2.5MBuL$	24.64	23.91	3.60	3.59	5.83	5.58	21.93	22.60	36.95	37.94
$UCl_4 \cdot 4VaL$	29.27	31.10	4.37	4.15	6.50	7.26	19.00	18.37	31.95	30.84
$UCl_4 \cdot 4CaL$	35.65	34.62	5.46	5.29	6.27	6.73	16.11	17.05	26.78	28.61
$UCl_4 \cdot 2.5MCaL$	31.37	30.12	4.85	4.66	4.91	5.02	19.71	20.34	33.35	34.13

Table 2. Diamagnetic susceptibility corrections

Complex	$\chi_{dia} \times 10^6$/emu
UCl_4·4BuL	−340.0
UCl_4·2.5MBuL	−291.5
UCl_4·4VaL	−387.5
UCl_4·4CaL	−442.0
UCl_4·2.5MCaL	−353.0

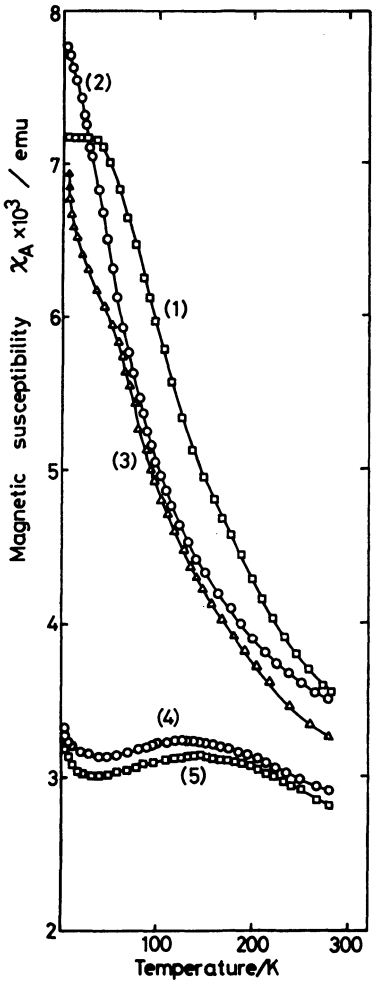

Fig. 1. Temperature dependence of magnetic susceptibility per gram atom. (1), UCl_4·4CaL; (2), UCl_4·4BuL; (3), UCl_4·4VaL; (4), UCl_4·2.5MBuL; (5), UCl_4·2.5MCaL.

2.5MBuL and UCl_4·2.5MCaL differ from the other three complexes having broad susceptibility maxima at 127 and 146 K respectively. Unsubstituted lactam complexes show different magnetic behavior at lower temperature, but show increasing susceptibilities with a decrease in the temperature from room temperature down to the temperature of liquid helium. Their paramagnetism can be explained by a model based on the crystalline field on the U(IV) ion.

Table 3 lists the Weiss contants and the effective Bohr magnetons in the temperature region where the data fit the Curie-Weiss law. The magnetic susceptibilities of UCl_4·2.5MBuL and UCl_4·2.5MCaL show maxima, indicating an antiferromagnetic-exchange interaction.

Table 3. Curie-Weiss constants and effective Bohr magnetons

Complex	Temperature range/K	θ/K	μ_{eff}/μ_B
UCl_4·4BuL	100 —r.t.	−257	2.76
UCl_4·2.5MBuL	200 —r.t.	−804	2.52
UCl_4·4VaL	100 —r.t.	−238	2.67
UCl_4·4CaL	75 —r.t.	−164	2.79
UCl_4·2.5MCaL	230 —r.t.	−387	2.47

a) Curie-Weiss law as $\chi_A = \frac{C}{T-\theta}$.

A dimeric structure for these complexes was assumed from their composition and the dimeric structures of complexes with similar compositions. UCl_4·2.5DMA has been considered to have a dimeric structure from its composition and from the measurement of its electric conductivity.[9–12] For the three bridges between two uranium ions, these are considered to be one ligand bridge and two chlorine ion bridges by Bagnall *et al.*,[12] while three ligand bridges are proposed by Gans.[13] Uranium(IV) chloride–*N*,*N*-dimethyl-*α*,*α*-diphenylacetamide (1/2.5) shows the temperature-independent paramagnetism characteristic of hexacoordinate U(IV) compounds; a dimeric structure with one ligand, dimethyl-diphenyl-acetamide, and two chlorine ions bridging two U(IV) ions has been proposed to account for the magnetic susceptibility.[4] Some transition-metal chloride complexes with lactam are considered to have dimer structures.[14,15] A dimer model is, therefore, assumed for complexes that have a magnetic-exchange interaction.

For the intradimer magnetic-exchange interaction, it is appropriate to use the isotropic spin Hamiltonian:

$$H_{ex} = -2J_{ex}\vec{S_1}\cdot\vec{S_2}, \quad (1)$$

where J_{ex} is the exchange integral for the interaction between uranium ions with spin operators $\vec{S_1}$ and $\vec{S_2}$. As each uranium(IV) ion has two unpaired spins, the spin angular momentum $S_1=S_2=1$. By substituting the energy levels obtained from the spin Hamiltonian (1) into the well-known van Vleck equation,[16] the magnetic susceptibility per gram of the atom is given as:

$$\chi_A = \frac{Ng^2\mu_B^2}{kT}\frac{5+\exp(-4J_{ex}/kT)}{5+3\exp(-4J_{ex}/kT)+\exp(-6J_{ex}/kT)} + N\alpha. \quad (2)$$

The value of $N\alpha$ is estimated by extrapolating the magnetic-susceptibility curve to the higher-temperature region. Then, the value of J_{ex} can be obtained from the temperature of maximum susceptibility. Susceptibilities calculated using these values, and assuming $g=2$ as in Part I, did not agree with the experimental results. Therefore, the effect of interdimer interaction was considered further.

For the complex that has a low symmetry field and $S>1/2$, zero-field splitting must be considered. Ginsberg *et al.* considered the effects of single-ion zero-field splitting on the magnetic susceptibility of nickel dimers.[17] They dealt with interdimer interactions by means of a molecular-field approximation. The Hamiltonian for this interaction is taken as $-2Z'J'_{ex}$

$\vec{S}_z\langle\vec{S}_z\rangle$. Here, $\vec{S}_z$ is the operator for the Z compounent of the dimer total spin, J'_{ex} is the effective interdimer exchange integral, and Z' is the coordination number of the dimer lattice. Therefore, the magnetic susceptibility per gram of the atom is:

$$\chi_A = \frac{Ng^2\mu_B^2}{3k}\left\{\frac{F_1}{T-4Z'J'_{ex}F_1} + \frac{2F'}{1-4Z'J'_{ex}F'}\right\} + N\alpha, \quad (3)$$

where

$$F' = F_2/D + 3C_2^2F_3/(3J_{ex}-\delta) + 3C_1^2F_4/(3J_{ex}+\delta),$$
$$F_1 = \{1 + \exp(4J_{ex}/kT) + 4\exp(4J_{ex}/kT)\exp(D/kT)\}/F_5,$$
$$F_2 = \{2\exp(4J_{ex}/kT)\exp(D/kT) + \exp(D/kT) - 1 - 2\exp(4J_{ex})/kT)\}/F_5,$$
$$F_3 = \{\exp(4J_{ex}/kT) - \exp(J_{ex}/kT)\exp(\delta/kT)\}/F_5,$$
$$F_4 = \{\exp(4J_{ex}/kT) - \exp(J_{ex}/kT)\exp(-\delta/kT)\}/F_5,$$
$$F_5 = 2 + \exp(D/kT) + \exp(J_{ex}/kT)\exp(-\delta/kT) + \exp(J_{ex}/kT)\exp(\delta/kT) + 2\exp(4J_{ex}/kT) + 2\exp(4J_{ex}/kT)\exp(D/kT),$$
$$\delta = [(3J_{ex} + D)^2 - 8J_{ex}D]^{1/2},$$
$$C_1 = 2(2)^{1/2}D/[(9J_{ex}-D+3\delta)^2+8D^2]^{1/2},$$
$$C_2 = (9J_{ex}-D+3\delta)/[(9J_{ex}-D+3\delta)^2+8D^2]^{1/2}.$$

The single-ion zero-field splitting parameter, D, was assigned an initial value of 10 cm^{-1}. The magnetic susceptibilities calculated by Eq. 3 using the parameters listed in Table 4 are shown in Fig. 2. Table 4 also lists the exchange parameters for UCl_4·2.5DMA and UCl_4·2.5DEA. In the temperature region of χ_{max}, the calculated values agreed well with the experimental magnetic susceptibilities. The discrepancy at lower temperatures is partly due to paramagnetic impurities, such as monomers. The calculation of the magnetic susceptibilities was not further refined, since the aim of this work was not a precise fit of the calculations with the experimental results, but the determination of the relation of the magnitude of the exchange parameter with the substituents on the ligand in the amide-addition complexes of UCl_4. It is noteworthy that UCl_4·2.5MBuL, whose χ_{max} temperature is lower than that of UCl_4·2.5MCaL; has a larger χ_{max} than the latter. This fact suggests that intradimer-exchange interaction is antiferromagnetic.

When a hydrogen bonded to a ligand-nitrogen atom is replaced by a methyl group, the number of lactam ligands coordinated with UCl_4 changes from 4 to 2.5 and the magnetic properties suggest intradimer-exchange interaction. Both complexes with half an integer-lactam molecule must be bridged dimers. The methyl group donates electron density to the nitrogen atom of the lactam ligand, so both the nitrogen and the oxygen atoms can bond to the U(IV) ion and the lactam ligand provides a path for the intradimer magnetic-super-exchange interaction.

Table 4. MAGNETIC-EXCHANGE INTERACTION PARAMETERS AND TIP[a] SUSCEPTIBILITIES FOR COMPLEXES

Complex	$2J_{ex}/cm^{-1}$	$Z'J'_{ex}/cm^{-1}$	$N\alpha$
UCl_4·2.5DMA[b]	−82.6	−64.0	970×10^{-6}
UCl_4·2.5DEA[b]	−77.0	−74.0	1240×10^{-6}
UCl_4·2.5MBuL	−86.8	−34.0	1010×10^{-6}
UCl_4·2.5MCaL	−99.4	−26.0	1000×10^{-6}

a) TIP: Temperature-independent paramagnetic. b) *Cf.* Part I.

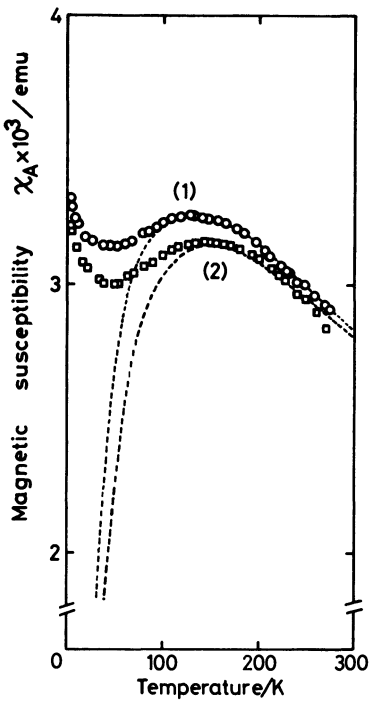

Fig. 2. Magnetic susceptibility *versus* temperature curve. (1), UCl_4·2.5MBuL; (2), UCl_4·2.5MCaL. ○, □; Experimental, ------; calculated.

Table 5. EFFECT OF THE SUBSTITUENT OF THE AMIDE MOLECULE ON THE MAGNETIC BEHAVIOR

Complexes in right-side column have the maximum of magnetic susceptibility *versus* temperature curve, while those on the left side are normally paramagnetic. Groups in parentheses are substituents.

UCl_4·4BuL	(H)	⟷ UCl_4·2.5MBuL	(CH_3)
UCl_4·4CaL	(H)	⟷ UCl_4·2.5MCaL	(CH_3)
UCl_4·6AA	(H, H)	⟷ UCl_4·2.5DMA[a]	(CH_3, CH_3)
UCl_4·4AAN	(Ph, H)	⟷ UCl_4·2.5DEA[a]	(C_2H_5, C_2H_5)
UCl_4·3DPA	(Ph, Ph)	⟷ UCl_4·4MA[a]	(CH_3, H)
		⟷ UCl_4·4EA[a]	(C_2H_5, H)
UCl_4·4BAM	(H, H)	⟷ UCl_4·3DMBA[a]	(CH_3, CH_3)
UCl_4·4BAN	(Ph, H)		
UCl_4·4AAN	(H, Ph)	⟷ UCl_4·3MAA[a]	(CH_3, Ph)
UCl_4·3DPA	(Ph, Ph)		

a) These complexes have been studied in Part I.

Table 5 lists complexes where magnetic-exchange interactions were found in the right-side column, and the remainder of the amide complexes on the left. Table 5 shows the correlation between *N*-methyl (ethyl) substitution and a magnetic-exchange interaction. The carbonyl oxygen of the amide ligand is the principal donor site, and the nonbonding electron pair on the nitrogen delocalizes into a π-molecular orbital involving oxygen, carbon, and nitrogen atoms. When a methyl group is substituted for a hydrogen on the nitrogen atom, the electron density on the nitrogen increases because of the electron-donating property of the methyl group.

For a large metal ion such as uranium, both oxygen and nitrogen coordinate and the amide ligand acts as a bridging group. As the electron-donating power of a methyl group is greater than that of an ethyl group, the temperature of the χ_{max} values of complexes with *N*-methyl-substituted amides is expected to be higher than that of complexes with *N*-ethyl-substituted amides. The experimental results coincide with this expectation. (Compare $UCl_4 \cdot 4MA$ and $UCl_4 \cdot 4EA$ and/or $UCl_4 \cdot 2.5DMA$ and $UCl_4 \cdot 2.5DEA$ in Part I.) It has been reported, on the basis of the vibrational and NMR spectra, that simultaneous coordination through both carbonyl oxygen and amide nitrogen may be present in $[Co(DMA)_6](ClO_4)_2$.[18]

The exchange interaction originates from an overlap of the wave functions of the unpaired electrons. Here, the superexchange interaction through the amide molecule between uranium ions must be considered.

The coordination number for the U(IV) ion is usually eight or six, but if the complex is hexacoordinate, it will have a constant paramagnetic susceptibility from room temperature corresponding to temperature-independent paramagnetism. When the complex has the coordination number of eight, it will show temperature-dependent paramagnetism. This magnetic behavior of uranium(IV) complexes can be explained on the basis of the crystalline-field theory. Thus, the present complexes are probably octacoordinated. Octacoordinated U(IV) complexes have either a dodecahedral or square antiprismatic field around the U(IV) ion, with the dodecahedral field occurring more often. Assuming a cubic coordination on the U(IV) ion, a probable structure for the $UCl_4 \cdot 3L$ complexes is shown in Fig. 3. In a field of cubic symmetry, seven 5f orbitals are split into a singlet, a_{2u}, and two triplets, t_{1u} and t_{2u}. The t_{1u} orbital is the lowest in energy. Each of the a_{2u}, t_{1u}, and t_{2u} orbitals has charge-density maximum in a certain direction. The t_{1u} orbital has a charge-density maximum in the direction toward the center of the cube-face, and this charge-density maximum is the largest among the three kinds of orbitals[19] (see Fig. 4). The t_{1u} orbital does not participate in the π-overlap with the coordinated oxygen or nitrogen atoms of the ligand, for this orbital is directed toward the center of the cube-face. However, the t_{1u} orbital is favored for the π-overlap with p_z, and this tendency is enhanced when the cubic coordination of the ligands actually becomes dodecahedral by up and down displacements of the corner oxygen and nitrogen atoms, as is shown in Fig. 3. The antiferromagnetic coupling of unpaired electrons of the U(IV) ions can be explained by the bridging of the amide ligands. The high temperature of χ_{max} suggests that the exchange interaction occurs *via* the π orbitals shown in Fig. 3, since the polarized spins in a π-system can couple at a distance with little attenuation[17] and can lead to strong superexchange interaction. A similar transmission of antiparallel spin coupling was found, for example, in the royal-blue modification of anhydrous copper(II) formate.[20] A proton-magnetic-resonance experiment now planned can provide evidence regarding the proposed π-system.[21]

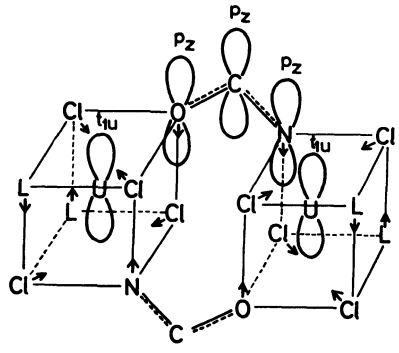

Fig. 3. Presumed structure for $UCl_4 \cdot 3L$ type complex in idealized form. For bridging amide molecules, only O=C–N is drawn, otherwise amide molecules are represented as L. If all ligands move to the directions shown by arrows, coordination polyhedron turns from cube to dodecahedron.

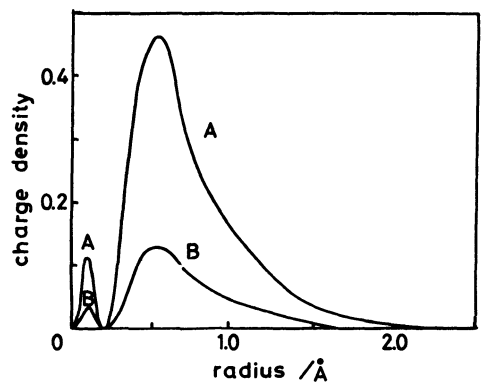

Fig. 4. Charge density distribution of 5f orbitals.
A: t_{1u} in the direction toward the center of cube-face,
B: a_{2u} in the direction toward the corner of cube and t_{2u} in its direction of charge density maximum.[19]

References

1) C. Miyake, Y. Hinatsu, and S. Imoto, *Bull. Chem. Soc. Jpn.*, **56**, 607 (1983).
2) T. Yoshimura, C. Miyake, and S. Imoto., *J. Nucl. Soc. Technol.*, **8**, 498 (1971).
3) J. G. H. du Preez, M. L. Gibson, and P. J. Steenkamp, *J. Inorg. Nucl. Chem.*, **36**, 579 (1974).
4) J. G. H. du Preez, M. L. Gibson, and C. P. J. van Vuuren, *J. South African Chem. Inst.*, **24**, 135 (1971).
5) T. Nakai, "Muki Kagaku Zensho XII-I Uranium," Maruzen, Tokyo (1960), p. 69.
6) H. St. Rade, *J. Phys. Chem.*, **77**, 424 (1973).
7) J. K. Dawson, *J. Chem. Soc.*, **1951**, 429.
8) L. N. Mulay, "Definitions of Units for Magnetic Terms in Theory and Applications of Molecular Paramagnetism," ed by E.A. Boudreaux and L.N. Mulay, John Wiley and Sons, N. Y. (1976).
9) G. Bombieri and K. W. Bagnall, *J. Chem. Soc., Chem. Commun.*, **1975**, 188.
10) K. W. Bagnall, A. M. Deane, T. L. Markin, P. S. Robinson, and M. A. A. Stewart, *J. Chem. Soc.*, **1961**, 1611.
11) K. W. Bagnall, D. Brown, and R. Colton, *J. Chem. Soc.*, **1964**, 2527.
12) K. W. Bagnall, D. Brown, P. J. Jones, and J. G. H. du Preez, *J. Chem. Soc.*, **1965**, 3594.
13) P. Gans, Ph. D. Thesis, London University (1964).

14) S. K. Madan and H. H. Denk, *J. Inorg. Nucl. Chem.*, **27**, 1049, (1965).
15) S. K. Madan and J. A. Sturr, *J. Inorg. Nucl. Chem.*, **29**, 1669 (1967).
16) J. H. van Vleck, "The Theory of Electric and Magnetic Susceptibilities," Oxford Univ. Press, London (1961).
17) A. P. Ginsberg, R. L. Martin, R. W. Brookes, and R. C. Sherwood, *Inorg. Chem.*, **11**, 2884 (1972).
18) B. B. Wayland, R. J. Fitzgerald, and R. S. Drago, *J. Am. Chem. Soc.*, **88**, 4600 (1966).
19) Sai-Kit. Chan, Proc. 2nd Int. Conf. Electr. Str. Actin., Wroclaw, Poland (1976), p. 327,
20) M. Inoue and M. Kubo, *Inorg. Chem.*, **9**, 2310 (1970).
21) C. Miyake, Y. Hinatsu, and S. Imoto, to be published.

Distribution and Chemical Behavior of 21 Elements in River Water in the Yakushima Island

Yoshiyuki TANIZAKI* and Sumiko NAGATSUKA
Tokyo Metropolitan Isotope Research Center, Fukazawa, Setagaya-ku, Tokyo 158
(Received May 28, 1982)

The concentrations of 21 elements dissolved in the river water collected from around the Yakushima Island were determined by a neutron activation analysis (NAA). From the analytical results, the distribution and chemical behavior of each element in the water were discussed. The chemical composition of the river water was nearly uniform all around the island, and the concentration of each element determined in this work was extremely close to the geochemical background value of river water, since our experimental area had scarcely any pollution. Among the 21 elements chlorine, sodium, and magnesium were mainly supplied into the river water from the ocean, while the others were chiefly driven from the rocks and their efflorescences in the drainage basin. The enrichment factors for the granitic earth crust (F_E-value) were very close to 1 for calcium, strontium, and zinc, while those of selenium, arsenic, tungsten, and antimony were much higher than 1. For the elements such as aluminium, iron, manganese, *etc.*, on the other hand, the F_E-values were very low. These differences in the F_E-values among the elements correspond to differences in their solubilities in the water.

The determination of multi-element concentrations in natural waters is of great importance to substantiate numerous theories on the geochemical migration of the chemical species on the earth surface. However, few articles have dealt with trace element concentrations in river water until recent years,[1-3] for the reason that the analytical methods for the determination of trace elements in the concentration less than part per billion (ppb) were generally quite complicated. More recent developments in instrumental neutron activation analysis (INAA) have facilitated the determination of multi-elements including trace elements. Using INAA, those concentrations in river water have been determined by many workers.[4-11] But no one has mentioned those in a natural freshwater which is perfectly free from pollutions by anthropogeneous sources, even though the analysis of such unpolluted water is very useful to evaluate the geochemical background value of natural water. In a previous paper,[12] it has been reported that the trace element concentrations in the river water collected from the Mikura Island were very close to a geochemical background value, since its basin was virtually unpolluted.

The Yakushima Island, one of the Nansei Islands, lies about 60 km south of Sata Point, the southernmost part of Kyushu, as shown in Fig. 1. It is supposed that the basin in the Island has scarcely any pollution as in the case of Mikura Island, for the reason that our experimental area is thinly populated and is far apart from any big town or industrial area. Furthermore, the streams in the Island flow with a rapid current throughout the year because of its steep topography and abundant rainfall.

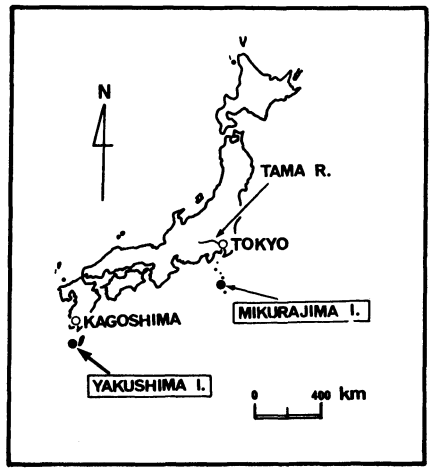

Fig. 1. Locality of the Yakushima Island.

In order to evaluate geochemical background values of river water, the concentrations of 21 elements in the water samples collected from 9 sites in the Island were determined using NAA.

Meanwhile, several workers[13-17] have reported on the chemical species of various elements dissolved in natural water and their solubilities. However, there is also no paper dealing with those of trace elements in unpolluted river water.

In this paper, therefore, the solubilities of trace elements in the river water are discussed; the relation between the enrichment factors for the granitic earth crust of those elements and their ionic potentials is emphasized.

Experimental

Water Sample. The Yakushima Island is composed of three geologic units, the Micocene Yakushima Granite, the Paleogene part of the Shimanto Group and the Quaternary deposits.[18,19] The Miocene Yakushima Granite is distributed most widely in the Island, especially in its basin, as can be seen in Fig. 2.

The river water samples were collected in December 1979 at nine sites in the basin of the Island. All the sampling sites are shown in Fig. 2.

The water samples were filtered within a few hours after the sampling, using a Type HA millipore filter with diameter 142 mm and pore size 0.45 μm. After the filtration, the samples were transferred to a 5-liter polyethylene bottle which was throughly washed with 10% nitric acid, followed by redistilled water, to remove trace element contaminations, and then acidified immediately with 30 ml of nitric acid (Super Special Grade) in order to avoid any adsorption of trace elements on the wall of the bottle.

For the analysis of chlorine, on the other hand, another 1

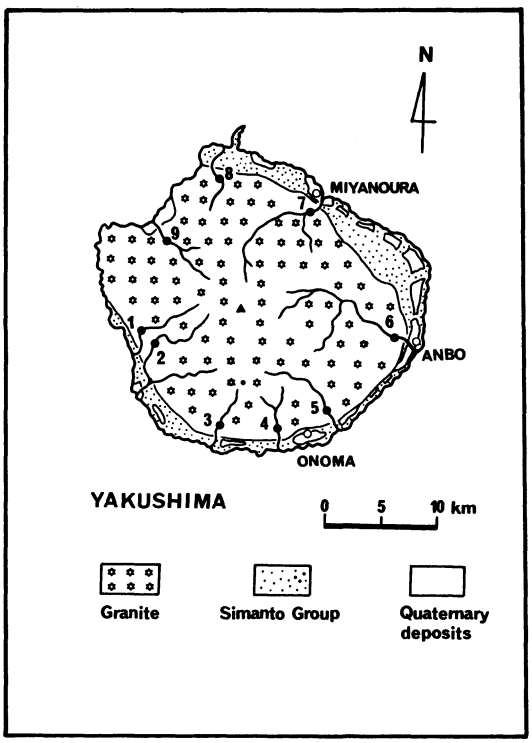

Fig. 2. Geological map of the Yakushima Island showing the sampling sites.

liter of the water sample was taken in another polyethylene bottle without the filtration and acidification.

Preparation of Irradiation Samples. For the NAA in this report, two kinds of irradiation samples, that is an evaporated residue sample and an iron(III) hydroxide coprecipitated one, were prepared from each water sample, according to the process reported in our previous papers.[5,8,20]

Four liters of the water sample were concentrated to 100 ml using a rotary evaporator. The concentrated water sample was then divided into two 50 ml portions.

One was dried on a Pyrex glass dish under an infrared lamp until the weight was constant. The residue was weighed and transferred into a polyethylene bag for neutron irradiation, and then heat-sealed.

The other was diluted with 100 ml of redistilled water, and then boiled for 30 min on a hot-plate after adding 0.5 ml of iron (III) chloride solution (Fe^{3+}: 10 mg/ml) and adjusting to pH 6 with aqueous ammonia. The iron (III) hydroxide precipitate was gathered on a piece of No. 5A filter paper with 5.5 cm in diameter and then rinsed with redistilled water ten times or more. After drying, the precipitate was transferred into another polyethylene bag together with the filter paper, and heat-sealed.

Irradiation and Gamma-counting. The sample and reference standard were encapsulated in a polyethylene capsule for all irradiations. The irradiation was performed by the TRIGA-Mark II Reactor of Rikkyo University, with a thermal neutron flux of 1.5×10^{12} n/cm^2 s. The gamma-spectrometer consists of a Ge(Li) coaxial detector of about 30 cm^3, with 2% efficiency and 2.8 keV resolution, and a 2048 and 4096 channel pulse height analyzer.

The evaporated residue sample was first irradiated for 1 minute to determine the elements induced the short-life nuclides such as Al(^{28}Al), Ca(^{49}Ca), Mg(^{27}Mg), Mn(^{56}Mn), Na(^{24}Na), and V(^{52}V), and these radioactivities were measured for 100 s by the spectrometer. One month later, the same sample was irradiated once more for 12 h to determine the elements induced the long-life nuclides such as Co(^{60}Co), Cr(^{51}Cr), Cs(^{134}Cs), Fe(^{59}Fe), Rb(^{86}Rb), Sb(^{124}Sb), Sc(^{46}Sc), Se(^{75}Se), Sr(^{85}Sr), and Zn(^{65}Zn). The measurement of these long-life activities were carried out for 50000 s after a cooling time of 2—4 weeks to reduce the short or medium-life nuclides.

The iron (III) hydroxide coprecipitate sample, on the other hand, was also irradiated for 12 h to determine the elements induced the medium-life nuclides such as As(^{76}As), La(^{140}La), Sm(^{153}Sm), and W(^{187}W), and after the cooling time of 1 d, these activities were measured for 1000 s.

Analysis of Chlorine. The concentration of chlorine in the river water samples was measured by means of Mohr's method.

Results and Discussion

The concentrations of 20 elements could be determined from the two irradiation samples by NAA. The recovery of several elements, such as arsenic, tungsten, *etc.* in water attendant upon the procedure of iron(III) hydroxide coprecipitation has been reported in the previous papers.[5,20,21]

In Tables 1—3, the concentrations of 21 elements determined in the river water collected from the Yakushima Island are listed, together with the statistical errors based on the gamma-counting.

These tables show that extraordinarily high concen-

TABLE 1. CONCENTRATIONS OF MAJOR ELEMENTS IN THE RIVER WATER COLLECTED FROM YAKUSHIMA ISLAND (units : ppm)

Sample No.	$WT^{a)}$ °C	pH	Conductivity $\mu\Omega^{-1}$ cm^{-1}	ER$^{b)}$	Cl	Na	Mg	Ca
1	10.0	7.4	28	42.5	7.9	5.0 ± 0.04	0.44 ± 0.11	1.1 ± 0.1
2	9.6	7.3	20	33.6	6.6	3.9 ± 0.04	0.34 ± 0.12	0.74 ± 0.08
3	11.4	7.0	23	38.9	7.2	5.0 ± 0.05	0.45 ± 0.11	0.96 ± 0.09
4	12.5	6.6	22	30.8	6.2	4.0 ± 0.04	0.51 ± 0.14	0.57 ± 0.08
5	9.5	6.6	15	26.2	4.5	2.8 ± 0.03	0.22 ± 0.10	0.42 ± 0.06
6	12.9	6.7	27	39.5	6.7	4.7 ± 0.05	0.41 ± 0.15	1.0 ± 0.1
7	11.3	6.6	23	34.7	7.0	3.8 ± 0.04	0.34 ± 0.11	0.59 ± 0.08
8	14.3	7.0	44	59.1	12.9	7.2 ± 0.05	0.99 ± 0.16	1.1 ± 0.1
9	11.7	7.1	32	46.0	8.3	5.0 ± 0.04	0.70 ± 0.12	1.2 ± 0.1
Average	11.5	6.9	26	39.0	7.5	4.6 ± 0.04	0.49 ± 0.12	0.85 ± 0.09

a) Water temperature. b) Amount of evaporated residue.

Table 2. Concentrations of minor elements in the river water collected from Yakushima Island (units : ppb)

Sample No.	Al	Sr	Fe	Zn	Rb	Mn	As	V
1	68 ± 1	13 ± 0.8	4.5 ± 1.1	1.5 ± 0.2	0.94 ± 0.06	0.36 ± 0.30	0.28 ± 0.02	0.11 ± 0.03
2	58 ± 2	13 ± 0.8	2.6 ± 1.0	1.0 ± 0.2	0.56 ± 0.06	0.77 ± 0.28	0.15 ± 0.02	0.04 ± 0.04
3	80 ± 1	9.0 ± 1.0	7.3 ± 1.2	0.7 ± 0.2	0.90 ± 0.07	0.33 ± 0.30	0.29 ± 0.02	0.10 ± 0.04
4	70 ± 2	6.2 ± 0.7	1.8 ± 1.2	1.7 ± 0.2	0.78 ± 0.06	0.54 ± 0.31	0.08 ± 0.01	0.05 ± 0.05
5	65 ± 1	6.7 ± 0.9	ND	1.1 ± 0.2	0.47 ± 0.06	0.31 ± 0.25	0.05 ± 0.01	0.02 ± 0.03
6	52 ± 2	12 ± 1	5.9 ± 1.1	1.4 ± 0.1	1.3 ± 0.1	1.2 ± 0.4	1.4 ± 0.1[a)]	0.07 ± 0.05
7	59 ± 1	9.2 ± 0.7	2.8 ± 0.5	0.9 ± 0.1	0.84 ± 0.07	0.41 ± 0.27	0.42 ± 0.02	0.02 ± 0.03
8	68 ± 2	17 ± 0.8	3.4 ± 1.3	0.7 ± 0.1	1.3 ± 0.1	0.86 ± 0.37	0 20 ± 0.03	0.08 ± 0.05
9	65 ± 1	17 ± 1	110 ± 3[a)]	1.3 ± 0.2	1.1 ± 0.2	88 ± 0.8[a)]	1.8 ± 0.04[a)]	0.09 ± 0.04
Average	65 ± 1	12 ± 0.8	4.0 ± 1.2	1.1 ± 0.2	0.91 ± 0.09	0.60 ± 0.31	0.21 ± 0.02	0.06 ± 0.04

a) These abnormal values are not included in the average values.

Table 3. Concentrations of trace elements in the river water collected from Yakushima Island (unit : ppt)

Sample No.	Cs	Cr	Se	La	W	Sb	Co	Sm	Sc
1	29 ± 2	ND	23 ± 5	28 ± 4	12 ± 3	10 ± 2	10 ± 1	7.4 ± 0.3	5.9 ± 0.2
2	29 ± 1	ND	26 ± 8	29 ± 3	8 ± 4	8 ± 1	23 ± 1	7.5 ± 0.3	5.8 ± 0.2
3	64 ± 2	46 ± 20	23 ± 8	23 ± 4	170 ± 5[a)]	17 ± 2	6.4 ± 0.8	8.1 ± 0.4	10 ± 0.2
4	58 ± 2	ND	10 ± 6	21 ± 3	28 ± 4	10 ± 1	8.4 ± 0.9	6.0 ± 0.3	6.9 ± 0.2
5	51 ± 2	ND	23 ± 6	23 ± 3	19 ± 3	9 ± 2	6.0 ± 0.9	7.2 ± 0.3	6.6 ± 0.2
6	100 ± 2	ND	31 ± 5	ND	820 ± 10[a)]	17 ± 2	13 ± 1	3.1 ± 0.4	3.1 ± 0.2
7	44 ± 2	ND	27 ± 5	18 ± 3	27 ± 5	11 ± 1	9.0 ± 0.8	5.2 ± 0.3	4.8 ± 0.2
8	48 ± 2	40 ± 20	69 ± 7	ND	25 ± 6	3 ± 1	13 ± 1	2.9 ± 0.4	3.6 ± 0.2
9	74 ± 3	ND	34 ± 8	39 ± 4	ND	29 ± 2	170 ± 2[a)]	16 ± 0.5	7.6 ± 0.3
Average	55 ± 2	43 ± 20	30 ± 6	26 ± 3	20 ± 4	13 ± 2	11 ± 1	7.0 ± 0.4	6.0 ± 0.2

a) These abnormal values are not included in the average values.

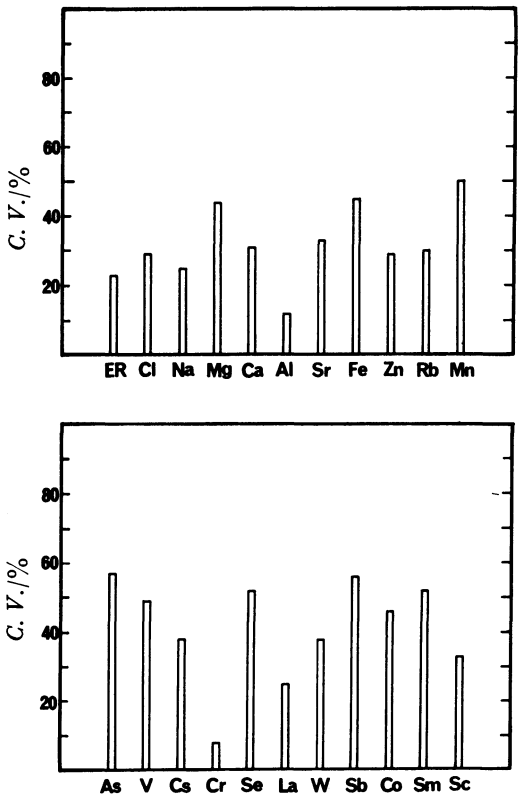

Fig. 3. The coefficients of variation of ER and 21 elements among the 9 sampling sites.

trations were given for heavy metal elements such as iron, manganese, arsenic, and cobalt at sampling site No. 9 (Nagata River), and high concentration of tungsten was found at the No. 3 (Yukawa River) and No. 6 (Anbo River). Utilizing the analytical results, but without these extraordinary values, the coefficients of variation (*C.V.*) were evaluated for 21 elements among all the sampling sites, by the next equation; the results are illustrated in Fig. 3.

$$\sigma = \sqrt{\sum(x_i - \bar{x})^2/n} \qquad (1)$$
$$C.V.(\%) = \sigma/\bar{x}$$

From Fig. 3, it was clarified that the coefficients of variation were less than 50% for almost all elements; those for the elements Cl, Na, Ca, Al, Sr, Zn, Rb, Cr, La, and Sc were less than 30%. These values are generally lower than those in the Tama River[5)] and the Mikura Island.[12)] Consequently, it can be said that the concentrations of almost all elements in the river water are nearly uniform all over the Island.

The basin in the Island had scarcely any pollution, as mentioned above, so that the values in the concentrations of various elements presented in Tables 1—3 are extremely close to the geochemical background value of the Yakushima's river water.

It is of interest to compare the concentrations of the elements in the Island water with those in river water collected from other districts, such as the drainage basin of the Tama River[5)] and the Mikura Island,[12)] so

TABLE 4. C_r-VALUES[a] FOR 21 ELEMENTS IN THE RIVER WATER COLLECTED FROM YAKUSHIMA ISLAND, MIKURAJIMA ISLAND,[12] AND THE TAMA RIVER[5]

	Yakushima Island	Mikurajima Island	Tama River
ER	1000	1000	1000
Cl	192	225	14
Na	118	117	40
Ca	22	28	131
Mg	13	17	25
Al	1.7	1.2	1.3
Sr	0.31	0.19	0.75
Fe	0.10	0.12	0.77
Zn	0.028	0.051	0.11
Rb	0.023	0.0071	0.011
Mn	0.015	0.017	0.023
As	0.0054	0.0025	0.035
V	0.0016	0.018	0.021
Cs	0.0014	0.00017	0.00052
Cr	0.0011	0.00056	0.0010
Se	0.00077	—	0.0013
La	0.00067	0.00032	0.0015
W	0.00051	0.00030	0.00041
Sb	0.00033	0.00031	0.0029
Co	0.00028	0.00031	0.00087
Sm	0.00018	0.00010	0.00031
Sc	0.00015	0.00021	—

a) The values are given in milligrams of each element per gram of the amount of evaporated residue (ER).

as to characterize the water quality of the Island. One has to keep in mind, however, that it is unsuitable to compare immediately each element concentration expressed in ppm, ppb and ppt because of their different sampling periods, geological features, *etc.* For this purpose, a relative concentration (C_r-value), using the average values, is evaluated by the next equation; this equation is given in the milligrams quantity of each element per the gram amount of evaporated residue (ER):

$$C_r = \frac{C_i}{C_{ER}} \times 1000, \tag{2}$$

where, C_i and C_{ER} mean the average concentrations of an element i and of the evaporated residue. The C_r-values for various elements in the three different districts are shown in Table 4. From Table 4, the following conclusions are drawn: No large difference in the C_r-values for most elements can be found between the two Islands, although there are some exceptions: the Yakushima Island water is more enriched in rubidium and caesium, and is deficient in vanadium in comparison with those in the Mikura Island water. The disagreement in the C_r-values for these three elements seems to be arise from the differences of their geological features, which is considered in the following way.

The Yakushima Island is mainly composed of the Miocene Yakushima Granite, as previous mentioned, while the Mikura Island is made up by the volcaniclastic rocks of Basalt and Andesite.[22] The concentration ratios of the former to the latter for rubidium, caesium and vanadium are 4.5, 9.2, and 0.11 respectively, provided the analytical values for two geochemical reference rock samples, JG-1 granodiorite and JB-1 basalt,[23] are utilized for the two different kind of rocks distributed in the two Islands. These values are close to the same ratios in the river water, 3.2, 8.2, and 0.089 respectively. Consequently, it could be said that the difference of the geological features has a large influence on the concentrations of these elements in the river water.

In the comparison with the amounts in the Tama River water, on the other hand, the Yakushima Island water is more enriched in chlorine, sodium, rubidium and caesium by 2—10 times. The high C_r-values for chlorine and sodium in the Island water can be explained by the assumption that both elements are easily supplied from the ocean; this will be discussed later. The highr C_r-values for rubidium and caesium in the Island water indicate that these elements tend to be derived from the Miocene Yakushima Granite, which is distributed extensively in the Island, as stated above.

Except these four elements, however, the C_r-values for most elements in the Island water are lower than those of the Tama River water by a factor of 2—10. This tendency is evident for the heavy metal elements such as iron, zinc, arsenic, vanadium, selenium, antimony, and cobalt.

It is well known that the difference of origin of the elements in rain water may be indicated by an enrichment factor for the earth's crust or the ocean, F_E or F_O.[24] The method is applicable not only to rain water, but also to the unpolluted river water.

$$F_E = \frac{C_{Ca}(\text{earth})}{C_{Ca}(\text{sample})} \times \frac{C_i(\text{sample})}{C_i(\text{earth})} \tag{3}$$

$$F_O = \frac{C_{Cl}(\text{ocean})}{C_{Cl}(\text{sample})} \times \frac{C_i(\text{sample})}{C_i(\text{ocean})} \tag{4}$$

Here, C_{Ca}, C_{Cl}, and C_i mean the concentrations of calcium, chlorine and some element i in the earth's crust, the ocean and the water sample, respectively. Calcium is chosen as the reference element for the F_E-values instead of the usually employed sodium, since at the Island sodium is mainly supplied from the ocean. Meanwhile, chlorine is used as the reference element for the F_O-values, because its main source is known to be the ocean.

In Eq. 3, the analytical values of various elements for JG-1[23] were employed in the place of those for the earth's crust, because the trace element concentrations of the Yakushima Granite have not been determined. For tungsten, however, the analytical value for international geochemical reference rock sample USGS G-1[25] was utilized, since the value for JG-1 has not been reported.

In Table 5, the enrichment factors (F_E- and F_O-value) are listed for 21 elements. From Table 5, it is recognized that the F_O-values are close to 1 for chlorine, sodium, and magnesium, and those for almost all of the elements except for above three elements are very high. This fact indicates that the origin of chlorine, sodium, and magnesium in the river water could be presumed to be the ocean, but for all of the elements other than chlorine, sodium, and magnesium their main sources should be

Table 5. Average enrichment factors F_E and F_O for various elements

	F_E	F_O
Cl	2400	1.0
Se	210	830
As	31	260
W	5.6	850
Na	3.6	1.2
Sb	2.4	110
Mg	2.0	0.98
Sr	1.2	2.2
Ca	1.0	5.3
Zn	0.60	590
Cs	0.11	470
Rb	0.094	7.0
V	0.054	87
Sm	0.031	31000
Co	0.031	190
Mn	0.027	3900
La	0.024	20000
Al	0.018	170000
Sc	0.015	3900
Cr	0.015	560
Fe	0.0055	3000

assumed to be elsewhere. The river water in the Island is virtually free from the anthropogeneous sources. Furthermore, the influence by naturally occurring organic substances such as humic acids appeared to be negligibly small in our experimental area because of th rocky river bed and abundant flow. Therefore, most of the elements other than the above three elements in the river water are derived from the rocks and their efflorescences in the drainage basin.

The F_E-values are close to 1 for calcium, strontium, and zinc; those for chlorine, selenium, arsenic, tungsten, sodium, antimony, and magnesium are much higher than 1. For aluminium, iron, manganese, *etc.* the F_E-values vanishingly low, as can be seen in Table 5. Chlorine, sodium, and magnesium, showed high F_E-values; these originated from the ocean, as stated above.

It is known that in natural water the elements such as calcium, strontium, zinc, *etc.* are present as divalent cations, and the elements such as aluminium, iron, chromium, *etc.* tend to exist as trivalent species. On the other hand, the great portion (70—100%) of arsenic and antimony are present as pentavalent species such as AsO_4^{3-} and SbO_4^{3-}.[26,27] For selenium and tungsten, it is assumed, according to the example of Garrels and Christ,[13] that those elements exist as hexavalent species, although the chemical species of those elements dissolved in natural water are probably either SeO_3^{2-} and WO_3^{2-} or SeO_4^{2-} and WO_4^{2-}.[28,29]

The relation between the F_E-values for various elements and their chemical valencies is demonstrated by Fig. 4, which is a plot of the logarithm of the F_E-value *versus* an ionic potential that is given in the ratio of chemical valency of the element to its radius.[30] In Fig. 4, it can be considered that the ordinate is one kind of measure of solubility, while the abscissa means the tendency of the cation to bond with anions.

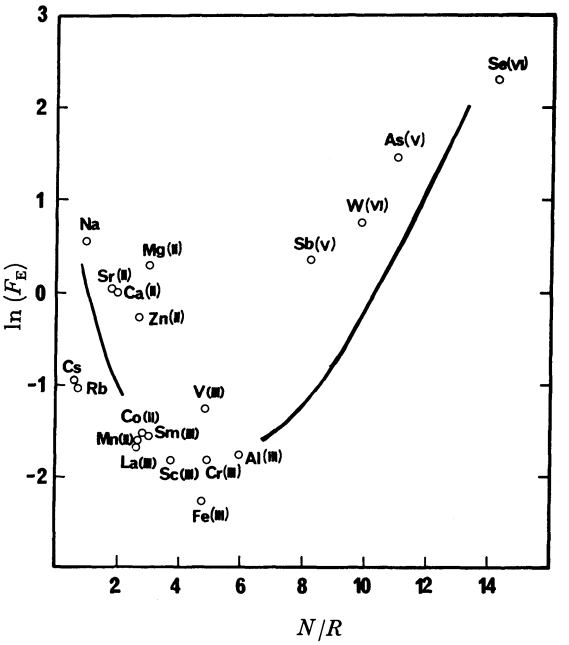

Fig. 4. Plot showing the relation between the logarithm of the enrichment factor (F_E-values) and the ionic potentials of cationic species. A parenthesized Roman numerals show chemical valency (N) of the elements easily formed under the natural conditions. Ionic radii (R) are employed from Shannon and Prewitte.[30]

The diagram shows the following general trends. The scattering pattern of each element in the diagram agrees with those reported by Garrels and Christ,[13] who have studied the behavior of various chemical species in sea water. The relatively high solubilities are found for the elements that form the divalent cations under the range of natural conditions, such as calcium, strontium, and zinc, while the elements that tend to form the trivalent ions such as aluminium, iron, chromium, scandium, *etc.* show very low solubilities. Such trivalent ions not only tend to interact with various anions to form soluble complexes, but also tend to form insoluble hydroxides or oxides in ordinary natural waters. It is well known that the transition elements such as iron, manganese, zinc, vanadium, chromium, cobalt, scandium, *etc.* are being held in the dissolved phase by complexation or chelation with dissolved organic substances in river water.[17,31,32] In our experimental area, however, it is supposed that these organic substances in the river water exist only in very small amounts, as stated above. Thus, the total solubilities for the elements which formed trivalent cations or for the transition elements are still held low in the Yakushima's water.

Zinc shows an exceptionally high solubility among the transition elements; it is extremely hard for zinc to be oxidized to trivalent cation, and easily dissolves in water as a divalent species such as $(Zn(H_2O)_6)^{2+}$.[33] The solubility of vanadium is slightly higher than those of the other transition elements, because a portion of vanadium exists as soluble pentavalent species such as $V_{10}O_{28}^{6-}$,[13] as in the case of arsenic and antimony.

On the other hand, for those elements that form small

penta and hexavalent species, such as selenium, arsenic, tungsten, and antimony, the solubilities have very high values, presumably because they react with oxygen to form metal-oxygen anions because of their high ionic potentials, as shown in Fig. 4.

Conclusion

Using NAA method, it was possible to obtain some knowledge about the distribution and chemical behavior of various elements in the river water in th Yakushima Island.

The analyzed values for the various element concentrations offered in this paper were close to the geochemical background value of river water, because our experimental area was free from any pollution by anthropogeneous sources. Thus, their values will serve satisfactorily as reference data for the concentrations of the elements dissolved in most river water.

The relation between the F_E-values and ionic potentials showed that the solubilities were relatively high for the elements that form the divalent cations in ordinary natural water, while those for the elements that tend to form trivalent ions were very low. For the elements that easily form the small high valent species, the solubilities were given in very high values. The term solubility indicates not only the tendency of each element to be supplied into the river water from the rocks, but the difficulty of being remove from the river water as deposits.

The geological structure of the Island is rather simple, and the Island forms a kind of closed system, since it is an isolated island. Furthermore, the flow of the water in each river is abundant throughout the year. Therefore, it was supposed that a kind of equilibrium was set up between the rocks and water in the basin as for the behavior of various chemical species, such as the dissolution, precipitation, adsorption, *etc.* These reasons made it easy to study the chemical behavior of the elements in the water.

For a general understanding, however, it would be necessary to evaluate the element concentrations much more than determined in this work, and to substantiate exactly the chemical species for various elements, and also to complete studies conducted on natural freshwaters collected from various different districts.

References

1) W. H. Durum and J. Haffty, *Geochim. Cosmochim. Acta*, **27**, 1 (1963).
2) P. D. Goulden and P. Brooksbank, *Anal. Chem.*, **46**, 1431 (1974).
3) S. Ramamoorthy and D. J. Kushner, *J. Fish. Res. Board Can.*, **32**, 1755 (1975).
4) T. Mamuro, Y. Matsuda, A. Mizohata, T. Takeuchi, and A. Fujita, *Radioisotopes*, **20**, 111 (1971).
5) Y. Tanizaki and S. Nagatsuka, *Nippon Kagaku Kaishi*, **1974**, 2094.
6) G. F. Clemente and G. G. Mastinu, *J. Radioanal. Chem.*, **20**, 707 (1974).
7) W. F. Merritt, *Can. J. Earth Sci.*, **12**, 850 (1975).
8) S. Nagatsuka and Y. Tanizaki, *Radioisotopes*, **25**, 375 (1976).
9) K. H. Lieser and V. Neitzert, *J. Radioanal. Chem.*, **31**, 397 (1976).
10) Y. Tanizaki and S. Nagatsuka, *Nippon Kagaku Kaishi*, **1977**, 667.
11) S. Habib and M. J. Minski, *J. Radioanal. Chem.*, **63**, 379, (1981).
12) Y. Tanizaki and S. Nagatsuka, *Radioisotopes*, **30**, 486, (1981).
13) R. M. Garrels and C. L. Christ, "Solutions, Minerals, and Equilibria," Harper and Row, New York (1965), Chap. 4.
14) G. E. Batley and T. M. Florence, *Mar. Chem.*, **4**, 347, (1976).
15) T. M. Florence, *Water Res.*, **11**, 681 (1977).
16) R. K. Skogerboe, S. A. Wilson, and J. G. Osteryoung, *Anal. Chem.*, **52**, 1960 (1980).
17) E. R. Sholkovitz and D. Copland, *Geochim. Cosmochim. Acta*, **45**, 181 (1981).
18) Y. Kawachi and T. Sato, *Neues Jahr. Mine Abh.*, **Bd. 132**, 136 (1978).
19) T. Sato and H. Nagahama, "Geology of the Yakushima-Seinanbu District, Quadrangle Series, scale 1 : 50000," Geol. Surv. Japan, (1979), p. 47.
20) S. Nagatsuka and Y. Tanizaki, *Radioisotopes*, **23**, 693 (1974).
21) S. Nagatsuka, H. Suzuki, and K. Nakajima, *Radioisotopes*, **20**, 305 (1971).
22) N. Isshiki, "Geology of the Mikurajima, Inambajima and Zenisu District, Quadrangle Series, Scale 1 : 50000," Geol. Surv., Japan (1980), p. 35.
23) A. Ando, H. Kurasawa, T. Ohmori, and E. Takeda, *Geochem. J.*, **8**, 175 (1974).
24) J. Bogen, *Atmos. Environ.*, **8**, 835 (1974).
25) F. J. Flanagan, *Geochim. Cosmochim. Acta*, **37**, 1189 (1973).
26) S. Gohda, *Bull. Chem. Soc. Jpn.*, **48**, 1213 (1975).
27) M. O. Andreae, *Anal. Chem.*, **49**, 820 (1977).
28) R. Massee, H. A. van der Sloot, and H. A. Das, *J. Radioanal. Chem.*, **35**, 157 (1977).
29) R. M. Garrels and C. L. Christ, "Solution, Minerals, and Equilibria," Harper and Row, New York (1965), pp. 421 and 426.
30) R. D. Shannon and C. T. Prewitt, *Acta. Crystallogr., Sect. B*, **25**, 925 (1969).
31) P. Benes, E. T. Gjessing, and E. Steinnes, *Water Res.* **10**, 711 (1976).
32) C. Steelink, *J. Chem. Educ.*, **54**, 599 (1977).
33) L. E. Orgel, "An Introduction to Transition-Metal Chemistry (Ligand-Field Theory)," Methuen and Co., Ltd., (1966), Chaps. 1 and 5.

Phase Behavior of 2-Butoxyethanols/Water/Oil Systems

Hironobu KUNIEDA
Department of Applied Chemistry, Faculty of Engineering, Yokohama National University, Tokiwadai 156, Hodogaya-ku, Yokohama 240
(Received June 11, 1982)

Synopsis. Phase diagrams of 2-isobutoxyethanol (D)/water (W)/decane (O) system were studied at 2.0, 8.2, 15.0, 19.0, and 19.8 °C. The addition of O lowers the critical solution temperature of the D–W system from 26.2 to 2.0 °C, at which temperature the critical solution curve ends with the lower critical end point (Kc). On the other hand, the addition of W raises the critical solution temperature of the O–D system to 19.8 °C at which the critical solution curve ends with another critical end point (Lc). A three-phase region consisting of O, D, and W phases appears in a temperature range between the two critical end temperatures.

Recently, similarity of phase behavior has been reported among some amphiphilic compound systems, such as an ionic surfactant/brine/(cosurfactant)/oil,[1,2] short-chain alcohol/brine/oil,[3] and nonionic surfactant/water/oil systems.[4] In these systems, an amphiphile changes from water-soluble (hydrophilic) to oil-soluble (lipophilic) with the increase in salt content or changing in temperature. In the transition range of phase behavior, there is a three-phase region in which an amphiphile phase coexists with a water phase and an oil phase in equilibrium.

In this paper, phase behavior of 2-isobutoxyethanol/water/oil system has been investigated around the temperatures of the three-phase region in order to compare with long-chain surfactant systems.

Experimental

Materials. Extra-pure-grade 2-isobutoxyethanol, 2-butoxyethanol, diethylene glycol hexyl ether, and hydrocarbons were obtained from Tokyo Kasei Kogyo Co. and were used with out further purifications.

Procedures for the determination of phase boundaries are described elsewhere.[5]

Results and Discussion

Phase Diagram of 2-Isobutoxyethanol/Water/Decane System. If temperature is taken as an axis perpendicular to a composition plane at constant pressure, the three-dimensional shape of a ternary system is a triangular prism and a horizontal section is the isobaric, isothermal section of the system, *i.e.*, the phase diagram of a three-component system. The phase diagrams of 2-isobutoxyethanol/water/decane system were determined at 2.0, 8.2, 15.0, 19.0, and 19.8 °C, and are shown in Figs. 1(a)—(e). The compositions are given in weight fractions. W, D, and O denote the water, 2-isobutoxyethanol, and oil phases, respectively.

The lower critical solution temperature of the binary

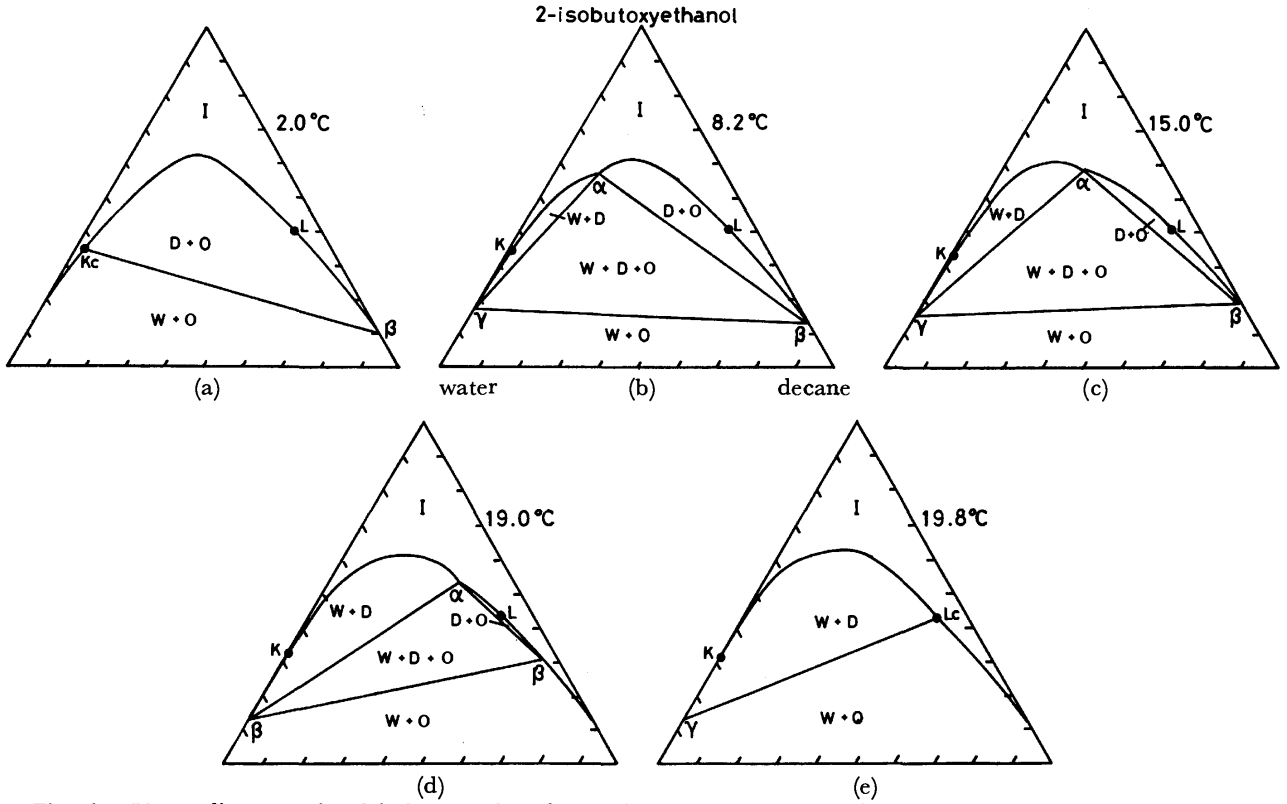

Fig. 1. Phase diagrams for 2-isobutoxyethanol/water/decane system at various temperatures.
O: an oil phase, W: a water phase, D: a 2-isobutoxyethanol phase, α, β, and γ: invariant points, K and L: plait points, Kc: the lower critical end point of W-D, Lc: the upper critical end point of O-D, I: one-phase region.

system of D–W is 26.2 °C, below which there are complete miscibilities in the binary systems of D–W and O–D. But, a large miscibility gap exists in the ternary system due to the poor mutual solubility of O and W. Plait points of the D–W and O–D phases in the three-component system are indicated by K and L. The locus of K in the triangular prism, *i.e.*, in the space of temperature and compositions, ends with the lower critical end point, Kc (water, 62.8 wt%; 2-isobutoxyethanol, 34.8 wt%; decane, 2.4 wt%) at 2.0 °C. On the other hand, the locus of L in the triangular prism ends at the upper critical end point Lc (water, 8 wt%; 2-isobutoxyethanol, 43 wt%; decane, 49 wt%) at 19.8 °C as is shown in Fig. 1(e). At the temperatures between the two critical end temperatures, a three-phase region consisting of O, D, and W phases appears due to the superposition of three-miscibility gaps; O+D, D+W, and O+W regions. The compositions of three coexisting liquid phases are invariant at constant temperature and pressure, and these points are indicated by α, β, and γ in Fig. 1. At the lower critical end temperature (LCET), W and D phases become identical on the line Kc-β, as is shown in Fig. 1(a). On the other hand, O and D phases merge on the line Lc-γ at the upper critical end temperature (UCET), as is shown in Fig. 1(e). The plait point K reaches the D–W axis at 26.2 °C, above which there is no plait point in the phase diagram.

The vertical section of the phase diagrams in Fig. 1 is shown in Fig. 2. The water/oil ratio is unity and the concentration of 2-isobutoxyethanol is plotted horizontally. Similar vertical sections of 2-butoxyethanol water/decane, diethylene glycol hexyl ether/water/decane and triethylene glycol octyl ether/water/decane[4] systems are also shown in Fig. 2. A three-phase region moves toward a water-oilaxis (left-hand axis) with the increase in the molecular size of an amphiphile. On the other hand, the temperature range of the three-phase region is little affected by the molecular size of an amphiphile, because the hydrophile-lipophile property

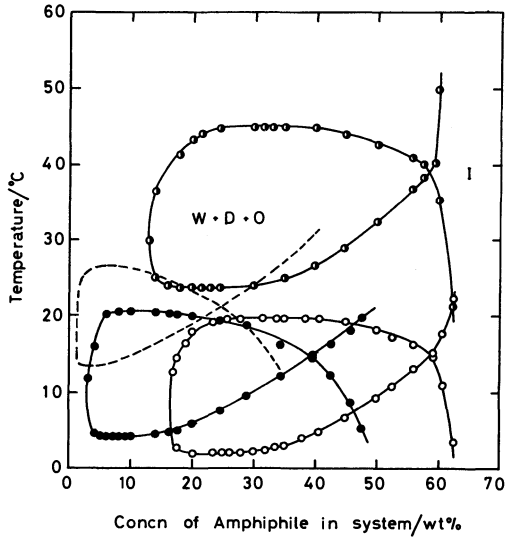

Fig. 2. The effect of the concentrations of an amphiphilic conpound on the equi-weight mixture of water and decane.
-○-: 2-Isobutoxyethanol system, -◑-: 2-butoxyethanol system. -●-: diethylene glycol hexyl ether system, ------: triethylene glycol octyl ether system.

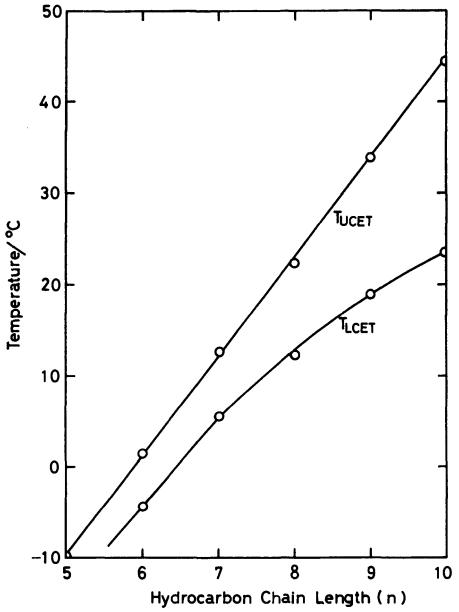

Fig. 3. The effect of hydrocarbon chain length of oil (C_nH_{2n+2}) on the critical end temperatures in the 2-butoxyethanol/water/oil systems.

of a nonionic amphiphile is related to the ratio of the hydrophilic and lipophilic portions.[6]

The Effect of Oil Size on the Difference in LCET and UCET. If three components are fixed, LCET and UCET are invariant at constant pressure. The lower and upper limits of a three-phase region in Fig. 2 correspond to LCET and UCET respectively. LCETs and UCETs in various 2-butoxyethanol/water/oil systems are shown in Fig. 3. With an decrease in the hydrocarbon chain-length of oil, the difference in LCET and UCET becomes smaller. If the two critical end temperatures coincide strictly, a tricritical phenomenon may be observed.[7] The degree of freedom (f) at a pth order critical point ($p=3$ at a tricritical point) is determined by the following equation;[8]

$$f = c - 2p + 3,$$

where c is the number of components. In a three-component system, $f=0$ holds at a tricritical pont, which is an invariant point in the space of temperature, pressure and compositions. Therefore, in order to observe a tricritical phenomenon, the pressure in a ternary system has to be changed.

The author thanks Prof. K. Shinoda for his stimulating discussions.

References

1) R. L. Reed and R. N. Healy, "Improved Oil Recovery by Surfactant and Polymer Flooding," ed by D. O. Shah and R. S. Schechter, Academic Press Inc., New York (1977), p. 383.
2) H. Kunieda and K. Shinoda, *J. Colloid Interface Sci.*, **75**, 601 (1980).
3) A. M. Bellocq, D. Bourbon, and B. Lemanceau, *J. Dispersion Sci. Tech.*, **2**, 27 (1981).
4) H. Kunieda and S. E. Friberg, *Bull. Chem. Soc. Jpn.*, **54**. 1010 (1981).
5) K. Shinoda and H. Kunieda, *J. Colloid Interface Sci.*, **42**, 381 (1973).
6) W. C. Griffin, *J. Soc. Cosmetic Chem.*, **1**, 311 (1949); **5**, 249 (1954).
7) B. Widom, *J. Phys. Chem.*, **77**, 2196 (1973).
8) J. Zernike, *Recl. Trav. Chim. Pays-Bas*, **68**, 585 (1949).

Study of the Mixed Solutions of an Anionic and a Nonionic Surfactant by Using the Azo-hydrazone Tautomerism of an Acidic Dye

Kenjiro MEGURO,* Yujin TABATA,† Naoki FUJIMOTO, and Kunio ESUMI
Department of Applied Chemistry, Faculty of Science, Science University of Tokyo, Kagurazaka, Shinjuku-ku, Tokyo 162
†*Nikko Chemicals Co., Ltd., Hasune, Itabashi-ku, Tokyo 174*
(Received June 11, 1982)

Synopsis. The absorbances of the azo-hydrazone tautomer of sodium 4-(*p*-sulfonatophenylazo)-1-naphthol-2-sulfonate dissolved in an aqueous solution of polyethylene glycol octyl dodecyl ether (8ED) were measured in the presence of various concentrations of sodium dodecyl sulfate (SDS). The existence of a mixed micellar region of SDS and 8ED in the bulk solution was confirmed by this azo-hydrazone tautomer method.

The present authors have previously reported the properties of mixed micelles between an anionic surfactant and a series of homogeneous polyethylene glycol dodecyl ethers (*n*ED) with no Poisson distribution and their dependence on the oxyethylenechain length.[1-4] The existence of a mixed micellar region in the bulk solution has been suggested from the finding that a long plateau appears on the surface-tension curve of nonionic surfactants in the presence of sodium dodecyl sulfate (SDS) at a constant concentration. Further, the authors have determined the cmc of mixed solutions of SDS and 7ED by the charge-transfer-solubilization method.

Recently, the cmc of nonionic surfactants has been determined spectroscopically by using the keto-enol tautomer of benzoylacetone or benzoylacetoanilide.[5,6] This method might also be used to elucidate the properties of mixed micelles. In this work, the properties of mixed micelles of SDS and polyethylene glycol octyl ether (8ED) were investigated by using an azo-hydrazone tautomer of sodium 4-(*p*-sulfonatophenylazo)-1-naphthol-2-sulfonate (PNDS) as one of the tautomers.

PNDS was prepared in the following way: Sulfanilic acid ($NH_2C_6H_4SO_3H$) was diazotized and coupled with potassium 1-naphthol-2-sulfonate ($HOC_{10}H_6SO_3K$). The PNDS thus obtained was purified by chromatography on Wakogel C-200, using a mixture of 1-butanol, acetic acid, and water as the eluent. The PNDS was dried at 100 °C under a vacuum. A homogeneous nonionic surfactant, polyethylene glycol octyl dodecyl ether (8ED) was supplied by the Nikko Chemicals Co., Ltd. This 8ED was highly pure, as was confirmed by gas-liquid chromatography, thin-layer chromatography, and cloud-point and surface-tension measurements. SDS as an anionic surfactant was synthesized by a modification of the method of Dreger *et al.*,[7] and subsequently purified by repeated recrystallizations from ethanol. The purity of SDS was confirmed by the absence of any minimum in the surface-tension diagram. The water used in all the experiments was purified by passing it through the MILL-Q Reagent-Grade Water System (Millipore, Ltd.) until its specific conductivity fell below $10^{-7}\ \Omega^{-1}$/cm. 2.5×10^{-5} mol dm^{-3} of PNDS in an aqueous solution was prepared, and then the surfactant solutions with various concentrations were prepared by dissolving a certain quantity of each surfactant into the PNDS aqueous solution in order to keep the concentration of PNDS constant. After the temperature of the samples had attained 25 °C, the absorption spectra of the samples were measured in a 1.0-cm quartz cell by means of a spectrophotometer (Model Hitachi ESP-3T).

It is well known that PNDS exists mostly in the hydrazone form in water and is tautomerised to the azo form in polar organic solvents.[8] To confirm this behavior, the absorption spectra of PNDS dissolved in water–ethanol mixtures were measured. It was seen that the spectrum of PNDS in water had an absorption band at 490 nm, where PNDS exists in the hydrazone form, while on the other hand, the spectrum in ethanol provides an absorption band at 410 nm which is attributed to the azo form. The absorbance of the hydrazone form decreased with an increase in the content of ethanol in the mixtures. Furthermore, an isobestic point was clearly observed at 435 nm. The above results support the idea that the azo-hydrazone tautomerism of PNDS exists in water–ethanol mixtures.

It is important to check whether or not an aggregation of PNDS exists in an aqueous solution, because dyes usually form aggregates, such as dimers, trimers, and higher oligomers.[9] When the absorbance of PNDS was plotted against the concentration of PNDS, the absorbances of PNDS in an aqueous solution and in ethanol both strictly obeyed Beer's law. This means that an aggregation, if any, of PNDS would occur to only a negligible extent in these solutions.

As the next step, the azo-hydrazone tautomerism of PNDS was examined in aqueous surfactant solutions.

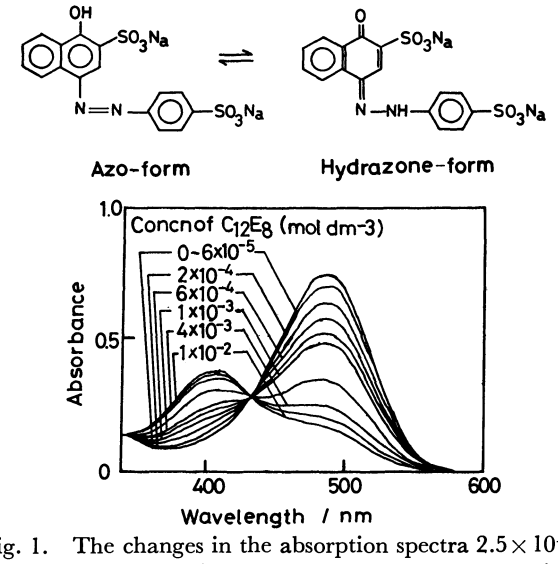

Fig. 1. The changes in the absorption spectra 2.5×10^{-5} mol dm^{-3} of PNDS as a function of the concentration of 8ED solution and the structure of PNDS.

The spectra of PNDS dissolved in surfactant solutions are expected to be different from those in water alone due to the interaction of the PNDS-surfactant. The changes in the absorption spectra of 2.5×10^{-5} mol dm^{-3} of PNDS as a function of the concentration of the 8ED solution and the structure of PNDS are shown in Fig. 1. The absorbance of the hydrazone form was constant until 7.0×10^{-5} mol dm^{-3}; thereafter, it decreased gradually with an increase in the concentration of 8ED. On the other hand, the absorbance of the azo form did not change until 6.5×10^{-5} mol dm^{-3} and then increased with an increase in the concentration of 8ED. Much as in the water–ethanol system, a sharp isobetic point was observed at 435 nm. Thus, the tautomerism from the hydrazone form to the azo form also proceeded in aqueous surfactant solutions. Further, it was found that the absorbances of the hydrazone form and of the azo form began to change near the cmc of 8ED.[10] This fact suggests that the tautomerism from the hydrazone form to azo form is related to a micellar phenomenon, since the absorbances of neither form changes below the cmc.

On the contrary, in the PNDS–SDS system, the absorbance of the hydrazone form decreased negligibly with an increase in the concentration of SDS from 0 to 20 mmol dm^{-3}, while the azo form in the spectrum did not appear at all in this concentration range. Since the cmc of SDS is 8 mmol dm^{-3}, the above result suggests that PNDS molecules are not solubilized into SDS micelles because, presumably, of an electric repulsion between PNDS anion molecules and SDS micelles. Thus, the properties of the mixed surfactant solutions of 8ED and SDS can be estimated by the utilization of the phenomenon that the azo-hydrazone tautomerism is not observed in an aqueous SDS solution, but only in an aqueous 8ED solution.

Figure 2 depicts the absorbances of PNDS *vs.* the concentration of 8ED in the presence of various concentrations of SDS. The concentration of 8ED at which the absorbance of the hydrazone form begins to decline is shifted to a higher concentration of 8ED with an increase in the concentration of SDS present in the mixtures. Similar behavior was observed in the change of the absorbance of the azo form in the mixtures of 8ED and SDS. This result can be interpreted as follows. The PNDS-anion molecules solubilized in 8ED micelles are expelled by the penetration of SDS into 8ED micelles due to electric repulsion; as a result, the mixed micelles of 8ED and SDS are formed. The present authors have previously reported[1,4] that the surface-tension curves of 8ED in the presence of SDS have a long plateau over a wide range of concentrations of 8ED and exhibit two break-points at lower and higher concentrations of 8ED. Further, they have pointed out[1,4] that the first break-points on the surface tension curves correspond to the cmc of mixed micelles of SDS and 8ED, while the second break-points indicate the existence of mixed micelles with excess 8ED. In general, the cmc of mixed micelles is well known to be lowered more than that of each single surfactant.[11–13] Although the present PNDS method does not provide the cmc values of mixed micelles of SDS and 8ED, it seems that the concentration

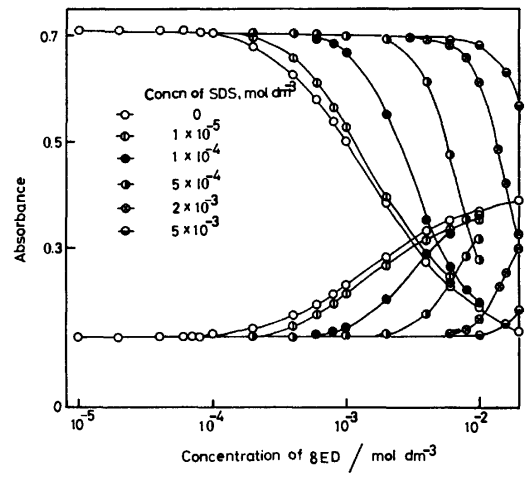

Fig. 2. The absorbances of PNDS *vs.* the concentration of 8ED in the presence of various concentrations of SDS.

region between the cmc of 8ED alone and the concentration of 8ED corresponding to that point at which the absorbance of the hydrazone form or the azo form begins to change is related, at least, to the presence of a mixed micelle of SDS and 8ED. The length of this region is extended with an increase in the concentration of SDS present in the mixtures. With further increase in the concentration of 8ED in the mixtures, the absorbance of the azo form or the hydrazone form begins to change. Since the concentration of 8ED corresponding to that at point which the absorbance of the azo form or the hydrazone form begins to change is correlated with the second break-point on the surface tension, PNDS might be solubilized into mixed micelles with excess 8ED in this concentration range.

Accordingly, the PNDS tautomer is a useful probe for elucidating the properties of mixed micelles of an anionic surfactant and a nonionic surfactant.

References

1) H. Akasu, M. Ueno, and K. Meguro, *J. Am. Oil Chem. Soc.*, **51**, 519 (1974).
2) K. Meguro, H. Akasu, and M. Ueno, *J. Am. Oil Chem. Soc.*, **53**, 145 (1976).
3) H. Akasu, A. Nishii, M. Ueno, and K. Meguro, *J. Colloid Interface Sci.*, **54**, 278 (1976).
4) Y. Takasawa, M. Ueno, and K. Meguro, *J. Colloid Interface Sci.*, **78**, 207 (1980).
5) N. Shoji, M. Ueno, and K. Meguro, *J. Am. Oil Chem. Soc.*, **53**, 165 (1976).
6) N. Shoji, M. Ueno, and K. Meguro, *J. Am. Oil Chem. Soc.*, **55**, 297 (1978).
7) E. E. Dreger, G. I. Keim, G. A. Miles, L. Shedlovsky, and J. Ross, *Ind. Eng. Chem.*, **36**, 610 (1944).
8) R. L. Reeves and R. S. Kaiser, *J. Org. Chem.*, **35**, 3670 (1970).
9) Y. Tanizaki and A. Ando, *Nippon Kagaku Zasshi*, **78**, 343 (1957).
10) K. Deguchi and K. Meguro, *J. Colloid Interface Sci.*, **38**, 596 (1972).
11) M. J. Schick and D. J. Manning, *J. Am. Oil Chem. Soc.*, **43**, 133 (1966).
12) H. Lange and K. H. Beck, *Kolloid Z. Z. Polym.*, **251**, 424 (1973).
13) J. H. Clint, *J. Chem. Soc., Faraday Trans. 1*, **71**, 1327 (1975).

The Relation between the Proton-induced Quenching Rate Constants and the Charge Densities of Aromatic Compounds[1)]

Haruo SHIZUKA* and Kinzo TSUTSUMI[2)]
Department of Chemistry, Gunma University, Kiryu, Gunma 376
(Received September 24, 1982)

Synopsis. A plot of log k_q' (the proton-induced quenching rate constants) *vs.* the charge densities P_Σ^* (or superdelocalizabilities S_Σ^*) in the excited state gave a straight line. The linear relation strongly supports the proton-induced quenching mechanism involving electrophilic protonation at the proper carbon atoms in the aromatic ring.[3)]

In previous papers,[4)] it has been shown that proton-induced fluorescence quenching competitive with proton transfer reactions is present (that is, the simple acid-base equilibrium cannot be accomplished in the excited state of aromatic amines) and the dynamic analyses containing the proton-induced quenching are, therefore, needed in order to obtain the correct pK_a^* values. The dynamic analyses by means of nanosecond (or picosecond) time-resolved spectroscopy with fluorimetry are applied to 1-pyrenylamine,[5)] phenanthrylamines,[6)] 1-anthrylamine,[7)] and naphthols.[8)] The Stuttgart group[9)] has supported our method to determine the pK_a^* values of naphthylamines. Similar experiments for excited naphthols have been reported by Harris and Selinger.[10)] The quenching mechanism induced by protons in polar media has been studied recently by this laboratory, and it is found that the fluorescence of aromatic compounds having an intramolecular CT structure is quenched effectively by protons and the proton-induced quenching is caused by electrophilic protonation at one of the carbon atoms of the aromatic ring leading to proton exchange (or isotope exchange).[3)] Hoytink[12)] and Waluk *et al.*[13)] have assumed a linear relationship between the logarithm of the protonation rate constant and π-electron density. It has been shown that the assumption fairly holds.[6)]

In the present paper, a plot of log k_p' (the proton-induced quenching rate constants) *vs.* the π-charge densities[14)] (or superdelocalizabilities)[15)] at the proper carbon atoms in the excited state of aromatic compounds was examined with the aid of a SCF-MO-CI method. The MO calculations of aromatic compounds were carried out by a semiempirical SCF-MO-CI method, which was described elsewhere.[11)] The calculations were performed by an electronic computer, HITAC 8800/8700, located at the Computer Center of the University of Tokyo. The rate constants k_q' for the proton-induced quenching are listed in Table 1.

Initially, the reaction parameter of the maximum charge density P_{max}^* (or superdelocalizability S_{max}^*) at the proper carbon atom of the aromatic compounds for the electrophilic protonation in the excited singlet state was used. A linear relation between log k_q' and P_{max}^* was derived: log $k_q'=22.73\,P_{max}^*-16.24$ (the correlation

TABLE 1. PROTON-INDUCED QUENCHING RATE CONSTANTS (k_q'),[a)] THE CHARGE DENSITIES (P_Σ^*),[b)] AND THE SUPERDELOCALIZABILITIES (S_Σ^*)[b)] OF AROMATIC COMPOUNDS

Compound	Quencher	Solvent	$k_q'/M^{-1}s^{-1}$	Ref.	$P_\Sigma^{*c)}$	$S_\Sigma^{*c)}$
1-Naphthylamine	H^+	5% CH_3CN in H_2O	8.9×10^9	4	2.274(5, 8)	0.4986(5, 8)
	D^+	5% CH_3CN in D_2O	6.0×10^9	4	2.274(5, 8)	0.4986(5, 8)
2-Naphthylamine	H^+	5% CH_3CN in H_2O	3.3×10^8	4	2.162(3, 5)	0.2867(5, 6)
	D^+	5% CH_3CN in D_2O	$1.9_6\times10^8$	4	2.162(3, 5)	0.2867(5, 6)
1-Anthrylamine	H^+	20% CH_3CN in H_2O	1.2×10^8	7	2.125(5, 9)	0.2956(3, 9)
	D^+	20% CH_3CN in D_2O	2.0×10^7	6	2.125(5, 9)	0.2956(5, 9)
1-Phenanthrylamine	H^+	10% CH_3CN in H_2O	1.6×10^8	6	2.070(7, 9)	0.2060(7, 9)
	D^+	10% CH_3CN in D_2O	5.4×10^7	6	2.070(7, 9)	0.2060(7, 9)
2-Phenanthrylamine	H^+	10% CH_3CN in H_2O	4.4×10^8	6	2.157(5, 7)	0.2148(5, 7)
	D^+	10% CH_3CN in D_2O	3.4×10^8	6	2.157(5, 7)	0.2148(5, 7)
3-Phenanthrylamine	H^+	10% CH_3CN in H_2O	9.3×10^7	6	2.081(4, 5)	0.2406(4, 5)
	D^+	10% CH_3CN in D_2O	4.4×10^7	6	2.081(4, 5)	0.2406(4, 5)
4-Phenanthrylamine	H^+	10% CH_3CN in H_2O	2.5×10^8	6	2.080(6, 8)	0.3094(6, 8)
	D^+	10% CH_3CN in D_2O	2.1×10^8	6	2.080(6, 8)	0.3094(6, 8)
9-Phenanthrylamine	H^+	10% CH_3CN in H_2O	1.9×10^8	6	2.102(5, 7)	0.2161(5, 7)
	D^+	10% CH_3CN in D_2O	1.6×10^8	6	2.102(5, 7)	0.2161(5, 7)
1-Pyrenylamine	H^+	20% CH_3CN in H_2O	3.7×10^7	5	2.123(4, 9)	0.2649(4, 9)
	D^+	20% CH_3CN in D_2O	1.4×10^7	5	2.123(4, 9)	0.2649(4, 9)
1-Naphthol	H^+	H_2O	7.5×10^8	8	2.202(5, 8)	0.1644(5, 8)
	D^+	D_2O	4.6×10^8	8	2.202(5, 8)	0.1644(5, 8)
1-Methoxynaphthalene	H^+	20% CH_3CN in H_2O	1.1×10^9	3	2.202(5, 8)	0.1644(5, 8)
	D^+	20% CH_3CN in D_2O	5.1×10^8	3	2.202(5, 8)	0.1644(5, 8)

a) The proton-induced quenching rate constants for the excited neutral species at 300 K. b) The two reactive positions were selected for determinatoin of the P_Σ^*(or S_Σ^*) value. For details see the text. c) The reactive state of all aromatic compounds in polar media is the lowest excited singlet state (^1L_a). The reactive positions are shown in parentheses.

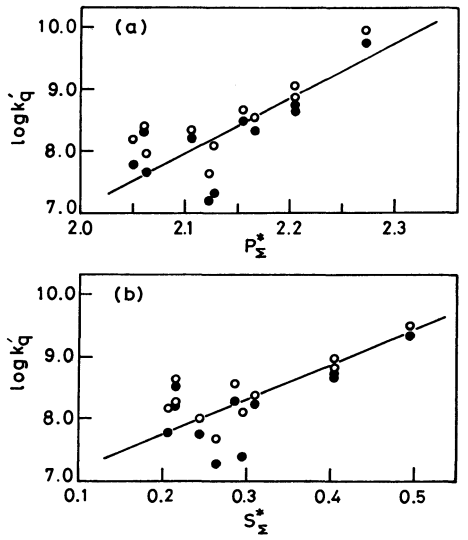

Fig. 1. Plots of (a) log k'_q *vs.* P^*_Σ and (b) log k'_q *vs.* S^*_Σ. ○: The H_2SO_4/H_2O system, ●: the D_2SO_4/D_2O system. The reactive positions were selected for determination of the P^*_Σ (or S^*_Σ) value. For details see the text.

coefficient $r=0.713$). However, lack of linear relation between log k'_q and S^*_{max} ($r=0.403$) was obtained. It is experimentally shown that the excited 1-methoxynaphthalene, for example, is attacked by protons mainly at the position 5 and slightly at the position 8.[3] Therefore, two reactive positions having larger P^* (or S^*) values in the lowest excited singlet state were selected from the carbon atoms as listed in Table 1. Figure 1 shows the plots of (a) log k'_q *vs.* P^*_Σ and (b) log k'_q *vs.* S^*_Σ, where P^*_Σ and S^*_Σ denote the summation values of charge densities and superdelocalizabilities at the two carbon atoms in the excited state, respectively. From Fig. 1, the following relations are obtained by the least squares method:

$$\log k'_q = 8.84\,P^*_\Sigma - 10.59 \qquad (r = 0.792), \qquad (1)$$

and

$$\log k'_q = 5.54\,S^*_\Sigma + 6.68 \qquad (r = 0.737). \qquad (2)$$

A plot of log k'_q *vs.* P^*_Σ (or S^*_Σ) where the reactive positions were expanded to three carbon atoms was also examined, and a straight line similar to that in Fig. 1 was obtained: $\log k'_q = 8.01\,P^*_\Sigma - 17.20$ ($r=0.785$); $\log k'_q = 5.13\,S^*_\Sigma + 8.12$ ($r=0.729$). From these results, the two reactive positions of the aromatic ring in the excited state may be adequate for determination of the P^*_Σ (or S^*_Σ) value. The linear relation in Fig. 1 strongly supports the mechanism that the proton-induced quenching is caused by electrophilic attack at one of carbon atoms of aromatic compounds.[3] Thus, one can approximately estimate the k'_q values for the proton-induced quenching of other aromatic compounds using Eq. 1 or 2.

References

1) Presented at the 45th National Meeting of the Chemical Society of Japan, Tokyo, April, 1982.
2) Department of Chemistry, Oyama Technical College, Oyama, Tochigi.
3) S. Tobita and H. Shizuka, *Chem. Phys. Lett.*, **75**, 140 (1980); H. Shizuka and S. Tobita, *J. Am. Chem. Soc.*, **104**, 6919 (1982).
4) K. Tsutsumi and H. Shizuka, *Chem. Phys. Lett.*, **52**, 485 (1977); *Z. Phys. Chem. (N. F.)*, **111**, 129 (1978).
5) H. Shizuka, K. Tsutsumi, H. Takeuchi, and I. Tanaka, *Chem. Phys.* **59**, 183 (1981).
6) K. Tsutsumi, S. Sekiguchi, and H. Shizuka, *J. Chem. Soc., Faraday Trans. 1*, **78**, 1087 (1982).
7) H. Shizuka and K. Tsutsumi, *J. Photochem.*, **9**, 334 (1978).
8) K. Tsutsumi and H. Shizuka, *Z. Phys. Chem. (N. F.)*, **122**, 129 (1980).
9) F. Hafner, J. Wörner, U. Steiner, and M. Hauser, *Chem. Phys. Lett.*, **72**, 139 (1980).
10) C. M. Harris and B. K. Selinger, *J. Phys. Chem.*, **84**, 891, 1366 (1980).
11) K. Tsutsumi, K. Aoki, H. Shizuka, and T. Morita, *Bull. Chem. Soc. Jpn.*, **44**, 3245 (1971).
12) G. J. Hoytink, *Recl. Trav. Chim. Rays-Bas.*, **11**, 885 (1957).
13) J. Waluk, A. Grabowska, and J. Lipinski, *Chem. Phys. Lett.*, **70**, 175 (1980).
14) C. A. Coulson and H. C. Longuet-Higgins, *Proc. R. Soc. London, Ser. A*, **191**, 39 (1947).
15) K. Fukui, T. Yonesawa, and C. Nagata, *Bull. Chem. Soc. Jpn.*, **27**, 423 (1954).

Preparation of Trifluoronitrosomethane

Teruo UMEMOTO* and Hideo TSUTSUMI
Sagami Chemical Research Center, Nishi-Ohnuma 4-4-1, Sagamihara, Kanagawa 229
(Received February 26, 1982)

Synopsis. Trifluoronitrosomethane was prepared in a good yield by pyrolysis of nitrosyl trifluoroacetate in a flow of nitrogen monoxide at 190 °C using refluxed perfluorotributylamine as a diluent.

Trifluoronitrosomethane (**1**)[1] is an industrially important material for the preparation of nitroso rubber.[2] There have been many investigations on the preparation of **1**.[2-4] Pyrolysis of nitrosyl trifluoroacetate (**2**)[5] in refluxed perfluorotributylamine has been adopted as a preparative method in spite of the low yield of **1**.[2,4] In the kinetic studies on the gas-phase thermal decomposition of **2**, Haszeldine *et al.* examined the effects of additives such as propene, **1**, and nitrogen monoxide under reduced pressure (about 10 mmHg = 1.33×10^3 Pa) and showed that the presence of nitrogen monoxide enhanced the formation of **1** while the presence of propene or **1** inhibited it.[6] The pyrolysis of **2** under reduced pressure was undesirable for the mass production of **1** because a large reactor was necessary for pyrolysis and was difficult to operate.

During our investigation of the pyrolysis of **2**, we found that **1** was obtained in a good yield when **2** was pyrolyzed in a flow of nitrogen monoxide at 190 °C using refluxed

$$\underset{\mathbf{2}}{CF_3COONO} \xrightarrow[\text{in a flow of NO}]{\Delta} \underset{\mathbf{1}}{CF_3NO} + CO_2$$

perfluorotributylamine as a diluent. Nitrogen monoxide could easily be removed from the gaseous products by introduction of oxygen into a stream of the gaseous products followed by washing with aqueous alkaline solution and **1** condensed in liquid nitrogen-isopentane traps as blue liquid (Fig. 1).

The influence of the flow rate of nitrogen monoxide on the yield of **1** was examined at a constant rate of addition of **2** (Table 1). The results show that the yield of **1** increases with an increase of the flow rate of nitrogen monoxide and reaches a maximum (77%) at the flow rate of 0.59 mmol/min. The decrease of the yield at the flow rates of more than 0.59 mmol/min is probably attributed to a shortage of the reaction time for **2** at such fast flow rates of nitrogen monoxide.

Table 1. Pyrolysis of **2** in the flow of nitrogen monoxide

Run	Addition rate of **2** mmol/min	Flow rate of NO mmol/min	Yield of **1**/%
1	1.1	0.09	44
2	1.1	0.18	56
3	1.1	0.45	75
4	1.1	0.59	77
5	1.1	0.89	52
6	1.1	1.79	44

The pyrolysis of **2** in the flow of nitrogen monoxide depressed the formation of by-products condensed in Dry Ice–acetone traps, while that without nitrogen monoxide yielded a large amount of by-products containing trifluoronitromethane and *O*-nitroso-*N*,*N*-bis(trifluoromethyl)hydroxylamine as components.[2,4]

Our procedure provides an efficient process for the preparation of **1** because of good yields as well as a flow system desirable for mass production.

Experimental

Nitrosyl Trifluoroacetate (2).[3d] *Caution*: Nitrosyl trifluoroacetate decomposes explosively at temperatures higher than about 100 °C.[3c]

Method A: Trifluoroacetic anhydride (155 ml, 1.1 mol) was added dropwise to dinitrogen trioxide (84 g, 1.1 mol) at −30 °C for 5 min. After stirring at −30 °C for 30 min and then at −5 °C for 3 h, the reaction mixture was distilled under reduced pressure to give **2** (230 g, 74%): bp 42—43 °C/82 mmHg (lit,[3c] 47 °C/94 mmHg).

Method B: Nitrosyl chloride (100 g, 1.54 mol) was condensed into a flask containing finely powdered silver trifluoroacetate (188 g, 0.85 mol) at −70 °C. Then the mixture was allowed to stand for 2 h at −20 °C and gradually warmed to room temperature. The excess of nitrosyl chloride was

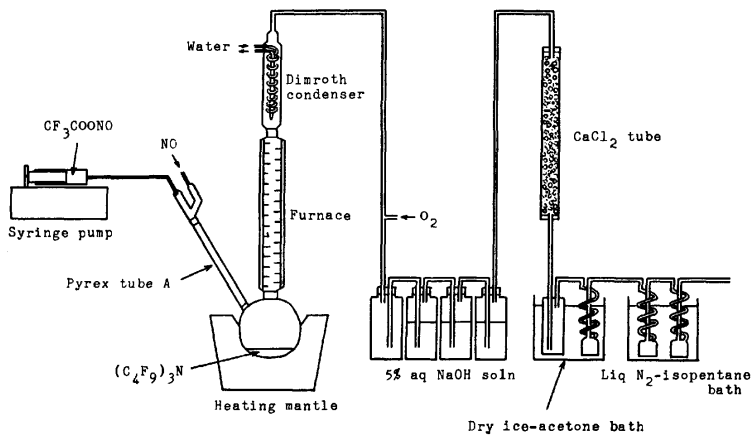

Fig. 1. Apparatus for pyrolysis of **2** in the flow of nitrogen monoxide.

removed and the residue distilled under reduced pressure to give **2** (87.7 g, 72%): bp 48 °C/92 mmHg.

*Trifluoronitrosomethane (**1**).* *Caution*: The pyrolysis must be carried out using a barricade in a hood for protection from a possible explosion hazard. The apparatus is shown in Fig. 1. The furnace is made of a Pyrex tube (2.5 cm × 50 cm, Vigreux tube) wrapped in an electrothermal heating tape controlled by a thermostat. The furnace was maintained at 190 °C. Trifluoroacetate **2** was added at a constant rate to a 500 ml-flask containing refluxed perfluorotributylamine (40 ml, bp 174 °C) through a Teflon tube by means of a syringe pump. A long Pyrex tube A (1.2 cm × 23 cm) is necessary to prevent an explosion of **2**. After the atmosphere in the furnace was replaced with nitrogen monoxide, the pyrolyses using 12.65 g of **2** were done under the conditions shown in Table 1. The results are summarized in Table 1. Oxygen was introduced to the apparatus at the same flow rate as that of nitrogen monoxide. The yields given in Table 1 are those of the product purified by distilling the blue liquid condensed in liquid nitrogen–isopentane traps. The properties of the product were in agreement with those of an authentic sample.

References

1) Toxic, blue gas of boiling point −84 °C.

2) M. C. Henry, C. B. Griffis, and E. C. Stump, "Fluorine Chemistry Reviews," ed by P. Tarrant, Marcel Dekker, Inc., New York (1967), Vol. 1, pp. 1—75.

3) a) R. N. Haszeldine, *J. Chem. Soc.*, **1953**, 2075; b) J. Banus, *ibid.*, **1953**, 3755; c) C. W. Tayler, T. J. Brice, and R. L. Wear, *J. Org. Chem.*, **27**, 1064 (1962); d) R. E. Banks, M. G. Barlow, R. N. Haszeldine, and M. K. McCreath, *J. Chem. Soc.*, **1966**, 1350, and references cited therein.

4) R. E. Banks, K. C. Eapen, R. N. Haszeldine, A. V. Holt, T. Myerscough, and S. Smith, *J. Chem. Soc., Perkin Trans. 1*, **1974**, 2532.

5) An explosive compound. See Ref. 3c.

6) R. Gibbs, R. N. Haszeldine, and R. F. Simmons, *J. Chem. Soc., Perkin Trans. 2*, **1972**, 773.

The Spectrophotometric Determination of Phosphate and Arsenate by Selective Extraction with Mixed Solvents

Junichi SHIDA,* Satoru KAKIZAKI, Yasuomi HOZUMI, Akiko ITOH, and (the late) Tsutomu MATSUO
Department of Applied Chemistry, Faculty of Engineering, Yamagata University, Jonan-4, Yonezawa, Yamagata 992
(Received July 15, 1982)

Synopsis. A spectrophotometric method for the simultaneous determination of phosphate and arsenate by selective solvent extraction was examined. First, molybdophosphate was extracted with 1-butanol–chloroform in the presence of molybdoarsenate, and then the molybdoarsenate in the aqueous phase was extracted with MIBK, followed by reduction directly in the organic phase to Molybdenum Blue.

Most methods for the determination of phosphate and arsenate are spectrophotometric methods, based on the formation of the yellow molybdophosphate and molybdoarsenate, followed by the reduction of these complexes to Molybdenum Blue. Arsenate interferes seriously with the determination of phosphate, since their chemical properties are similar.[1-3]

Previous studies of the separation of phosphate, silicate, arsenate, and germanate have shown that phosphate can be separated from mixtures of the four elements as the molybdophosphate by mixed-solvent extraction with (1+3) 1-butanol–chloroform[4] or (2+3) isobutyl alcohol–chloroform.[5]

Paul[6-9] has reported methods for the simultaneous determination of phosphorus, arsenic, silicon, and germanium as heteropoly-blue complexes. However, while simple, these methods lack precision, sensitivity, and rapidity. The present authors have now examined the separation of phosphate and arsenate by selective extraction with various mixed solvents. This paper will report a rapid, sensitive, and accurate method combining solvent extractions and spectrophotometry for the determination of phosphate and arsenate.

Experimental

Apparatus and Reagents. A Hitachi, model 139, spectrophotometer with 10-mm silica cells was used. An Iwaki, model S-L type KM, shaker was used to shake the separatory funnel. All the chemicals were of analytical-reagent grades and were stored in polyethylene bottles to prevent contamination by silica. The water was deionized after distillation.

Standard Phosphate Solution, 200 μg ml^{-1}: Dissolve 0.2198 g of potassium dihydrogenphosphate in water and dilute to 250 ml. This solution is then diluted as required to 2 μg P(V) ml^{-1} with water.

Standard Arsenate Solution, 200 μg As(V) ml^{-1}: Dissolve 0.2082 g of disodium hydrogenarsenate in water and dilute to 250 ml. This solution is then diluted as required to 10 μg As(V) ml^{-1} with water.

Ammonium Molybdate Solution, 0.1 M†: Dissolve 1.77 g of hexaammonium heptamolybdate tetrahydrate, $(NH_4)_6Mo_7O_{24}\cdot 4H_2O$ in water and dilute to 1 l.

Procedure. *a) Determination of Phosphate*: Transfer a 20-ml portion of the sample solution (previously neutralized) containing less than 20 μg P(V) and 50 μg As(V) into a 100-ml separatory funnel. Add 4 ml of 0.1 M molybdate solution, 5 ml of 0.5 M potassium chloride, and 3 ml of 2.5 M hydrochloric acid. Dilute with water to 25 ml, mix well, and allow to stand for 10 min. Then, add 10 ml of (7 : 13, v/v)1-butanol–chloroform and shake the funnel vigorously for 5 min with a mechanical shaker. After the phase separation, drain the organic phase into a 20-ml stoppered test tube containing *ca.* 2 g of anhydrous sodium sulfate. Transfer the organic solvent into a 10-ml silica cell, measure the absorbance at 310 nm against a reagent blank. Then, add 10 ml of (3 : 7, v/v) 1-butanol–chloroform to the originasl eparatory funnel, and repeat the extraction and measurement of the absorbance until the molybdophosphate is removed. Refer the total absorbance reading to a calibration curve obtained using a standard phosphate solution.

b) Determination of Arsenate:[10] Add 10 ml of isobutyl methyl ketone (MIBK) to an aqueous solution containing the molybdoarsenate by means of the procedure *a*) described above. Shake the funnel vigorously for 1 min and allow to stand for about 5 min to separate the phases. Discard the aqueous phase and wash the MIBK extract with 10 ml of (1+20)hydrochloric acid. Repeat the washing with 10 ml of (1+20)hydrochloric acid once more to remove the excess of molybdate. Transfer the MIBK extract into a 25-ml volumetric flask, add 4 ml of ethanol and 1 ml of 0.4 M tin(II) chloride, and dilute to the mark with ethanol. Mix well and allow to stand for 20 min. Measure the absorbance at 740 nm against a reagent blank.

Results and Discussion

Effect of the Hydrochloric-acid Concentration. The optimum acidity of the aqueous phase for he formation of the molybdophosphate was found to be 0.15—0.50 M

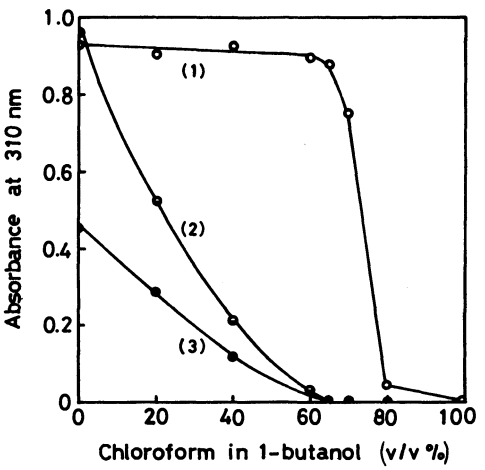

Fig. 1. Effect of the concentration of chlororm in 1-butanol on the extraction.
(1) P(V): 10 μg, (2) As (V): 40 μg, (3) As(V): 20 μg. [HCl]: 0.3 M, [Mo]: 1.6×10^{-2} M, reference: reagent blank.

† 1 M=1 mol dm^{-3}.

hydrochloric acid. Molybdoarsenate was extracted into MIBK in the same range as molybdophosphate. The concentration of 0.3 M hydrochloric acid in the initial solution was, therefore, chosen as the optimum.

Effect of the Concentration of Chloroform in 1-Butanol on the Extraction of Molybdophosphate and Molybdoarsenate. As is shown in Fig. 1, the optimum range was 60—65 v/v % chloroform in 1-butanol to separate the molybdophosphate from the molybdoarsenate. Therefore, 65 v/v% chloroform in 1-butanol, that is, (7 : 13, v/v) 1-butanol–chloroform, was used in the subsequent work. In order to remove the molybdophosphate completely, it was necessary to extract it twice or three times with 1-butanol–chloroform. When the molybdophosphate was extracted with 10 ml of 65 v/v% chloroform in 1-butanol, it was found that the concentration of chloroform in the organic phase turned to 70 v/v%. Then, for the second or third extraction, 70 v/v% chloroform in 1-butanol, that is, (3 : 7, v/v) 1-butanol–chloroform, was used.

The Choice of Extractant. Several mixed organic solvents (1-butanol–cyclohexane, MIBK–chloroform, MIBK-cyclohexane,[1] *etc.*) were examined as extractants. The considerations for the choice of the organic solvents to extract the molybdophosphate are as follows: (1) The solvent should have a greater specific gravity of the organic solvents than that of water, such a greater specific gravity being advantageous for the continuous extraction of molybdoarsenate; (2) the absorbance of reagent blank is low, and (3) it should be possible to separate the phases rapidly after shaking. The mixture of 1-butanol and chloroform was most suitable.

Calibration Curves. The calibration curves for the phosphate and arsenate obtained by the proposed procedure were linear in the ranges of 0—10 μg P(V) and 0—100 μg As(V), and the molar absorptivities, as calculated from the slope of the curve, were 3.0×10^4 $l\cdot mol^{-1}\cdot cm^{-1}$ (at 310 nm) and 1.6×10^4 $l\cdot mol^{-1}\cdot cm^{-1}$ (at 740 nm) respectively.

Recovery of Phosphate and Arsenate. The recovery of phosphate and arsenate in mixtures of the other was examined by the procedure previously described. The results are shown in Table 1. The values were means of the six determinations, and the coefficient of variation was 3—5%. A good recovery and reproducibility were obtained. At higher As(V) concentrations, however, As(V) caused positive error in the determination of P(V).

Table 1. Recovery of phosphorus(V) and arsenic(V)

Amount of elements added μg		Found μg		Recovery %	
P(V)	As(V)	P(V)	As(V)	P(V)	As(V)
4.0	100.0	4.4	98.0	110	98
4.0	50.0	4.2	50.0	105	100
6.0	40.0	6.0	40.8	100	102
20.0	50.0	19.6	51.0	98	102
6.0	15.0	6.0	15.3	100	102
15.0	12.0	14.7	12.0	98	100
20.0	10.0	19.6	10.2	98	102
20.0	6.0	20.0	5.9	100	98

Effect of Diverse Ions. The effect of silicate and germanate ions, which form heteropoly acids, was investigated on the absorbance produced from 6.0 μg P(V) by the proposed procedure. Less than a 2500-fold Si(IV) and a 120-fold Ge(IV) weight excess did not interfere.

References

1) T. Fujinaga, T. Hori, and Y. Kanada, *Bunseki Kagaku* **28**, 222 (1979).
2) H. Akaiwa, H. Kawamoto, and T. Takenouchi, *Nippon Kagaku Kaishi*, **1980**, 833.
3) J. Shida and T. Matsuo, *Bull. Chem. Soc. Jpn.*, **53**, 2868 (1980).
4) C. Wadelin and M. G. Mellon, *Anal. Chem.*, **25**, 1668 (1953).
5) T. Kiba and M. Ura, *Nippon Kagaku Zasshi*, **76**, 520 (1955).
6) J. Paul, *Anal. Chim. Acta*, **23**, 178 (1960).
7) J. Paul, *Mikrochim. Acta*, **1965**, 830.
8) J. Paul, *Mikrochim. Acta*, **1965**, 836.
9) J. Paul, *Anal. Chim. Acta*, **35**, 200 (1966).
10) JIS K 0102 (1974).

Optical Determination of Carboxylate Ions Utilizing Flocculation of Colloidal $Al(OH)_3$

Masayuki MUTO* and Yuko YAMAHACHI
Department of Chemistry, Faculty of Education, Wakayama University, Masago, Wakayama 640
(Received July 19, 1982)

Synopsis. Flocculation of colloidal $Al(OH)_3$ occurs by adding a suitable amount of Congo Red, and the supernatant liquid become scolorless. When some carboxylate ions are present in this colloidal mixture, the quantity of $Al(OH)_3$ decreases because of the formation of complexes, and then excess Congo Red gives a red color to the supernatant liquid. The indirect determination of some kinds of carboxylate ions was carried out by applying the measurement of optical absorption to the supernatant fraction.

An empirical method of measurement of the degree of fatigue was developed by Takeya and Kawada,[1] as described below. A mixture of alkaline Congo Red solution, aluminium potassium sulfate solution, and a body fluid (a serum or urine) was allowed to stand. After centrifugation of the colloidal liquid, the supernatant fraction was determined spectrophotometrically. According to their report, the supernatant fraction became colorless when water was used in place of body fluid. The reason that the supernatant became deep or light in color was, they reported, that the body fluid worked as a protective colloid toward colloidal $Al(OH)_3$.

We considered that the body fluid did not act as a protective colloid, but that carboxylate ions contained in the body fluid functioned as masking agents of Al^{3+}. That is, in the absence of body fluid, $Al(OH)_3$ is flocculated by a suitable amount of pigment anion and the supernatant fraction becomes colorless. However, in the presence of the body fluid, $Al(OH)_3$ decreases, Al^{3+} is masked by carboxylate ions contained in body fluid, and then excess Congo Red which takes no part in flocculation gives a red color to the supernatant fraction.

On the assumption described above, it became possible to determine indirectly carboxylate ion in solution in the suitable concentration range by the measurement of optical absorption of the supernatant fraction of the colloidal mixture.

Experimental

Reagent and Procedure. Takeya and Kawada's method[1] was modified. Aqueous solutions of carboxylate ions, citrate (0.1—1.2 mg/ml), oxalate (0.2—3.2 mg/ml) and lactate (2—32 mg/ml) were used as test solutions; all of these were used as sodium salts.

An aqueous mixture of 1 ml of test solution (including incremental amounts of carboxylate ions), 2 ml of 1.63 mM of aluminium potassium salfate solution, 2 ml of 0.35 mM of Congo Red solution and 2 ml of 4.5 mM of sodium hydroxide solution was allowed to stand for 2 h at 20 °C. In this mixture the Al^{3+}/OH^- is 1/2.76. After centrifugation, the supernatant fraction was measured spectrophotometrically at 490 nm.

Results and Discussion

As shown in Figs. 1—4, the curves of optical absorbance *vs.* content of carboxylate ions are somewhat similar to pH titration curves. In the lower concentration range of test solution, the curves are flat. In that flat part, Congo Red anion is strongly adsorbed. In the higher concentration range of test solution, the curves also appear flat. In the latter, carboxylate ion acts as a masking agent for a large amount of Al^{3+}, and it becomes hard for flocculation of $Al(OH)_3$ to occur.

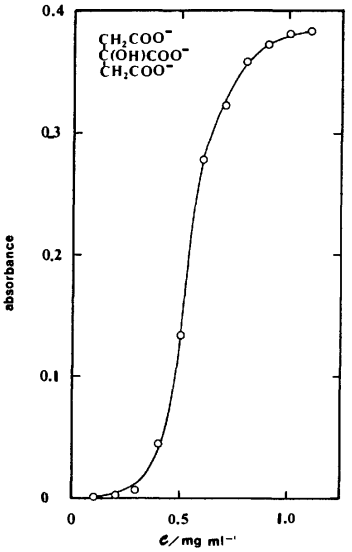

Fig. 1. Absorbance *vs.* content of citrate.

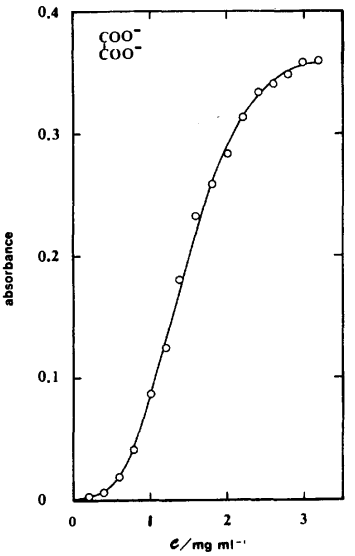

Fig. 2. Absorbance *vs.* content of oxalate.

As shown in Figs. 1—3, the more the number of COO^- and of other anionic groups in a carboxylate ion increases, the larger the masking effect towards Al^{3+} becomes; that is, carboxylate ions can act as chelating agents to Al^{3+}. Mono-dentate ligands, such as acetate and hippurate, are not suitable for this experiment,

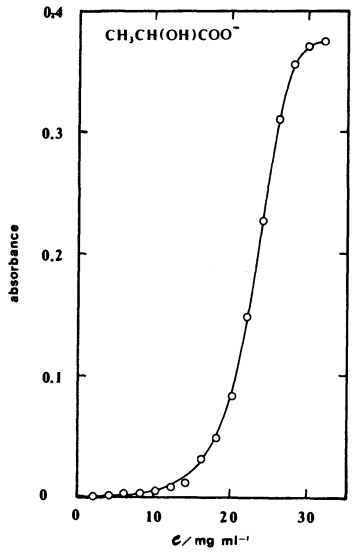

Fig. 3. Absorbance *vs.* content of lactate.

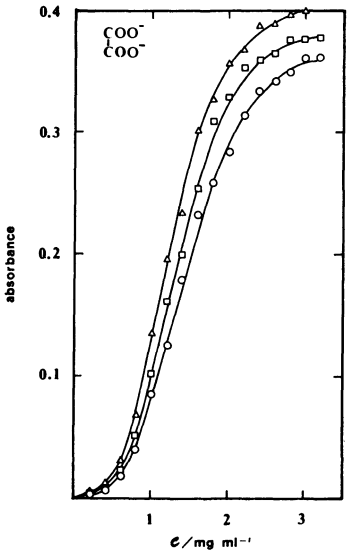

Fig. 4. The effect of temperature on absorbance. —△—: 10 °C, —○—: 20 °C, —□—: 30 °C.

because their masking abilities are very low.

The effect of temperature when oxalate is used as a sample is shown in Fig. 4. The slopes of the curves at lower (10 °C) and higher (30 °C) temperature become greater than that at the appropriate temperature (20 °C); this slope increase is not observed in the range 17—23 °C. At low temperature the formation of colloidal $Al(OH)_3$ is slow, while at high temperature its formation is fast, but the adsorption of pigment anion on the colloidal $Al(OH)_3$ occurs with difficulty. These tendencies are also observed for other carboxylate ions.

References

1) O. Takeya and T. Kawada, *Igaku To Seibutsugaku*, **4**, 230, 234, 244, (1943). Subsequently, more than 100 reports appeared which applied their method, *e.g.*, N. Matsumoto *Bull. Inst. Constit. Med., Kumamoto University*, **26**, 154 (1975); **29**, 429 (1979).

Palladium-catalyzed Reaction of Isoprene with Water in Presence of Carbon Dioxide and Base

Yoshio INOUE,* Michio SATO, Masaki SATAKE, and Harukichi HASHIMOTO
Department of Applied Chemistry, Faculty of Engineering, Tohoku University, Aramaki-Aoba, Sendai 980
(Received May 21, 1982)

Synopsis. Palladium(0)-catalyzed reaction of isoprene with water was enhanced by the presence of carbon dioxide and a base to give dimethyloctadienols. The same catalyst was found to dehydrate the dimethyloctadienols to afford the corresponding dimethyloctatrienes. The effect of acidity of water on the isoprene-water reaction was also studied.

Terpene alcohols such as geraniol and linalool are considered as made up of head-to-tail dimers of isoprene with the addition of a molecule of water. They occur in oil of rose and other flower essences and are important perfume ingredients.

It is known that the palladium-catalyzed reaction of butadiene with water to give octadienols is accelerated by the presence of carbon dioxide (CO_2).[1] The role of CO_2 is not clear. The possibility of the direct effect has been suggested. To synthesize terpene alcohols in one step from the corresponding reaction of isoprene with water is an interesting subject to be challenged. Usually the reactivity of isoprene is lower than that of butadiene and the reaction has been little studied.[2] Keim *et al.* investigated the reaction by palladium- or platinum-based system and found that the distribution of the isomeric terpenols were subtly influenced by catalyst metal, ligand, reaction temperature, and reaction time.[2a] Concerning the study on the catalytic fixation of CO_2 in 1,3-dienes,[3] we examined the isoprene-water reaction and found that the addition of a base such as $KHCO_3$ accelerated the reaction. The effect of acidity of water on the reaction was also studied.

Results and Discussion

Different from butadiene-water reaction, $Pd(PPh_3)_4$-catalyzed reaction of isoprene with water was very slow even in the presence of CO_2, and the main product was an isoprene dimer, 2,7-dimethyl-1,3,7-octatriene (**1**). But when a base such as $KHCO_3$ was added to the system, a considerable increase in the proportion of dimethyloctadienols was attained. Results are summarized in Table 1. The main alcohols formed were 2,7-dimethyl-1,7-octadien-3-ol (**2**) and 2,7-dimethyl-2,7-octadien-1-ol (**3**), tail-to-tail dimers of isoprene with addition of a molecule of water. The yield of head-to-tail type products, *i.e.*, 2,6-dimethyl-1,7-octadien-3-ol and 3,7-dimethyl-1,7-octadien-3-ol, was small (1—2%) by this catalyst system. It is reported that the addition of *p*-benzoquinone increased **3** in the yield by $Pd(PPh_3)_4$ catalyst.[2a] The reaction occurred from the reaction

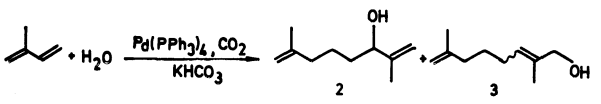

Table 1. Reaction of isoprene with water[a]

Base (mmol)	Isoprene conversion %	Isoprene dimer[b] (%)	C_{10}-Alcohol (%)	Yield/%[c] 2	3
—[d]	20	≈100	≈0	Trace	0
—	45	86	14	4	Trace
Me_3N(33)	74	67	33	12	4
Me_3N(30)[e]	64	52	48	17	4
$KHCO_3$(26)	76	54	46	19	6
$KHCO_3$(26)[d]	59	50	50	16	10
K_2CO_3(27)	79	71	29	12	6
Me_4NOH(5)	59	59	41	16	9

a) Isoprene, 45 mmol; $Pd(PPh_3)_4$, 0.2—0.3 mmol; water, 200—300 mmol; dioxane, 20 ml; CO_2, 40 atm(initial); 110—120 °C; 20 h. b) The main dimer was **1**. c) The yield is based on the isoprene charged (by gas chromatography). d) Without CO_2(under N_2 1 atm). e) Reaction temperature was 90 °C.

temperature 80 °C and the conversion of isoprene increased as the temperature was raised. Bases such as trimethylamine, tetramethylammonium hydroxide, and K_2CO_3 can be used as the co-catalyst. Interestingly $KHCO_3$ was effective by itself as co-catalyst without CO_2, whereas trimethylamine and K_2CO_3 were not effective. $Pd(diphos)_2$[diphos=$Ph_2PCH_2CH_2PPh_2$] scarecely showed the catalytic activity. Dioxane and diethylene glycol dimethyl ether were the best solvent tested. Tetrahydrofuran, 1,2-dimethoxyethane, and *t*-butyl alcohol, which were used for the butadiene-water reaction, were not so effective for the isoprene-water reaction. The same catalyst system accelerated also the butadiene-water reaction. For instance butadiene (180 mmol) and $KHCO_3$ (1 mmol) in 5 ml water gave 1,7-octadien-3-ol (13 mmol), 2,7-octadien-1-ol (49 mmol), and 1,3,7-octatriene (3 mmol) for 4 h reacton at 80 °C in dioxane by $Pd(PPh_3)_4$ (0.18 mmol) and CO_2 (40 atm), while 1,7-octadien-3-ol (7 mmol), 2,7-octadien-1-ol (44 mmol), and 1,3,7-octatriene (4 mmol) were produced under CO_2 pressure without $KHCO_3$.

Interestingly the base-added system catalyzed the dehydration of dimethyloctadienols to give the corresponding dimethyloctatrienes. For example dimethyloctadienols which were composed of **2** (2.8 mmol), **3** (0.7 mmol), and the other octadienols (0.6 mmol) afforded **1** (1.2 mmol) and the other dimers (1.2 mmol) on treatment with $Pd(PPh_3)_4$ (0.2 mmol), trimethylamine (19 mmol), and CO_2 (40 mmol) in dioxane (20 ml) and water (2.6 ml) at 120 °C for 20 h. Control experiments showed that both CO_2 and a base were necessary to the dehydration. This can partly explain the relatively low yield of dimethyloctadienols.

Co-existence of CO_2 and a base is a sort of buffer. The change of acidity of water may accelerate the reac-

Table 2. Effect of the acidity of water[a)]

Buffer solution (pH)	Ionic strength	Isoprene conversion %	Isoprene dimer (%)	C_{10}-Alcohol[b)] (%)
6.8[c)]	0.11	69	80	20
7.2[c)]	0.08	82	72	28
8.1[c)]	0.10	68	77	23
11.0[d)]	0.10	66	72	28
12.3[d)]	0.13	64	76	24

a) Isoprene, 45 mmol; $Pd(PPh_3)_4$, 0.2 mmol; buffer solution, 5 ml; dioxane, 20 ml; 110—120 °C; 20 h. b) The main alcohols were **2** and **3**. c) KH_2PO_4–Na_2HPO_4. d) KH_2PO_4–NaOH.

tion. So the effect of water acidity on the reaction was examined using several buffer solutions of various pH. Results are shown in Table 2. The reaction did not occur under pH 6 and almost no effect of ionic strength (μ) was observed between μ 0.11 and μ 2.7 at pH 6.8. A slight increase in the proportion of dimethyloctadienols was observed compared to the base-free system, and the proportion was almost constant (about 25%) between pH 6.8 and 12.3. When CO_2 was introduced to 40 atm at pH 6.8, it was improved to 43%. CO_2 in water exists mainly as the form of HCO_3^- in the pH range 7 to 10.[4)] Taking the novel effect of $KHCO_3$ on the isoprene-water reaction, the anion HCO_3^- is possibly playing an important part.[1)]

Experimental

The diene-water reaction was done in a 100 ml stainless-steel autoclave. Typically, isoprene (2.9 g, 43 mmol), $Pd(PPh_3)_4$ (0.36 g, 0.3 mmol), trimethylamine 30% solution (5.4 g), and dioxane (20 ml) were charged in it under an inert atmosphere. Then CO_2 was introduced up to 40 atm and the autoclave was heated at 112 °C for 20 h. After the reaction the organic layer was quantitatively analyzed by gas chromatography (FFAP, 2 m, 150 °C, helium as a carrier gas), showing the formation of 3,7-dimethyl-1,7-octadien-3-ol (0.2 mmol), 2,6-dimethyl-1,7-octadien-3-ol (0.4 mmol), **2** (2.4 mmol), and **3** (0.8 mmol) in addition to isoprene dimers (8.0 mmol). Separation of the octadienols formed from the reaction mixture was done by column chromatography (silica gel/benzene, then methanol). Individual alcohol was isolated by preparative gas chromatography (FFAP, 2 m, 185 °C, hydrogen as a carrier gas).

2,7-Dimethyl-1,7-octadien-3-ol (2): IR(neat); 3400, 1650, 890 cm^{-1}. NMR (CCl_4); δ 1.1 (1H, s), 1.4 (4H, m), 1.6 (6H, s), 1.8—2.1 (2H, m), 3.9 (1H, br), 4.55 (2H, s), 4.7 (2H, m). MS (*m/e*); 68, 71, 98, 111, 137, 139, 154 (M^+).

2,7-Dimethyl-2,7-octadien-1-ol (3): IR(neat); 3400, 1650, 890 cm^{-1}. NMR (CCl_4); δ 1.2 (1H, s), 1.55 (3H, s), 1.6 (3H, s), 1.9 (6H, m), 3.8 (2H, s), 4.5 (2H, s), 5.25 (1H, t).

3,7-Dimethyl-1,7-octadien-3-ol: IR(neat); 3400, 1650, 1000, 910, 890 cm^{-1}. NMR (CCl_4); δ 1.0 (1H, s), 1.1 (3H, s), 1.4 (4H, m), 1.6 (3H, s), 1.9 (2H, m), 4.55 (2H, s), 4.75—5.15 (2H, m), 5.45 (1H, m).

2,6-Dimethyl-1,7-octadien-3-ol: IR(neat); 3400, 1000, 900, 890 cm^{-1}. NMR (CCl_4); δ 0.96 (3H, d), 1.1 (1H, s), 1.3 (4H, m), 1.65 (3H, s), 2.0 (1H, br), 3.9 (1H, br), 4.7 (2H, s), 4.9 (2H, m), 5.3—5.6 (1H, m).

References

1) K. E. Atkins, W. E. Walker, and R. M. Manyik, *Chem. Commun.*, **1971**, 330.

2) a) W. Keim, A. Behr, and H. Rzehak, *Tenside Deterg.*, **16**, 113 (1979); b) L. I. Zakharkin, S. A. Babich, and I. V. Pisareva, *Izv. Akad. Nauk SSSR, Ser. Khim.*, **1976**, 1616.

3) Y. Sasaki, Y. Inoue, and H. Hashimoto, *J. Chem. Soc., Chem. Commun.*, **1976**, 605; *Bull. Chem. Soc. Jpn.*, **51**, 2375 (1978); Y. Inoue, S. Sekiya, Y. Sasaki, and H. Hashimoto, *J. Syn. Org. Chem. Jpn.*, **36**, 328 (1978); A. Musco, C. Perego, and V. Tartiari, *Inorg. Chim. Acta*, **28**, L141 (1978); A. Musco, *J. Chem. Soc., Perkin Trans. 1*, **1980**, 693; T. Ito, Y. Kindaichi, and Y. Takami, *Nippon Kagaku Kaishi*, **1979**, 1276.

4) K. Asada, "Tansangasu No Kagaku," ed by T. Osa, Kyoritsu Shuppan, Tokyo (1976), p. 137.

Esterification of Aromatic Carboxylic Acids with Alcohols Using 2-Chloro-3,5-dinitropyridine as a Condensing Agent

Seiji TAKIMOTO,* Naomi ABE, Yasushi KODERA, and Hiroshi OHTA
Department of Chemistry, Faculty of Science, Fukuoka University, 8-19-1 Nanakuma, Johnan-ku, Fukuoka 841-01
(Received May 26, 1982)

Synopsis. The reaction of 2-chloro-3,5-dinitropyridine (CDNP) with carboxylic acids and alcohols was examined, and it was found that CDNP was a useful condensing agent. Various esters were prepared in good yields.

It has been reported[1,2] that polynitrohalobenzenes are useful condensing agents for the ester synthesis. In continuation of our studies on the development of new condensing agents, we tried to use 2-chloro-3-nitropyridine, 2-chloro-5-nitropyridine, and 2-chloro-3,5-dinitropyridine (CDNP) and found that CDNP was a useful condensing agent for the preparation of esters.

In the first place, we searched for effective bases for the condensation of benzoic acid and 1-propanol using CDNP.

Pyridine and 4-dimethylaminopyridine (DMAP)[3] proved to give good results (94 and 93% yields, respectively).

Other bases such as triethylamine or 1,8-diazabicyclo-[5.4.0]undec-7-ene did not give good yields (56 and 17% yields, respectively).

In the next experiment, the reaction of benzoic acid with 1-propanol using CDNP was carried out in the presence of Lewis acid with the consideration that the coordination of Lewis acid to CDNP would form reactive species. Lewis acids such as $BF_3 \cdot OEt_2$, $TiCl_4$, $AgBF_4$, and AgCN, which are often used as efficient catalysts, gave only small amounts of the ester.

A significant solvent effect was observed in the condensation of 2,4,6-trimethylbenzoic acid and 1-propanol using CDNP in the presence of DMAP, the ester being obtained in 81% yield in acetonitrile, and 62% yield in dichloromethane as solvents.

Examples of esterification are shown in Table 1.

Benzoic acid was smoothly esterified in pyridine by the procedure in the experimental part. The esterification of sterically hindered 2,4,6-trimethylbenzoic acid with alcohols in pyridine was slow at room temperature. Consequently, the reactions were run by refluxing to give the desired esters in good yields (entries 6, 8, 9, and 11). It has been reported[2] that the esterification of 2,3,6-trimethylbenzoic acid with secondary or tertiary alcohols using 2-chloro-1,3,5-trinitrobenzene is difficult. In contrast, it was found that 2,4,6-trimethylbenzoic acid was esterified with tertiary alcohols such as 2-methyl-2-propanol or 3-ethyl-3-pentanol using CDNP (entries 13 and 15).

The esterification in acetonitrile using a limited amount of DMAP (2 mol equiv. per 1 mol of CDNP) did not give good results (entries 10, 12, 14, and 16) except for entry 7.

When 4-nitro- or 3,5-dinitrobenzoic acid was esterified, yields of the esters were satisfactory (entries 17—26).

On the other hand, when CDNP, benzoic acid, and pyridine were mixed in a 1 : 1 : 2 molar ratio under the absence of alcohol, benzoic anhydride was formed in 79% yield.

Although clear conclusions regarding the esterification reaction mechanism await further study, the main esterification reaction seems to proceed through the acid anhydrides presumably formed from the dinitropyridyl esters by the attack of carboxylate anions remaining in the mixture. However, the direct attack of alcohols on dinitropyridyl esters are considered to participate to varied extents.

TABLE 1. ESTERIFICATION OF CARBOXYLIC ACIDS

	Acid (1 mmol)	Alcohol (1.2 mmol)	Reaction conditions[a] base; temp/°C	Yield of ester/%
1	$C_6H_5CO_2H$	1-Propanol	Pyridine; r.t.	94[b]
2	$C_6H_5CO_2H$	Benzyl alcohol	Pyridine; r.t.	86[b]
3	$C_6H_5CO_2H$	2-Propanol	Pyridine; r.t.	89[b]
4	$C_6H_5CO_2H$	Cyclohexanol	Pyridine; r.t.	74[b]
5	$C_6H_5CO_2H$	2-Methyl-2-propanol	Pyridine; r.t.	70[b]
6	$2,4,6\text{-}(CH_3)_3C_6H_2CO_2H$	1-Propanol	Pyridine; 115	96[c]
7	$2,4,6\text{-}(CH_3)_3C_6H_2CO_2H$	1-Propanol	DMAP; r.t.	81[c]
8	$2,4,6\text{-}(CH_3)_3C_6H_2CO_2H$	Benzyl alcohol	Pyridine; 115	98[c]
9	$2,4,6\text{-}(CH_3)_3C_6H_2CO_2H$	2-Propanol	Pyridine; 115	90[c]
10	$2,4,6\text{-}(CH_3)_3C_6H_2CO_2H$	2-Propanol	DMAP; 82	53[c]
11	$2,4,6\text{-}(CH_3)_3C_6H_2CO_2H$	Cyclohexanol	Pyridine; 115	94[c]
12	$2,4,6\text{-}(CH_3)_3C_6H_2CO_2H$	Cyclohexanol	DMAP; 82	37[c]
13	$2,4,6\text{-}(CH_3)_3C_6H_2CO_2H$	2-Methyl-2-propanol	Pyridine; 115	91[c]
14	$2,4,6\text{-}(CH_3)_3C_6H_2CO_2H$	2-Methyl-2-propanol	DMAP; 82	30[c]
15	$2,4,6\text{-}(CH_3)_3C_6H_2CO_2H$	3-Ethyl-3-pentanol	Pyridine; 115	84[c,d]
16	$2,4,6\text{-}(CH_3)_3C_6H_2CO_2H$	3-Ethyl-3-pentanol	DMAP; 82	12[c]
17	$4\text{-}NO_2C_6H_4CO_2H$	1-Propanol	Pyridine; r.t.	88[e]
18	$4\text{-}NO_2C_6H_4CO_2H$	Benzyl alcohol	Pyridine; r.t.	76[e]
19	$4\text{-}NO_2C_6H_4CO_2H$	2-Propanol	Pyridine; r.t.	79[e]
20	$4\text{-}NO_2C_6H_4CO_2H$	Cyclohexanol	Pyridine; r.t.	82[e]
21	$4\text{-}NO_2C_6H_4CO_2H$	2-Methyl-2-propanol	Pyridine; 115	68[e]
22	$3,5\text{-}(NO_2)_2C_6H_3CO_2H$	1-Propanol	Pyridine; r.t.	73[e]
23	$3,5\text{-}(NO_2)_2C_6H_3CO_2H$	Benzyl alcohol	Pyridine; r.t.	92[e]
24	$3,5\text{-}(NO_2)_2C_6H_3CO_2H$	2-Propanol	Pyridine; r.t.	80[e]
25	$3,5\text{-}(NO_2)_2C_6H_3CO_2H$	Cyclohexanol	Pyridine; r.t.	88[e]
26	$3,5\text{-}(NO_2)_2C_6H_3CO_2H$	2-Methyl-2-propanol	Pyridine; 115	58[e]

a) All reactions were carried out for 30 min. b) Isolated yield of once distilled product. c) Isolated yield of purified product by filtration through a short column of silica gel employing chloroform as an eluant. d) Spectral data (NMR, IR) were consistent with the indicated structure. e) Yield of crude ester. All these crude crystalline esters gave the previously determined mp without further purification.

Experimental

All reagents employed were dried by appropriate methods Commercial 2-chloro-3,5-dinitropyridine (CDNP) was used without further purification.

Ester of Carboxylic Acids. The preparations of *t*-butyl 2,4,6-trimethylbenzoate and *t*-butyl 4-nitrobenzoate are described here as typical examples. To a mixture of 2,4,6-trimethylbenzoic acid (1 mmol, 164 mg) and 2-methyl-2-propanol (1.2 mmol, 114 μl) in pyridine (1 ml) under nitrogen atmosphere was added CDNP (1 mmol, 204 mg) with stirring at 115 °C. After stirring for 30 min, an 8% aqueous sodium hydrogencarbonate solution (20 ml), water (10 ml), and petroleum benzine (40 ml) were added to the reaction mixture, and the whole mixture was well stirred. The mixture was transferred into a separatory funnel and the petroleum benzine layer was separated. The aqueous phase was again extracted with petroleum benzine (20 ml). The combined petroleum benzine extracts were washed with water (10 ml) several times until the yellow color of the solution was removed. The

petroleum benzine layer was then washed twice with 2% hydrochloric acid (20 ml) and twice with water (10 ml), and dried over anhydrous sodium sulfate. The organic layer was concentrated, and the residue was purified by filtration through a short column of silica gel employing chloroform as an eluant. The desired ester (200 mg, 91%) was the only compound observed on solvent removal.

NMR ($CDCl_3$) $\delta = 1.58$ (s, 9H), 2.26 (s, 3H), 2.30 (s, 6H), 6.81 (s, 2H).

t-Butyl 4-nitrobenzoate is a solid, which was obtained directly after the reaction mixture was treated with an aqueous sodium hydrogencarbonate solution and washed with water.

The ester (152 mg, 68%) melted at 115—116 °C, pure enough before recrystallization. (lit,[4] mp 115.5 °C)

References

1) K. Inomata, H. Kinoshita, H. Fukuda, K. Tanabe, and H. Kotake, *Bull. Chem. Soc. Jpn.*, **51**, 1866 (1978).

2) S. Takimoto, J. Inanaga, T. Katsuki, and M. Yamaguchi, *Bull. Chem. Soc. Jpn.*, **54**, 1470 (1981).

3) G. Höfle, W. Steglich, and H. Vorbüggen, *Angew. Chem., Int. Ed. Engl.*, **17**, 569 (1978).

4) R. Adams, E. K. Rideal, W. B. Burnett, R. L. Jenkins, and E. E. Dreger, *J. Am. Chem. Soc.*, **48**, 1758 (1926).

Acid Decomposition of 5-Amino-1-vinyl-4,5-dihydro-1*H*-1,2,3-triazoles. A Novel Formation of 1-Amino-2-azabutadienes

Masato M. Ito, Yujiro Nomura,* Yoshito Takeuchi, and Shuji Tomoda
Department of Chemistry, College of General Education, The University of Tokyo, Komaba, Meguro-ku, Tokyo 153
(Received June 9, 1982)

Synopsis. Acid decomposition of 4-alkyl-5-dialkylamino-1-vinyl-4,5-dihydro-1*H*-1,2,3-triazoles gave N^1,N^1-dialkyl-N^2-vinylalkanamidines, which have 2-aza-1,3-butadiene skeleton, in fair yields.

We have previously reported the deamination of 5-amino-1-vinyl-4,5-dihydro-1*H*-1,2,3-triazoles (**1a**—**d**, R^3 =alkyl or aryl) to give the corresponding triazoles (**2a**—**d**).[1] Dihydrotriazoles (**1e**—**g**, R^3=H), however, were not deaminated under similar conditions.

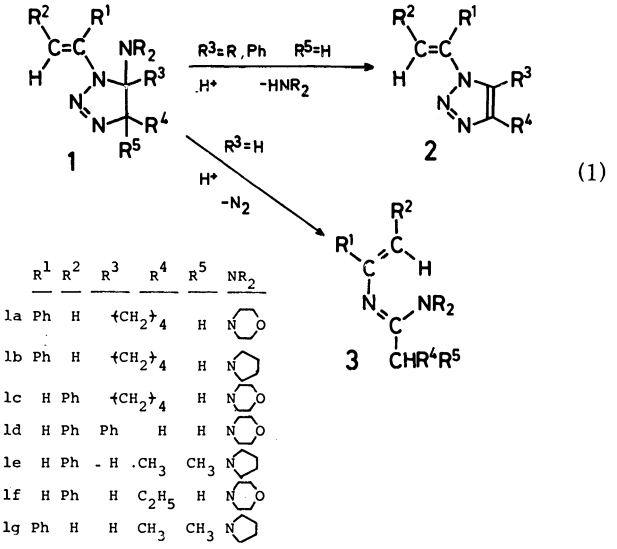

(1)

	R^1	R^2	R^3	R^4	R^5	NR_2
1a	Ph	H	$-(CH_2)_4-$		H	N⟨O
1b	Ph	H	$-(CH_2)_4-$		H	N⟨
1c	H	Ph	$-(CH_2)_4-$		H	N⟨O
1d	H	Ph	Ph		H	N⟨O
1e	H	Ph	H	CH_3	CH_3	N⟨
1f	H	Ph	H	C_2H_5	H	N⟨O
1g	Ph	H	H	CH_3	CH_3	N⟨

In the course of our study on nitrogen-extrusion reactions of the dihydrotriazoles (**1**), we noticed that acid decomposition of **1** (R^3=H) might give the corresponding N^2-vinylamidines (**3**) having a 2-aza-1,3 butadiene skeleton, so that the acid decomposition of **1e**—**g** was re-examined.

When the dihydrotriazoles (**1e, f**) were treated with 2 molar amounts of *p*-toluenesulfonic acid at 0 °C, **1** were decomposed with evolution of nitrogen to afford N^2-styrylamidines (**3e, f**) as slightly yellow oil in 46—64% yields.

Determination of the structure of **3e** and **3f** was based on the following spectral data. Mass spectra showed the existence of their molecular ion peak at *m/e* 242 and 258, respectively. In infrared spectra, no absorption corresponding to an N–H bond was observed, and absorption at about 1620 and 1600 cm^{-1} suggested the presence of C=C and C=N bonds. In ^1H and ^{13}C NMR, presence of a newly formed propyl or isopropyl group and an amidine carbon, in addition to a styryl and a 1-pyrrolidinyl or a morpholino group, was demonstrated by their characteristic signals (see Experimental).

Treatment of the dihydrotriazole (**1g**) with *p*-toluenesulfonic acid was also shown to give the corresponding

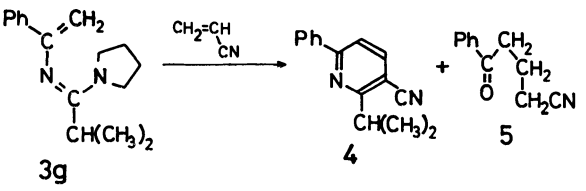

(2)

N^2-vinylamidine (**3g**) according to the NMR spectra of the crude product,[2] but attempted isolation of **3g** failed due to its sensitivity to moisture. After the acid in the reaction mixture was removed by neutralization with anhydrous potassium carbonate, the crude product was treated with excess acrylonitrile. Chromatographic separation of the product gave 2-isopropyl-6-phenylnicotinonitrile (**4**) and 5-oxo-5-phenylpentanenitrile (**5**) in 13 and 11% yields, respectively.

Both **4** and **5** were formed by reaction of **3g** with acrylonitrile. It is known that the nicotinonitrile derivative (**4**) is formed by [4+2] cycloaddition reaction of **3g**, formed by thermolysis of **1g** with acrylonitrile, followed by deamination and air oxidation.[2] The oxo nitrile (**5**) would be formed by Michael addition of the enamine moiety of **3g** to acrylonitrile followed by hydrolysis. Thus the formation of **3g** by acid decomposition of **1g** was certified.

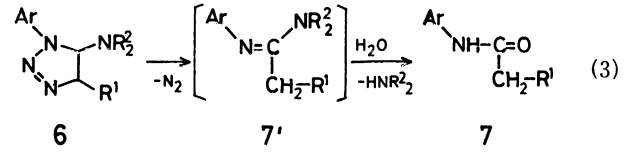

(3)

Fusco and coworkers reported that acid decomposition of 4-alkyl-1-aryl-5-dialkylamino-4,5-dihydro-1*H*-1,2,3-triazoles (**6**) gave *N*-arylamides (**7**).[3] They suggested the corresponding amidine (**7'**), which was not actually detected, as an intermediate (Eq. 3).

The present reaction demonstrated the formation of amidines by acid decomposition of 5-dialkylamino-4,5-dihydro-1*H*-1,2,3-triazoles, as well as gave a new route to 1-amino-2-aza-1,3-butadiene derivatives.

Experimental

General. Infrared spectra were determined on JASCO DS-403G and A-202 grating infrared spectrophotometers. Nuclear magnetic resonance spectra were determined on JEOL FX-90Q and Varian EM-390 spectrometers (splitting patterns in ^{13}C NMR data were obtained by off-resonance decoupling). Mass spectra were determined on a Hitachi RMU-6MG mass spectrometer.

4,5-Dihydro-1*H*-1,2,3-triazoles (**1**) were prepared from vinyl azides and enamines according to the previously reported method.[1] Solvents were distilled under anhydrous conditions before use.

2-Methyl-1-(1-pyrrolidinyl)-N-styryl-1-propanimine (3e). To a solution of 4,4-dimethyl-5-(1-pyrrolidinyl)-1-styryl-4,5-dihydro-1*H*-1,2,3-triazole (**1e**, 1.18 g, 4.4 mmol) in dry tetrahydrofuran (THF, 30 ml) was added a THF (30 ml) solution of anhydrous *p*-toluenesulfonic acid (1.57 g, 8.8 mmol) dropwise with stirring at 0 °C. Stirring was continued for further 30 min, until **1e** was completely consumed. Triethylamine (2 ml) was added and the solvent was removed *in vacuo*. After the residue was washed with diethyl ether (3×50 ml), it was alkalized with 5% aqueous solution (50 ml) of sodium hydrogencarbonate and was extracted with three portions (50 ml each) of diethyl ether. The ether layer was washed with saturated aqueous solution (50 ml) of sodium chloride and was dried over anhydrous magnesium sulfate. Removal of the ether *in vacuo* gave **3e** (243 mg, 46% yield) as slightly yellow oil: MS *m/e* 242 (M^+); IR (neat) 1620 and 1600 (C=C and C=N), and 940 cm^{-1} ($_H\rangle C{=}C\langle^H$); ^1H NMR ($CDCl_3$) δ 1.32 (6H, d, J=7 Hz), 1.83 (4H, m), 3.09 (1H, septet, J=7 Hz), 3.46 (4H, m), 6.14 (1H, d, J=13.5 Hz), 6.9—7.4 (5H, m), and 7.76 (1H, d, J=13.5 Hz); ^{13}C NMR ($CDCl_3$) δ 19.5 (q), 25.3 (t), 30.7 (d), 47.9 (t), 117.2 (d, PhCH=), 124.8 (d, *p*), 125.0 (d, *m*), 128.3 (d, *o*), 136.4 (d, =CHN), 139.3 (s, *ipso*), and 163.9 (s, C=N).

Found: *m/e* 242.1805. Calcd for $C_{16}H_{22}N_2$: M, 242.1783.

The amidine (**3e**) could not be induced to crystallize, and chromatographic separation caused decomposition; thus further purification was unsuccessful.

1-Morpholino-N-styryl-1-butanimine (3f). To a solution of 4-ethyl-5-morpholino-1-styryl-4,5-dihydro-1*H*-1,2,3-triazole (**1f**, 1.20 g, 4.20 mmol) in dry THF (40 ml) was added a THF (40 ml) solution of anhydrous *p*-toluenesulfonic acid (1.50 g, 8.40 mmol) dropwise with stirring at 0 °C. Stirring was continued for further 30 min, until **1f** was completely consumed. Then the solution was poured into 0.1 M hydrochloric acid (100 ml), and the solution was washed with diethyl ether (2×80 ml). After alkalization of the aqueous layer with excess sodium carbonate followed by extraction with diethyl ether (3×80 ml), the ether layer was washed with saturated aqueous solution (100 ml) of sodium chloride and was dried over anhydrous magnesium sulfate. Removal of the ether *in vacuo* gave **3f** (696 mg, 64% yield) as slightly yellow oil: MS *m/e* 258 (M^+); IR (neat) 1625 and 1600 (C=C and C=N), and 940 cm^{-1} ($_H\rangle C{=}C\langle^H$); ^1H NMR ($CDCl_3$) δ 0.96 (3H, t, J=7 Hz), 1.47 (2H, sextet, J=7 Hz), 2.21 (2H, t, J=7 Hz), 3.3—3.7 (8H, m), 6.30 (1H, d, J=13.5 Hz), 6.9—7.3 (5H, m), and 7.48 (1H, d, J=13.5 Hz); ^{13}C NMR ($CDCl_3$) δ 13.9 (q), 20.3 (t), 27.5 (t), 45.3 (t), 66.7 (t), 120.2 (d, PhCH=) 125.3 (d, *m*), 125.4 (d, *p*), 128.4 (d, *o*), 135.6 (d, =CHN), 138.6 (s, *ipso*), and 161.7 (s, C=N).

Found: *m/e* 258.1753. Calcd for $C_{16}H_{22}N_2O$: M, 258.1733.

The amidine (**3f**) could not be induced to crystallize, and attempted distillation *in vacuo* or chromatographic separation caused decomposition; thus further purification was unsuccesful.

Decomposition of 4,4-Dimethyl-1-(1-phenylvinyl)-5-(1-pyrrolidinyl)-4,5-dihydro-1H-1,2,3-triazole (1g). To a solution of **1g** (0.50 g, 1.9 mmol) in dry THF (30 ml) was added a THF (30 ml) solution of anhydrous *p*-toluenesulfonic acid (0.71 g, 4.0 mmol) dropwise with stirring at 0 °C. Stirring was continued for further 30 min until **1g** was completely consumed. Then anhydrous potassium carbonate (2.0 g) was added to the solution and stirring was continued overnight. After solid materials had been filtered off and the solvent had been removed *in vacuo*, acrylonitrile (3 ml) was added to the residue and the mixture was stirred for 2 d at room temperature. Excess acrylonitrile was removed and the silica gel preparative thin layer chromatography of the residue gave previously reported 2-isopropyl-6-phenylnicotinonitrile (**4**,[2] 54 mg, 13% yield) and 5-oxo-5-phenylpentanenitrile (**5**, 34 mg, 11% yield).

2-Isopropyl-6-phenylnicotinonitrile (4): Colorless crystals; mp 73.5—75.0 °C, lit, 75.5—76.5 °C.[2] Mixed melting point test with the authentic sample; mp 74.5—76.0 °C.

5-Oxo-5-phenylpentanenitrile (5): Colorless oil; MS *m/e* 173 (M^+); IR (neat) 2220 (C≡N) and 1685 cm^{-1} (C=O); ^1H NMR ($CDCl_3$) δ 2.09 (2H, quintet, J=6.5 Hz), 2.56 (2H, t, J=6.5 Hz), 3.17 (2H, t, J=6.5 Hz), 7.4—7.7 (3H, m), and 7.9—8.1 (2H, m); ^{13}C NMR ($CDCl_3$) δ 16.6 (t), 19.9 (t), 36.4 (t), 119.3 (s, C≡N), 128.0 (d), 128.7 (d), 133.4 (d), 136.6 (s), and 198.2 (s, C=O).

References

1) Y. Nomura, Y. Takeuchi, S. Tomoda, and M. M. Ito, *Bull. Chem. Soc. Jpn.*, **54**, 261 (1981).

2) Y. Nomura, Y. Takeuchi, S. Tomoda, and M. M. Ito, *Chem. Lett.*, **1979**, 187; *Bull. Chem. Soc. Jpn.*, **54**, 2779 (1981).

3) R. Fusco, G. Bianchetti, and D. Pocar, *Gazz. Chim. Ital.*, **91**, 933 (1961).

The Wallach Rearrangement of Some 4,4′-Disubstituted Azoxybenzenes

Ichiro SHIMAO* and Shigeru OAE†

Department of Industrial Chemistry, Faculty of Engineering, Toyama University, Takaoka, Toyama 933

†*Department of Chemistry, The University of Tsukuba, Sakura-mura, Niihari, Ibaraki 305*

(Received June 14, 1982)

Synopsis. The treatment of azoxybenzenes bearing electron-withdrawing substituents at 4,4′-positions with sulfuric acid gave the corresponding 2-hydroxyazobenzenes, together with 4′-substituted 4-hydroxyazobenzenes. The treatment of 4,4′-dimethoxyazoxybenzene with *p*-toluenesulfonic acid and acetic anhydride afforded 4,4′-dimethoxy-3-acetoxyazobenzene and 4,4′-dimethoxy-2-tosyloxyazobenzene as the main rearrangement products.

In the Wallach rearrangement of 4,4′-dialkylazoxybenzenes with sulfuric acid, the main product was not the *o*-hydroxyazo compound, but an abnormal product formed by the ipso nucleophilic attack on the ring carbon atom bearing the alkyl group.[1] Another abnormal rearrangement was also observed in the reaction of 4,4′-dihaloazoxybenzenes with sulfuric acid; in this reaction, however, the major products were the reduction products, *i.e.*, 4,4′-dihaloazobenzenes.[2] The pattern of the reaction of azoxybenzenes with strong acids seems to be markedly affected by the *p*-substituents.

We have now found another example of the ipso substitution reaction of 4,4′-disubstituted azoxybenzenes. That is, when 4,4′-dinitroazoxybenzene (**1**), 4,4′-diacetylazoxybenzene (**2**), and azoxybenzene-4,4′-dicarboxylic acid (**3**) were treated with sulfuric acid, not only the normal rearrangement products (**1a**—**3a**), but also the ipso rearrangement products (**1b**—**3b**), were obtained. The results are shown in Table 1.

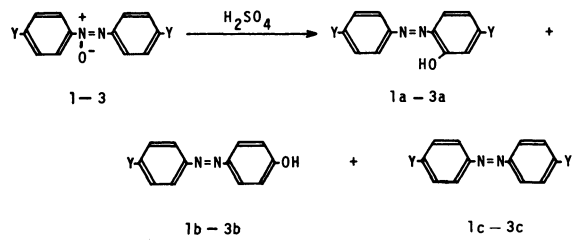

Compound **1** was found to rearrange in a normal fashion, giving preferentially 5-nitro-2-(*p*-nitrophenylazo)phenol (**1a**). This is a typical example of the Wallach rearrangement with sulfuric acid to give the ortho-rearranged azophenol.

The reaction of **2** gave 4-(*p*-acetylphenylazo)phenol (**2b**) as the main rearrangement product. When the aqueous solution was carefully concentrated in the work-up process, the characteristic odor of acetic acid was perceived. In the reaction of **3**, the evolution of carbon dioxide was observed when the reaction mixture was heated. These ipso substitution may be explained on the basis of the mechanistic scheme involving the initial formation of the dicationic inetermediate, $Ar\text{–}\overset{+}{N}\equiv\overset{+}{N}\text{–}Ar$, proposed previously.[1,2]

Table 1. Reactions of 4,4′-disubstituted azoxybenzenes with sulfuric acid

Azoxybenzene Y	Temp °C	Time h	Yield/% a	b	c	Recovered material/%
1 NO_2	100	3	54	11	4	27
2 $COCH_3$	70	5	2.5	46		31
3 COOH	100	1/3	29	49	9	

Although an acetyl group of **2** was readily removed, the reaction of *p*-acetylazoxybenzene (a mixture of *o*- and *p*-isomers) with sulfuric acid afforded **2b** (yield, 93%), without removing acetyl group. In this case, the nucleophilic attack of the hydrogen-sulfate ion on the dicationic intermediate occurs preferentially at the para position of the unsubstituted phenyl ring. This is different from the reaction of 4-*t*-butylazoxybenzene, in which 4-(phenylazo)phenol was formed as the main product.[3]

Several azoxybenzenes were treated with concentrated sulfuric acid at 100 °C for 20 min, and the yields of the recovered azoxy compounds (determination by gas-chromatographic analysis) were the following: **1**, 92%; **2**, 42%; 3,3′-dinitroazoxybenzene, 33%; **3**, 0%. The reaction is obviously retarded by the electron withdrawing substituent, in keeping with the kinetic results reported by Duffey and Hendley.[4]

Contrary to Cox and Buncel's description,[5] 4,4′-dimethoxyazoxybenzene (**4**) was found to react readily with 80% sulfuric acid. A black tarry substance was mainly formed, and only a small amount of 4,4′-dimethoxyazobenzene (**4c**) (yield, 2%) was isolated. However, no rearrangement product was obtained. Similary, 4-methoxyazoxybenzene did not give hydroxymethoxyazobenzene, but 4-methoxyazobenzene (34%) and 4-hydroxyazobenzene (0.5%) were obtained.

Meanwhile, the reaction of **4** with a mixture of *p*-toluene-sulfonic acid (TsOH) and acetic anhydride gave 4,4′-dimethoxy-3-acetoxyazobenzene (42%), 4,4′-dimethoxy-2-tosyloxyazobenzene (3.5%), and **4c** (32%) as the main products.

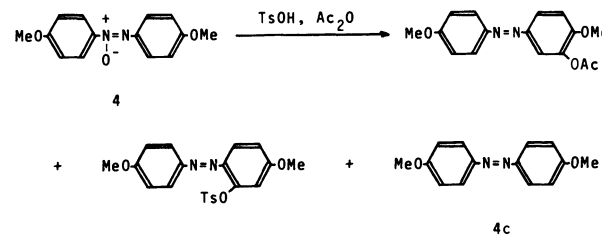

Under the same conditions, azoxybenzene gave 2- and 4-(tosyloxy)azobenzene as the main rearrangement products, while 4,4′-diacetoxyazoxybenzene gave *p*-acetoxyphenyl tosylate and hydroquinone diacetate.[6] The methoxyl group is a poor leaving group, and it can

stabilize the dicationic intermediate, $Ar-\overset{+}{N}\equiv\overset{+}{N}-Ar$. Hence, the rearrangement is believed to proceed very readily, without cleaving the azo linkage.

Thus, when 4-methoxyazoxybenzene was treated with TsOH and acetic anhydride, 4-methoxy-3-acetoxyazobenzene (38%), 4-methoxy-4′-tosyloxyazobenzene (5.6%), and 4-methoxyazobenzene (42%) were obtained as the main products.

Experimental

The reaction products were identified by a comparison of their properties with those of independently prepared samples.

The azoxy compounds, except **3**, were treated with sulfuric acid according to a procedure similar to those reported previously.[2] **1a**, mp 246—247 °C (from $CHCl_3$). Found: C, 49.85; H, 2.62; N, 19.29%. Calcd for $C_{12}H_8N_4O_5$: C, 50.00; H, 2.80; N, 19.44%. **2a**, mp 206—207 °C (from hexane–benzene). Found: C, 67.85; H, 5.08; N, 9.79%. Calcd for $C_{16}H_{14}N_2O_3$: C, 68.08; H, 5.00; N, 9.92%.

Reaction of 3 with Sulfuric Acid. A solution of **3** (0.5 g) in concentrated sulfuric acid (50 ml) heated at 100 °C for 20 min. The solution was poured into a large amount of cold water. The precipitates were filtered and then extracted with acetone. The extract gave **3b** (0.18 g); mp 270 °C (decomp). The acetone-insoluble material was added to a solution of H_2SO_4 (1 ml) in MeOH (30 ml). The suspension was refluxed for 24 h with stirring and then poured into cold water. The methyl ester was collected by filtration and then treated further with acetic anhydride and pyridine, as usual, to afford the acetate. The resulting esters were chromatographed on silica gel (benzene). The first fraction gave methyl 4-(*p*-methoxyphenylazo)benzoate (0.035 g); mp 170—171 °C (from MeOH). Found: C, 66.83; H, 5.31; N, 10.48%. Calcd for $C_{15}H_{14}N_2O_3$: C, 66.65; H, 5.23; N, 10.37%. The second fraction gave dimethyl azobenzene-4,4′-dicarboxylate (0.05 g); mp 242—243 °C. The third fraction gave dimethyl 2-acetoxyazobenzene-4,4′-dicarboxylate (0.18 g); mp 151—153 °C (from MeOH). Found: C, 60.77; H, 4.25; N, 8.08%. Calcd for $C_{18}H_{16}N_2O_6$: C, 60.66; H, 4.50; N, 7.87%.

Reaction of 4 with TsOH and Ac_2O. A solution of **4** (0.5 g) and $TsOH \cdot H_2O$ (5.0 g) (dehydrated by heating under reduced pressure) in Ac_2O (12.5 ml) was heated at 100 °C for 1 h. The reaction mixture was poured into a cold $NaHCO_3$ solution and then extracted with benzene. The extract was chromatographed on a silica-gel column (benzene). The first fraction gave **4c** (0.15 g); mp 168—169 °C. The second fraction gave 4,4′-dimethoxy-2-tosyloxyazobenzene (0.029 g); mp 100—101 °C. Found: C, 61.09; H, 4.87; N, 7.01%. Calcd for $C_{21}H_{20}N_2O_5S$: C, 61.15; H, 4.89; N, 6.79%. The tosylate was heated with a 30% NaOH solution at 100 °C for 3 h to give 4,4′-dimethoxy-2-hydroxyazobenzene (**4a**) (0.014 g); mp 137—138 °C. The third fraction was recrystallized from hexane–benzene to give 3-acetoxy-4,4′-dimethoxyazobenzene (0.20 g); mp 188—189 °C. The mother liquor was treated with 3% NaOH to give **4a** (0.008 g) and 3-hydroxy-4,4′-dimethoxyazobenzene; mp 177—178 °C (0.038 g). This azophenol was refluxed with dimethyl sulfate in acetone in the presence of K_2CO_3 for 6 h to yield 3,4,4′-trimethoxyazobenzene; mp 128—130 °C. Found: C, 66.36; H, 5.97; N, 10.29%. Calcd for $C_{15}H_{16}N_2O_3$: C, 66.16; H, 5.92; N, 10.28%.

Reaction of 4-Methoxyazoxybenzene with TsOH and Ac_2O. This reaction was carried out according to a procedure similar to those described above. Products: 4-methoxy-4′-tosyloxyazobenzene; mp 131.5—133 °C (from MeOH), 3-acetoxy-4-methoxyazobenzene; mp 112—113 °C (from hexane), 3-hydroxy-4-methoxyazobenzene; mp 95—97 °C (from hexane).

References

1) I. Shimao and S. Matsumura, *Bull. Chem. Soc. Jpn.*, **49**, 2294 (1976).

2) I. Shimao, K. Fujimori, and S. Oae, *Bull. Chem. Soc. Jpn.*, **55**, 546 (1982).

3) I. Shimao and S. Matsumura, *Bull. Chem. Soc. Jpn.*, **51**, 926 (1978).

4) D. Duffey and E. C. Hendley, *J. Org. Chem.*, **33**, 1918 (1968).

5) R. A. Cox and E. Buncel, "The Chemistry of the Hydrazo, Azo, and Azoxy Groups," ed by S. Patai, John Wiley and Sons, New York (1975), p. 812.

6) I. Shimao, K. Fujimori, and S. Oae, *Bull. Chem. Soc. Jpn.*, **55**, 1538 (1982).

The Reaction of *O*-Silylated Enolates of Carboxylic Esters and of Lactones with Aminomethyl Ethers Catalyzed by $ZnCl_2$

Tatsuo OIDA,* Shigeo TANIMOTO,* Hideyuki IKEHIRA, and Masaya OKANO
Institute for Chemical Research, Kyoto University, Uji, Kyoto 611

(Received June 22, 1982)

Synopsis. It was found that the reaction of *O*-silylated enolates of carboxylic esters and of lactones with aminomethyl ethers proceeds smoothly under a catalytic action of zinc chloride to afford the corresponding α-aminomethylated carboxylic esters or lactones, except only one case using *O*-silylated enolate of δ-valerolactone, in which the resultant α-aminomethyl-δ-valerolactone is somewhat unstable and undergoes decomposition, leading to the production of α-methylene-δ-valerolactone.

It is well known that Mannich salts and related compounds bearing a structural resemblance are excellent precursors of α-methylene carbonyl compounds.[1] In 1980 Miyano and his co-workers[1] were successful in preparing the Mannich salts of carbonyl compounds *via* *O*-silylated enolates of ketones and aldehydes by a combination of chloroiodomethane and *N,N,N',N'*-tetramethyldiaminomethane. More recently, Hosomi and his co-workers[2] were successful in preparing the salts by the reaction of *O*-silylated enolates of ketones with aminomethyl ethers catalyzed by the use of iodotrimethylsilane or trimethylsilyl trifluoromethanesulfonate. Though these mthods are found superior in many instances to the earlier procedures, such as those using preformed moisture-sensitive iminium salts[3] with enol silyl ethers, they involve the utilization of relatively expensive and not easily available reagents. With these considerations in mind, we have studied the reaction of *O*-silylated enolates of saturated carboxylic esters (**1**) with aminomethyl ethers (**2**) in the presence of easily available zinc chloride. The reaction proceeds smoothly at room temperature in acetonitrile to afford the corresponding α-aminomethyl carboxylic esters (**3**) in moderate yields; these esters are not readily, if at all, obtainable by other procedures (Table 1).

The reaction may involve the initial loss of the alkoxyl group of **2** to give the aminomethyl cation and its subsequent (or simultaneous) attack on **1**, accompanied by the release of the trimethylsilyl group.

When this procedure was extended to *O*-silylated enolates of δ-valerolactone, γ-butyrolactone, and methyl 3-butenoate (**4**, **5**, and **6**), somewhat different results were observed (Table 2).

It was recognized that, in the reaction of **4** with **2**, the initially formed α-aminomethyl-δ-valerolactones are

TABLE 1. REACTION OF *O*-SILYLATED ENOLATES OF SATURATED CARBOXYLIC ESTERS (**1**) WITH AMINOMETHYL ETHERS (**2**)

Silylated enolate	Amino ether[a]	Product	Yield[b] / %	Bp θ_b/°C (Torr)†	^{1}H-NMR (60 MHz, δ, $CDCl_3$)	MS (40 eV) *m/e*(M^+)
1a	**2a**	**3a** ($R'''=C_2H_5$)	52[c]	74—78 (5)	0.8—1.4 (m, 12H), 1.3—1.8 (m, 2H), 2.3—2.8 (m, 7H), 4.13(t, 2H)	201
1a	**2b**	**3a** ($R'''=CH_3$)	79	50—53 (6.5)	0.91 (t, 3H), 1.25 (t, 3H), 1.3—1.8 m, 2H), 2.19 (s, 6H), 2.3—2.8 (m, 3H), 4.14 (q, 2H)	173
1a	**2c**	**3a** ($R_2'''N=$O N)	51	62—65 (2.5)	0.89 (t, 3H), 1.25 (t, 3H), 1.3—1.8 (m, 2H), 2.1—2.7 (m, 7H), 3.60 (t, 4H), 4.13 (t, 2H)	215
1b	**2a**	**3b** ($R'''=C_2H_5$)	51	84—86 (18.5)	0.93 (t, 6H), 1.14s, 6H), 2.47 (q, 4H), 2.53 (s, 2H), 3.63 (s, 3H)	187
1b	**2b**	**3b** ($R'''=CH_3$)	32	77—81 (19)	1.21 (s, 6H), 2.28 (s, 6H), 2.50 (s, 2H), 3.70 (s, 3H)	159
1b	**2c**	**3b** ($R_2'''N=$O N)	64	84—88 (7)	1.14 (s, 6H), 2.3—2.7 (m, 4H), 2.43 (s, 2H), 3.4—3.8 (m, 4H), 3.60 (s, 3H)	201
1c	**2a**	**3c** ($R'''=C_2H_5$)	88	68—69 (6.5)	0.93 (t,9H), 1.33 (s, 3H), 1.1—2.0 (m, 2H), 2.25 (d, 1H), 2.49 (q, 4H), 2.73 (d, 1H), 3.61 (s, 3H)	201
1c	**2b**	**3c** ($R'''=CH_3$)	81	55—59 (7.5)	0.80 (t, 3H), 1.16 (s, 3H), 1.2—1.8 (m, 2H), 2.20 (s, 6H), 2.25 (d, 1H), 2.62 (d, 1H), 3.64 (s, 3H)	173
1c	**2c**	**3c** ($R_2'''N=$O N)	82	67—68 (3)	0.83 (t, 3H), 1.16 (s, 3H), 1.46 (q, 2H), 2.29 (d, 1H), 2.3—2.6 (m, 4H), 2.64 (d, 1H), 3.5—3.8 (m, 4H), 3.62 (s, 3H)	215
1d	**2a**	**3d** ($R'''=C_2H_5$)	90	118—121 (6.5)	0.91 (t, 6H), 0.7—1.8 (m, 8H), 1.8—2.3 (m, 2H), 2.43 (q, 4H), 2.48 (s, 2H), 3.63 (s, 3H)	227
1d	**2b**	**3d** ($R'''=CH_3$)	63	131—133 (26)	0.7—1.7 (m, 8H), 1.9—2.2 (m, 2H), 2.17 (s, 6H), 2.39 (s, 2H), 3.61 (s, 3H)	199
1d	**2c**	**3d** ($R_2'''N=$O N)	89	145—148 (6.5)	0.9—1.8 (m, 8H), 1.8—2.2 (m, 2H), 2.3—2.6 (m, 2H), 2.44(s, 2H), 3.5—3.7 (m, 4H), 3.63 (s, 3H)	241
1e	**2a**	**3e** ($R'''=C_2H_5$)	89	57—62 (3)	0.92 (t, 6H), 1.4—1.9 (m, 6H), 1.9—2.2 (m, 2H), 2.47 (q, 4H), 2.60 (s, 2H), 3.62 (s, 3H)	213
1e	**2b**	**3e** ($R'''=CH_3$)	62	35—36 (3)	1.4—2.3 (m, 8H), 2.20 (s, 6H), 2.52 (s, 2H), 3.64 (s, 3H)	185
1e	**2c**	**3e** ($R_2'''N=$O N)	91	91—94 (4)	1.4—2.0 (m, 6H), 2.0—2.3 (m, 2H), 2.3—2.7 (m, 4H), 2.55 (s, 2H), 3.6—3.8 (m, 4H) 3.64 (s, 3H)	227

a) **2a**: n-$C_2H_9OCH_2N(C_2H_5)_2$, **2b**: i-$C_2H_9OCH_2N(CH_3)_2$, **2c**: $C_2H_5OCH_2N$ O b) Yield of the isolated product based on **1**. c) When the reaction of **1a** with **2a** was accomplished by the following combination of a catalyst and a solvent under otherwise identical conditions, **3a** ($R'''=C_2H_5$) was obtained in the yields shown in parentheses: $ZnBr_2/CH_3CN$ (52%), $BF_3\cdot O(C_2H_5)_2/CH_3CN$ (43%), $AlCl_3/CH_3CN$ (34%), $TiCl_2/CH_3CN$ (26%), $ZnCl_2/CH_2Cl_2$ (43%), $ZnCl_2/C_6H_6$(45%), $ZnC_2/(C_2H_5)_2O$ (36%). d) Yield in the reaction using the CH_2Cl_2 solvent. †1 Torr≈133.322 Pa.

Table 2. Reaction of *O*-silylated enolates of δ-valerolactone, γ-butyrolactone, and methyl 3-butenoate (**4**, **5**, and **6**) with aminomethyl ethers (**2**)

O-Silylated enolate	Amino-methyl ether	Product[b]		Yield %[c]	Bp θ_b/°C (Torr)	MS(40 eV) *m/e*(M^+)
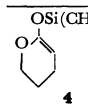 (**4**)	**2a**	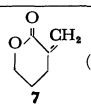 (**7**)		64	76—77 (6.5) [lit,[4] 56.5 (0.07)]	112
4	**2b**	**7**		31		
4	**2c**	**7**		49		
(**5**)	**2a**	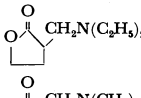	(**8a**)	35	59—62 (3)	171
5	**2b**	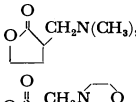	(**8b**)	40	54—57 (2.5) [lit,[5] 72—73(0.05)]	143
	c	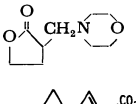	(**8c**)	60	Mp 134—135 (Hexane)	185
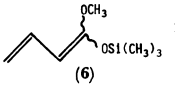 (**6**)	**2a**	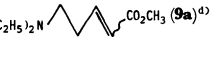	(**9a**)[d]	55[e]	49—50 (3)	185
6	**2b**	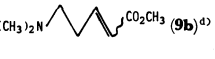	(**9b**)[d]	31[e]	50—51 (4)	157
6	**2c**	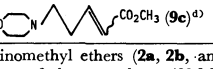	(**9c**)[d]	34[e]	76—77 (2.5)	199

a) The structures of the aminomethyl ethers (**2a**, **2b**, and **2c**) are shown in Table 1. b) The ^{1}H-NMR spectra of these products (60 MHz, δ, in $CDCl_3$) are as follows: **7**: 1.7—2.2(m, 2H), 2.5—2.8 (m, 2H), 4.36 (t, 2H), 5.4—5.7 (m, 1H), 6.2—6.5 (m, 1H). **8a**: 0.97 (t, 3H), 1.01 (t, 3H), 2.2—3.1 (m_2 9H), 4.1—4.5 (m, 2H). **8b**: 2.09 (s, 6H), 2.0—2.5 (m, 5H), 4.0—4.4 (m, 2H). **8c**: 2.0—3.0 (m, 2H), 3.5—3.8 (m, 4H), 4.0—4.5 (m, 9H). **9a**: 1.01 (t, 6H), 2.2—2.7 (m, 8H), 3.68 (s, 3H), 5.83 (d, 1H), 6.96 (dt, 1H). **9b**: 2.20 (s, 6H), 2.1—2.5 (m, 4H), 3.64 (s, 3H), 5.82 (d, 1H), 6.6—7.1 (m, 1H). **9c**: 2.3—2.6 (m, 8H), 3.5—3.8 (m, 4H), 3.68 (s, 3H), 5.84 (d, 1H), 6.7—7.2 (m, 1H). c) Yield of isolated product based on **4**, **5**, or **6**. d) Presumably, **9a**, **9b**, and **9c** are *trans*-isomers. e) Yield in the reaction using the CH_2Cl_2 solvent.

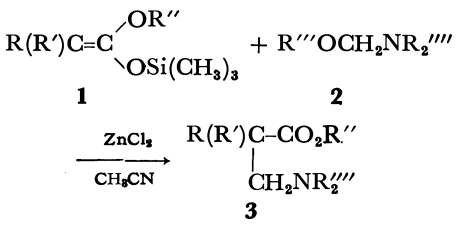

a: R=H, R′=R″=C_2H_5 **b**: R=R′=R″=CH_3
c: R=C_2H_5, R′=R″=CH_3 **d**: R(R′)=$-(CH_2)_5-$, R″=CH_3
e: R(R′)=$-(CH_2)_4-$, R″=CH_3

rather unstable under the present reaction conditions; therefore, they partially undergo decomposition, leading to the production of α-methylene-δ-valerolactone (**7**). The remaining α-aminomethyl-δ-valerolactones, unchanged during the reaction, were converted into **7** in the work-up procedure involving repeated distillation, which causes the thermal decomposition of the aminomethylated compounds (see Experimental section). In contrast, in the cases of **5**, α-aminomethyl-γ-butyrolactone (**8a**, **8b**, and **8c**) were isolated, suggesting that the aminomethylated compounds are stable under the given reaction conditions, as well as during distillation under reduced pressure. The reaction of **6** with **2** proceeded smoothly to afford the products **9a**, **9b**, and **9c** resulting from the attack on the γ-position of **6**.

The general availability of *O*-silylated enolates[6] from carboxylic esters and from lactones, and of aminomethyl ethers from secondary amines, formaldehyde, and primary alcohols, along with the simple work-up procedures required for these reactions, indicates that this procedure may provide a useful method for the preparation of α-aminomethylated carboxylic esters or lactones.

Experimental

Into a solution of zinc chloride (1.36 g, 10 mmol) in dry acetonitrile (20 ml), we added with stirring a mixture of an *O*-silylated enolate (10 mmol) and an aminomethyl ether (10 mmol). The stirring was continued at room temperature for about 24 h under nitrogen. The resultant reaction mixture was poured into dilute aq $NaHCO_3$ and extracted with ether. The ethereal solution was extracted with 5% aq HCl, and the resultant aq layer was basified with 5% NaOH. The basified aq phase was extracted with ether, then dried over $MgSO_4$ and evaporated *in vacuo* to give a residue. The distillation of this residue yielded the product. In the reaction using **4** as the starting substrate, the following work-up procedure was adopted: the resultant reaction mixture was poured into dilute aq Na_2CO_3 and extracted with ether. The ethereal solution was dried over $MgSO_4$ and evaporated *in vacuo* to give a residue, which was repeatedly distilled under reduced pressure.

References

1) S. Miyano, H. Hokari, A. Mori, and H. Hashimoto, *Chem. Lett.*, **1980**, 1213.
2) H. Hosomi, S. Iijima, and H. Sakurai, *Tetrahedron Lett.*, **22**, 547 (1982).
3) S. Danishefsky, T. Kitahara, R. McKee, and P. F. Schuda, *J. Am. Chem. Soc.*, **98**, 6715 (1976); J. Schreiber, H. Maag, N. Hashimoto, and A. Eschenmoser, *Angew. Chem.*, **83**, 355 (1971).
4) E. R. H. Jones, T. Y. Shen, and M. C. Whiting, *J. Chem. Soc.*, **1950**, 230.
5) C. R. Hutchinson, *J. Org. Chem.*, **39**, 1854 (1974).
6) C. Ainsworth, F. Chen, and Y.-N. Kou, *J. Organometal. Chem.*, **46**, 59 (1972); I. Paterson and I. Fleming, *Tetrahedron Lett.*, **1979**, 993; I. Fleming, J. Goldhill, and I. Paterson, *ibid.*, **1979**, 3205.

Structures of the [4+2] Bicyclic Adducts from the Diels-Alder Reaction of Methyl Coumalate with Isoprene

Takanao MATSUI,* Takeshi INOUE, Mitsuru NAKAYAMA,† and James D. WHITE††
Faculty of Engineering, Miyazaki University, Miyazaki 880
†*Faculty of Science, Hiroshima University, Hiroshima 730*
††*Department of Chemistry, Oregon State University, Corvallis, Oregon 97331, U. S. A.*
(Received July 5, 1982)

Synopsis. The preparation of 9- and 8-methyl-9-iodo-3-oxo-2-oxabicyclo[4.4.0]dec-4-ene-6,8-carbolactone and 8-methyl-3-oxo-2-oxabicyclo[4.4.0]deca-4,9-diene-6,8-carbolactone from the adducts (**2a** and **2b**) of methyl coumalate with isoprene confirmed the structures of the regioisomers, **2a** and **2b**.

With respect to our studies[1] on construction of the *cis* A, B ring junction of trichothecane-type sesquiterpenes, the cycloaddition of methyl coumalate (**1**) with isoprene was investigated for the preparation of a potential intermediate for these sesquiterpenoid syntheses.

Although the Diels-Alder reaction of **1** with isoprene was previously reported to produce a mixture of regioisomers (**2a** and **2b**),[2] no purification of the adducts has been made and the position of methyl substitution seems not to be confirmed. We have found that separation of the adducts by column chromatography on silica gel is unsuccessful, and the ^{1}H NMR spectra of the mixture showed homogeneous signals. Therefore, we tried to carry out the functionalization of **2a** and **2b** in order to confirm their structures.

The cycloaddition of **1** with isoprene at 110—120 °C in an autoclave afforded a mixture of bicyclic adducts (**2a** and **2b**) along with some other products. Hydrolysis of the regioisomeric mixture (the isomeric ratio was appoximately 10 : 1 as indicated by ^{13}C NMR integrals) with aqueous sodium hydroxide solution afforded the corresponding acids (**3a** and **3b**). Without separation and purification, a mixture of **3a** and **3b** was allowed to undergo iodolactonization. Column chromatography of the resultant iodolactones gave **4a** and **4b** in 10 : 1 ratio (63% yield from **2**). Their ^{1}H NMR spectra showed differences, such as the methylene proton signals, and each showed a characteristic pair of one proton quartets at δ 4.11, 4.59 (**4a**), and 4.36, 4.67 (**4b**), due to the methylidyne protons of C-1, C-8, and/or C-9. However, the assignments were ambiguous. The absence of a distinguishing feature between **4a** and **4b** prompted us to examine dehydrohalogenation of **4** as follows. Treatment of **4b** with 1,8-diazabicyclo-[5.4.0]undec-7-ene (DBU) in THF gave the desired **5b** in 91% yield. The structure of **5b** was confirmed by elemental analysis and spectral data. On the other hand, **4a** resisted an analogous elimination reaction, suggesting that the proton in an *anti* orientation with respect to the iodine is difficult to abstract by DBU due to the steric shielding by the C-9 methyl group.

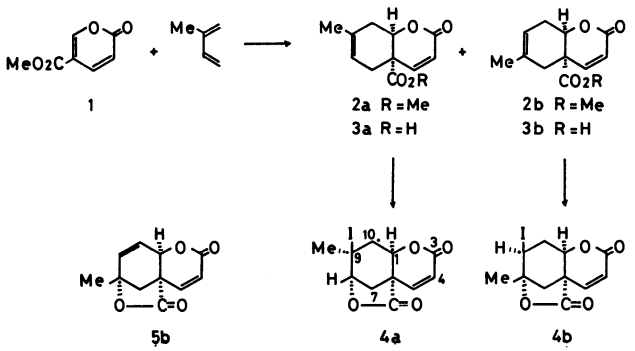

This result established that the structure of the major product of the Diels-Alder reaction corresponds to **2a**, which would be expected to provide a synthetic intermediate for the preparation of trichothecanes.

Experimental

All the melting points are uncorrected. IR spectra were recorded in $CHCl_3$ on a Hitachi 260-50 spectrophotometer. ^{1}H NMR spectra and ^{13}C NMR spectra were measured in $CDCl_3$ with a JEOL JNM MH-100 spectrometer (100 MHz) and a JEOL JNM-FX 60 Fourier Transform spectrometer (60 MHz) operating at 15.1 MHz, respectively. Chemical shifts are expressed in terms of δ values (ppm) relative to TMS as an internal standard. Mass spectra were recorded on a JEOL JMS-D 300S mass spectrometer with a direct inlet system operating at 70 eV. Column chromatography was performed with Merck silica gel (0.063 mm).

9- and 8-Methyl-6-methoxycarbonyl-2-oxabicyclo[4.4.0]*deca*-4,8-*dien-3-one (2a and 2b).* A mixture of 2.0 g (13 mmol) of methyl coumalate and 6 ml (60 mmol) of isoprene in 20 ml of benzene was heated at 110—120 °C for 18 h in an autoclave under N_2. After removal of the solvent and excess of the diene, the residue (3.0 g) was chromatographed on a silica gel with hexane–ethyl acetate (4 : 1) to afford a mixture of **2a** and **2b** as a colorless viscous oil, 0.93 g (32%). IR: 1740, 1720, 1640 cm^{-1}; ^{1}H NMR: 1.68 (3H, s, $-CH=\underline{C}CH_3$), 1.96—2.86 (4H, m, 2 $-CH_2-$), 3.76 (3H, s, $-CO_2CH_3$), 5.00 (1H, dd, J= 3, 5 Hz, C_1–H), 5.44 (1H, m, C_8– and/or C_9–H), 6.05 and 6.93 (each 1H, d, and J=11 Hz, C_4– and C_5–H); ^{13}C NMR: 22.9 (C_9–CH_3), 31.2, 29.1 (weak) and 33.7, 34.7 (weak) (C_7 and/or C_{10}), 45.8 (C_6), 52.9 ($CO_2\underline{C}H_3$), 76.1 and 75.1 (weak) (C_1), 117.8 and 117.4 (weak) (C_8), 120.9 (C_4), 131.2 (C_9), 149.9 (C_5), 163.4 (C_3), 171.8 ($\underline{C}O_2CH_3$); MS: *m/e* 222 (M^+). The other fractions gave the known product, tricyclo[3.2.1.0]octene derivative[2a] (1.0 g) and unidentified materials (0.4 g).

9- and 8-Methyl-9-iodo-3-oxo-2-oxabicyclo[*4.4.0*]*dec-4-ene-6,8-carbolactone (4a and 4b).* A mixture of 2.3 g (10.3 mmol) of **2** in 300 ml of 5% aqueous sodium hydroxide solution was stirred for 12 h at room temperature. The solution was acidified with 5% hydrochloric acid under ice-cooling and the mixture was extracted with $CHCl_3$. The extract was washed with brine and dried over Na_2SO_4. Removal of the solvent gave 2.0 g of crude acids (**3a** and **3b**). Without further purification, a mixture of the acids in 77 ml of 0.5 M aqueous sodium hydrogencarbonate solution was added to a solution of 6.35 g (25.0 mmol) of iodine and 12.8 g (76.6 mmol) of

potassium iodide in 38 ml of water. The mixture was allowed to stand in a dark room for 48 h with occasional shaking. The reaction mixture was extracted with CH_2Cl_2. The extract was washed with 5% aqueous sodium thiosulfate and brine, and dried over Na_2SO_4. The solvent was evaporated *in vacuo* to give 2.7 g of pale yellow solid, which was repeatedly chromatographed on a silica gel using CH_2Cl_2 as the eluent to afford 2.0 g of **4a** and 0.2 g of **4b**. **4a**: Mp 184.5—187.5 °C (recrystallized from CH_2Cl_2); IR: 1760, 1740 cm^{-1}; ^1H NMR: 1.66 (3H, s, C_9–CH_3), 2.40—2.70 (4H, m, 2 –CH_2–), 4.11 (1H, t, J=9 Hz, C_8–H), 4.59 (1H, dd, J=7, 10 Hz, C_1–H), 6.13 and 7.26 (each 1H, d, and J=11 Hz, C_4– and C_5–H); ^{13}C NMR: 22.5 (C_9–CH_3), 26.4 (C_9), 33.9 and 35.5 (C_7 and/or C_{10}), 43.4 (C_6), 74.5 (C_1), 84.3 (C_8), 122.3 (C_4), 143.6 (C_5), 161.9 (C_3), 169.6 (–CO_2– of C_6); MS: *m/e* 334 (M^+); Found: C, 39.60; H, 3.26%. Calcd for $C_{11}H_{10}O_4I$: C, 39.66; H, 3.03%. **4b**: Mp (decomp) 184—186 °C (recrystallized from CH_2Cl_2); IR: 1785, 1740 cm^{-1}; ^1H NMR: 1.79 (3H, s, C_8–CH_3), 2.0—3.2 (4H, m, 2 –CH_2–), 4.36 (1H, dd, J=2, 4 Hz, C_9–H), 4.67 (1H, dd, J=2, 3 Hz, C_1–H), 6.21 and 7.26 (each 1H, d, and J=11 Hz, C_4– and C_5–H); ^{13}C NMR: 20.7 (C_8–CH_3), 25.5 (C_9), 36.1 and 37.9 (C_7 and/or C_{10}), 49.4 (C_6), 73.6 (C_1), 86.7 (C_8), 123.5 (C_4), 144.4 (C_5), 161.0 (C_3), 169.2 (–CO_2– of C_6); MS: *m/e* 334 (M^+); Found: C, 39.64; H, 3.29%. Calcd for $C_{11}H_{10}O_4I$: C, 39.66; H, 3.03%.

Dehydrohalogenation of ***4a*** *and* ***4b***. To a solution of 100 mg (0.3 mmol) of **4b** in 10 ml of dry THF was added 0.13 ml (0.9 mmol) of DBU with stirring at 10 °C under N_2. After being stirred for 1 h at room temperature and for 30 min at 40—45 °C, the mixture was acidified with aqueous 5% hydrochloric acid under ice-cooling and taken up in benzene. The extract was washed with brine, dried over Na_2SO_4, and concentrated. The residue was chromatographed (benzene–ethyl acetate, 92 : 8) to give 56 mg (91%) of **5b** as a colorless solid. Mp 140—141 °C (recrystallized from benzene–hexane); IR: 1780, 1755, 1740, 1605 (weak) cm^{-1}; ^1H NMR: 1.67 (3H, s, C_8–CH_3), 2.28 and 2.52 (each 1H, d, and J=13 Hz, –CH_2–), 4.98 (1H, d, J=4 Hz, C_1–H), 6.03 (1H, dd, J=4, 10 Hz, C_{10}–H), 6.27, 6.39, and 7.02 (each 1H, d, and J=10 Hz, C_4–, C_9–, and C_5–H); ^{13}C NMR ($(CD_3)_2CO$): 22.9 (C_8–CH_3), 42.1 (C_7), 49.3 (C_6), 72.9 (C_1), 82.0 (C_8), 123.3 (C_4), 128.0 (C_{10}), 139.6 (C_9), 146.0 (C_5), 162.5 (C_3), 175.7 (–CO_2– of C_6); MS: *m/e* 206 (M^+); Found: C, 63.98; H, 4.92%. Calcd for $C_{11}H_{10}O_4$: C, 64.07; H, 4.89%; whereas an analogous reaction of **4a** with DBU led to recovery of the starting material, and to decomposition of **4a** under vigorous conditions.

References

1) J. D. White, T. Matsui, and J. A. Thomas, *J. Org. Chem.*, **46**, 3376 (1981).

2) a) T. Imagawa, N. Sueda, and M. Kawanisi, *Tetrahedron*, **30**, 2227 (1974); b) G. A. Kraus and K. Frazier, *J. Org. Chem.*, **45**, 4820 (1980).

Cyanation of 1-Halocycloalkenes Catalyzed by Tetracyanocobaltate(I). Convenient Synthesis of 1-Cyanocycloalkenes

Takuzo FUNABIKI,* Hirohito KISHI, Yoshihiro SATO, and Satohiro YOSHIDA
Department of Hydrocarbon Chemistry, Faculty of Engineering, Kyoto University, Kyoto 606
(Received July 30, 1982)

Synopsis. 1-Cyanocycloalkenes (1-cyanocyclopentene, -hexene, -heptene, and -octene) were readily synthesized by catalytic cyanation of the corresponding 1-halocycloalkenes with tetracyanocobaltate(I). Reactivities of methyl-substituted 1-chlorocyclohexenes were lower than that of 1-chlorocyclohexene, and 1-chloro-2-methylcyclohexene scarecely reacted. Hydrogenation and isomerization of 1-cyanocycloalkenes were observed only with 1-cyanocycloheptene and 1-cyano-6-methylcyclohexene, respectively.

Previously we have reported the convenient synthetic method of α,β-unsaturated nitriles by cyanation of vinyl halides with tetracyanocobaltate(I), which is formed in an aqueous alkaline solution of pentacyanocobaltate(II) under hydrogen atmosphere.[1] To extend the utility of this method, we have studied the reactivity of 1-halocycloalkenes. Alicyclic α,β-unsaturated nitriles serve as versatile intermediates in organic syntheses, and the methods of preparation of these nitriles may be applicable to the synthetic chemistry of natural products. The most conventional synthetic method of 1-cyanocycloalkenes is the addition of hydrogen cyanide to cycloalkanones to form cyanohydrins, which are dehydrated to nitriles.[2] This method was recently modified to a one-pot reaction by using trimethylsilyl cyanide.[3] Some other reactions have been reported mostly for synthesis of 1-cyanocyclohexene, but examples of synthesis of 1-cyanocyclopentene,[2a,b,e]-heptene,[2b,c,d] and -octene,[2c,3] are very few. The present reaction (Eq. 1) is applicable to 1-halocycloalkenes of various ring sizes, and high yields of 1-cyanocycloalkenes can be obtained under mild conditions from cycloalkenes or cycloalkanones as starting materials.

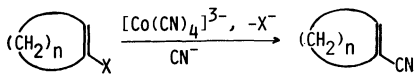

(1)

Results and Discussion

The reactions were performed in the same way as reported previously.[1] As shown in Table 1, 1-bromocycloalkenes were quantitatively converted into 1-cyanocycloalkenes. The reaction of 1-bromocyclopentene was fairly slower than other three bromides. The reaction proceeded catalytically, but the dropwise addition of the KCN solution at the controlled rate[1] was necessary for cyanation of a large excess of bromides as shown by the reaction of 1-bromocyclooctene. Interestingly, only 1-cyanocycloheptene was significantly hydrogenated. In the cyanation of alkenyl halides, the hydrogenation of acrylonitriles was observed with MeCH=CMeCN, but not with MeCH=CHCN, Me_2C=CHCN, and Me_2C=CMeCN.[1] The relation between the structure of acrylonitriles and facility for hydrogenation has not been clarified.

In order to find the effect of an alkyl substituent on the reactivity, we have studied the reactions of methyl-substituted 1-chlorocyclohexene. Results are shown in Table 2. 1-Chlorocyclohexene was cyanated at the similar rate to 1-bromocyclohexene, supporting that the reaction proceeds stepwise *via* a σ-vinyl cobalt complex and the C–X bond breaking is faster than the C–CN bond formation (Eqs. 2—4).[1] However, methyl-substituted 1-chlorocyclohexenes were less reactive than 1-chlorocyclohexene, regardless of the position of the methyl group, and, unexpectedly, 1-chloro-2-methylcyclohexene was hardly cyanated. In the case of alkenyl halides, the methyl substituent increased the reactivity of the halides, and the rapid reaction was observed with Me_2C=CHX and Me_2C=CMeX. The retardation effect of the methyl group observed with methyl-substituted 1-chlorocyclohexenes is not due to stabilization of the σ-complex (retarding the reaction (4)), but rather retardation or inhibition of the formation of the σ-complex. The result indicates that the rate of cyanation of alkyl-substituted 1-halocycloalkenes

Table 1. Cyanation of 1-bromocycloalkenes

$(CH_2)_n$ Br, n	Bromide[a]/Co	Time/h	Nitriles(mol %) Yield[b]	Composition $(CH_2)_n$ CN	Composition $(CH_2)_{n+1}$ CN
3	2	8	70(81)	100	
4	2	4.5	85(96)	100	
5	1	1.5	80(99)	63	37[d]
5	2	4.5	85(99)	66	34[d]
6	2	4.5	90(100)	95	5
6	10[c]	14	68(73)	99	1

a) Mole ratio. b) Total isolated and GLC (in parentheses) yields based on bromides. c) Alkaline KCN solution was added dropwise. d) Yield of the saturated nitrile increased with the elapse of time.

Table 2. Cyanation of 1-chlorocyclohexenes

Chloride[a]	Time/h	Products and Yield (mol %)[b] Nitriles	Yield
1-Cl-C_6H_9	4.5	1-CN-C_6H_9	70(78)
1-Cl-2-Me-C_6H_8	24	1-CN-2-Me-C_6H_8	Trace(4)
1-Cl-3-Me-C_6H_8	8	1-CN-3-Me-C_6H_8	75(85)
1-Cl-4-Me-C_6H_8	12	1-CN-4-Me-C_6H_8	70(78)
1-Cl-5-Me-C_6H_8	8	1-CN-5-Me-C_6H_8	75(85)
1-Cl-6-Me-C_6H_8	24	1-CN-6-Me-C_6H_8 (61%)+ 1-CN-2-Me-C_6H_8 (39%)	75(83)

a) C_6H_8 denotes cyclohexene. Chloride/ Co=2. b) Isolated and GLC yields (in parentheses) based on chlorides.

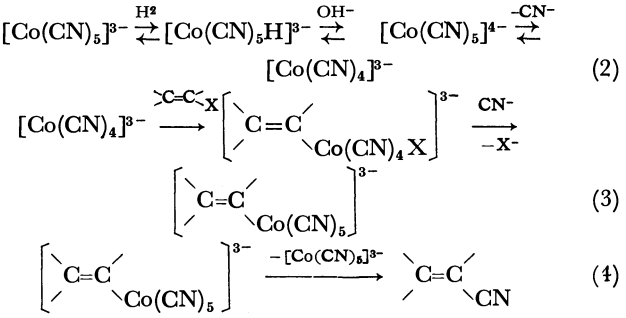

is affected not only by the reaction (4), but also (3).

We have proposed that the C–X bond cleavage and the C–Co bond formation proceeds by an oxidative addition process *via* an electron-transfer interaction.[1] The electron-transfer may take place by the interaction of Co(I) with the π^* orbital of the C–C bond. Since the electronic effect of the methyl substituent may be similar both in alkenyl and cycloalkenyl halides, the retardation by the methyl group must be due to the steric effect of the methyl and methylene hydrogens of the rigid cycloalkene ring, hindering the approach of $[Co(CN)_4]^{3-}$ to the C=C bond.

We have observed the isomerization of 1-cyano-6-methylcyclohexene to 1-cyano-2-methylcyclohexene. This is one of the very few examples of the double bond migration catalyzed by $[Co(CN)_5H]^{3-}$.[4] 1-Cyano-6-methylcyclohexene was selectively formed in the initial stage, but the cyanation became very slow when the isomerization became the predominant reaction. The isomerization proceeds irreversively probably *via* a σ-complex (Eq. 5), which was suggested by broad ^{1}H NMR peaks (δ=1.1—2.2) of the reaction solution prepared in D_2O. The isomerization can be used to synthesize 1-cyano-2-methylcyclohexene which can not be formed from 1-chloro-2-methylcyclohexene.

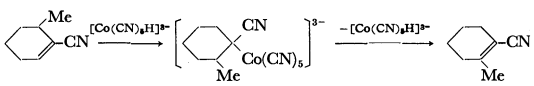

(5)

Experimental

1-Bromocycloalkenes were synthesized by dehydrobromination of α,β-dibromocycloalkanes[5] with KOH (1-bromocyclopentene),[6] $NaNH_2$-*t*-BuOH (1-bromocyclohexene),[7] and morpholine (1-bromocycloheptene and -octene).[8] 1-Chlorocyclohexenes were synthesized by chlorination of corresponding cyclohexanones with CCl_4/PPh_3,[9] and mixtures (1-chloro-2- and -6-methylcyclohexenes from 2-methylcyclohexanone, and 1-chloro-3- and -5-methylcyclohexenes from 3-methylcyclohexanone) were separated by a preparative GLC. Nitriles obtained here are known compounds (1-cyano-3- and -5-methylcyclohexenes have been reported as a mixture)[10] and gave satisfactory elemental analyses, and identified by IR (JASCO IRA-2, observed as neat films) and ^{1}H and ^{13}C NMR spectroscopy (JEOL FX-100, observed in $CDCl_3$).

Cyanation of 1-Halocycloalkenes. The reaction was performed in the same fassion as described previously.[1] A typical procedure was as follows: $CoCl_2$ (1.00 mmol, 0.130 g), KCN (4.95 mmol, 0.322 g) and KOH (2.0 mmol, 0.12 g) were placed in a 20 cm^3 two-necked flask equipped with a cold-finger. H_2O (5 cm^3) was added under hydrogen atmosphere at 45 °C, and the solution was stirred magnetically for 30 min. *1-Bromocyclopentene* (0.21 cm^3, 2.0 mmol) was added with a microsyringe through a serum cap. It took 8 h to cyanate the added bromide, and the reaction mixture was extracted with dichloromethane. Dichloromethane was evaporated, and the residue was distilled *in vacuo* with a Kügelrohr apparatus to give 1-cyanocyclopentene (0.13 g, 1.4 mmol) bp 95 °C/28 mmHg† (oven temperature); IR 2220 cm^{-1} (CN); ^{1}H NMR δ=1.99 (q, 2H), 2.54 (m, 4H), 6.66 (m, 1H); ^{13}C NMR δ=22.8 (t), 33.7 and 34.2 (t), 115.3 (s), 116.7 (s, CN), 128.9 (d). *1-Bromo* and *-chlorohexene* (2 mmol) yielded 1-cyanocyclohexene (0.18 g, 1.7 mmol) and 0.15 g, 1.4 mmol), respectively, bp 120 °C/28 mmHg; IR 2204 cm^{-1} (CN); ^{1}H NMR δ=1.65 (m, 4H), 2.20 (m, 4H), 6.62 (q,1H); ^{13}C NMR δ=20.7 (t), 21.4 (t), 25.7 (t), 112.3 (s), 119.7 (s, CN), 145.2 (d). *1-Bromo-cycloheptene* (2 mmol) yielded a mixture of 1-cyanocycloheptene and cyanocycloheptane (0.21 g): 1-Cyanocycloheptene bp 60 °C/2 mmHg; IR 2204 cm^{-1}; ^{1}H NMR δ=1.62 (s, br, 6H), 2.34 (m, 4H), 6.78 (t, 1H);^{13}C NMR δ=25.3, 26.2, 29.6, 31.3, and 31.6 (t), 117.6 (s), 120.9 (s, CN), 150.3 (d): *Cyanocycloheptane* bp 60 °C/2 mmHg; IR 2220 cm^{-1}; ^{1}H NMR δ=1.60 (m, 8H), 1.87 (m, 4H), 2.87 (tt, 1H); ^{13}C NMR δ=25.4 and 31.6 (t), 27.6 (t), 30.1 (s), 123.3 (s, CN). *1-Bromocyclooctene* (2 mmol) yielded 1-cyanocyclooctene and cyclooctane (95 : 5, 0.24 g); 1-cyanocyclooctene bp 75 °C/0.5 mmHg; IR 2210 cm^{-1}; ^{1}H NMR δ=1.53 (s, br, 8H), 2.31 (m, 4H), 6.60 (t, 1H); ^{13}C NMR δ=25.5, 26.0, 27.1, 27.8, 28.3, and 28.8 (t), 115.1 (s), 120.3 (s, CN), 148.1 (d). *1-Chloro-2-methylcyclohexene* scarecely reacted, but *1-chloro-3-*, *-4-*, and *-5-methylcyclohexenes* (2 mmol) yielded selectively corresponding 1-cyano(methyl)-cyclohexenes bp 125 °C/28 mmHg; 1-cyano-3-methylcyclohexene (0.18 g, 1.5 mmol) Found: C, 79.01; H, 9.20; N, 79.60%; Calcd for $C_8H_{11}N$: C, 79.29; H, 9.15; N, 11.56%; IR 2210 cm^{-1}; ^{1}H NMR δ=1.05 (d, 3H), 1.75 (m, 4H), 2.20 (m, 3H), 6.46 (tt, 1H); ^{13}C NMR δ=21.2, 25.8, and 34.5 (t), 27.6 (t), 28.8 (d), 111.9 (s), 119.7 (s, CN), 144.7 (d); 1-cyano-4-methylcyclohexene (0.17 g, 1.4 mmol) IR 2210 cm^{-1}; ^{1}H NMR δ=0.98 (d, 3H), 1.32 (m, 1H), 1.72 (m, 3H), 2.23 (m, 3H), 6.59 (m, 1H); ^{13}C NMR δ=21.3 (t), 26.6 (t), 27.0 (d), 29.5 (t), 33.9 (q), 112.0 (s), 119.6 (s,CN), 144.7 (d); 1-cyano-5-methylcyclohexene (0.18 g, 1.5 mmol) Found: C, 79.05; H, 9.30; N, 11.68%; Calcd for $C_8H_{11}N$: C, 79.29; H, 9.15; N, 11.56%; IR 2210 cm^{-1}; ^{1}H NMR δ=1.00 (d, 3H), 1.73 (m, 4H), 2.23 (m, 3H), 6.67 (m, 1H); ^{13}C NMR δ=20.3 (t and q), 26.6 (t), 29.3 (t), 30.8 (d), 111.7 (s), 119.7 (s,CN), 150.5 (d). *1-Chloro-6-methylcyclohexene* (2 mmol) yielded a mixture of 1-cyano-6- and -2-methylcyclohexenes (61: 39 after the 24 h reaction, 0.18 g, 1.5 mmol) bp 125 °C/28 mmHg; 1-cyano-6-methylcyclohexene IR 2205 cm^{-1}; ^{1}H NMR δ=1.19 (d, 3H), 1.69 (m, 4H), 2.15 (m, 3H), 6.60 (m, 1H); ^{13}C NMR δ=19.3 (t), 19.8 (q), 25.8 and 29.9 (t), 30.7 (d), 118.3 (s), 119.1 (s, CN), 145.0 (d); 1-cyano-2-methylcyclohexene IR 2202 cm^{-1}; ^{1}H NMR δ=1.63(m, 4H), 1.99 (s, 3H), 2.14 (m, 4H); ^{13}C NMR δ=21.5 (t), 21.6 (t), 23.0 (t), 27.1 (q), 31.3 (t), 106.2(s), 119.3 (s, CN), 153.4 (s).

† Throughout this paper 1 mmHg=133.322 Pa.

References

1) T. Funabiki, H. Hosomi, S. Yoshida, and K. Tarama, *J. Am. Chem. Soc.*, **104**, 1560 (1982).

2) a) S. M. McElvain and R. E. Starn, Jr., *J. Am. Chem. Soc.*, **77**, 4571 (1955); b) O. H. Wheeler and I. Lerner, *ibid.*, **78**, 63 (1956); c) J. Sicher, F. Sípoš, and J. Jonáš, *Collect. Czech. Chem. Commun.*, **26**, 262 (1961); *Chem. Abstr.*, **55**, 15372a (1961); d) K. C. Mathur, G. S. Saharia, *Indian J. Chem.*, **6**, 248 (1968); e) C. W. B. Cumper, S. K. Dev, and S. R. Landor, *J. Chem. Soc., Perkin Trans. 2*, **1973**, 537.

3) M. Oda, A. Yamamuro, and T. Watabe, *Chem. Lett.*, **1979**, 1427.

4) L. M. Jackman, J. A. Hamilton, and J. M. Lawlor, *J. Am. Chem. Soc.*, **90**, 1914 (1968).

5) H. R. Snyder and L. A. Brooks, *Org. Synth.*, Coll. Vol. II, 171 (1948).

6) P. I. Abell and C. Chiao, *J. Am. Chem. Soc.*, **82**, 3610 (1960).

7) P. Caubere and G. Coudert, *J. Chem. Soc., Chem. Commun.*, **1972**, 1289.

8) K. Schank and B. Eistert, *Chem. Ber.*, **99**, 1414 (1966).

9) N. Isaacs and D. Kirkpatrick, *J. Chem. Soc., Chem. Commun.*, **1972**, 443.

10) A. A. Petrov and A. F. Sapozhnikova, *J. Gen. Chem. (U.S.S.R)*, **18**, 424 (1948); *Chem. Abstr.*, **42**, 7221g (1948).

Studies of Aromatic Sesquiterpenes. IV.[1] The Synthesis of γ-Calacorene, Calamenene, and 4-Methoxyisocadalene

Kazuo ADACHI* and Masahito MORI
Osaka Institute of Technology, Omiya, Asahi-ku, Osaka 535
(Received August 28, 1982)

Synopsis. The Grignard reaction of 3,4-dihydro-4,7-dimethyl-1(2*H*)-naphthalenone with isopropylmagnesium bromide gave a 3 : 1 mixture of normal reaction product and α-isopropylidene ketone, from which, the title sesquiterpenes and 1,2-bis(3-isopropyl-4-methoxy-6-methyl-1-naphthyl)ethane were synthesized.

Some sesquiterpenes are dehydrogenated by heating with sulfur, selenium or palladium catalysts giving a parent hydrocarbon of the sesquiterpenes such as cadalene (**1**), which have been recently isolated[2] along with 4-methoxyisocadalene[3] (**2**) or other sesquiterpenes from *Heterotheca* species (Compositae). In the various path ways for synthesis of **1**, 3,4-dihydro-4,7-dimethyl-1(2*H*)-naphthalenone (**3**) have been employed as a key intermediate.[4] However, the isopropylated products of **3** by the Grignard reaction have not been investigated.

In this paper, it is described that the Grignard reaction products of **3** were dehydrated with formic acid giving a mixture of 1,2-dihydro-1,6-dimethylnaphthalene (**4**), γ-calacorene (**5**), and 3,4-dihydro-2-isopropylidene-4,7-dimethyl-1(2*H*)-naphthalenone (**6**). Calamenene (**7**) and 4-methoxyisocadalene (**2**) were synthesized from **5** and **6**, respectively.

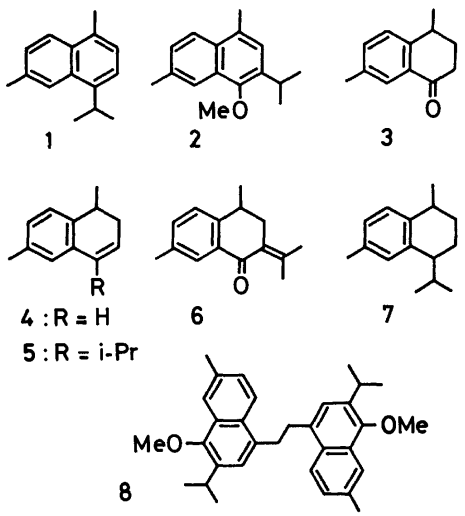

The ketone **3** was allowed to react with isopropylmagnesium bromide, and the dehydration of the reaction products gave a mixture of four components (**4**, **5**, and **6** including **3**). The formation of two hydrocarbons **4** and **5** indicates that the corresponding alcohols were respectively prepared by reductive reaction and normal addition of the Grignard reagent on **3**. Furthermore, any other isomers of the *endo*-olefin **5** were not observed. Therefore, an intermediate in the synthesis of cadalene (**1**) from **3** is γ-calacorene (**5**), which has been isolated from the wood of *Juniperus rigida*[5] and the Japanese hop (*Humulus lupulus* L.).[6] The structure of 3,4-dihydro-2-isopropylidene-4,7-dimethyl-1(2*H*)-naphthalenone (**6**) was confirmed by the comparison of its spectral data with those of 3,4-dihydro-2-isopropylidene-1(2*H*)-naphthalenone and the 4-methyl derivative.[7]

The catalytic hydrogenation of **5** afforded calamenene (**7**) in a mixture of diastereomers which consisted of *cis* (80%) and *trans* (20%) isomers on the basis of the ^{1}H-NMR (60 MHz), *i.e.*, the proton signals of two methyl groups in the isopropyl group indicated four pairs of doublets (d, at δ=0.74, 1.01, and 0.69, 0.98).[8] In the literature,[9] it has been reported that the reduction of α-calacorene afforded calamenene which consisted of about 40% of *cis*- and 60% of *trans*-isomers.

The unsaturated ketone **6** on isomerization with Pd–C catalysts and subsequent methylation with dimethyl sulfate afforded 4-methoxyisocadalene (**2**). The prism crystals (mp 165.5—166.0 °C) were obtained as a by-product of **2**, and its IR spectrum showed similar pattern with that of **2**. 1,2-Bis(3-isopropyl-4-methoxy-6-methyl-1-naphthyl)ethane (**8**) was proposed as the structure of this by-product on the basis of its NMR spectrum and the elementaly analysis. During the isomerization of **6**, a part of the reactant was dehydrogenatively dimerized to give **8**.

Experimental

The Grignard Reaction of Isopropylmagnesium Bromide on 3,4-Dihydro-4,7-dimethyl-1-(2H)-naphthalenone (3). The ketone **3** was synthesized from toluene in the same way as the synthesis of 3,4-dihydro-8-isopropyl-4,5-dimethyl-1(2*H*)-naphthalenone from *p*-cymene.[10]

A solution of **3** (10.0 g) in ether (25 ml) was added to the Grignard reagent prepared from Mg (4.2 g) and isopropyl bromide (23.0 g) in ether (150 ml). The reaction mixture was stirred for several hours in an ice bath, allowed to stand for over night, and then refluxed for 8 h. Acetone was added to destroy an excess reagent, and the reaction mixture was decomposed by adding a crushed ice and NH_4Cl. After removal of the solvent from the ethereal solution, the residue (14 g) was dehydrated by stirring with formic acid (70 ml) at 50 °C for 3 h. The reaction mixture was diluted with water and extracted with benzene. Removal of the solvent from the benzene extract and distillation of the residue gave 8.5 g of an oil, bp 94—146 °C/3 mmHg (1 mmHg=133.322 Pa), which was a mixture consisted of **4** (14.3%), **5** (54.8%), **3** (13.4%), and **6** (17.5%) (GC analysis). The oily mixture was separated into two fractions by successive elution with CCl_4 and ether through a silica-gel column. The hydrocarbon mixture eluted with CCl_4 was repeatedly distilled to separate **4** and **5**. The unsaturated ketone **6** in the ethereal eluates was freed from **3** over a silica-gel column chromatography.

1,2-Dihydro-1,6-dimethylnaphthalene (4): Oil, bp 96—97 °C/9 mmHg; IR: 1605, 1490, 1445, 880, 810, 695, and 670 cm^{-1}; NMR (CCl_4): δ=1.18 (3H, d, J=7 Hz, CH_3), about 2.2 (2H, m, CH_2), 2.23 (3H, s, CH_3), 2.78 (1H, m, J=7 Hz, >CH-),

5.81 (1H, dt, J=9 and 4 Hz), 6.32 (1H, dt, J=9 and 2 Hz), 6.73 and 6.88 (3H, each br, s).

γ-Calacorene (1,2-Dihydro-4-isopropyl-1,6-dimethylnaphthalene) (5): Oil, bp 125—126 °C/9 mmHg; IR: 1605, 1485, 1455, 1445, 1380, 1360, 880, 815, and 805 cm^{-1}; NMR (CCl_4): δ= 1.14 (9H, d, J=7 Hz, three CH_3), 2.17 (2H, m, CH_2), 2.30 (3H, s, CH_3), 2.82 (2H, m, J=7 Hz, two >CH–), 5.70 (1H, t, J=5 Hz, =CH–), 6.93 and 7.05 (3H, each br. s).

3,4-Dihydro-2-isopropylidene-4,7-dimethyl-1(2H)-naphthalenone (6): Oil, bp 127—128 °C/3 mmHg; IR: 1665, 1605, 1495, 1450, 1365, 1290, 1175, 820, and 785 cm^{-1}; NMR (CCl_4): δ= 1.24 (3H, d, J=7 Hz, CH_3), 1.90 (3H, br. s, vinyl-CH_3), 2.18 (3H, br. s, vinyl-CH_3), 2.35 (3H, s, CH_3), 2.73 (2H, br, CH_2), 3.00 (1H, m, >CH–), 7.02 (1H, d, J=8 Hz), 7.18 (1H, dd, J=8 and 2 Hz) and 7.82 (1H, br. s). Found: C, 84.01; H, 8.45%. Calcd for $C_{15}H_{18}O$: C, 84.07; H, 8.47%.

Calamenene (7). A solution of **5** (2.0 g) in ethanol (50 ml) was shaken with Pd–C (10%, 0.5 g) under a hydrogen atmosphere for 8 h. The catalysts were then removed by filtration, and the filtrate was evaporated to give an oil, which was distilled to afford **7** (1.9 g), bp 127—130 °C/10 mmHg, n_D^{20} 1.5262, d_4^{20} 0.9305; IR: 1615, 1495, 1455, 1380, 1370, 1360, and 815 cm^{-1}; NMR (CCl_4): δ=0.69 and 0.74 (3H, each d, J=7 Hz, CH_3), 0.98 and 1.01 (3H, each d, J=7 Hz, CH_3), 1.21 (3H, d, J=7 Hz, CH_3), 1.67 (4H, m), 2.23 (3H, s, CH_3), about 2.58 (3H, m, three >CH–) and 6.87 (3H, m). The resulting calamenene (**7**) showed a single peak on GC (a 2 m×3 mm Apiezon Grease L 30% on Cellite 545 column, He), but its NMR spectrum showed the presence of two isomers, *cis*-**7**: *trans*-**7**=4 : 1.

4-Methoxyisocadalene (2) and Its Dimerized Product (8). A mixture of the unsaturated ketone **6** (1.0 g) and Pd–C (10%, 0.5 g) in xylene (10 ml) was refluxed for 12 h. The catalysts were removed by filtration and the filtrate was evaporated. The residual oil was refluxed with K_2CO_3 (2.0 g) and dimethyl sulfate (1.6 g) in acetone (20 ml) for 8 h. After removal of the solvent, ammonia water (2 ml) was added and stirred to destroy an excess dimethyl sulfate at 50 °C for 30 min. The reaction mixture was diluted with water and then extracted with benzene. The benzene extract was washed with water, dried and evaporated to give an oil which was chromatographed over an alumina column. The hexane eluate wa evaporated to give an oil (0.9 g), from which, the precipitated crystals (0.3 g) of **8** were removed by filtration and the filtrate was purified by distillation to afford **2** (0.4 g), bp 128—130 °C/ 10 mmHg, n_D^{20} 1.5587. The IR and NMR spectra of **2** were superimposable with those of the authentic specimen.[1] *Picrate*: Orange brown needles, mp 90.5—91.5 °C (lit,[1] mp 90.5—91.5 °C).

1,2-Bis(3-isopropyl-4-methoxy-6-methyl-1-naphthyl)ethane (8): Prisms from petroleum ether, mp 165.5—166.0 °C; IR (KBr): 1620, 1600, 1565, 1510, 1455, 1440, 1405, 1350, 1225, 1195, 1090, 1060, 985, 880, and 815 cm^{-1}; NMR (CCl_4): δ=1.14 (12H, d, J=7 Hz, two $\langle^{CH_3}_{CH_3}$), 2.52 (6H, s, two CH_3), 3.35 (4H, s, two CH_2), 3.45 (2H, m, J=7 Hz, two >CH–), 3.80 (6H, s, two OCH_3), 6.85 (2H, s), 7.16 (2H, dd, J=9 and 2 Hz), 7.78 (2H, br. s) and 7.79 (2H, d, J=9 Hz). Found: C, 84.50; H, 8.42%. Calcd for $C_{32}H_{38}O_2$: C, 84.54; H, 8.43%.

References

1) Preceding paper: K. Adachi and N. Taniguchi, *Bull. Chem. Soc. Jpn.*, **55**, 1655 (1982).

2) F. Bohlmann and C. Zdero, *Chem. Ber.*, **109**, 2021 (1976); *Phytochemistry*, **18**, 1185 (1979); F. Bohlmann, C. Zdero, H. Robinson, and R. M. King, *ibid.*, **18**, 1675 (1979).

3) F. Bohlmann and W. Mailahn, *Chem. Ber.*, **114**, 1091 (1981).

4) W. S. Johnson and A. R. Jones, *J. Am. Chem. Soc.*, **69**, 792 (1947); K. Adachi, *Nippon Kagaku Kaishi*, **1972**, 985.

5) B. Tomita, Y. Hirose and Y. Nakatsuka, *Nippon Mokuzai Gakkaishi*, **15**, 48 (1969).

6) Y. Naya and M. Kotake, *Bull. Chem. Soc. Jpn.*, **42**, 2088 (1969).

7) K. Adachi, J. Tanaka, Y. Imai, and T. Okazaki, *Nippon Kagaku Kaishi*, **1980**, 62.

8) P. H. Ladwa, G. D. Joshi, and S. N. Kulkarni, *Indian J. Chem.*, **16B**, 853 (1978); J. D. Bunko, E. L. Ghisalberti, and P. R. Jefferies, *Aust. J. Chem.*, **34**, 2237 (1981).

9) N. H. Andersen, D. D. Syrdal, and C. Graham, *Tetrahedron Lett.*, **1972**, 905.

10) J. Tanaka and K. Adachi, *Nippon Kagaku Kaishi*, **1979**, 758.

Optical Resolution of Aspartic Acid by Using Copper Complexes of Optically Active Amino Acids

Kaoru HARADA* and Noriko FUJII
Department of Chemistry, The University of Tsukuba, Sakura-Mura, Niihari, Ibaraki 305
(Received August 30, 1982)

Synopsis. DL-Aspartic acid was resolved with high optical purity in the presence of an optically active amino acid copper complex. The mechanism of the optical resolution was explained by the competitive inhibition of crystallization.

We have reported a new method for the optical resolution of DL-aspartic acid by crystallization from a solution of DL-aspartic acid with a copper complex of optically active alanine, glutamic acid, and proline.[1,2] When the mixture was kept at a room temperature, the optically active aspartic acid copper complex crystallized spontaneously. The resolved aspartic acid had high optical purity and a configuration opposite to the optically active amino acid used in this resolution. This phenomenon had been explained as a stereoselective ligand exchange reaction.[1] However, the last communication confirmed that the proposed stereoselective ligand exchange did not represent the mechanism of these reactions, and that the phenomenon might be explained by the competitive inhibition of crystallization.[3]

L-Amino acid–Cu + DL-Asp → D-Asp–Cu ↓ crystallized
+ L-Asp + L-Amino acid ↓ in solution

This paper reports an optical resolution of DL-aspartic acid using a copper complex of the optically active amino acids other than those stated above. We also confirmed that the mechanism of the optical resolution of DL-aspartic acid was explained by competitive inhibition of crystallization.

Experimental

The optically active amino acids used in this experiment were D- or L-enantiomers of alanine, serine, threonine, valine, histidine, leucine, isoleucine, phenylalanine, methionine, glutamine, aspargine, lysine, and arginine. A solution (10 ml) of an optically active amino acid (2.5 mmol) was mixed with cupric carbonate ($CuCO_3 \cdot Cu(OH)_2 \cdot H_2O$, about 1.25 mmol) and was heated, and the solution was filtrated to remove the excess of cupric carbonate. DL-Aspartic acid (2.5 mmol) was dissolved in 10 ml of hot water and this was added to the solution of the amino acid copper complex and filtered. The solution was kept still at room temperature for 1 d. The crystallized optically active aspartic acid copper complex was collected by filtration. *N*-(trifluoroacetyl)aspartic acid isopropyl ester was prepared in the usual way. The enantiomeric ratios of the resolved aspartic acid were determined by gas chromatography (Hitachi 163 Gas Chromatograph) by using Chirasil-Val capillary glass column (Applied Science, U. S. A.).

Results and Discussion

The results of the resolution of racemic aspartic acid in the presence of copper ion and optically active amino acids (Ala, Ser, Thr, Val, and His) are summarized in Table 1. Racemic aspartic acid was successfully resolved in high optical purity. When L-amino acid was used, D-aspartic acid copper complex crystallized spontaneously. Whereas, L-aspartic acid copper complex precipitated by using D-amino acids as shown in Table 1. By using the other optically active amino acids (Leu, Ile, Phe, Met, $GluNH_2$, $AspNH_2$, Lys, and Arg), the resolution of DL-aspartic acid was not successful under the conditions described in the experimental section.

Table 2 shows the effect of D- or L-aspartic acid addition to the DL-aspartic acid resolution in the presence of a L-serine copper complex. The amount of D- or L-aspartic acid added to the solution was 1/10—1/2 in molar ratio of DL-aspartic acid. When D-aspartic acid was added to the aqueous mixtures of a L-serine copper complex and DL-aspartic acid, the time required for the crystallization was shorter than the case without addition of any other amino acid (control). And the amount of the crystallized copper complex and the

Table 1. Optical resolution of DL-Asp by using copper complexes of optically active amino acids

Optically active amino acid	Optically active aspartic acid copper complex			
	Crop (mg)	Recovery[a] %	Confign.	Optical purity/%
L-Ala	150	43.5	D	95
D-Ala	151	43.8	L	80
L-Ser	120	34.8	D	96
D-Ser	107	31.0	L	87
L-Thr	61	17.7	D	92
D-Thr	43	12.5	L	87
L-Val	68	19.7	D	100
D-Val	40	11.6	L	82
L-His	225	65.2	D	77

a) Recovery = $\frac{\text{isolated L-(or D-Asp)}}{\text{total L-(or D-Asp)}} \times 100$.

Table 2. Effect of D- or L-Asp addition to DL-aspartic acid resolution

L-Ser–Cu +DL-Asp	Crop (mg)	Recovery[a] %	D-Asp (%)	Time h
Control	120	34.8	98	25
+D-Asp (1/2)	180	52.2	100	18
+D-Asp (1/4)	170	49.3	100	18
+D-Asp (1/10)	160	46.4	100	18
+L-Asp (1/2)	83	24.1	75	25
+L-Asp (1/4)	84	24.3	96	25
+L-Asp (1/10)	75	21.8	97	25

a) Recovery = $\frac{\text{isolated L-(or D-Asp)}}{\text{total L-(or D-Asp)}} \times 100$.

Table 3. Seeding effect to DL-aspartic acid resolution using D-Ser or L-Ser–Cu complexes

	D-Ser–Cu+DL-Asp Seed			L-Ser–Cu+DL-Asp Seed		
	No	L	D[a)]	No	L[b)]	D
Crop (mg)	99	151	58	134	58	171
Recovery/%	28.7	43.8	16.8	38.9	16.8	49.6
Confign.	L	L	D	D	L	D
O.P./%	97	97	99	96	100	100
Time/h	10	2.5	2.5	20	2.5	2.5

Seed; L: L-Asp–Cu, D: D-Asp–Cu. a) 2nd crop; 77.4 mg (recovery: 22.4%), 92% L. b) 2nd crop; 114.8 mg (recovery: 33.3%), 97% D.

c) Recovery $= \frac{\text{isolated L-(or D-Asp)}}{\text{total L-(or D-Asp)}} \times 100.$

optical purity of aspartic acid both increased. The amount of the crystals increased 1.5 times compared with the control when the amount of L-aspartic acid was 1/2 molar ratio of DL-aspartic acid. However, by the addition of L-aspartic acid, the optical purity of the resolved aspartic acid decreased gradually. When the amount of L-aspartic acid reached 1/2 molar ratio of DL-aspartic acid, the optical purity of aspartic acid decreased to 75% and the amount of crystallized D-aspartic acid copper complex reduced to 40% of the control. Therefore, the results indicate that the newly added L-aspartic acid inhibits the crystallization of a D-aspartic acid copper complex.

We have reported that the racemic aspartic acid copper complex was resolved by seeding with a L- or D-aspartic acid copper complex.[4)] The effect of the seeding to this selective crystallization was studied and the results are summarized in Table 3. L- or D-Aspartic acid copper complex was added to the aqueous mixtures of a D-serine copper complex and DL-aspartic acid. Without seeding, L-aspartic acid copper complex crystallization took place in 10 h. When L-aspartic acid copper complex was added to the mixture as seed, the time required for the crystallization was shortened remarkably (2.5 h), and the amount of the crystallized complex increased. On the contrary, when D-aspartic acid copper complex was added to the mixtures, a small amount of optically active D-aspartic acid copper complex crystallized. After removal of D-aspartic acid copper complex, L-aspartic acid copper complex with high optical purity crystallized spontaneously in 24 h. The resolution of DL-aspartic acid by using L-serine copper complex was similar to that described above. Thus it was found that the seeding procedure crystallized optically active aspartic acid copper complex effectively when the configuration of the seeds have the same configuration as the first crop (Table 3 2nd and 6th columns), which was obtained without seeds. However, when the configuration of the seeds has the opposite configuration to the first crop, the seeds initiate the crystallization of small amount of optically active aspartic acid copper complex which has the same configuration as the seed. After removal of the crystallized complex from the solution, the optically active aspartic acid copper complex, which is favored to precipitate, was crystallized spontaneously.

These experiments indicate that the configuration of optically active amino acids determines the configuration of the crystallized optically active aspartic acid copper complex, and the configuration of the aspartic acid is opposite to the optically active amino acid used in the resolution. The mechanism of the optical resolution could be explained by the stereoselective inhibition of crystallization. When the DL-aspartic acid was resolved in the presence of D-serine copper complex, the solution was composed of L- and D-aspartic acid, D-serine and copper ions. The crystallization of L-aspartic acid copper complex is faster than that of D-aspartic acid copper complex in the presence of D-serine. The crystallization of D-aspartic acid copper complex was inhibited by the presence of D-serine copper complex in the solution. Because these two D-amino acid copper complexes have the same configuration and have stronger interaction between these two. Therefore the rate of the crystal growth is affected by the presence of the other optically active amino acid. The addition of L- or D-aspartic acid, and the seeding of L- or D-aspartic acid copper complex in the reaction mixture could also affect the rate of crystallization of optically active aspartic acid copper complex. All these results could support the competitive inhibition mechanism of crystallization proposed in this kind of the optical resolution of aspartic acid. This type of optical resolution could be applicable to other racemic compounds.

References

1) K. Harada, *Nature*, **205**, 590 (1965).
2) K. Harada and W. W. Tso, *Bull. Chem. Soc. Jpn.*, **45**, 2859 (1972).
3) K. Harada and T. Iwasaki, *Chem. Lett.*, **1972**, 1057.
4) K. Harada and S. W. Fox, *Nature*, **194**, 768 (1962).

Photolysis of Ozonides in the Gas Phase

Shiro HATAKEYAMA* and Hajime AKIMOTO
Division of Atmospheric Environment, National Institute for Environmental Studies, P.O. Tsukuba-gakuen, Ibaraki 305
(Received September 9, 1982)

Synopsis. Photolysis of four kinds of simple ozonides (ethene, propene, 2-butene, and isobutene ozonides) in the gas phase were carried out. The contribution of the double-β-scission mechanism was 4—13%. The main reaction path is proposed to be intramolecular hydrogen abstraction followed by radical forming unimolecular decomposition.

Ozonides are oxidants possibly present in photochemical smog since they are known to be formed in the gas-phase ozoneolefin reactions.[1,2] While photolytic decomposition is thought to be one of the degradation paths of ozonides in the atmosphere, photolysis of ozonide in gas phase has never been reported yet. Photolysis of ozonides in the liquid phase was suggested to proceed *via* a double-β-scission after the cleavage of oxygen-oxygen bond as follows.[3]

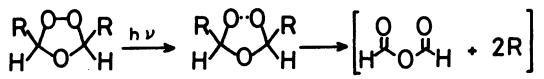

$$\longrightarrow \text{R-R} + \text{RH} + \text{HCOOH} + \text{CO} \quad (1)$$

Formic anhydride, however, has never been detected. In the present study, gas-phase photolysis of ozonides in near UV region was studied and the reaction mechanism is discussed.

Experimental

Ethene, propene, 2-butene, and isobutene ozonides (hereafter referred to as EO, PO, BO, and IO, respectively) were prepared by the reaction of ozone with ethene, propene, *cis*-2-butene, and isobutene, respectively, in isobutane at −78 °C. They were treated with K_2CO_3[4] and further purified with trap-to-trap distillation. UV spectrum of EO was obtained by use of Cary 17D spectrometer.

The photochemical reactor was an 11 L cylindrical quartz vessel (120 mm i.d., 1000 mm long) equipped with multi-reflection mirrors for long-path (40 m) Fourier transform infrared spectroscopy (LP-FTIR). Six Sun lamps (Toshiba FL 20 SE, $260 \leq \lambda \leq 400$ nm, $\lambda_{max}=310$ nm) surrounded the reactor coaxially. Ozonides (15—20 mTorr) (1 Torr = 133.32 Pa) were photolyzed in 1 atm of N_2 at 30±2 °C. Photolysis of BO without any buffer gas was also carried out. The irradiation time was 30 min, 1 h, 2 h, and 2 h for EO, PO, BO, and IO respectively. The concentrations of reactants and products were monitored by means of the LP-FTIR. The spectra were obtained with every 128 scans (scanning time was about 5 min) at a resolution of 1 cm^{-1}.

Results and Discussion

Products and their yields in the photolyses of ozonides are shown in Table 1. Formic anhydride which had been postulated as an intermediate in the liquid phase photolysis was detected for the first time as a product by means of gas-phase IR spectroscopy.

EO has a UV absorption (Fig. 1) due to peroxidic

Table 1. Molar percent yield of products in the photolysis of ozonides

	EO[a]	PO[b]	BO[c]	IO[c]
[Ozonide]$_0$/mTorr	16.66	18.77	18.47	19.83
$-\Delta$[ozonide]/mTorr	5.39	10.93	8.64	9.61
CO	69.8	43.5	40.4	49.6
CO_2	31.6	16.2	22.4	46.0
HCHO	44.8	19.8	—	19.2
HCOOH	54.0	21.3	6.4	18.8
CH_4	—	6.0	14.4	1.2
CH_3OH	—	6.6	10.4	14.4
CH_3CHO	—	13.5	24.4	—
CH_3COOH	—	9.2	18.8	8.2
C_2H_6	—	—	9.6	—
HCOOCHO	5.8	6.2	9.4	—
$CH_3COOCHO$	—	3.6	6.5	12.3
$CH_3COOCOCH_3$	—	—	2.4	—
CH_3COCH_3	—	—	—	30.0
CH_3COOCH_3	—	—	—	3.5
CH_2CO	—	1.2	1.0	—

a) Yields were obtained after 30 min irradiation. b) Yields were obtained after 1 h irradiation. c) Yields were obtained after 2 h irradiation.

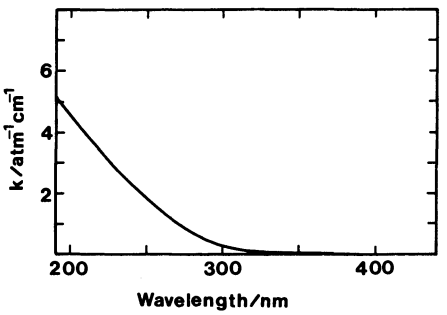

Fig. 1. Gas-phase UV spectrum of ethene ozonide.

O–O bond suggesting that the primary process of the photolysis of ozonides proceeds *via* the O–O bond rupture in an analogous way to peroxides.[5] Initial splitting of the O–O bond would be followed by unimolecular fragmentation or intramolecular hydrogen abstraction of the intermediate biradical, *e.g.*,

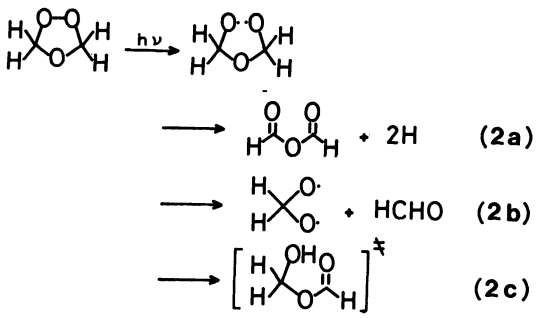

Energy diagram of this reaction sequence in the case

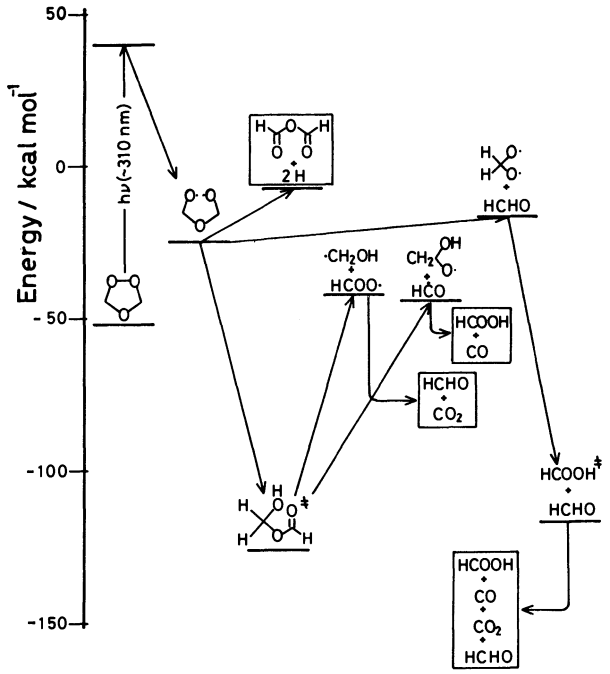

Fig. 2. Energy diagram of the photolysis of ethene ozonide.

of EO is schematically shown in Fig. 2. Heats of formation of the compounds shown in Fig. 2 are estimated by the method of Benson[6] except for OCH_2OCH_2O which is assumed to be $\approx$27 kcal mol^{-1} above ozonide on the basis of activation energy of thermal decomposition reported by Hull *et al.*[4] Reaction 2a is the double-β-scission process, which was suggested[3] to be the main reaction path in the liquid-phase photolysis of ozonides. The detection of formic anhydride in the photolysis of EO, PO, and BO established the participation of the double-β-scission also in the gas-phase photolysis of ozonides. Besides formic anhydride, acetic formic anhydride ($CH_3COOCHO$) was observed in the photolysis of PO, BO, and IO, and acetic anhydride ($CH_3COOCOCH_3$) was produced in the photolysis of BO. These facts indicate that not only alkyl groups but hydrogen atoms can also be released by the double-β-scission. This can account for the production of glutaric anhydride in the photolysis of cyclopentene ozonide in the liquid phase.[3]

Since further fragmentation of acid anhydride cannot occur on energetic basis (see Fig. 2), the contribution of the double-β-scission in the photolysis of ozonides under 1 atm of N_2 can be estimated based on the yields of the anhydrides to be 5.8, 9.8, 18.3, and 12.3% for EO, PO, BO, and IO, respectively. Thus, the contribution of double-β-scission increases as the number of CH_3 substituent group in the ozonides increases. Detection of CH_2CO and CH_3OH in the photolysis of PO and BO, and that of CH_3COOCH_3 in the photolysis of IO suggest the occurrence of the reaction of the type of Eq. 2b. This reaction involves C–O bond cleavage after O–O bond rupture and results in the production of aldehydes or ketones and methylenedioxy-type biradicals. Methylenedioxy biradical ($\cdot OCH_2O\cdot$) is known as an intermediate formed in the course of unimolecular reaction of the Criegee intermediate which is produced in ozone-olefin reactions.[7–9]

Observation of CH_2CO, CH_3OH, and CH_3COOCH_3 in this study may be explained by the contribution of this mechanism. However, the C–O bond cleavage cannot be the main reaction path since the fact that the sum of the yields of CO, CO_2, and HCOOH is much higher than that of HCHO in the photolysis of EO cannot be explained by this mechanism.

Another candidate for the reaction path is the reaction 2c followed by unimolecular decompositions. Such intramolecular hydrogen abstraction has been supposed to be the main route of the pyrolysis of ozonides both in the liquid phase[10] and in the gas phase.[4] Intramolecular hydrogen abstraction in alkoxyl radicals has also been noted by Carter and co-workers.[11]

If such intramolecular hydrogen abstraction occurs to give $HCOOCH_2OH$ as an intermediate in the photolysis of EO, the overall excess energy for the reaction 2c at the wavelength of 310 nm amounts to 166 kcal mol^{-1} as shown in Fig. 2. Therefore, following types of radical-forming unimolecular decomposition rather than the aldehyde-acid pair forming reaction would predominate in the gas-phase.

$$HCOOCH_2OH \rightarrow HOCH_2O + HCO \rightarrow HCOOH + H + HCO(H + CO) \quad (3a)$$

$$\rightarrow H_2COH + HCOO \rightarrow HCHO + CO_2 + 2H \quad (3b)$$

High yield of HCOOH, CO, and CO_2 as well as HCHO can be accounted for by this mechanism. Observation of CH_3COOH in the photolysis of PO, BO, and IO would also be explained by this mechanism.

References

1) H. Niki, P. D. Maker, C. M. Savage, and L. P. Breitenbach, *Chem. Phys. Lett.*, **46**, 327 (1977).

2) F. Su, J. G. Calvert, and J. H. Shaw, *J. Phys. Chem.*, **84**, 239 (1980).

3) P. R. Story, W. H. Morrison, III, T. K. Hall, J.-C. Farine, and C. E. Bishop, *Tetrahedron Lett.*, **1968**, 3291.

4) L. Hull, I. C. Hisatsune, and J. Heicklen, *J. Phys. Chem.*, **76**, 2659 (1972).

5) J. G. Calvert and J. N. Pitts, Jr., "Photochemistry," Wiley, New York (1966).

6) S. W. Benson, "Thermochemical Kinetics," 2nd ed, Wiley, New York (1976).

7) L. B. Harding and W. A. Goddard, III, *J. Am. Chem. Soc.*, **100**, 7180 (1978).

8) J. T. Herron and R. E. Huie, *J. Am. Chem. Soc.*, **99**, 5430 (1977).

9) J. T. Herron and R. E. Huie, *Int. J. Chem. Kinet.*, **10**, 1019 (1978).

10) P. R. Story, T. K. Hall, W. H.Morrison, III, and J.-C. Farine, *Tetrahedron Lett.*, **1968**, 5397.

11) W. P. L. Carter, K. R. Darnall, A. C. Lloyd, A. M. Winer, and J. N. Pitts, Jr., *Chem. Phys. Lett.*, **42**, 22 (1976).

Crystal Structures of (1,5-Cyclooctadiene)di-μ-methoxo-dirhodium(I) and Tetrakis(η^3-allyl)di-μ-hydroxo-dirhodium(III)

Isao TANAKA, Naoki JIN-NO, Takanori KUSHIDA, Noriyoshi TSUTSUI, Tamaichi ASHIDA,* Hiroharu SUZUKI,† Humio SAKURAI,† Yoshihiko MORO-OKA,† and Tsuneo IKAWA†

Department of Applied Chemistry, Faculty of Engineering, Nagoya University, Chikusa-ku, Nagoya 464

† *Research Laboratory of Resources Utilization, Tokyo Institute of Technology, 4259 Nagatsuta-cho, Midori-ku, Yokohama 227*

(Received April 28, 1982)

The crystal structures of (1,5-cyclooctadiene)di-μ-methoxo-dirhodium(I) and tetrakis(η^3-allyl)di-μ-hydroxo-dirhodium(III) were determined by the X-ray method. The former belongs to the triclinic space group $P\bar{1}$ with cell dimensions, $a=7.347(4)$, $b=6.471(3)$, $c=9.554(6)$ Å, $\alpha=87.06(4)$, $\beta=82.50(5)$ and $\gamma=77.98(4)°$. The space group of the latter is also $P\bar{1}$ but two crystallographically independent molecules exist in a cell with dimensions, $a=11.704(7)$, $b=9.793(6)$, $c=7.948(5)$ Å, $\alpha=113.49(5)$, $\beta=54.59(5)$, and $\gamma=110.99(5)°$. Both structures were determined by the heavy atom method and refined by the block-diagonal least-squares method. The final R values were 0.054 for the former and 0.075 for the latter. The coordination of the rhodium atom in the former compound is square planar, the cyclooctadiene ligand being regarded as a bidentate donor. The latter coordination is, in a formal sense, octahedral.

Some of the present authors recently reported the preparation of novel dioxygen complexes of palladium[1] and rhodium[2] which coordinated to both dioxygen and organic substrates, particularly olefins, by means of the anion exchange reaction of corresponding halogen-bridges complexes with potassium superoxide, and concurrently revealed the basic nature of the coordinated dioxygen. μ-Peroxo complexes of palladium and rhodium reacted with active methylene compounds of which pK_a values were less than 20 to result in the abstraction of the proton by the coordinated dioxygen. For example, treatment of μ-peroxo complexes with acetylacetone (pK_a 9), methyl acetoacetate (pK_a 11), dimethyl malonate (pK_a 13), and cyclopentadiene (pK_a 15) gave the acetylacetonato, methyl acetoacetate, dimethyl malonate and cyclopentadienyl complexes, respectively. With alcohols, amines and thiols, the μ-peroxo complexes also reacted to yield the corresponding μ-alkoxo, μ-amido, and μ-alkylthio complexes accompanied by the liberation of hydrogen peroxide. The alkoxo or hydroxo complexes having olefinic ligands have been studied with interest in recent years in connection with the alkoxy metallation reaction of the Wacker reaction.

This paper deals with two crystal structures of (1,5-cyclooctadiene)di-μ-methoxo-dirhodium(I), [{Rh(OMe)(1,5-cod)}$_2$], which was obtained by the reaction of [{RhO(1,5-cod)}$_2$] with methanol, and of tetrakis(η^3-allyl)di-μ-hydroxo-dirhodium(III), [{Rh(OH)(η^3-C_3H_5)$_2$}$_2$], which was prepared by the treatment of [{RhCl(η^3-C_3H_5)$_2$}$_2$] with potassium superoxide.[2]

Experimental

General. All reactions were run under positive pressure of dry nitrogen. Infrared spectra were recorded on a Shimadzu IR-27G or Hitachi Model 260-50 spectrometer. Proton magnetic resonance spectra were recorded on a Hitachi R-24B instrument. Chemical shifts are reported as δ values in parts per million relative to internal tetramethylsilane. Melting points were obtained on a Yanagimoto micro melting point apparatus. In experiments requiring dry solvents, benzene and ether were distilled from sodium benzophenon ketyl. Dichloromethane was distilled from diphosphorus pentaoxide. Methanol was distilled from magnesium turnings prior to use. Potassium superoxide, KO_2, (Ventron) was commercially available and used without further purification. Starting rhodium complexes, [{RhCl(1,5-cod)}$_2$] and [{RhCl(η^3-C_3H_5)$_2$}$_2$], were prepared by a standard procedure.

Preparation of [{*Rh(OMe)(1,5-cod)*}$_2$]. To a suspension of finely powdered potassium superoxide (3.48 g, 49 mmol) in 15 cm^3 of CH_2Cl_2 was added the solution of [{RhCl(1,5-cod)}$_2$] (2.10 g, 4.28 mmol) in 30 cm^3 of CH_2Cl_2 under an atmosphere of dry nitrogen at ambient temperature. The mixture was stirred for 4 h. Then the excess KO_2 together with the precipitated KCl were filtered off under nitrogen pressure. Concentration of the filtrate, followed by the addition of 30 cm^3 of pentane, gave [{RhO(1,5-cod)}$_2$] (1.30 g, 67%) as a yellowish brown microprisms. The [{RhO(1,5-cod)}$_2$] was then dissolved in 20 cm^3 of dry benzene. The addition of 1.0 cm^3 of freshly distilled methanol at room temperature instantaneously gave a yellow solution. Evaporation of the solvent followed by recrystallization from a mixed solvent of CH_2Cl_2 and CH_3OH (1:1 vol. ratio) gave [{Rh(OMe)(1,5-cod)}$_2$] as yellow prisms in a 50% yield (1.04 g) based on [{RhCl(1,5-cod)}$_2$]. IR and H-NMR spectral data and melting point agreed with those of the authentic sample. Elemental analysis was also consistent with the formula, $C_{18}H_{30}O_2Rh_2$. Calcd: C, 44.65; H, 6.24%. Found: C, 44.50; H, 6.45%.

Preparation of [{*Rh(OH)(η^3-C_3H_5)*$_2$}$_2$]. To a suspension of finely powdered KO_2 (718 mg, 10.1 mmol) in 10 cm^3 of CH_2Cl_2 was added the solution of [{RhCl(η^3-C_3H_5)$_2$}$_2$] (200 mg, 0.454 mmol) in 10 cm^3 of CH_2Cl_2 under nitrogen pressure at the ambient temperature. The resulting mixture turned to an orange solution, which was then stirred for 2 h. The excess KO_2 and the precipitated KCl were filtered off under nitrogen pressure and the filtrate was evaporated to dryness. The residue was dissolved in benzene and again filtered. The filtrate was concentrated to *ca.* 4 cm^3 and was allowed to cool to yield [{Rh(OH)(η^3-C_3H_5)$_2$}$_2$] as yellow prisms in a 70% (128 mg) yield; mp 129 °C (decomp). IR (KBr) OH 3580, 3549 cm^{-1}; ^{1}H-NMR ($CDCl_3$) 1.10 (br.d, 4H), 2.18 (br.d, 4H), 3.02 (br.d, 4H), 4.38 (m, 4H), 4.67 (br.s, 4H), −2.40 (br.s, 2H, OH). Found: C, 35.31; H, 5.40%. Calcd for $C_{12}H_{22}O_2Rh_2$: C, 35.66, H, 5.49%.

X-Ray Data Collection. The X-ray diffraction data were obtained with graphite monochromatized Mo $K\alpha$ ra-

Table 1. Crystal and experimental data

	[{Rh(OMe)-(1,5-cod)}$_2$]	[{Rh(OH)-(η^3-C_3H_5)$_2$}$_2$]
Chemical formula	$Rh_2C_{18}O_2H_{30}$	$Rh_2C_{12}O_2H_{22}$
Crystal system	triclinic	triclinic
Space group	$P\bar{1}$	$P\bar{1}$
Z	1	2
Cell dimensions		
a/Å	7.347(4)	11.704(7)
b/Å	6.471(3)	9.793(6)
c/Å	9.554(6)	7.948(5)
α/°	87.06(4)	113.49(5)
β/°	82.50(5)	54.59(5)
γ/°	77.98(4)	110.99(5)
D_m/g cm^{-3}	1.80	2.04
D_x/g cm^{-3}	1.82	2.02
Scan range $\Delta\omega$/°	$1.5+0.35\tan\theta$	$1.5+0.35\tan\theta$
Scan speed /° min^{-1} and background count time /s		
$0°<2\theta\leq40°$	10, 3	10, 3
$40°<2\theta\leq50°$	5, 6	5, 6
$50°<2\theta\leq60°$	2, 15	2, 15
Number of reflections	2154	3308
$2\theta_{max}$/°	60	60
Crystal size /mm^3	0.40×0.34×0.08	0.30×0.10×0.10

diation on a Rigaku four-circle diffractometer equipped with a rotating anode X-ray generator operated at 50 kV 120 mA. An ω-2θ continuous scanning technique was used for measuring integrated intensities. Background countings were made at each side of the scan. Other experimental details are listed in Table 1 together with the crystal data. Lorentz and polarization corrections were applied but no absorption correction was made.

Structure Determination and Refinement

Both structures were solved by the heavy atom method and refined by the block-diagonal least-squares procedure. Hydrogen atoms were located on difference Fourier maps with the help of geometrical consideration. Anisotropic thermal parameters were assigned to all the nonhydrogen atoms. Hydrogen positional parameters, as well as their isotropic thermal parameters which were made equal to B_{eq} of their carrier atoms, were not refined. The function minimized was $\Sigma\omega(\Delta F)^2$, with $\omega=a$ for $F_o=0$ and $\omega=[\sigma^2(F)+b|F_o|+c|F_o|^2]^{-1}$ for $F_o\neq0$, where $\sigma(F)$ is the estimated standard deviation based on counting statistics. The final R and parameters a, b, and c are 0.054, 0.68, −0.25, and 0.01 for [{Rh(OMe)(1,5-cod)}$_2$] and 0.075, 0.13, −0.06, and 0.01 for [{Rh(OH)(η^3-C_3H_5)$_2$}$_2$]. The atomic scattering factors were taken from the International Tables for X-Ray Crystallography.[3] The positional parameters are listed in Tables 2 and 3.[4]

Results and Discussion

[{Rh(OMe)(1,5-cod)}$_2$]. The molecule occupies a center of symmetry in the crystal. A stereo-

Table 2. Atomic positional (×10^4) and thermal parameters with their e.s.d.'s in parentheses for [{Rh(OMe)(1,5-cod)}$_2$]

Atom	x	y	z	B_{eq}/Å^2 a)
Rh	3988(0)	1582(0)	1253(0)	3.2(0)
O	3641(6)	701(6)	−711(6)	4.7(3)
C(1)	2091(9)	1353(9)	−1446(9)	4.8(4)
C(2)	4058(10)	1388(10)	3425(10)	4.1(3)
C(3)	4999(10)	2961(10)	2853(10)	4.6(4)
C(4)	4137(16)	5304(16)	3003(16)	7.7(7)
C(5)	2714(15)	6118(15)	2082(15)	8.0(7)
C(6)	2133(9)	4521(9)	1264(9)	4.3(4)
C(7)	1177(8)	2964(8)	1875(8)	4.0(3)
C(8)	606(11)	2722(11)	3436(11)	6.3(5)
C(9)	2147(13)	1789(13)	4253(13)	7.0(6)

a) The equivalent isotropic temperature factor.[12]

Table 3. Atomic positional (×10^4) and thermal parameters with their e.s.d.'s in parentheses for [{Rh(OH)(η^3-C_3H_5)$_2$}$_2$]

Atom	x	y	z	B_{eq}/Å^2
Rh(A)	84(0)	−1743(0)	−1526(0)	2.4(0)
Rh(B)	5047(0)	1785(0)	1306(0)	2.5(0)
O(A)	1484(6)	214(6)	−664(6)	2.8(2)
O(B)	6485(5)	200(5)	−1098(5)	2.5(2)
C(1A)	1683(10)	−3043(10)	−2954(10)	2.4(3)
C(2A)	421(10)	−3593(10)	−1212(10)	3.2(4)
C(3A)	−85(10)	−2647(10)	774(10)	3.2(3)
C(4A)	−1381(10)	−3162(10)	−2446(10)	3.2(4)
C(5A)	−169(9)	−2710(9)	−4226(9)	2.9(3)
C(6A)	257(9)	−1130(9)	−4101(9)	2.9(3)
C(1B)	6785(9)	3569(9)	583(9)	3.3(3)
C(2B)	5880(10)	3712(10)	82(10)	3.1(3)
C(3B)	5570(9)	2555(9)	−1359(9)	3.4(4)
C(4B)	3356(10)	2855(10)	4138(10)	3.5(3)
C(5B)	4293(10)	2738(10)	4607(10)	3.4(3)
C(6B)	4467(9)	1248(9)	4214(9)	3.2(4)

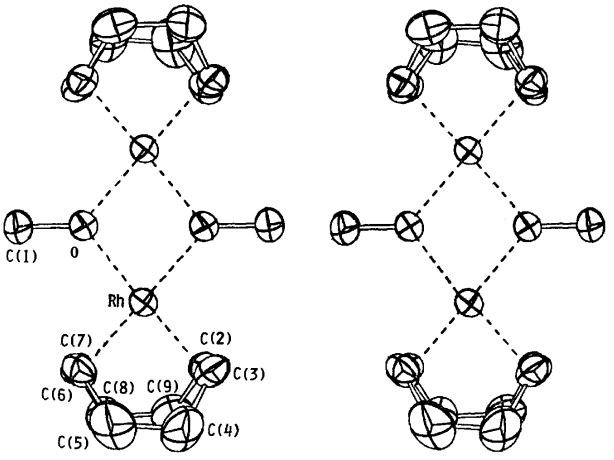

Fig. 1. A stereo drawing of [{Rh(OMe)(1,5-cod)}$_2$]. Thermal ellipsoids are scaled to include 50% probability level.

drawing of the molecule with the numbering of atoms is shown in Fig. 1. The coordination of the Rh atom is essentially square planar, the cyclooctadiene ligand being regarded as a bidentate donor. The geometry of the coordination plane of the Rh atom is given in Table 4. The molecule has an approximate D_{2h} (mmm) symmetry.

The bond lengths and angles are given in Table 5. The two Rh–O lengths, 2.051(5) and 2.063(5) Å, are similar to the values found in previous work, *e.g.* 2.054(5) and 2.066(5) Å for [Rh(acac)(1,5-cod)],[5] or 2.06 and 2.05 Å for [Rh(acac)$(CO)_2$].[6] The C–O length of 1.40(1) Å is shorter than the usual C–O single bond length, 1.43 Å. It indicates that this bond assumes a slight double bond character as a result of the coordination.

The cyclooctadiene ring acquires a tub form of approximate symmetry C_{2v} (2mm), the Rh–Rh vector being the twofold axis. The lengths of the two C=C double bonds participating in the coordination are 1.40(1) and 1.41(1) Å, which are in good agreement with the bond lengths of other complexes in the same situation: 1.41(1) Å for [Rh(acac)(1,5-cod)],[5] 1.44(7) Å for [{RhCl(1,5-cod)}$_2$],[7] or 1.40(1) Å for [Ni(1,5-cod)(duroq)] (duroq=duroquinone).[8] These are significantly longer than the corresponding lengths for the free molecule of 1,5-cyclooctadiene, 1.341 Å,[9] due to π-electron coordination. The two C(4)–C(5) and C(8)–C(9) single bonds have relatively shorter lengths 1.45(2) and 1.47(2) Å, which may be attributed to the larger thermal vibration of these atoms. The distance between the midpoint of the C(2)–C(3) bond and that of the C(6)–C(7) bond is 2.74 Å, which is similar to 2.74 Å for [Rh(acac)(1,5-cod)][5] but shorter than 2.91 Å for [Ni(1,5-cod)(duroq)].[8]

Table 4. The best plane and deviations (d/Å) of atoms from the plane in [{Rh(OMe)(1,5-cod)}$_2$][a]

$-0.5938X-0.6906Y+0.4129Z+2.1814=0$

Rh	0.00(1)	C(4)	−1.46(1)
O	0.02(1)	C(5)	−1.54(1)
M(1)	0.02(1)	C(6)	−0.71(1)
M(2)	0.00(1)	C(7)	0.70(1)
C(1)	0.13(1)	C(8)	1.54(1)
C(2)	0.72(1)	C(9)	1.60(1)
C(3)	−0.67(1)		

a) The plane is defined by Rh, O, M(1), and M(2), and their centrosymmetric equivalents; M(1) is the midpoint of the C(2)-C(3) bond and M(2) is that of C(6)-C(7). $X=ax+by\cos\gamma+cz\cos\beta$, $Y=by\sin\gamma-cz\cos\alpha^*\sin\beta$, $Z=cz\sin\alpha^*\sin\beta$.

Table 5. Bond lengths and angles in [{Rh(OMe)(1,5-cod)}$_2$][a]

Bond length	l/Å	Bond angle	θ/°
Rh-O	2.051(5)	O-Rh-O′	76.5(2)
Rh-O′	2.063(5)	O-Rh-M(1)	174.2(3)
Rh-M(1)	1.969(8)	O-Rh-M(2)	97.6(3)
Rh-M(2)	1.974(8)	O′-Rh-M(1)	97.8(3)
Rh-C(2)	2.080(8)	O′-Rh-M(2)	174.0(3)
Rh-C(3)	2.097(8)	M(1)-Rh-M(2)	88.1(3)
Rh-C(6)	2.096(8)	Rh-O-C(1)	128.0(5)
Rh-C(7)	2.094(7)	Rh-O-Rh′	103.5(2)
O-C(1)	1.40(1)	Rh′-O-C(1)	128.2(5)
C(2)-C(3)	1.40(1)	C(2)-C(3)-C(4)	122.2(8)
C(3)-C(4)	1.52(2)	C(3)-C(4)-C(5)	114.7(10)
C(4)-C(5)	1.45(2)	C(4)-C(5)-C(6)	116.1(11)
C(5)-C(6)	1.49(2)	C(5)-C(6)-C(7)	124.2(8)
C(6)-C(7)	1.41(1)	C(6)-C(7)-C(8)	124.0(7)
C(7)-C(8)	1.51(1)	C(7)-C(8)-C(9)	114.8(9)
C(8)-C(9)	1.47(2)	C(8)-C(9)-C(2)	115.1(9)
C(9)-C(2)	1.50(1)	C(9)-C(2)-C(3)	124.8(8)

a) Primed atoms refer to the centrosymmetric equivalents.

The molecular packing viewed along the a axis is shown in Fig. 2. None of the intermolecular distances is short enough to suggest any significant deviation from normal van der Waals interactions.

[{*Rh(OH)*(η^3-C_3H_5)$_2$}$_2$]. There are two crystallographically independent molecules (A and B) in the unit cell, each occupying the center of symmetry in the crystal. The molecular geometry and numbering scheme of atoms are shown in Fig. 3. The molecule has an approximate symmetry of C_{2h} (2/m) with the 2 axis coinciding with the Rh–Rh vector and the m plane passing through the two O atoms

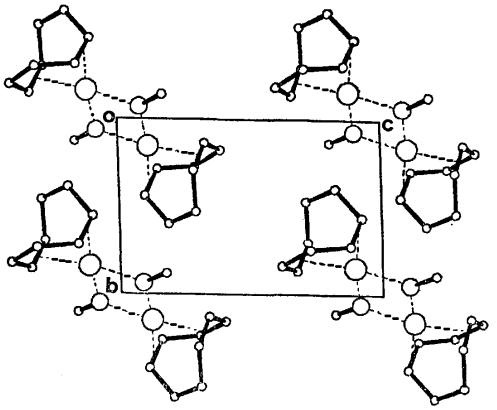

Fig. 2. Molecular packing of [{Rh(OMe)(1,5-cod)}$_2$].

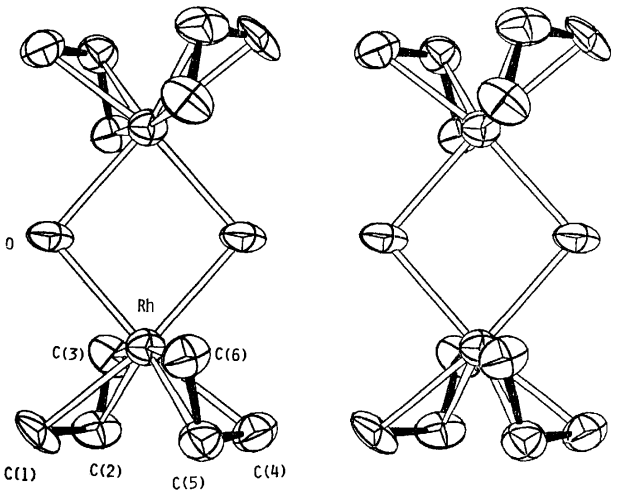

Fig. 3. A stereodrawing of [{Rh(OH)(η^3-C_3H_5)$_2$}$_2$].

Table 6. Bond angles involving Rh atom in $[\{Rh(OH)(\eta^3\text{-}C_3H_5)_2\}_2]$

Bond angle	θ/° A	θ/° B	Bond angle	θ/° A	θ/° B
O-Rh-O′	82.6(3)	80.9(3)	C(1)-Rh-C(3)	67.2(5)	67.3(5)
O-Rh-C(1)	87.6(4)	89.4(4)	C(1)-Rh-C(4)	104.8(5)	103.5(5)
O-Rh-C(2)	104.5(4)	105.4(4)	C(1)-Rh-C(5)	90.8(4)	90.4(5)
O-Rh-C(3)	85.4(4)	86.2(4)	C(1)-Rh-C(6)	108.3(3)	109.9(5)
O-Rh-C(4)	164.7(4)	163.8(4)	C(2)-Rh-C(3)	36.4(5)	36.9(4)
O-Rh-C(5)	134.5(4)	133.2(4)	C(2)-Rh-C(4)	90.8(5)	90.9(5)
O-Rh-C(6)	100.2(4)	99.2(3)	C(2)-Rh-C(5)	102.7(5)	103.0(5)
O′-Rh-C(1)	164.8(4)	163.9(4)	C(2)-Rh-C(6)	136.7(5)	137.9(4)
O′-Rh-C(2)	132.8(4)	132.5(4)	C(3)-Rh-C(4)	107.5(5)	108.0(5)
O′-Rh-C(3)	100.3(4)	99.1(4)	C(3)-Rh-C(5)	134.9(4)	135.7(5)
O-Rh-C(4)	86.9(4)	88.8(4)	C(3)-Rh-C(6)	172.8(4)	174.0(4)
O-Rh-C(5)	104.3(4)	105.7(4)	C(4)-Rh-C(5)	38.6(5)	38.4(5)
O′-Rh-C(6)	84.9(4)	84.4(3)	C(4)-Rh-C(6)	67.6(4)	67.1(5)
C(1)-Rh-C(2)	39.4(5)	38.5(5)	C(5)-Rh-C(6)	38.1(4)	38.3(4)

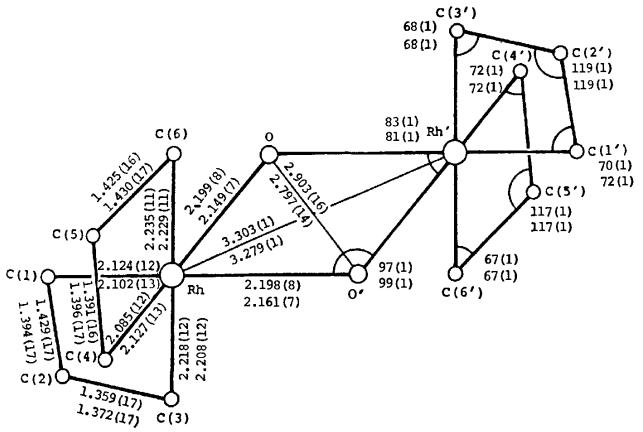

Fig. 4. The bond distances (l/Å) and angles (θ/°) in $[\{Rh(OH)(\eta^3\text{-}C_3H_5)_2\}_2]$.

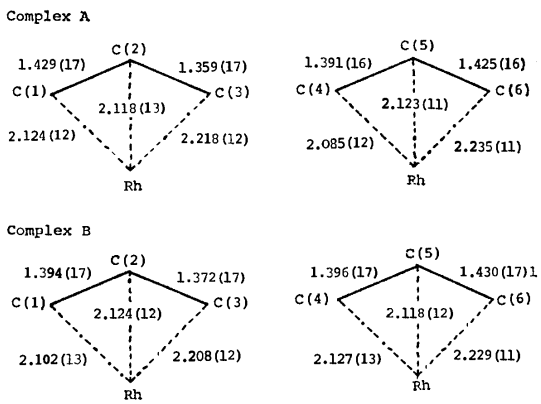

Fig. 5. The bond distances (l/Å) involving Rh and allyl group in $[\{Rh(OH)(\eta^3\text{-}C_3H_5)_2\}_2]$.

and perpendicular to the 2 axis. The bond lengths and angles are shown in Table 6 and Figs. 4 and 5.

The coordination of the Rh atom is, in a formal sense, octahedral, if either the two O atoms and the C(1), C(3), C(4), and C(6) atoms or the two O atoms and four midpoints of the C(1)–C(2), C(2)–C(3), C(4)–C(5), and C(5)–C(6) bonds are considered as the ligands. Two atoms C(1) and C(4) of two allyl groups lie roughly on the plane of the Rh and O atoms, and

Table 7. The best plane and deviations (d/Å) of atoms from the planes in $[\{Rh(OH)(\eta^3\text{-}C_3H_5)_2\}_2]$[a]

Rh(A) plane			
$0.2283X-0.5635Y+0.7939Z=0$			
Rh(A)	0.00(2)	C(2A)	1.41(3)
O(A)	−0.19(3)	C(3A)	2.09(3)
C(1A)	0.21(3)	C(5A)	−1.37(3)
C(4A)	−0.19(3)	C(6A)	−2.11(3)
RH(B) plane			
$0.6574X-0.3875Y+0.6463Z-3.8469=0$			
Rh(B)	0.00(1)	C(2B)	−1.43(2)
O(B)	0.18(1)	C(3B)	−2.10(2)
C(1B)	−0.26(2)	C(5B)	1.41(2)
C(4B)	0.26(2)	C(6B)	2.11(2)

a) The planes are defined by Rh, O, C(1), and C(4), and their centrosymmetric equivalents.

the best plane consisting of the Rh, O, C(1), and C(4) atoms and their centrosymmetric equivalents are given in Table 7 together with the deviations of atoms from that plane. The other two terminal atoms C(3) and C(6) of the allyl groups locate far from the plane on both sides. The bond angle C(3)–Rh–C(6) is 172.8(4)° and 174.0(4)° for the A and B molecules, respectively. The planes of four independent allyl groups, C(1A)–C(2A)–C(3A), C(4A)–C(5A)–C(6A), C(1B)–C(2B)–C(3B), and C(4B)–C(5B)–C(6B), make angles of 57.8(6)°, 59.5(6)°, 57.4(6)°, and 56.5(6)° with the above mentioned plane. These structural characteristics are similar to those found for $[\{RhCl(\eta^3\text{-}C_3H_5)_2\}_2]$[10] and $[\{RhBr(\eta^3\text{-}C_3H_5)_2\}_2]$,[11] in which halogen atoms take the place of the OH group of this molecule.

The mean length of the Rh–C(1) and Rh–C(4) bonds, 2.11 Å, is significantly shorter than that of Rh–C(3) and Rh–C(6), 2.22 Å; while that of Rh–C(2) and Rh–C(5) is 2.12 Å. This trend is seen also in $[\{RhCl(\eta^3\text{-}C_3H_5)_2\}_2]$[10] and $[\{RhBr(\eta^3\text{-}C_3H_5)_2\}_2]$.[11] On the other hand the mean length of C(1)–C(2) and C(4)–C(5) bonds, 1.40 Å, and that of C(2)–C(3) and C(5)–C(6), 1.40 Å, show no significant asymmetry in the C–C bonds.

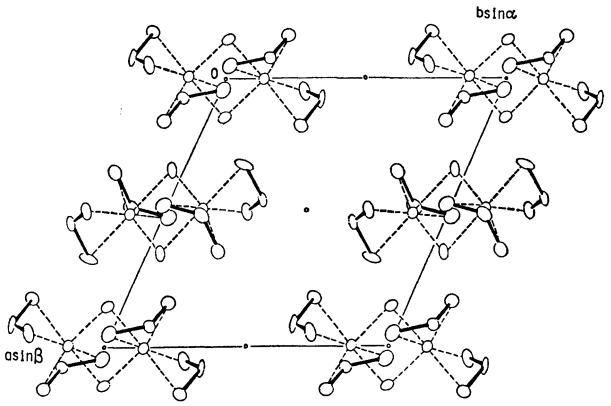

Fig. 6. Molecular packing of $[\{Rh(OH)(\eta^3\text{-}C_3H_5)_2\}_2]$.

The crystal structure is shown in Fig. 6. The molecule A locates at (0,0,0) and B locates at (0.5,0,0). Two Rh–Rh vectors of A and B are roughly parallel with each other, and a slight rotation of A around its Rh–Rh vector gives the orientation of B.

This work was supported in part by a Grant-in-Aid for Scientific Research No. 434024 from the Ministry of Education, Science and Culture.

References

1) a) H. Suzuki, K. Mizutani, Y. Moro-oka, and T. Ikawa, *J. Am. Chem. Soc.*, **101**, 748 (1979); b) P. J. Chung, H. Suzuki, Y. Moro-oka, and T. Ikawa, *Chem. Lett.*, **1980**, 63.

2) F. Sakurai, H. Suzuki, Y. Moro-oka, and T. Ikawa, *J. Am. Chem. Soc.*, **102**, 1749 (1980).

3) "International Tables for X-Ray Crystallography," The Kynoch Press, Birmingham (1974), Vol. IV, p. 71.

4) The F_o and F_c tables, anisotropic temperature factors and hydrogen positional parameters are kept as Document No. 8307 at the Chemical Society of Japan.

5) P. A. Tucker, W. Scutcher, and D. R. Russell, *Acta Crystallogr., Sect. B*, **36**, 592 (1975).

6) N. A. Bailey, E. Coates, G. B. Robertson, F. Bonati, and R. Ugo, *Chem. Commun.*, **1967**, 1041.

7) J. A. Ibers and R. G. Snyder, *Acta Crystallogr.*, **15**, 923 (1962).

8) M. D. Glick, and L. F. Dahl, *J. Organomet. Chem.*, **3**, 200 (1965).

9) L. Hedberg and K. Hedberg, Abstracts of Papers, National Meeting of the American Crystallographic Association, Bozeman, Montana, July 1964.

10) M. McPartlin and R. Mason, *Chem. Commun.*, **1967**, 16.

11) H. Pasternak, T. Glowiak, and F. Pruchnik, *Inorg. Chim. Acta*, **19**, 11 (1976).

12) W. C. Hamilton, *Acta Crystallogr.*, **12**, 609 (1959).

The Reactions of the Singlet NH Radicals with C_4 Olefins in the Liquid Phase

Jun-ichi HAMADA, Shigeru TSUNASHIMA,* and Shin SATO†

Department of Applied Physics, Tokyo Institute of Technology, Ookayama, Meguro-ku, Tokyo 152

†*Research Laboratory for Nuclear Reactors, Tokyo Institute of Technology, Ookayama, Meguro-ku, Tokyo 152*

(Received May 1, 1982)

The reactions of NH radicals with C_4 olefins, *trans*- and *cis*-2-butenes, 1-butene, and isobutene, were investigated by the photolysis of hydrogen azide in the liquid olefin at 0 °C and at the temperature of Dry Ice–methanol. Except for nitrogen and ammonia, amines and aziridines were found to be formed in good yield. 2-Butene-1-amine and *trans*-2,3-dimethylaziridine from *trans*-2-butene, 2-butene-1-amine and *cis*-2,3-dimethylaziridine from *cis*-2-butene, 3-butene-1- and 2-amines and 2-ethylaziridine from 1-butene, and 2-methyl-2-propene-1-amine and 2,2-dimethylaziridine from isobutene. These product formations were successfully explained by the insertion into the C–H bond and the addition to the double bond of olefin by the singlet NH radicals. In the case of 2-butene, no isomerized aziridine formation was observed. This result suggested that the triplet NH radicals rarely add to the double bond of olefin.

The reactions of NH radicals with lower olefins, ethylene and propene, have been reported.[1,2] The formations of aziridine and amine were explained by the addition and the insertion reactions of the singlet NH radicals, NH($a^1\Delta$), which were formed by the photolysis of hydrogen azide. The mechanism and the nature of the intermediate of these reactions have not yet been established. Amines are likely formed in an insertive attack of the NH singlet on the C–H bond of olefins as with paraffin.[3-7] For the aziridine formation, the following possibilities should be considered: (a) a concerted addition of the singlet NH radicals to the double bond of olefin, (b) an addition of the singlet NH radicals to the C atom of the double bond to form a singlet biradical, which is followed by the ring closure, and (c) a triplet biradical formation by the addition of the NH triplet, NH($X^3\Sigma^-$), followed by the spin inversion and ring closure. Aziridine formed by (a) process should retain the conformation of reactant; that is, cis isomer formation from cis olefin and trans isomer formation from trans olefin. Cis and trans isomer formations are expected from (b) and (c) processes, although the cis and trans ratio may depend on the nature of the biradicals and the experimental conditions.

The insertion and the addition reactions of O and CH_2, which are isoelectronic species of NH, have been extensively investigated.[8,9] In the reactions of methylene with 2-butene, it is well known that the singlet species add to the double bond of an olefin while they retain the stereospecificity, and the triplet species add without retaining stereospecificity.[10,11] Although O(^{1}D) adds to 2-butene while retaining the conformation of reactant,[12] O(^{3}P) gives *cis* and *trans* epoxide simultaneously. The cis and trans isomer ratio depended on the reaction temperature and/or the phase.[13,14]

In the previous paper,[1] the aziridine formation by the NH triplet was ignored in order to explain the concentration dependence of the ammonia formation. This explanation was based on the assumption that ammonia is formed by a hydrogen-atom abstraction from hydrogen azide. If ammonia is formed by the reactions of the NH singlet with olefin, the reaction of the NH triplet with olefin has to be included in the mechanism. If this is the case, both *cis*- and *trans*-aziridine formations may be expected in the reactions with *cis*- or *trans*-2-butene.

To continue such studies, we examined the photolyses of hydrogen azide in liquid *cis*- and *trans*-2-butenes, 1-butene, and isobutene at 0 °C and at the temperature of Dry Ice–methanol.

Experimental

The experimental methods and the apparatus used were essentially the same as those described in the previous paper.[1] Hydrogen azide was prepared and purified by the method already described.[1] Pure grade *trans*- and *cis*-2-butenes, 1-butene, and isobutene (Takachiho Shoji Co.) were used after having been distilled at a low temperature under vacuum. The mixture of hydrogen azide and olefin was prepared in a quartz tube (8 mm o.d.) or Pyrex tube (8 mm o.d.). The hydrogen azide solution was irradiated with a medium pressure mercury lamp (Wako Denki Co.) at 0 °C or at the temperature of Dry Ice–methanol. In the case of the quartz tube, a filter (Toshiba UV 27) was used to eliminate the light of wavelengths shorter than 250 nm.

After the irradiation, non-condensable products at −196 °C were analyzed with a combination of a Toepler pump, a gas buret, and a CuO furnace at 300 °C. The solvent hydrocarbon was evacuated at a temperature lower than −80 °C. Less volatile products, including unreacted hydrogen azide, were passed through a trap packed with NaOH coated glass wool, in order to decompose the quarternary ammonium salts which eventually formed.[4] The products thus obtained were analyzed with GLC, using a column packed with Amipack 124 (Gasukuro Kogyo Co., 3 m in length at 60 °C). Since authentic samples for the all products were not available, the sensitivity of an unavailable product i (S_i) was estimated from its retention time (Rt_i) using the relation: $S_i = a\,Rt_i + b$. The constants a and b were estimated using available amines and aziridines. Since the relation holds well for the amines and aziridines examined, the sensitivities, thus estimated, may be correct within an error of 30%.

The identification of the products was mainly done by the comparisons of their relative retention times and their mass spectra. The GC-mass spectrometer (Nichiden Varian, TE 600) was used. An NMR spectrometer (Varian, EM 390) was also used, using D_2O as a solvent.

Results

The photolyses of hydrogen azide in the liquid *cis*- and *trans*-2-butenes, 1-butene, and isobutene were examined at 0 °C or at the temperature of Dry Ice–methanol. In every case examined, nitrogen and ammonia were found to be formed, much as in the cases of ethylene and propene.[1] Neither methane nor hydrogen was detected. The less volatile products were subjected to the analysis by GLC after having been treated with NaOH. The results obtained are summarized as follows:

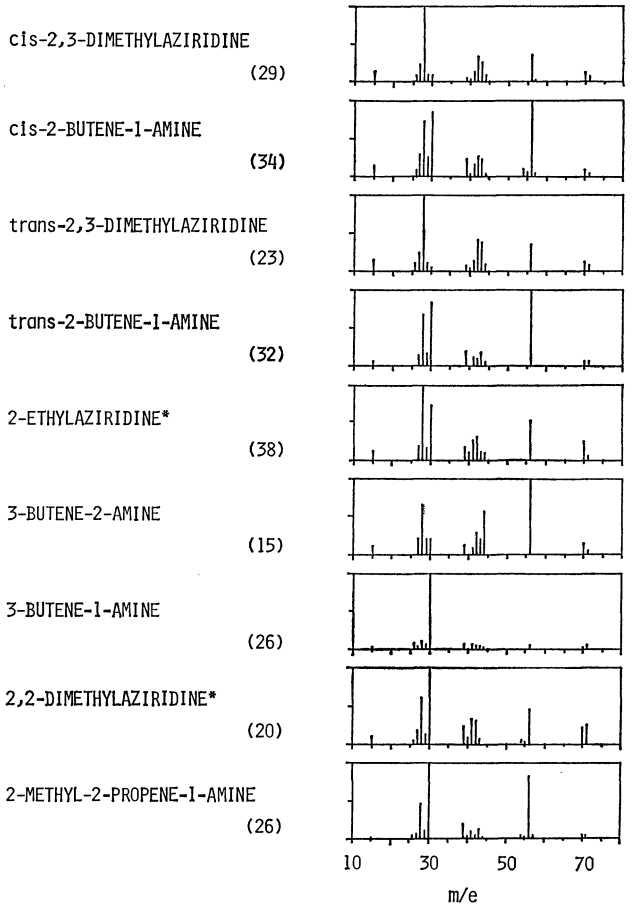

Fig. 1. The mass spectra of the products obtained in the photolyses of hydrogen azide in the liquid *cis*- and *trans*-2-butenes, 1-butene, and isobutene.
The values in the parentheses show the retention times (see Text). The mass spectrum of the compound with an asterisk could be compared with that reported.[18]. The abscissa shows the mass number.

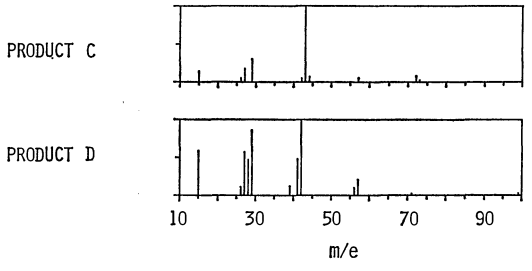

Fig. 2. The mass spectra of the products eluted at 22 min (product C) and 43 min (product D).
For the detail, see Text. The abscissa shows the mass number.

cis-*2-Butene.* In the case of *cis*-2-butene, 6 peaks were separated by GLC using a column of Amipack 124. Their retention times were 5, 15, 22, 29, 34, and 43 min. The main two peaks, which eluted at 29 and 34 min, were identified to be 2,3-dimethylaziridine and 2-butene-1-amine from the mass spectra shown in Fig. 1. The configuration of the aziridine was assigned to be cis isomer on the basis of its NMR spectrum, NMR(D_2O) δ 1.0 (3H, d, CH_3) and 2.1 (1H, m, CH), by the comparison with the reported values for *cis*- and *trans*-2,3-dimethylaziridine.[15] The mass spectra of the minor products eluted at 22 and 43 min are shown in Fig. 2. The 43 min product was tentatively assigned to be *s*-butyl azide. The product of 22 min could not be identified. The mass spectrum is apparently different from that of the product of 23 min obtained in the reaction of *trans*-2-butene. The product of 5 min was identified to be ethanamine by the comparison with the mass spectrum obtained using an authentic sample. The product eluted at 15 min gave the same mass spectrum as was obtained in the case of 1-butene (see later).

The yields of these products relative to that of nitrogen are shown in Table 1. The relative yields of the products were almost constant for the changes in the concentration of hydrogen azide and the irradiation time, except for ethanamine and *s*-butyl azide. The relative yield of ethanamine increased with an increase in the irradiation time. This trend suggested that this product was formed by the secondary reactions.

trans-*2-Butene.* In the case of *trans*-2-butene, 5 peaks were observed on the gas chromatogram. Their retention times were 5, 15, 23, 32, and 43 min. The main products eluted at 23 and 32 min were identified to be 2,3-dimethylaziridine and 2-butene-1-amine from their mass spectra shown in Fig. 1. The *cis-trans* configuration of the aziridine, NMR(D_2O) δ 1.0 (3H, d, CH_3) and 1.7 (1H, m, CH), was assigned to be in trans form by comparison with the reported values.[15] 2-Butene-1-amine formed from *trans*-2-butene, NMR-(D_2O) δ 1.7 (3H, d, CH_3), 3.3 (2H, d, CH_2), and 5.6 (m), eluted at 32 min, while the amine formed from *cis*-2-butene, NMR(D_2O) δ 1.6 (3H, d, CH_3), 3.2 (2H, d, CH_2), and 5.6 (m), eluted at 34 min. It is hard to assign the *cis-trans* configuration from the mass and NMR spectra. Since only one isomer could be obtained, the former was tentatively assigned to be in trans form and the latter to be in cis form. The products eluted at 5, 15, and 43 min were the same as those obtained in the case of *cis*-2-butene. The large peak of *trans*-2,3-dimethylaziridine probably masked the small peak eluted at 22 min obtained in the case of *cis*-2-butene; therefore, the amount of *trans*-2,3-dimethylaziridine was corrected by assuming that the relative yield of the product at 22 min is the same as that obtained in the case of *cis*-2-butene. No *cis*-2,3-dimethylaziridine formation was observed. Table 2 shows the relative yields of products obtained at the various concentrations of hydrogen azide, irradia-

TABLE 1. THE YIELDS OF PRODUCTS RELATIVE TO THAT OF NITROGEN OBTAINED IN THE PHOTOLYSIS OF HYDROGEN AZIDE IN THE LIQUID *cis*-2-BUTENE AT 0 °C[a]

$[HN_3]$ / mmol dm^{-3}	IT[b] / min	NH_3	*c*DMA (29)	*c*2B1A (34)	A (5)	B (15)	C (22)	D (43)
42	30	0.24	0.32	0.16	0.01	0.04	0.07	0
42	60	0.22	0.32	0.18	0.02	0.04	0.06	0
42	90	0.23	0.28	0.21	0.02	0.04	0.05	0
83	30	0.27	0.36	0.21	0.02	0.05	0.09	0.03
82	60	0.25	0.30	0.21	0.02	0.04	0.08	0.03
82	90	0.28	0.21	0.22	0.03	0.04	0.05	0.02
156	30	0.23	0.29	0.22	0.02	0.04	0.07	0.04
156	60	0.25	0.24	0.25	0.03	0.04	0.06	0.07
	Average	0.25 ±0.02	0.29 ±0.05	0.21 ±0.03		0.04 ±0.01	0.07 ±0.01	

a) A Pyrex cell was used. The abbreviations of products are *c*DMA=*cis*-2,3-dimethylaziridine and *c*2B1A=*cis*-2-butene-1-amine. A, B, and D were tentatively identified to be ethanamine, 3-butene-2-amine, and *s*-butyl azide respectively. For details, see Text. The values in the parentheses show the retention times of the products. b) IT=Irradiation time.

TABLE 2. THE YIELDS OF PRODUCTS RELATIVE TO THAT OF NITROGEN OBTAINED IN THE PHOTOLYSIS OF HYDROGEN AZIDE IN THE LIQUID *trans*-2-BUTENE[a]

$[HN_3]$ / mmol dm^{-3}	IT[b] / min	NH_3	*t*DMA (23)	*t*2B1A (32)	A (5)	B (15)	D (43)
41	30	0.20	0.38	0.16	0.01	0.04	0.03
42	60	0.21	0.33	0.16	0.02	0.04	0.02
42	90	0.20	0.33	0.19	0.02	0.04	0.02
83	30	—	0.25	0.15	0.02	0.04	0.04
81	60	0.25	0.30	0.18	0.03	0.03	0.04
81	90	0.29	0.30	0.27	0.04	0.04	0.04
84[c]	30	0.17	0.37	0.22	0.02	0.04	0.05
84[c]	60	0.18	0.33	0.21	0.04	0.04	0.06
99	60	0.27	0.32	0.26	0.04	0.04	0.06
150	60	0.24	0.24	0.24	0.05	0.04	0.18
211	90	0.25	—	0.25	0.05	—	0.16
211	150	0.27	—	0.24	0.06	0.03	0.09
	Average	0.23 ±0.04	0.31 ±0.05	0.21 ±0.04		0.04 ±0.01	

a) A Pyrex cell was used. The abbreviations of the products are *t*DMA=*trans*-2,3-dimethylaziridine and *t*2B1A=*trans*-2-butene-1-amine. A, B, and D are the same as shown in Table 1. Reaction temperature was 0 °C except indicated. The values in the parentheses show the retention times of the products. b) IT=Irradiation time. c) Reactions at the temperature of Dry Ice-methanol.

tion times, and the reaction temperatures. Much as in the case of *cis*-2-butene, the relative yields of the products were almost constant, except for ethanamine and *s*-butyl azide.

1-Butene. In the case of 1-butene, 6 peaks were separated on the gas chromatogram at 5, 15, 22, 26, 38, and 60 min. The main products eluted at 15, 26, and 38 min were identified to be 3-butene-2- and 1-amines and 2-ethylaziridine. The mass spectra of these products are shown in Fig. 1. The amount of the product eluted at 60 min was negligibly small and the identification could not be done. The products eluted at 5, 15, and 22 min were the same as those obtained in the cases of *cis*- and *trans*-2-butenes. The yield of ethanamine, however, was negligibly small. The relative yields of the products are shown in Table 3. Similar to the cases of *cis*- and *trans*-2-butenes, the relative yields were almost constant for the changes in the experimental conditions.

Isobutene. In the case of isobutene, four products were separated at 20, 26, 33, and 41 min. The products eluted at 20 and 26 min were identified to be 2,2-dimethylaziridine and 2-methyl-2-propene-1-amine from their mass spectra, shown in Fig. 1, and their NMR spectra. The products eluted at 33 and 41 min were negligibly small and were not identified. The yields of the products relative to nitrogen are shown in Table 4. In contrast to the cases of 2- and 1-butenes, the relative yields of 2,2-dimethylaziridine decreased with the increases in the irradiation time and the concentration of hydrogen azide. The difference in the reaction cell, quartz or Pyrex, did

Table 3. The yields of the products relative to that of nitrogen obtained in the photolysis of hydrogen azide in the liquid 1-butene at 0 °C

$[HN_3]$ / mmol dm^{-3}	IT[b] / min	NH_3	EA (38)	3B2A (15)	3B1A (26)	C (22)
83[c]	30	—	0.17	0.10	0.13	0.01
85[c]	60	0.29	0.19	0.12	0.16	0.02
85[c]	90	0.33	0.15	0.15	0.17	0.01
83[d]	30	0.22	0.23	0.08	0.15	0.03
154[c]	30	0.26	0.22	0.12	0.15	0.03
154[c]	60	0.26	0.21	0.15	0.17	0.02
Average		0.27 ±0.04	0.19 ±0.03	0.12 ±0.03	0.15 ±0.02	0.02 ±0.01

a) The abbreviations of the products are EA=2-ethylaziridine, 3B2A=3-butene-2-amine, and 3B1A=3-butene-1-amine. C was the same products obtained in the case of 2-butene, see Text. The values in the parentheses are the retention times of the products. b) IT=Irradiation time. c) A Pyrex cell was used. d) A quartz cell was used.

Table 4. The yields of the products relative to that of nitrogen obtained in the photolysis of hydrogen azide in the liquid isobutene[a]

$[HN_3]$ / mmol dm^{-3}	Cell[b]	IT[c] / min	NH_3	DMA (20)	2MPA (26)
11[d]	Q	20	0.15	0.42	0.26
16[e]	Q	20	0.18	0.41	0.23
32[d]	Q	20	0.19	0.42	0.25
33[e]	Q	20	0.19	0.43	0.23
47[e]	Q	20	0.20	0.37	0.23
63[e]	Q	40	0.29	0.25	0.28
63[e]	P	60	0.24	0.28	0.28
63[e]	P	90	0.25	0.17	0.27
64[e]	Q	20	0.22	0.38	0.24
64[e]	Q	60	0.24	0.16	0.28
65[e]	P	40	0.21	0.38	0.27
65[d]	Q	20	0.20	0.37	0.25
77[e]	Q	20	0.20	0.35	0.24
96[e]	Q	20	0.20	0.38	0.25
118[d]	Q	20	0.20	0.33	0.25
126[e]	Q	20	0.21	0.31	0.26
148[e]	Q	40	0.31	0.12	0.30
154[e]	Q	20	0.23	0.28	0.26
155[e]	P	30	0.22	0.14	0.26
157[e]	P	60	0.22	0.07	0.25

a) The abbreviation of the products are DMA=2,2-dimethylaziridine and 2MPA=2-methyl-2-propene-1-amine. The values in the parentheses are the retention times of the products. b) Two kinds of the cell were used: Q=quartz and P=Pyrex. c) IT=Irradiation time. d) Reactions at the temperature of Dry Ice–methanol. e) Reactions at 0 °C.

not make a difference in this trend, although the effective wavelengths of the light in the former are slightly shorter than those in the latter. These results suggested that the aziridine formed was decomposed by the secondary process. The relative yields of 2,2-dimethylaziridine at the zero irradiation time was estimated to be about 0.45 by the extrapolation.

Discussion

Main Products. In the photolyses of hydrogen azide in the liquid C_4 olefins, the main products observed were nitrogen, ammonia, amines, and aziridines. The formation of these products is expected from the reaction mechanism proposed in the previous paper.[1] The reaction mechanism proposed is shown as follows:

$$HN_3 + h\nu \longrightarrow {}^1NH + N_2 \quad (1)$$

$${}^1NH + Ol \longrightarrow \text{aziridine} \quad (2)$$

$$\longrightarrow \text{amine} \quad (3)$$

$$\longrightarrow {}^3NH + Ol \quad (4)$$

$${}^3NH + HN_3 \longrightarrow NH_2 + N_3 \quad (5)$$

$$NH_2 + HN_3 \longrightarrow NH_3 + N_3 \quad (6)$$

$$N_3 + Ol \longrightarrow OlN + N_2, \quad (7)$$

where ^1NH and ^3NH represent the NH radicals in the excited singlet state, $NH(a^1\Delta)$, and in the ground triplet state, $NH(X^3\Sigma^-)$, respectively. Ol stands for olefin.

Reaction 2 is the addition reaction of the NH singlet to the double bond of olefin: *cis*- or *trans*-2,3-dimethylaziridine from *cis*- or *trans*-2-butene, 2-ethylaziridine from 1-butene, and 2,2-dimethylaziridine from isobutene. The addition occurs by a concerted manner ((a) process); in fact, only *cis*-aziridine was formed from *cis*-2-butene and only *trans*-aziridine from *trans*-2-butene.

Reaction 3 is the insertion reaction of the NH singlet into the C–H bond of olefin: *cis*- or *trans*-2-butene-1-amine from *cis*- or *trans*-2-butene, 3-butene-1- and 2-amines from 1-butene, and 2-methyl-2-propene-1-amine from isobutene. These products were all observed to be formed in good yield.

Role of Triplet NH Radicals. The triplet NH radical formed by a deactivation, Reaction 4, is assumed to abstract a hydrogen atom from hydrogen azide, Reaction 5. The triplet NH radicals possess enough energy to abstract an allylic hydrogen atom from olefin:

$${}^3NH + Ol \longrightarrow NH_2 + R. \quad (8)$$

Reaction 8, however, may be unimportant at the low temperature since the activation energy of Reaction 8 is expected to be high. If Reaction 8 is important and the resultant allyl radical abstracts a hydrogen atom from hydrogen azide,

$$R + HN_3 \longrightarrow Ol + N_3, \quad (9)$$

Reaction 8 followed by Reaction 9 is indistinguishable from Reaction 5.[1]

In the cases of the triplet methylene and oxygen, the addition to the double bond of the olefin has been considered to be important.[8,9] The triplet NH radicals might add to the double bond of the olefin in this way:

$${}^3NH + Ol \longrightarrow \text{triplet biradical.} \quad (10)$$

If Reaction 10 competed with Reaction 5, the yield of ammonia would increase with an increase in the

concentration of hydrogen azide. The yield observed, however, was almost constant for the changes in the concentration. If Reaction 10 competed with Reaction 8, the observed concentration dependence could be explained. In this case, we should expect the difference in the yield of ammonia between ethylene and propene or butenes, since the number of allylic C–H bonds included is different. The yield of ammonia also should increase with the reaction temperature. The yield of ammonia, however, was almost constant for the changes in the reactant and also in the reaction temperature. This inconsistency could be eliminated by assuming that ammonia is formed by a reaction in which the NH singlet abstracts two hydrogen atoms from an olefin:

$$^1NH + Ol \longrightarrow NH_3 + \text{products.} \quad (11)$$

As was discussed in the previous paper, Reaction 11 is unlikely.[1]

If Reaction 10 be included in the mechanism, the triplet biradicals will form aziridine by a ring closure, as observed in the cases of methylene or oxygen:[8,9]

$$\text{triplet biradical} \longrightarrow \text{aziridine.} \quad (12)$$

The aziridine formed by Reaction 12 should contain two geometrical isomers in the case of 2-butene: *cis*- and *trans*-2,3-dimethylaziridine. The results obtained, however, were different from this expectation. Thus we may conclude that the triplet NH radicals rarely add to the double bond of olefin under the present experimental conditions. This conclusion is different from that obtained in the cases of the triplet CH_2 and O. The low reactivity of the NH triplet has recently been suggested by the *ab initio* calculation. Fueno calculated the activation energy of the reaction of the NH triplet with ethylene to be 57 kJ mol^{-1}.[16] For the reactions of the triplet O atoms with ethylene, the activation energy has been estimated to be about 6 kJ mol^{-1}.[17]

Material Balance. From the above reaction mechanism, Reactions 1—7, the following relation can be expected to hold between the relative yields of products:

$$(\text{aziridine} + \text{amine} + 3NH_3)/N_2 = 1.0. \quad (13)$$

Using the values shown in Tables 1—4, the left-hand-side of Eq. 13 was estimated to be 1.2, 1.2, 1.3, and 1.4 respectively for *cis*- and *trans*-2-butenes, 1-butene, and isobutene. In the above estimations, the yields of minor products were neglected. Although the detailed mechanism for the minor product formations cannot be specified at present, these products may probably result from OlN, the product of Reaction 7. In the cases of ethylene and propene, the similar product ratios were found to be 0.7 and 0.96 respectively[1] The small values were tentatively explained by neglecting the ethenamine formation. Ethenamine is a possible insertion product of the NH singlet into the vinylic C–H bond, but this compound is known to be unstable. In the cases of butenes, the sum of the relative yields, the left-hand-side of Eq. 13, were all larger than unity. This may be attributed to the large experimental errors, especially due to the indirect method of estimating the sensitivities of GLC and an incomplete reaction mechanism in which the formation of the minor products is neglected.

Relative Rate of the Insertion and the Addition. Using the values shown in Tables 1—4, the rate of the insertion into the allylic C–H bond can be estimated relative to that of the addition as follows: 0.7_1 (*cis*-2-butene), 0.6_7 (*trans*-2-butene), 0.5_2 (1-butene), and 0.5_7 (isobutene). The relative rate obtained with propene was 0.35.[1] Except for the case of 1-butene, the relative rate per bond was almost equal and about 0.1. In other words, the rate of the insertion into an allylic C–H bond is about 1/10 that of the addition to the double bond of olefin. The large insertion rate obtained with 1-butene may be explained by the fact that the allylic C–H bond of 1-butene is weaker than others.

The authors are much obliged to Professor Takeshi Nakai of this Institute for the NMR analyses.

References

1) T. Kitamura, S. Tsunashima, and S. Sato, *Bull. Chem. Soc. Jpn.*, **54**, 55 (1981).
2) M. E. Jacox and D. E. Milligan, *J. Am. Chem. Soc.*, **85**, 278 (1963).
3) J. R. McDonald, R. G. Miller, and A. P. Baronavski, *Chem. Phys.*, **30**, 133 (1978).
4) S. Tsunashima, M. Hotta, and S. Sato, *Chem. Phys. Lett.*, **64**, 435 (1979).
5) S. Tsunashima, J. Hamada, M. Hotta, and S. Sato, *Bull. Chem. Soc. Jpn.*, **53**, 2443 (1980).
6) J. Hamada, S. Tsunashima, and S. Sato, *Bull. Chem. Soc. Jpn.*, **55**, 1739 (1982).
7) O. Kajimoto and T. Fueno, *Chem. Phys. Lett.*, **80**, 484 (1981).
8) R. J. Cvetanović, *Adv. Photochem.*, **1**, 115 (1963).
9) "Carbenes," ed by R. A. Moss and M. Jones, Jr., I (1973) and II (1975), John Wiley & Sons, New York.
10) P. P. Gasper and G. S. Hammond, II, p. 207 of Ref. 9.
11) H. M. Frey and G. J. Kennedy, *J. Chem. Soc., Faraday Trans. 1*, **73**, 164 (1977).
12) O. Kajimoto and T. Fueno, to be submitted.
13) M. D. Scheer and R. Klein, *J. Phys. Chem.*, **73**, 597 (1969).
14) R. Klein and M. D. Scheer, *J. Phys. Chem.*, **74**, 613 (1970).
15) K. Hafner, W. Kaiser, and R. Puttner, *Tetrahedron Lett.*, **52**, 3953 (1964).
16) T. Fueno, 44th National Meeting of the Chemical Society of Japan, Okayama, October 1981, Abstr. No. S3Q06.
17) K. Sugawara, T. Kyogoku, and S. Sato, unpublished results.
18) "Registry of Mass Spectral Data," ed by E. Stenhagen, S. Abrahamsson, and F. W. McLafferty, John Wiley & Sons, New York (1974), Vol. 1, p. 23.

 © 1983 The Chemical Society of Japan Bull. Chem. Soc. Jpn., 56, 667—670 (1983)

Brønsted Relation for Hydrogen→Deuterium Exchange Reactions of Imidazole-bearing Molecules with Amino Groups

Toshiya ENDO,† Ichio SHIMADA,†† Fuyuhiko INAGAKI,††† and Tatsuo MIYAZAWA*

Department of Biophysics and Biochemistry, Faculty of Science, The University of Tokyo, Hongo, Bunkyo-ku, Tokyo 113

(Received June 16, 1982)

The base-catalyzed hydrogen→deuterium exchange rates of the imidazole C-2 protons were measured for the imidazole-bearing molecules with amino groups ($N^2H_2 \cdot Im$) in ^2H_2O at various pH. From the pH dependences of the pseudo-first-order rate constants, the second-order rate constants were obtained for the $N^2H_3^+ \cdot Im^2H^+$ species and for the equilibrium mixtures of the $N^2H_2 \cdot Im^2H^+$ and $N^2H_3^+ \cdot Im$ species. For both the $N^2H_3^+ \cdot Im^2H^+$ and $N^2H_2 \cdot Im^2H^+$ species, the second-order rate constants and microscopic dissociation constants of the imidazolium rings were found to satisfy the Brønsted relation, with concomitant estimation of the abundance ratio of the $N^2H_2 \cdot Im^2H^+$ and $N^2H_3^+ \cdot Im$ species. This abundance ratio was compared with that estimated from the pH dependence of proton chemical shifts.

The C-2 proton of imidazole ring is known to exchange with the hydrogen isotopes (deuterium or tritium) under mild condition by a base-catalyzed scheme.[1–3] For the hydrogen→tritium exchange reactions of imidazole-bearing molecules without amino groups, Minamino *et al.* have found that the second-order rate constants k_b and pK_a's of imidazole rings satisfy the Brønsted relation:

$$\log k_b = \alpha pK_a + \beta, \quad (1)$$

where α and β are the constants for this type of relation.[4]

For the determination of pK_a values the nuclear magnetic resonance (NMR) spectroscopy is useful. The second-order rate constants (k_b) for hydrogen→deuterium exchange reactions may also be measured by NMR, without radioisotope manipulations. Here it may be noted that (1) the rate constant k_b for hydrogen→deuterium exchange reaction may be different from that for hydrogen→tritium exchange reaction; (2) the pK_a value of imidazole ring in ^2H_2O solution is different from that in H_2O solution; (3) the correct k_b values may not be obtained by a simple relation (see Eq. 2) if the imidazole ring is in proximity to other positively-charged ionizable groups with pK_a values close to that of the imidazole ring.

In the present study a novel method for the Brønsted plots (log k_b *versus* pK_a) for hydrogen→deuterium exchange reactions of imidazole-bearing molecules with amino groups has been worked out. These Brønsted plots together with those for imidazole-bearing molecules with no amino groups give a single straight line, and the validity of the Brønsted relation has been confirmed.

Experimental

The imidazole-bearing molecules used in the present study are *trans*-urocanic acid, *N*-acetylhistidine methylamide, *N*-acetylhistidine, and imidazole-4-acetic acid with no amino groups, and histidine methylamide, histidylglycine, histidinol, histidine and histamine with amino groups. 270-MHz proton NMR spectra were recorded on a Bruker WH-270 spectrometer. pH values (direct pH-meter readings)[5] were measured by a Radiometer PHM-26 pH meter. pK_a values were obtained by the nonlinear least square analyses of the pH dependences of proton chemical shifts. The hydrogen→deuterium exchange reaction was carried out in ^2H_2O solution (0.2 M NaCl, 1 M=1 mol dm^{-3}) at 37 °C directly in the 5-mm glass NMR tubes. The intensity decay of the C-2 proton resonance was measured relative to the intensity of C-4 proton resonance, and the observed pseudo-first-order rate constant k_{obsd} were obtained from its semi-log plots.

Results and Discussion

Brønsted Plots for Imidazole-bearing Molecules with No Amino Groups. For the imidazole-bearing molecules with no amino groups, it was sufficient to do hydrogen→deuterium exchange experiments at a given pH (9—11). The second-order rate constant k_b was obtained from k_{obsd} by using the following equation:

$$k_{obsd} = \{k_\phi K_a/[^2H^+]\}/\{1+K_a/[^2H^+]\} \quad (2)$$

$$k_\phi = k_b K_w/K_a, \quad (3)$$

where K_a is the dissociation constant of the imidazolium ring and K_w is the ion product of H_2O ($10^{-13.6}$ at 37 °C). The results are shown in Table 1 and their Brønsted plots in Fig. 1. As clearly seen in Fig. 1, log k_b and pK_a values are correlated by a single straight line and thus satisfy the Brønsted relation ($\alpha=-0.76$ and $\beta=6.7$ in Eq. 1).[6]

Brønsted Plots for Imidazole-bearing Molecules with Amino Groups. For the imidazole-bearing molecules with amino groups (denoted as $N^2H_2 \cdot Im$), the time course of exchange reaction was followed at eight pH's in the range 3—12. For example, the pH dependence of k_{obsd} for histidine is shown in Fig. 2. Exchange reaction does not occur at the acidic pH indicating that acid (or ^2H_2O)-catalyzed exchange mechanism can be neglected. This pH dependence curve exhibits two inflections at pH's each corresponding to the pK_a's of the imidazolium ring and the amino group, as previously reported.[7,8]

For this case k_{obsd} is written as,

$$k_{obsd} = \frac{k_{\phi 1}K_{a1}/[^2H^+] + k_{\phi 2}K_{a1}K_{a2}/[^2H^+]^2}{1+K_{a1}/[^2H^+]+K_{a1}K_{a2}/[^2H^+]^2} \quad (4)$$

$$k_{\phi 1} = k_{b1}K_w/K_{a1} \quad (5)$$

† Present address: Department of Chemistry, College of Technology, Gunma University, Tenjin-cho, Kiryu 376.

†† Present address: Toray Research Center, Otsu 520.

††† Present address: Toray Research Center, Kamakura 248.

Table 1. Dissociation constant (K_a in M) and second-order rate constant (k_b in $s^{-1}M^{-1}$) for imidazole-bearing molecules without amino groups

Molecule		pK_a	$\log k_b$
A	*trans*-Urocanic acid	5.82	2.26
B	*N*-Acetylhistidine methylamide	6.45	1.79
C	*N*-Acetylhistidine	7.07	1.32
D	Imidazole acetic acid	7.55	0.93

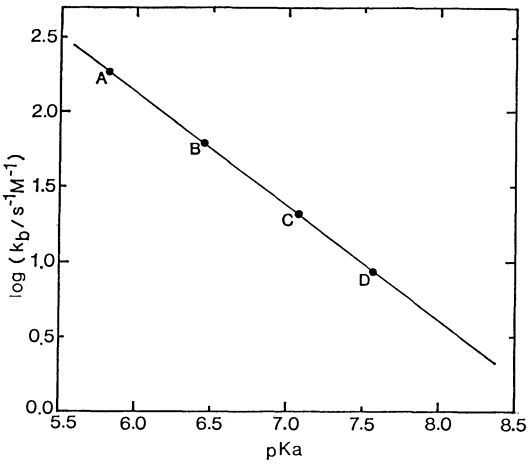

Fig. 1. Brønsted plots (k_b *versus* pK_a) for hydrogen→deuterium exchange reactions of imidazole-bearing molecules without amino groups.
For the notations A—D, see Table 1.

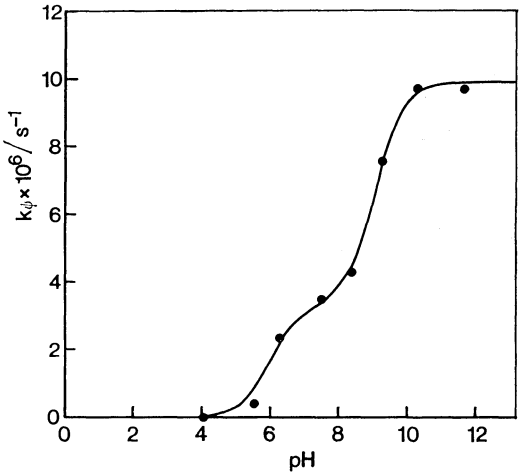

Fig. 2. pH dependence of the observed rate constant k_{obsd} for hydrogen→deuterium exchange reaction of histidine.

$$k_{\phi 2} = \rho k_{b2} K_w / K_{a2} \quad (6)$$

$$\rho/(1-\rho) = [N^2H_2 \cdot Im^2H^+]/[N^2H_3^+ \cdot Im], \quad (7)$$

where K_{a1} and K_{a2} are the first and second dissociation constants respectively, of $N^2H_3^+ \cdot Im^2H^+$, k_{b1} and k_{b2} are the second-order rate constants for the reaction of O^2H^- ion with $N^2H_3^+ \cdot Im^2H^+$ and $N^2H_2 \cdot Im^2H^+$ species respectively. Here it should be noted that the C_α–C_β rotamer populations of histidine compounds are not significantly perturbed by the ionization of the imidazole ring [J. Kobayashi, T. Higashijima, S. Sekido, and T. Miyazawa, personal communication]. By the use of Eqs. 4—7, the values of $k_{\phi 1}$ and $k_{\phi 2}$ were obtained by applying the nonlinear least-square method to the pH-dependence curves of k_{obsd}. These $k_{\phi 1}$ and $k_{\phi 2}$ were then used for calculating k_{b1} and ρk_{b2} (in $s^{-1}M^{-1}$) as shown in Table 2.

Table 2. Dissociation constants (K_{a1} and K_{a2} in M) and second-order rate constants (k_{b1} and k_{b2} in $s^{-1}M^{-1}$) for imidazole-amino bearing molecules

Molecule		pK_{a1}	$\log k_{b1}$	pK_{a2}	$\log \rho k_{b2}$
A	Histidine methylamide	5.45	2.44	7.42	1.02
B	Histidylglycine	5.84	2.10	7.62	0.85
C	Histidinol	5.90	2.10	8.90	−0.32
D	Histidine	6.06	2.08	9.16	−0.56
E	Histamine	6.18	2.07	9.92	−1.27

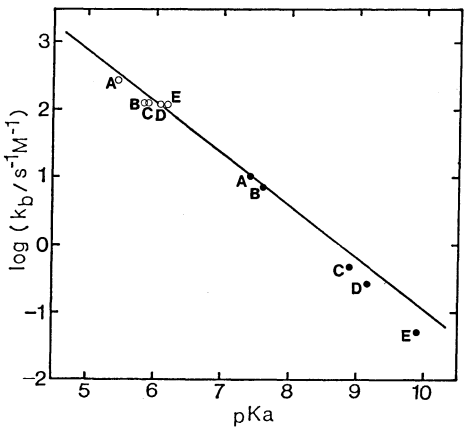

Fig. 3. Brønsted plots for hydrogen→deuterium exchange reactions of imidazole-amino-bearing molecules; ○ for k_{b1} *versus* K_{a1}; ● for ρk_{b2} *versus* K_{a2}.
For the notations A—E, see Table 2.

For this case the Brønsted plots of $\log k_{b1}$ and pK_{a1} (open circles in Fig. 3) show the tendency of slight deviations downward from the Brønsted line. The Brønsted plots of $\log \rho k_{b2}$ and pK_{a2} (closed circles in Fig. 3) lie also downward from the line.

Correction of Brønsted Plots Taking Account of Microscopic Equilibrium. The deviation from the Brønsted relation of the plots for imidazole-bearing molecules with amino groups (Fig. 3) indicates the necessity of taking into account the microscopic equilibrium. That is, the second-order rate constant k_{b1} for the $N^2H_3^+ \cdot Im^2H^+$ species should be correlated with the dissociation constant $K_1=(1-\rho)K_{a1}$ for the microscopic equilibrium $N^2H_3^+ \cdot Im^2H \rightleftarrows N^2H_3^+ \cdot Im + {}^2H^+$. The difference between pK_1 and pK_{a1} is equal to $\log [1/(1-\rho)]$. On the other hand, the second-order rate constant k_{b2} for the $N^2H_2 \cdot Im^2H^+$ species is to be correlated with the dissociation constant $K_2=K_{a2}/\rho$ for the microscopic equilibrium $N^2H_2 \cdot Im^2H^+ \rightleftarrows N^2H_2 \cdot Im + {}^2H^+$. The differences between $\log \rho k_{b2}$ and $\log k_{b2}$ and between pK_2 and pK_{a2} are both equal to $\log (1/\rho)$. In

Table 3. Dissociation constants (K_1 and K_2 in M), second-order rate constants (k_{b1} and k_{b2} in $s^{-1}M^{-1}$), and equilibrium constant (ρ) and its standard deviation (σ) for imidazole-amino-bearing molecules

Molecule		pK_1	$\log k_{b1}$	pK_2	$\log k_{b2}$	ρ (σ)
A	Histidine methylamide	5.71	2.44	7.07	1.37	0.45 (0.08)
B	Histidylglycine	6.10	2.10	7.27	1.20	0.45 (0.04)
C	Histidinol	5.97	2.10	8.08	0.50	0.15 (0.04)
D	Histidine	6.11	2.08	8.16	0.44	0.10 (0.02)
E	Histamine	6.19	2.07	8.22	0.43	0.02 (0.01)

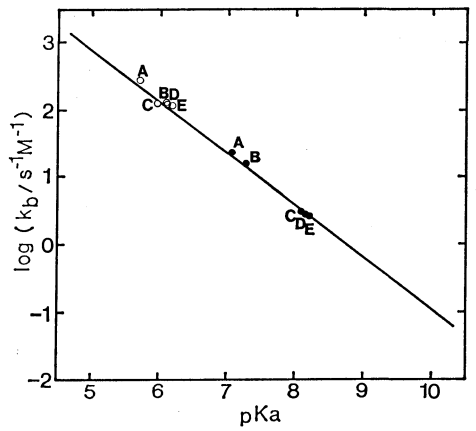

Fig. 4. Brønsted plots for hydrogen→deuterium exchange reactions of imidazole-amino-bearing molecules; ○ for k_{b1} *versus* K_1; ● for k_{b2} *versus* K_2. For the notations A—E, see Table 3.

fact, after adjusting the ratio ρ in the range 0—1, the Brønsted plots for k_{1b} (open circles in Fig. 4) and for k_{b2} (closed circles in Fig. 4) simultaneously lie close to the straight line, on the assumption that the imidazole-bearing molecules with amino groups follow the same Brønsted relation as obtained for the imidazole-bearing molecules with no amino groups. Thus, the values of ρ, pK_1, pK_2, and $\log k_{b2}$ were determined, as shown in Table 3, for the imidazole-bearing molecules with amino groups. The standard deviation for a pair of corrected Brønsted plots (pK_1, $\log k_{b1}$) and (pK_2, $\log k_{b2}$) is now smaller than that for a pair of uncorrected Brønsted plots (pK_{a1}, $\log k_{b1}$) and (pK_{a2}, $\log \rho k_{b2}$); the standard deviation is reduced from 0.12 to 0.091 for histidine methylamide, 0.28 to 0.08 for histidinol, 0.30 to 0.06 for histidine, and 0.44 to 0.08 for histamine.

It may be remarked that the second-order rate constant k_{b1} for the $N^2H_3^+ \cdot Im^2H^+$ species are 10—60 times as large as those (k_{b2}) for the $N^2H_2 \cdot Im^2H^+$ species, indicating that the reactivity of the imidazolium ring with O^2H^- ion is enhanced by the presence of the $N^2H_3^+$ groups in the proximity. Thus, as long as the base-catalyzed scheme is valid, the Brønsted relation applies to the second-order rate constants k_{b1} and k_{b2} with the concomitant estimation of the fractional population ρ of $[N^2H_2 \cdot Im^2H^+]$.

Comparison of ρ Estimated from the Brønsted-plot Correction with That from the pH Dependence of Proton Chemical Shifts. In the base catalyzed hydrogen→deuterium exchange reaction, O^2H^- ions react only with the species whose imidazole rings are protonated *i.e.* $N^2H_3^+ \cdot Im^2H^+$ and $N^2H_2 \cdot Im^2H^+$. This is the reason why we can estimate the microscopic equilibrium constant ρ (the fractional population of $[N^2H_2 \cdot Im^2H^+]$). ρ may be also determined from the pH dependences of proton chemical shifts if some reasonable assumptions are made.[9] One possible assumption is that the increase in the chemical shift upon protonation is equal to that of *N*-acetylhistidine methylamide[10] whether or not the neighboring amino group is protonated. This assumption allows us to calculate the chemical shifts for $N^2H_2 \cdot Im^2H^+$ (δ_{0+}) and $N^2H_3^+ \cdot Im$ (δ_{+0}) from the first and third limiting chemical shifts for $N^2H_2 \cdot Im$ (δ_{00}) and $N^2H^+_3 \cdot Im^2H^+$ (δ_{++}). Then ρ may be determined by using the relation $\rho = (\delta_+ - \delta_{+0})/(\delta_{0+} - \delta_{+0})$, where δ_+ is the second limiting shift obtained from the least-square fitting of the pH titration curve with the simple sum of two Henderson-Hasselbalch functions. Thus values of ρ were calculated for the five imidazole-bearing molecules with amino groups from the pH dependences of their C-2 and C-4 proton chemical shifts, and are listed in Table 4.

Table 4. Equilibrium constant (ρ) calculated from the pH dependences of C-2 and C-4 proton chemical shifts for imidazole-amino-bearing molecules

Molecule		ρ (C-2 proton)	ρ (C-4 proton)
A	Histidine methylamide	0.17	0.14
B	Histidylglycine	0.26	0.15
C	Histidinol	0.02	0.02
D	Histidine	0.03	0.06
E	Histamine	0.03	0.07

Now the values of ρ obtained by the two independent methods, the Brønsted-plot correction procedure (Table 3) and the analyses of the pH dependence of proton chemical shifts (Table 4), may be compared. Although ρ's in Table 4 are smaller than those in Table 3, the trend in ρ's among the five compounds is common to Table 3 and Table 4; histidine methylamide and histidinol have larger ρ's than the other three compounds. The differences in ρ's between Table 3 and Table 4 are probably due to that (1) the assumption used for calculating ρ in Table 4 is too simple because ρ's for C-2 proton chemical shifts differ from those for C-4 proton chemical shifts; (2) the accuracy of ρ in Table 3 is not sufficient for the critical discussion at present.

In conclusion, if an ionizable group with a pK_a

of 6—12 is in proximity to the imidazole ring, the pH dependence of the pseudo-first-order rate constant should be followed and be analyzed on the basis of microscopic equilibrium. Then the reactivity of the imidazole-ring C-2 proton may be compared on the Brønsted plots with those of imidazole-bearing molecules without such ionizable groups. Thus the validity of the Brønsted relation for the imidazole-bearing molecules even with amino groups was confirmed in the present study. This Brønsted relation will hopefully provide a basis for studying the perturbation on the reactivity of histidine residues in proteins.

References

1) J. D. Vaughan, Z. Mughrabi, and E. C. Wu, *J. Org. Chem.*, **35**, 1141 (1970).
2) H. Matsuo, M. Ohe, F. Sakiyama, and K. Narita, *J. Biochem. (Tokyo)*, **72**, 1057 (1972).
3) J. Markley, *Biochemistry*, **14**, 3546 (1975).
4) N. Minamino, H. Matsuo, and K. Narita, "Peptide Chemistry 1977," ed by T. Shiba, Protein Research Foundation, Osaka (1978), p. 85.
5) Generally p^2H is expressed as $p^2H = pH(\text{meter reading}) + 0.4 - \Delta pK_a$, where ΔpK_a is an isotope effect on the acidity constants of ionizable groups (A. Bundi and K. Wüthrich, *Biopolymers*, **18**, 285 (1979)) and is in the range *ca.* 0.5—0.7. However our discussion in the present study is valid without such an isotope correction, for we adopted pH(meter reading) in *all* the measurement and data interpretation *e.g.* in the measurements of pH dependence of exchange rate constants and proton chemical shifts.
6) T. Endo, F. Inagaki, K. Hayashi, and T. Miyazawa, *Eur. J. Biochem.*, **102**, 417 (1979).
7) J. H. Bradbury, B. E. Chapman, and F. A. Pellegrino, *J. Am. Chem. Soc.*, **95**, 6139 (1973).
8) J. H. Bradbury, B. E. Chapman, M. W. Crompton, R. S. Norton, and J. S. Teh, *J. Chem. Soc., Perkin Trans. 2*, **1980**, 693.
9) R. I. Shrager, J. S. Cohen, S. R. Heller, D. H. Sachs, and A. S. Schechter, *Biochemistry*, **11**, 541 (1972).
10) M. Tanokura, M. Tasumi, and T. Miyazawa, *Biopolymers*, **15**, 393 (1976).

 © 1983 The Chemical Society of Japan Bull. Chem. Soc. Jpn., 56, 671—675 (1983)

Infrared and Visible Absorption Spectra of Doped $(CH)_x$, $(CD)_x$, and Copolymers $[(C_2H_2)_{1-y}(C_2D_2)_y]_x$

Hitoshi Fujimoto, Masashi Tanaka,*,† and Jiro Tanaka

Department of Chemistry, Faculty of Science, Nagoya University, Chikusa-ku, Nagoya 464

†*Department of Chemistry, College of General Education, Nagoya University, Chikusa-ku, Nagoya 464*

(Received June 17, 1982)

Infrared and visible absorption spectra of $(CH)_x$, $(CD)_x$, and the copolymers $[(C_2H_2)_{1-y}(C_2D_2)_y]_x$ doped with Br_2 or I_2 were measured for various values of y between 0 and 1. By the doping, the $\pi\rightarrow\pi^*$ band located in the 19000 cm^{-1} region disappeared while several new bands were observed at 800—900-, 1000—1400-, and 5000-cm^{-1} regions. The absorption band shapes and the locations of the 5000- and 19000-cm^{-1} bands did not depend appreciably upon the value of y. The charged soliton induced vibrational bands were found at 870- and 1370-cm^{-1} in $(CH)_x$ and 1230-, 1100-, and 780-cm^{-1} in $(CD)_x$. In addition, another new bands were found around 570—660 cm^{-1} region by decreasing the temperature of the doped film to 160 K. These new bands were not shifted by the isotopic substitution. A plausible mechanism for the appearance of this band is suggested as an oscillation of trapped charged soliton around the negatively charged dopant. For the heavily doped $(CH)_x$ film, the gapless transition was observed and the optical conductivity was estimated by the Drude formula and was compared with the value obtained by a direct conductivity measurement.

Polyacetylene, $(CH)_x$, is one of the simplest linear conjugated polymers with a single chain structure and is a large band gap semiconductor. That is, pure $(CH)_x$ has the configuration of alternating single and double bonds and the $\pi\rightarrow\pi^*$ transition at about 19000 cm^{-1} indicates that the band gap exists due to the bond alternation in the polymer. However, Shirakawa, Heeger, and MacDiarmid and coworkers[1,2] found that this polymer undergoes dramatic increase in electrical conductivity upon exposure to vapors of chlorine, bromine, iodine, and arsenic pentafluoride. Furthermore, doping changes the color of thin films from reddish cupric to transparent blue. Such color change occurs by a new absorption band which may be due to charged soliton or free carrier and the suppression of the $\pi\rightarrow\pi^*$ interband transition. Many optical[3–7] and theoretical[8–10] studies have been presented hitherto to study the above-mentioned spectral changes, but the studies on the charged soliton state are not yet established. For instance, the new bands specific to the doped $(CH)_x$ are observed around 1370-, 1280-, and 870-cm^{-1}.[11–14] Doped $(CD)_x$ films also show additional bands which are located at 1230-, 1100-, and 780-cm^{-1}. These additional bands were assigned to the charged soliton-induced infrared absorption bands.[15–17] On the other hand Raman studies on $(CH)_x$ and $(CD)_x$ indicated that the bond alternation still remained or even enhanced after doping,[18] and ^{13}C NMR measurement did not show presence of Knight shift.[19]

In the present paper, we report the optical absorption spectra of Br_2 or I_2 doped $(CH)_x$, $(CD)_x$, and copolymers $[(C_2H_2)_{1-y}(C_2D_2)_y]_x$ and discuss the change of spectra with varying the y of deuterium composition. The temperature effect upon the 500—800 cm^{-1} band of these films was studied, and new bands were found just as were found in our earlier paper on the AsF_5 or Br_2 doped $(CH)_x$.[7]

Experimental

The copolymer films, $[(C_2H_2)_{1-y}(C_2D_2)_y]_x$, were prepared from the mixture of acetylene and acetylene-d_2 gases by Shirakawa's method.[20] Acetylene was purified before use by being passed successively through a concentrated sulfuric acid solution and Dry Ice-acetone traps. Acetylene-d_2 was prepared by adding heavy water to calcium carbide under vacuum. The isotopic contents were determined by partial pressure of C_2H_2 and C_2D_2.

The thin film was polymerized on the teflon frame with a 4×8 mm^2 hole and mounted in the Dewar vessel. Doping was accomplished by exposure of the film mounted in the Dewar vessel to bromine or iodine vapor. The extent of doping was controlled by measuring the four-probe d.c. conductivity of another thick film. After doping, the film was pumped out for at least 30 min and the infrared absorption of the film was measured with a Hitachi IR 260-50 (350—4000 cm^{-1}). Low temperature measurements were made by putting a liquid nitrogen into the Dewar vessel (see Fig. 1). For the visible absorption measurement, the thin film was polymerized on the inner surface of the 1 cm quartz cell and the absorption spectra of the films were measured with a Carl-Zeiss spectrophotometer (4000—45000 cm^{-1}) after doping.

The best fit of the calculated absorption spectrum to the observed spectrum of Br_2 doped $(CH)_x$ film was made on a FACOM M-200 computer of Nagoya University by using the SALS program.

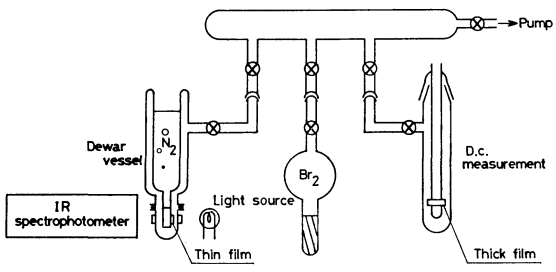

Fig. 1. Apparatus of the system of doping and IR absorption measurement.

Results and Discussion

Absorption Spectra of Thin $(CH)_x$ Films Doped with Br_2. Pure $(CH)_x$ film has a strong $\pi\rightarrow\pi^*$ band in the 19000 cm^{-1} region besides the C–H out-of-plane (740 cm^{-1} in *cis*-$(CH)_x$ and 1015 cm^{-1} in *trans*-$(CH)_x$) and the C–C–C deformation (446 cm^{-1} in *cis*-$(CH)_x$). Figures 2 and 3 show the change of spectra by doping:

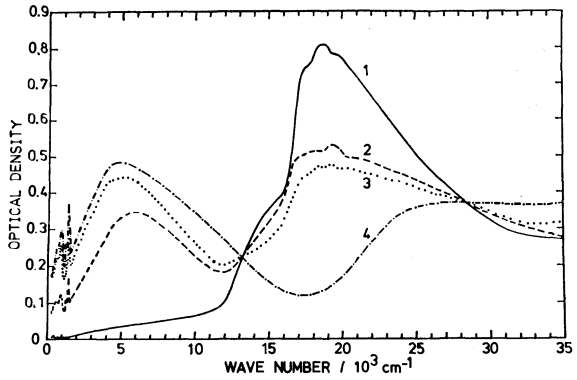

Fig. 2. Absorption spectra of the thin $(CH)_x$ films doped with Br_2.
1: Pure, 2: $\sigma \simeq 6\,\Omega^{-1}\,cm^{-1}$, 3: $\sigma \simeq 30\,\Omega^{-1}\,cm^{-1}$, 4: $\sigma \simeq 40\,\Omega^{-1}\,cm^{-1}$.

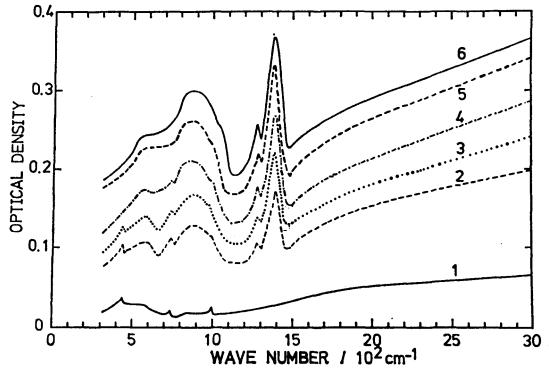

Fig. 3. IR absorption spectra of the thin $(CH)_x$ films doped with Br_2.
1: pure, 2: $\sigma \simeq 1\,\Omega^{-1}\,cm^{-1}$, 3: $\sigma \simeq 6\,\Omega^{-1}\,cm^{-1}$, 4: $\sigma \simeq 15\,\Omega^{-1}\,cm^{-1}$, 5: $\sigma \simeq 30\,\Omega^{-1}\,cm^{-1}$, 6: $\sigma \simeq 40\,\Omega^{-1}\,cm^{-1}$.

a new broad absorption band is observed over the wide region from 300- to 25000-cm^{-1}, while the $\pi \rightarrow \pi^*$ band at 19000 cm^{-1} is diminished and the absorption band of the Br_3^- ion appears in the 23000—35000 cm^{-1} region. Several new vibrational peaks are found at 1370-, 1280-, and 870-cm^{-1}, two of which were assigned by Mele and Rice[15] as the charged soliton-induced vibrations of C–C, C=C, and C–H bonds. Furthermore, the 1015 cm^{-1} band, which is the C–H out-of-plane band of *trans*-$(CH)_x$, is intensified although the 740- and 446-cm^{-1} bands assigned to the vibrational bands of *cis*-$(CH)_x$ are disappeared. This fact means that the doping induces the *cis-trans* isomerization of the $(CH)_x$ films.

Analysis of the Free Carrier Like Absorption Band of Heavily Br_2 Doped $(CH)_x$ Film. The observed optical density of thin films includes the contribution of the multiple reflection from the sample surface. Then, the absorption coefficient is determined from the observed transmittance as follows,[21]

$$T = \frac{(1-R)^2 e^{-\alpha d}}{1-R^2 e^{-2\alpha d}}, \tag{1}$$

where T is the observed transmittance, α the absorption coefficient, d the sample thickness, and R the surface reflectivity. Accordingly, the absorption coefficient is given by the following equation,

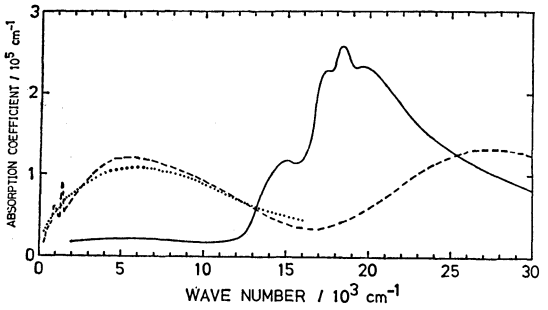

Fig. 4. Absorption spectra of pure and Br_2 doped $(CH)_x$.
——: Pure, ----: observed spectra of doped $(CH)_x$, ……: calculated spectra of doped $(CH)_x$.

$$\alpha = \frac{1}{d} \ln \left\{ \frac{(1-R)^2}{2T} + \left[\frac{(1-R)^4}{4T^2} + R^2 \right]^{1/2} \right\}. \tag{2}$$

As the surface reflectivity R corresponds to the measured reflectivity of the thick $(CH)_x$ film, the absorption spectra of pure and Br_2 doped thin $(CH)_x$ films are estimated as is shown in Fig. 4. Here, the thickness, d, of the film is determined by equating the maximum absorption coefficient of the 19000 cm^{-1} band to 2.58×10^5 cm^{-1}.[5] This value was determined by K-K transformations of the reflection spectra of pure thick films.

The absorption coefficient of the film, $\alpha(\omega)$, is expressed by using the complex dielectric constant, $\varepsilon(\omega)$, as follows,[5]

$$\alpha(\omega) = \frac{\sqrt{2}\,\omega}{c} \{(\varepsilon_1^2 + \varepsilon_2^2)^{1/2} - \varepsilon_1\}^{1/2}, \tag{3}$$

and,

$$\varepsilon(\omega) = \varepsilon_1(\omega) + i\varepsilon_2(\omega). \tag{4}$$

In the heavily doped $(CH)_x$ film, the 19000 cm^{-1} band corresponding to the interband transition disappears in the visible region and the broad band appears in the IR region having maximum at about 5500 cm^{-1}. The edge of the broad absorption band is not clearly found because of the overlapping with vibrational and soliton-induced bands. However, it seems to be decreasing less than 300 cm^{-1} with increasing doping, therefore the band gap seems to be closing at the final stage of doping.

Accordingly, if we suppose that the free carrier is formed by the heavy doping, then the complex dielectric constant will be given by a Drude type equation as,

$$\varepsilon(\omega) = \varepsilon_{core} - \frac{\omega_p^2}{\omega^2 + i\gamma\omega} \tag{5}$$

$$\varepsilon_1(\omega) = \varepsilon_{core} - \frac{\omega_p^2}{\omega^2 + \gamma^2}, \tag{6}$$

and,

$$\varepsilon_2(\omega) = \frac{\gamma}{\omega} \frac{\omega_p^2}{\omega^2 + \gamma^2}, \tag{7}$$

where ω_p is the plasma frequency and γ the band width.

For the heavily Br_2 doped $(CH)_x$ film, the parameters of Eqs. 6 and 7 are determined by the optimum fit of Eq. 3 to the experimental data of Eq. 2. The

best fit is obtained with $\hbar\omega_p=18200\,cm^{-1}$, $\gamma=8270\,cm^{-1}$, and $\varepsilon_{core}=2.77$. The calculated absorption spectrum based on these values is plotted for comparison with the experimental curve in Fig. 4. If we assume that the effective mass of the free carrier is equal to the electron mass, then the number of density, N, of the free carrier contributing to the metallic conduction is given as follows,

$$N=\frac{\omega_p^2 m_e}{4\pi e^2}. \tag{8}$$

Accordingly, the density of free carrier in the heavily doped $(CH)_x$ film is estimated as $3.0\times10^{21}\,cm^{-3}$. The total number of π-electron per unit volume was considered as $1.8\times10^{22}\,cm^{-3}$ from the specific gravity 0.4 g/cm^3 of $(CH)_x$ film.[3] Therefore, one-sixth of all π-electrons are considered to be susceptible to the optical exitation of gapless transition.

By using the values of ω_p and γ, the conductivity of the doped film shown in Fig. 4 is estimated as being $67\,\Omega^{-1}\,cm^{-1}$. The measured value was $40\,\Omega^{-1}\,cm^{-1}$; the agreement is reasonably good. The content of the dopant determined by chemical analysis was correlated with the conductivity, and the present heavily doped film includes 4% of tribromide ion (Br_3^-) per carbon atom. Therefore, one positive carbon atom or charged soliton may exist for twenty-five neutral atoms on an average. Since the probability density of the charged soliton spreads around the positive center, it is remarked that the π-electrons around the charged soliton may be responsible for the gapless transition.

Under the condition that the bond alternation exists in the chain, several mechanisms may be possible for the appearance of the gapless transition. One of them is based on the excitation of electrons around the positively charged soliton. Mele and Rice[8] have calculated the band structure of midgap state showing that the semiconductor to metal transition may occur by the heavy doping.

Absorption Spectra of Thin $(CD)_x$ Films Doped with Br_2. The spectra of the thin *cis*-$(CD)_x$ film are shown in Fig. 5, and the overall spectral change with Br_2 doping is illustrated in the order of increasing dopant concentration. The spectra observed in the near IR to visible region are similar to those of pure and Br_2 doped $(CH)_x$. That is, the strong peak around 19000 cm^{-1}, which is the $\pi\rightarrow\pi^*$ transition of the *cis* form, disappears and intense band grows up at 6000 cm^{-1} as a peak and its maximum moves to 4600 cm^{-1} at the final stage of doping. The position of the peak maxima shifts slightly to red by 200 cm^{-1} in $(CD)_x$ as compared to $(CH)_x$.

In Fig. 6 the spectral change in the IR region is shown with expanded scale. The tail of the 4600 cm^{-1} absorption band falls down gradually and it is overlapped with vibrational bands in the lower energy region. For the heavily doped film the low frequency part is enhanced and it appears to show a onset of the gapless transition. The new bands are observed at 1100- and 770-cm^{-1} regions with Br_2 doping. These bands are correlated with the 1370- and 870-cm^{-1} bands in $(CH)_x$, and the positions and the intensities of these bands are in excellent agreement with the calculation of Mele[16] and Etemad *et al.*[17] as shown in Fig. 6. This result is in conformity with Etemad's result, but our spectra show a shoulder at 1230 cm^{-1} which was predicted at 1270 cm^{-1} and was not clearly indicated in the earlier study.[17]

Temperature Dependence of Br_2 and I_2 Doped Thin Films. The changes of IR bands with temperature are measured in 160—300 K with Br_2 doped $(CD)_x$ and $(CH)_x$

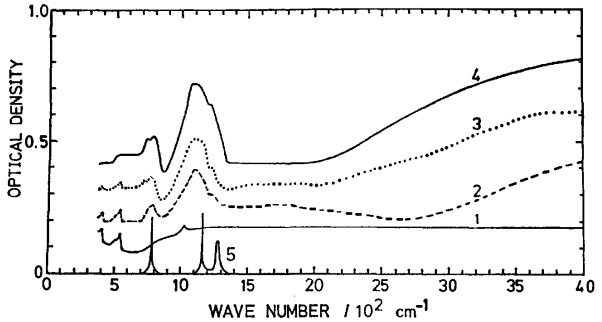

Fig. 6. IR absorption spectra of the thin $(CD)_x$ films doped with Br_2.
1: Pure, 2: $\sigma\simeq0.1\,\Omega^{-1}\,cm^{-1}$, 3: $\sigma\simeq1.3\,\Omega^{-1}\,cm^{-1}$, 4: $\simeq4\,\Omega^{-1}\,cm^{-1}$, 5: calculated by Mele and Rice.[16]

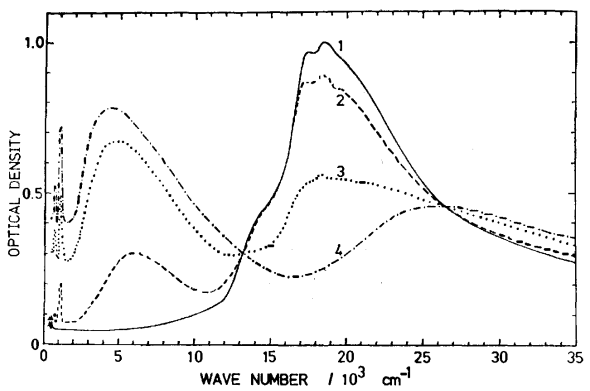

Fig. 5. Absorption spectra of the thin $(CD)_x$ films doped with Br_2.
1: Pure, 2: $\sigma\simeq0.1\,\Omega^{-1}\,cm^{-1}$, 3: $\sigma\simeq2\,\Omega^{-1}\,cm^{-1}$, 4: $\sigma\simeq4\,\Omega^{-1}\,cm^{-1}$.

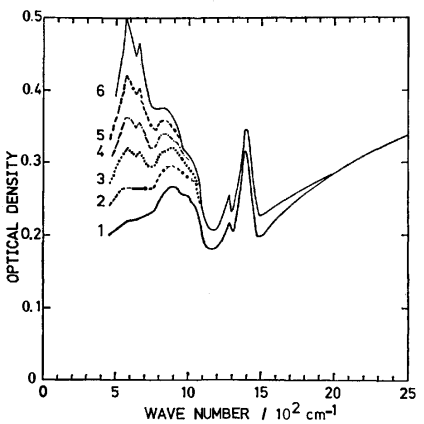

Fig. 7. Temperature dependence of the IR absorption spectra of the heavily Br_2 doped thin $(CH)_x$ film.
1: 300 K, 2: 280 K, 3: 260 K, 4: 230 K, 5: 200 K, 6: 140 K.

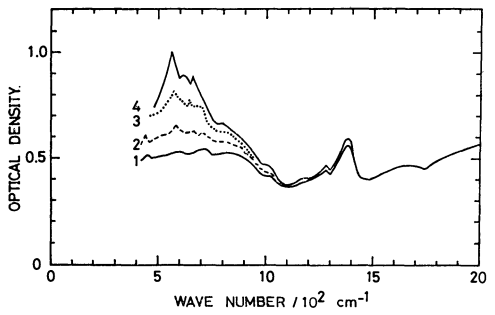

Fig. 8. Temperature dependence of the IR absorption spectra of the heavily I_2 doped thin $(CH)_x$ film. 1: 300 K, 2: 270 K, 3: 240 K, 4: 230 K.

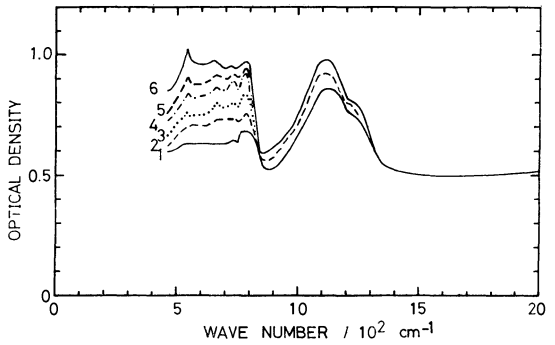

Fig. 9. Temperature dependence of the IR absorption spectra of the heavily Br_2 doped thin $(CD)_x$ film. 1: 300 K, 2: 280 K, 3: 260 K, 4: 240 K, 5: 220 K, 6: 160 K.

and I_2 doped $(CH)_x$. The spectral changes are illustrated in Figs. 7, 8, and 9. A common feature of spectral change is an appearance of new bands around 600 cm^{-1} region. It is remarkable that similar strong bands are observed with these films in spite of differences in isotopic species or chemical dopants. It should be remarked that the AsF_5 doped film showed the same spectral change in this region.[7]

In Fig. 7, the lower frequency bands around 400—1000 cm^{-1} are shown to be enhanced by cooling, and new peaks appear at 570- and 660-cm^{-1}. The 1370 cm^{-1} band and the broad absorption above 2000 cm^{-1} are not enhanced appreciably for this temperature range. In Fig. 8, the spectral change of the I_2 doped $(CH)_x$ film is illustrated, and the same peaks are found at 570- and 660-cm^{-1}. The Br_2 doped $(CD)_x$ film showed remarkably parallel spectral change by lowering the temperature; the broad bands around 500—800 cm^{-1} are enhanced and new peaks are found at 540- and 660-cm^{-1}. The deuterium substitution influences the new band as being found at slightly lower frequency. Moreover the skeletal vibration around 800 cm^{-1} is overlapped with new bands.

As regard to the origin of the new band, the predictions given by Mele and Rice[15] and Su, Schrieffer, and Heeger[22] on the soliton pinning mode should be mentioned. Mele and Rice[15] inferred that the far-infrared absorption may be found around 300—500 cm^{-1} by the pinning of the charged soliton, but they did not mention on the temperature effect on the soliton motion. Su, Schrieffer, and Heeger[22] have shown the pinning modes to appear at 560- and 720-cm^{-1}, and the lower one is due to the bound state of the charged soliton with the dopant and the higher one is a length or shape oscillation. The observed band positions are in excellent agreement with their calculations, but the assignment of the mode is difficult. The absence of isotopic effect indicates that the transition is essentially an electronic or the charged soliton's origin. The independence of the band position on the dopant species also support the soliton mechanism, because an impurity trapped bound state in the semiconductor is sensitive to acceptor species.[23]

The observed intensities of new bands are exceeding as compared to usual vibrational band. We have estimated the transition moment of the pinning mode of the charged soliton by a harmonic oscillator model with parameters given by Su, Schrieffer, and Heeger,[22] and the value was reasonable with their soliton mass of 6 m_e.

The absence of pinning mode at room temperature may be understood by the rapid motion of the charged soliton, because the energy of the pinning mode is dependent on the distance between the positively charged soliton and the dopant anion, and it might be smeared out at high temperature by the rapid motion. With decreasing the temperature, the charged soliton might be trapped at the proximity of anion, and the oscillatory motion will start around the anion.

IR Absorption Spectra of Thin Copolymers $[(C_2H_2)_{1-y}$-$(C_2D_2)_y]_x$ *Doped with* Br_2. In Fig. 10, the room temperature and low temperature absorption spectra of copolymers are shown for the following compositions: y=0, 0.2, 0.5, 0.8, and 1.0. The 870 cm^{-1} band in the Br_2 doped $(CH)_x$ (y=0) shifts to lower frequencies with increasing y. A more careful examination

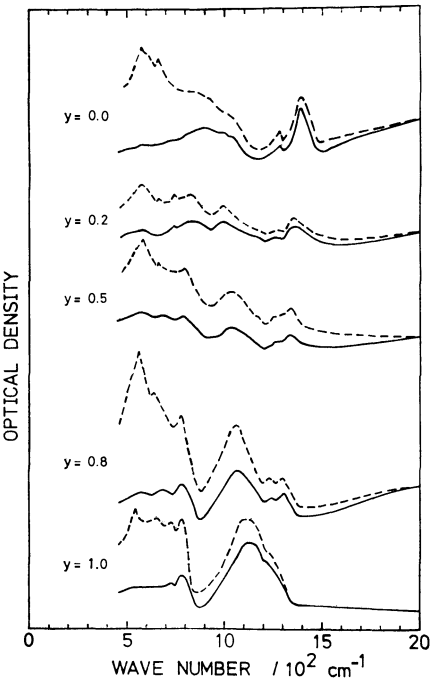

Fig.10. IR absorption spectra of copolymers $[(C_2H_2)_{1-y}$-$(C_2D_2)_y]_x$ doped with Br_2.
——: 300 K, ·····: 160 K.

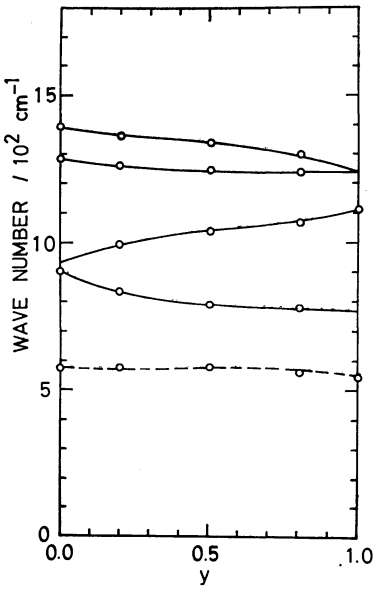

Fig.11. Mode frequencies *versus* composition, y, of Br_2 doped copolymers $[(C_2H_2)_{1-y}(C_2D_2)_y]_x$.
——: 300 K, ·····: 160 K.

reveals that this band shifts by about 100 cm^{-1} from 870 cm^{-1} at $y=0$ to 770 cm^{-1} at $y=1.0$ (Fig. 11). However, the frequency shifts of the 1370 cm^{-1} band in the Br_2 doped $(CH)_x$ ($y=0$) and the 1100 cm^{-1} band in the Br_2 doped $(CD)_x$ ($y=1.0$) show quite different behavior. That is, the 1370 cm^{-1} band in $(CH)_x$ and the 1100 cm^{-1} band in $(CD)_x$ shift to lower frequencies with increasing the isotopic substitution. As a result, the 1370 cm^{-1} band in $(CH)_x$ is not correlated directly with the 1100 cm^{-1} band in $(CD)_x$ at any composition y, as is shown in Fig. 11. This fact shows that these complicated spectral patterns should be analysed on the basis of the coupling of the C–H and C–D and C–C vibrations with π-electron transition of low energies occured with the charged soliton.

The authors would like to thank Mr. Toshiaki Noda and Mr. Gunzo Takamatsu for preparing the Dewar vessel for spectral measurement and the apparatus for the IR absorption measurement.

References

1) H. Shirakawa, E. J. Louis, A. G. MacDiarmid, C. K. Chiang, and A. J. Heeger, *J. Chem. Soc., Chem. Commun.*, **1977**, 578.
2) C. K. Chiang, M. A. Druy, S. C. Gau, A. J. Heeger, E. J. Louis, A. G. MacDiarmid, Y. W. Park, and H. Shirakawa, *J. Am. Chem. Soc.*, **100**, 1013 (1978).
3) C. R. Fincher, Jr., M. Ozaki, M. Tanaka, D. Peebles, L. Lauchlan, A. J. Heeger, and A. G. MacDiarmid, *Phys. Rev. B*, **20**, 1589 (1979).
4) M. Tanaka, A. Watanabe, and J. Tanaka, *Bull. Chem. Soc. Jpn.*, **53**, 645 (1980).
5) M. Tanaka, A. Watanabe, and J. Tanaka, *Bull. Chem. Soc. Jpn.*, **53**, 3430 (1980).
6) M. Tanaka, A. Watanabe, and J. Tanaka, *Chemica Scripta*, **17**, 131 (1981).
7) M. Tanaka, H. Fujimoto, and J. Tanaka, *Mol. Cryst. Liq. Cryst.*, **83**, 1107 (1982).
8) E. J. Mele and M. J. Rice, *Phys. Rev. B*, **23**, 5397 (1981).
9) J. L. Brédas, R. R. Chance, and R. Silbey, *J. Phys. Chem.*, **85**, 756 (1981).
10) J. J. Ritsko, *Phys. Rev. Lett.*, **46**, 849 (1981).
11) C. R. Fincher, Jr., M. Ozaki, A. J. Heeger, and A. G. MacDiarmid, *Phys. Rev. B*, **19**, 4140 (1979).
12) J. F. Rabolt, T. C. Clarke, and G. B. Street, *J. Chem. Phys.*, **71**, 4614 (1979).
13) I. Harada, Y. Furukawa, M. Tasumi, H. Shirakawa, and S. Ikeda, *J. Chem. Phys.*, **73**, 4746 (1980).
14) B. Francois, M. Bernard, and J. J. Andre, *J. Chem. Phys.*, **75**, 4142 (1981).
15) E. J. Mele and M. J. Rice, *Phys. Rev. Lett.*, **45**, 926 (1980).
16) E. J. Mele, *Mol. Cryst. Liq. Cryst.*, **77**, 25 (1981).
17) S. Etemad, A. Pron, A. J. Heeger, A. G. MacDiarmid, E. J. Mele, and M. J. Rice, *Phys. Rev. B*, **23**, 5137 (1981).
18) Y. Furukawa, I. Harada, M. Tasumi, H. Shirakawa, and S. Ikeda, *Chem. Lett.*, **1981**, 1489.
19) T. C. Clarke and J. C. Scott, *Solid State Commun.*, **41**, 389 (1982).
20) H. Shirakawa and S. Ikeda, *Polym. J.*, **2**, 231 (1971).
21) H. G. Lipson and A. Kahan, *Phys. Rev. A*, **133**, 800 (1964).
22) W. P. Su, J. R. Schrieffer, and A. J. Heeger, *Phys. Rev. B*, **22**, 2099 (1980).
23) E. Burstein, G. Picus, B. Henvis, and R. Wallis, *J. Phys. Chem. Solids*, **1**, 65 (1956).

Radical Formation through Curing Reaction of Epoxy Resins with 2,4,6-Trinitrophenol or 2,4,6-Trinitroresorcinol

Kazuro KAWAMURA

Department of Chemistry, National Defense Academy, 1-10-20, Hashirimizu, Yokosuka 239

(Received July 7, 1982)

Radicals formed spontaneously during the cure reaction of epoxy resins with 2,4,6-trinitrophenol (TNP) or 2,4,6-trinitroresorcinol (TNR) have been investigated using electron spin resonance (ESR) technique. The ESR spectrum of the radicals stabilized in the epoxy resins cured with TNP was a triplet and the other spectrum of the radicals in the epoxy resins cured with TNR was a triplet with high anisotropy. The triplet splittings and *g*-values were attributed to radicals of the type >N–Ȯ. The asymmetric line shapes of the triplet splittings caused by the ^{14}N coupling constant are induced by the slow motion of the radicals in the polymer. The presence of radicals of this type suggests the transfer of an oxygen of a nitro group of TNP or TNR during the cure reaction.

It has been known that phenols react with epoxy resins at elevated temperatures. The exact mechanism of the reaction has not been made sufficiently clear, but the reaction is likely to proceed through the formation of an intermediate oxonium ion:

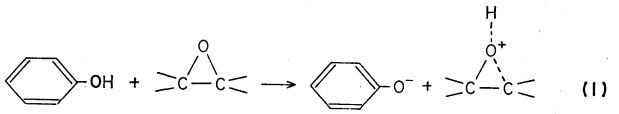

(1)

The resultant phenoxide ion may then react with the epoxy group. The carbonium ion from the oxonium complex may react with a hydroxyl group.[1,2]

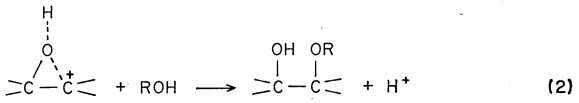

(2)

If polynitrophenols are used as the ring-opening agent of epoxy resins instead of phenols, reaction (1) may proceed easily because of the strong electron-attracting nature of nitro groups. In fact, the curing occurs by mixing TNP or TNR with the epoxy resins at room temperature.[3]

Recently it has been shown by ESR that radicals are generated during the cure reaction of the epoxy resins with TNP or TNR, and that they are stabilized in the cured resins. The process of radical formation through the cure reaction cannot be explained only from the ionic mechanism shown in the reactions (1) and (2). In the present study, we shall try to obtain some information about the radicals from ESR studies.

Experimental

Nitrophenols of extra pure commercial grade were purified by recrystallization. They were *o*-nitrophenol: mp 44—45 °C, *m*-nitrophenol: mp 96.5—97 °C, *p*-nitrophenol: mp 114—115 °C, 2,4-dinitrophenol: mp 113.0—113.5 °C, 2,6-dinitrophenol: mp 63—64 °C, and 2,4,6-trinitrophenol (TNP): mp 121.5—122.5 °C. 2,4,6-Trinitroresorcinol (TNR) was prepared by sulfonation and nitration of resorcinol: mp 174—175 °C. 2,2-Diphenyl-1-picrylhydrazyl (DPPH) of extra pure commercial grade was purified by recrystallization twice from benzene, and it was dried under reduced pressure at 80 °C: mp 139—140 °C.[4,5]

The epoxy resin was Shell Chemical Company Epikote 828 (diglycidyl ether of bisphenol A, mol wt. approx. 380).[2] 1,2-Epoxypropane was dried with calcium hydride and purified by distillation: bp 35 °C. 1-Chloro-2,3-epoxypropane (a commercial guaranteed reagent grade) was used without further purification.

ESR measurements were carried out with a JEOL X-band spectrometer, model JES-PE-1X, using 100 KHz magnetic field modulation. The *g*-value was measured by comparison with Mn^{2+} in MgO placed in the cavity close to the sample position. The *g*-value of Mn^{2+} was determined beforehand by comparison with the value of DPPH (g= 2.0036). The radical concentration of the sample was evaluated by the comparison of the double-integrated absorption intensity of the first-derivative spectrum with that of DPPH. Sample temperatures were controlled by a standard JES-VT-3A variable-temperature controller. The ESR measurements were made in air and in a vacuum. When the ESR was measured in a vacuum, the cured sample was ground and put into a standard sample-tube. The tube was sealed after evacuation by a vacuum-line system (10^{-4} Torr).

Results and Discussion

When 10—15 weight per cent of TNP or TNR was mixed with Epikote 828, the cure reaction proceeded at room temperature. ESR absorption was observed in these cure systems, as shown in Fig. 1. The Epikote 828–TNP system showed an asymmetrical triplet spectrum with an approximate 1:1:1 intensity distribution and centered at a position corresponding to g=2.007 (Fig. 1 (a)). The Epikote 828–TNR system also showed an asymmetrical triplet with g=2.006 (Fig. 1 (b)). These triplet spectra imply that the radicals formed have the odd electrons coupled strongly to the ^{14}N nuclei, and are most reasonably to be attributed to radicals of the type >N–Ȯ. The change of the line shape and the *g*-value with temperature was examined for the cured sample having a TNP content of 15 per cent. The sample was cooled from room temperature to −170 °C and then heated to 70 °C progressively in a vacuum. The ESR spectra at 70 °C and at −170 °C are shown in Figs. 2 (a) and (b). The component of the triplet at −170 °C was broadened and showed a line width of 18 G† and g=2.007 at the central position, while the spectrum at 70 °C was almost the same as that at room temperature and showed a line width of 8 G and g= 2.007. The difference in the line width is caused by the change of the motion of the radical molecules

† 1 G = 10^{-4} T.

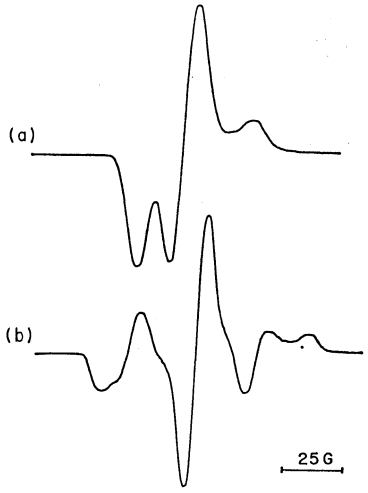

Fig. 1. ESR spectra of the radicals formed in the Epikoto 828–TNP system (a) and the Epikote 828–TNR system (b) at room temperature.

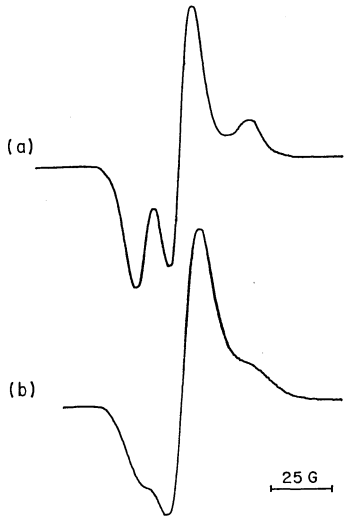

Fig. 2. Temperature dependence of ESR spectra of the radicals formed in the Epikote 828–TNP system. (a): 70 °C, (b): −170 °C.

in the cured resin. The same temperature dependence was seen on the Epikote 828–TNR system. The spectra shown in Figs. 1 and 2 agreed with the absorption pattern of nitroxide radicals when undergoing slow molecular motion, as has been investigated by the spin label technique.[6–10] According to this technique, the outer side lines of the spectrum in Fig. 1 (b) show that the radicals are arranged in parallel, and the inner side ones show that the radicals are arranged parpendicularly to the magnetic field. The splitting shows that the rotational motion of the radicals in the epoxy resin–TNR system is more limited than that of the radicals in the epoxy resin–TNP system. Neither spectra in Fig. 1 are resolved completely. A slow rotational motion of the radicals in the cured resin causes the poorly resolved and asymmetrical line shapes.

When TNP or TNR was mixed with other epoxy resins such as Epikote 812 (triglycidyl ether of glycerol) or Epikote 871 (diglycidyl ester of dimeric linoleic acid),[2] the cure reaction also proceeded at room temperature. In these cured resins the ESR spectra shown in Figs. 1 (a) and (b) were observed. However on adding TNP or TNR to monoepoxy compounds such as 1,2-epoxypropane or 1-chloro-2,3-epoxypropane, no ESR absorption occured. From these results, it is suggested that the radical formation and/or the accumulation result from a ring opening reaction of the epoxy resins which necessarily changes the resins to a high viscous state.

If mono- or dinitrophenol was mixed with Epikote 828 instead of TNP or TNR, the cure reaction scarcely proceeded at room temperature and these mixtures did not give the radicals. The mixtures were therefore heated in order to accelerate the cure reaction. The temperature was raised by 10 °C and left for 5 min. This process was repeated up to 300 °C. No ESR absorption was observed below 200 °C but a singlet spectrum due to carbonization appeared above 200 °C in each case. The result shows that not one or two but three nitro groups bonded to the benzene ring facilitate the radical formation.

The triplet spectra observed in the cure reactions of Epikote 828–TNP and Epikote 828–TNR systems may possibly be seen also in the nitrophenols alone. The ESR measurements of these nitrophenols were made under the same heating conditions as for the Epikote 828–nitrophenol mixtures. Mono- and dinitrophenols did not give the ESR absorption before carbonization, while TNP and TNR produced the radicals at 180—190 °C. Their ESR spectra are shown in Figs. 3 (a) and (b). These well resolved triplet spectra are observed both in a vacuum and in air. The spectra with an 1:1:1 intensity centered at a position corresponding to $g=2.006$ in Fig. 3 and an isotropic coupling constant of 28—30 G have been attributed to the radical $>N-\dot{O}$. This identification can be explained by the following facts: TNP decomposes slightly at 180 °C, and the g-value of the spectra almost agrees with the value of free spin. The intensity and the coupling constant of the spectra are the same as those of the radical $>N-\dot{O}$.[11,12] Therefore, it is appropriate to conclude that the radicals formed in

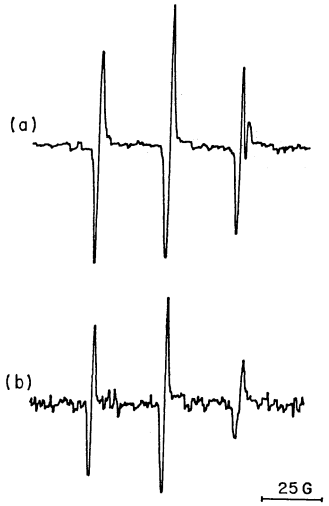

Fig. 3. ESR spectra of the radicals formed in TNP (a) and TNR (b) heated at 190 °C.

the epoxy resin cured with TNP or TNR coincide with those which appear by heating of TNP and TNR, although the radicals in the rigid state give the spectra in Fig. 1 and in the reverse case moving freely the radicals give the spectra in Fig. 3.

The changes in the absorption intensities (peak-to-peak height) of the center lines of the ESR spectra of the Epikote 828–TNP and Epikote 828–TNR systems as a function of time are shown in Figs. 4 and 5, respectively. The ESR absorption intensity of each system in Figs. 4 and 5 showed a maximum at 70 °C and the intensity changed little with time. The intensity curves above 70 °C in Fig. 4 clearly indicate a successive reaction A→B(radical)→C. On the other hand, the two steps-augmentation of the absorption intensity of the spectrum in Fig. 5 may imply that two hydroxyl groups of TNR take part in the ring-opening reaction of the epoxy groups.

More detailed investigations of the radicals formed in the Epikote 828–TNP system have been performed.

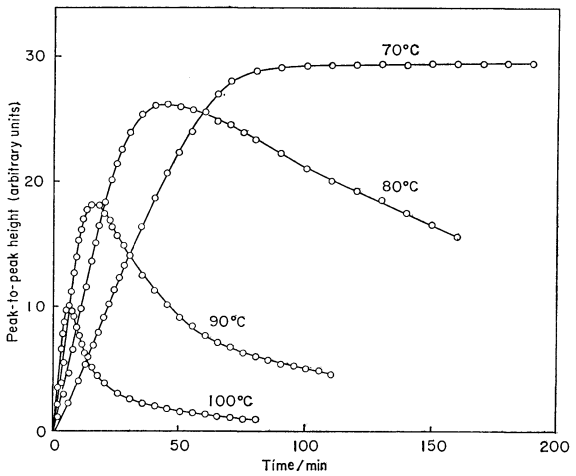

Fig. 4. Change in the intensities of ESR spectra of the radicals observed during the cure reaction of the Epikote 828–TNP system (Epikote 828/TNP=85/15) as a function of time.

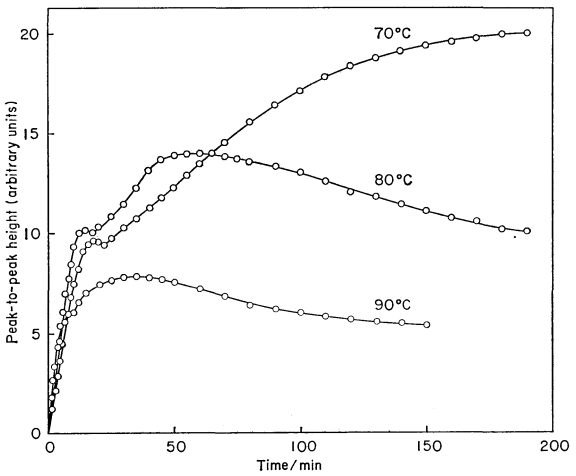

Fig. 5. Change in the intensities of ESR spectra of the radicals observed during the cure reaction of the Epikote 828–TNR system (Epikote 828/TNR=90/10) as a function of time.

Figure 6 shows the change of the absorption intensity of the center line of the triplet against the mixing ratio of TNP to the resin at 70 °C for 1 h. The ESR absorption appeared when the resin contains one per cent of TNP. When about 20 per cent of TNP was present, the ESR absorption showed a maximum. The absorption intensity of the cured resin which contained 15 per cent of TNP is equivalent to a radical concentration of 2×10^{17} spins/g.

The degree of cross-linking of Epikote 828 cured with TNP depends on the curing temperature, and is determined by the insolubility in acetone. The amount of the acetone-insoluble part of the cured resin which is mixed with 15 per cent of TNP is plotted against various temperatures as shown in Fig. 7. The absorption intensity of the ESR spectra of each cured resin is observed and plotted also in Fig. 7. As can be seen from the figure the change of these absorption intensities corresponds nicely to the amount of the acetone-insoluble part. That is, the more extensive the cross-linking is, the more the radicals are stabilized. At the temperature about 110 °C, the amount of acetone-insoluble part changes remarkably.

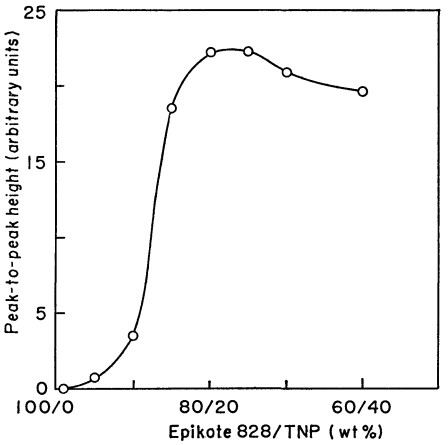

Fig. 6. Change in the intensities of ESR spectra of the radicals observed in the Epikote 828–TNP system by the treatment of 70 °C for 1 h at various ratios of mixing.

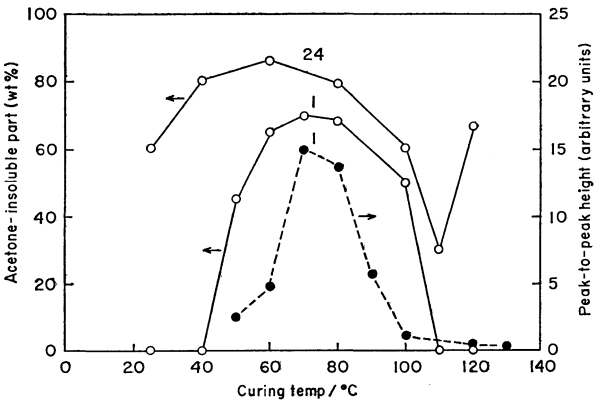

Fig. 7. Dependence of the acetone-insoluble parts and the ESR absorption intensities of Epikote 828 cured with 15 wt% of TNP at various temperatures. Numerals indicate cure time in hours.

This change of the acetone-insoluble part is caused by a ring-opening mechanism of Epikote 828 with TNP, and is explained by the following ring-opening reaction:

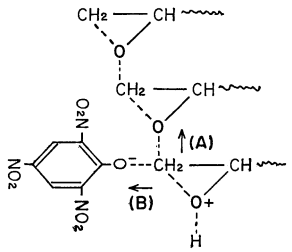

Scheme 1.

Scheme 1 implies that the ring-opening reaction has the character of a competitive reaction. When the reaction proceeds in the direction (A), more than to the direction (B), the cross-linked structure is formed directly. In the reverse case a linear product is formed at the first step, which is soluble in acetone. However many epoxy groups remain in this linear product and react with each other at elevated temperatures.[13] Finally the cross-linking occurs. It is considered that the reaction in the direction (A) proceeds at low temperature and the reaction in the direction (B) proceeds at high temperature. The latter mechanism can be supported by the fact that 2,4,6-trinitrophenyl propyl ether with hydroxyls was produced by the reaction of 1,2-epoxypropane with TNP.[14] However radical formation cannot be explained by this ionic mechanism in Scheme 1 which is almost the same as those of reactions (1) and (2). The radical formation during the cure reaction of the epoxy resins with TNP or TNR suggests that intermediate ions or radicals which appear in the high viscous reaction system promote transfer of the oxygen of a nitro group to an other position.

As the overall reaction under consideration is so complicated, the mechanism is not fully understood at present, but the ESR experiments show that the radical formation reaction must be taken into accout in interpreting the cure reaction discussed above.

References

1) L. Schechter and J. Wynstra, *Ind. Eng. Chem.*, **48**, 86 (1956).
2) H. Lee and K. Neville, "Handbook of Epoxy Resins," McGraw-Hill, Inc., New York (1967), pp. 5—16, 4—39.
3) Y. Nomura and K. Kawamura, *Kogyo Kayaku*, **28**, 20 (1967).
4) W. F. Watson, *J. Polym. Sci.*, **18**, 141 (1955).
5) J. E. Wertz, *Chem. Rev.*, **55**, 829 (1955).
6) G. B. Birrell, S. P. Van, and O. H. Griffith, *J. Am. Chem. Soc.*, **95**, 2451 (1973).
7) G. B. Birrell and O. H. Griffith, *J. Am. Chem. Soc.*, **95**, 8171 (1973).
8) M. Setaka and C. Lagercrantz, *J. Am. Chem. Soc.*, **97**, 6013 (1975).
9) Z. Veksli and W. G. Miller, *Macromolecules.*, **10**, 686 (1977).
10) M. Shiotani and J. Sohma, *Polym. J.*, **9**, 283 (1977).
11) K. Kawamura, *Kogyo Kayaku*, **39**, 313 (1978).
12) E. G. Rozantsev, "Free Nitroxyl Radicals," Plenum Press, New York (1970), p. 42.
13) K. Kawamura, *Kogyo Kayaku*, **34**, 105 (1973).
14) K. Kawamura, *Kogyo Kayaku*, **32**, 278 (1971).

Volumetric Study on the 1,3-Dipolar Cycloaddition Reaction of Diazodiphenylmethane with Several Olefins

Yosuke Yoshimura, Jiro Osugi, and Masaru Nakahara*

Department of Chemistry, Faculty of Science, Kyoto University, Oiwake-cho, Kitashirakawa, Sakyo-ku, Kyoto 606

(Received July 19, 1982)

A high pressure kinetic study was made of the 1,3-dipolar cycloaddition reaction of Ph_2CN_2 with dimethyl maleate (DMM), dimethyl fumarate (DMF), methyl acrylate (MA), maleonitrile (MN), fumaronitrile (FN), and acrylonitrile (AN) in toluene at 25 °C. The activation volumes (ΔV^*) at 1 bar obtained for DMM, DMF, MA, MN, FN, and AN are -23.4 ± 0.5, -22.3 ± 0.2, -19.8 ± 0.4, -21.5 ± 0.6, -21.0 ± 1.1, and -23.9 ± 0.5 cm^3 mol^{-1}, respectively. The reaction volume (ΔV) for the reaction between Ph_2CN_2 and DMM was determined dilatometrically by taking advantage of supersaturation of the cycloadduct in solution; $\Delta V=-24.5\pm0.5$ cm^3 mol^{-1} and $\Delta V^*/\Delta V=0.955$. The present volumetric information coupled with a kinetic analysis shows that Firestone's biradical mechanism is not the case; the concerted mechanism is supported. The experimental result is compared with that of a recent *ab initio* molecular orbital calculation with respect to the activation and reaction volumes.

One of the most fundamental thermodynamic quantities is the partial molal volume which is a function of the geometry and polarity of a molecule in solution. When this static viewpoint is taken to consider the transition state of a reaction in solution within the framework of the transition state theory,[1] the activation volume (ΔV^*), which reflects changes in the geometry and charge distribution of reacting molecules during the activation process, can be used as a criterion for distinguishing between some conceivable reaction mechanisms. Such an example is shown in a recent report on competitive 1,2- and 1,4-cycloadditions between tetracyanoethylene and *p*-methoxystyrene.[2]

In the present work, the approach mentioned above has been applied to another kind of cycloaddition, the 1,3-dipolar cycloaddition, for which two quite different mechanisms are proposed: Huisgen[3] has given a concerted mechanism on the basis of such experimental results as the stereospecificity, the reactivity sequence of dipolarophiles, the small solvent effect, and the large negative activation entropy which is similar in magnitude to that for the usual 1,4-cycloaddition (Diels-Alder) reaction, while Firestone[4] states that most of the experimental results are consistent with a two-step mechanism involving biradical intermediates. Recent molecular orbital calculations for the 1,3-dipolar cycloaddition between HCNO and HCCH also have led to different results on the mechanism depending on approximations used; the *ab initio* method[5] indicates a relatively symmetric transition state without an intermediate but the MINDO/3 method[6] a highly unsymmetric transition state with a zwitterionic intermediate.

Since the geometry of the cyclic transition state in the concerted mechanism differs significantly from that of the chainlike intermediate in the two-step mechanism, the volume profile is expected to play a decisively important role in the determination of mechanism of the 1,3-dipolar cycloaddition. As a typical 1,3-dipolar cycloaddition, the reaction of diazodiphenylmethane (Ph_2CN_2) with a series of olefins substituted by CN or $COOCH_3$ groups is chosen in the present study; the effect of temperature and solvent on the reaction rate is already clarified in a previous paper.[7]

Experimental

Ph_2CN_2 and dipolarophiles, such as dimethyl maleate (DMM), dimethyl fumarate (DMF), methyl acrylate (MA), maleonitrile (MN), fumaronitrile (FN), and acrylonitrile (AN), were prepared and purified in the same way as in the previous work.[7] Toluene was purified by the standard method.

The reaction rate at high pressure was determined by the batch method; it was required to prevent the compression heat from masking the pressure effect, so that the half-life period of the reaction was adjusted to 2—3 h by varying reactant concentrations. A dilute (10^{-3} to 10^{-1} mol dm^{-3}) reaction solution filled in a flexible Teflon capsule was put in a pressure bomb convenient for the quick recovery.[8] The recovered solution was analyzed in the same way as in the previous work.[7] The pressure was measured to ±2 kg cm^{-2} (1 kg cm^{-2}=0.9807 bar) by a Bourdon gauge (Heise) calibrated against a free piston gauge (Nagano P-3). The temperature was kept at 25.0 ± 0.05 °C.

For the dilatometric determination of the reaction volume, a pycnometer of the Lipkin-Davison type with a capacity of 4.7 cm^3 was employed, by which the relative volume change was measured to $\pm5\times10^{-5}$. The temperature was controlled to ±0.01 °C.

Results

The rates of the reactions studied obeyed the second-order rate law,

$$-\mathrm{d}[Ph_2CN_2]/\mathrm{d}t = k[Ph_2CN_2][\text{dipolarophile}], \quad (1)$$

where [ ], t, and k denote the concentration, the time, and the rate constant, respectively. The rate constants were determined from the second-order plots, *i.e.*, log $[Ph_2CN_2]/[\text{dipolarophile}]$ *vs.* t at each pressure; they are summarized in the middle columns of Table 1. According to the transition state theory, the pressure (P) effect on the rate constant allows us to determine the activation volume by

$$\left(\frac{\partial \ln k}{\partial P}\right)_T = -\frac{\Delta V^*}{RT} + \kappa, \quad (2)$$

where R, T, and κ are the gas constant, the temperature, and the isothermal compressibility of toluene,[9] respectively. A plot of the logarithmic values of k

TABLE 1. RATE CONSTANTS ($10^4\,k$/mol^{-1} dm^3 s^{-1}) AND ACTIVATION VOLUMES (ΔV^*/cm^3 mol^{-1}) FOR THE 1,3-DIPOLAR CYCLOADDITION OF Ph_2CN_2 IN TOLUENE AT 25 °C

Dipolarophile[a]	P/kg cm^{-2} 1	500	1000	1500	ΔV^*
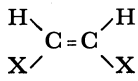 (DMM)	2.77±0.03	4.40±0.0	6.62±0.2	10.4±0.3	−23.4±0.5
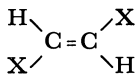 (DMF)	53.3±0.3	81.5±1.3	127±2	186±3	−22.3±0.2
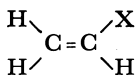 (MA)	19.8±0.2	28.2±0.7	42.0±0.8	59.5±0.8	−19.8±0.4
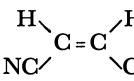 (MN)	25.0±0.1	39.0±0.3	56.0±0.5	82.0±1.2	−21.5±0.6
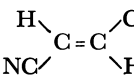 (FN)	9.97±0.05	16.7±0.2	22.1±0.2	32.3±0.7	−21.0±1.1
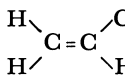 (AN)	9.72±0.06	15.2±0.3	22.9±0.2	34.0±1.0	−23.9±0.5

a) X=$COOCH_3$.

in Table 1 against pressure gives a straight line in each system. Applying Eq. 2 to such a linear relation, we can obtain the activation volume. The ΔV^* values thus obtained are listed in the last column of Table 1.

The values of ΔV^* in Table 1 are in the range of −20 to −24 cm^3 mol^{-1}, which are comparable with a value of −20 cm^3 mol^{-1} for another kind of 1,3-dipolar cycloaddition between a nitrile oxide and HCN in diisopropyl ether at 40 °C[10] but considerably larger than a value of −32 cm^3 mol^{-1} for the same kind of 1,3-dipolar cycloaddition between Ph_2CN_2 and a bicyclic olefin in toluene at 24.5 °C.[11] The small difference in ΔV^* between DMM and DMF might be ascribed to the steric hindrance by the bulky groups of $COOCH_3$, as already noticed in reactions of other kinds.[12,13] A similar trend is found previously for the activation entropy (ΔS^*).[7] The meaning of the obtained activation volumes will be discussed later in relation to the reaction mechanism.

The reaction volume (ΔV) has to be measured in some manner in order to establish the volume profile. However, since the 1,3-dipolar cycloaddition reactions of the dipolarophiles other than DMM are accompanied by a rapid consecutive reaction,[7] only the Ph_2CN_2–DMM system can be studied here. There is another problem: the cycloadduct (4,5-bis(methoxycarbonyl)-3,3-diphenyl-4,5-dihydro-3H-pyrazole) between Ph_2CN_2 and DMM has so low a solubility in toluene that we cannot determine its partial molal volume by the usual density measurement. Very fortunately, however, it turned out that when we employed the dilatometric method the solution could be highly supersaturated with respect to the product. If we assume that the volume change accompanying the 1,3-dipolar cycloaddition is independent of the concentration in the dilute solution, the following equation holds under the condition of $[Ph_2CN_2]=[DMM]$:

$$\frac{1}{A-x}-\frac{1}{A}=kt, \tag{3}$$

$$x=(m_t/m_\infty)A, \tag{4}$$

where A is the initial concentration of Ph_2CN_2, m_t, and m_∞ ($=\Delta V$) are the volume changes at t and $t=\infty$, respectively, and x is the amount of the consumed Ph_2CN_2. From Eqs. 3 and 4, we get

$$m_t=\frac{m_\infty}{1+1/kAt}. \tag{5}$$

Figure 1 shows the plot of m_t against $1/(1+1/kAt)$, and the linearity before the precipitation point indicates adequacy of the assumption utilized for deriving

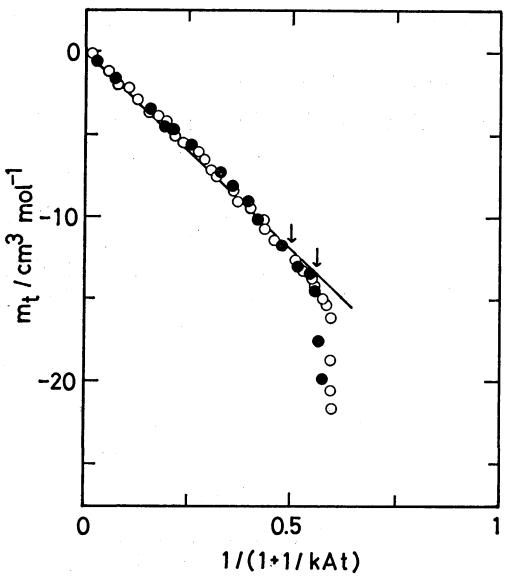

Fig. 1. Plot of Eq. 5.
●: A=0.168 mol dm^{-3}, ○: A=0.191 mol dm^{-3}. The arrows indicate the precipitation point at about 6 h; the left-hand one for A=0.168 mol dm^{-3}.

Eqs. 3 and 4. Applying the least-squares method to the linear portion of the plot, we obtained -24.5 ± 0.5 cm^3 mol^{-1} as ΔV for the 1,3-dipolar cycloaddition between Ph_2CN_2 and DMM. Probably, we can take this value as a representative one because ΔV^* does not differ so much from one dipolarophile to another as seen in Table 1.

Discussion

Biradical vs. *Concerted Mechanisms.* It is important to transform Firestone's idea on the reaction mechanism into a kinetic expression, before it is tested by the present volumetric investigation. His reaction scheme is given by

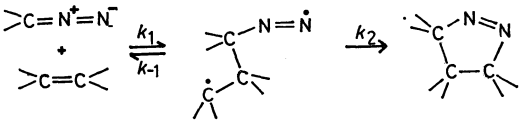

(6)

From the above scheme and the qualitative energy profile illustrated by him,[4] we get the following expression for the observed rate constant (k):

$$k = \frac{k_1 k_2}{k_{-1} + k_2} \tag{7}$$

$$= Kk_2, \tag{8}$$

where

$$K = k_1/k_{-1}, \tag{9}$$

$$k_1 \ll k_2 \ll k_{-1}. \tag{10}$$

From Eqs. 2 and 8, we have

$$\Delta V^* = \Delta V(K) + \Delta V^*(k_2), \tag{11}$$

where $\Delta V(K)$ and $\Delta V^*(k_2)$ are the reaction and the activation volumes correspoding to K and k_2, respectively. The cyclization step (k_2) of an extended biradical intermediate[14] would be diffusion controlled, the rate constant of which is inversely proportional to the bulk shear viscosity (η) of the solvent in the simplest approximation.[15] This approximation leads to

$$\Delta V^*(k_2) = RT(\partial \ln \eta/\partial P)_T, \tag{12}$$

which is 14.5 cm^3 mol^{-1} for toluene-d_8 at 25 °C; *cf.* 10.3 and 7.3 cm^3 mol^{-1} as activation volumes for the molecular and internal rotations, respectively.[16] By using $\Delta V^* = -23.4$ cm^3 mol^{-1} and $\Delta V^*(k_2) = 14.5$ cm^3 mol^{-1} in Eq. 11, we obtain -37.9 cm^3 mol^{-1} as a value of $\Delta V(K)$ for the Ph_2CN_2–DMM system, which is "smaller" than the reaction volume. This contradicts the stepwise bond formation in Firestone's mechanism; it is impossible that the bond formation due to the biradical cyclization is accompanied by as large a "positive" volume change as 13.4 cm^3 mol^{-1} ($=\Delta V - \Delta V(K)$). The value of -37.9 cm^3 mol^{-1} is also too small for the single-bond formation because no dramatic solvation can be expected for such a nonpolar intermediate; in fact, there is little solvent effect on this reaction.[7] Thus, Firestone's two-step mechanism is not supported by the present volumetric investigation.

The difference in the partial molal volume between the transition state and the cycloadduct is only 1.1 cm^3 mol^{-1} in the Ph_2CN_2–DMM system; $\Delta V^*/\Delta V = 0.955$. This indicates that the transition state resembles the product in regard to the geometry and suggests that the two bonds between the 1,3-dipole and dipolarophile develop to a large extent in the transition state. Such a resemblance is exhibited also by the usual 1,4-cycloaddition[17] which is considered to proceed *via* the concerted mechanism; *e.g.*, in the reaction between cyclopentadiene and DMF in 1-chlorobutane at 30 °C, $\Delta V^* = -32.7$ cm^3 mol^{-1} and $\Delta V = -36.7$ cm^3 mol^{-1} with $\Delta V^*/\Delta V = 0.891$.[18] The volumetric analogy between the two typical cycloadditions and the above-mentioned failure of Firestone's mechanism lead us to accept the concerted mechanism for the 1,3-dipolar cycloaddition.

Volume Profile. Figure 2 illustrates the volume profile of the 1,3-dipolar cycloaddition reaction between Ph_2CN_2 and DMM. The main features of the profile would not vary with the dipolarophile because of the similar values of ΔV^* in Table 1. It is interesting to compare the volume profile established experimentally for the 1,3-dipolar cycloaddition in solution with the theoretical one for the 1,3-dipolar cycloaddition between HCNO and HCCH in the gas phase.[5] When the van der Waals radii[19] of the relevant atoms are combined with the geometry determined by the *ab initio* method (double ζ basis set SCF), van der Waals volumes (V_W) of HCNO, HCCH, the transition state, and the product (isoxazole) are computed as 24.1, 23.1, 43.2, and 39.0 cm^3 mol^{-1}, respectively.[20] From these values we get changes in V_W accompanying the activation and reaction; $\Delta V_W^* = -4.0$ cm^3 mol^{-1} and $\Delta V_W = -8.2$ cm^3 mol^{-1} with $\Delta V_W^*/\Delta V_W = 0.49$. The theoretically predicted volumes for the transition state and the product are smaller than the volume of the reactants as a whole, but it seems that the predicted transition state is expanded relative to the product more than the one observed. If we bear it in mind that the packing fraction $\phi = V_W/V$ for most neutral

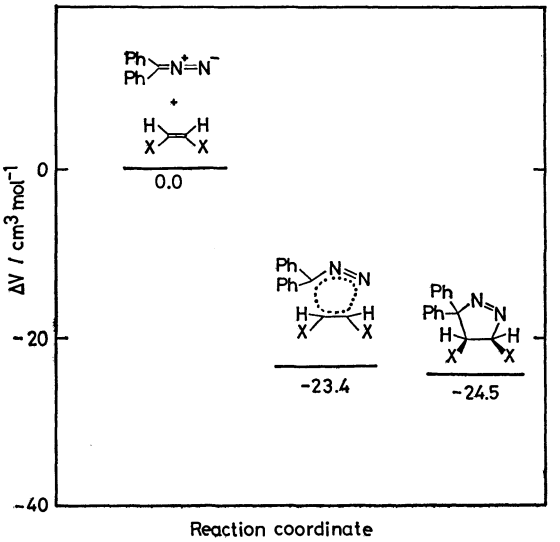

Fig. 2. The volume profile of the 1,3-dipolar cycloaddition between Ph_2CN_2 and DMM in toluene at 25 °C at 1 bar.
X=$COOCH_3$.

molecules are in the range of 0.5 to 0.6, a quantitative agreement between theory and experiment can be obtained; for example, one may take 0.5 and 0.6, respectively, for the reactants and the transition state to get $\Delta V^* = -22.4$ cm^3 mol^{-1}.[22] It is important to clarify how the activation and reaction volumes in the condensed phase are related to the theoretically calculated van der Waals volumes from the point of view of liquid theory in a further study.

Conclusion

The activation volumes for the 1,3-dipolar cycloaddition reactions of Ph_2CN_2 with olefins in toluene at 25 °C at 1 bar are in the range of -20 to -24 cm^3 mol^{-1}, and they are about 10 cm^3 mol^{-1} less negative than those for the usual 1,4-cycloaddition reactions. The partial molal volume of the transition state is close to that of the cycloadduct rather than to the sum of the partial molal volumes of the reactants. These observations are in favor of the concerted mechanism proposed by Huisgen without the volumetric information as obtained here. On the other hand, the product-oriented idea on the mechanism by Firestone that the 1,3-dipolar cycloaddition reaction proceeds *via* an extended-biradical intermediate does not succeed in explaining the pressure dependence of the rate constant. Although the *ab initio* molecular orbital calculation for the chemical reaction has so far been compared with the kinetic experiment with respect to energy, its comparison with respect to volume would serve as a tool for interpreting the experimentally obtained volumes of activation and reaction at the molecular level.

References

1) M. G. Evans and M. Polanyi, *Trans. Faraday Soc.*, **31**, 875 (1935).

2) Y. Uosaki, M. Nakahara, and J. Osugi, *Int. J. Chem. Kinet.*, (1983), in press.

3) R. Huisgen, *Angew. Chem.*, **75**, 742 (1963); *J. Org. Chem.*, **41**, 403 (1976).

4) R. A. Firestone, *J. Org. Chem.*, **33**, 2285 (1968); *Tetrahedron*, **39**, 3009 (1977).

5) A. Komornicki, J. D. Goddard, and H. F. Schaefer III, *J. Am. Chem. Soc.*, **102**, 1763 (1980).

6) M. J. S. Dewar, S. Olivella, and H. S. Rzepa, *J. Am. Chem. Soc.*, **100**, 5650 (1978).

7) Y. Yoshimura, J. Osugi, and M. Nakahara, *Bull. Chem. Soc. Jpn.*, **55**, 3325 (1982).

8) M. Nakahara, Y. Kumo-oka, and J. Osugi, *Bull. Chem. Soc. Jpn.*, **53**, 68 (1980).

9) F. I. Mopsik, *J. Chem. Phys.*, **50**, 2559 (1969).

10) M. Kurabayashi, K. Yanagiya, and M. Yasumoto, presented at the 19th High Pressure Conference of Japan, Sendai, Oct. 1978.

11) N. S. Isaacs and E. Rannala, *J. Chem. Soc., Perkin Trans. 2*, **1975**, 1555; N. S. Isaacs, "Liquid Phase High Pressure Chemistry," John Wiley & Sons, New York (1981), p. 227.

12) W. J. le Noble, *Prog. Phys. Org. Chem.*, **5**, 207 (1967).

13) K. E. Weale, "Chemical Reactions at High Pressure," Spon, London (1967), Chap. 7.

14) Firestone assumes that an extended form which plays an important role in his explanation of most important experimental results has the same energy as the cyclic one but is much more difficult to cyclize. Thus, an entropy factor related to the chance of intramolecular encounter of the radical ends is implicitly considered in his mechanism, which leads to the diffusion control.

15) P. Debye, *Trans. Electrochem. Soc.*, **82**, 265 (1942).

16) D. J. Wilbur and J. Jonas, *J. Chem. Phys.*, **62**, 2800 (1975).

17) The previous work[2] discloses an unusual 1,4-cycloaddition in which the transition state has the zwitterionic character to some extent and $\Delta V^*/\Delta V > 1$.

18) K. Seguchi, A. Sera, and K. Maruyama, *Bull. Chem. Soc. Jpn.*, **47**, 2242 (1974).

19) A. I. Kitaigorodsky, "Molecular Crystals and Molecules," Academic Press, New York (1973), Chap. 1; van der Waals radii for C, N, O, and H atoms are 180, 158, 153, and 117 pm, respectively.

20) Since overlapping of the van der Waals spheres of the atoms makes the calculation rather complicated, the spheres are divided into a large number of specimens with a dimension of about 5 pm in order to compute V_W by the numerical integration with an error of 0.1%. The molar volume (V) of isoxazole is 64.06 cm^3 mol^{-1} from its density,[21] and the ratio of V_W/V is 0.609 which is comparable with the corresponding quantities for many other nonpolar molecules.[19]

21) "Handbook of Chemistry and Physics," ed by R. C. Weast, CRC Press, Cleveland (1974), p. C-351.

22) It would be reasonable to take a larger packing fraction for the larger molecule in view of an analytical solution[23] of the Percus-Yevick equation for hard-sphere liquids,

$$\left(\frac{\partial \phi}{\partial V_W}\right)_{P,T} = \frac{P}{Nk_BT}\,\frac{(1-\phi)^3}{1+5\phi+9\phi^2-3\phi^3} > 0,$$

where P, N, k_B, and T are the pressure, the molecular number, the Boltzmann constant, and the temperature, respectively. Actually, such a trend is found when we calculate the ϕ values for normal alkane liquids using their molar volumes[24] and V_W obtained by the method employed here.

23) E. Thiele, *J. Chem. Phys.*, **39**, 474 (1963).

24) American Petroleum Institute, "Selected Values of Physical and Thermodynamic Properties of Hydrocarbons and Related Compounds," Project 44, Carnegie Press, Pittsburgh (1953).

Pressure and Temperature Effects on Octahedral-Tetrahedral Equilibria in Pyridine Solutions of Some Cobalt(II) Halides

Kazuo KOJIMA,* Minoru SAIDA, Masami DONOUE, and Jiro MATSUDA

Department of Chemistry, Faculty of Science and Engineering, Ritsumeikan University, Kita-ku, Kyoto 603

(Received August 23, 1982)

The visible absorption spectra of CoX_2 (X=Cl, Br) in pyridine solutions have been measured in the ranges 1 bar—3 kbar at room temperature, and ≈4—≈70 °C at 1 atm. The equilibrium, $[CoX_2(py)_2]$(tetrahedral)+ $2py \rightleftharpoons [CoX_2(py)_4]$(octahedral), is found to be followed over these pressure and temperature ranges. High pressure favors the octahedral species, with the volume changes, −41 cm³/mol for the chloride and ≈−30 cm³/mol for the bromide at 1 atm. The pressure dependence of the volume change is less for the bromide than for the chloride. High temperature, however, favors the tetrahedral species, with the heats of reaction, 57.3 and 60.7 kJ/mol for the chloride and the bromide, respectively. Some discussions on both the effects are also presented.

Although the effects of pressure on the ionic equilibria between tetrahedral and octahedral species of cobalt(II) in solutions have been studied quantitatively using spectrophotometric method,[1-4] there exist large discrepancies between their ΔV values, the volume changes accompanying the shift of the equilibria to the octahedral species side with increasing pressure. For example, for $CoCl_2$ in an ethanol solution, Kitamura[1] obtained ΔV to be −154 cm³/mol but Roariguez and Offen[2] −45 cm³/mol under atmospheric pressure at 25 °C, and for $CoBr_2$ in an acetone solution, Ishihara *et al.*[3] estimated ΔV to be −36 cm³/mol but later Ishihara[4] obtained −109 cm³/mol as a more accurate value. These discrepancies appear to arise from the following reason: More than two kinds of complexes exist in each solution, so that the separation of the spectra seems to be difficult.

In some pyridine solutions, the very simple equilibrium is known to exist only as follows:[5-7]

$$\underset{\text{(tetrahedral)}}{[CoX_2(py)_2]} + 2py \rightleftharpoons \underset{\text{(octahedral)}}{[CoX_2(py)_4]}, \quad (1)$$

where X=Cl, Br, or I. On the basis of the method of continuous variations, Katzin and Gebert[5] have shown that the main coordinated species is $[CoCl_2(py)_4]$, but some $[CoCl_2(py)_2]$ is also present in the pyridine solutions of $CoCl_2$. Katzin[6] measured the temperature variation of the absorbance of these solutions in the range 32—66 °C; the validity of Eq. 1 has been confirmed over this temperature range. By means of optical spectroscopy and electrical conductivity, King *et al.*[7] have established that the only equilibrium of Eq. 1 occurs in the solutions of compounds of the type $[CoX_2(py)_2]$ where X is Cl, Br, or I.

As a part of the study on the pressure and temperature effects on tetrahedral-octahedral configuration equilibria and on the structures of some complexes in solutions of cobalt(II) halides, the authors describe the pressure and temperature variations of the absorption spectra of $CoCl_2$ and $CoBr_2$ in pyridine solutions. The spectrophotometric method should be useful for these investigations because the visible spectra of both the species are separate and well-defined.

Experimental

The commercial chemical pure reagent (C. P. grade) $CoCl_2$ was dried under reduced pressure at about 105 °C for 12 h. $CoBr_2 \cdot 6H_2O$ (C. P. grade) was also dried to constant weight. After dried with anhydrous $CaSO_4$, the commercial guaranteed reagent grade pyridine was distilled.

A clamp-type optical cell[8] was used to measure the absorption spectra under high pressures. Silicone O-rings and aluminum gaskets were fitted at the connection parts of the cell to prevent corrosion by the pyridine solutions as well as pressure leaks. The spectra were determined on a Hitachi 340 spectrophotometer at room temperature.

For the measurements with temperature change, however, a Shimadzu model MPS-50L spectrophotometer was used. The maintenance of a constant temperature for an optical cell was effected by circulating water from a thermostat by means of a pump. The temperature was measured with a calibrated chromel-alumel thermocouple inserted in the sample solutions, being kept constant within 1.0 °C. A silicone-rubber lid was fitted to the sample cell to keep constant concentration of the solutions.

Results and Discussion

Pressure Effect. Figure 1 shows the absorption spectra of $CoCl_2$ in pyridine at high pressures. The spectrum at one atmosphere has three peaks at 500, 524, and 608 nm and three shoulders at about 571, 637, and 664 nm in agreement with the results of Katzin.[6] It can be seen that the two higher-energy peaks belong to a strong absorption band (O), the 608-nm peak and the shoulders do to another weak band (T); the O-band is assigned to the $^4T_{1g}(F) \rightarrow {}^4T_{1g}(P)$ transition of Co^{II} in the octahedral species $[CoCl_2(py)_4]$, and the T-band to the $^4A_2(F) \rightarrow {}^4T_1(P)$ transition of that in the tetrahedral one $[CoCl_2(py)_2]$.[3,5-7]

Although an isosbestic point appears at about 539 nm but is not well-defined, the equilibrium of Eq. 1 is found to be followed over this pressure range. The equilibrium shifts to the $[CoCl_2(py)_4]$ species side with increasing pressure, because the intensity of the O-band increases and that of the T-band decreases with increasing pressure. The O-band position scarcely changes but the 608-nm peak and the 637-nm shoulder shift slightly towards higher frequencies with pressure, which is probably due to a larger degree of distortion or compression in the species $[CoCl_2(py)_2]$ than in the other species $[CoCl_2(py)_4]$.

Figure 2 shows the absorption spectra of $CoBr_2$ in pyridine at high pressures. The spectrum at one atmosphere shows two peaks at 522 and 539 nm, and a shoulder at about 492 nm, which belong to an O'-

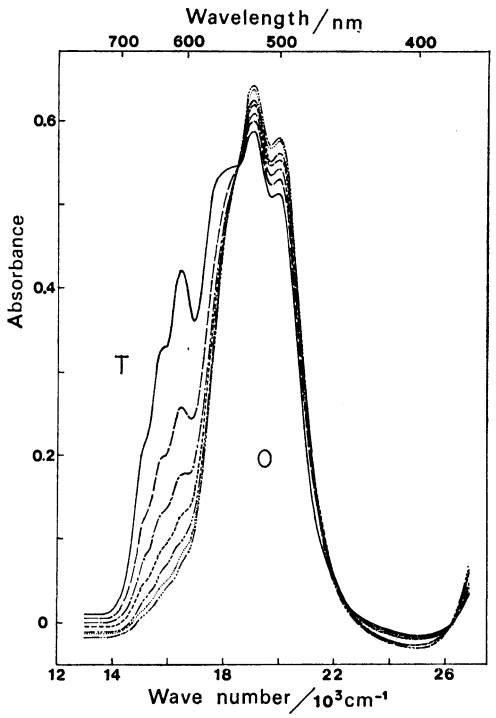

Fig. 1. Absorption spectra of $CoCl_2$ in pyridine at high pressures (25 °C), uncorrected for compression of solution.
Concn: 2.043×10^{-2} mol dm^{-3} (25 °C), optical path lenth: 1.6 cm.
——: 1 bar, — — —: 0.5 kbar, —·—: 1.0 kbar, ----: 1.5 kbar, — — —: 2.0 kbar, ·····: 2.6 kbar, —···—: 3.0 kbar.

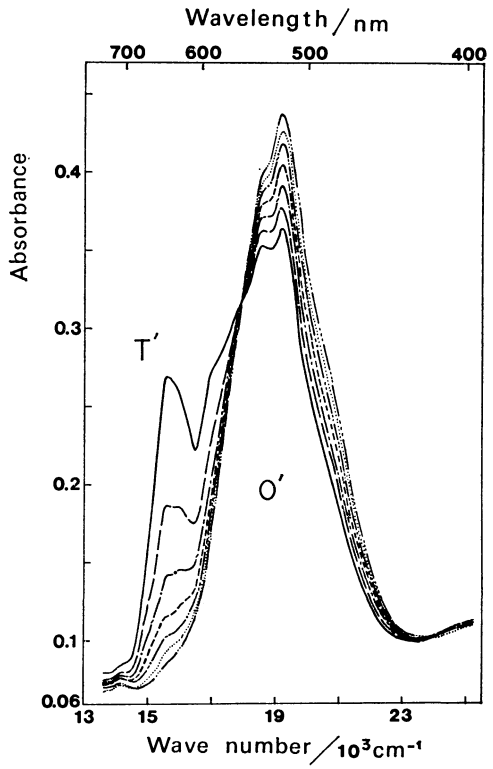

Fig. 2. Absorption spectra of $CoBr_2$ in pyridine at high pressures (20 °C), uncorrected for compression of solution.
Concn: 1.022×10^{-2} mol dm^{-3} (25 °C), optical path length: 1.6 cm.
——: 1 bar, — — —: 0.5 kbar, ——: 1.0 kbar, ----: 1.5 kbar, — — —: 2.0 kbar, ·····: 2.5 kbar, —···—: 3.0 kbar.

band. A peak at 643 nm, and shoulders at about 593, 629, and 711 nm are part of a T′-band. An isosbestic point is observed at about 564 nm. Since the spectra, as a whole, show similar pressure dependence to those of the chloride (Figs. 1 and 2), the equilibrium of Eq. 1 occurs also in the case of the bromide and shifts to the $[CoBr_2(py)_4]$ species side with increasing pressure. The 522-nm peak and the 492-nm shoulder increase in intensity more rapidly than the 539-nm peak, and consequently the O′-band changes its shape and shifts slightly to higher frequencies with increasing pressure, which the O-band scarcely shows (Fig. 1). $[CoBr_2(py)_4]$ may therefore be more distorted or compressed than $[CoCl_2(py)_4]$ probably for steric reasons.

Although for the compounds of the type $[CoX_2(py)_2]$, both the bonds of Co–X and Co–py were observed to be stronger in the chloride than in the bromide by spectroscopic[9–11] and calorimetric[12] methods, it is difficult to observe these differences in Figs. 1 and 2.

Now, we will estimate the volume change accompanying the shift of the equilibrium of Eq. 1 to the octahedral species side. In general, for an equilibrium existing in a diluted solution, the volume change (ΔV) is given by[13]

$$\Delta V = -RT\left(\frac{\partial \ln K}{\partial P}\right)_T + \Delta\nu\cdot\kappa\cdot RT, \qquad (2)$$

where K is the equilibrium constant expressed in terms of the molar concentration of each species, R is the gas constant, $\Delta\nu$ is the change in the number of the species due to the reaction, and κ is the isothermal compressibility of solvent.

Assuming that activity coefficient of each species equals to unity, the equilibrium constant for Eq. 1 is given by

$$K = \frac{c_{[CoX_2(py)_4]}}{c_{[CoX_2(py)_2]}\times c_{py}^2}. \qquad (3)$$

From Eqs. 2 and 3, we can obtain the volume change accompanying the shift of equilibrium of Eq. 1 to the octahedral species side, ΔV, as follows:

$$\Delta V = -RT\frac{d}{dP}\ln\left(\frac{c_{[CoX_2(py)_4]}}{c_{[CoX_2(py)_2]}}\right). \qquad (4)$$

Although we can not estimate the value, $\ln(c_{[CoX_2(py)_4]}/c_{[CoX_2(py)_2]})$, at a given pressure, we can obtain the pressure dependence of this value using the integrated intensities of the octahedral and the tetrahedral band, assuming that the absorbance observed under high pressures follows the Beer-Lambert law (it did at atmospheric pressure), and that the molar absorption coefficient (ε) and the optical path length do not change in this pressure range.

Figure 3 shows the plots of the logarithm of the ratio of both the integrated intensities for the chloride and the absorbances of the peaks for the bromide *vs.*

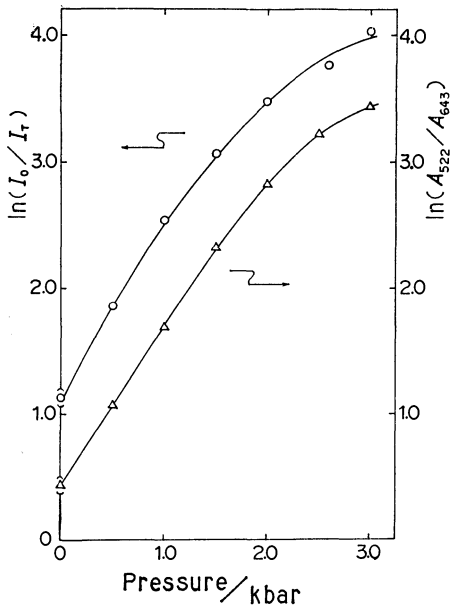

Fig. 3. Logarithm of the integrated-intensity ratio of the O-band to the T-band (I_O/I_T) for $CoCl_2$ and the ratio of the absorbance at 522 nm to that at 643 nm (A_{522}/A_{643}) for $CoBr_2$ *vs.* pressure.
○,△: Experimental, ——: calculated fitting curves.

Table 1. ΔV for $CoCl_2$ and $CoBr_2$ in pyridine solution

P / kbar	$-\Delta V$ / cm³ mol⁻¹	
	$CoCl_2$	$CoBr_2$
0.001	41	29
0.5	35	31
1.0	29	31
1.5	24	28
2.0	18	23
2.5	13	16
3.0	7	6

pressure. For the bromide, instead of the integrated intensities, the absorbances of the peaks at 522- and 643-nm are used, because of the rather changes of the O′-band shape with pressure as described above. These plots are fitted to the following equations by the least-squares method:

$$\ln\frac{I_O}{I_T} = 1.10 + 1.64P - 0.227P^2, \text{ for the chloride,}$$

$$\ln\frac{A_{522}}{A_{643}} = 0.446 + 1.17P + 0.143P^2 - 0.0665P^3, \text{ for the bromide.} \quad (5)$$

From Eqs. 4 and 5, the ΔV values are estimated and listed in Table 1. For the bromide, the absolute values of ΔV evaluated using the integrated intensities of the O′- and the T′-band are ≈5% larger than those in Table 1.

We can regard the ΔV value as the difference in the intrinsic volume between $[CoX_2(py)_4]$ and $[CoX_2(py)_2]$ solvated with two pyridine molecules. These intrinsic volumes, however, cannot be estimated at this

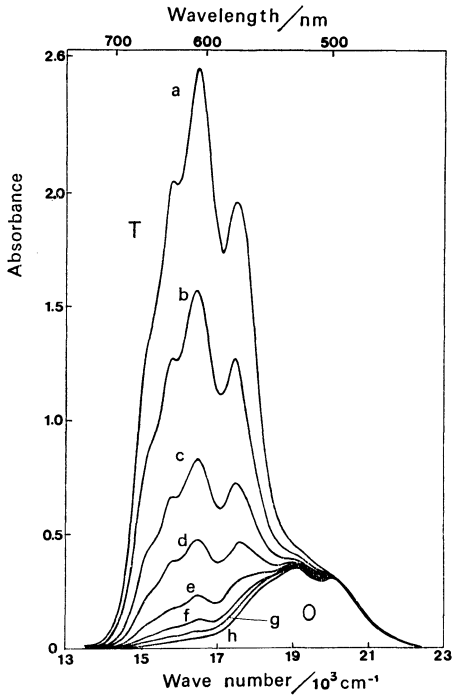

Fig. 4. Absorption spectra of $CoCl_2$ in pyridine at various temperatures (1 atm), uncorrected for thermal expansion of solution.
Concn: 2.043×10^{-2} mol dm^{-3} (25 °C), optical path length: 0.98 cm. a: 67.6 °C, b: 57.7 °C, c: 47.2 °C, d: 38.4 °C, e: 27.4 °C, f: 19.1 °C, g: 11.4 °C, h: 4.0 °C.

stage without the knowledge of the details of the structure of both complexes. The absolute value of ΔV at atmospheric pressure is smaller for the bromide (≈30 cm³/mol) than for the chloride (41 cm³/mol). This may be explained as follows; since the ionic radius of Br^- is larger than that of Cl^-, the volume difference between $[CoX_2(py)_4]$ and $[CoX_2(py)_2]$ is probably smaller for the bromide than for the chloride. Comparison with the chloride, the ΔV for the bromide changes almost linearly with pressure up to ≈1.5 kbar (Fig. 3 and Table 1).

Temperature Effect. Figure 4 shows the absorption spectra of $CoCl_2$ in pyridine at various temperatures. The intensity of the T-band increases steeply with increasing temperature; in particular, the 571- and 637-nm shoulders become well-resolved peaks. The O-band spectra, however, is insensitive against temperature change and covered by the T-band at high temperatures. This may be caused by the fact that $\varepsilon_{[CoCl_2(py)_2]}$ is much greater than $\varepsilon_{[CoCl_2(py)_4]}$.[14]

For $CoBr_2$, the corresponding spectra are shown in Fig. 5. The changes of these spectra quite resemble those of the chloride, except that in this case the 593-nm shoulder becomes a well-resolved peak.

Although no isosbestic point is found in each figure, for both the systems the equilibrium of Eq. 1 presumably occurs and shifts to the tetrahedral-species side with increasing temperature. The equilibrium constant K' is given by

$$K' = \frac{c_{[CoX_2(py)_2]}\times c_{py}^2}{c_{[CoX_2(py)_4]}}. \quad (6)$$

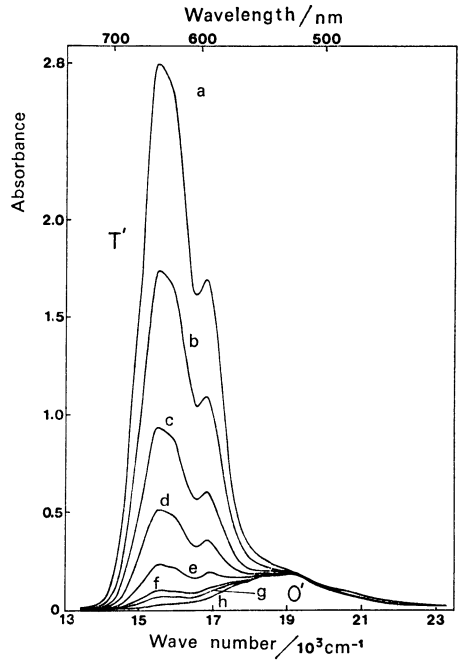

Fig. 5. Absorption spectra of $CoBr_2$ in pyridine at various temperatures (1 atm), uncorrected for thermal expansion of solution.
Concn: 1.022×10^{-2} mol dm^{-3} (25 °C), optical path length: 0.98 cm. a: 71.1 °C, b: 60.3 °C, c: 49.7 °C, d: 39.4 °C, e: 30.2 °C, f: 21.1 °C, g: 10.7 °C, h: 4.8 °C.

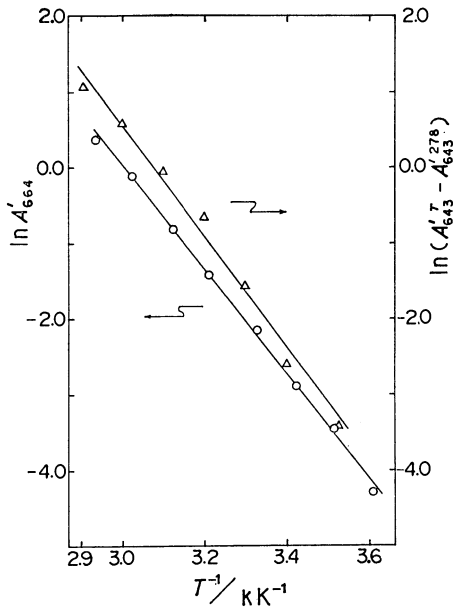

Fig. 6. Logarithm of the corrected absorbance for $CoCl_2$ (○) and for $CoBr_2$ (△) *vs.* reciprocal of absolute temperature.
A'^{278}_{643}, for example, denotes the absorbance at 643 nm and at 278 K corrected by approximate thermal expansion coefficient of pyridine. Solid lines are least-square fits to the data.

Because the concentrations of pyridine and $[CoX_2(py)_4]$ scarcely change, they can be assumed to be constant.[14] Therefore the change of K' can be followed by the intensity changes of the T'-band.

In Fig. 6, the logarithm of the corrected absorbance (A') of the 664-nm shoulder for the chloride and the 643-nm peak for the bromide is plotted against the reciprocal of absolute temperature. In order to correct the concentration, we used the approximate thermal expansion coefficient of pyridine (0.001[16]) over the temperature ranges. In order to express the intensity of the T-band, A' of the 664-nm shoulder is chosen, because there is little contribution of the intensity of the O-band at this wavelength. For the T'-band of the bromide, however, A' of the 643-nm peak subtracted out A'^{278}_{643} due to the O'-band is used. Linearities of the plots are obtained for both the halides. From each slope, the heat of reaction ΔH is estimated to be 57.3 for the chloride and 60.7 kJ/mol for the bromide. Since the similar ΔH values are obtained using the other peaks and shoulders for both cases, the equilibrium of Eq. 1 certainly occurs in each temperature range, and shifts to the $[CoX_2(py)_2]$ species side as temperature increases.

The ΔH value for the chloride is compatible with 56.1 kJ/mol obtained by Katzin.[6] Using the K' of 0.16 at 20 °C[15] and the ΔH of 57.3 kJ/mol, we can estimate ΔG to be $\approx$4.6 kJ/mol and $\Delta S\approx$0.18 kJ/(K mol), these values being comparable with the previous results.[6,7]

ΔH is a measure of the Co–py bond strength in $[CoX_2(py)_4]$. Clark and Williams[9] studied the far-infrared spectra of $[CoX_2(py)_4]$ complexes (X=Cl, Br, or I) by means of mull and assigned the strong band at about 215 cm^{-1} to the asymmetric Co–py vibration, because of the little dependence of its frequency on the type of halogen ion. King *et al.*[7] obtained ΔH for $[CoX_2(py)_4]$ (X=Cl, Br, or I) in chloroform solutions by calorimetric measurements. They were in the order of increase $Cl^-<Br^-<I^-$ and 63.6, 65.3, 69.5 kJ/mol, respectively. Though we lack ΔH for the iodide,** the order in halogen ion shown by King *et al.* is consistent with our result. The result seems to support their following explanation of this halogen ion order: Because I^- is most polarisable, charge is readily transferred to the metal along the σ-bond. This induces two opposite effects; one is to lower the effective electron affinity of Co^{II} towards pyridines, the Co–py bond strength being in the sequence $Cl^->Br^->I^-$, and the other is to enhance the release of non-bonding d-electrons of Co^{II} to antibonding pyridine π-orbitals (dative π-bonding); when the latter is superior to the former, the Co–py bond strengthens in the order $Cl^-<Br^-<I^-$.

The authors would like to thank Professor Keizo Suzuki and Professor Yoshihiro Taniguchi for their cooperation in making the clamp-type optical cell and for their valuable comments.

References

1) Y. Kitamura, *Rev. Phys. Chem. Jpn.*, **39**, 1 (1969).
2) S. Rodriguez and H. Offen, *Inorg. Chem.*, **10**, 2086 (1971).

**The experiment is in progress.

3) I. Ishihara, K. Hara, and J. Osugi, *Rev. Phys. Chem. Jpn.*, **44**, 11 (1974).
4) I. Ishihara, *Rev. Phys. Chem. Jpn.*, **48**, 27 (1978).
5) L. I. Katzin and E. Gebert, *J. Am. Chem. Soc.*, **72**, 5464 (1950).
6) L. I. Katzin, *J. Chem. Phys.*, **35**, 467 (1961).
7) H. C. A. King, E. Körös, and S. M. Nelson, *J. Chem. Soc., A*, **1963**, 5449.
8) K. Suzuki and M. Tsuchiya, *Bull. Chem. Soc. Jpn.*, **48**, 1701 (1975).
9) R. J. H. Clark and C. S. Williams, *Chem. Ind. (London)*, **1964**, 1317.
10) C. Postmus, K. Nakamoto, and J. R. Ferraro, *Inorg. Chem.*, **6**, 2194 (1967).
11) C. Postmus, J. R. Ferraro, A. Quattrochi, K. Shobatake, and K. Nakamoto, *Inorg. Chem.*, **8**, 1851 (1969).
12) G. Beech, C. T. Mortiner, and E. G. Tyler, *J. Chem. Soc., A*, **1967**, 925.
13) S. D. Hamann, "High Pressure Physics and Chemistry," ed by R. S. Bradley, Academic Press, New York (1965), Vol. 2, p. 131.
14) From $K'=0.16$ at 20 °C[15] and Fig. 4, we can roughly estimate $c_{[CoCl_2(py)_2]}/c_{[CoCl_2(py)_4]}\approx 950$ ($\approx$20 °C), ≈ 60 ($\approx$70 °C), and $\varepsilon_{[CoCl_2(py)_2]}/\varepsilon_{[CoCl_2(py)_4]}\approx 490$.
15) W. Libus and I. Uruska, *Inorg. Chem.*, **5**, 256 (1966).
16) R. F. Brunel and K. Van Bibber, "International Critical Tables," 1st ed, ed by E. W. Washburn *et al.*, McGraw-Hill Book Company, New York (1928), Vol. III, p. 28.

 © 1983 The Chemical Society of Japan Bull. Chem. Soc. Jpn., 56, 689—694 (1983)

Phase Equilibria in the La_2O_3–V_2O_3–V_2O_5 System at 1200 °C

Kenzo KITAYAMA,* Daizo ZOSHIMA,† and Takashi KATSURA

Department of Chemistry, Faculty of Science, Tokyo Institute of Technology, Ookayama, Meguro-ku, Tokyo 152

(Received February 5, 1982)

The phase equilibria in the La_2O_3–V_2O_3–V_2O_5 system were established at 1200 °C by changing oxygen partial pressures from −0.68 (air) to −13.00 in terms of $\log P_{O_2}$. In this system, $0.81La_2O_3 \cdot 0.19V_2O_5(La_{1.62}V_{0.38}O_{3.38})$, $3La_2O_3 \cdot V_2O_5(La_3VO_7)$, $0.71La_2O_3 \cdot 0.29V_2O_5(La_{1.42}V_{0.58}O_{3.58})$, $LaVO_4$, $LaVO_3$, V_nO_{2n-1} (n=2—7), and VO_2 were stable. $LaVO_3$, $LaVO_4$, $La_{1.62}V_{0.38}O_{3.38}$, La_3VO_7, and $La_{1.42}V_{0.58}O_{3.58}$ have nonstoichiometric compositions. On the basis of the phase equilibria, the Gibbs energies of the reactions:

$$31/50\ La_2O_3 + 19/50\ LaVO_3 + 19/100\ O_2 = La_{1.62}V_{0.38}O_{3.38}$$
$$50/31\ La_{1.62}V_{0.38}O_{3.38} + 12/31\ LaVO_3 + 6/31\ O_2 = La_3VO_7$$
$$21/50\ La_3VO_7 + 4/25\ LaVO_3 + 2/25\ O_2 = La_{1.42}V_{0.58}O_{3.58}$$
$$LaVO_3 + 1/2\ O_2 = LaVO_4$$

were determined to be −64.0, −55.8, −21.6, and −131.5 kJ respectively.

The phase equilibria in the Ln_2O_3–V_2O_3–V_2O_5 system (Ln=Sm, Lu, Er, and Gd) at 1200 °C have been established previously.[1-4] In these systems, the existence of V_nO_{2n-1} (n=2—7), VO_2, $LnVO_3$, and $LnVO_4$ were confirmed. In addition to the above vanadium oxides and lanthanoid vanadium oxides, in the Sm_2O_3–V_2O_3–V_2O_5 system, $Sm_{10}V_2O_{20}$ ($5Sm_2O_3 \cdot V_2O_5$); in the Lu_2O_3–V_2O_3–V_2O_5 system, $Lu_7V_3O_{16}$, $Lu_2V_2O_7$, and LuV_4O_8; in the Er_2O_3–V_2O_3–V_2O_5 system, $Er_8V_2O_{17}$ ($4Er_2O_3 \cdot V_2O_5$), and in the Gd_2O_3–V_2O_3–V_2O_5 system, $Gd_{1.62}V_{0.38}O_{3.38}$ ($0.81Gd_2O_3 \cdot 0.19V_2O_5$) were stable as ternary compounds. These diagrams, therefore, have shown different patterns as a result of the different coexisting compounds.

In the present study, we chose La_2O_3 as Ln_2O_3 because lanthanum has the largest ionic radius in the lanthanoid series.

In the La_2O_3–V_2O_3 system, the existence of $LaVO_3$ is well known,[5-8] but the system has not yet been completely studied. The crystallographic properties of $LaVO_3$ has been investigated by many researchers.[5-8] They say that $LaVO_3$, as well as $CeVO_3$, has a tetragonal crystal system, unlike the other orthorhombic $LnVO_3$ substances, although there has been report[8,9] that $CeVO_3$ has a cubic system.

Brusset *et al.*[10] studied the La_2O_3–V_2O_5 system in the temperature range from 600° to 1500 °C; they found that $4La_2O_3 \cdot V_2O_5$ was stable between La_2O_3 and $LaVO_4$ in the temperature range. However, their quench products of the composition usually contained three phases: $4La_2O_3 \cdot V_2O_5 + LaVO_4 + La_2O_3$, because of a sluggish reaction. They did not present any crystallographic data for $4La_2O_3 \cdot V_2O_5$, except a simple powder diffraction pattern (Fig. 2 in Ref. 10).

Much information pertinent to the crystal structure of $LaVO_4$ can be found in the recent literature.[11-14] Almost all lanthanoid vanadium(V) oxides crystallize in the zircon structure with a crystal symmetry of $I4_1/amd$.[15] The only exception is that of the $LaVO_4$ which has been known to have a monoclinic monazite structure with a crystal symmetry of $P2_1/n$.[16]

The objectives of the present study are: (1) to make a detailed phase diagram of the La_2O_3–V_2O_3–V_2O_5 system at 1200 °C in order to ascertain the stable ternary compounds under the present experimental conditions, (2) to calculate the standard Gibbs energy of the reactions found in the phase diagram, and (3) to ascertain whether or not there exists a linear relationship between the standard Gibbs energies of reactions and the ionic radius of the lanthanoid, as found in the Ln–Fe–O system.[17]

Experimental

Analytical-grade quantities of La_2O_3 (99.9%) and V_2O_5, obtained by heating the guaranteed grade of NH_4VO_3 at 500 °C in air for about 24 h, have been employed as the starting materials. The desired ratios of La_2O_3/V_2O_5 were obtained by mixing the appropriate quantities thoroughly in an agate mortar under ethyl alcohol. The mixtures thus obtained were treated by the procedures described in a previous report.[1] The apparatus and procedures for controlling the oxygen partial pressures, P_{O_2} (atm), and keeping a constant temperature, the method of thermogravimetry, the criterion for the establishment of an equilibrium, the method of lattice-constant determination, the method of the actual oxygen-partial-pressure measurement, and the method of chemical analysis are the same as those discussed in previous reports.[1,18-22]

The oxygen partial pressure of $10^{-13.00}$ was chosen as the reference oxygen partial pressure; that is, the weight of a sample in the atmosphere of $10^{-13.00}$ oxygen partial pressure was chosen as the reference weight throughout the present study.

Results and Discussion

Phase Equilibria. Eleven samples with La_2O_3/V_2O_5 mole ratios of 17/3, 31/9, 3/1, 29/11, 7/3, 13/7, 3/2, 1, 9/11, 7/13, and 1/4 were prepared to be used in the thermogravimetric experiment. In Fig. 1, the relationships between the oxygen partial pressure and the composition, W_{O_2}/W_T, are shown, where W_{O_2} is the weight gain of the samples from the reference weight at $\log P_{O_2} = -13.00$, while W_T is the total weight gain that the sample would get if the V_2O_3 in the sample had changed to V_2O_5. Thermogravimetric results of the six samples, 17/3, 31/9, 29/11, 7/3, 13/7, and 1/4, are shown as representative in Fig. 1.

As is shown in Fig. 1a to Fig. 1e, abrupt weight

† Present address: Eisai Co., Ltd., 6-10 Koishikawa-4 Chome, Bunkyo-ku, Tokyo 112.

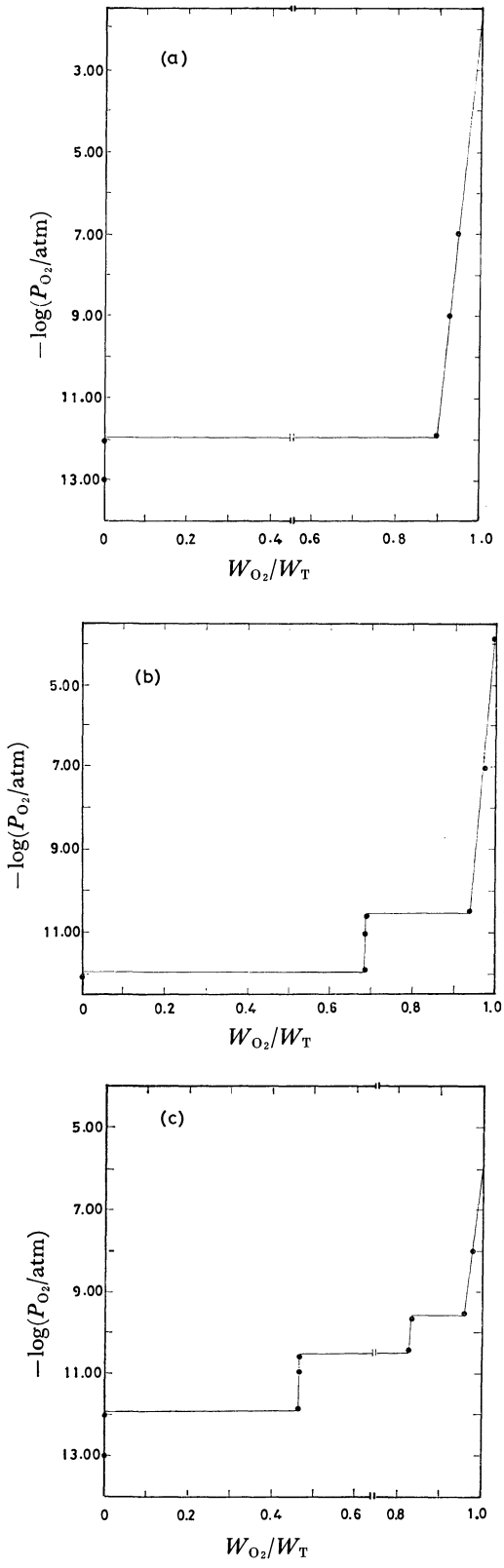

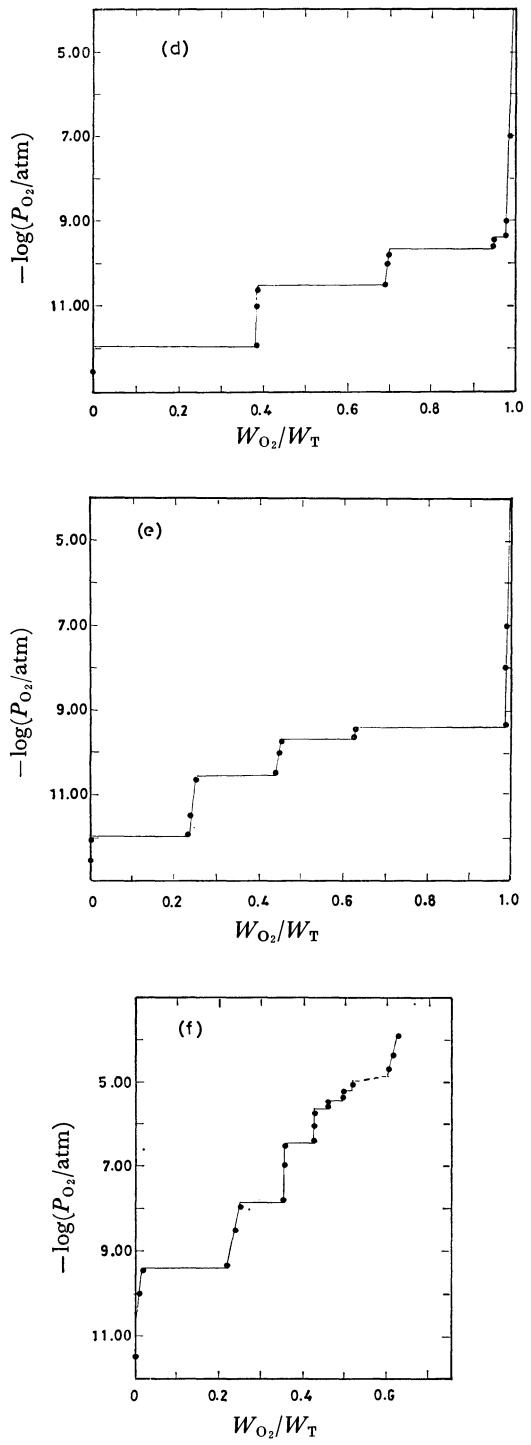

Fig. 1. The relationship between $-\log P_{O_2}$ and the weight gain (W_{O_2}/W_T) of the samples.
(a): $La_2O_3/V_2O_5=17/13$, (b): $La_2O_3/V_2O_5=31/9$, (c): La_2O_3 $V_2O_5=29/11$, (d): $La_2O_3/V_2O_5=7$ 3, (e): $La_2O_3/V_2O_5=13/7$, (f): $La_2O_3/V_2O_5=1/4$.

changes occured at 4 oxygen partial pressures, −11.95, −10.51, −9.68, and −9.35, in terms of $\log P_{O_2}$, in the samples in which the mole ratio is larger than unity. These values correspond to the equilibrium oxygen partial pressures of reactions that were found in the system and which are shown in Table 6. The last figure, $\log P_{O_2}=-9.35$, is lower than the value, -9.16 ± 0.05, previously presented by Nakamura *et al.*[6] for the same reaction at 1200 °C.

As is shown in Figs. 1d and 1e, the oxygen-partial-pressure range in which two phases, $LaVO_3$ and C, coexist is very narrow, about 0.3 in $\log P_{O_2}$, compared with the area of the other two phases. As is shown in Fig. 1f, samples with mole ratios lower than unity

Table 1. Identification of Phases

Starting materials (mol%)		$-\log(P_{O_2}/atm)$	Time h	Phases[a]
La_2O_3	V_2O_5			
85	15	12.50	6	$La_2O_3+LaVO_3$
		11.00	48	La_2O_3+A
		10.00	43	La_2O_3+A
		0.68	55	La_2O_3+A
80	20	10.00	33	A+B
77.5	22.5	12.50	6	$La_2O_3+LaVO_3$
		11.00	48	$A+LaVO_3$
		10.00	43	A+B
		0.68	55	A+B
72.5	27.5	12.50	6	$La_2O_3+LaVO_3$
		11.00	48	$A+LaVO_3$
		10.00	32	$B+LaVO_3$
		9.50	29	B+C
		0.68	55	B+C
60	40	12.50	6	$La_2O_3+LaVO_3$
		11.00	48	$A+LaVO_3$
		10.00	32	$B+LaVO_3$
		9.50	29	$C+LaVO_3$
		9.00	24	$C+LaVO_4$
		0.68	55	$C+LaVO_4$
35	65	12.00	7	$LaVO_3+V_2O_3$
		9.50	26	$LaVO_3+V_2O_3$
		8.00	27	$LaVO_4+V_2O_3$
		7.00	25	$LaVO_4+V_3O_5$
		5.75	34	$LaVO_4+V_4O_7$
		5.50	34	$LaVO_4+V_5O_9$
		5.30	40	$LaVO_4+V_6O_{11}$
		5.10	44	$LaVO_4+V_7O_{13}$
		4.50	48	$LaVO_4+VO_2$
20	80	12.00	7	$LaVO_3+V_2O_3$
		9.50	26	$LaVO_3+V_2O_3$
		8.00	27	$LaVO_4+V_2O_3$
		7.00	25	$LaVO_4+V_3O_5$
		5.75	34	$LaVO_4+V_4O_7$
		5.50	34	$LaVO_4+V_5O_9$
		5.30	40	$LaVO_4+V_6O_{11}$
		5.10	44	$LaVO_4+V_7O_{13}$
		4.50	48	$LaVO_4+VO_2$

a) A: $0.81La_2O_3\cdot0.19V_2O_5(La_{1.62}V_{0.38}O_{3.38})$, B: $3La_2O_3\cdot V_2O_5(La_3VO_7)$, C: $0.71La_2O_3\cdot0.29V_2O_5(La_{1.42}V_{0.58}O_{3.58})$.

show the similar pattern to those in the other systems[1,3,4] except for the oxygen partial pressure, log $P_{O_2}=-9.35$.

Table 1 shows the results of the identification of phases; in the first column is the composition of the starting materials; in the second, the experimental conditions of the oxygen partial pressure in terms of log P_{O_2}; in the third, the experimental duration, and in the last, the phases that are found in the quenched samples by means of an X-ray diffractometer using Cu $K\alpha$ radiation. The letters in the Phase are the abbreviations of the compounds which are shown in the lower part of the table. The abbreviations are the same as those in Tables 3 and 4 and in Fig. 2.

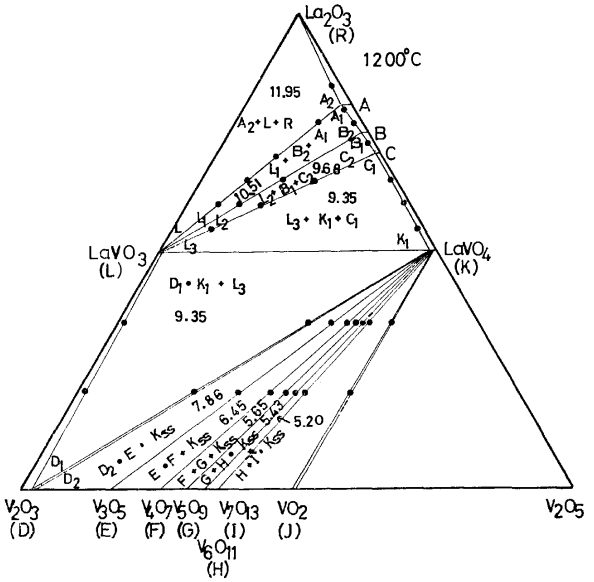

Fig. 2. Phase equilibria in the La_2O_3–V_2O_3–V_2O_5 system at 1200 °C.
Numerical values in the three solid phases regions are the oxygen partial pressures in $-\log P_{O_2}$ in equilibrium.
Abbreviations are the same as those in Tables 1, 2, and 3.

La_2O_3 is stable under the present experimental conditions, as has already been reported by Kimizuka and Katsura.[22]

Based upon the above experimental results, a phase diagram of the system at 1200 °C was drawn; it is shown in Fig. 2. The following phases are stable under the present experimental conditions, except for six compounds in the V_2O_3–V_2O_5 system, $LaVO_4$, and $LaVO_3$: La_2O_3(R), $La_{1.62}V_{0.38}O_{3.38}$(A), La_3VO_7 (B), and $La_{1.42}V_{0.58}O_{3.58}$(C). Compound A may correspond to the composition, $4La_2O_3\cdot V_2O_5$ that Brusset *et al.*[10] have reported, while Compound C may correspond to $7La_2O_3\cdot3V_2O_5$. Under the present experimental conditions, though these compounds have no round mole ratios such as are written above. The straight lines drawn by plotting the experimental points usually concentrate at the compositions presented above, even considering the experimental errors.

There are two possibilities to account for the deviations from the round mole ratios; one is the nonstoichiometry of the compounds toward the La_2O_3 side, and the other is systematic experimental errors in

Table 2. The relationships between the compositions and the oxygen partial pressures of solid solutions: $N_O/N_X=a\log P_{O_2}+b$

X	a	b
A	7.50×10^{-3}	0.0415
B	5.33×10^{-3}	0.0306
C	4.44×10^{-3}	0.0275
$LaVO_3$	0.0178	0.181
$LaVO_4$	6.64×10^{-3}	0.0325

TABLE 3. COMPOSITIONS, STABILITY RANGES IN OXYGEN PARTIAL PRESSURES, SYMBOLS, AND ACTIVITIES IN SOLID SOLUTIONS

Component	Composition	Symbol	$-\log(P_{O_2}/\text{atm})$	$\log a_i$
$La_{1.62}V_{0.38}O_{3.38}$	$La_{1.62}V_{0.38}O_{3.38}$	A	0.68[a]—5.53[b]	0.0772
	$La_{1.62}V_{0.38}O_{3.34}$	A_1	10.51	0.0308
	$La_{1.62}V_{0.38}O_{3.34}$	A_2	11.95	0
La_3VO_7	$La_3VO_{7.00}$	B	0.68[a]—5.74[b]	0.0303
	$La_3VO_{6.98}$	B_1	9.68	9.63×10^{-3}
	$La_3VO_{6.97}$	B_2	10.51	0
$La_{1.42}V_{0.58}O_{3.58}$	$La_{1.42}V_{0.58}O_{3.58}$	C	0.68[a]—6.19[b]	0.0135
	$La_{1.42}V_{0.58}O_{3.57}$	C_1	9.35	2.43×10^{-3}
	$La_{1.42}V_{0.58}O_{3.57}$	C_2	9.68	0
$LaVO_4$	$LaVO_{4.00}$	K	0.68[a]—4.89[b]	0.033
	$LaVO_{3.97}$	K_1	9.35	0
$LaVO_3$	$LaVO_{3.00}$	L	13.50[c]—10.57[b]	0
	$LaVO_{3.00}$	L_1	10.51	0.0136
	$LaVO_{3.01}$	L_2	9.68	0.0131
	$LaVO_{3.01}$	L_3	9.35	0.0111

a) The stability limit value in $\log P_{O_2}$ may be higher than -0.68 (air). b) These values are obtained by extrapolation using the experimental data. c) The stability-limit value in $\log P_{O_2}$ may be lower than this value.

the thermogravimetry. However, the following facts seem to eliminate both possibilities. For example, if the composition of Compound C were 7/3 in the La_2O_3/V_2O_5 mole ratio, no such sudden weight change would occur at $\log P_{O_2}=-9.35$ as shown in Fig. 1d; rather, it would show the same pattern as that of Fig. 1c. Also, we found compounds with round mole ratios, such as $3La_2O_3\cdot V_2O_5$(B), $4Er_2O_3\cdot V_2O_5$,[4] and $4Ho_2O_3\cdot V_2O_5$, in the Ho_2O_3–V_2O_3–V_2O_5 system in spite of using the same experimental techniques. On the other hand, $0.81Gd_2O_3\cdot0.19V_2O_5$ was found in the Gd_2O_3–V_2O_3–V_2O_5 system,[4] as has been described above.

Two new compounds, B and C, were found in the La_2O_3–V_2O_5 system. Kiparisov *et al.*[23] reported the existence of $3Er_2O_3\cdot V_2O_5$ at 1300 °C. However, the X-ray powder diffraction pattern of $3Er_2O_3\cdot V_2O_5$ is not similar to that of Compound B. No compound with a Ln_2O_3/V_2O_5 mole ratio of 7/3 or near it has yet been found in the another system.

Ternary compounds, A, B, C, $LaVO_3$, and $LaVO_4$ have nonstoichiometric compositions. The nonstoichiometry of the $LnVO_3$-type compound seems to be very rare, because the other compounds, $SmVO_3$, $LuVO_3$, $ErVO_3$, and $GdVO_3$, are stoichiometric under the same experimental conditions. It is still not clear whether or not $LaVO_3$ is the only special compound with a nonstoichiometric composition at 1200 °C. Nakamura *et al.*[6] pointed out the stoichiometry of $LaVO_3$ at 1000 °C in the oxygen pressure range from $10^{-12.8}$ to $10^{-21.1}$ bar, but they did not write anything about the composition of $LaVO_3$ at 1200 °C.

There are many two- and three-phase areas in Fig. 2. For example, the area that has the equilibrium oxygen partial pressure, -11.95 in $\log P_{O_2}$, has three phases; R, L, and A_2, that is the most reduced end-member of the solid solution A, and the area that has the compositions surrounded by the three points A_2, A, and La_2O_3, have two phases, $A_{ss}+La_2O_3$, in the oxygen partial pressure range from -11.95 to -0.68 in $\log P_{O_2}$. Here, A_{ss} means the solid solution of Compound A; its composition changes from A_2

TABLE 4. SPACINGS AND RELATIVE INTENSITIES OF COMPOUNDS B AND C

B		C	
d/Å	I/I_o	d/Å	I/I_o
9.596	10	7.629	21
9.017	12	5.700	10
7.658	10	3.8243	10
6.981	10	3.6632	16
4.514	10	3.3457	17
3.765	10	3.2994	67
3.6706	10	3.1935	50
3.3296	80	3.1768	100
3.1931	80	3.1544	52
3.1817	100	3.0717	14
3.0512	16	3.0449	21
2.9833	37	2.8586	17
2.9592	16	2.8256	17
2.8575	37	2.7692	31
2.7551	37	2.0584	19
2.1959	10	2.0059	34
2.1261	15	1.9663	21
2.0151	28	1.9111	10
2.0047	27	1.8554	10
1.9877	18	1.7717	12
1.9527	20		
1.9382	12		
1.9070	16		
1.7838	11		
1.7730	12		
1.7483	14		
1.7438	14		
1.7166	15		
1.7059	16		

to A depending upon the oxygen partial pressure.

As is shown in Fig. 2, the pattern of the present phase diagrm is new and different from the patterns of the other systems[1-4] established previously, because of the difference in the coexisting ternary compounds. That is, there are three compounds, A, B, and C, between La_2O_3 and $LaVO_4$ in this system. However, systems which contain Sm_2O_3,[1] Er_2O_3,[3] and Gd_2O_3[4] have one compound, although the compositions of the compounds are different from one another. On the other hand, three compounds were found in the Lu_2O_3-V_2O_3-V_2O_5 system,[2] though they did not appear between Lu_2O_3 and $LuVO_4$. We have not yet been able to find any rule for the appearance of compounds in the series or reasons why all these systems show different patterns.

The relationship between the composition, N_O/N_X, and the oxygen partial pressure of the solid solution, X, were determined using the thermogravimetric results. Here, N_O/N_X is the mole fraction ratio of oxygen to the component X, indicating the deviation from the component composition. Using the method of the least squares with a linear equation, $N_O/N_X = a \log P_{O_2} + b$, the a and b values for each solid solution were determined to be as shown in Table 2.

In Table 3, the compositions of the compounds, the stability ranges of the compounds in terms of log P_{O_2}, the symbols of the compounds, and the activities of the components in the solid solutions are tabulated. The activity of the components in the solid solutions is calculated with Gibbs-Duhem equations using the N_O/N_X *vs.* log P_{O_2} relations presented above. A detailed method of the calculation has been discussed in the paper of Kimizuka and Katsura.[21]

The assignment of indices for new compounds did not succeed. The data of relative intensities and spacings obtained by means of an X-ray diffractometer with powder samples are shown in Table 4. Because of the sluggish reactions, the samples used in this measurement were made in air by about 146 h heating at 1200 °C with four intermediate grindings in an agate mortar.

The lattice constants of the compounds A, $LaVO_3$ and $LaVO_4$, are tabulated in Table 5. The lattice constants of Sample A were successfully determined with the aid of the assignment of the indices of $4Tm_2O_3 \cdot V_2O_5$.[24]

Differences in the unit-cell dimensions are found in the two $LaVO_3$ samples quenched under different conditions of the oxygen partial pressure. Our values of the samples, made in the atmosphere of −9.45 in log P_{O_2}, are in good agreement with all those of authors previously cited except for one.[7]

As for the cell dimensions of $LaVO_4$, no differences are found in the two quenched samples. Three previous data are shown in Table 5, together with ours.

Calculation of the Standard Gibbs Energies of Reactions. On the basis of the present phase diagram, the standard Gibbs energies of reactions appearing in the system can be calculated by means of this equation; $\Delta G^\circ = -RT \ln K$, where R is the gas constant; T, the absolute temperature, and K, the equilibrium constant of each reaction. The equations of reactions, the equilibrium oxygen partial pressures for each reaction, and the ΔG° values obtained are shown in Table 6. The activities of each component in the solid solutions which are necessary for the calculation are listed in Table 3. The ΔG° value, −128.9 kJ, presented by

Table 5. Unit-cell dimensions of compounds

Compound	$-\log(P_{O_2}/\text{atm})$	a / Å	b / Å	c / Å	β / °	V / Å^3	Ref.
$La_{1.62}V_{0.38}O_{3.38}$	0.68	11.18±0.08	9.12 ±0.07	17.0 ±0.4	99.4±0.8	1709±39	Present
	11.50	11.20±0.08	9.07 ±0.06	16.9 ±0.5	99.2±0.5	1700±49	Present
$LaVO_4$	0.68	7.043±0.008	7.344±0.010	6.694±0.012	104.9±0.1	334.6±0.8	Present
	9.00	7.043±0.007	7.345±0.009	6.694±0.011	104.9±0.1	334.5±0.7	Present
		7.07	7.29	6.77	105		13
		7.03 ±0.03	7.34 ±0.03	6.69 ±0.03	105±0.5		24
		7.047	7.286	6.725	104.85		14
$LaVO_3$	(in H_2)	5.517±0.001		7.852±0.002		242.0±0.1	Present
	9.45	5.545±0.001		7.843±0.002		241.1±0.1	Present
		5.544		7.848			5
		5.547±0.002		7.840±0.003			6
		5.535		7.830		239.9	7
		5.546±0.005		7.827±0.005		240.7±0.1	9

Table 6. Gibbs free energies of reactions

	Reaction	$-\log(P_{O_2}/\text{atm})$	$-\Delta G^\circ$ / kJ
(1)	$31/50\ La_2O_3 + 19/50\ LaVO_3 + 19/100\ O_2 = La_{1.62}V_{0.38}O_{3.38}$	11.95	64.0
(2)	$50/31\ La_{1.62}V_{0.38}O_{3.38} + 12/31\ LaVO_3 + 6/31\ O_2 = La_3VO_7$	10.51	55.8
(3)	$21/50\ La_3VO_7 + 4/25\ LaVO_3 + 2/25\ O_2 = La_{1.42}V_{0.58}O_{3.58}$	9.68	21.6
(4)	$LaVO_3 + 1/2\ O_2 = LaVO_4$	9.35	131.5

Nakamura *et al.*[6] for reaction (4) is in fairly good agreement with ours, −131.5 kJ.

The $LnVO_3+1/2\ O_2=LnVO_4$ reaction is common in all the systems, and the ΔG° values for the reactions related to La, Sm,[1] Gd,[4] Er,[3] and Lu[2] were obtained as −131.5, −127.2, −127.7, −121.0, and −116.3 kJ respectively. Judging from the values obtained, the values seem to increase gradually as the atomic numbers increase from La to Lu, although the values for Sm and Gd are almost the same.

References

1) K. Kitayama and T. Katsura, *Bull. Chem. Soc. Jpn.*, **50**, 889 (1977).
2) K. Kitayama and T. Katsura, *Bull. Chem. Soc. Jpn.*, **51**, 1358 (1978).
3) K. Kitayama, T. Sugihara, and T. Katsura, *Bull. Chem. Soc. Jpn.*, **52**, 458 (1979).
4) K. Kitayama and T. Katsura, *Bull. Chem. Soc. Jpn.*, **55**, 1820 (1982).
5) H. Brusset, R. Mahe, and A. Deboiche, *C. R. Acad. Sci., Ser. C*, **274**, 1293 (1972).
6) T. Nakamura, G. Petzow, and L. J. Gauckler, *Mater. Res. Bull.*, **14**, 649 (1979).
7) G. J. McCarthy, C. A. Sipe, and K. E. McIlvried, *Mater. Res. Bull.*, **9**, 1279 (1974).
8) A. Wold and R. Ward, *J. Am. Chem. Soc.*, **76**, 1029 (1954).
9) V. G. Zubkov, G. V. Bazuev, and G. P. Shveikin, *Kristallografiya*, **25**, 180 (1980).
10) H. Brusset, F. Madaule-Aubry, B. Blanck, J. P. Glaziou, and J. P. Laude, *Can. J. Chem.*, **49**, 3700 (1971).
11) R. C. Ropp and B. Caroll, *J. Inorg. Nucl. Chem.*, **35**, 1135 (1973).
12) H. Brusset, F. Madaule-Aubry, R. Mahe, and C. Boursier, *C. R. Acad. Sci., Ser. C*, **273**, 455 (1971).
13) E. J. Baran and P. J. Aymonio, *Z. Anorg. Allg. Chem.*, **383**, 220 (1971).
14) C. E. Rice and W. R. Robinson, *Acta Crystallogr., Sect. B*, **32**, 2232 (1976).
15) J. A. Baglio and O. J. Sovers, *J. Solid State Chem.*, **3**, 458 (1971).
16) M. K. Carron, M. E. Morse, and K. T. Murata, *Am. Mineral.*, **43**, 985 (1958).
17) T. Katsura, K. Kitayama, T. Sugihara, and N. Kimizuka, *Bull. Chem. Soc. Jpn.*, **48**, 1809 (1975).
18) T. Katsura and H. Hasegawa, *Bull. Chem. Soc. Jpn.*, **40**, 561 (1967).
19) N. Kimizuka and T. Katsura, *J. Solid State Chem.*, **13**, 176 (1975).
20) T. Katsura and A. Muan, *Trans. AIME*, **230**, 77 (1964).
21) N. Kimizuka and T. Katsura, *J. Solid State Chem.*, **15**, 151 (1975).
22) N. Kimizuka and T. Katsura, *Bull. Chem. Soc. Jpn.*, **47**, 1801 (1974).
23) S. S. Kiparisov, R. A. Belyaev, V. V. Bondarenko, and V. P. Vyskubov, *Izv. Akad. Nauk SSSR, Neorg. Mater.*, **9**, 68 (1973).
24) H. Brusset, R. Mahe, and J. P. Laude, *Bull. Soc. Chim. Fr.*, **1973**, 495.

 © 1983 The Chemical Society of Japan Bull. Chem. Soc. Jpn., 56, 695—699 (1983)

Phase Equilibria in the Nd_2O_3–V_2O_3–V_2O_5 System at 1200 °C

Kenzo KITAYAMA,* Chikaaki MIZOKUCHI,† and Takashi KATSURA

Department of Chemistry, Faculty of Science, Tokyo Institute of Technology, Ookayama, Meguro-ku, Tokyo 152

(Received July 8, 1982)

Phase equilibria in the Nd_2O_3–V_2O_3–V_2O_5 system were established at 1200 °C by changing the oxygen partial pressures from −0.68 (air) to −12.50 in terms of log P_{O_2}. In this system, V_nO_{2n-1} (n=2—7), VO_2, Nd_2O_3, $NdVO_3$, $NdVO_4$, $0.81Nd_2O_3 \cdot 0.19V_2O_5$ ($Nd_{1.62}V_{0.38}O_{3.38}$, A), and $3Nd_2O_3 \cdot V_2O_5$ (Nd_3VO_7, B) were stable under the present experimental conditions. Compounds with Nd_2O_3/V_2O_5 mole ratios of 6/1 and 2/1 were not found under the present experimental conditions. Compounds A, Nd_3VO_7, $NdVO_3$, and $NdVO_4$ have nonstoichiometric compositions. The pattern of the phase diagram is different from those of other Ln_2O_3–V_2O_3–V_2O_5 systems that have previously been established by us. On the basis of the phase diagram, the Gibbs energies of the reactions:

(1) $31/50\ Nd_2O_3 + 19/50\ NdVO_3 + 19/100\ O_2 = Nd_{1.62}V_{0.38}O_{3.38}$

(2) $50/31\ Nd_{1.62}V_{0.38}O_{3.38} + 12/31\ NdVO_3 + 6/31\ O_2 = Nd_3VO_7$

(3) $NdVO_3 + 1/2\ O_2 = NdVO_4$

were determined to be −61.4, −47.4, and −128.9 kJ respectively. In the Nd_2O_3–V_2O_3 system, only $NdVO_3$ is stable under the present experimental conditions.

Phase equilibria in the Ln_2O_3–V_2O_3–V_2O_5 systems (Ln=Sm, Lu, Er, Gd, and La) at 1200 °C have been established.[1-5] In these systems, vanadium oxides V_nO_{2n-1} (n=2—7) and lanthanoid vanadium oxides, $LnVO_3$ and $LnVO_4$, were found to be stable in all systems. In addition to the above vanadium oxides and lanthanoid vanadium oxides, in Sm_2O_3–V_2O_3–V_2O_5 system, $Sm_{10}V_2O_{20}$ ($5Sm_2O_3 \cdot V_2O_5$); in the Lu_2O_3–V_2O_3–V_2O_5 system, $Lu_7V_3O_{16}$, $Lu_2V_2O_7$, and LuV_4O_8; in the Er_2O_3–V_2O_3–V_2O_5 system, $Er_8V_2O_{17}$ ($4Er_2O_3 \cdot V_2O_5$); in the Gd_2O_3–V_2O_3–V_2O_5 system, $Gd_{1.62}V_{0.38}O_{3.38}$ ($0.81Gd_2O_3 \cdot 0.19V_2O_5$), and in the La_2O_3–V_2O_3–V_2O_5 system, $La_{1.62}V_{0.38}O_{3.38}$($0.81La_2O_3 \cdot 0.19V_2O_5$), La_3VO_7 ($3La_2O_3 \cdot V_2O_5$), and $La_{1.42}V_{0.58}O_{3.58}$ ($0.71La_2O_3 \cdot 0.29V_2O_5$) have now been found to be stable under the same experimental conditions as the ternary compounds.

These phase diagrams, therefore, have shown different patterns as a result of the difference in coexisting compounds.

In the present study, Nd_2O_3 was chosen as the Ln_2O_3 because Nd_2O_3–$NdVO_4$ system has compounds with Nd_2O_3/V_2O_5 mole ratios of 6/1, 4/1, and 2/1; thus, we could expect a new type of phase diagram under the same experimental conditions.

Brusset *et al.*[6] studied the Nd_2O_3–V_2O_5 system in the temperature range from 600 to 1500 °C in air; they found two compounds, $4Nd_2O_3 \cdot V_2O_5$ and $6Nd_2O_3 \cdot V_2O_5$, besides $NdVO_4$, which is well known. Remizov *et al.*[7] also studied the same system from 645 to 1560 °C and found another two compounds, $2Nd_2O_3 \cdot V_2O_5$ and $Nd_2O_3 \cdot 2V_2O_5$. X-ray powder patterns in a simple form were shown for each compounds by both groups. The lattice constants for $NdVO_4$ have been determined by many researchers.[8-10]

In the Nd_2O_3–V_2O_3 system, only $NdVO_3$ was found; its crystallographic properties have been investigated by many researchers,[11-12] but the system has not been completely studied yet because of the instability of V_2O_3 in air.

The objectives of the present study are; (1) to make a detailed phase diagram of the Nd_2O_3–V_2O_3–V_2O_5 system at 1200 °C in order to establish the stable compounds under the present experimental conditions, (2) to calculate Gibbs energies of the reactions found in the established phase diagram, and (3) to ascertain whether or not there exists a linear relationship between the Gibbs energies of reactions and the ionic radius of the lanthanoid, as was found in the Ln–Fe–O system.[18]

Experimental

Analytical grades of Nd_2O_3 (99.9%) and V_2O_5, made by heating guaranteed-grade NH_4VO_3 at 500 °C in air for about 24 h, have been used as the starting materials. Desired Nd_2O_3/V_2O_5 ratios of the samples were obtained by mixing the appropriate quantities thoroughly in an agate mortar under ethyl alcohol. The mixtures thus obtained were treated by the procedures described in a previous report.[1] The apparatus and procedures for controlling the oxygen partial pressures and keeping a constant temperature, the method of thermogravimetry, the criterion for an equilibrium establishment, the method of actual oxygen-partial-pressure measurement, and the method of chemical analysis are the same as those reported in previous papers.[1,13-17]

The oxygen partial pressure of $10^{-12.50}$ was chosen as the reference oxygen partial pressure; that is, the weight of a sample in the atmosphere of $10^{-12.50}$ oxygen partial pressure was chosen as the reference weight throughout the present study.

Results and Discussion

Phase Equilibria. Nd_2O_3 is stable under the present experimental conditions.[18] Nine samples with Nd_2O_3/V_2O_5 mole ratios of 86/14, 80/20, 78/22, 70/30, 65/35, 60/40, 1, 25/75, and 10/90 were prepared to be used in the thermogravimetric experiment. The thermogravimetric results of the five samples with the mole ratios of 86/14, 80/20, 65/35, 1, and 10/90 are shown in Fig. 1 as representative. In Fig. 1 the ordinate is the oxygen partial pressure in log P_{O_2}, while the abscissa is the composition of the samples represented by W_{O_2}/W_T, where W_{O_2} is the weight gain of

† Present address: Hitachi Device Engineering Co. Ltd. 3350-2 Hayano, Mobara, Chiba 297.

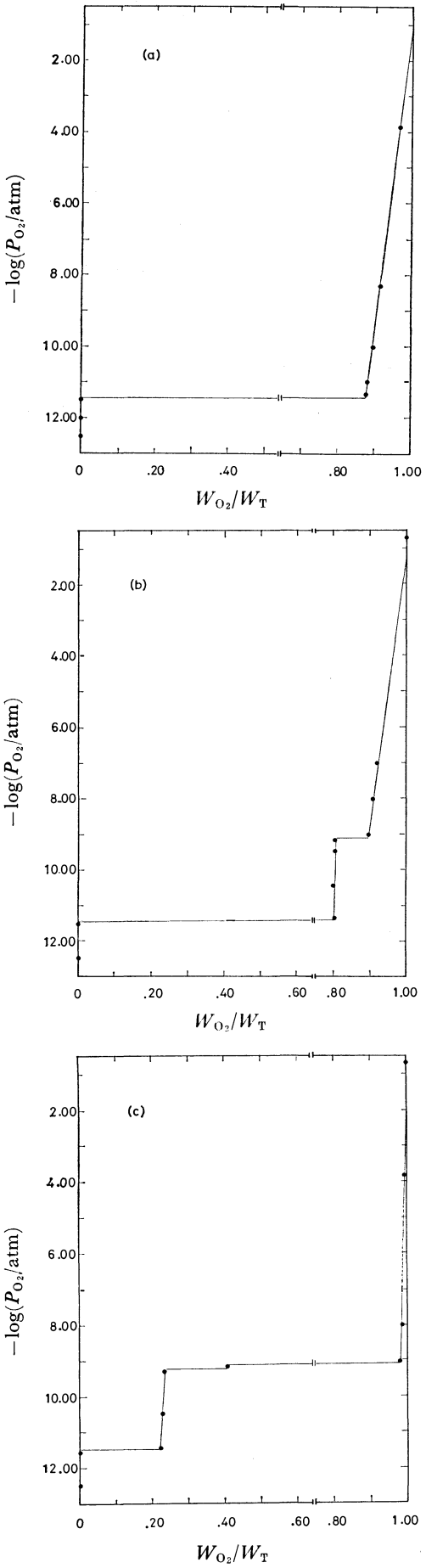

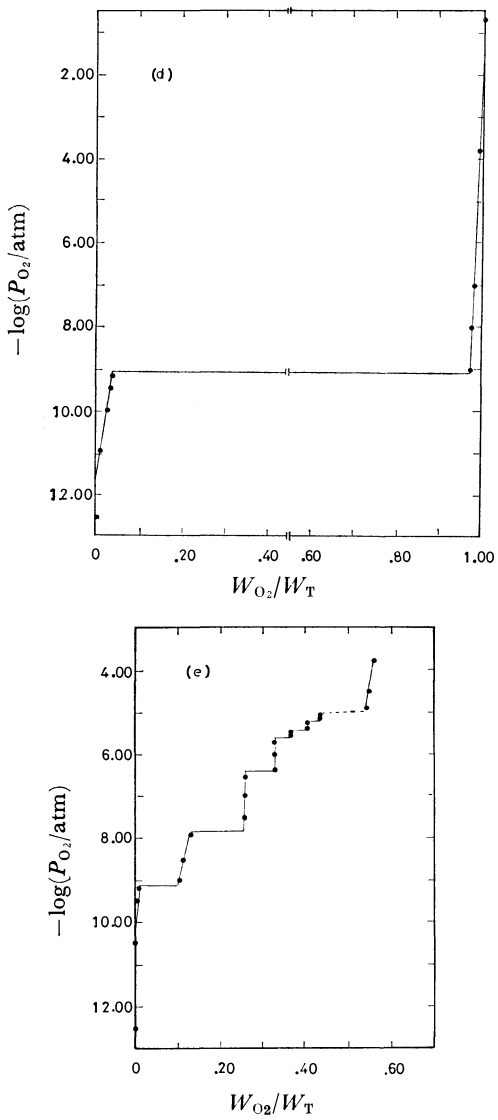

Fig. 1. The relationship between the oxygen partial pressure in $-\log P_{O_2}$ and the weight change of the samples in W_{O_2}/W_T, where W_{O_2} is the weight gain of the samples from the reference weight at $-\log P_{O_2}=12.50$ and W_T is the total weight gain that the samples would get if V_2O_3 in the samples had changed to V_2O_5.
(a): $Nd_2O_3/V_2O_5=86/14$, (b): $Nd_2O_3/V_2O_5=80/20$, (c): $Nd_2O_3/V_2O_5=65/35$, (d): $Nd_2O_3/V_2O_5=1$, (e): $Nd_2O_3/V_2O_5=10/90$.

the samples from the reference weight at $\log P_{O_2}=-12.50$, and where W_T is the total weight gain that the samples would get if V_2O_3 in the samples had been changed to V_2O_5.

As is shown in Figs. 1a to 1d, sudden weight changes occurred at 3 oxygen partial pressures, -11.45, -9.23, and -9.10, in $\log P_{O_2}$ in samples with Nd_2O_3/V_2O_5 mole ratios equal to unity and larger than unity. These figures correspond to the equilibrium oxygen partial pressures of reactions in the system shown in Table 5.

As is shown in Fig. 1c, the range of oxygen partial pressure in which $NdVO_3$ and Nd_3VO_7 coexist is very

Table 1. Identification of phases in quenched samples

Nd_2O_3 (mol%)	V_2O_5	$-\log(P_{O_2}/atm)$	Time / h	Phases[a)]
86	14	12.00	24	$Nd_2O_3+NdVO_3$
		10.00	24	Nd_2O_3+A
		9.00	28	Nd_2O_3+A
		0.68	30	Nd_2O_3+A
78	22	9.00	24	A+B
		0.68	24	A+B
70	30	12.00	24	$Nd_2O_3+NdVO_3$
		10.00	24	$A+NdVO_3$
		9.15	56	$B+NdVO_3$
		9.00	28	$B+NdVO_4$
		0.68	48	$B+NdVO_4$
60	40	12.00	24	$Nd_2O_3+NdVO_3$
		10.00	24	$A+NdVO_3$
		9.15	32	$B+NdVO_3$
		9.00	28	$B+NdVO_4$
		0.68	48	$B+NdVO_4$
25	75	11.00	8	$V_2O_3+NdVO_3$
		9.50	29	$V_2O_3+NdVO_3$
		8.50	25	$V_2O_3+NdVO_4$
		7.00	24	$V_3O_5+NdVO_4$
		6.00	43	$V_4O_7+NdVO_4$
		5.45	56	$V_5O_9+NdVO_4$
		5.25	50	$V_6O_{11}+NdVO_4$
		5.05	48	$V_7O_{13}+NdVO_4$
		4.50	40	VO_2+NdVO_4
10	90	11.00	8	$V_2O_3+NdVO_3$
		9.50	29	$V_2O_3+NdVO_3$
		8.50	25	$V_2O_3+NdVO_4$
		7.00	24	$V_3O_5+NdVO_4$
		6.00	43	$V_4O_7+NdVO_4$
		5.45	56	$V_5O_9+NdVO_4$
		5.25	50	$V_6O_{11}+NdVO_4$
		5.05	48	$V_7O_{13}+NdVO_4$
		4.50	40	VO_2+NVO_4

a) A: $Nd_{1.62}V_{0.38}O_{3.38}$, B: Nd_3VO_7.

narrow. This range is, indeed, too small for us to find Nd_3VO_7 in the early period of the thermogravimetric experiment. Throughout the experiment aimed at the identification of phases in the quenched samples, Compound Nd_3VO_7 was found as an unexpected phase.

As is shown in Fig. 1e, samples with mole ratios lower than unity showed patterns similar to those of the other systems[1,3–5] except for the oxygen partial pressure of $\log P_{O_2}=-9.10$, which correspond to the equilibrium oxygen partial pressure of the $NdVO_3+1/2\ O_2=NdVO_4$ reaction.

In Table 1, the results of the identification of phases are shown. In the first column is the composition of the starting materials in mol%; in the second, the experimental conditions of the oxygen partial pressure in terms of $\log P_{O_2}$; in the third, the experimental duration in hours, and in the last, phases that are found in the quenched samples by means of an X-ray powder diffractometer using Cu $K\alpha$ radiation. The

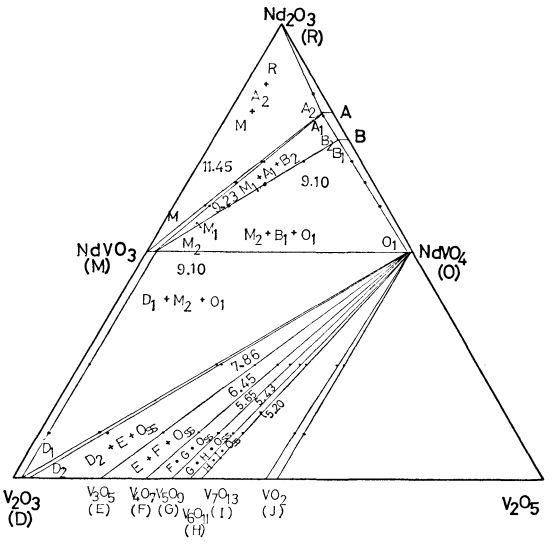

Fig. 2. Phase equilibria in the Nd_2O_3–V_2O_3–V_2O_5 system at 1200 °C. Numerical values in the three solid phases regions are the oxygen partial pressures in $-\log P_{O_2}$ in equilibrium. Abbreviations are the same as those in Tables 1 and 3. ss means the solid solution.

letters in the phases are abbreviations of the compounds shown in the lower part of the table. The abbreviations are the same as those of the other tables and figures in the present report.

Based upon the above experimental results, a phase diagram of the system at 1200 °C is shown in Fig. 2. The following phases are stable under the present experimental conditions, except for compounds in the V_2O_3–V_2O_5 system, $NdVO_3$, $NdVO_4$, and Nd_2O_3. The phases are: $Nd_{1.62}V_{0.38}O_{3.38}$ ($0.81Nd_2O_3\cdot 0.19V_2O_5$, A) and Nd_3VO_7 ($3Nd_2O_3\cdot V_2O_5$, B). Compounds with Nd_2O_3/V_2O_5 mole ratios of 6/1 and 2/1 were not found under the present experimental conditions. Compound A might have the composition, $4Nd_2O_3\cdot V_2O_5$, that Brusset *et al.*[6] and Remizov *et al.*[7] reported. However, under the present experimental conditions it has no round number of the mole ratio. The straight line drawn in Fig. 2 by plotting the experimental points is used to concentrate to the composition described above, even considering the experimental errors.

There are two possible explanations of why the deviation from the round number of the mole ratio occurred; one is the nonstoichiometry of the compound

Table 2. The relationship between the oxygen partial pressure and the composition of the solid solutions

N_O/N_X indicates the mole fraction ratio of oxygen to component X.

X	a	b
$Nd_{1.62}V_{0.38}O_{3.38}$	4.73×10^{-3}	4.16×10^{-3}
Nd_3VO_7	4.76×10^{-3}	8.10×10^{-3}
$NdVO_4$	2.67×10^{-3}	2.30×10^{-3}
$NdVO_3$	1.60×10^{-2}	0.183

$N_O/N_X=a\log P_{O_2}+b$.

TABLE 3. COMPOSITIONS, SYMBOLS, STABILITY RANGES IN OXYGEN PARTIAL PRESSURES, AND ACTIVITIES IN SOLID SOLUTIONS

Component	Composition	Symbol	$-\log(P_{O_2}/\text{atm})$	$\log a_i$
$Nd_{1.62}V_{0.38}O_{3.38}$	$Nd_{1.62}V_{0.38}O_{3.38}$	A	0.88[a]—0.68	0.132
$Nd_{1.62}V_{0.38}O_{3.88}$	$Nd_{1.62}V_{0.38}O_{3.34}$	A_1	9.23	0.0705
	$Nd_{1.62}V_{0.38}O_{3.33}$	A_2	11.45	0
Nd_3VO_7	$Nd_3VO_{7.00}$	B	1.70[a]—0.68	0.0674
	$Nd_3VO_{6.96}$	B_1	9.10	0.0023
	$Nd_3VO_{6.95}$	B_2	9.23	0
$NdVO_4$	$NdVO_{4.00}$	C	0.86[a]—0.68	0.0453
	$NdVO_{3.98}$	C_1	9.10	0
$NdVO_3$	$NdVO_{3.00}$	M	11.45[a]—12.50	0
	$NdVO_{3.035}$	M_1	9.23	−0.0203
	$NdVO_{3.037}$	M_2	9.10	−0.0221

a) These values were obtained by extrapolations using the experimental values.

toward the Nd_2O_3 side, and the other is experimental errors in the thermogravimetry. However, as shown in Fig. 1b, in which the results for $Nd_2O_3/V_2O_5=4/1$ are shown, a sudden change in the weight occurred at the oxygen partial pressure, −9.23 in $\log P_{O_2}$. Besides, this result has a good reproducibility. If the composition of Compound A was 4/1 in the Nd_2O_3/V_2O_5 mole ratio, such a weight change would not occur and there were be the same pattern as in Fig. 1a. Some might point out a systematic shift in the experimental points. To answer this, it is enough to show the existence of $3Nd_2O_3\cdot V_2O_5$. As has been described above, a compound with the same composition of A was found in the systems of both Gd and La.

A compound with a Ln_2O_3/V_2O_5 mole ratio of 3/1 was also found in the systems of La_2O_3,[5] Eu_2O_3,[19] and Sm_2O_3.[7]

Ternary compounds, A, Nd_3VO_7, $NdVO_3$, and $NdVO_4$ have nonstoichiometric compositions. The nonstoichiometry of the $LnVO_3$-type compound seems to be very rare. In this series, only $LaVO_3$[5] had a nonstoichiometric composition like $NdVO_3$. Judging from these two instances, the ionic radius seems to be effective. As is well known, La and Nd have ionic radii rather larger than the others in the lanthanoid series, although the crystal structure of $LaVO_3$ is different from that of $NdVO_3$. On the other hand, $SmVO_3$ is stoichiometric.[1]

There are many two-and three-phase areas in Fig. 2. For example, the area that has the equilibrium oxygen partial pressure of −9.10 in $\log P_{O_2}$ has three phases, B_1, M_2, and O_1; here, B_1 has the composition of the B solid solution at $\log P_{O_2}=-9.10$ and M_2 is the most oxidized end member of the solid solution M, while, on the other hand, O_1 is the most reduced end member of the solid solution O. The square area that is surrounded by points, B, B_1, O_1, and O, is a two-phase area, $B_{ss}+O_{ss}$, where ss indicates the solid solution.

As is shown in Fig. 2, the pattern of the present phase diagram is of a new type and is different from those of the previously reported systems because of the difference in the coexisting ternary compounds.

The relationship between the composition, N_O/N_X, and the oxygen partial pressure of the solid solution, X, were determined using the thermogravimetric results. Here, N_O/N_X is the mole fraction ratio of oxygen to a component X at a certain oxygen partial pressure; it indicates the deviation from the component composition. Using the method of the least squares with a linear equation, $N_O/N_X=a\log P_{O_2}+b$, the constants, a and b, for each solid solution were determined; they are shown in Table 2.

TABLE 4. COMPARISON OF SPACINGS AND RELATIVE INTENSITIES OF Nd_3VO_7 WITH THOSE OF La_3VO_7 AND $3Eu_2O_3\cdot V_2O_5$

Nd_3VO_7		La_3VO_7		$3Eu_2O_3\cdot V_2O_5$				
d/Å	I/I_o	d/Å	I/I_o	d/Å	I/I_o	h	k	l
3.266	88	3.330	80					
3.144	80	3.193	80	3.11	60	1	1	1
3.111	100	3.182	100	2.70	100	0	0	2
		3.051	16	1.93	30	2	2	0
2.919	35	2.983	37	1.799	30	0	0	3
		2.959	16	1.727	15	1	0	3
2.788	36	2.858	37	1.622	25	1	1	3
2.709	47	2.755	37					
		2.126	15					
1.970	37	2.015	28					
		2.005	27					
1.916	28	1.988	18					
1.867	20	1.953	20					

In Table 3, the compositions of the compounds at various oxygen partial pressures, the stability ranges of the compounds in terms of $\log P_{O_2}$, the symbols of the compounds, and the activities of the components in the solid solutions were calculated with Gibbs-Duhem equation using the N_O/N_X *vs.* $\log P_{O_2}$ relations described above. The method of the calculation has been discussed in detail in the paper of Kimizuka and Katsura.[16]

The attempted assignment of Miller indices for new compound was not successful. However, the values of the relative intensities and spacings that were obtained by means of an X-ray diffractometer with powder samples are shown in Table 4, together with $3Eu_2O_3\cdot V_2O_5$[19] and $3La_2O_3\cdot V_2O_5$.[5] The weak peaks

Table 5. Unit-cell dimensions of compounds, together with those in previous reports

Compound	$-\log(P_{O_2}/\text{atm})$	a/Å	b/Å	c/Å	β/°	V/Å^3	Ref.
$NaVO_4$	0.68	7.337±0.001		6.644±0.002		346.8±0.2	
	9.00	7.320±0.005		6.414±0.006		343.6±0.6	
		7.335		6.434			9
		7.3290		6.4355			10
		7.326		6.426			8
$NdVO_3$	12.00	5.443±0.005	5.566±0.003	7.736±0.004		234.4±0.3	
		5.451	5.575	7.740		235.2	11
		5.466	5.569	7.735		235.5	12
A	0.68	10.97±0.04	8.82 ±0.03	16.5±0.2	99.2±0.4	1570±17	
	11.30	10.94±0.04	8.79 ±0.03	16.3±0.2	99.2±0.4	1550±17	

Table 6. Gibbs free energies of reactions

	Reaction	$-\log(P_{O_2}/\text{atm})$	$\frac{-\Delta G^\circ}{\text{kJ}}$
(1)	$\frac{31}{50}Nd_2O_3 + \frac{19}{50}NdVO_3 + \frac{19}{100}O_2 = Nd_{1.62}V_{0.38}O_{3.38}$	11.45±0.07	61.4
(2)	$\frac{50}{31}Nd_{1.62}V_{0.38}O_{3.38} + \frac{12}{31}NdVO_3 + \frac{6}{31}O_2 = Nd_3VO_7$	9.23±0.03	47.4
(3)	$NdVO_3 + \frac{1}{2}O_2 = NdVO_4$	9.10±0.03	128.9

of Nd_3VO_7 and La_3VO_7 were omitted from the table. The pattern of Nd_3VO_7 is very similar to that of La_3VO_7, though its d-values are a little smaller than those of La_3VO_7, while the pattern of Eu_3VO_7 is different from those of Nd_3VO_7 and La_3VO_7.

The lattice constants of the A, $NdVO_3$ and $NdVO_4$ compounds are tabulated in Table 5. The lattice constants of Compound A were successfully determined with the aid of the assignment of indices of $4Tm_2O_3 \cdot V_2O_5$.[20] It is apparent from the table that the values of the lattice constants of $NdVO_4$ depend upon the oxygen partial pressures, and that those quoted in the table are intermediate in nature. The values of $NdVO_3$ are smaller than those of McCarthy *et al.*[11]

Calculation of Gibbs Energies of Reactions. On the basis of the present phase diagram, the Gibbs energies all of the reactions appearing in the system except those in the V_2O_3–V_2O_5 system can be calculated by means of this equation; $\Delta G^\circ = -RT \ln K$, where R is the gas constant; T, the absolute temperature, and K, the equilibrium constant of each reaction. The equation of the reactions, the equilibrium oxygen partial pressures for each reaction, and the ΔG° values calculated are shown in Table 6. The activities of each component in the solid solutions which are necessary for calculation are listed in Table 3.

References

1) K. Kitayama and T. Katsura, *Bull. Chem. Soc. Jpn.*, **50**, 889 (1977).
2) K. Kitayama and T. Katsura, *Bull. Chem. Soc. Jpn.*, **51**, 1358 (1978).
3) K. Kitayama, T. Sugihara, and T. Katsura, *Bull. Chem. Soc. Jpn.*, **52**, 458 (1979).
4) K. Kitayama and T. Katsura, *Bull. Chem. Soc. Jpn.*, **55**, 1820 (1982).
5) K. Kitayama, D. Zoshima, and T. Katsura, *Bull. Chem. Soc. Jpn.*, **56**, 689 (1983).
6) H. Brusset, F. Madaule-Aubry, B. Blanck, J. P. Glaziou, and J. P. Laude, *Can. J. Chem.*, **49**, 3700 (1971).
7) V. G. Remizov, A. K. Molodkin, V. M. Skorikov, and Yu. E. Bogatov, *Zh. Neorg. Khim.*, **21**, 1323 (1976).
8) V. A. Neumov, *Zh. Struk. Khim.*, **3**, 608 (1962).
9) M. Schwarz, *Z. Anorg. Allg. Chem.*, **323**, 44 (1963).
10) JCPDS, Card No. 15-769.
11) G. J. McCarthy, C. A. Sipe, and K. E. McIlvried, *Mater. Res. Bull.*, **9**, 1279 (1974).
12) T. Shinike, G. Adachi, and G. Shiokawa, *Denki Kagaku*, **48**, 258 (1980).
13) T. Katsura and H. Hasegawa, *Bull. Chem. Soc. Jpn.*, **40**, 561 (1967).
14) N. Kimizuka and T. Katsura, *J. Solid State Chem.*, **13**, 176 (1975).
15) T. Katsura and A. Muan, *Trans. AIME*, **230**, 77 (1964).
16) N. Kimizuka and T. Katsura, *J. Solid State Chem.*, **15**, 151 (1975).
17) N. Kimizuka and T. Katsura, *Bull. Chem. Soc. Jpn.*, **47**, 1801 (1974).
18) T. Katsura, K. Kitayama, T. Sugihara, and N. Kimizuka *Bull. Chem. Soc. Jpn.*, **48**, 1809 (1975).
19) S. S. Kiparisov, R. A. Belyaev, V. V. Bondrarenko, V. P. Vyskubov, *Izv. Akad. Nauk SSSR, Neorg. Mater.*, **9**, 68 (1973).
20) H. Brusset, R. Mahe, and J. P. Laude, *Bull. Soc. Chim. Fr.*, **1973**, 495.

Association of β-Diketones with Trioctylphosphine Oxide in Solvent Extraction Systems

Tatsuya SEKINE,* Takashi SAITOU, and Hiroto IGA
Department of Chemistry, Science University of Tokyo, Kagurazaka, Shinjuku-ku, Tokyo 162
(Received April 6, 1982)

Distribution of six β-diketones between hexane, benzene, carbon tetrachloride, or chloroform and 0.1 mol dm^{-3} aqueous perchlorate solutions has been measured in the presence of trioctylphosphine oxide (TOPO). The distribution ratio was, in many cases, enhanced by TOPO; this was explained in terms of association of the β-diketones and TOPO. The association constants were greater when the β-diketone was stronger as an acid and also in the following order of the diluent: $CHCl_3 < CCl_4 < C_6H_6 < C_6H_{14}$. It was concluded that, even though the effect was not very large, still correction for the decrease in the concentrations of both the β-diketone and TOPO is necessary for an accurate estimation of the equilibrium involved in solvent extraction of metal ions containing these two reagents, as in the synergistic solvent extraction of metal ions.

Synergistic solvent extraction of metal ions with mixtures of one chelating extractant and one solvating-type ligand has been found in several systems. The reason for the enhancement of the chelate extraction by additions of such a neutral ligand has been explained in terms of adduct formation of the metal chelate in the organic phase. The formation constants of such adducts can be calculated statistically from the enhancement of the extraction as a function of the ligand concentration. However, an association of the extractants in the organic phase is also possible and, in such a case, they should be taken into the account in order to analyse the extraction data.

In the present paper, the distribution of six β-diketones has been measured in several solvent extration systems as a function of trioctylphosphine oxide (TOPO) concentration in the organic phase. Four inert organic solvents were used as diluents of the reagents. The association equilibria of β-diketones and TOPO in the systems were determined from the distribution data. The effects of the chemical properties of the β-diketones and the diluents on the equilibria are discussed.

Experimental

The β-diketones studied are listed in Table 1 with their abbreviated nomenclatures. The β-diketones and TOPO were supplied by Dojindo & Co., Kumamoto. The organic diluents, sodium perchlorate, and perchloric acid were of analytical grade. Chloroform was washed three times with water before use.

Experiments were carried out in a thermostated room at 298 K. Stock β-diketone solutions were prepared by dissolving weighed amounts of each reagent into each diluent. The concentration of the β-diketone in the stock solutions of TFA and HFA was further checked by titration with a standard sodium hydroxide solution. A TOPO stock solution was also prepared in the same manner, and it was washed several times with water. Mixed solutions containing a β-diketone and TOPO at various concentrations were prepared from these stock solutions.

A portion of an organic solvent containing a β-diketone and TOPO and the same volume of an aqueous solution containing 0.010 mol dm^{-3} perchloric acid and 0.090 mol dm^{-3} sodium perchlorate were placed in a stoppered glass tube, agitated by a mechanical shaker, and centrifuged off. The aqueous phase of the experiments with BZA, BFA, or TTA was transferred into another tube and agitated with a portion of the same diluent containing no TOPO. The amount of the β-diketone thus extracted into the organic phase was determined from the optical absorption at 323(BFA in C_6H_{14}), 330(BFA in C_6H_6), 325(BFA in CCl_4), 305(BZA in C_6H_{14}), 310(BZA in C_6H_6), 307(BZA in CCl_4), 315(TTA in C_6H_{14}), 324(TTA in C_6H_6), and 319(TTA in CCl_4) nm, respectively. In the experiments with AA, TFA, and HFA, the amount in the aqueous phase was obtained by direct measurements of its UV absorption at 273, 280, and 305 nm, respectively, because their recovery in the organic phase was not quantitative by only a single extraction. The distribution ratio was calculated from the β-diketone concentration in the aqueous phase at equilibrium and from that in the initial organic phase.

Statistical

The β-diketones hereafter are represented by HA, and TOPO by L. The chemical species in the organic phase are denoted by a subscript "org", and those in the aqueous phase are given without any subscript.

The β-diketones (which are weak acids) in the aqueous phase may be both in the HA and A^- form, while those in the organic phase may be in the undissociated form HA as well as in the associated form with TOPO, HAL_n. Since n was found to be one or two in the present study and no species containing more than one HA was found, the distribution ratio of HA can generally be written as:

$$D = ([HA]_{org} + [HAL]_{org} + [HAL_2]_{org})/([HA] + [A^-]). \quad (1)$$

The dissociation constant and the two-phase distribution constant of the acid can be written as:

$$K_a = [H^+][A^-][HA]^{-1} \quad (2)$$

$$K_d = [HA]_{org}[HA]^{-1}, \quad (3)$$

and the distribution constant of the neutral ligand is:

$$K_d(L) = [L]_{org}[L]^{-1}. \quad (3')$$

The association equilibria of HA and L may be represented by:

$$\left.\begin{aligned} &HA_{(org)} + L_{(org)} \rightleftharpoons HAL_{(org)} \\ &\beta_{1(org)} = [HAL]_{org}[HA]_{org}^{-1}[L]_{org}^{-1} \end{aligned}\right\} \quad (4)$$

$$\left.\begin{aligned} &HA_{(org)} + 2L_{(org)} \rightleftharpoons HAL_{2(org)} \\ &\beta_{2(org)} = [HAL_2]_{org}[HA]_{org}^{-1}[L]_{org}^{-2} \end{aligned}\right\}. \quad (5)$$

In the absence and presence of L, the distribution ratio may be written as:

$$D_0 = [HA]_{org}/([HA]+[A^-]) = K_d/(1+K_a[H^+]^{-1}) \quad (6)$$

$$D = K_d(1+\beta_{1(org)}[L]_{org}+\beta_{2(org)}[L]_{org}^2)/(1+K_a[H^+]^{-1}). \quad (7)$$

When D in Eq. 7 is obtained at a certain $[H^+]$, D_0 at the same $[H^+]$ can be calculated by using the values of K_a and K_d; then the following equation can be written:

$$D/D_0 = 1 + \beta_{1(org)}[L]_{org} + \beta_{2(org)}[L]_{org}^2. \quad (8)$$

Both perchloric acid and sodium perchlorate are extractable with TOPO, but the extraction of the latter is negligible under the conditions of the present study, as can be calculated from the equilibrium constant:

$$K_{ex}(NaClO_4) = [NaL_3^+ClO_4^-]_{org}[Na^+]^{-1}[ClO_4]^{-1}[L]_{org}^{-3}. \quad (9)$$

When the solvent is hexane and when the total concentration of the salt is 1 mol dm^{-3}, this value of K_{ex} ($NaClO_4$) is $10^{1.01}$ and thus $[NaL_3^+ClO_4^-]_{org}$ should be less than 1×10^{-4} mol dm^{-3} when both $[Na^+]$ and $[ClO_4^-]$ are 0.1 mol dm^{-3} and $[L]_{org}$ is lower than 0.1 mol dm^{-3}.[1] When the salt concentration is 0.1 mol dm^{-3}, as in the present study, this value of the organic concentration of sodium perchlorate solvated with TOPO should be even lower.

The extraction equilibrium of perchloric acid is:[2]

$$\left.\begin{aligned} &H^+ + ClO_4^- + 2L_{(org)} \rightleftharpoons HClO_4L_{2(org)} \\ &K_{ex}(HClO_4) = [HClO_4L_2]_{org}[H^+]^{-1}[ClO_4^-]^{-1}[L]_{org}^{-2} \end{aligned}\right\}. \quad (10)$$

Since the volumes of both phases were always the same and the concentration of TOPO in the aqueous phase was very small, as is seen from the values of K_d(L) in Table 1, the following equations can be written:

$$\begin{aligned} &[L]_{org,init} \\ &= [L]_{org} + [HAL]_{org} + 2[HAL_2]_{org} + 2[HClO_4L_2]_{org} \\ &= [L]_{org}(1+\beta_{1(org)}[HA]_{org}) + 2[L]_{org}^2(\beta_{2(org)}[HA]_{org} \\ &\quad + K_{ex}(HClO_4)[H^+][ClO_4^-]) \end{aligned} \quad (11)$$

$$\begin{aligned} &[HA]_{org,init} \\ &= [HA]_{org} + [HAL]_{org} + [HAL_2]_{org} + [HA] + [A^-]. \end{aligned} \quad (12)$$

From the total concentration of the β-diketone in the equilibrated aqueous phase, the following equation can be obtained:

$$[HA]_{org} = K_d([HA]+[A^-])(1+K_a[H^+]^{-1})^{-1}. \quad (13)$$

Among the terms in Eqs. 10 to 12, the value of [HA] can be determined experimentally, $[HA]_{org}$ can be calculated as above, the constant $K_{ex}(HClO_4)$ can be determined by separate experiments in the absence of HA, while $[H^+]$ and $[ClO_4^-]$ may be determined experimentally. Then $\beta_{1(org)}$ and $\beta_{2(org)}$ can be determined with a succesive approximation approach by using a least squares computer program. The calculated value of $[L]_{org}$ at equilibrium can also be obtained when the best-fit values of these constants are computed in this way. The change in the distribution ratio of HA may be given by D/D_0 (*cf.* Eqs. 6 to 8) and the experimental data may be presented in a figure on the basis of Eq. 8.

When the diluent was hexane or carbon tetrachloride and the TOPO concentration was high, the extraction of perchloric acid was somewhat different from that expected from Eq. 10. This deviation could be explained by assuming extractions of trisolvate of the acid, more precise calculation should be possible by introducing these results into Eq. 11. However, since values of the constants in Eqs. 4 and 5 obtained after this correction were not very much different from those obtained by making no correction, all the calculations were made as follows. The data in these diluents were treated on the basis of the following equation:

$$\begin{aligned} &[L]_{org,init} - 2[HClO_4]_{org,obsd} \\ &\quad = [L]_{org} + [HAL]_{org} + 2[HAL_2]_{org}, \end{aligned} \quad (14)$$

where $[HClO_4]_{org,obsd}$ is the concentration of the extracted acid experimentally obtained by titration of the two phases in the absence of HA. Thus the error of the association constants in hexane and cabon tetrachloride could be a little larger than those in the other diluents.

The enhancement of the extraction of a β-diketone by an addition of TOPO can also be considered as an extraction of the β-diketone with TOPO. These extraction equilibria can be written as:

$$\left.\begin{aligned} &HA + L_{(org)} \rightleftharpoons HAL_{(org)} \\ &K_{ex1} = [HAL]_{org}[HA]^{-1}[L]_{org}^{-1} \end{aligned}\right\} \quad (15)$$

$$\left.\begin{aligned} &HA + 2L_{(org)} \rightleftharpoons HAL_{2(org)} \\ &K_{ex2} = [HAL_2]_{org}[HA]^{-1}[L]_{org}^{-2} \end{aligned}\right\}. \quad (16)$$

By introducing Eq. 3, Eqs. 15 and 16 can be rewritten as:

$$K_{ex1} = \beta_{1(org)} \times K_d \quad (17)$$

$$K_{ex2} = \beta_{2(org)} \times K_d. \quad (18)$$

Results and Discussion

The extractions of perchloric acid in 0.1 mol dm^{-3} (Na,H)ClO_4 ionic media with TOPO in the diluents were determined in the manner previously reported.[2] The extraction constants of the acid calculated from the present data are listed in Table 1.

The distribution data of each β-diketone in the four liquid-liquid systems were obtained as a function of $[HA]_{org,init}$, $[L]_{org,init}$, and $[H^+]$.

Figure 1 gives the increase in the distribution ratio as a function of the free TOPO concentration, computed in the way described in the preceding section. The solid curves are the calculated values obtained by introducing the association constants into Eq. 8. Each of the curves has two asymptotes. One of them has a slop zero and the other has a slop +1 or +2. This corresponds to the highest complex in the system, HAL or HAL_2. Since the calculated curves fit well with the experimental data, the constants in

TABLE 1. REAGENTS STUDIED

Abbreviated notation	Name	pK_a[a]	log K_d[b]				Remarks
			C_6H_{14}	C_6H_6	CCl_4	$CHCl_3$	
AA	Acetylacetone	8.67	−0.05	0.70	0.51	1.36	(1)
BZA	Benzoylacetone	8.39	2.30	3.02	2.81	3.64	(2)
TFA	Trifluoroacetylacetone	6.13	−0.54	0.04	−0.22	0.27	(3)
BFA	Benzoyltrifluoroacetone	6.03	1.75	2.61	2.39	2.84	(4)
TTA	2-Thenoyltrifluoroacetone	6.33	0.75	1.61	1.32	1.85	(5)
HFA	Hexafluoroacetylacetone	4.46	−2.04	−1.91	−1.92	−1.75	(6)
TOPO	Trioctylphosphine oxide	—	3.83	4.78	5.24	5.51	(7)

(1): 2,4-Pentanedione, (2): 1-phenyl-1,3-butanedione, (3): 1,1,1-trifluoro-2,4-pentanedione, (4): 4,4,4-trifluoro-1-phenyl-1,3-butanedione, (5): 4,4,4-trifluoro-1-(2-thienyl)-1,3-butanedione, (6): 1,1,1,5,5,5-hexafluoro-2,4-pentanedione, (7): log K_d of TOPO taken from Ref. 15. a) Taken from Ref. 14 when aqueous phase is 0.1 mol dm^{-3} $NaClO_4$. (b) log K_d of β-diketones taken from Ref. 14. log K_d of TOPO taken from Ref. 15 when aqueous phase is 0.1 mol dm^{-3} $NaClO_4$.

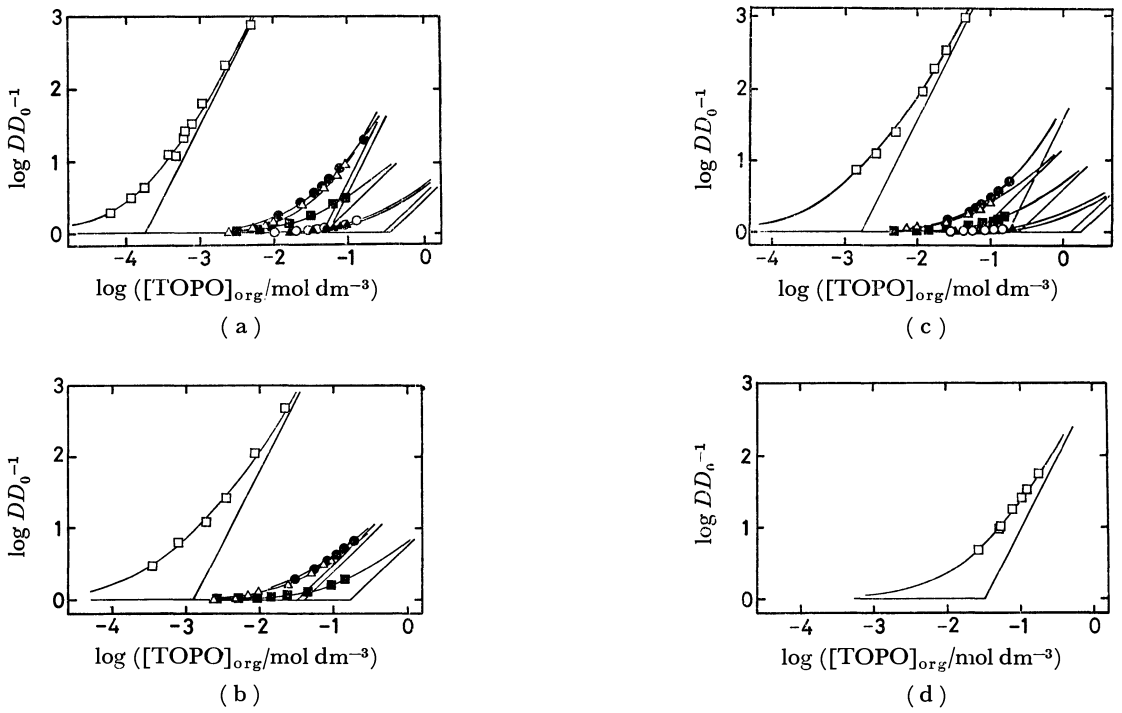

Fig. 1. Enhancement of distribution ratio as a function of calculated TOPO concentrations at equilibrium. The diluents are (a) C_6H_{14}, (b) C_6H_6, (c) CCl_4, and (d) $CHCl_3$. The β-diketones are AA(▲), BZA(○), TFA(●), BFA(■), TTA(△), and HFA(□). The curves are calculated by introducing the constants in Table 2 into Eq. 8. The straight lines are the asymptotes for the curves. Initial concentrations of the β-diketones (mol dm^{-3}) are as follows (The nomenclatures see Table 1).
(a): 1.0×10^{-4}(AA), 2.0×10^{-3}(BZA), 2.0×10^{-3} (TFA), 1.7×10^{-2} (BFA), 2.5×10^{-4}(TTA), and 2.0×10^{-2} (HFA), (b): 2.0×10^{-3}(TFA), 5.0×10^{-3}(TFA), 1.5×10^{-3}(TTA), and 2.0×10^{-2}(HFA), (c): 5.0×10^{-3}(AA), 2.0×10^{-2}(BZA), 2.0×10^{-3}(TFA), 5.0×10^{-3}(BFA), 7.5×10^{-4}(TTA), and 2.0×10^{-2}(HFA), (d): 2.0×10^{-2} (HFA).

Table 1 are reasonable.

The values of the equilibrium constants in Tables 1 and 2 may be summarized as follows.

(i) The distribution constants of TOPO are greater in the following order of the diluent: hexane<benzene<carbon tetrachloride<chloroform, while those of the β-diketones are greater in the order of hexane< carbon tetrachloride<benzene<chloroform.

(ii) The association constants between a certain β-diketone and TOPO are affected by diluent; it is greater in the order of chloroform<carbon tetrachloride<benzene<hexane, although the association constants of acetylacetone and benzoylacetone in benzene could not be determined in the range of the experimental error. This means that the tendency of the association is, in general, greater when the solvent-solute interactions are weaker. The order of $\beta_{n(org)}$ in the diluent, carbon tetrachloride<benzene, should indicate that the difference in the solvent-solute interactions of the β-diketones has a greater effect on

Table 2. Summary of equilibrium constants

		Diluents			
		C_6H_{14}	C_6H_6	CCl_4	$CHCl_3$
AA	$\log \beta_{1(org)}$	0.65	—[b]	−0.4	nil
	$\log K_{ex1}$	0.64	—[b]	0.12	nil
BZA	$\log \beta_{1(org)}$	0.62	—[b]	−0.3	nil
	$\log K_{ex1}$	2.65	—[b]	2.55	nil
TFA	$\log \beta_{1(org)}$	1.84	1.43	1.20	nil
	$\log \beta_{2(org)}$	2.40	nil	1.63	nil
	$\log K_{ex1}$	1.30	1.47	0.98	nil
	$\log K_{ex2}$	1.86	nil	1.41	nil
BFA	$\log \beta_{1(org)}$	1.37	0.83	0.59	nil
	$\log K_{ex1}$	3.12	3.44	2.98	nil
TTA	$\log \beta_{1(org)}$	1.62	1.46	1.18	nil
	$\log \beta_{2(org)}$	2.72	nil	nil	nil
	$\log K_{ex1}$	2.37	3.07	2.50	nil
	$\log K_{ex2}$	3.43	nil	nil	nil
HFA	$\log \beta_{1(org)}$	4.22	3.73	3.55	2.09
	$\log \beta_{2(org)}$	7.51	5.78	5.57	2.80
	$\log K_{ex1}$	2.18	1.82	1.63	0.34
	$\log K_{ex2}$	5.47	3.87	3.65	1.05
TOPO	$\log K_{ex}(HClO_4)$[a]	2.97	2.74	1.51	0.54[c]

a) For the extraction of perchloric acid with TOPO, the following constants were also obtained: $K_{ex}(HClO_4)_1 = [HClO_4(TOPO)]_{org}[H^+]^{-1}[ClO_4^-]^{-1}[TOPO]_{org}^{-1}$, $K_{ex}(HClO_4)_3 = [HClO_4(TOPO)_3]_{org}[H^+]^{-1}[ClO_4^-]^{-1}\times[TOPO]_{org}^{-3}$, $\log K_{ex}(HClO_4)_1 = 0.54(CHCl_3)$, $\log K_{ex}(HClO_4)_3 = 4.32(C_6H_{14})$, $2.60(CCl_4)$. b) Erroneous. c) Aq phase 1.0 mol dm^{-3} $NaClO_4$. Taken from Ref. 2.

the magnitude of the constant than the difference in those of TOPO.

(iii) When the solvent is chloroform, the association is observed only between HFA and TOPO. With the other β-diketones, a slight decrease in the distribution ratio with an increase in the TOPO concentration is observed.

(iv) Among the β-diketones in a certain given diluent, the association constant is larger when the K_a is higher (stronger as an acid).

The synergistic effect in metal extractions with β-diketones by TOPO or TBP is very well known, but such associations between the β-diketone and TBP or TOPO have not often been discussed quantitatively. The antagonistic effect caused by association of an acidic extractant and a neutral ligand was pointed out by Wang *et al.*[3,4] and also by Healy *et al.*[5,6] However, these reports gave only qualitative discussions. This problem has also been considered by several authors.[7–11] Recently, Khopkar and Mathur have discussed this problem on the basis of their experiments about solvent extraction of metal ions with TTA and TOPO[12] or TBP.[13] They described how the extraction curves in such synergistic systems can be well explained by assuming associations of the β-diketone and the neutral ligand. They determined the association constants between TTA and TBP or TOPO in those extraction systems and gave values $10^{0.57}$ and $10^{1.14}$ for the $\beta_{1(org)}$ of TTA with TBP and TOPO in xylene.

The observations in the present study can be explained by assuming that the β-diketone is extracted with the neutral ligand. As is seen from Eqs. 17 and 18, the extraction constant is the multiplication of K_d and $\beta_{n(org)}$. When pK_a values are similar, $\beta_{n(org)}$ may not be much different. Thus among a group of β-diketones of similar pK_a values, the magnitude of K_{ex1} and K_{ex2} should be dependent on the K_d values, which are higher when the molar volume is larger.

The extraction equilibria of metal ion M^{m+} in such synergistic systems can be written as:

$$M^{m+} + mA^- \rightleftharpoons MA_{m(org)};$$

$$K_{ex,m} = [MA_m]_{org}[M^{m+}]^{-1}[A^-]^{-m} \quad (19)$$

$$MA_{m(org)} + nL_{(org)} \rightleftharpoons MA_mL_{n(org)};$$

$$\beta_{m,n(org)} = [MA_mL_n]_{org}[MA_m]_{org}^{-1}[L]_{org}^{-n}, \quad (20)$$

and the enhancement of the metal extraction can be written as:

$$D/D_0 = 1 + \Sigma \beta_{m,n(org)}[L]_{org}^n, \quad (21)$$

where $D_0 = K_{ex,m}[A^-]^m$. When both $[A^-]$ and $[L]_{org}$ are lowerd by association, the value D/D_0 should be underestimated if no correction for the decreases in the concentrations would be made, and should cause an underestimation of the $\beta_{m,n(org)}$ values which were calculated by Eq. 21. At the same time, if no correction for the decrease in $[L]_{org}$ by associations with HA would be made, it should also cause an underestimation of $\beta_{m,n(org)}$. Thus although it seems to be necessary to recalculate the previously reported values of the adduct formation of metal chelate from such a standpoint, marked differences between the previous values and recalculated values should be found only in HFA–TOPO systems because the $\beta_{n(org)}$ are large enough to affect the results only in the HFA–TOPO systems. The differences will be slight in other systems.

The authors are grateful to Dr. J. N. Mathur for his valuable discussions about the association between 2-thenoyltrifluoroacetone and trioctylphosphine oxide.

References

1) S. Kusakabe and T. Sekine, *Bull. Chem. Soc. Jpn.*, **53**, 1759 (1980).
2) M. Niitsu and T. Sekine, *J. Inorg. Nucl. Chem.*, **37**, 1054 (1975).
3) S. M. Wang, W. R. Walker, and N. C. Li, *J. Inorg. Nucl. Chem.*, **28**, 875 (1966).
4) S. M. Wang, D. Y. Park, and N. C. Li, "Int. Solvent Extr. Conf., [Proc.]," ed by D. Dyrssen, O. Liljenzin, and J. Rydberg, North-Holland Publ. Co., Amsterdam (1967), p. 111.
5) T. V. Healy, D. F. Peppard, and G. W. Mason, *J. Inorg. Nucl. Chem.*, **24**, 1429 (1962).
6) T. V. Healy, "Int. Solvent Extr. Conf., [Proc.]," ed by A. S. Kertes and Y. Marcus, North-Holland Publ. Co., Amsterdam (1968), p. 257.
7) M. H. Konstantinova, *Dokl. Bolg. Akad. Nauk*, **30**, 1737 (1977).

8) M. H. Konstantinova, *Dokl. Bolg. Akad. Nauk*, **31**, 1011 (1978).
9) V. V. Ramakrishna and S. K. Patil, *Sep. Sci. Tech.*, **14**, 571 (1979).
10) T. Sekine and Y. Hasegawa, "Int. Solvent Extr. Conf., [Proc.]," ed by A. S. Kertes and Y. Marcus, North-Holland Publ. Co., Amsterdam (1968), p. 289.
11) C.-K. Wu, H. C. Kao, D.-F. Ching, K.-H. Hsu, W.-Q. Wang, and P.-C. Tsiang, *Pei-Ching Ta Hsueh Hsueh Pao, Tzu Jan. K'o Heueh Pom*, **1980**, 22; *Chem. Abstr.*, **95**, 31276k (1981).
12) P. K. Khopkar and J. N. Mathur, The Institute of Science Diamond Jubilee Celebrations, Symposium on "Solvent Extraction," 1980, S28.
13) P. K. Khopkar and J. N. Mathur, *J. Radioanal. Chem.* **60**, 131 (1980).
14) T. Sekine, Y. Hasegawa, and N. Ihara, *J. Inorg. Nucl. Chem.*, **35**, 3968 (1973).
15) K. Akiba and T. Kanno, *Kakuriken Kenkyu Houkoku*, **9**, 272 (1976).

Sodium Isotopic Exchange Rate between Disodium Zirconium(IV) Bis(orthophosphate) Trihydrate and Aqueous Solutions

Yasushi INOUE* and Yoshimune YAMADA

Department of Nuclear Engineering, Faculty of Engineering, Tohoku Universitv, Aramaki-aza-Aoba, Sendai 980

(Received June 25, 1982)

The sodium isotopic exchange rate between the large crystals of disodium zirconium(IV) bis(orthophosphate) trihydrate and aqueous solutions was determined radiochemically. The exchange proceeded quickly up to 5% of the total, followed by a slow process. The first step was attributed to the instantaneous attainment of the equilibrium between the imperfect surface layers of the crystals and the solution, and the second step was found to be controlled by the diffusion of sodium ions along the direction perpendicular to the layers consisting of zirconium atoms. The diffusion constant, D, was calculated with the equation obtained by Fick's diffusion law under the conditions of slab geometry and infinite solution volume. From the dependence of D on temperature, the activation energy for the diffusion was evaluated to be 101 kJ mol^{-1}.

Although the investigation of ion-exchange kinetics is very important for understanding the ion-exchange mechanism of crystalline zirconium(IV) bis(hydrogenphosphate) monohydrate (ZP), there has been only a little information up to date.[1–8] The measurement of the isotopic exchange rate of cations between the corresponding salt forms of ZP and aqueous solutions is especially interesting because it would provide the fundamental data which are useful for elucidating ion-exchange kinetics.

One of the outstanding studies made on this subject is that of Costantino *et al.*[8] They determined the isotopic exchange rate of sodium and potassium ions between the corresponding salt forms of powdered ZP, $M_2Zr(PO_4)_2\cdot 3H_2O$ (M=Na and K), and aqueous solutions and analyzed the data by the particle-diffusion mechanism. They assumed that the particles of the exchanger were spherically symmetrical, and succeeded in describing the rate law by one diffusion constant. In principle, however, the rate depends on the direction of diffusion because the crystal is not isomorphous, since it has a layered structure. Their assumption, therefore, is an approximation suitable for microcrystalline powders.

When large crystals having crystals shaped like thin platelets are used, the assumption made by Costantino *et al.* will be no longer valid. Hence, if macrocrystals, which have uniform in size are used and the rate is measured as a function of particle size, we can get a deeper insight into the isotopic exchange rate. This induced us to establish the conditions for preparing ZP with a large and uniform crystal size[9] and to obtain the information of phase stability of its disodium forms,[10] as reported previously. This information enables us to carry out the rate study more elaborately than before.

This paper deals with the results of the radiochemical experiments undertaken to measure the isotopic exchange rate of sodium ions between large crystals of $Na_2Zr(PO_4)_2\cdot 3H_2O$ and concentrated solutions of sodium salts.

Experimental

Preparation of $Na_2Zr(PO_4)_2\cdot 3H_2O$ Spiked with ^{22}Na. The crystals of $Na_2Zr(PO_4)_2\cdot 3H_2O$ prepared by the method recommended previously[9] were classified into four particle sizes: 48—70, 70—100, 100—145, and 145—250 mesh, by using Japan Industrial Standard sieves. The size of each fraction was then made more uniform by the sedimentation method with the equipment of Aly and Latimer.[11] The fraction of each uniform size was collected, dried in a desiccator over a saturated NaCl solution, and the particle size was measured with an optical microscope. The average size of each fraction is given in Table 1. $Na_2Zr(PO_4)_2\cdot 3H_2O$ thus obtained was then labeled with ^{22}Na by equilibrating 1 g of the sample with 10 cm^3 of 0.1 mol dm^{-3} NaOH solution containing ^{22}Na for two weeks at 40 °C. After being washed with distilled water, it was dried again to a constant weight over saturated NaCl solution. The product was verified to be homogeneously labeled at about 40 μCi/g (1 Ci=3.7×10^{10} Bq) and was used for the determination of the isotopic exchange rate.

Apparatus. The apparatus used for the measurements of the isotopic exchange rate is shown in Fig. 1. The sample is placed in a stainless steel cage fitted with a 400 mesh stainless steel screen on the openings at the side wall and the bottom. The cage was designed by modifying the device developed by Kressman and Kitchner;[12] the upper base of

Table 1. Particle size of the samples

No.	Mean crystal size/μm		
	Length	Width	Thickness
1	413±31	333±40	16±5
2	286±44	238±32	16±3
3	190±24	159±15	16±2
4	127±16	111±23	16±2

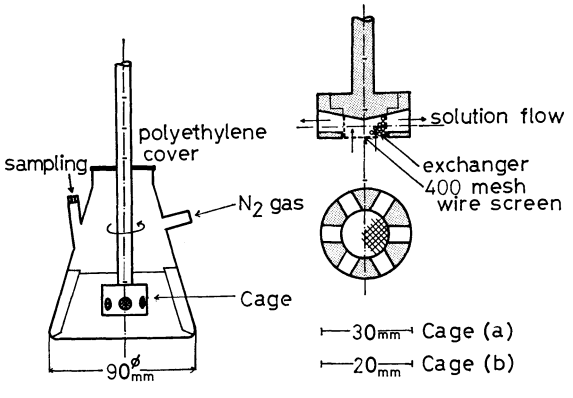

Fig. 1. Apparatus for the measurement of the isotopic exchange rate.

the inner surface was tapered and grooved so that no air might stay in the cage. This ensures the intimate contact of the exchanger with the solution. The cage is connected to the shaft of a stirrer and dipped into the solution in a conical beaker. The lower part of its wall is indented at three places to prevent the surface of the solution from becoming paraboloid when the solution is vigorously agitated by the stirrer. As it is rotated in the solution, the cage draws liquid from the bottom screen and discharges it through the side screen into the bulk of the solution; thus a very rapid stream of the solution passes through the sample placed inside the cage. The frequency of revolution was measured with a Yokogawa Model 2607 Photo Tachometer.

Measurements of the Isotopic Exchange Rate. All the experiments were performed in nitrogen atmosphere. A portion of 400 mg of the sample was placed in the cage and immersed into 200 cm^3 of the test solutions while the cage was rotated. The solution had been adjusted in advance to a constant temperature within ± 0.1 °C (below 50 °C), or within ± 0.2 °C (above 50 °C). Aliquots of the solution (about 0.2 cm^3) were taken out at appropriate time intervals in order to measure the radioactivity. A well-type NaI-(Tl)scintillation counter (Fuji Denki Model NHS-2) was used for the measurement of radioactivity. The time of contact of the solution with the exchanger was taken as the time elapsed between the immersion of the cage and the withdrawal of an aliquot of the solution.

The fractional attainment of equilibrium, $F=C_t/C_\infty$, was calculated from these results; here C_t is the total radioactivity of the solution at time t and C_∞ at $t=\infty$. C_∞ was calculated by the equation, $C_\infty=CM/(M+m)$, where C is the initial total radioactivity of the exchanger, and m and M are the total amounts of Na^+ ions in the exchanger and in the solution, respectively.

Results and Discussion

In order to determine the efficiency of agitation, the effect of the stirring rate and the size of the cage on the half-exchange time was examined for solutions of pH 11 having different $NaNO_3$ concentrations. In solutions as dilute as 0.01 mol dm^{-3} $NaNO_3$, the time required for half-exchange became shorter as the revolution rate increased, and became constant at 1000 min^{-1}. In more concentrated solutions, it was almost independent of the rate of revolution. This observation was irrespective of the diameter of the base screen of the cages used (17 and 12 mm): that is, the constant exchange rate is not due to the limiting hydrodynamic efficiency of the stirring. Furthermore, it was confirmed that no crystals were broken down during the agitation. From these results a revolution rate of 1400 min^{-1} was adopted throughout the subsequent experiments.

To make clear the rate controlling steps of the isotopic exchange, a plot of F against the square root of contact time t, was made for different experimental conditions. Figure 2 shows the comparison of the isotopic exchange rates in solutions of different sodium salts, indicating that no difference was observed in the rates for different anions in the solution. Figure 3 shows the influence of the sodium-ion concentration on the rate. When the concentration was higher than 0.5 mol dm^{-3}, the rate was independent of the sodium-ion concentration, and a linear relation between F and $\sqrt{t}$ held in the F range smaller than about 0.4, except for the initial portion of these plots. When the sodium-ion concentration was 0.01 mol dm^{-3}, however, the rate was much faster than that obtained for the solutions of higher concentrations than 0.5 mol dm^{-3}; in addition, linearity between F and $\sqrt{t}$ did not hold.

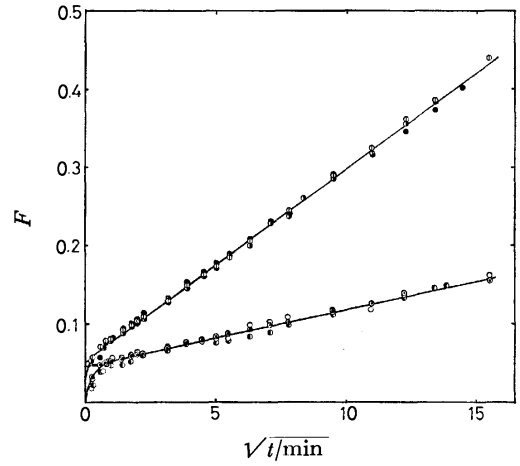

Fig. 2. Effect of anions on the isotopic exchange rate (sample 3).
T, 44.9 °C. ⓘ: 5 mol dm^{-3} $NaNO_3$ (pH 11), ◑: 5 mol dm^{-3} NaCl (pH 11), ●: 5 mol dm^{-3} NaOH.
T, 24.1 °C. ⊙: 0.5 mol dm^{-3} $NaNO_3$ (pH 11), ○: 0.5 mol dm^{-3} NaCl (pH 11), ◐: 0.5 mol dm^{-3} NaOH.

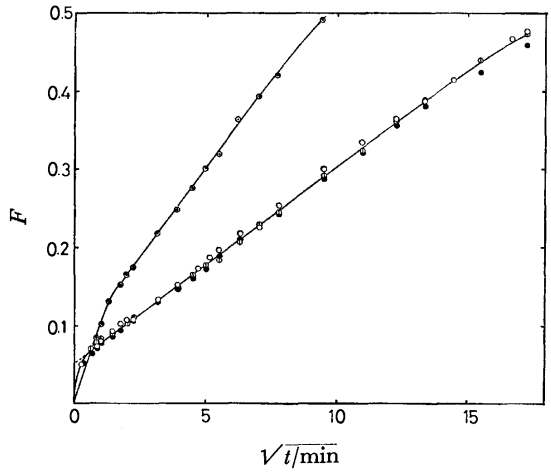

Fig. 3. Effect of Na^+ ion concentration on the isotopic exchange rate (sample 3).
pH 11. ⊙: 0.01 mol dm^{-3} $NaNO_3$, ○: 0.5 mol dm^{-3} $NaNO_3$, ⓘ: 5 mol dm^{-3} $NaNO_3$, ●: saturated $NaNO_3$.

The observations that the exchange rate is not affected by the revolution rate of the cage, by the kind of anions, or by the sodium-ion concentration, mean that the rate is controlled by the process within the particles. Moreover, the linearity of F *vs.* $\sqrt{t}$ in the F range smaller than 0.4 indicates that the particle diffusion is rate-controlling, and that the infinite solution-volume approximation is closely obeyed in this range, although the method of the rate measurement is for the limited solution-volume condition. The deviation from the linearity means that the assumption of the infinite solution-volume condition is no longer

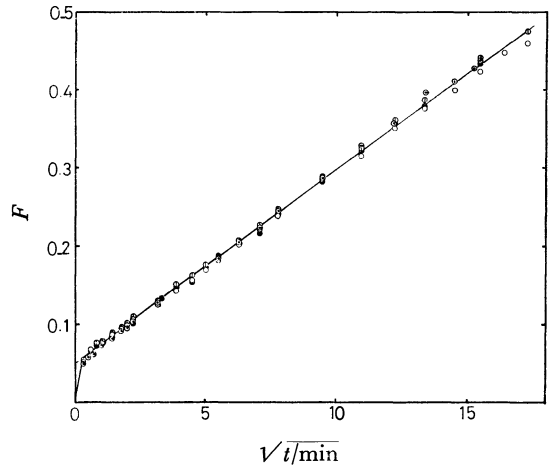

Fig. 4. Effect of particle size on the isotopic exchange rate.
T, 44.9 °C, 5 mol dm^{-3} $NaNO_3$. ⊙: Sample 1, ○: sample 2, ◑: sample 3, ●: sample 4.

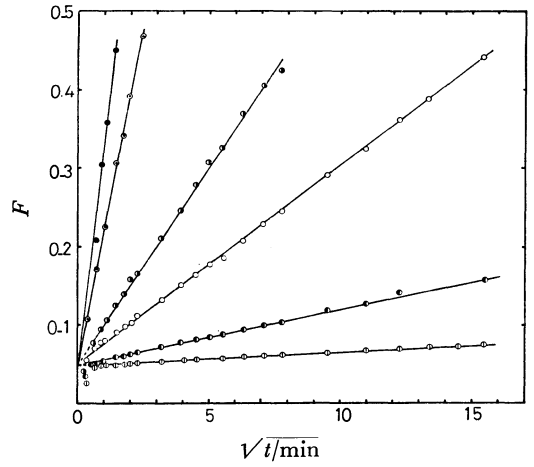

Fig. 5. Effect of temperature on the isotopic exchange rate (sample 3).
pH 11, 5 mol dm^{-3} $NaNO_3$. ●: 91.4 °C, ⊙: 79.8 °C, ◑: 57.9 °C, ○: 44.9 °C, ◐: 24.1 °C, ◑: 4.6 °C.

effective.

The effect of particle size on the rate was then studied. This is shown in Fig. 4, which indicates that the rate was not affected by the particle size of the samples employed. This observation can be explained as follows. The structure of $Na_2Zr(PO_4)_2 \cdot 3H_2O$ is a layered one similar to ZP: each layer consists of zirconium atoms lying very nearly in a plane and bridged by phosphate groups situated above and below the plane. Adjacent layers are arranged in such a way as to create zeolite-like cavities; these layers are interconnected by openings.[13] The diameters of the openings are 0.263 and 0.24 nm along the directions parallel and perpendicular to the layers, respectively. Since the sodium ion is small in size (0.19 nm), it can diffuse along both directions. Here, let us define the diffusion constants along the direction parallel and perpendicular to the layers respectively as D' and D, where D' is considered to be greater than D because of the difference in the diameters of the passages of ions. When D' is supposed to be very much greater than D, the isotopic exchange rate is determined by the diffusion along the direction parallel to the layers; accordingly, it must depend on the particle size of the samples. The experimental data, however, does not support this assumption. By assuming that D' is nearly equal to D, the diffusion along the direction parallel to the layers can be ignored, since the diffusion distance is much longer along this direction than along the direction perpendicular to the layers. As a result, the rate will be determined only by D. The independence of the rate on the particle size can reasonably be explained by this assumption since the thicknesses of the crystals are equal irrespective of the particle size.

The fractional attainment of equilibrium, therefore, can be obtained by solving the equation for diffusion in slabs immersed in a well-stirred solution under the infinite-solution volume condition:

$$F = 1 - \sum_{n=0}^{\infty} \frac{8}{(2n+1)^2\pi^2} \exp[-\beta(n+1/2)^2\pi^2 t] \quad (1)$$

where, $\beta = D\,l^{-1}$ and l is the half-length of the crystal in the direction perpendicular to the layers.[14,15]

When βt is smaller than 0.1, that is, when F is less than about 0.4, Eq. 1 can be approximated by a simpler form:

$$F = \frac{2}{\pi^{1/2}} \sqrt{\beta t} \quad (2)$$

which holds to a fairly good approximation.

The fractional attainment of equilibrium against square root of time was then studied as a function of temperature, as is shown in Fig. 5. The figure indicates that the slope of the linear relation between F and $\sqrt{t}$ increases with temperature. The straight lines, however, do not pass through the origin and always intersect the F axis at 0.05. This observation can be understood by considering that the defects of the crystal structure exist on the surface of the crystals and that the equilibrium between the surface region of the crystals and the solution is attained rapidly and then the diffusion into the bulk of the crystals proceeds. D was then calculated by taking consideration of the facts that 95% of total sodium ions in the crystals took part in the particle diffusion and that the effective length for diffusion was 95% of the actual crystal size.

When $\log D$ was plotted against $1/T$, good linearity was obtained, as is shown in Fig. 6. From the Arrhenius equation, $D = D_0 \exp(-E_a/RT)$, the activation energy E_a and the constant D_0 were determined. The value of E_a was 101 kJ mol^{-1} and $D_0 = 19$ m^2 s^{-1}. The present value of E_a is considerably higher than that given by Costantino *et al.*, 73 kJ mol^{-1}.[8] One explanation of this discrepancy is as follows. The activation energy of diffusion along the direction perpendicular to the layers is expected to be higher than that along the direction parallel to the layers, because the effective diameter of passage is smaller along the former than along the latter direction. The present value is related to the diffusion along the direction of the highest activation energy while Costantino's value resulted from some average of two diffusion con-

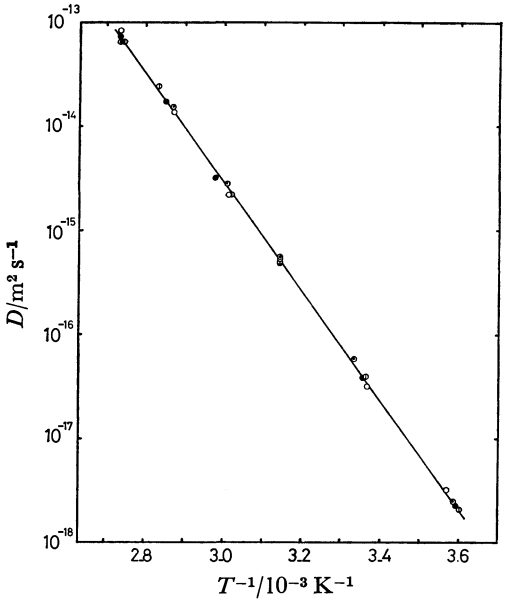

Fig. 6. Arrhenius plot for diffusion constant, D. pH 11, 5 mol dm^{-3} $NaNO_3$. ⊙: Sample 1, ○: sample 2, ◑: sample 3, ●: sample 4.

stants.

The experiments so far were performed with the dried exchanger which had been stored in a desiccator containing saturated NaCl solution. The same results were also obtained when the experiments were carried out by using the exchanger which had been equilibrated with distilled water. This fact offers a striking contrast between the trihydrate and high-temperature phases. The results for the latter phases will be reported later.

References

1) G. H. Nancollas and R. Paterson, *J. Inorg. Nucl. Chem.*, **22**, 259 (1961).
2) S. J. Harvie and G. H. Nancollas, *J. Inorg. Nucl. Chem.*, **30**, 273 (1968).
3) S. J. Harvie and G. H. Nancollas, *J. Inorg. Nucl. Chem.*, **32**, 3923 (1970).
4) A. Dyer and F. T. Ocon, *J. Inorg. Nucl. Chem.*, **33**, 3153 (1971).
5) A. Dyer and J. S. Gill, *J. Inorg. Nucl. Chem.*, **39**, 665 (1977).
6) A. Dyer and J. S. Gill, *J. Inorg. Nucl. Chem.*, **40**, 97 (1978).
7) A. Ruvarac, S. Milonjic, A. Clearfield, and J. M. Graces, *J. Inorg. Nucl. Chem.*, **40**, 79 (1978).
8) U. Costantino, L. Naszodi, L. Szirtes, and L. Zsinka, *J. Inorg. Nucl. Chem.*, **40**, 901 (1978).
9) Y. Inoue and Y. Yamada, *Bull. Chem. Soc. Jpn.*, **52**, 3528 (1979).
10) Y. Inoue and Y. Yamada, *Bull. Chem. Soc. Jpn.*, **55**, 792 (1982).
11) H. F. Aly and R. M. Latimer, *J. Inorg. Nucl. Chem.*, **29**, 2041 (1967).
12) T. R. E. Kressman and J. A. Kitchener, *Faraday Discuss. Chem. Soc.*, **7**, 90 (1949).
13) A. Clearfield, W. L. Duax, A. S. Medina, G. D. Smith, and J. R. Thomas, *J. Phys. Chem.*, **73**, 3424 (1969).
14) A. H. Wilson, *Philos. Mag.*, **39**, 48 (1948).
15) J. Crank, *Philos. Mag.*, **39**, 362 (1948).

 © 1983 The Chemical Society of Japan Bull. Chem. Soc. Jpn., 56, 709—714 (1983)

An Electron Transfer Chain Mechanism for Photoinduced Oxidative Addition of Alkyl Iodide to a Dimeric Rhodium(I) Complex under Low Energy Irradiation (553 nm)

Shunichi Fukuzumi, Nobuaki Nishizawa, and Toshio Tanaka*

Department of Applied Chemistry, Faculty of Engineering, Osaka University, Suita, Osaka 565

(Received July 23, 1982)

A dimeric Rh^{I} complex, $[Rh_2(dicp)_4]^{2+}$ (dicp=1,3-diisocyanopropane) was found to undergo a photoinduced oxidative addition with butyl iodide and isopropyl iodide in MeCN by 553 nm irradiation in high quantum yields, Φ=25.2 and 22.6, respectively. Electron acceptors (*p*-dinitrobenzene, *p*-benzoquinone, and chloranil) and radical scavengers (oxygen and isopentyl nitrite) act as inhibitors for the photoinduced oxidative addition, providing unambiguous evidence for a chain character of this reaction. The fluorescence quenching of $[Rh_2(dicp)_4]^{2+}$ by the electron acceptors as well as butyl iodide has also been examined. Based on the kinetics of the photochemical reactions in the absence or the presence of electron acceptors and radical scavengers, an electron transfer chain mechanism has been proposed. The formation of butyl radicals in the photoinitiation step was confirmed by the trap with oxygen to yield equimolar amounts of 1-butanol and butyraldehyde. The nature of the excited state of $[Rh_2(dicp)_4]^{2+*}$ ($^1A_{2u}$ or $^3A_{2u}$) involved in the photoinitiation step has also been discussed.

Oxidative additions of transition metal complexes with low-lying metal to ligand charge transfer (MLCT) excited states have recently merited a special attention as offering a possibility for photochemical energy storage.[1] There has, however, been reported only a few photochemical study on the oxidative additions of simple substrates such as alkyl halides and protic acids to transition metal complexes.[2] On the other hand, the thermal oxidative addition of organic halides to transition metal complexes have intensively been studied.[3] Although there is no simple generalization about the mechanisms of oxidative additions, some addition reactions of organic halides to transition metal complexes have been suggested to proceed *via* a radical chain process where the initiation step involves transfer of one electron rather than two electrons.[4] If such a radical chain process is initiated by light, the oxidative addition may be prompted photochemically with high quantum yields.

We have previously reported that a dimeric Rh^{I} complex, $[Rh_2(dicp)_4]^{2+}$ (dicp=1,3-diisocyanopropane), is an excellent one electron donor in the reactions with inorganic oxidants such as $[Fe(N\text{–}N)_3]^{3+}$ (N–N=2,2′-bipyridine and 1,10-phenanthroline).[5] The donor ability of $[Rh_2(dicp)_4]^{2+}$ would be further enhanced in the MLCT excited states, $[Rh_2(dicp)_4]^{2+*}$ ($^1A_{2u}$ or $^3A_{2u}$) formed by the irradiation of the lowest energy band which appears at 553 nm in MeCN.[6,7]

In this paper, we wish to report a photoinduced oxidative addition of butyl iodide (*n*-BuI) and isopropyl iodide (*i*-PrI) toward $[Rh_2(dicp)_4]^{2+*}$ by low energy irradiation (553 nm) under nitrogen atmosphere with exceptionally high quantum yields, Φ=25.2 and 22.6, respectively. The reaction mechanism is discussed based on the kinetics of the photochemical reactions in the absence or the presence of electron acceptors (*p*-dinitrobenzene, *p*-benzoquinone, and chloranil) as well as radical scavengers (oxygen and isopentyl nitrite). Electron transfer quenching of the fluorescence of $[Rh_2(dicp)_4]^{2+*}$ by the electron acceptors has also been examined to obtain the rate constants for the electron transfer reactions between $[Rh_2(dicp)_4]^{2+*}$ and the electron acceptors. A preliminary report of the present study has appeared.[8]

Experimental

Materials. Preparation of $[Rh_2(dicp)_4](BPh_4)_2$ (dicp=1,3-diisocyanopropane) was described previously.[5,8] Commercially available *n*-BuI and *i*-PrI were purified by distillation. Electron acceptors (chloranil, *p*-benzoquinone, *p*-dinitrobenzene, *m*-dinitrobenzene, methyl *p*-nitrobenzoate, *m*-nitrobenzaldehyde, *p*-chloronitrobenzene, nitrobenzene, diethyl fumarate, and benzophenone) and a radical scavenger (isopentyl nitrite) also obtained commercially were purified by the standard methods.[9] Acetonitrile used as a solvent was purified by distillation over P_2O_5 three times before use.

Photoinduced Addition of n-*BuI to* $[Rh_2(dicp)_4]^{2+}$ *under Nitrogen Atmosphere.* Butyl iodide (7.9 mmol) was dissolved in a MeCN solution (45 cm^3) of $[Rh_2(dicp)_4](BPh_4)_2$ (31 μmol) under nitrogen atmosphere in the dark. When the solution was irradiated by the visible light (an Ushio Model Ul-501C Xenon lamp) through a Toshiba glass filter O-55 transmitting the light $\lambda>550$ nm, the intensive violet color of the solution faded in a few minutes to turn yellow. The resulting solution was concentrated to one third volume under reduced pressure, followed by the slow addition of diethyl ether. A precipitate appeared was collected by filtration and recrystallized from MeCN to give brown crystals of $[Rh_2(dicp)_4(n\text{-Bu})(I)](BPh_4)_2$ in a 80% yield. Found C, 59.27; H, 4.95; N, 7.93%.[10] Calcd for $C_{72}H_{73}N_8B_2IRh_2$: C, 61.56; H, 5.24; N, 7.98%. ν(C≡N): 2200 and 2220 cm^{-1} (KBr pellet).

Photochemical Reaction of $[Rh_2(dicp)_4]^{2+}$ *with* n-*BuI under Oxygen Atmosphere.* Upon 1 min irradiation by the visible light ($\lambda>550$ nm) under oxygen atmosphere, a violet MeCN solution (*ca.* 1 cm^3) containing $[Rh_2(dicp)_4]^{2+}$ (0.83 μmol) and *n*-BuI (0.175 mmol) turned into deep green with concomitant disappearance of the absorption band of $[Rh_2(dicp)_4]^{2+}$ at 553 nm. The resulting solution contained equimolar amounts of 1-butanol and butyraldehyde (26% yield) as determined by GLC. The other products were obtained as a mixture of $[Rh_2(dicp)_4(n\text{-Bu})(I)]^{2+}$ (67%) and $[Rh_4dicp)_8(I)_2]^{4+}$ (16%), the composition of which was determined from their absorbances at λ_{max}; 407 nm ($\varepsilon=5.09\times10^5$ mol^{-1} dm^2) and 631 nm ($\varepsilon=8.71\times10^5$ mol^{-1} dm^2),[11] respectively.

Quantum Yield Determination. The visible light from an Ushio Model Ul-501C Xenon lamp was monochromatized with a Nikon G-250 monochromator. The incident light intensity at 553 nm was determined as 7.08×10^{-9} einsteins

min^{-1} by the use of a standard actinometer (potassium hexacyanoferrate(II))[12] under the same conditions as the photochemical experiments. Quantum yields Φ for the photoinduced oxidative addition of *n*-BuI and *i*-PrI to $[Rh_2(dicp)_4]^{2+}$ were then calculated by the equation $\Phi = R/In$, where R is the photochemical reaction rate determined from the disappearance of the 553 nm band due to $[Rh_2(dicp)_4]^{2+}$ and In is the light intensity absorbed by the reactants. In the absence of electron acceptors and radical scavengers, the quantum yields exhibited some decreasing dependence on the percent conversion and the initial values were taken by extrapolating the plots of Φ *vs.* time.

Fluorescence Quenching by Electron Acceptors. Fluorescence measurements were carried out using a Hitachi 650-10S fluorescence spectrophotometer. Relative fluorescence intensities of $[Rh_2(dicp)_4]^{2+*}$ at 656 nm were measured for MeCN solutions containing $[Rh_2(dicp)_4]^{2+}$ (2.7×10^{-4}—8.0×10^{-4} mol dm^{-3}) and a quencher at various concentrations. The absorption band due to $[Rh_2(dicp)_4]^{2+}$ ($\lambda_{max}=553$ nm) was not changed by the addition of quenchers with high concentrations ($>1\times10^{-1}$ mol dm^{-3}) except for chloranil and *p*-benzoquinone. In these cases, the presence of quenchers in high concentrations caused the slight red shift (≈10 nm) of the $[Rh_2(dicp)_4]^{2+}$ band, and thus the lower concentrations ($\ll1\times10^{-1}$ mol dm^{-3}) were used for the experiments of the fluorescence quenching in order to avoid the possible formation of the complexes with the ground state of $[Rh_2(dicp)_4]^{2+}$. Under such experimental conditions, the excitation wavelength agrees with the absorption maximum of $[Rh_2(dicp)_4]^{2+}$ where the quenchers used in this study have neither absorption nor emission. There was no change in the shape but intensity of the fluorescence spectrum of $[Rh_2(dicp)_4]^{2+*}$ by the addition of quenchers. The minimum slit width (1 mm) of the excitation light was chosen for the fluorescence quenching with *n*-BuI in order to avoid the facile photochemical reaction. The Stern-Volmer relationship (Eq. 1) between I_f^0/I_f and [Q] was obtained for each quencher,

$$I_f^0/I_f = 1 + K_q[Q], \quad (1)$$

where I_f^0 and I_f are relative fluorescence intensities in the absence and presence of a quencher, respectively, K_q is the quenching constant, and Q stands for the quencher. The quenching rate constant k_q was obtained by the relation $k_q = K_q\tau^{-1}$, where τ is the emission lifetime of $[Rh_2(dicp)_4]^{2+*}$ ($\tau=1.3$ ns[7]).

Results and Discussion

Photoinduced Oxidative Addition of n-*BuI to* $[Rh_2(dicp)_4]^{2+}$. Figure 1 shows the electronic absorption spectra of a MeCN solution containing $[Rh_2(dicp)_4]^{2+}$ (3.24×10^{-4} mol dm^{-3}) and *n*-BuI (1.75×10^{-1} mol dm^{-3}) before and after irradiation by the visible light through a filter transmitting the light $\lambda>550$ nm under nitrogen atmosphere. Since neither the shape nor intensity of the lowest energy band at 553 nm assigned to $^1A_{1g}\rightarrow{}^1A_{2u}$ transition of $[Rh_2(dicp)_4]^{2+}$ [6,7] has been changed by the addition of *n*-BuI which has no absorption band in the visible region, there seems to be no ground state complex formed between $[Rh_2(dicp)_4]^{2+}$ and *n*-BuI. The intense violet color ($\lambda_{max}=553$ nm) of the solution, however, faded upon irradiation for 1 min. The resulting yellow solution contains the oxidative adduct, $[Rh_2(dicp)_4](n\text{-Bu})(I)]^{2+}$ ($\lambda_{max}=407$ nm), as a main product and a small amount of $[Rh_4(dicp)_8(I)_2]^{4+}$ ($\lambda_{max}=631$ nm, 4.6×10^{-6} mol dm^{-3})[11] as well as octane (4.9×10^{-6} mol dm^{-3}) detected by GLC. No butane has been detected. Thus, the photochemical reaction of $[Rh_2(dicp)_4]^{2+}$ with *n*-BuI under nitrogen atmosphere involves a main path and a side path, as expressed by Eqs. 2 and 3, respectively. The thermal reaction of

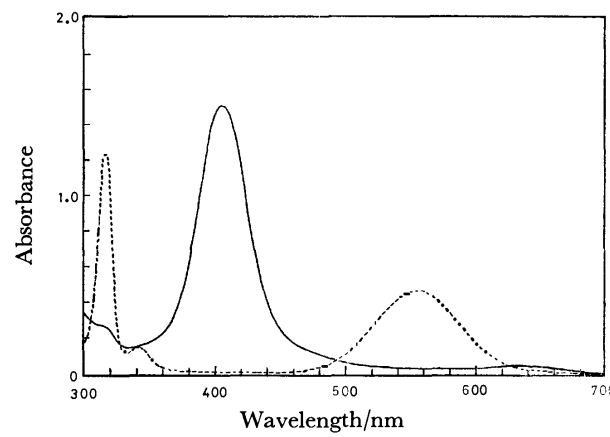

Fig. 1. Electronic absorption spectra of $[Rh_2(dicp)_4]^{2+}$ (3.23×10^{-4} mol dm^{-3}) in MeCN containing *n*-BuI (1.75×10^{-1} mol dm^{-3}) before irradiation (----) and after 1 min irradiation by the 553 nm light (——) under nitrogen atmosphere; 1 mm quartz cell.

$$[Rh_2(dicp)_4]^{2+} + n\text{-BuI} \xrightarrow[>550\,nm]{h\nu} [Rh_2(dicp)_4(n\text{-Bu})(I)]^{2+} \quad (2)$$

$$2[Rh_2(dicp)_4]^{2+} + 2n\text{-BuI} \xrightarrow[>550\,nm]{h\nu} [Rh_4(dicp)_8(I)_2]^{4+} + \text{Bu-Bu} \quad (3)$$

$[Rh_2(dicp)_4]^{2+}$ with *n*-BuI has been negligible in the extent under the conditions where the photochemical experiment was carried out since the rate of the thermal reaction was at least 10^3 times slower than that of the photochemical reaction.

The oxidative adduct in Eq. 2 was isolated as brown crystals of the tetraphenylborate salt, $[Rh_2(dicp)_4(n\text{-Bu})(I)](BPh_4)_2$. The infrared spectrum of the adduct in a KBr pellet showed two $\nu(C\equiv N)$ bands at 2200 and 2220 cm^{-1}, both of which are higher than the single $\nu(C\equiv N)$ frequency of $[Rh_2(dicp)_4](BPh_4)_2$ (2172 cm^{-1}) and lower than that of $[Rh_2(dicp)_4(I)_2]^{2+}$ (2227 cm^{-1}).[6] This is consistent with the structural formulation as *trans*-$[Rh_2(dicp)_4(n\text{-Bu})(I)](BPh_4)_2$ (**1**). The $[Rh_2(dicp)_4(n\text{-Bu})(I)]^{2+}$ cation in MeCN exhibits an intense absorption band at 407 nm ($\varepsilon=5.09\times10^5$ mol^{-1}

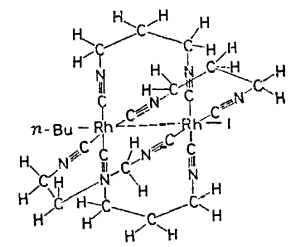

1

dm^2, Fig. 1), which is assigned to $\sigma \rightarrow \sigma^*$ transition in the Rh^{II}–Rh^{II} single bonded species as in the case of the MeI adduct, $[Rh_2(dicp)_4(Me)(I)]^{2+}$.[6]

The $[Rh_2(dicp)_4]^{2+}$ cation reacted with *i*-PrI as well under irradiation at 553 nm, yielding $[Rh_2(dicp)_4(i\text{-}Pr)(I)]^{2+}$ ($\lambda_{max}=414$ nm, $\varepsilon=6.16\times10^5$ mol^{-1} dm^2). The photochemical reaction of $[Rh_2(dicp)_4]^{2+}$ with MeI, however, could not be examined since the thermal oxidative addition of MeI to $[Rh_2(dicp)_4]^{2+}$ occurred appreciably upon mixing the reactants in the dark.[6]

Quantum Yields for the Photochemical Reaction of $[Rh_2(dicp)_4]^{2+}$ *with* n-*BuI.* Quantum yield Φ for the photochemical reaction of $[Rh_2(dicp)_4]^{2+}$ with *n*-BuI on irradiation with the 553 nm light under various conditions are listed in Table 1, which indicates that the Φ value for the reaction under nitrogen atmosphere increases with increasing the *n*-BuI concentration, and an exceptionally high quantum yield ($\Phi=25.2$) is achieved with the concentration of 1.75×10^{-1} mol dm^{-3}. The reaction with 1.0×10^{-1} mol dm^{-3} *i*-PrI also gives a similar high quantum yield (footnote b) in Table 1. Such high quantum yields strongly suggest that the photoinduced oxidative addition of $[Rh_2(dicp)_4]^{2+}$ with *n*-BuI as well as *i*-PrI is a chain process.

In order to elucidate the chain process, the effect of electron acceptors such as *p*-dinitrobenzene, *p*-benzoquinone, and chloranil on the quantum yields was examined. The quantum yields are drastically decreased (*e.g.*, from 25.2 to 0.87) by the addition of *p*-dinitrobenzene which is known as a powerful one electron acceptor.[13] Similarly, the decrease in the quantum yield is observed in the presence of *p*-benzoquinone and chloranil (Table 1). Oxygen, which is a typical radical scavenger, also reduces the quantum yield (Table 1). The addition of isopentyl nitrite which also is a radical scavenger[14] results in the reduction of the quantum yield although less effective than oxygen. Thus, the electron acceptors and radical scavengers act as inhibitors for the photoinduced oxidative addition of *n*-BuI to $[Rh_2(dicp)_4]^{2+}$, providing unambiguous evidence for the chain character of this process where strong one electron donors and radical species must be involved. The photoinitiation step of the chain process is discussed in the following section.

Fluorescence Quenching by Electron Transfer. The excitation of the lowest energy band (553 nm) of $[Rh_2(dicp)_4]^{2+}$ results in fluorescence ($\lambda_{max}=656$ nm, $h\nu_f=1.89$ eV, $\tau=1.3$ ns).[7] The fluorescence was efficiently quenched by the electron acceptors in Table 1 without change in the shape of the fluorescence spectrum.

Table 1. Quantum yields of the photoinduced oxidative addition of *n*-BuI to $[Rh_2(dicp)_4]^{2+}$ (7.6×10^{-4} mol dm^{-3}) in MeCN under 553 nm irradiation[a]

Additive (mol dm^{-3})	[*n*-BuI]/mol dm^{-3}	Φ
None	2.92×10^{-3}	1.9
None	1.75×10^{-2}	4.2
None	4.38×10^{-2}	6.8
None	8.76×10^{-2}	14.0
None	1.75×10^{-1}	25.2
None	1.00×10^{-1} [b]	22.6[b]
p-Dinitrobenzene		
5.23×10^{-2}	1.75×10^{-1}	1.0
1.11×10^{-1}	1.75×10^{-1}	0.87
p-Benzoquinone		
4.63×10^{-2}	1.75×10^{-1}	3.7
Chloranil		
2.56×10^{-2}	1.75×10^{-1}	7.5
Oxygen[c]	1.75×10^{-1}	3.2
Isopentyl nitrite		
1.49×10^{-2}	1.75×10^{-1}	15.6

a) Under a nitrogen atmospheric pressure unless otherwise noted. b) The addendum is *i*-PrI. c) Under an oxygen atmospheric pressure.

Table 2. Quenching rate constants (k_q) of the $[Rh_2(dicp)_4]^{2+*}$ fluorescence and reduction potentials (E^0_{red}) of electron acceptors

Quencher	E^0_{red}[a] *vs.* SCE / V	k_q / mol^{-1} dm^3 s^{-1}
Chloranil	0.01	1.6×10^{10}
p-Benzoquinone	−0.51	4.0×10^{10}
p-Dinitrobenzene	−0.69	1.8×10^{10}
m-Dinitrobenzene	−0.90	1.5×10^{10}
Methyl *p*-nitrobenzoate	−0.95	1.4×10^{10}
m-Nitrobenzaldehyde	−1.02	1.3×10^{10}
p-Chloronitrobenzene	−1.06	1.2×10^{10}
Nitrobenzene	−1.15	1.3×10^{10}
Diethyl fumarate	−1.50	6.8×10^{9}
Benzophenone	−1.86	5.9×10^{8}
Butyl iodide	b)	2.6×10^{8}

a) Taken from Ref. 15. b) The reduction is irreversible.

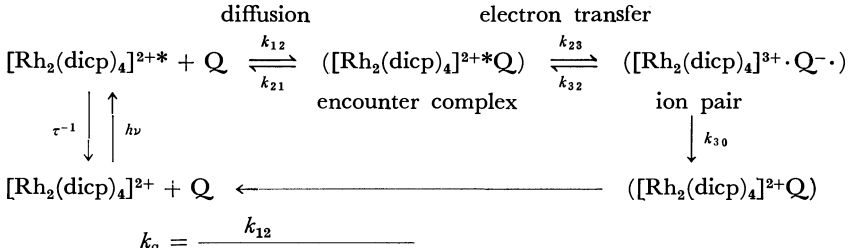

$$k_q = \frac{k_{12}}{1+\frac{k_{21}}{k_{23}}\left(1+\frac{k_{32}}{k_{30}}\right)} \quad (4)$$

Scheme 1.

Quenching rate constants of the $[Rh_2(dicp)_4]^{2+*}$ emission by various electron acceptors determined by the Stern-Volmer plots (see Experimental Section) are given in Table 2 together with the reduction potentials of the electron acceptors.

By analogy with the reaction scheme for fluorescence quenching by electron transfer in polar solvents reported previously,[16] the reaction of $[Rh_2(dicp)_4]^{2+*}$ with Q (quencher) may be shown in Scheme 1, according to which the quenching rate constant k_q is given by Eq. 4.[16] The free energy change of the actual electron transfer process, ΔG_{23}, (encounter complex→ion pair in Scheme 1) may be evaluated by Eq.5,[16]

$$\Delta G_{23} = E^0_{ox} - E^0_{red} + w_p - E_{0,0}, \quad (5)$$

where E^0_{ox} and E^0_{red} are the oxidation potential of $[Rh_2(dicp)_4]^{2+}$ and the reduction potential of electron acceptors, respectively, w_p is the work required to bring the product ions $[Rh_2(dicp)_4]^{3+}\cdot$ and $Q^{-}\cdot$ together to form the ion pair (Scheme 1),[17,18] and $E_{0,0}$ is the zero-zero transition energy between the ground state $[Rh_2(dicp)_4]^{2+}$ and the excited state $[Rh_2(dicp)_4]^{2+*}$. The $E_{0,0}$ value is obtained as 2.07 eV from the absorption spectrum (λ_{max}=553 nm, $h\nu$=2.24 eV) and the fluorescence spectrum (λ_{max}=656 nm, $h\nu_f$=1.89 eV) by the equation $E_{0,0}=(h\nu+h\nu_f)/2$.[16] Thus, the oxidation potential of the excited state $[Rh_2(dicp)_4]^{2+*}$ is decreased by 2.07 V relative to that of the ground state. Unfortunately, the oxidation potential of $[Rh_2(dicp)_4]^{2+}$ is unknown because the electrochemical oxidation is irreversible.[5] However, the peak potential E^p_{ox} of the cyclic voltammogram of $[Rh_2(dicp)_4]^{2+}$ (E^p_{ox}=0.92 V *vs.* SCE at the sweep rate of 0.1 V s^{-1})[5,19] gives the upper limit of the E^0_{ox} value. By using the w_p and $E_{0,0}$ values (−0.06 V[18] and 2.07 V, respectively), the upper limit of ΔG_{23} is then given as $\Delta G_{23} < -1.21 - E^0_{red}$. Thus, the quenching process by the electron acceptors except for diethyl fumarate and benzophenone in Table 2 (k_{23}) is exothermic and the reverse process (k_{32}) is thereby endothermic. Then, the relation $k_{30} \gg k_{32}$ may be valid since the free energy change of the back electron transfer to the ground state (k_{30}) is exceedingly negative. Under such a condition, Eq. 4 is reduced to Eq. 6. The

$$k_q = \frac{k_{12}k_{23}}{k_{23}+k_{21}} \quad (6)$$

quenching rate constants by the electron acceptors in Table 2 are thus close to the limiting value in Eq. 6, which is the diffusion rate constant, $k_{12}=2\times10^{10}$ mol^{-1} dm^3 s^{-1}.[16] The fluorescence of $[Rh_2(dicp)_4]^{2+*}$ is quenched also by *n*-BuI although the quenching rate constant k_q (2.6×10^8 mol^{-1} dm^3 s^{-1}) is smaller than those with the other electron acceptors in Table 2. Thus, the excited state $[Rh_2(dicp)_4]^{2+*}$ acts as an excellent electron donor toward various electron acceptors.

One electron transfer to *n*-BuI is known to result in the facile dissociation of the *n*-Bu–I bond, yielding butyl radicals.[20,21] The electron transfer quenching process shown in Eq. 7 is thus followed by the subsequent fast reaction expressed by Eq. 8, producing

$$([Rh_2(dicp)_4]^{2+*}n\text{-BuI}) \underset{k_{32}}{\overset{k_{23}}{\rightleftharpoons}} ([Rh_2(dicp)_4]^{3+}\cdot n\text{-BuI}^{-}\cdot) \quad (7)$$

$$([Rh_2(dicp)_4]^{3+}\cdot n\text{-BuI}^{-}\cdot \xrightarrow{\text{fast}} [Rh_2(dicp)_4(I)]^{2+}\cdot + n\text{-Bu}\cdot \quad (8)$$

butyl radicals, in competition with the back electron transfer to the ground state (k_{30} in Scheme 1). The presence of $[Rh_2(dicp)_4(I)]^{2+}\cdot$ and *n*-Bu· is supported from the formation of the coupling products, $[Rh_4(dicp)_8(I)_2]^{4+}$ and octane (Eq. 3), respectively, as described above.

Formation of Butyl Radicals in the Initiation Step. The formation of butyl radicals in the photoinitiation step (Eq. 8) is confirmed also by the effect of oxygen, which is a typical radical scavenger, on the photochemical reaction. The GLC analysis of the products in the photochemical reaction of $[Rh_2(dicp)_4]^{2+}$ (8.30×10^{-4} mol dm^{-3}) with *n*-BuI (1.75×10^{-1} mol dm^{-3}) by the irradiation ($\lambda>550$ nm) under oxygen atmosphere showed the formation of equimolar amounts of 1-butanol and butyraldehyde (26% based on the initial Rh concentration). A coupling product $[Rh_4(dicp)_8(I)_2]^{4+}$ also was obtained in a 33% yield, being close to those of 1-butanol and butyraldehyde. Thus, the stoichiometry of the photochemical reaction under oxygen may be given by Eq. 9. In the presence of oxygen, the butyl radicals should be trapped by oxygen molecules to yield butylperoxyl radicals (Eq. 10), which is known to undergo a bimolecular self-reaction, producing equimolar amounts of 1-butanol and butyraldehyde as well as oxygen (Eq. 11).[22] Thus, the formation of equimolar amounts of 1-butanol and butyraldehyde (Eq. 9) provides unambiguous evidence for

$$2[Rh_2(picp)_4]^{2+} + 2C_4H_9I + O_2 \xrightarrow[>550\,nm]{h\nu} [Rh_4(dicp)_8(I)_2]^{4+} + C_4H_9OH + C_3H_7CHO \quad (9)$$

$$C_4H_9\cdot + O_2 \longrightarrow C_4H_9O_2\cdot \quad (10)$$

$$2C_4H_9O_2\cdot \longrightarrow C_4H_9OH + C_3H_7CHO + O_2 \quad (11)$$

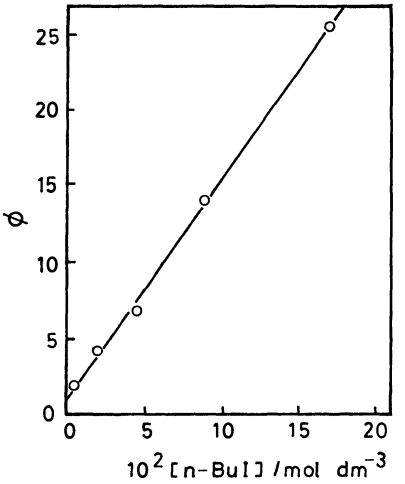

Fig. 2. Quantum yields for the photoinduced oxidative addition of *n*-BuI to $[Rh_2(dicp)_4]^{2+}$ (7.59×10^{-4} mol dm^{-3}) in MeCN at 298 K, as a function of the *n*-BuI concentration.

the formation of the butyl radicals in the photoinitiation step (Eq. 8). Oxygen molecules thus suppress the chain process to yield the oxidative adduct, where the butyl radical may act as a chain carrier, resulting in the reduction of the quantum yields (Table 1).

Kinetics and Mechanism of the Photoinduced Oxidative Addition. At a constant light intensity (7.08×10^{-9} einsteins min^{-1}) the quantum yield for the disappearance of $[Rh_2(dicp)_4]^{2+}$ in the photochemical reaction with *n*-BuI shows a linear dependence on the *n*-BuI concentration with the intercept of unity as shown in Fig. 2, from which Eq. 12 is derived,

$$\Phi = 1 + a[n\text{-BuI}], \tag{12}$$

where a is equal to 1.37×10^{2} mol^{-1} dm^3. A reaction scheme to account for the kinetic result (Eq. 12) is proposed as follows,

Initiation:

$$[Rh_2(dicp)_4]^{2+} + n\text{-BuI} \xrightarrow[h\nu]{\alpha In} [Rh_2(dicp)_4(I)]^{2+}\cdot + n\text{-Bu}\cdot \tag{13}$$

Propagation:

$$n\text{-Bu}\cdot + [Rh_2(dicp)_4]^{2+} \xrightarrow{k_1} [Rh_2(dicp)_4(n\text{-Bu})]^{2+}\cdot \tag{14}$$

$$[Rh_2(dicp)_4(n\text{-Bu})]^{2+}\cdot + n\text{-BuI} \xrightarrow{k_2} [Rh_2(dicp)_4(n\text{-Bu})(I)]^{2+} + n\text{-Bu}\cdot \tag{15}$$

Termination:

$$2[Rh_2(dicp)_4(n\text{-Bu})]^{2+}\cdot \xrightarrow{k_3} Bu\text{-}Bu + 2[Rh_2(dicp)_4]^{2+} \tag{16}$$

$$2[Rh_2(dicp)_4(I)]^{2+}\cdot \xrightarrow{k_4} [Rh_4(dicp)_8(I)_2]^{4+}, \tag{17}$$

Scheme 2.

where *In* is the light intensity absorbed by $[Rh_2(dicp)_4]^{2+}$ and α is the quantum yield for the photoinitiation step. The initiation step (Eq. 13) consists of the electron transfer quenching of $[Rh_2(dicp)_4]^{2+*}$ with *n*-BuI (Eq. 7) and the subsequent fast reaction to yield butyl radicals (Eq. 8). One of the propagation reactions (Eq. 15) also may consist of essentially the same reaction sequence as Eqs. 7 and 8, *i.e.*, an electron transfer from $[Rh_2(dicp)_4(n\text{-Bu})]^{2+}\cdot$ to *n*-BuI, followed by the facile fission of *n*-Bu–I bond to reproduce butyl radicals since the donor ability of $[Rh_2(dicp)_4(n\text{-Bu})]^{2+}\cdot$ is enhanced by the electron donating *n*-Bu group. The termination reactions (Eqs. 16 and 17) account for the coupling products in Eq. 3. The coupling of butyl radicals as a termination reaction is excluded since the rate-limiting step in the propagation process may be the reaction of $[Rh_2(dicp)_4(n\text{-Bu})]^{2+}\cdot$ with *n*-BuI (Eq. 15).[23]

Applying the steady-state approximation to the radical species involved in Scheme 2, the rate of the disappearance of $[Rh_2(dicp)_4]^{2+}$, $-d[Rh_2^{2+}]/dt$, is expressed as Eq. 18, from which the quantum yield Φ is given by Eq. 19. This equation is consistent with the kinetic result (Eq. 12) with respect to the dependence of the quantum yield on the *n*-BuI concentration. The comparison of Eq. 19 with Eq. 12 indicates that the quantum yield α for the photoinitiation step is *unity* and neither the back electron transfer to the ground state (k_{30} in Scheme 1) nor geminate recombination of the radical pair (Eq. 20) occurs in the photoinitiation step.

$$-\frac{d[Rh_2^{2+}]}{dt} = \alpha In + k_2\left(\frac{\alpha In}{2k_3}\right)^{1/2}[n\text{-BuI}] \tag{18}$$

$$\Phi = \alpha + k_2\left(\frac{\alpha}{2k_3 In}\right)^{1/2}[n\text{-BuI}] \tag{19}$$

$$([Rh_2(dicp)_4(I)]^{2+}\cdot n\text{-Bu}\cdot) \not\longrightarrow [Rh_2(dicp)_4(n\text{-Bu})(I)]^{2+} \tag{20}$$

The fluorescence quantum yield of $[Rh_2(dicp)_4]^{2+*}$ ($^1A_{2u}$) is 0.056[7] and therefore the remaining 94% of the excited species falls in the excited triplet state $^3A_{2u}$ by intersystem crossing. Then, the fluorescence quenching by *n*-BuI which is only 0.1% for the smallest concentration of *n*-BuI in Table 1 (2.92×10^{-3} mol dm^{-3})[24] cannot account for the high efficiency of the photoinitiation, $\alpha=1$. The much longer lifetime of the $^3A_{2u}$ state (8.5 μs)[7] than the $^1A_{2u}$ sate (1.3 ns) may, however, make it possible that the $^3A_{2u}$ sate is efficiently quenched by *n*-BuI with $\alpha=1$. The contribution of the lower excited states such as vibrationally excited state to the electron transfer reaction may be negligible since the donor ability of such states is much less than that of the $^3A_{2u}$ state. Thus, the excited state $[Rh_2(dicp)_4]^{2+*}$ involved in the photoinitiation step (Eq. 7) may be the triplet state ($^3A_{2u}$) rather than the singlet state ($^1A_{2u}$). The absence of the singlet geminate recombination of the radical pair (Eq. 20) also supports the electron transfer from the $^3A_{2u}$ state to *n*-BuI since the resultant triplet radical pair may diffusively separate without the singlet geminate recombination, yielding the free radicals (Eq. 8) which initiate the chain process (Eqs. 14 and 15).

It should be noted that a similar electron transfer chain mechanism has been proposed for some organic systems, *e.g.*, a substitution reaction of *p*-nitrobenzyl chloride with the sodium salt of 2-nitropropane which proceeds *via* a multi-stage chain sequence involving radical anions and free radicals as intermediates.[13,25] Recently, Chanon and Tobe in their excellent review[26] have formulated such chain reactions in the organic systems as the "DAISET" (Double Activation Induced by Single Electron Transfer) mechanism. The first activation results from the transfer of an electron to a molecular species (*e.g.*, Eq. 7); the second activation results from the build-up of a reaction chain capable of reproducing the species formed in the first step (*e.g.*, Eqs. 14 and 15). They have attempted to expand the "DAISET" mechanism in organic systems to some inorganic reactions in which the "DAISET" behavior is much less common, and have discussed a possibility of the existence of the "DAISET" mechanism in some reactions of d^8 square-planar complexes (*e.g.*, Rh^I). The present study thus provides an unique and unambiguous example of the "DAISET" mechanism in the inorganic counterpart.

References

1) A. W. Maverick and H. B. Gray, *Pure Appl. Chem.*, **52**, 2339 (1980); H. B. Gray, K. R. Mann, N. S. Lewis, J. A. Thich, and R. M. Richman, *Adv. Chem. Ser.*, **168**, 44 (1978).

2) W. C. Troger, G. L. Geoffroy, D. K. Erwin, and H. B. Gray, *J. Am. Chem. Soc.*, **100**, 1160 (1978); S. Otsuka and K. Ataka, *Bull. Chem. Soc. Jpn.*, **50**, 1118 (1977).

3) R. D. W. Kermitt and M. A. R. Smith, *Inorg. Reac. Mech.*, **3**, 451 (1974); J. Halpern, *Acc. Chem. Res.*, **3**, 386 (1970); R. Cramer, *ibid.*, **1**, 186 (1968); L. Vaska, *ibid.*, **1**, 335 (1968); R. Crabtree, *ibid.*, **12**, 331 (1979).

4) J. A. Osborn, "Organotransition Metal Chemistry," ed by Y. Ishii and M. Tsutsui, Plenum Press, New York (1976); A. V. Kramer, J. A. Labinger, J. S. Bradley, and J. A. Osborn, *J. Am. Chem. Soc.*, **96**, 7145 (1974); A. V. Kramer and J. A. Osborn, *ibid.*, **96**, 7832 (1974); M. J. S. Gyane, M. F. Lappert, S. J. Miles, and P. P. Power, *J. Chem. Soc., Chem. Commun.*, **1978**, 192.

5) S. Fukuzumi, N. Nishizawa, and T. Tanaka, *Bull. Chem. Soc. Jpn.*, **55**, 2892, 3482 (1982).

6) N. S. Lewis, K. R. Mann, J. G. Gordon II, and H. B. Gray, *J. Am. Chem. Soc.*, **98**, 7461 (1976).

7) S. J. Milder, R. A. Golbeck, D. S. Kliger, and H. B. Gray, *J. Am. Chem. Soc.*, **102**, 6761 (1980); V. M. Miskowski, G. L. Nobinger, D. S. Kliger, G. S. Hammond, N. S. Lewis, K. R. Mann, and H. B. Gray, *ibid.*, **100**, 485 (1978).

8) S. Fukuzumi, N. Nishizawa, and T. Tanaka, *Chem. Lett.*, **1982**, 719.

9) D. D. Perrin, W. L. F. Armarego, and D. R. Perrin, "Purification of Laboratory Chemicals," Pergamon Press, Elmsford, N. Y. (1968).

10) The smaller % C found in the elemental analysis could be caused by a partial decomposition of $[Rh_2(dicp)_4(n\text{-Bu})(I)](BPh_4)_2$ to $[Rh_2(dicp)_4(I)_2](BPh_4)_2$ during the isolation. A similar smaller % C has been reported in the isolation of $[Rh_2(dicp)_4(Me)(I)](BPh_4)_2$.[6]

11) The extinction coefficient of the absorption band due to $[Rh_4(dicp)_8(I)_2]^{4+}$ in MeCN was determined from the absorption spectrum of this cation prepared *in situ* as the mixture with $[Rh_2(dicp)_4(I)_2]^{2+}$ by the iodinolysis of $[Rh_2(dicp)_4]^{2+}$ in the dark. The concentration of $[Rh_4(dicp)_8(I)_2]^{4+}$ was determined by converting it to $[Rh_2(dicp)_4(I)_2]^{2+}$ ($\lambda_{max}=403$ and 467 nm, $\varepsilon=6.77\times10^5$ and 2.53×10^5 mol^{-1} dm^2, respectively) by irradiation of the visible light in the presence of excess iodine.

12) C. G. Hatchard and C. A. Parker, *Proc. R. Soc. London, Ser. A*, **235**, 518 (1956); J. G. Calvert and J. N. Pitts, "Photochemistry," Wiley, New York (1966), p. 783.

13) N. Kornblum, *Angew. Chem., Int. Ed. Engl.*, **14**, 734 (1975); R. C. Kerber, G. W. Urry, and N. Kornblum, *J. Am. Chem. Soc.*, **87**, 4520 (1965).

14) S. Fukuzumi and J. K. Kochi, *J. Am. Chem. Soc.*, **102**, 2141 (1980).

15) R. J. Klingler, K. Mochida, and J. K. Kochi, *J. Am. Chem. Soc.*, **101**, 6626 (1979); D. H. Geske, J. L. Ragle, M. A. Bambenek, and A. L. Balch, *ibid.*, **86**, 987 (1964); A. H. Maki and D. H. Geske, *ibid.*, **83**, 1852 (1961); F. M. Martens, J. W. Verhoven, R. A. Gase, U. K. Pandit, and Th. J. de Boer, *Tetrahedron*, **34**, 443 (1978).

16) D. Rehm and A. Weller, *Ber. Bunsenges. Phys. Chem.*, **73**, 834 (1969); D. Rehm and A. Weller, *Isr. J. Chem.*, **8**, 259 (1970).

17) The work term required to bring the reactants together to form the encounter complex has been neglected in Eq. 5.

18) C. R. Bock, T. J. Meyer, and D. G. Whitten, *J. Am. Chem. Soc.*, **97**, 2909 (1975).

19) The E^p_{ox} value *vs.* Ag/Ag^+ in Ref. 5 was corrected to that *vs.* SCE by adding 0.34 V.

20) P. B. Asycough and C. Thomson, *Trans. Faraday Soc.*, **58**, 1477 (1962); P. B. Asycough, "Electron Spin Resonance in Chemistry," Methuen, London (1967).

21) J. F. Garst, *Acc. Chem. Res.*, **4**, 400 (1971).

22) J. A. Howard, *Adv. Free Radical Chem.*, **4**, 49 (1972), and references cited therein.

23) If the rate-limiting step in the propagation process is the addition of *n*-Bu· to $[Rh_2(dicp)_4]^{2+}$ (Eq. 14), the quantum yield would be independent of the *n*-BuI concentration, which disagrees with the experimental result (Eq. 12).

24) By using the k_q value in Table 2, $k_q\tau[n\text{-BuI}]=1\times10^{-3}$.

25) G. A. Russell and W. C. Danen, *J. Am. Chem. Soc.*, **88**, 5563 (1966); G. A. Russell, *Chem. Soc. Spec. Publ.*, **24**, 271 (1970).

26) M. Chanon and M. L. Tobe, *Angew. Chem., Int. Ed. Engl.*, **21**, 1 (1982).

 © 1983 The Chemical Society of Japan Bull. Chem. Soc. Jpn., 56, 715—718 (1983)

Epilaurallene, a New Nonterpenoid C_{15}-Bromoallene from the Red Alga *Laurencia nipponica* Yamada[1)]

Minoru Suzuki, Kuniko Koizumi, Hajime Kikuchi, Teruaki Suzuki, and Etsuro Kurosawa*

Department of Chemistry, Faculty of Science, Hokkaido University, Sapporo 060

(Received July 1, 1982)

A new halogenated nonterpenoid C_{15}-compound, epilaurallene, has been isolated as a major constituent from the title alga along with several known compounds, and its structure was determined by the spectral and chemical methods. Epilaurallene is an epimer at C-4 of laurallene and was shown to possess *S*-configuration at C-4.

Within the Japanese species of genus *Laurencia* (Rhodomelaceae), *L. okamurai* Yamada (Mitsude-sozo) collected at various locations have contained laurinterol and debromolaurinterol as the characteristic major metabolites of this species.[2,3)] On the other hand, *L. nipponica* Yamada (Ura-sozo) have produced diverse terpenic and nonterpenic C_{15}-metabolites which seem to be mainly dependent upon the growth locality.[4)] As part of further studies on the constituents of *L. nipponica*, we examined a specimen collected at Tsukotan, near Oshoro Bay, Hokkaido, and isolated a new nonterpenoid C_{15}-bromoallene, designated as epilaurallene, as a major component. In this paper we describe the isolation and structural elucidation of this compound in full details.

Neutral methanol extracts obtained by the usual methods were submitted to repeated column and thin-layer chromatography to yield epilaurallene (**1**) together with known compounds, 10-bromo-α-chamigrene,[5)] laurene,[6)] (*E*)-γ-bisabolene 8,9-oxide,[7)] cycloeudesmol,[8)] (3*E*)-isolaureatin (T-laureatin),[9)] isolaureatin,[10)] and laureatin.[10)]

Epilaurallene (**1**), $C_{15}H_{20}O_2Br_2$ (*m/e* 313 and 311; M^+-Br), $[\alpha]_D^{25}$ +175° (*c* 1.00), mp 51—52 °C, showed the very similar IR ($CHCl_3$), ^1H NMR (200 MHz), and mass spectra to those of laurallene (**2**), which has previously been isolated from *L. nipponica* collected at Oshoro Bay and whose structure has been determined as **2** excluding the stereochemistry of C-4 and bromoallene moiety.[11)] However, the IR spectra of **1** and **2** in Nujol mulls were clearly distinguishable as shown in Fig. 1. Mixed mp of **1** and **2** revealed no depression, and instead higher mp (56—58 °C) than that of each compound. Furthermore, in the ^{13}C NMR spectra of **1** (Table 1) and **2**,[12)] fourteen of the fifteen carbon atoms showed the same chemical shifts while the remaining one carbon, which was assigned to C-4 by proton selective decoupling experiment, revealed the different chemical shift by 0.029 ppm. Above-mentioned data suggest that epilaurallene (**1**) would be an epimer at C-4 of laurallene (**2**). The structure of **1** was established by the following chemical reactions.

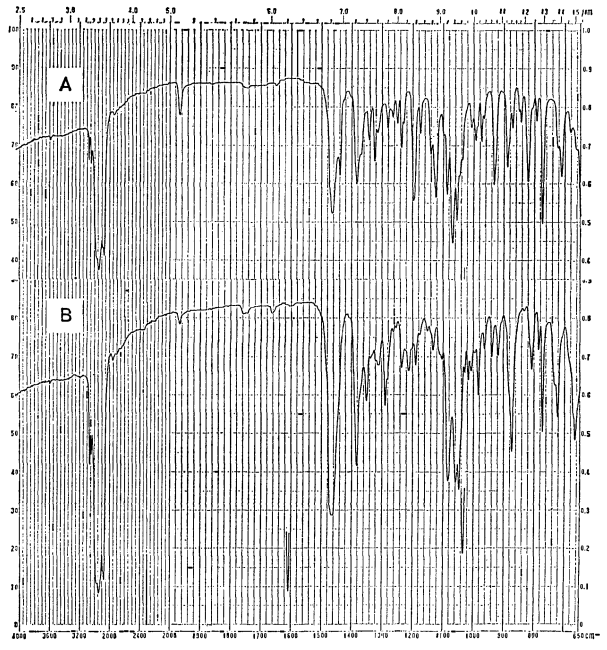

Fig. 1. IR (Nujol) spectra of (A) epilaurallene and (B) laurallene.

Hydrogenation of **1** with PtO_2 in ethanol gave two products, one of which was found to be identical with **3** previously derived from laurallene (**2**).[11)] Another hydrogenated product **4**, $C_{15}H_{27}O_2Br$ (*m/e* 277 and 275; $M^+-C_3H_7$), showed almost identical spectra (IR and ^1H NMR) with those of **5** also derived from **2**.[11)] Treatment of **4** with zinc in acetic acid and methanol

Table 1. ^{13}C NMR[a)] data for epilaurallene (**1**)

Carbon	δ[b)]	Multiplicity
1	74.224	d
2	201.036	s
3	102.693	d
4	73.552	d
5	39.448	t
6	82.925[c)]	d
7	79.830[c)]	d
8	30.571[d)]	t
9	129.469[e)]	d
10	127.396[e)]	d
11	29.374[d)]	t
12	73.406[e)]	d
13	57.960	d
14	28.148	t
15	11.241	q

a) Spectrum was recorded at 50.10 MHz. b) The δ values are in ppm downfield from TMS in $CDCl_3$. c) Assignments may be interconvertible. d), e) Assignments may be reversed.

afforded an unsaturated alcohol **6**, $C_{15}H_{28}O_2$ (*m/e* 240; M^+); ν_{max} 3400 and 970 cm^{-1}, δ 3.76 (1H, ddd, J=7, 7, and 3 Hz), 4.1—4.3 (2H, m), and 5.3—5.5 (2H, m), whose spectral data revealed the close resemblance to those of the reduction product **7** of **5**.[11] Compound **6**, when treated with carbon tetrabromide and triphenylphosphine in dry ether, gave a bromide **8**, $C_{15}H_{27}OBr$ (*m/e* 304 and 302; M^+); δ 3.7—4.1 (3H, m) and 5.2—5.5 (2H, m), whose IR spectrum indicated no hydroxyl absorption. Compound **8** was further subjected to Zn–AcOH–MeOH reduction followed by hydrogenation (PtO_2 in ethyl acetate) to yield 4-pentadecanol (**9a**), $C_{15}H_{32}O$ (*m/e* 210; M^+-H_2O), $[\alpha]_{589}^{25}$ +0.87° and $[\alpha]_{365}^{25}$ +3.55°, mp 43 °C; ν_{max} 3350 cm^{-1}, δ *ca.* 3.5 (1H, m). Acetylation of **9a** with acetic anhydride in pyridine gave the corresponding acetate **9b**, $C_{17}H_{34}O_2$ (*m/e* 227; $M^+-C_3H_7$), $[\alpha]_{589}^{25}$ +1.32° and $[\alpha]_{365}^{25}$ +4.25°; ν_{max} 1740 and 1240 cm^{-1}.

On the other hand, compound **3**, on treatment with Raney-Ni in ethanol and successive bromination with carbon tetrabromide and triphenylphosphine in ether, gave a bromide **10**, $C_{15}H_{29}OBr$ (*m/e* 306 and 304; M^+); ν_{max} 1132 and 1080 cm^{-1}, δ 3.3—3.9 (2H, m) and 4.14 (1H, ddd, J=10, 6, and 4 Hz). Moreover, treatment of **10** with zinc in acetic acid and methanol followed by hydrogenation (PtO_2 in ethyl acetate) afforded 4-pentadecanol (**11a**), $C_{15}H_{32}O$, mp 43—44 °C, $[\alpha]_{589}^{25}$ −0.74° and $[\alpha]_{365}^{25}$ −2.17°, which was further converted into the corresponding acetate **11b**, $C_{17}H_{34}O_2$, $[\alpha]_{589}^{25}$ −1.53° and $[\alpha]_{365}^{25}$ −5.60°. The IR, ^1H NMR, and mass spectra of **11a** and **11b** were identical with those of **9a** and **9b**, respectively. Mixed mp of **9a** and **11a** exhibited distinct depression (mp 38 °C).[13]

Since the (*R*)-configuration at C-12 in **3** is kept during the transformation procedure from **3** into **11a**, the configuration at C-4 in **11a** is *S*. Furthermore, 4-pentadecanol (**9a**) derived from **4** was apparently indicated to be an enantiomer of (*S*)-4-pentadecanol (**11a**) by comparison of the optical rotations of **9a**, **9b**, **11a**, and **11b** in different wavelength. Consequently, the stereochemistry at C-4 of epilaurallene (**1**) must be *S*-configuration, and hence the configuration at C-4 of laurallene (**2**) must be *R*.

In view of the strong positive rotations of **1** and **2**, which are due to their bromoallene moieties, the absolute configuration of the allene moiety in **1** and **2** would be assigned as *S* by application of Lowe's rule.[14] Thus, the structure of epilaurallene should be represented by formula **1**.

The finding of epilaurallene (**1**) in *L. nipponica* collected at Tsukotan, near Oshoro Bay, prompted us to reinvestigate the metabolites of Oshoro's specimens which have previously contained laurallene (**2**) as the main component. Surprisingly, fresh algae (coll. at several locations in Oshoro Bay, in April and May, 1982) displayed the existence of epilaurallene (**1**) as a major metabolite and absence of laurallene (**2**). These results appear to suggest that the major secondary metabolite(s) of *L. nipponica* sometimes changes or interconverts in a few years (or every year (?)).[15]

Experimental

All the melting points were uncorrected. The IR spectra were measured on a JASCO A-102 spectrometer. The ^1H NMR spectra were recorded on a JEOL FX-100 spectrophotometer, unless otherwise stated, TMS being used as an internal reference in $CDCl_3$. The ^{13}C NMR spectra were obtained with a JEOL FX-200 spectrophotometer in $CDCl_3$. The optical rotations were measured on a JASCO DIP-181 polarimeter in $CHCl_3$. Aluminium oxide (Merck, activity II-III) and silica gel (Merck, Kieselgel 60, 70—230 mesh) were used for column chromatography. Silica gel (Merck, Kieselgel GF_{254} (Type 60)) was used for preparative thin-layer chromatography. All known compounds were identified by comparison of the spectral data with those of the authentic specimens.

Isolation. *Laurencia nipponica* was collected in April, May, and June 1981, at Tsukotan, near Oshoro Bay,

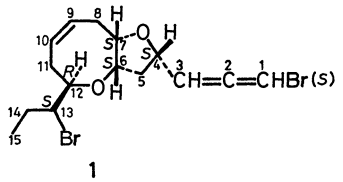

1

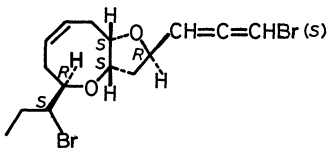

2

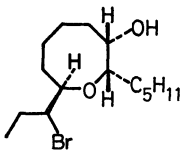

3

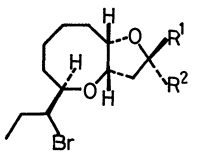

4: R^1=H, R^2=C_3H_7
5: R^1=C_3H_7, R^2=H

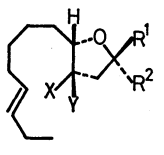

6: R^1=Y=H, R^2=C_3H_7, X=OH
7: R^1=C_3H_7, R^2=Y=H, X=OH
8: R^1=X=H, R^2=C_3H_7, Y=Br

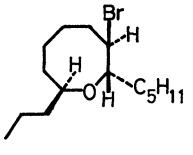

10

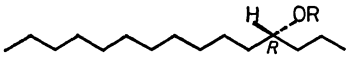

9a: R=H
9b: R=Ac

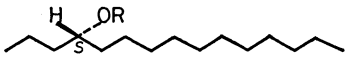

11a: R=H
11b: R=Ac

Hokkaido. The neutral methanol extracts (*ca.* 1% of the half-dried alga) obtained by the conventional methods were fractionated by column chromatography over alumina. The fraction eluted with hexane was chromatographed on silica-gel column to yield 10-bromo-α-chamigrene[5] (1% of the extracts) and laurene[6] (0.5%). The fraction eluted with benzene was repeatedly subjected to a combination of silica gel column and thin-layer chromatography to give a mixture of fatty acid esters (10%; main component, methyl palmitate), (3*E*)-isolaureatin[9] (1%), isolaureatin[10] (1%), laureatin[10] (3%), and (*E*)-γ-bisabolene 8,9-oxide[7] (2%). The fraction eluted with ether was further chromatographed on silica-gel column to yield epilaurallene (**1**) (25%), cycloeudesmol[8] (1%), and an unidentified alcohol (0.5%).

*Epilaurallene (**1**)*: Mp 51—52 °C (from hexane or MeOH); $[\alpha]_D^{25}$ +175° (*c* 1.00); IR (Nujol), ν_{max} 3060, 3025, 1959, 1190, 1120, 1085, 1065, 1053, 928, 818, 765, and 706 cm^{-1}; ^1H NMR (200 MHz), δ 1.09 (3H, t, *J*=7 Hz), 1.7—2.8 (8H, m), 4.0—4.2 (3H, m), 4.24 (1H, m), 4.85 (1H, m), 5.46 (1H, dd, *J*=5 and 5 Hz), 5.7—6.0 (2H, m), and 6.07 (1H, dd, *J*=5 and 2 Hz); MS, *m/e* (rel intensity) 313, 311 (2; M^+-Br), 275, 273 (58; $M^+-C_3H_2Br$), 193 (14; $M^+-C_3H_2Br-HBr$), 149 (9), 123 (15), 121 (15), 109 (31), 107 (75), 81 (30), 79 (100), 77 (38), 67 (69), 65 (29), 55 (56), and 41 (62).

Found: C, 45.94; H, 5.14; Br, 40.75%. Calcd for $C_{15}H_{20}O_2Br_2$: C, 45.88; H, 5.06; Br, 40.55%.

*Hydrogenation of **1**.* The hydrogenation of **1** (40 mg) was performed in EtOH over PtO_2-catalyst. After removal of the catalyst and the solvent, the residual oil was chromatographed on silica-gel column to give **3** (10 mg) and **4** (15 mg). The polar product **3**; colorless oil; $[\alpha]_D^{27}$ +11.1° (*c* 0.718); IR (film), ν_{max} 3450, 1285, 1213, 1128, 1107, 1090, 1053, 958, and 797 cm^{-1}; ^1H NMR, δ 0.89 (3H, br t, *J*=6 Hz), 1.06 (3H, t, *J*=7 Hz), and 3.5—4.1 (4H, m); MS, *m/e* 240 (1; M^+-HBr), 223, 221 (1), 199 (2), 141 (12), 123 (95), 83 (35), 81 (100), 67 (53), 55 (91), 44 (30), and 42 (50): These spectral data were consistent with those of one of the hydrogenation product **3** of laurallene (**2**).[11] The less polar product **4**; colorless oil; $[\alpha]_D^{27}$ +17.0° (*c* 1.17); IR (film), ν_{max} 1277, 1088, 1066, 920, and 795 cm^{-1}; ^1H NMR, δ 0.92 (3H, br t, *J*=6 Hz), 1.08 (3H, t, *J*=7 Hz), 3.6—4.2 (4H, m), and 4.35 (1H, m); MS, *m/e* 277, 275 (10; $M^+-C_3H_7$), 197 (68), 95 (35), 81 (53), 69 (43), 67 (21), 55 (92), 44 (31), and 42 (100).

*Conversion of **4** into **6**.* To a soln of **4** (96 mg) in MeOH (6 ml) containing 350 μl of acetic acid was added activated Zn-dust (350 mg), and the mixture was refluxed for 4 h. After cooling and filtering off Zn-dust, the mixture was extracted with ether. The ether soln was washed successively with water, 5% aqueous $NaHCO_3$, and water. After drying over Na_2SO_4, the solvent was removed to leave residual oil, which was purified by column chromatography on silica gel to afford **6** (72 mg); colorless oil; $[\alpha]_D^{25}$ +4.5° (*c* 1.57); IR, ν_{max} 3400, 1070, 1020, and 970 cm^{-1}; ^1H NMR, δ 0.93 (3H, br t, *J*=6 Hz), 0.96 (3H, t, *J*=7 Hz), 1.8—2.3 (4H, m), 3.76 (1H, ddd, *J*=7, 7, and 3 Hz), 4.1—4.3 (2H, m), and 5.3—5.5 (2H, m); MS, *m/e* 240 (3; M^+), 197 (4), 141 (4), 123 (13), 100 (12), 95 (14), 82 (86), 81 (39), 57 (100), 55 (53), and 42 (22).

*Conversion of **6** into **8**.* A soln of **6** (72 mg) in dry ether (8 ml) was refluxed with triphenylphosphine (160 mg) and carbon tetrabromide (200 mg) for 4 h in N_2 atmosphere and then cooled. The subsequent removal of the solvent gave a residual substance, which was purified by repeated column chromatography on alumina or silica gel to yield **8** (45 mg); colorless oil; $[\alpha]_D^{25}$ −8.6° (*c* 1.09); IR (film), ν_{max} 1091, 1028, and 977 cm^{-1}; ^1H NMR, δ 0.93 (3H, br t, *J*=6 Hz), 0.96 (3H, t, *J*=7 Hz), 1.8—2.2 (4H, m), 3.7—4.1 (3H, m), and 5.2—5.5 (2H, m); MS, *m/e* 304, 302 (1; M^+), 261, 259 (1), 223 (17), 135 (18), 95 (56), 81 (53), 69 (71), 67 (56), 55 (95), and 42 (100).

*4-Pentadecanol (**9a**) from **8**.* To a soln of **8** (45 mg) in MeOH (4 ml) containing 250 μl of acetic acid was added activated Zn-dust (300 mg), and the mixture was refluxed for 3 h. After being cooled and then filtered off, the mixture was extracted with ether. The ether soln was worked up as usual to give an oily residue, which was chromatographed on silica-gel column to yield an unsaturated alcohol (23 mg); colorless oil, IR (film), ν_{max} 3350, 1260, 1020, and 967 cm^{-1}; ^1H NMR, δ 0.93 (3H, br t, *J*=6 Hz), 0.96 (3H, t, *J*=7 Hz), *ca.* 3.5 (1H, m), and 5.2—5.6 (4H, m); MS, *m/e* 224 (0.2; M^+), 206 (1), 110 (33), 96 (26), 82 (34), 81 (34), 68 (48), 67 (50), and 55 (100). The hydrogenation of the unsaturated alcohol was carried out in ethyl acetate over PtO_2-catalyst. After removal of the catalyst and the solvent, the product was purified by column chromatography on silica gel to give **9a** (18 mg); colorless crystals; mp 43 °C; $[\alpha]_D^{25}$ +0.87° (*c* 1.87), $[\alpha]_{577}^{25}$ +1.04°, $[\alpha]_{546}^{25}$ +1.25°, $[\alpha]_{435}^{25}$ +2.30°, and $[\alpha]_{365}^{25}$ +3.55°; IR (Nujol), ν_{max} 3350 cm^{-1}; ^1H NMR, δ 0.8—1.0 (6H) and *ca.* 3.5 (1H, m); MS, *m/e* 210 (2; M^+-H_2O), 185 (19; $M^+-C_3H_7$), 97 (34), 73 (100; $M^+-C_{11}H_{23}$), and 55 (91).

*Acetylation of **9a**.* Acetylation of **9a** (15 mg) was carried out with acetic anhydride in pyridine in the usual manner. The acetylated product was purified by column chromatography on silica gel to give **9b** (13 mg); colorless oil; $[\alpha]_D^{25}$ +1.32° (*c* 1.06) and $[\alpha]_{365}^{25}$ +4.25°; IR (film), ν_{max} 1740, 1240, and 1020 cm^{-1}; ^1H NMR, δ 0.8—1.0 (6H), 2.04 (3H, s), and 4.88 (1H, dddd, *J*=6, 6, 6, and 6 Hz); MS, *m/e* 227 (1; $M^+-C_3H_7$), 210 (2; M^+-CH_3COOH), 115 (7; $M^+-C_{11}H_{23}$), 97 (5), 83 (4), 69 (4), 55 (6), and 43 (100).

*Conversion of **3** into **10**.* To a soln of **3** (110 mg) in EtOH (15 ml) was added freshly prepared W-7 Raney nickel (from 1.5 g of Al-Ni alloy) and then 2 M KOH (1 ml), and the mixture was refluxed for 2 h. After removal of the catalyst, water was added and the most of the solvent was evaporated under reduced pressure. The residue was extracted with ether, and the ether soln was washed with water, dried over Na_2SO_4, and evaporated to leave the debromo alcohol (78 mg); IR (film), ν_{max} 3420, 1125, 1075, 1046, 1012, and 948 cm^{-1}; ^1H NMR, δ 0.8—1.0 (6H) and 3.4—3.8 (3H, m); MS, *m/e* 242 (3; M^+), 82 (100), 57 (59), and 55 (56). Bromination of the above debromo alcohol (150 mg) was performed with triphenylphosphine (300 mg) and carbon tetrabromide (400 mg) in dry ether (10 ml) under the similar reaction conditions in the case of **6** to give **10** (105 mg); colorless oil; $[\alpha]_D^{27}$ −5.8° (*c* 0.24); IR (film), ν_{max} 1180, 1132, and 1080 cm^{-1}; ^1H NMR, δ 0.9—1.0 (6H), 3.3—3.9 (2H, m), and 4.14 (1H, ddd, *J*=10, 6, and 4 Hz); MS, *m/e* 306, 304 (1; M^+), 263, 261 (1), 125 (27), 82 (80), 69 (94), 55 (100), and 42 (8).

*(S)-4-Pentadecanol (**11a**) from **10**.* To a soln of **10** (105 mg) in MeOH (6 ml) containing 350 μl of acetic acid was added activated Zn-dust (200 mg), and the mixture was refluxed for 2 h. After the usual work-up, the resulting unsaturated alcohol was hydrogenated, without further purification, with PtO_2 in ethyl acetate and then purified by column chromatography on silica gel to give **11a** (48 mg); colorless crystals; mp 43—44 °C; $[\alpha]_D^{25}$ −0.74° (*c* 3.33), $[\alpha]_{577}^{25}$ −0.78°, $[\alpha]_{546}^{25}$ −0.92°, $[\alpha]_{435}^{25}$ −1.75°, and $[\alpha]_{365}^{25}$ −2.17°; The spectral properties were identical with those of **9a**.

*Acetylation of **11a**.* Acetylation of **11a** (18 mg) was carried out with acetic anhydride in pyridine by the usual method to give **11b** (15 mg); colorless oil; $[\alpha]_D^{25}$ −1.53° (*c* 1.57) and $[\alpha]_{365}^{25}$ −5.60°; The spectral properties were identical with those of **9b**.

References

1) Part 50 of "Constituents of Marine Plants." Part 49: K. Kurata, A. Furusaki, K. Suehiro, C. Katayama, and T. Suzuki, *Chem. Lett.*, **1982**, 1031.

2) M. Suzuki and E. Kurosawa, *Bull. Chem. Soc. Jpn.*, **52**, 3352 (1979); M. Suzuki and E. Kurosawa, *Tetrahedron Lett.*, **22**, 3853 (1981).

3) *L. okamurai* collected at Goza, Mie Pref., has contained laurinterol and debromolaurinterol as the minor components [H. Kigoshi, Y. Shizuri, H. Niwa, and K. Yamada, *Tetrahedron Lett.*, **22**, 4729 (1981)]. However, a red form of Goza's species contained these compounds as the major ones [Y. Shizuri, A. Yamada, and K. Yamada, 45th National Meeting of the Chemical Society of Japan, 1982, Abstracts II, p. 768].

4) K. Kurata, A. Furusaki, C. Katayama, H. Kikuchi, and T. Suzuki, *Chem. Lett.*, **1981**, 773; T. Suzuki, H. Kikuchi, and E. Kurosawa, *Bull. Chem. Soc. Jpn.*, **55**, 1561 (1982), and references cited therein.

5) M. Suzuki, A. Furusaki, and E. Kurosawa, *Tetrahedron*, **35**, 823 (1979).

6) T. Irie, T. Suzuki, Y. Yasunari, E. Kurosawa, and T. Masamune, *Tetrahedron*, **25**, 459 (1969).

7) T. Suzuki, H. Kikuchi, and E. Kurosawa, *Chem. Lett.*, **1980**, 1267.

8) T. Suzuki, A. Furusaki, H. Kikuchi, E. Kurosawa, and C. Katayama, *Tetrahedron Lett.*, **22**, 3423 (1981).

9) E. Kurosawa, A. Fukuzawa, and T. Irie, *Tetrahedron Lett.*, **1972**, 2121.

10) T. Irie, M. Izawa, and E. Kurosawa, *Tetrahedron*, **26**, 851 (1970).

11) A. Fukuzawa and E. Kurosawa, *Tetrahedron Lett.*, **1979**, 2797.

12) ^{13}C NMR data for laurallene (**2**); δ (50.10 MHz, $CDCl_3$) 201.036 (s), 129.469 (d), 127.396 (d), 102.693 (d), 82.925 (d), 79.830 (d), 74.224 (d), 73.581 (d), 73.406 (d), 57.960 (d), 39.448 (t), 30.571 (t), 29.374 (t), 28.148 (t), and 11.241 (q).

13) (±)-4-Pentadecanol: mp 36.3—37.5 °C; F. L. Breusch and S. Sokullu, *Chem. Ber.*, **86**, 678 (1953).

14) G. Lowe, *Chem. Commun.*, **1965**, 411; In the case of isolaurallene[16] and obtusallene-I,[17] which reveal the strong negative rotations and were shown to possess *R*-configuration at the bromoallene moiety by X-ray diffraction analysis, Lowe's rule can well be applied in order to determine the absolute stereochemistry of the bromoallene.

15) *L. nipponica* collected at Oshoro Bay in 1977—1980 unambiguously gave laurallene (**2**); private communication from Dr. Akio Fukuzawa.

16) K. Kurata, A. Furusaki, K. Suehiro, C. Katayama, and T. Suzuki, *Chem. Lett.*, **1982**, 1031.

17) P. J. Cox, S. Imre, S. Islimyeli, and R. H. Thomson, *Tetrahedron Lett.*, **23**, 579 (1982).

 © 1983 The Chemical Society of Japan Bull. Chem. Soc. Jpn., 56, 719—723 (1983)

Electrocatalytic Reduction Using Raney Nickel

Toshiro CHIBA,* Mitsuhiro OKIMOTO, Hiroshi NAGAI, and Yoshiyuki TAKATA†

Department of Applied Chemistry, Kitami Institute of Technology, Koen-cho 165, Kitami 090

†*Faculty of Engineering, Hokkaido University, Sapporo 060*

(Received July 3, 1982)

The Raney nickel catalyst was employed as a catalytic electrode in the electrohydrogenation of various unsaturated compounds, including ketones, aromatic aldehydes, Schiff's bases, oximes, nitriles, aromatic nitro compounds, olefins, and acetylenes. The hydrogen generated electrochemically was adsorbed and activated at the surface of the catalyst; it effectively hydrogenated these compounds, affording products which are very similar to those obtained in a normal catalytic hydrogenation with Raney nickel.

Although the Raney nickel (Ra/Ni) catalyst has been widely used as a catalyst in catalytic hydrogenation in the laboratory and on an industrial scale,[1] its application as a catalyst for electrochemical hydrogenation seems to have attracted very little attention.[2,3] Because of a large surface area and a high hydrogen-adsorption activity, Ra/Ni was expected to be applicable as a catalytic electrode. If the electrolytically generated hydrogen is directly used as a reducing agent at the surface of the catalyst, in the hydrogenation with Ra/Ni, it may be possible to avoid the use of an autoclave and comperessed hydrogen gas. Thus, we have attempted electrohydrogenation using a cathode made of nickel plate covered with Ra/Ni powder, and examined its reduction ability.

Results and Discussion

Preparative electrolyses were carried out in the cell depicted in Fig. 2. Almost all of the substrates were electrolyzed in methanol containing sodium methoxide under a constant current and at room temperature. The amount of the catalyst used was 2 g per 0.1 mol of the substrate.

At first, in preliminary experiments using benzophenone, the following facts were confirmed: a) when the Ra/Ni catalyst is omitted and the nickel plate alone is used as the cathode, the reduction of benzophenone to benzhydrol is extremely slow (the current efficiency is less than 10%); instead hydrogen is evolved; b) when the surface of the nickel plate is covered with the catalyst, the reduction proceeds essentially quantitatively, and c) if no current is passed through and hydrogen gas is bubbled through the catholyte in the presence of the catalyst, only about a 20% yield of benzhydrol is formed by the reaction over a period of 10 h. Apparently, Ra/Ni exerted an excellent electrode-catalytic effect.

Table 1 shows the results of the electrohydrogenation of various compounds.

All the ketones employed were effectively reduced predominantly to give the corresponding secondary alcohols. In these cases, hardly no glycols were detectable.[3] Analogous results were obtained with aromatic aldehydes;[4] however, aliphatic aldehydes could not be used since they formed aldol adducts in this medium.

Carbon-nitrogen unsaturated compounds, such as Schiff's bases,[5] nitriles,[6] and oximes,[7] were reduced equally well to the respective amines. The nonaqueous system of methanolic sodium methoxide appeared to be particularly favorable for the reduction of these compounds, which tend to involve C–N bond cleavage in an aqueous solution.[8] Either nitriles or oximes were electrolyzed in the presence of excess amounts of ammonia in order to suppress the formation of undesirable secondary amines.[9]

Under the same conditions, nitrobenzenes afforded anilines as the main products, along with a small amount of hydrodimers,[3,10] whereas aliphatic nitro compounds were not reducible. Probably, this was due to the formation of the anion of the aci-form in the basic solution, which prevented the reduction.[8]

According to this method, not only carbon-carbon conjugated double bonds with a carbonyl group, *etc.*,[11] but also isolated double bonds which are very resistant to conventional electrolytic reduction[12] could readily be hydrogenated. The selective reduction of acetylenes to olefins was not successful, however, since it always was attended by a subsequent reduction to alkanes.

Next, in order to examine the cathodic behavior of Ra/Ni, current-potential relationships were measured in a 0.1 mol dm^{-3} sodium methoxide–methanol solution.

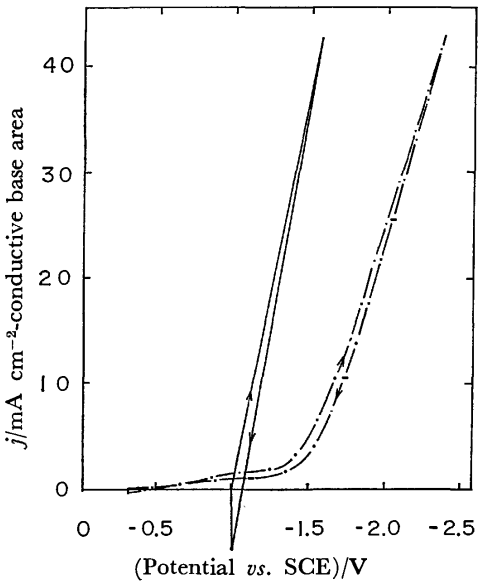

Fig. 1. Current-potential curves for 0.1 M NaOMe–MeOH. ——: at Ra/Ni cathode, ——: at Ni-plate cathode. Sweep rate of 0.1 V/s was used.

Table 1. Electrohydrogenation using Raney nickel catalyst[a)]

Starting material	Product[b)]	Consumed current F/mol	Isolated yield[c)] %	Isolation method	Bp θ_b/°C(mmHg) or Mp θ_m/°C Obsd[d)]	Ref.
[Ketones: $>C=O + 2H^+ + 2e^- \longrightarrow >CH\text{-}OH$]						
n-$C_3H_7COC_3H_7$	n-$C_3H_7CH(OH)C_3H_7$	3.4	71	A	153—154	154[17)]
n-$C_5H_{11}COCH_3$	n-$C_5H_{11}CH(OH)CH_3$	3.4	73	A	156—158	158—160[17)]
i-$C_4H_9COCH_3$	i-$C_4H_9CH(OH)CH_3$	2.8	75 (80)	A	129—131	130—131 (763)[17)]
=O	-OH	3.7	70 (97)	A	157—160	161[17)]
-$COCH_3$	-$CH(OH)CH_3$	3.4	82 (97)	A	93—94 (13)	98—99 (20)[17)]
-COC_2H_5	-$CH(OH)C_2H_5$	3.7	73	B	97—99 (12)	106—108 (18)[17)]
-CH_2COCH_3	-$CH_2CH(OH)CH_3$	3.4	70	B	95—98 (12)	219—221,[17)] 107 (15)[18)]
-CO- [e)]	-CH(OH)-	3.6	82 (90)	B	66—68 [MeOH]	69[17)]
-$COCH_2$-	-$CH(OH)CH_2$-	2.9	71	B	66—68 [Hexane]	67[17)]
[r-Keto acids]						
$CH_3COCH_2CH_2COOH$[f)]		2.8	73	B[g)]	85—86 (15)	83—84 (13)[17)]
-$COCH_2CH_2COOH$[f)]		2.8	80	B	38 [MeOH]	38[17)]
[Aldehydes: $-CHO + 2H^+ + 2e^- \longrightarrow -CH_2OH$]						
-CHO	-CH_2OH	2.2	70	B[h)]	91—92 (11)	93 (10)[17)]
CH_3- -CHO	CH_3- 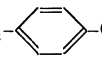 -CH_2OH	2.2	76	B[h)]	59—61 [Hexane]	61—62[17)]
CH_3O- -CHO	CH_3O- -CH_2OH	2.2	71	B[h)]	136—139 (12)	128—130 (8)[17)]
[f)]		2.2	83	B	80—83 [Benzene]	87[17)], 84[19)]
[Schiff's Bases: $-N=CH- + 2H^+ + 2e^- \longrightarrow -NHCH_2-$]						
n-$C_4H_9N=CHC_3H_7$	n-$C_4H_9NHC_4H_9$	2.8	79	C	156—160	159[17)]
n-$C_4H_9N=CH$-	n-$C_4H_9NHCH_2$-	2.8	75	C	107—109 (12)	226—230[20)]
-N=CH-	-$NHCH_2$-	2.8	74	C[i)]	213—215 [H_2O]	214—216[17)]
-$CH_2N=CH$-	-CH_2NHCH_2-	2.8	80	C[i)]	257—258 [H_2O]	256[17)]
[Nitriles: $-C\equiv N + 4H^+ + 4e^- \longrightarrow -CH_2NH_2$]						
n-C_4H_9CN[1)]	n-$C_5H_{11}NH_2$	5.4	72	C	103	104[17)]
n-$C_6H_{13}CN$[1)]	n-$C_7H_{15}NH_2$	5.1	76	C	154	155 (760)[17)]
$NC\{CH_2\}_4CN$[j,1)]	$H_2N\{CH_2\}_6NH_2$	10.0	70 (87)	k)	85 (15)	100 (20)[17)]
-CN[1)]	-CH_2NH_2	6.3	75	C	69—70 (12)	185[17)], 74/15[21)]
-CH_2CN[1)]	-$CH_2CH_2NH_2$	5.6	71	C	82—83 (12)	197—198[17)], 92—93 (19)[9)]
[Oximes: $=N\text{-}OH + 4H^+ + 4e^- \longrightarrow -NH_2$]						
=N-OH[1)]	-NH_2	6.7	65 (77)	C	131—134	134[17)]
-$C(=N\text{-}OH)$-CH_3[1)]	-$CH(NH_2)$-CH_3	6.7	62	C	71—72 (12)	87 (24)[17)], 80—81 (18)[22)]

TABLE 1. Continued.

Starting material	Product[b]	Consumed current F/mol	Isolated yield[c] %	Isolation method	Bp θ_b/°C(mmHg) or Mp θ_m/°C Obsd[d]	Ref.
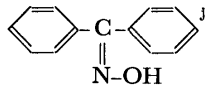 [j,l]	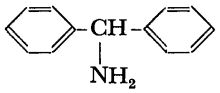	6.7	62	C	163—167(12)	175—176(23)[17]
[Nitro compounds: $-NO_2 + 6H^+ + 6e^- \longrightarrow -NH_2$]						
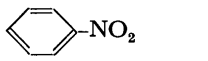	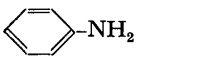	6.2	63(72)	C	75(12)	92(33)[17]
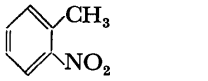	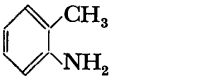	5.6	58(66)	C	83(12)	92(18)[17]
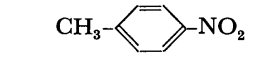	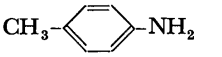	6.7	60(71)	C	40—43	42[17]
[Unsaturated hydrocarbons: $\overset{\diagdown}{C}=\overset{\diagup}{C} + 2H^+ + 2e^- \longrightarrow \overset{\diagdown}{CH}-\overset{\diagup}{CH}$]						
n-$C_6H_{13}CH=CH_2$	n-C_8H_{18}	3.2	66(76)	D	124—126	125.7[17]
n-$C_5H_{11}CH=CHCH_2$	n-C_8H_{18}	3.2	(70)			
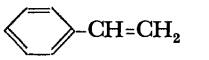	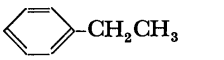	2.6	75(85)	D	133—135	136[17]
n-$C_6H_{13}C\equiv CH$	n-$C_6H_{13}CH=CH_2$	2.0	(11)	m, n)		
	n-C_8H_{18}		(39)			
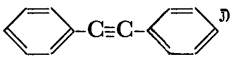 [j]	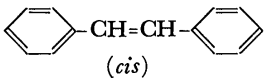 (*cis*)	5.6	(22)	m)		
	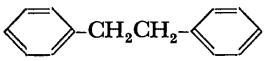		(60)			
[α,β-Unsaturated carboxylic acids]						
$CH_3CH=CHCOOH$[f]	n-C_3H_7COOH	2.8	60	B	156—160	162[17]
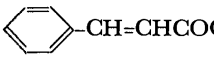 [f]	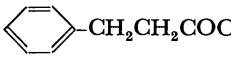	2.5	75	B	50—51 [Hexane]	48.5[11),17]

a) Anolyte: starting material (0.10 mol) in 150 ml of MeOH containing 0.15 mol of NaOMe. Raney nickel catalyst: 2 g. Constant current: 0.75 A. Temperature: *ca.* 15 °C. b) The products obtained were identified by a comparison of their phisical and IR-spectral data with those of authentic samples or with the literature data. c) Value in brackets refers to yield estimated by GLC. d) Boiling points and melting points are uncorrected. (1 mmHg≈133.322 Pa). e) 180 ml of methanol was used. f) Electrolyzed in 150 ml of a 1.67 mol dm^{-3} NaOH aq solution. g) Continuously extracted with diethyl ether for 12 h. h) The crude products were treated with a saturated sodium hydrogensulfite solution before distillation. i) Isolated as HCl-salt. j) 0.05 mol was used. k) After the removal of the methanol, the residue was diluted with 30 ml of water, refluxed for 10 h, and then continuously extracted with diethyl ether for 12 h. l) An excess amount of ammonia was added to the catholyte. m) Analytical samples were obtained by preparative GLC and were identified with authentic samples by NMR and mass spectroscopy. n) Unreacted acetylene was recovered in a yield of 44%.

As is shown in Fig. 1, the sodium methoxide–methanol electrolyte system was discharged at the potential of −1.0 V *vs.* SCE at a nickel-plate cathode covered with Ra/Ni, in contrast to the potential of −1.5 V at a nickel-plate cathode. Interestingly, in spite of an appreciable increase in the electrolytic current (10 A/dm^2-coductive base area), no evolution of hydrogen was observed, presumably because of a strong adsorption of hydrogen to the Ra/Ni electrode. In this system, the substrates employed, such as ketones and nitriles, showed no reduction waves below the potential of −1.0 V. Consequently, it was reasonable to assume that the reduction takes place by adsorbed hydrogen atoms which are electrolytically generated and activated under the catalytic influence. rather than by direct electron-transfer between the substrate and the electrode.

In conclusion, the Ra/Ni electrode brought about the hydrogenation of various compounds, and the course of the reaction resembled that taken by a normal catalytic hydrogenation with Ra/Ni and elemental hydrogen. It seemed to be especially attractive in that the reduction using Ra/Ni, which usually requires an increased temperature and pressure except for the use of Ra/Ni W-6, is possible at room temperature and atmospheric pressure,[14] while the hydrogenation of aromatic nuclei[15] or the hydrogenolysis of carbonyl groups of acid amides or esters was impossible. Application to compounds with two different functional groups is currently being undertaken, including the

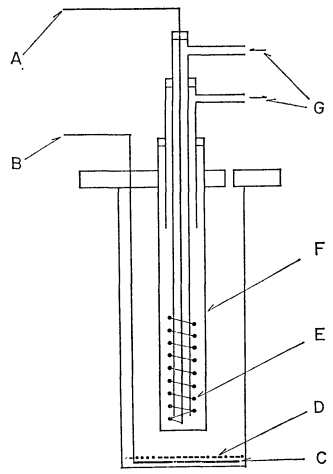

Fig. 2. Preparative scale electrolysis cell.
A: Lead to anode, B: lead to cathode, C: nickel plate, D: Raney nickel catalyst, E: platinum coil anode, F: ceramic cup, G: inlet and outlet of anolyte (to pump).

use of other Raney catalysts, *e.g.*, Ra/Co, Ra/Cu, and Ra/Fe.

Experimental

Apparatus. The preparative electrolyses were carried out in the two-compartment cell depicted in Fig. 2. On the bottom of the cathode compartment (200 ml), a conductive base of nickel plate ($\phi=5.0$ cm) is placed. As the anode compartment, a ceramic cup (2 mm wall thickness, 17 cm high, and 1.8 cm in diameter) is used; it is provided with a platinum coil anode and an inlet and outlet for the circulation of the anolyte. The cell is externally cooled with water.

Preparation of Raney Nickel Catalyst. In a 300-ml round-bottom flask, 4.0 g of Raney nickel alloy powder (Ni content, *ca.* 50%) is suspended in 40 ml of distilled water. Then, 6.5 g of sodium hydroxide pellets are added all at once. An exothermic reaction occurs with a vigorous evolution of hydrogen. After the evolution of hydrogen slows, the suspension is digested at 60 °C on a steam bath for 30 min with occasional shaking and then allowed to attain room temperature. The alkaline solution is decanted, and the nickel is washed three times with 50-ml portions of distilled water, followed by three washings with 25-ml portions of methanol. The Raney nickel catalyst obtained in this manner weighs about 2 g, and its activity is comparable to that of W-2.[16]

General Procedure. The cathode compartment is charged with 0.10 mol of a substrate dissolved in 150 ml of methanol containing 0.15 mol of sodium methoxide (unsaturated carboxylic acids, keto acids, and salicylaldehyde are electrolyzed in 150 ml of 1.67 mol dm^{-3} aqueous sodium hydroxide). Then, about 2 g of freshly prepared Raney nickel catalyst is added to the catholyte and allowed to settle on the nickel plate. The anolyte of the same concentration of methanolic sodium methoxide is circulated by pumping, and the current is turned on. During the electrolysis, the catholyte is occasionally stirred with a glass rod.

All electrolyses were conducted under a constant current of 0.75 A until almost all of the substrate has been consumed (1.1—1.8 of the theoretical current is passed through). After the reduction, the catholyte is filtered from the catalyst and treated as follows.

Work-up Procedure. A): The resulting catholyte is diluted to 2 volumes with methanol, and carbon dioxide is bubbled into the solution. The precipitated sodium carbonate is filtered off and washed with methanol (20 ml × 2). The filtrate and washings are combined and distilled.

B): After the removal of the solvent, the residue is acidified with 18% hydrochloric acid. The separated oily layer is extracted with diethyl ether (30 ml × 4), dried with magnesium sulfate, and distilled or recrystallized.

C): The reaction mixture is concentrated to 1/2 volume, acidified with 18% hydrochloric acid, and evaporated to dryness. The remaining solid is dissolved in water, washed thoroughly with diethyl ether, and made strongly alkaline with sodium hydroxide. The separated oily layer is extracted with diethyl ether (30 ml × 4), dried with sodium hydroxide, and distilled over a few pellets of sodium hydroxide.

D): The catholyte is poured into 2 volumes of water. The separated oily layer is extracted with hexane (30 ml × 4), washed with water, dried with anhydrous potassium carbonate, and distilled.

References

1) For example, see J. S. Pizey, "Synthetic Reagents," Ellis Horwood, Ltd., Chichester (1974), Vol. II, p. 175; R. Schröter, "Newer Methods of Preparative Organic Chemistry," Interscience Pub., Inc., New York (1948), p. 61.
2) B. Sakurai and T. Arai, *Bull. Chem. Soc. Jpn.*, **28**, 3873 (1962).
3) For the leading literature of the electrochemical reduction of organic compounds, see M. R. Rifi, "Technique of Electro-Organic Synthesis," ed by N. L. Weinberg, Wiley-Interscience, New York (1975), Part II, p. 83; "Organic Electrochemistry," ed by M. M. Baizer, Marcel Dekker, Inc., New York (1973); F. D. Popp and H. P. Schultz, *Chem. Rev.*, **62**, 19 (1962).
4) H. D. Law, *J. Chem. Soc.*, **89**, 1512 (1906); **91**, 748 (1907); **99**, 1113 (1911).
5) H. Lund, *Acta Chem. Scand.*, **13**, 249 (1959); A. J. Fry and R. G. Reed, *J. Am. Chem. Soc.*, **91**, 6448 (1969); see also R. A. Benkeser and S. J. Mels, *J. Org. Chem.*, **35**, 261 (1970).
6) M. Ohta, *Bull. Chem. Soc. Jpn.*, **17**, 485 (1942); F. Kawamura and S. Suzuki, *Nippon Kagaku Kaishi*, **55**, 476 (1952); *Chem. Abstr.*, **48**, 3167 (1954); S. Sawa, Japan Patent, 5019 (1951); *Chem. Abstr.*, **47**, 2617 (1953); T. Nonaka and K. Sugino, *J. Electrochem. Soc.*, **114**, 1255 (1967); Yu. D. Smirnov and A. P. Tomilov, *Zh. Org. Khim.*, **5**, 864 (1969); *Chem. Abstr.*, **71**, 38299h (1969).
7) H. Lund, *Tetrahedron Lett.*, **1968**, 3651; S. Swan, Jr., C.-Y. Chen, and H. D. Kerfman, *J. Electrochem. Soc.*, **99**, 460 (1952).
8) H. Lund, "The Chemistry of Carbon-Nitrogen Double Bond," ed by S. Patai, Wiley-Interscience, New York (1970), p. 505.
9) J. C. Robinson, Jr., and H. R. Snyder, *Org. Synth.*, Coll. Vol. III, 720 (1955).
10) S. Wawzonek, *Synthesis*, **1971**, 285.
11) A. W. Ingersoll, *Org. Synth.*, Coll. Vol. I, 311 (1941).
12) K. N. Campbell and B. K. Campbell, *Chem. Rev.*, **31**, 129 (1942); R. A. Benkeser and S. J. Mels, *J. Org. Chem.*, **34**, 3970 (1969).
13) K. N. Campbell and E. E. Young, *J. Am. Chem. Soc.*, **65**, 965 (1943); R. A. Benkeser and C. A. Tincher, *J. Org. Chem.*, **33**, 2727 (1968).

14) *Cf.* P. L. Cook, *J. Org. Chem.*, **27**, 3873 (1962).
15) L. L. Miller and L. Christesen, *J. Org. Chem.*, **43**, 2059 (1978); H. W. Sternberg, R. E. Markby, I. Wender, and D. M. Mohilner, *J. Am. Chem. Soc.*, **91**, 4191 (1969); R. A. Benkeser, E. M. Kaiser, and R. E. Lambert, *ibid.*, **86**, 5272 (1964).
16) H. R. Billica and H. Adkins, *Org. Synth.*, Coll. Vol. III, 176 (1955).
17) "Dictionary of Organic Compounds," 4th ed, ed by J. R. A. Pollack and R. Stevens, Eyre and Spottiswoode (Publishers), Ltd., Great Britain (1965).
18) M. S. Newman, *J. Am. Chem. Soc.*, **62**, 2295 (1940).
19) H. Adkins and H. I. Cramer, *J. Am. Chem. Soc.*, **52**, 4349 (1930).
20) A. Einhorn and H. Pfeiffer, *Justus Liebigs Ann. Chem.*, **310**, 225 (1900).
21) C. F. Winans and H. Adkins, *J. Am. Chem. Soc.*, **55**, 2051 (1933).
22) J. C. Robinson, Jr., and H. R. Snyder, *Org. Synth.*, Coll. Vol. III, 717 (1955).

Convenient Preparation of Dimethyl (Trifluoromethyl)malonate and Related Compounds

Nobuo Ishikawa* and Tsutomu Yokozawa

Department of Chemical Technology, Tokyo Institute of Technology, Ookayama, Meguro-ku, Tokyo 152

(Received July 12, 1982)

The preparative method for dimethyl (trifluoromethyl)malonate (**4**) from the adduct of perfluoro-2-methylpropene with methanol was improved, and several reactions of this base-sensitive substance were investigated. Alkylation of **4** was achieved by using CsF as a condensing agent, and the Michael addition on vinyl ketones proceeded in triethylamine–pyridine medium.

Organic molecules bearing a trifluoromethyl group have recently been drawing attention because of their possible biological activities.[1,2] One of the attractive methods for the preparation of this kind of compounds is to prepare some versatile intermediates carrying a trifluoromethyl group and to utilize them as building blocks. As one of these building blocks, (trifluoromethyl)malonic ester seemed to be useful because it would afford various trifluoromethylated aliphatic or heterocyclic compounds by the usual synthetic methods.

Dimethyl (trifluoromethyl)malonate (**4**) has already been prepared by Knunyants' group[3,4] from *F*-2-methylpropene (**1**), an extremely toxic perfluoroalkene gas. By their method, the adduct (**2**) of **1** with methanol, a stable liquid, was hydrolyzed with concd sulfuric acid, and the resulting ester (**3**) was subjected to alcoholysis in the presence of triethylamine to give **4**.

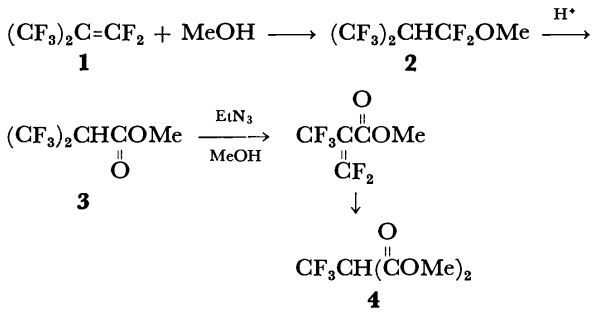

Another report form his group[5] also revealed the formation of **4** together with **3** and **6** from an enolate anion (**5**) generated by the reaction of **2** with triethylamine.

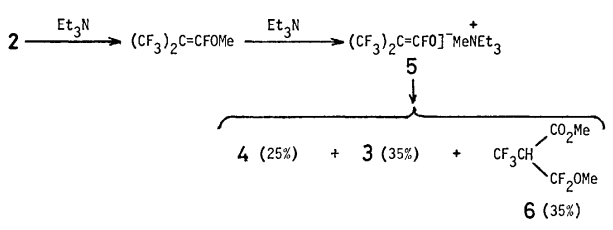

Although the reported yield of **4** is poor, the latter process, a one-step reaction from the adduct **2**, was more attractive to us and we were able to find the optimum conditions to produce **4** in sufficient yields. Some reactions of **4** including alkylations and Michael additions were examined. Although the results were not those which we had expected, we observed several interesting behaviors of **4** in its reaction mode.

Results and Discussion

Improved Preparation of 4. The adduct **2** was found to be readily converted to the enolate **5** in *N,N*-dimethylformamide by treating it with 2 mol of triethylamine, and **5** thus formed was subjected to methanolysis at room temperature. The major product was a ketene acetal **7**, formed together with a small amount of **6**. By treating the mixture with concd sulfuric acid **4** was obtained in a yield of 68% based on **2**.

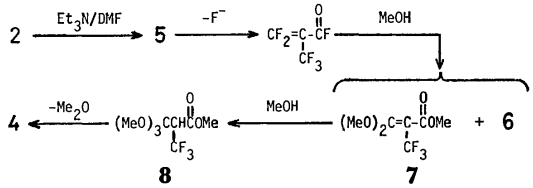

Alkylation of 4. Regarding the reactivities of (trifluoromethyl)malonic esters, it is known[4] that they are susceptible to the attack of an alkali, forming a terminal difluoromethylene compound (**10**) which is degraded to the nonfluorinated dimethyl malonate (**12**) *via* a carboxylic acid (**11**). This behavior makes the reaction of **4**, such as alkylation under alkaline conditions, impossible.

To avoid this degradation, cesium fluoride was used as a neutral proton-removing agent. The subsequent alkylation with an alkyl halide gave 2-alkyl-2-(trifluoromethyl)malonic ester (**13**) together with an addition product (**14**) of **9** and **10** as a by-product.

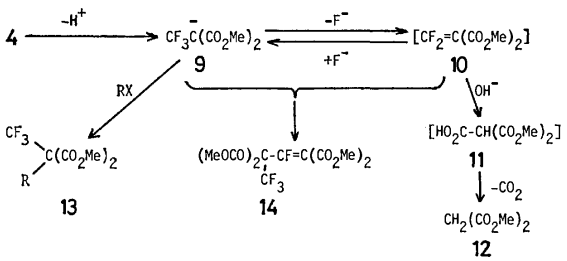

When potassium fluoride instead of cesium fluoride was used in this reaction, the formation of **14** was accelerated considerably. Particularly, in the reaction with benzyl or allyl bromide, the formation of alkylated product **13** was not observed (Table 1). This should be due to the stronger ionizing ability of CsF compared with that of KF. Thus, when CsF was used, the higher concentration of fluoride ions in the reaction

Table 1. Formation of **13** and **14**

RX	MF Yield/%[a]			
	CsF		KF	
	13	**14**	**13**	**14**
MeI	76	8	51	47
$PhCH_2Br$	22	44	—	82
$CH_2=CHCH_2Br$	19	58	—	90

a) Based on ^{19}F NMR signal intensities.

mixture would increase the amount of carbanion **9** rather than **10** in an equilibrium between them, resulting in the increase of the formation of alkylated product **13**. On the other hand, the lower concentration of fluoride ions in the case of KF, would rather favor the formation of the defluorinated intermediate **10** and the subsequent reaction with **9** forming **14** would occur instantly. In the absence of alkyl halides, we could obtain **14** in a good yield by the reaction of **4** with sodium hydride, a much stronger base containing no fluoride ion. A similar compound, tetraethyl ester, had been reported by Knunyants' group.[6]

The alkylation of **4** to give **13** was actually carried out by adding **4** gradually into a mixture of alkyl halide and CsF so that the formation of **14** would be significantly suppressed (Table 2).

Attempted decarboxylation of **13** by heating it with an alkali gave nonfluorinated alkylmalonic acid (**15**), presumably according to the following scheme.

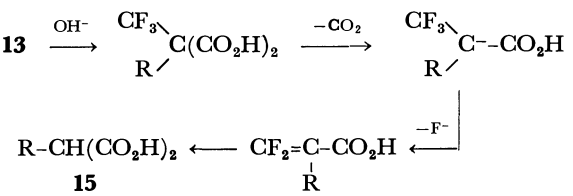

*Michael Addition of **4** to Vinyl Ketones.* As another kind of reactions utilizing the "activated hydrogen" of **4**, its addition to vinyl ketones was carried out. This Michael-type reaction using triethylamine and pyridine as a base and a solvent proceeded smoothly affording 3-oxoalkyl(trifluoromethyl)malonates (**16**) as shown in Table 3.

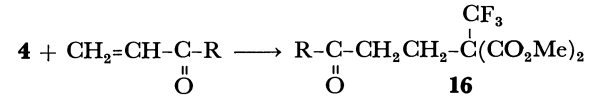

These derivatives of (trifluoromethyl)malonic esters are expected as useful intermediates for various organic compounds carrying a trifluoromethyl group. Studies for this purpose are now underway.

Experimental[7]

*Dimethyl (Trifluoromethyl)malonate, **4**.* Triethylamine (101.2 g, 1.0 mol) was added dropwise into a mixture of 1,1,3,3,3-pentafluoro-2-(trifluoromethyl)propyl methyl ether (**2**, the adduct of *F*-2-methylpropene with methanol) (116 g, 0.5 mol) and dried *N*,*N*-dimethylformamide (100 ml), keeping the temperature at 10—20 °C. After the addition, methanol (100 ml) was added dropwise into the mixture over a period of 40 min, during which the temperature was kept below 10 °C by cooling with an ice-bath. After being stirred for 70 min at that temperature, the reaction mixture was poured into water and the resultant oily layer was separated. The aqueous layer was subjected to ether extraction and the ethereal extract was combined with the oil and was dried over $MgSO_4$. After removal of the ether, conc. sulfuric acid (10 ml) was added to the residue and the mixture was stirred overnight at room temperature. After the mixture was poured on ice, the resulting oily material was separated, combined with the ethereal extract from the water layer, dried over $MgSO_4$ and subjected to distillation. (Trifluoromethyl)malonate (67.5 g), bp 65—66 °C/10 mmHg† (lit,[3] 72.5—73 °C/9 mmHg), was obtained in a yield of 68%. ^{19}F NMR: δ −11.1 (d, J_{H-F} 8.0 Hz). ^1H NMR: δ 4.11 (q, $CHCF_3$, J_{H-F} 8.0 Hz), 3.83 (s, CH_3). IR: 1755 (C=O) cm^{-1}.

*Dimethyl Methyl(trifluoromethyl)malonate (**13**, R=Me).* A mixture of dried CsF (9.11 g, 60 mmol), diglyme (41 ml), dimethyl (trifluoromethyl)malonate (4 g, 20 mmol), and methyl iodide (3.12 g, 22 mmol) was stirred overnight at room temperature. The reaction mixture was poured into

Table 2. Alkylation of **4** giving **13**, $RC(CF_3)(CO_2Me)_2$

RX	Reaction conditions: Solvent	Temp °C	Time h	Yield of **13** %	Bp θ_b/°C (mmHg)	NMR δ: ^{19}F[a] CF_3	^1H CO_2Me	^1H R	IR ν(CO) cm^{-1}	Found(%) C	Found(%) H	Calcd(%) C	Calcd(%) H
MeI	Diglyme	r.t.	12	60	63—65(10)	−7.5(s)	3.81(s)	1.66(s, CH_3)	1750	39.40	4.21	39.26	4.24
$PhCH_2Br$	Diglyme	70—75	2	45	91—94(0.3)	−12.2(s)	3.73(s)	3.50(s, CH_2) 7.29(s, ArH)	1745	53.58	4.49	53.80	4.51
$CH_2=CHCH_2Br$	Diglyme	70—75	2	47	90—94(9)	−10.6(s)	3.79(s)	2.85(d, CH_2)	1755	45.19	4.54	45.01	4.62

a) See Ref. 7.

Table 3. Michael addition of **4** to vinyl ketons giving **16**, $RC(O)CH_2CH_2C(CF_3)(CO_2Me)_2$

R in $RC(O)CH=CH_2$	Reaction conditions: Solvent	Temp °C	Time h	Yield of **16** %	Bp θ_b/°C (mmHg)	NMR δ: ^{19}F(neat)[a] CF_3	^1H (CCl_4) CO_2Me	^1H Me(R)	^1H CH_2CH_2	IR ν/cm^{-1} C=O	IR ν/cm^{-1} CO_2Me	Found(%) C	Found(%) H	Calcd(%) C	Calcd(%) H
Me	Pyridine	70	4	74	88—89(0.2)	−10.5(s)	3.82(s)	2.10(s)	2.22—2.69(m)	1720	1745	44.16	4.82	44.45	4.85
Et	Pyridine	70	4	66	89—91(0.2)	−10.7(s)	3.81(s)	1.04(t)	2.23—2.67(m)	1720	1750	46.18	5.36	46.48	5.36

a) See Ref. 7.

† 1 mmHg=133.322 Pa.

water and the resultant oily layer and the ether-extract from aqueous layer were combined and washed with water to remove diglyme. After drying over $MgSO_4$, the ether was evaporated and the residue was subjected to distillation, giving dimethyl methyl(trifluoromethyl)malonate (2.56 g, 60%), bp 63—65 °C/10 mmHg. ^{19}F NMR: δ −7.5 (s, $C\underline{F}_3$). ^1H NMR: δ 3.81 (s, 6H, $CO_2C\underline{H}_3$), 1.66 (s, $C\underline{H}_3$).

*Dimethyl Benzyl(trifluoromethyl)malonate (**13**, R=CH_2Ph).* Into a mixture of dried and powdered CsF (9.11 g, 60 mmol), benzyl bromide (8.55 g, 50 mmol), and diglyme (16 ml), a solution of dimethyl (trifluoromethyl)malonate (4.0 g) in diglyme (20 ml) was added at 70—75 °C over a period of 70 min. After being stirred for 50 min at that temperature, the reaction mixture was poured into water and worked up as usual. Benzyl(trifluoromethyl)malonate, **13** (R=CH_2Ph) (2.6 g, 45%) was distilled out at 91—94 °C/0.3 mmHg.

*Tetramethyl 2,4,4,4-Tetrafluoro-1-butene-1,1,3,3-tetracarboxylate (**14**).* Into a mixture of sodium hydride (0.36 g, 15 mmol) and *N,N*-dimethylformamide (5 ml), a solution of **4** (2.00 g, 10 mmol) in *N,N*-dimethylformamide (5 ml) was added dropwise with cooling the vessel in an ice-bath. After being stirred for 2 h at room temperature, the reaction mixture was poured into dilute aqueous HCl, and worked up as usual. Distillation under vacuum gave **13** (1.27 g, 70%), bp 122—124 °C/0.3 mmHg. Found: C, 40.74, H, 3.53%. Calcd for $C_8H_{12}O_8F_4$: C, 40.01; H, 3.36%. ^{19}F NMR: δ −15.1 (d, $C\underline{F}_3$), +10.7 (q, =C$\underline{F}$–). ^1H NMR: δ 3.77 (s, $C\underline{H}_3$), 3.87 (s, $C\underline{H}_3$), 3.90 (s, ($COC\underline{H}_3$)). IR: 1665 (C=C), 1750 (C=O) cm^{-1}.

Degradation of Dimethyl Methyl(trifluoromethyl)malonate. Into a methanolic solution of sodium methoxide prepared from sodium (0.46 g, 20 mmol) and dried methanol (10 ml), a solution of **4** (0.87 g) in methanol (4 ml) was added. After 3.5 h of stirring at room temperature, the reaction mixture was poured into dil aqueous HCl and worked up as usual. Removal of the ether gave pure dimethyl methylmalonate (0.39 g, 67%) which was identified by comparing its IR, ^1H NMR, and GLC data with those of an authentic sample.

*Dimethyl 1,1,1-Trifluoro-5-oxo-2,2-hexanedicarboxylate (**16**, R=Me).* A mixture of **4** (4.0 g, 20 mmol), methyl vinyl ketone (1.54 g, 22 mmol), triethylamine (0.30 g, 3 mmol), and pyridine (20 ml) was heated for 4 h at 70 °C. The reaction mixture was poured into water and worked up as usual. The adduct (3.97 g), bp 88—89 °C/0.2 mmHg, was obtained and identified in a similar way.

References

1) "Biochemistry Involving Carbon-Fluorine Bonds," ed by R. Filler, Am. Chem. Soc., Washington (1976).
2) N. Ishikawa, *Kagaku No Ryōiki*, **35**, 441 (1981).
3) I. L. Knunyants, S. T. Kocharyan, Yu. A. Cheburkov, M. D. Bargamova, and E. M. Rokhlin, *Dokl. Akad. Nauk SSSR*, **165**, 827 (1965).
4) N. P. Aktaev, O. G. Eremin, G. A. Sokol'skii, and I. L. Knunyants, *Izv. Akad. Nauk SSSR, Ser. Khim.*, **1977**, 1117.
5) S. T. Kocharyan, E. M. Rokhlin, and I. L. Knunyants, *Izv. Akad. Nauk SSSR, Ser. Khim.*, **1968**, 846.
6) I. L. Knunyants, U. Utebaev, E. M. Rokhlin, E. P. Luré, and E. I. Mysov, *Izv. Akad. Nauk SSSR, Ser. Khim.*, **1976**, 895.
7) All the ^{19}F NMR chemical shifts throughout this article are givin in δ ppm upfield from external trifluoroacetic acid.

Oxidative Dehydrogenation of Bis(salicylideneaminato)copper(II) Complex in Pyridine and Formation of 2-Cyanophenolato Complex

Takayuki MATSUSHITA* and Toshiyuki SHONO

Department of Applied Chemistry, Faculty of Engineering, Osaka University, Yamadaoka, Suita, Osaka 565

(Received February 8, 1982)

The copper(II) complex of salicylideneamine (salamH) reacts with molecular oxygen in pyridine to give the 2-cyanophenolato complex, $[Cu(2\text{-}CNphO)_2(py)_2]$, in good yield, where 2-CNphOH and py denote 2-cyanophenol and pyridine, respectively. This complex was characterized by the infrared and electronic spectra and by its magnetic susceptibilities, and was compared with the authentic complex, $[Cu(2\text{-}CNphO)_2(py)_2]$. The mechanism for the oxidation of the coordinated imino groups is discussed.

It is well known that copper(II) salts catalyze significantly the oxidation of organic substances by molecular oxygen.[1] Brackman *et al.*[2] have reported that the ammoxidation of alcohols and aldehydes catalyzed by copper(II) salts gives the corresponding nitriles in good yields, and have proposed that the imino function (RCH=NH) which formed by condensation of aldehyde with ammonia was oxidized to nitrile via an intermediate of an imino radical (RCH=N·), involving a Cu(II)/Cu(I) redox system. Misono *et al.*[3] have investigated the kinetics of the formation of benzonitrile from benzaldehyde and ammonia catalyzed by some copper compounds, and have proposed that benzilideneamine is an important intermediate. They have reported that 2-cyanophenol was formed by thermal decomposition of bis(salicylideneaminato)copper(II), $[Cu(salam)_2]$.[4]

The oxidative dehydrogenation of amino and alkylamino groups coordinated to metal ions has been reported.[5] Diamond *et al.*[6] have found that pentaammine(benzylamine)ruthenium(II) ion reacts with molecular oxygen to give pentaammine(benzonitrile)-ruthenium ion. Keene *et al.*[7] have reported that the complexes, $[Ru(bpy)_2(NH_2CH_2R)_2]^{+2}$($NH_2CH_2R$= allylamine, benzylamine, and butylamine) were oxidized chemically and electrochemically to give the corresponding bis(nitrile) complexes, $[Ru(bpy)_2(NCR)_2]^{+2}$ and proposed that the reactions proceed by initial oxidation of Ru(II) to Ru(III), followed by a series of stepwise dehydrogenation reactions which occur via the imine intermediate. Recently, the oxidative dehydrogenation of the coordinated secondary amine moieties to the copper atom has been reported for Cu(II)–4,4′-(ethane-1,2-diyldiimino)bis(pent-3-en-2-one) complex[8] and bi-Cu(I)–macrocyclic complex.[9]

In this paper we wish to report that $[Cu(salam)_2]$ reacts with molecular oxygen to give quantitatively the 2-cyanophenolato complex. This reaction should afford good information on the mechanism of the ammoxidation catalyzed by copper compounds.

Experimental

Preparation of Copper(II) Complexes with Salicylideneamine and Its Analogs. All the complexes with the Schiff bases used in this work were obtained by the method described in the literature. They are abbreviated as follows: Bis(salicylideneaminato)copper(II): $[Cu(salam)_2]$[10a]; bis(substituted salicylideneaminato)copper(II): $[Cu(X\text{-}salam)_2]$[10b], where X can be 5-Me, 3-Me, 3-MeO, 4-Cl, 5-Br, 5,6-Benzo, and 5-NO_2; bis[1-(*o*-hydroxyphenyl)ethylideneaminato)copper(II): $[Cu(hpam)_2]$[10c]; bis(*N*-methylsalicylideneaminato)-copper(II): $[Cu(N\text{-}Mesalam)_2]$[10c].

Isolation of Oxidized Products. Oxidized Product of [Cu(salam)$_2$]: A pyridine solution (300 cm^3) of $[Cu(salam)_2]$ (1.0 g) was kept at 70 °C, with dried air bubbled through it. The green solution turned brown gradually. The reaction was followed by monitering the visible absorption spectra of small portions of the solution at regular intervals. The spectral changes were no longer observed after *ca.* 7 h; the resulting solution was evaporated under reduced pressure. The brown solids were collected on a glass filter, washed with hexane, and dried *in vacuo*. The yield was quantitative. The product is soluble in pyridine (py), *N*,*N*-dimethylformamide (DMF), and dimethyl sulfoxide (DMSO), slightly soluble in dichloromethane, methanol, and benzene, but insoluble in water. This was reprecipitated from a mixture of pyridine and ether.

The oxidized product of $[Cu(salam)_2]$ could be obtained from the reaction between its pyridine solution and an aqueous solution of hydrogen peroxide (30%) at room temperature. This was identified to be the same product as the above. The reaction of $[Cu(salam)_2]$ with molecular oxygen in dioxane was found to give the pale brown product. This is soluble in pyridine, but insoluble in noncoordinating solvents; its formula is [Cu(2-CNphO)(OH)].

All the reaction conditions are summarized in Table 1, together with the empirical formulas of the products. The

Table 1. Oxidation conditions for copper(II) complexes and their products

Complex[a]	Solvent[b]	Temp °C	Time h	Atmosphere	Reaction product		
					Yield/%	Formula	Color
$[Cu(salam)_2]$	Pyridine	70	7	Air	95	$[Cu(2\text{-}CNphO)_2(py)_2]$	Greenish brown
$[Cu(salam)_2]$	Pyridine[c]	30	0.5	Air	90	$[Cu(2\text{-}CNphO)_2(py)_2]$	Greenish brown
$[Cu(salam)_2]$	Dioxane	70	7	Air	60	[Cu(2-CNphO)(OH)]	Pale brown
$[Cu(hpam)_2]$	Pyridine	80	10	Air	90	$[Cu(2\text{-}CNphO)_2(py)_2]$	Greenish brown
$[Cu(N\text{-}Mesalam)_2]$	Pyridine	110	100	O_2		No reaction	

a) Complex: 3 mmol. b) Solvent: 300 cm^3. c) Addition of aqueous H_2O_2 solution (30%, 6 mmol).

Table 2. Analytical data, magnetic moments, and ν(CN) frequencies for 2-cyanophenolato copper complexes

Complex	Found (%)			Calcd (%)			μ_{eff}[b]	ν(CN)[c]
	C	H	N	C	H	N	BM	cm^{-1}
[Cu(2-CNphO)$_2$(py)$_2$][a]	62.75	3.65	12.50	62.94	3.96	12.23	2.05	2220, 2205
[Cu(2-CNphO)$_2$(py)$_2$]	62.91	3.93	12.07	62.94	3.96	12.23	1.91	2220, 2205
[Cu(2-CNphO)$_2$(bpy)]	63.03	3.43	11.90	63.22	3.54	12.29	1.91	2220, 2208
[Cu(2-CNPhO)(OH)]	42.46	2.32	7.16	42.31	2.53	7.05	1.46	2238

a) Oxidized product. b) Measured at room temperature. c) Measured in Nujol mulls.
ν(CN): 2237 cm^{-1} for 2-CNphOH; 2205 cm^{-1} for 2-CNphONa.

analytical data for these products are given in Table 2, along with their magnetic moments determined at room temperature and the frequencies due to ν(CN).

Isolation of 2-Cyanophenol from the Oxidized Product of [Cu(salam)$_2$]. The oxidized product (0.1 g) of [Cu(salam)$_2$] was dissolved in pyridine (10 cm^3). A solution (100 cm^3) of 1 M (1 M=1 mol dm^{-3}) hydrochloric acid was added to it. Hydrogen sulfide gas was passed through the solution for 10 min, followed by passing nitrogen gas for 20 min. The black precipitates were filtered and washed with ether. The filtrate was extracted with ether (50 cm^3). The ethereal washings and extract were combined and dried over anhydrous sodium sulfate, and then evaporated under reduced pressure to yield tan-yellow solids. They were recrystallized from hexane to give white crystals. The yield was 0.04 g. This was identified to be 2-cyanophenol from the elemental analysis, infrared spectrum, and melting point (96.5 °C).

Preparation of 2-Cyanophenolato Complexes. Bis(2-cyanophenolato)bis(pyridine)copper(II), [Cu(2-CNphO)$_2$(py)$_2$]: This complex was obtained by a modification of the method described in the literature.[11] To an aqueous solution (20 cm^3) containing $CuSO_4 \cdot 5H_2O$ (0.75 g, 3 mmol) and pyridine (0.48 g, 6 mmol), an aqueous solution (15 cm^3) of 2-cyanophenol (0.72 g, 6 mmol) and sodium hydroxide (0.24 g, 6 mmol) was added dropwise with stirring. The olive green solids which precipitated were collected on a glass filter, and washed with water, and with small volumes of ethanol and ether, and then dried *in vacuo*. They were recrystallized from dichloromethane to give greenish brown crystals.

2,2′-Bipyridinebis(2-cyanophenolato)copper(II), [Cu(2-CNphO)$_2$(bpy)]. This complex was obtained in a similar way to that used for the above complex, using 2,2′-bipyridine in place of pyridine.

The analytical data for the 2-cyanophenolato complexes are given in Table 2, together with their magnetic moments determined at room temperature and the frequencies due to ν(CN).

Materials. All reagents were of reagent grade. The solvents were purified in the usual manner.

Measurements. The UV, VIS, and NIR spectra were recorded on a Hitachi 340 recording spectrophotometer. The diffused reflectance spectra were obtained by using the above instrument along with a Hitachi R-10 A integrating sphere unit and a NIR integrating sphere unit. The infrared spectra and magnetic susceptibilities were obtained by the method described elsewhere.[12]

Results and Discussion

We have found that a pyridine solution of [Cu(salam)$_2$] changed the color from green to greenish brown on being allowed to stand for a few days at room temperature under air. We are interested in the cause of such a color change.

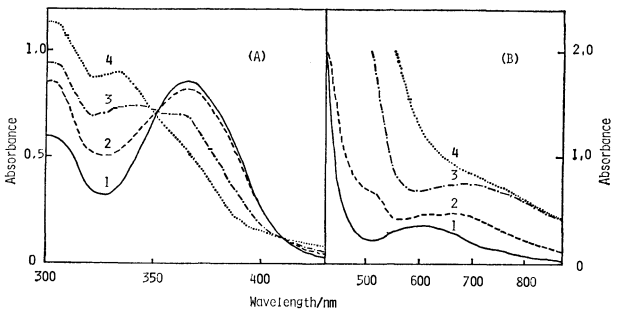

Fig. 1. Absorption spectral changes of pyridine solutions of [Cu(salam)$_2$] at 70 °C under air.
(A); [Complex]=8×10^{-5} M, 1): reaction time=0, 2): 265, 3): 325, 4): 385 min. (B); [Complex]=8×10^{-3} M, 1): reaction time=0, 2): 26, 3): 80, 4): 385 min. Cell length: 1 cm.

Absorption Spectral Changes. Figure 1 shows the absorption spectral changes of a pyridine solution of [Cu(salam)$_2$] at 70 °C under air. The absorption bands at 366 and 598 nm observed for the original spectrum can be assigned to charge-transfer and ligand field transitions, respectively. The absorption spectrum changes remarkably with time, showing the isosbestic points at 351 and 408 nm; the absorption band at 366 nm decreased in intensity and a new absorption band appeared at 333 nm (in Fig. 1-A), and the absorption band at 598 nm was shifted to lower energies with increasing the intensity around 500 nm (in Fig. 1-B). These spectral changes indicate that a marked change occurred in the coordinated ligand and the environment around the central copper atom.

Characterization of the Reaction Product. The analytical data for the reaction product of [Cu(salam)$_2$] in pyridine are in agreement with an empirical formula of [Cu(2-CNphO)$_2$(py)$_2$]. The magnetic moment is 2.05 BM. The electronic spectrum measured in pyridine shows an intense absorption band around 23000 cm^{-1} and a broad absorption band around 14000 cm^{-1} (Fig. 2). These bands can be assigned to a charge-transfer transition between the phenolic oxygen atom and copper atom and the ligand field transitions from higher energies.[13] Figure 3 shows the infrared spectra of [Cu(salam)$_2$] and its reaction product. In the latter compound, the absorption bands at 3280 and 1625 cm^{-1} are due to ν(N–H) and ν(C=N), re-

spectively, which were observed for $[Cu(salam)_2]$, disappeared and new absorption bands were observed at 2220 and 2205 cm^{-1} and at 1221, 1072, and 691 cm^{-1}. The bands at 2220 and 2205 cm^{-1} can be assigned to the stretching vibrations of nitrile group from their frequencies. The latter three bands can be assigned to the characteristic bands of the coordinated pyridine. These results indicate that the imino groups coordinated to the copper atom were oxidized to the nitrile groups by the oxidative dehydrogenation.

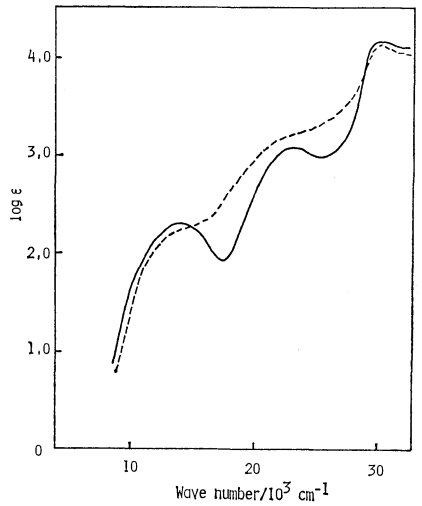

Fig. 2. Electronic spectra in pyridine.
---: Oxidized product of $[Cu(salam)_2]$ in pyridine,
——: authentic complex, $[Cu(2\text{-}CNphO)_2(py)_2]$.

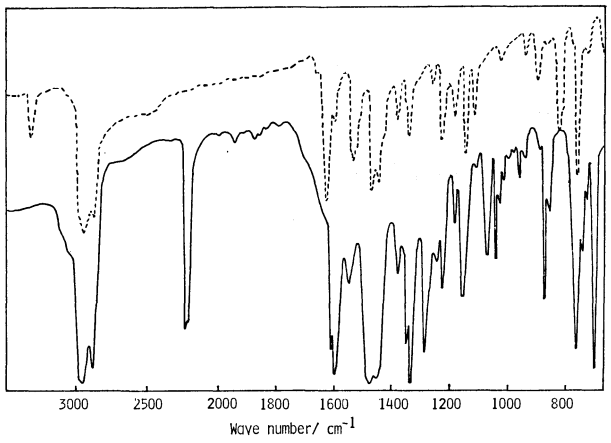

Fig. 3. Infrared spectra in Nujol mulls.
---: $[Cu(salam)_2]$, ——: oxidized product of $[Cu(salam)_2]$ in pyridine.

The authentic complex which was prepared by the reaction of $CuSO_4$, 2-cyanophenol, and pyridine has the same composition, formulated as $[Cu(2\text{-}CNphO)_2(py)_2]$, and shows the same infrared spectrum as that for the oxidized product (Table 2). In the electronic spectra, the absorption maxima for the oxidized product are in agreement with those for the authentic complex (Table 3). However, the intensities around 19000 cm^{-1} are slightly higher in the oxidized product than those in the authentic complex. This may be caused by the difference in orientation of the coordinated 2-cyanophenolato ligands between these complexes as shown below. A molecular model for them

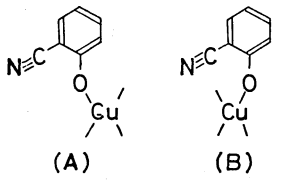

suggests that a free rotation of the 2-CNphO at the Cu–O bond is restricted by the coordinated pyridine molecules. Therefore, on the basis of steric repulsion, the form (A) is a possible configuration for the authentic complex. On the contrary, the form (B) may be maintained in the oxidized product, because the original $[Cu(salam)_2]$ has a *trans*-planar configuration. In this form, a planar configuration around the central copper atom may distort to a tetrahedral configuration by steric requirement. This is one reason why high intensities are observed in the oxidized product.

The magnetic moment of the authentic complex is a slightly lower value (1.91 BM) than that of the oxidized product. This may be caused by a slight difference between configurations of the authentic and the oxidized complexes, as mentioned above.

It should be noted that the doublet bands due to ν(CN) are observed for the 2-cyanophenolato complexes and both peaks are of equal intensity. Moreover, the C–O stretching vibrations of the coordinated 2-cyanophenol are observed around 1320 cm^{-1} as doublet bands. These results suggest that 2-cyanophenolato ligands coordinate to the copper atom in two different fashions. It has been reported that nitrile groups can coordinate to metal ions through either nitrogen atom or π-bond of nitrile.[14] In the former

Table 3. Electronic spectral data for 2-cyanophenolato copper complexes

Complex	Solvent	$\frac{\nu_{max}}{10^3\ cm^{-1}}$ (log ε)				
$[Cu(2\text{-}CNphO)_2(py)_2]$	Pyridine		14.0(2.23)	23.2(3.10)	30.3(4.15)	
	DMF	12.4 sh	14.4(1.86)	23.4(2.80)	30.3(3.38)	33.4(4.00)
	Solid	12.7 sh	16.2	23.1	31.1	33.1
$[Cu(2\text{-}CNphO)_2(py)_2]$[a]	Pyridine		14.4(2.20)	22.5(3.20)	30.5(4.11)	
	Solid	13.0 sh	15.8 sh	23.1	31.1	33.1
$[Cu(2\text{-}CNphO)_2(bpy)]$	Solid		15.9	23.1	30.0	34.1

a) Oxidized product. sh: Shoulder.

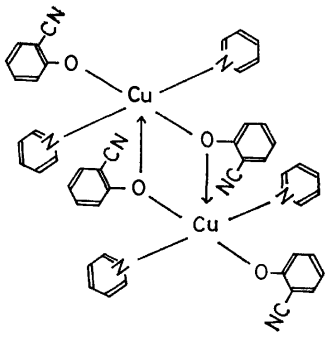

Fig. 4. Proposed structure for $[Cu(2\text{-}CNphO)_2(py)_2]$.

case, the ν(CN) frequencies shifted to higher energies than that of the free ligand, whereas in the latter case, they shifted to lower energies. In the present copper complexes, the ν(CN) frequencies are within a range of 2237 cm^{-1} for 2-CNphOH to 2205 cm^{-1} for 2-CNphONa (Table 2). This indicates that coordination of nitrile groups is not involved in these copper complexes. Therefore, we propose a binuclear structure for $[Cu(2\text{-}CNphO)_2(py)_2]$ as shown in Fig. 4 in which the copper atoms are bridged by the phenolic oxygen atoms. This structure could be easily broken up in pyridine solution. The infrared spectra taken on pyridine solutions of the oxidized and authentic complexes showed only one band due to ν(CN) at 2212 cm^{-1}. Such a binuclear structure has been revealed by X-ray analysis of [Cu(salen)], where salen denotes dianion of *N,N'*-disalicylideneethylenediamine, and its magnetic data (1.84 to 2.0 BM) are not inconsistent with the present results.[15] The facts that the original complex, $[Cu(salam)_2]$, has a *trans*-configuration[16] and that the two bands due to ν(CN) are of equal intensity suggest that a *trans*-form is probable for the oxidized complex, although either a *trans*- or *cis*-configuration is possible for $[Cu(2\text{-}CNphO)_2(py)_2]$. On the other hand, the complex, $[Cu(2\text{-}CNphO)_2(bpy)]$, may have a *cis*-configuration and the infrared spectrum shows two absorption bands due to ν(CN). Thus, this complex also may have a binuclear structure in the solid state.

Mechanism for Oxidative Dehydrogenation. In order to clarify the mechanism for the oxidative dehydrogenation of $[Cu(salam)_2]$ the following effects on the oxidation were investigated.

Solvent Effects: The $[Cu(salam)_2]$ complex was allowed to react with molecular oxygen in various solvents such as pyridine, dioxane, ethanol, and benzene under these conditions: The concentration of the complex was 8×10^{-5} M, at 70 °C, and under air. Absorption spectral changes were observed in the former three solvents, but no spectral change was observed in benzene. The time required for the oxidation increased in the order of: pyridine (4.5 h)<dioxane (5 h)<ethanol (20 h). The oxidized product could be obtained from the dioxane solution of $[Cu(salam)_2]$ and was identified to be [Cu(2-CNphO)(OH)], as mentioned in Experimental.

Effects of Added Bases: The oxidative dehydrogenation of $[Cu(salam)_2]$ in dioxane has been found to be accelerated by the addition of organic aromatic

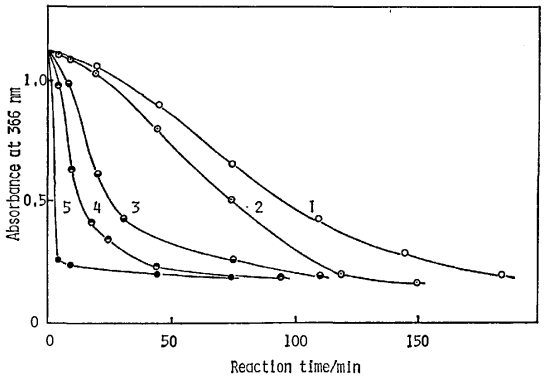

Fig. 5. Effects of added bases to dioxane solutions of $[Cu(salam)_2]$ on oxidation at 70 °C under air. Added bases; 1): none, 2): pyridine (10^{-3} M), 3): 2,2'-bipyridine (10^{-3} M), 4): bpy (10^{-2} M), 5): 1,10-phenanthroline (10^{-3} M). [Complex]=10^{-4} M, Cell length: 1 cm.

bases such as 1,10-phenanthroline (phen), 2,2'-bipyridine (bpy), and pyridine as shown in Fig. 5. The apparent reaction rates increased in the order of phen>bpy>py, and increased with an increase in concentration of the added base.

Concentration of Complex: The reaction of $[Cu(salam)_2]$ in pyridine was made by varying the concentration from 8×10^{-5} M to 1.6×10^{-3} M. All the reactions showed some induction periods. Thus, the maximal rate constants (k_{obsd}) were calculated graphically from the constant slopes after the induction periods obtained in the plots of $\ln(a-x)$ *vs.* reaction time, where a and x are the concentrations at time equal to t_0 and t, respectively, with assumption of the following equation:

$$[Cu(salam)_2] + O_2 \xrightarrow[py]{k_{obsd}} [Cu(2\text{-}CNphO)_2(py)_2] + 2H_2O. \quad (1)$$

A plot of $\log(k_{obsd})$ *vs.* $\log a$ shows a linear relation with a slope nearly equal to unity, as shown in Fig. 6. This indicates that the oxidative dehydrogenation of $[Cu(salam)_2]$ depends on the first order of the complex concentration. The induction periods are found to be decreased with an increase in the complex concentration.

Effects of Substituents on Aromatic Ring: Figure 7 shows the plots of the decreases in the complex concentration against reaction time. The complex concentration was calculated according to the following equation:

$$x = a(A_0-A_t)/(A_0-A_\infty), \quad (2)$$

where A_0, A_t, and A_∞ represent the absorbances at time equal to t_0, t, and at the final state, respectively. Clearly, the induction periods and the maximal rate constants are affected by the substituents on the aromatic ring; the electron-donating groups accelerate the reaction, whereas the electron-withdrawing groups retard it. The maximal rate constants increased in the order of 5-Me>3-Me>H>3-MeO>5-Br>4-Cl>5,6-Benzo>5-NO_2, as listed in Table 4. It should be noted that $[Cu(5\text{-}NO_2salam)_2]$ did not show any spectral changes under the same conditions.

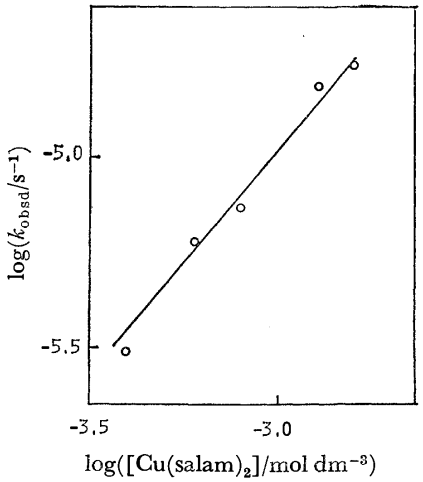

Fig. 6. A plot of log(k_{obsd}) *vs.* log[Cu(salam)$_2$].

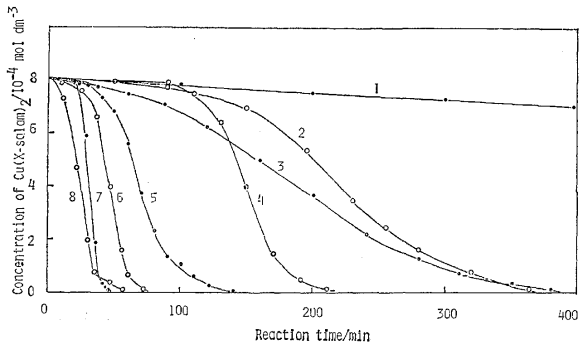

Fig. 7. Effects of substituents of [Cu(X-salam)$_2$] on oxidation in pyridine at 70 °C under air. [Complex]=8×10^{-4} M, 1): X=5-NO_2, 2): 4-Cl, 3): 5,6-Benzo, 4): 5-Br, 5): 3-MeO, 6): H, 7): 5-Me, 8): 3-Me.

TABLE 4. EFFECTS OF THE SUBSTITUENTS OF AROMATIC RING ON THE MAXIMAL RATE CONSTANTS AND THE INDUCTION PERIODS FOR THE OXIDATIVE DEHYDROGENATION OF [Cu(X-salam)$_2$] IN PYRIDINE AT 70 °C UNDER AIR

Substituent X	Maximal rate constant k_{obsd} / 10^{-4} s^{-1}	Induction period Time / min
5-Me	27.8	25
3-Me	15.2	8
H	13.5	40
3-MeO	8.8	50
5-Br	8.7	110
4-Cl	2.8	180
5,6-Benzo	2.1	95
5-NO_2	—	—

Concentration of complexes was 8×10^{-4} M.

Effects of Substituents on Nitrogen and Carbon Atoms of Imino Groups: Several copper(II) complexes, [Cu(hpam)$_2$], [Cu(*N*-Mesalam)$_2$], [Cu(salen)], and [Cu(*N*-OHsalam)$_2$], were made to react in pyridine at 70 °C under air, where *N*-OHsalamH denotes salicylaldehyde oxime. Among them, the carbon atom-substituted complex, [Cu(hpam)$_2$], gave the oxidized product, [Cu(2-CNphO)$_2$(py)$_2$], while the other nitrogen atom-substituted complexes did not show any oxidation under the above conditions. These results indicate that the oxidative dehydrogenation of [Cu(salam)$_2$] may be initiated by a splitting of the N–H bond of the coordinated imino groups.

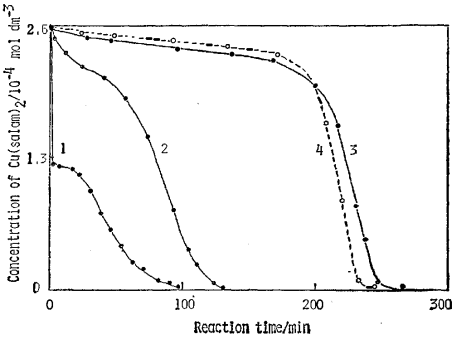

Fig. 8. Effects of added hydrogen peroxide on oxidation of [Cu(salam)$_2$] in pyridine at 70 °C under air. [Complex]=2.6×10^{-4} M, 1): [H_2O_2]=2.6×10^{-4} M, 2): 2.6×10^{-5} M, 3): 2.6×10^{-6} M, 4): no addition.

Effects of Addition of Hydrogen Peroxide: Figure 8 shows the plots for the oxidation of [Cu(salam)$_2$] *vs.* reaction time when various concentrations of hydrogen peroxide were added to the pyridine solutions of the complex at 70 °C under air. With the addition of an equimolar amount of hydrogen peroxide to the complex, a nearly half-mole of the complex was oxidized within 5 min, and the oxidation was completed within 100 min after showing a short induction period (curve 1). With the addition of one-tenth amount of hydrogen peroxide, the initial induction period disappeared, but the reaction rate retarded with time, and a fast oxidation again occurred after 50 min (curve 2). On the other hand, with the addition of one-hundredth of hydrogen peroxide, the reaction pattern (curve 3) was similar to the case of no addition (curve 4).

The available results suggest that the oxidative dehydrogenation of the coordinated imino groups in pyridine may occur according to the following scheme:

$$Cu(II)(R\text{-}CH{=}NH)_2 \rightleftharpoons Cu(I)(R\text{-}CH{=}\dot{N}H^+)(R\text{-}CH{=}NH) \quad (3)$$

$$Cu(I)(R\text{-}CH{=}\dot{N}H^+)(R\text{-}CH{=}NH) + O_2 \longrightarrow Cu(II)(R\text{-}CH{=}\dot{N})(R\text{-}CH{=}NH) + HO_2\cdot \quad (4)$$

$$Cu(II)(R\text{-}CH{=}\dot{N})(R\text{-}CH{=}NH) + HO_2\cdot \longrightarrow Cu(II)(R\text{-}CN)(R\text{-}CH{=}NH) + H_2O_2 \quad (5)$$

$$Cu(II)(R\text{-}CN)(R\text{-}CH{=}NH) + H_2O_2 \xrightarrow{py} Cu(II)(R\text{-}CN)_2(py)_2 + 2H_2O. \quad (6)$$

The initiation reaction is considered to be a thermal one-electron transfer from the imino nitrogen atom to the copper atom, as shown in Eq. 3. The induction periods observed in the oxidation investigated here may be due to the back reaction in Eq. 3, which is the oxidation of copper(I) to copper(II) by the imino radical. In the presence of molecular oxygen, the reactions shown in Eqs. 4 and 5 may occur in competetion with the above back reaction.

The effects of the added aromatic bases (Fig. 5) can be related to Eq. 3. That is, these bases can function as an acceptor of proton (H^+) liberated and as a promoter of electron transfer from the imino group to the copper atom by coordination. Thus the increasing order of the apparent reaction rates (phen> bpy>py) is not correlated to the order of the pK_a values (py>phen>bpy).

The substituent effects that the electron-donating groups on the aromatic ring accelerated the reaction rates and shortened the induction periods can be explained by taking account of Eqs. 3 and 4; the electron-donating groups may facilitate the electron transfers from the imino group to the copper atom (Eq. 3) and from the copper atom to molecular oxygen (Eq. 4). Such a behavior has been found in the autoxidation of the substituted phenylhydroxylamines.[17] And also the autoxidation of phenylhydroxylamine has been found to be accelerated by copper(II) ion.[18]

As described above, the oxidative dehydrogenation investigated here proceeded rapidly after showing induction periods. This indicates that the radical chain autoxidation may be involved in this system. The chain reaction may propagate by the direct attack of molecular oxygen to the imino radical and by the catalytic decomposition of hydrogen peroxide with the copper complex. A tentative scheme for the radical chain autoxidation is proposed, as follows:

$$Cu(II)(R\text{-}CH{=}\dot{N})(R\text{-}CH{=}NH) + O_2 \longrightarrow Cu(II)(R\text{-}CN)(R\text{-}CH{=}NH) + HO_2\cdot \quad (7)$$

$$Cu(II)(R\text{-}CN)(R\text{-}CH{=}NH) + HO_2\cdot \longrightarrow Cu(II)(R\text{-}CN)(R\text{-}CH{=}\dot{N}) + H_2O_2 \quad (8)$$

$$Cu(II)(R\text{-}CN)(R\text{-}CH{=}\dot{N}) + O_2 \longrightarrow Cu(II)(R\text{-}CN)_2 + HO_2\cdot \quad (9)$$

Decomposition of hydrogen peroxide

$$Cu(II)(R\text{-}CH{=}NH)_2 + H_2O_2 \longrightarrow Cu(I)(R\text{-}CH{=}NH)_2 + HO_2\cdot + H^+ \quad (10)$$

$$Cu(I)(R\text{-}CH{=}NH)_2 + H_2O_2 \longrightarrow Cu(II)(R\text{-}CH{=}NH)_2 + HO\cdot + HO^- \quad (11)$$

$$Cu(I)(R\text{-}CH{=}\dot{N}H^+)(R\text{-}CH{=}NH) + H_2O_2 \longrightarrow Cu(II)(R\text{-}CH{=}\dot{N})(R\text{-}CH{=}NH) + HO\cdot + H_2O \quad (12)$$

followed by abstraction of hydrogen atom with $HO_2\cdot$ and $HO\cdot$. The above reaction scheme is supported by the results that the reactions of $[Cu(salam)_2]$ with O_2^- [19] and H_2O_2 in pyridine occurred readily at room temperature.

In the catalytic decomposition of hydrogen peroxide, Sigel *et al.*[20] have found that coordinately saturated copper(II) complexes (four-coordinate complexes) are essentially inactive. And Kochi has pointed out that in the reaction of hydrogen peroxide catalyzed by iron ion the reaction represented in Eq. 13 is more facile than that represented in Eq. 14, because hydrogen peroxide is a strong oxidizing agent but only a mild reducing agent.[21]

$$Fe^{II} + H_2O_2 \longrightarrow Fe^{III} + HO\cdot + HO^- \quad (13)$$

$$Fe^{III} + H_2O_2 \longrightarrow Fe^{II} + HO_2\cdot + H^+ \quad (14)$$

Therefore, in the present oxidation, the reaction represented in Eq. 12 is considered to be more important than those represented in Eqs. 10 and 11.

As shown in Fig. 8, the initial induction period was made to disappear by the addition of an equimolar amount of hydrogen peroxide to the complex, but a short induction period was observed again after producing about a half oxidation of the complex. Furthermore, the catalytic amount of hydrogen peroxide ($[H_2O_2]$:[complex]=1:100) had no effect on the reaction. These results indicate that the radical chain sequence induced by decomposition of hydrogen peroxide may be not so long. These facts suggest that the rate-determining step in the present oxidative dehydrogenation of $[Cu(salam)_2]$ is the splitting of the N–H bond of the coordinated imino group, along with the reduction of copper(II) to copper(I), as shown in Eq. 3.

We have also found that $[Ni(salam)_2]$ and $[Co^{II}(salam)_2]$ were oxidized by molecular oxygen in pyridine to give their 2-cyanophenolato complexes. In the nickel complex, the severe conditions were required to obtain the fully oxidized product: for 120 h at 115 °C under O_2 1 atm. This suggests that the oxidative dehydrogenation of $[Ni(salam)_2]$ may be initiated by the electron transfer from the coordinated imino group to molecular oxygen without change in the oxidation state of the nickel ion. On the other hand, the oxidized product of $[Co^{II}(salam)_2]$ was obtained in the conditions similar to the case of $[Cu(salam)_2]$. In the cobalt complex, the initial reaction is considered to be the oxidation of Co(II) to Co(III) by molecular oxygen, followed by the stepwise dehydrogenation of the coordinated imino groups through a redox couple of Co(II)/Co(III) as in the copper case. Details on the oxidation of these Ni(II) and Co(II) complexes will be reported in the near future.

References

1) a) B. A. Marshall and W. A. Waters, *J. Chem. Soc.*, **1960**, 2392; b) K. Wuthrich and S. Fallab, *Helv. Chim. Acta*, **47**, 1440 (1964); **47**, 1609 (1964).

2) W. Brackman and P. J. Smit, *Recl. Trav. Chim. Pays-Bas*, **82**, 757 (1963).

3) A. Misono, T. Osa, and S. Koda, *Bull. Chem. Soc. Jpn.*, **40**, 912 (1967).

4) A. Misono and S. Koda, *Bull. Chem. Soc. Jpn.*, **41**, 2795 (1968).

5) C. J. Hipp and D. H. Busch, "Coordination Chemistry," ACS Monograph 174, ed by A. E. Martell, Am. Chem. Soc., Washington, D.C. (1978), Vol. 2, p. 435.

6) S. E. Diamond, G. M. Tom, and H. Taube, *J. Am. Chem. Soc.*, **97**, 2661 (1975).

7) F. R. Keene, D. J. Salmon, and T. Meyer, *J. Am. Chem. Soc.*, **98**, 1884 (1976).

8) S. Dilli and A. M. Maitra, *J. Chem. Soc., Chem. Commun.*, **1979**, 133.

9) M. G. Burnett, V. McKee, and S. M. Nelson, *J. Chem. Soc., Chem. Commun.*, **1980**, 829.

10) a) G. N. Tyson, Jr., and S. C. Adams, *J. Am. Chem. Soc.*, **62**, 1228 (1940); b) Prepared according to a); c) P. Pfeiffer and H. Glaser, *J. Prakt. Chem.*, **153**, 265 (1939).

11) J. F. Harrod, *Can. J. Chem.*, **47**, 637 (1969).
12) T. Matsushita and T. Shono, *Bull. Chem. Soc. Jpn.*, **54**, 3743 (1981).
13) E. W. Ainscough, A. G. Bingham, A. M. Brodie, J. M. Husbands, and J. E. Plowman, *J. Chem. Soc., Dalton Trans.*, **1981**, 1701.
14) B. N. Storhoff, *Coord. Chem. Rev.*, **23**, 1 (1977).
15) M. D. Hobday and T. D. Smith, *Coord. Chem. Rev.*, **9**, 311 (1972—1973).
16) H. S. Maslen and T. N. Waters, *Coord. Chem. Rev.*, **17**, 137 (1975).
17) Y. Ogata, Y. Sawaki, and T. Morimoto, *J. Am. Chem. Soc.*, **86**, 3854 (1964).
18) Y. Ogata and T. Morimoto, *J. Org. Chem.*, **30**, 597 (1965).
19) The reaction of $[Cu(salam)_2]$ with KO_2 was made in pyridine at room temperature in the presence of 18-crown-6. The oxidized product was obtained within an hour and identified to be $[Cu(2\text{-}CNphO)_2(py)_2]$.
20) H. Sigel and U. Müller, *Helv. Chim. Acta*, **49**, 671 (1966).
21) J. K. Kochi "Free Radicals," ed by J. K. Kochi, Wiley-Interscience, New York (1973), Vol. 1, p. 628.

The Ion-exchange Properties toward Hexaamminecobalt(III) and the Characterization of the Complex Cation Form of α-Zirconium Phosphate[1)]

Yoshitsugu HASEGAWA,* Seiichi KIZAKI, and Hiroshi AMEKURA

Department of Industrial Chemistry, Faculty of Technology, Tokyo University of Agriculture and Technology, Nakamachi, Koganei, Tokyo 184

(Received February 16, 1982)

The ion-exchange properties of α-zirconium phosphate have been investigated for the H^+–$[Co(NH_3)_6]^{3+}$ system. The ion-exchange process was examined by means of the variation in the pH values of the supernatant. α-Zirconium phosphate loaded with hexaamminecobalt(III) was also characterized by chemical analysis, X-ray diffractometry, infrared spectroscopy, and thermal analysis. In spite of the steric hindrance in the crystal structure of α-zirconium phosphate, the ion exchange proceeded gradually. About 30% of the hydrogen ions in α-zirconium phosphate were replaced by hexaamminecobalt(III). The interlayer distance of the exchanger expanded from 0.76 to 1.12 nm.

The ion-exchange properties of α-zirconium phosphate, $Zr(HPO_4)_2 \cdot H_2O$ (α-ZP), have been studied extensively, and its crystal structure has been determined.[2)] The structure is a layered one, and zeolitic-type cavities are present between layers. The cavities are connected by openings, the largest diameter being 0.264 nm.[3)] Hence, the ions of the ionic radius smaller than 0.133 nm can be easily taken up by α-ZP. However, larger cations, such as ammonium and tetra-alkyl-ammonium ions, and cobaltocene also exchange with the proton in α-ZP.[4,5)] These facts indicate that the ion exchange on α-ZP is not necessarily restricted by the size of the exchanging cation.

It has been known that α-ZP has not only catalytic activities, but also the possibility of use as a catalyst support. For example, Nozaki *et al.* have applied α-ZP to a catalyst for the dehydration of 2-propanol,[6)] and Hattori *et al.* studied the catalytic property and the acidity of α-ZP.[7)] Alberti pointed out that α-ZP loaded with a transition metal ion was promising as a catalyst.[8)] The copper form of α-ZP, $ZrCu(PO_4)_2$ was found to be active for the oxydation of carbon monoxide.[9)]

The ion-exchange reaction has been employed to prepare a highly dispersed metal-supported catalyst, especially when the metal is a member of the platinum group.[10)] Since many metal ions are not present in neutral pH solutions, a complex cation must be used for the ion exchange. The use of the metal-ammine complex is suitable, since the ammonia molecule is small and can easily be removed by heating.

In this work, the hexaamminecobalt(III)-hydrogen ion exchange was studied, and the α-ZP loaded with the hexaamminecobalt(III) ion (ZP-Co) was characterized by chemical analysis, X-ray powder diffraction, infrared spectroscopy, and thermal analysis.

Experimental

Preparation of α-ZP and Hexaamminecobalt(III) Trichloride. By the previously reported method α-ZP was prepared.[11)] When the zirconium dichloride oxide octahydrate used as a starting material included free hydrochloric acid, the salt was washed with acetone 2—3 times. The cobalt complex was prepared according to the literature.[12)] Identification was made by means of the X-ray diffraction pattern.[13)]

Ion Exchange. The ion-exchange experiments were carried out in batches. A weighed amount of α-ZP was placed in contact with the solution of hexaamminecobalt(III) in a thermostat bath. The concentration of the solution and the reaction temperature were varied. After the mixture has been shaken continuously or left to stand with a reflux condenser for a given period of time, the solid was centrifuged from the solution. The pH value of the supernatant was measured on a pH meter. Then, the solid was again added to a new solution of the complex. The process was repeated until the pH value of the supernatant became almost equal to that of the complex solution.

Analytical Procedure. The structural change in the exchanger during the ion exchange was measured by means of X-ray diffractometry. The patterns were recorded with a Rigaku Denki Geigerflex diffractometer, using Ni-filtered Cu $K\alpha$ radiation ($\lambda = 0.1542$ nm). The infrared (IR) spectra were measured on a JASCO DS-403G grating infrared spectrophotometer. The thermogravimetric (TGA) curve was obtained with a Shimadzu thermal analyser DT-30 at a heating rate of 10 °C/min in static air. The differential scanning calorimetric (DSC) data were obtained with a Rigaku differential scanning calorimeter under a helium stream to prevent the oxidation of the ammonia gas evolved at the surface of a platinum crucible.[14)]

The chemical analysis of the exchanger was carried out as follows. A weighed sample was decomposed with sodium peroxide. The precipitate was separated from the solution by filtration and then dissolved in hydrochloric acid. Zirconium was separated as cupferrate from cobalt and determined gravimetrically.[15)] Cobalt was titrated with a standardized EDTA solution, using xylenol orange as an indicator. Phosphorus was determined as magnesium pyrophosphate.[16)] Hydrogen and nitrogen were determined by elemental analysis.

Results and Discussion

Ion Exchange. To determine the optimum conditions of the ion exchange, the concentration of the complex cation and the reaction temperature were varied. The concentration range was from 0.025 to 0.2 mol dm^{-3}. The concentration of 0.025 mol dm^{-3} was equal to twice the ion-exchange capacity of the α-ZP used when the weighed amount of α-ZP was 500 mg and the volume of the solution was 100 cm^3. The concentration of 0.2 mol dm^{-3} was nearly equal to that of the saturated solution at 20 °C. Equilibrations were carried out at 25, 50, 75, and 90 °C.

In the first ion-exchange reaction at a given temperature, the equilibrium pH values of the supernatant solution were independent of the concentration of the complex cation. However, the pH values decreased at elevated temperatures. The hexaamminecobalt(III) ion is inert to the substitution of the ligand at room temperature, that is, the complex cation will persist for days. The hydrolysis of the complex cation took place at high temperatures. If the solution of the complex cation was heated at 75 or 90 °C, cobalt hydroxide was precipitated after 1.5 h or 15 min respectively. These facts indicate that, in the α-ZP–hexaamminecobalt(III) solution system, the ion exchange competes with hydrolysis at high temperatures. The change in pH values was steep at the end of ion exchange at 90 °C, and it was difficult to prevent the complex cation from hydrolyzing. The optimum experimental conditions were: concentration, 0.025 mol dm^{-3}, temperature, 75 °C, and reaction time, 1 h.

It is known that α-ZP and its salt forms have a layered structure, and that the interlayer distance depends on the size of the exchanging cation.[17] The structural change in the exchanger phase is usually examined by means of X-ray diffractometry. In an X-ray powder diffractogram, the peak due to the interlayer distance appears in the lowest angle region. Two peaks were observed at $2\theta=11.7°$ and 7.9° ($d=$ 0.76 and 1.12 nm) during the ion exchange, as is shown in Fig. 1. The former originated from the interlayer distance of α-ZP. The intensity of the X-ray reflection of the latter increased, while that of the former decreased, with an increase in the uptake of the complex cation. The precise interplanar spacings (d values) of ZP–Co are shown in Table 1.

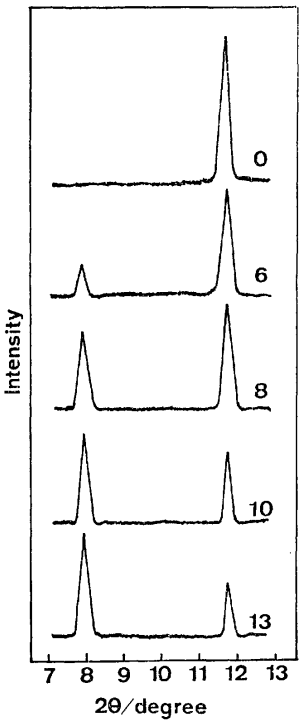

Fig. 1. Schematic diagrams of X-ray powder diffraction at the lowest angle region. Numbers in the figure represent the number of ion-exchange run.

Table 1. Interplanar spacings (d-values) of ZP-Co

d/nm	I/I_0
1.116	100
0.763	49
0.564	23
0.379	8
0.369	8
0.358	21
0.331	6
0.307	55
0.265	10
0.252	4
0.241	7
0.188	12

If the ammonia in the complex cation is abstracted directly by α-ZP or converted to the ammonium ion, thus contributing to the ion exchange, the ammonium form of α-ZP will be present. Since the interlayer distance of the ammonium form is 0.94 nm, the peak must be observed at $2\theta=9.4°$. This peak did not appear in powder diffractograms, however.

At the final stage of the ion exchange, the phase of α-ZP was still present (Table 1), indicating that not all the protons in α-ZP were replaced by $[Co(NH_3)_6]^{3+}$.

The IR spectra of ZP–Co and the ammonium form of α-ZP are shown in Fig. 2. The IR spectrum of α-ZP has been studied previously, and several bands have been assigned.[18] The absorption bands which appear in α-ZP are denoted by the symbol α in the figure. The ammonia in hexaamminecobalt(III) ion gave absorptions in the regions of 3000—3400, 1550—1650, 1300—1400, and 800—950 cm^{-1}.[19] It is clear that the spectrum of ZP–Co is composed of those of α-ZP and the hexaamminecobalt(III) ion, except for the region of 800—950 cm^{-1}, where the rocking vibrations are expected. According to Fujita *et al.*, the rocking mode is sensitive to the kinds of outer ions present and the hydrogen bonding, and the absorption band is shifted to higher frequencies by these effects.[20]

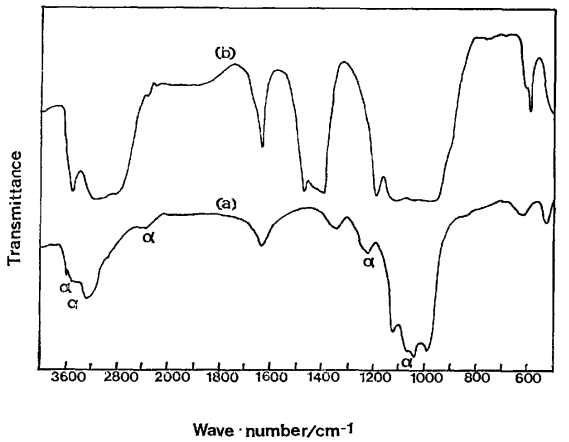

Fig. 2. IR spectra of (a) ZP-Co and (b) the ammonium form of α-ZP.

As is shown in Curve b, the ammonium ion of α-ZP gave strong and characteristic bands in the region of 1400—1500 cm^{-1}, but these bands were absent in Curve a. These facts indicate that the cobalt(III) ion was present as an ammine complex in the exchanger and that the ammonia molecules formed a hydrogen bond with the phosphate group; consequently, the rocking mode shifted to higher frequencies and overlapped with the absorption bands of phosphate.

In order to ascertain the ratio of cobalt to ammonia in ZP–Co, the composition was determined. Found: Zr, 23.8 (1.00); PO_4, 49.4 (1.99); Co, 4.53 (0.292); N, 6.40 (1.74); H, 2.68 (10.2); ignition loss, 22.6% (—). The values in parentheses are the molar ratio of each element to zirconium. It should be noted that the molar ratio of cobalt to ammonia is 1:5.96.

Figure 3 shows that ZP–Co was decomposed when heated in four steps. For each decomposition peak the presence of ammonia was examined by means of evolved gas analysis. Ammonia was detected at the third step. In static air, this decomposition was exothermic because of the oxidation of the evolved ammonia. The presence of zirconium pyrophosphate was confirmed by heating ZP-Co to about 900 °C (Fig. 4). This indicates that the unexchanged monohydrogen orthophosphate group (–HPO_4) was present in ZP–Co, was converted to pyrophosphate, and lost water at high temperatures.

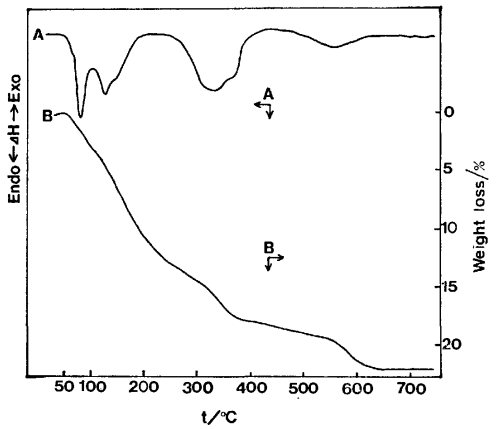

Fig. 3. DSC(A) and TGA(B) curves of ZP-Co.

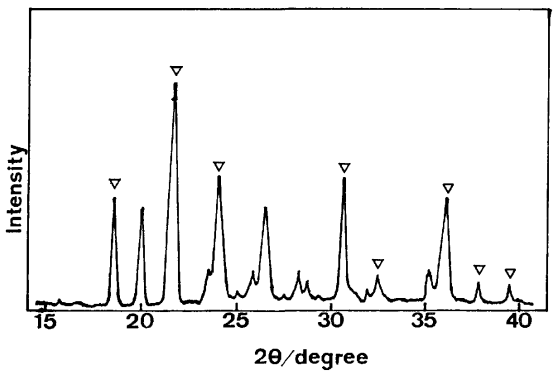

Fig. 4. Schematic diagram of X-ray powder diffraction pattern of the sample obtained by heating ZP-Co to about 900 °C. The symbol ▽ denotes the peak originating from ZrP_2O_7.

Assuming that the formula for ZP–Co is $Zr[Co(NH_3)_6]_m(H)_{2-3m}(PO_4)_2 \cdot nH_2O$ (m=0—2/3) and that the reduction of Co(III) does not occur, ZP–Co decomposes according to these reactions:

$$Zr[Co(NH_3)_6]_m(H)_{2-3m}(PO_4)_2 \cdot nH_2O \longrightarrow ZrCo_m(H)_{2-3m}(PO_4)_2(s) + 6mNH_3(g) + nH_2O(g)$$

$$ZrCo_m(H)_{2-3m}(PO_4)_2 \longrightarrow (1-3m/2)ZrP_2O_7(s) + 3m/2ZrCo_{2/3}(PO_4)_2{}^*(s) + (2-3m)/2H_2O(g)$$

(The compound marked with an asterisk could not be identified by means of its X-ray diffraction pattern.) The weight loss by heating is calculated by means of the following equations:

$$100\times(17.03\times6m+18.01\times n)/M_w = w_1(\%) \quad (1)$$

$$100\times[17.03\times6m+((2-3m)/2+n)\times18.01]/M_w = w_2(\%), \quad (2)$$

where M_w is the molecular weight of ZP-Co, and where w_1 and w_2 are the percentages of weight loss during heating to 420 and 900 °C respectively.

When the cobalt(III) ion in ZP–Co is reduced in the thermal decomposition, as in the case of $[Co(NH_3)_6]X_3$ (X=Cl, Br, I),[21] ZP–Co decomposes through these reactions:

$$Zr[Co(NH_3)_6]_m(H)_{2-3m}(PO_4)\cdot nH_2O \longrightarrow ZrCo_m(H)_{2-2m}(PO_4)_2(s) + 17m/3\,NH_3(g) + m/6N_2(g) + nH_2O(g)$$

$$ZrCo_mH_{2-2m}(PO_4)_2 \longrightarrow (1-m)ZrP_2O_7(s) + mZrCo(PO_4)_2{}^*(s) + (1-m)H_2O(g)$$

Thus, Eqs. 1 and 2 become:

$$100\times(17.03\times6m+18.01\times n-1.01\times m)/M_w = 100W/M_w = w_1\ (\%) \quad (3)$$

$$100\times[W+(1-m)\times18.01]/M_w = w_2\ (\%). \quad (4)$$

The experimental values agreed approximately with those calculated according to Eqs. 3 and 4 (Table 2). These facts indicate that the reduction of the cobalt(III) ocurred during heating.

TABLE 2. WEIGHT LOSS OF ZP-Co BY HEATING (%)

	Experimental	Calculated	
		Eqs. 1 and 2	Eqs. 3 and 4
420 °C	18.0	17.8	18.2
900 °C	22.6	20.5	21.7

In conclusion, the hexaamminecobalt(III)-hydrogen ion exchange partially proceeded in spite of the steric hindrance in the crystal structure of α-ZP. Cobalt(III) was present as a hexaammine complex cation in the exchanger.

The authors wish to express their thanks to Mr. Yukihiro Takekawa for the IR measurements and to Prof. Isao Tomita, Tokyo University of Fisheries, for the measurement of the TGA data.

References

1) Preceding paper: Y. Hasegawa and S. Kizaki, *Chem. Lett.*, **1980**, 241.
2) A. Clearfield and G. D. Smith, *Inorg. Chem.*, **8**, 431 (1969).
3) A. Clearfield, W. L. Duax, A. S. Medina, G. D. Smith, and J. R. Thomas, *J. Phys. Chem.*, **73**, 3424 (1969).
4) a) Y. Hasegawa and H. Aoki, *Bull. Chem. Soc. Jpn.*, **46**, 836 (1973). b) E. Michel and A. Weiss, *Z. Naturforsch., B*, **20**, 1307 (1965).
5) L. W. Johnson, *J. Chem. Soc., Chem. Commun.*, **1980**, 263.
6) F. Nozaki, T. Itoh, and S. Ueda, *Nippon Kagaku Kaishi*, **1973**, 674.
7) T. Hattori, A. Ishiguro, and Y. Murakami, *Nippon Kagaku Kaishi*, **1977**, 761.
8) G. Alberti, *Acc. Chem. Res.*, **11**, 163 (1978).
9) T. J. Kalman, M. Dudukovic, and A. Clearfield, *Adv. Chem. Ser.*, **133**, 654 (1974); *Chem. Abstr.*, **82**, 7891t (1975).
10) H. Arai, *Shokubai*, **19**, 365 (1977).
11) Y. Hasegawa and M. Kuwayama, *Bull. Chem. Soc. Jpn.*, **51**, 3485 (1978).
12) "Inorganic Synthesis," ed by W. C. Fernelius, McGraw-Hill, New York (1946), Vol II, pp. 216—217.
13) JCPDS Powder Diffraction file 21-862.
14) T. Flòra, *Acta Chem. Acad. Hung.*, **69**, 1 (1971).
15) Ref. 4 a.
16) I. M. Kolthoff and E. B. Sandell, "Textbook of Quantitative Inorganic Analysis," 3rd ed, McMillan, New York (1952), pp. 377—382.
17) G. Alberti and U. Costantino, *J. Chromatogr.*, **102**, 5 (1974) and the references cited therein.
18) S. E. Horsley, D. V. Nowell, and D. T. Stewart, *Spectrochim. Acta, Part A*, **30**, 535 (1974).
19) K. Nakamoto, "Infrared and Raman Spectroscopy of Inorganic and Coordination Compounds," 3rd ed, John Wiley & Sons, New York (1978), pp. 197—202.
20) J. Fujita, K. Nakamoto, and M. Kobayashi, *J. Am. Chem. Soc.*, **78**, 3295 (1956).
21) W. W. Wendlandt, *J. Inorg. Nucl. Chem.*, **25**, 545 (1963).

Lanthanoid Nitrate Complexes with Some Polyethylene Glycols and Glymes

Yoshiyuki HIRASHIMA,* Koji KANETSUKI, Ikuo YONEZU,
Kiyohito KAMAKURA, and Jiro SHIOKAWA
Department of Applied Chemistry, Faculty of Engineering, Osaka University, Yamada-oka, Suita, Osaka 565
(Received August 7, 1982)

Lanthanoid nitrates($Ln(NO_3)_3$) formed solid complexes with several polyethylene glycols and glymes. The compositions of the complexes were 1:1 (Ln:ligand) for triethylene glycol(EO3), tetraethylene glycol(EO4), pentaethylene glycol(EO5), and tetraglyme, 1:2 (Ln:ligand) for diethylene glycol, 2:1 for heptaethylene glycol, and 4:3 for pentaglyme and hexaglyme. Solid complexes were deposited also for hexaethylene glycol, but their compositions were not definitely determined. The solid complexes obtained here were all deliquescent. The deposition of the complexes was generally interfered with by water in the solution, and was not observed for some heavier lanthanoids when a small amount of water was present in the solution. The solubilities of the solid complexes with EO4 and EO5 increased with an increase in the atomic number of the lanthanoid, a fact suggesting a unique selectivity of the glycols. The infrared absorption bands of polyethylene glycols or glymes in the 1000—1150 cm^{-1} region became sharper upon the complexing of the glycols or glymes with lanthanoids; this sharpening can be explained by the change in the conformations in the ligand molecules.

Macrocyclic polyethers, so-called crown ethers, have been reported to form complexes with several cations.[1-4] The lanthanoid complexes of crown ethers have been reported, too.[5-8] King and Heckley suggested the possibility of the separation of lanthanoids by using crown ethers.[6] On the other hand, Yanagida *et al.* have reported the complexation of alkali and alkaline earth metals with noncyclic polyethers, polyethylene glycols and glymes.[9-11] Vögtle *et al.* have investigated the complexes of several noncyclic poly(oxyethylene) derivatives, which they call noncyclic crown ethers.[12-15] The lanthanoid complexes of polyethylene glycols have been reported by the present authors;[16] X-ray structure analyses indicate that polyethylene glycol molecules in the complexes assume ring-like structures similar to those of crown ethers,[17-19] suggesting that polyethylene glycols may have unique selectivities. The separation of lanthanoids with tetraethylene glycol by means of a fractional precipitation has been attempted on the basis of the fact that the yield of the lanthanoid complexes decreases as the atomic number of the lanthanoid increases.[20] Thus, polyethylene glycols may be promising reagents for the separation of lanthanoids. In the present work, lanthanoid complexes with several polyethylene glycols and glymes were isolated, and their properties were investigated.

Experimental

Materials. The lanthanoid nitrates were prepared by dissolving the corresponding oxides(>99.9% purity, Shin-Etsu Chemical Industry Co., Ltd.) into an excess of nitric acid. The solutions were concentrated on sand baths and then allowed to stand until the salts were deposited. The salts were dried at about 70 °C *in vacuo* for 6 h. The numbers of the hydrating water were 5—7.

The polyethylene glycols($HO(CH_2CH_2O)_nH$, EO*n*) and polyethylene glycol dimethyl ethers($CH_3O(CH_2CH_2O)_nCH_3$, glymes) used in this investigation were as follows: diethylene glycol (EO2, Wako Pure Chemicals Industries, Ltd.); triethylene glycol (EO3, Wako Pure Chemicals Industries, Ltd.); tetraethylene glycol(EO4, Tokyo Kasei Kogyo Co., Ltd.), and tetraethylene glycol dimethyl ether(tetraglyme, MeEO4Me, Tokyo Kasei Kogyo Co., Ltd.). They were all used after distillation. The penta-, hexa-, and heptaethylene glycols(EO5, EO6, and EO7) were offered by the Okahara Lab. (Department of Appled Chemistry of this Faculty). The pentaglyme and hexaglyme(MeEO5Me and MeEO6Me) were prepared by the method reported by Yanagida *et al.*[9]

Isolation of Solid Complexes of Lanthanoid Nitrates with Polyethylene Glycols and Glymes. A typical procedure for the preparation of solid complexes was as follows. About 1 mmol of a hydrous lanthanoid nitrate($Ln(NO_3)_3 \cdot nH_2O$, n= 5—7) in 10 cm^3 of ethyl acetate was mixed with about 1 mmol of a polyethylene glycol or a glyme in 10 cm^3 of ethyl acetate, after which the resulting solution was allowed to stand for a day. The solid complex deposited from the solution was filtered off, washed several times with 2 cm^3 of ethyl acetate, and then dried at about 60 °C *in vacuo* for 8 h. Each solution was dehydrated before mixing for the systems in which no solid complex was deposited, or in which the yield of the complex was low, by means of the method described above. The dehydration was carried out by refluxing each solution through a molecular-sieve layer. The composition of the solid complex deposited was not affected by dehydration. For the preparation of lanthanoid complexes with EO5, a solution of the lanthanoid nitrate was added to the EO5 solution under the conditions where there was always an excess of EO5.

Measurements of Infrared Spectra and Conductance. The infrared spectra were recorded on a Hitachi 260-10 spectrometer. The conductances of the solutions of the complexes were measured at 25.0±0.1 °C with a Yokogawa-Hewlett Packard Universal Bridge.

Measurements of Solubility. A flask containing 30 cm^3 of ethyl acetate and an appropriate amount of a solid complex was shaken in a water bath thermostatted at 25.0± 0.1 °C for 24 h or longer. The solid complex remaining undissolved was filtered off, and the concentration of the lanthanoid in the filtrate was determined by means of EDTA titration, with Xylenol Orange as an indicator.

X-Ray Powder Diffraction Analysis. The X-ray powder diffraction analysis was performed with a Rigaku Rotaflex diffractometer with a scintilation detector and Cu $K\alpha$ radiation (λ=1.5418 Å).

Results and Discussion

Isolation of Solid Complexes. The solid complexes of lanthanoid nitrates and yttrium nitrate with several

polyethylene glycols and glymes were isolated in this investigation. The well-defined complexes are listed in Tables 1—8, along with their analytical data. The solid complexes were deposited also for EO6, though they are not given in the tables because their compositions were not determined definitely. The solid complexes obtained here were all deliquescent. The deposition of the solid complexes was interfered with by water in the solution, and generally the solid complexes were not deposited for the heavier lanthanoids when the dehydration procedure was not carried out.

Table 1. Elemental analyses of $Ln(NO_3)_3 \cdot (EO2)_2$ complexes

Ln	Color	Found(Calcd)(%)			
		C	H	N	Ln
Pr	Pale green	17.69 (17.82)	3.78 (3.74)	7.84 (7.79)	26.0 (26.1)
Nd	Pale pink	17.45 (17.71)	3.75 (3.72)	7.70 (7.75)	26.6 (26.6)
Sm	White	17.57 (17.51)	3.75 (3.67)	7.72 (7.66)	27.2 (27.4)
Eu	White	17.61 (17.46)	3.79 (3.66)	7.45 (7.64)	27.4 (27.6)

Table 2. Elemental analyses of $Ln(NO_3)_3 \cdot EO3$ complexes

Ln	Color	Found(Calcd)(%)			
		C	H	N	Ln
La	White	14.99 (15.17)	2.70 (2.97)	8.84 (8.84)	28.7 (29.2)
Ce	White	14.93 (15.13)	2.77 (2.99)	8.67 (8.82)	29.2 (29.4)
Pr	Pale green	15.09 (15.11)	2.85 (2.96)	8.69 (8.81)	29.4 (29.5)
Nd	Pale pink	14.80 (15.00)	2.99 (2.94)	8.79 (8.75)	30.0 (30.0)
Sm	White	14.75 (14.81)	2.91 (2.90)	8.79 (8.64)	30.9 (30.9)
Eu	White	14.67 (14.76)	2.85 (2.89)	8.41 (8.61)	31.2 (31.1)
Gd	White	14.62 (14.61)	2.91 (2.86)	8.52 (8.52)	31.8 (31.9)
Tb	White	14.36 (14.56)	2.82 (2.85)	8.51 (8.49)	32.1 (32.1)
Dy	White	14.38 (14.45)	2.91 (2.83)	8.25 (8.43)	32.6 (32.6)
Ho	Pale orange	14.50 (14.38)	2.82 (2.82)	8.11 (8.39)	32.8 (32.9)
Er	Pale pink	14.80 (14.31)	2.86 (2.80)	7.80 (8.35)	33.5 (33.2)
Tm	White	14.24 (14.26)	2.77 (2.79)	8.30 (8.25)	33.1 (33.4)
Yb	White	14.26 (14.15)	2.78 (2.77)	8.35 (8.25)	34.4 (34.0)
Lu	White	13.92 (14.10)	2.81 (2.77)	8.07 (8.22)	34.1 (34.2)
Y	White	17.00 (16.95)	3.12 (3.33)	10.14 (9.88)	20.9 (20.9)

The Complexes with Diethylene Glycol(EO2): The solid complexes of $Ln(NO_3)_3 \cdot (EO2)_2$ (Ln; Pr, Nd, Sm, and Eu) were obtained as is shown in Table 1. Solid complexes were deposited also for the other lanthanoids and yttrium, but their compositions were not definitely determined. The ratios of metal/EO2 in such complexes ranged from 1/2 to 1/3.

The Complexes with Triethylene Glycol(EO3): Table 2 shows that EO3 formed 1:1 complexes with all the lanthanoids investigated and with yttrium. All the complexes were formulated as $Ln(NO_3)_3 \cdot EO3$, as is shown in Table 2, when the solid complexes were dried *in vacuo* at 80 °C. When the complexes were dried at room temperature (about 20 °C), however, the complex of lanthanum nitrate contained water and ethyl acetate, though the complexes of the other lanthanoid nitrates contained neither water nor ethyl acetate. The X-ray analysis of the complex of neodymium nitrate[19] has also indicated the absence of solvating water or a solvent. The deposition of the solid complexes seems to require the presence of a small amount of water in the solution. No solid complexes were obtained when the solutions were thoroughly dehydrated, and the deposition of the complexes was observed when a small amount of water was present. However, the presence of a large amount of water inhibited the deposition, as in the other EOn

Table 3. Elemental analyses of $Ln(NO_3)_3 \cdot EO4$ complexes

Ln	Color	Found(Calcd)(%)			
		C	H	N	Ln
La	White	18.37 (18.51)	3.55 (3.49)	7.89 (8.09)	26.6 (26.8)
Ce	White	18.75 (18.47)	3.65 (3.49)	8.22 (8.08)	26.8 (26.9)
Pr	Pale green	18.50 (18.44)	3.38 (3.48)	8.16 (8.06)	26.9 (27.0)
Nd	Pale pink	18.13 (18.32)	3.40 (3.46)	8.05 (8.01)	27.3 (27.5)
Sm	White	17.98 (18.11)	3.26 (3.42)	7.94 (7.92)	28.3 (28.3)
Eu	White	17.96 (18.05)	3.41 (3.41)	7.82 (7.90)	28.3 (28.6)
Gd	White	17.64 (17.88)	3.21 (3.38)	7.72 (7.82)	29.0 (29.3)
Tb	White	17.70 (17.82)	3.04 (3.37)	7.85 (7.79)	29.4 (29.5)
Dy	Pale yellow	17.74 (17.70)	3.21 (3.34)	7.60 (7.74)	29.7 (29.9)
Ho	Pale orange	17.63 (17.62)	3.32 (3.33)	7.65 (7.71)	30.0 (30.3)
Er	Pale pink	17.68 (17.55)	3.29 (3.31)	7.50 (7.67)	30.4 (30.5)
Tm	White	17.81 (17.50)	3.28 (3.30)	7.75 (7.65)	31.1 (30.8)
Yb	White	17.49 (17.36)	3.03 (3.29)	7.83 (7.59)	31.3 (31.3)
Lu	White	17.77 (17.30)	3.62 (3.27)	7.69 (7.57)	31.8 (31.5)
Y	White	20.37 (20.48)	3.96 (3.87)	8.73 (8.96)	18.9 (18.7)

complexes. These results suggest that water plays a part in the deposition of the complexes, but no further investigation was carried out.

The Complexes with Tetraethylene Glycol(EO4): Tetraethylene glycol(EO4) always formed a solid complex with the composition of $Ln(NO_3)_3 \cdot EO4$, irrespective of the mixing ratio or the mixing method of the solutions of the lanthanoid nitrate and EO4 (Table 3). The EO4 complexes were the least deliquescent of the complexes isolated in this investigation. These phenomena may be attributed to the fact that the chain length of EO4 is suitable for the 1:1 complex without any pronounced strain.[18]

The Complexes with Pentaethylene Glycol(EO5): Table 4 shows that the composition of well-defined complexes of EO5 are $Ln(NO_3)_3 \cdot EO5$. The 1:1 complex was deposited when there was an excess of EO5, while the ratio of Ln/EO5 in the complexes deposited was often larger than 1, ranging from 1.0 to 1.5 when the EO5 solution was added to the lanthanoid solution or when the mixing ratio of Ln/EO5 was larger than 1. However, only lanthanum nitrate always formed the 1:1 complex, regardless of the mixing conditions. This fact may be related to the fact that the ionic radius of lanthanum is the largest in the lanthanoids. The solid complexes were all hygroscopic; those of the heavier lanthanoids were more hygroscopic than those of the lighter lanthanoids, that of lutetium nitrate especially being so hygroscopic that the determination of the contents of C, H, and N was unsuccessful in the present method.

TABLE 4. ELEMENTAL ANALYSES OF $Ln(NO_3)_3 \cdot EO5$ COMPLEXES

Ln	Color	Found(Calcd)(%)			
		C	H	N	Ln
La	White	21.02 (21.33)	3.84 (3.94)	7.43 (7.46)	24.7 (24.7)
Ce	White	21.08 (21.28)	3.86 (3.93)	7.57 (7.44)	24.8 (24.8)
Pr	Pale green	21.41 (21.25)	3.90 (3.92)	7.46 (7.43)	24.9 (24.9)
Nd	Plale pink	20.96 (21.13)	3.85 (3.90)	7.37 (7.39)	25.2 (25.4)
Sm	White	20.60 (20.90)	3.63 (3.86)	7.19 (7.31)	26.0 (26.2)
Eu	White	20.60 (20.84)	3.85 (3.85)	7.17 (7.29)	26.4 (26.4)
Gd	White	20.49 (20.65)	3.85 (3.81)	7.20 (7.23)	26.9 (27.0)
Tb	White	20.57 (20.57)	3.79 (3.81)	7.23 (7.21)	27.3 (27.3)
Dy	Pale yellow	20.48 (20.45)	3.77 (3.79)	7.10 (7.16)	27.6 (27.7)
Ho	Pale orange	20.38 (20.12)	3.66 (3.77)	7.11 (7.13)	28.3 (28.0)
Er	Pale pink	20.30 (20.08)	3.76 (3.69)	7.11 (7.10)	28.3 (28.3)
Tm	White	20.17 (20.25)	3.74 (3.74)	7.21 (7.08)	28.7 (28.5)
Yb	White	20.04 (20.10)	3.65 (3.72)	7.03 (7.03)	29.0 (29.0)
Lu	White	—a) (20.04)	—a) (3.70)	—a) (7.01)	29.2 (28.1)

a) The contents of C, H, and N could not be determined because of great hygroscopy.

The Complexes with Heptaethylene Glycol(EO7): The 2:1 complexes were deposited for lanthanum and cerium. Table 5 shows the analytical data. For the other lanthanoids, the composition of the complex was not definitely determined or no solid complex was deposited. A heptaethylene glycol is considered to be bonded to two lanthanoid atoms because its chain length is too long to wrap around only one lanthanoid atom. The structures of the complexes prepared here are supposed to be similar to that of the 2:1 complex of merculy(II) chloride with hexaethylene glycol dimethyl ether reported by Iwamoto.[21]

The Complexes with Glymes: The 1:1 (Ln:glyme) complexes were deposited for tetraglyme (MeEO4Me), just as for EO3, EO4, and EO5, while the 4:3 complexes were deposited for pentaglyme (MeEO5Me) and hexaglyme (MeEO6Me). Tables 6, 7, and 8 show the complexes isolated in this investigation, together with the analytical data. The solid complexes of pentaglyme were deposited also for the lanthanoids which are not listed in Table 7, but their compositions were not defined well. Although there is a possibility that the 4:3 complexes prepared here were mixtures of the complexes with simple compositions, such as the 1:1 and 2:1 complexes, the 4:3 complex was always deposited for the system of praseodymium nitrate with pentaglyme, even when the mixing ratio of the nitrate to the glyme was varied from 1/4 to 4/1. Correspondingly, the possibility of the deposition of the mixture may well be neglected. The 4:3 complexes

TABLE 5. ELEMENTAL ANALYSES OF $[Ln(NO_3)_3]_2 \cdot EO7$ COMPLEXES

La	Color	Found(Calcd)(%)			
		C	H	N	Ln
La	White	17.19 (17.23)	2.83 (3.10)	8.72 (8.61)	28.05 (28.46)
Ce	White	16.99 (17.20)	3.09 (3.09)	8.52 (8.60)	28.44 (28.63)

TABLE 6. ELEMENTAL ANALYSES OF $Ln(NO_3)_3 \cdot$ MeEO4Me COMPLEXES

Ln	Color	Found(Calcd)(%)			
		C	H	N	Ln
La	White	21.75 (21.95)	4.10 (4.05)	7.55 (7.68)	25.0 (25.4)
Ce	White	21.68 (21.90)	4.06 (4.04)	7.52 (7.66)	25.1 (25.6)
Pr	Pale green	21.67 (21.87)	4.00 (4.04)	7.48 (7.65)	25.0 (25.7)
Nd	Pale pink	21.52 (21.74)	4.02 (4.01)	7.62 (7.60)	25.9 (26.1)
Sm	Pale yellow	21.35 (21.50)	3.92 (3.97)	7.35 (7.52)	26.1 (26.9)

Table 7. Elemental analyses of $[Ln(NO_3)_3]_4 \cdot [MeEO5Me]_3$ complexes

Ln	Color	Found(Calcd)(%)			
		C	H	N	Ln
La	White	19.63 (20.60)	3.77 (3.75)	7.51 (8.01)	26.0 (26.5)
Ce	White	20.32 (20.56)	3.66 (3.74)	7.89 (7.99)	26.4 (26.6)
Pr	Pale green	20.42 (20.52)	3.67 (3.73)	7.78 (7.98)	26.6 (26.8)
Nd	Pale pink	20.19 (20.42)	3.58 (3.71)	7.81 (7.93)	27.0 (27.2)
Sm	Pale yellow	20.13 (20.16)	3.74 (3.67)	7.78 (7.84)	27.8 (28.1)

Table 8. Elemental analyses of $[Ln(NO_3)_3]_4 \cdot [MeEO6Me]_3$ complexes

Ln	Color	Found(Calcd)(%)			
		C	H	N	Ln
La	White	22.24 (22.61)	3.83 (4.07)	7.22 (7.53)	24.9 (24.9)
Ce	White	22.19 (22.56)	4.07 (4.06)	7.47 (7.52)	25.0 (25.1)
Pr	Pale green	22.33 (22.53)	3.99 (4.05)	7.46 (7.51)	25.2 (25.2)
Nd	Pale pink	21.93 (22.40)	4.03 (4.03)	7.59 (7.46)	25.3 (25.6)

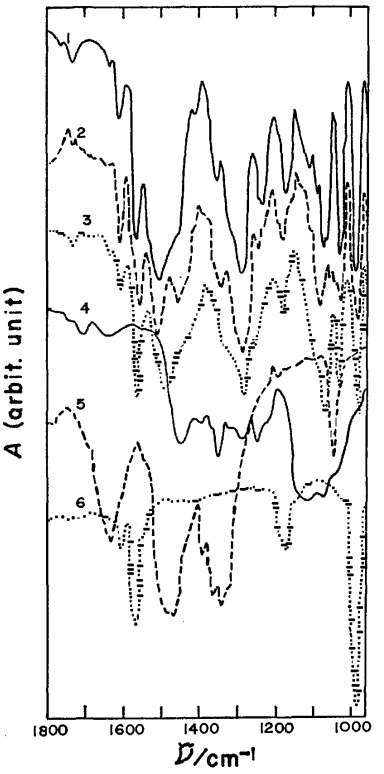

Fig. 1. IR spectra of neodymium nitrate, its complexes, EO4, and hexachlorobutadiene(HCB).
1: $Nd(NO_3)_3 \cdot EO3$ (HCB mull), 2: $Nd(NO_3)_3 \cdot EO4$ (HCB mull), 3: $Nd(NO_3)_3 \cdot EO5$ (HCB mull), 4: EO4 (liquid); 5: $Nd(NO_3)_3 \cdot 6H_2O$ (KBr pellet), 6: HCB (liquid).

of the lanthanoid nitrates have been reported also for crown compounds,[22] and the structure of the 4:3 complex of neodymium nitrate with 18-crown-6 ether has previously been reported;[23] *i.e.*, two different complex ions, the 1:1 complex cation $[Nd(NO_3)_2 \cdot 18\text{-crown-6}]^+$ and the complex anion containing no crown ether $[Nd(NO_3)_6]^{3-}$, are included in it.

Infrared Spectra of the Complexes. The infrared spectra of the solid complexes were similar to each other. In particular, there is little difference in the spectra among the complexes of individual lanthanoids with a given ligand (polyethylene glycol or glyme). The spectra of neodymium nitrate complexes with EO3, EO4, and EO5 are shown in Fig. 1 as typical examples, together with those of pure EO4, neodymium nitrate, and hexachlorobutadiene. Remarkable differences were observed between the complexes and the pure ligands in the 1000—1150 cm^{-1} region. The bands of the pure ligand (EO4 in Fig. 1) were broad in this region, while the bands became sharper in the case of the complexes. This change can be explained as follows: the ligand molecule can assume various conformations in a pure ligand; consequently, many bands appear in the spectra, overlapping each other, and resulting in broad bands, while the ligand molecule assumes a definite conformation in the complex. Accordingly, only the absorption bands corresponding to the conformation are observed, and the bands become sharp as a whole. A detailed discussion of similar phenomena in the merculy(II) chloride complexes has been reported by Iwamoto.[24] The absorption bands assigned to the coordinated nitrates were observed at about 1500 cm^{-1} and at about 1300 cm^{-1} for the complexes. There was no absorption band assigned to free nitrates at about 1380 cm^{-1} in the spectra of any of the complexes. According to the X-ray analyses of the neodymium nitrate complexes[17-19] three nitrates are all coordinated to a neodymium atom in the EO3 and EO4 complexes, while one nitrate is not coordinated in the EO5 complex. The results of the X-ray analyses are in agreement with the infrared spectra for the EO3 and EO4 complexes, but appear to be in conflict with that for the EO5 complex. According to the X-ray analyis, the uncoordinated nitrate in the EO5 complex assumes a C_{2v} symmetry rather than the D_{3h} one characteristic of a free nitrate. This fact explains the absence of the absorption band at about 1380 cm^{-1} in spite of the presence of the uncoordinated nitrate in the EO5 complexes.

Powder X-Ray Diffraction. The structures of neodymium nitrate complexes with EO3, EO4, and EO5 have been determined by the X-ray analyses of the single crystals.[17-19] The powder X-ray diffractions were measured for the complexes of the other lanthanoids as well as those of neodymium. Figure 2 shows some typical diffraction patterns. The diffraction patterns for the complexes of most of the lanthanoids with EO3, EO4, and EO5 were similar to those of the complexes of neodymium with the cor-

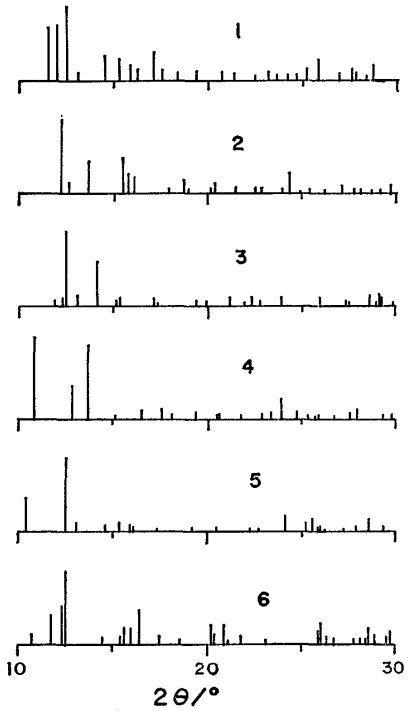

Fig. 2. X-Ray diffraction patterns of some lanthanoid complexes.
1: $La(NO_3)_3 \cdot EO3$, 2: $Nd(NO_3)_3 \cdot EO3$, 3: $Nd(NO_3)_3 \cdot EO4$, 4: $Er(NO_3)_3 \cdot EO4$, 5: $La(NO_3)_3 \cdot EO5$, 6: $Nd(NO_3)_3 \cdot EO5$.

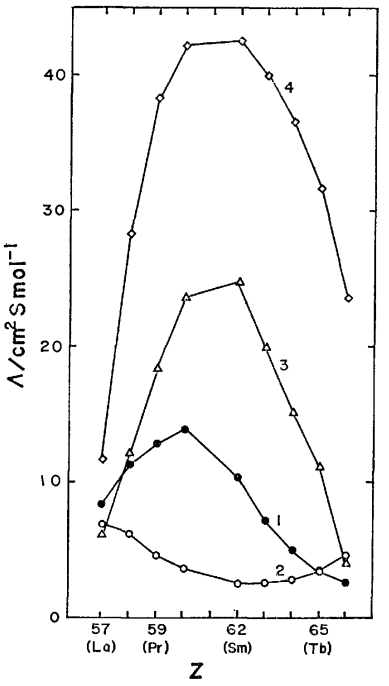

Fig. 3. Molar conductivities of lanthanoid nitrate complexes with EO3, EO4, and EO5 in acetone.
Concentration: 1 mmol/dm³, temp: 25 °C.
1: $Ln(NO_3)_3 \cdot nH_2O$, 2: EO3 complexes, 3: EO4 complexes, 4: EO5 complexes.

responding ligands. The complexes are expected to have structures similar to those of the neodymium complexes. The complexes of lanthanum and cerium with EO3 and EO5, and the complexes of terbium and the heavier lanthanoids with EO4 yielded patterns different from those of the corresponding neodymium complexes. These results suggest that the structures of the complexes are dissimilar to those of the neodymium complexes. The structures of the complexes are now being studied in detail by the present authors.

Electric Conductivities of the Solutions. Figure 3 shows the molar conductivities of the acetone solutions of the lanthanoid nitrate complexes of EO3, EO4, and EO5, together with those of the parent nitrates. All the values were lower than 45 S cm² mol⁻¹, suggesting that the complexes and the nitrates were essentially nonelectrolytes or dissociated as the 1:1 electrolytes.[25] The molar conductivities increased in the following order for a given lanthanoid: EO3 complex<parent nitrate<EO4 complex<EO5 complex. The mobility of the cation can reasonably be considered to decrease by complexing with any one of the glycols because of the increase in the size of the species. Therefore, the order of the conductivities described above is attributed to the difference in the degree of ionic dissociation among the complexes. According to the X-ray structure analyses of the complexes of neodymium nitrate, all the nitrates in the EO3 complex are bidentate, while one of the nitrates in the EO4 complex is unidentate and is uncoordinated in the EO5 complex, though the other two are bidentate. The degree of the dissociation is, therefore, expected to increase in this order: EO3 complex< EO4 complex<EO5 complex, since the ease of the dissociation of nitrates increases in this order: bidentate<unidentate<noncoordinated.

Solubilities of the Complexes. In the preparation of the solid complexes, the complexes of lighter lanthanoids appeared to be deposited more easily than those of heavier lanthanoids. This phenomenum is probably related to the difference in the solubilities between the complexes. Figures 4 and 5 show the solubilities of the EO4 complexes and the EO5 complexes respectively in ethyl acetate. The solubility generally increased with the increase in the atomic number of the lanthanoid both for the EO4 complexes and for the EO5 complexes, though some exceptions were observed (the heavier lanthanoids for the EO4 complexes and the lighter lanthanoids for the EO5 complexes). The observed solubilities shown in the figures are actually apparent ones, being affected not only by the solubilities of the undissociated complexes, but also by the stabilities of the complexes, for the complexes are probably, in part, dissociated in the solutions. The trend of the solubility shown in the figures implies an increase in the solubility of the undissociated complex and/or a decrease in the stability constant of the complex with an increase in the atomic number of the lanthanoid. The stability constants of the complexes with EO4 and EO5 may be expected to decrease with the increase in the atomic number of the lanthanoid; this tendency is contrary to those of the lanthanoid complexes with most other ligands, just as the stability constant of the lanthanoid complex with 18-crown-6 ether, which is similar in

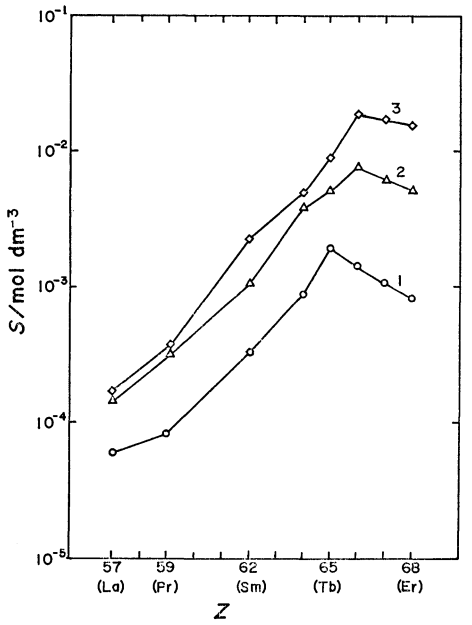

Fig. 4. Solubility(S) of $Ln(NO_3)_3 \cdot EO4$ complexes in ethyl acetate at 25 °C.
$[H_2O]$: 1. 0 mol/dm³, 2. 0.125 mol/dm³, 3. 0.25 mol/dm³.

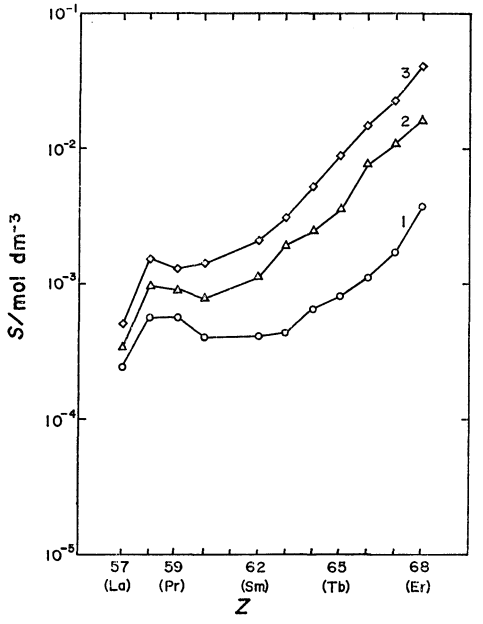

Fig. 5. Solubility(S) of $Ln(NO_3)_3 \cdot EO5$ complexes in ethyl acetate at 25 °C.
$[H_2O]$: 1. 0 mol/dm³, 2. 0.125 mol/dm³, 3. 0.25 mol/dm³.

molar structure to the complexes with EO4 and EO5, has been reported to decrease with the increase in the atomic number of the lanthanoid.[26] The anomalous behavior observed for terbium–erbium in the EO4 complexes and for lanthanum–praseodymium in the EO5 complexes is probably related to the difference in the crystal structures between those complexes and the other ones, as has been described above. The solubilities were increased by the presence of water in the solution for all the complexes. This result is in accordance with the fact that the deposition of the solid complexes was interfered with by water. The difference in the solubility among the complexes of individual lanthanoids with EO4 or EO5 suggests a new method for the mutual separation of lanthanoids by means of fractional precipitation.[20]

References

1) C. J. Pedersen, *J. Am. Chem. Soc.*, **89**, 2495, 7017 (1962); **92**, 386, 391 (1970).
2) J. J. Christensen, J. O. Hill, and R. M. Izatt, *Science*, **174**, 459 (1971).
3) C. J. Pedersen and H. K. Frensdorf, *Angew. Chem., Int. Ed. Engl.*, **11**, 16 (1972).
4) J. J. Christensen, D. J. Eatough, and R. M. Izatt, *Chem. Rev.*, **74**, 351 (1974).
5) A. Cassol, A. Seminaro, and G. De Paoli, *Inorg. Nucl. Chem. Lett.*, **9**, 1163 (1973).
6) R. B. King and D. R. Heckley, *J. Am. Chem. Soc.*, **96**, 3118 (1974).
7) M. Ciampolini and N. Nardi, *Inorg. Chim. Acta*, **32**, L9 (1979).
8) J.-C. G. Bünzli, D. Wessner, and H. T. T. Oanh, *Inorg. Chim. Acta*, **32**, L33 (1979).
9) S. Yanagida, K. Takahashi, and M. Okahara, *Bull. Chem. Soc. Jpn.*, **51**, 1294 (1978).
10) S. Yanagida, K. Takahashi, and M. Okahara, *Bull. Chem. Soc. Jpn.*, **50**, 1386 (1977).
11) S. Yanagida, K. Takahashi, and M. Okahara, *Bull. Chem. Soc. Jpn.*, **51**, 3111 (1978).
12) F. Vögtle and H. Sieger, *Angew. Chem.*, **89**, 410 (1977).
13) U. Heimann and F. Vögtle, *Angew. Chem.*, **90**, 212 (1978).
14) F. Vögtle and U. Heimann, *Chem. Ber.*, **111**, 2257 (1978).
15) W. Rasshofer, G. Oepen, and F. Vögtle, *Chem. Ber.*, **111**, 419 (1978).
16) Y. Hirashima and J. Shiokawa, *Chem. Lett.*, **1979**, 463.
17) Y. Hirashima, K. Kanetsuki, J. Shiokawa, and N. Tanaka, *Bull. Chem. Soc. Jpn.*, **54**, 1567 (1981).
18) Y. Hirashima, T. Tsutsui, and J. Shiokawa, *Chem. Lett.*, **1981**, 1501.
19) Y. Hirashima, T. Tsutsui, and J. Shiokawa, *Chem. Lett.*, **1982**, 1405.
20) Y. Hirashima, Y. Moriwaki, and J. Shiokawa, *Chem. Lett.*, **1980**, 1181.
21) R. Iwamoto, *Bull. Chem. Soc. Jpn.*, **46**, 1123 (1973).
22) J.-C. G. Bünzli and D. Wessner, *Helv. Chim. Acta*, **61**, 1454 (1978).
23) J.-C. G. Bünzli, B. Klein, D. Wessner, K. J. Schenk, G. Chapuis, G. Bombieri, and G. De Paoli, *Inorg. Chim. Acta*, **54**, L43 (1981).
24) R. Iwamoto, *Spectrochim. Acta, Part A*, **274**, 2385 (1971).
25) W. J. Geary, *Coord. Chem. Rev.*, **7**, 81 (1971).
26) R. M. Izatt, J. D. Lamb, J. J. Christensen, and B. L. Haymore, *J. Am. Chem. Soc.*, **99**, 8344 (1977).

Binuclear Metal Complexes. LI.[1] Synthesis and Characterization of the Tetrachloro-*o*-benzoquinone Adducts of Binuclear Iron(II) Complexes with 2-(Salicylideneamino)phenol and Its Substituted Homologs

Wakako KANDA, Masaaki NAKAMURA, Hisashi ŌKAWA,* and Sigeo KIDA
Department of Chemistry, Faculty of Science, Kyushu University 33 Hakozaki, Higashiku, Fukuoka 812
(Received August 9, 1982)

Binuclear iron(III) complexes Fe_2(R-R′-sap)$_2$(tcoq) have been prepared by the oxidation of binuclear iron(II) complexes Fe_2(R-R′-sap)$_2$ with tetrachloro-*o*-benzoquinone (TCOQ), where H_2(R-R′-sap) represents 2-(salicylideneamino)phenols with the substituent R on the salicylaldehyde ring and the R′ on the *o*-aminophenol ring. Magnetic measurements indicated the operation of an intramolecular antiferromagnetic spin-exchange interaction between the iron(III) ions, the exchange integrals being evaluated at -6——10 cm^{-1}. In both polarograms and cyclic voltammograms of these complexes, two redox processes attributable to Fe(III)–Fe(III) ⇌Fe(III)–Fe(II)⇌Fe(II)–Fe(II) were observed.

Previously we showed that binuclear manganese(II) complexes Mn_2(R-R′-sap)$_2$ of 2-(salicylideneamino)phenols (H_2(R-R′-sap); R and R′ being the substituents on the salicylaldehyde and the *o*-aminophenol rings, respectively) react with tetrachloro-*o*-benzoquinone (TCOQ) in an atmosphere of nitrogen to form binuclear manganese(III) complexes Mn_2(R-R′-sap)$_2$(tcoq), where two metal ions are bridged by the two phenolic oxygens of the Schiff bases in the equatorial plane and by the tetrachlorocatecholate group at the apical position (Fig. 1).[2] These complexes are very sensitive to moisture, hence decompose into Mn(R-R′-sap)$_2$ and Mn_2(R-R′-sap)$_2$ in an open atmosphere.[2]

As an extension of the above investigation, in this study we have prepared the binuclear iron(III) complexes Fe_2(R-R′-sap)$_2$(tcoq) and examined their properties in terms of Mössbauer spectroscopy, polarography, cyclic voltammetry and cryomagnetic measurements, in comparison with Mn_2(R-R′-sap)$_2$(tcoq) and binuclear iron(III) complexes related to the present complexes.

Experimental

Preparations. 2-(Salicylideneamino)phenol and its homologs were obtained by the reaction of salicylaldehyde or a substituted salicylaldehyde with 2-aminophenol or a substituted 2-aminophenol in the 1:1 mole ratio. In this study, the following ligands were used (*cf.* Fig. 1); 2-(salicylideneamino)phenol (H_2(sap)), 2-(5-methylsalicylideneamino)phenol (H_2(5-Me-sap)), 2-(salicylideneamino)-4-methylphenol (H_2(4′-Me-sap)), and 2-(salicylideneamino)-4-chlorophenol (H_2(4′-Cl-sap)).

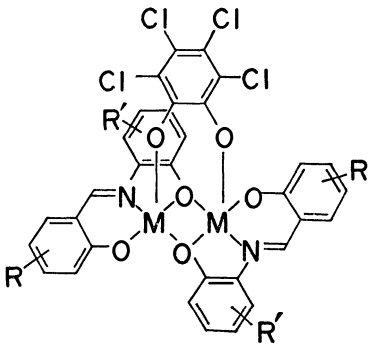

Fig. 1. Chemical structure of M_2(R-R′-sap)$_2$(tcoq) (M=Mn(III) and Fe(III)).

Binuclear iron(II) and iron(III) complexes, Fe_2(R-R′-sap)$_2$ and Fe_2(R-R′-sap)$_2X_2$ (X=Cl, Br), were prepared by the methods described in the literatures.[3,4]

Fe_2(R-R′-sap)$_2$(tcoq). Syntheses of the complexes were carried out in an atmosphere of nitrogen using a VAC Inert Atmosphere & Vacuum Deposition Equipment Model HE-43-2. The synthetic method for the complexes is exemplified by Fe_2(sap)$_2$(tcoq). A mixture of Fe_2(sap)$_2$ (0.50 g) and TCOQ (0.23 g) in absolute acetonitrile (20 cm^3) was refluxed for 5 h and then stirred overnight at room temperature. Black crystalline powder separated was collected, washed with a small amount of acetonitrile and dried *in vacuo*.

Elemental analyses of the complexes are given in Table 1.

Measurements. Elemental analyses of carbon, hydrogen, and nitrogen were carried out at the Service Center of Elemental Analysis Kyushu University. Analyses of iron were made with a Shimadzu Atomic Absorption-Flame Spectrometer Model AA-610S. Infrared spectra were measured with a Hitachi Infrared Spectrometer Model 215 on KBr disks. Mössbauer spectra were measured by the constant acceleration method at room temperature, using a cobalt 57 source (5 mCi) diffused into palladium foil. The velocity of the spectrometer was calibrated by the use of a pure iron foil enriched with iron-57, which was also used as a reference for the isomer shift values. All the Mössbauer parameters were obtained by computer calculations. Magnetic susceptibilities were measured by the Faraday method in the temperature range from liquid nitrogen temperature to room temperature. The apparatus was calibrated by the use of HgCo(NCS)$_4$.[5] Diamagnetic correction was made using Pascal's constants.[6] Effective magnetic moments were calculated by the equation, $\mu_{eff}=2.828(\chi_A \times T)^{1/2}$, where χ_A is the susceptibility per one iron atom corrected for diamagnetism. Electronic spectra were recorded on a Shimadzu UV-VISIBLE Recording Spectrometer Model UV-240 and Shimadzu Multipurpose Spectrophotometer Model MPS-5000 in dichloromethane. Polarograms and cyclic voltammograms were recorded with a Yanagimoto Voltammetric Analyzer Model P-1000 in dichloromethane containing 0.1 mol dm^{-3} tetrabutylammonium perchlorate as the supporting electrolyte. A three-electrode cell was used for measurements. The working electrode is a dropping mercury electrode for polarography and a glassy carbon for cyclic voltammetry. The auxiliary electrode and the reference electrode

Table 1. Elemental analyses of Fe_2(R-R′-sap)$_2$(tcoq)

	Found (%)				Calcd (%)			
	C	H	N	Fe	C	H	N	Fe
Fe(sap)$_2$(tcoq)·H_2O	47.87	2.51	3.82	13.7	48.16	2.53	3.51	14.0
Fe_2(5-Me-sap)$_2$(tcoq)·$2H_2O$	48.60	2.73	3.28	13.0	48.38	3.10	3.32	13.2
Fe_2(4′-Me-sap)$_2$(tcoq)·H_2O	49.75	2.94	3.52	13.3	49.44	2.92	3.39	13.5
Fe_2(4′-Cl-sap)$_2$(tcoq)·CH_3CN	45.80	2.23	4.50	12.3	45.89	2.15	4.72	12.6

were a platinum coil and a saturated calomel electrode, respectively. All the potentials were corrected by the use of ferrocene as an internal standard (Fc^+/Fc: $E_{1/2}=0.40$ V *vs.* NHE).[7]

Results and Discussion

Reaction of reddish brown Fe_2(R-R′-sap)$_2$ and TCOQ under nitrogen atmosphere yielded dark brown crystals. Elemental analyses suggested that these complexes contain (R-R′-sap)$^{2-}$, iron, and TCOQ in the ratio of 2:2:1. These complexes seem to be very stable in the open atmosphere, in contrast to the high sensitivity of Mn_2(R-R′-sap)$_2$(tcoq) to moisture. Infrared spectrum of Fe_2(sap)$_2$(tcoq) resembles that of Mn_2(sap)$_2$(tcoq), suggesting the similarity in the structure between them. The reactions of Fe_2(R-R′-sap)$_2$ with 9,10-phenanthrenequinone or 1,2-naphthoquinone instead of TCOQ gave no pure adducts.

In order to clarify the oxidation state and the spin state of the iron in Fe_2(R-R′-sap)$_2$(tcoq), the Mössbauer spectrum of Fe_2(sap)$_2$(tcoq) was measured at room temperature and is shown in Fig. 2. The quadrupole splitting (ΔE_q) and the isomer shift (δ) of this complex were determined to be 1.05 and 0.44 mm s^{-1}, respectively. It is known that the isomer shifts for most high-spin five-coordinate iron(III) complexes fall in the range 0.35—0.48 mm s^{-1}.[8,9] Thus, it is reasonable to assume that the iron in Fe_2(R-R′-sap)$_2$(tcoq) is in a high-spin state and of five-coordination. This suggests that the complexes possess the binuclear structure with the bridging tetrachlorocatecholate group at the apical position (Fig. 1).

The line-area ratio of the quadrupole doublet is estimated at 1:1, but the line-widths of the doublet are not identical; the positive side band (0.512 mm s^{-1}) is a little larger than that of the other band (0.425 mm s^{-1}). Similar asymmetry in quadrupole doublet has been found for [Fe(salen)Cl]$_2$ (salen^{2-}=*N*,*N*′-disalicylideneethylenediamine dianion) at 78 K, while its quadrupole doublet becomes nearly symmetric at 4.2 K.[4] According to Bergen *et al.* such asymmetry of Mössbauer doublet is attributable to the spin-spin relaxation.[10,11] Asymmetric quadrupole doublet was also observed for [Fe(salpa)Cl]$_2$ (salpa^{2-}=2-salicylideneamino-1-propanol dianion) and other binuclear iron(III) complexes.[9,12-14] In these complexes, spin-spin relaxation was regarded as the main reason for the asymmetric quadrupole splitting. Thus, it is likely that the asymmetric quadrupole doublet observed for Fe_2(sap)$_2$(tcoq) is also due to the spin-spin relaxation, although Mössbauer spectra at low temperatures are not measured.

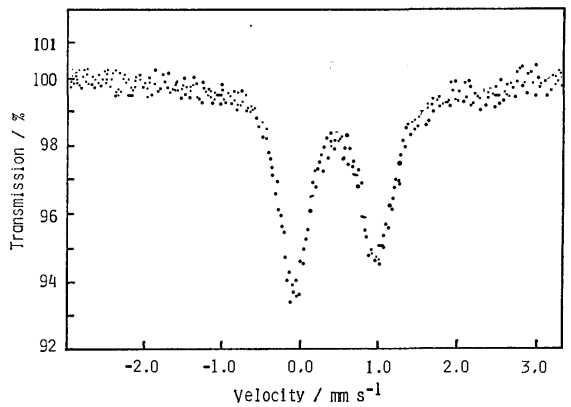

Fig. 2. Mössbauer spectrum of Fe_2(sap)$_2$(tcoq).

Magnetic susceptibilities of Fe_2(R-R′-sap)$_2$(tcoq) were measured in the temperature range 80—300 K. All of the complexes showed subnormal magnetic moments falling in the range 4.73—5.30 BM at room temperature (Table 2). Temperature-dependences of the magnetic moments suggested an operation of antiferromagnetic spin-exchange interaction between the metal ions. Based on the Heisenberg model ($\mathscr{H}=-2\Sigma J_{ij}S_iS_j$) and assuming no orbital contribution, the magnetic susceptibility equation for the Fe(III)-(S=5/2)-Fe(III)(S=5/2) system is given by

$$\chi_A=\frac{Ng^2\beta^2}{kT}\times\frac{55+30X^{10}+14X^{18}+5X^{24}+X^{28}}{11+9X^{10}+7X^{18}+5X^{24}+3X^{28}+X^{30}}+N\alpha$$
$$(X=\exp(-J/kT),$$

where χ_A represents magnetic susceptibility per iron atom and other symbols have their conventional meanings. Magnetic susceptibilities of the present complexes could be well interpreted in terms of this equation. A typical example of best-fits of magnetic susceptibilities to the theoretical curve is shown in Fig. 3. Magnetic parameters ($-J$ and g) thus determined are given in Table 2 (temperature-independent paramagnetism $N\alpha$ being assumed at zero). The exchange integrals range from -6 cm^{-1} to -10 cm^{-1}.

These integrals are close to the values of other di-μ-alkoxo or di-μ-phenoxo bridged binuclear iron(III) complexes so far reported.[4,15,16] It is particularly noticeable that the exchange integrals of the present complexes are essentially the same as those of $Fe_2(sap)_2X_2$ (X=Cl, Br).[4] This fact implies that the antiferromagnetic spin-exchange interaction in Fe_2(R-R′-sap)$_2$(tcoq) occurs *via* the phenolic oxygen bridge but not the tetrachlorocatecholate bridge.

Electronic spectra of the complexes Fe_2(R-R′-sap)$_2$-

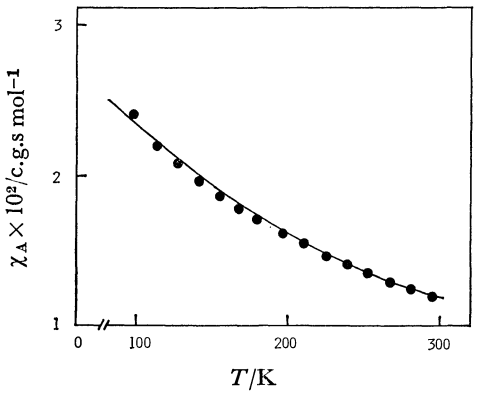

Fig. 3. Temperature variation of magnetic susceptibility for $Fe_2(sap)_2(tcoq)$. Solid curve is drawn based on the theoretical susceptibility equation using the parameters $g=1.98$, $-J=6.0$ cm^{-1} and $N\alpha=0$.

TABLE 2. EFFECTIVE MAGNETIC MOMENTS AT ROOM TEMPERATURE AND MAGNETIC PARAMETERS, J AND g, OF $Fe_2(R\text{-}R'\text{-}sap)_2(tcoq)$

	μ_{eff}/BM (T/K)	J/cm^{-1}	g
$Fe_2(sap)_2(tcoq)$	5.30(295.2)	−6	1.98
$Fe_2(5\text{-Me-sap})_2(tcoq)$	4.75(296.6)	−10	2.00
$Fe_2(4'\text{-Me-sap})_2(tcoq)$	5.00(296.1)	−8	2.00
$Fe_2(4'\text{-Cl-sap})_2(tcoq)$	5.30(297.8)	−6	1.98

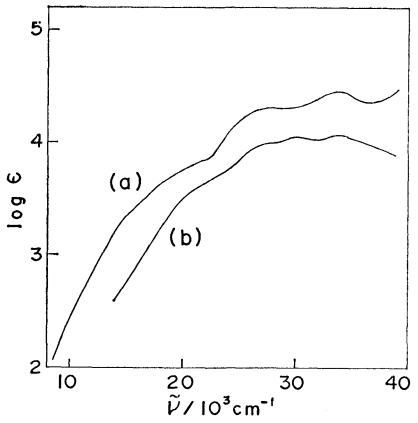

Fig. 4. Electronic spectra of (a)$Fe_2(sap)_2(tcoq)$ and (b) $Fe_2(sap)_2Cl_2$ in dichloromethane.

(tcoq) in dichloromethane are practically the same as each other, and were characterized by a strong absorption around 15×10^3 cm^{-1}, which is absent in the spectrum of $Fe_2(sap)_2Cl_2$. The spectrum of $Fe_2(sap)_2$-(tcoq) is shown in Fig. 4. The spectrum of $Fe_2(sap)_2$-Cl_2 is also shown for comparison. It is likely that the band at 15×10^3 cm^{-1} is due to the charge transfer band between iron(III) and tetrachlorocatecholate oxygen.

Electrochemical properties of the present complexes were investigated by means of polarography and cyclic voltammetry The complexes are stable in dichloromethane, judging from the fact that the electronic spectra obey Beer's law. Thus, electrochemical measurements were carried out in dichloromethane. All the complexes showed two quasi-reversible redox waves.

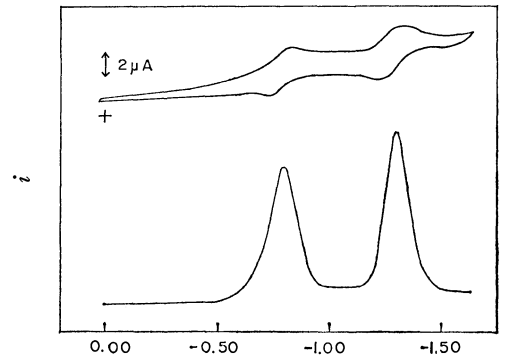

Fig. 5. Cyclic voltammogram (above) and differential pulse polarogram (below) of $Fe_2(5\text{-Me-sap})_2(tcoq)$.

TABLE 3. REDOX POTENTIALS $E_{1/2}$ (V vs. NHE) OF $Fe_2(R\text{-}R'\text{-sap})_2(tcoq)$

	DPP		CV	
	1st	2nd	1st	2nd
$Fe_2(sap)_2(tcoq)$	−0.77	−1.27	−0.91	−1.28
$Fe_2(5\text{-Me-sap})_2(tcoq)$	−0.86	−1.36	−0.83	−1.32
$Fe_2(4'\text{-Me-sap})_2(tcoq)$	−0.84	−1.34	−0.85	−1.35
$Fe_2(4'\text{-Cl-sap})_2(tcoq)$	−0.90	−1.26	−0.91	−1.30

DPP: Differential pulse polarogram, CV: cyclic voltammogram.

Differential pulse polarogram and cyclic voltammogram of $Fe_2(5\text{-Me-sap})_2(tcoq)$ are shown in Fig. 5. Half-wave potentials ($E_{1/2}$), which were determined from differential pulse polarogram and from the arithmetic mean of the cathodic and anodic peaks (E_{pc} and E_{pa}) of cyclic voltammogram, are given in Table 3.

Since binuclear zinc(II) complexes $Zn_2(R\text{-}R'\text{-sap})_2$ do not show any redox process in the range 0——1.8 V, the redox processess observed for $Fe_2(R\text{-}R'\text{-sap})_2$-(tcoq) can be attributed to those at the metal center. The first reduction occured at the potential −0.77——0.90 V and the second reduction at −1.26——1.36 V. The log (i/i_d-i) *vs.* E plots revealed that each process involves one-electron transfer. Based on these facts, we may tentatively attribute the first process to Fe(III)–Fe(III)⇌Fe(III)–Fe(II) and the second process to Fe(III)–Fe(II)⇌Fe(II)–Fe(II). It is to be noted that the redox potentials of $Fe_2(R\text{-}R'\text{-sap})_2(tcoq)$ are practically independent of the substituents R and R′ on the ligand, while the redox potentials of Mn(R-R′-sap)$_2$[2] and Zr(R-R′-sap)$_2$[17] are reported to be markedly dependent on the substituents.

In order to compare the electrochemical property of $Fe_2(R\text{-}R'\text{-sap})_2(tcoq)$ with that of $Fe_2(R\text{-}R'\text{-sap})_2X_2$, cyclic voltammograms of $Fe_2(sap)_2Cl_2$ and $Fe_2(sap)_2$-Br_2 were measured. The cyclic voltammograms, however, involved some complicated waves which could be hardly analyzed. It seems that $Fe_2(sap)_2X_2$ is partly dissociated or decomposed in solution.

Contrary to the step-wise redox behavior of $Fe_2(R\text{-}R'\text{-sap})_2(tcoq)$, $Mn_2(sap)_2(tcoq)$ showed only one redox couple attributable to the process Mn(III)–Mn(III)⇌

Mn(II)–Mn(II).[2] The present complexes Fe_2(R-R′-sap)$_2$(tcoq) are insensitive to moisture, while the manganese(III) complexes Mn_2(R-R′-sap)$_2$(tcoq) are very sensitive to moisture. It seems that the difference in sensitivity to moisture between Fe_2(R-R′-sap)$_2$(tcoq) and Mn_2(R-R′-sap)$_2$(tcoq) is due to their different electrochemical properties.

The authors are grateful to Associate Professor Yonezo Maeda and Dr. Tetsuaki Nishida of Kyushu University for the measurements and useful discussion of Mössbauer spectra.

References

1) Binuclear Metal Complexes. L: M. Mikuriya, H. Ōkawa, and S. Kida, *Inorg. Chim. Acta*, in press.
2) H. Ōkawa, M. Nakamura, and S. Kida, *Bull. Chem. Soc. Jpn.*, **55**, 466 (1982).
3) F. Maggio, T. Pizzino, and V. Romano, *Inorg. Nucl. Chem. Lett.*, **10**, 1005 (1974).
4) A. Bergen, K. S. Murray, B. O. West, and A. N. Buckley, *J. Chem. Soc., A*, **1969**, 2051.
5) B. N. Figgis and R. S. Nyholm, *J. Chem. Soc.*, **1959**, 331.
6) F. E. Mabbs and D. J. Marchin, "Magnetism and Transition Metal Complexes," Chapman and Hall, London (1973), p. 5.
7) H. M. Koepp, H. Wendt, and H. Strehlow, *Z. Electrochem.*, **64**, 483 (1960).
8) N. N. Greenwood and T. C. Gibb, "Mössbauer Spectroscopy," Chapman and Hall, London (1971), pp. 91, 162.
9) G. J. Long, J. T. Wrobleski, R. V. Thundathil, D. M. Sparlin, and E. O. Schlemper, *J. Am. Chem. Soc.*, **102**, 6040 (1980).
10) M. Blume, *Phys. Rev. Lett.*, **14**, 96 (1965).
11) M. Blume, *Phys. Rev. Lett.*, **18**, 305 (1967).
12) J. A. Bertrand, J. L. Breece, A. R. Kalyanaraman, G. J. Long, and W. A. Baker, Jr., *J. Am. Chem. Soc.*, **92**, 5233 (1970).
13) K. S. Murray, *Coord. Chem. Rev.*, **12**, 1 (1974).
14) S. L. Kessel and D. N. Hendrickson, *Inorg. Chem.*, **19**, 1883 (1980).
15) M. Gerloch, J. Lewis, F. E. Mabbs, and A. Richards, *J. Chem. Soc., A*, **1968**, 112.
16) C. S. Wu, G. R. Rossman, H. B. Gray, G. S. Hammond, and H. J. Schgar, *Inorg. Chem.*, **11**, 990 (1972).
17) M. Nakamura, H. Okawa, and S. Kida, Presented at the Meeting of the Kyushu and Chugoku-shikoku Branches of Chemical Society of Japan, Kagoshima, November 22, 1981.

Analysis for the Oligomerization Mechanism of Styrene by Field Desorption Mass Spectrometry

Jun SAITO,* Junji HARA,† Shozo TODA,†† and Shigeyuki TANAKA†††

Central Research Laboratory, Mitsui Toatsu Chemicals, Inc., 1190 Kasama, Totsuka-ku, Yokohama 247

† *Hara Polymer Consultant Office, 593-13 Terabun, Kamakura 248*

†† *Department of Agricultural Chemistry, Faculty of Agriculture, The University of Tokyo, 1-1-1 Yayoi, Bunkyo-ku, Tokyo 113*

††† *Department of Industrial Chemistry, Faculty of Engineering, The University of Tokyo, 7-3-1 Hongo, Bunkyo-ku, Tokyo 113*

(Received August 11, 1982)

Measurements were made of field desorption mass spectra of normal and deuterated styrene oligomers synthesized in various alkylbenzenes. Several series of molecular ion peaks are observed in both the spectra. From a comparison between them we have identified oligomers' end groups and derived formation mechanisms for individual molecular species. It has been clarified that molecular species independent of solvents are produced through chain transfer of propagating radicals to styrene dimers. Analysis for the polymerization mechanism of styrene as well as characterization of polymer molecules has been successfully performed by field desorption mass spectrometry.

Field desorption mass spectrometry (FD-MS) has been recognized as a very powerful tool for determination of molecular weights and structural characterization of nonvolatile compounds.[1] Recently, FD-MS has been applied also to examining various synthetic oligomers or polymers which consist of homologous mixtures, and its potentials for characterizing polymers have been demostrated.[2-4] However, until now the applicability of FD-MS to polymer chemistry has been restricted to determination of molecular weight distributions and molecular species.

Bevington[5] proposed from results in kinetic studies that radicals generated through reaction of Diels-Alder adducts with styrene monomers should react as an initiator in the thermally initiated polymerization of styrene. Similar results were obtained in a study[6] with considerations of isotope effect in the case of deuterated styrene.

In our previous works using the FD-MS,[7,8] we discussed on the telomerization of styrene oligomers to a chain transfer agent of 1,1,3,3,5,5-hexamethylhexanethiol and identified molecular species generated by the chain transfer in the thermal polymerization. In this investigation, we have been able to analyze successfully the mechanism of the thermally-initiated polymerization of styrene on the basis of FD-MS spectra of normal and deuterated styrene oligomers.

Experimental

Sample Preparation. Normal styrene monomer, toluene, ethylbenzene, propylbenzene, and isopropylbenzene were all commercial chemicals and used after distillation. Deuterated styrene monomer was obtained from Merck Sharp & Dohme Co., Ltd. and used without purification.

The oligomerization of normal or deuterated styrene was carried out by heating a sealed glass tube containing normal or deuterated styrene in solvent (molar ratio 1/100) at 200 °C for 2 h.

Apparatus. Mass spectrometry was performed on a JEOL-JMS D-300 double focusing mass spectrometer with a combined field desorption/field ionization/electron impact ion source, connected to a JMA 2000S mass data analysis system. The FD emitter used was a 10 μm tungsten wire with carbon needles. The oligomer sample was dissolved in chloroform (about 1 mg/0.5 ml) and loaded on the emitter by the normal dipping technique. The calibration of magnetic field current was done with perfluorokerosene or perfluoropoly(propylene oxide) as the reference *via* the EI mode. The accelerating voltage was either 3 or 2 kV. The instrumental resolution, $M/\Delta M$, was *ca.* 1000 (10% valley). The emitter current was increased linearly in the range 0—25 mA at the rate of 2 mA/min. The cathode potential was 5.5 kV. All FD-MS spectra were recorded as a sum of stored spectra.

Results and Discussion

Figures 1 and 2 show FD-MS spectra in the m/z region 250—800 for normal and deuterated styrene oligomers synthesized in ethylbenzene, respectively. It is seen from Fig. 1 that four series of molecular ion-peak patterns are distinguished by each mass number "104", which is the repetitive unit interval of a normal styrene. These series of peaks are at $92+104n$ (m/z 300—404—508—612), $208+104n$ (m/z 312—416—520—624), $106+104n$ (m/z 314—418—522—626), and $222+104n$ (m/z 326—430—534—638), where n is an integer corresponding to the degree of polymerization. Then, they are generally formulated as "$K+104n$," where K is a constant and is equivalent to the sum of both the mass numbers of the head and tail end groups. In the case of deuterated styrene, five series are also expressed in the same way as normal styrene oligomers except for the repetitive unit interval "107" being applicable to deuterated styrene; the five series are at $94+107n$ (m/z 308—415—522—629), $106+107n$ (m/z 320—427—534—641), $210+107n$ (m/z 317—424—531—638), $214+107n$ (m/z 321—428—535—642), and $226+107n$ (m/z 333—440—547—654). They are generally formulated as "$K+107n$."

Figures 3 and 4 show FD-MS spectra in the m/z region 400—500 for normal and deuterated styrene oligomers synthesized in toluene, ethylbenzene, propylbenzene, and isopropylbenzene. Each oligomer peak in Figs. 3 and 4 is also classified in the above-mentioned way. These results are summarized in Tables 1 and 2 for normal and deuterated styrenes, respec-

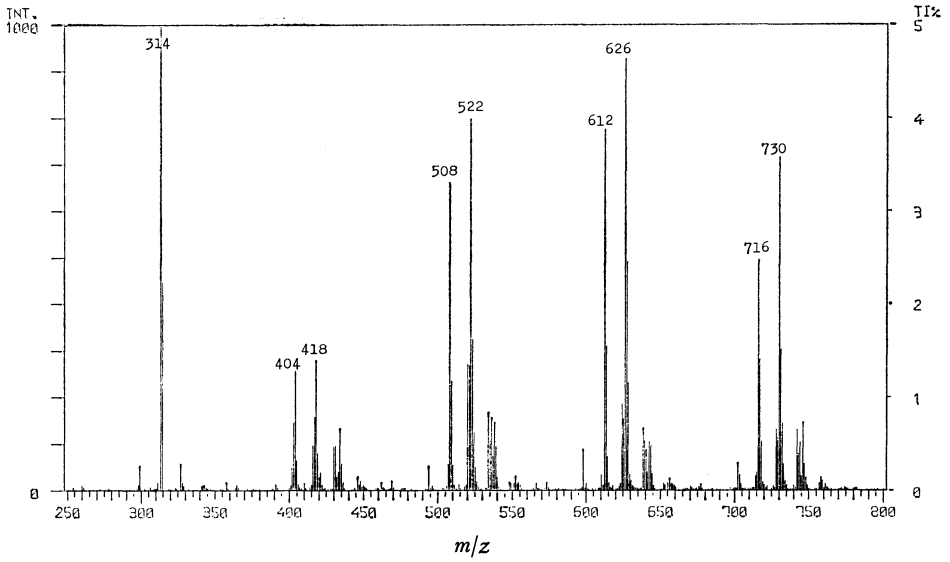

Fig. 1. FD-MS spectrum of normal styrene oligomers synthesized in ethylbenzene.

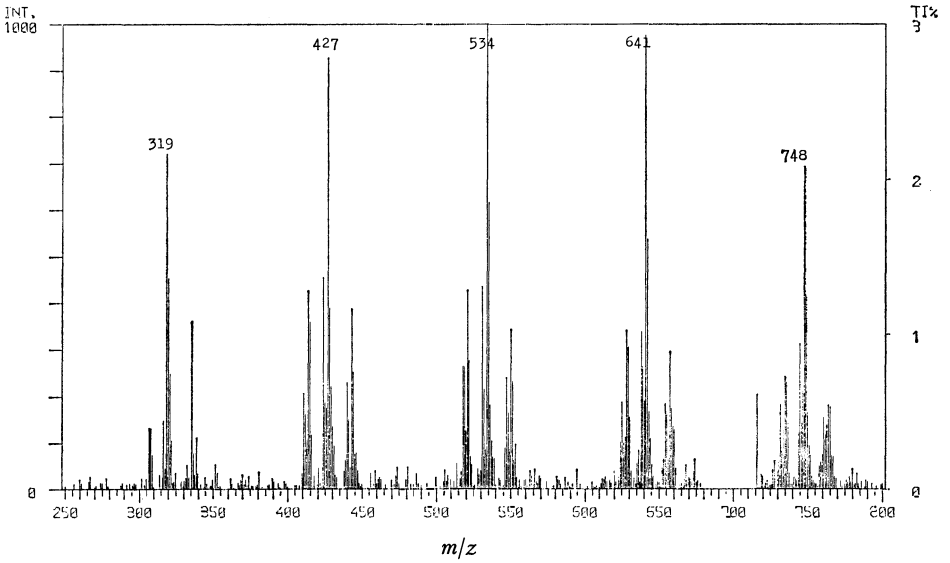

Fig. 2. FD-MS spectrum of deuterated styrene oligomers synthesized in ethylbenzene.

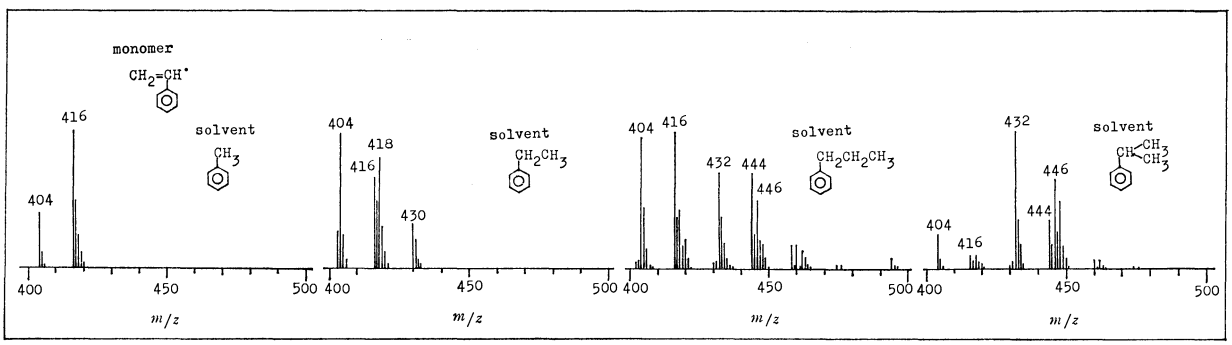

Fig. 3. FD-MS spectra (m/z; 400—500) of normal styrene oligomers synthesized in various solvents.

tively.

According to the reasonable proposal on the initiation mechanism for the thermal polymerization of styrene by Mayo[9] and Kopecky and Evani,[6] the first step is the Diels-Alder dimerization to form styrene dimers (SD) according to

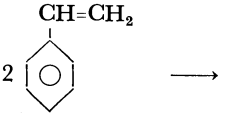

(1)

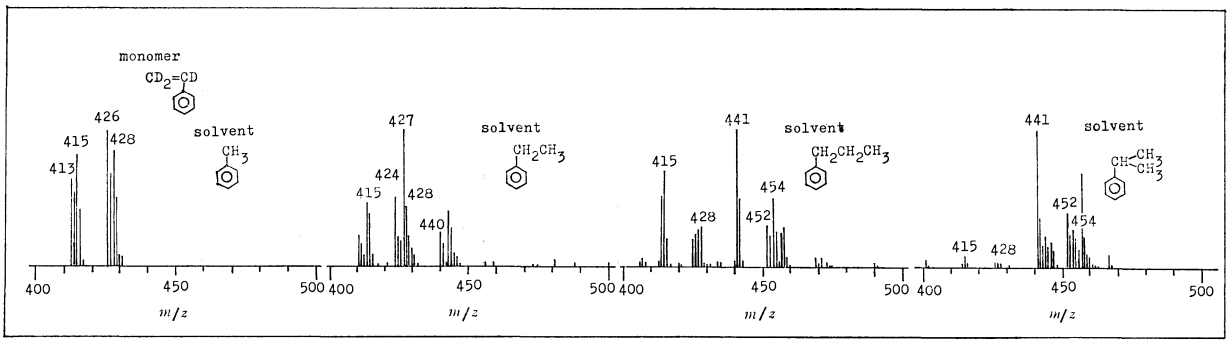

Fig. 4. FD-MS spectra (m/z; 400—500) of deuterated styrene oligomers synthesized in various solvents.

TABLE 1. MASS NUMBERS OF THE SPECIES DERIVED FROM THE PROPOSED MECHANISM FOR NORMAL STYRENE OLIGOMERS

Solvent	Head group		Tail group: ·H 1	Tail group: ·CH_2CH=CH-⟨○⟩ 117
Toluene	⟨○⟩-$\dot{C}H_2$	91	$92+(104)_n$	$208+(104)_n$
	⟨○⟩-$\dot{C}H_2$	91	$92+(104)_n$	$208+(104)_n$
Ethylbenzene	⟨○⟩-$\dot{C}HCH_3$	105	$106+(104)_n$	$222+(104)_n$
	⟨○⟩-$\dot{C}H_2$	91	$92+(104)_n$	$208+(104)_n$
Propylbenzene	⟨○⟩-$\dot{C}HCH_2CH_3$	119	$120+(104)_n$	$236+(104)_n$
	⟨○⟩-$\dot{C}H_2$	91	$92+(104)_n$	$208+(104)_n$
Isopropylbenzene	⟨○⟩-$\dot{C}(CH_3)_2$	119	$120+(104)_n$	$236+(104)_n$
	⟨○⟩-$\dot{C}H_2$	91	$92+(104)_n$	$208+(104)_n$

TABLE 2. MASS NUMBERS OF THE SPECIES DERIVED FROM THE PROPOSED MECHANISM FOR DEUTERATED STYRENE OLIGOMERS

Solvent	Head group		Tail group: ·H 1	Tail group: ·CD_2CD=CD-⟨○⟩ 121
Toluene	⟨○⟩-$\dot{C}H_2$	91	$92+(107)_n$	$212+(107)_n$
	⟨○⟩-$\dot{C}D_2$	93	$94+(107)_n$	$214+(107)_n$
Ethylbenzene	⟨○⟩-$\dot{C}HCH_3$	105	$106+(107)_n$	$226+(107)_n$
	⟨○⟩-$\dot{C}D_2$	93	$94+(107)_n$	$214+(107)_n$
Propylbenzene	⟨○⟩-$\dot{C}HCH_2CH_3$	119	$120+(107)_n$	$240+(107)_n$
	⟨○⟩-$\dot{C}D_2$	93	$94+(107)_n$	$214+(107)_n$
Isopropylbenzene	⟨○⟩$C(\dot{C}H_3)_2$	119	$120+(107)_n$	$240+(107)_n$
	⟨○⟩-$\dot{C}D_2$	93	$94+(107)_n$	$214+(107)_n$

In a subsequent step, SD reacts with a third styrene monomer in a molecule-induced homolysis to produce two kinds of radicals according to

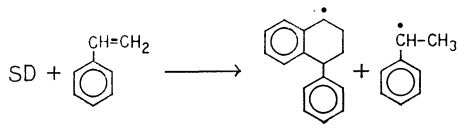
(2)

These two radicals then initiate polymerization, and under our experimental conditions employing circumstances with much more solvent, it is expected that the propagation radicals stimulate the chain transfer to solvent molecules (SH) and furthermore that solvent radicals with hydrogen atom abstracted should play a major role as a reinitiator according to

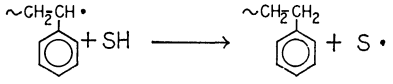
(3)

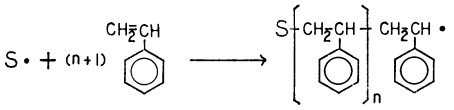
(4)

On the basis of the dependency of reactivity on the kind of solvents, the mass numbers of normal styrene oligomers with K's 92, 106, and 120 in Table 1 are assigned to the molecular species

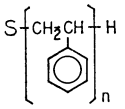
(5)

It is shown in Table 2 that such series as have the same K's are observed in deuterated styrene oligomers as well. On the contrary, existence of such molecular species as are independent of the kind of solvents is indicated which have K's 92 and 208 for normal styrene oligomers and 94 and 214 for deuterated ones in Tables 1 and 2, respectively.

Though with no detailed discussion on the mechanism of the chain transfer, Pryor and Coco[10] pointed out from a computer simulation that the propagation mechanism for the thermal polymerization of styrene should be related to the chain transfer of SD and that at 60 °C the chain transfer constant, Cm*, for SD was 10^2—10^3 times higher than that for any aromatic hydrocarbon solvents used here. In our present investigation, the chain transfer to the solvent could occur with a rather high probability because of the low concentration of styrene monomer (below 1 mol%).

In order to explain the appearance of molecular species given in Tables 1 and 2, it is assumed that the chain transfer of propagating radicals to SD should follow the reaction sequences

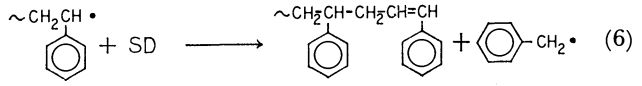
(6)

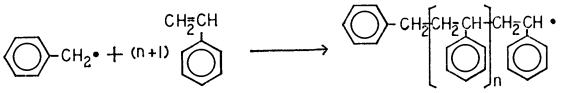
(7)

Thus, if the propagating radicals encounter SD, the SD makes a cleavage into benzyl and 3-phenyl-2-propenyl radicals, and then the 3-phenyl-2-propenyl radicals are combined with the propagating radicals, while the benzyl radicals only contribute to the reinitiation process. According to this assumption and considering the chain transfer to solvents, it may be expected that there should exist two head groups and two tail groups, and therefore that the four molecular species represented by Formula 5 and the following formulas should be observed in FD-MS spectra.

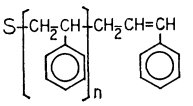
(8)

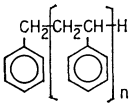
(9)

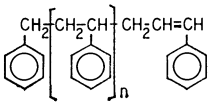
(10)

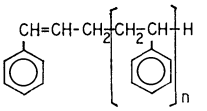
(11)

Indeed, our experimental results may support the proposed mechanism. Furthermore, it is clarified that the abstraction reaction of a benzyl group through the chain transfer to SD dose not occur, as evidenced by the fact that no such molecular species as shown by Formula 11 appears in any FD-MS spectra.

In Figs. 3 and 4, besides the peaks attributed to the chemical structures for Formulas 5 and 8—10, molecular ion peaks independent of the kind of solvents, whose K's correspond to 182, 210, and 238, are observed. They are thought as being produced by the recombination termination between the propagating radicals, since there are generally two termination processes, that is, recombination and disproportionation, and moreover it was reported that the probability of the recombination termination for styrene is nearly 100%.[11] Other intense peaks in Figs. 1 and 2 are observed at 312 and 321 for normal and deuterated styrene oligomers, respectively. These peaks are assigned to the molecular species formed in the trimerization of monomers. These results are in agreement with the fact that the radical pair produced in the reaction between SD and styrene monomers should generate the cage reaction to form trimeric products concertedly against the chain initiation.[12]

In conclusion, it was proved from a detailed analysis of molecular ion peaks observed in FD-MS spectra that some kinds of reactions were generated in the styrene polymerization. They are radical telomerization to solvents and SD and recombination termination and cage reaction between initiating or propagating radicals. Thus, it has been found that the

* SD may be considered as such intermediates:

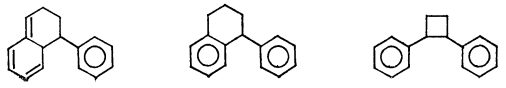

FD-MS is effective for the investigation on the polymerization mechanism. However, it is not sufficient to discuss the quantitative analysis owing to the bad reproducibility of peak intensities. In near future, if high sensitive measurement in the high mass region becomes available, the whole polymerization mechanism might get clarified and confirmed more accurately.

References

1) H. D. Beckey and H. R. Schulten, *Angew. Chem., Int. Ed. Engl.*, **14**, 403 (1975); T. Matsuo, Y. Itagaki, and I. Katakuse, *Shitsuryo Bunseki*, **29**, 2 (1981).
2) J. Saito, S. Toda, and S. Tanaka, *Shitsuryo Bunseki*, **28**, 175 (1980); *J. Thermosetting Plastics Jpn.*, **2**, 72 (1981).
3) R. P. Lattimer, D. J. Harmon, and G. E. Hansen, *Anal. Chem.*, **52**, 1808 (1980); *Macromolecules*, **14**, 776 (1981).
4) G. M. Neumann, P. G. Cullis, and P. J. Derrick, *Z. Naturforsch., A*, **35**, 1090 (1980); A. G. Craig, P. G. Cullis, and P. J. Derrick, *Int. J. Mass Spectrom. Ion Phys.*, **38**, 297 (1981).
5) J. C. Bevington, *Fortschen. Hochpolym. Forsch.*, **2**, 1 (1960).
6) K. R. Kopecky and S. Evani, *Can. J. Chem.*, **47**, 4049 (1969).
7) J. Saito, S. Toda, and S. Tanaka, *Bunseki Kagaku*, **30**, 706 (1981).
8) J. Saito, J. Hara, S. Toda, and S. Tanaka, *Chem. Lett.*, **1982**, 311.
9) F. R. Mayo, *J. Am. Chem. Soc.*, **90**, 1289 (1968).
10) W. A. Pryor and J. H. Coco, *Macromolecules*, **3**, 500 (1970).
11) J. C. Bevington and H. W. Melville, *J. Polym. Sci.*, **12**, 449 (1952).
12) W. G. Brown, *Makromol. Chem.*, **128**, 130 (1969).

 © 1983 The Chemical Society of Japan Bull. Chem. Soc. Jpn., 56, 753—757 (1983)

Aromatic Nucleophilic Substitution. XVI.[1] Stopped-flow Kinetics of Formation and Decomposition of 1,3- and 1,1-Disubstituted Anionic σ Complexes in Reactions of 1-Dimethylamino-2,4-dinitronaphthalene with Potassium Alkoxides in Dimethyl Sulfoxide–Alcohol

Shizen Sekiguchi,* Noboru Tone, Toshio Takei, and Noboru Tomoto†

Department of Chemistry, Gunma University, Kiryu, Gunma 376

† *Department of Chemistry, Miyazaki University, 1-1-1 Kirishima, Miyazaki, Miyazaki 880*

(Received June 10, 1982)

Reactions of 1-dimethylamino-2,4-dinitronaphthalene with potassium methoxide or ethoxide were carried out in DMSO–CH_3OH or DMSO–C_2H_5OH (90:10 v/v), respectively, where the 1,3-disubstituted anionic σ complexes were first rapidly formed, undergoing isomerizations to the 1,1-disubstituted anionic σ complexes. Rates and activation parameters were determined by kinetic studies using stopped-flow and conventional spectrophotometers. The rate constant (25 °C) for the formation of 1,3-disubstituted one in DMSO–CH_3OH is about half that in DMSO–C_2H_5OH, whereas the rate constant (25 °C) for its decomposition is more than twice that in DMSO–C_2H_5OH. The apparent pseudo-first-order rate constant for the formation of 1,1-disubstituted anionic σ complex in DMSO–CH_3OH depends upon the methoxide ion concentration, whereas that in DMSO–C_2H_5OH is almost independent of the ethoxide ion concentration. The mechanism is discussed on the basis of activation parameters.

In our previous work[1] we reported detailed kinetics of reactions of 1-dialkylamino-2,4-dinitronaphthalenes with potassium methoxide in DMSO–CH_3OH, where 1,3-disubstituted anionic σ complexes are first formed, undergoing isomerizations to 1,1-disbustituted ones according to

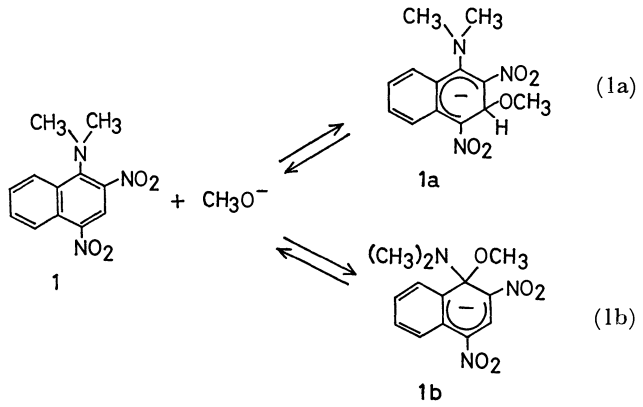

Thus we found that the kind of the 1-dialkylamino groups and the DMSO content in the mixed solvent will affect the rate of formation and decomposition of 1,3- (**1a**) and 1,1-disubstituted anionic σ complexes (**1b**).

Therefore, replacement of potassium methoxide by potassium ethoxide would be expected to affect the rates of formation and decomposition of both complexes.

This paper reports a comparison of the results obtained in the case of potassium ethoxide with those in the case of potassium methoxide in order to elucidate further the reaction mechanism.

Results

Absorption Spectra. Upon addition of excess ethanolic C_2H_5OK to 1-dimethylamino-2,4-dinitronaphthalene (**1**) in DMSO–C_2H_5OH (90:10 v/v), the solution was colored red instantly (Fig. 1): Curve b, for the formation of a complex (**2a**, corresponding to **1a**), was first obtained, which was then gradually changed into Curve d due to the formation of a complex (**2b**, corresponding to **1b**). The time-dependent spectral change is clearly interpreted on the basis of the reaction paths defined by

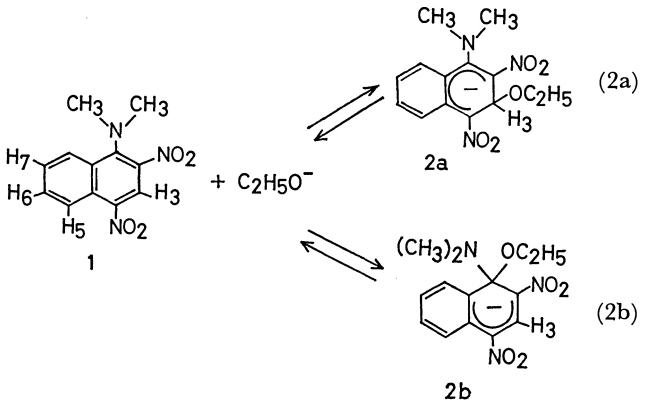

On the other hand, NMR spectrometry, which is generally recognized useful for elucidating structures of anionic σ complexes,[2,3] also showed that the process (Eq. 2) is valid: Just after addition of ethanolic C_2H_5OK (1.19×10^{-4} mol) to a DMSO solution (0.4 ml) of **1** (1.15×10^{-4} mol) at room temperature, the solution turned red at once, suggesting the formation of a complex. Just after addition, H_3 sharp singlet ($\delta=8.70$) of **1** shifted upfield ($\delta=6.27$, H_3 of **2a**). Fast sweep time (500 Hz/50 s) and fast procedures are indispensable for detecting spectral changes. One minute and a half after addition, a new singlet, due to H_3 of **2b**, appeared at $\delta=9.26$ at the expense of the singlet at $\delta=6.27$ which appeared faintly.

It is thus expected that the discrete kinetics of formation and decomposition of **2a** and **2b** is possible.

Kinetic Runs. Let us rewrite Eq. 2 in a form convenient for quantitative discussion as follows:

$$\mathbf{1} + C_2H_5O^- \underset{k_{-1}}{\overset{k_1}{\rightleftharpoons}} \mathbf{2a}, \quad (3a)$$

$$\mathbf{2a} \underset{k_{-2}}{\overset{k_2}{\rightleftharpoons}} \mathbf{2b}, \quad (3b)$$

$$K_1 = \frac{k_1}{k_{-1}}, \quad K_2 = \frac{k_2}{k_{-2}}.$$

According to the results of UV-VIS and NMR spectra, the reaction will occur in two distinct stages: The chemical transformations responsible for the first (Spectrum a→b) and second spectral changes (Spectrum b→c→d), to be termed Stage I and Stage II, respectively. The Stage I reaction (**1**⇄**2a**) is much faster than the Stage II reaction (**1**⇄**2b**). Accordingly, in treating the Stage I kinetics, the Stage II reaction can be neglected; the Stage I reaction goes to completion in a few tenths of a second (Table 1), making negligible the possible kinetic effect from the Stage II reaction.

Stage I. The pseudo-first-order rate constant, k_ψ, for the attainment of an equilibrium (K_1) is the sum of forward and reverse components.[4] For the Stage I reaction the kinetic expression (Eq. 4)

$$k_\psi = k_1([C_2H_5O^-]+[\mathbf{1}]) + k_{-1} \quad (4)$$

$$k_\psi = k_1[C_2H_5O^-] + k_{-1} \quad (5)$$

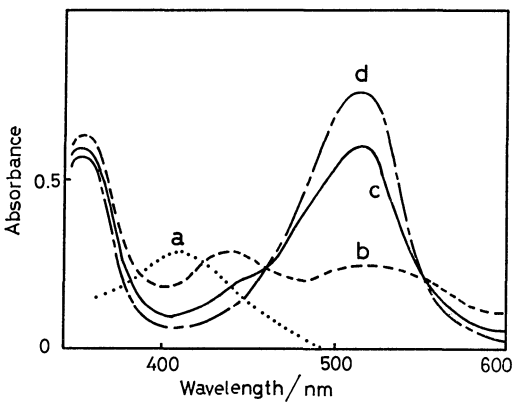

Fig. 1. Spectral change relevant to the reaction of 1-dimethylamino-2,4-dinitronaphthalene (**1**) with C_2H_5OK in DMSO–C_2H_5OH (90:10 v/v) at room temperature.
a: **1** (3.5×10^{-5} M) (1 M=1 mol dm^{-3}), b: just after addition of C_2H_5OK (4.42×10^{-3} M), c: 15 min after addition, d: 90 min after addition.

should hold. Under the actual condition $[C_2H_5O^-]\gg[\mathbf{1}]$, Eq. 4 is simplified to Eq. 5.[5]

As a result, k_1 and k_{-1} are estimated from the slope and intercept in the linear dependence of k_ψ on $[C_2H_5O^-]$ (not shown). Table 1 shows the dependence of k_ψ on the ethoxide ion concentration, including the estimated rate and equilibrium constants. Table 2

TABLE 1. RATE AND EQUILIBRIUM CONSTANTS FOR THE FORMATION AND DECOMPOSITION OF 1,3-DISUBSTITUTED ANIONIC σ COMPLEXES FORMED FROM 1-DIMETHYLAMINO-2,4-DINITRONAPHTHALENE (**1**) AND POTASSIUM ALKOXIDES IN (90:10 v/v) AT 25 °C

[ROK] / M	k_ψ[b] / s^{-1}	k_1[c] / M^{-1} s^{-1}	$10\,k_{-1}$[c] / s^{-1}	K_1[d] / M^{-1}
		DMSO–CH_3OH[a]		
10^3[CH_3OK]				
2.16	1.95±0.07			
3.53	2.94±0.09			
6.35	4.66±0.03			
7.20	5.08±0.06			
8.10	5.49±0.10			
8.80	6.05±0.05	607±12[e]	6.98±1.44[e]	940± 230[e]
9.90	6.70±0.06			
11.0	7.37±0.05			
12.0	8.00±0.04			
13.0	8.60±0.07			
14.0	9.27±0.08			
		DMSO–C_2H_5OH[a]		
10^3[C_2H_5OK]				
3.25	3.98±0.05			
4.13	5.11±0.05			
6.50	7.77±0.42			
6.88	8.60±0.07			
9.63	12.0 ±0.1			
9.75	11.6 ±0.1	1190±25	3.00±0.16	4380±1400
12.3	15.2 ±0.7			
15.1	18.5 ±0.1			
16.3	19.5 ±0.5			
17.8	20.0 ±0.7			
19.5	23.0 ±0.8			

a) [**1**]=2.0×10^{-4} M; μ=0.05 ($KClO_4$). b) Measured at 565 nm by the stopped-flow method. c) Calculated from Eq. 5. d) Calculated from $K_1=k_1/k_{-1}$. e) Although the values are a little different from those in Table 1 in Ref. 1, they are more rigorous because of the broader range of [CH_3OK] adopted for the measurement.

Table 2. Temperature dependence of rate constants for the formation and decomposition of 1,3-disubstituted anionic σ complex formed from 1-dimethylamino-2,4-dinitronaphthalene (**1**) and potassium ethoxide in DMSO-C_2H_5OH (90 : 10 v/v)[a]

Temp °C	k_1 [b] $M^{-1}s^{-1}$	k_{-1} [c] s^{-1}	K_1 [d] M^{-1}
15	519± 8	0.10±0.02	5420±1160
25	1190±25	0.30±0.16	4380±1400
35	2430±20	—[e]	—[e]
40	3510±60	—[e]	—[e]

a) $[\mathbf{1}]_0=2.0\times10^{-4}$ M; $\mu=0.05$ M ($KClO_4$). For the results of the reaction of **1** with CH_3OK, see Table 2 in Ref. 1. b) Calculated from Eq. 5. c) Calculated from Eq. 5. d) Calculated from $K_1=k_1/k_{-1}$. e) Not calculated owing to too large errors.

Table 3. Kinetic and thermodynamic parameters for the formation and decomposition of 1,3-disubstituted anionic σ complexes in DMSO-ROH (90:10 v/v) at 25 °C

	DMSO-CH_3OH[a]	DMSO-C_2H_5OH
$k_1/M^{-1}s^{-1}$	607±12	1190±25
$10k_{-1}/s^{-1}$	6.98±1.44	3.00±0.16
K_1/M^{-1}	940±230	4380±1400
ΔH_1^*/kcal mol^{-1}	10.6±2.5	10.8±2.2
ΔS_1^*/e.u.	−10.0±7.4	−8.3±4.5
ΔH_{-1}^*/kcal mol^{-1}	13.4±3.7	—
ΔS_{-1}^*/e.u.	−14.1±11.9	—

a) Cited from Ref. 1.

shows the dependence of k_1, k_{-1}, and K_1 on reaction temperature.

The kinetic and activation parameters obtained from the Arrhenius plot (not shown) are summarized in Table 3.

Stage II. As shown in Fig. 1, the first spectral change (**1**⇄**2a**) can be followed by stopped-flow spectrophotometry, whereas the second one (**2a**⇄**1**⇄**2b**) can be measured by usual spectrophotometry. As a result, the Stage I reaction is very fast compared with the Stage II one, because the time scale of measurement by stopped-flow spectrophotometry is extremely short compared with that by usual spectrophotometry. Therefore, the Stage I reaction can be treated as a fast mobile equilibrium, with shift almost entirely to the right, in treatments of the Stage II kinetics.

As to the rate of the Stage II reaction, the kinetic expression derivable from Eq. 3 should take account of the possibility that the substrate may be split between **1** and **2a**. Putting $[\mathbf{1}]_{st}=[\mathbf{1}]+[\mathbf{2a}]$ and with K_1 standing for the equilibrium constant for the Stage I reaction, one obtains

$$k_{obsd} = k_{-2} + \frac{k_2[C_2H_5O^-]}{1+K_1[C_2H_5O^-]}, \quad (6)$$

where k_{obsd} is the pseudo-first-order rate constant for the Stage II reaction, and k_2 and k_{-2} the rate constants for the forward and reverse reactions.

From Eq. 6, the dependence of k_{obsd} on $[C_2H_5O^-]$ would afford a curvilinear relationship, in which the curve would not pass through the origin. If the k_{-2} value can be obtained by extrapolation from the relationship between k_{obsd} and $[C_2H_5O^-]$, one may derive the following equation by substituting the value into Eq. 6 and rearranging:

$$\frac{1}{k_{obsd}-k_{-2}} = \frac{1}{k_2[C_2H_5O^-]} + \frac{K_1}{k_2}. \quad (7)$$

Thus, k_2 and K_1 can be obtained from the slope and intercept in the plot of $1/(k_{obsd}-k_{-2})$ against $1/[C_2H_5O^-]$. In the inversion plot the k_{-2} value was determined so that the best linear relationship might be established. Therefore, there might be some ambiguity in the k_{-2} values.

Table 4 shows the dependence of k_{obsd} on the alkoxide concentration, including the estimated rate and equilibrium constants. The relationships (Eqs. 6 and 7) hold for the reaction of **1** with CH_3O^- [1] (Figs. 2 and 3). It is clear, however, that the k_{obsd} values hardly depend upon $[C_2H_5O^-]$.

Discussion

Activation Parameters of Stage I. The difference between the k_1 values depends upon the ΔS_1^* rather than the ΔH_1^* values, although the ΔH_1^* and ΔS_1^* values compensate each other (Table 3). This relationship reasonably arises from the difference between the structures of the transition states leading to **1a** and **2a**. The transition state leading to **2a** would resemble the intermediate **2a** less closely than does the one leading to **1a**; the $C_2H_5O\cdots C_1$ (naphthalene)

Table 4. Rate constant for the formation and decomoosition of 1,1-disubstituted anionic σ complex formed from 1-dimethylamino-2,4-dinitronapthalene (**2**) and potassium ethoxide in DMSO-C_2H_5OH (90:10 v/v) at 25 °C[a]

$10^3[C_2H_5OK]$ M	$10^3 k_{obsd}$ s^{-1}	$(k_2/K_1)+k_{-2}$ [b] s^{-1}
1.00	3.06	
1.22	3.08	
1.30	3.07	
2.00	3.12	
2.44	3.23	
2.61	3.31	
3.00	3.15	
3.66	3.15	
3.91	3.38	$3.18\pm0.16\times10^{-3}$
4.00	3.22	
4.88	3.16	
5.00	3.24	
6.10	3.19	
6.52	3.22	
7.83	3.19	
8.00	3.14	
9.13	3.15	
9.76	3.10	

a) $[\mathbf{2}]_0=3.96\times10^{-5}$ M; $\mu=0.05$ M ($KClO_4$). Measured at λ_{max} 519 nm. For the results of the reaction of **1** with CH_3OK, see Table 4 in Ref. 1. b) The $(k_2/K_1)+k_{-2}$ value is the average of k_{obsd}'s.

bond would be less closer to the covalent bond (C_2H_5O–C_1) in **2a**. This situation would likely originate from the higher nucleophilicity of $C_2H_5O^-$. As a result, the free energy ΔG_1^* ($=\Delta H_1^* - T\Delta S_1^*$) for the forward reaction (Eq. 2a) is less than the free energy ΔG_1^* for the forward reaction (Eq. 1a) due to more delocalization of the negative charge donated by $C_2H_5O^-$.

Stage II. As described previously, the rate expression for Stage II is as shown in Eq. 6. Equation 6 is consistent with the results for the reaction of **1** with CH_3O^- (Fig. 2). The k_{-2} value can be determined by extrapolation of $1/[CH_3O^-]\rightarrow 0$. The inversion plot using the k_{-2} value (Eq. 7) shows a good linearity (Fig. 2).

For the reaction of **1** with $C_2H_5O^-$, however, the k_{obsd} values hardly depend upon $[C_2H_5O^-]$ at the ethoxide ion concentrations studied (Fig. 3). The results could rationally be interpreted as follows: The K_1 value for the reaction of **1** with $C_2H_5O^-$ was determined to be 4380 M^{-1} (1 M=1 mol dm^{-3}). Accord-

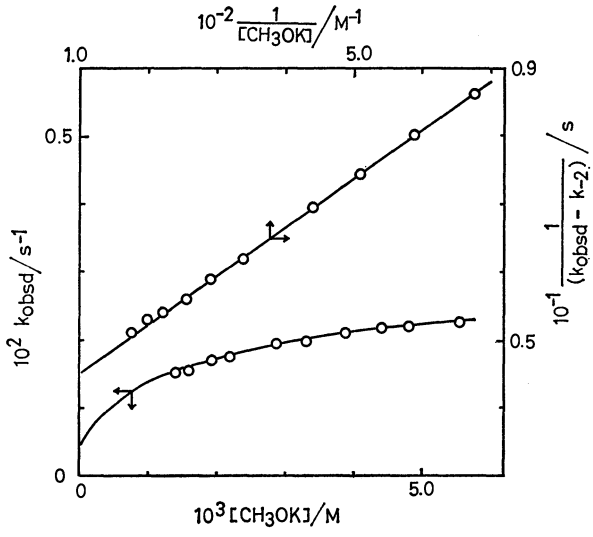

Fig. 2. Relationships between k_{obsd} and $[CH_3OK]$ and between $1/(k_{obsd}-k_{-2})$ and $1/[CH_3OK]$ in naphthalene (**1**) with CH_3OK in DMSO-CH_3OH (90:10 v/v) at 25 °C [cited from Ref. 1]: $[\mathbf{1}]_0$ 3.20×10^{-5} M; μ 0.05 M ($KClO_4$).

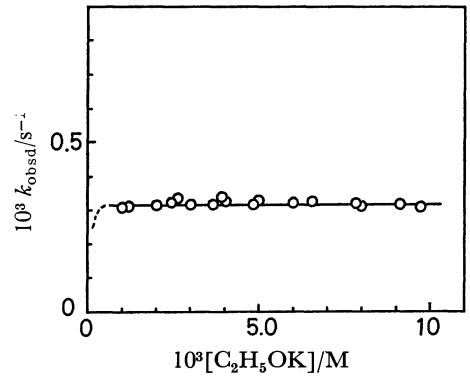

Fig. 3. Relationship between k_{obsd} and $[C_2H_5OK]$ in the reaction of 1-dimethylamino-2,4-dinitronaphthalene (**1**) with C_2H_5OK in DMSO-C_2H_5OH (90:10 v/v) at 25 °C.

ing to this value, $K_1[C_2H_5O^-]$ varies from *ca.* 4 to *ca.* 43 (Table 4). In Eq. 6, then, $1+K_1[C_2H_5O^-]$ is nearly equal to $K_1[C_2H_5O^-]$ except for the $[C_2H_5O^-]$ range 1.00 to 1.30×10^{-3} M. As a result, k_{obsd} is equal to $k_{-2}+(K_2/K_1)$ (Fig. 3). Accordingly, in the case of **1** with $C_2H_5O^-$, too, the reaction will proceed as shown in Eq. 3.

It is of interest to compare our results with those of Millot and Terrier,[7] who carried out a kinetic study of the reaction of **2** with potassium methoxide in DMSO-CH_3OH (90:10 v/v) at 20 °C and proposed the sequences

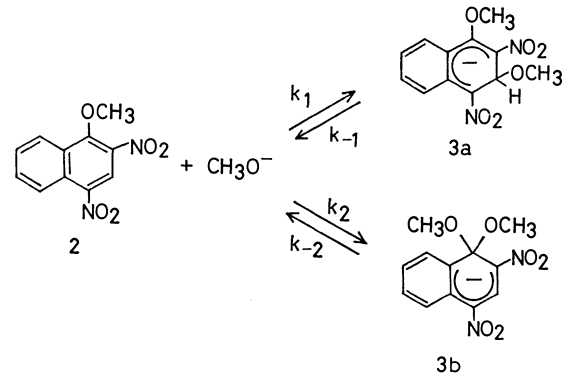

The values they specified are as follows: k_1 7800 M^{-1} s^{-1}; k_{-1} 8.5 s^{-1}; K_1 916 M^{-1}; k_2 2100 M^{-1} s^{-1}; k_{-2} too small to be decided.

With the Stage I reactions (Eqs. 1a, 2a, and 8a), the k_1 and k_{-1} values for the reaction of **2** with CH_3O^- are the largest, but the K_1 values are similar in both cases (Eqs. 1a and 8a), whereas the K_1 value for the reaction of **1** with $C_2H_5O^-$ (Eq. 2a) is much larger than those in the other cases (Eqs. 1a and 8a). Further, the k_1(**3a**)/k_1(**1a**) and k_{-1}(**3a**)/$k^{-}{}_1$(**1a**) ratios are *ca.* 12, whereas the k_1(**3a**)/k_1(**2a**) and k_{-1}(**3a**)/k_{-1}(**2a**) ratios are *ca.* 6.6 and *ca.* 28, respectively. That is to say, in the former cases (Eqs. 1a and 8a) the k_1 and k_{-1} ratios are quite the same, whereas in the latter (Eq. 2a) the k_1 ratio is about one seventh the k_{-1} ratio. The difference arises from the fact that the free energy (ΔG_1^*) for the reaction of **1** with $C_2H_5O^-$ is the least among the three cases (Eqs. 1a, 2a, and 8a) and, then, the complex **2a** is the most stable as described above.

In conclusion, it is confirmed that the reactions of 1-dialkylamino-2,4-dinitronaphthalenes with alkoxides will proceed according to Eq. 1 and that the larger the nucleophilicity of alkoxides is, the stabler are the anionic σ complexes.[7]

Experimental

NMR spectra were recorded on a Varian A-60D spectrometer and UV-VIS absorption spectra on a Hitachi Model 200-10 spectrophotometer.

Materials. Compound **1** was prepared according to the method described previously.[7] A small amount of calcium hydride was added to commercial dimethyl sulfoxide, which was then distilled under reduced pressure prior to use. Commercial potassium perchlorate of special grade was used without further purification,

Rate Measurement. As regards the kinetics of formation and decomposition of 1,3-disubstituted anionic σ complex, the transmittance of the complex was measured in order to estimate the apparent pseudo-first-order rate constants (k_{ψ}) with a thermostated Union RA-1300 Stopped-Flow Analyser (Union Giken). The kinetic measurements for the formation and decomposition of 1,1-disubstituted ones (k_{obsd}) were made with a thermostated Hitachi Model 200-10 Spectrophotometer.

This research was supported in part by a Grant-in-Aid for Scientific Research No. 455330 from the Ministry of Education, Science and Culture.

References

1) Part XV: S. Sekiguchi, T. Takei, K. Matsui, N. Tone, and N. Tomoto, *Bull. Chem. Soc. Jpn.*, **54**, 3009 (1981).
2) M. J. Strauss, *Chem. Rev.*, **70**, 667 (1970).
3) S. Sekiguchi, *Yuki Gosei Kagaku Kyokai Shi*, **36**, 633 (1978).
4) K. J. Laidler, "Chemical Kinetics," McGraw-Hill Book Co., New York (1965), p. 19.
5) Strictly speaking, $[C_2H_5O^-]_e$ and $[\mathbf{2}]_e$ (the suffix e represents the concentration at the attainment of equilibrium) should be substituted for $[C_2H_5O^-]$ and [**2**].[4]
6) S. Sekiguchi, T. Hirose, K. Okada, K. Matsui, and T. Aizawa, *Research Report of the Asahi Glass Foundation for the Countribution to Industrial Technology*, **27**, 221 (1975).
7) F. Millot and F. Terrier, *Bull. Soc. Chim. Fr.*, **1971**, 3897.

Mechanism of the Photochemical and Thermal Wolff Rearrangement of 2-Diazo-1,3-dicarbonyl Compounds

Hideo Tomioka,* Norihiro Hayashi, Tsuneo Asano, and Yasuji Izawa
Department of Industrial Chemistry, Faculty of Engineering, Mie University, Tsu, Mie 514

(Received July 12, 1982)

Thermolysis and photolysis of 2-diazo-1,3-dicarbonyl compounds were investigated as a function of methanol concentration. As the methanol concentration decreased, methyl group migration increased concomitant with the suppression of O–H insertion into methanol, whereas aryl group migration was essentially unaltered with the methanol concentration. The results are interpreted as indicating that aryl migration occurs directly from the excited state of diazo compounds, but that methyl migration takes place in the singlet carbene in competition with O–H insertion.

The Wolff rearrangement of α-diazo carbonyl compounds has received continuous interests,[1] since the reaction has not only found wide use as the crucial step in the Arndt-Eistert synthesis, but also attracted much interests industrially as a photoresist process.[2] Although the Wolff rearrangement has been the subject of numerous mechanistic investigations,[1] a satisfactory rationalization of this reaction has been achieved only recently. Since Kaplan and Meloy[3] have shown that diazo ketones exist as an equilibrium mixture of *s-cis* and *s-trans* forms as a result of hindered internal rotation about central C–C bond, the crucial question related to the mechanism of the Wolff rearrangement seems to be whether the reactive intermediate is a free keto carbene or the diazo ketone itself. We have recently suggested[4] that the Wolff rearrangement to form ketene takes place directly from the diazo ketone in some cases, whereas singlet keto carbene undergoes either characteristic carbenic reactions, *e.g.*, insertion, or gives rise to ketene. The mechanisms have been shown[4] to account for the relative efficiency of other competing reactions of more complicated polyfunctional diazo compounds. The relative migratory aptitude established[5] with 2-diazo-1,3-dicarbonyl compounds should be re-examined in this respect since it has been generally assumed that only free keto carbene is involved in the migration. The relative migratory aptitudes of individual groups have been reported[1,5] to be sensitive to the method in which the reaction is conducted. Thus, the following series is generally valid for the thermal reaction:

$$H > Ph > Me > R_2N > RO.$$

In the photochemical variant, Ph and Me change places:

$$H > Me > Ph > R_2N > RO.$$

To date, no reasonable scheme to explain the difference has appeared. Thus, we have examined the thermolysis and photolysis of 2-diazo-1,3-dicarbonyl compounds in more detail in order to get deeper insight into the nature of migration.

Results and Discussion

A solution of 2-diazo-1-phenyl-1,3-butanedione (**1a**) in methanol-dioxane was decomposed in Pyrex tubes either photochemically or thermally as detailed in the Experimental section. GC analysis of the product mixture revealed the presence of two rearranged products (**2** and **3**) arising from the migration of both Ph and Me groups, O–H insertion (**4**) and double hydrogen-abstraction products (**5**) of carbene (Eq. 1). The

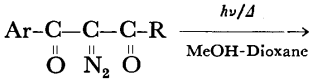

1

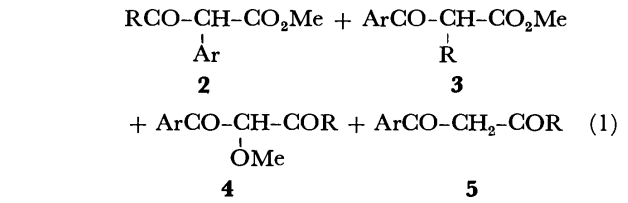

2 **3** **4** **5** (1)

a: Ar=Ph, R=Me, **c**: Ar=*p*-MeO-C_6H_4, R=Me,
b: Ar=*p*-Br-C_6H_4, R=Me, **d**: Ar=Ph, R=OEt

product identifications and distributions were determined by GC and/or NMR using authentic samples. As summarized in Table 1, the product distributions were sensitive to the concentration of methanol. Thus,

Table 1. Photolysis and thermolysis of 2-diazo-1-phenyl-1,3-butanedione (**1a**)[a]

hν or *Δ*	MeOH (%)	Additives	Yield/%[b]			
			2	**3**	**4**	**5**
hν[c]	100		12.5	23.9	27.4	h)
	100	Q[d]	11.5	26.2	27.2	h)
	100	S[e]	2.4	10.9	31.5	h)
	10		11.8	32.7	15.9	h)
	5		12.4	36.1	12.8	h)
	3		14.4	44.2	8.3	h)
	1		15.2	47.2	2.7	h)
Δ[f]	100		32.4	13.4	6.4	h)
	100	BPO[g]	1.9	h)	h)	82.0
	10		31.0	24.4	7.1	h)
	5		29.2	26.3	5.2	h)
	3		28.7	28.2	3.3	h)
	1		28.9	30.3	1.0	h)

a) Reactions were performed on a 10 mM solution of **1** in dioxane in sealed Pyrex tubes. b) Determined by GC. c) Irradiations were carried out at 10 °C with 300 W high-pressure Hg lamp. d) Ten-fold excess of 1,3-pentadiene was added as a triplet quencher. e) Five-fold excess of 4-methylbenzophenone was added. f) Thermolyses were carried out at 80±1 °C. g) One-fifth of benzoyl peroxide was added. h) Trace.

in both photolytic and thermal runs, as the methanol concentration decreased, Me group migration product **3** increased concomitant with the suppression of the O–H insertion product **4**, whereas phenyl group migration product **2** was essentially unaltered with the methanol concentration. Similar trends were also observed for other 2-diazo-1,3-diketones (**1b, c**) as summarized in Table 2. Although the high incidence of Me as opposed to Ar migration was generally observed for the photochemical Wolff rearrangement regardless of the methanol concentration, Ar and Me change places for the thermal run as the methanol concentration decreased. Consequently, at high methanol concentration where the Wolff rearrangement has been generally carried out, the apparent relative migratory aptitudes of Me and Ar groups are not same in the thermal and photochemical Wolff rearrangements, but the trends become similar at the lower concentration regardless of the way in which the reaction is conducted.

Table 2. Photolysis and thermolysis of 2-diazo-1,3-dicarbonyl compounds (**1**)[a]

1	*hν* or *Δ*	MeOH(%)	Yield/%[b]		
			2	**3**	**4**
1b	*hν*[c]	100	9.6	44.3	17.3
		10	7.9	47.3	12.1
		5	9.0	51.7	11.6
		3	9.3	53.0	7.6
		1	9.0	54.8	2.7
	Δ[d]	100	21.3	20.0	5.7
		10	15.3	37.7	11.5
		5	14.6	40.6	9.7
		3	14.7	43.1	7.8
		1	15.3	45.9	2.7
1c	*hν*[c]	100	6.6	26.0	22.5
		10	9.2	43.4	12.9
		5	9.1	49.6	10.1
		3	9.2	53.7	7.9
		1	10.2	65.5	3.1
	Δ[d]	100	18.9	11.4	2.9
		10	17.9	31.4	f)
		5	17.0	32.7	f)
		3	17.0	36.0	f)
		1	16.9	38.3	f)
1d	*hν*[c]	100	58.2	0	37.6
		100[e]	12.1	0	45.4
		10	68.8	0	22.6
		5	76.3	0	2.5
		3	76.8	0	1.5
		1	80.1	0	f)
	Δ[d]	100	23.8	0	5.4
		10	20.6	0	1
		5	20.3	0	1
		3	21.6	0	1
		1	18.5	0	f)

a)—d) They are defined in Table 1. e) Five-fold excess of 4-methylbenzophenone was added. f) Trace.

It is very important to examine the origin of the effect of the methanol concentration on the relative migratory aptitude. The above data indicate that Me migration **3** and O–H insertion products **4** arise from a common intermediate (A), while Ar migration product **2** is derived from a different intermediate (B). In order to obtain information on the multiplicity of the intermediates, the effects of triplet sensitizer and quencher were studied. When the photolysis of **1a** was carried out in the presence of 4-methylbenzophenone, formation of **2** was greatly reduced whereas **3** as well as **4** were still formed in moderate yields. One may propose that the intermediate A may be the triplet carbene, since it is generally accepted[6] that photosensitized decomposition of a diazo compound circumvents the formation of the singlet carbene and generates exclusively the triplet carbene *via* energy transfer and loss of N_2 from the resulting triplet precursor diazo compound. The substantial formation of **3** and **4** in the direct irradiation, then, suggests that the triplet carbene would be formed either *via* a rapid intersystem crossing from the initially generated singlet carbene or *via* dissociation from the triplet diazo compound **1**, probably formed by the intersystem crossing from the singlet excited state. If this were the case, one would expect that the addition of 1,3-pentadiene, an efficient quencher for both triplet carbene and triplet excited states,[1] should cause considerable suppression of the formation of **3** and **4**. No change in the product ratio was, however, observed even in the presence of a high concentration of this quencher. This clearly eliminates the triplet carbene as a possible intermediate A for **3** and **4**. It is generally accepted,[1,7] on the other hand, that the key intermediate leading to the O–H insertion product (*e.g.*, **4**) is singlet carbene, and hydroxylic reagents have been shown[8] to be efficient quenchers for singlet carbene. Thus, the structure for the intermediate A that best fits into these data is that of a singlet carbene.

What is then the intermediate B? It is quite important to note here that there has been accumulating evidence[3,4,9,10] on the mechanism of the Wolff rearrangement which shows that there is a pathway which does not include the singlet carbene but favors the migration accompanied by loss of N_2 directly from the excited diazo compound. It is tempting to suggest the excited (either photochemically or thermally)

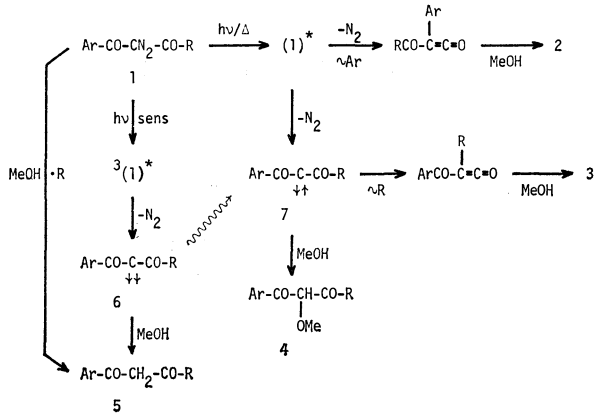

Scheme 1.

1 as the most likely intermediate B for **2**. Suppression of **2** by the photosensitization which circumvents the formation of the excited singlet **1** also supports the above assignment.

On the basis of the above assignments, a reasonable mechanism which explains the data is given in Scheme 1. Thus, **1** is excited either thermally or photochemically to its excited state which can give rise to the Ph migration product directly or dissociate to give N_2 and singlet carbene (**7**). The singlet carbene **7** subsequently undergoes either Me migration or O–H insertion into alcohol. Appreciable formation of **3** and **4** from the singlet carbene **7** even in the sensitized decomposition can be interpreted as indicating that intersystem crossing of the triplet carbene to the singlet is possible, as has frequently been observed in other analogous carbene systems, *e.g.*, $:CHCOCH_3$,[9] $:CHCONEt_2$,[4] and :CHCN.[9] No prominent formation of the characteristic triplet product in the sensitized photolysis is interpreted as indicating that intersystem crossing of the triplet carbene to the singlet is significant and its rate is substantially greater than its overall rate. It has been generally accepted[1] that one of the characteristic product from the triplet carbene is the double hydrogen-abstraction product **5**. Thermolysis of **1** in the presence of benzoyl peroxide (BPO) resulted in almost exclusive formation of **5**. This indicates that **5** is formed mainly *via* radical-induced[11] decomposition of **1** itself, but not from the triplet carbene **6** in this case.

There remains the question of the factors which control the two competitive processes from the excited diazo compounds. One explanation must include Kaplan and Meloy's suggestion[3] that diazo ketones exist as an equibrium mixture of *s-cis* and *s-trans* forms as a result of hindered internal rotation about the central C–C bond. In the investigation of photochemical processes of several α-diazo monocarbonyl compounds, we have suggested[4] that the Wolff rearrangement to form ketene takes place directly from the singlet excited state of the *s-cis* conformer, whereas that of the *s-trans* conformer dissociates N_2 to generate singlet keto carbene which either undergoes characteristic carbenic reactions, *e.g.*, O–H insertion, or gives rise to ketene.

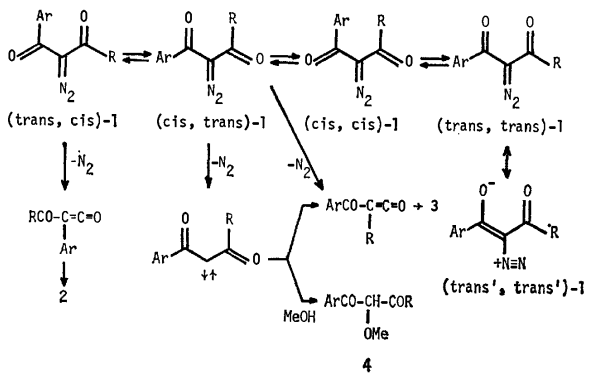

Scheme 2.

Thus, the ratio of the Wolff rearrangement to the competing carbenic processes is shown to be roughly proportional to the ground state population of *s-cis* and *s-trans* conformers. If one assumes here a coplanar molecule for **1** as a result of resonance contribution, one would expect four possible rotamers for **1** (Scheme 2). The influence of steric and electrostatic effects exerted between the Ar, R, C=O, and $C=N_2$ groups causes variations in the relative energy of four conformers and, therefore, in their populations.[12] Electrostatically, conformers (*trans, cis*), (*cis, trans*), and (*cis, cis*) are favorable as a result of electrostatic attraction, whereas (*trans, trans*) is less stable due to the repulsion between two C=O groups, as is predicted from the canonical form (*trans', trans'*). Sterically, on the other hand, (*trans, trans*) would suffer from steric repulsion in the Ar–N_2–R groups, all in a cis relationship, and in (*cis, cis*), the nonbonding repulsion between Ar and R would be severe. Thus, one would expect that conformers (*trans, cis*) and (*cis, trans*) would be more stable than (*trans, trans*) and (*cis, cis*). The conformer (*trans, cis*) presents a favorable situation for Ar migration to occur in its excited state, since migrating and leaving groups in this conformer are situated in positions with respect to each other which permit the migration. In the (*cis, trans*) conformer, on the other hand, Me migration accompanied by loss of N_2 would be expected to occur in its excited state. Experimental results suggest, however, that main pathway from this conformer is dissociation of N_2 to generate singlet carbene in which Me migration occurs in competition with the O–H insertion. The reason for this difference lies partly in the difference in inherent migratory ability between Me and Ph groups. A concerted process with Ph migration and loss of N_2 would be favored[13] by donation of more labile π-electron to the diazo carbon and by the stabilization of a transition state (or short-lived intermediate) through bridging delocalization. Since such stabilization is not attained in Me migration, dissociation of N_2 occurs before Me group shifts to the diazo carbon.

The dependence of the product ratio, **2**/(**3**+**4**), on the method of reaction reflects, at least in part, the influence of the temperature on the relative population of each conformer. It has been reported,[14] for example, that photolysis of diazo ketone $RCOC(CH_2R')N_2$ yields the α,β-unsaturated ketone as the major product at room temperature; however, at higher temperature, the ketene rearrangement product is obtained. The results are similarly explained by assuming that the higher energy conformations are more populated as the temperature is raised. The product distributions in Tables 1 and 2 indicate that (*cis, trans*) conformers are preferred for **1a**—**c**. Apparent decrease in this conformer for **1d** can be attributable to a finite activation energy to migration of the alkoxyl group which is known[1] to be an inefficient migrating group. This group did not migrate at all either in the excited diazo compound or in the singlet carbene even in the absence of an efficient trap for the singlet carbene, *i.e.*, methanol. It is also important to note that the singlet carbene generated thermally undergoes Me migration more readily than that generated photolytically as opposed to the O–H insertion. This is explained in terms of the activation energy difference

between two processes. Alternatively, a part of Me migration would occur directly in the excited state in thermal run.

From the data, we propose a reasonable reaction scheme to explain why Me and Ph migrations take place in the trend of relative migratory aptitude as the method of reaction is changed. We wish to point out that the ground state population of rotational isomers and nature of migration (carbenic or diazo) are definitely related to the apparent relative migratory aptitude in 2-diazo-1,3-dicarbonyl compounds. These factors have not been taken into account in the literature.

Experimental

Instrumentation. UV spectra were recorded on a Hitachi 220-S spectrophotometer. IR spectra were measured on a JASCO IR-G recording spectrometer, and ^{1}H NMR spectra were determined with a JEOL JNM-MH-100 NMR spectrometer in $CDCl_3$ with Me_4Si as an internal reference. GC analyses were performed on a Yanagimoto Model G-180 instrument with flame ionization detector using 80 cm×4.0 mm column packed with (A) 5% PEG 20 M and (B) 5% Silicone SE-GE on 60—80 mesh Diasolid L.

Materials. 2-Diazo-1,3-dicarbonyl compounds **1a—d** were conveniently prepared[13] by diazo-group transfer from *p*-toluenesulfonyl azide to the appropriate dicarbonyl compounds and purified through a short silica-gel column. Authentic samples for product identification were prepared according to the literature procedures. Thus, Ar migration products **2a—c** were prepared by the condensation[15] of ethyl acetate with the corresponding benzyl cyanides, followed by methanolysis[16] of the resulting cyanide. Phenylmalonate **2d** was obtained by stepwise esterification of phenylmalonic acid.[17] Me migration products **3a—c** were synthesized[18] by the reaction of methyl propionate with the corresponding methyl benzoates. OEt migration product **3d** was obtained in the photolysis of methyl diazobenzoylacetate in ethanol. O–H insertion products **4a—c** were obtained in the reaction[19] of acetic anhydride with the corresponding α-methoxyacetophenone in the presence of $BF_3 \cdot OEt_2$. **4d** was isolated in the irradiation of **1d** in methanol.

Photolysis and Thermolysis of 1. All irradiations were carried out with a Halos 300 W high-pressure mercury lamp with a water-cooled jacket. In a typical procedure, 0.05 mmol of **1** was added to 5.0 cm^3 of a mixture of methanol and dioxane in Pyrex tubes. The sample was then degassed, sealed, and irradiated until all of the diazo compound was destroyed. Thermolysis was done in a sealed Pyrex tube in an oil bath thermostated at 80±1 °C. Control experiments ruled out the interconversion of the products during the reaction. Product identification and yields were determined mainly by GC. The product ratio was also determined by NMR. CF_3CO_2H was used as solvent for NMR to prevent the enolization of products. The product ratios determined by both methods were generally in good agreement.

References

1) For review see: W. Kirmse, "Carbene Chemistry," Academic Press, New York (1971), p. 475; R. A. Moss and M. Jones, Jr., "Carbenes," Wiley, New York (1973), Vol, 1, p. 117; H, Meier and K. P. Zeller, *Angew. Chem., Int. Ed. Engl.*, **14**, 32 (1975); W. Ando, "The Chemistry of Diazonium and Diazo Groups," ed by S. Patai, Wiley, New York (1978), Vol. 1, p. 341; W. M. Jones, "Rearrangements in Ground and Excited State," ed by P. de Mayo, Academic Press, New York (1980), Vol. 1, p. 95.

2) See, for example, M. S. Dinaburg, "Photosensitive Diazo Compounds," Focal Press, New York (1964); W. S. Deforest, "Photoresist Materials and Processes," McGraw-Hill, New York (1975).

3) F. Kaplan and G. K. Meloy, *J. Am. Chem. Soc.*, **88**, 950 (1966). See also, F. Kaplan and M. L. Mitchell, *Tetrahedron Lett.*, **1979**, 759.

4) H. Tomioka, H. Okuno, and Y. Izawa, *J. Org. Chem.*, **45**, 5278 (1980); See also, H. Tomioka, H. Kitagawa, and Y. Izawa, *ibid.*, **44**, 3072 (1979); H. Tomioka, M. Kondo, and Y. Izawa, *ibid.*, **46**, 1090 (1981).

5) K.-P. Zeller, H. Meier, and E. Müller, *Tetrahedron*, **28**, 5831 (1972).

6) H. D. Roth and M. L. Manion, *J. Am. Chem. Soc.*, **97**, 779 (1975), and references cited therein.

7) See for recent spectroscopic evidence, J. J. Zupancic and G. B. Schuster, *J. Am. Chem. Soc.*, **102**, 5958 (1980).

8) K. B. Eisenthal, N. J. Turro, M. Aikawa, J. A. Butcher, Jr., C. Dupuy, G. Hefferon, W. Hetherington, G. M. Korenowski, and M. J. McAuliffe, *J. Am. Chem. Soc.*, **102**, 6565 (1980).

9) H. D. Roth and M. L. Manion, *J. Am. Chem. Soc.*, **98**, 3392 (1976); H. D. Roth, *Acc. Chem. Res.*, **10**, 85 (1977).

10) T. DoMinh, O. P. Strausz, and H. E. Gunning, *J. Am. Chem. Soc.*, **91**, 1261 (1969).

11) L. Horner and H. Schwarz, *Justus Liebigs Ann. Chem.*, **747**, 1 (1971).

12) S. Sorrio, "The Chemistry of Diazonium and Diazo Groups," ed by S. Patai, Wiley, New York (1978), Vol. 1, p. 96.

13) G. Heyes and G. Holt, *J. Chem. Soc., Perkin Trans. 1*, **1973**, 1206.

14) V. Franzen, *Justus Liebigs Ann. Chem.*, **602**, 199 (1957).

15) P. L. Julian, J. J. Oliver, R. H. Kimball, A. B. Pike, and G. D. Jefferson, *Org. Synth.*, Coll. Vol. II, 487 (1943).

16) R. H. Kimball, G. D. Jefferson, and A. B. Pike, *Org. Synth.*, Coll. Vol. II, 284 (1943).

17) A. A. Morton, F. Fallwell, Jr., and L. Palmer, *J. Am. Chem. Soc.*, **60**, 1426 (1938).

18) E. E. Royals, *J. Am. Chem. Soc.*, **70**, 489 (1948).

19) J. Munch-Petersen and C. R. Hauser, *J. Am. Chem. Soc.*, **71**, 770 (1949).

Conversions of Carbonyl Compounds *via* Their Polymeric Sulfonylhydrazones into Alkenes, Alkanes, and Nitriles

Hiroyoshi KAMOGAWA,* Asami KANZAWA, Masahiro KADOYA, Takeshi NAITO, and Masato NANASAWA

Department of Applied Chemistry, Yamanashi University, Takeda 4, Kofu, Yamanashi 400

(Received July 13, 1982)

Resins consisting of cross-linked poly(styrene-divinylbenzene) matrices functionalized with hydrazinosulfonyl groups react with aldehydes and ketones to form the sulfonylhydrazone derivatives. The extent of the reaction is sensitive to the type of resin and the bulk of the carbonyl compound. When heated strongly under alkaline conditions, the sulfonylhydrazones release the corresponding alkenes; upon the $NaBH_4$ or $LiAlH_4$ treatment, they also release the corresponding alkanes; and, upon refluxing in methanol with potassium cyanide, they release nitriles containing one additional carbon atom.

The preparation of poly(*p*-vinylphenylsulfonylhydrazine) (**1**) and its use as a diazene source have been previously reported.[1,2]

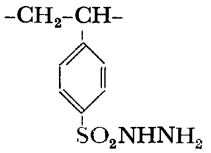

1

Our present interest was in exploring the potential of **1** as a possible polymer reagent for converting aldehydes and ketones into alkenes, alkanes, and nitriles *via* their hydrazones with **1**.

Results and Discussion

The polymers employed as starting reagents for this investigation were commercially available, macroreticular and gel-type styrene (St)–divinylbenzene (DVB) copolymers (**2**) (Table 1).

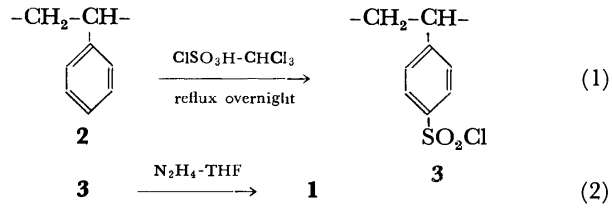

(1)

(2)

Each material (**2**) is readily converted, by refluxing it overnight in a solution of chlorosulfuric acid in chloroform, to the intermediate copoly(St- and DVBsulfonyl chloride) (**3**; 93—100% yield) (Eq. 1), and thence by the action of hydrazine–THF solutions to **1** (77—91% yield) (Eq. 2).

As can be seen in Table 1, macroreticular resins **2** (Nos. 1 and 2) provided higher conversions to **3** and thence to **1** than did gel-type resin **2** (No. 3).

Alternatively, the polymer **1** was prepared by the polymerization of the *p*-vinylphenylsulfonylhydrazine (**6**) synthesized starting with sodium *p*-styrenesulfonate (**4**) *via* sulfonyl chloride (**5**) (Eq. 3).

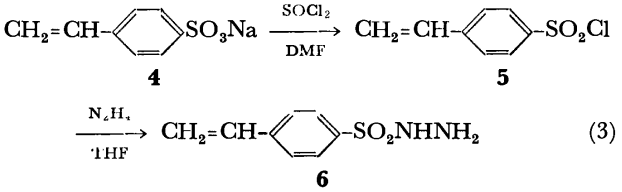

(3)

An attempt to synthesize **6** by the alkaline dehydrobromination of the *p*-(2-bromoethyl)phenylsulfonylhydrazine synthesized starting with (2-bromoethyl)benzene as in polymer (Eqs. 1 and 2) failed, presumably because of the high alkali-susceptibility of the prod-

Table 1. Preparation of copoly(*p*-vinyl- and divinylphenylsulfonylhydrazone) (**1**)

No.	Polymer **2**	Polymer **3** Sulfonyl-chloride (mol%)[d]	Polymer **1** Sulfonyl-hydrazine (mol%)[e]
1	Macroreticular St-DVB copolymer[a]	100	91
2	Macroreticular St-DVB copolymer[b]	97	87
3	Gel-type St-DVB copolymer[c]	93	77

a) Aldrich: 19,215-5. b) Containing 6% DVB (Mitsubishi Kasei). c) Containing 8% DVB (Mitsubishi Kasei). d) By weight increase. e) By CHN-analyses.

Table 2. Reaction of aldehydes and ketones with copoly(*p*-vinyl- and divinylphenylsulfonylhydrazine) (**1**)

No.	Polymer **1**[a]	Aldehyde or ketone	Polymer **7** Sulfonylhydrazone (mol%)[b]
1	1	Cyclohexanone	94
2	2	Cyclohexanone	86
3	3	Cyclohexanone	Trace[c]
4	2	4-Methylcyclohexanone	64[d]
5	1	Dibenzyl ketone	90
6	2	Dibenzyl ketone	41
7	2	Cyclododecanone	38[d]
8	2	Camphor	No reaction[d]
9	2	Camphor	15[e]
10	2	Acetophenone	72
11	2	Benzophenone	58
12	2	Heptanal	79
13	3	Heptanal	Trace[c]
14	2	Cyclohexanecarbaldehyde	72
15	2	Benzaldehyde	71

a) No. in Table 1. b) By weight increase. c) 3 h-reflux; carbonyl compound/polymer **1** = 2/1 mol/mol. d) 5 h-reflux in methanol. e) 5 h-reflux in methanol containing 0.5% hydrochloric acid.

uct, **6**.

The reaction of the polymer **1** with aldehydes and ketones in refluxing ethanol to produce the corresponding hydrazones **7** (Eq. 4) provided varied results (Table 2).

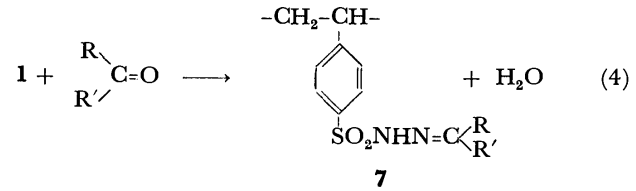

(4)

7

These results suggest that some of the hydrazinosulfonyl groups are in an environment too crowded to accommodate the hydrocarbon residues of bulky carbonyl compounds, even in the macroreticular form. Thus, cyclododecanone and camphor, typical bulky ketones, provided reactions of a low extent (Nos. 7, 8, and 9). The polymer **1**-3 with a gel structure also provided poor results (Nos. 3 and 13), presumably because of a lack of a swelling property for ethanol.

The polymeric arylsulfonylhydrazones (**8**) thus prepared were decomposed in the following two ways (Eqs. 5 and 6).

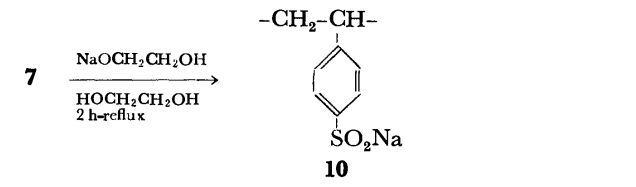

(5)

10 **8**

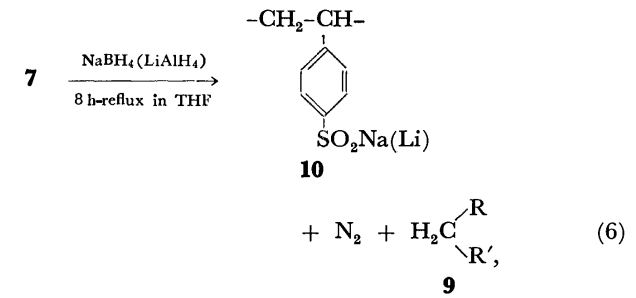

(6)

10 **9**

where R″ denotes the substituent attached to the α-carbon atom of the original carbonyl compound.

It is known that tosylhydrazones react with a solution of sodium in ethylene glycol to give diazo compounds, which subsequently decompose with the elimination of nitrogen to form alkenes.[3] This reaction was applied to the polymer **7** with the intention of converting carbonyl compounds to the corresponding alkenes (Eq. 5). Thus, a polymeric sulfonylhydrazone was dispersed in ethylene glycol containing a large excess of sodium, and the mixture was stirred under reflux for 2 h. The alkene (**8**) thus generated was extracted with either carbon tetrachloride or ether. The results are given in Table 3. The apparent low value obtained for the hydrazone with cyclohexanone (**7**-1) seems to be caused partly by the loss of the low-boiling product, cyclohexene, by evaporation during the reaction and the subsequent isolation process,

Table 3. Decomposition of copoly(*p*-vinyl- and divinylphenylsulfonylhydrazone) (**7**)

Sulfonylhydrazone[a] (**7**)	Alkene (**8**) by Eq. 5 (mol%)	Alkane (**9**) by Eq. 6 (mol%)/**7**
1	Cyclohexene, 9%	—
4	—	Methylcyclohexane, 13%, (19%)[b]
5	1,3-Diphenyl-1-propene, 77%	—
6	—	1,3-Diphenylpropane, 31%, (26%)[b]
7	Cyclododecene, 40%	—
9	—	Bornane, 6%, (0.8%)[b]
11	—	Diphenylmethane, 18%, (16%)[b]
15	—	Toluene, 11%, (9%)[b]
16[c]	—	Propylbenzene, 27%, (27%)[b]

a) No. in Table 2. b) With gel-type resin. c) With benzylacetone for the polymer **1**-2.

since cyclohexanone tosylhydrazone gave cyclohexene almost quantitatively under similar reaction conditions.[3] Another cause of decrease in the yield of alkene is the formation of alkane, presumably due to the production of diazene from the remaining hydrazinosulfonyl group (**1**) in **7** and the subsequent hydrogenation of the alkene,[1] as is indicated in Eq. 7:

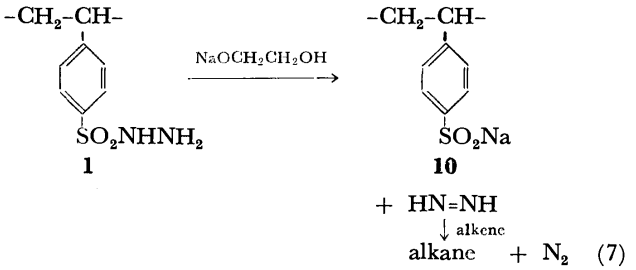

(7)

1 **10**

The production of alkanes could be recognized by means of the mass and ^{1}H-NMR spectra in all instances. Since the IR spectra of the resins which had been subjected to the procedure of Eq. 5 indicated no absorptions at 1320 and 1160 cm^{-1} attributable to hydrazones or hydrazines, but indicated every evidence of sodium poly(styrenesulfinate) (**10**), including a strong absorption at 960 cm^{-1},[4] the decomposition of **7** appears to take place completely under the present experimental conditions. The results of elemental analyses indicating the absence of nitrogen also support this conclusion.

Another way of decomposition, that indicated in Eq. 6, is also known for tosylhydrazones,[5] which are reduced with sodium borohydride or lithium aluminium hydride to liberate alkanes under relatively mild conditions, thereby constituting a general way of converting carbonyl compounds to alkanes. Thus, a polymeric sulfonylhydrazone **7** was dispersed in THF, and the mixture was refluxed for 8 h in the presence of a large excess of $NaBH_4$ ($LiAlH_4$ for **7**-11 and **7**-15).

The experimental conditions adopted here were the standard ones for low-molecular weight analogs.[5] Table 3 also indicates the results thus obtained. The relatively low yields of alkanes and the generally small differences between macroreticular and gel-type resins may indicate that the rate of reaction is governed by the permeation and diffusion of reductant $NaBH_4$ or $LiAlH_4$ into resin beads. Judging together with the fact that the IR spectra for macroreticular resins after the decomposition still indicate the absorptions attributable to the remaining hydrazones, it is likely that the reaction takes place mainly at the inner surfaces of resin beads, thereby indicating a poor permeability of the reductant under the present experimental conditions, although satisfactory yields were obtained for low-molecular weight analogs under these conditions.

The third trial carried out on the polymeric sulfonylhydrazine reagents (**1**) was the conversion of aldehydes and ketones *via* their hydrazones (**7**) into nitriles containing one additional carbon atom, as is indicated below:

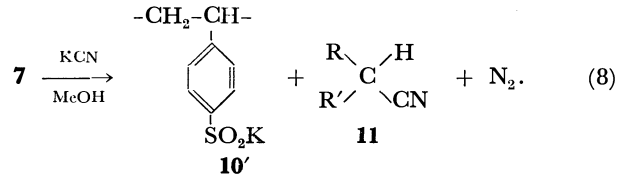

(8)

The reaction is also known for arylsulfonylhydrazones,[6] and mild reaction conditions have been established. Thus, polymeric sulfonylhydrazone **7** was dispersed in methanol, and the mixture was refluxed with stirring in the presence of a large excess of potassium cyanide to liberate nitrile (**11**). A refluxing lasting approximately 72 h, twice as long as that for low-molecular weight analogs in homogeneous methanolic solutions,[6] was necessary to effect the complete decomposition of macroreticular **7**, as judged from the IR spectra. Table 4 summarizes the obtained results.

In spite of the complete decomposition of **7**, the yields of nitrile isolated are generally lower than those for the corresponding tosylhydrazones, even with macroreticular resins. Particularly in the case of **7**-11, a nucleophilic attack of the solvent methanol of the sp^2-carbon atom of the hydrazone resulted in the production of methyl diphenylmethyl ether, with the absence of the expected product. In other sulfonylhydrazones with macroreticular resins, however, the expected nitriles were isolated to appreciable extents, leaving potassium poly(styrenesulfinate) (**10′**). The macroreticular potassium poly(styrenesulfinate) thus produced was oxidized with aqueous bromine to afford poly(styrenesulfonic acid), which was then treated with chlorosulfuric acid to afford poly(styrenesulfonyl chloride) (**3**) almost quantitatively. This resin, **3**, could be reused as effectively as the fresh resins from **2**.

Table 4. Conversion of aldehydes and ketones into nitriles

Sulfonylhydrazone[a] (**7**)	Nitrile (**11**) by Eq. 8 (mol%)/**7**
2	Cyclohexanecarbonitrile, 20%
3	Cyclohexanecarbonitrile, 0%
10	2-Phenylpropionitrile, 7%
11	Diphenylacetonitrile, 0%
12	Octanenitrile, 22%
13	Octanenitrile, 3%
14	Cyclohexylacetonitrile, 20%
15	Phenylacetonitrile, 12%

a) No. in Table 2.

The production of poly(styrenesulfinates) (**10** and **10′**) is common to all the reactions (Eqs. 5, 6, and 8) investigated here. Good reusability and the easy separation of **10** or **10′** from the low-molecular weight decomposition products constitute the advantages of this type of polymer reagent, although the rates and extents of the reactions of Eqs. 5, 6, and 8 are generally inferior to those of the corresponding low-molecular weight analogs.

Experimental

The infrared (IR), ^{1}H-NMR, and mass spectra were recorded on a Hitachi 215 spectrophotometer, a JNM-PMX 60 spectrometer, and a Hitachi RMU-6M spectrometer respectively. The elemental analyses were done with a Perkin-Elmer 240 instrument.

Copoly(styrene- and divinylbenzenesulfonyl chloride) (3). A copoly(styrene-divinylbenzene) (**2**; 2.6 g, 25 mmol) was stirred in chloroform (100 ml) and then chlorosulfuric acid (20 ml, 250 mmol) was added dropwise. The mixture was subsequently stirred overnight under reflux, with the exclusion of moisture. The mixture was then filtered, and the resin was stirred for 30 min successively in chloroform (100 ml) and acetonitrile (100 ml), followed by thorough washing with water and vacuum drying to a constant weight. The results thus obtained are given in Table 1. The IR spectra of the products (**3**) indicated absorptions at 1170 and 1370 cm^{-1} characteristic of the sulfonyl chloride.

Copoly(p-vinyl- and divinylphenylsulfonylhydrazine) (1). The polymer **3** (4.05 g, 20 mmol) was stirred in THF (150 ml) externally cooled in an ice bath, after which hydrazine hydrate (5.7 ml, 80 mmol) was added dropwise. The reaction mixture was then stirred for further 30 min. The resin was filtered off, stirred in iced 1 mol dm^{-3} hydrochloric acid (150 ml) for 30 min, filtered, washed with water, further stirred in iced 1 mol dm^{-3} sodium hydrogencarbonate (150 ml), filtered, washed again with water, stirred in cold water for 30 min, filtered, and finally dried. The results thus obtained are also given in Table 1. The IR spectra of the products (**1**) indicated absorptions at 1150 and 1310 cm^{-1} characteristic of the sulfonylhydrazine, with the absence of that at 1370 cm^{-1} (sulfonyl chloride).

p-Styrenesulfonyl Chloride (5). A mixture of thionyl chloride (50 ml), 4-*t*-butylcatechol (0.3 g), and anhydrous *N,N*-dimethylfomamide (DMF; 60 ml) was stirred in an ice bath. Sodium *p*-styrenesulfonate (**4**; Tokyo Kasei; 20 g, 86 mmol) was added in small portions, and the mixture was stirred for 3 h to afford a homogeneous solution; it was then left to stand for 24 h in a refrigerator. The reaction mixture was then poured into ice water (300 ml) and extracted twice with benzene (each 200 ml). The extract was washed twice with water (each 200 ml), dried over anhydrous sodium sulfate, and concentrated on a rotary evaporator below 40 °C. Upon drying *in vacuo*, a pale yellow liquid was obtained in a 95% yield. Found: C, 47.01; H, 3.88%. Calcd for $C_8H_7O_2SCl$: C, 47.41, H, 3.48%. IR ($CHCl_3$) 1580

(aryl), 1360 (S=O), 980, 910 (vinyl) cm^{-1}. NMR ($CDCl_3$) δ=5.7 (d, 1H, $C\underline{H}_2$=CH-), 6.1 (d, 1H, $C\underline{H}_2$=CH-), 6.9 (q, 1H, CH_2=C$\underline{H}$-), 7.6—8.3 (q, 4H, ArH). Mass (*m/e*) 202 (M^+).

p-*Vinylphenylsulfonylhydrazine* (**6**). Hydrazine hydrate (3 ml, 50 mmol) was dropped with stirring into a solution of **5** (4 g, 20 mmol) in THF (20 ml), cooled in an ice bath. The turbid mixture was stirred for further 15 min and then poured into 200 ml of water with vigorous stirring. Stirring was continued for a while to separate a crude product, which was purified by dissolution in a small amount of THF and subsequent precipitation into hexane to afford fine colorless needles (mp 90—92 °C) in a 75% yield. Found: C, 48.46; H, 5.20; N, 14.11%. Calcd for $C_8H_{10}N_2SO_2$: C, 48.47; H, 5.08; N, 14.13%. IR (KBr) 3250 (NH_2, NH), 1600 (Ar), 1310, 1150 (SO_2), 1620, 1000, 930 (vinyl) cm^{-1}. NMR (DMSO-d_6+$CDCl_3$) δ=3.9 (b, 2H, NH_2), 5.6 (d, 1H, $C\underline{H}_2$=CH-), 6.1 (d, 1H, $C\underline{H}_2$=CH-), 7.0 (q, 1H, CH_2=C$\underline{H}$-), 7.9 (q, 4H, ArH), 7.5—9.0 (b, 1H, NH). Mass (*m/e*) 198 (M^+, 13), 42 (100).

Polymer **1** *Obtained by the Polymerization of* **6**. A solution of **4** (0.89 g) and α,α'-azobisisobutyronitrile (40 mg) in DMF (10 ml) was put into a glass ampoule, which was then evacuated, filled with nitrogen, and sealed in a conventional manner. Polymerization was carried out at 50 °C for 48 h. The contents of the ampoule were precipitated into methanol to isolate a white powder in an 80% conversion. The polymer was soluble in DMF and dimethyl sulfoxide and afforded a value of the intrinsic viscosity [η] of 0.22 dl/g in DMF at 30 °C. The IR (KBr) spectrum of the polymer was essentially identical with that of **1** with absorptions at 1310 and 1150 cm^{-1} characteristic of the sulfonylhydrazine.

*Formation of Copoly(*p*-vinyl- and divinylphenylsulfonylhydrazones)* (**7**). In a typical example corresponding with No. 2 in Table 2, a solution of cyclohexanone (2.72 ml, 26.3 mmol) in ethanol (70 ml) was added to a vacuum-dried polymer, **1**-2 (3.47 g, 17.5 mmol). The mixture was heated under reflux for 0.5 h, with the exclusion of the moisture. The resin was then filtered off, stirred in methanol (100 ml) for 30 min, filtered, washed thoroughly with methanol, and dried *in vacuo* to a constant weight.

The same reaction conditions were applied to other carbonyl compounds, unless otherwise noted.

The IR spectra of all the polymers thus obtained indicated absorptions at 1620 (C=N), 1600 (Ar), 1320, and 1150 (SO_2) cm^{-1}.

Decomposition of **7** *by Alkali (Eq. 5).* Hydrazone **7** (1 g) was stirred in ethylene glycol (10 ml). Sodium (0.30 g) was added, and the mixture was heated under reflux for 2 h with stirring. The mixture was diluted with water (50 ml) and extracted with carbon tetrachloride or ether. The organic layer was washed with water, dried over anhydrous sodium sulfate, and concentrated on a rotary evaporator below 40 °C. The presence of alkene in the residue was confirmed by a study of the IR [1600—1640 cm^{-1} (C=C)] and mass spectra, and its content was determined from ^{1}H-NMR [δ=5—6 (CH=CH)].

The results thus obtained are given in Table 3. The IR spectra of the resins after alkaline decomposition indicated absorptions at 1600 (Ar), 1010, and 960 cm^{-1}, with the absence of those at 1320 and 1150 cm^{-1}. Elemental analyses indicated the absence of nitrogen.

Decomposition of **7** *with Reduction (Eq. 6).* Hydrazone **7** (10 mmol) was stirred in THF (70 ml), $NaBH_4$ (3.0 g, 80 mmol) was added, and the mixture was heated under reflux for 8 h with stirring. The mixture was then poured into iced dilute hydrochloric acid and extracted with ether. The organic layer was washed with water, dried over anhydrous sodium sulfate, and concentrated on a rotary evaporator. The presence of alkane in the residue was confirmed by a study of the IR and mass spectra, and its content was determined from ^{1}H-NMR. Table 3 also gives the results thus obtained, where $LiAlH_4$ was used in place of $NaBH_4$ for the hydrazone **7** from aromatic carbonyl compounds (**7**-11 and **7**-15).

Decomposition of **7** *with Production of Nitriles (Eq. 8).* Hydrazone **7** (5 mmol) was stirred in methanol (70 ml), potassium cyanide (0.98 g, 15 mmol) was added, and the mixture was heated, under gentle reflux, for 72 h. After water (70 ml) had then been added, the product was extracted with dichloromethane (140 ml) and the extract was washed with saturated aqueous sodium hydrogencarbonate (100 ml) and water (50 ml). The dried (Na_2SO_4) organic layer was concentrated on a rotary evaporator. The presence of nitrile in the residue was cofirmed by a study of the IR 2200—2250 cm^{-1} (CN) and mass spectra, and its content was determined from ^{1}H-NMR. The IR spectra of the resins after decomposition indicated absorptions at 1600, 1010, and 960 cm^{-1}, with the absence of those at 1150 and 1320 cm^{-1}.

Recycling of Used Resins. The macroreticular potassium poly(styrenesulfinate) (**10'**; 5 mmol) left after the decomposition of the polymers **7**-2 according to Eq. 8 was stirred in an aqueous solution of bromine (2.4 g in 100 ml) at room temperature for 1 h. The potassium poly(styrenesulfonate) thus produced was filtered, washed thoroughly with water, and dried. The polymer was then stirred in chlorosulfuric acid (20 g) at 80 °C for 8 h. The mixture was filtered with a glass filter, and the resin was washed successively with two 100 ml-portions of dichloromethane and THF, and dried to regenerate poly(styrenesulfonyl chloride) (**3**) almost quantitatively. The resin **3** thus obtained was then subjected to the same reaction procedures as those used for fresh resin **3** to afford hydrazine **1** and thence cyclohexanone hydrazone **7**. The yield of cyclohexanecarbonitrile generated by the decomposition following Eq. 8 was 22%, based on **7**.

The resin **10**, obtained after decomposition by Eq. 5, was subjected to the same regeneration procedures as above, and the resin **3** thus regenerated was converted again to hydrazone **7**-5, which was subsequently decomposed following Eq. 5 to afford 1,3-diphenyl-1-propene in a 75% yield.

Acknowledgement is made to Mitsubishi Chemical Industries, Ltd., for providing the resins used.

References

1) D. W. Emerson, R. R. Emerson, J. E. M. Sorensen, and J. E. Turek, *J. Org. Chem.*, **44**, 4634 (1979).
2) F. Gaviña, P. Gil, and B. Palazón, *Tetrahedron Lett.*, **1979**, 1333.
3) W. R. Bamford and T. S. Stevens, *J. Chem. Soc.*, **1952**, 4735.
4) H. Kamogawa, T. Hayashi, and M. Nanasawa, *Chem. Lett.*, **1976**, 419.
5) L. Caglioti, *Org. Synth.* **52**, 122 (1972).
6) J. Jiricny, D. M. Orere, and C. B. Reese, *J. Chem. Soc., Perkin Trans. 1*, **1980**, 1487.

Studies of Bitter Peptides from Casein Hydrolyzate. I. Synthesis of Bitter Peptide BPIa Corresponding to Arg-Gly-Pro-Pro-Phe-Ile-Val from Casein Hydrolyzate by Alkaline Proteinase of *Bacillus subtilis*[1)]

Hiroshi Fukui, Hidenori Kanehisa, Norio Ishibashi, Ichizo Miyake, and Hideo Okai*

Department of Fermentation Technology, Faculty of Engineering, Hiroshima University, Shitami, Saijo-cho, Higashihiroshima 724

(Received July 19, 1982)

A bitter heptapeptide BPIa was synthesized and compared with the natural peptide, isolated by Minamiura *et al.* from casein hydrolyzate, by means of thin layer chromatography, paper electrophoresis, and carboxymethylcellulose column chromatography. All results for the two peptides matched very closely each other. The synthetic BPIa has an extremely bitter taste with its threshold value 0.05 mM. It is one of the most bitter compounds such as phenylthiourea and quinine.

In recent years, many people have investigated chemical properties of various bitter peptides. Some bitter peptides have been isolated from natural foodstuffs such as cheese, natto, sake, and cocoa.[2–5)] In addition, some workers have reported that hydrolysis of proteins with proteolytic enzymes is usually accompanied by formation of bitter taste.[6–9)] Minamiura *et al.*[8,9)] isolated bitter peptides from casein hydrolyzate by alkaline proteinase of *Bacillus subtilis*, and determined their amino acid sequences as shown in Fig. 1.

BPIa Arg-Gly-Pro-Pro-Phe-Ile-Val

BPIb Leu-Val-Pro-Arg-Tyr-Phe-Gly-----

BPIc Val-Tyr-Pro-Phe-Pro-Pro-Gly-Ile-Asn-His

BPII cyclo-(Trp-Leu-Trp-Leu)

Fig. 1. Amino acid sequence of bitter peptides from casein hydrolyzate by Minamiura *et al.*[8,9)]

Although they reported that these peptides possessed a strong bitter taste, they did not report any other characteristics of these peptides. In connection with studies of the relationship between chemical structure and bitter taste, Shiba and Nunami[10)] synthesized some cyclic oligopeptides, including Minamiura's BPII (cyclo-tryptophylleucyltryptophylleucyl). The results indicated that the structure of Minamiura's BPII was actually cyclo-tryptophylleucyl. They also reported that the threshold value of the synthetic cyclo-tryptophylleucyl was 0.063 mM (1 M=1 mol dm^{-3}). The value of the peptide anhydride is the same as that of phenylthiourea and quinine. They are one of the most bitter compounds known.

As for the linear decapeptide BPIc, one of the authors synthesized and compared it with natural BPIc. Details will be described in another investigation.[11)] The present paper deals with synthesis of BPIa, measurement of its threshold value of bitter taste, and comparison between natural and synthetic BPIa.

The synthetic route for BPIa is shown in Fig. 2. *N*-(*t*-Butoxycarbonyl)isoleucine was coupled with valine benzyl ester by means of the mixed anhydride method to form *N*-(*t*-butoxycarbonyl)isoleucylvaline benzyl ester (**1**). Removal of the *t*-butoxycarbonyl group from **1** with hydrogen chloride in dioxane afforded the corresponding dipeptide ester hydrochloride (**2**). Compound **2** was coupled with *N*-(*t*-butoxycarbonyl)phenylalanine by the mixed anhydride method to yield acyltripeptide ester (**3**). Removal of the *t*-butoxycarbonyl group from **3** with hydrogen chloride in dioxane afforded the corresponding tripeptide ester hydrochloride (**4**). *N*-(*t*-Butoxycarbonyl)proline and proline benzyl ester were condensed to yield *N*-(*t*-butoxycarbonyl)prolylproline benzyl ester (**5**) by the dicyclohexylcarbodiimide method. Hydrogenation of **5** easily gave the corresponding acid (**6**). Compounds **6** and **4** were condensed by the same method as was used in the preparation of **1**, and the resulting acylpentapeptide ester (**7**) was converted to the corresponding pentapeptide ester hydrochloride (**8**) by action of hydrogen chloride in dioxane. Saponification of N^{a}-benzyloxycarbonyl-N^{G}-nitroarginylglycine benzyl ester (**9**), derived from N^{a}-benzyloxycarbonyl-N^{G}-nitroarginine and glycine benzyl ester by the mixed anhydride method, gave the corresponding acid (**10**). Compounds **10** and **8** thus obtained were condensed by the dicyclohexylcarbodiimide method to yield the fully protected BPIa (**11**). Catalytic hydrogenation of **11** in methanol–acetic acid (1:1, v/v) gave a heptapeptide BPIa. The synthetic BPIa and its intermediates were subjected to measurement for melting point and specific rotation. Their purity was confirmed by thin layer chromatography on two and/or three solvent systems and by elemental analyses. The homogeneity of the final product was also confirmed by amino acid analysis, paper electrophoresis, and carboxymethylcellulose column chromatography.

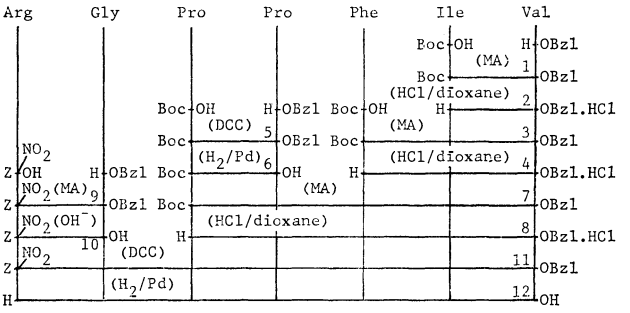

Fig. 2. Synthesis of BPIa.

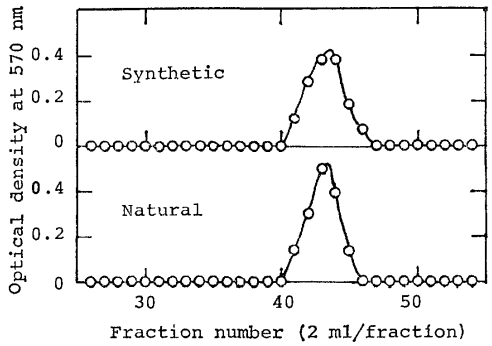

Fig. 3. Carboxymethylcellulose column chromatography of synthetic and natural BPIa.
Solvent: 0.2 M pyridinium acetate, pH 5.0.

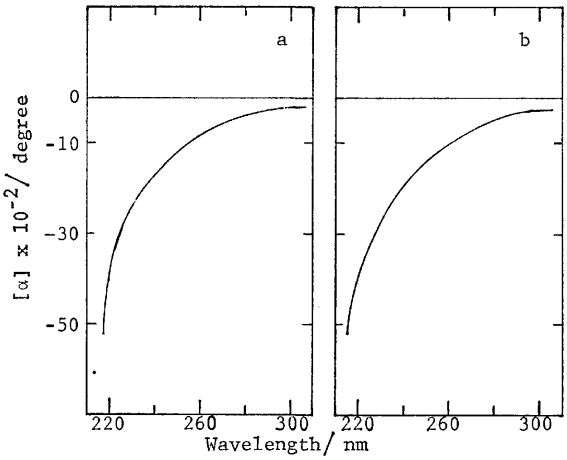

Fig. 4. ORD curves of synthetic BPIa.
Solvent: a; water, b; ethanol.

The synthetic BPIa was then compared with natural BPIa[12] isolated by Minamiura *et al.* Both compounds gave a single spot and identical R_f value on thin layer chromatography. The mobility of synthetic BPIa was indistinguishable from that of natural BPIa on paper electrophoresis. Both compounds also gave the same pattern on carboxymethylcellulose column chromatography as shown in Fig. 3. The ORD curves of synthetic BPIa measured in both aqueous and ethanol solutions are presented in Fig. 4. In both media BPIa exhibited similar curves.

The bitterness of synthesized BPIa was organoleptically determined *via* panel evaluation by four people; the threshold value of BPIa was found 0.05 mM. It is one of the most bitter compounds that are known now.

Dumas *et al.*[13] determined the whole primary structure of bovine β-casein which contains a partial sequence of -Arg^{202}-Gly-Pro-Phe-Pro-Ile-Ile-Val^{209} in the C-terminal portion. Although Minamiura's BPIa cannot be found in the structure of Dumas' formula, it is similar to the C-terminal of that formula. Hashimoto *et al.*[14] synthesized a heptapeptide, H-Gly-Pro-Phe-Pro-Ile-Ile-Val-OH, corresponding to the C-terminal portion (203—209) and compared it with the natural peptide isolated from tryptic hydrolyzate of casein. He reported that the two peptides matched closely each other and supported Dumas' formula. In the same laboratory, Aoyagi and Izumiya[15] suggested, from a result that H-Arg-Gly-Pro-Phe-Pro-Ile-OH (202—207) of Dumas' formula possessed a bitter taste, that Minamiura's BPIa is to be changed so as to correspond to the C-terminal of that formula. However, we submit that Minamiura's findings are indentical with our own as shown herein. Therefore, we suggest that the sequence should be converted at this stage of investigation for the correct C-terminal sequence of β-casein.

Experimental

All the melting points are uncorrected. The thin layer chromatography was carried out on Merck silica gel G. The developing solvents used were 1) 1-butanol-acetic acid-pyridine-water (4:1:1:2, v/v), 2) 1-butanol-acetic acid-water (4:2:1, v/v), and 3) chloroform-methanol (5:1, v/v). Spots of materials possessing free amino group on a thin layer plate were detected by spraying ninhydrin, and those with blocked amino group, by spraying 25% hydrogen bromide in acetic acid and then ninhydrin. Optical rotations were measured on a JASCO automatic polarimeter, DIP-SL type. Amino acid analysis was performed with a Hitachi amino acid analyzer, KLA-5 type. Prior to analysis, compounds were dried over phosphorus pentaoxide at 66 °C and 2 mmHg (1 mmHg=133.332 Pa) for 2 h.

Synthesis of BPIa. N-*(t-Butoxycarbonyl)isoleucylvaline Benzyl Ester (1)*: Boc-Ile-OH·DCHA (9.08 g, 22 mmol) was dissolved in ethyl acetate (150 ml), and 1 M sulfuric acid (50 ml) was added to the mixture with stirring. The organic layer was washed with water and dried over anhydrous sodium sulfate. The solution was concentrated to dryness *in vacuo*, and the oily residue was dissolved in tetrahydrofuran (40 ml) and *N*-methylmorpholine (2.2 ml, 20 mmol). Ethyl chloroformate (2.0 ml, 20 mmol) was added to the mixture at −5 °C. After 10 min, a solution of H-Val-OBzl·TsOH (7.59 g, 20 mmol) and *N*-methylmorpholine (2.2 ml, 20 mmol) in chloroform (40 ml) was added to the mixture. The reaction mixture was stored in an ice bath for 1 h, and then at room temperature overnight. The mixture was evaporated *in vacuo*, and the oily residue was dissolved in ethyl acetate. The solution was washed successively with water, 4% citric acid, 4% sodium hydrogencarbonate, and water, and then dried over anhydrous sodium sulfate. The filtrate was evaporated *in vacuo*. The oily residue was crystallized with petroleum ether; yield 5.67 g (67%); mp 93—94 °C (lit,[14] 89—91 °C); $[\alpha]_D^{20}$ −50.0° (*c* 1, methanol) (Lit,[14] −48° (*c* 1.9, ethanol)); R_f^1 0.98, R_f^2 0.98, and R_f^3 0.93.

Found: C, 65.56; H, 8.61; N, 6.61%. Calcd for $C_{23}H_{36}O_5N_2$: C, 65.69; H, 8.63; N, 6.66%.

Isoleucylvaline Benzyl Ester Hydrochloride (2): To a solution of **1** (4.21 g, 20 mmol) in dioxane (10 ml) 4 M hydrogen chloride in dioxane (40 ml) was added. The solution was allowed to stand at room temperature. After 1 h, the solution was evaporated *in vacuo*. The residual oil was solidified with ether: yield 3.36 g (95%); mp 154—155 °C; $[\alpha]_D^{20}$ −11.0° (*c* 1, methanol); R_f^1 0.80, R_f^2 0.90, and R_f^3 0.47.

Found: C, 60.30; H, 8.18; N, 7.72%. Calcd for $C_{18}H_{29}O_3N_2Cl$: C, 60.57; H, 8.19; N, 7.85%.

N-*(t-Butoxycarbonyl)phenylalanylisoleucylvaline Benzyl Ester (3)*: This was prepared from Boc-Phe-OH·DCHA (4.91 g, 11 mmol) and **2** (3.57 g, 10 mmol) in the same way as described above. The product was solidified from ether–petroleum

ether: yield 5.16 g (91%); mp 148 °C; $[\alpha]_D^{20}$ −48.5° (*c* 1, methanol); R_f^1 0.99, R_f^2 0.99, and R_f^3 0.85.

Found: C, 67.93; H, 8.10; N, 7.48%. Calcd for $C_{32}H_{45}O_6N_3$: C, 67.70; H, 7.99; N, 7.40%.

*Phenylalanylisoleucylvaline Benzyl Ester Hydrochloride (**4**)*: This was prepared from **3** (5.68 g, 10 mmol) by the same procedure as described for the preparation of **2**: yield 4.96 g (98%); mp 231 °C; $[\alpha]_D^{20}$ −37.0° (*c* 1, methanol); R_f^1 0.92, R_f^2 0.94, and R_f^3 0.78.

Found: C, 64.28; H, 7.70; N, 8.17%. Calcd for $C_{27}H_{38}O_4N_3Cl$: C, 64.33; H, 7.60; N, 8.34%.

N-*(t-Butoxycarbonyl)prolylproline Benzyl Ester (**5**)*: To a suspension of Boc–Pro–OH (4.30 g, 20 mmol), H–Pro–OBzl·HCl (5.32 g, 22 mmol) and *N*-methylmorpholine (2.42 ml, 22 mmol) in acetonitrile (60 ml), dicyclohexylcarbodiimide (4.50 g, 22 mmol) was added at 0 °C with stirring. The reaction mixture was stirred at 0 °C for 3 h and then at room temperature overnight. *N,N'*-Dicyclohexylurea was filtered off and the filtrate was evaporated *in vacuo*. The oily residue was dissolved in ethyl acetate and the solution was washed successively with water, 4% citric acid, 4% sodium hydrogencarbonate, and water. The solution was dried over anhydrous sodium sulfate and evaporated *in vacuo*. The residual oil weighed 8.0 g (100%). Deber *et al.*[16] also obtained this compound as an oily form: R_f^1 0.96 and R_f^3 0.79.

N-*(t-Butoxycarbonyl)prolylproline (**6**)*: Compound **5** (8.0 g, 20 mmol, oily form) was dissolved in methanol (50 ml) and hydrogenated in the presence of palladium black at room temperature for 48 h. The catalyst was removed by filtration and the filtrate was evaporated *in vacuo*. The residue was crystallized from ether–petroleum ether. It was recrystallized from hot ethyl acetate: yield 4.60 g (74%); mp 177—180 °C (lit,[17] 187—187.5 °C); $[\alpha]_D^{20}$ −121.5° (*c* 1, methanol); R_f^1 0.70, R_f^2 0.93, and R_f^3 0.48.

Found: C, 57.41; H, 7.67; N, 8.84%. Calcd for $C_{15}H_{24}O_5N_2$: C, 57.67; H, 7.74; N, 8.79%.

N-*(t-Butoxycarbonyl)prolylprolylphenylalanylisoleucylvaline Benzyl Ester (**7**)*: Compounds **6** (1.56 g, 5 mmol) and **4** (2.52 g, 5 mmol) were coupled by the same method as described for the preparation of **1**: yield 3.49 g (92%); mp 109—110 °C; $[\alpha]_D^{20}$ −101.0° (*c* 1, methanol); R_f^1 0.96, R_f^2 0.99, and R_f^3 0.67.

Found: C, 66.46; H, 7.83; N, 8.97%. Calcd for $C_{42}H_{59}O_8N_5$: C, 66.22; H, 7.81; N, 9.19%.

*Prolylprolylphenylalanylisoleucylvaline Benzyl Ester Hydrochloride (**8**)*: Compound **7** (3.80 g, 5 mmol) was treated in the same way as described for the case of **2**: yield 3.40 g (97%); mp 191 °C; $[\alpha]_D^{20}$ −99.0° (*c* 1, methanol); R_f^1 0.81, R_f^2 0.50, and R_f^3 0.45.

Found: C, 63.82; H, 7.45; N, 10.25%. Calcd for $C_{37}H_{52}O_6N_5Cl$: C, 63.64; H, 7.51; N, 10.03%.

N^{α}-*Benzyloxycarbonyl-*N^{G}*-nitroarginylglycine Benzyl Ester (**9**)*: To a solution of Z–Arg(NO_2)–OH (7.06 g, 20 mmol) and *N*-methylmorpholine (2.2 ml, 20 mmol) in tetrahydrofuran (20 ml), ethyl chloroformate (2.0 ml, 20 mmol) was added at −5 °C. After 10 min, a solution of H–Gly–OBzl·TsOH (6.74 g, 20 mmol) and *N*-methylmorpholine (2.2 ml, 20 mmol) in *N,N*-dimethylformamide (20 ml) was added to the mixture. The reaction mixture was stored in an ice bath for 1 h, and then at room temperature overnight. The mixture was evaporated *in vacuo*. The precipitate which was formed upon addition of water to the residue was collected, washed with 0.5 M hydrochloric acid, 4% sodium hydrogencarbonate, and water, and dried. It was dissolved in *N,N*-dimethylformamide (10 ml) and solidified with ethyl acetate–ether: yield 8.70 g (87%); mp 150—151 °C (lit,[18] 145—147 °C); $[\alpha]_D^{20}$ −3.5° (*c* 1, *N,N*-dimethylformamide) (lit,[18] −14.7° (*c* 1, methanol)); R_f^1 0.95, R_f^2 0.99, and R_f^3 0.66.

Found: C, 55.31; H, 5.69; N, 16.79%. Calcd for $C_{23}H_{28}O_7N_6$: C, 55.19; H, 5.64; N, 16.79%.

N^{α}-*Benzyloxycarbonyl-*N^{G}*-nitroarginylglycine (**10**)*: To a suspension of **9** (5.00 g, 10 mmol) in methanol (20 ml), 1 M sodium hydroxide (12 ml, 12 mmol) was added. The mixture was allowed to stand at room temperature. After 3 h, the mixture was evaporated *in vacuo* and 2 M hydrochloric and (7 ml) was added to it. The precipitate thus obtained was collected and washed with water. It was recrystallized from hot ethanol: yield 3.72 g (91%); mp 110—112 °C (Lit,[19] 112 °C); $[\alpha]_D^{20}$ −10.0° (*c* 1, methanol) (lit,[20] −10° (methanol)); R_f^1 0.81, R_f^2 0.85, and R_f^3 0.07.

Found: C, 46.69; H, 5.58; N, 20.66%. Calcd for $C_{16}H_{22}O_7N_6$: C, 46.82; H, 5.40; N, 20.48%.

N^{α} *- Benzyloxycarbonyl -* N^{G} *- nitroarginylglycylprolylprolylphenylalanylisoleucylvaline Benzyl Ester (**11**)*: To a solution of **10** (0.82 g, 2 mmol) in *N,N*-dimethylformamide (10 ml), dicyclohexylcarbodiimide (0.45 g, 2 mmol) was added at 0 °C. After 20 min, a solution of **8** (1.39 g, 2 mmol) and *N*-methylmorpholine (0.22 ml, 2 mmol) in chloroform (10 ml) was added to it. The reaction mixture was stirred at 0 °C for 3 h and then at room temperature overnight. *N,N*-Dicyclohexylurea was removed by filtration, and the filtrate was diluted with ethyl acetate. The solution was washed successively with 0.5 M hydrochloric acid, 4% sodium hydrogencarbonate, and water, dried over anhydrous sodium sulfate, and evaporated *in vacuo*. The residue was solidified with ether. The product was dissolved in methanol (2 ml) and solidified with ethyl acetate–ether: yield 1.45 g (69%); mp 120 °C; $[\alpha]_D^{20}$ −44.0° (*c* 1, *N,N*-dimethylformamide); R_f^1 0.86 and R_f^3 0.64.

Found: C, 60.46; H, 6.71; N, 14.62%. Calcd for $C_{53}H_{71}O_{12}N_{11}$: C, 60.38; H, 6.79; N, 14.62%.

*Arginylglycylprolylprolylphenylalanylisoleucylvaline Diacetate (**12**)*: A solution of **11** (1.05 g, 1 mmol) in methanol—acetic acid (1:1, 10 ml) was hydrogenated in the presence of palladium black at room temperature for 48 h. The catalyst was removed by filtration and the filtrate was evaporated *in vacuo*. The residue was crystallized by the aid of acetone. It was recrystallized from methanol–ether: yield 0.76 g (97%); $[\alpha]_D^{20}$ −92.5° (*c* 1, water); R_f^1 0.59. The spot was detected by Sakaguchi reagent as well as ninhydrin. Amino acid analysis:[21] Arg 1.06; Gly 1.07; Pro 1.83; Phe 1.11; Ile 1.00; Val 1.05.

Found: C, 55.60; H, 7.71; N, 15.34%. Calcd for $C_{38}H_{60}O_8N_{10}2CH_3COOH$: C, 55.74; H, 7.57; N, 15.48%.

Comparison of Synthetic and Natural BPIa. Thin Layer Chromatography: Both compounds gave a single spot with the R_f^1 value 0.59.

Paper Electrophoresis: This was carried out under the following conditions: paper, Toyo Roshi No. 51 A chromatography paper; solvent, pyridine–acetic acid–water (10:0.4:90, v/v) (pH 6.4); voltage gradient, 15 V/cm; charge period, 2 h. The mobility of synthetic BPIa was 7.8 cm and indistinguishable from that of natural BPIa.

Carboxymethylcellulose Column Chromatography: A portion (*ca.* 1 mg) of synthetic or natural BPIa was dissolved in 0.3 ml of 0.2 M pyridinium acetate (pH 5.0). The solution was applied to a column (1.0 cm × 60 cm) of carboxymethylcellulose. Elution was carried out with the same solvent and 2 ml fractions were collected at a flow rate of 8 ml h^{-1}. The peptide content was determined by the method described by Yemm and Cocking.[22] The results shown in Fig. 3 indicate that the pattern of chromatogram of synthetic BPIa

is indistinguishable from that of natural one.

ORD Measurement: This was performed with a JASCO spectropolarimeter Model ORD/UV-5 over a range 215—300 nm. A cell of path length 0.1 cm was used and runs were made at ambient temperature. Patterns in both aqueous and ethanol solutions are shown in Fig. 4.

Sensory Test: The bitterness of the synthetic BPIa was organoleptically determined *via* panel evaluation by four people. A series of solutions of decreasing concentration was prepared in which each solution was half as strong as its proceeding one. Before testing the sample, the mouth was thoroughly rinsed with deionized water. The sample size was usually 2—3 ml. The sample solution was held in the mouth for *ca.* 10 s and then spit out, and the threshold value of the sample was determined. The threshold value of synthetic BPIa was 0.05 mM, the same as that of phenylthiourea and quinine.

The authors wish to express their thanks to Dr. Noshi Minamiura of Osaka City University for his kind offer of the natural sample of BPIa. Thanks are also due to Associate Professor Tetsuo Kato of Kyushu University for the ORD measurements, and Dr. Shinji Okumura of Ajinomoto Co. Inc., for supplying some amino acids.

References

1) The abbreviations recommended by the IUPAC-IUB commission of Biochemical Nomenclature (*J. Biol. Chem.*, **247**, 977 (1972)) have been used. Amino acid symbols except glycine denote L-configuration. Additional abbreviations: DCHA, dicyclohexylamine; TsOH; *p*-toluenesulfonic acid.

2) T. S. Hamilton, R. D. Hill, and H. von Leeuwen, *Agric. Biol. Chem.*, **38**, 375 (1974).

3) K. Maekawa and S. Tamai, Abstracts of paper, 36th National Meeting of Agricultural Chemical Society of Japan, Tokyo, April 1965.

4) K. Takahashi, M. Tadenuma, K. Kitamoto, and S. Sato, *Agric. Biol. Chem.*, **38**, 927 (1974); O. Tajima and S. Sato, *Rept. Inst. Phys. Chem.*, **40**, 259 (1964).

5) W. Pickenhangen and P. Dietrich, *Helv. Chim. Acta*, **58**, 1078 (1975).

6) M. Yamashita, S. Arai, and M. Fujimaki, *Agric. Biol. Chem.*, **33**, 321 (1969); S. Arai, M. Yamashita, H. Kato, and M. Fujimaki, *ibid.*, **34**, 729 (1970).

7) T. Matoba, R. Hayashi, and T. Hata, *Agric. Biol. Chem.*, **34**, 1235 (1970).

8) N. Minamiura, Y. Matsumura, J. Fukumoto, and T. Yamamoto, *Agric. Biol. Chem.*, **36**, 588 (1972).

9) N. Minamiura, Y. Matsumura, and T. Yamamoto, *J. Biochem. (Tokyo)*, **72**, 841 (1972).

10) T. Shiba and K. Nunami, *Tetrahedron Lett.*, **1974**, 509.

11) A preliminary account has been reported: H. Kanehisa, H. Okai, and S. Oka, "Proceedings of the 13th Sympodium on Peptide Chemistry," ed by S. Yamada, Protein Research Foundation, Osaka (1976), pp. 72—76 and H. Kanehisa, *Bull. Chem. Soc. Jpn.*, submitted.

12) Natural BPIa was offered from Dr. N. Minamiura.

13) B. Ribadeau Dumas, C. Brignon, F. Grosclade, and J. C. Mercier, *Eur. J. Biochem.*, **25**, 505 (1972).

14) A. Hashimoto, H. Aoyagi, and N. Izumiya, *Bull. Chem. Soc. Jpn.*, **53**, 2926 (1980).

15) H. Aoyagi and N. Izumiya, *Bull. Chem. Soc. Jpn.*, **50**, 2387 (1977).

16) C. M. Deber, F. A. Borey, J. P. Carver, and E. R. Blout, *J. Am. Chem. Soc.*, **92**, 6191 (1970).

17) G. R. Pettit and S. K. Das Gupta, *Can. J. Chem.*, **45**, 1600 (1967).

18) M. Fujino and O. Nishimura, *Chem. Pharm. Bull.*, **17**, 1937 (1969).

19) K. Suzuki and T. Abiko, *Chem. Pharm. Bull.*, **16**, 1997 (1968).

20) P. M. Scopes, K. B. Welfold, and G. T. Young, *J. Chem. Soc.*, **1965**, 782.

21) The synthetic BPIa was hydrolyzed with 6 M hydrochloric acid in a sealed tube at 110 °C for 60 h. Molar ratios of amino acids are based on the isoleucine value.

22) E. W. Yemm and E. C. Cocking, *Analyst*, **80**, 209 (1955).

Coenzyme Models. 33. Evidence for Retro-acyloin Condensation as Catalyzed by Thiazolium Ion and Cationic Micelle. Oxidative Trapping of the "Active Aldehyde" Intermediates by Flavin

Seiji SHINKAI,* Youichiro HARA, and Osamu MANABE

Department of Industrial Chemistry, Faculty of Engineering, Nagasaki University, Nagasaki 852

(Received July 28, 1982)

N-Hexadecylthiazolium bromide(HxdT) in the CTAB micelle, which is known as an excellent catalytic system for acyloin condensation of aldehydes, catalyzes the reverse reaction (*i.e.*, retro-acyloin condensation) to give aldehydes from α-ketols *via* the active aldehyde intermediates. The existence of the novel, HxdT-mediated process was proposed on the basis of an experimental discovery that flavin (3-methyltetra-*O*-acetylriboflavin: MeFl), which is capable of oxidatively trapping the active aldehyde intermediates, is reduced by α-ketols such as acetoin and 3-hydroxy-3-methyl-2-butanone in the micellized HxdT solution. It was further substantiated by detection of acetaldehyde in the final reaction mixture. Based on the disappearance rate of the absorbance of MeFl, we spectrophotometrically estimated the rate constants for the retro-acyloin condensation. Similarly, biacetyl, the monohydrated species of which is analogous to α-ketol, afforded acetaldehyde and acetic acid in the micellized HxdT solution, the rate constant being greater by factors of 10^2—10^3 than those for α-ketols. The relevance of the retro-acyloin condensation to biological systems (*e.g.*, the mechanism of transketolase catalysis) is discussed.

Recently, it has been established that some flavin-dependent enzymes employ carbanion intermediates during the course of the oxidation of bound substrates.[1-3] In previous publications of this series,[4-7] we have demonstrated that the application of the biochemical concept "flavin oxidation of carbanion" to organic chemistry is very useful in exploring a new class of oxidation reactions. For example, flavin is rapidly reduced according to zero-order kinetics in cyanide-catalyzed benzoin condensation,[4] thiazolium-catalyzed acyloin condensation,[5,7] and thiol-catalyzed rearrangement of glyoxals,[6] which all proceed *via* the carbanionic intermediates. The role of flavin oxidation in thiazolium-catalyzed reactions is also discussed by Yano *et al.*[8] The product analyses of these systems showed that the reactions are readily diverted to the oxidation reactions in the presence of flavin as an oxidative trapping agent. Similarly, the "active aldehydes" afforded from aldehydes and the conjugate bases of thiazolium ions are oxidized by nitrobenzene,[9] acridine and its analogues,[10] disulfides,[11] and nitrosobenzene.[12] In Scheme 1, we illustrated a typical example for flavin trapping in thiazolium-mediated acyloin condensation, in which the key intermediate **1** is rapidly oxidized by flavin to yield the corresponding carboxylic acid.[5]

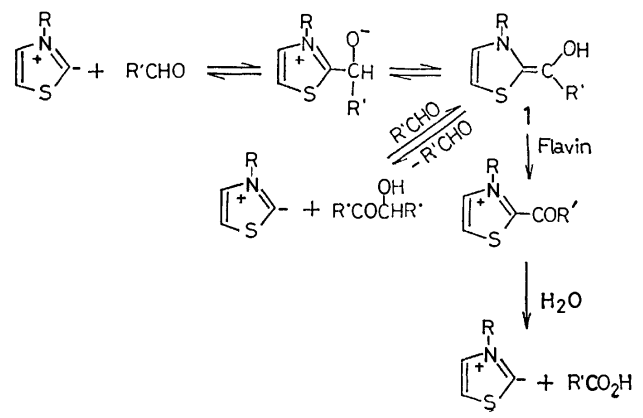

Scheme 1.

It is a well-known fact that the conjugate bases of thiazolium ions (vitamin B_1 analogues) catalyze acyloin condensation as cyanide ion catalyzes benzoin condensation.[13] To the best of our knowledge, however, there is no clear evidence as to whether the conjugate bases catalyze the reverse reaction (retro-acyloin condensation) to afford aldehydes from α-ketols. It occurred to us that if the retro-acyloin condensation is catalyzed by thiazolium ions, the transient intermediates **1** would be rapidly trapped by flavin. In the enzymatic system, the mechanism of transketolase which requires thiamine pyrophosphate(TPP) as a co-factor and catalyzes the cleavage of xylulose 5-phosphate or D-fructose 6-phosphate in its early stage is analogous to that of the retro-acyloin condensation.[14-16] Christen and Gasser[17] have reported that the 1,2-dihydroxyethyl–TPP intermediates (analogues of **1**) formed from these substrates in the active site of the enzyme can be oxidatively trapped by hexacyanoferrate(III). Based on flavin-trapping of **1** from α-ketols, we here report evidence that *N*-hexadecylthiazolium bromide(HxdT) bound to the CTAB(hexadecyltrimethylammonium bromide) micelle catalyzes not only the acyloin condensation[13,18] but also the retro-acyloin condensation.

Results and Discussion

Flavin Oxidation of α-Ketols and Analogues in Micellized HxdT Solution. We have used 3-methyltetra-*O*-acetylriboflavin(MeFl) and HxdT in the cationic CTAB solution. The kinetic measurements of the flavin oxidation were carried out at 30 °C under anaerobic conditions(N_2). The reaction was followed spectrophoto-

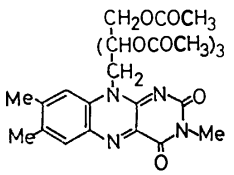

MeFl

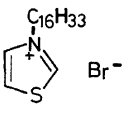

HxdT

metrically by monitoring the disappearance of the absorption band of MeFl at 448 nm (ε 12200). Since the active aldehydes rapidly reduce MeFl,[5,8] the production of **1** from the substrates, if it occurs, can be immediately detected as a decrease in the absorption band.

In an anaerobic aqueous solution containing HxdT (1 mM) and CTAB (10 mM), MeFl was reduced by acetoin, benzoin, 3-hydroxy-3-methyl-2-butanone (HMB), 3-hydroxy-3-phenyl-2-butanone(HPB), and biacetyl, but the reaction with benzil and 4,4′-dichlorobenzil was not detected. As reported in the thiazolium-mediated flavin oxidation of aldehydes,[5] the zero-order decrease of the 448 nm band was observed for the initial stage of the reaction and lasted up to, for example, 40% reaction for acetoin (0.1 M). We noticed, however, that acetoin and benzoin in the CTAB micelle solution reduce MeFl even in the absence of HxdT. The reductant in this system is a 1,2-enediolate which is formed by base-catalyzed deprotonation of these "carbon acids" (Eq. 1).[19-21] Thus, the rates

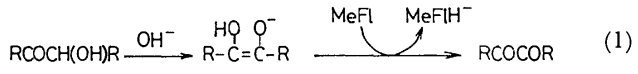

(1)

observed in the micellized HxdT solution (v_{obsd}) are expressed as the sum of the base-catalyzed term (v_{base}) and the HxdT-catalyzed term (v_{HxdT}) (Eq. 2),

$$v_{obsd} = v_{base} + v_{HxdT}, \quad (2)$$

where v_{base} is the rate of the flavin reduction in the CTAB micelle solution and v_{obsd} is that in the presence of both HxdT and the CTAB micelle.

We found that the base-catalyzed deprotonation of benzoin is so fast in the CTAB micelle that the accurate determination of v_{HxdT} from Eq. 2 is rather difficult. The facile deprotonation of benzoin is due to the acidity of benzoin as carbon acid. On the other hand, the v_{base} of acetoin was relatively slow, the v_{obsd} being greater by a factor of 6.1 than the v_{base}. From Eq. 2, we thus determined the v_{HxdT} which is responsible for the HxdT-mediated retro-acyloin condensation. More unequivocal evidence was obtained from the reaction with HMB and HPB since the base-catalyzed deprotonation is not the case in these substrates. In fact, MeFl was not reduced at all by HMB and HPB in the CTAB micelle. On the other hand, the reduction of MeFl occurred on the addition of HxdT to the micelle solution. We thus determined the v_{HxdT} ($=v_{obsd}$) directly. Biacetyl, the monohydrated species of which is an analogue of α-ketol, also reduced MeFl in the micellized HxdT solution, the rate being much faster than that of α-ketols.

For the specification of the reaction order, the HxdT-catalyzed rates (v_{HxdT}) were determined as a function of the concentration of HxdT (0.2—2 mM) or substrates (for the concentration ranges see Table 1). It was found that the rates are first-order with respect to HxdT and substrates under these experimental conditions. The HxdT-catalyzed rates were thus given by Eq. 3. The $k_{2,app}$ values are summarized in Table 1.

$$v_{HxdT} = k_{2,app}[S]^{1.0}[HxdT]^{1.0}[MeFl]^{0} \quad (3)$$

The examination of this table reveals that (i) in aqueous solution, the thiazolium-mediated reduction of MeFl occurs only in the presence of the cationic micelle, (ii) the $k_{2,app}$ for $CH_3COC(OH)(CH_3)X$ series increases with increasing electron-withdrawing nature of X (*i.e.*, $CH_3<H<C_6H_5$), (iii) the reaction with biacetyl is much faster than that with analogous α-ketols, the rate constant being greater by factors of 10^2—10^3, and (iv) benzil and 4,4′-dichlorobenzil are totally unreactive. The effect of the substituents (ii) will be discussed later. The remarkable reactivity difference between biacetyl and benzil analogues is ascribed to the steric effect. For example, we have found that the micellized thiazolium ions is capable of catalyzing the decarboxylation of pyruvic acid but not that of 4-chlorobenzoylformic acid.[5] Both results suggest that the carbonyl group next to a phenyl ring is sterically deactivated in the thiazolium-mediated reactions.

As a summary of the foregoing results, one can safely conclude that the "active aldehydes" are produced from α-ketols and biacetyl in the micellized HxdT solution. In other words, it implies that the retro-acyloin condensation is mediated by micellized thiazolium ions. Subsequently, we carried out the product analyses of these reaction systems.

Product Analyses of the HxdT-mediated Retro-acyloin Condensation Systems. If HxdT-mediated retro-acyloin condensation takes place, 1 mol of acetoin afford

Table 1. Apparent second-order rate constants ($10^3 k_{2,app}$ M^{-1} s^{-1}) for the oxidation of α-ketols and analogues[a]

Substrate(S)	[S] / mM	CTAB / mM	pH	$10^3 k_{2,app}$ / M^{-1} s^{-1}
$CH_3COCH(OH)CH_3$	30—200	10	7.8	0.149
$CH_3COC(OH)(CH_3)_2$	30—200	10	7.8	0.0116
$CH_3COC(OH)(CH_3)_2$[b]	30—200	0	7.8	No reaction
$CH_3COC(OH)(CH_3)C_6H_5$	10— 50	10	7.8	2.05
$CH_3COCOCH_3$	0.5—3.0	10	7.8	21.8
$CH_3COCOCH_3$	0.5—3.0	10	8.0	27.6
$C_6H_5COCOC_6H_5$	0.2—2.0	10	8.0	No reaction
$4\text{-}ClC_6H_4COCOC_6H_4Cl(4-)$	0.2—2.0	10	8.0	No reaction

a) 30 °C, [HxdT] = 1.00 mM, [MeFl] = 5.00×10^{-5} M. pH was adjusted with 0.01 M phosphate. b) *N*-Benzylthiazolium bromide(1.00 mM) was used instead of HxdT.

2 mol of acetaldehyde, and 1 mol of 3-hydroxy-3-methyl-2-butanone affords 1 mol of acetaldehyde and 1 mol of acetone. The reactions were carried out at 30 °C in anaerobic (N_2) ampuls. After 1 d, we treated the final reaction solution with 2,4-dinitrophenylhydrazinc[22] and analyzed the products as their hydrazone derivatives by using high-pressure liquid chromatography(HPLC). On the other hand, acetic acid was analyzed by GLC before the treatment with 2,4-dinitrophenylhydrazine. The results are summarized in Table 2. The examination of Table 2 reveals that the expected products are detected in the micellized HxdT solution, whereas no such product is afforded in the absence of HxdT. The yields of these products are relatively low, however. The low yields would be ascribed to the consumption of acetaldehyde (or acetone) by aldol-type condensation. In fact, we confirmed in a separate study that the concentration of acetaldehyde decreases with time in the CTAB micelle solution. These data support that HxdT in the CTAB micelle is capable of catalyzing the retro-acyloin condensation. It is now obvious, therefore, that the reduction of MeFl observed in the kinetic measurements is attributable to the reaction of MeFl with the active aldehydes (**1**) afforded from these substrates (see Scheme 1).

Table 3 shows that in the micellized HxdT solution biacetyl is converted to acetaldehyde and acetic acid. This reaction, the socalled biacetyl mutase reaction, has been found by Mizuhara and Oono.[23] The quantitative scission of 1 mol biacetyl gives 1 mol of acetic acid and 1 mol of acetaldehyde (Eq. 4). As shown in Table 3, however, the yield of acetic acid is much higher than that of acetaldehyde. The relatively low yield of acetaldehyde is again attributed to the consumption by aldol-type condensation. The yield of acetic acid calculated on the basis of HxdT was 190%. This

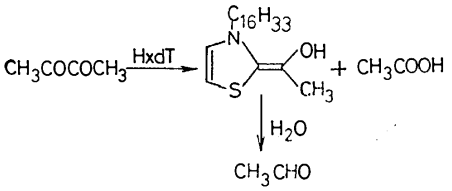

(4)

implies that HxdT acts as a recycle catalyst. It is presumed that this reaction also proceeds *via* the active aldehyde intermediate.[23] In fact, biacetyl in the micellized HxdT solution reduces MeFl (*vide supra*), indicating the formation of the active aldehyde from biacetyl and HxdT. We added flavin to the reaction system, and carried out the product analysis. Entry 3 in Table 3 shows that in the presence of FMN(flavin mononucleotide) the yield of acetaldehyde is lowered, while that of acetic acid is significantly enhanced. It seems likely, therefore, that the added FMN diverts (at least partially) the reaction route from the biacetyl mutase to the oxidation. The incompleteness of the trapping efficiency is related to the following experimental difficulties. When the reaction is carried out under aerobic conditions where FMN serves as recycle oxidation catalyst, hydrogen peroxide formed through the reoxidation process of reduced FMN also oxidizes biacetyl to acetic acid (see entry 4 in Table 3). This makes the reaction system very complex. In order to preclude the oxidation by hydrogen peroxide, one has to carry out the reaction under anaerobic conditions and enhance the flavin concentration. However, MeFl is not so soluble in the reaction medium while water-soluble FMN caused the precipitation of CTAB at its high concentration. Thus, the flavin trapping in the present system could be demonstrated only qualitatively.

TABLE 2. PRODUCT ANALYSES OF HxdT-MEDIATED RETRO-ACYLOIN CONDENSATION OF ACETOIN AND HMB[a]

Entry	Substrate	HxdT (mM)	Product(%)[b]	
			CH_3CHO	$(CH_3)_2CO$
1	$CH_3COCH(OH)CH_3$	5	9.8	Trace (<1)
2	$CH_3COC(OH)(CH_3)_2$	5	7.8	14
3	$CH_3COC(OH)(CH_3)_2$	0	Trace (<0.1)	Trace (<1)

a) 30 °C, pH 7.4 with 0.01 M phosphate, 1 d, anaerobic (N_2), [substrate] = 100 mM, [CTAB] = 30 mM. b) Acetaldehyde and acetone were recovered as their 2,4-dinitrophenylhydrazone derivatives and the yields were determined by HPLC. The yields were calculated on the basis of HxdT.

TABLE 3. PRODUCT ANALYSES OF HxdT-MEDIATED REACTION OF BIACETYL[a]

Entry	HxdT (mM)	Flavin (mM)	CTAB (mM)	Product(%)[b]	
				CH_3CHO	CH_3CO_2H
1	0	0	30	0	0
2	5	0	30	10	190
3	5	10[c]	30	6.4	510
4[d]	0	0	10	0	(5.8 mM)

a) 30 °C, pH 7.4 with 0.01 M phosphate, 1 d, anaerobic (N_2), [biacetyl] = 100 mM. b) Acetaldehyde was recovered as its 2,4-dinitrophenylhydrazone derivative and analyzed by HPLC. Acetic acid was analyzed by GLC. The yields were calculated on the basis of HxdT. c) [FMN] = 10.0 mM. d) [$CH_3COCOCH_3$] = 30.0 mM, [H_2O_2] = 30 mM.

Comments on the Mechanism of Thiazolium-mediated Biacetyl Scission. Here, we wish to consider the mechanism of the HxdT-mediated biacetyl scission. Mizuhara and Oono,[23] who found for the first time that thiamine would catalyze the biacetyl mutase reaction, proposed that the mutase reaction begins with the reaction of thiamine and biacetyl enolate to give ketene and **1**. However, the mechanism involving the ketene production is now considered to be most improbable.[24] Here, two possible mechanisms come to mind: one is the reaction analogous to retro-acyloin condensation which occurs from the monohydrated form of biacetyl directly affording acetic acid and **1** (Eq. 5), and the other is the mechanism similar to that proposed for cyanide-ion catalyzed C–C bound scission of α,β-diketones (*e.g.*, benzil)[25,26] (Eq. 6). It

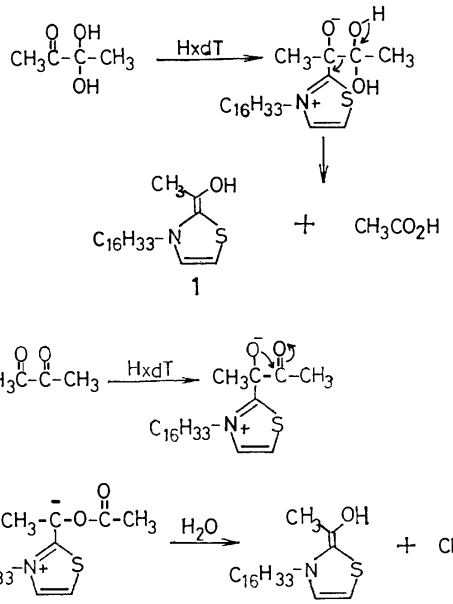

(5)

1

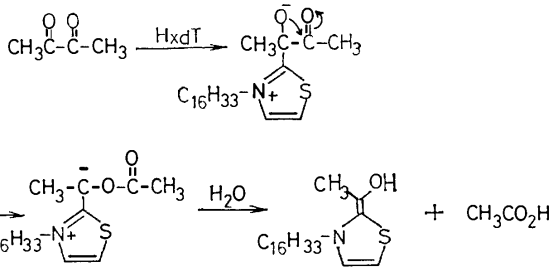

(6)

is not easy to distinguish between these two mechanisms by conventional kinetic methods. Based on the flavin trapping of **1**, we could determine the rate constant for biacetyl scission as well as those of α-ketol scission. Since biacetyl is extensively hydrated in aqueous solution,[27] one may regard diacetyl as a substrate with X=OH in $CH_3COC(OH)(CH_3)X$ series. We noticed that the plot of Taft's σ_I[28] *vs.* $\log k_{2,app}$ of $CH_3COC(OH)(CH_3)X$ holds a good linear relationship (r=0.97) (Fig. 1). Here, one has to take it into account that $k_{2,app}$ in the micellar system is affected not only by the reactivity of the substrate but also by the partition of the substrate between the micelle and the bulk water phase. We carried out the same reaction in a homogeneous solution (methanol) in the presence of strong base (DBU: 1,8-diazabicyclo[5.4.0]-undec-7-ene). As shown in Fig. 1, the plot for X=CH_3, H, and phenyl again held a good straight line (r=0.99). The finding suggests that in the present case the partition would not provide a significant influence upon the rate constant. Thus, the involvement of the plot for X=OH in a single straight line implies that the mechanism of biacetyl scission would be similar to that of the retro-acyloin condensation.

Conclusion. The present study establishes that

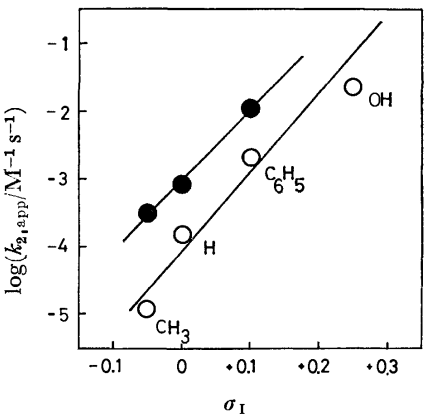

Fig. 1. Plot of σ_I for $CH_3COC(OH)(CH_3)X$ *vs.* log $k_{2,app}$. ○, Rate constants for the micellar system cited from Table 1. ●, Rate constants for the reaction in methanol, where [MeFl]=3.30×10^{-5} M, [*N*-benzylthiazolium bromide]=1.10×10^{-3} M, [DBU]=5.30×10^{-3} M. The $k_{2,app}$ is defined as v_{obsd}/[thiazolium ion][substrate]. In methanol, $k_{2,app}=3.08\times10^{-4}$ $M^{-1}s^{-1}$ for X=CH_3, 8.09×10^{-4} $M^{-1}s^{-1}$ for X=H, and 1.10×10^{-2} $M^{-1}s^{-1}$ for X=C_6H_5.

the micellized thiazolium ion is capable of catalyzing not only the acyloin condensation but also the retro-acyloin condensation. Obviously, the thiazolium-mediated acyloin condensation is reversible. The finding suggests an important insight into the mechanism of the early stage of the transketolase catalysis. We are now devoting our research effort toward the application of this concept to transketone reaction in the model system.

Experimental

Materials. Preparations of the following compounds were described previously: MeFl,[29] HxdT,[5] *N*-benzylthiazolium bromide,[5] and 4,4′-dichlorobenzil.[5] Acetoin, 3-hydroxy-3-methyl-2-butanone, and biacetyl were purchased from Tokyo Kasei Co. Ltd. and were distilled before use. 3-Hydroxy-3-phenyl-2-butanone was prepared from biacetyl and benzene in the presence of $AlCl_3$ according to the method of Wegmann and Dahn.[30]

Kinetic Measurements. The kinetic measurements of the micellar system were carried out at 30 °C under anaerobic (N_2) conditions in 3 vol% of aqueous ethanol. The details of the method were described previously[4,5]. Similarly, the kinetic measurements in methanol were carried out at 30 °C under anaerobic (N_2) conditions. The details of the reaction conditions are recorded in a caption to Fig. 1.

Product Analyses. The reactions for the product analyses were carried out at 30 °C in anaerobic (N_2) sealed ampuls. The detailed conditions were recorded in Table 2. Acetic acid was analyzed by GLC (Shimadzu GC-Mimi I: column, Silicone GE SE-30). To analyze acetaldehyde and acetone, the solution was treated with an excess of 2,4-dinitrophenylhydrazine,[22] and both the precipitate and the filtrate were subjected to HPLC analysis (Shimadzu LC-3: column, Merck Lichrosorb RP-18). The hydrazone derivatives of acetaldehyde and acetone were mainly present in the filtrate. Their yields were determined by comparing the integrated intensity of the peaks with that of the authentic samples.

The authors thank Miss. Y. Kusano and Miss K. Ueda for helpful technical assistance.

References

1) T. C. Bruice, *Progr. Bioorg. Chem.*, **4**, 1 (1976); *Acc. Chem. Res.*, **13**, 256 (1980).
2) C. Walsh, *Ann. Rev. Biochem.*, **47**, 881 (1978); *Acc. Chem. Res.*, **13**, 148 (1980); C. T. Walsh, A. Schonhruun, and R. H. Abeles, *J. Biol. Chem.*, **246**, 6855 (1971); C. T. Walsh, E. Krödel, V. Massey, and R. H. Abeles, *ibid.*, **248**, 1946 (1973).
3) D. J. Kosman, "Bioorganic Chemistry," ed by E. E. van Tamelen, Academic Press, New York (1977), Vol. 2, p. 175.
4) S. Shinkai, T. Ide, and O. Manabe, *Chem. Lett.*, **1978**, 538; S. Shinkai, T. Yamashita, and O. Manabe, *J. Chem. Soc., Chem. Commun.*, **1979**, 301; S. Shinkai, T. Yamashita, Y. Kusano, T. Ide, and O. Manabe, *J. Am. Chem. Soc.*, **102**, 2335 (1980).
5) S. Shinkai, T. Yamashita, Y. Kusano, and O. Manabe, *Tetrahedron Lett.*, **20**, 2543 (1980); *J. Org. Chem.*, **45**, 4947 (1980); S. Shinkai, Y. Hara, and O. Manabe, *J. Polym. Sci., Polym. Chem. Ed.*, **20**, 1097 (1982).
6) S. Shinkai, T. Yamashita, Y. Kusano, and O. Manabe, *Chem. Lett.*, **1979**, 1323; *J. Am. Chem. Soc.*, **103**, 2070 (1981).
7) S. Shinkai, T. Yamashita, and O. Manabe, *Chem. Lett.*, **1981**, 961; S. Shinkai, T. Yamashita, Y. Kusano, and O. Manabe, *J. Am. Chem. Soc.*, **104**, 563 (1982).
8) Y. Yano, Y. Hoshino, and W. Tagaki, *Chem. Lett.*, **1980**, 749.
9) J. Castells, H. Llitjos, and M. Moreno-Manas, *Tetrahedron Lett.*, **1977**, 205.
10) H. Inoue and K. Higashiura, *J. Chem. Soc., Chem. Commun.*, **1980**, 549.
11) W. H. Rastetter, J. Adams, J. W. Frost, L. J. Nummy, J. E. Frommer, and K. B. Roberts, *J. Am. Chem. Soc.*, **101**, 2752 (1979).
12) M. D. Corbett and B. R. Chipko, *Bioorg. Chem.*, **9**, 273 (1980).
13) R. Breslow, *J. Am. Chem. Soc.*, **79**, 1762 (1957).
14) Y. Shain and M. Gibbs, *Plant Physiol.*, **48**, 325 (1971).
15) S. Asami and T. Akazawa, *Biochemistry*, **16**, 2202 (1977).
16) J. W. Bradbeer and E. Racker, *Fed. Proc.*, **20**, 88 (1961).
17) P. Christen and A. Gasser, *Eur. J. Biochem.*, **107**, 73 (1980).
18) W. Tagaki and H. Hara, *J. Chem. Soc., Chem. Commun.*, **1973**, 891; Y. Yano, Y. Tamura, and W. Tagaki, *Bull. Chem. Soc. Jpn.*, **53**, 740 (1980); J. C. Seehan and T. Hara, *J. Org. Chem.*, **39**, 1196 (1974); R. C. Cookson and R. M. Lane, *J. Chem. Soc., Chem. Commun.*, **1976**, 804.
19) S. Shinkai, T. Kunitake, and T. C. Bruice, *J. Am. Chem. Soc.*, **96**, 7140 (1974).
20) S. Shinkai and T. Kunitake, *J. Chem. Soc., Perkin 2*, **1976**, 980; *Polym. J.*, **9**, 423 (1977); S. Shinkai, *J. Polym. Sci., Polym. Chem. Ed.*, **17**, 3905 (1979).
21) T. C. Bruice and J. Taulane, *J. Am. Chem. Soc.*, **98**, 7769 (1976); T. W. Chan and T. C. Bruice, *ibid.*, **99**, 2389 (1977).
22) R. L. Shriner, R. C. Fuson, and D. Y. Curtin, "The Systematic Identification of Organic Compounds," Wiley, New York (1956), p. 218.
23) S. Mizuhara and K. Oono, *Proc. Jpn. Acad.*, **27**, 705 (1951).
24) T. C. Bruice and S. Benkovic, "Bioorganic Mechanisms," Benjamin, New York (1966), p. 200.
25) F. Jourdan, *Ber.*, **16**, 658 (1883).
26) H. Kwart and M. M. Baevsky, *J. Am. Chem. Soc.*, **80**, 580 (1958) and references cited therein.
27) R. P. Bell and A. O. McDougall, *Trans. Faraday Soc.*, **56**, 1281 (1960).
28) R. W. Taft, Jr., *J. Phys. Chem.*, **64**, 1805 (1960); R. W. Taft, Jr., E. Price, I. R. Fox, I. C. Lewis, K. K. Andersen, and G. T. Davis, *J. Am. Chem. Soc.*, **85**, 709, 3146 (1963).
29) S. Shinkai, S. Yamada, and T. Kunitake, *Macromolecules*, **11**, 65 (1978).
30) J. Wegmann and H. Dahn, *Helv. Chim. Acta*, **29**, 101 (1946).

The Synthesis of 2,7-Bis(dimethylamino)pyrene and -tetrahydropyrene and the Electrical Conductivities of Their Complexes[1)]

Naomi UEDA, Bunji NATSUME, Kazumi YANAGIUCHI, Yoshiteru SAKATA,*
Toshiaki ENOKI,† Gunzi SAITO,† Hiroo INOKUCHI,† and Soichi MISUMI*
The Institute of Scientific and Industrial Research, Osaka University, Ibaraki, Osaka 567
† *The Institute for Molecular Science, Okazaki, Aichi 444*

(Received August 9, 1982)

New π-donors containing a pyrene or a tetrahydropyrene ring were synthesized by means of a unique transannular reaction of the corresponding [2.2]metacylcophane derivatives. The CT complexes of these donors with a series of TCNQ derivatives different in electron affinity were prepared, and their electrical conductivities on single crystals were measured. The highest conductivity (0.36 Ω^{-1} cm^{-1}) was that of the tetrahydropyrene derivative–TCNQ complex. It was reconfirmed that the partial charge-transfer from a donor to an acceptor is very important for high conductivity.

A wide variety of charge-transfer (CT) complexes with a metal-like conductivity have recently been prepared. Many such highly conductive CT complexes or salts are composed of chalcogen atom-containing π-donors like TTF. Several heterocyclic donors containing one or two nitrogen atoms in condensed-ring systems also give highly conductive CT complexes, *e.g.*, *N*-methylphenazinium–TCNQ[2)] and quinolinium–TCNQ[3)] complexes.

On the other hand, a fairly high conductivity (2 Ω^{-1} cm^{-1} with a compressed sample) has been reported for the TCNQ complex of a diamino derivative of a carbocyclic hydrocarbon, 1,6-diaminopyrene.[4)] The conductivity of a single crystal can usually be expected to be increased by 10^2 times the conductivity on the corresponding pressed pellet. This excellent conductivity prompted us to prepare the complex of 2,7-bis(dimethylamino)pyrene **1**, which has a higher symmetry (D_{2h}) than 1,6-diaminopyrene (C_{2h}). Bis(dimethylamino)tetrahydropyrene **2**, a precursor in the present synthetic course for **1**, is also interesting in connection with the study[5)] of the relationship between the conductivity and the crystal structure of a series of benzidine–TCNQ complexes.

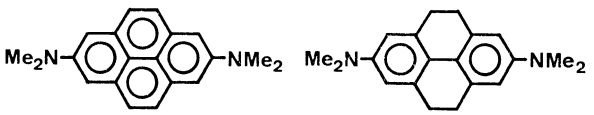

1 **2**

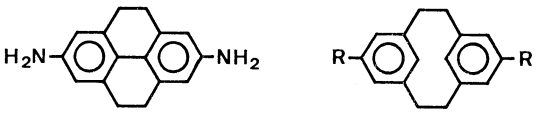

3

4 R = CH_2Br
5 R = CHO
6 R = CO_2H
7 R = NH_2
8 R = NMe_2

Results and Discussion

Synthesis. Because of the high electron density at the 1-position in the highest occupied molecular orbital (HOMO), pyrene is much more subjected to electrophilic substitution at this position than the others. Therefore, it is difficult to prepare 2,7-disubstituted pyrene by the electrophilic substitution reaction of pyrene itself. Furthermore, the solubility of pyrene derivatives is generally low in usual organic solvents. These facts forced us to choose a synthetic route which leads to the substituted pyrene chromophore in the final step.

According to the literature,[6)] 5,13-bis(bromomethyl)-[2.2]metacyclophane **4** was prepared *via* four steps starting from mesitylene. The Sommelet reaction of **4** was carried out in the usual manner to give **5** in a 72% yield. The oxidation of **5** with potassium permanganate gave **6** quantitatively. The Curtius reaction of **6** *via* acid chloride, acid azide, and isocyanate yielded a diamino compound **7** in a 64% yield. The diamine **7** was converted to **8** with dimethyl sulfate in an 86% yield.

The ready transformation of substituted [2.2]metacyclophane to the tetrahydropyrene framework has been reported by Allinger *et al.*[7)] and by Sato *et al.*[8)] Since then, this unique reaction has been utilized by several groups in the synthesis of substituted tetrahydropyrenes and pyrenes.[9)] We also have been employed this elegant reaction as a key step in the synthesis of **1**—**3**. Thus, the transannular dehydrogenative ring contraction of **7** and **8** with DDQ gave **3** (93% yield) and **2** (96% yield) respectively. The tetrahydro compound **2** was further dehydrogenated with Pd–C in boiling decalin to yield **1** in a 49% yield. The complexation of **1**—**3** was carried out with π-acceptors, such as TCNQ derivatives and chloranil. Single crystals of these CT complexes were obtained by the diffusional method or by recrystallization. The details will be described in the experimental part. The donor-to-acceptor ratio was determined by elemental analysis to be 1:1 for all the complexes.

Cyclic Voltammetry. Cyclic voltammetry was carried out in acetonitrile containing 0.1 M** of tetraethylammonium perchlorate as a supporting electrolyte and with an SCE reference electrode. The voltammograms of **1**—**3** are shown in Fig. 1. In each curve in the figure, two oxidation waves are observed. Both waves of **2** and **3** and the first wave of **1** are reversible,

** 1 M = 1 mol dm^{-3}.

whereas the second one of **1** is irreversible. The half-wave potentials ($E_{1/2}$) of these compounds are summarized in Table 1, together with those of the reference compounds, **9**—**11**. Of the three new donors, **2** shows the lowest value, one which is close to that of the powerful donor **11**. It should be pointed out that the value of **2** is lower by 0.20 V than that of **10**. This observation is particularly surprising in view of the fact that **2** and **10** have the same chromophore, 4,4'-diaminobiphenyl. A similar extent of difference (0.12 V) was also observed between the potentials of **3** and **9**. These data clearly indicate that the planar structure of a biphenyl chromophore forced by two ethylene chains plays an important role in lowering the oxidation potential. Furthermore, the value of **2** remains lower than that of **1**, which has a more condensed aromatic ring than the biphenyl. This might be interpreted as follows. The electron density at the 2- and 7-positions of pyrene at the HOMO level is zero. Hence, the ionization potential of the pyrene is subject to only a small influence of the substituents attached to these positions. The SCF-CI calculation by Nogami[10] showed that the ionization potentials of 1,6-, 1,8-, and 2,7-diaminopyrenes are 6.63, 6.64, and 7.39 eV respectively, supporting the interpretation stated above.

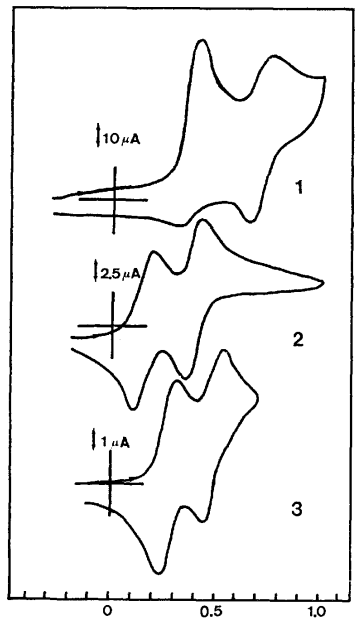

Fig. 1. Cyclic voltammograms of compounds, **1**, **2**, and **3**, in CH_3CN using Et_4NClO_4 as a supporting electrolyte.

Table 1. Half-wave potentials $E_{1/2}$ of **1**—**3** **9**—**11**

	($E^1_{1/2}$ *vs.* SCE)/V	($E^2_{1/2}$ *vs.* SCE)/V
1	0.37	0.71
2	0.14	0.38
3	0.31	0.49
9	0.43	0.69
10	0.34	0.52
11	0.04	0.63

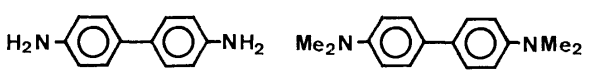

9 **10**

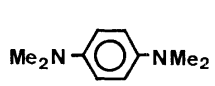

11

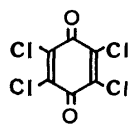

13

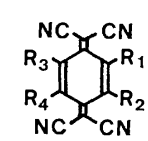

12 a $R_1 = R_2 = R_3 = R_4 = H$
b $R_1 = R_2 = R_3 = R_4 = F$
c $R_1 = F, R_2 = R_3 = R_4 = H$
d $R_1 = R_3 = Me, R_2 = R_4 = H$
e $R_1 = R_3 = OMe, R_2 = R_4 = H$

In order to evaluate a relative acceptor strength, we determined the half-wave reduction potentials of six π-acceptors, TCNQ **12a**, $TCNQ(F)_4$ **12b**,[11] TCNQ(F) **12c**,[12] $TCNQ(Me)_2$ **12d**,[11] $TCNQ(OMe)_2$ **12e**,[11] and chloranil **13**, as is shown in Table 2.

Infrared Spectra. The frequencies of C≡N stretching vibrations of CT complexes are shown in Table 3, together with those of composite acceptors and their potassium salts. With these values, the degree of charge-transfer (ρ) in the complexes was calculated according to this equation:[13]

$$\rho = (\nu^{acc}_{C\equiv N} - \nu^{com}_{C\equiv N})/(\nu^{acc}_{C\equiv N} - \nu^{salt}_{C\equiv N})$$

Table 2. Half-wave potentials $E_{1/2}$ of **12** and **13**

	($E^1_{1/2}$ *vs.* SCE)/V	($E^2_{1/2}$ *vs.* SCE)/V
12b	0.50	−0.04
12c	0.22	−0.33
12a	0.12	−0.43
12d	0.05	−0.42
12e	−0.08	−0.55
13	−0·06	−0.82

Table 3. Wavenumbers of $\nu_{C\equiv N}$ in acceptors **12**, their K^+ salts, and CT complexes with **1**—**3** and degree of charge transfer (ρ) in the complexes[a]

Donor	Acceptor	$\nu^{acc}_{C\equiv N}$/cm^{-1}	$\nu^{com}_{C\equiv N}$/cm^{-1}	$\nu^{salt}_{C\equiv N}$/cm^{-1}	ρ
1	**12a**	2220	2210	2185	0.29
1	**12d**	2225	2205	2185	0.50
2	**12a**	2220	2200	2185	0.57
2	**12b**	2220	2195	2195	1.00
2	**12c**	2215	2190	2180	0.71
2	**12d**	2225	2210	2185	0.38
2	**12e**	2205	2200	2180[b]	0.20
3	**12a**	2220	2195	2185	0.71
3	**12d**	2225	2210	2185	0.63

a) $\nu^{acc}_{C\equiv N}$, $\nu^{com}_{C\equiv N}$, and $\nu^{salt}_{C\equiv N}$ are C≡N stretching vibrations of **12**, CT complexes, and K^+ salts respectively. b) Value of sodium salt.

Table 4. Electrical conductivities (σ) at room temperature and activation energies (E_a) of CT complexes of **1**—**3** and related donors on single crystals

	$\sigma/\Omega^{-1}\,cm^{-1}$	E_a/eV
1—**12a**	1.95×10^{-5}	0.32
1—**12d**[a]	2.86×10^{-11}	0.52
1—**13**[a]	5.13×10^{-13}	0.95
2—**12a**	0.358	0.50
2—**12b**	6.90×10^{-6}	0.37
2—**12c**	1.05×10^{-2}	0.53
2—**12d**	8.26×10^{-5}	0.19
2—**12e**	2.38×10^{-6}	0.31
2—**13**	1.01×10^{-10}	—[b]
3—**12a**[a]	5.30×10^{-7}	0.53
3—**12d**[a]	5.46×10^{-9}	0.53
3—**13**	5.52×10^{-10}	0.53
10—**12a**	6.49×10^{-6}	0.32
9—**12a**[a]	6.99×10^{-12}	0.54[5]

a) Compressed pellet. b) The activation energy could not be determined because the very weak current was hard to detect.

The values are summarized in the same table, showing the distribution of ρ values between unity and 0.20. A linearity is obtained when the ρ values of the complexes **1**—**12** are plotted against the half-wave potentials, $E^1_{1/2}$, of the acceptors in Table 2. This reveals a close relationship between these two values.

Electrical Conductivity. All the complexes show typical semiconducting behavior in the temperature range measured. Table 4 summarizes the electrical conductivities (σ) of these complexes on a single crystal at room temperature and the activation energies (E_a) based on the temperature dependence of the resistivities. The data on **9**–TCNQ given by Takahashi *et al.*[5] are included for purposes of comparison. In contrast to the high conductivity of 1,6-diaminopyrene-TCNQ on a compressed sample, the value of **1**–TCNQ is lower, even on a single crystal. This may be due to the relatively high $E^1_{1/2}$ value of **1**, as may be seen in Table 1. On the other hand, **2** with low $E^1_{1/2}$ value forms better conducting CT complexes than does **1**. It is noteworthy that, of the fourteen CT complexes in the table, **2**–TCNQ showed the highest conductivity, larger by 10^5 times than that of **10**–TCNQ, despite bearing the same diaminobiphenyl chromophore in **2** and **10**. A difference of similar extent (10^5) was also observed between **3**–TCNQ and **9**–TCNQ. Possibly these results are mainly due to the difference in the oxidation potential between **2** and **10** or between **3** and **9**, as may be seen in Table 1, and partly due to the different packing in a crystal, based on the different extent of planarity between biphenyl and tetrahydropyrene chromophores, although the molecular structures of these complexes are not yet known.

In Fig. 2 the conductivities of a series of complexes of **2** are plotted against the $E^1_{1/2}$ values of the acceptors. A noticeable point is that the conductivity of **2**–TCNQ is the highest. Not only the weaker acceptors, but also stronger acceptors than TCNQ itself diminish the conductivities of the complexes with **2**. In other words, the introduction of substituents to the TCNQ ring results in a decrease in the conductivities of the complexes, apart from the kind of the substituent. This fact clearly indicates that the incomplete electron transfer[14] from a donor to an acceptor has a significant effect on the high conductivity of the charge-transfer complexes.

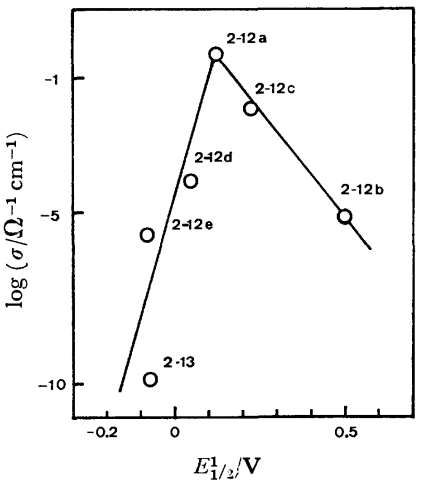

Fig. 2. Plots of conductivities of complexes, **2**—**12** and **2**—**13**, *vs.* $E^1_{1/2}$ of acceptors.

Experimental

All the melting points are uncorrected. The IR, NMR, MS, and electronic spectra were recorded with a Hitachi EPI-G2 and a Hitachi 345, a JEOL JNM-FX-100 (100 MHz for ^{1}H), a Hitachi RMU-7, and a Hitachi EP3-3T spectrometer respectively.

The cyclic voltammetry was carried out at room temperature under argon using the combination of a generator, Hokuto HB-107A, and a potentiostat, Hokuto HA-104. A glassy carbon electrode (Yanagimoto P-13) was used as the anode, and platinum wire was used as the counter electrode.

The electrical resistances for the pressed pellet and for the single crystal were measured with the two probe methods in the region from room temperature down to the temperature where an electrometer (Keithley 616) reached the lower limit of the detectable current (10^{-14} A). The electrical constants were obtained using silver paint (Du Pont 4817). The sizes of the single crystals were measured with a profile projector, Nikon V-24B.

[2.2]Metacyclophane-5,13-dicarbaldehyde (5). To a solution of 5,13-bis(bromomethyl)[2.2]metacyclophane **4**[6] (6.17 g, 15.6 mmol) in chloroform (60 ml) was added hexamethylenetetramine (5.10 g, 35.9 mmol), then the mixture was refluxed for 4 h. After cooling, a precipitate (ammonium salt) was collected and dried. A solution of this salt in 50% acetic acid (80 ml) was refluxed for 15 h. The crystals thus yielded were collected, washed with water, and dried. The subsequent recrystallization of the product from acetone gave **5** (2.98 g, 72% yield).

5: Colorless needles; mp 235—236.5 °C. ^{1}H NMR ($CDCl_3$) δ=3.23, 3.30 (d, J=8 Hz, 8H, CH_2), 4.52 (t, J=2 Hz, 2H, inner ArH), 7.65 (d, J=2 Hz, 4H, outer ArH), 10.04 (s, 2H, CHO). IR (Nujol mull) 2800, 2720, 1690 cm^{-1}.

Found: C, 81.57; H, 5.89%. Calcd for $C_{18}H_{16}O_2$: C,

Table 5. Properties and analytical data of CT complexes of **1**—**3**

Complex	Solvent	Yield %	Found (Calcd)[c] (%) C	H	N	Cl	Mp θ_m/°C	Remarks	Size/mm^3 [d]
1—**12a**[a]	CH_3CN	95	78.03 (78.03)	4.76 (4.91)	16.94 (17.06)		decomp>230	Fine black needles	0.048×0.040×2.553
1—**12d**[a]	CH_3CN	89	78.73 (78.44)	5.26 (5.42)	15.89 (16.14)		decomp>248	Fine dark brown needles	2×2×0.97[e]
1—**13**[b]	Benzene	84	58.48 (58.45)	3.64 (3.77)	5.13 (5.24)	26.39 (26.54)	decomp>280	Black micro-crystals	2.5×2.5×1.01[e]
2—**12a**[a]	CH_3CN	92	77.66 (77.39)	5.67 (5.68)	17.15 (16.92)		decomp>223	Long dark violet columns	0.197×0.198×4.687
2—**12b**[a]	CH_3CN	62	67.10 (67.60)	4.07 (4.25)	14.78 (14.78)		187—189	Dark bluish green needles	0.127×0.687×2.826
2—**12c**[a]	CH_3CN	71	74.72 (74.69)	5.19 (5.29)	16.45 (16.33)		201—203	Dark purple needles	0.120×0.129×3.859
2—**12d**[b]	THF	82	77.63 (77.83)	6.14 (6.15)	15.72 (16.02)		207—208	Dark violet needles	0.048×0.040×1.194
2—**12e**[b]	CH_3CN	55	73.22 (73.36)	5.82 (5.79)	15.20 (15.10)		181—183	Long dark violet columns	0.090×0.076×1.847
2—**13**[b]	THF	75	57.88 (58.01)	4.49 (4.49)	5.04 (5.20)	26.55 (26.34)	decomp>340	Long black columns	0.123×0.019×1.122
3—**12a**[b]	CH_2Cl_2	82	76.05 (76.35)	4.33 (4.58)	18.82 (19.08)		decomp>170	Dark violet needles	2.522×2.522×1.601[e]
3—**12d**[b]	CH_2Cl_2	82	76.72 (76.90)	5.04 (5.16)	18.03 (17.94)		183.5—185	Black needles	2.534×2.534×0.459[e]
3—**13**[b]	CH_2Cl_2	71	55.00 (54.80)	3.55 (3.34)	5.97 (5.81)	29.65 (29.41)	decomp> 142	Long black columns	2.519×2.519×0.364[e]
10—**12a**[a]	CH_3CN	80	75.39 (75.65)	5.16 (5.44)	18.75 (18.90)		219—222	Dark violet needles	0.066×0.062×2.294

a) Prepared by diffusional method. b) Prepared by mixing and recrystallization. c) Values are calculated assuming that the donor-to-acceptor ratio is 1:1. d) Crystal sizes used for measurement of electrical conductivity. e) Sizes of pellet (radius×radius×thickness).

81.79; H, 6.10%.

[2.2]Metacyclophane-5,13-dicarboxylic Acid (6). An aqueous solution (125 ml) of potassium permanganate (4.0 g, 25.3 mmol) was stirred with a solution of dialdehyde **5** (2.5 g, 9.46 mmol) at 60—70 °C for a period of 2 h. After the addition was over, the mixture was stirred for a further hour. To the solution was added 10% aqueous sodium hydroxide (80 ml), and the insoluble material was filtered off. The filtrate was acidified with dil hydrochloric acid. The precipitate was collected, washed with water, and dried to give 2.6 g (93%) of **6**.

6: Mp >350 °C. IR (Nujol mull) 1690 cm^{-1}. MS *m/e* 296 (M^+).

5,13-Diamino[2.2]metacyclophane (7). A mixture of dicarboxylic acid **6** (2.6 g, 8.8 mmol) and thionyl chloride (60 ml) was refluxed for 4 h, and the excess thionyl chloride was distilled off. The acid chloride thus obtained was dissolved in THF (80 ml). To the stirred, ice-cooled solution was added an aqueous solution (19 ml) of sodium azide (1.35 g, 20.8 mmol). After additional stirring at room temperature for 1 h, water was added to the solution. The precipitate was collected by filtration, washed with water, and dried. The acid azide is fairly stable and can be handled safely at room temperature. A solution of the azide in benzene (60 ml) was refluxed for 4 h. After cooling, 18 ml of conc hydrochloric acid was added, and the mixture was refluxed for 1 h under nitrogen. The benzene was then removed, and the insoluble material was filtered off. The filtrate was neutralized with aqueous sodium hydroxide. The crystals thus deposited were collected by filtration and washed with water to give 1.33 g (64%) of **7**.

7: Colorless prisms from benzene-hexane; mp 232—233 °C with dec. ^{1}H NMR ($CDCl_3$) δ=2.08, 2.91 (d, J=8 Hz, 8H, CH_2), 4.06 (t, J=1.5 Hz, 2H, inner ArH), 6.40 (d, J=1.5 Hz, 4H, outer ArH). IR (Nujol mull) 3400, 3290, 3190 cm^{-1}.

Found: C, 80.36; H, 7.49; N, 11.87%. Calcd for $C_{16}H_{18}N_2$: C, 80.63; H, 7.61; N, 11.75%.

5,13-Bis(dimethylamino)[2.2]metacyclophane (8). To a mixture of **7** (1.70 g, 7.1 mmol) and sodium hydrogencarbonate (4.47 g, 53.2 mmol) in 70 ml of water-THF (3:4) was added dimethyl sulfate (6.08 g, 48.3 mmol) at 0 °C under nitrogen. Stirring was continued at room temperature for 2 h and then at 65—70 °C for 20 min. After cooling, 2-aminoethanol (7 ml) was added, and the mixture was heated at 120 °C (bath temperature) for 9 h with stirring. The THF was then distilled off, and the residue was extracted with dichloromethane. The extracts were washed with a saturated aqueous solution of sodium chloride and dried over $MgSO_4$. After the removal of the solvent, the crude product was passed through a short column of alumina with chloroform–benzene (1:1). Recrystallization from methanol gave 1.79 g (86%) of pure **8**.

8: Mp 208—209 °C. ^{1}H NMR ($CDCl_3$) δ=2.14, 2.97 (d, J=7.8 Hz, 8H, CH_2), 2.96 (s, 12H, Me), 4.04 (t, J=1.2 Hz, 2H, inner ArH), 6.48 (d, J=1.2 Hz, 4H, outer ArH). IR (Nujol mull) 1595 cm^{-1}.

Found: C, 82.26; H, 8.47; 9.29%. Calcd for $C_{20}H_{26}N_2$: C, 82.15; H, 8.27; N, 9.58%.

2,7-Diaminotetrahydropyrene (3). To a stirred solution of **7** (200 mg, 0.84 mmol) in benzene (50 ml) was added a solution of dichlorodicyano-*p*-benzoquinone (DDQ) (190 mg) in benzene (40 ml). After additional stirring for 1 h at room temperature and the removal of the benzene, an

aqueous solution of 10% sodium hydroxide was added and the mixture was extracted with dichloromethane. The extracts were washed with a saturated sodium chloride solution and dried. The subsequent removal of the solvent gave 190 mg (95%) of **3**.

3: Colorless microcrystals by sublimation; mp 242—243 °C with decomp. ^{1}H NMR ($CDCl_3$) δ=2.75 (s, 8H, CH_2), 6.40 (s, 4H, ArH). IR (Nujol mull) 3440, 3390, 3180, 1630, 1610 cm^{-1}.

Found: C, 81.32; H, 6.82; N, 11.85%. Calcd for $C_{16}H_{16}N_2$: C, 81.11; H, 6.66; N, 11.90%.

2,7-Bis(dimethylamino)tetrahydropyrene (2). a): The methylation of **3** with dimethyl sulfate was done in a manner similar to that used in the synthesis of **8**. The crude product was passed through a short column of alumina. Further purification by sublimation gave 224 mg (96%) of **2**.

2: Colorless prisms; mp 142—143 °C. ^{1}H NMR ($CDCl_3$) δ=2.84 (s, 8H, CH_2), 2.96 (s, 12H, CH_3), 6.49 (s, 4H, ArH). UV (MeOH) 220 (ε 3.86×10^4), 321 (3.53×10^4), 333 nm (2.96×10^4).

Found: C, 82.32; H, 8.36; N, 9.69%. Calcd for $C_{20}H_{24}N_2$: C, 82.15; H, 8.27; N, 9.58%.

b): The transannular reaction of **8** with DDQ was carried out in a manner similar to that described for **3**. The crude product was purified by column chromatography with silica gel and dichloromethane-benzene (1:1) and then by recrystallization from methanol (93% yield).

2,7-Bis(dimethylamino)pyrene (1). A mixture of **2** (630 mg, 2.15 mmol), Pd-C (1.378 g), and decalin (50 ml) was refluxed under nitrogen for 1 h. After the filtration of the Pd-C, 2 mol dm^{-3} hydrochloric acid was added to the filtrate. The aqueous layer separated was made basic with 10% sodium hydroxide, extracted with dichloromethane, and the organic layer was dried. After the removal of the solvent, the residue was chromatographed on silica gel containing 10% of water with benzene. Recrystallization from benzene gave 304 mg (49%) of **1**.

1: Yellowish orange columns; mp 222—223 °C with dec. ^{1}H NMR ($CDCl_3$) δ=3.19 (s, 12H, CH_3), 7.55 (s, 4H, ArH), 7.88 (s, 4H, ArH). UV (MeOH) 289 (ε 1.31×10^5), 314 (1.51×10^4), 328 (1.20×10^4), 344 (2.49×10^4), 443 nm (3.29×10^3). IR (Nujol mull) 1605 cm^{-1}.

Found: C, 83.26; H, 7.18; N, 9.56%. Calcd for $C_{20}H_{20}N_2$: C, 83.30; H, 6.99; N, 9.71%.

Preparation of Single Crystals of CT Complexes. a) Difusional Method: In one side of an H-type glass tube was placed **2** (29 mg, 0.1 mmol), and in the other side, TCNQ (20 mg, 0.1 mmol). The apparatus was then gradually filled with acetonitrile under nitrogen and allowed to stand in the dark for 20 d. The black column crystals produced at the middle part of the apparatus were collected, washed with acetonitrile, and dried (46 mg, 95%).

b) Recrystallization: Two solutions of **2** (10 mg, 0.07 mmol) and $TCNQ(Me)_2$ (15 mg, 0.07 mmol) in an equal amount (10 ml) of acetonitrile were mixed at room temperature. The precipitate was collected and recrystallized from THF to give 28 mg (82%) of **2**-$TCNQ(Me)_2$ as dark violet needles.

Single crystals of the other complexes were prepared according to method *a*) or *b*). The data of the elemental analyses, melting points, colors, shapes, and crystal sizes of the complexes are summarized in Table 5.

The present work was supported by a Grant-in-Aid for Scientific Research (No. 543009) from the Ministry of Education, Science and Culture, for which the authors are grateful.

References

1) Preliminary report: B. Natsume, N. Nishikawa, T. Kaneda, Y. Sakata, S. Misumi, T. Enoki, and H. Inokuchi, *Chem. Lett.*, **1981**, 601.

2) L. R. Melby, *Can. J. Chem.*, **43**, 1448 (1965).

3) W. J. Siemons, P. E. Bierstedt, and R. G. Kepler, *J. Chem. Phys.*, **39**, 3523 (1963); L. R. Melby, R. J. Harder, W. R. Hertler, W. Mahler, R. E. Benson, and W. E. Mochel, *J. Am. Chem. Soc.*, **84**, 3374 (1962).

4) H. Scott, P. L. Kronick, P. Chairge, and M. M. Lakes, *J. Phys. Chem.*, **69**, 1740 (1965).

5) N. Takahashi, K. Yakushi, K. Ishii, and H. Kuroda, *Bull. Chem. Soc. Jpn.*, **49**, 182 (1976).

6) T. Umemoto, S. Satani, Y. Sakata, and S. Misumi, *Tetrahedron Lett.*, **1975**, 3159.

7) N. L. Allinger, B. J. Gorden, S.-H. Hu, and R. A. Ford, *J. Org. Chem.*, **32**, 2272 (1967).

8) T. Sato, S. Akabori, S. Muto, and K. Hata, *Tetrahedron*, **24**, 5557 (1968).

9) T. Umemoto, T. Kawashima, Y. Sakata, and S. Misumi, *Tetrahedron Lett.*, **1975**, 463, 1005; T. Umemoto, T. Kawashima, Y. Sakata, S. Misumi, *Chem. Lett.*, **1975**, 837; J. Y. Becker, L. L. Miller, V. Boekelheide, and T. Morgan, *Tetrahedron Lett.*, **1976**, 2939; T. Kawashima, T. Otsubo, Y. Sakata, and S. Misumi, *ibid.*, **1978**, 5115; M.-R. Maxfield, D. O. Cowan, A. N. Bloch, and T. O. Poehler, *Nouv. J. Chim.*, **3**, 647 (1979).

10) T. Nogami, unpublished work. We wish to thank Dr. Nogami, Faculty of Engineering, Osaka University, for his kind communication of unpublished data.

11) R. C. Wheland and E. L. Martin, *J. Org. Chem.*, **40**, 3101 (1975).

12) J. P. Ferraris and G. Saito, *J. Chem. Soc., Chem. Commun.*, **1978**, 992.

13) J. S. Chappell, A. N. Bloch, W. A. Bryden, M. Maxfield, T. O. Poehler, and D. O. Cowan, *J. Am. Chem. Soc.*, **103**, 2442 (1981).

14) G. Saito and J. P. Ferraris, *Bull. Chem. Soc. Jpn.*, **53**, 2141 (1980); J. B. Torrence, *Acc. Chem. Res.*, **12**, 79 (1979).

Stereochemistry of the Palladium-catalyzed Hydrogenation of 3-Oxo-4-ene Steroids. V.[1] A Kinetic Study in Basic and Acidic Media

Shigeo NISHIMURA,* Yasuhiro MOMMA, Hideo KAWAMURA, and Michio SHIOTA†

Department of Industrial Chemistry, Tokyo University of Agriculture and Technology, Koganei, Tokyo 184

† *Department of Chemistry, Ochanomizu University, Bunkyo-ku, Tokyo 112*

(Received August 13, 1982)

Effects of the β-methyl group at C-10 and some oxygen functions (=O, OH, OAc) at C-11, C-17, and C-20 on the rates of hydrogenation of 3-oxo-4-ene steroids have been studied with palladium catalyst in pyridine or THF/HBr as solvent. In contrast to the hydrogenation in pyridine, the rate in THF/HBr was greatly depressed by the presence of 10β-methyl group. The reactivity of the steroids was enhanced by the oxygen functions, in particular, by 11, 17-dioxo group. The effects of the substituents are discussed from a mechanistic consideration based on the obtained results.

The stereochemistry of catalytic hydrogenation of cyclic α,β-unsaturated ketones to saturated ketones has been of wide interest from the viewpoint of stereoselective synthesis as well as from the mechanistic interpretation of the results.[2] Although a considerable body of studies has been described in literature, in particular, in the fields of 3-oxo-4-ene steroids and bicyclo[4.4.0]dec-1-en-3-one ($\Delta^{1(8a)}$-2-octalone), the mechanistic interpretations proposed do not appear to be sufficient to explain the stereochemical outcomes under various reaction conditions. This may be due to a rather complex nature of the reaction. The polar character of the unsaturated system is susceptible to a variety of factors which can influence the stereochemistry of hydrogenation, including the problem of 1,2- and 1,4-addition of hydrogen. Of these factors the most important is the effects of bases and acids.

As well known, 3-oxo-4-ene steroids are stereoselectively hydrogenated to 3-oxo-5β steroids in basic media.[3] The stereoselectivity, however, is not always satisfactory in these compounds with oxo and hydroxy functions at C-11, C-17, and C-20. The use of 4-methoxypyridine as a solvent has been found most effective for these compounds.[1] On the other hand, the addition of hydrobromic acid to acetic acid or, better, to tetrahydrofuran greatly increases the yields of 3-oxo-5β compounds from 19-nor-3-oxo-4-ene steroids.[1] The results on 19-nor steroids in acidic media are in line with those reported in the hydrogenation of 2-octalone where high yields of *cis*-2-decalone are obtained under acidic conditions.[4] In basic media, however, the results are not always consistent with those on 2-octalone in which the stereoselectivity is usually low under basic conditions.[2] Since 19-nor-3-oxo-4-ene steroids are very similar to 2-octalone in their A/B ring structures, a comparable study on 19-nor and 10β-methyl steroids allows an estimation of the effect of the angular methyl group more directly. Since the kinetic aspect of the hydrogenation of these steroids is little known, we have investigated the rates of hydrogenation of various steroids with or without 10β-methyl group in basic and acidic media in order to know the effect of the angular methyl group as well as the effect of some oxygen functions at C-11, C-17, and C-20.

Results

Hydrogenation in Basic Medium. Seven 3-oxo-4-enes (**1a—g**) and three 19-nor-3-oxo-4-enes (**2c—e**) (see Table 1) have been hydrogenated in pyridine as a solvent at 25 °C and atmospheric pressure with palladium black as a catalyst. The hydrogenation was zero order in the concentration of the steroids and the zero-order kinetics held until the most portion of the steroids had been hydrogenated. The steroids have also been hydrogenated competitively in a 1:1 mixture of an appropriate pair of the compounds. The relative reactivity of a compound to cholest-4-en-3-one (**1a**), (R/R_{1a}), was obtained by employing the relationship of Eq. 1,

$$\log (C^\circ/C) = (R/R_{1a}) \log (C^\circ_{1a}/C_{1a}), \quad (1)$$

where C° and C represent the concentrations of the compound at the initiation and a given time, respectively, and the subscript 1a refers to cholest-4-en-3-one. Most of the values were obtained in competitive hydrogenation of a compound with **1a**, but in some cases, because of difficulty in analysis, the ratios were determined indirectly by competitive hydrogenation with another compound which was in turn hydrogenated competitively with **1a**. From the values obtained in individual and competitive hydrogenations, the ratios of adsorption coefficients, b/b_{1a}, were calculated from the relationship: $R/R_{1a}=(k/k_{1a})(b/b_{1a})$, where k/k_{1a} denotes the ratio of the rate of hydrogenation of a steroid to that of **1a** in individual hydrogenations. The results are summarized in Table 1. It is seen from the results that the rate of hydrogenation is generally enhanced by the oxygen functions at C-11, C-17, and C-20 which tend to lower the selectivity to 5β except the 17β-acetoxy group in **1c**. This trend is most prominently seen in the case of **1g** with 11,17-dioxo group where the rate of hydrogenation is 4 times as great as that of **1a** and the selectivity to 5β is as low as 32%. Since the relative reactivity of **1g** to **1a**, R_{1g}/R_{1a}, is 10, it results that the value for b_{1g}/b_{1a} is 2.5. Thus the compound **1g** is more strongly adsorbed to the catalyst than **1a**. With the compounds having the other oxygen functions, any tendency of strong adsorption over **1a** was not indicated. The reactivities of 19-nor steroids in individual hydrogenations are not much different from those of the corresponding 10β-methyl analogs, but the relative reac-

Table 1. Hydrogenation of 3-oxo-4-ene and 19-nor-3-oxo-4-ene steroids in pyridine[a)]

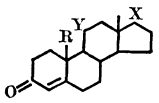

1: R=Me
2: R=H

Compd	X	Y	10^4k / mol min^{-1} g-cat^{-1}	$k^{b)}/k_{1a}$	$R^{b)}/R_{1a}$	$b^{b)}/b_{1a}$	Selectivity to 5β/(%)
1a	β-C_8H_{17}	H	1.0	1.0	1.0	1.0	99
1b	H	H	1.2	1.2	1.3	1.1	95
1c	β-OAc	H	1.8	1.8	2.0	1.1	98.5
1d	β-OH	H	2.1	2.1	1.8	0.87	93
1e	=O	H	2.4	2.4	2.2	0.92	92.5
1f	β-Ac	H	2.6	2.6	1.8	0.72	86
1g	=O	=O	4.1	4.1	10[c)]	2.5	32
2c	β-OAc	H	1.8	1.8 (0.99)	1.9 (0.95)	1.1 (0.96)	95
2d	β-OH	H	2.4	2.4 (1.1)	2.7 (1.5)	1.1 (1.3)	85
2e	=O	H	2.8	2.8 (1.2)	4.2 (1.9)	1.5 (1.6)	89

a) The compound was hydrogenated in 0.0316 M solution (1.8 ml) with 3 mg of palladium catalyst at 25 °C and atmospheric pressure. In competitive hydrogenation an equimolar mixture of two compounds was hydrogenated in 0.0316 M solution. b) The figures in parentheses indicate the values for 19-nor steroids relative to the corresponding 10β-methyl analogs. c) Obtained from $R_{1g}/R_{2e}(2.4)$ and $R_{2e}/R_{1a}(4.2)$.

Table 2. Hydrogenation of 3-oxo-4-ene and 19-nor-3-oxo-4-ene steroids in tetrahydrofuran and hydrobromic acid[a)]

Compd[b)]	X	Y	10^4k / mol min^{-1} g-cat^{-1}	$k^{c)}/k_{1a}$	$R^{c)}/R_{1a}$	$b^{c)}/b_{1a}$	Selectivity to 5β/(%)
1a	β-C_8H_{17}	H	0.98	1.0	1.0	1.0	98.5
1b	H	H	0.98	1.0	1.0	1.0	94
1c	β-OAc	H	0.98	1.0	1.5	1.6	97
1d	β-OH	H	1.5	1.5	1.7	1.1	78
1e	=O	H	1.4	1.4	3.2	2.3	84
1f	β-Ac	H	1.8	1.8	2.1	1.2	79
1g	=O	=O	2.6	2.7	5.4	2.0	30
2c	β-OAc	H	13	13 (13)	26 (18)	2.1 (1.3)	99.9
2d	β-OH	H	12	12 (8.1)	24 (14)	2.0 (1.7)	98
2e	=O	H	13	13 (9.3)	66[d)] (21)	5.1 (2.3)	98

a) The compound was hydrogenated in 1.8 ml of THF containing 0.2 μl of concd HBr (48%). For the other conditions see the footnote a) in Table 1. b) For the compound structure, see Table 1. c) The figures in parentheses indicate the values for 19-nor steroids relative to the corresponding 10β-methyl analogs. d) Obtained from $R_{2e}/R_{1f}(31.5)$ and $R_{1f}/R_{1a}(2.1)$.

tivities in competitive hydrogenations are somewhat greater in the cases of **2d** and **2e**, indicating slightly stronger adsorption of these 19-nor steroids. The selectivity to 5β is always lower with 19-nor steroids than with the corresponding 10β-methyl analogs, although differences are not so great.

Hydrogenation in Acidic Medium. The results of the hydrogenation in tetrahydrofuran and hydrobromic acid are summarized in Table 2. The hydrogenation was zero order in concentration of steroids. Similar to the hydrogenation in pyridine, the oxygen functions enhance the reactivity of the steroids and lower the selectivity to 5β. As observed in pyridine, 11,17-dioxo steroid **1g** showed the greatest reactivity and afforded the lowest yield of 5β-product. High reactivities of **1g** and **1e** are more pronounced in competitive hydrogenation than in individual hydrogenation and this suggests that under acidic condition 11- and 17-oxo groups may contribute to adsorption to the catalyst probably at the α-face. In contrast to the hydrogenation in pyridine, the rates of hydrogenation of 19-nor steroids are all far greater than those of the corresponding 10β-methyl analogs. The selectivity to 5β is also much higher for the 19-nor steroids where the yields of 5β-products were almost quantitative.

Discussion

The Effect of 10β-Methyl Group. The course of catalytic hydrogenation of α,β-unsaturated ketones over palladium catalysts has been discussed in several papers with respect to product stereochemistry.[2,4-7] It appears likely that in basic or acidic conditions hydrogen adds *via* 1,4, rather than 1,2, to the unsaturated system. In the case of 3-oxo-4-ene steroids, the formation of 5β-compounds increases in both basic and acidic media, while with 2-octalone high stereoselectivity to the *cis* isomer was obtained only in acidic medium.[2]

As seen from the results in Table 1, the reactivities of 19-nor-steroids **2c**, **2d**, and **2e** are almost the same with or only slightly larger than those of the corresponding 10β-methyl analogs. The stereoselectivity to 5β always decreases with the 19-nor steroids, although the degree of the decrease is not great (98.5→95% with **2c**; 93→85% with **2d**; 92.5→89% with **2e**). In view of the rather small effects of 10β-methyl group on the rate and the product stereochemistry, it would be reasonable to assume that the transition state which may control the product is in an sp^3-like conformation at C-5. In this conformation, the formation of 5α isomer would be more favorable for 19-nor steroids than for 10β-methyl steroids, because in the transition state leading to 5α isomers the interaction between an axial 2β-hydrogen and 10β-methyl group lacks in 19-nor steroids (see Fig. 1). On the other hand, at the transition state leading to 5β isomers (Fig. 2), the energy difference between both series of the steroids would be rather small, because 10β-methyl group takes an equatorial conformation with respect to the ring A. Rather small differences in reactivities between 19-nor and 10β-methyl steroids would thus be plausible if we consider that the major products are 5β isomers for both series of the steroids. Accordingly, the increase in the formation of 5α isomers with 19-nor steroids is considered to be due to an increase in the rate of formation of 5α isomers.

In contrast to the results in pyridine, 19-nor steroids are hydrogenated much more rapidly in tetrahydrofuran/hydrobromic acid than the corresponding 10β-methyl steroids (Table 2). This result strongly suggests that in the presence of acid the product controlling transition state is in an sp^2-like conformation at C-5 and the attack of hydrogen from the β-face to C-5 is strongly hindered by 10β-methyl group. Almost exclusive formation of 5β isomers from 19-nor steroids in the presence of acid is thus considered to be a result of a great increase in the rate of β-addition of hydrogen. It is further noted that some favorable β-face adsorption in 19-nor steroids may also contribute to the increase of 5β-products.

The Effects of Functional Groups. It is well known that the stereochemistry of hydrogenation of 3-oxo-4-ene steroids is considerably influenced by the substituents which are located far from the reaction site.[8] The nature of the substituent effect, however, has not clearly been understood yet. Some models for explaining it have been discussed, *e.g.*, by Kirk and Hartshorn.[6] Henbest and coworkers have pointed out some similarities in the substituent effects between catalytic hydrogenation and alkaline epoxidation of 3-oxo-4-ene steroids.[9,10]

The results on the kinetic study (Tables 1 and 2) indicate that the compounds having the oxygen functions which may decrease the 5β/5α ratio of product are generally more reactive than those not carrying such functions (compare **1d**, **1e**, **1f**, and **1g** with **1a** and **1b**). The only exception to this is the case of **1c** in pyridine where the rate of hydrogenation is greater than that of **1a** or **1b** and the selectivity to 5β is very high. The compound **1g** with 11,17-dioxo group is noteworthy in that in both basic and acidic media it is definitely more reactive and affords considerably lower yields of 5β-product, than the other compounds investigated. In general, the effects of the oxygen functions are very similar in basic and acidic conditions, as shown in Fig. 3. Since the high stereoselectivity to 5β is obtained in both basic and acidic conditions which can assist polarized adsorption

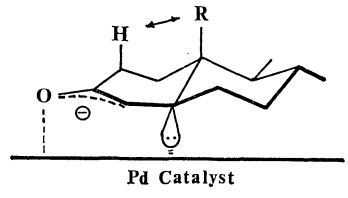

Fig. 1. The transition state leading to 5α-product in an sp^3-like conformation at C-5 (R=Me or H).

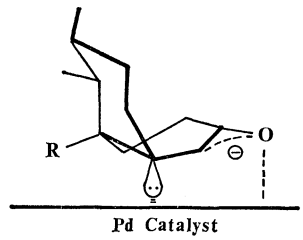

Fig. 2. The transition state leading to 5β-product in an sp^3-like conformation at C-5 (R=Me or H).

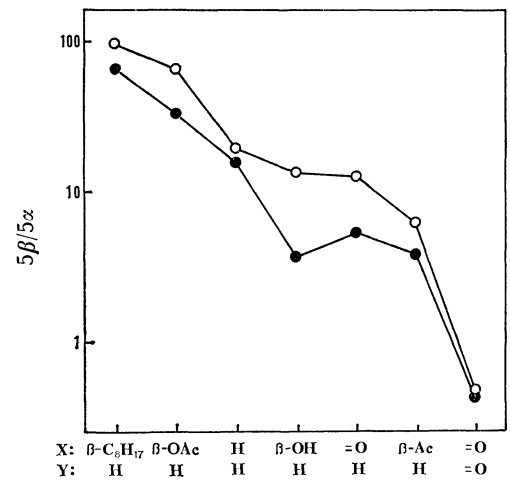

Fig. 3. Effects of substituents on 5β/5α ratio of product.
○: Hydrogenation in pyridine; ●: hydrogenation in THF/HBr.

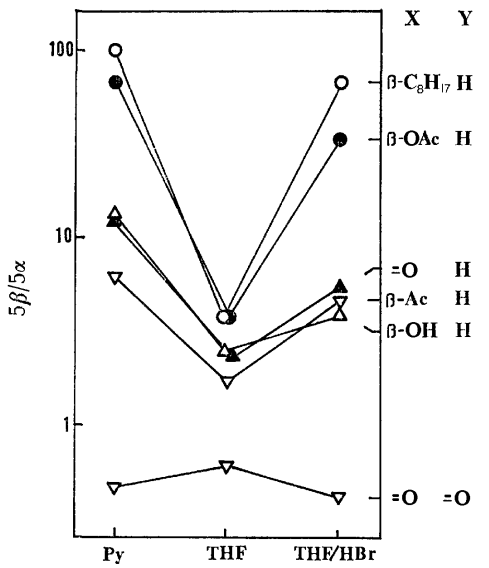

Fig. 4. Effects of media on 5β/5α ratio of product.

of the substrate onto the catalyst, it would be reasonable to consider that the electron-attractive oxygen functions may act in opposition to the π-electron polarization toward 3-oxo group, as suggested by Kirk and Hartshorn for the formation of a 4β,5β-bonded surface complex. Further, it is supposed that the interaction of the substrate with pyridine or hydrogen bromide would be stronger in a polarized state and under such circumstances the rate of hydrogenation would be depressed.[11] Hence the hydrogenation in a less polarized state would result in an increased rate as well as a decreased 5β/5α ratio of the product, as it is supposed to be the case with **1g**. This explanation is further supported by the fact that with **1g** the 5β/5α ratio of the product obtained in tetrahydrofuran was not much different from those observed in pyridine or in tetrahydrofuran and hydrobromic acid, while with other compounds the 5β/5α ratios distinctly increased in pyridine and tetrahydrofuran/hydrobromic acid, compared to those in tetrahydrofuran (see Fig. 4).

Experimental

General. All hydrogenations were carried out at 25 °C and atmospheric pressure in a small glass apparatus driven vibrationally. The compound to be hydrogenated (0.0569 mmol) was added in a solution after the catalyst (3 mg) had been shaken with hydrogen in the reaction medium for 20 min. The combined volume of the solution was 1.8 ml. In competitive hydrogenation an equimolar mixture of 0.0285 mmol of each compound was hydrogenated. Hydrogen bromide was added as a THF solution after the catalyst had been shaken with hydrogen for 20 min, and the mixture was further shaken with hydrogen for 30 min prior to the addition of the compound. The reaction mixture was taken into a microsyringe through a silicone rubber plug in the course of hydrogenation and analyzed by GLC using OV-17 as a stationary phase.

Solvent. Pyridine was treated with Raney nickel, dried over potassium hydroxide, and then distilled. THF was purified using $LiAlH_4$ as described previously.[1]

Catalyst. The palladium black used as the catalyst was prepared by reduction of palladium hydroxide in water.[12]

The authors are grateful to Teikoku Hormone Manufacturing Co. for the gift of androst-4-en-3-one and to the Mitsubishi Chemical Industries Co. for the supply of androst-4-ene-3,17-dione and 19-norandrost-4-ene-3,17-dione. This work was partially supported by a Grant-in-Aid for Scientific Research (C)(No. 57540279) from the Ministry of Education, Science and Culture.

References

1) Part IV: N. Tsuji, J. Suzuki, M. Shiota, I. Takahashi, and S. Nishimura, *J. Org. Chem.*, **45**, 2729 (1980).
2) For a review, see R. L. Augustine, *Adv. Catal.*, **25**, 56 (1976).
3) H. J. E. Loewenthal, *Tetrahedron*, **6**, 269 (1959).
4) R. L. Augustine, D. C. Migliorini, R. E. Foscante, C. S. Sodano, and M. J. Sisbarro, *J. Org. Chem.*, **34**, 1075 (1969).
5) M. G. Combe, H. B. Henbest, and W. R. Jackson, *J. Chem. Soc., C*, **1967**, 2467.
6) D. N. Kirk and M. P. Hartshorn, "Steroid Reaction Mechanisms," Elsevier Publishing Co., New York (1968), p. 81.
7) T. Lolek, I. Malunowicz, and A. Mironowicz, *Polish J. Chem.* **53**, 453 (1979).
8) K. Mori, K. Abe, M. Washida, S. Nishimura, and M. Shiota, *J. Org. Chem.*, **36**, 231 (1971) and references cited therein.
9) H. B. Henbest and W. R. Jackson, *J. Chem. Soc., C*, **1967**, 2459.
10) H. B. Henbest, W. R. Jackson, and I. Malunowicz, *J. Chem. Soc., C*, **1967**, 2469.
11) Pyridine and hydrogen bromide are both catalyst poisons and may also contribute to the depression in the rate as such.
12) S. Nishimura, M. Ishige, and M. Shiota, *Chem. Lett.*, **1977**, 535.

The Hydroxylation of β-Terpineol and Its Acetate with the Cultured Cells of *Nicotiana tabacum*

Takayuki SUGA,* Ym Sook LEE, and Toshifumi HIRATA

Department of Chemistry, Faculty of Science, Hiroshima University, Higashisenda-machi, Naka-ku, Hiroshima 730

(Received August 16, 1982)

The biotransformation of *c*-4-*p*-menth-8(9)-en-*r*-1-ol (β-terpineol) and its acetate with the cultured suspension cells of *Nicotiana tabacum* were tested. It was found that the cultured cells have the ability to hydroxylate not only the allylic positions of the C-C double bond of these substrates, but also their terminal carbon-carbon double bond. The hydroxylation at the 4-position of their allylic positions was stereospecific, affording a *trans*-1,4-diol.

The biochemical capability of plant cells to metabolize foreign substrates and/or convert them into more useful substances is of considerable interest. In such a status, we recently investigated the transformation of monoterpenoid alcohols and ketones with the cultured cells of *Nicotiana tabacum* "Bright Yellow," and found that the tobacco cells have the ability not only to reduce stereoselectively the carbon–carbon double bond adjacent to the carbonyl group of carvone as well as the carbonyl group,[1] but also to hydroxylate regioselectively the allylic position of the carbon-carbon double bond of linalool.[2] Also, the cultured cells were found to have the ability to hydrolyze the acetoxyl group of linalyl acetate, dihydrolinalyl acetate, and α-terpinyl acetate, but the cells scarcely show such an ability to γ-terpinyl acetate.[3] To generalize how the transformation patterns depend on the type of the functional group of the substrates and the structure around the functional group, we now have investigated the biotransformation of *c*-4-*p*-menth-8(9)-en-*r*-1-ol (β-terpineol) (**1**) and its acetate (**2**). The result was in part outlined in the preliminary communication.[4] This paper will give a full detail of the result.

Results and Discussion

Callus tissues induced from the stem of *N. tabacum* "Bright Yellow" were used in this work. The callus tissues were cultured in Murashige and Skoog's medium[5] with continuous shaking for 3—4 weeks and then the monoterpenoids were administered to the cultures. The cultures were then incubated at 25 °C for 7—10 d with shaking in the dark.

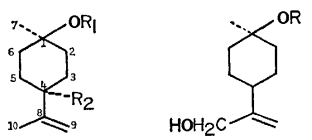

1: $R_1=R_2=H$
2: $R_1=Ac$, $R_2=H$
4: $R_1=H$, $R_2=OH$
8: $R_1=Ac$, $R_2=OH$

3: R=H
7: R=Ac

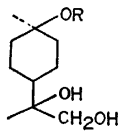

5: R=H
6: R=Ac

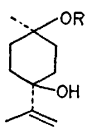

9: R=H
10: R=Ac

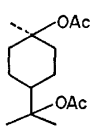

11

c-4-*p*-Menth-8(9)-en-*r*-1-ol (**1**) was transformed into three products, *c*-4-*p*-menth-8(9)-ene-*r*-1,10-diol (**3**), 4-*p*-menth-8(9)-ene-*r*-1,*t*-4-diol (**4**), and *c*-4-*p*-menthane-*r*-1,8,9-triol (**5**), which were characterized as follows. The major product (**3**) was indicated to be a 10-hydroxylated derivative of **1** on the basis of the fragment ion peaks at *m/z* 155.1042 (M^+-CH_3, $C_9H_{15}O_2$), 152.1185 (M^+-H_2O, $C_{10}H_6O$), and 134.1096 ($M^+-2\times H_2O$, $C_{10}H_{14}$) in the high resolution mass spectrum, the hydroxyl stretching bands at 3635 (primary) and 3618 cm^{-1} (tertiary) in the IR spectrum, and the ^1H NMR signal at δ 4.12 due to a hydroxymethyl group instead of the 10-methyl signal of **1**. Identity of the product **3** with *c*-4-*p*-menth-8(9)-ene-*r*-1,10-diol was established by comparisons of its spectral data with those of an authentic sample, which was prepared by oxidation of *r*-1-acetoxy-*c*-4-*p*-menth-8(9)-ene (**2**) with SeO_2 followed by hydrolysis of the oxidation product. On the other hand, the product **4** was established to be 4-*p*-menth-8(9)-ene-*r*-1,*t*-4-diol on the basis of comparisons of its spectral data with those of the literature[6-8] and those of an authentic sample. Identity of the product **5** with *c*-4-*p*-menthane-*r*-1,8,9-triol was established by comparisons of its TLC, IR and mass spectra with those of the authentic sample prepared by oxidation of **2** with OsO_4 followed by reduction with $LiAlH_4$.

The biotransformation of *r*-1-acetoxy-*c*-4-*p*-menth-8(9)-ene (**2**) with the cells yielded three products, **6**, **7**, and **8**. The ^1H NMR spectrum of **6** revealed a new signal at δ 3.47 due to a hydroxymethyl group with the disappearance of the signal of the terminal ethylenic linkage of **2**. Its mass spectrum exhibited the ion peaks at *m/z* 199 (M^+-CH_2OH), 139 ($M^+-CH_2OH-AcOH$), and 121 ($M^+-CH_2OH-AcOH-H_2O$). These data indicated the product **6** to be *r*-1-acetoxy-*c*-4-*p*-menthane-8,9-diol. Identity of the product with the diol was established by direct comparisons of its IR, ^1H NMR, and mass spectra with those of the authentic sample prepared by oxidation of **2** with OsO_4.[9] The formation of the diol (**6**) indicates the occurrence of hydroxylation of the terminal ethylenic linkage of **2**. On the other hand, the products **7** and **8** were identified as *r*-1-acetoxy-*c*-4-*p*-menth-8(9)-en-10-ol and *r*-1-acetoxy-4-*p*-menth-8(9)-en-*t*-4-ol, respectively, by direct comparisons of their physical and spectral data with those of the

Table 1. Biotransformation of *c*-4-*p*-menth-8(9)-en-*r*-1-ol (**1**) and its acetate (**2**) by the cultured cells of *N. tabacum*

Substrates	Products	Yield/%[a]
c-4-*p*-Menth-8(9)-en-*r*-1-ol (**1**)	*c*-4-*p*-Menth-8(9)-ene-*r*-1,10-diol (**3**)	13.1
	4-*p*-Menth-8(9)-ene-*r*-1,*t*-4-diol (**4**)	6.1
	c-4-*p*-Menthane-*r*-1,8,9-triol (**5**)	0.8
r-1-Acetoxy-*c*-4-*p*-menth-8(9)-ene (**2**)	*r*-1-Acetoxy-*c*-4-*p*-menthane-8,9-diol (**6**)	14.7
	r-1-Acetoxy-*c*-4-*p*-menth-8(9)-en-10-ol (**7**)	9.8
	r-1-Acetoxy-4-*p*-menth-8(9)-en-*t*-4-ol (**8**)	8.4

a) The weight percent of the products per the administered substrates.

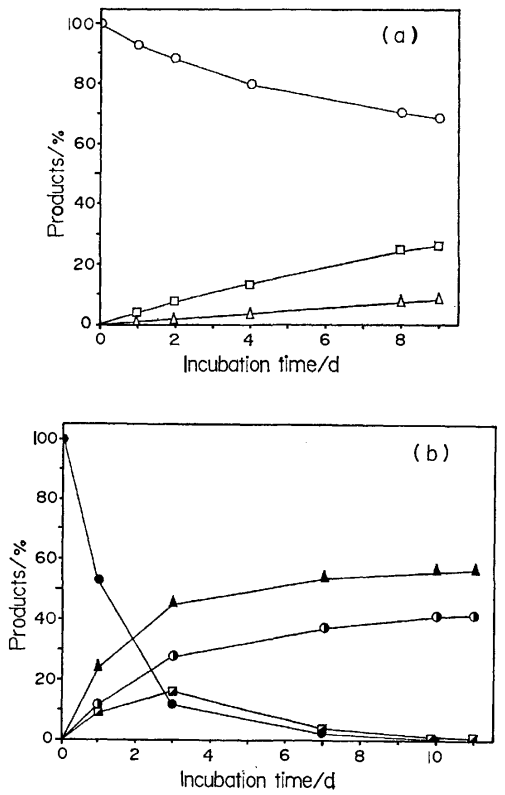

Fig. 1. The time-courses in the biotransformation of **1** (a) and **2** (b) by the cultured cells of *N. tabacum*. ○: **1**, ●: **2**, □: **3**, △: **4**, ▲: **6**, ◪: **7**, and ◑: **8**.

authentic samples, which had been prepared following to the reported procedure.[6,7] The yields of the transformation products are given in Table 1. The time-courses in the biotransformation of β-terpineol (**1**) and its acetate (**2**) with the cultured suspension cells were followed, and it was found that the transformation of **2** is more rapid than that of **1**. The products **3**, **4**, **6**, and **8** gradually increased in their amounts with the lapse of the incubation time, but, after the amounts of the product **7** became maximum at the 3-d incubation, it gradually decreased; this is probably due to the further conversion of **7** to another product. In spite of careful and repeated TLC and GLC analyses, no *cis*-1,4-glycols (**9** and **10**) were found in the reaction mixtures obtained at each regular interval in the time-course experiment. This fact indicates that the hydroxylation with the tobacco suspension cells is more stereoselective than that with SeO_2, which is known to convert **2** into *r*-1-acetoxy-4-*p*-menth-8(9)-en-*t*-4-ol (**8**) and its *cis*-isomer (**10**) in the ratio of 6:5.[6]

Thus, it has been clarified that β-terpineol (**1**) and its acetate (**2**) are hydroxylated not only at the allylic positions of the ethylenic linkage but also at the ethylenic linkage itself by the tobacco cultured suspension cells. However, in contrast to the predominant hydroxylation at the ethylenic linkage in the case of β-terpinyl acetate (**2**), only a small amount of β-terpineol (**1**) is hydroxylated at the ethylenic linkage. The hydroxylation of the 4-position of **1** and **2** is stereospecific and arises from the direction *trans* to the 1-hydroxyl or 1-acetoxyl group. Our recent studies on the biotransformation of carvone[1] showed that its carbon-carbon double bond adjacent to the carbonyl group was reduced, but its terminal carbon-carbon double bond remained unchanged. However, the terminal ethylenic linkage of β-terpinyl acetate (**2**) was hydroxylated to an appreciable extent. It is fascinating to note that the biotransformation pattern of the foreign substrates depends on the functional group of the substrate administered and the structure around the functional group.

Experimental

Analytical (0.25 mm thick) and preparative TLC (0.75 mm thick) were carried out on a silica-gel plate (Merck, Type 60, GF_{254}). GLC analyses were performed on an instrument equipped with an FID and a glass column (3 mm×2 m) packed with 15% DEGS, 2% OV-17, or 2% OV-101 on Chromosorb W (AW-DMCS; 80—100 mesh) by programming the column temperature at 100—200 °C with a rate of 3 °C/min for DEGS and at 90—250 °C, 2 °C/min for OV-17 and OV-101. The areas of the peaks on the gas-liquid chromatogram were calculated by use of a Shimadzu C-R1A Chromatopac recording data processor for chromatography. GC-MS were recorded on a mass spectrometer which was installed with a gas chromatograph equipped with an OV-101 capillary column (0.28 mm×50 m) at 80—210 °C with a rate of 3 °C/min using an EI ion source at 20 eV. ^1H NMR spectra were taken at 60 or 90 MHz for $CDCl_3$ solutions with TMS as an internal reference. FT-IR spectra were obtained on a JIR-40X FT-IR spectrophotometer.

Preparation of the Materials Used for Substrates. Following the method described in the literature,[10,11] *r*-1-acetoxy-*c*-4-*p*-menth-8(9)-ene (**2**) was prepared by pyrolysis of terpin diacetate (**11**) (n_D^{25} 1.4510, d_4^{25} 1.0217), which was derived from terpin hydrate[12] by acetylation, followed by purifications by column chromatography on 10% $AgNO_3$-silica gel with a hexane-EtOAc mixture with increasing EtOAc from 0 to 5% and then by distillation under a reduced pressure: bp 71 °C/3.5 mmHg, 1 mmHg≈133.322 Pa; n_D^{25} 1.4569; d_4^{25} 0.9414 (lit,[10] bp 81—82 °C/4 mmHg; n_D^{25} 1.4562; d_4^{25}

0.9411); >99.8% pure on GLC; IR (neat) 1737 (OAc), 3084, 1644, and 892 cm^{-1} (>C=CH_2); ^1H NMR ($CDCl_3$) δ=1.47 (3H, s, 7-CH_3), 1.69 (3H, bs, 10-CH_3), 1.99 (3H, s, OAc), and 4.69 (2H, bs, >C=CH_2). Found: C, 73.29; H, 10.24%. Calcd for $C_{12}H_{20}O_2$: C, 73.43; H, 10.27%.

c-4-*p*-Menth-8(9)-en-*r*-1-ol (**1**) was prepared from **2** by hydrolysis with 2.5% ethanolic KOH soln, followed by purification by preparative TLC on silica gel with hexane–EtOAc (7:3, v/v): mp 30.5—30.8 °C (lit,[7] 28—30 °C); >99.9% pure on GLC; IR (neat) 3400 (OH), 3095, 1648, and 890 cm^{-1} (>C=CH_2); ^1H NMR ($CDCl_3$) δ=1.23 (3H, s, 7-CH_3), 1.72 (3H, bs, 10-CH_3), and 4.70 (2H, bs, >C=CH_2). Found: C, 77.74; H, 11.73%. Calcd for $C_{10}H_{18}O$: C, 77.86; H, 11.76%.

Feeding of the Monoterpenoids to the Tobacco Suspension Cells. The callus tissues used in this study were induced from the stem of *Nicotiana tabacum* "Bright Yellow" and have been maintained for about 8 years. Just prior to use for this work, the callus tissue was transplanted to freshly prepared Murashige and Skoog's medium[5] (100 ml per 300 ml-conical flask) containing 2 ppm 2,4-dichlorophenoxyacetic acid and 3% sucrose, and it was grown with continuous shaking for 3—4 weeks at 25 °C in the dark. After the substrate (10 mg per one flask; total 250—400 mg) had been added to the suspension cultures (about 50—70 g cells per one flask), the cultures was incubated at 25 °C for 7—10 d on a rotary shaker (70 min^{-1}) in the dark.

Isolation and Identification of the Products. The suspension cells were filtered off and triturated with MeOH. Removal of the solvent from the methanol solution gave an extract, which was again extracted with $CHCl_3$. On the other hand, the culture medium separated from the mass of the cells was extracted with $CHCl_3$. The two $CHCl_3$ extracts were put together, since they exhibited the same behavior on TLC and GLC. Transformation products **3**, **4**, and **6**—**8** were isolated from the combined $CHCl_3$ extract by preparative TLC on silica gel with hexane–EtOAc (1:2 or 7:3, v/v), and identified by direct comparisons of their physical constants, TLC, GLC, and spectral data with those of synthetic specimens prepared as described below.

In the case of β-terpineol (**1**), the aqueous layers separated from the $CHCl_3$ solution were put together, and the combined aqueous solution (850 ml) was exactly neutralized and concentrated into 50 ml by lyophilization. The concentrated aqueous solution was extracted continuously with EtOAc for 17 h by use of a liquid-liquid extractor. Triol **5** was isolated from the EtOAc extract by preparative TLC (0.5 mm thick) on silica gel with EtOAc–MeOH (97:3, v/v), and identified by direct comparisons of its TLC, IR and mass spectra with those of a synthetic sample. To confirm the complete extraction of the triol **5** from the aqueous solution, the residue (6.20 g) obtained from the residual aqueous solution by lyophilization was extracted with MeOH (50 ml×2), and then the sirup (3.75 g) obtained from the MeOH solution on evaporation was subjected to the analytical TLC. However, no spot of the triol (**5**) was observed.

The yields of the products were as shown in Table 1, and the physical constants and spectral data of the products were as follows.

c-*4*-p-*Menth-8(9)-ene*-r-*1,10-diol (3)*: Mp 75.0—76.2 °C (from hexane); IR (KBr) 3327 (OH) and 3100, 1652, and 901 cm^{-1} (>C=CH_2); IR (1.8×10^{-3} M, CCl_4) 3635 (primary OH), 3618 (tertiary OH); ^1H NMR ($CDCl_3$) δ=1.24 (3H, s, 7-CH_3), 4.12 (2H, bs, -CH_2OH), 4.92 and 5.01 (2H, each d, >C=CH_2); MS (70 eV), *m/z* (rel intensity) 155 (6), 152 (33), 137 (12), 134 (20), 119 (17), 109 (34), 94 (33), 84 (34), 71 (66), 55 (30), and 43 (100); High-resolution MS *m/z* 155.1042 (M^+-CH_3, $C_9H_{15}O_2$), 152.1185 (M^+-H_2O, $C_{10}H_6O$), and 134.1096 ($M^+-2\times H_2O$, $C_{10}H_{14}$).

4-p-*Menth-8(9)-ene*-r-*1*,t-*4-diol (4)*: Mp 139—140 °C (from hexane) (lit,[8] 140—141 °C); IR (KBr) 3357 (OH), 3098, 1641, and 895 cm^{-1} (>C=CH_2); IR (4.1×10^{-3} M, CCl_4) 3617 cm^{-1} (tertiary OH); ^1H NMR ($CDCl_3$) δ=1.27 (3H, s, 7-CH_3), 1.83 (3H, bs, 10-CH_3), 4.82 and 5.05 (2H, m, >C=CH_2); MS (70 eV), *m/z* (rel intensity) 170 (M^+, 10), 155 (13), 152 (23), 137 (24), 123 (38), 109 (31), 98 (100), 84 (38), 73 (53), 69 (59), and 43 (74); High-resolution MS *m/z* 155.1086 (M^+-CH_3, $C_9H_{15}O_2$), 152.1207 (M^+-H_2O, $C_{10}H_{16}O$), and 134.1109 ($M^+-2\times H_2O$, $C_{10}H_{14}$).

c-*4*-p-*Menthane*-r-*1,8,9-triol (5)*: FT-IR (neat) 3355 (OH), 1453, 1380, 1168 1048 (C–O), 900 cm^{-1}; MS (70 eV), *m/z* (rel. intensity) 157 (1), 155 (1.5), 152 (1), 149 (1), 139 (35), 121 (3), 109 (3), 95 (18), 81 (20), 75 (9), 71 (20), 55 (13), and 43 (100); High-resolution MS *m/z* 157.1238 (M^+-CH_2OH, $C_9H_{17}O_2$), 139.1124 ($M^+-H_2O-CH_2OH$, $C_9H_{15}O$), and 121.1005 ($M^+-2\times H_2O-CH_2OH$, C_9H_{13}).

r-*1-Acetoxy*-c-*4*-p-*menthane-8,9-diol (6)*: n_D^{25} 1.4749; IR (neat) 3421 (OH) and 1727 cm^{-1} (OAc); ^1H NMR ($CDCl_3$) δ=1.09 (3H, s, 10-CH_3), 1.46 (3H, s, 7-CH_3), 1.99 (3H, s, OAc), and 3.47 (2H, dd, J=16 and 11 Hz, -CH_2OH); MS (70 eV), *m/z* (rel intensity) 199 (0.5), 155 (2), 152 (4), 139 (49), 135 (5), 121 (11), 95 (26), 82 (26), 75 (17), and 43 (100); High-resolution MS *m/z* 152.1172 ($M^+-AcOH-H_2O$, $C_{10}H_{16}O$), 139.1119 ($M^+-AcOH-CH_2OH$, $C_9H_{15}O$), 135.1173 ($M^+-AcOH-H_2O-OH$, $C_{10}H_{15}$), and 121.1027 ($M^+-AcOH-CH_2OH-H_2O$, C_9H_{13}).

r-*1-Acetoxy*-c-*4*-p-*menth-8(9)-en-10-ol (7)*: n_D^{25} 1.4764 (lit,[6] n_D^{25} 1.4757); IR (neat) 3427 (OH), 1728 (OAc), and 3100, 1651, and 898 cm^{-1} (>C=CH_2); ^1H NMR ($CDCl_3$) δ=1.48 (3H, s, 7-CH_3), 2.00 (3H, s, OAc), 4.19 (2H, bs, -CH_2OH), 4.75 and 5.01 (2H, m, >C=CH_2); MS (70 eV), *m/z* (rel intensity) 194 (M^+-H_2O, 1), 152 (20), 137 (20), 134 (27), 121 (14), 119 (26), 109 (27), 106 (27), 94 (30), 84 (28), 79 (26), and 43 (100). The structure of **7** was further confirmed by its conversion to *c*-4-*p*-menth-8(9)-ene-*r*-1,10-diol (**3**) (mp 74.0—76.0 °C) on reduction with $LiAlH_4$ in dry ether. The diol (**3**) was identified by direct comparisons of the IR and ^1H NMR spectra with those of an authentic specimen.

r-*1-Acetoxy-4*-p-*menth-8(9)-en*-t-*4-ol (8)*: Mp 88.5—89.5 °C (from hexane) (lit,[6] 88—89 °C); IR (KBr) 3480 (OH), 1708 (OAc), 3100, 1642, and 905 cm^{-1} (>C=CH_2); ^1H NMR ($CDCl_3$) δ=1.49 (3H, s, 7-CH_3), 1.78 (3H, m, 10-CH_3), 1.99 (3H, s, OAc), 4.79 and 5.02 (2H, m, >C=CH_2); MS (70 eV), *m/z* (rel intensity) 171 (2), 152 (50), 137 (19), 124 (30), 123 (55), 119 (7), 111 (23), 109 (28), 97 (40), 84 (45), 69 (59), and 43 (100). The structure of **8** was further confirmed by its conversion to 4-*p*-menth-8(9)-ene-*r*-1,*t*-4-diol (**4**) (mp 135—139 °C; lit,[8] 140—141 °C) on reduction with $LiAlH_4$ in dry ether. Identification of **4** was performed by direct comparisons of its spectra (IR and ^1H NMR) with those of an authentic sample.

Time-courses in the Biotransformation of 1 and 2. The substrate (10 mg) was administered to each of five flasks containing 100 ml of the precultured suspension. The cultured mixtures were worked up at a regular time interval in the same manner as described above. The oily product (5—10 mg) obtained from the $CHCl_3$ extract was dissolved in 0.4 ml of ethyl acetate to subject to GLC. Components of the product were identified by co-TLC and co-GLC with authentic samples and then by GC-MS measurements. The yields of the products were determined on the basis of the peak areas on GLC, and expressed as relative percent to the whole products extracted, as shown in Fig. 1.

Preparation of the Authentic Samples. *Preparation of* ***7***, ***8***, *and* ***10***: Following the method described in the literature,[7] *r*-1-acetoxy-*c*-4-*p*-menth-8(9)-ene (**2**) (2.46 g) was oxidized with SeO_2 (0.75 g) dissolved in a mixture of *t*-BuOH (6.0 g) and benzene (8 ml) at 40—50 °C for 9 h under a nitrogen atmosphere. The reaction mixture was subjected to preparative TLC with hexane–EtOAc (7:3, v/v) to give *r*-1-acetoxy-*c*-4-*p*-menth-8(9)-en-10-ol (**7**) (0.11 g; n_D^{25} 1.4769), *r*-1-acetoxy-4-*p*-menth-8(9)-en-*t*-4-ol (**8**) (0.31 g; mp 88.5—89.5 °C), and *r*-1-acetoxy-4-*p*-menth-8(9)-en-*c*-4-ol (**10**) (0.25 g; n_D^{25} 1.4778).

Preparation of ***3*** *and* ***4***: *c*-4-*p*-Menth-8(9)-ene-*r*-1,10-diol (**3**) (22 mg; mp 75.0—76.0 °C) and 4-*p*-menth-8(9)-ene-*r*-1,*t*-4-diol (**4**) (31 mg; mp 139—140 °C) were obtained from **7** (30 mg) and **8** (45 mg) by reduction with $LiAlH_4$ in dry ether for 3 h at 0 °C, respectively.

Preparation of **6**: Following the procedure described in the literature,[9] β-terpinyl acetate (**2**) (0.196 g) was oxidized with osmium tetraoxide (0.275 g) in a mixture of ethyl ether (20 ml) and pyridine (0.4 ml) at room temp for 2 d to give brownish precipitates. The precipitates were filtered off and hydrolyzed with a sodium hydroxide solution (1%) in the presence of mannitol. *r*-1-Acetoxy-*c*-4-*p*-menthane-8,9-diol (**6**) (0.190 g, n_D^{25} 1.4736) was isolated from the reaction mixture by preparative TLC with hexane–EtOAc (3:7, v/v).

Preparation of ***5***: *c*-4-*p*-Menthane-*r*-1,8,9-triol (**5**) (48 mg) was obtained from **6** (68 mg) by reduction with $LiAlH_4$ in dry ether for 8 h at 0 °C: mp 118.0—118.5 °C (from EtOAc) (lit,[13] 118—118.5 °C); FT-IR (neat) 3355 (OH), 1453, 1380, 1168, 1048 (C–O), 900 cm^{-1}; ^1H NMR ($CDCl_3$) $\delta=1.10$ (3H, s, 10-CH_3), 1.16 (3H, s, 7-CH_3), and 3.36 (2H, d, $J=3.7$ Hz, -$C\underline{H}_2OH$); ^{13}C NMR ($CDCl_3$) $\delta_c=$ 74.9(s), 69.1(s), 68.3(t), 44.1(d), 38.8(t, 2×C), 31.4(q), 22.8(t), 21.8(t), and 20.7(q); MS (70 eV), *m/z* (rel intensity) 157 (1), 155 (1.5), 152 (1), 149 (2), 139 (39), 121 (3), 109 (3), 95 (19), 81 (17), 75 (9), 71 (19), 55 (10), and 43 (100).

The present work was supported in part by a Grant-in-Aid for Developmental Scientific Research 384030 (1978, to T. S.) and by it for Scientific Research No. 56540323 (1981, to T. H.), from the Ministry of Education, Science and Culture.

References

1) T. Hirata, H. Hamada, T. Aoki, and T. Suga, *Phytochemistry*, **21**, 2209 (1982).
2) T. Suga, T. Hirata, Y. Hirano, and T. Ito, *Chem. Lett.*, **1976**, 1245; T. Hirata, T. Aoki, Y. Hirano, T. Ito, and T. Suga, *Bull. Chem. Soc. Jpn.*, **54**, 3527 (1981).
3) T. Suga, T. Hirata, Y. S. Lee, H. Hamada, M. Futatsugi, and T. Aoki, The 24th Symposium on the Chemistry of Natural Products, Osaka, October 1981, Abstr., p. 513.
4) T. Suga, T. Aoki, T. Hirata, Y. S. Lee, O. Nishimura, and M. Utsumi, *Chem. Lett.*, **1980**, 229.
5) T. Murashige and F. Skoog, *Physiol. Plant*, **15**, 473 (1962).
6) T. Tahara and Y. Sakuda, *Yukagaku*, **25**, 161 (1976).
7) Y. Sakuda, *Nippon Kagaku Zasshi*, **81**, 1891 (1960).
8) Y. Sakuda, *Nippon Kagaku Zasshi*, **82**, 117 (1961).
9) D. Y. Curtin, E. E. Harris, and E. K. Meislich, *J. Am. Chem. Soc.*, **74**, 2901 (1952).
10) T. Aratani and T. Matsuura, *J. Sci. Hiroshima Univ., Ser. A*, **20**, 191 (1957).
11) Y. S. Lee, T. Hirata, T. Aoki, and T. Suga, *J. Sci. Hiroshima Univ., Ser. A*, **45**, 407 (1982).
12) T. Suga, T. Hirata, and T. Aoki, *Bull. Chem. Soc. Jpn.*, **55**, 914 (1982).
13) J. L. Simonsen, "The Terpenes," Cambridge Univ. Press, London (1947), Vol. I, p. 267.

Aryliminodimagnesium Reagents. V. The Reaction with Bifunctional Nitroarenes

Masao Ōkubo,* Hiroyuki Aratani, Takayuki Gondō, and Kōji Koga
Department of Chemistry, Faculty of Science and Engineering, Saga University, Honjō-machi, Saga 840

(Received September 1, 1982)

The reactions of *p*-methylphenyliminodimagnesium reagent (*p*-$MeC_6H_4N(MgBr)_2$) with *p*- and *m*-dinitrobenzenes, bis(*p*-nitrophenyl)methane, bis(*p*-nitrophenyl) sulfide and ether, *p*- and *m*-nitrobenzaldehydes as well as 4-nitro-4′-methylbenzophenone were investigated. *p*-Dinitrobenzene, which is the strongest electron-acceptor among the substrates used, gave *ca.* 30% combined yield of bis(azoxy) and azoxy azo products. The oxidative coupling product, 4,4′-dimethylazobenzene, was isolated in 20—30% yields. About 60% combined yield of the bis(azoxy) and azoxy azo products was obtained in the same reaction with *m*-dinitrobenzene, which is less electron-accepting than the *p*-isomer. In the reaction of bis(*p*-nitrophenyl)methane, bis(*p*-nitrophenyl) sulfide and ether with five molar amounts of the reagent, *ca.* 70% combined yields of bis(azoxy), azoxy azo, and bis(azo) products were obtained. On the treatment of the nitrobenzaldehydes and the nitrobenzophenone, in contrast, the reaction took place exclusively on the nitro group. The results are discussed in terms of the electron-accepting ability of substrates.

The aryliminodimagnesium reagents ($ArN(MgBr)_2$, aryl-IDMg) condense with diaryl ketones to give the anils (Scheme 1),[1,2] and also with nitroarenes to give azoxy- and azoarenes (Scheme 2).[3,4] On the basis of the previous results,[1–4] the IDMg reaction with an aromatic dinitro compound is expected to provide a new route for the one step preparation of the corresponding bis(azoxy) and bis(azo) compounds. The expectation was verified in the reaction of *p*-methylphenyl-IDMg with *p*- and *m*-dinitrobenzenes (**1** and **2**), bis(*p*-nitrophenyl)methane (**3**), bis(*p*-nitrophenyl) sulfide (**4**) and ether (**5**).

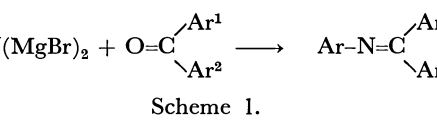

Scheme 1.

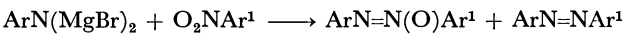

Scheme 2.

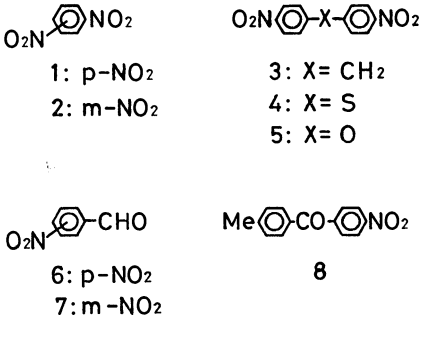

Similarly, the treatment of *p*- and *m*-nitrobenzaldehydes (**6** and **7**) as well as 4-nitro-4′-methylbenzophenone (**8**) with the same reagent is also expected to afford the corresponding azoxy azomethines and azo azomethines. Even by use of an excessive amount of the reagent, however, the reaction took place exclusively on the nitro group and not on the carbonyl group.

In this paper, the results of the IDMg reaction with the bifunctional nitro compounds, **1**—**8**, will be reported and explained in terms of their relative electron-accepting ability.

Results and Discussion

IDMg Reaction with p- *and* m-*Dinitrobenzenes.* In the reaction of *p*-dinitrobenzene, **1**, with five or six molar equivalents of *p*-methylphenyl-IDMg, the expected bis(azoxy) (**9a**), azoxy azo (**9b**), and bis(azo) (**9c**) products were obtained (Scheme 3 and Table 1).

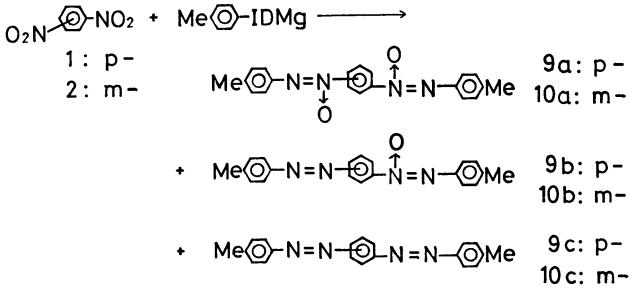

Scheme 3.

The yields of the deoxygenative condensation products; **9a**, **9b**, and **9c**, are affected by the reaction conditions, especially by the temperature at which the addition is done (Expts 1—5). The yields were poor when the addition was carried out at 0 °C, and were improved by the addition at −78 °C. The formation of 4,4′-dimethylazobenzene is due to the oxidative coupling of the reagent molecules,[3] and that of an unidentifiable black material is due to the polymerization of the substrate initiated by one-electron reduction.[3] Their formation is reasonable, since the substrate **1** is highly electron-accepting.[5] The possible nitro azoxy product was not detected even by the treatment with the smaller excess of the reagent (Expt 2).

The reaction with *m*-dinitrobenzene, **2**, was carried out by adding its solution at −78 °C (Expts 6 and 7). The less electron-accepting **2**[5] gave the better combined yield of the bis(azoxy) (**10a**) and azoxy azo (**10b**) products, which were deoxygenated to afford **10b** and **10c**, respectively, by the treatment with

Table 1. Distribution of products in the reaction of p-MeC_6H_4-IDMg with p- and m-dinitrobenzenes

Expt No.	Substrate	[IDMg]/[Substrate]	Addition		Yields/%				
			Manner[a]	Temp °C	**9a**	**9b**	**9c**	(p-MeC_6H_4N=)$_2$	Recovered **1**
1	**1**	5	N	0	6	5	0	32	9
2	**1**	3	N[b]	0	−0	−0	−0	20	50
3	**1**	5	N	−78	20	13	0	17	10
4	**1**	6	R	0	0	6	18	23	16
5	**1**	6	R	−78	26	11	0	25	3
					10a	**10b**	**10c**		Recovered **2**
6	**2**	5	N	−78	43	15	0	18	—
7	**2**	10	N	−78	0	17	29	26	—

a) N and R designate "normal" and "reverse" additions respectively. b) The diluted THF solutions of the reagent and the substrate were used.

Table 2. Distribution of products in the reaction of p-MeC_6H_4-IDMg with bis-(p-nitrophenyl) compounds

Substrate	Yields/%[a]			
	Bis(azoxy)	Azoxy azo	Bis(azo)	(p-MeC_6H_4N=)$_2$
3($X=CH_2$)	26	31	9	25
4(X=S)	29	30	8	22
5(X=O)	27	32	10	29

a) Five molar equivalents of the reagent were used.

a larger excess of the reagent. The better yields of the condensation products in the reaction of **2** than those in the reaction of **1** suggests the importance of the combination of the electron-accepting and -donating abilities of the reactants.[6]

IDMg Reaction with Bis(p-nitrophenyl)methane, Bis(p-nitrophenyl) Sulfide and Ether. The bis(p-nitrophenyl) compounds, **3**, **4**, and **5**, the two nitro groups of which are located on the different phenyl groups, gave high combined yields of the corresponding bis(azoxy), azoxy azo, and bis(azo) products, **11a—c**, **12a—c**, and **13a—c** (Scheme 4 and Table 2).

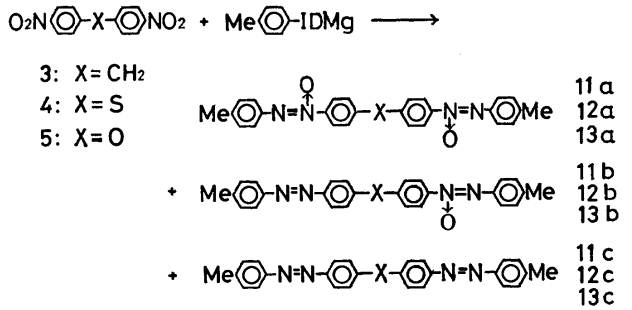

Scheme 4.

The high combined yield of the products is ascribed to the moderate electron-accepting ability of **3**, **4**, and **5**. The electron-accepting effects of the individual nitro groups seem to be additive, but not synergic as in the case of **1**, since the formation of the unidentifiable black material is negligible and that of 4,4′-dimethylazobenzene *per* one nitro group is comparable to that obtained in the case of monofunctional nitroarenes.[3] The effect of the central atoms, C, S, and O, of the substrates on the distribution of the three types of the products is negligible.

The good result of the reaction of Scheme 4 forced the authors to examine the preparation and the reaction of bis(iminodimagnesium) reagents. An attempt to prepare the reagent from p-phenylenediamine by treating it with four molar equivalents of EtMgBr was unsuccessful: a voluminous white precipitate appeared and hardly any evolution of ethane[1] was observed. In contrast, bis(p-aminophenyl) ether gave the bis(iminodimagnesium) reagent. Its reaction with p-nitrotoluene(1.6 mol equiv., Scheme 5) gave the corresponding bis(azoxy) product (**14a**, 12%) and azoxy azo product (**14b**, 13%), which were isomeric with **13a** and **13b** respectively. A 22% of the substrate was recovered in this case.

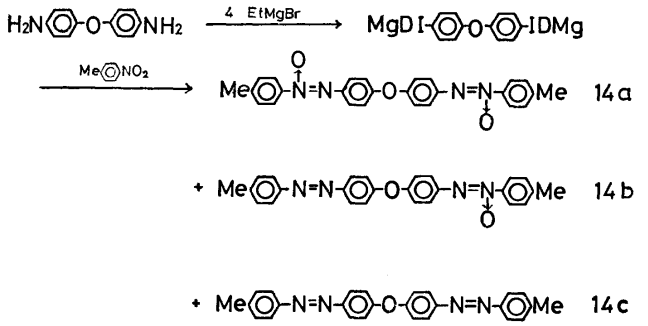

Scheme 5.

IDMg Reaction with Nitrobenzaldehydes and a Nitrobenzophenone. It should be noted that the IDMg reaction with the substrates having nitro and carbonyl groups took place exclusively on the nitro group. The reaction of p-nitrobenzaldehyde, **6**, with five molar

Table 3. Distribution of products in the reaction of p-MeC_6H_4-IDMg with p- and m-nitrobenzaldehydes

Substrate	[IDMg]/[Substrate]	Reaction time/h	Yields/%		
			Azoxy aldehyde	Azo aldehyde	(p-MeC_6H_4N=)$_2$
			15a	**15b**	
6	5	3	30	25	13
			16a	**16b**	
7	8	6	0	82	18

Table 4. Analytical data and physical constants of products

Product No.	Mp θ_m/°C	Formula	Found(Calcd)(%)			NMR data, δ in $CDCl_3$
			C	H	N	
9a	145—147.5	$C_{20}H_{18}N_4O_2$	69.61 (69.36)	4.98 (5.20)	16.09 (16.18)	8.52(4H, s), 8.26 and 7.38(8H, ABq), 2.46 (6H, s).
9b	185—189.5	$C_{20}H_{18}N_4O$	72.62 (72.73)	5.62 (5.45)	17.10 (16.97)	8.54 and 8.08(4H, ABq), 8.27 and 7.96(4H, ABq), 7.50—7.30(4H, ABq), 2.48(3H, s), 2.45 (3H, s).
9c	209.5—213	$C_{20}H_{18}N_4$	76.55 (76.43)	5.80 (5.73)	17.65 (17.83)	8.10(4H, s), 7.92 and 7.36(8H, ABq), 2.46 (6H, s).
10a	164—165.5	$C_{20}H_{18}N_4O_2$	69.56 (69.36)	5.08 (5.45)	16.21 (16.18)	9.18(1H, m), 8.50—8.46(2H, m), 8.14 and 7.24(8H, ABq), 7.56(1H, m), 2.40(6H, s).
10b	124.5—128	$C_{20}H_{18}N_4O$	72.78 (72.73)	5.56 (5.45)	17.19 (16.97)	8.76(1H, m), 8.38—7.44(7H, m), 7.36—7.16 (4H, m), 2.38(6H, s).
10c	131—133.5	$C_{20}H_{18}N_4$	76.37 (76.43)	5.69 (5.73)	17.94 (17.83)	8.08—7.60(8H, m), 7.30(4H, d), 2.38(6H, s).
11a	169—173	$C_{27}H_{24}N_4O_2$	74.25 (74.31)	5.38 (5.50)	12.93 (12.84)	8.30(8.10) and 7.18(8H, ABq), 8.10(8.30) and 7.18(8H, ABq), 4.08(2H, s), 2.40(6H, s).
11b	190—198	$C_{27}H_{24}N_4O$	76.98 (77.14)	5.77 (5.71)	13.43 (13.33)	8.32—8.06(4H, m), 7.94—7.79(4H, m), 7.42 —7.20(8H, m), 4.10(2H, s), 2.40(6H, s).
11c	231—233	$C_{27}H_{24}N_4$	80.25 (80.20)	5.89 (5.94)	13.86 (13.86)	7.96—7.82(8H, m), 7.46—7.26(8H, m), 4.16 (2H, s), 2.44(6H, s).
12a	171—174	$C_{26}H_{22}N_4O_2S$	68.81 (68.72)	4.92 (4.85)	12.29 (12.33)	8.30(8.16) and 7.48(8H, m), 8.16(8.30) and 7.30 (8H, m), 2.42(6H, s).
12b	182.5—185	$C_{26}H_{22}N_4OS$	71.29 (71.23)	4.13 (5.02)	12.92 (12.78)	8.32—8.04(4H, m), 7.92—7.74(4H, m), 7.60 —7.40(8H, m), 2.41(3H, s), 2.38(3H, s).
12c	218—220.5	$C_{26}H_{22}N_4S$	74.02 (73.93)	5.38 (5.21)	13.21 (13.27)	7.92(7.86) and 7.52(8H, ABq), 7.86(7.92) and 7.32(8H, ABq), 2.42(6H, s).
13a	150—154	$C_{26}H_{22}N_4O_3$	71.29 (71.23)	4.97 (5.02)	12.91 (12.78)	8.28(8.06) and 7.24(8H, ABq), 8.06(8.28) and 7.08(8H, ABq), 2.38(6H, s).
13b	159—163.5	$C_{26}H_{22}N_4O_2$	74.02 (73.93)	5.25 (5.21)	13.31 (13.27)	8.38—7.72(8H, m), 7.34—7.02(8H, m), 2.42 (3H, s), 2.40(3H, s).
13c	215—218	$C_{26}H_{22}N_4O$	76.91 (76.84)	5.39 (5.41)	13.82 (13.79)	7.90(7.78) and 7.26(8H, ABq), 7.78(7.90) and 7.14(8H, ABq), 2.42(6H, m).
14a	166—172	$C_{26}H_{22}N_4O_3$	71.32 (71.23)	5.09 (5.02)	12.91 (12.78)	8.32(8.20) and 7.28(8H, ABq), 8.20(8.32) and 7.16(8H, ABq), 2.40(6H, m).
14b	172—176.5	$C_{26}H_{22}N_4O_2$	74.04 (73.93)	5.10 (5.21)	13.32 (13.27)	8.42—8.20(4H, m), 8.02—7.80(4H, m), 7.40 —7.10(8H, m), 2.44(6H, s).
15a[a]	—	—	—	—	—	10.16(1H, s), 8.50 and 8.02(4H, ABq), 8.20 and 7.30(4H, ABq), 2.42(3H, s).
15b[a]	—	—	—	—	—	10.04(1H, s), 8.96(4H, s), 7.83 and 7.28(4H, ABq), 2.42(3H, s).
16b[a]	—	—	—	—	—	9.80(1H, s), 8.24—6.90(8H, m), 2.36(3H, s).
17	175—179	$C_{21}H_{19}NO$	76.73 (76.60)	5.81 (5.77)	12.68 (12.76)	8.56(1H, s), 8.04(4H, s), 7.84 and 7.32(4H, ABq), 7.24 and 6.96(4H, ABq), 3.84(3H, s), 2.44(3H, s).
18	153—155	$C_{21}H_{18}N_2O_2$	76.30 (76.36)	5.39 (5.45)	8.55 (8.48)	8.56 and 7.99(4H, ABq), 8.29 and 7.39(4H, ABq), 7.84 and 7.39(4H, ABq), 2.54(3H, s), 2.50(3H, s).
19	136—139	$C_{21}H_{19}NO$	83.75 (83.72)	6.44 (6.31)	4.72 (4.65)	7.90 and 7.06(4H, ABq), 7.84 and 7.34(4H, ABq), 7.16(4H, s), 5.94(1H, broad s), 2.42 (3H, s), 2.34(3H, s).

a) The azoxy and azo aldehydes, **15a**, **15b**, and **16b**, were identified by NMR; they were not purified. They were used for converting into the imino compounds.

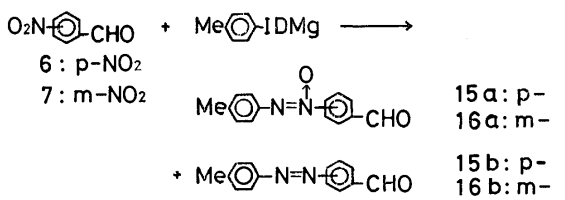

Scheme 6.

equivalents of *p*-methylphenyl-IDMg gave the corresponding azoxy and azo aldehydes, **15a** and **15b** (Scheme 6 and Table 3). Even by use of eight molar equivalents of the reagent, *m*-nitrobenzaldehyde, **7**, afforded solely an excellent yield of the azo aldehyde, **16b**. Neither azoxy azomethine nor azo azomethine were detected. In an attempt to convert the isolated **15b** into the corresponding azo azomethine by treating with the more electron-donating *p*-methoxyphenyl-IDMg, the substrate was recovered unchanged. The expected azo azomethine, **17**, was prepared quan-

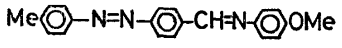

17

titatively by the treatment of **15b** in refluxing dry benzene with *p*-methoxyaniline in the presence of *p*-toluenesulfonic acid.[7] For the purpose of converting an aromatic aldehyde into the aldimine, the IDMg method is not advisable:[2] *p*-chlorobenzaldehyde was converted into the aldimine in only a 32% yield by the treatment with 1.2 molar equivalents of *p*-methylphenyl-IDMg.

The inertness of the carbonyl functional group is consistent with the fact that the one-electron reduction of nitro-substituted benzophenones gives the ESR spectra assigned to the benzoyl-substituted nitrobenzene anion radicals.[9] The higher oxidizing ability of nitroarenes compared with that of diaryl ketones[10] also supports the present result.

4-Nitro-4′-methylbenzophenone, **8**, also gave products which originated from the reactions exclusively on the nitro group by the treatment with five molar equivalents of *p*-methylphenyl-IDMg (Scheme 7). The normal condensation product, **18**, and the replacement product, **19**, were obtained in 38% and

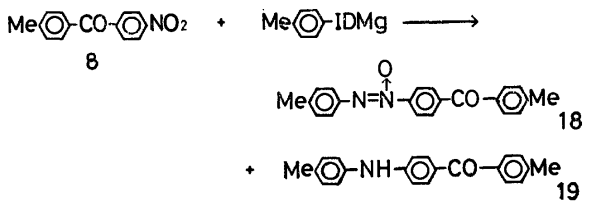

Scheme 7.

28% yields, respectively; the oxidative coupling product, 4,4′-dimethylazobenzene, was also isolated in 21% yield. The formation of **19** is reasonable, since the nitro group is responsible for the replacement in the reaction of 4-nitroquinoline *N*-oxide and related compounds with alkali alkoxides and alkanethiolates.[11] The present result, however, may be the first example for the replacement of nitro group in organomagnesium reactions.

All the results obtained in the reactions of Schemes 1—7 are preliminary ones, but they show the important role of the electron-accepting ability of the substrates.

Experimental

The melting points are uncorrected.

The bifunctional nitro compounds **1**—**7** were obtained commercially. The nitrobenzophenone, **8**, was prepared by p-nitrobenzoylation of toluene by the Friedel-Crafts method.

The procedures for the reactions and for the isolation of products were reported previously.[1-4]

The melting points, the results of elemental analyses, and the NMR data of the products **9**—**19** are summarized in Table 4. Among the NMR data, several aromatic proton signals consisting of two or three AB quartets are not assigned and the δ values are given in parentheses.

The support of this work by research grants from the Ministery of Education, Science and Culture (C-56540307) is gratefully acknowledged.

References

1) M. Ōkubo and S. Ueda, *Bull. Chem. Soc. Jpn.*, **53**, 281 (1980).
2) M. Ōkubo, S. Hayashi, M. Matsunaga, and Y. Uematsu, *Bull. Chem. Soc. Jpn.*, **54**, 2337 (1981).
3) M. Ōkubo, T. Takahashi, and K. Koga, *Bull. Chem. Soc. Jpn.*, **56**, 199 (1983).
4) M. Ōkubo and K. Koga, *Bull. Chem. Soc. Jpn.*, **56**, 203 (1983).
5) C. E. Bennett and P. J. Elving, *Collect. Czech. Chem. Commun.*, **76**, 3213 (1960).
6) M. Ōkubo and Y. Uematsu, *Bull. Chem. Soc. Jpn.*, **55**, 1121 (1982).
7) J. A. Castellano, J. E. Goldmacher, L. A. Barton, and J. S. Kane, *J. Org. Chem.*, **33**, 3501 (1968).
8) L. A. Bigelow and H. Eatough, *Org. Synth.*, Coll. Vol. I, 80 (1941).
9) K. Maruyama and T. Otsuki, *Bull. Chem. Soc. Jpn.*, **41**, 444 (1968).
10) P. Zuman, "Substituent Effects in Organic Polarography," Plenum Press, New York (1967), Chap. 3, p.55.
11) A. R. Katrizky and J. M. Lagowski, "Chemistry of the Heterocyclic *N*-Oxides," Academic Press, London (1971), p. 435.

The Ion-exchange Chromatography of Imino Derivatives of Glycine

Katsuhiro KAWASHIRO,* Shiro MORIMOTO, and Hideyuki YOSHIDA

Department of Chemical Engineering, Faculty of Engineering, Tokushima University, Minamijosanjima, Tokushima 770

(Received April 15, 1982)

The resolution of the six imino derivatives of glycine (Gly) by ion-exchange chromatography is described. The imino compounds included iminodiacetonitrile (**1**), iminodiacetamide (**2**), iminodiacetic acid (**3**), α-(cyanomethylamino)acetamide (**4**), α-(cyanomethylamino)acetic acid (**5**), and α-(carbamoylmethylamino)acetic acid (**6**). A mixture of **1**—**6** was chromatographed along with Gly, glycinamide, aminoacetonitrile, and NH_3 with an automatic amino acid analyzer using Aminex A-4 resin column (0.25ϕ × 50 cm) and sodium citrate buffers. When the initial buffer of pH 3.25 was changed to pH 6.50 15 min after beginning the analysis, these ten components were completely resolved. The analysis was completed in about 4.5 h. The stability of **1**, **4**, and **5** in aqueous media at room temperature was also studied.

In connection with chemical evolution, Ponnamperuma and Woeller[1] demonstrated that aminoacetonitrile (AAN) could be formed by an electric discharge through an anhydrous mixture of methane and ammonia (a simulated Jovian atmosphere) which was considered to resemble the primitive atmosphere of the Earth. Consequently, the role of AAN in aqueous media, as a precursor to polypeptides and amino acids, became of primary importance.[2-4] Chadha *et al.*[3] studied the reaction of AAN in aqueous solutions of pH 9. When the reaction products were examined by ion-exchange chromatography, peptides such as diglycine were not detected. After the reaction products were hydrolyzed and derivatized for gas chromatography, they identified glycine (Gly), iminodiacetic acid (**3**), and a small amount of nitrilotriacetic acid by gas chromatography-mass spectrometry. Recently, we investigated the reaction of AAN in aqueous ammoniacal solutions. When the reaction mixtures were examined by ion-exchange chromatography, a number of ninhydrin reactive products were eluted along with Gly and glycinamide (Gly-NH_2). On the basis of the results obtained by Chadha *et al.*[3,4] these products were considered to be imino derivatives of Gly, as shown in Fig. 1. Therefore, the resolution of these imino compounds by ion-exchange chromatography was necessary for identification and determination of the reaction products of AAN.

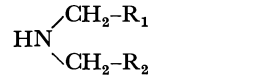

1: $R_1=R_2=C{\equiv}N$
2: $R_1=R_2=CONH_2$
3: $R_1=R_2=COOH$
4: $R_1=C{\equiv}N$, $R_2=CONH_2$
5: $R_1=C{\equiv}N$, $R_2=COOH$
6: $R_1=CONH_2$, $R_2=COOH$

Fig. 1. Imino derivatives of Gly.

Since an automatic amino acid analyzer based on ion-exchange chromatography was first devised by Spackman *et al.*[5] in 1958, not only the resolution of amino acids and related compounds but also analysis time has been much improved by many investigators. However, substances analyzed by this method have been limited to those of biological origin such as hydrolyzates of proteins, physiological fluids, and tissue extracts.[6] This paper deals with the resolution of **1**—**6** by ion-exchange chromatography.

Results and Discussion

Ion-exchange Chromatography. The six imino compounds, that is, iminodiacetonitrile (**1**), iminodiacetamide (**2**), **3**, α-(cyanomethylamino)acetamide (**4**), α-(cyanomethylamino)acetic acid (**5**), and α-(carbamoylmethylamino)acetic acid hydrobromide (**6**·HBr) were prepared in the present study as the authentic samples for ion-exchange chromatography. The latter three (**4**, **5**, and **6**·HBr) are new compounds.

Because AAN was considered to give not only the imino compounds (**1**—**6**) but also hydrolysis products such as Gly, Gly-NH_2, and NH_3 in aqueous media, the resolution of a synthetic mixture of these ten compounds with an amino acid analyzer was examined.

Figure 2 illustrates the resolution of them with a pH 3.25—6.50 sodium citrate buffer system. All the ten components were completely resolved from each other and the analysis time was about 4.5 h. A column of 0.25ϕ × 50 cm packed with a Bio-Rad spherical resin, Aminex A-4 (8% crosslinkage; particle size 20± 4 μm) was found to be adequate for the present analysis. Among the basic components, **4** was always eluted at the break-through point of the second buffer. The buffer change time of 15 min was found to be optimum; the elutions with a buffer change time longer than 15 min or shorter than 15 min, resulted in merely a

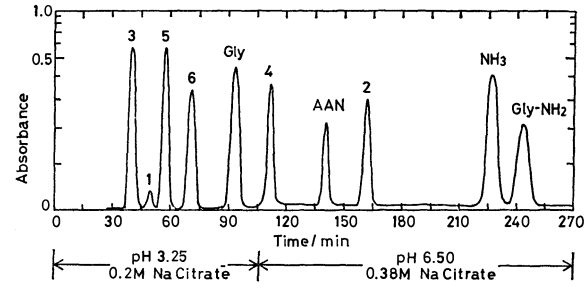

Fig. 2. Ion-exchange chromatogram of a mixture of imino derivatives of Gly (**1**—**6**) and related compounds. Conditions of chromatography are described in the Experimental Section. Charge amount of each component, 0.1 μmol. Elution was started using a pH 3.25 citrate buffer. A buffer change was made after 15 min to pH 6.50, and the break-through of the pH 6.50 buffer was observed at 108 min.

longer analysis time or the poor resolution of Gly and **4**, respectively.

As shown in Fig. 2, the components were eluted in a regular manner. Namely, compounds with the same *N*-substituent group (X) were eluted in the order of X–NH–CH_2–COOH (carboxylic acid), X–NH–CH_2–CN (nitrile), and X–NH–CH_2–$CONH_2$ (amide). For example, the compounds having carboxymethyl as an *N*-substituent group (X=CH_2–COOH) were eluted in the order of **3**, **5**, and **6**. The only exception is the case of the compounds (X=CH_2–CN), which were eluted in the order of **1** (nitrile), **5** (carboxylic acid), and **4** (amide). This reversed elution order of **1** and **5** could be explained in terms of the increased acidity of **1** due to a strong electron-attracting effect of the two cyano groups.

Figure 3 shows the elution behavior of the basic components with a pH 3.25—6.50 or a pH 3.25—5.28 citrate buffer system. Elution with a pH 3.25 buffer alone (D) resulted in a significantly longer analysis time, with the complete overlap of AAN and Gly–NH_2. The basic components, except for AAN and **2**, were eluted at almost constant positions regardless of the pH of a second buffer, so long as the buffer

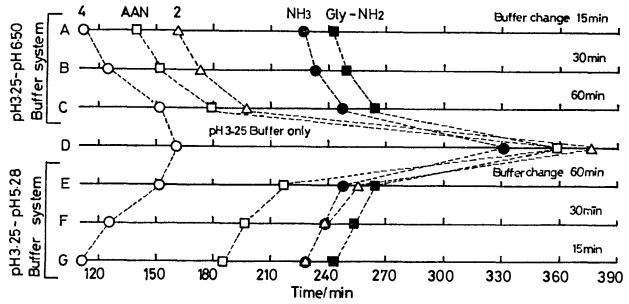

Fig. 3. Elution behavior of the basic components with various buffer systems.
Conditions of chromatography are described in the Experimental Section.

Table 1. Elution times and relative color constants of imino derivatives of Gly and related compounds[a)]

Compound	Elution time/min	Relative color constant[b)]
3	41	1.07
1	50	0.064
5	57	1.11
6	71	0.65
Gly	94	1.00
4	112	0.79
AAN	140	0.39
2	162	0.65
NH_3	227	1.23
Gly–NH_2	243	0.72

a) Conditions of chromatography are described in the Experimental Section. Elution was started using a pH 3.25 citrate buffer. A buffer change was made after 15 min to pH 6.50. b) The color constant refers to peak area per μmol of a compound. The peak area was calculated according to the conventional $H \times W$ method (Ref. 5). The color constant of Gly was 93.7 μmol^{-1}.

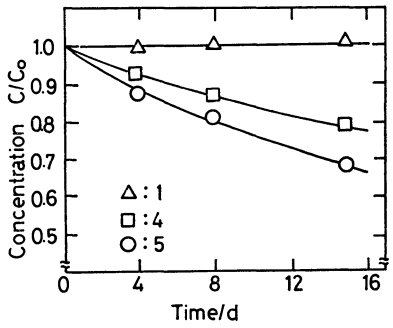

Fig. 4. Decomposition of α-amino nitriles (**1**, **4**, and **5**) in aqueous media (1 mM) at room temperature.

change time was unchanged. The elution times of AAN and **2** were very sensitive to the pH of a second buffer. Their elution was retarded remarkably with the pH 5.28 buffer, resulting in the poor resolution of NH_3, **2**, and Gly–NH_2 (E) or the complete overlap of NH_3 and **2** (F and G), in comparison with the elution with the pH 6.50 buffer. In this way, the basic components could be successfully resolved from each other by the use of the pH 3.25—6.50 buffer system.

Table 1 shows the elution times and the relative color constants of the ten components. It was evident that the color constant of **1** with ninhydrin was extremely poor compared with the other imino compounds, although the time of heating in the reaction bath of the amino acid analyzer was designed to be about 30 min.

Stability of the Imino Compounds in Aqueous Media. Among the imino compounds, α-amino nitriles such as **1**, **4**, and **5** were thought to be unstable in aqueous media due to the reverse Strecker reaction. Figure 4 shows the rate of decomposition of them in aqueous solutions (1 mM) (1 M=1 mol dm^{-3}) at room temperature. **4** and **5** were unstable and decomposed to 20.2 and 31.5%, respectively, in 15 d. Since **4** and **5** yielded Gly–NH_2 and Gly as the decomposition products, respectively, the unstability could be explained in terms of the reverse Strecker reaction as follows:

$$HN\begin{matrix}\diagup CH_2\text{–}CN \\ \diagdown CH_2\text{–}Y\end{matrix} + H_2O \longrightarrow H_2N\text{–}CH_2\text{–}Y + CH_2O + HCN$$

(Y=$CONH_2$ or COOH)

Unlike **4** and **5**, **1** was stable under these conditions. Hence, in the case of such unstable compounds, it is desirable to calibrate an amino acid analyzer with freshly prepared standard solutions.

Experimental

All the melting points were determined with a Yanagimoto micro melting point apparatus and were not corrected. IR spectra were taken with a Hitachi Model 285 Infrared spectrophotometer. ^{1}H-NMR spectra were measured with a Hitachi R-24B spectrometer using TMS as an internal reference. Thin layer chromatography was carried out on silica gel 60 F_{254}(Merck) using the following solvent system: *n*-BuOH–AcOH–H_2O (4:1:1, v/v). *S*-(*p*-methoxybenzyloxycarbonyl)-4,6-dimethyl-2-pyrimidinethiol(Z(OMe)–SDP) and

25% HBr–AcOH were obtained from Protein Research Foundation.

Ion-exchange Chromatography. Ion-exchange chromatography was carried out with a Sibata amino acid analyzer AA-600 under the following conditions: column, 0.25ϕ × 50 cm packed with Aminex A-4(Bio-Rad, 8%-crosslinked, sulfonic acid type cation exchange resin, particle size 20± 4 μm); flow rate of an eluent, 6 ml/h; flow rate of a ninhydrin solution,[5] 3 ml/h; jacket temperature, 30 °C; chart speed, 120 mm/h. Absorbance at 570 nm was measured by continuous photometry. Sodium citrate buffers of pH 3.25 (0.2 M Na), pH 5.28(0.35 M Na), and pH 6.50(0.38 M Na) were used as eluents. The former two buffers were obtained from Wako Pure Chemical Industries, Ltd. The pH 6.50 buffer was prepared according to the method of Moore *et al.*[7] using caprylic acid instead of phenol. Elution was started with the pH 3.25 buffer and the initial buffer was changed to a second buffer(pH 5.28 or 6.50) at an appropriate later time. A calibrated equimolar(0.1 μmol) mixture of the imino compounds(**1**—**5**, and **6**·HBr), Gly, Gly–NH_2·HBr, AAN·1/2 H_2SO_4, and NH_4·1/2 SO_4 was applied on the column of the amino acid analyzer.

Aminoacetonitrile Neutral Sulfate(AAN·1/2 H_2SO_4). Concd H_2SO_4(25.5 g, 0.25 mol) was gradually added to ethanol (EtOH) (125 ml). The temperature of the solution rose, but it was adjusted to 65—70 °C. Methyleneaminoacetonitrile (MAAN)[8] (34 g, 0.5 mol) was added gradually to it. In the beginning, MAAN dissolved, but after a certain point it ceased to dissolve. The mixture was warmed for 1 h(60 °C) on a water bath, and then kept in a refrigerator overnight. The precipitates were dissolved in H_2O(100 ml) and the undissolved material(MAAN) was removed by filtration. The product was precipitated by the addition of EtOH(600 ml) to the filtrate and then recrystallized from H_2O–EtOH; yield, 20 g(38%); mp, 160 °C(decomp)(lit,[9] mp, 165 °C); R_f, 0.27. Found: C, 23.03; H, 4.72; N, 26.76%. Calcd for $C_2H_5N_2O_2S_{0.5}$: C, 22.85; H, 4.79; N, 26.68%.

*Iminodiacetonitrile (**1**).* A solution of freshly distilled HCN(70 ml, 1.81 mol) and concd H_2SO_4(1 ml) in methanol (MeOH) (175 ml), was added to a suspension of MAAN (119 g, 1.75 mol) in MeOH (70 ml). The resulting suspension was warmed for 3 h(60 °C), and then refluxed at 75 °C for a further 30 min on a water bath, in a draft chamber. After the reaction mixture had been cooled to room temperature, the precipitates(MAAN) were removed by filtration. When the filtrate was cooled to 0 °C, **1** precipitated; this was processed with charcoal and then recrystallized from EtOH; yield, 85.7 g(52%); mp, 76—77 °C(lit,[10] 75 °C); R_f, 0.62.

*Iminodiacetamide (**2**).* A solution of dimethyl iminodiacetate hydrochloride(1.97 g, 10 mmol) in MeOH(15 ml) was treated with triethylamine (Et_3N) (1.4 ml, 10 mmol) at 0 °C. When diethyl ether(Et_2O) (60 ml) was added to the resulting solution, Et_3N·HCl precipitated and was removed by filtration. The filtrate was evaporated to give an oil (dimethyl iminodiacetate). Ammonolysis of the crude oil according to the method of Jongkees[11] gave **2**, which was recrystallized from MeOH: yield, 0.85 g(65%); mp, 141—143 °C(lit,[11] 143 °C); R_f, 0.17.

*Iminodiacetic Acid (**3**).* A solution of Gly(18.8 g, 0.25 mol) and chloroacetic acid(23.6 g, 0.25 mol) in 3 M LiOH (250 ml) was allowed to stand at room temperature for 6 d. When the solution was acidified with 6 M HCl(60 ml) under cooling, crystals precipitated; these were collected by filtration. The crystals(yield, 12.5 g; mp, 152—154 °C) were identified to be nitrilotriacetic acid by elementary analysis(Found: C, 37.53; H, 4.72; N, 7.47%. Calcd for $C_6H_9NO_6$: C, 37.70; H, 4.75; N, 7.33%. Lit,[12] mp, 142 °C). The filtrate was concentrated to give a syrup, which was dissolved in a minimum amount of H_2O. The half volume of the solution was applied on a column(Amberlite CG-120, acid form, 2ϕ × 90 cm), and then eluted with H_2O. The fractions containing **3** were collected and evaporated to give **3**. The remaining solution was also treated similarly. Recrystallization was performed from H_2O–EtOH; yield, 12.8 g(39%); mp, 225—228 °C(lit,[13] 225 °C); R_f, 0.09.

*α-(Cyanomethylamino)acetamide (**4**).* A mixture of Gly–NH_2·HBr(5.27 g, 34 mmol) and formalin(2.7 ml, 34 mmol) was cooled below 0 °C on an ice salt bath, and then a solution of NaCN(1.64 g, 34 mmol) in a minimum amount of H_2O was added dropwise with stirring. After the addition was completed, the stirring was continued for 3 h. The reaction mixture was extracted with ethyl acetate(AcOEt) (40 ml × 7), and the extract was dried (Na_2SO_4), filtered, and then evaporated to give **4**, which was recrystallized from AcOEt–Et_2O; yield, 0.90 g(27%); mp, 124—126 °C; R_f, 0.41: IR (KBr), 3380(NH), 2225(C≡N), and 1650 cm^{-1} (amide I); NMR(DMSO-d_6), δ=7.24, 7.05(2H, br, $CONH_2$), 3.63(2H, s, CH_2), 3.14(2H, s, CH_2), and 2.81(1H, br, NH). Found: C, 42.25; H, 6.07: N, 37.18%. Calcd for $C_4H_7N_3O$: C, 42.47; H, 6.24; N, 37.14%.

*Ethyl α-(Cyanomethylamino)acetate (**7**).*[14] A mixture of glycine ethyl ester hydrochloride(41.9 g, 0.3 mol) and formalin(25 ml, 0.3 mol) was cooled below 0 °C, and a solution of NaCN(14.7 g, 0.3 mol) in H_2O(30 ml) was added dropwise with stirring. After the addition was completed, the stirring was continued for 4 h. The reaction mixture was extracted with Et_2O(30 ml × 2), and the ethereal extract was dried (Na_2SO_4), filtered, and then evaporated to give a pale yellowish oil; yield, 32 g(75%); R_f, 0.49; NMR($CDCl_3$), δ= 4.20(2H, q, J=7 Hz, $C\underline{H}_2CH_3$), 3.59(2H, s, CH_2), 3.49 (2H, s, CH_2), 2.31(1H, s, NH), and 1.27(3H, t, J=7 Hz, $CH_2C\underline{H}_3$); ion-exchange chromatography (a pH 3.25—5.28 buffer system with the buffer change of 30 min), elution time 137 min.

*N-(p-Methoxybenzyloxycarbonyl)-α-(cyanomethylamino) acetic Acid Dicyclohexylammonium Salt (**8**·DCHA).* A mixture of **7** (7.10 g, 50 mmol), Z(OMe)–SDP(9.13 g, 30 mmol), and Et_3N(7 ml, 50 mmol) in $CHCl_3$ (50 ml) was stirred for 24 h at room temperature. The reaction mixture was washed with H_2O(25 ml × 5) and the $CHCl_3$ layer was dried(Na_2SO_4), filtered, and then evaporated to give a brown oil. The oily ethyl *N*-(*p*-methoxybenzyloxycarbonyl)-α-(cyanomethylamino)acetate was taken up in acetone(20 ml) and saponified as follows. 1 M NaOH(30 ml) was added to it and the resulting solution was stirred at room temperature for 2 h. After being acidified to pH 3 with 1 M HCl, the solution was extracted with AcOEt(50 ml × 5). The extract was washed with H_2O(50 ml × 3), dried(Na_2SO_4), filtered, and then evaporated to give a brown oil. The oil was dissolved in AcOEt(20 ml) and treated with DCHA(5 ml). When the solution was kept in a deep freezer overnight, **8**·DCHA precipitated and was recrystallized from $CHCl_3$–Et_2O; yield, 2.3 g(17%); mp, 152—154 °C; R_f, 0.61; IR (KBr), 2750—2400(NH_2^+), 2230(C≡N), and 1630 cm^{-1} (COO^-); NMR($CDCl_3$), δ=8.53(2H, br, NH_2^+), 7.45—6.70(4H, m, aromatic), 5.06(2H, s, CH_2O), 4.38(2H, s, CH_2), 3.90(2H, s, CH_2), 3.78(3H, s, OCH_3), and 2.90, 1.87—1.20(22H, m, cyclohexyl). Found: C, 65.12; H, 8.30; N, 8.86%. Calcd for $C_{25}H_{37}N_3O_5$: C, 65.34; H, 8.11; N, 9.14%.

*α-(Cyanomethylamino)acetic Acid (**5**).* To a suspension

of **8**·DCHA(1.0 g, 2.2 mmol) in AcOEt(50 ml) was added 0.2 M H_2SO_4 dropwise with shaking until the solution became free of suspended material. The AcOEt layer was washed with H_2O(20 ml×3), dried (Na_2SO_4), filtered, and then evaporated to give a pale brown oil. When the oil was dissolved in trifluoroacetic acid(3 ml) at 0 °C, the solution turned red. After 5 min, anisole(1 ml) was added to the solution; the mixture became colorless on standing at room temperature for 30 min. Et_2O(20 ml) was added and the precipitates were dissolved in H_2O(20 ml). After the undissolved materials had been removed by filtration, the filtrate was concentrated to a small volume. On the addition of EtOH and a large amount of Et_2O, free **5** precipitated; yield, 80 mg(32%); mp, 142—144 °C; R_f, 0.21: IR(KBr), 2750—2500(NH_2^+), 2250(C≡N, weak), and 1580 cm^{-1} (COO^-); NMR(DMSO-d_6), δ=6.48(2H, br, NH_2^+), 3.65 (2H, s, CH_2), and 3.31(2H, s, CH_2). Found: C, 41.95; H, 5.34; N, 24.91%. Calcd for $C_4H_6N_2O_2$: C, 42.11; H, 5.30; N, 24.55%.

*α-(Carbamoylmethylamino)acetic Acid Hydrobromide (**6**·HBr).* **8** prepared by decomposition of its DCHA salt(1.0 g, 2.2 mmol), was treated with anhydrous 25% HBr–AcOH(1.5 ml) at room temperature to give a clear solution with the evolution of CO_2. After 30 min, crystals were precipitated by the addition of Et_2O(30 ml); these were dissolved in H_2O (5 ml). After filtration, the solution was concentrated to a small volume and EtOH(10 ml) was added. When the solution was kept in a deep freezer, **6**·HBr precipitated and was recrystallized from H_2O–EtOH; yield, 180 mg (38%); mp, 211—213 °C; R_f, 0.42; IR(KBr), 2750—2600 (NH_2^+), 1740(COOH), and 1680 cm^{-1}(amide I); NMR (DMSO-d_6), δ=8.90(2H, br, NH_2^+), 7.90, 7.54(2H, br, $CONH_2$), 3.91(2H, s, CH_2), and 3.77(2H, s, CH_2). Found: C, 22.82; H, 4.39; N, 13.20%. Calcd for $C_4H_9N_2O_3Br$: C, 22.55; H, 4.26; N, 13.15%.

Decomposition of the Imino Compounds. An aqueous solution of each imino compound(1 mM) was prepared and allowed to stand at room temperature. An aliquot(0.1 ml) of the solution was analyzed with the amino acid analyzer at appropriate intervals. Decomposition products were identified by comparing their elution times with those of the authentic samples. **4** and **5** yielded Gly–NH_2(19.3%) and Gly(26.5%), respectively, on decomposition with H_2O in 15 d. The other imino compounds were found to be stable under these conditions.

References

1) C. Ponnamperuma and F. Woeller, *Curr. Mod. Biol.*, **1**, 156 (1967).
2) R. E. Moser and C. N. Matthews, *Experientia*, **24**, 658 (1968).
3) M. S. Chadha, L. Replogel, J. Flores, and C. Ponnamperuma, *Bioorg. Chem.*, **1**, 269 (1971).
4) G. H. Loew, M. S. Chadha, and S. Chan, *J. Theor. Biol.*, **35**, 359 (1972).
5) D. H. Spackman, W. H. Stein, and S. Moore, *Anal. Chem.*, **30**, 1190 (1958).
6) K. Maruyama and N. Shindo, *J. Chromatogr.*, **143**, 137(1977) and references cited therein.
7) S. Moore, D. H. Spackman, and W. H. Stein, *Anal. Chem.*, **30**, 1185 (1958).
8) R. Adams and W. D. Langley, *Org. Synth.* Coll. Vol. I, 355 (1943).
9) A. Klages, *Ber.*, **36**, 1506 (1903). Aminoacetonitrile hydrogen sulfate(AAN·H_2SO_4) was prepared first from MAAN and H_2SO_4 (1 equiv.), and then converted to AAN·1/2 H_2SO_4 by the treatment of aq. $BaCO_3$(0.5 equiv.).
10) J. R. Bailey and D. F. Snyder, *J. Am. Chem. Soc.*, **37**, 938 (1915). **1** was prepared from MAAN and anhydrous HCN in a pressure flask at room temperature for 24 h, in the presence of a catalytic amount of concd HCl.
11) W. J. A. Jongkees, *Recl. Trav. Chim. Pays-Bas*, **27**, 287 (1909).
12) J. V. Dubsky, *Ber.*, **49**, 1041 (1916).
13) W. Eschweiler, *Justus Liebigs Ann. Chem.*, **278**, 229 (1894). **3** was prepared by refluxing **1** in aq $Ba(OH)_2$.
14) H. Scheibler and H. Neef, *Ber.*, **59**, 1500 (1926).

Anion-catalyzed Phase-transfer Catalysis. I. Application to Diazo-coupling Reactions

Hidetoshi Iwamoto,† Masaji Yoshimura,** Takaaki Sonoda, and Hiroshi Kobayashi*

Research Institute of Industrial Science, Kyushu University 86, Kasuga, Fukuoka 816

† *Department of Molecular Science and Technology, Graduate School of Engineering Sciences, Kyushu University 39, Kasuga, Fukuoka 816*

(Received September 17, 1982)

Anion-catalyzed phase-transfer catalysis was evidenced in the diazo-coupling reactions of the arenediazonium ion with a range of diazophile components in liquid-liquid- and liquid-solid two-phase systems. The tetrakis[3,5-bis(trifluoromethyl)phenyl]borate ion was effective as an anionic catalyst to accelerate the reactions. Comparisons of the reaction rates in the two-phase system with those in solution systems indicated that the acceleration was due to the increased activity of the cationic reagent, partly by solubilization and partly by the dehydration of such cationic species in the nonpolar organic phase.

A great number of studies of phase-transfer catalysis (PTC) have appeared in the literature during the last decade.[1] All but a few applications thus far reported have been nucleophilic or base-mediated reactions catalyzed by an oleophilic organic cation, such as the tetraalkylammonium ion or the crown ether–metal complex. An electrophilic reaction may also proceed in a PTC manner if an appropriate anionic catalyst is provided. A few examples of this class have been verified in some reactions of the arenediazonium ion,[2] though such attempts at verification have not always been successful. This seems to have been due to the lack of an efficient anionic catalyst suitable for this purpose. In fact, very few stable organic anions have been known except for the conjugate bases of organic acids. Among them we directed our attention to the tetraphenylborate (TPB) anion as a possible anionic phase-transfer catalyst. The structural features of TPB were considered to be that the negative charge was formally localized on the central boron atom and that the hydrophilic-anion center was shielded by lipophilic phenyl ligands configured in a tetrahedrally symmetrical array.[3] Various types of homolog and their salts are conveniently discussed in the literature.

In the anion-catalyzed PTC process, the reactions were generally acid-mediated, and the leaving group upon the reaction was a proton or protonated species. In this respect, the catalyst anion had to be stable enough in an acid medium. Also, the reaction should be conducted in a nonpolar organic solvent immiscible with water in a manner like that formerly used in the traditional PTC process.

The TPB anion was, however, highly susceptible to proton-catalyzed decomposition,[4] and its solubility in nonpolar organic solvents was not always satisfactory for a phase-transfer catalyst.[5] Therefore, our efforts were focussed on improving the drawback of chemical instability[6] and, at the same time, attaining a higher solubility into the organic media by virtue of introducing a trifluoromethyl group on the phenyl rings of TPB.[7]

During the course of our studies aimed to producing the present tetrakis[3,5-bis(trifluoromethyl)phenyl]borate (TFPB) anion,[8] an application of the PTC process was reported in the acid-mediated hydrolysis of esters by the use of an ordianry TPB anion as a phase-transfer catalyst,[9] though it was shortly thereafter revealed to be false;[10] TPB is not long-lasting in such acid media.

The present paper will describe phase-transfer catalyzed diazo-coupling reactions, in which a typical onium ion acts as an electrophile, by the use of TFPB as a catalyst in two-phase systems consisting of a non-donating, inert organic phase and a solid or an aqueous one.[11] It should be noted that the present catalyst was contrived to be more oleophilic and especially durable in acid media than the parent TPB anion; sodium TFPB remained intact for more than 9 h in a vigorously stirred two-phase system of dichloromethane and 4 mol dm^{-3} sulfuric acid, and the second-order rate constants of the acid-catalyzed hydrolysis of TFPB and TPB salts in aqueous ethanol were 1.3×10^{-4} and 1.6×10^{-3} mol^{-1} dm^3 s^{-1} at 25 °C respectively. Under the present experimental conditions, therefore, the great majority of TFPB anions remain in the organic phase, and one can neglect the acid-catalyzed decomposition of TFPB by the proton which is liberated on the electrophilic aromatic substitution.

Results and Discussion

Diazo-coupling in a Liquid-solid PTC System. The dissolution of benzenediazonium tetrafluoroborate (**1**) into a benzene solution was followed by monitoring the absorbance of **1** at 300 nm. The absorbance of a supernatant containing sodium TFPB increased with the lapse of time and attained saturation within 1 h, while the dissolution rate varied with the fineness of the powdered **1**. Without the addition of sodium TFPB, we observed no indication of **1** being dissolved in the solvent; the absorbance was kept at nothing.

The suspension of the powdered **1** in a benzene solution of twice the molar amount of *N*,*N*-dimethylaniline (**2**) gave no color change, even upon vigorous agitation. The addition of a 20% molar amount of sodium TFPB to the suspension with moderate stirring at room temperature caused a rapid red-color development, where the added sodium TFPB was dissolved in the solution.[12] A 1-h reaction then afforded the coupling

** Present address: The Central Research Institute, Mitsui-Toatsu Chemical Co., Ltd., Kasama, Tozuka-ku, Yokohama 247.

product, 4-dimethylaminoazobenzene (**3**), in an 86% yield. In a similar manner, twice the molar amount of phenol (**4**) gave 4-hydroxyazobenzene (**5**) in a quantitative yield after a 3-h reaction in the presence of twice the molar amount of 2,6-dimethylpyridine (**6**). No diazo-coupling with phenol in the organic phase proceeded without the addition of a base such as **6**.[13]

The acceleration of the diazo-coupling rate can be attributed predominantly to the dissolution of the arenediazonium ion into the solvent by ion-pairing with the TFPB anion. The coupling reactions in the absence of the TFPB anion were negligible, though possibly taking place on the surface of the solid diazonium salt (**1**).

Diazo-coupling in a Liquid-liquid PTC System. In a two-phase system consisting of an aqueous 4-nitrobenzenediazonium tetrafluoroborate (**7**) and a dichloromethane solution of an equimolar amount of 9-ethylcarbazole (**8**), the vigorous agitation of the two-phase mixture resulted in a faint red coloration after a while, but no more color was developed by further, prolonged agitation. The addition of one-fifteenth the molar amount of sodium TFPB to the mixture immediately turned it dark red. The two-phase system formed no emulsion and was separated into two layers as soon as agitation stopped. After 3 h of continuous, vigorous stirring, the diazonium test by *N,N*-dimethylaniline was negative to the aqueous phase, and then the coupling product was isolated in an 80% yield. In a similar manner, the reactions of **7** with two kinds of diphenylamines, **9** and **10**, and three kinds of anisole derivatives, **11**, **12**, and **13**, gave the corresponding coupling products. The results are summarized in Table 1. A comparison of the latter three examples seemed to suggest a rather large substituent effect of diazophile components upon the reaction rate and yield. It is worthwhile noting that the coupling of **7** with **8** was found to afford the coupling product in a yield of less than a 2% after a 5-h reaction when the reaction was carried out in aqueous acetic acid.[14] From the comparisons of the yield and the reaction period, one can readily notice the efficiency of the present PTC system.

Diazotization and diazo-coupling could be conducted successively in one pot without any isolation of diazonium salt. The process was exemplified by PTC, consisting of a dichloromethane solution of **8** and an aqueous solution of 4-nitrobenzenediazonium salt, in the presence of a 1% molar amount of sodium TFPB. The conversion attained up to 94%, based upon the amount of sodium nitrite added after the 5-h reaction at room temperature. This procedure can provide a convenient method of diazo-coupling in general; it might be especially useful in reactions with the diazonium salts, which are too labile to be isolated.

Table 1. Phase-transfer catalyzed diazo-coupling in an aqueous-CH_2Cl_2 two-phase system[a]

Diazophile	Reaction time h	Yield[b] %
9-Ethylcarbazole (**8**)	3	80
Diphenylamine (**9**)	2	76
N-Methyldiphenylamine (**10**)	3	85
Anisole (**11**)	48	10[c,d]
m-Methylanisole (**12**)	12	50[d]
m-Methoxyanisole (**13**)	2	85[e]

a) The reaction was carried out at room temperature. b) Yield of the isolated product. c) A 10-fold molar excess of the diazophile was added. d) The aqueous phase was buffered at pH 7. e) The aqueous phase was not buffered, and the aqueous phase was found to be acid after the reaction.

Diazo-coupling in Homogeneous Phases. Kinetics and Mechanism. In connection with the diazo-coupling in liquid-liquid two-phase systems, the reaction rates were examined in homogeneous solution phases of aqueous and non-donating inert organic solvents separately. A solution of arenediazonium TFPB in such an organic solvent was prepared by ion exchange between the corresponding arenediazonium tetrafluoroborate in the solid state and sodium TFPB dissolved in the organic solvent to be examined. The kinetics of the diazo-coupling reaction of *N,N*-dimethylaniline (**2**) with benzenediazonium salt was followed under the pseudo-first-order conditions in the latter. A general expression of the reaction rate was given by Eq. 1, with the assumption that no exchange of the diazonium ion occurred between the ion pair of BF_4^- and that of $TFPB^-$ in the solution phase;

$$d[\text{Product}]_t/dt = k_1'[ArN_2^+ \cdot TFPB^-] + k_1''[ArN_2^+ \cdot BF_4^-], \quad (1)$$

where k_1' and k_1'' were the conditional rate constants concerning the respective diazonium salts. The ratio of $[ArN_2^+ \cdot BF_4^-]_{t=0}/[ArN_2^+ \cdot TFPB^-]_{t=0}$ in chloroform, for example, was estimated, from the ratio of $[\text{Product}]_{t=\infty}$ in the absence of the TFPB anion to that in the presence of the same anion, to be about 5%.

In the absence of TFPB salt, the first term was zero, irrespective of the reaction medium; then, assuming $[\text{Product}]_{t=0}=0$, we obtained:

$$\ln([\text{Product}]_{t=\infty}) - \ln([\text{Product}]_{t=\infty} - [\text{Product}]_t) = k_1''t. \quad (2)$$

Excellent pseudo-first-order kinetic plots were obtained according to Eq. 2 with a correlation coefficient (γ) greater than 0.99 in each system of the tetrafluoroborate with **2** as well as **4**.

An examination of the rate constants indicated that the reactions in dry organic solvents were second-order in **2**, while in aqueous buffers it was first-order also in **2**. These kinetic orders, in accordance with Bartsch's observation,[15] indicate that, in the dry organic phase, the reaction rate is determined by the stage of deprotonation from a σ-complex, and that the reaction requires an equimolar amount of the proton-accepting base, as is observed in the diazo-coupling of phenol in a solid-liquid PTC system. In the aqueous phase, the formation of the σ-complex would be the rate-determining step, and the subsequent deprotonation would proceed rapidly, promoted by a large excess of the water base. When the reaction was conducted in a wet chloroform which had been saturated in advance with an aqueous buffer such as would occur in an actual liquid-liquid PTC

Table 2. Rate constants of the diazo-coupling of *N,N*-dimethylaniline with benzenediazonium tetrafluoroborate (**1**) and -TFPB (**11**) in aqueous and organic solvents at 25 °C

Solvent	Third-order rate constant, k_3/mol^{-2} dm^6 s^{-1}		Second-order rate constant, k_2/mol^{-1} dm^3 s^{-1}
	1	**11**	**1**
Benzene	c)	7.1×10^4	—
Chloroform			
anhydrous	2.9×10^4	4.6×10^5	—
wet[a]	1.02×10^3	—	1.6
Aqueous buffer[b]	—	—	1.7×10^{-1}

a) Saturated with the aqueous buffer at 25 °C (*ca.* 6×10^{-2} mol dm^{-3} of water). b) pH 7.02. c) Not measurable due to the low solubility of **1**.

system, the kinetic behavior was again first-order in benzenediazonium salt, while the overall reaction order in **2** was not a simple one. Instead, the kinetic data were consistent with the rate expression of a sum of two terms, one being first-order, and the other, second-order, in **2**. The two terms conceivably correspond to the respective deprotonating paths simultaneously taking place in the solution, the former, to that by the water base present in the wet organic phase, and the latter, to that by **2** itself. The rate constants thus obtained are summarized in Table 2.

Comparisons of the rate constants concerning the fluoroborate (**1**) indicate that the k_3 in wet chloroform was reduced to 1/30 of that in the dry solvent, while the k_2 in the aqueous buffer was lowered to 1/15 of that in the wet chloroform, despite the increase in the water base in the former; the reduced reactivity can be ascribed to the stabilization of the cationic reagent due to hydration in such wet media.

It can also be seen that the presence of TFPB in a benzene solution caused a distinct difference in the reaction rate, since practically no arenediazonium ion was transferred into the organic phase without the TFPB catalyst. Also, a comparison of k_3 values of **1** and **11** in dry chloroform solutions indicates that the coupling reaction with the diazonium ion paired with TFPB proceeded about sixteen times faster. Comparisons of the k_1' and k_1'' values in the reactions with phenol of an equal concentration reveal a parallel tendency, with the rate three times faster. If the ratio of $[ArN_2^+\cdot BF_4^-]_{t=0}/[ArN_2^+\cdot TFPB^-]_{t=0}$ is taken into account, the contribution due to the second term in Eq. 1 can be neglected in practice. The observed acceleration caused by TFPB is presumably to be ascribed to the larger size of the counter anion upon ion pairing in nonpolar organic solvents.[16]

Kinetics and Mechanism of PTC. The kinetics in the solution phases suggested that the reaction scheme

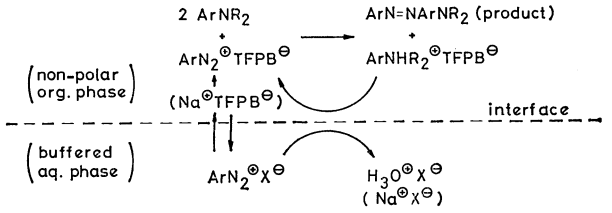

Fig. 1. PTC scheme of diazo-coupling reaction in a two-phase system.

of the present PTC cycle was as is illustrated in Fig. 1. At the beginning of the reaction, the diazonium ion was exchanged for the sodium ion of the catalyst at the interface, solubilized into the organic phase, and coupled with the diazophile dissolved therein, to give a product of azo dye;

$$(Na^+\cdot TFPB^-)_{org} + (ArN_2^+)_{aq} \overset{K_1}{\rightleftharpoons} (ArN_2^+\cdot TFPB^-)_{org} + (Na^+)_{aq}, \quad (3)$$

where

$$K_1 = [ArN_2^+\cdot TFPB^-]_{org}[Na^+]_{aq}/[Na^+\cdot TFPB^-]_{org}[ArN_2^+]_{aq} \quad (4)$$

and

$$[ArN_2^+\cdot TFPB^-]_{org} + [Diazophile]_{org} \xrightarrow{k_2} [Product]_{org} + [H_3O^+\cdot TFPB^-]_{org}, \quad (5)$$

where we assumed a slow coupling reaction relative to the mass-transfer between the two phases under an efficient stirring; the rate expression was then given by Eq. 6:

$$d[Product]_{org}/dt = k_2[ArN_2^+\cdot TFPB^-]_{org}[Diazophile]_{org}. \quad (6)$$

The liberated proton, which was in the form of an oxonium ion or some other protonated species, formed an ion pair with the TFPB anion to be transported to the interface; the proton was thrown out of the organic phase in exchange for the diazonium ion, which was used in the next PTC cycle:

$$[H_3O^+\cdot TFPB^-]_{org} + [ArN_2^+]_{aq} \overset{K_2}{\rightleftharpoons} [ArN_2^+\cdot TFPB^-]_{org} + [H_3O^+]_{aq}, \quad (7)$$

where

$$K_2 = [ArN_2^+\cdot TFPB^-]_{org}[H_3O^+]_{aq}/[H_3O^+\cdot TFPB^-]_{org}[ArN_2^+]_{aq}. \quad (8)$$

Provided the thermodynamic activities of the sodium and diazonium ions were maintained constant throughout the reaction period in an aqueous buffer, then the ratios of $[Na^+]_{aq}/[ArN_2^+]_{aq}$ and $[H_3O^+]_{aq}/[ArN_2^+]_{aq}$ were constant; they are represented by the symbols of Φ_1 and Φ_2 respectively.

Since the initial concentration of TFPB, Q_0, was given by Eq. 9, the concentration of the diazonium ion in the organic phase, $[ArN_2^+\cdot TFPB^-]_{org}$, was derived to be constant, as is given in Eq. 10, by com-

bining Eqs. 4, 8, and 9:

$$Q_0 = [Na^+ \cdot TFPB^-]_{org} + [ArN_2^+ \cdot TFPB^-]_{org} + [H_3O^+ \cdot TFPB^-]_{org}, \quad (9)$$

$$[ArN_2^+ \cdot TFPB^-]_{org} = Q_0/(\Phi_1/K_1 + \Phi_2/K_2 + 1). \quad (10)$$

In other words, the diazonium ion in the organic phase was supplied from the aqueous phase so fast, relative to the consumption rate by the reaction, that the concentration of the ion pair of $ArN_2^+ \cdot TFPB^-$ in the organic phase could be maintained at a steady level. Consequently, the reaction became apparently first-order only in the diazophile in the organic phase, as is expressed in Eq. 11:

$$d[Product]_{org}/dt = k_{app}[Diazophile]_{org}, \quad (11)$$

where;

$$k_{app} = k_2 Q_0/(\Phi_1/K_1 + \Phi_2/K_2 + 1) = k_2' Q_0. \quad (12)$$

Equation 12 indicated that the apparent first-order rate constant, k_{app}, was linearly proportional to the catalyst concentration, Q_0.

Since the total moles of diazophile and product was always equal to the initial moles of diazophile, the rate equation was then given by Eq. 13 or by Eq. 14 of an integrated form:

$$d[Product]_{org}/dt = k_{app}([Diazophile]_{org,0} - [Product]_{org}), \quad (13)$$

$$\ln([Diazophile]_{org,0}/([Diazophile]_{org,0} - [Product]_{org})) = k_{app}t. \quad (14)$$

The resulting formulations in the present process are quite analogous to those derived by Starks for the traditional cation-catalyzed PTC process.[17] The only essential difference is that each ionic species has a sign of charge which is opposite to that of the corresponding one in the traditional process.

Conditions such as those which Eqs. 11 and 13 were premised on could be accomplished in the diazo-coupling of 9-ethylcarbazole (**8**) in dichloromethane with a ten-fold excess of 4-nitrobenzenediazonium tetrafluoroborate (**7**) in an aqueous buffer in the presence of sodium TFPB if the reaction mixture was stirred at a speed such that the stirring was no longer rate-limiting.

The effect of stirring in the two-phase system is shown in Fig. 2. The initial rates were compared at various stirring speeds in the reaction of **8** with **1** in dichloromethane under an apparently first-order condition in **8**. The results indicated that, at a stirring speed higher than 400 min^{-1}, the reaction was no longer of an interfacial phenomena.

The kinetics of the formation of the azo dye from **7** and **8** was followed by monitoring the absorbance at 430 nm at 25.0 °C. Apparent first-order kinetic plots, mostly covering more than one half-life of the diazophile, were obtained with a correlation coefficient (γ) greater than 0.99, as is summarized in Table 3. The apparent rate constants thus obtained were linearly proportional to the catalyst concentration with a γ value of 0.998 in its range from 5.15×10^{-5} to 2.00×10^{-4} mol dm^{-3}, consistent with Eq. 12; the gradient of the correlation line gave the overall k_2' value of 8.9 mol^{-1} dm^3 s^{-1} in the present PTC system.

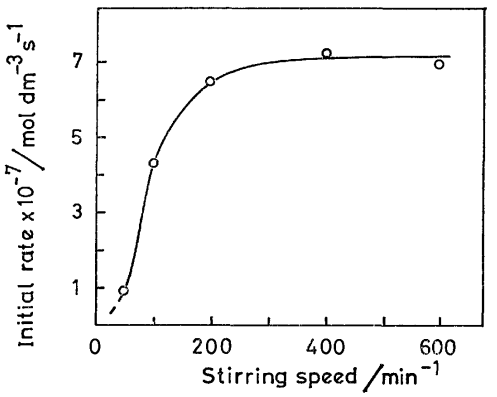

Fig. 2. Dependence of the initial reaction rate upon the stirring speed in the two-phase system.

The kinetics of the present model reactions in the two-phase system, though the diazophile and diazonium components examined fell within a rather limited range, indicated the catalyst turnover in the course of the PTC cycle and a remarkable acceleration of the *C*-coupling rate in non-donating organic solvents, irrespective of the reactivity of the diazophile component. Recently Griffiths and his co-workers reported on diazo-coupling in the PTC manner by the use of dodecylbenzenesulfonate (DBS) in a dichloromethane-aqueous buffer two-phase system.[2b] The DBS in their system, however, seems not always efficient as a phase-transfer catalyst; *e.g.*, PTC using DBS took 48 h to obtain a 44% yield from **8** and 4-nitrobenzenediazonium chloride, showing a great difference from the result of the present one-pot operation. A lower catalytic efficiency of DBS is consistent with the steric effect of an uncrowded anionic center of the sulfonate, which would favor the formation of a tight ion pair in nonpolar organic solvents and would consequently, decrease the reactivity of the counter cation. Also, they mentioned that, upon the diazo-coupling with arylamines in an anion-catalyzed PTC manner, the nucleophilicity of the amino nitrogen might affect the reaction site so as to cause *N*-coupling prior to *C*-coupling. However, such reaction behavior was unlikely so far as we have examined the present system; instead, *N*-coupling was seemingly observed only in

Table 3. Apparent first-order rate constants, k_{app}, in the diazo-coupling of 4-nitrobenzenediazonium salt with 9-ethylcarbazole in the two-phase system

$[TFPB^-]/10^{-5}$ mol dm^{-3}	5.15	7.7	10.0	15.0	20.0
Observed range of conversion/%	41	54	57	72	85
$k_{app}/10^{-4}$ s^{-1}	4.3	7.2	9.5	13.3	17.9
γ	0.992	0.996	0.996	0.998	0.995

cases of the absence of an effective proton-accepting base.

Experimental

Diazo-coupling in Liquid-solid PTC Systems. Into a stirred suspension of powdered benzenediazonium tetrafluoroborate (**1**)[18] (50 mg, 0.26 mmol) in benzene (10 ml) we added *N,N*-dimethylaniline (**2**) (66 mg, 0.55 mmol). The mixture was then colored pale yellow, but prolonged stirring caused no further reaction and gave no coupling product. Into a stirred mixture of the same compositions we added sodium TFPB (48 mg, 0.05 mmol). The mixture immediately turned red. We then kept stirring it at room temperature for 1 h. The resulting benzene layer was evaporated to dryness. The residual red solid was chromatographed on a silica-gel column; the fraction eluted with hexane gave yellow, crystalline 4-dimethylaminoazobenzene (49 mg, 86% yield) melting at 118 °C.[19]

The reaction with phenol was conducted in a similar manner except that an equimolar amount of 2,6-dimethylpyridine was added as a proton-accepting base. 4-Hydroxyazobenzene was obtained from a chromatographic fraction eluted with dichloromethane on a silica-gel column. Mp 154 °C.[20] The yield was quantitative when a double molar amount of phenol was used.

Diazo-coupling in Liquid-liquid PTC Systems. A mixture of an aqueous solution (25 ml) of 4-nitrobenzenediazonium tetrafluoroborate (**7**)[21] (70 mg, 0.3 mmol) and a dichloromethane solution (25 ml) of 9-ethylcarbazole (**8**) (55 mg, 0.3 mmol) and sodium TFPB (20 mg, 0.02 mmol) were agitated by means of a screw propeller rotating at 700 min^{-1} [22] for 3 h at room temperature; the aqueous layer was then negative to a diazonium test by *N,N*-dimethylaniline. The organic layer was evaporated to dryness. 9-Ethyl-3-(4-nitrophenylazo)carbazole (80 mg) was isolated from a chromatographic fraction eluted with dichloromethane on a silica-gel column. Recrystallization from methanol–dichloromethane gave red needles melting at 180—182 °C.[14] Found: C, 69.53; H, 4.72; N, 16.15%; *m/e*, 344 (M^+). The yield is tabulated in Table 1, together with those of the following reactions.

The reactions with diphenylamine (**9**) and *N*-methyldiphenylamine (**10**) were conducted in a similar manner to give 4-(4-nitrophenylazo)diphenylamine[23] of dark red needles melting at 160 °C[23] from methanol–dichloromethane (Found: C, 67.65; H, 4.15; N, 17.50%; *m/e*, 318 (M^+)) and 4-(4-nitrophenylazo)-*N*-methyldiphenylamine[24] of red needles melting at 174—175 °C from methanol-dichloromethane. Found: C, 68.46; H, 5.00; N, 16.79%; *m/e*, 332 (M^+). Calcd for $C_{19}H_{16}N_4O_2$: C, 68.66; H, 4.85; N, 16.86 %; M, 332. UV_{max} (CH_2Cl_2) 474 nm (ε 31900); ^{13}C-NMR ($CDCl_3$) δ=114.29, 122.77, 124.68, 125.61, 125.93, 126.22, 129.93, 144.99, 147.10, 147.62, 152.63, and 156.61; ^{1}H-NMR ($CDCl_3$) δ=3.40 (3H, s, =N-CH_3), 6.78 (2H of =N-C_6H_4-N_2-, d, J=5 Hz), 7.27 (5H, m, =N-C_6H_5), 7.77 (2H of =N-C_6H_4-N_2-, d, J=5 Hz), 7.80 (2H of -N_2-C_6H_4-NO_2, d, J=4.5 Hz), and 8.22 (2H of -N_2-C_6H_4-NO_2, d, J=4.5 Hz). The ^{1}H- and ^{13}C-NMR spectra were compatible with the assigned structure.

The reactions with anisoles were conducted in a mixture of 10 ml of a dichloromethane solution and 10 ml of an aqueous solution buffered with disodium hydrogenphosphate and potassium dihydrogenphosphate (2.0×10^{-3} mol dm^{-3} each) at pH 7.02. Each product was obtained from a chromatographic fraction eluted with dichloromethane on a silica-gel column. 4-(4-Nitrophenylazo)anisole; yellow crystallites melting at 140 °C.[25] MS: *m/e*, 257 (M^+). 4-(4-Nitrophenylazo)-3-methylanisole; red fibriles melting at 138 °C.[26] MS: *m/e*, 271 (M^+). 4-(4-Nitrophenylazo)-3-methoxyanisole; red fibriles melting at 155 °C.[27] Found: C, 58.28; H, 4.66; N, 14.56%; *m/e*, 287 (M^+).

Diazo-coupling in Liquid-liquid PTC System by One-pot Operation. The aqueous solution of diazonium salt was prepared by the addition of an aqueous sodium nitrite (0.170 g, 2.47 mmol, in 2 ml of water) to a solution of 4-nitroaniline (0.386 g, 2.80 mmol) in 2 mol dm^{-3} hydrochloric acid (7 ml) at 0 °C. After 1.5-h stirring, a nitrous acid test by the use of potassium iodide and starch was negative. The diazonium salt solution was stirred vigorously, together with a dichloromethane solution (20 ml) of 9-ethylcarbazole (**8**) (0.501 g, 2.57 mmol) and sodium TFPB (20 mg, 2.15×10^{-2} mmol). The absorbance of the azo dye was monitored at 430 nm. After a 5-h reaction, a diazonium test using *N,N*-dimethylaniline was negative to the aqueous phase, and the absorbance attained a plateau. The yield of azo dye was estimated by the absorbance to be 94%, based upon the amount of sodium nitrite added.

Kinetics in Solution Phases. A suspension of the diazonium salt (**1**) (10 mg, 0.05 mmol) in benzene or chloroform (50 ml) was shaken for 1 h at 25 °C with or without the addition of sodium TFPB (5 mg), the amount of which had previously been confirmed to be enough for the saturation in benzene,[12] while it dissolved completely in chloroform. The residual solid was filtered off if present. The benzene filtrate or chloroform solution was diluted with the same solvent to 10 times the original volume when TFPB was added. No dilution was needed in the absence of TFPB. An aliquot (2.00 ml) was placed in a septum-capped 10-mm photometric cell previously maintained at 25.0 °C. The absorbance was monitored immediately after the addition of a diazophile solution (1.00 ml) into the cell through the septum by means of a syringe.

The key bands for the determination of azo dyes in benzene and chloroform solutions were as follows: λ_{max} and (ε) for 4-dimethylaminoazobenzene, 410 nm (28000) and 410 nm (26000) respectively, and those for 4-hydroxyazobenzene, 345 nm (24000) and 345 nm (20000), respectively. The former azobenzene showed an ε value of 19000 at λ_{max} of 410 nm in a methanol–water (6:4 in volume) mixture; this value was used for the kinetic determinations of the azo dye in an aqueous solution buffered at pH 7.02. The resulting azo dye was less soluble in the aqueous solution, and the absorbance was followed until the reaction mixture became cloudy.

The kinetic dependence upon the concentration of *N,N*-dimethylaniline was examined in benzene, chloroform, and aqueous solutions, where the concentration ranges examined were 2.12—5.30×10^{-4}, 8—40×10^{-4}, and 1.0—5.0×10^{-3} mol dm^{-3} respectively; otherwise, the concentration was 3.80×10^{-4} mol dm^{-3}. Phenol (3.80×10^{-4} mol dm^{-3}) as a diazophile was added, together with an equimolar amount of 2,6-dimethylpyridine as a proton-accepting base. Plottings according to Eqs. 1 and 2 afforded k_1' value of 8.7×10^{-3} s^{-1} (γ=0.998) and k_1'' value of 2.7×10^{-3} s^{-1} (γ=0.991).

Kinetics in Liquid-liquid PTC Systems. An aqueous solution (25 ml) of 4-nitrobenzenediazonium tetrafluoroborate (**7**) (12 mg, 2.0×10^{-3} mol dm^{-3}), buffered with disodium hydrogenphosphate and potassium dihydrogenphosphate (2.0×10^{-3} mol dm^{-3} each) at pH 7.02 and a dichloromethane solution (25 ml) of 9-ethylcarbazole (**8**) (2.05×10^{-4} mol dm^{-3}) and sodium TFPB (5.15—20.0×10^{-5} mol dm^{-3}), both previously maintained at 25.0 °C, were put together all at once and stirred by means of a screw propeller rotating

at 700 min^{-1}. Every 2.0 min stirring was stopped, and a 100-μl portion was taken out of the dichloromethane layer. The aliquot was poured into the same solvent (3.0 ml), previously placed in a photometric cell, to determine the absorbance at 430 nm. The production of azo dye was plotted against the time lapse according to Eq. 14 to give the k_{app} for systems of different TFPB concentrations. The results are summarized in Table 3.

The plotting of k_{app} against the concentration of sodium TFPB gave a linear relationship with a γ value of 0.998, the gradient of the correlation line being 8.93 mol^{-1} dm^3 s^{-1}.

The authors wish to thank Professors Yukito Murakami and Toyoki Kunitake in the Department of Organic Synthesis, Kyushu University, for their informative criticism and advice in the discussion of the results.

References

1) a) W. P. Weber and G. W. Gokel, "Phase Transfer Catalysis in Organic Synthesis," Springer Verlag, Berlin (1977); b) C. M. Starks and C. Liotta, "Phase Transfer Catalysis. Principles and Techniques," Academic Press, New York (1978); c) E. V. Dehmlow and S. S. Dehmlow, "Phase Transfer Catalysis," Verlag Chemie, Weinheim (1980).

2) a) A. R. Butler and P. T. Shepherd, *J. Chem. Res. (M)*, **1978**, 4464; b) M. Ellwood, J. Griffiths, and P. Gregory, *J. Chem. Soc., Chem. Commun.*, **1980**, 181; c) D. E. Rosenberg, J. R. Beadle, S. H. Korzeniowski, and G. W. Gokel, *Tetrahedron Lett.*, **21**, 4141 (1980).

3) T. Davis and L. A. K. Staveley, *Trans. Faraday Soc.*, **53**, 19 (1957).

4) J. N. Cooper and R. E. Powell, *J. Am. Chem. Soc.*, **85**, 1590 (1963).

5) IUPAC, "Solubility Data Series, Vol. 18, Tetraphenylborates," ed by O. Popovych, Pergamon Press, Oxford (1981).

6) J. T. Vandeberg, C. E. Moore, F. P. Cassaretto, and H. Posvic, *Anal. Chim. Acta*, **44**, 175 (1969).

7) R. A. Coburn and A. J. Solo, *J. Med. Chem.*, **19**, 748 (1976); M. E. Wolff and C. Hansch, *ibid.*, **17**, 898 (1974).

8) The synthesis and physicochemical properties of TFPB salts were partly presented at the 6th Symposium on Fluorine Chemistry held at Tokyo in 1980. More details will be published elsewhere.

9) D. W. Armstrong and M. Godat, *J. Am. Chem. Soc.*, **101**, 2489 (1979).

10) S. Snipes and A. W. Herriott, *J. Am. Chem. Soc.*, **101**, 6441 (1979).

11) A preliminary communication appeared in *Chem. Lett.*, **1981**, 579.

12) Sodium TFPB was soluble in benzene up to 5.7×10^{-5} mol dm^{-3} at 25 °C.

13) The coupling reaction with diazophile components other than arylamine, when carried out in nonpolar solvents, required some additional deprotonating agent to make the reaction proceed; this is in accordance with those carried out in an anhydrous solution phase,[15] which is also described below. Organic bases, such as pyridine and aliphatic amines, were purposely not employed, since the diazonium ion attacked the nitrogen atom of these bases to give an *N*-coupling product[28] or some related transforms.[29]

14) H. Gilman and J. B. Honeycutt, Jr., *J. Org. Chem.*, **22**, 563 (1957).

15) P. N. Juri and R. A. Bartsch, *J. Org. Chem.*, **44**, 143 (1979).

16) P. N. Juri and R. A. Bartsch, *J. Org. Chem.*, **45**, 2028 (1980).

17) Ref. 1b, p. 37.

18) M. F. W. Dunker, E. B. Starkey, and G. L. Jenkins, *J. Am. Chem. Soc.*, **58**, 2308 (1936).

19) M. R. Brode, I. L. Seldin, P. E. Spoerri, and G. M. Wyman, *J. Am. Chem. Soc.*, **77**, 2762 (1955), and the references cited therein.

20) O. Oddo and E. Puxeddu, *Chem. Ber.*, **38**, 2755 (1905).

21) E. B. Starkey, *Org. Synth.*, Coll. Vol. II, 225 (1950).

22) At this stage, the reaction mixtures were stirred at 700—1000 min^{-1} by the use of the same apparatus as that used in the kinetic measurements, on the basis of the knowledge about the effect of stirring speed obtained in the traditional cation-catalyzed PTC system.[1b]

23) E. Sawicki, *J. Org. Chem.*, **22**, 915 (1957); R. Meldola, *J. Chem. Soc.*, **43**, 440 (1883).

24) This compound was cited in Eur. Pat. Appl. 28464 (1981) by M. Ellwood, P. Gregory, and J. Griffiths [*Chem. Abstr.*, **95**, 134370r (1981)]. The melting point, though differing somewhat from ours, is described as 160—161 °C, while the visible absorption maximum is similar to ours, appearing at 471 nm with an ε value of 31870.

25) D. Schulte-Frohlinde, *Justus Liebigs Ann. Chem.*, **612** 138 (1956); O. Schmidt, *Chem. Ber.*, **38**, 3208 (1905).

26) K. v. Auwers and F. Michaelis, *Chem. Ber.*, **47**, 1296 (1914).

27) K. H. Meyer and S. Lenhardt, *Justus Liebigs Ann. Chem.*, **398**, 77 (1913).

28) J. R. Penton and H. Zollinger, *J. Chem. Soc., Chem. Commun.*, **1979**, 819; T. P. Ahern and K. Vaughan, *ibid.*, **1973**, 701.

29) R. A. Abramovitch and J. G. Saha, *Tetrahedron*, **21**, 3297 (1965); P. Burri, H. Loewenschuss, H. Zollinger, and G. K. Zwolinski, *Helv. Chim. Acta*, **57**, 395 (1974).

Reaction of the Azomethine Moiety Buried in Bilayer Membranes[1)]

Yoshio Okahata,† Reiko Ando, and Toyoki Kunitake*
Department of Organic Syntheis, Faculty of Engineering, Kyushu University, Higashi-ku, Fukuoka 812
(Received September 22, 1982)

The reaction with water and amines of the azomethine moiety that is part of single-chain ammonium amphiphiles was examined. These amphiphiles form stable bilayer aggregates when they have the alkyl tail of C_7 or C_{12}. The reaction with water of the bilayer-forming amphiphiles ceases at the hydration stage and are 10—2000 times slower than those of the amphiphiles which do not form bilayers and undergo hydrolytic cleavage. The reactivity of the azomethine moiety in bilayers decreases with increasing distance from the membrane surface. The Arrhenius plots for the bilayer-forming amphiphiles show discontinuities at temperatures corresponding to phase transition of the respective bilayer (T_c). The apparent activation energy is larger at temperatures below T_c than at temperatures above T_c. This suggests that water penetration is facilitated in the fluid bilayer. The reaction with amines was affected by their solubility in the bilayer matrix, and poly(ethylenimine) gave a much reduced reaction rate when the azomethine moiety was buried deep in the bilayer matrix.

Organic reactions in the bilayer membrane matrix are attracting increasing attention in recent years, since the highly-organized bilayer matrix offers unique media for controlling reactions. A variety of double-chain surfactants have been shown to produce stable bilayer aggregates in dilute aqueous solution.[2-5)] Physicochemical properties of these bilayer membranes are intrinsically the same as those of the biolipid bilayer and, therefore, their unique properties have been examined in relation to catalysis of some organic reactions.[6)]

We showed previously that single-chain ammonium amphiphiles which possess the *N*-benzylideneaniline moiety (C_n–BB–C_m–N^+) in the hydrophobic portion produce stable bilayer aggregates in water.[7,8)] The aggregate morphology changes extensively with the molecular structure of the amphiphile. For instance, the stable bilayer structure is apparently not formed when the length of the alkyl tail is shorter than C_7. The linear amphiphiles (C_n–BB–N^+ and C_n–BB–C_m–N^+, n=7,12) form multi-walled bilayer vesicles, whereas an amphiphile with the bent rigid segment (p-C_{12}–BB–m-C_4–N^+) gives tubular aggregates.

The variation in morphology necessarily leads to the change in the packing and/or location of the *N*-benzylideneaniline moiety in the aggregate, which, in turn, may produce changes in its reactivity.

The bilayer aggregates of C_n–BB–C_m–N^+ are stable in neutral and alkaline solution; however, they slowly decompose in acidic media due to reaction at the *N*-benzylideneaniline moiety. This group readily reacts with amine nucleophiles, and the reactivity may also depend on the aggregate morphology. We describe in this paper reactions of the azomethine moiety that is part of the bilayer structure. The relation between aggregate morphology and reactivity, once established, would give important means to control organic reactions in aqueous media.

Experimental

Syntheses of amphiphiles containing the *N*-benzylideneaniline moiety(C_n–BB–N^+, C_n–BB–C_m–N^+) and aggregation behavior of these amphiphiles have been reported elsewhere.[7,8)] Electron microscopy was performed by using a Hitachi H-500 instrument.[7)] Differential scanning calorimetry was carried out with a Daini-Seikosha SSC-560 instrument. Sample solutions(1—2 wt%, 0.02—0.05 M)(1 M=1 mol dm^{-3}) were sealed in silver pans and the thermal measurement was repeated from 3 °C to 90 °C at a rate of 2 °C/min. The detail is described elsewhere.[9)]

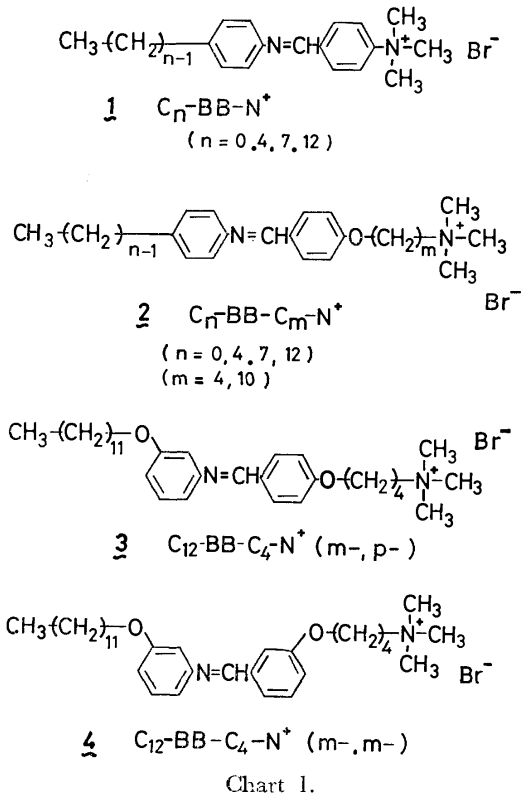

Chart 1.

Acid hydrolyses of aqueous C_n–BB–C_m–N^+ were performed usually at 30 °C, pH 5.5(0.02 M phosphate buffer) and μ=0.02(KCl). A stock solution(10^{-3}—10^{-2} M) of an amphiphile was prepared by sonication(Branson Sonifier 185) in a weakly alkaline solution(pH 9), and the reaction was initiated by adding 0.1—0.01 ml of this solution to an acidic buffer solution. The course of reaction was followed by disappearance of the absorption due to the azomethine linkage(-CH=N-) at 320 nm with a Hitachi 200 spectrophotometer. Pseudo first-order kinetics were observed up to at least 70—80% completion of the reaction, and apparent rate constants(k_{obsd}) were estimated. The pH

† Present address: Department of Polymer Science, Tokyo Institute of Technology, O-okayama, Meguro-ku, Tokyo 152.

of the reaction medium was maintained within ±0.05 during the reaction(HM-10B digital pH meter, Toa Electronics). The reaction with amines was followed in the same way.

Results

The Course of Reaction. The time course of the spectral change due to reaction of the C_{12}–BB–C_4–N^+ bilayer aggregate is shown in Fig. 1. C_{12}–BB–C_4–N^+ possesses absorption maxima at 280 nm and 320 nm. The latter peak that is attributable to the azomethine linkage[10,11] diminished with time. The absorption maximum and the spectral pattern were not influenced by the alkyl chain length (C_n and C_m). C_{12}–BB–C_4–N^+ in 50 v/v% EtOH–H_2O where the amphiphile does not form the bilayer aggregate gave the same spectral change as that of Fig. 1. It means that the spectra of C_n–BB–C_m–N^+ and C_n–BB–N^+ are not affected by the aggregate formation. Therefore, the spectrum of the amphiphile and the course of reaction are concluded to be identical irrespectively of the bilayer formation.

Acid hydrolysis of the azomethine linkage is initiated by proton addition to nitrogen followed by the rate-limiting nucleophilic attack of H_2O or OH^-, as shown in Eq. 1.[12] It is assumed that the same mechanism operates in the aqueous micelle[13] and in liquid crystalline media.[14]

$$-CH{=}N- \underset{\text{fast}}{\overset{H^+}{\rightleftharpoons}} -CH{=}\overset{+}{N}H- \underset{\text{slow}}{\overset{H_2O}{\rightleftharpoons}} -\underset{\displaystyle OH}{\underset{|}{CH}}-NH- \rightleftharpoons$$

$$-\underset{\displaystyle O^-}{\underset{|}{CH}}-\overset{+}{N}H_2- \rightleftharpoons -CHO + H_2N- \qquad (1)$$

Disappearance of the azomethine absorption at 320 nm that is used for following the reaction does not assure completion of Eq. 1. In the case of BB–N^+ and C_4–BB–C_4–N^+ which do not form bilayers, thin-layer chromatography of the reaction mixture indicated formation of the corresponding amines and aldehydes, and therefore, the reaction proceeds to completion according to Eq. 1. On the other hand, in the bilayer system, the reaction appears to stop at the hydration step from the following reasons: (1) The bilayer structure remains in electron micrographs after the reaction, as discussed below (Fig. 4b); (2) equimolar mixtures of the product amines and aldehydes do not give clear solution under the same conditions, although the reaction mixture remains clear after the reaction is over; (3) when the homogeneous reaction mixture is mixed with concentrated hydrochloric acid and refluxed, the product amine and aldehyde separate as white precipitates. Therefore, the reaction stops at the intermediate stage without the acid treatment. For these reasons, hydrolysis and hydration will not be discriminated in the subsequent discussion as long as the kinetics are concerned.

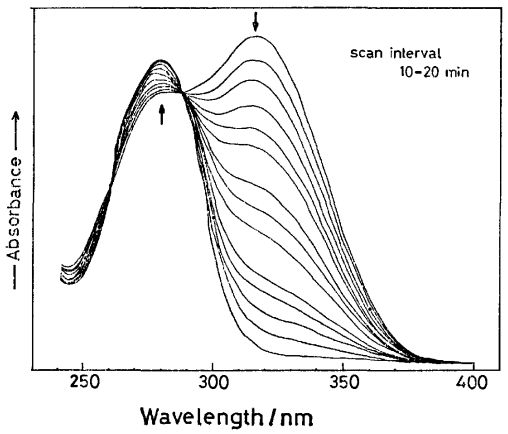

Fig. 1. Spectral change due to reaction of aqueous C_{12}–BB–C_4–N^+ bilayer.
30 °C, pH 3.4 (0.02 M acetate buffer), μ=0.02 (KCl), [C_{12}–BB–C_4–N^+]=1.0×10^{-4} M.

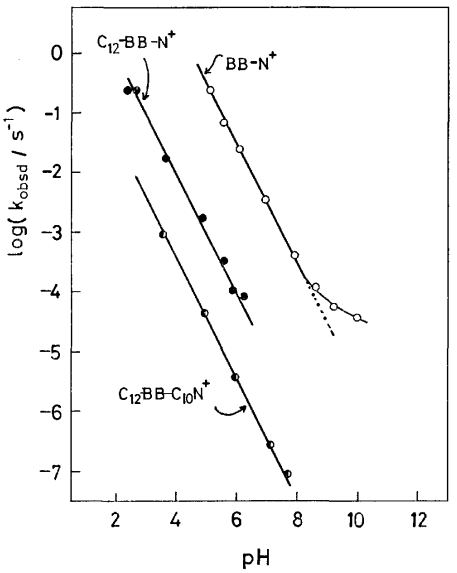

Fig. 2. pH-rate profiles of the reaction of C_n–BB–C_m–N^+.
30 °C, 0.02 M acetate buffer (pH 2—5), 0.02 M phosphate buffer (pH 6—7), 0.02 M borate buffer (pH 7—9), μ=0.02 (KCl), [C_{12}–BB–C_{10}–N^+]=6.0×10^{-5} M, [C_{12}–BB–N^+]=6.0×10^{-5} M, [BB–N^+]=6.0×10^{-4} M.

The pH-rate profile of the azomethine reaction was examined at pH 2 to 10 and those of BB–N^+, C_{12}–BB–N^+, and C_{12}–BB–C_{10}–N^+ are shown in Fig. 2 as typical examples. In all cases, log k_{obsd} decreases linearly with the slope of −1 at pH 2 to 8. This is consistent with the above-mentioned supposition that the reaction proceeds *via* the specific acid catalysis (Eq. 1). The upward curvature for BB–N^+ at pH 8—10 indicates the involvement of water or hydroxide catalysis. The catalytic effect of the basic buffer species (HBO_3^-, HPO_4^-, and $CH_3CO_2^-$) was negligibly small and the effective nucleophilic species is limited to water at buffer concentrations of 0.005 to 0.02 M. The subsequent experiments were conducted at pH 5.5 because of the experimental convenience.

Electron Microscopy. It is expected that the reaction alters the aggregate morphology drastically. An electron micrograph for an aqueous solution of C_{12}–BB–C_4–N^+ (5×10^{-3} M) is shown in Fig. 3a, which indicates the presence of multi-walled vesicles. A reacted sample for electron microscopy was obtained as follows: One ml of the same aqueous solution as that

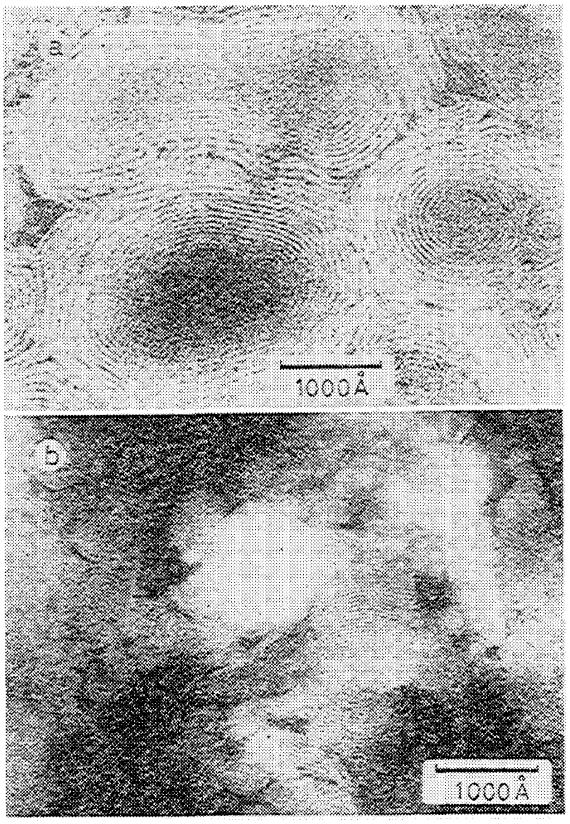

Fig. 3. Electron micrographs before (a) and after (b) reaction of C_{12}-BB-C_4-N^+ aggregates with water. Initial magnification, ×50,000, stained by uranyl acetate.

used for the rate measurement was adjusted to pH 1—2 by adding one drop of concentrated hydrochloric acid, and maintained at room temperature for 1 h. Complete disappearance of the absorption at 320 nm was confirmed, and the solution was stained with aqueous uranyl acetate (1 wt%). An electron micrograph for this sample is shown in Fig. 3b. The lamellar structure is preserved even after complete disappearance of the azomethine linkage.

As mentioned above, the acid-catalyzed reaction supposedly ceases to proceed at the hydration step of Eq. 1. The bilayer assemblage of the hydrated intermediate may suppress the subsequent cleavage step. It is interesting to note that the hydrogenation product of this amphiphile, **5**, gives tubular aggregates, in contrast to formation of lamellar aggregates by the hydration product.

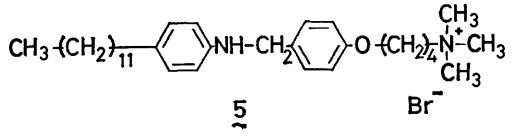

5

Chart 2.

Amphiphile Structure and Reaction Rate. Figure 4 illustrates the dependence of the reaction rate on the amphiphile concentration. In Fig. 4a is given the concentration dependence for three amphiphiles whose total alkyl lengths (C_n+C_m) are 10 to 12. They react more slowly than BB-N^+ which does not have the

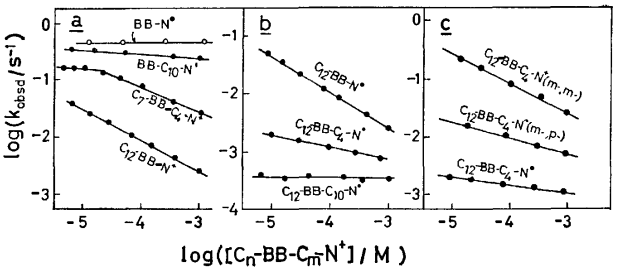

Fig. 4. Concentration dependence of the rate constant. 30 °C, pH 5.5±0.1 (0.02 M phosphate buffer), μ= 0.02 (KCl).

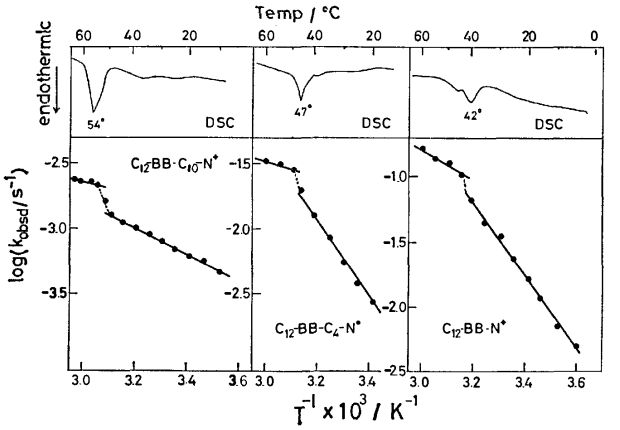

Fig. 5. Arrhenius plots of the reaction and DSC curves of C_{12}-BB-C_m-N^+ bilayers.
Reaction conditions: pH 4.3 (0.02 M acetate buffer), 0.02 M KCl, [C_{12}-BB-C_m-N^+]=6.1×10^{-5} M DSC samples: [C_{12}-BB-C_m-N^+]=1—2 wt% (2—5×10^{-2} M).

alkyl chain. It is interesting that the reaction rate varies considerably among the three amphiphiles in spite of their closely-related structures (only the distribution of the alkyl chain is different). The reaction rate is suppressed when the alkyl chain is localized in the tail portion (C_{12}-BB-N^+), but it is not so when the alkyl chain is localized in the spacer portion (BB-C_{10}-N^+). Figure 4b compares log k_{obsd} for C_{12}BB-C_m-N^+ in which the spacer length is varied. The rate as well as concentration dependence become smaller as the spacer is lengthened. The influence of the pattern of alkyl substitution at the rigid segment is shown in Fig. 4c. The meta substitution makes these amphiphiles more vulnerable to reaction than the para substitution.

Effect of Temperature. Reactions of aqueous bilayers of C_{12}-BB-C_m-N^+ (m=0, 4, 10) were performed at 0—60 °C. The corresponding Arrhenius plots are shown in Fig. 5. The three Arrhenius plots are made of two linear portions. The inflection regions are 40—45 °C, 45—50 °C, and 50—55 °C for C_{12}-BB-C_m-N^+ (m=0, 4, and 10), respectively. These temperature regions agree very closely to the endothermic region observed in the DSC measurement. The endothermic peaks are derived from the crystal-to-liquid crystal phase transition of the bilayer membrane.[7] Thus, the anomaly in the Arrhenius plots reflects the change

in the membrane physical state. In agreement with this supposition, aqueous BB–C_{10}–N^+ which does not form the bilayer structure and correspondingly gives no DSC peak gave linear Arrhenius plots.

Effect of Reaction Media. The reaction of C_{12}–BB–C_m–N^+ (m=0, 4, and 10) was examined in the bilayer matrix of dihexadecyldimethylammonium bromide ($2C_{16}N^+2C_1$), in the aqueous hexadecyltrimethylammonium bromide (CTAB) micelle, and in 50 v/v% EtOH–H_2O. The results are summarized in Table 1, in comparison with those of the single-component bilayer membrane. The k_{obsd} value decreased with increasing spacer lengths, when C_{12}-BB–C_m–N^+ were allowed to react as single-component bilayer membranes, in the $2C_{16}N^+2C_1$ bilayer or in the CTAB micelle. In contrast, the influence of the spacer length cannot be seen in the reaction in 50 v/v% EtOH–H_2O, and the k_{obsd} value is much larger in this medium than in other media. C_{12}–BB–C_m–N^+ would be molecularly dispersed in 50 v/v% EtOH–H_2O, and the azomethine moiety should be equally exposed to acid in spite of different spacer lengths, leading to the lack of the spacer effect. The observed influence of the spacer length in the other three media clearly indicates that C_{12}–BB–C_m–N^+ molecules are more or less organized in these media.

Table 1. Reaction of C_{12}-BB-C_m-N^+ (m=0, 4, and 10) in various microenvironments[a]

Medium	$10^4 \times k_{obsd}/s^{-1}$		
	C_0	C_4	C_{10}
Water	220	44	1.3
Aqueous $2C_{16}N^+2C_1$ bilayer	120	23	1.0
Aqueous CTAB micelle	480	100	8.2
50 v/v% EtOH-H_2O	1200	1400	1300

a) 30 °C, pH 5.5 (0.02 M phosphate buffer) μ=0.02 (KCl) [C_{12}-BB-C_m-N^+]=1.0×10^{-4}, [CTAB]=1.0×10^{-3} M, [$2C_{16}N^+2C_1$]=1.0×10^{-3} M.

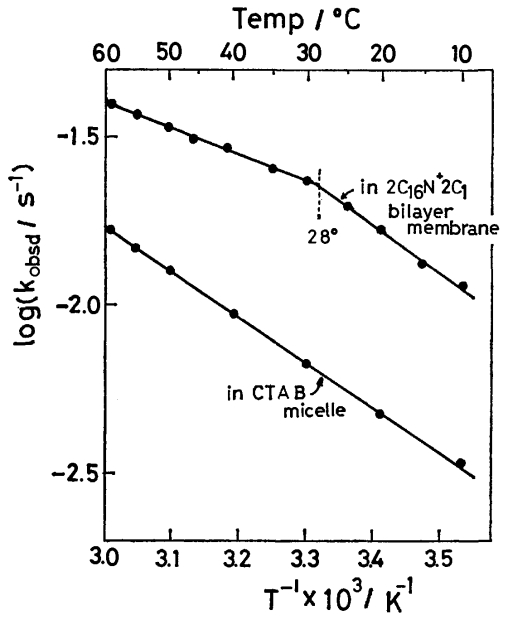

Fig. 6. Arrhenius plots of the reaction of C_{12}-BB-C_{10}-N^+ in the CTAB micelle and in the $2C_{16}N^+2C_1$ bilayer. 30 °C, pH 2.2, 0.02 M KCl, [C_{12}-BB-C_{10}-N^+]=6.0×10^{-5} M, [CTAB]=[$2C_{16}N^+2C_1$]=1.0×10^{-3} M.

Figure 6 illustrates the Arrhenius plots for the reaction of C_{12}–BB–C_{10}–N^+ in the $2C_{16}N^+2C_1$ bilayer and in the CTAB micelle. In the latter system the linear plots are observed, but the former system gives an inflection at *ca.* 28 °C. This temperature agrees with that of the crystal-to-liquid crystal phase transition of the $2C_{16}N^+2C_1$ bilayer.[9]

Reaction with Amines. Primary amines readily undergo the exchange reaction with Schiff bases. The exchange reaction with the azomethine moiety of aqueous C_{12}–BB–C_m–N^+ (m=0, 4, and 10) was examined in the presence of excess amines. The results are summarized in Fig. 7. The overall rate (k_{all} term) of disappearance of the azomethine moiety was corrected for the water reaction in the absence of amines (k_{obsd} term). Poly (ethylenimine) used is commercially available (MW 60000) and contains 25% primary, 50% secondary, and 25% tertiary amino groups.[15]

The rate constant increases linearly with the amine concentration, indicating occurrence of clean second-order reaction. The spacer length exerts relatively small influences in the reaction with benzylamine. The spacer effect is more apparent with dodecylamine as attacking nucleophile, although the reaction rates are smaller. In the case of poly(ethylenimine), the reactivities of C_{12}–BB–C_m–N^+ (m=4 and 10) are much smaller than that of C_{12}–BB–C_m–N^+ (m=0).

Discussion

Mode of Aggregation and Reactivity. The aggregation behavior of single-chain amphiphiles has been shown to be determined by five structural elements.[8] They are (1) flexible tail, (2) rigid segment, (3) hydrophilic head group, (4) spacer group, and (5) additional interacting group. In the case of the amphiphiles used in this study, three structural elements (length of flexible tail, spacer length and the mode of substitution at the rigid segment) are responsible for the change in the aggregation behavior.

The rate constants(k_{obsd}) at the amphiphile concentration of 1.0×10^{-4} M are summarized in Table 2, together with the aggregation behavior. The predom-

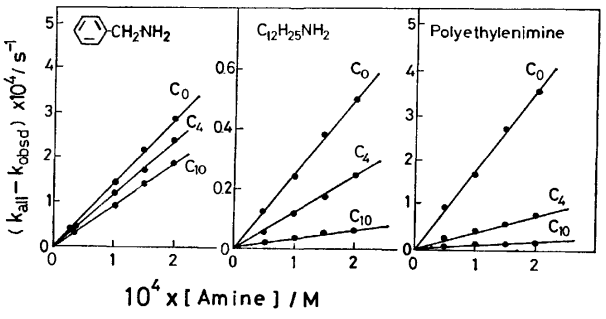

Fig. 7. Reaction of amines with C_{12}-BB-C_m-N^+ bilayers.
30 °C, pH 6.0 (0.02 M phosphate buffer), 0.02 M KCl, [C_{12}-BB-C_m-N^+]=1.0×10^{-3} M, [amine]=1.0×10^{-2} M. Unit mole is used for the polymer.

Table 2. Aggregation behavior and reactivity of C_n-BB-C_m-N^+ in water

Amphiphile	$10^3 \times$ CMC / M	Aggregate weight ($\times 10^{-4}$ dalton)	Electron micrograph	$10^4 \times k_{obsd}$[b] / s^{-1}
C_{12}-BB-C_{10}-N^+	0.01	1000	Vesicle and lamella	1.2
C_{12}-BB-C_4-N^+	0.01	400	Vesicle	44
C_{12}-BB-N^+	0.01	400	Multi-walled vesicle	220
C_7-BB-C_{10}-N^+	0.02	2000	Vesicle	7.4
C_7-BB-C_4-N^+	0.01	2000	Finger-print like	620
C_7-BB-N^+	0.06	800	Finger-print like	1000
C_4-BB-C_{10}-N^+	0.33	600	No structure	2500
C_4-BB-C_4-N^+	0.16	800	No structure	1800
C_4-BB-N^+	0.22	10	No structure	4800
BB-C_{10}-N^+	>10	400	No structure	2500
BB-N^+	>10	<1	No structure	4500
C_{12}-BB-C_4-N^+(*m*-, *p*-)	0.01	60	Rod	92
C_{12}-BB-C_4-N^+(*m*-, *m*-)	0.01	70	Pre-rod and partial lamella	450

a) Aggregation behaviors are mostly quoted from Refs. 8 and 9. b) 30 °C, pH 5.5±0.1, μ=0.02(KCl), [C_n-BB-C_m-N^+] = 1.0×10^{-4} M.

inant factors which govern the reaction rate are (1) the extent of bilayer assemblage as determined by the tail length and the pattern of substitution at the rigid segment, and (2) the distance of the reacting group from the membrane surface as determined by the spacer length. The bilayer structure is not developed for the azomethine amphiphiles with alkyl tails shorter than C_7. These amphiphiles give largest k_{obsd} values (0.2—0.5 s^{-1}). It is noteworthy that C_4–BB–C_m–N^+ (m=4 and 10) and BB–C_{10}–N^+ are among the most reactive amphiphiles in spite of their extensive aggregation (though bilayer is not formed). This means that simple aggregation without amphiphile orientation do not lead to rate suppression. Comparisons shown in Figs. 4a and 4c also point to the same conclusion. Three amphiphiles (BB–C_{10}–N^+, C_7–BB–C_4–N^+ and C_{12}–BB–N^+) of Fig. 4a possess similar amounts of the alkyl chain and form equally huge aggregates (aggregate weight, 4—20 millions). However, their reactivities change drastically due to varying extents of orientation. The reactivities of amphiphiles with different patterns of substitution are compared in Fig. 4c. The molecular orientation in the aggregate as examined by electron microscopy becomes less ordered, as the meta substitution increases. The reaction rate becomes greater accordingly.

The influence of the distance of the reacting group from the membrane surface is found in Table 2 for several combinations. In the series of C_{12}–BB–C_m–N^+ (m=0, 4, and 10) which all give fully developed bilayers, the reaction rate decreases as the spacer becomes longer (see also Fig. 4b). The same trend is found for a series of less developed bilayers: C_7–BB–C_m–N^+ (m=0, 4, and 10). The spacer effect is similarly noticed when amphiphiles C_{12}–BB–C_m–N^+ are buried in the $2C_{16}N^+2C_1$ bilayer matrix and in the CTAB micelle (Table 1), but it totally disappears in 50 v/v% EtOH–H_2O. The ordered structure may persist in the CTAB micelle.

Additional examples of the spacer effect are obtained for Schiff-base exchange reaction of the azomethine bilayer with amines. As shown in Fig. 7, the reaction rate decreases with increasing spacer lengths, and the extent of the spacer effect (rate difference) varies with the structure of amines. Benzylamine produces the smallest spacer effect and the rate difference is largest for poly(ethylenimine). Benzylamine should be incorporated into the bilayer matrix relatively nonspecifically; hence, small spacer effects. Dodecylamine is expected to align better in the membrane matrix. This factor would lead to larger differences in relative rate. Poly(ethylenimine) is highly water-soluble, and would not readily penetrate into the bilayer matrix. In consistence with this supposition, the azomethine moiety near the membrane surface (no spacer) reacts much faster with the polymer than those buried in the membrane (spacer: C_4 and C_{10}).

As for the reactant orientation in the bilayer matrix, Czarniecki and Breslow examined the photosensitized hydrogen abstraction by benzophenones in the dihexadecyl phosphate bilayer.[16] They showed the bilayer lamella produced better orientation of the reagents than the bilayer vesicle, although the difference was not remarkable.

Membrane Physical State and Reactivity. The Arrhenius plots of the azomethine reaction show discontinuity near the phase transition of the respective membrane (Fig. 5). When the reaction was carried out in the $2C_{16}N^+2C_1$ bilayer, an inflection in the Arrhenius plots was found at T_c of the matrix membrane (Fig. 6). No inflection was observed in the CTAB micelle. Figure 8 is schematic illustrations of the membrane physical state. The component molecules are highly aligned and the molecular movement is suppressed in the gel(crystalline) state. However, the alignment becomes less ordered and the alkyl chain can assume multiple conformations in the liquid-crystalline state, although the bilayer structure is maintained. This change in the membrane physical state could produce the reactivity difference, and discontinuities observed in the Arrhenius plots (Fig. 5) may be related to coexistence of the two physical states during phase transition.

Table 3 summarizes the apparent activation energy

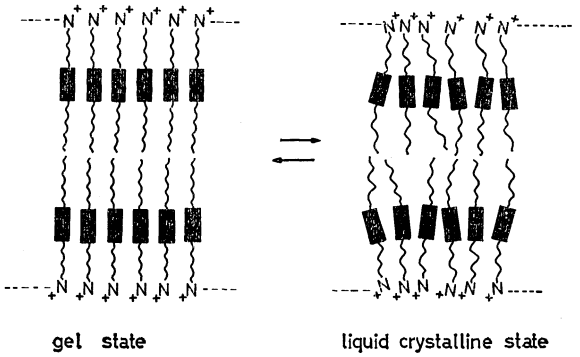

Fig. 8. Schematic illustrations of the phase transition of the C_n–BB–C_m–N^+ bilayer membrane.

Table 3. Apparent activation energy of the reaction of C_{12}-BB-C_m-N^+ aggregates

Aggregate	E_a/kJ mol^{-1} Below T_c	Above T_c	ΔE_a
C_{12}-BB-N^+ bilayer	67	20	56
C_{12}-BB-C_4-N^+ bilayer	54	11	45
C_{12}-BB-C_{10}-N^+ bilayer	19	7.5	12
C_{12}-BB-C_{10}-N^+ in $2C_{16}N^+2C_1$ bilayer	16	12	4.2
C_{12}-BB-C_{10}-N^+ in CTAB micelle	(13)		—

E_a of the reaction. In all the three single-component bilayers, the activation energy is greater in the temperature region below T_c than above T_c. This is not unexpected results, since the azomethine reactivity would certainly be suppressed in the rigid membrane matrix. In several reactions where reactants are buried in the membrane matrix, the activation energy increased in the temperature below T_c. For example, E_a was 167 and 84 kJ/mol at temperatures below and above T_c, respectively, in the case of proton abstraction of Eq. 2.[17] Nucleophilic displacement of a phosphate ester by hydroxamates (Eq. 3) gave similar E_a difference (88 and 59 kJ/mol)[18]

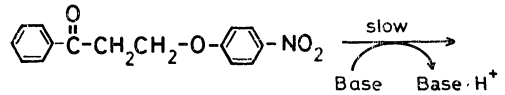

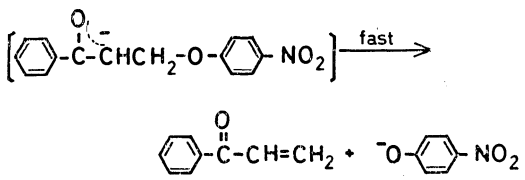

(2)

In the present system, the E_a values observed at temperatures above T_c are small and, correspondingly, its variation among different bilayers (C_{12}–BB–C_m–N^+, m=0, 4, and 10) is small. The E difference is much greater at temperatures below T_c. In both cases, E_a values become smaller as the spacer length is increased, and the E_a difference due to phase transition (ΔE_a) is 58 kJ/mol for the C_{12}–BB–N^+ bilayer and is only 12 kJ/mol for the C_{12}–BB–C_{10}–N^+ bilayer. It has been pointed out that longer spacers lead to stabilization of the bilayer structure.[8] The rate constant of the azomethine reaction decreases with the spacer length (Table 1). Thus, it is suggested that the temperature dependence is diminished for well-developed bilayers or when the reacting moiety is buried deep in the matrix. Interestingly, the concentration dependence of the reaction rate shows a pattern (Fig. 4b) analogous to that of the temperature effect in that the reaction of the C_{12}–BB–C_{10}–N^+ bilayer gives a much reduced concentration dependence relative to that of the C_{12}–BB–N^+ bilayer.

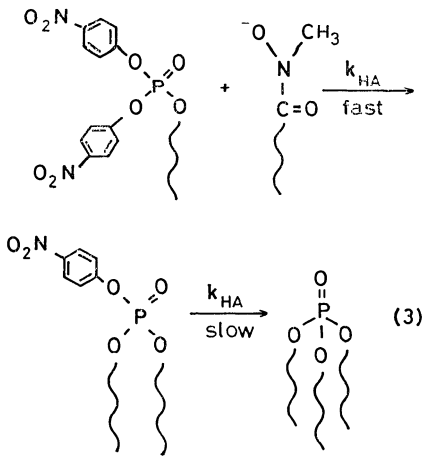

(3)

When C_{12}–BB–C_{10}–N^+ is buried in the $2C_{16}N^+2C_1$ matrix, the reactivity is much enhanced and an inflection in the Arrhenius plots is observed near T_c of the matrix membrane. The enhanced reactivity suggests that the cluster formation of C_{12}–BB–C_{10}–N^+, if present, is not significant. The inflection observed at T_c of the matrix membrane, not at T_c of the substrate itself, is not inconsistent with the cluster formation.

Conclusion

It is established in this investigation that the reactivity of a functional group is governed by molecular orientation (bilayer formation) in the aggregate, and if bilayer is formed, by distance from the membrane surface and membrane physical state. These results would provide valuable information on peculiar reactivities associated with bilayer characteristics.

References

1) Contribution No. 670 from the Department of Organic Synthesis.

2) T. Kunitake and Y. Okahata, *J. Am. Chem. Soc.*, **99**, 3860 (1977); *Chem. Lett.*, **1977**, 1337; T. Kunitake, Y. Okahata, K. Tamaki, F. Kumamaru, and M. Takayanagi, *ibid.*, **1977**, 387.

3) T. Kunitake and Y. Okahata, *Bull. Chem. Soc. Jpn.*, **51**, 1877 (1978).

4) Y. Okahata, S. Tanamachi, M. Nagai, and T. Kunitake, *J. Colloid Interface Sci.*, **82**, 401 (1981).

5) For reviews; T. Kunitake, *J. Macromol. Sci. Chem.*, **A13**, 587 (1979); J. H. Fendler, *Acc. Chem. Res.*, **13**, 7 (1980).

6) For a review, T. Kunitake and S. Shinkai, *Adv. Phys. Org. Chem.*, **17**, 435 (1980).
7) T. Kunitake and Y. Okahata, *J. Am. Chem. Soc.*, **102**, 549 (1980).
8) T. Kunitake, Y. Okahata, M. Shimomura, S. Yasunami, and K. Takarabe, *J. Am. Chem. Soc.*, **103**, 5401 (1981).
9) Y. Okahata, R. Ando, and T. Kunitake, *Ber. Bunsenges. Phys. Chem.* **85**, 789 (1981).
10) E. H. Cordes and W. P. Jencks, *J. Am. Chem. Soc.*, **84**, 832 (1962).
11) R. L. Reeves, *J. Am. Chem. Soc.*, **84**, 3332 (1962).
12) W. P. Jencks, "Catalysis in Chemistry and Enzymology," McGraw-Hill, New York, N. Y. (1969), Chap. 3.
13) M. T. A. Behme and E. H. Cordes, *J. Am. Chem. Soc.*, **87**, 260 (1965).
14) W. E. Bacon, *Mol. Cryst. Liq. Cryst.*, **67**, 101 (1981).
15) L. E. Davis, "Water-soluble Resins," ed by R. L. Davidson and M. Sittig, Reinhold Publ. New York, (1968), p. 1216; G. M. Lukovkin, V. S. Pshezhetsky, and G. A. Murtazaeva, *Eur. Polym. J.*, **9**, 559 (1973).
16) M. F. Czarniecki and R. Breslow, *J. Am. Chem. Soc.*, **101**, 3675 (1979).
17) Y. Okahata, S. Tanamachi, and T. Kunitake, *Nippon Kagaku Kaishi*, **1980**, 442.
18) Y. Okahata, H. Ihara, and T. Kunitake, *Bull. Chem. Soc. Jpn.*, **54**, 2072 (1981).
19) Y. Okahata, H. Ihara, and T. Kunitake, *J. Am. Chem. Soc.*, submitted.

 © 1983 The Chemical Society of Japan Bull. Chem. Soc. Jpn., 56, 809—814 (1983)

Restricted Rotation Involving the Tetrahedral Carbon. XLVII. The "Positive" and the "Negative" Buttressing Effects on the Rotational Barriers in 9-(1,1-Dimethyl-2-phenylethyl)-1-halotriptycenes[1)]

Gaku YAMAMOTO, Masahiko SUZUKI, and Michinori ŌKI*

Department of Chemistry, Faculty of Science, The University of Tokyo, Bunkyo-ku, Tokyo 113

(Received October 9, 1982)

9-(1,1-Dimethyl-2-phenylethyl)-1,2,3,4-tetrahalotriptycenes (halogen=F, Cl, and Br) were synthesized and the kinetic studies of the rotational isomerization were made. The obtained data were compared with those for the corresponding 1-halo derivatives. The equilibrium constants (±*sc*/*ap*) for the tetrahalo compounds are smaller than those for the respective monohalo counterparts. The tetrafluoro compound isomerizes twice slower than the monofluoro one at 240 °C, showing the "positive" buttressing effect. Contrarily, the tetrachloro and the tetrabromo compounds isomerize 13 and 100 times, respectively, faster than the corresponding monohalo compounds at 175 °C, exhibiting the "negative" buttressing effect. These intriguing phenomena are discussed in terms of the molecular deformation in these congested compounds, which affects both the ground state and the transition state for rotation.

In 1934, Chien and Adams found that the presence of a substituent in 3′-position considerably reduces the rate of racemization of the optically active 2-carboxy-2′-methoxy-6-nitrobiphenyl (**1**),[2)] the degree of retardation being dependent on the 3′-substituent. The origin of the effect was not fully understood at that time. Later, Rieger and Westheimer found that 2,2′-diiodo-5,5′-dicarboxybiphenyl (**2a**) racemizes 30,000 times faster than 2,2′,3,3′-tetraiodo-5,5′-dicarboxybiphenyl (**2b**),

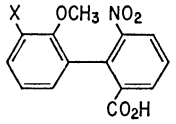

1

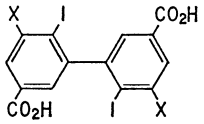

2a: X=H
2b: X=I

the enthalpies of activation being 21.0 and 27.3 kcal mol^{-1} (1 cal=4.18 J), respectively.[3)] These enthalpy values were satisfactorily reproduced by calculation in their pioneering works on molecular mechanics. The calculation revealed the origin of the retarding effects of the *m*-substituents, which is now recognized as the buttressing effect. In the planar transition state for racemization, the ortho groups bend away from each other to relieve the steric strain. Presence of a group in the neighboring meta position prevents the bending to some extent by "buttressing" the *o*-substituent, thus raising the transition state energy. The ground state in these compounds is considered almost free of strain, and the buttressing by the *m*-substituents docs not appreciably affect the ground state energy. Therefore, the buttressing effect operates to increase the energy barrier to racemization, which we refer to as the "positive" buttressing effect.

The buttressing effect on the energy barrier to internal rotation about an sp^2-sp^2 single bond is generally positive, because the ground state of the molecule is not much affected by the introduction of a buttressing substituent. However, when internal rotation about an sp^2-sp^3 or sp^3-sp^3 bond is concerned, the situation is somewhat different because the ground state usually suffers from some congestion.

If a substituent is introduced into the neighborhood of a congested site, it would increase the congestion and would raise the ground state energy. Since an energy barrier to rotation is a difference in energies between the ground and the transition states, if the change in the ground state energy is not negligible, it is possible that the buttressing effect either raises or lowers the barrier. The transition state is naturally more congested than the ground state and hence the buttressing effect should operate more effectively in the transition state than in the ground state: this results in the "positive" buttressing effect on the energy barrier, as is commonly observed.

Some examples of the buttressing effect on the energy barrier to rotation about an sp^2-sp^3 bond are known. The buttressed compound **3b** showed a higher barrier to rotation of the dichloromethyl group than **3a** ($\Delta G^{\ddagger}_{298}$: 15.4 *vs.* 14.9 kcal mol^{-1}).[4)] We observed the positive buttressing effect in 9-arylfluorenes (**4**) as

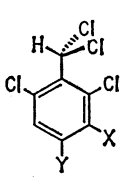

3a: X=H, Y=Cl
3b: X=Cl, Y=H

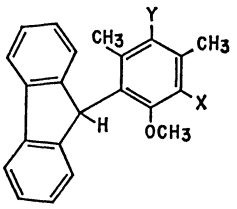

4

well. Free energies of activation for rotation at 329 K are 25.0 kcal mol^{-1} if X=Y=H, 25.9 kcal mol^{-1} if X=H and Y=Br, 26.5 kcal mol^{-1} if X=Br and Y=H, and 27.2 kcal mol^{-1} if X=Y=Br.[5)]

Though not definite, there are a few examples of the "negative" buttressing effect, namely, the lowering of the barrier by the presence of a buttressing substituents, in the literature. The barrier to racemization of optically active **5** decreases by the introduction of methyl groups in *m*-positions ($\Delta G^{\ddagger}_{298}$: 22.8 *vs.* 22.1 kcal mol^{-1}).[6)] Since there are two C–C$_{ar}$ bonds about which internal rotation is restricted, the observed barriers may not be mechanistically simple, although the authors attributed the retardation to the increase in the ground state energy.[6)] In compounds **6**, the

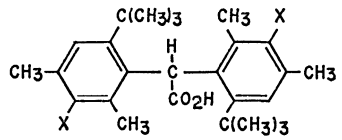

5: X=H or CH_3

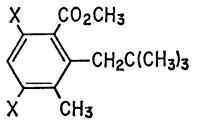

6: X=H or CH_3

rotational barrier of the neopentyl group is reduced by the presence of buttressing methyl groups ($\Delta G^{\ddagger}_{398}$: 14.6 *vs.* 13.8 kcal mol^{-1}).[7] In this case, the barrier reduction was ascribed to the change in conformation of the ester group because the ester moiety can no longer be coplanar with the benzene ring in the presence of the neighboring methyl group. The barrier to exchange of the diastereotopic *o*-methyl groups was suggested to be higher in compound **7** than in **8**.[8]

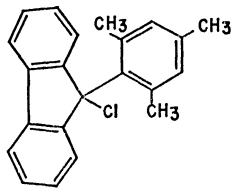

7

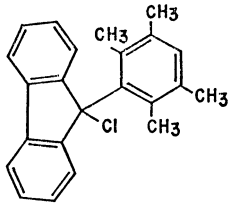

8

This fact was interpreted by the original authors in terms of sterically accelerated ionization followed by ion-pair return.[8] This conclusion was questioned from the results in solvent effect studies: the barriers showed no appreciable solvent dependence.[9] Thus one of the remaining possibilities is the restricted rotation about the C_9–C_{ar} bond which is subjected to the "negative" buttressing effect.

Several examples of the buttressing effect in sp^3-sp^3 systems have been found during the course of our studies on rotational barriers in 9-substituted triptycene derivatives. Dynamic NMR studies revealed that the barrier to the $+sc \rightleftarrows -sc$ interconversion in **9b** is 2.0

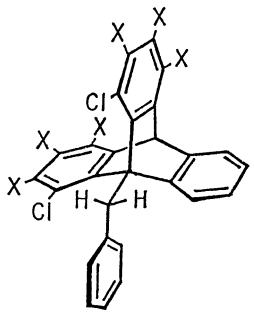

9a: X=H
9b: X=Cl

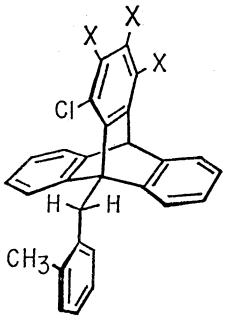

10: X=H or Cl

kcal mol^{-1} higher than in **9a** ($\Delta G^{\ddagger}_{c}$: 18.1 kcal mol^{-1} at 100 °C *vs.* 16.1 kcal mol^{-1} at 60 °C).[10] This suggests that the buttressing effect destabilizes the transition state to a greater extent than the ground state. A similar but less remarkable trend was also observed in the stereodynamics of compounds **10**.[11]

Recently we found an interesting dependence of the energy barrier to rotation upon the *peri*-substituent in 9-*t*-alkyltriptycenes.[12,13] In a series of 9-(1,1-dimethyl-2-phenylethyl)triptycene derivatives (**11**—**17**), the

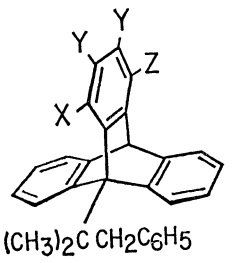

	X	Y	Z
11	H	Cl	H
12	F	H	H
13	Cl	H	H
14	Br	H	H
15	OCH_3	H	OCH_3
16	CH_3	H	CH_3
17	CF_3	H	H
18	F	F	F
19	Cl	Cl	Cl
20	Br	Br	Br

compounds with small *peri*-substituents, **12** and **15**, show higher barriers ($\Delta G^{\ddagger}_{500}$: 43.2 and 42.5 kcal mol^{-1}, respectively) than the *peri*-unsubstituted derivative **11** ($\Delta G^{\ddagger}_{500}$: 40.4 kcal mol^{-1}), but the *peri*-chloro compound **13** has almost the same barrier ($\Delta G^{\ddagger}_{500}$: 40.4 kcal mol^{-1}) as **11** and those with the even bulkier *peri*-substituent, **14**, **16**, and **17**, have lower barriers than **11**, the barrier height decreasing in this order ($\Delta G^{\ddagger}_{500}$: 39.2, 38.4, and 33.8 kcal mol^{-1}, respectively).[13] This implies that the presence of a bulky *peri*-substituent destabilizes the transition state to a lesser extent than the ground state.

It seemed interesting to investigate how the buttressing effect affects the energy barrier in these circumstances. We report in this paper the kinetic studies on the rotational barriers in 9-(1,1-dimethyl-2-phenylethyl)-1,2,3,4-tetrahalotriptycenes (**18**—**20**) to provide clear examples of the "negative" buttressing effect, comparing the data with those for the 1-halo counterparts **12**—**14** reported before.[13] The "positive" and the "negative" buttressing effects observed are discussed in terms of the molecular deformation in this highly congested system.[14]

Results

Syntheses. The tetrahalotriptycenes **18**—**20** were synthesized by reactions of 9-(1,1-dimethyl-2-phenylethyl)anthracene (**21**) with tetrahalobenzynes **22a**—**22c**. Tetrafluoro- and tetrabromobenzynes were generated by pyrolysis of the corresponding tetrahalo-2-diazoniobenzoates prepared from the respective anthranilic acids, while tetrachlorobenzyne was generated by pyrolysis of pentachlorophenyllithium prepared from hexachlorobenzene and butyllithium.[15] Reaction of either **22b** or **22c** with **21** afforded the *ap* atropisomer of the respective triptycene as a sole product.[17] Tetrafluorobenzyne (**22a**) reacted with **21** to give two products in a 3:2 ratio. The major product was the desired triptycene *ap*-**18**, and the minor one was assigned to a 1,4-adduct **23** by the ^{1}H NMR spectrum. As the chromatographic separation of **23** from *ap*-**18** seemed tedious, isolation of *ap*-**18** was performed by oxidative degradation of **23** with potassium permanganate followed by chromatography. The $\pm sc$ rotamers of **18**—**20** were isolated in pure forms from the equilibrated mixture of the rotamers by column chromatography. In each case, the $\pm sc$ rotamer eluted faster than the corresponding *ap* rotamer, in sharp contrast with the behavior exhibited by the 1-halo derivatives **12**—**14**, where the *ap* rotamers eluted faster.[13]

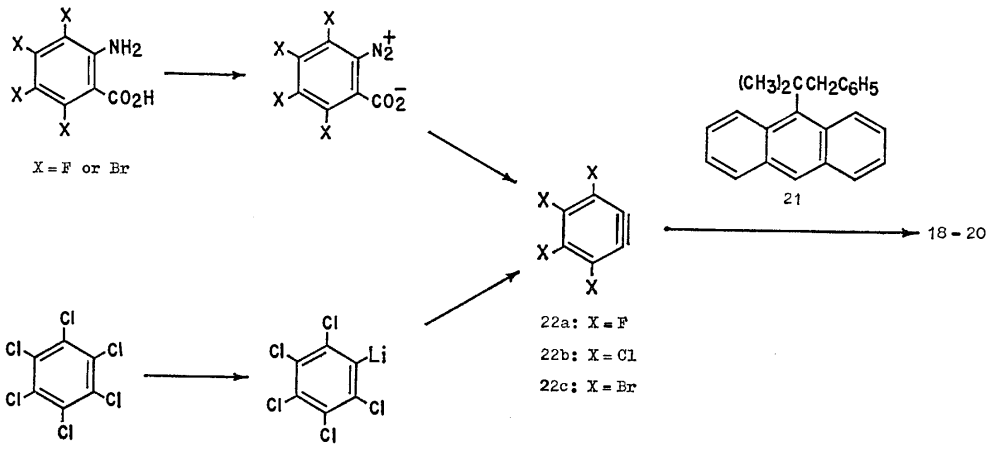

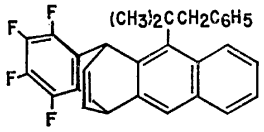

23

Kinetics. Kinetic measurements of rotamer isomerization were performed in 1-chloronaphthalene solutions according to the procedure described before.[13] Equilibrium and rate constants at several temperatures and the free energies of activation therefrom are compiled in Table 3. Allowance for the degeneracy of the $\pm sc$ rotamers is made in the calculations of the van't Hoff and the Eyring parameters, which are given in Table 1. Table 2 shows a comparison of the data with those of the 1-halo counterparts. Comparison is made at 240 °C for the fluoro pair and at 175 °C for the chloro and the bromo pairs. The reference temperatures are chosen because they are nearly the midpoints of the temperature range in which the kinetic measurements were made for each pair.

Discussion

Buttressing Effect on the Ground State Properties. A 9-*t*-alkyltriptycene is a highly congested molecule with some of the atoms in 9-*t*-alkyl group locating within the sum of the van der Waals radii from the triptycyl skeleton. Substitution at a *peri*-position increases the congestion so that the C_9–C_{alkyl} bond is forced to bend away from the *peri*-substituent. This feature was actually observed in the X-ray structure of 9-*t*-butyl-1,2,3,4-tetrachlorotriptycene.[18] It deserves to mention here that the 1,2,3,4-tetrachlorobenzo group is almost planar including the chloro groups. It would not have been possible to discuss the buttressing effect if the chloro groups deviated seriously from coplanarity. We assume the compounds in question take the similar structure. Then 9-(1,1-dimethyl-2-phenylethyl)-1,2,3,4-tetrahalotriptycenes (**18**—**20**) are supposed to be more crowded than the corresponding 1-halo compounds (**12**—**14**) in the vicinity of the axis bond.

A long-range spin-spin coupling is observed between the 1-fluorine and protons in the $\pm sc$-methyl group in any of the fluorine-containing atropisomers.[19] The coupling constant is larger in a tetrafluoro rotamer (9.2 Hz in *ap*-**18**, and 8.3 Hz in $\pm sc$-**18**) than in the corresponding monofluoro one (8.4 Hz in *ap*-**12** and 7.9 Hz in $\pm sc$-**12**), which may be the consequence of the closer proximity between the methyl group and the 1-fluorine in the tetrafluoro rotamers than in the monofluoro counterparts.

The buttressing effect in the ground state is manifested in the rotamer equilibrium. Table 2 shows that the equilibrium constants ($\pm sc/ap$) for the tetrahalo compounds are slightly smaller than those for the monohalo counterparts regardless of the kind of halogen. Increase in congestion by the presence of the buttressing halogens should cause a greater destabilization of the $\pm sc$ rotamer than the *ap* because the former has the bulkier benzyl group in the $\pm sc$ site. Thermodynamic data on **11**—**17** show that the equilibrium constant monotonously decreases as the bulkiness of the *peri*-substituent becomes larger. In this context, the buttressing effect in the ground state is understood as the increase in the effective bulkiness of the *peri*-halogen substituent in the tetrahalo compounds relative to the respective monohalo ones.

Buttressing Effect on the Rotational Barriers. Phenomenological Aspects: Plotting the barriers to rotation in 1-substituted 9-(1,1-dimethyl-2-phenylethyl)triptycenes **11**—**17** against the bulkiness (van der Waals radius) of the 1-substituent, we find a maximum at the 1-fluoro compound **12** and a gradually descending curve as the bulkiness increases.[13] This will imply that in compounds with a *peri*-substituent bulkier than fluorine, the presence of a buttressing substituent should lower the barrier, exhibiting the negative buttressing effect.

The tetrachloro compound **19** isomerizes 13 times faster than the monochloro counterpart **13** at 175 °C with the barrier drop of 2.3 kcal mol^{-1}, manifesting the negative buttressing effect. Even more conspicuous negative effect is found in the tetrabromo compound **20**, which isomerizes 100 times faster than the monobromo one **14** at 175 °C, the drop in the free energy of activation being 4.1 kcal mol^{-1}. Appearance of the negative effect in these compounds are in line with the expectation discussed above. A greater magnitude of the effect in the tetrabromo compound **20** than in the tetrachloro one **19** is also reasonable on the ground

TABLE 1. THERMODYNAMIC AND KINETIC PARAMETERS FOR 9-(1,1-DIMETHYL-2-PHENYLETHYL)-1,2,3,4-TETRAHALOTRIPTYCENES[a]

Compound	ΔH° / kcal mol^{-1}	ΔS° [b] / eu	ΔH^* / kcal mol^{-1}	ΔS^* [b] / eu
18	0.29±0.43	−0.2±0.8	41.1±0.3	−5.7±0.6
19	1.45±0.02	0.2±0.1	32.6±0.5	−11.5±1.2
20	1.70±0.10	0.4±0.3	30.7±0.1	−8.8±0.3

a) Obtained from the data shown in Table 3. b) Degeneracy of $\pm sc$ rotamers is taken into account.

TABLE 2. COMPARISON BETWEEN THE TETRAHALO AND THE MONOHALO COMPOUNDS

Compound	Temp / °C	K	k_1 / s^{-1}	ΔG^* / kcal mol^{-1}	$\Delta\Delta G^*$ / kcal mol^{-1}	$k_1(X_4)/k_1(X)$
18	240	1.35	1.9×10^{-6}	44.0	0.7	0.5
12[a]	240	1.53	3.8×10^{-6}	43.3		
19	175	0.44	3.6×10^{-6}	37.8	−2.3	13
13[a]	175	0.52	2.8×10^{-7}	40.0		
20	175	0.37	1.1×10^{-4}	34.7	−4.1	100
14[a]	175	0.43	1.1×10^{-6}	38.8		

a) Ref. 13.

TABLE 3. THERMODYNAMIC AND KINETIC DATA

$$ap \underset{k_{-1}}{\overset{2k_1}{\rightleftharpoons}} \pm sc \quad K=2k_1/k_{-1}$$

Compound	Temp / °C	K	k_1 / s^{-1}	ΔG^* / kcal mol^{-1}	Bath liquid
18	258	1.35	7.40×10^{-6}	44.1_6	Diphenyl ether
	246	1.35	2.88×10^{-6}	44.1_2	Diethylene glycol
	238	1.36	1.55×10^{-6}	44.0_4	Quinoline
	226.5	1.33	5.99×10^{-7}	43.9_8	Hexylbenzene
19	208	0.49	4.80×10^{-5}	38.1_2	Nitrobenzene
	196	0.47	2.01×10^{-5}	37.9_6	1,2-Ethanediol
	184.5	0.45	7.62×10^{-6}	37.8_9	1,2-Propanediol
	162	0.42	1.20×10^{-6}	37.5_8	Mesitylene
20	202[a]	0.40			Silicone oil
	175	0.37	1.12×10^{-4}	34.6_9	Decane
	166	0.35	5.47×10^{-5}	34.6_0	Mesitylene
	157	0.33	2.49×10^{-5}	34.5_4	Bromobenzene
	133	0.30	2.87×10^{-6}	34.3_2	Chlorobenzene

a) Only the equilibrium constant is obtained.

mentioned above, because both the buttressing and the buttressed halogens are bulkier in **20** than in **19**.

As for the tetrafluoro compound **18**, it is difficult to predict *a priori* the sign of the buttressing effect, since the 1-fluoro compound **12** gives a maximal barrier in the series of compounds **11**—**17**: the introduction of a buttressing substituent could lower the barrier, if a phantom substituent smaller than fluorine gives a real maximum in the series, and the reverse could occur if a phantom substituent a little bulkier than fluorine gives a maximum. In practice, the tetrafluoro compound **18** isomerizes twice slower than the monofluoro one **12** at 240 °C, exhibiting a small positive buttressing effect. This fact is an indication that a compound with a *peri*-substituent slightly bulkier than fluorine, if existed, should give a maximal barrier in a series of 1-substituted 9-(1,1-dimethyl-2-phenylethyl)triptycenes.

Analysis of the Barrier: Although the simple explanation in terms of the increase in the effective bulkiness of the *peri*-halogen substituent is possible for the observed buttressing effect, it turns out to be too rough in some cases. For example, the equilibrium constant for the tetrachloro compound **19** (0.44 at 175 °C) is almost identical with that for the monobromo compound **14** (0.43), and hence we can say that the 1-chlorine in **19** has almost the same effective bulkiness as the 1-bromine in **14**. However, the rotational barrier in **19** is lower than that in **14** by 1.0 kcal mol^{-1}. This implies that the buttressing effect on the energy barrier operates somewhat differently from that on the ground state and thus we must consider the effect on the transition state in some detail.

We have developed a hypothesis which uses a rigid rotor model to explain the observed dependence of the barrier on the bulkiness of the 1-substituent; that is, the lowering of the barrier with the increasing bulkiness of the *peri*-substituent should at least partly ascribed to lowering of the transition state energy.[13] The hypothesis states that a bulky *peri*-substituent in-

duces the deformation of the molecule typically manifested in the tilting of the axis bond of the 9-substituent away from the *peri*-substituent. If this feature is retained during the rotation about the axis bond, the maximal eclipsing interactions between the β-groups of the 9-substituent and the *peri*-substituent or hydrogens do not occur simultaneously at the three sites but sequentially with some time lags. Therefore, the transition state is not destabilized to such an extent that would be expected from the bulkiness of the *peri*-substituent, causing the decrease in the barrier. As the *peri*-substituent becomes bulkier, these time lags should become larger and hence the barrier should become lower, which was actually observed.

However this hypothesis still fails to explain the differential behavior observed in compounds **14** and **19**. The fact that **19** has a lower barrier to rotation than **14** suggests that the transition state for rotation in **19** is more "stabilized" than that in **14** relative to the respective ground state. A possible rationalization may be as follows. In order to relieve a large congestion in the transition state, 9- and *peri*-substituents further bend away from each other. While the 1-bromo group in **14** is prone to easy in-plane bending away from the 9-substituent, the bending of the 1-chloro group in **19** is restricted because of the buttressing effect. Hence the axis bond of the 9-substituent in **19** suffers a greater additional tilting than that in **14** on going from the ground to the transition state. This results in the larger time lags between the maximal eclipsing interactions in the transition state and thus the lower barrier in **19** than in **14**.

Thus we have to admit that the molecule is subjected to further deformation in the course of internal rotation for the better understanding of the buttressing effect. We conclude that the negative buttressing effect is originated from the fact that the transition state for rotation is less destabilized than the ground state upon introduction of a buttressing substituent.

Experimental

Melting points are not corrected. ^{1}H NMR spectra were obtained on a Hitachi R-20B (60 MHz) or a Varian EM-390 (90 MHz) spectrometer with tetramethylsilane as an internal reference. ^{19}F NMR spectra were recorded on a Varian EM-390 at 84.67 MHz with hexafluorobenzene as an internal reference, and the chemical shifts are given in ppm downfield from C_6F_6.

ap-*9-(1,1-Dimethyl-2-phenylethyl)-1,2,3,4-tetrafluorotriptycene* (ap-**18**). A solution of 1.05 g (5 mmol) of 1,2,3,4-tetrafluoroanthranilic acid[20] in 15 mL of dry acetone was added dropwise to a boiling solution of 764 mg (2.46 mmol) of 9-(1,1-dimethyl-2-phenylethyl)anthracene (**21**)[21] and 1 mL of isopentyl nitrite in 20 mL of dichloromethane during the course of 1 h. The mixture was heated under reflux for 1 h and evaporated. The residue was chromatographed through an alumina column. The desired triptycene *ap*-**18** and a by-product, which was assigned to the 1,4-adduct (**23**) by its ^{1}H NMR [($CDCl_3$, δ): 1.80 (3H, s), 1.86 (3H, s), 3.33 and 3.67 (2H, AB-q, J=13.2 Hz), 5.42 (1H, td J=1.7 and 6.0 Hz), 5.99 (1H, br d, J=6.2 Hz), 6.34 (1H, ddd, J=1.6, 6.2, and 7.2 Hz)], eluted together, which weighed 519 mg (47%). The mixture was dissolved in 20 mL of acetone and chilled to 0 °C, to which a solution of 190 mg of potassium permanganate in 15 mL of water was added dropwise. The mixture was stirred at 0 °C for 2 h and evaporated. The residue was extracted with dichloromethane and chromatographed through an alumina column with hexane as eluent affording 208 mg (19% based on **21**) of *ap*-**18** as colorless crystals, mp 192—194 °C (from benzene–hexane). Found: C, 78.76; H, 5.08%. Calcd for $C_{30}H_{22}F_4$: C, 78.59; H, 4.84%. ^{1}H NMR ($CDCl_3$, δ): 2.04 (6H, d, J=9.2 Hz), 3.87 (2H, s), 5.74 (1H, br d, J=1.6 Hz), 6.9—7.7 (11H, m), 8.08 (2H, m). ^{19}F NMR ($CDCl_3$): 2.96 (t, J=19.5 Hz, 2-F), 3.59 (ddd, J=22.0, 19.4, and 5.3 Hz, 3-F), 12.80 (dd, J=22.0 and 13.7 Hz, 4-F), 38.05 (br, 1-F).

±sc-*9-(1,1-Dimethyl-2-phenylethyl)-1,2,3,4-tetrafluorotriptycene* (±sc-**18**). The equilibrated mixture of the rotamers was chromatographed on alumina with hexane as eluent. The ±*sc* rotamer eluted faster than the *ap*, and was recrystallized from tetrahydrofuran–hexane, mp 203—204 °C. Found: C, 78.88; H, 4.66%. Calcd for $C_{30}H_{22}F_4$: C, 78.59; H, 4.84%. ^{1}H NMR ($CDCl_3$, δ): 1.95 (3H, d, J=8.3 Hz), 2.09 (3H, s), 2.61 (1H, d, J=14.1 Hz), 3.97 (1H, dd, J=14.1 and 2.4 Hz), 5.70 (1H, br d, J=1.6 Hz), 6.9—7.7 (12H, m), 7.81 (1H, m). ^{19}F NMR ($CDCl_3$): 3.24 (t, J=19.8 Hz, 2-F), 4.03 (ddd, J=22.9, 19.8, and 6.1 Hz, 3-F), 12.79 (dd, J=22.9 and 13.4 Hz, 4-F), 40.40 (br, 1-F).

ap-*1,2,3,4-Tetrachloro-9-(1,1-dimethyl-2-phenylethyl)triptycene* (ap-**19**). To a suspension of 3.68 g (12.9 mmol) of hexachlorobenzene in 200 mL of diethyl ether was added dropwise a solution of 13 mmol of butyllithium in hexane at −78 °C. The mixture was stirred at −78 °C until the solid had disappeared, to which an ethereal solution of 1.5 g (4.84 mmol) of **21** was added dropwise. The mixture was allowed to slowly warm up to room temperature, and then heated under reflux for 2 h. Column chromatography on alumina with hexane–benzene as eluent gave a mixture of *ap*-**19** and unidentified by-products, presumably polychlorobiphenyls. Repeated chromatographies and recrystallizations from tetrahydrofuran–methanol afforded a pure sample of *ap*-**19**, mp 283—285 °C. Found: C, 68.73; H, 4.25; Cl, 26.79%. Calcd for $C_{30}H_{22}Cl_4$: C, 68.72; H, 4.23; Cl, 27.05%. ^{1}H NMR ($CDCl_3$, δ): 2.36 (6H, s), 3.81 (2H, s), 6.12 (1H, s), 7.0—7.6 (11H, m), 8.08 (2H, m).

±sc-*1,2,3,4-Tetrachloro-9-(1,1-dimethyl-2-phenylethyl)triptycene* (±sc-**19**). The equilibrated mixture of the rotamers was chromatographed on alumina with benzene–hexane as eluent. ±*sc*-**19** eluted faster than *ap*-**19**. Recrystallization from tetrahydrofuran–hexane afforded pure ±*sc*-**19**, mp 231—232 °C. Found: C, 68.71; H, 4.17; Cl, 26.64%. Calcd for $C_{30}H_{22}Cl_4$: C, 68.72; H, 4.23; Cl, 27.05%. ^{1}H NMR ($CDCl_3$, δ): 2.12 (3H, s), 2.37 (3H, s), 4.13 and 4.37 (2H, AB-q, J=15.2 Hz), 6.11 (1H, s), 6.9—7.7 (11H, m), 7.92 (1H, m), 8.16 (1H, m).

ap-*1,2,3,4-Tetrabromo-9-(1,1-dimethyl-2-phenylethyl)triptycene* (ap-**20**). A solution of 2.7 g (6 mmol) of tetrabromoanthranilic acid[22] in 10 mL of 1,2-dimethoxyethane (DME) was added dropwise to a boiling solution of 486 mg (1.56 mmol) of **21** and 1 mL of isopentyl nitrite in 20 mL of DME during the course of 2.5 h. The mixture was heated under reflux for 1 h, evaporated and chromatographed on alumina with dichloromethane–hexane as eluent, affording 194 mg (18%) of *ap*-**20**, mp 291—293 °C (from tetrahydrofuran–hexane). Found: C, 51.30; H, 2.88%. Calcd for $C_{30}H_{22}Br_4$: C, 51.32; H, 3.16%. ^{1}H NMR ($CDCl_3$, δ): 2.51 (6H, s), 3.75 (2H, s), 6.24 (1H, s), 7.0—7.6 (11H, m), 8.10 (2H, m).

±sc-*1,2,3,4-Tetrabromo-9-(1,1-dimethyl-2-phenylethyl)triptycene*

(±sc-20). Addition of hexane to the equilibrated mixture of rotamers of **20** in 1-chloronaphthalene caused selective crystallization of *ap*-**20**, leaving the ±*sc*-enriched mixture in the mother liquor, which was chromatographed on alumina with hexane as eluent. The ±*sc* rotamer eluted slightly faster than the *ap*. The fractions containing almost pure ±*sc*-**20** was evaporated and recrystallized from tetrahydrofuran–hexane, affording a pure sample of ±*sc*-**20**, mp 223—225 °C. Found: C, 51.57; H, 3.28; Br, 45.55%. Calcd for $C_{30}H_{22}Br_4$: C, 51.32; H, 3.16; Br, 45.52%. ^{1}H NMR ($CDCl_3$, δ): 2.01 (3H, s), 2.57 (3H, s), 4.08 and 4.67 (2H, AB-q, J=15.5 Hz), 6.23 (1H, s), 6.9—7.7 (11H, m), 7.95 (1H, m), 8.15 (1H, m).

Kinetic Measurements. The experimental procedures described before[13] were followed. Relative populations of the rotamers were obtained by integrating the 1-fluorine signals for **18** and the *gem*-dimethyl signals for **19** and **20**. The liquids used for the boiling bath were shown in Table 3. The equilibrium constant for **20** at 202 °C was obtained in a conventional silicone oil bath.

References

1) Part XLVI: G. Yamamoto and M. Ōki, *J. Org. Chem.*, in press.

2) S. L. Chien and R. Adams, *J. Am. Chem. Soc.*, **56**, 1787 (1934).

3) M. Rieger and F. H. Westheimer, *J. Am. Chem. Soc.*, **72**, 19 (1950); F. H. Westheimer, "Calculation of the Magnitude of Steric Effects" in "Steric Effects in Organic Chemistry," ed by M. S. Newman, Wiley, New York, (1956), Chap. 12.

4) B. J. Fuhr, B. W. Goodwin, H. M. Hutton, and T. Schaefer, *Can. J. Chem.*, **48**, 1558 (1970); M. A. H. Stewart, T. Schaefer, H. M. Hutton, and C. M. Wong, *ibid.*, **49**, 1085 (1971).

5) M. Aoki, M. Nakamura, and M. Ōki, *Bull. Chem. Soc. Jpn.*, **55**, 2512 (1982).

6) O. S. Akkerman and J. Coops, *Recl. Trav. Chim. Pays-Bas*, **86**, 755 (1967).

7) A. J. M. Reuvers, A. Sinnema, T. J. Nieuwstad, F. van Rantwijk, and H. van Bekkum, *Tetrahedron*, **27**, 3713 (1971).

8) E. A. Chandross and C. F. Sheley, Jr., *J. Am. Chem. Soc.*, **90**, 4345 (1968).

9) A. Rieker and H. Kessler, *Tetrahedron Lett.*, **1969**, 1227.

10) G. Yamamoto and M. Ōki, *Bull. Chem. Soc. Jpn.*, **54**, 473 (1981).

11) G. Yamamoto and M. Ōki, *Bull. Chem. Soc. Jpn.*, **54**, 481 (1981).

12) S. Otsuka, T. Mitsuhashi, and M. Ōki, *Bull. Chem. Soc. Jpn.*, **52**, 3663 (1979); S. Otsuka, G. Yamamoto, T. Mitsuhashi, and M. Ōki, *ibid.*, **53**, 2095 (1980).

13) G. Yamamoto, M. Suzuki, and M. Ōki, *Bull. Chem. Soc. Jpn.*, **56**, 306 (1983).

14) Preliminary reports have been published: G. Yamamoto, M. Suzuki, and M. Ōki, *Angew. Chem., Int. Ed. Engl.*, **20**, 607 (1981); *Chem. Lett.*, **1980**, 1523.

15) Generation of **22a** from pentafluorophenyllithium[16a] and of **22b** from tetrachloro-2-diazoniobenzoate[16b] is well documented and the choice of the precursors in our experiments was simply based on the ready availability of the precursors. Generation of **22c** from hexabromobenzene and butyllithium is also reported[16c] but does not seem to be generally applicable.

16) a) J. P. N. Brewer, H. Heaney, S. V. Ley, and T. Ward, *J. Chem. Soc., Perkin Trans. 1*, **1974**, 2688; b) H. Heaney and J. M. Jablonski, *J. Chem. Soc., C*, **1968**, 1895; c) D. J. Berry and B. J. Wakefield, *ibid.*, **1969**, 2342.

17) Stereoselective formation of the *ap* atropisomers in the reactions of benzynes with the anthracene **21** is well documented. See for example: G. Yamamoto and M. Ōki, *Bull. Chem. Soc. Jpn.*, **48**, 3686 (1975).

18) M. Mikami, K. Toriumi, M. Konno, and Y. Saito, *Acta Crystallogr., Sect. B*, **31**, 2474 (1975).

19) Details of the long-range ^{1}H–^{19}F spin-spin couplings in triptycene derivatives will be discussed elsewhere: G. Yamamoto and M. Ōki, in preparation.

20) N. Ishikawa, T. Tanabe, and T. Ohashi, *Nippon Kagaku Kaishi*, **1972**, 202.

21) G. Yamamoto, M. Nakamura, and M. Ōki, *Bull. Chem. Soc. Jpn.*, **48**, 2592 (1975).

22) H. Heaney, K. G. Mason, and J. M. Sketchley, *J. Chem. Soc., C*, **1971**, 567.

 © 1983 The Chemical Society of Japan Bull. Chem. Soc. Jpn., 56, 815—817 (1983)

Acyl Transfer from *S*-Monoacyldihydrolipoamide to Benzylamine in the Presence of Oxidizing Agents

Yoko Nambu,* Takeshi Endo, and Makoto Okawara

Research Laboratory of Resources Utilization, Tokyo Institute of Technology, Nagatsuta, Midori-ku, Yokohama 227

(Received October 26, 1982)

Acyl transfer reaction from *N*-benzyl-8-*S*-(*p*-nitrobenzoyl)dihydrolipoamide to benzylamine was enhanced with oxidizing agents such as cobalt(II) ion or a soluble flavin under an oxygen atmosphere or with di-4-pyridyl disulfide, accompanied by the formation of *N*-benzyllipoamide.

Lipoic acid is known to work as an acyl carrier in the oxidative decarboxylation of α-keto acids in living systems through formation of active acyl intermediates, 6-*S*-acyldihydrolipoic acids which in turn acylate coenzyme A, and subsequent oxidation of the resultant dihydrolipoic acid to lipoic acid, enzymatically.

We have already reported that 8-*S*-monoacyldihydrolipoamides were synthesized by the reductive acylation of lipoamide with tributylphosphine in high yields (Eq. 1).[1]

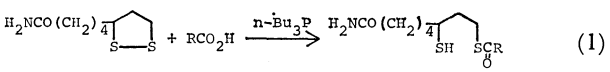

(1)

Further, we have found that acyl transfer from *S*-monoacyldihydrolipoamides to amine was accelerated by silver ion more effectively than that from *S,S'*-diacyl derivatives, caused by the activation of acyl group by silver ion bound to the neighboring mercapto group.

On the other hand, the acyl transfer from hydroquinone monobenzoates to alcohols has been reported to proceed oxidatively by use of oxidizing agents such as Ce^{4+}, Tl^{3+}, NBS, or Br_2,[3] and by electrochemical oxidation.[4]

These results suggested us to investigate the acyl transfer from *S*-monoacyldihydrolipoamide to amines in the presence of oxidizing agents for thiols, expecting that the activation of acyl group through two-electron oxidation of neighboring mercapto group to form amide and lipoamide. Various kinds of oxidizing agents are considered to be applied to the present case. However, by using some oxidizing agents which form S radicals rather than S cations from thiols, the dimerization of *S*-monoacylated dithiols might precede the activation of acyl groups, as reported in the iodine oxidation of 8-*S*-acetyldihydrolipoic acid in methanol[5] (Scheme 1).

We now report the acyl transfer from *N*-benzyl-8-*S*-(*p*-nitrobenzoyl)dihydrolipoamide (**1**) to benzylamine (**2**) in the presence of oxidizing agents such as an active flavin (**5**),[6] metal salts,[7] and di-4-pyridyl disulfide (4-PDS),[8] which are known to oxidize thiols to disulfides *via* the formation of complexes or adducts between oxidizing agents and thiols (Eq. 2).

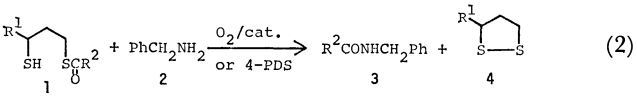

(2)

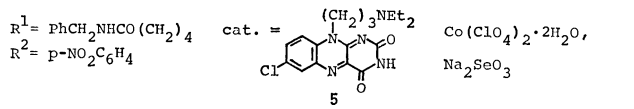

Experimental

^{1}H-NMR spectra were recorded on a JEOL-PMX 60 NMR spectrometer using tetramethylsilane as an internal reference.

N-Benzyl-8-*S*-(*p*-nitrobenzoyl)dihydrolipoamide (**1**) and *N*-benzyl-*S,S'*-bis(*p*-nitrobenzoyl)dihydrolipoamide were prepared by the methods reported previously.[2b] An active flavin (**5**) was also prepared according to the procedure of King *et al.*[9] GLC analyses were carried out on a JEOL-1100 gas chromatograph (10% SE-30, stainless-steel column, 220 °C, N_2 carrier gas).

*Acyl Transfer Reaction from Monoacyl Derivative **1** to Benzylamine (**2**) in the Presence of Cobalt(II) Perchlorate as Catalyst.* To a THF solution (3 ml) of **1** (20 mg, 0.045 mmol) and amine **2** (0.1 ml, 0.9 mmol) was added cobalt(II) perchlorate (1.2 mg, 0.004 mmol) under an oxygen atmosphere and stirred for 15 h at room temperature. The reaction mixture was poured into ethyl acetate (50 ml), and the solution was washed with 0.1 M† HCl and saturated aqueous NaCl, then dried over $MgSO_4$. The solvent was removed under reduced pressure to obtain a solid residue. ^{1}H-NMR spectrum of the residue in $CDCl_3$ was measured to show a quantitative formation of *N*-benzyl-*p*-nitrobenzamide (**3**) and *N*-benzyllipoamide (**4**) compared with the authentic samples. The yield of amide **3** was calculated from the ratio of the ^{1}H-NMR signal of benzyl proton in **3** (δ=4.6) to the sum of benzyl protons in **1** and **4** (δ=4.4) to be 100% (Fig. 1). The residue obtained in the scale up experiment (two times of the above procedure) was chromatographed on silica gel with ethyl acetate to obtain amide **3** (18 mg, 78%) and **4** (19 mg, 71%). Authentic sample of **3** was prepared from *p*-nitrobenzoyl chloride and benzylamine mp 142.5—143.5 °C (from ethanol) (lit,[10] 141—142.5 °C); NMR ($CDCl_3$): δ 4.6 (2H, d, J=5.8 Hz, $PhCH_2$), 5.9 (1H, s, NHCO), 7.4 (5H, s, C_6H_5), 8.1 (4H, q, J=9.2 Hz, *p*-$NO_2C_6H_4$). Amide **4** was prepared by the method reported previously.[2c] NMR ($CDCl_3$): δ 1.5—2.0 (8H, m, $>CH_2$), 3.2 (2H, t, 5-membered CH_2–SS), 3.6 (1H, m, CH–SS), 4.4 (2H, d, J=5.7 Hz,

† 1 M = 1 mol dm^{-3}.

$PhCH_2$), 5.9 (1H, s, NHCO), 7.3 (5H, s, C_6H_5).

In case of other catalysts or 4-PDS, the reaction was carried out in the same procedure as described above.

Kinetic measurements were carried out by GLC analyses of the reaction solutions operated in the same way described above at 30 °C in the presence of *N*-cyclohexyl-*p*-nitrobenzamide as an internal standard for GLC analyses.

Acyl Transfer Reaction from Monoacyl Derivative **1** *to Methanol in the Presence of Oxidizing Agents.* The reaction was carried out in the same way as described above. Methanol (1 ml, 24 mmol) and triethylamine (0.13 ml, 0.9 mmol) were added instead of amine **2** and allowed to react for 15 h at room temperature. The residue was chromatographed on silica gel with ethyl acetate as eluent to afford methyl *p*-nitrobenzoate (**8**) identical with the authentic sample prepared from *p*-nitrobenzoyl chloride and methanol. The yield of ester **8** was calculated from the ratio of ^{1}H-NMR signal of methyl proton in **8** (δ=4.0) to that of benzyl protons in **1** and **4** (δ=4.4).

Results and Discussion

The acyl transfer reaction was carried out by treating monoacyl derivative **1** with excess benzylamine (**2**) in tetrahydrofuran (THF) in the presence of some oxidizing catalysts under an oxygen atmosphere, or in the presence of 4-PDS under a nitrogen atmosphere at 30 °C. The progress of the reaction was followed by GLC analyses of the acyl transfer product, *N*-benzyl-*p*-nitrobenzamide (**3**), in the reaction solution (Fig. 1). In every case, the formation of **3** followed first-order kinetics, and pseudo first-order rate constants, *k*, were obtained from the slopes of the first-order plots (Table 1). The yields of **3** were determined by ^{1}H-NMR method by carrying out the acyl transfer reaction at room temperature for 15 h, and the results were summarized in Table 1 together with those obtained by treating a diacyl derivative, *N*-benzyl-*S*,*S*′-bis(*p*-nitrobenzoyl)dihydrolipoamide, with amine **2**.

In the presence of excess amine **2**, amide **3** was obtained in 55% yield without oxidizing agents. No or slight enhancement was observed by bubbling oxygen gas into the reaction mixture or by adding a catalytic amount of Co(II) ion under a nitrogen atmosphere. On the other hand, the acyl transfer reaction was promoted by adding catalytic amounts of flavin (**5**), Co(II), or Se(IV) ion to the reaction mixture of monoacyl derivative **1** and amine **2** under an oxygen atmosphere, as observed both in the rate enhancements and the increase of yields in Table 1. Co(II)

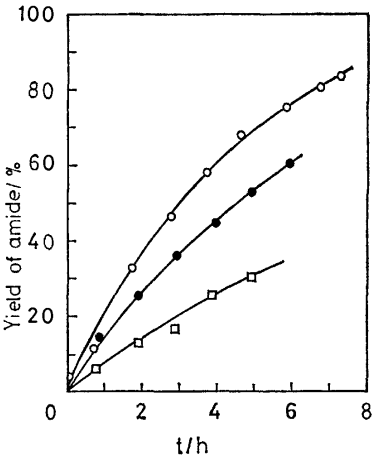

Fig. 1. Effects of oxidizing agents on the acyl transfer reaction from monoacyl derivative **1** to benzylamine (**2**) in THF (3 ml) at 30 °C; **1** 0.045 mmol, **2** 0.9 mmol,
○: 4-PDS (0.045 mmol), ●: Co(II) (0.004 mmol)/O_2, □: no catalyst/N_2.

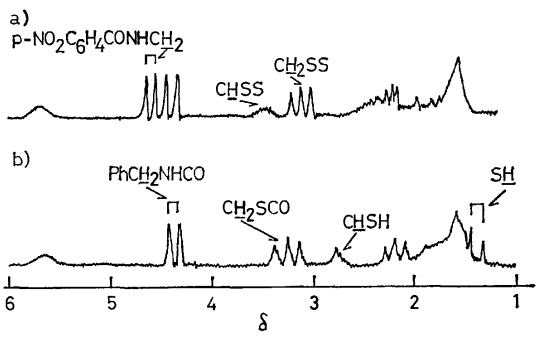

Fig. 2. ^{1}H-NMR spectra obtained by Co(II) catalyzed acyl transfer from monoacyl derivative **1** to benzylamine (**2**).
a): Reaction products, b): **1**.

Table 1. Acyl transfer reaction from *S*-acyl derivatives to benzylamine (**2**)[a]

Acyl derivative	Oxidizing agent	Yield of **3**/%[b]	$k\times10^3$/min^{-1} [c]
Monoacyl deriv. **1**	None (N_2)	55	0.91
	O_2	53	1.03
	N_2/$Co(ClO_4)_2\cdot2H_2O$	59	1.20
	O_2/$Co(ClO_4)_2\cdot2H_2O$	100	2.00
	O_2/**5**	80	1.67
	O_2/Na_2SeO_3	64	
	4-PDS	100	2.37
Diacyl deriv.[d]	None (N_2)	50	
	O_2	53	
	O_2/$Co(ClO_4)_2\cdot2H_2O$	63	

a) Conditions; monoacyl deriv. **1** 0.045 mmol (diacyl deriv. 0.023 mmol), amine **2** 0.9 mmol, cat. 0.004 mmol (4-PDS 0.045 mmol), THF 3 ml, room temperature, 15 h. b) Yields were determined by ^{1}H-NMR method as mentioned in experimental section. c) Kinetic measurements were carried out at 30 °C. d) *N*-Benzyl-*S*,*S*′-bis(*p*-nitrobenzoyl)dihydrolipoamide.

ion was the most effective catalyst to lead to the quantitative formation of amide **3** in the present reaction conditions. The ^{1}H-NMR spectrum of the products in the presence of Co(II) ion was shown in Fig. 2. Proton signal of mercapto group in **1** at $\delta=1.4$ (1H, d) disappeared completely by the reaction and new signals at $\delta=3.2$ (2H, d, $PhCH_2N$) appeared which suggested the quantitative formation of *N*-benzyllipoamide (**4**) accompanying the acyl transfer. However, only slight enhancement was observed by Co(II) ion catalyst in case of the acyl transfer reaction from diacyl derivative. Co(II) ion is known to catalyze the oxidation of dithiols to cyclic disulfides by oxygen effectively by way of complex formation.[7] It is presumed therefore that Co(II) ion catalyzed the acyl transfer oxidatively through the activation of acyl group by way of the complex formation with monoacyl derivative **1** as shown in Eq. 3.

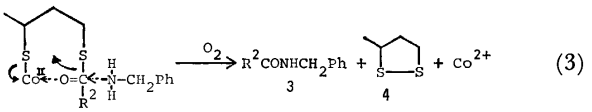

(3)

In the oxidation of dithiols by flavins, Loechler *et al.*[9] proposed the formation of a thiol-*C*(4a)-flavin adduct (**6**). Also in the present flavin catalyzed reaction, flavin (**5**) presumably enhanced the acyl transfer reaction oxidatively by the formation of adduct intermediate (**7**), and the reduced flavin formed might be reoxidized by oxygen to work catalytically.

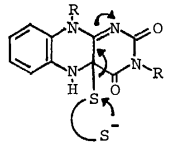

6

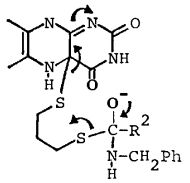

7

In he presence of 4-PDS as an oxidizing agent, acyl transfer reaction was enhanced most effectively to result in the quantitative formation of amide **3** and lipoamide **4**. The formation of 4(1*H*)-pyridinethione was ascertained from the UV spectrum of the reaction mixture (λ_{max}, 350 nm). Further 4-PDS is known to form reactive mixed disulfides with thiols very easily.[8] Therefore, the mechanism shown in Scheme 2 is proposed for the 4-PDS promoted acyl transfer reaction.

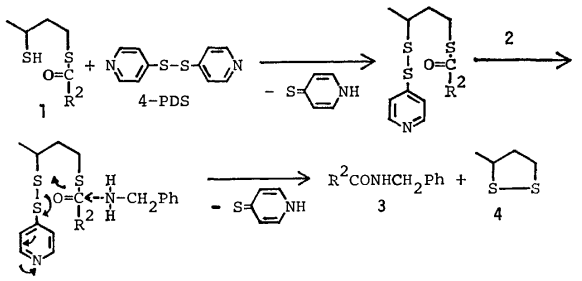

Scheme 2.

Table 2. Acyl transfer reaction from monoacyl derivative **1** to methanol[a]

Oxidizing agent	Yield of **8**/%[b]
None (N_2)	24
O_2/$Co(ClO_4)_2\cdot 2H_2O$	26
4-PDS	22
I_2	21

a) Conditions; monoacyl derivative **1** 0.045 mmol, methanol 24 mmol, Et_3N 0.9 mmol, cat. 0.004 mmol (4-PDS 0.045 mmol, I_2 0.05 mmol), room temperature, 15 h. b) Yields were determined by ^{1}H-NMR method as mentioned in experimental section.

The effect of oxidizing agents was further examined in case of the acyl transfer reaction from monoacyl derivative **1** to methanol. The reaction was carried out in the presence of various kinds of oxidizing agents and triethylamine (Et_3N). The results are shown in Table 2. No enhancement was observed for the formation of methyl *p*-nitrobenzoate (**8**) by adding oxidizing agents in the present reaction conditions, contrary to the reported results[5] where methanol was used as a solvent. The SH proton signal disappeared completely in ^{1}H-NMR spectrum of the reaction products. These results suggested that the dimerization of monoacyl derivative **1** preceded the enhancement of acyl transfer reaction in case of acyl transfer to weak nucleophiles such as alcohols.

The results in this study suggest that lipoamide might work as an acyl carrier in the synthesis of amides from carboxylic acids and amines by combining both the reductive acylation (Eq. 1) and the oxidative acyl transfer reaction (Eq. 2). We are planning to apply these reactions to a lipoamide immobilized on polystyrene beads to get a polymeric acyl carrier which is capable of recycle uses.

References

1) Y. Nambu, T. Endo, and M. Okawara, *J. Polym. Sci., Polym. Chem. Ed.*, **19**, 1937 (1981).
2) a) M. Okawara, A. Fujimoto, and T. Endo, *Isr. J. Chem.*, **17**, 264 (1978); b) Y. Nambu, T. Endo, and M. Okawara, *Bull. Chem. Soc. Jpn.*, **54**, 3433 (1981); c) Y. Nambu, T. Endo, and M. Okawara, *J. Polym. Sci., Polym. Chem. Ed.*, **18**, 2793 (1980).
3) V. M. Clark, M. R. Eraut, and D. W. Hutchinson, *J. Chem. Soc., C*, **1969**, 79.
4) R. W. Johnson, M. D. Bednarski, B. F. O'Leary, and E. R. Grover, *Tetrahedron Lett.*, **22**, 3715 (1981).
5) M. Takagi, S. Goto, R. Ishihara, and T. Matsuda, *J. Chem. Soc., Chem. Commun.*, **1976**, 993.
6) I. M. Gasoigne and G. K. Radda, *Biochem. Biophys. Acta*, **131**, 498 (1967).
7) C. C. Tsen and A. L. Tappel, *J. Biol. Chem.*, **233**, 1230 (1958).
8) D. R. Grassetti and J. F. Murray, *Arch. Biochem. Biophys.*, **119**, 41 (1967).
9) E. L. Loechler and J. C. Hollocher, *J. Am. Chem. Soc.*, **102**, 7312, 7322 (1980); **97**, 3235 (1975).
10) R. Huisgen and H. Reimlinger, *Justus Liebigs Ann. Chem.*, **599**, 161 (1956).

^{31}P NMR Study of Active Species for Ethylene Dimerization in σ-Aryl Nickel Complex–$AgClO_4$

Yoshimasa Ishimura, Ken-ichi Maruya,* Yoshiyuki Nakamura, Tsutomu Mizoroki, and Atsumu Ozaki

Research Laboratory of Resources Utilization, Tokyo Institute of Technology, 4259 Nagatsuta, Midori-ku, Yokohama 227

(Received February 24, 1982)

$[NiBr(\sigma\text{-}C_6F_5)(PPh_3)_2]$ and $[NiCl(\sigma\text{-}C_6Cl_5)(PPh_3)_2]$ are active for ethylene dimerization in the presence of $AgClO_4$. The activity increases with increase in the amount of $AgClO_4$ and reaches maximum at $AgClO_4$/Ni-complex=2. Addition of excess $AgClO_4$ leads to marked decrease in activity with $[NiBr(\sigma\text{-}C_6F_5)(PPh_3)_2]$ but a little decrease with $[NiCl(\sigma\text{-}C_6Cl_5)(PPh_3)_2]$. ^{31}P NMR spectra of the active solution showed new resonance peaks due to $[Ni(ClO_4)(\sigma\text{-}C_6X'_5)(PPh_3)_2]$ and $[Ni(ClO_4)(\sigma\text{-}C_6X'_5)(PPh_3)]$ (X'=F,Cl), accompanying formation of AgX (X=Br,Cl) and $[Ag(ClO_4)(PPh_3)]$. Thus the role of $AgClO_4$ is to abstract halide anion and/or triphenylphosphine. The amount of $[Ni(ClO_4)(\sigma\text{-}C_6X'_5)(PPh_3)]$ is in good correlation with the rate of dimerization, which suggests this species to be catalytically active.

It has been shown that σ-aryl(halogeno)bis(triphenylphosphine)nickel(II), $[Ni(\sigma\text{-aryl})X(PPh_3)_2]$, is active for the dimerization of ethylene[1] and for the codimerization of ethylene with styrene[2] or 1,3-butadiene[3] in the presence of ether-boron trifluoride (1/1), $Et_2O\cdot BF_3$. During the course of our study on the effect of aryl ligands and $Et_2O\cdot BF_3$ on the dimerization, it has been found that $Et_2O\cdot BF_3$ combined with chloro(σ-pentachlorophenyl) bis (triphenylphosphine) nickel(II), $[NiCl(\sigma\text{-}C_6Cl_5)(PPh_3)_2]$, in the catalyst system can be effectively replaced by silver perchlorate, $AgClO_4$.[4] In the $[Ni(\sigma\text{-aryl})X(PPh_3)_2]$–$Et_2O\cdot BF_3$ system, the role of $Et_2O\cdot BF_3$ was suggested to form BF_3X^- and to abstract the phosphine ligand,[1] but no evidence to prove this has been reported. On the other hand, $AgClO_4$ is not so sensitive to water as $Et_2O\cdot BF_3$ and $[NiCl(\sigma\text{-}C_6Cl_5)(PPh_3)_2]$ is stabler than other σ-arylnickel(II) complexes such as $[NiBr(\sigma\text{-}C_6H_5)(PPh_3)_2]$ and $[NiBr(\sigma\text{-1-naphthyl})(PPh_3)_2]$.[5] The system comprising $[NiCl(\sigma\text{-}C_6Cl_5)(PPh_3)_2]$ and $AgClO_4$ is suitable to investigate the effects.

When chlorobis(methyldiphenylphosphine or dimethylphenylphosphine) (σ-pentachlorophenyl)nickel(II), $[NiCl(\sigma\text{-}C_6Cl_5)(PR_3)_2]$ (PR_3=$PMePh_2$ or PMe_2Ph), is treated with $AgClO_4$ in the presence of the ligand (L) such as lutidine, carbon monoxide, or water the corresponding cationic complex, $[Ni(\sigma\text{-}C_6Cl_5)(L)(PR_3)_2]ClO_4$ is isolated.[6,7] The reaction of the triphenylphosphine analogue, $[NiCl(\sigma\text{-}C_6Cl_5)(PPh_3)_2]$, with $AgClO_4$ is, however, too complicated to isolate the corresponding cationic complex, since the addition of excess $AgClO_4$ results in formation of triphenylphosphine–silver complex.[7] This suggests that $AgClO_4$ replaces the halide anion of the nickel complex with perchlorate anion and at the same time abstracts the triphenylphosphine ligand. Both bromobis (triphenylphosphine) (σ-pentafluorophenyl) nickel(II), $[NiBr(\sigma\text{-}C_6F_5)(PPh_3)_2]$,[8] and $[NiCl(\sigma\text{-}C_6Cl_5)(PPh_3)_2]$[4] are active for the dimerization of ethylene in the presence of $AgClO_4$. The reaction of $AgClO_4$ with $[NiBr(\sigma\text{-}C_6F_5)(PPh_3)_2]$ was investigated by means of ^{31}P NMR spectroscopy, suggesting a coordinatively unsaturated nickel complex, $[Ni(ClO_4)(\sigma\text{-}C_6F_5)(PPh_3)]$, to be an active species for the dimerization of ethylene.[8] This report is concerned with investigation of the reaction of $AgClO_4$ with $[NiCl(\sigma\text{-}C_6Cl_5)(PPh_3)_2]$ by means of ^{31}P NMR spectroscopy in addition to re-examination of the reaction with $[NiBr(\sigma\text{-}C_6F_5)(PPh_3)_2]$; the active species for the dimerization of ethylene is described.

Experimental

Materials. The preparation of nickel complexes and the purification of solvents were conducted in a nitrogen atmosphere, and they were kept under nitrogen. $[NiBr(\sigma\text{-}C_6F_5)(PPh_3)_2]$[9] and $[NiCl(\sigma\text{-}C_6Cl_5)(PPh_3)_2]$[10] were prepared according to the literature. Solvents were dried with diphosphorus pentaoxide (dichloromethane, chlorobenzene, and *o*-dichlorobenzene), metallic sodium (tetrahydrofuran and toluene), or metallic magnesium (ethanol) before distillation. Ethylene was distilled *in vacuo* at the Dry Ice temperature. Exact measurement of the amount of $AgClO_4$ was very hard because of its hygroscopicity. $AgClO_4$ was evacuated in a two-necked flask (50 ml) of known weight at 60 °C for 5 h, after which the flask was filled with nitrogen and weighed. It was kept as a toluene solution of 0.1, 0.2, or 0.5 mol/l.

Ethylene Dimerization. A typical reaction was performed as follows. To an *o*-dichlorobenzene solution (5 ml) of $[NiBr(\sigma\text{-}C_6F_5)(PPh_3)_2]$ (16.6 mg, 0.02 mmol) was added a toluene solution (0.2 ml) of $AgClO_4$ (0.1 mol/l). The solution was kept stirred at room temperature for 1 h, during which the color turned from yellow to reddish brown accompanying a formation of white precipitate. Then ethylene was introduced at 0 °C at 67 kPa of initial pressure and the pressure change was followed. After 1 h of the reaction the volatile material in the reaction flask was transferred into a sampling tube cooled at −196 °C *in vacuo* and analyzed by gas chromatography. The products corresponded to a butene mixture of equilibrium composition and no hexene was detected.

^{31}P NMR Measurements. ^{31}P NMR spectra were obtained on an Electron Optics Laboratory FX-100 spectrometer capable of operating in the pulsed Fourier transform mode at 40.26 MHz. In a typical experiment a toluene solution of $AgClO_4$ was added to a dichloromethane solution (2 ml) of $[NiBr(\sigma\text{-}C_6F_5)(PPh_3)_2]$ (33.2 mg, 0.04 mmol). The solution was filtered to remove the silver bromide formed before being put into an ampule. The chemical shifts were reported in ppm from the external PPh_3 reference (−5.86 ppm from 85% H_3PO_4).

Quantitative measurements were performed using $[NiCl(\sigma\text{-}$

$C_6Cl_5)(PPh_3)_2]$. To a chlorobenzene solution (2 ml) of the nickel complex (17.3 mg, 0.02 mmol) was added a toluene solution of $AgClO_4$. After stirring the solution at room temperature for 1 h, benzene-d_6 (0.2 ml) was added and the solution was filtered to remove the silver chloride. A chlorobenzene solution of triphenylphosphine was sealed into a capillary tube, which was fixed in the NMR tube. The integrated peak area was corrected by use of known concentrations of $[NiCl(\sigma\text{-}C_6Cl_5)(PPh_3)_2]$ in chlorobenzene. Amounts of the complexes and silver-phosphine complexes were evaluated by using the same correction factor as for $[NiCl(\sigma\text{-}C_6Cl_5)(PPh_3)_2]$.

Results and Discussion

Ethylene Dimerization with $[NiBr(\sigma\text{-}C_6F_5)(PPh_3)_2]$. Figure 1 shows a typical time course of ethylene dimerization catalyzed by $[NiBr(\sigma\text{-}C_6F_5)(PPh_3)_2]$-$AgClO_4$ system. Since the total yield of the butene

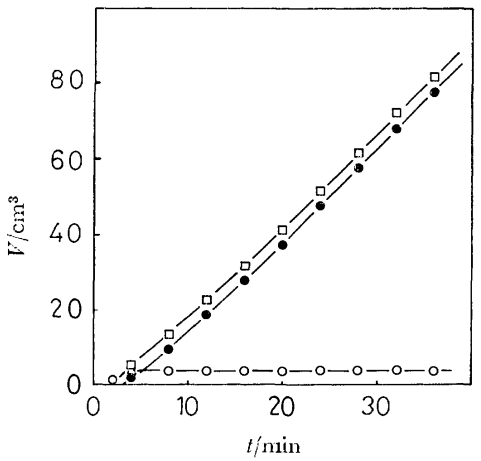

Fig. 1. Time course of ethylene absorption.
$[NiBr(\sigma\text{-}C_6F_5)(PPh_3)_2]$ (0.02 mmol) and $AgClO_4$ (0.04 mmol) in dichloromethane (5 ml) soln, reaction temp 0 °C, initial ethylene pressure 67 kPa.
○: Without $AgClO_4$, □: with $AgClO_4$, ●: reacted ethylene.

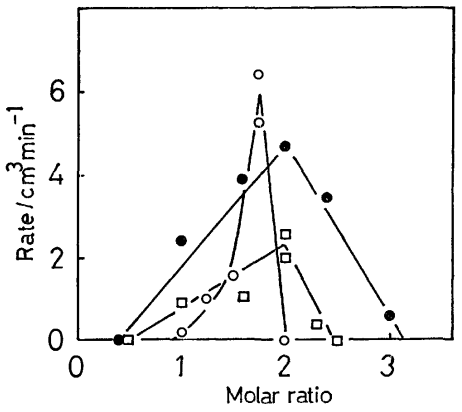

Fig. 2. Rate of ethylene dimerization as a function of molar ratio $AgClO_4$/Ni-complex at 0 °C.
a □: $[NiBr(\sigma\text{-}C_6F_5)(PPh_3)_2]$ (0.02 mmol) in *o*-di chlorobenzene (5 ml) soln, b ●: $[NiBr(\sigma\text{-}C_6F_5)(PPh_3)_2]$ (0.05 mmol) in *o*-dichlorobenzene (5 ml) soln, c ○: $[NiBr(\sigma\text{-}C_6F_5)(PPh_3)_2]$ (0.02 mmol) in dichloromethane (5 ml) soln.

mixture exceeded 97% and no other products such as hexene were detected, the rate of the absorption of ethylene corresponds to that of the ethylene dimerization. Thus the rate of dimerization is easily derived from a constant slope in Fig. 1. Figure 2 shows the dependence of the dimerization rate of ethylene in an *o*-dichlorobenzene solvent on the molar ratio of the nickel complex to $AgClO_4$. It can be seen that the catalyst does not show any activity at molar ratios smaller than 0.5. The catalytic activity increases with increase in the molar ratio from 0.5 to 2 and reaches the highest value at the molar ratio of 2. Beyond this ratio the catalytic activity decreases with increase in the ratio. The rate of dimerization depends also on the concentration of the nickel complex, but the dependence is not so simple. The higher concentration of the nickel complex results in the wider effective range of molar ratio, where the catalyst system is sufficiently active even at higher molar ratios than 2.5. When the same reaction was carried out in dichloromethane, the effective range was limited to 1 to 2 and the highest activity was obtained at the molar ratio of 1.75 (Fig. 2c). These results show that the molar ratio range for the catalyst system effective for the reaction is dependent on both the concentration of the nickel complex and the solvent used.

In order to clarify the effective component in the catalyst system, the reaction of the nickel complex with $AgClO_4$ was examined. When a toluene solution (0.2 ml) of $AgClO_4$ (0.1 mmol) was added to a dichloromethane solution (4 ml) of $[NiBr(\sigma\text{-}C_6F_5)(PPh_3)_2]$ (83 mg, 0.10 mmol), 16.0 mg of AgBr (85% based on the nickel complex) was precipitated. This shows that the following reaction is almost completed:

$$[NiBr(\sigma\text{-}C_6F_5)(PPh_3)_2] + AgClO_4 \longrightarrow [Ni(ClO_4)(\sigma\text{-}C_6F_5)(PPh_3)_2] + AgBr. \quad (1)$$

An addition of more than 0.2 mmol of $AgClO_4$ resulted in a formation of light greenish brown precipitate and a decoloration of the solution. The aqueous solution of the precipitate reacted with dimethylglyoxime to give a reddish brown precipitate. These results suggest that the addition of excess $AgClO_4$ decomposes the nickel complex to reduce the dimerization activity.

^{31}P NMR Spectra of $[NiBr(\sigma\text{-}C_6F_5)(PPh_3)_2]$-$AgClO_4$ *System.* The dichloromethane solution of $[NiBr(\sigma\text{-}C_6F_5)(PPh_3)_2]$ with or without $AgClO_4$ was monitored by ^{31}P NMR at −30 and −80 °C. As shown in Fig. 3b, the addition of an equimolar amount of $AgClO_4$ to the nickel complex leads to the disappearance of the resonance peak at 30.5 ppm due to the original nickel complex and to the appearance of a new resonance peak at 27.1 ppm. Since the reaction of $AgClO_4$ with the nickel complex at this molar ratio is expressed by Reaction 1, the new resonance peak at 27.1 ppm can be assigned to $[Ni(ClO_4)(\sigma\text{-}C_6F_5)(PPh_3)_2]$. Further addition of $AgClO_4$ up to 1.5 of molar ratio resulted in both the decrease in the resonance peak at 27.1 ppm and the increase in a resonance peak at 34.7 ppm along with the appearance of three broad resonance peaks at 13.3, 21.7, and 25.4 ppm (Fig. 3c). At the ratio of 2, the resonance peak

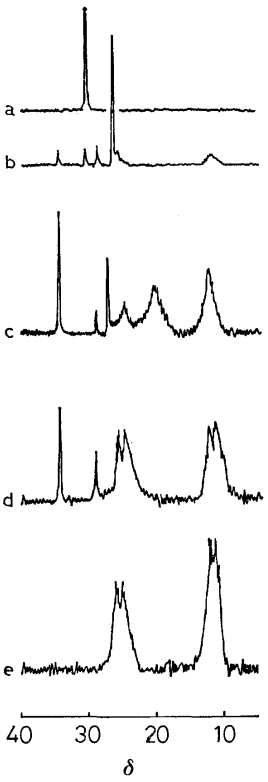

Fig. 3. ^{31}P NMR spectra of catalyst solution (0.02 mmol cat. ml) with different molar ratio $AgClO_4$/Ni-complex at −30 °C in dichloromethane (2 ml) soln. Molar ratios are as follows: a; zero, b;1, c;1.5, d;2, e;3.

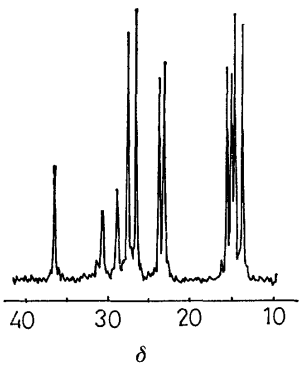

Fig. 4. ^{31}P NMR spectrum of Fig. 3 (c) at −80 °C.

at 27.1 ppm disappeared accompanying the decrease in the resonance peak at 34.7 ppm with the growth of the broad resonance peaks remaining (Fig. 3e). This sample gave eight sharp resonance peaks at −80 °C instead of broad ones. These resonance peaks are assigned to a couple of double doublet peaks due to (perchloro)(triphenylphosphine)silver(I), $[Ag(ClO_4)(PPh_3)]$, at 20.5 ppm ($^1J_{^{107}Ag,P}$=499.24 Hz, $^1J_{^{109}Ag,P}$ =577.34 Hz) and (perchloro)bis(triphenylphosphine)-silver(I), $[Ag(ClO_4)(PPh_3)_2]$, at 19.2 ppm ($^1J_{^{107}Ag,P}$= 317.97 Hz, $^1J_{^{109}Ag,P}$=367.80 Hz) according to the litterature,[11,12] where the broadness was induced by rapid exchange of the coordinated PPh_3. The disappearance of the resonance peak at 21.7 ppm in Figs. 3d and 3e may be ascribable to the transformation

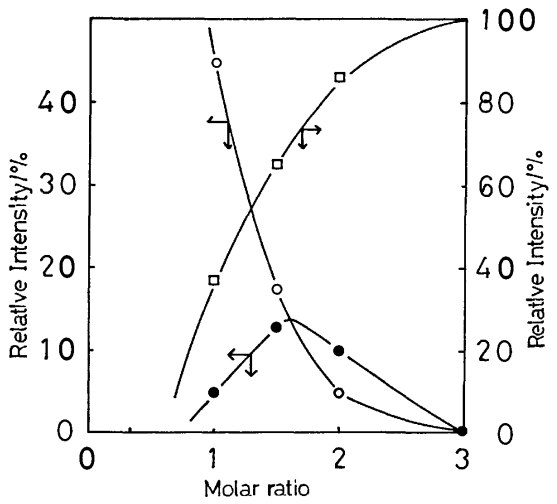

Fig. 5. Changes in relative intensities of resonances as a function of molar ratio $AgClO_4$/Ni-complex. □: Broad resonance peaks, ○: 27.1 ppm, ●: 34.7 ppm.

of $[Ag(ClO_4)(PPh_3)_2]$ into $[Ag(ClO_4)(PPh_3)]$ with increase in $AgClO_4$. The formation of these silver–phosphine complexes suggests the presence of a coordinatively unsaturated nickel complex according to the following reaction:

$$[Ni(ClO_4)(\sigma\text{-}C_6F_5)(PPh_3)_2] + AgClO_4 \longrightarrow [Ni(ClO_4)(\sigma\text{-}C_6F_5)(PPh_3)] + [Ag(ClO_4)(PPh_3)]. \quad (2)$$

Thus, the sharp resonance peak at 34.7 ppm in Figs. 3b, c, and d would be assigned to $[Ni(ClO_4)(\sigma\text{-}C_6F_5)(PPh_3)]$. The changes in relative intensity of the resonance peaks shown in Fig. 3 with increase in $AgClO_4$ added are summarized in Fig. 5. The intensity change of the resonance peak at 34.7 ppm well corresponds to the change in the dimerization rates shown in Fig. 2, suggesting that $[Ni(ClO_4)(\sigma\text{-}C_6F_5)(PPh_3)]$ would be an active species. The decrease in the active species must come from the abstraction of the second PPh_3 accompanied by the decomposition of the nickel complex, because the addition of excess $AgClO_4$ resulted in the formation of the precipitate of Ni(II) salts. The reason for the dependences of the dimerization rate on the solvent and the concentration of the nickel complex in higher molar ratios than 2 is not clear.

Ethylene Dimerization with $[NiCl(\sigma\text{-}C_6Cl_5)(PPh_3)_2]$. $[NiCl(\sigma\text{-}C_6Cl_5)(PPh_3)_2]$ as well as $[NiBr(\sigma\text{-}C_6F_5)(PPh_3)_2]$ is active for the ethylene dimerization in the presence of $AgClO_4$. As shown in Fig. 6, the rate of dimerization increases with increase in the molar ratio of $AgClO_4$ to $[Ni(ClO_4)(\sigma\text{-}C_6Cl_5)(PPh_3)_2]$, and reaches the highest at around 2 of the ratio in a similar manner as $[NiBr(\sigma\text{-}C_6F_5)(PPh_3)_2]$. However, differing from $[NiBr(\sigma\text{-}C_6F_5)(PPh_3)_2]$, the rate decreases only slightly with increase in the ratio up to 5. ^{31}P NMR spectra of the chlorobenzene solution of $[NiCl(\sigma\text{-}C_6Cl_5)(PPh_3)_2]$ and $AgClO_4$ showed three sharp resonance peaks at 25.0, 26.4, and 28.6 ppm due to nickel complexes along with two broad ones due to $[Ag(ClO_4)(PPh_3)]$. The resonance peak at 26.4 ppm is the one of the original nickel complex. As with

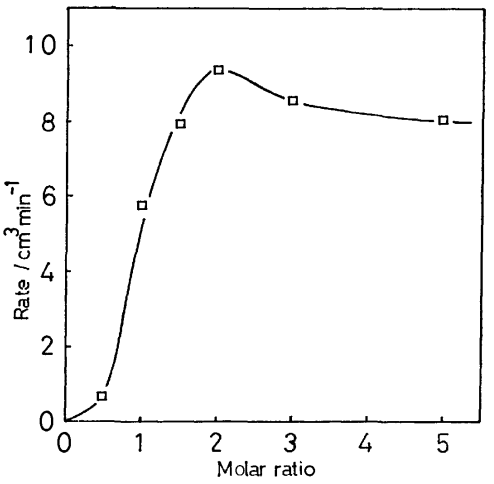

Fig. 6. Rate of ethylene dimerization as a function of molar ratio AgClO$_4$/Ni-complex.
[NiCl(σ-C$_6$Cl$_5$)(PPh$_3$)$_2$] (0.02 mmol) in chlorobenzene (2 ml) soln, react. temp 0 °C, initial ethylene pressure 67 kPa.

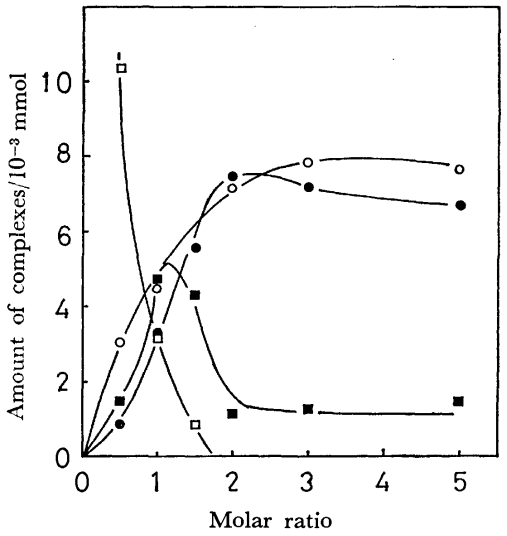

Fig. 7. Changes in the amount of complexes as a function of molar ratio AgClO$_4$/Ni-complex.
□: [NiCl(σ-C$_6$Cl$_5$)(PPh$_3$)$_2$], ■: [Ni(ClO$_4$)(σ-C$_6$Cl$_5$)-(PPh$_3$)$_2$], ●: [Ni(ClO$_4$)(σ-C$_6$Cl$_5$)(PPh$_3$)], ○: [Ag-(ClO$_4$)(PPh$_3$)].

the case of [NiBr(σ-C$_6$F$_5$)(PPh$_3$)$_2$], the resonance peak at 25.0 ppm can be assigned to [Ni(ClO$_4$)(σ-C$_6$Cl$_5$)-(PPh$_3$)$_2$] because the peak intensity was the highest at the molar ratio of 1. The resonance peak at 28.6 ppm would be assigned to [Ni(ClO$_4$)(σ-C$_6$Cl$_5$)(PPh$_3$)], because the intensity increases with compensation of the resonance peak at 25.0 ppm. Figure 7 shows the dependence of the intensity of the resonance peak at 28.6 ppm on the molar ratio, where the material balances of PPh$_3$ as estimated from each resonance peak

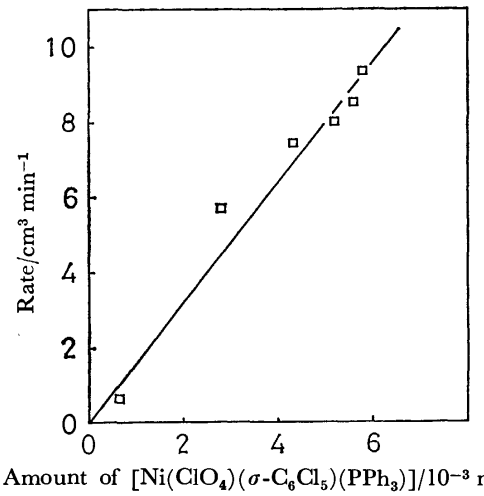

Fig. 8. Relationship between amount of [Ni(ClO$_4$)(σ-C$_6$Cl$_5$)(PPh$_3$)] and the rate of ethylene dimerization.

are not complete. This incompleteness is probably because of a loss caused in the procedure of filtration of the solution followed by ampuling the samples.

The dependence of the amount of [Ni(ClO$_4$)(σ-C$_6$Cl$_5$)(PPh$_3$)] on the molar ratio is analogous to the rate change shown in Fig. 6. Figure 8 shows the dependence of the rate on the amount of [Ni(ClO$_4$)-(σ-C$_6$Cl$_5$)(PPh$_3$)]. The clear linear relationship would suggest that [Ni(ClO$_4$)(σ-C$_6$Cl$_5$)(PPh$_3$)], which can afford two vacant sites on the nickel atom by dissociating the perchlorate anion, is an active species for the dimerization of ethylene. Although a real active species may be such a nickel hydride complex as has been assumed in the [Ni(σ-aryl)X(PPh$_3$)$_2$]-Et$_2$O·BF$_3$ system,[1] we have no evidence for the presence of any hydride species at present.

References

1) K. Maruya, T. Mizoroki, and A. Ozaki, *Bull. Chem. Soc. Jpn.*, **45**, 2255 (1972).
2) N. Kawata, K. Maruya, T. Mizoroki, and A. Ozaki, *Bull. Chem. Soc. Jpn.*, **47**, 413 (1974).
3) N. Kawata, K. Maruya, T. Mizoroki, and A. Ozaki, *Bull. Chem. Soc. Jpn.*, **47**, 2003 (1974).
4) T. Koike, K. Kawakami, K. Maruya, T. Mizoroki, and A. Ozaki, *Chem. Lett.*, **1977**, 551.
5) J. Chatt and B. L. Shaw, *J. Chem. Soc.*, **1960**, 1718.
6) M. Wada, *Inorg. Chem.*, **14**, 1415 (1975).
7) M. Wada and K. Oguro, *Inorg. Chem.*, **15**, 2346 (1976).
8) Y. Ishimura, K. Maruya, Y. Nakamura, T. Mizoroki, and A. Ozaki, *Chem. Lett.*, **1981**, 675.
9) J. R. Phillips, D. T. Rosevear, and F. G. A. Storn, J. *Organomet. Chem.*, **2**, 455 (1964).
10) J. M. Coronas and J. Sales, *J. Organomet. Chem.*, **94**, 107 (1975).
11) R. G. Goel and P. Pilon, *Inorg. Chem.*, **17**, 2876 (1978).
12) E. L. Muetterties and C. W. Alegranti, *J. Am. Chem. Soc.*, **95**, 6386 (1972).

The ESR Spectrum of a π Cation Radical Trapped in a Single Crystal of Chloro(tetraphenylporphyrinato)cobalt(III)

Masahiro KOHNO,* Hiroaki OHYA-NISHIGUCHI,† Kiyoko YAMAMOTO,†† and Tosio SAKURAI††

JEOL Ltd., Akishima, Tokyo 196

† *Department of Chemistry, Faculty of Science, Kyoto University, Sakyo-ku, Kyoto 606*

†† *The Institute of Physical and Chemical Research, Wako, Saitama 351*

(Received March 20, 1982)

The electron-spin-resonance (ESR) spectra of three paramagnetic species trapped in single crystals of chloro(tetraphenylporphyrinato)cobalt(III) have been observed at 77 K. Using the ESR parameters obtained, one of them has been identified as the $[Co^{III}(tpp)]^{2+}\cdot(Cl^-)_2$ π cation radical, and the other two species, as $[Co^{II}(tpp)]$ which are influenced by axial ligation. From the angular variations in the hfcc due to the ^{59}Co, ^{14}N, and ^{35}Cl in the π cation radical, it has been found that the unpaired electron resides on the a_{2u} porphyrin π orbital and polarizes the Co and Cl atomic orbitals through a spin-polarization mechanism. Finally, the radical formation mechanisms in solution are briefly discussed, based on the results obtained from the single-crystalline measurements.

The role of the porphyrin-cation radicals in the chemical and biological behavior of metalloporphyrins has become very important. In the enzymatic reaction of horse-radish peroxidase (HRP) with peroxide, for example, it has been pointed out that the HRP I has an electronic configuration of Fe(IV) ($S=1$), with the porphyrin ring forming an a_{2u} π cation radical.[1] On the other hand, Dolphin *et al.*[2] showed how the organic macrocycles play important roles in biochemical systems in addition to those of the centrally coordinated metals.

It has been previously shown by ^1H FT-NMR[3] and ESR studies[4] that diamagnetic chloro(tetraphenylporphyrinato)cobalt(III) (**A**) (Fig. 1) in chlorinated solvents changes partially into paramagnetic species upon thermal and light activations. The formation of this species in the solutions occurs reversibly, with small enthalpy differences. This species was identified as a π cation radical of cobalt(III) tetraphenylporphyrin, $[Co^{III}(tpp)]^{2+}\cdot(Cl^-)_2$, using an electrochemical ESR technique[5]. The formation of the cation radical under ambient conditions can, therefore, be closely related to the enzymatic reactions of the metalloporphyrins mentioned above.

In the course of a crystallographic investigation of **A**[6] it was expected that the crystals grown from a solution including such paramagnetic species may trap the species. It may, therefore, be appropriate to elucidate in detail the electronic structure and the mechanism of its formation in solutions by using the single crystals trapping the species. In agreement with this expectation, we have succeeded in observing the ESR spectra of paramagnetic species trapped in the single crystals, one of which has been identified as the π cation radical. In order to clarify further the electronic structure of the radical, we have carried out a detailed ESR investigation of the single crystals.

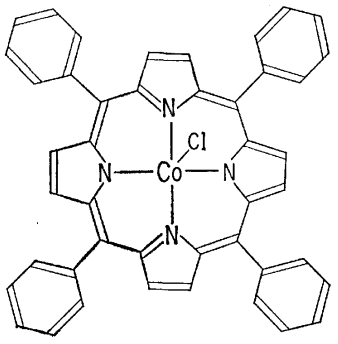

Fig. 1. Chloro($\alpha,\beta,\gamma,\delta$-tetraphenylporphyrinato)cobalt(III).

In this paper we will first describe the ESR parameters obtained from the angular dependences of the ESR spectra due to the paramagnetic species in the single crystals of **A**. Second, the electronic structure of the cation radical will be discussed in detail based on the parameters thus obtained and those in solutions reported previously. Finally, the mechanisms of its formation in solutions will be presented in relation to that of HRP I.

Experimental

A was prepared by using a method previously reported.[6] The compound obtained from the methanol solution was dissolved in chloroform or dichloromethane, and the solvent was allowed to evaporate slowly to yield violet and lustrous crystals of **A**. The purity of the crystals obtained was examined by means of elemental analysis and visible-spectrum measurements (Found: C, 73.40; H, 4.20; N, 7.84; Co, 8.24; Cl, 5.06%. λ_{max} (ε) in CH_2Cl_2: 544 nm(13200) and 406 nm(112000)). The spontaneous evaporation of the solvent gave crystals of various external forms; obelisk, pyramid, and bulky shapes. Previously the results of a X-ray analysis of the obelisk crystals were reported.[6] The successive refinement of the structure analysis[7] of these crystals made clear the existence of oxygen at the 6th ligand position.

Their crystal parameters, as determined by the X-ray diffraction method, are listed in Table 1. The pyramid and obelisk crystals were submitted to the ESR measurements. In the case of the obelisk crystal, the c axis was perpendicular to the porphyrin plane and parallel to the Co–Cl bond, which corresponds to the molecular symmetry axis and coincides with the long crystal axis. The basal plane of the pyramid crystal coincides with the molecular plane and is perpendicular to the c axis. The relationships between the a and b axes and the external forms are illustrated in Fig. 2. The angle between the a axis and one of the molecular symmetry axes parallel to the Co–N bond was 15°.[6] Such crystal habits were utilized for the single-crystal

Table 1. Crystal parameters of $Co^{III}(tpp)Cl$

Form	System	Lattice constants a/Å	c/Å	U/Å^3	Space group	Z	D_o	D_c
Obelisk	Tetragonal	13.693(2)	9.701(2)	1818.9(6)	14	2	1.34_7	1.324
Pyramid	Tetragonal	13.450(5)	9.792(3)	1771.4(11)	14	2	1.35_6	1.359

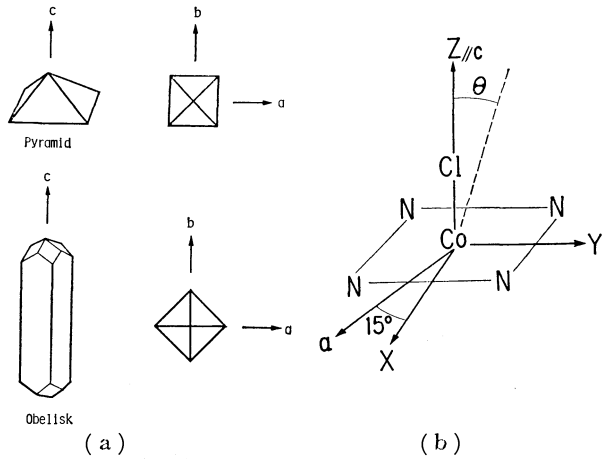

Fig. 2. (a) Crystal axis in pyramid and obelisk type crystals of A. (b) Relationship between crystal axis and molecular axis.

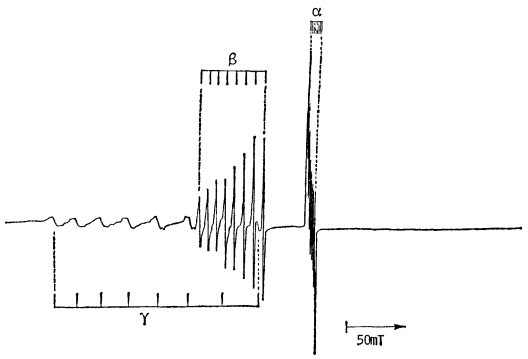

Fig. 3. The ESR spectrum of paramagnetic species trapped in a pyramid type single crystal of **A** at 77 K ($H_0 \perp c$).
Note that three paramagnetic species, α, β, and γ are clearly distinguished.

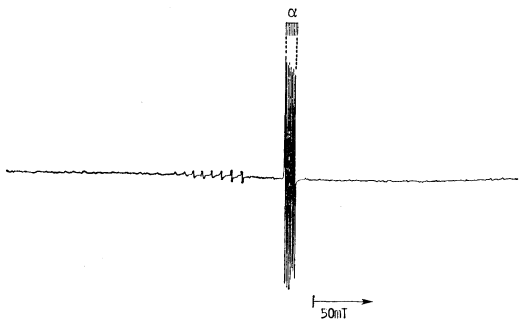

Fig. 4. The ESR spectrum of paramagnetic species trapped in an obelisk type single crystal of A at 77 K ($H_0 \perp c$).
Note that the gain of the ESR observation is about 10 times larger than that of Fig. 3.

ESR measurements. Typical sizes of the obelisk and pyramid crystals used for the measurements were $0.1 \times 0.1 \times 0.3$ cm^3 and $0.2 \times 0.2 \times 0.1$ cm^3 respectively.

The ESR spectra were recorded on a JEOL X-band FE-3X ESR spectrometer. The spin concentrations of the paramagnetic species were determined from a comparison of the intensity of the signals with that of 2,2,6,6-tetramethyl-4-hydroxyl-1-piperidyl oxyl (98%) used as a standard. In order to obtain the ESR parameters of the paramagnetic species, the resonance magnetic field and the microwave frequency of each absorption line were measured using a JEOL ES-FC-4 NMR gaussmeter and a Takeda Riken TR5211 frequency counter respectively. The ESR parameters were determined by the best fitting of the experimental data with an equation derived by the second-order perturbation theory.[8] The computer simulation for the hyperfine structure analysis was carried out using a JEOL ES-9835 computer system.

Results and Discussion

The ESR Spectra of the Paramagnetic Species in the Single Crystal of A. It has already been determined from the magnetic susceptibility measurements that **A** is diamagnetic in the range from 77 K to room temperature.[6] Therefore, the ESR signals obtained from the crystals are regarded as those due to paramagnetic species trapped in the diamagnetic matrix. Figure 3 shows the ESR spectrum of the paramagnetic species in a pyramid crystal of **A** with the crystal setting of $H_0 \perp c$ at 77 K. The spectrum is composed of three signals, each of which has the hyperfine (hf) structure characteristic of ^{59}Co with $I=7/2$. Their microwave power and the temperature dependences of the signal intensities were different from one another. Therefore the spectrum was regarded as a superposition of the hf patterns due to three different species. Hereafter, we will call them α, β, and γ species, from right to left in the spectrum shown in Fig. 3. The relative intensities of these signals, that is, the relative amounts of these species, depended on the conditions of the crystallization and the external forms. The signal intensities due to these species in the pyramid crystal were of comparable orders of magnitude. On the other hand, the spectrum obtained from the obelisk crystal showed mainly the hf pattern due to the α species, as is shown in Fig. 4.

The angular variations in the absorption lines due to these species were measured on a plane including the c axis and on the ab plane which corresponds to the molecular plane of porphyrin. Table 2 lists the observed parameters of ^{59}Co in these species. The parameters obtained from the pyramid and obelisk crystals coincided with each other within the range of experimental errors. The g values of the β and γ

species are very similar to those of Co^{II}(tpp) in H_2-(tpp),[9] they are also listed in Table 2. The results are good enough to conclude that the β and γ species correspond to Co^{II}(tpp) in H_2(tpp), although the hfcc are a little different. The small deviations from the data reported earlier[9] may be due to slightly different perturbations from the axial ligands. The electronic configurations of Co^{2+} are very sensitive to axial ligands, as has already been pointed out.[10] The details of the discussion of the electronic structures of these species will be published elsewhere. The existence of the Co^{II} species in the crystals means their formation in solution, which provides an important clue to the mechanism of the formation of the π cation radical in solution, as will be described in the last section.

π Cation Radical of Cobalt(III) Tetraphenylporphyrin. The angular dependences of the ESR spectra of the α species were observed in the obelisk and pyramid crystals. The hf structure due to the α species in the pyramid crystal overlapped with those due to the β and γ species. Fortunately, the obelisk crystal showed mainly the signals due to the α species. Therefore, the angular dependence of the spectrum was measured by using the obelisk crystal.

The angular-dependent spectra of the α species on the ab plane and on the plane including the c axis are shown in Fig. 5. The spectra about the c axis (Fig. 5a) are angular-independent and have only eight hf lines due to ^{59}Co with an appreciably broad line width, the g value and the hfcc of ^{59}Co being 1.9980± 0.0001 and 1.25 mT respectively. On the other hand, in Fig. 5b, the eight hf lines for $H_0 \perp c$ gradually coalesce into one broad distorted line, as the angle between the direction of the magnetic field and the c axis, (θ), increases. The coalesced line at about θ= 40—50° splits into many lines at the higher angles. The small, sharp line at the center is due to an impurity in the crystal. It should be noted here that the g value is constant within the range of experimental errors (±0.0001) in this experiment. The spectrum for $H_0//c$ consists of 28 lines with a line-width (ΔH) of about 0.3 mT and with g=1.9981±0.0001. The spectrum simulation was carried out using one cobalt $a_{^{59}Co}$= 1.13 mT, four nitrogens $a_{^{14}N}$=0.56 mT, two chlorines $a_{^{35}Cl}$=0.57 mT ($a_{^{37}Cl}$=0.50 mT), and ΔH=0.40 mT,

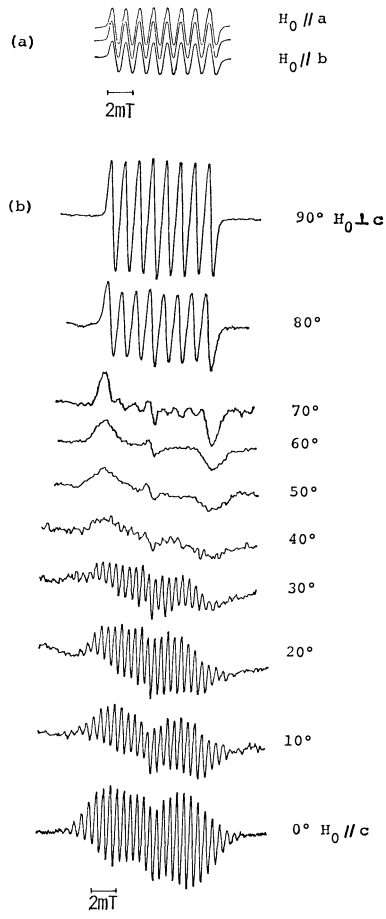

Fig. 5. The angular dependent ESR spectra of α species, (a): rotation about c axis, (b): rotation from the c axis to an axis perpendicular to the c axis.

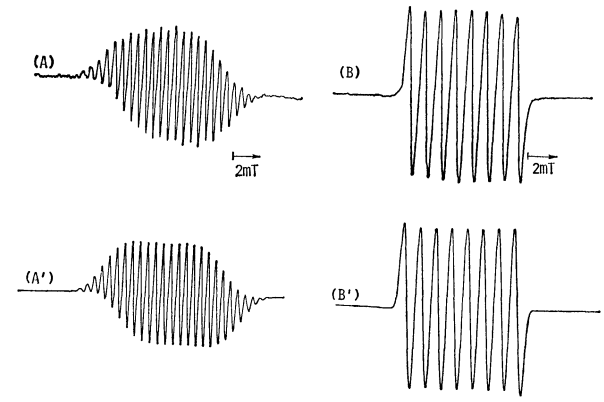

Fig. 6. The ESR spectra of the α species trapped in a single crystal of A at 77 K, (A) at $H_0//c$ and (B) at $H_0 \perp c$.
Simulation (A') assumes one cobalt a_{Co}=1.13 mT, four nitrogens a_N=0.56 mT, and two chlorines $a_{^{35}Cl}$= 0.57 ($a_{^{37}Cl}$=0.50) mT and (B') assumes one cobalt a_{Co}=1.18 mT.

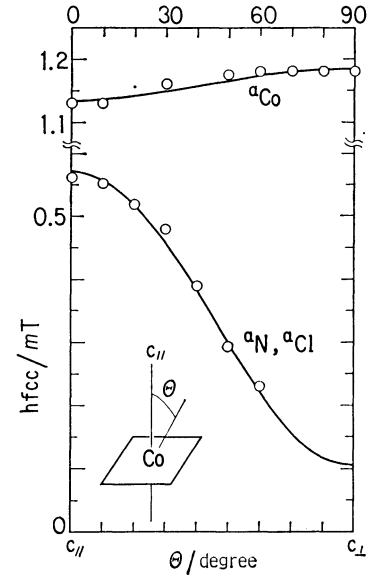

Fig. 7. The angular dependent hfcc of cobalt, nitrogen, and chlorine atoms.
○: Observed value, ——: calculated value.

TABLE 2. ESR PARAMETERS OF PARAMAGNETIC SPECIES TRAPPED IN THE SINGLE CRYSTALS OF **A**

Species	$g_\perp$	$g_{//}$	A_{Co} 10^{-4} cm^{-1}		A_N 10^{-4} cm^{-1}		A_{Cl} 10^{-4} cm^{-1}		
			$A_\perp$	$A_\parallel$ c)	$A_\perp$	$A_\parallel$ c)	$A_\perp$	$A_\parallel$ c)	
α, $[Co^{III}(tpp)]^{2+}(Cl^-)_2$	1.9980 (±0.0001)	1.9981 (±0.0001)	12 (±0.1)	10 (±0.1)	0.9 (±0.1)	5.2 (±0.1)	1.0 (±0.1)	5.2 (±0.1)	a)
β	2.5273 (±0.0003)	1.9964 (±0.0003)	97 (±3)	105 (±3)					a)
γ	3.241 (±0.001)	1.745 (±0.001)	401 (±3)	192 (±3)					a)
Co^{II}(tpp) in H_2(tpp)	2.505	2.034	92	115					b)
Co^{II}(tpp) in H_2(tpp)	3.322	1.798	395	197					b)

a) This work. b) Ref. 9. c) The parallel direction of A values of Co, N, and Cl coincides with the z axis of the molecule.

which led to the best fit to the experimental data. The simulation spectra are shown in Fig. 6. The simulation at various angles was successively carried out by changing the parameters mentioned above, shown in Fig. 7, as functions of θ. The hfcc values of ^{14}N and $^{35}Cl(^{37}Cl)$ have a maximum at $\theta=0°$ ($H_0//c$) and a minimum at $\theta=90°$ ($H_0\perp c$), but that of ^{59}Co is almost independent of θ; its small anisotropic part has a maximum at $\theta=90°$ ($H_0\perp c$). The principal values of g and hfcc are also summarized in Table 2.

The g value obtained was isotropic and very close to that of the free electron (2.0023). The difference in these values is probably due to contributions from unoccupied orbitals of the cobalt atom. The isotropic parts of the ^{59}Co, ^{14}N, and $^{35}Cl(^{37}Cl)$ were also very close to those of the π cation radical of Co^{III}(tpp) obtained by the electrochemical oxidation of Co^{II}(tpp) of **A**.[5] Therefore, one can, from these data, identify the α species as the π cation radical of Co^{III}(tpp) coordinated by two chlorines.

Electronic Structure of the π Cation Radical of $[Co^{III}(tpp)]^{2+\cdot}$. It was well established that the neutral species Co^{II}(tpp) is paramagnetic, with an effective electron spin of 1/2 and with a square-planar $3d^7$ configuration, $(3d_\pi)^4$ $(3d_{xy})^2$ $(3d_{z^2})$. In the present case, the β and γ species showed the ESR parameters characteristic of this configuration. On the other hand, as we reported previously,[5] the π cation radical of $[Co^{III}(tpp)]^{2+\cdot}$, generated by electrochemical oxidations of Co^{II}(tpp) or **A** in solutions, has an electronic configuration described by a combination of diamagnetic Co^{3+} and paramagnetic tpp ligands, $(3d_\pi)^4$ $(3d_{xy})^2$ $(a_{2u})^1$. The a_{2u} π orbital has a spin distribution characterized by an appreciable localization (76%) at meso-carbons, followed by a 20% spin density at four nitrogens. This spin distribution of the π cation radical was experimentally confirmed by the observation of the angular dependent hfcc values of cobalt and four nitrogen atoms, $a_{Co}(\theta)$ and $a_N(\theta)$, in the single crystal, as is shown in Fig. 7.

The $a(\theta)$ is expressed by a combination of the isotropic (A_{iso}) and the anisotropic (A_{aniso}) parts of the hfcc:

$$a(\theta) = A_{aniso}(3\cos^2\theta - 1) + A_{iso} \quad (1)$$

$$A_{iso} = (A_\parallel + 2A_\perp)/3 \quad (2)$$

where $A_\parallel$ and $A_\perp$ are the values of $a(\theta)$ at $\theta=0°$ and 90° respectively. The best fit of the equations to the experimental values, as is shown in Fig. 7, has lead to the values of $A^N_{iso}=0.26$ mT and $A^N_{aniso}=0.15$ mT. A^N_{iso} is very close to that of $[Co^{III}(tpp)]^{2+\cdot}(Cl^-)_2$ in solution (0.28 mT). This confirms the appropriateness of the identification of the α species as the π cation radical. From $A^N_{iso}=0.26$ mT, the spin density at the 2s orbital of nitrogen is calculated as $0.26/55.7=0.0047$ by using a theoretically estimated hfcc.[11] The anisotropic part in Eq. 1 provides also useful information about the contribution of the nitrogen orbitals to the a_{2u} orbital. First, $a_N(\theta)$ has a maximum at $\theta=0°$. This means that the axis of the $2p_z$ orbital of the nitrogen coincides with the c axis of the crystal. Second, the A^N_{aniso} is another measure of the spin density on the nitrogen $2p_z$ orbital. When we use the hfcc of the nitrogen $2p_z$ orbital of 1.7 mT[11] the spin density of one of the four nitrogen atoms ($\rho^N_{2p_z}$) is estimated as 0.088. This value coincides with that obtained from the spectra in solution (5 to 10%).

The chlorine hfcc showed the same angular dependence as the nitrogens; thus $A^{Cl}_{iso}=0.26$ mT and $A^{Cl}_{aniso}=0.15$ mT. A similar estimation of the spin density on the chlorine atom has lead to the values of $\rho^{Cl}_{3s}=0.0016$ and $\rho^{Cl}_{3p_z}=0.029$.[11] It should be noted here that the spin polarization in the $3p_z$ orbital is dominant. Although numerous ESR studies have revealed interactions of diamagnetic cations with aromatic anion radicals,[12] it was not until recently that the opposite interaction of diamagnetic anions with cation radicals[13] was detected. In order to clarify the mechanism of the interaction, it is instructive to compare the A^{Cl}_{iso} and A^N_{iso} in our system with those in some analogous systems, $[M^{II}(tpp)]^{+\cdot}Cl^-$: 0.152 and 0.151 mT for M=Mg, 0.162 and 0.166 mT for M=Zn, and 0.185 and 0.182 mT for M=Cd,[13] respectively. These data show clearly that A^{Cl}_{iso} depends linearly on A^N_{iso}, as in the case of A^{Co}_{iso} with A^N_{iso} reported previously. Therefore, it is concluded that the chlorine hfcc results from the spin polarization by the π electron on the nitrogen atoms.

The unpaired π electron on the nitrogen $2p_z$ orbital polarizes the four nonbonding orbitals of the nitrogens. A combination of these orbitals with total symmetry mixes well with the $3d_{z^2}$ and 4s orbitals of the cobalt atom. The ^{59}Co hfcc ($A^{Co}_{Iso}=1.16$ and $A^{Co}_{aniso}=-0.03$ mT) showed a small angular dependence, different from those due to ^{14}N and ^{35}Cl. The estimated spin densities, ρ^{Co}_{4s} and $\rho^{Co}_{3d_{x^2-y^2}}$ at the cobalt nucleus were $1.16/130.8=0.009$ and $-0.03/7.65=-0.04$ respectively, which were estimated based on the values of the hfcc calculated for the Co^0 configuration of $3d^74s^2$.[11] The spin density at the cobalt nucleus is of the same order of magnitude as those at the two chlorine nuclei. This means that the polarizations at these nuclei are a result of the first-order in the perturbation induced by the unpaired electron which resides on the nitrogen π orbital. Therefore, the other possibility that the electrons at the two chlorine nuclei are polarized through the cobalt atom, of the second-order in the effect, can be neglected. Figure 8 shows a schematical drawing of the spin polarization mentioned above with capable atomic orbitals. In summary, the unpaired π electron on four nitrogen atoms polarizes the electrons on two chlorine nuclei and the cobalt nucleus through the spin-polarization mechanism, the orders of the polarization being about 0.03 and 0.01 respectively.

On the Mechanism of the Cation Radical Formation. As described in the previous papers,[3,4] the π cation radical is formed by thermal activation in the chlorinated solvents. The formation of the species occurs reversibly with small enthalpy differences (ΔH). From the exponential portion of the temperature dependences of the spin concentration, ΔH was estimated to be 4 kJ mol^{-1} in tetrachloroethane and 10 kJ mol^{-1} in dichloromethane.[4] These results may indicate phenomenologically an equilibrium between the paramagnetic species (α, β, and γ) and the diamagnetic species, (**A**):

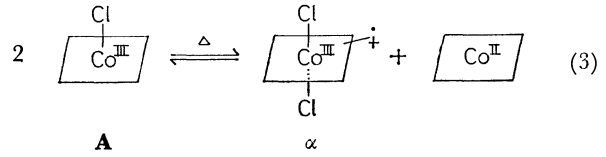

(3)

From the ESR measurements described above, it has been found that the crystals grown from the chlorinated solvents trap Co^{II}(tpp) (β and γ) in addition to the π cation radical (α). This fact apparently supports the hypothesis of Eq. 3. However, the detailed examination of Eq. 3 provides several possibilities as to the elementary reactions. The existence of oxygen in the atmosphere and the natural-light irradiation over the procedure of the sample preparations also induce the radical formation.

In conclusion, it should be understood that the observation of three paramagnetic species in our systems supports the apparent equilibrium of Eq. 3 described as a result of several reactions undetectable by the ESR techniques.

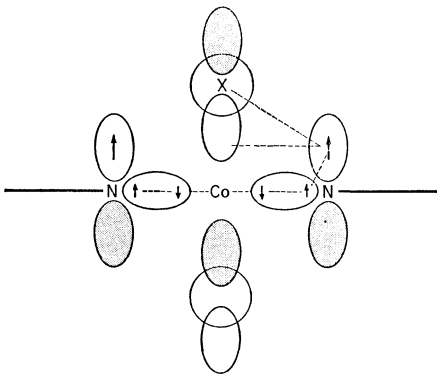

Fig. 8. Schematical drawing about the spin polarization on the cobalt, nitrogen, and halogen atoms in $[Co^{III}(tpp)]^{2+}\cdot(X^-)_2$.

References

1) G. H. Loew and Z. S. Herman, *J. Am. Chem. Soc.*, **102**, 6173 (1980), and the other references cited therein.
2) D. Dolphin, A. W. Addison, M. Cairns, R. K. Dinello, N. P. Farrell, B. R. James, D. R. Paulson, and C. Welborn, *Int. J. Quant. Chem.*, **16**, 311 (1979).
3) K. Yamamoto, J. Uzawa, and T. Chijimatsu, *Chem. Lett.*, **1979**, 89.
4) K. Yamamoto, M. Kohno, and H. Ohya-Nishiguchi, *Chem. Lett.*, **1981**, 255.
5) H. Ohya-Nishiguchi, M. Kohno, and K. Yamamoto, *Bull. Chem. Soc. Jpn.*, **54**, 1923 (1981).
6) T. Sakurai, K. Yamamoto, H. Naito, and N. Nakamoto, *Bull. Chem. Soc. Jpn.*, **49**, 3042 (1976).
7) T. Sakurai and K. Yamamoto, Proceedings of the 30th Annual Meeting of Coordination Chemistry (1980), p. 106.
8) G. Bleaney, *Philos. Mag.*, **42**, 441 (1951).
9) J. M. Assour, *J. Chem. Phys.*, **43**, 2477 (1965).
10) W. C. Lin, "Electron Spin Resonance and Electronic Structure of Metalloporphyrins," in "The Porphyrins," ed by D. Dolphin, Academic Press, New York and London (1979), Vol. 4, p. 355.
11) K. Kuwata and K. Ito, "Denshi-spin-kyomei Nyumon," Nankodo, Tokyo (1980), Chap. 2.
12) For example, F. Gerson, "High Resolution ESR Spectroscopy," John Wiley & Sons and Verlag Chemie (1970), p. 137.
13) J. Fajer and M. S. Davis, "Electron Spin Resonance of Porphyrin π Cations and Anions," in "The Porphyrins," ed by D. Dolphin, Academic Press, New York and London (1979), Vol. 4, p. 198, and the other references cited therein.

 © 1983 The Chemical Society of Japan Bull. Chem. Soc. Jpn., 56, 827—830 (1983)

Viscosities of Aqueous Solutions of Alkanoic Acids

Koichiro MIYAJIMA,* Masahiro SAWADA, and Masayuki NAKAGAKI

Faculty of Pharmaceutical Sciences, Kyoto University, Yoshida-shimoadachi-cho, Sakyo-ku, Kyoto 606

(Received April 1, 1982)

Viscosities of aqueous solutions of alkanoic acids including formic acid were measured by an Ostwald type viscometer at 15, 25, and 35 °C, and the viscosity B-coefficient and the temperature dependence of B-coefficient, dB/dT, were calculated. From the signs and the magnitudes of B_{st}, increment of B-coefficient arising from the change of water structure, and dB/dT, it was concluded that formic acid was a hydrophilic structure breaker, while acetic acid was neither a structure maker nor a structure breaker. Both propionic acid and butyric acid were the hydrophobic structure makers. The mechanism of structure breaking effect of carboxyl group was briefly discussed.

Various nonelectrolytes which have the groups such as –OH, $-NH_2$, and >CO form the hydrogen bond with water molecules in aqueous solutions, and more or less cause the change of the structure of water depending on the size and shape of the molecule. Urea and monosaccharides, for instance, are typical nonelectrolytes capable of hydrogen bond formation with water molecules. But their effects on the structure of water are quite different. Urea increases the water activity,[1] while glucose decreases it in aqueous solution.[2] This fact seems to be related to the geometry of the hydrogen bond between nonelectrolyte molecule and water molecule, and that between water molecules. Carboxyl group is also capable of forming hydrogen bond. Judging from the conformation of carboxyl group, the orientation of hydrogen bonds between carboxyl group and water molecules would not fit the orientation of hydrogen bond in the tridymite-like structure of water.

In a previous paper,[3] the effects of alkanoate ions on the structure of water were investigated by measuring the viscosities of aqueous solutions and it was concluded that the structure making effects of alkanoate ions did not arise from the hydration of carboxylate groups by the electrostriction, but from the hydrophobic hydration of alkyl groups. In other words, carboxylate group hardly influences the structure of water.

From these points of view, the viscosities of aqueous solutions of a homologous series of alkanoic acids including formic acid were determined at various temperatures. Based on the viscosity B-coefficients and their temperature dependences, the effects of alkanoic acids on the structure of water were discussed.

Experimental

Materials. Reagent grade alkanoic acids and hydrochloric acid were purchased from Nakarai Chemical Co. Ltd., and were used without further purification. These compounds were dissolved in water purified by redistillation and deionization with ion exchange resin.

Method. Viscosity measurement was carried out by an Ostwald type viscometer with an efflux time of *ca.* 360 s for water at 25 °C. Efflux time was measured with the Seiko stop watch 89 T to 0.01 s. At least five readings of the efflux time with variations not exceeding ±0.05 s were taken for each solution. Kinetic correction of viscometer was made by using the following equation:

$$\eta/d = \alpha t - \beta/t,$$

where η and d are the viscosity and density of the solution, t the efflux time in second. Pure water at 15, 25, and 35 °C was used as standard, and linear relation was obtained between η/dt and $1/t^2$. The values of α and β obtained from the intercept and the slope were 2.628×10^3 cP g^{-1} cm^3 s^{-1} and 15.00 cP g^{-1} cm^3 s, respectively. The effect of kinetic correction on the relative viscosity was observed in the high concentration region, and the difference of η_{rel} values before and after correction were within 0.3—0.5%. The temperature of the thermostat bath was controlled within ±0.03 °C.

Results

The relative viscosity, η_{rel}, of a nonelectrolyte solution below 0.1 mol dm^{-3} is expressed by Eq. 1.

$$\eta_{rel} = \eta/\eta_0 = 1 + Bc, \quad (1)$$

where η and η_0 are the viscosities of solution and solvent, respectively, and B is the viscosity B-coefficient, and c is the concentration in mol dm^{-3}. At higher concentration than 0.1 mol dm^{-3}, η_{rel} of nonelectrolyte is described by Eq. 2.

$$\eta_{rel} = 1 + Bc + Dc^2, \quad (2)$$

where D is a characteristic constant of the solute.

Alkanoic acid dissociates into proton and alkanoate anion in water. The alkanoic acids used in this experiment are formic acid, acetic acid, propionic acid and butyric acid, and their pK_a values are between 3.7—4.9 at 25 °C. Therefore, in dilute solution of alkanoic acid the dissociated ions also contribute to the viscosity of the solution. To remove the contribution of the dissociated species from the solution viscosity, two kinds of experiments were carried out. The viscosity of each alkanoic acid dissolved in 0.01 mol dm^{-3} aqueous solution of hydrochloric acid was determined by using 0.01 mol dm^{-3} of hydrochloric acid as a reference solution. The B-coefficient of the alkanoic acid was obtained from Eq. 3.

$$\eta/\eta_{HCl} = 1 + B'c, \quad (3)$$

where η and η_{HCl} are the viscosity of 0.01 mol dm^{-3} HCl solution of the alkanoic acid and that of 0.01 mol dm^{-3} HCl solution, respectively. B'-coefficient in Eq. 3 is the B-coefficient of alkanoic acid in aqueous 0.01 mol dm^{-3} HCl solution, where the amount of dissociated species of alkanoic acid is negligible. As shown in Fig. 1, linear relationships were obtained

Table 1. B and D coefficients of alkanoic acids at various temperatures

	T/°C	HCOOH	CH_3COOH	C_2H_5COOH	C_3H_7COOH
B'/mol^{-1} dm^3	25	0.032	0.111	0.184	—
B/mol^{-1} dm^3	15	0.032	0.120	0.204	0.281
	25	0.035	0.113	0.185	0.247
	35	0.037	0.106	0.168	0.226
D/mol^{-2} dm^6	15	−0.003	0.004	0.016	0.046
	25	−0.003	0.002	0.013	0.038
	35	−0.005	0.002	0.013	0.030

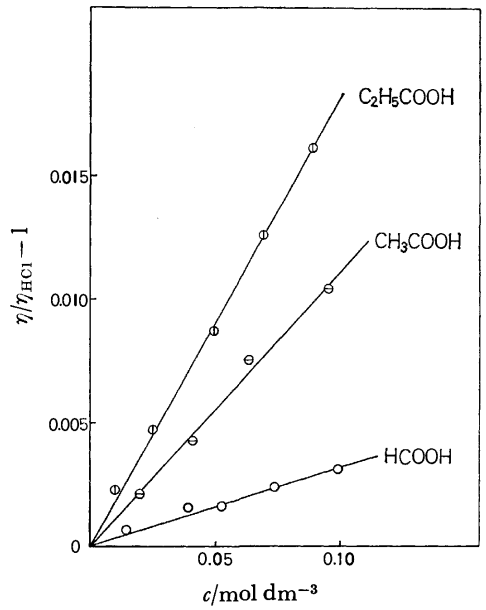

Fig. 1. Relationships between $\eta/\eta_{HCl}-1$ and c for alkanoic acids at 25 °C.
○: HCOOH, ⊖: CH_3COOH, ⓘ: C_2H_5COOH.

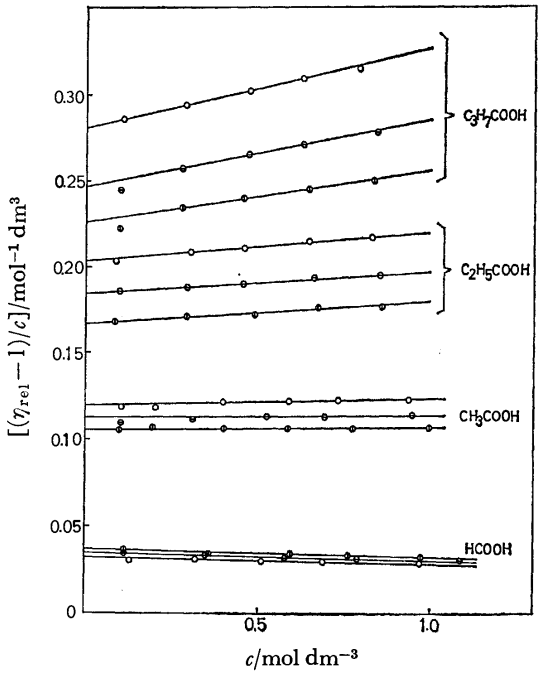

Fig. 2. Relationships between $(\eta_{rel}-1)/c$ and c for alkanoic acids at various temperatures.
○: 15 °C, ⊖: 25 °C, ⓘ: 35 °C.

between $(\eta/\eta_{HCl}-1)$ and c. B' values obtained from the slope are shown in Table 1.

At higher concentration than 0.1 mol dm^{-3}, where the concentration of dissociated species is considered to be negligible as compared to the undissociated species, Eq. 2 was applied to the determination of B-coefficients. Linear relationships were obtained between $(\eta/\eta_0-1)/c$ and c at 15, 25, and 35 °C as seen in Fig. 2. B and D coefficients obtained from the intercepts and the slopes are shown in Table 1. B values agree with B' values for three alkanoic acids at 25 °C, indicating that at higher concentration than 0.1 mol dm^{-3} the contribution of dissociated species to B-coefficient is negligible. Consequently it is evident that B and D values obtained from the measurements in high concentration region are those for undissociated species. These B values at 25 °C are also in fair agreement with Rupley's values,[4] which were calculated from the η values described in International Critical Table.

As stated previously,[3] B value of nonelectrolyte consists of two terms, B_{size} and B_{st}. B_{size} is the contribution of hydrodynamic obstruction effect of solute to B value and is usually evaluated from Einstein's viscosity equation for spherical colloidal particle on the assumption that the effective rigid volume of the solute is equal to the partial molal volume of the solute at infinite dilution. Thus B_{st}, the contribution of solute to the structure of water, is determined from Eq. 4.

$$B_{st} = B - 0.0025\overline{V}^\circ, \quad (4)$$

where $\overline{V}^\circ$ is generally the partial molal volume of solute at infinite dilution, but in this case we used the partial molal volume of undissociated species as $\overline{V}^\circ$.[9] B value *vs.* $\overline{V}^\circ$ curves for alkanoate ions and alkanoic acids are shown in Fig. 3 together with Einstein's relation (0.0025 $\overline{V}^\circ$). The solutes with the points above the dotted line are considered to be structure makers. B_{st} values obtained from Eq. 4 are shown in Table 2.

Another and more reliable criterion for the judgement of the solute effect on the structure of water is the sign and magnitude of temperature dependence of B value, dB/dT.[3] The values of dB/dT of four kinds of alkanoic acids at 25 °C obtained from the slopes in Fig. 4 are shown in Table 2 together with the values of B, B_{st}, and $\overline{V}^\circ$.

Discussion

As for formic acid, the sign of B_{st} is negative, while the sign of dB/dT is positive, indicating that it is a

TABLE 2. B, B_{st}, dB/dT, AND $\overline{V}^\circ$ OF ALKANOIC ACIDS AT 25 °C

	HCOOH	CH_3COOH	C_2H_5COOH	C_3H_7COOH
B/mol^{-1} dm^3	0.035	0.113	0.185	0.247
B_{st}/mol^{-1} dm^3	−0.052	−0.017	0.015	0.035
(dB/dT)/mol^{-1} dm^3 K^{-1}	0.0003	−0.0007	−0.0018	−0.0027
$\overline{V}^\circ$/cm^3 mol^{-1} a)	34.7	51.9	67.9	84.7

a) Ref. 9.

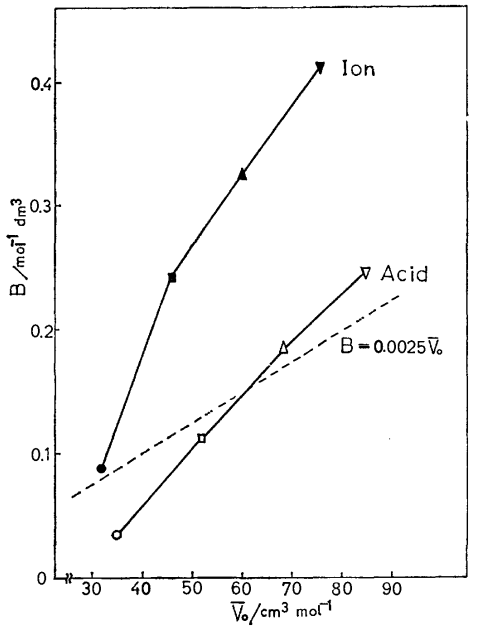

Fig. 3. Relationships between B-coefficients and $\overline{V}^\circ$ at 25 °C.
○: HCOOH, □: CH_3COOH, △: C_2H_5COOH, ▽: C_3H_7COOH, ●: $HCOO^-$, ■: CH_3COO^-, ▲: $C_2H_5COO^-$, ▼: $C_3H_7COO^-$.

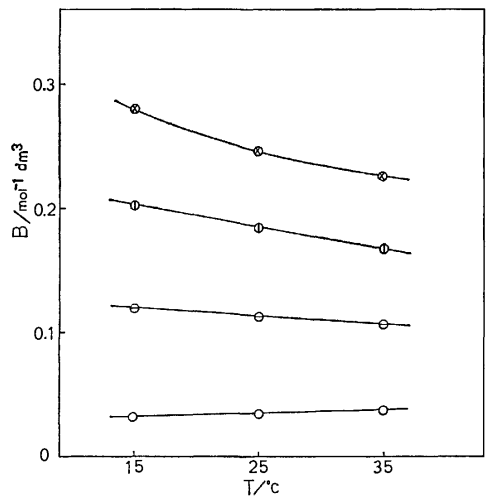

Fig. 4. Temperature dependences of B-coefficients for alkanoic acids.
○: HCOOH, ⊖: CH_3COOH, ⊕: C_2H_5COOH, ⊗: C_3H_7COOH.

structure breaker. The result that both values of B_{st} and of dB/dT for acetic acid are negative seems to be inconsistent with the criterion that structure maker has the positive sign of B_{st} and negative sign of dB/dT, and *vice versa* for structure breaker. However, judging from the absolute values of B_{st} and dB/dT, acetic acid may be neither a structure maker nor a structure breaker. Applying the criterion to propionic acid and butyric acid, both fall under the category of structure maker. The signs and magnitudes of B_{st} and dB/dT for a homologous series of alkanoic acids indicate that structure making effect of propionic acid and butyric acid originates from the hydrophobic group and not from the carboxyl group, because structure making effect of alkanoic acids increases with alkyl chain-length, and because formic acid with no alkyl group is clearly a structure breaker. From the similar study for sodium alkanoates, methyl group of acetate ion was found to increase the structure of water.[3] Therefore carboxyl group should be a structure breaker. The structure breaking effect of carboxyl group compensates for the structure making effect of methyl group in acetic acid, because the values of B_{st} and dB/dT are nearly zero for acetic acid. Propionic acid and butyric acid are hydrophobic structure makers.

D-coefficients of four alkanoic acids at 15, 25, and 35 °C are shown in Table 1. The variations of D-coefficients with alkyl chain-length and temperature are similar to those of B-coefficients except the temperature dependence of the coefficients for formic acid. Thomas extended the Einstein equation and showed that for colloidal suspensions the η_{rel} is given by[5]

$$\eta_{rel} = 1 + 2.5\phi + 10.05\phi^2$$
$$= 1 + 2.5\times10^{-3}Vc + 10.05\times10^{-6}V^2c^2, \quad (5)$$

where ϕ and V are the volume fraction and the molar volume of solute and c the concentration of solute in mol dm^{-3}. By assuming that $D=10.05\times10^{-6}\,\overline{V}^{\circ\,2}$, the values of D-coefficients at 25 °C were found to be 0.012, 0.027, 0.046, and 0.072 for formic acid, acetic acid, propionic acid, and butyric acid, respectively. Thomas's relation predicts the correct order of D-coefficient. But the magnitudes are too large, especially for formic acid and acetic acid. This fact suggests that D-coefficient relates to the volume of the solute, but another effect also contributes to the magnitude of D-coefficient.

Desnoyers *et al.*[6] pointed out that the solute-solute structural interaction and the solute-solvent interaction which were not accounted for by Bc term would greatly influence the magnitude of D-coefficient. As stated above, the structure making effects of propionic acid and butyric acid come from the hydrophobic hydration of alkyl-chain. The hydrophobic hydration increases with the solute concentration, resulting in the increase

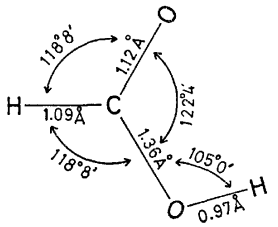

Fig. 5. Molecular structure of formic acid.

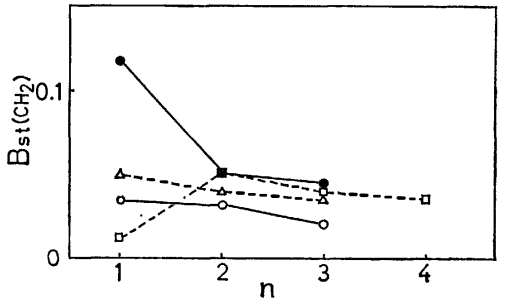

Fig. 6. Relationships between $B_{st}(CH_2)$ and alkyl-carbon numbers for various alkyl derivatives at 25 °C.
●: $H(CH_2)_nCOO^-$, ○: $H(CH_2)_nCOOH$, □: $H(CH_2)_nNH_3^+$ [a], △: $H(CH_2)_nCONH_2$ [b].
a) Calculated from the data in Ref. 10, b) Ref. 11.

of the solution viscosity and consequently D-coefficient of solute. Such a structural interaction increases with alkyl chain-length and decreases with the increase of temperature. The small values of D-coefficients for formic acid and acetic acid may be due to an absence of such interaction.

Carboxyl group forms hydrogen bond with water like urea and saccharides. It is, however, important whether the formation of hydrogen bond between carboxyl group and water molecule promote the hydrogen bond between water molecules. The structure breaking effect of carboxyl group may be related to its molecular structure. The orientation of hydrogen bond in pure water may be tetrahedral as seen in the tridymite structure of ice. The molecular structure of formic acid is shown in Fig. 5 as a typical example of carboxyl group.[7] Roughly speaking, all atoms are in a plane, and three bond angles around the central carbon atom are nearly 120°. The structure of carboxyl group of alkyl homologous is similar to that of formic acid. Such a configuration of carboxyl group can hardly fit with the tridymite-like structure of water. In other words, the formation of hydrogen bonds between carboxyl group and adjacent water molecules would cause the disruption of hydrogen bond network of water. The situation is quite similar to urea.

The contribution of a methylene group to the value of B_{st} estimated from Eq. 6 is shown in Fig. 6.

$$B_{st}(CH_2) = B_{st}[H(CH_2)_nX] - B_{st}[H(CH_2)_{n-1}X], \quad (6)$$

where X is the terminal functional group shown in Fig. 6. The $B_{st}(CH_2)$ value of the methylene group adjacent to the terminal ionic group was more influenced than that of nonionic group. The small value of $B_{st}(CH_2)$ of methylammonium ion reflects the strong electrostriction of ammonium ion as pointed out by Zana.[8] It seems that the values of $B_{st}(CH_2)$ of these four kinds of alkyl derivatives converge to around 0.02—0.03 with increase of alkyl carbon chain.

In conclusion, carboxyl group is a weak structure breaker in contrast to carboxylate group, which is neither a structure maker nor a structure breaker. As for the alkanoic acids, the structure breaking effect of carboxyl group compensates for the hydrophobic structure making effect of methyl group of acetic acid, and alkanoic acids with more than two methylene groups become hydrophobic structure makers.

References

1) R. H. Stokes, *J. Phys. Chem.*, **70**, 1188 (1966).
2) O. O. Bonner and W. H. Breazeale, *J. Chem. Eng. Data*, **10**, 325 (1965).
3) K. Miyajima, M. Sawada, and M. Nakagaki, *Bull. Chem. Soc. Jpn.*, **55**, 3101 (1982).
4) J. A. Rupley, *J. Chem. Phys.*, **68**, 2002 (1964).
5) D. G. Thomas, *J. Colloid Sci.*, **20**, 267 (1965).
6) J. E. Desnoyers and G. Perron, *J. Solution Chem.*, **1**, 199 (1972).
7) "Table of Interatomic Distances and Configuration in Molecules and Ions," ed by L. E. Sutson, The Chemical Soc., London (1958).
8) R. Zana, *J. Phys. Chem.*, **81**, 1817 (1977).
9) F. J. Millero, "Water and Aqueous Solution," ed by R. A. Horne, John Wiley, New York (1972), Chap. 13, p. 572.
10) J. E. Desnoyers, M. Arel, and P-A. Leduc, *Can. J. Chem.*, **47**, 547 (1969).
11) T. T. Herskovits and T. M. Kelly, *J. Phys. Chem.*, **77**, 381 (1973).

 © 1983 The Chemical Society of Japan Bull. Chem. Soc. Jpn., 56, 831—837 (1983)

A Comparison between Ruthenium and Palladium with Regard to the Chemisorption of Carbon Monoxide on Metal Clusters Using Molecular Orbital Calculations

Masahiro KOBAYASHI

Research Laboratory of Resources Utilization, Tokyo Institute of Technology, 4259 Nagatsuta-cho, Midori-ku, Yokohama, 227

(Received April 14, 1982)

Self-consistent charge extended Hückel calculations for systems consisting of 1—3 CO molecules chemisorbed on 8-atom and 10-atom clusters of Ru and Pd are reported. The binding energies and overlap populations between Pd and C are always smaller than those between Ru and C. It was found that the multiple types of bondings between 2—3 CO and a surface metal atom were less stable for Pd than for Ru.

Ruthenium and palladium exhibit different properties in CO adsorption, though they are the same type of platinum metal.

It is firmly established for Pd that the ratio of CO molecules chemisorbed to the surface atoms (CO/M_s) is less than unity and that there are two types of bonding (linear and bridge) between CO and surface metal atoms.[1]

We showed recently, however, that the ratio of chemisorbed CO molecules to the total metal atoms of Ru-supported catalysts was more than unity; consequently, CO molecules form multiple bonds with the surface atoms in the following manner:[2,3]

Hereafter, the (a) and (b) types will be called "twin" and "trine" respectively, and Ru^1, "multivalent metal atom", for the sake of convenience.

Further support has been afforded to our proposal that the stoichiometry of CO/Ru_s is more than unity using hydrogen uptake measurements.[4,5] Taylor[4] and Dalla Betta[5] found that the atomic ratio of the hydrogen uptake to the surface Ru atoms (H/Ru_s) was almost 1. This stoichiometry was confirmed by an examination of the data reported by Kubicka[6] and the new data obtained in the present laboratory.

The uptake of H_2 and CO obtained by using the same Ru–SiO_2 catalysts as in previous papers[2,3] and the calculated CO/H (molecule/atom) are summarized in Table 1. The CO/H values of Ru catalysts supported on various other carriers; Al_2O_3 as given by Dalla Betta,[7] TiO_2 as given by Tauster *et al.*,[8] and active carbon *etc.*, as given by Vannice and Garten,[9] have values greater than 1. These data are also summarized in Table 1. This means that CO molecules more than 1 combine with a surface Ru atom.

The IR studies of chemisorbed CO on Ru show that two CO molecules form the twin-type coordination with a Ru atom which is positively charged.[10,11] Thus, the charge or electronic properties of surface metal atoms would be influenced by CO chemisorption of the twin or trine type.

Politzer and Kasten successfully explained the characteristic features of electronic-charge transfer in the systems of Ni_n–CO, where the n values ranged from 1 to 9, by using the self-consistent-charge (SCC) approximation in the extended Hückel method.[12] The present investigation has been undertaken with the purpose of elucidating the difference between Pd and Ru catalysts in these CO-chemisorbed states in relation to the electronic charge transfer by means of the SCC extended Hückel approximation.

Procedure

Model Clusters. The crystal lattice of Pd metal is face-center-cubic (fcc), while that of Ru metal is hexagonal close-packed (hcp). The calculations have been performed for 10-atom clusters, as is shown in

TABLE 1. HYDROGEN AND CO ADSORPTION ON VARIOUS Ru CATALYSTS

Catalysts		t/°C	H_2[ml(stp)/g]	t/°C	CO[ml(stp)/g]	CO/H	Ref.
0.367(mg-atoms/g) Ru-SiO_2-35-1		100	1.52	−78	9.93	3.27	
				150	11.28	3.71	
0.186	2	100	1.10	−78	6.77	3.08	
0.093	3	100	0.60	−78	4.57	3.81	
0.047	4	100	0.40	−78	2.55	3.19	
			H_2(μmol/g)		CO(μmol/g)		
5% Ru-Al_2O_3		21	82.7	21	373	2.3	7
0.5% Ru-Al_2O_3		21	15.1	21	116	3.8	7
0.23% Ru-Al_2O_3		21	9.3	21	57.3	3.1	7
2% Ru/TiO_2		r.t.	3.0	r.t.	7.2	1.2	9
5% Ru/Al_2O_3		r.t.	17.4	r.t.	35	1.01	9
4% Ru/C		r.t.	38	r.t.	160	2.11	9
2% Ru-TiO_2(reduction temp 200 °C)		25	H/M=0.23	25	CO/M=0.64	2.78	8
(reduction temp 500 °C)		25	H/M=0.06	25	CO/M=0.11	1.83	8

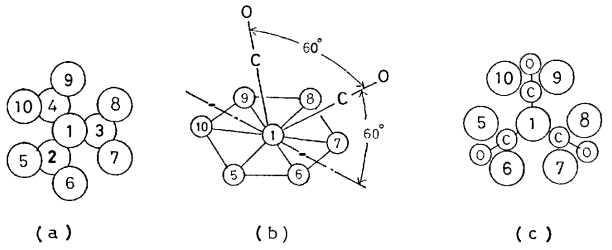

Fig. 1. Models for 10-atom cluster (a), M_{10}-$(CO)_2$ (b), and M_{10}-$(CO)_3$ (c).

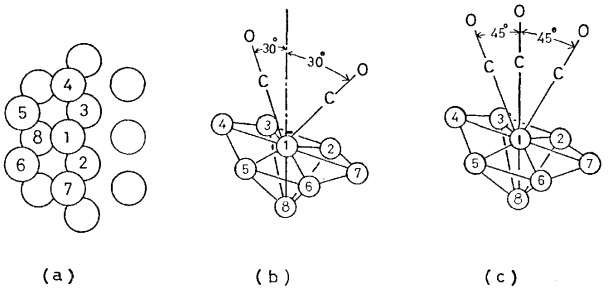

Fig. 2. Models for 8-atom cluster (a), M_8-$(CO)_2$ (b), and M_8-$(CO)_3$ (c).

Fig. 1(a). The atoms numbered 1 and 5—10 constitute the surface of Pd(111) or Ru(001). The atoms numbered 2, 3, and 4 correspond to the second layer.

It is presumed that the metal particles which are highly dispersed have the step sites, as is shown in Fig. 2(a). The model of the 8-atom cluster was also adopted. The atoms numbered 1, 4, and 7 constitute the edge of a stepped Pd(111) or Ru(001) surface. The 2, 3, and 8 atoms are second-layer with respect to the 1 and 4—7 atoms.

All the CO molecules bond to a central atom (numbered 1 in Figs. 1 and 2) through carbon atoms. In the present paper, models of the CO chemisorbed clusters are expressed, such as M_{10}–CO and M_8-$(CO)_2$. M is meant by Pd or Ru. The subscripts 10 and 8 indicate the clusters of Figs. 1 and 2 respectively. The subscripts of CO show the numbers of CO molecules adsorbed on the atom 1.

In M_{10}–CO, the C and O atoms are taken on the C_3-axis of C_{3v} symmetry. In M_{10}-$(CO)_2$ of Fig. 1 (b), two pairs of C and O are taken on the σ_h-plane of C_s symmetry, with the C–M–C angle of 60°. In M_{10}-$(CO)_3$ of Fig. 1(c), three pairs of C and O are taken on each of the three σ_v-planes of C_{3v} symmetry. Three C and atom 1 form a regular tetrahedral arrangement.

In M_8–CO, the atoms numbered 8, C, and O are taken on the C_2-axis of the C_{2v} symmetry. In M_8-$(CO)_2$ of Fig. 2 (b), the 1, 4, 7, and 8 atoms and two pairs of C and O are taken on one of the two σ_v-planes of the C_{2v} symmetry, with the C–M–C angle of 60°. In M_8-$(CO)_3$ of Fig. 2 (c), one of three CO is taken on the C_2-axis of the C_{2v} symmetry, with the C–M–C angle of 45°.

All the nearest-neighbor distances between metal atoms are taken as metallic values of 2.65 Å and 2.75 Å for Ru and Pd respectively. The Ru–C bond length is taken as 2.00 Å, which is close to that of 1.92 Å in $Ru_3(CO)_{12}$.[13] The two kinds of Pd–C bond length are taken as 2.00 Å for the sake of comparison with Ru, and as 2.25 Å; this brought about a desirable density of states in comparison with the UPS spectra. Palladium carbonyl complexes to be referred to for the Pd–C bond length are lacking. The C–O bond length is taken as 1.15 Å, which is identical with Politzer and Kasten's report[12] and close to the 1.128 Å of free CO.

Calculation. Computation was carried out by using the SCC extended Hückel method. Each molecular orbital, Ψ_i, is written as a linear combination of the occupied valence orbitals of various atoms:

$$\Psi_i = \sum_{jk} C_{ijk}\phi_{jk},$$

where ϕ_{jk} is an atomic orbital j on the atom k.

The diagonal elements of the Hamiltonian matrix, H_{ii}, are given in terms of the valence-state ionization energy according to the procedure of Basch, Viste, and Gray:[14]

$$-H_{ii} = A+BQ,$$

where Q is the charge on the atom. Basch *et al.*[14] applied A and B as functions of the average electron configuration as well as the atomic orbitals, but in the present paper A and B were adopted as functions of the atomic orbitals only, because of the difficult convergence and because of the insufficient spectroscopic data on Ru and Pd.[15] The A and B determined by spectroscopic data[15] as well as other input data are listed in Table 2.

The overlap elements, S_{ij}, were culculated by using Slater orbitals. The interactions among all the nearest-neighbor atoms are taken into account. The orbital exponents (ζ) obtained by Clementi *et al.*[16,17] were adopted except for 5s and 5p. The ζ_{5p} of Ru or Pd is lacking in Clementi's table,[17] but ζ_{5p} was postulated to be equal to ζ_{5s} according to Slater's rule. The ζ_{5s} and ζ_{5p} of Pd or Ru were determined as the minimum values so as not to give rise to negative eigenvalues of the determinant S_{ij}, since negative ones were produced when Clementi's ζ_{5s} was adopted. The ζ_{5s} and ζ_{5p} of Ru are accidentally coincident to those of Pd in two significant figures.

The off-diagonal elements of the Hamiltonian matrix were approximated by using Cusachs formula:[18]

$$H_{ij} = (1/2)S_{ij}(2-|S_{ij}|)(H_{ii}+H_{jj})$$

The calculation generally went through 5—35 iterations, giving a Mulliken charge distribution varying by less than 0.01 on each atom between successive cycles. As did Rein, Fukuda, Win, and Clark, we used the damping parameter in the iteration process to avoid divergence or oscillation;[19] convergence was forced by changing this damping parameter.

The density of states (DOS) was calculated from the converged coefficients, C_{ijk}, in every occupied level and multiplied by the Gaussian function, with a standard deviation of 2.0 eV. In the present paper, energy levels are expressed in values relative to the highest occupied molecular orbital (HOMO), which is taken as zero or the Fermi level (E_f). Fassaert and van der Avoird's paper[20] was referred to.

TABLE 2. PARAMETERS OF THE CALCULATION

Orbital exponents								
	Ru		Pd			C		O
4d	3.2032		3.4044		2s	1.6083		2.2458
5s, 5p	2.6		2.6		2p	1.5679		2.2266
	Ru		Pd			C		O
(eV)	A	B	A	B		A	B	A	B
4d	10.78	4.36	12.43	11.54	2s	16.60	19.48	32.37	16.78
5s	7.36	8.05	8.33	7.99	2p	11.26	6.49	15.84	17.36
5p	5.91	5.36	3.70	7.06					
								A[a]	B[a]
					2s			32.37	13.28
					2p			15.84	13.44

a) In negative charge of Q.

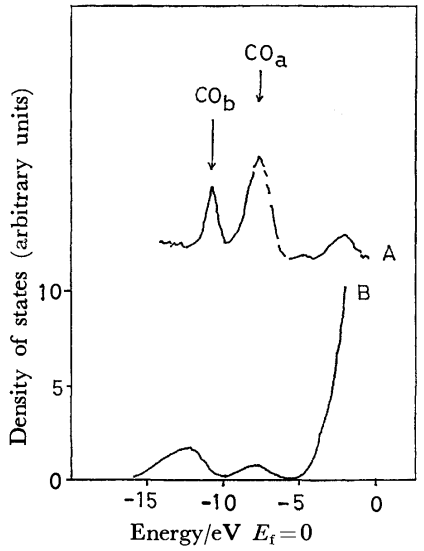

Fig. 3. Comparison between density of states for Ru_{10}–CO and UPS spectra of CO-covered Ru(001) surface. (A): UPS (He_{II}) spectra of Ru(001) covered 15 Langmuir CO, (B): density of states calculated for Ru_{10}–CO.

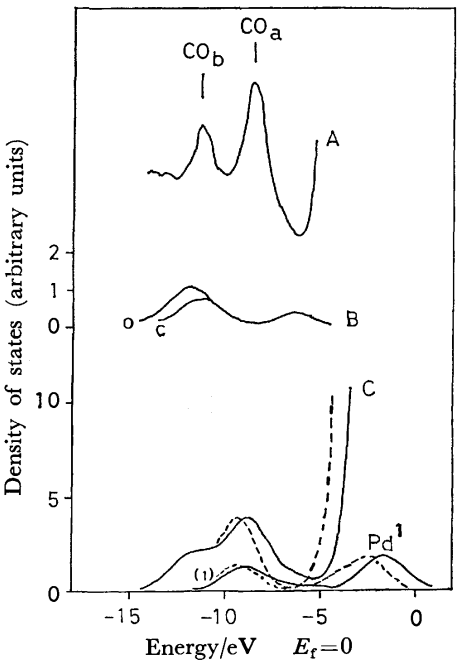

Fig. 4. Comparison between density of states for Pd_{10}–CO and UPS spectra of CO adsorbed Pd(111). (A): UPS (He_{II}) spectra of Pd(111) exposed to 2×10^{-7} Torr of CO, (B): density of states for C and O calculated in Pd_{10}–CO; (C): density of states for the whole and for central Pd^1 in Pd_{10}–CO (——) and Pd_{10} (----).

There were great differences in the total energies (ground states) of various models. It should be noted that the convergent states in the SCC approximation are not necessarily minimum in energy. The total energies will not be discussed in the present paper.

Results and Discussion

Density of States (DOS). The DOS values for Ru_{10}–CO are shown in Fig. 3, along with the UPS spectra of CO adsorbed Ru(001).[21] The DOS of the Ru_{10} cluster almost overlaps with that of Ru_{10}–CO over −5 eV and almost equals zero under −5 eV, so the DOS line is omitted in Fig. 3. The results of calculation agree with the UPS spectra on the CO_a band (−7.6 eV).

The DOS for Pd_{10}–CO (Pd–C=2.25 Å) and the Pd_{10} cluster are shown in Fig. 4, along with the UPS spectra of CO-adsorbed Pd(111).[22] In the case of Pd–C= 2.00 Å, the higher band (−7 or −6 eV) in the DOS of CO is very small; hence, the figure is omitted. The results of calculation agree with the UPS spectra on the CO_b band (−11.2 eV). The higher band (CO_a) in the DOS of CO (B in Fig. 4) agrees with the 5σ level obtained by Chen *et al.* in the SCF-XαSW calculation for Pd_5–CO.[23]

The DOS of the Ru_{10} cluster scarcely differs from that of Ru_{10}–CO, but the DOS of the Pd_{10} cluster (C in Fig. 4) has two important characteristcs. First, the DOS of the Pd_{10} cluster is widespread over a range lower than that of Ru_{10} and changes to a higher range upon adsorbing CO. Secondly, about half of the DOS of Pd^1 exists in a range lower than −5 eV, and this DOS is not influenced by the presence of CO. These

two characteristcs suggest that electrons of Pd_{10} are more stable and that fewer electrons take part in bonding with CO compared with Ru_{10}. This difference will be discussed numerically in the next section.

Population Analysis. Mulliken's atomic gross population (AGP), the atomic net population (ANP), the atomic bond population (ABP), and the atomic orbital-bond population (AOBP) were analyzed by using the converged C_{ijk} values. All the ANP properly have values less than the numbers of the valence electron on the atom. All the ABP of all the models except for Pd_{10}-$(CO)_3$ are positive, but negative ABP of Pd-Pd were contained in the Pd_{10}-$(CO)_3$; consequently, it can be presumed that such a state of chemisorption as in this model is not possible.

In the 10-atom cluster, M_{10}-$(CO)_2$ has C_s symmetry, unlike the other models. In the 8-atom cluster, M_8-$(CO)_3$ contains two different pairs of C and O atoms. Consequently, a detailed comparison among the same metal and the same cluster was omitted.

In AGP, the 10-atom cluster and 8-atom cluster systems are summarized in Tables 3 and 4 respectively. All the AGP of C (AGP-C) in the adsorbed CO are greater than the 3.695 of free CO. In Ru, all the AGP-C are greater than 4 (valence electrons of C). These results indicate the presence of an overall transfer of electrons from Ru to C, a so-called "back donation." In Pd_{10}-CO, the AGP-C of Pd-C=2.25 Å is greater than 4 and that of Pd-C=2.00 Å. This corresponds to the result of DOS presented above; that is, in Pd-C=2.00 Å, the higher band in DOS of CO is very small. The AGP-C values of Pd_{10}-$(CO)_2$, Pd_8-$(CO)_2$, and Pd_8-$(CO)_3$ are smaller than in all other models. The back donation can be taken as a measure of the strength of the bond between metal and carbon, so that the strength of the bond between a multivalent Pd and two or three C may be weak.

In the 8-atom cluster, all the AGP of oxygen have values greater than 6; that is, oxygen atoms have negative charges. This agrees with the general tendency found by another investigation.[12] In the 10-atom cluster, these AGP values of oxygen are less than 6. This suggests that the 8-atom cluster gives more suitable results of calculation.

In the AGP of a central atom, Ru^1 or Pd^1, without CO, those of the 8-atom cluster are greater than those of the 10-atom cluster, and they (8-atom cluster) are greater than the number of each valence electron (Ru: 8, Pd: 10). The transfer of electrons from the nearest-neighbor atoms to a central atom occurs and facilitates the back donation. Consequently, the step site (8-atom cluster) forms stronger bonds between metal and C, and also forms twin or trine easily. The values AGP−8.00 of Ru^1 are always greater than the values

TABLE 3. THE ATOMIC GROSS POPULATION OF C, O, AND CENTRAL METAL ATOM IN THE 10-ATOM CLUSTERS

	CO[a]	M_{10}[b]	M_{10}-CO	M_{10}-$(CO)_2$[c]	M_{10}-$(CO)_3$
Ru^1 [d]	—	7.900	7.972	8.507	7.931
C	3.695	—	4.040	4.137	4.224
O	6.305	—	5.689	6.433	5.632
Pd-C=2.00 Å					
Pd^1 [d]	—	9.227	9.389	9.923	—
C	3.695	—	3.867	3.758	—
O	6.305	—	5.514	6.294	—
Pd-C=2.25 Å					
Pd^1 [d]	—	9.227	9.491	9.945	—
C	3.695	—	4.123	3.743	—
O	6.305	—	5.747	6.294	—

a) Free CO. b) Metal cluster. c) AGP of C or O are the average values of two different atoms in C_s symmetry. d) Central atom numbered 1 in Fig. 1.

TABLE 4. THE ATOMIC GROSS POPULATION OF C, O, AND CENTRAL METAL ATOM IN THE 8-ATOM CLUSTERS

	CO[a]	M_8[b]	M_8-CO	M_8-$(CO)_2$	M_8-$(CO)_3$[c]
Ru^1 [d]	—	8.107	8.310	8.401	8.493
C	3.695	—	4.238	4.143	4.079
O	6.305	—	6.470	6.441	6.421
Pd-C=2.00 Å					
Pd^1 [d]	—	10.005	9.971	9.925	9.938
C	3.695	—	3.962	3.722	3.741
O	6.305	—	6.350	6.322	6.300
Pd-C=2.25 Å					
Pd^1 [d]	—	10.005	9.962	9.997	9.958
C	3.695	—	3.924	3.687	3.726
O	6.305	—	6.357	6.312	6.294

a) Free CO. b) Metal cluster. c) AGP of C or O are the averages of two different atoms which are located in the center and at the side. d) Central atom numbered 1 in Fig. 2.

AGP -10.00 of Pd[1] in all models. This indicates that the Ru–C bonding is more stable than that of Pd–C.

The binding energy (E_b) between the central metal atom and C, and the C–O stretching frequencies (ν) in various models are summarized in Table 5. The ν of C–O were evaluated by fitting the equation given by Baerends and Ros[24] to the ABP of CO. Except for M_{10}–CO and Ru_8–CO, the calculated ν values are close to the experimental values (1900—2200 cm^{-1}), so the SCC approximation seems reasonable. The discrepancies in the ν values of M_{10}–CO and Ru_8–CO are ascribed to Baerends's equation,[24] which was derived from carbonyl complexes. These complexes contain 4—6 CO, and neither Pd nor Ru was dealt with as a transition metal atom in the Baerends's paper.[24]

The binding energy, E_b is the E_{ab} value proposed by Pople *et al.*[25] These $|E_b|$ values decrease with an increase in the number of CO; that is, the bonding of twin or trine is weaker than linear bonding. The E_b values of Pd–C=2.00 Å properly have greater negative values than those of Pd–C=2.25 Å because of their shorter bond lengths. The E_b values of Ru–C always have greater negative values than the E_b values of Pd–C, and the E_b values of Pd–C=2.25 Å, which gives a result closer to the UPS spectra, are particularly small negative values, less than half those of Ru–C. On the whole, it is clear that the bonding of Pd–C, especially the bonding of twin or trine, is more unstable than that of Ru–C.

The ABP between the central metal atom and C in various models are summarized in Table 6, while the ABP between C and oxygen in various models are summarized in Table 7. The total ABP of Ru–C have greater values than those of Pd–C in each model. Contrary to the case of metal-C, the total ABP of CO in Ru are always smaller than those in Pd. The total ABP of CO in each model are always smaller than those of free CO. This shows that the overall increase in electron density between metal and C causes a decrease in the electron density between C and oxygen; this tendency agrees with the well-known description of transition-metal complexes involving car-

Table 5. C–O stretching frequencies and binding energies in 8-atom and 10-atom clusters

	M_{10}–CO	M_{10}–$(CO)_2$[a]	M_{10}–$(CO)_3$	M_8–CO	M_8–$(CO)_2$	M_8–$(CO)_3$[b]
Ru–C=2.00 Å ν/cm^{-1}	1234	1923		1852	1915	1982
Pd–C=2.00 Å ν/cm^{-1}	1611	2219		2062	2217	2233
Pd–C=2.25 Å ν/cm^{-1}	1620	2240		2096	2256	2253
Ru–C=2.00 Å E_b/eV	−1.94	−1.57	−1.44	−2.68	−1.80	−1.52
Pd–C=2.00 Å E_b/eV	−1.73	−1.32		−2.14	−1.25	−1.06
Pd–C=2.25 Å E_b/eV	−0.83	−0.67		−1.02	−0.67	−0.61

a) The averages of two different atoms in C_s symmetry. b) The averages of the central and side atoms.

Table 6. Atomic bond population between the 1 atom and carbon atoms in various clusters

		M_{10}–CO	M_{10}–$(CO)_2$[a]	M_{10}–$(CO)_3$	M_8–CO	M_8–$(CO_2)_2$	M_8–$(CO)_3$[b]
Ru–C=2.00 Å	σ	0.478	0.348	0.304	0.405	0.352	0.285
	π	0.161	0.181	0.125	0.231	0.183	0.160
	Total	0.639	0.528	0.429	0.635	0.535	0.445
Pd–C=2.00 Å	σ	0.429	0.208		0.274	0.208	0.184
	π	0.078	0.075		0.113	0.074	0.066
	Total	0.507	0.283		0.388	0.282	0.250
Pd–C=2.25 Å	σ	0.320	0.150		0.179	0.152	0.136
	π	0.026	0.038		0.055	0.034	0.034
	Total	0.347	0.187		0.234	0.186	0.170

a) The averages of two different atoms in C_s Symmetry. b) The averages of the central and side atoms.

Table 7. Atomic bond population between C and O

		CO[a]	M_{10}–CO	M_{10}–$(CO)_2$[b]	M_{10}–$(CO)_3$	M_8–CO	M_8–$(CO)_2$	M_8–$(CO)_3$[c]
Ru–C=2.00 Å	σ	0.614	0.478	0.602	0.448	0.600	0.600	0.600
	π	0.715	0.048	0.468	−0.124	0.423	0.463	0.506
	Total	1.329	0.526	1.070	0.324	1.023	1.063	1.105
Pd–C=2.00 Å	σ	0.614	0.463	0.613	—	0.647	0.600	0.605
	π	0.715	0.292	0.656	—	0.549	0.657	0.666
	Total	1.329	0.755	1.268	—	1.196	1.256	1.271
Pd–C=2.25 Å	σ	0.614	0.431	0.626	—	0.652	0.605	0.621
	π	0.715	0.304	0.667	—	0.570	0.681	0.676
	Total	1.329	0.734	1.293	—	1.222	1.285	1.297

a) Free CO. b) The averages of two different atoms in C_s symmetry. c) The averages of the central and side atoms.

TABLE 8. ATOMIC ORBITAL BOND POPULATION BETWEEN THE 1 ATOM AND C IN VARIOUS CLUSTERS

		M_{10}-CO	M_{10}-$CO)_2$[a]	M_{10}-$(CO)_3$	M_8-CO	M_8-$(CO)_2$	M_8-$(CO)_3$[b]
Ru-C=2.00 Å	4d	0.040	0.227	0.060	0.233	0.187	0.153
	5s	0.201	0.160	0.149	0.194	0.163	0.136
	5p	0.398	0.140	0.220	0.209	0.185	0.156
Pd-C=2.00 Å	4d	0.012	0.055		0.101	0.063	0.063
	5s	0.175	0.239		0.225	0.195	0.163
	5p	0.320	0.021		0.062	0.024	0.024
Pd-C=2.25 Å	4d	−0.004	0.027		0.042	0.023	0.026
	5s	0.090	0.124		0.139	0.130	0.111
	5p	0.261	0.037		0.054	0.033	0.033

a) The averages of two different atoms in C_s symmetry. b) The averages of the central and side atoms.

bonyl groups. In the 8-atom cluster, the total ABP of CO and ν increase, while those of metal-C decrease, with the number of CO. This tendency agrees with the view reported by Davydov and Bell[11] concerning the band shift of the IR spectra.

The ABP of π-orbitals in Pd–C are less than half those of Ru–C in every model. Since the ABP of π-orbitals result from the back donation of electrons from metals, the greater values of the ABP of π-orbitals as well as the total ABP in Ru–C show that Ru adsorbs CO more strongly than Pd.

The steep falls of the ABP (π-orbitals) in Pd_8-$(CO)_2$ and Pd_8-$(CO)_3$ and of the total ABP in Pd_{10}-$(CO)_2$ seem to explain why no experimental data of twin or trine types of CO chemisorption in Pd exist.

The AOBP between the 1 atom and C in various models are summarized in Table 8. In the AOBP of metal-C, remarkable differences between Pd and Ru are observed. The AOBP of the 4d-orbital in Ru–C are always more than double those in Pd–C. It seems an important factor for the stabilization of the bonding, especially, the bonding of twin or trine, that 4d-orbitals take part in the bond formation between metal and carbon. In Pd–C, the AOBP of 5s or 5p are greater than those of 4d. In the calculation of Chen *et al.*[23] for Pd_5–CO by the SCF-XαSW method, the ratio of the charge density in s, p, and d orbitals is 1:1:2. In the present calculations, the result for Pd_8–CO is close to that for Pd_5–CO obtained by Chen *et al.*[23] The great charge density of the d-orbital obtained by Chen *et al.*[23] arises from their taking the four Pd atoms as nearest neighbors. In the three hypothetical models Pd_8-$(CO)_2$, Pd_8-$(CO)_3$, and Pd_{10}-$(CO)_2$, the AOBP of 4d-orbitals are very small compared with Pd_8–CO. This is why twin or trine do not exist in CO-adsorbed Pd metal. The small AOBP of the 4d-orbital in Pd_{10}–CO have not yet been solved.

C–C Interaction. In the calculations described above, the overlap elements among carbon atoms were not taken into account. Further calculations were performed by placing the overlaps between carbon atoms in the matrix elements according to the following scheme of M_8-$(CO)_2$ and M_{10}-$(CO)_2$:

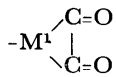

The various atomic populations of 10-atom and 8-atom clusters are summarized in Tables 9 and 10 respectively. The M^1–C bond length is taken as the same 2.00 Å in both Ru and Pd metals. The C–C bond length also results in a value of 2.00 Å when the M_8-$(CO)_2$ and M_{10}-$(CO)_2$ are used as models.

TABLE 9. THE ATOMIC POPULATION[a] OF M_{10}-$(CO)_2$ WITH A C–C BOND

Metal	AGP		Total ABP		AOBP	(M^1-C)
Ru	Ru^1	8.424	Ru-C	0.440	4d	0.181
	C	4.250	C-O	0.952	5s	0.092
	O	6.482	C-C	0.487	5p	0.166
Pd	Pd^1	9.945	Pd-C	0.228	4d	0.080
	C	4.132	C-O	1.010	5s	0.116
	O	6.368	C-C	0.541	5p	0.033

a) The values of carbon and oxygen are averages of two different atom in C_s symmetry.

TABLE 10. THE ATOMIC POPULATION OF M_8-$(CO)_2$ WITH A C–C BOND

Metal	AGP		Total ABP		AOBP	(M^1-C)
Ru	Ru^1	8.313	Ru-C	0.442	4d	0.184
	C	4.266	C-O	0.953	5s	0.097
	O	6.478	C-C	0.499	5p	0.160
Pd	Pd^1	9.904	Pd-C	0.232	4d	0.086
	C	4.089	C-O	1.014	5s	0.121
	O	6.356	C-C	0.561	5p	0.024

In all the evidence, the case taking the C–C overlap shows the same tendency as the preceding case taking no C–C overlap. The same discussion as in the preceding sections therefore holds.

The ABP of the C–C bond of the Pd cluster are greater than those of Ru contrary to the ABP of M^1–C. This is coincident with the tendency of the C–O bond.

The binding energies, E_b, values of M^1–C (E_{M-C}), of C–O (E_{C-O}), and of C–C (E_{C-C}) are summarized in Table 11. The $|E_{C-O}|$ and $|E_{C-C}|$ values of Ru are smaller than those of Pd. This tendency is comparable to that of ABP.

Concluding Remarks

Generally speaking, the experimental results show that no CO chemisorption of the twin or trine type is found on Pd, but is found on Ru metal.

Table 11. The binding energy of carbon atom in 8-atom and 10-atom clusters with a C–C bond

Cluster		E_{C-M}/eV	E_{C-O}/eV	E_{C-C}/eV
10-atom	Ru	−1.28	−8.87	−1.11
	Pd	−1.07	−10.58	−1.47
8-atom	Ru	−0.94	−8.86	−1.41
	Pd	−0.55	−10.42	−1.85

Calculations for the model Pd_{10}–$(CO)_3$ cluster gave negative ABP among the Pd atoms, suggesting that there is no trine type CO adsorption on the 10-atom Pd cluster.

From a comparison of Ru with Pd concerning twin-type adsorption on the 8-atom and 10-atom clusters, stability differences in bonding between two CO molecules and these metals were deduced, as is shown by the following inequality relationships:

1. AGP of $Ru^1 > 8$ (valence electron numbers of Ru)
   AGP of $Pd^1 < 10$ (valence electron numbers of Pd)
   This shows that an over-all donation to Ru^1 occurs more easily than to Pd^1.
2. AGP of C in Ru > 4
   AGP of C in Pd < 4
   This shows that an over-all back donation from Ru metal occurs more easily than from Pd metal.
3. (Total ABP of Ru–C) > (total ABP of Pd–C)
4. (AOBP of 4d in Ru–C) $\gg$ (AOBP of 4d in Pd–C)
5. ($|E_b|$ of Ru–C) > ($|E_b|$ of Pd–C)

All five of these relationships indicate that the twin-type CO adsorption on 8-atom and 10-atom Ru clusters are more stable than those on Pd. Thus, the calculated results account well for the experimental observations.

References

1) R. P. Eischens and W. A. Plinskin, *Adv. Catal.*, **10**, 1 (1958); R. P. Eischens, S. A. Francis, and W. A. Plinskin, *J. Phys. Chem.*, **60**, 194 (1956); *J. Chem. Phys.*, **22**, 1786 (1954).
2) M. Kobayashi and T. Shirasaki, *J. Catal.*, **28**, 289 (1973).
3) M. Kobayashi and T. Shirasaki, *J. Catal.*, **32**, 254 (1974).
4) K. C. Taylor, *J. Catal.*, **38**, 299 (1975).
5) R. A. Dalla Betta, *J. Catal.*, **34**, 57 (1974).
6) H. Kubicka, *J. Catal.*, **12**, 223 (1968).
7) R. A. Dalla Betta, *J. Phys. Chem.*, **79**, 2519 (1975).
8) S. J. Tauster, S. C. Fung, and R. L. Garten, *J. Am. Chem. Soc.*, **100**, 170 (1978).
9) M. A. Vannice and R. L. Garten, *J. Catal.*, **63**, 255 (1980).
10) M. F. Brown and R. D. Gonzalez, *J. Phys. Chem.*, **80**, 1731 (1976).
11) A. A. Davydov and A. T. Bell, *J. Catal.*, **49**, 332 (1977).
12) P. Politzer and S. D. Kasten, *J. Phys. Chem.*, **80**, 385 (1976).
13) R. Mason and A. I. M. Rae, *J. Chem. Soc.*, *A*, **1968**, 778.
14) H. Basch, A. Viste, and H. B. Gray, *J. Chem. Phys.*, **44**, 10 (1966).
15) C. E. Moore, "Atomic Energy Levels," Natl. Bur. Stand. (U. S.), (1949), Vol. 1; (1958), Vol. 3.
16) E. Clementi and D. L. Raimondi, *J. Chem. Phys.*, **38**, 2686 (1963).
17) E. Clementi, D. L. Raimondi, and W. P. Reinhardt, *J. Chem. Phys.*, **47**, 1300 (1967).
18) L. C. Cusachs, *J. Chem. Phys.*, **43**, s157 (1965).
19) R. Rein, N. Fukuda, H. Win, and G. A. Clarke, *J. Chem. Phys.*, **45**, 4743 (1966).
20) D. J. M. Fassaert and A. van der Avoird, *Surface Sci.*, **55**, 291 (1976).
21) D. Menzel, *J. Vac. Sci. Technol.*, **12**, 313 (1975).
22) D. R. Lloyd, C. M. Quinn, and N. V. Richardson, *Solid State Commun.*, **20**, 409 (1976).
23) B.-H. Chen, D. C. Foyt, and J. M. White, *Surface Sci.*, **67**, 218 (1977).
24) E. J. Baerends and P. Ros, *Mol. Phys.*, **30**, 1735 (1975).
25) J. A. Pople and G. A. Segal, *J. Chem. Phys.*, **44**, 3289 (1966).

Conformational Changes of the Poly(α-L-glutamic acid)-Cu(II) Macromolecular Complexes in the pH Range of 4—7. A Light Scattering Study with Emphasis on Aggregation and Helix-coil Transitions

Tsutomu MASUJIMA†

Faculty of Science, Hiroshima University, Higashisenda-machi, Naka-ku, Hiroshima 730

(Received April 15, 1982)

The overall conformational changes of the macromolecular complex between poly(α-L-glutamic acid), poly(Glu), and Cu(II) in 0.15 M NaCl were investigated by means of the light scattering method at three mixing ratios of Glu residues to Cu^{2+}, R, (32, 16, and 8) in the pH range of 4—7. The root-mean-square radius of gyration and the weight-averaged molecular weight of poly(Glu) were determined by means of the Zimm plot, and those pH dependences show that the poly(Glu) shrinks in the course of the coil-to-helix transition and that it forms aggregates at pH values lower than 4.7, where helix formation is almost completed. In the presence of Cu^{2+} ions, the bound Cu(II) accelerates the shrinking of the poly(Glu) conformation and induces the aggregation in a high pH region, where the helix is imperfect. With the aid of theoretical treatments in the text, the aggregation scheme in the helix region was disclosed to be side-by-side, in which a 70—95% length of a helix overlaps one another. All these results and the pH dependence of the radius of gyration per poly(Glu) molecule were discussed in relation to the complex formation between Cu(II) and poly(Glu).

The poly(α-L-glutamic acid), poly(Glu), has been used extensively as a model substance of the proteins. Thus, the systems including both poly(Glu) and the transition-metal ions are interesting as models of the metallo-proteins or of the materials of the functional metal-polymer complex, and so they have been studied extensively.[1-19] In these transition-metal ions, the Cu(II) was shown to be rather unique in the induction of the conformational changes in poly(Glu),[2,11,14,16,17,19] the strength of the binding,[13,15-17] and the complicated complex formations.[12-18] Our recent work has clarified that three classes of complexes predominate either in the helix or extended-coil region, in the helix-coil intermediate transition region, or in the low-pH region, where the helix formation has already been completed.[15] The characteristic formation of the complex should be correlated with the conformational changes of poly(Glu). Since no definite conformation, however, was observed in the helix-coil intermediate region, a study of the conformational changes from other points of veiw is needed. One important point of view is that of the overall conformations of poly(Glu). The light scattering method is useful for this purpose, because it can discriminate the aggregation and the change in the scale of poly(Glu) by the use of the weight-averaged molecular weight, M_w, and the z-averaged root-mean-square radius of gyration, $\langle s^2 \rangle_z^{1/2}$, of poly(Glu) respectively.

Aqueous solutions of poly(Glu) or poly(Glu)–Cu(II) have been studied slightly by means of the light scattering method.[18,20,21] These studies have, though, been related to the aggregation[18,20] or have been only of the random coil of poly(Glu).[21] In the present study, poly(Glu)–Cu(II) macromolecular complexes at various pHs and various mixing ratios of Glu residues to Cu^{2+}, R, in 0.15 M (1 M=1 mol dm^{-3}) NaCl were investigated. With the observed values of M_w and $\langle s^2 \rangle_z^{1/2}$, the pH dependence of the overall conformational changes in poly(Glu) and the effect of Cu(II) binding on this changes were determined from the points of view of aggregation and the compactness of the poly(Glu) molecule. Furthermore, with the aid of some theoretical treatments developed (Theoretical), the equilibrium and the scheme (*e.g.*, side-by-side or head-to-tail) of aggregation, and the participation of H^+ ions in the aggregation were analyzed. Finally, the pH dependence of the extension per poly(Glu) molecule in the presence of Cu(II) was discussed in relation to the characteristic complex formations between poly(Glu) and Cu(II).

Experimental

Materials and Preparations of Poly(Glu) and Poly(Glu)–Cu(II) Solutions. Sodium poly(Glu), hereafter denoted simply as poly(Glu), was the same sample as has been described elsewhere.[11] The other chemicals were all of a reagent grade and were used without further purification. The preparation of the poly(Glu) and poly(Glu)–Cu(II) solutions prior to dialysis was the same as has been described previously.[15] The mixing ratio, R, defined as the molar residue concentration of poly(Glu) to the total concentration of Cu^{2+} ions, was adjusted by changing the amount of Cu^{2+} ions. Freshly redistilled, dust-free water was used for all preparations of solutions. The sample solutions were dialyzed against 2 l of a 0.15 M NaCl solution for 48 h. For a Cu^{2+} containing sample, an adequate amount of Cu^{2+} ions was also added to the outer-side solution prior to dialysis in order to diminish the change in the R of the inner-side solution in the course of dialysis. In this case, the concentration of the unbound Cu^{2+} was calculated on the basis of the data of equilibrium dialysis.[15] For the pH adjustment of a sample at a low pH (<4.5), H^+ ions were added indirectly from the outer-side solution in order to prevent the precipitation of poly(Glu). The dialyzed sample (inner side) was diluted with the outer-side dialysis solution when the concentration dependence of light scattering and the refractive index were measured. All the sample solutions were clarified by a careful and slow flow rate (1—3 ml/min) filtration[22] through a pair of 23 mmϕ Fuji micro filters FM-22 (0.22 μm pore) (Fuji Photo Film Co., Ltd., Japan), which adsorbed slight proteins (less than 1 μg/cm^2). The concentrations of poly(Glu) in all the samples after the light-scattering and refractive-index measurements were deter-

† Present address: Institute of Pharmaceutical Sciences, Hiroshima University School of Medicine, Kasumi 1-2-3, Minami-ku, Hiroshima 734.

mined by means of the micro-Biuret method with a precision of ±1% or less.[23] The value of 151.1 g/mol was used as the Glu residue mass throughout the experiments.

Light Scattering and Differential Refractive Index Measurements. The light scattering (L.S.) photometer was a Shimadzu type PG-21 apparatus, with a Takeda Riken digital multimeter, type TR-6855. The incident-light beam of the 436 nm wavelength of the Hg lamp was used. The cross section of the beam was 4×12 mm^2. The calibration of the instrument was achieved by the use of the freshly distilled benzene and standard polyethylene oxide of molecular weights of 8×10^4 and 15×10^4 (Toyo Soda SE-8 and SE-15 respectively; Toyo Soda Co., Ltd., Japan). The reference value of the R_{90} of benzene was 46.5×10^{-6} cm^{-1} (25 °C).[24] The intensities of the vertical and horizontal components of the scattered light at a given angle, θ, with a vertically polarized incident beam, $V_v(\theta)$ and $H_v(\theta)$ respectively, were calculated by means of the scattered-light intensities (without an analysing polarizer) with vertically (θ=30—135°), $U_v(\theta)$, and horizontally (90° only), $U_h(90)$, polarized incident beams as follows:[25,26]

$$V_v(\theta) = U_v(\theta) - H_v(\theta) \quad (1)$$

$$H_v(\theta) = U_h(90)/2. \quad (2)$$

Tomimatsu's method was followed for the correction of the back reflection of the cylindrical cell (38 mmϕ) (in a water jacket).[27] All L.S. measurements were carried out at 25±0.1 °C. The contributions of Cu^{2+} ions and the optical absorption of poly(Glu)–Cu(II) solutions ($\varepsilon\simeq20$ at most at 436 nm) to the scattered-light intensity were negligible.[28]

The differential refractive index, dn/dc, of a sample solution at 436 nm and at 25±0.1 °C was determined by the use of a Shimadzu differential refractometer (the Debye type) which has been modified in some respects. The method of detecting the slit image was changed to that with the photomultiplier. The Debye cell was capped to prevent the evaporation of the solvent, and the optical bench below the photomultiplier box was thermostated. In the measurements of both L.S. and dn/dc, the outer-side dialysis solution was used as a blank solution. The pH variation in the sample solution in the course of dilution was less than ±0.02 at pH≤5.5 and less than ±0.04 at pH>5.5.

The pH values of the sample solutions were determined on a Hitachi-Horiba Model N-5 pH meter after the L.S. and dn/dc measurements.

Theoretical

General Aggregation Models and the Variation in M_w. Two typical models can be assumed, called;
a) open association;

$$\begin{aligned} &M_1 + M_1 \overset{K_1}{\rightleftharpoons} M_2 \\ &M_2 + M_1 \overset{K_2}{\rightleftharpoons} M_3 \\ &\cdots\cdots\cdots\cdots \\ &M_{n-1} + M_1 \overset{K_{n-1}}{\rightleftharpoons} M_n \\ &\cdots\cdots\cdots\cdots \end{aligned} \quad (3)$$

and b) closed association;

$$nM_1 \overset{K'}{\rightleftharpoons} M_n, \quad (4)$$

where M_n is the n-mer of poly(Glu) and where K or K' is the equilibrium constant of association.[29] Since the precipitation of poly(Glu) is observed at pH values lower than 3.5, the aggregation process of poly(Glu) molecules seems to be of the former type, in which the value of n increases indefinitely. Since no definite correlating function has been found among the K values, all the steps in the open association are assumed to be equivalent, *i.e.*, identical K values, for a mathematically rigorous model;[29]

$$K_1 = K_2 = \cdots = K_n = \cdots = K. \quad (5)$$

This model implies an independence of the equilibrium constants from the degree of association.[29] Thus,

$$(K_1\cdot K_2\cdot \cdots \cdot K_{n-1} =)K^{n-1} = \frac{\gamma_n[M_n]}{(\gamma_1[M_1])^n}, \quad (6)$$

where γ_n is the activity coefficient of n-mer. As Ogston and Winzor showed in their theoretical study, $\gamma_n/{\gamma_1}^n$ in Eq. 6 can be regarded as 1 because of the self-cancellation of the activity coefficients in the equilibrium expression for the association of charged spherical or rod-shaped polymers.[30] In this case, Eq. 6 can be treated simply as;[31]

$$[M_n] = K^{n-1}[M_1]^n = [M_1]Y^{n-1}, \quad (7)$$

where

$$Y = K[M_1]. \quad (8)$$

The variation in $[M_n]/[M_1]$ with n at various parameters of Y is shown in Fig. 1. The figure shows that the weight-averaged molecular weight can be determined by the use of Y. The total molar concentration of unimers, C_0, included in unimers and multimers is;

$$C_0 = [M_1] + 2[M_2] + \cdots + n[M_n] + \cdots. \quad (9)$$

By combining Eqs. 7 and 9, we obtain;

$$C_0 = \frac{[M_1]}{(1-K[M_1])^2} = \frac{[M_1]}{(1-Y)^2}, \quad (10)$$

when $|Y|<1$. The weight-averaged molecular weight, M_w, which can be determined experimentally is;

$$M_w = \frac{M_1^2[M_1]\sum n^2(K[M_1])^{n-1}}{M_1C_0}, \quad (11)$$

when combined with Eq. 10, Eq. 11 was reduced;[29]

$$\frac{M_w}{M_1} = \frac{1+K[M_1]}{1-K[M_1]} = \frac{1+Y}{1-Y}. \quad (12)$$

These equations show that the observed values of M_w

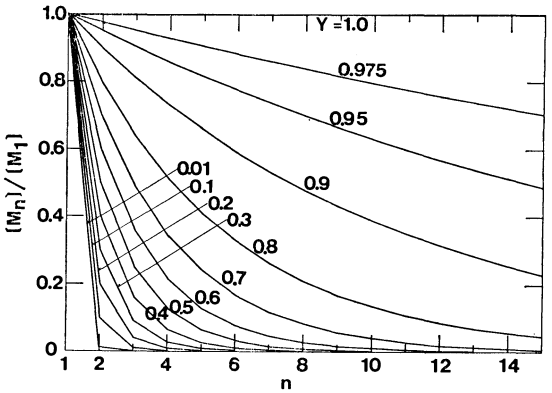

Fig. 1. The distribution curve of the molar concentration ratio of n-mer to unimer *vs.* n in the aggregated system at various assumed values of $Y(=K[M_1])$.

and M_1 give the value of Y by means of Eq. 12; then, with the values of Y and C_0, the values of $[M_1]$ and subsequently K can be determined by the use of Eqs. 8 and 10.

pH-Dependent Aggregation Models and the Variation in M_w. As will be shown later, the aggregation of poly(Glu) depends on the pH. This phenomenon shows that the binding of H^+ ions contributes to the aggregation. If the binding of mH^+ ions advances the one step of the open association, the following association process can be assumed as a first approximation;

$$\begin{aligned} &M_1' + M_1' + mH^+ \overset{K''}{\rightleftharpoons} M_2' \\ &M_2' + M_1' + mH^+ \overset{K''}{\rightleftharpoons} M_3' \\ &\cdots\cdots\cdots\cdots \\ &M_{n-1}' + M_1' + mH^+ \overset{K''}{\rightleftharpoons} M_n' \\ &\cdots\cdots\cdots\cdots . \end{aligned} \tag{13}$$

Then, just as in the preceding section,

$$[M_n'] = K''^{n-1}[M_1']^n((\gamma_{H^+}[H^+])^m)^{n-1}, \tag{14}$$

where γ_{H^+} is the activity coefficient of the H^+ ion. In this case, the following treatment is the same as in the previous open-association model when we regard Y as;

$$Y = K''[M_1'](\gamma_{H^+}[H^+])^m (= Y_H). \tag{15}$$

By combining Eqs. 14 and 10, we obtain;

$$\frac{Y_H}{(1-Y_H)^2} = C_0K''(\gamma_{H^+}[H^+])^m. \tag{16}$$

On electrochemical detection, $pH = -\log(\gamma_{H^+}[H^+])$. Thus,

$$\log\left(\frac{Y_H}{(1-Y_H)^2}\right) = \log(C_0K'') - m\cdot pH. \tag{17}$$

When we plot the pH dependence of the $\log(Y_H/(1-Y_H)^2)$, which can be determined by the data of M_w and M_1, the straight line gives the value of m from the slope and that of K'' from the intercept. When the curved plot is obtained, this model is unsuitable. Both K'' and m can be determined by the use of the two sets of data of M_w and pH by Eq. 17, but they should be nominal values in the curved plot.

Variation in the Mean-square Radius of Gyration in the Aggregate System. The variation in the mean-square radius of gyration, $\langle s^2\rangle_z$, with aggregation is more complicated than that of the M_w, because the variation in $\langle s^2\rangle_z$ is affected by the conformations of the polymer and $\langle s^2\rangle$ is z-averaged. In general,

$$\langle s^2\rangle_z = \frac{\sum n^2M_1^2Y^{n-1}\langle s_n^2\rangle}{\sum n^2M_1^2Y^{n-1}}, \tag{18}$$

where the open association is assumed and $\langle s_n^2\rangle$ is the mean-square radius of the gyration of the n-mer with the molecular weight of M_n. In the following, the conformation of the polymer should be assumed prior to the analysis.

1) Aggregation of Helices. In the association of helices, when the σ part (in length) of a helix overlaps with the unimer or multimer of the helix in a side-by-side or head-to-tail scheme, the length of the multimer, L, can be related with that of the unimer helix, L_1, by;

$$L = L_1(1+(n-1)(1-\sigma)). \tag{19}$$

Since the $\langle s_1^2\rangle$ of a helix equals $L_1^2/12$,[32] the $\langle s^2\rangle$ of aggregated n-helices, $\langle s_n^2\rangle$, is;

$$\langle s_n^2\rangle = \frac{L_1^2(1+(n-1)(1-\sigma))^2}{12} \tag{20}$$

$$= \langle s_1^2\rangle(1+(n-1)(1-\sigma))^2. \tag{21}$$

At $\sigma=0$, the head-to-tail aggregation scheme is assumed; on the other hand, at $\sigma=1$, the perfect side-by-side scheme is assumed. By combining Eqs. 18 and 21, we obtain;

$$\frac{\langle s^2\rangle_z}{\langle s_1^2\rangle} = \frac{\sum n^2Y^{n-1}(1+(n-1)(1-\sigma))^2}{\sum n^2Y^{n-1}}. \tag{22}$$

For the various σ values, the $(\langle s^2\rangle_z/\langle s_1^2\rangle)^{1/2}$ was calculated; it is plotted against Y and M_w/M_1 in Fig. 2 (a and b), which shows that the relation between $(\langle s^2\rangle_z/\langle s_1^2\rangle)^{1/2}$ and M_w/M_1 is almost linear.

2) Aggregation in the Helix-Coil Transition Region. Since the conformation of poly(Glu) changes in the helix-coil region, a general estimation of $\langle s^2\rangle_z$ is needed.

$$\langle s^2\rangle = \text{const}\cdot M^q, \tag{23}$$

where $q=2/3$, 1, and 2 for spheres, a Gaussian coil, and a thin rod respectively;[31] thus,

$$\frac{\langle s_n^2\rangle}{\langle s_1^2\rangle} = \left(\frac{M_n}{M_1}\right)^q (= n^q). \tag{24}$$

By combining Eqs. 18 and 24, we obtain;

$$\frac{\langle s^2\rangle_z}{\langle s_1^2\rangle} = \frac{\sum n^{2+q}Y^{n-1}}{\sum n^2Y^{n-1}}. \tag{25}$$

In Fig. 3, the value of $(\langle s^2\rangle_z/\langle s_1^2\rangle)^{1/2}$ is plotted against M_w/M_1 at the various q values assumed. In this case, it should be noted that there is an implicit assumption that $\langle s_n^2\rangle$ increases additively with n, just like the increment in the $\langle s^2\rangle$ of the unimers at various molecular-weights. When the association and the conformational changes occur simultaneously, the $(\langle s^2\rangle_z/$

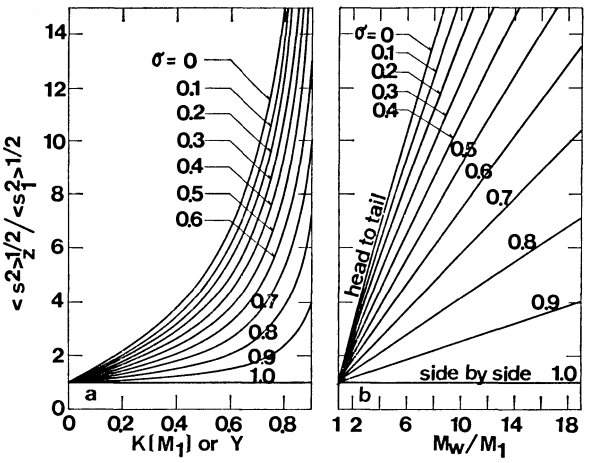

Fig. 2. The dependence of $\langle s^2\rangle_z^{1/2}/\langle s_1^2\rangle^{1/2}$ on (a) Y $(=K[M_1])$, and (b) M_w/M_1, at various overlapping parameters of σ, when the aggregation of helices is assumed to be the scheme of Eq. 22. The summation was carried out from $n=1$ to 100.

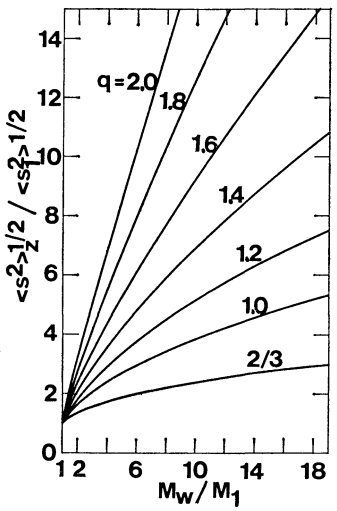

Fig. 3. The dependence of $\langle s^2\rangle_z^{1/2}/\langle s_1^2\rangle^{1/2}$ on M_w/M_1 at various conformational parameters of q, when the poly(Glu) is assumed to aggregate in the helix-coil transition region according to the scheme of Eq. 25. The summation was carried out from $n=1$ to 100.

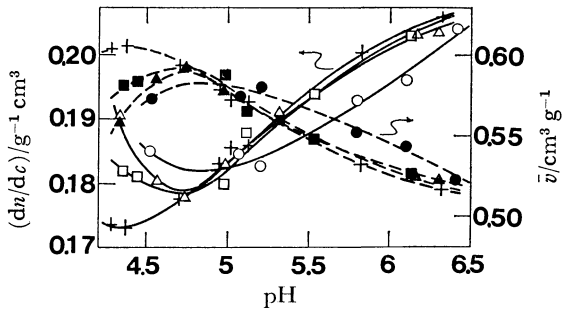

Fig. 4. The pH dependence of dn/dc (solid lines) and the partial specific volume (dashed lines) of poly(Glu) in 0.15 M NaCl solutions at various R of ∞ (poly-(Glu) only) (crosses), 32 (squares), 16 (triangles), and 8 (circles).

$\langle s_1^2\rangle)^{1/2}$ *vs.* M_w/M_1 curves will be very complicated.

Results and Discussion

pH Dependence of dn/dc and the Partial Specific Volume. Figure 4 shows the pH dependence of dn/dc and the partial specific volume, $\bar{v}$, of poly(Glu) in a 0.15 M NaCl solution at various R values. The value of $\bar{v}$ was calculated by means of Heller's equation using dn/dc;[33]

$$\bar{v} = 1.069 - 2.679\ (dn/dc), \tag{26}$$

as will be detailed in a subsequent paper.[19] The increment in $\bar{v}$ with the helix formation was interpreted as showing voids formed in the helix conformation and/or a change in the hydration of water accompanied by the transition.[34] In every case of R, almost all (more than 95%) the Cu^{2+} ions bind with poly(Glu) at pH values higher than 5, and then dissociate with a lowering of the pH.[15] The binding of the Cu^{2+} ion instead of two Na^+ ions should increase the n value; however, the value of dn/dc in the presence of Cu^{2+} ions decreases at a low R. Thus the decrease in dn/dc (increment of $\bar{v}$) in pH 5—6.5 at $R=8$ should be due to the helix formation of poly(Glu) induced by Cu(II).[15] The decrease in $\bar{v}$ at a low pH may show the exclusion of hydrated water on the aggregate formation. With the value of dn/dc and the Rayleigh ratio, the M_w and $\langle s^2\rangle_z^{1/2}$ of poly(Glu) were determined according to Zimm's method.[35]

Zimm Plots of Poly(Glu) at Various R and pH Values. The Rayleigh ratio, which is corrected for the optical anisotropy, $R'(\theta)$, was determined as follows:[25,26]

$$R'(\theta) = R_{V_V}(\theta) - (4/3)R_{V_h}(\theta). \tag{27}$$

Then,

$$K^*c/R'(\theta) = (1/M_w)(1+(16\pi^2/3\lambda^2)\langle s^2\rangle_z \times \sin^2(\theta/2)) + 2A_2c, \tag{28}$$

where K^* is the optical constant, c is the concentration of poly(Glu) (g/ml), λ is the wavelength of the incident beam (cm), and A_2 is the second virial coefficient.

Figure 5 shows the Zimm plots of poly(Glu) solutions at various R values and at pH 6.1—6.3. The almost linear plots seem to show that the molecular-weight distribution of the sample is rather narrow,[32] which is consistent with the results of electric birefringence ($M_w/M_n=1.13$).[36] The values of M_w obtained were 1.06×10^5, 1.22×10^5, and 1.79×10^5, the $\langle s^2\rangle^{1/2}$ values were 290, 250, and 210 Å, and the $A_2\times10^3$ values were 2.9, 1.5, and 0.93 at $R=\infty$, 16, and 8 respectively. The increment of M_w with the addition of Cu(II) shows the participation of Cu(II) in the formation of the aggregate at a high pH, while the decrease in $\langle s^2\rangle_z^{1/2}$ shows that the bound Cu(II) induces the shrinking of the poly(Glu) conformation.

Figure 6 shows the Zimm plot for poly(Glu) at various R values and at low pH (4.28—4.52), where the formation of the helix is completed.[15] The curvilinear plots should show that the molecular-weight distribution is dispersive or that the unimer and multimer of poly(Glu) coexist under these conditions.[32] However, the negative A_2 which is frequently seen in the aggregate systems was not observed, and the plot was almost linear in the experimented-on concentration

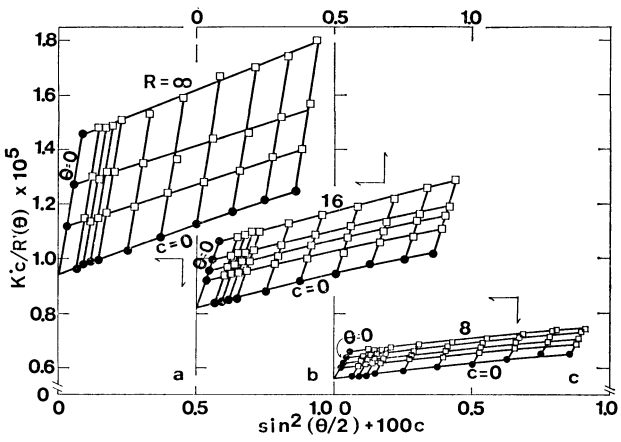

Fig. 5. The Zimm plots for poly(Glu) in 0.15 M NaCl solutions at high pH regions in (a) the absence ($R=\infty$) (pH 6.32) and (b,c) the presence of Cu^{2+} ions ((b) $R=16$ (pH 6.16) and (c) 8 (pH 6.09)).

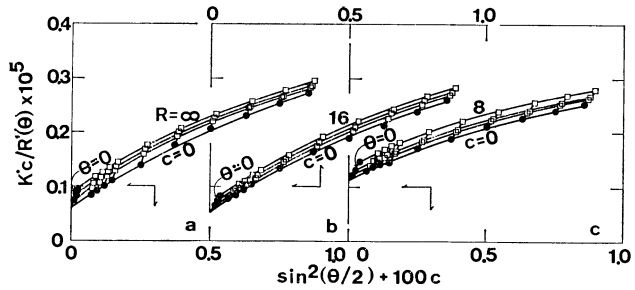

Fig. 6. The Zimm plots for poly(Glu) in 0.15 M NaCl solutions at low pH regions in (a) the absence (pH 4.28) and (b,c) the presence of Cu^{2+} ions ((b) $R=16$ (pH 4.34), and (c) 8 (pH 4.52)).

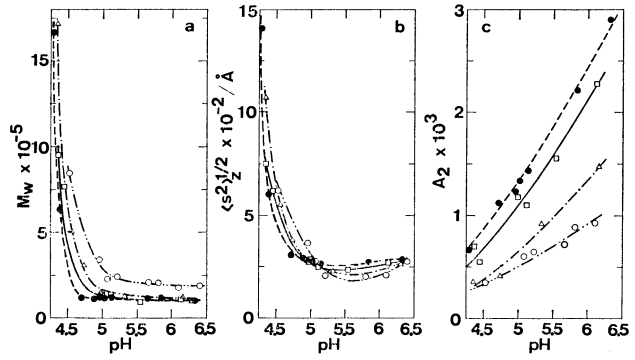

Fig. 7. The pH variation of (a) weight-averaged molecular weight, M_w, (b) z-averaged root-mean square of radius of gyration, $\langle s^2\rangle_z^{1/2}$, and (c) second virial coefficient, A_2, of poly(Glu) in the absence (--●--) and the presence ($R=32$ (—□—), 16 (—·△—·), and 8 (—··○—··)) of Cu^{2+} ions.

range. This may be mainly due to the large equilibrium constant of association[29] (noted later) of this system, in which the associated polymers hardly dissociate from each other with the decrease in the concentration. The value of A_2 was then determined by the slope of the linear region of the $\theta=0$ curve from the high concentration in the Zimm plot. The obtained values of M_w were 1.67×10^6, 1.72×10^6, and 8.47×10^5, while those of $\langle s^2\rangle_z^{1/2}$ were 1410, 1070, and 621 Å and those of $A_2\times10^3$ were 0.67, 0.36, and 0.35, at $R=\infty$, 16, and 8 respectively. In this pH range, the increment of M_w at any R shows that the aggregation of helices is induced by bound H^+ and Cu(II) ions.

pH Dependence of M_w, $\langle s^2\rangle_z^{1/2}$, and A_2. The values of M_w, $\langle s^2\rangle_z^{1/2}$, and A_2 thus determined at various R and pH values are plotted against the pH in Fig. 7. When the A_2, was not determined, the values of M_w and $\langle s^2\rangle_z^{1/2}$ were determined according to Eq. 27 with the light scattering data at one concentration and the interpolated A_2 value. Figure 7(a) shows the M_w *vs.* pH curves. The value of M_w is almost constant at pH values higher than 5.5 and at $R=\infty$ and 32. The M_w data in this region were averaged to 1.07×10^5, which was assumed to be the M_w of the unimer of poly(Glu), *i.e.*, M_1. The increment in M_w from this value means the aggregate formation. In the absence of Cu(II), the aggregation is formed rather drastically at pH values lower than 4.7, and the value of M_w increases to 1.67×10^6 at pH 4.28. With the addition of Cu(II) in a poly(Glu) solution, the starting pH of aggregate formation shifted to the high pH range at about 5, 6, and higher than 6.5 (not determined) at $R=32$, 16, and 8 respectively. The bound Cu(II) induces the aggregate formation of poly(Glu) at high pH values where the helix formation is imperfect. The M_w *vs.* pH curves at various R values seem finally to overlap with each other at some low pH value, because the Cu(II) dissociates from poly(Glu) with a lowering of the pH.[15]

Parallel with the M_w change, the variation in $\langle s^2\rangle_z^{1/2}$ with the pH is shown in Fig. 7(b). At $R=\infty$, the value of $\langle s^2\rangle_z^{1/2}$ decreases in the course of the transition from random coil to helix and then increases with the formation of helix and aggregation. In the presence of Cu^{2+} ions, $\langle s^2\rangle_z^{1/2}$ further decreases in the intermediate helix-coil transition region. The bound Cu(II) seems to induce the shrinking of the poly(Glu) conformation in the helix-coil region. In the low pH range, the value of $\langle s^2\rangle_z^{1/2}$ increases with further aggregate formation. The difference between the pH dependence of M_w and $\langle s^2\rangle_z^{1/2}$ at low pH values (in Figs. 7(a) and (b)) will be discussed later in relation to the aggregation scheme.

For the sample which has been dialyzed in equilibrium, the expression for A_2 is;

$$A_2=\frac{10^3}{2M_p^2}\left(\frac{Z^{*2}}{2m'}+\frac{\partial\ln\gamma_p^*}{\partial c}\right), \tag{29}$$

where Z^* is the number of charges on the polymer, γ_p^* is the activity coefficient of the polymer, and m' is the concentration of the salt (mol dm^{-3}) at equilibrium.[37] Since the A_2 is identical for the unimer and the multimer,[38,39] M_p in Eq. 29 can be regarded as M_1. When we assume that the first Donnan term in Eq. 29 mainly contributes to the A_2 value, the number of effective charges on a poly(Glu) unimer can be estimated to be 140—69, 130—61, 100—47, and 80—49, at $R=\infty$($\alpha\cdot=0.94$—0.24), 32 ($\alpha\cdot=0.80$—0 21), 16 ($\alpha\cdot=0.75$—0.15), and 8 ($\alpha\cdot=0.73$—0.15) respectively, where $\alpha\cdot$ is the degree of dissociation of Glu residues unbound by H^+ and Cu^{2+}.[15] The values of Z^* show a tendency to decrease with a lowering of the pH and are parallel with the $\alpha\cdot$. However, the Z^* values are 2 to 5 times smaller than the number of charges on a polymer, which were estimated by the degree of dissociation. This should show qualitatively that the charge-suppression effect by the salt-ion binding is included in the A_2 value and that the decrease in A_2 in Fig. 7(c) with a lowering of the pH and R should be a charge-neutralization effect caused by the binding of the Cu^{2+} and H^+ ions. However, the second term of Eq. 29 could not be determined by this study. Since it has been reported that the activity coefficient of poly(Glu) increases with the polymer concentration (positive second term in Eq. 29),[40] the real values of Z^* should be smaller than the values noted above.

The Equilibrium of the Aggregate Formation of Poly(Glu). With the data shown above, a more detailed discussion of the equilibrium of aggregation and its scheme can be given in combination with the theoretical treatment.

Since the M_w varies depending on the pH, Eq. 13 can be adopted for the analysis of the aggregation equilibrium. Since only two data of M_w at $R=\infty$ were available in the aggregation region, two simultaneous equations according to Eq. 17 were solved to determine the values of m and K''. The data of M_w at pH 4.28 and 4.38 give the number of H^+ ions, *i.e.*, m, to be 18.8 which should take part in the one-step association. With the aid of the value of C_0 ($=1.97\times10^{-6}$ mol of poly(Glu) unimer/dm^3), the log K'' can be estimated to be 87.9. This K'' value may be quite large but still reasonable, because the term of $((\gamma_{H^+}[H^+])^m)^{-1}$ contributes to this value, as may be seen in Eqs. 15 and 16. Since more than 62% of the Glu residues are discharged by H^+ binding at this pH,[15] the number of H^+ unbound Glu residues resting on a helix is less than 269 ($=(1-0.62)\times107000/151.1$). Thus, more than 3.5% ($=(18.8/2/269)\times100$) of the H^+ unbound Glu residues on a helix should be discharged by H^+ for the advance of the one-step association at pH 4.28—4.38. The contribution of Cu^{2+} ions to the aggregation, however, can not be estimated by this analysis, because the competitive binding between H^+ and Cu^{2+} ions to poly(Glu)[15] makes this analysis complicated. The attractive forces for the association of poly(Glu) may be hydrogen bonding between protonized carboxyl groups as in polymethacrylate,[41] intermolecular chelation by Cu(II), and hydrophobic interaction.

Aggregation Scheme, Side-by-side or Head-to-tail. Such an induction of aggregation by H^+ and Cu(II) binding suggests that helices associate in a side-by-side scheme, judging from the binding region of H^+ and Cu(II) on a helix. In order to determine whether the aggregation scheme is side-by-side or head-to-tail, $\langle s^2\rangle_z^{1/2}$ and M_w are correlated and the plots are fitted to the theoretical curves as shown in Fig. 8. Prior to this analysis, $\langle s_1^2\rangle^{1/2}$ should be assumed. The results of the viscosity study showed that the helix of poly(Glu) in 0.15 M NaCl is a slightly fat α-helix, with its long axis 640—1200 Å long (minor axis 10—18 Å),[19] in which the length of the α-helix of 1063 Å is included. In Fig. 8, the plots of $\langle s^2\rangle_z^{1/2}/\langle s_1^2\rangle^{1/2}$ *vs.* M_w/M_1, which were determined by means of the data at a helical content over 90%, are dispersed around the theoretical curves at $\sigma=0.7$—0.8 and $\sigma=0.9$—0.95, depending on the assumed helix types, with long axes of 640 (the upper group of points) and 1200 Å (the lower group of points) respectively, but irrespective of R. This shows that each helix in the multimer overlaps to each other in side-by-side, attached with a 70—95% length of a helix. This means that almost all of the bound Cu(II) is surrounded by helices of poly(Glu) in this case. Thus, it can form the characteristic complex with poly(Glu) ligands, as will be discussed later.

On the other hand, it is difficult to analyze the aggregation scheme in the helix-coil transition region with Eq. 24, because the conformation of the poly(Glu) unimer is not identical; it changes from a helix to not only a rather extended coil, but also to a compact coil, especially in the presence of Cu^{2+} ions, as has been shown above or in an subsequent viscosity study.[19]

However, in the helix-coil region, the increase in M_w is only 2—3 fold at most. Thus, the curve of $\langle s^2\rangle_z^{1/2}/\langle s_1^2\rangle^{1/2}$ *vs.* M_w/M_1 can be regarded as almost linear in the M_w/M_1 range of 1—3 as may be seen in Fig. 3. Since the curves of $\langle s^2\rangle_z^{1/2}/\langle s_1^2\rangle^{1/2}$ *vs.* M_w/M_1 for the aggregation of helices are also linear, as is shown in Fig. 2, the $\langle s^2\rangle_z^{1/2}/n$ value ($n=M_w/M_1$) was obtained; it should be a measure of the extension per poly(Glu) molecule.

The pH Dependence of $\langle s^2\rangle_z^{1/2}/n$ and the Complex Formation. Figure 9(a) shows the pH dependence of $\langle s^2\rangle_z^{1/2}/n$ at various values of R. In the absence of the Cu^{2+} ion and at around pH 5.5, poly(Glu) molecules shrink in the course of transition from a random coil to a helix, and at pH values lower than 4.7, they form the aggregate. Since the aggregate is of the side-by-side form, the $\langle s^2\rangle_z^{1/2}/n$ value does not increase additively with n; thus, $\langle s^2\rangle_z^{1/2}/n$ decreases with the low-

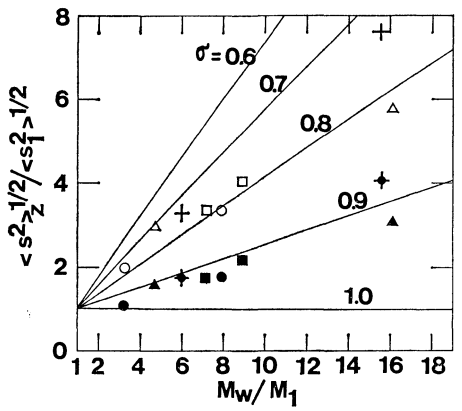

Fig. 8. The dependence of the observed data of $\langle s^2\rangle_z^{1/2}/\langle s_1^2\rangle^{1/2}$ on the values of M_w/M_1 of poly(Glu) at low pH region and at various R(∞ (crosses), 32 (squares), 16 (triangles), and 8 (circles)).
The $\langle s_1^2\rangle^{1/2}$ was assumed to be $640/\sqrt{12}$ Å (open symbols) or $1200/\sqrt{12}$ (filled symbols) Å. The solid lines are theoretical curves which were shown in Fig. 2(b).

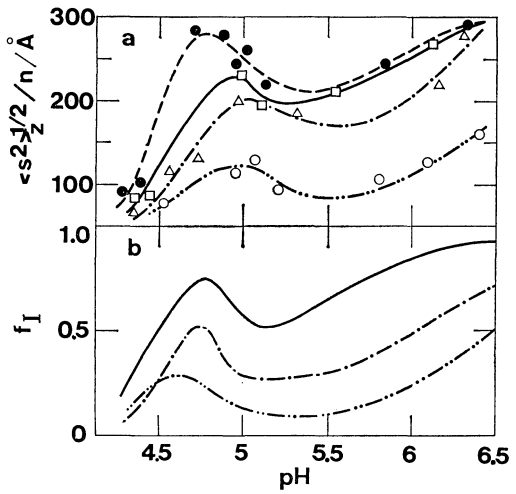

Fig. 9. The comparison of pH dependence of (a) root-mean-square radius of gyration divided by n, $\langle s^2\rangle_z^{1/2}/n$, and (b) the fraction of Complex I, f_I, from the Ref. 15: $R=\infty$ (--, ●), 32 (——, □), 16 (—·, △), and 8 (—··, ○).

ering of the pH because of one-sided increase in n. In the presence of Cu(II), $\langle s^2\rangle_z^{1/2}/n$ further decreases over the entire pH range. It seems that the bound Cu(II) induces the further shrinking of poly(Glu) and/or changes its conformation to a near-spherical type, whose model shows the small slope of the $\langle s^2\rangle_z^{1/2}/\langle s_1^2\rangle^{1/2}$ *vs.* n curve shown in Fig. 3.

It is interesting to compare the pH variation in $\langle s^2\rangle_z^{1/2}/n$ with that in the fraction of one of the three classes of poly(Glu)–Cu(II) complexes, *i.e.*, f_I (the fraction of Complex I in Ref. 15), which was clarified by the spectroscopic method.[15] The curves in both figures are almost parallel to each other. In the region where f_I decreases from 1.0 in Fig. 9(b), Complexes II and III are predominant instead of I in the pH ranges at around 5—5.5 and below 5 respectively.[15] This should show that Complex II appears when the poly(Glu) shrinks in the helix-coil intermediate transition region, while Complex III appears in parallel with the aggregate formation. The Cu(II) which is surrounded by the ligands of poly(Glu) in the intra- and inter-molecular fashions should form the chelates characteristic of its coordination field, *i.e.*, the species, number, and symmetry of the ligand field, like the complexes proposed in Ref. 15. The chelation is different from that of Complex I, in which Cu(II) seems to bind the extended coil or helix of poly(Glu). This interpretation is quite consistent with all our previously reported results.[11,13–15]

Conclusion

It was concluded that, in addition to the helix-coil transition, the conformation of poly(Glu) shrinks in the course of the helix-coil transition and forms an aggregate of helices in the low-pH range. The shrinking and the aggregate formation of poly(Glu) induce the chelation of Cu(II) to poly(Glu) residues in intra- and inter-molecular fashions, and *vice versa*. It is quite consistent that, in Complexes II and III, the Cu(II) binds to the side-chain carboxylate groups which are remote from, and independent of, each other on a single polymer strand or on different ones, as is shown by stoichiometric analysis.[15] Thus, this work further confirms our conclusions that the Cu(II) binds to the nearest-neighbor ligands on the extended coil or the helix portion of the polymer (Complex I), or that it binds to the ligands in the compact coil of poly(Glu)–Cu(II) (Complex II) while, in the low-pH range, Cu(II) binds to the ligands of the helical poly(Glu) in the multistranded aggregate (Complex III).[11,13–15]

The author would like to express his deep gratitude to Associate Professor Kiwamu Yamaoka of Hiroshima University for his helpful discussions and continuous encouragement in the course of this study.

A preliminary work (Light Scattering of Poly(Glu)–Cu(II) Solutions without Equilibrium Dialysis) was presented at the Annual Meeting of the Chemical Society of Japan in the Chugoku and Shikoku Areas (at Ube) in 1979.

References

1) A. L. Jacobson, *Biopolymers*, **1**, 269 (1963).
2) H. Takesada, H. Yamazaki, and A. Wada, *Biopolymers*, **4**, 713 (1966).
3) Y. Hibino and S. Sugai, *Rep. Prog. Polym. Phys. Jpn.*, **11**, 513 (1968).
4) H. Sigel and G. Blauer, *Helv. Chim. Acta*, **51**, 1246 (1968).
5) S. Yamashoji, H. Yoshida, and G. Kajimoto, *Yukagaku*, **25**, 128 (1976).
6) J. A. Marinsky, *Coord. Chem. Rev.*, **19**, 125 (1976).
7) O. Iwaki, K. Hikichi, M. Kaneko, S. Shimizu, and T. Maruyama, *Polym. J.*, **4**, 623 (1973).
8) M. Branca, M. E. Marini, and B. Pispisa, *Biopolymers*, **15**, 2219 (1976).
9) T. Hiraoki, A. Tsutsumi, K. Hikichi, and M. Kaneko, *Rep. Prog. Polym. Phys. Jpn.*, **19**, 527 (1976).
10) T. Hiraoki, M. Kaneko, and K. Hikichi, *Rep. Prog. Polym. Phys. Jpn.*, **21**, 525 (1978).
11) K. Yamaoka and T. Masujima, *Bull. Chem. Soc. Jpn.*, **52**, 1286 (1979).
12) T. Hiraoki, M. Kaneko, and K. Hikichi, *Polym. J.*, **11**, 397 (1979).
13) K. Yamaoka and T. Masujima, *Polym. J.*, **11**, 889 (1979).
14) S. Noji and K. Yamaoka, *Macromolecules*, **12**, 1110 (1979).
15) T. Masujima and K. Yamaoka, *Biopolymers*, **19**, 477 (1980).
16) N. Imai and J. A. Marinsky, *Macromolecules*, **13**, 275 (1980).
17) M. Koide and E. Tsuchida, *Makromol. Chem.*, **182**, 359 (1981).
18) M. Koide and E. Tsuchida, *Makromol. Chem.*, **182**, 367 (1981).
19) T. Masujima, K. Yamaoka, and J. Hori, *Bull. Chem. Soc. Jpn.*, **56**, (1983) in press.
20) Y. Tomimatsu, L. Vitello, and W. Gaffield, *Biopolymers*, **4**, 653 (1966).
21) R. B. Hawkins and A. Holzer, *Macromolecules*, **5**, 294, (1972).
22) W. H. Kulicke and R. Kniewske, *Macromol. Chem., Rapid Commun.*, **1**, 719 (1980).
23) R. F. Itzhaki and D. M. Gill, *Anal. Biochem.*, **9**, 401 (1964).
24) J. P. Kratohvil, G. Dezelic, M. Kerker, and E. Matijevic, *J. Polym. Sci.*, **57**, 59 (1962).
25) H. Utiyama and M. Kurata, *Bull. Inst. Chem. Res. Kyoto Univ.*, **42**, 128 (1964).
26) H. Utiyama, "Light Scattering From Polymer Solutions," ed by M. B. Huglin, Academic Press, London (1972), Chap. 4.
27) Y. Tomimatsu and K. J. Palmer, *J. Phys. Chem.*, **67**, 1720 (1963).
28) B. A. Brice, G. C. Nutting, and M. Halmer, *J. Am. Chem. Soc.*, **75**, 824 (1953).
29) H. G. Elias, "Light Scattering From Polymer Solutions," ed by M. B. Huglin, Academic Press, London (1972), Chap. 9.
30) A. G. Ogston and D. J. Winzor, *J. Phys. Chem.*, **79**, 2496 (1975).
31) E. T. Adams, Jr., *Biochemistry*, **4**, 1646 (1965).
32) P. Kratochvil, "Light Scattering From Polymer Solutions," ed by M. B. Huglin, Academic Press, London (1972), Chap. 7.
33) W. Heller, *J. Polym. Sci., Part A-2*, **4**, 209 (1966).

34) H. Noguchi and J. T. Yang, *Biopolymers*, **1**, 359 (1963).
35) B. H. Zimm, *J. Chem. Phys.*, **16**, 1099 (1948).
36) K. Yamaoka and K. Ueda, *J. Phys. Chem.*, **86**, 406 (1982).
37) M. Nakagaki and K. Ikeda, "Hikari Sanran Jikkenho," ed by M. Nakagaki and H. Inagaki, Nankodo, Tokyo (1965), Chap. 10.
38) H. Edelhoch, E. Katchalski, R. H. Mayburv, W. L. Hughes, Jr., and J. T. Edsall, *J. Am. Chem. Soc.*, **75**, 5058 (1953).
39) R. Townend and S. N. Timasheff, *J. Am. Chem. Soc.*, **82**, 3168 (1960).
40) M. Sugimura, T. Okubo, and N. Ise, *Polymer Preprints, Japan*, **31**, 654 (1982).
41) N. A. Kuznetsov, Z. A. Roganova, and A. L. Smolyanski, *Vysokomol. Soedin., Ser. A*, **20**, 791 (1978).

Pressure Effect on Transference Numbers for KCl in Ethanol–Water Mixtures at 25 °C

Masakatsu Ueno,* Shōgo I, and Kiyoshi Shimizu

Department of Applied Chemistry, Faculty of Engineering, Doshisha University, Karasuma Imadegawa, Kamigyo-ku, Kyoto 602

(Received May 6, 1982)

Cation transference numbers for 0.02 mol dm^{-3} KCl in 0-, 5-, 10-, 15-, 20-, and 30-mol% ethanol–water mixtures were determined by the moving boundary method at 25 °C up to 1500 kg cm^{-2} (1 kg cm^{-2}=0.9807×10^5 Pa). The cation transference number, t_+, initially increases with increasing ethanol content up to 10—15 mol% and then decreases at all the pressures studied. In water and ethanol–water mixtures below 20 mol%, t_+ at the definite solvent decreases with increasing pressure. The decreasing rate becomes smaller as the ethanol content increases, and the tendency is reversed finally at 30 mol%. To account for the variation of t_+ with solvent composition and pressure, specific interactions between the ions and solvent have been taken into consideration.

When we study ionic conductances, transference numbers are required to split electrolyte conductances into the ionic components without any assumptions. There have been several reports on the pressure effect on transference numbers in water,[1–6] but none in alcohol–water mixtures. Ionic conductances in alcohol–water mixtures are needed to elucidate the ionic transport process, in particular in relation to the liquid structure. Numerous properties of alcohol–water mixtures show a extremum in the water-rich region, which may be a reflection of increased solvent structure.[7] The solvent structure is also affected by pressure and temperature as well as by solvent composition.

In the previous paper,[8] conductances of potassium halides in water were measured at high pressure. Here, to provide a basis from which to investigate how the pressure dependence of ionic conductances of K^+, Cl^-, and other ions varies with the ethanol content in ethanol–water mixtures, we carried out the transference number measurements for KCl in the mixed solvents up to 30 mol% ethanol at 25 °C up to 1500 kg cm^{-2}. The results are compared with the Zwanzig dielectric friction theory,[9] which gives one important step to a more quantitative theory.

Experimental

Chemicals and Solutions. Ethanol of guaranteed reagent grade (Nakarai Chemical Co., Ltd.) was dried with Molecular Sieves (3A, Nakarai) and purified by distillation under a nitrogen atmosphere. Fractionally distilled ethanol had a density of 0.7853 g cm^{-3}, and showed a water content of 0.05 wt% in the Karl Fischer test. Its conductivity was less than 3×10^{-7} Ω^{-1} cm^{-1}. Conductivity water was prepared by passing distilled water through a mono-bed ion-exchange resin. Its conductivity was about 1.2×10^{-6} Ω^{-1} cm^{-1}. Potassium chloride salt of high purity was obtained from Merck and dried above 130 °C. Aqueous mixtures up to 30 mol% ethanol were prepared by weighing; the solutions of 0.02 mol dm^{-3} KCl were made by use of measuring flasks. The concentrations of the solutions at high pressure were corrected with the densities of the aqueous mixtures.[10,11]

Apparatus. Cation transference numbers at high pressure were determined by the moving boundary method with an autogenic-type cell equipped with a cadmium anode and a silver–silver chloride cathode, as shown in Fig. 1. The boundary movement was followed by measuring the change in resistance between platinum probe electrodes separated by 3 cm and sealed into 2 mm i.d. hard glass tube. The resistance was measured by a Yanagimoto MY8 type a.c. bridge. A constant current was supplied by a direct current stabilizer (Metronics 691B type), and measured periodically during electrolysis by potentiometric measurement (a Shimadzu digital potentiometer) of a potential drop across a 100-Ω standard resistor, connected in series with the moving boundary cell. The small current of 0.15 mA was used to minimize the effect of heat developed from electrolysis. A stop-watch was used to measure the time during which the current flowed.

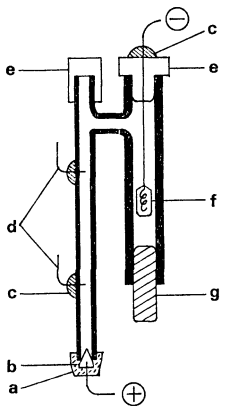

Fig. 1. High pressure autogenic cell for the measurement of the transference number.
a: DeKotinsky, b: cadmium anode, c: Araldite, d: probe electrode, e: Teflon cap, f: silver–silver chloride cathode, g: glass piston.

Conductivities of solvents and solutions were determined by using a syringe-type cell which is described elsewhere.[12]

Pressure generated by means of a hand pump was measured to ±3 kg cm^{-2} by a calibrated Bourdon gauge (Nagano Keiki Seisakusho, Ltd.). The oil pressure in the pressure vessel was transmitted to the solution by a glass piston of the syringe. The temperature of the oil bath in which the pressure vessel was immersed was kept constant at 25± 0.03 °C.

Determination of the Transference Number. The apparent cation transference number, t_+', can be calculated from the equation:[13]

$$t_+' = \frac{\Delta V C F}{i \Delta t}, \quad (1)$$

where ΔV is the volume (cm^3) swept out by the boundary

during time Δt (s) at i (mA) of current, C is the concentration of solution (mol dm^{-3}), and F is the Faraday constant. Considering the change in resistance between probe electrodes $\Delta R(\Omega)$ when the boundary moves upward, Eq. 1 can be transformed to the following equation:[1,5]

$$t_+' = \frac{VCF}{i(R_2-R_1)}\frac{\Delta R}{\Delta t}, \quad (2)$$

where V is the volume (cm^3) between the probe electrodes, and R_1 and R_2 are the resistances (Ω) when the uniform glass tube between the probe electrodes is occupied by KCl solution only and by $CdCl_2$ solution only, respectively. V was determined by calibration runs at 1 atm and 25 °C with 0.02 mol dm^{-3} KCl aqueous solution and by taking Longsworth's value of $t_+=0.4901$.[13] V's at high pressure were corrected with the compressibilities of Pyrex glass.[14] The variation of the resistance between the probe electrodes with time is shown in Fig. 2 for a typical run.

The transference number corrected for the solvent conductivity and volume change at the anode, t_+, is calculated from the following equation:[15]

$$t_+ = (t_+'-C\Delta\overline{V})\left(1+\frac{\kappa^\circ}{\kappa}\right). \quad (3)$$

Here,

$$\Delta\overline{V} = 0.5V^\phi(CdCl_2) - t_+V^\phi(KCl) - 0.5V_m(Cd), \quad (4)$$

and κ° and κ are the solvent and solution conductivities, and V^ϕ and V_m are the apparent molar volume and the molar volume, respectively. The volume correction term is small for dilute solution, so it was neglected.

Estimation of the Experimental Error. From Eq. 2, an estimate can be made of the magnitude of the error. The concentration may be affected through possible contamination with the high pressure system. The volume between probe electrodes, V, was determined within 0.1%. The error for the resistance measurements due to diffusion was about 0.08%. The variation of the current for a given run was within 0.01%. The slope of the resistance *versus* time curve had an error of about 0.05%, when approximately ten points were used for determining the slope. Considering these possible errors in the determined parameters, the transference number given by our measurements should be accurate within 0.3%.

Results and Discussion

Transference numbers obtained are listed in Table 1. The present results at 1 atm are compared with those by other workers.[16–19] As shown in Fig. 3, above 10 mol% our results are higher by 0.8% than those by Erdey-Grúz and Majthényi[16] and lower by 0.8% than those by Fratiello and Kay,[18] and Esteso and Grandoso.[19]

As can be seen in Fig. 4, t_+ has a maximum around 10—15 mol% at all the pressures studied. The solvent composition where t_+ exhibits a maximum slightly shifts to the ethanol-rich region with increasing pressure. In water and aqueous mixtures below 20 mol%, t_+ at the definite solvent decreases with increasing pressure. The decreasing rate becomes smaller as the ethanol content increases, and the tendency is reversed finally at 30 mol%. Since transference numbers for K^+ ion in KCl solutions are close to 0.5, there is very little concentration dependence.[20] In the present discussion, we assume that the variation of t_+ with solvent composition and pressure is equal to that at infinite dilution, t_+°.

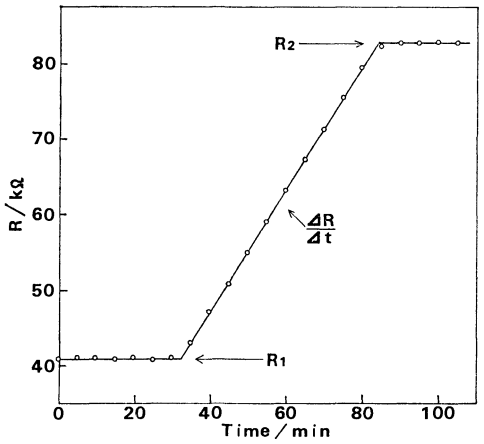

Fig. 2. A typical plot of resistance against time. 5 mol%, 25 °C, 500 kg cm^{-2}.

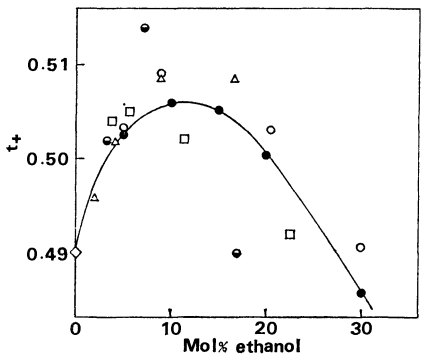

Fig. 3. Variation of the transference number for K^+ ion with mol% of ethanol at 1 atm and 25 °C.
●: Present work, □: Ref. 16, ◒: Ref. 17, ○: Ref. 18, △: Ref. 19, ◇: Ref. 13.

Table 1. Cation transference numbers for 0.02 mol dm^{-3} KCl in ethanol-water mixtures at 25 °C under pressure

p / kg cm^{-2}	Mol% of ethanol					
	0	5	10	15	20	30
1	0.4901[a]	0.5025(4)[b]	0.5060(7)	0.5052(6)	0.5004(5)	0.4856(5)
500	0.4859(5)	0.4983(8)	0.5034(4)	0.5034(5)	0.4992(8)	0.4869(7)
1000	0.4809(5)	0.4951(7)	0.5020(5)	0.5023(6)	0.4984(6)	0.4875(6)
1500	0.4785(5)	0.4918(5)	0.5001(6)	0.5014(7)	0.4979(7)	0.4889(7)

a) Ref. 13. b) The numbers in parentheses are 10^4 times the standard deviation of repeated runs.

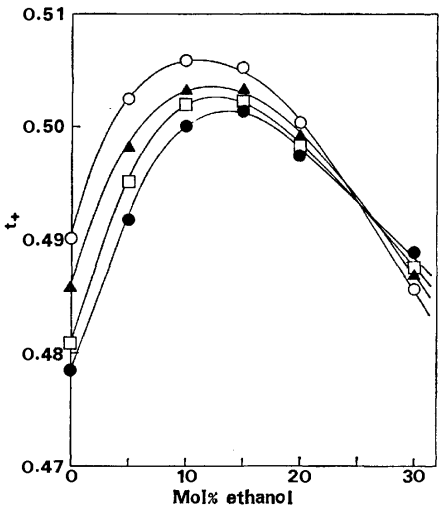

Fig. 4. Variation of the transference number for K^+ ion with mol% of ethanol at various pressures.
○: 1 atm, ▲: 500 kg cm^{-2}, □: 1000 kg cm^{-2}, ●: 1500 kg cm^{-2}.

To investigate the variation of the transference number with solvent composition, the experimental results are compared with the Zwanzig dielectric friction theory,[9] which is based on a continuum model for solvent. It is expressed by Eq. 5 for the slipping case:

$$\lambda_i^\circ = \frac{eF}{\eta(4\pi r_i + \phi r_i^{-3})}, \tag{5}$$

where,

$$\phi = \frac{3}{4}\left(\frac{e^2\tau}{\eta}\right)\frac{(\varepsilon_o - \varepsilon_\infty)}{\varepsilon_o(2\varepsilon_o + 1)}. \tag{6}$$

Here, λ_i°, r_i, e, η, τ, ε_o, and ε_∞ are the molar conductance of the monovalent ion at infinite dilution, the radius of the ion, the protonic charge, the solvent viscosity, the solvent dielectric relaxation time, the low and the infinite frequency dielectric constants, respectively. From the definition,

$$t_+^\circ = \frac{\lambda^\circ(K^+)}{\lambda^\circ(K^+) + \lambda^\circ(Cl^-)}. \tag{7}$$

Examination of Eqs. 5 and 7 shows that t_+° decreases with increasing ϕ, if r_i is taken to be the crystallographic radius of the ion.[21] By using the values of τ,[22] ε_o,[23] and η[24] at 0-, 20-, and 30-mol% at 1 atm, and with the assumption that ε_∞ is equal to that of water,[25] the calculated value of ϕ in Eq. 6 is shown to increase with increasing ethanol content. That is, t_+° should decrease with increasing ethanol content, which does not agree with the experimental results seen in Fig. 4. Kay *et al.*[26] also pointed out that the initial increase in ionic Walden products with ethanol content can not be explained qualitatively by the Zwanzig theory. Therefore, it is necessary to consider specific interactions between the ions and solvent.

As is reviewed by Franks and Ives,[7] the addition of ethanol to water initially increases the degree of structure of the solvent and then decreases it. From a wide variety of thermodynamic and transport data, both K^+ and Cl^- ions are classified as structure breakers in hydrogen-bonded solvents. If the structure-breaking effect of K^+ ion is larger than that of Cl^- ion, the structural excess mobility of K^+ ion is greater than that of Cl^- ion.[27] The effect is more pronounced in more highly structured solvents. Since the degree of structure of the aqueous mixtures is enhanced in the water-rich region containing up to about 10 mol%, the mobility of K^+ ion becomes progressively faster with respect to Cl^- ion. The initial increase in t_+ obtained with increasing ethanol content would be primarily ascribed to the relative structure-breaking properties of these two ions.

Zwanzig theory can not also account for the pressure dependence of the transference number in water. With the values of ε_o[28] and η,[29] and with the assumption that the pressure dependence of τ at 20 °C[30] is equal to that at 25 °C and ε_∞ is invariant under compression, ϕ in Eq. 6 is shown to decrease with increasing pressure. That is, t_+° in Eq. 7 should increase with increasing pressure, which is in contradiction to the experimental results.

To interpret the pressure dependence of the transference number in water, the effect of pressure to break the water structure may be taken into consideration.[4] As pressure weakens the hydrogen bonds and decreases the degree of structure of water, the structural excess mobility of K^+ ions may decrease relatively more than that of Cl^- ions with increasing pressure. Consequently, the cation transference number may decrease with increasing pressure. In the mixed solvents containing a small amount of ethanol, the decreasing rate of the cation transference number is expected to be larger than in pure water. However, this is not in conformity with the experimental results. Other specific interactions between the ions and solvent must be considered.

The orientation of solvent molecules around the negative ion, Cl^-, may be different from that around the positive ion, K^+. The ion-solvent interaction of K^+ ion is mostly dominated by the ion-dipole interaction, while that of Cl^- ion involves the additional contribution of hydrogen bonds.[31] The hydrogen bonds between water molecules and Cl^- ions may be broken down by pressure, and the degree of the hydration of Cl^- ion may decrease slightly with increasing pressure. The decrease of the cation transference number in water with increasing pressure was ascribed to this pressure effect.[5] Water molecules in alcohol-water mixtures are more basic than in pure water.[32] The contribution of hydrogen bonds between water molecules and Cl^- ion would be smaller in ethanol-water mixtures than in pure water. Therefore, the decreasing tendency of the cation transference number with pressure would become weaker with an increase in ethanol content. At 30 mol%, the specific interaction between water molecules and Cl^- ions would be insignificant.

Further conductivity measurements for KCl and various electrolytes at high pressure will reveal the ion-solvent interactions more thoroughly.

References

1) F. T. Wall and S. J. Gill, *J. Phys. Chem.*, **59**, 278 (1955),

2) F. T. Wall and J. Berkowitz, *J. Phys. Chem.*, **62**, 87 (1958).
3) G. J. Hills, P. J. Ovenden, and D. R. Whitehouse, *Discuss. Faraday Soc.*, **39**, 207 (1965).
4) R. L. Kay, K. S. Pribadi, and B. Watson, *J. Phys. Chem.*, **74**, 2724 (1970).
5) Y. Matsubara, K. Shimizu, and J. Osugi, *Nippon Kagaku Kaishi*, **1973**, 1817.
6) J. Osugi, M. Nakahara, Y. Matsubara, and K. Shimizu, *Rev. Phys. Chem. Jpn.*, **45**, 23 (1975).
7) F. Franks and D. J. G. Ives, *Quart. Rev. London*, **20**, 1 (1966).
8) K. Shimizu and N. Tsuchihashi, *Rev. Phys. Chem. Jpn.*, **49**, 18 (1979).
9) R. Zwanzig, *J. Chem. Phys.*, **52**, 3625 (1970).
10) G. S. Kell, "Water," ed by F. Franks, Plenum, New York (1972), Vol. 1, Chap. 10.
11) M. Yusa, G. P. Mathur, and R. A. Stager, *J. Chem. Eng. Data*, **22**, 32 (1977).
12) M. Ueno, M. Nakahara, and J. Osugi, *Rev. Phys. Chem. Jpn.*, **47**, 25 (1977).
13) D. A. MacIness and L. G. Longsworth, *Chem. Rev.*, **11**, 171 (1932).
14) L. H. Adams, *J. Am. Chem. Soc.*, **53**, 3769 (1931).
15) J. R. Gwyther, M. Spiro, R. L. Kay, and G. Marx, *J. Chem. Soc., Faraday Trans. 1*, **72**, 1419 (1976); J. R. Gwyther and M. Spiro, *ibid.*, **72**, 1410 (1976).
16) T. Erdey-Grúz and L. Majthényi, *Acta Chim. Hung.*, **20**, 73 (1959).
17) B. J. Yager and P. Y. Smith, *J. Chem. Eng. Data*, **17**, 446 (1972).
18) A. Fratiello and R. L. Kay, *J. Solution Chem.*, **3**, 857 (1974).
19) M. A. Esteso and D. M. Grandoso, *J. Chem. Eng. Data*, **25**, 398 (1980).
20) R. L. Kay and J. L. Dye, *Proc. Natl. Acad. Sci. U.S.A.*, **49**, 5 (1963).
21) L. Pauling, "The Nature of the Chemical Bond," 3rd ed, Cornell University, New York (1960), Chap. 13.
22) D. E. Buck, *U. S. Govt. Res. Develop. Rept.*, **40**, 59 (1965).
23) G. Åkerlöf, *J. Am. Chem. Soc.*, **54**, 4125 (1932).
24) R. L. Kay and T. L. Broadwater, *J. Solution Chem.*, **5**, 57 (1976).
25) J. B. Hasted, "Water," ed by F. Franks, Plenum, New York (1972), Vol. 1, Chap. 7.
26) R. L. Kay, G. P. Cunningham, and D. F. Evans, "Hydrogen-Bonded Solvent Systems," ed by A. K. Convington and P. Jones, Taylor and Francis Ltd., London (1968), pp. 249—260.
27) R. L. Kay and G. A. Vidulich, *J. Phys. Chem.*, **74**, 2718 (1974).
28) K. R. Srinivasan and R. L. Kay, *J. Chem. Phys.*, **60**, 3645 (1974).
29) J. B. Cappi, Ph. D. Thesis, London University (1964); K. E. Bett and J. B. Cappi, *Nature*, **207**, 620 (1965).
30) R. Pottel and E. Asselborn, *Ber. Bunsenges. Phys. Chem.*, **83**, 29 (1979).
31) M. Nakahara, K. Shimizu, and J. Osugi, *Nippon Kagaku Zasshi*, **92**, 785 (1971).
32) D. Feakins, "Physico-Chemical Processes in Mixed Aqueous Solvents," ed by F. Franks, Heinemann Educational Books Ltd., London (1967), pp. 71—90.

Electronic Structure and Spectra of Organic Dye Anions of Uranine and Eosin Y

Koichi HIRANO

Department of Chemistry, Miyagi University of Education, Aramaki-aoba, Sendai 980

(Received May 14, 1982)

The excited states of the organic dye anions of Uranine and Eosin Y are invesitigated by the semi-empirical SCF-MO-CI calculations. The two-center core integral values of the C–Br bond (−0.20 eV) were determined. Agreement between the calculated and observed spectra was satisfactory. The first intense bands of these dye anions can be assigned to the HOMO→LUMO transition band arising from the local excitation of xanthene ring. The second bands are interpreted as the overlap of the two transition bands for the xanthene ring and for the residual π-systems.

Because of the interest in the metachromatic changes exhibited by many dye ions,[1–5] we have made experimental studies on the solvato-chromic effects of several xanthene dyes.[6] We analyzed the solvent effects on the Eosin Y spectra using the modified McRae's theory,[7] and determined separately the values of the dispersion shift and the hydrogen bond shift.[8] In addition, an attempt was made to estimate the electrostatic shifts for Eosin Y anion by means of Hückel MO perturbation theory.[9] It was concluded that quantitative knowledge about the electronic transitions of the solute dye ions is needed to obtain a deeper understanding of the solvato-chromic effects. For xanthene dyes including Uranine and Eosin Y, however, very little is known about the nature of the electronic transitions.

The main aim of this invesitigation is to gain information about the electronic transitions of Uranine and Eosin Y anions. For this purpose, the lower excited states of the anions of Uranine ($URAN^{2-}$) and Eosin Y ($EOSY^{2-}$) were invesitigated using semi-empirical SCF-MO-CI calculations.

Theoretical

Methods and Models. The Pariser-Parr-pople type of SCF-MO calculations[10,11] with limited D–CI were employed. In these calculations, singly-excited configurations higher than the ground configuration by 10 eV, and doubly-excited configurations higher than the ground configuration by 18—25 eV, were taken into account. The equal charge sharing models (see Fig. 1), in which a formal negative charge is equally shared between the two oxygen atoms O (24) and O(25), were considered for each of the anions. The attached benzene ring with a carboxy group cannot rotate freely around the C(14)–C(15) linkage, because of its steric hindrance.[12] We determined the dihedral angle to be $\theta=73°$ from the sum of the van der Waals radi of C(3) and C(23).[13] The molecular geometry used were assumed as follows: All bond angles equal to 120° and C(14)–C(15)=1.51,[14] C(21)–C(22)=1.24, C(21)–C(23)=1.24,[15] C(5)–O(24)=1.26, C(10)–O(25)=1.26,[16] C(3)–Br(26)=1.89,[17,18] C(6)–O(7)=1.39, and aromatic C–C bond lengths equal to 1.39 Å.

Parametrization. One-center-core and repulsion integrals W's, γ_{rr}'s were evaluated from the valence state ionization potentials and electron affinities. Two-center-core integrals, β_{rs}'s were calculated by the Wolfsberg-Helmholtz's formula.[19] Taking account of the rotation of the benzene ring, the two-center core integral for the C(14)–C(15) bond was formulated by Eq. 1;

$$\beta_{14,15} = \frac{K}{2} S_{14,15}(\theta=0°)\{W_{14}+W_{15}\}\cos\theta, \qquad (1)$$

where, θ is the dihedral angle, $S_{14,15}$ the overlap integral between C(14) and C(15), and K a constant taken to be 0.96 when β_{CC} in benzene is −2.39 eV. For the carbonyl and carboxy oxygen, $W_O^{-1/2}$ is taken as the arithmetic mean of W_O and $W_{O(-)}$; $W_{O(-)}$ is determined by a method identical with that previously reported by Nishimoto and Förster.[20] The two-center-repulsion integrals γ_{rs} were evaluated by the Nishimoto-Mataga's formula.[21] In the present calculations, the Br atom is assumed to participate in the pi-electronic system with a 4p lone electron-pair.

However, we have no available parameters for the atom, so we determined that parameter by following procedure. A one-center-core integral W_{Br} is estimated from the second ionization potential of the free Br atom.[22] The one-center-repulsion integral, γ_{BrBr}, and the effective nuclear charge, Z_{eff}, were evaluated by Morita-Dewer's formula.[23] The two-

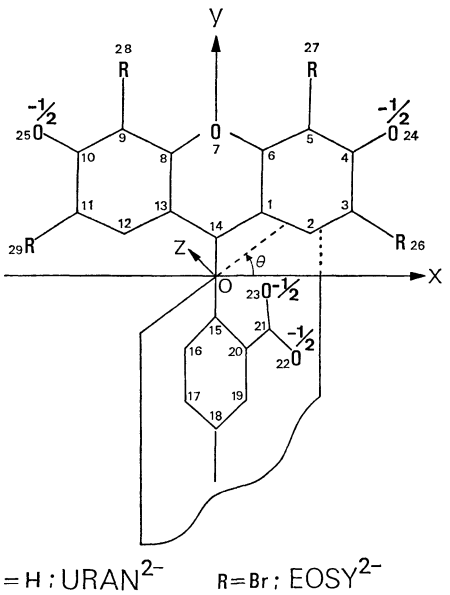

Fig. 1. Nuclear skelton and coordinate of an equal charge sharing model of $URAN^{2-}$ and $EOSY^{2-}$ anions. Dihedral angle θ is measured clockwise from the plane of the xanthene ring.

Table 1. Parameters

Core	W_{rr}/eV[a]	$\langle rr\|rr\rangle$/eV[b]	Q_r[c]	Z_r^{eff} [d]	A_r/Å[e]
C^+	11.22	10.06	1.00	3.25	1.358
O^+	17.70	15.23	1.00	4.08	0.9453
O^{2+}	33.90	18.93	2.00	5.65	0.7606
$O^{-1/2}$	17.70	15.23	1.00	4.08	0.9453
$O^{(-)}$	17.70	15.23	1.00	4.08	0.9453
Br^{2+}	21.60	13.80	2.00	4.21	1.043

a) W_{rr}: Valence-state ionization potential. b) $\langle rr|rr\rangle$: One-center repulsion integral. c) Q_r: Core charges on atom r. d) Z_r^{eff}: Effective nuclear charge. e) A_r: $A_r=14.398/\langle rr|rr\rangle$ (Å).

center-core integral, β_{CBr}, was regarded as a parameter. Preliminary calculations were made by changing β_{CBr}, from -0.1 to -1.0 eV; an appropriate value of this parameter was determined as $\beta_{CBr}=-0.2$ eV. This value is lower than that estimated for 3-bromophenanthrenquinone molecule by Kuboyama *et al.*[24] A major source of this difference is that in negative ions, the pi-electrons are much more weakly bound and the spatial distribution of the electrons is more diffuse.[25,26]

Subsequently the correct β_{CBr} would be lower in magnitude than that estimated from a Slater type 4p orbital. The parameters finally employed were listed in Table 1.

Experimental

Uranine and Eosin Y obtained commercially were purified in the manner described previouly.[6] Wako Junyaku, Spectro grade, acetonitrile was used without further purification.

Visible and ultraviolet absorption spectra were measured on a Shimadzu UV200-S spectrophotometer. All the measurements were carried out at 25.0 °C.

Results and Discussion

Characteristics of Molecular Orbitals. The SCF-MO energy levels considered in CI calculation are illustrated in Fig. 2. One of interesting features found in the energy-level diagrams is that the HOMO of $URAN^{2-}$ is localized on C=O, whereas that of $EOSY^{2-}$ is localized both on C=O and Br. This indicates that in $EOSY^{2-}$ C=O and Br make dominant contributions to the lower energy excitations arising from the HOMO to the appropriate unoccupied MO's.

Another feature found in the energy diagram for $EOSY^{2-}$ is that the four new levels that originated from the 4p Br orbitals are closely located just below the HOMO level, so that the HOMO level is slightly destabilized. This orbital energy destabilization produces a red shift in the lowest energy absorption band of $EOSY^{2-}$ in comparison with that of $URAN^{2-}$.

Transition Energies and Oscillator Strengths. The calculated and experimental transition energies and oscillator strengths were shown in Table 2, where the calculations without D-CI are also shown for the sake of comparision. Agreement between the calculated and experimental values is satisfactory, excepting the oscillator strength for the lowest transitions of both

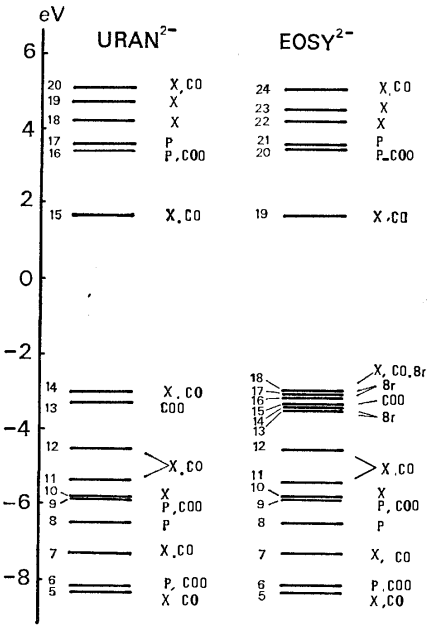

Fig. 2. MO energy-level diagrams for $URAN^{2-}$ and $EOSY^{2-}$, together with the orbital character. Symbol P and X designate the MO of phenyl and xanthene groups, respectively.

dye anions. As is shown in the table, the D-CI procedure does not always reduce the value of oscillator strengths, but it does enhance that value. This unexpected result may be partly ascribable to the fact that in our calculations, the number of doubly-excited configurations is not sufficiently large.

MO Coefficient Diagrams. The ground and excited state functions Ψ_J ($J=0$, $a,b,c,..$) are listed in Table 3. In the table, the configurations whose weight of mixing is larger than 2.0%, are given. On the basis of the main terms of the ground state functions, the MO coefficient diagrams associated with the excitations $\Psi_{t\to m}$'s$\leftarrow\Psi_G$ can be constructed from the one electron molecular orbitals of ϕ_t and ϕ_m as is shown in Figs. 3—4.

Electronic Spectra of $URAN^{2-}$. The calculated and observed spectrum of an acetonitrile solution of $URAN^{2-}$ are shown in Fig. 5. In the absorption spectrum of an acetonitrile solution of $URAN^{2-}$, we can see four π—π^* transition bands at 19.5, 32.5, 37.2, and 43.9×10^3 cm^{-1}. The additional tail at lower energy side ($22—23\times10^3$ cm^{-1}) may be ascribed to the singly ionized species.[27] The first high intensity visible band (1) is assigned to the transition $\Psi_a\leftarrow\Psi_0$, designated by line (a), which is mainly contributed by a HOMO→LUMO transition arising from the local excitation of xanthene ring (Fig. 3). The second weaker band (2), is regarded as the overlap of the two different types of transitions $\Psi_b\leftarrow\Psi_0$ and $\Psi_c\leftarrow\Psi_0$, denoted by (b) and (c): $\Psi_b\leftarrow\Psi_0$ Originates from the excitation of the attached benzene ring with carboxy group, whereas $\Psi_c\leftarrow\Psi_0$ originates from the excitation of the xanthene ring (Fig. 3). The third band (3) may be regarded as the superposition of the two transitions (d) and (e), although this assignment may not be unique. The predicted polarization direc-

Table 2. Transition energies ($\Delta E(10^3\,cm^{-1})$), oscillator strengths (f) and polarization($\phi°$)

URAN^{2-}

Transition	S-CI			D-CI			Obsd	
	ΔE	f [a]	ϕ [b]	ΔE	f [a]	ϕ [b]	ΔE	f
a	22.3	1.642	1.6	22.3	1.655	1.7	19.5	0.251
b	30.9	0.065	−72	31.1	0.065	−72		
c	33.0	0.172	−87	33.2	0.172	−87	32.5	0.081
d	36.1	0.361	−83	36.3	0.363	−83		
e	38.1	0.136	56	37.3	0.132	71	37.2	0.092
f	48.2	0.096	−31	48.4	0.097	31	43.9	0.670

EOSY^{2-}

Transition	S-CI			D-Cl			Obsd	
	ΔE	f [a]	ϕ [b]	ΔE	f [a]	ϕ [b]	ΔE	f
a	20.6	1.130	0.73	20.2	1.360	1.6	18.9 19.3[c]	0.427
b	20.9	0.300	3.2					
c	21.9	0.070	−0.14	22.0	0.069	−7.9		
d	23.1	0.079	−8.0	23.2	0.082	−6.1		
e	30.9	0.064	−72	31.3	0.065	−72	31.2	0.144
f	32.8	0.132	−88	32.9	0.118	−88		
g	34.2	0.113	−90	33.9	0.132	−85		
h	36.2	0.165	90	36.3	0.146	85	38.2	0.294
i				44.1	0.141	86	41.2	0.765

a) Oscillator strength greater than 0.05. b) The polarization vector is projected along the z-axis and angle ϕ was taken in a right-handed sense against the x-axis. c) For gaseous EOSY^{2-} determined from the spectral solvent effects.[3]

Table 3. Ground and excited wave functions of URAN^{2-} and EOSY^{2-}

URAN^{2-}	EOSY^{2-}
$\Psi_0=0.999\Psi_G$ [a] $+\cdots$	$\Psi_0=0.999\Psi_G+\cdots$
$\Psi_a=0.985\Psi_{14\to15}+\cdots$	$\Psi_a=0.951\Psi_{18\to19}+0.206\Psi_{17\to19}+\cdots$
$\Psi_b=0.988\Psi_{13\to16}+\cdots$	$\Psi_c=0.981\Psi_{14\to19}+0.137\Psi_{16\to19}+\cdots$
$\Psi_c=0.880\Psi_{12\to15}-0.272\Psi_{14\to18}+\cdots$	$\Psi_d=0.991\Psi_{13\to19}+\cdots$
$\Psi_d=0.837\Psi_{14\to18}+0.345\Psi_{11\to15}-0.275\Psi_{10\to15}+\cdots$	$\Psi_e=0.989\Psi_{15\to20}+\cdots$
$\Psi_e=-0.661\Psi_{14\to19}+0.646\Psi_{10\to15}-0.255\Psi_{14\to18}+\cdots$	$\Psi_f=0.829\Psi_{12\to19}-0.320\Psi_{18\to24}+\cdots$
$\Psi_f=0.901\Psi_{12\to18}+0.362\Psi_{14\to19}+\cdots$	$\Psi_g=0.783\Psi_{11\to19}-0.453\Psi_{12\to19}-0.342\Psi_{18\to22}+\cdots$
$\Psi_g=0.862\Psi_{9\to16}-0.395\Psi_{8\to17}-\cdots$	$\Psi_h=-0.568\Psi_{18\to23}-0.510\Psi_{18\to22}+0.280\Psi_{14\to22}-0.255\Psi_{16\to22}+\cdots$
	$\Psi_i=0.853\Psi_{9\to19}-0.254\Psi_{17\to22}+\cdots$
	$\Psi_j=0.585\Psi_{17\to22}-0.499\Psi_{16\to23}+0.351\Psi_{13\to21}+\cdots$

a) G: Ground configuration.

tion of transition (*a*) is along the x-axis and those of (*b*) and (*c*) are along the y-axis. This agree well with the prediction based on the fluorescence polarization measurements.[28]

Electronic Spectra of EOSY^{2-}. The absorption spectra of acetonitrile solution of EOSY^{2-} and URAN^{2-} generally resemble (Figs. 5, 6): There are four π—π^* transition bands at 18.9, 31.2, 38.2, and 41.2×10^3 cm^{-1} (Fig. 6). The first intense band (1) shows a small red shift in comparision with the corresponding band of URAN^{2-}. This is interpreted in terms of orbital destabilization due to the substituent effect with bromine. This band is assigned to the transition $\Psi_a\leftarrow\Psi_0$ mainly contributed by a HOMO→LUMO transition, arizing from the local excitation of the xanthene ring. A chracteristic feature of this transition is that on going from Ψ_0 to Ψ_a, a substantial amount of charge transfer from the carbonyl oxygen ($-0.127e$) and from the bromine substituents ($-0.229e$) into the xanthene ring, especially the central carbon atom C(14), the latter being primary (Fig. 4). The second weaker band (2) is regarded as the overlap of the transitions $\Psi_e\leftarrow\Psi_0$ and $\Psi_f\leftarrow\Psi_0$ denoted by (*e*) and (*f*). Transition $\Psi_e\leftarrow\Psi_0$ has almost the same nature as that of $\Psi_b\leftarrow\Psi_0$ for URAN^{2-} which has been already been described. Transition $\Psi_f\leftarrow\Psi_0$, however, is somewhat different in nature from that of $\Psi_c\leftarrow\Psi_0$ for URAN^{2-}: On going from Ψ_0 to Ψ_f, the charge tend to move away from the xanthene ring to the carbonyl oxygen (Fig. 4). The third band (3) may be assigned to the superposition of the transitions (*g*) and (*h*), however, the fourth band (4) cannot be assigned to the calculated transitions.

Neither the transition energies nor the oscillator

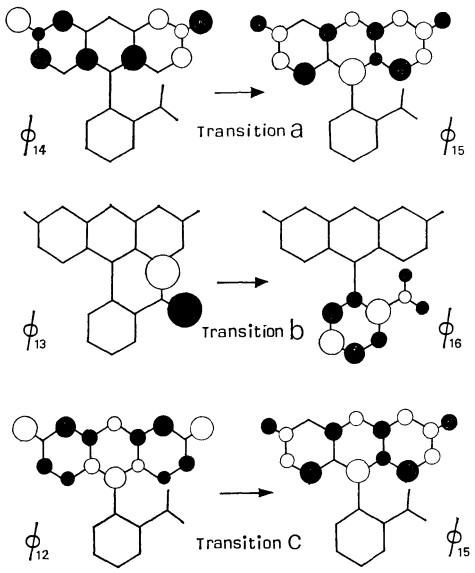

Fig. 3. Schematic representation of MO coefficients for $URAN^{2-}$ associated with three lowest excitations.

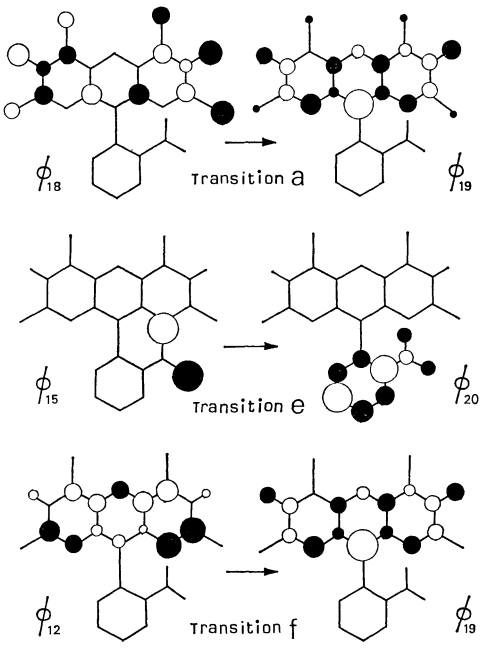

Fig. 4. Schematic representation of MO coefficients for $EOSY^{2-}$ associated with three lowest excitations.

strengths were affected by changes of the dihedral angle θ. This is consistent with the transitional characteristics of these dye anions.

We wish to express our hearty thanks to the members of the Computer Center Tohoku University for their kind cooperations and advice. This work supported in part by a scientific Research Grant from the Ministry of Education, Science and Culture, Japan (No. 538029).

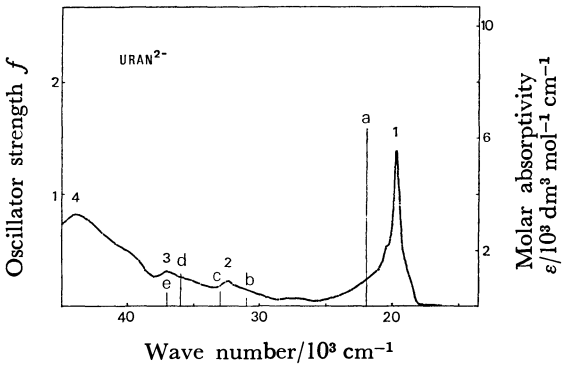

Fig. 5. Absorption spectrum of $URAN^{2-}$ in acetonitrile solution at 25.0 °C; 1.14×10^{-5} mol dm^{-3}.
The vertical lines represent the calculated transition energies and oscillator strengths greater than 0.05.

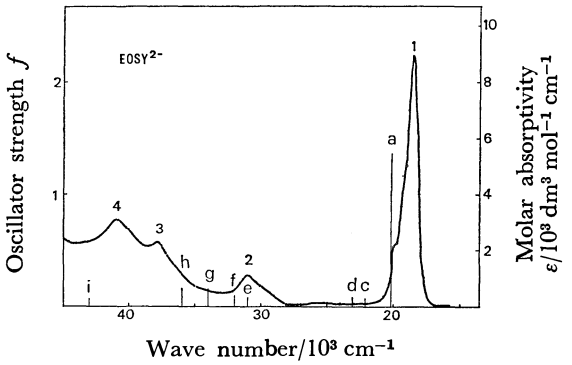

Fig. 6. Absorption spectrum of $EOSY^{2-}$ in acetonitrile solution at 25 °C; 1.49×10^{-5} mol dm^{-3}.
The vertical lines represent the calculated transition energies and oscillator strengths greater than 0.05.

References

1) P. Ehrlich, *Arch. Mikroskop. Anat. Entwick.*, **1877**, 13.
2) L. Michaelis and S. Granick, *J. Am. Chem. Soc.*, **67**, 1212 (1945).
3) H. Terayama, *Kagaku No Ryoiki*, **1**, 17 (1947).
4) M. Koizumi and N. Mataga, *J. Am. Chem. Soc.*, **75**, 483 (1953).
5) K. Hirano, *Biophysics (Seibutu-Buturi)*, **19**, 38 (1979).
6) K. Hirano, *Nippon Kagaku Kaishi*, **1974**, 1823.
7) K. Hirano, *Nippon Kagaku Kaishi*, **1978**, 481.
8) K. Hirano, *Nippon Kagaku Kaishi*, **1980**, 675.
9) K. Hirano, *Nippon Kagaku Kaishi*, **1976**, 361.
10) R. Pariser and R. G. Parr, *J. Chem. Phys.*, **21**, 446 (1953).
11) J. A. Pople, *Trans. Faraday Soc.*, **49**, 1375 (1953).
12) S. E. Sheppard, *Rev. Mod. Phys.*, **14**, 317 (1942).
13) J. Silverman and N. F. Yannori, *J. Chem. Soc., B*, **1967**, 194.
14) H. Suzuki, *Bull. Chem. Soc. Jpn.*, **32**, 1340 (1959).
15) J. M. Skinner, G. M. D. Stewart, and J. C. Speakman, *J. Chem. Soc.*, **1954**, 180.
16) The bond length of C=O's were estimated from the SCF pi-bond order, according to C. A. Coulson, *Proc. R. Soc. London, Ser. A*, **169**, 413 (1939).
17) T. Sato. M. Shiro, and H. Koyama, *J. Chem. Soc., B*, **1962**, 935.
18) M. Tabata, Y. Takada, and A. Suzuki, *Chem. Lett.*, **1972**, 1092.

19) M. Wolfsberg and L. Helmholtz, *J. Chem., Phys.*, **20**, 837 (1952).
20) K. Nishimoto and L. Förster, *J. Phys. Chem.*, **72**, 914 (1968).
21) N. Mataga and K. Nishimoto, *Z. Phsik. Chem. Neue Folge*, **13**, 140 (1957).
22) C. E. Moor, "Atomic Energy Levels," National Burau of Standers, Washington (1949), Circ. No. 467, Vol. I—III.
23) M. J. S. Dewer and T. Morita, *J. Am. Chem. Soc.*, **91**, 796 (1969).
24) A. Kuboyama, F. Kobayashi, and S. Morokuma, *Bull. Chem. Soc. Jpn.*, **48**, 1245 (1975).
25) H. Tsubomura and S. Sunakawa, *Bull. Chem. Soc. Jpn.*, **40**, 2463 (1967).
26) A. H. Zimmerman, R. Gygax, and J. I. Brauman, *J. Am. Chem. Soc.*, **78**, 5595 (1978).
27) F. M. Abdel-Halim, R. M. ISSA, M. S. El-Ezaby, and A. A. Hasein, *Z. Phys. Chem. Neue Folge*, **73**, 50 (1970).
28) A. Wrazeesinska, *Acta Physik. Polan.*, **4**, 486 (1935).

The Adsorption of Tetramethylurea at the Mercury/Water Interface

Osamu IKEDA,* Hiroyuki JIMBO, and Hideo TAMURA

Department of Applied Chemistry, Faculty of Engineering, Osaka University, 2-1 Yamadaoka, Suita, Osaka 565

(Received June 1, 1982)

The adsorption of tetramethylurea (TMU) at the mercury/water interface was studied by means of differential capacity measurements. TMU was found to take three different orientations, depending on the surface excess and the charge sign of the electrode. These orientations could not be explained simply by the orientation of the TMU dipole in the electric field or by the hydrophobic interaction between the methyl groups of TMU and the electrode, but it was explained on the basis of interactions between TMU and water molecules, and on the basis of the TMU molecules themselves in the adsorption layer and an electronic polarization effect of the nitrogen atoms in TMU. A few water-adsorption models were compared in an attempt to estimate the dipole moment of the TMU molecule at the interface.

It has been shown in a recent paper[1] that tetramethylthiourea (TMTU) at the mercury/aqueous solution interface takes a vertical orientation with the sulfur atom on the electrode, in a manner similar to thiourea.[2] Such an orientation was explained on the basis of the hydrophobicity of the sulfur atom and the high electronic polarizability of the >C=S bond. In order to make these points clearer, it is desirable to study the adsorption behavior of tetramethylurea (TMU), in which the sulfur atom of tetramethylthiourea (TMTU) is displaced by the oxygen atom with a lower electronic polarizability and a higher hydrophilicity, compared to that of the sulfur atom. It is also interesting to see how the dipole moment of TMU, lower than those of other ureas,[3] is reflected in the adsorption behavior.

The adsorption behavior of organic compounds at the mercury/aqueous solution interface[4] is usually elucidated by a determination of the adsorption isotherm and by the change in the potential drop across the inner layer, $\Delta_2^M\phi$, due to adsorption. In the case of organic compounds with a polar group, a somewhat accurate orientation can be estimated from the change in $\Delta_2^M\phi$ due to adsorption. It has seldom been tried, however, to estimate the dipole moment of an adsorbed molecule because of the uncertainty in the potential drop due to adsorbed water dipoles, Δg^w_{dipole}. Parsons and his co-workers[5] first evaluated the dipole moment of an urea molecule at the mercury/water interface after the establishment of the water-adsorption model.[6] Studies along this direction seem to be important for a better understanding of the double-layer structure and property, and of their effects on the electrode kinetics.

The accurate evaluation of the dipole moment of an adsorbed molecule demands an accurate Δg^w_{dipole} as a function of the electric field. Several water-adsorption models[7] have been proposed, along with Δg^w_{dipole} as a function of the surface charge density. Aside from the idea contained in each model, however, the agreement in the values of Δg^w_{dipole} is not so good among models. In this study, the Bockris-Habib (B-H) model,[8] the "experimental" model by Trasatti (T-model),[9] and the Damaskin-Frumkin (D-F) model[10] were taken up and compared in the evaluation of the dipole moment of an adsorbed TMU molecule.

Experimental

An analytical reagent grade of tetramethylurea (TMU) was used, it was vacuum-distilled twice before use. The sodium fluoride was of a high-purity reagent grade (Merck, ultrapure) and was used without further purification. The water and mercury were triply distilled before use. Nitrogen deoxygenated by passing it through copper meshes heated to 400 °C was used for deaeration and then blown over the solution. An aqueous 0.5 M NaF solution (1 M=1 mol dm^{-3}) was used as the supporting electrolyte. Eleven different concentrations of TMU were prepared to cover 2×10^{-3} M and 1×10^{-1} M.

The differential capacity, C, was measured at 25±0.1 °C using a dropping mercury electrode and by a method similar to that of Hills and Payne.[11] The measurement was carried out at 7.2 s after the birth of a mercury drop whose total life was about 13 s in pure 0.5 M NaF and at several frequencies, f, with an amplitude of 5 mV. The equilibrium capacities were obtained by extrapolating the linear relation of C against $f^{1/2}$ at a constant potential to $f=0$. A vertical capillary as the test electrode was prepared by drawing a Pyrex glass tube and was siliconed on the internal wall by passing through a vapor of dimethyldichlorosilane for several seconds. A KCl-saturated calomel electrode (SCE) and a cylindrical platinum plate, with a mercury drop at the center, were used as the reference and the counter electrode respectively. The mercury height from the reservior to the capillary tip was 1.4 m. The flow rate of mercury was determined by weighing mercury recovered during a given time.

The potential of zero charge, E_z was measured using a streaming electrode,[12] while the interfacial tension at the E_z, γ_z was measured by the maximum bubble pressure method following Schiffrin.[13] Most of the parameters essential to the analysis of the adsorption were derived by the double integration of the equilibrium capacity-potential curves using a computer program.

No corrections for the medium effects[14,15] on the activity of the supporting electrolyte or for the activity coefficient of the adsorbate[16] were taken into consideration.

Results and Discussion

Differential Capacity-potential Curves. Figure 1 shows the equilibrium differential capacity-potential curves measured with several concentrations of TMU. Two adsorption-desorption peaks are observed, but the shape of the peak at more negative potentials becomes higher and narrower than that at more positive po-

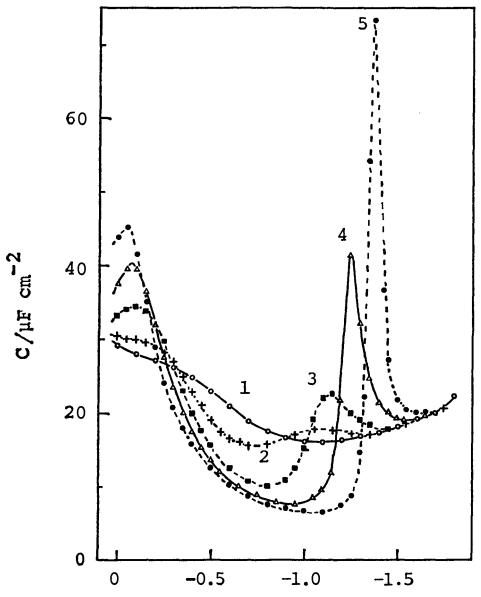

Fig. 1. Differential capacity-potential curves (extrapolated to zero frequency) of the mercury electrode in 0.5 M aqueous NaF solutions containing TMU at 25 °C.
Concentration of TMU (mM): (1) 0 (base solution, 0.5 M NaF), (2) 5, (3) 20, (4) 50, and (5) 100.

TABLE 1. DATA OF E_z AND γ_z

C_{TMU} / mol l^{-1}	E_z vs. SCE / V	γ_z / mN m^{-1}
0 (0.5 M NaF)	−0.432	426.8
0.002	−0.418	426.3
0.003	−0.412	426.0
0.005	−0.401	425·3
0.007	−0.392	424.8
0.010	−0.379	423.5
0.015	−0.362	422.4
0.020	−0.347	421.4
0.030	−0.324	419.5
0.050	−0.296	416.6
0.070	−0.278	414.4
0.100	−0.259	412.2

tentials with an increase in the concentration of TMU. This suggests that the attractive interaction among adsorbed molecules at more negative potentials is stronger than that at more positive potentials.[17]

Data of E_z and γ_z. Table 1 summarizes the data of E_z and γ_z. Positive shift of E_z with an increase in the concentration of TMU, C_{TMU}, was observed, as opposed to the negative shift of E_z in TMTU.[1] The orientation of TMU at E_z is expected to differ from that of TMTU.

Surface Excess. The surface excess, Γ, at a constant charge density, σ, was evaluated by means of the following relation: $\Gamma=-(1/RT)(\partial\xi/\partial\ln C_{TMU})$, where ξ is the Parsons function ($\xi=\gamma+\sigma E$).[18]

Figure 2 shows the variation in Γ at different concentrations of TMU with the surface charge density. The maximum of surface excess, Γ_{max}, was shifted toward a negative charge density with an increase in the concentration.

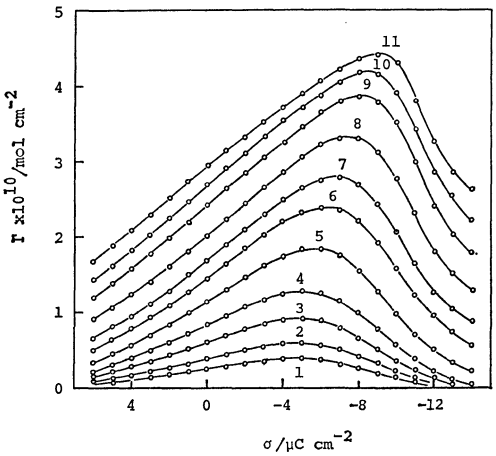

Fig. 2. Variation of surface excess of TMU with charge density at various concentrations.
Concentration of TMU (mM): (1) 2, (2) 3, (3), 5, (4) 7, (5) 10, (6) 15, (7) 20, (8) 30, (9) 50, (10) 70, and (11) 100.

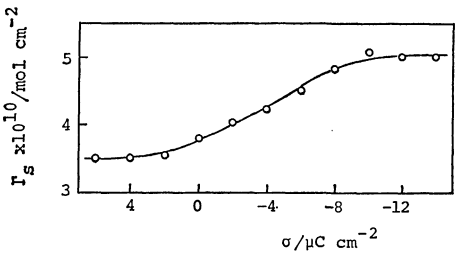

Fig. 3. Variation of Γ_s with surface charge density.

Figure 3 shows the surface excess at saturation, Γ_s, which was obtained by an extrapolation of the plot of $1/\Gamma$ against $1/C_{TMU}$ at a constant charge density to $1/C_{CMU}=0$. We observed two extreme values of Γ_s, namely, 3.5×10^{-10} mol dm^{-2} and 5.0×10^{-10} mol cm^{-2}, at positive and negative extremes of the surface charge density respectively.

Potential Drop across the Inner Layer, $\Delta_2^M\phi$. The value of $\Delta_2^M\phi$ was evaluated using this relation; $\Delta_2^M\phi=E-E_z-\Delta_S^2\phi$, where E and E_z are the potential at a constant charge density and the potential of zero charge for the electrolyte solution without any specific adsorption of ions (−0.432 V *vs.* SCE,[19]) respectively, and where $\Delta_S^2\phi$ is the potential drop across the diffuse layer at a constant charge density, which was calculated using the Gouy-Chapman theory.[20] The $\Delta_2^M\phi$ defined above corresponds to Grahame's rational potential difference.[20]

Figure 4 shows the change in $\Delta_2^M\phi$ due to the adsorption of TMU. The relations between $\Delta_2^M\phi$ and Γ for $\sigma\geqslant2$ μC cm^{-2} were linear, while those for $\sigma<2$ μC cm^{-2} were also linear at a lower surface excess, but were curved at a higher surface excess. When an adsorption isotherm can be described by the two series capacitor (TSC) model,[21] where the free energy

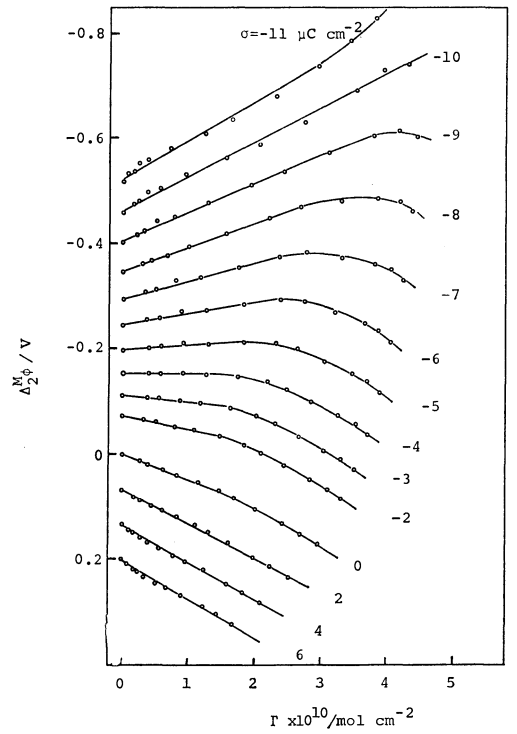

Fig. 4. Change in the potential drop across the inner layer due to adsorption of TMU.
Charge density is indicated by each line.

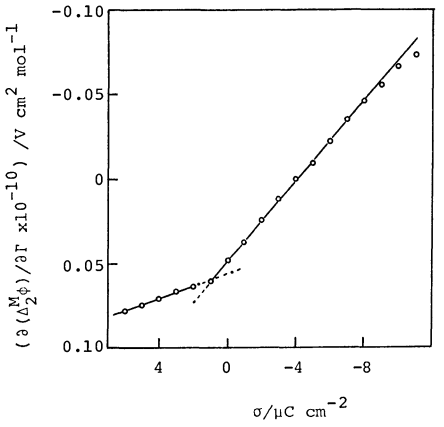

Fig. 5. Relation between $\partial(\Delta_2^M\phi)/\partial\Gamma$ obtained for the region where linear $\Delta_2^M\phi$-Γ relations were observed in Fig. 4 and the surface charge density.

of adsorption is a function of the charge density, a linear relation between $\Delta_2^M\phi$ and Γ should be observed for a constant orientation. In this sense, the linear portion of the $\Delta_2^M\phi-\Gamma$ curves in Fig. 4 can be assumed to result from a constant orientation based on the TSC model.

The magnitude of the positive shift of $\Delta_2^M\phi_{\sigma=0}$ with Γ for TMU is much larger than that of pyrazine[22] or ethylene glycol,[23] which are known as compounds with a small effective normal dipole moment, which means that the normal component of the dipole moment to the electrode surface is small. This suggests that TMU at a higher surface excess is adsorbed through an orientation with the positive end of the dipole toward the electrode surface.

Figure 5 shows the relation between the slope of the linear portion of the $\Delta_2^M\phi-\Gamma$ curves in Fig. 4 and the surface charge density. Two straight lines with different slopes are observed in Fig. 5. This indicates that the adsorption of TMU for $\sigma<2$ μC cm^{-2} and that for $\sigma\geqslant2$ μC cm^{-2} can not be described by the same isotherm. Since the charge of the maximum adsorption, σ_{max}, is defined as σ at $(\partial\Delta_2^M\phi/\partial\Gamma)=0$,[4] the former is the adsorption with $\sigma_{max}=-15$——17 μC cm^{-2}, which was elucidated by an extrapolation, and the slope, $\partial(\partial\Delta_2^M\phi/\partial\Gamma)/\partial\sigma=3.87\times10^{10}$ mV cm^4 μC^{-1} mol^{-1}, while the latter is the adsorption with $\sigma_{max}=-4$ μC cm^{-2} and the slope of 11.83×10^{10} mV cm^4 μC^{-1} mol^{-1}.

Adsorption Isotherm and Free Energy of Adsorption. In order to determine the adsorption isotherm of TMU, various adsorption isotherms were examined using Γ in the region where linear portions were observed on the $\Delta_2^M\phi-\Gamma$ curves in Fig. 4; it was found that the adsorption of TMU could be described by the Frumkin isotherm:

$$\beta x = [\theta/(1-\theta)]\exp(-2\alpha\theta), \quad (1)$$

where β is the adsorption coefficient defined by $\exp(-\Delta\bar{G}^\circ/RT)$ containing the free energy of adsorption at zero coverage, $\Delta\bar{G}^\circ$, x is the molar fraction of the adsorbate, θ is the coverage, and α is the interaction parameter.

The Frumkin isotherm plot in Fig. 6 is drawn with respect to the regions where the linear $\Delta_2^M\phi-\Gamma$ relations were observed in Fig. 4, namely, $\sigma=-10$ μC cm^{-2} and $\sigma\geqslant2$ μC cm^{-2}. The coverage was evaluated using Γ_s in Fig. 3; that is, $\Gamma_s=5.0\times10^{-10}$ mol cm^{-2} for $\sigma=-10$ μC cm^{-2} and $\Gamma_s=3.5\times10^{-10}$ mol cm^{-2} for $\sigma\geqslant2$ μC cm^{-2}. It is thought from Fig. 6 that the adsorption of TMU in $\sigma\geqslant2$ μC cm^{-2} can be described by the Frumkin isotherm with $\Gamma_s=3.5\times10^{-10}$ mol cm^{-2} and $\alpha=-0.25$. The deviation of the points at a lower coverage from a linear relation may be affected by a different adsorption, which will be discussed later. On the other hand, the adsorption of TMU at $\sigma=-10$ μC cm^{-2} could not be described

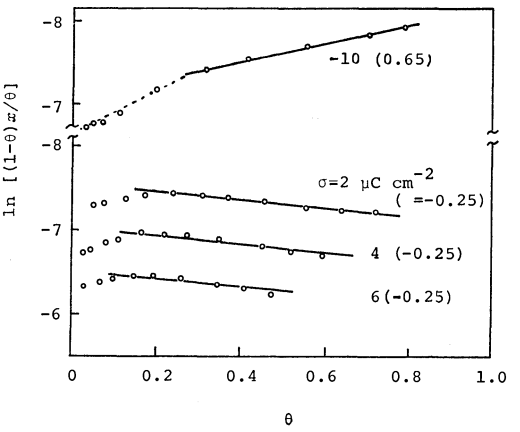

Fig. 6. Test of the Frumkin isotherm with Γ_s varing with surface charge density.
Charge density is indicated by each line, and the values in the parentheses represent the interaction parameter, α.

by a single isotherm throughout the coverage. The linear $\Delta_2^M\phi - \Gamma$ relation at $\sigma = -10$ μC cm^{-2} in Fig. 4 seems to be an incidental result. Probably, a change in the orientation or a mixed adsorption occurs with an increase in the surface excess at this charge density.

At a higher surface excess, the interaction parameter, which is shown in the parentheses of Fig. 6, was negative for $\sigma \geqslant 2$ μC cm^{-2}, but was positive at $\sigma = -10$ μC cm^{-2}. This difference in α at positive and far negative charges is compatible with the explanations given for the adsorption-desorption peaks in Fig. 1.

On the other hand, at a lower coverage in $\sigma < 2$ μC cm^{-2}, the Γ_s seems to be different from the Γ_s shown in Fig. 3, because the latter is obtained by weighing the data at a higher surface excess. In order to estimate the Γ_s for a lower coverage, the following equation was used:[28]

$$\partial(\Delta_2^M\phi)/\partial\Gamma = -RT[\partial \ln \beta/\partial(\sigma - \sigma_{max})], \quad (2)$$

with a previously verified precondition that β is a function of the charge density. If a quadratic dependence of ln β on the charge density is assumed, Eq. 2 can be rearranged to Eq. 3:

$$\partial[\partial(\Delta_2^M\phi)/\partial\Gamma]/\partial(\sigma - \sigma_{max}) = -2RT[\partial \ln \beta/\partial(\sigma - \sigma_{max})^2]. \quad (3)$$

The left-hand side of Eq. 3 has already been estimated as the experimental slope for $\sigma < 2$ μC cm^{-2} in Fig. 5. Therefore, several Γ_s values were chosen and varied step-by-step until the ln β values obtained satisfy Eq. 3. The final value of Γ_s estimated in this way was 3.4—3.5 × 10^{-10} mol cm^{-2}; the average was used in the subsequent analysis. Figures 7 and 8 show the Frumkin isotherm plot using the Γ_s finally estimated and the relation between ln β and $(\sigma - \sigma_{max})^2$ respectively. The satisfactory result with respect to Eq. 3 indicates that the assumption of the quadratic

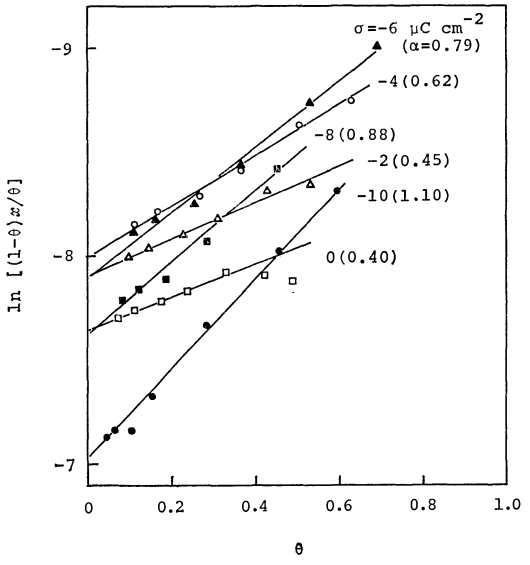

Fig. 7. The Frumkin isotherm plot using a constant $\Gamma_s = 3.45 \times 10^{-10}$ mol cm^{-2}.
Charge density is indicated by each line, and the values in the parentheses represent the interaction parameter, α.

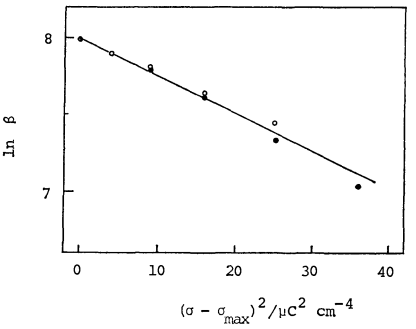

Fig. 8. Test of a quadratic dependence of ln β on the surface charge density.
Here open and closed circles correspond to ln β for $\sigma > \sigma_{max}$, and $\sigma < \sigma_{max}$ ($\sigma_{max} = -4$ μC cm^{-2}), respectively.

dependence of ln β on the charge density and the estimated value of Γ_s are generally reasonable. The value of α shown in the parentheses of Fig. 7 were always positive, but changed with the surface charge density. According to the view of Pulidori and his co-workers,[27] the observed lowering of the positive α with an increase in the surface charge density means that the attractive interaction between TMU and water molecules becomes stronger, or that the attractive interaction among TMU molecules themselves becomes weaker with an increase in the surface charge density. So long as a constant orientation is assumed for the adsorption at a lower coverage, the fact that the attractive interaction varies with the charge density on the electrode suggests that adsorbed TMU molecules interact with the neighboring water structure, which also varies with the charge density.

Orientation Models of TMU. The following three fundamental orientations can be considered on the basis of the results presented thus far: (I) Orientation at a lower coverage in the region of $\sigma < 2$ μC cm^{-2}. This orientation takes $\Gamma_s = 3.45 \times 10^{-10}$ mol cm^{-2} and $\sigma_{max} = -4.0$ μC cm^{-2}, which suggests an orientation with a small effective normal dipole moment,[23] and it has positive interaction parameter. This will be a horizontal orientation where the >C=O group is approximately parallel to the electrode surface. (II) Orientation in the region of $\sigma \geqslant 2$ μC cm^{-2}. This orientation takes $\Gamma_s = 3.5 \times 10^{-10}$ mol cm^{-2} and $\sigma_{max} = -15 \sim -17$ μC cm^{-2}, which suggests an orientation with a large positive effective normal dipole moment, and it has negative interaction parameter. This will be a vertical orientation where the >C=O group is approximately vertical to the electrode surface. (III) Orientation at a higher coverage in the region of very negative charges. This orientation takes $\Gamma_s = 5.0 \times 10^{-10}$ mol cm^{-2} and has a positive interaction parameter because of lateral attractive interaction among the TMU dipoles in the adsorption layer.[26] This will also be a horizontal orientation where the >C=O group is nearly parallel to the electrode surface, but the occupied area is different from that of the (I) orientation.

The molecular structure of TMU, unlike that of urea,[27] has been considered to be non-planar because

of a steric repulsion. The single NMR signal of the CH_3 proton of TMU[28] is attributed to an internal rotation of the two $(CH_3)_2N-$ groups, which relieve the steric repulsion. In spite of its similar molecular structure[29] and the internal rotation property,[30] the dipole moment of TMU,[3] 11.6×10^{-30} C m, is greatly different from that of TMTU,[31] 15.7×10^{-30} C m. The dipole moment of TMU is smaller than that of urea,[3] 15.2×10^{-30} C m, but is rather close to that of acetone,[32] 9.7×10^{-30} C m. The lower dipole moment of TMU compared with that of TMTU may be attributable to a slightly deeper pyramidal structure of TMU about N atoms.[29] The most simple and unambiguous explanation, however, is a minor contribution of the conjugate system of $^+N{=}C{-}O^-$ to the dipole moment of TMU.[33] This leads to a consideration that the possibility of the distribution of a positive charge on N atoms is small.

In considering the orientation of TMU on the electrode, three possible extreme molecular conformations[30] were taken into account, and the average was taken for the projected area. Figure 9 shows the models corresponding to the three orientations, (I), (II), and (III). The projected areas of the rectangles enclosing a molecule were (I) 0.481, (II) 0.474, and (III) 0.332 nm^2, while the corresponding Γ_s values were (I) 3.45, (II) 3.5, and (III) 5.0×10^{-10} mol cm^{-2}. The averages of the molecular height, X_1, were estimated to be (I) 0.58, (II) 0.58, and (III) 0.62 nm.

Evaluation of the Dipole Moment of the TMU Molecule at the Interface. From the evaluation of the dipole moment of TMU adsorbed at the interface, we next attempted to confirm the three orientation models and to verify that the variation in the interaction parameter attributable to the charge density with respect to the (I) orientation is caused by the interaction with the neighboring water structure, not by a slight change in the orientation which leads to a change in the lateral attractive interaction among TMU dipoles.

The orientation of organic compounds with a polar group can be determined by the evaluation of the dipole moment of an adsorbed molecule using the following equation, which is similar to that derived by Parsons and his co-workers,[5] and by Damaskin and Frumkin:[34]

$$\Delta(\Delta_2^M\phi) = \theta[(\Gamma_s P_1/\varepsilon_1 - \Gamma_s n P_0/\varepsilon_0) + \sigma(1/K_1^i - 1/K_0^i)], \quad (4)$$

where ε, P, and K^i are the permittivity of the inner layer, the dipole moment of an adsorbed molecule, and the integral inner-layer capacity respectively, where n is the number of water molecules displaced by an adsorbate molecule, and where the subscripts 1 and 0 denote the inner layers saturated with adsorbate and water respectively.

The term $-\Gamma_s n P_0/\varepsilon_0$ in Eq. 4 is equal to the potential drop across the inner layer due to water dipoles, Δg^w_{dipole}. In the evaluation of the dipole moment of TMU, one can use several water-adsorption models[7] in which the value of Δg^w_{dipole} is given as a function of the charge density. The Bockris and Habib model was used in this study for the comparison of the results of TMU with those of TMTU.[1] In addition, the T-model[9] and the D-F model[10] were also applied to Eq. 4; the results will be compared below with those from the B-H model.

The integral inner-layer capacity in Eq. 4 should be $K^{i(ion)}$ as a result of free charges on the electrode; it is free from any contribution by dipoles, $K^{i(dipole)}$.[38] When the B-H model was applied to Eq. 4, $K_0^{i(ion)}$ was evaluated by substituting the K_0^i determined ex-

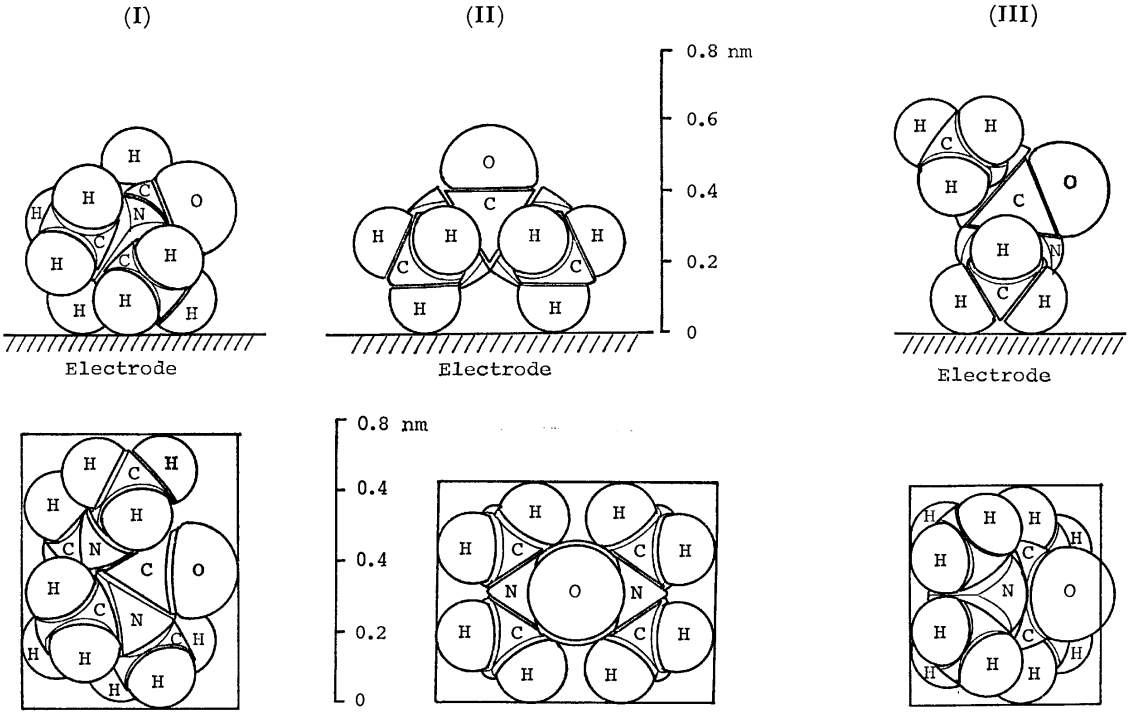

Fig. 9. Scale drawings of an adsorbed TMU molecule through the orientations, (I), (II), and (III). Upper and lower figures show the side and the top views, repectively. Rectangle enclosing a molecule means the projected area.

perimentally and the $1/K_0^{i(\text{dipole})}=8.0\times10^{-3}$ cm^2 μF^{-1} from the B-H model into this relation: $1/K_0^i=1/K_0^{i(\text{ion})}-1/K_0^{i(\text{dipole})}$. When the T and D-F models are applied to Eq. 4, the constant $K_0^{i(\text{ion})}$ values, 17 and 16 μF cm^{-2}, specified by each model were used. On the other hand, $K_1^{i(\text{ion})}$ was assumed to be equal to K_1^i.

For the evaluation of P_1 using Eq. 4, it is further necessary to estimate K_1^i and ε_1 as functions of the charge density. The values of K_1^i were obtained by plotting first the integral inner layer capacity at different surface excesses, K^i, against Γ, and then by extrapolating the plot to each Γ_s, as is shown in Fig. 10. The values of K_1^i for the (I) orientation were, however, obtained by extrapolating a linear relation between $1/K^i$ and Γ at each charge density to $\Gamma_s=3.45\times10^{-10}$ mol cm^{-2}. The values of ε_1 were calculated by substituting K_1^i and the molecular height, X_1, into this relation; $\varepsilon_1=X_1\cdot K_1^i$. Regarding orientations at full coverage in the region of $0\geqslant\sigma\geqslant-10$ μC cm^{-2}, X_1 was estimated by assuming a weighted average between the (II) orientation with $\Gamma_s=3.5\times10^{-10}$ mol cm^{-2} and $X_1=0.58$ nm, and the (III) orientation with $\Gamma_s=5.0\times10^{-10}$ mol cm^{-2} and $X_1=0.62$ nm, for the measured Γ_s in Fig. 3. The above assumption is based on the observation that the Γ_s in Fig. 3 changes from the Γ_s of the (II) orientation to the Γ_s of the (III) orientation with a decrease in the surface charge density.

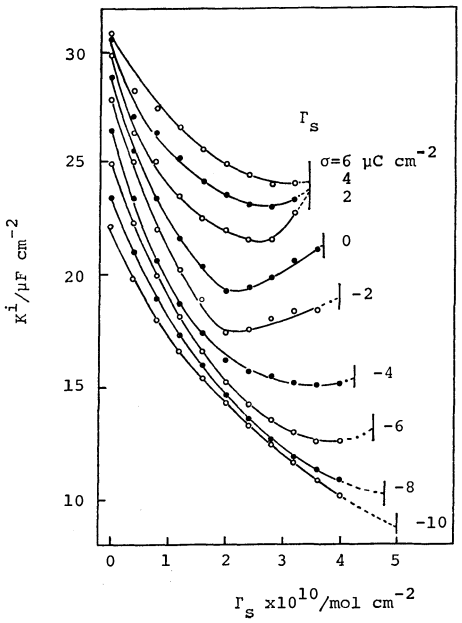

Fig.10. Plot of the integral inner-layer capacity against the surface excess at different surface charge density. Charge density is indicated by each line. Short vertical line represents Γ_s at each surface charge density.

The P_1, ε_1, and K_1^i values finally evaluated are summarized in Table 2, along with K_0^i and $K_0^{i(\text{ion})}$. The result with respect to P_1 indicates that the angles of the C=O bond axis to the electrode surface are about 25°, 90°, and 30° for the (I), (II), and (III) orientations respectively. The models in Fig. 9 were approximately confirmed by the evaluation of the dipole moment of TMU. Since the P_1 for the (I) orientation is almost constant, irrespective of the charge density, it seems most likely that the variation in the interaction parameter with the charge density is not caused by a slight change in the orientation, but by an interaction with neighboring water structure. It was further observed that the P_1 for the (II) orientation was almost the same as that measured on the basis of the polarization phenomena in the bulk of the solution, 11.6×10^{-30} C m.[3]

In summary, the adsorption behavior of TMU can be interpreted as follows. The principal orientation of the TMU adsorbed from lower concentrations is the (I) orientation, which is governed by an interaction with the neighboring water structure. With an increase in the surface excess, however, this orientation changes into the (II) or (III) orientation, depending on the charge sign of the electrode. The orientation at full coverage in the region of $0\geqslant\sigma\geqslant-8$ μC cm^{-2} is a mixture of (II) and (III). The (I) orientation was quite similar to that of urea.[5]

Since the dipole moment of TMU acts along the C^+–O^- bond axis, the observed orientations deviate from those expected from the polarity. For example, the (II) orientation is the most probable orientation at a negative electric field, but it was not observed. Such an deviation from the expectation is often observed,[1,2,36,37] however, and this suggests that the electric field is effective for a short-range interaction, but not for a long-range interaction. The polarity of TMU was not an important factor governing the adsorption behavior. The scarcity of the positive charge on N atoms attributable to a weak conjugation is con-

Table 2. Various inner-layer parameters at saturation with TMU and water

σ/μC cm^{-2}	6	4	2	0	−2	−4	−6	−8	−10
K_0^i/μF cm^{-2}	30.8	30.5	29.8	28.8	27.8	26.4	24.9	23.4	22.1
$K_0^{i(\text{ion})}$/μF cm^{-2}	24.7	24.5	24.1	23.4	22.7	21.8	20.8	19.7	18.8
(I) Constant orientation with $\Gamma_s=3.45\times10^{-10}$ mol cm^{-2}									
K_1^i/μF cm^{-2}	—	—	—	14.5	13.2	12.2	11.8	11.5	11.3
$\varepsilon_1\times10^{11}$/F m^{-1}	—	—	—	8.4	7.6	7.1	6.8	6.6	6.6
$P_1\times10^{30}$/C m	—	—	—	5.5	5.0	5.0	5.3	5.3	5.5
(II) Variable orientation with $\Gamma_s=(3.5\text{—}5.0)\times10^{-10}$ mol cm^{-2}									
$\Gamma_s\times10^{10}$/mol cm^{-2}	3.5	3.5	3.5	3.7	4.0	4.3	4.6	4.8	5.0
K_1^i/μF cm^{-2}	24.2	24.0	23.4	21.3	18.6	15.4	13.2	10.2	8.8
$\varepsilon_1\times10^{11}$/F m^{-1}	14.0	13.8	13.6	12.5	11.1	9.3	8.1	6.3	5.5
$P_1\times10^{30}$/C m	11.9	11.5	11.5	11.1	10.6	9.3	8.3	7.5	6.1

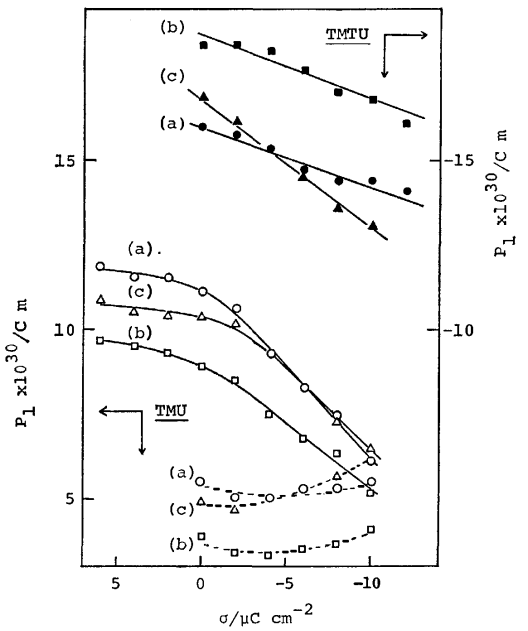

Fig.11. Comparison of P_1 estimated from different water-adsorption models.
(a) B-H model, (b) T-model, and (c) D-F model. Open and closed symbols correspond to TMU and TMTU, respectively.

sidered to be a main cause of the observed adsorption behavior, namely, an attractive interaction between electrons on N atoms and the positive charge on the electrode, and a repulsive interaction at a very negative charge density in addition to the lateral attractive interaction among TMU dipoles in the adsorption layer.

P_1 Evaluated from Different Water-adsorption Models. It is important to use an appropriate Δg^{w}_{dipole} value for the evaluation of P_1 using Eq. 4; it is also important to know the precise orientation state of the adsorbate on the molecular level. Aside from the different ideas contained in the water-adsorption models, as has already been mentioned, the values of Δg^{w}_{dipole} are different among the models. Figure 11 shows the P_1 values of TMU evaluated using the B-H model, the D-F model, and the T model. The results with TMTU[1)] are also plotted in the same figure. A positive (negative) value of P_1 means an orientation with the positive (negative) end of the dipole toward the electrode. In general, the dipole moment of an organic molecule adsorbed around $\sigma=0$ μC cm^{-2} seems to be nearly the same as that measured on the basis of the polarization phenomena in the bulk of the solution. In this sense, the B-H model seems to give reasonable P_1 values for TMU and TMTU.

The difference in P_1 value among the three models was not so large as was expected from the difference in the Δg^{w}_{dipole}, probably because of a compensation action due to $K_0^{1(ion)}$. Strictly speaking, however, the following features are recognized. The way of the variation in P_1 with the charge density between the B-H model and the T model is almost the same, but the values of P_1 are different. On the contrary, the way of the variation in P_1 with the charge density between the B-H model and the D-F model is somewhat different, but the values of P_1 are approximately the same.

References

1) O. Ikeda, H. Jimbo, and H. Tamura, *J. Electroanal. Chem.*, **137**, 127 (1982).
2) R. Parsons, *Proc. R. Soc. London, Ser. A*, **261**, 79 (1961).
3) Cl. Béguin and T. Gäumann, *Helv. Chim. Acta*, **45**, 1971 (1958).
4) S. Trasatti, *J. Electroanal. Chem.*, **53**, 335 (1974).
5) R. Parsons, R. Peat, and R. M. Reeves, *J. Electroanal. Chem.*, **62**, 151 (1975).
6) R. Parsons and P. C. Symons, *Trans. Faraday Soc.*, **64**, 1077 (1968).
7) S. Trasatti, "Modern Aspects of Electrochemistry," Plenum Press, New York (1979), Vol. 13, p. 81.
8) J. O'M Bockris and M. A. Habib, *Electrochim. Acta*, **22**, 41 (1977).
9) S. Trasatti, *J. Electroanal. Chem.*, **64**, 128 (1975).
10) B. B. Damaskin and A. N. Frumkin, *Electrochim. Acta*, **19**, 173 (1974).
11) G. J. Hills and R. Payne, *Trans. Faraday Soc.*, **61**, 316 (1965).
12) D. C. Grahame, E. M. Coffin, J. P. Cummings, and M. A. Poth, *J. Am. Chem. Soc.*, **74**, 1207 (1952).
13) D. J. Schiffrin, *J. Electroanal. Chem.*, **23**, 168 (1969).
14) A. De Battisti and S. Trasatti, *J. Electroanal. Chem.*, **54**, 1 (1974).
15) D. M. Mohilner and H. Nakadomari, *J. Phys. Chem.*, **77**, 1594 (1973).
16) D. M. Mohilner, L. W. Browman, S. J. Freeland, and H. Nakadomari, *J. Electrochem. Soc.*, **120**, 1658 (1973).
17) B. B. Damaskin, O. A. Petrii, and V. V. Batrakov, "Adsorption of Organic Compounds on Electrodes," Plenum Press, New York (1971), p. 84.
18) R. Parsons, *Trans. Faraday Soc.*, **51**, 1518 (1955).
19) P. Delahay, "Double Layer and Electrode Kinetics," Interscience, New York (1965), p. 23.
20) D. C. Grahame, *Chem. Rev.*, **41**, 441 (1947).
21) A. N. Frumkin, B. B. Damaskin, and A. A. Survila, *J. Electroanal. Chem.*, **16**, 493 (1968).
22) B. E. Conway, H. P. Dhar, and S. Gottesfeld, *J. Colloid Interface Sci.*, **43**, 303 (1973).
23) S. Trasatti, *J. Electroanal. Chem.*, **28**, 257 (1970).
24) R. Parsons, *Trans. Faraday Soc.*, **55**, 999 (1959).
25) F. Pulidori, G. Borghesani, R. Pedriali, A. De Battisti, and S. Trasatti, *J. Chem. Soc., Faraday Trans. 1*, **74**, 79 (1978).
26) J. O'M Bockris, E. Gileadi, and K. Müller, *Electrochim. Acta*, **12**, 1301 (1967).
27) J. E. Worsham, Jr., H. A. Levy, and S. W. Peterson, *Acta Crystallogr.*, **10**, 319 (1957).
28) R. J. Niedzielski, R. S. Drago, and R. L. Middaugh, *J. Am. Chem. Soc.*, **86**, 1694 (1964).
29) L. Fernholt, S. Samdal, and R. Seip, *J. Mol. Struct.*, **72**, 217 (1981).
30) F. A. L. Anet and M. Ghiaci, *J. Am. Chem. Soc.*, **101**, 6857 (1979).
31) A. Luttrinhaus and J. Grohman, *Z. Naturforsch., B*, **10**, 365 (1955).
32) J. D. Swalen and C. C. Costain, *J. Chem. Phys.*, **31**, 1562 (1959).
33) M. Schafer and C. Curran, *Inorg. Chem.*, **5**, 265 (1966).
34) B. B. Damaskin and A. N. Frumkin, *J. Electroanal. Chem.*, **34**, 191 (1972).
35) S. Trasatti, *J. Electroanal. Chem.*, **64**, 128 (1973).
36) L. M. Baugh and R. Parsons, *J. Electroanal. Chem.*, **41**, 311 (1973).
37) G. J. Hills, D. J. Schiffrin, and T. Solomon, *J. Electroanal. Chem.*, **41**, 41 (1973).

The Effect of the Difference in the Oxidation State of the Second Component Added to MoO_3 on the Generation of the Acidic Property

Mamoru Ai

Research Laboratory of Resources Utilization, Tokyo Institute of Technology, 4259 Nagatsuta, Midori-ku, Yokohama 227

(Received June 11, 1982)

The effect of the difference in the oxidation state of the second component added to MoO_3 on the generation of acidic sites was studied with regard to Sn^{2+}—Sn^{4+}, Fe^{2+}—Fe^{3+}, Cr^{3+}—Cr^{6+}, and Cu^{+}—Cu^{2+}. It was found that a markedly lager amount of acidic sites is generated by the combination of Sn^{2+}, Fe^{2+}, or Cr^{3+} with MoO_3 than by that of Sn^{4+}, Fe^{3+}, or Cr^{6+} respectively. As a general feature of metal-oxide combination, it is proposed that the addition of a metal ion in a lower oxidation state to MoO_3 brings about a markedly more significant acidity generation than that of a metal ion in a higher oxidation state. An explanation to account for the results was attempted in relation to the reducing function of the second component.

It is widely known that a combination of different metal oxides sometimes induces a significant acidity-generation and that this character of metal oxides has actually been applied to the preparation of a catalyst. For understanding the acidity-generation, an explanation has been proposed by Tanabe *et al.* based on the acidity-basicity data for many binary-oxides.[1,2]

However, it still seems difficult to understand the acidity-generation in the case of transition-metal oxides in which the oxidation state is variable. It is, therefore, important to find some general rules effective for predicting the acidity-generation of mixed oxides containing transition-metal oxides, such as MoO_3, V_2O_5, WO_3, and U_3O_8.

It was found in studying Sn–Mo oxides[3] that the acidity-generation is markedly affected by the oxidation state of tin in the starting material as well as by the method of catalyst preparation. This finding led us to a prediction that the acidity-generation is related to the oxidation state of the second component added to a transition-metal oxide.

In the present study, MoO_3 was chosen as the first component, and the effect of the oxidation state of the second component was studied with regard to Sn^{2+}—Sn^{4+}, Fe^{2+}—Fe^{3+}, Cr^{3+}—Cr^{6+}, and Cu^{+}—Cu^{2+}.

Experimental

Catalysts. The catalysts used in this study were nine kinds of MoO_3–X_nO_m with different X/Mo ratios, where X refers to four different metals. They were prepared as follows.

Mo–Sn Oxides: The required quantity of either $SnCl_2$ or $SnCl_4$ was dissolved in water. To this solution, a dilute aqueous ammonia solution was added to precipitate the corresponding hydroxide. After filtering and washing, the paste-like hydroxide was added to an aqueous solution of $(NH_4)_6Mo_7O_{24}\cdot 4H_2O$, and 10 to 20 mesh pumice was mixed with the solution; then the mixture was evaporated with stirring. The amount of pumice was about 500 ml per g atom of metal. The catalyst was calcined under flowing oxygen at 500 °C for 4 to 5 h. The catalysts were denoted as MoO_3–Sn^{2+} and MoO_3–Sn^{4+} respectively.

Mo–Fe Oxides: As the starting materials we used iron(II) oxalate dihydrate, $FeC_2O_4\cdot 2H_2O$, for Fe^{2+} and ammonium tris(oxalato) ferrate(III) trihydrate, $(NH_4)_3Fe(C_2O_4)_3\cdot 3H_2O$, for Fe^{3+}. Aqueous solutions of each compound were mixed with a solution of $(NH_4)_6Mo_7O_{24}\cdot 4H_2O$. Pumice was then added to the solution or slurry thus obtained. The further procedures were the same as those used in the case of Mo–Sn oxides. The catalysts were denoted as MoO_3–Fe^{2+} and MoO_3–Fe^{3+} respectively.

Mo–Cr Oxides: $Cr(NO_3)_3\cdot 9H_2O$ and CrO_3 were used as the starting materials. The further procedures were the same as above. The catalysts were denoted as MoO_3–Cr^{3+} and MoO_3–Cr^{6+}.

Mo–Cu Oxides: As the starting materials we used CuCN and CuCl for Cu^{+} and $Cu(CH_3CO_2)_2\cdot H_2O$ for Cu^{2+}. The catalysts were denoted as MoO_3–CuCN, MoO_3–CuCl, and MoO_3–Cu^{2+} respectively.

Catalytic-activity Measurements. The vapor-phase dehydration of 2-propanol and the oxidation of propylene and methanol were carried out in an ordinary continuous-flow system. The reactor and the experimental procedures were the same as those employed in previous works.[4–7]

Results

Mo–Sn Oxides. The effect of the difference in the oxidation state of tin on the specific surface area was checked by the BET method using nitrogen at −196 °C. As may be seen in Fig. 1, the surface area

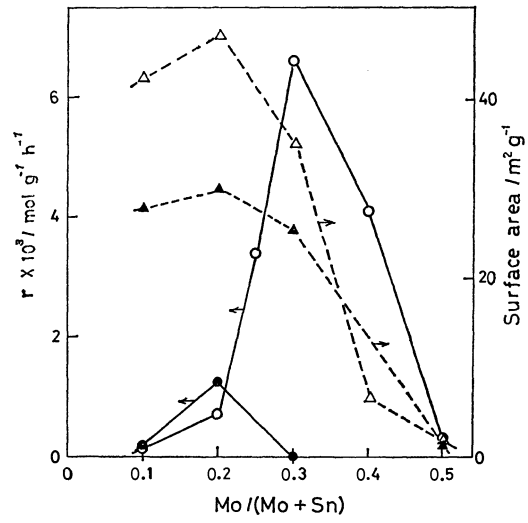

Fig. 1. Surface area and catalytic activity for dehydration of 2-propanol.
r=Rate at 160 °C and 1.7 vol% 2-propanol in air.
○,△: MoO_3–Sn^{2+}, ●,▲: MoO_3–Sn^{4+}.

of both the MoO_3–Sn^{2+} and MoO_3–Sn^{4+} systems are of the same order of magnitude and vary in the same way with an increase in the Mo content; that is, they pass through a maximum at Mo/(Mo+Sn) atomic ratio=0.2 and then sharply decline with the Mo-content at Mo/(Mo+Sn)>0.4.

As a measure of the acidity of a catalyst, the catalytic activity for the dehydration of 2-propanol was chosen for convenience as in the previous studies.[4-6] The initial rate of dehydration was measured at low conversion levels. The rate at 160 °C is plotted as a function of the catalyst composition in Fig. 1. As has been reported earlier,[5] a dramatically high acidity is obtained in the case of the MoO_3–Sn^{2+} catalyst at the Mo/(Mo+Sn) atomic ratio of 0.3, while the generation of acidic sites is much less remarkable in the case of the MoO_3–Sn^{4+} catalysts.

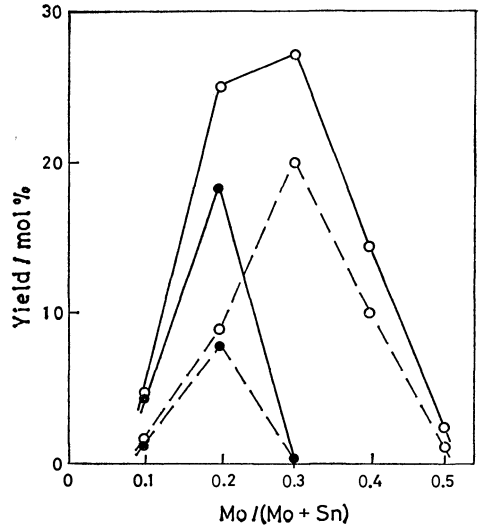

Fig. 2. Yield of acetone in the oxidation of propylene. Feed rates=propylene-20/oxygen-15/nitrogen-24/water vapor-104 ml/min (at 25 °C), catalyst used=20 g, full line=at 240 °C, broken line=at 190 °C, ○: MoO_3–Sn^{2+}, ●: MoO_3–Sn^{4+}.

As another example of an acid-catalyzed reaction, the oxyhydration of propylene to acetone was chosen.[8] The yields of acetone obtained from the MoO_3–Sn^{2+} and MoO_3–Sn^{4+} catalysts are plotted in Fig. 2. The results are well consistent with those shown in Fig. 1, suggesting the validity of these results.

Mo–Fe Oxides. The specific surface areas of the MoO_3–Fe^{2+} and MoO_3–Fe^{3+} systems are compared in Fig. 3. The surface area of the MoO_3–Fe^{3+} system is a little greater than that of the MoO_3–Fe^{2+} system, though the surface areas of both the systems pass through a broad maximum at Mo/(Mo+Fe) atomic ratio=0.2 with an increase in the Mo-content.

As an index of the acidity of the catalyst, the initial rate of 2-propanol dehydration at 200 °C is plotted as a function of the catalyst composition in Fig. 3. The acidity of the MoO_3–Fe^{2+} catalyst is much higher than that of the MoO_3–Fe^{3+} catalysts.

As another example of an acid-catalyzed reaction, the oxidation of methanol to formaldehyde was chosen.[7] The rates of formaldehyde formation at 260 °C obtained from the two series of catalysts are plotted in Fig. 4. The activity for methanol oxidation varies in the same way as that for 2-propanol dehydration, also suggesting the validity of the results.

Mo–Cr Oxides. Figure 5 shows the surface areas of the MoO_3–Cr^{3+} and MoO_3–Cr^{6+} systems. They are of the same order of magnitute, except for the Mo/(Mo+Cr^{3+})=0.9 catalyst.

The initial rate of 2-propanol dehydration at 200 °C is plotted in Fig. 6. The acidity of the MoO_3–Cr^{3+} catalysts is much higher than that of the MoO_3–Cr^{6+} catalysts, though the acidity of the two systems vary in the same way with an increase in the Mo-content. It is interesting to note that the maximum

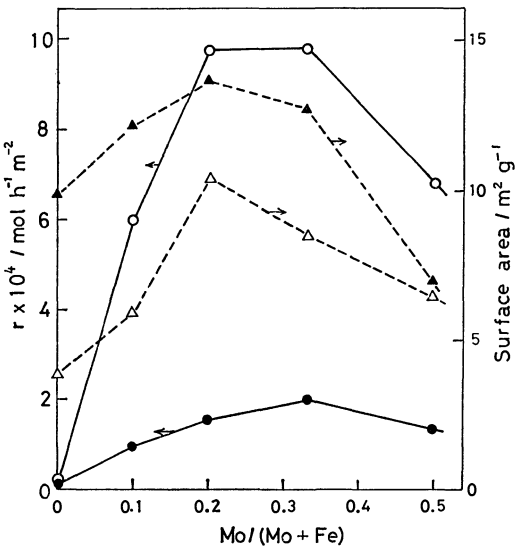

Fig. 3. Surface area and catalytic activity for dehydration of 2-propanol.
r=Rate at 200 °C and 1.7 vol% 2-propanol in air, ○,△: MoO_3–Fe^{2+}, ●,▲: MoO_3–Fe^{3+}.

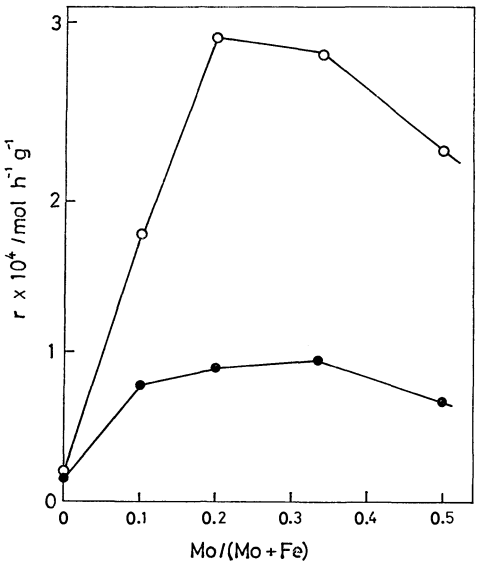

Fig. 4. Catalytic activity for oxidation of methanol to formaldehyde.
r=Rate at 260 °C and 6.3 vol% methanol in air, ○: MoO_3–Fe^{2+}, ●: MoO_3–Fe^{3+}.

Table 1. Dehydration of 2-propanol over Mo-Cu oxide catalysts[a)]

Catalyst (mole ratio) MoO_3–CuCN	Conversion %	Catalyst (mole ratio) MoO_3–CuCl	Conversion %	Catalyst (mole ratio) MoO_3–Cu^{2+}	Conversion %
100— 0	3.0	100— 0	3.0	100— 0	3.0
90—10	3.0	90—10	3.0	90—10	5.0
80—20	3.0	80—20	2.7	80—20	5.0
67—33	2.0	67—33	2.5	67—33	8.0
50—50	2.0	50—50	2.3	50—50	8.0
		33—67	1.0	33—67	2.0

a) Temperature=200 °C, catalyst used=10 g, 2-propanol=1.7 vol% in air, total flow=1.0 l/min.

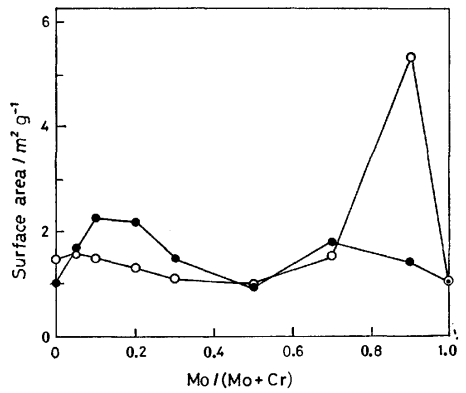

Fig. 5. Surface area of the MoO_3–Cr^{3+} and MoO_3–Cr^{6+} catalysts.
○: MoO_3–Cr^{3+}, ●: MoO_3–Cr^{6+}.

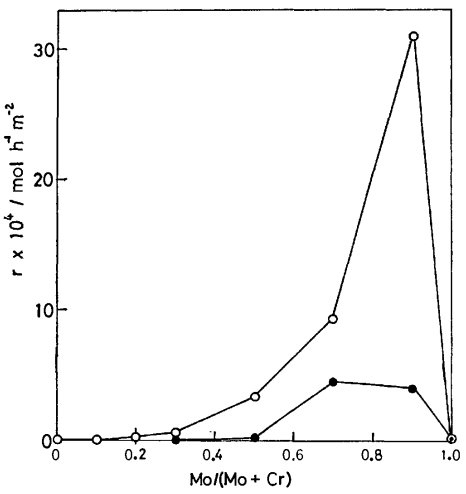

Fig. 6. Catalytic activity for dehydration of 2-propanol.
r=Rate at 200 °C and 1.7 vol% 2-propanol in air.
○: MoO_3–Cr^{3+}, ●: MoO_3–Cr^{6+}.

acidity occurs in Mo-rich regions, unlike the cases of the Mo–Sn and Mo–Fe oxides.

Mo–Cu Oxides. The rate of 2-propanol dehydration was measured at 200 °C for three series of Mo–Cu catalysts, *i.e.*, the MoO_3–CuCN, MoO_3–CuCl, and MoO_3–Cu^{2+} systems. As may be seen in Table 1, the catalytic activity is very low, regardless of the kind and amount of copper compounds. It is concluded that new acidic sites are not generated by the combination of copper with molybdenum. It is, therefore, impossible to ascertain the effect of the difference in the oxidation state of copper.

Discussion

From the experimental findings, it can be deduced as a general feature of metal-oxide combination that the addition of a metal ion in a lower oxidation state to molybdenum oxide brings about a markedly more significant acidity-generation than that of a metal ion in a higher oxidation state, though the surface area is changed only a little with the difference in the oxidation state.

As a possible explanation for this feature of metal-oxide combination, we would like to consider as follows. The combination of a metal ion in a lower oxidation state, which can act as a reductant and so has a special affinity for an oxidant such as the molybdenum ion, induces a reduction of the molybdenum ion, resulting in the generation of an anion vacancy on the molybdenum ion. Possibly, a kind of valence control may take place as a result of the combination, though the situation is much more complex than in the case when oxides of nontransition metals are mixed. On the other hand, it may be hard for the anion vacancy to form with the combination of the metal ion in a higher oxidation state with molybdenum, because the additive metal ion is lacking in the reducing function.

It has already been reported that the reduction of Mo–Al oxide by hydrogen brings about a marked increase in the acidity and that this acidity generation is explained by the formation of an anion vacancy on the molybdenum ion.[9–11)]

This view is also supported by the finding that the combination of other metal ions having no reducing function, such as Al^{3+}, Si^{4+}, and Zn^{2+}, brings about a much lower acidity-generation than that of Sn^{2+}, Fe^{2+}, or Cr^{3+}.[12)]

Actually, the colors of the MoO_3–Sn^{2+} and MoO_3–Fe^{2+} catalysts are darker than the corresponding MoO_3–Sn^{4+} and MoO_3–Fe^{3+} catalysts, even after calcination in an oxygen atmosphere, suggesting the presence of the molybdenum ion in lower oxidation states. It is interesting to note that the reduced molybdenum cannot be reoxidized by the heat treatment in gaseous oxygen.

There may naturally exist other factors deciding the acidity-generation in a combination of transition-metal oxides. For example, the composition showing a max-

imum acidity is different depending on the second components, and the acidity-generation is not observed in the case of the combination of Cu^+ and Cu^{2+} with MoO_3. This study will be followed by a second part in which other factors deciding the acidity-generation will be studied, based on data for various kinds of mixed oxides.

References

1) K. Tanabe, T. Shibata, T. Kiyoura, and J. Kitagawa, *Bull. Chem. Soc. Jpn.*, **47**, 1064 (1974).
2) K. Shibata, T. Kiyoura, J. Kitagawa, and K. Tanabe, *Bull. Chem. Soc. Jpn.*, **46**, 2985 (1973).
3) M. Ai, Preprint, 41th Disc. Meeting, Catal. Soc. Jpn., Toyama, 1977, p. 184.
4) M. Ai and S. Suzuki, *J. Catal.*, **30**, 362 (1973).
5) M. Ai, *J. Catal.*, **40**, 327 (1975).
6) M. Ai, *J. Catal.*, **52**, 16 (1978).
7) M. Ai, *J. Catal.*, **54**, 426 (1978).
8) Y. Takita, A. Ozaki, and Y. Morooka, *J. Catal.*, **27**, 185 (1972).
9) W. H. Hall and W. E. Massoth, *J. Catal.*, **34**, 41 (1974).
10) W. E. Massoth, *J. Catal.*, **36**, 164 (1975).
11) S. Yamadaya, T. Kabe, M. Oba, and Y. Miki, *Nippon Kagaku Kaishi*, **1976**, 227.
12) M. Ai, unpublished data.

A Conductance Study of 18-Crown-6 and Dibenzo-18-crown-6 Complexes with K^+ in Various Solvents

Yasuyuki TAKEDA

Department of Chemistry, Faculty of Science, Chiba University, Yayoi-chō, Chiba 260

(Received July 7, 1982)

Limiting ionic molar conductivities ($\lambda°$) of 18-crown-6 (18C6) and dibenzo-18-crown-6 (DB18C6) complexes with K^+ in several protic and aprotic solvents have been determined at 25 °C. The crystal ionic radius of 18C6 complex with K^+ is nearly identical with that of tetrabutylammonium ion ($(n\text{-}C_4H_9)_4N^+$). For CH_3OH, the mobility of the 18C6 complex with K^+ is nearly equal to that of $(n\text{-}C_4H_9)_4N^+$. However, for H_2O, the former is much larger than the latter, but the contrary is true for aprotic solvents. Walden products of 18C6 complexes with K^+ for the solvents are nearly equal to each other. For acetonitrile and DMSO, the $\lambda°$ value of the DB18C6 complex with K^+ is smaller than those for the tetrapentylammonium ion ($(n\text{-}C_5H_{11})_4N^+$) and for the tetraisopentylammonium ion ($(i\text{-}C_5H_{11})_4N^+$). For nitrobenzene and propylene carbonate, that of the DB18C6 complex with K^+ is smaller than those of $(n\text{-}C_5H_{11})_4N^+$ and $(i\text{-}C_5H_{11})_4N^+$, respectively. In contrast to the case of the aprotic solvents, the $\lambda°$ value of the DB18C6 complex with K^+ for CH_3OH is nearly equal to those of $(n\text{-}C_5H_{11})_4N^+$ and $(i\text{-}C_5H_{11})_4N^+$. Walden products of the DB18C6 complexes with K^+ for the solvents are nearly equal to each other. From the above data, it appears that a solute which contains a unit of 18C6 in its structure does not enforce a hydrogen-bonded structure for a protic solvent.

Stabilities and selectivities on complexation of 18-crown-6 (18C6) and dibenzo-18-crown-6 (DB18C6) with alkali metal ions in various solvents have been studied in detail.[1–5] However, the behavior of these crown ether complexes in various solvents has scarcely been investigated systematically.

In the present work, limiting ionic molar conductivities of 18C6 and DB18C6 complexes with K^+ in several protic and aprotic solvents have been determined at 25 °C; the limiting ionic molar conductivities of the crown ether complexes have been compared with those of tetraalkylammonium ions in order to investigate the behavior of the crown ether complexes in the solutions.

Experimental

Materials. 18-Crown-6 (Nisso Co., Ltd.) was recrystallized three times from acetonitrile and dried at 70 °C in a vacuum oven before use. DB18C6 (Aldrich Chemical Co., Inc.) was dissolved in chloroform, and filtered while hot. It was then recrystallized four times from benzene and dried at 60 °C in a vacuum oven prior to use. Potassium perchlorate and chloride were obtained from Merck Japan Ltd. The potassium perchlorate was recrystallized twice from water and dried at 150 °C in a vacuum oven prior to use. The potassium chloride was used without further purification. The method of purification of *N,N*-dimethylformamide (DMF),[5] methanol,[6] and propylene carbonate[3] was as has previously been described. Acetonitrile and dimethyl sulfoxide (DMSO) were allowed to stand in contact with molecular sieves for several days. The acetonitrile was then distilled twice and DMSO twice under nitrogen at about 1.8 kPa. In the case of each of these five solvents, the middle 70% of the distillate was used. The water contents of the purified acetonitrile, propylene carbonate, DMF, and DMSO determined by means of the Karl Fischer titration were less than 0.01%, and, in the case of CH_3OH, less than 0.03%. The conductivities of these final products of acetonitrile, propylene carbonate, H_2O, CH_3OH, DMF, and DMSO were less than 2×10^{-7}, 5×10^{-8}, 5×10^{-7}, 2×10^{-7}, 3×10^{-7}, and 8×10^{-8} Ω^{-1} cm^{-1}, respectively.

Apparatus and Procedure. The conductance measurements were made on a Fuso conductivity apparatus, model 362A, in a water bath thermostated at 25±0.005 °C. Three cells were used with cell constants of 0.059707, 0.093936, and 0.20461 cm^{-1}. The experimental procedure to obtain complex-formation constants and limiting ionic molar conductivities of 18C6 and DB18C6 complexes with a potassium ion was described in the previous paper.[3]

Results and Discussion

The procedure for obtaining the complex-formation constants, K_{ML^+}, and limiting ionic molar conductivities, $\lambda°$, of 18C6 and DB18C6 complexes with K^+ was the same as that described in the previous study.[3] M^+ and L denote an alkali metal ion and a crown ether respectively. In this work, it is assumed that the association between a cation and an anion is negligible under these highly dilute experimental conditions and that crown ethers form 1:1 complexes with K^+. Since concentrations of crown ethers were kept low ($<2.0\times10^{-3}$ M; 1 M=1 mol dm^{-3}) during these experiments, corrections for viscosity changes were neglected. The K_{ML^+} and the limiting molar conductivity, $\Lambda°$, values of 18C6 and DB18C6 complexes with potassium salts in various solvents are listed in Table 1.

As can be seen from Table 2, in the cases of K^+, 18C6 and DB18C6 complexes with K^+, the $\lambda°$ value decreases with an increase in the size of the cation for each solvent system. It is interesting to note that the 1,7,10,16-tetraoxa-4,13-diazacyclooctadecane ((2,2)) complex with K^+ is more mobile than the 18C6 complex with K^+ in acetonitrile, although the size and cavity size of (2,2) are nearly the same as those of 18C6. The author cannot explain this phenomenon at present. Both dibenzo-24-crown-8 (DB24C8) and DB18C6 have two benzene rings, and DB24C8 is larger than DB18C6. However, the $\lambda°$ value of DB24C8 complex with K^+ in propylene carbonate is nearly equal to that of DB18C6 complex. Since DB24C8 has a flexible structure and a large cavity, the potassium ion trapped in the cavity is surrounded by DB24C8. Thus, the potassium ion held in the DB24C8

Table 1. K_{ML^+} and Λ° values of 18C6 and DB18C6 complexes with potassium salts in various solvents at 25 °C

Solvent	Crown ether-Salt	K_{ML^+} / mol^{-1} dm^3	Λ° / Ω^{-1} cm^2 mol^{-1}
CH_3CN	18C6-$KClO_4$	5.2×10^5	163
	DB18C6-$KClO_4$	6.3×10^4	157
PC[a)]	18C6-$KClO_4$	1.6×10^{6} [3)]	27.1$_9$ [3)]
	DB18C6-$KClO_4$	1.4×10^{5} [4)]	25.$_6$
H_2O	18C6-KCl	1.11×10^{2} [2)]	101.$_7$
CH_3OH	18C6-KCl	1.2×10^6	92.$_3$
	DB18C6-KCl	1.2×10^5	87.$_9$
DMF	18C6-$KClO_4$	2.0×10^{4} [5)]	77.$_4$ [5)]
	DB18C6-$KClO_4$	6.3×10^{2} [4)]	75.$_1$
DMSO	18C6-$KClO_4$	1.9×10^3	34.$_6$
	DB18C6-$KClO_4$	3.3×10^2	32.$_8$

a) Propylene carbonate.

cavity may be effectively screened by DB24C8. On the contrary, since DB18C6 has a rigid structure and an optimum cavity size for K^+, solvent molecules may be able to interact with central K^+ in the DB18C6 cavity in the direction perpendicular to the plane of the DB18C6. This is the reason why the mobilities of the DB24C8 and the DB18C6 complexes with K^+ in propylene carbonate are nearly equal.

The crystal ionic radius of 18C6 complex with K^+ (4.9 Å[3)]) is nearly identical with that of tetrabutylammonium ion, $(n\text{-}C_4H_9)_4N^+$, (4.94 Å[20)]). For CH_3OH, the mobility of the 18C6 complex with K^+ is nearly equal to that of $(n\text{-}C_4H_9)_4N^+$; however, for H_2O, the former is much larger than the latter, contrary to the aprotic solvents (acetonitrile, DMF, DMSO, and propylene carbonate) (Table 2). In the case of $(n\text{-}C_4H_9)_4N^+$, the surface charge of the central nitrogen atom is effectively shielded by four butyl groups, while, for the 18C6 complex with K^+, K^+ trapped in the 18C6 cavity is exposed to solvent molecules on two axial sides of the 18C6 plane. Thus, the interaction between cation and solvent dipole seems to be stronger for 18C6 complex with K^+ than for $(n\text{-}C_4H_9)_4N^+$. Consequently, since the aprotic solvents have no hydrogen-bonded structures, $(n\text{-}C_4H_9)_4N^+$ is more mobile than 18C6 complex with K^+ in these aprotic solvents. In hydrogen-bonding solvents such as H_2O and CH_3OH, enforcement of a hydrogen-bonded structure for hydrophobic butyl groups of $(n\text{-}C_4H_9)_4N^+$ decreases the mobility of $(n\text{-}C_4H_9)_4N^+$. Although the 18C6 complex with K^+ would undergo specific solvation than $(n\text{-}C_4H_9)\ N^+$ much more strongly as is stated above and, moreover, hydrogen bonds between protic solvent molecules and ether oxygen atoms of 18C6 would decrease the mobility of the 18C6 complex with K^+, the 18C6 complex is much more mobile than $(n\text{-}C_4H_9)_4N^+$ in H_2O and is nearly as mobile as $(n\text{-}C_4H_9)_4N^+$ in CH_3OH (Table 2). This indicates that the 18C6 complex with K^+ in H_2O and CH_3OH does not enforce the hydrogen-bonded structure around the complexed ion like $(n\text{-}C_4H_9)_4N^+$ does. This is supported by the data in Table 3. As can be seen from Table 3, Walden products of 18C6 complexes with K^+ for the solvents are nearly equal to each other, while, that of $(n\text{-}C_4H_9)_4N^+$ for H_2O is much smaller than those of $(n\text{-}C_4H_9)_4N^+$ for the other solvents and those of $(n\text{-}C_4H_9)_4N^+$ for the other solvents are nearly identical. Judging from the above observations, the 18C6 complex with K^+ appears to act as a structure breaker in hydrogen-bonding solvents, and the complex shows almost the same behavior for transport phenomena in all the solvents in Table 3. The ratio of λ° value of the 18C6 complex with K^+ to that of $(n\text{-}C_4H_9)_4N^+$ for H_2O (1.3) is much larger than that for CH_3OH (1.0) (Table 2). This may reflect a difference in characteristics of hydrogen bonds for H_2O and CH_3OH. Since H_2O forms three-dimentional structures *via* hydrogen bonding, while, CH_3OH can form only one-dimentional structures *via* hydrogen bonding, the effect of hydrogen-bonded structure enforcement on the mobility of $(n\text{-}C_4H_9)_4N^+$ appears to be much greater for H_2O than for CH_3OH.

As can be seen from Table 2, for acetonitrile and DMSO, the λ° value of DB18C6 complex with K^+ is smaller than those of tetrapentylammonium ion ($(n\text{-}C_5H_{11})_4N^+$) and tetraisopentylammonium ion ($(i\text{-}C_5H_{11})_4N^+$); for nitrobenzene and propylene carbonate, that of DB18C6 complex with K^+ is smaller

Table 2. λ° values in various solvents at 25 °C

	λ°/Ω^{-1} cm^2 mol^{-1}							
	C_2H_5OH	CH_3OH	$C_6H_5NO_2$	CH_3CN	DMF	DMSO	PC[a)]	H_2O
K^+	23.55[7)]	52.44[7)]	17.53[8)]	83.6[9)]	30.6$_5$ [5)]	14.69[10)]	11.9$_8$ [3)]	73.55[7)]
18C6-K^+	—	39.$_9$	—	59	24.$_6$ [5)]	10.$_0$	8.9$_1$ [3)]	25.$_3$
DB18C6-K^+	18.40[11)]	35.$_5$	9.6[12)]	53	22.$_3$	8.$_2$	7.$_3$	—
(2,2)-K^+	—	—	—	62.4[13)]	—	—	—	—
DB24C8-K^+	—	—	—	—	—	—	7.4$_2$ [3)]	—
$(n\text{-}C_4H_9)_4N^+$	19.67[14)]	38.94[7)]	11.9[15)]	61.4[9)]	26.9[16)]	11.2$_9$ [16)]	9.32[16)]	19.31[7)]
$(n\text{-}C_5H_{11})_4N^+$	—	34.8[17)]	10.6[18)]	55.1[19)]	—	10.41[20)]	—	—
$(i\text{-}C_5H_{11})_4N^+$	—	35.2$_6$ [21)]	—	57.24[8)]	—	10.61[20)]	8.185[22)]	—
$(n\text{-}C_7H_{15})_4N^+$	14.93[14)]	—	—	—	—	9.18[20)]	—	—
ClO_4^-	—	—	—	103.7[9)]	52.8$_5$ [5)]	24.52[10)]	18.2$_3$ [16)]	67.2[23)]
Cl^-	—	52.36[7)]	—	—	—	—	—	76.39[7)]

a) Propylene carbonate.

TABLE 3. WALDEN PRODUCTS AND VISCOSITIES (η_0) AT 25 °C

	C_2H_5OH	CH_3OH	$C_6H_5NO_2$	CH_3CN	DMF	DMSO	PC[a]	H_2O
η_0/mP*	10.84[14]	5.42[24]	18.11[24]	3.39[24]	7.96[24]	19.6[24]	25.3[24]	8.903[24]
18C6-K^+	—	0.21_6	—	0.20	0.19_5[5]	0.19_6	0.22_5[3]	0.22_5
DB18C6-K^+	0.1995[11]	0.19_2	0.17[12]	0.18	0.17_7	0.16	0.18	—
$(n\text{-}C_4H_9)_4N^+$	0.2132[14]	0.211[7]	0.216[15]	0.208[9]	0.214[16]	0.221[16]	0.236[16]	0.1719[7]

* 1 P=0.1 Pa s. a) Propylene carbonate.

than those of $(n\text{-}C_5H_{11})_4N^+$ and $(i\text{-}C_5H_{11})_4N^+$, respectively. In contrast to the cases of aprotic solvents, the λ° value of DB18C6 complex with K^+ for CH_3OH is nearly equal to those of $(n\text{-}C_5H_{11})_4N^+$ and $(i\text{-}C_5H_{11})_4N^+$. For DMSO, the DB18C6 complex with K^+ is not so mobile as tetraheptylammonium ion ($(n\text{-}C_7H_{15})_4N^+$), and contrary holds for C_2H_5OH. The fact that, for every aprotic solvent, the DB18C6 complex with K^+ is less mobile than these tetraalkylammonium ions can be attributed to the fact that the former would undergo specific solvation much more strongly than the latter, as is stated above. The results for protic solvents indicate that the effect of hydrogen-bonded structure enforcement on the mobility is very much larger for these tetraalkylammonium ions than for the DB18C6 complex with K^+. Walden products of DB18C6 complexes with K^+ are nearly equal to each other (Table 3). Thus, it seems that the behavior of the DB18C6 complex with K^+ for transport phenomena is much the same in the various solvents.

From the above discussion, it appears that a solute which contains a unit of 18C6 in its structure does not enforce hydrogen-bonded structure of a protic solvent.

References

1) D. F. Evans, S. L. Wellington, J. A. Nadis, and E. L. Cussler, *J. Solution Chem.*, **1**, 499 (1972).
2) H. Høiland, J. A. Ringseth, and T. S. Brun, *J. Solution Chem.*, **8**, 779 (1979).
3) Y. Takeda, H. Yano, M. Ishibashi, and H. Isozumi, *Bull. Chem. Soc. Jpn.*, **53**, 72 (1980).
4) I. M. Kolthoff and M. K. Chantooni, Jr., *Anal. Chem.*, **52**, 1039 (1980).
5) Y. Takeda, *Bull. Chem. Soc. Jpn.*, **54**, 3133 (1981).
6) Y. Takeda and H. Yano, *Bull. Chem. Soc. Jpn.*, **53**, 1720 (1980).
7) R. L. Kay and D. F. Evans, *J. Phys. Chem.*, **70**, 2325 (1966).
8) J. F. Coetzee and G. P. Cunningham, *J. Am. Chem. Soc.*, **87**, 2529 (1965).
9) C. H. Springer, J. F. Coetzee, and R. L. Kay, *J. Phys. Chem.*, **73**, 471 (1969).
10) R. Gopal and J. S. Jha, *J. Phys. Chem.*, **78**, 2405 (1974).
11) M. S. Frant and J. W. Ross, *Science*, **167**, 987 (1970).
12) T. Iwachido, M. Kimura, and K. Tōei, *Chem. Lett.*, **1976**, 1101.
13) S. Kulstad and L. Å. Malmsten, *J. Inorg. Nucl. Chem.*, **42**, 573 (1980).
14) D. F. Evans and P. Gardam, *J. Phys. Chem.*, **72**, 3281 (1968).
15) C. R. Wischonke and C. A. Kraus, *J. Am. Chem. Soc.*, **69**, 2472 (1947).
16) N. Matsuura, K. Umemoto, and Y. Takeda, *Bull. Chem. Soc. Jpn.*, **48**, 2253 (1975).
17) R. L. Kay, C. Zawoyski, and D. F. Evans, *J. Phys. Chem.*, **69**, 4208 (1965).
18) E. G. Taylor and C. A. Kraus, *J. Am. Chem. Soc.*, **69**, 1731 (1947).
19) A. C. Harkness and H. M. Daggett, Jr., *Can. J. Chem.*, **43**, 1215 (1965).
20) D. E. Arrington and E. Griswold, *J. Phys. Chem.*, **74**, 123 (1970).
21) R. L. Kay, D. F. Evans, and G. P. Cunningham, *J. Phys. Chem.*, **73**, 3322 (1969).
22) L. M. Mukherjee, D. P. Boden, and R. Liendauer, *J. Phys. Chem.*, **74**, 1942 (1970).
23) A. D'Aprano, *J. Phys. Chem.*, **75**, 3290 (1971).
24) G. J. Janz and R. P. T. Tomkins, "Nonaqueous Electrolytes Handbook," Academic Press, New York and London (1972), Vol. 1.

 © 1983 The Chemical Society of Japan Bull. Chem. Soc. Jpn., 56, 869—872 (1983)

Mechanism of Chlorine Catalytic Oxidation of CO in the Gas Phase

Tomohiro OHTA

Department of Environmental Sciences, Tokyo Metropolitan Research Laboratory of Public Health, Hyakuninchō, Shinjuku-ku, Tokyo 160

(Received July 14, 1982)

The mechanism of the title reaction is determined under steady state conditions by the irradiation of the mixtures of Cl_2, CO, O_2, and N_2 at 300 K with black blue fluorescence lamps using infrared spectroscopy. The pressure dependence of the ratio of the formation rate of carbon dioxide to that of phosgene($COCl_2$) and the other results indicated that the oxidation of CO proceeded *via* intermediates ClCO and $ClC(O)O_2$ as the termolecular process rather than the bimolecular oxidation by ClOO and/or ClO. The ratio of the competitive reactions of chloroformyl radicals, k_8/k_{9a}, was found to be $(6.5\pm0.4)\times10^{-2}$ in the total pressure range from 30 to 755 Torr (1 Torr=133 Pa); $ClCO+Cl_2\rightarrow COCl_2+Cl$ (8), $ClCO+O_2\rightarrow ClC(O)O_2$* (9a). And also, the ratio of the competitive reactions of the vibrationally excited intermediates, k_{9b}/k_{9c}, was $(3.4\pm0.3)\times10^{18}$ molecule/cm^3; $ClC(O)O_2^*\rightarrow ClCO+O_2$ (9b), $ClC(O)O_2^*+M\rightarrow ClC(O)O_2+M$ (9c). The role of this reaction in the stratosphere is discussed and estimated to be unimportant.

Accumulation of CO_2 in the atmosphere has been discussed to affect the temperature of the erath in future.[1] In addition to the direct emission of CO_2 by combustion, breathing, and respiration, the chemical oxidation of CO is believed to occur in the atmosphere. The major pathway is the oxidation by OH radicals.[2] Catalytic oxidation cycle of Cl atoms, which are formed from the ultraviolet photolysis of chlorofluorocarbons in the stratosphere, may contribute to the conversion as another possible path. And any reaction involving Cl atoms is essential to understand chlorine reaction in the atmosphere.

The oxidation of CO by Cl atoms in the presence of O_2 was found as early as 1930's.[3,4] Brenschede,[5] in illuminating mixtures of CO, O_2, and Cl_2, found the ratio of formed CO_2 to formed $COCl_2$ to be given by Eq. 1,

$$\frac{[CO_2]}{[COCl_2]} = A\frac{[O_2]_0}{[Cl_2]_0}, \quad (1)$$

where A increases with total pressure at first rapidly and then slowly. But his interpretation on mechanism involved uncertainty, because he did not analyze the pressure dependence behavior and the value of the proportionality constant in terms of kinetics. A probable mechanism for chlorine catalytic oxidation of CO is Reaction 2 and/or 3 as proposed by Prinn,[6] but very little information is available on the rate constant involving ClO_x. The other is Reaction 4 proposed by Spence *et al.*[7] by observing $ClC(O)OONO_2$ as an oxidation product of the ultraviolet irradiation of Cl_2, NO_2, and CO mixtures in air, though the possibility of Reaction 2 and/or 3 is not excluded from their experiments.

$$ClOO + CO \longrightarrow ClO + CO_2 \quad (2)$$

$$ClO + CO \longrightarrow Cl + CO_2 \quad (3)$$

$$Cl + CO \longrightarrow ClCO \xrightarrow[O_2]{} ClC(O)O_2 \longrightarrow ClCO_2 \longrightarrow Cl + CO_2 \quad (4)$$

In this paper, we try to analyze the relation (1) to get more information on the mechanism of the reaction system by irradiating the mixture of Cl_2, CO, O_2, and N_2 with varying the initial conditions and add some facts that supports the mechanism involving ClCO and $ClC(O)O_2$. And also the role of the reaction in the atmosphere is discussed.

Experimental

Chlorine from a cylider (Fujimoto Sanso) was pumped through a trap immersed in isopentane-liquid nitrogen bath (160 °C). The condensed fraction was used for the experiments. CO, O_2, and N_2 form research grade steel cylinders were used without further purification. Experimental apparatus was described previously.[8] In brief, reactant gases Cl_2, CO, and O_2 and inert gas N_2 were mixed in a 10 cm Pyrex-body infrared absorption cell of 4 cm diameter (window was NaCl). The cell was mounted in the sample beam of the infrared spectrometer. Two 20-W black blue light lamps irradiated into the cell from 7 cm above at 27±1 °C. Concentration-time profile of the products, CO_2 and $COCl_2$, increased lineary within the irradiation time of 50 s. Thus, measurement of the initial rates was made after light exposure of less than 30 s duration. The concentration was determined by measuring the peak intensity. The peak and absorption coefficients used were the same as those in the previous publication except $COCl_2$. $COCl_2$ was measured by the more sensitive absorption at 852 cm^{-1} in this work.

Results and Discussion

It is well confirmed by early works[9] that when mixtures of CO, Cl_2, and O_2 are illuminated with light which is absorbed by Cl_2, part of CO is changed to $COCl_2$ and part to CO_2, and that, at relatively high pressures of O_2, CO_2 formation occurs almost exclusively, whereas at low O_2 pressures $COCl_2$ formation is predominant.

The mechanism of the formation of $COCl_2$ is well established by Burns and Dainton[10] to be the reactions (5) to (8) in this system. In the later work by Jacox and Milligan,[11] the formation of chloroformyl radical, ClCO, from the reaction of Cl with CO was confirmed using an argon matrix by infrared spectroscopy.

$$Cl_2 + h\nu \longrightarrow 2Cl \quad (5)$$

$$Cl + CO + M \rightleftharpoons ClCO + M \quad (6, -6)$$

$$ClCO + Cl \longrightarrow Cl_2 + CO \quad (7)$$

$$ClCO + Cl_2 \longrightarrow COCl_2 + Cl \quad (8)$$

As a first series of experiment, each initial pressure of Cl_2 and O_2 was held constant at 10 Torr (1 Torr=133 Pa) and CO pressure was varied while keeping

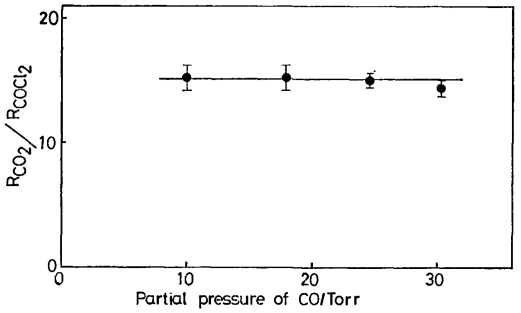

Fig. 1. The function, R_{CO_2}/R_{COCl_2}, *vs.* partial pressure of CO in the photolysis of $Cl_2/CO/O_2/N_2$; $[Cl_2]_0=[O_2]_0=10$ and [total pressure]$_0=755$ Torr.

the total pressure at 755 Torr. The value R_{CO_2}/R_{COCl_2} was plotted against the partial pressure of CO (Fig. 1). The value was independent on the partial pressure of CO as found in the previous work.[5] If the reaction intermediates ClOO and/or ClO were important for the CO oxidation, Cl would have two competitive paths: one is the association with O_2 to form CO_2 *via* Reactions 2 and/or 3 and the other is association with CO to form $COCl_2$ *via* Reactions 6 and 8, R_{CO_2}/R_{COCl_2} would decrease as the initial pressure of CO increases. Thus, the oxidation of CO seems to occur *via* the intermediate ClCO, not *via* ClOO or ClO.

Then, the effect of the total pressure on the ratio of the initial formation rates, R_{CO_2}/R_{COCl_2}, was examined at total pressure ranging from 30 to 755 Torr by changing the amount of added N_2 to a mixture of 10 Torr of Cl_2, 10 Torr of CO, and 10 Torr of O_2. The infrared spectra were taken after filling N_2 up to 755 Torr following the photolysis, since IR intensities of CO and CO_2 depend on the total pressure. The logarithm of R_{CO_2}/R_{COCl_2} is plotted against that of the total pressure (Fig. 2). Typical fall-off behavior is appeared in the figure. Since stripping reaction such as Reaction 8 is not usally pressure dependent, the observed pressure effect is due to the pressure dependence in the CO_2 formation process, and this reaction seems to proceed *via* a stabilized adduct ($ClC(O)O_2$) from a vibrationally excited intermediate ($ClC(O)O_2$*). High pressure limit appears a little above the highest pressure used in our experiment, and it is higher than the limit observed for $C_2H_5+O_2$ by Plumb and Ryan[11] as expected from the consideration of the number of degrees of freedom.

Consequently, let us assume the following reaction mechanism involving ClCO and $ClC(O)O_2$.

$$ClCO + O_2 + M \longrightarrow ClC(O)O_2 + M \quad (9)$$

$$ClC(O)O_2 + ClC(O)O_2 \longrightarrow 2ClCO_2 + O_2 \quad (10)$$

$$ClCO_2 \longrightarrow Cl + CO_2 \quad (11)$$

In order to make some estimation for the fall-off region, the combination reaction 9 is decomposed into the steps 9a to 9c.

$$ClCO + O_2 \longrightarrow ClC(O)O_2^* \quad (9a)$$

$$ClC(O)O_2^* \longrightarrow ClCO + O_2 \quad (9b)$$

$$ClC(O)O_2^* + M \longrightarrow ClC(O)O_2 + M \quad (9c)$$

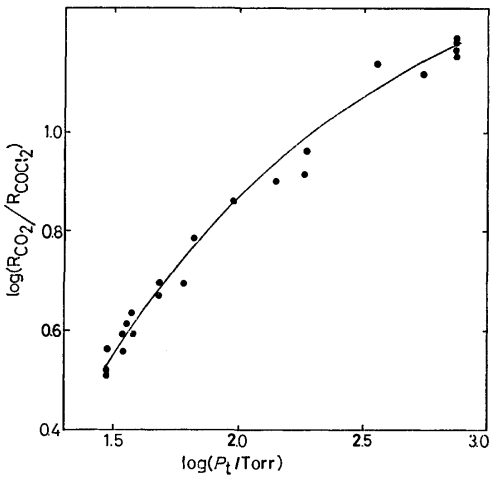

Fig. 2. Total pressure (P_t) dependence of the function, R_{CO_2}/R_{COCl_2} in the photolysis of $Cl_2/CO/O_2/N_2$; $[Cl_2]_0=[O_2]_0=[CO]_0=10$ Torr.

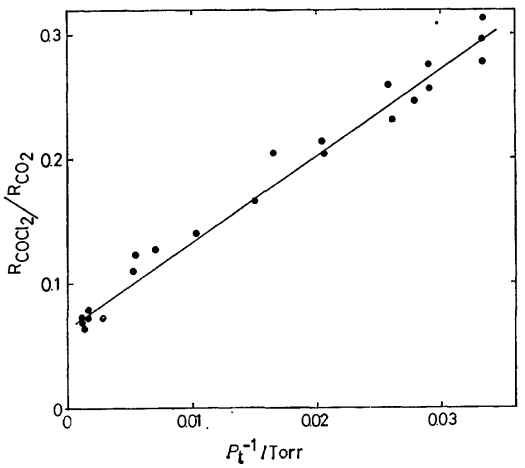

Fig. 3. The function, R_{COCl_2}/R_{CO_2} *vs.* inverse of total pressure (P_t) in the photolysis of $Cl_2/CO/O_2/N_2$; $[Cl_2]_0=[CO]_0=[O_2]_0=10$ Torr.

The steady state treatment with respect to $ClC(O)O_2$* gives,

$$[ClC(O)O_2^*] = \frac{k_{9a}[ClCO][O_2]}{k_{9b}+k_{9c}[M]}. \quad (12)$$

The formation rate of CO_2 is expressed by Eq. 13, if we apply the steady state treatment also to $ClC(O)O_2$ and $ClCO_2$.

$$R_{CO_2} = k_{9c}[ClC(O)O_2^*][M] = \frac{k_{9a}k_{9c}[ClCO][O_2][M]}{k_{9b}+k_{9c}[M]} \quad (13)$$

And,

$$R_{COCl_2} = k_8[ClCO][Cl_2]. \quad (14)$$

Then,

$$\frac{R_{COCl_2}}{R_{CO_2}} = \frac{[Cl_2]}{[O_2]}\left(\frac{k_8}{k_{9a}}+\frac{k_8k_{9b}}{k_{9a}k_{9c}[M]}\right). \quad (15)$$

To correlate Eq. 15 with the pressure dependence, the value, R_{COCl_2}/R_{CO_2}, from the same data used in Fig. 2 is replotted *vs.* inverse of total pressure (Fig. 3). The plots gave a straight line which is fit by

Eq. 15 under our experimental conditions. Assume $[Cl_2]/[O_2]$ is 1 during the course of the irradiation in the experiment of total pressure variation, since the initial concentration of Cl_2 and O_2 were 10 Torr and the photolysis did not exceed 10% of the reactants. We obtained the values of k_8/k_{9a} and $k_8k_{9b}/k_{9a}k_{9c}$ from the intercept and the slope in Fig. 3, respectively.

$$k_8/k_{9a} = (6.45\pm0.41)\times10^{-2}\ \text{Torr} \quad (16)$$

$$k_8k_{9b}/k_{9a}k_{9c} = (6.89\pm0.21)\ \text{Torr}, \quad (17)$$

where error is a standard deviation of the least-squares analysis.

Then,

$$k_{9b}/k_{9c} = (108\pm8)\ \text{Torr} = (3.4\pm0.3)\times10^{18}\ \text{molecule/cm}^3 \quad (18)$$

Eq. 16 and the literature value,[10] $k_8=2.91\times10^{-14}$ cm^3 molecule^{-1} s^{-1} at 300 K, gives $k_{9c}=4.51\times10^{-13}$ cm^3 molecule^{-1} s^{-1}. The k_{9a} value is ten times smaller than the rate constant for a similar recombination $C_2H_5+O_2\rightarrow C_2H_5O_2$* reported by Plumb and Ryan.[12] It is also important to note that $ClCO+O_2$ addition (9a) is faster than the competing reaction of Cl abstraction by ClCO from Cl_2 (8).

To evaluate the obtained value of Eq. 18, 3.4×10^{18} molecule/cm^3, k_{9b} and k_{9c} may be estimated from a quantum RRK theory for unimolecular decomposition of energized molecule. Necessary parameters are assumed as: the proportionality constant is to be 10^{14} s^{-1} from the Arrhenius A factor for the unimolecular decomposition of alkyl-O_2[13]: the bond strength of $ClC(O)$–O_2 is 28 kcal/mol from that of alkyl-O_2[13]: the geometrical mean frequency is guessed at 640 cm^{-1} by assigning 600 Cl–C st. from $ClC(O)CH_3$ in Ref. 14, 1800 for C=O st. from $ClC(O)OONO_2$ in Ref. 7, 1200 for C–O st. in Ref. 15, 880 for O–O st. from HO_2NO_2 in Ref. 16, 400 for O–O–C bend,[15] 420 for O=C–O,[15] 360 for O=C–Cl,[15] and 400 for O–C–Cl,[15] all in units of cm^{-1}. If we choose 9 as the number of effective oscillators, k_{9b} is about 10^8 s^{-1}. By substituting k_{9b} in Eq. 18, k_{9c} becomes 3×10^{-11} cm^{3}molecule^{-1} s^{-1}. Although we do not have enough knowledge what value less than 9 is proper for the number of effective oscillations, the k_{9c} derived from crude calculation is near collision frequency under our experimental conditions. Hence, the value (18) obtained here appears reasonable.

Next, we find k_8/k_9 at 755 Torr from the equations obtained. From Reaction 9,

$$R_{ClC(O)O_2} = k_9[ClCO][O_2][M] = R_{CO_2}. \quad (19)$$

From the comparison of Eq. 19 with 13,

$$k_{9a} = \frac{k_{9a}\,k_{9c}}{k_{9b}+k_{9c}[M]}. \quad (20)$$

From this,

$$\frac{k_8}{k_9} = \frac{k_8}{k_{9a}}\left(\frac{k_{9b}}{k_{9c}}+[M]\right). \quad (21)$$

By substituting the values of $k_8/k_{9a}=6.45\times10^{-2}$ and $k_{9b}/k_{9c}=107$ Torr found before,

$$\frac{k_8}{k_9} = 0.0645(107+[M]). \quad (22)$$

When [M]=755 Torr, k_8/k_9 is calculated to be 55.6 Torr.

Rollefson, in the previous work,[17] assumed Reaction 23 in place of the set of the Reactions 9, 10, and 11. He disregarded the pressure effect on the products distribution and obtained the value 0.2 for k_8/k_{23} by finding that the number of moles of Cl_2 and O_2 reacting to be equal when the Cl_2 pressure was five times that of oxygen.

$$ClCO + O_2 \longrightarrow CO_2 + ClO. \quad (23)$$

The ratio k_8/k_{23} by Rollefson corresponds to $k_8/(k_9[M])$ in our mechanism. Since he did not show the total pressure of each run, we guess mean value for the total pressure [M] as 50 Torr from the list of the partial pressure of three reactants. Then, $k_8/(k_9[M])$ becomes 0.2 that agrees very well with the results shown by Rollefson.

In order to compare the derived value of k_8/k_9 with the value obtained experimentally at constant total pressure, we determined A in Eq. 1 in different initial conditions. First, by keeping the constant total pressure of 755 Torr and the initial concentration of Cl_2 and CO at 10 Torr, the pressure of O_2 was varied. Plot of the values of R_{CO_2}/R_{COCl_2} against the initial pressure of O_2 gave a straight line (Fig. 4). From the relations (14) and (19),

$$\frac{R_{CO_2}}{R_{COCl_2}} = \frac{k_9[M]}{k_8[Cl_2]}[O_2]. \quad (24)$$

The relation (24) fits to the line. The slope is 1.48, which corresponded to $k_9[M]/(k_8[Cl_2])$. Thus,

$$k_8/k_9 = 51.0\ \text{Torr}. \quad (25)$$

Secondly, by keeping the total pressure, initial pressure of CO and O_2 constant, 755, 10, and 10 Torr, respectively, the partial pressure of Cl_2 was varied. The plot of the value of R_{COCl_2}/R_{CO_2} against the partial pressure of Cl_2 gave also a straight line with a slope of 0.00645 (Fig. 5). The slope must be equal to $k_8/(k_9[M][O_2])$. Then,

$$k_8/k_9 = 48.7\ \text{Torr}. \quad (26)$$

In view of the consumption of O_2 and Cl_2 during the irradiation that will cause error, the value 55.6 Torr

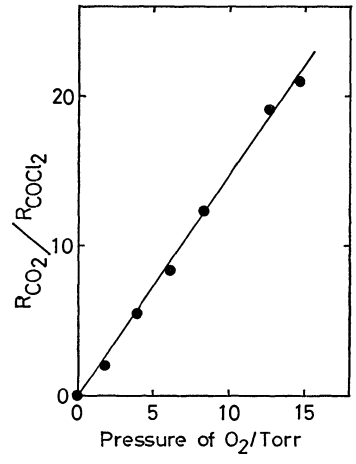

Fig. 4. The function, R_{CO_2}/R_{COCl_2} *vs.* partial pressure of O_2 in the photolysis of $Cl_2/CO/O_2/N_2$; $[Cl_2]_0=[CO]_0=10$ and $[\text{total pressure}]_0=755$ Torr.

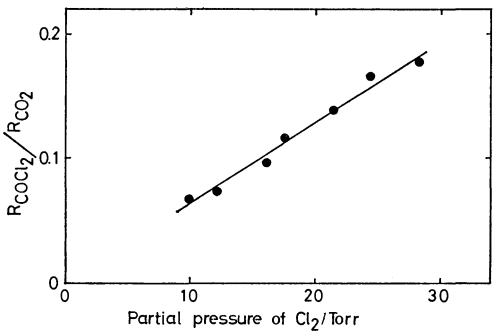

Fig. 5. The function, R_{COCl_2}/R_{CO_2} *vs.* partial pressure of Cl_2 in the photolysis of $Cl_2/CO/O_2/N_2$; $[CO]_0 = [O_2]_0 = 10$ and [total pressure]$_0$ = 755 Torr.

for k_8/k_9 determined from the assumption of termolecular process agrees with the results (25) and (26) obtained from the different experiments.

In consideration of all the points discussed above, the termolecular process via ClCO and $ClC(O)O_2$ is confirmed to be the major pathway for the oxidation of CO by Cl atoms at the pressure range of 30 to 755 Torr.

It is of interset to discuss the role of this termolecular reaction in the atmosphere. The most important reaction of Cl in the stratosphere is beleived to be Reaction 27, whose rate constant is $2.7 \times 10^{-11} \exp(-257/RT)$ cm^3 molecule^{-1} s^{-1}.[18]

$$Cl + O_3 \longrightarrow ClO + O_2 \qquad (27)$$

k_6 was determined to be $10^{14.5}$ cm^6 molecule^{-2} s^{-1} or 8.73×10^{-34} cm^6 molecule^{-2} s^{-1} at 300 K by Clark *et al.*[19] Since the Arrhenius parameters for the rate constant was not given, let us compare k_{27} with $k_6[M]$ at 300 K and 1 atmospheric pressure to get a rough idea on the role of ClCO mechanism in the stratosphere: k_{27} is 10000 times larger than $k_6[M]$. In the upper atmosphere at low pressure, $k_6[M]$ becomes smaller, and moreover, the concentration of ozone is higher than that of CO in the region.[20,21] Thus, Reaction 27 is predominant over Reaction 6. Even when ClCO is formed and becomes adduct, $ClC(O)O_2$*, it dissociates very easily, since the atmospheric density is too low to make three-body reaction effective. Therefore, the oxidation of CO by Cl catalytic cycle is not important in the atmosphere.

The author is grateful to Professor Ikuzo Tanaka, Tokyo Institute of Technology, Professor Okitsugu Kajimoto, The University of Tokyo and Haruo Tsuruta, Yokohama Research Institute for Environmental Protection, for helpful discussions. He also thanks Dr. Isao Mizoguchi for his interest and encouraging.

References

1) S. Watanabe and R. T. Wetherald, *J. Atmos. Sci.*, **24**, 241 (1967).
2) H. Levey, II, *Science*, **173**, 141 (1971).
3) S. Lenher and G. K. Rollefson, *J. Am. Chem. Soc.*, **52**, 500 (1930).
4) M. Bodenstein, S. Lenher, and C. Wagner, *Z. Physk. Chem.*, **B3**, 459 (1929).
5) W. Brenschede, *Z. Phys. Chem.*, **40B**, 237 (1938); **41B**, 254 (1938).
6) P. G. Prinn, "Physics and Chemistry of Upper Atmosphere," ed by B. M. McCormac, Rediel, Dordrechet, Holland (1973).
7) J. W. Spence, E. O. Edney, and P. L. Hanst, *Chem. Phys. Lett.*, **56**, 478 (1978).
8) T. Ohta and I. Mizoguchi, *Int. J. Chem. Kinet.*, **12**, 717 (1980).
9) W. A. Noyes, Jr., and P. A. Leighton, "Photochemistry of Gases," Dover Publication Inc., New York (1941) and references therein.
10) W. G. Burns and F. S. Dainton, *Trans. Faraday Soc.*, **48**, 39 (1952).
11) M. E. Jacox and D. E. Milligan, *J. Chem. Phys.*, **43**, 866 (1965).
12) I. C. Plumb and K. R. Ryan, *Int. J. Chem. Kinet.*, **13**, 1011 (1981).
13) S. W. Benson, *J. Am. Chem. Soc.*, **87**, 972 (1965).
14) T. Shimanouchi, "Analysis of Infrared Spectra," Nankodo, Tokyo (1960) in Japanese.
15) S. W. Benson, "Thermochemical Kinetics," 2nd ed, Wiley, New York (1976).
16) A. C. Baldwin and D. M. Golden, *J. Phys. Chem.*, **82**, 644 (1978).
17) G. K. Rollefson, *J. Am. Chem. Soc.*, **55**, 148 (1933).
18) R. T. Watson, *J. Phys. Chem. Ref. Data*, **6**, 871 (1977).
19) T. C. Clark, M. A. A. Clyne, and D. H. Stedmsn, *Trans. Faraday Soc.*, **62**, 3354 (1966).
20) A. J. Kruger and R. A. Minzner, *J. Geophys. Res.*, **81**, 4477 (1976).
21) P. Fabian, R. Borchers, K. H. Weiler, U. Schmidt, A. Voltz, D. H. Ehhalt, W. Seiler, and F. Muller, *J. Geophys. Res.*, **84**, 3149 (1979).

Conductimetric Study of the Ion Pair Formation in Mixtures of Bivalent Metal Nitrates and Sodium Sulfate in Aqueous Solutions

Shunzo KATAYAMA,* Kazuko TANAKA, and Reita TAMAMUSHI

Inorganic Chemistry Laboratory, The Institute of Physical and Chemical Research, Wako, Saitama 351

(Received September 7, 1982)

The conductance behavior of electrolyte mixtures was investigated for the systems of bivalent metal nitrates and sodium sulfate in aqueous solutions of high ionic strengths ($I \geq 0.3$ mol dm^{-3}) at 25 °C. Significant deviations of the measured conductivities from the additivity were observed in all the systems, which can be attributed to the ion pair formation of the bivalent metal ion with sulfate ion. The conditional formation constants, K_c, were determined by means of computer analysis of the deviation; K_c-values at each ionic strength were found to decrease in the sequence Cd > Mn ≃ Ni ≃ Co ≃ Zn > Mg.

The measurement of electrolytic conductivity of mixtures of two electrolytes provides a valuable method of studying the ionic interaction. The conductance behavior of binary mixtures of 1-1, 2-1, and 2-2 type electrolytes was studied by Rysselberghe *et al.*[1,2] and by Davies.[3,4] Recently, Fisher[5] reported about the ion association in mixtures of 0.005 mol dm^{-3} $MgCl_2$ and 0.005 mol dm^{-3} Na_2SO_4 solutions as a function of pressure.

In our previous works,[6,7] the continuous variation method was applied to the determination of the ion pair formation constants of $[Co(NH_3)_6]^{3+}\cdot SO_4^{2-}$, $[Co(en)_3]^{3+}\cdot SO_4^{2-}$, $[Co(en)_3]^{3+}\cdot(Maleate)^{2-}$, and $[Co(en)_3]^{3+}\cdot(Fumarate)^{2-}$ from the conductivity measurement of mixtures. Good agreement of the results obtained for $[Co(NH_3)_6]^{3+}\cdot SO_4^{2-}$ with those of Jenkins and Monk[8] suggests that the conductivity measurement of mixtures is a useful method for determining formation constants.

The application of the conductimetric continuous variation method to the determination of formation constants appears to have the advantage that the measured quantities can be analysed, in principle, without relying on the quantitative validity of the theoretical equation of conductivity; this advantage is particularly important when the method is applied to systems of higher ionic strengths.[9]

This paper deals with the determination of ion pair formation constants of bivalent metal ions (Mg^{2+}, Mn^{2+}, Co^{2+}, Ni^{2+}, Zn^{2+}, and Cd^{2+}) with sulfate ion at 25 °C in aqueous solutions of apparent ionic strengths 0.3—6 mol dm^{-3} from the conductivity measurements of electrolytic solution mixtures.

Experimental

Materials and Preparation of Solutions. $Mg(NO_3)_2\cdot 6H_2O$, $Mn(NO_3)_2\cdot 6H_2O$, $Co(NO_3)_2\cdot 6H_2O$, $Ni(NO_3)_2\cdot 6H_2O$, $Zn(NO_3)_2\cdot 6H_2O$, $Cd(NO_3)_2\cdot 4H_2O$, and Na_2SO_4 of analytical reagent grade were used without further purification. The purity of the samples was determined by chemical analysis of the components. The analysis gave results which were in good agreement with the theoretical values.

Solutions of different concentrations were prepared by using conductivity water (conductivity $< 2.0\times10^{-7}$ Ω^{-1} cm^{-1} at 25 °C).

Conductivity Measurements. Electrolytic conductivities of mixtures were measured by mixing the solutions of the same ionic strength at various volume fractions. A conductance-linear-bridge, operated at 1000 Hz, was used for conductivity measurements as described in previous papers.[10,11] The resistance readings of the bridge were calibrated by the substitution method with a precision decade resistance box (Dekastat RS-624, Electro Scientific Industries; accuracy ±0.005%). Three conductivity cells designed for solutions of moderate and high conductivities were used. The cell constants were determined to be 11.093 cm^{-1}, 35.422 cm^{-1}, and 97.349 cm^{-1} by using standard potassium chloride solutions. The reproducibility of the conductivity measurements was better than 0.05%. All measurements were carried out in a water–ethylene glycol mixture bath of 25.000± 0.003 °C, which was electrically grounded.

Results and Discussion

Analysis of Conductivity of Electrolyte Mixtures.[6] Let us consider the conductivity of a solution prepared by mixing volume ϕV of a solution of molar concentration, c_1, of MA_2 (M: bivalent metal, A: NO_3) and volume $(1-\phi)V$ of a solution of molar concentration, c_2, of N_2B (N: Na, B: SO_4) to give the solution of total volume V; the concentrations, c_1 and c_2, are adjusted so that the apparent ionic strength of the mixtures is independent of volume fraction, ϕ (in the present study $c_1 = c_2 = c$).

The conductivity, κ_{calcd}, of the mixture calculated by using the additivity rule is given by

$$10^3\kappa_{calcd} = z_M\lambda_M c\phi + z_A\lambda_A 2c\phi + z_N\lambda_N 2c(1-\phi) + z_B\lambda_B c(1-\phi), \quad (1)$$

where z is the charge number of ionic species, and λ the ionic equivalent conductivity at the ionic strength of the mixture. If the following ion pair formation is assumed in the mixture:

$$M^{2+} + B^{2-} \rightleftharpoons M^{2+}\cdot B^{2-},$$

the observed conductivity, κ_{obsd}, of the mixture is given by

$$10^3\kappa_{obsd} = z_M\lambda_M(c\phi - [M^{2+}\cdot B^{2-}]) + z_A\lambda_A 2c\phi + z_N\lambda_N 2c(1-\phi) + z_B\lambda_B(c(1-\phi) - [M^{2+}\cdot B^{2-}]), \quad (2)$$

where $[M^{2+}\cdot B^{2-}]$ is the concentration of ion pairs $M^{2+}\cdot B^{2-}$. The deviation, $\Delta\kappa$, of the observed conductivity from additivity is given by

$$10^3\Delta\kappa = 10^3\kappa_{obsd} - 10^3\kappa_{calcd} = -(z_M\lambda_M + z_B\lambda_B)[M^{2+}\cdot B^{2-}]. \quad (3)$$

The deviation $\Delta\kappa$ is then represented by the equation:[6]

$$10^3\Delta\kappa = \Delta\lambda[c+K_c^{-1} - \sqrt{(c+K_c^{-1})^2-4c^2\phi(1-\phi)}]/2, \quad (4)$$

where

$$\Delta\lambda = -(z_M\lambda_M+z_B\lambda_B), \quad (5)$$

and where K_c is the conditional formation constant of $M^{2+}\cdot B^{2-}$ as given by

$$K_c = \frac{[M^{2+}\cdot B^{2-}]}{[M^{2+}][B^{2-}]}. \quad (6)$$

A set of K_c and $\Delta\lambda$ values giving the best fit between the observed and calculated $\Delta\kappa$ values can be determined by computer calculation.

Conductivities of Mixtures in the Absence of Specific Ionic Interactions. The difficulty involved in the conductimetric continuous variation method consists in the fact that the deviation of the observed conductivity from additivity may be caused not only by specific ionic interactions but also by the non-specific effect of the added ions on the mobility of the ions.[12,13] In the present study, the deviation due to the non-specific effect was examined with mixtures of simple electrolytes, in which no specific individual effects is expected.

The conductivities of ($KCl+KNO_3$) and ($KCl+NaCl$) mixtures at apparent ionic strengths $I_{app}=2$ mol dm^{-3} gave slightly smaller values than those expected from additivity; the deviation reached the maximum value of about 0.7% at the volume fraction $\phi=0.5$, as shown in Fig. 1 (curves (1) and (2)). The conductivity of ($Mg(NO_3)_2+Na_2SO_4$) mixtures of $I_{app}=3$ mol dm^{-3}, however, showed a large deviation from additivity of about 12% at $\phi=0.5$ on account of the ion pair formation between Mg^{2+} and SO_4^{2-} (Fig. 1, curve (3)).

Theoretically, the conductivity of electrolyte mixtures is never strictly additive, because of the effect of added ions on the time of relaxation[13]; in our present systems, however, this effect is shown to be negligibly small in comparison with the specific individual effect as seen from Fig. 1. In the following discussion, therefore, the deviation of the observed conductivities from additivity was attributed entirely to the ion pair formation of bivalent metal ion with sulfate ion, the ion association between the bivalent metal ion and nitrate ion and that between sodium ion and sulfate ion being neglected for the sake of simplicity.

Ion Pair Formation Constants of Bivalent Metal Ions with Sulfate Ion. In mixtures of bivalent metal nitrate and sodium sulfate, a large deviation of the measured conductivity from additivity was observed at each ionic strength, as shown by curve (3) in Fig. 1. The conductivities of the mixtures were always smaller than those expected from additivity and showed an extreme at $\phi=0.5$ in each system. Conductivities, κ, of mixtures and the deviation, $\Delta\kappa$, of the observed conductivities from calculated values are shown in Tables 1—6 as a function of the volume fraction, ϕ, of the bivalent metal nitrate. In our present systems, the volume changes of mixing were smaller than about 0.1% and were neglected in the calculation of $\Delta\kappa$.

The conditional formation constants of ion pair, K_c, were determined by analysing the $\Delta\kappa$ values according to Eq. 4. Table 7 summarizes the values of K_c thus determined for $M^{2+}\cdot SO_4^{2-}$ at various ionic strengths. For the six mixtures studied, the K_c values at 25 °C decrease in the sequence: Cd>Mn≃Ni≃Co≃Zn>Mg.

The conditional formation constants at sufficiently low ionic strengths can be estimated from the knowledge of the thermodynamic association constant K_A[10,14,15] and the activity coefficient $y_\pm$ according to the following equations:

$$K_c = K_A y_\pm, \quad (7)$$

$$\log y_\pm = -A|z_M z_B|I^{1/2}/(1+BaI^{1/2}), \quad (8)$$

where A and B are the Debye-Hückel constants and a is the ion-size parameter. Under the assumption that Eqs. 7 and 8 could be satisfied in solutions of

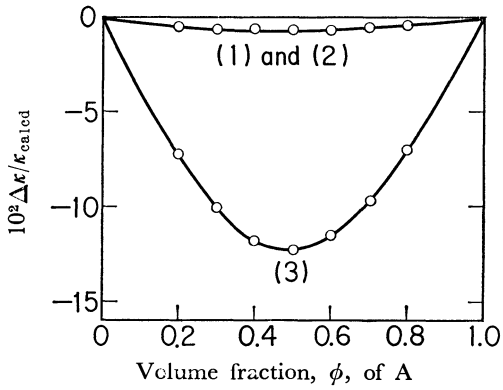

Fig. 1. Deviations, $\Delta\kappa$, of the observed conductivities of mixtures from additivity (25 °C).
(1): $KCl(A)+KNO_3(B)$ mixtures, $I_{app}=2$ mol dm^{-3};
(2): $KCl(A)+NaCl(B)$ mixtures, $I_{app}=2$ mol dm^{-3};
(3): $Mg(NO_3)_2(A)+Na_2SO_4(B)$ mixtures, $I_{app}=3$ mol dm^{-3}.

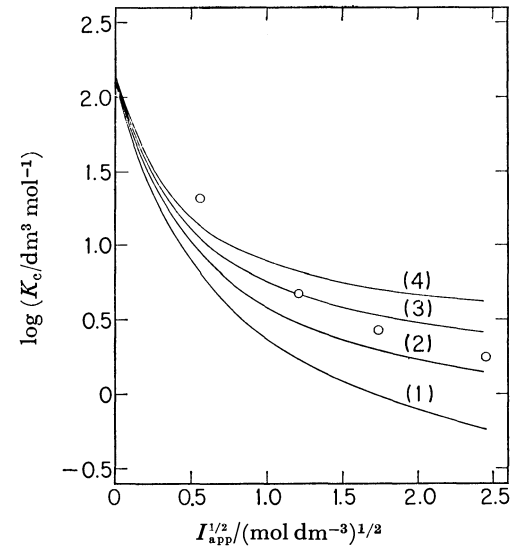

Fig. 2. Experimental (open circle ○) and calculated (solid line —) formation constants for ion pair $Mg^{2+}\cdot SO_4^{2-}$ as a function of apparent ionic strength: a/nm= 0.4 (1), 0.5 (2), 0.6 (3), and 0.7 (4); $K_A=135$ dm^3 mol^{-1}.[10]

Table 1. Conductivities, $\kappa/\Omega^{-1}\,cm^{-1}$, of $(Mg(NO_3)_2+Na_2SO_4)$ mixtures and deviations, $\Delta\kappa/\Omega^{-1}\,cm^{-1}$, of the observed conductivities from calculated values as a function of the volume fraction, ϕ, of $Mg(NO_3)_2$ at various apparent ionic strengths, I_{app}/mol dm^{-3}

ϕ	$10^3\kappa$	$10^3\Delta\kappa$	$10^3\kappa$	$10^3\Delta\kappa$	$10^3\kappa$	$10^3\Delta\kappa$	$10^3\kappa$	$10^3\Delta\kappa$
	(I_{app}=0.3)		(I_{app}=1.5)		(I_{app}=3)		(I_{app}=6)	
0	16.325	—	59.25	—	93.77	—	125.62	—
0.2	15.538	−1.017	56.95	−4.25	90.14	−7.33	119.33	−10.76
0.3	15.285	−1.385	56.39	−5.78	89.31	−10.01	117.36	−14.97
0.4	15.165	−1.621	56.36	−6.78	89.32	−11.85	116.69	−17.87
0.5	15.189	−1.712	56.97	−7.14	90.47	−12.55	117.73	−19.07
0.6	15.384	−1.632	58.26	−6.82	92.83	−12.05	120.66	−18.38
0.7	15.722	−1.409	60.19	−5.86	96.35	−10.38	125.46	−15.81
0.8	16.204	−1.043	62.70	−4.33	100.86	−7.72	131.87	−11.64
1.0	17.477	—	68.97	—	112.28	—	147.98	—

Table 2. Conductivities, $\kappa/\Omega^{-1}\,cm^{-1}$, of $(Mn(NO_3)_2+Na_2SO_4)$ mixtures and deviations, $\Delta\kappa/\Omega^{-1}\,cm^{-1}$, of the observed conductivities from calculated values as a function of the volume fraction, ϕ, of $Mn(NO_3)_2$ at various apparent ionic strengths, I_{app}/mol dm^{-3}

ϕ	$10^3\kappa$	$10^3\Delta\kappa$	$10^3\kappa$	$10^3\Delta\kappa$	$10^3\kappa$	$10^3\Delta\kappa$	$10^3\kappa$	$10^3\Delta\kappa$
	(I_{app}=0.3)		(I_{app}=1.5)		(I_{app}=3)		(I_{app}=6)	
0	16.325	—	59.25	—	93.77	—	125.62	—
0.2	15.327	−1.251	55.91	−5.18	88.40	−8.55	117.10	−11.19
0.3	14.998	−1.707	54.94	−7.07	86.82	−11.72	114.19	−15.43
0.4	14.830	−2.002	54.64	−8.29	86.33	−13.80	112.63	−18.32
0.5	14.850	−2.109	55.17	−8.69	87.25	−14.47	113.03	−19.26
0.6	15.076	−2.009	56.55	−8.23	89.63	−13.68	115.56	−18.06
0.7	15.497	−1.715	58.73	−6.97	93.33	−11.56	119.94	−15.01
0.8	16.078	−1.261	61.54	−5.08	98.08	−8.40	125.59	−10.69
1.0	17.592	—	68.46	—	109.66	—	138.95	—

Table 3. Conductivities, $\kappa/\Omega^{-1}\,cm^{-1}$, of $(Co(NO_3)_2+Na_2SO_4)$ mixtures and deviations, $\Delta\kappa/\Omega^{-1}\,cm^{-1}$, of the observed conductivities from calculated values as a function of the volume fraction, ϕ, of $Co(NO_3)_2$ at various apparent ionic strengths, I_{app}/mol dm^{-3}

ϕ	$10^3\kappa$	$10^3\Delta\kappa$	$10^3\kappa$	$10^3\Delta\kappa$	$10^3\kappa$	$10^3\Delta\kappa$	$10^3\kappa$	$10^3\Delta\kappa$
	(I_{app}=0.3)		(I_{app}=1.5)		(I_{app}=3)		(I_{app}=6)	
0	16.325	—	59.25	—	93.77	—	125.62	—
0.2	15.356	−1.224	56.12	−4.96	88.69	−8.22	117.74	−10.50
0.3	15.038	−1.670	55.23	−6.77	87.20	−11.28	115.09	−14.46
0.4	14.874	−1.962	55.01	−7.91	87.09	−12.96	113.83	−17.03
0.5	14.899	−2.065	55.58	−8.26	88.01	−13.61	114.38	−17.79
0.6	15.126	−1.965	56.96	−7.79	90.39	−12.79	116.81	−16.67
0.7	15.542	−1.677	59.09	−6.58	94.03	−10.72	120.89	−13.90
0.8	16.116	−1.231	61.80	−4.79	98.57	−7.75	126.13	−9.97
1.0	17.602	—	68.42	—	109.46	—	138.72	—

Table 4. Conductivities, $\kappa/\Omega^{-1}\,cm^{-1}$, of $(Ni(NO_3)_2+Na_2SO_4)$ mixtures and deviations, $\Delta\kappa/\Omega^{-1}\,cm^{-1}$, of the observed conductivities from calculated values as a function of the volume fraction, ϕ, of $Ni(NO_3)_2$ at various apparent ionic strengths, I_{app}/mol dm^{-3}

ϕ	$10^3\kappa$	$10^3\Delta\kappa$	$10^3\kappa$	$10^3\Delta\kappa$	$10^3\kappa$	$10^3\Delta\kappa$	$10^3\kappa$	$10^3\Delta\kappa$
	(I_{app}=0.3)		(I_{app}=1.5)		(I_{app}=3)		(I_{app}=6)	
0	16.325	—	59.25	—	93.77	—	125.62	—
0.2	15.307	−1.236	55.91	−5.03	88.45	−8.10	117.34	−10.38
0.3	14.959	−1.693	54.96	−6.83	86.89	−11.06	114.49	−14.28
0.4	14.772	−1.989	54.66	−7.97	86.45	−12.89	113.06	−16.76
0.5	14.779	−2.091	55.17	−8.31	87.33	−13.40	113.41	−17.47
0.6	14.988	−1.991	56.48	−7.84	89.56	−12.56	115.63	−16.30
0.7	15.392	−1.696	58.57	−6.60	93.00	−10.51	119.45	−13.53
0.8	15.955	−1.242	61.22	−4.79	97.31	−7.60	124.38	−9.65
1.0	17.415	—	67.70	—	107.69	—	136.13	—

TABLE 5. CONDUCTIVITIES, $\kappa/\Omega^{-1}\,cm^{-1}$, OF $(Zn(NO_3)_2+Na_2SO_4)$ MIXTURES AND DEVIATIONS, $\Delta\kappa/\Omega^{-1}\,cm^{-1}$, OF THE OBSERVED CONDUCTIVITIES FROM CALCULATED VALUES AS A FUNCTION OF THE VOLUME FRACTION, ϕ, OF $Zn(NO_3)_2$ AT VARIOUS APPARENT IONIC STRENGTHS, I_{app}/mol dm^{-3}

ϕ	$10^3\kappa$	$10^3\Delta\kappa$	$10^3\kappa$	$10^3\Delta\kappa$	$10^3\kappa$	$10^3\Delta\kappa$	$10^3\kappa$	$10^3\Delta\kappa$
	(I_{app}=0.3)		(I_{app}=1.5)		(I_{app}=3)		(I_{app}=6)	
0	16.325	—	59.25	—	93.77	—	125.62	—
0.2	15.326	−1.230	56.08	−5.01	88.79	−8.20	118.09	−10.87
0.3	14.992	−1.680	55.18	−6.83	87.36	−11.24	115.71	−14.93
0.4	14.812	−1.975	54.93	−8.00	87.05	−13.16	114.69	−17.62
0.5	14.823	−2.080	55.48	−8.38	88.05	−13.77	115.49	−18.49
0.6	15.038	−1.981	56.87	−7.91	90.46	−12.97	118.29	−17.36
0.7	15.441	−1.693	59.03	−6.67	94.09	−10.95	122.75	−14.57
0.8	16.008	−1.242	61.75	−4.87	98.69	−7.96	128.60	−10.40
1.0	17.481	—	68.46	—	109.87	—	142.34	—

TABLE 6. CONDUCTIVITIES, $\kappa/\Omega^{-1}\,cm^{-1}$, OF $(Cd(NO_3)_2+Na_2SO_4)$ MIXTURES AND DEVIATIONS, $\Delta\kappa/\Omega^{-1}\,cm^{-1}$, OF THE OBSERVED CONDUCTIVITIES FROM CALCULATED VALUES AS A FUNCTION OF THE VOLUME FRACTION, ϕ, OF $Cd(NO_3)_2$ AT VARIOUS APPARENT IONIC STRENGTHS, I_{app}/mol dm^{-3}

ϕ	$10^3\kappa$	$10^3\Delta\kappa$	$10^3\kappa$	$10^3\Delta\kappa$	$10^3\kappa$	$10^3\Delta\kappa$	$10^3\kappa$	$10^3\Delta\kappa$
	(I_{app}=0.3)		(I_{app}=1.5)		(I_{app}=3)		(I_{app}=6)	
0	16.325	—	59.25	—	93.77	—	125.62	—
0.2	15.133	−1.317	55.21	−4.66	87.32	−6.58	116.55	−5.95
0.3	14.710	−1.803	53.84	−6.34	85.09	−8.88	112.90	−8.06
0.4	14.454	−2.122	53.13	−7.36	83.85	−10.19	110.13	−9.28
0.5	14.418	−2.221	53.21	−7.59	83.69	−10.42	108.55	−9.31
0.6	14.593	−2.108	54.07	−7.04	84.63	−9.54	107.99	−8.32
0.7	14.984	−1.780	55.57	−5.85	86.43	−7.81	108.16	−6.60
0.8	15.532	−1.295	57.55	−4.18	88.81	−5.50	108.73	−4.47
1.0	16.952	—	62.35	—	94.44	—	110.10	—

TABLE 7. CONDITIONAL FORMATION CONSTANTS, K_c/dm^3 mol^{-1}, OF $M^{2+}\cdot SO_4^{2-}$ AT 25 °C IN AQUEOUS SOLUTIONS OF VARIOUS APPARENT IONIC STRENGTHS, I_{app}

Ion pair	I_{app}/mol dm^{-3}			
	0.3	1.5	3.0	6.0
$Mg^{2+}\cdot SO_4^{2-}$	20.6	4.6	2.6	1.7
$Mn^{2+}\cdot SO_4^{2-}$	26.3	6.1	3.5	2.7
$Co^{2+}\cdot SO_4^{2-}$	28.8	6.1	3.2	2.2
$Ni^{2+}\cdot SO_4^{2-}$	28.8	6.1	3.4	2.3
$Zn^{2+}\cdot SO_4^{2-}$	28.1	6.2	3.4	2.2
$Cd^{2+}\cdot SO_4^{2-}$	31.7	7.4	3.8	3.1

higher ionic strengths, the conditional formation constants for ion pair $Mg^{2+}\cdot SO_4^{2-}$ were calculated and are shown in Fig. 2 as a function of ionic strength. The calculation was made at different a-values, the most probable value of a being considered to be about 0.5—0.6 nm.[10] Similar results were obtained for the other systems investigated. It is rather surprising that the experimental values are not very much different from the values estimated by using Eqs. 7 and 8, even at the highest apparent ionic strength (6 mol dm^{-3}).

References

1) P. V. Rysselberghe and L. Nutting, *J. Am. Chem. Soc.*, **59**, 333 (1937).
2) P. V. Rysselberghe, S. W. Grinnell, and J. M. Carlson, *J. Am. Chem. Soc.*, **59**, 336 (1937).
3) C. W. Davies, *J. Chem. Soc.*, **1938**, 448.
4) C. W. Davies, *Endeavour*, **4**, 114 (1945).
5) F. H. Fisher, *J. Solution Chem.*, **7**, 897 (1978).
6) S. Katayama and R. Tamamushi, *Bull. Chem. Soc. Jpn.*, **43**, 2354 (1970).
7) S. Katayama and R. Tamamushi, *Bull. Chem. Soc. Jpn.*, **44**, 1812 (1971).
8) I. L. Jenkins and C. B. Monk, *J. Chem. Soc.*, **1951**, 68.
9) C. W. Davies, "The Structure of Electrolytic Solutions," ed by W. J. Hamer, John Wiley and Sons, Inc., New York (1959), p. 24.
10) S. Katayama, *Bull. Chem. Soc. Jpn.*, **46**, 106 (1973).
11) K. Takahashi, S. Katayama and R. Tamamushi, *Rep. I.P.C.R.*, **49**, 13 (1973).
12) C. W. Davies, "Ion Association," Butterworth, London (1962), pp. 27—31.
13) H. S. Harned and B. B. Owen, "The Physical Chemistry of Electrolytic Solutions," Reinhold Publishing Corp., New York (1967), pp. 200—203.
14) S. Katayama, *J. Solution Chem.*, **5**, 241 (1976).
15) S. Katayama, *Rep. I.P.C.R.*, **53**, 212 (1977).

 © 1983 The Chemical Society of Japan Bull. Chem. Soc. Jpn., 56, 877—880 (1983)

Hydrates of Organic Compounds. VII. The Effect of Anions on the Formation of Clathrate Hydrates of Tetrabutylammonium Salts

Haruo NAKAYAMA

Department of Chemistry, Faculty of Engineering, Yokohama National University, Tokiwadai, Hodogaya-ku, Yokohama 240

(Received September 13, 1982)

Phase diagrams of the binary mixtures of tetrabutylammonium salt $[(n\text{-}C_4H_9)_4N]_nX$ ($X=NO_2$, NO_3, BrO_3, ClO_3, IO_3, ClO_4, MnO_4, and NCS for $n=1$; $X=CO_3$, SO_4, WO_4, and CrO_4 for $n=2$; and $X=PO_4$ for $n=3$) with water were determined over the temperature range between -10 and $+50$ °C. From these diagrams the following results were obtained: (1) the formation of a clathrate-like hydrate for salts having such anions as NO_2^-, NO_3^-, BrO_3^-, ClO_3^-, IO_3^-, SO_4^{2-}, and PO_4^{3-} was newly confirmed; (2) the melting point of the clathrate hydrate of the salt with monovalent anion was appreciably influenced by the kind of anion; (3) in the hydrates of the salt having either di- or trivalent anions, the melting points were relatively high and were only slightly affected by the kind of anion; (4) the crystal structure of these hydrates was essentially the same as that of the tetrabutylammonium fluoride hydrate, judging from the hydration numbers; (5) the solubilities in water of both permanganate and perchlorate were markedly lower than that of the iodide; and (6) in the thiocyanate system a phase separation into two liquid phases was observed at temperatures higher than $+3.5$ °C. The effect of a monovalent anion on the stability of the clathrate hydrate was discussed in connection with the conventional partial molal volume of the anion.

Such quaternary ammonium salts as tetrabutylammonium halides[1,2-6] and tetraisopentylammonium halides,[1,2,4-6] are now widely known to form a clathrate-like hydrate, similar to so-called "gas hydrates."[7] In these hydrates, each alkyl group of the quaternary ammonium cation is surrounded by a polyhedron constructed by hydrogen-bonded water molecules. In general, the stability of these quaternary ammonium salt hydrates is affected by two factors: (1) the length and the shape of the alkyl group of the quaternary ammonium cation and (2) the kind of anion. Although the effect of an alkyl group has been extensively investigated in previous papers,[4,5] we have no sufficient data to draw any conclusion as to the influence of an anion on the stability of the hydrate, except that tetrabutyl(or tetraisopentyl)ammonium salts having such anions as F^-, Cl^-, Br^-, HCO_3^-, CrO_4^{2-}, WO_4^{2-}, and HPO_4^{2-} were reported to be able to form stable clathrate hydrates.[1] However, even the existence of some of these hydrates is dubious for the reasons described in the following experimental section.

In this paper, from the phase diagrams for thirteen binary systems consisting of tetrabutylammonium salt–water, the effect of anions on the formation of the clathrate hydrates has been examined. The information about what kind of anion can contribute to the formation of the clathrate hydrate and to what extent the melting point of the hydrate is affected by the kind of anion will be of great value for an application of these hydrates, for example, (1) as a heat reservoir utilizing the heat evolved or absorbed when their states change and (2) for highly selective separation of a specific anion from an aqueous solution containing several kinds of anions through the formation of a mixed clathrate hydrate.[8]

Experimental

Materials. Aqueous solutions of the tetrabutylammonium salts, except for perchlorate and permanganate, were prepared by reaction between tetrabutylammonium iodide and the corresponding silver salt in water, followed by filtration of AgI precipitate. Tetrabutylammonium iodide was synthesized by reacting tributylamine with butyl iodide in ethyl acetate and was purified by recrystallization from ethyl acetate–acetone mixture. Such silver salts as $AgNO_3$, $AgClO_3$, $AgIO_3$, Ag_2WO_4, Ag_2SO_4, and Ag_2CrO_4 were purchased from Tokyo Kasei Kogyo Co. Ltd. and were used without further purification. The other silver salts, like $AgNO_2$, AgNCS, $AgBrO_3$, Ag_2CO_3, and Ag_3PO_4, were prepared by mixing an aqueous solution of $AgNO_3$ with the corresponding sodium salt solution. These slightly soluble salts were filtered off, washed with cold water, and used in a wet state.

We attempted and failed to prepare such silver salts as $AgHCO_3$, $AgHSO_4$, AgH_2PO_4, and Ag_2HPO_4. When a sodium hydrogencarbonate solution was mixed with a silver nitrate solution, a yellowish white solid was precipitated with evolution of gas, which was presumably carbon dioxide, indicating that the solid was Ag_2CO_3 rather than $AgHCO_3$. The X-ray diffraction pattern of the solid thus obtained was exactly the same as that of Ag_2CO_3 (ASTM 12-766). The white precipitate obtained from the reaction of a silver nitrate solution and a $NaHSO_4$ solution was also believed to be Ag_2SO_4 instead of $AgHSO_4$, since a supernatant solution became highly acidic, indicating a liberation of hydrogen ion, and the X-ray diffraction pattern of the solid thus obtained gave a similar pattern to that of Ag_2SO_4 (ASTM 7-203) although the diffraction intensities corresponding to $l=3$ were relatively low as compared to those of Ag_2SO_4. Similarly, the yellow solid which was formed by mixing a silver nitrate solution with either a NaH_2PO_4 or a Na_2HPO_4 solution was also concluded to be Ag_3PO_4 from the following reasons: (1) a supernatant solution became highly acidic (pH $\approx$2.5) and the amount of a NaOH solution required to neutralize the supernatant solution agreed very closely with that calculated on the assumption that all the hydrogen, which was initially contained in each phosphate ion, was completely dissociated into hydrogen ion in the supernatant mixture; (2) when an excess amount of $AgNO_3$ solution was reacted with a known amount of each phosphate solution (NaH_2PO_4 or Na_2HPO_4), the silver ion content remaining in the supernatant mixture was reasonably explained by assuming that the precipitate was Ag_3PO_4 in both cases; and (3) their X-ray diffraction patterns were exactly the same as that of Ag_3PO_4 (ASTM 6-505).

Therefore, the existence of hydrates of $(n\text{-}C_4H_9)_4NHCO_3$

and of $[(n\text{-}C_4H_9)_4N]_2HPO_4$, reported by McMullan and Jeffrey,[1] is dubious since they reported that these salts were prepared by a reaction of tetrabutylammonium iodide with the corresponding silver salts.

Tetrabutylammonium perchlorate was prepared by mixing a tetrabutylammonium bromide solution with an aqueous $NaClO_4$ solution, and purified by recrystallization from water. Tetrabutylammonium permanganate was prepared by mixing a tetrabutylammonium chloride solution with a $KMnO_4$ solution, followed by filtration of the mixture and washing it with cold water.

Measurements and Analyses. Phase diagrams for the binary systems of water–tetrabutylammonium salt, except for perchlorate, permanganate and thiocyanate, were determined in the same manner as described in the previous paper[5] (an ampoule method). The concentrations of mother solutions were mostly determined by measuring the water content using the Karl Fischer titration method on a MK-AII apparatus (Kyoto Electronics Manufacturing Co.). For mother solutions containing anions which interfered with the Karl Fischer titration method, the concentrations were determined by one of the following methods: (1) titration by a standard sodium tetraphenylborate solution for the nitrite and iodate solutions; (2) titration by 0.1 mol dm^{-3} hydrochloric acid solution for the carbonate solution; and (3) ordinary iodometry[9] for the chromate solution. The titration method using a sodium tetraphenylborate was carried out in the following way. A sample containing about 1×10^{-4} equivalent was diluted with water to about 15 cm^3. After addition of 0.5 cm^3 of 0.05 wt% Bromophenol Blue solution (indicator), 10 cm^3 of chloroform and 10 cm^3 of 0.1 mol dm^{-3} NaOH solution in this order, the whole mixture was stirred vigorously with a magnetic stirrer for about 15 m. Then the solution was titrated with a 0.02 M $(C_6H_5)_4$-BNa solution, which had been standarized with a known amount of pure $(n\text{-}C_4H_9)_4NI$, until the color in the lower chloroform phase changed from blue to colorless.

The phase diagrams of the systems containing such sparingly soluble salts as perchlorate and permanganate were determined by measuring the solubility of each solid in water at various temperatures.[5] The concentration of perchlorate solution was determined gravimetrically after evaporating a known amount of the solution to dryness at 50 °C under reduced pressure. The concentration of permanganate solution was determined by a standard iodometric method.[9] The phase diagram of the thiocyanate system, in which a liquid-liquid phase separation occurred, was determined by measuring the respective concentrations of the two liquid phases which were in equilibrium with each other at a given temperature. The concentration determination of thiocyanate ion was carried out by a standard KNCS titration method (the Volhard method).[9]

Results and Discussion

(1) Clathrate Hydrate Formation of Tetrabutylammonium Salts Having Monovalent Anions. The solid-liquid phase diagrams for the binary systems, water–$(n\text{-}C_4H_9)_4NX$, where $X=NO_2$, NO_3, ClO_3, BrO_3, and IO_3, are shown in Fig. 1. The logarithm of the concentration expressed in mole fraction (X) is plotted against the reciprocal of the absolute temperature. The temperature expressed in ordinary Celsius units is shown on the upper side of the figure. For comparison, Fig. 1 includes the phase diagram of the tetrabutylammonium fluoride–water system reported earlier.[5]

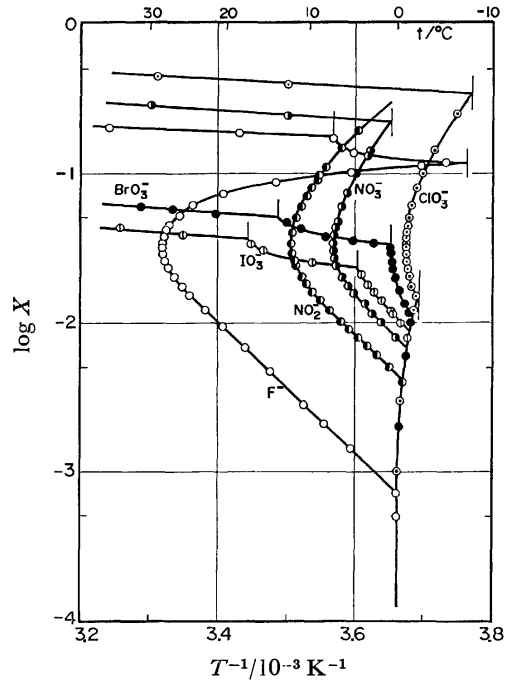

Fig. 1. Solid-liquid phase diagrams for the water–$(n\text{-}C_4H_9)_4NX$ systems.
○: X=F, ◐: $X=NO_2$, ◑: $X=NO_3$, ●: $X=BrO_3$, ⊙: $X=ClO_3$, ⓘ: $X=IO_3$.

Table 1. Melting points and hydration numbers of tetrabutylammonium salt clathrate hydrates

Anion	Mp θ_m/°C	Hydration number
F^-	28.3[5,6]	30±1[5,6]
NO_2^-	11.5	29±2
NO_3^-	7.3	30±1
ClO_3^-	−0.9	30±2
BrO_3^-	0.8 (incongruent)	—
IO_3^-	4.9 (incongruent)	—
CO_3^{2-}	18.3	66±2
SO_4^{2-}	12.6	64±2
CrO_4^{2-}	12.7 (13.6[1])	66±2 (65—68[1])
WO_4^{2-}	15.0 (15.1[1])	64±2 (60—63[1])
PO_4^{3-}	17.8	100±4

Figure 1 clearly shows that the three salts with $X=NO_2$, NO_3, and ClO_3 can form clathrate-like hydrates similar to that of the fluoride although their congruent melting points are considerably lower than that of the fluoride hydrate. The congruent compositions of these three hydrates are almost the same as that of the fluoride hydrate. This suggests that these newly found hydrates have the same crystal structure as that of the fluoride hydrate.[3] The melting points and the hydration numbers calculated from their congruent compositions are summarized in Table 1, together with those previously reported.[4-6]

The phase diagrams for the bromate and iodate systems resemble each other and are different from those of the other salts. They show the existence of three types of solid phases other than ice over the

temperature range studied. The incongruent melting points and corresponding compositions are 0.8 °C, X= 0.032 and 14.0 °C, X=0.050 for the bromate and 4.9 °C, X=0.024 and 17.3 °C, X=0.034 for the iodate, respectively. Of these phases, the ones which are stable over a low temperature interval of −2.1—+0.8 °C for the bromate and of −1.5—4.9 °C for the iodate seem to be clathrate hydrates, since not only the temperature dependence of the solubility curves of these two phases but also their morphological appearance is quite similar to those of the other clathrate hydrates. The incongruent melting points of the two hydrates are also given in Table 1. As is obvious from Fig. 1, these incongruent melting points are very close to their hypothetical congruent melting points since the incongruent composition is comparable to that of the hydrate itself ($X \simeq 0.033$).

As pointed out above, the melting points of these hydrates are considerably lower than that of, for example, the fluoride hydrate,[4-6] indicating that the hydrogen-bonded water lattice within the hydrate solid is markedly distorted by the presence of the anion, which is polyatomic and consequently more bulky than a simple anion such as a fluoride ion. Generally, it is hardly possible to evaluate quantitatively the effect of anions on the lattice distortion, because of the lack of any precise knowledge about the behavior of anions within the lattice, for example, about the possibility of hydrogen-bond formation between an oxygen atom of the anion and a hydrogen atom of the water molecule included in the lattice. Here we simply discuss the effect of the geometrical size of an anion on the lattice distortion of the hydrate from the following point of view. Firstly, as an estimation of the effective size of an anion within the hydrate crystal, it would be appropriate to refer to an ionic volume in an aqueous solution rather than its intrinsic (crystallographic) volume, since the anion present in the hydrate solid is undoubtedly surrounded by many water molecules, as if it were in an aqueous solution. Secondly, the ionic volume in an aqueous solution which we can use quantitatively is a conventional partial molal ionic volume at infinite dilution, $\overline{V}^{\circ}_{conv}$, based on the assumption that the partial molar volume of hydrogen ion at infinite dilution is 0 cm^3/mol.[10]

In Fig. 2 the melting point of each hydrate, which may be considered an indication of the stability of the hydrate, is tentatively plotted against the $\overline{V}^{\circ}_{conv}$ of the respective anions at 25 °C including halide and hydroxide hydrates already reported.[11] The melting points of both iodate and bromate hydrates are estimated from the temperature dependence of their solubility curves, which are shown in Fig. 1. It is obvious from this figure that the melting point of the hydrate decreases almost linearly with increasing the $\overline{V}^{\circ}_{conv}$, indicating that the stability of the hydrate is to a considerable extent governed by the distortion effect of the anion. The relationship found in Fig. 2 could also be used to estimate the melting point of the hydrate of tetrabutylammonium salt having a monovalent anion not examined in this study. It is interesting to note that Fig. 2 can reasonably explain the fact that tetrabutylammonium salts having large anions[10] such as I^-

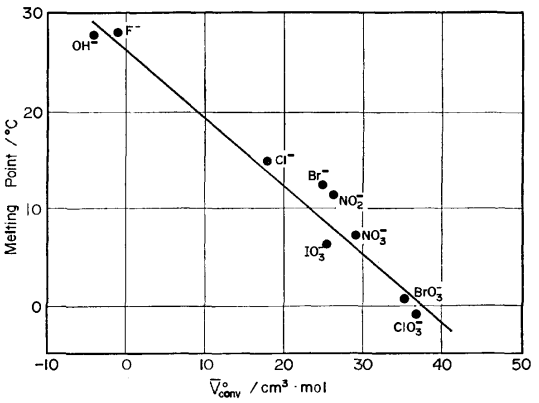

Fig. 2. Relationship between the melting points and the conventional partial molal anionic volumes in the clathrate hydrates of tetrabutylammonium salts with monovalent anions.

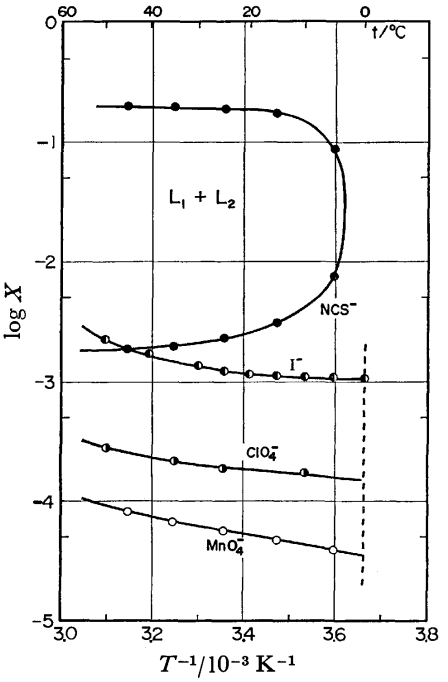

Fig. 3. Solid-liquid and liquid-liquid phase diagrams for the water-(n-$C_4H_9)_4NX$ systems.
◐: X=I, ○: X=MnO_4, ◑: X=ClO_4, ●: X=NCS.

($\overline{V}^{\circ}_{conv}$=36.22 cm^3/mol), NCS^-($\overline{V}^{\circ}_{conv}$=35.7 cm^3/mol), MnO_4^-($\overline{V}^{\circ}_{conv}$=42.5 cm^3/mol) and ClO_4^- ($\overline{V}^{\circ}_{conv}$= 44.12 cm^3/mol) cannot form stable clathrate hydrates.

The phase diagrams for systems which do not form hydrates are shown in Fig. 3 in the same way as in Fig. 1. This figure includes the phase diagram of the water–(n-$C_4H_9)_4NI$ system[5] for comparison. The characteristics of this figure are summarized as follows: (1) the solubilities in water of both permanganate and perchlorate are considerably lower than that of the iodide, which is well known to be a sparingly soluble salt (for example, at 25 °C, the solubilities are 0.112 wt%, 0.345 wt%, and 2.447 wt%[5] for permanganate, perchlorate, and iodide, respectively); and (2) a phase separation into two liquid phases occurs in

the thiocyanate system with lower critical solution temperature of +3.5 °C.

(2) Clathrate Hydrate Formation of Tetrabutylammonium Salts Having Di- and Trivalent Anions. The solid-liquid phase diagrams for the binary systems, water–$[(n\text{-}C_4H_9)_4N]_2Y$, where $Y=CO_3$, SO_4, WO_4, and CrO_4, and water–$[(n\text{-}C_4H_9)_4N]_3PO_4$, are shown in Fig. 4. This figure clearly shows that all the salts studied can form clathrate hydrates which melt congruently. Their melting points and hydration numbers are also listed in Table 1. Of these hydrates, the carbonate, sulfate, and phosphate hydrates are newly confirmed in this study. The data for both chromate and tungstate hydrates are in good agreement with those reported earlier,[1] although some discrepancy in the melting point of the chromate hydrate is seen.

It is interesting to note that these hydrates are fairly stable, as compared with those of the salts with monovalent anion mentioned in the previous section. This fact indicates that the distortion effect of the anion on the water lattice within the hydrate crystal is relatively small. One reason for this will be the fact that the number of anion per one $(n\text{-}C_4H_9)_4N^+$ cation is reduced to either a half or a third of the above mentioned case. An approximately linear relationship between the melting point and the $\overline{V}°_{conv}$ of anion, found for the salts with monovalent anion (Fig. 2), cannot be seen in this series of hydrates, since their melting points vary only over a limited range of temperature (13—18 °C), whereas the $\overline{V}°_{conv}$'s widely vary from −4.3 cm³/mol[10] for CO_3^{2-} ion to 25.7 cm³/mol[10] for WO_4^{2-} ion. This suggests that the distortion on the water lattice due to the introduction of divalent (or trivalent) anion is not the dominant factor which determines the stability of the hydrate. The slight difference in stability of these hydrates seems to be governed by such factors as either geometrical shape of the anion or slight difference in the ability of hydrogen-bond formation of the oxygen atom of the anion with a water molecule.

Judging from the hydration numbers listed in Table 1, the crystallographic structure of these hydrates is believed to be essentially the same as that of the salts with monovalent anion since the numbers of water molecules per one $(n\text{-}C_4H_9)_4N^+$ cation are approximately equal. The fact that the number of water molecules per one $(n\text{-}C_4H_9)_4N^+$ cation in the hydrates of salts with either di- or trivalent anions, around 33, is slightly larger than 30 found in the series of salts with monovalent anion, will be reasonable since the number of water molecules which construct the clathrate lattice must increase in order to fill the vacant space arising from the decrease in the number of anions.

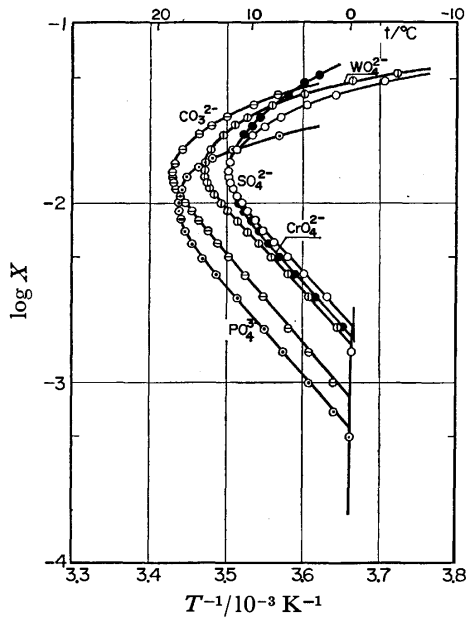

Fig. 4. Solid-liquid phase diagrams for the water–$[(n\text{-}C_4H_9)_4N]_2Y$ and water–$[(n\text{-}C_4H_9)_4N]_3PO_4$ (⊙) systems.
⊖: $Y=CO_3$, ○: $Y=SO_4$, ●: $Y=CrO_4$, ⓘ: $Y=WO_4$.

The present work was supported by the Asahi Glass Foundation for Industrial Technology and by a Grant-in-Aid for Scientific Research from the Ministry of Education, Science and Culture No. 57540240.

References

1) R. McMullan and G. A. Jeffrey, *J. Chem. Phys.*, **31**, 1231 (1959).
2) D. Feil and G. A. Jeffrey, *J. Chem. Phys.*, **35**, 1863 (1961).
3) R. K. McMullan, M. Bonamico, and G. A. Jeffrey, *J. Chem. Phys.*, **39**, 3295 (1963).
4) H. Nakayama and K. Watanabe, *Bull. Chem. Soc. Jpn.*, **49**, 1254 (1976).
5) H. Nakayama, *Bull. Chem. Soc. Jpn.*, **54**, 3717 (1981).
6) H. Nakayama, *Bull. Chem. Soc. Jpn.*, **55**, 389 (1982).
7) M. von Stackelberg and H. R. Müller, *Z. Elektrochem.*, **58**, 25 (1954).
8) H. Nakayama, M. Asano, Y. Nakajima, and K. Hanno, *Nippon Kagaku Kaishi*, **1983**, 269.
9) F. P. Treadwell and W. T. Hall, "Analytical Chemistry," John Wiley, New York (1963), Vol. 2.
10) F. J. Millero, "The Partial Molar Volumes of Electrolytes in Aqueous Solutions," in "Water and Aqueous Solutions," ed by R. A. Horne, Wiley-Interscience, London (1972), Chap. 13, pp. 519—595.
11) H. Nakayama, *Bull. Chem. Soc. Jpn.*, **52**, 52 (1979).

 © 1983 The Chemical Society of Japan Bull. Chem. Soc. Jpn., 56, 881—887 (1983)

Reactions of the Octahedral Bis(α-diketone dioximato)iron(II) Complexes with Carbon Monoxide and Benzyl Isocyanide

Yoshihiro Sasaki

Institute for Chemical Research, Kyoto University, Uji, Kyoto 611

(Received February 5, 1982)

The reactions of bis(α-diketone dioximato)iron(II) coordinated by two nitrogeneous base molecules (X) with carbon monoxide and benzyl isocyanide were studied kinetically in chloroform; here α-diketone dioxime= 2,2′-difurylglyoxime (H_2fr) and dimethylglyoxime (H_2dg). The reactions proceeded reversibly through a dissociative mechanism. For the reaction $Fe(Hfr)_2(X)_2 \underset{k_{-1}}{\overset{k_1}{\rightleftharpoons}} Fe(Hfr)_2(X)+X$, plots of log k_1 *vs.* pK_a (K_a: dissociation constant of conjugate acid of base) for pyridines gave a negative correlation. The log k_1 values of 4-cyanopyridine and 4-acetylpyridine systems were smaller and that of 2,6-dimethylpyridine system larger than predicted by their pK_a values. Imidazole and 1-methylimidazole were more inert than pyridines. For the reaction $Fe(Hfr)_2(X)+CO \underset{k_{-2}}{\overset{k_2}{\rightleftharpoons}} Fe(Hfr)_2(X)(CO)$, log k_{-2} *vs.* pK_a plots for sterically unhindered pyridines showed a linear relationship, but the basicity of pyridine bases did not affect the CO dissociation processes very much. 2-Methylpyridine, 2,4-dimethylpyridine, and 2,6-dimethylpyridine facilitated the dissociation of CO slightly as compared with pyridine. Imidazole and 1-methylimidazole allowed CO to be more inert and piperidine more labile than pyridines. The dissociation of the base was significantly affected by the change of substituents in α-diketone dioxime, and the dissociation of CO was slightly affected by the change of substituents. The reaction behavior was discussed on the basis of the activation parameters and infrared data.

Many investigations have been reported on axial ligand substitution reactions in six-coordinated iron(II) complexes containing macrocyclic ligands.[1–12] In such complexes the equatorial positions are occupied by four nitrogen atoms of the macrocycles and the axial sites by the ligands taking part in the observed rate processes. All the complexes investigated so far are able to bind carbon monoxide reversibly at the sixth position. The reactions proceed through a dissociative mechanism involving a five-coordinated intermediate which is very reactive. The binding processes of five-coordinated iron(II) porphyrins with bases and CO, which are related to biological functions of hemoproteins, have been studied using flash- or laser-photolysis techniques.[13–16] On the other hand, studies of axial ligand substitution reactions for six-coordinated iron(II) complexes with macrocycles may offer useful information on the dissociative processes of axial ligands such as nitrogeneous bases, CO, and O_2 in iron(II) porphyrins.

Octahedral bis(α-diketone dioximato)iron(II) containing a nitrogeneous base possesses a similar structure to that of iron(II) porphyrins and is able to bind CO reversibly.[17,18] Vaska and Yamaji have studied reactions of bis(diphenylglyoximato)iron(II) with CO; they proposed that the reactions proceed *via* a five-coordinated intermediate.[19] Pang and Stynes have reported the rate parameters for dissociation of base, CO, and benzyl isocyanide in bis(dimethylglyoximato)-iron(II) systems at low and high temperatures.[20] In the reaction systems studied so far, pyridine, 1-methylimidazole, and piperidine have been used as bases.[2,3,5,20] The factors regulating such reactions are not sufficiently understood. The reactivity of iron atom in these complexes is thought to be affected by the properties of the axial ligand as well as by the properties of the equatorial macrocycle. In this study, the reactions of bis(2,2′-difurylglyoximato)iron(II), $Fe(Hfr)_2(X)_2$ (X=base), with CO and benzyl isocyanide have been investigated in order to reveal the basicity effect and the steric effect of axial ligands on the reactions, and the reactions of bis(dimethylglyoximato)iron(II), $Fe(Hdg)_2(X)_2$ (X=pyridine and 1-methylimidazole), with CO have been re-examined in order to compare them with $Fe(Hfr)_2(X)_2$–CO systems.

Experimental

Materials. Pyridine (py), 2-methylpyridine (2-mepy), 4-methylpyridine (4-mepy), 2,6-dimethylpyridine (2,6-me_2py), 2,4-dimethylpyridine (2,4-me_2py), 3,4-dimethylpyridine (3,4-me_2py), 4-acetylpyridine (acpy), 3-chloropyridine (3-clpy), 1-methylimidazole (meim), butylamine (buam), and piperidine (pip) were distilled from KOH solutions prior to use. 4-Cyanopyridine (cnpy) and 4-dimethylaminopyridine (dmnpy) were purified by recrystallization. 2,2′-Difurylglyoxime (H_2fr), dimethylglyoxime (H_2dg), and imidazole (im) of guaranteed grade were used without further purification. 4-Chloropyridine (4-clpy) was prepared from 4-chloropyridine hydrochloride according to Lavalette *et al.*[16] Solutions of 4-clpy in chloroform were stored in a refrigerator. Guaranteed grade chloroform was used as solvent and carbon monoxide was obtained commercially. Benzyl isocyanide (bzlnc) was prepared according to the procedure described by Ugi and Meyer.[21]

Preparation of Complexes. Iron(II) dimethylglyoxime complexes, $Fe(Hdg)_2(X)_2$ (X=py and meim), and some iron(II) 2,2′-difurylglyoxime complexes, $Fe(Hfr)_2(X)_2$ (X= py, meim, 4-mepy, and cnpy), were prepared according to the methods reported previously.[22] $Fe(Hdg)_2(X)(CO)$ and $Fe(Hdg)_2(X)$(bzlnc) (X=py and meim) were prepared according to the procedures described by Pang and Stynes.[20]

$Fe(Hfr)_2$(3-clpy)$_2$: Methanol–water solutions of Mohr's salt (0.4 g) and 2,2′-difurylglyoxime (0.4 g) were mixed together under a nitrogen atmosphere and then 3-chloropyridine (2 ml) was added to the mixture. The pH value of the mixed solution was adjusted to about 7 by adding an aqueous NaOH solution to precipitate reddish brown crystals.

TABLE 1. ANALYTICAL DATA OF NEW COMPLEXES

Compound	Found(Calcd)(%)			
	C	H	N	Cl
$Fe(Hfr)_2(3\text{-clpy})_2$	49.42	2.98	11.66	
	(49.95)	(3.08)	(11.65)	
$Fe(Hfr)_2(acpy)_2$	54.77	4.37	11.35	
	(55.45)	(3.83)	(11.41)	
$Fe(Hfr)_2(3,4\text{-me}_2py)_2$	57.24	4.21	11.90	
	(57.63)	(4.55)	(11.86)	
$Fe(Hfr)_2(dmnpy)_2$	53.92	4.55	14.63	
	(55.29)	(4.64)	(15.18)	
$Fe(Hfr)_2(im)_2H_2O$	47.59	3.34	17.12	
	(48.16)	(3.73)	(17.19)	
$Fe(Hfr)_2(py)(CO)$	51.92	3.22	11.45	
	(51.93)	(3.19)	(11.65)	
$Fe(Hfr)_2(meim)(CO)$	49.07	3.43	14.30	
	(49.68)	(3.34)	(13.91)	
$Fe(Hfr)_2(3\text{-clpy})(CO)$	49.31	3.44	9.62	
	(49.12)	(2.85)	(11.02)	
$Fe(Hfr)_2(py)(bzlnc)\text{-}CH_2Cl_2$	52.32	3.56	11.24	9.44
	(52.66)	(3.64)	(10.84)	(9.14)
$Fe(Hfr)_2(meim)(bzlnc)$	55.21	3.90	14.22	
	(55.42)	(3.93)	(14.14)	
$Fe(Hfr)_2(3\text{-clpy})(bzlnc)$	54.31	3.49	11.36	3.50
	(54.67)	(3.48)	(11.60)	(4.89)
$Fe(Hfr)_2(buam)(bzlnc)$	55.42	4.47	11.94	
	(56.15)	(4.71)	(12.28)	

$Fe(Hfr)_2(py)(CO)$: A solution of $Fe(Hfr)_2(py)_2H_2O$ (700 mg) in dichloromethane (200 ml) was stirred for 12 h under a CO atmosphere in the dark and concentrated to about 25 ml by bubbling CO. The brown crystals were precipitated by the addition of petroleum ether (70 ml) to the concentrated solution.

$Fe(Hfr)_2(py)(bzlnc)CH_2Cl_2$: $Fe(Hfr)_2(py)_2H_2O$ (500 mg) was added to 50 ml of dichloromethane containing benzyl isocyanide (350 mg) and pyridine ($\approx 10^{-3}$ mol dm^{-3}). The solution was stirred for 6 h and concentrated to about 20 ml by bubbling N_2. Petroleum ether (70 ml) was added to the solution to precipitate the black crystals.

$Fe(Hfr)_2(acpy)_2$, $Fe(Hfr)_2(3,4\text{-me}_2py)_2$, $Fe(Hfr)_2(dmnpy)_2$, $Fe(Hfr)_2(im)_2$, $Fe(Hfr)_2(meim)(CO)$, $Fe(Hfr)_2(3\text{-clpy})(CO)$, $Fe(Hfr)_2(meim)(bzlnc)$, $Fe(Hfr)_2(3\text{-clpy})(bzlnc)$, and $Fe(Hfr)_2(buam)(bzlnc)$ were prepared by the procedures described above. The analytical results of these new complexes are shown in Table 1.

Physical Measurements. Visible spectra were obtained on a Hitachi 323 automatic recording spectrophotometer, equipped with a thermostated cell-holder and connected with a vacuum line. Infrared spectra were measured in Nujol mull or KBr disk with a Perkin-Elmer 521 spectrophotometer.

$Fe(Hfr)_2(X)_2$, $Fe(Hdg)_2(X)_2$, and Carbonyl Complex Samples. Solutions of $Fe(Hfr)_2(X)_2$ (X=py, 4-mepy, cnpy, 3-clpy, acpy, dmnpy, 3,4-me_2py, im, and meim) ($\approx 3\times10^{-4}$ mol dm^{-3}) and $Fe(Hdg)_2(X)_2$ (X=py and meim) ($\approx 6\times10^{-4}$ mol dm^{-3}) were prepared by dissolving isolated complexes in chloroform containing a large excess of the bases to prevent oxidation of the complexes. Solutions of the other 2,2′-difurylglyoxime complexes (X=buam, 2-mepy, 2,4-me_2py, 2,6-me_2py, 4-clpy, and pip) ($\approx 3\times10^{-4}$ mol dm^{-3}) were prepared by dissolving $Fe(Hfr)_2(3\text{-clpy})_2$ or $Fe(Hfr)_2(py)_2$ in chloroform containing the bases. Carbonyl complexes were prepared by bubbling CO through bis(base) complex solutions for 2—4 h.

Kinetics. For the reactions of Fe(α-diketone dioximato)$_2$(X)$_2$ with CO or bzlnc, a 0.3 ml portion of a bis(base) complex solution was syringed into a serum-capped chloroform solution (2.7 ml) over 1 atm. CO or 10^{-3}—5×10^{-3} mol dm^{-3} bzlnc. The substitution reaction of Fe(α-diketone dioximato)$_2$(X)(CO) with base (X) was carried out by syringing 0.3 ml of a carbonyl complex solution bubbled with N_2 for 2 min into chloroform containing a large excess of base ([X]$>10^{-1}$ mol dm^{-3}) or into base (2.7 ml). The kinetic measurement was made by monitering the absorbance change at a constant temperature (±0.2 °C). The experimental conditions, where the axial ligands were kept in large excess against the complexes ($\approx 3\times10^{-5}$ mol dm^{-3}), gave rise to pseudo-first-order rate constants. The rate constant, k_{obsd}, was evaluated from the $\ln(A-A_\infty)$ *vs.* time plots, which were linear or at least 3-half-lives.

Results and Discussion

$Fe(Hfr)_2(X)_2$ (X=py, 4-mepy, 3-clpy, cnpy, acpy, 3,4-me_2py, dmnpy, im, and meim) and $Fe(Hdg)_2(X)_2$ (X=py and meim) were synthesized in methanol–water (1:1 volume ratio) containing a large excess of the bases. The complexes were oxidized readily in chloroform, but the oxidation was suppressed by the presence of the bases. The H_2fr complexes were more stable than the H_2dg complexes. The other H_2fr complexes (X=pip, 2-mepy, 2,4-me_2py, and 2,6-me_2py) were oxidized immediately in methanol–water containing a large excess of the bases, but the complexes in chloroform were fairly stable in the presence of the bases. The carbonyl and bzlnc complexes in solution displayed photodissociation of CO and bzlnc, respectively. The preparation of $Fe(Hfr)_2(cnpy)(CO)$ and $Fe(Hfr)_2(cnpy)(bzlnc)$ was not successful, since they were very photosensitive. The bzlnc complexes were too stable in the dark to study the dissociation process of bzlnc at 25 °C.

The data of the visible spectra are shown in Table 2. The assignments of the bands for the bis(base) complexes were reported previously.[17,22-25] The bands at longer and shorter wavelengths were assigned to charge transfers from iron to α-diketone dioxime and from iron to pyridine ring, respectively. The bis(base) complexes of meim, im, buam, and pip did not exhibit the second band. The first band shifted to longer wavelengths with increasing basicity of the axial base. The axial ligation of CO and bzlnc, being good π-acceptors, gave rise to a band at short wavelength, and the position was not much affected by trans base. This may mean that the band in the CO and bzlnc complexes can be assigned to charge transfer from iron to CO and to bzlnc, respectively.

The infrared stretching frequencies for the CO and bzlnc complexes are given in Table 3. The CO stretches in the CO complexes occurred at lower wave numbers than that for free CO (ν_{CO}=2143 cm^{-1}). The ν_{CO} for the H_2dg complexes was smaller (by ≈20 cm^{-1}) than that for the H_2fr complexes. If we consider the ν_{CO} for the CO complexes as an indication of the ability of the π back-donation from iron to

Table 2. Absorption maxima of visible spectra of octahedral bis(2,2′-difurylglyoximato)iron(II) and bis(dimethylglyoximato)iron(II) complexes

Compound	λ/nm ($10^{-3}\varepsilon$) L=base		L=CO		L=bzlnc	
Fe(Hfr)$_2$(dmnpy)(L)	330	(29.2)	610	(19.1)	440 (16.6)	—
Fe(Hfr)$_2$(3,4-me$_2$py)(L)	369	(13.4)	578	(23.8)	435 (18.5)	—
Fe(Hfr)$_2$(4-mepy)(L)	370	(12.5)	576	(23.6)	437 (17.9)	494 (22.2)
Fe(Hfr)$_2$(py)(L)	380	(9.3)	568	(22.9)	436 (17.1)	494 (19.6)
Fe(Hfr)$_2$(4-clpy)(L)	398	(8.7)	561	(21.2)	436 (16.0)	—
Fe(Hfr)$_2$(acpy)(L)	514[a]	(15.4)	554	(24.3)	436 (17.4)	—
Fe(Hfr)$_2$(3-clpy)(L)	406	(7.8)	555	(22.7)	436 (17.4)	491 (21.7)
Fe(Hfr)$_2$(cnpy)(L)	512[a]	(16.9)	542	(21.8)	437 (15.2)	488 (18.7)
Fe(Hfr)$_2$(2,6-me$_2$py)(L)	380	(9.7)	571	(22.4)	435 (17.8)	—
Fe(Hfr)$_2$(2,4-me$_2$py)(L)	370	(11.6)	575	(21.4)	435 (16.9)	—
Fe(Hfr)$_2$(2-mepy)(L)	380	(9.2)	567	(22.6)	435 (17.3)	—
Fe(Hfr)$_2$(pip)(L)	—		606	(23.0)	445 (17.3)	—
Fe(Hfr)$_2$(buam)(L)	—		592	(23.0)	439 (20.9)	499 (20.9)
Fe(Hfr)$_2$(meim)(L)	—		591	(18.4)	434 (14.0)	494 (19.4)
Fe(Hfr)$_2$(im)(L)	—		589	(20.1)	431 (16.4)	493 (21.6)
Fe(Hdg)$_2$(py)(L)	410	(7.7)	511	(8.7)	391 (4.0)	—
Fe(Hdg)$_2$(meim)(L)	—		529	(7.8)	388 (4.5)	—

Solvent: chloroform. a) Shoulder.

Table 3. Infrared frequencies of CO and NC in carbonyl and benzyl isocyanide complexes

Compound[a]	$\tilde{\nu}$/cm^{-1} py	meim	3-clpy	buam
Fe(Hfr)$_2$(X)(CO)	2013	2010	2027	
Fe(Hdg)$_2$(X)(CO)	1988	1990		
Fe(Hfr)$_2$(X)(bzlnc)	2165	2162	2179	2161
Fe(Hdg)$_2$(X)(bzlnc)	2146	2142		

a) X=base.

CO, the H_2dg systems are seen to better than the H_2fr systems. This is expected, based on the greater inductive effect of the methyl group compared with that of the furyl group. The ν_{CO} values of the 3-clpy complexes were larger (by $\approx$15 cm^{-1}) than those of the py and meim complexes, which means that the strength of σ-donor property of trans base also affects significantly the π-bonding between iron and CO. Behavior of the NC stretching frequencies of the bzlnc complexes was more complicated: The ν_{NC} values of the H_2fr complexes were larger and those of the H_2dg complexes smaller than that of free bzlnc (ν_{NC}=2153 cm^{-1}).[26] This seems to be related to the two resonance forms of isocyanides:

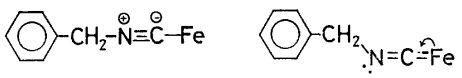

a b

In form a, bzlnc acts as a σ-donor ligand; this type of bonding is characterized by a shift of the ν_{NC} to higher frequency upon complex formation. In form b, bzlnc acts as a π-acceptor; this type of bonding occurs preferably with transition metals by making a π back-donation from metal to the ligand.[27] Thus

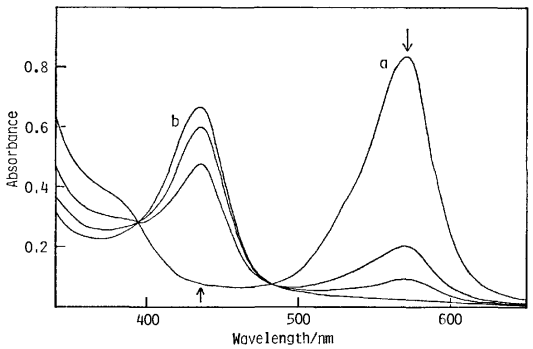

Fig. 1. Time dependence of spectra for Fe(Hfr)$_2$(2,6-me$_2$py)$_2$–CO system in chloroform at 25 °C. [Fe(Hfr)$_2$(2,6-me$_2$py)$_2$]=3.73×10^{-5} mol dm^{-3}, [2,6-me$_2$py]=4.00×10^{-2} mol dm^{-3}, CO: 1 atm. b: after 19 min.

the behavior of ν_{NC} observed in this study shows that form a is dominant in the H_2fr complexes.

The visible spectral change of the CO– and bzlnc–Fe(Hfr)$_2$(X)$_2$ systems with time exhibited two isosbestic points. As a typical example, the spectra of Fe(Hfr)$_2$(2,6-me$_2$py)$_2$–CO and Fe(Hfr)$_2$(2,6-me$_2$py)-(CO)–2,6-me$_2$py systems are shown in Figs. 1 and 2. Two excellent isosbestic points were found at 394 and 481 nm, suggesting that the following reversible reaction takes place without oxidation of the bis(2,6-me$_2$py) complex:

$$\mathrm{Fe(Hfr)_2(X)_2 + L \underset{K}{\rightleftharpoons} Fe(Hfr)_2(X)(L) + X,} \quad (1)$$

where X=base, L=CO or bzlnc, and K is an equilibrium constant. The reaction 1 is to pass through a five-coordinated intermediate (dissociative mechanism), as reported in other systems:

$$\mathrm{Fe(Hfr)_2(X)_2 \underset{k_{-1}}{\overset{k_1}{\rightleftharpoons}} Fe(Hfr)_2(X) + X,} \quad (2)$$

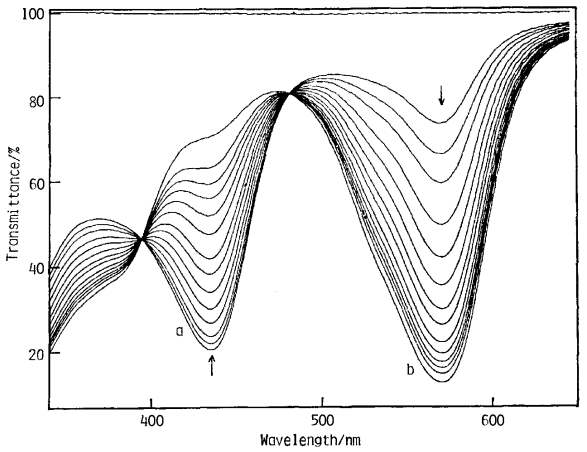

Fig. 2. Time dependence of spectra for $Fe(Hfr)_2(2,6\text{-}me_2py)(CO)$–2,6-$me_2$py system in chloroform at 25 °C. $[Fe(Hfr)_2(2,6\text{-}me_2py)(CO)]=4.03\times10^{-5}$ mol dm^{-3}, $[2,6\text{-}me_2py]=7.25\times10^{-1}$ mol dm^{-3}. b: after 310 min.

$$Fe(Hfr)_2(X) + L \underset{k_{-2}}{\overset{k_2}{\rightleftharpoons}} Fe(Hfr)_2(X)(L). \quad (3)$$

If we assume a steady-state concentration for the five-coordinated intermediate and neglect k_{-2}, the CO or bzlnc complex-formation rate constant, k_{obsd}, can be represented by:

$$k_{obsd}^{-1} = (1/k_1)(1+(k_{-1}/k_2)([X]/[L])). \quad (4)$$

Plots of k_{obsd}^{-1} *vs.* [X]/[CO] for several $Fe(Hfr)_2(X)_2$–CO systems are shown in Fig. 3. The solubility of CO in chloroform was taken as that in toluene at 25 °C (6.5×10^{-3} mol dm^{-3} atm^{-1}).[5,28] The plots for all the base systems gave good straight lines. The visible spectra of the $Fe(Hdg)_2(X)_2$–CO systems changed with an excellent isosbestic point. The plots of k_{obsd}^{-1} *vs.* [X]/[CO] gave also good straight lines (Fig. 4). The parameters k_1 and k_{-1}/k_2 were determined from the intercepts and the slopes. The intercept of pip in Fig. 3 and that of py in Fig. 4 were too small to allow us to estimate k_1.

The kinetic data were estimated by the least-squares method, and the equilibrium constants were calculated from the kinetic data. Several equilibrium constants were obtained experimentally and consistent with those calculated. The activation parameters were estimated from the kinetic data at 20, 25, and 30 °C.

The rate constants and the activation parameters for the $Fe(Hfr)_2(X)_2$–CO systems are given in Tables 4 and 5, respectively. Figure 5 shows the relationship between the rate constants and pK_a (K_a: dissociation constant of conjugate acid of the base). The $\log k_1$ values of the pyridines increased with decreasing basicity of the bases. But the $\log k_1$ values of cnpy and acpy were smaller and that of 2,6-me_2py was larger than predicted by their pK_a values. The imidazoles were more inert, and buam and pip more labile than predicted by their pK_a values. The sterically unhindered pyridines gave rise to ΔH_1^* values of the same degree in magnitude ($\approx$105 kJ mol^{-1}).[29] The decreased ΔH_1^* valuc of 4-clpy may be due to the polymerizing property of the base.[30] The steric effect on

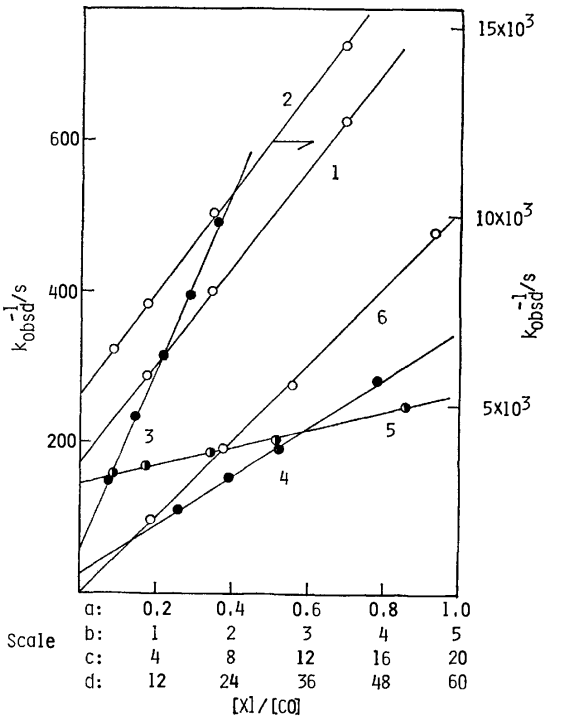

Fig. 3. Plots of k_{obsd}^{-1} *vs.* [X]/[CO] for $Fe(Hfr)_2(X)_2$–CO systems.
Scale a: X=py (1) and meim (2). Scale b: X=cnpy (3) and 3-clpy (4). Scale c: X=2,6-me_2py (5). Scale d: X=pip (6).

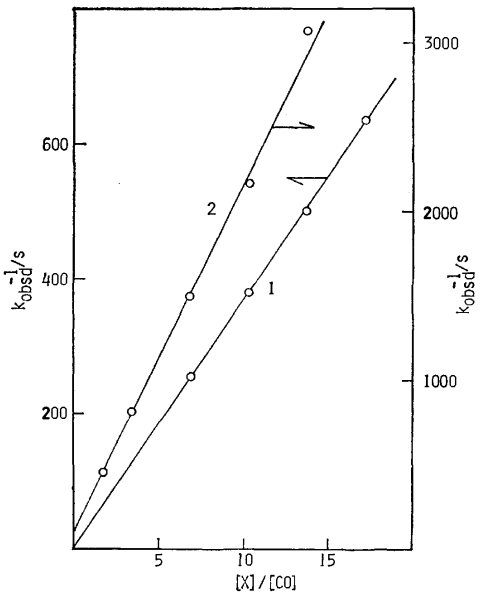

Fig. 4. Plots of k_{obsd}^{-1} *vs.* [X]/[CO] for $Fe(Hdg)_2(X)_2$–CO systems.
X=py (1) and meim (2).

the dissociation of the pyridines in the $Fe(Hfr)_2$ systems very little. The decreased ΔH_1^* values of the sterically hindered pyridines may support the steric hindrance by the methyl group in α position. The small steric effect is in striking contrast to that on dissociation of imidazoles in iron(II) phthalocyanine system, in which 2-methylimidazole is about 12700 times labile than

Table 4. Rate constants of axial ligand dissociation for Fe(Hfr)$_2$(X)$_2$-CO system in chloroform at 25 °C

Base (X)	10^3k_1/s^{-1}	10^4k_{-2}/s^{-1}	k_{-1}/k_2	K[a]	
4-Dimethylaminopyridine	0.55±0.02	0.35±0.01	1.3	12	
3,4-Dimethylpyridine	3.36±0.03	0.736±0.005	2.3	20	
4-Methylpyridine	2.24±0.01	0.675±0.001	2.4	14	15[b]
Pyridine	5.2±0.3	1.06±0.05	3.1	16	18[b]
4-Chloropyridine	9.4±0.4	1.2±0.2	3.6	21	
3-Chloropyridine	37±5	1.77±0.05	2.3	91	32[b]
4-Acetylpyridine	4.53±0.05	1.23±0.05	3.1	12	
4-Cyanopyridine	16±2	2.1±0.1	3.7	21	25[b]
2,4-Dimethylpyridine	2.47±0.05	1.04±0.05	0.03	740	
2,6-Dimethylpyridine	6.83±0.08	1.23±0.05	0.04	1390	
2-Methylpyridine	5.7±0.4	1.12±0.05	0.05	1020	
1-Methylimidazole	0.178±0.005	0.192±0.005	2.5	4	
Imidazole	0.47±0.01	0.18±0.01	2.7	10	
Piperidine	>150	11.1±0.1	—	106[c]	
Butylamine	5.3±0.2	1.8±0.2	1.5	20	

a) Calculated from k_1, k_{-2} and k_{-1}/k_2. b) Obtained experimentally. c) Calculated from $k_{-1}/(k_1k_2)$ and k_{-2}.

Table 5. Activation parameters of axial ligand dissociation reactions in Fe(Hfr)$_2$(X)$_2$-CO systems at 25 °C

Base (X)	ΔH_1^* / kJ mol^{-1}	ΔS_1^* / J mol^{-1} K^{-1}	ΔH_{-2}^* / kJ mol^{-1}	ΔS_{-2}^* / J mol^{-1} K^{-1}
4-Dimethylaminopyridine	105±5	46±17	103±7	15±23
3,4-Dimethylpyridine	106±2	64±7	106±2	30±7
4-Methylpyridine	102±2	46±8	105±2	25±8
Pyridine	106±2	67±8	108±7	42±25
4-Chloropyridine	75±8	−33±33	100±4	13±13
3-Chloropyridine	107±10	85±33	108±2	46±8
4-Acetylpyridine	95±6	28±19	100±2	15±5
4-Cyanopyridine	90±2	21±8	92±8	−2±29
2,4-Dimethylpyridine	103±5	26±8	100±8	7±28
2,6-Dimethylpyridine	97±9	19±15	100±7	16±23
2-Methylpyridine	90±2	13±6	106±1	34±4
1-Methylimidazole	112±2	50±8	109±10	17±33
Imidazole	120±3	93±11	110±3	34±11
Piperidine	—	—	95±11	17±38
Butylamine	103±2	59±8	105±4	33±13

Solvent: chloroform.

imidazole.[2] The dissociation of 1,2-dimethylimidazole in Fe(Hfr)$_2$ system also was too fast to study on a conventional spectrophotometer. Therefore, it seems that the steric effect for both systems may be affected by the difference in rigidity of the macrocycles as well as by some difference in the axial ligation property of pyridine and imidazole. π-Receptive groups such as cyano and acetyl groups in pyridine ring decreased the ΔH_1^* value. If we consider ΔH_1^* as the binding energy between iron and base, the π-receptive groups in pyridine ring are seen to weaken the bond between iron and base. The ΔS_1^* values of cnpy, acpy and the sterically hindered pyridines were rather small, as compared with those of the other pyridines. The increased lability of buam and pip may be attributed to the inability of those bases to undergo dπ-π interaction, in addition to the steric repulsion in the pip system.[31] The imidazoles were more inert and gave rise to larger ΔH_1^* values than the pyridines. This may be explained in terms of π-basicity of the imidazoles,[32] although we could not find good evidence of the dπ-π interaction between iron and imidazole ring in the infrared data of the CO and bzlnc complexes.

The log k_2 values of the sterically unhindered pyridines also increased slightly with decreasing basicity of the bases. The sterically hindered pyridines allowed CO to be a little more labile than predicted by their pK_a values. The small steric effect is in striking contrast to the results for imidazole systems of iron(II) phthalocyanine and chelated hemes, in which 2-methylimidazole allows CO to be about 20 times more labile than imidazole.[2,14] The CO in the imidazole systems was 5 times more inert and the CO in the pip system 10 times more labile than that in the py system. The sterically unhindered pyridines

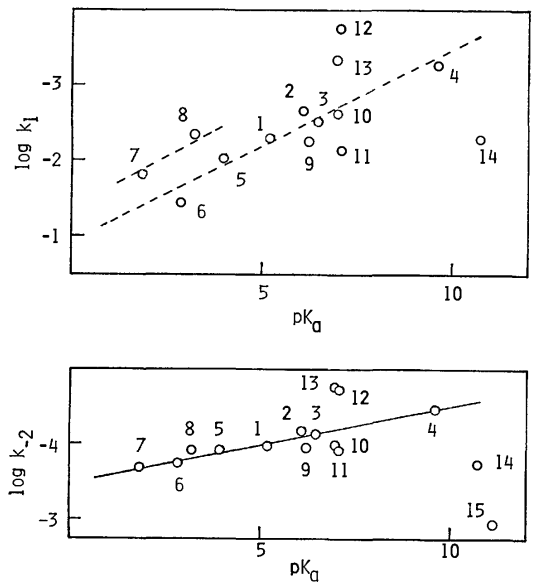

Fig. 5. Plots of $\log k_1$ and $\log k_{-2}$ *vs.* pK_a.
1: py, 2: 4-mepy, 3 3,4-me$_2$py, 4: dmnpy, 5: 4-clpy, 6: 3-clpy, 7: cnpy, 8: acpy, 9: 2-mepy, 10: 2,4-me$_2$py, 11: 2,6-me$_2$py, 12: meim, 13: im, 14: buam, 15: pip.

gave rise to ΔH^*_{-2} values of the same degree in magnitude ($\approx$105 kJ mol^{-1}), which were roughly equal to the ΔH_1^* values. The ΔH^*_{-2} values of the sterically hindered pyridines and those of cnpy and acpy, being π-acceptors, were smaller than 105 kJ mol^{-1}. If factors favoring π back-donation facilitate electron transfer from metal to ligand, π-receptive bases are expected to weaken the dπ-π interaction between iron and CO. This is presumably supported by the small ΔH^*_{-2} values of cnpy and acpy. The ΔH^*_{-2} values of the imidazoles were slightly larger and the ΔH^*_{-2} value of pip smaller than that of py. The ΔS^*_{-2} values were smaller than the corresponding ΔS_1^* values, which results in greater inertness of CO compared with that of the bases. The bases used in this study are strong dipoles (1.2 D for pip—4.3 D for dmnpy), and the five-coordinated intermediate assumed here may have an electric dipole moment (complex dipole moment) along the direction of axial ligand since the iron in the intermediate is found to lie out of the plane of the equatorial ligands. Therefore, it is expected that the activation potential for a dissociative process of base may be contributed to some extent by the long range electrostatic repulsion between the base dipole and the induced complex dipole.[33] On the other hand, the electric dipole moment of CO is very small (0.1 D), suggesting that the activation potential for the dissociation process of CO may be greatly contributed by a short range electron-exchange interaction between iron and CO. If we assume that the Δr ($=r^*-r_0$) value for a dissociation of base is larger than that for the dissociation of CO, where r_0 and r^* are the distances between iron and the leaving ligand in the initial complexes and their transition states, and that the activation entropy is due partially to the Δr values, the dissociation of bases may give rise to larger ΔS^* than that of CO. This rough estimation is consistent with the results obtained in this study.

The dissociation rates of CO in the Fe(Hfr)$_2$ systems did not correlate with the CO stretching frequencies in Table 3, as found in heme systems previously.[34] This suggests that both σ electron donation and π back-donation contribute to the stability of CO complexes, but the CO stretching frequency is sensitive to changes in the π back-donation of CO complexes.

The k_{-1}/k_2 ratios obtained in this study are comparable in magnitude to those for iron(II) phthalocyanine and iron(II) diphenylglyoxime systems.[2,19] On the other hand, the ratio for the sterically hindered pyridine systems was far too small. The steric effect on k_{-1}/k_2 ratio is presumably related to the structure of the five-coordinated intermediate. The result of k_{-1}/k_2 ratio in the pyridine systems is also in striking contrast to that in imidazole systems of iron(II) phthalocyanine, where the ratio of 2-methylimidazole is comparable to that of imidazole.[2] The values of equilibrium constant, K, estimated in this study were roughly equal in magnitude. But the K values of the sterically hindered pyridines were much larger; this resulted from the decreased k_{-1}/k_2 ratio.

The rate constants and the activation parameters for the Fe(Hdg)$_2$(X)$_2$–CO systems are given in Table 6. The Fe(Hdg)$_2$ systems gave rise to k_1 values about 50 times larger than those in the Fe(Hfr)$_2$ systems. The CO in the Fe(Hdg)$_2$ complexes was about twice as inert as that in the Fe(Hfr)$_2$ complexes. The ΔH_1^* value of Fe(Hdg)$_2$(meim)$_2$ was smaller than that of Fe(Hfr)$_2$(meim)$_2$, but the ΔH^*_{-2} and ΔS^*_{-2} values of Fe(Hdg)$_2$(py)(CO) were larger than those of Fe(Hfr)$_2$(py)(CO). The change of the ΔH_1^* values suggests that the bond between iron and axial base (mainly σ bond) in Fe(Hdg)$_2$ complexes is weaker than that in Fe(Hfr)$_2$ complexes, as expected by the greater inductive effect of methyl group than that of furyl group. The result that the dissociation of CO is not much affected by the electronic effect of the substituents is consistent with that reported recently in some chelated hemes.[5] These suggest that stability of CO complexes is determined by both σ electron donation and π back-donation. The increased ΔH^*_{-2} value

TABLE 6. RATE CONSTANTS AND ACTIVATION PARAMETERS FOR AXIAL LIGAND DISSOCIATION IN Fe(Hdg)$_2$(X)$_2$–CO SYSTEMS AT 25 °C

Base (X)	10^3k_1/s^{-1}	10^4k_{-2}/s^{-1}	k_{-1}/k_2	K	ΔH^* / kJ mol^{-1}	ΔS^* / J mol^{-1} K^{-1}
Pyridine	>120	0.401±0.005	—	680[a]	ΔH^*_{-2}=131±4	ΔS^*_{-2}=112±13
1-Methylimidazole	10.3±0.6	0.119±0.005	2.1	410[b]	ΔH_1^*=104±9	ΔS_1^*=66±29

Solvent: chloroform. a) Calculated from $k_{-1}/(k_1k_2)$ and k_{-2}. b) Calculated from k_1, k_{-2}, and k_{-1}/k_2.

Table 7. Rate constants of axial ligand dissociation for Fe(Hfr)$_2$(X)$_2$-bzlnc systems at 25 °C

Base (X)	$10^3k_1/s^{-1}$	k_{-1}/k_2
Pyridine	4.9±0.3	1.1
4-Methylpyridine	2.24±0.01	0.9
3-Chloropyridine	46±18	0.8
4-Cyanopyridine	17±2	1.3
1-Methylimidazole	0.183±0.001	0.8
Imidazole	0.48±0.01	—
Butylamine	5.6±0.2	0.5

of Fe(Hdg)$_2$(py)(CO) is presumably due to better ability of π back-bonding formation of Fe(Hdg)$_2$ complexes, as concluded on the basis of the infrared data.

The rate constants for several Fe(Hfr)$_2$(X)$_2$–bzlnc systems are summarized in Table 7. The k_1 values for the Fe(Hfr)$_2$(X)$_2$–bzlnc systems were in agreement with those for the Fe(Hfr)$_2$(X)$_2$–CO systems; this is good evidence of the dissociative mechanism assumed in this study. The k_{-1}/k_2 ratios for the bzlnc systems were 1/3 in magnitude, compared with those for the corresponding CO systems. This means that the k_2 values of the bzlnc systems are 3 times larger than those of the CO systems. The bzlnc complexes were much more stable than the CO complexes.

The author wishes to thank to Dr. Tadashi Okamoto for helpful discussions.

References

1) D. V. Stynes and B. R. James, *J. Chem. Soc., Chem. Commun.*, **1973**, 325.
2) D. V. Stynes and B. R. James, *J. Am. Chem. Soc.*, **96**, 2733 (1974).
3) C. J. Weschler, D. L. Anderson, and F. Basolo, *J. Am. Chem. Soc.*, **97**, 6707 (1975).
4) D. A. Sweigart, *J. Chem. Soc., Dalton Trans.*, **1976**, 1476.
5) B. R. James, K. J. Reimer, and T. C. T. Wong, *J. Am. Chem. Soc.*, **99**, 4815 (1977).
6) D. V. Stynes, *Inorg. Chem.*, **16**, 1170 (1977).
7) I. W. Pang and D. V. Stynes, *Inorg. Chem.*, **16**, 2192 (1977).
8) J. G. Jones and M. V. Twigg, *J. Chem. Soc., Dalton Trans.*, **1978**, 1709.
9) D. E. Hamilton, T. J. Lewis, and N. K. Kildahl, *Inorg. Chem.*, **18**, 3364 (1979).
10) C. E. Holloway, D. V. Stynes, and C. P. J. Vuik, *J. Chem. Soc., Dalton Trans.*, **1979**, 124.
11) J. Martinsen, M. Miller, D. Trojan, and D. A. Sweigart, *Inorg. Chem.*, **19**, 2162 (1980).
12) C. Ercolani, F. Monacelli, G. Pennesi, G. Rossi, E. Antonini, P. Ascenzi, and M. Brunori, *J. Chem. Soc., Dalton Trans.*, **1981**, 1120.
13) J. Geibel, J. Cannon, D. Campbell, and T. G. Traylor, *J. Am. Chem. Soc.*, **100**, 3575 (1978).
14) D. K. White, J. B. Cannon, and T. G. Traylor, *J. Am. Chem. Soc.*, **101**, 2443 (1979).
15) T. G. Traylor, D. K. White, D. H. Campbell, and A. P. Berzinis, *J. Am. Chem. Soc.*, **103**, 4932 (1981).
16) D. Lavalette, C. Tetreau, and M. Momentear, *J. Am. Chem. Soc.*, **101**, 5395 (1979).
17) B. A. Jillot and R. J. P. Williams, *J. Chem. Soc.*, **1958**, 462.
18) K. Bowman, A. P. Gaughan, and Z. Dori, *J. Am. Chem. Soc.*, **94**, 727 (1972).
19) L. Vaska and T. Yamaji, *J. Am. Chem. Soc.*, **93**, 6673 (1971).
20) I. W. Pang and D. V. Stynes, *Inorg. Chem.*, **16**, 590 (1977).
21) I. Ugi and R. Meyer, *Chem. Ber.*, **93**, 239 (1960).
22) Y. Sasaki, *Bull. Inst. Chem. Res., Kyoto Univ.*, **58**, 244 (1980).
23) N. Sanders and P. Day, *J. Chem. Soc., A*, **1969**, 2303.
24) C. Matsumoto, Y. Yamane, and K. Shinra, *Nippon Kagaku Zasshi*, **89**, 44 (1968).
25) Y. Yamane, I. Masuda, and K. Shinra, *Bull. Chem. Soc. Jpn.*, **44**, 1581 (1971).
26) The ν_{NC} value for free bzlnc is slightly larger than that reported in Ref. 21.
27) F. Millich, *Chem. Rev.*, **72**, 101 (1972).
28) A. Seidell, "Solubilities of Inorganic and Metal Organic Compounds," 3rd ed, D. Van Nostrand Co., New York, N.Y. (1970), Vol. 1, p. 218.
29) The activation parameters of 3-clpy differ from the data in the preliminary report (*Chem. Lett.*, **1981**, 1117). The difference may be due to impurities in 3-clpy.
30) H. S. Mosher, "Heterocyclic Compounds," ed by R. C. Elderfield, Wiley, New York (1950), Vol. 1, p. 516.
31) L. J. Radonovich, A. Bloom, and J. L. Hoard, *J. Am. Chem. Soc.*, **94**, 2073 (1972).
32) C. K. Chang and T. G. Traylor, *J. Am. Chem. Soc.*, **95**, 8477 (1973).
33) The existence of such an electrostatic repulsion may be supported by the result that the rate constants for association of the pyridines in chelated heme systems are correlated to the electric dipole moments of the bases, where one base B (imidazole or pyridine) is covalently linked to the TPP macrocycle (Fe(II)TPP-B). See Ref. 16.
34) C. K. Chang and D. Dolphin, *Proc. Natl. Acad. Sci. U.S.A.*, **73**, 3338 (1976).

The Formation of Needle-like Particles of $x CoFe_2O_4 \cdot (1-x)Fe_3O_4$ with $x \leq 0.2$

Masao KIYAMA* and Toshio TAKADA

Institute for Chemical Research, Kyoto University, Uji, Kyoto 611

(Received February 12, 1982)

An experimental study was made of the oxidation with air of alkaline suspensions containing needle-like Fe_3O_4 particles and slight amounts of $Co_{1/3}/Fe_{2/3}(OH)_2$ at temperatures between 60 and 90 °C, together with the properties of the resulting oxidation products. It has been found that the H_c (coercivity) values of the products were greatly affected by both the excess NaOH concentration and the oxidation temperature—*i.e.*, the two essential factors in determining the difference in the properties of a cobalt ferrite layer coated on the Fe_3O_4 particles, that these values increased with the heat treatment *in vacuo* of the products within the temperature range of 200 to 450 °C, without decreasing the saturation magnetization values, and that the H_c increment was mainly governed by the Co content.

Needle-like particles of γ-Fe_2O_3, containing a slight amount of Co(II), have been widely used as a ferromagnetic material for high-density recording tapes. The coercivity (coercive force), H_c, of γ-Fe_2O_3 particles has been known to become greater with an increase in the shape anisotropy.[1] The γ-Fe_2O_3 particles become magnetically harder—*i.e.*, the H_c increase, by either the adsorption of Co(II)[2,3] or the epitaxial coating of cobalt ferrite[3-5] on their surfaces, with the participation of the properties of a surface magnetic anisotropy.

The precipitate of $Co_{x/3}Fe_{1-x/3}(OH)_2$, prepared by adding an excess NaOH solution to a mixed solution of Co(II) and Fe(II) salts, can transform itself by oxidation into a ferromagnetic precipitate consisting of cubic $Co_xFe_{3-x}O_4$ particles, whose H_c value is governed by the conditions of oxidation.[6] As has been known, the difference in the lattice constant between Fe_3O_4 and cobalt ferrite is appreciably small relative to that between γ-Fe_2O_3 and cobalt ferrite.

The present authors considered that the use of Fe_3O_4 particles instead of γ-Fe_2O_3 would contribute to the ease of the epitaxial coating of cobalt ferrite, with a consequent attainment of a magnetically harder material. The authors have found that magnetic properties of the products prepared by subjecting aqueous suspensions containing needle-like Fe_3O_4 particles and slight amounts of $Co_{1/3}Fe_{2/3}(OH)_2$ to oxidation were greatly affected by the conditions of oxidation.

This paper is an account of the properties of such products and of the conditions for the formation of $x CoFe_2O_4 \cdot (1-x)Fe_3O_4$ with $0.2 \geq x$, featuring greater H_c values created by coating cobalt ferrite on the surfaces of needle-like Fe_3O_4 particles.

Experimental

A number of α-FeO(OH) samples, each consisting of needle-like particles, were prepared as follows. Alkaline suspensions (each 3 dm^3) of $Fe(OH)_2$, which had been prepared by mixing aqueous solutions of $FeSO_4$ and NaOH (both of an analytical grade), were heated and then oxidized at 40 °C by bubbling CO_2-eliminated air into them at various constant rates until the precipitate of $Fe(OH)_2$ completely disappeared. The oxidation method for these suspensions was the same as that previously reported.[7] The yellowish precipitates of α-FeO(OH) were separated by filtration, washed well with water, treated with acetone, and then dried at 70 °C in air. The mean particle size of the α-FeO(OH) samples was estimated from the BET surface area, S, which had been measured using nitrogen; it could successfully be controlled in the S range between 20 and 45 $m^2 g^{-1}$ by varying the concentrations of Fe(II) and of the excess NaOH in the starting suspension, and the air-flow rate.

The α-FeO(OH) samples were then directly reduced in hydrogen at 330 °C to Fe_3O_4. The Fe_3O_4 sample with the highest H_c value (Fig. 1(b)), which had been prepared from the α-FeO(OH) sample with $S = 30\ m^2 g^{-1}$ (Fig. 1(a)), was selected from the Fe_3O_4 samples and used as the starting ferromagnetic material. The α-FeO(OH) sample (Fig. 1(a)) was prepared by bubbling air at a constant rate of 500 dm^3/h for 20 h into the individual 3-dm^3 suspensions, each containing 0.22 M(1 M = 1 mol dm^{-3}) $Fe(OH)_2$ and 1.25 M excess NaOH; the resulting suspensions were mixed and subjected to further treatment.

The starting suspensions, consisting of the particles of Fe_3O_4 and the hydroxides of Co(II) and Fe(II), were prepared in each 4-dm^3 spherical flask, as will be described. $FeSO_4 \cdot 7H_2O$ and $CoSO_4 \cdot 7H_2O$(both of an analytical grade) in the required amounts were dissolved in the atomic ratio of 1:2 into 1 or 2 dm^3 of water, followed by the dispersion of the Fe_3O_4 sample (60—100 g) in the mixed solution. The Fe(II) and Co(II) in the black suspension were precipitated by adding an excess of NaOH to the acidic suspension. Each alkaline suspension in the flask was diluted with water to 3 dm^3, quickly heated to the desired temperature, and then stirred in air with a mechanical stirrer for 3 to 5 h until the precipitate of $Co_{1/3}Fe_{2/3}(OH)_2$ has been completely transformed by oxidation into $CoFe_2O_4$. The construction

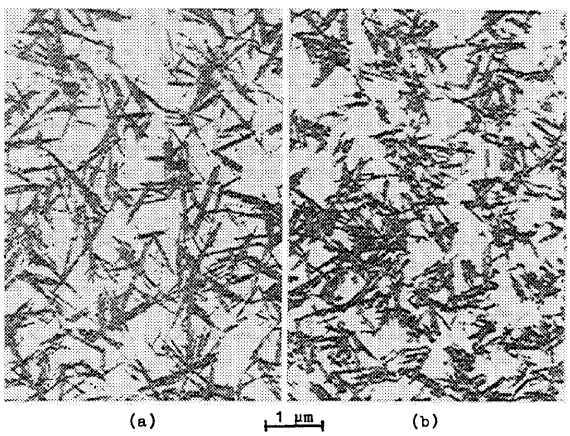

Fig. 1. Fe_3O_4 particles(b) obtained by subjecting α-FeO(OH) particles(a) to direct reduction in H_2 at 330 °C.

Table 1. Properties of some typical $x CoFe_2O_4 \cdot (1-x)Fe_3O_4$ samples prepared at various oxidation temperatures, t, and excess NaOH concentrations

Sample	Excess NaOH (mol dm^{-3})	t/°C	x	S/m^2 g^{-1}	M_s/emu g^{-1}	H_c/Oe
A	1.54	90	0.12	16.3	85	588
B	0.50	90	0.07	17.0	85	521
C	0.02	90	0.12	18.1	83	480
D	1.54	80	0.07	17.5	86	580
E	1.54	60	0.07	18.1	85	536

of the flask for the oxidation was the same as has previously been described, except that the stirrer was inserted in place of an air-introducing tube.[7] The Co-ion contents in the oxidation products were controlled by varying the mixing ratio of the Fe_3O_4 and $Co_{1/3}Fe_{2/3}(OH)_2$. The oxidation products with the $x CoFe_2O_4 \cdot (1-x)Fe_3O_4$ composition were filtered, washed well with water, treated with acetone, and then dried at 50 °C under reduced pressure.

Five kinds of $x CoFe_2O_4 \cdot (1-x)Fe_3O_4$ samples, selected from the numerous samples, were packed into brass cylinders 6 cm in length and 0.6 cm in diameter with packing densities, p (g/cm^3), ranging from 0.1 to 1.2. Some samples with $p<0.5$ had to be immersed in paraffin. After the sample had been magnetized up to 4 kOe (1 Oe$=1000/4\pi$ A m^{-1}) in a solenoid, the demagnetization curve was taken at room temperature with a self-recording permeameter. An inspection of these curves indicated that the H_c values of each sample were independent of the p for $p<0.5$, as could be anticipated from an earlier publication.[8] For $p \geq 0.5$, the H_c values manifested a decrease of $-100p$, regardless of the difference in kind of samples, presumably due to the use of the same starting material.

Exactly the same samples were also packed in brass cylinders 0.6 cm in diameter and 0.2 cm in height in the $0.6 \leq p \leq 0.9$ range. Magnetic measurements with these samples were carried out at room temperature in a magnetic field up to 10 kOe using a vibrating sample magnetometer (VSM). The H_c values for each of these samples were found to be lowered approximately $-50p$ with an increase in the p. In this case, the difference in saturation-magnetization, M_s, values for each sample was within 0.5 emu g^{-1} (1 emu g$^{-1}=4\pi 10^{-4}\rho$ Wb m^{-2}, where ρ=specific gravity in units of 10^3 kg m^{-3}).

As a result of normalizing for $p=0.5$ the H_c values for each sample with $p \geq 0.5$, after these values had been obtained using the previously mentioned two methods, it has been found that the difference between the two sets of normalized H_c values could be held within 15 Oe. Magnetic measurements of the remaining samples were also made using a VSM at room temperature in 10 kOe. The H_c values normalized for $p=0.5$ are presented in the present paper.

The cobalt and iron-ion contents of some samples were determined by atomic absorption after the samples had been dissolved in a HCl solution. The Fe(II) content in the Fe_3O_4 sample was decided by titrating with $KMnO_4$ after it had been dissolved in a mixed solution of H_2SO_4 and H_3PO_4 under a nitrogen atmosphere.

Results and Discussion

The H_c values of the Fe_3O_4 samples prepared from the α-FeO(OH) samples with $S \leq 25$ and $S \geq 35$ m^2 g^{-1} were found to be less than the H_c value of the Fe_3O_4 sample (Fig. 1(b)) prepared from the α-FeO(OH) sample with $S=30$ m^2 g^{-1} (Fig. 1(a)). This was due to the formation of microscopic pores in each needle-like particle (for $S \leq 25$) or the decrease in the shape anisotropy (for $S \geq 35$ m^2 g^{-1}). The starting ferromagnetic material with $S=18.0$ m^2 g^{-1} (Fig. 1(b)) contained 26% Fe(II) of the total iron ions, and its H_c and M_s values were 467 Oe and 87 emu g^{-1} respectively.

The conditions for the formation of five typical samples with the $x CoFe_2O_4 \cdot (1-x)Fe_3O_4$ composition and their magnetic properties at room temperature are given in Table 1, together with the S values. Table 1 demonstrates that, with the increase in the excess NaOH concentration and the elevation of the oxidation temperature, the H_c value increases and the S value decreases.

According to our electron-microscopic observation, no cubic particles could be detected with Samples A and D. This indicates that the $Co_{1/3}Fe_{2/3}(OH)_2$ was almost entirely changed by oxidation to $CoFe_2O_4$ on the surfaces of the needle-like Fe_3O_4 particles. The fact that cubic particles 0.05—0.1 μm in size were intermingled in Samples B, C, and E demonstrates that part or all of the $Co_{1/3}Fe_{2/3}(OH)_2$ was transformed into $CoFe_2O_4$ off the surfaces.

Insoluble oxides suspended in an aqueous solution are known, in general, to be electrically charged by adsorbing H^+ or OH^- ions. At pH values greater than the point of zero charge (PZC), the metal ions that have been combined only with O^{2-} ions are known to be formed in the subsurface of an oxide such as Fe_2O_3[9] or ZnO[10] by the dissociation of surface protons, thus providing the insoluble particles with negatively charged sites, whose number becomes greater with an increase in the pH.

In the present experiments, it is presumed that the metal ions, probably bivalent, in the alkaline-suspension medium tend to be adsorbed at negatively charged sites where the iron ions combined only with O^{2-} ions exist in the subsurfaces of needle-like particles of Fe_3O_4, whose PZC is 6.55 at 25 or 5.4 at 90 °C.[11] It is considered from these results that the surface area coated with the Fe(II) and Co(II) on the needle-like particles becomes wider with an increase in the excess NaOH concentration and that a rise in the oxidation temperature facilitates the formation of $CoFe_2O_4$.

Some samples, each divided into several parts and enclosed in glass tubes under a reduced pressure of 1.33×10^{-3} Pa, were heat-treated at temperatures between 200 and 600 °C for 4 h and then allowed to cool to room temperature. Figure 2 shows a plot of the H_c values of two typical samples A and D, *vs.* the heat-treated temperature to demonstrate that the

Table 2. Properties of some typical samples subjected to heat treatment at 400 °C *in vacuo*

Sample	A	B	C	D	E
$S/m^2\,g^{-1}$	16.0	16.9	14.9	15.8	17.1
H_c/Oe	920	603	687	701	632

H_c values become greater upon heat treatment, even at such low temperatures as 200 °C. It has been found that there was no marked difference in M_s values between samples A and D for heat-treatment temperatures≤450 °C, except that the M_s for 500 °C became less than that for 450 °C due to the formation of α-Fe_2O_3.

As is indicated in Table 2, the S and H_c values of the five samples prepared at 400 °C *in vacuo* become less than and higher than those of the original samples, respectively. As is evident from a comparison of Tables 1 and 2, the increase in H_c is mainly governed by the Co content.

The H_c values were also measured with the original samples, A and D, and their heat-treated samples under the magnetic fields of 10 and 20 kOe within the temperature range from 77 to 350 K. Figure 3 is a plot of [H_c] (ratio of H_c at various measuring temperatures, T, to that at 295 K) against T/K.

The temperature dependence of [H_c] for the other original samples was substantially the same as for the original samples, A and D, regardless of the conditions of oxidation and the Co(II) content. From the gradual variations in [H_c] with the temperature for the original samples, the H_c increase at room temperature may be attributed to the participation of the effect of the magnetic-surface anisotropy caused by the formation of the cobalt ferrite layer on the surface of Fe_3O_4 particles, as has previously been described for γ-Fe_2O_3 ones.[3] The H_c increase at room temperature would be determined by the properties of a ferrite layer coated on the surfaces, notably the percentage of the surface coverage, and the homogeneity and thickness of the ferrite layer, governed by the conditions of oxidation.

The cobalt ferrite layer coated on the surfaces presumably possesses a Co(II) concentration gradient similar to that of the cubic particles of ferrite formed outside the needle-like particles.[6] The reason for the differences in the temperature dependence and in the H_c increase at room temperature among the five kinds of samples prepared by heat treatment *in vacuo* can be attributed to the facts that some of the fine cubic particles of $CoFe_2O_4$ form a ferrite layer on the needle-like particles of Fe_3O_4 and that the participation of the crystal anisotropy effect of Co(II) attributable to the internal diffusion of part of the Co(II) ions into the needle-like particles becomes predominant with the tendency towards the uniform concentration of Co(II) ions in the coated ferrite layer.

The authors wish to thank Messrs. T. Kusuda (this Institute), Y. Enoki (Matsushita Electric Industrial Co., Ltd.), and N. Horiishi (Toda Kogyo Co., Ltd.) for their extensive assistance in conducting a number of experiments.

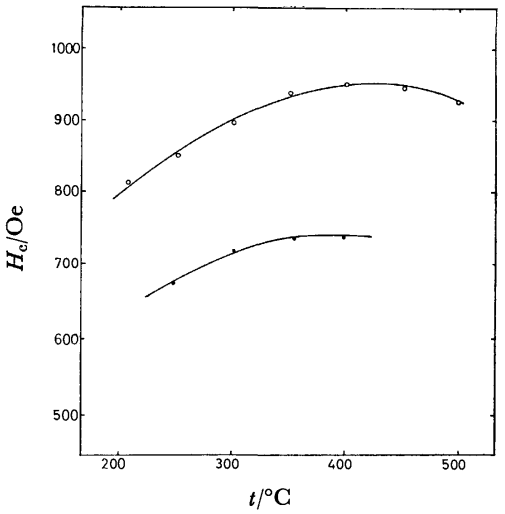

Fig. 2. Plot of coercivity, H_c, as a function of heat treatment temperatures *in vacuo* for samples A(○) and D(●).

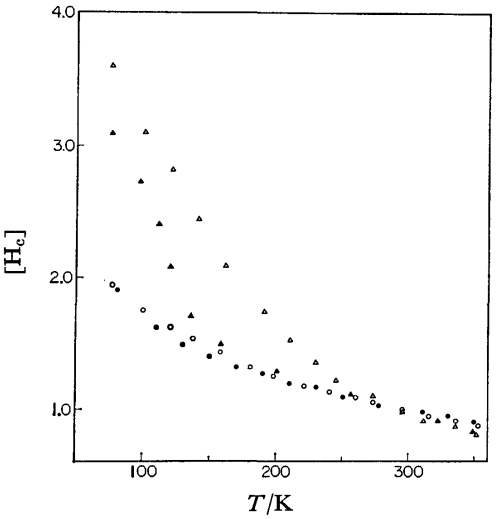

Fig. 3. Plot of relative coercivity, [H_c], as a function of measuring temperatures for original samples A(○) and D(●) and their heat-treated samples A(△) and D(▲) prepared at 300 and 400 °C *in vacuo*, respectively.

References

1) A. H. Morrish and L. A. K. Watt, *J. Appl. Phys.*, **29**, 1029 (1958).
2) Y. Tokuoka, S. Umeki, and Y. Imaoka, *J. Phys. (Paris)*, **38**, Cl-337 (1977).
3) H.-L. Lo and W. Gung, *J. Appl. Phys.*, **50**, 2414 (1979).
4) M. Kishimoto, T. Sueyoshi, J. Hirata, M. Amemiya, and F. Hayama, *J. Appl. Phys.*, **50**, 450 (1979).
5) K. Sumiya, T. Matsumoto, S. Watani, and F. Hayama, *J. Phys. Chem. Solid*, **40**, 1097 (1979).
6) M. Kiyama, *Bull. Chem. Soc. Jpn.*, **51**, 134 (1978).
7) M. Kiyama, *Bull. Chem. Soc. Jpn.*, **47**, 1646 (1974).
8) L. A. K. Watt and A. H. Morrish, *J. Appl. Phys.*, **31**, 72s (1960).
9) G. A. Parks and P. L. de Bruyn, *J. Phys. Chem.*, **66**, 967 (1962).
10) H. F. A. Trimbos and H. N. Stein, *J. Colloid Interface Sci.*, **77**, 397 (1980).
11) P. H. Tewari and A. W. Mclean, *J. Colloid Interface Sci.*, **40**, 267 (1972).

Synthesis and Characterization of a New Family of Binuclear Nickel(II) Complexes with a Terephthaloyl or Isophthaloyl Bridge

Naohide MATSUMOTO,* Akira HIRANO, and Akira OHYOSHI

Department of Industrial Chemistry, Faculty of Engineering, Kumamoto University, Kurokami 2-39-1, Kumamoto 860

(Received June 24, 1982)

A new family of binuclear nickel(II) complexes with a terephthaloyl or isophthaloyl bridge have been prepared by the electrophilic substitution reaction of (11,13-dimethyl-1,4,7,10-tetraaza-10,12-cyclotridecadienato)-nickel(II) ($Ni(Me_2[13]dienatoN_4)]^+$) or (12,14-dimethyl-1,4,8,11-tetraaza-11,13-cyclotetradecadienato)nickel(II) ($[Ni(Me_2[14]dienatoN_4)]^+$) containing a nucleophilic center at the γ-carbon and terephthaloyl chloride or isophthaloyl chloride. The complexes were characterized by elemental analyses, infrared spectra, ^1H NMR spectra, electronic spectra, and conductivity measurements.

Binuclear metal complexes are of much current interest as models for active sites[1-8] in biological systems such as cytchrome oxidase, hemerythrin, hemocyanin, and laccase. In such complexes, two metal ions are positioned in close proximity by the ligand framework to promote substrate binding between them. Recently binuclear complexes with a flexible chain or a bridging moiety such as *p*-xylene or *m*-xylene have been developed to mimic the reactivity to molecular oxygen and carbon monooxide of hemocyanin,[9-11] since it has been reported that hemocyanin consists of a rather flexible binuclear unit.[12] We wish now to report a new family of ligands with a terephthaloyl or isophthaloyl bridge as their nickel(II) complexes, whose possible structure can be described as face-to-face species and has a substrate binding site. In our previous papers,[13,14] we have reported the synthesis, properties, and crystal structure of the substituted mononuclear nickel(II) complexes (**2**), which have been prepared by the electrophilic substitution reaction of $[Ni(Me_2[Z]dienatoN_4)]^+$ (**1**) ($Z=13$, 14) with the *p*-substituted benzoyl chlorides, as shown in Fig. 1. The binuclear nickel(II) complexes reported here have been prepared by a similar reaction procedure for the substituted mononuclear complexes by using terephthaloyl chloride or isophthaloyl chloride, instead of benzoyl chloride (Fig. 1). The complexes were characterized by elemental analyses, infrared spectra, ^1H NMR spectra, electronic spectra, and conductivity measurements. The properties of the binuclear complexes have been compared with those of the mononuclear complexes.

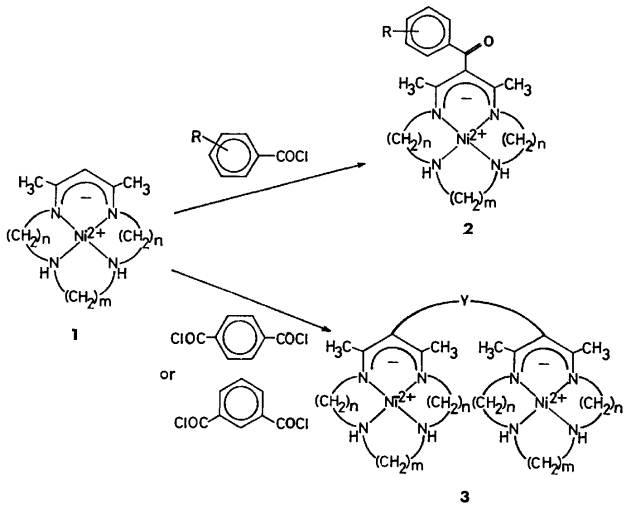

Fig. 1. Reaction scheme from parent complex (**1**) to substituted mononuclear complex (**2**) and binuclear complex (**3**).
1: $[Ni(Me_2[Z]dienatoN_4)]^+$($Z=13$, $n=m=2$, $Z=14$, $n=2$, $m=3$), **2**: $[Ni(Me_2E[Z]dienatoN_4)]^+$(E=benzoyl, *p*-methylbenzoyl, *m*-methylbenzoyl), **3**: $(Ni_2ter[Z])^{2+}$ or $(Ni_2iso[Z])^{2+}$.

Experimental

Physical Measurements. Visible and ultraviolet spectra were obtained with a Hitachi 323 spectrophotometer, while infrared spectra were recorded as KBr disks or Nujol mulls with a Shimadzu IR-410 spectrophotometer. The 100 MHz ^1H NMR spectra were recorded on a JEOL MH 100 spectrometer. The solvent used was CD_3CN and in all cases shift measurements were relative to tetramethylsilane. Elemental analysis was performed at the Technical Service Center of Kumamoto University. The thermogravimetric analysis(TGA) was carried out on a Shimadzu TGC 20 type microthermobalance at the heating rate of 5° min^{-1} using *ca.* 10 mg of the sample for each run, according to a method in the literature.[15] Conductivity measurements were carried out on a Denki Kagaku AOC-10 in methanol.

Syntheses. Parent Nickel(II) Complexes (1): (11,13-Dimethyl-1,4,7,10-tetraaza-10,12-cyclotridecadienato)nickel-(II) bromide hemihydrate, $[Ni(Me_2[13]dienatoN_4)]Br\cdot 0.5H_2O$; (12,14-Dimethyl-1,4,8,11-tetraaza-11,13-cyclotetradecadienato)nickel(II) bromide monohydrate, $[Ni(Me_2[14]dienatoN_4)]Br\cdot H_2O$; (12,14-dimethyl-1,4,8,11-tetraaza-11,13-cyclotetradecadienato)nickel(II) iodide monohydrate, $[Ni(Me_2[14]dienatoN_4)]I\cdot H_2O$: These parent complexes were prepared by the method of S. C. Cummings *et al.*,[16] and identified by elemental analyses.

Substituted Mononuclear Nickel(II) Complexes (2). [11,13-Dimethyl-12-(*p*-methylbenzoyl)-1,4,7,10-tetraaza-10,12-cyclotridecadienato]nickel(II) hexafluorophosphate, $[Ni(Me_2p\text{-}MeBzyl[13]dienatoN_4)]PF_6$; [12,14-dimethyl-13-(*p*-methylbenzoyl)-1,4,8,11-tetraaza-11,13-cyclotetradecadienato]nickel-(II) hexafluorophosphate hemihydrate, $[Ni(Me_2p\text{-}MeBzyl[14]dienatoN_4)]PF_6\cdot 0.5H_2O$: The complexes were prepared by the method described previously,[14] and identified by elemental analyses. [11,13-Dimethyl-12-(*m*-methylbenzoyl)-1,4,7,10-tetraaza-10,12-cyclotridecadienato]nickel(II) iodide, the hexafluorophosphate salt, [12,14-dimethyl-13-(*m*-methylbenzoyl)-1,4,8,11-tetraaza-11,13-cyclotetradecadienato]nickel-(II) tetrafluoroborate and the perchlorate salt were first prepared in this work in a similar manner to $[Ni(Me_2p\text{-}MeBzyl[13]dienatoN_4)]PF_6$[14] in order to compare their properties with those of the binuclear complexes with a isophthaloyl bridge, and abbreviated as $[Ni(Me_2m\text{-}MeBzyl$-

TABLE 1. ELEMENTAL ANALYTICAL DATA AND SELECTED INFRARED FREQUENCIES WITH THEIR ASSIGNMENTS FOR MONONUCLEAR AND BINUCLEAR COMPLEXES

Complex	Found (Calcd) (%)			$\tilde{\nu}$/cm^{-1}		
	C	H	N	NH	C=O	C=C or C=N
[Ni(Me$_2$*m*-MeBzyl[13]dienatoN$_4$)]I·0.5H$_2$O	44.01(43.71)	5.42(5.41)	10.55(10.73)	3040	1640	1542
[Ni(Me$_2$*m*-MeBzyl[13]dienatoN$_4$)]PF$_6$	43.15(42.97)	5.41(5.12)	10.50(10.55)	3250	1638	1553
[Ni(Me$_2$*m*-MeBzyl[14]dienatoN$_4$)]BF$_4$·H$_2$O	47.60(47.57)	6.05(6.19)	11.16(11.09)	3150, 3230	1638	1556
[Ni(Me$_2$*m*-MeBzyl[14]dienatoN$_4$)]ClO$_4$·H$_2$O	46.66(46.41)	5.97(6.04)	10.81(10.82)	3150, 3200	1638	1555
(Ni$_2$ter[13])Br$_2$·4H$_2$O	40.50(40.13)	5.75(5.84)	12.50(12.48)	3070, 3140	1622	1542
(Ni$_2$ter[13])(PF$_6$)$_2$	37.78(37.69)	5.12(4.64)	11.72(11.67)	3264	1636	1545
(Ni$_2$iso[13])I$_2$·2H$_2$O	37.71(37.69)	4.92(5.06)	11.67(11.71)	3065	1635	1545
(Ni$_2$ter[14])Br$_2$·3H$_2$O	42.28(42.33)	5.83(5.94)	12.20(12.33)	3050, 3140	1618	1544
(Ni$_2$ter[14])I$_2$·2H$_2$O	39.16(39.06)	4.96(5.28)	11.38(11.38)	3070, 3160	1618	1546
(Ni$_2$ter[14])(ClO$_4$)$_2$·0.5CH$_2$Cl$_2$	42.28(42.33)	5.27(5.22)	12.20(12.30)	3160, 3210	1624	1547
(Ni$_2$ter[14])(BF$_4$)$_2$	43.81(43.39)	5.61(5.68)	12.68(12.65)	3160, 3230	1622	1547
(Ni$_2$ter[14])(PF$_6$)$_2$·2CH$_2$Cl$_2$	35.26(35.29)	4.54(4.54)	9.90(9.71)	3250	1632	1549
(Ni$_2$iso[14])I$_2$·H$_2$O	39.74(39.79)	5.21(5.21)	11.58(11.60)	3030	1623	1538
(Ni$_2$iso[14])(ClO$_4$)$_2$·CH$_2$Cl$_2$	40.81(40.53)	5.23(5.15)	11.91(11.46)	3190	1630	1542
(Ni$_2$iso[14])(BF$_4$)$_2$·2H$_2$O	42.61(42.52)	5.88(5.79)	12.23(12.48)	3220, 3060	1636	1546
(Ni$_2$iso[14])(PF$_6$)$_2$	39.10(39.06)	4.90(4.92)	11.25(11.39)	3240	1640	1548

[13]dienatoN$_4$)]I, [Ni(Me$_2$*m*-MeBzyl[13]dienatoN$_4$)]PF$_6$, [Ni(Me$_2$*m*-MeBzyl[14]dienatoN$_4$)BF$_4$, and [Ni(Me$_2$*m*-MeBzyl[14]dienatoN$_4$)]ClO$_4$, respectively.

Binuclear Nickel(II) Complexes with a Terephthaloyl or Isophthaloyl Bridge (3). μ-[12,12′-Terephthaloyl-bis(11,13-dimethyl-1,4,7,10-tetraaza-10,12-cyclotridecadienato)]dinickel(II) hexafluorophosphate (abbreviated as (Ni$_2$ter[13])(PF$_6$)$_2$). To a solution of [Ni(Me$_2$[13]dienatoN$_4$)]Br·0.5H$_2$O (15 mmol) containing 30 mmol of triethylamine in 200 cm^3 of dichloromethane was added dropwise a solution of 7.5 mmol terephthaloyl chloride in 150 cm^3 dichloromethane during 1 h with vigorous stirring at room temperature. After the completion of the addition, the solution was refluxed for 6 h and then evaporated to dryness under reduced pressure. The resultant orange-red viscous oil was dissolved in 50 cm^3 of water and filtered. The pH of the solution was adjusted to 10 with 6 mol dm^{-3} NaOH. The solution was added dropwise to 30 cm^3 of a saturated aqueous solution of ammonium hexafluorophosphate. After standing for several hours in a refrigerator, a deep-red crystalline material precipitated, it was collected and dried *in vacuo* over P_2O_5 overnight.

The other binuclear nickel(II) complexes were prepared according to the procedure described above, by using the corresponding parent complex, terephthaloyl chloride or isophthaloyl chloride and the sodium salt of the counter anion. The binuclear complexes prepared in this study are as follows: (Ni$_2$ter[13])Br$_2$, (Ni$_2$ter[13])(PF$_6$)$_2$, (Ni$_2$iso[13])I$_2$, (Ni$_2$ter[14])Br$_2$, [Ni$_2$ter[14])I$_2$, (Ni$_2$ter[14])(ClO$_4$)$_2$, (Ni$_2$ter[14])I$_2$, (Ni$_2$iso[14])(ClO$_4$)$_2$, (Ni$_2$iso[14])(BF$_4$)$_2$, and (Ni$_2$ter[14])(PF$_6$)$_2$, where (Ni$_2$ter[13])$^{2+}$, (Ni$_2$iso[13])$^{2+}$, (Ni$_2$ter[14])$^{2+}$, and (Ni$_2$iso[14])$^{2+}$ denote μ-[12,12′-terephthaloyl-bis(11,13-dimethyl-1,4,7,10-tetraaza-10,12-cyclotridecadienato)]dinickel(II), μ-[12,12′-isophthaloyl-bis(11,13-dimethyl-1,4,7,10-tetraaza-10,12-cyclotridecadienato)]dinickel(II), μ-[13,13′-terephthaloyl-bis(12,14-dimethyl-1,4,8,11-tetraaza-11,13-cyclotetradecadienato)]dinickel(II), and μ-[13,13′-isophthaloyl-bis(12,14-dimethyl-1,4,8,11-tetraaza-11,13-cyclotetradecadienato)]dinickel(II), respectively.

Results and Discussion

Synthesis. As shown in Fig. 1, the binuclear nickel(II) complexes have been prepared by the electrophilic substitution reaction of the parent complex [Ni(Me$_2$[*Z*]dienatoN$_4$)]$^+$ (*Z*=13, 14) **1** with terephthaloyl chloride or isophthaloyl chloride by the similar reaction procedure for the substituted mononuclear complexes (**2**). The advantages of the present synthetic route for the preparation of bimetallic complex with a bridging group are as follows: (1) Since the complex is derived from the reaction of the parent complex [Ni(Me$_2$[*Z*]dienatoN$_4$)]$^+$ (**1**) containing a coordinated metal center and terephthaloyl chloride or isophthaloyl chloride as a bridging moiety, structural parameters associated with the macrocyclic metal complex and the bridging moiety such as macrocyclic ring size and the orientation of two MN$_4$ planes can be varied independently. (2) Since the parent complex and terephthaloyl chloride or isophthaloyl chloride contain a nucleophilic center and two electrophilic centers, respectively, binuclear species can be obtained easily and selectively without the formation of monomeric and polymeric species.

Elemental analytical data are given in Table 1. As indicated by the elemental analyses, the binuclear nickel(II) complexes tend to crystallize as solvate. The water and dichloromethane as a crystal solvent were detected by thermo-gravimetric analyses (TGA), where the thermal process has a weight change corresponding to the loss of the approximately quantitative molecules of water or dichloromethane estimated by the elemental analyses. The weight loss was observed at 70—100 °C and 40—70 °C for the water and the dichloromethane, respectively.

Infrared Spectra. Some selected infrared frequencies and their assignments are given in Table 1. Infrared spectra of the products differ from those of the

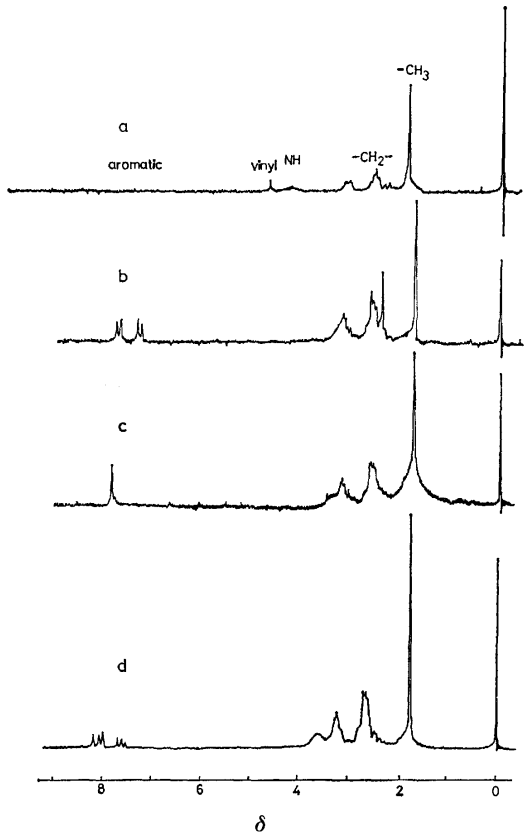

Fig. 2. ^{1}H NMR spectra in CD_3CN of (a) [Ni(Me_2-[14]dienatoN$_4$)]I·H_2O, (b) [Ni(Me_2*p*-MeBzyl[14]dienatoN$_4$)]PF_6, (c) (Ni_2ter[14])$(ClO_4)_2$·0.5CH_2Cl_2, (d) (Ni_2iso[14])$(ClO_4)_2$·CH_2Cl_2.

parent complex [Ni(Me_2[*Z*]dienatoN$_4$)]$^+$, most notably in the appearance of the intense band at *ca.* 1630 cm^{-1} which can be assigned to C=O stretching mode characteristic for the complexes containing a benzoyl group.[13,17,18] Two intense bands of the starting material terephthaloyl chloride (1780, 1724 cm^{-1}) or isophthaloyl chloride (1760, 1730 cm^{-1}) which are assigned to C=O stretching mode are absent in the products. The same feature was also observed for the reactants and the products in the mononuclear system,[13,14] indicating the completion of the substitution reaction and consistent with the formation of the binuclear species.

The NH frequency in a series of the binuclear complexes (Ni_2ter[14])X_2 (X=Br, I, ClO_4, BF_4, PF_6) as well as that of the substituted mononuclear complexes shifts to lower energy in the order of the basicity of the counter anion, Br<I<ClO_4<BF_4<PF_6. As the same phenomenon observed for the parent complexes [Ni(Me_2[*Z*]dienatoN$_4$)]X (X=Br, I, SCN, NO_3, BF_4, PF_6, *Z*=13, 14) was explained due to the hydrogen bond between the secondary amine nitrogen atom and the counter anion[16] and the existence of the hydrogen bond was confirmed by the X-ray analysis of [Ni(Me_2[14]dienatoN$_4$)]Br·H_2O,[13] the shift observed for the binuclear complexes can be also considered due to the hydrogen bond.

^{1}H NMR Spectra. Proton magnetic resonance spectra of the binuclear nickel(II) complexes, along with the substituted mononuclear complexes and the parent complex are shown in Fig. 2. The spectrum consists of four distinct regions with resonances attributable to methyl (singlet), methylene (multiplet), aromatic, and NH (broad) protons. As anticipated, the vinyl proton resonance at the γ-carbon of the parent complex has disappeared in the binuclear and substituted mononuclear complexes, since the electrophilic substitution reaction takes place at the γ-carbon. The methyl proton signal of the binuclear and substituted mononuclear complexes is shifted to a higher magnetic field than that of the parent complex. This can be attributed to the ring current effect of the benzene ring and the shielding effect of the carbonyl group of the substituent, because it has been confirmed for [Ni(Me_2*p*-MeBzyl[13]dienatoN$_4$)]PF_6 by single-crystal X-ray analysis[14] that the substituent is nearly perpendicular to the unsaturated six-membered chelate ring to which the methyl groups are attached.

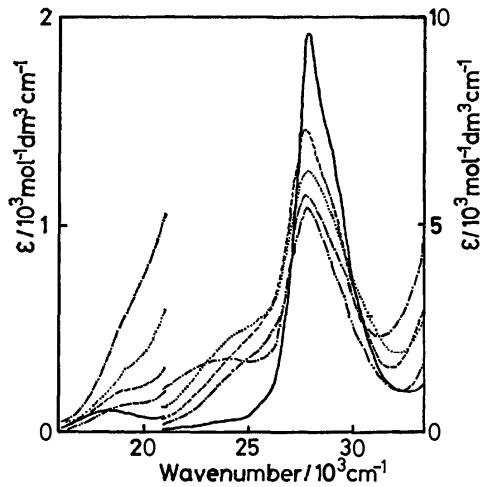

Fig. 3. Absorption spectra in methanol of [Ni(Me_2[14]-dienatoN$_4$)]PF_6·0.5H_2O(——), [Ni(Me_2*p*-MeBzyl[14]-dienatoN$_4$)]I(—··—), [Ni(Me_2*m*-MeBzyl[14]dienato-N$_4$)]BF_4·H_2O(----), (Ni_2ter[14])Br_2·3H_2O(—·—), (Ni_2iso[14])$(BF_4)_2$·H_2O(·····).

Electronic Spectra. Visible and ultraviolet spectra of the complexes were obtained on 10^{-3}—10^{-4} mol dm^{-3} solutions in methanol or acetonitrile. The spectra of the parent complex, the substituted mononuclear complex, and the binuclear complexes are shown in Fig. 3. Electronic spectra of some of the binuclear complexes, especially those of the 13-membered complexes, were not measured due to the sparing solubility. The spectra of the substituted mononuclear complex and the binuclear complex consist of a broad band in the visible region assignable to the d-d transition with an extinction coefficient on the order of *ca.* (100—500)×10^3 mol^{-1} dm^3 cm^{-1} which resembles the d-d transition of other square planar nickel(II) complexes.[19] There are also several peaks in the ultraviolet region assignable to the charge-transfer bands. As shown in Fig. 3, when the substituent of the electron withdrawing group, such as benzoyl group, is replaced at the γ-carbon, the d-d transition band shifts to higher energy and a new band with an extinction coefficient *ca.* (2000—3000)×10^3 mol^{-1} dm^3 cm^{-1} appears at (23—

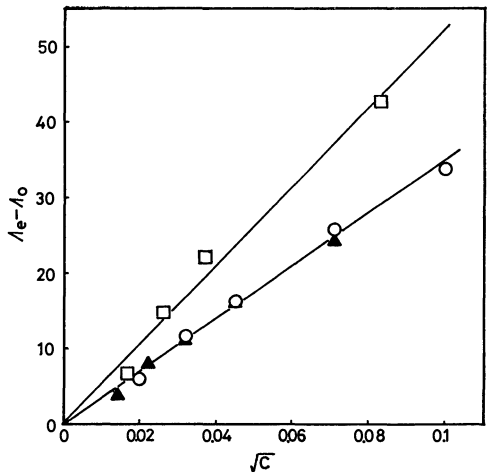

Fig. 4. Onsager plots for parent, substituted mononuclear, and binuclear nickel(II) complexes in methanol.
(a): $[Ni(Me_2[14]dienatoN_4)]I \cdot H_2O$(○), (b): $[Ni(Me_2p\text{-}MeBzyl[13]dienatoN_4)]PF_6$(▲), (c): $(Ni_2iso[14])I_2 \cdot H_2O$(□).

$25) \times 10^3$ cm^{-1}.

Molar Conductivity. The molar conductance was measured in methanol as a function of concentration, and the Onsager plots are shown in Fig. 4. For the parent complex $[Ni(Me_2[14]dienatoN_4)]I \cdot H_2O$ and the substituted mononuclear complex $[Ni(Me_2p\text{-}MeBzyl[13]dienatoN_4)]PF_6$, Onsager plots show the slopes of 351 and 349 S mol^{-1} cm$^{3.5}$ and the Λ_0 values of 114 and 98 S cm^2, respectively, in which their slopes are somewhat higher than the expected value for 1:1 electrolytes.[20,21] On the other hand, Onsager plots of the binuclear complex $(Ni_2iso[14])I_2 \cdot H_2O$ gave a slope of 525 S mol^{-1} cm$^{3.5}$ and the Λ_0 value of 114 S cm^2, which are in the expected range for 2:2 electrolytes.[20,21]

Based on the above described results, it was established that the binuclear complexes are formed, while the detailed structure remains uncertain for the present. The crystal structure determination of $(Ni_2iso[14])I_2 \cdot H_2O$ is in progress in our laboratory.

The authors are grateful to Mrs. K. Wakizaka and T. Hara for their assistance in part of the experiments.

References

1) D. H. Busch, G. G. Christoph, L. L. Zimmer, S. C. Jackels, J. J. Grzybowski, R. C. Callahan, M. Kojima, K. A. Holter, J. Mocak, N. Herron, M. Chavan, and W. P. Schammel, *J. Am. Chem. Soc.*, **103**, 5107 (1981).
2) M. J. Gunter, L. N. Mander, K. S. Murray, and P. E. Clark, *J. Am. Chem. Soc.*, **103**, 6784 (1981).
3) A. E. Martin and J. E. Bulkowski, *J. Am. Chem. Soc.*, **104**, 1434 (1982).
4) V. Mckee, J. V. Dagdigian, R. Bau, and C. A. Reed, *J. Am. Chem. Soc.*, **103**, 7000 (1981).
5) J. T. Landrum, D. Grimmett, K. J. Haller, W. R. Scheidet, and C. A. Reed, *J. Am. Chem. Soc.*, **103**, 2640 (1981).
6) N. Oishi, Y. Nishida, and S. Kida, *Chem. Lett.*, **1981**, 1031.
7) M. Suzuki, H. Kanatomi, and I. Murase, *Chem. Lett.*, **1981**, 1745.
8) W. Kanda, M. Nakamura, H. Okawa, and S. Kida, *Bull. Chem. Soc. Jpn.*, **55**, 471 (1982).
9) J. E. Bulkowski, P. L. Burk, M. F. Ludmann, and A. Osborn, *J. Chem. Soc., Chem. Commun.*, **1977**, 498.
10) J. Powell and C. J. May, *J. Am. Chem. Soc.*, **104**, 2636 (1982).
11) J. Birker, H. Hendriks, and J. Reedijk, *Inorg. Chim. Acta*, **55**, L17 (1981).
12) J. M. Brown, L. Powers, B. Kimcaid, J. A. Larrabee, and T. G. Spiro, *J. Am. Chem. Soc.*, **102**, 4210 (1980).
13) N. Matsumoto, K. Wakizaka, and A. Ohyoshi, *Bull. Chem. Soc. Jpn.*, **55**, 3165 (1982).
14) N. Matsumoto and A. Ohyoshi, *Bull. Chem. Soc. Jpn.*, **56**, 134 (1983).
15) A. Ohyoshi, S. Hiraki, T. Odate, S. Kohata, and J. Oda, *Bull. Chem. Soc. Jpn.*, **48**, 230 (1975).
16) S. C. Cummings and R. T. Sievers, *Inorg. Chem.*, **9**, 1131 (1970).
17) N. Matsumoto, M. Imaizumi, and A. Ohyoshi, *Bull. Chem. Soc. Jpn.*, **55**, 3170 (1982).
18) J. A. Streeky, D. G. Pillsburry, and D. H. Busch, *Inorg. Chem.*, **19**, 3148 (1980).
19) A. B. P. Lever, "Inorganic Electronic Spectroscopy," Elsevier, Amsterdam (1968).
20) R. D. Feltham and R. G. Hayter, *J. Chem. Soc., A*, **1964**, 4587.
21) R. G. Hayter, *J. Am. Chem. Soc.*, **84**, 3046 (1962).

 © 1983 The Chemical Society of Japan Bull. Chem. Soc. Jpn., 56, 895—898 (1983)

Potentiometric Study of Heteropolyanion Formation from Dimethylarsinate and Molybdate Anions in Acidic Aqueous Solution

Hironobu TAKAHAMA and Yukiyoshi SASAKI*

Department of Chemistry, Faculty of Science, The University of Tokyo, Hongo, Bunkyo-ku, Tokyo 113

(Received August 10, 1982)

The equilibria, $p\mathrm{H}^+ + q\mathrm{MoO_4}^{2-} + r(\mathrm{CH_3})_2\mathrm{AsO_2}^- = (\mathrm{H}^+)_p(\mathrm{MoO_4}^{2-})_q[(\mathrm{CH_3})_2\mathrm{AsO_2}^-]_r$ were studied by the use of a glass electrode in 1 M Na(Cl) ionic medium at 25 °C. The data were explained by assuming two heteropolyanions of the compositions, $(p,q,r)=(6,4,1)$ and $(7,4,1)$ with the formation constants $\log \beta_{6,4,1}=39.80\pm0.02$ and $\log \beta_{7,4,1}=46.03\pm0.01$.

Heteropolymolybdates containing organic derivatives of arsenic acid have been investigated by using preparative, X-ray crystallographic and NMR techniques,[1–7] but our knowledge about their solution states and the conditions of their formation is still fairly limited.

In order to clarify the formation equilibria of these compounds in solutions, studies of these compounds in aqueous solutions by the use of potentiometric techniques were planned in this laboratory.

As the first subject of study, the system in the title was chosen because it appeared simpler than others such as a $\mathrm{H^+}$–$\mathrm{MoO_4}^{2-}$–$\mathrm{RAsO_3}^{2-}$ mixture from which at least four different polyanions have been separated as crystals.[1–5]

Heteropolymolybdates containing dimethylarsinate was first studied by Rosenheim in 1913.[6] He reported the preparation of the guanidinium, barium, and potassium salts of the anion $\mathrm{H[As(OH)_2(CH_3)_2(Mo_2O_7)_2]^{2-}}$. These syntheses have recently been reproduced in Georgetown University and in this laboratory and the guanidinium compound was formulated as $(\mathrm{NC_3H_6})_2\cdot[(\mathrm{CH_3})_2\mathrm{AsMo_4O_{14}(OH)}]\cdot\mathrm{H_2O}$. The structure shown in Fig. 1 was determined by the single crystal X-ray diffraction technique.[1,2]

The position of the hydrogen atom shown in Fig. 1 was confirmed by the neutron diffraction work by Pope *et al.*[7] However, the pH titration of this compound by sodium hydroxide showed no evidence of the dissociation of this proton.[2]

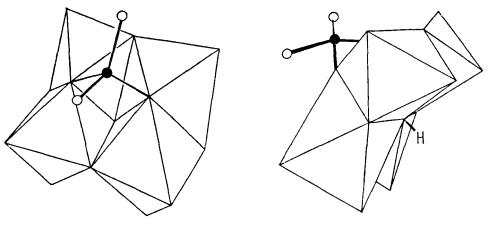

Fig. 1. Polyhedra model of $[(\mathrm{CH_3})_2\mathrm{AsMo_4O_{14}OH}]^{2-}$. ○: $\mathrm{CH_3}$, ●: As.

Symbols and Equations

Symbols. h=free hydrogen ion concentration; H=total analytical hydrogen ion concentration over the zero level $\mathrm{MoO_4}^{2-}$, $(\mathrm{CH_3})_2\mathrm{AsO_2}^-$, and $\mathrm{H_2O}$; B=total molybdenum concentration; b=concentration of free $\mathrm{MoO_4}^{2-}$ ion; C=total arsenic concentration; c=free $(\mathrm{CH_3})_2\mathrm{AsO_2}^-$ ion concentration; (p,q,r)=the composition of the ternary polyanion, $(\mathrm{H}^+)_p(\mathrm{MoO_4}^{2-})_q[(\mathrm{CH_3})_2\mathrm{AsO_2}^-]_r$.

Equations. The equilibria in the solution phase can be written as follows:

$$p\mathrm{H}^+ + q\mathrm{MoO_4}^{2-} + r(\mathrm{CH_3})_2\mathrm{AsO_2}^- = (\mathrm{H}^+)_p(\mathrm{MoO_4}^{2-})_q[(\mathrm{CH_3})_2\mathrm{AsO_2}^-]_r, \quad (1)$$

$$\beta_{pqr} = \frac{\{(\mathrm{H}^+)_p(\mathrm{MoO_4}^{2-})_q[(\mathrm{CH_3})_2\mathrm{AsO_2}^-]_r\}}{(\mathrm{H}^+)^p(\mathrm{MoO_4}^{2-})^q[(\mathrm{CH_3})_2\mathrm{AsO_2}^-]^r}. \quad (2)$$

From the mass action law and the mass balances, we can derive the next relationships in the case of binary complexes.

$$H = h + \sum_1^p \sum_1^q p\beta_{pq}h^p b^q, \quad (3)$$

$$B = b + \sum_1^p \sum_1^q q\beta_{pq}h^p b^q, \quad \text{or} \quad C = c + \sum_1^p \sum_1^r r\beta_{pr}h^p c^r. \quad (4)$$

For ternary systems, we have the equations,

$$H = h + \sum_1^p \sum_1^q \sum_1^r p\beta_{pqr}h^p b^q c^r, \quad (5)$$

$$B = b + \sum_1^p \sum_1^q \sum_1^r q\beta_{pqr}h^p b^q c^r, \quad (6)$$

$$C = c + \sum_1^p \sum_1^q \sum_1^r r\beta_{pqr}h^p b^q c^r. \quad (7)$$

Experimental

Chemicals. Stock solutions were prepared from twice recrystallized $\mathrm{Na_2MoO_4\cdot 2H_2O}$ and $\mathrm{Na(CH_3)_2AsO_2\cdot 2H_2O}$ of the special grade (Wako Chemicals). Sodium chloride of "primary standard" quality (Matsunaga Chemicals) was used after heating at 150 °C.

Apparatus. A glass electrode of TOA Electronics, HGS-2005 type, a Kawai-type half-cell[8] connected with a titration vessel and a Data Precision Digital Multimater were used for the potentiometry. All the titrations were performed by the use of an automated titrator equipped with a pair of Metrohm Multi Dosimat E 415 burettes which was designed and made[9] by the late Dr. Olle Ginstrup.

Potentiometric Titration. All the measurements were carried out at 25±0.1 °C in the ionic medium of 1 M Na(Cl), as potentiometric titrations of sodium molybdate and/or sodium dimethylarsinate with hydrochloric acid. The concentration of the sodium ion was maintained constant at 1 M.

The potentials of the cell electrode was registered four times at each point with intervals of 5 min to ±0.01 mV and the quick attainment of the equilibrium within ±0.1 mV was ascertained. No precipitation was observed during

TABLE 1. EQUILIBRIUM CONSTANTS OF BINARY COMPLEXES $(H^+)_p[(CH_3)_2AsO_2^-]_r$ AND $(H^+)_p(MoO_4^{2-})_q$
The standard deviations $3\sigma(\beta)$ and $\sigma(H)$ were defined and calculated according to Ref. 11.

(p,r)	$\log \beta_{p,r} \pm 3\sigma(\beta)$	U_{min}	$\sigma(H)$
(1,1)	6.08±0.01	19.19	0.40
(2,1)[a]	7.77±0.01		
(p,q)	$\log \beta_{p,q} \pm 3\sigma(\beta)$	U_{min}	$\sigma(H)$
(1,1)	3.53±0.01	292.35	0.846
(2,1)	7.64±0.06		
(8,7)	52.84±0.04		
(9,7)	57.25±0.06		
(10,7)	60.92±0.03		
(11,7)	63.30±0.05		
(10,8)	65.75±0.01		
(11,8)	67.76±0.01		
(12,8)	69.69±0.01		

a) $(CH_3)_2As(OH)_2^+$.

the series of titrations. The potential in mV of the cell, −Ag,AgCl/1 M NaCl/equilibrium solution/glass electrode+, is expressed as follows:

$$E = E_0 + 59.16 \log h + E_j, \quad (8)$$

where E_0 is an experimental constant and E_j (liquid junction potential)$=j \cdot h$. The values of E_0 and E_j were obtained by an independent titration of 1 M NaCl by HCl in the same medium.

The data were obtained as $H(\log h)_B$ and $H(\log h)_C$. At first, binary systems, H^+-molybdate and H^+-dimethylarsinate were studied to compute the equilibrium constants of these binary complexes which are required for further analyses of the ternary systems.

In the case of dimethylarsinate, 123 points were obtained in four titrations and used in the calculations, the concentration was chosen between 30 and 50 mM and the $-\log h > 1.8$. In the case of the H^+-molybdate system 416 points were obtained from 13 titrations at the $-\log h > 1.6$, the concentrations were between 20 and 50 mM.

In the next step, mixed solutions of molybdate and dimethylarsinate were titrated. The molybdate concentrations were between 40 and 14 mM and the B/C ratios were 1.0, 1.3, 1.5, and 3.0. All the solutions were colorless. About 40 points were obtained from each titration and twelve sets of data containing 459 points in total were collected and used for analyses.

Analysis

The method of analysis and nomenclature proposed by Pettersson were used.[12]

The computer program LETAGROP version ETITR[10,11] was used to find the complexes present and the equilibrium constants which give the best fitting of the experimental data with theoretical titration curves drawn by Eq. 5. In the least squares treatments, the determined values of h are assumed to be always correct and the function to be minimized is $U=\Sigma(H_{calcd}-H)^2$.

Binary System. Table 1 shows the composition and the equilibrium constants together with the minimum value of U and $\sigma(H)=[U_{min}/(m-n)]^{1/2}$, where m and n stand for the number of experimental points, of constants varied, respectively.

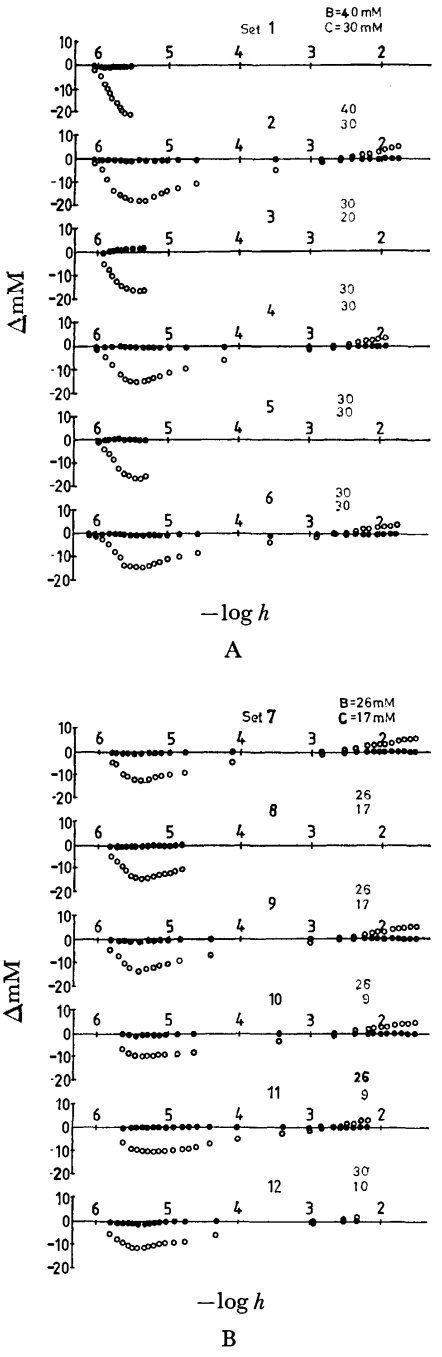

Fig. 2. Residual diagrams of 12 titrations.
○: Only binary species assumed, ●: binary and ternary complexes, (6,4,1) and (7,4,1) are taken into account.

Ternary System. The potentiometric data of the ternary systems are best illustrated as "residual diagrams" shown in Fig. 2. At each $-\log h$ measured, the "residual" defined by $\Delta=(H_{calcd}-H)$ was calculated assuming that only binary complexes are present. The constants given in Table 1 were used. The deviations of unfilled symbols from the abscissa suggest that at least one ternary complex is formed. To spare the computation time, only 96 points (sets 10—12) were used at the beginning to find (p,q,r), the composition of the polyanions formed.

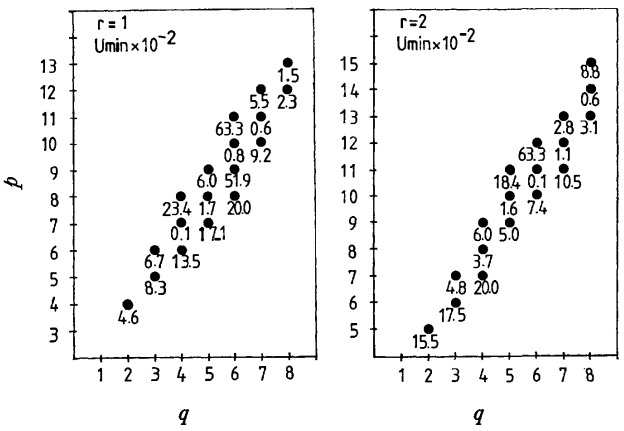

Fig. 3. Error squares sums $U_{min} \times 10^{-2}$ for various p,q,r combinations.

Table 2. The final results of the (p,q,r) analyses by the use of LETAGROP version ETITR
For one, two, and three complexes equilibria.

(p,q,r)	$U_{min} \times 10^{-2}$	$\sigma(H)$	$\log \beta_{p,q,r} \pm 3\sigma(\beta)$
(7,4,1)[a]	2.43	0.73	46.07±0.01
(10,6,1)	96.05	1.45	66.23
(11,7,1)	7.70	1.30	73.30±0.03
(11,6,2)	8.07	1.33	74.17±0.03
(14,8,2)	11.58	1.58	94.37±0.03
(14,7,3)	21.93	2.19	95.89±0.03
(7,4,1)	2.47	0.74	46.04±0.01
(10,6,1)			72.63±0.06
(7,4,1)	2.44	0.73	46.06±0.01
(11,7,1)			71.30±0.06
(7,4,1)	3.84	0.91	45.94±0.02
(11,6,2)			65.50±0.10
(6,4,1)[b]	1.78	0.62	39.80±0.02
(7,4,1)			46.03±0.01
(7,4,1)	2.43	0.73	46.07±0.01
(8,4,1)			44.02±0.02
(6,4,1)[c]			39.81±0.09
(7,4,1)	1.78	0.62	46.03±0.01
(8,4,1)			45.44±0.10
(6,4,1)			40.25±0.06
(7,4,1)	3.94	0.93	44.82±0.06
(10,6,1)			66.13±0.06
(6,4,1)			39.82±0.09
(7,4,1)	3.10	0.63	45.93±0.09
(11,7,1)			72.03±0.09

a) The combinations, (15,8,3) and (10,6,1) giving high values of $U_{min} \times 10^{-2}$ (43.8 and 96.0 respectively) were omitted. b) Assumption of (6,4,1) and (7,4,1) polyanions in equilibrium explains the data most satisfactorily. c) Addition of one more complex (8,4,1) does not improve the agreement. The constants obtained do not make sense either.

As is visualized in Fig. 3, among 91 combinations of p,q and r tested, the species, (7,4,1), (10,6,1), (11,7,1), (11,6,2), (14,8,2), (14,7,3), and (15,8,3) give the U_{min} values lower than 100. In the course of the least squares treatment, preliminary values of the formation constants were also obtained. The final analyses were started from these values of (p,q,r) and $\beta_{p,q,r}$ by using all the points (sets 1—12) and the cases of coexistence

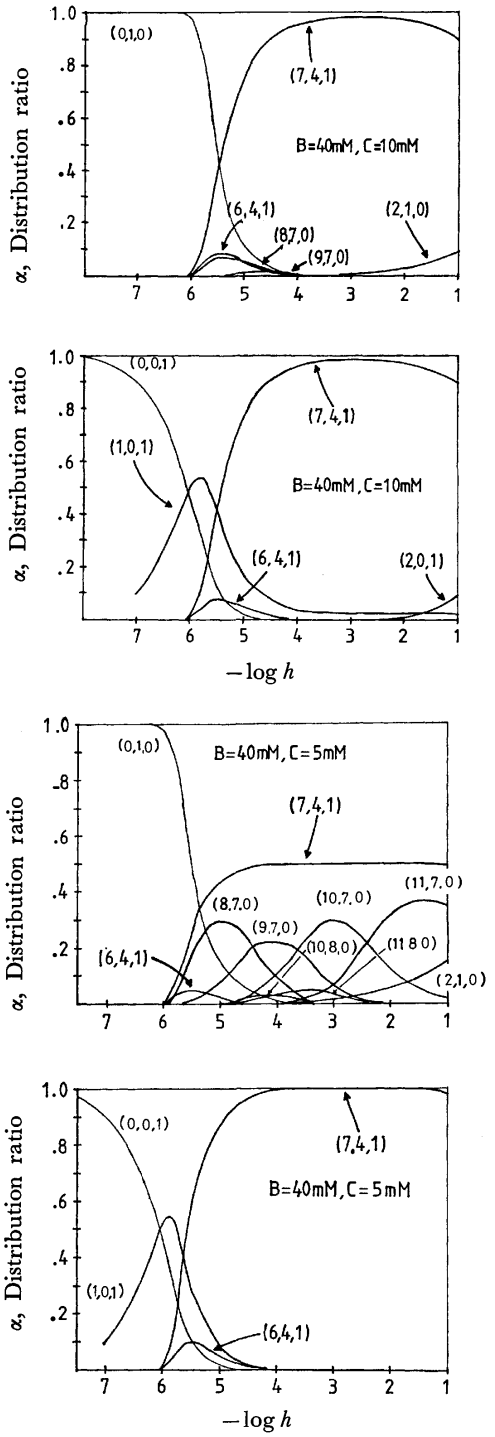

Fig. 4. Distribution diagrams of complexes $\alpha(\log h)$ for B and C, defined as the ratio between molybdenum in complexes and total molybdenum or arsenic in polyanions and total arsenic.

of two or three species were also tested.

Results and Discussion

Table 2 shows that the species, (6,4,1) and (7,4,1) are formed in solutions with the following formation constants, $\log \beta_{6,4,1} = 39.80 \pm 0.02$ and $\log \beta_{7,4,1} = 46.03 \pm 0.01$.

The possibility of the third complex was excluded

since this assumption did not make the $\sigma(H)$ value lower. The filled symbols in Fig. 2 represent the residuals calculated assuming the binary and ternary systems. These correspond to the F_o-F_c table in X-ray crystallography. They deviate very little from 0 in all the $-\log h$ region suggesting that our assumption is correct.

In order to visualize the equilibria in solution, the concentration ratio of the complexes are plotted against $-\log h$ in Fig. 4. The polyanion (7,4,1) predominates in the $-\log h$ range between 1 and 5, when $B=40$ and $C=10$ and this result agrees with the UV spectra.[2]

The possibility that the minor product, (6,4,1) could be a "ghost" derived from an error in E_0 or in stability constants of isopolymolybdates was ruled out. In the concentration range studied, $B/C<3$ and $C>9$ mM isopolymolybdates are always minor species in solutions; their stabilities have very little effect on the computation of heteropoly complexes formed and their equilibrium constants. However, such a condition as simulated in Fig. 4b would be unfavorable for accurate equilibrium studies. The composition of the polyanion, (7,4,1) in solution agrees with that found in crystals as shown in Fig. 1, and very probably the structure may be the same in both phases.

The proton attached to an oxygen atom bridging four molybdenum atoms was acidic with $pK_a=6.23$, but the unprotonated species exists only in a small amount in a narrow $-\log h$ range between 5 and 6, and the acidic form is always predominating. It was thus shown that the binding of a proton to that oxygen atom is an essentially important factor to stabilize the polyanion.

This is understandable from the structural point of view. In general, OH forms longer Mo–O bonds than O and the (6,4,1) anion must be more unstable than (7,4,1), because of the strong repulsion between four molybdenum atoms of short Mo–Mo distances caused by the short Mo–O bonds.

Similar equilibrium studies using methyl- and phenylarsonate are proceeding in this laboratory.

The authors are deeply indebted to Prof. N. Ingri of the University of Umeå, Sweden for his encouragement and supports in many ways to start the solution chemistry work in Tokyo. Thanks are also due to the late Dr. O. Ginstrup for building the automatic titrator and to Dr. L. Lyhamn for his advise in the implementation and use of the program, LETAGROP version ETITR.

Dr. L. Petterson has kindly read through the manuscript and given us many valuable comments.

References

1) K. Y. Matsumoto, *Bull. Chem. Soc. Jpn.*, **52**, 3284 (1979).
2) K. M. Barkigia, L. M. Rajkovic, M. T. Pope, and C. O. Quicksall, *J. Am. Chem. Soc.*, **97**, 4146 (1975).
3) W. Kwak, L. M. Rajkovic, J. K. Stallick, M. T. Pope, and C. O. Quicksall, *Inorg. Chem.*, **15**, 2778 (1976).
4) W. Kwak, L. M. Rajkovic, M. T. Pope, C. O. Quicksall, K. Y. Matsumoto, and Y. Sasaki, *J. Am. Chem. Soc.*, **99**, 6464 (1977).
5) K. M. Barkigia, L. M. Rajkovic-Blazer, M. T. Pope, and C. O. Quicksall, *Inorg. Chem.*, **20**, 3318 (1981).
6) A. Rosenheim, R. Bilecki, *Chem. Ber.*, **4**, 543 (1913).
7) K. M. Barkigia, L. M. Rajkovic, M. T. Pope, E. Prince, and C. O. Quicksall, *Inorg. Chem.*, **19**, 2531 (1980).
8) H. Tsukuda, T. Kawai, M. Maeda, and H. Ohtaki, *Bull. Chem. Soc. Jpn.*, **48**, 691 (1975).
9) O. Ginstrup, *Chem. Instrum.*, **4**, 141 (1973).
10) P. Brauner, L. G. Sillén, R. Whiteker, *Arkiv Kemi*, **31**, 365 (1969).
11) L. G. Sillén, *Acta Chem. Scand.*, **16**, 159 (1962); L. G. Sillén and B. Warnqvist, *Arkiv Kemi*, **31**, 341 (1969).
12) L. Pettersson, *Acta Chem. Scand.*, **25**, 1959 (1971).

Mössbauer Studies of Thermal Decomposition of Hexaamminecobalt(III) Hexacyanoferrate(III) and Hexaamminecobalt(III) Hexachloroferrate(III) in Air and in Nitrogen Atmosphere

Ajaib Singh BRAR,*,† Sarvjit BRAR, and Sarjit Singh SANDHU
Chemistry Department, Guru Nanak Dev University, Amritsar-143005, India
(Received January 23, 1981)

Thermal decomposition of hexaamminecobalt(III) hexacyanoferrate(III) (**1**) and hexaamminecobalt(III) hexachloroferrate(III) (**2**) in air as well as in nitrogen atmosphere was studied by using Mössbauer spectroscopy, TGA, DTA, IR spectroscopy, and magnetic susceptibility measurement. **1**, when heated in air, is stable up to 200 °C and then converted into hexacyanoferrate(II) and finally to ferrites; in inert atmosphere iron metal and carbides are formed above 400 °C. **2** in air is reduced to iron(II) species and finally to ferrites; in inert atmosphere ligand exchange takes place forming cobalt(II) chloride. A mechanism is proposed for the decompositions of **1** and **2**.

Mössbauer spectroscopy is a very helpful tool for the investigation of change in the oxidation state of intermediates.[1-3] Sanyal and Dass[4] used DTA and TGA to study thermal decomposition of iron(III) tris(oxalato)-ferrate(III) tetrahydrate. Gallagher and Shurey[5] applied DTA, TGA, and the Mössbauer effect for studying thermal decomposition of europium hexacyanoferrate(III) and ammonium europium hexacyanoferrate(II). Recently, evidence has been given by Gibb[6] from Mössbauer spectroscopy for an orbitally degenerate ground state in hexaamminecobalt(III) hexacyanoferrate(III). Peev and Kurtev[7] reported that solid state decomposition of iron complexes gives ferrites, which are useful because of their semiconducting properties as well as catalytic properties. They reported a change in Mössbauer parameters with catalytic properties of ferrites. The aim of the present paper is to study thermal decomposition of hexaamminecobalt(III) hexacyanoferrate(III) and hexaamminecobalt (III) hexachloroferrate(III) and to disclose effects of ligand on thermal decomposition patterns, by using Mössbauer spectroscopy, TGA, DTA, IR spectra, and magnetic susceptibility measurements.

Experimental

Hexaamminecobalt(III) hexacyanoferrate(III) (**1**) and hexaaminecobalt(III) hexachloroferrate(III) (**2**) were prepared by the methods described in Refs. 6 and 8, respectively. For **2** a solution of hexaamminecobalt(III) trichloride (0.0016 mol) in 3.4 mol dm^{-3} HCl was treated with an aqueous solution of $FeCl_3 \cdot 6H_2O$ (0.005 mol) at 70 °C. The precipitates thus obtained were washed with ethanol and ether and dried in a vacuum desiccator. **1** was obtained as yellow needle-like crystals from a mixed aqueous solution of hexaamminecobalt-(III) trichloride and potassium hexacyanoferrate(III).

IR spectra were recorded on a Mom-2000 spectrophotometer (Hungarian Optical Works) in the range 4000—700 cm^{-1} and magnetic susceptibility was measured by Gouy's method using Hg $[Co(SCN)_4]$ as calibrant. TGA and DTA thermograms were recorded in air at Chemistry Department, I.I.T., Bombay.

For thermal decomposition, **1** or **2** was heated in silica crucibles in a tubular furnace at 100, 200, 300, 400, 500, and 700 °C for 3 h in air or under a flowing nitrogen atmosphere. The nitrogen used for arranging inert atmosphere was purified by passage through copper heated at 300 °C and then through traps of anhydrous calicum chloride and potassium hydroxide. The temperature of the furnace was measured by a small chromel-alumel thermocouple connected to a portable potentiometer (Toshniwal Industries (P), Ltd., India). The sample was heated at a specified temperature for 3 h in air, or under a flowing nitrogen atmosphere. The rate of heating was kept 10 °C/min. The variation in temperature was ±5 °C. The experimental detail of our Mössbauer investigation was described in Refs. 9 and 10. Values for isomer shift were determined with reference to the natural iron.

TABLE 1. MÖSSBAUER PARAMETERS, ISOMER SHIFT (δ) AND QUADRUPOLE SPLITTING (Δ) OF HEXAAMMINECOBALT(III) HEXACYANOFERRATE(III) (**1**), AND HEXAAMMINECOBALT(III) HEXACHLOROFERRATE(III) (**2**) AND THEIR THERMAL DECOMPOSITION PRODUCTS

Complex		δ[a] or Δ/mm s^{-1} at				
		25 °C(R.T.)	200 °C in air	300 °C in air	500 °C in air	700 °C in air
$Co(NH_3)_6Fe(CN)_6$	δ	0.12±0.03	0.31±0.03	0.33±0.09	0.33±0.09	0.33±0.09
	Δ	0.35±0.03	0.75±0.03	—	—	—
				HI=492 kOe	HI=492 kOe	HI=492 kOe
$Co(NH_3)_6(FeCl_6)$	δ	0.41±0.03	0.38±0.03	0.31±0.09	0.31±0.09	0.33±0.09
	Δ	—	—	—	—	—
				HI=514 kOe	HI=506 kOe	HI=502 kOe

a) All the values of isomer shift refer to the natural iron.

† Present address: Chemistry Department, Indian Institute of Technology, New Delhi-110016, India.

Results and Discussion

The Mössbauer spectrum of **1** (at 25 °C) indicates an isomer shift value −0.12 mm/s and a quadrupole splitting 0.35 mm/s. The relatively small value of quadrupole doublet is as expected from a distorted trigonal symmetry at the Fe site[6] (Fig. 1a). Infrared frequencies and magnetic measurements confirm the formation of **1** since they are in agreement with the values given in Refs. 11 and 12. The TGA thermogram of the complex in air does not show any weight loss up to 200 °C (Fig. 2), whereas in the DTA thermogram there is an exothermic peak at 175°C and another exothermic peak at 278 °C (Fig. 3). The Mössbauer spectrum of the sample heated at 200 °C for 15 min shows formation of hexacyanoferrate(II) as identified by a single absorption band having an isomer shift value −0.14 mm/s (Fig. 4). There is another doublet due to the parent complex and a six-line pattern associated with magnetic hyperfine splitting. The intensity of magnetic field at the nucleus is 492 kOe (1 Oe=(1000/4π) A m^{-1}), which is only slightly lower than that for normal α-Fe_2O_3. These observations reveal that on heating at this temperature a part of hexacyanoferrate(III) is reduced to hexacyanoferrate-(II), while decomposition to α-Fe_2O_3 occurs concurrently.

1 was heated at 200 °C for 3 h. The Mössbauer spectrum of this sample shows a doublet (Fig. 1b) which has a quadrupole splitting of 0.79 mm/s and an isomer shift of 0.31 mm/s. These values are typical of the tervalent iron of $CoFe_2^{III}O_4$ in the superparamagnetic state. The value of isomer shift shows that the complex has the iron in high spin state. Mössbouer spectra of the samples thermally decomposed at 300, 500, and 700 °C in air are given in Fig. 5. The spectrum of the sample heated at 300 °C shows a six-line pattern due to magnetic hyperfine splitting which has an isomer shift value 0.33 mm/s. It also exhibits a doublet due to superparamagnetism, indicating the formation of $CoFe_2^{III}O_4$. The Mössbauer parameters of α-Fe_2O_3 and

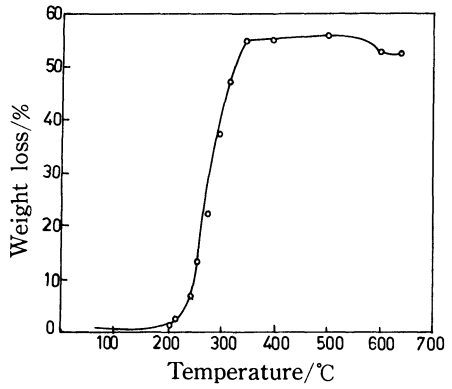

Fig. 2. TGA thermogram of hexaamminecobalt(III) hexacyanoferrate(III) in air.

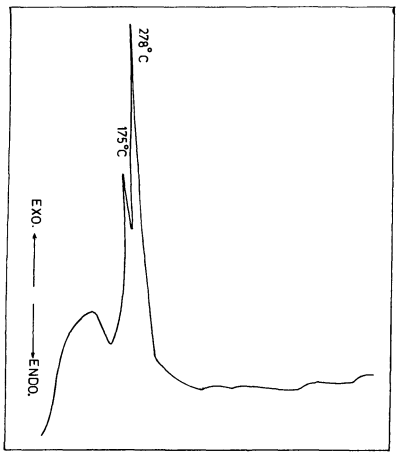

Fig. 3. DTA thermogram of hexaamminecobalt(III) hexacyanoferrate(III) in air.

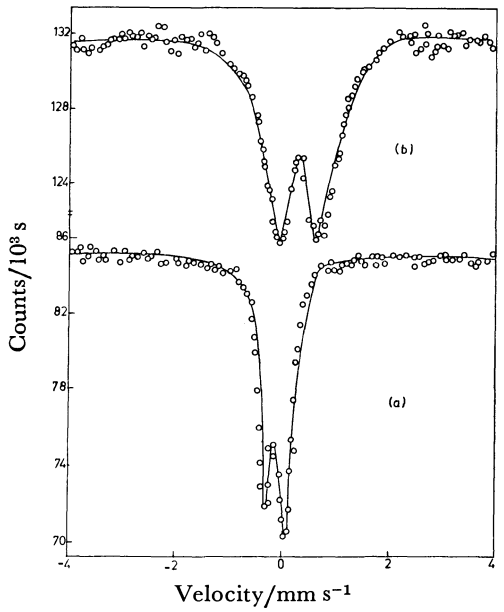

Fig. 1. (a) Mössbauer spectrum of hexaamminecobalt-(III) hexacyanoferrate(III) at room temperature (25 °C). (b) Mössbauer spectrum of hexaamminecobalt-(III) hexacyanoferrate(III) heated in air at 200 °C for 3 h.

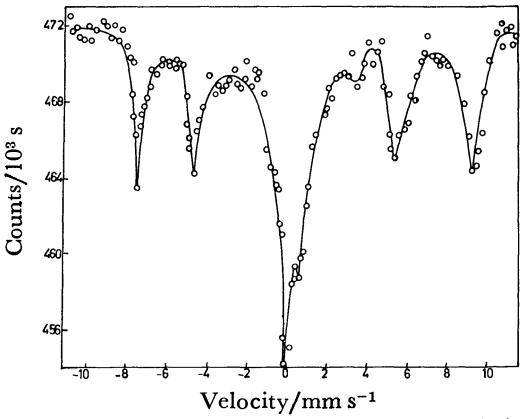

Fig. 4. Mössbauer spectrum of hexaamminecobalt(III) hexacyanoferrate(III) in air at 200 °C for 15 min.

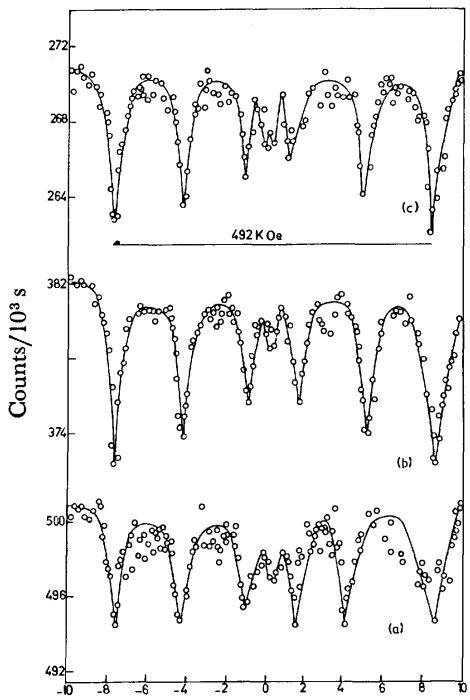

Fig. 5. (a) Mössbauer spectrum of hexaamminecobalt-(III) hexacyanoferrate(III) heated in air at 300 °C for 3 h. (b) Mössbauer spectrum of hexaamminecobalt(III) hexacyanoferrate(III) heated in air at 500 °C for 3 h. (c) Mössbauer spectrum of hexaamminecobalt(III) hexacyanoferrate(III) heated in air at 700 °C for 3 h.

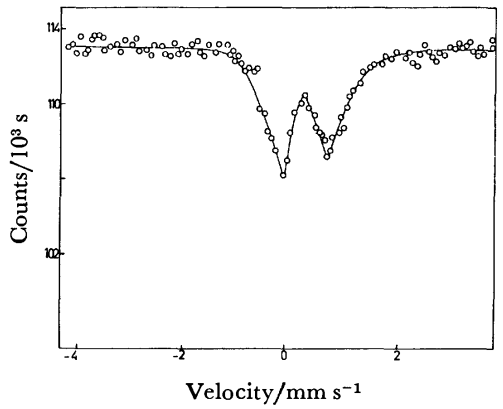

Fig. 6. Mössbauer spectrum of hexaamminecobalt(III) hexacyanoferrate(III) heated under nitrogen at 300 °C for 3 h.

$CoFe_2^{III}O_4$ are almost identical with each other at room temperature and any different sites are not resolved in ferrite, the intensity of magnetic field at the nucleus being about 510 kOe[13-15] in both the compounds. However, we assign the six-line pattern to $CoFe_2^{III}O_4$ since cobalt is available at this stage.

On further heating up to 700 °C, no remarkable change was found in the nature of this sample. The weight loss at 350 °C is 55%, which shows formation of ferrites. The DTA peak at 278 °C is considered to be due to oxidation of the complex (Fig. 3).

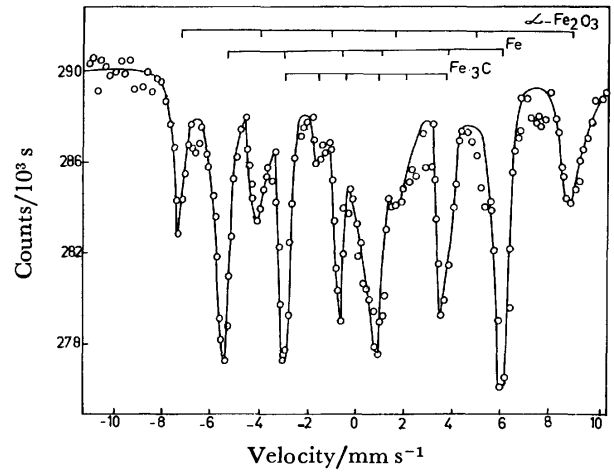

Fig. 7. Mössabauer spectrum of hexaamminecobalt(III) hexacyanoferrate(III) heated heated under nitrogen at 400 °C for 3 h.

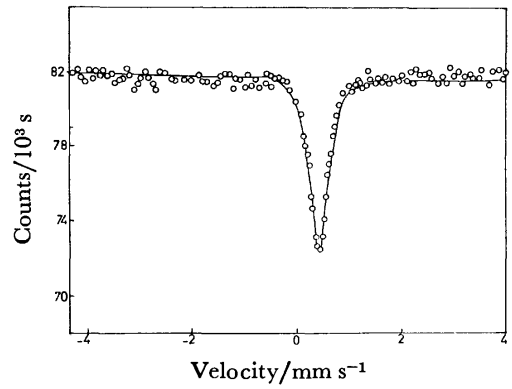

Fig. 8. Mössbauer spectrum of hexaamminecobalt(III) hexachloroferrate(III) at room temperature (25 °C).

1 was heated under a flowing oxygen-free nitrogen atmosphere. No change was found in values for isomer shift and quadrupole splitting up to 200 °C. At 300 °C the sample gives a higher value of isomer shift 0.37 mm/s and a value of quadrupole splitting 0.63 mm/s, which may be due to ligand exchange (Fig. 6). Frequency $\gamma(C\equiv N)$ in the infrared region shows the splitting having absorption bands at 2250 and 2125 cm^{-1}, and the band at 3200 cm^{-1} may be due to NH_3 stretching, in support of the exchange mechanism. On further heating, Mössbauer spectra show formation of iron metal, iron carbide, and a small quantity of ferrite, as shown in Fig. 7. Oxidation takes place only after the sample has been exposed to air to make the strip for recording Mössbauer spectrum. Formation of these products was confirmed also by magnetic measurements.

The Mössbauer spectrum of **2** (at 25 °C) shows a single line absorption band having an isomer shift 0.41 mm/s (with respect to the natural iron) and a line width 0.40 mm/s which indicates a cubic symmetry around the iron atoms, and the electron density is the same in all the d-orbitals of iron(III) (Fig. 8). The value of isomer shift shows that the complex is in a high spin (+3) oxidation state. Infrared frequencies

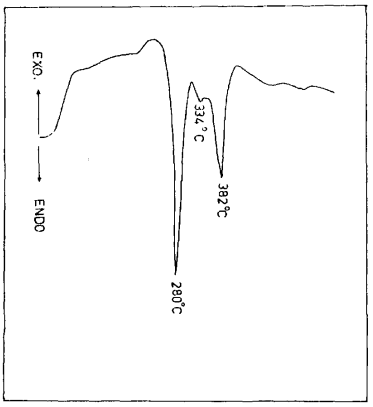

Fig. 9. DTA thermogram of hexaamminecobalt(III) hexachloroferrate(III) in air.

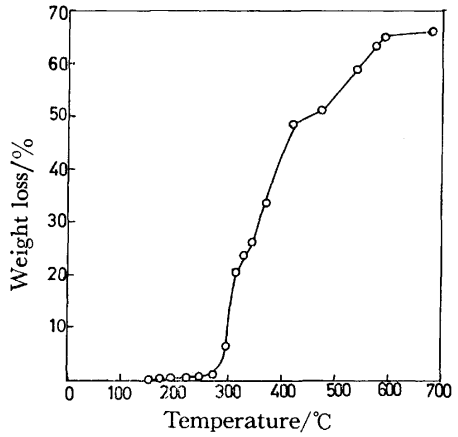

Fig. 10. TGA thermogram of hexaamminecobalt(III) hexachloroferrate(III) in air.

and ω_{eff} show formation of the above complex. The DTA thermogram shows an endothermic peak at 280 °C, very small endothermic peak at 334 °C, and a peak at 382 °C (Fig. 9). The TGA thermogram shows that there is no weight loss up to 270 °C, over which a weight loss occurs, as shown in Fig. 10. It is evident from the DTA and TGA data that this complex is stable up to 270 °C.

2 heated at 300 °C for 15 min gives a Mössbauer spectrum having an absorption band with an isomer shift 0.42 mm/s due to $FeCl_6^{3-}$ moeity and another doublet with an isomer shift 1.27 mm/s and a quadrupole splitting 1.69 mm/s due to Fe^{2+}, along with the magnetic hyperfine splitting of low intensity due to ferrite already mentioned (Fig. 11a). Thus it is clear that iron(III) is reduced to iron(II) and then oxidized to $CoFe_2^{III}O_4$.

The Mössbauer spectrum of the sample heated at 300 °C for 3 h in air shows a six-line pattern having a value of isomer shift 0.21 mm/s, as shown in Fig. 11b. The intensity of the magnetic field is 514 kOe, which agrees well with that of $CoFe_2O_4$. There was no observable change found in the spectra of the samples heated up to 700 °C (Figs. 11b and c). The magnetic moment of the sample at room temperature is 5.9 BM ($\psi_g = 32.7 \times 10^{-6}$). The ψ_g values of the samples at 200 and 300 °C are 37.6×10^{-6} and 51.61×10^{-6} cgs,

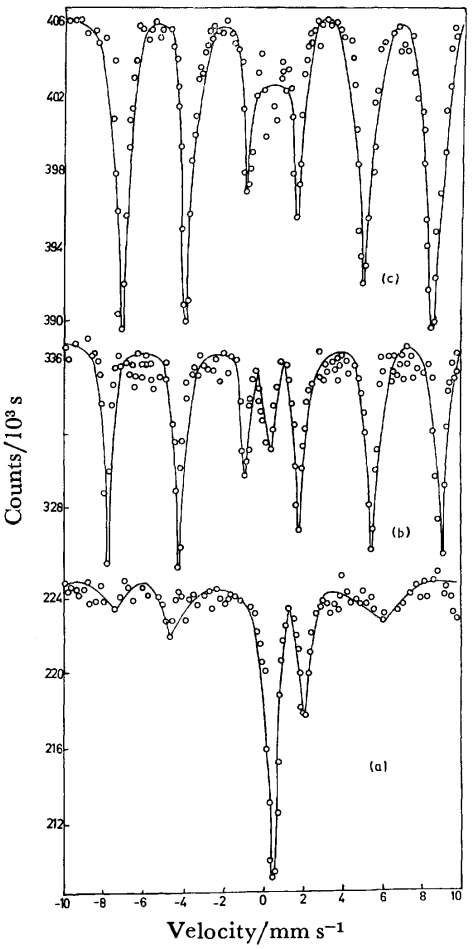

Fig. 11. (a) Mössbauer spectrum of hexaamminecobalt(III) hexachloroferrate(III) heated in air at 300 °C for 15 min. (b) Mössbauer spectrum of hexaamminecobalt(III) hexachloroferrate(III) heated in air at 300 °C for 3 h. (c) Mössbauer spectrum of hexaamminecobalt(III) hexachloroferrate(III) heated in air at 700 °C for 3 h.

respectively. The samples heated at 400, 500, and 700 °C are highly paramagnetic and are attracted towards the magnet. The IR spectrum of the sample heated at 300 °C shows a peak at 3100—3300 cm^{-1} due to ν(N–H), a peak at 1600 cm^{-1} due to δ_{asy}(N–H), and a peak at 1400 cm^{-1} δ_{sym}(N–H), which shows the presence of ammonia at this temperature. Thus it is shown that the parent complex is present in the mixture along with the ferrites. There is, however, no absorption band in the range 4000—700 cm^{-1} with the samples heated at higher temperatures, which shows complete decomposition of the complex into ferrites. This is supported by magnetic susceptibility data. DTA and TGA thermograms also show elimination of ammonia and the chloride group by giving endothermic peaks at 334 and 382 °C. The samples for Mössbauer measurement were first heated at 300 °C and then at a higher constant temperature for 3 h, so that decomposition products were formed at a little lower temperature than expected in DTA and TGA. The weight loss is also in agreement with the formation of ferrites.

In the case of **2** in inert atmosphere, the sample was

found stable up to 300 °C. On further heating, for example, up to 400 °C, ligand exchange takes place. Even with the maximum care to avoid the samples from being exposed to air, they got fully oxidized when taken out of the furnace to make the strip for Mössbauer spectral recording. A chemical analysis of these pinkish products shows presence of cobalt(II) chloride, which is highly hygroscopic, absorbs water from air, and oxidizes the sample quickly. This is why the spectrum of the sample heated at 500 °C in inert atmosphere shows a ferrite pattern (Since we had no arrangement for recording Mössbauer spectra with sample kept in the furnace in nitrogen atmosphere, the experimental information obtainable was limited to what has been given above.).

From the above investigations it is clear that patterns of decomposition and products formed depend on ligands and atmospheres employed, as expected. For both the complexes the temperature of decomposition in air is lower than in inert atmosphere. The temperature of decomposition for **1** is comparable to the temperature of thermal decomposition for alkali metal hexacyanoferrate(III). But the temperature of decomposition for **2** is higher than those for hexacyanoferrate(III) complexes. **1** is reduced to ferrate(II) around 200 °C and on further heating to higher temperatures ferrites are formed in air, whereas iron metal and carbides are formed in inert atmosphere. In the case of **2**, on the other hand, the products formed under inert atmosphere are readily oxidizable and hygroscopic, absorb moisture and oxygen from air, and get oxidized partially to ferrites. In earlier investigations,[16] in a preparation of cobalt oxides from carbonates in vacuum, cobalt oxides prepared at 300 °C were observed to take oxygen from air and to change in color from grey to black. This type of oxidation of cobalt also results in formation of ferrites. Ligand exchange takes place at 300 °C forming cobalt(II) chloride, which was confirmed from its violet pink color and by chemical analysis. The products when exposed to air absorbed water from air, and iron and cobalt are oxidized to ferrites. This may be due to the high surface reactivity of small particles of the powdered iron and cobalt metals (The ferrites and mixed oxides formed by the decomposition of the abovementioned complexes are useful in industry because of their semiconducting as well as catalytic activities.).

Although the mechanism of solid state decomposition is complex, the present information furnished from Mössbauer, infrared, and magnetic measurements, differential thermal analysis, and thermogravimetric analysis, allows us to deduce the following paths of decomposition in air for **1** and **2**:

$$4[Co(NH_3)_6][Fe(CN)_6] \xrightarrow[15\,min]{200\,^\circ C} [Co(NH_3)_6]_4[Fe(CN)_6]_3 + {}^1/_2Fe_2O_3 + 3(CN)_2,$$

$$[Co(NH_3)_6]_4[Fe(CN)_6]_3 + {}^1/_2Fe_2O_3 \xrightarrow[air]{350\,^\circ C} Co_2O_3 + 2CoFe_2^{III}O_4 + 9(CN)_2 + 24NH_3,$$

$$2[Co(NH_3)_6][FeCl_6] \xrightarrow[15\,min]{300\,^\circ C} 2[Co^{II}(NH_3)_6][Fe^{II}Cl_4] + 2Cl_2,$$

$$2[Co(NH_3)_6][Fe^{II}Cl_4] \xrightarrow[air]{400\,^\circ C} CoFe_2^{III}O_4 + {}^1/_2Co_2O_3 + 12NH_3 + 4Cl_2.$$

The percentage weight loss calculated for the decomposition of **1** effected by 15 min heating at 200 °C is 9%, corresponding to 2% weight loss in TGA. The higher value of weight loss is due to the heating time being longer than in TGA. The weight loss for the second step is 57.2% which is in agreement with the TGA value (55%) for decomposition. In the case of **2** the weight loss calculated for the first step is 15% which is higher than the TGA value (10%) due to longer heating time. The weight loss calculated for the second step is 63% which is in agreement with the TGA value (65%) for the thermal decomposition. The temperature of decomposition is higher in the case of **2**, which indicates that the ligand has a great effect on the thermal stability of the complex.

References

1) T. C. Gibb and N. N. Greenwood, "Mössbauer Spectroscopy," Chapman and Hall, London (1971), p. 173.
2) P. K. Gallagher, "Applications of Mössbauer Spectroscopy," ed by R. L. Cohen, Academic Press, New York (1976), p. 199.
3) D. Raj and J. Danon, *J. Inorg. Nucl. Chem.*, **37**, 2039 (1975).
4) T. K. Sanyal and N. N. Dass, *J. Inorg. Nucl. Chem.*, **42**, 811 (1980).
5) P. K. Gallaghar and F. Shrey, *Thermal Analysis*, **2**, 1910 (1977).
6) T. C. Gibb, *J. Chem. Soc., Dalton Trans.*, **19**, 1910 (1977).
7) T. Peev and K. Kurtev, *Bulg. J. Phys.*, **6**, 535 (1979).
8) W. E. Hatfield, C. Robert, F. Basolo, Whyman, and R. Fay, *Inorg. Synth.*, **11**, 47 (1968).
9) A. S. Brar, S. Brar, and S. S. Sandhu, *Radiochem. Radioanal. Lett.*, **44**, 155 (1980).
10) A. S. Brar, and B. S. Randhawa, *Bull. Chem. Soc. Jpn.*, **54**, 3166 (1981).
11) K. Nakamoto, "Infrared Spectra of Inorganic and Coordination Compounds," Wiley Interscience, New York (1970), p. 155.
12) J. Craszar and Annafelvegi, *Acta Chim. Acad. Sci. Hung.*, **47**, (i, 37—52), (1966).
13) I. Dezsi, A. Z. Hryn Kiewicz, and D. S. Kulgawizuk, *Acta Phys. Pol.*, **24**, 283 (1963).
14) W. J. Schulle, S. Shtrikman, and D. Treves, *J. Appl. Phys.*, **36**, 1010 (1965).
15) M. Eibscheitz and S. Shtrikman, *J. Appl. Phys.*, **39**, 997 (1968).
16) A. S. Brar and L. D. Ahuja, *J. Colloid Interface Sci.*, **50**, 195 (1975).

Analytical Extraction of Uranium with TOPO from Sea Water

Sandro Degetto,* Mario Faggin, Anna Moresco, and Livio Baracco
I.C.T.R.-C.N.R., Cso Stati Uniti-35100 Padova, Italy
(Received June 23, 1982)

A distribution study was carried out on the extraction behaviour of uranium in sea water using solutions of TOPO in cyclohexane. The influence of various factors (time, pH, TOPO concn in the organic phase, nitrate or chloride concentration in the aqueous phase and volumetric ratio between the two phases) on the extractability of uranium was investigated. In view of the results obtained, the best conditions for a quantitative recovery were selected. The application of the results to fluorimetric determination of uranium is also reported.

Phosphine oxides are among the most powerful neutral ligands towards uranyl complexes.[1] In particular TOPO (trioctylphosphine oxide) has been widely used in liquid-liquid extraction systems and many application to uranium separation have been reported.[2–8] In the present work a systematic investigation on the extractability of uranium from sea water with TOPO in cyclohexane is reported and selected conditions for a quantitative recovery are recommended.

In view of the results obtained a method for the determination of uranium in sea water by fluorimetric analysis is proposed. The analytical method is simple, rapid and gives reliable and highly reproducible results.

Experimental

Materials. Trioctylphosphine$^-$=(TOPO), Merck product, was used without further purification. Cyclohexane, hydrochloric and nitric acids were C. ERBA analytical grade products.

Instruments. pH measurements were performed with a Metrohom E603 and fluorimetric determinations with a FLUPAD-U fluorimeter equipped with a low current, low noise, selected preamplifier and a very high stability circuit for H. V. power switching supply. In addition, the temperature is controlled in order to avoid drifts in the electronic components response.

Uranium Standard Solutions. Aliquots of a stock solution containing 100 mg of uranium (as uranyl nitrate) per litre of 6 M HNO_3, are diluted with the same acid to give standard solution containing 10100 or 1000 g l^{-1} uranium.

Procedure. Sea water samples were filtered on 0.45 μm Millipore. Sea water collected near the shore at Jesolo (Venice) poured into polyethylene containers was used in most experiments. Uranium content of each stock was accurately determined and the results were always near to an average of 3.0 g l^{-1}. All salinity values of the samples were between 29 and 32 g l^{-1}.

The sea water samples properly acidified with HCl or HNO_3 were thoroughly mixed with solutions of TOPO in cyclohexane at various concentrations and with different volumetric ratios between the two phases (organic phase and aqueous phase). The mixed solutions attain equilibrium rather rapidly. The two phases were allowed to separate (10—20 min) and the uranium content determined in the aqueous or/and in the organic phase by a method described in a previous report[9] and by the present method.

Results and Discussion

Effect of Time. The equilibration time depends on the exchange surface and therefore on the efficiency of mixing of the two phases. In an experiment the extent of uranium extraction from 2 l of sea water 0.5 M in HNO_3 by 80 ml 2.5% TOPO soln in cylohexane was studied. The two phases were allowed to stand carefully separated in a cylindric vessel (internal diameter 9.4 cm) and analysed for uranium from time to time. The rate of equilibration was very low (the equilibrium was attained in more than 15 d) whereas when the two phases were thoroughly mixed by magnetic stirring, equilibrium was rapidly attained (about 10′—20′). In view of these results in all the following experiments an excess time of 1 h was adopted.

Effect of pH. The pH values of sea water show some diurnal and seasonal variation with a mean value 8.3—8.5 at the surface.[10] In these conditions uranium is not extracted by the organic solution of TOPO owing to the very high stability of the uranyl tricarbonate complex ($\log \beta_3 = 21.54$)[11] in which the carbonat anions fully engage the coordination sphere of the oxo cation UO_2^{2+}. On adding an acid (HCl or HNO_3) the $UO_2(CO_3)^{4-}$ complex is progressively destroyed (the maximum stability for this species is at about pH 8.5, whereas it is at 7 for $UO_2(CO_3)_2^{2-}$ and at 6 for neutral species $UO_2(CO_3)$), and the extractant TOPO can more easily enter the coordination sphere of the oxo cation.

In Figs. 1a and 1b the effect of acidification of the sea water solutions with HCl and HNO_3 is reported. It can be seen that up to pH 2.5 the % U extraction is almost independent of the kind of acid used.

The effects observed at lower pH when the molarity of the added acid is increased will be discussed later. The meaning of the maxima presented by curves a and b of Fig. 1 can be interpreted bearing in mind that:

i) The TOPO is capable of capturing uranium from the aqueous phase only when the species are coordinated to neutral donors (in practice water molecules), it cannot compete with anionic species whose coordinating ability is higher by many orders of magnitude.

ii) The nature of the extractant phase makes the extraction of charged species difficult.

Therefore it is likely that at the higher pH side of the "bell" the non extractability of the uranium is due to the presence of almost only one species, the coordinatively saturated $UO_2(CO_3)_3^{4-}$, whereas the low % extraction values obtained at low pH are related to the prevailing presence of the charged solvated UO_2^{2+}.

It is reasonable to suppose that the maximum observed

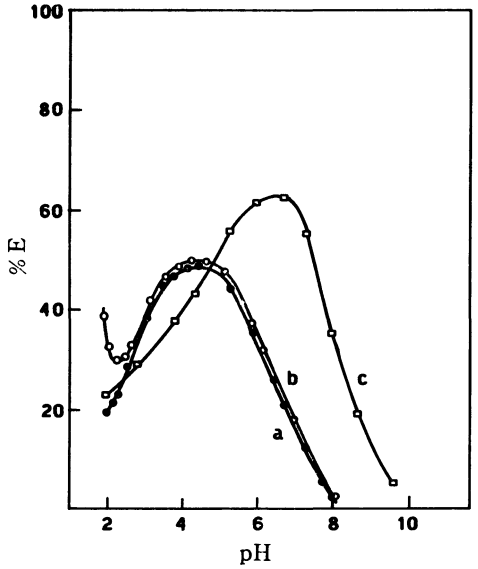

Fig. 1. Effect of pH value on the extraction of uranium.
a: HCl added, b: HNO_3 added, c: carbonates absent. Organic phase/aqueous phase: 0.04, organic phase: 0.5% TOPO soln.

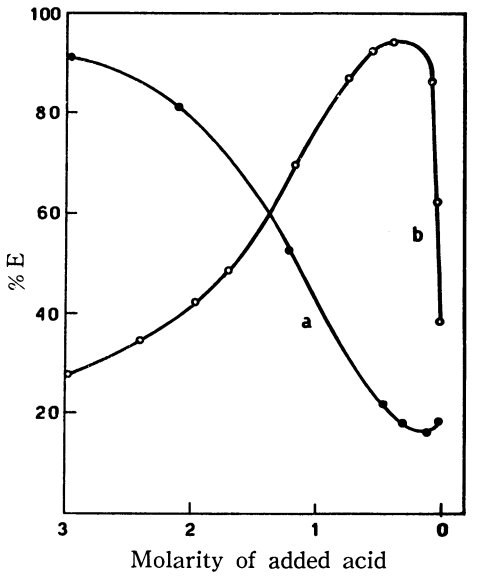

Fig. 2. Effect of increased acid concentration on the extraction of uranium.
a: HCl added, b: HNO_3 added. Organic phase/aqueous phase: 0.04, organic phase: 0.5% TOPO soln.

at about pH 4.5 is due to the presence of neutral uranium complexes containing hydrogen carbonate and hydroxide anions.

The role of carbonates on the extraction ability of TOPO is more evident considering the curve c of Fig. 1 obtained in the absence of carbonate species. In this case also, the maximum (at about pH 6.5) would correspond to the extraction of neutral species (hydroxo or chlorohydroxo complexes) but in this particular case coordinatively unsaturated but charged species, as for instance $(UO_2)_3(OH)_5^+$ and $(UO_2)_4(OH)_7^+$, in which the single charge is widely distributed could contribute to the extractability of uranium.

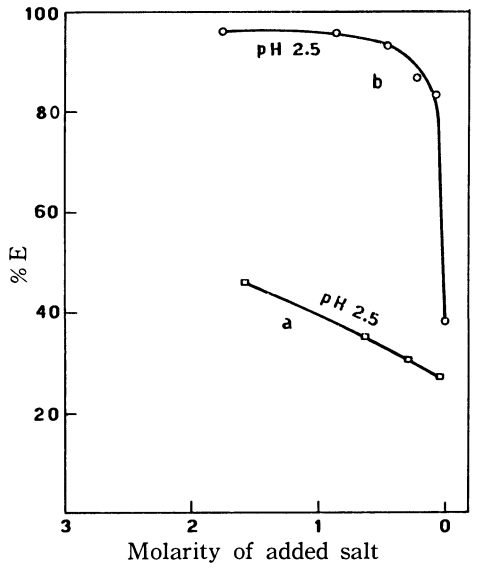

Fig. 3. Effect of added salts on the extraction of uranium at constant pH value.
a: Chloride added, b: nitrate added. Organic phase/aqueous phase: 0.04; organic phase: 0.5% TOPO soln.

The formation constants of the above mentioned hydroxo complexes are in fact very high and compared well with those of carbonato complexes.[12] As far as the extraction mechanism is concerned there exists in this case, (in addition to the usual type of coordination $R_3P{=}O{\rightarrow}U$), the possibility of interaction, through hydrogen bonding of the oxygen of TOPO with the hydrogen atom of a coordinated hydroxyl group.[3,13]

Effect of Chloride and Nitrate Concentration. The extraction curves a and b of Fig. 1 behave differently at pH lower than 2.5 as the molarity of the added acid is increased.

In Fig. 2 the %E of uranium *vs.* the molarity of the HCl or HNO_3 added, up to 3 M, is reported. On adding HCl the extraction yield continuously increases, but HNO_3 presents a second bell shaped curve with a rather sharp maximum at about 0.4 M HNO_3.

The result reported in Fig. 3, the effects of increasing molarity of added Cl^- or NO_3^- at constant pH (2.5), throw some light on this behaviour.

The observed results can be interpreted taking into account:

i) The type of complexes formed by uranyl ion with the anionic species *i.e.* : $UO_2(NO_3)^+$, $UO_2(NO_3)_2$, $UO_2(NO_3)_3^-$ and the analogous series with Cl^- up to $UO_2Cl_4^{2-}$.

ii) The competition of the proton for the oxygen of TOPO

As regards the complex species, the same considerations mentioned above (for carbonate complexes) can be applied. However, up to molarity 2 for NO_3^- and even higher for Cl^- (see Fig. 3). The problem of the competition of TOPO with the anionic species in coordinating the uranyl does not exist.

Comparing curves (b) of Figs. 2 and 3 the importance of the second factor ii) is evident.

The formation of the species TOPO–HNO_3[14] sharply

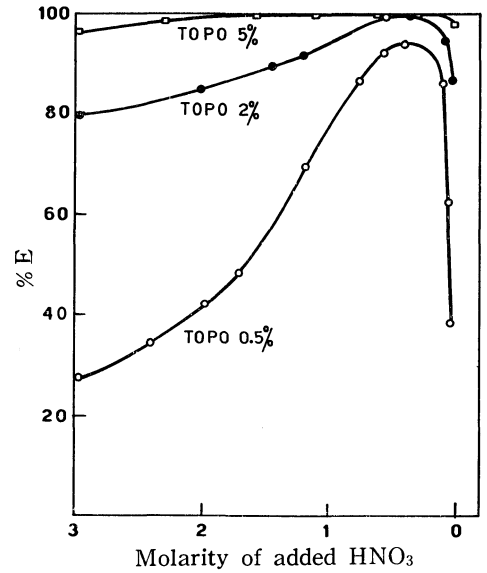

Fig. 4. Effect of TOPO concn in the organic phase on the extraction of uranium at various HNO_3 molarity. Organic phase/aqueous phase: 0.04.

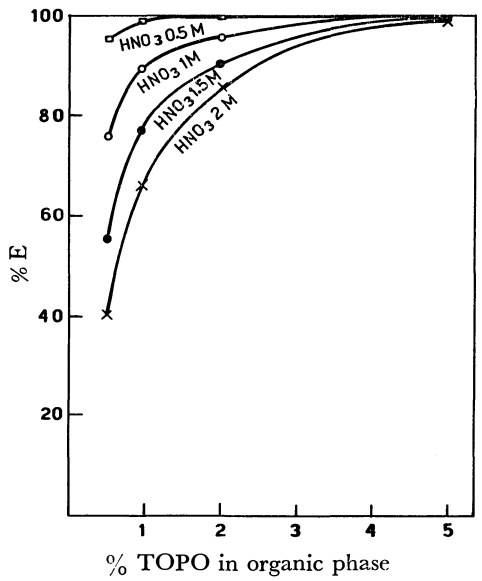

Fig. 5. Effect of TOPO concn in the organic phase on the extraction of uranium. Curves at constant HNO_3 molarity.
Organic phase/aqueous phase: 0.04.

decreases the equilibrium concentration of the free TOPO in the organic layer.

This effect appears to be less important for HCl as the curves a in Figs. 2 and 3 show an increase in % E with both increasing acidity and chloride concentration. Titrations with NaOH of the acids extracted by TOPO into the organic phase indicate that the extraction of HNO_3 is much more favoured compared to HCl.

Effect of TOPO Concentration. In Fig. 4 are reported a series of extraction curves at constant concentration of TOPO in the organic phase and constant volumetric ratio of the two phases. These results show dramatic change in uranium extractability at higher concentrations of HNO_3.

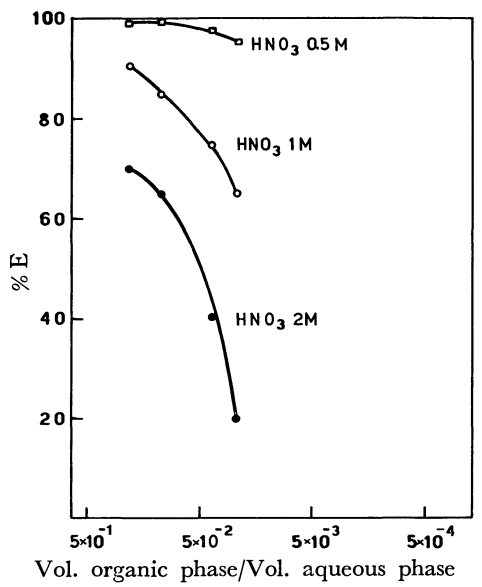

Fig. 6. Effect of the volumetric ratio between the organic and aqueous phases. Curves at constant HNO_3 molarity. Organic phase: 0.5% TOPO soln.

As can be seen from Fig. 4, for organic phase/aqueous phase=0.04, (*i.e.* 4 ml of organic phase per 100 ml of sea water), there is a rather large range of molarity (0.1—1.3 M) for which a 5% TOPO solution gives an extraction yield>99%. The same results can be represented in a different way (see Fig. 5) by curves showing the effects of % TOPO in the organic phase at constant HNO_3 molarity.

Effect of the Volumetric Ratio between the Two Phases. In order to have a complete picture of the situation and to identify the best conditions for quantitative extraction, the final factor considered was the effect of a volumetric ratio change between aqueous and organic phase. These results are reported in Fig. 6 in which the extractant solution is 0.5% TOPO and the organic phase/aqeous phase ratios ranged from 16/100 to 2/100.

The Analytical Method

It is evident from the above results that it is quite simple to reach an essentially complete (>99%) extraction of uranium from sea water in a single-batch contact. As this procedure could be easily applicable for U determination on a routine basis, we examined the possibility of directly measuring the fluorescence of the uranium extracted, (without any supplementary separation), by use of a pellet with a high carbonate flux.

It is well known that in spite of its high sensitivity the fluorimetric method suffers from some disadvantages. First there is the possibility that the uranium fluorescence may be quenched by a number of heavy metals. Secondly there is the need to control carefully the operating conditions. As regards the second point we have already shown[9] that the variability of the results observed in preparing and measuring the pellets from standard uranium samples was from 0.4% for 0.07 μg U up to 2% for 0.007 μg U in easily reproducible conditions.

Thus, high errors are likely to be mainly related to the chemical treatment of the samples.

We have now rechecked these earlier results using a new fluorimeter, of our own design, in which, owing to the very high linearity of instrumental response is possible to obtain a straight line calibration curve for the whole range 0.001—0.1 g U which should satisfy all the needs of environmental or biological samples. The fluorescence signals of the pellets obtained (starting from standard uranium samples) now show a reproducibility better than 1% over the whole range (average of six determinations).

The instrumental response is easily controlled routinely before every series of measurements by a set of quartz buttons containing different appropriate amounts of uranium.

The reliability of such a system tested over two years was excellent.

The procedure recommended for the analysis of uranium entails the following steps:

1°) Filtration of the sea water samples on 0.45 μm Millipore and acidification with concentrated HNO_3 (4 ml per 100 ml sea water).

2°) Addition to the sea water of a 5% TOPO solution in cyclohexane up to a volumetric ratio organic phase/aqueous phase 4×10^{-2}.

3°) Efficient mixing of the two phases (by magnetic stirring) in a tightly closed glass container for about 1 h. (The shape of the container should facilitate the separation of the small organic phase).

4°) At this point an adequate fraction of the organic phase (possibly containing $(1—4)\times10^{-8}$ g of uranium) is transferred onto the platinum dish, brought to dryness by an IR lamp and then heated for a few seconds over a Bunsen burner in order to destroy completely the organic materials. This operation is quite difficult to do without losses as the organic materials tend to lined the rim of the dish. After many attempts we realized that the simplest way to overcome these difficulities is a back extraction of U by a 15% aqueous solution of $(NH_4)_2CO_3$ volume to volume. This step is quantitative within a few minutes of stirring and can be easily performed in a small test-tube.

An aliquot of the carbonate phase is now transferred to the dish by a pipette (without the need to separate the phases) and the sample is treated as reported above.

5°) Preparation of the pellet with a high carbonate flux namely 10% NaF, 40% K_2CO_3, 50% Na_2CO_3. The distance of the head of the Bunsen burner from the platinum dish is adjusted to give a fusion time of about 90″ and the heating is then continued for 30″ more. In such conditions the temperature of the fused salts does not exceed 600—630 °C.

6°) After cooling the dishes the pellets are easily taken off, inserted in a measuring plate and stored for half an hour in a desiccator thermostatted at 25 °C before measurements are made.

None of these steps appears to be "critical," the overall analytical reproducibility for some sea water samples is reported in Table 1.

The reproducibility observed is strictly related, in our opinion, to the almost 100% yield of each step and the use of convenient volume measuring apparatus. As regards the precision of the measurements this is related to the first disadvantage mentioned above for the fluorimetric method, namely the quenching effect.

In the present case such effects are quite small or even absent, owing to the low concentration of any quencher and to the selection resulting from the two extraction steps (see Table 1). As a matter of fact it was difficult to detect (even qualitatively), by X-ray fluorescence analysis, the presence of very low quantities of Fe, Ni, Cu, Zn, and Pb in samples fifty times more concentrated than those normally used for analysis. Anyhow as the quenching effect is known to be proportional to the quantity of quenchers present but independent of the amount of uranium[15] it is possible, even with samples other than sea water, to apply the spiking technique even on a routine basis by adding directly to the platinum dishes different known amounts of uranium.

This simplified procedure can only be applied however when (as in the present case) the procedure warrants an overall extraction yield >99%. In our opinion it is in fact extremely difficult to obtain a good reproducibility of lower extraction yields without any supplementary technique such as, for instance, the isotopic dilution method.

The minimum time interval required between the receipt of a sample and the analytical result (average of

Table 1. Uranium content of some samples of natural waters taken at surface

Sample	U found ($\mu g\ l^{-1}$) using the spiking technique[a]	Quenching effect[b]
Adriatic Sea at shore near Jesolo (Venice) in the period 1979—1982	2.91±0.07	0.99
	3.07±0.08	1.01
	3.28±0.09	0.97
	2.84±0.06	0.98
Mediterranean Sea, at shore Taranto (1981)	3.32±0.09	0.99
Tyrrhene Sea off shore of Piombino (1981)	3.15±0.07	1.02
Atlantic Ocean, at shore, Asilah (Maroc) 1981	3.36±0.06	0.97
Pacific Ocean, at shore, Bay of Monterey, California (1981)	2.81±0.05	0.95
Piave River (Noventa di Piave) 1981	0.72±0.04	0.73
Brenta River (Strá) 1982	0.64±0.05	0.85

a) The values reported are the mean of six results with the relative mean error. b) Expressed as the ratio of the values obtained without and with spiking of the samples.

six determinations) is about 4 h, and the size of sample normally required is 50 ml.

We thank Dr. J.S. Coe (King's College, London) for helpful discussion, V. Corrado and G. Agostini for technical assistance.

References

1) S. Degetto, L. Baracco, and G. Manangoni, *J. Chem. Soc., Dalton Trans.*, **1976**, 1645.
2) R. J. Baltisberger, *Anal. Chem.*, **36**, 2369 (1964).
3) M. Niitsu and Sekine, *J. Inorg. Nucl. Chem.*, **38**, 1057 (1976).
4) G. Ting and T.-W. Lee, *Radiochim. Acta*, **28**, 103, (1981).
5) K. Shakir and S. G. Beheir, *Chimia*, **33**, 192 (1979).
6) R. Shabana and H. Ruf, *Radiochim. Acta*, **23**, 117 (1976).
7) G. W. Mason, S. McCarty, and D. F. Peppard, *J. Inorg. Nucl. Chem.*, **24**, 976 (1962).
8) F. T. Bunus, V. C. Domocus, and P. Dumitrescu, *J. Inorg. Nucl. Chem.*, **40**, 117 (1978).
9) U. Croatto, S. Degetto, and L. Baracco, *Ann. Chim.*, **68**, 53 (1978).
10) J. P. Riley and R. Chester, "Introduction to Marine Chemistry," Academic Press, London (1971), p. 143.
11) S. O. Cinneide, J. P. Scanlan, and M. J. Hynes, *J. Inorg. Nucl. Chem.*, **37**, 1013 (1975).
12) R. N. Sylva and M. R. Davidson, *J. Chem. Soc., Dalton Trans.*, **1979**, 465.
13) M. Niitsu and T. Sekine, *J. Inorg. Nucl. Chem.*, **38**, 1053 (1976).
14) A. M. Rozen, Z. I. Nikolotova, N. A. Kartasheva, and L. A. Kasumova, *Russ. J. Inorg. Chem.*, **23**, 62 (1978).
15) G. R. Price, R. J. Ferretti, S. Schwart, *Anal. Chem.*, **25**, 322 (1953).

A Kinetic Study on the Oxychlorination of Benzene

Jesus Blanco,* Pedro Avila, and Francisco Vicente Melo
Instituto de Catálisis y Petroleoquimica†, Serrano, 119, Madrid-6, Spain
(Received March 19, 1982)

Gas-phase benzene oxychlorination was carried out over a $CuCl_2$–$CeCl_3/Al_2O_3$ catalyst. A kinetic model is proposed which permits us to obtain a rate equation capable of reproducing experimental results. The presence of cerium in the catalyst increases the reaction rate and maintains the conversion level for a long time. It seems that this element facilitates copper reoxidation by making the total rate independent of the partial pressure of oxygen and stabilizes the active phase of the catalyst.

Oxychlorination is one of the most interesting ways of consuming the HCl surplus produced in conventional hydrocarbon chlorination processes.

A considerable number of kinetic studies on catalytic hydrocarbon oxychlorination are found in the paper by Allen and Clark.[1] The reported data relate mainly to hydrocarbons to be oxychlorinated, reaction temperature, nature of catalyst, and whether reaction takes place in the liquid or gas phase. Most of this information relates, however, to aliphatic hydrocarbons, particularly ethylene, whereas the information about oxychlorination of aromatics in the gas phase is scarce, being restricted to the works of Solomoniv *et al.*[2] on toluene oxychlorination, Shutenkova and Gor'kova,[3] and Blanco *et al.*[4,5] on benzene, and Altuglu and Roberts[6] on chlorobenzene. In the case of chlorobenzene, using a $CuCl_2$–$LiCl/Al_2O_3$ catalyst at 200 °C,[6] the authors claimed that the Deacon reaction should not be included in the overall mechanism, and that the rate limiting step would be the formation of an activated complex compound between the hydrocarbon and adsorbed oxygen: $C_6H_5ClO^*$. Blanco *et al.* have published reports of studies on benzene oxychlorination using $CuCl_2$/alumina[7,8] and $CuCl_2$–KCl/alumina.[4,5] In these studies they have pointed out the existence of an interaction between copper cations and OH groups of the support.

Lately they have developed a series of catalysts containing copper and cerium chlorides on alumina that exhibit greater activity than copper chloride or mixtures of copper and alkali metal chlorides.

In this communication, the behaviour of these $CuCl_2$–$CeCl_3/Al_2O_3$ catalysts has been studied for the oxychlorination of benzene, and the results are compared with kinetic data previously reported.

Experimental

Apparatus. The experiments were carried out at atmospheric pressure in a conventional fixed-bed flow catalytic reactor described elsewhere.[9] The exit gases from the reactor pass through a condenser where the liquid products are collected, and then through a water adsorption column to remove unreacted HCl. The chlorinated products in the organic condensate were analyzed by GLC in a column (6.5 mm × 4.2 m) of SE. 30 Silicone rubber on Chromosorb P (60—80 mesh). Complete balance of C, H_2, and Cl_2 was confirmed for each experiment.

Catalyst. The catalyst used in this work was prepared by impregnation of gamma-Al_2O_3 (EPA, high purity, containing $Fe_2O_3 \leqslant 0.05\%$; $SiO_2 \leqslant 0.5\%$; $Na_2O \leqslant 0.01\%$; $K_2O \leqslant 0.05\%$; LOI = 7.0%) with aqueous solutions of $CuCl_2$–$2H_2O$ (Carlo Erba) and $CeCl_3 \cdot 7H_2O$ (BDH), and drying at 110 °C for 2 h. The alumina support was previously treated at 400 °C in air for 12 h.

The catalyst obtained has surface area 152 m^2/g, pore volume 0.351 cm^3/g, average pore radius 55 Å, and metal contents 0.42×10^{-3} g-atom Cu/g cat. and 0.40×10^{-3} g-atom Ce/g cat., as determined by atomic absorption spectrophotometry, equivalent to about 2.7 wt% Cu and 6.1 wt% Ce. The E.D.A.X. analysis showed that both elements are totally mixed and uniformly distributed throughout the support.

Results and Discussion

Exploratory runs were initially performed in order to define the range of experimental conditions in which the rate is not limited by mass transfer. A test carried out with the reactor packed with support alone gave no detectable conversion.

The effect of reaction temperature and contact time on rate and selectivity was studied with a stoichiometric feed mixture according to the equation

$$C_6H_6 + HCl + \frac{1}{2}O_2 \longrightarrow C_6H_5Cl + H_2O.$$

The operation conditions employed were: reaction temperature, T, 230—300 °C; pressure, P, 700±10 mmHg (1 mmHg = 133.322 Pa); weight of catalyst, W, 1—12 g; catalyst size, 1—2 mm; benzene feed, F_b, $(1.125—2.25) \times 10^{-3}$ mol min^{-1}; feed composition, $C_6H_6 : HCl : O_2 : N_2 = 1 : 1 : 0.5 : 1.9$ molar ratio; and Reynold Number, 20—40.

The catalyst was dispersed over 2—3 mm carborundum particles in order to obtain a bed of 25 cm. In this way the actual reaction temperature was only 1 °C off the desired value over more than 90% of the catalyst bed.

The results obtained are summarized in Table 1, where total benzene conversion (mol of benzene reacted per 100 mol of benzene fed) and product selectivities (mol of each product formed per 100 mol of benzene reacted) are shown.

These results clearly indicate that the maximum benzene conversion to be attained with the stoichiometric feed ratio is about 70%, since part of the starting HCl and O_2 is consumed in the production of higher chlorinated compounds (dichloro- and trichlorobenzene); to avoid this limitation, a series of experiments was carried out at 270 °C with amounts of HCl and O_2

† Formerly called Instituto Rocasolano.

Table 1. Effect of reaction temperature and contact time on benzene conversion and selectivity

Temp °C	Pressure total atm	W/F_b[a] g min mol^{-1} (Benzene)	Conversion mol %	Selectivity/mol%			
				C_6H_5Cl	p-$C_6H_4Cl_2$	o-$C_6H_4Cl_2$	$C_6H_3Cl_3$
300	0.929	444	25.1	83.4	11.8	4.7	0.2
300	0.922	889	42.9	79.3	14.6	5.8	0.4
300	0.921	1778	57.9	71.9	19.7	7.7	0.6
300	0.932	3556	64.1	69.4	21.5	8.4	0.8
300	0.929	7111	66.4	65.9	24.1	9.0	1.0
270	0.928	444	11.5	92.3	5.6	2.1	0.0
270	0.925	889	22.3	87.7	8.3	4.0	0.0
270	0.929	1333	32.0	87.1	9.4	3.4	0.0
270	0.930	1778	40.7	81.5	11.7	6.5	0.2
270	0.930	3556	56.7	74.4	19.0	6.1	0.5
270	0.922	5333	65.1	69.9	22.1	7.6	0.4
270	0.926	7111	69.1	66.3	24.2	8.7	0.8
250	0.925	889	12.2	94.2	4.3	1.5	0.0
250	0.933	1778	17.2	92.8	5.2	1.9	0.0
250	0.930	3556	38.1	87.1	9.6	3.4	0.0
250	0.932	5333	47.8	79.5	15.1	5.2	0.2
250	0.922	10667	57.1	74.6	18.5	6.5	0.3
230	0.934	3556	14.7	93.9	4.5	1.5	0.0
230	0.928	5333	19.9	93.0	5.1	1.9	0.0
230	0.931	8889	27.2	89.8	7.6	2.5	0.0

a) Feed molar ratio is stoichiometric to the formation of C_6H_5Cl.

Table 2. Effect of contact time on benzene conversion and selectivity[a]

Pressure total atm	W/F_b g min mol^{-1} (Benzene)	Conversion mol%	Selectivity/mol%			
			C_6H_5Cl	p-$C_6H_4Cl_2$	o-$C_6H_4Cl_2$	$C_6H_3Cl_3$
0.930	444	11.2	91.5	6.2	2.3	0.0
0.928	889	26.2	8..6	12.1	5.8	0.2
0.934	1778	34.8	82.8	12.3	4.6	0.3
0.932	3556	59.4	69.7	21.8	7.8	0.7
0.933	7111	78.3	54.1	32.4	11.7	1.8
0.934[b]	254	4.9	—	72.4	26.8	0.8
0.930[b]	507	10.2	—	72.3	26.6	1.0
0.930[b]	4064	56.8	—	71.6	24.0	4.4

a) Feed molar ratio is stoichiometric to the formation of dichlorobenzene. Temperature of reaction is 270±1 °C. b) Experiments carried out with C_6H_5Cl in the feed instead of benzene.

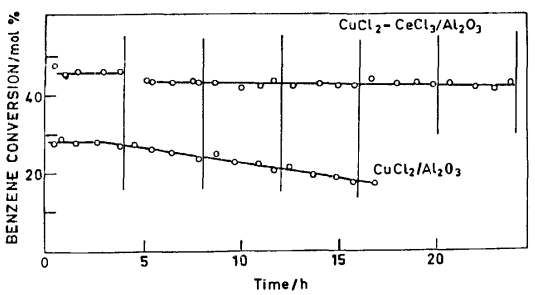

Fig. 1. Accelerated life test carried out at 330±1 °C with W/F_b=444 g min mol^{-1} (benzene) for $CuCl_2$-$CeCl_3$/Al_2O_3 and $CuCl_2/Al_2O_3$ catalysts.

in the feed corresponding to the stoichiometric ratio for the formation of dichlorobenzene. The results are shown in Table 2, together with another series of experiments in which chlorobenzene was the starting material and HCl and O_2 were fed in stoichiometric ratio to produce dichlorobenzene.

Finally, the influence of operation time on catalyst activity was examined by performing an accelerated life test at 330 °C, with the conditions of W/F_b 444 g min (mol benzene)$^{-1}$, atmospheric pressure, and feed molar ratio C_6H_6 : HCl : O_2 : N_2=1 : 1 : 0.5 : 1.9. The system was put in operation for 4 h a day during 6 d. The results of conversion *vs.* time on stream are plotted in Fig. 1. The upper curve corresponds to the catalyst studied in this work while the lower one corresponds to a catalyst containing only $CuCl_2$ on Al_2O_3, which was prepared by substituting the $CeCl_3$ by the equivalent amount of $CuCl_2$.

For the analysis of the experimental results the following reaction scheme is proposed:

$$C_6H_6 + HCl + \frac{1}{2}O_2 \rightleftharpoons C_6H_5Cl + H_2O,$$

$$C_6H_5Cl + HCl + \frac{1}{2}O_2 \rightleftharpoons C_6H_4Cl_2 + H_2O,$$

$$C_6H_4Cl_2 + HCl + \frac{1}{2}O_2 \rightleftharpoons C_6H_3Cl_3 + H_2O,$$

in which no distinction is made between the *o*- and *p*-dichlorobenzene, as far as their rates of formation and urther reaction is concerned. This simplifying assumption can be reasonably introduced on the basis of the experimental data that showed a constant molar ratio of both isomers at all conversion levels of para/ortho= 2.7±0.2.

According to the above scheme, different rate equations were tested by considering several orders of reaction for the various compounds taking part in the process, and different rate controlling steps. A mathematical fitting of the experimental data to the various equations was carried out through analytical integration of the different sets of rate equations by using a 4th order Runge-Kutta method, and the values of the parameters were estimated through nonlinear regression analysis by using also duplicate runs.

The optimized parameter was the variance of correlation defined by

$$\sigma^2 = \frac{\sum_{i=1}^{N}\sum_{j=1}^{N'}(x_{ij}(\text{exp}) - x_{ij}(\text{theor}))^2}{N \times N' - N''},$$

where N is the number of points, N' the number of yields by point, and N'' the number of parameters to be determined.

The experimental error resulting from repeated experiments was estimated by

$$\varepsilon = \frac{\sum_{i=1}^{N}\sum_{j=1}^{N'}\sum_{k=1}^{N''}(x_{ijk}(\text{exp}) - x_{ij}(\text{average}))^2}{N' \times N - N'''} = 0.24 \times 10^{-3},$$

where N''' is the number of average values.

The best fit was obtained with the following set of Langmuir-Hinshelwood type equations:

Benzene disappearance: $$-\frac{dx}{d\left(\frac{W}{F_b}\right)} = \frac{k_1 P_{C_6H_6}}{(1+K_A P_{H_2O})^2},$$

Chlorobenzene formation:

$$\frac{dx_1}{d\left(\frac{W}{F_b}\right)} = \frac{k_1 P_{C_6H_6}}{(1+K_A P_{H_2O})^2} - \frac{k_2 P_{C_6H_6Cl}}{(1+K_A P_{H_2O})^2},$$

Dichlorobenzene formation:

$$\frac{dx_2}{d\left(\frac{W}{F_b}\right)} = \frac{k_2 P_{C_6H_5Cl}}{(1+K_A P_{H_2O})^2} - \frac{k_3 P_{C_6H_4Cl_2}}{(1+K_A P_{H_2O})^2},$$

Trichlorobenzene formation:

$$\frac{dx_3}{d\left(\frac{W}{F_b}\right)} = \frac{k_3 P_{C_6H_4Cl_2}}{(1+K_A P_{H_2O})^2}.$$

Table 3 shows the values of the different kinetic parameters obtained at various temperatures. From these values a similar apparent activation energy is obtained for the oxychlorination of benzene (19.5±0.3 kcal/mol) and chlorobenzene (20.1±0.3 kcal/mol), the small difference being probably due to the "deactivation" of the aromatic ring by the presence of the chlorine atom.

Table 3. Rate constants and variance of the correlation obtained at different temperatures

Temp °C	$k_1\times10^4$	$k_2\times10^4$	$k_3\times10^5$	K_A	σ^2
230	2.753	1.802	—	8.142	2.078×10^{-6}
250	7.028	4.344	—	3.696	2.223×10^{-4}
270	13.97	9.203	9.621	1.422	2.228×10^{-4}
300	30.42	20.87	20.51	0.9466	2.205×10^{-4}

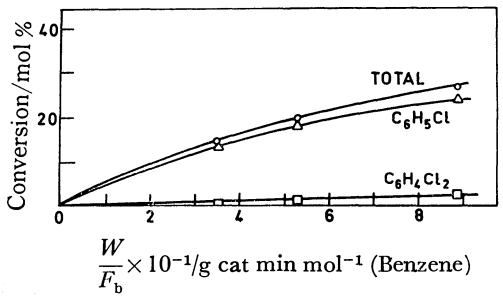

Fig. 2. Experimental results and calculated curves based on the proposed equations at 230±1 °C: △, conversion of benzene; △, C_6H_5Cl formation; □, $C_6H_4Cl_2$ formation.

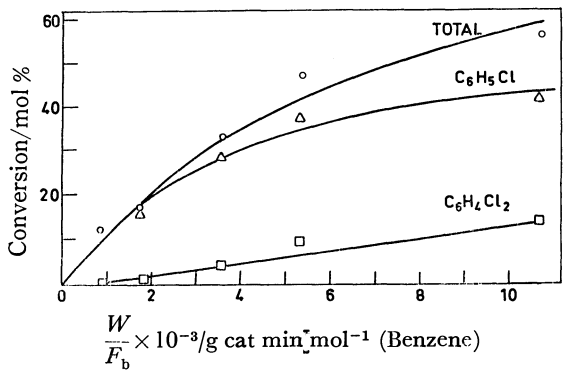

Fig. 3. The same title with Fig. 2 except that the temperature is 250±1 °C.

The variation of K_A with temperature can be related to the heat of adsorption of water on the surface of catalyst, which has a negative effect on the rates, possibly by partially blocking the active sites.

The ratio between the correlation variance and the experimental error was lower than the Fisher parameter[10] $F_{(32,21)}$ for 90%=1.71.

The experimental conversion data obtained as different temperatures are compared in Figs. 2—5 with those calculated by using the proposed equations (continuous lines). These equations reproduce the experimental values satisfactorily the data obtained at 300 °C, where the consumption of HCl and O_2 produced a dramatic decrease in their partial pressures. The dotted line corresponds to the 90% consumption of HCl and O_2. Under these conditions the catalyst may also undergo a change in its active phase composition.

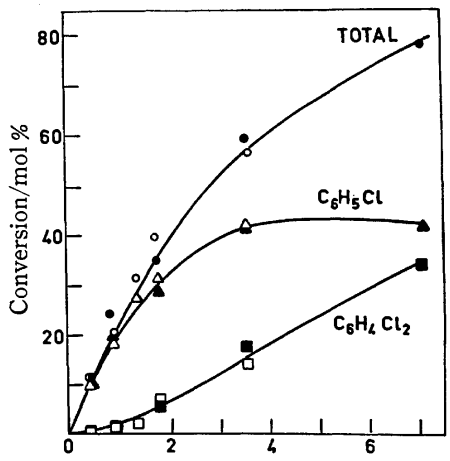

Fig. 4. The same title with Fig. 2 except that the temperature is 270±1 °C. The full points correspond to experiments with a feed molar ratio stoichiometric to the $C_6H_4Cl_2$ formation.

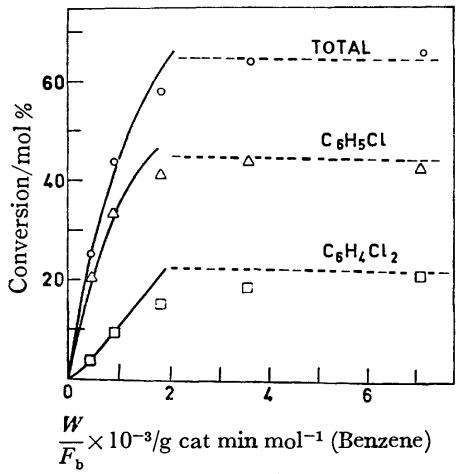

Fig. 5. The same title with Fig. 2 except that the temperature is 300±1 °C. The dotted line corresponds to 90% and O_2 consumption.

The fitness of the experimental data, obtained by replacing benzene will chlorobenzene as feedstock (Table 2), appears in Fig. 6. The use of the parameter values shown in Table 3 gives calculated conversions slightly smaller than the experimental ones. This difference may be due to an effect caused by the benzene adsorption which was neglected in the proposed equations. In any cases, the deviations fell within the experimental error.

According to the proposed equations, the process may be considered independent of the partial pressures of oxygen and hydrogen chloride, the reaction rate being only a function of the partial pressures of the hydrocarbon and water.

In Table 4, the kinetic equations published in previous papers are listed together with the one proposed in this study. As can be seen, when $CuCl_2$ and $CuCl_2$–alkali chloride supported catalysts are used, the reaction rate depends on the partial pressure of oxygen, but in the

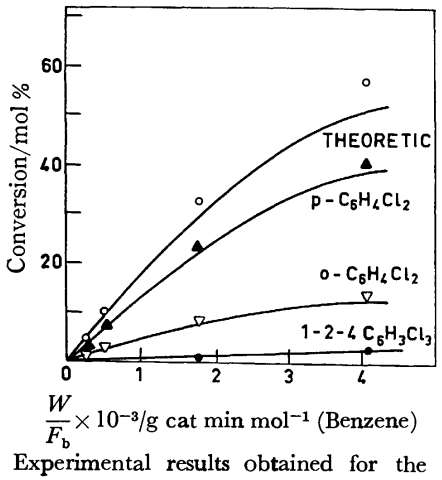

Fig. 6. Experimental results obtained for the chlorobenzene oxychlorination and calculated curves based on the proposed equations at 270±1 °C: ○, conversion of C_6H_5Cl; △, p-$C_6H_4Cl_2$ formation; ▽, o-$C_6H_4Cl_2$ formation; ●, 1,2,4-$C_6H_3Cl_3$ formation.

Table 4. Rate equations obtained for the oxychlorination of aromatic hydrocarbons will different catalysts

Reference	Catalyst	Rate equation
11	$CuCl_2/Al_2O_3$	$r=\frac{k_1P_{HC}\cdot k_2P_{O_2}^{1/2}}{k_1P_{HC}+k_2P_{O_2}^{1/2}}$
5	$CuCl_2$–KCl/Al_2O_3	$r=kP_{HC}\cdot P_{O_2}^{1/2}$
6	$CuCl_2$–$LiCl/Al_2O_3$	$r=\frac{k_1P_{HC}\cdot P_{O_2}^{1/2}}{(1+k_2P_{HC}+k_3P_{O_2}^{1/2})^2}$
This study	$CuCl_2$–$CeCl_3/Al_2O_3$	$r=\frac{k_1P_{HC}}{(1+K_AP_{H_2O})^2}$

case of $CuCl_2$–$CeCl_3/Al_2O_3$ this relation is no longer applicable.

The presence of cerium seems to facilitate the copper reoxidation step by making the overall rate higher and also independent of the partial pressure of oxygen. Moreover, the life test results indicate that the cerium in these catalysts not only increases the reaction rate but also maintains the conversion level for a longer time. This effect may be due to the formation of Cu and Ce complex compounds on the alumina surface,[12] which are more stable and therefore less likely to undergo the decomposition to $CuCl_2$, a phenomenon considered to be the main reason for the deactivation of these catalysts.[8]

References

1) J. A. Allen and A. J. Clark, *Rev. Pure and Appl. Chem.*, **21**, 145 (1971).

2) A. B. Solomonov, P. P. Gertsen, and A. N. Ketov, *Zh. Prikl. Khim.*, **43**, 162, 471 (1970).

3) T. V. Shutenkova and S. A. Gor'kova, *Khim. Vysokomol Soedin Neftekhim.*, **1975**, 56.

4) J. Blanco, R. Blanco, A. Cortés and J. Soria, Proc. of the 5th Int. Cong. of Catal. Florida, North Holland Pub. Co. (1973), p. 905.

5) J. Blanco, R. Blanco and E. Hermana, *Otd. Khim. Nauki, Bulg. Akad. Nauk. VI.*, **2**, 321 (1973).

6) S. Altuglu and R. W. Roberts, *Ind. Eng. Chem. Proc. Res. Dev.*, **12**, 2, 160 (1973).
7) J. Blanco, J. Fayos, J. F. Garćia de la Banda, and J. Soria, *J. Catal.*, **31**, 257 (1973).
8) P. Avila, J. Blanco, J. L. Garćia-Fierro, S. Mendioroz and J. Soria, Proc. of the 7th Int. Cong. of Catal. Tokyo., B-25 (1980).
9) J. Blanco, R. Blanco and E. Hermana, *ANQUBU*, **67**, 11, 1119 (1971).
10) D. M. Himmelblau, "Process, Analysis by Statistical Methods," John Wiley and Sons, Inc., New York (1968), p. 432.
11) C. Cuenca, Doct. Thesis. Comp. Univ. Madrid, Dec. 1973.
12) P. Avila, J. Blanco, and J. Soria, Proc. of 7th Symp. Iber. Cat. La Plata, Argentina, 1980.

Barium Manganate. A Versatile Oxidant in Organic Synthesis

Habib FIROUZABADI* and Zohreh MOSTAFAVIPOOR
Chemistry Department, Shiraz University, Shiraz, Iran
(Received July 19, 1982)

Preparation of barium manganate in large-scale is discussed. It is also shown that this reagent is capable of oxidizing organic substrates, converting alcohols to their corresponding carbonyl compounds, aromatic amines to their corresponding azo compounds, hydroquinone to *p*-benzoquinone, benzylamine to benzaldehyde, and triphenylphosphine to its oxide in good yields. Saturated hydrocarbons, unsaturated hydrocarbons, unsaturated ketones, and saturated amines are not affected by this reagent in a reasonable reaction time.

Among many oxides and oxoanions of manganese, only manganese dioxide[1] and potassium permanganate[2] have extensively studied in the oxidation of organic compounds. Recently several permanganates; potassium permanganate "dicyclohexyl-18-crown-6",[3] benzyltriethylammonium permanganate,[4] tetrabutylammonium permanganate,[5,6] bis(pyridine)silver permanganate[7] have been prepared and used in the oxidations of organic substrates in organic solvents. Manganates are also of interest in the oxidation of organic compounds but, very little attention has been paid to their properties in organic oxidation reactions. There have been few reports available in the literature in which potassium manganate is used as an oxidant.[8,9] Very recently basic strontium manganic manganate[10] has also been used in the oxidation of alcohols to their corresponding carbonyl compounds in organic media.

Lately in a communication we introduced barium manganate in heterogeneous system as a good oxidizing agent for the oxidation of alcohols and indicated its advantages over manganese dioxide.[11] Here we discuss the large-scale preparation of this reagent with some modification to our previously reported procedure.[11] We have also extended our studies to the oxidation of different groups of organic compounds.

Results and Discussion

Barium manganate was prepared as following: 1) 2 mol of potassium hydroxide were fused with 1 mol of manganese dioxide at 350 °C to produce dark green potassium manganate.[12] 2) 1 mol of potassium manganate was added while being stirred to a warm solution of 1 mol of barium hydroxide at pH=7. The dark blue crystals of barium manganate[13] were collected and dried at 100 °C for 24 h.

Oxidation with barium manganate, prepared by this method, gives reproducible results without requiring

TABLE 1. COMPARISON OF OXIDATION OF SOME ORGANIC COMPOUNDS WITH $BaMnO_4$ AND MnO_2

No.	Substrate	Product	$BaMnO_4$		MnO_2	
			Reaction time/h	Yield/%	Reaction time/h	Yield/%
1	Aniline	Azobenzene	0.5	90	6	87[14]
2	*p*-Toluidine	4,4′-Dimethylazobenzene	1.5	67	6	87[14]
3	*m*-Nitroaniline	3,3′-Dinitroazobenzene	2.5	55	24	0[14]
4	*o*-Nitroaniline	2,2′-Dinitroazobenzene	24	0	24	0[14]
5	Benzyl alcohol	Benzaldehyde	1.5	90	3	26.7[15]
6	Benzhydrol	Benzophenone	0.5	100	2	87[14]
7	*p*-Nitroaniline	4,4′-Dinitroazobenzene	2.5	30	24	0[14]
8	1-Naphthylamine	1,1′-Azonaphthalene	4.5	25	24	0[14]
9	*p*-Chloroaniline	4,4′-Dichloroazobenzene	1.5	80	6	87[14]
10	*o*-Phenylenediamine	2,2′-Diaminoazobenzene	0.5	60	4	50[18]
11	Benzylamine	Benzaldehyde	1	95	24	34[19]
12	Hydroquinone	*p*-benzoquinone	0.3	75	0.5	38[14]
13	Diphenylmethane	Tetraphenylethane	3	0	2	49[14]
14	Triphenylphosphine	Triphenylphosphine oxide	2	100	5	75[14]
15	2,4-Dinitrophenylhydrazine	*m*-Dinitrobenzene	1.5	50	5	50[14]
16	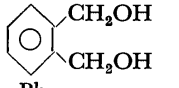	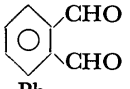	3	80	5	45[16]
17	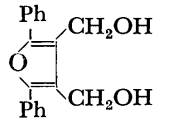	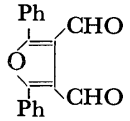	4	90	17	20—40[16,17]
18	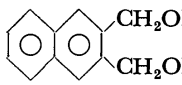	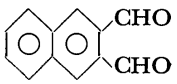	12	87	8	50[16]

Table 2. Oxidation of alcohols with $BaMnO_4$

No.	Substrate	Product	Mp θ_m/°C (n_D^{20})	$BaMnO_4$		
				Reaction time/h	Yield/%	Oxidant/Reactant
1	Citronellol	Citronellal	(1.4590)	24	85—90	5
2	PhCH: $CHCH_2OH$	PhCH: CHCHO	(1.6220)	0.75	100	4
3	PhCH: $CHCHOHCH_3$	PhCH: $CHCOCH_3$	36—40	3	50	5
4	PhCH: $CHCHOHCH_3$	PhCH: $CHCOCH_3$	36—40	0.75	80	10
5	1-Pentanol	1-Pentanal	(1.3945)	24	50	10
6	Cyclohexanol	Cyclohexanone	(1.4500)	24	50—60	10
7	1-Tetradecylol	1-Tetradecylal	—	6	30	5
8	Benzyl alcohol	Benzaldehyde	(1.5455)	0.15	90	1
9	Furfuryl alcohol	Furfural	(1.5244)	0.15	75	2
10	Piperonol	Piperonal	35—38	1.5	60	5
11	*p*-Nitrobenzylalcohol	*p*-Nitrobenzaldehyde	106	4.5	60	2
12	Benzhydrol	Benzophenone	58	0.5	100	2
13	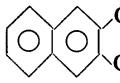	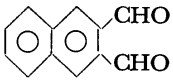	112—115	12	87[a]	10
14	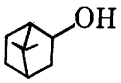		170—173	15	90[a]	5
15	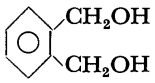	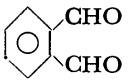	54	3	80	10
16	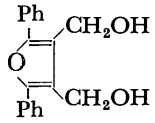	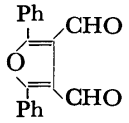	126—128	4	90	10
17	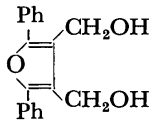	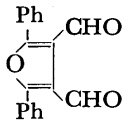	126—128	16	80[a]	10
18	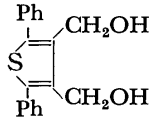	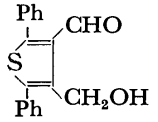	114—116	3	85	10
19	PhCHOHC≡CPh	PhCOC≡CPh	110—113	4	80	10
20	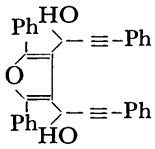	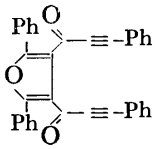	165—166	4	70	10
21	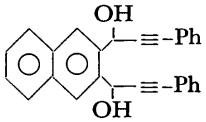	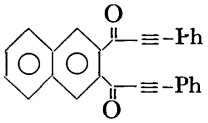	119—120	5	80[a]	10

a) In dichloromethylene.

further activation, while oxidation reaction with manganese dioxide is not reproducible in many aspects.[1] This reagent is indefinitely stable, active, and could be stored for months under dried condition. According to our finding barium manganate is a good reagent in organic synthesis whenever both the rate and the selectivity of the reaction are concerned. To our view this reagent is a good substitute for manganese dioxide in many respects. First, its preparation and isolation is much easier than of active manganese dioxide. Second, the ratio of substrates to manganese dioxide can range from 1 : 5 to 1 : 50.[1] This ratio for barium manganate in our investigation ranged from 1 : 1 to 1 : 10, which makes the isolation of the oxidation product from the solid oxidizing material easier and more practical. Third, the oxidation reactions of organic compounds under investigation with barium manganate were usually faster and resulting higher yields than those obtained from manganese dioxide. The results obtained are summarized in Table 1. Barium manganate reacts very mildly and selectively in dry organic solvents, *e.g.* dichloromethane and benzene, either at room temperature, or under reflux conditions. The rate of reaction under reflux conditions

Table 3. Oxidation of amines with $BaMnO_4$

No.	Substrate	Product	Mp θ_m/°C (n_D^{20})	$BaMnO_4$ Reaction time/h	$BaMnO_4$ Yield/%	$BaMnO_4$ Oxidant/Reactant
1	2-Nitro-4-chloroaniline	2,2′-Dinitro-4,4′-dichloroazobenzene	220—221	2	8	5
2	Aniline	Azobenzene	66—68	0.5	90	3
3	*m*-Toluidine	3,3′-Dimethylazobenzene	49—50	1.5	46	5
4	*p*-Toluidine	4,4′-Dimethylazobenzene	138—140	1.5	67	5
5	*o*-Toluidine	2,2′-Dimethylazobenzene	52—54	1.5	66	5
6	*m*-Nitroaniline	3,3′-Dinitroazobenzene	148—150	2.5	55	5
7	*o*-Nitroaniline	—	—	24	0	5
8	*p*-Nitroaniline	4,4′-Dinitroazobenzene	220—222	2.5	30	5
9	1-Naphthylamine	1,1′-Azonaphthalene	187—189	4.5	25	5
10	*m*-Chloroaniline	3,3′-Dichloroazobenzene	99—100	2	67	5
11	*p*-Chloroaniline	4,4′-Dichloroazobenzene	220—221	1.5	80	5
12	*m*-Methoxyaniline	3,3′-Dimethoxyazobenzene	73—75	2	50	5
13	*o*-Phenylenediamine	2,2′-Diaminoazobenzene	132—133	0.5	60	5
14	Benzylamine	Benzaldehyde	(1.5454)	1	95	2
15	2,4-Dinitrophenylhydrazine	*m*-Dinitrobenzene	86—88	1.5	50	5

Table 4. Miscellaneous oxidation with $BaMnO_4$

No.	Substrate	Product	Mp θ_m/°C	$BaMnO_4$ Reaction time/h	$BaMnO_4$ Yield/%	$BaMnO_4$ Oxidant/Reactant
1	Hydroquinone	*p*-Benzoquinone	112—114	0.3	75	2
2	Diphenylmethane	—	—	3	0	2
3	Styrene	—	—	2	0	2
4	Toluene	—	—	3	0	5
5	Triphenylphosphine	Triphenylphosphine oxide	150—154	2	100	5
6	1-Heptylamine	—	—	3	0	4
7	PhCH: $CHCOCH_3$	—	—	4	0	4
8	PhCH: CHCOH	—	—	3	0	4

is much faster.

Benzylic alcohols were converted to the corresponding carbonyl compounds without further oxidation. In the oxidation of diols; (16 and 18) in Table 2 in addition to the isolation of corresponding aldehydes a small amount of the corresponding lactone was also isolated. Allyl alcohols were also very reactive and produced their carbonyl compounds in good yields. 2-Alkyn-1-ols were very reactive and were oxidized very easily to their corresponding carbonyl compounds in good yields. Saturated alcohols were oxidized rather slowly with difficulty. In some cases even after 24 h only fifty percent conversion were observed (Table 2).

Aromatic amines with nitro groups substituted on the aromatic ring and 1-naphthylamine gave none to low yields of their corresponding azo compounds. In these cases manganese dioxide is reported to be quite unreactive.[14] The other aromatic amines were quite reactive and their corresponding azo compounds were produced very easily. Benzylamine was converted to benzaldehyde very rapidly (Table 3).

Triphenylphosphine was converted very easily and rapidly to triphenylphosphine oxide, 2,4-dinitrophenylhydrazine to *m*-dinitrobenzene, and hydroquinone to *p*-benzoquinone. The oxidation of a few hydrocarbons, unsaturated ketones, and saturated amines were also investigated. They were unreactive towards this reagent (Table 4).

Experimental

General. All yields refer to isolated products. Products were characterized by comparison with authentic sample (IR spectrum, thin layer, gas chromatography, melting point, and refractive index). All reactions proceeded in benzene, unless otherwise indicated.

Preparation of Potassium Manganate. Potassium hydroxide (2 mol) were thoroughly mixed with manganese dioxide (1 mol) and left in an oven at 350 °C for 3 h. The fused green potassium manganate was discharged and used for the preparation of barium manganate.

Preparation of Barium Manganate. In a (500 ml) flask, barium hydroxide (7 g, 0.041 mol) was added to distilled water (100 ml) and pH was adjusted to 7 with dilute hydrochloric acid. To the resulting warm solution, 8.6 g (0.043 mol) of potassium manganate was added with stirring. The colour of the reaction mixture immediately changed to dark purple. The reaction mixture was filtered with suction and the dark blue crystals were washed for several times with distilled water. The resulting crystals were put in an oven at 100 °C for 24 h, to produce active barium manganate in 60% yield. Found: Ba, 52.85%. Calcd for $BaMnO_4$: Ba, 53.58%.

General Procedure for the Conversion of Alcohols to Their Aldehydes and Ketones. To a solution of alcohol (0.01 mol) in dry

benzene (30 ml), in a (100 ml) round-bottomed flask, equipped with a condenser and magnetic stirrer, barium manganate (0.05—0.1 mol) was added and refluxed for 1/2-24 h the reaction mixture was filltered with suction and the solid material was washed with dichloromethane for several times. The filterates were added together and evaporated. The resulting material was chromatographed on silica-gel column eluted with benzene. Evaporation of the solvent afforded pure carbonyl compound in 50—100% yield (Table 2).

General Procedure for the Conversion of Aromatic Amines to Their Corresponding Azo Compounds. In a round-bottomed flask (100 ml), equipped with a condenser and magnetic stirrer, amine (0.01 mol) in dry benzene (30 ml) was mixed with barium manganate (0.03—0.05 mol) and refluxed for 0.5 to 4.5 h. The reaction mixture was filtered with suction. The solid material was washed with dichloromethane for several times. The filterates were added together and evaporated. The resulting material was chromatographed on either silica gel or neutral alumina column eluted with benzene. Evaporation of the solvent afforded the azo compound in 0—90% yield (Table 3).

Conversion of 2,4-Dinitrophenylhydrazine to m-*Dinitrobenzene.* In a round-bottomed flask (100 ml) equipped with a condenser and magnetic stirrer, 2,4-dinitrophenylhydrazine (0.01 mol) in dry benzene (30 ml) was mixed with barium manganate (0.05 mol) and refluxed for 1.5 h. The reaction mixture was filtered with suction and the solid material was washed with dichloromethane for several times. The filterates were added together and evaporated. The resulting material was chromatographed on neutral alumina column eluted with benzene. Evaporation of the solvent afforded *m*-dinitrobenzene in 50% yield (Table 4).

Conversion of Benzylamine to Benzaldehyde. In a round-bottomed flask (100 ml) equipped with a condenser and magnetic stirrer, benzylamine (0.01 mol) in dry benzene (30 ml) was mixed with barium manganate (0.02 mol) and refluxed for 1 h. The reaction mixture was filtered with suction. The solid material was washed with dichloromethane for several times. The filterates were added together and evaporated. The resulting material was chromatographed on silica-gel column eluted with benzene. Evaporation of the solvent afforded benzaldehyde in 95% yield (Table 4).

Conversion of Hydroquinone to p-*Benzoquinone.* In a round-bottomed flask (100 ml) equipped with a condenser and magnetic stirrer, hydroquinone (0.01 mol) in dry benzene (30 ml) was mixed with barium manganate (0.02 mol) and refluxed for 20 min. The reaction mixture was filtered with suction. The solid material was washed with dichloromethane for several times. The filterates were added together and evaporated. The resulting material was chromatographed on silica-gel column eluted with benzene. Evaporation of the solvent afforded *p*-benzoquinone in 75% yield (Table 4).

Conversion of Triphenylphosphine to Triphenylphophine Oxide. In a round-bottomed flask (100 ml) equipped with a condenser and magnetic stirrer, triphenylphosphine (0.01 mol) in dry benzene (30 ml) was mixed with barium manganate (0.05 mol) and refluxed for 2 h. The reaction mixture was filtered with suction. The solid material was washed with dichloromethane for several times. The filterates were added together and evaporated. The resulting material was chromatographed on silica-gel column eluted with benzene. Evaporation of the solvent afforded triphenylphosphine oxide in 100% yield (Table 4).

We are thankful to Shiraz University Jehad Council for the Partial support of this work and also Mr. J. Toofan for the elemental analysis.

References

1) A. J. Fatiadi, *Synthesis*, **65**, 133 (1976).
2) L. F. Fieser and M. Fieser, "Reagent for Organic Synthesis," Wiley, New York (1967), Vol. 1.
3) D. J. Sam and H. E. Simmons, *J. Am. Chem. Soc.*, **94**, 4024 (1972).
4) H. J. Schmidt and H. J. Schafer, *Angew. Chem., Int. Ed. Engl.*, **18**, 68 (1979).
5) T. Sala and M. V. Sargent, *J. Chem. Soc., Chem. Commun.*, **1978**, 253.
6) A. W. Herriott and D. Picker, *Tetrahedron Lett.*, **1974**, 1511.
7) H. Firouzabadi, B. Vessal, and M. Naderi, *Tetrahedron Lett.*, **23**, 1847 (1982).
8) R. Stewart, *J. Am. Chem. Soc.*, **79**, 3057 (1957).
9) W. Rigby, *J. Chem. Soc.*, **1956**, 2452.
10) H. Firouzabadi and N. Maleki, *Iranian J. Sci. Tech.*, in press.
11) H. Firouzabadi and E. Ghaderi, *Tetrahedron Lett.*, **1978**, 839.
12) H. I. Schlesinger, R. D. Mullinix, and S. Popoff. *J. Ind. Eng. Chem.*, **11**, 317 (1919).
13) *Inorg. Synth.* Vol XI, 58 (1968).
14) M. Z. Barakat, M. F. Abdel-Wahab, and M. M. El-Sadr, *J. Chem. Soc.*, **1956**, 4685.
15) K. Nakagawa, R. Konaka, and T. Nakata, *Bull. Chem. Soc. Jpn.*, **35**, 1597 (1962).
16) In our laboratory we have observed the indicated yields.
17) A. Verine and Y. Lepage, *Bull. Soc. Chim. Fr.*, **1973**, 1154.
18) I. Bahatnagar and M. V. George, *J. Org. Chem.*, **33**, 2407 (1968).
19) R. J. Highet and W. C. Wildman, *J. Am. Chem. Soc.*, **77**, 4399 (1955).

Catalytic Alkylation, Sulphonation, and Heteroarylation of Some Bicyclic Pyrazolines in Solid-Liquid Two Phase Systems

Ahmed Kamal EL-SHAFEI,* Ahmed Mahmoud EL-SAYED, and Ali Ali KHALAF†
Chemistry Department, Faculty of Sciences, Sohag University, Sohag, Egypt
†*Chemistry Department, Faculty of Sciences, Assiut University Assiut, Egypt*
(Received March 29, 1982)

The reaction of some bicyclic pyrazolines with alkyl halides, aryl sulphonyl chlorides as well as with some N–H and S–H containing heterocycles is affected in solid-liquid two phase systems using a catalyst. The catalytic cycle is described, the purity of the obtained products is checked using TLC and their structure is confirmed by a combination of chemical and spectroscopic methods.

It has been recognized recently[1] that numerous N–H acidic compounds can be conveniently alkylated in the presence of concentrated aqueous sodium hydroxide or potassium hydroxide solutions and quaternary ammonium salts as catalysts. The catalytic method has been used for alkylation of aziridine,[2] phenothiazine,[3] pyrrole,[4] indole,[4–7] and its derivatives,[5] diphenylamine,[4] carbazole,[4] some amides,[8] and phenylhydrazones of aldehydes and ketones.[9] These reactions take place in liquid-liquid two phase system in which both phases, aqueous sodium hydroxide and organic reactants (neat or in nonpolar solvent) are mutually immiscible. This catalytc two phase (CTP) system offers numerous advantages over other bases such as NaH, $NaNH_2$, and *t*-BuOK *inter alia* elimination of hazardous and expensive reactants, anhydrous organic solvents, *etc.*

Despite many advantages, the CTP system has some limitations, one of them being the hydrolytic activity of concentrated aqueous alkali. However, it has been reported that many reactions with C–H acidic compounds can be efficiently carried out using anhydrous sodium or potassium carbonate as bases.[9–11] In these cases the reactions proceed in liquid-solid two phase systems, organic reactants neat (if liquids) or in aprotic solvents form the organic phase in which solid sodium or potassium carbonate is suspended. In these systems reactions are catalyzed by tetraalkylammonium salts or crown ethers. The catalysts are unable to transfer carbonate anions (CO_3^{2-}) into the organic phase,[12] thus solid-liquid phase-transfer phenomena are probably not involved here. It is more plausible that the first step, namely proton abstraction, takes place on the surface of the solid carbonate (see Fig. 1). The anions formed then migrate into the organic phase as ion pairs with the catalyst cation. Since several reports indicated the pharmacological importance[13–16] of some bicyclic pyrazolines, we report here the synthesis of some new derivatives of 7-benzylidene-3,3a,4,5,6,7-hexahydro-3-phenyl-2*H*-indazole (**1**) using solid-liquid two phase transfer system. This method offers a convenient synthetic means due to the comparative stability of such compounds.[17] Compound **1** was obtained by refluxing 2,6-dibenzylidenecyclohexanone with hydrazine hydrate in methanol.

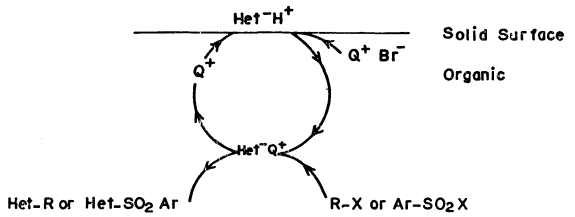

Fig. 1. Catalytic two phase solid-liquid cycle.

The alkylation and sulphonation of **1** in CTP system

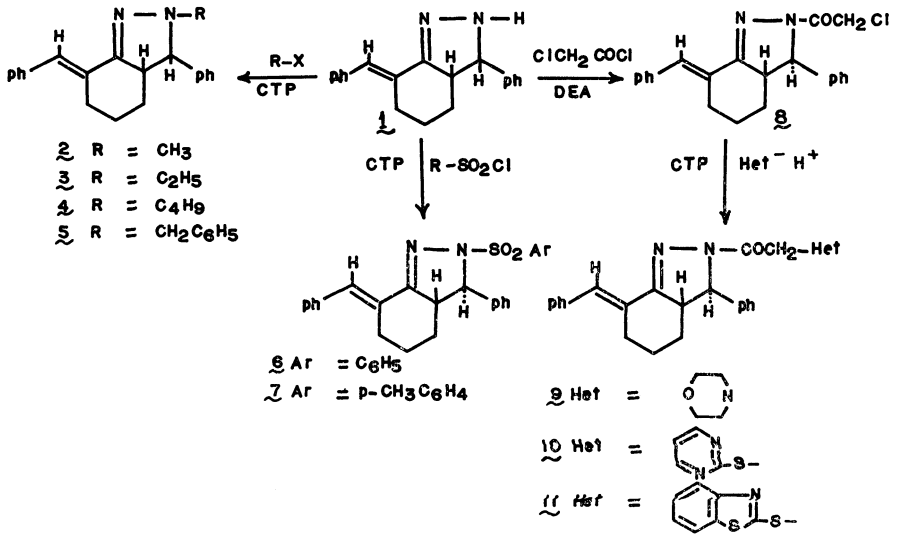

Scheme 1.

Table 1. Preparation of alkylated, sulphonated, and heteroarylated bicyclic pyrazolines using CTP system

Product	Reaction conditions: Temperature °C	Reaction conditions: Time h	Yield %	Mp θ_m/°C	Mol formula (Mol wt.)	Calcd (Found) (%): C	H	N	TLC R_f
1	See experimental		82	84—86	$C_{20}H_{20}N_2$ (288)	83.33 (83.21)	6.94 (7.06)	9.72 (9.80)	0.6[a]
2	33	2.5	65	233—235	$C_{21}H_{22}N_2$ (302)	83.44 (83.37)	7.28 (7.31)	9.27 (9.29)	0.2
3	33	2.5	74	164—165	$C_{22}H_{24}N_2$ (316)	83.54 (83.59)	7.59 (7.62)	8.86 (8.78)	0.1
4	33	4	61	103—105	$C_{24}H_{28}N_2$ (344)	83.72 (83.83)	8.13 (8.09)	8.13 (8.19)	0.3
5	33	3	82	137—138	$C_{27}H_{26}N_2$ (378)	85.71 (85.68)	6.87 (6.85)	7.40 (7.29)	0.7
6	33	2	87	210	$C_{26}H_{24}N_2SO_2$ (428)	72.89 (72.96)	5.60 (5.64)	6.54 (6.48)	0.7
7	33	2	82	226—227	$C_{27}H_{26}N_2SO_2$ (442)	73.30 (73.41)	5.88 (5.92)	6.33 (6.42)	0.7
8	See experimental		43	151—153	$C_{22}H_{21}N_2OCl$ (364.5)	72.42 (72.60)	5.76 (5.69)	7.68 (7.56)	0.2
9	40	2	75	90—92	$C_{26}H_{29}N_3O_2$ (415)	75.18 (75.09)	6.98 (7.06)	10.12 (10.04)	0.7
10	33	4	66	218	$C_{26}H_{24}N_4SO$ (440)	70.90 (70.99)	5.45 (5.39)	12.72 (12.86)	0.3
11	33	4	58	165	$C_{29}H_{25}N_3S_2O$ (495)	70.30 (70.22)	5.05 (5.12)	8.48 (8.31)	0.6

a) Eluted in CH_2Cl_2.

Table 2. ^{1}H-NMR spectral data of the prepared bicyclic pyrazoline derivatives using CTP system

Compound	NMR δ
1	7.50—7.05 (m, 10H, Ar), 6.9 (m, 1H, =CH), 6.50 (s, 1H, NH), 4.35 (t, 1H, N-CH), 3.0—0.90 (m, 7H, aliph.) (DMSO-d_6)
2	7.68—7.18 (m, 10H, Ar), 7.10 (m, 1H, =CH), 4.85 (t, 1H, N-CH), 3.55 (s, 3H, CH_3), 3.30—0.9 (m, 7H, aliph.) (CF_3COOD)
3	7.65—7.00 (m, 11H, Ar+=CH), 5.0 (t, 1H, N-CH), 3.30—0.9 (m, 12H, aliph.) (CF_3COOD)
4	7.60—6.80 (m, 11H, Ar+=CH), 4.80 (t, 1H, N-CH), 3.30—0.60 (m, 16H, aliph.) (CF_3COOD)
5	7.67—6.68 (m, 16H, Ar+=CH), 4.55 (t,, 1H, N-CH), 3.80 (s, 2H, CH_2), 3.30—0.95 (m 7H, aliph.) (CF_3COOD)
6	8.10—7.00 (m, 16H, Ar+=CH), 5.60 (t, 1H, N-CH), 3.35 (m, 7H, aliph.) (pyridine-d_5)
7	8.15—7.05 (m, 15H, Ar+=CH), 4.25 (t, 1H, N-CH), 3.15—0.80 (m, 10H, aliph.+p-CH_3) (pyridine-d_5)
8	7.55—7.10 (m, 10H, Ar), 7.00 (s, 1H, =CH), 5.00 (t,1H, N-CH), 3.48 (t, 2H, CH_2), 3.00—1.00 (m, 7H, aliph.) ($CDCl_3$)
9	7.40—7.00 (m, 11H, Ar+=CH), 4.80 (t, 1H, N-CH), 3.82—3.15 (m, 8H, aliph.), 3.10—0.75 (m, 9H, aliph.+CH_2) ($CDCl_3$)
10	8.92—8.68 (m, 3H, pyrimidine), 7.68—6.70 (m, 11H, Ar+=CH), 4.83 (t, 1H, N-CH), 3.45—0.75 (m, 9H, aliph. +CH_2) (CF_3COOD)
11	7.95—6.85 (m, 15H, Ar+=CH+2-benzothiazolyl-), 4.80 (t, 1H, N-CH), 3.35—0.80 (m, 9H, aliph.+CH_2) (CF_3COOD)

was affected in potassium carbonate-acetone using tetrabutylammonium bromide (TBAB) as a catalyst. Time of the reaction at the appropriate temperature was summarized in Table 1. The reactions were monitored by TLC and the identity of the obtained products was based on both microanalytical and NMR data. The starting bicyclic pyrazoline **1** was chloroacetylated by stirring an equimolar mixture of **1** and chloroacetyl chloride in benzene at 18 °C for 1 h. The *N*-chloroacetylpyrazoline derivative **8** was effectively used as an alkylating agent to some N–H and S–H containing heterocycles, namely, morpholine, 2-mercaptopyrimidine, and 2-mercaptobenzothiazole. The reactions were performed in CTP system (K_2CO_3/acetone/TBAB) where the corresponding dehydrochlorinated products **9**, **10**, and **11**, respectively were obtained in fair yields. Figure 1 illustrate the catalytic cycle where Het^- corresponds to cations derived from N–H or S–H containing heterocycles used in CTP reactions, Q^+ to tetrabutylammonium cation and R^+ to

alkyl or *N*-acetylpyrazolinyl cations.

Experimental

Melting points are uncorrected and were determined using a Kopfler bank. ^{1}H-NMR spectra were obtained on a Varian EM 360 A or NV 14 spectrometer at 60 MHz or at 100 MHz using TMS as an internal standard, chemical shifts are expressed in ppm. Qualitative thin layer analyses were carried out using nanoplates (10 cm × 10 cm, HPTLC, 5 μm silica) with nitromethane as eluent.

Catalytic Two Phase Alkylation and Sulphonation of N–H Containing Compound ***1****. General Procedure*: To a mixture of compound **1** (0.05 mol) and potassium carbonate (0.05 mol) in acetone (70 ml) an equimolar amount of alkyl halide or aryl sulphonyl chloride (0.05 mol) was added. The mixture was treated with a catalytic amount of tetrabutylammonium bromide (TBAB) (0.001 mol), and vigorously stirred at the appropriate temperature (see Table 1) over periods of time ranging between 2—6 h. After completion of the reaction (TLC) the mixture was filtered off, dried ($MgSO_4$), evaporated *in vacuo* and the residual solid was crystallized from the appropriate solvent.

Synthesis of N-*Chloroacetyl Bicyclic Pyrazoline Derivative* ***8****.* To a solution of 0.01 mol of compound **1**, 0.015 mol of *N,N*-diethylaniline in 50 ml of benzene, 0.012 mol of chloroacetyl chloride in few ml of benzene was gradually added under efficient stirring, the reaction mixture was stirred at 18 °C for 1 h and was then evaporated *in vacuo*. The obtained solid was washed with water followed by petroleum ether 60—80 °C, dried and crystallized from dioxane.

Reaction of N-*Chloroacetylpyrazoline Derivative* ***8*** *with N–H and S–H Containing Heterocycles Using CTP System. General Procedure*: Compound **8** (0.05 mol) along with 0.05 mol of potassium carbonate in acetone (70 ml) was treated with 0.05 mol of morpholine, 2-mercaptopyrimidine, or 2-mercaptobenzothiazole, in presence of a catalytic amount of TBAB (0.001 mol). The reaction mixture was vigorously stirred at the appropriate temperature for a certain time (see Table 1). After filtration the mixture was dried ($MgSO_4$), evaporated *in vacuo* to give the desired products **9**, **10**, or **11**.

References

1) R. Gallo, H. J-M Dou, and P. Hassanaly, *Bull. Soc. Chim. Belg.* **90**, 849 (1981).
2) M. Maurette, A. Lopez, R. Martino, and A. Lattes, *C. R. Acad. Sci., Ser. C*, **282**, 599 (1976).
3) H. Wunderlich, W. Lugenheim, A. Stark, and G. Detrekoi, *Pharmazie*, **21**, 57 (1966).
4) A. Jonczyk and M. Makosza, *Rocz. Chem.*, **49**, 1203 (1975).
5) N. N. Suvorov, Y. J. Smushkevich, V. S. Velezheva, V. S. Rozhkov, and S. V. Simakov, *Khim. Geterotsikl. Soedin.*, **1976**, 191.
6) A. Barco, S. Benetti, G. P. Pollini, and P. G. Baraldi, *Synthesis*, **1976**, 124.
7) V. Bocchi, G. Casnati, A. Dossena, and F. Villani, *Synthesis*, **1976**, 414.
8) R. Brehme, *Synthesis*, **1976**, 113.
9) A. Jonczyk, J. Wlostowska, and M. Makosza, *Synthesis*, **1976**, 795.
10) D. A. White, *Synth. Commun.*, **7**, 559 (1977) and references cited therein.
11) R. M. Boden, *Synthesis*, **1975**, 784.
12) M. Fedorynski, K. Wojciechowski, Z. Matacz, and M. Makosza, *J. Org. Chem.*, **43**, 4682 (1978).
13) J. Krapcho and C. Turk (Squibb, E. R. and Sons. Inc.) U. S. Patent 3 957 762 (cl. 260—240D; Co 7D 231/56) 18 May 1976, Appl. 469, 171, 13 May 1974; *Chem. Abstr.*, **85**, 63066b (1976).
14) J. Krapcho and C. Turk, Ger. Offen 2 521 299 (cl O and D), 27 Nov. 1975, U. S. Appl. 469, 171, 13 May 1974; *Chem. Abstr.*, **84**, 59455q (1976).
15) J. Krapcho and C. Turk, (Squibb, E. R. and Sons Inc.) U. S. Patent 4 004 007 (cl. 424—246); (07D 487/OZ), 18 Jan. 1977, Appl. 603, 222, 8 August 1975; *Chem. Abstr.*, **86**, 171443b (1977).
16) J. Krapcho and C. Turk, *J. Med. Chem.*, **22**, 207 (1979).
17) Gy. Oszbach and D. Szabo, *Acta Chim. Acad. Sci. Hung.*, **86**, 449 (1975).

© 1983 The Chemical Society of Japan

NOTES

Bull. Chem. Soc. Jpn., 56, 921—922 (1983)

Absorption Intensity of Charge-transfer Transition between Ion Radicals in One-dimensional System of Crystalline Ion Radical Salts

Yôichi IIDA

Department of Chemistry, Faculty of Science, Hokkaido University, Sapporo 060

(Received August 16, 1982)

Synopsis. The charge-transfer interaction between ion radicals in crystalline ion radical salts was examined with one-dimensional Hubbard model. The intensity of charge-transfer absorption in crystal electronic spectra was estimated with both simple and complex ion radical salts. This approach was then applied to simple cation radical salt of Phenothiazine$^+ \cdot Br^-$ and complex cation radical salt of (Phenothiazine)$_2^+ \cdot Br^-$.

Much attention has been paid to the charge-transfer interaction in one-dimensional system of crystalline ion radical salts.[1-5] In simple ion radical salts where each ion radical carries one unpaired electron, the planar ion radical molecules are known to form, in themselves, a plane-to-plane stacking into one-dimensional column so as to make a large overlap between their half-occupied molecular orbitals. The electronic spectrum of crystalline simple salt differs distinctly from the monomer spectrum of the radical ion, but shows a charge-transfer transition between ion radicals in the low-energy region.[1-4] On the other hand, in crystalline complex ion radical salts, ion-radical and its parent neutral molecules are known to stack together to form regular one-dimensional column, where each molecular site is occupied by less-than-one unpaired electron. The electronic spectrum of complex salt is somewhat different from that of simple salt. Usually, the spectrum of complex salt shows two kinds of charge-transfer absorptions.[1,5] One arises from the electronic transition between ion radical and its parent neutral molecule, and the other, from the electronic transition between ion radicals. Although the latter transition is similar to the charge-transfer transition in simple salt, there may be a marked difference in the absorption intensity. In the present paper, we shall derive the absorption intensity of the charge-transfer transition between ion radicals in simple and complex ion radical salts and apply it to certain ion radical salts.

First, we consider the charge-transfer absorption in simple ion radical salts. In previous papers,[3] we applied the one-dimensional half-occupied Hubbard model to the segregated column of ion radicals. This model is a simplification of the real crystal and is expressed by two parameters I and T. $T(<0)$ is the transfer matrix element which describes hopping of an unpaired electron between adjacent molecular ion radical sites, while $I(>0)$ is the on-site Coulomb repulsion between two electrons with up and down spins on the same molecule. This model can well explain the reason why the absorption due to the charge-transfer transition between ion radicals is observable in simple ion radical salts. The previous paper described that the total intensity of the charge-transfer absorption per unit volume, A, was given by[3]

$$A = \frac{n\pi e^2}{4a} I(at)^2 \left(1 - \frac{3}{8}t^2 + \cdots\right), \quad (1)$$

where n is the number of one-dimensional columns per unit area perpendicular to the column axis, e is the electric charge, a is the lattice separation in one-dimensional column and $t=2T/I$. Hereafter, we only consider the case of $|t|\to 0$ limit and neglect the terms higher than t^4 in Eq. 1. Then, we obtain

$$A = \frac{n\pi e^2}{4a} I(at)^2 = \frac{n\pi e^2 a^2}{a} \cdot \frac{T^2}{I}. \quad (2)$$

Since a is the lattice separation, $(1/a)$ gives the number of sites per unit length in one-dimensional column. Therefore, (n/a) in Eq. 2 gives the number of sites (ion radical molecules) per unit volume in crystalline ion radical salt, being denoted by $N=n/a$. Then, A is expressed by $A=N\pi e^2 a^2 T^2/I$. Note that N is also equal to the number of unpaired electrons, because each ion radical carries one unpaired electron. The magnitude of A is rewritten by $A=N\pi e^2 a^2 J/2$, where $J=2T^2/I$ is an antiferromagnetic spin exchange parameter between adjacent unpaired electrons in one-dimensional column.[4]

It has been experimentally known that the charge-transfer interaction between ion radicals gives an antiferromagnetic Heisenberg chain of ion radical salt and that those ion radical salts which possess large J values show strong charge-transfer absorption intensities.[3] These experimental results can be well understood in terms of $A=N\pi e^2 a^2 J/2$. Here, A is proportional not only to the number of unpaired electrons, N, in the system but also to the magnitude of J. The latter can be explained in the following way. Since the charge-transfer interaction occurs mostly between adjacent ion radicals, the charge-transfer transition can only take place if the unpaired electrons of adjacent ion radicals in the ground state are antiparallel. In this case, the charge-transfer excited state corresponds to occupation of two electrons with up and down spins on the same site of ion radical molecule. If the unpaired electrons of adjacent ion radicals in the ground state are parallel, the charge-transfer transition is forbidden because of Pauli's exclusion principle. Thus, the absorption intensity of charge-transfer transition is closely related to the strength for aligning two unpaired electron spins of adjacent ion radicals antiparallel, and this strength corresponds to the magnitude of J.

On the basis of this discussion, we consider the charge-transfer transition between ion radicals in complex ion radical salts. As was mentioned, we assume a regular one-dimensional column composed of ion radical and its parent neutral molecule. Each mole-

cular site is occupied by less-than-one unpaired electron, the average number of unpaired electron per site being denoted by ρ, $(0 \leq \rho \leq 1)$. Then, we can apply one-dimensional less-than-half occupied Hubbard model to such a column. Here, we again use the parameters of I, T and a, which are common to those used in half-occupied Hubbard model. If we denote N as the total number of molecular sites (ion radicals + parent neutral molecules), the number of unpaired electrons is given by $N\rho$. As for the spin exchange interaction, Shiba and Klein-Seitz have shown that the magnetic susceptibility of a uniform stack of less-than-half occupied molecules ($\rho < 1$) is related to the magnetic susceptibility of a uniform stack of half-occupied molecules ($\rho = 1$) in simple ion radical salts.[6,7] If the value of I is much larger than that of $|T|$, the less-than-half occupied one-dimensional Hubbard model becomes equivalent to an antiferromagnetic Heisenberg chain with exchange interaction,

$$J = \frac{2T^2\rho}{I}\left(1 - \frac{\sin 2\pi\rho}{2\pi\rho}\right). \quad (3)$$

As was mentioned, the absorption intensity of charge-transfer transition between ion radicals is proportional not only to the number of unpaired electrons but also to the magnitude of J. If we apply this approach to the absorption intensity, A, of less-than-half occupied system of complex ion radical salts, we have $A \propto N\rho J = (2NT^2\rho^2/I)(1 - \sin 2\pi\rho/(2\pi\rho))$. As our model requires, if $\rho = 1$, A should become identical with $N\pi e^2a^2T^2/I$ in simple ion radical salts. This condition means that A of complex ion radical salts is given by $A = (N\pi e^2a^2T^2\rho^2/I)(1 - \sin 2\pi\rho/(2\pi\rho))$. In this equation, if $\rho \to 0$, that is, if average unpaired electron density approaches zero, the magnitude of A tends to zero, and we can observe no charge-transfer absorption in such a system. The value of A becomes greatest at $\rho = 1$, so that we obtain maximum intensity of the charge-transfer absorption in simple ion radical salt. On the other hand, if $|T| \to 0$, that is, if no charge-transfer interaction acts between adjacent ion radicals, the magnitude of A also tends to zero, and no charge-transfer absorption appears in such a case.

Let us apply this approach to certain crystalline ion radical salts. For example, we take a simple cation radical salt of Phenothiazine$^{+\cdot}$ Br^- and a complex cation radical salt of (Phenothiazine)$_2^{+\cdot}$ Br^-. The crystal electronic spectrum of the simple salt was measured by the present author,[2] while that of the complex salt, by Doi and Matsunaga.[5] The simple salt shows a strong low-energy band at 12900 cm^{-1}, which was assigned to the charge-transfer transition between phenothiazine cation radicals.[4] The one-dimensional half-occupied Hubbard model was applied to the system of the simple salt, and the parameter values of $I =$ 12900 cm^{-1} and $T = -2500$ cm^{-1} were estimated. On the other hand, the complex salt shows two charge-transfer absorptions at 5200 cm^{-1} and 12600 cm^{-1}.[5] The former was assigned to the transition from neutral phenothiazine to its cation radical, while the latter, to the transition between the cation radicals. We discuss only the latter absorption. Application of regular one-dimensional less-than-half occupied Hubbard model to the complex salt gave values of $I = 12900$ cm^{-1}, $T = -2500$ cm^{-1} and $\rho = 1/2$.[4] We denote the intensities of the charge-transfer absorptions per mol for the simple and complex salts as A(simple) and A(complex), respectively. The molecular sites per mol for the simple and complex salts are $N = N_A$ (Avogadro's number) and $N = 2N_A$, respectively. As for the lattice separation, we have no data on the crystal structures, and assume common value of a for both the salts. By putting those parameter values into the equation of A, the ratio of A(complex)/A(simple) was calculated as 1/2. Therefore, the intensity of the charge-transfer absorption of the complex salt at 12600 cm^{-1} appears to be half of that of the simple salt at 12900 cm^{-1}.

References

1) Y. Iida, *Bull. Chem. Soc. Jpn.*, **42**, 71, 637 (1969).
2) Y. Iida, *Bull. Chem. Soc. Jpn.*, **44**, 663 (1971).
3) Y. Iida, *Bull. Chem. Soc. Jpn.*, **50**, 1445 (1977); **52**, 2791 (1979).
4) Y. Iida, *Bull. Chem. Soc. Jpn.*, **53**, 2397 (1980); **54**, 921 (1981).
5) S. Doi and Y. Matsunaga, *Bull. Chem. Soc. Jpn.*, **48**, 3747 (1975).
6) H. Shiba, *Phys. Rev. B*, **6**, 930 (1972).
7) D. J. Klein and W. A. Seitz, *Phys. Rev. B*, **10**, 3217 (1974).

The Quenching of the OH ($^2\Sigma^+$) Produced in the H_2–O_2 Reaction by Collision with Ar

Yoshiaki HIDAKA,* Hiroyuki KAWANO, and Masao SUGA
Department of Chemistry, Faculty of Science, Ehime University, Bunkyo-cho, Matsuyama 790

(Received November 14, 1981)

Synopsis. H_2–O_2 mixtures highly diluted with Ar were heated to temperatures in the range of 1200—1800 K behind reflected shock waves. The OH*-emission intensity was then measured to determine its quenching-rate constant upon collision with Ar; this constant was found to be about 1/164 of that in the case of H_2O.

The ultraviolet-band system OH ($^2\Sigma^+$—$^2\Pi$) is the most prominent feature in the emission spectra of flames sustained by the oxidation of hydrogenous compounds. A number of studies have been made to clarify the mechanism of OH* ($^2\Sigma^+$) formation in various systems. The collisional quenching of OH* has also been studied by several authors.[1–6] It has been reported that the quenching effect of H_2O is considerably larger than those of other species, while that of Ar is very small. The quenching cross-sections (Q) of Ar reported are very scattered ($Q<0.01$—$Q<2$Å^2),[1,6] even though scarcely cross-sections at high temperatures have been reported. In this report, we will describe OH* emission measurements in the H_2–O_2 reaction, measurements undertaken in order to determine the quenching-rate constant by Ar.

Experimental

The apparatus and procedures are essentially the same as have been described previously.[7–9] Emission was monitored with a Hamamatsu R-306 photomultiplier through an interference filter ($\lambda_{max}=305.5$ nm, half-width=15 nm) located behind a quartz window of the shock tube and through two slits with widths of 0.14 and 0.17 mm, separated by a cylindrical tube.

The computer calculation was carried out based on the Gear-type integration of the set of differential equations describing the chemical kinetics under constant-density conditions for reflected shock waves.

The compositions of the reaction mixtures were:

(A) 0.50% H_2, 0.25% O_2, 99.25% Ar,
(B) 1.00% H_2, 1.00% O_2, 98.00% Ar.

The H_2, O_2, and Ar, specified as 99.9%, 99.9%, and 99.99% pure respectively, were obtained from commercial cylinders and were used without further purification. The initial pressures of the mixtures were about 0.13 atm.

Results and Discussion

Two mixtures, (A) and (B), were heated to temperatures in the range of 1200—1800 K behind reflected shock waves. The typical OH* emission profiles observed with these two mixtures, (A) and (B), are shown in Fig. 1, which also shows the computed [OH*] profiles. Since one volt of the signal corresponds to 4.9×10^{-15} mol cm^{-3} of [OH*] under our experimental conditions,[9] the observed OH* emission intensity can readily be converted into the OH* concentration. In Fig. 2, a plot of $\log I_B/I_A$ *vs.* T is shown, together with the simulation results, where I_A and I_B are the maximum OH* emission intensities measured with Mixtures (A) and (B) respectively.

The OH* formed in the H_2–O_2 reaction may disappear by quenching:

$$OH^* + M = OH + M, \quad (1)$$

and by emission:

$$OH^* = OH + h\nu. \quad (2)$$

The reverse reaction (−1) is the thermal-excitation process, which contributes much less than the chemical excitation pathway at temperatures below 2000 K.[11] The reverse reaction (−2) is the self-absorption process, the extinction coefficient of which is small enough for to be disregarded.[11] Therefore, aside from quenching effects, the OH*-emission intensity observed below 2000 K may be assumed to be proportional to the chemiluminescent OH* concentration. For computations, the value of $k_2=1.4\times10^6$ s^{-1} [12] is used as the rate constant of Reaction (2).

Reaction (3) is adopted as the OH*-formation process attributable to a chemical excitation:[9]

$$H + O + M = OH^* + M, \quad (3)$$

whose rate constant is assumed to have the value of $k_3=1.2\times10^{13}\exp(-6940/RT)$ cm^6 mol^{-2} s^{-1}.[9] The maximum concentration ratios, $\alpha=[OH^*]_B/[OH^*]_A$, calculated for the two mixtures, (A) and (B), are independent of k_3, which is changed by a factor of 10. The value of α is also independent of the mechanism of the OH*-formation reaction (bimolecular or termolecular reaction). Computations are performed by using a mechanism including:

(a) 14 reactions and their rate constants for the H_2–O_2 reaction reported by Olson and Gardiner,[10] and

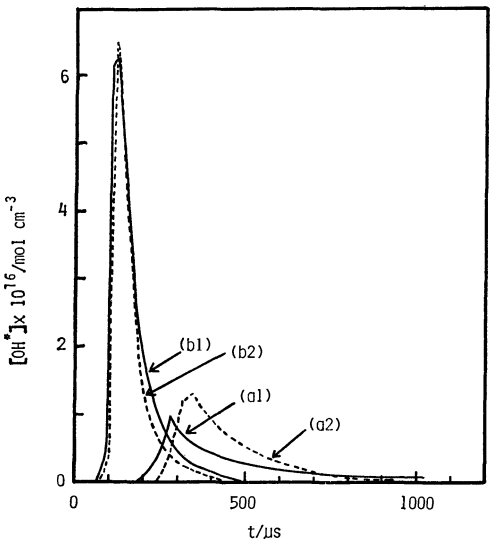

Fig. 1. Comparison of observed OH* emission profiles with [OH*] profiles computed by using $k_1(M=Ar)=5.2\times10^{10}T^{0.5}$ and $k_1(M=H_2O)=8.6\times10^{12}T^{0.5}$.
Profile (a1): observed at 1400 K with Mixture (A),
Profile (a2): computed at 1400 K for Mixture (A),
Profile (b1): observed at 1358 K with Mixture (B),
Profile (b2): computed at 1358 K for Mixture (B).

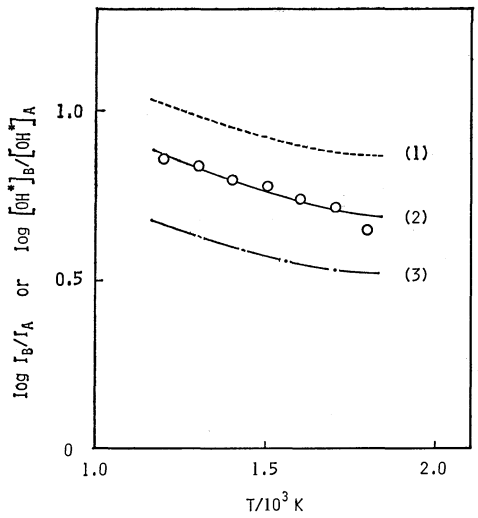

Fig. 2. Temperature dependence of the observed maximum OH* emission intensity ratio (open circle) and of the maximum OH* concentration ratio calculated for Mixtures (A) and (B).
Curve (1): $[OH^*]_B/[OH^*]_A$ calculated by using $k_1(M=Ar)=4.2\times10^{11}T^{0.5}$. Curve (2): $[OH^*]_B/[OH^*]_A$ calculated by using $k_1(M=Ar)=5.2\times10^{10}T^{0.5}$ and $k_1(M=H_2O)=8.6\times10^{12}T^{0.5}$. Curve (3): $[OH^*]_B/[OH^*]_A$ calculated by using $k_1(M=H_2O)=8.6\times10^{12}T^{0.5}$.

(b) 3 reactions (1)—(3) and their rate constants as described above.

In the present system, this relation holds: $I_B/I_A=[OH^*]_B/[OH^*]_A$, where I_A and I_B are the maximum OH*-emission intensities measured with Mixtures (A) and (B) respectively.

Fluorescence measurements (Reaction (1)) in the burnt gases in a lean acetylene-oxygen flame have revealed that the collision cross-sections for quenching by O_2, H_2O, and Ar are 7, 35, and below 2 Å^2 respectively.[1] Of these cross-sections, it is concluded that k_1 $(M=H_2O)=8.6\times10^{12}T^{0.5}$, k_1 $(M=O_2)=1.5\times10^{12}T^{0.5}$, and k_1 $(M=Ar)=4.2\times10^{11}T^{0.5}$ cm^3 mol^{-1} s^{-1} as the rate constants of Reaction (1). Since species such as H_2, O, OH, and H are also present in the reaction system, the quenching by them should also be taken into account. As k_1 $(M=H_2)$ at room temperature, values in the range of 3.6×10^{12}—7.6×10^{13} cm^3 mol^{-1} s^{-1} have been reviewed.[13] Since the quenching data against H, O, and OH as collision partners with OH* have not been reported, it is assumed that H_2, OH, H-atoms, and O-atoms have the same quenching rate as O_2. When we assume that k_1 $(M=Ar)=5.2\times10^{10}T^{0.5}$ cm^3 mol^{-1} s^{-1}, kinetic analysis under our experimental conditions shows that the Ar gas plays a dominant role for the OH* quenching, and that the quenching by O_2, H_2, OH, H, and O is negligible in comparison with those by H_2O and Ar (see Ref. 9). Hence, the quenching reactions by O_2, H_2, OH, H, and O were disregarded in the final computations. When M in Reaction (1) is assumed to be H_2O, the calculated value of α is always smaller than that observed. When M is Ar, on the other hand, the value of α is always larger than that observed, as may be seen in Fig. 2. By trial and error, it has been found that a curve calculated assuming that k_1 $(M=H_2O)/k_1$ $(M=Ar)=164$ fits the experimental data best, as shown in Fig. 2. Consequently, the collision cross-section ratio, $Q(H_2O)/Q(Ar)$, is 140. When the quenching-rate constant of H_2O is assumed to be $8.6\times10^{12}T^{0.5}$ cm^3 mol^{-1} s^{-1} (Q=35 Å^2),[1] that by Ar is $5.2\times10^{10}T^{0.5}$ cm^3 mol^{-1} s^{-1} (Q=0.25 Å^2). In Fig. 1, the typical emission profiles observed in the (A) and (B) mixtures are compared with the [OH*] profiles computed. The maxima of the calculated [OH*] are slightly larger than those observed in both mixtures, while the maxima computed for some runs were found to be slightly smaller than the observed ones. Consequently, the profiles calculated with the expression $k_1=5.2\times10^{10}T^{0.5}$ (M=Ar) are concluded to fit the experimental results best.

Carrington[1] has reported that the quenching cross-section of Ar over the temperature range of 850—1500 K is less than 2 Å^2, which corresponds to k_1 $(M=Ar)<1.2\times10^{13}$ cm^3 mol^{-1} s^{-1}.[13] This upper-limit value is much larger than values at room temperature[13] and is consistent with our observation.

The quenching by inert monoatomic gases is generally accepted to be inefficient compared with that by bi- or triatomic gas molecules. If the smallest value recommended by Schofield[13] is assumed at room temperature, our observation of the larger value at high temperatures must lead to the conclusion that $k_1(M=Ar)$ is strongly dependent on the temperature. Assuming that a large kinetic energy of OH*+Ar collision is required to reach a crossing point of the potential curves of OH*+Ar and OH+Ar, $k_1(M=Ar)$ increases at a higher temperature. However, no significant temperature-dependence of k_1 could be found under our temperature conditions (1200—1800 K). Such independence of $k_1(M=Ar)$ conflicts with the quenching mechanism described above. In order to solve this difficulty, an experiment for the reliable determination of $k_1(M=Ar)$ is desired over a wide temperature range from room temperature to several thousand K.

References

1) T. Carrington, *J. Chem. Phys.*, **30**, 1087 (1959).
2) V. N. Kondrat'ev, "Chemical Kinetics of Gas Reactions," Pergamon Press, New York (1964).
3) R. G. Bennett and F. W. Dalby, *J. Chem. Phys.*, **40**, 1414 (1964).
4) H. P. Hooymayers and C. Th. J. Alkemade, *J. Quant. Spectry. Radiative Transfer*, **7**, 495 (1967).
5) M. Kaneko, Y. Mori, and I. Tanaka, *J. Chem. Phys.*, **48**, 4468 (1968).
6) D. Kley and K. H. Welge, *J. Chem. Phys.*, **49**, 2870 (1968).
7) Y. Hidaka, T. Kataoka, and M. Suga, *Bull. Chem. Soc. Jpn.*, **47**, 2166 (1974).
8) Y. Hidaka, T. Nishi, and M. Suga, *Bull. Chem. Soc. Jpn.*, **49**, 2007 (1976).
9) Y. Hidaka, S. Takahashi, H. Kawano, M. Suga, and W. C. Gardiner, Jr., *J. Phys. Chem.*, **86**, 1429 (1982).
10) D. B. Olson and W. C. Gardiner, Jr., *Combust. Flame*, **32**, 151 (1978).
11) W. C. Gardiner, Jr., K. Morinaga, D. L. Ripley, and T. Takeyama, *Phys. Fluids Supplement*, **1**, 120 (1969).
12) K. R. German, *J. Chem. Phys.*, **62**, 2584 (1975).
13) K. Schofield, *J. Phys. Chem. Ref. Data*, **8**, 723 (1979).

Hydrogen Evolution from Alkaline Formaldehyde Solution

Hiroshi Okamoto,* Masayuki Katsumoto, and Tetsuichi Kudo
Central Research Laboratory, Hitachi Ltd., 1-280, Higashi-Koigakubo, Kokubunji, Tokyo 185
(Received May 10, 1982)

Synopsis. Hydrogen is evolved from an alkaline solution of formaldehyde in the presence of a tungsten carbide catalyst at room temperature under atmospheric pressure. Neither platinum nor palladium shows any catalytic activity to this reaction. The hydrogen evolution competes with the Cannizzaro reaction.

Much attention has been paid to hydrogen as a fuel of a post-petroleum clean energy system. If hydrogen could be made available in desired quantities without great effort or equipment, this energy system would become more feasible. Formaldehyde in an alkaline solution has been found to yield hydrogen at room temperature under atmospheric pressure when tungsten carbide (WC) is used as a catalyst. This new type of reaction might satisfy some of the above requirements. Moreover, a hydrogen energy system including formaldehyde is related to an efficient utilization of coal since formaldehyde is produced from coal. The present note describes and discusses experimental results of a preliminary investigation on the new reaction.

When WC (0.5 g) was added to a formaldehyde (1 mol dm^{-3}) solution containing 2 mol dm^{-3} NaOH at around room temperature under atmospheric pressure, a gas was evolved after an induction period of about 1 min as shown in Fig. 1. The evolved gas was identified with pure hydrogen gas by gas chromatography (with molecular sieves 5A column and TCD). As Fig. 1 shows, the hydrogen evolution rate decreases with increasing reaction time. This tendency is more predominant at higher reaction temperatures. The hydrogen evolution rate calculated from the amount of hydrogen evolved for 5 min after the beginning of the evolution was greater for the higher temperature. An activation energy estimated was about 36 kJ mol^{-1}.

No change was observed in the X-ray diffraction of WC after the reaction, indicating that it worked as a catalyst.

The relation between the hydrogen evolution rate and the hydroxide ion concentration under conditions where the initial formaldehyde concentration was 2 mol dm^{-3} and the reaction temperature was maintained at 20 °C, is shown in Fig. 2. The evolution rate increased linearly until the concentration was increased to 2 mol dm^{-3}. Above this value, the rate decreased slightly.

The dependence on the formaldehyde concentration of the evolution rate observed at 20 °C with the hydroxide ion concentration of 2 mol dm^{-3}, is shown in Fig. 3. The rate increased when the formaldehyde concentration was increased up to 2 mol md^{-3}. However, further increases in the concentration decreased the rate.

No hydrogen was evolved when benzaldehyde, acetaldehyde, paraldehyde, acetone, methanol, or formic acid was used in place of formaldehyde. No hydrogen evolution was observed either in an acidic formaldehyde solution. Thus, the hydrogen evolution must occur only in an alkaline formaldehyde solution. Therefore, the conceivable reaction is written as

$$HCHO + OH^- = HCOO^- + H_2. \quad (1)$$

The total amount of hydrogen evolved from a solution containing 26 mmol formaldehyde and 26 mmol NaOH was 10 mmol. If only reaction 1 proceeded

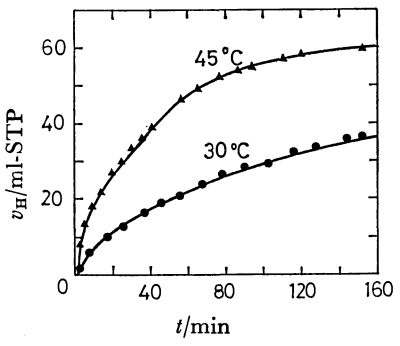

Fig. 1. Hydrogen evolution volume *vs.* time under at mospheric pressure.
v_H: Hydrogen evolution volume in ml-STP, formaldehyde concentration: 1 mol dm^{-3}, hydroxide ion concentration: 2 mol dm^{-3}, WC weight: 0.5 g.

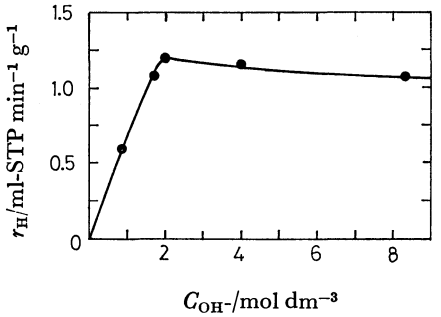

Fig. 2. Dependence of hydrogen evolution rate on hydroxide ion concentration at 20 °C.
r_H: Hydrogen evolution rate measured at 5 min after the beginning of the evolution, formaldehyde concentration: 2 mol dm^{-3}.

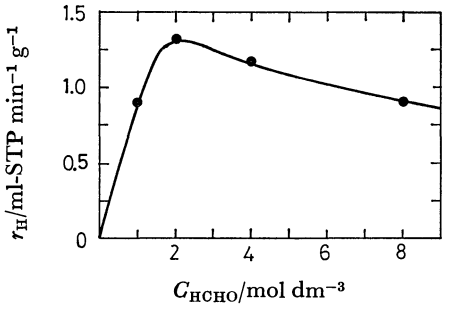

Fig. 3. Dependence of hydrogen evolution rate on formaldehyde concentration at 20 °C.
Hydroxide ion concentration: 2 mol dm^{-3}.

in the reaction solution, the total hydrogen amount must have been 26 mmol. This discrepancy can be explained as follows. In the reaction system, the Cannizzaro reaction

$$2HCHO + OH^- = CH_3OH + HCOO^- \quad (2)$$

must compete with the hydrogen evolution. Thus, the total amount of hydrogen is smaller than that calculated on the basis of only reaction 1.

Sodium formate and methanol were found except for formaldehyde in the reaction solution by Raman spectroscopy. This is consistent with reactions 1 and 2.

The standard Gibbs energy difference of reaction 1 is $-47.7\ kJ\ mol^{-1}$.[1] Therefore, the forward reaction in reaction 1 is thermodynamically easy to proceed. With an acidic formaldehyde or alkaline methanol solution, the standard free energy difference is positive or slightly negative as follows:[1]

$$HCHO + H_2O = HCOOH + H_2$$
$$\Delta G^0 = 10.9\ kJ\ mol^{-1}, \quad (3)$$

$$CH_3OH = HCHO + H_2 \quad \Delta G^0 = 44.9\ kJ\ mol^{-1}, \quad (4)$$

$$CH_3OH + OH^- = HCOO^- + 2H_2$$
$$\Delta G^0 = -0.7\ kJ\ mol^{-1}. \quad (5)$$

Thus, the forward reactions in reactions 3—5 are thermodynamically almost difficult to proceed. By comparing the free energy difference in reaction 1 with that for reaction 3, the motive force for hydrogen evolution is considered to be the heat of neutralization

$$OH^- + HCOOH = HCOO^- + H_2O$$
$$\Delta G^0 = -58.6\ kJ\ mol^{-1}. \quad (6)$$

To find catalysts effective to the hydrogen evolution other than WC, carbides, nitrides, borides, oxides, sulfides, and transition metals of all the groups from III B to VIII B were tested at room temperature with an aqueous solution of 2 mol dm^{-3} formaldehyde concentration and 1.6 mol dm^{-3} hydroxide ion concentration. It was found that Mo_2C, W_2C, (Mo,W)C, Mo_2N, W_2B_5, WB_4, WB_2, Mo, and W were active. It can be pointed out that only the compounds of the VI B group elements have catalytic activities. Among them, WC was most active. It was interesting that platinum black and palladium black were inactive. WC often behaves as a platinum-like catalyst[2,3] due to its similar catalytic activity and electronic structure. However, WC catalyzes the reaction that platinum does not. Since WC is known to be a catalyst for the anodic oxidation of hydrogen,[4] ammonia synthesis,[5] and other reactions,[6] it is a very promising material to replace precious metal catalysts.

References

1) W. M. Latimer, "Oxidation Potentials," 2nd ed, Prentice-Hall, Inc., N. J. (1952).

2) R. B. Levy, and M. Boudart, *Science*, **181**, 547 (1973).

3) L. H. Bennett, J. R. Cuthill, A. J. McAlister, N. E. Erickson, and R. E. Watson, *Science*, **184**, 563 (1974).

4) H. Binder, A. Koeling, and G. Sandstede, *Am. Chem. Soc., Div. Fuel Chem., Prepr.*, **13**, 99 (1969).

5) G. S.-Ekloff, D. Baresel, and W. Salholz, *J. Catal.*, **43**, 353 (1976).

6) For example, ethylene hydrogenation: I. Kojima, E. Miyazaki, Y. Inoue, and I. Yasumori, *J. Catal.*, **59**, 472 (1979); hydrogen oxidation at rt: R. B. Levy and M. Boudart, *Science*, **181**, 547 (1973); liquid phase hydrogenation: G. Horányi, G. Vértes, and Gy. Fézler, *Z. Phys. Chem. N. F.*, **83**, 322 (1973).

Dependence of Electric Polarizability of Rodlike DNA in Aqueous Solutions on Ionic Strength as Studied by Electric Dichroism and Birefringence. A Comparison between Experimental and Theoretical Results

Kiwamu YAMAOKA,* Koichiro MATSUDA, and Kaoru TAKARADA
Faculty of Science, Hiroshima University, Higashisenda-machi, Naka-ku, Hiroshima 730
(Received July 23, 1982)

Synopsis. Orientation of a sonicated DNA fragment in aqueous solutions containing sodium chloride (0.2—4 mmol/dm^3) by an external electric field was discussed in terms of counterion-induced electric moments by using the electric dichroism and birefringence data experimentally determined at limiting low field strengths.

Ample evidence indicates that highly charged DNA in aqueous solutions can be oriented by an external electric field.[1-3] In previous studies of electric dichroism (ED) and electric birefringence (EB), we have shown that the electric field orientation of sonicated DNA fragments (sDNA) obeys the Kerr law in the low field strength region under diverse conditions.[4,5] This result is in good agreement with recent reports by other workers.[6-10] The orientation of sDNA has been attributed to the interaction between the ionized site and counterion and the applied field. Detailed analyses have shown, however, that the polyion behaves as if it possesses both a permanent dipole moment and a covalent polarizability anisotropy.[4-7] Thus, this electric dipole has been termed either the pseudo-[4,5,9] or quasi-permanent dipole[11] or the saturated induced dipole.[12] The electric moment was recently shown to result from the fast polarization of the "bound" counterion.[4,7] For the understanding of the polyelectrolyte property of DNA, its field-orientation mechanism should be fully clarified. Since the counterion-induced dipole is affected by the added simple ions, we examined the dependence of the steady-state ED and EB at limiting low electric field on the ionic strength (thus, saturation of the counterion-induced dipole moment could be avoided). We also present a critical comparison of observed results with recent theoretical developments.[13-15]

Experimental

Materials and Measurements. The sDNA sample is the same as before.[5] In order to adjust the counterion (Na^+) concentration, the sDNA solution was dialyzed at 4 °C for at least 48 hours against distilled water containing sodium chloride at the desired level. Both ED and EB were measured at 7 °C.[5] The observed data were expressed with the parallel (specific) dichroism, $\Delta A_\parallel/A$ at 260 nm, and the specific birefringence, $\Delta n/C$ at 535 nm.[5] At limiting low field strengths, E, the following expression generally holds for charged polyions:

$$\frac{(\Delta A_\parallel/AE^2)_{E^2\to 0}}{(\Delta A_\parallel/A)_s} = \frac{(\Delta n/CE^2)_{E^2\to 0}}{(\Delta n/C)_s} = \frac{1}{15}\left[\left(\frac{\mu_3}{kT}\right)^2 + \frac{\Delta\alpha^t}{kT}\right], \quad (1)$$

where $(\Delta A_\parallel/A)_s$ and $(\Delta n/C)_s$ are the corresponding quantities at limiting high fields, μ_3 is the permanent dipole moment along the symmetry axis, and $\Delta\alpha^t$ is the polarizability anisotropy, which is generally the sum of the covalent (*i.e.*, electronic and atomic) and ionic polarizabilities ($\Delta\alpha^t = \Delta\alpha^c + \Delta\alpha^i$).

Results and Discussion

Dependence of ED and EB on Added Sodium Ions. In the added-salt concentration range of 0.2—4 mM (1 M=1 mol/dm^3), values of $\Delta A_\parallel/A$ and $\Delta n/C$ for the rodlike sDNA sample are proportional to the second power of electric field in the limiting low field region. The results are given in Table 1. The linear portions in the plots of these values against E^2 become narrower and the magnitudes are larger at lower concentrations of added salt (*cf.* Figs. 1 and 2 of Ref. 5). Values of $(\Delta A_\parallel/A)_s$ and $(\Delta n/C)_s$ are nearly independent of the added-salt concentration,[5] *i.e.*, the optical part in Eq. 1 is constant. Therefore, the electric parameter should be responsible for the variation of the observed limiting-low-field quantities with salt concentration. Since the double-helical DNA possesses no permanent dipole moment under ordinary conditions ($\mu_3=0$ in Eq. 1), the variation of $(\Delta A_\parallel/AE^2)_{E^2\to 0}$ and $(\Delta n/CE^2)_{E^2\to 0}$ should result from the change in the electric polarizability $\Delta\alpha^t$, in particular the ionic polarizability $\Delta\alpha^i$. Values of $\Delta\alpha^t$ decrease with the increase in added-salt concentration, and are given in Table 1. Their magnitude is of the order of 10^{-16} cm^3, in good agreement with reported values.[5-7,9,12]

In Fig. 1, values of $(\Delta A_\parallel/AE^2)_{E^2\to 0}$ and $(\Delta n/CE^2)_{E^2\to 0}$ are plotted against the total concentration of sodium ions, $[Na^+]_t$, *i.e.*, the sum of those ions from the added sodium chloride and from the counterions of DNA-phosphates. In Fig. 1, values of $(\Delta A_\parallel/AE^2)_{E^2\to 0}$ at

Table 1. Values of $(\Delta A_\parallel/AE^2)_{E^2\to 0}$ at 260 nm and $(\Delta n/CE^2)_{E^2\to 0}$ at 535 nm of a sonicated DNA sample at various concentrations of added sodium chloride [NaCl] at 7 °C [a]

[NaCl] / mM	$\left(\frac{\Delta A_\parallel}{AE^2}\right)_{E^2\to 0}\times 10^2$ / (kV/cm)$^{-2}$	$\left(\frac{\Delta n}{CE^2}\right)_{E^2\to 0}\times 10^3$ / M^{-1}(kV/cm)$^{-2}$	$\Delta\alpha^t\times 10^{16}$ / cm^3 [b]
0.2	−1.33	−0.36	10.4(9.37)[c]
1.0	−0.75	−0.22	6.68(6.99)[c]
2.0	−0.39	—	3.43[d]
4.0	−0.23	—	2.02[d]

a) The concentrations of DNA, C, in nucleotide units are 0.17—0.18 mM. b) 1 cm^3 = 1.113 × 10^{-16} F m^2. c) Values in the parentheses are obtained with the limiting low-field strength birefringence. d) Value of $(\Delta A_\parallel/A)_s$ is −0.593.

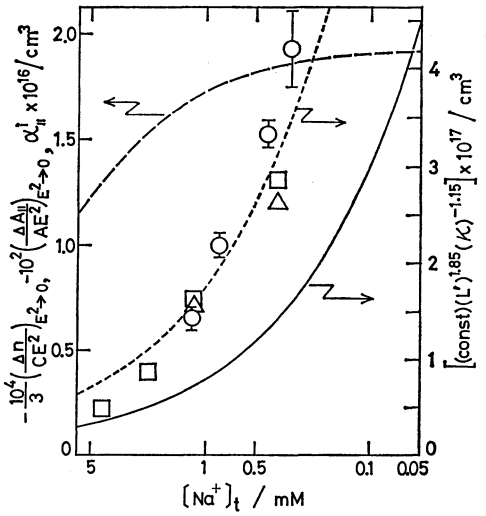

Fig. 1. Dependence of the measured limiting low-field dichroism, birefringence, and the theoretical electric polarizabilities of rodlike sDNA solutions on the total concentration of sodium ions, $[Na^+]_t$. Experimental values: $(\Delta A_\parallel/AE^2)_{E^2\to 0}$ (□) in this work and (○) cited in Ref. 9, and $(\Delta n/CE^2)_{E^2\to 0}$ (△) in (kV/cm)$^{-2}$. Theoretical curves: Fixman's polarizability (——) was calculated from Eq. 2 with the parameters: $q_1 = -q_2 = 1$ and $\gamma^2 = 28.52 \times 10^{12} C_1$, where C_1 (mol/dm^3) is the bulk concentration of Na^+. Rau and Charney's polarizabilities (——), for which the (const) is unity, and (----), for which the (const) is 2.2, were calculated from Eq. 3. Dielectric constant is 80 and temperature is 280 K. The $[Na^+]_t$ includes the concentration of DNA in nucleotide units.

270 nm for a nearly identical sDNA sample are also plotted. They were calculated from published values of $(\Delta A_\parallel/A)$ (*cf.* Fig. 1 of Ref. 9) but they agree well with the present data, which were obtained with an entirely different apparatus.

Comparison between Experimental and Theoretical Results. Recently, Manning derived an expression for the parallel component ionic polarizability $\alpha^1_\parallel$ on the basis of the ion condensation model.[16] The slight dependence of this theoretical $\alpha^1_\parallel$ on ionic strength is, however, in opposition to experimental results.[7,9,13] More recently, Fixman proposed an expression for electric polarizability (with his own notations):[14]

$$\alpha^1_\parallel \equiv \frac{\mu}{E_0} = \frac{2q_1KDL}{(q_1-q_2)\gamma^2}\left[1-\frac{\tanh(\gamma L)}{\gamma L}\right], \qquad (2)$$

where $K=[2\ln(4L/a)-(14/3)]^{-1}$. Approximating the B-DNA form for the present sDNA sample regardless of salt concentrations (a=13 Å, L=319.6 Å),[5] we have calculated the polarizability in Eq. 2 as a function of concentrations of added sodium chloride. The result is shown by a dashed curve in Fig. 1. This curve *decreases* monotonously but in a *convex* fashion with increasing salt concentrations in the range< 6 mM.

Another theoretical advance has been made lately by Rau and Charney.[15] By calculating the electric moment for an electric field-induced polarization of a Debye-Hückel ion atmosphere, they show that the polarizability along a charged rod, $\alpha^1_\parallel$, is approximately proportional to the half length of the rod, L'(=319.6 Å), and to the Debye-Hückel shielding parameter κ (with their own symbolism):[15]

$$\alpha^1_\parallel = (\mathrm{const})(L')^{1.85}(\kappa)^{-1.15}. \qquad (3)$$

As a function of the ionic strength of NaCl, we have calculated the quantity $(L')^{1.85}(\kappa)^{-1.15}$ and plotted it in Fig. 1 (solid curve). This curve, too, *decreases* monotonously and in a *concave* fashion with the increase in the total sodium concentration. The curve is nearly parallel to experimental values of the limiting low-field dichroism and birefringence. To visualize this trend quantitatively, the solid curve was shifted upward by multiplying a factor of 2.2 (shown by the dotted curve); the agreement with the experimental points is good.

In summary, the effect of ionic strength on observed limiting low-field dichroism or birefringence now appears to be explicable reasonably well by the Debye-Hückel ion atmosphere polarization concept. Another test for the Fixman *vs.* the Rau and Charney model may reside on measurements of ED, EB, or dielectric constants as a function of temperature, since the polarizability in Eq. 2 is temperature-independent but that in Eq. 3 is inversely proportional to temperature. A remaining question on the counterion-induced dipole moment is to assess the contribution from the condensed or "bound" counterions.[8,13] This contribution would be most prominent, if it exists, in the DNA solution in which no excessive salt ions are present. Values of, *e.g.*, $(\Delta A_\parallel/AE^2)_{E^2\to 0}$ may show an asymptotic trend in salt-free solutions. Measurements of ED or EB of rodlike sDNA under such conditions are highly desirable.

References

1) E. Fredericq and C. Houssier, "Electric Dichroism and Electric Birefringence," Clarendon Press, Oxford (1973).
2) N. C. Stellwagen, "Molecular Electro-Optics," ed by C. T. O'Konski, Marcel Dekker, New York (1978), Part 2, Chap. 18; M. Shirai, *ibid.*, Chap. 19.
3) For proceedings, B. R. Jennings, Ed. "Electro-Optics and Dielectrics of Macromolecules and Colloids," Plenum Press, New York (1979); "Molecular Electro-Optics," ed by S. Krause, Plenum Press, New York (1981).
4) K. Yamaoka and K. Matsuda, *Macromolecules*, **13**, 1558 (1980); **14**, 595 (1981).
5) K. Matsuda and K. Yamaoka, *Bull. Chem. Soc. Jpn.*, **55**, 1727 (1982). Also see references cited therein.
6) N. C. Stellwagen, *Biopolymers*, **20**, 399 (1981).
7) J. G. Elias and D. Eden, *Macromolecules*, **14**, 410 (1981).
8) D. Balasubramanian and E. Charney, *J. Phys. Chem.*, **85**, 1943, (1981).
9) E. Charney and K. Yamaoka, *Biochemistry*, **21**, 834 (1982).
10) S. Diekmann, W. Hillen, M. Jung, R. D. Wells, and D. Pörschke, *Biophys. Chem.*, **15**, 157 (1982).
11) T. Fujikado, R. Hayakawa, and Y. Wada, *Biopolymers*, **18**, 2303 (1979).
12) S. Sokerov and G. Weill, *Biophys. Chem.*, **10**, 161 (1979).
13) E. Charney, K. Yamaoka, and G. S. Manning, *Biophys. Chem.*, **11**, 167 (1980).
14) M. Fixman, *Macromolecules*, **13**, 711 (1980).
15) D. C. Rau and E. Charney, *Biophys. Chem.*, **14**, 1 (1981).
16) G. S. Manning, *Biophys. Chem.*, **9**, 65 (1978).

Intensity Enhancement Caused by Complex Formation between Pyrene and Alcohols

Akira NAKAJIMA

Department of Electronic Engineering, Faculty of Engineering, Saitama Institute of Technology, Okabe, Saitama 369-02

(Received July 31, 1982)

Synopsis. The enhancement of the weak 0-0 band in the absorption spectrum of pyrene has been observed using various mixtures of cyclohexane and alcohols. The relations of the absorption coefficients with the alcohol concentrations have been studied on the assumption of 1:1 complex formation between pyrene and alcohols. The association constants for the hydrogen-bonded complexes have been estimated to be of a reasonable order of magnitude (0.1—0.4 mol^{-1} dm^3).

Growing interest has been shown in the investigations of the microenvironments in micellar and membraneous systems. For spectroscopic studies of the structures and mechanisms in these systems a variety of molecular probes[1] have been employed with appreciable success. It has been demonstrated[2-4] that pyrene (and other related aromatic hydrocarbons) can also be used as such a probe. It may be said however that pyrene has a unique character in that one can utilize not only the overall intensities of its emission and absorption spectra but also the variations of their vibronic structures in various media.

The enhancement of weakly allowed vibronic bands in the absorption and fluorescence spectra of pyrene in polar solvents was first studied by this author[5] and a number of investigations[3,6-9] have so far been undertaken for the purpose of elucidation and application of this phenomenon.

Recently Lianos and Georghiou[10] have studied the systems of pyrene and alcohols in nonpolar solutions by infrared spectroscopy and fluorescence decay analysis and shown that the intensity enhancement arises from the formation of stoichiometric complexes. As reported previously, the present author[11,12] has observed that the weak 0-0 band of pyrene in a nonpolar solvent can gain considerable intensity on addition of a polar solvent and indicated that the large initial increase can be explained by the complex formation between pyrene and polar molecules.

In this work, the enhancement of the 0-0 band has been studied employing various mixtures of nonpolar and polar solvents; cyclohexane was used as a nonpolar component, while 2-methyl-2-propanol, ethanol, and phenol were adopted as polar components. An attempt has been made to interpret the enhancement in terms of 1:1 complex formation between pyrene and the alcohols or phenol and to estimate the association constants.

Experimental

GR grade pyrene obtained from Wako Pure Chemical Industries was recrystallized repeatedly from ethanol. Checking by the absorption spectra indicated no impurity absorption present in the spectral range studied. Spectrograde cyclohexane from Kanto Chemical Co. was used without further purification. Ethanol and 2-methyl-2-propanol were purified by fractional distillations after drying. Phenol was recrystallized many times from the melt.

The solutions were carefully prepared by the volumetric method from various mixtures of cyclohexane and alcohols or phenol with a constant concentration of pyrene (2.99×10^{-3} mol dm^{-3}).

The absorption spectra were recorded at room temperature on a Shimadzu 210A double-beam spectrophotometer, with a slit width for 0.5 nm resolution and at a scan speed of 50 nm/min. In the lowest electronic transition of pyrene the absorption coefficient for the 0-0 band (around 371 nm), which has been found to be most sensitive to the solvent polarity, has been measured by varying the alcohol concentrations. The variation of the band width in different solvents has been observed to be relatively small (less than 3%), of which no account has been taken.

The preparations of the solutions and the measurements were repeated several times, especially at lower alcohol concentrations, followed by averaging the measured values to compensate volumetric and instrumental errors.

Results and Discussion

The observed relations between the absorption coefficients for the 0-0 band (ε) and the concentrations of alcohols or phenol (C_A) are shown in Fig. 1. From the figure it should be noticed that relatively large increases in ε can be observed at lower C_A and changes in the higher C_A region are appreciable. In pure cyclohexane ε is small with a value of 135.0 (mol^{-1} dm^3 cm^{-1}), while its value increases to 226.0 in 2-methyl-2-propanol and 276.3 in ethanol. The general tendency of the increase seems to be explained in terms of the solvent polarity and has been considered on the basis of the bulk properties of solvents.[5] However, recent studies[10-12] have indicated that the formation of complexes occurs considerably. In particular, Lianos and Georghiou[9] have concluded that the enhancement is the result of the reduction of the molecular symmetry caused by the 1:1 complex formation between pyrene and alcohols.

Accordingly, it may be assumed also in this study that the intensity enhancement is primarily induced by the formation of weak 1:1 complexes between pyrene and alcohols or phenol. Thus, an equilibrium is postulated among a pyrene molecule P, an alcohol or phenol molecule A, and a complex PA as follows

$$P + A \overset{K}{\rightleftharpoons} PA.$$

Here the association constant K is given by

$$K = \frac{[PA]}{[P][A]}$$

with the additional conditions:

$$[P] + [PA] = C_P$$
$$[A] + [PA] = C_A$$

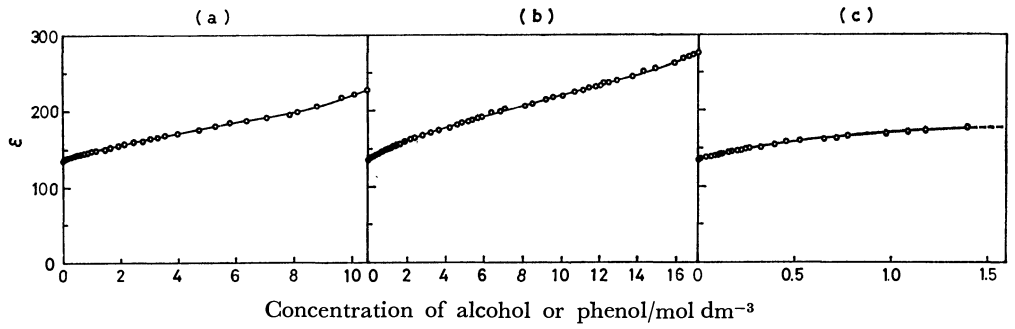

Fig. 1. Relations between the absorption coefficient for the 0-0 band of pyrene and the concentrations of (a) 2-methyl-2-propanol, (b) ethanol, and (c) phenol.

TABLE 1. THE ASSOCIATION CONSTANTS AND ABSORPTION COEFFICIENTS FOR THE SYSTEMS OF PYRENE IN ALCOHOL- OR PHENOL-CYCLOHEXANE MIXTURES, WITH SOME RELEVANT PROPERTIES OF ALCOHOLS AND PHENOL

Compound	D[a,c]	μ[b,c]	pK_a[c]	K/mol^{-1} dm^3	ε_C/mol^{-1} dm^3 cm^{-1}
2-Methyl-2-propanol	12.47	1.66	19	0.22±0.06	208.5±18
Ethanol	24.55	1.66	15.9	0.14±0.07	261.6±23
Phenol	9.78	1.45	10.02	0.43±0.04	275.8±12

a) Dielectric constant. b) Dipole moment in Debye units. c) J. A. Riddick and W. B. Bunger, "Technique of Chemistry, Vol. 3, Organic Solvent," 3rd ed, Wiley-Interscience, New York (1970).

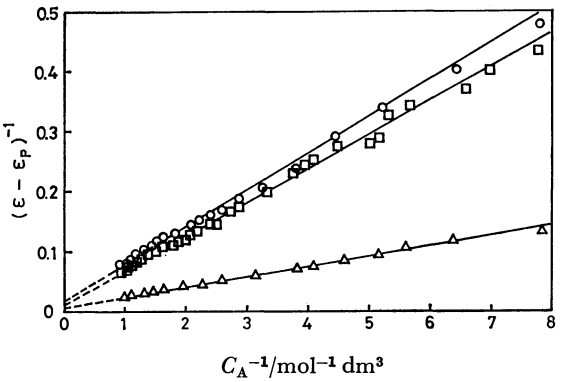

Fig. 2. Plots of $(\varepsilon-\varepsilon_P)^{-1}$ *vs.* C_A^{-1} for 2-methyl-2-propanol–cyclohexane (○), ethanol–cyclohexane (□), and phenol–cyclohexane (△) solutions. ε_P is taken as the absorption coefficient in pure cyclohexane.

where C_P and C_A are the total concentrations of pyrene and alcohol or phenol, respectively.

The absorbance measured at the wavelength for the 0-0 band can be expressed as

$$A = \varepsilon_P l\,[P] + \varepsilon_C l\,[PA],$$

where ε_P and ε_C denote the absorption coefficients for free pyrene and the complex, respectively, and l is the optical path length (1 cm).

Provided that C_A is much larger than C_P ($=2.99\times 10^{-3}$ mol dm^{-3}), [A] is approximated to C_A, and the following relation[12] can be derived between C_A and the apparent absorption coefficient $\varepsilon=A/C_Pl$:

$$\frac{1}{\varepsilon-\varepsilon_P} = \frac{1}{\varepsilon_C-\varepsilon_P} + \frac{1}{(\varepsilon_C-\varepsilon_P)KC_A}.$$

Thus, a plot of $1/(\varepsilon-\varepsilon_P)$ *vs.* $1/C_A$ should give a straight line, from the intercept and slope of which the values of ε_C and K can be determined.

Figure 2 shows such plots for the systems of pyrene in various alcohol- or phenol-cyclohexane mixtures. Because of the condition $C_A \gg C_P$ and much complicated interactions at higher C_A, the concentration range effective for plots should be considerably narrowed (roughly $0.1<C_A<1$). As shown in Fig. 2, fairly good linear relationships have been obtained, a fact which indicates that the stoichiometry corresponds to 1:1 complexation in the lower concentration region. From the values of the slopes and intercepts, the association constants K and the absorption coefficients ε_C have been estimated, as listed in Table 1. The values of K obtained are in good order-of-magnitude agreement with those ($\lesssim 1$ mol^{-1} dm^3) estimated by Lianos and Georghiou,[10] though more accurate determinations are difficult because of unavoidable experimental errors. Similar values have been obtained using aprotic polar solvents.[12]

It can be seen from Table 1 that the K and ε_C values bear no direct relation to the dielectric constants or dipole moments; they seem to be rather correlated with the acidities, which may imply that hydrogen-bonded complexes are formed between pyrene and phenol or alcohols.[10]

References

1) L. Brand and J. R. Gohlke, *Ann. Rev. Biochem.*, **41**, 843 (1972).
2) A. Nakajima, *Bull. Chem. Soc. Jpn.*, **50**, 2473 (1977).
3) K. Kalyanasundaram and J. K. Thomas, *J. Am. Chem. Soc.*, **99**, 2039 (1977).
4) P. Lianos, A. K. Mukhopadhyay, and S. Georghiou, *Photochem. Photobiol.*, **32**, 415 (1980).
5) A. Nakajima, *Bull. Chem. Soc. Jpn.*, **44**, 3272 (1971).
6) A. Nakajima, *Bull. Chem. Soc. Jpn.*, **46**, 2602 (1973).
7) A. Nakajima, *J. Lumin.*, **8**, 266 (1974).
8) A. Nakajima, *J. Lumin.*, **11**, 429 (1976).
9) P. Lianos and S. Georghiou, *Photochem. Photobiol.*, **30**, 355 (1979).
10) P. Lianos and G. Georghiou, *Photochem. Photobiol.*, **29**, 843 (1979).
11) A. Nakajima, *Spectrochim. Acta, Part A*, **30A**, 860 (1974).
12) A. Nakajima, *Spectrochim. Acta, Part A*, **38A**, 693 (1982).

Thermodynamic Study on Solvent Extraction of Sodium and Potassium Picrates by Benzo-15-crown-5

Yasuyuki TAKEDA

Department of Chemistry, Faculty of Science, Chiba University, Yayoi-chō, Chiba 260

(Received August 20, 1982)

Synopsis. In order to obtain enthalpy and entropy changes for extraction of sodium and potassium picrates by benzo-15-crown-5 (B15C5) between benzene and water, the overall extraction equilibrium constants for the 1:1:1 complexes of B15C5 with the salts were determined at various temperatures. The enthalpy and entropy changes for both the systems are all large and negative.

For the evaluation of complexing ability of a crown ether for various metal ions, solvent extraction is a facile and useful method. Many overall extraction equilibrium constants for various crown ether–metal ion systems have been reported up to date. In some of these works,[1-4] the role of crown ether in the extraction process has been discussed in detail by analyzing the overall extraction equilibrium constant on the basis of constituent equilibria: the stability and extractability of crown ether–metal ion complex, and the distribution coefficient of crown ether itself. For further investigation on the role of crown ether in the extraction process, it is very important to obtain enthalpy and entropy changes for the extraction reaction of a crown ether with a metal ion. However, there is very little data on enthalpy and entropy changes.[5,6]

In the present study, in order to obtain enthalpy and entropy changes for the extraction of sodium and potassium picrates by benzo-15-crown-5 (B15C5) between benzene and water, the overall extraction equilibrium constants for the 1:1:1 complexes of B15C5 with the salts have been determined at various temperatures.

Experimental

The method of purification of B15C5 (Merck Japan Ltd.) has been described in a previous paper.[7] Concentrations of alkali metal hydroxides and picric acid solutions were determined by means of acid and basic titrations, respectively. Analytical-grade benzene was washed twice with distilled water. A benzene phase of B15C5 (1.9×10^{-4}—3.5×10^{-3} M; 1 M = 1 mol dm^{-3}), and an aqueous phase of the alkali metal hydroxide (4.6×10^{-3}—1.4×10^{-2} M) and picric acid ($(3.2—4.1)\times10^{-3}$ M) in a stoppered glass tube (30 ml) were shaken in a thermostated water bath for 40 min and centrifuged. The initial volume of each phase was 10 ml in all cases. Extractions were conducted at pH 11.1—11.8. The picrate in the benzene phase was back-extracted into 8 ml of 0.01 M NaOH aqueous solution, and the picrate concentration was determined at 356 nm by means of a Shimadzu UV-200 spectrophotometer ($\varepsilon=1.45\times10^{4}$ cm^{-1} M^{-1}). In control experiments, there was no detectable extraction in the absence of B15C5. Extractions for sodium and potassium picrates by B15C5 were conducted at 25, 28, 31, 34, and 37 ± 0.3 °C, and 19, 22, 25, 28, and 31 ± 0.3 °C, respectively.

Results

When an aqueous solution of alkali metal ion (M^+) and picrate ion (A^-) and a benzene solution of crown ether (L) are equilibrated, the equilibrium constants may be defined by

$$K_{ex} = [MLA]_o/[M^+][L]_o[A^-], \quad (1)$$

$$K_{D,L} = [L]_o/[L], \quad (2)$$

$$K_{ML} = [ML^+]/[M^+][L], \quad (3)$$

$$K_{ex'} = [MLA]_o/[ML^+][A^-], \quad (4)$$

where the subscript "o" and the lack of subscript designate the organic and aqueous phases, respectively. Thus, K_{ex} can be written as

$$K_{ex} = K_{ML}K_{ex'}K_{D,L}^{-1}. \quad (5)$$

The distribution ratio of the alkali metal may be represented by

$$D = [MLA]_o/([M^+]+[ML^+]). \quad (6)$$

In the case of $[M^+]\gg[ML^+]$, Eq. 6 becomes

$$D = K_{ex}[L]_o[A^-]. \quad (7)$$

$\mathrm{Log}(D/[A^-])$ *vs.* $\log[L]_o$ plots show a linear relationship with a slope of 1 in every case. This indicates that B15C5 forms a 1:1 complex with the alkali metal ion. The values of $[L]_o$ and $[A^-]$ in Eq. 7 were calculated by

$$[L]_o = [L]_t - [MLA]_o, \quad (8)$$

$$[A^-] = [HA]_t - [MLA]_o, \quad (9)$$

where the subscript "t" denotes the total concentration.

As can be seen from Fig. 1, the $\log K_{ex}$ *vs.* T^{-1} plots for NaA– and KA–B15C5 systems show a linear relationship. The enthalpy change ($\Delta H°$) and the

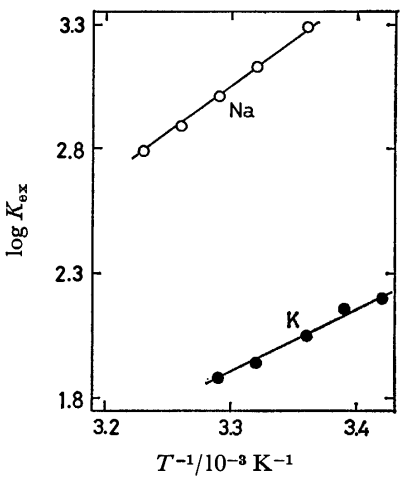

Fig. 1. $\log K_{ex}$ *vs.* T^{-1} plots for sodium picrate- and potassium picrate–B15C5 systems.

Table 1. Thermodynamic quantities

Temp/°C	$\log K_{ex}$	
	Na(B15C5)A	K(B15C5)A
19	—	2.26
22	—	2.16
25	3.29	2.05
28	3.13	1.94
31	3.01	1.88
34	2.89	—
37	2.79	—

	Na(B15C5)A	K(B15C5)A
$\Delta G°$/kJ mol^{-1} (at 25 °C)	−19	−12
$\Delta H°$/kJ mol^{-1}	−74	−50
$T\Delta S°$/kJ mol^{-1} (at 25 °C)	−55	−38

entropy change ($\Delta S°$) were calculated from these data by using the following equations: $\Delta G° = -RT\ln K_{ex}$ and $\Delta G° = \Delta H° - T\Delta S°$ where $\Delta G°$ denotes the free energy change. These thermodynamic quantities are listed in Table 1.

Discussion

It may be seen from Table 1 that overall extraction reactions for B15C5 are all exothermic and the $\Delta S°$ values are all negative. For both Na^+– and K^+–B15C5 systems, the very great $-\Delta H°$ value is canceled by the very large $-T\Delta S°$ value, resulting in the small $-\Delta G°$ value and the relatively low preference of Na^+ over K^+. A similar tendency as mentioned above is found in extractions for sodium and potassium picrates–dibenzo-18-crown-6 systems (benzene/water).[5] It is interesting that the $-\Delta H°$ and $-\Delta S°$ values of Na^+, which fits much more closely into the B15C5 cavity than K^+, are much greater than those of K^+.

The values of enthalpy ($\Delta H°_{ML}$) and entropy changes ($\Delta S°_{ML}$) for the complexation reaction of B15C5 with K^+ in H_2O are −9.75 kJ mol^{-1} and −26 J K^{-1} mol^{-1}, respectively,[8] both the $\Delta H°_{ML}/\Delta H°$ and $\Delta S°_{ML}/\Delta S°$ ratios being only 0.2. Thus, the contributions of $\Delta H°_{ML}$ and $\Delta S°_{ML}$ to $\Delta H°$ and $\Delta S°$ are small, respectively. Since the $K_{D,L}$ value scarcely varies (19—21) in the range 19—37 °C, the contributions of enthalpy and entropy changes of this process to $\Delta H°$ and $\Delta S°$ may be very small, respectively. It thus appears that, for the KA–B15C5 system, the magnitudes of $\Delta H°$ and $\Delta S°$ are determined primarily by those of enthalpy and entropy changes of the process related to Eq. 4, respectively.

The author wishes to thank Professor Shizuo Fujiwara, Chiba University, for his valuable discussion.

References

1) Y. Takeda and H. Katō, *Bull. Chem. Soc. Jpn.*, **52**, 1027 (1979).
2) T. Sekine, K. Shioda, and Y. Hasegawa, *J. Inorg. Nucl. Chem.*, **41**, 571 (1979).
3) Y. Takeda and H. Gotō, *Bull. Chem. Soc. Jpn.*, **52**, 1920 (1979).
4) Y. Takeda and F. Takahashi, *Bull. Chem. Soc. Jpn.*, **53**, 1167 (1980).
5) A. Sadakane, T. Iwachido, and K. Tōei, *Bull. Chem. Soc. Jpn.*, **48**, 60 (1975).
6) K. Kimura, T. Tsuchida, T. Maeda, and T. Shono, *Talanta*, **27**, 801 (1980).
7) Y. Takeda, Y. Wada, and S. Fujiwara, *Bull. Chem. Soc. Jpn.*, **54**, 3727 (1981).
8) R. M. Izatt, R. E. Terry, D. P. Nelson, Y. Chan, D. J. Eatough, J. S. Bradshaw, L. D. Hansen, and J. J. Christensen, *J. Am. Chem. Soc.*, **98**, 7626 (1976).

Wetting of Coal by Aqueous Surfactant Solutions

Kunio Esumi,* Kenjiro Meguro, and Hidemasa Honda

Department of Applied Chemistry and Institute of Colloid and Interface Science, Science University of Tokyo, Kagurazaka, Shinjuku-ku, Tokyo 162

(Received September 3, 1982)

Synopsis. The rates of wetting of coals of various carbon content by aqueous anionic surfactant solutions were measured. It was found that the rates of wetting increased with increasing concentration of the anionic surfactant in solution and further, the addition of electrolyte significantly promoted the rates of wetting. The presence of the electrolyte on the surface of coal after wetting was confirmed by the zeta potential measurement.

Wettability of coal[1-3] has been investigated to understand mechanisms of coal flotation, coal dust suppression, and coal–oil mixture. Recently, a coal–water mixture has been receiving attention as a fuel source. Thus, extensive studies have been made of the nature of adsorption of surfactants[4] on coal to understand stability of coal–water mixture. Glanville and Wightman[5] have reported that rates of wetting of coal by aqueous surfactant solution are influenced by addition of dipositive metal ions. Acceleration of wettability of coal into aqueous solution is one of the factors necessary to prepare a stable coal–water mixture.

In this note, the wetting behavior of coals of various carbon content by aqueous anionic surfactant solution is discussed by measuring the wetting rates, the zeta potential of the coals and the surface tension of aqueous anionic surfactant solutions.

Experimental

Materials. The coals used in this study were Yallourn, Taiheiyo, Miike, and Hon-gay which were sieved between 60 and 100 mesh. Their pertinent properties have been described elsewhere.[4]

Sodium 1,2-bis(2-ethylhexyloxycarbonyl)ethanesulfonate (Aerosol OT), sodium 1,2-bis(2-methylpentyloxycarbonyl)ethanesulfonate(Aerosol MA), and sodium 1,2-bis[diamyl(mixture of 2-methylbutyl and 3-methylbutyl)oxycarbonyl] ethanesulfonate (Aerosol AY) were obtained from the American Cyanamid Co. They were used without further purification. The metal salts used were obtained as laboratory grade reagents.

The water used was purified by passing through Milli-Q Reagent-Grade Water Systems until its specific conductivity fell below $10^{-7}\,\Omega^{-1}\,cm^{-1}$.

Measurements. To estimate rates of wetting of coal, sink times were measured for 0.30 g of coal gently deposited on the surface of the aqueous surfactant solution. Tests were carried out in a room maintained at 25±2 °C. The time taken for the last trace of unwetted coal particles to break through the surface of the aqueous surfactant solution was measured with a stopwatch. The average value of four or five run was taken as the final sink time. The standard deviation was 15%. The rate of wetting of coal was evaluated as the surface area of coal wetted per second.

The zeta potential of coal particles after exposure to the aqueous surfactant solution was measured using a Pen Kem Laser 500 Zeta Potential. The surface tension of the solution was measured using a Wilhelmy-type tensiometer at 25 °C.

Results and Discussion

Figure 1 shows the rates of wetting of coals of various carbon content by the aqueous surfactant solutions. It is seen that the rates of wetting are increased with the concentration of the surfactant. Furthermore, it is noteworthy that the behavior of rates of wetting of coals of various carbon content by Aerosol OT is different from those by Aerosol MA and Aerosol AY. Although it is known that the rate of wetting is a function of surface tension of the solution,[6] the surface tensions of the three Aerosol surfactant solutions were almost the same at each cmc in this study. Here, each cmc was as follows: Aerosol OT, 2.76; Aerosol MA, 15; Aerosol AY, 34 mmol dm^{-3}. Therefore, the differences among the three surfactants might be explained by diffusion rates and orientation of surfactants at the coal surfaces rather than by a surface tension effect. The surfactants having short-chain hydrophobic groups, such as Aerosol MA and Aerosol AY, are generally[6] believed to have faster rates of diffusion to and orientation at coal surfaces than that with long-chain hydrophobic groups like Aerosol OT. Especially, such a difference in the rates of wetting is apparent on relatively high carbon content coals, such as Miike and Hon-gay.

Since addition of electrolyte to the aqueous surfactant solution would be expected to have a considerable effect on the wetting of coals, the effect of electrolyte on the rate of wetting of coals was examined. The results are depicted in Fig. 2. In Aerosol OT-electrolyte system, the addition of electrolyte to Aerosol OT promoted the rates of wetting of all the coals tried. In particular, the addition of strontium chloride gave the most effective result. Similar results were obtained for systems of Aerosol MA-electrolyte and Aerosol AY-electrolyte. The addition of a tripositive electrolyte, such as lanthanum nitrate, was not so effective on the rate of wetting of coals as that of

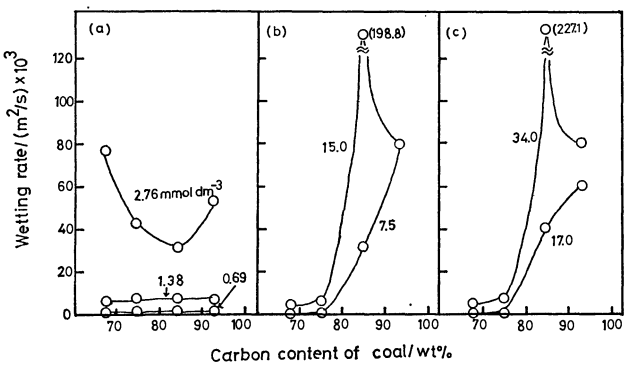

Fig. 1. The rates of wetting of coals with various carbon content by the aqueous surfactant solutions.
(a): Aerosol OT, (b): Aerosol MA, (c) Aerosol AY.

Table 1. The surface tensions of aqueous aerosol surfactant solutions with and without electrolyte

Sample(concn/mmol dm^{-3})	Surface tension / dyn cm^{-1} (at 25 °C)
Aerosol OT(0.69)	39.0
Aerosol OT(0.69)-$SrCl_2$(0.26)	25.5
Aerosol OT(0.69)-$La(NO_3)_3$(0.26)	26.5
Aerosol OT(0.69)-$ZnCl_2$(0.26)	27.6
Aerosol OT(0.69)-$CaCl_2$(0.26)	27.7
Aerosol OT(0.69)-$MgCl_2$(0.26)	28.0
Aerosol MA(7.5)	41.7
Aersol MA(7.5)-$La(NO_3)_3$(0.26)	31.4
Aerosol MA(7.5)-$SrCl_2$(0.26)	37.5
Aerosol AY(34)	32.6
Aerosol AY(34)-$La(NO_3)_3$(0.26)	28.0
Aerosol AY(34)-$SrCl_2$(0.26)	32.3

a dipositive electrolyte. The surface tensions of Aerosol surfactants with and without electrolyte are tabulated in Table 1. The addition of electrolyte, particularly strontium chloride, reduced the surface tension of Aerosol OT surfactant significantly. Thus, the electrolyte that decreased the surface tension of the surfactant solution increased its rate of wetting of coal. In Aerosol MA and Aerosol AY systems, the rates of wetting of coals were promoted by the addition of electrolyte, although the ratio of electrolyte to surfactant is different for each system.

Further, to elucidate the interaction of coal surfaces and the surfactant with and without the electrolyte, the zeta potentials of coal particles after their exposure to the solutions were measured. The results are shown in Fig. 3. The zeta potential of coal particles after the exposure to the Aerosol surfactant solution containing electrolyte was less negative than that in the Aerosol surfactant solution alone. This implies that dipositive or tripositive ions are present on the coal surface. Accordingly, it follows that the adsorption of dipositive or tripositive ions promotes the rate of wetting of coal by Aerosol surfactant solution.

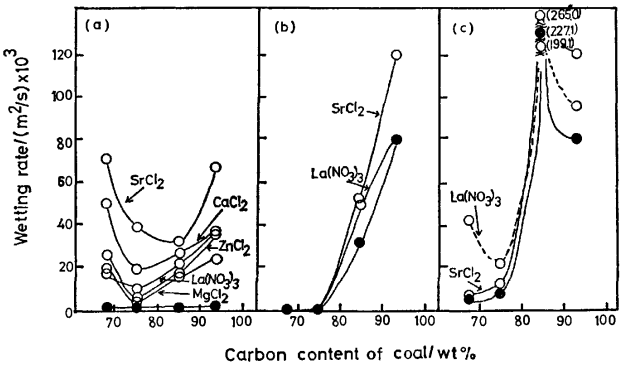

Fig. 2. The rates of wetting of coals with various carbon content by the aqueous surfactant solutions with (○) and without (●) electrolyte. The concentration of electrolyte is 0.26 mmol dm^{-3}.
(a): Aerosol OT, 0.69 mmol dm^{-3}, (b): Aerosol MA, 7.5 mmol dm^{-3}, (c): Aerosol AY, 34 mmol dm^{-3}.

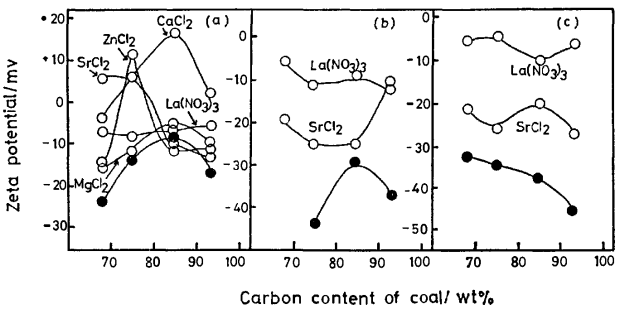

Fig. 3. The zeta potentials of coal samples shown in Fig. 2.

References

1) T. Murata, *Nippon Kogyo Kaishi*, **94**, 547 (1980).
2) J. O. Glanville and J. P. Wightman, *Fuel*, **59**, 557 (1980).
3) D. T. Hornsby and J. Leja, *Colloids and Surfaces*, **1**, 425 (1980).
4) K. Esumi, K. Meguro, and H. Honda, *Bull. Chem. Soc. Jpn.*, **55**, 3021 (1982).
5) J. O. Glanville and J. P. Wightman, *Fuel*, **58**, 819 (1979).
6) M. J. Rosen, "Surfactants and Interfacial Phenomena," Wiley-Interscience (1978).

Zeta Potentials of Metal Oxides Coated with Titanate Coupling Agents in Aqueous Solution

Kunio Esumi*, Toshio Suzuki, and Kenjiro Meguro

Department of Applied Chemistry and Institute of Colloid and Interface Science, Science University of Tokyo, Kagurazaka, Shinjuku-ku, Tokyo 162

(Received October 19, 1982)

Synopsis. The zeta potentials of metal oxide surfaces coated with titanate coupling agents were measured as a function of pH in the suspensions. The treatment by titanium(IV) isopropoxide tris(2-methylheptadecanoate) on the metal oxides, such as iron oxide, titanium dioxide, and silica, provided lower zeta potential values over a wide pH range than those of untreated samples. On the other hand, the treatment of the samples by titanium(IV) tris[2-(2-aminoethylamino)ethoxide] isopropoxide rendered the surfaces more cationic. Further, it was found that the titanate coupling layer was almost removed from the surfaces after one day they were immersed in aqueous solution.

Silane coupling agents[1,2] for modifying many fillers have been used to improve the bonding between reinforcements and polymer matrix. Recently, as coupling agents, titanate coupling agents[3] have been attractive for chemical bridges between the interface of an inorganic substrate and the polymer. It is believed that titanate coupling agents form a monomolecular layer on the inorganic substrate providing polymer compatibility and a reduction in the water of hydration and air voids in the inorganic substrate. Accordingly, it seems important to elucidate the interaction between the surface of inorganic substrate treated with titanate coupling agents and aqueous solution.

For this purpose, in this work, the zeta potentials of inorganic substrates treated with titanate coupling agents were measured as a function of pH in aqueous solution.

Experimental

Materials. Two titanate coupling agents, such as titanium(IV) isopropoxide tris(2-methylheptadecanoate) and titanium(IV) tris[2-(2-aminoethylamino)ethoxide] isopropoxide, were kindly supplied by Ajinomoto Co., and were used without further purification. Metal oxides employed were titanium dioxide(rutile type), iron oxide, and silica supplied by Teikoku Chemicals, Titan Chemicals, and Nippon Aerosil Co, respectively.

Procedure. Coating of titanate coupling agents on metal oxide surfaces was carried out with about 3 wt% solution of titanate coupling agents in an organic solvent. For titanium(IV) isopropoxide tris(2-methylheptadecanoate), hexane was used as a solvent and 2-propanol for titanium(IV) tris[2-(2-aminoethylamino) ethoxide] isopropoxide. Then, the metal oxide was added and stirred into the titanate coupling agent solution for 20 min at room temperature. The metal oxide coated with the titanate coupling agent was collected and dried in an oven at 80 °C for 20 min.

Measurements of zeta potential for the metal oxides before and after their titanate coupling agent treatments were made using a Pen Kem Laser 500 Zeta Potential. The pH of the suspension was adjusted with HCl or NaOH.

Results and Discussion

When metal oxides are treated with titanate coupling agents consisting hydrophilic and hydrophobic groups, it is considered that the hydrophilic group of the coupling agent is oriented to the surface of metal oxide and as a result, the treated surface shows hydrophobicity due to exposure of hydrophobic group to outward.

The stability of untreated and titanate coupling agent treated metal oxide suspensions was compared visually in small beakers. The untreated metal oxides were readily dispersible in aqueous solution by gentle shaking, while the treated metal oxides were initially aggregated and floated on the surface of water. However, they dispersed when the suspensions were treated in an ultrasonic cleaning bath.

Figure 1 depicts zeta potentials of untreated and

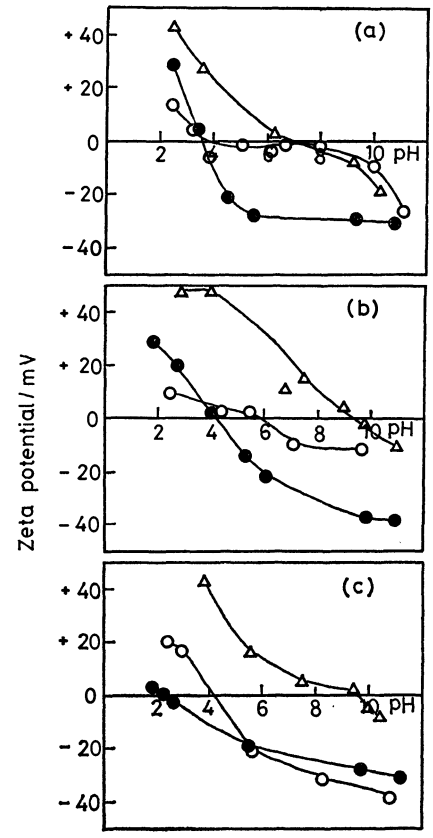

Fig. 1. Zeta potentials of untreated and titanate coupling agents treated metal oxides as a function of pH in suspensions: (a) iron oxide, (b) titanium dioxide (rutile type), (c) silica; (●) untreated, (○) titanium-(IV) isopropoxide tris(2-methylheptadecanoate), (△) titanium(IV) tris[2-(2-aminoethylamino)ethoxide]isopropoxide.

titanate coupling agents treated metal oxides as a function of pH in aqueous suspensions. It can be seen from Fig. 1 that the magnitude of zeta potentials for iron oxide and titanium dioxide treated with titanium-(IV) isopropoxide tris(2-methylheptadecanoate) was smaller in a pH range from 2 to 12 than that of untreated samples. In case of silica, the zeta potential treated with titanium(IV) isopropoxide tris(2-methylheptadecanoate) showed a similar behavior as a function of pH to that of untreated samples. This result may suggest that titanium(IV) isopropoxide tris(2-methylheptadecanoate) does not provide a strong coating on the surface of silica. On the other hand, the zeta potentials of all the samples treated with titanium-(IV) tris[2-(2-aminoethylamino)ethoxide] isopropoxide were much positively over a wide pH range than those of untreated samples. As a result, the zero point of charge (ZPC) of their treated samples shifted to much higher values. Similar behavior has been observed[4] in change of the zeta potential of metal oxides treated with aminosilane coupling agents.

It is also important to study the stability of deposited titanate coupling agent layers on the metal oxides in aqueous solution. For this purpose, the samples treated with two kinds of titanate coupling agents were allowed to stand for one day in aqueous solution at a some pH value and then the zeta potential was measured. The results are given in Fig. 2. The zeta potentials of metal oxides treated with the titanate coupling agents in the suspensions after one day became near the value of the untreated metal oxides as a function of pH in the suspensions. These results indicate that the titanate coupling agent layer was almost removed from the metal oxide surface after one day it was immersed in aqueous solution. Thus, it is suggested that the attachment of titanate coupling agent layer on the surface of metal oxide is not strong in aqueous solution. On the other hand, it has been reported[4] that the zeta potentials of iron oxide, titanium dioxide(rutile type), and silica treated with aminosilane coupling agents were not significantly changed even after one day storage in aqueous solution at a some pH value.

Thus, zeta potential measurement is a useful method to elucidate surface properties of metal oxides treated with titanate coupling agents.

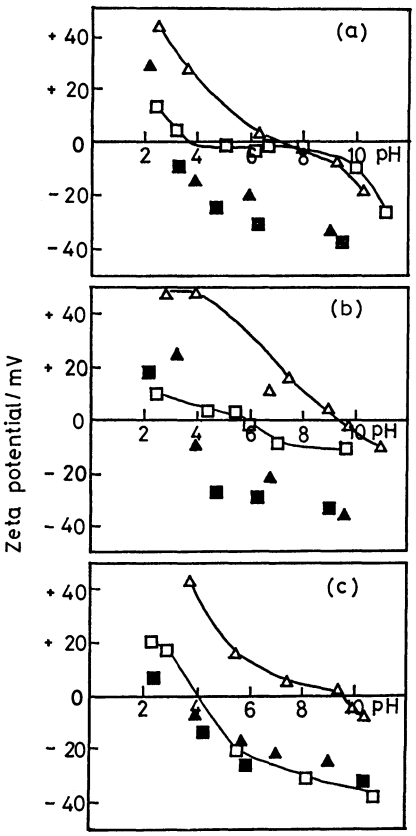

Fig. 2. Effect of storage on zeta potential of metal oxides treated with titanate coupling agents as a function of pH in suspensions: (a) iron oxide, (b) titanium dioxide(rutile type), (c) silica; (□) titanium(IV) isopropoxide tris(2-methylheptadecanoate), (△) titanium(IV) tris[2-(2-aminoethylamino)ethoxide]isopropoxide. Open mark refers to immediate measurement and closed mark to measurement after one day.

References

1) P. W. Erickson and E. P. Plueddemann, "Composite Materials," Academic Press, New York (1974), Vol. 6, Chap. 6, p. 1.

2) M. R. Rosen, *J. Coat. Technol.* **50**, 70 (1978).

3) Bulletin KR-0278=7 Rev. #2, "Titanate Coupling Agents for Filled Polymers," Kenrich Petrochemicals, Inc.

4) K. Esumi and K. Meguro, *Bull. Chem. Soc. Jpn.*, **56**, 331 (1983).

Laser Stark Spectroscopy of AsH_3 Using 9.4 and 10.6 μm CO_2 Laser

Kuniaki NAKAGAWA,† Yoshifumi UEDA, and Kozo KUCHITSU*

Department of Chemistry and Department of Physics, Faculty of Science, The University of Tokyo, Hongo, Bunkyo-ku, Tokyo 113

(Received October 27, 1982)

Synopsis. Perturbation-allowed transitions of the ν_2 and ν_4 bands of AsH_3 were observed. About 100 Stark components were assigned to six $\Delta(k-l)=0$, six $\Delta(k-l)=\pm3$, and three $\Delta(k-l)=\pm6$ transitions. The Stark patterns and hyperfine splittings were used for confirming the assignment.

Since AsH_3 is a nearly spherical top, the rotational energy levels with various k values for a given J value are very close to one another. This near degeneracy increases the importance of various interactions which are usually insignificant, and it enables observation of the transitions that follow the selection rule, $\Delta(k-l)=\pm3n$ $(n=1,2,\cdots)$. The $\Delta(k-l)=\pm3$ transitions have been observed in the rotational spectrum of AsH_3 in the vibrational ground state.[1-3] In the vibrationally excited states, accidental degeneracies of rotation-vibration levels of the same rovibrational symmetry are also caused by the first-order Coriolis effect and possibly by the near degeneracy of vibrational levels. Transitions with $\Delta(k-l)=\pm3$ in the ν_1 and ν_3 bands of AsH_3 have thus been observed by infrared spectroscopy.[4] Recently, Scappini and Oka[5] observed and assigned the $\Delta(k-l)=\pm3$ transitions in the ν_2 and ν_4 bands by infrared-radiofrequency double resonance. The ν_2 and ν_4 bands are much more complicated than the ν_1 and ν_3 bands by the strong Coriolis interaction between them and are difficult to be assigned definitely. However, they assigned the transitions on the basis of the observed hyperfine patterns.

In the present note, laser Stark spectroscopy was used to observe and assign the $\Delta(k-l)=\pm3n$ transitions in the ν_2 and ν_4 bands. The present assignment has been confirmed by well-resolved Stark splitting patterns. The sensitivity of the spectrometer[6] was such that a number of weak forbidden transitions became detectable.

The Stark spectra were observed up to the field strength of 300 esu (90 kV/cm) with 9.4 and 10.6 μm band CO_2 laser following the $\Delta m_J=0$ and ±1 selection rules. About 1000 Stark components were observed, and about 100 components were assigned to those of 15 transitions. The assigned transitions are listed in Table 1.

The Stark shift for a certain level, J, k, m_J, of AsH_3 is mainly caused by the first-order effect. The first-order Stark shift, $\Delta\nu$, of the J', k', $m_J'\leftarrow J''$, k'', m_J'' transition frequency is given by

$$\Delta\nu = -(\varepsilon/h)[\mu' k' m_J'/J'(J'+1) - \mu'' k'' m_J''/J''(J''+1)], \quad (1)$$

where μ is the electric dipole moment and ε is the applied electric field. The relative signs of k', m_J', k'', and m_J'' are especially important for the assignment of the $\Delta(k-l)\neq0$ transitions. For simple designation of their relative signs, quantum numbers K' for $|k'|$, L for $(k'l)/K'$, and K'' for $(k'k'')/K'$ are used in the present note. Assignments of the transitions were confirmed by the following two criteria: First, all the observed patterns of the Stark components, $\Delta m_J=0$ or $\Delta m_J=\pm1$, must be explained consistently. Second, if a splitting is observed, it must agree with that estimated. The hyperfine splittings were calculated by using a formula for the strong-field case[7] with reported eQq values.[5,8]

It was thus possible to confirm the assignment of the $\Delta(k-l)=\pm3$ transitions by taking into account the relative signs of the quantum numbers mentioned above as in the rotational $\Delta k=\pm3$ transitions.[1] All the components, for which the splittings were estimated to exceed their Doppler widths, were actually resolved with splittings consistent with the estimations. Two of the three observed $\Delta(k-l)=\pm6$ transitions, which involve the $|k-l|=3$ levels, need further consideration in regard to the A_1-A_2 splitting of the levels. However, it was possible to explain their Stark patterns approximately by assuming the A_1-A_2 splitting to be zero (*i.e.*, by simply applying Eq. 1). This assumption is valid for the case in which the magnitude of the Stark shift of the levels is considerably larger than that of the A_1-A_2 splitting.

The difference between the Stark shift of the $\Delta(k-l)=\pm6$ transition and that of the normal $\Delta(k-l)=0$ transition is given by Eq. 1 with the relative signs of k', k'', l', and l'' chosen adequately. This equation shows that the magnitude of the Stark shift of the former transition is larger than that of the latter; this facilitates observation of perturbation-allowed transitions by laser Stark spectroscopy.

The Stark shifts of the observed transitions, given in Table 1, were calculated by diagonalization of a matrix, in which Coriolis interaction between ν_2 and ν_4 was taken into account, by use of the molecular constants determined by Olson *et al.*[4] for the ground state and by Sarka *et al.*[9] for the ν_2 and ν_4 states. However, the results were essentially equal to those calculated by the first-order equation (1). The dipole moments for the ν_2 and ν_4 states were assumed to be equal to that for the ground state, $\mu=0.22$ D.[1] Errors in the calculated shifts are mainly caused by the uncertainty in these values. The total uncertainty of the Stark shift is estimated to be less than 10% of the shift itself. As for the zero-field transition frequencies of the two $\Delta(k-l)=\pm6$ transitions mentioned above, neglect of the A_1-A_2 splitting is not adequate, because the magnitude of the splitting can be larger than the uncertainty in the Stark shift. Since the magnitude of the A_1-A_2 splitting is not exactly known, only approximate first-order values derived from the assumption that there is no A_1-A_2 splitting are listed

† Present address: Department of Physics, Toyama University, Gofuku, Toyama 930.

Table 1. Assigned transitions for the ν_2 and ν_4 bands of AsH_3

Transition[a]						Laser line[b]	Stark component[c]		Stark field	Calculated shift	Zero-field transition
J'	K'	L	J''	K''	$\Delta(k-l)$		$M \leftarrow M''$		esu	cm^{-1}	cm^{-1}
2	1	0	1	1	0	10P (44)	0	1	192.4	−0.106	920.935(11)[e]
5	4	0	4	4	0	10P (22)	3	4	200.7[d]	0.089	942.295(9)
6	5	0	5	5	0	10P (14)	4	5	47.5[d]	−0.019	949.498(2)
5	3	1	6	2	0	10R (4)	5	4	146.9	−0.049	964.818(5)
5	4	−1	5	5	0	10R (44)	5	5	110.6[d]	0.037	989.610(4)
9	9	1	9	8	0	9P (44)	9	9	241.8	−0.026	1023.216(3)
6	1	0	5	−2	±3	10P (18)	6	5	43.0	0.023	945.957(2)
8	6	1	9	2	±3	10P (18)	8	8	275.2[d]	−0.150	946.131(15)
8	0	0	7	3	±3	10P (4)	7	7	249.0	−0.104	957.904(10)
6	5	1	5	1	±3	9P (10)	6	5	126.9[d]	0.078	1055.548(8)
7	3	1	6	5	±3	9R (8)	6	6	230.6[d]	−0.105	1070.567(10)
8	6	1	7	2	±3	9R (12)	8	7	131.6[d]	0.062	1073.217(6)
7	5	1	8	−2	±6	10P (10)	7	8	197.9	−0.186	953.066(19)
4	2	−1	5	−3	±6	10P (4)	4	5	108.9		(957.91)[f]
3	2	−1	4	−3	±6	10R (4)	3	4	59.8		(964.70)

a) Transitions with $L=0$ and $L=\pm1$ correspond to the ν_2 (A_1) and ν_4 (E) bands, respectively. b) 10: 10.6 μm CO_2 laser, 9: 9.4 μm CO_2 laser. c) A typical $M' \leftarrow M''$ component is listed for each transition. d) Hyperfine splitting is resolved. The listed field values correspond to the centers of the doublets. e) Number in parentheses represents estimated uncertainty in units of 10^{-3} cm^{-1}. f) Estimated from the assumption that there is no A_1-A_2 splitting.

in Table 1.

The obtained zero-field transition frequencies were analyzed in combination with the reported infrared frequencies.[9] The results of a least-squares analysis were essentially the same as that obtained by the infrared data alone. A further analysis of the strong Coriolis interaction between ν_2 and ν_4 and a larger number of accurate spectroscopic data are needed for a more precise determination of the molecular constants. We note that there is no overlapping between the transitions assigned by Scappini and Oka[5] and those assigned in the present study. This is probably because of the difference in the characteristic ranges of applicability of these techniques; radiofrequency-infrared double resonance is more suitable for observing transitions that are relatively close to the laser frequencies, whereas laser Stark patterns can be resolved and assigned more easily for transitions that are separated farther from the laser lines. In this context, laser Stark spectroscopy provides data complementary to RF-IR double resonance spectroscopy.

The authors wish to thank Professor Takeshi Oka for his helpful comments.

References

1) F. Y. Chu and T. Oka, *J. Chem. Phys.*, **60**, 4612 (1974).
2) D. A. Helms and W. Gordy, *J. Mol. Spectrosc.*, **69**, 473 (1978).
3) A. V. Burenin, V. P. Kazakov, A. F. Krupnov, A. A. Mel'nikov, and S. M. Shapin, *J. Mol. Spectrosc.*, **94**, 253 (1982).
4) W. B. Olson, A. G. Maki, and R. L. Sams, *J. Mol. Spectrosc.*, **55**, 252 (1975).
5) F. Scappini and T. Oka, *J. Mol. Spectrosc.*, **85**, 390 (1981).
6) Y. Ueda and K. Shimoda, "Proceedings of the Second Laser Spectroscopy Conference," ed by S. Haroche, J. C. Pebay-Peyroula, T. W. Hänsch, and S. E. Harris, Springer-Verlag, Berlin (1975), p. 186.
7) W. Gordy and R. L. Cook, "Microwave Molecular Spectra," Interscience (1970), p. 317.
8) P. Helminger, E. L. Beeson, Jr., and W. Gordy, *Phys. Rev. A*, **3**, 122 (1971).
9) K. Sarka, D. Papoušek, and K. N. Rao, *J. Mol. Spectrosc.*, **37**, 1 (1971).

Production of Hydrogen by Photochemical Splitting of Water Using Diammonium Tetrathiomolybdate as Photocatalyst

A. Bhattacharya, J. Basu, K. Das, R. G. Bhattacharyya, A. B. Chatterjee, and K. K. Rohatgi-Mukherjee*

Department of Chemistry, Jadavpur University, Calcutta-32, India

(Received December 11, 1981)

Synopsis. Hydrogen gas is generated at the cathode when the anode compartment of a photogalvanic cell anode/$(NH_4)_2MoS_4$(aq, satd.)//5 M HCl (aq)/cathode is illuminated. The photocurrent generated rises slowly with time and reaches a limiting value. A mechanism is suggested involving the conversion of Mo(VI) to Mo(V) and the formation of OH radicals, as evidenced by development of paramagnetism on irradiation. Although the photocatalyst is susceptible to hydrolysis, it can be easily regenerated by passing H_2S.

Transition metal complexes are known to sensitize photodissociation of water to produce hydrogen, a potential fuel. Recently[1] it has been shown that hexakis(alkylammonium)heptamolybdate catalyzes the photochemical splitting of water, but the efficiency of the system is very low since the photocatalyst absorbs in the UV region only. Herein is described the photogalvanic generation of hydrogen gas using diammonium tetrathiomolybdate as the photocatalyst. This compound absorbs in the visible region (λ_{max}=467.3 nm)[2] and, therefore, may be more effective from the standpoint of solar energy utilisation.

Experimental

$(NH_4)_2MoS_4$ was synthesized by following the method available in the literature[3] and was characterized by analytical, as well as spectral data.[2] The IR spectra were measured as KBr pellets using a Perkin Elmer 597 IR spectrophotometer and the UV-visible spectra were measured using a Perkin Elmer Hitachi 200 model instrument. The photocatalyst was preserved in the dark and always a freshly prepared solution was used. The photogalvanic cell consisted of two half-cells connected by a KCl-agar salt bridge. A saturated solution of $(NH_4)_2MoS_4$ was used as the photoactive anolyte and a 5 M HCl solution as the dark catholyte. A Pt-foil or a carbon rod (obtained from a flashlight dry cell) was used as the anode. The cathode was a Pt-wire which was subsequently replaced by platinized Pt and Cu wires. The H_2 gas generated at the dark cathode was collected in an inverted microburette over the cathode wire. The solutions of different pH were prepared from reagent grade NH_4Cl and NH_4OH.

The anode compartment was illuminated by a 1 kW halogen lamp, heating effect being minimised[4] by placing a saturated solution of Na_2SO_4 contained in a 10 cm thick cell, in between the compartment and the light source. The short circuit current was measured by using a Keithley model 616 digital electrometer. A Guoy type magnetic balance was used to measure the paramagnetic susceptibility generated on irradiation of the $(NH_4)_2MoS_4$ solution. A 15% (w/v) aqueous solution of $NiCl_2$, $6H_2O$ was used as the callibrant.

Results and Discussion

The photogalvanic cell can be represented as follows: anode/$(NH_4)_2MoS_4$ (aq, satd.)//5 M HCl/cathode.

On irradiation of the anode compartment hydrogen is generated at the cathode. The amount of hydrogen generation depends on the anode and cathode materials. Effect of changing the cathode material (Table 1) clearly reflects the relative ease of hydrogen evolution on platinized Pt, bright Pt, and Cu as determined by the respective overvoltage. Platinized Pt is known to be a better electrocatalyst than bright Pt for this reaction, whereas Cu is much inferior. However, the increase in the rate of hydrogen production on replacing a Pt-foil by a carbon rod of approximately the same surface area (*ca.* 7.5 sq. cm) can arise due to two different reasons: (i) Difference in the catalytic activities of carbon and Pt for the anode reaction, (ii) the active surface area of carbon may be much greater than the measured 'apparent' surface area due to its somewhat porous nature. This question is sorted out later. The quantum efficiencies of hydrogen production, as given in Table 1, are not monochromatic values and hence, can be considered as the lower limits of actual efficiencies under the given conditions. These values are based on the number of average photons in the visible range received by the anolyte solution which is measured by Reinecke's salt actinometry.[5] The quantum yield of its photoaquation has been assumed to be 0.3 over the entire visible region of the spectrum.[5]

The measurement of the short circuit current, with and without illumination, is more convenient and can provide more quantitative information regarding the mechanism of the overall process. The results are presented in Table 2. Apparently, the greater 'true' surface area of carbon seems to explain the increased efficiency of hydrogen production. Since the ratios of the dark and photo current densities of Pt and carbon are observed to be nearly the same, the effect appears not due to any difference in their catalytic activities. The data in Table 2 are based on apparent surface areas. However, a slow rise of the photocurrent to a limiting

Table 1. Effect of cathode and anode material on the rate of hydrogen generation

Anode	Cathode	Light intensity / E h^{-1}	Volume of H_2 / cm^3 h^{-1}	Quantum efficiency
Pt-foil	Bright Pt	4.8×10^{-4}	0.06	0.011
	Platinized Pt	4.8×10^{-4}	0.1	0.019
Carbon rod	Bright Pt	1.3×10^{-3}	0.25	0.017
	Platinized Pt	1.3×10^{-3}	0.5	0.034
	Copper	1.3×10^{-3}	Negligible	—

Table 2. Short circuit current densities with and without illumination

Anode	Short circuit current density/μA cm^{-2}		
	Dark	Illuminated	Photo
Pt-foil	2.0	12.0	10.0
Carbon rod	16.0	96.0	80.0

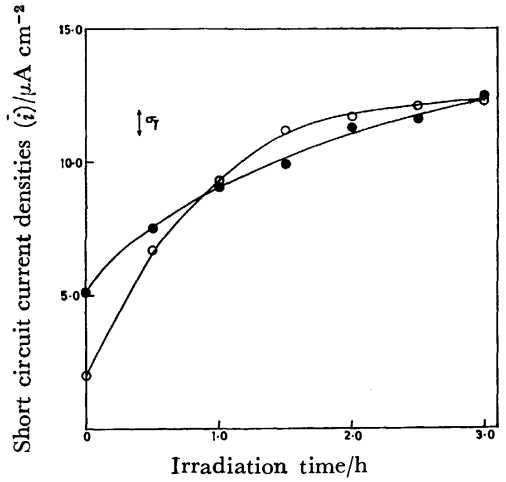

Fig. 1. Rise of short circuit current densities with irradiation time in solutions of pH 8 (○) and pH 10 (●).

value (Fig. 1) seems to indicate a competitive step in the overall reaction mechanism and a consequent slow build up of electroactive material in the anode compartment.

Following Yamase and Ikawa,[1] a sequence of steps, somewhat analogous to those in molybdate system, may be proposed:

$$(1)\ (MoS_4)^{2-} \xrightarrow{h\nu} [(MoS_4)^{2-}]^*$$

$$(2)\ [(MoS_4)^{2-}]^* + H_2O \rightarrow (MoS_3SH)^{2-} + \cdot OH$$

$$(3)\ (MoS_3SH)^{2-} + \cdot OH \rightarrow (MoS_4)^{2-} + H_2O$$

anode $(4)\ (MoS_3SH)^{2-} \rightarrow (MoS_4)^{2-} + H^+ + e$

cathode $(5)\ H^+ + e \rightarrow 1/2\ H_2$.

This sequence assumes the step (3) to be competitive with the anode reaction. Once a steady state concentration of $(MoS_3SH)^{2-}$, in which Mo is in its +5 oxidation state as against +6 state in $(MoS_4)^{2-}$, is reached the photocurrent attains its limiting value. The main water-splitting reaction according to the above mechanism is seen to be

$$H_2O \rightarrow \cdot OH + H^+ + e.$$

Carbon is known to be a better heterogeneous catalyst than Pt[6] for the combination of ·OH radicals leading to the formation of H_2O_2 and O_2 successively as follows:

$$\cdot 2HO \rightarrow H_2O_2 \rightarrow H_2O + 1/2\ O_2.$$

Consumption of ·OH radicals in this way should indirectly favour the anode reaction and thus, may be partly responsible for the observed higher efficiency of carbon than Pt apart from the surface area consideration.

Further evidence in support of the said mechanism is obtained by following the change in the magnetic property of an aqueous solution of $(NH_4)_2MoS_4$ on irradiation. On exposure to light the solution develops paramagnetism as expected if Mo(V) species and OH· radicals are produced, which reaches a limiting value after 1.5 h (Fig. 2). The striking similarity of the rise in photocurrent and growth of paramagnetism with time places the validity of our tentative reaction scheme on a firmer basis. The % conversion of $(MoS_4)^{2-}$ has been calculated from the experimental paramagnetic susceptibility measurements of the irradiated solution and the theoretically computed values for $(NH_4)_2MoS_3SH$ and ·OH taking into consideration the 'spin only' magnetic moments. The decay curves obtained after switching off the light source are also identical in pattern. However, while the photogenerated paramagnetism disappears almost completely within one and a half hour or so, much longer time, even overnight, is necessary for the short circuit current to return to its initial *i.e.*, dark value. Admittedly, at present we are unable to account for this observation quantitatively.

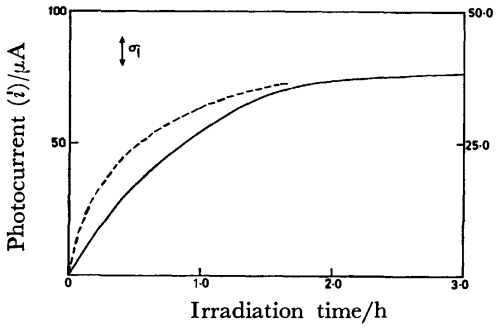

Fig. 2. Rise of photocurrent (solid curve) and growth of paramagnetism (dotted curve) with irradiation time.

All the above experiments were performed in solutions of pH around 8 as the photocatalyst is stable in alkaline solutions only. However, $(NH_4)_2MoS_4$ undergoes a slow hydrolysis in aqueous solution according to the following reaction where stepwise replacement of S atoms by O atoms occurs.

$$(NH_4)_2MoS_4 + nH_2O \rightarrow (NH_4)_2MoO_nS_{4-n} + nH_2S\ [n=1,2,3,4]$$

A part of the resulting H_2S may dissolve and dissociate to give HS^- and S^{2-} ions. Although the dissociation constants are very small in acid solutions (1.1×10^{-7} and 1×10^{-4} respectively) these may increase appreciably with the increase in pH of the solution. Thus, the redox couple H_2S/S may be established at higher pH as S has a tendency to dissolve in alkaline solution, containing excess of S^{2-}, forming polysulphides. The redox potential of the reaction

$$2H^+ + S + 2e \rightarrow H_2S$$

at pH 7 is 0.14 V.[6] We have observed that at pH 10 the dark short circuit currents have appreciably higher values leading to some amount of hydrogen production even in the dark. This seems possible in view of the negative Nernst potential calculated for the couple H_2S/S at these higher pH values. However, the photoeffect remains essentially of the same nature (Fig. 1). Due to this slow hydrolysis, occasional 'reactivations' by passing H_2S has been found to be necessary to use $(NH_4)_2MoS_4$ as a catalyst for photodissociation of water over long periods of time.

Financial support from UGC, New Delhi is gratefully acknowledged

References

1) T. Yamase and T. Ikawa, *Inorg. Chim. Acta*, **37**, L 529 (1979) and relevant references therein.

2) E. Diemann and A. Mueller, *Coord. Chem. Rev.*, **10**, 79 (1973).

3) G. Kruss, Leibigs. *Ann. Chem.*, **225**, 29 (1884).

4) S. Marks, *Solar Energy*, **25**, 255 (1980); D. R. Biswas, *ibid*, **19**, 99 (1977).

5) E. E. Wegner and A. W. Adamson, *J. Am. Chem. Soc.*, **88**, 394 (1966).

6) D. J. G. Ives and G. J. Janz, "Reference Electrodes," Academic Press (1961).

Preparation of Tetraethylammonium Hexamolybdate by the Use of Extraction Method

Katsuo MURATA,* Etsuko YAMAMOTO, and Shigero IKEDA

Department of Chemistry, Faculty of Science, Osaka University 1-1 Machikaneyama-cho, Toyonaka, Osaka 560

(Received April 30, 1982)

Synopsis. It was found that cyclohexanone selectively extracts hexamolybdate from weakly acidic solutions. Tetraethylammonium hexamolybdate was prepared as precipitate in the extracted phase by the addition of alcoholic tetraethylammonium chloride solution. This compound was confirmed to be $[(C_2H_5)_4N]_2Mo_6O_{19}$ by elementary analysis and Raman measurements.

Alkylammonium salt of hexamolybdate was at first prepared from the acidified aqueous molybdate solutions by the use of precipitation and recrystallization.[1] However, it has not been claimed that $Mo_6O_{19}^{2-}$ species is present in the aqueous molybdate solutions.[2] The authors found a small amount of hexamolybdate ion in the acidified molybdate solutions,[3] which was selectively extracted into cyclohexanone. This finding revealed a new extracting procedure for preparation of hexamolybdate salt.

Experimental

Reagent and Apparatus. A molybdenum solution was prepared from sodium molybdate $Na_2MoO_4 \cdot 2H_2O$ of analytical reagent grade and was standardized by gravimetric method of oxinate.[4] Polynuclear molybdate complexes were produced by means of acidification of this molybdate solution.

Extraction procedure is as follows. Ten ml of acidified molybdate solution and equal volume of cyclohexanone were shaken for 20 min. The molybdenum content of the aqueous solutions before and after extraction was determined by atomic absorption spectrometry.[5] Tetraethylammonium hexamolybdate was obtained as precipitate by the addition of alcoholic tetraethylammonium chloride solution to the extracted phase.

Raman spectra were taken with a JASCO Model R750 Raman Spectrophotometer with a triple monochromator by using 514.5 nm line of Ar^+ laser as the excitation source.

Results and Discussion

Heteropolymolybdic acid has been easily extracted by oxygen-containing solvents such as ethers, alcohols, esters, and ketones,[6] but isopolymolybdic acid is not extracted so well by these solvents.[7] The present authors found a good solvent for the extraction of isopolymolybdic acid. Cyclohexanone can efficiently extract yellow polynuclear molybdate from the weakly acidic solutions. The extraction curves for the acidified molybdate solutions of 100, 10, and 1 mM were shown in Fig. 1. The abscissa indicates Z value (the molar ratio of reacted H^+ ion to initially present MoO_4^{2-} ions in the polymerization reaction of molybdate) of molybdate solutions, which exhibits approximately polymerization degree of polynuclear molybdate.[2] It can be seen that each extraction curve

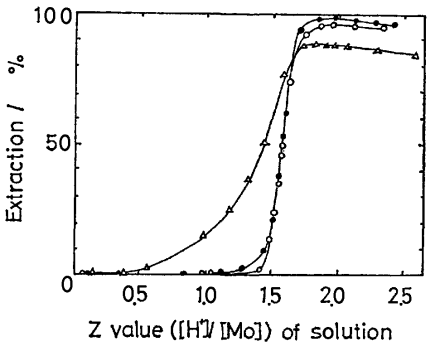

Fig. 1. Extraction curves plotted against Z value of solutions.
—○—: $[Mo]=1.0\times10^{-1}$ M, —●—: $[Mo]=1.0\times10^{-2}$ M, —△—: $[Mo]=1.0\times10^{-3}$ M.

Table 1. Elementary analysis of some extracts and the calculated values

	Found[a] (%)			Calculated (%)	
	(A)	(B)	(C)	$[(C_2H_5)_4N]_2Mo_6O_{19}$	$[(C_2H_5)_4N]_4Mo_8O_{26}$
C	16.67	16.97	17.17	16.86	7.06
H	3.51	3.55	3.57	3.54	5.88
N	2.45	2.50	2.42	2.46	3.95
Mo	49.26	50.23	49.79	50.49	54.18

a) The extracts (A), (B), and (C) were prepared from acidic solutions of pH 2.24(Z=1.58), pH 1.87(Z=1.67), and pH 0.97(Z=2.34), respectively, and then the products were precipitated as tetraethylammonium salt.

$$7\,MoO_4^{2-} + 8\,H^+ \rightleftharpoons Mo_7O_{24}^{6-} + 4\,H_2O \qquad Z = 1.14 \quad (1)$$

$$8\,MoO_4^{2-} + 12\,H^+ \rightleftharpoons Mo_8O_{26}^{4-} + 6\,H_2O \qquad Z = 1.50 \quad (2)$$

$$6\,MoO_4^{2-} + 10\,H^+ \rightleftharpoons Mo_6O_{19}^{2-} + 5\,H_2O \qquad Z = 1.67 \quad (3)$$

shows a similar range of Z value for the optimum extraction as shown in Fig. 1. It is expected from the steep rise of the extractability about Z=1.5 that octamolybdate or hexamolybdate might be concerned with this extraction. The authors could obtain a solid yellow extract as precipitate from the organic phase by the addition of 1% methanol solution of tetraethylammonium chloride. In order to clarify the extracted species, three kinds of extracts were obtained by means of the extraction from different acidic solutions followed by the precipitation as tetraethylammonium salt. Table 1 gives the results of elementary analysis. Three kinds of extracts show similar results. Moreover, these results are close to the calculated value

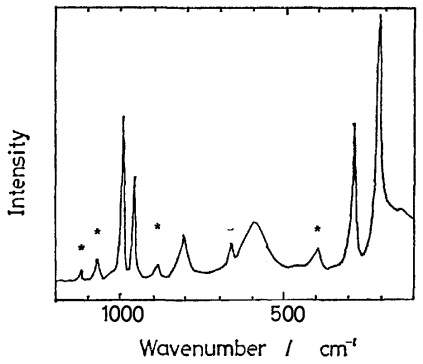

Fig. 2. Raman spectrum of the extract (B), which was obtained by extracting from pH 1.87 ($Z=1.67$) and then precipitating as tetraethylammonium salt in cyclohexanone.
*Raman lines are attributed to tetraethylammonium group.

of hexamolybdate, not octamolybdate. Therefore, these results indicate that the extracted species would be hexamolybdate. Figure 2 shows Raman spectrum of the extract (B). It exhibits four intense Raman lines at 990, 963, 286, and 210 cm^{-1}. Raman lines marked with an asterisk are attributed to tetraethylammonium group. This Raman spectrum resemble closely to that of tetrabutylammonium hexamolybdate $[(C_4H_9)_4N]_2Mo_6O_{19}$, which was previously prepared by means of precipitation from acidified aqueous solution and then recrystallization with acetone.[8] Thus the Raman spectrum also indicates that the extract (B) is hexamolybdate. Raman spectra of acidified molybdate solutions, however, are different from those of solid hexamolybdate. The authors found only small amounts of hexamolybdate ion in the weakly acidic solution ($Z=1.56$—2.05).[3] Consequently, the precipitate obtained from these solutions always contains small amounts of hexamolybdate and large amounts of other molybdate, and recrystallization is necessary to obtain pure hexamolybdate. The yield of hexamolybdate is small. In contrast to this, the extraction method by the use of cyclohexanone results in the production of hexamolybdate with a high yield. The extraction of hexamolybdate is so selective that recrystallization is not required. Since the formation of $Mo_6O_{19}^{2-}$ species is limited to a small extent in the weakly acidic solutions, a longer time of 20 minutes is needed to attain the extraction equilibrium. But this extraction method is better to obtain pure solid hexamolybdate than the previous preparative method by the use of precipitation procedure alone from the weakly acidic solution.

The authors wish to express their thanks to Professor Yukiyoshi Sasaki, the University of Tokyo, for his helpful discussions.

References

1) J. Fuchs and K. F. Jahr, *Z. Naturforsch., Teil B*, **23**, 1380 (1968).
2) K. Tytko and O. Glemser, *Adv. Inorg. Chem. Radiochem.*, **19**, 239 (1976).
3) K. Murata and S. Ikeda, *Spectrochim. Acta*, in press.
4) M. Borrel and R. Paris, *Anal. Chim. Acta*, **4**, 267 (1950).
5) H. Oguro, *Bunseki Kagaku*, **23**, 1362 (1974).
6) C. Wadelin and M. G. Mellon, *Anal. Chem.*, **25**, 1668 (1953).
7) T. Fujinaga, T. Hori, and Y. Kaneda, *Bunseki Kagaku*, **27**, 395 (1978).
8) R. Mattes, H. Bierbusse, and J. Fuchs, *Z. Anorg. All. Chem.*, **385**, 230 (1971).

Properties of Alkali-free Magnesium Phosphate Glass Membranes Containing Silver Oxide and Their Application to the Ammonia Selective Electrode

Tsuyoshi NOMURA* and Genkichi NAKAGAWA

Laboratory of Analytical Chemistry, Nagoya Institute of Technology, Gokiso-cho, Showa-ku, Nagoya 466

(Received June 7, 1982)

Synopsis. The properties of magnesium phosphate glass and the potential response of its membrane to ammonia were studied. The most suitable glass composition for the ammonia selective electrode is $5Ag_2O$–$50P_2O_5$–$40MgO$–$5Al_2O_3$. The potential-concentration curve of the electrode exhibits a slope of about 48 mV/decade for the ammonia-concentration range of (10^{-2}—10^{-6}) mol/dm^3.

Various types of alkali silicate glasses containing Al_2O_3 or B_2O_3 have been investigated as materials of the ion selective electrode, and they were used for the measurement of alkali metal ions, Ag^+, Cu^+,[1,2] and the ammonium ion.[3] The ammonia selective electrode consists of a hydrophobic gas-permeable membrane and pH electrode.[4,5] Truesdell and his co-workers[6] found that the glass containing P_2O_5 and Fe_2O_3 as the major constituents can be applied to the ion-selective electrode for alkaline earth cations. According to Eisenman's suggestion,[7] the replacement of aluminium in the sodium-almino-silicate glass by phosphorus would be expected to lead to anion-exchange properties and a response to anionic substances. This paper will describe the composition of alkali-free magnesium phosphate glasses, the durability of glasses against water, and the application of the electrode membrane to ammonia.

Experimental

Preparation of Glass Membrane. Orthophosphoric acid (85%), silver carbonate, tetramagnesium tricarbonate dehydroxide, and aluminium hydroxide were used to prepare the alkali free magnesium phosphate glasses. Mixtures of the chemicals were placed in a quartz evaporating dish and evaporated to dryness. The cake was finely powdered, it was then melted at 1350 °C for 90 min in a platinum crucible, and the melt was poured into a circular hollow of a graphite plate. The final composition of the glass usually deviates from the initial composition because of the loss of phosphoric acid by vaporization during melting.[8] From the determination of P_2O_5 as $Mg_2P_2O_7$ or $AlPO_4$ by the gravimetric method, the volatillization loss of P_2O_5 was found to be about 5 weight % of the initial orthophosphoric acid content from 45 to 55 mol% P_2O_5 glass. Therefore, under all the experimental conditions, the orthophosphoric acid content in the initial materials were established to be about 5 weight % in excess of the calculated amount. To form the electrode, disks (11—12) mm in diameter and (0.4—0.6) mm thick were cut from the glass pellet.

Measurement of the Membrane Potentials. The cell scheme used for the investigation was as follows:

SCE	0.1 mol/dm^3 $NaNO_3$	Glass membrane	Sample soln containing 5×10^{-4} mol/dm^3 NaOH	Agar bridge	0.1 mol/dm^3 $NaNO_3$	SCE
	Ion-selective electrode					

The membrane potentials for ammonia and other anions or compounds were measured in a solution containing 5×10^{-4} mol/dm^3 sodium hydroxide at pH about 10.4 at 20 °C.

TABLE 1. DURABILITY OF GLASSES AGAINST WATER

Glass composition	Solubility in water (mg mm^{-2})	Ratio
$5Ag_2O$–$50P_2O_5$–$45MgO$	3.87×10^{-3}	1.00
$5Ag_2O$–$50P_2O_5$–$40MgO$–$5Al_2O_3$	1.45×10^{-3}	0.37
$25Ag_2O$–$50P_2O_5$–$20MgO$–$5Al_2O_3$	3.11×10^{-3}	0.80
$5Ag_2O$–$50P_2O_5$–$35MgO$–$10Al_2O_3$	1.08×10^{-3}	0.28

From the dissociation constant[9] of the ammonium ion, $K=a_{H^+}\cdot a_{NH_3}/a_{NH_4^+}=10^{-9.25}$, the concentration of the ammonium ion becomes very small at pH values above 10.0. Therefore, the temperature being constant, we can write the glass membrane potential, E, as the following equation:

$$E = \text{Const} - K\log a_{NH_3}, \quad (1)$$

where a_{NH_3} denotes the activity of ammonia and K is the slope of the calibration graph.

The activities of various anions were derived from the concentration by means of the activity coefficients tabulated by kielland.[10]

Durability of Glass against Water. Glass film (about 0.3 g) (surface area, 3×10^2 mm^2) was weighted and placed in a 100-ml portion of distilled water, and then allowed to stand for 60 d at about 30 °C. The durability was measured by the weight loss per unit of area of the glass membrane.

Results and Discussion

Glass-forming Region and Durability of Glass against Water. A glass-forming region in the MgO–P_2O_5 system was found at the composition with a MgO contents of less than 55 mol %. This was in agreement with that found in the previous studies.[11] The same result was observed with the Ag_2O–P_2O_5 system.

Table 1 shows the durability of various glasses against water. With an increase in the amount of Al_2O_3 in the glass composition, the solubility of glass decreased. It can be decided that the durability of glasses is produced by the formation of the –P–O–Al– linkage.[12] However, the melting point for the glass formation becomes very high when the Al_2O_3 content increases to more than about 15 mol %.

Potential Response of the Magnesium Phosphate Glass Membrane Electrode. Figure 1 shows the potential response of the $5Ag_2O$–$50P_2O_5$–$40MgO$–$5Al_2O_3$ glass membrane for various anions or compounds in solutions containing 5×10^{-4} mol/dm^3 sodium hydroxide.

In the case of the alkali silicate glass electrode, cation exchange is the basis for the Nicolsky-Eisenman interpretation.[7] As is shown in Fig. 1, on the contrary, it became clear that this glass shows the properties of the anionic response.

The response for ammonia was linear over the range of (10^{-2}—10^{-5}) mol/dm^3, and had a slope of a 48 mV/decade change in the ammonia concentration at 20

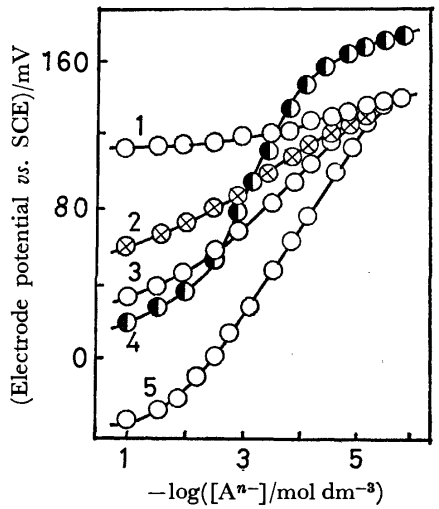

Fig. 1. Potential response of the $5Ag_2O$–$50P_2O_5$–$40MgO$–$5Al_2O_3$ gass electrode.
Here, 5×10^{-4} mol/dm^3 sodium hydroxide was used as the electrolyte solution except for the measurement of hydroxide ion.
1: SO_4^{2-}, 2: Cl^-, 3: NO_3^-, 4: OH^-, 5: NH_3.

°C. Below 10^{-5} mol/dm^3 and above 10^{-2} mol/dm^3, however, the a_{NH_3}-potential graph deviates from linearity.

When the ammonia concentration increases from 10^{-6} to 10^{-2} mol/dm^3, the electrode potential attains a constant value within a minute, but the concentration of ammonia decreases in the same concentration range, the dynamic response time[13] becoming 10 to 20 min.

Response Behavior of Glass Membranes of Various Compositions. The glass electrode containing only MgO and P_2O_5 shows a small response to ammonia. This suggests that no carrier ions which produce the potential response to ammonia, such as the silver ion, are present in the glass composition.

Both the selectivity coefficient of ammonia for other anions and the durability against water decrease with an increase in the Ag_2O content in the glass composition. For the variation in Ag_2O content, the selectivity coefficient of ClO_4^- is found to be $10^{-1.5}$ in Ag_2O content of 15 mol% and $10^{-1.0}$ at 25 mol%, while that of NO_3^- is found to be $10^{-1.5}$ at 15 mol% and $10^{-1.2}$ at 25 mol% respectively.

From these results, it can be concluded that the glass composition of $5Ag_2O$–$50P_2O_5$–$40MgO$–$5Al_2O_3$ is the most suitable for an ammonia selective electrode.

Selectivity Coefficient of Ammonia for the Other Anions or Compounds. The method for the determination of the selectivity coefficients, $K_{NH_3\cdot A}$, is based on the electrode-potential measurements in a mixed solution containing ammonia and the interfering ion, A.[14] The electrode potential of the mixture is expressed by the following equation:

$$E' = \text{Const} - K\log(a_{NH_3}+K_{NH_3\cdot A}\cdot a_A), \quad (2)$$

where $K_{NH_3\cdot A}$ is the selectivity coefficient for A over ammonia and a_A is the activity of an interfering anion or compound A. In the case of $E=E'$, by combining Eqs. 1 and 2 $K_{NH_3\cdot A}$ is obtained by means of the following equation:

$$K_{NH_3\cdot A} = a_{NH_3}/a_A. \quad (3)$$

Therefore, the values of $K_{NH_3\cdot A}$ are obtained by measuring the electrode potential in solutions containing a fixed quantity (10^{-2} mol/dm^3) of the interfering anion or compound and a varied concentration of ammonia.

The selectivity coefficient and the potential slope for each anion or compound obtained using the $5Ag_2O$–$50P_2O_5$–$40MgO$–$5Al_2O_3$ glass electrode are listed in Table 2.

Table 2. Selectivity coefficient for anions or compounds

Anions or compounds	Slope (mV/pC)	Selectivity coefficient
NH_3	48	1
ClO_4^-	37	1.6×10^{-2}
NO_3^-	38	2.1×10^{-2}
OH^-	45	7.4×10^{-2}
Cl^-	32	8.4×10^{-3}
SCN^-	44	8.4×10^{-2}
$CH_3CO_2^-$	30	6.5×10^{-3}
SO_4^{2-}	12	1.4×10^{-3}
$S_2O_3^{2-}$	38	2.1×10^{-2}
Pyridine	33	9.8×10^{-3}
Ethylenediamine	40	5.8×10^{-2}
Triethanolamine	39	5.2×10^{-2}
Urea	14	2.5×10^{-3}

In comparing the pH glass electrode coated by a hydrohobic gas-permeable membrane,[4] the preparation and the operation of the electrode is more simplified, and the effect of interfering species, such as pyridine and urea, is less.

We wish to thank Prof. Yoshihiro Abe for his valuable advice.

References

1) G. Eisenman, R. Bates, G. Mattock, and S. M. Friedman, "The Glass Electrode," Interscience, New York (1965), p. 222.
2) G. A. Rechnitz, *Chem. Eng. News*, **12**, 146 (1967).
3) G. G. Guilbault, R. K. Smith, and J. G. Montalvo, Jr., *Anal. Chem.*, **41**, 600 (1969).
4) T. R. Gilbert and A. M. Clay, *Anal. Chem.*, **45**, 1757 (1973).
5) P. L. Bailey and M. Riley, *Analyst*, **100**, 145 (1975).
6) A. H. Truesdell and A. M. Pommer, *Science*, **142**, 1292 (1963).
7) G. Eisenman, *Biophys. J., Part* 2 *Suppl.*, **1962**, 259.
8) A. Naruse, Y. Abe, and Y. Inoue, *Yogyo Kyokai Shi*, **76**, 36 (1968).
9) L. G. Sillen and A. E. Martell, "Stability Constants of Metal Ion Complexes," The Chemical Society, London (1964), p. 149.
10) J. Kielland, *J. Am. Chem. Soc.*, **59**, 1675 (1937).
11) A. Kishioka, M. Hayashi, and M. Kinoshita, *Bull. Chem. Soc. Jpn.*, **49**, (1976) 3032.
12) Y. Abe, *Zairyo Kagaku*, **11**, 311 (1974).
13) K. Toth and E. Pungor, *Anal. Chim. Acta*, **64**, 417 (1973).
14) G. E. Baiulescu and V. V. Cosofret, "Applications of Ion-Selective Membrane Electrode in Organic Analysis," John Wiley & Sons, New York (1977), p. 17.

^{197}Au-Mössbauer Spectroscopic Studies of Monomeric and Trimeric Gold(I) Azolates

Motomi KATADA,* Kumiko SATO, Yoshio UCHIDA, Seiichiro IIJIMA,**
Hirotoshi SANO, H. H. WEI,† Hiroshi SAKAI,†† and Yutaka MAEDA††

Department of Chemistry, Faculty of Science, Tokyo Metropolitan University, Fukasawa, Setagaya-ku, Tokyo 158
† *Department of Chemistry, Tamkang University, Tamsui, Taiwan 251, Republic of China*
†† *Research Reactor Institute, Kyoto University, Kumatori-cho, Sennan-gun, Osaka 590-04*

(Received August 19, 1982)

Synopsis. The identical chemical state of three gold atoms in trimeric gold(I) azolates and the Au(I)–Au(III) mixed-valence state in their iodine adducts, $Au_3(az)_3I_2$, were confirmed by means of ^{197}Au-Mössbauer spectroscopy.

^{197}Au-Mössbauer spectroscopy is one of the most useful techniques in the structural diagnosis of gold(I) compounds because the Mössbauer parameters are very sensitive to the number and nature of ligands coordinated with the gold atom.

Recently, stable gold(I) derivatives of several azoles have been prepared by Minghetii *et al.*[1] A nine-membered-ring structure containing three gold atoms in a molecule has been suggested in several cases. Some of these trimeric compounds react with iodine to give mixed-valence compounds.

It is our purpose to confirm the trimeric structure and mixed-valence state of gold in several iodine adducts, $Au_3(az)_3I_2$. The present paper will describe the results obtained by ^{197}Au-Mössbauer spectroscopy for monomeric and trimeric gold(I) derivatives of several azoles and their iodine adducts.

Experimental

Materials. The $Au_3(az)_3$ (az=pyrazolato, (pz); 3,5-dimethylpyrazolato, (3,5-Me_2-pz); 3,5-dimethyl-4-iodopyrazolato, (3,5-Me_2-4-I-pz); or benzo-1,2,3-triazolato, (btaz)), $Au_3(3,5\text{-}Me_2\text{-}pz)_3I_2$, $Ph_3PAu(btaz)$, and $Ph_3PAu(3,5\text{-}Me_2\text{-}pz)$ were prepared by following the method described in the literature.[1] The $Au_3(pz)_3I_2$ was prepared by a method similar to that described in Ref. 1. The purity of the samples was checked by elemental analysis.

Measurements. ^{197}Au-Mössbauer spectroscopic measurements were carried out with a source and an absorber, both cooled to 18 K by using a constant acceleration-type spectrometer accompanied with a pure-Ge diode detector. Details of the ^{197}Au-Mössbauer spectroscopy were described in our previous study.[2] All the values of isomer shifts are referred to metallic gold at 18 K. The precision of the Mössbauer parameters obtained is within ±0.04 mm/s.

Results and Discussion

Mössbauer parameters, such as the isomer shift (*IS*), the quadrupole splitting (*QS*), and the half-width (Γ_{exp}), are summarized in Table 1, while some typical spectra are shown in Fig. 1. The values of *IS* and *QS* for $Ph_3PAu(btaz)$ are smaller than those of $Ph_3Au(3,5\text{-}Me_2\text{-}pz)$. This may be ascribed to the reduction of the σ-donating ability of nitrogen by the fused benzene ring. The Mössbauer parameters of monomeric gold(I) azolates are similar to those of the same type of compounds, $[Ph_3PAuL]^+$ (L=C_5H_5N, $C_5H_{10}NH$, or $[N_3]^-$), reported previously.[3,4]

In trimeric gold(I) azolates, the Mössbauer spectra consist of a single doublet, indicating that the three gold atoms in a molecule have an identical chemical state. This means that these compounds have a nine-membered-ring structure. Therefore, in trimeric compounds, the azole acts as an exobidentate *N,N'*-ligand,

Table 1. Mössbauer parameters of gold(I) azolates and their iodine adducts

Compound		*IS* / mm s^{-1}	*QS* / mm s^{-1}	Γ_{exp} / mm s^{-1}
$Ph_3PAu(btaz)$		4.38	8.32	2.04
$Ph_3PAu(3,5\text{-}Me_2\text{-}pz)$		4.78	9.00	1.95
$Au_3(btaz)_3$		3.44	6.98	2.35
$Au_3(pz)_3$		3.41	7.35	2.11
$Au_3(3,5\text{-}Me_2\text{-}pz)_3$		3.28	7.39	2.37
$Au_3(3,5\text{-}Me_2\text{-}4\text{-}I\text{-}pz)_3$		3.41	7.42	2.70
$Au_3(pz)_3I_2$	Au(I)	3.40	7.43	2.18
	Au(III)	3.31	3.67	2.06
$Au_3(3,5\text{-}Me_2\text{-}pz)_3I_2$	Au(I)	3.57	7.82	2.23
	Au(III)	3.40	3.92	2.14

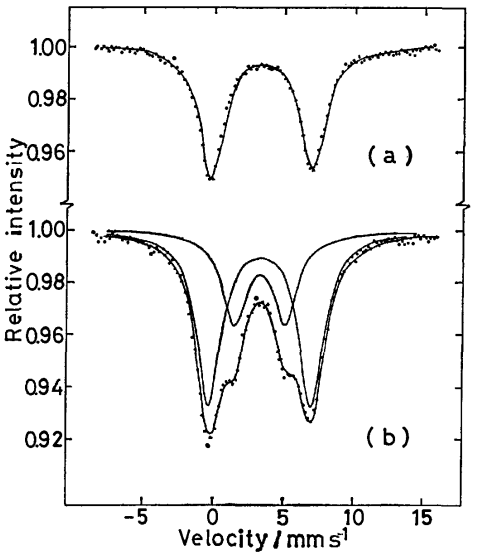

Fig. 1. Mössbauer spectra of (a) $Au_3(pz)_3$ and (b) $Au_3(pz)_3I_2$.
The full lines are least-squares fits of Lorentzians. The areal intensity ratio, $R=A_+/A_-$ was 0.96 for top spectrum. The lines of each pair for bottom spectrum were constrained to have equal intensities and widths.

** Present address: Research Institute for Polymers and Textiles, Yatabe-Higashi, Ibaraki 305.

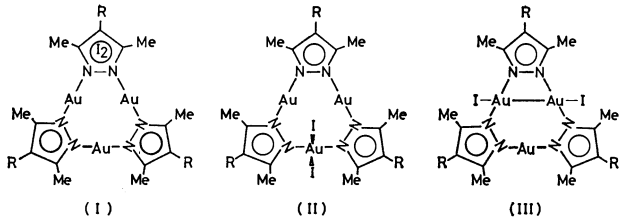

Fig. 2. Possible structures for iodine adducts (from Ref. 1).

forming a cyclic structure. Since the σ-donating ability of the azole ligand is smaller than that of triphenylphosphine, both the *IS* and *QS* values can be expected to decrease for the trimeric compound. A similar trend of the decrease in *IS* and *QS* values is observed on going from $[Ph_3PAuL]^+$ to $[AuL_2]^+$ (L=C_5H_5N, $C_5H_{10}NH$, or $[N_3]^-$).[3,5]

Trimeric gold(I) azolates are stable to air, moisture, and heat and are sparingly soluble in most organic solvents. Those compounds are very stable toward alkalis and acids, but the reaction of trimeric gold(I) azolates with iodine is carried out readily in chloroform and gives only 1:1 adducts, even in the presence of excess iodine. Three kinds of possible structures for these adducts were proposed by Minghetti *et al.* (*cf.* Fig. 2). Based on the results of the visible, IR, and ^{1}H-NMR spectra, they suggested for the adducts the type-II structure. The ^{197}Au-Mössbauer spectra of $Au_3(pz)_3I_2$ and $Au_3(3,5\text{-}Me_2\text{-}pz)_3I_2$ in the present studies show the presence of at least two different sites or oxidation states of gold. A typical spectrum of $Au_3(pz)_3I_2$ is shown in Fig. 2b. The estimated Mössbauer parameters for the adducts are listed in Table 1. One of the sets of parameters is almost the same as that of the original materials. From the Mössbauer parameters, the set is assigned to the Au(I) site which is not attached by iodine. The other set of Mössbauer parameters is very different from the original materials.

In ^{197}Au-Mössbauer spectroscopy, a linear relationship between the observed *IS* and *QS* values has been established for many gold(I) and gold(III) compounds.[6] The average of the literature values is given by:

$$QS = 1.74IS - 2.27 \text{ mm/s for Au(III)}, \quad (1)$$

and:

$$QS = 1.06IS + 3.80 \text{ mm/s for Au(I)}, \quad (2)$$

where the *IS* data are given relative to Au foil.

By using the *IS* data of the new peak components found in $Au_3(pz)_3I_2$ and $Au_3(3,5\text{-}Me_2\text{-}pz)_3I_2$ in Eq. 1, we can estimate the expected values of *QS* as 3.49 and 3.65 mm/s respectively for the adducts. A comparison of these values with the observed values in Table 1 suggests that the Mössbauer parameters of the gold atoms in the other site in the adducts are assigned to gold(III). Furthermore, the area intensity ratio of the absorption line of Au(I) and Au(III) sites is about 2:1. Thus, it may be concluded that the adducts with iodine are Au(I)–Au(III) mixed-valence compounds and have the type-II structure, as has been suggested by Minghetti *et al.*

A part of this work has been carried out under the Visiting Researcher's Program of Kyoto University Research Reactor Institute.

References

1) G. Minghetti, G. Banditelli, and F. Banati, *Inorg. Chem.*, **18**, 658 (1979).
2) M. Katada, Y. Uchida, K. Sato, H. Sano, H. Sakai, and Y. Maeda, *Bull. Chem. Soc. Jpn.*, **55**, 444 (1982).
3) P. G. Jones, A. G. Maddock, M. J. May, M. M. Muir, and A. F. Williams, *J. Chem. Soc., A*, **1977**, 1434.
4) J. S. Charlton and D. I. Nichols, *J. Chem. Soc., A*, **1970**, 1484.
5) H. D. Bartunik, W. Potzel, R. L. Mössbauer, and G. Kaindl, *Z. Phys.*, **240**, 1 (1970).
6) P. Gütlich, R. Link, and A. Trautwein, "Mössbauer Spectroscopy and Transition Metal Chemistry," Springer-Verlag, Berlin (1978), p. 201.

The Solvent Extraction-Spectrophotometric Determination of Perchlorate Ions with Monoethynolog of Malachite Green[1)]

Shuzo AKIYAMA,* Kenichiro NAKASHIMA, Shin'ichi NAKATSUJI, Makiko HAMADA, and Yayoi IZAKI

Faculty of Pharmaceutical Sciences, Nagasaki University, 1-14 Bunkyomachi, Nagasaki 852

(Received September 18, 1982)

Synopsis. By the use of a new reagent, 1,1-bis(*p*-dimethylaminophenyl)-3-phenyl-2-propynylium chloride, *i.e.*, one of the ethynologs of Malachite Green, micro amounts of perchlorate ions could be extracted into chlorobenzene and determined spectrophotometrically. Beer's law holds over the range of 4×10^{-6}—2.5×10^{-5} M (M=1 mol dm^{-3}); $\varepsilon=4.0\times10^{4}$ dm^3 mol^{-1} cm^{-1} at 690 nm.

The study of the synthesis and the properties of the ethynologs of triphenylmethane dyes has been developed and has demonstrated that the introduction of an acetylenic bond into such a classical dye system causes a large bathochromic shift in the longest wavelength.[2)]

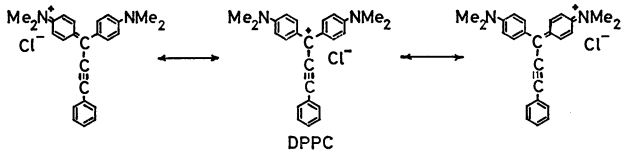

For the application of the effect to analytical chemistry, one of the monoethynologs of Malachite Green, *i.e.*, 1,1-bis(*p*-dimethylaminophenyl)-3-phenyl-2-propynylium chloride (DPPC), was newly prepared and examined in order to determine micro amounts of perchlorate ions by means of solvent-extraction spectrophotometry.[3)]

Experimental

Apparatus. The spectrophotometric measurements were made with Shimadzu UV-300 and UV-150 spectrophotometers.

Materials. *Synthesis of DPPC.* Dried hydrogen chloride was bubbled through a solution of 1,1-bis(dimethylaminophenyl)-3-phenyl-2-propyn-1-ol[2)] (0.500 g, 0.0014 M) in toluene (150 ml) for 15 min. The resulting dark green solution was concentrated *in vacuo* to give crude crystals, which were then recrystallized from the same solvent: deep green crystals,[4)] 0.439 g, 81%; mp 85 °C.

Found; C, 67.76; H, 6.72; N, 5.73%. Calcd for $C_{25}H_{25}N_2Cl\cdot3H_2O$; C, 67.80; H, 7.01; N, 6.33%. MS (*m/e*): 353 (M−Cl⁻); UV λ (H_2O) 645 nm (ε=18500).

Buffer (Potassium Phosphate Solution). Various kinds of pH solutions were made by the use of potassium dihydrogenphosphate (1 M), sulfuric acid (0.1 M), and sodium hydroxide (1 M).

Solvents. Chlorobenzene was purified by distillation. All the other reagents were of an analytical grade and were used without further purification.

Procedure. Place an aliquot of the standard potassium perchlorate solution (1×10^{-5}—6.25×10^{-4} M) into a 25-ml calibrated flask. Add 5 ml of a potassium phosphate buffer (1 M, pH 3.5) and 2 ml of a DPPC aqueous solution (1×10^{-3} M). Dilute the solution to the mark with distilled water. Take 10 ml of the above solution, transfer it into a 100-ml separatory funnel, and shake with 10 ml of chlorobenzene for 3 min. Filter the organic layer after 15 min and measure the absorbance at 690 nm in a 1-cm cell against the reagent blank or chlorobenzene as a reference.

Results and Discussion

The absorption spectra of the chlorobenzene extract containing the ion pair obtained by the above procedure are shown in Fig. 1. The wavelength of the maximum absorption occurs at 690 nm.

The effect of the pH value on the absorbance was examined in the range of pH 0.5 to 10. As is shown in Fig. 2, constant absorbances were obtained in the pH region from 2 to 4, from which the buffer solution of pH 3.5 was used.

The concentration of DPPC to 1.6×10^{-5} M of perchlorate was confirmed by using 8×10^{-5} M for the determination.

The effect of the shaking time in the extraction was examined to give a constant absorbance from 2 to 10 min.

The absorbance of the extract of perchlorate did not change at all for 1 h.

Various organic solvents (chlorobenzene, benzene, nitrobenzene, toluene, chloroform, 1,2-dichloroethane, and carbon tetrachloride) were tested for the extrac-

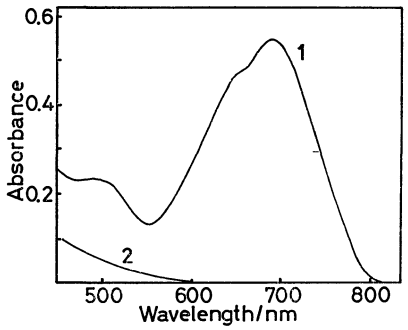

Fig. 1. Absorption spectra of 1,1-bis(*p*-dimethylaminophenyl)-3-phenyl-2-propynylium perchlorate (DPPP). 1: DPPP complex against chlorobenzene, 2: reagent blank against chlorobenzene, ClO_4^-: 1.4×10^{-5} M.

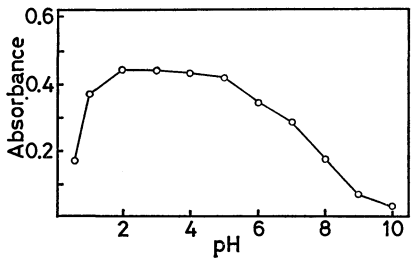

Fig. 2. Effect of pH. ClO_4^-: 1.2×10^{-5} M.

Table 1. Effects of diverse ions

Ion	Added as	Concentration/M	Absorbance
None	—	—	0.425
ClO_3^-	$KClO_3$	1.2×10^{-4}	0.422
BrO_3^-	$KBrO_3$	1.2×10^{-4}	0.434
IO_3^-	KIO_3	1.2×10^{-4}	0.457
IO_4^-	KIO_4	1.2×10^{-6}	0.418
Cl^-	KCl	1.2×10^{-3}	0.435
Br^-	KBr	1.2×10^{-3}	0.433
I^-	KI	1.2×10^{-6}	0.438
NO_3^-	$NaNO_3$	1.2×10^{-5}	0.420
SCN^-	KSCN	1.2×10^{-6}	0.423
SO_4^{2-}	Na_2SO_4	2.4×10^{-5}	0.427

ClO_4^- added: 1.2×10^{-5} M.

tion. Subsequently, chlorobenzene was chosen because it showed a small blank value and the largest absorbance difference at 690 nm between the ion pair and the blank.

On the basis of the above results, a standard procedure was evolved, by which the linear calibration graph was obtained in the range from 4×10^{-6} to 2.5×10^{-5} M of perchlorate. The practical absorptivity was 4.0×10^4 dm^3 mol^{-1} cm^{-1}. The coefficient of variation for the ten replicated experiments was satisfactory (2.20% for 1.6×10^{-5} M of perchlorate).

The interferences due to various ions were also examined, as is shown in Table 1. The periodate, iodide, and thiocyanate caused considerable errors. It is worth noting that the characteristic larger red shift (*ca.* 100 nm) due to the effect of an acetylenic bond larger than Crystal Violet[3] has been observed. The absorptivity was about one-half of that for Crystal Violet; however, the sensitivity and the reproducibility were quite good in this method. DPPC is useful enough as an analytical reagent for perchlorates.[5]

The authors wish to thank Miss Atsuko Yamaguchi for helping with the experiments.

The financial support of this work by a Grant-in-Aid for Scientific Research (No. 56470022) from the Ministry of Education, Science and Culture is gratefully acknowledged.

References

1) Development and Application of Organic Analytical Reagents, Part II. Part I: S. Nakatsuji, R. Nakano, M. Kawano, K. Nakashima, and S. Akiyama, *Chem. Pharm. Bull.*, **30**, 2467 (1982).

2) S. Akiyama, K. Yoshida, M. Hayashida, K. Nakashima, S. Nakatsuji, and M. Iyoda, *Chem. Lett.*, **1981**, 311.

3) For the related works using cationic triphenylmethane dyes, see a) S. Uchikawa, *Bull. Chem. Soc. Jpn.*, **40**, 798 (1967); b) S. Motomizu, S. Fujiwara, and K. Tôei, *Anal. Chem. Acta*, **128**, 185 (1981).

4) The chloride was found to be very hygroscopic; this fact was also demonstrated with the elemental-analyses data.

5) Good recovery yields were obtained in the determination of perchlorates by using the above calibration graph: $NaClO_4$(recovery yield, 103.6%; standard deviation, 0.91; $n=5$), NH_4ClO_4(102.5%; 1.05; 5), and 60% $HClO_4$(98.6%; 1.34; 5).

An Odorless Preparative Method of Sulfides and Thiocarboxylic *S*-Esters Using 3-(Alkylthio)-1,2-benzisothiazole 1,1-Dioxide

Hiroyuki YAMADA, Hideki KINOSHITA, Katsuhiko INOMATA, and Hiroshi KOTAKE*

Department of Chemistry, Faculty of Science, Kanazawa University, Kanazawa 920

(Received April 30, 1982)

Synopsis. It was found that sodium salt of 1,2-benzisothiazole-3(2*H*)-thione 1,1-dioxide (thiosaccharin) readily reacted with alkyl halide affording 3-(alkylthio)-1,2-benzisothiazole 1,1-dioxide (**3**). Treatment of **3** with piperidine produces the corresponding alkanethiol *in situ* quantitatively and subsequent treatment with various electrophiles gives the corresponding sulfides and thiocarboxylic *S*-esters in good yields.

Recently the herbicidal and fungicidal properties of 3-substituted 1,2-benzisothiazole 1,1-dioxide have been noted,[1,2] and the preparation of such compounds was performed by the reaction of 3-chloro-1,2-benzisothiazole 1,1-dioxide with an alcohol or thiol in the presence of base.[2] Generally, thiols have unpleasant odor, therefore the development of odorless equivalent of thiols would be convenient. We have found that 3-(alkylthio)-1,2-benzisothiazole 1,1-dioxide (**3**), which is prepared from the sodium salt (**2**) of thiosaccharin (**1**) and alkyl halides is an efficient synthetic equivalent of alkanethiols. 3-(Alkylthio)-1,2-benzisothiazole 1,1-dioxide (**3**) was prepared upon treatment of **2** with 1.1 equivalent of halide in excellent yields as shown in Table 1 (Eq. 1). Odorless compounds **3** reacted

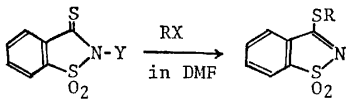

(1)

1 Y=H
2 Y=Na

3(BID-SR)

with secondary amines stoichiometrically. The reaction of **3** with piperidine produces the corresponding alkanethiols smoothly *in situ*. Subsequently treatment with electrophiles gives the corresponding sulfides in one-pot reaction. Treatment with acid chlorides led

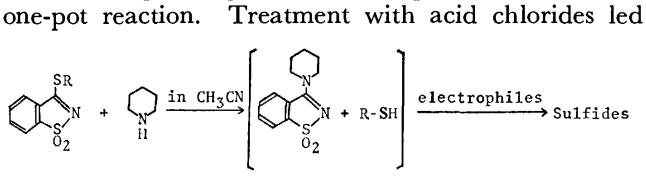

3

to the corresponding thiocarboxylic *S*-esters in high yields. In the same manner, the reactions with other electrophiles such as α,β-unsaturated carbonyl compounds, alkyl halides and epoxide also give satisfactory results. As mentioned above, it is clear that readily available **3** is a useful equivalent of the corresponding thiol.

Experimental

*Preparation of 3-(Alkylthio)-1,2-benzisothiazole 1,1-Dioxides (**3a—g**).* Typically, to a solution of **2** (663 mg, 3 mmol) in DMF (2 ml) was added a solution of benzyl bromide (564 mg, 3.3 mmol) in DMF (2 ml) at room temperature under nitrogen. After stirring for 3 h, water was added to the reaction mixture. The precipitate was recrystallized from ethanol and dichloromethane to give 3-(benzylthio)-1,2-benzisothiazole-1,1-dioxide (**3a**) (791 mg, 93%), whose structure was established by comparison with the authentic sample prepared by the reaction of 3-(chloro)-1,2-benzisothiazole 1,1-dioxide with benzenemethanethiol in the presence of triethylamine in CH_3CN (Mp, IR). **3a**: Mp 141.0—142.0 °C; IR (KBr) 1587, 1320, 1163 cm^{-1}; Found: C, 57.82; H, 3.94; N, 4.75%. Calcd for $C_{14}H_{11}NO_2S_2$: C, 58.11; H, 3.83; N, 4.85%. **3b**: Mp 144.5—145.5 °C; IR (KBr) 1587, 1312, 1163 cm^{-1}: Found: C, 59.34; H, 4.14, N, 4.75%. Calcd for $C_{15}H_{13}NO_2S_2$: C, 59.40, H, 4.32; N, 4.62%. **3c**: Mp 129.5—130.5 °C; IR (KBr) 1587, 1328, 1166 cm^{-1}; Found: C, 61.12; H, 4.31; N, 4.38%. Calcd for $C_{16}H_{13}NO_2S_2$: C, 60.93; H, 4.15; N, 4.44%. **3d**: Mp 114.0—115.0 °C; IR (KBr) 3067, 1497, 1325, 1235, 1167, 990, 930, 784 cm^{-1}; Found: C, 50.37; H, 3.81; N, 5.82%. Calcd for $C_{10}H_9NO_2S_2$: C, 50.19; H, 3.79; N, 5.86%. **3e**: Mp 168.0—169.0 °C; IR (KBr) 3257, 1493, 1319, 1157 cm^{-1}; Found: C, 50.63; H, 2.85; N, 5.73%. Calcd for $C_{10}H_7NO_2S_2$: C, 50.62; H, 2.97; N, 5.90%. **3f**: Mp 234.5—235.5 °C; IR (KBr) 2247, 1504, 1318, 1163 cm^{-1}; Found: C, 45.47; H, 2.30; N, 11.97%. Calcd for $C_9H_6N_2O_2S_2$: C, 45.39; H, 2.54; N, 11.76%. **3g**: Mp 227.5—228.5 °C; IR (KBr) 1488, 1316, 1170, 1156, cm^{-1}; Found: C, 45.30; H, 3.17; N, 6.53%. Calcd for $C_8H_7NO_2S_2$: C, 45.08; H, 3.31; N, 6.57%.

TABLE 1. PREPARATION OF 3-(ALKYLTHIO)-1,2-BENZISOTHIAZOLE 1,1-DIOXIDE (**3**) FROM THE SODIUM SALT (**2**) AND HALIDES

RX	Time/h	**3a—g**	Yield/%
$PhCH_2Br$[b]	3	**3a**	93
$PhCH_2CH_2Br$[c]	11	**3b**	82
$PhCH{=}CHCH_2Cl$[c]	3.5	**3c**	84
$CH_2{=}CHCH_2Br$[b]	3	**3d**	87
$CH{\equiv}CCH_2Br$[b]	4	**3e**	80
$N{\equiv}CCH_2Cl$[b]	3.5	**3f**	85
CH_3I[b]	3	**3g**	89

a) The reactions performed in DMF. b) Room temp. c) 50 °C.

*Preparation of Thiocarboxylic S-Esters (**4a—h**).* Typically, to a solution of 3-(methylthio)-1,2-benzisothiazole 1,1-dioxide (3 g) (211 mg, 1 mmol) in CH_3CN (3 ml) was added an CH_3CN solution of piperidine (85 mg, 1 mmol) at −18 °C under N_2. After 20 min a solution of benzoyl chloride (169 mg, 1.2 mmol) in CH_3CN (1.5 ml) was added followed by the addition of a solution of triethylamine (121 mg, 1.2 mmol) in CH_3CN (1.5 ml). The mixture was kept at −18 °C for 1.5 h and gradually warmed to room temperature. The solvent was removed *in vacuo* to give a residue. A crude material was subjected to preparative TLC (benzene) to give pure **4d** (138 mg, 91%). **4a**: Oil; *m/e* 178 (M^+); IR (neat) 1656, 1200, 901, 673 cm^{-1}; NMR ($CDCl_3$) δ 3.70 (2H, d, J=7.0 Hz), 4.96—5.48 (2H, m), 5.55—6.26 (1H, m), 7.15—8.11 (5H, m). **4b**: Oil; *m/e* 176 (M^+); IR (neat) 3300, 1660, 1205, 911, 680 cm^{-1}; NMR ($CDCl_3$)

TABLE 2. PREPARATION OF THIOCARBOXYLIC *S*-ESTERS (**4**) AND SULFIDES (**5**) FROM BID-SR (**3**) AND ELECTROPHILES

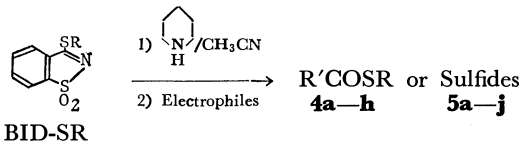

BID-SR

BID-SR	Electrophile	Product	Yield/%
3d	PhCOCl	$PhCOSCH_2CH=CH_2$[a] (**4a**)	95[3]
3e	PhCOCl	$PhCOSCH_2C\equiv CH$[a] (**4b**)	91[4]
3f	PhCOCl	$PhCOSCH_2C\equiv N$[a] (**4c**)	89
3g	PhCOCl	$PhCOSCH_3$[a] (**4d**)	91
3a	CH_3COCl	CH_3COSCH_2Ph[b] (**4e**)	94[5]
3a	$PhCH_2COCl$	$PhCH_2COSCH_2Ph$[b] (**4f**)	92[6]
3a	$CH_3(CH_2)_2COCl$	$CH_3(CH_2)_2COSCH_2Ph$[b] (**4g**)	94[7]
3a	$(CH_3)_3CCOCl$	$(CH_3)_3CCOSCH_2Ph$[c] (**4h**)	33[8]
3a	$CH_3COCH=CH_2$	$CH_3COCH_2CH_2SCH_2Ph$[d] (**5a**)	quant.[9]
3b	$CH_3COCH=CH_2$	$CH_3COCH_2CH_2SCH_2CH_2Ph$[d] (**5b**)	87
3c	$CH_3COCH=CH_2$	$CH_3COCH_2CH_2SCH_2CH=CHPh$[d] (**5c**)	92
3a	$CH_2=CHCHO$	$PhCH_2SCH_2CH_2CHO$[d,e] (**5d**)	92[10]
3a	$CH_3CH=CHCHO$	$PhCH_2SCH(CH_3)CH_2CHO$[d,e] (**5e**)	89[10]
3a	$PhCH=CHCH_2Cl$	$PhCH_2SCH_2CH=CHPh$[c] (**5f**)	88
3a	$(CH_3)_2CHBr$	$PhCH_2SCH(CH_3)_2$[c] (**5g**)	81[11]
3a	$CH_3(CH_2)_3CH_2I$	$PhCH_2S(CH_2)_4CH_3$[c] (**5h**)	89[11]
3a	$PhCH_2Br$	$PhCH_2SCH_2Ph$[c] (**5i**)	90[12]
3a		PhCH-CH(OH)Ph (**5j**) (erythro)	quant.

a) Condition: −18 °C—room temp, 90 min. b) Room temp, 5 min. c) Room temp, 1.5 h. d) Room temp, 4.5 h. e) Room temp, 5 h. f) Triethylamine used as a base in **4a—h**, DBU used in **5a—i**, 2.4 equiv. of 1 M NaOH used in **5j**. g) They were isolated as 2,4-dinitrophenylhydrazone derivatives.

δ 2.22 (1H, t, J=2.6 Hz), 3.83 (2H, d, J=2.6 Hz), 7.23—8.17 (5H, m). **4c**: Oil; *m/e* 177 (M^+); IR (neat) 2985, 1667, 1211, 911 cm^{-1}; NMR ($CDCl_3$) δ 3.85 (2H, s), 7.26—8.07 (5H, m). **4d**: Oil; *m/e* 152 (M^+); IR (neat) 1650, 1195, 902, 673 cm^{-1}; NMR ($CDCl_3$) δ 2.45 (3H, s), 7.17—8.07 (5H, m). **4e**: Oil; *m/e* 166 (M^+); IR (neat) 1680, 1126, 697 cm^{-1}; NMR ($CDCl_3$) δ 2.32 (3H, s), 4.10 (2H, s), 7.24 (5H, s). **4f**: Mp 39.5—40.5 °C; *m/e* 242 (M^+); IR (KBr) 1672, 1014, 697 cm^{-1}; NMR ($CDCl_3$) δ 3.71 (2H, s), 3.99 (2H, s), 7.07 (5H, s), 7.14 (5H, s). **4g**: Oil; *m/e* 194 (M^+); IR (neat) 2959, 1680, 982, 697 cm^{-1}; NMR ($CDCl_3$) δ 0.91 (3H, t, J=7.0 Hz), 1.66 (2H, t,q. J=7.2, J=7.0 Hz), 2.49 (2H, t, J=7.2 Hz), 4.03 (2H, s), 7.12 (5H, s). **4h**: Oil; *m/e* 208 (M^+); IR (neat) 2690, 1672, 949, 697 cm^{-1}; NMR ($CDCl_3$) δ 1.24 (9H, s), 4.03 (2H, s), 7.20 (5H, s).

*Addition of Thiols to α,β-Unsaturated Carbonyl Compounds (**5a—e**).* Typically, to a solution of 3-(cinnamylthio)-1,2-benzisothiazole 1,1-dioxide (**3c**) (154 mg, 0.5 mmol) in CH_3CN (1 ml) was added a CH_3CN solution of piperidine (43 mg, 0.5 mmol) under N_2 at room temperature. After 30 min a solution of methyl vinyl ketone (38 mg, 0.5 mmol) in CH_3CN (1.5 ml) was added dropwise and then after 3 h a drop of triethylamine was added. The reaction mixture was stirred for additional 1.5 h and evaporated *in vacuo*. Purification with preparative TLC (benzene–ethyl acetate=10:1 v/v) gave **5a** (101 mg, 92%). **5a**: Oil; *m/e* 194 (M^+); IR (neat) 1700, 1408, 1353, 693 cm^{-1}; NMR ($CDCl_3$) δ 2.09 (3H, s), 2.62 (4H, s), 3.69 (2H, s), 7.26 (5H, s). **5b**: Oil; *m/e* 208 (M^+); IR (neat) 2920, 1709, 1355, 690 cm^{-1}; NMR ($CDCl_3$) δ 2.12 (3H, s), 2.69 (4H, s), 2.80 (4H, s), 7.17 (5H, s). **5c**: Oil; *m/e* 220 (M^+); IR (neat) 3035, 2933, 1712, 1361, 963 cm^{-1}; NMR ($CDCl_3$) δ 2.08 (3H, s), 2.67 (4H, s), 3.25 (2H, d, J=6.0 Hz), 6.12 (1H, t, d, J=6.0, 15.6 Hz), 6.35 (1H, d, J=15.6 Hz),7.03—7.47 (5H, m).

Compounds (**5d—e**) were not stable to silica gel purification and then characterized as 2,4-dinitrophenylhydrazones, respectively. **5d**: Mp 99.0—99.5 °C (from EtOH); Found: C, 53.24; H, 4.42; N, 15.53%. Calcd for $C_{16}H_{16}N_4O_4S$: C, 53.32; H, 4.48; N, 15.55%. **5e**: Mp 65.0—65.5 °C (from EtOH); Found: C, 54.40; H, 4.69; N, 14.94%. Calcd for $C_{17}H_{18}N_4O_4S$: C, 54.43; H, 4.85; N, 14.96%.

*Preparation of the Sulfides (**5f—i**).* Typically, to a suspension of 3-(benzylthio)-1,2-benzisothiazole 1,1-dioxide (**3a**) (142 mg, 0.5 mmol) in CH_3CN (1 ml) was added a solution of piperidine (43 mg, 0.5 mmol) in CH_3CN (1 ml) under N_2. After stirring for 20 min, a solution of DBU (92 mg, 0.6 mmol) in CH_3CN (1 ml) was added followed by the addition of a solution of benzyl bromide (102 mg, 0.6 mmol) in CH_3CN (1 ml). The reaction mixture was stirred for 5 h and worked up in the usual way. Preparative TLC (hexane–benzene=5:2 v/v) gave pure **5i** (96 mg, 90%). **5f**: Oil; *m/e* 240 (M^+); IR (neat) 3049, 1496, 961 cm^{-1}; NMR ($CDCl_3$) δ 3.21 (2H, d, J=6.4 Hz), 3.62 (2H, s), 6.11 (H, t, d, J=6.4, 15.4 Hz), 6.20 (1H, d, J=15.4 Hz), 6.92—7.74 (10H, m). **5g**: Oil; *m/e* 166 (M^+); IR (neat) 2950, 1484, 1443, 1374, 685 cm^{-1}; NMR ($CDCl_3$) δ 1.23 (6H, d, J=6.6 Hz), 2.68 (1H, q, J=6.6 Hz), 3.67 (2H, s), 7.19 (5H, s). **5h**: Oil; *m/e* 194 (M^+); IR (neat) 2920, 1481, 1443, 685 cm^{-1}; NMR ($CDCl_3$) δ 0.63—1.82 (9H, m), 2.37 (2H, t, J=7.0 Hz), 3.63 (2H, s), 7.18 5H, s). **5i**: Oil; *m/e* 214 (M^+); IR (neat) 3012, 1488, 1445, 685 cm^{-1}; NMR ($CDCl_3$) δ 3.53 (4H, s), 7.20 (10H, s). **5j**: Mp 107—108 °C; IR (KBr) 3390, 1595, 1445, 1046 cm^{-1}; NMR ($CDCl_3$) δ 2.31 (1H, bs), 3.29 (2H, s), 3.80 (1H, d, J=6.4 Hz), 4.85 (1H, d, J=6.4 Hz), 6.71—7.61 (15H, m); Found: C, 78.79; H, 6.26%. Calcd for $C_{21}H_{20}OS$: C, 78.71; H, 6.29%.

References

1) Y. Suzuki, K. Matsumoto, M. Iwata, S. Seki, and T. Watanabe, Jpn. Kokai Tokkyo Koho, 1978-59029 (Cl. A 01 N 9/14), May 27, 1978; Y. Suzuki, S. Seki, T. Watanabe, and Y. Sekizawa, *ibid.*, 1978-66424 (Cl. A 01 N 9/14), Jun. 13, 1978; Y. Suzuki, S. Seki, T. Watanabe, and Y. Sekizawa, *ibid.*, 1979-35217 (Cl. A 01 N 9/02), Mar. 15, 1979.

2) G. L. Bachman, J. W. Baker, and D. P. Roman, *J. Pharm.*, **67**, 1323 (1978).

3) S. G. Smith, *J. Am. Chem. Soc.*, **83**, 4285 (1961).

4) K. Sato and O. Miyamoto, *Nippon Kagaku Zasshi*, **77**, 1409 (1956).

5) J. H. Chapman and L. N. Owen, *J. Chem. Soc.*, **1950**, 579.

6) L. S. Godinho and H. J. C. Neves, *Rec. Port. Farm.*, **23**, 592 (1973).

7) R. A. Nyquist and W. J. Potts, *Spectrochim. Acta*, **1959**, 514.

8) Y. Yokoyama, T. Shioiri, and S. Yamada, *Chem. Pharm. Bull.*, **1977**, 25 (9), 2423 (Eng.).

9) M. Tanaka, M. Sashio, Y. Shimodori, and M. Murata, *Kogyo Kagaku Zasshi*, **59**, 577 (1956).

10) J. R. Catsh, A. H. Cook, A. R. Graham, and I. Heilbron, *J. Chem. Soc.*, **1947**, 1609.

11) I. J. Buchi, M. Prost, H. Eichenberger, and R. Lieberherr, *Helv. Chim. Acta*, **35**, 1527 (1952).

12) R. Mozingo, D. E. Wolf, S. A. Harris, and K. Folkers, *J. Am. Chem. Soc.*, **65**, 1013 (1943).

Photoinduced Alcoholysis of Trihaloacetyl Group

Yasuji IZAWA, Katsuhiro ISHIGURO, and Hideo TOMIOKA*

Department of Industrial Chemistry, Faculty of Engineering, Mie University, Tsu, Mie 514

(Received June 29, 1982)

Synopsis. Photolysis of trichloroacetamide in non-degassed methanol gave methyl oxanilate (13—44%), along with carbamate (3—20%) and amine (4—12%). Similar irradiation of other trichloroacetyl derivatives of aliphatic ketone, aldehyde, and acetate afforded only radical product. The results are interpreted in terms of the mechanism involving electron transfer of the radical pair.

There has been increasing interest paid recently to photolysis of alkyl and alkenyl halides,[1-4] because, contrary to the earlier belief that only radical intermediates are involved, it becomes clear that cationic, as well as free radical, intermediates play an important role in the solution-phase photochemistry of these halides. During an effort[5-7] to generate α-oxo carbonium ion we found[8,9] that photolysis of α,α,α-trihaloacetophenone in alcohols gave a new photoalcoholysis product, benzoylformate, which was apparently derived from nucleophilic trapping of ionic species. Since thermal (dark) nucleophilic attack of alcohol on trihaloacetyl group is known to occur exclusively at carbonyl function to give benzoate (haloform reaction), the present photoalcoholysis is quite important not only from the standpoint of the reaction mechanism but also from synthetic viewpoints. Thus we have examined the photolysis of other trihaloacetyl compounds in alcohol.

Results and Discussion

Irradiation of a non-degassed solution of trichloroacetoanilide (**1a**) in methanol through a Pyrex filter for 4 h afforded methyl oxanilate (**2a**, 25.9%), along with methyl phenylcarbamate (**3a**, 12.5%) and aniline (**4a**, 12.3%). The similar reactions were found to

$$\underset{\mathbf{1}}{RNHC(=O)CCl_3} \xrightarrow[MeOH]{h\nu} \underset{\mathbf{2}}{RNHC(=O)CO_2Me} + \underset{\mathbf{3}}{RNHCO_2Me} + \underset{\mathbf{4}}{RNH_2} \quad (1)$$

a: R=C_6H_5, **b**: R=*p*-$MeOC_6H_4$, **c**: R=*p*-MeC_6H_4
d: R=*p*-ClC_6H_4, **e**: R=$PhCH_2$, **f**: R=H

occur with other trichloroacetoanilides as summarized in Table 1. The photoalcoholysis was also applicable to trichloroacetamide (**1e**, **f**). This is in marked contrast with that observed for trihalo-ketone where only aromatic ketone derivatives undergo photoalcoholysis to give formate (*vide infra*). Oxanilate **2** and carbamate **3** were apparently formed *via* nucleophilic trapping by methanol of cationic species resulting from C–Cl and C–CO bond fission in heterolytic way, respectively. Amine **4** was derived from radical species since trichloroacetaldehyde was detected in the reaction mixture.

Irradiation of hexachloroacetone (**5a**) in methanol did not result in the formation of expected alcoholysis product, *i.e.*, methyl trichloroacetate or trichloropyruvate. Tribromoacetaldehyde (**5b**) also did not lead to the alcoholysis upon irradiation in methanol. The main product in these photolyses was reduction (radical) product. For example, dibromoacetaldehyde was obtained in more than 90% yield in the photolysis of **5b**. Irradiation of methyl trihaloacetate (**6a**, **d**) in methanol through quartz resulted in the formation of the reduction product *i.e.*, dihaloacetate. GC analysis showed that neither dimethyl oxalate nor carbonate was detected in the reaction mixtures. When aryl ester (**6b**, **c**) was similarly irradiated, phenol was isolated as a main product (70—80%), but no photoalcoholysis product was detected.

Table 1. Photoreaction of **1** in methanol[a]

1	(R)	Irradiation time / h	Yield/%[b] 2	3	4
1a	(C_6H_5)	4	28.9	12.5	12.3
1b	(*p*-$MeOC_6H_4$)	5	43.7	15.8	10.3
1c	(*p*-MeC_6H_4)	4	36.9	13.4	11.9
1d	(*p*-ClC_6H_4)	18	21.1	14.8	10.2
1e	($PhCH_2$)	20	28.5	20.2	3.5
1f	(*c*-C_6H_{11})	20	13.0	3.1	8.2

a) Irradiations were carried out in a Pyrex tube until all starting amide was consumed. b) Isolated yield.

$$\underset{\mathbf{5}}{CX_3C(=O)R} \qquad \underset{\mathbf{6}}{CX_3C(=O)OR}$$

a: X=Cl, R=CCl_3, **b**: X=Br, R=H

a: X=Cl, R=Me, **b**: X=Cl, R=C_6H_5, **c**: X=Cl, R=*p*-MeC_6H_4, **d**: X=Br, R=Me

The results indicated that the photoalcoholysis of $COCX_3$ to $COCO_2R$ is applicable to trihaloacetamide group, but not to aliphatic trihalo-ketone, -aldehyde, and trihaloacetate. This is in contrast with that observed for photoalcoholysis of simple halides, where not only arylalkyl halide, *e.g.*, benzyl halide,[1,3] but also more simple alkyl and cycloalkyl halides[2] efficiently undergo photoalcoholysis to give ether and/or olefins along with radical products. In their interesting work on photosolvolysis of alkyl iodide Kropp *et al.*[2] have proposed that ionic intermediates are not produced directly from the photoexcited state, but that the photoexcited state decays by homolysis to a radical pair, which may undergo radical reactions or electron transfer to afford an ion pair as shown in Eq. 2. We

$$R\text{–}X \xrightarrow{h\nu} [R\cdot X\cdot] \xrightarrow[\text{transfer}]{\text{electron}} [R^+X^-] \quad (2)$$

have also suggested[8,9] that photoalcoholysis and photoreduction of trihaloacetophenone (**7**) are coupled

through the common intermediacy of the radical pair (**8**) and that benzoylformate is formed *via* spontaneous (dark) alcoholysis of initial photoalcoholysis product, *i.e.*, α-alkoxy-α,α-dihaloacetophenone (**11**). The ratio of heterolytic products to the radical (reduction) products is then influenced by lifetime of the radical pair **8**, since the radical pair must have a lifetime to permit electron transfer to compete with diffusion of the radical

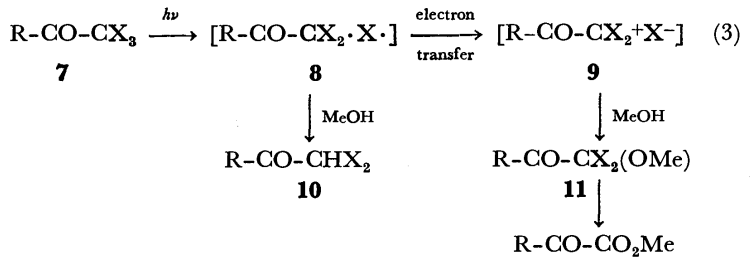

(3)

components from the caged pair. The present results then suggest that only radical pair generated from trihaloacetophenone and trihaloacetamide has sufficient lifetime for electron transfer to occur, while that derived from aliphatic trihalo derivatives undergoes predominant hydrogen abstraction before electron transfer occurs. Alternatively, an α-oxo dihalo carbonium ion generated from trihaloacetophenone and trihaloamide may be stabilized by non-bonded interaction of phenyl and amide nitrogen. This will facilitate electron transfer process to generate the α-oxo dihalo carbonium ion which may be otherwise very unfavorable.

Experimental

Materials. α,α,α-Trichloroacetamide **1a—f** was prepared by the reaction of hexachloroacetone with amine according to the literature procedure.[10] Tribromoacetaldehyde **5b** was obtained by treatment[11] of paraldehyde with excess bromine. Aryl trichloroacetate **6b**, **6c** was synthesized by the Schotten-Baumann reaction of trichloroacetyl chloride with phenol. Methyl tribromoacetate **6d** was obtained by esterification of the corresponding acid. All other trihalo compounds were obtained from commercial source. Oxanilate **2** and carbamate **3** were prepared by the reaction of amine with dimethyl oxalate[12] and methyl chloroformate,[13] respectively.

Irradiation of Trichloroacetamide in Methanol. In a typical run, a solution of trichloroacetamide (1 mmole) in methanol (200 ml) was placed in a Pyrex tube and irradiated with a high-pressure, 300W, Hg lamp with a water-cooled jacket. The progress of the reaction was monitored by TLC. The irradiated mixtures were concentrated on a rotary evaporator and extracted with ether-water. Acidification of the aqueous layer, followed by ether extraction gave amine. The ethereal solutions were concentrated and chromatographed on 2.0 cm × 30 cm silica gel (Woelm, Activity III) column with $CHCl_3$ as eluant to give oxanilate **2** and carbamate **3**, all of which showed the same NMR spectra and GC retention time as authentic samples.

Irradiation of Other Trihaloacetyl Compounds in Methanol. Irradiations were carried out as outlined above. Identifications of photoproducts were done either by GC comparison with authentic samples or by isolation followed by spectroscopic determination.

References

1) S. J. Cristol and T. H. Bindel, *J. Org. Chem.*, **45**, 951 (1980), and references cited therein.
2) P. J. Kropp, G. S. Poindexter, N. J. Pienta, and D. C. Hamilton, *J. Am. Chem. Soc.*, **98**, 8135 (1976), and references cited therein.
3) D. C. Appleton, B. Brocklehurst, J. McKenna, J. M. McKenna, S. Thackeray, and A. R. Walley, *J. Chem. Soc., Perkin Trans. 2*, **1980**, 87.
4) T. Kitamura and S. Kobayashi, *Tetrahedron Lett.*, **1979**, 1619.
5) P. C. Purohit and H. R. Sonawane, *Tetrahedron*, **37**, 873 (1980) and references cited therein.
6) H. Tomioka, Y. Izawa, and Y. Ogata, *Tetrahedron*, **24**, 5739 (1968).
7) Y. Izawa, H. Tomioka, M. Kutsuna, and Y. Toyama, *Bull. Chem. Soc. Jpn.*, **52**, 3465 (1979).
8) Y. Izawa, H. Tomioka, M. Natsume, S. Beppu, and H. Tsujii, *J. Org. Chem.*, **45**, 4835 (1980).
9) Y. Izawa, K. Ishiguro, and H. Tomioka, *Bull. Chem. Soc. Jpn.*, in press.
10) B. Sukornick, *Org. Synth.*, Coll. Vol. V, 1074 (1973).
11) F. A. Long and J. W. Howard, *Org. Synth.*, Coll. Vol. II, 87 (1943).
12) J. S. Pierce, C. D. Lunsford, R. W. Raiford, Jr., J. L. Rush, and D. W. Riley, *J. Am. Chem. Soc.*, **73**, 2595 (1951).
13) W. W. Hartman and M. R. Brethen, *Org. Synth.*, Coll. Vol. II, 278 (1943).

Catalytic Activity of $PdCl_2$ Complexes Having Sulfur Compounds as Ligands

Katsuyuki OGURA,* Teruki AIZAWA, Koichiro UCHIYAMA, and Hirotada IIDA

Department of Synthetic Chemistry, Faculty of Engineering, Chiba University, Yayoicho 1-33, Chiba 260

(Received July 8, 1982)

Synopsis. The $PdCl_2$ complexes coordinated with methyl *p*-tolyl sulfoxide (1:2), methylthiomethyl *p*-tolyl sulfoxide (1:2), and 1,3-bis[(*p*-tolylsulfinyl)methylthio]propane (1:1) as ligands were prepared. Among these complexes, bis(methyl *p*-tolyl sulfoxide)palladium dichloride catalyzed effectively cyclotrimerization of diphenylethyne and rearrangement of 3-acetoxy-1-tridecene to 1-acetoxy-2-tridecene.

Sulfur-containing compounds are well known to coordinate strongly to many kinds of metals or metal salts and to poison metallic catalysts, and there are several reports[1] for catalytic reactions using metal complexes with sulfur compounds as ligands. Now we wish to report preparation of three types of $PdCl_2$ complexes (**1**, **2**, and **3**) containing methyl *p*-tolyl sulfoxide (**4**), methylthiomethyl *p*-tolyl sulfoxide (**5**), and 1,3-bis[(*p*-tolylsulfinyl)methylthio]propane (**6**) as ligands, and their catalytic activities for cyclotrimerization of diphenylethyne and rearrangement of 3-acetoxy-1-tridecene.

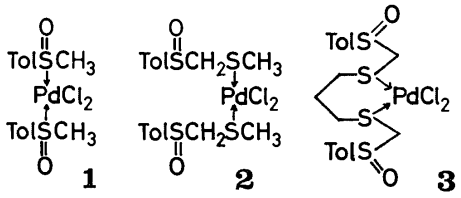

1 **2** **3**

Complexes **1**, **2**, and **3** were easily obtained by simple stirring of $PdCl_2$ and sulfur compounds **4**, **5**, and **6**, respectively, in CH_2Cl_2 at room temperature. Their structures were assigned by their elemental analyses and IR spectra.[2] The absorption of sulfinyl stretching of **1** appears at a higher frequency (1148 cm^{-1})[5] than that (1030 cm^{-1}) of **4** itself, indicating that the lone-pair electrons of the sulfur atom coordinates to $PdCl_2$. Whereas, **2** and **3** showed their sulfinyl absorptions at 1050 cm^{-1} and 1045 cm^{-1}, respectively, in accord with the assigned structures. We also prepared the $PdCl_2$ complex (**1***) with optically active (*R*)-methyl *p*-tolyl sulfoxide (**4***) as a ligand. The protons of the sulfinyl methyl group of **1*** were observed as a relatively sharp singlet in the NMR spectrum, while those of **1** appeared as a very broad signal as shown in Fig. 1, implying that **1** consisted of two diastereomeric isomers (*dl* and *meso* forms) and underwent fast ligand-exchange in solution.

Next, the catalytic activities of the thus prepared complexes were examined for cyclotrimerization of diphenylethyne (**7**) to form hexaphenylbenzene (**8**).[6] To a solution of **7** in CH_2Cl_2, was added the complex (**1**, **2**, or **3**) (0.03 mol equiv.) and the resulting solution was stirred at 30 °C for 24 h. The yield of **8** based on the used complex was 405% for **1**, 40% for **2**, and 13% for **3**. When insoluble $PdCl_2$ was utilized, **8** was obtained in only 25% yield. These

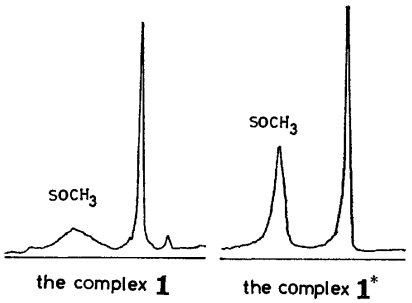

Fig. 1. ^1H NMR signals of methyl protons of complexes **1** and **1***.

facts indicate that, in the complex **3**, ligand (**6**) coordinates to $PdCl_2$ strongly enough to retard the cyclotrimerization.

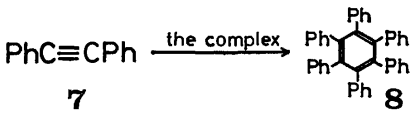

7 **8**

Recently, $(CH_3CN)_2PdCl_2$ was disclosed to promote the rearrangement of 1-alken-3-yl acetates.[7] We also found that **1** catalyzed the conversion of 3-acetoxy-1-tridecene (**9**) to 1-acetoxy-2-tridecene (**10**). When a solution of **9** and **1** (0.03 mol equiv.) in CH_2Cl_2 was stirred at 30 °C for 2 h, a 1:2.1 mixture of **9** and **10** was obtained in a total yield of 92%. Since the ratio remained unchanged even after a prolonged reaction time (16 h), and the similar treatment of **10** afforded a mixture of **9** and **10** in a comparable ratio (1:2.2), it was shown that **9** and **10** were in equilibrium under the present conditions. Although **2** exhibited slight effects on the rearrangement of **9** into **10** (**9**:**10**=10:1 after 149 h), **3** did not promote the rearrangement at all. This tendency seems to be in good relationship with the coordinating strength of the ligand. Furthermore, complex (**1***) with optically active (*R*)-methyl *p*-tolyl sulfoxide was employed in the above rearrangement. Stirring a solution of **9** and **1*** (0.03 mol equiv.) in CH_2Cl_2 gave a mixture of **9** and **10** (1:2.1), but the remained **9** was optically inactive. This phenomenon may be reasonably explained by complete ligand-displacement of **1*** with **9** to produce complex (**12**). For appearance of the optical activity in the remained **9**, complex (**11**) containing both **9** and **4*** must be produced. Hence, we investigated the catalytic rearrangement of **9** in the coexistence of **4***. In the reaction using 0.03 mol equiv. of $PdCl_2$ and

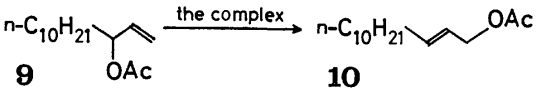

9 **10**

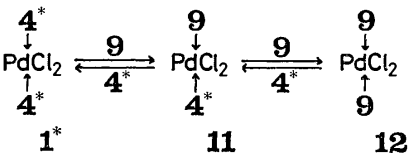

1.0 or 2.0 mol equiv. of **4*** (at room temperature for 8—16 h), no rearrangement took place. When 0.5 mol quiev. of **4*** was used, the rearrangement proceeded slowly and a 10:1 mixture of **9** and **10** was obtained after 16 h. The remained **9** exhibited an optical purity of 2%. This indicates that enantioselectivity in the initial ligand-displacement of **1*** with racemic **9** is approximately 20%.

Thus we have shown that methyl *p*-tolyl sulfoxide (**4**) can coordinate to $PdCl_2$ to make it soluble in CH_2Cl_2, and thus-formed complex (**1**) catalyzes efficiently cyclotrimerization of **7** and rearrangement of **9** to **10** by means of ligand-displacement.

Experimental

The melting points were measured by a Yamagimoto micro melting point apparatus and were uncorrected. The ^1H NMR spectra were taken with a Hitachi R-600 spectrometer, and the IR spectra were recorded on a JASCO A-200 spectrometer. Optical rotations were measured on a JASCO DIP-140 polarimeter.

Bis(methyl p*-tolyl sulfoxide)palladium Dichloride (**1**) and Bis-(methylthiomethyl* p*-tolyl sulfoxide)palladium Dichloride (**2**).* To a solution of **4** (232 mg: 1.50 mmol) in CH_2Cl_2 (10 ml), was added $PdCl_2$ (116 mg: 0.654 mmol), and the resulting mixture was stirred at room temperature for 1 d. Evaporation and recrystallization from benzene-hexane gave **1** as orange crystals (167 mg: 53%): mp 121—122 °C; ^1H NMR ($CDCl_3$): δ 2.42 (6H, s), 3.09 (6H, broad), 7.40 (4H, d, J= 8 Hz), and 7.74 (4H, d, J=8 Hz); IR (KBr): 1148 cm^{-1}. Found: C, 39.60; H, 4.03%. Calcd for $C_{16}H_{20}Cl_2O_2PdS_2$: C, 39.56; H, 4.15%.

In a similar manner, complex **1*** was prepared as orange crystals: mp 75—76 °C (from benzene-hexane).

Complex **2** was analogously obtained in 95% yield: yellow crystals; mp 147—148 °C (from hexane-CH_2Cl_2); ^1H NMR ($CDCl_3$): δ 2.43 (6H, s), 2.67 (6H, s), 4.00 (2H, d, J=13.6 Hz), 4.28 (2H, d, J=13.6 Hz), 7.38 (4H, d, J=8 Hz), and 7.58 (4H, d, J=8 Hz); IR (KBr): 1050 cm^{-1}. Found: C, 37.35; H, 4.17. Calcd for $C_{18}H_{24}Cl_2O_2PdS_4$: C, 37.41; H, 4.19.

*Complex (**3**) of $PdCl_2$ with 1,3-Bis[(*p*-tolylsulfinyl)methylthio]-propane.* To a solution of **6** (300 mg: 0.727 mmol) in CH_2Cl_2 (10 ml), was added $PdCl_2$ (129 mg: 0.728 mmol) and the resulting mixture was stirred at room temperature for 1 d. Evaporation and recrystallization from CH_2Cl_2-hexane afforded **3** as yellow crystals (328 mg: 77%): mp 141—142 °C; ^1H NMR ($CDCl_3$): δ 1.59 (2H, broad s), 2.41 (6H, s), 2.79—3.28 (4H, m), 3.99 (1H, d, J=13 Hz), 4.09 (1H, d, J=13 Hz), 4.67 (1H, d, J=13 Hz), 4.74 (1H, d, J=13 Hz), 7.34 (4H, d, J=8 Hz), and 7.54 (4H, d, J=8 Hz); IR (KBr): 1045 cm^{-1}. Found: C, 38.29; H, 4.05%. Calcd for $C_{19}H_{24}Cl_2O_2PdS_4$: C, 38.68; H, 4.10%.

*Cyclotrimerization of Diphenylethyne (**7**).* To a solution of **7** (200 mg) in CH_2Cl_2 (5 ml), was added **1**, **2**, **3**, or $PdCl_2$ (0.03 mmol equiv. to **7**), and the resulting mixture was stirred at 30 °C for 1 d. Evaporation and chromatography on silica gel [hexane and benzene-CH_2Cl_2 (1:1)] gave **8** as a colorless solid which was identified by comparison of its IR spectrum with that of the authentic sample.[8] The yields of **8** (the recovered **7**) using **1**, **2**, **3**, and $PdCl_2$ were 73.3 mg (127 mg), 7.3 mg (194 mg), 2.4 mg (193 mg), and 4.6 mg (186 mg), respectively. The value in parentheses means the yield of the recovered **7**.

*Rearrangement of 3-Acetoxy-1-tridecene (**9**).* Starting material **9** was prepared by the lit.[9] procedure. Rearrangement product **10** was obtained by the reaction of 1-bromo-2-tridecene (908 mg: 3.48 mmol) with AcOK (425 mg: 4.33 mmol) and KI (8 mg) in AcOH (10 ml) at 80 °C for 11 h, which gave a mixture of **9** and **10** (1:5.05) (617 mg: 74%): a colorless oil; IR (neat): 1742 cm^{-1}. Found: C, 75.07; H, 11.52%. Calcd for $C_{15}H_{28}O_2$: C, 74.95; H, 11.74%. ^1H NMR ($CDCl_3$) of **10** ($CDCl_3$): δ 0.90 (3H, diffused t), 1.31 (18H, broad s), 2.01 (3H, s), 4.51 (2H, d, J=5 Hz), and 5.57 (2H, m).

To a solution of **9** (200 mg) in CH_2Cl_2 (10 ml), was added **1** (12 mg: 0.03 mol equiv.), and the resulting mixture was stirred at 30 °C for 2 h under nitrogen atmosphere. Evaporation and chromatography on silica gel [benzene-hexane (1:1)] gave a mixture (184 mg) of **9** and **10**, the ratio of which was determined to be 1:2.1 by a GLC analysis [Silicone DC 550 column (1 m)/nitrogen gas carrier (1 kg/cm^2)/160 °C].

*Rearrangement of **9** in the Coexistence of **4***.* After $PdCl_2$ (8.8 mg) was added to a solution of **4*** (129 mg) in CH_2Cl_2 (5 ml) and the resulting mixture was stirred at room temperature for 3 h, **9** (400 mg) was added together with CH_2Cl_2 (15 ml). The mixture was further stirred for 16 h at room temperature. Evaporation and chromatography gave a mixture (382 mg) of **9** and **10** (10:1) which showed α_D of 0.022± 0.002 ($CHCl_3$, *c* 15.1), *i.e.* $[\alpha]_D$ of 0.16. The optical purity of the remained **9** was calculated to be 2.0%, from the lit.[9] value ($[\alpha]_D$ +7.28 for (*R*)-**9** of 91.8% e.e.).

References

1) B. R. James and R. S. McMillan, *Can. J. Chem.*, **55**, 3927 (1978) and the references cited therein.

2) At the present time, the data for the geometric isomerism of **1** and **2** are not available, but these complexes are thought to have *trans*-geometry by analogy to the already reported facts that the geometry of $PdCl_2$ complex having a sulfide[3] or a sulfoxide[4] as a ligand is *trans*.

3) R. J. H. Clark and G. Natile, *J. Chem. Soc., A*, **1970**, 659.

4) W. Kitching and C. J. Moore, *Inorg. Nucl. Chem. Lett.*, **4**, 691 (1968).

5) J. H. Price, A. N. Williamson, R. F. Schramm, and B. B. Wayland, *Inorg. Chem.*, **11**, 1280 (1972).

6) The catalytic cyclotrimerization of alkynes to produce benzene derivatives has been intensively studied: C. W. Bird "Transition Metal Intermediates in Organic Synthesis," Logos Press, London, 1967; P. M. Maitlis "The Organic Chemistry of Palladium, "Academic Press, New York (1971); P. N. Rylander, "Organic Synthesis with Novel Metal Catalysts," Academic Press, New York (1973); J. Tsuji, "Organic Synthesis by Means of Transition Metal Complexes," Springer-Verlag, West Berlin and Heidelberg (1975); P. M. Maitlis, *Acc. Chem. Res.*, **9**, 93 (1976).

7) L. E. Overman and F. M. Knoll, *Tetrahedron Lett.*, **1979**, 321.

8) L. F. Fieser, *Org. Synth.*, Coll. Vol. V, 604 (1973).

9) H. Ohta and H. Tetsukawa, *Agric. Biol. Chem.*, **44**, 863 (1980).

The Crystal Structure of the 1-(2-Carboxyethyl)uracil : Phenethylamine (1 : 1) Complex[1]

Toshimasa Ishida,* Keizo Yamamoto, and Masatoshi Inoue
Osaka College of Pharmacy, 2-10-65 Kawai, Mastubara, Osaka 580

(Received August 4, 1982)

Synopsis. The crystal of the title complex is monoclinic, with a space group of Cc, $a=5.678(1)$, $b=33.814(7)$, $c=8.058(2)$ Å, $\beta=103.42(1)°$, and $Z=4$. The two component molecules are linked to each other by hydrogen bonds between the amino and carboxyl groups. No prominent interaction was observed between benzene and uracil rings.

In effort to obtain information bearing on the nature of the interactions between nucleic acid bases and protein side groups, various studies have been done by using the model systems containing these components. As a result, the stacking interaction, as well as hydrogen bonding, with nucleic-acid bases has been found to be essential for the aromatic amino acids.[2-5]

As part of the program aimed at exploring, at atomic resolution, the possible geometrical features of the interaction, we prepared the crystals of the 1:1 complex between 1-(2-carboxyethyl)uracil (CEU) and phenethylamine (PEA) as a model for uracil–phenylalanine interaction. The present paper will report its X-ray crystal structure.

Experimental

CEU, synthesized from uracil and acrylonitrile by the Ueda and Fox method[6] (mp 186—187 °C), was added to a 50% ethanol aqueous solution containing an equimolar amount of PEA.. Transparent platelet crystals were obtained by slow evaporation at room temperature. Although oscillation and Weissenberg photographs showed the space group to be Cc or C2/c, it was assumed to be noncentrosymmetric Cc from the statistical distribution of the normalized structure factors. The crystal data are as follows: $a=5.678(1)$, $b=33.814(7)$, $c=8.058(2)$ Å, $\beta=103.42(1)°$, $Z=4$, $D_m=1.344(1)$, $D_x=1.347$ g cm^{-3}, μ(Cu $K\alpha$)$=8.315$ cm^{-1}, $F(000)=648$. A total of 1297 independent intensity data were collected on a Rigaku four-circle diffractometer with graphite-monochromated Cu $K\alpha$ radiation using the ω-2θ scan technique (sin $\theta/\lambda \leqq 0.588$ Å^{-1}) with a scan speed of 4°/min and a scan width of 1.2°; they were corrected for the Lorentz and polarization factors, but not for the absorption effects (crystal size: $0.4\times0.3\times0.4$ mm^3).

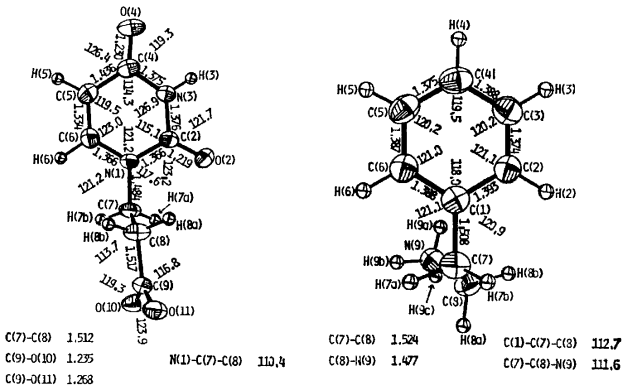

Fig. 1. Atomic numbering of the CEU:PEA complex with the bond lengths (l/Å) and angles (ϕ/°) of non-hydrogen atoms.
E.s.d.'s are 0.003 to 0.004 Å for lengths and 0.2 to 0.3° for angles. This figure also represents the molecular conformations projected onto the uracil and benzene rings.

The structure was solved by the direct method with the MULTAN program.[7] All the non-hydrogen atoms appeared clearly in the E-map, while the hydrogen atoms were found on a difference Fourier map. The R value was finally reduced to 0.029 by the block-diagonal least-squares refinement using the HBLS V program,[8] with anisotropic thermal parameters for non-hydrogen atoms and isotropic ones for hydrogen atoms. The quantity minimized was $\Sigma w(|F_o|-|F_c|)^2$. In the final refinements, the following weighting scheme was used: $w=0.3$ for $F=0.0$, $w=1.0$ for $0.0<F_o\leqq22.0$, and $w=1.0/[1.0+0.464(F_o-22.0)]$ for $F_o>22.0$. All the numerical calculations were carried out on an ACOS-900 computer at the Computation Center of Osaka University. The final positional parameters and equivalent isotropic temperature factors for non-hydrogen atoms are listed in Table 1.[9]

Results and Discussion

The bond lengths and angles for non-hydrogen atoms are given in Fig. 1. The dimensions of the uracil ring are comparable with the published data.[10] The ring is almost planar, with a maximum deviation of 0.014(3) Å at C(4), and the atoms attached to the ring except H(3) lie almost on the plane. The bond sequence of N(1)–C(7)–C(8)–C(9)–O(11) forms a fully

Table 1. Fractional coordinates and isotropic temperature factors of non-hydrogen atoms

The B values are the equivalent isotropic temperature factors calculated from the deposited anisotropic thermal parameters(B_{ij}) using this equation: $B_{eq}=4/3(B_{11}a^2+B_{22}b^2+B_{33}c^2+acB_{13}\cos\beta)$.

Atom	x	y	z	B_{eq}/Å^2
CEU				
N(1)	0.1547(3)	0.05736(5)	0.1367(2)	2.6
C(2)	0.0277(4)	0.08577(6)	0.0326(3)	2.6
O(2)	0.1016(3)	0.11942(4)	0.0255(2)	3.7
N(3)	−0.1933(4)	0.07383(6)	−0.0645(3)	3.1
C(4)	−0.2980(5)	0.03718(7)	−0.0639(3)	3.6
O(4)	−0.5024(4)	0.03150(6)	−0.1530(3)	5.2
C(5)	−0.1510(5)	0.00898(7)	0.0473(4)	4.2
C(6)	0.0648(5)	0.01999(7)	0.1407(3)	3.7
C(7)	0.3938(4)	0.06855(7)	0.2453(3)	3.0
C(8)	0.3634(4)	0.08753(8)	0.4089(3)	3.3
C(9)	0.5976(4)	0.10321(6)	0.5203(3)	2.6
O(10)	0.7908(3)	0.09612(6)	0.4808(3)	4.0
O(11)	0.5805(3)	0.12337(5)	0.6496(2)	3.0
PEA				
C(1)	0.3822(4)	0.20447(6)	−0.0697(3)	2.9
C(2)	0.2422(5)	0.21917(7)	0.0373(3)	3.3
C(3)	0.3022(5)	0.21176(8)	0.2097(4)	3.7
C(4)	0.5060(5)	0.18946(7)	0.2807(3)	3.8
C(5)	0.6478(5)	0.17502(7)	0.1774(4)	3.7
C(6)	0.5868(4)	0.18259(7)	0.0035(3)	3.3
C(7)	0.3066(5)	0.21043(7)	−0.2600(3)	3.4
C(8)	0.0909(4)	0.18485(7)	−0.3440(3)	3.3
N(9)	0.1377(3)	0.14254(6)	−0.3039(2)	2.9

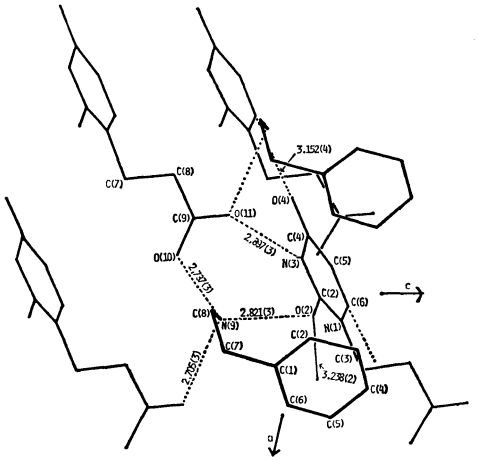

Fig. 2. The molecular arrangement of CEU and PEA in the crystal projected along the b-axis.
The broken lines represent the hydrogen bondings, and the thin line shows the short contact between the O(2) atom of CEU and the benzene ring of PEA.

extended *trans-zigzag* chain, and the torsion angles of C(2)–N(1)–C(7)–C(8), N(1)–C(7)–C(8)–C(9), and C(7)–C(8)–C(9)–O(11) are 84.9(3), −174.8(2), and 172.3(2)° respectively. The carboxyl group makes an angle of 100.6(1)° with the uracil ring. The bond distances and angles of the carboxyl group are in the range of the ionized form.[11]

The bond lengths and angles of PEA are in good agreement with those of phenethylamine[12] and L-phenylalanine.[13] The C–C bond lengths within the benzene ring are in the range of 1.374(4) to 1.393(4) Å (average value of 1.384 Å); this value is slightly shorter than that of the standard aromatic ring (1.395(3) Å).[11] Three hydrogen atoms of H(9a)–H(9c) are tetrahedrally bound to the N(9) atom, indicating the amino group to be in a cationic form. The plane of the aminoethyl group makes an angle of 96.1(1)° with the benzene ring, and the torsion angle of C(1)–C(7)–C(8)–N(9) is −55.3(3)°, in contrast to that of phenethylamine (=−171.1°).

The molecular arrangement projected along the b-axis is shown in Fig. 2. The hydrogen-bond lengths and angles are given in Table 2. In this complex, a salt bridge is formed between the anionic carboxyl group of CEU and the cationic amino group of PEA; the CEU and PEA molecules are linked to each other by three N–H···O hydrogen bonds between the amino nitrogen and carbonyl or carboxyl oxygen atoms [N(9)···O(2), N(9)···O(10) and N(9)···O(11)]. On the other hand, the N(3) of CEU at (x,y,z) is hydrogen-bonded to the O(11) atom of the same molecule translated at $(-1+x, y, -1+z)$, and the O(4) atom is hydrogen-bonded to the C(6) atom translated by the c-glide plane, which forms the *trans-zigzag* connection along the c-axis.

Although the hydrophobic and/or stacking interaction between the aromatic rings was suggested from the solubility study of the phenylalanine–uridine interaction,[14] there was no specific interaction in this crystal; the dihedral angle between the benzene and uracil rings is almost at a right angle [89.1(1)°]. The hydrogen bonds between the acid and amine might be preferable to any specific interaction of the uracil base and the benzene ring.

However, it is of interest to note that the O(2) atom of CEU points to the center of the benzene ring of PEA, with the distance of 3.238(2) Å, and that the angle of the C(2)–O(2) bond to the ring is 74.0°. Even though this distance is slightly longer than the van der Waals separation (3.1 Å), the possibility of interaction between the polarizable π-electron system and the polar carbonyl oxygen atom cannot be disregarded.

Table 2. Hydrogen-bond distances(l/Å) and angles (ϕ/°)

Donor (D)	Acceptor (A)	D----A	H---A	D-H---A
N(3) (CEU)[1]	O(11) (CEU)[2]	2.897(3)	2.00(4)	168(4)
C(6) (CEU)[1]	O(4) (CEU)[3]	3.152(4)	2.16(4)	156(3)
N(9) (PEA)[1]	O(2) (CEU)[1]	2.821(3)	1.92(3)	172(3)
N(9) (PEA)[1]	O(11) (CEU)[4]	2.705(3)	1.77(3)	175(3)
N(9) (PEA)[1]	O(10) (CEU)[1]	2.787(3)	1.85(4)	177(3)

Symmetry code
1) x, y, z 2) $-1+x, y, -1+z$ 3) $1+x, -y, 1/2+z$ 4) $x, y, -1+z$

References

1) This work is Part I of "X-Ray Structural Studies of the Interaction between the Components of Protein and Nucleic Acid."
2) V. Wray and K. G. Wagner, *Z. Naturforsh., Teil. C*, **32**, 315 (1977).
3) E. J. Gabbay, P. D. Adawadkar, and W. D. Wilson, *Biochemistry*, **15**, 146 (1976).
4) C. Héléne and G. Lancelot, *Prog. Biophys. Mol. Biol.*, **39**, 1 (1982).
5) D. Voet, *J. Am. Chem. Soc.*, **102**, 2071 (1980).
6) T. Ueda and J. J. Fox, *J. Org. Chem.*, **29**, 1762 (1964).
7) P. Main, S. E. Hull, L. Lessinger, G. Germain, J. P. Declercq, and M. M. Woolfson, MULTAN78. A System of Computer Programs for the Automatic Solution of Crystal Structures from X-ray Diffraction Data. (1978). University of York, England, and Louvain, Belgium.
8) T. Ashida, HBLS V, The Universal Crystallographic Computing System-Osaka. The Computation Center of Osaka University (1979), p. 53.
9) Lists of the F_o and F_c factors, the anisotropic thermal parameters of non-hydrogen atoms, the coordinates and isotropic temperature factors of hydrogen atoms, the bond lengths and angles involving hydrogen atoms, the equations of least-squares planes of the uracil, carboxyl, and benzene moieties, together with the displacement of atoms from the plane(in Å), and the selected torsion angles are deposited as Document No. 8310 at the Office of the Bulletin of the Chemical Society of Japan.
10) D. Voet and A. Rich, *Prog. Nucleic Acid Res. Mol. Biol.*, **10**, 183 (1970).
11) O. Kennard, "International Tables for X-ray Crystallography," Kynoch Press, Birmingham (1968), Vol. III, pp. 275—276.
12) P. G. Tsoucaris, *Acta Crystallogr.*, **14**, 909 (1961).
13) A. R. Alkaraghouli and T. F. Koetzle, *Acta Crystallogr., Sect. B*, **31**, 2461 (1975).
14) P. D. Thomas and S. K. Podder, *FEBS Lett.*, **96**, 90 (1978).

Preparation of Red Organic Pigment with Phenylated Silica Gel as Core

Mituru SUZUKI, Seisirô ITÔ,* and Tosihide KUWAHARA

Department of Applied Chemistry, Faculty of Science and Engineering, Kinki University, Kowakae, Higashiosaka, Osaka 577

(Received August 9, 1982)

Synopsis. The silanols on the surface of silica gel were chlorinated and a phenyl group was introduced onto the silica gel (≡Si–C_6H_5) by phenylating with phenyllithium. The surface group was derived to a structure similar to Sudan I by nitration, reduction, diazotization, and coupling (with 2-naphthol). The prepared pigment showed approximately the same color as Sudan I, and had very good resistance to water.

We have studied the introduction of alkoxyl groups onto silica gel (as model powder), silica, and titanium oxide by treating with aromatic alcohols [C_6H_5–$(CH_2)_n$–OH], and succeeded in the preparation of red or yellow pigments with metal oxides as core, by deriving the surface alkoxyl group to a structure similar to Sudan I (azo dyestuff) or tartrazine (food color).[1-3] But the surface groups of pigments were lost with hydrolysis in boiling water, because the surface groups were alkoxyl groups.

In this paper, silica gel was used as the reaction model; the surface silanols were chlorinated and a phenyl group was introduced onto the surface of silica gel by the reaction with phenyllithium. Pigment with the same color as Sudan I was prepared by deriving the surface phenyl group to a structure similar to Sudan I, by nitration, reduction, diazotization, and coupling with 2-naphthol.

Experimental

Silica gel (Wakogel C-200) was used as in the previous reports.[1,2] Thionyl chloride and benzene (commercial guaranteed reagent grade) were used after purification.[4] Phenyllithium solution (in cyclohexane–diethyl ether) (Aldrich Chemical Company's reagent) and diethyl ether (anhydrous) (Dotite reagent) were used. Chlorination and phenylation were performed according to one of the methods reported by Wartmann and Deuel:[5] 20 g of silica gel dried sufficiently at 110 °C was added to the mixture of 500 g of benzene and 160 ml of thionyl chloride, and was chlorinated by refluxing under stirring for 3 h. Benzene and thionyl chloride were distilled out and then the chloride of the silica gel was dried under 20 Torr (1 Torr=133.322 Pa) at 60 °C for 2 h. And 700 ml of 0.5 mol/l phenyllithium solution (in the mixture of cyclohexane and diethyl ether) was dropped slowly under cooling by ice bath, and the silica gel was phenylated by heating at 40 °C under stirring for 1 h. After the phenylation, the contents were added into about 500 ml of methanol to decompose the excess phenyllithium which did not react, and were filtered, washed (with methanol, water, and acetone) and vacuum dried (50 °C); the resulting sample was called phenylated. Nitration,[1,2] reduction,[2] diazotization,[1,2] and coupling[1,2] methods were the same as the previous reports.[1,2] The samples of each stage were called nitrated sample, reduced sample, and pigmented sample (which was coupled after diazotization).

IR spectrum and ultimate analysis of carbon and nitrogen were measured for the confirmation of the structure of surface group and the investigation of the character of the surface. The methods and conditions of measurements were the same as in the previous report.[2]

Results and Discussion

An IR spectrum of silica gel treated with phenyllithium after chlorination was shown in Fig. 1. Silica gel treated with phenyllithium exhibits 1420 and 700 cm^{-1} bands which are attributed to Si–C_6H_5. The strength of a 950 cm^{-1} band corresponding to the surface silanols of silica gel[6] decreased slightly. So it was confirmed that the surface silanols were phenylated, and the surface phenyl group was bonded directly to silicon atom on silica gel, as reported by Wartmann and Deuel.[5] The number of introduced phenyl groups calculated by carbon content (Table 1) is 2.76×10^{20} g^{-1}.

Then the phenylated sample was nitrated, reduced, diazotized, and coupled with 2-naphthol to prepare the red pigmented sample. The surface groups were separated from the silica gel core at each stage; their

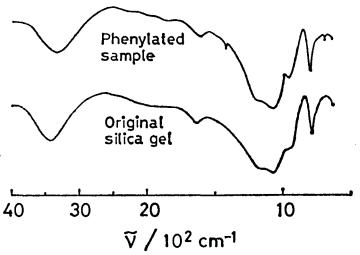

Fig. 1. IR spectra of original and phenylated silica gels.

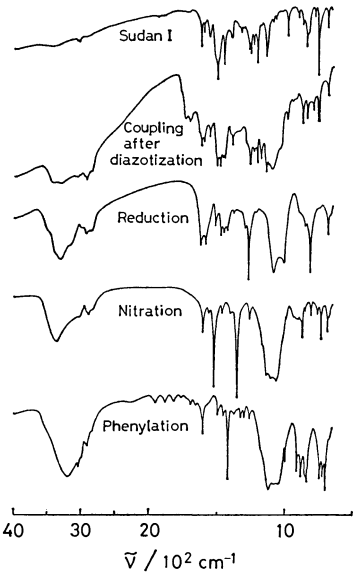

Fig. 2. IR spectra of the surface groups separated from the each sample.

IR spectra are shown in Fig. 2. The core silica gels of samples at each stage were dissolved with hot sodium hydroxide solution and the separated organic surface groups were extracted with ether. The ether extraction from the phenylated sample exhibits absorption bands in the neighborhood of 3000 (weak), 1600 (sharp), 1500 (weak), 1450 (weak), and 700 cm^{-1} (sharp) positions due to aromatic nucleus and also at 1420 (strong), 1120 (strong, shoulder), and 700 cm^{-1} (sharp) due to $Si–C_6H_5$. The bands at 3350 (broad) and 850 cm^{-1} (strong) are due to silanols and those at 1100—1000 cm^{-1} (strong) are due to Si–O–Si. After drying and calcination of the ether extraction part, white ash (SiO_2) remained. These results confirmed that the phenyl group is directly bonded to silicon atom, and that the Si–C bond in $\equiv Si–C_6H_5$ was very stable and did not split even under a severe condition such as in a hot alkali treatment. The ether extraction from the nitrated sample was found to exhibit absorption bands at 1520 (strong) and 1340 cm^{-1} (strong) and 870 cm^{-1} (sharp) positions, the former two bands being due to aromatic nitro group and third one to C–N stretching vibration. This means that the nitro group was introduced on the surface phenyl group. In the extraction from the reduced sample, the bands of the nitro group disappeared and the bands due to aromatic primary amine newly appeared in 3450 (broad), 3350 (broad), 1620 (strong), and 1280 cm^{-1} (strong) positions. The spectrum pattern of pigmented sample which was prepared *via* coupling after diazotization agreed with the pattern of Sudan I. So it was presumed that the surface group was derived to a structure similar to Sudan I by the aforementioned procedure. The strong bands at 1100—1000 cm^{-1} positions, as stated for the phenylated sample, was absorption due to Si–O–Si. The results mean that the red pigment with silica gel as core can be prepared according to the reaction scheme shown in Fig. 3. The pigmented sample showed approximately the same red color as Sudan I, azo dyestuff.

Results of the final analysis for the samples of each stage are shown in Table 1. Values found for the ratio of carbon and nitrogen contents (N/C) almost agreed with calculated values, but were slightly less than the calculated ones. So it was presumed that a small portion of the surface phenyl groups did not react in the further procedure and remained unchanged. The carbon and nitrogen contents of the pigmented sample did not show any decrease after refluxing in water for 5 h. And discoloration also did not occur at all after the refluxing. These results mean that the pigmented samples prepared by this procedure have great resistance to water.

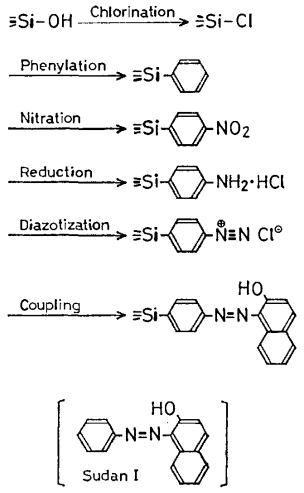

Fig. 3. Postulated reaction scheme.

Table 1. Results of ultimate analysis

Samples	C (%)	N (%)	N/C	
			Found	Calcd
Phenylated sample	3.31	0	—	—
Nitrated sample	3.38	0.55	0.16	0.19
Reduced sample	3.25	0.46	0.14	0.19
Pigmented sample	6.08	0.63	0.10	0.15

References

1) M. Suzuki, S. Itô, and T. Kuwahara, *Chem. Lett.*, **1981**, 1785.
2) M. Suzuki, S. Itô, and T. Kuwahara, *Shikizai Kyokai Shi*, **55**, 280 (1982).
3) M. Suzuki, S. Itô, and T. Kuwahara, *Shikizai Kyokai Shi*, **56**, 73 (1983).
4) L. F. Fieser, "Fieser Yûki-kagaku Zikken," tr by Y. Hirata and K. Nakanishi, Maruzen, Tokyo (1974), pp. 267, 341.
5) J. Wartmann and H. Deuel, *Helv. Chim. Acta*, **42**, 1166 (1959).
6) H. Utsugi, *Nippon Kagaku Kaishi*, **1972**, 2237.

The Formation of Vinyl Sulfides by the Cleavage of the Carbon-Sulfur Bond in Dithioacetals with $CuCl_2$

Tatsuo OIDA,* Shigeo TANIMOTO,* Hideyuki IKEHIRA, and Masaya OKANO
Institute for Chemical Research, Kyoto University, Uji, Kyoto 611

(Received August 14, 1982)

Synopsis. The elimination of arene- and alkanethiol from diaryl and dialkyl dithioacetals, in the presence of copper(I) or copper(II) salt plus tertiary amine, to produce the corresponding aryl and alkyl vinyl sulfides, respectively, has been studied. The employment of a combination of 2 mol equiv. of $CuCl_2$ and 2 mol equiv. of *N,N*-diisopropylethylamine is most favorable.

Cohen and co-workers have reported that, in the presence of *N,N*-diisopropylethylamine, the benzene complex of copper(I) trifluoromethanesulfonate promotes the removal of benzenethiol from the unsaturated or vinylogous diphenyl dithioacetals to produce 1,3-butadienes substituted with a phenylthio group.[1,2] Prior to this work, Mukaiyama and co-workers have found that, in the presence of 2,6-lutidine, the $CuCl_2$-induced reaction of benzaldehyde diethyl dithioacetal with malononitrile in tetrahydrofuran proceeds smoothly to afford the condensation product, benzylidenemalononitrile.[3] They have also found that $CuCl_2$ together with CuO can convert a wide variety of 1,3-dithiane derivatives into the corresponding carbonyl compounds.[4] Since all of these reactions appear to involve a reaction mechanism in which the alkylthio or arylthio group is liberated from the dithioacetal molecule, it can be concluded that, in the presence or absence of tertiary amine, copper(I) or copper(II) salt effects the cleavage of one or two carbon-sulfur bonds in dithioacetals. With these considerations in mind, we have studied the elimination of arene- and alkanethiol from several diaryl and dialkyl dithioacetals, in the presence of copper(I) or copper(II) salt plus tertiary amine, to produce the corresponding aryl and alkyl vinyl sulfides.

In preliminary experiments, phenylacetaldehyde diphenyl dithioacetal (**1a**) and two molar amounts of *N,N*-diisopropylethylamine in benzene[5] were heated at reflux temperature with stirring for 24 h without any reaction occurring. When copper(I) or copper(II) salt was added to the mixture, the expected reaction took place to afford phenyl styryl sulfide (**2a**) and phenyl disulfide (**3a**).

$$\underset{\mathbf{1}}{(RS)_2CHCHR'R''} \xrightarrow[\text{benzene}]{CuX_n,\ \text{tertiary amine}} \underset{\mathbf{2}}{RSCH{=}CR'R''} + 1/2\ \underset{\mathbf{3}}{RSSR}$$

a: R=R'=C_6H_5, R''=H
b: R=C_6H_5, R'=*n*-C_3H_7, R''=H
c: R=C_6H_5, R'=R''=CH_3
d: R=C_6H_5, R'=CH_2=CH–, R''=H
e: R=C_6H_5, R'=CH_2=C(CH_3)–, R''=H
f: R=$C_6H_5CH_2$, R'=C_6H_5, R''=H
g: R=CH_3, R'=C_6H_5, R''=H
h: R=C_2H_5, R'=C_6H_5, R''=H

Table 1 shows that, among these copper(I) and copper(II) salts, only anhydrous $CuCl_2$ is available for the elimination and that even in the case with $CuCl_2$ the use of an excess or a deficiency of this salt causes a significant decrease in the yield.

We then examined the possibility of substituting the other tertiary amines for the *N,N*-diisopropylethylamine employed in the above experiments. Thus when **1a** and two molar amounts of $CuCl_2$ in benzene were heated at reflux temperature with stirring for 24 h, in the presence of a variety of tertiary amines, **2a** and **3a** were obtained in the yields shown in Table 2, together with unchanged **1a**.

As can be seen from Table 2, the addition of tertiary amine is unessential to promote the formation of **2a**, since the yield of **2a** in the absence of any tertiary amine is nearly equal to that obtained in the cases where 2 mol equiv. of *N,N*-diisopropylethylamine or 2,6-lutidine was used. However, it is noteworthy that

Table 1. Reaction of phenylacetaldehyde diphenyl dithioacetal (**1a**) with various copper(I) and copper(II) salts in the presence of *N,N*-diisopropylethylamine

1a 0.2 mmol, *N,N*-diisopropylethylamine 0.4 mml, benzene 20 ml. Reaction conditions: 24 h reflux.

Run	Additive (CuX_n) (equiv.)	Yield/%		Recovered **1a** (%)[a]
		2a[a]	**3a**[a]	
1	None	0	0	
2	$CuCl_2$ (0.5)	7	2	82
3	$CuCl_2$ (1)	9	10	81
4	$CuCl_2$ (2)	49	42	47
5	$CuCl_2$ (4)	2	92	0
6	$CuCl_2$ (1)+CuCl (1)	17	17	72
7	CuCl (2)	12	20	78
8	$Cu(OAc)_2$ (2)	8	7	82
9	$CuBr_2$ (2)	11	95	0
10	$Cu(CN)_2$ (2)	0	0	
11	$CuCl_2 \cdot 2H_2O$	0	0	

a) Determined by GLC using *p*-terphenyl as internal standard.

Table 2. Reaction of phenylacetaldehyde diphenyl dithioacetal (**1a**) with $CuCl_2$ in the presence of a variety of tertiary amines

1a 0.2 mmol, $CuCl_2$ 0.4 mmol, benzene 20 ml. Reaction conditions: 24 h reflux.

Run	Additive (tertiary amine) (equiv.)	Yield/%		Recovered **1a** (%)[a]
		2a[a]	**3a**[a]	
1	None	46	66	25
2	*N,N*-Diisopropylethylamine (1)	40	54	44
3	*N,N*-Diisopropylethylamine (2)	49[b]	42[b]	47[b]
4	*N,N*-Diisopropylethylamine (4)	25	31	64
5	*N,N*-Diisopropylethylamine (8)	5	12	87
6	Triethylamine (2)	6	12	88
7	Pyridine (2)	3	4	95
8	2,6-Lutidine (2)	48	32	47
9	DBU[c] (2)	12	73	0
10	$CuCl_2 \cdot$(pyridine)$_2$ (2)	0	0	

a) Determined by GLC using *p*-terphenyl as internal standard. b) These valuesare identical to those for Run 4 given in Table 1. c) 1,8-Diazabicyclo-[5.4.0]undec-7-ene.

Table 3. Reaction of several dithioacetals (**1a—h**) with $CuCl_2$ in the presence of *N,N*-diisopropylethylamine

Dithioacetal 0.2 mmol, $CuCl_2$ 0.4 mmol; *N,N*-diisopropylethylamine 0.4 mmol, benzene 20 ml. Reaction conditions: 36 h reflux.

Run	Starting dithioacetal	Products (yield/%)[b]	Recovered dithioacetal (%)	Analytical data of product: Found (Calcd) (%) C	H	MS(40 eV) *m/e* M^+
1	**1a**	**2a** (79)	14	78.95(79.20)	5.51(5.70)	212
2	**1b**	**2b** (63)	20	73.96(74.10)	8.05(7.91)	178
3	**1c**	**2c** (77)	10	73.01(73.12)	7.08(7.36)	164
4	**1d**	**2d** (30)	<2	73.88(74.03)	6.04(6.21)	162
5	**1e**	**2e** (36)	<2	75.21(74.95)	6.84(6.86)	176
6	**1f**	**2f** (90)	4	79.40(79.60)	6.09(6.23)	226
7	**1g**	**2g** (54)	26	71.83(71.95)	6.53(6.71)	150
8	**1h**	**2h** (79)	9	73.06(73.12)	7.21(7.36)	164

a) Except **2c**, these products seem to be a mixture of *trans*-isomer and *cis*-isomer in small amounts. The isolation of **3**, which was produced together with **2**, was omitted because of its minor importance. The ^{1}H-NMR spectra (60 MHz, δ, in CCl_4) are as follows: **2a**: 6.41(d, 1H, J=17 Hz), 6.68(d, 1H, J=17 Hz), 7.0—7.7(m, 10H). **2b**: 0.96(t, 3H, J=6 Hz), 1.0—1.8(m, 2H), 1.9—2.4(m, 2H), 5.5—6.3(m, 2H), 7.1—7.3(m, 5H). **2c**: 1.86(s, 6H), 5.86(s, 1H), 7.0—7.3(m, 5H). **2d**: 4.7—5.2 (m, 2H), 6.1—6.7(m, 3H), 7.1—7.5(m, 5H). **2e**: 1.83(s, 3H), 5.86(d, 1H, J=1 Hz), 6.35(d, 1H, J=1 Hz), 6.60(d, 1H, J=10 Hz), 7.17(d, 1H, J=10 Hz), 7.0—7.5(m, 5H). **2f**: 3.70(s, 2H), 6.16(d, 1H, J=15 Hz), 6.48(d, 1H, J=15 Hz), 7.0—7.3(m, 10H). **2g**: 2.22(s, 3H), 6.18(d, 1H, J=17 Hz), 6.69(d, 1H, J=17 Hz), 7.1—7.4(m, 5H). **2h**: 1.23(t, 3H, J=7 Hz), 2.4—2.9(m, 2H), 6.18(d, 1H, J=17 Hz), 6.45(d, 1H, J=17 Hz), 7.0—7.5(m, 5H). b) Yield of isolated product based on **1**.

simply by adding 2 mol equiv. of the tertiary amine to the reaction mixture the proportion of recovered **1a** can be increased to 47% from 25%. An advantage of the employment of the tertiary amine lies in that it suppresses the occurrence of undesirable side reaction. Presumably, an obvious difference in yields of **2a** between the former case and the latter case using 2 mol equiv. of the tertiary amine should be observed if the reaction time is extended over 24 h. On the other hand, the use of a large excess of *N,N*-diisopropylethylamine results in a significant decrease in yield of **2a**. The addition of 2 mol equiv. of triethylamine or pyridine also diminished the yield of **2a**, presumably due to the complex formation between the amine and $CuCl_2$. The inactivity of such a complex is easily understandable if we consider the finding that the pre-formed 1:2 complex between $CuCl_2$ and pyridine does not promote the reaction.

This information concerning the elimination of benzenethiol from **1a** in benzene to produce **2a** could help in accomplishing the conversion of the other dithioacetals (**1**) into the corresponding vinyl sulfides (**2**). Thus, when diaryl and dialkyl dithioacetals in benzene were heated at reflex temperature with stirring for 36 h in the presence of 2 mol equiv. of $CuCl_2$ and 2 mol equiv. of *N,N*-diisopropylethylamine, the moderately good yields of the corresponding aryl and alkyl vinyl sulfides were obtained toegther with disulfides (**3**), suggesting that our procedure is fairly general for this type of elimination reaction. Table 3 shows the results obtained with **1b—h**, including **1a**, as the starting substrate.

Experimental

1a, **1b**, **1c**, **1d**, and **1e** were synthesized in yields of 99, 93, 88, 99, and 91%, respectively, by the reaction of lithiated formaldehyde diphenyl dithioacetal in tetrahydrofuran with each of benzyl bromide, butyl bromide, isopropyl bromide, allyl bromide, and 2-methylallyl chloride.[6] **1g** was prepared in yield of 60%, by the same procedure, from lithiated formaldehyde dimethyl dithioacetal and benzyl bromide. **1f** and **1h** were synthesized in yields of 96 and 90%, respectively, by the *p*-toluenesulfonic acid-promoted interchange reaction of phenylacetaldehyde dimethyl acetal in benzene with α-toluenethiol and with ethanethiol.

Reactions Summarized in Table 1. The copper(I) or copper(II) salt used for each run is listed in Table 1. To a suspension of the salt in 20 ml of benzene were added 0.2 mmol of phenylacetaldehyde diphenyl dithioacetal (**1a**) and 0.4 mmol of *N,N*-diisopropylethylamine under nitrogen. The mixture was heated at reflux temperature with stirring for 24 h. Thirty ml of water was added and the organic layer was separated and subjected to GLC.

Reactions Summarized in Table 2. The tertiary amines used were noted in Table 2. To a suspension of 0.4 mmol of $CuCl_2$ in 20 ml of benzene were added 0.2 mmol of phenylacetaldehyde diphenyl dithioacetal (**1a**) and the tertiary amine under nitrogen. The mixture was heated as above, and similarly worked up. The obtained organic layer was subjected to GLC.

Reactions Summarized in Table 3. To a suspension of 0.4 mmol of $CuCl_2$ in 20 ml of benzene were added 0.2 mmol of a dithioacetal (**1**) and 0.4 mmol of *N,N*-diisopropylethylamine under nitrogen. After the addition was complete, the mixture was heated at reflux temperature with stirring for 36 h. Thirty ml of water and 50 ml of saturated aqueous solution of NH_4Cl were added, and the mixture was extracted with several portions of ether. The combined ethereal extracts were dried, filtered, and concentrated *in vacuo* to give a residue. The products were isolated by column chromatography on silica gel, using 20% benzene–hexane or 10% chloroform–hexane as the eluent.

References

1) T. Cohen, A. J. Mura, Jr., D. W. Shull, E. R. Fogel, R. J. Ruffner, and J. R. Falck, *J. Org. Chem.*, **41**, 3218 (1976), and references therein.

2) T. Cohen and Z. Kosarych, *Tetrahedron Lett.*, **21**, 3955 (1980), and references therein.

3) T. Mukaiyama, K. Narasaka, and H. Hokonoki, *J. Am. Chem. Soc.*, **91**, 4315 (1969).

4) K. Narasaka, T. Sakashita, and T. Mukaiyama, *Bull. Chem. Soc. Jpn.*, **45**, 3724 (1972).

5) In preliminary experiments, it was found that benzene is the most suitable solvent for this reaction.

6) Fröling and Arens found that formaldehyde dialkyl dithioacetal can be metallated easily with $NaNH_2$ or $LiNH_2$ in liquid ammonia and subsequently converted to dialkyl dithioacetals of higher aldehydes by trapping the metallated compound with alkyl halides: A. Fröling and J. F. Arens, *Recl. Trav. Chim. Pays-Bas*, **81**, 1009 (1962).

Palladium-catalyzed Reaction of 4′-Iodobenzocrown Ethers with Acetylenes. Convenient Synthesis of Alkyl-substituted Benzocrown Ethers and Bis(benzocrown ether)s *via* Alkynyl-substituted Benzocrown Ethers

Kiyoshi KIKUKAWA,* AkitoABE, Fumio WADA, and Tsutomu MATSUDA

Department of Organic Synthesis, Faculty of Engineering, Kyushu University, Hakozaki, Higashi-ku, Fukuoka 812

(Received September 11, 1982)

Synopsis. 4′-Iodobenzo-15-crown-5 and -18-crown-6 were alkynylated by heptyne, propargyl alcohol, 1,7-octadiyne and acetylene in good yields with use of $Pd(PPh_3)_2Cl_2$ and CuI as catalysts. The latter two acetylenes gave bis(crown ether)s in one step. Hydrogenation of the alkynylated benzocrown ethers gave 4′-heptyl, 4′-(3-hydroxypropyl)-benzocrown ethers and bis(benzocrown ether)s connected with ethylene or octamethylene linkage.

Functionalized benzocrown ethers have received much attention through not only their modified nature of complexation with cations, but also their specialized utility for analytical[1] and pharmaceutical applications,[2] and as potential intermediates for other functionalized crown ethers, such as polymer-bound crown ethers[3] or bis(crown ether)s.[4] Since halogenation and nitration of benzocrown ethers at 4′-position can be carried out with excellent yields, the transformation of halo[5] or nitro group[6] on benzocrown ethers is one of the promising methods to obtain the functionalized benzocrown ethers. Alkenylated benzocrown ethers have been synthesized by palladium-catalyzed reaction of 4′-halobenzocrown ethers with olefins, such as styrene or acrylic acid and its derivatives.[5] The alkenylation of haloarenes with simple olefins such as 1-octene, however, gives a mixture of regioisomers, *i.e.*, 1-aryloctenes and 2-aryloctenes.[7] Whereas there is no ambiguity of the substituted position in the palladium-copper-catalyzed alkynylation of iodoarenes by terminal acetylenes.[8]

Now we wish to report a convenient transformation of 4′-iodobenzocrown ethers to the alkylbenzocrown ethers and bis(benzocrown ether)s *via* the alkynylated benzocrown ethers.

Results and Discussion

*Alkynylation of 4′-Iodobenzocrown Ethers (**1**).* A solution of a 4′-iodobenzocrown ether(**1**), 1-heptyne, $Pd(PPh_3)_2Cl_2$, and CuI in diethylamine was refluxed for 24 h under nitrogen (Eq. 1).

After evaporation of diethylamine from the reaction mixture, the residue was purified by passing it through a short alumina column with chloroform as eluent.

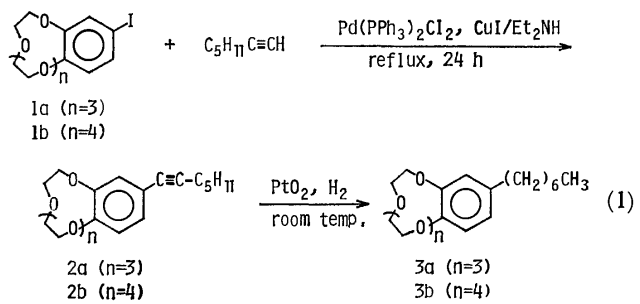

(1)

On being conducted at room temperature as the alkynylation of iodobenzene in the original report,[8] the reaction did not proceed to lead recovery of **1**. Longer reaction time (for 2 d), however, reduced the yield. The use of triethylamine or morpholine instead of diethylamine did not give **2**. Purification of

Table 1. Hydrogenation of alkynylated benzocrown ethers

Products	*n*	Yield[a] %	Mp θ_m/°C	Found (Calcd) (%) C	H
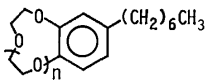	3	76	Oil	68.58, (68.82,	9.30 9.35)
	4	84	Oil	66.65, (67.30,	9.33 9.32)
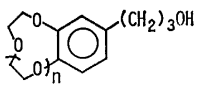	3	70	45.3—48.3	62.30, (62.56,	8.14 8.03)
	4	68	Oil	61.25, (61.61,	8.18 8.16)
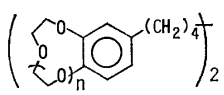	3	76	97.1—99.9	66.72, (66.85,	8.55 8.41)
	4	69	88.4—89.4	65.93, (65.38,	8.76 8.50)
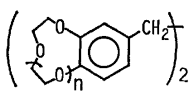	3	75	106.5—108.7	63.97, (64.04,	7.67 7.52)
	4	69	87.6—89.4	62.71, (62.76,	7.80 7.74)

a) Isolated and purified yields based on alkynylated benzocrown ethers.

1 by recrystallization from heptane was found to be essential to obtain good yields, and the present reaction did not proceed when **1** was purified only by column chromatography (alumina–chloroform).

The reaction of **1** with propargyl alcohol and 1,7-octadiyne under the same reaction conditions gave the following compounds, **4** and **5**, respectively. Introduction of acetylene gas to a hot solution of **1**, Pd(PPh_3)$_2Cl_2$, CuI and diethylamine for 3 h gave the bis(benzocrown ether) (**6**). The alkynylated benzocrown ethers in general were obtained in excellent yields, irrespective of the nature of acetylenes.

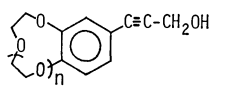

4a (n=3)
4b (n=4)

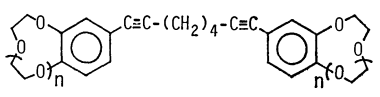

5a (n=3)
5b (n=4)

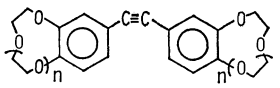

6a (n=3)
6b (n=4)

Hydrogenation of Alkynylated Benzocrown Ethers. The alkynylated benzocrown ethers were effectively hydrogenated by atmospheric hydrogen under PtO_2 catalysis at room temperature (Eq. 1). Typical results are summarized in Table 1.

Since **1** is easily obtained from benzocrown ethers in a good yield, the present method provides a convenient route to prepare functionalized benzocrown ethers, especially a new type of bis(benzocrown ether)s connected with polymethylene linkage.

Experimental

Materials. 1-Heptyne, 1,7-octadiyne, propargyl alcohol, PPh_3, $PdCl_2$, CuI, and PtO_2 were used as received. Diethylamine and methanol were distilled before use. 4′-Iodobenzocrown ethers[9] and Pd(PPh_3)$_2Cl_2$[10] were prepared by the published methods, respectively. 4′-Iodobenzocrown ethers were purified by recrystallization from heptane.

General Procedure. A solution of a **1** (1.0 mmol), an acetylene derivatives (1.2 mmol as ethynyl unit), Pd(PPh_3)$_2Cl_2$ (0.01 mmol), and CuI (0.04 mmol) in diethylamine (10 ml) was refluxed for 24 h under nitrogen. When acetylene was used, acetylene gas was passed through a solution of **1**, Pd(PPh_3)$_2Cl_2$ and CuI in diethylamine under gentle reflux. After removal of diethylamine under reduced pressure, the residue was purified by chromatography (alumina–chloroform) or recrystallization from hexane. In the case of 4′-alkynylated benzo-18-crown-6s which were obtained in *ca.* 61—83% yields, however, small amounts of unknown impurities (2—5%) could not be removed even after purification was repeated several times, although hydrogenation of the crude crown ethers gave easily the corresponding pure hydrogenated products. Therefore the structure of 4′-alkynylated benzo-18-crown-6s was confirmed by both the IR & NMR spectra and elemental analysis of the corresponding hydrogenated crown ethers.

Analytical data of 4′-alkynylbenzo-15-crown-5s are as follows.

*4′-(1-Heptynyl)benzo-15-crown-5(**2a**)*: Yield 87%, oil, NMR ($CDCl_3$) δ=0.93 (–CH_3, t, 3H), 1.15—1.80 (–CH_2–, m, 6H), 2.05—2.55 (–C≡C–CH_2–, t, 2H), 3.50—4.25 (–OCH_2CH_2O–, m, 16H), 6.45—6.91 (aromatic protons, m, 3H), Found: C, 69.06; H, 8.29%. Calcd for $C_{21}H_{30}O_5$: C, 69.59; H, 8.34%.

*4′-(3-Hydroxy-1-propynyl)benzo-15-crown-5(**4a**)*: Yield 73%, mp 118.9—120.3 °C, NMR ($CDCl_3$) δ=2.05 (–OH, s, 1H), 4.4 (–C≡C–CH_2–O–, s, 2H), 3.5—4.3 (–OCH_2CH_2O–, m, 12H), 6.6—7.1 (aromatic protons, m, 3H). Found: C, 63.44; H, 6.93%. Calcd for $C_{17}H_{22}O_6$: C, 63.34; H, 6.88%. **5a**: Yield 88%, mp 108.5—110.7 °C, NMR ($CDCl_3$) δ=1.50—1.95 (–CH_2–, m, 4H), 2.10—2.60 (–C≡C–CH_2–, m, 4H), 3.45—4.15 (–OCH_2CH_2O–, m, 32H), 6.45—6.95 (aromatic protons, m, 6H), Found: C, 67.33; H, 7.37%. Calcd for $C_{36}H_{46}O_{10}$: C, 67.69; H, 7.26%. **6a**: Yield 98%, mp 125.4—127.0 °C, NMR ($CDCl_3$) δ=3.6—4.3 (–OCH_2CH_2O–, m, 32H), 6.6—7.2 (aromatic protons, m, 6H). Found: C, 64.33; H, 6.94%. Calcd for $C_{30}H_{38}O_{10}$: C, 64.50; H, 6.86%. The C≡C stretching of the alkynylated benzocrown ethers was generally not observed, except **4a**(2220 cm^{-1}) and 4′-(3-hydroxy-1-propynyl)benzo-18-crown-6 (2220 cm^{-1}).

Hydrogenation of the alkynylated benzocrown ethers was carried out by atmospheric hydrogen with PtO_2 in methanol at room temperature. After removal of solvent and catalyst, the products were easily purified by chromatography (alumina–chloroform) or recrystallization from hexane, The structure of 4′-alkylbenzocrown ethers was also confirmed by IR, NMR, and elemental analysis.

References

1) H. Nakamura, H. Nishida, M. Takagi, and K. Ueno, *Bunseki Kagaku*, **31**, E 131 (1982).

2) G. R. Brown and A. J. Foubister, *J. Med. Chem.*, **22**, 997 (1979).

3) E. Blasius and P. G. Maurer, *Makromol. Chem.*, **178**. 649 (1977).

4) F. Wada, R. Arata, T. Goto, K. Kikukawa, and T. Matsuda, *Bull. Chem. Soc. Jpn.*, **53**, 2061 (1980).

5) K. Kikukawa, S. Takamura, H. Hirayama, H. Namiki, F. Wada, and T. Matsuda, *Chem. Lett.*, **1980**, 511.

6) K. Kikukawa, K. Nagira, and T. Matsuda, *Bull. Chem. Soc. Jpn.*, **50**, 2207 (1977); W. H. Feigenbaum and R. H. Michel, *J. Polymer Sci., A-1*, **9**, 817 (1971).

7) R. F. Heck, *Acc. Chem. Res.*, **12**, 146 (1979). K. Kikukawa, K. Nagira, F. Wada, and T. Matsuda, *Tetrahedron*, **37**, 31 (1981).

8) K. Sonogashira, Y. Toda, and N. Hagihara, *Tetrahedron Lett.*, **50**, 4467 (1975).

9) E. M. Hyde, B. L. Shaw, and I. Shephered, *J. Chem. Soc., Dalton*, **1978**, 1696.

10) M. R. Kharasch, R. C. Seyler, and F. R. Mayo, *J. Am. Chem. Soc.*, **60**, 882 (1938).

Primary Structure and Molecular Evolution of Intestinal Calcium-binding Protein

Yôichi IIDA

Department of Chemistry, Faculty of Science, Hokkaido University, Sapporo 060

(Received September 18, 1982)

Synopsis. The primary structure and the molecular evolution of protein were examined with bovine and porcine intestinal calcium-binding protein (ICaBP). The amino acid sequence of this protein was compared with that of ancestral calmodulin, which had been predicted as the most ancient form in the family of calcium-binding proteins.

Much attention has been paid to the structure and properties of calcium-binding proteins.[1] These proteins interact reversibly with Ca^{2+} to form a protein–Ca^{2+} complex, whose activity is controlled by the cellular flux of Ca^{2+}. They can regulate other enzymatic reactions and cellular processes, thus playing an important role in various biological systems. Of the calcium-binding proteins so far studied, calmodulin (CaM) is the most widely distributed throughout eukaryotes. The highly conserved structure observed in various CaM which had been isolated from phylogenetically diverse species suggests that CaM is probably the most ancient in the family of calcium-binding proteins.[2] In previous papers,[3,4] we examined the primary structure and the molecular evolution of CaM taken from phylogenetically diverse species. One notable feature of the primary structure of CaM is its internal homology. It can be subdivided into four domains having a similar amino acid sequence. This homology implies that the primary structure of CaM should have been elongated by twice events of intragenic duplication. Making use of this internal homology, we could predict, to some extent, the amino acid sequence of ancestral CaM,[3] which is supposed to be the most ancient form of CaM.

On the other hand, another kind of high-affinity calcium-binding proteins has been identified in the intestinal mucosae of a variety of animals, including reptiles, amphibians, birds and mammals.[5,6] These proteins have been shown to exhibit a dependency on vitamin D or its metabolites. Intestinal calcium-binding protein (ICaBP) is an acidic protein with molecular weight of 9000, and appears to bind two Ca^{2+} ions per molecule. Although the molecular role of ICaBP is not known, it is likely that this protein functions analogously to CaM, *i.e.* by conferring calcium sensitivity to another enzymatic reaction.

The amino acid sequence of bovine ICaBP was recently determined by Fullmer *et al.*,[6] while that of porcine ICaBP, by Hofmann *et al.*[5] For the complete amino acid sequences, refer to those references. In the following, we compare the amino acid sequences between ICaBP and the ancestral CaM, and examine the molecular evolution of ICaBP. In connection with this, we also discuss the internal sequence homology of ICaBP itself.

According to our previous analysis,[3] the ancient form of CaM was supposed to be ···HC···HC···, where HC (half-calmodulin) is the amino acid sequence given by Fig. 1, and where HC has two domains of calcium-binding sites. In the sequence of HC, the brackets show amino acid residues which cannot be determined by our analysis. At the birth of CaM, doubling of HC (*i.e.*, ···HC···HC···) occurred through intragenic duplication, resulting in the four calcium-binding sites of CaM. If ICaBP arises from ancestral CaM through evolution, the amino acid sequence of ICaBP will have homology to that of ancestral CaM. Since ICaBP has two calcium-binding sites, we compared the sequences of bovine ICaBP and ···HC··· (former or latter half of ancestral CaM). This result is also shown in Fig. 1, where we found a strong homology between the two sequences. In this figure, solid-line boxes indicate positions for which the amino acid residues of the two sequences are identical, while dashed-line boxes, positions for which the two amino acids are related by functionally conservative replacements. Note that most of the positions of solid-line boxes corresponds to the putative calcium-binding residues as predicted by the Kretsinger model.[7] This fact implies that, in both of ICaBP and CaM, the calcium-binding residues are particularly conservative against evolution. If there occurs significant

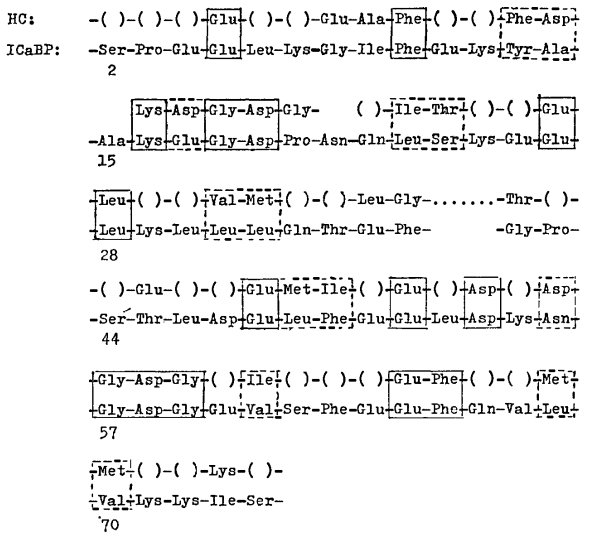

Fig. 1. Comparison of amino acid sequences between ancestral half-calmodulin (HC) and bovine intestinal calcium-binding protein (ICaBP).
Solid-line boxes indicate positions for which the amino acid residues of the two sequences are identical, while dashed-line boxes, positions for which the two amino acids are related by functionally conservative replacements. The sequence of HC was taken from Ref. 3, while that of bovine ICaBP, from Ref. 6. Brackets in HC show amino acids which could not be determined by the analysis described in Ref. 3. Numbers shown in ICaBP indicate positions of amino acid residues as given by Ref. 6.

change of those residues, it will give rise to the loss of calcium-binding function. Thus, the calcium-binding residues have to be highly conservative against evolution.

The strong homology of amino acid sequences between ICaBP and ···HC··· implies that ICaBP should have arisen from ancestral CaM. It was also found that, in order to obtain maximum homology, two amino acid residues of –Ala– and –Asn– should be inserted at positions 15 and 21, respectively, in the sequence of ICaBP, as is shown in Fig. 1. Occurrence of this insertion event in the course of the ICaBP molecular evolution was also supported by examining the internal homology of ICaBP in the following.

As for the homology between ICaBP and ···HC···, a question may arise why the length of the ICaBP sequence is half of that of ancestral CaM. As was mentioned, ICaBP has two domains of calcium-binding sites, while CaM, four domains. If the common ancestor of ICaBP and CaM is the ancient form of ···HC···HC···, the following evolutionary process must have taken place. Since the birth of CaM, CaM has had evolutionary changes and has accumulated accepted point mutations. In the course of evolution, however, several copies of CaM gene have been created by gene duplication, and one of them changed into ICaBP gene at certain time. This change was more drastic than point mutation of amino acid residues. Deletion of former or latter half of the amino acid sequence took place in CaM, and the remaining half of the sequence became ICaBP. The time of such creation of ICaBP may probably be the time when the common ancestor of amphibians, reptiles, birds and mammals appeared, because ICaBP's are found only in the intestines of those animals. After divergence from CaM, ICaBP has received independently accepted point mutations and two amino acid insertions of –Ala– and –Asn– as mentioned above. In Fig. 1, the amino acid sequence of HC is considered as the original one. Then, in ICaBP, those amino acid residues which are no longer identical with those of HC correspond to the residues which have received accepted point mutations. The insertion of two amino acid residues in ICaBP should have taken place after the divergence from CaM, because no such amino acid insertion is detected in CaM. Note that several other copies of CaM gene diverged into various related proteins, such as troponin C, to form the family of calcium-binding proteins.

As for the ancestor of ICaBP, a question may arise if there is any possibility that the ancestor of ICaBP may not be ···HC···HC··· but may be HC itself. However, this possibility can be rejected because of the following reasons. (1) ICaBP is distributed only in the intestines of amphibians, reptiles, birds and mammals. On the other hand, there is an evidence that HC had been living before the birth of ancestral CaM.[3] If the ancestor of ICaBP is not CaM but HC, the descendant protein of HC should be distributed widely in phylogenetically diverse species including fungi and plants. (2) Evolutionary rate of ICaBP is much more rapid than that of CaM. It is very hard to consider that such a rapidly changing protein may be originated from so early living HC. (3) There is another example of calcium-binding protein which has lost long amino acid sequence. Parvalbumin, which also arose from CaM, lost a quarter of the whole sequence.[7]

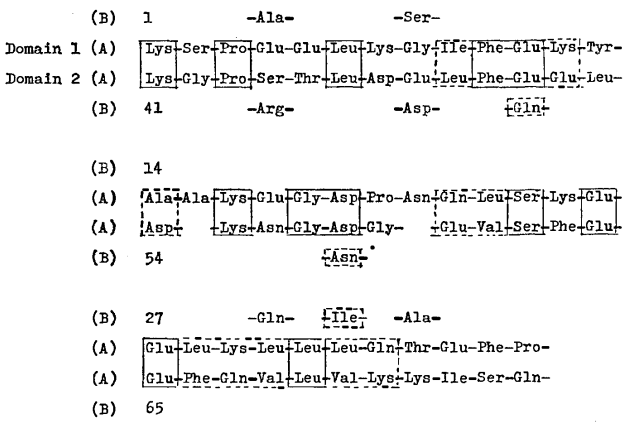

Fig. 2. Internal homology of amino acid sequences of bovine (A) and porcine (B) intestinal calcium-binding proteins (ICaBP).
In each case, the former half (Domain 1) and the latter half (Domain 2) of the sequence are compared. For solid-line boxes, dashed-line boxes and numbers given in the figure, see the caption of Fig. 1. The sequence data were taken from Refs. 5 and 6.

Finally, the amino acid sequence of ICaBP is also found to possess internal homology, that is, the former half of the sequence is very similar to the latter half. This is shown with bovine and porcine ICaBP in Fig. 2. Again, in this case, insertion of two amino acid residues of –Ala– and –Asn– is necessary to obtain maximum homology. The internal homology of ICaBP is well explained if we consider that CaM can be subdivided into four domains with similar amino acid sequences and that ICaBP corresponds to the former or latter half of the CaM sequence.

References

1) See, for example, "Calcium-Binding Proteins and Calcium Function," ed by R. H. Wasserman *et al.*, North-Holland Inc., New York (1977).
2) N. Y. Cheung, *Science*, **207**, 19 (1980).
3) Y. Iida, *J. Mol. Biology*, **159**, 167 (1982).
4) Y. Iida, *Bull. Chem. Soc. Jpn.*, **55**, 2683 (1982).
5) T. Hofmann, M. Kawakami, A. J. W. Hitchman, J. E. Harrison and K. H. Dorrington, *Can. J. Biochem.*, **57**, 737 (1979).
6) C. S. Fullmer and R. H. Wasserman, *J. Biol. Chem.*, **256**, 5669 (1981).
7) R. H. Kretsinger and C. E. Nockolds, *J. Biol. Chem.*, **248**, 3313 (1973); R. H. Kretsinger and C. D. Barry, *Biochem. Biophys. Acta*, **405**, 40 (1975).

Benzocyclobutenes Part 8.[1] Geometrical Isomerism of Arylhydrazones of Benzocyclobutene-1,2-dione

Mark Edward CRACKNELL, Michael Charles GOODLAND, and John Frederick William McOMIE*
School of Chemistry, The University, Bristol BS8 1TS, England
(Received June 28, 1982)

Synopsis. Four mono(arylhydrazone)s of benzocyclobutene-1,2-dione (BBD) have been prepared in which the aryl group is 2,4-dinitrophenyl, 4-bromophenyl, phenyl, and 4-nitrophenyl. The first three have been separated into their *E*- and *Z*-isomers whose configurations are assigned on the basis of spectra and R_f values. Improvements in the preparation of BBD from 1,2-dibromo-1,2-dihydrobenzocyclobutene are described.

During studies on reactions of 5,10-diazabenzo-*b*-biphenylene it was found that hydrolysis of this compound with hydrochloric acid in the presence of 2,4-dinitrophenylhydrazine gave the mono(2,4-dinitrophenylhydrazone) of benzocyclobutene-1,2-dione (BBD) (**1**) as a mixture of *E*- and *Z*-isomers.[2] BBD was known to give a bis(2,4-dinitrophenylhydrazone) but attempts to prepare mono-derivatives with hydrazine and tosylhydrazine had given the 1(2*H*)-phthalazinones **2** and **3** respectively.[3] We describe here an improved preparation of BBD and the preparation from it of four monoarylhydrazones also the separation of three of them into their geometrical isomers and the assignment of their configuration.

The monoarylhydrazones were made by treating BBD with one equivalent of the appropriate arylhydrazine. With each reagent a mixture of the *E*- and *Z*-isomers was obtained and those from 2,4-dinitrophenyl-, 4-bromophenyl-, and phenyl-hydrazine were separated by preparative TLC. The mixture of isomers from 4-nitrophenylhydrazine could not be separated. 4-Bromophenylhydrazine gave a variable yield of the 1(2*H*)-phthalazinone **4** (as well as the *E*- and *Z*-hydrazones) depending on the reaction conditions. The structure of the phthalazinone **4** follows from its analysis and its IR spectrum ($\nu_{C=O}$ 1660 and $\nu_{C=N}$ 1595 cm^{-1}; ν_{N-H} was absent) which agrees with that of the 2-tosyl-1(2*H*)-phthalazinone **3** ($\nu_{C=O}$ 1695 and $\nu_{C=N}$ 1600 cm^{-1}). Furthermore the NMR spectrum of compound **4** showed a singlet at δ 8.29 for the azomethine proton and the spectrum did not change when D_2O was added to the solvent, thus confirming the absence of an NH group.

Assignment of Configuration. Our assignments are based on the work of Nashima and co-workers[4] who studied the geometrical isomerism of the 2,4-dinitrophenylhydrazones of four esters of pyruvic acid. They found that in each pair of geometrical isomers the *Z*-isomer (having an intramolecular hydrogen bond between the imino hydrogen and the ester carbonyl group) has the higher R_f value, the longer wavelength of the absorption maximum in the UV/visible spectrum, and the lower C=O and N–H stretching frequencies in the IR spectrum. Our results, shown in the Table 1, are consistent with those of the Japanese workers. Unfortunately most of our compounds were too sparingly soluble in dichloromethane to observe the weak N–H stretching bands. The NMR spectra of each pair of isomers should provide confirmation of the assignments since the hydrogen bonded imine proton should resonate well downfield of the non-hydrogen bonded imine proton. This effect was found by Nashima and co-workers but we were unable to obtain information about the δ_{NH} values, except for compound **9**, because of the low solubility of the arylhydrazones in $CDCl_3$ and CD_3COCD_3. We did not try more polar solvents because they are known to favour interconversion of isomers.[5]

In the above discussion we have tacitly assumed that the *Z*-isomers **5**, **7**, and **9** contain intramolecular N–H···O hydrogen bonds. Scale drawings of these isomers (based on the crystal structure of BBD[6]) show that the relevant N to O distance is about 3.3 Å which is just within the limits for an N–H···O bond (2.6—3.3 Å).[7] However the angle subtended by the atoms N, H, and O can be 134° to 123° depending on the values (from 109° to 120°) chosen for the NNH angle.

TABLE 1. PHYSICAL PROPERTIES OF (*Z*)- AND (*E*)-MONO(ARYLHYDRAZONE)S

Compound	R_f value (CH_2Cl_2/silica gel)	λ_{max}/nm (CH_2Cl_2)	$\nu_{C=O}$/cm^{-1} (CH_2Cl_2)
5	0.35	418	1768
6	0.30	382	1793
7	0.70	434	1760
8	0.50	407	1787
9	0.70	432	1760
10	0.50	408	1782

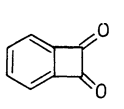

(1)

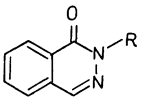

(2) R = H
(3) R = 4-$MeC_6H_4SO_2$-
(4) R = 4-BrC_6H_4-

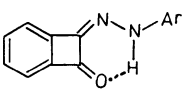

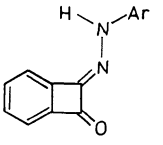

(5) Ar = 2,4-dinitrophenyl (6)
(7) Ar = 4-bromophenyl (8)
(9) Ar = phenyl (10)

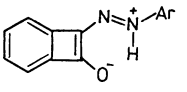

(11)

According to Speakman[7] when the angle NHO becomes less than 140° "genuine hydrogen bonding must become minimal." Nevertheless the physical properties of isomers **5**, **7**, and **9**, compared with those of isomers **6**, **8**, **10**, do suggest intramolecular hydrogen bonding. The actual bond angles in these *Z*-isomers may be more favourable than the scale drawings suggest. Furthermore there is the possibility that the canonical form **11** makes a small but significant contribution which would strengthen the hydrogen bond.

Experimental

IR and UV spectra were measured as solutions in dichloromethane. Some of the UV spectra are qualitative because of the sparing solubility of the arylhydrazones in this solvent. The ^{1}H NMR spectra were recorded on a Varian HA-100 spectrometer. Petroleum refers to light petroleum (bp 60—80 °C). TLC was carried out on silica gel M. F. C. (Hopkin and Williams). The product compositions were estimated from the size of spots on TLC and are therefore very approximate.

Improved Preparation of Benzocyclobutene-1,2-dione. 1,2-Dibromo-1,2-dihydrobenzocyclobutene[8] was freed from iodine-containing impurities by keeping a solution of it (100 g) and bromine (20 g) in carbon tetrachloride (600 ml) for 24 h, preferably in sunlight. The solution was then washed with aqueous sodium hydrogensulfite, dried and distilled in vacuo. A solution of the purified dibromide (20 g) in carbon tetrachloride (300 ml) was irradiated by two 200-W tungsten-filament light bulbs placed under the flask: the heat from the bulbs kept the liquid boiling. Bromine (27.2 g) was added dropwise during 2 h and heating/irradiation was continued for 16 h more. The solvent and excess of bromine were removed under reduced pressure. The residual solid (32.5 g) was recrystallized from petroleum and gave 1,1,2,2-tetrabromo-1,2-dihydrobenzocyclobutene (28.9 g, 90%), mp 118—119 °C (lit,[9] mp 117—118 °C, yield 65%). The tetrabromide was hydrolysed to BBD as previously described.[9]

Benzocyclobutenedione Mono(2,4-dinitrophenylhydrazone). BBD (34 mg) was added to a warm solution of 2,4-dinitrophenylhydrazine (50 mg) in 5 M HCl (5 ml) and the mixture was warmed on a water bath at 60—70 °C for 30 min. The mixture was cooled and the mixture of *E*- and *Z*-isomers (70 mg, 89%) was collected, mp 228—240 °C (the previously recorded[2] mp 249—250 °C was an error). TLC using CH_2Cl_2 showed that the mixture contained roughly equal amounts of both isomers which were separated by preparative TLC (CH_2Cl_2–petroleum, 3:2). The band with the higher R_f value gave the (*Z*)-dinitrophenylhydrazone **5** as an orange solid, mp 235—240 °C; IR 1768 and 1713 cm^{-1}; UV λ_{max} (qualitative) 236, 258 sh, 400, and 418 nm. Found: M$^+$, 312.050. Calcd for $C_{14}H_8N_4O_5$: M, 312.049. The band with the lower R_f value gave the (*E*)-dinitrophenylhydrazone **6** as orange crystals, mp 238—239 °C; IR 1793, 1713, 1615, and 1600 cm^{-1}; UV λ_{max} 236 (log ε 3.96), 256 sh (3.86), and 382 (4.08) nm. Found: M$^+$, 312.050.

Benzocyclobutenedione Mono(4-bromophenylhydrazone). BBD (34 mg) was added to a warm solution of 4-bromophenylhydrazine hydrochloride (54 mg) in 4 M HCl (10 ml) and the mixture was warmed on a water bath at 60—70 °C for 30 min. Next day the solid (51 mg) was collected. The mixture was separated into three components by preparative TLC (elution with CH_2Cl_2). The band with the highest R_f value (0.7) gave the (*Z*)-4-bromophenylhydrazone **7** as a yellow-orange solid, mp 205—206 °C; IR 1760, 1595, and 1070 cm^{-1}; UV λ_{max} (qualitative), 259, 295 sh, 315 sh, 339, and 434 nm. Found: M$^+$, 301.985 and 299.988. Calcd for $C_{14}H_9BrN_2O$: M, 301.987 and 299.987. The band with R_f value 0.5 gave the (*E*)-4-bromophenylhydrazone **8** as yellow-orange crystals, mp 219—220 °C (from ethanol) as major product; IR 1787 and 1570 cm^{-1}; UV λ_{max} 258 (log ε 4.26), 342 (4.10), and 407 (4.12) nm. Found: C, 56.1; H, 3.1; N, 9.4%. Calcd for $C_{14}H_9BrN_2O$: C, 55.8; H, 3.0; N, 9.3%. The band with the lowest R_f value (0.3) gave 2-(4-bromophenyl)-1(2*H*)-phthalazinone **4**, mp 168—169 °C; IR (Nujol) 1657 and 1595 cm^{-1}; UV λ_{max} 236 (log ε 4.42), 270 (3.89), and 303 (3.97) nm; NMR ($CDCl_3$) δ 8.50 (m, H-8), 8.29 (s, H-4), 7.83 (m, H-5,6,7), and 7.62 (s, H-2′,3′,5′,6′). Found: C, 55.6; H, 3.1; N, 9.1%. Calcd for $C_{14}H_9BrN_2O$: C, 55.8; H, 3.0; N, 9.3%. The ratio of *E*- to *Z*-isomer was always about 7 : 1 but the yield of phalazinone increased from about 20 to about 40% when the mixture was heated for longer times.

Benzocyclobutenedione Mono(4-nitrophenylhydrazone). This was made in the same way as the mono(2,4-dinitrophenylhydrazone). The crude product (78% yield) was freed from impurities by soxhlet extraction with acetone to give the mono(4-nitrophenylhydrazone) as yellow crystals, mp 265—266 °C; IR (Nujol) 3360, 3080, 1766, and 1747 cm^{-1}. Found: C, 62.9; H, 3.4; N, 15.7%. Calcd for $C_{14}H_9N_3O_3$: C, 62.9; H, 3.4; N, 15.8%. TLC (CH_2Cl_2) showed two yellow spots very close together but it was impossible to separate the *E*- and *Z*-isomers by preparative TLC.

Benzocyclobutenedione Mono(phenylhydrazone). BBD (67 mg) in hot ethanol (1 ml) was added to a solution of phenylhydrazine hydrochloride (73 mg) and sodium acetate (100 mg) in hot water (2 ml), and the mixture warmed on a water bath at 50—60 °C for 2 h. After cooling, the orange-yellow solid (59 mg) was collected. Examination by TLC (CH_2Cl_2) showed one major component (yellow spot, R_f 0.50) with a small component (orange spot, R_f 0.70) in the ratio of about 9 : 1. Recrystallization from ethanol gave the (*E*)-phenylhydrazone **10** as yellow needles, mp 180—183 °C; IR 1782, 1600, and 1042 cm^{-1} (in Nujol N-H stretch at 3310 cm^{-1}); UV λ_{max} 228 (log ε 4.10), 249 (4.09), 290 (3.79), 332 (4.01), and 408 (3.91) nm. Found: C, 75.5; H, 4.3; N, 12.3%. Calcd for $C_{14}H_{10}N_2O$: C, 75.7; H, 4.5; N, 12.6%.

Refluxing a solution of the crude (*E*)-phenylhydrazone (73 mg) in acetic acid (2 ml) increased the amount of orange component (R_f 0.70) in the mixture. Evaporation of the solution followed by preparative TLC (elution with CH_2Cl_2) gave the (*Z*)-phenylhydrazone **9** (20 mg) as red crystals, mp 122—135 °C which recrystallized above 140° to give a mixture of *E*- and *Z*-isomers (confirmed by TLC) as yellow needles, mp 170—178 °C; IR 3350, 3050 (br), 1760, and 1600 cm^{-1}; UV λ_{max} 252 (log ε 4.01), 258 (4.02), 293 (3.88), 334 (4.20), and 432 (4.05) nm; NMR ($CDCl_3$) δ 9.20 (br s, N-H), 7.9—6.7 (m, Ar-H′ s). Found: N, 12.6%. Calcd for $C_{14}H_{10}N_2O$: N, 12.6%.

References

1) N. P. Hacker, J. F. W. McOmie, J. Meunier-Piret, and M. Van Meerssche, *J. Chem. Soc., Perkin Trans. 1*, **1982**, 19.

2) J. W. Barton, M. C. Goodland, K. J. Gould, J. Hadley, and J. F. W. McOmie, *Tetrahedron*, **34**, 495 (1978).

3) M. P. Cava and R. P. Stein, *J. Org. Chem.*, **31**, 1866 (1966).

4) T. Nashima, F. Ishibashi, M. Iwamoto, Y. Aihara, S. Anzai, and G. Yamano, *Bull. Chem. Soc. Jpn.*, **50**, 539 (1977).

5) G. H. Yoder, S. Kennedy, and F. A. Snavely, *J. Org. Chem.*, **43**, 1077 (1978).

6) F. H. Allen and J. Trotter, *J. Chem. Soc., B*, **1970**, 916.

7) J. C. Speakman, "The Hydrogen Bond," The Chemical Society Monographs for Teachers (1975), No. 27.

8) M. P. Cava, A. A. Deana, and K. Muth, *J. Am. Chem. Soc.*, **81**, 6458 (1959).

9) M. P. Cava and K. Muth, *J. Org. Chem.*, **27**, 757 (1962).

Reaction of α,α-Bis(trimethylsilyl)phenylthiomethyllithium with (Chloromethyl)oxiranes. Synthesis of 1-Alkyl-3-phenylthio-3-trimethylsilyl-1-trimethylsiloxycyclobutanes

Takeshi TAKEDA,* Satoru NAITO, Kazuo ANDO, and Tooru FUJIWARA

Department of Industrial Chemistry, Faculty of Technology, Tokyo University of Agriculture and Technology, Koganei, Tokyo 184

(Received August 31, 1982)

Synopsis. The cyclobutanes of the title are produced in good yields by means of the reaction of the title.

Recently many rearrangement reactions with migration of organosilyl group have been studied and a variety of useful methods for the synthesis of carbonyl compounds and silyl enol ethers have been reported.[1] Although the 1,4-silyl group shift from carbon to oxygen is especially an interesting process and would be utilized for the preparation of various γ-trimethylsiloxy carbanions, only a few examples such as reactions of oxiranes with lithium enolate of *N,N*-dimethyl-2-trimethylsilylacetamide,[2] lithium salt of trimethylsilylacetonitrile,[3] and α-(trimethylsilyl)phenylsulfonylmethyllithium[4] have so far been reported.

In the course of our study on reactions using α-thio carbanions, it was found that the cyclobutane derivatives (**3**) were selectively produced by a reaction of the α,α-bis(trimethylsilyl)carbanion (**1**) with (chloromethyl)oxiranes (**2**)[5] which involves the process of 1,4-silyl group shift.

When α,α-bis(trimethylsilyl)phenylthiomethyllithium (**1**) prepared from the corresponding sulfide with butyllithium at 0 °C was allowed to react with **2** in THF at the same temperature, 1-phenylthio-1-trimethylsilyl-3-trimethylsiloxycyclobutanes (**3**) and 3-phenylthio-3-trimethylsilyl-1-cyclobutanols (**4**) were obtained in good yields (Table 1). This reaction may proceed by the initial addition of the anion (**1**) at the less substituted site to the oxirane (**2**), followed by the 1,4-migration of silicon and cyclization, as shown in the following scheme:

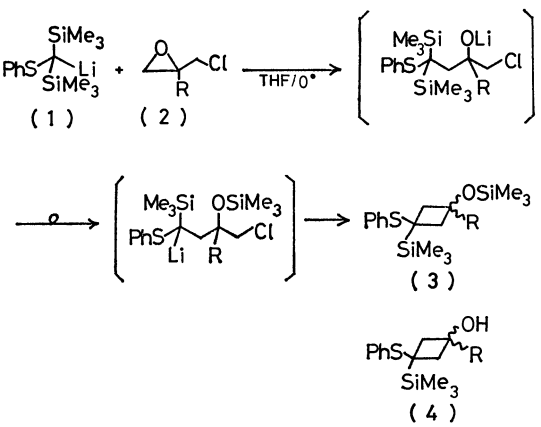

Scheme 1.

Experimental

Reaction of Epichlorohydrin (2) with α,α-Bis(trimethylsilyl)-phenylthiomethyllithium (1). To a THF (6 ml) solution of bis(trimethylsilyl)methyl phenyl sulfide (537 mg, 2 mmol) was added a hexane solution of butyllithium (2.2 mmol) at 0 °C. After stirring for 30 min, THF (2 ml) solution of epichlorohydrin (204 mg, 2.2 mmol) was added to the reaction mixture and stirred for 2 h. The reaction was quenched with a phosphate buffer solution (pH 7) and subjected to extraction with dichloromethane. The extract was dried over Na_2SO_4 and concentrated under reduced pressure. The residue was chromatographed on silica gel (AcOEt–hexane) and trimethylsiloxycyclobutane (**3a**) (238 mg, 37%) and cyclobutanol (**4a**) (205 mg, 41%) were isolated. **3a**: viscous oil; IR (neat) 2950, 1580, 1471, 1248, 1128, 841, 747, and 692 cm^{-1}; ^1H NMR (CCl_4) $\delta=-0.08$ (s, 9H), 0.07 (s, 9H), 1.73—2.65 (m, 5H), 3.57—4.13 (m, 1H), and 7.13—7.66 (m, 5H). **4a**: viscous oil; IR (neat) 3330, 2950, 1580, 1472, 1248, 1117, 840, 748, and 692 cm^{-1}; ^1H NMR (CCl_4) $\delta=0.04$ and 0.08 (2s, 9H), 1.73—2.70 (m, 4H), 2.70—2.93 (br s, 1H), 3.65—4.11 (m, 1H), and 7.09—7.65 (m, 5H). Found: C, 61.91; H, 8.05; S, 12.76%. Calcd for $C_{13}H_{20}OSSi$: C, 61.85; H, 7.99; S, 12.70%.

By a similar procedure, the cyclobutanes (**3b—f** and **4f**) were obtained. **3b**: viscous oil; IR (neat) 2960, 1584, 1474, 1249, 1173, 840, 748, and 693 cm^{-1}; ^1H NMR (CCl_4) $\delta=$ 0.05 (s, 18H), 1.02 (s, 3H), 2.03—2.67 (m, 4H), and 6.97—7.52 (m, 5H). Found: C, 60.38; H, 8.94; S, 9.48%. Calcd for $C_{17}H_{30}OSSi_2$: C, 60.29; H, 8.93; S, 9.47%. **3c**: viscous oil; IR (neat) 2955, 1582, 1437, 1248, 1162, 837, 747, and 692 cm^{-1}; ^1H NMR (CCl_4) $\delta=0.05$ (s, 18H), 0.48—0.84 (m, 3H), 0.96—1.38 (m, 2H), 2.02—2.59 (m, 4H), and 7.02—7.48 (m, 5H). Found: C, 61.37; H, 8.87; S, 8.94%. Calcd for $C_{18}H_{32}OSSi_2$: C, 61.30; H, 9.15; S, 9.09%. **3d**: viscous oil; IR (neat) 2955, 1581, 1438, 1249, 1137, 838, 748, and 693 cm^{-1}; ^1H NMR (CCl_4) $\delta=0.04$ (s, 18H), 0.62—1.38 (m, 9H), 1.99—2.62 (m, 4H), and 7.01—7.47 (m, 5H). **3e**: viscous oil; IR (neat) 2955, 1583, 1439, 1250, 1134, 843, 749, and 697 cm^{-1}; ^1H NMR (CCl_4) $\delta=0.08$ and 0.12 (2s, 18H), 1.21—1.75 (m, 4H), 2.05—2.78 (m, 6H), and 6.71—7.57 (m, 10H). **3f**: viscous oil; IR (neat) 2950, 1582, 1438, 1249, 1129, 845, 745, and 694 cm^{-1}; ^1H NMR (CCl_4) $\delta=-0.32$ (s, 9H), 0.16 (s, 9H), 2.82 (s, 4H), and 6.60—7.36 (m, 10H). **4f**: mp 107—108 °C (hexane–benzene); IR (KBr) 3460, 2960, 1571, 1253, 1127, 851,

TABLE 1.

Entry	R	Yield/% 3	Yield/% 4
a	H	37	41
b	CH_3	73	—
c	CH_3CH_2	58	—
d	$CH_3(CH_2)_3$	53	—
e	$Ph(CH_2)_2$	74	—
f [a]	Ph	30	5

a) Acetophenone and phenyl 1-(trimethylsilyl)vinyl sulfide were isolated as by-products.

752, and 700 cm^{-1}; ^1H NMR (CCl_4) δ=0.17 (s, 9H), 1.58 (s, 1H), 2.72 (s, 4H), and 6.57—7.49 (m, 10H). Found: C, 69.48; H, 7.40; S, 9.68%. Calcd for $C_{19}H_{24}OSSi$: C, 69.46; H, 7.36; S, 9.76%.

References

1) For example: K. Sachdev and H. S. Sachdev, *Tetrahedron Lett.*, **1976**, 4223; H. J. Reich, J. J. Rusek, and R. E. Olson, *J. Am. Chem. Soc.*, **101**, 2225 (1979); I. Kuwajima and M. Kato, *Tetrahedron Lett.*, **21**, 623 (1980); D. J. Ager, *ibid.*, **22**, 587 (1981); I. Kuwajima and R. Takeda, *ibid.*, **22**, 2381 (1981); C. P. Casey, C. R. Jones, and H. Tukada, *J. Org. Chem.*, **46**, 2089 (1981).

2) R. P. Woodbury and M. W. Rathke, *J. Org. Chem.*, **43**, 1947 (1978).

3) I. Matsuda, S. Murata, and Y. Ishii, *J. Chem. Soc., Perkin Trans. 1*, **1979**, 26; I. Matsuda, S. Murata, and Y. Izumi, *Bull. Chem. Soc. Jpn.*, **52**, 2389 (1979).

4) M. Isobe, M. Kitamura, and T. Goto, *Tetrahedron Lett.*, **1979**, 3465.

5) F. Johnson, J. P. Panella, and A. A. Carlson, *J. Org. Chem.*, **27**, 2241 (1962).

 © 1983 The Chemical Society of Japan Bull. Chem. Soc. Jpn., 56, 969—979 (1983)

Importance of Work Terms in the Free Energy Relationship for Electron Transfer

Shunichi Fukuzumi† and Jay K. Kochi*

Department of Chemistry, Indiana University, Bloomington, Indiana 47405, U.S.A.

(Received July 2, 1982)

The rates of arene and alkene brominations and mercurations, Diels-Alder cycloaddition as well as alkylmetal cleavages by electrophiles, electron acceptors and free atoms can be quantitatively analyzed in terms of the driving force for electron transfer. The single, unified free energy relationship for all of these rather disparate chemical processes relates the activation free energy to the standard free energy change for electron transfer and the work term for ion-pair formation. The latter is evaluated from charge transfer spectral data of the electron donor-acceptor complexes formed as transient intermediates. The large variations in the apparent Brönsted slopes from unity to even negative values in these systems can be readily attributed to changes in the work terms arising from steric effects in ion-pair formation.

Electron transfer mechanisms are receiving increased attention in a wide variety of reactions previously formulated as more conventional ionic or concerted processes. Let us consider for example such conventional transformations as (1) the addition of halogen to alkenes, (2) aromatic substitution, (3) Diels-Alder reactions, and (4) halogenolysis of organometals. The activation process for each is commonly represented by a single step shown in the following classical examples:

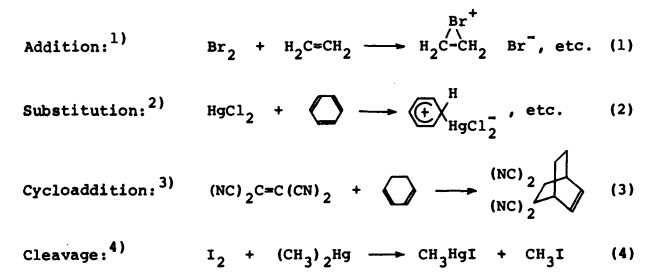

[Note that the activation processes in Eqs. 1 and 2 are subsequently followed by one or more rapid steps to afford the final products.]

The same transformations can be represented by an alternative two-step mechanism in which electron transfer is rate-limiting, *i.e.*,

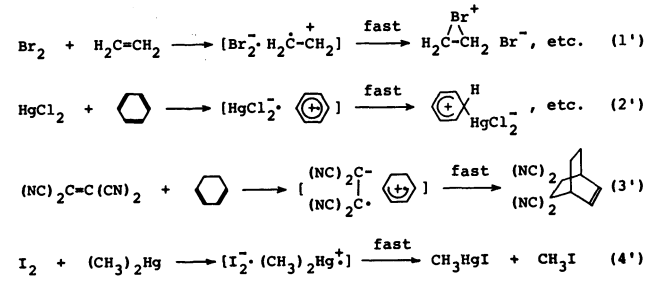

In this formulation, the followup steps are sufficiently rapid to render the initial electron transfer to be part of an overall irreversible transformation. Such mechanisms have been referred to as SET, or single electron transfer,[5,6] since they derive their driving force from one component (A=Br_2, $HgCl_2$, $(NC)_2C{=}C(CN)_2$, I_2) acting as an one-electron acceptor relative to the other component (D=$H_2C{=}CH_2$, C_6H_6, C_6H_8, $(CH_3)_2Hg$) which is then considered to be the electron donor.[7]

Since electron transfer mechanisms such as these are likely to be considered with increasing frequency in organic and organometallic chemistry, we wish to present in this paper the quantitative relationship between the rate of the reaction and the energetics of the electron transfer process. Such a free energy relationship (FER) would provide a better means to evaluate electron transfer mechanisms and also to facilitate their further analysis.

Mechanistic Formulation of Electron Transfer. Importance of the Work Term

The viability of the electron transfer mechanism is usually evaluated in the light of the standard potentials E^0 for each redox couple, *i.e.*, E^0_{ox} for the oxidation of the donor ($D \rightarrow D^+ + e$) and E^0_{red} for the reduction of the acceptor ($A + e \rightarrow A^-$). Thus the general reaction scheme for an irreversible process is represented by:[8]

$$D + A \overset{K_{DA}}{\rightleftharpoons} [D\ A] \overset{k_{et}}{\longrightarrow} [D^+A^-] \overset{fast}{\longrightarrow} \text{Products}, \quad (5)$$

in which electron transfer in the encounter complex [D A] is rate-limiting. This scheme is particularly applicable to systems which lie in the endergonic region of the driving force [*i.e.*, where the standard free energy change, $\Delta G^0 \gg 0$]. The observed second-order rate constant k_{obsd} is then given by:

$$k_{obsd} = k_{et}K_{DA}, \quad (6)$$

where K_{DA} is the formation constant of the complex and k_{et} is the intramolecular rate constant for electron transfer. The thermochemical cycle for an irreversible electron transfer in the highly endergonic region[9,10] is schematically illustrated below. In such a highly endergonic region, the activation free energy for electron transfer ΔG^* in the encounter complex is considered to be equal to the free energy change for the ion pair formation, and thus given by Eq. 10 (Scheme 1),[10]

$$\Delta G^* = \Delta G^0 + w_p - w_r, \quad (7)$$

where ΔG^0 corresponds to the standard free energy

† Present address: Department of Applied Chemistry, Faculty of Engineering, Osaka University, Suita, Osaka 565.

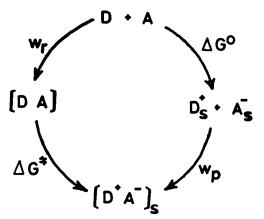

Scheme 1.

change of the redox process: $D+A \rightarrow D^+ + A^-$, and the work terms w_p and w_r represent the energy required to bring together the products and reactants, respectively, to within the mean separation r_{DA} in the ion pair $[D^+ A^-]$. The observed second-order rate constant in Eq. 6 can be expressed in terms of the activation free energy for electron transfer ΔG^* in the encounter complex and the work term w_r as:[11]

$$k_{obsd} = \frac{\kappa T}{h} \exp\left[-\frac{(\Delta G^* + w_r)}{RT}\right]. \quad (8)$$

The combination of Eqs. 7 and 8 affords the free energy relationship for electron transfer as:

$$\log k_{obsd} = -\frac{1}{2.3\,RT}(\Delta G^0 + w_p) + C_1, \quad (9)$$

where $C_1 = \log(\kappa T/h)$ is taken as 12.8 at 298 K. Since the free energy change for electron transfer ΔG^0 is obtained from the standard potentials of the acceptor and donor [*i.e.*, $\Delta G^0(\text{in V}) = E^0_{ox} - E^0_{red}$], the free energy relationship in Eq. 9 may be represented by an equivalent form in Eq. 10,

$$\log k_{obsd} = -\frac{1}{2.3\,RT}(E^0_{ox} + w_p) + \text{Constant}, \quad (10)$$

when one is dealing with a series of electron transfer reactions with a fixed acceptor.[12] Thus Eqs. 9 and 10 state that the observed rate constant ($\log k_{obsd}$) for electron transfer can be expressed as the sum of the standard free energy change (ΔG^0) and the work term of the products (w_p). Previous considerations of electron transfer have tended to focus only on the magnitude of ΔG^0, without explicitly taking account the energetics of the ion pair $[D^+ A^-]$ formation, *i.e.*, the work term w_p.[13,16] Such an oversimplication is perhaps understandable if one considers the experimental difficulty of directly evaluating the work terms of ion pairs by the usual procedures. The problem is severely compounded by exceedingly short lifetimes of the transient ion-pairs which must be involved in irreversible electron transfer. We now wish to discuss how the observation of charge-transfer spectra in these systems can be used to evaluate such ion-pairing energies.

Evaluation of the Work Term from Charge-transfer Spectral Data

The intermolecular interaction leading to the precursor complex in Scheme 1 is reminiscent of the electron donor-acceptor or EDA complexes formed between electron donors and acceptors.[18] The latter is characterized by the presence of a new absorption band in the electronic spectrum. According to the Mulliken charge-transfer (CT) theory for weak EDA complexes, the absorption maximum $h\nu_{CT}$ corresponds to the vertical (Franck-Condon) transition from the neutral ground state to the polar excited state.[19,20]

$$[D\ A] \xrightarrow{h\nu_{CT}} [D^+A^-]^* \quad (11)$$

The asterisk identifies an excited ion pair with the same mean separation r_{DA} as that in the precursor or EDA complex. The thermo-chemical cycle for such a charge-transfer transition is schematically illustrated below. The

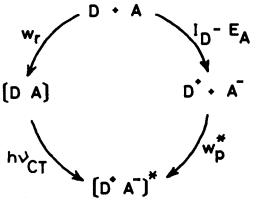

Scheme 2.

vertical ionization potential of the electron donor is represented by I_D, and the electron affinity of the acceptor by E_A.

The charge-transfer Scheme 2 is akin to the adiabatic electron transfer cycle in Scheme 1. In this case the work term w_p^* required to bring the products D^+ and A^- together to the mean separation r_{DA} in the CT excited state is given by:

$$w_p^* = h\nu_{CT} - I_D + C_2, \quad (12)$$

where $C_2 = E_A + w_r$ and considered to be constant for a fixed acceptor.[21] In the limit of simple ion-pair interactions, the work term is largely coulombic, *i.e.*, $w_p^* \cong -e^2/r_{DA}$.

The charge-transfer spectral data listed in Table 1 relate to the various donors and acceptors pertinent to the various reactions described in Eqs. 1—4. In order to assess these systems quantitatively, we relate the work term w_p^* to that of a reference donor w_p^{0*}, since each series in Table 1 involves a fixed acceptor. This comparative procedure allows the acceptor component in a given series to drop out by cancellation, and it follows from Eq. 12 that:[27]

$$\Delta w_p^* = w_p^* - w_p^{0*} = \Delta h\nu_{CT} - \Delta I_D. \quad (13)$$

In Eq. 13, $\Delta h\nu_{CT}$ refers to the relative CT transition energy with a common acceptor, and ΔI_D is the difference in the ionization potentials of the donor and the chosen reference. Thus by selecting a reference donor, we can express all changes in the ion-pairing energies in the CT excited state (including steric, distortional and other effects in the D/A pair) by a single, composite energy term Δw_p^*.

The values of Δw_p^* for a series of EDA complexes are listed in Table 1, together with the ionization potentials of the donors. The reference donor in each series is appropriately designated.

The relative work term Δw_p^* evaluated from the data in Table 1 and Eq. 13 is plotted in Fig. 1 against the ionization potential of the donor for each series of EDA complexes in Table 1. Several features in Fig. 1 are noteworthy. First, the magnitude and the variation of

TABLE 1. CHARGE-TRANSFER TRANSITION ENERGIES AND THE VARIATION OF THE WORK TERM w_p^* OF VARIOUS ELECTRON DONOR-ACCEPTOR COMPLEXES[a]

Donor	I_D / eV	Acceptor	$h\nu_{CT}$ / eV	Δw_p^* / eV
Anthracenes[b]				
1 Anthracene	7.33	TCNE	1.65	0.42
2 9-(Me)anthracene	7.17	TCNE	1.50	0.43
3 9-(Et)anthracene	7.19	TCNE	1.52	0.43
4 9-(Br)anthracene	7.38	TCNE	1.74	0.46
5 9,10-(Me_2)anthracene	7.04	TCNE	1.38	0.44
6 9,10-(Br_2)anthracene	7.44	TCNE	1.77	0.43
7 Benz(α)anthracene	7.47	TCNE	1.76	0.39
Alkylmetals[c]				
8 Me_4Pb	8.90	TCNE	3.01	0.21
9 Me_3PbEt	8.65	TCNE	2.89	0.34
10 Me_2PbEt_2	8.45	TCNE	2.73	0.38
11 $MePbEt_3$	8.26	TCNE	2.59	0.43
12 Et_4Pb	8.13	TCNE	2.52	0.49
13 Me_4Sn	9.69	TCNE	3.59	0†
14 n-Bu_4Sn	8.76	TCNE	2.98	0.32
Arenes[d]				
1 C_6H_6	9.23	Br_2	4.32	0.05
2 MeC_6H_5	8.82	Br_2	4.15	0.29
3 EtC_6H_5	8.76	Br_2	4.15	0.35
4 i-PrC_6H_5	8.69	Br_2	4.13	0.40
5 $MeOC_6H_5$	8.39	Br_2	3.73	0.30
6 o-$Me_2C_6H_4$	8.56	Br_2	4.00	0.40
7 m-$Me_2C_6H_4$	8.56	Br_2	3.97	0.37
8 p-$Me_2C_6H_4$	8.44	Br_2	4.13	0.65
9 1,3,5-$Me_3C_6H_3$	8.40	Br_2	3.79	0.35
Alkenes[e]				
10 $H_2C{=}CH_2$	10.52	Br_2	5.14	−0.42
11 $H_2C{=}CHMe$	9.74	Br_2	4.64	−0.14
12 $H_2C{=}CHEt$	9.63	Br_2	4.61	−0.06
13 $H_2C{=}CH(n\text{-}Pr)$	9.52	Br_2	4.56	0†
14 $H_2C{=}CMe_2$	9.24	Br_2	4.27	−0.01
15 $H_2C{=}CMe(Et)$	9.15	Br_2	4.21	0.02
16 (Z)-MeCH=CHMe	9.12	Br_2	4.25	0.09
17 (E)-MeCH=CHEt	9.04	Br_2	4.24	0.16
18 (E)-MeCH=CH(t-Bu)	8.91	Br_2	4.04	0.09
19 $H_2C{=}CH(t\text{-}Bu)$	9.45	Br_2	4.51	0.02
20 $Me_2C{=}CMe(Et)$	8.21	Br_2	3.57	0.32
21 $Me_2C{=}CMe_2$	8.27	Br_2	3.61	0.30
22 $Me_2C{=}CMe(n\text{-}Pr)$	8.19	Br_2	3.55	0.32
23 $Me_2C{=}CMe(n\text{-}Bu)$	8.15	Br_2	3.52	0.33
24 Cyclohexene	8.95	Br_2	4.16	0.17
Alkylmetals[f]				
25 Me_4Sn	9.69	Br_2	4.73	0†
26 Et_4Sn	8.90	Br_2	4.43	0.49
27 n-Pr_4Sn	8.82	Br_2	4.43	0.57
28 n-Bu_4Sn	8.76	Br_2	4.43	0.66
29 i-Pr_4Sn	8.46	Br_2	4.25	0.75
30 s-Bu_4Sn	8.45	Br_2	4.22	0.73
31 i-Bu_4Sn	8.68	Br_2	4.41	0.69
Alkenes[e]				
1 $H_2C{=}CH(n\text{-}Pr)$	9.52	$Hg(OAc)_2$	5.08	0†
2 $H_2C{=}CH(n\text{-}Bu)$	9.48	$Hg(OAc)_2$	5.06	0.02
3 $H_2C{=}CH(n\text{-}C_6H_{13})$	9.43	$Hg(OAc)_2$	5.04	0.05
4 Cyclohexene	8.95	$Hg(OAc)_2$	4.80	0.29
5 Cycloheptene	8.81	$Hg(OAc)_2$	4.78	0.41
6 (Z)-Cyclooctene	8.97	$Hg(OAc)_2$	4.84	0.31
7 $H_2C{=}CH(t\text{-}Bu)$	9.45	$Hg(OAc)_2$	5.08	0.07
8 (E)-MeCH=CH(t-Bu)	8.91	$Hg(OAc)_2$	4.84	0.37
9 $MeCH{=}CMe_2$	8.68	$Hg(OAc)_2$	4.68	0.44
10 $Me_2C{=}CMe_2$	8.27	$Hg(OAc)_2$	4.52	0.69
Alkylmetals[g]				
11 Me_4Sn	9.69	$HgCl_2$	5.27	0†
12 Et_4Sn	8.90	$HgCl_2$	5.08	0.60
13 n-Pr_4Sn	8.82	$HgCl_2$	5.10	0.70
14 n-Bu_4Sn	8.76	$HgCl_2$	5.12	0.78
15 i-Bu_4Sn	8.46	$HgCl_2$	5.10	0.84
16 i-Pr_4Sn	8.45	$HgCl_2$	5.14	1.10
17 s-Bu_4Sn	8.68	$HgCl_2$	5.12	1.09

a) The reference donor is designated by †. b) From Ref. 26. c) From Ref. 22. d) From Ref. 25. e) From Ref. 24. f) From Ref. 23c. g) From Ref. 23b.

the work term depends strongly on the electron donor as well as the acceptor. Thus w_p^* is rather constant for TCNE when it interacts with various substituted anthracene donors (Fig. 1a), but it decreases significantly as the ionization potential of the organometal donors increases (Fig. 1b). Furthermore, the variation in w_p^* is the largest with organometals, when considered among other donors such as arenes and alkenes. With a particular series of donors, the variation of w_p^* is the largest with the mercury(II) complexes $Hg(OAc)_2$ and $HgCl_2$, among other acceptors such as TCNE and Br_2.

We associate such variations in the work term w_p^* with changes in the mean separation r_{DA} in the EDA complexes. Qualitatively, such changes may be viewed as steric effects which hinder the close approach of the acceptor and the donor.[28] For example, the constancy of w_p^* for the substituted anthracene donors accords with the minor steric perturbation since a substituent is expected to exert on a large π-donor such as a polycyclic aromatic network. By contrast, bulky substituents on alkylmetals can effect large changes in w_p^* owing to the localized nature of the interaction in these σ-donors.[29,30]

Free Energy Relationship for Electron Transfer from the CT Work Terms

Taken all together, the relationships in Fig. 1 graphically underscore the marked variation in the work term w_p^* in the excited ion pair (Scheme 2) as a result of the structural changes in the various donor-acceptor pairs. Moreover the interrelationship between encounter and EDA complexes implies that the work term w_p in the adiabatic ion pair (Scheme 1) can be subject to similar variations arising from structural changes in the donor-acceptor pair. Indeed, we previously showed how the variation of the work terms in the adiabatic ion pairs can parallel those in the excited ion pairs.[17] In order

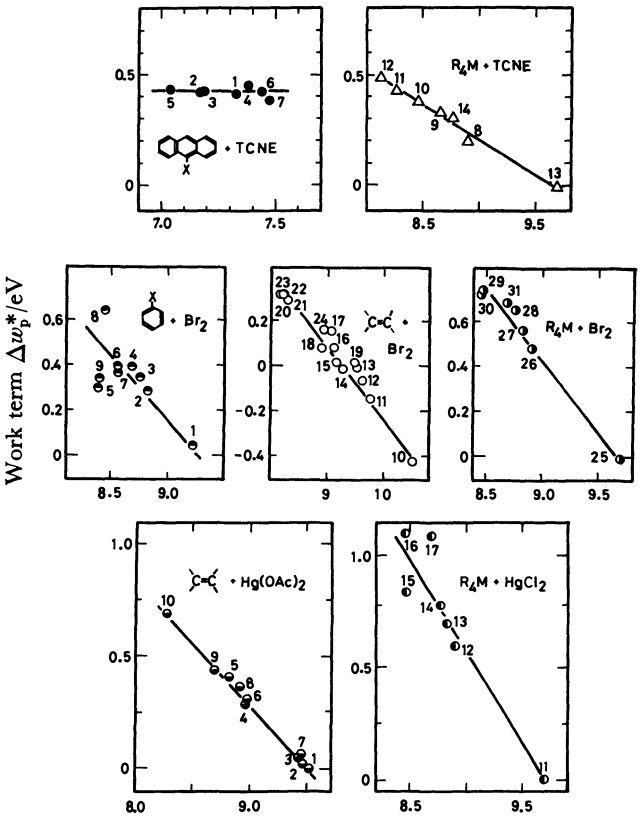

Fig. 1. Variation of the work term w_p* evaluated for the various electron donor-acceptor complexes. The numbers refer to the donors listed in Table 1.

to establish this connection, we initially examined the electron-transfer kinetics of a series of alkylmetal donors R_4M with the inorganic oxidant hexachloroiridate(IV), which is known to effect one-electron transfer, *i.e.*,[31]

$$IrCl_6^{2-} + R_4M \xrightarrow{k} [IrCl_6^{3-}\ R_4M^+]. \quad (14)$$

We next examined the electron transfer kinetics of the same series of alkylmetal donors with the organic electron acceptor tetracyanoethylene, for which the rate-limiting step had been previously established as:[21,32]

$$TCNE + R_4M \xrightarrow{k} [TCNE^-\ R_4M^+]. \quad (15)$$

In both series of electron transfer processes, the free energy relationship was found to be:

$$\log k = -\frac{1}{2.3\,RT}[E^0_{ox} + \Delta w_p^*] + \text{Constant}, \quad (16)$$

where E^0_{ox} is the standard potential for the alkylmetal donor, and the work term Δw_p^* was evaluated from the charge transfer spectral data of the EDA complex [TCNE R_4M] according to Eq. 13.[17,27,33] Thus the experimental free energy relationship in Eq. 16 is equivalent to that (Eq. 10) obtained from Scheme 1.[34]

The successful derivation of this linear free energy relationship encourages us to now apply it to the series of reactions in Eqs. 1—4 which have been variously described as either an electrophilic or a concerted process. Thus let us first consider anthracene cycloaddition with TCNE,

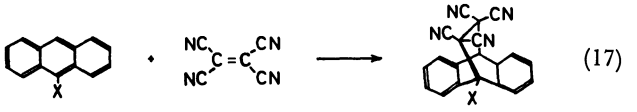

(17)

in the light of alkylmetal insertion,

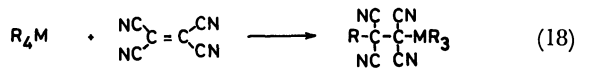

(18)

In the following sections, we will also describe how the same treatment applies to diverse reactions of molecular bromine, mercury(II), and atomic iodine with arene, alkene, and alkylmetal donors.

Diels-Alder Cycloaddition of Anthracenes and Organometal Cleavage with Tetracyanoethylene. New, transient absorption bands are observed immediately upon mixing (1) a series of substituted anthracenes or (2) a series of tetraalkyllead and tin compounds with tetracyanoethylene in either 1,2-dichloroethane or chloroform solutions.[26] With both series of donors, the disappearance of the CT bands coincides with the product formation given in Eqs. 17 and 18. Moreover, the rates of reaction in both series follow second-order kinetics overall—first-order in TCNE and first-order in the anthracenes or the alkylmetals. For convenience, the second-order rate constants are relisted in Table 2 together with the standard potentials E^0_{ox} of the anthracenes and the alkylmetals.

In Fig. 2a, we find a direct relationship between the E^0_{ox} of anthracenes and alkylmetals and their reactivity [$\log(k_{obsd}/M^{-1}\,s^{-1})$; 1 M=1 mol dm^{-3}] toward TCNE.

TABLE 2. SECOND-ORDER RATE CONSTANTS FOR THE REACTIONS OF SUBSTITUTED ALKYLMETALS AND ANTHRACENES WITH TETRACYANOETHYLENE. THE STANDARD POTENTIALS E^0_{ox} OF THE DONORS

Donor	E^0_{ox}/V	$\log(k_{obsd}/M^{-1}\,s^{-1})$	$E^0_{ox}+\Delta w_p^*$/eV
Alkylmetals[a]			
1 Me_4Pb	1.22	−1.49	1.43
2 Me_3PbEt	1.08	−0.28	1.42
3 Me_2PbEt_2	0.97	0.49	1.35
4 $MePbEt_3$	0.87	1.08	1.30
5 Et_4Pb	0.79	1.68	1.28
6 Me_4Sn	1.66	−4.82	1.66
7 *n*-Bu_4Sn	1.14	−2.04	1.46
Anthracenes[b]			
8 Anthracene	0.95	0.52	1.37
9 Benz(α)anthracene	1.05	−1.51	1.44
10 9-(Me)anthracene	0.79	3.04	1.22
11 2-(Me)anthracene	0.89	0.54	1.32
12 9-(Et)anthracene	0.81	2.51[c]	1.24
13 9-(*n*-Pr)anthracene	0.82	2.43[c]	1.25
14 9-(*i*-Pr)anthracene	0.86	1.74[c]	1.29
15 9-(*t*-Bu)anthracene	0.84	1.95[c]	1.27
16 9-(Br)anthracene	0.94	−0.51	1.40
17 9,10-(Me_2)anthracene	0.65	4.60[c]	1.09

a) In acetonitrile at 298 K from Ref. 22. b) In acetonitrile at 298 K from Ref. 26, unless noted otherwise. c) In carbon tetrachloride.

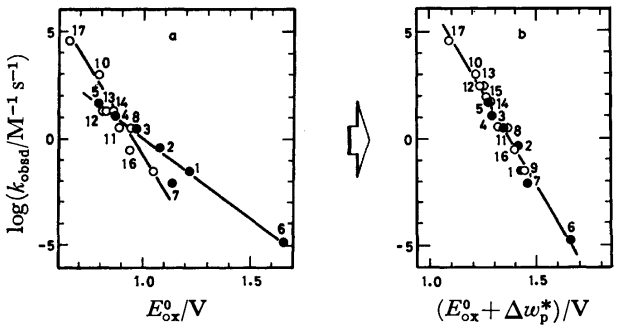

Fig. 2. (a) Free energy relationships for the Diels-Alder reaction of anthracenes (○) and the insertion reaction of alkylmetals (●) with TCNE. (b) Unified free energy relationship with the work term according to Eq. 16. Donors identified by the numbers in Table 2.

The experimental plot shows two linear, but separate correlations described by Eqs. 19 and 20.

Alkylmetal-TCNE:

$$\log k_{obsd} = -\frac{1}{2.3RT}(0.96\,E^0_{ox}) + 16. \quad (19)$$

Alkylmetal-TCNE:

$$\log k_{obsd} = -\frac{1}{2.3RT}(0.45\,E^0_{ox}) + 7.6. \quad (20)$$

It is noteworthy that the two different correlations in Fig. 2a emerge as a single correlation when the work term Δw^*_p is included. The result in Fig. 2b is a linear free energy relationship,[35]

$$\log k_{obsd} = -\frac{1}{2.3RT}(E^0_{ox} + \Delta w^*_p) + \text{Constant}, \quad (16)$$

which applies to both anthracene cycloaddition and alkylmetal insertion. Note the line in Fig. 2b is arbitrarily drawn with a slope of $-1/2.3RT$ to emphasize the fit of both sets of data to Eq. 16.[36] Such an unification is remarkable since these processes clearly represen-inherently dissimilar reaction types. Thus the Diels-Alder reaction is usually considered to involve a concerted [2π+4π] cycloaddition,[3] whereas the alkylmetal insertion requires a multistep scission of a σ carbon-metal bond.[22] The applicability of Eq. 16 to such diverse processes as anthracene cycloaddition and alkylmetal insertion derives from a correspondence of the work term variation, *i.e.*, $\Delta w^*_p = \Delta w_p$.[34]

It must be emphasized that the values of w^*_p are obtained from the independent measurements of the ionization potentials and the CT transition energies in Eq. 12. As such, the constancy of Δw^*_p for the anthracenes in Fig. 1a indicates that the relative rates of cycloaddition with TCNE are solely determined by E^0_{ox}. Thus these Diels-Alder reactions can be classified as irreversible electron transfer processes in which the mean separations in the ion pairs are constant. Indeed the apparent Brönsted slope of nearly unity in Eq. 19 accords with an endergonic electron transfer process.[9,37,38]

Bromination of Arenes, Alkenes, and Alkylmetals. Molecular bromine forms transient EDA complexes with a variety of π-donors (arenes and alkenes)[24,25] as well as σ-donors (alkylmetals).[23] The decay of the charge-transfer bands has been shown to coincide with the bromination of the donor molecules, as given by Eqs. 21—23.

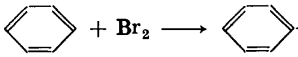
(21)[39]

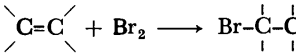
(22)[24]

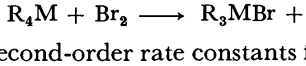
(23)[23]

The second-order rate constants for the arene and alkene brominations have been reported[40] in acetic acid and are relisted in Table 3, together with the second-order rate constants for alkylmetal brominolysis in carbon tetrachloride.[23c] Since the standard potentials of the donors are not known, we used the general relationship in Eq. 24[43,44] to evaluate E^0_{ox} in these solvents.

$$E^0_{ox} = I_D + \Delta G^s - C \quad (24)$$

Table 3. Second-order rate constants for the reactions of alkylmetals, alkenes, and arenes with bromine. The standard potentials E^0_{ox} of donors

Donor	E^0_{ox}/V	log(k_{obsd}/M^{-1} s^{-1})	E^0_{ox}+Δw^*_p/eV
Alkylmetals[a]			
1 Me_4Sn	2.36	−3.72	2.36
2 Et_4Sn	1.77	−1.60	2.26
3 n-Pr_4Sn	1.71	−1.96	2.28
4 n-Bu_4Sn	1.66	−1.89	2.32
5 i-Pr_4Sn	1.44	−0.57	2.19
6 s-Bu_4Sn	1.43	−1.19	2.16
7 i-Bu_4Sn	1.61	−2.62	2.30
Alkenes[b]			
8 H_2C=CH_2	2.66	−0.66	2.24
9 H_2C=CHMe	2.29	1.25	2.15
10 H_2C=CHEt	2.25	1.46	2.19
11 H_2C=CH(n-Pr)	2.19	1.22	2.19
12 H_2C=CMe_2	2.06	3.18	2.05
13 H_2C=CMe(Et)	2.02	3.52	2.04
14 (Z)-MeCH=CHMe	2.00	3.09	2.09
15 (E)-MeCH=CHEt	1.97	3.25	2.13
16 (E)-MeCH=CH(t-Bu)	2.02	2.48	2.11
17 H_2C=CH(t-Bu)	2.15	1.01	2.17
18 Me_2C=CMe(Et)	1.57	5.92	1.89
19 Me_2C=CMe_2	1.57	5.76	1.87
20 Me_2C=CMe(n-Pr)	1.56	5.58	1.88
21 Me_2C=CMe(n-Bu)	1.57	5.62	1.90
22 Cyclohexene	1.96	2.53	2.13
Arenes[c]			
23 C_6H_6	2.82	−11.63	2.87
24 MeC_6H_5	2.41	−8.85	2.70
25 EtC_6H_5	2.35	−8.97	2.70
26 i-PrC_6H_5	2.28	−9.22	2.68
27 $MeOC_6H_5$	1.98	−2.37	2.28
28 o-$Me_2C_6H_4$	2.15	−7.90	2.55
29 m-$Me_2C_6H_4$	2.15	−5.89	2.52
30 p-$Me_2C_6H_4$	2.03	−8.23	2.68
31 1,3,5-$Me_3C_6H_3$	1.99	−3.35	2.34

a) In carbon tetrachloride at 298 K from Ref. 23c. b) In acetic acid at 298 K from Refs. 40 and 41. c) In acetic acid at 298 K from Refs. 40 and 42.

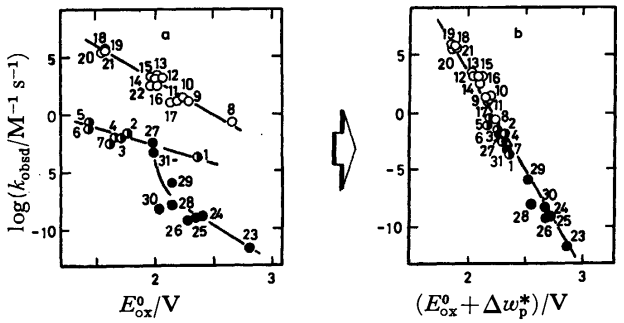

Fig. 3. Brominations. (a) Free energy relationships for arenes (●), alkenes (◑), and alkylmetals (○), as donors identified in Table 3. (b) Unified free energy relationship including the work term as described by Eq. 16.

The free energy change ΔG^s represents the solvation of the donor cation relative to the neutral donor, and are evaluated in Table 6 (see Appendix). C is a constant which includes the potential of the reference electrode on the absolute scale and the junction potential.[44] The relevant values of E^0_{ox} are included in Table 3.

The relationship between the rates of electrophilic bromination ($\log k_{obsd}$) and the standard potentials (E^0_{ox}) of the arene, alkene, and alkylmetal donors is shown in Fig. 3a.[35] Although a rough linear correlation exists for each series,[45] there is no clearcut interrelationship among any of them. However, if the variation of the work term Δw^*_p derived from the CT data in Table 1 is included, the three separate relationships in Fig. 3a become a single correlation. The result in Fig. 3b is the same linear free energy relationship previously expressed in Eq. 16.[46] Indeed the line in Fig. 3b is arbitrarily drawn with a slope of $-1/2.3RT$ to emphasize the correlation of the data with Eq. 16.

Mercuration of Alkenes and Mercurolysis of Alkylmetals. Systems with Large Steric Variations: Transient charge transfer bands are immediately observed when mercury(II) complexes such as mercuric acetate and chloride are mixed with a series of alkene, arene, and alkylmetal donors.[23b,24] The disappearance of the EDA complex of mercury(II) acetate and an alkene is accompanied by the addition reaction in Eq. 25.

$$\text{C=C} + \text{Hg(OAc)}_2 \xrightarrow[\text{MeOH}]{} \text{AcOHg-C-C-OMe} + \text{HOAc} \qquad (25)$$

The rate of this oxymercuration follows overall second-order kinetics in protic solvents such as methanol.[24]

The observed second-order rate constants ($\log k_{obsd}$) for the oxymercuration of various alkenes are collected in Table 4 together with the values of the standard potentials (E^0_{ox}) for the alkene donors in methanol.[47] It is interesting to note that the rates of oxymercuration of electron rich alkenes such as trimethyl- and tetramethylethylene are actually slower than those of normal alkenes such as 1-pentene and 1-octene. Such a trend for $\log k_{obsd}$ to generally decrease with the lowering of E^0_{ox} is in marked contrast to the results in Figs. 2a and 3a. Moreover, the plot of $\log k_{obsd}$ and E^0_{ox} affords the rather random, "buckshot" pattern shown in Fig. 4a. Nonetheless such a nondescript appearance of the data is transformed into the linear correlation shown in Fig. 4b when the work term variation Δw^*_p is included. Although the correlation in Fig. 4b has considerable scatter (owing to the experimental difficulties in the measurement of w^*_p and the limited range of rates), the fit of the data to the line which describes the general free energy relationships of Eq. 16 is unmistakable.[35]

The same relationship applies to the CT interaction of alkylmetals with mercuric chloride leading to the complete scission of a R-M bond,[48] *i.e.*,

TABLE 4. SECOND-ORDER RATE CONSTANTS FOR THE ELECTROPHILIC REACTIONS OF MERCURY(II) COMPLEXES WITH ALKENES AND ALKYLMETALS

	Donor	Acceptor	E^0_{ox}/V	$\log (k_{obsd}/M^{-1} s^{-1})$	$E^0_{ox}+\Delta w^*_p$/eV
	Alkenes[a]				
1	H_2C=CH(n-Pr)	$Hg(OAc)_2$	2.04	1.26	2.04
2	H_2C=CH(n-Bu)	$Hg(OAc)_2$	2.03	1.34	2.05
3	H_2C=CH(n-C_6H_{13})	$Hg(OAc)_2$	2.01	1.30	2.06
4	Cyclohexene	$Hg(OAc)_2$	1.86	0.26	2.15
5	Cycloheptene	$Hg(OAc)_2$	1.78	0.11	2.19
6	(Z)-Cyclooctene	$Hg(OAc)_2$	1.84	−2.28	2.15
7	H_2C=CH(t-Bu)	$Hg(OAc)_2$	2.01	−0.80	2.08
8	(E)-MeCH=CH(t-Bu)	$Hg(OAc)_2$	1.81	−3.00	2.18
9	MeCH=CMe_2	$Hg(OAc)_2$	1.73	0.83	2.17
10	Me_2C=CMe_2	$Hg(OAc)_2$	1.52	−1.96	2.21
	Alkylmetals[b]				
1	Me_4Sn	$HgCl_2$	1.66	0.38	1.66
2	Et_4Sn	$HgCl_2$	1.22	−1.80	1.82
3	n-Pr_4Sn	$HgCl_2$	1.18	−2.43	1.88
4	n-Bu_4Sn	$HgCl_2$	1.14	−2.42	1.92
5	i-Bu_4Sn	$HgCl_2$	1.10	−3.25	1.94
6	i-Pr_4Sn	$HgCl_2$	0.98	−5.30	2.08
7	s-Bu_4Sn	$HgCl_2$	0.97	−6.15	2.06

a) In methanol at 298 K from Ref. 24. b) In acetonitrile at 298 K from Ref. 48.

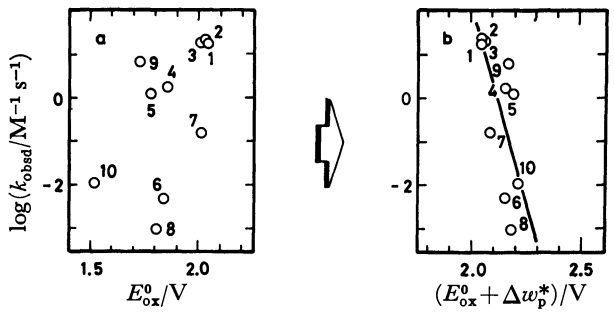

Fig. 4. Oxymercuration of Alkenes. (a) Variation of the rate constant with the standard potentials of the alkene donors identified in Table 4. (b) Unified free energy relationship by inclusion of the work term. The line is arbitrarily drawn with a slope of $-1/2.3RT$ to emphasize the correlation with Eq. 16.

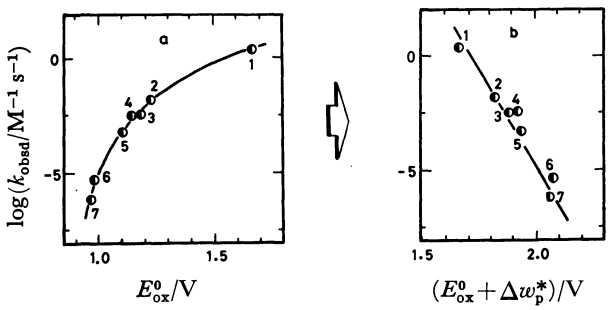

Fig. 5. Alkylmetal Cleavage with $HgCl_2$. (a) Plot of the rate (log k_{obsd}) and the oxidation potentials of the alkylmetal donors identified in Table 4. (b) Unified free energy relationship in which the line is drawn with a slope of $-1/2.3RT$ to emphasize the agreement of the data with Eq. 16.

$$R_4M + HgCl_2 \longrightarrow R_3MCl + RHgCl. \quad (26)$$

Such a cleavage process differs fundamentally from the addition process in Eq. 25, but the rate data listed in Table 4 follows a similar inverse relationship with E^0_{ox}. Thus the apparent Brönsted slope α (which varies with E^0_{ox} in the curved relations shown in Fig. 5a) is clearly negative for these cleavage reactions. Again when the work term Δw^*_p is included with E^0_{ox}, the curved free energy relationship with negative slopes is transformed into the linear correlation in Fig. 5b.

Despite the strong dissimilarity of the addition and the cleavage processes described in Eqs. 25 and 26, they both abide by the same linear free energy relationship described by Eq. 16 when the variation of the work term Δw^*_p is specifically included as a part of the driving force. Moreover, the influence of the work term is sufficiently strong in both of these mercurations to actually invert the negative Brönsted slopes to the unified correlation in Eq. 16. Such an effect underscores the large steric variations extant in these systems. Before commenting on this point further, we wish to describe the application of the free energy relationship to a system in which the CT spectral information is unavailable.

Homolytic Substitution of Alkylmetals by Iodine Atom. The photochemically induced iodinolysis of alkylmetals has been shown to proceed by a radical chain mechanism in which the homolytic S_H2 reaction in Eq. 27 is rate-limiting.[49] The homolytic rate constant (k) for

$$R_4M + I\cdot \xrightarrow{k} R_3MI + R\cdot, \quad (27)$$

the iodinolysis of the various tetraalkyltin compounds in Table 5 have been evaluated relative to tetramethyltin (k_0), and the relative rates (log k/k_0) are plotted in Fig. 6a against E^0_{ox} of the alkylmetal donors.

Table 5. Relative reactivity of alkylmetals in S_H2 cleavage reactions with iodine atom. The stand ardpotentials E^0_{ox} of alkylmetals in carbon tetrachloride[a]

Alkylmetals	E^0_{ox} / V	log (k/k_0)	$E^0_{ox}+\Delta w^*_p$ / eV
1 Me_4Sn	2.36	0	2.36
2 Et_4Sn	1.77	1.71	2.24
3 *n*-Pr_4Sn	1.71	1.69	2.26
4 *n*-Bu_4Sn	1.66	1.71	2.31
5 *i*-Pr_4Sn	1.44	1.58	2.28
6 *s*-Bu_4Sn	1.43	1.68	2.22
7 *i*-Bu_4Sn	1.61	1.01	2.25

a) At 298 K from Ref. 49.

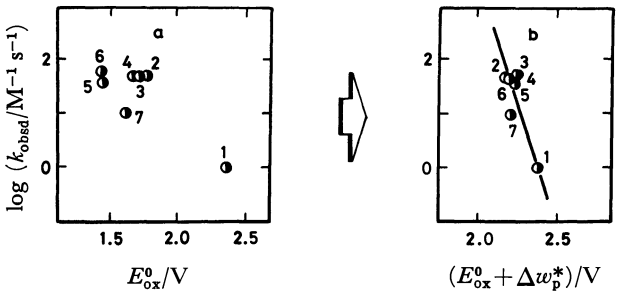

Fig. 6. Homolytic Iodinolysis of Alkylmetals. (a) Variation of the relative rates log (k/k_0) of cleavage of the alkylmetals in Table 5 by iodine atom. (b) Unified free energy relationship with the line arbitrarily drawn with a slope of $-1/2.3RT$ according to Eq. 16.

The charge-transfer spectral data for the EDA complexes in this system are unavailable owing to the transient character of the iodine atom. Thus the values of the work term w^*_p which were previously obtained from the analogous EDA complexes of molecular iodine,[23a] *i.e.*, [R_4M I_2], have been substituted in Table 5. Indeed the resulting free energy correlation shown in Fig. 6b provides a reasonable fit to the general relationship in Eq. 16.[35]

The successful transferal of work terms w^*_p derived from the spectra of *molecular* iodine complexes for use with *atomic* iodine complexes indicates that these acceptors in fact share features in common, despite the substantial difference in the values of their electron affinities (*i.e.*, for I_2, E_A=1.60 eV and for I·, E_A=3.06 eV).[23a] Indeed the steric effects of iodine donors, in both molecular and atomic forms, should be sufficiently similar to render the mean separations in the complexes [R_4M I_2] and [R_4M I·] and therefore the work terms equivalent.[50,51]

The examples in the foregoing sections illustrate how

a knowledge of the standard redox potentials and the ion-pair work terms provides a unified free energy relationship (Eq. 16) for the rates of electron transfer in quite different chemical systems. Since the apparent Brönsted slope α,[52] which measures the dependence of the reaction rate (log k_{obsd}) on the standard free energy change (ΔG^0) for electron transfer, *i.e.*, $\alpha = \partial \Delta G^* / \partial \Delta G^0$, differs from system to system (see Figs. 2a, 3a, 4a, and 5a) we wish to inquire now into the origin of this variation.

Significance of the Brönsted Slope in Electron Transfer

Linear free energy relationships have been extensively studied for electron transfer and related reactions in both inorganic and organic systems.[53,54] For highly endergonic reactions, the Brönsted slope α, is close to unity.[10,55] In many cases, however, the more or less linear plots of ΔG^* (or a related quantity such as the rate constant log k_{obsd}) and ΔG^0 (or some related quantity such as the polarographic $E_{1/2}$ potentials[56]) have been observed with slopes significantly less than unity (*e.g.*, typically $0.1 < \alpha < 0.5$) in systems showing irreversible electron transfer in the endergonic region.[57,58] Such contradictions have led to the explanation that electron transfer is not complete in the transition state. As such, the diminished Brönsted slope would correspond to the fraction of charge transfer in the activated complex.[59] Alternatively, the small Brönsted slopes may be ascribed to large intrinsic barriers ΔG_0^* for electron transfer,[60] since the limit of α will be 0.5 for a sufficiently large value of ΔG_0^*.[8,61] For the latter, α is not related to the fractional charge transfer which is taken to be unity in all cases, but it cannot readily explain those cases with $\alpha < 0.5$.

In this light, our observations of apparent Brönsted slopes which span the limit of $\alpha = 1$ (Fig. 2a) to $\alpha \approx 0$ (Fig. 3a) cannot be easily reconciled with either explanation especially if one includes the examples (Figs. 4a and 5a) in which the apparent Brönsted slopes are actually negative. However, it clearly follows from the electron transfer cycle in Scheme 1 that the work term w_p must be explicitly included in the free energy relationship. Such a FER is expressed by Eq. 7, and the intrinsic Brönsted slope is accordingly evaluated as:[52]

$$\alpha = \frac{\partial \Delta G^*}{\partial \Delta G^0} = 1 + \frac{\partial w_p}{\partial \Delta G^0} \qquad (28)$$

It is important to emphasize that the Brönsted slope is not a meaningful quantity without a knowledge of the variation of w_p from system to system. Indeed the systems shown in Figs. 2a and 3a, for which the apparent Brönsted slopes lie in the range $0 < \alpha < 1$, are those in which variation in the work term is $-1 < (\partial w_p / \partial \Delta G^0) < 0$. Furthermore when the variation of the work term is large enough such that $(\partial w_p / \partial \Delta G^0)$ is less than -1 in Eq. 28, the apparent Brönsted slope will become negative, as observed in Figs. 4a and 5a. In other words the variation of the work term is largely responsible for the magnitudes of the apparent Brönsted slopes in Figs. 2a, 3a, 4a, and 5a.

The right sides of Figs. 2—6 represent the unified free energy relationship in Eq. 16 and uniformly support the use of the CT work term w_p^* in the experimental verification of the thermochemical cycle in Scheme 1 (Eq. 7). Thus the work term w_p^* is sufficient to unify all those systems with small and even negative values of the apparent Brönsted slope into a single general relationship in Eq. 16. At this juncture, we might enquire as to why the work term evaluated from the CT interaction in Scheme 2 serves as such an adequate representation of the adiabatic work term in Scheme 1.

By employing the *variation* of the work term Δw_p^* in Eq. 16, we are actually focussing in large part on the electrostatic interaction in the ion pair, since the other structural factors drop out by cancellation in the comparative procedure used in Eq. 13.[63] Thus the contribution to Δw_p^* consists largely of a coulombic potential (*i.e.*, $-e^2/r_{DA}$) in which the mean separation r_{DA} in the ion pair is the determinant factor. It is then likely that steric effects which mediate the magnitude of r_{DA} in the EDA complex, and thus the CT excited ion-pair state, parallel those in the adiabatic ion pair in Schemes 2 and 1, respectively.

Summary and Conclusions

The varied reactions of the donors and acceptors in Eqs. 1—4 can be quantitatively analyzed by the free energy relationship in Eq. 10, in which the variation of the work term Δw_p in the adiabatic ion pair can be evaluated from the variation of the work term Δw_p^* of the CT excited ion pair. The values of Δw_p^* are readily obtained from the charge-transfer spectra of the transient electron donor-acceptor complexes extant in these systems. The activation processes are governed by the combination of two terms; the standard free energy change E^0 for electron transfer (*i.e.*, $D + A \rightarrow D^+ + A^-$) and the work term of the products w_p (*i.e.*, the interaction energy in the ion pair $[D^+ A^-]$). The importance of the work term lies in the mean separation r_{DA} of the ion pair which is mediated by the steric effects in both donor and the acceptor. The work term variation is experimentally observed in systems showing apparent Brönsted slopes[52] α of substantially less than unity.

For a series of donors reacting with a *fixed acceptor*, the variation in the work term generally increases in the order: anthracenes $\ll$ benzenes $<$ alkenes $<$ alkylmetals. Similarly, for a series of acceptors acting upon a *fixed donor*, the variation in the work term generally increases in the order: TCNE $<$ Br_2 $<$ HgX_2. Thus the interaction of anthracenes with TCNE leading to the Diels-Alder adduct is the least subject to steric effects. Accordingly, the Brönsted slope in the free energy relationship is close to unity, even without specifically taking into account the work term. At the other extreme, the interaction of alkylmetals with HgX_2 is strongly influenced by steric effects. If the work terms are neglected, the apparent Brönsted slope is actually negative. Such variations in α strongly underscore the importance of evaluating work terms in the development of free energy relationships for electron transfer, especially in those systems which

proceed by an inner-sphere pathway.

Appendix

Evaluation of Solvation Energies of Donor Cations in Different Solvents. The solvation energies of arene cations are constant ($\Delta G^s = -2.01$ eV) for the solvents used in this study.[26] The difference in the solvation of $\Delta\Delta G^s$ of alkene and arene cations in acetonitrile was previously obtained from the outer-sphere electron transfer rates of a series of iron(III) oxidants with various alkenes and arenes.[40] The values of $\Delta\Delta G^s$ in other solvents were evaluated relative to those in acetonitrile, with the aid of the modified Born equation,

$$\Delta\Delta G^s = (1-1/\varepsilon)(1-1/\varepsilon_0)^{-1}\,\Delta\Delta G^s_0, \qquad (29)$$

where ε and ε_0 are the dielectric constants of the solvent and acetonitrile, respectively, and $\Delta\Delta G^s_0$ is the value in acetonitrile.

The values of $\Delta\Delta G^s$ for the alkylmetal donors in acetonitrile were reported previously. Those in carbon tetrachloride are evaluated by Eq. 29. The values of $\Delta\Delta G^s$ are listed in Table 6, together with the values of E^0_{ox} evaluated from Eq. 30.

$$E^0_{ox} = I_D + \Delta\Delta G^s - 2.01 - C \qquad (30)$$

Table 6. The evaluation of solvation energies of donor cations relative to arene cations. The standard potentials E^0_{ox} of donors in various solvents

Donor	$-\Delta\Delta G^s$/V		E^0_{ox}/V
Alkylmetals	CH_3CN[a]	CCl_4[b]	CCl_4[c]
Me_4Sn	1.62	0.92	2.36
Et_4Sn	1.27	0.72	1.77
n-Pr_4Sn	1.23	0.70	1.71
n-Bu_4Sn	1.21	0.69	1.66
i-Pr_4Sn	1.07	0.61	1.44
s-Bu_4Sn	1.07	0.61	1.43
i-Bu_4Sn	1.17	0.66	1.61
Alkenes	CH_3CN[d]	HOAc[b]	HOAc[a]
$H_2C{=}CH_2$	1.69	1.45	2.66
$H_2C{=}CHMe$	1.21	1.04	2.29
$H_2C{=}CHEt$	1.13	0.97	2.25
$H_2C{=}CH(n\text{-Pr})$	1.07	0.92	2.19
$H_2C{=}CMe_2$	0.99	0.77	2.06
$H_2C{=}CMe(Et)$	0.84	0.72	2.02
(*Z*)-MeCH=CHMe	0.82	0.71	2.00
(*E*)-MeCH=CHEt	0.77	0.66	1.97
(*E*)-MeCH=CH(*t*-Bu)	0.73	0.48	2.02
$H_2C{=}CH(t\text{-Bu})$	1.03	0.89	2.15
$Me_2C{=}CMe(Et)$	0.27	0.23	1.57
$Me_2C{=}CMe_2$	0.34	0.29	1.57
$Me_2C{=}CMe(n\text{-Pr})$	0.25	0.22	1.56
$Me_2C{=}CMe(n\text{-Bu})$	0.20	0.17	1.57
Cyclohexene	0.68	0.58	1.96
Arenes	CH_3CN[e]	HOAc[e]	HOAc[a]
C_6H_6	2.01	2.01	2.82
MeC_6H_5	2.01	2.01	2.41
EtC_6H_5	2.01	2.01	2.35
i-PrC_6H_5	2.01	2.01	2.28
$MeOC_6H_5$	2.01	2.01	1.98
o-$Me_2C_6H_4$	2.01	2.01	2.15
m-$Me_2C_6H_4$	2.01	2.01	2.15
p-$Me_2C_6H_4$	2.01	2.01	2.03
1,3,5-$Me_3C_6H_3$	2.01	2.01	1.99

a) Calculated from Eq. 30. b) Calculated from Eq. 29. c) From Ref. 17. d) From Ref. 40. e) From Ref. 26.

The authors wish to thank the National Science Foundation for financial support.

References

1) See for example, P. B. D. de la Mare and R. Bolton "Electrophilic Addition to Unsaturated Systems," Elsevier New York (1966); G. H. Schmid and D. G. Garratt, "Chemistry of Alkenes," ed by J. Zabicky, Wiley-Interscience, New York (1977), Vol. 3.

2) L. M. Stock, "Aromatic Substitution Reactions," Prentice-Hall, Englewood Cliffs, N. J. (1968); R. O. C. Norman and R. Taylor, "Electrophilic Substitution of Benzenoid Compounds," American Elsevier, New York (1965).

3) A. Wasserman, "Diels-Alder Reactions," Elsevier, New York (1965); J. Sauer and R. Sustmann, *Angew. Chem., Int. Ed. Engl.*, **19**, 779 (1980).

4) D. S. Matteson, "Organometallic Mechanisms," Academic Press, New York (1974); M. Gielen, *Acc. Chem. Res.*, **6**, 198 (1973); F. R. Jensen and B. Rickborn, "Electrophilic Substitution of Organomercurials," McGraw-Hill Book Co., New York (1968).

5) For example, see E. C. Ashby, A. B. Goel, R. N. DePriest, and H. S. Prasad, *J. Am. Chem. Soc.*, **103**, 973 (1981) and related papers; F. G. Bordwell and A. H. Clemens, *J. Org. Chem.*, **46**, 1035 (1981).

6) A wide variety of photochemical processes involving electron transfer in the quenching of excited states is also known. For inorganic examples, see G. L. Geoffroy and M. S. Wrighton, "Organometallic Photochemistry," Academic Press, New York (1979); "Concepts of Inorganic Photochemistry," ed by A. W. Adamson and D. D. Fleischauer, Wiley, New York (1975) for some leading references. For some recent organic systems, see F. D. Lewis, T.-I. Ho, and J. T. Simpson, *J. Am. Chem. Soc.*, **104**, 1924 (1982); J. L. Stavinoha and P. S. Mariano, *ibid.*, **103**, 3136, 3148 (1981); G. B. Schuster, *Acc. Chem. Res.*, **12**, 366 (1979) and related papers.

7) J. K. Kochi, "Organometallic Mechanisms and Catalysis," Academic Press, New York (1978), Part 3.

8) See F. Scandola, V. Balzani, and G. B. Schuster, *J. Am. Chem. Soc.*, **103**, 2519 (1981).

9) In the endergonic limit, the activation barrier for electron transfer corresponds to the energetics of ion pair formation (see Ref. 10). In qualitative terms, this equality is tantamount to a restatement of the Hammond postulate [G. S. Hammond, *J. Am. Chem. Soc.*, **77**, 334 (1955)].

10) R. A. Marcus, *J. Phys. Chem.*, **72**, 891 (1968).

11) The Boltzmann constant is κ and the Planck constant is h.

12) Note that the contribution from the acceptor drops out by cancellation in such a series.

13) For outer-sphere electron transfer mechanisms, it is a common practice to neglect the work term of the product, especially if the ions have like charges (see Ref. 14). However, the importance of w_p has been noted in outer-sphere reactions with ions of opposite charges (see Ref. 15).

14) R. J. Klingler and J. K. Kochi, *J. Am. Chem. Soc.*, **103**, 5839 (1981).

15) A. Haim and N. Sutin, *Inorg. Chem.*, **15**, 476 (1976).

16) In inner-sphere electron transfer for which interaction energies can be large, the neglect of the work term w_p is not justified. For the mechanistic distinction between outer-sphere and inner-sphere electron transfer, see the discussion in Ref. 17.

17) S. Fukuzumi, C. L. Wong, and J. K. Kochi, *J. Am.*

Chem. Soc., **102**, 2928 (1980).
18) R. Foster, "Organic Charge-Transfer Complexes," Academic Press, New York (1969).
19) For the theory, see a) R. S. Mulliken, *J. Am. Chem. Soc.*, **74**, 811 (1952); *J. Phys. Chem.*, **56**, 801 (1952); b) R. S. Mulliken and W. B. Person, "Molecular Complexes," Wiley-Interscience, New York (1969).
20) For the experimental verification, see N. Mataga and M. Ottolenghi, "Molecular Association," ed by K. Foster, Academic Press, New York (1979), Vol. 2, p. 31.
21) The formation constants K_{DA} for the weak EDA complexes are small and considered as rather constant compared with the magnitude of the change in I_D and $h\nu_{CT}$ (Refs. 22—26).
22) a) S. Fukuzumi, K. Mochida, and J. K. Kochi, *J. Am. Chem. Soc.*, **101**, 5961 (1979); b) H. C. Gardner and J. K. Kochi, *ibid.*, **98**, 2460 (1976); c) J. Y. Chen, H. C. Gardner, and J. K. Kochi, *ibid.*, **98**, 6150 (1976).
23) a) S. Fukuzumi and J. K. Kochi, *J. Phys. Chem.*, **84**, 608, 617 (1980); b) S. Fukuzumi and J. K. Kochi, *ibid.*, **85**, 648 (1981); c) S. Fukuzumi and J. K. Kochi, *ibid.*, **84**, 2246, 2254 (1980).
24) S. Fukuzumi and J. K. Kochi, *J. Am. Chem. Soc.*, **103**, 2783 (1981).
25) S. Fukuzumi and J. K. Kochi, *J. Org. Chem.*, **46**, 4116 (1981).
26) S. Fukuzumi and J. K. Kochi, *Tetrahedron*, **38**, 1035 (1982).
27) In previous papers (Refs. 22—26), we used the notation ΔE instead of Δw_p^*. In this paper, we use the notation Δw_p^* to emphasize the relationship to Δw_p in Eqs. 9 and 10. Since the photoexcitation of EDA complexes is a vertical process, the CT transition energies $h\nu_{CT}$ do not include a major change in solvation during the excitation. The minor contribution of the solvent effects on $h\nu_{CT}$ which has been measured in inert solvents (Refs. 22—26) is cancelled out in the relative values of Δw_p^* in Eq. 13.
28) Note that the sign of the work term w_p^* is negative.
29) The HOMO of these alkylmetals is a sigma bonding orbital [T. P. Fehlner, J. Ulman, W. A. Nugent, and J. K. Kochi, *Inorg. Chem.*, **15**, 2544 (1976)].
30) For example, the difference between w_p^* for *s*-Bu_4Sn and that for Me_4Sn in their $HgCl_2$ complexes is as large as 1.10 eV, which corresponds to 106 kJ mol^{-1}. Such a large difference in work terms corresponds to a factor of 3.6×10^{18} in the rates of reaction if Δw_p^* is simply equated to Δw_p in Eq. 9.
31) H. C. Gardner and J. K. Kochi, *J. Am. Chem. Soc.*, **97**, 1855 (1975).
32) H. C. Gardner and J. K. Kochi, *J. Am. Chem. Soc.*, **97**, 5026 (1975).
33) In Ref. 17, values of $(E^0_{ox}+w_p/F)$ were reported. The work term w_p for the electron transfer between $[FeL_3]^{3+}$ and the alkylmetals is neglected here, since the outer-sphere work term w_p with ions of the same charge is negligible (see Ref. 13).
34) Note that the constants in Eqs. 10 and 16 are different, since w_p and Δw_p^* represent absolute and relative work terms, respectively. The equivalency implies that $\Delta w_p = w_p - w_p^0 = \Delta w_p^*$, where w_p^0 is the *absolute* work term of the reference system.
35) Although the error bars are not included in the figures, the correlation and trends are to be conservatively considered to 2 significant digits.
36) When E^0 is given in V (or eV), the Brönsted a corresponds to the slope of -16.9 in the plot between log k_{obsd} and E^0 at 298 K, *i.e.*, $23.04\times10^3/2.3RT=16.9$ (1 V=23.04 kcal mol^{-1}, R=1.987 cal mol^{-1} K^{-1}, T=298 K).
37) Since the reduction potential of TCNE is 0.22 V *vs.* SCE, the standard free energy change for electron transfer ΔG^0 is in the range of 9.9 kcal mol^{-1} for 9,10-Me_2-anthracene and $\approx$33 kcal mol^{-1} for Me_4Sn.
38) By way of contrast, note that the apparent Brönsted slope for the insertion reaction of alkylmetals with TCNE is only 0.45, despite the large positive value (Ref. 17) of ΔG^0. The explanation for the difference is discussed in the last section (*vide infra*). Furthermore, the same Brönsted slope has been reported in Ref. 31 for the more conventional electron transfer reaction of hexachloroiridate(IV) with the same series of alkylmetals (compare Eqs. 14 and 15).
39) S. Fukuzumi and J. K. Kochi, *J. Am. Chem. Soc.*, **103**, 7240 (1981).
40) S. Fukuzumi and J. K. Kochi, *J. Am. Chem. Soc.*, **104**, 7599 (1982).
41) A. Modro, G. H. Schmid, and K. Yates, *J. Org. Chem.*, **42**, 3673 (1977); M. F. Ruasse, J. E. Dubois, and A. Argile, *ibid.*, **44**, 1173 (1979).
42) H. C. Brown and L. M. Stock, *J. Am. Chem. Soc.*, **79**, 1421 (1957); L. M. Stock and H. C. Brown, *ibid.*, **82**, 1942 (1960); R. M. Keefer, A. Ottenberg, and L. J. Andrews, *ibid.*, **78**, 255 (1956).
43) a) M. E. Peover, *Electroanal. Chem.*, **2**, 1 (1967); b) B. Case, "Reactions of Molecules at Electrodes," ed by N. S. Hush, Wiley-Interscience, New York (1971), p. 125.
44) a) R. C. Larson, R. T. Iwamoto, and R. N. Adams, *Anal. Chim. Acta*, **25**, 371 (1961); b) The value of C for the Ag/$AgClO_4$ reference in CH_3CN is 4.70 V, which is decreased by 0.30 V relative to the SCE reference electrode.
45) The apparent Brönsted slope in Fig. 3a is 0.37 for alkylmetals, 0.17 for alkenes, and 0.54 for arenes.
46) The unification of the reactions of alkylmetals with Br_2 in CCl_4 and the reactions of olefins and arenes in HOAc in Fig. 3b implies that the solvation term for Br_2^- in CCl_4 is about equal to that in HOAc.
47) See Table 6 in the Appendix.
48) S. Fukuzumi and J. K. Kochi, *J. Am. Chem. Soc.*, **102**, 7290 (1980).
49) S. Fukuzumi and J. K. Kochi, *J. Org. Chem.*, **45**, 2654 (1980).
50) The similarity between I_2 and I· in charge-transfer interactions has been examined with alkyl iodides as donors [R. L. Strong and J. A. Kaye, *J. Am. Chem. Soc.*, **98**, 5460 (1976); R. L. Strong and F. Venditti, Jr., *Chem. Phys. Lett.*, **46**, 546 (1977)].
51) There are other instances in which Δw_p^* determined indirectly has been successfully employed in FERs. For example, the values of Δw_p^* employed in the FER for the inner-sphere oxidation of alkylmetals by hexachloroiridate(IV) in Eq. 14 were obtained from the CT spectral data of [R_4M TCNE] complexes (see Ref. 17).
52) We define the apparent Brönsted slope for an electron transfer process to be the dependence of the rate (log k_{obsd}) on the standard free energy change ΔG^0 of the redox couple. It is to be contrasted with the intrinsic Brönsted slope, which is obtained from a consideration of all contributions to the driving force, including the work terms, as in Eq. 28.
53) a) N. Sutin, "Inorganic Biochemistry," ed by G. Eichorn, Elsevier, Amsterdam (1973), p. 611; b) H. Taube, "Electron Transfer Reactions of Complex Ions in Solution," Academic Press, New York (1970); c) W. L. Reynolds and R. W. Lummy, "Mechanism of Electron Transfer," Ronald Press, New York (1966); d) R. G. Wilkins, "The Study of Kinetics and Mechanism of Reactions of Transition Metal Complexes," Allyn and Bacon, Boston (1974); e) V. Balzani, F. Bolletta, M. T. Gandolfi, and M. Maestri, *Top. Curr. Chem.*, **75**, 1 (1978).

54) a) E. Mentasti, E. Pelizzetti, and C. Baiocchi, *J. Chem. Soc., Dalton Trans.*, **1977**, 132; b) E. Pelizzetti, E. Mentasti, and C. Baiocchi, *J. Phys. Chem.*, **80**, 2979 (1976); c) M. G. Kuzmin N. A. Sadovskii, and I. V. Soboleva, *Chem. Phys. Lett.*, **71**, 232 (1980); d) K. Okamoto, K. Takeuchi, O. Murai, and Y. Fujii, *J. Chem. Soc., Perkin Trans. 2*, **1979**, 490; e) E. Pelizzetti, M. Woods, and J. C. Sullivan, *Inorg. Chem.*, **19**, 524 (1980); f) A. J. Audsley, G. R. Quick, and J. S. Littler, *J. Chem. Soc., Perkin Trans. 2*, **1980**, 557; g) F. T. T. Ng and P. M. Henry, *J. Am. Chem. Soc.*, **98**, 3606 (1976); h) I. B. Afaıias'ev, S. V. Prigoda, T. Ya. Maltseva, and G. I. Samokhvalov, *Int. J. Chem. Kinet.*, **6**, 643 (1974); i) E. Vogelmann, S. Schreiner, W. Rauscher, and H. E. A. Kramer, *Z. Phys. Chem. (Neue Folge)*, **101**, 321 (1976); j) T. J. Kemp and L. J. A. Martins, *J. Chem. Soc., Perkin Trans. 2*, **1980**, 1708; k) J. Eriksen and C. S. Foote, *J. Phys. Chem.*, **82**, 2659 (1978).

55) a) R. D. Levine, *J. Phys. Chem.*, **83**, 159 (1979); b) See also E. S. Lewis, C. C. Shen, and R. A. More O'Ferrall, *J. Chem. Soc., Perkin Trans. 2*, **1981**, 1084.

56) For a relationship between the potential measurements of electrochemically irreversible processes and E^0_{ox}, see R. J. Klingler and J. K. Kochi, *J. Am. Chem. Soc.*, **102**, 4790 (1980); *J. Phys. Chem.*, **85**, 1731 (1981).

57) a) H. Shizuka, T. Saito, and T. Morita, *Chem. Phys. Lett.*, **56**, 519 (1978); b) H. Shizuka, M. Nakamura, and T. Morita, *J. Phys. Chem.*, **84**, 989 (1980); c) S. Bank and D. A. Juckett, *J. Am. Chem. Soc.*, **97**, 567 (1975); d) T. W. Chan and T. C. Bruice, *ibid.*, **99**, 7287 (1977).

58) A number of correlations between log k and the ionization potentials of donor molecules have been reviewed for various electrophilic reactions by F. Freeman, *Chem. Rev.*, **75**, 439 (1975).

59) a) C. Walling, *J. Am. Chem. Soc.*, **102**, 6854 (1980); b) F. Scandola and V. Balzani, *ibid.*, **101**, 6140 (1979).

60) The intrinsic barrier represents the activation free energy for electron transfer when $\Delta G^0+w_p-w_r=0$. As a concept, it is most useful for outer-sphere reactions, since there are theoretical models available for its calculation (for a review, see R. D. Cannon, "Electron Transfer Reactions," Butterworths, London (1980)). However, theoretical models are not available for the calculation of ΔG_0^* for inner-sphere reactions.

61) Most FERs (Ref. 62) predicts $\alpha=0.5$ for large values of ΔG_0^*, or its equivalent.

62) a) D. Rehm and A. Weller, *Ber. Bunsenges. Phys. Chem.*, **73**, 834 (1969); *Isr. J. Chem.*, **8**, 259 (1970); b) M. D. Evans and M. Polanyi, *Trans. Faraday Soc.*, **32**, 1333 (1936); **34**, 11 (1938); c) R. A. Marcus, *Ann. Rev. Phys. Chem.*, **15**, 155 (1964); d) N. Agmon, *Int. J. Chem. Kinet.*, **13**, 333 (1981).

63) For a discussion of this important point, see S. Fukuzumi and J. K. Kochi, *J. Am. Chem. Soc.*, **102**, 2141 (1980).

64) a) Ref. 26; b) V. D. Parker and O. Hammerich, *Acta Chem. Scand.*, **B31**, 883 (1977); c) O. Hammerich and V. D. Parker, *J. Am. Chem. Soc.*, **96**, 4289 (1974); d) B. S. Jensen and V. D. Parker, *ibid.*, **97**, 5211 (1975).

65) a) W. M. Latimer, K. S. Pitzer, and C. M. Slansky, *J. Chem. Phys.*, **7**, 108 (1939); b) R. M. Noyes, *J. Am. Chem. Soc.*, **84**, 513 (1962); c) J. F. Coetzee and J. J. Campion, *ibid.*, **89**, 2513 (1967); d) M. Tanaka, *Inorg. Chem.*, **15**, 2325 (1976).

66) The dielectric constants of various solvents are listed in I. A. Koppel and V. A. Palm, "Advances in Linear Free Energy Relationships," ed by N. B. Chapman and Y. Shorter, Plenum Press, London (1972), Chap. 5.

Phase Behavior and Tricritical Phenomena in a Bile Salt System

Hironobu KUNIEDA* and Kōzō SHINODA
Department of Applied Chemistry, Faculty of Engineering, Yokohama National University, Tokiwadai 156, Hodogaya-ku, Yokohama 240
(Received July 22, 1982)

A three-phase region consisted of a water (W), a surfactant (D) and an oil (O) phases was found in a sodium taurocholate (NaTC)/brine/co-surfactant (monoglyceride or its model compound)/oil (triglyceride) system. A required concentration of cosurfactant to produce the three-phase region was decreased with increasing salinity. The three-phase region becomes narrower and finally vanishes with decreasing salinity at constant temperature or with the rise in temperature at constant salinity in a NaTC/brine/glycerol mono (2-ethylhexyl) ether/glycerol tris (2-ethylhexanoic) ester system. Since the critical end points of O–D and D–W phases approach and coincide in the system, the three-phase region disappears at a tricritical point at which three coexisting liquid phases become identical. According to the phase rule, there is a line of tricritical points in the space of T and compositions in this five-component system and it moves toward higher temperatures with the increase in salinity. Therefore, the three-phase region exists at temperatures below the tricritical temperature at constant salinity.

In a three-fluid-phase system (a liquid-liquid-gas type or a liquid-liquid-liquid type), two fluid phases become identical in the presence of a third phase at a critical end point.[1-3] There are two kinds of critical end phenomena as is shown schematically in Figs. 1(a) and (b). One is the critical phenomenon between upper (A) and middle (B) phases, and the other is that between middle (B) and lower (C) phases. But, the critical phenomenon between upper and lower phases is not observed in the presence of the middle phase.[4] If these two critical end points coincide each other, three coexisting phases become identical at a high-order critical point, *i.e.*, a tricritical point as is shown in Fig. 1(c).[1-4] This kind of critical phenomenon has been observed in some systems.[5-9]

In a surfactant/water/oil system, three coexisting liquid phases consisted of a water (W), a surfactant (D) and an oil (O) phases appear under certain conditions. For example, a three-phase region is observed at a certain temperature range in a nonionic surfactant/water/oil system and its upper limit corresponds to a critical end temperature of O–D phases, while its lower limit is that of D–W phases.[10-12] The equilibrium of three coexisting phases in a surfactant system at atmospheric pressure is shown schematically in Fig. 2.[10-12] The orientation of X axis corresponds to the oil–water ratio and that of Y axis corresponds to the concentration of surfactant. The Z axis is perpendicular to the plane (X–Y plane) of a three-phase triangle and it corresponds to temperature in a nonionic surfactant system. In Fig. 2(a), K and L are critical curves of D–W and O–D which exist outside the three-phase region and terminate at respective critical end points Kc and Lc. Curves, α, β, γ, are the loci of D, O, and W phases forming a three-phase triangle. The points on α and β curves coincide at Lc point at which O and D phases become identical. The critical mixture of O–D is in

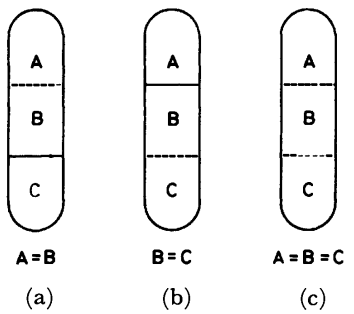

Fig. 1. Schematic figures of critical end points, (a), (b), and a tricritical point, (c).
(a): A and B phases become identical in the presence of C phase, (b): B and C phases become identical in the presence of A phase, (c): A, B, and C phases become identical at a tricritical point.

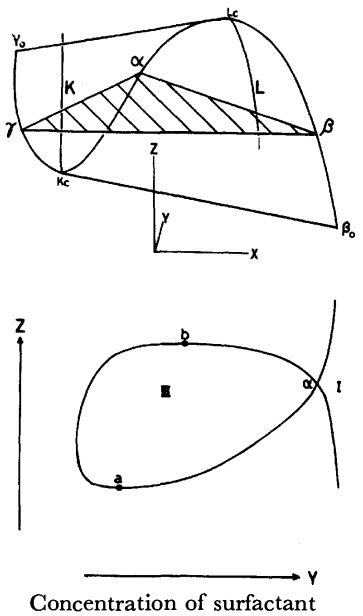

Fig. 2. (a) Schematic diagram of three coexisting phases in a surfactant/water/oil system at constant pressure. Curves α, β, and γ show the loci of compositions of a surfactant(D), and oil(O), and a water(W) phases forming a three-phase region. K and L are the critical curves of D–W and O–D phases. Lc and Kc are the critical end points of D–W and O–D. One of three-phase triangles is shown. (b) Vertical section of Fig. 2(a) at equal amount of water–oil. Points a and b are the intersections of this plane and Kc-β_o, Lc-γ_o lines respectively. The orientation of X axis is vertical to this plane. III is the three-phase region.

equilibrium with W phases (γ_0 point) on the Lc-γ_0 line which is called a critical tie line.[13] Therefore, the critical end phenomenon as is shown in Fig. 1(a) occurs on this line. Similarly the critical end phenomenon occurs on another critical tie line, Kc-β_0 on which the phenomenon in Fig. 1(b) is observed. A three-phase region exists between two critical tie lines.

Vertical section (Z–Y plane) of Fig. 2(a) at a composition of equal amount of water and oil is also shown in Fig. 2(b).[10–12] A three-phase region exists inside a closed loop. Point **a** is the intersection of this plane and a critical tie line Kc-β_0 in Fig. 2(a). Point **b** is that of this plane and Lc-γ_0 line.

If these two critical end points strictly coincide, a tricritical phenomenon as is shown in Fig. 1(c) occurs. But, in a nonionic surfactant systems, it may not appear at atmospheric pressure, because a tricritical point is an invariant point in the space of T, P and compositions in a three-component system.[4,12] On the other hand, similar three-phase region appears in an ionic surfactant/brine/(co-surfactant)/oil system.[10,14–17] In these systems, one or two degrees of freedom increase in comparison with a nonionic surfactant system so that it seems to be easier to find a tricritical phenomenon despite of the difficulty of determining X, Y, Z axes exactly. Although the solution behavior of surfactant in a water–oil system is generally very complicated due to formation of a liquid crystalline phase,[18,19] it is known that there is no liquid crystalline phase in a bile salt system.[19] Therefore, a three-phase region and tricritical phenomenon may appear in a bile salt/brine/co-surfactant(monoglyceride)/oil(triglyceride) system, which can be regarded as a model of biological system.

Experimental

Materials. Sodium taurocholate (NaTC) was obtained from Sibma Chemicals Co. Its purity is above 98%. 3-(2-ethylhexyloxy)-1,2-propanediol (glycerol mono(2-ethylhexyl) ether, MEH) and 3-(*cis*-9-octadecenyloxy)-1,2-propanediol (glycerol monooleyl ether, MO) were obtained from Nikko Chemicals Co. and their purities are above 99%. 1,2,3-propanetriyl tris(2-ethylhexanoate) (glycerol tris(2-ethylhexanoic) ester, TEH) was obtained from Nisshin Seiyu Co. (above 97%) Extra-pure-grade 1,2,3-propanetriyl tris(*cis*-9-octadecenoate) (triolein, TO) was obtained from Nakarai Chemicals Co. Extrapure-grade *cis*-9-octadecenoic acid (oleic acid, OA) and 2,3-dihydroxypropyl dodecanoate (monolaurin, ML) were obtained from Tokyo Kasei Kogyo Co. These reagents were used without further purifications.

Procedures. Various amounts of brine, oil, surfactant and co-surfactant were sealed in ampoules. A series of ampoules kept in a thermostat were well shaken and left at constant temperature from 1 d to one week depending on the stability of solution and the three-phase boundary and the change in volumes of respective phases were determined.

Results and Discussion

Phase Behavior in Sodium Taurocholate (NaTC)/Brine/Co-surfactant/Oil Systems. Figure 3 shows three-phase regions consisted of a water (W), a surfactant (D) and an oil (O) phases in various systems of NaTC/brine/co-surfactant/oil at 35 °C. The concentration of NaTC is 3 wt%/system and (co-surfactant+oil)/brine ratio is unity. The weight percent of co-surfactant, *i.e.*, co-surfactant/(oil+co-surfactant)is plotted vertically and the salinity is plotted horizontally. At constant salinity, D phase is separated from W phase in the presence of O phase with the increase in co-surfactant content and a three-phase region appears. With further increase in co-surfactant content, D and O phases dissolve each other and the three-phase region turns to a two-phase system. The required concentration of co-surfactant to produce a three-phase region becomes low at high salinity. These results completely correspond with that in an ordinary ionic surfactant/brine/co-surfactant/oil system.[16] The change in solution behavior of NaTC from water-soluble to oil-soluble as a function of the concentration of co-surfactant corresponds to that of a nonionic surfactant/water/oil system as a function of temperature.[10,20,21] It is known that solubilization of oil or water in a surfactant solution reaches maximum and ultralow interfacial tensions are attained around a three-phase region due to critical solution phenomena of O–D and D–W phases.[11,21] The solubilization of MEH–TEH mixture in an aqueous NaTC solution has been determined and is shown in Fig. 4. It is clear that the optimum ratio of oil–co-surfactant is very important for large solubilization and the solution behavior of NaTC is highly affected by salinity.

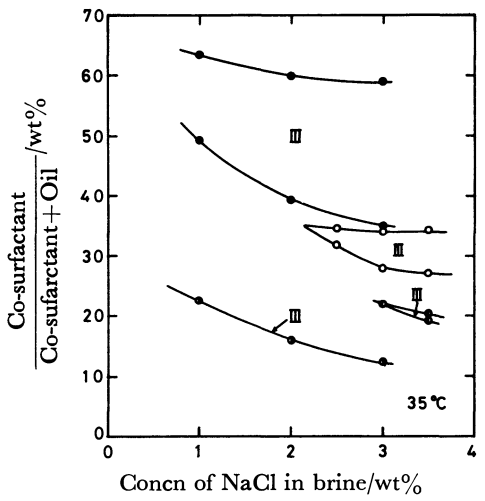

Fig. 3. The effect of salinity on the required concentration of co-surfactant to produce a three-phase region in a NaTC/brine/co-surfactant/oil system at 35 °C. The concentration of NaTC is 3 wt%/system and (oil+co-surfactant)/brine ratio is unity. III, the three-phase region.

	co-surfactant	oil
●	MO	TO
○	MEH	TEH
◐	MEH	OA
◑	ML	OA

The Effect of Salinity and Temperature on the Three-phase Region. Three-phase regions become narrower and finally diminishes with the decrease in salinity in the systems of NaTC/brine/MEH/TEH and NaTC/brine/MEH/OA as is shown in Fig. 3. In order to clarify this

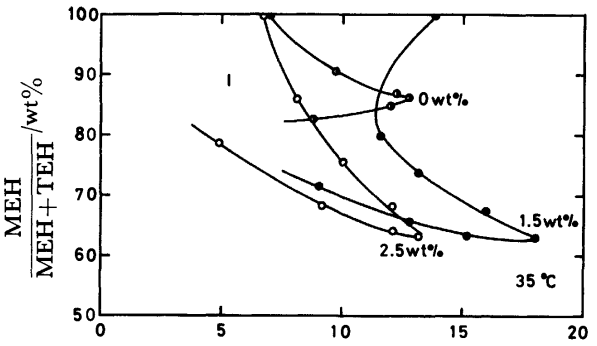

Fig. 4. The effect of NaCl on the solubilization of (TEH +MEH) mixture in brines containing 5 wt% of NaTC at 35 °C. The numerical values indicate concentrations of NaCl in brine.

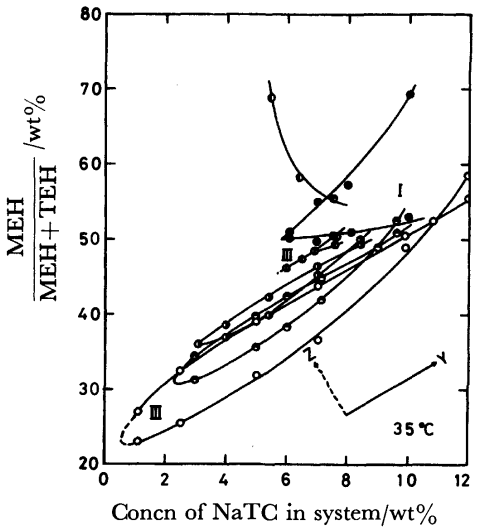

Fig. 5. The effect of NaCl on the three-phase region in NaTC/brine/MEH/TEH system at 35 °C. (MEH+ TEH)/brine ratio is unity. The three-phase region becomes very narrow at 1.5 wt% NaCl.
◐: 0 wt% NaCl, ●: 1 wt% NaCl, ◑: 1.5 wt% NaCl, ◑: 2 wt% NaCl, ◓: 2.5 wt% NaCl, ○: 3.5 wt% NaCl.

phenomenon, the effect of the concentration of NaTC on the three-phase region has been determined at 35 °C in the NaTC/brine/MEH/TEH system and is shown in Fig. 5. The vertical axis is the same as that of Fig. 3 and the concentration of NaTC in system is plotted horizontally. A three-phase region changes to one-phase region with increasing NaTC content, because O and W phases dissolve into D phase. On the other hand, the volume of D phase is decreased and finally, diminishes at the left-hand boundary of the three-phase region. Since inorganic salt is practically soluble only in water, brine can be regarded as a pseudo one component, then a pseudo four-component system of ionic surfactant/ brine/co-surfactant/oil is represented by a tetrahedron at constant temperature and salinity as is shown in Fig. 6. In this pseudo four-component system, degree of freedom of respective regions is the same as that in a nonionic surfactant/water/oil system as is shown in Fig. 2

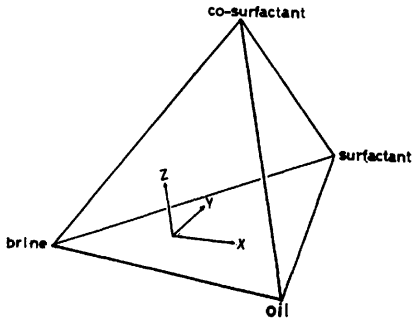

Fig. 6. Composition tetrahedron at constant T and P in a pseudo four-component system.

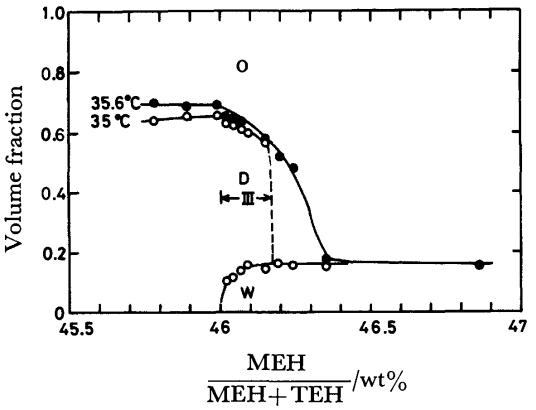

Fig. 7. The effect of $\frac{\text{MEH}}{\text{MEH+TEH}}$ on the volume fractions of respective phases at 1.5 wt% NaCl. The three-phase region diminishes at 35.6 °C. (MEH+TEH)/ brine ratio is unity. The concentration of NaTC is 6 wt%/system.

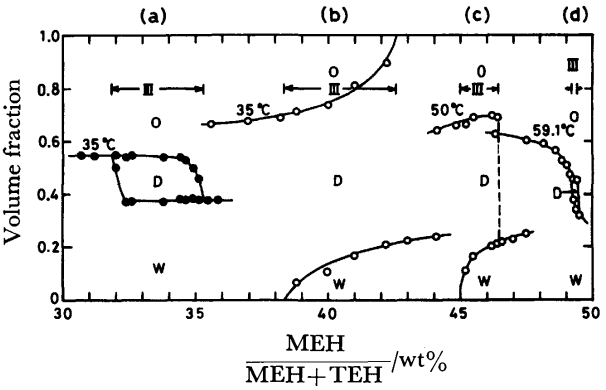

Fig. 8. The effect of temperature and the concentration of co-surfactant on the volume fractions of respective phases at various temperatures in a NaTC/brine(2.5 wt% NaCl)/MEH/TEH system. The concentrations of NaTC are 6 wt%/system (○) and 3 wt%/system (●).

because temperature and salinity are fixed. Therefore, two critical end points are invariant points and two critical tie lines are also fixed in a composition tetrahedron. Accordingly X, Y, Z, coordinate system similar to that in Fig. 2 can be taken in this tetrahedron. The orientation of Y axis in Fig. 5 corresponds to that in Fig. 2, because the volume fraction of D phase is in-

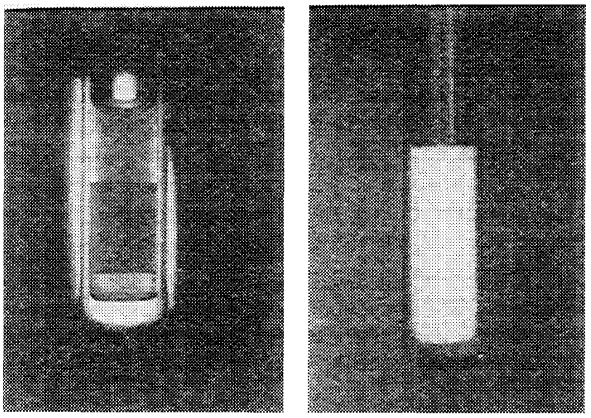

(a) (b)

Fig. 9. The photographs of the three coexisting phases near the tricritical point at 35 °C in transmitted light (a) and in scattered light (b). (NaTC, 6 wt%/system. (MEH+TEH)/brine (1.5 wt% NaCl) is unity. MEH/(MEH+TEH) is 46.05 wt%.)

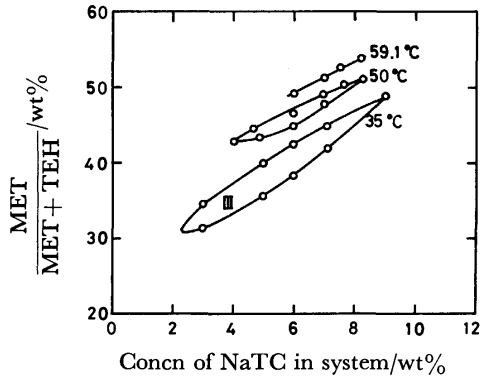

Fig. 10. The effect of temperature on the three-phase region at constant salinity (2.5 wt% NaCl) in a NaTC/brine/MEH/TEH system. The three-phase region vanishes slightly above 59.1 °C. (MEH+TEH)/brine ratio is unity.

creased in this direction. The three-phase region becomes narrower with the decrease in salinity and vanishes slightly below 1.5wt% NaCl. The change in volume fractions of respective phases as a function of co-surfactant content is shown in Figs. 7 and 8(a), (b) at 35 °C. As is shown in Figs. 8(a) and (b), when the concentration of NaTC is low (3 wt%), D phase dissolves into O or W phase and disappers at the right- or left-hand boundaries of the three-phase region. On the other hand, when the concentration of NaTC is high (6 wt%), O or W phase dissolves into D phase and disappears at those boundaries. This means that the critical end phenomena between O–D or D–W phases occur in the presence of a third phase (W or O phase) at a concentration of NaTC between 3—6 wt% on the curve in Fig. 5.[10,11,16] Those points correspond to the intersection between the plane of Fig. 5 and the critical tie lines in a composition tetrahedron (*cf.* points **a** and **b** in Fig. 2). Therefore, Z axis in Fig. 5 corresponds to that in Fig. 2 but is not completely in parallel with the plane of Fig. 5 as described later. Since these two points exist on the closed curve of Fig. 5, the width of a three-phase region at respective salinity represents the relative distance between two critical tie lines and it corresponds to the difference in critical end temperatures in a nonionic surfactant system. As is shown in Fig. 5, that distance shortens with the decrease in salinity and at last becomes zero slightly below 1.5 wt% NaCl at constant temperature (35 °C). In other words, the three-phase region in the composition tetrahedron becomes smaller and smaller with decreasing in salinity. Therefore, a tricritical point exists slightly below 1.5 wt% NaCl. In fact, all three coexisting phases show critical opalescence at 1.5 wt% NaCl as is shown in Fig. 9.

On the other hand, at constant salinity (2.5 wt% NaCl), a three-phase region also becomes narrow and vanishes with the rise in temperature as is shown in Fig. 10. The change in volume fractions of respective phases at 35, 50, and 59.1 °C are also shown in Figs. 8(b), (c), and (d). Hence, it is considered that a tricritical point also exists slightly above 59.1 °C at 2.5 wt% NaCl. From these results, a tricritical point shifts toward higher temperatures with increasing salinity.

Correlation between a Tricritical Phenomenon and the Degree of Freedom.[22] If the number of components are increased, a tricritical phenomenon can be observed more easily. The degree of freedom (f) of pth order critical point is expressed by following relation.[22]

$$f = c - 2p + 3, \quad (1)$$

where p is the number of phases becoming identical, and c is the number of components. Therefore, at a tricritical point, $f=c-4$ at constant pressure. This means that there is a line of tricritical points in the space of T and compositions in a five component system and it becomes an invariant point when temperature or composition of one component is fixed. In other words, a tricritical temperature is invariant at constant salinity, while the salinity at a tricritical point is invariant at constant temperature.

The Shape of a Three-phase Region Near the Tricritical Point. Figure 11 shows the shape of the three-phase region at 1.5 wt% NaCl on the plane almost perpen-

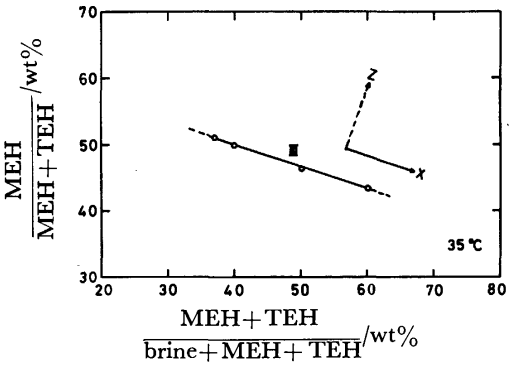

Fig. 11. The effect of (MEH+TEH)/brine ratio on the three-phase region in a NaTC/brine(1.5 wt% NaCl)/MEH/TEH system at 35 °C. The concentration of NaTC in system is 6 wt%. This figure is almost perpendicular to the plane of Fig. 5 in a composition tetrahedron.

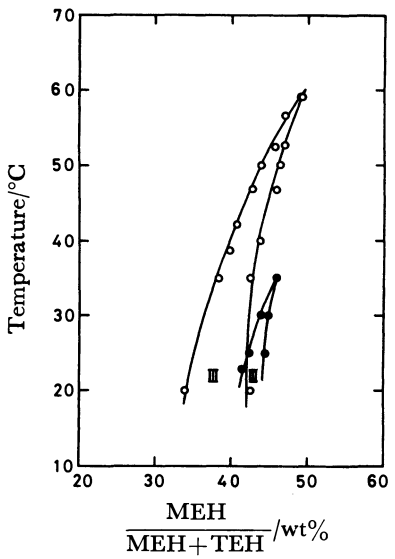

Fig. 12. The effect of temperature on the three-phase region in a NaTC/brine(●, 1.5 wt% NaCl; ○, 2.5 wt% NaCl)/MEH/TEH system. The concentration of NaTC in system is 6 wt%. (MEH+TEH)/brine ratio is unity. The three-phase region vanishes in the vicinity of a tricritical temperature.

dicular to that in Fig. 5 in the composition tetrahedron at 1.5 wt% NaCl. X axis and Y axis are approximately parallel to the respective figures. But Z axis in the figures is the projection of true axis on respective planes judging from Figs. 5 and 11. Although we could not determine the edges of the three-phase region in Fig. 11 because of their narrownesses, it is clear that near the tricritical point, the order of the sizes of the three-phase region in three directions is X>Y>Z. As described before, a three-phase region shrinks to a point, *i.e.*, a tricritical point in a composition tetrahedron with the rise in temperature at constant salinity or with increasing salinity at constant temperature. Griffiths predicted theoretically the shape of a three-phase region as a function of temperature in his coordinate system ξ_1, ξ_2, ξ_3, which is intrinsic to the figure of a three-phase region.[1] Present coordinate system, X, Y, Z, approximately corresponds with his system near a tricritical point.[1,2] According to his theory, the dimensions of the three-phase region vanish at different rates. The size in the ξ_1 direction diminishes proportionally to $(T_{Tcp}-T)^{1/2}$, that in the ξ_2 direction vanishes proportionally to $(T_{Tcp}-T)$ and that in the ξ_3 direction disappears proportionally to $(T_{Tcp}-T)^{3/2}$, where T_{Tcp} is a tricritical temperature.[1,2] Therefore, on approach to the tricritical point the region first becomes flat (the size in the ξ_3 (or Z) direction shrinks), then slender (that in the ξ_2 (or Y) direction shrinks) and finally of vanishing length (that in the ξ_1 (or X) direction shrinks).[1,2] His prediction is qualitatively in correspondence with the NaTC system as is shown in Figs. 5 and 11.

Correlation between a Tricritical Point and a Three-phase Region. As described before, a tricritical point is shifted to higher temperatures with increasing salinity. Accordingly, at fixed salinity, a three-phase region exists at temperatures below the tricritical temperature as is shown in Fig. 12. If the salinity is approached to zero, the tricritical temperature becomes below 0 °C and the three-phase region cannot be observed. This is the reason why it is difficult to obtain a three-phase region in an ionic surfactant/water/co-surfactant/oil system without adding salt.

The authors wish to thank Mr. M. Tanaka for his technical assistance.

References

1) R. B. Griffiths, *J. Chem. Phys.*, **60**, 195 (1974).
2) J. C. Lang, Jr., and B. Widom, *Physica*, **81A**, 190 (1975).
3) M. L. McGlashan, "Chemical Thermodynamics," Academic Press Inc., London (1979), Chap. 17.
4) B. Widom, *J. Phys. Chem.*, **77**, 2196 (1973).
5) J. Specovius, M. A. Leiva, R. L. Scott, and C. M. Knobler, *J. Phys. Chem.*, **85**, 2313 (1981).
6) G. S. Radyshevskaya, N. I. Nikurashina, and R. V. Mertslin, *J. Gen. Chem. USSR*, **32**, 673 (1962).
7) I. R. Krickevskii, G. D. Efremova, R. O. Pryanikova, and A. V. Serebryakova, *Russ. J. Phys. Chem.*, **37**, 1046 (1963).
8) G. D. Efremova and A. V. Shvarts, *Russ. J. Phys. Chem.*, **40**, 486 (1966).
9) R. B. Griffiths, *Phys. Rev. Lett.*, **24**, 715 (1970).
10) H. Kunieda and S. E. Friberg, *Bull. Chem. Soc. Jpn.*, **54**, 1010 (1981).
11) H. Kunieda and K. Shinoda, *Bull. Chem. Soc. Jpn.*, **55**, 777 (1982).
12) H. Kunieda, *Bull. Chem. Soc. Jpn.*, **56**, 625 (1983).
13) B. M. Knickerbocker, C. V. Pesheck, H. T. Davis, and L. E. Scriven *J. Phys. Chem.*, **86**, 393 (1982).
14) P. A. Winsor, "Solvent Properties of Amphiphilic Compounds," Butterworths, London (1950), p. 68.
15) R. L. Reed and R. N. Healy, "Improved Oil Recovery by Surfactant and Polymer Flooding," ed by D. O. Shah and R. S. Schecther, Academic Press Inc., New York (1977), p. 383.
16) H. Kunieda and K. Shinoda, *J. Colloid Interface Sci.*, **75**, 601 (1980).
17) H. Kunieda and K. Shinoda, *Yukagaku*, **29**, 676 (1980).
18) H. Kunieda and K. Shinoda, *J. Dispersion Sci. Tech.*, **3**, 233 (1982).
19) P. Ekwall, L. Mandell, and K. Fontell, *Mol. Cryst. Liquid Cryst.*, **8**, 157 (1969).
20) K. Shinoda and H. Saito, *J. Colloid Interface Sci.*, **26**, 70 (1968).
21) K. Shinoda and H. Kunieda, *J. Colloid Interface Sci.*, **42**, 381 (1973).
22) J. Zernike, *Recl. Trav. Chim. Pays-Bas*, **68**, 585 (1949).

Electrochemical Properties of Electrochemically Polymerized Polypyrrole Film in the Dark and under Light Irradiation

Tooru INOUE* and Toshihiro YAMASE
Research Laboratory of Resources Utilization, Tokyo Institute of Technology, 4259 Nagatsuta-cho, Midori-ku, Yokohama 227
(Received August 2, 1982)

Polypyrrole films prepared on Pt or SnO_2 through electrochemical oxidative polymerization of pyrrole were characterized with respect to electroconductivity by photoelectrochemical measurements. Redox reactions of solution species such as methyl viologen, hydroquinone, oxygen, Cu^{2+}, I^-, and Br^- occur on these electroconductive films. Light excitation of the film with wavelengths shorter than 550 nm results in observable cathodic photocurrent at the potential region more negative than 0.0 V *vs.* Ag. The polypyrrole film is a p-type semiconductor with a bandgap energy of *ca.* 2.2 eV and is stable during redox reactions.

Many works on photoelectrochemical processes have recently been carried out from the standpoint of solar energy conversion to electrical energy and/or chemical energy. There have been intensive studies on semiconductor transducers such as photoelectrodes, composed of TiO_2, CdS, GaP, GaAs, Si, *etc.*, for electrochemical photocells.[1-7]

Thin-layer-coated semiconductor electrodes with dyes,[8,9] metal complexes,[10-12] and organic polymers[13-15] such as Rhodamine B, thiacyanine, chlorophyll, Cu-phthalocyanine, $Ru(bpy)_3^{3+}$, and polypyrrole have been developed as photoelectrodes for electrochemical systems. Fan *et al.*,[13] Simon *et al.*,[14] and Skotheim *et al.*[15] have reported that an Si electrode coated with polypyrrole film is stabilized against photodegradation by the SiO_2 layer formation on Si surface so as to provide an electrochemical photocell capable of supplying stable photocurrent for a long period.

Organic polymers such as polyacetylene $(CH)_x$, poly(sulfur nitride) $(SN)_x$, and polypyrrole $(Pyr)_x$ have been synthesized as promising electrical conductors and their electrical and optical properties have been investigated.[13-21] Diaz *et al.*[17] have reported on electrochemical preparation and behavior of polypyrrole films on a Pt electrode. The polypyrrole films show a metallic conductivity and redox reactions of ferrocene, nitrobenzene, and chloranil occur on the surface of these films.

This paper describes spectral observations during polypyrrole film formation, redox reactions of methyl viologen, hydroquinone, oxygen, Cu^{2+}, I^-, and Br^-, and photocathodic reactions under light irradiation. The polypyrrole film shows an electrical conductivity like a metal or semiconductor electrode. Especially, under light irradiation with wavelengths shorter than 550 nm the polypyrrole film shows cathodic photocurrent under cathodic polarization, so that the film is considered to have a p-type semiconducting property with a bandgap energy of *ca.* 2.2 eV. The polypyrrole film is discussed from the viewpoint of the traditional theory of semiconductors.

Experimental

A Pt electrode and an optically-transparent SnO_2 electrode were employed as substrate electrode for pyrrole polymerization. For the pretreatment of the Pt electrode, the potential of Pt was scanned several times between −0.2 and 1.3 V *vs.* SCE in order to get a clean Pt surface. The SnO_2 electrode was rinsed with a dilute H_2SO_4 aqueous solution and methanol before use.

Polypyrrole film was formed on the electrode by electrochemical oxidation of pyrrole in an electrochemical glass cell with an Ag reference electrode and a Pt counter electrode, a potensiostat system (Hokuto Denko Co. Model HA301) being employed. The solution used for the polymerization was acetonitrile with 0.1 M (1 M = 1 mol dm^{-3}) pyrrole and 0.1 M Bu_4NClO_4. As for the polymerization, the electrode potential was initially polarized at 1.3 V *vs.* Ag in order to produce a cationic radical[17] of pyrrole, $pyrrole^+$. Then to let the $pyrrole^+$ polymerize with other pyrroles, the electrode potential was kept at 1.0 V for several minutes or scanned between −0.5 and 1.0 V *vs.* Ag. For the polypyrrole films in the photoelectrochemical study, the polymerization was carried out *via* oxidation with current charges from 10 to 100 milli coulombs (mC).

For the electrochemical measurement the light source was a 500 W Xe lamp (Ushio Electric Co.) with a glass cut-filter $\lambda(<350$ nm cut-off). Absorption spectra of polypyrrole films in the course of polymerization were measured with an SnO_2 electrode which was attached on the front of a box-type cell settled in the spectrometer. The light intensity dependence of cathodic photocurrents was measured with neutral density filters. Current-potential characteristics were observed by employing a potensiostat with a function generator. Measurements of action spectra of photocurrents were carried out by use of a synchrotrack lock-in amplifier and a light chopper (NF Circuit Design Block Co.). A grating monochromator (Nikon G-250) was employed for the wavelength selection on the light from the 500 W Xe lamp.

Chemicals used in this study were all of reagent grade and used without further purification. Electrolyte solutions were deaerated with a purified nitrogen purge during experiment.

Results and Discussion

Pyrrole was oxidized at the Pt electrode in the acetonitrile solution containing 0.1 M Bu_4ClO_4 (TBAP). Figure 1 shows the current-potential curves obtained in the course of the pyrrole polymerization. At first, the electrode was polarized at 1.2 V *vs.* Ag, where a pyrrole cationic radical was formed. Then the pyrrole was polymerized at the potentials above 1.0 V. In the first cycle of potential under the polarization between −0.5 and 1.0 V, the anodic (I_{pa}) and cathodic peak currents

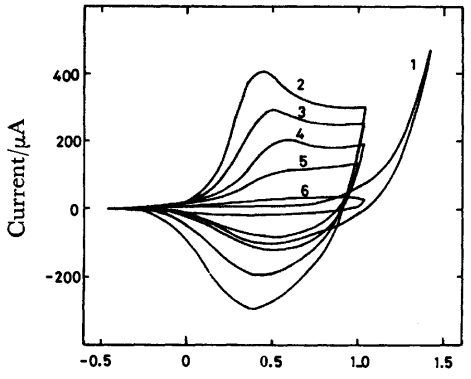

Fig. 1. Current-potential curves in the course of the oxidative polarization of pyrrole in an acetonitrile solution with 0.1 M pyrrole and 0.1 M TBAP. Potential sweep rate is 30 s/V. 1; 1st sweep, 2; 3rd, 3; 5th, 4; 8th, 5; 10th, 6; 50th.

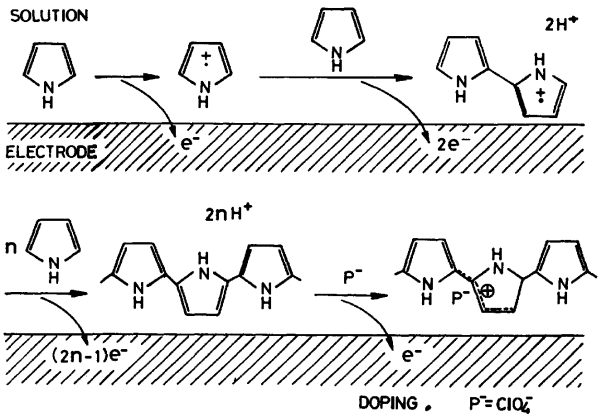

Fig. 2. Schematic illustration of a polypyrrole film prepared by the electrolytic oxidation.

(I_{pc}) appear at the potentials E_{pc} and E_{pa}, respectively where I_{pa}=411 μA at E_{pa}=0.42 V, I_{pc}=395 μA at E_{pc}=0.3 V, and I_{pc}/I_{pa}=0.96. From these data, the redox reactivity of pyrrole may be considered reversible. This anodic current is due to the oxidation during the polymerization of pyrrole accompanying a ClO_4^- doping into the polypyrrole film matrix.[18] The anodic and cathodic currents decrease with increasing number of potentials cyclings, due to increase in film thickness.

The polymerization reaction under an anodic polarization of an electrode can take place accompanying a doping of ClO_4^- anion, leading to the formation of pyrrole cation radical-ClO_4^- pair, and is controlled by the charge amount of anodic current. That is, the concentration of ClO_4^- as a dopant controls the electrical conductivity of the film from 0.1 to 10 Ω^{-1} cm^{-1}. The polypyrrole film formation is schematically illustrated in Fig. 2.

The thickness of polypyrrole was increased and its blue color deepened with increasing electrolytic charge amount. Absorption spectra of the polypyrrole film on an optically transparent SnO_2 electrode in the course of the polymerization are shown in Fig. 3 as a function of the electrolytic charge amount. The absorbance in

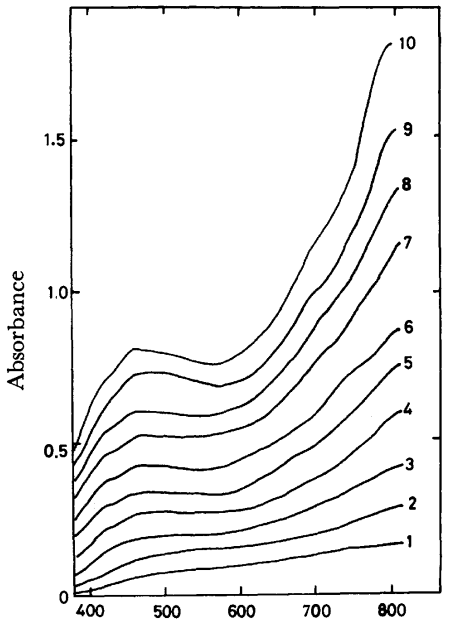

Fig. 3. Absorption spectra of the polypyrrole films prepared on a SnO_2 electrode as a function of the oxidation charges. 1; 12.4 mC/cm^2, 2; 19.1, 3; 26.0, 4; 35.5, 5; 43.0, 6; 47.3, 7; 66.1, 8; 75.2, 9; 83.2, 10; 97.0.

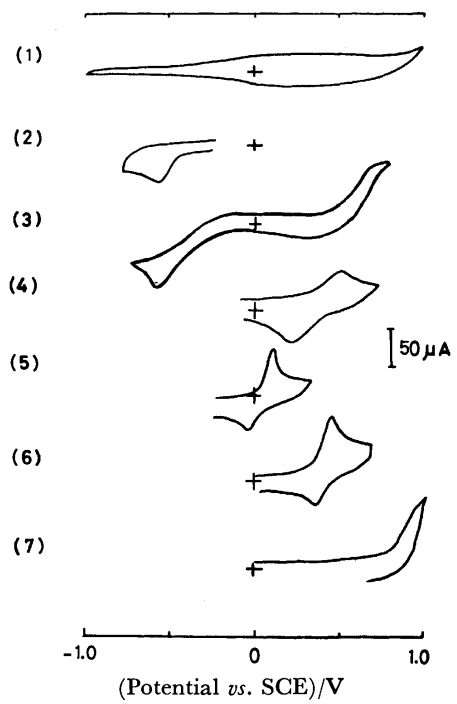

Fig. 4. Current-potential curves at the polypyrrole film electrode in the aqueous solution (0.1 M $NaClO_4$) with various redox agents. (1) without redox agent, (2) 1 mM MV^{2+}, (3) 1 mM H_2Q, (4) *ca.* 1 mM O_2, (5) 1 mM Cu^{2+}, (6) 1 mM I^-, (7) 1 mM Br^-.

the visible region, especially at wavelengths longer than 600 nm, increases with increase in the oxidation charge amount.

Figure 4 shows current-potential curves which were

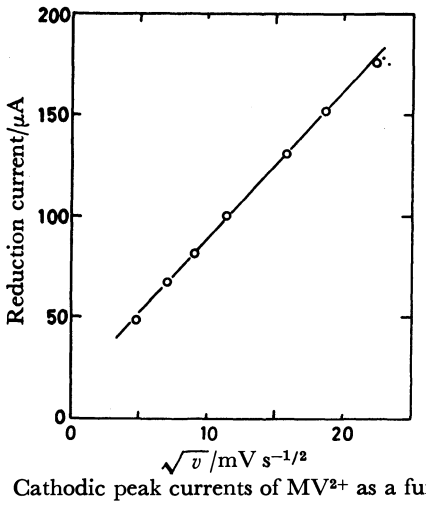

Fig. 5. Cathodic peak currents of MV^{2+} as a function of potential sweeping rate (v).

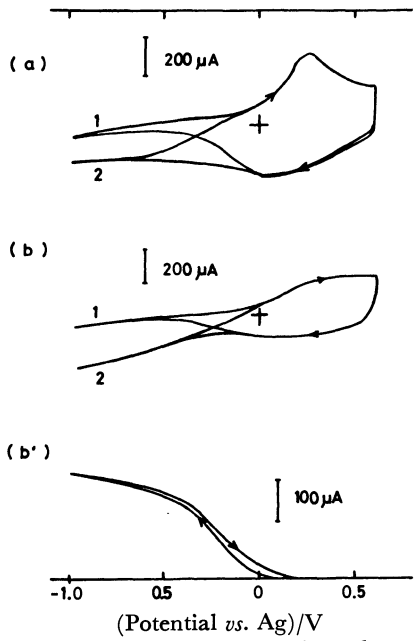

Fig. 6. Current-potential curves at the polypyrrole film in a solution with 0.1 M TBAP in the dark (1) and under light irradiation (2). (a) At the film prepared with the charge of 23.4 mC (1200 Å thickness), (b) at the film prepared with the charge of 30.0 mC (1500 Å thickness), (b') a photocurrent-potential curve at the film (b).

obtained with the Pt electrode with the polypyrrole film in the presence or absence of various redox agents such as methyl viologen (MV^{2+}), hydroquinone (H_2Q), O_2, Cu^{2+}, I^-, and Br^- in solution. The presence of redox agents brings about increase in the anodic and cathodic currents. Especially, the redox agents H_2Q, Cu^{2+}, and I^- can exchange electrons with the polypyrrole electrode surface, resulting in reversible voltammograms. Oxygen can be reduced on this film surface. Therefore, the polypyrrole film doped with ClO_4^- can be considered to have electrical conducting characteristics which are similar to those of metallic electrodes. Diaz *et al.*[17,18] have reported that redox agents such as ferricinium and that redox reactions for these redox agents are reversible on this film electrode.

Figure 5 shows cathodic peak currents as a function of the sweeping rate of potential. The linear relationship of the plot indicates that the charge transfer reaction is controlled by the MV^{2+} diffusion toward the polypyrrole electrode surface. The diffusion constant of MV^{2+} in Fig. 5 is 4.8×10^{-6} cm^2 s^{-1}, a little smaller than the value of 1.38×10^{-5} cm^2 s^{-1} obtained with a Pt electrode in an acetonitrile solution.[22] This discrepancy between the diffusion constants may result from surface constitution of the polypyrrole film.

Figure 6 shows current-potential curves obtained under light irradiation for the polypyrrole films which were prepared by applying charge amounts of (a) 23.4 mC and (b and b$^-$) 30.0 mC for oxidative polymerization with resulting film thicknesses of *ca.* 1200 and 1500 Å, respectively; in these preparations cathodic photocurrents were observed at cathodic potentials more negative than 0.0 V *vs.* Ag. Cathodic photocurrents at the potential of -1.0 V were 120 μA for (a) and 260 μA for (b), reaching a maximum value with the film corresponding to *ca.* 40 mC, as established from variation in the relationship between light absorption and resistance of the film with film thickness. Hysteresis of photocurrent is observed during cyclic potential scanning, as shown in Fig. 6(b'). This may be explained in terms of the concentration of the dopant, that is, the film composition depends on the flow of dopant ClO_4^- which directs from the polypyrrole film into the solution at the cathodic current observed and in the reverse direction at the anodic current.

In the aqueous solution with 0.1 M $NaClO_4$, current-potential characteristics of the redox agents are similar to those in the acetonitrile solution; the non-Faradaic current is a little larger in the former solution than in the latter. The onset potential for cathodic photocurrent is 0.3 V *vs.* SCE.

For interpretation of the electrochemical behavior and photoresponse of polypyrrole film, the following physical properties need to be taken into account: The electrical property of organic polymers such as polyacetylene, polypyrrole, and poly(sulfur nitride) is controlled by the π-electron distribution for polymer, as schematically illustrated in Fig. 7. A polymer film with perfectly localized π-electrons (Fig. 7(1)) has no or a low conducting property because the π-electrons over the polymer are trapped in deep wells of electronic potential in double bonds. According to the traditional semiconductor theory, the energy diagram can be represented as being equal to the one for an intrinsic semiconductor with a large bandgap energy E_g. On the contrary, the polymer film with fully delocalized π-electrons (Fig. 7(2)) has a high conducting property because the π-electrons are distributed over the polymer chain.

For the film involved in the charge transfer doping of an anion (P^-) (Fig. 7(3)), an acceptor is induced to appear removal of one π-electron from one π-bond of the polymer under the requirement of electrical neutrality and causes localized distortion of the π-electrons on the polymer. The nonlinear wave function of the positively-charged localized region is called a soliton.[23,24]

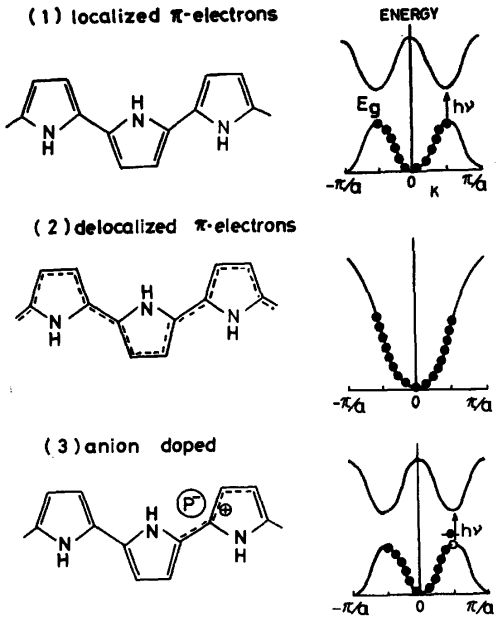

Fig. 7. Schematic diagram of the energy bands of the polypyrrole film where the energy diagram is governed by the electron distribution spreading over the polypyrrole linkage. Electroconductivity of the film with localized π-electrons is quite low because of the large bandgap energy E_g, on the contrary, that of the film with delocalized π-electrons is high because of no bandgap energy. A dopant forms a state within the bandgap resulting in an increase in the conductance.

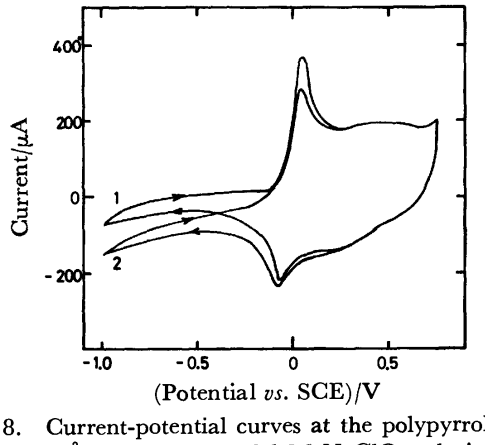

Fig. 8. Current-potential curves at the polypyrrole film of 1000 Å thickness in a 0.1 M $NaClO_4$ solution with 1 mM $CuCl_2$. 1; in the dark, 2; under light irradiation.

The spreading mode of a soliton determines the electrical conductivity of polymer. The soliton density increases with increase in the dopant concentration, enhancing the electrical conductivity of polymer. The polypyrrole film with ClO_4^- anions doped may be considered to be a p-type semiconductor with positive acceptor sites in its bandgap.

The dopant transfer into and out of polymer, allowed to occur by anodic and cathodic polarization, respectively, in the course of potential cycling, can change the acceptor density in the polymer; under cathodic polarization the polymer has a high conductivity. The

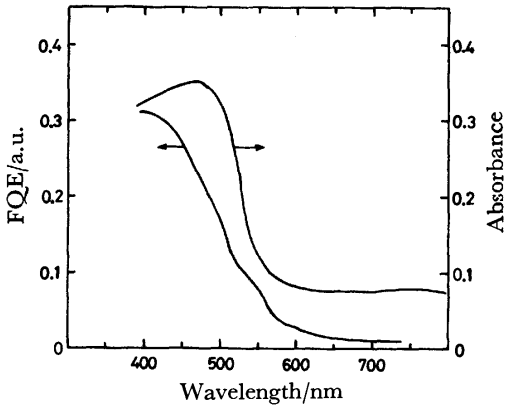

Fig. 9. Actionspectrum of the formal quantum efficiency (FQE) of cathodic photocurrents observed at the polypyrrole film electrode at -1.0 V *vs.* Ag in an acetonitrile solution and the absorption spectrum of the polyrrole film polarized at -1.0 V. FQE denotes the current efficiency against the amount of the incident photons.

hysteresis illustrated in Fig. 6(b') is presumed to be due to a conductivity difference between the anodic and cathodic polarizations.

Figure 8 shows current-potential curves for the polypyrrole electrode in an aqueous solution with 0.001 M $CuCl_2$ and 0.1 M $NaClO_4$ under light irradiation. The current-potential curve in the dark (a) has a couple of anodic and cathodic current peaks around 0.0 V *vs.* SCE, representing an occurrence of the reversible redox reaction of Cu^{2+}/Cu^+

$$Cu^{2+} + e^- \rightleftarrows Cu^+. \quad (1)$$

When the polypyrrole electrode is irradiated with light, cathodic photocurrent appears at negative potentials than 0.3 V. For curve (b) in Fig. 8, the anodic current peak for the oxidation of Cu^+ to Cu^{2+} is larger than the one in the dark (a). The photoinduced increase in anodic current is attributed to the increase in the Cu^+ concentration on the surface due to the reduction by photogenerated conduction band electrons. Because an electron-hole pair produced in a photoexcited polypyrrole film can be separated by the electric field generated by the cathodic polarization, the electron produced reduces the oxidized form (Cu^{2+}) on the film surface. Therefore, it is inferred that the polypyrrole film electrode can act as an active photocathode for the redox reaction of solution species.

The action spectrum of cathodic photocurrents at the potential of -1.0 V *vs.* SCE is shown in Fig. 9, were the action spectrum coincides well with the absorption spectrum of polypyrrole film referring to a photoabsorption due to π-π^* transition at wavelengths shorter than 550 nm. From this result, the bandgap energy of the p-type semiconducting polypyrrole film is estimated to be about 2.2 eV. The action and absorption spectra of the film observed at -1.0 V are different from the absorption spectrum of the film observed at 1.0 V, as seen from Fig. 3. This electrochromic property of the polypyrrole film arises from conformation change of the polymer based on the ClO_4^- doping with electrode

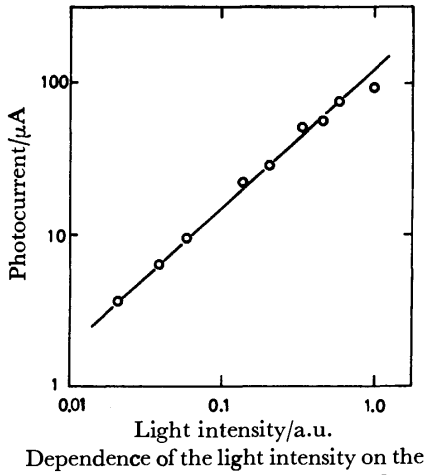

Fig. 10. Dependence of the light intensity on the cathodic photocurrents observed at the polypyrrole film electrode polarized at −1.0 V *vs.* Ag in an acetonitrile solution with 0.1 M TBAP and 2 mM MV^{2+} under light irradiation with wavelengths longer than 430 nm.

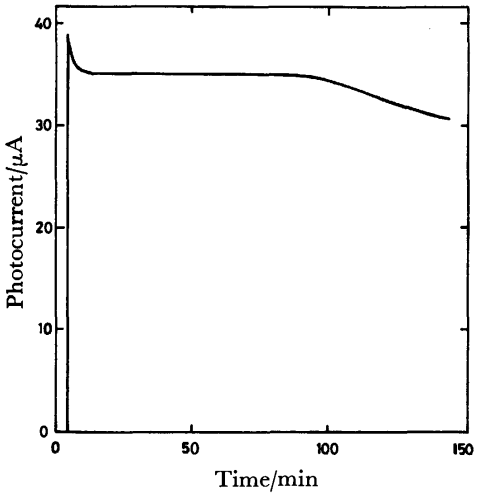

Fig. 11. Time dependence of the cathodic photocurrent observed at the polypyrrole film (500 Å thickness) polarized at −1.0 V *vs.* Ag in an acetonitrile solution with 2 mM MV^{2+}.

polarization.

Figure 10 shows the light intensity dependence of cathodic photocurrent which was observed at −1.0 V *vs.* Ag in an acetonitrile solution. The cathodic photocurrent increases in a linear relationship with a slope of *ca.* 0.9 with increasing light intensity. It follows that the carrier formation is of one photon. The quantum efficiency of the photocurrent is around 0.01.

Figure 11 shows the time dependence of cathodic photocurrent. Photocurrents flow with fair stability but decrease by 15% after a 120 min irradiation. The charge required for the polypyrrole film preparation and the photocurrent charge for 120 min are 10 and 250 mC, respectively. The result suggests that the polypyrrole film works stably under the restriction that the ratio of cathodic photocurrent charge to polymerization charge should be less than 20, although the photocurrent decreases gradually over about 2 h.

Conclusion

The polypyrrole film was formed on Pt and SnO_2 electrodes through an oxidation of pyrrole accompanying a radical linking and an anion doping. The polypyrrole film is capable of electrical conduction based on the solution effect that a doped anion (ClO_4^- in this study) affects the distribution of π-electron densities in the polypyrrole linkage.

Redox reactions of solution species occur on the polypyrrole film electrode. Under visible light irradiaton at $\lambda < 550$ nm, the polypyrrole film electrode shows a p-type semiconducting property, resulting in cathodic photocurrent evolution due to reduction of solution species.

p-Type semiconducting polypyrrole films with high conductance can be developed which are applicable to photoelectrodes in photoelectrochemical cells and to electrochromic devices.[25]

We thank Mr. Koji Asano for the technical assistance in the electrochemical experiments.

References

1) A. Fujishima and K. Honda, *Nature*, **238**, 37 (1972).
2) A. Fujishima, T. Inoue, and K. Honda, *J. Am. Chem. Soc.*, **101**, 5582 (1979).
3) T. Inoue, C. Weber, A. Fujishima, and K. Honda, *Bull. Chem. Soc. Jpn.*, **53**, 334 (1980).
4) T. Inoue, T. Watanabe, A. Fujishima, K. Honda, and K. Kohayakawa, *J. Electrochem. Soc.*, **124**, 719 (1977).
5) A. B. Ellis, J. B. Bolts, S. W. Kaiser, and M.S. Wrighton, *J. Am. Chem. Soc.*, **99**, 2848 (1977).
6) B. A. Parkinson, A. Heller, and B. Miller, *J. Electrochem. Soc.*, **126**, 954 (1979).
7) T. Skotheim, I. Lundstrom, A. E. Delahay, F. J. Kampas, and P. E. Vanier, *Appl. Phys. Lett.*, **40**, 281 (1982).
8) M. Fujihira, N. Ohnishi, and T. Osa, *Nature*, **268**, 226 (1977).
9) W. Arden and P. Fromherz, *J. Electrochem. Soc.*, **127**, 370 (1980).
10) H. Tributsch and M. Calvin, *Photochem. Photobiol.*, **14**, 95 (1971).
11) N. Minami, T. Watanabe, A. Fujishima, and K. Honda, *Ber. Bunsenges. Phys. Chem.*, **83**, 476 (1979).
12) P. K. Ghosh and T. S. Spiro, *J. Am. Chem. Soc.*, **102**, 5543 (1980).
13) F. F. Fan, B. L. Wheeler, A. J. Bard, and R. N. Noufi, *J. Electrochem. Soc.*, **128**, 2042 (1981).
14) R. A. Simon, A. J. Ricco, and M. S. Wrighton, *J. Am. Chem. Soc.*, **104**, 2031 (1982).
15) T. Skotheim, I. Lundstrom, and J. Prejza, *J. Electrochem. Soc.*, **128**, 1625 (1981).
16) S. N. Chan, A. J. Heeger, Z. Kiss, A. G. MacDiarmid, S. C. Gau, and D. L. Peebles, *Appl. Phys. Lett.*, **36**, 96 (1980).
17) A. F. Diaz, K. K. Kanazawa, J. I. Castillo, and J. A. Logan, *Polym. Sci. Tech.*, **15**, 149 (1981).
18) A. F. Diaz, J. I. Castillo, J. A. Logan, and W. Y. Lee, *J. Electroanal. Chem. Interfacial Electrochem.*, **129**, 115 (1981).
19) T. Yamase, H. Harada, S. Ikeda, and H. Shirakawa, *Bull. Chem. Soc. Jpn.*, **54**, 2817 (1981).
20) A. Watanabe, M. Tanaka, and J. Tanaka, *Bull. Chem. Soc. Jpn.*, **54**, 2278 (1981).

21) M. Tanaka, A. Watanabe, and J. Tanaka, *Bull. Chem. Soc. Jpn.*, **53**, 645 (1980).
22) T. Osa and T. Kuwana, *J. Electroanal. Chem. Interfacial Electrochem.*, **22**, 389 (1969).
23) C. R. Fincher, Jr., M. Ozaki, A. J. Heeger, and A. G. MacDiarmid, *Phys. Rev. B*, **19**, 4140 (1979).
24) W. P. Su, J. R. Schrieffer, and A. J. Heeger, *Phys. Rev. Lett.*, **42**, 1698 (1979).
25) T. Inoue and T. Yamase, to be submitted.

 © 1983 The Chemical Society of Japan Bull. Chem. Soc. Jpn., 56, 991—996 (1983)

A Potential-step Chronoamperometric Study of Ion Transfer at the Water/Nitrobenzene Interface

Tadaaki KAKUTANI, Toshiyuki OSAKAI, and Mitsugi SENDA*

Department of Agricultural Chemistry, Faculty of Agriculture, Kyoto University, Kyoto 606

(Received August 2, 1982)

Potential-step chronoamperometry, cyclic voltammetry, and chronopotentiometry have been applied to the study of the transfer of the tetramethylammonium (TMA^+) ion across the interface between a 0.1 mol dm^{-3} lithium chloride aqueous solution and a 0.1 mol dm^{-3} tetrabutylammonium tetraphenylborate nitrobenzene solution. An analysis of the current-time and current-potential curves obtained by means of potential-step chronoamperometry indicates that the transfer of the TMA^+ ion across the water/nitrobenzene interface is a reversible diffusion-controlled process, which can be explained by the theory of the chronoamperometry of a reversible charge transfer at the electrode surface. The values of the diffusion coefficient of the TMA^+ ion in the aqueous phase and of the reversible half-wave potential of the TMA^+ ion transfer, as determined by means of potential-step chronoamperometry, agreed well with those determined by means of cyclic voltammetry and chronopotentiometry.

Recently there has been growing interest in electrochemical phenomena occurring at the interface between oil and water or two immiscible liquids (for reviews, see Refs. 1, 2, and 3). Electrochemical information on the charge (ion or electron) transfer at the liquid-liquid interface is important for a better understanding of the solvent extraction of ions, of liquid membrane ion-selective electrodes, and of the biological membrane and its model systems. Although several electrochemical techniques have been developed for studying the ion transfer at the interface between two immiscible electrolyte solutions (chronopotentiometry with the stationary interface,[4] cyclic voltammetry with the stationary interface,[5,6] and d.c. polarography with the electrolyte dropping electrode[7-9]), the further development of experimental approaches to the electrochemistry of the ion transfer at the interface seems highly desirable. In this work we have applied potential-step chronoamperometry to the study of the tetramethylammonium (TMA^+) ion transfer at the stationary water/nitrobenzene interface. The electrochemical data obtained by this techniques were then compared with those obtained by cyclic voltammetry and chronopotentiometry.

Experimental

Chemicals. The tetrabutylammonium tetraphenylborate (TBATPB) was prepared by the equimolar addition of an aqueous solution of tetrabutylammonium bromide to an aqueous solution of sodium tetraphenylborate and purified by repeated recrystalizations from acetone. The lithium chloride was a Merck product of the "spurapur" grade. The tetramethylammonium bromide (TMABr) and tetrabutylammonium chloride (TBACl) were analytical reagent-grade products of the Nakarai Chemicals Co. These reagents were used as received. Analytical-grade nitrobenzene was shaken with neutral alumina overnight; after the filtration of the suspension, the filtrate was fractionally distilled under a vacuum. The central 60% fraction of the distillate was collected and washed with triply distilled water. Triply distilled water was also used to prepare the aqueous electrolyte solutions.

Electrochemical Measurements. The transfer of the TMA^+ ion across the interface between a 0.1 mol dm^{-3} TBATPB nitrobenzene solution (Phase II in Cell A) and a 0.1 mol dm^{-3} LiCl aqueous solution containing $(0.5—2)\times 10^{-3}$ mol dm^{-3} TMABr (Phase III in Cell A) was studied. The electrolytic cell assembly is shown in Fig. 1. The test interface, *i.e.*, the water/nitrobenzene interface to be studied for the transfer of the TMA^+ ion, is formed in a glass tube A. A flat and reproducible water/nitrobenzene interface, with an area of 0.159 cm^2, can be formed by treating with dimethyldichlorosilane the inner surface of the tube A that will come in contact with nitrobenzene.[10] The potential difference across the test interface was controlled by a four-electrode potentiostat,[5,10] with two reference electrodes and two counter electrodes. The reference electrode for the nitrobenzene phase, RE2, was an Ag/AgCl/0.1 mol dm^{-3} TBACl (water) electrode which was connected to the nitrobenzene phase by means of a Luggin capillary filled with the 0.1 mol dm^{-3} TBATPB nitrobenzene solution. The reference electrode for the aqueous phase, REl, was an Ag/AgCl electrode immersed in an aqueous phase containing 0.1 mol dm^{-3} LiCl. Accordingly, the cell to be studied can be expressed by:

$$\begin{array}{l}\overset{\text{I}}{\text{(RE2) Ag|AgCl|0.1 mol dm}^{-3}\text{ TBACl(W)}}\\ \overset{\text{II}}{\text{|0.1 mol dm}^{-3}\text{TBATPB(N)}}\\ \left|\begin{array}{l}\overset{\text{III}}{(0.5-2)\times 10^{-3}\text{ mol dm}^{-3}\text{ TMABr}}\\ \qquad\qquad\qquad\qquad\qquad\text{(W)}\\ \qquad+\text{ 0.1 mol dm}^{-3}\text{ LiCl}\end{array}\right.\\ \overset{\text{IV}}{\text{|0.1 mol dm}^{-3}\text{ LiCl(W)|AgCl|Ag(REl).}}\quad\text{(A)}\end{array}$$

As the counter electrodes, Ag/AgCl electrodes with a large surface area (>4 cm^2) were used. One of the counter electrodes, CEl, was immersed in the aqueous phase, while the other, CE2, was immersed in a 0.1 mol dm^{-3} TBACl aqueous solution which was connected to the nitrobenzene phase through sintered glass. The location of the tip of the Luggin capillary of the reference electrode was adjusted by using a manipulator, Narishige BC-4; the distance, d_W, between the tip of the Luggin capillary of REl and the test interface, and the distance, d_N, between the tip of the Luggin capillary of RE2 and the test interface, were accurately measured by means of a travelling microscope, PIKA Seiko Co., Model PRM-2XYZ. Usually d_N and d_W were set at 0.2 mm and 1.0 mm respectively. Then the resistance of the electrolyte-solution column between the tips of the two Luggin capillaries, REl and RE2, r_s, was estimated to be 180 Ω, as calculated from the conductivities of the electrolyte solutions and the area of the test interface. The conductivities of the 0.1 mol dm^{-3} LiCl aqueous solution and the 0.1 mol dm^{-3} TBATPB nitrobenzene solution were

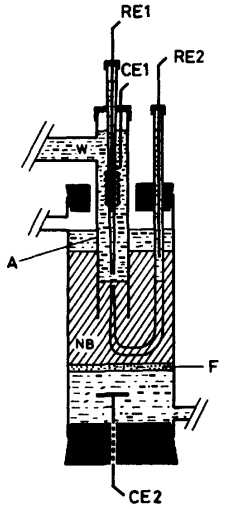

Fig. 1. Electrolytic cell. W: Water phase; NB: nitrobenzene phase; A: glass tube; RE1 and RE2: reference electrodes; CE1 and CE2: counter electrodes; F: sintered glass.

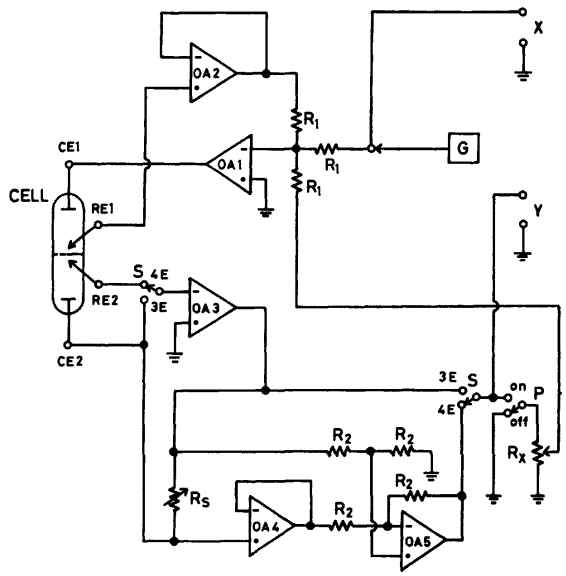

Fig. 2. Electronic circuit of the four-electrode potentiostat with the cell system. G: Sweep and step function generator; X and Y: X- and Y-axis inputs of recorder; RE1 and RE2: reference electrodes; CE1 and CE2: counter electrodes; OA1 to OA5: operational amplifiers, Burr Brown 3112/12C; R_s: current-measuring resistor, variable; R_1 and R_2: resistor, 10 kΩ; S: switch, in position 4E for the four-electrode potentiostat operation and in position 3E for the three-electrode potentiostat operation; P: switch, in on position for positive feedback for iR compensation; R_x: resistor for positive feedback, adjustable.

determined to be 9.48×10^{-3} and 1.12×10^{-3} Ω^{-1} cm^{-1} respectively at 25 °C.

For potential-step chronoamperometry and cyclic voltammetry, a four-electrode potentiostat,[10] to which a Yanako Model PE21-TB2S potentiostat was remodelled, and a function generator, Nikko Keisoku Model NFG-3, were used. Figure 2 shows the basic electronic circuit of the four-electrode potentiostat, with the cell system. The current-time curves of the potential-step chronoamperometry were recorded using both a transient memory, Union Giken System 71-02, and an X-Y recorder, Yokogawa 3077. The cyclic voltammograms were recorded with the same X-Y recorder. For chronopotentiometry, the current across the two counter electrodes (CE1 and CE2) of the cell in Fig. 1 was controlled using a conventional, laboratory-made galvanostat,[10,14] and the potential difference across the test interface was measured by means of the two reference electrodes (RE1 and RE2), using a laboratory-made, high-input-impedance differential amplifier and an X-Y recorder, Yokogawa 3077. All the electrochemical measurements were performed at 25±2 °C.

Results

In the following remarks, the potential applied to the cell A, E, is defined as the potential difference between the two reference electrodes, RE1 and RE2, *i.e.*, $E=E_{RE1}-E_{RE2}$. The flow of the positive charge from the aqueous to the nitrobenzene phase is considered as the positive current.

Potential-step Chronoamperometry. In this method, a potential step $\Delta E=E-E_i$, E_i being the initial potential where the current due to the ion transfer is negligible, is applied to the test interface at time $t=0$, and the resulting current, i, is recorded against t. For studying the TMA^+ ion transfer from the aqueous to the nitrobenzene phase, E_i was set at 200 mV. Figure 3 shows an example of the current-time curves of the TMA^+-ion transfer from the aqueous to the nitrobenzene phase. The currents measured at various E's, when corrected for the base current, were inversely proportional to $t^{1/2}$ at $t>0.1$ s, as is shown in Fig. 4. This indicates that the transfer of the TMA^+ ion from the aqueous to the nitrobenzene phase is a diffusion-controlled process at $t>0.1$ s. Figure 5 shows a plot of the current measured at $t=10$ s, $I_{t=10\,s}$, against

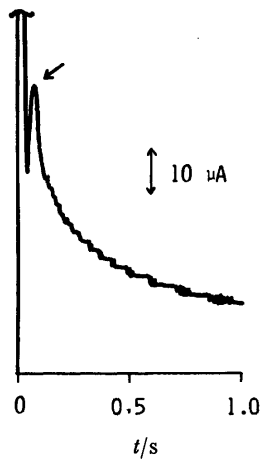

Fig. 3. Chronoamperometric current-time(i-t) curve of TMA^+ ion transfer from the aqueous to the nitrobenzene phase at $E=0.38$ V for 0.5×10^{-3} TMA^+ in 0.1 mol dm^{-3} LiCl aqueous solution. A transient oscillation of the current (as indicated by an arrow) was sometimes observed, depending on the solution resistance and ion transfer impedance at the interface, at the initial part of i-t record.

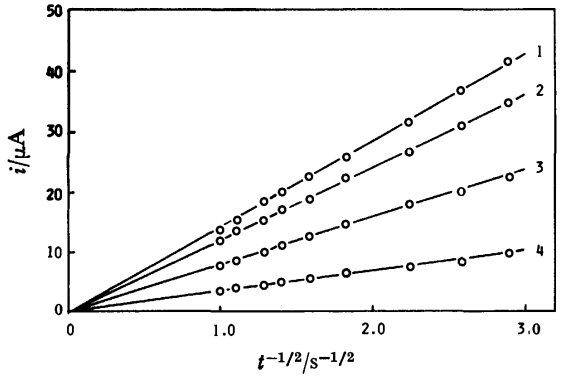

Fig. 4. Plots of i, corrected for the base current, against $t^{-1/2}$ for 0.5×10^{-3} mol dm^{-3} TMA$^+$ ion in 0.1 mol dm^{-3} LiCl aqueous solution. E: (1) 0.38, (2) 0.35, (3) 0.32, (4) 0.29 V.

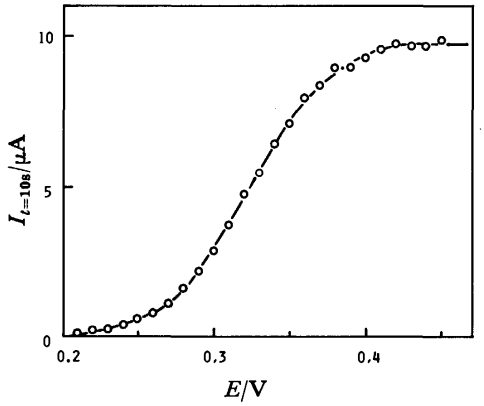

Fig. 5. Plot of $I_{t=10s}$, corrected for the base current, against E for 1×10^{-3} mol dm^{-3} TMA$^+$ ion in 0.1 mol dm^{-3} LiCl aqueous solution.

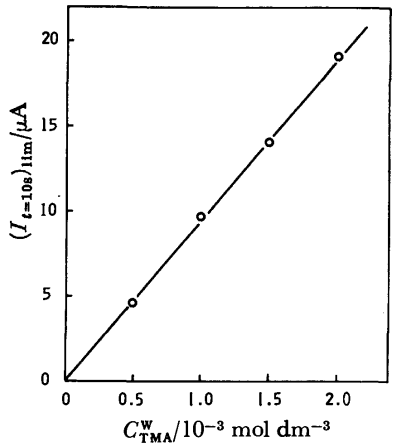

Fig. 6. Dependence of limiting current, $(I_{t=10s})_{lim}$, on the bulk concentration of TMA$^+$ ion, C^W_{TMA}, in 0.1 mol dm^{-3} LiCl aqueous solution.

E for 10^{-3} mol dm^{-3} TMABr in a 0.1 mol dm^{-3} LiCl aqueous solution; it gives a well-defined current-potential ($I_{t=10s}-E$) curve, with the limiting current, $(I_{t=10s})_{lim}$, and the half-wave potential, $E_{1/2}$, for the transfer of the TMA$^+$ ion from the aqueous to the nitrobenzene phase. In the present case (d_N=0.2 mm, d_W=1.0 mm, and t=10 s), the ohmic drop due to r_s was estimated to be always less than 4 mV, even for the 2.0×10^{-3} mol dm^{-3} TMA$^+$ ion in the aqueous phase. Accordingly, no correction for the ohmic drop was made. The limiting current was proportional to the bulk concentration of the TMA$^+$ ion in the aqueous phase, as is shown in Fig. 6. Figure 7 shows a logarithmic analysis of the wave, giving a straight line with the slope of 60 mV. The half-wave potential was 0.32 V, independently of the bulk concentration of the TMA$^+$ ion. These results indicate that the $I_{t=10s}-E$ curve of the TMA$^+$ ion transfer has the same characteristics as a reversible d.c. polarographic wave:

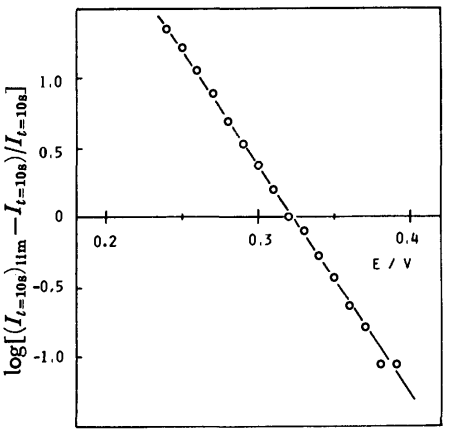

Fig. 7. Logarithmic analysis of the current-potential ($I_{t=10s}-E$) curve shown in Fig. 5.

$$E = E^r_{1/2,j} + (RT/z_jF)\ln[I_{t=t_s}/((I_{t=t_s})_{lim} - I_{t=t_s})], \quad (1)$$

where $E^r_{1/2,j}$ is the reversible half-wave potential of the j ion (here, j=TMA$^+$); z_j the ionic valence of the j ion, and $I_{t=t_s}$, the ion-transfer current at $t=t_s$ (here, t_s=10 s).

The limiting current at $t=t_s$, $(I_{t=t_s})_{lim}$, due to the diffusion-controlled j ion transfer from the aqueous to the nitrobenzene phase should be given by the Cottrell equation:[11]

$$(I_{t=t_s})_{lim} = z_jFA(D^W_j/\pi t_s)^{1/2}C^W_j, \quad (2)$$

where A is the surface area; C^W_j, the bulk concentration, and D^W_j the diffusion coefficient of the j ion in the aqueous phase (W). The application of this equation to the plot in Fig. 6 yielded the diffusion coefficient of the TMA$^+$ ion in the aqueous phase, D^W_{TMA}. The values of $E^r_{1/2,TMA}$ and D^W_{TMA} as determined by means of potential-step chronoamperometry are summarized in Table 1.

Cyclic Voltammetry. Figure 8 shows cyclic voltammograms of the 2×10^{-3} mol dm^{-3} TMA$^+$ ion in the aqueous phase. The positive-current peak on the forward polarization and the negative-current peak on the following backward polarization correspond, respectively, to the transfer of the TMA$^+$ ion from the aqueous to the nitrobenzene phase and its transfer back to the aqueous phase. The voltammograms were influenced by the solution resistance, r_s. The peak potentials of the positive and negative currents, E_{pa} and E_{pc}, varied linearly with d_N, as is shown in Fig. 9.[10] The slopes of

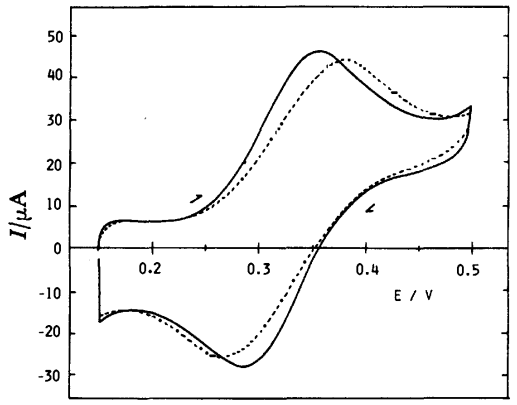

Fig. 8. Cyclic voltammograms for the transfer of 2×10^{-3} mol dm^{-3} TMA^+ ion from 0.1 mol dm^{-3} LiCl aqueous solution to 0.1 mol dm^{-3} TBATPB nitrobenzene solution and back at $v=20$ mV s^{-1}. Solid line: measured at $d_N=0.2$ mm and $d_W=1.0$ mm. Dotted line: measured at $d_N=d_W=1.0$ mm.

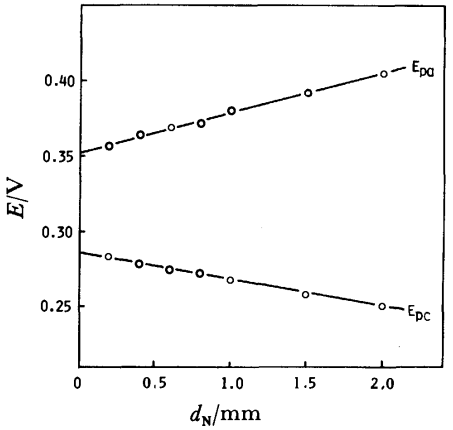

Fig. 9. Plots of the peak potentials of the positive and negative current, E_{pa} and E_{pc}, against d_N for 2×10^{-3} mol dm^{-3} TMA^+ ion in 0.1 mol dm^{-3} LiCl aqueous solution. d_W: 1.0 mm; v: 20 mV s^{-1}.

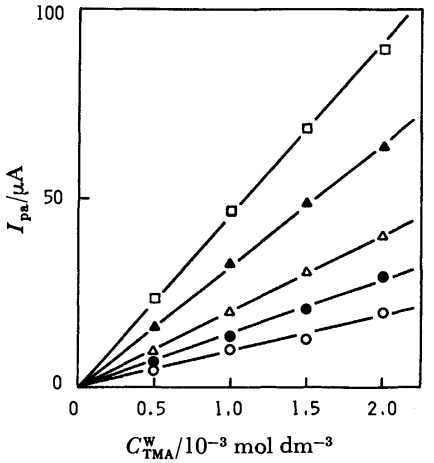

Fig. 10. Dependence of the positive peak current of cyclic voltammogram of TMA^+ ion transfer, I_{pa}, on the bulk concentration of TMA^+ ion, C^W_{TMA}, in 0.1 mol dm^{-3} LiCl aqueous solution. v: (○) 5, (●) 10, (△) 20, (▲) 50, and (□) 100 mV s^{-1}.

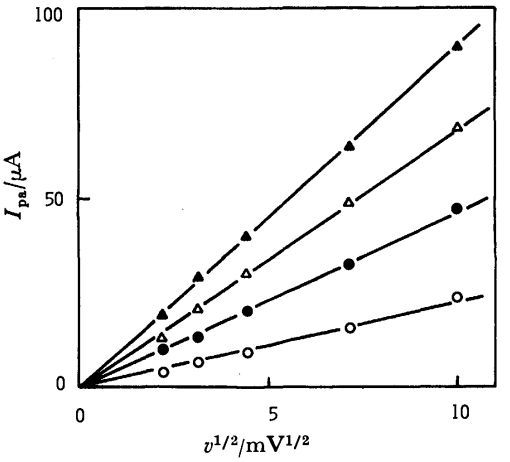

Fig. 11. Dependence of the positive peak current of cyclic voltammogram of TMA^+ ion transfer, I_{pa}, on the voltage scan rate, v. C^W_{TMA}: (○) 0.5×10^{-3}, (●) 1.0×10^{-3}, (△) 1.5×10^{-3}, and (▲) 2.0×10^{-3} mol dm^{-3}.

the linear plots gave 636 Ω mm^{-1} (average of these two plots) for the resistance per mm of the nitrobenzene-solution column; this value agreed well with the calculated value of 563 Ω mm^{-1}. The extrapolation of E_{pa} and E_{pc} to $d_N=0$ should yield the peak potentials corrected for the ohmic drop in the nitrobenzene phase. Correction for the ohmic drop in the nitrobenzene as well as the aqueous phase yielded the corrected peak potentials, $E_{pa,corr}$ and $E_{pc,corr}$, which were independent of both the concentration of the TMA^+ ion in the aqueous phase, C^W_{TMA}, in the range between 0.5×10^{-3} and 2×10^{-3} mol dm^{-3} and the scan rate, v, in the range between 5 and 100 mV s^{-1}. The corrected peak separations, $\Delta E_{p,corr}=E_{pa,corr}-E_{pc,corr}$, were 60 mV over the scan-rate range of 5 to 100 mV s^{-1} for all the concentration of the TMA^+ examined. When $r_s=180$ Ω ($d_N=0.2$ mm and $d_W=1.0$ mm), the positive peak current, I_{pa}, was proportional to the concentration of the TMA^+ ion and to the square root of the voltage-scan rate (see Figs. 10 and 11). Similarly, the negative peak current, I_{pa}, was proportional to the concentration of the TMA^+ ion in the aqueous phase and to the square root of the voltage-scan rate (data are not shown). These results indicated that the transfer of the TMA^+ ion across the water/nitrobenzene interface was a diffusion-controlled process over the scan-rate range from 5 to 100 mV s^{-1}. Accordingly, the theory of the voltammetry of a reversible charge transfer at the electrode surface[11] was used to analyse the cyclic voltammetric data. The reversible half-wave potential (or the midpoint potential between $E_{pa,corr}$ and $E_{pc,corr}$) and the diffusion coefficient of the TMA^+ ion in the aqueous phase, as determined by cyclic voltammetry, are given in Table 1.

Chronopotentiometry. Figure 12 shows chronopotentiometric potential-time ($E-t$) curves with the current reversal at various current densities for the transfer of the TMA^+ ion from the aqueous to the nitrobenzene phase and its transfer back to the aqueous phase. The transition times were inversely proportional to the square of the current density over the range from

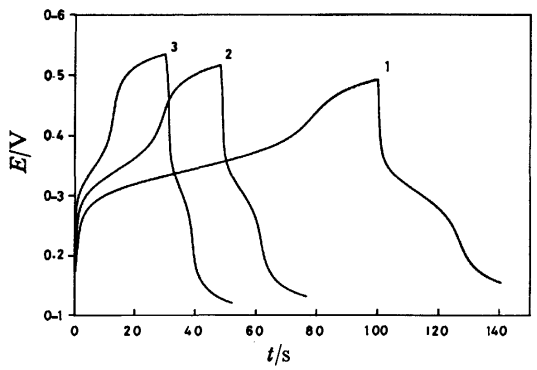

Fig. 12. Chronopotentiometric potential-time curves with current reversal for TMA^+ ion transfer across the water/nireobenzene interface for 1×10^{-3} mol dm^{-3} TMA^+ ion in 0.1 mol dm^{-3} LiCl aqueous solution. The current density: (1) 31.4, (2) 62.9, and (3) 94.3 μA cm^{-2}.

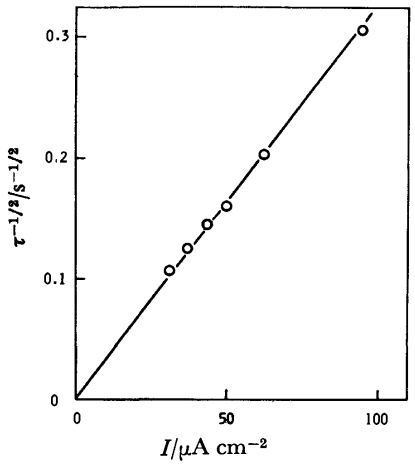

Fig. 13. Dependence of the chronopotentiometric transition time of TMA^+ ion transfer from the aqueous to the nitrobenzene phase, τ, on the current density, I, for the transfer of 1×10^{-3} mol dm^{-3} TMA^+ ion from 0.1 mol dm^{-3} LiCl aqueous solution to 0.1 mol dm^{-3} TBATPB nitrobenzene solution.

Table 1. Half-wave potential for the transfer of TMA^+ ion across water/nitrobenzene interface and diffusion coefficient of TMA^+ ion in the aqueous phase as determined by three electrochemical methods

Method	$E^r_{1/2,TMA}$ / V	D^w_{TMA} / 10^{-5} cm^2 s^{-1}
Potential-step chrononoamperometry	0.32	1.2
Cyclic voltammetry	0.32	1.1
Chronopotentiometry	0.32	1.3

31.4 to 94.3 μA cm^{-2} (Fig. 13). Thus, the chronopotentiometric behavior was interpreted by means of the theory of the chronopotentiometry of a reversible charge transfer at the electrode surface.[11] The reversible half-wave potential and the diffusion coefficient of the TMA^+ ion in the aqueous phase, as determined from the chronopotentiometric data, are given in Table 1.

All three methods yielded the same values of the half-wave potential for the transfer of the TMA^+ ion across the water/nitrobenzene interface and of the diffusion coefficient of the TMA^+ ion in the aqueous phase.

Discussion

We shall define the standard ion-transfer potential of the j ion across the water(W)/nitrobenzene(N) interface, $\Delta^w_N\phi^\ominus_j$, by:

$$\Delta^w_N\phi^\ominus_j = -\Delta G^{\ominus,N\to W}_{tr,j}/z_jF, \quad (3)$$

where $\Delta G^{\ominus,N\to W}_{tr,j}$ is the standard Gibbs free energy of the transfer of the j ion from the nitrobenzene to the aqueous phase. Then, $E^r_{1/2,j}$ is given by:

$$E^r_{1/2,j} = \Delta^w_N\phi_{1/2,j} + \Delta E_{ref}, \quad (4)$$

$$\Delta^w_N\phi_{1/2,j} = \Delta^w_N\phi^\ominus_j + (RT/z_jF)\ln(\gamma^N_j\sqrt{D^w_j}/\gamma^w_j\sqrt{D^N_j}), \quad (5)$$

where ΔE_{ref} is the constant which depends only on the reference electrode system, and where γ^N_j and γ^w_j are the activity coefficients of the j ion in the nitrobenzene and aqueous phases respectively. For the reference electrodes, RE1 and RE2, used here, ΔE_{ref} in Eq. 4 is given by:

$$\Delta E_{ref} = -\Delta\phi_L + E_{Ag/AgCl/0.1\ mol\ dm^{-3}\ LiCl(W)} - E_{Ag/AgCl/0.1 mol\ dm^{-3}\ TBACl(W)}, \quad (6)$$

where $\Delta\phi_L(=\phi^w_I-\phi^N_{II})$ is the potential difference between a 0.1 mol dm^{-3} TBACl aqueous solution(I) and a 0.1 mol dm^{-3} TBATPB nitrobenzene solution(II). Since $\Delta^w_N\phi^\ominus_{TPB}$ is extremely positive compared with $\Delta^w_N\phi^\ominus_{TBA}$, while $\Delta^w_N\phi^\ominus_{Cl}$ is extremely negative compared with $\Delta^w_N\phi^\ominus_{TBA}$, $\Delta\phi_L$ is given in a good approximation by:[10,12]

$$\Delta\phi_L = \Delta^w_N\phi^\ominus_{TBA} + (RT/F)\ln(\gamma^N_{TBA}C^N_{TBA}/\gamma^w_{TBA}C^w_{TBA}), \quad (7)$$

where γ^α_{TBA} and C^α_{TBA} (α=N and W) are the activity coefficient and the concentration of the TBA^+ ion respectively in the nitrobenzene(N) and aqueous(W) phases. The validity of Eq. 7 for the interface between the 0.1 mol dm^{-3} TBACl aqueous solution and the 0.1 mol dm^{-3} TBATPB nitrobenzene solution was proved by measuring the electromotive force, E_{emf}, of the following cell:

$$\begin{array}{l} \overset{I}{Ag|AgCl|0.1\ mol\ dm^{-3}TBACl(W)} \\ \overset{II}{|0.1\ mol\ dm^{-3}\ TBATPB(N)|} \\ \left|\begin{array}{c} \overset{III}{x\ mol\ dm^{-3}\ TBACl} \\ (0.1-x) mol\ dm^{-3}\ LiCl \end{array}\right. (W) \left| AgCl \right| Ag \end{array} \quad (B)$$

for 0.02 mol dm^{-3} $\leq x\leq$ 0.1 mol dm^{-3}; E_{emf} depended linearly on $\ln(C^{III}_{TBA}/C^{I}_{TBA})$, with a slope of 26 mV ($=RT/F$).[10] Upon assuming that $E_{Ag/AgCl/0.1\ mol\ dm^{-3}\ LiCl(W)} - E_{Ag/AgCl/0.1\ mol\ dm^{-3}\ TBACl(W)} \approx 0$, we obtain:

$$\begin{aligned} E^r_{1/2,TBA} &= \Delta^w_N\phi^\ominus_{TMA} + (RT/F)\ln(\gamma^N_{TMA}\sqrt{D^w_{TMA}}/\gamma^w_{TMA}\sqrt{D^N_{TMA}}) \\ &\quad - \Delta^w_N\phi^\ominus_{TBA} - (RT/F)\ln(\gamma^N_{TBA}C^N_{TBA}/\gamma^w_{TBA}C^w_{TBA}) \quad (8) \\ &\approx \Delta^w_N\phi^\ominus_{TMA} - \Delta^w_N\phi^\ominus_{TBA} + (RT/F)\ln(\sqrt{D^w_{TMA}}/\sqrt{D^N_{TMA}}) \end{aligned}$$

since $C^N_{TBA}=C^w_{TBA}=0.1$ mol dm^{-3}, and $\ln(\gamma^N_{TMA}\gamma^w_{TBA}/\gamma^w_{TMA}\gamma^N_{TBA})\approx 0$. The standard ion-transfer potentials of the TMA^+ and TBA^+ ions, as estimated from the ionic distribution coefficient data, are given[13] as $\Delta^w_N\phi^\ominus_{TMA} - \Delta^w_N\phi^\ominus_{TBA} = 0.283$ V, which is 40 mV more negative than

the present result of $E^{\circ}_{1/2,\mathrm{TMA}}=0.32$ V. This difference cannot be explained by the $(RT/F)\ln(\sqrt{D}^{\mathrm{W}}_{\mathrm{TMA}}/\sqrt{D}^{\mathrm{N}}_{\mathrm{TMA}})$ terms. It seems premature to discuss the origin of this discrepancy.

The potential-step chronoamperometry appears a promising technique for the investigation of the charge-transfer processes at the interface between two immiscible electrolyte solutions.

References

1) A. Watanabe and H. Tamai, *Hyomen*, **13**, 67 (1975).
2) J. Koryta, *Electrochim. Acta*, **24**, 293 (1978).
3) M. Senda and T. Kakutani, *Hyomen*, **18**, 535 (1980).
4) C. Gavach and F. Henry, *J. Electroanal. Chem. Interfacial Electrochem.*, **54**, 361 (1974).
5) Z. Samec, V. Mareček, J. Koryta, and M. W. Khalil, *J. Electroanal. Chem. Interfacial Electrochem.*, **83**, 393 (1977).
6) Z. Samec, V. Mareček, and J. Weber, *J. Electroanal. Chem. Interfacial Electrochem.*, **100**, 841 (1979).
7) J. Koryta, P. Vaný́sek, and M. Březina, *J. Electroanal. Chem. Interfacial Electrochem.*, **67**, 263 (1976).
8) J. Koryta, P. Vaný́sek, and M. Březina, *J. Electroanal. Chem. Interfacial Electrochem.*, **75**, 211 (1977).
9) Z. Samec, V. Mareček, J. Weber, and D. Homolka, *J. Electroanal. Chem. Interfacial Electrochem.*, **99**, 385 (1979).
10) M. Senda, T. Kakutani, and T. Osakai, *Denki Kagaku*, **49**, 322 (1981).
11) P. Delahay, "New Instrumental Methods in Electrochemistry," Interscience, New York (1954), Chaps. 3, 6, and 8.
12) L. Q. Hung, *J. Electroanal. Chem. Interfacial Electrochem.*, **115**, 159 (1980).
13) J. Rais, *Collect. Czeck. Chem. Commun.*, **36**, 3253 (1971).
14) D. T. Sawyer and J. L. Roberts, "Experimental Electrochemistry for Chemists," Wiley, New York (1974), Chap. 5.

 © 1983 The Chemical Society of Japan Bull. Chem. Soc. Jpn., 56, 997—1001 (1983)

The Adsorption of Polypeptides on Polystyrene Latices and Their Effects on Colloid Stability

Kunio FURUSAWA,* Hidetoshi SAKAI, Noribumi WATANABE, and Norio TOMOTSU
The University of Tsukuba, Department of Chemistry, Sakura-Mura, Ibaraki 305
(Received August 7, 1982)

The adsorption behavior of poly(L-lysine) and poly(L-glutamic acid) on negatively and positively charged latices was examined in combination with their stabilizing effects on the latex dispersion. It was realized that the polypeptide adsorption was, to a large extent, determined by the coulombic interaction between the polypeptide and the charged surface, and by the conformational change (helix-coil transition) in the polypeptide in the solution. The flocculation behavior of the dispersion in the presence of polypeptide was also explained reasonably by taking account of the results of electrophoretic measurements of the polypeptide-coated particles.

The stability of a colloid dispersion can be widely modified by adding polymer molecules. Especially, a partially ionic polymer is important as a flocculant in various practical fields.[1] As for the mechanism of destabilization to the dispersion by a polymer, two principal ideas have been proposed. One is the bridging effect,[2] which is built up between the particles containing an adsorbed polymer layer. Under this mechanism, loops and tails in the adsorption layer play an important role. Another mechanism is based on the charge neutralization of the particles by the adsorption of oppositely charged polyelectrolytes.[3] The problem is that these two mechanisms for destabilization are not independent; rather, the colloid stability is practically determined by the combined action of these two effects.[4]

Poly(L-lysine)(PLL) and poly(L-glutamic acid)(PLG) are typical cationic and anionic polypeptides, and the study of molecular conformation, *i.e.*, the helix-coil transition in solution, has been examined extensively. According to Chou *et al.*,[5] the helix-coil transition of PLL is brought about by the change in pH from around pH 11, where the polymer is helix, to pH$<$8, where the helix content is zero and where all the molecules take an extended form. On the other hand, the PLG takes the helical conformation in the pH$<\approx$5.5 range and is changed to a random or a stretched structure in the pH$>$6 range.

In this work, PLL and PLG were used as adsorbates and the adsorption behavior was examined by combining their flocculation effects on the latex dispersion. As the colloidal dispersion, several polystyrene latices of different polarities were used to suppress the effects of electrostatic interaction. The main object in this work is to clarify the following problems:

a) What is the principal mechanism of destabilization (or stabilization) in the present system?

b) How does the helix-coil transition influence the adsorption phenomena?

c) How does the destabilization (or stabilization) appear in the different conformations of the polymers?

Working with well-defined latices of different characters as adsorbents will assist in gaining a better understanding of these ends.

Experimental

Materials. To emphasize the polarity of the substrate, three kinds of polystyrene latices were employed. Latex-A was prepared by the usual Kotera-Furusawa-Takeda method.[6] Latex-B was made by incorporating a small amount of an ionic comonomer, sodium *p*-vinylbenzeulsulfonate, into a polystyrene chain according to Juang *et al.*[7] The charge density of Latex-B is much higher than that of Latex-A. Latex-C consists of amphoteric lat prepared by the method described by Homola *et al.*[8] The characterization data for these samples are shown in Table 1. All the latices were prepared by the use of an emulsifier-free system to reduce the spurious effects of surface-active substance. Also, the use of buffers has been avoided in order to obtain a clean system.

Table 1. Characterization data of polystyrene lattices

Sample	Diameter (2a) / A	Surface charge σ_0 / $\mu C\ cm^{-2}$	ζ-Potential/mV (25 °C, 10^{-3} M KCl) pH 4.5	pH 10
Later-A	5260	3.1	−39	−42
Latex-B	1600	9.0	−67	−70
Latex-C	1950	—	+38	−17

The hydrobromide of PLL was purchased from the Sigma Chemical Co. Ltd. (U. S. A.) and had the reported molecular weights of 4000, 32500, and 57500 respectively. The hydrobromide form was converted to the hydrochloride form by dissolving the PLL in distilled water and by dialyzing them exhaustively against 0.01 M HCl (1 M=1 mol dm^{-3}) and then against distilled water to remove the excess chloride ions.

The sodium salt of PLG was obtained from the Ajinomoto Co., Ltd. (Yokohama, Japan); the molecular weight was determined by the supplier to be 42000 from viscosity measurements.

The other reagents were commercially available and of an analytical grade. All the solutions of these materials were made with deionized and distilled water, using an all-Pyrex apparatus.

Electrophoresis. The electrophoretic mobilities of the bare latex particles were determined at various pH values in an aqueous solution of 1×10^{-3} M KCl at 25 °C. The measurements were performed in a Rank Brothers Microelectrophoresis apparatus (MK-2) using a rectangular glass cell. The ζ-potential was derived following the method of Wiersema *et al.*[9] Polymer-coated particles for electrophoretic measurements were prepared as follows: A dilute latex suspension (*ca.* 0.01 wt%) controlled at a definite pH in 10^{-3} M KCl was mixed immediately with an equal volume of the polypeptide solution (C_p=0.2 mg/dm^{-6}) which gave enough plateau adsorption. After the mixture had been left standing for 2 h at room temperature, the electrophoretic mobilities of the polymer-coated particles were determined by using the same technique with bare particles. The results for Latex-A

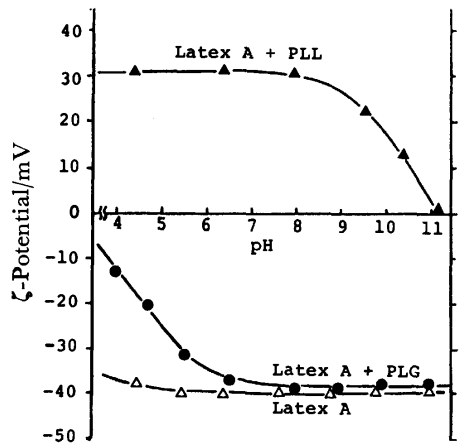

Fig. 1. ζ-Potentials of Latex-A (—△—), PLL-covered Latex-A(—▲—), and PLG-covered Latex-A(—●—) (M_{PLL}=57500, M_{PLG}=42000, 10^{-3} M KCl, 25 °C).

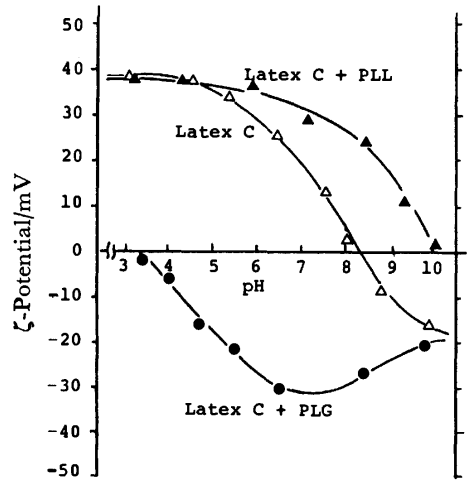

Fig. 2. ζ-Potentials of Latex-C (—△—), PLL-covered Latex-C (—▲—), and PLG-covered Latex-C (—●—) (M_{PLL}=57500, M_{PLG}=42000, 10^{-3} M KCl, 25 °C).

and -C covered by PLL and PLG are shown in Figs. 1 and 2 respectively, along with the data for the respective bare particles.

Adsorption Experiments. In glass-stoppered vials (5 ml), 2 ml of a latex suspension was added to 2 ml of the polypeptide solution. Prior to mixing, both the solutions were brought to the same pH and KCl concentration without using any buffers. The vials were rotated end-over-end for 5 h. The suspension was then centrifuged for 30 min at 25000 g. The concentration of polypeptide in the supernatant as well as in the initial solution was determined by analytical methods, *i.e.*, by the Ninhydrin method for L-lysine and PLL and by the Microbiuret method for PLG. From the difference in the concentrations before and after the adsorption process, the amounts of adsorption per unit of surface area (A_p) was calculated. All the measurements were made at a constant temperature of 25 °C.

Flocculation Experiments. In the flocculation experiments using polyelectrolyte as a flocculant, careful attention must be paid to the method of mixing the polymer solution and the colloid dispersion, because the adsorption of polyelectrolyte on a charged surface is usually very rapid and irreversible.[10] Here, the mixing was performed as follows: Five-ml portions of KCl solutions of various concentrations were added carefully on top of a latex suspension (C_{solid}=0.4 wt%, 2 ml) in such a way that a sharp boundary between the dispersion and the salt solution was formed. Thereafter, on top of these, 2-ml portions of polymer solutions of different contents were added using a pipet. After rotating end-over-end ($10\ min^{-1}$) for 2 h, the system was left to stand for 20 h in order to allow the flocculated particles to settle out. Then, the extinction of supernatant was measured using a Jasco Digital Spectrophotometer (Uvidec-410) at a wavelength of 550 nm. The critical flocculation concentration (CFC) was defined as the salt concentration at which the absorbance of the supernatant was reduced to 50% of the original. The ionic strength was varied using KCl, while all the experiments were carried out at a constant temperature of 25 °C.

Direct Observation of Flocculating States. The flocculating states of latex particles were examined visually by means of a direct-observation technique.[11] The optical microscope used was a lateral-type metallurgical microscope with a magnification of 1500, Type-Mg, Olympus Optical Co., Ltd. (Tokyo, Japan). Some amounts of the latex sample prepared by the same procedure as were used in the flocculation experiments were charged into the observation cell, made of a Pyrex glass tube, 100 mm high and 15 mm in diameter, with a thin glass window at its lower end. The sample was observed through the window by means of the oil-immersion method.

Results and Discussion

Adsorption Behavior. Figure 3 shows the adsorption isotherms of L-lysine on Latex-A, -B, and -C at different pH values in a 10^{-3} M KCl solution. In all the systems, the isotherms have low affinities, with small plateaus. In the acidic medium, Latex-A and -B have electrical signs opposite that of the adsorbate, but Latex-C has the same sign. As may be seen in the figure, the experimental results show the same behavior as would be anticipated from the estimation of the elec-

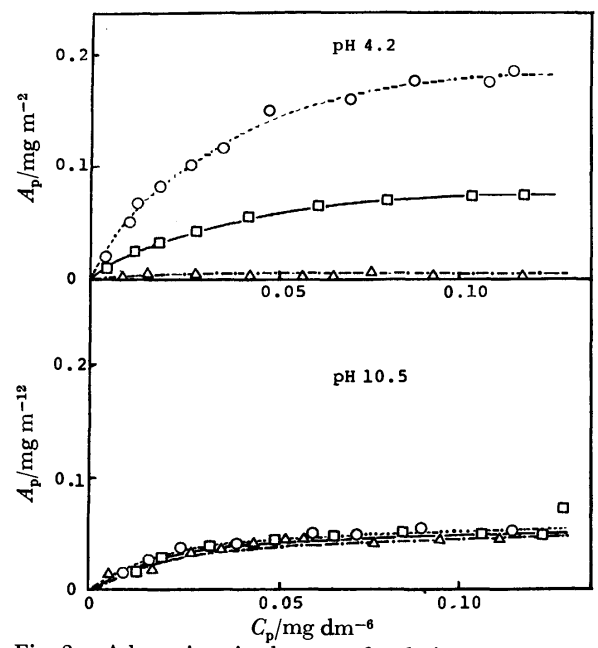

Fig. 3. Adsorption isotherms of L-lysine on Latex-A (—□—), Latex-B (—○—), and Latex-C (—△—) (10^{-3} M KCl, 25 °C).

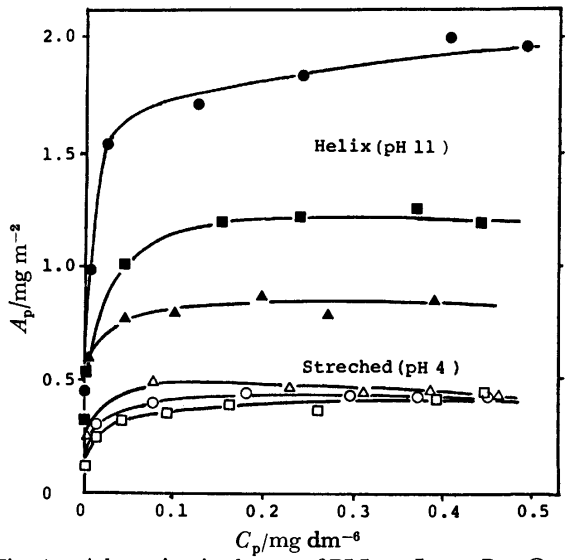

Fig. 4. Adsorption isotherms of PLL on Latex-B. Open symbols; pH 4, filled symbols; pH 11, —○—; M_{PLL}= 57500, —□—; M_{PLL}=32500, —△—; M_{PLL}=4000 (10^{-3} M KCl, 25 °C).

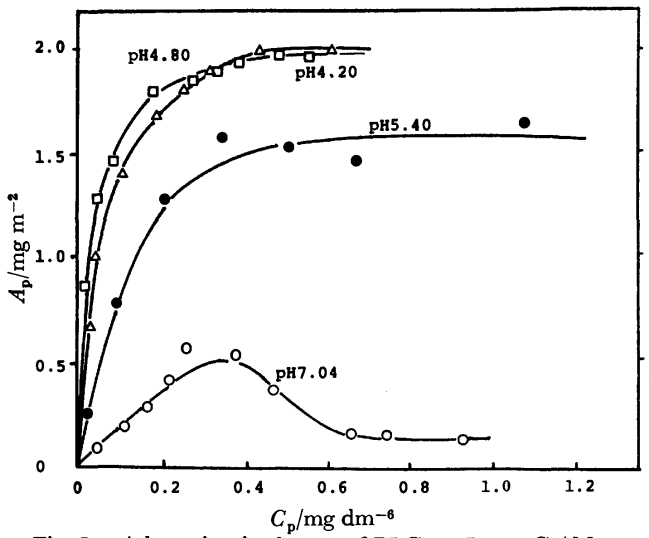

Fig. 5. Adsorption isotherms of PLG on Latex-C (M_{PLG} =42000, 10^{-3} M KCl 25 °C).

trostatic interaction: *i.e.*, Latex-C gives no adsorption, and -A and -B, 0.06_8 mg/m^2 and 0.18 mg/m^2 respectively, values which accord with the calculated values (0.06_4 mg/m^2, 0.18_6 mg/m^2), assuming an equimolar reaction between $-OSO_3^-$ on the latex surface and NH_3^+ in the peptide. In the basic condition (pH 10.5), however, all the latices have a nearly constant plateau (*ca.* 0.05 mg/m^2) which would seem to be based on the deionization of the lysine molecule in the alkaline solution.

As may be seen in Fig. 4, the adsorption isotherms of PLL have a high affinity, with a well-defined plateau. In the acidic solution, the plateau is independent of the molecular weight, which indicates the adsorption in a flat conformation, *i.e.*, with trains only. According to a theoretical study of the molecular model of polypeptide,[12] it may be possible for PLL to take two kinds of conformation in extreme cases: *i.e.*, A fully extended

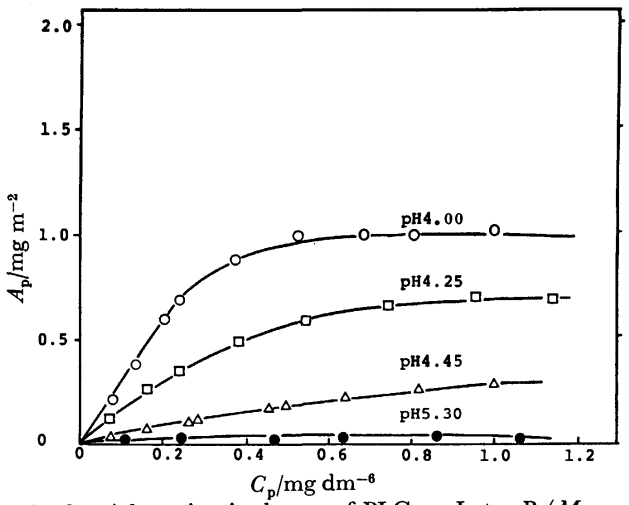

Fig. 6. Adsorption isotherms of PLG on Latex-B (M_{PLG} =42000, 10^{-3} M KCl 25 °C).

conformation, and a compact one. Using these molecular dimensions, the maximum monolayer coverages for these two configurations would amount to 0.41 mg/m^2 and 0.61 mg/m^2 respectively. The plateau value (0.48 mg/m^2) obtained by the present experiments in the acidic medium suggests that PLL molecules would be adsorbed by an intermediate form of these extreme conformations. According to the electrophoretic measurements of the PLL-coated particles (which can be estimated from Fig. 1 for Latex-A), a charge reversal of the original latex particles has occurred at the saturated PLL adsorption (the same result has been reported by Corry[13]). It is indicated that a more positive charge due to PLL than the negative charge on the latices is accumulated on the surface. Though such a superequivalent adsorption, which indicates that the chain effect of the adsorbed polymer overcomes the electrostatic instability, has been observed frequently in polyelectrolyte-colloid systems, the occurrence in the present PLL adsorption with trains only is very interesting as showing a new singularity of polymer adsorption.

The PLL adsorption in the basic medium, however, shows a specific nature. According to the double-layer capacitance measurements on charged silver iodide surfaces in the presence of various oligo- and polypeptide molecules, the helical form in the solution of PLL persists in the adsorbed state.[12] Therefore, the increased plateau values at pH 11 in Fig. 4 may be recognized to be based on the stiff structure of the helical conformation of PLL. When stiff rods of a helical form adsorb on a solid surface, they can either lie flat on the surface or stand on end. The resulting molecular-weight dependence of the plateau adsorption, as may be seen in Fig. 4, suggests that they are adsorbed vertically on the ends of the rods. This is surprising: A detailed analysis of this point will be discussed in the next paper of this series.

Figures 5 and 6 show examples of the adsorption isotherm of PLG on Latex-B and -C. In Fig. 5, in which adsorbate and adsorbent have opposite electric charges at pH values lower than 8.5, the isotherms again exhibit

a high plateau with a steep initial slope, but, as a special feature, an additional reduction of A_p is found at pH 7.04. This reduction is probably due to a partial flocculation of the latex particles: *i.e.*, Under these conditions, the latex particles used as adsorbates become unstable and lose their apparent adsorbable areas. In contradistinction to Fig. 5, the isotherms of Fig. 6 (PLG–Latex-B system) are of a low-affinity type, and the plateaus are much influenced by the pH value. Such behavior may be explained as a consequence of coulombic interaction and the helix-coil transition of PLG. The importance of the coulombic interaction and the helix-coil transition in the polypeptide adsorption can be illustrated by plotting the plateau adsorption (A_{pm}) as a function of the pH value in the medium. Figure 7 shows the A_{pm}(pH) curves for four systems, *i.e.*, PLL–Latex-B, PLL–Latex-C, PLG–Latex-B, and PLG–Latex-C. We can realize that the A_{pm}(pH) curves for PLL–Latex-B and PLG–Latex-C are related symmetrically to the vertical line at pH 7.5. The same trend is also found in the A_{pm}(pH) curves for PLL–Latex-C and PLG–Latex-B. These two trends show that A_{pm} is, to a large extent, determined by the coulombic interaction between the polypeptide and the charged surface. Especially, the first trend indicates that the helical structures of both the polypeptides exert the same influence on the adsorption behavior under the relevant conditions.

Flocculation Behavior. The stability of polymer-coated particles and the conformation of the adsorbed polymer are closely related. By this sense, the study of the stability of polymer-coated particles is instructive with regard to the conformation of the adsorbed polymer. In Fig. 8, the dependence of the critical flocculation concentration (CFC) on the PLL dosage is given for two medium conditions, *i.e.*, the streched-induced conditions (pH 4) and the helix-induced conditions (pH 11). In pH 4, a sharp decrease in the CFC is observed, after which the CFC increases slowly again. Thereafter, the CFC is kept at a constant value (*ca.* 200 mmol/dm^3 of KCl), which is rather lower than

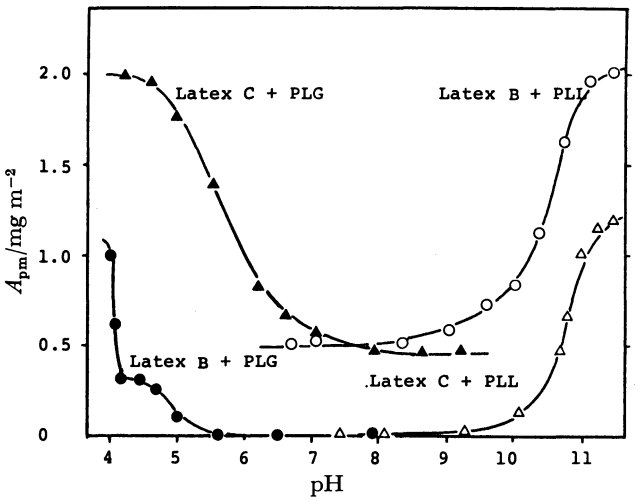

Fig. 7. Relation between the plateau adsorption (A_{pm}) and the medium pH (M_{PLL}=57500, M_{PLG}=42000, 10^{-3} M KCl, 25 °C).

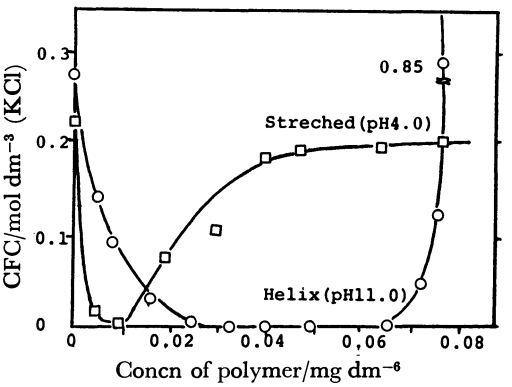

Fig. 8. Dependence of the CFC on the polymer concentration (Polymer; M_{PLL}=57500, Colloid; Latex-B, 25 °C).

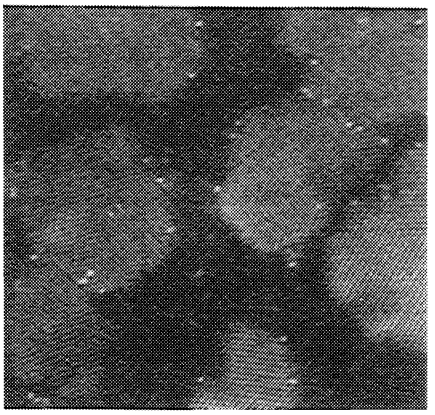

Fig. 9. Microphotograph showing latex aggregates with ordered structure (Polymer; M_{PLL}=57500, Colloid; Latex-A).

the CFC for the bare particles of Latex-B. It is indicative that at pH 4, the adsorption layer of PLL does not confer any steric stabilization on the particles, but brings about the charge reversal in the diffuse double-layer which is shown in Fig. 1. Furthermore, it is known that the narrow flocculation range seen in Fig. 8 does not correspond to the polymer concentration for making an effective interparticle bridging, but does correspond to the charge neutralization performed by the adsorption of PLL with the opposite electrical charge. On the other hand, the CFC in the helix-induced pH stays at a low value for a long period after decreasing slowly from the CFC of bare particles. This phenomena seems to be due to the adsorption of uncharged helix molecules, while the broad range of polymer dosage for flocculation corresponds to the high capacity of polymer adsorption under those conditions (see Fig. 4). Also, the appearance of strong stabilization in the high-polymer dosage may be explained as a result of the thicker adsorption layer. The helical rods of PLL are adsorbed vertically on the latex surface, and their denser (and thicker) adsorption layer throughly resist direct contact with the latex particles.

Formation of Aggregates With an Ordered Structure. Usual latex sediments appear milky white and clusters with an irregular structure are visible under an optical

microscope. Under some conditions, however, especially in concentrated PLL solutions, some latex sediment with a brilliant iridescence is formed. It has been shown that such latex sediments are built up by the large aggregates with an ordered structure.[14] As may be seen in Fig. 9, the particles in the aggregates are arranged in a hexagonal array and seem to be in face-to-face contact. On the formation of such aggregates in the PLL–Latex-A system, the following special features are found:

a) Ordered aggregates are formed only at pH values lower than 8, which are the stretched or random coil-induced conditions for the PLL.

b) In a 10^{-3} M KCl solution, the aggregates were formed in the concentration range of PLL from 0.1—0.6 mg/dm^{-6}. In order to produce the same aggregates in the more concentrated solution of KCl, we must prepare the aggregates in more concentrated PLL solutions.

c) The ordered aggregates were also observed in the system of PLG–Latex-C. In this combination, however, the aggregating capacity was very limitted.

Though, from these results, only a very little can be said about the mechanism of this phenomena, the appearance of such characteristic aggregates suggests that some attractive interaction (perhaps some bridging attraction) is working between the particles covered by the flat adsorption layer of polypeptide.

The authors wish to thank Professor J. Lyklema, Agricultural University, Wageningen, The Netherlands, for his advice and cooperation.

References

1) A. J. Anthoney, P. H. King, and C. W. Randall, *J. Appl. Polym. Sci.*, **19**, 37 (1975).
2) V. K. La Mer and T. H. Healy, *Rev. Pure Appl. Chem.*, **13**, 112 (1963).
3) D. J. Williams and R. H. Ottewill, *Kolloid Z. Z. Polym.*, **243**, 141 (1971).
4) B. Vincent, *Adv. Colloid Interface Sci.*, **4**, 226 (1974).
5) P. Y. Chou and H. A. Scheraga, *Biopolymers*, **10**, 657 (1971).
6) A. Kotera, K. Furusawa, and Y. Takeda, *Kolloid Z. Z. Polym.*, **237**, 677 (1970).
7) M. S. Juang and I. M. Krieger, *J. Polym. Sci.*, **14**, 2089 (1976).
8) A. Homola and R. O. James, *J. Colloid Interface Sci.*, **59**, 123 (1977).
9) P. H. Wiersema, A. L. Loeb, and J. Th. G. Overbeek, *J. Colloid Interface Sci.*, **22**, 78 (1966).
10) J. Gregory, *J. Colloid Interface Sci.*, **42**, 448 (1973).
11) A. Kose, M. Ozaki, K. Takano, Y. Kobayashi, and S. Hachisu, *J. Colloid Interface Sci.*, **44**, 330 (1973).
12) H. A. Van der Schee and J. Lyklema, "The effect of Polymers on Dispersion Properties," ed by Th. F. Tadros, Academic Press, London (1982), p. 82.
13) W. D. Corry, *J. Colloid Interface Sci.*, **63**, 151 (1978).
14) A. Kose and S. Hachisu, *J. Colloid Interface Sci.*, **46**, 460 (1974).

Prediction of Adsorbability of Organic Compounds from Aqueous Solution on Activated Carbon by Means of the Linear Free-energy Relationship

Ikuo ABE,* Katsumi HAYASHI, Mutsuo KITAGAWA,† and Tsuneaki HIRASHIMA
Osaka Municipal Technical Research Institute, Morinomiya, Joto-ku, Osaka 536
†*Society for Activated Carbon Research, Morinomiya, Joto-ku, Osaka 536*
(Received August 16, 1982)

A method is presented for predicting the adsorbability of a wide variety of organic compounds from aqueous solution onto an activated carbon. The method, which is based on the linear free-energy relationship, requires only the solute's molecular refraction and the number of hydrophilic functional groups. The molecular refraction represents the free energy contribution by the solute-adsorbent interaction and the number of hydrophilic functional groups represents that by the solute-solvent interaction.

The ability to predict the adsorbability for a given adsorbent from a knowledge of the physical properties of the adsorbate is an important objective in adsorbent-adsorbate interaction research. In our preceding papers,[1-5] the methods for prediction of the adsorption isotherms of organic compounds from aqueous solution onto activated carbons were discussed. The adsorption isotherms of aliphatic monofunctional compounds,[3] amino acids,[4] and saccharides[5] could be predicted from the molecular refraction alone. The prediction method was applicable to activated carbons with different adsorptive capacities. Manes *et al.* applied the Polanyi adsorption potential theory to adsorption from solution onto activated carbon.[6-8] The Polanyi methods of predicting adsorption isotherms requires the solute's solubility, refractive index, and molar volume. McGuire and Suffet, using the separable formalism of the partial solubility parameters, defined a net adsorption energy for the adsorption of solute from a dilute solution onto adsorbent.[9] The method requires the solute's solubility parameter and molar volume.

Here we describe a method using the linear free-energy relationships which are widely used as tools for investigating chemical similarity.[10]

Experimental

The adsorbent used (Pittsburgh Activated Carbon Co., grade CAL activated carbon) and the experimental techniques were the same as described in a previous paper.[11] All of the adsorbates came from commercial sources (stated minimum assay 99%) and were used without further purification.

Results and Discussion

The adsorption equilibria of 57 organic compounds from aqueous solution onto CAL activated carbon at 25 °C were measured. Table 1 shows the amount adsorbed, k(mg/g), at very low equilibrium concentration, 1 mg/l, including data for 45 compounds from the literatures.

By assuming that the adsorbed molecules behave ideally at the low concentration, the Gibbs free energy change for the adsorption process, ΔG, is calculated experimentally by the following equation:

$$\Delta G = -RT\ln(k/V), \quad (1)$$

where V is the volume of adsorption phase (pore volume).[11-13] This equation indicates that the value

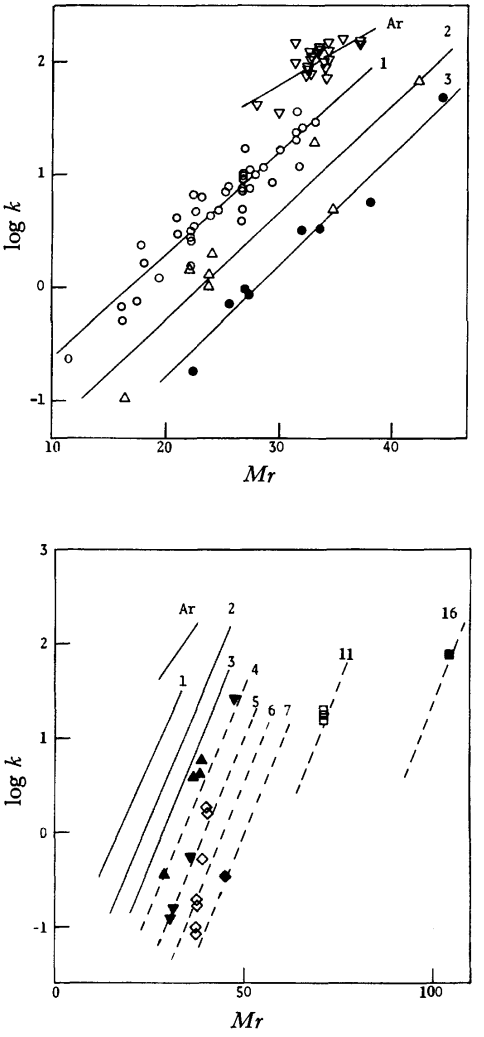

Fig. 1. Relationship between log k and molecular refraction. The values in figure are the number of hydrophilic functional group, Nf. The lines 1—3 and Ar (aromatics) are from linear least-squares analysis of the data points. $Nf=1$: log $k=0.09125Mr-1.530$ ($r=0.9259$, $s=0.1882$, $F=240.3$, $t=15.50$***), $Nf=2$: log $k=0.09521Mr-2.185$ ($r=0.9375$, $s=0.3253$, $F=43.58$, $t=6.601$***), $Nf=3$: log $k=0.09899Mr-2.773$ ($r=0.9751$, $s=0.1769$, $F=115.8$, $t=10.76$***), Ar: log $k=0.05885Mr+0.04096$ ($r=0.6665$, $s=0.1360$, $F=17.59$, $t=4.194$***), $Nf=1$: ○; $Nf=2$: △; $Nf=3$: ●; $Nf=4$: ▲; $Nf=5$: ▼; $Nf=6$: ◇; $Nf=7$: ◆; $Nf=11$: □; $Nf=16$: ■; Ar: ▽.

TABLE 1. AMOUNT ADSORBED, k, OF 102 ORGANIC COMPOUNDS FROM AQUEOUS SOLUTION ONTO CAL ACTIVATED CARBON AT AN EQUILIBRIUM CONCENTRATION, 1 mg/l, AND NUMBER OF HYDROPHILIC FUNCTIONAL GROUPS, Nf, IN AN ADSORBATE MOLECULE

Compound No.	Adsorbate	k/mg g^{-1}	Nf	Ref.
1	1-Propanol	0.745	1	11
2	1-Butanol	3.20	1	11
3	1-Pentanol	10.5	1	11
4	1-Hexanol	25.6	1	11
5	2-Methyl-1-propanol	2.75	1	
6	2-Butanol	2.49	1	
7	2-Methyl-2-propanol	1.48	1	
8	3-Methyl-1-butanol	9.58	1	
9	2-Pentanol	9.89	1	
10	3-Pentanol	6.67	1	
11	2,2-Dimethyl-1-propanol	3.66	1	
12	2-Methyl-2-butanol	6.91	1	
13	Cyclopentanol	4.69	1	
14	Cyclohexanol	7.93	1	
15	2-Methyl-1-butanol	8.98	1	
16	3-Methyl-2-butanol	4.76	1	
17	Acetaldehyde	0.229	1	11
18	Propionaldehyde	0.663	1	11
19	Butyraldehyde	3.15	1	11
20	Valeraldehyde	8.35	1	11
21	Propylamine	1.18	1	
22	Butylamine	4.21	1	
23	Pentylamine	11.9	1	
24	Hexylamine	28.2	1	
25	Methyl acetate	1.78	1	11
26	Ethyl acetate	3.60	1	11
27	Propyl acetate	12.0	1	11
28	Butyl acetate	26.5	1	11
29	Isopropyl acetate	7.04	1	
30	Isobutyl acetate	11.0	1	
31	Diethyl ether	5.14	1	11
32	Dipropyl ether	19.4	1	11
33	Acetone	0.484	1	11
34	2-Butanone	4.66	1	11
35	2-Pentanone	7.43	1	11
36	2-Hexanone	16.7	1	11
37	Cyclopentanone	6.71	1	
38	Cyclohexanone	9.96	1	
39	Propionic acid	2.59	1	11
40	Butyric acid	7.04	1	11
41	Valeric acid	19.2	1	11
42	Hexanoic acid	42.3	1	11
43	Glycine	0.0994	2	4
44	L-Leucine	4.84	2	4
45	2-Ethoxyethanol	2.17	2	
46	2-Butoxyethanol	22.0	2	
47	2-(Hexyloxy)ethanol	68.0	2	
48	1,4-Butanediol	0.978	2	
49	1,2-Butanediol	1.41	2	
50	1,4-Dioxane	1.59	2	
51	L-Glutamine	3.37	3	4
52	L-Threonine	0.953	3	4
53	L-Serine	0.175	3	4
54	L-Glutamic acid	3.47	3	4
55	L-Aspartic acid	0.943	3	4
56	L-Methionine	5.43	3	4
57	Diethylene glycol	0.783	3	
58	2-(2-Butoxyethoxy)-ethanol	52.9	3	
59	L-Histidine	6.44	4	4
60	2-Desoxy-D-ribose	0.360	4	5
61	Triethylene glycol	4.39	4	
62	Triethanolamine	4.56	4	
63	D-(+)-Xylose	0.162	5	5
64	D-(−)-Arabinose	0.132	5	5
65	L-(+)-Rhamnose	0.587	5	5
66	Tetraethylene glycol	29.2	5	
67	D-(+)-Glucose	0.185	6	5
68	D-(+)-Mannose	0.104	6	5
69	D-(−)-Fructose	0.0940	6	5
70	D-(+)-Galactose	0.202	6	5
71	α-Methyl D-glucoside	1.73	6	5
72	α-Methyl D-mannoside	1.95	6	5
73	D-(−)-Mannitol	0.570	6	5
74	Perseitol	0.371	7	
75	(+)-Maltose	19.8	11	5
76	(+)-Sucrose	18.3	11	5
77	(+)-Lactose	20.9	11	5
78	Raffinose	83.5	16	
79	Chlorobenzene	101	0	
80	Benzoic acid	77.2	1	
81	Phenol	37.7	1	
82	Aniline	32.4	1	
83	Anisole	109	1	
84	*o*-Methoxyphenol	130	2	
85	*m*-Methoxyphenol	101	2	
86	*p*-Methoxyphenol	158	2	
87	*o*-Nitrophenol	122	1	
88	*m*-Nitrophenol	128	1	
89	*p*-Nitrophenol	137	1	
90	*o*-Chlorophenol	103	1	
91	*m*-Chlorophenol	108	1	
92	*p*-Chlorophenol	135	1	
93	*o*-Cresol	90.3	1	
94	*m*-Cresol	76.1	1	
95	*p*-Cresol	84.3	1	
96	*o*-Hydroxybenzoic acid	65.0	2	
97	*m*-Hydroxybenzoic acid	83.9	2	
98	*p*-Hydroxybenzoic acid	99.0	2	
99	*o*-Hydroxyacetophenone	143	2	
100	*p*-Hydroxyacetophenone	135	2	
101	*m*-Aminophenol	158	2	
102	*p*-Bromophenol	166	1	

of log k may represent the adsorbability associated with the free energy change.

In the linear free-energy relationship models, the logarithm of activity is expressed as a linear function of physicochemical parameters. The method is based on multiple linear regression analysis. The expression for the free energy change of the adsorption process may be given by the following equation:

$$\Delta G = \Delta G_{js} - \Delta G_{ls} - \Delta G_{jl}, \quad (2)$$

where ΔG is the net free energy change, ΔG_{js} is that associated with the solute-adsorbent interaction, ΔG_{is} the solvent-adsorbent interaction, ΔG_{ji} the solute-solvent interaction, and the subscripts i, j, and s refer to solvent, solute, and adsorbent, respectively. In the case of the adsorption from water, ΔG_{is} is identical for each adsorbate and consequently the following relation may be derived:

$$\Delta G = \Delta G_{js} - \Delta G_{ji} - \text{const.} \quad (3)$$

Each of these terms can be estimated with a knowledge of the physicochemical properties of each species. The ΔG_{js} term is mainly affected by the hydrophobic effect because the surface of activated carbon is hydrophobic. The driving force for the adsorption by hydrophobic effect is the dispersion component of the Van der Waals forces. This adsorptive interaction is strongly dependent on the polarizability of the solute. Since the polarizability of a molecule is proportional to the molecular refraction (Mr), ΔG_{js} can be expressed in terms of molecular refraction. Assuming that the ΔG_{ji} term is identical for each adsorbate, the following equation may be derived:

$$\log k = A_1 Mr + A_0, \quad (4)$$

where A_1 and A_0 are constant. Figure 1 shows a plot of log k *vs.* Mr for 102 organic compounds. A good linear relationship was obtained within each family of compounds with the same number of hydrophilic functional groups (Nf). The correlation coefficient(r) for compounds **1**—**42** with $Nf=1$ was 0.926, $r=0.938$ for compounds **43**—**50** with $Nf=2$, and $r=0.975$ for compounds **51**—**58** with $Nf=3$. The adsorbability of aliphatic compounds decreased with an increase in the number of hydrophilic functional groups in a solute molecule. This indicates that the ΔG_{ji} term in Eq. 3 affects the adsorbability.

The free energy change for the solution process was calculated by Amidon *et al.*.[14] The molecular surface area for 158 aliphatic hydrocarbons, olefins, alcohols, ethers, ketones, aldehydes, esters, and fatty acids were computed and correlated with the aqueous solubilities. The expression was:

$$\log S = \theta_1 \cdot TSA + \theta_2 \cdot IFG + \theta_0, \quad (5)$$

where S is the aqueous solubility, TSA is the total surface area, and IFG is the functional group index (zero for hydrocarbons and unity for a monofunctional compound). From the coefficients for the IFG term, the free energy contribution of functional group to the solution process (ΔG_{sol}) may be calculated. The values of ΔG_{sol} for each functional group are −4090——4310 cal/mol. This suggests that for the functional groups (–OH, –O–, >C=O, –CHO, –COO–, and –COOH) the free energy contributions per one functional group to the ΔG_{ji} term is nearly equal. Therefore, the ΔG_{ji} term may be related to the number of the functional group regardless of the kind. Thus:

$$\log k = A_1 Mr + A_2 Nf + A_0, \quad (6)$$

where A_1, A_2, and A_0 are constant. The data of compounds **1**—**78** were given to a NEC PC-8001 computer to determine the A_1, A_2, and A_0 values by means of multiple regression analysis. The regression equation is:

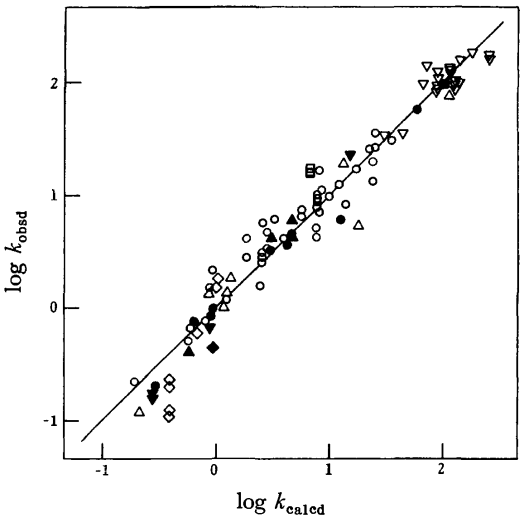

Fig. 2. Relationship between log k observed and log k calculated using Eq. 9.

$$\log k = 0.1089\, Mr - 0.4919\, Nf - 1.520. \quad (7)$$

The correlation coefficient r was 0.9355, the standard deviation s was 0.2596, the F-value representing the over-all goodness of fit was 262.7, and the t-values in the Student test were 22.87*** (for 0.1089) and −21.17*** (for −0.4919). The asterisk, ***, represents that the significant level of the regression coefficient is 0.1%. The results of statistical test indicate that Eq. 7 is statistically significant.

It can be seen from Fig. 1 and Table 1 that the adsorbability of aromatic compounds is higher than the other compounds in spite of the presence of hydrophilic functional groups in a molecule. The phenomena can be explained by the electronic effects and the resonance effects. The solubility of aliphatic compounds increases markedly with an increase in the number of hydrophilic functional groups in a molecule, while the solubility of aromatic compounds does not appreciably increase because of the resonance effects. This suggests that the ΔG_{ji} term can not be related to Nf for aromatics. The high adsorbability of aromatics can be accounted for by the strong interaction with π-electrons in the graphitic structure of an activated carbon. Therefore, ΔG for aromatics must be distinguished from that for aliphatics. Equation 6 has been changed to the following equation:

$$\log k = A_1 \cdot Mr + A_2 \cdot D \cdot Nf + A_0, \quad (8)$$

where D is the dummy variable being zero for aromatics and unity for aliphatics. From the data of 102 compounds in Table 1, a statistical analysis yields the following results:

$$\log k = 0.1044\, Mr - 0.4694 D \cdot Nf - 1.450 \quad (9)$$

($r=0.9642$, $s=0.2409$, $F=654.4$, $t(0.1044)=33.85$***, $t(-0.4694) = -34.29$***).

Figure 2 shows the relationship between log k observed and log k calculated using Eq. 9. These results indicate that the adsorbability of many compounds can be predicted from the molecular refraction and the number of hydrophilic functional group. Since the physical constants Mr and Nf can be easily obtained, the above

method for predicting adsorbability is simpler and more accurate than the other methods.

References

1) I. Abe, K. Hayashi, and M. Kitagawa, *Bull. Chem. Soc. Jpn.*, **54**, 3857 (1981).
2) I. Abe, K. Hayashi, M. Kitagawa, and T. Urahata, *Bull. Chem. Soc. Jpn.*, **53**, 1199 (1980).
3) I. Abe, K. Hayashi, and M. Kitagawa, *Bull. Chem. Soc. Jpn.*, **54**, 2810 (1981).
4) I. Abe, K. Hayashi, and M. Kitagawa, *Bull. Chem. Soc. Jpn.*, **55**, 687 (1982).
5) I. Abe, K. Hayashi, and M. Kitagawa, *Carbon*, in press.
6) M. Manes and L. J. E. Hoffer, *J. Phys. Chem.*, **73**, 584 (1969).
7) D. A. Wohleber and M. Manes, *J. Phys. Chem.*, **75**, 61 (1971).
8) M. R. Rosenes, M. Ozcan, and M. Manes, *J. Phys. Chem.*, **80**, 2586 (1976).
9) I. H. Suffet and M. J. McGuire, "Activated Carbon Adsorption of Organics from the Aqueous Phase," Ann Arbor Science Publishers, MI (1980).
10) N. B. Chapman and J. Shorter, "Correlation Analysis in Chemistry," Plenum Press, New York (1978).
11) I. Abe, K. Hayashi, M. Kitagawa, and T. Urahata, *Bull. Chem. Soc. Jpn.*, **52**, 1899 (1979).
12) F. E. Bartell, T. L. Thomas, and Y. Fu, *J. Phys. Chem.*, **55**, 1456 (1951).
13) I. Abe, K. Hayashi, M. Kitagawa, and T. Urahata, *Nippon Kagaku Kaishi*, **1980**, 545.
14) G. L. Amidon, S. H. Yalkowsky, S. T. Anik, and S. C. Valvani, *J. Phys. Chem.*, **79**, 2239 (1975).

The Absorption Spectra of Monolayers of Fluorescent Probes and the Orientations of Their Chromophores

Kazunori MATSUKI* and Hideo FUKUTOME
Department of Physics, Faculty of Science, Kyoto University, Sakyo-ku, Kyoto 606
(Received August 16, 1982)

The UV absorption spectra of monolayers of 12-(9-anthrylcarbonyloxy)octadecanoic acid (12-AS), 2-(9-anthrylcarbonyloxy)hexadecanoic acid (2-AP), and 2-octadecylamino-6-naphthalenesulfonic acid (ONS) were measured at normal incidence and the polarized spectra at 45° incidence. New peaks which were absent in the spectra of their solutions were observed in the polarized spectra at 45° incidence. The orientation of their chromophores in the monolayers were investigated by means of the dichroic ratios obtained from their polarized spectra. These monolayers were found to consist of H-aggregates where chromophores are oriented nearly perpendicularly to the monolayer plane and molecules in a monomer-like state where the chromophores are rather randomly oriented. The molecular axes of 12-AS, 2-AP, and ONS were found to be oriented uniaxially against the normals of their monolayer planes in the ranges 0—7°, 0—21°, and 0—34°, respectively.

Fluorescent probes have been widely used to study the behavior of lipids and proteins in natural and model membranes.[1] Cadenhead *et al.* showed that 12-(9-anthrylcarbonyloxy)octadecanoic acid (12-AS), 2-(9-anthrylcarbonyloxy)hexadecanoic acid (2-AP), and 2-octadecylamino-6-naphthalenesulfonic acid (ONS) form stable and condensed monolayers at the air-water interface.[2,3] Their chromophores will probably interact strongly in these monolayers. Therefore, their monolayer spectra are expected to differ remarkably from their solution spectra. The absorption spectra of these monolayers, however, have not been measured yet and information about the orientation of their chromophores in the monolayers is lacking although Teissie *et al.* studied the fluorescence of 12-AS monolayers.[4]

In this paper the polarized absorption spectra of monolayers of 12-AS, 2-AP, and ONS were measured in order to get information about the interactions and the orientations of their chromophores in monolayers.

Experimental

Materials. 12-AS, mp 79 °C (lit, 78.5 °C[2]) and crystalline dipalmitoyl-L-α-phosphatidylcholine (DPPC) were purchased from Sigma Chemicals Co., stearic acid (standard for elementary analysis) from Merck Co., and 2-AP, mp 96 °C (lit, 91—92 °C[2] and 94 °C[5]) from Molecular Probe Inc. ONS (Nakarai, S.P.-grade) was recrystallized from chloroform–methanol (2 : 1, v/v).[6] The purity of ONS was checked by TLC on precoated plates (Merck, Kieselgel 60 F_{254}) in chloroform–methanol (1 : 1, v/v). It revealed a single spot both under UV light to visualize fluorescent species and in iodine vapor to check nonfluorescent contaminants. All the above chemicals, except stearic acid, were stored in the dark about −20 °C in a desiccator. Hexane, ethanol, methanol, and chloroform were spectroscopic grade (Nakarai). Dichloroacetic acid (Nakarai, E.P.-grade) was distilled under vacuum. These chemicals were used without further purification unless otherwise stated. Twice-distilled water (pH=5.0—5.5) was used in all the experiments. Optically flat quartz plates (50×24×0.8 mm³) were obtained from Kōno Seisakusho (Kyoto).

Methods. The UV absorption spectra of 12-AS, 2-AP, and ONS in organic solvents were recorded on a UV-180 spectrophotometer (Shimadzu Co.). The absorption spectra of their monolayers were measured with a high-sensitivity spectrophotometer using the single-beam and sample in-sample out technique.[7] It was constructed in our laboratory.[8]

In the measurements of the polarized absorption spectra at 45° incidence, a polarizer (a Glan-Thomson prism made of calcite) was set before the plate in such a manner as to make the plane of polarization parallel to the plane of incidence (p-spectrum) or perpendicular to it (s-spectrum).[7]

The Blodgett method[9] was used for preparing spectroscopic samples of monolayers. A monolayer was spread on twice-distilled water at 23±1 °C by dropping a solution(5—10 mg/10 cm³). Spreading solvents were hexane–ethanol (10 : 1, molar ratio)[2] for 12-AS and 2-AP, and chloroform–dichloroacetic acid (9.6 : 0.4, v/v)[3] for ONS. Surface pressure was applied to the monolayer by using oleic acid (30 mN/m), ethyl myristate (20 mN/m), or a mixture of ethyl myristate and liquid paraffin (16 mN/m)[10] as a piston oil. One monolayer was transferred on each side of the lower half of the clean quartz plate.

The details of cleaning the quartz plate were described previously.[8]

Results and Discussion

In the high-sensitivity spectrophotometer with the single-beam and sample in-sample out technique used in this study, the measured absorption includes the apparent absorption due to the difference in reflectivity between the monolayer and the plate and to the inhomogeneousness in the quartz plate as described before.[8] Since 12-AS, 2-AP, and ONS have a stearic acid-like chain, the apparent absorption of their monolayers can be canceled out by subtracting the apparent absorption of a monolayer of stearic acid. In all the spectra shown in this paper this correction for the apparent absorption was made.

The polarized absorption spectra at normal and 45° incidences were measured in order to investigate the anisotropy of the monolayers. In the case of the normal incidence, the spectra of the monolayers were examined with the plane of polarization set at the angles 0°, ±45°, and 90° against the direction of the withdrawal of the plate from the monolayer at the air-water interface. All the monolayers examined showed no significant difference in the polarized spectra at normal incidence. This indicates that no anisotropy exists in the layer plane. In the case of the 45° incidence, however,

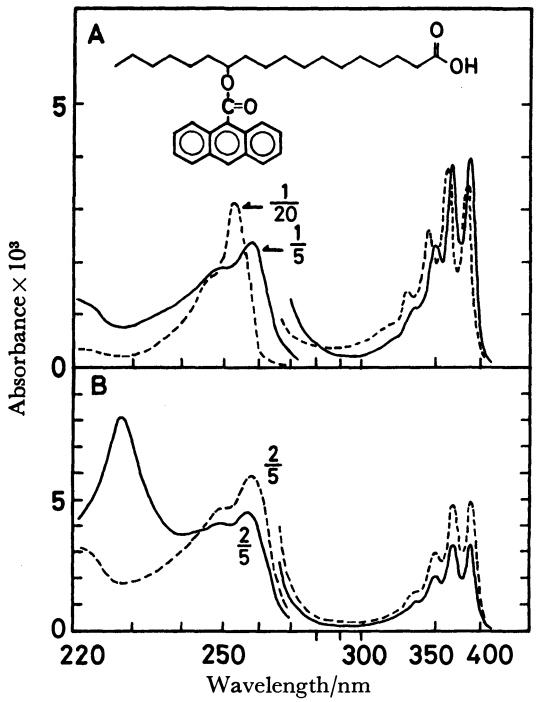

Fig. 1. Absorption spectra of the 12-AS monolayer spread on twice-distilled water and transferred to a quartz plate under the surface pressure of 16 mN/m. The correction for apparent absorptions was made as described in text.

(A) Absorption of the monolayer at normal incidence (n-spectrum) (——) and absorption in solution in an arbitrarily chosen scale (------). (B) Polarized spectra of the monolayer at 45° incidence. The plane of polarization was parallel to the plane of incidence (p-spectrum) (——) or perpendicular to it (s-spectrum) (------).

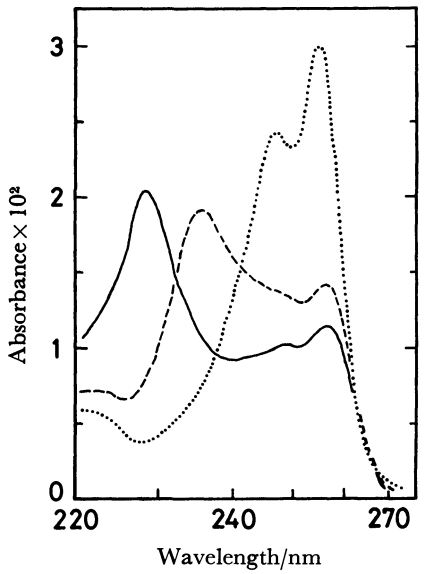

Fig. 2. P-Spectra of the monolayers of 12-AS mixed with DPPC. The monolayers were spread on twice-distilled water and transferred to a quartz plate under the surface pressure of 16 mN/m. The molar ratio of 12-AS to DPPC was 1 : 0 (——), 3 : 2 (------), or 1 : 4 (·····). The absorbances were normalized so as to give the same concentration of 12-AS per area.

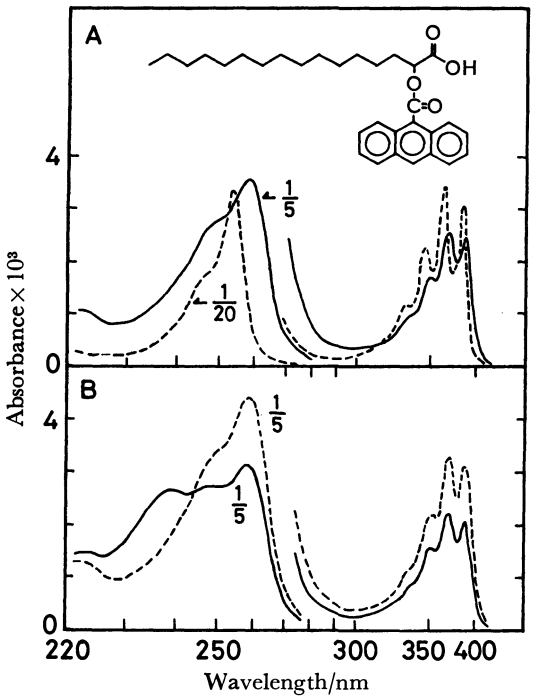

Fig. 3. Absorption spectra of the 2-AP monolayer spread on twice-distilled water and transferred to a quartz plate under the surface pressure of 20 mN/m. The notations are the same as those in Fig. 1.

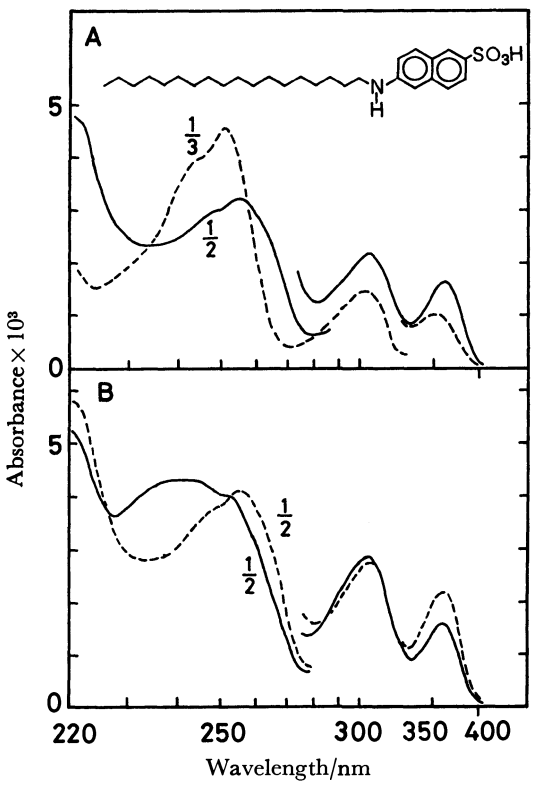

Fig. 4. Absorption spectra of the ONS monolayer spread on twice-distilled water and transferred to a quartz plate under the surface pressure of 30 mN/m. The notations are the same as those in Fig. 1.

remarkable differences between the p- and s-spectra were observed. These indicate that the molecules in all the monolayers are oriented uniaxially. The apparent

TABLE 1. SPECTRAL DATA AND ORIENTATION ANGLES OF THE MONOLAYERS

Compound	λ_{max}/nm		R_{app}[a]	R[a]	θ/°	γ/°
	Monolayer	Solution[b]				
12-AS	229	—	≈0	≈0	≈0	≈0
	257	253	1.306±0.002	1.094±0.002	60—62	
	333	328	—	—	—	
	348	343	1.447±0.008	1.215±0.007	70—73	0—7
	366	361	1.521±0.005	1.278±0.004	79—83	
	386	380	1.542±0.001	1.295±0.001	85—90	
2-AP	239	—	≈0	≈0	≈0	≈0
	258	254	1.418±0.008	1.187±0.007	68—75	
	334	329	—	—	—	
	350	344	1.435±0.003	1.205±0.002	70—76	0—21
	367	362	1.470±0.007	1.234±0.006	72—84	
	387	381	1.495±0.009	1.256±0.008	75—90	
ONS	241	—	≈0	≈0	≈0	≈0
	255	252	—	—	—	
	306	305	0.957±0.013	0.803±0.011	34—45	0—34
	360	351	1.400±0.010	1.176±0.009	66—90	

a) The average of the results for two samples prepared independently. b) Solvent: hexane for 12-AS and 2-AP, methanol for ONS.

dichroic ratio, $R_{app}=A_s/A_p$, was obtained from A_s and A_p, the absorbances of the s- and p-spectra, which were corrected for the apparent absorption as has been described above. The true dichroic ratio, R, corrected for the interference effect[7] was calculated from R_{app} as described before.[8]

Figures 1 to 4 show the observed absorption spectra in solution and those of the monolayers of 12-AS, 2-AP, and ONS which are corrected for the apparent absorption. Table 1 lists the positions of the absorption peaks in the solution and monolayer spectra and the apparent and true dichroic ratios. A new band which was absent in the solution spectra and in the spectra at the normal incidence appeared in all the p-spectra at the 45° incidence. This band seems to arise from the excitonic interaction among chromophores on formation of aggregates in the monolayers as will be discussed in detail later.

The absorption spectra of 12-AS and 2-AP in hexane closely resemble that of anthracene. The longer wavelength bands with fine vibronic structures can be assigned to the ^1L_a transition and the intense bands at shorter wavelength to the ^1B_b transition.[11]

The nonpolarized spectrum at the normal incidence (n-spectrum) of the 12-AS monolayer was similar to its solution spectrum though it was slightly red-shifted (Fig. 1). This shift appears to be due to a solvatochromic effect. In the polarized spectra at the 45° incidence, a new absorption band which was absent in the solution spectra appeared at 229 nm in the p-spectrum. The s-spectrum had no peak corresponding to this new band and showed the same pattern as the n-spectrum. This shows that the transition moment of the new 229 nm band is oriented nearly perpendicularly to the layer plane. The p-spectra of the monolayers of 12-AS mixed with DPPC were measured in order to clarify the origin of the 229 nm band. As can be seen from Fig. 2, the 229 nm band was shifted toward the 257 nm band and its absorption intensity was decreased whereas the intensity of the 257 nm band was increased as 12-AS was diluted with DPPC. The band at 333—386 nm showed no significant changes, and so these spectra are not shown in Fig. 2. The marked concentration dependence of the 229 nm band in the mixed monolayer of 12-AS and DPPC shows that it is a band blue-shifted from the ^1B_b band by the excitonic interaction on formation of aggregates where the chromophores are arranged regularly. The shift of the 229 nm band seen in Fig. 2 can be explained if the size of the aggregates is decreased as 12-AS in the monolayer is diluted.[12] The direction of the transition moment of the ^1B_b band of anthracene is parallel to its long axis according to the data obtained by Inoue *et al.*[13] The p-polarization of the 229 nm band shows that the aggregates formed in the monolayer are H-aggregates.[14] In those H-aggregates, the long axes of the anthracene moieties of 12-AS are oriented parallel to each other and perpendicularly to the layer plane. This explains the blue shift of the ^1B_b band in the H-aggregates.[12]

The 257 nm band in the 12-AS monolayer has the peak position and the band shape similar to the 253 nm band in solution, so it can be obviously assigned to the ^1B_b transition. Its polarization is small as seen from the true dichroic ratio given in Table 1. Its intensity increased as the intensity of the blue-shifted band in the H-aggregates decreased upon dilution of 12-AS. These observations show that the 257 nm band corresponds to the ^1B_b transition in 12-AS molecules with a different state of the chromophores from the H-aggregates. It is most likely that the chromophores in the state are oriented rather randomly. We call this state the monomer-like state. Therefore, the 12-AS monolayer appears to consist of the H-aggregates and the molecules in the monomer-like state. Heesemann reported absorption spectra similar to those in our study in the monolayers of surface-active azo and stilben dyes.[15] The H-aggregates in the 12-AS monolayer seem to correspond to the "microdomains" termed by

Teissie *et al.*[4]

The band at 333—386 nm in the 12-AS monolayer can be assigned to the ^1L_a transition because its peak positions and vibronic structure resemble those of 12-AS in solution. The ^1L_a band of the H-aggregates seems to be almost unchanged and superposed on that of the monomer-like state because no new peaks appeared near this wavelength region. The direction of the transition moment of the ^1L_a band is parallel to the short axis of anthracene and is orthogonal to the transition moment of the ^1B_b band according to Inoue *et al.*[13] This means that the transition moment of the 333—386 nm band is nearly parallel to the monolayer plane in the H-aggregates. The absence of observable excitonic shift in this band might mean that the short axes of the anthracene moieties are not regularly arranged but randomly oriented in the H-aggregates. However, we can not eliminate the possibility of a regular arrangement of the chromophores. The excitonic spectral shift is proportional to the square of the magnitude of the transition moment in the point dipole approximation of excitonic interaction.[16] The spectral shift of the ^1B_b band in the H-aggregates is 28 nm (=257 nm−229 nm). The magnitude of the transition moment of the ^1L_a band is found to be about 1/17 of that of the ^1B_b band from their absorbances in the solution spectrum. The spectral shift of the ^1L_a band in the H-aggregates is estimated from this relative magnitude of the transition moment to be less than 0.3 nm even if the transition moments are completely parallel arranged. Such a small shift can not be detected with our spectrophotometer even if there is no solvatochromic effect. Therefore, we can not discriminate which of the two possibilities is the case that the anthracene moieties in the H-aggregates are stacked or that their short axes are randomly oriented.

The chromophores in the 12-AS monolayer are oriented uniaxially as stated above. The orientation angles of the molecules were calculated by assuming the same model as used in a previous paper.[8] Let γ be the angle between the normal of the layer plane and the principal axis of the molecule and θ be the angle between the transition moment and the principal axis of the molecule. Then, the θ and γ angles to give a fixed value of the true dichroic ratio R make a curve in the θ-γ plane.[8] We show in Fig. 5 the θ-γ curves to give the observed values of R for the absorption peaks in the 12-AS monolayer. In the band at 229 nm, R can be regarded as ≈ 0 because there is no peak corresponding to it in the s-spectrum. The θ and γ angles clearly become $\approx 0°$ in this case, and so its curve is not shown in Fig. 5. The calculation for the peak at 333 nm was not done because it seems unreliable owing to the smallness of the absorbance and the presence of an overlap of the neighboring absorption bands. The dichroic ratio of the 257 nm band belongs only to the monomer-like state. In the 348-, 366-, and 386-nm peaks, it should be noted that their dichroic ratios are the averages of those of the H-aggregates and of the monomer-like state. It is difficult to separate the spectrum of the monomer-like state from that of the H-aggregates because of the overlap of their spectra. The γ angle

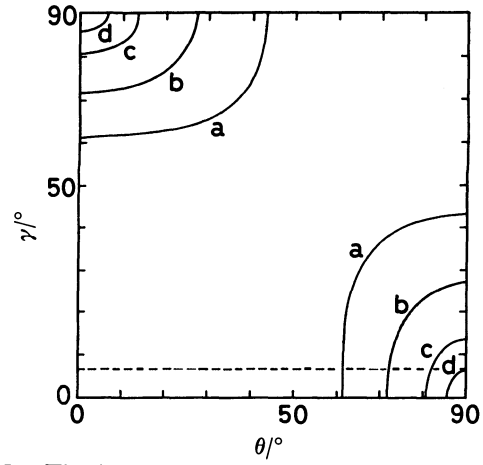

Fig. 5. The θ-γ curves to give the observed values of the true dichroic ratio R in the 12-AS monolayer. Curve a: for the 257 nm band, b: 348 nm band, c: 366 nm band, d: 386 nm band. The broken line indicates the upper limit of γ.

of the monomer-like state was then assumed to be equal to that of the H-aggregates. This means that the 12-AS monolayer is regarded as a homogeneous monolayer as long as fatty acid chains concern though it is a heterogeneous monolayer in chromophore arrangement. Then, the γ angle must have the same value for all the band. Hence, the θ's for each band are obtained from the points where each curve intersects the line of a constant value of γ in Fig. 5. The admissible ranges of γ are determined as 0—7° and 85—90° from the curve d where the permissible range of γ is the narrowest in the four curves. The range, γ=85—90°, is inadequate because it means that the alkyl chains of 12-AS molecules are almost parallel to the water surface. Therefore, we adopt the range, γ=0—7°. This is consistent with the result, $\gamma \approx 0°$, obtained from the polarization of the 229 nm band in the H-aggregates.

The admissible ranges of θ are summarized in Table 1. The ranges of θ for the vibronic peaks in the 348—386 nm band indicate that the direction of the transition moment of this band is roughly parallel to the short axis of the anthracene moiety in agreement with the ^1L_a assignment. Let us assume that the short axes of the anthracene moieties in the monomer-like state are isotropically distributed (R=1) and those in the H-aggregates are fully parallel to the layer plane. Then, the molar ratio of 12-AS molecules in the H-aggregates is estimated to be 98% from the observed R value of 1.295 for the 386 nm band. The dichroic ratio, R, of this band in the H-aggregates is assumed to be 1.299, the theoretical value for γ=0° and θ=90°. This high value of the molar ratio of the H-aggregates is unreasonable because the 257 nm band of the monomer-like state has a considerable absorption intensity. Therefore, the assumption of isotropic distribution of the short axes of the anthracene moieties in the monomer-like state is not valid and they are likely to be oriented much more parallel to the layer plane.

The admissible range of θ is 60—62° for the ^1B_b band at 257 nm. Cadenhead *et al.* suggested that the an-

thracene moiety of 12-AS is parallel to its alkyl chain at the area/molecule about 40 Å².[2] In the H-aggregates, the orientation of the anthracene moiety obtained from the polarized spectra agrees with their suggestion because $\theta \approx 0°$ for the 229 nm band. The θ angle obtained from the 257 nm band, however, indicates that the anthracene moiety fairly twists against the molecular axis in the monomer-like state. This suggests that the anthracene moiety makes an internal rotation around the –CO–C– bond when the molecules in the monomer-like state are transformed into the H-aggregates.

The n-spectrum of the 2-AP monolayer also showed a red-shift compared with its solution spectrum (Fig. 3). This shift may be ascribed to the solvatochromic effect. A new absorption band which was absent in the solution spectrum appeared at 239 nm in the p-spectrum at the 45° incidence but s-spectrum showed no peak corresponding to this band. This indicates that the transition moment of the new band is oriented nearly perpendicularly to the layer plane. The 239 nm band can be assigned to the excitonic band blue-shifted from the ^1B_b band at 258 nm similarly to the 229 nm band of 12-AS. The 2-AP monolayer also appears to consist of the H-aggregates and the molecules in the monomer-like state. The spectral shift of the chromophores in the H-aggregates is smaller than that in the 12-AS monolayer. This may be due to that the excitonic interaction among the chromophores of 2-AP is weaker than that in the 12-AS monolayer because 2-AP makes a more expanded monolayer than 12-AS.[2] The 334—387 nm band may be assigned to the ^1L_a transition. The ^1L_a band of the H-aggregates appears to be almost unchanged and superposed on that of the monomer-like state because no new peaks appeared near this wavelength region. This is the situation also similar to the 12-AS case.

The orientation angles of the molecules in the 2-AP monolayer were calculated by the similar manner to the 12-AS case. In the 239 nm band, R can be regarded as ≈ 0 because there is no peak corresponding to it in the s-spectrum. Hence, γ and θ in this band should be $\approx 0°$. The calculation for the peak at 334 nm was not done for the same reason as the peak at 333 nm in the 12-AS molayer. For the bands at 258-, 350-, 367-, and 387-nm, the admissible ranges or γ and θ were estimated by drawing the θ-γ curves which give the observed values of R. These curves are very similar to those in Fig. 5, and they are not shown. The γ angle of the monomer-like state was also assumed to be equal to that of the H-aggregates. Then, we obtain the admissible ranges of γ as 0—21° and 75—90°. We adopt the former range as the physically reasonable one. The admissible ranges of θ are summarized in Table 1. The ranges of θ for the peaks in the 350—387 nm band indicate that the direction of their transition moments are roughly parallel to the short axis of the anthracene moiety. It should also be noted that the dichroic ratio of a peak in the band is an average of those of the H-aggregates and of the monomer-like state. The assumption of completely random distribution of the transition moments in the monomer-like state again leads to an unreasonably high fraction of the H-aggregates, 86%, from the observed R value of the 387 nm band, 1.256. Hence, the short axes of the anthracene moieties in the monomer-like state are not distributed isotropically but more parallel to the layer plane.

The range of θ is 68—75° for the 258 nm band but $\approx 0°$ for the 239 nm band. This suggests that the anthracene moiety of 2-AP also makes an internal rotation around the –CO–C– bond at the transformation from the monomer-like state to the H-aggregates. The anthracene moiety of 2-AP is very close to its hydrophilic group. The internal rotation of the anthracene moiety is likely to be sterically hindered by the water surface especially when $\theta \approx 0°$. Therefore, formation of H-aggregates seems to be harder in the 2-AP monolayer than in the 12-AS monolayer. The relative intensity of the 239 nm band to the 258 nm band in the 2-AP monolayer is smaller than that of the 229 nm band to the 257 nm band in the 12-AS monolayer (Figs. 1 and 3). This means that the fraction of the H-aggregates in the 2-AP monolayer is smaller than that in the 12-AS monolayer. This observation is consistent with the above mentioned structural feature of the 2-AP molecule.

The absorption spectra of the ONS monolayer are shown in Fig. 4. The solvent for the solution spectra was methanol because ONS was almost insoluble in hexane. A new absorption peak which was absent in the solution spectrum also appeared at 241 nm in the p-spectrum of the ONS monolayer. The transition moment of this band seems to be oriented nearly perpendicularly to the layer plane because its s-spectrum contained no peak corresponding to it. The peak at 241 nm was shifted toward the 255 nm band as the ONS monolayer was diluted with DPPC. Therefore, the 241 nm band is due to the H-aggregates and the ONS monolayer consists of the H-aggregates and the molecules in the monomer-like state similarly to the 12-AS and 2-AP monolayers. The 306- and 360- nm bands are little changed from those of the monomer-like state on formation of the H-aggregates because no new peak appeared near these bands.

The orientation angles of γ and θ in the ONS monolayer were estimated by the similar manner as above. In the 241 nm band, R can be regarded as ≈ 0 because there is no peak corresponding to it in the s-spectrum, and γ and θ in the H-aggregates are $\approx 0°$. The calculation for the 255 nm band was not done because its dichroic ratio could not be reliably measured owing to a large overlap with the 241 nm band in the p-spectrum. The orientation angles were tentatively estimated from the observed R values of the 306- and 360-nm bands. The γ angle in the monomer-like state and that in the H-aggregates were assumed to be the same. The θ-γ curves which give R's of the two bands are shown in Fig. 6. The admissible range of γ is estimated to be 0—34° from the curve b. The ranges of θ for the 306- and 360-nm bands are obtained as 34—45° and 66—90°, respectively. Badley *et al.* estimated θ from comparison of related compounds as 55° (=90°—35°) for the 360 nm band.[17] Their estimation is consistent with ours if the structure of ONS with respect to the bond C–N–C is as shown in Fig. 4. The curves in Fig. 6, however, were obtained from the

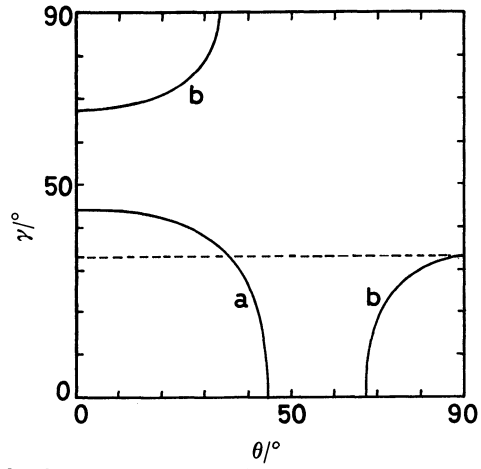

Fig. 6. The θ-γ curves to give the observed values of the true dichroic ratio R in the ONS monolayer. Curve a: for the 306 nm band, b: 360 nm band. The broken line indicates the upper limit of γ.

observed values of R which were the averages for the H-aggregates and the monomer-like state. Since no theoretical and experimental data about the directions of the transition moment of the chromophore of ONS are available, it is difficult to get further information about the orientation of the chromophores in the monomer-like state. By the way, the chromophore of ONS itself is the hydrophilic group at the end of the molecule. Another model for the orientation of ONS molecules is possible where their alkyl chains are randomly oriented independently of the uniaxial arrangement of their chromophores. The ONS monolayer, however, was transferred to the quartz plate under the surface pressure of 30 mN/m where the pressure-area isotherm of the ONS monolayer was steeply rising.[3] It seems unlikely that the alkyl chains in the ONS monolayer are randomly oriented because the surface pressure of the monolayer in such a steeply rising phase of the pressure-area isotherm is mostly produced by solid-like packing of long chains of surface-active molecules. Therefore, the model used by us seems to be plausible.

The pure monolayers of 12-AS, 2-AP, and ONS emitted blue fluorescence when excited by UV light. It was visible even to the naked eye. The fluorescence may provide further information about the H-aggregates and the monomer-like state in these monolayers. Roberts *et al.* reported that Langmuir films of short-chain derivatives of anthracene diplayed interesting electric conduction effects.[18] Electrical properties of 12-AS and 2-AP monolayers may also be worthy of a study.

We would like to thank Dr. Benedikt M. J. Kellner for kindly sending us the data of the isotherms of the 12-AS and 2-AP monolayers when mixed with DPPC at 22—23 °C and for kindly informing us that 2-AP is obtainable from Molecular Probes, Inc.

References

1) G. K. Radda, "Methods in Membrane Biology," ed by E. D. Korn, Plenum Press, New York (1975), Vol. IV, pp. 97—188.
2) D. A. Cadenhead, B. M. J. Kellner, K. Jacobson, and D. Papahadjopoulos, *Biochemistry*, **16**, 5386 (1977).
3) B. M. J. Kellner and D. A. Cadenhead, *Biochim. Biophys. Acta*, **513**, 301 (1978).
4) J. Teissie, J-F. Tocanne, and A. Baudras, *Eur. J. Biochem.*, **83**, 77 (1978).
5) M. D. Barratt, R. A. Badley, and R. B. Leslie, *Eur. J. Biochem.*, **48**, 595 (1974).
6) A. S. Waggoner and L. Stryer, *Proc. Natl. Acad. Sci. U. S. A.*, **67**, 579 (1970).
7) H. Kuhn, D. Möbius, and H. Bücher, "Physical Methods of Chemistry," ed by A. Weissberger and B. W. Rossiter, Wiley-Interscience, New York (1972), Vol. I, Pt. III B, Chap. VII.
8) K. Matsuki, Y. Nagahira, and H. Fukutome, *Bull. Chem. Soc. Jpn.*, **53**, 1817 (1980). Instead of $\log_{10}(e/100)$ on p. 1818 28th line on left row, read $(\log_{10}e)/100$.
9) K. B. Blodgett, *J. Am. Chem. Soc.*, **56**, 495 (1934); **57**, 1007 (1935).
10) A. Norris and J. W. J. Taylor, *J. Chem. Soc.*, **1938**, 1719.
11) H. B. Klevens and J. R. Platt, *J. Chem. Phys.*, **17**, 470 (1949).
12) V. Czikklely, H. D. Forsterling, and H. Kuhn, *Chem. Phys. Lett.*, **6**, 207 (1970).
13) H. Inoue, T. Hoshi, T. Masamoto, J. Shiraishi, and Y. Tanizaki, *Ber. Bunsenges. Phys. Chem.*, **75**, 441 (1971).
14) G. R. Bird, K. S. Norland, A. E. Rosenoff, and H. B. Michaud, *Photogr. Sci. Eng.*, **12**, 196 (1968).
15) J. Heesemann, *J. Am. Chem. Soc.*, **102**, 2167 (1980).
16) E. G. McRae and M. Kasha, "Physical Processes in Radiation Biology," ed by L. Augenstein, Academic Press Inc., New York and London (1964), pp. 23—42.
17) R. A. Badley, W. G. Martin, and H. Schneider, *Biochemistry*, **12**, 268 (1973).
18) G. G. Roberts, T. M. McGinnity, W. A. Barlow, and P. S. Vincett, *Thin Solid Films*, **68**, 223 (1980).

Selective Adsorption of Alkylbenzenesulfonates on Quaternized Crosslinked Poly(4-vinylpyridine)

Nariyoshi KAWABATA,* Eisuke NATSUHARA, Ichiro HIGUCHI, and Jun-ichi YOSHIDA
Laboratory of Environmental Chemistry, Department of Chemistry, Faculty of Polytechnic Science, Kyoto Institute of Technology, Matsugasaki, Sakyo-ku, Kyoto 606
(Received August 21, 1982)

Selective ion-exchange adsorption of a series of alkylbenzenesulfonate ions (C_nBS^-) on a series of crosslinked poly(*N*-alkyl-4-vinylpyridinium bromide) (C_mVP) and crosslinked poly(*N*-benzyl-4-vinylpyridinium bromide) (BVP) was investigated based upon the selectivity coefficient of the resins for C_nBS^- relative to Br^- which was expressed as $K_{Br^-}^{C_nBS^-}$. In the adsorption of C_nBS^- of $n<8$, the selectivity coefficient linearly increased with the number of carbon atoms of the alkyl chain, n, of C_nBS^-, which was ascribed to the hydrophobic interaction between the alkyl chain of C_nBS^- and the resin. In the adsorption of C_nBS^- of $n>8$, however, the selectivity coefficient did not increase with n, which was explained in terms of a steric effect. The selectivity coefficient also increased with the number of carbon atoms of the alkyl chain, m, of C_mVP, but saturation was also observed for the adsorption on C_mVP of $m>12$. In the adsorption of C_nBS^- of $n<8$ on BVP, significant influence of the degree of quaternization was not observed. In the adsorption of $C_{12}BS^-$, however, BVP of lower degree of quaternization showed a much larger selectivity than that of BVP of higher degree of quaternization. The observation indicated that steric repulsion between C_nBS^- ions adsorbed on the surface of the resin played a crucial role.

Adsorption of organic materials by polymeric adsorbents is of considerable interest.[1] In a previous paper,[2] crosslinked poly(*N*-benzyl-4-vinylpyridinium bromide) (BVP) was reported to be an excellent polymeric adsorbent for removal of sodium dodecylbenzenesulfonate from aqueous solution. Although the adsorption proceeded by ion-exchange mechanism, the adsorption capacity was scarcely affected by the presence of inorganic anions such as chloride, sulfate, and hydroxide ions. Extremely high selectivity of BVP for alkylbenzenesulfonate ion provided strong motivation for understanding of the nature of such adsorption. In this study, selectivities of BVP and a series of crosslinked poly(*N*-alkyl-4-vinylpyridinium bromide) (C_mVP, here m is the number of carbon atoms of the alkyl group) for a series of alkylbenzenesulfonate ions (C_nBS^-, here n is the number of carbon atoms of the alkyl group) were determined, and an attempt has been made to indicate which factors operate in determining the selectivity.

Experimental

Materials. Sodium dodecylbenzenesulfonate ($C_{12}BS$) of high purity (special grade for the test of synthetic detergent) was supplied from Wako Pure Chemical Industries, Japan. Sodium benzenesulfonate (C_0BS) was supplied from Nakarai Chemicals, Japan. Sodium ethylbenzenesulfonate (C_2BS) was supplied from Tokyo Kasei Kogyo Co., Japan. These sodium alkylbenzenesulfonates (C_nBS) were used without further purification. Sodium butylbenzenesulfonate (C_4BS), sodium hexylbenzenesulfonate (C_6BS), and sodium octylbenzenesulfonate (C_8BS) were prepared according to the literature procedure[3] with minor modifications, and purified by recrystallization from hot methanol before use.

^1H NMR spectra of these C_nBS were obtained with a Varian T-60A spectrometer in dimethyl-d_6 sulfoxide using tetramethylsilane as an internal standard. Aromatic protons showed distinct AB-type quartets. This result indicated that para isomers were predominant and the presence of ortho and meta isomers was not significant. Aliphatic protons showed the presence of only one methyl group in each C_nBS. This result indicated that the normal alkyl groups were predominant and the presence of branched alkyl groups was not significant.

Table 1. Degree of quaternization and ion exchange capacity of resins

Resin	Degree of quaternization/%	Ion exchange capacity/mequiv. g^{-1}
BVP	89	2.85
BVP′	32	1.51
C_4VP	71	2.77
C_8VP	55	2.09
$C_{12}VP$	36	1.44
$C_{16}VP$	20	0.92

Relative amounts of aromatic and aliphatic protons were also consistent with the prescribed structure.

Crosslinked poly(4-vinylpyridine) containing 72 mol% of 4-vinylpyridine was prepared by a copolymerization of 4-vinylpyridine with divinylbenzene followed by grinding and sifting to 60—80 mesh as described previously.[4] Quaternization of the copolymer with benzyl bromide in benzene (60 °C 4 h) yielded crosslinked poly(*N*-benzyl-4-vinylpyridinium bromide) (BVP).[2] Quaternization of the copolymer with a series of alkyl bromides was carried out in a similar fashion (60 °C, 40 h) to yield crosslinked poly(*N*-alkyl-4-vinylpyridinium bromide) (C_mVP). The resins thus obtained were washed with benzene, methanol, and water before the adsorption test. Degree of quaternization and ion exchange capacities of the resins were determined by titration with standard $AgNO_3$ solution using eosin as the indicator, after the reaction with excess aq $NaNO_3$ (Table 1).

Deionized water was used throughout the experiments. Other chemicals were used as obtained commercially.

Equilibrium Adsorption Test. Equilibrium adsorption tests were conducted by placing weighed quantities of the resin and an aqueous solution of sodium alkylbenzenesulfonate and sodium bromide (total concentration 0.1 M) in a 100-cm^3 Erlenmeyer flask equipped with a mechanical stirrer at 30 ± 1 °C. After the mixture reached equilibrium, the concentration of alkylbenzenesulfonate ion was determined based upon the absorptivities at 260 nm using Shimadzu UV-100-02 spectrophotometer. Concentration of bromide ion was determined by titration with standard $AgNO_3$ solution using eosin as the indicator.

Results and Discussion

Selectivities of several quaternized crosslinked poly(4-vinylpyridine) (BVP and C_mVP) for a series of alkylbenzenesulfonate ions (C_nBS^-) were determined by equilibrium adsorption tests. The selectivities were determined relative to bromide ion because of the following reasons. The bromide form of the quaternized crosslinked poly(4-vinylpyridine) can be obtained more easily than the corresponding chloride form since the quaternization with alkyl bromide proceeds more smoothly than that with alkyl chloride. Although the bromide form of the polymer can be transformed into the chloride form or sulfate form by ion-exchange process, it is difficult to confirm the completeness of the transformation. Incomplete transformation might result in a large experimental error in determination of selectivities. The selectivity coefficients, $K_{Br^-}^{C_nBS^-}$, were calculated by use of the following relationship.[5]

$$K_{Br^-}^{C_nBS^-} = \frac{(\text{mmol } C_nBS^- \text{ in resin})}{(\text{mmol } Br^- \text{ in resin})} \times \frac{[Br^-]}{[C_nBS^-]}, \quad (1)$$

where $[Br^-]$ is the molar concentration of bromide ion in the solution and $[C_nBS^-]$ is the molar concentration of alkylbenzenesulfonate ion. The selectivity coefficients somewhat varied with the molar fraction of alkylbenzenesulfonate ion in the resin, x, which was defined as follows:

$$x = \frac{(\text{mmol } C_nBS^- \text{ in resin})}{(\text{mmol } C_nBS^- \text{ in resin}) + (\text{mmol } Br^- \text{ in resin})}. \quad (2)$$

The dependency of $K_{Br^-}^{C_nBS^-}$ on x is illustrated in Fig. 1. Therefore, discussions were made based on the values of $K_{Br^-}^{C_nBS^-}$ at $x=0.5$, which were determined from the plots of log $K_{Br^-}^{C_nBS^-}$ *vs.* x.

Influence of Alkyl Chain Length of Alkylbenzenesulfonates. With increasing alkyl chain length of alkylbenzenesulfonate ions, *i.e.*, when the value of n of C_nBS^- increased, the competition between alkylbenzenesulfonate ion and bromide ion for the ion-exchange sites strongly favored the adsorption of the former. In order to evaluate the influence of alkyl chain length more quantitatively, log $K_{Br^-}^{C_nBS^-}$ of BVP was plotted against the number of carbon atoms, n, of the alkyl chain of C_nBS^-. In the cases where $n<8$, log $K_{Br^-}^{C_nBS^-}$ of BVP increased linearly with n as shown in Fig. 2. It holds widely that the standard free energy change for transfer of hydrocarbon chains from aqueous solution to other phase varied in proportion to the number of carbon atoms. This relationship has been explained in terms of hydrophobic interactions of the hydrocarbon chain.[6] On this basis, it may be reasonably considered that hydrophobic interaction between the resin and the alkyl chain of C_nBS^- is responsible for the increase in selectivity with the length of alkyl chain.

The standard free energy change for the transfer of alkylbenzenesulfonate ion from aqueous solution to the resin phase (ΔG) is correlated to the selectivity coefficient as follows:[7]

$$-RT\delta(\ln K_{Br^-}^{C_nBS^-})/\delta n = \delta\Delta G/\delta n + \Pi\delta V_{C_nBS^-}/\delta n, \quad (3)$$

where Π is the swelling pressure of the resin and $V_{C_nBS^-}$ is partial molar volume of C_nBS^-. The linear part of Fig. 2 gave a value for $RT\delta(\ln K_{Br^-}^{C_nBS^-})/\delta n$ of approximately 2400 J mol^{-1}. Similar values (*ca.* 2200 J mol^{-1}) were reported for the adsorption of aliphatic carboxylate anion on anion exchange resins.[7]

On the other hand, in the cases where $n>8$, log $K_{Br^-}^{C_nBS^-}$ did not increase with n. Steric factor seemed to be responsible for the results, since hydrophobic interaction is expected to increase with further increase in the alkyl chain length. As the alkyl chain length of C_nBS^- increased, steric repulsion between the adsorbed sulfonate ions would increase, which might compensate for the increase in hydrophobic interaction. Steric repulsion between the polymer matrix and the sulfonate ions also seemed to be important.

As has been mentioned above, steric effect seemed to

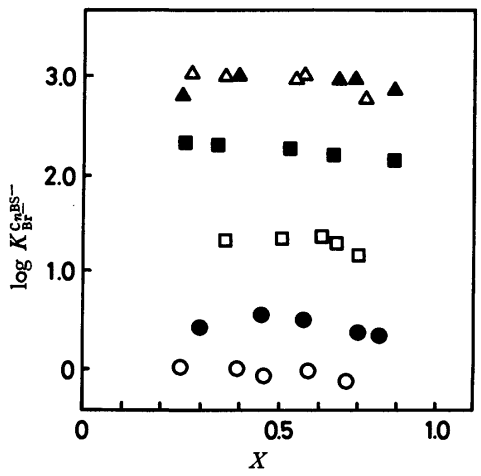

Fig. 1. Variation of selectivity coefficients of BVP resin for a series of alkylbenzenesulfonate ions (C_nBS^-) with molar fraction of C_nBS^- in resin.
○: C_0BS^-, ●: C_2BS^-, □: C_4BS^-, ■: C_6BS^-, △: C_8BS^- ▲: $C_{12}BS^-$. Degree of quaternization of BVP was 89%.

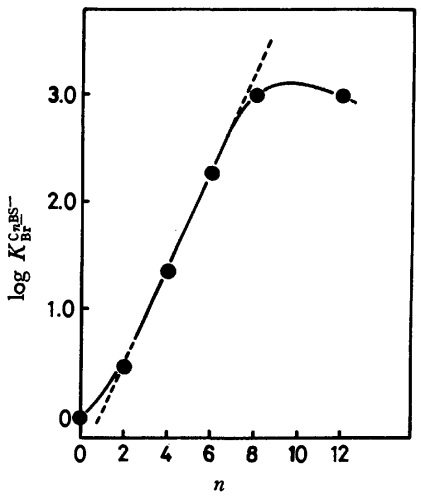

Fig. 2. Variation of selectivity coefficients of BVP resins for a series of alkylbenzenesulfonate ions (C_nBS^-) with a number of alkyl carbon atoms of C_nBS^-. Degree of quaternization of BVP was 89%.

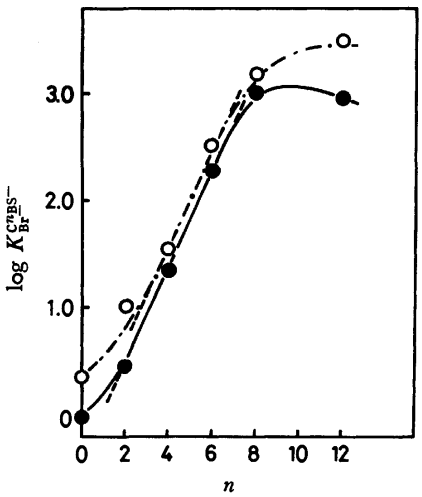

Fig. 3. Variation of selectivity coefficients of BVP resins for a series of alkylbenzenesulfonate ions (C_nBS^-) with a number of alkyl carbon atoms of C_nBS^-. Influence of degree of quaternization.
●: Degree of quaternization, 89%, ○: Degree of quaternization, 32%.

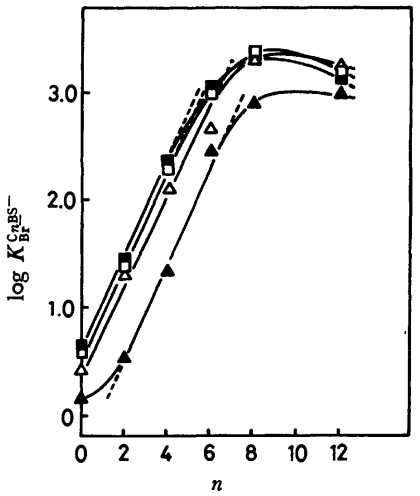

Fig. 4. Variation of selectivity coefficients of C_mVP resins for a series of alkylbenzenesulfonate ions (C_nBS^-) with a number of alkyl carbon atoms of C_nBS^-.
▲: C_4VP, △: C_8VP, □: $C_{12}VP$, ■: $C_{16}VP$.

play an important role in the adsorption. Since steric repulsion between the adsorbed alkylbenzenesulfonate ions was expected to be reduced if the ion exchange sites were separated by enough distances from each other, the influence of degree of quaternization of the resin was examined. Thus, the adsorption tests were carried out with BVP of lower degree of quaternization (32%) and that of higher degree of quaternization (89%). Figure 3 shows the selectivity coefficients obtained for these resins. No significant difference was observed between their selectivities for C_nBS^- of $4<n<8$. In these cases steric repulsion between the adsorbed alkylbenzenesulfonate ions seemed to be insignificant. However, in the case of the adsorption of $C_{12}BS^-$, the selectivity coefficient of BVP of lower degree of quaternization was much higher than that of BVP of higher degree of quaternization. In the latter case, the alkyl chain of $C_{12}BS^-$ was presumably long enough to cause steric repulsion between the adsorbed $C_{12}BS^-$ ions, whereas in the former case such steric repulsion might be reduced by separation of ion exchange sites on the surface of the resin.

Influence of alkyl chain length of alkylbenzenesulfonate ions was also examined in the case of the adsorption on a series of crosslinked poly(*N*-alkyl-4-vinylpyridinium bromide) (C_mVP). In Fig. 4 are shown the plots of log $K_{Br^-}^{C_nBS^-}$ of C_mVP against the number of carbon atoms, n, of C_nBS^-. In the cases where $n<8$, log $K_{Br^-}^{C_nBS^-}$ of each C_mVP also increased linearly with n, which was ascribed to the hydrophobic interaction between the alkyl chain of C_nBS^- and the resin. Although the degree of quaternization of these C_mVP was not equal, Fig. 3 shows that the linearity of the plot of log $K_{Br^-}^{C_nBS^-}$ *vs.* n was not influenced by the degree of the quaternization. The linearity of Fig. 4 gave a value of 2400 J mol^{-1} for $RT\delta(\ln K_{Br^-}^{C_nBS^-})/\delta n$.

Influence of Alkyl Chain Length of Resins. Since hydrophobic interaction between the alkyl chain of the

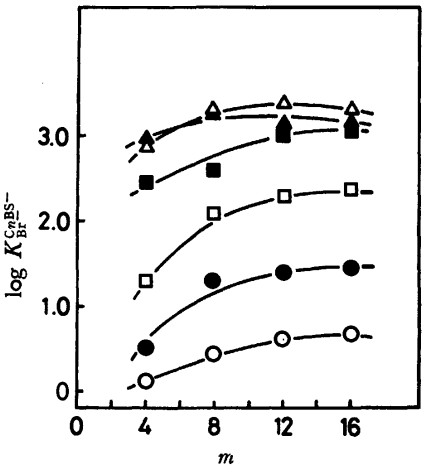

Fig. 5. Variation of selectivity coefficients of C_mVP resins for a series of alkylbenzenesulfonate ions (C_nBS^-) with a number of alkyl carbon atoms of C_mVP.
○: C_0BS^-, ●: C_2BS^-, □: C_4BS^-, ■: C_6BS^-, △: C_8BS^-, ▲: $C_{12}BS^-$.

C_nBS^- ion and the resin was suggested to play an important role in the adsorption, the influence of the hydrophobicity of the resin was then examined. Thus the selectivities of a series of crosslinked poly(*N*-alkyl-4-vinylpyridinium bromide) (C_mVP) were plotted against the number of carbon atoms, m, of the alkyl chain attached to the resin. As can be seen in Fig. 5, log $K_{Br^-}^{C_nBS^-}$ increased with m, which may be attributed to the hydrophobic interaction mentioned above. In the cases where $m>12$, however, saturation of the selectivity coefficients was observed. This may be ascribable to the steric effect as discussed above. It should be noted here that in the case of the adsorption of $C_{12}BS^-$, the selectivity coefficient did not vary appreciably with the value of m. Probably the alkyl chain of $C_{12}BS^-$ was long enough to cause significant steric repulsion even in the case of the resins having a short alkyl chain such as C_4VP and C_8VP.

References

1) B. R. Kim, V. L. Snoeyink, and F. M. Saunders, *J. Water Pollut. Control Fed.*, **48**, 120 (1976).

2) N. Kawabata and T. Morigaki, *Environ. Sci. Technol.*, **14**, 1089 (1980).

3) S. R. Sander and W. Karo, "Organic Functional Group Preparations," Academic Press, New York and London (1968), Vol. I, p. 511.

4) N. Kawabata and K. Ohira, *Environ. Sci. Technol.*, **13**, 1396 (1979).

5) R. L. Gustafson and J. A. Lirio, *Ind. Eng. Chem., Prod. Res. Dev.*, **7**, 116 (1968).

6) C. Tanford, "The Hydrophobic Effect: Formation of Micelles and Biological Membranes," John Wiley & Sons, New York (1980), pp. 5—20.

7) a) J. Gregory and M. J. Semmens, *J. Chem. Soc., Faraday Trans. 1*, **68**, 1045 (1972); b) M. Semmens and J. Gregory, *Environ. Sci. Technol.* **8**, 834 (1974).

^{129}I Mössbauer Effect in Several π-σ Charge Transfer Complexes of Iodine

Hiroshi SAKAI,* Tomochika MATSUYAMA, Hitoshi YAMAOKA, and Yutaka MAEDA
Research Reactor Institute, Kyoto University, Kumatori, Sennan-gun, Osaka 590-04

(Received September 6, 1982)

The ^{129}I Mössbauer spectra at 16 K have been measured for the π-σ charge transfer complexes of iodine with benzene, coronene, perylene, and poly(*p*-phenylene). It is suggested that the benzene–iodine complex in benzene prepared by slow cooling consists of alternate benzene and iodine molecules with the six-fold axial symmetry. The Mössbauer spectrum for the coronene–iodine complex (1 : 1) shows only one chemical state of iodine. The acceptor orbital is described by only the σ_u-antibonding molecular orbital of iodine. The extent of charge transfer in the complex is estimated to be $0.06e^-$ in the electronic ground state. In the poly(*p*-phenylene)–iodine complex the iodine exists as almost a free molecule, indicating that the interaction between the phenylene ring and iodine is very weak.

Iodine is a typical electron acceptor and forms charge transfer (CT) complexes with various electron donor molecules.[1-3] In particular, benzene–iodine (Bz–I_2) is one of the most typical π-σ CT complexes and has been extensively treated with many experimental and theoretical investigations. However, the geometrical configuration and the electronic state of the Bz–I_2 complex are not fully understood. Two conflicting models, "resting model" and "axial model," are proposed from various experimental methods such as IR,[4] MCD,[5,6] and ^{129}I Mössbauer[7-9] spectroscopies in addition to the theoretical treatments.[10-14] From the ^{129}I Mössbauer spectroscopic studies, it is found that the iodine in benzene exhibits an anomalously high value of the quadrupole coupling constant (e^2Qq) compared to that of the free iodine molecule.[7,8] Furthermore, the same tendency is found in methylated benzene-iodine complexes.[9,15]

Shibuya[16] determined the crystal and molecular structure of the coronene–iodine (1 : 1) complex by X-ray diffraction. He reported that each iodine molecule was situated between two coronene molecules and that its axis was almost normal to the plane of the coronene molecule, although it was not coincident with the C_{3v} axis of the coronene molecule. This is the only iodine-containing π-σ complex of which the molecular structure is determined. It is therefore worthwhile to compare the ^{129}I Mössbauer spectrum of Bz–I_2 with that of coronene–I_2. Recently Teitelbaum, Ruby, and Marks[17] performed the ^{129}I Mössbauer effect measurement of the perylene–iodine (2 : 3) complex, which is an organic semiconductor with relatively high electrical conductivity ($\approx 10^{-1}$ S/cm).[18,19] They reported from the ^{129}I Mössbauer and the resonance Raman spectra that the perylene–iodine complex was not a well-known molecular complex, such as coronene–iodine, but rather a partially oxidized, mixed-valence compound. We have also studied the ^{129}I Mössbauer effect of the perylene–iodine (2 : 3) complex in order to elucidate the charge state and the configuration of the iodine. A comparison of the Mössbauer results of the coronene–iodine and perylene–iodine complexes will provide some information about the CT bonding formation and the electrical conductivity.

Poly(*p*-phenylene) has attracted much interest because of an increase of the electrical conductivity from about 10^{-12} S/cm of the undoped polymer to 5×10^2 S/cm with the doping of arsenic pentafluoride (AsF_5).[20] It is expected that iodine-doped poly(*p*-phenylene) may also exhibit high electrical conductivity in analogy with the iodine-doped polyacetylene. However, Mainthia *et al.*[21] were unsuccessful in obtaining conductivities higher than 4×10^{-5} S/cm.

In this paper we report ^{129}I Mössbauer effect studies on the aromatic hydrocarbon–iodine (π-σ type) complexes such as benzene–iodine, coronene–iodine (1 : 1), and perylene–iodine (2 : 3) complexes. Furthermore, iodine-doped poly(*p*-phenylene) was also studied in order to elucidate the charge state and the configuration of iodine.

Experimental

All the absorber samples were prepared from Na^{129}I in Na_2SO_3 solution. After oxidizing the iodide with 3 mol dm^{-3} H_2SO_4 and 10% H_2O_2, the resulting molecular iodine ($^{129}I_2$) was extracted with benzene. The benzene solution was washed thoroughly with water and passed through a Teflon filter to eliminate a slight amount of water. The benzene solution of iodine was slowly cooled in a Teflon sample holder and used for the ^{129}I Mössbauer effect measurement as such. The other complexes, coronene–iodine (1 : 1) and perylene–iodine (2 : 3), were prepared by using the procedure of Kommandeur and Hall.[18] In the case of the coronene–iodine complex a large excess of iodine was used for preparation in order to get the brown needle-like crystals in high yields. Since these complexes decompose gradually in air, the products were immediately transferred into Teflon sample holders and kept in liq. N_2 until the Mössbauer measurement.

Poly(*p*-phenylene) was synthesized by polymerization of benzene with the $AlCl_3$–$CuCl_2$ system.[22] Iodine doping was performed by immersing the poly(*p*-phenylene) powder in hexane solution of $^{129}I_2$ at room temperature for 1 d. The content of iodine was estimated to be about 0.01 atoms per the polymer unit, $[(C_6H_4)I_{0.01}]$, from an increase of weight. The molecular iodine was doped very little in this polymer compared with arsenic pentafluoride (AsF_5).[20]

The Mössbauer source in the ^{66}Zn ^{129}Te form was prepared by irradiation of a 150 mg ^{66}Zn ^{128}Te compound at a flux of 2×10^{13} neutrons/cm^2 s for one hour in the Kyoto Univ. Reactor (KUR). The apparatus used for Mössbauer measurements was described in our previous paper.[23]

Results and Discussion

Benzene–Iodine Complex. An ^{129}I Mössbauer spec-

trum of iodine dissolved in benzene at 16 K is shown in Fig. 1. The spectrum was analyzed by the least-square fitting method, as indicated by the solid line. The obtained Mössbauer parameters, such as the quadrupole coupling constant (e^2Qq), the asymmetry parameter (η), the isomer shift (δ), and the line width (2Γ) are given in Table 1 together with the results of Bukshpan *et al.*[8] The e^2Qq value was converted to the ^{127}I nucleus by using the ground state quadrupole moment ratio $^{129}Q/^{127}Q=+0.70121$.[24]

As shown in Table 1, the value of $e^2Qq=-2341\pm13$ MHz is higher and the value of $\delta=0.84\pm0.02$ mm/s is lower than those for the free iodine molecule in inert matrices. Bukshpan *et al.* have observed the same tendency, but their values are slightly different from ours. The slight difference may come from the cooling procedure and the measuring temperature of the sample, that is, Bukshpan *et al.* have prepared the sample by rapid cooling and measured at liq. He temperature, while in our case the sample has been prepared by slow cooling and measured at 16 K. The value $\eta=0$ agrees with that of Bukshpan *et al.*[8] As shown in Fig. 1, only one chemical species of iodine was observed in the benzene-iodine frozen solution. Furthermore, no broadening of the line width was observed in the octet lines compared with the other spectra of crystalline materials. These observations suggest that the Bz–I_2 complex exists as n : n chains of alternate halogen and benzene molecules with the axial configuration in the benzene frozen solution in a similar manner to the

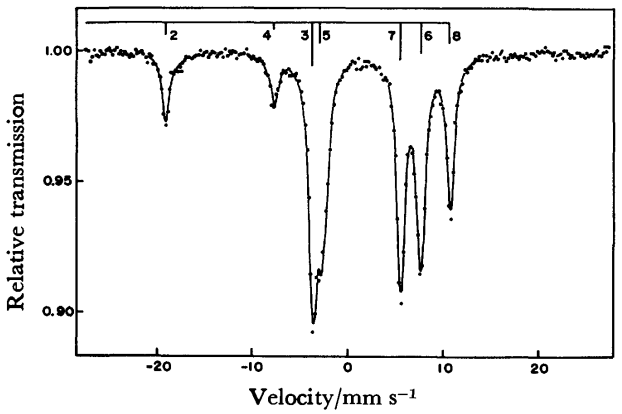

Fig. 1. ^{129}I Mössbauer spectrum of the benzene-iodine complex in the benzene frozen solution at 16 K.

Bz–Br_2 and Bz–Cl_2 crystalline complexes.[25] In contrast, Wynter *et al.*[15] argued from the large value of the asymmetry parameter ($\eta=0.18$) that the *p*- and *o*-xylene-iodine complexes had the resting configuration.

In our previous paper[9] we discussed the electronic state of the Bz–I_2 complex by assuming axial geometry. Comparing the high value of e^2Qq and the low value of δ with those for the free iodine molecule, we found that the CT bonding orbital consisted of an *spd* hybrid orbital of iodine. The contribution of the *5d*-character to the CT bond formation was dependent on the extent of CT. This extent was not directly evaluated from the δ value. From the values of e^2Qq and δ in Table 1, and Eqs. 9 and 10 in Ref. 9, we obtain the *s*- and *d*-characters of the CT bonding orbital to be 0.8% and 8%, respectively, by assuming the extent of CT to be 0.06. This result indicates that the contribution of the *s*- and *d*-characters in the CT bond formation can not be ignored in the case of the Bz–I_2 complex.

Coronene–Iodine Complex. The ^{129}I Mössbauer spectrum of the coronene–iodine (1 : 1) crystalline complex at 16 K is shown in Fig. 2. The Mössbauer parameters obtained by analyzing the spectrum in the same manner as the Bz–I_2 complex are presented in Table 1. The spectrum shows only one chemical species of iodine, as expected from the crystal structure determined by an X-ray diffraction method.[16] The intensities of the absorption peaks are deviated from the ideal ones ($\eta=0$), which are proportional to the square of the Clebsch-Gordan coefficient $|CG|^2$.[26,27] This deviation may be due to: (i) the saturation effect and (ii), the preferred orientation. The first effect depends on the absorber thickness. If the absorber is too thick, the intense peak will be relatively weakened. In our case, the absorber thickness was about 20 mg ^{129}I/cm^2, which seemed to be too thick. Since the coronene–iodine complex is a needle-like crystal, the second possibility is also not ignored.

Both values of e^2Qq and δ for the coronene–iodine complex are lower than those for free iodine molecule. This result suggests that the acceptor orbital of the iodine molecule is only the σ_u-antibonding molecular orbital, as is generally accepted. In this case we can apply the following relationship between δ and *5p* electron populations:[7]

$$\delta(\text{mm/s}) = 1.5\,h_p - 0.54\ (\text{ZnTe source}), \qquad (1)$$

Table 1. The Mössbauer parameters for the π-σ charge transfer complexes of iodine

	e^2Qq[a] / MHz	η	δ / mm s^{-1}	2Γ / mm s^{-1}	U_p[b]	h_p[c]	Ref.
I_2 in CS_2	-2288 ± 20	0	0.96 ± 0.03	1.08	1.00	1.00	
Benzene–I_2	-2341 ± 13	0	0.84 ± 0.02	1.10	1.02	0.92	
Benzene–I_2	-2380 ± 25	0	0.77 ± 0.03		1.04	0.87	8
Coronene–I_2	-2216 ± 13	0.06	0.92 ± 0.02	1.12	0.97	0.97	
Phenazine–I_2	-2223 ± 20	0.06	0.93 ± 0.02		0.97	0.98	29
Poly(*p*-phenylene)–I_2	-2296 ± 13	0	0.94 ± 0.02	1.26	1.00	0.99	

a) The e^2Qq values are converted to ^{127}I. b) $U_p=-e^2Qq_{obsd}/e^2Qq_{at}$, $e^2Qq_{at}=2292.7$ MHz. c) $\delta=1.5\,h_p-0.54$ mm s^{-1}, relative to ZnTe source.

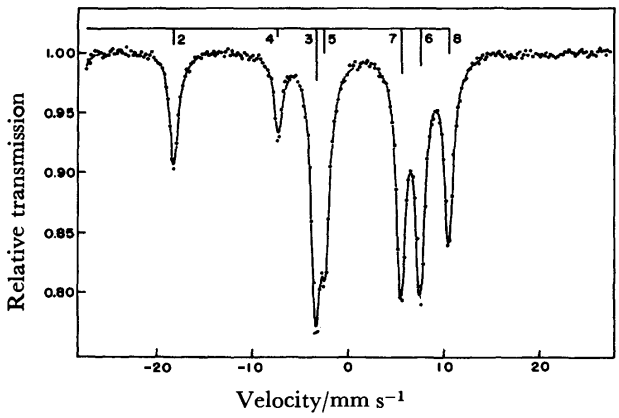

Fig. 2. ^{129}I Mössbauer spectrum of the crystalline coronene–iodine complex at 16 K.

where h_p is the number of p-holes in the $5s^25p^6$ configuration. Substituting the δ value to Eq. 1, we get $h_p=0.97$. It corresponds to the charge transfer of 0.06 electrons from the coronene molecule to the iodine molecule. On the other hand, the charge density localized on each iodine atom is also estimated from the value of e^2Qq according to the Townes and Dailey treatment.[26-28]

$$U_p \equiv -e^2Qq_{obsd}/e^2Qq_{at} \approx 1 - s^2 \pm i - \pi, \quad (2)$$

where U_p is the number of the unbalanced p electrons, s^2 and i are the amount of s-hybridization and the ionic character, respectively, and π is the double bond character and/or the intermolecular bond. The atomic iodine quadrupole coupling constant, e^2Qq_{at}, is equal to 2292.7 MHz. With $e^2Qq=-2216\pm13$ MHz we get $U_p=0.97$. The value obtained is in good agreement with the h_p value. This agreement means that the I–I bond in this complex consists of a pure p_σ bond and the acceptor orbital can be described by only the σ_u-antibonding molecular orbital of the iodine molecule. This is also supported by the small η value.

Although the number of transferred electrons (0.06 e^-) is nearly equal to that for the Bz–I_2 complex, the electronic state of the iodine molecule is appreciably different from that for the Bz–I_2 complex. This result may be attributable to the difference of the geometrical configuration in the two complexes. In the case of the coronene–iodine complex, the axis of the iodine molecule is perpendicular to the coronene molecular plane but is not coincident with the six-fold axis of coronene, as shown in Fig. 3.[16] In the benzene–iodine complex, the iodine molecule is symmetrically situated along the six-fold axis of the benzene molecule.

The values of e^2Qq, δ, and η for the coronene–iodine complex are very close to those for the n-σ type complex of phenazine–iodine[29] which consists of the infinite chains of alternate phenazine and iodine molecules (in Table I). This fact suggests that the mechanism and the bond formation of the charge transfer are not essentially different between the π-σ and n-σ type complexes made up of the infinite alternative chain.

Perylene–Iodine Complex. The ^{129}I Mössbauer spectrum obtained for the perylene–iodine (2 : 3)

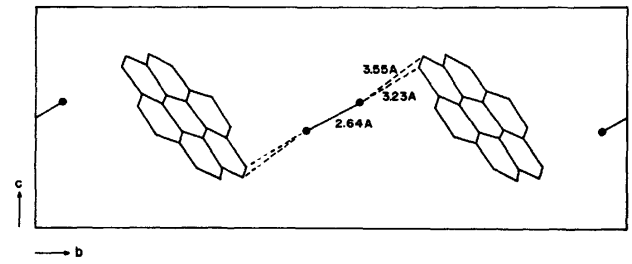

Fig. 3. Molecular structure of the coronene–iodine complex. The black circle represents the iodine atom.

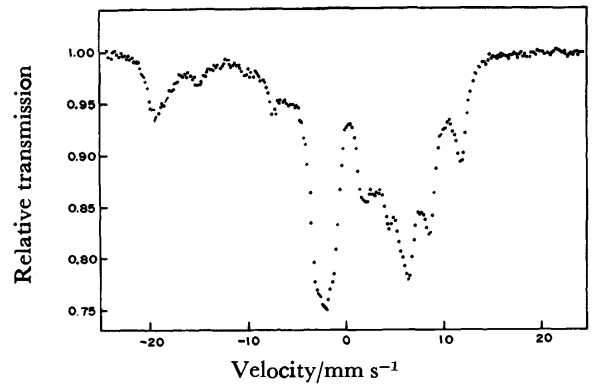

Fig. 4. ^{129}I Mössbauer spectrum of the crystalline perylene–iodine complex at 16 K.

crystalline complex (≈40 mg $^{129}I/cm^2$) at 16 K is presented in Fig. 4. This spectrum has quite complicated features and is clearly different from those of the π-σ charge transfer complexes such as the benzene-iodine and coronene–iodine complexes. It is suggested from the spectrum that the iodine present in the perylene–iodine (2 : 3) complex exists as polyiodides or mixtures of the triiodide ion (I_3^-) and the molecular iodine (I_2). The possibility for the presence of the iodide ion (I^-) is immediately ruled out by finding no single peak at about −0.5 mm/s. The spectrum is very similar to one observed at liq. He temperature by Teitelbaum *et al.*[17] They were successful in analyzing their spectrum into five chemically different iodine sites which consisted of two interacting I_2 units and a distorted I_3^- ion. Their analysis was also supported from the result of the resonance Raman spectra.

There is little doubt that the perylene–iodine complex is not a normal molecular complex but rather an ionic, mixed-valence compound. On the other hand, the coronene–iodine complex is a typical molecular complex which consists of infinite stacks of alternate coronene and iodine molecules (Fig. 3). This difference in the complex formation may first be explained on the basis of the ionization potential of the donor molecules. That is, the ionization potential of perylene (6.85 eV) is much lower than that of coronene (7.50 eV).[30] For many of the solid complexes formed between the donors having lower ionization potential and the acceptors having higher electron affinity, there is a tendency to form ionic, radical salts which show some paramagnetic

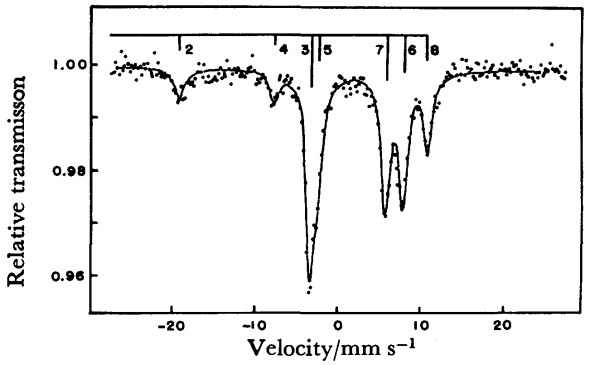

Fig. 5. ^{129}I Mössbauer spectrum of the poly(*p*-phenylene)-iodine complex at 16 K.

behavior and have high electrical conductivities.

Poly(p-phenylene)-Iodine Complex. Figure 5 shows the ^{129}I Mössbauer spectrum for the poly(*p*-phenylene)-iodine complex ($\approx$5 mg ^{129}I/cm^2) at 16 K. The solid line represents the best fitted curve obtained by the least square method. The Mössbauer parameters obtained are given in Table 1. The spectrum shows only one kind of iodine species and the values of e^2Qq and δ are in good agreement with those for the free iodine molecule. Consequently, the iodine doped in poly(*p*-phenylene) exists as almost free iodine molecules. It is then concluded that the iodine molecule interacts little with the phenylene ring. This finding well explains the following experimental results: (i) the electrical conductivity for poly(*p*-phenylene) does not increase with doping of iodine ($\approx 10^{-4}$ S/cm) as much as observed in the case of AsF_5-doping; (ii) the value of the conductivity for the iodine-doped poly(*p*-phenylene) decreases under dynamic vacuum.[20,21] The apparent activation energy for electrical conductivity is also high for Br_2 doping sample ($\approx$0.3 eV).

On the other hand, Matsuyama *et al.*[31] and Kaindl *et al.*[32] found from the ^{129}I Mössbauer spectroscopy that the iodine doped in polyacetylene existed as the chemical forms of I_3^- and/or I_5^- ions. The electrical conductivity for polyacetylene increases drastically with doping of iodine ($\approx 10^2$ S/cm).[33] The activation energy also decreases from 0.3 eV for undoped to $\approx$0.01 eV for iodine-doped polyacetylene. The difference in the doping process between poly(*p*-phenylene) and polyacetylene may be interpreted in terms of the ionization potential of each polymer. For doping of the very strong electron acceptor AsF_5, both polymers indeed exhibit the high electrical conductivity: $\approx 10^2$ S/cm for poly(*p*-phenylene)[20] and $\approx 10^3$ S/cm for polyacetylene.[34]

The authors wish to thank Profs. Takenobu Higashimura and Iwao Shibuya in the Research Reactor Institute, Kyoto University, for their helpful discussions and encouragements. This work was partly supported by a Grant-in-Aid for Scientific Research No. 56540259 from the Ministry of Education, Science and Culture.

References

1) R. S. Mulliken and W. B. Person, "Molecular Complexes," Wiley, New York (1969).
2) R. Foster, "Organic Charge-Transfer Complexes," Academic Press, London (1969).
3) "Spectroscopy and Structure of Molecular Complexes," ed by J. Yarwood, Plenum Press, London (1973).
4) See, for example, L. Fredin and B. Nelander, *J. Am. Chem. Soc.*, **96**, 1672 (1974) and the references cited therein.
5) A. G. El-Kourasky and R. Gimter, *J. Chem. Soc., Faraday Trans. 2*, **72**, 1860 (1976).
6) T. J. Barton, R. Grinter, and A. J. Thomson, *Chem. Phys. Lett.*, **66**, 252 (1979).
7) S. Bukshpan, C. Goldstein, and T. Sonnino, *J. Chem. Phys.*, **49**, 5477 (1968).
8) S. Bukshpan, C. Goldstein, T. Sonnino, L. May, and M. Pasternak, *J. Chem. Phys.*, **62**, 2606 (1975).
9) H. Sakai, Y. Maeda, S. Ichiba, and H. Negita, *J. Chem. Phys.*, **72**, 6192 (1980).
10) R. S. Mulliken, *J. Am. Chem. Soc.*, **72**, 600 (1950); **74**, 811 (1952).
11) S. Aono, *Prog. Theor. Phys.*, **22**, 313 (1959).
12) M. W. Hanna and D. E. Williams, *J. Am. Chem. Soc.*, **90**, 5358 (1968).
13) E. G. Cook, Jr., and J. C. Schug, *J. Chem. Phys.*, **53**, 723 (1970).
14) J. McHale, A. Banerjee, and J. Simons, *J. Chem. Phys.*, **69**, 1406 (1978).
15) C. I. Wynter, Y. W. Chow, and A. Mukerji, *J. Chem. Phys.*, **72**, 5412 (1980).
16) I. Shibuya, *Bussei*, **2**, 636 (1961).
17) R. C. Teitelbaum, S. L. Ruby, and T. J. Marks, *J. Am. Chem. Soc.*, **101**, 7568 (1979).
18) J. Kommandeur and F. R. Hall, *J. Chem. Phys.*, **34**, 129 (1961).
19) T. Uchida and H. Akamatsu, *Bull. Chem. Soc. Jpn.*, **34**, 1015 (1961).
20) D.M. Ivory, G. G. Miller, J. M. Sowa, L. W. Shacklette, R. R. Chance, and R. H. Baughman, *J. Chem. Phys.*, **71**, 1506 (1979); L. W. Shacklette, R. R. Chance, D. M. Ivory, G. G. Miller, and R. H. Baughman, *Synth. Metals*, **1**, 307 (1979).
21) S. B. Mainthia, P. L. Kronick, H. Ur, E. F. Chapman, and M. M. Labes, *Polym. Prepr.*, **4**, 208 (1963).
22) P. Kovacic and J. Oziomek, *Macromol. Synth.*, **2**, 23 (1966).
23) H. Sakai, T. Matsuyama, Y. Maeda, and H. Yamaoka, *J. Chem. Phys.*, **75**, 5155 (1981).
24) R. Livingston and H. Zeldes, *Phys. Rev.*, **90**, 609 (1953).
25) O. Hassel and K. O. Strømme, *Acta Chem. Scand.*, **12**, 1146 (1958); **13**, 1781 (1959).
26) M. Pasternak, *Symp. Faraday Soc.*, **1**, 119 (1967).
27) H. deWaard, "Mössbauer Effect Data Index 1973," ed by J. G. Stevens and V. E. Stevens, IFI/Plenum Press, New York (1974), p. 447.
28) S. L. Ruby and G. K. Shenoy, "Mössbauer Isomer Shifts," ed by G. K. Shenoy and F. E. Wagner, North-Holland, Amsterdam (1978), Chap. 9b.
29) S. Ichiba, H. Sakai, H. Negita, and Y. Maeda, *J. Chem. Phys.*, **54**, 1627 (1971).
30) F. A. Matsen, *J. Chem. Phys.*, **24**, 602 (1956).
31) T. Matsuyama, H. Sakai, H. Yamaoka, Y. Maeda, and H. Shirakawa, *Solid State Commun.*, **40**, 563 (1981).
32) G. Kaindl, G. Wortmann, S. Roth, and K. Menke, *Solid State Commun.*, **41**, 75 (1982).
33) See, for example, C. K. Chiang, Y. W. Park, A. J.

Heeger, H. Shirakawa, E. J. Louis, and A. G. MacDiarmid, *J. Chem. Phys.*, **69**, 5098 (1978) and the references cited therein.

34) A. G. MacDiarmid and A. J. Heeger, *Synth. Metals*, **1**, 101 (1979).

 © 1983 The Chemical Society of Japan Bull. Chem. Soc. Jpn., 56, 1021—1024 (1983)

Isotope Effect on the Emission Cross Section and Translational Energy of Excited Hydrogen Atoms Produced in Electron-Hydrogen Chloride Collisions

Morihide HIGO,† Satsuo KAMATA,† and Teiichiro OGAWA*

Department of Molecular Science and Technology, Kyushu University, Kasuga, Fukuoka 816

†*Faculty of Engineering, Kagoshima University, Korimoto, Kagoshima 890*

(Received September 6, 1982)

The Balmer-α, β, γ lines of the excited hydrogen atoms ($n=3$, 4, 5) produced in e-HCl and DCl collisions have been measured in the energy range of 30—300 eV. The average translational energies of H* and D* are 4—5 eV at higher electron energies and 2—2.5 eV at lower electron energies; no appreciable isotope effect is found for the translational energy. The relative emission cross section of D* and H* shows an isotope effect and this effect is larger in the lower electron energy range; σ_D/σ_H's are 0.74 for $n=3$, 0.71 for $n=4$ and 0.78 for $n=5$ at 30 eV. These results show that there are two groups of the excited hydrogen atoms and their relative cross sections vary with the electron energy. The existence of the isotope effect indicates a competing decay process in the repulsive excited states of HCl.

Electron-impact excitation of a hydride molecule leads to the formation of an excited hydrogen atom (H*). The translational energy[1-6] of H* and its distribution[7-16] have clarified the highly excited states and their dissociation mechanism. The Rydberg states converging to the ionic states which produce H^+ play an important role for the formation of H*; comparison of the translational energy distributions of H* with those of H(HR) and H^+ justifies an extension of the core-ion model to the low-Rydberg emissive atoms.[10-14,16] Curve crossing between potential curves is involved in the formation of the excited hydrogen atom.[9-11,13,16]

The translational energy distribution of H*($n=4$) from HCl has two major components; their peaks lie at about 5 eV (the fast component) and 2.5 eV (the slow component).[9] The former is important at higher electron energies, whereas the latter is important at lower electron energies. The production mechanism of the fast component has been assigned to dissociation through Rydberg states converging to the $^2\Pi$ state of HCl^+, and that of the slow component to excitation to Rydberg states converging to the $^4\Pi$, $^4\Sigma^-$ and/or $^2\Sigma^-$ states of HCl^+ followed by curve crossing and succeeding dissociation through those converging to the $^2\Sigma^+$ state.[9]

The investigation of the isotope effect in the emission cross section of H*(D*)[1,15,17-22] is equally important for the elucidation of the molecular dissociation dynamics and for their theoretical interpretation.[23,24] In our previous paper,[20] it has been shown that the isotope effect of H*(D*)($n=4,5,6$) from HCl(DCl) exists even in the repulsive Rydberg states at an electron energy of 300 eV, and principal quantum number dependence has been discussed.

In the present paper, we have observed the Balmer-α,β,γ lines from HCl and DCl at various electron energies, and measured the average translational energy of H*(D*)($n=3,4,5$) and the isotope effect of their emission cross sections in order to discuss the mechanism of dissociative excitation of hydrogen chloride.

Experimental

The apparatus consists of a stainless-steel collision chamber, a 1.26 m monochromator and a photon counting system. The details of the collision chamber have been published previously.[25] The mixture of HCl (99.7%, Tsurumi Souda) and DCl (99%, Merk) gases were jetted into the collision region and collided with electrons. The base pressure was of the order of 10^{-7} Torr (1 Torr≈133.322 Pa) and the operating pressure was of the order of 10^{-4} Torr.

The spectra were measured with a Spex 1269 monochromator equipped with a 1200 grooves/mm grating blazed at 500 nm. Photons were detected with an HTV R585 photomultiplier for the Balmer-β and γ lines or with a cooled HTV R649 photomultiplier for the Balmer-α line, and were counted with an NF PC545A photon counter.

Measurements were carried out where the intensity of the Balmer radiation was proportional to both the gas pressure and the electron-beam current. The energy of the electron was calibrated with the threshold of N_2^+ (3914 Å) at 18.75 eV and its energy resolution was ±1 eV.

Results and Discussion

Average Translational Energy. Collisions between HCl(DCl) and electrons give the excited H*(D*) atoms. The spectra of the Balmer-α,β,γ lines observed at an angle of 90° with respect to the electron beam and at various electron energies are shown in Figs. 1—3, respectively. The line shape depends on the electron energy; it becomes narrower with decreasing the electron energy.

The true width of the Balmer line, $\delta\lambda_t$, was calculated from the observed half-width, $\delta\lambda_{obsd}$, by the following relation:[5]

$$\delta\lambda_{obsd}^2 = \delta\lambda_t^2 + S^2 + a^2, \quad (1)$$

where S is the resolution of the monochromator and a the fine structure splitting.[26] The results are shown in Table 1. The uncertainty is mainly caused by random experimental fluctuation. The true width obtained here agrees well with that observed at higher resolution (0.033 Å) in our previous measurement[9] as shown in parentheses in Table 1.

At lower gas pressures, the spectral line shape of the emissive atom is determined by the Doppler effect[26] and, thus, has information on the velocity. The translational energy distribution can be calculated from the

Table 1. The corrected half-widths ($\delta\lambda_t$/Å) of the Balmer lines of the excited hydrogen and deuterium atoms in electron-hydrogen chloride collisions

Electron energy/eV	Balmer-α		Balmer-β		Balmer-γ	
	H	D	H	D	H	D
300	1.21	0.89	0.96 (0.96) [a)]	0.72	0.88	0.62
200	1.23	0.92	0.98	0.72	0.89	0.61
100	1.23	0.89	0.96 (0.99)	0.70	0.88	0.61
50	1.18	0.89	0.94 (0.92)	0.68	0.83	0.57
40	1.09	0.79	0.84 (0.76)	0.60	0.71	0.49
35	0.97	0.75	0.73	0.50	0.61	0.44
30	0.85	0.67	0.68 (0.72)	0.48	0.55	0.42

a) Calculated from the Balmer-β line taken at a high resolution (0.033 Å).[9)]
The uncertainties are about 5 and 7% for higher electron energies ($\geq$50 eV) and lower electron energies, respectively.

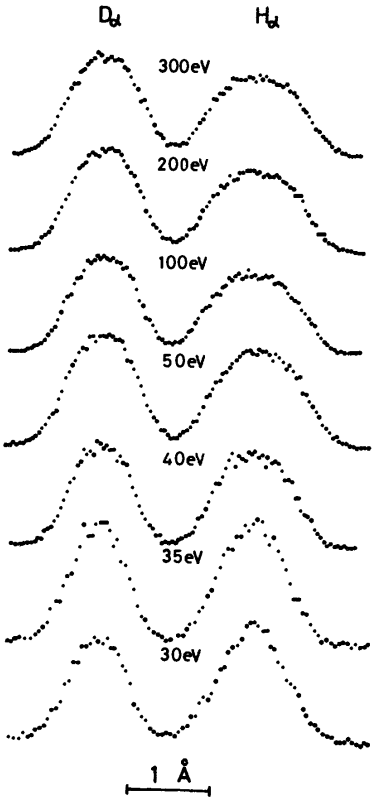

Fig. 1. The spectra of the Balmer-α lines produced in e-HCl and DCl collisions observed at 90° with respect to the electron beam. Spectral resolution: 0.32 Å. Electron-beam current: 220—770 μA. Operating pressure: (1.0—4.0) × 10^{-4} Torr.

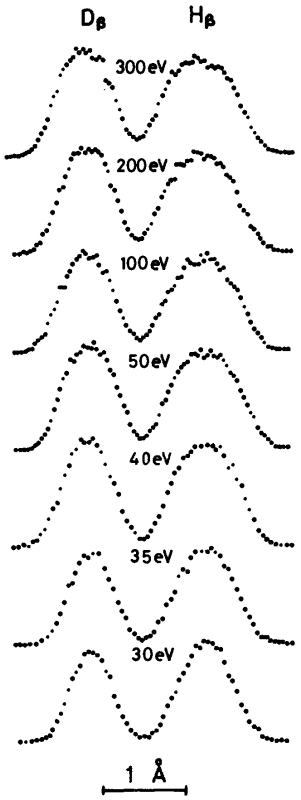

Fig. 2. The Spectra of the Balmer-β lines produced in e-HCl and DCl collisions. Spectral resolution: 0.31 Å. Electron-beam current: 420—740 μA. Operating pressure: (1.5—4.0) × 10^{-4} Torr.

line shape taken at a high optical resolution.[7,9)] Since resolution used here was not good enough to obtain the distribution, we have calculated the average translational energy instead of its distribution.

The average translational energy, E, of H* and D* was calculated by the following equation by assuming the distribution of the velocity to be a delta function:[3-6,15)]

$$E = mc^2/8 \cdot (\delta\lambda_t/\lambda_0)^2, \quad (2)$$

where m is the mass of H*(D*), c the velocity of light and λ_0 the characteristic wavelength of its radiation. The results are shown in Table 2. The electron energy dependence is similar for all of them. The average translational energy of the H*(n=4) is in agreement with the peak of the distribution. Neither the isotope effect nor the dependence on the principal quantum number is clear in the average translational energy of H*(D*) within the experimental uncertainty.

The similarity in both the translational energies of H*(D*) (n=3,4,5) and their electron energy dependence obtained in this measurement indicates that the excited states and their dissociation mechanisms for the formation of H*(n=3,5) and D*(n=3,4,5) are similar

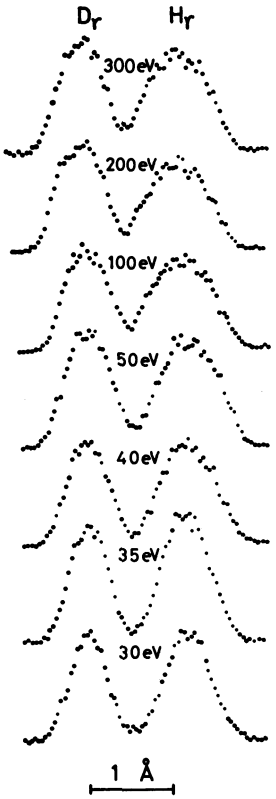

Fig. 3. The spectra of the Balmer-γ lines produced in e-HCl and DCl collisions. Spectral resolution: 0.31 Å. Electron-beam current: 360—820 μA. Operating pressure: $(1.5—4.0)\times10^{-4}$ Torr.

Table 2. Average translational energies (E/eV) of the excited hydrogen and deuterium atoms produced in electron-hydrogen chloride collisions

Electron energy/eV	Balmer-α		Balmer-β		Balmer-γ	
	H	D	H	D	H	D
300	4.0	4.4	4.6	5.1	4.8	4.8
200	4.2	4.6	4.8	5.1	5.0	4.7
100	4.1	4.4	4.6	4.8	4.8	4.6
50	3.8	4.3	4.4	4.6	4.3	4.0
40	3.3	3.4	3.5	3.6	3.1	3.0
35	2.5	3.1	2.6	2.5	2.3	2.4
30	2.0	2.5	2.3	2.3	1.9	2.2

The uncertaintities are about 10 and 15% for higher electron energies (≥50 eV) and lower electron energies, respectively.

to those of H*(n=4).[9] This finding is consistent with the core-ion model.[27] Thus, it is concluded for all of n=3,4,5 of H* and D* that the repulsive Rydberg states converging to the $^2\Pi$ state of $HCl^+(DCl^+)$ produce the fast component and the slightly repulsive Rydberg states which cross the $^2\Sigma^+$ state produce the slow component.

It can generally be concluded that the translational energy for a single component has no isotope effect since the potential curve is common. The traslational energy of H*(D*)(n=3) at higher electron energies, however, is somewhat smaller than those of others. This may suggest that the slow component has a relatively larger

Table 3. Relative emission cross sections (σ_D/σ_H) of the Balmer lines of the excited hydrogen atoms in electron-hydrogen chloride collisions

Electron energy/eV	Balmer-α	Balmer-β	Balmer-γ	Balmer-δ
300	0.90	0.84 (0.83) [a]	0.86 (0.87) [a]	(0.93) [a]
200	0.91	0.87	0.89	
100	0.90	0.83	0.84	
50	0.90	0.84	0.82	
40	0.87	0.81	0.80	
35	0.81	0.69	0.76	
30	0.74	0.71	0.78	

a) Ref. 20. The uncertainty is estimated to be about 7%.

contribution for the formation of H*(D*)(n=3) even at higher electron energies; singlet Rydberg states converging to the $^2\Sigma^-$ states may be involved in such a process.

Isotope Effect on the Emission Cross Section. The relative emission cross section (σ_D/σ_H) has been obtained by comparing the areas of its spectrum. The results are shown in Table 3, with values measured in our previous paper[20] in parentheses. The main sources of uncertainty are random experimental fluctuation (5%), the sample preparation (4%) and the line overlap between H* and D*(2%). The cascade effect has been neglected; this effect has been estimated to be small for the Balmer-α line and negligible for the other Balmer lines by electron impact on H_2.[17,28]

The relative emission cross section shows an isotope effect ($\sigma_D/\sigma_H<1$), which depends on the electron energy as the translational energy does. Since the isotope effect for a single dissociation process is expected to be independent of the electron energy,[21,22] this dependence shows that two or more processes are involved for the formation of H*(D*) and that their relative cross sections vary with the electron energy. This is consistent with the result obtained in the translational energy.

Rydberg states converging to the $^2\Pi$ state are highly repulsive and produce the fast component. Dissociation and autoionization are main competing decay processes in these repulsive excited states. Since the heavier nuclei of DCl separate more slowly along the repulsive potential curve, more DCl molecules autoionize before they dissociate to neutral atoms (D*+Cl). Such a velocity dependent isotope effect has also been observed in the formation of H*(D*) from $H_2(D_2)$,[11,13] and $CHCl_3(CDCl_3)$[15] by electron impact.

Repulsive Rydberg states which cross the $^2\Sigma^+$ state produce the slow component. Its isotope effect is larger than that of the fast component; however, its n dependence is not clear. The probability for curve crossing depends on the velocity of nuclei[29] and the slower motion of DCl results in a larger probability for curve crossing. In addition to competition with autoionization, the probability difference can induce an isotope effect, which may be dependent on n. An n dependence of the isotope effect for the formation of H*(D*) has been observed in the case of CH_3CN (CD_3CN),[1] $H_2(D_2)$,[21,22] and $CHCl_3(CDCl_3)$.[15]

The authors thank Junichi Kurawaki and Yasuhiro Ueda for their cooperation and Professor Nobuhiko Ishibashi of Kyushu University for his encouragement. The present study was partially supported by a Grant-in-Aid for Scientific Research from the Ministry of Education, Science and Culture.

References

1) I. Tokue, I. Nishiyama, and K. Kuchitsu, *Chem. Phys. Lett.*, **35**, 69 (1975).
2) T. Ogawa, F. Masumoto, and N. Ishibashi, *Chem. Lett.*, **1976**, 207.
3) R. S. Freund, J. A. Schiavone, and D. F. Brader, *J. Chem. Phys.*, **64**, 1122 (1976).
4) K. Ito, N. Oda, Y. Hatano, and T. Tsuboi, *Chem. Phys.*, **21**, 203 (1977).
5) M. Higo, T. Ogawa, and N. Ishibashi, *Chem. Lett.*, **1977**, 739.
6) N. Kouchi, M. Ohno, K. Ito, N. Oda, and Y. Hatano, *Chem. Phys.*, **67**, 287 (1982).
7) T. Ogawa, and M. Higo, *Chem. Phys. Lett.*, **65**, 610 (1979).
8) I. Nishiyama, T. Kondow, and K. Kuchitsu, *Chem. Phys. Lett.*, **68**, 333 (1979).
9) M. Higo and T. Ogawa, *Chem. Phys.*, **44**, 279 (1979).
10) T. Ogawa and M. Higo, *Chem. Phys.*, **52**, 55 (1980).
11) M. Higo and T. Ogawa, *Chem. Phys.*, **56**, 15 (1981).
12) T. Ogawa, J. Kurawaki, and M. Higo, *Chem. Phys.*, **61**, 181 (1981).
13) M. Higo, S. Kamata, and T. Ogawa, *Chem. Phys*, **66**, 243 (1982).
14) T. Ogawa and J. Kurawaki, *Bull. Chem. Soc. Jpn.*, **55**, 2271 (1982).
15) T. Ogawa, F. Miyoshi, and M. Higo, *Bull. Chem. Soc. Jpn.*, **55**, 1790 (1982).
16) J. Kurawaki, K. Ueki, M. Higo, and T. Ogawa, *J. Chem. Phys.*, **78**, 3071 (1983).
17) D. A. Vroom and F. J. de Heer, *J. Chem. Phys.*, **50**, 537; 580 (1969).
18) I. Fujita, M. Hatada, T. Ogawa, and K. Hirota, *Bull. Chem. Soc. Jpn.*, **44**, 1751 (1971); K. Hirota, M. Hatada, and T. Ogawa, *Int. J. Radiat. Phys. Chem.*, **8**, 205 (1976).
19) G. A. Khayrallah, *Phys. Rev. A*, **13**, 1989 (1976); G. R. Möhlmann, F. J. de Heer, and J. Los, *Chem. Phys.*, **25**, 103 (1977); C. Karolis and E. Harting, *J. Phys. B*, **11**, 357 (1978).
20) T. Ogawa, M. Higo, M. Toyoda, and N. Ishibashi, *Chem. Lett.*, **1978**, 493.
21) M. Higo and T. Ogawa, *Chem. Phys. Lett.*, **75**, 271 99 (1980).
22) M. Higo, S. Kamata, and T. Ogawa, *Chem. Phys.*, **73**, 99 (1982).
23) R. L. Platzman, *Vortex*, **23**, 372 (1962).
24) R. S. Berry and S. E. Nielsen, *Phys. Rev. A*, **1**, 395 (1970).
25) T. Ogawa, N. Yamami, M. Tsuji, and Y. Nishimura, *Bull. Chem. Soc. Jpn.*, **54**, 1203 (1981).
26) H. E. White, "Introduction to Atomic Spectra," McGraw-Hill, New York (1934).
27) J. A Schiavone, K. C. Smyth, and R. S. Freund, *J. Chem. Phys.*, **63**, 1043 (1975).
28) M. Ortiz and J. Campos, *J. Chem. Phys.*, **72**, 5635 (1980).
29) L. D. Landau, and E. M. Lifschitz, Quantum Mechan-·cs, Nonrelativistic Theory," Pergamon, London (1965).

Cyclopropanation of Electron-deficient Olefins with Dibromomethane by Ni(0) Complexes and Zinc

Hiroyoshi KANAI,* Nobuyuki HIRAKI, and Shigeki IIDA
Department of Hydrocarbon Chemistry, Faculty of Engineering, Kyoto University, Sakyo-ku, Kyoto 606
(Received September 7, 1982)

A new method for the synthesis of cyclopropane derivatives is described. It involves treatment of electron-deficient olefins with dibromomethane in the presence of Ni(0) complex/zinc/Lewis acid (or alkali halide) systems. $Ni(PPh_3)_4/Zn/ZnBr_2$ system was effective for the cyclopropanation of methyl acrylate and acrylonitrile, but was ineffective for that of methyl vinyl ketone and acrylaldehyde. $Ni(COD)_2/Zn/NaI$ system was applicable to the cyclopropanation of methyl vinyl ketone as well as to that of methyl acrylate and acrylonitrile. Alternative catalytic systems which were easy to handle were exploited, involving *in situ* generated Ni(0) complexes prepared from $NiBr_2(PPh_3)_2$ and zinc, or nickel bromide, sodium iodide, zinc, and an olefin. Catalytic amounts of nickel compounds are sufficient for the cyclopropanation of methyl acrylate, acrylonitrile, and methyl vinyl ketone, but a 1 : 2 nickel : acrylaldehyde mole ratio results in the best yield. A mechanism is proposed which involves metallacyclobutane as an intermediate.

The Simmons-Smith reaction provides a convenient synthesis of cyclopropane derivatives.[1] Copper has been found to act as an agent for a similar reaction.[2] The metal-carbenoid intermediates of these reactions are electrophilic so that electron-rich olefins are more susceptible to the reactions than electron-deficient ones. Modifications of zinc couples have enabled less reactive *gem*-dihalides and olefins to react: The zinc–copper couple prepared by treating granular zinc with a hot acetic acid solution of copper(II) acetate[3a] and zinc powder prepared by lithium reduction of zinc chloride[3b] can be used in the reactions involving unreactive *gem*-dihalides, and zinc–silver couple can improve yields in the reactions of electron-deficient olefins.[4] However, cyclopropane derivatives of acrylonitrile and acrylaldehyde have been obtained in very low or no yields. We have found a new method for the synthesis of cyclopropane derivatives by the reactions of electron-deficient olefins with dibromomethane by nickel(0) complexes and zinc.[5]

$$CH_2{=}CHY + CH_2X_2 + Zn \xrightarrow[\text{or NaI}]{\text{Ni(0)/Lewis acid}} \quad (1)$$

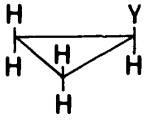

$+ ZnX_2$

X = Br, I; Y = CO_2CH_3, CN, $COCH_3$, CHO.

Experimental

General. All reactions involving organometallic reagents were carried out under a nitrogen atmosphere. Tetrahydrofuran (THF) was refluxed over sodium, distilled, and stored in a nitrogen atmosphere. Methyl acrylate, acrylonitrile, methyl vinyl ketone, and acrylaldehyde were distilled and stored in N_2 and in a refrigerator. The zinc powder provided by E. Merck was used without further purification. Other chemicals were commercially available and were used without further purification. $Ni(PPh_3)_4$[6] and $Ni(COD)_2$[7] (COD= 1,5-cyclooctadiene) were prepared by literature methods. Analysis and purification of cyclopropanes were run on a Shimadzu 6A gas chromatograph using analytical and preparative columns (PEG, 20% on Celite 545).

Reactions of Olefins with Dibromomethane in the Presence of Ni(0) Complexes and Zinc. In a 100 ml two-necked flask were placed zinc powder (8 mmol) and additives. Tetrahydrofuran (10 ml), an olefin (10 mmol), a Ni(0) complex (0.05—0.90 mmol), and dibromomethane (5 mmol) were added and the reaction mixture was stirred at room temperature for a given period of time.

Reactions of Olefins with Dibromomethane in the Presence of in situ *Generated $Ni(PPh_3)_3$ and Zinc.* In a two-necked flask were placed $NiBr_2(PPh_3)_2$ (0.5 mmol), PPh_3 (0.5 mmol), and zinc (8 mmol). Tetrahydrofuran (10 ml) was added and the mixture was stirred at room temperature. After a few minutes, the color changed from green first to yellow and soon to red-brown. The yellow color is due to the formation of $NiBr(PPh_3)_3$,[8] which is subsequently reduced to red-brown $Ni(PPh_3)_3$.[9] After 30 min, an olefin (10 mmol) and dibromomethane (5 mmol) were added and the mixture was stirred at r.t. for 24 h.

Reactions of Olefins with Dibromomethane in the Presence of in situ *Generated Nickel(0) Complexes and Zinc.* Nickel bromide (0.25—5.0 mmol), alkali halide (0—10 mmol), and zinc powder (8 mmol) were placed in the standard reaction flask. Tetrahydrofuran (10 ml) and an olefin (10 mmol) were added. The mixture was stirred and turned brown in a few minutes. After 20—30 min, dibromomethane (5 mmol) was added and the mixture was stirred at r.t. for a given period of time. If necessary, the flask was thermostated at the desired temperature before dibromomethane was added.

All cyclopropane derivatives were isolated with a Shimadzu 6A preparative gas chromatograph. Their NMR spectra and gas chromatograms agreed well with those of the authentic samples.

Results

Cyclopropanation of Electron-deficient Olefins with Dibromomethane by Ni(0) Complexes and Zinc. Electron-deficient olefins such as methyl acrylate, acrylonitrile, and methyl vinyl ketone (abbreviated as MA, AN, and MVK, respectively) were allowed to react with dibromomethane in the presence of Ni(0) complexes ($Ni(PPh_3)_4$ or $Ni(COD)_2$) to give cyclopropane drivatives.[5] The addition of Lewis acids or sodium iodide is necessary for the reactions. The effects of zinc bromide and sodium iodide on the cyclopropanation of MA, AN, and MVK are shown in Table 1. No cyclopropanation

TABLE 1. CYCLOPROPANATION OF ELECTRON-DEFICIENT OLEFINS WITH DIBROMOMETHANE BY Ni(0) COMPLEX/ZINC/LEWIS ACID (OR SODIUM IODIDE) SYSTEMS[a]

Olefin[b]	Catalytic system: Ni(0) complex (mmol)		Additive (mmol)		Zn (mmol)	Yield[c] of cyclopropane %
MA	$Ni(PPh_3)_4$	0.05	$ZnBr_2$	0.57	8.1	51
		0.10	$ZnBr_2$	0.10	8.1	84[d]
		0.10	$ZnBr_2$	0.61	5.0	27
		0.10	$ZnBr_2$	0.69	8.1	55
		0.10	$ZnBr_2$	0.56	12	79
		0.50	$ZnBr_2$	0.16	8.1	86[e]
		0.50	$ZnBr_2$	1.0	8.2	23
		0.61	NaI	4.4	8.0	24
	$Ni(COD)_2$	0.79	$ZnBr_2$	0.50	8.0	14
		0.43	NaI	4.0	8.0	63
		0.66	phen[f] / NaI	0.5 / 5.0	8.1	21
AN	$Ni(PPh_3)_4$	0.90	$ZnBr_2$	0.95	8.0	18
		0.40	NaI	1.0	8.0	33
		0.37	NaI	6.0	8.0	50
	$Ni(COD)_2$	0.30	$ZnBr_2$	0.51	8.0	14[g]
		0.58	NaI	4.1	8.0	21
MVK	$Ni(PPh_3)_4$	0.41	$ZnBr_2$ / NaI	1.1 / 6.0	8.0	4.1
	$Ni(COD)_2$	0.43	$ZnBr_2$	0.51	8.0	20
		0.65	NaI	4.1	8.1	39
		0.43	bpy[h] / NaI	0.53 / 4.0	8.0	28

a) A mixture of an olefin (10 mmol), dibromomethane (5 mmol), Ni(0) complex, Zn, and Lewis acid or sodium iodide in THF (10 ml) was stirred at r.t. for 24 h. b) MA: Methyl acrylate; AN: acrylonitrile; MVK: methyl vinyl ketone. c) Vpc yield based on CH_2Br_2. d) 48 h. e) 46 h. *f*) phen: 1,10-Phenanthroline. g) 18 h. h) bpy: 2,2'-Bipyridyl.

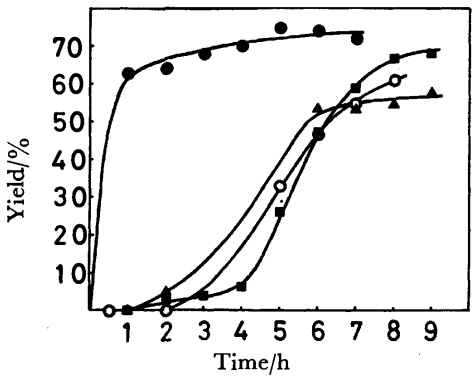

Fig. 1. Time dependence of the yields of methyl cyclopropanecarboxylate in the reaction of MA (10 mmol) with dibromomethane (5 mmol) in THF (10 ml) by the following systems; ○: $Ni(PPh_3)_4$ (0.5)/Zn (8.1)/$ZnBr_2$ (0.56); ▲: $Ni(PPh_3)_4$ (0.3)/Zn (8.1)/$ZnBr_2$ (0.15); ■: $Ni(PPh_3)_4$ (0.1)/Zn (12)/$ZnBr_2$ (0.56); ●: $Ni(COD)_2$ (0.5)/Zn (8.2)/NaI (5.0) where the number in parentheses is given as mmol values.

occurred in the absence of nickel complexes. The yields of methyl cyclopropanecarboxylate slightly increased with an increase in the amount of $Ni(PPh_3)_4$. Although zinc bromide is essential for the reaction, its increase lowers the yield. Lewis acids such as zinc chloride and iodide, and aluminium chloride were also effective,[5] but tin(IV) chloride was ineffective. Sodium iodide played a role similar to that of Lewis acids. In $Ni(PPh_3)_4$/Zn/$ZnBr_2$ or NaI system cyclopropane derivatives from MA, AN, and MVK were obtained in good, moderate, and very low yields, respectively.

The reaction of AN and MVK with dibromomethane gave cyclopropane derivatives in the presence of $Ni(COD)_2$ and NaI.[5] Zinc is required for the cyclopropanation of MA, AN, and MVK by the $Ni(COD)_2$/$ZnBr_2$ system. Sodium iodide is more effective than zinc bromide. An advantage of sodium iodide is the lack of retardation of the reaction by its excess. In $Ni(COD)_2$/Zn/NaI system a further addition of ligands *e.g.* PPh_3, 2,2'-bipyridyl (bpy), 1,10-phenanthroline (phen), lowered the yields of cyclopropanes.

The induction periods were observed in the cyclopropanation of MA by $Ni(PPh_3)_4$/Zn/$ZnBr_2$ system (Fig. 1). The decrease in the amount of $ZnBr_2$ shortens the induction period. It takes about 24 h for the consumption of dibromomethane since the rates after 6 h are very slow. With the elapse of time, zinc bromide is produced (Eq. 1), resulting in a gradual inhibition. On the other hand, the initial rate is very fast in the cyclopropanation of MA by $Ni(COD)_2$/Zn/NaI system. Three-quarters of the total yield is obtained in less than one hour.

Cyclopropanation of Electron-deficient Olefins with Dibromomethane by in situ Generated Ni(0) Complexes and Zinc. When $NiBr_2(PPh_3)_2$ was reduced with zinc in the presence of PPh_3, $Ni(PPh_3)_3$, or $Ni(PPh_3)_4$ was produced *via* $NiBr(PPh_3)_3$.[8b,9] The method serves a double

$$NiBr_2(PPh_3)_2 + PPh_3 \xrightarrow{Zn} NiBr(PPh_3)_3$$
$$\xrightarrow{Zn} Ni(PPh_3)_3 \quad \xrightarrow{PPh_3} Ni(PPh_3)_4 \quad + ZnBr_2 \qquad (2)$$

TABLE 2. CYCLOPROPANATION OF METHYL ACRYLATE AND ACRYLONITRILE WITH DIBROMOMETHANE BY THE *in situ* GENERATED $Ni(PPh_3)_3$/Zn SYSTEM[a]

Olefin	X in $NiX_2(PPh_3)_2$	PPh_3 mole ratio to Ni	Conversion of CH_2Br_2 %	Yield[b] of cyclopropane %
MA	Br	1.0	100	73
	Br[c]	3.0	100	63
	Br[c]	5.0	100	44
	Br[c,d]	1.0	77	6.6
	Br[e,f]	1.0	96	45
	I[g]	1.0	100	18
	I[g,h]	1.0	100	52
AN	Br	1.0	100	49

a) To the *in situ* generated $Ni(PPh_3)_{3-4}$ from $NiBr_2(PPh_3)_2$ (0.5 mmol), PPh_3, and Zn (8 mmol) in THF (10 ml) were added an olefin (10 mmol) and dibromomethane (5 mmol) and the mixture was stirred at r.t. for 24 h. b) Vpc yield based on CH_2Br_2. c) 25 h. d) Mn powder (8 mmol) was used instead of Zn. e) CH_3CN (10 ml) was used as solvent. f) 18 h. g) CH_2I_2 was used instead of CH_2Br_2. h) 0 °C.

Table 3. Cyclopropanation of electron- deficient olefins with dibromomethane by the *in situ* generated Ni(0) complex/Zn/NaI systems

Olefin	$NiBr_2$ (mmol)	NaI (mmol)	Temp °C	Time h	Conversion of CH_2Br_2 %	Yield[d] of cyclopropane %
MA	0.5	0	r.t.	24	100	9.9
	0.5	10	r.t.	24	100	67
	1.0	10	r.t.	20	100	73
	1.0	10	0	24	100	90
	1.0[c]	10	0	69	100	83
	3.0	10	r.t.	20	100	71
AN	0.25	6	20	43	100	62
	0.5	1	r.t.	24	100	35
	0.5	6	20	43	100	70
	1.0	6	0	42	100	92
	1.0	6	20	43	100	67
	1.0	6	25	66	98	53
	1.0	KI 7	r.t.	96	41	26
	2.0	6	20	43	98	74
MVK	0.5	LiI 7	0	64	56	7
	0.5	7	0	67	100	58
	0.5	10	0	96	72	67
	0.5	KI 7	0	93	31	16
	1.0	6	r.t.	65	100	78
	1.0	10	r.t.	52	100	82
	1.0	10	0	96	100	97
	5.0	10	0	163	71	67
AC[d]	1.0	5	r.t.	46	64	46
	1.0	LiBr 5	r.t.	48	41	tr
	1.0	LiI 5	r.t.	48	56	36
	1.0	KI 5	r.t.	48	6	3
	1.0[e]	5	r.t.	48	39	30
	1.0[f]	5	r.t.	120	31	17
	1.0	10	r.t.	48	83	60
	3.0	5	r.t.	46	77	71
	5.0	5	r.t.	46	93	81
	5.0	5	r.t.	120	—	48

a) To Ni(0)–olefin complex prepared *in situ* from $NiBr_2$, an olefin (10 mmol), NaI, and Zn (8 mmol) in THF (10 ml) was added dibromomethane (5 mmol); the mixture was stirred for a given period of time. b) Vpc yield based on CH_2Br_2. c) MA (20 mmol), CH_2Br_2 (10 mmol), Zn (15 mmol), and THF (20 ml). d) AC: Acrylaldehyde. e) 1,2-Dimethoxyethane (10 ml) was used as solvent. f) Acetonitrile (10 ml) was used as solvent. g) CH_2I_2 (5 mmol) was used instead of CH_2Br_2.

purpose: The *in situ* generated $Ni(PPh_3)_3$ contaminates the zinc bromide formed, and then catalytic species are completely supplied in Eq. 2 in the presence of excess of zinc.

In the *in situ* generated $Ni(PPh_3)_3$/Zn system, the cyclopropane derivatives from MA was obtained in high yields and that from AN was obtained in moderate yields, but no cyclopropanes from MVK and acrylaldehyde (abbreviated as AC) were produced (Table 2).

Tetrahydrofuran is the most suitable solvent among several examined: The yield decreased in acetonitrile and none was obtained in benzene and diethyl ether.

Dibromomethane gave higher yields than diiodomethane. The yield increased appreciably for reactions with diiodomethane at 0 °C. No reaction occurred with dichlomethane. Zinc could be replaced by manganese, which was a milder reductant, to give a drop in the yield.

We have exploited an alternative catalytic system for $Ni(COD)_2$/Zn/NaI system (Table 3). When the mixture of nickel bromide, sodium iodide, and zinc was stirred in THF in the presence of an electron-deficient olefin, a red-brown solution was obtained after a few minutes. Dibromomethane was added and aliquots were analyzed at various times. A cyclopropane derivative was gradually produced with the elapse of time, in contrast to the case of the $Ni(COD)_2$/Zn/NaI system. This may be due to the slow rate of the formation of a Ni(0)–olefin complex.[10,11] The amount of sodium iodide needed for the reaction is nearly that of the cyclopropane derivative produced. Further addition of sodium iodide brought a slight increase of the yield. Sodium iodide is the most favorable promoter among the alkali halides investigated.

The yields were almost invariable or rather decreased for the cyclopropanation of MA, AN, and MVK with

an increase in the amount of nickel bromide. However the highest yield was obtained at a 1 : 2 nickel : olefin mole ratio for the cyclopropanation of AC. Lower temperatures gave higher yields of cyclopropane derivatives, due to the decrease of the ethylene formation.[12]

Discussion

The cyclopropanation of electron-deficient olefins with *gem*-dihalides by Ni(0) complex/Zn/Lewis acid systems has some characteristics different from the Simmons-Smith reaction:[1,3,4] (1) Electron-deficient olefins are more susceptible than electron-rich ones; (2) dibromomethane is more suitable than diiodomethane; (3) no cyclopropanation occurs in diethyl ether.

The first requisite for the cyclopropanation of electron-deficient olefins with dibromomethane is the formation of Ni(0)–olefin complexes which are not too much stabilized. Twice as much olefin as dibromomethane was used to complete the reaction of the latter. Ni(0) complexes in the form of $Ni(olefin)_2$ are isolated for olefins with highly electron-deficient groups such as CN, CHO, and $COCH_3$.[10,11] $Ni(MA)_2$ has not been isolated, but its formation in solution may be conceivable on the basis of the results in Tables 1 and 3. The Ni(0) complex of MA is suitably stabilized by further coordination of PPh_3. On the other hand, cyclopropanation of AN, MVK, and AC was inhibited in the presence of PPh_3, bpy, and phen. The inhibition may be caused by the increased stabilization due to their coordination,[13,14] or because olefins are expelled from the sphere of coordination when dibromomethane oxidatively adds to the Ni(0)–olefin complexes.[15] No reaction occurred with electron-rich olefins such as cyclohexene and vinyl acetate because of the absence of nickel–olefin complexes.[14b,17] No cyclopropanation occurred with α- or β-methyl-substituted olefins with polar groups such as methyl crotonate, methyl methacrylate, methacrylonitrile, and 4-methyl-3-penten-2-one due to their weak coordination to nickel complexes.[14b]

The reaction of ethylene with dibromomethane in the presence of Ni(0)–PPh_3 or –bpy complex gives large amounts of propylene and very little cyclopropane.[12] No olefinic products were obtained in the presence of electron-deficient olefins and dibromomethane by Ni(0) complex/Zn/Lewis acid (or sodium iodide) systems.[18] Methylene species formed from dibromethane and Ni(0) complexes[12] or alkylnickel complexes[19] have been thought to be nickel–carbene complexes on the basis of the reactions between metal–carbene complexes and olefins or alkyl groups.[20]

Metallacyclobutane complexes produced from metal–carbene species and olefins are key intermediates for the metathesis of olefins.[21] Metallacyclobutanes undergo metathesis, cyclopropanation, and olefin formation, which are affected by the nature of metals, carbene species, and olefins.[22] The reaction of metal–carbenes and electron-deficient olefins gives reductive elimination products rather than metathesis ones.[20b,c] It seems reasonable to assume that the cyclopropane derivatives from the reactions of electron-deficient

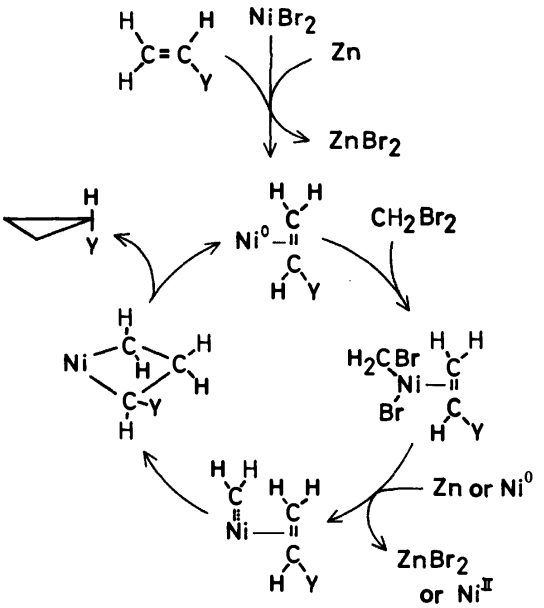

Scheme 1.

olefins and dibromomethane by Ni(0) complex/Zn/Lewis acid (or sodium iodide) systems are produced *via* nickellacyclobutanes. We have not been able to detect any nickel–carbene species.

We propose a mechanism for the cyclopropanation *via* nickellacyclobutane intermediates which are formed from Ni(0)–olefin complexes and dibromomethane. Dibromomethane oxidatively adds to a nickel metal center followed by debromination with a reduced nickel complex or zinc to produce a nickel–methylene complex. The role of Lewis acids or sodium iodide has not been clarified. Lewis acids are necessary cocatalysts in some metathesis reactions.[23] Grubbs *et al.* have found that Me_2AlCl or $AlCl_3$ interacts with titanacyclobutane to facilitate its isomerization and C–C bond cleavage.[24] Lewis acids such as zinc halides and aluminium chloride effectively promoted the cyclopropanation, but their excess hindered the reaction and lengthened the induction period. The basicity of low-valent transition-metal complexes is manifested in many examples.[25] Lewis acids may form adducts involving nickel complexes to saturate coordination sites and/or to deactivate nickel complexes. An excess of sodium iodide, which is the most effective alkali halide, is desirable, but an excess of lithium iodide is not. It is not clear now whether sodium iodide plays the same role as Lewis acids do.

Suitable solvents such as THF may give stabilization to Ni(0)–olefin and/or nickel–carbene and/or nickellacyclobutane complexes by interacting the nickel metal center, and may be easily replaced by olefins. The interaction of Lewis acids with THF may not be neglected completely.[26]

References

1) H. E. Simmons, T. L. Cairns, S. A. Vladuchick, and C. M. Hoiness, *Org. React.*, **20**, 1 (1973).

2) a) N. Kawabata, I. Kamemura, and M. Naka, *J. Am. Chem. Soc.*, **101**, 2139 (1979); b) N. Kawabata and M. Tanimoto, *Tetrahedron*, **36**, 3517 (1980); c) N. Kawabata, S. Yano, J. Hashimoto, and J. Yoshida, *Bull. Chem. Soc. Jpn.*, **54**, 2539 (1981).

3) a) E. Legoff, *J. Org. Chem.*, **29**, 2048 (1964); b) R. D. Rieke, P. Tsu-Jung Li, T. P. Burns, and S. T. Uhm, *ibid.*, **46**, 4323 (1981).

4) J. M. Denis, C. Girard, and J. M. Conia, *Synthesis*, **1972**, 549.

5) H. Kanai and N. Hiraki, *Chem. Lett.*, **1979**, 761.

6) R. A. Schunn, *Inorg. Synth.*, **13**, 124 (1972).

7) F. Guerrieri and G. Salerno, *J. Organomet. Chem.*, **114**, 339 (1976).

8) a) P. Heimbach, *Angew. Chem.*, **76**, 586 (1964); b) H. Kanai, K. Kushi, K. Sakanoue, and N. Kishimoto, *Bull. Chem. Soc. Jpn.*, **53**, 2711 (1980).

9) C. A. Tolman, W. C. Seidel, and D. H. Gerlach, *J. Am. Chem. Soc.*, **94**, 2669 (1972).

10) G. N. Schrauzer, *J. Am. Chem. Soc.*, **81**, 5310 (1959); *Chem. Ber.*, **94**, 642 (1961).

11) R. van der Linde and B. Bogdanović, Proc. Int. Conf. Organomet. Chem., 4th, 1969 U8 (1969).

12) S. Takahashi, Y. Suzuki, K. Sonogashira, and N. Hagihara, *Chem. Lett.*, **1976**, 515.

13) H. P. Fritz and G. N. Schrauzer, *Chem. Ber.*, **94**, 650 (1961).

14) a) A. Yamamoto and S. Ikeda, *J. Am. Chem. Soc.*, **89**, 5989 (1967); b) T. Yamamoto, A. Yamamoto, and S. Ikeda, *ibid.*, **93**, 3360 (1971).

15) We thank a referee who suggested the release of an olefin as an alternative reason for the inhibition. $Ni(olefin)_2L_n + CH_2Br_2 \rightarrow BrNi(CH_2Br)L_n + 2$ olefin. The presence of PPh_3 prevents AN from remaining coordinated to nickel when $Ni(AN_2)(PPh_3)$ is reacted with allyl bromide.[16]

16) M. Dubini and F. Montino, *J. Organomet. Chem.*, **6**, 188 (1966).

17) C. A. Tolman, *J. Am. Chem. Soc.*, **96**, 2780 (1974).

18) We found the formation of an olefin product in the cyclopropanation. A small amount of methyl (*E*)-4-methyl-2-pentenoate was produced from MA and 2,2-dibromopropane.

19) T. Yamamoto, *J. Chem. Soc., Chem. Commun.*, **1979**, 1003.

20) a) F. J. Brown, *Prog. Inorg. Chem.*, **27**, 1 (1980); b) P. G. Gassman and T. H. Johnson, *J. Am. Chem. Soc.*, **98**, 6058 (1976); c) M.D. Cooke and E. O. Fischer, *J. Organomet. Chem.*, **56**, 279 (1973).

21) a) R. H. Grubbs, *Prog. Inorg. Chem.*, **24**, 1 (1978); b) T. Ikariya and S. Yoshikawa, *Kagaku No Ryoiki*, **36**, 456 (1982).

22) H. Yamazaki and Y. Wakatsuki, "*Kagaku Sosetsu*, No. 32," ed by the Chemical Society of Japan, Japan Scientific Societies Press, Tokyo (1981), p. 161.

23) a) F. N. Tebbe, G. W. Parshall, and G. S. Reddy, *J. Am. Chem. Soc.*, **100**, 3611 (1978); b) F. N. Tebbe, G. W. Parshall, and D. W. Ovenall, *ibid.*, **101**, 5074 (1979); c) D. M. Singleton and D. J. Eatough, *J. Mol. Catal.*, **8**, 175 (1980).

24) K. C. Ott, J. B. Lee, and R. H. Grubbs, *J. Am. Chem. Soc.*, **104**, 2942 (1982).

25) V. Lokshin, A. G. Ginzburg, and E. B. Nazarova, *Usp. Khim.*, **49**, 223 (1980).

26) F. N. Tebbe and R. L. Harlow, *J. Am. Chem. Soc.*, **102**, 6149 (1980).

Conformational Changes of the Poly(α-L-glutamic acid)-Cu(II) Macromolecular Complexes in the pH Range 4—7. A Comparative Study by Means of Viscosity and Circular Dichroism[1)]

Tsutomu MASUJIMA,† Kiwamu YAMAOKA,* and Jin-ichiro HORI
Faculty of Science, Hiroshima University, Higashisenda-machi, Naka-ku, Hiroshima 730
(Received September 16, 1982)

Intrinsic viscosity, [η], and far-UV circular dichroism, CD, were measured at 25 °C for poly(α-L-glutamic acid), poly(Glu), solutions in 7.5 mM and 150 mM NaCl in the presence and the absence of copper(II) ions over the pH range 4—7, where poly(Glu) undergoes two conformational transitions. The first is the well-known helix-coil transition and the second, which is followed by completion of the helix, was attributed to the formation of aggregates. The pH dependence of [η] and molar ellipticity was analyzed with the two-state model. The helix-coil transition can not be represented by the all-or-none process. The aggregation mode of helices is predominantly the side-by-side type in 7.5 mM NaCl, but probably a mixture of the side-by-side and the head-to-tail types in 150 mM NaCl. The hydrodynamic shapes of poly(Glu) and its Cu(II)-complexes were calculated with ellipsoid, cylinder, and straight chain element models. The so-called random-coil form is an extended-coil in 7.5 mM NaCl at higher pH. The poly(Glu) helix is probably slightly shortened as compared with the α-helix.

Among the transition metal ions which bind to poly(α-L-glutamic acid), poly(Glu), the copper ion is unique in that it induces the conformational change of poly(Glu).[2-18)] Our recent studies[11-14)] have clarified that three classes of the Cu(II)–Glu residue complexes are present, and that the formation of these complexes is related to the conformational change of the poly(Glu) backbone. A light scattering study has revealed the formation of poly(Glu) aggregates in both the absence and the presence of Cu^{2+} ions in the low pH region.[18)] While the viscosity of poly(Glu) has often been measured,[19-24)] few attempts were made to interpret the conformational changes in terms of the hydrodynamic shape. For example, Go *et al.* have noted, on a qualitative basis, that the variation of the intrinsic viscosity, [η], of poly(Glu) with pH reflects several distinct changes in the backbone conformation.[20,21)] The present viscometric work aims at the quantitative interpretation of the overall conformational changes of poly(Glu) in the absence and the presence of Cu^{2+} ions. For this purpose, the variations of [η] were correlated with changes of the far-UV circular dichroism, CD, under closely paralleled conditions. Thus, the overall hydrodynamic shapes of poly(Glu) in the absence and the presence of Cu^{2+} ions could be compared with optically determined conformational changes. With reference to the previous light scattering results, we present some quantitative discussions on the axial ratio of the rodlike poly(Glu) helix, the possible aggregation mode, and the effects of the concentrations of Cu^{2+} ions and sodium chloride.

Experimental

Materials and Preparations of Sample Solutions. The sodium salt of poly(Glu), hereafter denoted simply as poly(Glu), was described elsewhere.[11)] The degree of polymerization, DP_w, of the sample for viscosity was 708,[18)] and the one for CD was nominally 610.[14)] Other chemicals were of reagent grade and used without further purification. In a given poly(Glu) or poly(Glu)–Cu(II) solution, the final concentration of HCl plus NaCl was kept constant at 7.5 mM (1 M=1 mol dm^{-3}) or 150 mM. The mixing ratio, R, was defined in the same manner as before and adjusted by changing the amount of Cu^{2+}.[11)]

Measurements. A modified Ubbelohde-type viscometer was used at 25±0.01 °C. The flow times were 264.1 and 265.9 s, respectively, for the 7.5 and 150 mM NaCl solutions which were used as solvents. A sample poly(Glu) solution (5 ml, [Glu]=8 mM) was diluted up to twentyfold by the stepwise addition of the NaCl solution to the viscometer. The initial concentration of [Glu] was reduced to 1 mM at pH values lower than 4.6 to avoid precipitation. Since no buffer reagent was used, values of pH of a given polymer solution vary slightly upon dilution. The relation between the shift of pH and the dilution of the poly(Glu) concentration was predetermined outside the viscometer, and utilized to correct the observed values of the reduced viscosity, η_{sp}/c, for an initially set pH, where c is the mass concentration of poly(Glu) in g/100 cm^3. The pH-corrected values of η_{sp}/c were then extrapolated to zero concentration to obtain [η] at the given initial pH as

$$\eta_{sp}/c = [\eta] + k_2c. \quad (1)$$

Linear extrapolations by the least-square method were possible in all cases, except for the poly(Glu) solutions in 7.5 mM NaCl at pH higher than 5, for which the Fouss plot[25)] also produced nonlinear curves. In these cases, the most likely extrapolated values were taken for [η]. The pH of sample solutions was measured on a Hitachi-Horiba N-5 pH meter under the same conditions as used for the viscosity; the measurement of the CD spectra has been described elsewhere.[11)]

Partial Specific Volume. The partial specific volume of the poly(Glu) in the presence and the absence of Cu^{2+} ions, $\bar{v}$, in the 150 mM NaCl solution was calculated with the aid of Eq. 2[26)] by using the value of the refractive index increment, dn/dc, at 436 nm.[18)]

$$\bar{v} = \left(\frac{n_1^2+2}{n_1^2-1}\right)k - \frac{6n_1}{(n_1^2+2)(n_1^2+1)}\left(\frac{dn}{dc}\right), \quad (2)$$

where n_1 is a refractive index increment of the poly(Glu) solution in 150 mM NaCl and k is the specific refraction of the solute prior to mixing with solvent. The value of k was determined to be 0.223 from Eq. 2 with a value of 0.604 for $\bar{v}$ of the poly(Glu) solution in 200 mM NaCl at a pH of 4.42[23)] and with a value of 0.1734 for dn/dc of the poly(Glu) solution

† Present address: Institute of Pharmaceutical Sciences, Hiroshima University School of Medicine, Kasumi 1-2-3, Hiroshima 734.

in 150 mM NaCl at the same pH.[18] The value of k was assumed to be constant at other R and pH values. The dependence of $\bar{v}$ on pH was assumed to be the same for the two poly(Glu) solutions, in 7.5 mM and 150 mM NaCl, for a particular value of R.

Results and Discussion

Dependence of Viscosity on pH. Figure 1 summarizes the intrinsic viscosity and the coefficient k_2 for the poly(Glu) solutions in the presence and the absence of Cu^{2+} ions. When the plot of η_{sp}/c *vs.* c is curved, k_2 was determined from the initial slope of the curved line. Values of $[\eta]$ and k_2 in 7.5 mM NaCl decrease sharply with the decrease in pH. The large value of k_2 indicates that the electrostatic interaction between ionized poly(Glu) ions is poorly suppressed at the low ionic strength; hence, the polyion may be in the highly extended-coil form in the neutral pH range. Qualitatively, the sharp decrease of $[\eta]$ in the pH region between 7 and 5.6 may be ascribed to the change from the extended- to the less extended-coil, mainly because of charge neutralization by added hydrogen ions.[20,21] An apparent plateau region for $[\eta]$ between pH 5.6 and 5.1 may also be attributed to the formation of helix for poly(Glu).[20,21] These views must, however, be verified on a quantitative basis (see below). A further decrease in $[\eta]$ after the completion of the helix (pH 5.1) may reflect the formation of aggregates.[17,18,27-30] The higher contents of Cu^{2+} ions ($R=8$) result in the lower values of $[\eta]$ over the entire pH region. This decrease should be an effect of the bound Cu(II), because almost all Cu^{2+} ions are bound to poly(Glu) at pH higher than 5.[14]

For poly(Glu) solutions in 150 mM NaCl, the behavior of $[\eta]$ is quite different from the above.[20-22] The expansion of the poly(Glu) backbone chain by the charge repulsion of ionized Glu residues is less marked at the higher ionic strength. Values of $[\eta]$ and k_2 are small, k_2 being nearly constant over the entire pH region. Each $[\eta]$ *vs.* pH curve shows a minimum at pH about 5. The curves are similar to each other in the presence and the absence of Cu^{2+} ions, but values of $[\eta]$ decrease with the decrease in R.

Far-UV CD of Poly(Glu) and Its Cu(II)-Complexes. Figure 2 shows typical far-UV CD spectra of poly(Glu) in 150 mM NaCl solutions in the presence and the absence of Cu^{2+} ions. The general characteristics are nearly the same as those in 7.5 mM NaCl solutions.[11] The CD spectra of poly(Glu) show an isoelliptic point at 203.5 nm in the pH range 7.76—4.35; however, they

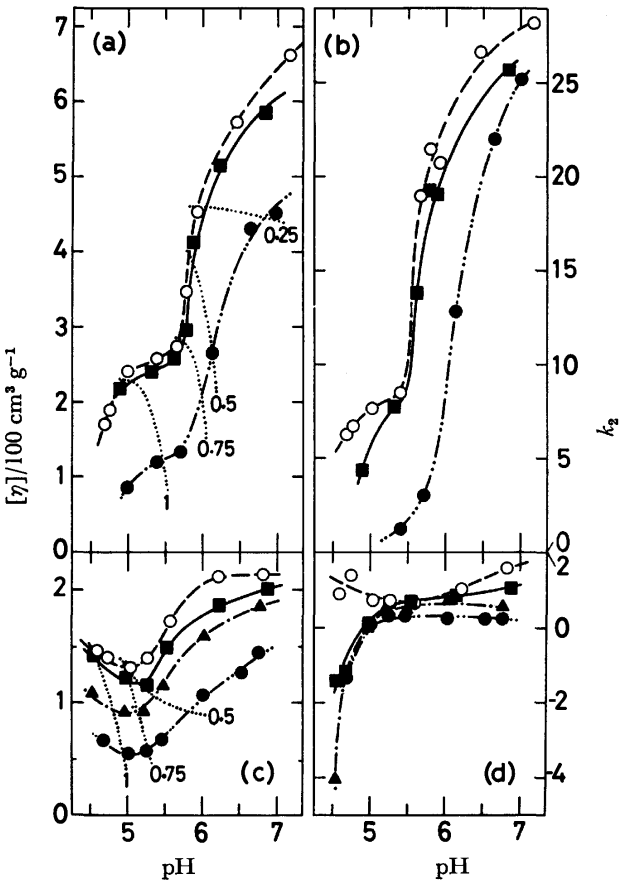

Fig. 1. The pH dependence of the intrinsic viscosity, $[\eta]$, and the increment of reduced viscosity, k_2, for poly(Glu) and poly(Glu)-Cu(II). (a) and (b) at 7.5 mM NaCl and (c) and (d) at 150 mM NaCl. Values of R are ∞ (poly(Glu) only) (——○), 32 (——■), 16 (——▲), and 8 (——●). Dotted curves indicate the helix fraction f_h as given by numerals.

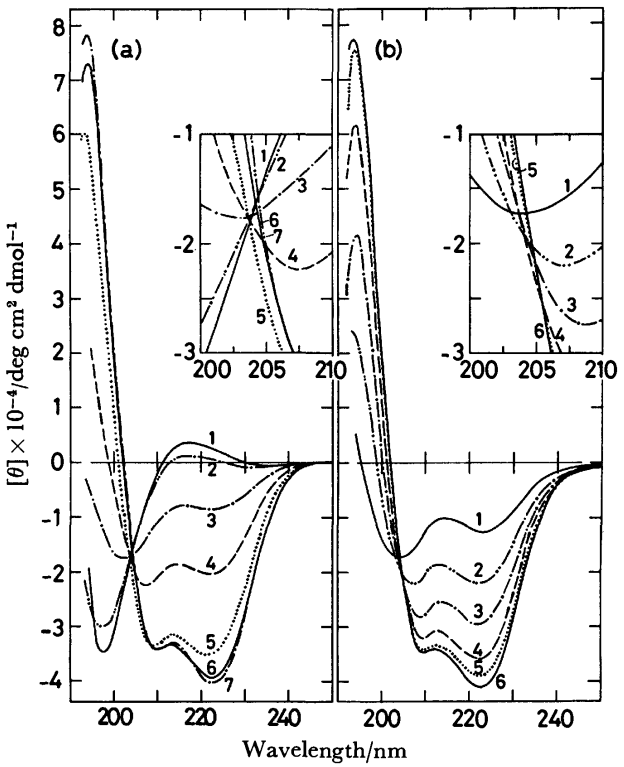

Fig. 2. The far-UV circular dichroism spectra of poly(Glu) at various pH in the absence (a) and the presence ($R=8$) of Cu^{2+} ions (b) at 150 mM NaCl. Values of pH are: (a) 7.76 for 1, 5.68 for 2, 5.21 for 3, 5.07 for 4, 4.57 for 5, 4.28 for 6, and 4.19 for 7; (b) 6.40 for 1, 5.53 for 2, 5.16 for 3, 4.90 for 4, 4.71 for 5, and 4.48 for 6. Inserts are the enlargement of the $[\theta]$ *vs.* wavelength plots in the neighborhood of isoelliptic points.

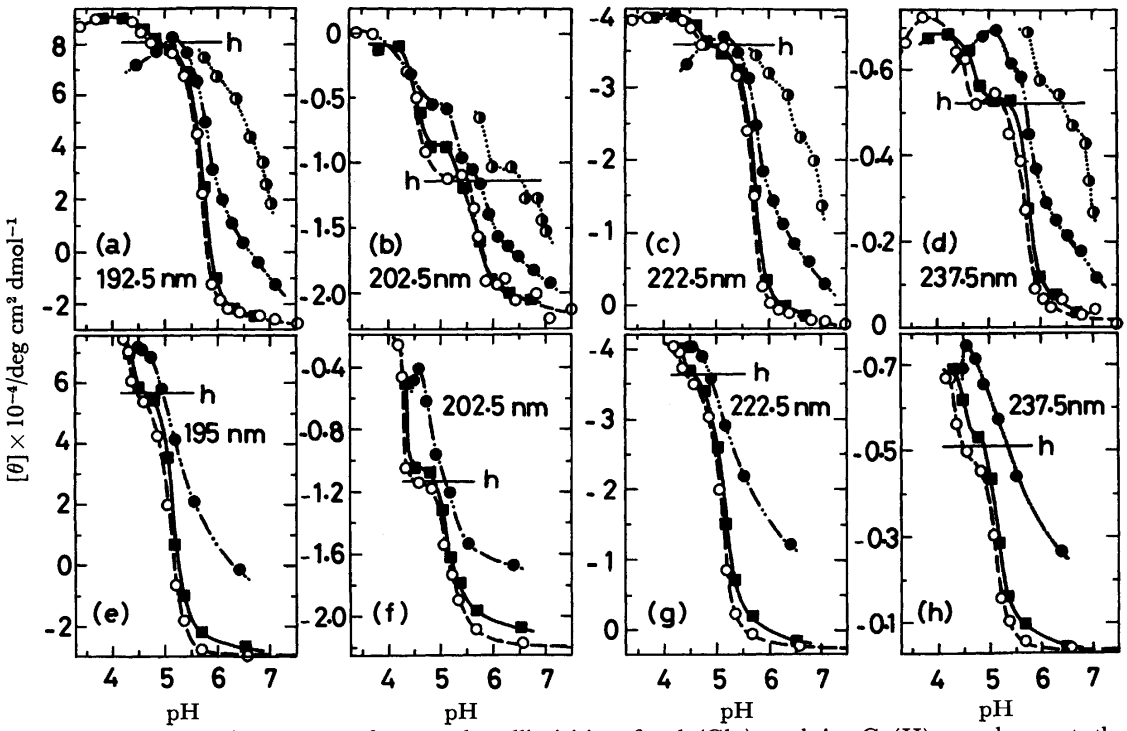

Fig. 3. The pH dependence of the molar ellipticities of poly(Glu) and its Cu(II)-complexes at the selected wavelengths at 7.5 mM ((a)—(d)) and 150 mM ((e)—(h)) NaCl. Values of R are ∞ (— — ○), 32 (——■),8 (—·—●), and 4 (·····◑). The horizontal line in each figure is the value of $[\theta]$ for which $f_h=1$.

deviate from this point at pH's lower than 4.3, showing a larger negative peak at 222.5 nm. The CD spectra of poly(Glu)–Cu(II) complexes show the isoelliptic point only in a limited pH range above 4.5 ($R=32$) or 5.16 ($R=8$). The presence of an isoelliptic point in a family of CD spectra indicates that each observed spectrum can be decomposed into two component-spectra: the helix and the coil spectra in this case.[31] The steady deviation of the isoelliptic point to higher wavelengths indicates that another conformational change is likely to occur at pH lower than 4.28 for poly(Glu) and lower than 5.6 for poly(Glu)–Cu(II). It is now clear that this spectral feature is related to the formation of aggregate helices, as observed by light scattering measurements.[18] The possible contribution of the extrinsic CD band of the bound Cu(II) to the observed molar ellipticity, $[\theta]$, is ruled out, since the CD spectra of poly(Glu) alone show the same kind of deviation.[11]

The dependence of $[\theta]$ on pH was examined at some selected wavelengths to estimate the fraction of helix formed in the poly(Glu) backbone in the presence and the absence of Cu^{2+} ions. Figure 3 shows the plots of $[\theta]$ *vs.* pH for poly(Glu) and its Cu(II)–complexes in 7.5 mM and 150 mM NaCl solutions. A two-step change in $[\theta]$ is clearly observed at each selected wavelength. (The choice of a wavelength often enlarges or conceals the stepwise change.) These two stepwise changes are less overlapped for solutions of lower ionic strength and higher R, but tend to merge to each other, as the amounts of Na^+ and Cu^{2+} ions increase.

The helix fraction, f_h, for poly(Glu) at a given pH may be calculated by the conventional method as[11,14]

$$f_h = \frac{[\theta]^c_\lambda - [\theta]_\lambda}{[\theta]^c_\lambda - [\theta]^h_\lambda}, \tag{3}$$

where $[\theta]^c_\lambda$ and $[\theta]^h_\lambda$ are the molar ellipticities of the pure coil and the pure helix states at the wavelength, λ, and $[\theta]_\lambda$ is the observed molar ellipticity of the poly-(Glu) solution at a given pH. It has been amply documented in the literature that unique assignments of values for $[\theta]^h_\lambda$ and $[\theta]^c_\lambda$ are difficult even for the standard polypeptides, poly(Glu) and poly(L-lysine);[32] however, to retain internal consistency throughout, we selected the molar ellipticity at the onset of the second transition (the one on the lower pH side) for the value of $[\theta]^h_\lambda$ and the molar ellipticity at the highest observed pH 7.76 for $[\theta]^c_\lambda$. Values of $[\theta]^h_\lambda$ are indicated by the horizontal lines in Fig. 3. The helix fraction for the poly(Glu)–Cu(II) complex was also calculated with the above values of $[\theta]^h_\lambda$ and $[\theta]^c_\lambda$. The values of pH, for which $f_h=1$, 0.75, 0.5, 0.25, and 0, were evaluated from the f_h *vs.* pH plots at several wavelengths and averaged for poly(Glu) solutions in 7.5 mM and 150 mM NaCl in the absence and the presence of Cu^{2+} ions.

In order to compare the CD data with the intrinsic viscosity, the f_h *vs.* pH plots must be evaluated at infinitely diluted poly(Glu) concentrations. This was done by making use of a previous report by Nitta *et al.*[33] Their results showed that the f_h *vs.* pH plots shift toward the higher pH side by 0.14 in pH-unit for poly(Glu) in 7.5 mM NaCl, but remain unshifted in 150 mM NaCl. In Fig. 1, the helix fractions thus estimated at infinite dilution (dotted lines) are indicated; hence, comparison

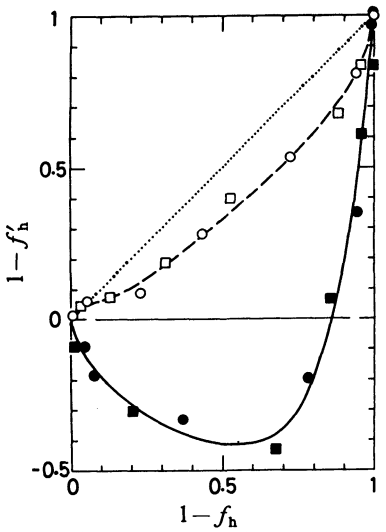

Fig. 4. Comparison of the helix fraction, f'_h, from the intrinsic viscosity with the helix fraction, f_h, from CD for poly(Glu) and poly(Glu)-Cu(II) at $R=\infty$ and 32 and at 7.5 mM (a) and 150 mM NaCl (b). For (a), $[\eta]_h=2.40$ and $[\eta]_c=6.50$ ($R=\infty$, ○) and $[\eta]_h=2.25$ and $[\eta]_c=6.50$ ($R=32$, □). For (b), $[\eta]_h=1.52$ and $[\eta]_c=2.13$ ($R=\infty$, ●) and $[\eta]_h=1.45$ and $[\eta]_c=2.13$ ($R=32$, ■). $[\eta]$'s are in 100 cm^3 g^{-1}.

of the helix fraction with the intrinsic viscosity is now possible for poly(Glu) and poly(Glu)-Cu(II) systems.

Helix Fraction and Hydrodynamic Behavior. (i) Helix-coil Transition and Viscosity: If a poly(Glu) solution contains only pure helix-polyions (the mass concentration of c_h) and pure coil-polyions (c_c), the observed reduced viscosity, $\langle\eta_{sp}\rangle/c$, where $c=c_h+c_c$, and the intrinsic viscosity, $\langle[\eta]\rangle$, may be written as[34]

$$\frac{\langle\eta_{sp}\rangle}{c}=\frac{[\eta]_h c_h+(k_2)_h c_h^2}{c}+\frac{[\eta]_c c_c+(k_2)_c c_c^2}{c}, \tag{4}$$

$$\text{and } \lim_{c\to 0}\frac{\langle\eta_{sp}\rangle}{c}=\langle[\eta]\rangle=f'_h([\eta]_h-[\eta]_c)+[\eta]_c, \tag{5}$$

where $f'_h=c_h/c$, and $[\eta]_h$ and $[\eta]_c$ are the intrinsic viscosities of the unaggregated (single-stranded) helix-polyion and the extended coil-polyion, respectively, while $(k_2)_h$ and $(k_2)_c$ are the corresponding coefficients in Eq. 1. Values of $(1-f'_h)$ were calculated with $[\eta]_h$, $[\eta]_c$, and $\langle[\eta]\rangle$, and are plotted against $(1-f_h)$ in Fig. 4, values of $(1-f_h)$ being calculated from Eq. 3. The values of $(1-f'_h)$ for poly(Glu) and poly(Glu)-Cu(II) do not fit those of $(1-f_h)$ over the entire helix-coil transition region. This result confirms that the helix-coil transition cannot be represented *hydrodynamically* by the all-or-none process of the two-state model. Hence, both partly helical and partly coil portions are contained in each polyion chain in this transition region.

(ii) Viscosity and Aggregation Process of Helices: Light scattering studies have shown that the molecular weight of poly(Glu) and poly(Glu)-Cu(II) increases very rapidly with lowering pH,[18,28] while the viscosity of poly(Glu) tends to increase or decrease in the same pH range depending on ionic strength (Fig. 1). Therefore, it is now beyond doubt that some aggregation process is involved in the pH region where the formation of helix

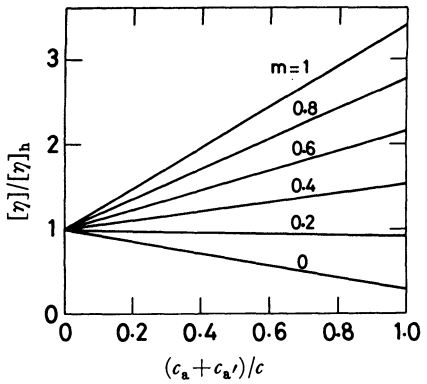

Fig. 5. The theoretical variations of $[\eta]/[\eta]_h$ with the ratio of concentrations of aggregated helices, $c_a+c_{a'}$, to the total concentration of helices, c. The parameter m is $c_{a'}/(c_a+c_{a'})$. For $m=1$ (the head-to-tail type), $L_{a'}=2124$ Å and $2b_{a'}=2b=13$ Å, and for $m=0$ (the side-by-side type), $L_a=1062$ Å and $2b_a=26$ Å, and for unaggregated helix, $L=1062$ Å and $2b=13$ Å being assumed.

is nearly completed. Aggregated helices appear to be quite cohesive against dilution, since extrapolation of scattered light intensity[18] or reduced viscosity to zero concentration of poly(Glu) exhibits no strong tendency of molecular dissociation. The mode of aggregation should be reflected on the pH dependence of $\langle[\eta]\rangle$ or $\langle\eta_{sp}\rangle/c$. Two extreme modes may be represented by the side-by-side and the head-to-tail association schemes. Here, the observed intrinsic viscosity, $\langle[\eta]\rangle$, is given as

$$\frac{\langle[\eta]\rangle}{[\eta]_h}=\frac{c_h}{c}+\frac{c_a}{c}\cdot\frac{[\eta]_a}{[\eta]_h}+\frac{c_{a'}}{c}\cdot\frac{[\eta]_{a'}}{[\eta]_h}, \tag{6}$$

where $[\eta]_a$ and $[\eta]_{a'}$, are the intrinsic viscosities for the aggregated helices of the side-by-side (unprimed) and the head-to-tail (primed) types ($c=c_h+c_a+c_{a'}$). For the rigid rodlike aggregated helix (the n-mer) consisting of n single-stranded helices (monomers), the values of $[\eta]_a$ or $[\eta]_{a'}$ may be calculated with Eq. 7 (see the later sections for detail), together with the appropriate numerical values for the length L and the diameter $2b$.

In order to illustrate the viscometric behavior in the helix-aggregate region (Fig. 1), we utilize Eq. 6 for an assumed simple system of the monomer-dimer equilibrium. Figure 5 shows that the quantity $\langle[\eta]\rangle/[\eta]_h$ decreases with formation of the side-by-side aggregates, but increases with formation of the head-to-tail aggreates. This result is qualitatively in accord with the observed relationship between $[\eta]$ and pH in Fig. 1, indicating that the aggregated poly(Glu) or poly(Glu)-Cu(II) helices are predominantly the side-by-side type in 7.5 mM NaCl, but probably a mixture of both this and the head-to-tail type with a slight chain overlap in 150 mM NaCl. Interchain hydrogen bonds of the acetate dimer type, chelation by Cu(II),[14] and hydrophobic bonds between undissociated side-chain carboxyl groups belonging to different poly(Glu) chains are all attractive forces, favoring formation of the aggregated helices. Indeed, these structures are supported by CPK atomic model building. We are at present unable to specify if the aggregation is the all-or-none process, as

assumed in the present discussion, or if it resumes the open association process, in which aggregated helices elongate lengthwise and become thicker in diameter simultaneously, with lowering of the pH. This is partly because the fractional change of formed aggregates with pH cannot be evaluated by the CD method, in contrast with the result for the helix-coil region (Fig. 4).

Hydrodynamic Shape of Poly(Glu) and Cu(II)-Complexes. Since the two-state model is inadequate for the pH-variation of $[\eta]$, the hydrodynamic shape of poly(Glu) in the presence and the absence of Cu^{2+} ions must be estimated, by use of appropriate models, from values of $[\eta]$ and $\bar{v}$. In the following calculation, the poly(Glu) sample is assumed to be monodisperse as regards the molecular weight.[35]

(i) Undeformable Ellipsoid and Cylindrical Models: As a coarse approximation, the shapes of the poly(Glu) and its Cu(II)-complexes may be assumed by the undeformable prolate ellipsoid of revolution with the axial ratio $p(=a/b)$, where a is the major semi-axis and b is the minor semi-axis. Simha's equation may be employed:[36]

$$[\eta] = \bar{v}\left\{\frac{p^2}{15[\ln(2p)-m]} + \frac{p^2}{5[\ln(2p)-m+1]} + \frac{14}{15}\right\}, \quad (7)$$

where $m=1.5$ for the ellipsoid of revolution, and $m=1.8$ for a long cylinder. Since the results for values of p are almost the same, only the case of ellipsoid is shown in Fig. 6. The apparent axial ratios decrease with the increase in helix fraction. Thus, the hydrodynamic shape of poly(Glu) may be interpreted as being changed from the extended-coil ($p \simeq 160$) to the less extended-coil in the 7.5 mM NaCl solutions and from the less extended- to the shrunk- or compact-coil in 150 mM NaCl solutions, probably because of charge neutralization by added protons and Cu^{2+} ions (especially, at low values of R), and because of charge suppression by added Na^+ ions (in the case of 150 mM NaCl).

If an appropriate value is assigned to b, the length of the cylindrical or ellipsoidal macroion, L, may be estimated. Two extreme values of 10 Å and 16 Å are used for $2b$ in the present calculation. (The distance between the α-carbon and the oxygen of the side chain carboxylate is about 8 Å.) Figure 7 summarizes the results, in which "extended-coil" indicates the upper limit of the length of the polyion in its most extended-form (2560 Å). This limiting value is given by the length of a Glu residue (3.62 Å) multiplied by the weight-average degree of polymerization (708), which was obtained from light scattering.[18] The lengths of the poly(Glu) coil in 7.5 mM NaCl and at neutral pH are in the range of 1500—2400 Å, depending on the hydrodynamic diameter $2b$. This result indicates that the backbone chain is rather elongated in 7.5 mM NaCl, and that the poly(Glu) ions are not in the so-called random-coil state. (This is the reason why we use the term extended-coil). In 150 mM NaCl solution, the

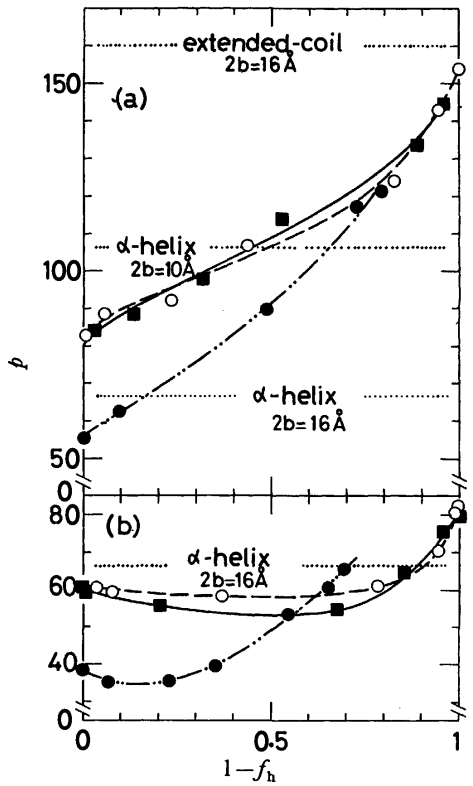

Fig. 6. The dependence of the axial ratio p on the helix fraction f_h of poly(Glu) and poly(Glu)-Cu(II) at 7.5 mM (a) and 150 mM NaCl (b). Values of R are ∞ (——○), 32 (——■), and 8 (——●).

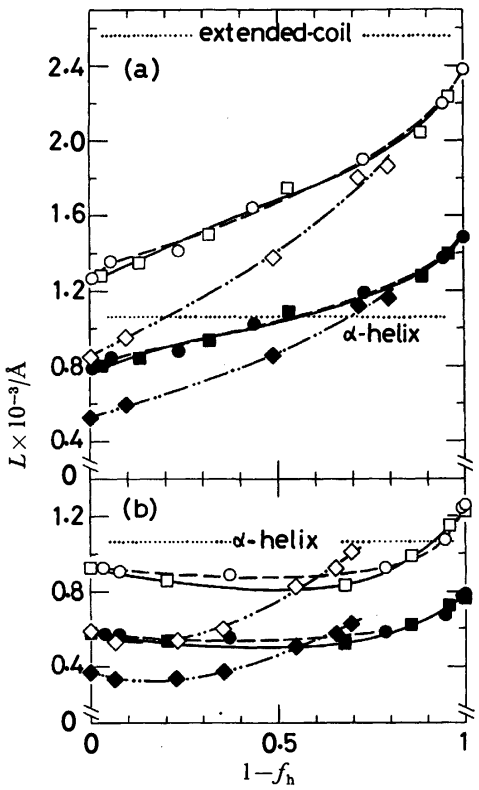

Fig. 7. The dependence of the length of poly(Glu) and poly(Glu)-Cu(II), L, calculated with the cylindrical model on the helix fraction f_h at 7.5 mM (a) and 150 mM NaCl (b). Values of R are ∞ (circles), 32 (squares), and 8 (diamonds). Two extreme values of 10 Å (filled symbols) and 16 Å (open symbols) are assumed for $2b$. The dashed lines indicate the length of α-helix (1062 Å) and that of extended-coil (2560 Å), these lengths being independent of values of $2b$.

poly(Glu) coil is much less extended even at neutral pH.

The possible length for the α-helix is also indicated in Fig. 7 with the horizontal lines, by using a value of 1.5 Å per Glu residue for the axial translation. It is clear that the overall length of the poly(Glu) chain calculated from the viscometric data critically depends on the choice of values of $2b$.[35] If the unhydrated and unaggregated α-helix is assumed for the conformation of poly(Glu), the value of $2b$ would be 13 ± 1 Å in 7.5 mM NaCl, but it would be an unrealistically large value of 20 ± 1 Å in 150 mM NaCl (Fig. 7). On the other hand, the most likely value of $2b$ is probably 11 ± 1 Å, as judged from CPK atomic model building for the unhydrated α-helix. Hence, if poly(Glu) or its Cu(II)-complexes are rigid and rodlike in shape at or near the completion of helix (f_h=0.9—1.0), the helical conformation should not be perfectly α-helical. It should be a slightly shortened helix in the low salt concentration, the length per residue, L/res, being about 1.3 Å instead of 1.5 Å. A more distinct deviation from the α-helix is evident in 150 mM NaCl, the L/res being about 1.0 Å. The effect of bound Cu(II) on the L/res value is also quite large. An alternative interpretation of the results in the helix region (f_h=0.9—1.0) is given as follows: The conformation of poly(Glu) and its Cu(II)-complexes is not perfectly rigid, but is partially broken or semi-flexible even at or near the 100% helix content in aqueous solutions.

(ii) Wormlike Model: As a typical example, Kuhn's straight element model is examined:[37]

$$[\eta] = \frac{A_m d^2 N_A}{M_g} \cdot \frac{0.43\,Z}{-1.6+2.3\log(A_m/d_h)+\sqrt{d/A_m}\sqrt{z}}, \quad (8)$$

where A_m is the length of the straight line chain element, d and M_g are, respectively, the actual length and the molecular weight of the monomeric unit, Z is the degree of polymerization, d_h is the hydrodynamic thickness, and N_A is Avogadro's number. The value of d_h was again assumed to be 10—16 Å under the same consideration as above. The value of d in Å is given by Eq. 9 as a function of helix fraction; the α-helix (at f_h=1) and the most extended chain (at f_h=0) are assumed.

$$d = 1.5f_h + 3.62(1-f_h). \quad (9)$$

The dependence of A_m on f_h is shown in Fig. 8. In the coil region, the length of each straight line chain element is about 200 Å at 7.5 mM NaCl, whereas it is about 80 Å at 150 mM NaCl. The extension of the coil conformation due to the charge repulsion of ionized carboxylate groups is suppressed by the excess salt ions. The smaller value of A_m at R=8 may be explained as being due to the bound Cu(II) folding the backbone chain by the charge suppression and chelation.[11-14] For the $R=\infty$ and 32 solutions, the shortest straight chain elements are 180—190 Å, a value about 15-fold smaller than the contour length, in the region where $0.1<f_h<0.4$, and for the R=8 solution the A_m value is about 150 Å in $0.6<f_h<0.8$ region. Values of A_m depend on the salt conditions greatly. This result should be taken as indicating that the formation of partial helices in the helix-coil region causes a poly(Glu) chain to contract, and that each straight chain element

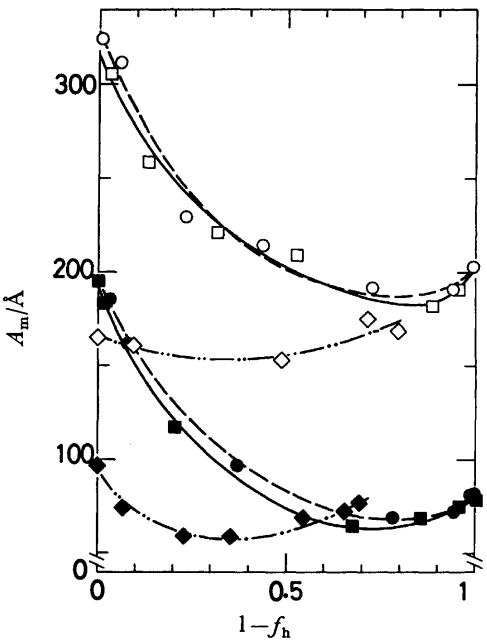

Fig. 8. The dependence of the straight chain element A_m of poly(Glu) chain on pH at 7.5 mM (open symbols) and 150 mM NaCl (filled symbols). Values of R are ∞ (circles), 32 (squares), and 8 (diamonds). The d_h value of 10 Å was used in these calculations.

becomes shorter with more of such elements at a higher salt concentration. As the longer helices are formed at higher f_h, values of A_m increase; however, these values should be only nominal in the high f_h region where this model is unsuitable.

Conclusion

The helix fraction estimated from the far-UV CD data does not correspond linearly to the helix fraction evaluated from viscometric data. Thus the all-or-none conformational transition is unlikely to occur in aqueous added-salt solutions of poly(Glu) and its Cu(II) complexes. At the same helix fraction, the overall conformations of poly(Glu) and poly(Glu)-Cu(II) are not necessarily the same, but depend on pH and the concentrations of Na^+ and Cu^{2+} ions. At a low concentration of salt, the poly(Glu) chain is in an extended-coil in the neutral pH region and the aggregated helices are likely to be of the side-by-side type in the low pH region. At a high salt concentration, the conformation of poly(Glu) seems to be compact in the helix-coil intermediate region. The added Cu^{2+} ions also accelerate the shrinking of poly(Glu) conformation by inducing helix fragments. This shrinking effect should result from intra- and inter-molecular chelations of Cu(II),[14,18] and thus it can be correlated to the appearance of the characteristic absorption band in the helix-coil intermediate region.[11-14]

References

1) Macromolecule-Metal Ion Complexes. IX. For the preceding paper, see Ref. 14.

2) A. L. Jacobson, *Biopolymers*, **2**, 207 (1964).

3) H. Takesada, H. Yamazaki, and A. Wada, *Biopolymers*, **4**, 713 (1966).
4) Y. Hibino and S. Sugai, *Rep. Prog. Polym. Phys. Jpn.*, **11**, 513 (1968).
5) H. Sigel and G. Blauer, *Helv. Chim. Acta*, **51**, 1246 (1968).
6) S. Inoue, K. Yamaoka, and M. Miura, *Bull. Chem. Soc. Jpn.*, **45**, 1314 (1972).
7) S. Inoue, K. Yamaoka, and M. Miura, *J. Sci. Hiroshima Univ., Ser. A*, **39**, 27 (1975).
8) S. Yamashoji, H. Yoshida, and G. Kajimoto, *Yukagaku*, **25**, 128 (1976).
9) J. A. Marinsky, *Coord. Chem. Rev.*, **19**, 125 (1976).
10) T. Hiraoki, M. Kaneko, and K. Hikichi, *Polym. J.*, **11**, 397 (1979).
11) K. Yamaoka and T. Masujima, *Bull. Chem. Soc. Jpn.*, **52**, 1286 (1979).
12) K. Yamaoka and T. Masujima, *Polym. J.*, **11**, 889 (1979).
13) S. Noji and K. Yamaoka, *Macromolecules*, **12**, 1110 (1979).
14) T. Masujima and K. Yamaoka, *Biopolymers*, **19**, 477 (1980).
15) N. Imai and J. A. Marinsky, *Macromolecules*, **13**, 275 (1980).
16) M. Koide and E. Tsuchida, *Makromol. Chem.*, **182**, 359 (1981).
17) M. Koide and E. Tsuchida, *Makromol. Chem.*, **182**, 367 (1981).
18) T. Masujima, *Bull. Chem. Soc. Jpn.*, **56**, 838 (1983).
19) P. Doty, A. Wada, J. T. Yang, and E. R. Blout, *J, Polym. Sci.*, **23**, 851 (1957).
20) Y. Go, Y. Kondo, and K. Aoyama, *Kobunshi Kagaku*, **25**, 344 (1968).
21) Y. Go, Y. Kondo, E. Yamabe, and T. Okumura, *Kobunshi Kagaku*, **25**, 477; 548 (1968).
22) V. E. Bychkova, O. B. Ptitsyn, and T. V. Barokaya, *Biopolymers*, **10**, 2161 (1971).
23) Y. Tadokoro, K. Kawahara, H. Ochiai, and I. Murakami, *Rep. Prog. Polym. Phys. Jpn*, **21**, 585 (1978).
24) H. Kanehiro, J. Komiyama, M. Satoh, and T. Iijima, *Nippon Kagaku Kaishi*, **1980**, 254.
25) R. M. Fouss and U. P. Strauss, *J. Polym. Sci.*, **3**, 246; 602 (1948).
26) W. Heller, *J. Phys. Chem.*, **76**, 2437 (1972).
27) T. M. Schuster, *Biopolymers*, **3**, 681 (1965).
28) Y. Tomimatsu, L. Vitello, and W. Gaffield, *Biopolymers*, **4**, 653 (1966).
29) J. Y. Cassim and J. T. Yang, *Biochem. Biophys. Res. Commun.*, **26**, 58 (1967).
30) B. R. Jennings, G. Spach, and T. M. Schuster, *Biopolymers*, **6**, 635 (1968).
31) K. Yamaoka and T. Matsuda, *Bull. Chem. Soc. Jpn.*, **53**, 968 (1980).
32) N. Greenfield, B. Davidson, and D. Fasman, *Biochemistry*, **6**, 1630 (1967); J. Y. Cassim and J. T. Yang, *Biopolymers*, **9**, 1475 (1970); J. R. Parrish, Jr., and E. R. Blout, *ibid.*, **10**, 1491 (1971); Y-H. Chen, J. T. Yang, and H. M. Martinez, *Biochemistry*, **11**, 4120 (1972).
33) K. Nitta, M. Yoneyama, and N. Ohno, *Biophys. Chem.*, **3**, 323 (1975).
34) C. Wolff, A. Silberberg, Z. Priel, and M. N. Layec-Raphalen, *Polymer*, **20**, 281 (1979).
35) K. Yamaoka and K. Ueda, *J. Phys. Chem.*, **86**, 406 (1982).
36) R. Simha, *J. Phys. Chem.*, **44**, 25 (1940).
37) H. Kuhn, W. Kuhn, and A. Silberberg, *J. Polym. Sci.*, **14**, 193 (1953).

 © 1983 The Chemical Society of Japan Bull. Chem. Soc. Jpn., 56, 1037—1040 (1983)

A Kinetic Study on the Conformational Change of Bovine Serum Albumin Induced by Sodium Dodecyl Sulfate

Kunio TAKEDA

Department of Applied Chemistry, Faculty of Science, Okayama University of Science, 1-1 Ridai-cho, Okayama 700

(Received September 16, 1982)

Stopped-flow measurements were made on the conformational change of bovine serum albumin induced by sodium dodecyl sulfate in a buffer solution containing 3.33 mmol/dm^3 NaH_2PO_4 and 3.56 mmol/dm^3 Na_2HPO_4 (pH 7.0, μ=0.014). The protein adopted a conformation with a smaller helical content than the original native state (helix to coil transition) upon the addition of the surfactant. The rate of transition depended strongly on the surfactant concentration. The results were compared with those of conformational changes of other proteins, in which a helical structure increased in the surfactant solution (coil to helix transition). It is noticeable that the value of the activation entropy is negative in the helix to coil transition, as compared with its positive and large values in the coil to helix transition. It seems that the binding of the surfactant to the protein causes the transition to only a particular conformation of the protein *via* each individual process.

The interactions of surfactants with proteins are interesting *per se*, and so have been extensively investigated.[1,2] However, kinetic studies of the interactions have been neglected. Recently, the kinetic aspects of these interactions have been studied by Wyn-Jones and his coworkers.[3-5] They paid attention to the behavior of the surfactant molecules associated with their binding to macromolecules. Conformational changes of protein polypeptides induced by the binding of surfactants are also interesting. With respect to the conformational changes of proteins, the addition of ionic surfactants such as sodium dodecyl sulfate (SDS) causes either an increase or a decrease of helix content, depending on the nature of the proteins.[6-13] More recently, Takeda and his coworkers have studied the kinetic aspects of the conformational changes of a synthetic homopolypeptide[14,15] and the increase of the helix content of some proteins[16,17] in surfactant solutions. They reported characteristic processes in which the native conformation directly turns to a particular conformation without passing through other conformations.

In this work, a kinetic study was carried out on the conformational change of bovine serum albumin (BSA), which had been reported to adopt a conformation with a smaller helix content than its native state upon the addition of ionic surfactants such as SDS.[9-13]

Experimental

Crystalline BSA and SDS have been described elsewhere.[12] The concentration of the protein was determined spectrophotometrically using $E^{1\%}_{cm}$=6.8 at 280 nm.[18] A sodium phosphate buffer of pH 7.0 was exclusively used (μ=0.014). The final concentrations of NaH_2PO_4 and Na_2HPO_4 in the buffer were 3.33×10^{-3} and 3.56×10^{-3} M (1 M=1 mol/dm^3). The critical micelle concentration of the SDS was determined by the electric conductance method to be 8.3×10^{-3} M in pure water and 5.6×10^{-3} M in the buffer (25 °C).

Static measurements of ultraviolet absorbance were made with a Hitachi double-beam spectrophotometer, Model 220A. The absorbance stopped-flow measurements were carried out with a stopped-flow apparatus, RA-401 of Union Giken Co. equipped with a kinetic data processor, RA-450. The circular dichroism measurements were made with a JASCO J-500A spectropolarimeter equipped with a JASCO DP-501 data processor.[12]

Throughout the measurements, the protein concentration was kept at 1.0×10^{-5} M. The aqueous solution of the protein was used within 6 h of preparation.

Results

Prior to the stopped-flow measurements, the conformational change of the BSA was examined by circular dichroism measurements. Figure 1 shows the circular dichroic spectra of the protein in the absence and the presence of SDS. All of the spectra showed a double negative maximum, which is characteristic of an α-helical structure, although the magnitude of the ellipticity decreased with an increase of SDS. The protein did not lose all of its helical structure[19] and had a constant magnitude of ellipticity above 7.0 mM SDS. However, the predominant loss of the helix content occurs up to 3.5 mM, as seen in Fig. 1. The ultraviolet absorbance change accompanying the conformational change of the protein is shown in Fig. 2. The blue-shift was observed and the difference spectrum had a positive peak around 265 nm and a negative one at 288 nm.

The stopped-flow measurements were carried out at these two wavelengths. Representative time depend-

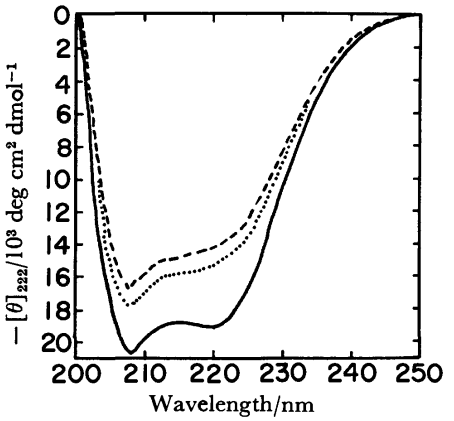

Fig. 1. Typical circular dichroic spectra of BSA in the absence (solid curve) and the presence of 3.5 mM (dotted curve) and 7.0 mM (dashed curve) SDS at 25 °C. These spectra were obtained over 8 repetitions.

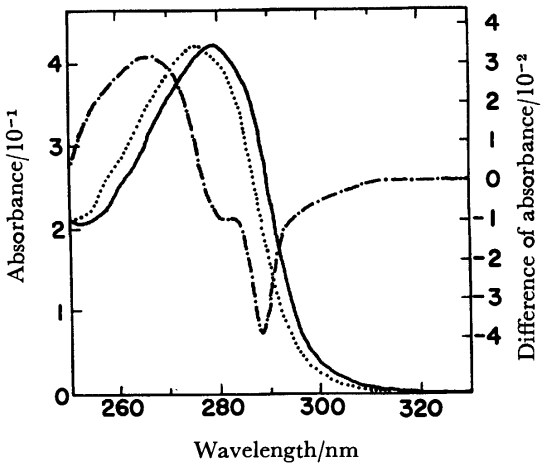

Fig. 2. Typical absorbance spectra of BSA in the absence (solid curve) and the presence of 7.0 mM SDS (dotted curve) and the difference spectrum of them (dot-dashed curve) at 25 °C.

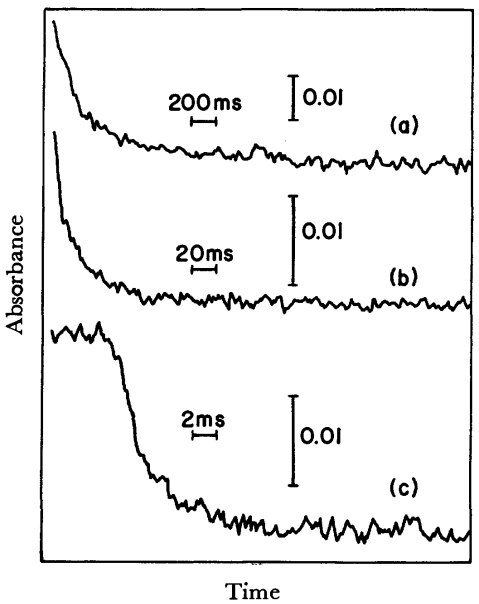

Fig. 3. Representative time courses of absorbance changes at 288 nm. Final concentrations of BSA and SDS were 1.0×10^{-5} M and 3.5 (a), 5.0 (b), and 10.0 mM (c), respectively. The trace (c) is the average of 4 repetitions.

ances of the absorbance changes are shown in Fig. 3. As expected from the absorbance change in Fig. 2, the absorbance decreased with time at 288 nm (as seen in Fig. 3) and increased at 265 nm (not shown here). As clearly recognized in Fig. 3, the rate of the absorbance change became faster with an increase of SDS. Unfortunately, the rate of the conformational change of BSA was too fast to be measured by a circular dichroism stopped-flow method.[14-17] However, it was apparent in previous work[16,17] that the absorbance stopped-flow measurements give identical rates with those obtained by the circular dichroism stopped-flow ones, and the behavior of chromophores such as tryptophan and tyrosine is useful in following the conformational

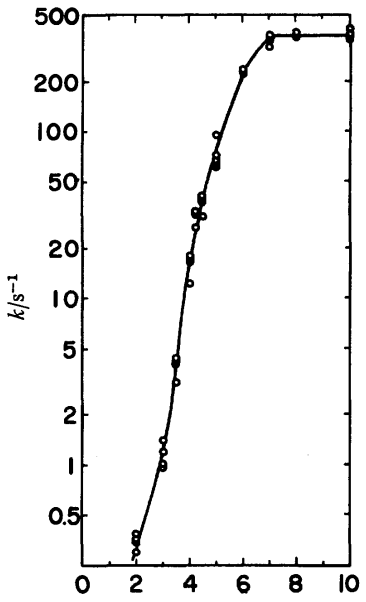

Fig. 4. SDS concentration dependance of rate constant, k, at 25 °C.

TABLE 1. KINETIC PARAMETERS FOR CONFORMATIONAL CHANGES OF PROTEINS IN SDS SOLUTION

	Temperature/°C	Helix to Coil (BSA)	Coil to Helix (δ-Chymotrypsin)
	20	240	0.085
k/s^{-1}	25	370	0.29
	30	470	0.70
ΔH^*/kJ mol^{-1}		48	140
ΔS^*/J K^{-1} mol^{-1}		−34	160

changes of proteins. This is also emphasized when we take account of a similarity of the SDS concentration dependance of the absorption coefficient of the protein at 288 nm to that of the residue ellipticity at 222 nm.[12] Therefore, the absorbance change with time is considered to correspond to the rate of the conformational change of the protein. The first-order rate constant, k, was obtained by the usual treatment.[14] The SDS concentration dependance of k is represented in Fig. 4. The rate constant, k, sharply increased with an increase of the SDS concentration and attained a constant value around 7 mM SDS. The temperature dependance of k was examined at 10 mM SDS in order to evaluate activation parameters of the conformational change. The activation parameters, ΔH^* and ΔS^*, were calculated in the usual manner.[17] Table 1 shows the activation parameters together with those for the conformational change of delta-chymotrypsin.[17]

Discussion

Kinetic studies were made on the conformational change of BSA induced by SDS. The protein loses some parts of the helical conformation (termed the helix to coil transition). This conformational change accompanies the change of the ultraviolet absorbance, as seen

in Fig. 2. The rate constant, k, of the conformational change was obtained by the absorbance changes with time. The value of k strongly depends on the SDS concentration, indicating that the greater the degree of the conformational change, the faster the rate of the conformational change. This tendency also appears in a conformational change of delta-chymotrypsin, in which the helix content increases upon the addition of SDS (termed the coil to helix transition).[17]

The next two processes may be expected for conformational changes of proteins in a solution of surfactant such as SDS,

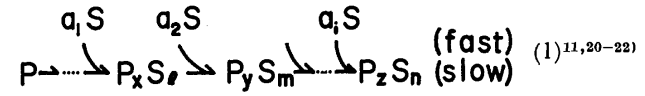

(1)[11,20-22]

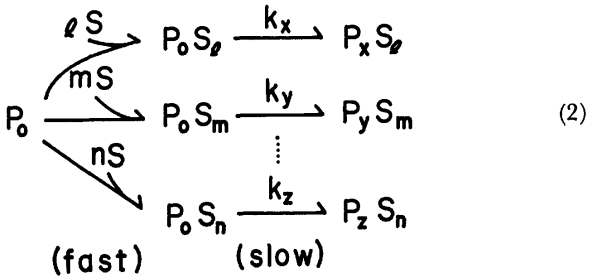

(2)

where P_0: a native protein, S: a surfactant molecule, a_i: a particular number, P_xS_l, P_yS_m,$\cdots$, P_zS_n: complexes (the helix content decreases in the order of x, y, $\cdots$, z in this case), l, m, n: binding numbers of surfactants to a protein, k_x, k_y, k_z: rate constants. In this case, the protein designated by P_0 has the most abundant helical conformation and the complex designated by P_zS_n has the least helix content. If the conformational change proceeds *via* reaction (1) which has been often assumed for the formation of these complexes,[11,20-22] the longest time is required for the transition from P_0 to P_zS_n. However, the transition to P_zS_n with the least helical conformation is faster than those to the intermediate species, as seen in Fig. 4. As discussed before, a protein cannot adopt various different conformations as reaction intermediates in the presence of a ceratin quantity of SDS.[17] This is because the surfactants rapidly bind to a protein,[3-5,23] causing the transition only to a particular conformation of the protein. Reaction (2) indicates that the binding of the surfactant to a protein is completed before the conformational change of the protein,[24] and that the conformation of the protein changes together with the many surfactant molecules bound to it. The bulky hydrophobic groups of the surfactant are obliged to come into maximal contact with the hydrophobic parts of the other surfactants and the protein polypeptide. The saturated binding of SDS would reduce the freedom of choice in adopting a final conformation. On the contrary, the protein with the unsaturated binding of SDS may take much time to choose a final conformation, because this situation necessarily needs more redistribution of the bound surfactants to unoccupied binding sites than in the saturated binding stage. As a result, the rate of the conformational change seems to become faster with an increase of the bound surfactant. It is considered that the conformation of a protein does not change *via* the process expressed by the reaction (1). The reaction (2) appears to be suitable for the understanding of the kinetic aspects of the conformational change of a protein induced by a surfactant such as SDS.

SDS binding to the BSA proceeds in two steps.[12] Under the present condition, the initial binding of about 115 mol of SDS per mole of BSA completes around 4 mM of total SDS and the second binding of a further 90 mol of SDS goes to completion around 7 mM of total SDS (see Fig. 5 in Ref. 12). It is noticeable that the rate constant, k, becomes constant above 7 mM SDS where the binding of SDS saturates (Fig. 4). The stepwise natures of the SDS binding and the conformational change of the protein must be correlated with the fact that the protein has at least two independent domains.[25-29] Jones *et al.* have proposed that the binding initially occurs mainly to the C-terminal section of BSA and then the more stable N-terminal part begins to be bound.[29] In the light of their proposal, it seems that the conformational change occurs only in the C-terminal part of the protein in the initial binding stage (below about 4 mM SDS under the present condition). The rate of the conformational change in the saturated binding stage is faster by two or three orders of magnitude than those in the initial binding stage, as seen in Fig. 4. However, the difference between the rates of conformational changes would not relate to the original stabilities of the C- and N-terminal sections of the protein because of the following reason. Since all of the bindings to both the C- and N-terminal parts occur at the same time in the time scale of the conformational change as mentioned above, the conformations of all of the parts are forced to change together and simultaneously in the sense of reaction (2).

One of the purposes of this work is to make clear distinctions between the helix to coil and the coil to helix transitions. The value of k for the helix to coil transition increases more sharply with an increase of the SDS concentration (Fig. 4), compared with those of k for the other transition.[16,17] In addition, the rate of the helix to coil transition is clearly faster than those of the other one as seen in Table 1, although few kinetic studies have been made on the conformational changes of proteins. The difference between both the transitions is also distinct in their kinetic parameters, as seen in Table 1. The value of ΔH^* for the helix to coil transition is about one-third of that of the other. In particular, it should be noted that the value of ΔS^* is negative in the helix to coil transition, while it is positive and large in the other one. As discussed previously,[17] in the case of the conformational changes induced by the surfactant, the entropic change must reflect not only the folding and unfolding of the protein polypeptide, but also both the rearrangement of the surfactants bound to the polypeptide and the solvent-ordering around the hydrophobic groups of the surfactant exposed to an aqueous environment. Therefore, it seems that the former contribution to the entropic change is

defeated by the latter two of the surfactants, which must be negative, in the activation state of the conformational change of the BSA. It has been considered that a large-scale conformational change of protein-surfactant complex occurs in the coil to helix transition, that is, a part of the polypeptide chain is unfolded, followed by a continuous refolding in the activation state.[17] Compared with this, the helix to coil transition may proceed in a rather simple way.

The kinetic studies of conformational changes of polypeptides made to date[14-17] have strongly suggested that, when a certain number of surfactants bind to a protein, the native conformation of the protein directly transforms into another particular conformation without passing through any intermediate conformation such as may be induced below the binding number mentioned above. This is quite a different feature from the sense of reaction (1) which may be favorable for an interpretation of the gradual growth of complexes.

References

1) C. Tanford, *Adv. Protein Chem.*, **23**, 121 (1968).
2) J. Steinhardt and J. A. Reynolds, "Multiple Equilibria in Protein," Academic Press, New York (1969), pp. 239—302.
3) D. M. Bloor, W. Knoche, and E. Wyn-Jones, "Techniques and Applications of Fast Reactions in Solution," ed. by W. J. Gettins and E. Wyn-Jones, D. Reidel Publishing Co., Holland (1979), pp. 265—270.
4) J. Gettins, C. Gould, D. G. Hall, P. L. Jobling, J. E. Rassing, and E. Wyn-Jones, *J. Chem. Soc., Faraday Trans. 2*, **76**, 1535 (1980).
5) D. M. Bloor and E. Wyn-Jones, *J. Chem. Soc., Faraday Trans. 2*, **78**, 657 (1982).
6) B. Jirgensons, *J. Biol. Chem.*, **242**, 912 (1967).
7) A. H. Hunt and B. Jirgensons, *Biochemistry*, **12**, 4435 (1973).
8) B. Jirgensons, *Macromol. Chem., Rapid Commun.*, **2**, 213 (1981).
9) W. J. Leonard, Jr., and J. F. Foster, *J. Biol. Chem.*, **236**, PC 73 (1961).
10) R. V. Decker and J. F. Foster, *Biochemistry*, **5**, 1242 (1966).
11) J. A. Reynolds, S. Herbert, H. Polet, and J. Steinhardt, *Biochemistry*, **6**, 937 (1967).
12) K. Takeda, M. Miura, and T. Takagi, *J. Colloid Interface Sci.*, **82**, 38 (1981).
13) K. Aoki, H. Okabayashi, S. Maezawa, T. Mizuno, M. Murata, and K. Hiramatsu, *Biochim. Biophys. Acta*, **703**, 11 (1982).
14) K. Takeda, A. Iba, and K. Shirahama, *Bull. Chem. Soc. Jpn.*, **54**, 1793 (1981).
15) K. Takeda, A. Iba, and K. Shirahama, *Bull. Chem. Soc. Jpn.*, **55**, 985 (1982).
16) K. Takeda and S. Takagi, *Agric. Biol. Chem.*, **45**, 777 (1981).
17) K. Takeda, *Bull. Chem. Soc. Jpn.*, **55**, 1335 (1982).
18) H. A. Sober and R. A. Harte (eds), "Handbook of Biochemistry (Selected Data for Molecular Biology)," 2nd ed, CRC Press, Cleveland, Ohio (1970), p. C-71.
19) These findings are in qualitative agreement with earlier results.[13-15,17]
20) J. Oakes, *J. Chem. Soc., Faraday Trans. I*, **70**, 2200 (1974).
21) A. Ray, J. A. Reynolds, H. Polet, and J. Steinhardt, *Biochemistry*, **5**, 2606 (1966).
22) J. A. Reynolds, J. P. Gallagher, and J. Steinhardt, *Biochemistry*, **9**, 1232 (1970).
23) K. Takeda, *Bull. Chem. Soc. Jpn.*, **55**, 2547 (1982).
24) The binding processes of surfactants to proteins are considered to consist of successive bimolecular steps on a very short time scale. Refer to the following: N. Muller, "Solution Chemistry of Surfactants," ed by K. L. Mittal, Plenum Press, New York (1979), Vol. 1, pp. 267—295.
25) T. P. King, *Arch. Biochem. Biophys.*, **156**, 509 (1973).
26) M. C. Hilak, B. J. M. Harmsen, W. G. M. Braam, J. J. M. Joordens, and G. A. J. Van Os, *Int. J. Pept. Protein Res.*, **6**, 95 (1974).
27) R. C. Feldhoff and T. Peters, Jr., *Biochemistry*, **14**, 4508 (1975).
28) M. J. Pallansch and D. R. Briggs, *J. Am. Chem. Soc.*, **76**, 1396 (1954).
29) M. N. Jones, H. A. Skinner, and E. Tipping, *Biochem. J.*, **147**, 229 (1975).

 © 1983 The Chemical Society of Japan Bull. Chem. Soc. Jpn., 56, 1041—1044 (1983)

On the Effect of the Finite Size of the Solvent Molecule in Dielectric Friction Theory

Shi-aki Hyodo,*,† Unpei Nagashima,†† and (the late) Tsunetake Fujiyama
Institute for Molecular Science, Myodaiji, Okazaki 444
†*Department of Chemistry, Faculty of Science, Tokyo Metropolitan University, Setagaya-ku, Tokyo 158*
††*Department of Chemistry, Faculty of Science, Hokkaido University, Sapporo 060*
(Received September 17, 1982)

By considering the charge distribution function around the ion, the effect of the finite size of the solvent molecule can be introduced in the homogeneous dielectric continuum model. A very simple and useful model is presented. The results of this model are compared quantitatively with the experimental Walden products of some simple cations in water, methanol, ethanol, acetone, and acetonitrile solutions, and found to be satisfactory.

There has been a lot of theoretical work on the dielectric friction using the continuum model.[1-5] It has been shown that some of these theories succeed qualitatively.[6-7] Most of the authors of these works regarded the surrounding medium as a dielectric continuum extending up to the surface of the ion. Due to this assumption, dielectric continuum theories do not consider the short range order around the ion correctly. The finite size of the solvent molecule has not yet been properly treated in dielectric continuum theories.

In this article, we will develop a dielectric continuum model without empirical parameters by taking the finite size of the solvent radius into consideration. By introducing the similar treatment of the molecular theory by Wolynes[8] into the dielectric continuum model, we can achieve a very simple and useful model for the dielectric friction theory. We will show that this model is successful for some ion-solvent systems.

Description of the Dielectric Drag Coefficient

We will start from the consideration of the polarization of a volume element at point $\boldsymbol{r}$ due to the electric field originating from the ion. The force exerted on the ion by this induced polarization at point $\boldsymbol{r}$, $\boldsymbol{f}(\boldsymbol{r})$, can be written as[8]

$$\boldsymbol{f}(\boldsymbol{r}) = -2q^2 \frac{\varepsilon_0 - \varepsilon_\infty}{4\pi\varepsilon_0^2} \frac{\boldsymbol{r}}{r^5}, \tag{1}$$

where q is the charge of the ion, ε_0 the static (low frequency) dielectric constant of the solvent, ε_∞ the optical (infinite frequency) dielectric constant of the solvent, and $r=|\boldsymbol{r}|$.

On the other hand, when the ion moves in a potential with relaxation time τ_d, the drag coefficient, $\Delta\zeta$, originating from this electrostatic interaction is expressed by[8]

$$\Delta\zeta = k\tau_d. \tag{2}$$

Here k is the force constant of this potential and the harmonic potential is assumed. This constant, k, can be derived from the differential coefficient of the total electrostatic force, $\boldsymbol{F}$, which acts on the ion, when the ion is displaced a small distance δz from the center of this potential. Namely,

$$k = \left(\frac{\partial \boldsymbol{F}}{\partial z}\right)_{z=0}, \tag{3}$$

where the total force, $\boldsymbol{F}$, is expressed by the sum of the contribution of the polarizations, $\boldsymbol{f}(\boldsymbol{r})$, which are induced on each volume element. When we carry out this summation, we must consider the charge distribution around the ion. For the use of Eq. 1, we will introduce the charge distribution function $\rho(\boldsymbol{r})$ which is normalized in such a way that $\rho(\boldsymbol{r})$ is equal to 1 at large r. Therefore, k can be expressed by the following equation:

$$k = \int \mathrm{d}^3\boldsymbol{r}\rho(\boldsymbol{r})\left(\frac{\partial f(\boldsymbol{r})}{\partial z}\right)_{z=0} = \int_0^\infty \mathrm{d}r \int_\Omega \mathrm{d}\Omega\rho(\boldsymbol{r})\left(\frac{\partial f(\boldsymbol{r})}{\partial z}\right)_{z=0}, \tag{4}$$

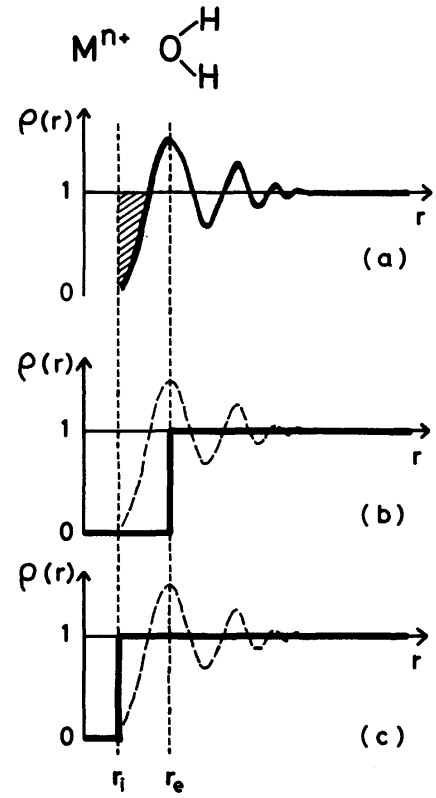

Fig. 1. Schematic charge distribution function around the ion, $\rho(r)$. (a) "Exact" charge distribution. The shaded region indicates the underestimated region of the previous works. (b) Step-wise charge distribution for $r_e=R_{M-O}$. (Eq. 5) (c) Charge distribution for the previous works.

where d^3r is the differential volume element and $d\Omega$ is the angular part of the differential volume element. Considering the effect of the finite size of the solvent radius corresponds to the consideration of the oscillation of $\rho(r)$ (see Fig. 1). In Wolynes' treatment, $\rho(r)$ was calculated by the molecular dynamics method. It can be seen that the distribution function of their model was selected strictly. By introducing a suitable model, we can take the effect of the oscillation of $\rho(r)$ into the continuum theory. For simplicity, we will take the step function for $\rho(r)$ as

$$\rho(r) = \rho(r) \begin{cases} = 0 & \text{for } r < r_e \\ = 1 & \text{for } r \geq r_e, \end{cases} \quad (5)$$

where r_e is the first peak position of the charge distribution function contributing to the induced polarization. This step function, Eq. 5, can take roughly the effect of the first trough of $\rho(r)$ which is shown by the shaded region of Fig. 1-a. The value of $\rho(r)$ at the first peak is larger than 1 and that at the second trough is smaller than 1, *etc.* Therefore, the use of the step function, Eq. 5, possibly underestimates the effect of the first peak and overestimates that of the second trough, *etc.* But these effects partly cancel with each other. So we can use this equation as a first approximation.

By referring to Eq. 5, the drag coefficient, $\Delta\zeta$, is expressed by the following equation:

$$\begin{aligned} \Delta\zeta &= \tau_d \int_0^\infty dr \int_\Omega d\Omega \rho(r) \left(\frac{\partial f(r)}{\partial z}\right)_{z=0} \\ &= \tau_d \int_{r_e}^\infty dr \int_\Omega d\Omega \left(\frac{\partial f(r)}{\partial z}\right)_{z=0} \\ &= \frac{2}{3} q^2 \frac{\varepsilon_0 - \varepsilon_\infty}{{\varepsilon_0}^2} \frac{\tau_d}{{r_e}^3}. \end{aligned} \quad (6)$$

If we replace r_e with the radius of the ion in Eq. 6, this formula will be identical with the results obtained by Zwanzig's theory,[4] which can be regarded as the essence of the dielectric friction theories.

The values of r_e can be obtained from the distance between the center of the ion and the center of the atom that belongs to the first nearest neighbor molecules, *i.e.*, in the case of the aqueous solution, the distance between the ion and the oxygen atom, R_{M-O}. We can take the R_{M-O} data of some of the electrolyte aqueous solutions from X-ray diffraction analyses.[9-14] The R_{M-O} data from the X-ray studies agree well with the sum of the crystalline ion radius and the van der Waals' radius of an oxygen atom.

Results and Discussion

We will examine Eq. 6 with the R_{M-O} values which are used for r_e. R_{M-O} values are taken as the sum of the crystalline ion radius and the van der Waals' radius of the nearest atom of the first nearest neighbor molecule. The other parameters used in the following results are taken from Refs. 15—23. The results of the calculations using the Walden product,[24] $\lambda_0\eta$, are shown in Figs. 2 and 3 in the case of aqueous solutions. Here λ_0 is limiting ionic equivalent conductance: $\lambda_0 = Fq/\zeta$ (F is the Faraday constant) and $\zeta = 4\pi\eta r_i + \Delta\zeta$ (η is the bulk viscosity of the solvent). The results in the case of the solution of some other solvents are also shown in Figs. 4 and 5.

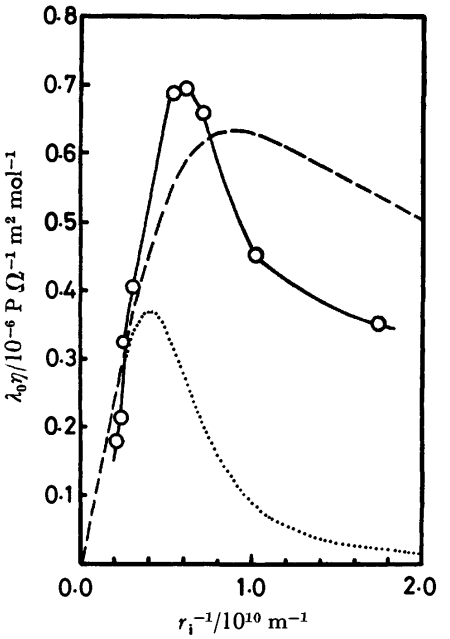

Fig. 2. Experimental (—○—) and calculated (----; $r_e = R_{M-O}$, ·····; $r_e = r_i$) Walden products for the alkali metal and tetraalkylammonium ions in water solutions. The experimental values indicate Li^+, Na^+, K^+, Rb^+, Cs^+, $(CH_3)_4N^+$, $(C_2H_5)_4N^+$, $(C_3H_7)_4N^+$, and $(C_4H_9)_4N^+$, from right side to left side [1 P=0.1 Pa s (in the unit of the vertical axis)].

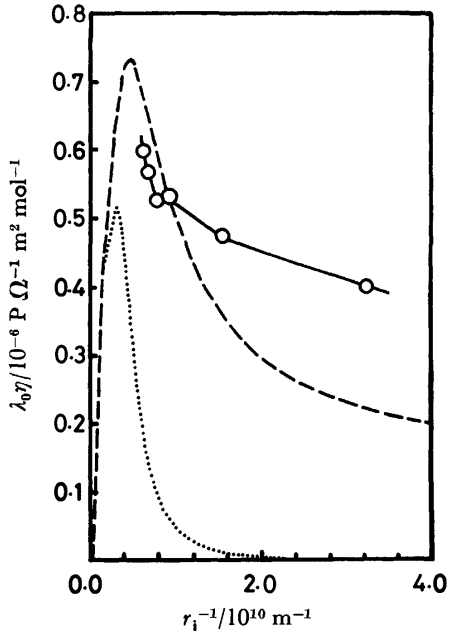

Fig. 3. Experimental (—○—) and calculated (----; $r_e = R_{M-O}$, ·····; $r_e = r_i$) Walden products for the alkaline earth metal ions in water solutions. The experimental values indicate Be^{2+}, Mg^{2+}, Sr^{2+}, Ba^{2+}, and Ra^{2+}, from right side to left side [1 P=0.1 Pa s (in the unit of the vertical axis)].

Figure 2 shows the observed[15,16] and calculated $\lambda_0\eta$

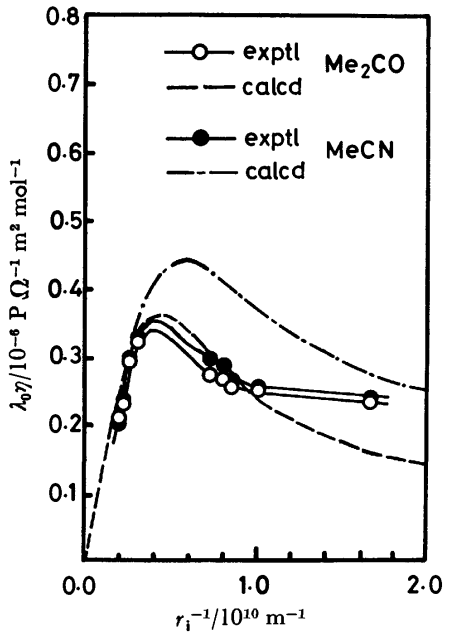

Fig. 4. Experimental and calculated Walden products for the alkali metal and tetraalkylammonium ions in acetone (Me_2CO) and acetonitrile (MeCN) solutions. The experimental values indicate Li^+, Na^+, K^+, Rb^+, Cs^+, $(CH_3)_4N^+$, $(C_2H_5)_4N^+$, $(C_3H_7)_4N^+$, and $(C_4H_9)_4N^+$, from right side to left side [1 P=0.1 Pa s (in the unit of the vertical axis)].

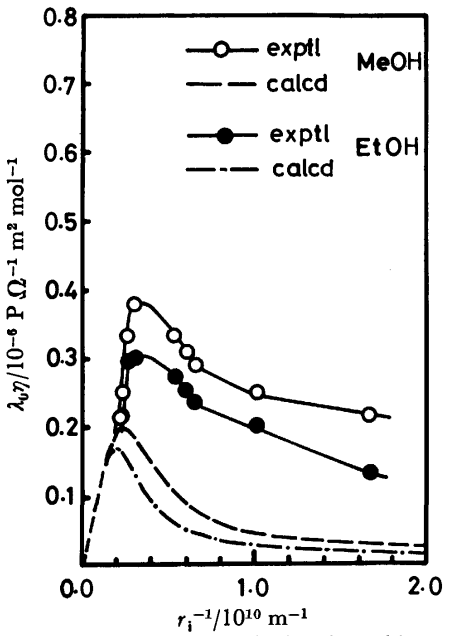

Fig. 5. Experimental and calculated Walden products for the alkali metal and tetraalkylammonium ions in methanol (MeOH) and ethanol (EtOH) solutions. The experimental values indicate Li^+, Na^+, K^+, Rb^+, Cs^+, $(CH_3)_4N^+$, $(C_2H_5)_4N^+$, $(C_3H_7)_4N^+$, and $(C_4H_9)_4N^+$, from right side to left side. The experimental value of $(C_4H_9)_4N^+$ in ethanol solution is lacked [1 P=0.1 Pa s (in the unit of the vertical axis)].

values for the aqueous solutions of some (1+) ions. It can be seen from Fig. 2 that the calculated values agree well with the observed ones. Figure 2 shows also the calculated values using Zwanzig's formula[4] ($r_e=r_i$). Fig. 3 shows the data of the Walden products for the aqueous solutions of some (2+) ions. It shows better agreement than the case of (1+) ions, except for Be^{2+} and Mg^{2+} ions. We can see from this fact that the contribution of the electrostatic interaction will be the main effect for the case where the ion has larger electronic charge than a (1+) ion with the same radius. Figure 4 shows the observed[15,16,18] and calculated Walden products of the (1+) ions dissolved in acetone or acetonitrile. They agree well, as is the case in water. In the case of methanol and ethanol, however, our results do not agree with the observed results,[15,16] as shown in Fig. 5.

Latimer *et al.*[25] and Stokes[26] discussed the problem of the short range order around the ion on the solvation enthalpy. Considering the small region around the ion whose dielectric constant is different from the "bulk" dielectric constant, they have corrected the Born's equation[1] and fitted the calculated solvation enthalpy to the observed one. It is surely important for the ionic mobility problem also that the physical properties around the ion are different from "bulk" ones. But these treatments have some empirical parameters such as the size of the region. Therefore, in this article, we will discuss the ionic mobility problem without such empirical parameters and consider the importance of the charge distribution around the ion.

Wolynes *et al.* gave the results of their molecular theory on the ionic mobility problem.[8] Our results for the case of water and acetonitrile agree well with theirs. It is surprising that a very simple description of the charge distribution function such as Eq. 5 can express the force exerted on the ion well. The advantage of our approach is that it needs only simple parameters.

A theory that regards the surrounding medium as a dielectric continuum extending up to the surface of the ion, like Zwanzig's,[4] is not sufficient. For example, such a theory gives a Walden product of Li^+ ion about 20 times smaller than the one observed in water solution. As compared with this, our treatment of dielectric friction using the very simple charge distribution function agree quite well with observed data quantitatively. This indicates that the short range order around the ion is important for electrostatic interaction. This can be anticipated from the consideration of the r_e dependence of $\Delta\zeta$ in Eq. 6. The same situation occurs in the other dielectric friction theories.[1-3,5,6]

In contrast with the good agreement of the case of water solution *etc.*, our model for the methanol or ethanol solution does not agree with experimental data quantitatively. An effort to make agreement by varying the R_{M-O} value results in physically unreasonable figures. Therefore, some other effect must be involved in these alcohols. The dielectric relaxation times of methanol (69 ps) and ethanol (144 ps) are 1—2 orders larger than that of water (9.3 ps).[16,17] This indicates that some other relaxation time governs the exerted force relaxation, *e.g.*, the translational relaxation time pointed out by Wolynes.[8] The disagreement of our calculation for methanol and ethanol (Fig. 5) may correspond to this possibility.

The calculated Walden products of Be^{2+} and Mg^{2+} of aqueous solution do not agree with observed ones as well as those for the other (2+) ions (Fig. 3). The ionization potential (IP) data[27] suggests the existence of the specific interaction between Be^{2+} or Mg^{2+} and water molecules. The electron affinities of Be^{2+} (18.2 eV) and Mg^{2+} (15.0 eV) are larger than the first IP of water molecule (12.8 eV). Therefore, it is possible that the charge transfer from water molecule to the Be^{2+} or Mg^{2+} ion occurs in the aqueous solutions. This fact suggests that there are two types of cations, *i.e.* Be^{+} or Mg^{+} and H_2O^{+} ion, in these aqueous solutions. The *ab initio* SCF calculation of Mg^{2+}–H_2O system[28] indicates that the charge transfer from H_2O to Mg^{2+} occurs. The atomic population of Mg^{2+} obtained from this calculation is 10.058.

The results shown here indicate that the charge distribution function must be used when we consider the dielectric friction quantitatively. For closer quantitative discussion, the exact (and/or experimental) charge distribution function is necessary. But the simple treatment of the charge distribution like Eq. 5 is sufficient to describe the dielectric friction quantitatively. This fact suggests that the consideration of the electrostatic interaction at the short range order around the ion is important for the macroscopic dielectric friction theories.

The authors would like to thank Prof. P. G. Wolynes of the Univ. of Illinois and Prof. Y. Udagawa of the Institute for Molecular Science for helpful discussions and a critical reading of this manuscript.

References

1) M. Born, *Z. Physik*, **1**, 221 (1920).
2) R. M. Fuoss, *Proc. Natl. Acad. Sci. U. S. A.*, **45**, 807 (1959).
3) R. H. Boyd, *J. Chem. Phys.*, **35**, 1281 (1961); **39**, 2376 (1963).
4) R. Zwanzig, *J. Chem. Phys.*, **38**, 1603 (1963); **52**, 3625 (1970).
5) J. Hubbard and L. Onsager, *J. Chem. Phys.*, **67**, 4850 (1977); J. Hubbard, *ibid.*, **68**, 1649 (1978).
6) G. Atkinson and Y. Mori, *J. Phys. Chem.*, **71**, 3523 (1967).
7) N. Takisawa, J. Osugi, and M. Nakahara, *J. Phys. Chem.*, **85**, 3582 (1981).
8) P. G. Wolynes, *J. Chem. Phys.*, **68**, 473 (1978); P. Colonomos and P. G. Wolynes, *ibid.*, **71**, 2644 (1979).
9) A. H. Narten, F. Vaslow, and H. A. Levy, *J. Chem. Phys.*, **58**, 5017 (1973).
10) M. Maeda and H. Ohtaki, *Bull. Chem. Soc. Jpn.*, **48**, 3755 (1975).
11) G. W. Brady, *J. Chem. Phys.*, **28**, 464 (1958).
12) R. M. Lawrence and R. F. Kruh, *J. Chem. Phys.*, **47**, 4758 (1967).
13) J. N. Albright, *J. Chem. Phys.*, **56**, 3783 (1972).
14) R. Caminti, G. Licher, G. Piccaluga, and G. Pinna, *Chem. Phys. Lett.*, **47**, 275 (1977).
15) R. L. Kay and D. F. Evans, *J. Phys. Chem.*, **70**, 2325 (1966) and its references.
16) R. L. Kay, "Water A Comprehensive Treatise," ed by F. Frank, Plenum Press, New York (1973), Vol. 3, Chap. 4, and its references.
17) M. W. Sagal, *J. Chem. Phys.*, **36**, 2437 (1962).
18) "Landolt-Boernstein Tabllen," II Band, 7 Teil, Elektriche Eigenschaften II, Springer-Verlag, Berline (1960).
19) J. Timmermans, "Physico-Chemical Constants of Pure Organic Compounds," Elsevier, Amsterdam (1950).
20) J. Calderwood and C. P. Smyth, *J. Am. Chem. Soc.*, **78**, 1295 (1956).
21) F. J. Moore and I. B. Johns, *J. Am. Chem. Soc.*, **63**, 3336 (1941).
22) R. D. Shannon and C. T. Frewitt, *Acta Crystallogr., Sect. B*, **25**, 925 (1969).
23) L. Pauling, "The Nature of Chemical Bond," 3rd ed, Cornel Univ. Press, Ithaca, New York (1960).
24) P. Walden, *Z. Phys. Chem.*, **55**, 207, 246 (1906).
25) W. M. Latimer, K. S. Pitzer, and C. M. Slansky, *J. Chem. Phys.*, **7**, 108 (1939).
26) R. H. Stokes, *J. Am. Chem. Soc.*, **86**, 979, 982 (1964).
27) C. E. Moore, "Atomic Energy Levels," NBS (1971), Vol. 1.
28) S. Hyodo, unpublished results.

Vibration-rotation Spectra of Formamides

Yoko SUGAWARA,† Yoshiaki HAMADA, and Masamichi TSUBOI*
Faculty of Pharmaceutical Sciences, University of Tokyo, Hongo, Bunkyo-ku, Tokyo 113
(Received October 6, 1982)

Taking advantage of the Fourier transform infrared (FTIR) spectrophotometry in accumulating a very weak available radiation, which comes out from a multiple-reflection-type gas-cell (17 m), we have been able to record the infrared absorption spectrum of formamide ($HCONH_2$ or $DCONH_2$) at room temperature, where its vapor pressure is only 0.1 Torr (1 Torr≈133.322 Pa) in the order of magnitude. From an analysis of the rotational structure (resolution 0.5 cm^{-1}) of the C-H stretching band, a revised set of parameters has been obtained. A Q-branch analysis was made for the $v=2\leftarrow0$ and $v=3\leftarrow1$ bands (resolution 0.24 cm^{-1}) of the amino wagging vibration, where v is its vibrational quantum number. The rotational constants $A-B$ were determined to be 2.0269 cm^{-1} for the $v=2$ state and 1.9990 cm^{-1} for the $v=3$ state, and the transition frequencies 657.7_5 cm^{-1} for $v=2\leftarrow0$ and 769.8_5 cm^{-1} for $v=3\leftarrow1$. On the basis of these new parameter values, a discussion was made of the amino wagging coordinate of this molecule.

The molecular structure of formamide is now precisely known through a microwave study of Hirota *et al.*[1] as well as previous investigations cited by them. The microwave spectrum was observed, not only for the ground-state molecule, but also for a few lower-lying vibrational excited states. It is desirable, however, to observe its vibration-rotation transitions directly by the infrared spectroscopy, to ellucidate intramolecular potential and vibration-rotation interaction in detail. Thanks to the recent FTIR (Fourier transform infrared spectrophotometry) technique, we have succeeded for the first time in observing vibration-rotation spectrum of formamide at room temperature. At room temperature, the vapor pressure of formamide is very low (only 0.1 Torr in the order of magnitude), and an optical path as long as 17 m which is obtained by the use of a multiple-reflection-type gas cell is needed. This causes a very low infrared radiation energy available. By accumulating (1000 times, for example) interferograms of such a weak radiation, however, we could reach a sufficiently good spectrum.

Previous works of the infrared spectrum of formamide vapor were all done at higher temperatures; for example, at 126 °C[2] or 180 °C.[3] At these temperatures, some disturbing emissions, hot-band absorptions, and impurity bands (from decomposition products, *etc.*) may often be generated from the sample system.

Experimental

$HCONH_2$ was purchased from Inumaru Co., Ltd. and $DCONH_2$ from Merck Sharp and Dohme, Canada Ltd. These were used after being dried in vacuum. The sample was placed in a multiple-reflection cell of Wilks Scientific Corporation. Its optical path was set at 17.25 m. Infrared absorption measurement was made with a Nicolet 7199 FT-IR system. The resolution was set at 1.0 cm^{-1} (Figs. 1 and 2), at 0.5 cm^{-1} (Fig. 3), or at 0.24 cm^{-1} (Figs. 4 and 5). For each spectral measurement, the interferometer was scanned 1000 times, and each interferogram was accumulated for Fourier transform.

Results and Interpretations

Whole Vibrational Spectrum. In Figs. 1 and 2, the whole spectra (4000—400 cm^{-1} region) of $HCONH_2$ and $DCONH_2$ are reproduced with a lower dispersion.

For many bands, the fine structures are found to be rather simple. If the band is of A-type or A-B hybrid, the central Q-branch is readily identified. When the Q-branch peaks are sharp enough, the frequencies of such peaks were determined with errors less than ±0.2 cm^{-1}. Therefore, the fundamental frequencies of such bands were determined rather precisely without any detailed analyses (although a slight difference between

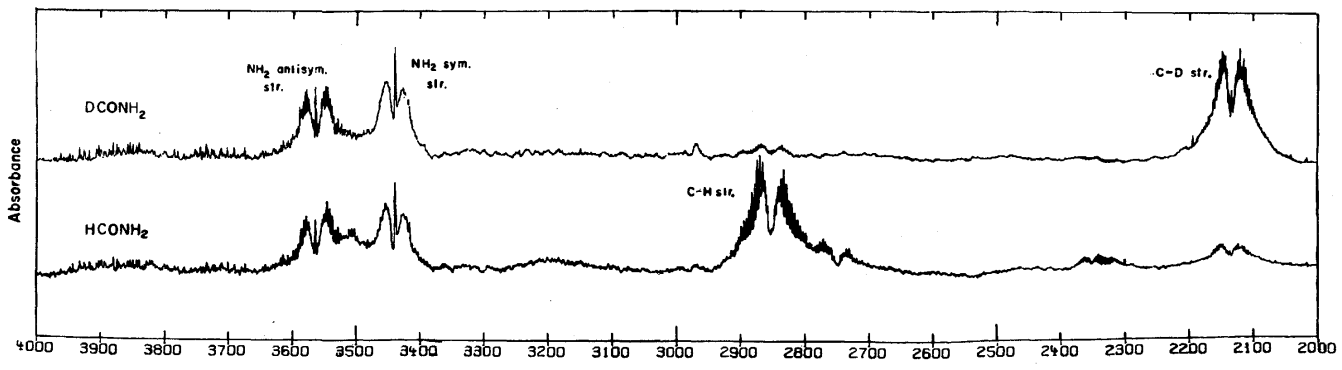

Fig. 1. Infrared absorption spectra (4000—2000 cm^{-1} range) of $HCONH_2$ and $DCONH_2$ in gaseous states. Pressure, vapor pressure at 20 °C. Optical path length, 17.25 m. Resolution, 1.0 cm^{-1}.

† Present address: The Institute of Physical and Chemical Research, Wako, Saitama 351

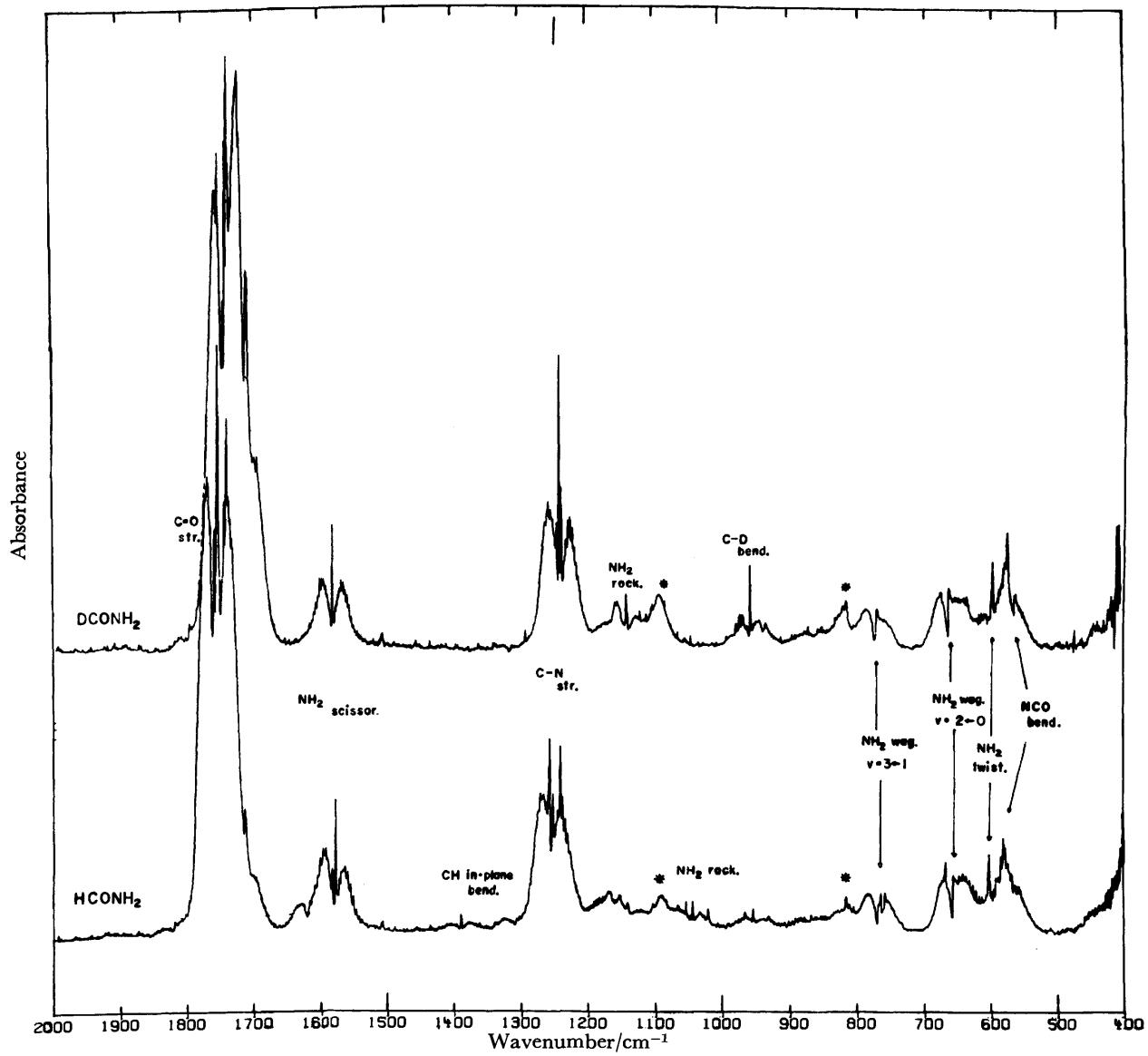

Fig. 2. Infrared absorption spectra (2000—400 cm^{-1} range) of $HCONH_2$ and $DCONH_2$ in gaseous states. Pressure, vapor pressure at 20 °C. Optical path length, 17.25 m. Resolution, 1.0 cm^{-1}. The peaks with* are probably due to impurity.

the Q-peak and band center frequencies must be taken into account). For other bands, however, some ambiguity (given in the footnotes of Table 1) remains in locating the band centers, and therefore in fixing the fundamental frequencies with any greater accuracy than ± 1 cm^{-1}. In Table 1, the fundamental frequencies are listed with these uneven accuracies. The data in the table will be useful in a detailed study of the force field of this molecule in its completely free state.[4]

CH Stretching Band. The band at 2854 cm^{-1}, assignable to the C–H stretching vibration of $HCONH_2$, is an example of what shows relatively simple structure, as shown in Fig. 3. This is a nearly pure B-type band. This is understandable because the C–H bond is directed nearly along the B axis of the molecule. The band consists of a progression of peaks assignable to Q-branch clusters, whose J-structures are not resolved because $\bar{B}'-\bar{B}''$ is small. Evans[2] reported his analysis of this progression with a lower resolution, and we now revise it as follows: Our new K-numbering is given in Fig. 3; this was fixed by forming combination differences for a few trial sets of assignments. As may be seen in the figure, ${}^{R}Q_9$ and ${}^{P}Q_{11}$ peaks are both broader and lower than the neighboring peaks. This probably means that the upper $K'=10$ state has an anomaly. Such a correspondence (of ${}^{R}Q_9$ and ${}^{P}Q_{11}$), on the other hand, may be taken as another support to the assignment. By assuming that the rotational energy is given by $(A-\bar{B})K^2-D_KK^4$, combination relation,

$$({}^{R}Q_K-{}^{P}Q_K)/4K = (A'-\bar{B}') + D_K(2K^2+2) \qquad (1)$$

is derived, where the centrifugal distortion constant D_K is assumed to have an equal value in the upper state to that in the lower state. By the use of this relation, the upper state rotational constant $A'-\bar{B}'$ has been determined to be 2.060 ± 0.003 cm^{-1}, and $D_K=(0.38\pm 0.04)\times 10^{-4}$ cm^{-1}. From a similar combination relation, the lower state rotational constant $A''-\bar{B}''$ came out to be 2.070 ± 0.003 cm^{-1}, which is in agreement with what was determined by the microwave spectroscopy

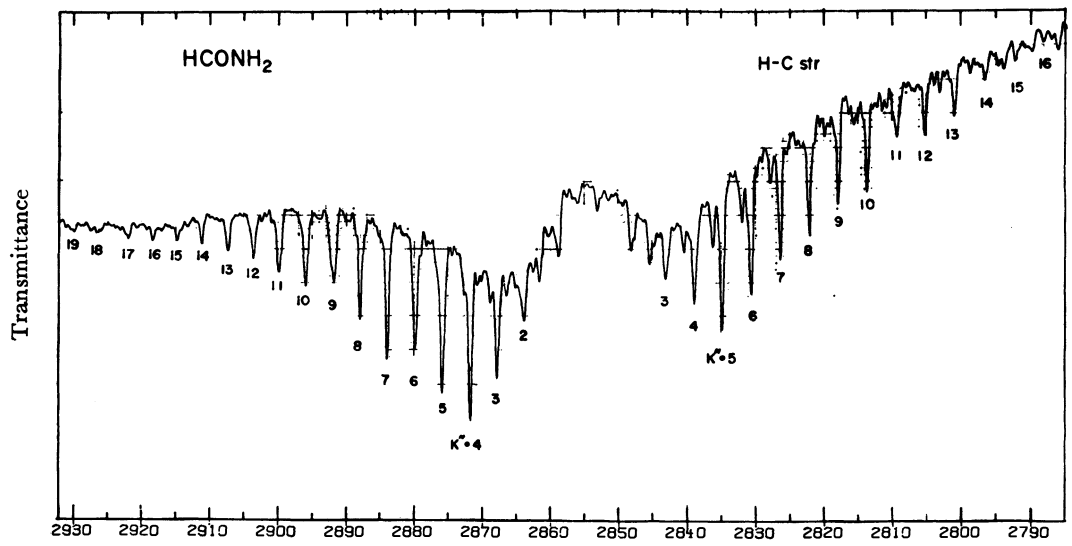

Fig. 3. Fine structure of the absorption band of $HCONH_2$ at 2854 cm^{-1} assignable to the C–H stretching vibration. At the vapor pressure of 20 °C. Optical path length, 17.25 m. Resolution, 0.5 cm^{-1}.

Table 1. Observed frequencies assignable to the fundamental vibrations of $HCONH_2$ and $DCONH_2$

Frequency ν/ cm^{-1}		Assignment[a]
$HCONH_2$	$DCONH_2$	
In-plane modes		
3563.5	3563.2	NH_2 antisym. stretching
3439.3	3437.8	NH_2 sym. stretching
2853.6		CH stretching
	2135.0	CD stretching
1754.1	1739.6	CO stretching
1576.9	1582.4	NH_2 scissoring
1390.2		CH bending
	955.0	CD bending
1258.2	1241.8	CN stretching
1045.6[b]	1142.4	NH_2 rocking
581[c]	563[c]	NCO bending
Out-of-plane modes		
1021.2[d]		CH out-of-plane deformation
	——[e]	CD out-of-plane deformation
602.8[c]	591.4[c]	NH_2 twisting
(288.7)[f]		NH_2 wagging

a) Ref. 4. b) Band shape is anomalous, probably for a Coriolis coupling with the $v=3$ level of NH_2 wagging. c) NCO bending and NH_2 twisting levels are considered to be involved in a Coriolis interaction, and therefore no reliable band center determination is possible for these bands in our present resolution. d) The assignment is not sufficiently supported. e) CD out-of-plane deformation band is considered to be too weak for our present observation or hidden under another band. f) Not observed in the present study. This is what was observed by King[3].

(2.0705 cm^{-1}). Finally, the band center frequency has been determined with a considerable precision: $\nu_0 = 2853.63 \pm 0.10$ cm^{-1}.

Overtone Bands of Amino Wagging Vibration. King[3] observed the far-infrared spectrum of $HCONH_2$ in the 200—450 cm^{-1} region, and found three peaks at 288.7, 368.6, and 401 cm^{-1}. These were assigned by Hirota *et al.*[1] respectively to the $v=1\leftarrow0$, $2\leftarrow1$, and $3\leftarrow2$ transitions of the amino wagging vibration. They also proposed[1] to assign a band at 660 cm^{-1} reported by King[3] to $v=2\leftarrow0$ and that at 770 cm^{-1} to $v=3\leftarrow1$ of the amino wagging vibration. These two bands have been observed in our present study with a higher resolution (0.24 cm^{-1}) and with an expanded wavenumber scale. The results are reproduced in Figs. 4 and 5. It is readily seen that both of these are primarily A-type bands; P and R progressions with apparent average spacings of about 0.7 cm^{-1}, which is nearly equal to $2\bar{B}$, are recognized. It is noticeable that the central Q-branch absorption shows a distinct K-structure in each of these two bands. This fact means that the rotational constant $A-\bar{B}$ is appreciably different in the upper amino wagging state from that in the lower state. The K-numbering given in Figs. 4 and 5 was fixed by calculating simulation spectra with a number of trial sets of rotational constants, and by comparing the calculated intensity distribution among the Q-branch lines with what was observed. The calculation was made with a HITAC M200-H in the Computer Center, University of Tokyo, by the use of programs BC2 and ENVLOP written by Dr. T. Nakagawa, and our own plotter program. The frequency of each of these ${}^{Q}Q_K$ peaks is approximately given by

$$ {}^{Q}Q_K = \nu_0 + [(A'-\bar{B}')-(A''-\bar{B}'')]K^2, \qquad (2) $$

and practically independent of the $\bar{B}'$ and $B'-C'$ values. Because the $A''-\bar{B}''$ values (for $v=0$ and 1) are known,[1] the band center ν_0 and $A'-\bar{B}'$ are readily fixed:

$\nu_0 = 657.7_5$ cm^{-1} for the $v = 2 \leftarrow 0$ band,

$\nu_0 = 769.8_5$ cm^{-1} for the $v = 3 \leftarrow 1$ band,

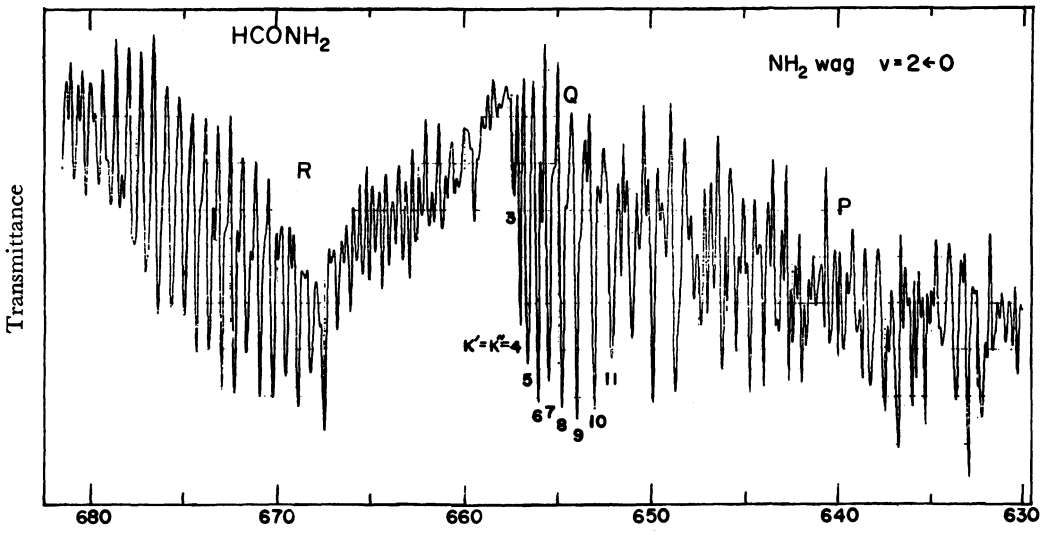

Fig. 4. Fine structure of the absorption band of $HCONH_2$ at 658 cm^{-1} assignable to the $v=2\leftarrow0$ transition of the amino wagging vibration. At the vapor pressure of 20 °C. Optical path length, 17.25 m. Resolution, 0.24 cm^{-1}.

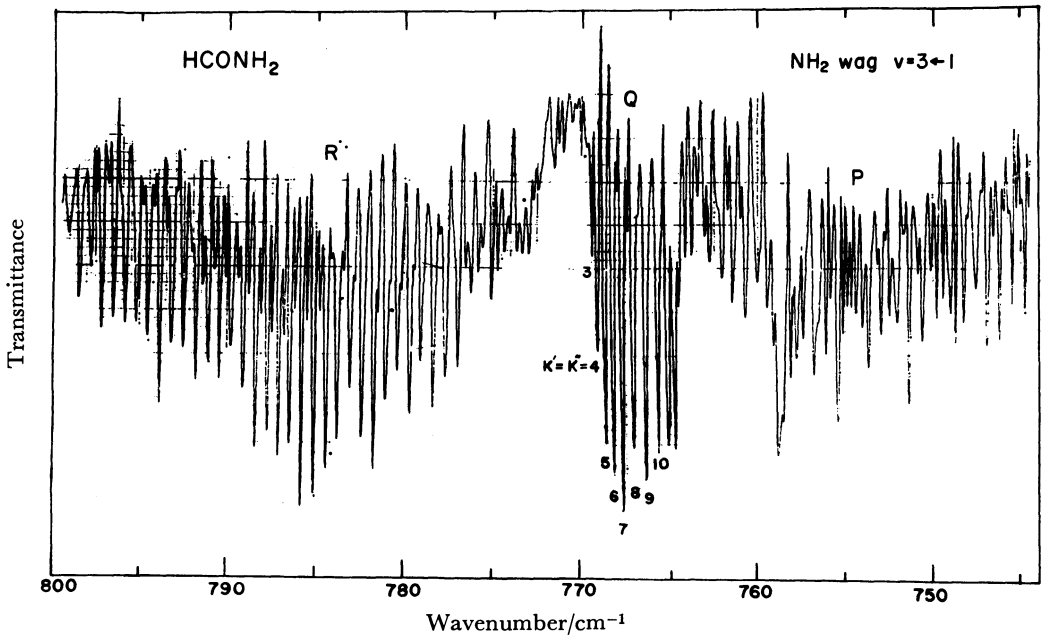

Fig. 5. Fine structure of the absorption band of $HCONH_2$ at 770 cm^{-1} assignable to the $v=3\leftarrow1$ transition of the amino wagging vibration. At the vapor pressure of 20 °C. Optical path length, 17.25 m. Resolution, 0.24 cm^{-1}.

$A - \bar{B} = 2.0269\ cm^{-1}$ for the $v = 2$ state,

and

$A - \bar{B} = 1.9990\ cm^{-1}$ for the $v = 3$ state.

It should be pointed out that an anomaly in the Q-branch progression of the $v=3\leftarrow1$ band is apparent at $K=11$, 12, and a few subsequent K values. Here, the spacings are smaller than they ought to be and intensity distribution is also different from what is expected (see Fig. 5). This is considered to be caused by an A axis ($\Delta K=0$) Coriolis coupling between the $v=3$ level (A'', at 1058 cm^{-1}) of the amino wagging vibration, now in question, and the first excited state (A', at 1045 cm^{-1}) of the amino rocking vibration. If the $A-\bar{B}$ value in the latter state is assumed to be 2.0719 cm^{-1} (equal to the $A-\bar{B}$ value of the ground vibrational state), the accidental coincidence of the unperturbed rotational levels should take place at about $K=14$ of the two vibrational states. The observed band shape of the 1045 cm^{-1} band is also anomalous.

Next an estimation of the $\bar{B}'$ values was made. The $\bar{B}'$ value is reflected in the apparent spacing of the P branch progression. Because of the K-structure of each P branch ($\Delta J=-1$) transition, however, the apparent spacing is not simply correlated to the rotational constants $\bar{B}'$. We have to repeat trial calculation with a

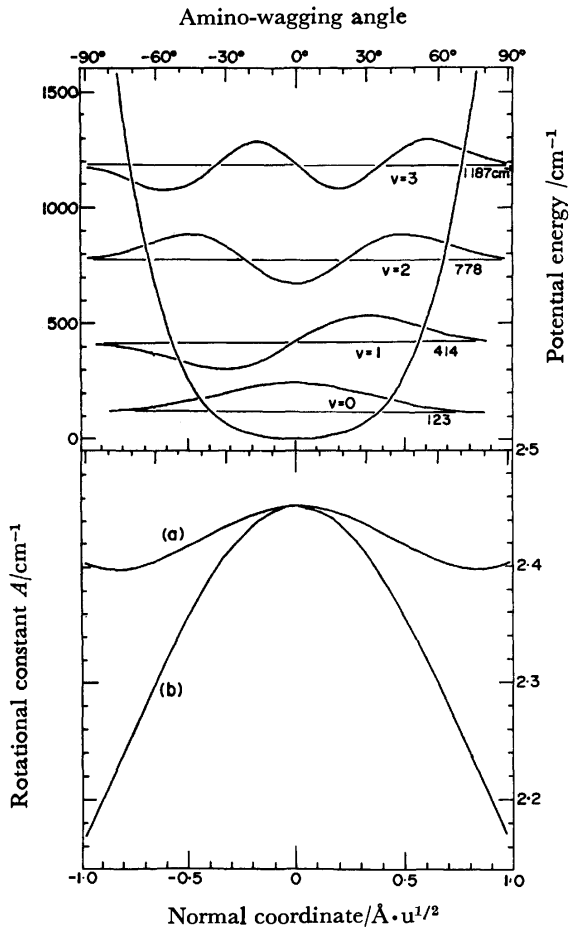

Fig. 6. (Upper) Amino wagging potential function, energy levels, and eigenfunctions of $HCONH_2$. (Lower) Rotational constant A as a function of amino wagging coordinate τ. (a) Calculated on an assumption that, in the "amino wagging motion," only the angle between the OCN plane and the bisector of $\angle$HNH changes, while all the bond lengths and bond angles (except CNH's) are kept unchanged. (b) Calculated by Eq. 5, which was derived to fit the calculated A_v's to the observed (A_v's).

trial $\bar{B}'$ value and with the known $A'-\bar{B}'$ value. Calculation indicates, for example, that in the 670—680 cm^{-1} spectral range 20 main spacings should be involved if $\bar{B}$ (at $v=2$) is assumed to be 0.3505 cm^{-1}, 17 spacings for $\bar{B}$ ($v=2$)=0.3518 cm^{-1}, 15 for $\bar{B}$ ($v=2$)=0.3537 cm^{-1}, and 14 for $\bar{B}$ ($v=2$)=0.3547 cm^{-1}. In the observed spectrum, there are 15 spacings involved in this spectral range (see Fig. 4). In this way we may reach a conclusion that $\bar{B}$ (at $v=2$)=0.3537$\pm$0.0005 cm^{-1}. Likewise, by examining the P branch progression in the 780—790 cm^{-1} spectral range, we know that $\bar{B}$ (at $v=3$)=0.3534$\pm$0.0005 cm^{-1}.

Discussion

One of the interesting problems in the formamide molecule is concerned with the large amplitude motion along the amino wagging coordinate. It has nearly been established that the equilibrium conformation of the molecule is planar.[1] The arrangement of the amino wagging levels (which has now been precisely determined) indicates, however, that the potential function (V) of this out-of-plane motion is severely anharmonic. It involves the fourth power of the amino wagging coordinate (τ) besides the quardratic term, and it is approximately given as,

$$V = V_2\tau^2 + V_4\tau^4. \quad (3)$$

A Hamiltonian with this potential was solved as will be detailed below, and by a least squares fit for the four energy levels ($v=0$, 1, 2, and 3) the coefficients were fixed as $V_2=156$ cm^{-1}/radian^2 and $V_4=410$ cm^{-1}/radian^4. This is close to what Hirota *et al.*[1] gave, but this gives a slightly better fit for the observed levels with $v=2$ and 3. The eigenvalues and eigenfunctions $\phi_v(\tau)$. of the amino wagging Hamiltonian with the potential energy of Eq. 3 are illustrated in the upper half of Fig. 6. In the calculation, the Hamiltonian matrix was represented by the use of proper harmonic oscillator basis functions. If the order of matrix is taken sufficiently large, the eigenvalues and eigenfunctions of lower levels are found independent of the frequency of the basis harmonic oscillator itself. For example, the eigenvalues and eigenfunctions of the lower four levels, shown in Fig. 6, were obtained by diagonalizing a 40×40 Hamiltonian matrix in the representation of the harmonic oscillator with its frequency 156 cm^{-1}. These were found to be exactly equal (over the four significant figures) to those obtained by diagonalizing a 40×40 matrix in the representation of the harmonic oscillator with 300 cm^{-1}.

Let us now proceed with an examination of the amino wagging coordinate, τ. Let us assume, for trial, that τ is equal to the angle between the OCN plane and the bisector of $\angle$HNH. The rotational constant A has been calculated, for trial, at various τ values (0°—90°) by keeping all the bond lengths and bond angles (other than $\angle$CNH's) at the values given by Hirota *et al.*[1] The result is shown in the lower portion of Fig. 6 (curve (a)). On the basis of this $A-\tau$ relation, the average rotational constant at each wagging level can be calculated by

$$A_v = \int_{-\pi}^{\pi} \phi_v(\tau)A(\tau)\phi_v(\tau)d\tau, \quad (4)$$

where $v=0$, 1, 2, and 3. The result is given in the fifth column of Table 2. As may be seen here, the calculated A_v's show desperate disagreement with the observed A_v's. This means that the actual amino wagging motion is greatly different from the mere out-of-plane motion of the NH_2 triangle.

We next inquire: what $A-\tau$ relation can fit the observed A_v values (for $v=0$, 1, 2, and 3)? By expressing A by a power series of τ, a least squares fit resulted in the following expression:

$$A = 2.4520 - 0.1555\tau^2 + 0.01667\tau^4, \quad (5)$$

where A is given in cm^{-1} and τ in radian. This $A-\tau$ relation is shown by curve (b) in Fig. 6. The A_v values obtained by Eq. 4 with this $A-\tau$ relation (Eq. 5) are given in the last column of Table 2. The fit of the calculated A_v values to the observed A_v has certainly been improved. Comparing the curve (a) with (b) in Fig. 6, we now conclude that a large displacement along the amino wagging coordinate causes a great lowering of

TABLE 2. ROTATIONAL CONSTANTS (IN cm^{-1}) OF $HCONH_2$

Vibrational level[a)]	$A-B$ observed	B observed	A observed	A calculated (a)[c)]	A calculated(b)[d)]
$v=0$	2.071873[b)]	0.3537024[b)]	2.425575[b)]	2.4435	2.4298
1	2.039523[b)]	0.3534253[b)]	2.392948[b)]	2.4314	2.3955
2	2.0269	0.353_7	2.380_6	2.4254	2.3737
3	1.9990	0.353_4	2.352_4	2.4206	2.3557

a) v is the vibrational quantum number of the amino wagging vibration. b) Determined by Hirota *et al.*[1] by microwave spectroscopy. c) Calculated from the A-τ relation given by the curve (a) of Fig. 6 by Eq. 4. d) Calculated from the A-τ relation given by the curve (b) of Fig. 6 by Eq. 4.

A value (*i.e.*, a great increase of the moment of inertia I_A); the amount of lowering is much greater than that expected for a simple out-of-plane bending of the NH_2 triangle. In other words, this bending motion must be accompanied by appreciable amounts of stretching of some bonds and opening of some angles. Such a coupling of the out-of-plane wagging and in-plane modes may be mainly caused, as Hirota *et al.*[1] pointed out, by anharmonic potential constants. As they also showed, a coupling may partly be caused by a Coriolis force. It should be pointed out, however, that the partner level of an A axis Coriolis coupling should have A'' symmetry for the $v=2$ wagging level (A'), whereas A' symmetry for the $v=3$ wagging level (A'').

This work was partly done in the Institute for Molecular Science, Myodaiji, Okazaki 444, in the period (April 1979—March 1981) in which M. Tsuboi was an Adjunct Professor there. We wish to express our sincere thanks to Professor E. Hirota, late Professor T. Fujiyama, Mr. S. Hyodo, and Mr. S. Sofue for their kind help and valuable discussions. This work was supported by the Joint Studies Program (1980—1981) of the Institute for Molecular Science. Some of our preliminary experiments were made in Faculty of Pharmaceutical Sciences, University of Tokyo, by the use of a Digilab FTS-14 system. In this experiment, we thank Professor S. Tanaka and Dr. T. Matsui (Faculty of Engineering, University of Tokyo) for their kindness in our use of their Wilks multiple reflection cell.

References

1) E. Hirota, R. Sugisaki, C.J. Nielsen, and G.O. Sørensen, *J. Mol. Spectrosc.*, **49**, 251 (1974).
2) J. C. Evans, *J. Chem. Phys.*, **22**, 1228 (1954); **31**, 1435 (1959).
3) S. T. King, *J. Phys. Chem.*, **75**, 405 (1971).
4) Y. Sugawara, Y. Hamada, A. Y. Hirakawa, M. Tsuboi, S. Kato, and K. Morokuma, *Chem. Phys.*, **50**, 105 (1980).

 © 1983 The Chemical Society of Japan Bull. Chem. Soc. Jpn., 56, 1051—1056 (1983)

Cobalt(III) Complexes with Quadridentate Ligands. III.[1] The Preparation and Properties of the Salicylato or Dichloro(quadridentate amine)cobalt(III) Complexes

Yoshihisa YAMAMOTO,* Hiroko KUDO, and Eiko TOYOTA

Faculty of Pharmaceutical Sciences, Higashi Nippon Gakuen University, Ishikari-Tobetsu, Hokkaido 061-02

(Received July 20, 1982)

In the ^{1}H and ^{13}C NMR spectra of *trans*- or *cis*-dichloro(quadridentate amine)cobalt(III) chloride hydrates, $[CoCl_2L]Cl \cdot nH_2O$ (L: 2,2,2-tet(trien) (**1a**), 2,3,2-tet (**1b**), 3,2,3-tet (**1c**), and 3,3,3-tet (**1d**)), the signals of their methylene protons and methylene carbons have been assigned to the individual methylene protons and methylene carbon of the coordinated quadridentate amine ligands. The order of ^{1}H and ^{13}C chemical shift of their methylene protons and methylene carbon is as follows:

$$NH_2\underline{CH_2}(CH_2)_n\underline{CH_2}NH\underline{CH_2}- < NH_2\underline{CH_2}(CH_2)_n\underline{CH_2}NH < NH_m\underline{CH_2}\underline{CH_2}\underline{CH_2}NH \quad \begin{pmatrix} m: 1 \text{ or } 2 \\ n: 0 \text{ or } 1 \end{pmatrix}$$

NH-side methylene protons (or carbon); NH_2-side methylene protons (or carbon); Center methylene protons (or carbon)

Thus, the signal of the center methylene protons (or carbon) of the coordinated quadridentate amine ligands appears at higher field than that of the NH-side methylene protons (or carbon). *cis*-β_1-Salicylato(3,7-diazanonane-1,9-diamine)cobalt(III) chloride hydrate, *cis*-β_1-[Co(sal)(2,3,2-tet)]Cl·H_2O (**3b**), and *cis*-β_2-salicylato(quadridentate amine)cobalt(III) chloride hydrates, *cis*-β_2-[Co(sal)L]Cl·nH_2O (L: 2,3,2-tet (**4b**), 3,2,3-tet (**4c**) and 3,3,3-tet (**4d**)) have been isolated from a reaction mixture of sodium salicylate or salicylic acid and **1b—d**. The properties of **3b** and **4b** are similar to those of the previously reported complexes **3a** (L: 2,2,2-tet, β_1-form) and **4a** (L: 2,2,2-tet, β_2-form), respectively. Those of **4c** are similar to those of **4d**. Complex **4d** is the most unstable complex among **4a—d**. This property is attributable to the center methylenes of the coordinated quadridentate amine ligands.

Many investigations of metal complexes with quadridentate amine ligands, *e.g.*, with 2,2,2-tet(trien), 2,3,2-tet, and 3,3,3-tet, have been reported especially in the field of stereochemistry[2-7] and NMR spectra.[7-13] In the NMR spectra, the investigations of methylene protons and methylene carbons of the coordinated quadridentate amine ligands in complexes have received little attention. This is probably because the methylene proton and methylene carbon signals of the coordinated quadridentate amine ligands are close together, and they have not previously assigned separately.

Previous paper[11] has been concerned with the preparation and properties of the *cis*-β_1 and *cis*-β_2-[Co(sal)(2,2,2-tet)]Cl·H_2O. The present paper deals with the assignments of the methylene protons and methylene carbons of the coordinated quadridentate amine ligands of *trans*- or *cis*-$[CoCl_2L]Cl \cdot nH_2O$ (L: 2,2,2-tet, 2,3,2-tet, 3,2,3-tet, and 3,3,3-tet) on their NMR spectra, and deals with the preparation and properties of the *cis*-β_1-[Co(sal)(2,3,2-tet)]Cl·H_2O, and *cis*-β_2-[Co(sal)L]Cl·nH_2O (L: 2,3,2-tet, 3,2,3-tet, and 3,3,3-tet).

Results and Discussion

cis-*α*-*Dichloro(3,6-diazaoctane-1,8-diamine)cobalt(III) Chloride*, *[$CoCl_2$(2,2,2-tet)]Cl (**1a**) and* trans-*Dichloro(quadridentate amine)cobalt(III) Chloride Hydrates*, *[$CoCl_2$-L]Cl·nH_2O L: 2,3,2-tet*, n=*2.5 (**1b**)*; *L: 3,2,3-tet*, n=*1 (**1c**)*; *and L: 3,3,3-tet*, n=*1 (**1d**)*: The ^{1}H NMR spectra of **1a—d** were measured in 0.01 and 1.8 mol dm^{-3} D_2SO_4. The methylene proton signals of the coordinated quadridentate amine ligands in **1a—d** can be divided into three groups at 1.5—2.4, 2.3—3.0, and 2.8—3.8 ppm as shown in Fig. 1 and Table 1. The signals (1.5—2.4 ppm) at highest field of **1b—d** can be assigned to the center methylene protons ($NHCH_2C\underline{H_2}$-$CH_2NH_{1\text{ or }2}$) of the ligands, because the total number of the center methylene protons of **1b**, **1c**, and **1d** is 2, 4, and 6, respectively. The signals at 2.3—3.0 ppm (4H) of **1a**, **1b**, and **1d** can be assigned to the NH_2-side methylene protons ($NHCH_2(CH_2)_nC\underline{H_2}NH_2$ *n*: 0 or 1), and the signals (2.8—3.8 ppm, 8H) at a low field of **1a**, **1b** and **1d** are assigned to the NH-side methylene protons ($-C\underline{H_2}NHC\underline{H_2}(CH_2)_nCH_2NH_2$ *n*: 0 or 1) of the quadridentate ligands. The difference of chemical shifts of the NH_2 and NH-side methylene protons can be attributed to the properties of the terminal NH_2 and secondary NH. Thus, the order of the ^{1}H chemical shifts is given as Scheme 1.

$$NH_2CH_2(CH_2)_n\underline{CH_2}NH\underline{CH_2}- < NH_2\underline{CH_2}(CH_2)_nCH_2NH < NH_m\underline{CH_2}\underline{CH_2}CH_2NH \quad \begin{pmatrix} m: 1 \text{ or } 2 \\ n: 0 \text{ or } 1 \end{pmatrix}$$

NH-side methylene protons; NH_2-side methylene protons; Center methylene protons

Scheme 1.

The ^{1}H NMR spectra of the *trans*-dichloro(2,2,2-tet)-cobalt(III) chloride hydrate hydrochloric acid, *trans*-$[CoCl_2$(2,2,2-tet)]Cl·H_2O·HCl (**2a**), could not be measured in DMSO-d_6, CF_3COOH, 0.01, 0.1 and 1.8 mol dm^{-3} D_2SO_4, because of isomerization to the *cis*-form. The chemical shifts of the terminal NH_2 protons and secondary NH protons of **1a—d** are collected in Table 1.

The ^{13}C NMR spectra of **1b—d** were measured in D_2O. Both the signal at 28.8 ppm of **1b** and that at 23.5 ppm of **1d** can be assigned to the center methylene carbon (C-5) of the quadridentate ligands as shown in

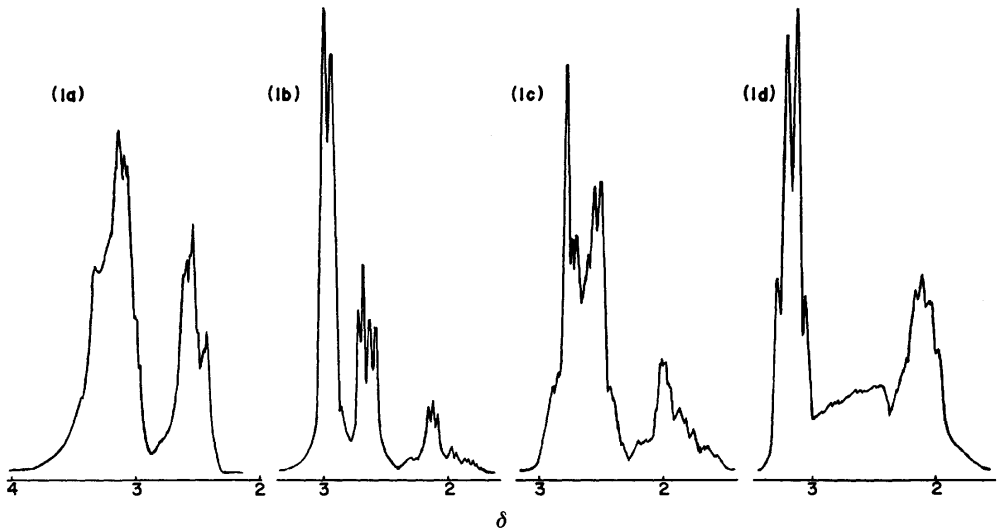

Fig. 1. The ^{1}H NMR spectra of **1a**—**d** complexes. (**1a**): *cis*-*a*-[$CoCl_2$(2,2,2-tet)]Cl in 0.01 mol dm^{-3} D_2SO_4. (**1b**): *trans*-[$CoCl_2$(2,3,2-tet)]Cl·2.5H_2O in 0.01 mol dm^{-3} D_2SO_4. (**1c**): *trans*-[$CoCl_2$(3,2,3-tet)]Cl·H_2O in 0.01 mol dm^{-3} D_2SO_4. (**1d**): *trans*-[$CoCl_2$(3,3,3-tet)]Cl·H_2O in 1.8 mol dm^{-3} D_2SO_4.

TABLE 1. ^{1}H NMR SPECTRA OF COMPLEXES **1a**—**d**. **3a**. **3b**. AND **4a**—**d**

Complex No.	Center methylene protons $NHCH_2\underline{CH_2}CH_2NH_2$ $NHCH_2\underline{CH_2}CH_2NH$ δ	NH_2-side methylene protons $NHCH_2\underline{CH_2}NH_2$ $NHCH_2CH_2\underline{CH_2}NH_2$ δ	NH-side methylene protons $-\underline{CH_2}NHCH_2CH_2NH_2$ $-CH_2NH\underline{CH_2}CH_2\underline{CH_2}NH_2$ δ	$[NH_2]$ $N(1)H_2$ δ	$[NH]$ $N(4)H_q$ δ	N(3)H δ	[N(2)H+Salicylato] N(2)H δ	[N(2)H+Salicylato] Salicylato δ	Solvents
1a	—	2.3—2.9(4H)	2.9—3.8(8H)	[5.6(4H)]	[6.1(2H)]				1
1b	1.7—2.4(2H)	2.4—2.8(4H)	2.8—3.3(8H)	[5.3(4H)]	[6.0(2H)]				1
1c	1.5—2.3(4H)	2.3—3.0(12H)		[4.9(4H)]	[5.9(2H)]				1
1d	1.7—2.4(6H)	2.4—3.0(4H)	3.0—3.4(8H)	[4.7(4H)]	[5.1(2H)]				2
3a[a]	—	2.39—3.76(12H)		4.34(1H) 4.57(1H)	4.81(1H) 5.23(1H)	6.20(1H)	6.51(1H)	6.66—8.00(4H)	2
3b	1.68—2.29(2H)	2.29—3.30(12H)		4.12(2H)	5.13(3H)		6.25(1H)	6.51—7.89(4H)	2
4a[a]	—	2.38—2.80(3H)	2.80—3.80(9H)	4.34(2H)	4.76(1H) 5.21(1H)	6.07(1H)	[6.49—7.97(5H)]		2
4b	1.71—2.01(2H)	2.01—2.45(3H)	2.45—3.18(9H)	4.35(2H)	4.86(2H)	5.20(1H)	6.32(1H)	6.55—7.85(4H)	2
4c	1.44—1.97(4H)	1.97—2.40(3H)	2.40—3.20(9H)	3.32(1H) 4.14(1H)	4.71(2H)	5.12(1H)	6.31(1H)	6.57—7.92(4H)	2
4d	1.48—2.24(9H)		2.24—3.23(9H)	3.54—3.97(1H)	3.97—4.93(4H)		5.21(1H)	6.57—7.91(4H)	2

Solvents: 1) 0.01 mol dm^{-1} D_2SO_4; 2) 1.8 mol dm^{-3} D_2SO_4.
Standard: internal DSS. a) Ref. 11.

TABLE 2. ^{13}C NMR SPECTRA OF COMPLEXES **1b**—**d** AND **4a**—**d**

Complex No.	Center methylene carbon δ		NH_2-side methylene carbon δ	NH-side methylene carbon δ	
	C-5	C-2 and C-8	C-1 and C-9	C-3 and C-7,	C-4 and C-6
1b	28.8	—	43.3	55.6	49.1
1c	—	27.7	39.8	49.4	53.3
1d	23.5	24.6	37.5	45.6	45.6
4a	—	—	[42.0, 47.5]	[48.3, 49.7,	52.1, 52.7]
4b	23.6	—	43.1	[51.0, 55.3]	[45.7, 47.2]
4c	—	[21.9, 27.2]	[37.0, 38.5]	[45.2, 47.6]	[48.3, 52.9]
4d	22.9	[24.5, 26.3]	[37.8, 38.8]	[47.3, 49.5,	50.4, 52.8]

Solvent: D_2O, internal dioxane (δ=67.4 ppm). [ ]: The chemical shifts could not be assigned to the individual methylene carbon.

Fig. 2. The signals at 27.7 ppm of **1c** and at 24.6 ppm of **1d** can be assigned to the center methylene carbons (C-2 and C-8) of the ligands. In the **1d** complex, the intensity ratio of the two signals at 37.5 and 45.6 ppm is 1 : 2. The signal at 37.5 ppm can be assigned to the NH_2-side methylene carbons (C-1 and C-9) of the coordinated 3,3,3-tet ligand, and the signal at 45.6 ppm can be assigned to the NH-side methylene carbons (C-3, C-4, C-6, and C-7) of that ligand. Thus, the signal of the NH_2-side methylene carbons of the quadridentate ligands is observed at higher field than that of the NH-side methylene carbons. The signal at 49.1 ppm of **1b** may be assigned to C-4 and C-6 methylene carbons (neighboring methylene carbons of center

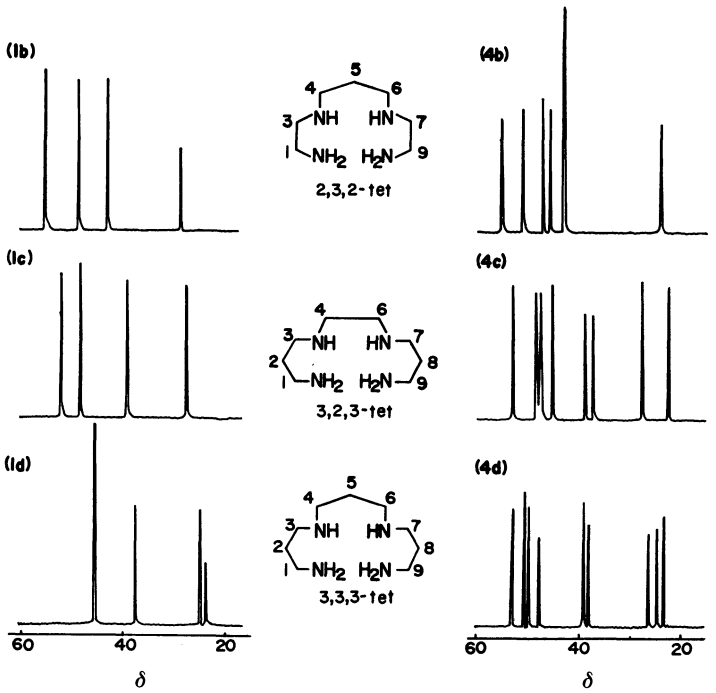

Fig. 2. The ^{13}C NMR spectra of **1b—d** and **4b—d** complexes in D_2O. (**1b**): *trans*-[$CoCl_2$(2,3,2-tet)]Cl·2.5H_2O. (**1c**): *trans*-[$CoCl_2$-(3,2,3-tet)]Cl·H_2O. (**1d**): *trans*-[$CoCl_2$(3,3,3-tet)]Cl·H_2O. (**4b**): *cis*-β_2-[Co(sal)(2,3,2-tet)]Cl·2H_2O. (**4c**): *cis*-β_2-[Co(sal)(3,2,3-tet)]-Cl·3H_2O. (**4d**): *cis*-β_2-[Co(sal)(3,3,3-tet)]Cl·H_2O.

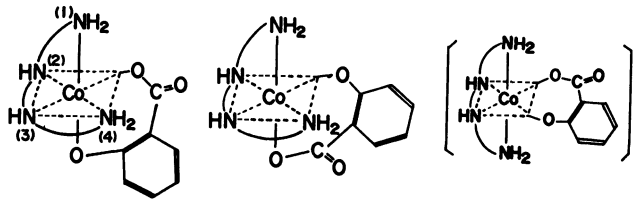

β_1 β_2 α

Fig. 3. The *cis*-α, β_1 and β_2 configurations of [Co(sal)-(quadridentate amine)]Cl·nH_2O.

methylene carbon of C-5) of coordinated 2,3,2-tet ligand, and the signal at 49.4 ppm of **1c** is assigned to C-3 and C-7 methylene carbons of coordinated 3,2,3-tet ligand. Thus, the order of the ^{13}C chemical shifts of the methylene carbon signals of the quadridentate ligands in **1b—d** is given as Scheme 2. This order is similar to that of ^1H NMR spectra. The ^{13}C NMR spectral data are collected in Table 2.

$NH_2CH_2\underline{C}H_2NH\langle NH_2CH_2CH_2\underline{C}H_2NH$
$NHCH_2\underline{C}H_2NH\rangle NHCH_2CH_2\underline{C}H_2NH$

NH-side methylene carbon

$\langle NH_2\underline{C}H_2CH_2NH$
$NH_2\underline{C}H_2CH_2CH_2NH\rangle$

NH_2-side methylene carbon

$\langle NH_2CH_2\underline{C}H_2CH_2NH\langle NHCH_2\underline{C}H_2CH_2NH$

Center methylene cabon

Scheme 2.

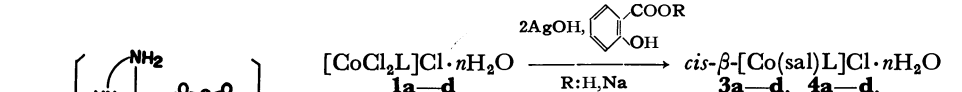

[$CoCl_2$L]Cl·nH_2O (**1a—d**) → *cis*-β-[Co(sal)L]Cl·nH_2O (**3a—d**, **4a—d**,)

	Form	L	*n*
3a		2,2,2-tet	1
3b	β_1	2,3,2-tet	1
3c		3,2,3-tet	
3d		3,3,3-tet	
4a		2,2,2-tet	1
4b	β_2	2,3,2-tet	2
4c		3,2,3-tet	3
4d		3,3,3-tet	1

cis-β_1-*Salicylato(quadridentate amine)cobalt(III) Chloride Hydrate(**3a—d**), and* cis-β_2-*Salicylato(quadridentate amine)-cobalt(III) Chloride Hydrates (**4a—d**)*: Complexes **3b** and **4b—d** have been isolated from a reaction mixture of AgOH, salicylic acid or sodium salicylate and **1b—d**. Salicylato(quadridentate amine)cobalt(III) complexes have three isomeric forms of *cis*-α, *cis*-β_1, and *cis*-β_2 as shown in Fig. 3. The α-form could not be obtained at pH 2—8.[7] The separation of β_1 and β_2-forms was attempted by using ion exchange resin.[11,14] The isolation of **3c** and **3d** from the reaction mixtures was difficult. Complexes **3b** and **4b—d** are soluble in water, acid solvents, DMSO and methanol, but are insoluble in the common organic solvents.

The IR spectra of **3b** and **4b—d** showed 4—5 absorption bands in the 3000—3300 cm^{-1} region and 6 absorption bands in the 990—1100 cm^{-1} region as

TABLE 3. SOME PHYSICAL PROPERTIES OF **3b** AND **4b—d** COMPLEXES

Complex No.	IR spectra $\tilde{\nu}$/cm^{-1} 990—1100 cm^{-1}	Absorption bands λ/nm	ε	Electric conductivity of aqueous solution S cm^2 equiv.$^{-1}$
3b	1005(s), 1017(sh), 1025(vs)	333	2210[1]	106
	1055(vs), 1070(sh), 1087(s)	530	224	
4b	1000(s), 1014(s), 1022(vs)	333	2540[1]	98
	1036(vs), 1060(vs), 1090(vs)	525	241	
4c	1018(m), 1029(s), 1040(vs)	335	2420[1]	100
	1048(vs), 1058(s), 1077(m)	533	217	
4d	985(m), 1028(vs), 1038(s)	335	2400[1]	96
	1050(s), 1068(sh), 1092(m)	550	189	

Solvent: 1) H_2O.

shown in Table 3. This indicates that these complexes assume the β-form.[11,15,16]

The ^{1}H NMR spectra of **3a**, **3b**, and **4a—d** were measured in 1.8 mol dm^{-3} D_2SO_4. The signals of the center methylene protons, NH_2-side methylene protons and NH-side methylene protons of **4a—d** have been assigned by the comparison with those of **1a—d**. In complexes **4b—d**, the intensity ratio of two methylene proton signals at 2.0—2.4 and 2.2—3.2 ppm of the quadridentate ligands is 3 : 9, *i.e.*, one proton in the NH_2-side methylene protons shifts to the region (2.2—3.2 ppm) of the NH-side methylene protons. Those properties are similar to those[11,12] of **4a** (β_2-form). The methylene proton signals (2.2—3.3 ppm) of the coordinated 2,3,2-tet ligand in **3b** are similar to those of **3a** (β_1-form). Thus, the isomeric form of **3b** is *cis*-β_1-form and that of **4b—d** is *cis*-β_2-form. The signals of amine protons and salicylato protons of the coordinated ligands in **3b** and **4b—d** have been assigned by comparison with those of **3a** and **4a** complexes,[11] and are collected in Table 1. These amine proton signals disappeared in heavy water containing NaOH. In the ^{13}C NMR spectra of **4b—d** in D_2O, there have been observed 6—9 signals for the quadridentate ligands and 7 signals for the salicylato ligand. The spectrum of **4c** is similar to that of **4d** as shown in Fig. 2. The chemical shifts of the salicylato ligand in **4b—d** are similar to those of **4a**.[17] The chemical shifts of the quadridentate ligands in **4a—d** are difficult to assign to the individual carbon atoms, but regions of the chemical shifts of center methylene, NH_2-side methylene and NH-side methylene carbons are around 22—27, 37—48, and 45—55 ppm, respectively as shown in Table 2.

The absorption spectra of **4a—d** in H_2O showed two absorption bands at 333 nm (specific absorption band) and at 520—550 nm (first absorption band) as shown in Fig. 4. The ε of both the absorption bands of **4a—d** decreases with the increase of the total number of center methylene carbons of the quadridentate ligands, and their first absorption band shifts from 520 nm (**4a**) to 550 nm (**4d**) as shown in Fig. 4. In the **4a—d** complexes, their colors in the solid state are russet (**4a** and **4b**), pink-violet (**4c**) and dark-brown (**4d**). Their melting points are 240—244 °C (**4a**, **4b**), 231—233 °C (**4c**) and 190—192 °C (**4d**). Their yields of synthesis are 84% for **4a**, 61% for **4b**, 43% for **4c**, and 27% for

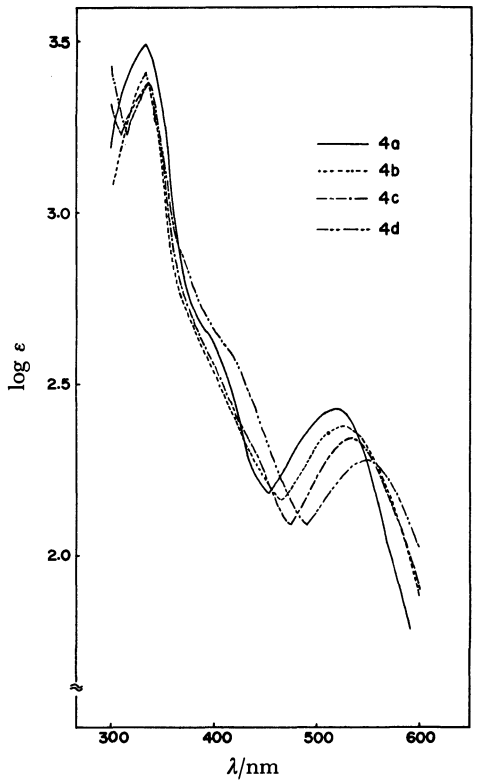

Fig. 4. The absorption spectra of **4a—d** complexes in H_2O. (**4a**): *cis*-β_2-[Co(sal)(2,2,2-tet)]Cl·H_2O. (**4b**): *cis*-β_2[Co(sal)(2,3,2-tet)]Cl·2H_2O. (**4c**): *cis*-β_2-[Co(sal)-(3,2,3-tet)]Cl·3H_2O. (**4d**): *cis*-β_2-[Co(sal)(3,3,3-tet)]-Cl·H_2O.

4d. The *cis*-β_1 complexes of **4a** and **4b** are isolated from the reaction mixtures, but those of **4c** and **4d** could not be isolated. From the above results, the properties of **4b** are seen to be very similar to those of **4a**, though those of **4c** are similar to those of **4d**. Complex **4d** is the most unstable complex among **4a—d**. In the **3b** complex, the color (russet), melting point (≈238 °C) and yield (≈5%) are similar to those of **3a**.[11,12] These properties are attributable to the center methylenes of the quadridentate ligands. All complexes are diamagnetic. The NMR, IR, absorption spectral data and electric conductivity of the aqueous solutions are collected in Table 1—3.

Experimental

Measurements. The NMR spectra were recorded with an FX-60 apparatus (JEOL) for ^{13}C NMR and an R-40 apparatus (Hitachi) for ^{1}H NMR. The visible absorption spectra were recorded with a Shimadzu MPS-5000 recording spectrophotometer. The magnetic susceptibilities were measured by Faraday's method using a magnetic balance (Shimadzu) at room temperature. The pH was measured with a Corning pH-meter M-125. The electric conductivity of an aqueous solution was determined by the use of a conductmetric meter, CM-30 (Shimadzu) at room temperature.

Preparation of Complexes. trans-*Dichloro(3,6-diazaoctane-1,8-diamine(trien))cobalt(III) Chloride Hydrate Hydrochloric Acid (**2a**)* and cis-α-*Dichloro(3,6-diazaoctane-1,8-diamine(trien))cobalt (III) Chloride (**1a**)* were prepared by the Sargeson's method.[10,18]

trans-*Dichloro(3,7-diazanonane-1,9-diamine)cobalt(III) Chloride 2.5 Hydrate (**1b**)* and trans-*Dichloro(4,7-diazadecane-1,10-diamine)cobalt(III) Chloride Hydrate (**1c**)* were prepared by the Bosnich's method.[19,20]

trans-*Dichloro(4,8-diazaundecane-1,11-diamine)cobalt(III) Chloride Hydrate (**1d**)*: Eighteen cubic centimeters of a methanol solution of the tetramine of 3 g (15.9 mmol) were added to 9 cm^3 of an aqueous solution of cobalt(II) chloride hexahydrate of 3.79 g (15.9 mmol). To this solution, was airated 3 h, 4.5 cm^3 of 35% hydrochloric acid was added. The solution was stirred for 1 h and concentrated in a rotary evaporator. The precipitated green complex was filtered. Acetone was added to an aqueous solution of the green complex. Then, precipitated **1c** complex was filtered and dried. Yield: 4.43 g (75.0%). Found: C, 30.06; H, 7.41; N, 15.22; Cl, 28.72%. Calcd for $CoC_9H_{26}N_4OCl_3$ (MW 371.63) C, 29.09; H, 7.05; N, 15.08; Cl, 28.62%. Mp 228—230 °C.

cis-β_1-*Salicyclato(3,7-diazanonane-1,9-diamine)cobalt(III) Chloride Hydrate (**3b**)* and cis-β_2-*Salicylato(3,7-diazanonane-1,9-diamine)cobalt(III) Chloride Dihydrate (**4b**)*: Complex 1b of 5.0 g (13.49 mmol) was added to moistened fresh AgOH, which was made from silver nitrate (4.58 g, 26.96 mmol) and potassium hydroxide (1.52 g, 27.10 mmol). The mixture was stirred in the solid state for several minutes, then 10 cm^3 of water was added to the mixture. The mixture was stirred for about 30 minutes at 60 °C, the precipitated silver chloride filtered off and washed with a small amount of water. To the reddish violet filtrate was added 1.86 g (13.47 mmol) of salicylic acid. The solution was warmed to 50 °C. The reddish brown complex thus precipitated was filtered off, washed with EtOH and acetone, dried in a desiccator over silica gel, and recrystallized from water. Separation of β_1 (**3b**) and β_2 (**4b**) form was carried out by the method described in the previous paper,[11] but the length of the large column of cation-exchange resin (Dowex 50W-X2) was about 18 cm. Yields: 0.26 g (4.7%) for **3b**, 3.5 g (60.8%) for **4b**. Found **3b**: C, 41.22; H, 6.48; N, 13.51; Cl, 9.03%. Calcd for $CoC_{14}H_{26}N_4O_4Cl$ (MW 408.78) C, 41.14; H, 6.41; N, 13.71; Cl, 8.67%. Found **4b**: C, 39.13; H, 6.80; N, 13.47; Cl, 8.41%. Calcd for $CoC_{14}H_{28}N_4O_5Cl$ (MW 426.79) C, 39.40; H, 6.61; N, 13.13; Cl, 8.31%. Mp 237—239 °C for **3b**, 242—244 °C for **4b**.

cis-β_2-*Salicylato(4,7-diazadecane-1,10-diamine)cobalt(III) Chloride Trihydrate (**4c**)*: Complex **1c** (5.0 g, 13.98 mmol) was added to moistened fresh AgOH (3.5 g, 28.0 mmol). The mixture was stirred in the solid state for several minutes, then, 10 cm^3 of water was added to the mixture. The mixture was stirred for about 30 min at 60 °C, the precipitated silver chloride was filtered and washed with a small amount of water. To the reddish violet filtrate, sodium salicylate (2.24 g, 13.99 mmol) was added. The solution was warmed at 50 °C. The precipitated complex was filtered off, washed with EtOH and acetone, dried in a desiccator over silica gel, and recrystallized from water. Yield: 2.75 g (42.9%). Found: C, 39.41; H, 6.88; N, 12.50; Cl, 6.60%. Calcd for $CoC_{15}H_{32}N_4O_6Cl$ (MW 458.83) C, 39.27; H, 7.03; N, 12.21; Cl, 7.73%. Mp 231—233 °C.

cis-β_2-*Salicylato(4,8-diazaundecane-1,11-diamine)cobalt(III) Chloride Hydrate (**4d**)*: The brown complex was prepared from the reaction mixture of **1d** (5.0 g, 13.45 mmol), fresh AgOH (1.68 g, 13.46 mmol), water (about 10 cm^3), and sodium salicylate (2.08 g, 12.99 mmol) according to the preparation method of **4c**. From the brown complex, **4d** was isolated by using column chromatography of alumina. On elution with water, the bands of the complex split into four components. The complex obtained from the first band was rechromatographed with methanol eluent. The methanol solution of the first band was concentrated and dried over silica gel, the **4d** complex was recrystallized from water–acetone, twice. Yield: 1.6 g (27.2%). Found: C, 44.41; H, 7.26; N, 12.62; Cl, 7.10%. Calcd for $CoC_{16}H_{30}N_4O_4Cl$ (MW 436.83) C, 43.99; H, 6.92; N, 12.83; Cl, 8.12%. Mp 190—192 °C.

cis-β_1-*Salicylato(4,7-diazadecane-1,10-diamine)cobalt(III) Chloride (**3c**)* and cis-β_1-*Salicylato(4,8-diazaundecane-1,11-diamine)-cobalt(III) Chloride (**3d**)*: Attempts to isolate the complexes **3c** and **3d** from their reaction mixture were unsuccesful, because the bands of the **3c** and **3d** on the column of ion-exchange resin were very small.

References

1) Part I: Ref. 14, Part II: Ref. 11.
2) T. Ito, M. Sugimoto, K. Toriumi, and H. Ito, *Chem. Lett.*, **1981**, 1477.
3) D. A. Buckingham, P. J. Cresswell, R. J. Dellaca, M. Dwyer, G. J. Gainsford, L. G. Marzilli, I. E. Maxwell, Ward T. Robinson, A. M. Sargeson, and K. R. Turnbull, *J. Am. Chem. Soc.*, **96**, 1713 (1974).
4) N. C. Payne, *Inorg. Chem.*, **12**, 1151 (1973).
5) R. K. Wismer, and R. A. Jacobson, *Inorg. Chim. Acta.*, **7**, 477 (1973).
6) H. C. Freeman, and I. E. Maxwell, *Inorg. Chem.*, **8**, 1293 (1969).
7) B. F. Anderson, J. D. Bell, D. A. Buckingham, P. J. Cresswell, G. J. Gainsford, L. G. Marzilli, G. B. Robertson, and A. M. Sargeson, *Inorg. Chem.*, **16**, 3233 (1977).
8) L. F. Lindoy and H. W. Louie, *Inorg. Chem.*, **20**, 4186 (1981).
9) B. Bosnich, J. M. Harrowfield, and H. Boucher, *Inorg. Chem.*, **14**, 815 (1975).
10) A. M. Sargeson and G. H. Searle, *Inorg. Chem.*, **6**, 787 (1967).
11) Y. Yamamoto and E. Toyota, *Bull. Chem. Soc. Jpn.*, **52**, 2540 (1979).
12) Y. Yamamoto, E. Toyota, and N. Mitsudera, *Bull. Chem. Soc. Jpn.*, **53**, 3517 (1980).
13) S. Utsuno, Y. Sakai, Y. Yoshikawa, and H. Yamatera, *J. Am. Chem. Soc.*, **102**, 6903 (1980).
14) Y. Yamamoto and E. Toyota, *Chem. Pharm. Bull.*, **26**, 2275 (1978).
15) D. A. Buckingham and D. Jones, *Inorg. Chem.*, **4**, 1387 (1965).
16) D. A. Buckingham, M. Dwyer, G. J. Gainsford, V. Janson Ho, L. G. Marzilli, Ward T. Robinson, A. M. Sargeson, and K. R. Turnbull, *Inorg. Chem.*, **14**, 1739 (1975).
17) Y. Yamamoto, *Bull. Chem. Soc. Jpn.*, **51**, 2894 (1978).

18) "Shin Jikken Kagaku Koza," ed by the Chemical Society of Japan, Maruzen, Tokyo (1977), Vol. 8, Chap. 3, p. 1446.
19) B. Bosnich, R. D. Gillard, E. D. Mckenzie, and G. A. Webb, *J. Chem. Soc.*, *A*, **1966**, 1331.
20) "Shin Jikken Kagaku Koza," ed by the Chemical Society of Japan, Maruzen, Tokyo (1977), Vol. 8, Chap. 3, p. 1453.

 © 1983 The Chemical Society of Japan Bull. Chem. Soc. Jpn., 56, 1057—1059 (1983)

Preparation and ^{119}Sn NMR Spectra of Coordination Compounds of Di-*t*-butyltin(IV) Derivatives

Junzo Otera,* Toru Yano, and Kazunori Kusakabe
Okayama University of Science, Ridai-cho, Okayama 700
(Received September 16, 1982)

Di-*t*-butyltin bis(chelates) were prepared and characterized in comparison with dimethyltin analogs. ^{119}Sn NMR spectra show a six-coordinate configuration for the acetylacetonate, tropolonate, and oxinate; a nonchelating structure is partially involved in the 2-methyloxinate and dialkyldithiocarbamates. Di-*t*-butyltin dichloride gives no isolable adducts with monodentate ligands; however, the Job's continuous variation method using ^{119}Sn NMR spectra has revealed that complexations with 2 : 1 and/or 1 : 1 donor/Sn molar ratios occur in ether. It has been concluded that *t*-butyl group reduces the acceptor property of tin by means of both inductive and steric effects.

Despite extensive preparative and spectroscopic investigations on coordination compounds of dimethyltin(IV) derivatives,[1] rather few studies have been made on the other diorganotin analogs except some diphenyltin(IV) compounds, because IR and NMR spectroscopies are not so powerful means for these compounds. However, X-ray studies have revealed that the configulation was varied in some cases where methyl groups attached to tin were replaced by phenyl groups,[2] and therefore, it seems of interest to investigate other organotin analogs. *t*-Butyl group, possessing increased electron donating ability and bulkiness, seems to be appropriate for evaluating the effect of alkyl group on coordination behavior. Unfortunately, however, only a few coordination compounds of *t*-butyltin(IV) derivatives have been prepared,[3] and no systematic studies on these compounds have been made.

The most popular dimethyl- and diphenyltin(IV) compounds known so far involve diorganotin bis(chelates), $R_2Sn(Ch)_2$ (Ch=chelating ligands), and molecular complexes of diorganotin dihalides with monodentate donors. For $Me_2Sn(Ch)_2$, we have shown the usefulness of ^{119}Sn NMR spectra for elucidating the coordination about tin.[4-7] In this paper, we wish to report the preparation of di-*t*-butyltin bis(chelates), *t*-$Bu_2Sn(Ch)_2$, for which characterization was carried out by means of ^{119}Sn FT NMR spectroscopy. Interaction of *t*-Bu_2SnCl_2 with monodentate ligands in solution will also be described.

Experimental

^{119}Sn and ^{1}H NMR spectra were measured in the FT and CW modes, respectively, as reported previously.[4-7] Chemical shifts are relative to Me_4Sn and Me_4Si for ^{119}Sn and ^{1}H NMR spectra, respectively, and positive signs indicate downfield shifts from the reference. UV spectra were measured with a Hitachi Model 285 spectrophotometer equipped with 1 cm quartz cells. All the solvents were purified by standard methods. *t*-Bu_2SnCl_2 was prepared by a slightly modified Grignard method.[8] The employment of THF in place of ether as solvent resulted in an improvement of yield from 4 to 15%. Abbreviations for ligands are as follows: acac=acetylacetonate, trop=tropolonate, oxin=oxinate (or 8-quinolinolate), meox=2-methyloxinate (or 2-methyl-8-quinolinolate), mdtc and edtc=dimethyl- and diethyldithiocarbamate, DMSO=dimethyl sulfoxide, HMPA=hexamethylphosphoric triamide, DMF=*N*,*N*-dimethylformamide, and Py=pyridine.

Preparation of t-$Bu_2Sn(Ch)_2$. To a methanol solution (10 cm^3) of CH_3ONa (1 mmol) was added Hacac (100 mg, 1 mmol). After stirring for 1 h at room temperature, *t*-Bu_2SnCl_2 (152 mg, 0.5 mmol) in methanol (5 cm^3) was added to this solution. The reaction mixture was stirred for 2 h and subjected to evaporation *in vacuo*. The precipitates thus obtained were extracted with hexane (10 cm^3). After addition of a few drops of Hacac, the hexane solution was concentrated to 2 cm^3. Cooling this concentrated solution in a Dry Ice–methanol bath gave *t*-$Bu_2Sn(acac)_2$ (**1**) as colorless crystals: yield 100 mg (41%). All operations were carried out in an inert atmosphere because **1** decomposes easily in air.

t-$Bu_2Sn(trop)_2$ (**2**), *t*-$Bu_2Sn(oxin)_2$ (**3**), and *t*-$Bu_2Sn(meox)_2$ (**4**) were prepared similarly in 25—55% yields. Recrystallization of these compounds was effected from CH_2Cl_2–hexane in air.

t-$Bu_2Sn(mdtc)_2$ (**5**) and *t*-$Bu_2Sn(edtc)_2$ (**6**) were prepared by mixing mdtcNa (359 mg, 2 mmol) or edctNa (451 mg, 2 mmol) in methanol (10 cm^3) with *t*-Bu_2SnCl_2 (304 mg, 1 mmol) in CH_2Cl_2 (5 cm^3). The pure sample was obtained by recrystallization from CH_2Cl_2–hexane in yields of 308 mg (65%) and 434 mg (82%), respectively. Melting points and analytical data of the compounds thus obtained are summarized in Table 1.

The Job's continuous variation method[9,10] was used under the condition that the total concentration of *t*-Bu_2SnCl_2 and a ligand was 1 M (1 M=1 mol dm^{-3}) in ether. The ligands employed were distilled from CaH_2 before use.

Attempted Isolation of Adducts. *t*-Bu_2SnCl_2 (304 mg, 1 mmol) and DMSO (156 mg, 2mmol) were stirred in ether (3 cm^3) at room temperature for 30 min. After addition of 3 cm^3 hexane, the solution was cooled at −78 °C to give white precipitates, which were filtered out and dried (100 mg). The NMR spectrum of the precipitates in CCl_4 exhibited two methyl proton signals at δ=2.45 (DMSO) and 1.41 (*t*-Bu), but no reproducible results were obtained with respect to their integral ratios, which varied between 12 : 20 and 12 : 28 in

Table 1. Melting points and analytical data of *t*-$Bu_2Sn(Ch)_2$

	Ch	Mp θ_m/°C	Found (Calcd) (%) C	H	N
1	acac	101—103	50.23(50.15)	7.67(7.48)	
2	trop	166—168	55.58(55.62)	5.95(5.94)	
3	oxin	199—202	59.60(59.91)	5.77(5.80)	5.40(5.38)
4	meox	207—208	60.70(61.00)	6.04(6.58)	5.01(5.08)
5	mdtc	174—176	35.56(35.52)	6.37(6.39)	5.98(5.92)
6	edtc	100—102	40.87(40.83)	7.23(7.23)	5.38(5.29)

repeated preparations, indicating coexistence of 2 : 1 and 1 : 1 adducts. Employment of 4 equiv. DMSO also gave similar results. When other monodentate ligands were treated in an analogous manner, no adducts were obtained,only t-Bu_2SnCl_2 being recovered after cooling at −78 °C.

Results and Discussion

t-Bu₂Sn(Ch)₂. All chelates were prepared as analytically pure crystalline compounds from t-Bu_2SnCl_2 and sodium salts of ligand anions, and were fairly stable in air except the acetylacetonato complex, which decomposes easily on exposure to air both in the solid state and in solution. The ^1H and ^{119}Sn NMR spectral parameters of these compounds are summarized in Table 2, in which the deviations in $^3J(^{119}Sn-H)$ and $\delta(^{119}Sn)$ values from those in the corresponding dimethyltin analogs are given as Δ_1 and Δ_2. Evidently, the $^3J(^{119}Sn-H)$ value in t-$Bu_2Sn(Ch)_2$ is constantly increased by 30—40 Hz from the $^2J(^{119}Sn-H)$ value in $Me_2Sn(Ch)_2$, except for the 2-methyloxinato complex **4**

Table 2. ^1H and ^{119}Sn NMR spectral parameters of t-$Bu_2Sn(Ch)_2$ in CCl_4

Compound	$\delta(CH_3-C-Sn)$ ppm	$^3J(^{119}Sn-H)$ Hz	Δ_1[a] Hz	$\delta(^{119}Sn)$ ppm	Δ_2[b] ppm
1	1.01	130.6	31.3	−486	−120
2	1.18	111.4	39.2	−326	−134
3	1.13	107.2	36.0	−338	−105
4	1.03	109.4	20.4	−311	−83
5	1.53	119.3	35.3	−255	+89
6	1.55	119.6	35.6	−262	+76

a) $\Delta_1 = {}^3J(^{119}Sn-H)$ (t-$Bu_2Sn(Ch)_2$) $- {}^2J(^{119}Sn-H)$ ($Me_2Sn(Ch)_2$). b) $\Delta_2 = \delta(^{119}Sn)$ (t-$Bu_2Sn(Ch)_2$) $- \delta(^{119}Sn)$ ($Me_2Sn(Ch)_2$).

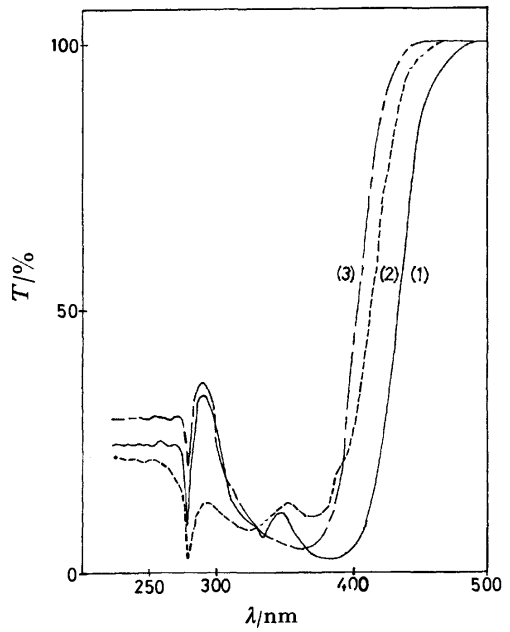

Fig. 1. UV spectra of $R_2Sn(oxin)_2$ and $R_2Sn(meox)_2$ in benzene. (1) t-$Bu_2Sn(oxin)_2$: λ_{max} 386 nm (ε 5200), (2) t-$Bu_2Sn(meox)_2$: λ_{max} 320 nm (ε 3800) and 370 nm (ε 3400), (3) $Me_2Sn(meox)_2$: λ_{max} 365 nm (ε 3900).

(*vide infra*). Since the latter value can be correlated linearly with the C–Sn–C bond angle,[4] it may be said that the $^3J(^{119}Sn-H)$ value in t-$Bu_2Sn(Ch)_2$ also increases with increasing C–Sn–C bond angle. It should be noted, however, that the $^3J(^{119}Sn-H)$ value cannot necessarily be correlated with the coordination mode.[4]

By contrast, a great discrepancy was found for Δ_2. The $\delta(^{119}Sn)$ values in t-$Bu_2Sn(Ch)_2$ shifted upfield by 105—134 ppm from those in corresponding $Me_2Sn(Ch)_2$ for the acetylacetonato **1**, tropolonato **2**, and oxinato **3** complexes. Since the chelation of ligands in these compounds is confirmed on the basis of IR spectra for **1** (ν(C=O) 1590 cm^{-1})[10] and **2** (ν(C=C) 1592 and ν(C=O) 1497 cm^{-1})[12] and UV spectrum for **3** (Fig. 1),[13] the upfield shifts mentioned above has been brought about simply by the replacement of methyl group by t-butyl group. On the other hand, the magnitude of the upfield shift is moderately reduced in the 2-methyloxinato complex **4**. As shown in Fig. 1, the UV spectrum of **4** exhibits two peaks at 320 and 370 nm assignable to nonchelating and chelating structures, respectively, while the dimethyltin counterpart gives rise to a single peak at 365 nm. As a result, the $\delta(^{119}Sn)$ value apparently reflects this coordination behavior. In $Me_2Sn(Ch)_2$, when Ch was changed from oxin to meox, $\delta(^{119}Sn)$ was shifted downfield (from −273 to −228 ppm).[6] Introduction of a methyl group into the α-position of the quinoline ring resulted in expansion of the C–Sn–C bound angle, though a slightly weakened chelation being maintained; that is, a considerable steric repulsion is operative between methyl groups attached to tin and the quinoline ring. Accordingly, a strong steric interaction between t-butyl groups and methyl groups in **4** is reasonably assumed to prevent nitrogen from coordinating to tin.

Quite surprisingly, the $\delta(^{119}Sn)$ values in the dialkyldithiocarbamato complexes **5** and **6** lie downfield relative to those in corresponding dimethyltin compounds. Since we have revealed that the $\delta(^{119}Sn)$ value in organotin chelates is shifted downfield as the coordination number of tin decreases,[7] the above results may be interpreted in terms of coexistence of a nochelating structure with the chelating structure. In general, t-$Bu_2Sn(Ch)_2$ was found to involve a fairly weak chelation as compared with $Me_2Sn(Ch)_2$.

Interactions of t-Bu₂SnCl₂ with Monodentate Ligands. Me_2SnCl_2 forms molecular complexes with various monodentate ligands with 2 : 1 and/or 1 : 1 donor/Sn stoicheometry. For example, DMSO, HMPA, and Py afford quite stable 2 : 1 adducts, while DMF gives

Table 3. ^1H and ^{119}Sn NMR spectral parameters of t-Bu_2SnCl_2 in donor solvents

Solvent	$\delta(CH_3-C-Sn)$ ppm	$^3J(^{119}Sn-H)$ Hz	$\delta(^{119}Sn)$ ppm
CCl_4	1.43	112.8	56
DMSO	1.36	125.0	−147
HMPA	1.42	122.0	−153
DMF	1.38	118.0	−99
Py	1.39	117.0	30

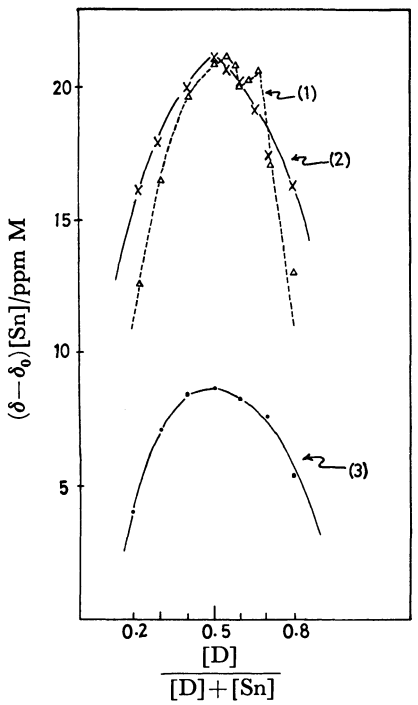

Fig. 2. Job's plots for t-Bu_2SnCl_2–monodentate ligand system in ether at total concentration of 1 M. (1) DMSO (2) HMPA (3) DMF.

both 2 : 1 and 1 : 1 adducts.[1b] Here we have studied the coordinating behavior of these ligands towards t-Bu_2SnCl_2. When t-Bu_2SnCl_2 and a ligand were mixed in hexane in various molar ratios, no adducts were obtained. Treatment of DMSO with t-Bu_2SnCl_2 in molar ratios more than 2 : 1 in ether, followed by addition of hexane and cooling at −78 °C, yielded white precipitates. The ^1H NMR spectrum, however, showed that these precipitates consisted of 2 : 1 and 1 : 1 adducts. Accordingly, we have investigated whether some kind of interaction exists in solution. In Table 3 are listed the $^3J(^{119}Sn–H)$ and $\delta(^{119}Sn)$ values of t-Bu_2SnCl_2 in the donor solvents. The increase in ^3J ($^{119}Sn–H$) values from that in CCl_4 indicates occurrence of donor-acceptor interactions. In line with this, the $\delta(^{119}Sn)$ values in DMSO, HMPA, and DMF shifted 150—200 ppm upfield relative to the one in CCl_4, while a slight shift was observed in Py. This is quite unexpected because Py is classified as the most favorite ligand for Me_2SnCl_2 to afford the 2 : 1 adduct.[1] In the hope of elucidating the stoicheometry of the interaction in solution, the Job's continuous variation method was applied. When hexane was employed as a solvent, $\delta(^{119}Sn)$ shifted only 10 ppm at most, so that a reliable Job's plot could not be drawn. Then, ether was used, which resulted in a shift by more than 50 ppm. Evidently, the shift was not caused by the coordination of ether since $\delta(^{119}Sn)$ of t-Bu_2SnCl_2 in ether (55 ppm) gave no evidence for solvation. Therefore, it can be concluded that the interaction is favored in polar medium. The Job's plots in ether are illustrated in Fig. 2. DMSO gave rise to both 2 : 1 and 1 : 1 complexations but HMPA and DMF only to the 1 : 1 stoicheometry

$$t\text{-}Bu_2SnCl_2 \overset{D}{\rightleftharpoons} t\text{-}Bu_2SnCl_2\cdot D \overset{D}{\rightleftharpoons} t\text{-}Bu_2SnCl_2\cdot 2D. \quad (1)$$

It is apparent from these findings that the acceptor property of tin is considerably reduced in t-Bu_2SnCl_2. Since a consultation with the molecular model showed little steric interaction for t-Bu_2SnCl_2–DMSO and t-Bu_2SnCl_2–DMF systems, the reduction of acceptor property may be attributable to the inductive effect of the t-butyl group. On the other hand, a significant interaction between t-butyl groups and N-methyl groups is induced on coordination of HMPA. Both t-Bu_2SnCl_2–DMSO and t-Bu_2SnCl_2–HMPA systems are comparable in stability constant for the 1 : 1 complexation, judging from the $(\delta-\delta_0)$[Sn] values in the Job's plot which are proportional to stability constants.[9] The $\delta(^{119}Sn)$ values of t-Bu_2SnCl_2 in these systems (Table 3) are consistent with this postulation. Therefore, the absence of the 2 : 1 complexation of HMPA is accounted for by the steric reason.

In summary, di-t-butyltin(IV) compounds showed various differences in coordination behavior from dimethyltin analogs. The reduced acceptor property of tin in the former compounds is primarily caused by the inductive effect of t-butyl groups. However, in some cases where bulky ligands are involved, it was found that the steric factor also is important.

References

1) R. Okawara and M. Wada, *Adv. Organomet. Chem.*, **5**, 137 (1967); V. S. Petrosyan, N. S. Yashina, and O. A. Reutov, *ibid.*, **14**, 63 (1976).
2) J. A. Zubieta and J. J. Zuckerman, *Prog. Inorg. Chem.*, **24**, 257 (1978).
3) M. Gielen and J. Topart, *Bull. Soc. Chim. Belg.*, **84**, 13 (1975).
4) J. Otera, T. Hinoishi, Y. Kawabe, and R. Okawara, *Chem. Lett.*, **1981**, 273.
5) J. Otera, T. Hinoishi, and R. Okawara, *J. Organomet. Chem.*, **202**, C93 (1980).
6) J. Otera, *J. Organomet. Chem.*, **221**, 57 (1981).
7) J. Otera, A. Kusaba, T. Hinoishi, and Y. Kawasaki, *J. Organomet. Chem.*, **228**, 223 (1982).
8) H. H. Huang, K. M. Hui, and K. K. Chiu, *J. Organomet. Chem.*, **11**, 515 (1968).
9) K. Roth, M. Grosse, and D. Rewicki, *Tetrahedron Lett.*, **1972**, 435.
10) J. Otera, T. Shiomi, K. Murakami, and Y. Kawasaki, *Bull. Chem. Soc. Jpn.*, **54**, 2964 (1981).
11) Y. Kawasaki and T. Sasaki, *Chem. Lett.*, **1979**, 279.
12) M. Komura, T. Tanaka, and R. Okawara, *Inorg. Chim. Acta*, **2**, 321 (1968).
13) K. Kawakami and R. Okawara, *J. Organomet. Chem.*, **6**, 249 (1966).

A Nuclear Magnetic Resonance Study of the Kinetics of Ligand Exchange Reactions in Uranyl Complexes. III. Dimethyl Sulfoxide Exchange in Bis(β-diketonato)(dimethyl sulfoxide)dioxouranium(VI)

Yasuhisa IKEDA, Hiroshi TOMIYASU, and Hiroshi FUKUTOMI*

Research Laboratory for Nuclear Reactors, Tokyo Institute of Technology, O-okayama, Meguro-ku, Tokyo 152

(Received September 30, 1982)

The exchange reactions of dimethyl sulfoxide (DMSO) with $UO_2(acac)_2dmso$ and $UO_2(dbm)_2dmso$ (acac= acetylacetonate, dbm=dibenzoylmethanate) have been studied by the NMR method in CD_3COCD_3 and CD_2Cl_2. In CD_3COCD_3, rates of DMSO exchange for these complexes are independent of the free DMSO concentrations. Rate constants (s^{-1}) at 25 °C and activation parameters ΔH^* (kJ mol^{-1}) and ΔS^* (J K^{-1} mol^{-1}) are 2.36×10^2, 45.8 ± 0.8, -46.6 ± 2.9 for $UO_2(acac)_2dmso$, and 3.92×10^2, 44.5 ± 0.4, -46.2 ± 2.1 for $UO_2(dbm)_2dmso$, respectively. In CD_2Cl_2, the exchange rates are dependent on the free DMSO concentration. For $UO_2(acac)_2dmso$, rate$=(k_d+k_IK_{OS}[DMSO])[UO_2(acac)_2dmso]/(1+K_{OS}[DMSO])$, where $k_d(25\ °C)=1.02\times10^2\ s^{-1}$, $\Delta H^*=47.9\pm5.2$ kJ mol^{-1}, and $\Delta S^*=-46.6\pm11.2$ J K^{-1} mol^{-1}, and $k_I(25\ °C)=1.01\times10^3\ s^{-1}$, $\Delta H^*=35.4\pm12.4$ kJ mol^{-1}, and $\Delta S^*=-69.7\pm20.5$ J K^{-1} mol^{-1}, and $K_{OS}(10\ °C)=4.6\pm2.1\ M^{-1}$ (M=mol dm^{-3}). For $UO_2(dbm)_2dmso$, rate$=(k_1+k_2[DMSO])[UO_2(dbm)_2dmso]$, where $k_1(25\ °C)=1.74\times10^2\ s^{-1}$, $\Delta H^*=29.6\pm2.2$ kJ mol^{-1}, $\Delta S^*=-104\pm9$ J K^{-1} mol^{-1}, and $k_2(25\ °C)=1.62\times10^3\ M^{-1}\ s^{-1}$, $\Delta H^*=34.9\pm0.6$ kJ mol^{-1}, and $\Delta S^*=-67.2\pm2.4$ J K^{-1} mol^{-1}. The D and I mechanisms are proposed for the DMSO exchange in these complexes.

Recently, the kinetics of the ligand exchange reactions for $UO_2L_n^{2+}$, where $n=4$ and L is water[1] or hexamethylphosphoric triamide (hmpa),[2] and $n=5$ and L is *N,N*-dimethylacetamide(dma),[3] trimethyl phosphate(tmp) and triethyl phosphate(tep),[4] dimethyl sulfoxide (dmso),[5] *N,N*-dimethylformamide(dmf),[6] and *N*-methylacetamide(nma),[7] have been studied by NMR. However, only a few studies have been concerned with ligand exchange in uranyl chelate complexes.[8,9] The uranyl β-diketonato complexes, $UO_2(\beta\text{-diketonato})_2L$ (L=adduct ligands), have been of particular interest among these chelate complexes in view of their role in the extraction of uranyl ions.[10-14]

This paper will deal with the kinetics of DMSO exchange in $UO_2(acac)_2dmso$ (acac=acetylacetonate) and $UO_2(dbm)_2dmso$ (dbm=dibenzoylmethanate) by NMR. At the same time the structure of these complexes will be determined, since it has not been reported whether the pentagonal bipyramidal structure which was found by the X-ray study of crystalline $UO_2(acac)_2\text{-}H_2O$[15,16] remains unchanged in solution.

Experimental

Synthesis of Complexes. The $UO_2(acac)_2dmso$ complex was prepared by dissolving $UO_2(acac)_2H_2O$ in warm DMSO. The $UO_2(acac)_2H_2O$ complex was prepared according to the procedure of Comyns *et al.*[17] The $UO_2(acac)_2dmso$ solution was cooled and the resultant orange crystals were filtered and dried *in vacuo* for 1 d. The $UO_2(dbm)_2dmso$ complex was prepared by mixing DMSO with diethyl ether solution of $UO_2(dbm)_2H_2O$ which was synthesized by mixing an aqueous solution of uranyl(VI) acetate dihydrate (1 mol) with an ethanolic solution of dibenzoylmethane (2 mol).[18] The resultant orange crystals were filtered, washed with diethyl ether and dried *in vacuo* for 1 d. The composition of these complexes was determined by elemental analysis. The results are as follows: Calcd for $UO_2(acac)_2dmso$: C, 26.38; H, 3.69%. Found: C, 26.49; H, 3.66%. Calcd for $UO_2(dbm)_2dmso$: C, 48.37; H, 3.55; S, 4.03%. Found: C, 48.32; H, 3.52; S, 4.08%. Elemental analysis of the complexes was carried out in the Institute of Physical and Chemical Research.

Other Materials. Acetone-d_6(CD_3COCD_3, Merck 99.8%) and dichloromethane-d_2 (CD_2Cl_2, Merck 99%), which were used as solvents, were dried over 3A and 4A molecular sieves (Wako Pure Chemical Ind. Ltd.), respectively. Dimethyl sulfoxide (Wako Pure Chemical Ind. Ltd.) was distilled *in vacuo*, followed by distillation with molecular sieves, and stored over 3A molecular sieves. Acetylacetone (Wako Pure Chemical Ind. Ltd.) was used without further purification.

Preparation of Samples. Sample solutions in the appropriate solvent were prepared by weighing sample substances in a 1 cm^3 volumetric flask and some of each solution was placed in an NMR sample tube and sealed. All samples were prepared in a glove box filled with dried nitrogen. Proper precautions were taken to minimize the probability of photochemical redox reactions.

Measurement of NMR and IR Spectra. The measurements of the ^1H NMR spectra were carried out at 100 MHz on a JEOL JNM-MH 100 NMR spectrometer and JEOL JNM-FX 100 FT-NMR spectrometer equipped with a JNM-VT-3B temperature controller. Infrared spectra of the $UO_2(acac)_2\text{-}dmso$ complex in CD_3COCD_3 and CD_2Cl_2 were recorded in the 200—4000 cm^{-1} range by using a JASCO DS-701G IR spectrometer.

Kinetic Analysis. The kinetic parameters were calculated by using a program on the assumption of a two-site exchange process.[19] Input parameters for this program are the chemical shifts and the linewidths at half amplitude of each signal of the coordinated and free sites at −60 °C where no exchange was observed, the site populations, and appropriate life-times (τ-values). The experimental spectra are compared with the calculated spectra and the best-fit τ-values are determined. All computations were carried out with a Hitach M-200 computer.

Results and Discussion

The Structure of $UO_2(acac)_2dmso$ in Solutions. The ^1H NMR spectra in DMSO and CD_3COCD_3 mixtures including $UO_2(acac)_2dmso$ at −25 and 40 °C are shown in Fig. 1. In the spectrum at −25 °C, the signals of (a) and (d) can be assigned to be the methyl protons and 3-H protons of the coordinated acac, respectively. The signals (b) and (c) are the methyl

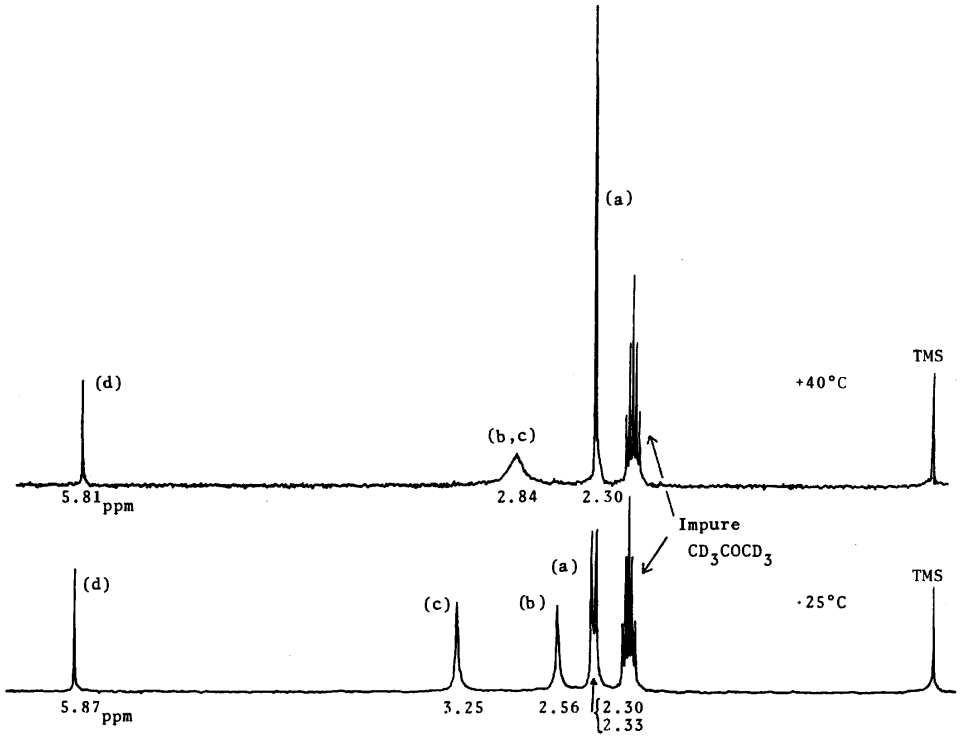

Fig. 1. ^{1}H NMR spectra of a solution consisting of $UO_2(acac)_2$dmso (0.0298 M), DMSO (0.0294 M), and CD_3COCD_3 (13.4 M) at −25 and 40 °C, respectively.

protons of the free and coordinated DMSO, respectively. A comparison of the integrated areas for (b) and (c) indicates that one DMSO molecule is coordinated to each uranyl ion. The area ratio of (a) to (c) to (d) was 6 : 3 : 1, the signal of (d) being used as a standard. The ratio was constant in solutions of various compositions. These facts indicate that two acetylacetonate ions and one DMSO molecule coordinate to uranyl ion. The separation of the methyl protons for coordinated acac means that these methyl groups are not geometrically identical. This may be explained by assuming the structure of this complex to be pentagonal bipyramidal like the crystal structure of the $UO_2(acac)_2H_2O$ complex,[15,16] because in such a structure the methly protons of coordinated acac exist in two different magnetic circumstances, with one near and one distant from the coordinated DMSO. The fact that the 3-H proton of the coordinated acac has a single peak also supports the proposed structure. In CD_2Cl_2, similar phenomena were also obseved in the ^{1}H NMR spectra.

The IR measurements for $UO_2(acac)_2$dmso were made in CD_3COCD_3 and CD_2Cl_2. The results are given in Table 1. The S=O stretch of the uranyl complex in CD_3COCD_3 and CD_2Cl_2 is observed at 1010 cm^{-1}, which is 45 cm^{-1} lower than the 1055 cm^{-1} observed in pure DMSO. Cotton and Francis[20] have shown that the S=O stretching frequency of sulfoxide in complexes decreases when coordination occurs through oxygen. Hence, it is concluded that one DMSO molecule is coordinated through oxygen in this complex. In addition, it was found that the two acetylacetonate ions were coordinated as bidentate ligands, because only one band corresponding to the carbonyl vibration was observed at frequencies less than 1600 cm^{-1}, which is the characteristic frequency of the carbonyl vibration for chelated metal β-diketone complexes.[21]

Table 1. Characteristic IR stretching frequencies for $UO_2(acac)_2$dmso in solution

Solvent	ν_3(O=U=O) cm^{-1}	ν(S=O) cm^{-1}	ν(C–O) cm^{-1}
CD_3COCD_3	905	1010	1517
CD_2Cl_2	908	1010	1570

The Structure of $UO_2(dbm)_2$dmso in Solutions. Figure 2 shows the ^{1}H NMR spectra of $UO_2(dbm)_2$dmso in DMSO and CD_3COCD_3 mixtures at −30 and 30 °C. At −30 °C, the signals (a) and (b) can be assigned to be the methyl protons of the free and coordinated DMSO, respectively. The signals (c) and (d) are the 3-H protons and the protons on benzene rings of the coordinated dbm, respectively. The area ratio of (d) to (c) to (b) was 10 : 1 : 3 and the ratio was constant in solutions of various composition. The signal for the 3-H protons of the coordinated dbm is a single peak as seen in Fig. 2. These ^{1}H NMR spectra in solutions containing $UO_2(dbm)_2$dmso indicate that two dibenzoylmethanate ions and one DMSO molecule coordinate to uranyl ion. Therefore, the structure of $UO_2(dbm)_2$dmso is presumed to be pentagonal bipyramidal which is the same as that of $UO_2(acac)_2$dmso.

DMSO Exchange in $UO_2(acac)_2$dmso. It is noted from Fig. 1 that DMSO exchanges between coordinated and free sites, because the methyl proton signals of the coordinated and free DMSO are observed at −25 °C, while only a single methyl proton signal for DMSO is observed at 40 °C. In addition, coalescence of the methyl proton signal for coordinated acac at 40 °C may

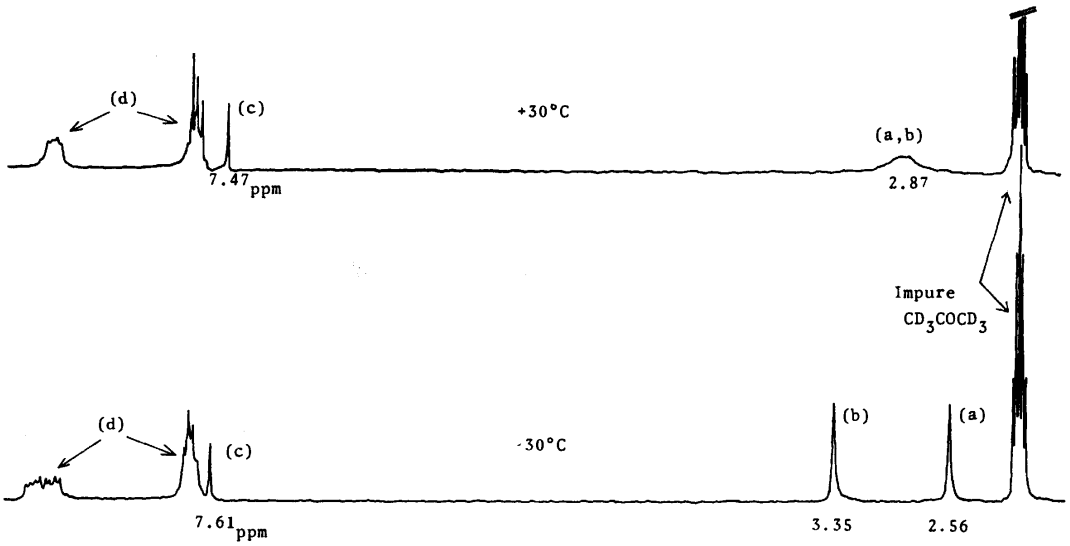

Fig. 2. ^{1}H NMR spectra of a solution consisting of $UO_2(dbm)_2dmso$ (0.0117 M), DMSO (0.0115 M), and CD_3COCD_3 (13.5 M) at −30 and 30 °C, respectively.

TABLE 2. SOLUTION COMPOSITION AND KINETIC PARAMETERS FOR THE EXCHANGE OF DMSO IN $UO_2(acac)_2$ dmso

Solution	$[UO_2(acac)_2dmso]$ / 10^{-2} M	[DMSO][a] / M	$[CD_3COCD_3]$ / M	$[CD_2Cl_2]$ / M	ΔH^* / kJ mol^{-1}	ΔS^* / J K^{-1} mol^{-1}	k_{ex}(25 °C)[b] / 10^2 s^{-1}
i	2.98	0.0294	13.4		45.8± 0.4	−44.9± 1.7	2.89
ii	4.65	0.151	13.2		45.8± 0.8	−46.6± 2.9	2.36
iii	4.58	0.243	13.2		39.5± 0.8	−68.9± 2.9	2.07
iv	4.70	0.321	13.0		41.6± 1.7	−60.5± 5.9	2.43
v	1.79	0.0282		15.7			
vi	3.53	0.0320		15.6	k_d path		
vii	4.05	0.0563		15.4	47.9± 5.2	−46.6±11.2	1.02
viii	7.78	0.0870		15.4	k_I path		
ix	10.5	0.239		14.5	35.4±12.4	−69.7±20.5	10.1

a) Added as DMSO. b) Calculated values from ΔH^* and ΔS^* at 25 °C.

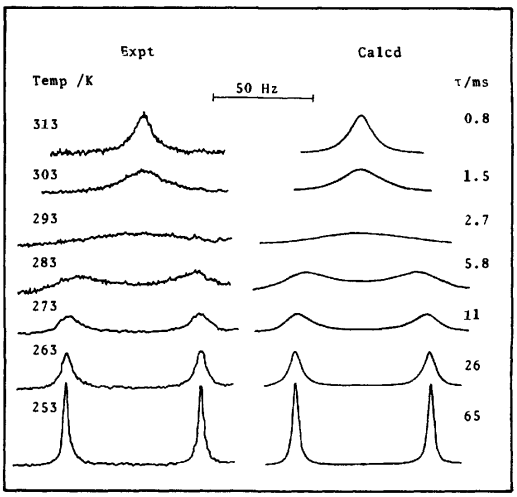

Fig. 3. Experimental (left side) and best-fit calculated lineshapes of a solution consisting of $UO_2(acac)_2dmso$ (0.0298 M), DMSO (0.0294 M), and CD_3COCD_3 (13.4 M). Temperatures and best-fit τ-values are shown at left and right sides of the figure, respectively.

be attributed to intermolecular DMSO exchange or intramolecular exchange for this complex.[22] The ^{1}H NMR measurements for DMSO methyl protons were carried out at various temperatures in order to examine in detail the change in lineshape. Results are shown in Fig. 3. The temperature dependence of the spectra is consistent with the results of previous work dealing with the DMSO exchange in $UO_2(dmso)_5^{2+}$.[5] The best-fit τ-values at each temperature were obtained by the method described in the Experimental Section. The calculated lineshapes are shown in Fig. 3 together with the corresponding best-fit τ-values.

The first-order rate constants, k_{ex}, for the DMSO exchange in $UO_2(\beta$-diketonato$)_2$dmso were calculated from the following equations:

$$\tau = \tau_c P_f = \tau_f P_c \quad (1)$$

$$k_{ex} = 1/\tau_c = \text{rate}/[UO_2(\beta\text{-diketonato})_2dmso] = (kT/h)\exp(-\Delta H^*/RT)\exp(\Delta S^*/R), \quad (2)$$

where the τ_c and τ_f are the mean life-times of the coordinated and free sites, respectively and P_c and P_f refer to the mole fractions of the coordinated and free DMSO, respectively. The rate constants, k_{ex}, were

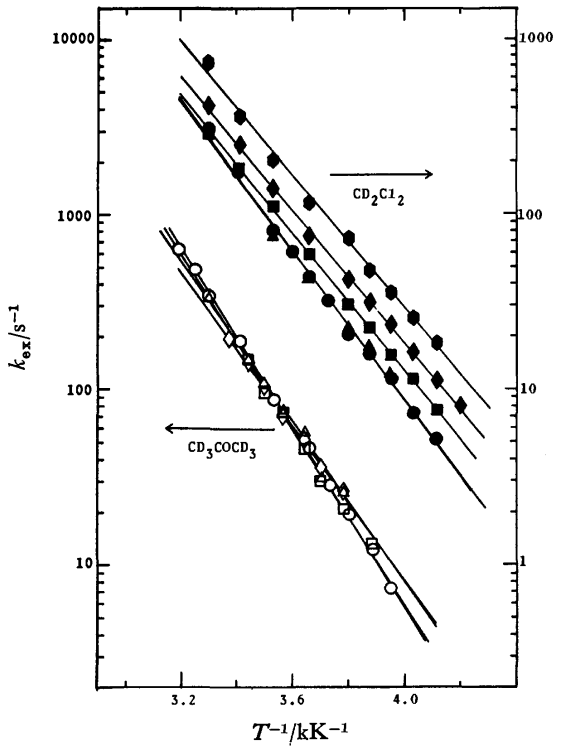

Fig. 4. Semilogarithmic plots of k_{ex} against the reciprocal temperature for the exchange of DMSO in UO_2-(acac)$_2$dmso in CD_3COCD_3 and CD_2Cl_2. The symbols of ○, △, □, ◇, ●, ▲, ■, ◆, and ⧫ correspond to i, ii, iii, iv, v, vi, vii, viii, and ix solutions in Table 2.

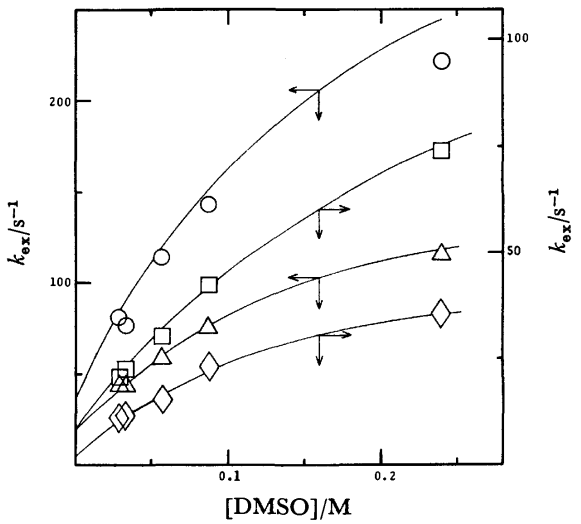

Fig. 5. Plots of k_{ex} *vs.* [DMSO] for the exchange of DMSO in UO_2(acac)$_2$dmso in CD_2Cl_2. ○: 10 °C; △: 0 °C; □: −10 °C; ◇: −20°C.

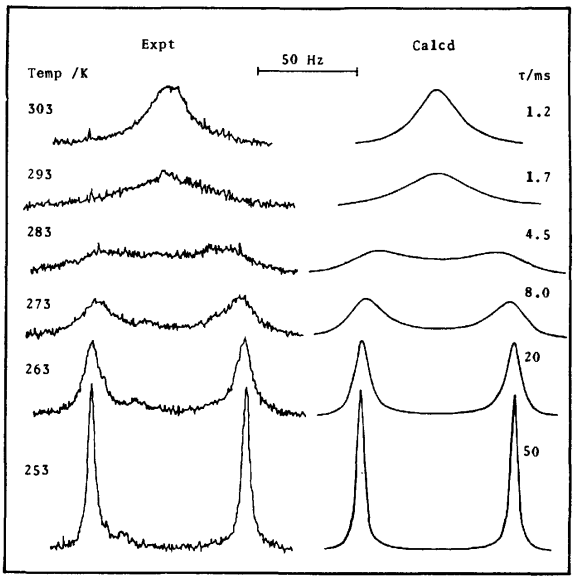

Fig. 6. Experimental (left side) and best-fit calculated lineshapes of a solution consisting of UO_2(dbm)$_2$dmso (0.0117 M), DMSO (0.0115 M), and CD_3COCD_3 (13.5 M). Temperatures and best-fit τ-values are shown at left and right sides of the figure, respectively.

obtained for various solutions listed in Table 2. In Fig. 4, the values of k_{ex} are plotted semilogarithmically against the reciprocal temperature. The activation parameters obtained from Fig. 4 are listed in Table 2. It can be seen from Table 2 and Fig. 4 that the rates of DMSO exchange in CD_3COCD_3 are independent of the free DMSO, while those of the DMSO exchange in CD_2Cl_2 depend on the concentration of free DMSO. The values of k_{ex} in the CD_2Cl_2 system were plotted against the DMSO concentration as shown in Fig. 5. This figure indicates that the rate of DMSO exchange in CD_2Cl_2 does not obey a simple linear relationship with the DMSO concentration.

DMSO Exchange in UO_2(dbm)$_2$dmso. It can be also expected from Fig. 2 that the DMSO exchanges

Table 3. Solution composition and kinetic parameters for the exchange of DMSO in UO_2(dbm)$_2$dmso

Solution	[UO_2(dbm)$_2$dmso] / 10^{-2} M	[DMSO][a] / M	[CD_3COCD_3] / M	[CD_2Cl_2] / M	$\Delta H^{\ddagger}$ / kJ mol^{-1}	$\Delta S^{\ddagger}$ / J K^{-1} mol^{-1}	k_{ex}(25 °C)[b] / 10^2 s^{-1}
i	1.17	0.0115	13.5		44.5±0.8	−47.9±2.5	3.37
ii	2.64	0.0384	13.3		44.5±0.4	−46.2±2.1	3.92
iii	3.10	0.0678	13.1		43.3±0.4	−50.8±2.1	3.68
iv	6.37	0.0627		14.8			
v	6.39	0.124		14.8	k_1 path		
vi	6.37	0.266		14.8	29.6±2.2	−104.2±8.6	1.74
vii	6.36	0.376		14.7	k_2 path		
viii	6.31	0.499		14.7	34.9±0.6	−67.2±2.4	16.2/M^{-1}

a) Added as DMSO. b) Calculated values from $\Delta H^{\ddagger}$ and $\Delta S^{\ddagger}$ at 25 °C.

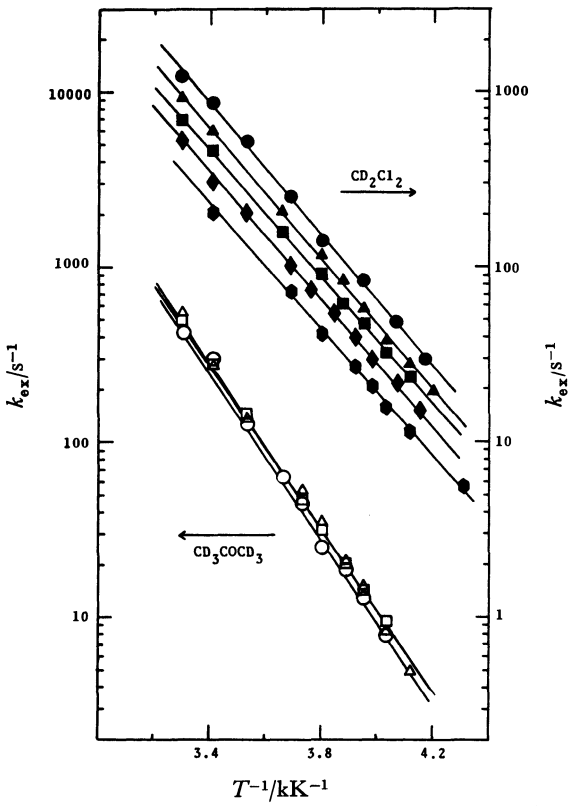

Fig. 7. Semilogarithmic plots of k_{ex} against the reciprocal temperature for the exchange of DMSO in $UO_2(dbm)_2dmso$ in CD_3COCD_3 and CD_2Cl_2. The symbols of ○, △, □, ⧫, ◆, ■, ▲, and ● correspond to i, ii, iii, iv, v, vi, vii, and viii solutions in Table 3.

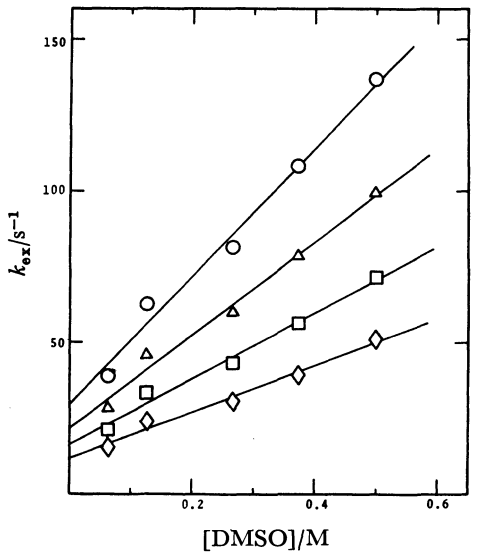

Fig. 8. Plots of k_{ex} *vs.* [DMSO] for the exchange of DMSO in $UO_2(dbm)_2dmso$ in CD_2Cl_2. ○: −10 °C; △: −15 °C; □: −20 °C; ◇: −25 °C.

between the coordinated and free sites with $UO_2(dbm)_2$-dmso in a DMSO and CD_3COCD_3 mixture, because the signal of the DMSO methyl protons changes from two signals at −30 °C to one signal at 30 °C. More detailed spectral changes with temperature are shown in Fig. 6 for the temperature region from −20 to 30 °C.

TABLE 4. THE VALUES OF k_1 AND k_2 AT VARIOUS TEMPERATURES FOR THE EXCHANGE OF DMSO IN $UO_2(dbm)_2dmso$ IN CD_2Cl_2

Temp / °C	k_1 / $10\ s^{-1}$	k_2 / $10^2\ M^{-1}\ s^{-1}$
−10	2.91±0.44	2.12±0.14
−15	2.18±0.33	1.53±0.11
−20	1.62±0.25	1.09±0.08
−25	1.19±0.18	0.76±0.06

The coalescence of the coordinated and free DMSO signals was also observed at high temperature. The best-fit τ-values at each temperature were determined by the same method as mentioned before and the calculated lineshapes are also shown in Fig. 6. The first-order exchange rate constants, k_{ex}, were calculated by Eqs. 1 and 2. The k_{ex} values obtained for the solutions listed in Table 3 were plotted semilogarithmically against the reciprocal temperature (Fig. 7). The activation parameters are given in Table 3. As can be seen in Fig. 7 and Table 3, the rate of DMSO exchange in CD_3COCD_3 is independent of the free DMSO concentration, while the rate in CD_2Cl_2 is dependent on the concentration of free DMSO. A plot of k_{ex} values which were obtained in CD_2Cl_2 against the free DMSO concentration is linear (Fig. 8) and results in the following equation.

$$k_{ex} = k_1 + k_2[\mathrm{DMSO}] \quad (3)$$

The values of k_1 and k_2 were, respectively, obtained from the intercepts and the slopes of the plots from Fig. 8 by means of the least-squares method, and are shown in Table 4. The activation parameters for these paths are given in Table 3.

Possible Mechanism. It was found that the rate of the DMSO exchange reactions in $UO_2(acac)_2dmso$ and $UO_2(dbm)_2dmso$ in CD_3COCD_3 is independent of the free DMSO. This fact suggests that the DMSO exchange process for these complexes in CD_3COCD_3 proceeds through either the D or the I mechanism.[23]

In the D mechanism, the exchange process is expressed as

$$UO_2(\beta\text{-diketonato})_2dmso + DMSO^* \xrightarrow[\text{slow}]{k_d}$$
$$UO_2(\beta\text{-diketonato})_2 + DMSO + DMSO^* \xrightarrow[\text{fast}]{}$$
$$UO_2(\beta\text{-diketonato})_2dmso^* + DMSO. \quad (4)$$

In this mechanism, the rate-determining step is the dissociation of the coordinated DMSO from $UO_2(\beta$-diketonato$)_2dmso$ and an intermediate of reduced coordination number, $UO_2(\beta$-diketonato$)_2$, is formed. Thus, k_{ex} is given as

$$k_{ex} = k_d. \quad (5)$$

In the I mechanism, overall processes are represented as

$$UO_2(\beta\text{-diketonato})_2dmso + DMSO^* \underset{\text{fast}}{\overset{K_{os}}{\rightleftharpoons}}$$
$$UO_2(\beta\text{-diketonato})_2dmso\cdots DMSO^* \xrightarrow[\text{slow}]{k_1}$$

$$UO_2(\beta\text{-diketonato})_2dmso^*\cdots DMSO \xrightarrow[fast]{} UO_2(\beta\text{-diketonato})_2dmso^* + DMSO, \quad (6)$$

where K_{os} is the formation constant of the outer-sphere complex, $UO_2(\beta$-diketonato$)_2$dmso$\cdots$DMSO*, and k_I is the interchange rate constant between DMSO molecules in the first coordination sphere and those in the second coordination sphere. Since the rate-determining step is the k_I path, k_{ex} is given by Eq. 7.

$$k_{ex} = k_I K_{os}[DMSO]/(1+K_{os}[DMSO]) \quad (7)$$

If $K_{os}[DMSO] \gg 1$, Eq. 7 can be simplified as $k_{ex}=k_I$ and the exchange rate of DMSO becomes independent of DMSO. This mechanism also appears to be compatible with the results of the DMSO exchange in $UO_2(acac)_2$dmso and $UO_2(dbm)_2$dmso in CD_3COCD_3.

Although the D or I mechanism can not be distinguished by the form of the rate law, the I mechanism seems to be unlikely for the following reasons. In the I mechanism, the condition $K_{os}[DMSO] \gg 1$ is required and hence $K_{os} \gg 100\ M^{-1}$ should be satisfied over the concentration range in the present experiments. However, such a value of $K_{os}(\gg 100\ M^{-1})$ is too large considering the normal association constant between uncharged molecules. The D mechanism, on the other hand, might be supported by the fact that some uranyl complexes, *e.g.* $UO_2(H_2O)_4^{2+}$ [1,24,25] $UO_2(hmpa)_4^{2+}$ [2,26] exist in solution as a tetragonal bipyramid.

Another mechanism, where the rate-determining step is the ring-opening of one of the coordinated acac groups, might be proposed. However, this mechanism can be ruled out since the rate constant for ring-opening is about 2.04 s^{-1} at 25 °C in o-$C_6H_4Cl_2$ [27] which is much smaller than that observed for the DMSO exchange reaction.

For the DMSO exchange reaction for $UO_2(acac)_2$-dmso in CD_2Cl_2, the observed first-order rate constants, k_{ex}, depend on the free DMSO concentrations but not linearly as shown in Fig. 5. This fact might suggest that the DMSO exchange in this system proceeds through both the D and I mechanisms. From Eqs. 4 and 6, k_{ex} is given by Eq. 8.

$$k_{ex} = \frac{k_d + k_I K_{os}[DMSO]}{1+K_{os}[DMSO]} \quad (8)$$

If $K_{os}[DMSO] \ll 1$, Eq. 8 can be simplified as $k_{ex}=k_d+k_I K_{os}[DMSO]$. This corresponds to the region of low DMSO concentration in Fig. 8, where k_{ex} changes linearly with DMSO concentration. If $K_{os}[DMSO] \gg 1$, k_{ex} is close to k_I. This is consistent with the fact that the k_{ex} values approach the limiting values at high DMSO concentrations. The values of k_d, k_I, and K_{os} were calculated by using the nonlinear least-squares method for Eq. 8 and are listed in Table 5. The experimental data are in close agreement with the calculated best-fit lines, which are shown in Fig. 5 as solid lines. The activation parameters for k_d and k_I were obtained from the data for various temperatures and are shown in Table 2.

Table 5. The values of k_d, k_I, and K_{os} at various temperatures for the exchange of DMSO in $UO_2(acac)_2$ dmso in CD_2Cl_2

Temp / °C	k_d / s^{-1}	k_I / $10^2\ s^{-1}$	K_{os} / M^{-1}
10	35.5±6.1	4.47±1.17	4.6±2.1
0	18.5±0.8	1.86±0.45	5.9±0.4
−10	8.38±0.44	1.65±0.08	3.1±0.2
−20	2.85±0.67	0.57±0.01	6.2±0.5

As can be seen in Fig. 8, the DMSO exchange in $UO_2(dbm)_2$dmso behaves similar to that observed for $UO_2(acac)_2$dmso in CD_2Cl_2 except for the plots being linear even at the high DMSO concentration range. In spite of the linear relationship of k_{ex} against the DMSO concentration, the A mechanism [23] seems to be unlikely, because the size of dbm is much larger than that of acac and the associative attack of the DMSO molecule should be sterically restricted for the dbm complex. If a similar mechanism (combination of the D and I mechanisms) as proposed for $UO_2(acac)_2$dmso In CD_2Cl_2 is assumed, the condition of $K_{os}[DMSO] \ll 1$ should be satisfied over the range of DMSO concentrations from 0.0627 to 0.499 M. This means that K_{os} for $UO_2(dbm)_2$dmso and DMSO is at least fivefold smaller than that between $UO_2(acac)_2$dmso and DMSO. Considering the bulky size of dbm compared with that of acac, such a value of K_{os} might be expected to be reasonable.

The difference in exchange processes which were observed in two different solvents, CD_3COCD_3 and CD_2Cl_2, may primarily be attributed to the difference in affinity of these solvents for uranyl complexes. Acetone has a relatively large basicity compared with dichloromethane on the basis of Gutmann's donor number [28] and tends to solvate the second coordination spheres of uranyl complexes under the present experimental conditions. It may be predicted that in the case of DMSO exchange in CD_3COCD_3, solvation by CD_3COCD_3 assists the dissociation of DMSO from the first coordination sphere, instead of the free DMSO in the bulk solvent being involved in the activated complex. The dielectric constant of acetone (20.7) is larger than that of dichloromethane (8.93), and hence smaller K_{os} values are expected in CD_3COCD_3 than in CD_2Cl_2.

Table 6. Kinetic parameters for the exchange of DMSO in various uranyl complexes in CD_3COCD_3

Complex	Mechanism	ΔH^* / kJ mol^{-1}	ΔS^* / J K^{-1} mol^{-1}	k_{ex}(25 °C) / s^{-1}
$UO_2(dmso)_5^{2+}$	D	53.8±2.4	6.3±14.5	5.53×10^3
	A	39.1±1.7	−28.1± 5.0	$3.22\times10^4/M^{-1}$
$UO_2(acac)_2$ dmso	D	45.8±0.8	−46.6± 2.9	2.36×10^2
$UO_2(dbm)_2$ dmso	D	44.5±0.4	−46.2± 2.1	3.92×10^2

Nevertheless, much larger values of k_{ex} in CD_3COCD_3 may support the above solvent assisted mechanism.

In spite of the DMSO exchange reactions in $UO_2(acac)_2dmso$ and $UO_2(dbm)_2dmso$ proceeding through the D and I mechanisms, large negative activation entropies are observed. This may be due to the solvent effect as suggested by Bennetto and Caldin.[29,30] They suggested that even though the exchange reaction proceeds dissociatively, ΔS^* may have negative values from the contribution of the solvent rearrangement around the metal complexes.

It is interesting to compare the DMSO exchange reactions in $UO_2(dmso)_5^{2+}$, $UO_2(acac)_2dmso$, and $UO_2(dbm)_2dmso$. The kinetic parameters of these DMSO exchange reactions in CD_3COCD_3 are summerized in Table 6. In the case of $UO_2(dmso)_5^{2+}$, the exchange rate is much faster than for the other complexes. This is consistent with general expectation that if the exchange reaction proceeds through an associative process, the reaction rate should be reduced significantly with crowding at the reaction site. It is quite reasonable that the bulky chelating ligands, acac and dbm, may hinder the approach of free DMSO to the first coordination sphere of the uranyl complex. This result may support the notion that the A mechanism is the major process for $UO_2(dmso)_5^{2+}$ in contrast with the D type processes for $UO_2(acac)_2dmso$ and $UO_2(dbm)_2dmso$.

The authors wish to thank Professor Gilbert Gordon of Miami University and Professor Thomas W. Swaddle of the University of Calgary for their helpful discussions.

References

1) Y. Ikeda, S. Soya, H. Tomiyasu, and H. Fukutomi, *J. Inorg. Nucl. Chem.*, **41**, 1333 (1979).
2) G. J. Honan, S. F. Lincoln, and E. H. Williams, *Inorg. Chem.*, **17**, 1855 (1978).
3) R. P. Bowen, S. F. Lincoln, and E. H. Williams, *Inorg. Chem.*, **15**, 2126 (1976).
4) J. Crea, R. Digiusto, S. F. Lincoln, and E. H. Williams, *Inorg. Chem.*, **16**, 2825 (1977).
5) Y. Ikeda, H. Tomiyasu, and H. Fukutomi, *Bull. Res. Lab. Nucl. Reactors.*, **4**, 47 (1979).
6) R. P. Bowen, G. J. Honan, S. F. Lincoln, T. M. Spotswood, and E. H. Williams, *Inorg. Chim. Acta*, **33**, 235 (1979).
7) G. J. Honan, S. F. Lincoln, and E. H. Williams, *J. Chem. Soc., Dalton Trans.*, **1979**, 1220.
8) A. Vasilescu, *Rev. Roum. Chim.*, **20**, 951 (1975).
9) K. Bokolo, J. J. Delpuech, L. Rodehüsen, and P. R. Rubini, *Inorg. Chem.*, **20**, 992 (1981).
10) T. V. Healy, D. F. Peppard, and G. W. Mason, *J. Inorg. Nucl. Chem.*, **24**, 1429 (1962).
11) T. V. Healy and J. R. Ferraro, *J. Inorg. Nucl. Chem.*, **24**, 1449 (1962).
12) Y. Baskin and J. R. Ferraro, *J. Inorg. Nucl. Chem.*, **30**, 241 (1968).
13) M. S. Subramanian and A. Viswanatha, *J. Inorg. Nucl. Chem.*, **31**, 2575 (1969).
14) J. M. Haigh and D. A. Thornton, *J. Inorg. Nucl. Chem.*, **33**, 3001 (1971).
15) E. Frasson, G. Bombieri, and C. Panattoni, *Nature*, **202**, 1325 (1964).
16) E. Frasson, G. Bombieri, and C. Panattoni, *Coord. Chem. Rev.*, **1**, 145 (1966).
17) A. E. Comyns, B. M. Gatehouse, and E. Wait, *J. Chem. Soc.*, **1958**, 4655.
18) L. Sacconi and G. Giannoni, *J. Chem. Soc.*, **1944**, 2368.
19) E. L. Eliel and N. L. Allinger, *Top. Stereochem.*, **3**, 97 (1968).
20) F. A. Cotton and R. Francis, *J. Am. Chem. Soc.*, **82**, 2986 (1960).
21) K. Nakamoto, "Infrared and Raman Spectra of Inorganic and Coordination Compounds," John Wiley and Sons, Inc., New York (1978).
22) Y. Ikeda, H. Tomiyasu, and H. Fukutomi, 3rd Symposium on Solution Chemistry, Tokyo, Oct. 1980, Abstr. p. 213.
23) C. H. Langford and H. B. Gray, "Ligand Substitution Processes," Benjamin, London (1974).
24) A. Fratiello, V. Kubo, R. E. Lee, and R. E. Schuster, *J. Phys. Chem.*, **74**, 3726 (1970).
25) A. Fratiello, V. Kubo, and R. E. Schuster, *Inorg. Chem.*, **10**, 744 (1971).
26) A. Fratiello, G. A. Vidlich, C. Cheng, and V. Kubo, *J. Solution Chem.*, **1**, 433 (1972).
27) Y. Ikeda, H. Tomiyasu, and H. Fukutomi, 30th Symposium on Coordination Chemistry, Tokyo, Oct. 1980, Abstr. p. 56.
28) V. Gutmann and R. Schmid, *Coord. Chem. Rev.*, **12**, 263 (1974).
29) H. P. Bennetto and E. F. Caldin, *J. Chem. Soc., A*, **1971**, 2198.
30) E. F. Caldin and H. P. Bennetto, *J. Solution Chem.*, **2**, 217 (1973).

Preparation and Circular Dichroism Spectra of *trans*-Dichlorocobalt(III) Complexes with (2-Aminoethyl)diphenylphosphine and Related Ligands. Crystal Structures of *trans*(Cl,Cl), *cis*(P,P)-$[CoCl_2\{NH_2CH_2CH_2P(C_6H_5)_2\}_2]\cdot 1/2[CoCl_4]$ and -$[CoCl_2\{NH_2CH_2CH_2P(C_4H_9)(C_6H_5)\}_2]ClO_4$

Isamu KINOSHITA,† Yasuno YOKOTA,† Keiji MATSUMOTO,† Shun'ichiro OOI,† Kazuo KASHIWABARA, and Junnosuke FUJITA*

Department of Chemistry, Faculty of Science, Nagoya University, Chikusa-ku, Nagoya 464
†*Department of Chemistry, Faculty of Science, Osaka City University, Sumiyoshi-ku, Osaka 556*

(Received October 7, 1982)

Green *trans*-dichlorocobalt(III) complexes with a variety of achiral and chiral (2-aminoalkyl)phosphines have been prepared and characterized. The crystal structures of $[CoCl_2\{(2\text{-aminoethyl})diphenylphosphine\}_2]1/2[CoCl_4]$ and $[CoCl_2\{(R)\text{-}(2\text{-aminoethyl})butylphenylphosphine\}_2]ClO_4$ have been determined by X-ray analyses. Both complex cations have a distorted octahedral coordination with two Cl atoms in the *trans* positions and two P (and N) atoms in the *cis* positions. The Co–N distances (2.02—2.05 Å) are 0.05—0.07 Å longer than the usual Co(III)–N distance, and the P–Co–P angles are widened (99.4 and 103.1°) on account of bulky substituents on the phosphorus atoms. The circular dichroism spectra of $[CoCl_2\{(2\text{-aminoethyl})diphenylphosphine\}_2]ClO_4$ (space group $P3_221$) in Nujol mull and the complexes with chiral (aminoalkyl)phosphines in methanol solutions have been recorded and compared with those of related complexes.

In a previous paper,[1] we have reported the preparation, and some spectroscopic and chemical properties of the $[CoCl_2\{NH_2CH_2CH_2P(C_6H_5)_2\}_2]X$ (X=Cl^- or ClO_4^-) complex. The complex has a green color characteristic of the *trans*(Cl,Cl) configuration. However, no clear evidence was obtained for assigning the geometrical configuration of the phosphorus (or nitrogen) donor atoms, *trans*(P,P) or *cis*(P,P). This paper deals with crystal structures of two green complexes, $[CoCl_2\{NH_2CH_2CH_2P(C_6H_5)_2\}_2]1/2[CoCl_4]$ and $[CoCl_2\{(R)\text{-}NH_2CH_2CH_2P(C_4H_9)(C_6H_5)\}_2]ClO_4$, determined by X-ray structure analyses. The latter complex is chiral and shows circular dichroism (CD). The perchlorate salt of the former complex, the structure of which could not be solved because of the twin crystal, crystallizes in the chiral space group $P3_221$ and also exhibits CD in the solid state. This paper includes CD spectra of those and several complexes of the same *trans*-dichloro-type formed with related optically active (aminoalkyl)phosphine ligands.

The ligands used in this study and the abbreviations are as follows; (2-aminoethyl)diphenylphosphine, $NH_2CH_2CH_2P(C_6H_5)_2$=edpp; (2-aminoethyl)dimethylphosphine, $NH_2CH_2CH_2P(CH_3)_2$ = edmp; (*S*)-(2-aminopropyl)diphenylphosphine, (*S*)-$NH_2CH(CH_3)CH_2P(C_6H_5)_2$ = *S*-pdpp; (*R*)-(2-aminoethyl) butylphenylphosphine, (*R*)-$NH_2CH_2CH_2P(C_4H_9)(C_6H_5)$ = *R*-ebpp; (*S*)-2-(diphenylphosphinomethyl)pyrrolidine, (*S*)-$CH_2CH_2CH_2NHCHCH_2P(C_6H_5)_2$=*S*-prdpp; (*S*(C),*R*(P))- and (*S*(C),*S*(P))-2-(butylphenylphosphinomethyl)-pyrrolidine, (*S*(C), *R*(P))- and (*S*(C), *S*(P))-$CH_2CH_2CH_2NHCHCH_2P(C_4H_9)(C_6H_5)$ = *S*(C),*R*(P)- and *S*(C),*S*(P)-prbpp. The notation of the absolute configurations, *R* and *S*, for the chiral phosphorus atom of a free ligand is reversed upon coordination to the cobalt(III) ion.[2] In this paper, however, we use the same notation for a coordinating ligand as that when it is free.

Experimental

Preparations. Free (aminoalkyl)phosphines were prepared according to methods reported and handled under nitrogen atmosphere until they formed air-stable cobalt(III) complexes; edpp,[3] edmp,[4] *S*-pdpp,[5] *R*-ebpp,[6] *S*-prdpp,[7] and *S*(*C*), *R*(P)- and *S*(C), *S*(P)-prbpp.[8]

$[CoCl_2(edpp)_2]ClO_4$ and $[CoCl_2(edpp)_2]1/2[CoCl_4]$. The perchlorate was prepared by the method reported in a previous paper.[1]

The perchlorate (100 mg) was dissolved in methanol (40 cm³), and 5 cm³ of concd hydrochloric acid was added. On standing at room temperature the solution gave green needles of $[CoCl_2(edpp)_2]Cl\cdot HCl\cdot H_2O$ (38 mg). Found: C, 49.86; H, 5.20; N, 4.12%. Calcd for $C_{28}H_{35}N_2OP_2Cl_4Co$: C, 49.58; H, 5.20; N, 4.13%.

The crystals were dissolved again in methanol and $CoCl_2\cdot 6H_2O$ (8 mg) was added. The solution was evaporated slowly by standing at room temperature to give dark green plates of $[CoCl_2(edpp)_2]1/2[CoCl_4]$ which were subjected to X-ray analysis. Found: C, 48.02; H, 4.84; N, 4.09%. Calcd for $C_{28}H_{32}N_2P_2Cl_4Co_{1.5}$: C, 48.82; H, 4.68; N, 4.07%.

$[CoCl_2(edmp)_2]Cl\cdot H_2O$ and $[CoCl_2(edmp)_2]ClO_4\cdot 1/2\ NaClO_4$. The chloride was prepared by two methods. *Method 1*: To a methanol solution (50 cm³) of $CoCl_2\cdot 6H_2O$ (238 mg, 1 mmol) was added edmp (210 mg, 2 mmol) under nitrogen atmosphere, and then the mixture was stirred in the air for 6 h. The resulting brown solution was diluted with water and poured onto an SP-Sephadex column. The product adsorbed was eluted with a 0.01 mol/dm³ NaCl solution, and the eluate was evaporated to dryness under reduced pressure. The residue was extracted with ethanol. The extract was allowed to evaporate slowly at room temperature, giving blue-green crystals of $[CoCl_2(edmp)_2]Cl\cdot H_2O$. Yield: *ca.* 10%.

Method 2: An *N*,*N*-dimethylformamide solution (50 cm³) of *cis*-$[CoCl_2(en)_2]Cl$ (en: ethylenediamine) (285 mg, 1 mmol) was mixed with a methanol solution (10 cm³) of edmp (105 mg, 1 mmol), and the mixture was stirred for 6 h. The resulting solution was diluted and chromatographed by the same method as the above to give the complex. Yield: *ca.* 7%. Found: C, 24.12; H, 6.54; N, 6.95%. Calcd for $C_8H_{26}N_2OP_2Cl_3Co$: C, 24.42; H, 6.66; N, 7.12%. No dichloro complex was

TABLE 1. CRYSTAL DATA AND EXPERIMENTAL DETAILS

	Compound	
	$[CoCl_2(R\text{-ebpp})_2]$-$ClO_4$	$[CoCl_2(edpp)_2]$-1/2$[CoCl_4]$
Crystal system	Orthorhombic	Monoclinic
Space group	$P2_12_12$	$C2/c$
a/Å	18.30(1)	29.52(2)
b/Å	17.83(1)	14.517(5)
c/Å	9.496(7)	16.928(6)
β/°		119.29(4)
Z	4	8
D_m/g cm^{-3}	1.38	1.45
D_c/g cm^{-3}	1.39	1.45
μ(Mo $K\alpha$)/cm^{-1}	9.7	12.9
Crystal size/mm^3	0.20×0.23×0.35	0.18×0.28×0.50
Scan type	ω	ω
Scan speed/° s^{-1}	0.033	0.025
Scan range/°	1.0+0.2 tan θ	1.0+0.2 tan θ
Background count/s^{-1}	15	20
$2\theta_{max}$/°	55	50
No. of unique data ($F_0^2>2\sigma(F_0^2)$)	3271	3493
Minimized function	$\sum w(F_o-\|F_c\|)^2$	$\sum w(F_o-\|F_c\|)^2$
Weight	$1/\sigma^2$ (F_o)	$1/\sigma^2$ (F_o)
$R_1=\sum\Delta F/F_o$	0.069	0.062
$R_2=[\sum w\Delta F^2/\sum wF_0^2]^{1/2}$	0 090	0.078
Convergence maximum shift (Δ/σ)	0.5	0.12
Peak hight in the final difference synthesis/e Å^{-3}	1.0	0.14

obtained when treated with 2 mmol of edmp, yellow $[Co(en)_{3-n}(edmp)_n]^{3+}$ complexes being formed.

The perchlorate was obtained by adding $NaClO_4$ to a solution of the chloride in the minimum amount of ethanol, and recrystallized from ethanol and diethyl ether. Found: C, 19.62; H, 4.92; N, 5.67%. Calcd for $C_8H_{24}N_2O_6P_2Cl_{3.5}CoNa_{0.5}$: C, 19.20; H, 4.83; N, 5.59%.

$[CoCl_2(S\text{-pdpp})_2]ClO_4$, $[CoCl_2(R\text{-ebpp})_2[ClO_4]$, $CoCl_2(S\text{-prdpp})_2]ClO_4\cdot H_2O$, $[CoCl_2(S(C), R(P)\text{-prbpp})_2]ClO_4\cdot 1/2\ H_2O$, and $[CoCl_2(S(C), S(P)\text{-prbpp})_2]ClO_4\cdot H_2O$. These complexes were prepared by a method similar to that for the edpp complex. The *R*-ebpp, and *S*(C), *R*(P)- and *S*(C), *S*(P)-prbpp ligands were obtained from their palladium(II) complexes by the method reported.[6] Found for $[CoCl_2(S\text{-pdpp})_2]ClO_4$: C, 50.07; H, 5.63; N, 3.44%. Calcd for $C_{30}H_{36}N_2O_4P_2Cl_3Co$: C, 50.33; H, 5.07; N, 3.91%. Found for $[CoCl_2(R\text{-ebpp})_2]ClO_4$: C, 44.39; H, 6.20; N, 4.32%. Calcd for $C_{24}H_{40}N_2O_4P_2Cl_3Co$: C, 44.50; H, 6.22; N, 4.32%. Found for $[CoCl_2(S\text{-prdpp})_2]ClO_4\cdot H_2O$: C, 51.75; H, 5.56; N, 3.31% Calcd for $C_{34}H_{42}N_2O_5P_2Cl_3Co$: C, 51.96; H, 5.39; N, 3.56%. Found for $[CoCl_2(S(C), R(P)\text{-prbpp})_2]ClO_4\cdot 1/2H_2O$: C, 48.45; H, 6.31; N, 4.30%. Calcd for $C_{30}H_{49}N_2O_{4.5}P_2Cl_3Co$: C, 48.89; H, 6.70; N, 3.80%. Found for $[CoCl_2(S(C), S(P)\text{-prbpp})_2]ClO_4\cdot H_2O$: C, 47.68; H, 6.32; N, 4.44%. Calcd for $C_{30}H_{50}N_2O_5P_2Cl_3Co$: C, 48.30; H, 6.76; N, 3.76%.

Spectral Measurements. Absorption and CD spectra were recorded on a Hitachi 323 spectrophotometer and a JASCO J-40CS spectropolarimeter, respectively.

X-Ray Analyses. X-Ray analyses of $[CoCl_2(edpp)_2]1/2[CoCl_4]$ and $[CoCl_2(R\text{-ebpp})_2]ClO_4$ were performed. Space groups and approximate unit-cell dimensions were determined from oscillation and Weissenberg photographs taken with Cu $K\alpha$ radiation. Crystal data and experimental details are given in Table 1.

Intensity data were collected at room temperature on a Philips PW1100 automated diffractometer by the use of graphite-monochromated Mo $K\alpha$ radiation. The intensities of three standard reflections of each compound showed no appreciable decay throughout the data collections. An absorption collection was applied for the ebpp complex, but not for the edpp complex. The maximum and minimum transmission factors are 1.34 and 1.30, respectively. Relative structure factors were calculated by use the program written

TABLE 2. FRACTIONAL COORDINATES AND TEMPERATURE FACTORS FOR *trans*-$[CoCl_2(edpp)_2]1/2[CoCl_4]$
Standard deviations of the least significant figures are given in parentheses.

Atom	x	y	z	B_{eq}/Å^2	Atom	x	y	z	B_{eq}/Å^2
Co(2)	0.11496(4)	0.2336(1)	0.0896(1)	3.16(4)	N(2)	0.0915(3)	0.2241(6)	−0.0440(4)	4.5(3)
Cl(1)	0.0416(1)	0.3099(2)	0.0547(1)	4.5(1)	C(3)	0.1152(4)	0.3861(7)	−0.0392(5)	4.9(4)
Cl(2)	0.1848(1)	0.1503(2)	0.1160(2)	4.1(1)	C(4)	0.1152(4)	0.2913(8)	−0.0795(6)	5.4(4)
N(1)	0.0748(3)	0.1149(5)	0.0714(6)	5.5(4)	P(2)	0.1517(1)	0.3679(2)	0.0843(1)	3.0(1)
C(1)	0.1226(4)	0.0980(6)	0.2375(7)	5.5(5)	C(17)	0.1432(3)	0.4745(5)	0.1342(5)	3.1(3)
C(2)	0.0707(4)	0.0823(7)	0.1526(8)	6.4(5)	C(18)	0.0941(3)	0.5185(6)	0.0898(6)	4.4(4)
P(1)	0.1374(1)	0.2212(1)	0.2370(1)	3.3(1)	C(19)	0.0876(3)	0.5982(6)	0.1318(7)	5.0(4)
C(5)	0.0994(3)	0.2820(6)	0.2797(5)	3.3(3)	C(20)	0.1268(4)	0.6316(7)	0.2121(7)	5.0(4)
C(6)	0.0935(3)	0.3779(6)	0.2684(5)	3.5(3)	C(21)	0.1750(3)	0.5864(7)	0.2544(6)	4.7(4)
C(7)	0.0683(3)	0.4279(6)	0.3070(6)	4.1(3)	C(22)	0.1829(3)	0.5073(6)	0.2145(6)	3.7(3)
C(8)	0.0489(3)	0.3791(7)	0.3565(6)	4.9(3)	C(23)	0.2197(3)	0.3709(6)	0.1133(5)	3.3(3)
C(9)	0.0541(3)	0.2833(7)	0.3661(6)	4.3(3)	C(24)	0.2346(4)	0.4066(7)	0.0514(7)	5.3(4)
C(10)	0.0790(3)	0.2349(6)	0.3270(5)	3.8(3)	C(25)	0.2893(4)	0.4108(7)	0.0805(8)	5.7(5)
C(11)	0.2040(3)	0.2395(6)	0.3261(5)	4.0(3)	C(26)	0.3258(3)	0.3832(6)	0.1654(7)	5.0(4)
C(12)	0.2429(4)	0.1715(8)	0.3454(7)	6.2(5)	C(27)	0.3105(3)	0.3483(6)	0.2253(7)	5.1(4)
C(13)	0.2931(4)	0.1891(9)	0.4085(6)	7.2(5)	C(28)	0.2572(3)	0.3403(6)	0.2000(6)	4.1(3)
C(14)	0.3075(4)	0.272(1)	0.4519(7)	7.5(5)	Co(1)	0.50000(0)	0.4093(1)	0.25000(0)	4.1(1)
C(15)	0.2713(4)	0.3402(9)	0.4365(7)	6.8(5)	Cl(3)	0.4368(1)	0.4909(2)	0.1341(2)	5.0(1)
C(16)	0.2179(3)	0.3231(7)	0.3710(6)	4.6(3)	Cl(4)	0.4646(1)	0.3195(2)	0.3162(2)	8.0(1)

TABLE 3. FRACTIONAL COORDINATES AND TEMPERATURE FACTORS FOR *trans*-[$CoCl_2$(*R*-ebpp)$_2$]ClO_4
Standard deviations of the least significant figures are given in parentheses.

Atom	*x*	*y*	*z*	B_{eq}/Å^2	Atom	*x*	*y*	*z*	B_{eq}/Å^2
Co	0.1524(1)	0.0768(1)	−0.0185(1)	3.19(2)	C(8)	0.1142(5)	0.3183(5)	−0.462(1)	6.9(4)
Cl(3)	0.4037(1)	0.3656(1)	−0.3517(3)	5.1(1)	C(9)	0.187(1)	0.3105(7)	−0.413(1)	6.0(6)
O(1)	0.3398(1)	0.4025(1)	−0.3368(3)	19.4(1)	C(10)	0.2112(5)	0.2422(5)	−0.3563(9)	4.6(2)
O(2)	0.4011(4)	0.2851(4)	−0.3413(9)	11.0(2)	P(2)	0.1663(5)	0.1913(6)	0.072(1)	3.5(3)
O(3)	0.4492(6)	0.3944(6)	−0.248(1)	10.5(3)	C(11)	0.2581(6)	0.2219(7)	0.116(1)	3.8(4)
O(4)	0.4346(4)	0.3833(4)	−0.4802(8)	16.7(2)	C(12)	0.3033(6)	0.2479(6)	0.006(1)	4.4(3)
Cl(1)	0.0377(6)	0.1063(7)	−0.082(1)	4.0(3)	C(13)	0.3752(5)	0.2688(6)	0.039(1)	4.6(3)
Cl(2)	0.2620(1)	0.0398(1)	0.0560(2)	4.6(1)	C(14)	0.4012(5)	0.2637(5)	0.171(1)	6.2(2)
N(1)	0.1342(6)	−0.0309(5)	−0.085(1)	4.6(3)	C(15)	0.3573(5)	0.2395(5)	0.284(1)	5.7(3)
C(1)	0.1471(4)	0.0179(5)	−0.3263(9)	5.0(2)	C(16)	0.2838(5)	0.2199(6)	0 253(1)	5.6(3)
C(2)	0.1622(5)	−0.0496(7)	−0.228(1)	6.2(3)	C(17)	0.2887(6)	0.0936(6)	−0.267(1)	6.2(3)
N(2)	0.1113(1)	0.0462(1)	0.1724(2)	4.5(1)	C(18)	0.1223(6)	0.2697(6)	−0.011(1)	4.5(3)
C(3)	0.1185(5)	0.1809(6)	0.239(1)	5.2(3)	C(19)	0.3096(6)	0.0795(6)	−0.426(1)	6.2(2)
C(4)	0.1308(5)	0.0959(5)	0.2886(9)	6.0(2)	C(20)	0.3888(8)	0.0608(9)	−0.440(2)	9.5(4)
P(1)	0.1902(5)	0.0989(5)	−0.238(1)	3.4(2)	C(21)	0.409(1)	0.042(1)	−0.602(2)	13.7(6)
C(5)	0.1602(1)	0.1806(1)	−0.3318(3)	3.8(1)	C(22)	0.1233(7)	0.3441(8)	0.078(2)	7.9(3)
C(6)	0.0878(5)	0.1903(6)	−0.379(2)	4.0(9)	C(23)	0.0785(9)	0.4048(9)	0.017(2)	10.3(4)
C(7)	0.0648(6)	0.2535(5)	−0.439(1)	5.2(4)	C(24)	0.018(2)	0.396(2)	0.056(3)	24(1)

by Hornstra and Stubbe.[9]

The structures were solved by the conventional Patterson and Fourier techniques. The parameters were refined by the block-diagonal least-squares method. The six carbon atoms of the two butyl groups were isotropically refined because they were disordered. The atomic scattering factors of the Co, Cl, P, O, N, and C atoms were taken from the reference.[10] The real part of the anomalous dispersion corrections were applied for the Co, Cl, and P atoms. The absolute configuration of the ebpp complex could not be determined, since the Weissenberg photographs taken with Cu *Ka* radiation showed no appreciable difference in intensities of any Bijvoet pairs.

The atomic coordinates are listed in Tables 2 and 3.

The F_o-F_c tables and anisotropic thermal parameters are preserved by the Chemical Society of Japan (Document No. 8314). The computation were carried out by the FACOM 230-60 computer at Osaka City University and the ACOS 700 computer at the Crystallographic Research Center, Institute for Protein Research, Osaka University. The programs used included local versions of the UNICS[11] and ORTEP II.[12]

Results and Discussion

Crystal Structures of [$CoCl_2$(*edpp*)$_2$]*1/2*[$CoCl_4$] (*A*) *and* [$CoCl_2$(R-*ebpp*)$_2$]ClO_4 (*B*). Figures 1 and 2 show the X-ray structures of the complex cations in **A** and **B**, respectively. Both cations have a distorted octahedral coordination with two Cl atoms in the *trans* positions and two P (and N) atoms in the *cis* positions. The complex cation in **A** has an approximate two-fold axis running through the Co atom and the mid point of the P···P edge. Thus both edpp chelate rings form the same $\delta\delta$ or $\lambda\lambda$ chiral conformation, although the crystal has the achiral space group C2/c, comprising of an equal amount of the $\delta\delta$ and $\lambda\lambda$ conformers. The corresponding perchlorate salt crystallizes in the chiral space group $P3_221$ (or $P3_121$), and all the chelate rings in a crystal should have the same chirality (*vide infra*). Complex **B** contains the optically active ebpp ligand. The absolute configuration of the ligand could not be determined by the X-ray method (Experimental), but has been assigned conclusively to *R* from CD studies of the Pd(II)–dichloro complex of this ligand and the corresponding *S*(C),*S*(P)- and *S*(C),*R*(P)-prbpp complexes.[6] The absolute configuration of the *S*(C),*S*(P)-prbpp complex was determined by the X-ray method.[8] The two *R*-ebpp chelate rings take enantiomeric conformations to each other, δ and λ and the two phenyl (or butyl) groups are disposed in the opposite directions to each other from the plane formed with the two chelate rings. The selected bond distances and angles are given in Tables 4 and 5.

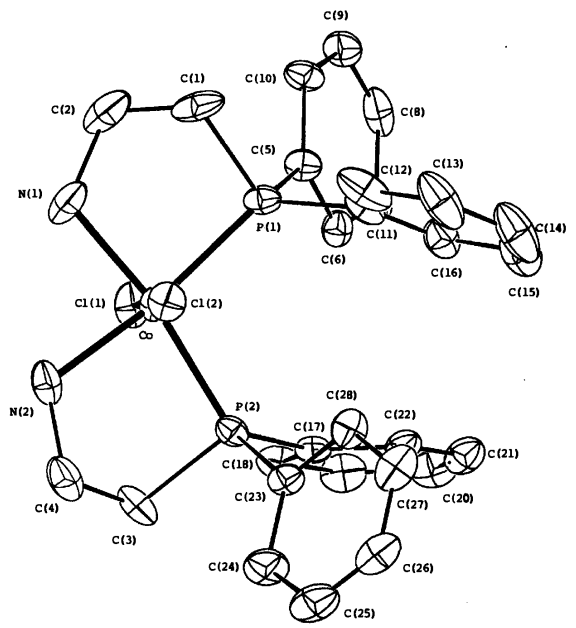

Fig. 1. The *trans*(Cl, Cl), *cis*(P, P)-[$CoCl_2$(edpp)$_2$]$^+$ ion viewed along the Cl–Co–Cl axis. The thermal ellipsoids are drawn at the 30% probability level.

The average Co–P distance in **B** is slightly shorter

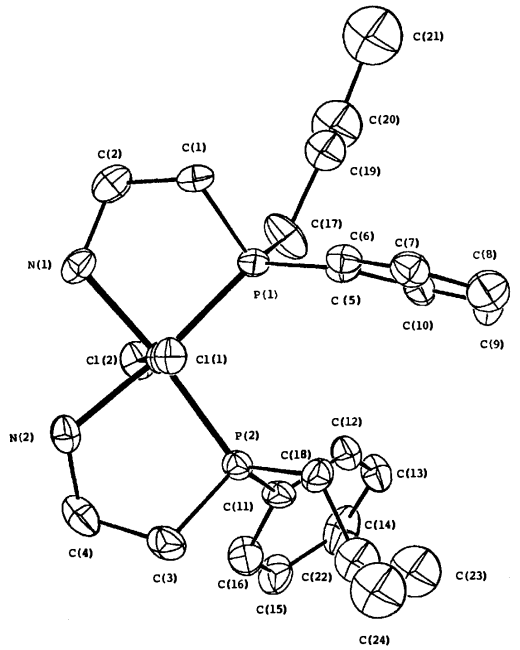

Fig. 2. The *trans*(Cl, Cl), *cis*(P, P)-$[CoCl_2(R\text{-ebpp})_2]^+$ ion viewed along the Cl-Co-Cl axis. The thermal ellipsoids are drawn at the 30% probability level, except for C(24) which is represented by a sphere with arbitrary radius.

than that in **A**, although the difference is not significant in view of the e.s.d.'s. These distances are 0.03—0.10 Å shorter than the Co(III)–P distances found for unidentate phosphine complexes.[13] The Co–N distances range from 2.02 to 2.05 Å which are 0.05—0.07 Å longer than the usual Co(III)–N distance. The lengthening of the Co–N bond has been found in *fac*-$[Co(edmp)_3]Br_3\cdot 3H_2O$ (Co–N=2.04 Å).[4] Such elongation of the Co–N distance is ascribable to the trans influence of phosphine ligands.

The chelate P–Co–N angles in both complexes are less than 90° and similar to the N–Co–N angles in Co(III) complexes of en and its derivatives.[14] In the chelate rings, the average P–C distance of 1.84 Å is *ca.* 0.30 Å longer than the N–C distance. The Co–P–C angle is *ca.* 9—10° smaller than the tetrahedral angle, while the Co–N–C angle is *ca.* 6° greater than the tetrahedral one.

For bis- and tris(aminoalkyl)phosphine complexes, the two phosphino groups tend to prefer the *cis* positions as have been found in the present complexes and *fac*-$[Co(edmp)_3]^{3+}$.[4] No fraction indicative of the *trans*-(P,P) isomer was obtained in column chromatography. The *cis* disposition of the phosphino groups seems to be unfavorable in view of the inter-ligand overcrowding among bulky substituents on the P atoms. However, such overcrowding appears to be alleviated by i) widenning the P–Co–P angle to 103.1° (**A**) and 99.4° (**B**), and ii) varing the Co–P-substituent angle (116°—122°) so as to keep inter-ligand contact distance normal. Such large deviations from the normal angle would cause strain in the ligand. The *cis* preference of the phosphino groups at the expence of the strain of the

TABLE 4. SELECTED BOND LENGTHS AND ANGLES IN *trans*-$[CoCl_2(edpp)_2]1/2[CoCl_4]$[a]

Bond length	*l*/Å		*l*/Å
Co(2)-Cl(1)	2.239(3)	P(2)-C(17)	1.838(9)
Co(2)-Cl(2)	2.240(3)	P(2)-C(23)	1.817(9)
Co(2)-P(1)	2.255(3)	N(1)-C(2)	1.52(2)
Co(2)-P(2)	2.254(3)	C(1)-C(2)	1.52(1)
Co(2)-N(1)	2.028(8)	C(1)-P(1)	1.842(9)
Co(2)-N(2)	2.020(7)	N(2)-C(4)	1.49(2)
P(1)-C(5)	1.831(10)	C(3)-C(4)	1.54(2)
P(1)-C(11)	1.819(7)	C(3)-P(2)	1.843(8)
Bond angle	*φ*/°		*φ*/°
Cl(1)-Co(2)-Cl(2)	175.8(1)	C(2)-C(1)-P(1)	105.9(6)
Cl(1)-Co(2)-N(1)	87.9(3)	Co(2)-P(1)-C(1)	98.1(4)
Cl(1)-Co(2)-P(1)	93.1(1)	Co(2)-P(1)-C(5)	119.6(2)
Cl(1)-Co(2)-N(2)	88.9(2)	Co(2)-P(1)-C(11)	121.3(4)
Cl(1)-Co(2)-P(2)	89.1(1)	C(5)-P(1)-C(11)	103.0(4)
Cl(2)-Co(2)-N(1)	89.1(3)	N(2)-Co(2)-P(2)	85.6(2)
Cl(2)-Co(2)-P(1)	89.6(1)	Co(2)-N(2)-C(4)	115.8(5)
Cl(2)-Co(2)-N(2)	87.9(2)	N(2)-C(4)-C(3)	107.8(9)
Cl(2)-Co(2)-P(2)	93.5(1)	C(4)-C(3)-P(2)	104.4(6)
N(1)-Co(2)-N(2)	85.2(4)	Co(2)-P(2)-C(3)	98.2(3)
P(1)-Co(2)-P(2)	103.1(1)	Co(2)-P(2)-C(17)	122.2(3)
N(1)-Co(2)-P(1)	86.2(3)	Co(2)-P(2)-C(23)	120.0(3)
Co(2)-N(1)-C(2)	115.4(6)	C(17)-P(2)-C(23)	103.6(4)
N(1)-C(2)-C(1)	108.6(10)		
		Cl(3)-Co(1)-Cl(4)	110.1(1)
		Cl(3)-Co(1)-Cl(3′)	117.0(1)
		Cl(3)-Co(1)-Cl(4′)	104.7(1)
		Cl(4)-Co(1)-Cl(4′)	110.2(2)

a) Primed atoms are those in the equivalent position $(1-x, y, (1/2)-z)$.

Table 5. Selected bond lengths and angles in *trans*-[$CoCl_2$(*R*-ebpp)$_2$]ClO_4

Bond length	*l*/Å		*l*/Å
Co–Cl(1)	2.248(2)	C(1)–P(1)	1.845(10)
Co–Cl(2)	2.227(3)	N(2)–C(4)	1.46(1)
Co–P(1)	2.235(3)	C(3)–C(4)	1.60(2)
Co–P(2)	2.229(3)	C(3)–P(2)	1.823(10)
Co–N(1)	2.048(7)	P(1)–C(5)	1.792(9)
Co–N(2)	2.037(8)	P(1)–C(17)	1.825(10)
N(1)–C(2)	1.50(2)	P(2)–C(11)	1.815(9)
C(1)–C(2)	1.55(1)	P(2)–C(18)	1.794(9)
Bond angle	*φ*/°		*φ*/°
Cl(1)–Co–Cl(2)	175.0(1)	C(2)–C(1)–P(1)	105.1(7)
Cl(1)–Co–N(1)	89.1(2)	Co–P(1)–C(1)	98.8(3)
Cl(1)–Co–N(2)	87.5(2)	Co–P(1)–C(5)	120.7(3)
Cl(1)–Co–P(1)	89.8(1)	Co–P(1)–C(17)	115.7(4)
Cl(1)–Co–P(2)	89.8(1)	C(5)–P(1)–C(17)	105.8(5)
Cl(2)–Co–N(1)	88.1(2)	N(2)–Co–P(2)	86.8(2)
Cl(2)–Co–N(2)	88.3(2)	Co–N(2)–C(4)	114.8(6)
Cl(2)–Co–P(1)	94.0(1)	N(2)–C(4)–C(3)	108.6(8)
Cl(2)–Co–P(2)	92.7(1)	C(4)–C(3)–P(2)	106.5(7)
N(1)–Co–N(2)	87.8(3)	Co–P(2)–C(3)	100.8(3)
P(1)–Co–P(2)	99.4(1)	Co–P(2)–C(11)	117.9(3)
N(1)–Co–P(1)	85.9(2)	Co–P(2)–C(18)	119.5(3)
Co–N(1)–C(2)	115.7(6)	C(11)–P(2)–C(18)	106.4(4)
N(1)–C(2)–C(1)	108.3(8)		

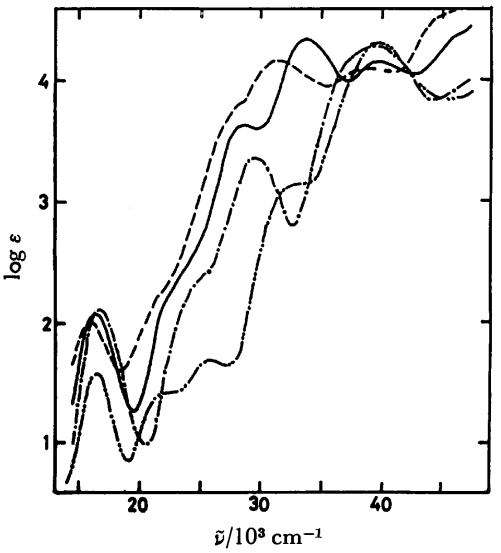

Fig. 3. Absorption spectra of *trans*(Cl, Cl), *cis*(P, P)-[$CoCl_2L_2$]$^+$ in methanol, L: edpp (------), edmp (·–·–), *R*-ebpp (——),-and *trans*-[$CoCl_2$(*S*-pn)$_2$]$^+$ (-·-·-) in methanol.

ligand suggests that the *trans*(P,P) configuration is unfavorable because of the mutual trans influence of P atoms.

The complex ions in **A** and **B** have a very similar coordination geometry, but there is a slight difference between the structural parameters. The P–Co–P angle in **B** is 3.7° smaller than that in **A**. All of the inter-ligand distances among substituents on the P atoms in **B** are longer than 4.0 Å, but some of them in **A** are less than 4.0 Å (*ca.* 3.7 Å). These facts indicate that the

Table 6. Absorption (AB) and CD spectral data in the d-d transition region

trans(Cl, Cl)-type complex	$\tilde{\nu}_{AB}/10^3$ cm^{-1} (log ε)	$\tilde{\nu}_{CD}/10^3$ cm^{-1} (Δε)
[$CoCl_2$(edpp)$_2$]$^+$	15.9(2.03)	
	21.5(2.1)sh	
[$CoCl_2$(edmp)$_2$]$^+$	16.6(2.14)	
	23.8(2.2)sh	
[$CoCl_2$(*S*-pdpp)$_2$]$^+$	16.1(1.92)	15.5(+1.75)
		17.2(−0.67)
	21.5(2.0)sh	21.9(−3.25)
[$CoCl_2$(*R*-ebpp)$_2$]$^+$	16.3(2.08)	15.9(+1.27)
		18.2(−0.06)
	23.0(2.3)sh	23.4(−2.80)
[$CoCl_2$(*S*-prdpp)$_2$]$^+$	15.5(2.02)	15.0(+1.77)
		16.7(−0.92)
	21.5(2.1)sh	20.5(−1.39)
[$CoCl_2${*S*(C), *R*(P)-prbpp}$_2$]$^+$	15.9(1.85)	15.4(+0.88)
		17.3(−0.36)
		20.7(+0.32)
	22.7(2.5)sh	22.7(−0.18)
[$CoCl_2${*S*(C), *S*(P)-prbpp}$_2$]$^+$	15.9(1.94)	14.6(+0.05)
		16.4(−0.59)
	22.7(2.5)sh	23.8(+0.82)sh
[$CoCl_2$(*S*-pn)$_2$]$^+$	16.3(1.60)	16.5(−0.81)
	22.0(1.43)	21.5(+0.11)
	25.7(1.69)	

Solvent: methanol. sh: shoulder

–P(C_4H_9)(C_6H_5) group is smaller in bukiness than the –P(C_6H_5)$_2$ group. This is in accord with the cone angle for these groups.[15] On the other hand, the –P(C_4H_9)-(C_6H_5) group should be more basic than the –P(C_6H_5)$_2$ one, since in phenylphosphines, replacement of a phenyl substituent by an alkyl one generally increases basicity of a phosphine.[16] Thus the smaller and more basic –P(C_4H_9)(C_6H_5) group would form a stronger Co–P bond and hence would exert stronger trans influence on a trans ligand than the case of the –P(C_6H_5)$_2$ group. Indeed, the Co–P bonds in **B** are shorter than those in **A**, while the Co–N bonds in **B** are longer than those in **A**, although the differences are less significant on the statistical ground.

Nonbonded distances in both crystals are normal. The shortest hydrogen bond length is 3.01(1) Å [N-(NH_2)···O(ClO_4)] in the *R*-ebpp complex, and 3.37(1) Å [N(NH_2)···Cl($CoCl_4$)] in the edpp complex.

The geometry of green [$CoCl_2$(edmp)$_2$]$^+$ has not yet been determined. However, this complex ion should also have the *cis*(P,P) configuration in view of the small size and strong basicity of the –P(CH_3)$_2$ group. Other aminoalkyl-diphenyl- and -butylphenyl-phosphine complexes prepared in this study can be assigned to the *cis*(P,P) configuration. In fact, all the complexes show absorption spectral patterns very similar to one another (*vide infra*).

Absorption and CD Spectra. Figure 3 shows absorption spectra of the edpp, *R*-ebpp, and edmp complexes together with that of *trans*-[$CoCl_2$(*S*-pn)$_2$]$^+$ (*S*-pn=(*S*)-1,2-propanediamine), and Table 6 lists the spectral data in the region of 15000 to 25000 cm^{-1} (the

d-d transition region). All the (aminoalkyl)phosphine complexes exhibit a medium intensity band at *ca.* 16000 cm^{-1}. This band should correspond to the split component, Ia of the first d-d band of the *S*-pn complex, since the complexes have the *trans*(Cl,Cl), *cis*(P,P) configuration as stated previously, and ligand field strength of these (aminoalkyl)phosphines are similar to or a little stronger than that of *S*-pn.[5] The absorption maxima of these bands are shifted to the high energy side in the order of edpp<*R*-ebpp<edmp complexes. This order is the same as that found for bis(ethylenediamine)complexes of these ligands.[4] The absorption intensities increase in the same order, but it is reverse to that of the bis(ethylenediamine)complexes.

The Ib component and the second d-d bands are observed as shoulders (21000—24000 cm^{-1}) by overlapping of the strong bands (26000—29000 cm^{-1}) which can be assigned to the Co–Cl charge transfer bands.[17] The bands at 31450 and 33600 cm^{-1} of the edpp and *R*-ebpp complexes, respectively, and the shoulder at *ca.* 36500 cm^{-1} of the edmp complex can be assigned to the Co–P charge transfer bands, since the corresponding bis(ethylenediamine) complexes of these phosphine ligands also show similar strong bands at nearly the same wavenumbers. The bands at *ca.* 40000 cm^{-1} can be assigned to another Co–Cl charge transfer band from a comparison with the spectrum of the *S*-pn complex.[17]

As stated previously, the green $[CoCl_2(edpp)_2]ClO_4$ complex crystallizes in the chiral space group. Figure 4a shows the solid CD spectrum of this complex dispersed in Nujol in the d-d transition region. The spectral pattern quite resembles that of *trans*(Cl,Cl)-$[CoCl_2(S\text{-pdpp})_2]^+$ in methanol (Fig. 4b). The *S*-pdpp complex has two sources of optical activity, the chiral carbon atom and the chiral conformation of the chelate ring. However, the similarity in the two CD spectra indicates that the optical activity of both complexes arises mainly from the chiral conformation of the chelate ring. The *S*-pdpp ligand will be stabilized in the δ conformation with the methyl group disposed equatorially. Thus the chelate rings in the edpp complex given in Fig. 4a should be of the δ conformation. In Fig. 4c is given the CD spectrum of *trans*-$[CoCl_2(S\text{-pn})_2]^+$ in methanol for comparison. The *S*-pn chelate ring also forms the same δ conformation. However, the spectrum is different to a large extent from those of the *S*-pdpp and edpp complexes.

Figure 5 compares CD spectra of the *S*-pdpp and *S*-prdpp complexes in methanol. Both CD spectra are similar over the whole region, in particular, in the Ia band region. The *S*-prdpp chelate ring should be fixed in the δ conformation, producing a new chiral source on the nitrogen atom (*S*) stereoselectively.[18] Thus it is presumed that the *S*-pdpp chelate ring is conformationally stable in the δ form, and that the vicinal effect of the chiral nitrogen atom in the *S*-prdpp complex is small.

Figure 6 shows CD spectra of a diastereomeric pair of the *S*(C),*S*(P)- and *S*(C),*R*(P)-prbpp complexes. The nitrogen atoms in these isomers are also chiral to form the *S* configuration. The spectra exhibit the main CD bands with different signs in the Ia band region and are almost enantiomeric to each other in the high energy

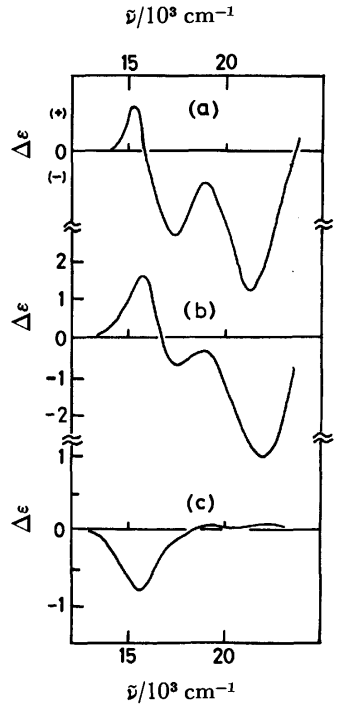

Fig. 4. CD spectra of (a) *trans*(Cl, Cl), *cis*(P, P)-$[CoCl_2(edpp)_2]ClO_4$ in Nujol mull, (b) *trans*(Cl, Cl), *cis*(P, P)-$[CoCl_2(S\text{-pdpp})_2]^+$ in methanol, and (c) *trans*-$[CoCl_2(S\text{-pn})_2]^+$ in methanol.

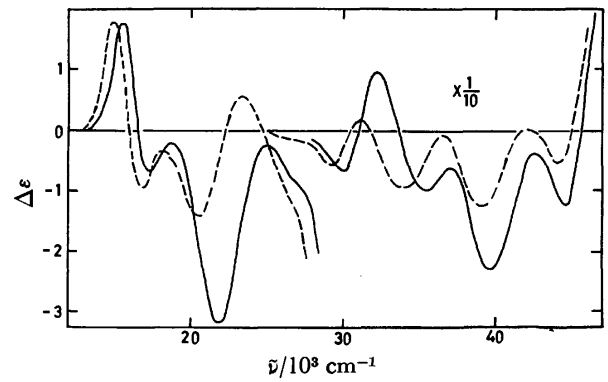

Fig. 5. CD spectra of *trans*(Cl, Cl), *cis*(P, P)-$[CoCl_2L_2]^+$ in methanol, L: *S*-pdpp (——), *S*-prdpp (------).

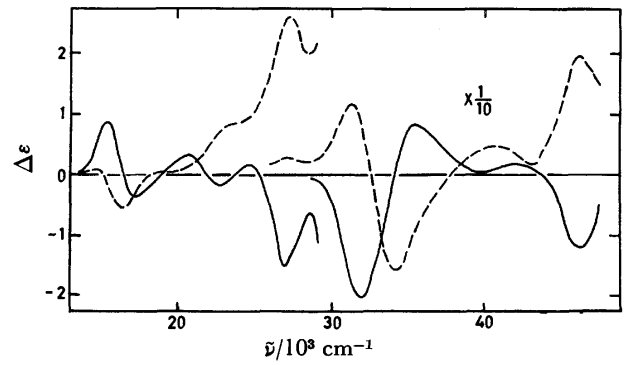

Fig. 6. CD spectra of *trans*(Cl, Cl), *cis*(P, P)-$[CoCl_2L_2]^+$ in methanol, L: *S*(C), *R*(P)-prbpp (——), *S*(C), *S*(P)-prbpp (------).

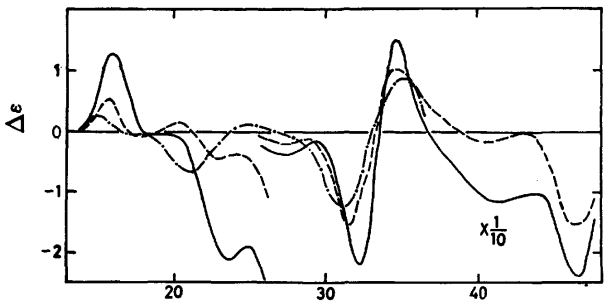

Fig. 7. CD spectra of *trans*(Cl, Cl), *cis*(P, P)-[$CoCl_2$(*R*-ebpp)$_2$]$^+$ (——) and *trans*(Cl, Cl), *trans*(CH_3, CH_3)-[$CoCl_2${(*R*)-*N*-methylethylenediamine}$_2$]$^+$ (·–·–·)[20] in methanol. The vicinal CD curve (------) for the *R*(P)-ligand obtained from CD curves of a pair of diastereomers, *trans*(Cl, Cl)*cis*(P, P) complexes of *S*(C), *R*(P)- and *S*(C), *S*(P)-prbpp (1/2[Δε{*S*(C), *R*(P)-isomer}-Δε{*S*(C), *S*(P)-isomer}]).

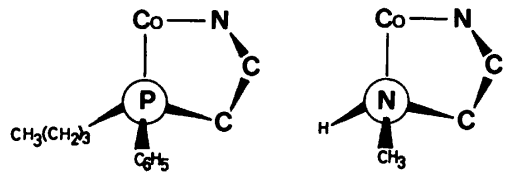

S-configuration *R*-configuration

Fig. 8. Absolute configuration of donating phosphorus and nitrogen atoms.

region. Thus it is suggested that the vicinal effect of the chiral phosphorus atom is considerably large in these complexes. The vicinal effect of the (*R*)-phosphorus atom can be estimated from the observed CD spectra by calculating 1/2[Δε{*S*(C),*R*(P)-isomer}—Δε{*S*(C),*S*-(P)-isomer}]. The result is compared with the CD spectrum of the *R*-ebpp complex, in which the chiral phosphorus atom is the sole source of optical activity (Fig. 7). Both curves are similar, although there is some difference in strength. In Fig. 7 these curves are compared with the CD spectrum of *trans*(Cl,Cl), *trans*-(CH_3, CH_3)-[$CoCl_2${(*R*)-*N*-methylethylenediamine}$_2$]$^+$ in methanol.[19,20] The CD curve calculated for the vicinal effect of the (*R*)-nitrogen atom in *trans*(Cl,Cl), *trans*(C_2H_5,C_2H_5)-[$CoCl_2${(2*S*)-2-amino-4-azahexane}$_2$]$^+$ is also very similar to the CD spectrum of the (*R*)-*N*-methylethylenediamine complex.[21] The absolute configuration of the *R*-ebpp ligand is denoted as *S* upon coordination, as stated previously. Thus the (*S*)-phosphorus and (*R*)-nitrogen donor atoms in the *trans*-dichloro-type complex shown in Fig. 8 induce the vicinal effect of the positive sign in the Ia band region.

For the *R*-ebpp complex, the two chelate rings in crystals are diastereomeric to have *R*(δ) and *R*(λ) chiralities, indicating a small energy difference between the two chiral forms of the ring. In solution the chelate ring would exist in the two forms in a similar amount. Hence the CD spectrum of the *R*-ebpp complex would involve a small vicinal effect of the chiral conformation, δ and λ. This is supported by the fact that the spectrum is similar to the vicinal CD curve of the (*R*)-phosphorus atom obtained from a pair of diastereomeric prbpp complexes.

References

1) M. Atoh, I. Kinoshita, K. Kashiwabara, and J. Fujita, *Bull. Chem. Soc. Jpn.*, **55**, 3179 (1982).
2) R. S. Cahn, C. K. Ingold, and V. Prelog, *Angew. Chem., Int. Ed. Engl.*, **5**, 385 (1966).
3) K. Issleib and D. Haferburg, *Z. Naturforsch., B*, **20**, 916 (1965).
4) I. Kinoshita, K. Kashiwabara, J. Fujita, K. Matsumoto, and S. Ooi, *Bull. Chem. Soc. Jpn.*, **54**, 2683 (1981).
5) K. Kashiwabara, I. Kinoshita, T. Ito, and J. Fujita, *Bull. Chem. Soc. Jpn.*, **54**, 725 (1981).
6) I. Kinoshita, K. Kashiwabara, and J. Fujita, *Bull. Chem. Soc. Jpn.*, **53**, 3715 (1980).
7) I. Ogata, F. Mizukami, Y. Ikeda, and M. Tanaka, Japan Patent Kokai, **76**, 43754 (1976).
8) I. Kinoshita, K. Kashiwabara, J. Fujita, T. Yamane, H. Ukai, and T. Ashida, *Bull. Chem. Soc. Jpn.*, **52**, 1413 (1979).
9) J. Hornstra and B. Stubbe, PW 1100 Data Processing Program, Philips Research Laboratories, Eindhoven Holland.
10) "International Tables for X-Ray Crystallography," Kynoch Press, Birmingham (1974), Vol. IV, pp. 71 and 148.
11) "The Universal Crystallographic Computation Programs," Crystallographic Society of Japan (1969).
12) C. K. Johnson, Report ORNL-5138, Oak Ridge National Laboratory, Oak Ridge, TN 1976.
13) For example, P. J. Toscano and L. G. Marzilli, *Inorg. Chem.*, **18**, 421 (1979); L. Randaccio, N. Bresciani-Pahor, P. J. Toscano, and L. G. Marzilli, *J. Am. Chem. Soc.*, **102**, 7373 (1980).
14) For example, M. Iwata, K. Nakatsu, and Y. Saito, *Acta Crystallogr., Sect. B*, **25**, 2562 (1969).
15) C. A. Tolman, *Chem. Rev.*, **77**, 183 (1977); *J. Am. Chem. Soc.*, **92**, 2956 (1970).
16) C. A. Tolman, *J. Am. Chem. Soc.*, **92**, 2953 (1970).
17) H. Yamatera, *J. Inorg. Nucl. Chem.*, **15**, 50 (1960).
18) T. Yasui, J. Hidaka, and Y. Shimura, *Bull. Chem. Soc. Jpn.*, **39**, 2417 (1966).
19) D. A. Buckingham, L. G. Marzilli, and A. M. Sargeson, *Inorg. Chem.*, **7**, 915 (1968).
20) M. Kojima and T. Ishii, *Inorg. Nucl. Chem. Lett.*, **10**, 1095 (1974).
21) T. Kitamura, M. Saburi, and S. Yoshikawa, *Inorg. Chem.*, **16**, 585 (1977).

 © 1983 The Chemical Society of Japan Bull. Chem. Soc. Jpn., 56, 1074—1079 (1983) [Vol. 56, No. 4

Simultaneous Multielement Determination of Major, Minor, and Trace Elements in Soil and Rock Samples by Inductively Coupled Plasma Emission Spectrometry.

Hiroaki TAO,† Yasuo IWATA,†† Tetsuya HASEGAWA, Yukihiro NOJIRI,†††
Hiroki HARAGUCHI,* and Keiichiro FUWA

Department of Chemistry, Faculty of Science, University of Tokyo, Bunkyo-ku, Tokyo 113

(Received October 9, 1982)

A simple and convenient analytical method for simultaneous multielement determination of soil and rock samples has been investigated by inductively coupled plasma emission spectrometry. Spectral interferences due to major elements were examined in detail, and the correction coefficients for minor and trace elements were estimated for correction of matrix effects. The determinations of minor and trace elements as well as major elements could be performed without matrix matching of the standard solutions. The present method investigated has been applied to the analysis of various soil and rock samples, and the analytical results have been compared with those obtained by atomic absorption spectrometry.

An inductively coupled plasma (ICP) is an efficient excitation source in emission spectrochemical analysis for major, minor and trace elements in various samples.[1] As has been extensively studied,[2-8] ICP optical emission spectrometry (ICP-OES) provides high sensitivities for a variety of elements, wide linear dynamic ranges of calibration curves, and less chemical and ionization interferences, along with simultaneous multielement detection capability. However, spectral interferences with major elements in samples, which originate from spectral line overlapping, stray light or scattering due to strong emission lines, and continuous emission backgrounds, are severe problems in the determination of trace elements.[9,10] Usually in conventional analyses, the concentrations of major elements in sample solutions and those in standard solutions are matched as closely as possible in order to compensate the matrix effects. This experimental procedure requires the different sets of standard solutions for samples with different matrices, and so it is not easily applicable to or convenient for rapid analysis of a number of samples. The soil or rock samples have been analysed by ICP-OES.[11-16] Since the matrix compositions of soil or rock samples are complicated, spectral interferences mentioned above should be carefully corrected for accurate analyses. In addition, the chemical reagents used for digestion are often prone to contamination and physical interference as well as spectral interference. Generally, acid digestion is preferable to alkali fusion in the viewpoints of contamination from chemicals used and nebulization interference. Hence, acid digestion method has been employed in the present experiment.

Furthermore, we have investigated a conventional method for analysis of digested soil and rock samples without matrix-matching of major elements. The changes of background intensities for trace elements at the monitored wavelengths due to major elements are estimated as the correction coefficients for background correction. The background correction method examined is applied to the analysis of soil and rock samples, and the analytical values are compared with those obtained by atomic absorption spectrometry.

Experimental

Instruments. An ICP emission spectrometer (Mode Plasma Atomcomp Mk II) from Jarrell-Ash Co. was used with a crossflow type nebulizer. The instrumental components and operating parameters for the emission measurements are summarized in Table 1. The solution was fed to the nebulizer through a Teflon capillary tube. The analytical lines employed are shown in Table 2. The calibration curves were made by joining the points for the blank and standard with the straight lines.

Chemicals and Standard Solutions. All the chemicals used were of analytical or spectrochemical reagent grade. Commercially available standard solutions (1000 μg/ml) for atomic absorption spectrometry (Wako Pure Chemicals Co.) were used for the stock solutions except for K, Na, Be, P, Pb, Sc and Y, which were prepared from proper compounds or metals according to the recommended methods.[17] Working standard solutions for calibration curves were simply prepared by mixing and/or diluting the stock solutions in four groups. The combinations of elements for working standard solutions

TABLE 1. INSTRUMENTATION AND OPERATING PARAMETERS

ICP spectrometer	Jarrell-Ash Plasma Atomcomp MkII
Frequency	27.12 MHz
Output power	1.1 kW
Coolant gas	argon 16.0 l/ml
Auxiliary gas	argon 0.8 l/ml
Carrier gas	argon 1.0 l/ml
Nebulizer	cross-flow type
Observation height	17 mm above work coil
Polychromator	Paschen-Runge type (75 cm focal length)
Grating	2400 grooves/mm
Reciprocal linear dispersion	0.54 nm/mm at 270 nm
Entrance slitwidth	25 μm
Exit slitwidth	50 μm (100 μm for Na and K)
Monochromator	Ebert type (50 cm focal length)

† Present address: National Research Institute for Pollution and Resources, Yatabe, Ibaraki 305.

†† Present address: Ichikawa Laboratory, Nippon Engelhard, Ltd., Nakakokubun, Ichikawa, Chiba 272.

††† Present address: National Institute for Environmental Studies, Yatabe, Ibaraki 305.

TABLE 2. COMPOSITIONS OF MIXED STANDARD SOLUTIONS FOR CALIBRATION CURVES AND ANALYTICAL WAVELENGTHS

Standard I			Standard II			Standard III			Standard IV		
	Concn	Wavelength		Concn	Wavelength		Concn	Wavelength		Concn	Wavelength
	$\mu g\ ml^{-1}$	nm		$\mu g\ ml^{-1}$	nm		$\mu g\ ml^{-1}$	nm		$\mu g\ ml^{-1}$	nm
Al	500	I 308.2	As	5	I 193.6	Be	5	II 313.0	Si	50	I 288.2
Ca	100	II 317.9	Ba	5	II 483.4	Bi	5	I 223.0[a]			
Fe	300	II 259.9	Cr	5	II 205.5[a]	Cd	5	I 228.8[a]			
K	40	I 766.5	Ga	1	I 417.2	Co	5	II 228.6			
Mg	40	II 279.1	Mn	5	II 257.6	Cu	5	I 324.7			
Na	30	I 589.0	P	5	I 214.9[a]	La	5	II 398.8			
Ti	30	II 334.9	Pb	5	II 220.3	Mo	5	II 202.0			
			Sr	5	II 421.5	Ni	5	II 231.6[a]			
			V	1	II 292.4	Sb	5	I 217.5			
			Zr	2	II 343.7	Sc	5	II 361.3			
						Sn	5	I 189.9			
						Y	5	II 371.0			
						Zn	5	I 213.8[a]			

a) 2nd order.

are summarized in Table 2.

Standard I is composed of major elements in usual soil samples, and these concentrations are similar to the average values of the digested solutions of soil samples. Standards II and III are composed of minor and trace elements. Standard IV for Si was prepared to check the suitability of the digestion procedure, because incomplete digestion resulted in abnormally high concentration of Si in the digested solutions.

In order to minimize the variation of the nebulization efficiency due to the differences of the viscosities of the solutions, the acid contents in each standard solution were adjusted to be 3% $HClO_4$ and HCl so as to match those in the digested sample solutions.

Digestion Procedure. About 0.5 g of powdered soil or rock sample was dried at 110 °C for 4 h, and taken into a Teflon beaker. Ten ml of concd HNO_3 was added in the beaker, and heated to near dryness on a hot plate at 200 °C. Five ml of HF was added into the dried residue, and heated again to dryness. After cooling, 3 ml of HNO_3 and 5 ml of $HClO_4$ were added, and heated for about 3 h until white fume of $HClO_4$ appeared. The digested sample was diluted with 20 ml of distilled water and 3 ml of HCl, and filtered with a 5 A filter paper. Finally, the filtrate was filled up to 100 ml with water.

According to the digestion procedure described above, the final concentration of $HClO_4$ was about 3%, and the content of total salts (major components) was less than 0.5%. As mentioned earlier, the concentrations of $HClO_4$ in the standard solutions were adjusted to be 3%. It was reported that the spectral interferences by major elements were linear in the concentration range of the total salts less than 0.5%.[16] It should be noted that the decomposition of oxide minerals such as chromite and zircon by the digestion method above may not be complete. In general, however, the contents of such minerals in soil samples are not significant.

Results and Discussion

Detection Limits and Recoveries. The detection limits, average contents of minor and trace elements in soils,[18] and the recoveries of elements in the digestion procedure are summarized in Table 3. The detection limits were defined as the analyte concentrations equivalent to twice the standard deviations of the background emission intensities in the presence of major elements at the average concentration levels in the soil samples. The detection limits were obtained under the compromised operating conditions shown in Table 1. The compromised conditions were chosen to make the detection limits as low as possible and to avoid the spectral interferences of major elements as much as possible.

TABLE 3. DETECTION LIMITS, ELEMENTAL CONTENTS OF SOIL, AND ANALYTICAL RECOVERIES

Element	Detection limit ($\mu g\ ml^{-1}$)	Detection limit for soil ($\mu g\ g^{-1}$)	Average[a] content in soil $\mu g\ g^{-1}$	Recovery %
As	0.4	80	6	102.4
Ba	0.001	0.2	500	100.4
Be	0.0006	0.12	6	101.6
Bi	0.04	8	—	99.6
Cd	0.004	0.8	0.06	103.3
Co	0.02	4	8	102.9
Cr	0.008	1.6	100	102.3
Cu	0.004	0.8	20	104.3
Ga	0.05	10	30	104.5
La	0.02	4	30	100.5
Mn	0.005	1	850	93.5
Mo	0.02	4	2	98.3
Ni	0.02	4	40	102.2
P	0.2	40	650	99.9
Pb	0.2	40	10	99.5
Sb	0.1	20	—	101.1
Sc	0.002	0.4	7	99.1
Sn	0.04	8	10	98.4
Sr	0.003	0.6	300	100.0
V	0.01	2	100	101.7
Y	0.004	0.8	50	99.8
Zn	0.007	1.4	50	104.3
Zr	0.01	2	300	106.2

a) Cited from Ref. 18.

Table 4. Correction coefficients for spectral interferences of major elements at emission lines of minor and trace elements[a)]

Element	Major elements						
	Al	Ca	Fe	K	Mg	Na	Ti
Sn	1.60	—	0.318	—	0.063	—	5.10
As	23.9	—	2.92	—	0.206	—	0.400
Mo	1.17	—	0.187	—	0.067	—	0.042
Cr	0.354	—	0.052	—	0.026	—	0.026
Zn	0.038	—	0.048	0.031	0.052	0.031	0.117
P	1.48	0.199	1.84	—	0.819	—	0.367
Sb	1.01	—	1.78	0.030	0.248	0.037	0.344
Pb	1.21	—	0.563	—	0.259	—	1.81
Bi	0.046	—	0.291	—	0.351	—	2.15
Co	0.024	—	0.181	—	0.048	0.001	1.256
Cd	0.006	—	0.032	—	0.018	—	0.013
Ni	—	—	0.232	—	0.230	—	0.036
Mn	0.187	0.009	0.134	—	0.015	—	0.038
V	0.027	0.025	0.297	—	0.264	0.011	0.587
Be	—	—	—	—	—	—	0.007
Cu	0.006	0.007	0.031	0.005	0.009	0.002	1.73
Zr	0.003	0.016	0.093	—	—	0.007	0.081
Sc	—	—	0.004	0.002	0.007	0.004	0.016
Y	—	0.009	0.010	—	—	0.003	0.085
La	0.015	0.633	0.008	—	0.002	0.016	0.123
Ga	0.017	0.213	0.263	—	—	—	5.81
Sr	—	0.005	0.001	—	—	0.001	0.001
Ba	0.001	0.002	0.005	—	—	0.001	0.005

a) Spectral interference is expressed as the analyte concentration (ng/ml) equivalent to the background emission intensity which is provided with 1 μg/ml of major element.

Table 5. Effects of major elements on net intensities of minor and trace elements

Element	Net intensity without major elements[a)]	Net intensity with major elements[a)]	Relative intensity[b)]
Sn	8540	8750	1.02
As	10820	10940	1.01
Mo	2090	2110	1.01
Cr	9850	10140	1.03
Zn	22510	23320	1.04
P	1450	1380	0.95
Sb	6500	6470	0.99
Pb	9650	9120	0.94
Bi	5900	6190	1.05
Co	9920	10150	1.02
Cd	3360	3360	1.09
Ni	4760	4760	1.00
Mn	2700	2750	1.02
V	1520	1540	1.02
Be	18770	17680	0.94
Cu	12390	14270	1.15
Zr	3450	3210	0.93
Sc	3770	3670	0.97
Y	14330	12890	0.90
La	4780	4750	0.99
Ga	16900	15020	0.89
Sr	11450	11630	1.02
Ba	11400	11590	1.02

a) The values when each element is aspirated at the concentration given in Table 2. All intensities are shown as the arbitrary unit. b) Relative intensity is expressed as the ratio of net intensities observed without and with major elements.

The detection limits for soil, which were converted as the minimal detectable contents in soil samples from the detection limits for the standard solutions, are also shown in the second column of Table 3. It can be seen from Table 3 that the determinations of elements except for As, Bi, Cd, Mo, Pb, and Sb are possibly made in terms of soil samples.

The recoveries summarized in Table 3 were obtained by digesting about 0.5 g of soil sample with 50 μg of each element added, and measuring the emission intensities simultaneously. The recovery values obtained were good enough to apply the present method to the soil analysis.

Spectral Interferences. The changes of background intensities due to major elements were investigated by observing intensity profiles near analytical lines of minor and trace elements. The profiles were obtained by moving a refractor quartz plate behind the entrance slit. The profile measurements allowed to distinguish the emission signals caused by spectral interferences from those due to impurities. Consequently, the spectral interference due to major elements such as Al, Ca, Fe, K, Mg, Na, and Ti were estimated as correction coefficient expressed as the analyte concentration (ng/ml) equivalent to the background emission intensity which is provided with 1 μg/ml of each major element. The results are summarized in Table 4. For example, the interference with 1000 μg/ml of Al is equivalent to 23.9 μg/ml of As. The largeness of the interference is generally dependent on the operating conditions of the instrument, especially on the RF power. Therefore, the interference data such as those shown in Table 4 should be estimated under each operating condition and also with each instrument.

The effects of major elements on emission intensities of minor and trace elements were observed as the changes of net intensities at various emission lines with and without major elements. The results are shown in Table 5, along with relative intensities. In the experiment, the concentrations of major, minor and trace elements were the same as those shown in Table 2. As can be seen in Table 5, the changes of net intensities caused by major elements are negligibly small at the tested concentrations of minor and trace elements except for Ga, Zr, Cd, Cu, and Y. However, such changes must be carefully examined at the lower concentrations of analytes.

In order to make accurate background correction, the linearity of the spectral interferences with the major element concentration must be investigated at each emission line. The interferences of Ti and K with Cu are, for example, shown in Fig. 1. The interference at Cu I 324.7 nm caused by Ti is proportional to the Ti concentration, while that by K is not. Generally, the interferences were proportional to the concentration of major elements (Al, Ca, Fe, Mg, and Ti) at the level

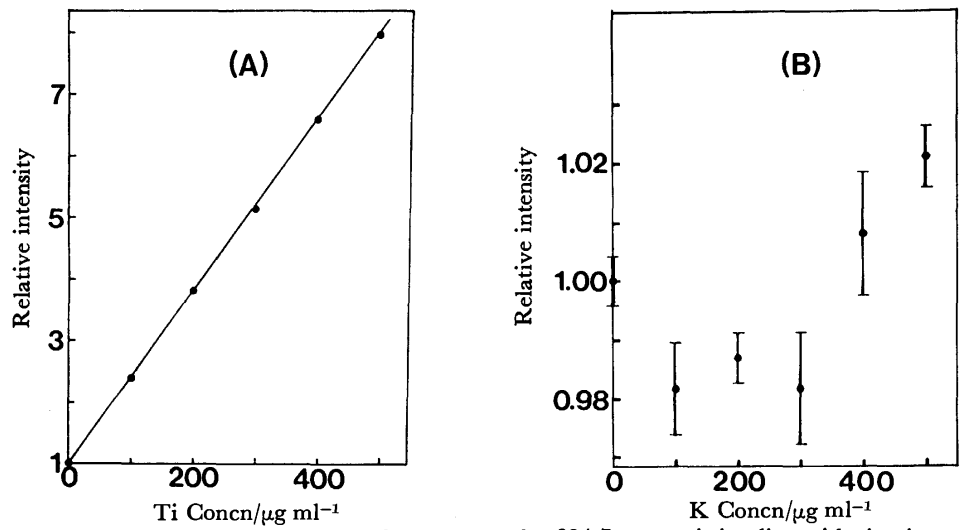

Fig. 1. Spectral interference of copper at the 324.7 nm emission line with titanium and potassium. (A) Interference of titanium, (B) interference of potassium.

Table 6. Additivity of interferences of major elements

Interfering element	Concentration μg ml⁻¹	Apparent intensity[a] Cr	Cu	La
Al	100	74.5	1	4
Ca	100	−4.5	1.5	115
Fe	100	13	9	5
K	100	−6.5	−4	−4
Mg	100	6.5	4	3.5
Na	100	−9.5	−2.5	−3
Total interference[b]		73.5	9	120.5
Total interference without Na and K[c]		89.5	15.5	127.5
Observed interference of mixed solution[d]		91	14	115

a) The values are the apparent intensities (arbitrary unit) caused by 100 μg/ml of each interfering element. b) Sum of the apparent intensities caused by 6 interfering elements. c) Sum of the apparent intensities caused by 4 interfering elements (Al, Ca, Fe, Mg). d) Observed apparent intensity of mixed solution.

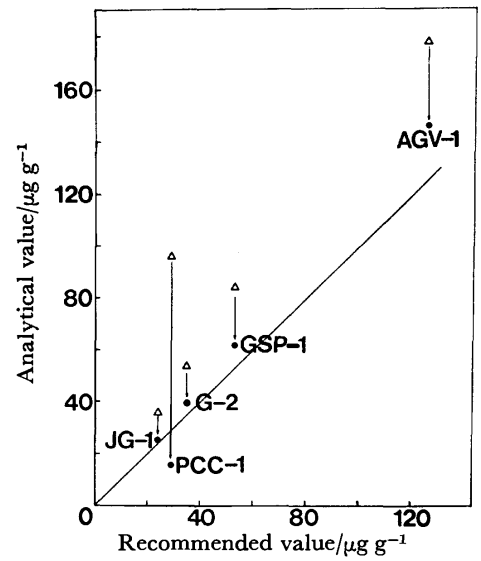

Fig. 2. Correlations of recommended values for vanadium in rock samples with analytical values obtained by ICP-OES. △: Observed value, ●: corrected value.

less than 500 μg/ml. On the other hand, the linearity of spectral interferences was not found in the case of Na and K, but the interferences due to Na and K were rather small compared to those due to other major elements, or sometimes negative for most minor and trace elements. This result suggests that the interferences due to Na and K are physical ones caused by nebulization changes. In most cases, however, the interferences due to Na and K could be neglected in the background correction except for the case at their high concentration levels.

The additivity of the spectral interferences due to major elements, when the mixed solution of major elements are aspirated, should be also examined for the background correction. In Table 6, the sum of the apparent intensities at the emission lines of Cr, Cu, and La caused by 100 μg/ml of each major element is compared with those caused by the mixed solution which contains all the major elements at the level of 100 μg/ml. As can be seen from Table 6, the interferences due to major elements without Na and K is more similar to the observed interference of the mixed solution than that due to all major elements including Na and K.

Standardization of Analytical Method. The present analytical method was standardized by analysing some standard rock samples of which elemental compositions were known. It is, also, desirable to analyse standard soil samples, but such standard soil samples have not been available yet. The rock samples studied are AGV-1, GSP-1, G-2, and PCC-1 from the United States Geological Survey, and JG-1 from the Geological Survey of Japan.

The correlation between the analytical and recommended values for V in the standard rock samples are shown in Fig. 2, where the observed and corrected

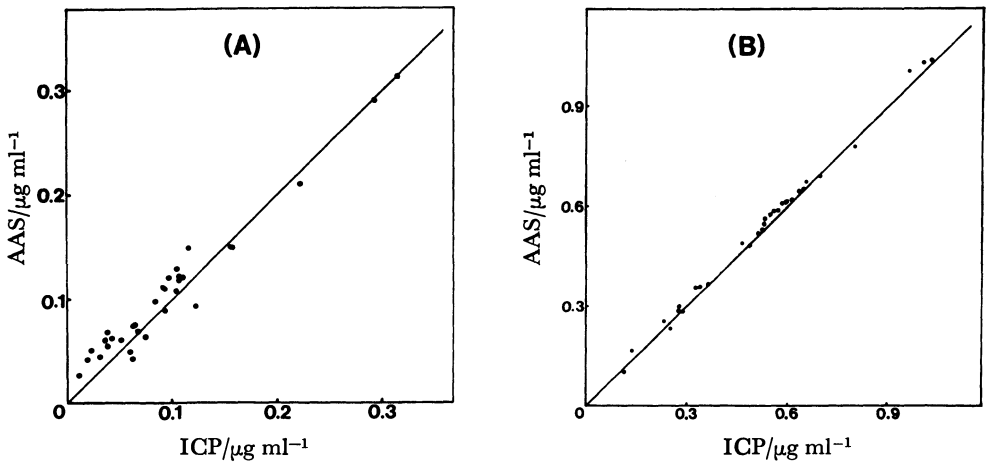

Fig. 3. Correlations of analytical results for cobalt and zinc in soil samples obtained by ICP-OES and AAS. (A) Cobalt, (B) zinc.

Table 7. Analytical results of rock sample (G-2)

Element	Reported values[a]	ICP-OES		AAS
		Observed values	Corrected values	Observed values
	μg g⁻¹	μg g⁻¹	μg g⁻¹	μg g⁻¹
Al	81500	80300	80300	77100
Ca	13900	13500	13400	13400
Fe	18500	21100	21100	17300
K	37400	36700	36500	36500
Mg	4600	4500	4500	4120
Na	30200	29600	29400	30200
Ti	3000	3100	3100	3690
Be	2.6	3.1	3.0	
Ba	1870	1850	1850	
Cr	7	40	8.0	
Cu	11.7	13	8.9	8.9
Ga	22.9	73	25.4	
La	96	103	91	
Mn	260	310	267	260
P	610	690	560	
Pb	31.2	140	30.2	26.3
Sr	479	467	467	
V	35.4	53.6	39.6	
Zn	85	111	107	95

a) Cited from Ref. 19.

values are indicated as △ and ●, respectively. As can be seen in Fig. 2, most of the corrected values agree well with the recommended values reported in the literature. In the case of PCC-1, the lower value for V was obtained, compared with the recommended value. Since the content of Mg in PCC-1 is relatively high (1200 μg/ml), the over-correction might be made. When the concentrations of some major elements are high like in the case of PCC-1, the over-correction of the spectral interferences is generally made because of the deviation from the linearity of the interference at the high concentration range of major elements.[20]

Analytical results for the standard rock sample G-2 by the present method are shown in Table 7, along with the results obtained by atomic absorption spectrometry (AAS) and the reported values. It can be seen from Table 7 that the present data are almost consistent with those in the literature values for most elements. Thus the present method is well standardized for the rock and soil samples with complicated matrices.

Application to Simultaneous Multielement Determinations of Soil Samples. The present ICP-OES method has been applied to the simultaneous multielement determinations of 40 soil samples from South-East Asian countries. No adjustment of the operating parameters were required during the experimental period for total analysis time of 3 h. The analytical results for some elements were cross-checked with those obtained by AAS. In Fig. 3, the correlations of analytical results obtained for Zn and Co by ICP-OES are shown, respectively.

The extensive data shown in Table 7 and Figs. 2 and 3 suggest that a single set of the calibration standard solutions (see Table 2) suffices for the quantitative determination of the elements at the minor and trace concentration levels in a variety of sample matrices. It should, however, be noted here that the matrix matching of acid contents and the background correction for major elements are strongly recommended for accurate determination of minor and trace elements, when ICP-OES is applied.

The authors express their thanks to Dr. Hideaki Kai in the Kyushu Unive rsity for his providing soil samples This research was supported by Grant-in-Aid for Environmental Science under Grand No. 56030019 from the Ministry of Education, Science and Culture.

References

1) "ICP Emission Spectrometry," ed by K. Fuwa and H. Haraguchi, Nanko-do, Tokyo (1980).
2) V. A. Fassel and R. N. Kniseley, *Anal. Chem.*, **46**, 1110A (1974).
3) R. M. Barnes, *CRC. Crit. Rev. Anal. Chem.*, **7**, 203 (1978).
4) S. Greenfield, H. M. McGeachin, and P. B. Smith, *Talanta*, **23**, 1 (1976).
5) V. A. Fassel, *Science*, **202**, 183 (1978).
6) V. A. Fassel, *Anal. Chem.*, **51**, 1290A (1979)

7) P. W. J. M. Boumans, *Fresenius' Z. Anal. Chem.*, **299**, 337 (1979).
8) S. Greenfield, *Analyst (London)*, **105**, 1032 (1980).
9) R. K. Winge, V. A. Fassel, R. N. Kniseley, E. Dekalb, and W. J. Haas, Jr., *Spectrochim. Acta, Part B*, **32**, 327 (1977).
10) R. K. Winge, V. A. Fassel, V. J. Peterson, and M. A. Floyd, *Appl. Spectrosc.*, **36**, 210 (1982).
11) S. A. Sinex, A. Y. Cantillo, and G. R. Hetz, *Anal. Chem.*, **52**, 2342 (1980).
12) N. R. McQuaker, D. F. Brown, and P. O. Klucker, *Anal. Chem.*, **51**, 1083 (1979).
13) J. N. Walsh, *Spectrochim. Acta, Part B*, **35**, 107 (1980).
14) H. Uchida, T. Uchida, and C. Iida, *Anal. Chim. Acta*, **116**, 433 (1980).
15) J. A. C. Broekaert, F. Leis, and K. Laqua, *Spectrochim. Acta, Part B*, **34**, 167 (1979).
16) J. R. Garbarino and H. E. Taylor, *Appl. Spectrosc.* **33**, 220 (1979).
17) JIS K 102 (1974).
18) H. J. M. Bowen, "Trace Elements in Biochemistry," Academic Press, New York (1966).
19) F. J. Flanagan, *Geochim. Cosmochim. Acta*, **37**, 1189 (1973).
20) R. L. Dahlquist and J. W. Knoll, *Appl. Spectrosc.*, **32**, 1 (1978).

A Cation-exchange Study of the Hydrolysis of Tracer Concentrations of Polonium(IV)

Hideo SUGANUMA,* Itsuhachiro HATAYE, and Yoshimasa TAKASHIMA†
Radiochemistry Research Laboratory, Shizuoka University, 836, Ooya, Shizuoka 422
†*Department of Chemistry, Faculty of Science, Kyushu University, 33, Hakozaki, Higashi-ku, Fukuoka 812*
(Received October 12, 1982)

A cation-exchange method was used for determining the average cationic charge of polonium species present in hydrolytic equilibrium in solutions. This method is based on measurements of the distribution ratio of polonium at a constant internal hydrogen-ion concentration of the cation-exchanger phase. In 1.0 mol dm^{-3} (H,Na)ClO_4 and 1.0 mol dm^{-3} (H,Na)NO_3 solutions at $-\log[H^+]=1.0$, tracer concentrations of polonium(IV) were found to exist in the mean chemical forms of $Po(OH)_{3.43}^{0.53+}$ and $Po(OH)_{2.83}(NO_3)_{0.60}^{0.57+}$, respectively. The formation of cationic polymerized species was also estimated in region of $4\leqq -\log[H^+]$ in a 1.0 mol dm^{-3} (H,Na)ClO_4 solution.

In polonium compounds, it has been reported that the oxidation numbers of plonium are ± 2, $+3$, $+4$, and $+6$.[1] The quadrivalent state was assigned to a large portion of polonium in every pH region.[2-4] With respect to polonium in solution, the solvent-extraction study of polonium in strongly acidic solutions has been reported by several workers.[5-9] The present authors have investigated the hydrolysis of polonium(IV) ions in the pH region through solvent extraction with dithizone–CCl_4 solutions.[10-12] The dependence of the chemical behavior of polonium on the pH of the solution clearly showed the importance of the hydrolytic processes. Paper chromatography was also used to study the chemical state of polonium in nitrate solutions.[13,14] The results showed appreciable variations in chemical species with the storage time and with the hydrogen-ion concentrations of the polonium solutions. Koch and Schmidt have studied the hydrolysis of polonium in perchlorate solutions by the cation-exchange method.[2] There have been some other reports of ion exchange on polonium,[15-19] but the results, derived from the ion-exchange behavior of polonium, have not indicated the well-defined chemical species for polonium in each solution. In continuation of the preceding work on polonium,[10-12,14] we have now studied the mean chemical species of polonium in 1.0 M (H,Na)ClO_4 (1 M=1 mol dm^{-3}) and 1.0 M (H,Na)NO_3 solutions at $-\log[H^+]=1.0$ with the cation-exchange method.

Experimental

Reagents. The water and reagents used were all purified to the highest degree, especially to overcome the difficulties hitherto experienced as a result of contamination. Bio-Rad AG 50W-X8 was the cation-exchange resin employed in this study. The H-form resin, 100—200 mesh, was washed three times alternatively with 1 M HCl and 1 M NaCl to remove impurities (finally converted to the Na-form), washed with water sufficiently, and dried in air. A part of the polonium (^{210}Po) imported from the Radiochemical Centre, Amersham, England, was used by diluting it to the appropriate concentration with a 1.0 M (H, Na)ClO_4 or 1.0 M (H, Na)NO_3 solution.

Measurements of the Distribution Ratio. Twenty ml (1 ml=1 cm^3) of a 1.0 M (H, Na)ClO_4 or 1.0 M (H, Na)NO_3 solution containing definite amounts of polonium was mixed with 0.3 g of a cation exchanger in a test tube with a stopper and then shaken at room temperature until the partition equilibrium was attained. A 5-ml portion of the aqueous phase was pipetted into a scintillation vial containing 5 ml of a scintillator (Dotite Scintisol 500, Dojindo Lab.), shaken sufficiently, and then subjected to measurements of its α-activity. Because it is difficult to count the activity of the resin phase with the same counting efficiency as the aqueous phase with a liquid scintillation counter, the α-activity of the resin phase ($\bar{A}$) was calculated using $\bar{A}=A_{aq}^{\circ}-A_{aq}$, where A_{aq}° is the initial activity of the aqueous phase before shaking and where A_{aq} is the activity of the aqueous phase after shaking. The distribution ratio of polonium, D, is given as follows:

$D=(\bar{A}$/gram of air-dried resin)/(A_{aq}/ml of aqueous phase).

In each case, the multiple ion-exchange procedures were repeated by using the same test tube on a solution with a definite hydrogen-ion concentration and definite amounts of polonium; the data obtained in the first half were discarded, and only the reproducible data in the other half were taken. As D is influenced by the extent of the dehydration of air-dried resin, a definite water content must be kept in the series of experiments.

Results and Discussion

Adsorption of Polonium onto Test Tube. The inside surfaces of the test tubes used were, in advance, sufficiently and repeatedly equilibrated with respect to the adsorption of polonium with 20 ml of a 1.0 M (H,Na)-ClO_4 solution containing polonium (1.56×10^5 cpm) at $-\log[H^+]=1.2$. After the test tube containing a freshly prepared 1.0 M (H,Na)ClO_4 solution (20 ml, 1.56×10^5

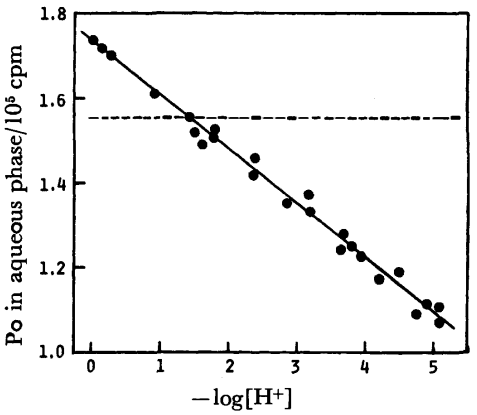

Fig. 1. The adsorption and desorption of polonium onto/from the test tube. The test tubes were in advance equilibrated with 20 ml of ^{210}Po solution (1.56×10^5 cpm, 1.0 M (H, Na)ClO_4) at $-\log[H^+]=1.2$.

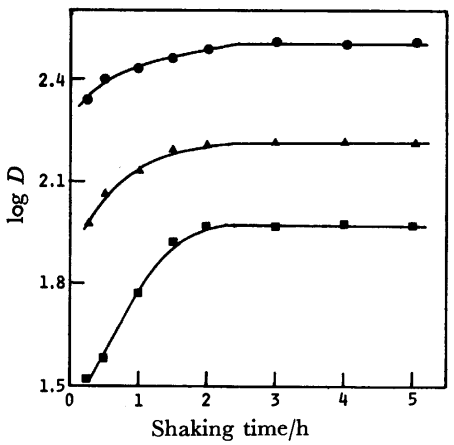

Fig. 2. The effect of shaking time on the cation-exchange equilibrium. ●; 1.0 M $HClO_4$ solution, ▲; 1.0 M (H, Na)ClO_4 solution ($-\log[H^+]=1.95$), ■; 1.0 M (H, Na)ClO_4 solution ($-\log[H^+]=3.95$).

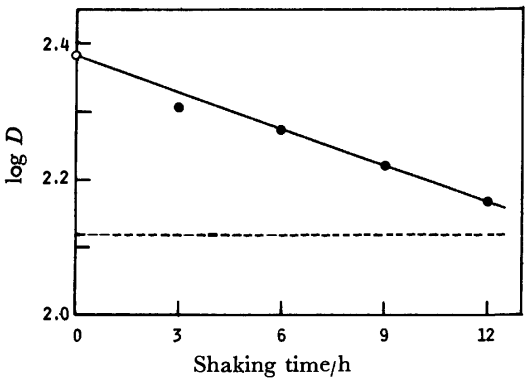

Fig. 3. The time-dependence of desorption from the resin (Bio-Rad AG 50W-X8, 100—200 mesh).
After the partion system (20 ml of ^{210}Po solution of 1.0 M (H, Na)ClO_4 at $-\log[H^+]=3.54$, 0.3 g resin) attained equilibrium, the time-dependence of desorption was measured in the solution whose quarter volume was replaced by the fresh solution free from polonium. (The broken line indicates the D in the equilibrium state.)

cpm), with pH values varying from 0 to 5, had been shaken for 3 h, the activity of the aqueous phase was measured. The results are shown in Fig. 1. Those results indicate that polonium is leached from the glass wall in a higher acidity than $-\log[H^+]=1.2$ and, moreover, adsorbed onto it in a lower acidity. Therefore, the reproducible results of D should be obtained in the cation-exchange study of polonium only when the distribution equilibrium is set up among the resin phase, the glass wall of the test tube, and the aqueous phase in a definite hydrogen-ion concentration.

Time Required for Partition Equilibrium. As is shown in Fig. 2, the sorption of polonium onto Bio-Rad AG 50W-X8 (0.3 g) reaches equilibrium within 3 h in 1.0 M (H,Na)ClO_4 solutions at $-\log[H^+]=0$, 1.95, and 3.95 respectively. Accordingly, the partition system was shaken for more than 3 h in all the experiments in order to attain equilibrium.

Time Dependence of Desorption from the Resin. After the partition system (20 ml of ^{210}Po solution and 0.3 g resin) had attained equilibrium at $-\log[H^+]=3.54$, the time dependence of the desorption was measured in a solution whose quater volume had been replaced by a newly prepared solution containing no polonium. From the results shown in Fig. 3, we can see that the distribution ratio decreases slowly toward equilibrium again in 1.0 M (H,Na)ClO_4 at $-\log[H^+]=3.54$ and that the rate of desorption of polonium from the resin is smaller than that of sorption onto the resin. At any rate, it seems that the sorption reaction of polonium with the resin proceeds reversibly.

Dependence of Selectivity Coefficients of Polonium Species on the Hydrogen-ion Concentration. We have previously reported that polonium was present in the chemical forms of $Po(OH)_3^+$ and $Po(OH)_4$ in a 1.0 M (H,Na)-ClO_4 solution in region of $0 \leq -\log[H^+] \leq 6$.[10] In general, as the ionic strength in the resin phase is higher than in a solution equilibrated with it, the less hydrolyzed species, such as $Po(OH)_2^{2+}$, should be present in the resin, when the hydrolysis reaction on polonium is suppressed. Therefore, the distribution ratio, D, is expressed as follows:

$$D = \frac{[Po^{4+}]_R + [Po(OH)^{3+}]_R + [Po(OH)_2^{2+}]_R + [Po(OH)_3^+]_R + [Po(OH)_4]_R}{([Po(OH)_3^+] + [Po(OH)_4])} \quad (1)$$

$$= K_{H^+}^{Po(OH)_3^+} \times \frac{[H^+]_R}{[H^+]} \times \frac{(K_{-3}[OH^-]_R^{-3} + K_{-2}[OH^-]_R^{-2} + K_{-1}[OH^-]_R^{-1} + 1 + K_1[OH^-]_R)}{(1 + K_1[OH^-])}, \quad (2)$$

where $K_{H^+}^{Po(OH)_3^+}$ (selectivity coefficient) $= \frac{[Po(OH)_3^+]_R[H^+]}{[Po(OH)_3^+][H^+]_R}$ for the reaction, $Po(OH)_3^+ + \overline{H^+} = \overline{Po(OH)_3^+} + H^+$, $K_n = [Po(OH)_{3+n}^{1-n}]/\{[Po(OH)_3^+][OH^-]^n\}$ for the reaction, $Po(OH)_3^+ + nOH^- = Po(OH)_{3+n}^{1-n}$, and $\overline{K_n} = [Po(OH)_{3+n}^{1-n}]_R/\{[Po(OH)_3^+]_R[OH^-]_R^n\}$ for the reaction, $\overline{Po(OH)_3^+} + n\overline{OH^-} = \overline{Po(OH)_{3+n}^{1-n}}$, where species and $[species]_R$ refer to the species in the resin phase and its concentration respectively. It is difficult to determine the selectivity coefficients between hydrogen ions in macro amounts and a definite polonium species in trace amounts. The constancy of its selectivity coefficients was, therefore, examined by replacing that of the selectivity coefficients between Na^+ and H^+, both present in macro amounts in solution. The selectivity coefficient ($K_{Na^+}^{H^+}$) was evaluated from the exchange capacity of the resin (2.581 mequiv./g) and the hydrogen-ion concentration of solutions before/after the ion-exchange reaction. The hydrogen-ion concentration was determined by titration with a standard solution (0.1 M NaOH) for $-\log[H^+]<1.1$ and by measuring with a pH meter for $-\log[H^+]>1.1$. The results are shown in Fig. 4. Taking into account the activity coefficient for the hydrogen-ion concentration in case of the titration,[20] it seems that $K_{Na^+}^{H^+}$ is constant in the region of $0.3<-\log[H^+]<3$.

Dependence of the Distribution Ratio on the Hydrogen-ion Concentration. The distribution ratio of polonium is plotted in Fig. 5 as a function of the hydrogen-ion concentration in a 1.0 M (H,Na)ClO_4 solution. As is shown in the figure, the $\partial \log D/\partial(-\log[H^+])$ slope is negative for $0<-\log[H^+]<3$, naught for $3<-\log[H^+]<4$, and positive for $4<-\log[H^+]<5$. As the condition

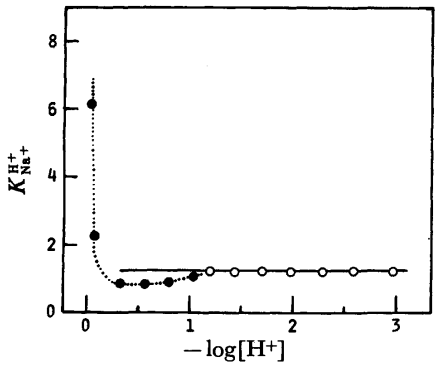

Fig. 4. The dependence of the selectivity coefficient ($K_{Na^+}^{H^+}$) on the hydrogen-ion concentration in 1.0 M (H, Na)ClO_4 solution. The hydrogen-ion concentration was determined by the titration method (●) or with a pH meter (○).

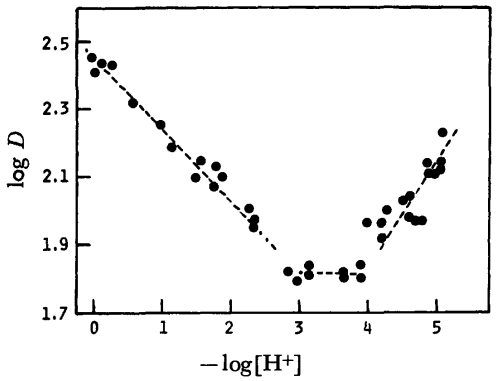

Fig. 5. The dependence of the distribution ratio of polonium on the hydrogen-ion concentration in 1.0 M (H, Na)ClO_4 solution after shaking for 4 h.

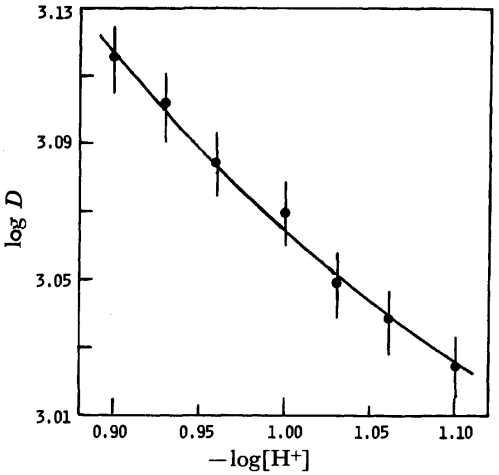

Fig. 6. The dependence of the distribution ratio of polonium on the hydrogen-ion concentration measured at a constant resin acidity.

TABLE 1. COMPOSITIONS OF THF EQUILIBRATING SOLUTION IN 100 ml

$-\log[H^+]$ of aqueous phase	1.00 M $HClO_4$ (ml)	1.00 M $NaClO_4$* or 1.80 M $NaClO_4$** (ml)	H_2O (ml)	$[ClO_4^-]$ of aqueous phase/M
0.90	12.59	66.81*	20.60	0.794
0.93	11.75	73.35*	14.90	0.851
0.96	10.96	80.23*	8.81	0.912
1.00	10.00	90.00*	—	1.000
1.03	9.33	54.36**	36.31	1.072
1.06	8.71	58.94**	32.35	1.148
1.10	7.94	65.53**	26.53	1.259

of resin in the partition system of cation exchange is changed by varying the hydrogen-ion concentration of the aqueous phase, the variation in log D does not always indicate a change in the chemical species. However, if the selectivity coefficient between polonium species and H^+ is invariant, it can be assumed that the variation in D indicates the change in the chemical species of polonium. The increase in D for $4<-\log[H^+]$ implies the variation in the selectivity coefficient and/or the increase in the cationic polonium species. From the results of the paper chromatography on polonium in nitrate solutions stored for a month or more,[14] it has been indicated that hydrolyzed polynuclear cationic species of polonium might exist for $-\log[H^+]=4.7$—6.6. Consequently, the formation of cationic polymers of polonium after shaking for 4 h can be assumed in the region of $4<-\log[H^+]<5$. On the other hand, the decrease in D for $0.3<-\log[H^+]<3$ indicates a decrease in the cationic polonium species, by analogy with the results of solvent extraction and paper chromatography.[10,14]

The Mean Charge of Polonium Species in 1.0 M (H,Na)-ClO_4 Solutions at $-log[H^+]=1.0$. As the constancy of $K_{H^+}^{Po(OH)_n^{4-n+}}$ in the region of $0.3<-\log[H^+]<3$ has been assumed from $K_{Na^+}^{H^+}$ as is shown in Fig. 4, the distribution ratio, D, was determined under the condition of a constant hydrogen-ion concentration in the resin phase. If the hydrogen-ion concentration in the resin phase is constant, D in Eq. 2 may be simplified as follows:

$$D = \text{constant} \times ([H^+]+K_1Q_W)^{-1}, \quad (3)$$

where $Q_W=[H^+][OH^-]$.

To determine the charge of the polonium species from the distribution ratio at $-\log[H^+]=1.0$ under the condition of a definite ionic strength in (H,Na)ClO_4 solutions, D was, in practice, determined by using the equilibrating solutions shown in Table 1.[21] In Fig. 6, we plot log$D$ as a function of $-\log[H^+]$ in solution. The slope of a tangent line as the mean charge of polonium, that is, the value of -4 plus n_{OH} (number of OH^- ligands combining to a polonium atom), was obtained as -0.45 ± 0.08 at $-\log[H^+]=1.0$. The value of n_{OH} was calculated to be 3.55, slightly larger than 3.43, the value obtained by solvent-extraction study at $-\log[H^+]=1.0$.[10] It is assumed that the true tangential slope at $-\log[H^+]=1.0$ in the cation-exchange method should be larger than the value obtained, for the ionic strength in a higher acidity should be slightly lower than that at $-\log[H^+]=1.0$ (to promote the hydrolysis) and higher in a lower acidity (to depress it). The value of n_{OH}, judging from these facts, may be close to 3.43, result from solvent extraction;[10] hence, the mean chemical form can be estimated to be $Po(OH)_{3.43}^{0.57+}$.

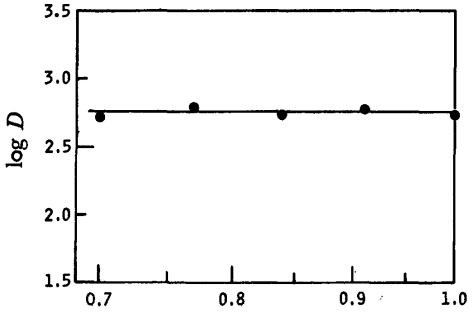

Fig. 7. The effect of the nitrate ion on the distribution ratio of polonium in the cation exchange. The $-\log[H^+]$ of the aqueous phase was kept constant to 1.0.

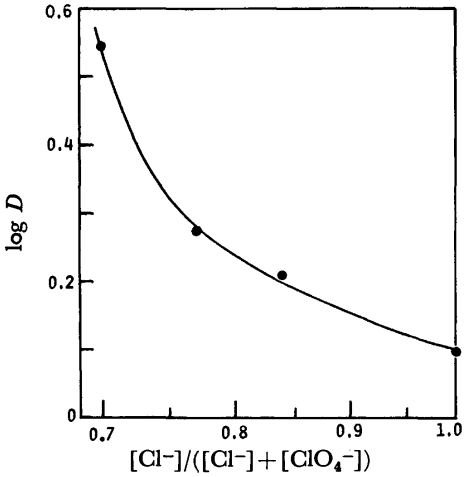

Fig. 8. The effect of the chloride ion on the distribution ratio of polonium in the cation exchange. The $-\log[H^+]$ of the aqueous phase was kept constant to 1.0.

The Mean Charge of Polonium Species in 1.0 M (H,Na)-NO_3 Solutions at $-\log[H^+]=1.0$. In general, the slope of $\log D$ *vs.* $\log\{[NO_3^-]/([NO_3^-]+[ClO_4^-])\}$ in 1.0 M (H,Na)(NO_3,ClO_4) solutions at $-\log[H^+]=1.0$ indicates the difference in the mean charge of the polonium species between 1.0 M (H,Na)NO_3 and 1.0 M (H,Na)ClO_4 solutions at $-\log[H^+]=1.0$. We have determined the slope by varying the mole fractions of the NO_3^- ion, as is shown in Fig. 7. As the slope indicates nearly 0, the mean charge of polonium species in 1.0 M (H,Na)NO_3 at $-\log[H^+]=1.0$ is almost identical with that in 1.0 M (H,Na)ClO_4 at $-\log[H^+]=1.0$. Because it is improbable that the polonium species is polymerized in the shaking period, only the coordination of nitrate ions to polonium should be taken into account. The mean number of NO_3^- combining to a polonium atom being 0.60 at $-\log[H^+]=1.0$,[10,11] the mean chemical form may be $Po(OH)_{2.83}(NO_3)_{0.60}^{0.57+}$ in 1.0 M (H,Na)NO_3 solutions. A similar experiment was carried out with 1.0 M (H,Na)(Cl,ClO_4) solutions at $-\log[H^+]=1.0$. The results are shown in Fig. 8. The distribution ratio of polonium rapidly decreases with an increase in the mole fraction of Cl^- ions, reaching a small value in a 1.0 M (H,Na)Cl solution at $-\log[H^+]=1.0$. This result indicates the formation of negatively charged species and is consistent with the results of solvent extraction.[12] The mean charge of the polonium species in 1.0 M (H,Na)Cl solutions must be further determined by using an anion-exchange method.

The authors are very grateful to Associate Professor Hirohiko Waki of Kyushu University for his valuable suggestions, especially with regard to the ion-exchange method.

References

1) K. W. Bagnall, "Chemistry of the Rare Radioelements, Polonium-Actinium," Butterworths, London (1957), pp. 25 and 51.
2) V. H. Koch and H. Schmidt, *Z. Naturforsch., B*, **18**, 936 (1963).
3) I. E. Starik, N. I. Ampelogova, and B. S. Kuznetsov, *Radiokhimiya*, **6**, 519 (1964).
4) N. I. Ampelogova, *Radiokhimiya*, **17**, 68 (1974).
5) T. Ishimori, *Bull. Chem. Soc. Jpn.*, **27**, 520 (1954).
6) K. W. Bagnall and D. S. Robertson, *J. Chem. Soc.*, **509** (1957).
7) M. Haissinsky and E. Pluchet, *J. Inorg. Nucl. Chem.*, **28**, 2861 (1966).
8) N. Matsuura, A. Ouchi, and M. Kojima, *Bull. Chem. Soc. Jpn.*, **34**, 411 (1961).
9) I. E. Starik and N. I. Ampelogova, *Radiokhimiya*, **3**, 261 (1961).
10) I. Hataye, H. Suganuma, M. Sakata, and Y. Nagame, *J. Inorg. Nucl. Chem.*, **43**, 2101 (1981).
11) I. Hataye, H. Suganuma, and M. Sakata, *J. Inorg. Nucl. Chem.*, **43**, 2575 (1981).
12) H. Suganuma and I. Hataye, *J. Inorg. Nucl. Chem.*, **43**, 2511 (1981).
13) I. S. Kirin and V. M. Zaitsev, *Radiokhimiya*, **10**, 42 (1968).
14) H. Suganuma, K. Ito, and I. Hataye, *J. Radioanal. Chem.*, **62**, 125 (1981).
15) J. Danon and A. A. L. Zamith, *J. Phys. Chem.*, **61**, 431 (1957).
16) I. E. Starik, N. I. Ampelogova, and B. S. Kuznetsov, *Radiokhimiya*, **6**, 524 (1964).
17) I. E. Starik, N. I. Ampelogova, and B. S. Kuznetsov, *Radiokhimiya*, **7**, 199 (1965).
18) N. I. Ampelogova, *Radiokhimiya*, **15**, 813 (1973).
19) N. I. Ampelogova, *Radiokhimiya*, **16**, 56 (1974).
20) J. Kielland, *J. Am. Chem. Soc.*, **59**, 1675 (1937).
21) H. Waki, Y. Hisazumi, and S. Ohashi, *J. Inorg. Nucl. Chem.*, **39**, 349 (1977).

 © 1983 The Chemical Society of Japan Bull. Chem. Soc. Jpn., 56, 1084—1088 (1983) [Vol. 56, No. 4

Phase Equilibria in the Tm_2O_3-V_2O_3-V_2O_5 System at 1200 °C

Kenzo KITAYAMA* and Takashi KATSURA

Department of Chemistry, Faculty of Science, Tokyo Institute of Technology, Ookayama, Meguro-ku, Tokyo 152

(Received November 13, 1982)

Phase equilibria in the Tm_2O_3-V_2O_3-V_2O_5 system were established at 1200 °C; the oxygen partial pressure was varied −0.68 (air) to −12.50 atm in terms of log Po_2. In this system, V_nO_{2n-1} (n=2—7), VO_2, Tm_2O_3, $TmVO_3$, $TmVO_4$, $Tm_8V_2O_{17}$ ($4Tm_2O_3 \cdot V_2O_5$), $Tm_7V_3O_{16}$ were stable under the present experimental conditions. The pattern of the phase diagram is different from those of other Ln_2O_3-V_2O_3-V_2O_5 systems (Ln=Sm, Lu, Er, Gd, La, and Nd) that were already established. Compounds $TmVO_3$, $TmVO_4$, $Tm_8V_2O_{17}$, $Tm_7V_3O_{16}$, V_2O_3, and VO_2 have nonstoichiometric compositions. On the basis of the established phase diagram, the Gibbs energies of the reactions,

(1) $2\,Tm_2O_3 + 3\,TmVO_3 + 1/2\,O_2 = Tm_7V_3O_{16}$
(2) $TmVO_3 + 1/2\,O_2 = TmVO_4$
(3) $5/3\,Tm_2O_3 + 2/3\,Tm_7V_3O_{16} + 2/3\,O_2 = Tm_8V_2O_{17}$
(4) $Tm_7V_3O_{16} + O_2 = 5/3\,TmVO_4 + 2/3\,Tm_8V_2O_{17}$

were determined to be −132, −119, −157, and −228 kJ, respectively. The relationship between the ionic radius and ΔG° of the reactions, $LnVO_3 + 1/2\,O_2 = LnVO_4$, is linear, provided that lanthanum and the lanthanoid can be divided into two groups.

Phase equilibria in the Ln_2O_3-V_2O_3-V_2O_5 systems (Ln=Sm, Lu, Er, Gd, La, and Nd) at 1200 °C have been established.[1-6] The oxygen partial pressure was changed from −0.68 to −12.50 or −13.00 atm in terms of log Po_2. We succeeded in obtaining the Gibbs energies of the reactions which appeared in the systems and the crystallographic data of the ternary compounds and the activities of the components in the solid solutions. These established phase diagrams showed the different patterns as a result of the differences of the compounds coexisting under the experimental conditions.

In the present study, Tm_2O_3 was chosen as the Ln_2O_3, because the system might show as interesting a pattern as that of the Lu_2O_3 system.[2] The pyrochlore type compound, $Tm_2V_2O_7$, is well known[7] and its physical properties were studied by many researchers.[7-10]

The Tm_2O_3-V_2O_5 system was studied by Brusset *et al.*[11] in the temperature range from 600 °C to 1500 °C in air. They found two compounds, $4Tm_2O_3 \cdot V_2O_5$ ($Tm_8V_2O_{17}$) and $5Tm_2O_3 \cdot V_2O_5$, besides $TmVO_4$ which is well known. The crystallographic properties of $TmVO_4$ were studied by Brusset *et al.*[11] and Schwarz[12] and those of $Tm_8V_2O_{17}$ by Brusset *et al.*[13] and Ustalova *et al.*[14]

In the Tm_2O_3-V_2O_3 system, only $TmVO_3$ was found; its crystallographic properties were investigated by many researchers.[15-16] But the system has not been completely studied yet on account of the instability of V_2O_3 in air

The objectives of the present study are to (1) make the detailed phase diagram of the Tm_2O_3-V_2O_3-V_2O_5 system at 1200 °C in order to determine the stable compounds under the present experimental conditions, to (2) calculate the Gibbs energies of the reactions found in the established phase diagram, and to (3) ascertain whether or not there is a linear relationship between the Gibbs energies of reactions and the ionic radii of the lanthanoid elements, as found in the Ln-Fe-O system.[17]

Experimental

Analytical grades of Tm_2O_3 (99.9%) and V_2O_5, which was made by heating the guaranteed grade of NH_4VO_3 at 500 °C in air for about 24 h, have been used as the starting materials. Desired Tm_2O_3/V_2O_5 ratios of samples were obtained by mixing the appropriate quantities thoroughly in an agate motar under ethyl alcohol. The mixtures thus obtained were treated by the procedures described in the previous report.[1] The apparatus and procedures for controlling the oxygen partial pressures, keeping a constant temperature, the method of thermogravimetry, the criterion for an equilibrium establishment, the method of the actual oxygen partial pressure measurement, and the method of the chemical analysis are the same as those reported in the previous papers.[1,18-22]

The oxygen partial pressure −12.50 atm in terms of log Po_2 was chosen as the reference oxygen partial pressure; that is, the weight of a samples in the atmosphere of $10^{-12,50}$ atm of oxygen partial pressure was chosen as the reference weight thorough the present experiment.

Results and Discussion

Phase Equilibria. Tm_2O_3 is stable under the present experimental conditions.[23] Eleven samples with Tm_2O_3/V_2O_5 mole ratios 84/16, 8/2, 77/23, 74/26, 7/3, 65/35, 6/4, 1, 3/7, 2/8, and 1/9 were prepared to be used in the thermogravimetric experiment. The thermogravimetric results of the four samples with mole ratios, 84/16, 74/26, 65/35, and 3/7 are shown in Fig. 1 as representative. In Fig. 1, the ordinate is the oxygen partial pressure (atm) in log Po_2 and the abscissa is the composition of the samples represented by Wo_2/W_T, where Wo_2 is the weight gain of the samples from the reference weight at log Po_2=−12.50, and W_T is the total weight gain that the samples would get if V_2O_3 in the samples had changed to V_2O_5. Figure 1 shows the different patterns. That is, Fig. 1a had two sudden weight changes at log Po_2=−8.10 and −9.37, Fig. 1b three at log Po_2=−7.70, −8.10, and −9.37, Fig. 1c also three at −7.70, −8.47, and −9.37. Figure 1d shows the same pattern as those of the previous

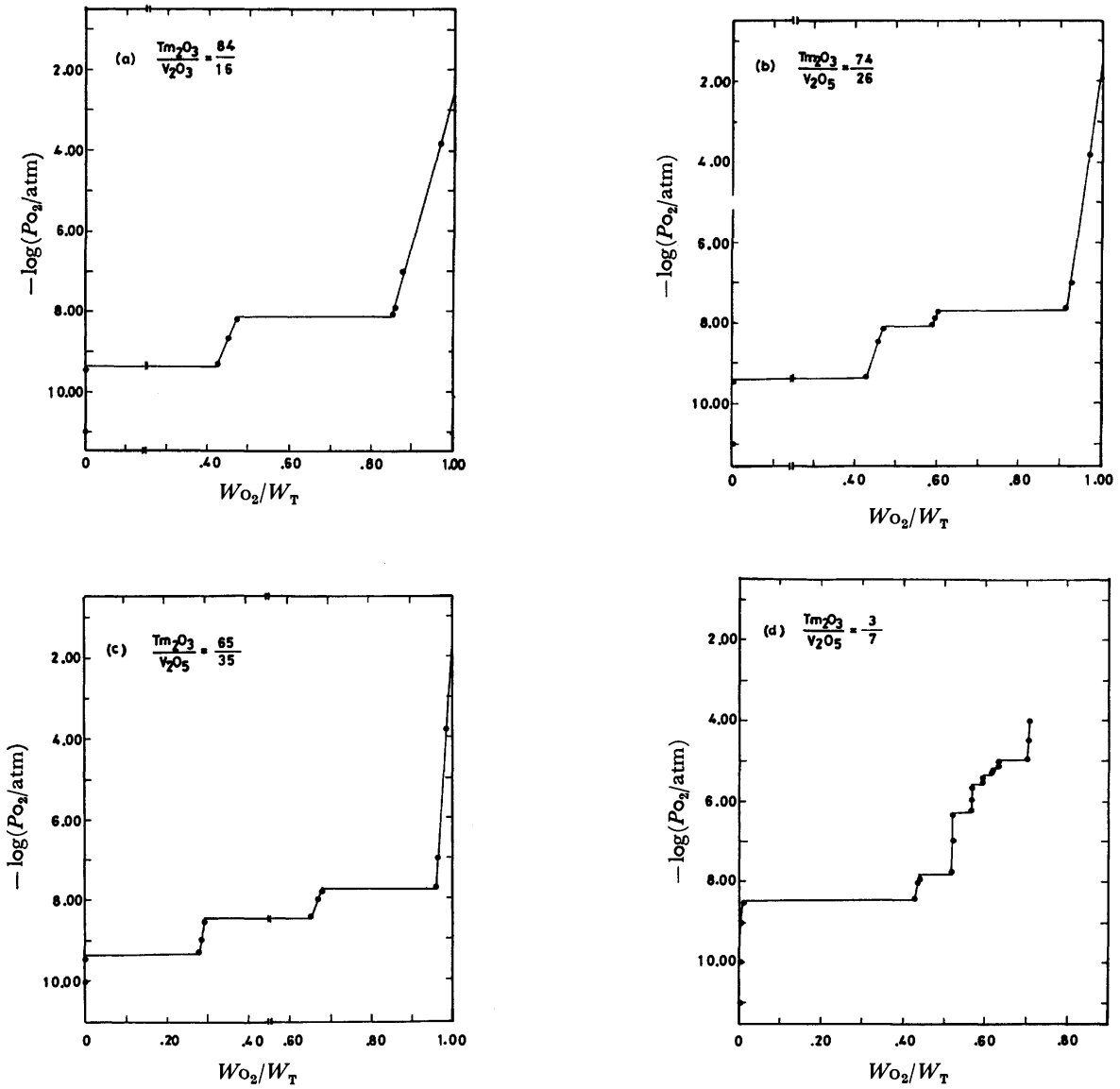

Fig. 1. The relationships between $-\log P_{O_2}$ (atm) and the weight gains, W_{O_2}/W_T, of the samples. (a): $Tm_2O_3/V_2O_5=84/16$, (b): $Tm_2O_3/V_2O_5=74/26$, (c): $Tm_2O_3/V_2O_5=65/35$, (d): $Tm_2O_3/V_2O_5=3/7$.

reports[1,3-6] except one change at the oxygen partial pressure $\log P_{O_2}=-8.47$ that corresponds to the equilibrium oxygen partial pressure of a reaction, $TmVO_3+1/2\ O_2=TmVO_4$. These oxygen partial pressures also correspond to the equilibrium oxygen partial pressures of reactions in the system, as will be shown in Table 5.

In Table 1, the results of the identification of phases are shown. In the first column are shown the compositions of the strating materials in mol%, in the second the experimental conditions of the oxygen partial pressure in terms of $\log P_{O_2}$ (atm), in the third the experimental durations in hours, and in the last the phases that are found in the quenched samples by X-ray powder diffractometer using Cu $K\alpha$ radiation.

Based upon the above thermogravimetric results and the results of the identification of phases, a phase diagram of the system was drawn and is shown in Fig. 2. The following phases are stable under the present experimental conditions, omitting compounds in the V_2O_3–V_2O_5 system and Tm_2O_3 : $TmVO_4$, $TmVO_3$, $4Tm_2O_3\cdot V_2O_5$ ($Tm_8V_2O_{17}$, A), and $Tm_7V_3O_{16}$ (L). The compound $5Tm_2O_3\cdot V_2O_5$, which was reported[11] as a stable compound together with $4Tm_2O_3\cdot V_2O_5$ in air in the Tm_2O_3–V_2O_5 system, and the pyrochlore type $Tm_2V_2O_7$ were not found under the present experimental conditions.

The present phase diagram is different from those of the other systems[1-6] on account of the different coexisting compounds. That is, the Sm_2O_3–V_2O_3–V_2O_5 system has a ternary compound, $5Sm_2O_3\cdot V_2O_5$; the Lu_2O_3–V_2O_3–V_2O_5 system contains $Lu_7V_3O_{16}$, $Lu_2V_2O_7$, and LuV_4O_8; the Er_2O_3–V_2O_3–V_2O_5 system $4Er_2O_3\cdot V_2O_5$; the Gd_2O_3–V_2O_3–V_2O_5 system $0.81Gd_2O_3\cdot 0.19V_2O_5$; the La_2O_3–V_2O_3–V_2O_5 system $0.81La_2O_3\cdot 0.19V_2O_5$, $3La_2O_3\cdot V_2O_5$, and $0.71La_2O_3\cdot 0.19V_2O_5$; and the Nd_2O_3–V_2O_3–V_2O_5 system contains $0.81Nd_2O_3\cdot 0.19V_2O_5$ and $3Nd_2O_3\cdot V_2O_5$.

TABLE 1. IDENTIFICATION OF PHASES

Tm_2O_3 (mol %)	V_2O_5	$-\log (P_{O_2}/atm)$	Time / h	Phases
84	16	10.00	23	$Tm_2O_3 + TmVO_3$
		9.00	27	$Tm_2O_3 + Tm_7V_3O_{16}$
		7.00	30	$Tm_2O_3 + Tm_8V_2O_{17}$
		0.68	38	$Tm_2O_3 + Tm_8V_2O_{17}$
77	23	10.00	23	$Tm_2O_3 + TmVO_3$
		9.00	27	$Tm_2O_3 + Tm_7V_3O_{16}$
		8.00	48	$Tm_8V_2O_{17} + Tm_7V_3O_{16}$
		7.00	30	$Tm_8V_2O_{17} + TmVO_4$
60	40	10.00	23	$Tm_2O_3 + TmVO_3$
		9.00	27	$TmVO_3 + Tm_7V_3O_{16}$
		8.20	42	$TmVO_4 + Tm_7V_3O_{16}$
		7.00	30	$Tm_8V_2O_{17} + TmVO_4$
30	70	9.00	27	$V_2O_3 + TmVO_3$
		8.20	42	$V_2O_3 + TmVO_4$
		7.00	31	$V_3O_5 + TmVO_4$
		6.00	40	$V_4O_7 + TmVO_4$
		5.45	60	$V_5O_9 + TmVO_4$
		5.25	60	$V_6O_{11} + TmVO_4$
		5.05	47	$V_7O_{13} + TmVO_4$
		4.50	38	$VO_2 + TmVO_4$
10	90	8.80	27	$V_2O_3 + TmVO_3$
		7.90	47	$V_2O_3 + TmVO_4$
		7.00	31	$V_3O_5 + TmVO_4$
		6.00	40	$V_4O_7 + TmVO_4$
		5.45	60	$V_5O_9 + TmVO_4$
		5.25	60	$V_6O_{11} + TmVO_4$
		5.05	47	$V_7O_{13} + TmVO_4$
		4.50	38	$VO_2 + TmVO_4$

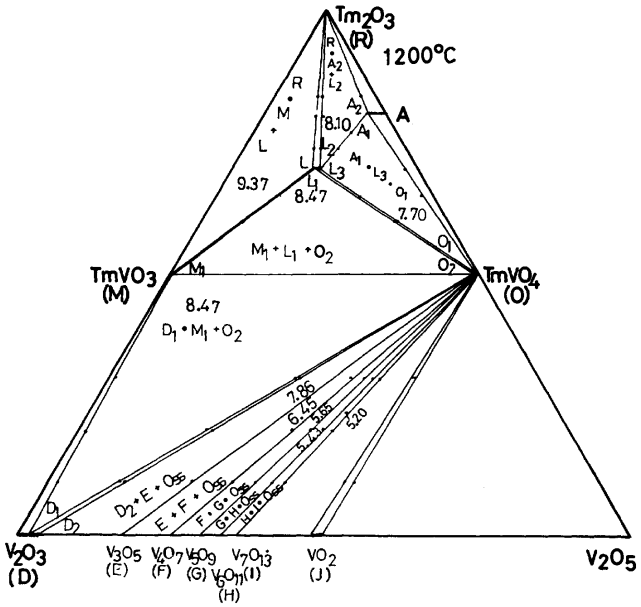

Fig. 2. Phase equilibria in the Tm_2O_3–V_2O_3–V_2O_5 system at 1200 °C. Numerical values in the three solid phases regions are the equilibrium oxygen partial pressure in $-\log P_{O_2}$. Abbreviations are the same as thosein Table 3.

The compound $Tm_7V_3O_{16}$ is a new compound, although the atomic ratio is analogous to the compound $Lu_7V_3O_{16}$ that was found by us thorough the study of the Lu_2O_3–V_2O_3–V_2O_5 system.[2] Both compounds, $Tm_7V_3O_{16}$ and $Lu_7V_3O_{16}$, have a similar powder X-ray diffraction pattern, as shown in Fig. 3, but we could not yet determine the crystallographic system. The spacing and relative intensities which were obtained

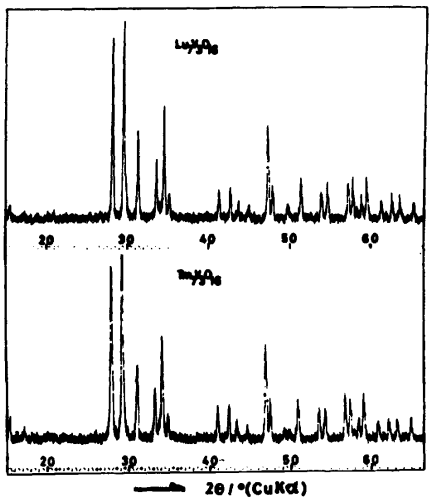

Fig. 3. The X-ray powder pattern of $Tm_7V_3O_{16}$ together with $Lu_7V_3O_{16}$.

TABLE 2. SPACINGS AND RELATIVE INTENSITIES OF THE COMPOUND, $Tm_7V_3O_{16}$

d/A	I/I_o	d/A	I/I_o
5.78	12	1.8536	7
3.20	98	1.7968	27
3.05	100	1.7121	20
2.878	44	1.6923	22
2.695	33	1.6229	29
2.624	58	1.6068	24
2.576	16	1.5799	11
2.206	21	1.5651	27
2.136	18	1.5237	12
2.092	12	1.4941	13
1.9380	59	1.4727	13
1.9175	23	1.4384	13

TABLE 3. COMPOSITIONS, SYMBOLS, STABILITY RANGES IN OXYGEN PARTIAL PRESSURES, AND ACTIVITIES OF COMPONENTS IN SOLID SOLUTIONS

Component	Composition	Symbol	$-\log (P_{O_2}/atm)$	$\log a_i$
$TmVO_4$	$TmVO_{4.00}$	O	0.68—7.70[a]	≈0
	$TmVO_{3.987}$	O_1	7.70	≈0
	$TmVO_{3.985}$	O_2	8.47	0
$TmVO_3$	$TmVO_{3.00}$	M	12.50—9.37	≈0
	$TmVO_{3.00}$	M_1	8.47	0
$Tm_8V_2O_{17}$	$Tm_8V_2O_{17.0}$	A	0.68—1.83[a]	0.02
	$Tm_8V_2O_{16.72}$	A_1	7.70	0.06
	$Tm_8V_2O_{16.68}$	A_2	8.10	0
$Tm_7V_3O_{16}$	$Tm_7V_3O_{16.3}$	L	9.37	0
	$Tm_7V_3O_{16.4}$	L_1	8.47	−0.152
	$Tm_7V_3O_{16.7}$	L_2	8.10	−0.235
	$Tm_7V_3O_{16.6}$	L_3	7.70	−0.329

a) These values were obtained by extrapolating the experimental values.

Table 4. Unit cell dimensions of the compounds

Sample	$-\log (Po_2/atm)$	$\frac{a}{A}$	$\frac{b}{A}$	$\frac{c}{A}$	$\frac{\beta}{°}$	$\frac{V}{A^3}$	Ref.
$TmVO_4$	0.68	7.071 ± 0.001		6.260 ± 0.001		313.0 ± 0.1	Present
		7.071 ± 0.003		6.263 ± 0.003		313.1	12
		7.062 ± 0.002		6.252 ± 0.003			11
$TmVO_3$	12.00	5.243 ± 0.001	5.581 ± 0.001	7.551 ± 0.001		220.9 ± 0.	Present
		5.237	5.573	7.545		220.2	15
		5.248	5.575	7.548		220.8	16
$Tm_8V_2O_{17}$	7.00	10.42 ± 0.02	8.30 ± 0.02	16.07 ± 0.06	98.1 ± 0.2	137.7 ± 6	Present
		10.440 ± 0.003	8.328 ± 0.003	16.069 ± 0.010	98.23 ± 0.03		13

Table 5. Gibbs energies of reactions

Reaction	$-\log (Po_2/atm)$	$\frac{-\Delta G°}{kJ}$
(1) $2\,Tm_2O_3 + 3\,TmVO_3 + 1/2\,O_2 = Tm_7V_3O_{16}$	9.37 ± 0.05	132 ± 1
(2) $TmVO_3 + 1/2\,O_2 = TmVO_4$	8.47 ± 0.05	119 ± 1
(3) $5/3\,Tm_2O_3 + 2/3\,Tm_7V_3O_{16} + 2/3\,O_2 = Tm_8V_2O_{17}$	8.10 ± 0.07	157 ± 2
(4) $Tm_7V_3O_{16} + O_2 = 5/3\,TmVO_4 + 2/3\,Tm_8V_2O_{17}$	7.70 ± 0.07	228 ± 2

by the X-ray powder diffractometer are shown in Table 2.

Compounds $Tm_8V_2O_{17}$, $Tm_7V_3O_{16}$, $TmVO_3$, $TmVO_4$, V_2O_3, and VO_2 have nonstoichiometric compositions. The relationship between a composition, N_O/N_Y, and the oxygen partial pressure of the solid solution, Y that means an arbitary component, were determined using the thermogravimetric results. Here, N_O and N_Y are the mole fractions of oxygen and of the component Y. Using the method of the least squares with a linear equation, $N_O/N_Y = a \log Po_2 + b$, the constants a and b for each solid solution were determined as follows: for $Tm_8V_2O_{17}$ 0.10 and 0.49 and for $Tm_7V_3O_{16}$ 0.17 and 0.186. As for the solid solutions $TmVO_4$ and $TmVO_3$, the composition ranges are too narrow to obtain such equations. Especially, the nonstoichiometric ranges of $TmVO_3$ are very small, although the width of ranges is a little exaggerated in Fig. 2. V_2O_3 and VO_2 were already discussed in the previous report.[1]

In Table 3, the compositions of the compounds at various oxygen partial pressures, stability ranges of the compounds in terms of $\log Po_2$, the symbol of the compounds, and the activities of the component in the solid solutions at distinct oxygen partial pressures are tabulated. The activities of the components in the solid solutions were calculated with the Gibbs-Duhem equation using the thermogravimetric results of the N_O/N_Y *vs.* $\log Po_2$ relations described above. A detailed method of the calculation has been discussed in the paper of Kimizuka and Katsura.[21] Since solid solution ranges of $TmVO_4$ and $TmVO_3$ were too small to get the general equations of N_O/N_Y *vs.* $\log Po_2$, we took the activities of components $TmVO_4$ and $TmVO_3$ as unity over the whole range of compositions.

Lattice constants of the compounds $TmVO_4$, $TmVO_3$, and $Tm_8V_2O_{17}$ are tabulated in Table 4. Our values are in good agreement with those quoted in the Table.

Calculation of Gibbs Energies of Reactions. On the basis of the present phase diagram, Gibbs energies of the reactions represented in the system, except those in the partial system V_2O_3-V_2O_5, can be calculated by the equation $\Delta G° = -RT \ln K$, where R is the gas constant, T the absolute temperature, and K the equilibrium constant of each reaction. Chemical reactions, the equilibrium oxygen partial pressure for each reaction, and $\Delta G°$ values calculated are shown in Table 5. Activities of each component of the solid solutions, which are necessary for the calculations, are tabulated in Table 3.

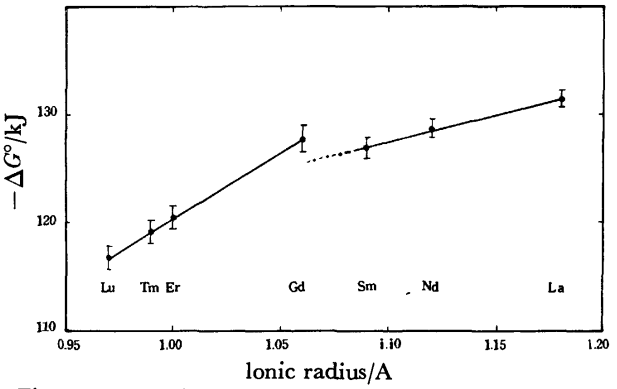

Fig. 4. The relationship between the ionic radius in 8 coordination number and the Gibbs energy of reaction, $LnVO_3 + 1/2\,O_2 = LnVO_4$.

The relationship between $\Delta G°$ and Ionic Radius. In the series of the Ln_2O_3-V_2O_3-V_2O_5 system, the common reaction $LnVO_3 + 1/2\,O_2 = LnVO_4$ appear in all the systems. So it is very interesting to correlate the $\Delta G°$ with some properties of this lanthanoid element. As mentioned above, we reported a linear relation between the $\Delta G°$ values of the formation of perovskite from Ln_2O_3, iron, and oxygen and the tolerance factor. In Fig. 4, is shown the relationship between the ionic radius of the lanthanoid element with coordination number 8[24] of $LnVO_4$ and $\Delta G°$ values. Unlike the case of Ln–Fe–O system, it seems to seperate to two groups:

the so-called heavy lanthanoid series and the so-called light one and they show a linear relationship with a rule that ΔG° values decrease with increasing the atomic radius. This pattern is similar even if the abscissa is changed to the radius of coordination number 12[25] of $LnVO_3$ or to the tolerance factor. As is well known, $LaVO_3$ has a tetragonal crystal system and $LaVO_4$ has a monoclinic system. The linear relation fits well even for La, in spite of the difference of crystal system. This means that the difference of the crystal system does not affect the energies of such a reaction.

References

1) K. Kitayama and T. Katsura, *Bull. Chem. Soc. Jpn.*, **50**, 889 (1977).
2) K. Kitayama and T. Katsura, *Bull. Chem. Soc. Jpn.*, **51**, 1358 (1978).
3) K. Kitayama, T. Sugihara, and T. Katsura, *Bull. Chem. Soc. Jpn.*, **52**, 458 (1979).
4) K. Kitayama and T. Katsura, *Bull. Chem. Soc. Jpn.*, **55**, 1820 (1982).
5) K. Kitayama, D. Zoshima, and T. Katsura, *Bull. Chem. Soc. Jpn.*, **56**, 689 (1983).
6) K. Kitayama, C. Mizokuchi, and T. Katsura, *Bull. Chem. Soc. Jpn.*, **56**, 695 (1983).
7) G. W. Bazuev, O. V. Makarova, V. Z. Oboldin, and G. P. Shveikin, *Dokl. Akad. Nauk SSSR*, **230**, 869 (1976).
8) T. Shin-ike, G. Adachi, and J. Shiokawa, *Mater. Res. Bull.*, **12**, 1149 (1977).
9) J. E. Greedan, *Mater. Res. Bull.*, **14**, 13 (1979).
10) L. Soderholm and J. E. Greedan, *Mater. Res. Bull.*, **17**, 707 (1982).
11) H. Brusset, F. Madaule-Aubry, B. Blanck, J. P. Glaziou, and J. P. Laude, *Can. J. Chem.*, **49**, 3700 (1971).
12) H. Schwarz, *Z. Anorg. Allg. Chem.*, **323**, 44 (1963).
13) H. Brusset, R. Mahe, and J. P. Laude, *Bull. Soc. Chim. Fr.*, **1973**, 495.
14) O. N. Ustalova, G. A. Rykova, V. M. Skorikov, and I. V. Tananaev, *Zh. Neorg. Khim.*, **25**, 1223 (1980).
15) G. J. McCarthy, C. A. Sipe, and K. E. McIlvried, *Mater. Res. Bull.*, **9**, 1279 (1974).
16) T. Shin-ike, G. Adachi, and J. Shiokawa, *Denki Kagaku*, **48**, 258 (1980).
17) T. Katsura, K. Kitayama, T. Sugihara, and N. Kimizuka, *Bull. Chem. Soc. Jpn.*, **48**, 1809 (1975).
18) T. Katsura and H. Hasegawa, *Bull. Chem. Soc. Jpn.*, **40**, 561 (1967).
19) N. Kimizuka and T. Katsura, *J. Solid State Chem.*, **13**, 176 (1975).
20) T. Katsura and A. Muan, *Trans. AIME*, **230**, 77 (1964).
21) N. Kimizuka and T. Katsura, *J. Solid State Chem.*, **15**, 151 (1975).
22) N. Kimizuka and T. Katsura, *Bull. Chem. Soc. Jpn.*, **47**, 1801 (1974).
23) T. Katsura, T. Sekine, K. Kitayama, T. Sugihara, and N. Kimizuka, *J. Solid State Chem.*, **23**, 43 (1978).
24) R. D. Shannon and C. T. Prewitt, *Acta Crystallogr., Sect. B*, **25**, 925 (1969).
25) G. P. Espinosa, *J. Chem. Phys.*, **37**, 2344 (1962).

 © 1983 The Chemical Society of Japan Bull. Chem. Soc. Jpn., 56, 1089—1094 (1983)

Retentive Friedel-Crafts Alkylation of Benzene with Optically Active 2-Chloro-1-phenylpropane and 1-Chloro-2-phenylpropane

Shinji MASUDA,*,† Tadashi NAKAJIMA,†† and Sohei SUGA††

†*Ashikaga Institute of Technology, Ashikaga 356*

††*Department of Industrial Chemistry, Faculty of Technology, Kanazawa University, Kodatsuno, Kanazawa 920*

(Received June 15, 1982)

Alkylations of benzene with both (−)-2-chloro-1-phenylpropane (**1**) and (+)-1-chloro-2-phenylpropane (**2**) in the presence of Lewis acid gave the same products: (−)-1,2-diphenylpropane (**3**), 1,1-diphenylpropane, and polymeric materials. In these reactions, (−)-**3** was obtained in 45—100% optical yield and was not racemized under the conditions used. These results reveal that the reaction from **1** to **3** proceeds with retention of configuration and that from **2** to **3** with inversion. The stereochemistry of the alkylation with **1** is elucidated by the mechanism involving a neighboring phenyl π-assisted cation; benzene attacks only the β-carbon of **1** from the side on which the previously attached chloride anion is located. The result of the reaction with **2** can be explained by a process involving the 1,2-shift of phenyl group in the ionization step of **2**, followed by the formation of the same intermediate as in the reaction with **1**. The mechanism of the overall reaction is discussed.

Since the discovery of the Friedel-Crafts reaction with high stereospecific integrity,[1] many reports have been published during the past decade.[2] Most of these stereospecific reactions resulted in the inversion of configuration at the reaction center of the alkylating reagent. Although the Friedel-Crafts reactions have been expected to proceed through a free carbonium ion,[3] the stereospecific examples reported so far indicate that the intermediate cation exists as a tight ion pair with the counterion or as a complex with the Lewis acid used. The validity of such an assumption can be justified by recent stereochemical results on the alkylations of benzene with (+)-2-butanol[4] and (+)-2-chlrobutane;[5] both reactions proceeded with inversion of configuration to give 2-phenylbutane in 27—40% optical yield. Thus, it is expected that the stereospecificity in the Friedel-Crafts reaction using optically active alkylating reagent can be enhanced if the reaction condition was controlled so as not to cause the isomerization of the starting material or the product.

The reaction with inversion of configuration has often been studied. But there have been few studies on the Friedel-Crafts alkylation with retention of configuration. Sprung,[6] Hart,[7] and their co-workers reported that optically active *s*-butyl phenyl ether and α-phenylethyl *p*-tolyl ether rearranged intramolecularly in the presence of a Lewis acid to the corresponding *o*-alkylphenol with retention of configuration. These reactions are in a sence aromatic alkylations with retention. However, when the alkyl phenyl ether was conducted with phenol, the reaction proceeded intermolecularly to give a totally racemic product.[8] Thus, this stereochemical result (retention) of forcing the reaction to be intermolecular has not been reported so far.

In a preliminary account, we demonstrated that the alkylation of benzene with (−)-2-chloro-1-phenylpropane (**1**) by a Lewis acid catalyst proceeded with complete retention of configuration to give (−)-1,2-diphenylpropane (**3**) and that the reaction with (+)-1-chloro-2-phenylpropane (**2**) gave the same product with inversion, as shown in Scheme 1.[2e] The former reaction is the first example of a retentive Friedel-Crafts alkylation which proceeds intermolecularly. In the present paper, we have undertaken a broader investigation of stereochemistry in the Friedel-Crafts alkylation of benzene with (−)-**1** and (+)-**2**, and we discuss the reaction mechanism.

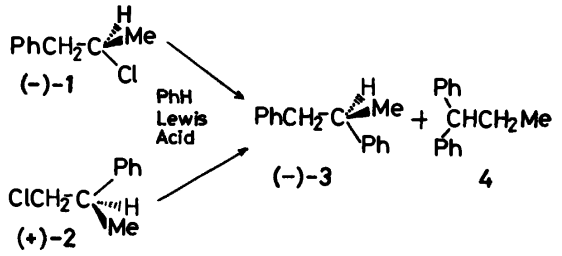

Scheme 1.

Results and Discussion

Both (−)-2-chloro-1-phenylpropane (**1**) and (+)-1-chloro-2-phenylpropane (**2**) reacted with benzene in the presence of 0.1 equivalent of $AlCl_3$ or $FeCl_3$ at −20—40 °C to give the same products: (−)-1,2-diphenylpropane (**3**), 1,1-diphenylpropane (**4**), and polymeric materials. The results under various conditions are summarized in Tables 1 and 2. The structures of **3** and **4** were identified by IR and NMR spectroscopies, and by comparing the retention time of their gas chromatograms with those of authentic samples. The isomer ratio of **3**/**4** was determined by NMR analysis. The optical rotations were taken on the mixture of **3** and **4**, since the two isomers could not be isolated in pure form.[9] The optical yields of the reactions were calculated from the optical purities of the starting materials, the reported rotation of **3**,[4] and the isomer ratio of **3**/**4** in the mixture obtained. The maximum rotation ($[\alpha]_D$) of optically active **1** was evaluated to be +23.9° on the basis of the rotation power of (+)-**1** derived by a series of reaction from optically pure (+)-propylene oxide, as mentioned in the experimental section.[10]

The absolute configurations of (−)-**1**, (+)-**2**, and (−)-**3** have been established to be R,[10] R,[11] and R,[12] respectively. Thus, it is apparent that the reaction from **1** to **3** proceeded with retention of configuration and

Table 1. Alkylation of benzene with (−)-2-chloro-1-phenylpropane (1) in the presence of Lewis acid[a)]

1 $[\alpha]_D^{25}$[b)] °	Lewis acid	Temp °C	Time h	Alkylated product: Yield[b)] %	Isomer (%)[d)] 3	4	$[\alpha]_D^{25}$[e)] °	Optical yield of 3[f)] %
−18.4	$AlCl_3$	20	0.3	74	81	19	−27.7	69
−18.4	$AlCl_3$	0	1.0	62	76	24	−37.8	100
−20.0	$AlCl_3$	−20	2.0	71	80	20	−41.7	96
−20.0	$FeCl_3$	40	0.3	62	46	54	−12.5	50
−20.0	$FeCl_3$	20	1.0	67	53	47	−20.2	70
−20.0	$FeCl_3$	0	3.0	61	61	35	−30.1	86
0.0	$FeCl_3$	−20	8.0	51	73	27	—	—

a) Molar ratio; 1: Lewis acid: C_6H_6=1 : 0.1 : 30—40. Carbon disulfide was added in the reaction below 5 °C. b) Measured in $CHCl_3$ (*c* 5). Maximum rotation of (−)-1: $[\alpha]_D^{25}$−23.9° (*c* 5, $CHCl_3$). c) Based on 1 used. d) Determined by NMR analysis. e) Rotations were taken on the mixture of 3 and 4, (*c* 5, $CHCl_3$). f) Calculated from the optical purity of 1 used, the reported rotation of 3 ($[\alpha]_D^{25}$+63.5° (*c* 2.34, $CHCl_3$)[4)]), and the isomer ratio of 3/4.[9)]

Table 2. Alkylation of benzene with (+)-1-chloro-2-phenylpropane (2) in the presence of Lewis acid[a)]

2 $[\alpha]_D^{25}$[b)] °	Lewis acid	Temp °C	Time h	Alkylated product: Yield[c)] %	Isomer (%)[d)] 3	4	$[\alpha]_D^{25}$[e)] °	Optical yield of 3[f)] %
14.0	$AlCl_3$	20	0.5	70	86	14	−26.3	51
14.0	$AlCl_3$	0	1.0	60	75	25	−45.0	100
14.0	$AlCl_3$	−20	1.5	65	76	24	−40.3	88
13.5	$FeCl_3$	40	0.2	55	46	54	−14.5	55
14.0	$FeCl_3$	20	1.0	64	52	48	−21.9	71
14.0	$FeCl_3$	0	3.0	60	65	35	−32.0	83
13.5	$FeCl_3$	−20	8.0	61	75	25	−40.2	97

a) Molar ratio; 2; Lewis acid: C_6H_6=1 : 0.1 : 30—40. Carbon disulfide was added in the reaction below 5 °C. b) Measured in $CHCl_3$ (*c* 5). Maximum rotation of (+)-2: $[\alpha]_D^{25}$+14.9° (neat), see Experimental section. c) Based on 2 used. d) Determined by NMR analysis. e) Rotations were taken on the mixture of 3 and 4, (*c* 5, $CHCl_3$). f) Calculated from the optical purity of 2 used, the reported rotation of 3 (see footnote f in the table 1), and the isomer ratio of 3/4.[9)]

that from 2 to 3 with inversion of configuration at the asymmetric carbon. The $AlCl_3$ catalyzed reaction at 0 °C revealed the highest (complete) stereospecificity. When the reaction was carried out in the presence of $FeCl_3$ or at elevated temperature, considerable racemization of 3 was observed. On the whole, increasing temperature tends to decrease the magnitude of the optical yield of 3 and the isomer ratio of 3/4.

Thus, the stereochemistry (retention) of the alkylation using 1 may be interpreted by a mechanism involving an intermediate (5) of the phenonium ion type, in which benzene attacks only β-carbon of the two bridged carbon atoms from the opposite side of the bulky phenyl ring (the side on which the previously attached chloride anion is located); (Scheme 2).

On the other hand, the stereochemistry of the reaction using 2 indicates that the migration of the phenyl group on C_α to the adjacent carbon takes place simultaneously with the departure of the chlorine atom and then the same phenonium ion (5) as mentioned above was formed prior to the attack of benzene. In connection with this observation, we had found previously that (+)-2 was converted stereospecifically into (−)-1 by trace amounts of Lewis acid.[2e)] If the chlorine atom of 2 was directly replaced with a phenyl group, as suggested by Brown *et al.*,[13)] the alkylation of benzene with (+)-2 should give (+)-3; this does not accord with the result obtained here.

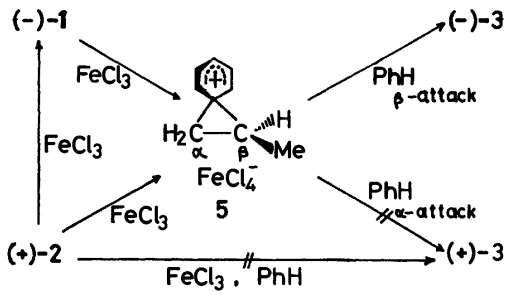

Scheme 2.

The existence of a phenonium ion has recently been recognized on the basis of studies on the rates and products of acetolysis of *threo*-2-aryl-1-methylpropyl brosylate with a number of different substituents,[14)] and has been confirmed spectroscopically to be a stable symmetrically bridged ion in superacid medium,[15)] although there were many controversies over the past two decades.[16)] McMahon *et al.*[17)] also have concluded that the Friedel-Crafts alkylation of toluene with 2-

Table 3. Alkylation of *p*-xylene with **1** and **2** the presence of $FeCl_3$[a]

Starting chloride	Temp °C	Time h	Alkylated product Yield[b] %	Isomer (%)[c] **6**	**7**
1	40	0.2	83	54	46
1	20	1.0	88	67	33
1	0	3.0	81	74	26
2	30	0.5	85	61	39
2	0	3.0	87	76	24

a) Molar ratio; **1** (or **2**): $FeCl_3$: *p*-xylene=1 : 0.1 : 35 b) Based on starting chloride. c) Determined by NMR analysis.

phenylethyl-1-^{14}C chloride proceeded *via* a symmetric phenyl bridged intermediate. In our experiment, if the phenyl ring in the intermediate is equally bonded to both the α and β carbons and if the benzene attacks equally both these carbons, the product (**3**) would not be optically active; such an intermediate must yield a racemic product.

In order to confirm the reaction site in the intermediate, both **1** and **2** were allowed to react with *p*-xylene in the presence of $FeCl_3$. These two reactions gave the same products: 1-phenyl-2-(2,5-dimethylphenyl)propane (**6**) and 1-phenyl-1-(2,5-dimethylphenyl)-propane (**7**), in 80—90% yield. However, no amount of 1-(2,5-dimethylphenyl)-2-phenylpropane (**8**) was detected at all, as shown in Table 3. The process from **2** to **6** involves the 1,2-shift of phenyl group on C_β of **2** to the adjacent carbon, accompanied by the attack of *p*-xylene to the β-carbon. Thus, it is evident that both reactions using **1** and **2** proceed through the same intermediate, in which the β-carbon is attacked exclusively by aromatics.

Accordingly, much of the positive charge in the intermediate resides on the β-carbon, and the participation of phenyl group to that carbon seems to be of the π-bridged type (**9**)[18] (or unsymmetrically bridged type)[19] rather than of symmetrically σ-bridged type (**5**) mentioned above, as shown in Scheme 3. Furthermore, the above result excludes the rapid equilibration between the secondary cation (**9**) and the primary one (**9'**) although such an interconversion between the above two cations is still controversial.[18,19]

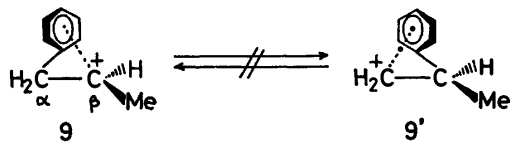

Scheme 3.

The stereospecificity of both reactions using **1** and **2** decreased remarkably with a rise in the reaction temperature, as mentioned above (Tables 1 and 2). In order to estimate the net stereospecificity of these reactions, one must know whether the starting chloride or the product is racemized in the course of reaction. Optically

Table 4. Treatment of (−)-**3** with $FeCl_3$ in benzene at 30 °C[a]

Time h	Specific rotation[b]/° Before reaction	After reaction
0.5	−24.7	−24.7
1.5	−24.7	−24.6
2.5	−24.7	−24.5
5.0	−24.7	−24.1

a) Molar ratio; (−)-**3**: $FeCl_3$: C_6H_6=1 : 0. 1 : 35. b) Measured in $CHCl_3$ (*c* 5) at 25 °C.

active alkylbenzenes having the asymmetric carbon atom attached to a benzene ring undergo rapid racemization under Friedel-Crafts conditions.[20] The racemization process has been considered to be due to a hydride transfer reaction through a free carbonium ion. In order to ascertain the possibility of such a process, (−)-**3** was treated with $FeCl_3$ in benzene at 30 °C. The result in Table 4 shows that the specific rotation of (−)-**3** remained unchanged before and after the reaction. Furthermore, no rearrangement of **3** to **4** was observed in this treatment. Thus, it turns out that the lesser stereospecificity in the reaction at elevated temperature can not be attributed to the successive racemization of the product. The greater optical stability of **3** than of alkylbenzenes such as 2-phenylbutane[20b] may be interpreted as the following considerations. The first is on the basis of a steric factor for the abstraction of hydrogen of the β-carbon of **3**. If the α-phenyl group of **3** assists the departure of the β-hydrogen as a hydride ion anchimerically, **3** should have the conformation in which two bulky phenyl and methyl groups are next to each other, in the transition state of reaction, as presented in Scheme 4. Such a conformation,

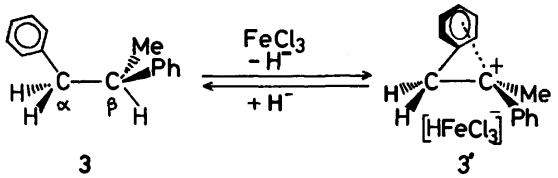

Scheme 4.

however, is unfavorable due to the steric hindrance, and thus the β-hydrogen may not be removed under the condition used. The second involves the formation of π-bridged cation such as **3'** yielded by the removal of the β-hydrogen of **3**. If the hydrogen was abstracted with the aid of $FeCl_3$ or a positive ion (R^+), the phenyl group on C_α would participate with β-carbon to form the π-bridged cation (**3'**), and a reverse attack of hydride ion would take place on the β-carbon from the opposite side of the assisting phenyl group to give (−)-**3** again. Thus, the configuration of (−)-**3** would remains unchanged during the reaction. In this stage, however, it is not clear which explanation is more reasonable.

Next, we examined the possibility of simultaneous racemization of the starting chloride (**1**) by observing

Table 5. The net stereospecificity in the alkylation of benene with (+)-1 in the presence of Lewis acid

(+)-1 $[\alpha]_D^{25b)}$ °	Lewis acid	Temp °C	Time min	Conversion[c] %	Recovered 1 $[\alpha]_D^{25b)}$ °	Recovered 1 Remaining optical activity/%	Alkylated products Isomer (%)[d] 3	Alkylated products Isomer (%)[d] 4	Alkylated products $[\alpha]_D^{25e)}$ °	Net stereo-[f] specificity %
21.2	$AlCl_3$	5	4	65	21.0	99	80	20	43.8	100
21.2	$FeCl_3$	30	25	80	16.5	78	50	50	17.9	70
21.2	$FeCl_3$	5	120	45	19.6	92	61	39	31.0	94

a) Molar ratio; (+)-1: Lewis acid: C_6H_6=1 : 0.15 : 35. b, c, d, and e) See footnotes b, c, d, and e in Table 1, respectively. f) Calculated by the reported method.[2d)]

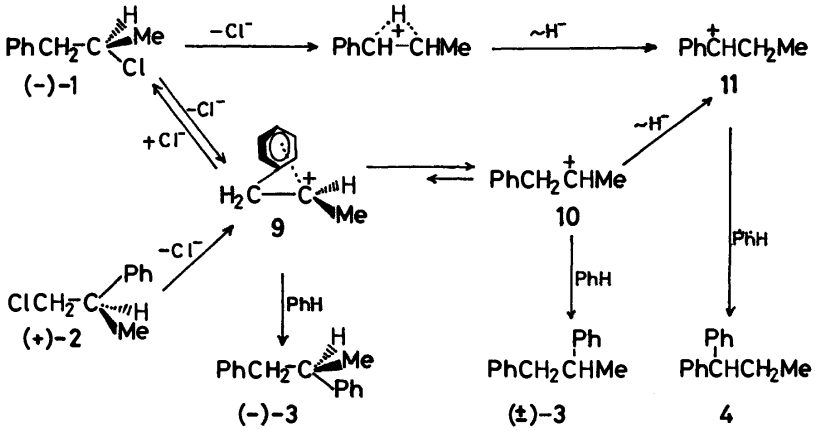

Scheme 5. Lewis acid and its conjugated base are abbreviated for conciseness.

the optical activity of that recovered before the completion of reaction. As can be seen from Table 5, the racemization of (−)-**1** is evident in the reaction catalyzed by $FeCl_3$, especially at elevated temperature. Thus, the lesser stereospecificity at these conditions depends on the simultaneous racemization of the starting chloride. This may be explained in terms of the formation of an open carbonium ion such as 2-phenyl-1-methylethyl-cation (**10**)[21)] followed by an internal return as shown in Scheme 5. Then, the net stereospecificity of reaction was estimated on the basis of the remaining optical activity of **1** and the extent of alkylation observed at the same reaction time according to the method described previously.[2d)] The net stereospecificity of the reaction catalyzed by $FeCl_3$ decreased from 94 to 70% with the rise of temperature from 5 to 30 °C. This result suggests that the alkylation of benzene with **1** involves both intermediates, **9** and **10**, and that the latter plays a rather important role at elevated temperatures.

Consequently, the overall reaction can be illustrated as in Scheme 5. The precursor of 1,1-diarylpropane (**4** or **7**) seems to be 1-phenylpropyl cation (**11**) formed through two distinct pathways; the first path involves the hydride participation in minor competition with the phenyl participation accompanied by ionization of **1**, and the second involves the carbonium ion rearrangement of **10** to **11** (1,2-hydride shift). At the lower reaction temperature, the rate of the reaction (**9**→**10**) is so much slower than those of reactions (**9**→**3**, and **1**→**11**) that the total reaction from **1** to **3** proceeds with high stereospecificity, and the formation of **4** is suppressed. On the contrary, the reversible reaction from **9** to **10** is accelerated by increasing the reaction temperature so that the racemization of **9** takes place easily, which leads to the formation of (±)-**3**. Thus, the stereospecificity in the reaction from **1** to **3** decreases under the high temperature conditions. Furthermore, the formation of **4** is enhanced because of the easy rearrangement of **9** to **10**. The isomer ratio of **6**/**7** in the reaction of *p*-xylene with **1** (or **2**) is lower than that of **3**/**4**. This depends on the higher reactivity (higher basicity) of *p*-xylene toward the intermediate cations than that of benzene.

The Friedel-Crafts alkylation of benzene with **1** in the presence of Lewis acid resembles the solvolysis of 2-phenyl-1-methylethyl tosylate in trifluoroacetic acid with complete retention of configuration.[19)] The solvolysis of all primary and most secondary 2-arylalkyl system has been suggested to proceed through discrete aryl-assisted (retention) and solvent-assisted (inversion) pathways.[14)] However, our Friededl-Crafts alkylation does not involve the latter path in the solvolysis reaction.

Experimental

The optical rotations were taken on a JASCO DIP-SL polarimeter with use of 0.05 and 0.1 dm cells at 25 °C. The NMR spectra were recorded on a JEOL PS-100 spectrometer. The chemical shifts are given in ppm downfield from internal TMS. The IR spectra were determined on a JASCO DS-301 spectrometer. Gas chromatograph analyses (GC) were carried out on a 3 m column of 10% Carbowax 20 M on Diasolid L with Shimadzu DC-6A and GC-3A instruments. All the boiling points are uncorrected.

Benzene was washed with concentrated sulfuric acid and then water, distilled after drying on calcium chloride, and stored over sodium wire. *p*-Xylene was purified by fractional distillation and stored over sodium wire. Other solvents were dried and distilled before use.

Preparation of Optically Active Chlorophenylpropanes. *(+)-2-Chloro-1-phenylpropane (1)*: A solution of (+)-propylene oxide (11.6 g, 0.2 mol, $[\alpha]_D^{25}$ +7.96° (c 5, $CHCl_3$))[2b] in ether (50 ml) was added dropwise into an etheral solution of phenyllithium (0.25 mol). The resulting mixture was stirred at room temperature for 4 h, and then quenched by the slow addition of water. After the organic layer was separated, the aqueous layer was extracted with ether. The combined organic solution was dried over sodium sulfate and concentrated. The resulting yellow oil was distilled under reduced pressure to give a distillate (20.3 g), bp 103—108 °C/17 Torr.* The distillate was subjected to column chromatography on silica gel. Elution with hexane afforded biphenyl (0.7 g) and then that with chloroform gave (−)-1-phenyl-2-propanol in 66% yield (18 g), bp 102—105 °C/19 Torr, $[\alpha]_D^{25}$ −37.57° (*c* 5, $CHCl_3$), [lit,[19] $[\alpha]_D$ +38.69° (*c* 13.4, $CHCl_3$)].

To a stirred solution of the above optically active alcohol (10 g, 74 mmol) in pyridine (10 ml) was added thionyl chloride (9.6 g, 81 mmol) at such a rate that the temperature did not exceed 5 °C. After the addition was complete, the mixture was heated at 65 °C for 6 h, and poured into water. The organic layer was separated and the water layer was extracted with three portions of ether. The combined organic mixture was washed with water, dilute hydrochloric acid, saturated sodium chloride, 6% sodium hydrogencarbonate and water, successively. After drying over sodium sulfate, ether was removed. The residual liquid was distilled under reduced pressure to give (+)-**1** in 68% yield (7.8 g), bp 91 °C/17 Torr, $[\alpha]_D^{25}$ +21.85° (neat), $[\alpha]_D^{25}$ +23.19° (*c* 5, $CHCl_3$). Provided that this chlorination step proceeded with complete inversion, the optical purity of (+)-**1** obtained is evaluated to be 97.1%. Thus the maximum rotation was calculated to be $[\alpha]_D^{25}$ +23.88° [lit,[10] $[\alpha]_{25}^{D}$ −24.9° (neat)]. IR (neat): 1605 (skeltal vibration of phenyl ring), 760 and 700 (δ CH, monosubstituted phenyl), and 610 cm^{-1} (νC–Cl, secondary chloride). NMR ($CDCl_3$, 10%): δ=1.41 (d, *J*=7.6 Hz, 3H, $-CH_3$), 2.92 (m, 2H, $-CH_2-$), 4.10 (m, 1H, -CH=), 7.10 (m, 5H, phenyl). (−)-**1**; The solution of (+)-1-chloro-2-phenylgropane (**2**) (5.0 g, 32 mmol, $[\alpha]_D^{25}$ +14.0°) in dichloroethane (20 ml) was added dropwise to a stirred mixture of anhydrous iron(III) chloride (50 mg, 0.3 mmol) and 1,2-dichloroethane (20 ml) at room temperature. The resulting mixture was stirred at 65 °C for 2 h, and then poured onto a mixture of crushed ice (15 g) and concentrated hydrochloric acid (15 g). The organic layer was separated and the aqueous layer was extracted with two 15 ml portions of 1,2-dichloroethane. The combined organic solution was washed with water, 6% sodium hydrogencarbonate and water, successively, and then dried over sodium sulfate. After removal of the solvent, the residue was distilled under reduced pressure to give (−)-**1** in 70% yield, $[\alpha]_D^{25}$ −20.0° (*c* 5, $CHCl_3$). IR and NMR spectra of (−)-**1** were identical to those of (+)-**1** obtained above.

(+)-1-Chloro-2-phenylpropane (2): The reaction of (+)-2-phenyl-1-propanol (13.6 g, 0.1 mol, $[\alpha]_D^{25}$ +15.7° (neat), 94% optically pure)[2b] with thionyl chloride (9.6 g, 0.1 mol) in pyridine gave (+)-**2** in 80% yield (7.8 g). Bp 94 °C/18 Torr, $[\alpha]_D^{25}$ +14.0° (neat). Thus, the maximum rotation was evaluated to be $[\alpha]_D^{25}$ +14.9° (neat). IR (neat): 1605 (skeltal vibration of phenyl ring), 700 and (δCH, monosubstituted phenyl), and 645 cm^{-1} (νC–Cl, primary chloride). NMR: δ=1.38 (d, *J*=7.4 Hz, 3H, $-CH_3$), 3.20 (m, 1H, -CH=), 3.50 (m, 2H, $-CH_2-$), 7.14 (m, 5H, phenyl).

Reaction Procedures. *Method A*: A slurry of pulverized anhydrous aluminium chloride (60 mg, 0.45 mmol) in dry benzene (12 ml) and carbon disulfide (4 ml) was cooled to 0 °C in a three-necked 100 ml flask equiped with a thermometer, an additional funnel, and a drying tube. To this stirred mixture was added a solution of (−)-**1** or (+)-**2** (0.7 g, 45 mmol) in benzene (3 ml) carefully over a period of 2 min at 0 °C. The resulting mixture was stirred at 0±0.5 °C for 1 h and then poured onto a mixture of crushed ice (5 g) and concentrated hydrochloric acid (5 ml). The benzene layer was separated and the aqueous layer was extracted with two 10 ml portions of benzene. The combined organic solution was washed with dilute hydrochloric acid, water, 6% sodium hydrogencarbonate solution and water, successively, and then dried over anhydrous sodium sulfate. After removal of the solvent, the residue was distilled under reduced pressure to give a distillate (bp 150—155 °C/20 Torr.) and high boiling materials. The distillate was shown to be a mixture of **3** and **4** by NMR analysis. The structure of these products was confirmed by the spectroscopic comparison with their authentic samples (see below). The optical rotations and the isomer ratio of **3**/**4** were determined on this distillate.[9]

The alkylation of *p*-xylene with **1** and **2** were also carried out in the same way as those of benzene and gave a mixture of **6** and **7** in 80—90% yield, bp 158—163 °C/15 Torr.

Details of reaction conditions and results are given in Tables 1, 2, and 3.

Method B: In order to estimate the net stereospecificity of the reaction, the experiment was carried out as follows. To a cooled suspension (below 0 °C) of $FeCl_3$ (0.45 mmol) in benzene (15 ml) was added, all at once, a solution of (+)-**1** (45 mmol) in benzene (3 ml), and the reaction mixture was stirred at the prescribed temperature for the prescribed period (see Table 5). After the reaction was quenched by an addition of water, the resulting benzene solution was subjected to gas chromatography to determine the conversion percent, and then worked up as mentioned above. The unreacted starting chloride and the product were separated by fractional distillation. The results are summarized in Table 5.

Preparation of Authentic Samples. *1,2-Diphenylpropane (3)* was prepared by a series of reactions as follows: 2-Phenylpropionic acid, prepared from 2-phenylpropanol[22] by the silver nitrate oxidation, was converted into 2-phenylpropionyl chloride by the reaction with phosphoryl chloride. The acylation of benzene with the acid chloride obtained above yielded 1,2-diphenyl-1-propanone. The above ketone was reduced according to the method[23] of Clemmensen to give 1,2-diphenylpropane (**3**). Bp 155 °C/20 Torr. IR (neat): 1325 (δCH, $-CH_3$), 700 and 755 cm^{-1} (δCH, monosubstituted phenyl). NMR: δ=1.17 (d, *J*=6.4 Hz, 3H, $-CH_3$), 2.80 (m, 2H, $-CH_2-$), 2.86 (m, 1H, -CH=), 7.10 (m, 10H, 2 phenyl).

1,1-Diphenylpropane (4) was prepared by the alkylation of benzene with 3-phenyl-1-propene in the presence of aluminium chloride at 5 °C, bp 160 °C/18 Torr. IR (neat): 700 and 740 cm^{-1} (δCH, monosubstituted phenyl). NMR: δ=0.88 (t, *J*=8.0 Hz, 3H, $-CH_3$), 2.20 (q, *J*=8.0 Hz, 2H, $-CH_2-$), 3.72 (t, *J*=8.0 Hz, -CH=), 7.11 (s, 10H, 2 phenyl).

1-Phenyl-2-(2,5-dimethylphenyl)propane (6) was prepared by the alkylation of *p*-xylene with **1** in the presence of aluminium chloride at −20 °C. Although the reaction gave a trace amount of **7** as a by-product, the fractional distillation of the mixture gave **6**, bp 169 °C/14 Torr. IR: 810 and 880 (δCH, 1,2,5-trisubstituted phenyl), 700 and 750 cm^{-1} (δCH, monosubstituted phenyl). NMR: δ=1.18 (d, *J*=7.8 Hz, 3H, $-CH_3$), 2.26 (s, 3H, *ortho*-CH_3), 2.37 (s 3H, *meta*-CH_3), 2.86

* 1 Torr≈133.322 Pa

(d, J=7.8 Hz, 2H, -CH_2-), 3.20 (m, 1H, -CH=), 7.00 (m, 3H, 1,2,5-trisubstituted phenyl), 7.18 (s, 5H, phenyl).

1-Phenyl-1-(2,5-dimethylphenyl)propane (7) was prepared by the alkylation of *p*-xylene with 3-phenyl-1-propene in the presence of aluminium chloride at 5 °C. Bp 174 °C/15 Torr. IR (neat): 880 and 810 (δCH, 1,2,5-trisubstituted phenyl), 760 and 700 cm^{-1} (δCH, monosubstituted phenyl). NMR: δ= 0.88 (t, J=8.0 Hz, 3H, -CH_3), 2.25 (s, 3H, *meta*-CH_3), 3.82 (t, J=8.0 Hz, 1H, -CH=), 6.90 (m, 3H, 1,2,5-trisubstituted phenyl), 7.05 (s, 5H, phenyl).

1-(2,5-Dimethylphenyl)-2-phenylpropane (8) was prepared by the Clemmensen reduction of 1-(2,5-dimethylphenyl)-2-phenyl-1-propanone obtained from the reaction of *p*-xylene with 2-phenyl propionyl chloride. **8**: Bp 182 °C/15 Torr. IR: 880 and 810 (δCH, 1,2,5-trisubstituted phenyl), 760 and 700 cm^{-1} (δCH, monosubstituted phenyl). NMR: δ=1.20 (d, J=7.4 Hz, 3H, -CH_3), 2.13 (s, 3H, *ortho*-CH_3), 2.18 (s, 3H, *meta*-CH_3), 2.78 (m, 2H, -CH_2-), 2.86 (m, H, -CH=). 7.00 (m, 3H, 1,2,5-trisubstituted phenyl), 7.18 (s, 5H, phenyl).

References

1) J. I. Brauman and A. J. Pandell, *J. Am. Chem. Soc.*, **89**, 5421 (1967).

2) a) J. I. Brauman and A. Solladie-Cavallo, *J. Chem. Soc., Chem. Commun.*, **1968**, 1124; b) T. Nakajima, S. Suga, T. Sugita, and K. Ichikawa, *Tetrahedron*, **25**, 1807 (1969); c) T. Nakajima, Y. Nakamoto, and S. Suga, *Bull. Chem. Soc. Jpn.*, **48**, 960 (1974); d) T. Nakajima, S. Masuda, S. Nakashima, T. Kondo, Y. Nakamoto, and S. Suga, *ibid.*, **52**, 2377 (1979); e) S. Masuda, T. Nakajima, and S. Suga, *J. Chem. Soc., Chem. Commun.*, **1974**, 954; f) S. Masuda, M. Seigi, T. Nakajima, and S. Suga, *ibid.*, **1980**, 86; g) M. Segi, M. Takebe, S. Masuda, T. Nakajima, and S. Suga, *Bull. Chem. Soc. Jpn.*, **55**, 167 (1982).

3) a) C. C. Price and M. Lund, *J. Am. Chem. Soc.*, **62**, 3105 (1940); b) R. L. Burwell, Jr., and S. Archer, *ibid.*, **64**, 1032 (1942); c) A. Streitwieser, Jr., and P. J. Stang, *ibid.*, **87**, 4953 (1965).

4) P. A. Spanninger and J. L. von Rosengerg, *J. Am. Chem. Soc.*, **91**, 1970, 1973 (1972).

5) S. Suga, M. Segi, K. Kitano, S. Masuda, and T. Nakajima, *Bull. Chem. Soc. Jpn.*, **54**, 3611 (1981).

6) M. N. Sprung and E. S. Wallis, *J. Am. Chem. Soc.*, **56**, 1715 (1934).

7) H. Hart and R. Elia, *J. Am. Chem. Soc.*, **76**, 3031 (1954).

8) W. I. Gilbert and E. S. Wallis, *J. Org. Chem.*, **5**, 184 (1940).

9) In order to confirm the validity of the optical yield observed, we examined the dependence of the value of $[\alpha]_D$ of **3** on the ratio of **3**/**4**. Some samples having different ratios of **3**/**4** were prepared by adding pure **4** to a mixture of **3** and **4** in the ratio of 83 : 17($[\alpha]_D$ of **3**, −63.0°). The specific rotation of **3** in these samples was calculated to give an almost constant value with an error of about 2.3% as follows: [ratio of **3**/**4**, $[\alpha]_D$ of (**3**+**4**), $[\alpha]_D$ of **3**]; [68 : 32, −41.9°, −62.1°], [58 : 42, −36.9°, −63.6°], [51 : 49, −31.3°, −61.3°], [42 : 58, −26.5°, −63.2°]. Thus the optical yields of **3** listed on the table **1**, **2**, and **4** seem to be accurate.

10) J. Kenyon, H. Philips, and V. P. Pitman, *J. Chem. Soc.*, **1935**, 1072.

11) P. A. Leven, R. E. Marker, and A. Rothen, *J. Biol. Chem.*, **100**, 589 (1933).

12) R. A. Barns and B. R. Juliano, *J. Am. Chem. Soc.*, **85**, 6462 (1959).

13) H. C. Brown and M. Grayson, *J. Am. Chem. Soc.*, **75**, 6285 (1953); H. Jungk, C. R. Smoot, and H. C. Brown, *ibid.*, **78**, 2185 (1956).

14) a) For a review: C. J. Lancelot, D. J. Cram, and P. v. R. Schleyer, "Carbonium ions," ed by G. A. Olah and P. v. R. Schleyer, Wiley-Interscience, New York (1972), Vol. 3, p. 1347; b) F. L. Schat, III, C. J. Lancelot, and P. v. R. Schleyer, *J. Am. Chem. Soc.*, **100**, 228 (1978).

15) a) G. A. Olah, M. B. Comisarow, E. Namanworth, and B. Ramsey, *J. Am. Chem. Soc.*, **89**, 5259 (1967); b) G. A. Olah and R. D. Porter, *ibid.*, **93**, 6877 (1971).

16) For a review: H. C. Brown, "The Nonclassical Ion Problem" Plenum Press, New York (1977), p. 47.

17) M. A. McMahon and S. C. Bunce, *J. Org. Chem.*, **29**, 1515 (1964).

18) H. C. Brown, R. Bernheimer, and C. J. Kim, and S. E. Scheppele, *J. Am. Chem. Soc.*, **89**, 370 (1967).

19) J. H. Nordlander and W. J. Kelly, *J. Am. Chem. Soc.*, **91**, 996 (1969).

20) a) R. L. Burwell and A. D. Shields, *J. Am. Chem. Soc.*, **77**, 2766 (1955); b) E. L. Eliel, P. H. Wilken, and F. T. Fang, *J. Org. Chem.*, **22**, 231 (1957).

21) G. A. Olah, R. J. Spear, and D. A. Forsyth, *J. Am. Chem. Soc.*, **99**, 2615 (1977).

22) C. Allen and J. Van Allan, *Org. Synth.*, **24**, 82 (1944).

23) E. L. Martin, *Org. React.*, **1**, 155 (1942).

The Use of Grignard Reagents in Carbohydrate Synthesis.[1] The Synthesis of Branched-chain Deoxy Sugars and Their Anomerizations

Masajiro KAWANA,* Tetsuo KORESAWA, and Hiroyoshi KUZUHARA
The Institute of Physical and Chemical Research, Wako, Saitama 351

(Received June 18, 1982)

The reactions of methyl 5-*O*-benzyl-2-*O*- and -3-*O*-tosyl-β-D-ribofuranosides with methylmagnesium iodide gave, in one-step, 2-deoxy-3-*C*- and 3-deoxy-2-*C*-methyl branched-chain sugars, respectively. These sugars were anomerized with Grignard reagents; the thermodynamically more stable anomers were converted preferentially into the respective less stable anomers.

Recently, one of the authors has reported that methyl 5,6-*O*-cyclohexylidene-3-*O*-mesyl-α- and -β-D-allofuranosides reacted with Grignard reagents to give 3-deoxy or 3-deoxy-2-*C*-methyl-branched-chain sugars in one-step.[2] These reactions proceeded through 2-keto sugars which were formed *via* eliminations of the mesyloxy groups and 1,2-hydride shifts on the furanose rings. In the course of these studies, it has also been found that methyl glycofuranosides were anomerized by the use of the Grignard reagents.[3] The proposed mechanism consisted of the furanose-ring opening-reclosure by the coordination of sugar oxygens to the magnesium atoms of the reagents.

In this paper we would like to report an extention of these deoxygenation reactions to the tosylates of methyl 5-*O*-benzyl-D-ribofuranosides (**1**), and to report the anomerization of the deoxygenated products obtained therefrom.

The starting materials, methyl 5-*O*-benzyl-2-*O*- and -3-*O*-tosyl-D-ribofuranosides (**2** and **3**), were prepared from **1** by two methods **A** and **B**: the former was the conventional way and the latter involved the activation of hydroxyl groups of **1** with dibutyltin oxide.[4] The results are summarized in Scheme 1. Method **B** was superior to **A** in regioselective tosylation of the hydroxyl group at C-2 and in almost avoiding any production of 2,3-di-*O*-tosylates (**4**).

Treatment of **3**β with 3.4 mol equiv. of MeMgI gave methyl 5-*O*-benzyl-3-deoxy-2-*C*-methyl-β-D-*threo*-pentofuranoside (**5**β) and its C-2 epimer (**6**β) in 81 and 6% yields, respectively (Scheme 2). The structure of **5**β was confirmed by chemical conversion to a known compound, 5-*O*-benzyl-1,2-*O*-cyclohexylidene-3-deoxy-2-*C*-methyl-β-D-*threo*-pentofuranose (**10**).[5] The same reaction on **2**β gave methyl 5-*O*-benzyl-2-deoxy-3-*C*-methyl-β-D-*threo*-pentofuranoside (**7**β) and its C-3 epimer (**8**β) in 57 and 2.5% yields, respectively. In addition, an α-anomer (**8**α, 19%) and a small amount of an open-chain product (**9**, 5%) were isolated; these results suggested that 2-deoxy furanosides were easily anomerized under the Grignard reaction conditions. Debenzylation of **7**β afforded methyl 2-deoxy-3-*C*-methyl-β-D-*threo*-pentofuranoside (**11**), which, without further purifications, was converted into a 3,5-*O*-isopropylidene derivative (**12**), thus indicating the 3,5-*cis* structure of the hydroxyl functions of **7**β.

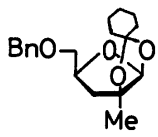

10

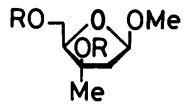

11 : R=H
12 : R=>C(CH₃)₂

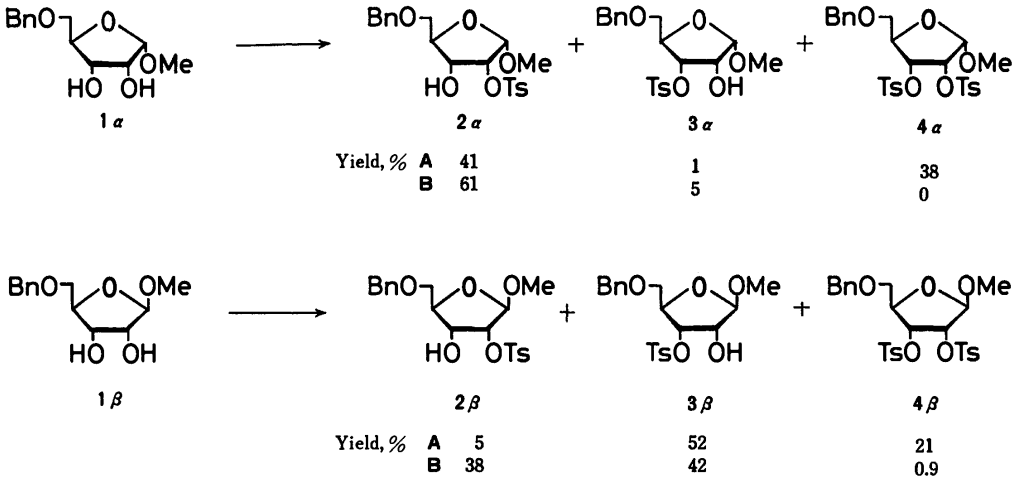

Method **A**: TsCl (1.4 equiv.), Pyr, 0 °C, 24 h.
Method **B**: 1) Bu_2SnO, MeOH; 2) TsCl (1 equiv.), Pyr–DMF–PhH, 0 °C, 50 min.
Bn=$C_6H_5CH_2$–. Ts=*p*-$CH_3C_6H_5SO_2$–.

Scheme 1.

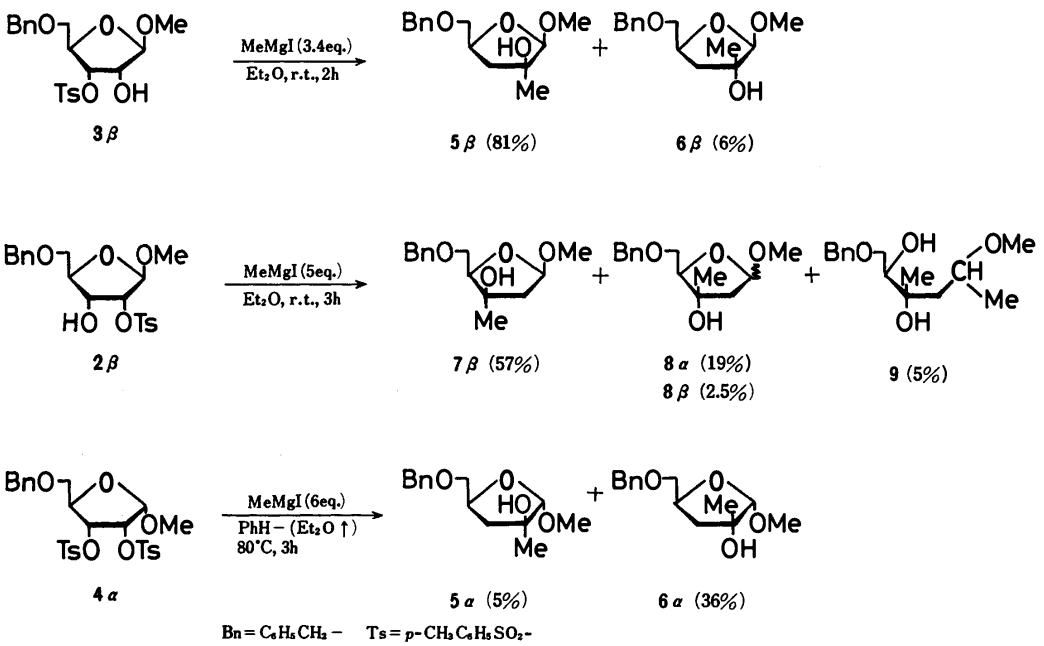

Scheme 2.

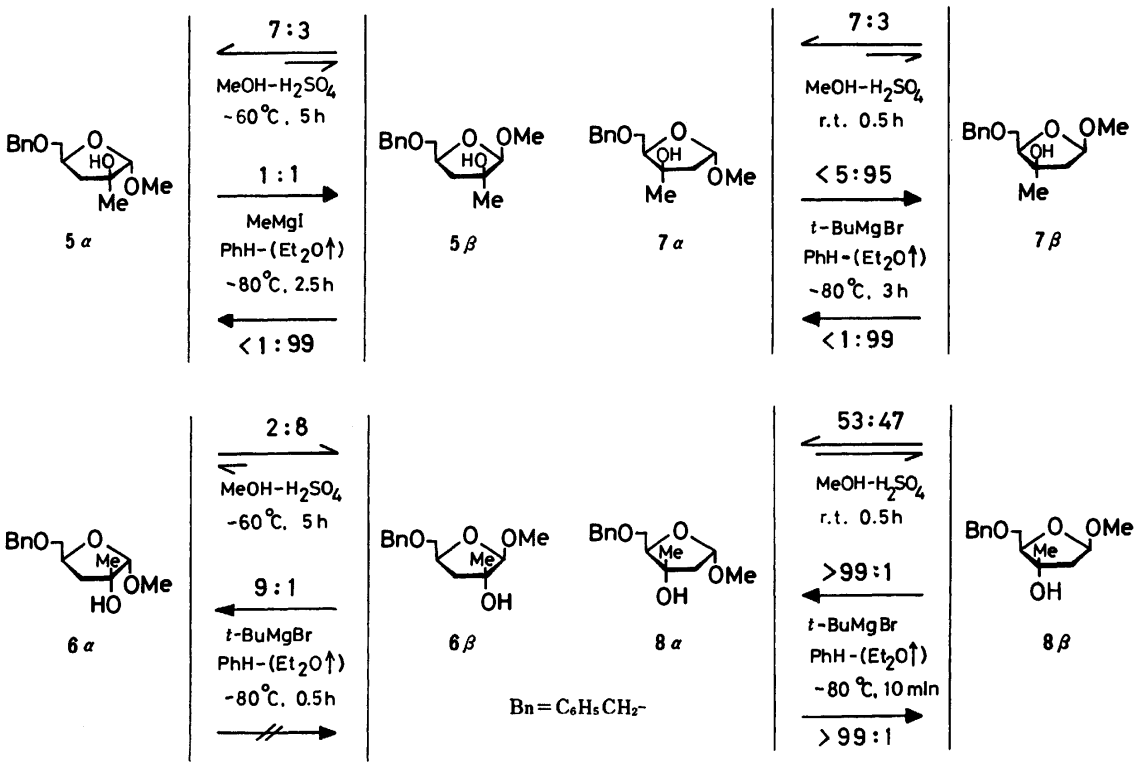

Scheme 3.

The reaction of **2***α* with MeMgI did not proceed even under refluxing conditions: An insoluble complex was formed when **2***α* was added to the Grignard reagent.

We attempted to use the ditosylate derivatives, **4***α* and **4***β*, in the present reactions, in the hope that one of the tosyl groups would selectively be cleaved to form a monotosylate derivative, which, in turn would react with the Grignard reagent to give the deoxy compounds *via* a keto sugar. A mixture of **4***α* and MeMgI in benzene–ether was treated at *ca.* 80 °C to produce the expected compound, **6***α*, although in low yield. However, starting from **4***β*, we could not isolate any desired products.

The branched-chain deoxy sugars thus obtained were subjected to the anomerization reaction with an acid as well as with the Grignard reagents (Scheme 3). In the acidic anomerization of the 3-deoxy sugars, the anomers which have 1,2-*trans* oxygen functions always predominated over the 1,2-*cis* counterparts under equilibrating conditions because of the repulsion of the

Table 1. The physical properties and elemental analyses of the sugar derivatives

Compound	Mp θ_m/°C	$[\alpha]_D$/° (c, $CHCl_3$)	Temp/°C	Formula	Found (%) C	H	S
2α	Syrup	+54.0 (1.0)	21	$C_{20}H_{24}O_7S$[a]	58.83	5.72	7.86
2β	Syrup	−11.2 (1.0)	22		58.70	5.93	7.62
3α	Syrup	+77.4 (0.8)	27		58.80	5.97	7.82
3β	Syrup	+5.1 (1.4)	22		58.65	5.76	7.78
4α	87.0—87.5[c]	+44.7 (1.0)	25	$C_{27}H_{30}O_9S_2$[c]	57.48	5.37	11.37
4β	88.5—89.5[b]	+31.9 (1.3)	25		57.69	5.35	11.34
5α	Syrup	+112 (1.0)	21	$C_{14}H_{20}O_4$[e]	66.64	8.17	
5β	40—42[f]	−56.7 (1.0)	20		66.46	7.87	
6α	Syrup	+69.0 (1.1)	25		66.55	7.95	
6β	Syrup	−72.4 (1.0)	20		66.52	7.97	
7α	Syrup[g]	+102 (1.0)	21		66.67	8.21	
7β	Syrup	−50.7 (1.0)	23		66.68	8.02	
8α	Syrup	+108 (0.6)	19		66.70	8.03	
8β	Syrup	−54.8 (0.7)	20		66.58	7.98	
9	Syrup	+11.7 (1.0)	20	$C_{15}H_{24}O_4$[h]	66.98	9.03	
10	49—50[f,i]	−22.4[i] (1.6)	25	$C_{19}H_{26}O_4$	71.75	8.20	
12	Syrup	−110 (0.6)	24	$C_{10}H_{18}O_4$	59.33	9.08	

a) Calcd: C, 58.81; H, 5.92; S, 7.85%. b) Recrystallized from benzene–hexane. c) Calcd: C, 57.64; H, 5.34; S, 11.40%. d) Distilled at *ca.* 143 °C (bath temperature)/2 mmHg. e) Calcd: C, 66.64; H, 7.99%. f) Crystallized on cooling. g) Distilled at 138—144 °C (bath temperature)/2 mmHg. h) Calcd: C, 67.13; H, 9.02%. i) Lit, (Ref. 5): 47—48 °C; $[\alpha]_D^{20}$ −22.6° (*c* 2.6, $CHCl_3$).

1,2-*cis* oxygen functions. On the other hand, in the case of the 2-deoxy sugars, the anomers having 1,3-*trans* oxygen functions were not always favorable; the equilibrated solution of **8** consisted of a mixture of **8α** and **8β** in a ratio of 53 : 47.

The anomerization of each anomer of the deoxy compounds with the Grignard reagents was carried out using a large excess of *t*-BuMgBr (MeMgI for **5**) in a mixture of benzene–ether. The ether was allowed to distill out from the reaction mixture: under these conditions, a lot of precipitates came out as the ether was lost, so that the reaction mixture became heterogeneous. In the case of **5α**, the anomerization with *t*-BuMgBr was very slow under the conditions used. However, when MeMgI was used instead of *t*-BuMgBr, **5α** was anomerized to give a 1 : 1 anomeric mixture. Starting from **5β**, slight anomerization was observed under the same conditions.

On the other hand, the anomerization of **6β** with *t*-BuMgBr was very fast to give a 9 : 1 mixture of the α- and β-anomers. The reverse reaction (from **6α** to **6β**) did not proceed; thus a one-way anomerization[3] was observed in this case.

It is noted that the 3-deoxy sugars, **5** and **6**, were anomerized predominantly with the Grignard reagents from the thermodynamically more stable 1,2-*trans* anomers to the less stable 1,2-*cis* counterparts. In the case of the 2-deoxy sugars, the anomerization of the 1,3-*trans* anomers, **7α** and **8β**, with *t*-BuMgBr also proceeded smoothly to result in the preferred formation of the 1,3-*cis* anomers, **7β** and **8α**, respectively.

The ^{1}H NMR spectral data of the branched-chain deoxy sugars are summarized in Table 2; these data are consistent with the structures. The methoxyl or methylene (at C-5) protons located next to the branching methyl group in a *cis* manner resonated at higher field than those in a *trans* relation presumably because of the shilding effect of the branching methyl group. These differences in chemical shifts were diagnostic for determining the configuration of the hydroxyl groups at the branching points.

The signs of the specific rotations of the above described deoxy sugars which have the β-D-configuration were negative, whereas the corresponding α-anomers showed positive signs. These phenomena were compatible with those for the methyl pentofuranosides reported earlier.[3,6]

Experimental

The melting points were determined with a Yamato capillary-melting point apparatus and were uncorrected. The ^{1}H NMR spectra were recorded on a JEOL PS-100 NMR spectrometer, with tetramethylsilane as the internal standard The optical rotations were measured on a Perkin-Elmer Model 241MC polarimeter.

Merck silica gel GF_{254} was used for the TLC, and the compounds were detected by heating after spraying them with a methanol–sulfuric acid–*p*-methoxybenzaldehyde (85 : 10 : 5, v/v) mixture. Merck silica gel 60 (0.063—0.29 mm) was utilized for the column chromatography. The elemental analyses were performed by this Institute.

The Grignard reagents, MeMgI and *t*-BuMgBr, were prepared from magnesium and the corresponding alkyl halide in dry ether, and the Grignard reactions were carried out in dry solvents under an atmosphere of dry nitrogen.

The ^{1}H NMR spectral data of the compounds are listed in Table 2, while their physical properties and the results of their elemental analyses are summarized in Table 1.

The Tosylation of Methyl 5-O-Benzyl-α- and -β-D-ribofuranosides (1α and 1β). Some of the results and reaction conditions are described in Scheme 1 and Table 1.

Method A: To a cold (0—5 °C) solution of **1α** (4.32 g, 17.6 mmol)[3] or **1β** (8.94 g, 35.2 mmol)[3] in dry pyridine (60 or

TABLE 2. THE ^{1}H NMR SPECTRA OF THE SUGAR DERIVATIVES

Compound	δ (in $CDCl_3$)
2α	2.40 (3H, s, C-CH_3), 2.8 (1H, br s, OH), 3.33 (3H, s, OMe), 3.50 (2H, d, J=4 Hz, H-5,5′), 3.97 (1H, dd, $J_{2,3}$=5.5 Hz, $J_{3,4}$=2 Hz, H-3), 4.16 (1H, br m, H-4), 4.39 and 4.47 (2H, ABq, J=11 Hz, CH_2Ph), 4.67 (1H, dd, $J_{1,2}$=4 Hz, $J_{2,3}$=5.5 Hz, H-2), 4.85 (1H, d, $J_{1,2}$=4 Hz, H-1), 7.3—7.8 (9H, m, phenyl protons)
2β	2.43 (3H, s, C-CH_3), 2.21 (1H, d, J=8 Hz, OH), 3.24 (3H, s, OMe), 3.59 (2H, m, H-5,5′), 4.0—4.4 (2H, m, H-3 and H-4), 4.54 (2H, s, CH_2Ph), 4.66 (1H, dd, $J_{1,2}$=1 Hz, $J_{2,3}$=5 Hz, H-2), 4.83 (1H, d, $J_{1,2}$=1 Hz, H-1), 7.2—7.8 (9H, m, phenyl protons)
3α	2.44 (3H, s, C-CH_3), 2.70 (1H, d, J=7 Hz, OH), 3.45 (3H, s, OCH_3), 3.5 (2H, m, H-5, 5′), 4.0—4.4 (2H, m, H-3 and H-4), 4. 48 (2H, m, CH_2Ph), 4.71 (1H, dd, J=7 Hz and J=3 Hz, H-3), 4.87 (1H, d, $J_{1,2}$=4 Hz, H-1), 7.2—7.8 (9H, m, phenyl protons)
3β	2.30 (3H, s, C-CH_3), 3.04 (1H, d, J=4 Hz, OH), 3.25 (3H, s, OCH_3), 3.4 (2H, m, H-5,5′), 4.1—4.4 (2H, m, H-2 and H-4), 4.37 (2H, m, CH_2Ph), 4.8 (1H, m, H-3), 4.82 (1H, s, H-1), 7.1—7.8 (9H, m, phenyl protons)
4α	2.40 (6H, s, C-CH_3×2), 3.26 (3H, s, OCH_3), 3.54 (2H, d, J=2 Hz, H-5,5′), 4.33 (1H, m, H-4), 4.46 (2H, d, J=3 Hz, CH_2Ph), 4.60 (1H, dd, $J_{1,2}$=4 Hz, $J_{1,2}$=7 Hz, H-2), 4.8 (1H, m, H-3), 4.76 (1H, d, $J_{1,2}$=4 Hz, H-1), 7.2—7.8 (13H, m, phenyl protons)
4β	2.36 and 2.43 (6H, each s, C-CH_3×2), 3.22 (3H, s, OCH_3), 3.26 (1H, dABq, $J_{5,5'}$ =11 Hz, $J_{4,5'}$=4 Hz, H-5) and 3.48 (1H, dABq, $J_{5,5'}$ =11 Hz, $J_{4,5'}$=3 Hz, H-5′), 4.2 (1H, m, H-4), 4.30 and 4.38 (2H, ABq, J=13 Hz, CH_2Ph), 4.72 (1H, br d, J=4 Hz, H-2), 4.9 (1H, m, H-3), 4.95 (1H, br s, H-1), 7.1—7.8 (13H, m, phenyl protons)
5α	1.34 (3H, s, C-CH_3), 1.89 (1H, dABq, $J_{3,3'}$=14 Hz, $J_{3,4}$=4 Hz, H-3) and 2.23 (1H, dABq, $J_{3,3'}$=14 Hz, $J_{3',4}$=10 Hz, H-3′), 3.36 (3H, s, OCH_3), 3.48 and 3.78 (2H, dABq, J=11 Hz, J=2 Hz, H-5,5′), 4.36 (1H, m, H-4), 4.57 and 4.71 (2H, ABq, J=12 Hz, CH_2Ph), 4.60 (1H, s, H-1), 7.35 (5H, s, phenyl protons)
5β	1.34 (3H, s, C-CH_3), 1.77 (1H, dABq, $J_{3,3'}$=12 Hz, $J_{3,4}$=10 Hz, H-3) and 2.01 (1H, dABq, $J_{3,3'}$=12 Hz, $J_{3',4}$=7 Hz, H-3′), 2.84 (1H, br s, OH), 3.42 (3H, s, OCH_3), 3.48 (2H, m, H-5.5′), 4.2 (1H, m, H-4), 4.57 (2H, s, CH_2Ph), 4.36 (1H, s, H-1), 7.32 (5H, s, phenyl protons)
6α	1.36 (3H, s, C-CH_3), 1.74 and 2.04 (2H, dABq, $J_{3,3'}$=13 Hz, $J_{3,4'}$=8 Hz, H-3,3′), 2.99 (1H, br s, OH), 3.49 (3H, s, OCH_3), 3.4—3.5 (2H, m, H-5,5′), 4.4 (1H, m, H-4), 4.57 (2H, s, CH_2Ph), 4.52 (1H, s, H-1), 7.32 (5H, s, phenyl protons)
6β	1.33 (3H, s, C-CH_3), 1.72 (1H, dABq, $J_{3,3'}$=13 Hz, $J_{3,4}$=9 Hz, H-3) and 1.97 (1H, dABq, $J_{3,3'}$=13 Hz, $J_{3,4}$=7 Hz H-3′), 1.88 (1H, s, OH), 3.30 (3H, s, OCH_3), 3.45 (2H, m, H-5,5′), 4.4 (1H, m, H-4), 4.57 (2H, s, CH_2Ph), 4.51 (1H, s, H-1), 7.29 (5H, s, phenyl protons)
7α	1.40 (3H, s, C-CH_3), 1.91 (1H, dABq, $J_{2,2'}$=14 Hz, $J_{1,2}$=4 Hz, H-2) and 2.29 (1H, dABq, $J_{2,2'}$=14 Hz, $J_{1,2'}$=6 Hz, H-2′), 3.09 (1H, s, OH), 3.39 (3H, s, OCH_3), 3.7—3.9 (3H, m, H-4 and H-5,5′), 4.58 (2H, s, CH_2Ph), 5.11 (1H, dd, $J_{1,2}$=4 Hz, $J_{1,2'}$=6 Hz, H-1), 7.32 (5H, s, phenyl protons)
7β	1.36 (3H, s, C-CH_3), 2.06 (2H, m, H-2,2′), 2.21 (1H, s, OH), 3.37 (3H, s, OCH_3), 3.7 (2H, m, H-5,5′), 3.9 (1H, m, H-4), 4.60 (2H, s, CH_2Ph), 5.00 (1H, psued t, J=3 Hz, H-1), 7.33 (5H, m, phenyl protons)
8α	1.33 (3H, s, C-CH_3), 2.04 (2H, m, H-2,2′), 3.66 (1H, s, OH), 3.43 (3H, s, OCH_3), 3.49 (2H, m, H-5,5′), 4.17 (1H, psued t. J=5 Hz, H-4), 4.52 (2H, s, CH_2Ph), 5.07 (1H, dd, J=6 Hz, J=2 Hz, H-1), 7.32 (5H, s, phenyl protons)
8β	1.38 (3H, s, C-CH_3), 1.93 (1H, dABq, $J_{2,2'}$=14 Hz, $J_{1,2}$=4 Hz, H-2) and 2.29 (1H, dABq, $J_{2,2'}$=14 Hz, $J_{1,2'}$=6 Hz, H-2′), 2.17 (1H, s, OH), 3.38 (3H, s, OCH_3), 3.55 (2H, d, J=6 Hz, H-5,5′), 4.00 (1H, psued t, J=6 Hz, H-4), 4.56 (2H, s, CH_2Ph), 5.04 (1H, dd, $J_{1,2}$=4 Hz, $J_{1,2'}$=6 Hz, H-1), 7.34 (5H, s, phenyl protons)
9	1.12, 1.13, 1.18, and 1.19 (6H, m, C(OH)C<u>H</u>$_3$ and CHC<u>H</u>$_3$), 1.3—1.9 (2H, m, C<u>H</u>$_2$CH), 3.32 and 3.35 (3H, each s, 53 : 47, OCH_3), 3.5—3.9 (4H, m, $BnOCH_2$, C<u>H</u>OH, and CHOMe), 4.17 (1H, d, J=6 Hz, CHO<u>H</u>), 4.58 (2H, s, CH_2Ph), 4.34 (5H, s, phenyl protons)
10	1.50 (3H, s, C-CH_3), 2.03 and 2.15 (2H, dABq, $J_{3,3'}$=14 Hz, $J_{3,4}$=8 Hz, H-3,3′), 1.2—1.8 (10H, m, cyclohexane ring protons), 3.58 and 3.66 (2H, dABq, J=10 Hz, J=6 Hz, H-5,5′), 4.24 (1H, m, H-4), 4.59 (2H, s, CH_2Ph), 5.35 (1H, s, H-1), 7.32 (5H, s, phenyl protons)
12	1.44 and 1.48 (6H, each s, isopropyl protons), 2.00 (1H, dABq, $J_{2,2'}$=14 Hz, $J_{1,2}$=6 Hz, H-2) and 2.26 (1H, dABq, $J_{2,2'}$=14 Hz, $J_{1,2'}$=2 Hz, H-2′), 3.38 (3H, s, OCH_3), 3.7—4.1 (3H, m, H-4 and CH_2Ph), 4.98 (1H, dd, $J_{1,2}$=6 Hz, $J_{1,2'}$=2 Hz,H-1)

120 ml), there was added tosyl chloride (4.70 g, 24.6 mmol or 9.20 g, 48.3 mmol), respectively. Each mixture was stirred at 0—5 °C for a few hours, and then allowed to stand in a refrigerator at the same temperature overnight. The usual work-up gave a syrupy mixture, which was purified by silica-gel column chromatography with benzene–ethyl acetate (9 : 1) to afford **4α** (3.77 g, 38%), **3α** (0.05 g, 1%), and **2α** (2.96 g, 41%) from **1α**, or to give **4β** (4.14 g, 21%), **2β** (0.69 g, 5%), and **3β** (7.34 g, 52%) from **1β**.

Method B:[4] A mixture of **1α** or **1β** (508 mg, 2 mmol) and dibutyltin oxide (498 mg, 2 mmol) in methanol (7 ml) was heated at 75—80 °C (bath temperature) for 3 h with stirring.

The methanol was removed by co-evaporation with benzene. The residue was dissolved in hot benzene (5 ml) and *N,N*-dimethylformamide (5 ml), and a solution was cooled to 0—5 °C. Pyridine (180 mg) was added, followed by addition of tosyl chloride (382 mg, 2 mmol), and the mixture was stirred at 0—5 °C for 30 min. Aqueous sodium hydrogencarbonate was added, and the mixture was extracted with ether. The usual work-up gave a syrup, which was chromatographed on a silica-gel column with benzene–ethyl acetate (9 : 1) to provide **3***α* (42 mg, 5%) and **2***α* (502 mg, 61%) from **1***α*, or to afford **4***β* (10 mg, 0.9%), **2***β* (310 mg, 38%), and **3***β* (347 mg, 42%) from **1***β*.

*Methyl 5-O-Benzyl-3-deoxy-2-C-methyl-β-*D-threo-*pentofuranoside (5β) and Methyl 5-O-Benzyl-3-deoxy-2-C-methyl-β-*D-erythro-*pentofuranoside (6β).* To a cold solution of MeMgI (11.6 mmol) in ether (30 ml), there was added **3***β* (1.4 g, 3.43 mmol) in benzene (5 ml) over a period of 5 min. The mixture was stirred at room temperature for 2 h. After cooling, aqueous ammonium chloride was added and the mixture was extracted with ether. The extract was washed with water and dried ($MgSO_4$). Evaporation of the solvent gave a syrup, which was chromatographed on a silica-gel column with benzene–ethyl acetate (9 : 1) to give **5***β* (700 mg, 81%) and **6***β* (50 mg, 6%).

*Methyl 5-O-Benzyl-3-deoxy-2-C-methyl-α-*D-erythro-*pentofuranoside (6α).* A solution of **4***α* (819 mg, 1.45 mmol) in benzene (3 ml) was added to a stirred solution of MeMgI (11.6 mmol) in benzene (15 ml) and ether (15 ml) at room temperature. After the mixture in a flask without a refluxing condenser had been heated at 80—85 °C (bath temperature) to remove the ether for 1 h, the flask was fitted with the refluxing condenser and the heating was continued for 45 min. After cooling, aqueous ammonium chloride was added, and the mixture was extracted with ether. The extract was washed with water, dried ($MgSO_4$), and concentrated to give a syrup, which was chromatographed on a silica-gel column with benzene–ethyl acetate (9 : 1) to give the starting material (80 mg, 10%), an unidentified crystalline compound (225 mg), **5***α* (17 mg, 5%), and **6***α* (130 mg, 36%). These compounds (**5***α* and **6***α*) were identical with the samples prepared from the Grignard anomerization of **5***β* and **6***β*, respectively.

*Methyl 5-O-Benzyl-2-deoxy-3-C-methyl-β-*D-threo-*pentofuranoside (7β), Methyl 5-O-Benzyl-2-deoxy-3-C-methyl-α-*D-erythro-*pentofuranoside (8α), and Its β-Anomer (8β), and the Open-chain Product (9).* To a solution of MeMgI (16 mmol) in ether (20 ml), there was added a solution of **2***β* (1.29 g, 3.2 mmol) in benzene (10 ml) at room temperature over a period of 15 min. The mixture was stirred at this temperature for 80 min. The usual work-up gave a syrupy mixture, which was chromatographed on a silica-gel column with benzene–ethyl acetate (9 : 1) to afford **7***β* (455 mg, 57%), **8***α* (150 mg, 19%), **9** (40 mg, 5%), and **8***β* (20 mg, 2.5%).

*5-O-Benzyl-1,2-O-cyclohexylidene-3-deoxy-2-C-methyl-β-*D-threo-*pentofuranose (10).* A mixture of **5***β* (130 mg, 0.52 mmol), cyclohexanone (0.4 ml), and concd sulfuric acid (38 mg) in dry benzene (2 ml) was stirred at room temperature for 30 min. After cooling, aqueous sodium hydrogencarbonate was added under vigorous stirring, and the mixture was extracted with ether. The extract was washed with water and dried ($MgSO_4$). Evaporation of the solvent and an excess of the cyclohexanone by co-evaporation with toluene gave a syrup, which was chromatographed on a silica-gel column with benzene–ethyl acetate (4 : 1) to give **10** (96 mg, 59%). Its physical properties were identical with those of an authentic sample.[5]

*Methyl 2-Deoxy-3,5-O-isopropylidene-3-C-methyl-β-*D-threo-*pentofuranose (12).* A solution of **7***β* (188 mg, 0.75 mmol) in methanol (10 ml) was hydrogenated in the presence of 10%Pd–C (130 mg) under hydrogen atmosphere at ordinary pressure for 3.5 h. The usual work-up gave a syrup, which was chromatographed on a silica-gel column with chloroform–methanol (49 : 1) to afford almost pure methyl 2-deoxy-3-*C*-methyl-*β*-D-*threo*-pentofuranoside (**11**; 119 mg, 98%) as a syrup. This product was used, without further purification, for the isopropylidenation. A mixture of **11** (54 mg, 0.33 mmol), 2,2-dimethoxypropane (0.5 ml), and pyridinium *p*-toluenesulfonate (10 mg)[7] in acetone (1 ml) was stirred at room temperature for 2.5 h. After cooling, aqueous sodium hydrogencarbonate was added, and the mixture was extracted with ether. The extract was washed with water, dried ($MgSO_4$), and concentrated to give a syrup, which was purified by silica-gel column chromatography with benzene–ethyl acetate (1 : 1) to provide **12** (46 mg, 69% from **11**).

The Anomerization of the Branched-chain Deoxy Sugars with an Acid. The ratio of *α*- and *β*-anomers in an equilibrium was determined on the basis of the ^1H NMR spectroscopy; these results are summarized in Scheme 3.

From 5β: A mixture of **5***β* (880 mg, 3.5 mmol) and concd sulfuric acid (250 mg) in methanol (40 ml) was heated at 60—65 °C (bath temperature) for 5 h. An equilibrium was reached within 5 h, judging from TLC and ^1H NMR spectroscopic analyses. After cooling, calcium hydroxide (300 mg) was added and the mixture was stirred vigorously. The undissolved materials were filtered through a Celite pad and washed with methanol. The combined filtrate and washing were concentrated, and the residue (**5***α* : **5***β*=7 : 3) was chromatographed on a silica-gel column with benzene–ethyl acetate (9 : 1) to give **5***α* (568 mg, 65%) and **5***β* (248 mg, 28%).

From 6α: A mixture of **6***α* (32 mg, 0.13 mmol), concd sulfuric acid (80 mg) in methanol (13 ml) was treated under the same conditions as described for the acid anomerization of **5***β* to give a 1 : 4 mixture (29 mg) of **6***α* and **6***β*.

From 7β: A mixture of **7***β* (400 mg, 1.59 mmol) and concd sulfuric acid (120 mg) in methanol (35 ml) was stirred at room temperature for 30 min. Within this time an equilibrium was reached. The mixture was treated in a manner similar to that described for the acid anomerization of **5***β* to give a syrupy mixture (**7***α* : **7***β*=7 : 3), which was chromatographed on a silica-gel column with benzene–ethyl acetate (85 : 15) to afford **7***β* (104 mg, 26%) and **7***α* (250 mg, 63%).

From 8α: A mixture of **8***α* (30 mg, 0.12 mmol), concd sulfuric acid (40 mg) in methanol (12 ml) was treated under the same conditions as described for the acid anomerization of **7***β* to afford a 53 : 47 mixture (28 mg) of **8***α* and **8***β*.

The Anomerization of the Branched-chain Deoxy Sugars with the Grignard Reagents. The ratio of the *α*- and *β*-anomers was determined by means of the ^1H NMR spectroscopy; the results are summarized in Scheme 3.

From 5α: To a solution of MeMgI (2.4 mmol) in ether (5 ml) and benzene (10 ml), there was added a solution of **5***α* (120 mg, 0.48 mmol) in benzene (2 ml), and the mixture was heated at 80—85 °C (bath temperature) to remove the ether for 2.5 h. The usual work-up gave a syrupy mixture (**5***α* : **5***β* =1 : 1; 126 mg), the TLC analyses of which indicated that this contained a small amount of degradation products.

From 5β: To a solution of MeMgI (2.4 mmol) in benzene (10 ml) and ether (5 ml), there was added a solution of **5***β* (128 mg, 0.51 mmol) in benzene (2 ml), and the mixture was treated in a manner similar to that described for the Grignard anomerization of **5***α*. The product (**5***α* : **5***β*=<1 : 99; 126 mg) contained a small amount of decomposed materials.

From 6α: A solution of **6***α* (57 mg, 0.23 mmol) in benzene (2 ml) was added to a stirred solution of *t*-BuMgBr (4.8 mmol) in benzene (10 ml) and ether (5 ml) at room temperature, and the mixture was heated at 80—85 °C (bath temperature) for

30 min with stirring to remove the ether. No anomerization was observed by means of TLC analyses. The usual work-up recovered the starting material (50 mg).

From **6**β: A solution of **6**β (130 mg, 0.52 mmol) in benzene (2 ml) was added to a stirred solution of *t*-BuMgBr (4.8 mmol) in benzene (10 ml) and ether (5 ml), and the mixture was treated under the same conditions as those described for the Grignard anomerization of **6**α. The work-up gave a syrup (**6**α : **6**β=9 : 1), which was chromatographed on a silica-gel column with benzene–ethyl acetate (85 : 15) to give **6**α (93 mg, 72%) and **6**β (8 mg, 6%). The former anomer was identical with a sample prepared from **4**α and MeMgI.

From **7**α: To a stirred solution of *t*-BuMgBr (4.8 mmol) in benzene (10 ml) and ether (5 ml), there was added to solution of **7**α (130 mg, 0.52 mmol) in benzene (2 ml) at room temperature; the mixture was heated at 80—85 °C to remove the ether for 3 h with stirring. The usual work-up gave an anomeric mixture (**7**α : **7**β=$<$5 : 95; 131 mg).

From **7**β: The sugar derivative **7**β (130 mg, 0.52 mmol) was treated under the same conditions as described for the Grignard anomerization of **7**α to provide an anomeric mixture (**7**α : **7**β=$<$1 : 99; 112 mg).

From **8**α: The sugar derivative **8**α (43 mg, 0.17 mmol) was treated with *t*-BuMgBr (4.8 mmol) under the same conditions as described for the Grignard anomerization of **7**α, except that the reaction time was 10 min. The work-up recovered the starting material (43 mg), which contained a trace amount of 8β and of unidentified by-products, judging from TLC analyses.

From **8**β: The sugar derivative **8**β (38 mg, 0.15 mmol) was treated with *t*-BuMgBr (4.8 mmol) under the same conditions as described for the Grignard anomerization of **8**α to give **8**α (39 mg), which contained a trace amount of **8**β and of unidentified by-products.

We wish to thank Dr. Haruo Homma and his staff for the elemental analyses, and Dr. Jun Uzawa and Mrs. Tamiko Chijimatsu for measuring the ^{1}H NMR spectra. We are also grateful to Dr. Hiroshi Ohrui for his valuable discussions.

References

1) Portions of this work have been reported at the 44th National Meeting of the Chemical Society of Japan, Okayama, Oct. 1981.

2) M. Kawana and S. Emoto, *Tetrahedron Lett.*, **1975**, 3395; *Chem. Lett.*, **1977**, 597; *Bull. Chem. Soc. Jpn.*, **53**, 222 (1980).

3) M. Kawana and S. Emoto, *Tetrahedron Lett.*, **1978**, 1561; M. Kawana, H. Kuzuhara, and S. Emoto, *Bull. Chem. Soc. Jpn.*, **54**, 1492 (1981).

4) D. Wagner, J. P. H. Verheyden, and J. G. Moffatt, *J. Org. Chem.*, **39**, 24 (1974).

5) H. Ohrui and S. Emoto, *Agric. Biol. Chem.*, **40**, 2267 (1976).

6) S. J. Angyal, *Carbohydr. Res.*, **77**, 37 (1979).

7) M. Miyashita, A. Yoshikoshi, and P. A. Grieco, *J. Org. Chem.*, **42**, 3772 (1977).

 © 1983 The Chemical Society of Japan Bull. Chem. Soc. Jpn., 56, 1101—1106 (1983)

Metalloenzyme Models. Divalent Metal Ion Catalyzed Hydrolysis of *p*-Nitrophenyl Picolinate in the Presence of Imidazoles and Pyridines Having Hydroxyl Groups in Their Side Chains

Kenji Ogino, Katsuhiko Shindo, Tooru Minami, Waichiro Tagaki,* and Toshio Eiki†

Department of Applied Chemistry, Faculty of Engineering, Osaka City University, Sugimoto 3, Sumiyoshi-ku, Osaka 558

†Department of Chemistry, Faculty of Technology, Gunma University, Kiryu, Gunma 376

(Received June 28, 1982)

Rate constants for hydrolysis of *p*-nitrophenyl picolinate at 25 °C in the pH range 6.5—8.5 were measured in the absence and presence of divalent metal ions (Ni(II), Zn(II), Co(II), Ca, Mg) and substituted imidazoles or pyridines as ligands having alcoholic hydroxyl groups in their side chains. In the presence of either metal ion or ligand, the rate is slow and the pseudo-first-order rate constant (k_{obsd}) increases linearly in a first-order manner with respect to the concentration of metal ion or ligand until it gives the second-order rate constant, k_M or k_L, respectively. In the presence of both a metal ion (Ni(II) or Zn(II)) and a ligand, rate increase is remarkable for some ligands and the increase in k_{obsd} values constructs saturation curves with respect to increase in either metal ion or ligand concentration. The saturation curves were analyzed based upon rate equations formulated by assuming the formation of 1 : 1 complex of metal ion and ligands as the catalyst, leading to evaluation of the association constant K for complexes and the second-order rate constant k_c for the reaction of complex with substrate. Values of k_{obsd}, k_c, and K are dependent greatly upon the structure of ligands and pH. The ligands complexed with Zn(II) ion appear to be simple but highly active models of hydrolytic metalloenzymes.

Metal ion catalyzed reactions of carboxylic acid derivatives have been extensively investigated in recent years as model reactions of metalloenzymes such as carboxypeptidase A, carbonic anhydrase, and related enzymes.[1-6] It is now well known that a zinc ion is coordinated to two imidazoles and one carboxyl group at the active site of carboxypeptidase A[7-12] and to three imidazole groups at the active site of carbonic anhydrase.[13-16] In these enzymes, the zinc ion is considered to serve as a primary catalytic center for bringing substrate and nucleophile together through formation of a coordination complex, and to activate the substrate carbonyl group toward the action of the nucleophile in carboxypeptidase A or to activate the water molecule in the reversible hydration of carbon dioxide in carbonic anhydrase. In related alkaline phosphatases, the zinc ion appears to activate the serine hydroxyl group.[17,18] Thus it is important for model studies to examine the cooperativity in catalysis between the imidazolyl and hydroxyl groups in the presence of metal ion.

Most of model studies so far conducted are related to intramolecular catalysis, making use of substrates designed to be susceptible to the attack by nucleophile either intramolecularly or intermolecularly through complexation with metal ion.[19] However, there have been known only a few examples of metal ion catalyzed acyl-transfer reactions between coordinated ligands. Breslow *et al.* discovered that the zinc or nickel ion complex of (*E*)-2-pyridinecarbaldehyde oxime, alone[20] or attached to the cyclodextrin moiety,[21] is a remarkably active catalyst for the hydrolysis of esters. Sigman and Jorgensen[22] demonstrated that zinc ion catalyzes the *trans*-esterification between *p*-nitrophenyl picolinate and *N*-(2-hydroxyethyl)ethylenediamine. Very recently, bis(imidazolyl)cyclodextrin[23] and some triimidazolyl derivatives[24] were reported to be effective ligands for the modeling of carbonic anhydrase. However, even in these examples the cocatalysis by imidazolyl and hydroxyl groups has not yet been examined. Furthermore, it should be noted that the catalytic activity of these known complexes is by no means enzymic. Thus complexes more active by several orders should be designed in order to obtain really enzymic artificial enzymes. It has been reported, though with a few examples, that metal-bound imidazolate and hydroxide ions are very reactive nucleophiles.[25]

In our recent communications,[26,27] we reported that *N*-substituted 2-(hydroxymethyl)imidazole-Zn^{2+} ion complexes are much more active catalysts than the above 2-pyridinealdoxime-Zn^{2+} complex for the hydrolysis of *p*-nitrophenyl picolinate. The coexistence of imidazole and hydroxyl groups appears to be essential for the development of catalytic activity, indicating that the system is a simple but good model for the hydrolytic metalloenzymes.

In the present paper, we wish to report a full account of our previous communication[26] as well as results of a further extention including a finding of some more powerful ligands. Activities of ligands **2**—**12** were examined in the presence of divalent metal ions Ni^{2+}, Zn^{2+}, Co^{2+}, Ca^{2+}, and Mg^{2+} for the hydrolysis of *p*-

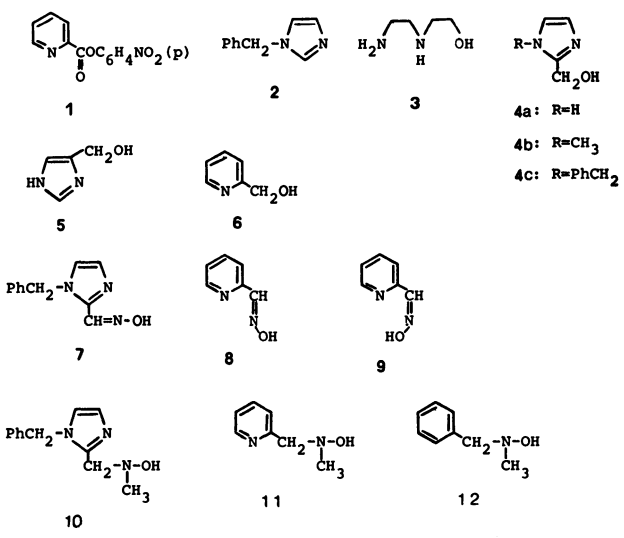

nitrophenyl picolinate (**1**). These ligands may be classified into two groups: One contains 2-aminomethylamino, imidazolyl, or pyridyl groups as the primary coordination site to bind metal ion, and the other contains alcoholic hydroxyl, aldoxime hydroxyl, or hydroxyamino hydroxyl group as the reacting nucleophile in acyl-transfer reaction.

Results and Discussion

Ligand Hydroxyl Group in Catalysis. Rates of reaction were determined by observing the release of *p*-nitrophenol from the substrate **1** spectrophotometrically. In all cases, under the condition of excess ligand over the substrate, good pseudo-first-order rate constants (k_{obsd}) were obtained up to completion of reaction. Part of the results are shown in Table 1. The table indicates that the uncatalyzed buffer rate constant is $k_0=1.0\times10^{-3}$ min^{-1} at pH 7.05 and 25 °C. In the presence of 1.33×10^{-3} mol dm^{-3} Zn^{2+} ion, the rate increased about 30-fold. This rate increase was little affected by addition of such a ligand as **2** having no hydroxyl group or **12** which is a poor ligand toward Zn^{2+} ion. In the absence of metal ion, the rate enhancement by ligand alone was relatively small, although some of hydroxyl-group bearing ligands showed some enhanced reactivity. At any rate, a large rate enhancement was observed only when ligands with both hydroxyl and neighboring nitrogen groups such as **3**—**11** were used in the presence of either Ni^{2+}, Zn^{2+}, or Co^{2+} ion.

Pseudo-first-order kinetics were also observed under the condition of five molar excess of substrate over the ligand for all the ligands except **3** and **9**, indicating the reaction to occur catalytically. In the case of (*Z*)-2-pyridinecarbaldehyde (**9**), the reaction proceeded in a biphasic manner in which the release of *p*-nitrophenol was initially rapid and then slowed down. Such a biphasic behavior is an evidence for a two-step process involving, in this case, the acylation of the hydroxyl group of catalyst followed by the rate determining deacylation to regenerate the catalyst.[1-3,28] In the case of **3**, as already demonstrated by Sigman and Jorgensen,[22] the second deacylation step was so slow that the reaction ceased in effect at the first acylation step.

The above observation that hydroxyl group is necessary for the enhanced generation and detection of acylated intermediates in **3** and **9**, strongly suggests that catalyses by those ligands with which direct evidence for formation of such acylated intermediates is lacking also occur through the two-step process.

Kinetic Equation. The rates were dependent on both metal ion and ligand concentrations. In the case of *N*-benzylimidazole (**2**) having no hydroxyl group, the k_{obsd} values were found to be given by

$$k_{obsd} = k_o + k_L[L] + k_M[M] + k_{M\cdot L}[L][M], \quad (1)$$

where k_0 is the rate constants due to the buffer, k_L and k_M are the second-order rate constants due to ligand (L) and metal ion (M), respectively, and $k_{M,L}$ is the third-order rate constant for the cocatalysis of metal ion and ligand. The observed values for **2** are $k_L=7.98$ mol^{-1} dm^3 min^{-1}, $k_M=15.3$ mol^{-1} dm^3 min^{-1}, and $k_{M,L}=9.72\times10^3$ mol^{-2} dm^6 min^{-1} at pH 7 and 25 °C.

For other ligands having hydroxyl groups, the rates tended to be saturated with increasing metal ion concentration, as exemplified in Fig. 2 for the case of 1-benzyl-2-(hydroxymethyl)imidazole (**4c**). The figure indicates that in the absence of metal ion, the k_{obsd} values are linear to the ligand concentration with $k_L=1.68$ mol^{-1} dm^3 min^{-1} smaller than the above k_L value for **2**. The saturation curves in Fig. 1 can be analyzed by assuming the formation of 1 : 1 complex of metal ion and ligand according to the kinetic scheme of reactions 2—4 and the set of Eqs. 5—7 for derived rates:

Table 1. Pseudo-first-order rate constants ($k_{obsd}\times10^3$/min^{-1}) for *p*-nitrophenol release from *p*-nitrophenyl picolinate **1** in the presence of metal ion and ligand under the condition of [ligand]$\gg$[1][a]

L	M^{2+}					
	None	Ni^{2+}	Zn^{2+}	Co^{2+}	Ca^{2+}	Mg^{2+}
None	1.0	41.1	28.5	23.2	17.1	2.6
2	11.6	—	49.2	—	—	—
3	9.1	134	136	51.3	13.2	9.5
4a	—	—	381[b]	—	—	—
4b	—	—	1008[b]	—	—	—
4c	3.2	1230	2120	268	7.33	13.7
5	—	—	55[b]	—	—	—
6	—	—	242[b]	—	—	—
7	57.4	—	1390	—	75.6	61.9
8	34.1	2590	1570	—	35.4	34.7
9	14.0	525	2530	—	16.6	15.9
10	25.0	718	23500	11700	33.0	40.8
11	18.3	332	14400	4870	20.9	17.8
12	8.8	79.4	24.4	20.3	9.0	8.9

a) Observed at 25 °C, pH 7.05 (0.1 mol dm^{-3} 2,6-lutidine-HNO_3 buffer), $\mu=0.2$ (KNO_3), [L]=[M]=1.33×10^{-3} mol dm^{-3} mol dm^{-3}, and [1]=1×10^{-4} mol dm^{-3}. b) [L]=1.0×10^{-3} mol dm^{-3} and [M]=1.33×10^{-3} mol dm^{-3}.

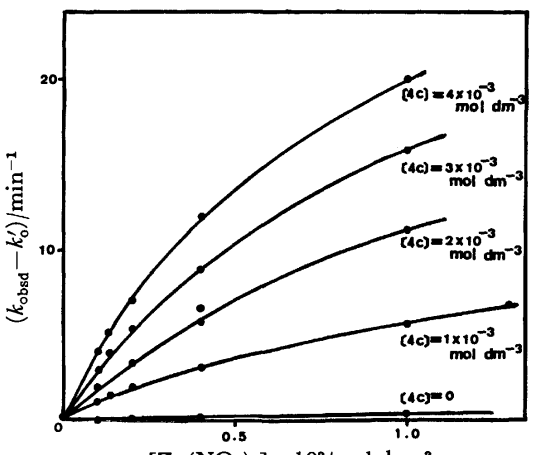

Fig. 1. Plots of pseudo-first-order rate constants for the release of *p*-nitrophenol from **1** as a function of zinc ion concentration; see Table 1 for other reaction conditions.

$$M + L \overset{K}{\rightleftharpoons} \text{complex}, \quad (2)$$

$$S + \text{complex} \xrightarrow{k_c} \text{products}, \quad (3)$$

$$S \xrightarrow{k_o'} \text{products}, \quad (4)$$

$$k_o' = k_o + k_L[L] + k_M[M], \quad (5)$$

$$k_{obsd} = k_o' + \frac{k_c K[L]_T[M]_T}{1+K([L]_T+[M]_T)}, \quad (6)$$

$$\frac{1}{k_{obsd}-k_o'} = \frac{1}{k_c[L]_T} + \frac{1+K[L]_T}{k_c K[L]_T} \cdot \frac{1}{[M]_T}, \quad (7)$$

where L, M, k_o, k_L, and k_M are as defined for Eq. 1, S refers to the substrate, $[L]_T$ and $[M]_T$ are the total concentrations of ligand and metal ion, respectively, K is the association constant between metal ion and ligand and k_C is the catalytic second-order rate constant for the reaction of complex with substrate **1**. A more detailed reaction scheme may involve the complexation between metal ion and substrate, or the formation of ternary complex between the three components (M,L,S). However, such additional complexation equilibria appear to be unimportant, since as mentioned above, the rate was linear to the metal ion concentration in the absence of ligands, indicating that the association constant for the formation of metal ion (Ni^{2+} or Zn^{2+}) and substrate complex is small as compared to that of metal ion and ligand complex.

The above 1 : 1 stoichiometry with the complexation of Eq. 2 was also confirmed for the ligand **4c** by looking at the kinetic version of Job plots shown in Fig. 2. The figure indicates that for both Ni^{2+} and Zn^{2+} ions the plot of k_{obsd} values as a function of mole fraction of **4c** gives a maximum at the mole fraction of 0.5, which corresponds to the 1 : 1 stoichiometry for the kinetically active species.

Saturation curves similar to the one exemplified in Fig. 1 were also obtained for other ligands, although appropriate concentration ranges of metal ion and ligand for kinetics depended on the magnitude of K and k_C values as illustrated in Fig. 3. Based on Eq. 7, three linear plots, *i.e.*, $1/(k_{obsd}-k_o')$ *vs.* $1/[M]_T$, 1/(intercept) *vs.* $[L]_T$, and the slope *vs.* $1/[L]_T$, were obtained for each pair of ligand and metal ion by changing $[M]_T$ and $[L]_T$ and these plots allowed the evaluation of k_C and K. The results of calculation are summarized in Table 2. The table indicates that (*E*)-2-pyridinecarbaldehyde(**8**)-Zn^{2+} ion complex is fairly active in harmony with the activity reported in the literature.[19h,20,21,29] The table also shows that 1-benzyl-2-(*N*-hydroxymethylaminomethyl)imidazole (**10**) and 2-(*N*-hydroxymethylaminomethyl)pyridine (**11**) are more active ligands than **8**. However, for more quantitative comparison, pH dependency of the rate should be examined.

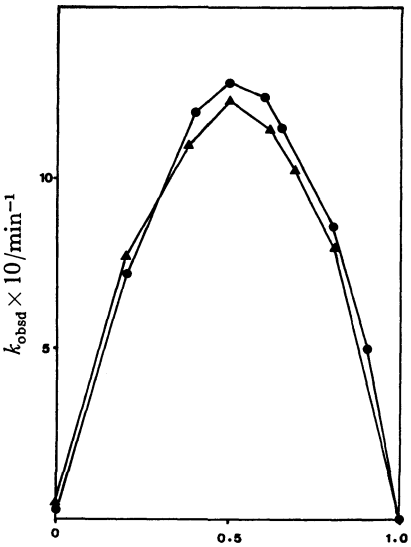

Fig. 2. Job plots for the ligand **4c** and Zn^{2+} and Ni^{2+}. ●: **4c**–Zn^{2+}, $[L]+[M]=2.6\times10^{-3}$ mol dm^{-3}, ▲: **4c**–Ni^{2+}, $[L]+[M]=2\times10^{-3}$ mol dm^{-3}.

pH-Rate Profile. Figure 4 shows plots of log k_{obsd} *vs.* pH for the same reaction conditions as given in Table 1 except for the pH. The figure indicates that both Ni^{2+} and Zn^{2+} ion complexes of **8** yield saturation curves with inflection points at around pH's 6 and 8, respectively. These saturation curves are most likely

Table 2. Association constants (K) and second-order rate constants (k_L and k_C) for *p*-nitrophenol release from *p*-nitrophenyl picolinate (**1**) in the presence of ligand (L) and metal ion (M)[a]

L–M	k_L / mol^{-1} dm^3 min^{-1}[b]	k_C / mol^{-1} dm^3 min^{-1}	K / mol^{-1} dm^3	k_CK or $k_{M\cdot L}$ / mol^{-2} dm^6 min^{-1}
2–Zn^{2+}	7.98	—	—	9.72×10^3
4a–Zn^{2+}	—	2.56×10^3	142	364×10^3
4b–Zn^{2+}	—	8.13×10^3	104	846×10^3
4c–Zn^{2+}	1.68	10.0×10^3	162	1620×10^3
4c–Zn^{2+}	1.68	8.3×10^3	110	913×10^3
5–Zn^{2+}	—	0.31×10^3	95	29.5×10^3
6–Zn^{2+}	—	1.26×10^3	178	224×10^3
8–Zn^{2+}	42.0	4.0×10^3	559	224×10^3
8–Ni^{2+}	—	6.3×10^3	1120	7080×10^3
9–Ni_2^{2+}	12.0	40.0×10^3	44	1760×10^3
10–Zn^{2+}	16.1	27.8×10^3	563	15650×10^3
11–Zn^{2+}	12.1	12.5×10^3	1260	15790×10^3

a) Observed at 25 °C, pH 7.05 (0.1 mol dm^{-3} 2,6-lutidine–HNO_3 buffer), $\mu=0.2$ (KNO_3), $[\mathbf{1}]=1\times10^{-4}$ mol dm^{-3}, and $[L]=[M^{2+}]=1.33\times10^{-3}$ mol dm^{-3}. b) $k_M=15.3$ mol^{-1} dm^3 min^{-1} (see text).

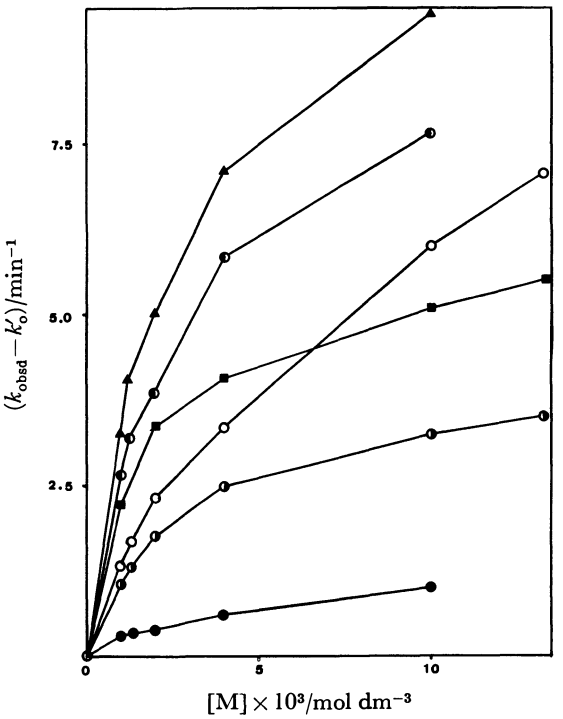

Fig. 3. Plots of $(k_{obsd}-k_o')$ as a function of metal ion concentration in the presence of the various ligand. ○: **4c**–Zn^{2+}, [**4c**]=3×10⁻⁴ mol dm⁻³, ●: **6**–Zn^{2+}, [**6**]=1×10⁻³ mol dm⁻³, ◑: **8**–Zn^{2+}, [**8**]=1×10⁻³ mol dm⁻³, ■: **8**–Ni^{2+}, [**8**]=1×10⁻³ mol dm⁻³, ▲: **10**–Zn^{2+}, [**10**]=3×10⁻⁴ mol dm⁻³, ◐: **11**–Zn^{2+}, [**11**]=3×10⁻⁴ mol dm⁻³.

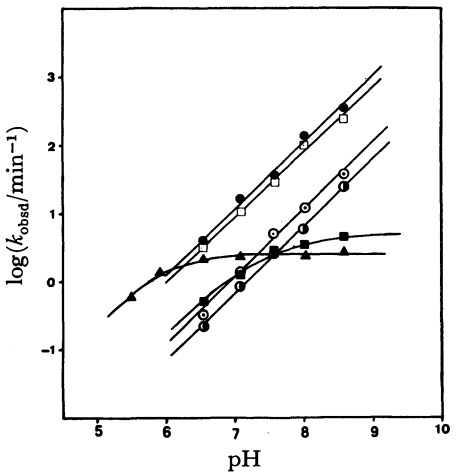

Fig. 4. Plots of k_{obsd}-*vs.* pH for the relase of *p*-nitrophenol from **1** in the presence of 1.33×10⁻³ mol dm⁻³ ligand and 1.33×10⁻³ mol dm⁻³ metal ion; see Table 1 for other reaction conditions. ◑: **4c**–Ni^{2+}, ⊙: **4c**–Zn^{2+}, ■: **8**–Zn^{2+}, ▲: **8**–Ni^{2+}, ●: **10**–Zn^{2+}, □: **11**–Zn^{2+}.

to represent the ionization of hydroxyl group complexed with Ni^{2+} or Zn^{2+} ion. The pK_a 8.6 was assigned to the ionization of hydroxyl group of the latter complex.[20] The lower pH for the ionization of the Ni^{2+} ion complex than that of the Zn^{2+} ion complex suggests that the ligand **8** coordinates to Ni^{2+} ion more tightly than to Zn^{2+} ion, in conformity with the larger K value (1120 mol dm⁻³) for the Ni^{2+} ion complex than that for the Zn^{2+} ion complex (559 mol dm⁻³) at pH 7.05, as shown in Table 2.

All the other five complexes, except for those of **8**, gave linear plots with slopes close to unity in the pH range 6.5—8.5. The ligands **10** and **11** having hydroxyamino hydroxyl group are about tenfold more active than **4c** which has a hydroxymethyl group. These linear plots also seem to represent ionization of hydroxyl groups, although their pK_a values must be higher than 8.5. Unfortunately, it was difficult to use higher pH's due to precipitation of metal hydroxide. For this reason, effects of pH on K and k_c values at higher pH's were not examined further. Nevertheless, the data in Fig. 4 together with others may suffice for qualitative discussion on the relationship among catalytic activity, ligand structure, and nature of metal ion.

Effects of Metal Ion and Ligand Structure on the Mechanism of Catalyses. Table 1 indicates that the activity of metal ions at pH 7 in the absence of ligand is in the order $Ni^{2+}>Zn^{2+}>Co^{2+}>Ca^{2+}>Mg^{2+}$. This order may be reasonable if considered on the basis of the ligand affinity of a pyridine base like **1** toward these metal ions. In the absence of metal ion, the activity of ligands is in the order **8**>**10**>**11**>**3**>**4c**. These activities are enhanced 10^2—10^3 times in the presence of Ni^{2+}, Zn^{2+}, or Co^{2+} ion. Ions Ca^{2+} and Mg^{2+} seem to have no activating effect. It is of interest to note that the activating effect of Ni^{2+} ion is somewhat different from those of Zn^{2+} and Co^{2+} ions, in such a manner that in the presence of Ni^{2+} ion the activity order of ligands is **8**>**4c**>**10**>**11**>**3**, which is changed to **10**>**11**>**4c**>**8**>**3** in the presence of Zn^{2+} or Co^{2+} ion. As is clear from Fig. 5, the reactivity order is also pH-dependent. At higher pH's, the difference in reactivity becomes larger between the complexes of **8** and those of the others.

It is most likely that a metal ion activates ligand hydroxyl group by coordination. Comparison of (*E*)- and (*Z*)-oxime **8** and **9** is of interest. The association constants in Table 2 indicate that **8** forms much more stable complexes with Ni^{2+} ion than **9**, presumably because in **8** the two nitrogen atoms are in a coplanar position favorable for chelation with a metal ion, in contrast to **9** (compare the structures **13** and **14**). The activity of complex itself (k_c value), however, is much larger for **9** than for **8**, presumably because the hydroxyl group is bonded to the metal ion much more tightly in **9** (**14**) than in **8** (**13**). Similarly the diamine **3** must form a much stabler complex with Zn^{2+} ion than **4c** (**15** *vs.* **16**), but the resulting activation of hydroxyl group in the former complex is not so large as in the latter complex. Such activation may also be influenced by the nature of nitrogen ligand, such as whether it is aliphatic or aromatic. It is interesting to note with Table 2 that in each pair of **4c**–Zn^{2+} and **6**–Zn^{2+} and **10**–Zn^{2+} and **11**–Zn^{2+}, the imidazole ligands give larger k_c values, whereas the pyridine ligands give larger K values than those of the other. It is also important to note that 2-(hydroxymethyl)imidazole–**4a**–Zn^{2+} ion complex is more active than 4-(hydroxymethyl)-imidazole–**5**–Zn^{2+} ion complex. Moreover, it should be pointed out that the activity of **10**–Zn^{2+} ion complex

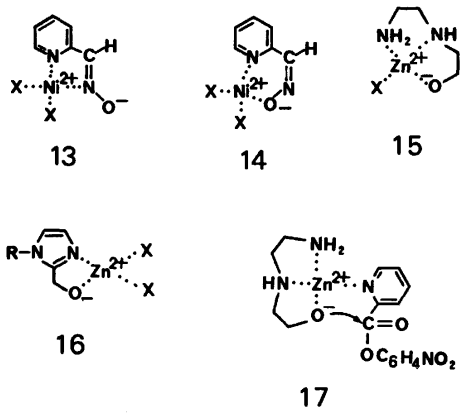

is really remarkable as compared to those of known examples in the literature.[20–22]

Sigman and Jorgensen[22] proposed the formation of a reactive ternary complex **17** composed of Zn^{2+} ion, **3** and **1** in the transesterification reaction between **1** and **3**. In this ternary complex the Zn^{2+} ion perturbs the pK_a (estimated to be 8.4) of the hydroxyethyl group of **3** to provide a high concentration of the effective nucleophile, which in turn acts as a template to orient **1** for the intracomplex nucleophilic attack of the ionized hydroxyethyl group on the carbonyl group of **1**. The importance of the formation of the intracomplex for the catalysis was shown by the inability of the **3**–Zn^{2+} ion complex to catalyze the transesterification of *p*-nitrophenyl acetate or *p*-nitrophenyl nicotinate which are unable to form any intracomplex. We also observed a similar substrate specificity in the present systems of **4c**–Zn^{2+} and **10**–Zn^{2+} ion complexes. Thus the formation of the ternary complex **18b**, analogous to **17**, is also conceivable for the catalysis by the **10**–Zn^{2+} ion complex illustrated in Scheme 1. However, as mentioned earlier, such a complex as **18b** should be very low in concentration as compared to the 1 : 1 complex of **18a**. It is rather more reasonable to consider that the Zn^{2+} ion stabilizes the tetrahedral addition intermediate **18c** through which the acylated intermediate **18d** is formed. As already mentioned, the Zn^{2+} ion must also catalyze the deacylation of **18d**. The complex **18e** may explain how the hydroxide ion bound on Zn^{2+} ion facilitates the deacylation through the formation of another tetrahedral intermediate **18f**. Alternatively, the Zn^{2+} ion may act as an electrophile to assist the carbonyl attack by hydroxide ion as illustrated in **18g**, although it is difficult to distinguish between the two mechanisms (**18e** and **18g**) kinetically. Whichever mechanism is true, the breakdown of the tetrahedral intermediate **18f** into products should also be fast for an effective catalysis to occur.

In summary, we have disclosed that the ligands **4c**, **10**, and **11**, when complexed with a metal ion such as Zn^{2+}, Ni^{2+}, or Co^{2+} ion, become highly active toward the hydrolysis of *p*-nitrophenyl picolinate (**1**). The catalysis is most likely to occur through formation of a ternary complex in the transition state or in reactive intermediates. The metal ion in such a complex serves to activate ligand hydroxyl group for nucleophilic attack and to orient the substrate into a favorable position to undergo the reaction. Future interesting subjects are how to incorporate these complexes into more sophisticated systems, such as micellar systems, as active centers of artificial metalloenzymes, although some serious problems still remain to be solved such as how to activate inert substrates.

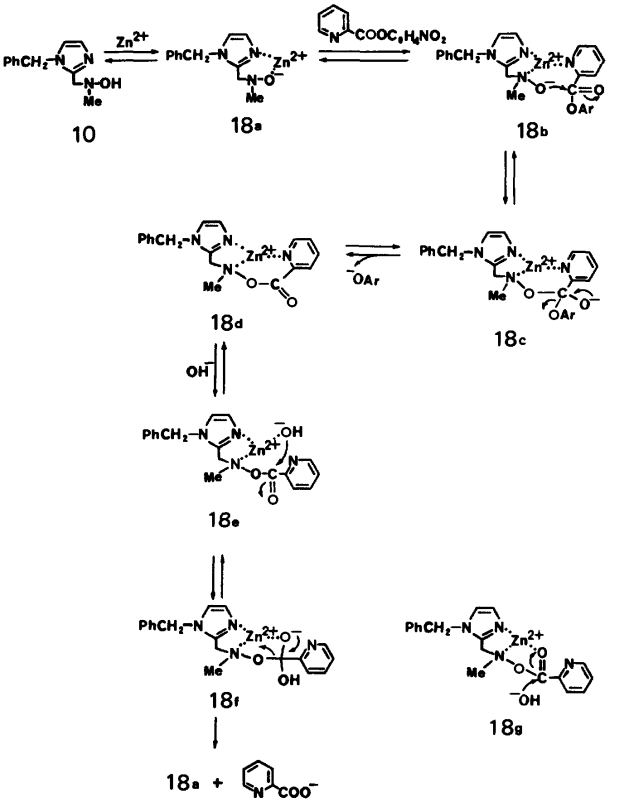

Scheme 1. Mechanism of hydrolysis of **1** catalyzed by **10**–Zn^{2+} complex.

Experimental

Materials. The water used for kinetic experiments was obtained by distilling deionized water. Buffer reagents, HEPES (2-[4-(2-hydroxyethyl)-1-piperazinyl]ethanesulfonic acid), MES (2-morpholinoethanesulfonic acid), KNO_3, hydrochloric acid, nitric acid, *etc.* were commercial extra pure reagents. Commercially available 2,6-lutidine, *N*-ethylmorpholine, *N*-(2-hydroxyethyl)ethylenediamine (**3**), and 2-(hydroxymethyl)pyridine (**6**) were distilled twice prior to use. Acetonitrile was distilled twice from phosphorus pentaoxide. Commercially available metal salts, $Zn(NO_3)_2 \cdot 6H_2O$, $Ni(NO_3)_2 \cdot 6H_2O$, $Co(NO_3)_2 \cdot 6H_2O$, $Ca(NO_3)_2 \cdot 4H_2O$, and $Mg(NO_3)_2 \cdot 6H_2O$, were used without further purification. *p*-Nitrophenyl picolinate (**1**) was prepared and purified according to the literature procedure.[22] (*E*)-2-Pyridinecarbaldehyde (**8**) was a commercial reagent (Wako Pure Chem.) and was purified by recrystallization from chloroform–hexane. *N*-Benzyl-2-(hydroxymethyl)imidazole (**4c**) was prepared by heating *N*-benzylimidazole and 30% aqueous solution of formaldehyde in an autoclave at 120 °C for 18 h. The resulting mixture was evaporated to dryness and the residue was crystallized after treatment with charcoal from ethyl acetate and white cubes were obtained. These crystals were recrystallized from ethyl acetate and dried: mp 96—97 °C; ^1H NMR ($CDCl_3$) δ=4.60 (2H, s), 4.9 (1H, br s), 5.20 (2H, s), 6.77

(1H, d, J=1.5 Hz), 6.82 (1H, d, J=1.5 Hz), and 7.15—7.30 (5H, m). 1-Benzyl-2-imidazolecarbaldehyde oxime (**7**) was synthesized by slowly adding 1-benzyl-2-imidazolecarbaldehyde and hydroxylamine hydrochloride to a methanol–water (1 : 1 volume ratio) containing sodium carbonate at room temperature. Extraction, drying over magnesium sulfate, concentration *in vacuo*, and column chromatographic separation yielded product **7**: mp 170—171 °C; ^{1}H NMR ($CDCl_3$–$(CD_3)_2SO$) δ=5.55 (2H, s), 7.05 (1H, d, J=1.5 Hz), 7.10 (1H, d, J=1.5 Hz), 7.20—7.35 (5H, m), 8.18 (1H, s), and 11.5 (1H, s). *syn*-Pyridinealdoxime (**9**) was obtained by a photoisomerization of (*E*)-2-pyridinecarbaldehyde oxime (**8**) using a 150 W high-pressure Hg lamp through a Pyrex filter for 30 h. The usual work-up and thin layer chromatographic separation yielded the recovered starting material **8** and (*Z*)-oxime **9**: mp 91—92 °C; ^{1}H NMR ($CDCl_3$) δ=7.3—8.1 (3H, m), 8.68 (1H, s), 8.54—8.65 (1H, m), and 11.25 (1H, br s). 1-Benzyl-2-(*N*-hydroxymethylaminomethyl)imidazole (**10**) was synthesized as follows: *N*-Benzyl-2-chloromethylimidazole hydrochloride, which was obtained by chlorination of **4c** with thionyl chloride, was added to a methanol–water (1 : 5 volume ratio) containing excess amounts of *N*-methylhydroxylamine hydrochloride and sodium carbonate. The usual work-up procedure gave colorless needles of **10**: mp 91—93 °C; ^{1}H NMR ($CDCl_3$) δ=3.30 (1H, s), 4.48 (2H, s), 5.17 (2H, s), 6.88 (1H, d, J=1.5 Hz), and 6.99 (1H, d, J=1.5 Hz). 2-(*N*-Hydroxymethylaminomethyl)pyridine (**11**) was also prepared similarly to **10** and obtained as colorless needles: mp 92—94 °C; ^{1}H NMR δ=2.68 (3H, s), 3.92 (2H, s), 7.00—7.75 (4H, m), 8.0 (1H, br s), and 8.45—8.55 (1H, m). *N*-Hydroxy-*N*-methylbenzylamine (**12**) was obtained by treatment of benzyl chloride with *N*-methylhydroxylamine: mp 41—42 °C; ^{1}H NMR ($CDCl_3$) δ=2.45 (3H, s), 3.66 (2H, s), 7.28 (5H, s), and 8.12 (1H, br s).

Kinetic Measurements. Kinetic runs were generally conducted on a Hitachi 220 spectrophotometer equipped with a thermostated cell compartment. A Hitachi-Horiba pH meter/F-7ss was used for pH determination on buffer and reaction mixtures. The kinetic run was initiated by introducing 10—30 μl of ester stock solution into 3 ml of the buffer solution containing the metal ion and ligand at desired concentrations and maintained at 25 °C. The stock solution contained 1.0—3.0$\times 10^{-2}$ mol dm^{-3} ester in acetonitrile. The ionic strength was maintained at 0.1 mol dm^{-3} with KNO_3. The rate of hydrolysis of *p*-nitrophenyl picolinate (**1**) was obtained by following the appearance of liberated *p*-nitrophenol at 400 nm. The reaction followed a pseudo-first-order kinetics for at least 3 half-lives. Rate constants and derived kinetic parameters were evaluated by a nonlinear least-squars programs.

This research was supported in part by a Grant-in-Aid for Special Project Research from the Ministry of Education, Science and Culture.

References

1) T. C. Bruice and S. J. Benkovic, "Bioorganic Mechanism," Benjamin, New York (1966), Vol. 1.
2) W.P. Jencks, "Catalysis in Chemistry and Enzymology," McGraw-Hill, New York (1969).
3) M. L. Bender, "Mechanism of Homogeneous Catalysis from Protons to Proteins," Wiley-Interscience, New York (1971).
4) A. Mildvan, *Enzyme*, **2**, 446 (1970).
5) J. E. Coleman, in "Progress in Bioorganic Chemistry," ed by E. T. Kaiser and F. J. Kezdy, Wiley-Interscience, New York (1971), Vol. 1, p. 159.
6) "Inorganic Biochemistry," ed by G. L. Eichhorn, Elsevier, Amsterdam (1973), Vol. 1.
7) W. N. Lipscomb, *Acc. Chem. Res.*, **3**, 81 (1970).
8) W. N. Lipscomb, *Enzyme*, **3**, 1 (1971).
9) F. A. Quiocho and W. N. Lipscomb, *Adv. Protein Chem.*, **25**, 1 (1971); D. C. Rees and W. N. Lipscomb, *Proc. Natl. Acad. Sci. U. S. A.*, **78**, 5455 (1981).
10) W. N. Lipscomb, *Tetrahedron*, **30**, 1725 (1974).
11) E. T. Kaiser and B. L. Kaiser, *Acc. Chem. Res.*, **5**, 219 (1972).
12) Ref. 6, Chap. 15, p. 438.
13) S. Lindskog, L. E. Henderson, K. K. Kannan, A. Liljas, P. O. Nyman, and B. Strandberg, *Enzyme*, **5**, 587 (1971).
14) Y. Pocker and S. Starkanen, *Adv. Enzymol.*, **47**, 149 (1978).
15) B. Nostrand, I. Vaara, and K. K. Kannan, "Isozymes I," ed by C. L. Markert, Academic Press, New York (1975), p. 575.
16) Ref. 6, Chap.16, p. 488.
17) Y. W. Reid and I. B. Wilson, *Enzyme*, **4**, 373 (1971).
18) T. G. Spiro, in Ref. 6, p. 549.
19) a) R. Breslow, D. E. McClure, R. S. Brown, and J. Eisenach, *J. Am. Chem. Soc.*, **97**, 194 (1975); b) R. Breslow and D. E. McClure, *ibid.*, **98**, 258 (1976); c) T. H. Fife and V. L. Squillacote, *ibid.*, **99**, 3762 (1977); d) T. H. Fife and V. L. Squillacote, *ibid.*, **100**, 4787 (1978); e) T. H. Fife, T. J. Przystas, and V. L. Squillacote, *ibid.*, **101**, 3017 (1979); f) T. H. Fife and T. J. Przystas, *ibid.*, **102**, 7297 (1980); g) J. T. Groves and R. M. Dias, *ibid.*, **101**, 1033 (1979); h) J. Suh, M. Cheong, and M. P. Suh, *ibid.*, **104**, 1654 (1982); i) R. M. Propst III and L. S. Trzupek, *ibid.*, **103**, 3233 (1981).
20) R. Breslow and D. Chipman, *J. Am. Chem. Soc.*, **87**, 4195, (1965).
21) R. Breslow and L. E. Overman, *J. Am. Chem. Soc.*, **92**, **1075** (1970).
22) D. S. Sigman and C. T. Jorgensen, *J. Am. Chem. Soc.*, **94**, 1724 (1972).
23) I. Tabushi, Y. Kuroda, and A. Mochizuki, *J. Am. Chem. Soc.*, **102**, 1152 (1980).
24) R. S. Brown, N. J. Curtis, and J. Huguet, *J. Am. Chem. Soc.*, **103**, 6953 (1981); C. C. Tang, D. Davalian, and R. Breslow, *ibid.*, **98**, 3918 (1978).
25) J. M. Harrowfield, V. Norris, and A. M. Sargeson, *J. Am. Chem. Soc.*, **98**, 7282 (1976).
26) T. Eiki, S. Kawada, K. Matsushima, M. Mori, and W. Tagaki, *Chem. Lett.*, **1980**, 997.
27) T. Eiki, M. Mori, S. Kawada, K. Matsushima, and W. Tagaki, *Chem. Lett.*, **1980**, 1431.
28) M. L. Bender and T. H. Marshall, *J. Am. Chem. Soc.*, **90**, 201 (1968).
29) G. J. Lloyd and B. S. Cooperman, *J. Am. Chem. Soc.*, **93**, 4883 (1971); C. Hsu and B. S. Cooperman, *ibid.*, **98**, 5652 (1976).

 © 1983 The Chemical Society of Japan Bull. Chem. Soc. Jpn., 56, 1107—1112 (1983)

Synthetic Control by Internal Interaction. The Intramolecular Diels-Alder Reactions of Furan Derivatives and α, β-Unsaturated Amides

Toyonori TAKEBAYASHI, Nobuharu IWASAWA, and Teruaki MUKAIYAMA*

Department of Chemistry, Faculty of Science, The University of Tokyo, Hongo, Bunkyo-ku, Tokyo 113

(Received July 23, 1982)

An efficient method for the acceleration of the intramolecular Diels-Alder reaction was established utilizing the internal interaction——the internal hydrogen bonding and the internal coordination of a magnesium salt. The intramolecular Diels-Alder reaction between nitrofuran derivatives and various acrylic acid derivatives give good yields of the cycloadducts when internal hydrogen bonding is present. When cyclic α,β-unsaturated amides are employed as dienophile, the corresponding cycloadducts are obtained in high yield utilizing internal coordination of a magnesium salt.

The intramolecular Diels-Alder reaction is one of the most expedient methods for the stereoselective construction of polycyclic systems and is often employed as a key step for the total synthesis of various complex natural products.[1] In general, the intramolecular Diels-Alder reaction profits from entropical factors due to the spatial proximity of the reaction parameters, and many examples are known that verify this feature. However, it is sometimes difficult to obtain the cycloadducts even in the intramolecular Diels-Alder reaction. For example, furan is known as a relatively unreactive diene because of its aromaticity, and only a few examples on the intramolecular Diels-Alder reactions of furan derivatives with reactive dienophiles such as fumaric acid or acrylic acid derivatives have been reported.[2] Then we assumed that even in the unfavorable combination of dienes and dienophiles such as furan moiety and sterically hindered acrylic acid derivatives, it would be possible to obtain the corresponding cycloadducts by manipulating some artificial control on the reaction. Based on these assumptions, we have explored an efficient method for the acceleration of the intramolecular Diels-Alder reaction utilizing the intramolecular interactions —that is, the internal coordination of a magnesium salt and the internal hydrogen bonding.[3,4]

In the present paper, we wish to report this new concept for the acceleration of the intramolecular Diels-Alder reaction between furan derivatives and various sterically hindered α,β-unsaturated amides in detail.

Results and Discussion

It is well known that electron-rich dienes and electron-deficient dienophiles react easily to afford the cycloadducts in good yields. On the other hand, electron-deficient dienes preferentially react with dienophiles substituted with electron-donating groups, that is, the Diels-Alder reaction with "inverse electron demand."[5] Of these reactants, electron-deficient dienes, only a few papers related to dienes substituted with the strongly electron-withdrawing groups such as nitro group have been noted.[6] Notably, there has been only one example of the Diels-Alder reaction of nitrofuran with maleic anhydride reported by Van Campen *et al.*,[7] though they were unable to isolate the corresponding cycloadduct. It seems that, in this case, the cycloaddition reaction is impossible, as both nitrofuran and maleic anhydride are strongly electron-deficient. So the promotion of the reaction of this unfavorable combination of diene and dienophile was undertaken based on the intramolecular interaction taking the intramolecular Diels-Alder reaction between nitrofuran (*i.e.* the electron-deficient diene) and α,β-unsaturated amides (*i.e.* the electron-deficient dienophile), as a model.

In the first place, *N*-(5-nitrofurfuryl)-*N*-(2-hydroxyphenyl)acrylamides (**5**), the Diels-Alder reagents, were prepared from 5-nitrofurfural (**1**) and 2-hydroxyaniline (**2**) as shown in Eq. 1.

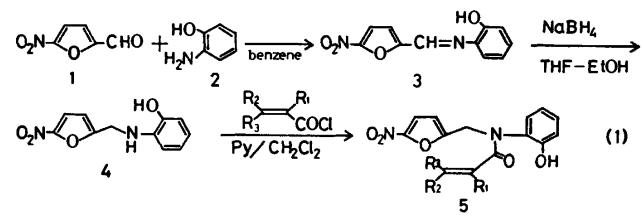

(1)

With the expectation that the formation of internal chelate complex **6** would bring both diene and dienophile groups to come closely to promote the cycloaddition reaction effectively, the reaction of the magnesium salt of amide **5** was examined, and the results are summarized in Table 1.

As shown in Table 1, cycloadducts **7a—c** were obtained only in 44—58% yield,[8] though starting material **5** was consumed completely and several minor products were detected on the thin-layer chromatography. This result indicates that the cycloaddition reaction might be accelerated by the formation of

Table 1. The Diels-Alder reaction of **5** with magnesium salt

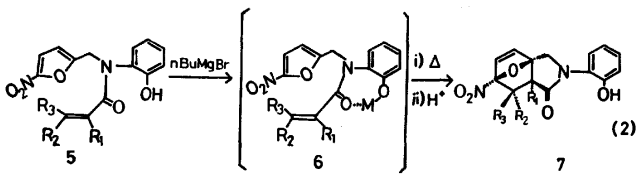

(2)

Amide	R_1	R_2	R_3	Solvent	Reaction time/h	Yield of **7** %
5a	CH_3	H	H	Benzene	3	46
				Benzene	7	57
5b	H	CH_3	H	Toluene	7	47
				Toluene–THF	9	42
5c	H	CH_3	CH_3	Toluene	7	48
				Toluene–THF	9	44

internal chelate, but some difficulties arose because of side reactions caused by the presence of a nitro group. Then the cycloaddition reaction of amide **5**, without converting to its magnesium salt, was tried on the assumption that the internal hydrogen bonding would be sufficient for the effective promotion of the cycloaddition reaction. Amides **5a**, **8**, and **9** were prepared to compare the reactivity, and to determine the existence and the role of the internal hydrogen bonding, and their reactions were examined under the same conditions (Eq. 3).

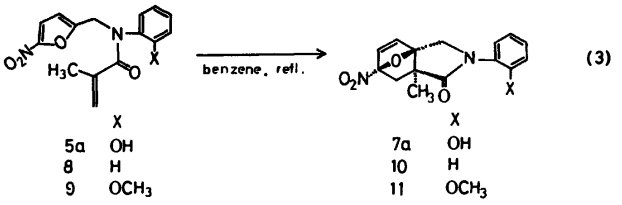

(3)

When a benzene solution of amide **5a** was refluxed for 7 h, adduct **7a** was obtained in 75% yield, but amides **8** and **9**, in which there is no internal hydrogen bonding, gave adducts **10** and **11** in only 30 and 11% yields, respectively, under the same conditions. Further, the existence of the internal hydrogen bonding in amide **5a** was supported by its IR spectra, that is, the absorptions of the carbonyl group of **5a**, **8**, and **9** are at 1600, 1650, and 1650 cm^{-1}, respectively.

These results indicate that the internal hydrogen bonding performs an important part on the acceleration of this cycloaddition reaction as expected.

Among possible conformers of amide **5a**, only conformer **12**, in which the diene and the dienophile approach closely, leads to the cycloaddition reaction.[2)]

In this case, it is apparent that the internal hydrogen bonding of the phenolic hydrogen to the carbonyl oxygen is sufficient to fix the conformation of this molecule to favorable conformer **12** (Eq. 4).

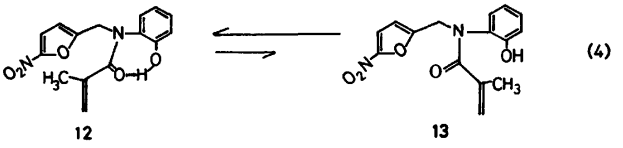

(4)

The yield of adduct **7a** increased to 94% when the reaction was performed in refluxing toluene. Similar reactions with other sterically hindered α,β-unsaturated amide **5** were tried, and adducts **7** were obtained in good yields as shown in Table 2.

The intramolecular cycloaddition reaction between furan moiety and cyclic α,β-unsaturated amide gives the tetracyclic compounds in one step, which are useful for the construction of polycyclic system. Moreover, there is no report on the intramolecular Diels-Alder reaction using the cyclic α,β-unsaturated amide as dienophile, probably because of its high steric hindrance. Then we next tried the cycloaddition reaction between furan derivatives and 1-cyclohexenecarboxamide utilizing the internal interaction—that is, the internal hydrogen bonding or the internal coordination of the metal salt. *N*-Furfuryl-*N*-(2-hydroxyphenyl)-1-cyclohexenecarboxamide (**14**) was prepared from 2-furoyl chloride (**15**) and 2-hydroxyaniline (**2**) as shown in Eq. 6.

TABLE 2. THE DIELS-ALDER REACTION OF **5**

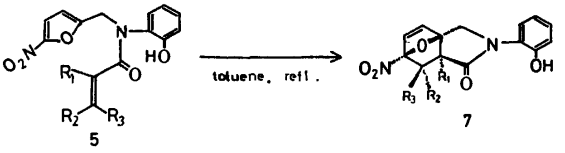

(5)

Amide	R_2, R_1, R_3	Reaction time/h	Yield of **7**/%
5a		7	94
b		9	93
c		9	73
d		7	96
e		9	30

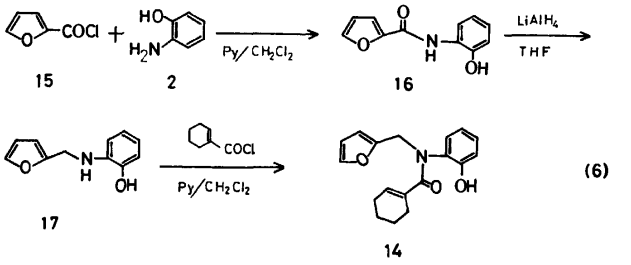

(6)

With starting material **14** in hand, we then examined the reaction of amide **14** and its magnesium salts based on the same assumption described above (Eq. 7).

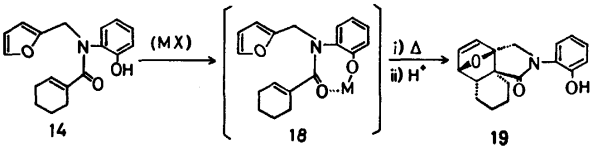

(7)

When amide **14** was heated in the refluxing benzene or toluene, only a trace of the cycloadduct was detected. Then, amide **14** was converted to its magnesium salt by the treatment with the Grignard reagent, and the reaction was performed in refluxing toluene. And, in this case, the reaction was effectively accelerated to afford cycloadduct **19** in 38% yield. To increase the yield of **19**, the effect of the solvent was examined. The results are summarized in Table 3. As shown in this Table, remarkable increase in the yield of cycloadduct **19** was not observed. Moreover, the effect of the reaction time was also investigated. When the reaction was continued for 14 h, the yield of cycloadduct **19** increased to 41%. However, longer reaction time decreased the yield of cycloadduct **19**, and only 14% yield of **19** was obtained, when the reaction was run

Table 3. The effect of reaction temperature[a)]

Solvent	Reaction temp/°C	Reaction time/h	Yield of **19** %
Benzene	Reflux	7	Trace
Toluene	Reflux	7	38
Xylene	Reflux	7	18
Cumene	115—120	7	17
DMF	Reflux	5	—
DMF–Benzene (4 : 1)	115—120	7	9
DMF–Toluene (1 : 1)	120—125	7	11
Toluene–THF (25 : 2)	107	7	16

a) Magnesium chloride was used as the metal salt.

Table 4. The reaction with various metal salts[a)]

Metal salt	Reaction time/h	Yield of **19**/%
–OMgCl	7	39
–OMgBr	7	30
–OZnCl	11.5	32
$-OAlCl_2$	9	Trace
$-OB(C_2H_5)_2$	10	25
$-OBBr_2$	7	—

a) The reaction was carried out in refluxing toluene.

for 33.5 h. We also found that starting material **14** was recovered in 30% yield, when the magnesium salt of cycloadduct **19** was refluxed in toluene for 7 h. This result indicates that the reaction is an equilibrating one and both cycloaddition reaction and the retro Diels-Alder reaction proceed concurrently at high temperature. And this could partly explain the rather moderate yield of cycloadduct **19** in this reaction.

Finally, we examined other metal salts such as Zn, Al, and B, which are thought to be stronger Lewis acids than Mg. However, as shown in Table 4, the use of these metal salts rather decreased the yield of adduct **19**.

It is well known that the Diels-Alder reaction is accelerated by the Lewis acid,[9)] but, at the same time, side reactions such as polymerization often occur, because both dienes and dienophiles are rather unstable under the acidic conditions.[10)] And in this case magnesium which is regarded as a week Lewis acid, is most favorable, that is, strong enough to accelerate the reaction effectively but not too strong to cause the side reactions. Further, the cycloaddition reaction of other cyclic α,β-unsaturated amides were examined. Molecular models show that in the case of 1-cyclohexenecarboxamide **14**, the axial protons in the cyclohexene ring seem to disturb the approach of the furan ring, and it is assumed that more planar cyclic α,β-unsaturated amides would show higher reactivity in the cycloaddition reaction. Based on this assumption, 1-cyclopentenecarboxamide derivative **20** and 1,5-cyclohexadienecarboxamide derivative **23** were prepared, and their reactivities were examined under the various reaction conditions. The results are summarized in Tables 5 and 6.

As clearly shown in these Tables, these two compounds show higher reactivity than the 1-cyclohexenyl derivative, and the corresponding cycloadducts were obtained in high yields by forming the internal chelate complexes

Table 5. The Diels-Alder reaction of **20**[a)]

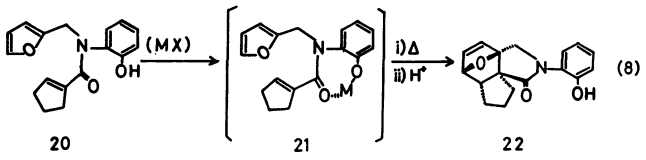

(8)

20 **21** **22**

Metal salt	Solvent	Reaction time/h	Yield of **22**/%
None	Benzene	7	18
–OMgBr	Benzene	7	65
None	Toluene	7	51
–OMgBr	Toluene	1	85
–OMgCl	Toluene	1	84
–OMgI	Toluene	1	84
–OZnCl	Toluene	1	21
–OMgBr	DME	1	31

a) The reaction was carried out under reflux temperature.

Table 6. The Diels-Alder reaction of **23**[a)]

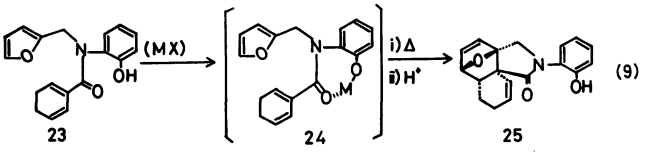

(9)

23 **24** **25**

Metal salt	Solvent	Reaction time/h	Yield of **25** %
None	Toluene	10	Trace
–OMgBr	Toluene	7	52
	Toluene–THF[b)]	5	75
–OMgCl	Toluene–THF[b)]	5	77

a) The reaction was carried out under reflux. b) THF was added to dissolve the magnesium salt of **23** and the reaction solution was heated to reflux at 107.5 °C.

of magnesium. These results indicate that steric hindrance of the dienophile remarkably affects the reactivity of the intramolecular Diels-Alder reaction, and that by employing coordinating property of magnesium ingeniously, dramatic acceleration of the reaction could be achieved.

In conclusion, it is noted that an efficient and general method is established for the acceleration of the intramolecular Diels-Alder reaction by employing internal hydrogen bonding or the internal coordination of a magnesium salt. By employing this method, various cycloadducts, which cannot be obtained in the previous intramolecular Diels-Alder reaction, have become available in high yields.

Experimental

Measurements. All the melting points were uncorrected. NMR spectra were recorded with a Hitachi R-24B spectrometer. IR spectra were measured with a Hitachi EPI-G2 spectrometer. Mass spectra were measured with a JEOL JMS 01-SG spectrometer.

Materials. All organic solvents used were distilled according to the general methods and stored over sodium metal or molecular sieves as a drying agent.

2-Hydroxy-N-(5-nitrofurfurylidene)aniline (3). 2-Hydro-

xyaniline (2.02 g, 18.5 mmol) was added to the benzene solution (20 ml) of 5-nitrofurfural (2.59 g, 18.4 mmol) at room temperature. A yellow precipitate was formed immediately. After 30 min the precipitate was filtered and recrystallized from benzene to afford **3** as yellow needles (3.73 g, 88%). Mp 158 °C (decomp) (benzene); IR (KBr) 3360, 3160, 1625, 1525, and 1332 cm^{-1}; NMR (DMSO-d_6) δ=6.25—7.53 (6H, m), 8.48 (1H, s), 8.70 (1H, broad); Found: C, 56.91; H, 3.30; N, 11.96%; Calcd for $C_{11}H_8N_2O_4$: C, 56.90; H, 3.47; N, 12.07%.

N-(2-Hydroxyphenyl)-5-nitrofurfurylamine (4). 2-Hydroxy-*N*-(5-nitrofurfurylidene)aniline (**3**) (3.22 g, 13.9 mmol) was dissolved in 165 ml of THF and 66 ml of 95% ethanol. The mixture was cooled to −35—−40 °C. The solution of sodium borohydride (0.79 g, 20.8 mmol) dissolved in 0.8—1.3 ml water and 9 M (1 M=1 mol dm^{-3}) hydrochloric acid were alternately added dropwise to the stirred solution so that pH 6—8 was maintained. During the addition, care was taken to maintain the temperature between −35 and −45 °C. After the addition of the sodium borohydride was complete, the solution was stirred at −35 °C for 1.5 h and hydrolyzed with water. After being acidified with acetic acid–ethanol solution to pH 3—4, the mixture was neutralized with 6 M sodium hydroxide. To the solution dichloromethane was added and the organic layer was washed with water, dried over Na_2SO_4, and the solvent was evaporated *in vacuo*. The residue was purified by silica-gel column chromatography using benzene–ethyl acetate (5 : 1) and amine **4** was obtained (2.72 g, 70%; unstable to light). Mp 85 °C; IR (KBr) 3320, 3130, 1490, and 1350 cm^{-1}; NMR ($CDCl_3$) δ=4.33 (2H, s), 4.63 (2H, broad), 6.30 (1H, d, J=4 Hz), 6.37—6.70 (4H, m), 7.07 (1H, d, J=4 Hz).

N-(5-Nitrofurfuryl)-N-(2-hydroxyphenyl)methacrylamide (5a). To a solution of amine **4** (0.82 g, 3.76 mmol) in 10 ml of dichloromethane and dry pyridine (0.43 g, 5.46 mmol) was added dropwise methacryloyl chloride (0.48 g, 4.55 mmol) in 5 ml of dichloromethane at −20 °C under an argon atmosphere. After the addition was complete, the reaction mixture was stirred at room temperature for 3 h. Then the organic layer was washed with 2 M hydrochloric acid and water. After being dried over Na_2SO_4, the solvent was evaporated *in vacuo* and the residue was purified by silica-gel column chromatography using benzene–ethyl acetate (5 : 1) and amide **5a** was obtained as yellow needles (0.77 g, 71%). Mp 146—147 °C (dichloromethane); IR (KBr) 3250, 1605, 1590, and 1350 cm^{-1}; NMR (DMSO-d_6) δ=1.75 (3H, s), 4.67 (1H, m), 4.90 (3H, m), 6.48 (1H, d, J=4 Hz), 11.10 (1H, broad); Found: *m/e* 302.0943. Calcd for $C_{15}H_{14}N_2O_5$: M, 302.0903. By similar procedure amides **5b—e**, **8**, and **9** were also prepared. **5b**: Mp 170—171 °C (dichloromethane); IR (KBr) 3200, 1605, 1580, and 1360 cm^{-1}; NMR (DMSO-d_6) δ=1.73 (3H, dd, J=7 and 2 Hz), 4.47 (1H, d, J=14 Hz), 5.15 (1H, d, J=14 Hz), 5.62 (1H, d, J=14 Hz), 6.29—7.25 (7H, m), 9.33 (1H, s); Found: *m/e* 302.0917. Calcd for $C_{15}H_{14}N_2O_5$: M, 302.0902, **5c**: Mp 163—164 °C (dichloromethane); IR (KBr) 3230, 1605, 1580, and 1360 cm^{-1}; NMR (DMSO-d_6) δ=1.35 (3H, s), 2.07 (3H, s), 4.42 (1H, d, J=16 Hz), 5.13 (1H, d, J=16 Hz), 5.35 (1H, m), 6.28—7.20 (6H, m), 9.22 (1H, s); Found: *m/e* 316.1054. Calcd for $C_{16}H_{16}N_2O_5$: M, 316.1059. **5c**: Mp 154—155 °C (dichloromethane); IR (KBr) 3200, 1605, 1560, and 1350 cm^{-1}; NMR (DMSO-d_6) δ=1.35—2.35 (6H, m), 4.40 (1H, d, J=14 Hz), 5.03 (1H, d, J=14 Hz), 5.62 (1H, m), 6.18—7.52 (6H, m), 9.35 (1H, s); Found: *m/e* 328.1048. Calcd for $C_{17}H_{16}N_2O_5$: M, 328.1059. **5e**: Oil; IR ($CHCl_3$) 3340, 1620, 1500, and 1360 cm^{-1}; NMR ($CDCl_3$) δ=0.90—2.70 (8H, m), 4.82 (2H, s), 5.82 (1H, s), 6.35 (1H, d, J=4 Hz), 6.50—7.40 (6H, m). **8**: Oil; IR (liquid) 1650, 1490, and 1350 cm^{-1}; NMR ($CDCl_3$) δ=1.73 (3H, s), 4.73 (2H, s), 5.30 (2H. s), 6.40 (1H, d, J=4 Hz), 6.82—7.47 (6H, m). **9**: Mp 97—98 °C (dichloromethane); IR 1650, 1500, and 1350 cm^{-1}; NMR ($CDCl_3$) δ=1.42 (3H, s), 3.72 (3H, s), 4.88 (4H, m), 6.35 (1H, d, J=4 Hz), 6.57—6.90 (5H, m).

Intramolecular Diels-Alder Reaction.[8] *2,3,3a,6,7,7a-Hexahydro-2-(2-hydroxyphenyl)-7a-methyl-6-nitro-3a,6-epoxy-1H-isoindol-1-one (7a).* After the toluene solution (20 ml) of amide **5a** (100 mg, 0.33 mmol) was refluxed for 7 h, the solvent was evaporated. The residue was purified by silica-gel column chromatography to afford cycloadduct **7a** (94 mg, 94%). Mp 221—222 °C (dichloromethane); IR (KBr) 3400, 1650, 1540, and 1360 cm^{-1}; NMR (DMSO-d_6) δ=1.20 (3H, s), 1.88 (1H, d, J=12 Hz), 6.28—7.28 (6H, m), 9.20 (1H, s); Found: *m/e* 302.0872. Calcd for $C_{15}H_{14}N_2O_5$: M, 302.0903. By similar procedure the intramolecular Diels-Alder reaction of amides **5b—e**, **8**, and **9** were performed to afford cycloadducts **7b—e**, **10**, and **11**. **7b**: Mp 207—208 °C (dichloromethane); IR (KBr) 3060, 1650, 1550, and 1380 cm^{-1}; NMR (DMSO-d_6) δ=1.18 (3H, d, J=7 Hz), 2.67—3.20 (2H, m), 3.57 (1H, d, J=12 Hz), 4.47 (1H, d, J=12 Hz), 6.28—7.28 (6H, m), 9.27 (1H, s); Found: *m/e* 302.0899. Calcd for $C_{15}H_{14}N_2O_5$: M, 302.0903. **7c**: Mp 189—190 °C (dichloromethane); IR (KBr) 3300, 1645, 1545, and 1370 cm^{-1}; NMR (DMSO-d_6) δ=1.22 (3H, s), 1.25 (3H, s), 2.95—3.55 (1H, m), 3.85 (1H, d, J=12 Hz), 4.48 (1H, d, J=12 Hz), 6.28—7.28 (6H, m), 9.32 (1H, s); Found: *m/e* 316.1107. Calcd for $C_{16}H_{16}N_2O_5$: M, 316.1061. **7c**: Mp 225—226 °C (dichloromethane); IR (KBr) 3200, 1665, 1550, and 1370 cm^{-1}; NMR (DMSO-d_6) δ=1.08—1.98 (6H, m), 3.08—3.42 (1H, m), 3.90 (1H, d, J=12 Hz), 4.52 (1H, d, J=12 Hz), 6.32—7.32 (6H, m), 9.33 (1H, s); Found: *m/e* 328.1055. Calcd for $C_{17}H_{16}N_2O_5$: M 328.1059, **7e**: Mp 200—201 °C (dichloromethane); IR (KBr) 3300. 1650, 1540, and 1370 cm^{-1}; NMR (DMSO-d_6) δ=0.65—2.12 (8H, m), 2.98—3.48 (1H, m), 3.92 (1H, d, J=12 Hz), 4.50 (1H, d, J=12 Hz), 6.35—7.32 (6H, m), 9.45 (1H, s); Found: *m/e* 342.1208. Calcd for $C_{18}H_{18}N_2O_5$: M, 342.1217. **10**: Mp 132—133 °C. (benzene–cyclohexane); IR (KBr) 1696, 1550, and 1360 cm^{-1}; NMR ($CDCl_3$) δ=1.18 (3H, s), 2.27 (1H, d, J=12 Hz), 3.23 (1H, d, J=12 Hz), 4.27 (2H, d, J=4 Hz), 6.67 (2H, d, J=2 Hz), 6.90—7.68 (5H, m); Found: C, 62.94; H, 4.83; N, 9.59%; Calcd for $C_{15}H_{14}N_2O_4$: C, 62.93; H, 4.93; N, 9.79%. **11**: Mp 162—163 °C (dichloromethane); IR (KBr) 1695, 1530, and 1340 cm^{-1}; NMR ($CDCl_3$) δ=1.25 (3H, d, J=2 Hz), 1.90 (1H, d, J=10 Hz), 2.87 (1H, d, J=10 Hz), 3.78 (3H, s), 3.93 (1H, d, J=12 Hz), 4.43 (1H, d, J=12 Hz), 6.47—6.80 (6H, m); Found: C, 60.53; H, 5.00; N, 8.80%; Calcd for $C_{16}H_{16}N_2O_5$: C, 60.75; H, 5.10; N, 8.86%.

N-(2-Hydroxyphenyl)-2-furancarboxamide (16). Under an argon atmosphere 2-furoyl chloride (22.9 g, 0.18 mol) was added to the suspension of 2-hydroxyaniline (19.1 g, 0.18 mol) and dry triethylamine 35 ml in 400 ml dichloromethane at 0—5 °C and the mixture was stirred at room temperature for 2 h. After 2 M hydrochloric acid was added to the mixture to afford amide **16** (20.2 g, 57%), a white precipitate formed was filtered. The filtrate was extracted with dichloromethane and the extract was washed with water. The organic layer was dried over Na_2SO_4 and evaporated. The residue was recrystallized from benzene to afford amide **16** (8.76 g, 25%). Mp 165—166 °C (benzene); IR (KBr) 3390, 3100, and 1635 cm^{-1}; NMR ($CDCl_3$) δ=6.37—7.47 (7H, m), 8.00 (1H, m), 8.83 (1H, broad); Found: C, 65.05; H, 4.37; N, 7.01%; Calcd for $C_{11}H_9NO_3$: C, 65.02; H, 4.46; N, 6.89%.

N-(2-Hydroxyphenyl)-2-furfurylamine (17). Under an argon atmosphere, amide **16** (25.0 g, 0.12 mol) in 220 ml THF solution was added dropwise to the suspension of $LiAlH_4$ (6.1 g, 0.16 mol) in 30 ml of THF at −5—0 °C. After the mixture was refluxed for 1 h, saturated sodium sulfate solution was

added cautiously in an ice-cold bath. The precipitate was filtered and washed with ethyl acetate. The filtrate was washed with 2 M hydrochloric acid and neutralized with sodium hydrogencarbonate, and then extracted with ethyl acetate. The organic layer was dried over Na_2SO_4 and the solvent was evaporated *in vacuo*. The residue was distilled and amine **17** was obtained as a colorless oil (2.80 g, 80%). Bp 110 °C/0.2 mmHg (1 mmHg≈133.322 Pa); mp 62 °C; IR (liquid) 3340 and 1610 cm^{-1}; NMR ($CDCl_3$) δ=4.12 (2H, s), 5.25 (2H, s), 6.03 (2H, m), 6.33—6.70 (4H, m), 7.10 (1H, s).

*N-Furfuryl-N-(2-hydroxyphenyl)-1-cyclohexenecarboxamide (**14**).* To a solution of amine **17** (1.42 g, 7.50 mmol) in 20 ml of dichloromethane and dry pyridine (0.89 g, 11.26 mmol) 1-cyclohexenecarbonyl chloride (1.40 g, 7.54 mmol) in 14 ml of dichloromethane was added dropwise at −20 °C under an argon atmosphere. After the addition was complete, the mixture was stirred at room temperature for 3 h. Then the organic layer was washed with 2 M hydrochloric acid and water. After being dried over Na_2SO_4, the solvent was evaporated and the residue was recrystallized from benzene and amide **14** was obtained as white needles (1.85 g, 83%). Mp 171—172 °C (benzene); IR (KBr) 3400 and 1610 cm^{-1}; NMR ($CDCl_3$) δ=1.02—1.67 (4H, m), 1.67—2.33 (4H, m), 4.82 (2H, s), 5.67—6.00 (1H, m), 6.10 (2H, m), 6.60—7.33 (6H, m); Found: C, 72.68; H, 6.41; N, 4.45%; Calcd for $C_{18}H_{19}NO_3$: C, 72.70; H, 6.44; N, 4.71%. By similar procedure amide **20** was prepared. **20**: Mp 114—115 °C (benzene); IR (KBr) 3130 and 1610 cm^{-1}; NMR ($CDCl_3$) δ= 1.28—2.50 (6H, m), 4.78 (2H, s), 5.85 (1H, m), 6.07 (2H, m), 6.52—7.40 (6H, m); Found: C, 72.26; H, 6.07; N, 4.84%; Calcd for $C_{17}H_{17}NO_3$: C, 72.06; H, 6.05; N, 4.94%.

*N-Furfuryl-N-(2-hydroxyphenyl)-1,5-cyclohexadienecarboxamide (**23**).* To 1-methyl-2-chloropyridinium tosylate (1.95 g, 6.5 mmol) in 15 ml of dichloromethane was added a mixture of amine **17** (1.00 g, 5.30 mmol), 1,5-cyclohexadienecarboxylic acid[11] (0.67 g, 5.42 mmol) and triethylamine (0.87 g, 13.11 mmol) in 40 ml of dichloromethane. After being stirred overnight at room temperature under an argon atmosphere, 2 M hydrochloric acid (10 ml) was added to the reaction mixture and the resulting mixture was washed with water (20 ml) three times. The organic layer was dried over Na_2SO_4 and concentrated under the reduced pressure. Amide **23** was isolated after separation by silica-gel column chromatography using benzene–ethyl acetate (5 : 1) (0.48 g, 30%). Mp 139—140 °C (cyclohexane–benzene); IR (KBr) 3150 and 1610 cm^{-1}; NMR ($CDCl_3$) δ=1.92 (4H, m), 4.86 (2H, m), 5.27—6.33 (5H, m), 6.43—7.33 (6H, m); Found: C, 72.97; H, 5.63; N, 4.64%; Calcd for $C_{18}H_{17}NO_3$: C, 73.20; H, 5.80; N, 4.74%.

Intramolecular Diels-Alder Reaction Using Halophenoxy Magnesium Salt.[8] *1,2,3,3a,6,6a,7,8,9,10-Decahydro-(2-hydroxyphenyl)-3a,6-epoxybenz[d]isoindol-1-one (**19**).* To a solution of amide **14** (100.3 mg, 0.337 mmol) in 3 ml of THF was added dropwise butylmagnesium chloride (0.39 ml, 0.86 mol dm^{-3} ether solution) at −78 °C under an argon atmosphere. After the solution being concentrated under the reduced pressure at room temperature, toluene (30 ml) was added and the reaction mixture was refluxed for 14 h under an argon atmosphere. To the solution was added 2 M hydrochloric acid (10 ml), and the organic layer was extracted with dichloromethane. The extract was washed with water and dried over Na_2SO_4. The solution was concentrated under the reduced pressure. Cycloadduct **21** was isolated after separation by the thin-layer chromatography using benzene–ethyl acetate (5 : 1) (44.0 mg, 44%). Mp 138—139 °C (cyclohexane); IR (KBr) 3180 and 1660 cm^{-1}; NMR ($CDCl_3$) δ=0.50—2.10 (8H, m), 2.83 (1H, d, J=5 Hz), 3.58 (1H, d, J=12 Hz), 4.10 (1H, d, J=12 Hz), 4.85 (1H, d, J=5 Hz), 6.37 (2H, s), 6.53—6.97 (4H, m), 7.88 (1H, broad); Found: C, 72.71; H, 6.46; N, 4.77%; Calcd for $C_{18}H_{19}NO_3$: C, 72.70; H, 6.44; N, 4.71%. By similar procedures the intramolecular Diels-Alder reaction of amides **20** and **23** were performed to afford cycloadducts **22** and **25**. **22**: Mp 182—183 °C (benzene); IR (KBr) 3500 and 1670 cm^{-1}; NMR ($CDCl_3$) δ=1.33—2.32 (6H, m), 2.93—3.43 (1H, m), 3.97 (1H, d, J=12 Hz), 4.43 (1H, d, J=12 Hz), 4.87 (1H, d, J=5 Hz), 6.42 (2H, s), 6.63—7.30 (4H, m), 8.18 (1H, s); Found: C, 72.17; H, 6.15; N, 4.90%; Calcd for $C_{17}H_{17}NO_3$: C, 72.06; H, 6.05; N, 4.94%. **25**: Mp 151—152 °C (benzene); IR (KBr) 3450 and 1650 cm^{-1}; NMR ($CDCl_3$) δ=0.90—2.22 (4H, m), 2.67—3.22 (1H, m), 3.87 (1H, d, J=11 Hz), 4.38 (1H, d, J=11 Hz), 4.82 (1H, d, J=4 Hz), 5.43 (1H, d, J=10 Hz), 5.85 (1H, m), 6.20 (2H, s), 6.43—7.20 (4H, m), 7.87 (1H, s); Found: C, 73.18; H, 5.77; N, 4.90%; Calcd for $C_{18}H_{17}NO_3$: C, 73.20; H, 5.80; N, 4.74%.

References

1) W. Oppolzer, *Angew. Chem., Int. Ed. Engl.*, **16**, 10 (1977).

2) a) H. W. Gschwend, M. J. Hillman, B. Kisis, and R. K. Rodebaugh, *J. Org. Chem.*, **41**, 104 (1976); b) K. A. Parker and M. R. Adamechuk, *Tetrahedron Lett.*, **1978**, 1689.

3) T. Mukaiyama, T. Tsuji, and N. Iwasawa, *Chem. Lett.*, **1979**, 697.

4) T. Mukaiyama and T. Takebayashi, *Chem. Lett.*, **1980**, 1013.

5) J. Sauer, *Angew. Chem., Int. Ed. Engl.*, **5**, 211 (1966); **6**, 16 (1967).

6) N. N. Podogornova, E. S. Lipina, and U. V. Perekalin, *Nauchn. Dokl., Gertsenovskie Cheteniva*, **27**, 22 (1974); *Chem. Abstr.*, **85**, 192214x (1976); D. Alkeksiev, I. Mladenov, E. Lipina, and V. Perekalin, *Izv, Khim.*, **9**, 439 (1976); *Chem. Abstr.*, **87**, 84587d (1977); c) T. Severin and I. Ipack, *Chem. Ber.*, **109**, 3541 (1976).

7) M. G. Van Campen and J. R. Johnson, *J. Am. Chem. Soc.*, **55**, 430 (1933).

8) Only one of two stereoisomers was obtained. In this case, based on models and spectral analogy, the exo mode cyclization (trans ring junction) was preferred. The coupling constant between proton Ha and Hb in adducts **19**, **22**, and **25** are 5, 5, and 4 Hz, respectively, suggesting a dihedral angle of 40° or 45° (according to models, the corresponding angle for the alternative structure would be about 90° resulting in no spin-spin coupling) (Fig. 1). These results agree with

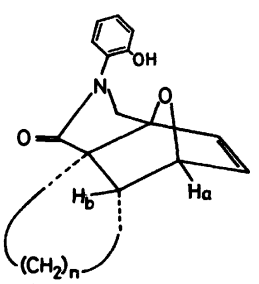

Fig. 1. Stereochemistry of cycloadducts.

spectral data presented by K. A. Parker[2b] for a related set of compounds. In the case of nitrofuran derivatives, we cannot tell the stereochemistry of the formed cycloadduct from the coupling constant becase a nitro group is present in the place of Ha proton. But in the intramolecular Diels-Alder reaction of furan derivatives, it is well known[2,12] that only the exo mode

of cycloadducts are formed, and, in this case also, we assume that only the exo mode of cycloaddition was preferred.

9) P. Yates and P. Eaton, *J. Am. Chem. Soc.*, **82**, 4436 (1960).
10) G. I. Fray and R. Robinson, *J. Am. Chem. Soc.*, **83**, 249 (1961).
11) H. Plieninger and G. Ege, *Chem. Ber*, **94**, 2088 (1961).
12) D. Bilovic, *Croat. Chem. Acta*, **40**, 15 (1968); D. D. Sternbach and D. M. Rossana, *Tetrahedron Lett.* **23**, 303 (1982).

The Reductive Coupling of Organic Halide Using Hydrazine and a Palladium Amalgam Catalyst. II.[1] Homocoupling of Haloarene with Arylhydrazine

Riichiro NAKAJIMA,* Masaji KINOSADA,† Takashi TAMURA, and Tadashi HARA
Department of Chemical Engineering, Faculty of Engineering, Doshisha University, Karasuma Imadegawa Kamikyo-ku, Kyoto 602
(Received July 28, 1982)

The function of palladium chloride in the reaction of an arylhydrazine with a haloarene was found to differ from those of other metal salts; palladium chloride was reduced with arylhydrazine, and the palladium metal produced was again oxidized with haloarene to give palladium halide. Thus the reductive coupling of haloarene occurred in the presence of a catalytic amount of palladium chloride. Addition of mercury(II) chloride promoted this reaction. The reaction of *o*-, *m*-, and *p*-bromotoluene with the corresponding tolylhydrazine gave the corresponding bitolyl in 99, 112, and 115% yield, respectively, based on the haloarene.

Monoarylhydrazines are readily oxidized like hydrazine itself by a variety of reagents, the products varying with the oxidant used. For example, when oxidation is effected by either silver(I) oxide, mercury(II) oxide,[2] or lead(IV) acetate[3] in aromatic solvents, an arylhydrazine is converted smoothly into the corresponding biaryl; bromo- or chlorobenzene reacted with phenylhydrazine to give bromo- or chlorobiphenyls without displacement of halogen. On the other hand, Bacon *et al.*[4] have observed catalytic effects of small amounts of phenylhydrazine on the coupling of bromo- or iodonitroarene with copper(I) oxide, but details are not clear. The present study has, therefore, been carried out in order to examine the reaction of haloarene with arylhydrazine in the presence of a palladium catalyst because in the latter case phenylhydrazine is anticipated to play the role of hydrazine in the Busch reaction. The reductive homocoupling of both iodo- and bromoarenes occurs in the presence of a palladium amalgam catalyst and arylhydrazines to give the corresponding halogen-free biaryls in good yield.

Results and Discussion

As Table 1 shows, when halobenzene (25.0 mmol) was treated with phenylhydrazine (10.0 mmol) in the presence of a catalytic amount (2 mol%) of palladium prepared *in situ* from palladium chloride in refluxing methanol for 6 h, the reductive coupling of bromo- or iodobenzene with phenylhydrazine occurred to give biphenyl. In contrast to the behavior of chlorobenzene, no phenylation of bromo- or iodobenzene occurred.

TABLE 1. COUPLING OF HALOBENZENE WITH PHENYLHYDRAZINE BY THE USE OF PALLADIUM METAL OR A PALLADIUM AMALGAM

Halobenzene	Yield of biphenyl/%[a]	
	Pd	Pd-Hg
Chlorobenzene	11.7[b]	7.8[b]
Bromobenzene	61.8	96.6
Iodobenzene	62.2	105.7

a) Based on halobenzene used. b) Traces of chlorobiphenyls were also formed.

† Present address: Toyo Kasei Kogyo Co. Ltd., 2900, Sonecho Takasago 676.

This coupling was promoted by addition of mercury(II) chloride.

It has long been known that the formation of biphenyl arises not only by oxidation of phenylhydrazine with metal oxides, metal acetates, *etc.*, but also by reductive coupling of halobenzenes with metals. To determine the source of the biphenyl, one of the aromatic rings in Eq. 1 was labeled with a substituent to distinguish it from the other.

$$ArX + ArNHNH_2 \xrightarrow{\text{Pd or Pd-Hg}} ArAr, \textit{ etc.} \quad (1)$$

The aryl group in the biaryls was derived mostly from the haloarene, independent of the presence of substituent, as listed in Table 2. When a palladium amalgam catalyst was used, about 75% of *p*-halotoluene was converted to 4,4′-dimethylbiphenyl, the remainder being consumed in the reaction with phenylhydrazine to give 4-methylbiphenyl and toluene. However, the homocoupling of *p*-bromotoluene was scarcely observed in the absence of a palladium catalyst and a large portion of bromotoluene was recovered. These results clearly indicate that the formation of the biaryl occurs mostly by the reductive coupling of haloarene, *i.e.*, Eq. 2.

$$2ArX + Pd \longrightarrow ArAr + PdX_2 \quad (2)$$

Evidently the palladium(II) halide formed *in situ*, as described in Eq. 2, was also reduced with arylhydrazine, because both the palladium(II) salt and the mercury(II) salt used were recovered as the metals. It is known that the oxidation of phenylhydrazine with metal oxide in halobenzene yields benzene, biphenyl, azobenzene, and halobiphenyls, and the formation of these compounds can be explained in terms of a radical mechanism.[3,4] However, in the present system no halobiphenyls were obtained and one of the biphenyls isolated was formed by the displacement of halogen with the aryl group derived from arylhydrazine. These results can be best explained by the mechanism *via* arylhydrazine-palladium halide complex[5] (Eq. 3).

$$2NH_2NHPh + PdX_2 \longrightarrow PdX_2(NH_2NHPh)_2 \xrightarrow{-2HX\ -2H^+} \begin{cases} \longrightarrow 2PhH(\text{and/or } Ph_2+H_2)+2N_2+Pd \\ [Pd(NH{=}NPh)_2] \longrightarrow 2NH{=}NPh + Pd \\ \xrightarrow{+2ArX} 2ArPh + 2HX + 2N_2 + Pd \end{cases} \quad (3)$$

TABLE 2. REACTION OF HALOARENE WITH ARYLHYDRAZINE

ArX (12.5 mmol)	ArNHNH$_2$ (12.5 mmol)	Catalyst (0.5 mmol)	Biaryls(mmol)		
			Ar$_2$	ArAr	Ar$_2$
p-Bromotoluene[a)]	Phenylhydrazine	None	0.10		0.48
p-Bromotoluene	Phenylhydrazine	Pd	1.69	1.11	0.63
p-Bromotoluene	Phenylhydrazine	Pd–Hg	4.75	1.51	0.79
Bromobenzene	*p*-Tolylhydrazine hydrochloride	Pd–Hg	2.56	1.03	0.04
p-Iodotoluene	Phenylhydrazine	Pd	2.73	0.73	0.17
Iodobenzene	*p*-Tolylhydrazine hydrochloride	Pd	3.43	1.89	0.41
p-Iodotoluene	Phenylhydrazine	Pd–Hg	4.83	1.64	0.75

a) A large portion of bromotoluene was recovered.

TABLE 3. HOMOCOUPLING OF ORGANIC BROMIDE WITH ARYLHYDRAZINE IN THE PRESENCE OF A PALLADIUM AMALGAM CATALYST

Organic bromide	Arylhydrazine	Coupling products and yield/%[a)]
o-Bromotoluene	*o*-Tolylhydrazine hydrochloride	2,2′Dimethylbiphenyl/99[b)]
m-Bromotoluene	*m*-Tolylhydrazine hydrochloride	3,3′-Dimethylbiphenyl/112[b)]
p-Bromotoluene	*p*-Tolylhydrazine hydrochloride	4,4′-Dimethylbiphenyl/115[b)]
4-Bromo-*o*-xylene	3,4-Xylylhydrazine hydrochloride	3,3′4,4′-Tetramethylbiphenyl/88.4
1-Bromonaphthalene	Phenylhydrazine	1,1′-Binaphthyl/50.2 1-Phenylnaphthalene[c)] Biphenyl/6.4
2-Bromonaphthalene	Phenylhydrazine	2,2′-Binaphthyl/71.2 2-Phenylnaphthalene/4.7 Biphenyl/5.4
2-Bromopyridine	Phenylhydrazine	2,2′Bipyridyl/42[b)] 2-Phenylpyridine/0.6 Biphenyl/1.8
2-Bromothiophene	Phenylhydrazine	2,2′-Bithienyl/41.7 2-Phenylthiophene[c)] Biphenyl/1.4

a) Yield based on organic bromide used except that of biphenyl and determined by GLPC. b) Isolated yield.
c) Not measured.

Consequently, the present reaction is a Busch-type reaction because arylhydrazine acts as a reducing agent and then the reductive homocoupling of haloarene proceeds in the presence of the palladium catalyst.

According to the present method, both iodo- and bromoarenes could be used as the starting materials for the preparation of biaryls. The previous method[1)] gave satisfactory yields of biaryls only when iodoarene was used and, therefore, the utility of the present method was examined in the coupling of bromoarenes (Table 3). Usually traces of arylamine, azoarene, and hydrazoarene, which are well known as the decomposition products of arylhydrazine, were detected, but these compounds were easily separated from the biaryls. Bromotoluenes and bromoxylene reacted with tolyl- and xylylhydrazine, respectively, to give the corresponding biaryls in high yield. 2,2′-Disubstituted biphenyl, which is difficult to prepare by ordinary symmetrical biaryl syntheses with haloarenes except the Ullmann reaction, was also obtained without the formation of 2,3′-isomer.[6)] Although the Busch reaction has been used when the Ullmann reaction is inefficient for the preparation of biaryl, the Busch reaction of bromonaphthalene[7)] and 2-bromopyridine[8)] has been inefficient. Treatment of bromonaphthalene, or bromopyridine with phenylhydrazine gave the corresponding binaphthyl or bipyridyl accompanying of small amounts of phenylnaphthalene or phenylpyridine, and biphenyl, which were easily removed at the isolation/purification stage, and the yield was higher than the previous one.[7,8)] Bithienyl was also prepared by the present method, but the yield is still somewhat modest. These results were always superior to those obtained under the Busch reaction conditions.

Experimental

Materials. The reagents used were commercial reagent grade materials except those noted below. 4-Bromo-*o*-xylene and 3,4-dimethylphenylhydrazine were prepared from 3,4-dimethylaniline according to the method of Bigelow,[9)] and Coleman,[10)] respectively. The following authentic samples were also prepared in accordance with the method given in the literature; 4-methylbiphenyl,[11)] 2,2′-, 3,3′-, and 4,4′-dimethylbiphenyl,[1)] 1,1′-, and 2,2′-binaphthyl,[12)] 2-phenylnaphthalene,[13)] and 2,2′-bithienyl.[14)]

Reductive Coupling of Halobenzene with Phenylhydrazine.

Pd Catalyst: A mixture of halobenzene (25.0 mmol), $PdCl_2$ (0.50 mmol), phenylhydrazine (10.0 mmol), and NaOH (100 mmol) was stirred in refluxing MeOH (12 ml) for 6 h. The resulting mixture was filtered, and the residual metal was washed with benzene, and subsequently water. The organic layer separated from the aqueous layer was concentrated by rotary evaporation under reduced pressure, and analyzed by GLPC and GC–MS. The products exhibited spectral characteristics in accord with those of known samples.

Pd–Hg Catalyst: The reaction was carried out as described above except that both $PdCl_2$ (0.50 mmol), and $HgCl_2$ (0.50 mmol) were used in place of $PdCl_2$.

Reaction of Haloarene with Arylhydrazine. A mixture of haloarene (12.5 mmol), arylhydrazine (12.5 mmol), and NaOH (125 mmol) was refluxed in 16 ml of MeOH in the presence or absence of the catalyst (0.50 mmol of $PdCl_2$, or 0.50 mmol of $PdCl_2$ and 0.50 mmol of $HgCl_2$) for 9 h with stirring. The resulting mixture was worked up as described above.

Synthesis of Biaryls. The following procedure for the synthesis of 2,2′-dimethylbiphenyl is representative. A mixture of *o*-bromotoluene (25.0 mmol), *o*-tolylhydrazine hydrochloride (15.0 mmol), $PdCl_2$ (0.50 mmol), $HgCl_2$ (0.50 mmol), and NaOH (125 mmol) was refluxed in 16 ml of MeOH for 6 h with stirring. The resulting mixture was treated as above,

and after analysis the concentrated organic layer was distilled *in vacuo* using a ball tube distillation apparatus to give 2,2'-dimethylbiphenyl (12.4 mmol, 99%).

2,2'-Bipyridyl: A mixture of 2-bromopyridine (25.0 mmol), phenylhydrazine (15.0 mmol), $PdCl_2$ (0.50 mmol), $HgCl_2$ (0.50 mmol), NaOH (125 mmol), and MeOH (16 ml) was processed as above. The distillate gave bipyridyl together with a small amount of phenylpyridine and biphenyl. This distillate (or the concentrated organic layer) was steam-distilled from iron(II) solution buffered at pH 4.4 to remove biphenyl and phenylpyridine, and the residue was then steam-distilled from a strongly basic medium to give 2,2'-bipyridyl (5.3 mmol, 42%) as crystals, mp 66.5—68.0 °C.

We wish to thank Messrs. M. Aoyama and T. Ikeda for their assistance in the experimental work. The present work was partially supported by the Asahi Glass Foundation For Industrial Technology.

References

1) Part I of this series: R. Nakajima, Y. Shintani, and T. Hara, *Bull. Chem. Soc. Jpn.*, **53**, 1767 (1980).
2) R. L. Hardie and R. H. Thomson, *J. Chem. Soc.*, **1957**, 2512.
3) J. B. Aylward, *J. Chem. Soc., C*, **1969**, 1663.
4) R. G. R. Bacon, S. G. Seeterram, and O. J. Stewart, *Tetrahedron Lett.*, **1967**, 2003; R. G. R. Bacon and O. J. Stewart, *J. Chem. Soc., C*, **1969**, 301.
5) J. Dehand, J. Jordanov, and M. Pfeffer, *J. Chem. Soc., Dalton Trans.*, **1976**, 1553; J. Dehand and M. Pfeffer, *Bull. Soc. Chim. Fr.*, **1974**, 2782; *Chem. Abstr.*, **82**, 179826s (1975.)
6) The absence of mercury resulted in the formation of 2,3'-dimethylbiphenyl and in the decrease of the yield of bitolyls; the same effects of mercury have been noted previously on the coupling of *o*-iodotoluene using hydrazine.[1]
7) M. Busch and W. Schmidt, *Ber.*, **62**, 2612 (1927); M. Busch and W. Weber, *J. Prakt. Chem.*, **146**, 1 (1936).
8) G. J. Moore, Ger. Offen. 2230562 (1973).
9) L. A. Bigelow, *Org. Synth.*, Coll. Vol. I, 136 (1956).
10) G. H. Coleman, *Org. Synth.*, Coll. Vol. I, 442 (1956).
11) W. E. Bachmann and R. A. Hoffman, "Organic Reactions," ed by R. Adams, John Wiley and Sons, Inc., New York (1944), Vol. II, p. 247.
12) D. A. Shirley, "Preparation of Organic Intermediates," John Wiley and Sons, Inc., New York (1951), p. 33.
13) J. C. W. Evans and C. F. H. Allen, *Org. Synth.*, Coll. Vol. II, 517 (1943).
14) R. Nakajima and T. Hara, 45th National Meeting of the Chemical Society of Japan, Tokyo, April 1982, Abstr. No. 2C12.

Studies of Bitter Peptides from Casein Hydrolyzate. II.[1] Syntheses of Bitter Peptide Fragments and Analogs of BPIa (Arg-Gly-Pro-Pro-Phe-Ile-Val) from Casein Hydrolyzate[2]

Ken Otagiri, Ichizo Miyake, Norio Ishibashi, Hiroshi Fukui, Hidenori Kanehisa, and Hideo Okai*

Department of Fermentation Technology, Faculty of Engineering, Hiroshima University, Shitami, Saijo-cho, Higashihiroshima 724

(Received August 23, 1982)

In order to investigate the relationship between bitterness and chemical structure of BPIa, eleven kinds of fragments and analogs of BPIa were synthesized. des-Gly^2-BPIa and des-Pro^4-BPIa exhibited extremely bitter taste. However, the pentapeptide (Arg-Gly-Pro-Pro-Phe) of BPIa possessed weak bitterness. The bitterness exhibition of BPIa probably derived from the spatial structure of its molecule.

In the previous paper[1] and the preliminary reports,[3,4] the authors described the synthesis of the bitter peptide BPIa (Arg-Gly-Pro-Pro-Phe-Ile-Val) which was isolated by Minamiura *et al.*[5] and found that the peptide possesses extremely bitter taste, such as quinine and phenylthiourea. They also reported that the bitter taste exhibited by BPIa was associated with its characteristic conformation. In this paper, we describe the synthesis of eleven kinds of peptides as shown in Table 1 to investigate the participation of constituent amino acid residues of BPIa in producing the strong bitter taste.

Table 1. The threshold value for bitter taste of the synthetic peptides

	Compound	T.V.[b] / mM	Rcaf.[c]
(1)	Arg–Gly–Pro–Pro–Phe–Ile	0.025	40.00
(2)	Arg–Gly–Pro–Pro–Phe	2.30	0.43
(3)	Arg–Gly–Pro	13.00	0.08
(4)	Arg–Gly	10.00	0.10
(5)	Ile–Val	12.50	0.08
(6)	Phe–Ile–Val	1.50	0.67
(7)	Pro–Phe–Ile–Val	0.30	3.33
(8)	Pro–Pro–Phe–Ile–Val	1.20	0.83
(9)	Gly–Pro–Pro–Phe–Ile–Val	1.20	0.83
(10)	Arg–Pro–Pro–Phe–Ile–Val	0.08	12.50
(11)	Arg–Gly–Pro–Phe–Ile–Val	0.05	20.00
(12)	Arg–Gly–Pro–Pro–Phe–Ile–Val[a]	0.05	20.00

a) BPIa. b) Threshold value. c) The ratio of caffeine.

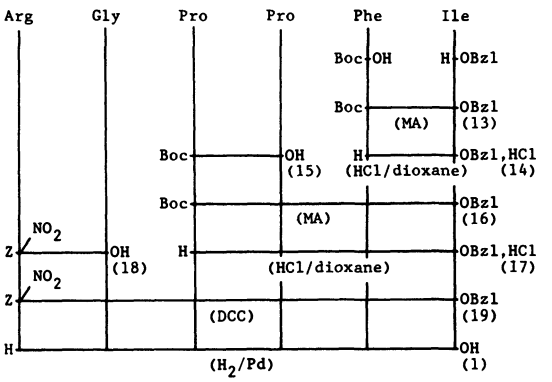

Fig. 1. The synthetic route of Arg–Gly–Pro–Pro–Phe–Ile.

In connection with the syntheses, the BPIa intermediates, as had been reported in the previous paper,[1] were efficiently employed. The synthetic route of the hexapeptide (Arg-Gly-Pro-Pro-Phe-Ile) is shown in Fig. 1. *N*-(*t*-Butoxycarbonyl)phenylalanine was coupled with isoleucine benzyl ester by the mixed anhydride method to yield *N*-(*t*-butoxycarbonyl)phenylalanylisoleucine benzyl ester (**13**). After treatment of the protected dipeptide with hydrogen chloride, the dipeptide benzyl ester hydrochloride (**14**) and *N*-(*t*-butoxycarbonyl)prolylproline (**15**) were coupled by the mixed anhydride method to yield *N*-(*t*-butoxycarbonyl)prolylprolylphenylalanylisoleucine benzyl ester (**16**). The *t*-butoxycarbonyl group was removed from the protected tetrapeptide with hydrogen chloride and the resulting tetrapeptide benzyl ester hydrochloride (**17**) was acylated with N^a-benzyloxycarbonyl-N^G-nitroarginylglycine (**18**) by the dicyclohexylcarbodiimide method to yield N^a-benzyloxycarbonyl-N^G-nitroarginylglycylprolylprolylphenylalanylisoleucine benzyl ester (**19**). The protected hexapeptide was hydrogenated in the presence of palladium black to give the desired hexapeptide (H-Arg-Gly-Pro-Pro-Phe-Ile-OH) (**1**).

The synthetic route to compounds **2**, **3**, and **4**, compounds **6**, **7**, and **11**, and compounds **8**, **9**, and **10** are shown in Fig. 2, 3, and 4 respectively. However, the details of the synthetic route to those peptides is uneventful and is described in the experimental part. The purity of the synthetic peptides and their intermediates was confirmed by thin-layer examinations in two solvent systems and by elemental analyses.

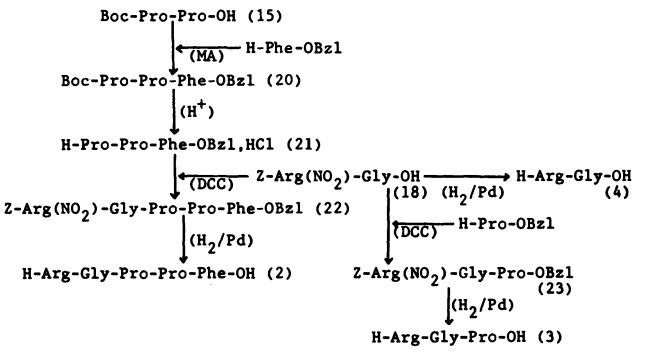

Fig. 2. The synthetic route of compound **2**, **3**, and **4**.

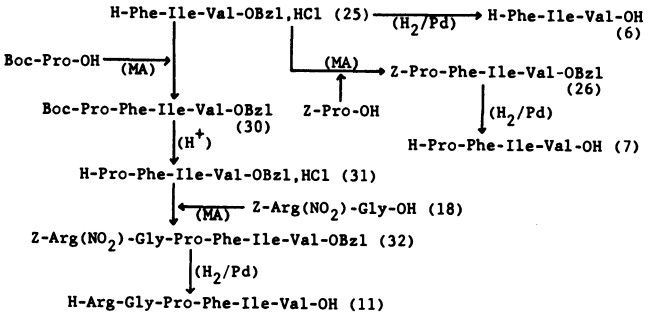

Fig. 3 The synthetic route of compounds **6**, **7**, and **11**.

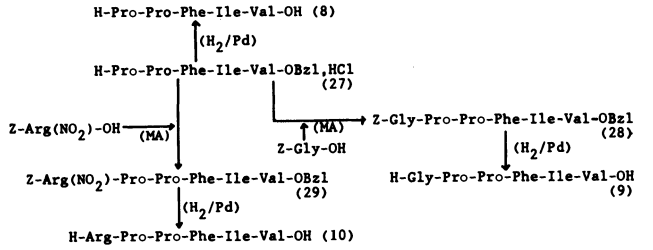

Fig. 4. The synthetic route of compounds **8**, **9**, and **10**.

The bitterness of the synthetic peptides were organoleptically determined by panel evaluation with five people (Table 1). As far as the N-terminal fragments of BPIa, compounds **2**—**4** exibited a weak bitter taste, but the hexapeptide (**1**) exhibited a strong bitter taste of the same level as BPIa. On the other hand, the C-terminal fragments of BPIa **5**—**9** that lack the arginine residue also exhibited a slightly bitter taste. These findings indicated that the L-arginine residue in the N-terminal and at least two hydrophobic amino acid residues in the C-terminal group are necessary for an intense bitter taste exhibition.

In order to confirm the participation of the strong bitter taste exhibition from the glycine residue at the 2-position and the L-proline residue at the 3-position, the bitterness of des-Gly^2-BPIa (**10**) and des-Pro^4-BPIa (**11**) were compared with that of BPIa. Both of these peptides exhibited a strong bitter taste of the same level as BPIa (Table 1). The results indicated that the glycine residue at the 2-position in BPIa is not always necessary, but the L-proline residue at the 3-position is necessary for an intense bitter taste exhibition.

Then, the authors measured circular dichroism (CD) and optical rotatory dispersion (ORD) of the synthetic peptides above mentioned. The CD curves of compounds **1** and **11** afforded a similar shape of BPIa, but those of compound **2** afforded a different shape from that of BPIa as shown in Fig. 5. The ORD curve of compound **10** afforded a similar shape to that of BPIa.[3)]

From the results described above, the strong bitter taste exhibition of BPIa is caused by its characteristic conformation. Furthermore, in this report, we will propose the following requirements for the strong bitter taste exhibition of BPIa; (a) at least six amino acid residues are necessary, (b) the proline residue at the 3-position must have the L-configuration and (c) the number of hydrophobic amino acid residues in the C-terminal is not important.

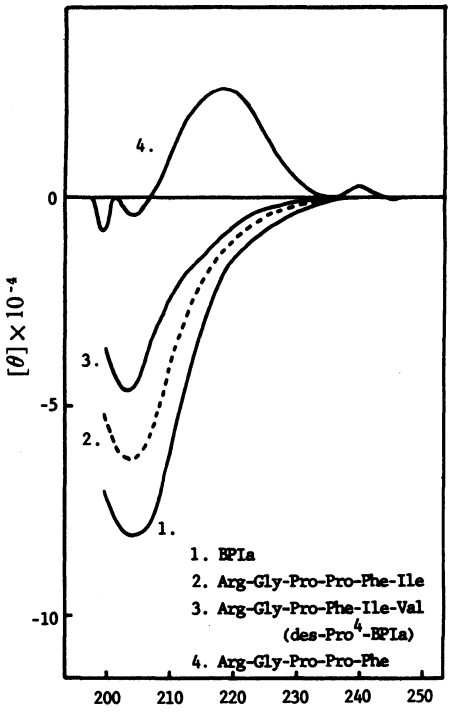

Fig. 5. CD curves of synthetic peptides in water.

Experimental

All the melting points are uncorrected. Thin-layer chromatography was carried out with Merck silica gel 60G. Developing solvents commonly used were (1) 1-butanol–acetic acid–pyridine–water (4 : 1 : 1 : 2, v/v) and (2) chloroform–methanol (5 : 1, v/v). Materials possessing a free amino group on a thin-layer plate were detected by spraying with ninhydrin. Compounds with blocked amino groups were detected by spraying with 25% hydrogen bromide in acetic acid and then with ninhydrin. The optical rotations were measured on an Union PM-101 polarimeter.

Boc–Phe–Ile–OBzl (13). To a solution of Boc–Phe–OH·DCHA[6)] (9.83 g, 22 mmol) in THF (20 ml), ECF (2.0 ml, 20 mmol) and NMM (2.2 ml, 20 mmol) were added at −5 °C. After 10 min, a solution of H–Ile–OBzl·TsOH[7)] (7.87 g, 20 mmol) and NMM(2.2 ml, 20 mmol) in chloroform (20 ml) was added. The reaction mixture was stirred in an ice bath for an hour, then at room temperature overnight. The mixture was evaporated *in vacuo*, and the oily residue was dissolved in ethyl acetate. The solution was washed with water, 4% citric acid, 4% sodium hydrogencarbonate, and water successively, then dried over anhydrous sodium sulfate. Sodium sulfate was removed by filtration, and the filtrate was evaporated *in vacuo*. The oily residue was crystallized with ether–petroleum ether: yield 9.04 g (96%); mp 87—88 °C $[\alpha]_D^{20}$ −18° (*c* 1, MeOH); R_f^1 0.99 and R_f^2 0.54. Found: C, 69.35; H, 7.69; N, 6.01%. Calcd for $C_{27}H_{36}O_5N_2$: C, 69.20; H, 7.74; N, 5.98%.

H–Phe–Ile–OBzl·HCl (14). To a solution of **13** (2.34 g, 5 mmol) in dioxane (10 ml), 4 M HCl(1 M=1 mol dm^{-3})/dioxane (20 ml) was added. The reaction mixture was allowed to stand at room temperature. After 2 h, the solution was evaporated *in vacuo*. The compound was obtained as an oily form: yield 1.86 g (92%); R_f^1 0.81 and R_f^2 0.68.

Boc–Pro–Pro–Phe–Ile–OBzl (16). Boc–Pro–Pro–OH[1)] (**15**) (1.56 g, 5 mmol) and **14** (1.86 g, 4.8 mmol) were coupled

by the same method as has been described for the preparation of **13** This compound was obtained as an oily form: yield 2.89 g (92%); R_f^1 0.97 and R_f^2 0.67.

H-Pro-Pro-Phe-Ile-OBzl·HCl (17). Compound **16** (2.89 g, 4.5 mmol) was treated as has been described in the case of **14**. This compound was obtained as an oily form: yield 2.50 g (88%); R_f^1 0.81 and R_f^2 0.59.

Z-Arg(NO$_2$)-Gly-Pro-Pro-Phe-Ile-OBzl (19). To a solution of Z-Arg(NO$_2$)-Gly-OH[1] (1.64 g, 4 mmol) in DMF (20 ml), DCC (0.81 g, 4 mmol) was added at 0 °C. After 10 min, to the mixture, a solution of **17** (2.50 g, 4 mmol) and NMM (0.44 ml, 4 mmol) in chloroform (20 ml) was added. The mixture was cooled at 0 °C for an hour and allowed to stand overnight at room temperature. The DCUrea was removed by filtration, and the filtrate was evaporated *in vacuo*. The oily residue was dissolved in ethyl acetate and the solution was washed with water, 2% hydrochloric acid, 4% sodium hydrogencarbonate, and water successively. The solution was dried over anhydrous sodium sulfate. Sodium sulfate was removed by filtration, and the filtrate was evaporated *in vacuo*. The residue was crystallized with ether-petroleum ether: yield 2.71 g (74%); mp 111—112 °C; $[\alpha]_D^{20}$ −87° (*c* 1, MeOH); R_f^1 0.91 and R_f^2 0.54. Found: C, 60.51; H, 6.53; N, 14.72%. Calcd for $C_{48}H_{62}O_{11}N_{10}$: C, 60.36; H, 6.56; N, 14.67%.

H-Arg-Gly-Pro-Pro-Phe-Ile-OH (1). A solution of **19** (1.24 g, 1.3 mmol) in methanol (2 ml) and acetic acid (2 ml) was hydrogenated in the presence of palladium black at room temperature for 72 h. The catalyst was removed by filtration, the filtrate was evaporated *in vauco*. The residue was crystallized with acetone: yield 0.72 g (74%) hygroscopic form; R_f^1 0.68 and R_f^2 0.00.

Boc-Pro-Pro-Phe-OBzl (20). Compound **15** (3.12 g, 10 mmol) and H-Phe-OBzl·TsOH[7] (4.28 g, 10 mmol) were coupled by the same method as has been described for the preparation of **13**: yield 5.22 g (95%) oily form; R_f^1 0.98 and R_f^2 0.78.

H-Pro-Pro-Phe-OBzl·HCl (21). Compound **20** (5.22 g, 9.5 mmol) was treated as has been described in the case of **14**: yield 4.25 g (92%); mp 84—86 °C; $[\alpha]_D^{20}$ −115.5° (*c* 1, H_2O); Found: C, 56.35; H, 6.01; N, 16.53%. Calcd for $C_{28}H_{35}O_8N_7$: C, 56.26; H, 5.91; N, 16.41%.

H-Arg-Gly-Pro-OH·HCl (3). Compound **23** (1.50 g, 2.50 mmol) was treated as has been described in the case of **1**: yield 0.43 g (66%) hygroscopic form; R_f^1 0.12.

H-Arg-Gly-OH·2AcOH (4). Z-Arg(NO$_2$)-Gly-OH (**19**) (1.00 g, 2 mmol) was treated as has been described in the case of **1**: yield 0.43 g (76%); $[\alpha]_D^{20}$ +36.7° (*c* 2, H_2O); R_f^1 0.21. Found: C, 42.35; H, 4.50; N, 20.36%. Calcd for $C_{16}H_{11}O_5N_5\cdot 2CH_3COOH$: C, 42.22; H, 4.44; N, 20.52%.

Z-Ile-Val-OH (24). To a solution of Z-Ile-OSu (3.60 g, 10 mmol) in dioxane (10 ml), a solution of H-Val-OH (1.32 g, 11 mmol), Et_3N (2.0 ml, 11 mmol) in water (15 ml) was added at room temperature. After 20 h, the mixture was evaporated *in vacuo*. The oily residue was dissolved in 8% sodium hydrogencarbonate and the solution washed with ether. The aqueous layer was acidified with 10% citric acid. The oily residue was extracted with ethyl acetate. The solution was dried over anhydrous sodium sulfate. Sodium sulfate was removed by filtration, and the filtrate was evaporated *in vacuo*. The oily residue was crystallized with ether: yield 2.86 g (81%); mp 133—134 °C; $[\alpha]_D^{20}$ +7.0° (*c* 1, DMF); R_f^1 0.87. Found: C, 62.36; H, 7.77; N, 7.62%. Calcd for $C_{19}H_{28}O_5N_2$: C, 62.62; H, 7.74; N, 7.69%.

H-Ile-Val-OH (5). Compound **24** (1.77 g, 5 mmol) was treated as has been described in the case of **1**: yield 1.02 g (89%); $[\alpha]_D^{20}$ +12.5° (*c* 1, H_2O); R_f^1 0.81. Found: C, 57.06; H, 9.76; N, 12.08%. Calcd for $C_{11}H_{22}O_3N_2$: C, 57.36; H, 9.63; N, 12.17%.

H-Phe-Ile-Val-OH (6). H-Phe-Ile-Val-OBzl·HCl[1] (**25**) (1.51 g, 3 mmol) was treated as has been described in the case of **1**; yield 0.91 g (80%); $[\alpha]_D^{20}$ +10.5° (*c* 0.5, H_2O); R_f^1 0.77. Found: C, 61.39; H, 8.19; N, 10.74%. Calcd for $C_{20}H_{31}O_4N_3\cdot 2/3\ H_2O$: C, 61.67; H, 8.37; N, 10.79%.

Z-Pro-Phe-Ile-Val-OBzl (26). Z-Pro-OH[10-12] (0.59 g, 2 mmol) and **25** (1.01 g, 2 mmol) were coupled by the same method as has been described for the preparation of **13**: yield 1.15 g (85%); mp 196 °C; $[\alpha]_D^{20}$ −57.1° (*c* 1, $CHCl_3$); R_f^1 0.99. Found: C, 67.97; H, 7.32; N, 7.98%. Calcd for $C_{40}H_{50}O_7N_4\cdot 1/2\ H_2O$: C, 67.87; H, 7.12; N, 7.92%.

H-Pro-Phe-Ile-Val-OH (7). Compound **26** (0.91 g, 1.3 mmol) was treated as has been described in the case of **1**: yield 0.54 g (88%); $[\alpha]_D^{20}$ −51.7° (*c* 0.5, H_2O); R_f^1 0.70. Found: C, 57.41; H, 7.84; N, 10.48%. Calcd for $C_{25}H_{38}O_5N_4\cdot 1/2\ CH_3COOH\cdot 2H_2O$: C, 57.76; H, 8.20; N, 10.36%.

H-Pro-Pro-Phe-Ile-Val-OH (8). H-Pro-Pro-Phe-Ile-Val-OBzl·HCl[1] (0.69 g, 1 mmol) was treated as has been described in the case of **1**: yield 0.47 g (82%); mp 182 °C; $[\alpha]_D^{20}$ −122.0° (*c* 0.7, H_2O); R_f^1 0.61. Found: C, 60.54; H, 7.90; N, 11.14%. Calcd for $C_{30}H_{45}O_6N_5\cdot CH_3COOH$: C, 60.82; H, 7.83; N, 11.09%.

Z-Gly-Pro-Pro-Phe-Ile-Val-OBzl (28). Z-Gly-OH[13-15] (0.32 g, 1.5 mmol) and H-Pro-Pro-Phe-Ile-Val-OBzl·HCl (**27**) (0.90 g, 1.3 mmol) were coupled by the same method as has been described for the preparation of **13**: yield 1.02 g (93%); mp 78—82 °C; $[\alpha]_D^{20}$ −54.0° (*c* 1, DMF); R_f^1 0.93 and R_f^2 0.66. Found: C, 65.55: H, 7.13: N, 9.62%. Calcd for $C_{47}H_{60}O_9N_6\cdot 1/2H_2O$: C, 65.80; H, 7.17; N, 9.80%.

H-Gly-Pro-Pro-Phe-Ile-Val-OH (9). Compound **28** (0.80 g, 0.94 mmol) was treated as has been described in the case of **1**: yield 0.46 g (77%): $[\alpha]_D^{20}$ −133.5° (*c* 1, H_2O); R_f^1 0.75. Found: C, 57.53; H, 7.68; N, 12.31%. Calcd for $C_{32}H_{48}O_7N_6\cdot 2H_2O$: C, 57.81; H, 7.88; N, 12.64%.

Z-Arg(NO$_2$)-Pro-Pro-Phe-Ile-Val-OBzl (29). Z-Arg(NO$_2$)-OH[16,17] (0.54 g, 1.5 mmol) and **27** (1.04 g, 1.5 mmol) were coupled by the same method as has been described for the preparation of **13**: yield 1.06 g (73%); mp 104—107 °C; $[\alpha]_D^{20}$ −60.2° (*c* 0.6, EtOH); R_f^1 0.96. Found: C, 61.00; H, 6.89; N, 13.44%. Calcd for $C_{50}H_{68}O_{10}N_{10}\cdot H_2O$: C, 60.83; H, 7.15; N, 13.19%.

H-Arg-Pro-Pro-Phe-Ile-Val-OH·2AcOH (10). Compound **29** (0.76 g, 0.8 mmol) was treated as has been described in the case of **1**: yield 0.60 g (95%); mp 139—141 °C; $[\alpha]_D^{20}$ −114.0° (*c* 1, H_2O); R_f^1 0.66. Found: C, 54.34; H, 7.48; N, 14.43%. Calcd for $C_{36}H_{57}O_7N_9\cdot 2CH_3COOH\cdot 2H_2O$: C, 54.34; H, 7.87; N, 14.25%.

Boc-Pro-Phe-Ile-Val-OBzl (30). Boc-Pro-OH[19,20] (2.15 g, 10 mmol) and **25** (5.04 g, 10 mmol) were coupled by the same method as has been described for the preparation of **13**: yield 6.06 g (91%); mp 111—112 °C; $[\alpha]_D^{20}$ −83° (*c* 1, MeOH); R_f^1 0.98 and R_f^2 0.88. Found: C, 67.01; H, 7.92; N, 8.39%. Calcd for $C_{37}H_{52}O_7N_4$: C, 66.84; H, 7.88; N, 8.43%.

H-Pro-Phe-Ile-Val-OBzl·HCl (31). Compound **30** (1.99 g, 3 mmol) was treated as has been described in the case of **14**: yield 1.71 g (95%); mp 90 °C (decomp); $[\alpha]_D^{20}$ −66° (*c* 1, MeOH); R_f^1 0.88 and R_f^2 0.61. Found: C, 63.99; H, 7.29; N, 9.36%. Calcd for $C_{32}H_{44}O_5N_4\cdot HCl$: C, 63.93; H, 7.38; N, 9.32%.

Z-Arg(NO$_2$)-Gly-Pro-Phe-Ile-Val-OBzl (32). Z-Arg-(NO$_2$)-Gly-OH (**21**) (0.41 g, 1 mmol) and **31** (0.60 g, 1 mmol) were coupled by the same method as has been described for the preparation of **13**: yield 0.72 g (75%); mp 175—180 °C; $[\alpha]_D^{20}$ −24° (*c* 1, DMF); R_f^1 0.88 and R_f^2 0.74. Found: C,

60.12; H, 6.74; N, 14.52%. Calcd for $C_{48}H_{64}O_{11}N_{10}$: C, 60.23; H, 6.74; N, 14.64%.

H–Arg–Gly–Pro–Phe–Ile–Val–OH (11). Compound **32** (0.50 g, 0.52 mmol) was treated as has been described in the case of 1: yield 0.27 g (69%); $[\alpha]_D^{20}$ −114° (*c* 1, H_2O); R_f^1 0.74 and R_f^2 0.00. Found: C, 55.21; H, 7.95; N, 16.81%. Calcd for $C_{33}H_{53}O_7N_9 \cdot CH_3COOH \cdot 1/2\ H_2O$: C, 55.53; H, 7.72; N, 16.66%.

We would like to acknowledge helpful discussion with Professor Sakuzo Fukui of Hiroshima University. We also wish to thank Associate Professor Michio Kondo of Saga University for the CD measurement and Dr. Shinji Okumura of Ajinomoto Co. Inc., for supplying some amino acids.

References

1) Part I. H. Fukui, H. Kanehisa, N. Ishibashi, I. Miyake, and H. Okai, *Bull. Chem. Soc. Jpn.*, **56**, 766 (1983).

2) The abbreviations recommended by the IUPAC-IUB commission of Biochemical Nomenclature (*J. Biol. Chem.*, **247**, 977 (1972)) have been used. Amino acid symbols except glycine denote the L-configuration. Additional abbreviations: AcOH, acetic acid; DCC, dicyclohexylcarbodiimide; DCUrea, *N,N'*-dicyclohexylurea; DMF, *N,N*-dimethylformamide; ECF, ethyl chloroformate; EtOH, ethanol; Et_3N, triethylamine; MA, mixed anhydride; MeOH, methanol; NMM, *N*-methylmorpholine; TsOH, *p*-toluenesulfonic acid; THF, tetrahydrofuran.

3) H. Okai, "Peptide Chemistry 1976," ed by T. Nakajima, Protein Research Foundation, Osaka (1977), p. 139.

4) K. Otagiri, I. Miyake, K. Kouge, T. Shigenaga, H. Fukui, H. Kanehisa, and H. Okai, "Peptide Chemistry 1981," ed by T. Shioiri, Protein Research Foundation, Osaka (1982), p. 75.

5) N. Minamiura, Y. Matsumura, J. Fukumoto, and T. Yamamoto, *Agric. Biol. Chem.*, **36**, 588 (1972).

6) M. Fujino and C. Hatanaka, *Chem. Pharm. Bull.* (Tokyo), **15**, 2015 (1967).

7) L. Zervas, M. Winitz, and J. P. Greenstein, *J. Org. Chem.*, **749**, 90 (1971).

8) R. E. Newman and E. L. Smith, *J. Biol. Chem.*, **193**, 97 (1951).

9) J. Ramachandran and C. H. Li, *J. Org. Chem.*, **28**, 173 (1963).

10) W. Grassmann and E. Wünsch, *Chem. Ber.*, **91**, 462 (1958).

11) E. Schröder, *Ann. Chem.*, **692**, 241 (1966).

12) A. Berger, J. Kutz, and E. Katchalski, *J. Am. Chem. Soc.*, **76**, 5552 (1954).

13) M. Bergmann, L. Zervas, *Chem. Ber.*, **65**, 1192 (1932).

14) D. F. Detar, R. Silverstein, and F. F. Rogers, Jr., *J. Am. Chem. Soc.*, **88**, 1024 (1966).

15) F. H. C. Stewart, *Aust. J. Chem.*, **18**, 1699 (1965).

16) H. Gibian and E. Schröder, *Ann. Chem.*, **642**, 145 (1961).

17) K. Hofmann, W. D. Peckham, and A. Rheiner, *J. Am. Chem. Soc.*, **78**, 238 (1956).

18) G. W. Anderson and A. C. McGregor, *J. Am. Chem. Soc.*, **79**, 6180 (1957).

19) E. Bayer, G. Jung, and H. Hagenmaier, *Tetrahedron*, **24**, 4853 (1968).

Sesquiterpenoid Constituents of the Liverwort *Frullania brotheri* STEPH.

Reiji TAKEDA,* Yoshimoto OHTA, and Yoshio Hirose
Suntory Institute for Bioorganic Research, Wakayama-dai, Shimamoto-cho, Mishima-gun, Osaka 618
(Received August 26, 1982)

Two new sesquiterpene lactones, (+)-β-frullanolide and (+)-brothenolide, have been isolated from the liverwort *Frullania brotheri* STEPH. One of them, (+)-brothenolide, has an allergenic property. The absolute structures of these lactones have been established by spectroscopic analysis and chemical transformation.

It is well-known that a number of sesquiterpene lactones have been isolated from the liverwort belonging to Frullaniacea and that some of them have an allergenic property.[1] In the course of our investigation on terpene constituents of the liverwort, we examined the constituents of *Frullania brotheri* STEPH. collected in Wakayama Prefecture around Mt. Ohto in June 1976 and isolated two new sesquiterpene lactones, (+)-β-frullanolide (**1**) and (+)-brothenolide (**2**), one of which, **2**, had an allergenic property. This paper deals in detail with the structural determination of (+)-β-frullanolide and (+)-brothenolide.[2]

Column chromatographic separation on SiO_2 and $AgNO_3$-SiO_2 of the ether extract of the fresh material gave lactones **1** and **2**. (+)-β-Frullanolide (**1**), mp 165—167 °C, $[\alpha]_D$ +178°, was obtained as colorless needles. The molecular formula $C_{15}H_{20}O_2$ of **1** was determined by the appearence of a molecular ion peak at 232.1453 in the high resolution mass spectrum (HR-MS). The IR spectrum ($CHCl_3$) showed an α,β-unsaturated γ-lactone absorption bands at 1760 and 1670 cm^{-1} and an exocyclic methylene absorption band at 910 cm^{-1}. The ^1H NMR spectrum ($CDCl_3$) indicated the presence of one tertiary methyl group (δ 0.92), four exocyclic methylene protons (δ 4.92, 5.09, 5.52, and 6.07) and one methine proton (δ 4.58) adjacent to oxygen. In the decoupling experiments of **1**, irradiation at δ 5.09 (14-H_B) collapsed the proton of 5-H at δ 2.01 and the allylic methylene protons (3-$H_{A,B}$) at δ 2.1—2.5 to sharp peaks, respectively. Also irradiation of 6-H at δ 4.56 collapsed a doublet of 5-H to a singlet and collapsed a multiplet of 7-H to sharp peaks. Furthermore, irradiation at δ 2.88 (7-H) converted a pair of doublets at δ 5.52 and 6.07 due to exocyclic methylene protons (13-$H_{A,B}$) into a pair of singlets and doublet of doublets at δ 4.58 (6-H) into a doublet. These results indicated that β-frullanolide (**1**) had the partial structure **1a**. When the ^1H NMR spectrum of **1** was compared with those of eudesmanolides,[3] it was similar to them. From these results, we assumed that lactone **1** had an eudesmanolide skeleton, as shown by structure **1**. This assumption was confirmed by a partial synthesis from costunolide (**3**)[4] according to the following pathway (Chart 1).

Costunolide (**3**), isolated from costus root oil, was cyclized with thionyl chloride to give the cyclocostunolide mixture[5] from which β-cyclocostunolide **4** was separated by column chromatography on 10% $AgNO_3$-SiO_2. This compound was identified as β-cyclocostunolide **4** with authentic spectra.[5] Next, this compound was converted to **5** by ethanolysis with Na_2CO_3 in ethanol. The IR spectrum showed hydroxyl and ester

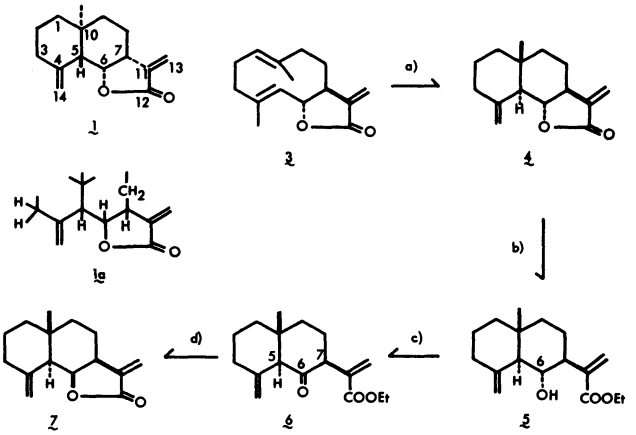

Chart 1. $SOCl_2$/pyridine, b) Na_2CO_3/EtOH, c) Jones reagent, d) $NaBH_4$/MeOH.

absorption bands at 3460 and 1715 cm^{-1}. In the ^1H NMR spectrum, the signals due to an ethyl group as the ester function at δ 1.30 and 4.23 were observed. The alcohol thus obtained was oxidized with Jones reagent to give keto ester **6**. The IR spectrum showed bands at 1718 cm^{-1} due to carbonyl groups and at 910 cm^{-1} due to an exocyclic methylene. In the ^1H NMR spectrum of **6**, the signals of 5-H and 7-H were observed at lower field (5-H: δ 3.08, s; 7-H: 3.67, t, J=10.0 Hz) than those of **5** (5-H: δ 1.90, d, J=11.0 Hz; 7-H: 2.60, dt, J=6.0 and 11.0 Hz). These results and the absence of a hydroxyl absorption in the IR and the signal of 6-H in the ^1H NMR of **6** indicated that hydroxyl group at C-6 was oxidized to keto group. Reduction of keto ester **6** with $NaBH_4$ in methanol gave a *cis* lactone **7**: $[\alpha]_D$ −161.8°.

Compound **7** was identified in every respect with (+)-β-frullanolide except for chiroptical property, CD (MeOH) $\Delta\varepsilon_{254}$+1.5 for **7** *vs.* $\Delta\varepsilon_{254}$−1.5 for **1** (Fig. 1). (+)-β-Frullanolide is fully represented by structure **1**.

(+)-Brothenolide (**2**), mp 113—114 °C, $[\alpha]_D$ +153.0°, CD (MeOH) $\Delta\varepsilon_{255}$−1.6, was obtained as colorless needles. The molecular formula $C_{15}H_{20}O_2$ of **2** was determined by HR-MS together with the ^{13}C and ^1H NMR data. The IR spectrum ($CHCl_3$) showed bands at 3040 cm^{-1} due to a cyclopropane ring, and at 1760 and 1660 cm^{-1} due to an α,β-unsaturated γ-lactone. The ^1H NMR spectrum ($CDCl_3$) showed the signals of two tertiary methyl groups (δ 1.11, s and 1.36, s), one proton on the cyclopropane ring (δ 0.38, t, J=3.6 Hz), two olefinic protons (δ 5.52, d, J=0.6 and 6.09, d, J=0.6 Hz), one allylic methine (δ 2.72, m) and one methine proton (δ 4.76, dd, J=3.0 and 4.8 Hz) adjacent to oxygen. The ^{13}C NMR spectrum ($CDCl_3$)

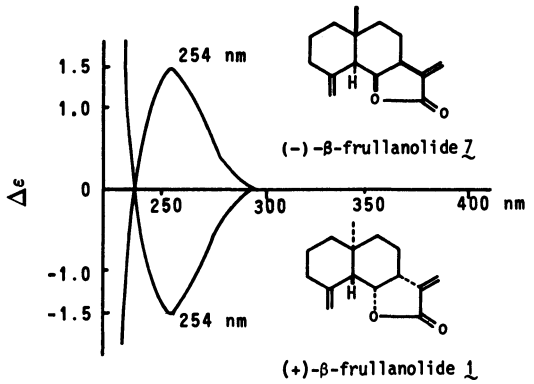

Fig. 1. CD spectra of (+)- and (−)-β-frullanolide.

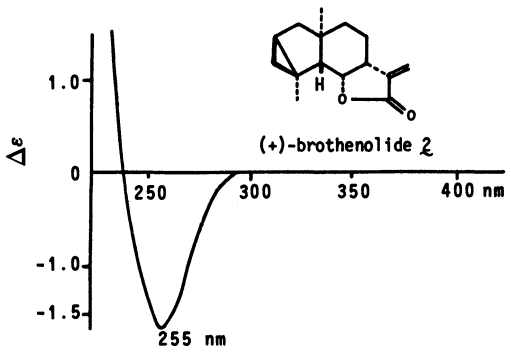

Fig. 2. CD spectrum of (+)-brothenolide.

also indicated the signals of α,β-unsaturated γ-lactone: C=O, δ 171.3; C-, 141.8; $=CH_2$, 119.5 and -O-CH, 77.8.

Hydrogenation of **2** with Pd/C in EtOH yielded a dihydro compound **8** (*m/z* 234). The ^1H NMR spectrum indicated the signal of a secondary methyl group at δ 1.06 instead of the protons of the exocyclic methylene in the spectrum of **2**. This compound was further reduced[6] with PtO_2 in EtOH-AcOH to give a tetrahydro compound **9** (*m/z* 236, $C_{15}H_{24}O_2$). The IR spectrum indicated the absence of a cyclopropane ring absorption and the presence of *gem*-dimethyl absorption bands at 1380 and 1370 cm^{-1}. In the ^1H NMR spectrum, a signal of a tertiary methyl group was observed in place of the protons on the cyclopropane ring. This fact showed that one of the two methyl groups in **2** should be attached to the cyclopropane ring. The presence of the partial structure **2a** was indicated by the above result, and the results of double irradiation experiments in the ^1H NMR spectrum of **2** with the aid of shift reagent. The signal of the proton at 7-H appeared as a multiplet which collapsed to a broad doublet of doublets (J=7.0 and 10.2 Hz) on irradiation of 6-H. In addition, irradiation of the signal of 6-H converted the doublet of 5-H into a singlet. The fact that 7-H is coupled to the 8α- and 8β-H's with J=7.0 and 10.2 Hz indicated that it is axial. Thus the $J_{6,7}$ value of 4.8 Hz shows that 6-H is equatorial. Therefore, the γ-lactone ring must be *cis*-fused at C-6 and C-7. The reduction of **9** with LAH afforded a diol **10**, the IR spectrum of which showed the presence of hydroxyl groups at 3500 and 3430 cm^{-1}. The ^1H NMR spectrum showed the signals of methylene protons adjacent to oxygen as primary alcohol at δ 3.44 and 3.56. The diol **10** was acetylated with acetic anhydride and pyridine at room temperature to give monoacetate **11**, the IR spectrum of which showed bands at 3510 and 1720 cm^{-1} due to the hydroxyl group and the carbonyl group, respectively. The ^1H NMR spectrum showed also the signals of the acetoxymethyl group at δ 2.06 and the $-C\underline{H}_2-OAc$ group at δ 3.94 and 4.24. The monoacetate **11** was oxidized with Jones reagent to yield a corresponding keto compound **12**. The IR spectrum indicated the presence of a 6-membered ring ketone at 1715 cm^{-1}. Furthermore, in the decoupling experiments of **2** using 360 MHz NMR, irradiation of 1-H_A at δ 0.83 collapsed the doublet of doublets of 1-H_B (δ 1.77) to a doublet, and a multiplet of 2-H (δ 1.22) to a sharp peak. In addition, irradiation of 3-H_A (δ 0.38) collapsed the doublet of doublets of 3-H_B (δ 0.93) to a doublet, and 2-H (δ 1.22) to sharp peak. This result indicated that brothenolide (**2**) had a partial structure **2b**. All these data show that the new sesquiterpene lactone **2** is most favorably represented by formula **2**. The fact that the CD Cotton effects of lactones **1** and **2** have the same signs (Figs. 1 and 2) shows that they belong to the same chiroptical series.[7]

Table 1. Chemical shift of the methyl groups (in δ)

	4-CH_3	4-CH_2D	10-CH_3
11-d_2	1.20	1.17	1.03
12-d_2	1.34	1.07	0.91

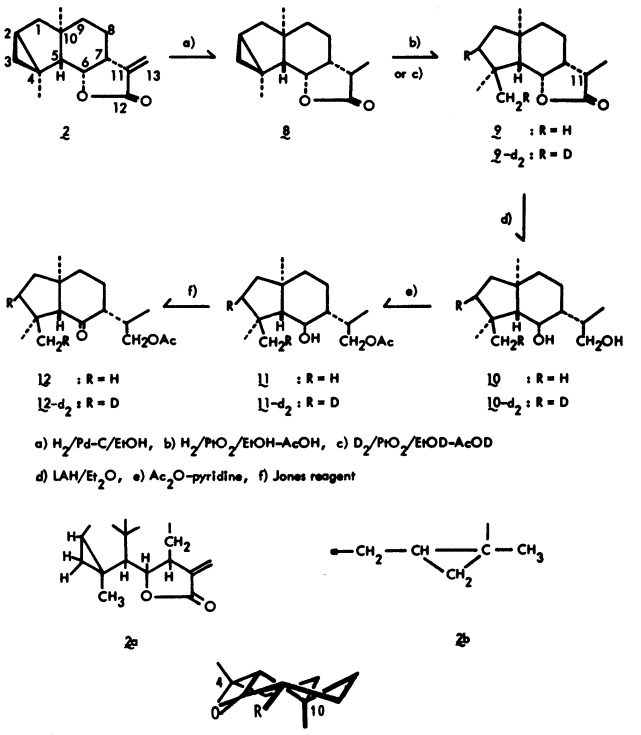

Chart 2.

The β-configuration of the cyclopropane ring was determined as follows. Reduction of dihydrobrothenolide **8** with deuterium instead of hydrogen (see above) in EtOD-AcOD, followed by LAH treatment and acetylation gave **11**-d_2 (the dideuterio derivative of **11**).

The ^1H NMR spectrum of **11** showed three tertiary methyl signals at δ 1.17, 1.20, and 1.03, one of which, at δ 1.17, appeared as a CH_2D signal in **11**-d_2. Oxidation of **11**-d_2 with Jones reagent gave **12**-d_2, the ^1H NMR spectrum of which showed the signals of two tertiary methyl groups at δ 1.34 and 0.91, and a tertiary CH_2D group at δ 1.07. The chemical shifts of CH_3 and CH_2D groups of **11**-d_2 and **12**-d_2 are shown in Table 1. One methyl peak at δ 1.20 in **11**-d_2 underwent a low field shift to δ 1.34 in **12**-d_2 whereas the other methyl peaks at δ 1.17 and 1.03 in **11**-d_2 shifted to δ 1.07 and 0.91 in **12**-d_2. These shifts of methyl peaks were explained by the difference of anisotropic effects between 6α-OH and 6-keto function. The methyl signals at δ 1.17, 1.20, and 1.03 in **11**-d_2 were therefore assigned to 4β-Me, 4α-Me, and 10-Me groups, respectively.

Molecular model **12a** clearly shows that 4-Me group (δ 1.34) should have the α-configuration since it is in-plane in relation to the carbonyl group. The CH_2D group in **11**-d_2 is thus β-oriented, and therefore, the cyclopropane methylene group is also β-oriented in brothenolide (**2**).

Experimental

All melting points are uncorrected. IR spectra were measured with a Hitachi EPI-G2 spectrometer, ^{13}C NMR spectra with a JEOL FX-100 (25.0 Hz) spectrometer, ^1H NMR spectra with a JEOL FX-100 (100 MHz), a Nicolet NT-360 (360 MHz), or a Hitachi R-20B (60 MHz) spectrometer in deuteriochloroform solution containing tetramethylsilane as an internal standard, low resolution mass spectra with a Hitachi RMU-6 mass spectrometer and high resolution mass spectra with a JEOL-JMS 01SG-2, with direct inlet system operating at 70 eV. CD spectra were measured with a JASCO J-20 spectrometer. For column chromatography Kieselgel 60 (E. Merck, Darmstadt) was used. Thin-layer chromatography (TLC) was carried out on Kieselgel GF_{254} (E. Merck, Darmstadt) in 0.25 mm thickness.

Isolation. The fresh material (100 g) of *Frullania brotheri* Steph. collected in Wakayama Prefecture around Mt. Ohto in June 1976 was extracted with ether at room temperature. The ether extract (1.8 g) was chromatographed on SiO_2. Elution with $CHCl_3$ gave a lactone mixture that was subjected to further column chromatography on SiO_2 impregnated with 10% $AgNO_3$. Elution with hexane–Et_2O (20 : 1) yield a fraction of (+)-brothenolide. Next, elution with ether gave crude (+)-β-frullanolide.

(+)-β-Frullanolide (1). The crude material was recrystallized from hexane–EtOAc to yield colorless needles (**1**, 40 mg), mp 165—167 °C, $[\alpha]_D$ +178.0° (*c* 1.17, $CHCl_3$); CD, $\Delta\varepsilon_{254}$ −1.5 (*c* 0.012, MeOH); IR ($CHCl_3$) 1760, 1670, and 910 cm^{-1}; ^1H NMR δ 0.92 (3H, s, 10-CH_3), 4.58(1H, dd, J=4.5 and 3.0 Hz, 6-H), 4.92 (1H, br. s, 14-H_A), 5.09 (1H, br. s, 14-H_B), 5.52 (1H, d, J=0.6 Hz, 13-H_A), and 6.07 (1H, d, J=0.6 Hz, 13-H_B); ^{13}C NMR δ 18.3 (q), 23.0 (t), 24.6 (t), 34.7 (t), 37.5 (t), 38.8 (t), 41.4 (d), 43.0 (t), 50.9 (d), 77.8 (d), 109.7 (t), 119.0 (t), 141.7 (s), 145.7 (s) and 170.8 (s); MS *m/z* (%) 232 (93, M^+), 217 [100, $(M-CH_3)^+$], 176 (35), 171 (34), 91 (46), and 79 (37). Found: *m/z* 232.1453. Calcd for $C_{15}H_{20}O_2$: M, 232.1445.

Isolation of (+)-Brothenolide (2). The crude fraction was recrystallized from hexane–EtOAc to give colorless needles (**2**, 270 mg), mp 113—114 °C, $[\alpha]_D$ +153.0° (*c* 1.14, $CHCl_3$); CD, $\Delta\varepsilon_{255}$ −1.6 (*c* 0.012, MeOH); IR ($CHCl_3$) 3040, 1760, 1660 cm^{-1}; ^1H NMR (360 MHz) δ 0.38 (1H, t, J=3.6 Hz, 3-H_A), 0.83 (1H, br. dd, J=3.6 and 12.5 Hz, 1-H_A), 0.93 (1H, dd, J=3.6 and 8.7 Hz, 3-H_B), 1.06 (1H, d, J=3.0 Hz, 5-H), 1.11 (3H, s, 10-CH_3), 1.22 (1H, m, 2-H), 1.22 (1H, m, 9-H_B), 1.36 (3H, s, 4-CH_3), 1.47 (1H, m, 8-H_A), 1.60 (1H, ddd, J= 3.0, 4.2, and 12.6 Hz, 9-H_B), 1.72 (1H, dd, J=7.5 and 12.5 Hz, 1-H_B), 2.72 (1H, m, 7-H), 4.76 (1H, dd, J=3.0 and 4.8 Hz, 6-H), 5.52 (1H, d, J=0.6 Hz, 13-H_A), and 6.09 (1H, d, J=0.6 Hz, 13-H_B); ^{13}C NMR δ 20.4 (q), 20.9 (q), 25.5 (t), 25.9 (d), 26.6 (s), 34.1 (t), 35.7 (t), 40.5 (d), 46.3 (t), 50.4 (s), 56.5 (d), 77.8 (d), 119.5 (t), 141.8 (s), and 171.3 (s); MS *m/z* (%) 232 (8, M^+), 217 [100, $(M-CH_3)^+$], 199 (39), 171 (44), 145 (31), 119 (45), 91 (41), and 79 (28). Found: *m/z* 232.1472. Calcd for $C_{15}H_{20}O_2$: M, 232.1445.

Isolation of Costunolide (3). Costus root oil (3 g) was chromatographed on SiO_2, and eluted with $CHCl_3$ to give costunolide (**3**, 270 mg), colorless needles, mp 104—105 °C (recrystallized from hexane), $[\alpha]_D$ +127.0° (*c* 1.05, $CHCl_3$). The IR, NMR, and mass spectra, and $[\alpha]_D$ value of **3** were found to be identical with those of known (+)-costunolide.[4]

Cyclization of Costunolide (3). A solution of costunolide (270 mg) in $CHCl_3$ (50 ml) containing $SOCl_2$ (0.1 ml) was kept at room temperature for 1 h. After removal of solvent under vacuum, the resulting residue was chromatographed on 10% $AgNO_3$–SiO_2. Elution with hexane–EtOAc (5 : 1) gave β-cyclocostunolide (160 mg), colorless needles, mp 67—68 °C (recrystallized from EtOH), $[\alpha]_D$ +175.3° (*c* 0.93, $CHCl_3$). The IR, NMR, and mass spectra, and $[\alpha]_D$ value were identical with those of known (+)-β-cyclocostunolide.[5]

Ethanolysis of β-Cyclocostunolide (4). 0.05 M (1 M=1 mol dm^{-3}) Na_2CO_3 aqueous solution (0.2 ml) was added to a solution of β-cyclocostunolide (150 mg) in EtOH (10 ml), and the mixture was kept at room temperature for 2 d. The reaction mixture was diluted with H_2O, evaporated to remove EtOH under reduced pressure and extracted with ether. Ether layer was washed with H_2O and dried over Na_2SO_4. After removal of solvent under reduced pressure, the resulting residue was chromatographed on SiO_2. Elution with $CHCl_3$ gave hydroxy ester **6**, colorless needles, mp 95—96 °C (recrystallized from hexane), $[\alpha]_D^{20}$ +25.2° (*c* 0.92, $CHCl_3$); IR ($CHCl_3$) 3460 and 1715 cm^{-1}; ^1H NMR δ 0.83 (3H, s, 10-CH_3), 1.30 (3H, t, J=8.0 Hz, $OCH_2C\underline{H}_3$), 1.90 (1H, d, J=11.0 Hz, 5-H), 2.60 (1H, dt, J=6.0 and 11.0 Hz, 7-H), 3.92 (1H, t, J= 11.0 Hz, 6-H), 4.23 (2H, q, J=8.0 Hz, $OC\underline{H}_2CH_3$), 4.68 (1H, br. s, 14-H_A), 4.96 (1H, br. s, 14-H_B), 5.69 (1H, br. s, 13-H_A), and 6.27 (1H, br. s, 13-H_B); MS *m/e* (%) 278 (trace, M^+), 232 [53, $(M-EtOH)]^+$], 217 (33), 123 (61), and 81 (100). Found: *m/z* 278.1864. Calcd for $C_{17}H_{26}O_3$: 278.1869.

Oxidation of 5 with Jones Reagent. A few drops of Jones reagent were added slowly to a stirred solution of **5** (80 mg) in acetone (10 ml) at 0 °C, and the mixture was further stirred for 2 d at room temperature. The reaction mixture was treated in the usual way to give a residue which was chromatographed on SiO_2. Elution with $CHCl_3$ gave keto compound **6**, colorless needles, mp 64 °C (recrystallized from hexane), $[\alpha]_D^{22}$ +10.6° (*c* 1.0, $CHCl_3$); IR ($CHCl_3$) 1718, 1640, and 910 cm^{-1}; ^1H NMR δ 0.83 (3H, s, 10-CH_3), 1.27 (3H, t, J=8.0 Hz, $OCH_2C\underline{H}_3$), 3.08 (1H, s, 5-H), 3.63 (1H, t, J=10.0 Hz, 7-H), 4.18 (1H, q, J=8.0 Hz, $OC\underline{H}_2CH_3$), 4.98 (1H, br. s, 14-H_A), 5.54 (1H, br. s, 13-H_A), 5.88 (1H, br. s, 14-H_B), and 6.32 (1H, br. s, 13-H_B); MS *m/z* (%) 276 (55, M^+), 230 [92, $(M-EtOH)^+$], 175 (89), 135 (100), and 107 (97). Found: *m/z* 276.1714. Calcd for $C_{17}H_{24}O_3$: M, 276.1706.

Reduction of 6 with $NaBH_4$. After $NaBH_4$ (4.4 mg) was added to an ice-cooled solution of **6** (26 mg) in MeOH (0.3 ml), the mixture was stirred at room temperature for 2 h. The

reaction mixture was diluted with H_2O and extracted with CH_2Cl_2. The CH_2Cl_2 layer was treated in the usual way to give a residue (20 mg) which was chromatographed on TLC (solvent system; hexane–EtOAc=10 : 1). Colorless needles (**7**, 8 mg) were obtained by recrystallization from hexane–EtOAc, mp 164—165 °C, $[\alpha]_D$ −161.8° (*c* 0.64, $CHCl_3$); CD, $\Delta\varepsilon_{254}$ +1.5 (*c* 0.012, MeOH). Found: *m/z* 232.1449. Calcd for $C_{15}H_{20}O_2$: M, 232.1445. The IR, NMR and mass spectra were found to be identical with those of (+)-β-frullanolide (**1**).

Hydrogenation of Brothenolide (2). Lactone **2** (25 mg) and palladium charcoal (10 mg) in EtOH (2 ml) were stirred under hydrogen atmosphere at room temperature for 3 h. The catalyst was removed by filtration and the solvent was evaporated to give a residue (25 mg), which was purified by recrystallization from hexane (**8**, 18 mg). Colorless needles, mp 105—106 °C; IR ($CHCl_3$) 3040 and 1770 cm^{-1}; ^1H NMR δ 0.32 (1H, t, *J*=3.6 Hz, 3-H_A), 1.06 (3H, d, *J*=7.0 Hz, 11-CH_3), 1.18 (3H, s, 10-CH_3), 1.36 (3H, s, 4-CH_3), and 4.53 (1H, dd, *J*=3.0 and 4.8 Hz, 6-H); MS *m/z* (%) 234 (7, M^+), 219 [100, $(M-CH_3)^+$], 161 (57), 145 (71), and 107 (45). Found: *m/z* 234.1613. Calcd for $C_{15}H_{22}O_2$: M, 234.1608.

Hydrogenation of Dihydro Lactone (8). Dihydro lactone **8** (20 mg) and platinum catalyst (prepared from platinum oxide; 10 mg) in EtOH (1.5 ml) and AcOH) (0.3 ml) were stirred under hydrogen atmosphere at room temperature for 8 h. The reaction mixture was filtered and the filtrate was evaporated under reduced pressure to give a residue (21 mg). Tetrahydro lactone **9** was obtained by recrystallization from hexane, (**9**, 15 mg), colorless needles, mp 138—140°C; IR (CCl_4) 1780, 1380, and 1370 cm^{-1}; ^1H NMR δ 1.04 (3H, s), 1.07 (3H, s), 1.17 (3H, s), 1.20 (3H, d, *J*=6.6 Hz, 11-CH_3), and 4.52 (1H, dd, *J*=3.0 and 4.8 Hz, 6-H); MS *m/z* (%) 236 (1.5, M^+), 221 [16, $(M-CH_3)^+$], 177 (43), 147 (62), 123 (40 , 109 (100), and 107 (69). Found: *m/z* 236.1762. Calcd for $C_{15}H_{24}O_2$: M, 236.1751.

Reduction of Tetrahydro Lactone (9) with Lithium Aluminium Hydride. After a solution of LAH (10 mg) in dry Et_2O (2 ml) was added to an ice-cooled solution of tetrahydro lactone **9** (12 mg) in dry ether (2 ml), the mixture was kept at room temperature for 3 h. The reaction mixture was treated in the usual way to give a residue (15 mg) which was chromatographed on SiO_2. Elution with $CHCl_3$–MeOH (15 : 1) gave a diol compound (**10**, 10 mg), colorless viscous oil, IR (film) 3500, 3430, and 1045 cm^{-1}; ^1H NMR δ 0.98 (3H, d, *J*=7.0 Hz, 11-CH_3), 1.02 (3H, s), 1.19 (6H, s), 3.44 (1H, dd, *J*=5.0 and 12.0 Hz, $\underline{H}_A$CH-OH), 3.56 (1H, dd, *J*=6.5 and 12.0 Hz, HC$\underline{H}_B$-OH), and 4.14 (1H, br. s, 6-H); MS *m/z* (%) 240 (trace, M^+, $C_{15}H_{28}O_2$), 222 [43, $(M-H_2O)^+$], 209 (100).

Acetylation of Diol Compound (10). A solution of diol **10** (10 mg) in dry pyridine (2 ml) and Ac_2O (1 ml) was kept at room temperature for 3 h. The reaction mixture was treated in the usual way to give a residue (13 mg), which was purified by SiO_2 column chromatography using $CHCl_3$ to give monoacetate, (**11**, 8 mg), colorless viscous oil, IR (film) 3510, 1720, and 1370 cm^{-1}; ^1H NMR δ 1.03 (3H, s, 10-CH_3), 1.06 (3H, d, *J*=7.0 Hz, 11-CH_3), 1.17 (3H, s, 4-CH_3), 1.20 (3H, s, 4-CH_3), 2.06 (3H, s, $COCH_3$), 3.94 (1H, dd, *J*=7.5 and 11.0 Hz, 12-H_A), 4.18 (1H, br. s, 6-H), and 4.24 (1H, dd, *J*=2.1 and 11.0 Hz, 12-H_B); MS *m/z* (%) 282 (5, M^+, $C_{17}H_{30}O_3$), 142 (58), 141 (100), and 140 (42).

Oxidation of Acetate (11) with Jones Reagent. A drop of Jones reagent was added to a solution of **11** (10 mg) in acetone (1 ml) at 0 °C, and the mixture was further stirred for 3 h at room temperature. The reaction mixture was treated in the usual way to give a residue (10 mg), which was chromatographed on TLC using $CHCl_3$ to afford keto acetate, (**12**, 6 mg), colorless viscous oil, IR (film) 1735 and 1715 cm^{-1}; ^1H NMR δ 0.91 (3H, s, 10-CH_3), 0.98 (3H, d, *J*=7.0 Hz, 11-CH_3), 1.07 (3H, s, 4-CH_3), 1.34 (3H, s, 4-CH_3), 2.03 (3H, s, $COCH_3$), 2.12 (1H, s, 5-H), 2.24 (1H, m, 7-H), 3.93 (1H, dd, *J*=7.1 and 11.0 Hz, 12-H_A), and 4.09 (1H, dd, *J*=2.1 and 11.0 Hz, 12-H_B); MS *m/z* (%) 280 (17, M^+, $C_{17}H_{28}O_3$), 265 [36, $(M-CH_3)^+$], and 220 [100, $(M-60)^+$].

Preparation of D-Labelled Compounds (9-d_2), (11-d_2), and (12-d_2). Dihydro lactone **8** (10 mg) and platinum catalyst (prepared from platinum oxide; 5 mg) in EtOD (1.5 ml) and AcOD (0.3 ml) were stirred under deuterium atmosphere at room temperature for 8 h. The reaction mixture was filtered and the filtrate was evaporated *in vacuo* to give a residue which was chromatographed on TLC using $CHCl_3$ to give **9**-d_2 (7 mg), MS *m/z* (%) 238 (1, M^+, $C_{15}H_{22}D_2O_2$), and 110 (100); IR (CCl_4) 1780, 1380, and 1370 cm^{-1}; ^1H NMR δ 1.04 (3H, s, 10-CH_3), 1.08 (2H, s, 4-CH_2D), 1.16 (3H, s, 4-CH_3), 1.20 (3H, *J*=6.5 Hz, 11-CH_3), and 4.51 (1H, br. s, 6-H).

Conversion of 9-d_2 into 11-d_2. A mixture of **9**-d_2 (7 mg) and LAH (10 mg) in dry ether (3 ml) was stirred at room temperature for 3 h. The reaction mixture was treated in the usual way. The residue was treated with acetic anhydride (0.5 ml) and pyridine (1 ml) at room temperature for a day and then worked up in the usual way. The resulting residue was chromatographed on TLC using $CHCl_3$ to yield **11**-d_2, (4 mg); MS *m/z* (%) 284 (54, M^+, $C_{17}H_{28}D_2O_3$), 269 [31, $(M-CH_3)^+$] and 209 (100); IR (film) 3500, 1720 and 1380 cm^{-1}; ^1H NMR δ 1.03 (3H, s, 10-CH_3), 1.06 (3H, d, *J*=7.0 Hz, 11-CH_3), 1.17 (2H, s, 4-CH_2D), 1.20 (3H, s, 4-CH_3), 2.06 (3H, s, $COCH_3$), 3.94 (1H, dd, *J*=7.5 and 11.0 Hz, 12-H_A), 4.18 (1H, br. s, 6-H), and 4.24 (1H, dd, *J*=2.1 and 11.0 Hz, 12-H_B).

Oxidation of 11-d_2 with Jones Reagent. To a solution of **11**-d_2 (4 mg) in acetone (1 ml) was added a drop of Jones reagent at 0 °C. The mixture was stirred for a day at room temperature, and then worked up in the usual way. The residue was chromatographed on TLC using $CHCl_3$ to afford **12**-d_2 (2 mg), MS *m/z* (%) 282 (32, M^+, $C_{17}H_{26}D_2O_3$), 267 [28, $(M-CH_3)^+$], and 222 [100, $(M-60)^+$]; IR (film) 1735 and 1715 cm^{-1}; ^1H NMR δ 0.91 (3H, s, 10-CH_3), 0.98 (3H, d, *J*=7.0 Hz, 11-CH_3), 1.07 (2H, s, 4-CH_2D), 1.34 (3H, s, 4-CH_3), 2.03 (3H, s, $COCH_3$), 2.13 (1H, s, 5-H), 2.24 (1H, m, 7-H), 3.93 (1H, dd, *J*=7.1 and 11.0 Hz, 12-H_A), and 4.09 (1H, dd, *J*=2.1 and 11.0 Hz, 12-H_B).

We wish to thank Dr. Tsutomu Kodama of Ottemon Gakuin High School for identification of *Frullania brotheri* Steph., Prof. Tetsuro Fujita of Tokushima Univ. for bioassay of brothenolide, Mr. Hiroshi Nii of Nagaoka Perfumery Co. Ltd., for providing the Costus root oil, and Prof. Yoshinori Asakawa Tokushima-Bunri Univ. for supply of costunolide.

References

1) H. Knoche, G. Ourisson, G. W. Perold, J. Foussereau and J. Maleville, *Science*, **166** 239 (1969); J. D. Connolly and I. M. S. Thornton, *Phytochemistry*, **12**, 631 (1973); Y. Asakawa, J. C. Muller, G. Ourisson, J. Foussereau, and G. Ducombs, *Bull. Soc. Chim. Fr.*, **1976**, 1465. Y. Asakawa, G. Ourisson, and T. Aratani, *Tetrahedron Lett.*, **1976**, 3967; K. R. Markham and L. J. Porter, "Progress in Phytochemistry," ed by L. Reinhold, J. B. Harborne, and T. Swain, Pergamon Press, London (1978), Vol. 5, p. 181.

2) R. Takeda, Y. Ohto, and Y. Hirose, *Chem. Lett.*, **1980**, 1461.

3) H. Yoshioka, T. J. Mabry, and B. N. Timmermann,

"Sesqui-terpene Lactones," The University of Tokyo, Press, Tokyo (1973).
4) V. Herout and F. Sorm, *Chem. Ind.*, **1959**, 1067.
5) R. W. Doskotch and F. S. El-Feraly, *J. Org. Chem.*, **35**, 1928 (1970).
6) K. Takeda, M. Ikuta, and M. Miyawaki, *Tetrahedron*, **20**, 2991 (1964).
7) W. Stocklin, T. G. Waddel, and T. A. Geissman, *Tetrahedron*, **26**, 2397 (1970).

Sesquiterpenoid Constituents of the Liverwort, *Ptychanthus striatus* (LEHM. et LINDENB.) NEES

Reiji TAKEDA,* Hideo NAOKI, Takashi IWASHITA, Kosei MIZUKAWA, Yoshio HIROSE, Toshimasa ISIDA,† and Masatoshi INOUE†

Suntory Institute for Bioorganic Research, Wakayama-dai, Shimamoto-cho, Mishima-gun, Osaka 618

†*Osaka College of Pharmacy, 2-10-65 Kawai, Matsubara, Osaka 580*

(Received October 25, 1982)

Four sesquiterpenoids, striatene, striatol, β-monocyclonerolidol and ptychanolide, were isolated from the liverwort *Ptychanthus striatus* (LEHM. et LINDENB.)NEES. Their structures have been established by spectroscopic analysis and chemical transformation. Three of them, striatene, striatol and β-monocyclonerolidol, are interesting in terms of the evolution of the liverwort from the algae.

Previously, a number of compounds have been isolated from the liverwort belonging to Jungermanniales.[1] In the course of our investigation on the terpene constituents of the liverwort, we examined the constituents of *Ptychanthus striatus* (LEHM. et LINDENB.) NEES and isolated four new sesquiterpenes, striatene, striatol, β-monocyclonerolidol and ptychanolide together with two known sesquiterpenes, deoxopinguisone[2] and pinguisanene.[3] Three of them, striatene, striatol and β-monocyclonerolidol are interesting in terms of the evolution of the liverwort and the algae. Asakawa *et al.*[3] have reported the identification of mono- and sesquiterpene hydrocarbons, *e.g.* α-pinene, β-pinene, camphene, calamenene, and α-copaene, from the same liverwort. This paper deals in detail with the structural determination of striatene, striatol, β-monocyclonerolidol[4] and ptychanolide.[5]

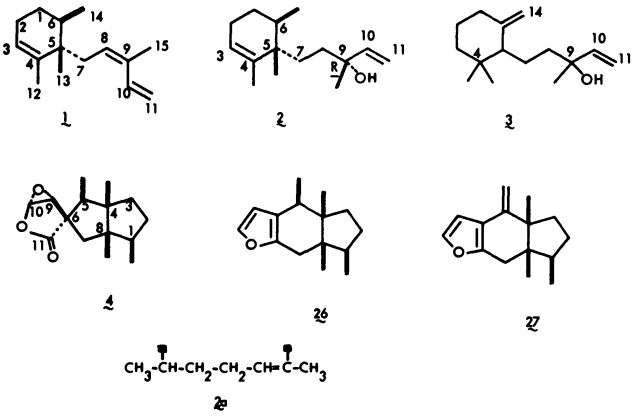

Chart 1.

Striatene (**1**), striatol (**2**), and ptychanolide (**4**) were isolated from the acetone extract of the dry material collected in Tokushima Prefecture in August 1979 by column chromatography on SiO_2 using hexane (F-1) and $CHCl_3$ (F-2 and F-3), while striatene (**1**), β-monocyclonerolidol (**3**), and ptychanolide (**4**) were isolated from the dry material collected in Nara Prefecture in November 1979 by similar procedure.

Striatene (**1**), $[\alpha]_D$ +72.7°, was obtained as a colorless oil by preparative GC of the hydrocarbon fraction. The molecular weight by HR-MS together with the ^1H and ^{13}C NMR data indicated the molecular formula to be $C_{15}H_{24}$. Its IR (1600 cm^{-1}) and UV (λ_{max} 238 nm, ε 24400) spectra showed the presence of conjugated diene system. The IR (1640 and 990 cm^{-1}) and ^1H NMR (δ 5.25, 5.28, and 6.91) spectra also showed characteristic bands and signals due to vinyl groups. Moreover, the ^1H NMR spectrum showed signals due to a tertiary methyl at δ 0.96, a secondary methyl at δ 0.92, two olefinic methyls at δ 1.69 and 1.88, two trisubstituted double bonds at δ 5.34 and 5.56, and an allylic methylene at δ 2.18 and 2.49.

Striatol (**2**), $[\alpha]_D$ +49.5°, was also obtained as a colorless oil by rechromatography on $AgNO_3$-SiO_2 of F-2. The molecular formula $C_{15}H_{26}O$ of **2** was determined by HR-MS together with the ^1H and ^{13}C NMR data. The IR (3400, 1640, 990, and 880 cm^{-1}) spectrum showed bands due to hydroxyl, trisubstituted double bond and vinyl groups. The olefinic functions were further supported by ^1H [δ 5.41 (3-H), 5.09, 5.26 (11-$H_{A,B}$), and 5.92 (10-H)], and ^{13}C NMR (δ 124.0, 145.1, 139.3, and 111.4) spectra. Moreover, ^1H NMR spectrum showed signals due to a secondary methyl at δ 0.87, two tertiary methyls at δ 0.88 and 1.29, and an olefinic methyl at δ 1.59. Treatment of **2** with $POCl_3$ in dry pyridine yielded two trienes, one of which was identified as striatene (**1**) by GLC, IR, and MS. The above spectral data together with this result indicated that striatene and striatol have the same monocyclic carbon skeleton. The presence of the partial structure **2a** was indicated by the results of double irradiation experiments in the ^1H NMR spectrum of **2** using $Eu(fod)_3$. Irradiation of the signal of 6-CH_3 converted a triplet of quartets of 6-H into a triplet (J=6.1 Hz). The fact that 6-H is coupled to 1α- and 1β-H's with J=6.1 Hz indicates it is equatorial. Also, irradiation of 1-H_A collapsed the multiplet of 2-H_A to a sharp peak and a triplet of quartets of 6-H to a doublet of quartets. Further, irradiation of the signal due to 2-H_A collapsed a broad singlet due to 3-H and a multiplet due to 1-H_A to sharp peaks.

Striatene (**1**) was oxidized with *m*-chloroperbenzoic acid (MCPBA) in CH_2Cl_2 at 0 °C to give two monoepoxides **5** and **6**, the UV spectra of which indicated absorption maximum at 238 nm (ε 19500) due to a conjugated diene. The ^1H NMR spectra of epoxides **5** and **6** indicated signals of four olefinic protons (**5**: δ 5.08, 5.21, 5.35, and 6.73; **6**: 5.06, 5.20, 5.67, and 6.82) and a methine proton (**5**: δ 3.01; **6**: 2.77) attached to an epoxy ring. These results indicated that the double

bonds at C_3/C_4 was epoxidized. The stereochemistry of oxirane rings in **5** and **6** were determined by ^1H NMR using shift reagent, *i.e.*, two protons of α-epoxide **6** at C-7 underwent a much larger shift than those of β-epoxide **5**, thus showing that the oxirane ring and side chain in **6** have a *cis* relation, while those of in **5** have a *trans* relation. The presence of the C_6 side chain was suggested by the mass spectra of **1** and **5**, and ^1H NMR of **5**. Namely, the mass spectra contained intense ions at *m/z* 123 (M−81) for **1**, *m/z* 139 for **5** and *m/z* 81 for both compounds originating by cleavage of the C-5/C-7 bond. Furthermore, in the ^1H NMR spectrum of **5**, irradiation at δ 5.21 (8-H) collapsed the allylic methylene at δ 2.15 (7-H_A) and 2.41 (7-H_B) to AB type doublets and the olefinic methyl protons (9-CH_3) at δ=1.86 to a sharp peak. These results indicated that the C_6 side chain in **1** is 3-methyl-1,3-pentadiene. In the ^1H NMR of **2** with the aid of shift reagents [Eu(fod)$_3$], the proton at C-6 together with the CH_3 group at C-4 were observed to have larger shifts than CH_3 groups at C-5 and C-6. In the NOE experiments of benzoate **9** (described below), a 2.7% NOE was observed on the 6-CH_3 group (axial) upon irradiation of 5-CH_3.[6] These results indicated that 6-H and the hydroxyl-containing side chain have a *cis* relation. The geometry of 8-ene in **1** was determined by NOE experiment. An 11% NOE was observed on 8-H upon irradiation of 9-CH_3, *i.e.*, the 8-ene is *Z*. These results lead to structures **1** and **2** for striatene and striatol, respectively.

The absolute configurations of **1** and **2** were determined in the following way. Hydrogenation of monoepoxide **5** with Pd/C gave tetrahydro compound **7**, the IR spectrum of which showed the absence of double bond absorption. The ^1H NMR spectrum indicated signals of two secondary and one primary methyl groups at δ 0.74, 0.84, and 0.88. Compound **7** was treated with diethylamine and *n*-BuLi[7] in dry ether to give **8** which was then reacted with *p*-bromobenzoyl chloride in dry pyridine to yield the corresponding monobenzoate **9**. The IR spectrum exhibited bands at 1718, 1640, and 890 cm^{-1} due to an ester group and an exocyclic methylene group. The ^1H NMR spectrum indicated the presence of a methine proton adjacent to an oxygen (δ 5.57), exocyclic methylene protons (δ 4.76 and 5.08) and protons on an aromatic ring (δ 7.59 and 7.97). The fact that 3-H is coupled to 2-$H_{A,B}$ with J=5.3 and 10.9 Hz indicates that it is axial. The signal of 6-H at δ 1.67 appeared as a triple quartet, (J=4.8 and 6.6 Hz) which collapsed to triplet (J=4.8 Hz) on irradiation of 6-CH_3. This fact indicates that 6-H is equatorial. In the NOE experiments of **9**, an 11% NOE is observed on 12-H_A upon irradiation of 5-CH_3, *i.e.*, 5-CH_3 is equatorial. From these results the conformation of this compound was determined to be as shown by **9a**. Harada *et al.* reported that the absolute configuration of cyclic allylic alcohols can be determined nonempirically by the CD exciton chirality method.[8] Application of this method to benzoate **9**, $\Delta\varepsilon_{241}$+3.1, shows that the exocyclic double bond and the 3-OCOPh group constitute a positive chirality as shown in **9b**. Thus, the absolute configuration of striatene is as shown in structure **1**.

The configuration of the *t*-OH group in **2** was determined by taking (*R*)-(−)-linalool (**10**) as the reference sample. Namely, it was found that the *p*-bromobenzoates of striatol and (*R*)-(−)-linalool both show negative Cotton effects at 252 nm (in MeOH), **2b** $\Delta\varepsilon_{252}$−0.4 and **10a** $\Delta\varepsilon_{252}$−0.5. This establishes the C-9 configuration in **2** to be *R*. Recently, Gonnella *et al.*[9] have shown that the benzoate method described above for cyclic compounds is extensible to acyclic secondary allylic alcohols, namely, that the benzoate of acyclic allylic moiety **11** exhibits a positive CD. The present results including that of linalool show that the method is applicable to *t*-OH system **12** as well (because the methyl group is smaller than other alkyl substituents).

β-Monocyclonerolidol (**3**), $[\alpha]_D$ +3.2°, was obtained as a colorless oil by rechromatography on $AgNO_3$-SiO_2

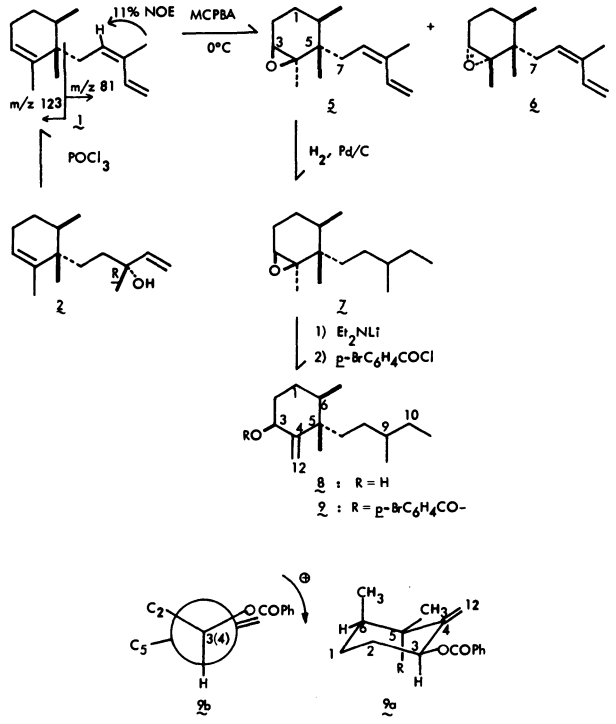

Chart 2.

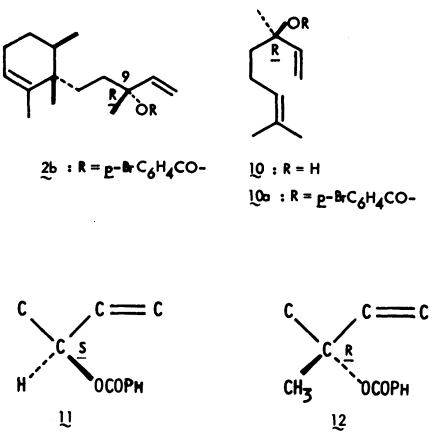

Chart 3.

of F-2′. The molecular formula $C_{15}H_{26}O$ of **3** was determined by HR-MS together with the ^1H and ^{13}C NMR data. The IR spectrum showed the presence of a hydroxyl group at 3400 cm^{-1}, a vinyl group at 1645 and 990 cm^{-1}, and an exocyclic methylene group at 890 cm^{-1}. The ^1H NMR spectrum indicated signals of *gem*-dimethyl groups at δ 0.84 and 0.92, a tertiary methyl group on a carbon bearing hydroxyl at δ 1.27, an exocyclic methylene group at δ 4.53 and 4.75, and vinyl groups at δ 5.02, 5.18, and 5.91. The mass spectrum indicated intense ion peaks at *m/z* 123 (M−18−81) and *m/z* 81 as observed in **1** and **2**. The fact indicates that **3** also has a C_6 side chain. From these results together with biogenetic consideration, we assumed that **3** had a monocyclonerolidol skeleton as shown by structure **3**. This assumption was confirmed by partial synthesis of **3** from α-ionone.

Hydrogenation of commercial (±)-α-ionone **13** with Pd/C in 1.5% KOH-EtOH gave the hydrogenated mixture, from which dihydroionone **14** was separated by column chromatography on SiO_2. Dihydroionone **14** exhibited the molecular ion peak at *m/z* 194 in its mass spectrum. The IR spectrum exhibited bands at 1710 and 810 cm^{-1} due to a carbonyl group and a trisubstituted double bond. The ^1H NMR spectrum indicated the presence of an olefinic methyl group (δ 1.66) and a trisubstituted double bond (δ 5.31). The reaction of **14** with ethylene glycol and TsOH yielded acetal **15**, the ^1H NMR spectrum of which exhibited a signal due to the acetal group at δ 3.90. The IR spectrum showed the absence of a carbonyl group. Next, irradiation of acetal **15** in ether containing 10% phenol with a 450 W-Hg lamp[10] afforded a mixture of **16** and starting material **15**. Then, this mixture was hydrolyzed with TsOH in THF containing H_2O to give a ketone mixture, **16a** and **14**, from which the exocyclic isomer **16a** was separated by column chromatography on $AgNO_3$-SiO_2. The IR spectrum showed exocyclic methylene absorption bands at 1640 and 885 cm^{-1}, and a carbonyl absorption band at 1710 cm^{-1}. The ^1H NMR spectrum also suggested the presence of an exocyclic methylene group at δ 4.49 and 4.74. The exocyclic isomer **16a** was reacted with vinylmagnesium bromide (prepared from vinyl bromide and magnesium in THF) in dry THF to give the racemic alcohol **17**. The NMR, IR, and mass spectra of **17** were identical with those of β-monocyclonerolidol (**3**).

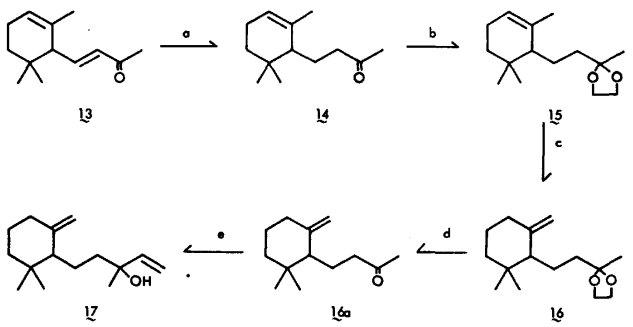

Chart 4.

a) H_2, pd/C, 1.5% KOH-EtOH; b) Ethylene glycol, TsOH c) 10% Penol/ether, *hν*(450 W); d) TsOH, THF THF; e) CH_2=CHMgBr, THF.

On the basis of distribution of terpenoids, Asakawa and co-workers[11] have noted that liverwort are closely related to algae. The fact that the skeletal structures of **1**—**3** are identical with α- and β-snyderol,[12] microcionin,[13] *etc.*[14] which have been found in marine algae and in marine animals feeding on algae, supports the notion that liverworts have evolved from algae.

Ptychanolide (**4**), mp 143—144 °C, $[\alpha]_D$ +23.2° was obtained as a colorless needles by recrystallization of F-2 and 2′. The molecular formula $C_{15}H_{22}O_3$ of **4** was determined by the appearance of a molecular ion peak at 250.1565 in the HR-MS. The IR spectrum showed the presence of a γ-lactone absorption band at 1780 cm^{-1} and the absence of hydroxyl absorptions. The ^1H NMR spectrum indicated signals due to two secondary CH_3 groups at δ 0.84 and 0.98, two tertiary CH_3 groups at δ 0.79 and 0.93, an isolated methylene group at δ 1.39 and 1.99, and two methine protons adjacent to oxygen at δ 3.55 and 5.52. The ^{13}C NMR spectrum also suggested the presence of a γ-lactone group at δ 76.1 and 179.8. Hence the remaining oxygen atom was attributed to an ether linkage. Treatment of the lactone **4** with 10% H_2SO_4 in acetone afforded the diol lactone **18**. The IR spectrum showed bands at 3500 and 1770 cm^{-1} due to hydroxyl and γ-lactone groups. The ^1H NMR spectrum indicated signals of two methine protons adjacent to oxygen at δ 4.13 and 5.62 which were coupled with each other. The formation of an α-glycol from an ether indicates that the diol is derived from an epoxide. The lactone **4** was reduced with LAH in dry ether to triol **19**, the ^1H NMR spectrum of which showed signals of five protons adjacent to oxygen at δ 3.64, 3.72, 3.76, 3.84, and 3.92. In decoupling experiments, irradiation at δ 3.92 collapsed the two double doublets of the $-C\underline{H}_2OH$ group at δ 3.72 and 3.76 to AB type doublets. This result and assignments of *J* values suggested that a hydroxymethyl group at C-11 and 1,2-diol system at C-9 and C-10 are attached to a quaternary carbon. Hence, the γ-lactone must form a spiro linkage at C-6 and the epoxy ring is attached to the γ-lactone ring.

Oxidation of triol **19** with $NaIO_4$ gave aldehyde **20**, M^+ *m/z* 224 ($C_{14}H_{24}O_2$), the IR spectrum of which showed bands at 3560, 3450, and 1715 cm^{-1} due to hydroxyl and formyl group. The ^1H NMR spectrum indicated signals of two protons adjacent to an oxygen as primary alcohol at δ 3.55 and 3.94, and proton of formyl group at δ 9.69 instead of three protons adjacent to oxygen in **19**. Aldehyde **20** was further oxidized with MCPBA in CH_2Cl_2, followed by hydrolysis with Al_2O_3 to yield diol **21** (M^+, *m/z* 212; $C_{13}H_{24}O_2$). Its IR spectrum showed the presence of a hydroxyl absorption band at 3325 cm^{-1} and the absence of carbonyl absorption. The diol **21** was oxidized further with $NaIO_4$ to the corresponding ketone **22** which exhibited a molecular ion peak at 180 ($C_{12}H_{20}O$) in the mass spectrum. The IR spectrum indicated the presence of a five-membered ring ketone (1740 cm^{-1}). These results establish that ptychanolide **4** has a spiro lactone moiety at C-6. Reduction of ketone **22** with LAH in dry ether afforded alcohols **23** and **24**, the ^1H NMR

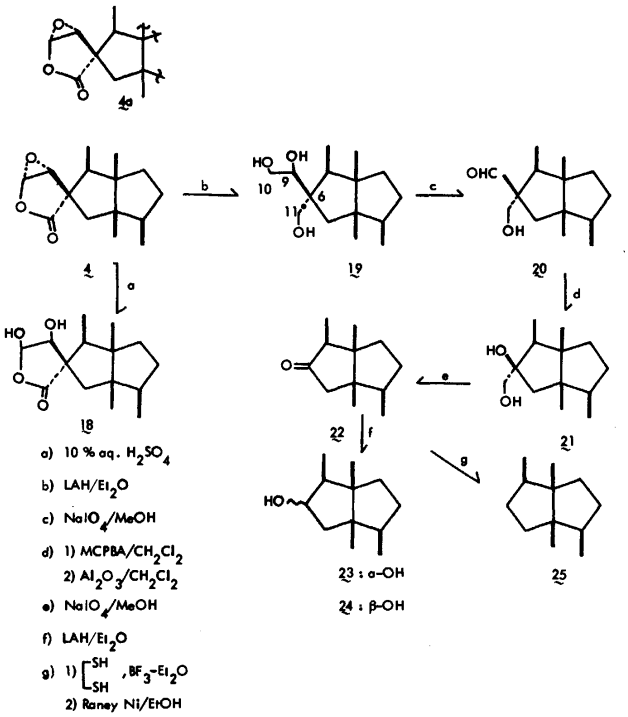

Chart 5.

spectra of which showed signals of protons on carbons bearing hydroxyl groups (**23**: δ 3.77; **24**: 4.20), respectively. In the decoupling experiments of **23**, irradiation of 6-H as a double triplet collapsed a pair of double doublets of 7-CH_2 at δ 1.49 and 1.79 to a pair of doublets and a double quartet of 5-H at δ 1.74 to a quartet. This fact indicated that the OH function was flanked by a methylene group and secondary CH_3 group. Namely, ptychanolide has a partial structure **4a**. Ketone **22** was treated with 1,2-ethanedithiol to give the corresponding thioacetal which was desulfurized with Raney Ni in EtOH to yield the volatile hydrocarbon **25**. Its mass spectrum showed a molecular ion peak at 166 ($C_{12}H_{22}$). However, the ^1H and ^{13}C NMR spectra showed only the signals of two methyl groups and five protons, and those of six carbons, respectively. Therefore, the hydrocarbon **25** has the symmetric bicyclo[3.3.0]octane skeleton. The above results indicate that ptychanolide is represented by formula **4** (planar).

The stereostructure of ptychanolide (**4**) was determined by X-ray analysis. The colorless transparent crystals of **4**, which were recrystallized from hexane-EtOAc, belong to orthorhombic with space group $p2_12_12_1$. The crystal data are as follows: $C_{15}H_{22}O_3$, M_r= 250.16, a=6.514(1), b=19.376(4), c=10.543(3) Å, v= 1330.7(5) Å^3, Z=4, D_m=1.233 (1), D_x=1.249 g cm^{-3}. X-Ray diffraction intensities were measured by Rigaku automatic diffractometer with graphite-monochromated Cu $K\alpha$ radiation using a θ-2θ scan mode and a scan rate of 4°/min. Stationary background counts (5 s each) were taken at both limits of each scan (scan width in 2θ: 1.2+0.15 tanθ). A total of 1344 unique reflections were measured to the limit 2θ=130°. Lorentz and polarization corrections were applied, but no absorption correction was made because of the small size of the used crystal (dimension: 0.3×0.4×0.2 mm^3). The X-ray intensities of four standard reflections monitored at 100 reflection intervals showed no evidence of structural deterioration during the data collection.

Table 1. Atomic coordinates (× 10^4) of nonhydrogen atoms of **4**

Atom	x	y	z
C1	4160 (11)	977 (3)	5420 (6)
C2	3997 (11)	237 (3)	5870 (8)
C3	5405 (11)	162 (4)	7049 (8)
C4	6291 (8)	886 (3)	7297 (6)
C5	4842 (9)	1322 (3)	8111 (6)
C6	5179 (8)	2073 (3)	7648 (6)
C7	6138 (9)	2006 (3)	6283 (6)
C8	6217 (8)	1238 (3)	5977 (5)
C9	6445 (9)	2549 (3)	8451 (6)
C10	5357 (11)	3181 (4)	8584 (6)
C11	3183 (9)	2479 (3)	7560 (6)
C12	3899 (12)	1056 (4)	3983 (8)
C13	8035 (10)	1071 (4)	5107 (7)
C14	8450 (10)	842 (4)	7867 (7)
C15	4977 (12)	1232 (4)	9551 (7)
O16	5529 (7)	2767 (3)	9630 (4)
O17	3428 (7)	3132 (2)	7980 (5)
O18	1566 (6)	2293 (2)	7122 (5)

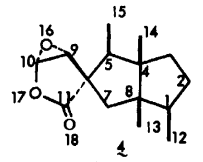

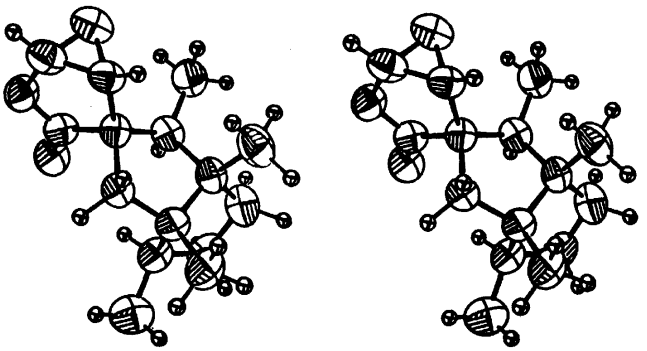

Fig. 1. Perspective drawing of ptychanolide **4**.

The structure was solved by the direct methods with program MULTAN78.[15] An E-map, calculated using 200 reflections ($|E|>1.40$) with the phase set of the highest combined figure of merit (=2.86), revealed the positions of all nonhydrogen atoms. These coordinates were refined by a full-matrix least-squares method with isotropic temperature factors and then by a block-diagonal least-squares method with anisotropic ones. All hydrogen atoms could be located from a difference Fourier map and these were included in a further refinement with isotropic temperature factors. The final R value was 0.078. The final positional parameters with their estimated standard deviations of nonhydrogen atoms are listed in Table 1.

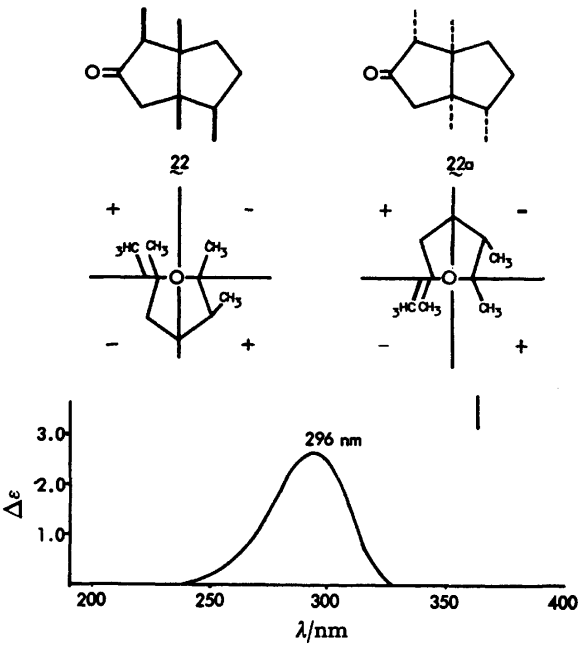

Fig. 2. CD spectrum of **22**.

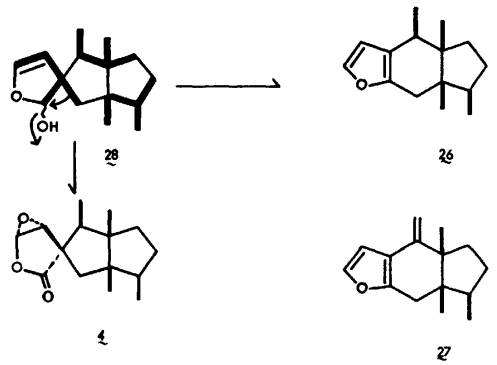

Chart 6.

The atomic scattering factors for all atoms were taken from "International Tables for X-Ray Crystallography."[16] All numerical calculations were carried out on an ACOS-700 computer at the Computation Center of Osaka University using *UNICS* program.[17] The stereostructure of **4** is shown in Fig. 1. The relative stereostructure of ptychanolide (**4**) was thus clarified. Furthermore, the keto compound **22** showed a positive Cotton effect at 295 nm in the CD spectrum (Fig. 2). The positive sign of the Cotton effect can be understood by application of the octant rule[18] to the cyclopentanone system, as visualized in octant projection formula **22** and **22a**. This leads to the absolute configuration shown for **22** which is corroborated by the established configuration of congeners **26**[2,19] and **27**.[3] Thus, the absolute structure of ptychanolide is shown by formula **4**.

The biogenesis of the pinguisone type sesquiterpenoids represented by deoxopinguisone **26** and pinguisanene **27** is as yet not clear. However, the isolation of ptychanolide **4** from the same liverwort suggests that they are derived from an intermediate such as **28**.

Experimental

All melting points are uncorrected. IR spectra were measured with a Hitachi EPI-G2 spectrometer, ^{13}C NMR spectra with a JEOL FX-100 (25.0 MHz) spectrometer, ^1H NMR spectra with a JEOL FX-100 (100 MHz), a Nicolet NT-360 (360 MHz) or a Hitachi R-20B (60 MHz) spectrometer in deuteriochloroform solution containing tetramethylsilane as an internal standard, low resolution mass spectra with a Hitachi RMU-6 mass spectrometer and high resolution mass spectra with a JEOL 01SG-2, with direct inlet system operating at 70 eV. CD spectra were measured with a JASCO J-20 spectrometer. An analytical GC was performed with a Hitachi 163-type apparatus equipped with a Thermon 600T glass capillary column, and preparative GC with Varians model 90 fitted OV-17 on Chromosorb-W, operated at 150°. Kieselgel 60 (E. Merck, Darmstadt) and Silica CC-7 special (Mallinckrodt) were used for column chromatography. Thin-layer chromatography (TLC) was carried out on Kieselgel GF_{254} (E. Merck, Darmstadt) in 0.25 mm thickness.

Extraction and Isolation. The dry material (100 g) of *Ptychanthus striatus* (Lehm. et Lindenb.) Nees collected in Wakayama Prefecture around Kosa-cho in March 1980 was extracted with acetone at room temperature. Acetone was evaporated under vacuum and the concentrate was extracted with $CHCl_3$. The $CHCl_3$ extract (6.6 g) was subjected to column chromatography over SiO_2. The fraction eluted with hexane gave sesquiterpene hydrocarbons (F-1) containing striatene (**1**), deoxopinguisone (**26**), and pinguisanene (**27**). The fraction eluted with $CHCl_3$ yielded crude ptychanolide (**4**) (F-2) and crude striatol (**2**) (F-3). Also, F-1′, F-2′, and F-3′ were isolated from the acetone extract of the dry material (100 g) collected in Nara Prefecture around Ikadaba in November 1979 by a similar procedure.

Striatene (**1**) was isolated from hydrocarbon fractions, F-1 and F-1′, by preparative GC, as a colorless oil (**1**, 200 mg from F-1 and F-1′, respectively), $[\alpha]_D^{22}$ +72.7° (*c* 1.19, $CHCl_3$), IR (film) 1640, 1600, 990, 810 cm^{-1}; UV (cyclohexane) 232 (sh), 238 (ε 24400) and 245 (sh) nm; ^1H NMR δ 0.92 (3H, d, J=6.5 Hz, 6-CH_3), 0.96 (3H, s, 5-CH_3), 1.69 (3H, br.s, 4-CH_3), 1.88 (3H, br.s, 9-CH_3), 2.18 (1H, dd, J=6.0, 16.0 Hz, 7-H_A), 2.49 (1H, dd, J=8.0, 16.0 Hz, 7-H_B), 5.25 (1H, dd, J=1.6, 10.5 Hz, 11-H_A), 5.28 (1H, dd, J=1.6, 17.3 Hz, 11-H_B), 5.34 (1H, m, 8-H), 5.56 (1H, t-like, 3-H), and 6.91 (1H, dd, J=10.5, 17.3 Hz, 10-H); ^{13}C NMR δ 16.0 (q), 19.2 (q), 20.0 (q), 20.7 (q), 25.3 (t), 27.1 (t), 34.2 (t), 34.2 (d), 40.7 (s), 113.2 (t), 124.4 (d), 128.1 (d), 134.0 (d), 133.2 (s), and 139.1 (s); MS *m/z* (%) 204 (7, M^+), 123 [100, $(M-81)^+$] and 81 (25). Found: *m/z* 204.1866. Calcd for $C_{15}H_{24}$: M, 204.1856.

Epoxidation of Striatene (1). The solution of *m*-chloroperbenzoic acid (390 mg) in CH_2Cl_2 (5 ml) was added to an ice-cooled solution of **1** (300 mg) in CH_2Cl_2 (5 ml) and the mixture was stirred for 40 min at 0 °C. The reaction mixture was treated in the usual way to give residue (190 mg), which was chromatographed on 10% $AgNO_3$–SiO_2 (Mallinckrodt, CC-7). Elution with CH_2Cl_2–EtOAc (20 : 1) gave β-epoxide **5** (55 mg) as a colorless oil. Successive elution with the same solvent gave α-epoxide **6** (10 mg) as a colorless oil.

β-Epoxide 5: IR (film) 1640, 1600, 980, 900 cm^{-1}; UV (cyclohexane) 237 nm (ε 19500); ^1H NMR δ 0.75 (3H, d, J=6.5 Hz, 6-CH_3), 0.92 (3H, s, 5-CH_3), 1.26 (3H, s, 4-CH_3), 1.86 (3H, br.s, 9-CH_3), 2.15 (1H, dd, J=5.5, 17.0 Hz, 7-H_A), 2.41 (1H, dd, J=7.5, 17.0 Hz, 7-H_B), 3.01 (1H, br.s, 3-H), 5.08 (1H, dd, J=1.5, 10.5 Hz, 11-H_A), 5.21 (1H, t-like, 8-H), 5.35 (1H, dd, J=1.5, 17.5 Hz, 11-H_B), and 6.73 (1H, dd, J=10.5, 17.5 Hz, 10-H); MS *m/z* (%) 220 (3, M^+, $C_{15}H_{24}O$), 205 [8, $(M-CH_3)^+$], 139 [98, $(M-81)^+$], 109 (92), 95 (100), 81 (99), 43 (98).

α-Epoxide 6: IR (film) 1645, 1605, 980, 900 cm^{-1}; UV

(cyclohexane) 238 nm (ε 18000); ^{1}H NMR δ 0.72 (3H, d, J=6.5 Hz, 6-CH_3), 0.91 (3H, s, 5-CH_3), 1.27 (3H, s, 4-CH_3), 1.86 (3H, br.s, 9-CH_3), 2.36 (2H, br.s, 7-$H_{A,B}$), 2.77 (1H, t, J=1.5 Hz, 3-H), 5.06 (1H, dd, J=1.5, 10.5 Hz, 11-H_A), 5.20 (1H, dd, J=1.5, 17.5 Hz, 11-H_B), 5.67 (1H, br.t, J=4.0 Hz, 8-H), and 6.82 (1H, dd, J=10.5, 17.5 Hz, 10-H); MS m/z (%) 220 (trace, M^+, $C_{15}H_{24}O$), 139 [17, $(M-81)^+$], 95 (30), 81 (20), 43 (100).

Hydrogenation of β-Epoxide ***5***. β-Epoxide **5** (10 mg) and 10% palladium charcoal (10 mg) in EtOH (1 ml) were stirred under hydrogen atmosphere at room temperature for 5 h. The catalyst was removed by filtration and the solvent was evaporated to give a residue (11 mg), which was chromatographed on SiO_2. Elution with $CHCl_3$ yielded tetrahydro epoxide **7** (7 mg), colorless oil, ^{1}H NMR δ 0.74 (3H, d, J=6.5 Hz, s-CH_3), 0.84 (3H, d, J=7.5 Hz, s-CH_3), 0.86 (3H, s, 5-CH_3), 0.88 (3H, t, J=6.6 Hz, 10-CH_3), 1.24 (3H, s, 4-CH_3), and 2.96 (1H, br.s, 3-H); MS m/z (%) 224 (12, M^+, $C_{15}H_{28}O$), 209 [31, $(M-CH_3)^+$], 103 (100), 85 (98), 43 (76).

Conversion of ***7*** *into Benzoate* ***9***. Commercial butyllithium (0.3 ml, 15% solution in hexane) was added to a solution of diethylamine (36.5 mg) in dry ether (1 ml). Tetrahydro epoxide **7** (18 mg) in dry ether (1 ml) was then added and the mixture was refluxed for 3 h. The reaction mixture was poured into NaCl aqueous solution and extracted with ether. The ether layer was treated in the usual way to give residue (14 mg), which was treated with *p*-bromobenzoyl chloride (20 mg) in dry pyridine (2 ml) at room temperature for a day. The reaction mixture was treated in the usual way to give a residue, which was chromatographed on SiO_2. Elution with hexane–EtOAc (20 : 1) gave benzoate **9** (8 mg), colorless viscous oil, IR (film) 1718, 1640, 890 cm^{-1}; UV (MeOH) 205.5, 244 nm (ε 16900, 17500); CD, $\Delta\varepsilon_{241}$ +3.06 (c 0.145, MeOH); ^{1}H NMR δ 0.82 (3H, t, J=6.6 Hz, 10-CH_3), 0.83 (3H, d, J=6.6 Hz, 9-CH_3), 0.90 (3H, d, J=6.7 Hz, 6-CH_3), 1.01 (3H, s, 5-CH_3), 1.67 (1H, tq, J=4.8, 6.6 Hz, 6-H), 4.76 (1H, br.s, 12-H_A), 5.08 (1H, br.s, 12-H_B), 5.57 (1H, dd, J=5.3, 10.9 Hz, 3-H), 7.59 (2H, aromatic protons) and 7.98 (2H, aromatic protons); MS m/z (%) 408, 406 (trace, M^+, $C_{22}H_{31}O_2Br$), 323, 321 [45, 47, $(M-85)^+$], 185, 183 [92, 91, $(p$-$BrC_6H_4CO)^+$], 122 (100), 93 (69).

Benzoylation of (R)-(−)-Linalool ***(10)***. The mixture of (*R*)-(−)-linalool (**10**) (20 mg) isolated from Ho leaf oil and *p*-bromobenzoyl chloride (20 mg) in dry pyridine (1 ml) was kept at room temperature for 2 d. The reaction mixture was treated in the usual way to yield a residue, which was chromatographed on SiO_2. Elution with $CHCl_3$ gave a benzoate **10a** (15 mg), colorless oil, IR (film) 1720, 1645, 910, 830 cm^{-1}; UV (EtOH) 206.5, 244.5 nm (ε 14500, 16400); CD, $\Delta\varepsilon_{252}$ −0.54 (c 2.5, EtOH); ^{1}H NMR δ 1.57, 1.62 (3H each, br.s), 1.68 (3H, s, 6-CH_3), 1.76—2.28 (4H, 4-$H_{A,B}$, 5-$H_{A,B}$), 5.12 (1H, m, 3-H), 5.17 (1H, dd, J=1.2, 10.0 Hz, 8-H_A), 5.23 (1H, dd, J=1.2, 17.5 Hz, 8-H_B), 6.07 (1H, dd, J=10.0, 17.5 Hz, 7-H), 7.52 (2H, aromatic protons) and 7.85 (2H, aromatic protons); MS m/z (%) 185, 183 [100, 98 (p-BrC_6H_4)$^+$], 136 (43).

Isolation of Striatol ***(2)***. Fraction 3 (F-3) was rechromatographed on 10% $AgNO_3$–SiO_2 eluted with hexane–EtOAc (10 : 1) to yield colorless viscous oil (**2**, 70 mg), $[\alpha]_D^{22}$ +49.5° (c 1.2, $CHCl_3$); IR (film) 3400, 1640, 990, 800 cm^{-1}; ^{1}H NMR δ 0.87 (3H, d, J=6.5 Hz, 6-CH_3), 0.88 (3H, s, 5-CH_3), 1.29 (3H, s, 9-CH_3), 1.59 (3H, br.s, 4-CH_3), 5.09 (1H, dd, J=1.6, 10.5 Hz, 11-H_A), 5.26 (1H, dd, J=1.6, 17.5 Hz, 11-H_B), 5.41 (1H, m, 3-H) and 5.92 (1H, dd, J=10.5, 17.5 Hz, 10-H); ^{13}C NMR δ 15.7 (q), 19.0 (q), 21.0 (q), 27.6 (q), 25.4 (t), 27.0 (t), 30.1 (t), 36.5 (t), 33.2 (d), 40.0 (s), 73.1 (s), 111.4 (t), 124.0 (d), 145.1 (d), 139.3 (s); MS m/z (%) 204 [17, $(M-18)^+$], 123 [100, $(M-81)^+$], 81 (44). Found: m/z 222.1994, Calcd for $C_{15}H_{26}O$: M, 222.2004.

Benzoylation of Striatol ***(2)***. A solution of striatol **2** (10 mg) and *p*-bromobenzoyl chloride (10 mg) in dry pyridine (1 ml) was kept at room temperature for 2 d. The reaction mixture was treated in the usual way to give a residue, which was purified by SiO_2 column chromatography using hexane–EtOAc (15 : 1) to afford benzoate **2b** (7 mg), colorless viscous oil, IR (film) 1720, 1645, 980, 800 cm^{-1}; UV (EtOH) 206, 244.5 nm (ε 16000, 18000); CD, $\Delta\varepsilon_{252}$ −0.4 (c 2.7, EtOH), ^{1}H NMR δ 0.81 (3H, d, J=7.0 Hz, 6-CH_3), 0.81 (3H, s, 5-CH_3), 1.59 (3H, br.s, 4-CH_3), 1.69 (3H, s, 9-CH_3), 5.17 (1H, dd, J=1.6, 10.5 Hz, 11-H_A), 5.22 (1H, dd, J=1.6, 17.5 Hz, 11-H_B), 5.40 (1H, m, 3-H), 6.03 (1H, dd, J=10.5, 17.5 Hz, 10-H), 7.53 (2H, aromatic protons) and 7.85 (2H, aromatic protons); MS m/z (%) 185, 183 [100, 98 (p-BrC_6H_4CO)$^+$], 204 (20), 123 (95), 81 (30).

Isolation of β-Monocyclonerolidol ***(3)***. Fraction 3′ (F-3′) was purified by column chromatography on 10% $AgNO_3$–SiO_2 using hexane–EtOAc (10 : 1) to give β-monocyclonerolidol (**3**, 70 mg), colorless viscous oil, $[\alpha]_D^{25}$ +3.2° (c 0.66, $CHCl_3$); IR (film) 3400, 1645, 990, 890 cm^{-1}; ^{1}H NMR δ 0.84, 0.92 (3H each, s, *gem*-dimethyl at C-4), 1.27 (3H, s, 9-CH_3), 4.53 (1H, br.s, 14-H_A), 4.75 (1H, br.s, 14-H_B), 5.02 (1H, dd, J=1.6, 10.5 Hz, 11-H_A), 5.18 (1H, dd, J=1.6, 17.5 Hz, 11−H_B), and 5.91 (1H, dd, J=10.5, 17.5 Hz, 10H); ^{13}C NMR δ 20.4 (q), 26.4 (q), 27.7 (q), 23.7 (t), 28.5 (t), 32.4 (t), 36.2 (t), 41.1 (t), 54.5 (d), 35.0 (s), 73.3 (s), 109.0 (t), 111.4 (t), 145.4 (d), 149.3 (s); MS m/z (%) 204 [25, $(M-H_2O)^+$], 189 (40), 123 [100, $(M-18-81)^+$], 109 (43), 93 (43), 81 (75). Found: m/z 222.1992. Calcd for $C_{15}H_{26}O$: M, 222.2004.

Hydrogenation of α-Ionone ***(13)***. The mixture of α-ionone **13** (500 mg) and Pd/C (50 mg) in EtOH containing 1.5% KOH was stirred under hydrogen atmosphere at room temperature for 4 h. The reaction mixture was filtered and the filtrate was neutralized with 5% aqueous HCl, diluted with H_2O, and extracted with ether. The ether layer was treated in the usual way to give a residue, which was chromatographed on SiO_2. Elution with $CHCl_3$ yielded dihydroionone **14** (190 mg), colorless oil, IR (film) 1710, 810 cm^{-1}; ^{1}H NMR δ 0.88, 0.93 (3H each, s, *gem*-dimethyl), 1.66 (3H, br.s, $=C(CH_3)$), 2.12 (3H, s, $COCH_3$), 5.31 (1H, m, $=CH$); MS m/z (%) 194 (4, M^+, $C_{13}H_{22}O$), 176 [23, $(M-CH_3)^+$], 161 [17, $(M-30)^+$], 136 [80, $(M-15-43)^+$], 121 (100), 43 (84).

Acetalization of Dihydroionone ***14***. A solution of dihydroionone **14** (500 mg) in benzene (40 ml) containing ethylene glycol (6 ml) and TsOH (0.13 g) was stirred at reflux with a Dean-Stark trap for 12 h. The reaction mixture was washed with aqueous $NaHCO_3$ and H_2O, and dried over Na_2SO_4. The solvent was removed *in vacuo* to give a residue (580 mg), which was chromatographed on SiO_2. Elution with $CHCl_3$ gave acetal **15** (400 mg), colorless oil, IR (film) 1650, 1060, 860 cm^{-1}; ^{1}H NMR δ 0.86, 0.92 (3H each, s, *gem*-dimethyl) 1.30 (3H, s,), 1.66 (3H, br. s, $=C(CH_3)$), 3.90 (4H, s), 5.27 (1H, br.s, $H\diagdown=$); MS m/z (%) 238 (1, M^+, $C_{15}H_{26}O_2$), 223 [2, $(M-CH_3)^+$], 136 (25), 87 [100, 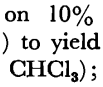], 43 (19).

Irradiation of Acetal ***15***. A solution of acetal **15** (2 g) in ether (270 ml) containing phenol (30 g) was irradiated with 450 W-Hg lamp for 3 h. The reaction mixture was passed an Al_2O_3 column by elution with ether. The ether fraction was evaporated under vacuum to give a residue (1.5 g), which was chromatographed on 10% $AgNO_3$–SiO_2 to yield β-isomer **16** (550 mg) and starting material **15** (600 mg). β-Isomer **16**,

colorless oil, IR (film) 1640, 1070, 890 cm^{-1}; ^1H NMR δ= 0.84, 0.94 (3H each, s, *gem*-dimethyl), 1.31 (3H, s, $\overline{\text{O}}\text{>}$-$CH_3$), 3.92 (4H, s), 4.52, 4.73 (1H each, br.s, $=\langle^{H}_{H}$); MS *m/z* (%) 238 (58, M^+, $C_{15}H_{26}O_2$), 223 [100, $(M-CH_3)^+$], 178 (73), 176 (93), 161 (97), 136 (98), 87 [99, $(CH_3\langle^{O-}_{O-}\rangle)^+$]. 43 (70).

Hydrolysis of Acetal **16**. The mixture of acetal **16** (300 mg) and TsOH (20 mg) in THF (10 ml) and H_2O (1 drop) was kept at room temperature for 2 d. The reaction mixture was diluted with H_2O and extracted with CH_2Cl_2. The CH_2Cl_2 layer was treated in the usual way to afford a residue (250 mg), which was purified by SiO_2 column chromatography using CH_2Cl_2 to yield ketone **16a** (190 mg), colorless oil, IR (film) 1710, 1640, 885 cm^{-1}; ^1H NMR δ 0.94, 0.96 (3H each, s, *gem*-dimethyl), 2.00 (3H, s, $-COCH_3$), 4.49, 4.74 (1H each, br. s, $=\langle^{H}_{H}$); MS *m/z* (%) 194 (2, M^+, $C_{13}H_{22}O$), 176 [25, $(M-CH_3)^+$], 161 (27), 136 (59), 121 (68), 43 (100).

Grignard Reaction of Ketone **16a**. After a solution of ketone **16a** (250 mg) in dry THF (5 ml) was added dropwise to a stirred solution of vinylmagnesium bromide (prepared from 3 g of vinyl bromide and 720 mg of Mg in 10 ml of dry THF) at room temperature, the mixture was heated under reflux for 3 h. The reaction mixture was then decomposed by addition of a saturated solution of NH_4Cl. The water layer was extracted with ether and the ether extract dried over Na_2SO_4. The solvent was evaporated under vacuum to give a residue, which was chromatographed on SiO_2. Elution with $CHCl_3$ yielded alcohol **17** (123 mg).

The IR, NMR, and mass spectra were found to be identical with those of β-monocyclonerolidol (**3**).

Isolation of Ptychanolide (**4**). The crude ptychanolide (F-2 and F-2′) was recrystallized with hexane–EtOAc to yield colorless needles (**4**, 270 mg, 120 mg), mp 143—144 °C, $[\alpha]_D^{24}$ +23.2° (*c* 0.47, $CHCl_3$); IR (KBr) 1780 cm^{-1}; ^1H NMR δ 0.79, 0.93 (3H each, s, 4-CH_3, 8-CH_3), 0.84 (3H, d, J=7.7 Hz, 1-CH_3), 0.98 (3H, d, J=7.7 Hz, 5-CH_3), 1.3—1.4 (2H, m, 2-H_A, 3-H_A), 1.39 (1H, d, J=13.6 Hz, 7-H_A), 1.71 (1H, m, 2-H_B), 1.87 (1H, m, 3-H_B), 1.99 (1H, d, J=13.6 Hz, 7-H_B), 2.38 (1H, m, 1-H), 2.61 (1H, q, J=7.7 Hz), 3.55 (1H, d, J= 2.4 Hz, 9-H and 5.52 (1H, d, J=2.4 Hz, 10-H); ^{13}C NMR δ 10.7 (q), 14.5 (q), 16.7 (q), 18.4 (q), 31.0 (t), 35.5 (t), 44.6 (t), 42.0 (d), 50.0 (d), 54.4 (s), 55.3 (s), 56.3 (s), 57.5 (d), 76.1 (d), 179.8 (s); MS *m/z* (%) 250 (6, M^+), 235 [13, $(M-CH_3)^+$], 205 (24), 109 (100). Found: *m/z* 250.1565. Calcd for $C_{15}H_{22}O_3$: M, 250.1564.

Hydrolysis of Ptychanolide (**4**). After 10% aqueous H_2SO_4 was added to a solution of ptychanolide **4** (20 mg) in acetone (2 ml) at 0 °C, the mixture was kept at room temperature for 3 h. The reaction mixture was diluted with H_2O and extracted with $CHCl_3$. The $CHCl_3$ layer was washed with a saturated solution of $NaHCO_3$ and H_2O, and dried over Na_2SO_4. The solvent was removed under reduced pressure to give residue (24 mg), which was chromatographed on SiO_2. Elution with $CHCl_3$–MeOH (15 : 1) gave diol lactone **18** (17 mg), colorless powder, IR ($CHCl_3$), 3500, 1770 cm^{-1}; ^1H NMR δ 0.84 (3H, d, J=7.5 Hz, 1-CH_3), 0.80, 0.91 (3H each, s, 4-CH_3, 8-CH_3), 1.07 (3H, d, J=7.5 Hz, 5-CH_3), 2.67 (1H, q, J=7.5 Hz, 5-H), 4.13 (1H, d, J=2.0 Hz, 9-H) and 5.62 (1H, d, J=2.0 Hz, 10-H); MS *m/z* (%) 268 (trace, M^+, $C_{15}H_{24}O_4$), 250 [4, $(M-H_2O)^+$], 193 (100), 165 (98), 109 (97), 55 (32).

Reduction of Ptychanolide (**4**) *with Lithium Aluminium Hydride*. A solution of ptychanolide **4** (75 mg) in dry ether (2 ml) was added to an ice-cooled solution of LAH (100 mg) in dry ether (4 ml). After addition, the reaction mixture was stirred at room temperature for 2 h followed by the usual work-up afforded a residue. The residue was chromatographed on SiO_2 using $CHCl_3$–MeOH (15 : 1) to give triol **19** (75 mg). recrystallization of triol **19** from MeOH yielded colorless plates, mp 118—119 °C, $[\alpha]_D^{28}$ −40.0° (*c* 1.04, $CHCl_3$); IR ($CHCl_3$) 3420, 3250 cm^{-1}; ^1H NMR δ 0.69, 0.82 (3H each, s, 4-CH_3, 8-CH_3), 0.81 (3H, d, J=7.7 Hz, 1-CH_3), 1.16 (3H, d, J=7.7 Hz, 5-CH_3), 1.10 (1H, d, J=13.6 Hz, 7-H_A), 1.42 (1H, d, J=13.6 Hz, 7-H_B), 2.15 (1H, q, J=7.7 Hz, 5-H), 2.65, 3.20 (1H each, m, OH), 3.26 (1H, br.s, OH), 3.64, 3.84 (1H each, AB type, J=14.4 Hz, $-C\underline{H}_2OH$), 3.72 (1H, dd, J= 7.2, 14.4 Hz, $-CH-HC\underline{H}-OH$), 3.76 (1H, dd, J=4.0, 14.4 Hz, $-CH-HC\underline{H}-OH$) and 3.92 (1H, dd, J=4.0, 7.2 Hz, $-C\underline{H}-(OH)-CH_2OH$); MS *m/z* (%) 225 [75, $(M-31)^+$], 207 (80), 189 (58), 109 (100). Found: C, 69.98; H, 11.04%. Calcd for $C_{15}H_{28}O_3$: C, 70.27; H, 11.01%.

Oxidation of Triol **19** *with* $NaIO_4$. A solution of $NaIO_4$ (25 mg) in H_2O (1 ml) was added to a solution of triol **19** (20 mg) in MeOH (1 ml) and the mixture was stirred at room temperature for 3 h. The reaction mixture was diluted with H_2O and extracted with ether. The residue after usual treatment was chromatographed on SiO_2 and elution with $CHCl_3$–MeOH (25 : 1) afforded aldehyde **20** (16 mg), colorless oil, $[\alpha]_D^{25}$ −3.3° (*c* 0.42, $CHCl_3$); IR (film) 3560, 3450, 1715 cm^{-1}; ^1H NMR δ 0.81 (6H, s, 4-CH_3, 8-CH_3), 0.89 (3H, d, J=7.5 Hz, 1-CH_3), 0.92 (3H, d, J=7.5 Hz, 5-CH_3), 3.55, 3.94 (1H each, d, J=11.0 Hz, $C\underline{H}_2OH$) and 9.69 (1H, s, CHO); MS *m/z* (%) 224 (2, M^+), 206 [15, $(M-H_2O)^+$], 195 (51), 181 (100), 109 (90). Found: *m/z* 224.1771. Calcd for $C_{14}H_{24}O_2$: M, 224.1768.

Oxidation of Aldehyde (**20**) *with MCPBA*. A solution of aldehyde **20** (16 mg) in CH_2Cl_2 (1 ml) was added to a solution of MCPBA (20 mg) and the mixture stirred at room temperature for a day. Then the reaction mixture was treated with Al_2O_3 for 30 min. Al_2O_3 was removed by filtration and the solvent was evaporated to give a residue, which was purified by column chromatography on SiO_2. Elution with $CHCl_3$–MeOH (15 : 1) gave diol **21** (12 mg), colorless oil, $[\alpha]_D^{23}$ −18.4° (*c* 0.57, $CHCl_3$); IR (film) 3325, 1050 cm^{-1}; ^1H NMR δ 0.88 (3H, d, J=7.5 Hz, 1-CH_3), 0.89, 0.93 (3H each, s, 4-CH_3, 8-CH_3), 0.90 (3H, d, J=7.5 Hz, 5-CH_3), 1.47 (1H, d, J= 13.5 Hz, 7-H_A), 1.92 (1H, d, J=13.5 Hz, 7-H_B), 3.42 (2H, AB q, J=11.0 Hz, $-C\underline{H}_2OH$); MS *m/z* (%) 212 (3, M^+, $C_{13}H_{24}O_2$), 194 [5, $(M-H_2O)^+$], 181 [100, $(M-31)^+$], 163 (62), 137 (53), 109 (97).

Oxidation of Diol **21** *with* $NaIO_4$. A solution of $NaIO_4$ (20 mg) in H_2O (1 ml) was added to a MeOH (1.5 ml) solution of diol **21** (17 mg) and the mixture was stirred at room temperature for a day. The reaction mixture was diluted with H_2O and extracted with hexane. The solvent was removed under vacuum to give a residue (15 mg), which was chromatographed on SiO_2. Elution with CH_2Cl_2 yielded ketone **22** (9 mg), colorless oil, CD, $\Delta\varepsilon_{295}$ +2.6 (*c* 0.0115, MeOH); IR (film) 1740 cm^{-1}; ^1H NMR δ 0.81, 0.87 (3H each, s, 4-CH_3, 8-CH_3), 0.93, 0.95 (3H each, d, J=7.5 Hz, 1-CH_3, 5-CH_3), 1.55 (1H, d, J=13.5 Hz, 7-H_A), 2.32 (1H, d, J=13.5 Hz, 7-H_B) and 2.27 (1H, q, J=7.5 Hz, 5-H); MS *m/z* (%) 180 (82, M^+, $C_{12}H_{20}O$), 165 [33, $(M-CH_3)^+$], 123 (46), 109 (100), 82 (88).

Reduction of Ketone **22** *with Lithium Aluminium Hydride*. A mixture of ketone **22** (9 mg) and LAH (20 mg) in dry ether (3 ml) was stirred at room temperature for 2 h. The reaction mixture was treated in the usual way to give a residue (9 mg), which was purified by column chromatography on SiO_2. Elution with $CHCl_3$ gave a minor alcohol **24** (2 mg), colorless oil, IR (film) 3430 cm^{-1}; ^1H NMR δ 0.84, 0.90 (3H each, s, 4-CH_3, 8-CH_3), 0.84 (3H, d, J=7.7 Hz, 1-CH_3), 0.91 (3H, d,

J=7.7 Hz, 5-CH_3), 1.42 (1H, dd, J=5.4, 13.6 Hz, 7-H_A), 1.95 (1H, dd, J=7.2, 13.6 Hz, 7-H_B), 1.77 (1H, m, 1-H), 1.87 (1H, dq, J=7.2, 7.7 Hz, 5-H) and 4.20 (1H, dt, J=5.4, 7.2 Hz, 6-H). Successive elution with the same solvent gave a major alcohol **23** (5 mg), colorless oil, IR (film) 3450 cm^{-1}; ^1H NMR δ 0.75 (6H, s, 4-CH_3, 8-CH_3), 0.84 (3H, d, J=7.7 Hz, 1-CH_3), 0.91 (3H, d, J=7.7 Hz, 5-CH_3), 1.49 (1H, dd, J=7.7, 13.6 Hz, 7-H_A), 1.74 (1H, dq, J=9.4, 7.7 Hz, 5-H), 1.79 (1H, dd, J=7.7, 13.6 Hz, 7-H_B), 2.01 (1H, tq, J=7.2, 8.1 Hz, 1-H), 3.77 (1H, dt, J=9.4, 7.7 Hz, 6-H); MS m/z (%) 164 [32, $(M-H_2O)^+$], 149 [100, $(M-18-15)^+$].

*Conversion of Ketone **22** into Hydrocarbon **25**.* A mixture of ketone **22** (10 mg) in 1,2-ethanedithiol (0.1 ml) and BF_3–Et_2O (2 drops) was kept at room temperature for 2 h. The reaction mixture was poured into ice-water, and extracted with ether. The ether layer was washed with a saturated solution of $NaHCO_3$ and H_2O, and dried over Na_2SO_4. The solvent was removed under vacuum to give a residue, which was desulfurized with Raney Ni (W-4, 50 mg) in EtOH (1.5 ml) under reflux for 2 h. The reaction mixture was filtered and the filtrate was diluted with H_2O, and extracted with pentane. The solvent was removed with N_2 gas to give a colorless residue, which was subjected to GC separation to yield hydrocarbon **25** (4 mg), colorless oil, ^1H NMR δ 0.73 (6H, s, 4-CH_3, 8-CH_3), 0.83 (6H, d, J=7.7 Hz, 1-CH_3, 5-CH_3), 1.27 (2H, m, 3-H_A, 7-H_A), 1.30 (2H, m, 2-H_A, 6-H_A), 1.50 (2H, m, 3-H_B, 7-H_B), 1.73 (2H, m, 2-H_B, 6-H_B), and 1.85 (2H, m, 1-H, 5-H); ^{13}C NMR δ 15.0, 18.0, 31.7, 37.5, 44.4, 53.7; MS m/z (%) 166 (9, M^+, $C_{12}H_{22}$), 151 [51, $(M-CH_3)^+$], 109 (61), 84 (100).

We wish to thank Dr. Jiro Hasegawa of Kyoto Univ. for identification of *Ptychanthus striatus* (LEHM. et LINDENB.) NEES, to Professor Yoshinori Asakawa of Tokushima Bunri Univ. for supply of deoxopinguisone and Professor Koji Nakanishi of our institute director for many discussions.

References

1) V. Benesova, Z. Samek, V. Herout, and F. Sorm, *Coll. Czech. Chem. Comm.*, **34**, 582 (1969); H. Knoche, G. Ourisson, G. W. Perold, J. Foussereau, and J. Maleville, *Science*, **166**, 239 (1969); S. Huneck, *J. Hattori Bot. Lab.*, **43**, 468(1972); N. H. Andersen, B. Shunk, and C. R. Costin, *Experimentia*, **29**, 645 (1973); S. Hayashi and A. Matsuo, *Hikobia*, **7**, 125 (1975); C. Suire, *Rev. Bryol. Lichen.*, **41**, 105 (1975); Y. Asakawa, T. Takemoto, M. Toyota, and T. Aratani, *Tetrahedron Lett.*, **1977**, 1407; "Progress in Phytochemistry," ed by L. Reinhold, J. B. Harborne, and T. Swain, Pergamon Press, London (1978), Vol. 5, p. 181.

2) S. M. Krutov, Z. Samek, V. Benesova, and V. Herout, *Phytochemistry*, **12**, 1405 (1973).

3) Y. Asakawa, C. Suire, M. Toyota, N. Tokunaga, T. Takemoto, S. Hattori, and M. Mizutani, *J. Hattori Bot. Lab.*, **46**, 77 (1980).

4) R. Takeda, R. Mori, and Y. Hirose, *Chemistry Lett.*, **1982**, 1625.

5) R. Takeda, H. Naoki, T. Iwashita, and Y. Hirose, *Tetrahedron Lett.*, **22**, 5307 (1981).

6) The present result was confirmed by NOE difference spectrum.

7) C. L. Kissel and B. Rickborn, *J. Org. Chem.*, **37**, 2060 (1972).

8) N. Harada, J. Iwabuchi, Y. Yokota, H. Ueda, and K. Nakanishi, *J. Am. Chem. Soc.*, **103**, 5590 (1981).

9) N. C. Gonnella, K. Nakanishi, V. S. Martin, and K. B. Sharpless, *J. Am. Chem. Soc.*, **104**, 3775 (1982).

10) P. J. Kropp and H. J. Krauss, *J. Am. Chem. Soc.*, **89**, 5199 (1967); S. G. Levine and B. Gopalakrishnan, *Tetrahedron Lett.*, **1979**, 699.

11) Y. Asakawa, N. Tokunaga, M. Toyota, T. Takemoto, and C. Suire, *J. Hattori Bot. Lab.*, **45**, 395 (1979).

12) B. M. Howard and W. Fenical, *Tetrahedron Lett.*, **1976**, 41.

13) G. Cimino, S. D. Stefano, A. Gueriero, and L. Minale, *Tetrahedron Lett.*, **1975**, 3723.

14) G. Cimino, S. D. Stefano, A. Gueriero, and L. Minale, *Tetrahedron Lett.*, **1975**, 1417, 1425; R. J. Capon, E. L. Ghisalberti, and P. R. Jefferies, *Aust. J. Chem.*, **34**, 1775 (1981).

15) P. Main, S. E. Hull, L. Lessinger, G. Germain, J. P. Declercq, and M. M. Woolfson (1978). MULTAN78, A System of Computer Pograms for the Automatic Solution of Crystal Structures from X-ray Diffraction Data. University of York, England, and Louvain, Belgium.

16) "International Tables for X-Ray Crystallography," Kynoch Press, Birmingham (1974), Vol. IV.

17) The Universal Crystallographic Computing System (1979). Library of Programs, Osaka University, Computing Center.

18) W. Moffitt, R. B. Woodward, A. Moscowitz, W. Klyne, and C. Djerassi, *J. Am. Chem. Soc.*, **83**, 4013 (1961); "Natural Products Chemistry," ed by K. Nakanishi, T. Goto, S. Ito, S. Natori, and S. Nozoe, Kodansha, Tokyo and Academic Press, N. Y., London (1974), Vol. 1, p. 28.

19) A. Corbella, P. Gariboldi, G. Jommi, F. Orsini, A. DeMarco, and A. Immirzi, *J. Chem. Soc., Perkin Trans. I*, **1974**, 1875.

 © 1983 The Chemical Society of Japan Bull. Chem. Soc. Jpn., 56, 1133—1138 (1983)

Mechanism for the Oxidative Cleavage of Electron-deficient Acetylenes with Alkaline Hydrogen Peroxide[1]

Yasuhiko SAWAKI,* Hiroshi INOUE, and Yoshiro OGATA
Department of Applied Chemistry, Faculty of Engineering, Nagoya University, Chikusa-ku, Nagoya 464
(Received August 26, 1982)

4-Phenyl-3-butyn-2-one (**1a**) was effectively cleaved by alkaline hydrogen peroxide to afford benzoic and acetic acids. The rate ratio for the addition of HOO^- and HO^- to **1a** resulted in $k_{HOO^-}/k_{HO^-}=1400$, which is comparable to that of benzylideneacetone. The major reaction of the cleavage proceeds *via* benzoylacetone. As a minor pathway, α-keto oxirene intermediate is formed and rearranges only to α-benzoylpropionate in a different way from the corresponding diketo carbene. α-Keto esters are found to be converted by HOO^- to α-alkoxy ketones *via* a novel oxidative substitution of ester group. Methyl phenylpropiolate is oxidized by HOO^- similarly as **1a**. The mechanism is discussed on the basis of oxirene intermediate inconvertible to keto carbene.

The peroxy acid oxidation of acetylenes is understood much less than that of olefins;[2] its mechanism has been discussed in relation to oxirene and keto carbene intermediates.[2,3] The two intermediates are also interested theoretically[4a,b] since oxirenes are anti-aromatic 4π-electron species.[4c] Recently, we have reported that oxirene intermediates produced from phenylacetylenes and peroxy acid are further oxidized or rearrange to ketenes (Eq. 1), but are not convertible to keto carbenes.[5]

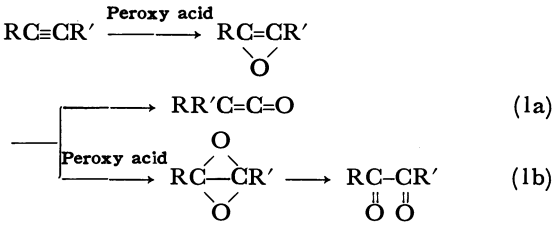

Acetylenes are known to be less reactive toward electrophiles but more reactive toward nucleophiles than olefins.[6] Although the epoxidation of α-keto olefins with alkaline hydrogen peroxide is well known,[7] few is known about the nucleophilic oxidation of acetylenes by peroxides. We were interested in the alkaline hydrogen peroxide oxidation of electron-deficient acetylenes,[8] and herein wish to summarize our mechanistic study on the facile C–C cleavage. A study on similar cleavage of acetylenes has appeared,[9] but mechanistic details are still unclear.

Results and Discussion

Oxidative Cleavage of Acetylenes with HOO^-. An attempted oxidation of phenylacetylene with alkaline hydrogen peroxide (HOO^-) was ineffective, but electron-deficient acetylenes are smoothly cleaved by HOO^-. Thus, the oxidation of 0.1 M 4-phenyl-3-butyn-2-one (**1a**) with 1 M H_2O_2 and 0.2 M NaOH in 50% EtOH was complete within 2 h at room temperature (1 M=1 mol dm^{-3}). One molar acetylene consumed

$$\underset{\textbf{1a}}{PhC{\equiv}CCOMe} \xrightarrow{HOO^-} \underset{95\%}{PhCO_2H} + \underset{93\%}{MeCO_2H} + \underset{48\%}{CO_2} \qquad (2)$$

three moles of H_2O_2, affording high yields of benzoic and acetic acids; the yield of CO_2 was not quantitative and formic acid was detectable.

Similar oxidation of methyl phenylpropiolate ($PhC{\equiv}CCO_2Me$, **1b**) with excess HOO^- afforded $PhCO_2H$ (99%) and CO_2 (96%). Here, 96% yield of CO_2 does not mean quantitative one since **1b** possesses two carbons available for decarboxylation. As the excess amount of H_2O_2 was decreased, the hydrolysis of **1b** became a major path and the resulting propiolate ion was quite stable toward HOO^-. 55—70% yields of C–C cleavage has been reported for the case of 4-phenyl-3-butyn-2-ones,[9] but present results indicate that almost quantitative cleavage may be accomplished by using excess H_2O_2 in aqueous alcohols.

Kinetics. The rate of addition of HOO^- to acetylene **1a** was determined in water by following the decrease of **1a** using excess H_2O_2. The rate increased linearly with $[HO^-]$ up to pH 11, reaching a constant value at pH>12 and pK_a of H_2O_2 is 11.37; hence the rate quation satisfies Eq. 3.

$$v = k_2[PhC{\equiv}CCOMe][HOO^-] \qquad (3)$$

The rate constants, $10\,k_2$, for **1a** are 1.04, 1.39, 1.97, 2.50, and 3.47 $M^{-1}\,s^{-1}$ at 15.0, 20.0, 25.0, 30.0, and 35.0 °C, respectively, at pH 11.2 (Na_2CO_3 buffer). For comparison, the epoxidation rate of benzylideneacetone (**2**) was also determined; $10\,k_2$=1.40, 1.76, 2.32, 3.03, and 3.79 $M^{-1}\,s^{-1}$, respectively. The resulting activation parameters are listed in Table 1.

The addition rate of HO^- (0.05—0.28 M) for **1a** to form benzoylacetone was found to be a combination of two- and third-order kinetics (Eq. 4).

$$v = \{k_2[HO^-]+k_3[HO^-]^2\}[PhC{\equiv}CCOMe] \qquad (4)$$

The third-order kinetics suggest a base-catalysis by second HO^- ion, *i.e.*, an attack with $HO^-\cdots HO^-$. Similar third-order kinetics are known for nucleophilic additions[11] such as hydrolysis[12] and aminolysis[13] of esters.

It is generally accepted that acetylenes are more susceptible to nucleophilic attacks than olefins.[6] But acetylene **1a** and olefin **2** have rates of similar magnitude for both additions of HOO^- and HO^-. A small kinetic differences between **1a** and **2** lies in the change in activation parameters; while the activation enthalpy (ΔH^*) for acetylene **1a** is slightly higher than olefin **2**, entropy requirement for **1a** is substantially smaller. The larger entropy loss for olefin **2** is probably due to the rather restricted orientation in the Michael addition

TABLE 1. KINETIC DATA FOR THE ADDITION OF HOO^- AND HO^- TO PhC≡CCOMe (**1a**) AND PhCH=CHCOMe (**2**) IN WATER AT 25.0 °C[a)]

Substrate	Nucleophile	k_2 / $M^{-1}\,s^{-1}$	k_3 / $M^{-2}\,s^{-1}$	ΔH^* / kcal mol^{-1}	ΔS^* / e.u.	α-Effect
1a	HOO^-	1.67×10^{-1}		11.0	−18	1.39×10^3
	HO^-	1.20×10^{-4}	8.5×10^{-3}			
2	HOO^-	2.20×10^{-1}		9.1	−24	1.92×10^3
	HO^-	1.14×10^{-4}	2.2×10^{-4}			

a) The oxidation was conducted with 5×10^{-5} M substrate and 2—10 mM H_2O_2 in an aqueous buffer of 0.1 M Na_2CO_3. The addition reaction of HO^- was carried out with 5×10^{-5} substrate and and 0.05—0.3 M NaOH. The rates were monitored by the decrease of UV absorbance of **1a** or **2**. Notations for k_2 and k_3 are shown in Eqs 3 and 4.

TABLE 2. OXIDATION: OF ACETYLENES AND RELATED COMPOUNDS WITH ALKALINE H_2O_2[a)]

Substrate (S)	S : H_2O_2	Products (%)[b)]					
		$PhCO_2H$	**3**	**4**	**5**	**6a**	Others
PhC≡CCOMe (**1a**)	1 : 1	46	24	3	2	2	$PhCO_2Me$ (1%), Adducts (28%)[c)]
	1 : 5	92	5	6	2	1	
	1 : 0	0	12	0	0	0	MeOH adducts (70%)[c)]
	1 : 1[d)]	40	22	6	2	<1	e)
	1 : 1[f)]	50	17	6	2	<1	e)
$PhCOCH_2COMe$ (**3**)	1 : 1	27	73[g)]	0	0	0	
	1 : 5	71	14[g)]	0	0	0	
$PhCOCH(Me)CO_2Me$ (**7a**)	1 : 1	19	0	11	17	33	
	1 : 5	32	0	11	16	16	
	1 : 0	0	0	≈10	10	0	Recovered **7a** (80%)
$MeCOCH(Ph)CO_2Me$ (**7c**)	1 : 5	22	0	0	0	39[h)]	$PhCH_2COMe$ (16%); $PhCH_2CO_2Me$ (2%)
	1 : 0	0	0	0	0	0[h)]	$PhCH_2CO_2Me$ (85%)
PhC≡CCO_2Me (**1b**)	1 : 1	45			1[i)]	5[j)]	$PhCO_2Me$ (22%); PhC≡CCO_2H (20%)
	1 : 5	56			1[i)]	0[j)]	$PhCO_2Me$ (6%); PhC≡CCO_2H (25%)
	1 : 0	0			0[i)]	0[j)]	Adduct[k)] (10%); **1b**[g)] (90%)
$PhCOCH_2CO_2Me$ (**7b**)	1 : 1	34			3[i)]	19[j)]	Recovered **7b** (33%)
	1 : 5	70			3[i)]	14[j)]	
	1 : 0	0			0[i)]	0[j)]	Recovered **7b** (100%)

a) Reaction with 0.02 M substrate and 0.1 M MeONa at 20—25 °C for 1 h. b) Products were determined by GLC and/or NMR. c) Ph(MeO)C=CHCOMe; cis : trans ratio being 7 : 3. d) Reaction in EtOH. e) Not determined. f) Reaction in *i*-PrOH. g) Recovered. h) **6c**. i) Acetophenone. j) **6b**. k) Ph(MeO)C=$CHCO_2Me$; cis : trans ratio of *ca.* 1 : 1.

to the planar olefin. On the other hand, the addition to linear acetylenic moiety of **1a** requires smaller restriction on orientation, thus lowering entropy loss in attaining the transition state.

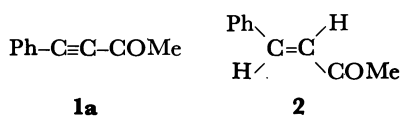

1a **2**

The rate ratio of HOO^- *vs* HO^- is known to exhibits a large α-effect;[14] *e.g.*, the α-effect in the addition to nitriles is in the range of 3000—10000.[15] The ratios k_{HOO^-}/k_{HO^-} for the present reaction are 1400 and 1900 for acetylene **1a** and olefin **2**, respectively (Table 1). A trend has been noted that nucleophilic additions to sp carbon exhibit a larger α-effect than addition to sp^2 carbon.[16] But no significant difference was found between acetylene **1a** (*i.e.*, sp carbon) and olefin **2** (*i.e.*, sp^2 carbon). It seems that there is no single factor to govern the α-effect, although several explanations have been noted on the origin of the effect.[17]

Intermediates. In order to clarify the oxidation mechanism, searches for intermediates were carried out with 1 h reaction in MeOH. GLC, NMR, and GC-MS analyses indicated several intermediates during the oxidation with HOO^- (Table 2). Considerable amounts of adducts with solvent MeOH were produced when **1a** : H_2O_2 was 1 : 1, but became negligible with **1a** : H_2O_2=1 : 5. Products from **1a** and HOO^- are shown in Eq. 5; major intermediates were benzoylacetone **3** and α-benzoylpropionic acid **4**. Minor byproducts were propiophenone **5** and α-methoxypropio-

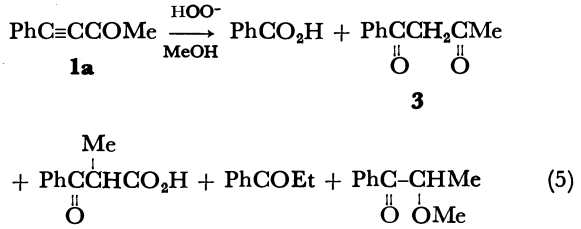

1a **3**

4 **5** **6a** (5)

phenone **6a**, both of which were shown to be produced from methyl α-benzoylpropionate (**7a**) by a control experiment.

The reaction of methyl phenylpropiolate (**1b**) with HOO⁻ afforded, in addition to benzoic and phenylpropiolic acids, methyl benzoate, acetophenone, and α-methoxyacetophenone in MeOH (Table 2). Again, control experiments revealed that the latter two products

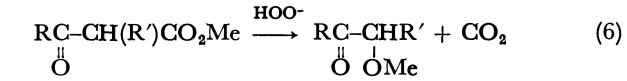

(6)

7 **6**

a, R=Ph, R′=Me
b, R=Ph, R′=H
c, R=Me, R′=Ph

are formed from methyl benzoylacetate (**7b**) and HOO⁻. Thus the formation of α-alkoxy ketones (**6**) from β-keto esters is a novel oxidative substitution of ester group (Eq. 6). The yield of **6** is 33, 19, and 39% from **7a**, **7b**, and **7c**, respectively. For the case of **7b**, its reaction with MeONa alone yielded methyl phenylacetate *via* MeO⁻-catalyzed deacylation.

Decomposition of Diazo Diketone. In the decomposition of α-diazo ketones, ketocarbene-ketocarbene interconversions have been proved experimentally, where oxirenes are often supposed to be an intermediate (Eq. 7).[18] On the other hand, it is reasonable to assume

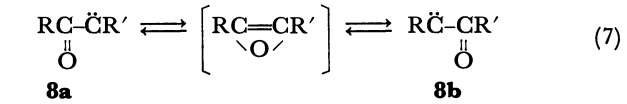

(7)

8a **8b**

that acetylenes are attacked electrophilically by peroxy acid to form oxirenes in analogy with olefin epoxidation.[3,5] Likewise, a generation of oxirene intermediate is conceivable in the present nucleophilic oxidation of acetylene **1a** or **1b** with HOO⁻.[9] In order to check the intermediacy of oxirene and/or keto carbene, the decomposition of 2-diazo-1-phenyl-1,3-butanedione (**9**) was carried out in alcohols (Table 3). Major products *via* carbene **10** were rearranged esters (**11** and **12**), O–H inserted diketones **13** and **14** (Eq. 8), diketone **14** being formed *via* O–H insertion of isomerized keto carbene from **10**. Benzoylacetone **3**, a hydrogen abstraction

Table 3. Photolysis and thermolysis of diazo ketone (**9**)[a]

Solvent	Conditions	Products (%)[b]				
		11	**12**	**13**	**14**	**3**
MeOH	*hν*(>290 nm)/8 h	26	13	26	≈10	0
	hν(290 nm)/N_2/8 h	26	11	28	≈13	0
	hν(254 nm)/4 h	21	11	20	≈3	0
	Δ(80 °C)/4 h	15	28	21	≈10	<1
EtOH	*hν*(>290 nm)/5 h	30	11	17	≈3	≈1
	hν(254 nm)/5 h	38	13	10	≈11	≈3
	Δ(95 °C)/4 h	16	27	16	≈12	8

a) A solution of 0.02 M **9** was photolyzed at room temperature or thermolyzed under air unless noted otherwise. b) Products were detemined by NMR, GLC, and GC-MS. The structure of diketone **14** was deduced from its GC-MS spectra although it could not be isolated.

product, was negligible in MeOH (Eq. 8). The product ratios were not changed largely by changing the decomposition conditions, *e.g.*, wavelength of irradiating light,[19] air, or temperature. Somewhat different ratio

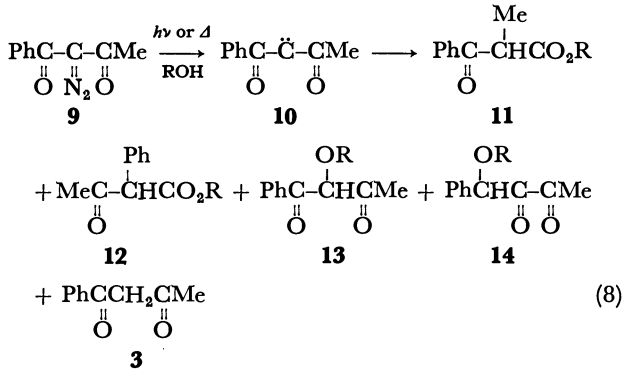

(8)

9 **10** **11** **12** **13** **14** **3**

of products has been reported for the photolysis of **9**.[21] The present values are more accurate since the reaction mixture was analyzed directly by NMR and GLC. At any rate, it is apparent that β-diketone **3** is not formed in MeOH and the Wolff rearrangement afforded two products **11** and **12** by methyl and phenyl migration.

Oxidation Mechanism. One of mechanistic points for the HOO⁻ oxidation of electron-deficient acetylenes lies in the intermediacy of oxirene and/or keto carbene. As noted above, acetylbenzoylcarbene **10** affords two products *via* the Wolff rearrangement (*i.e.*, **11** and **12** by Me and Ph migration), but benzoylacetone **3** is not formed in MeOH. In contrast, major primary products for the reaction of **1a** and HOO⁻ are β-diketone **3** and rearranged ester **7a**, which is converted to hydrolyzed acid **4**, propiophenone **5**, and α-methoxypropiophenone (**6a**) (Eq. 5). It is noteworthy that any products (*e.g.*, methyl phenylacetate or α-methoxybenzyl methyl ketone (**6c**)) were not detectable. Therefore, keto carbene (*e.g.*, **10**) is not involved in the HOO⁻ oxidation of **1a**, excluding an equilibrium reaction such as Eq. 7. This is consistent with our recent results not involving ketocarbene in the electrophilic oxidation of phenylacetylenes with peroxy acid.[5] According to calculation by MINDO/3 method oxirene is more stable than keto carbene,[22] but more rigorous ab initio methods leads to a reverse result.[23] Our previous[5] and present studies suggest a rearrangement *via* oxirene itself and a significant energy barrier in isomerization between oxirene and keto carbene.

A reasonable pathway for the nucleophilic oxidation of **1a** would then be formulated as Scheme 1. The addition of HOO⁻ to **1a** produces **15a**, which cyclizes to form α-keto oxirene **16** or is protonated to yield adduct **15b**.[24] For the case of olefinic ketones, the cyclization to epoxides is very facile.[7] But for acetylenic ketones the cyclization to oxirene **16** would be significantly retarded owing to its large strain energy.[25]

Recently we have reported that the migration aptitude in oxirene rearrangement (*i.e.*, H≫Me>Ph) is in line with that of the Wolff rearrangement of keto carbene.[5] In fact, the rearrangement of ketocarbene **10** afforded two products **11** and **12** by Me and Ph migration, respectively. In contrast, the present oxidation of **1a** with HOO⁻ yielded only **7a** as a rearranged product.

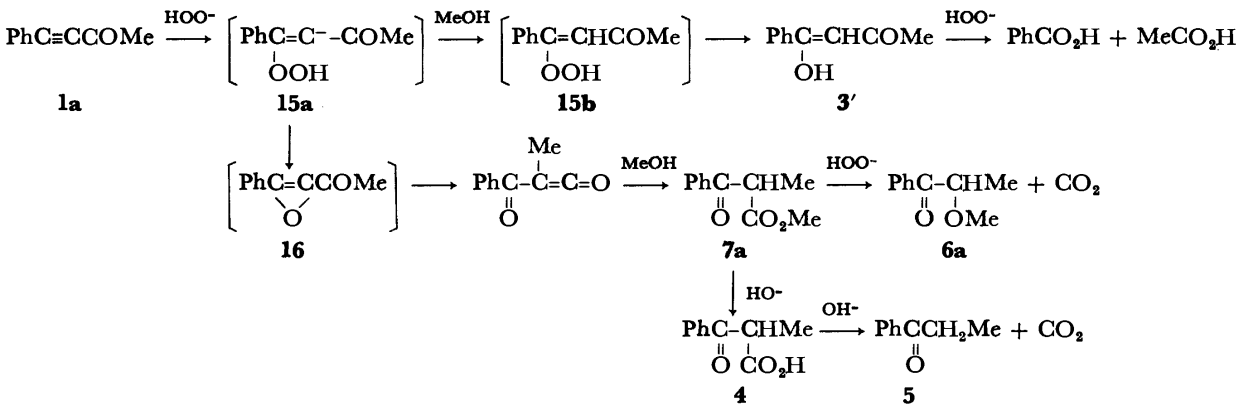

Scheme 1.

This is comprehensible because oxirene **16** is unsymmetrically substituted and the two groups are attacked to different migration origins, *i.e.*, methyl group to carbonyl and phenyl group to oxirene. Methyl migration in oxirene **16** affords β-benzoyl ester **7a** *via* ketene. Subsequent decarboxylation of β-keto acids is well known.[26]

The novel reaction of β-keto esters with HOO^- to afford α-alkoxy ketones is interesting mechanistically. An appropriate scheme for this oxidative substitution is outlined in Eq. 9, which is somewhat similar to the ring contruction of β-diketones with H_2O_2 (*e.g.*, the synthesis of cyclopentanecarboxylic acid from α-acylcyclohexanone).[27]

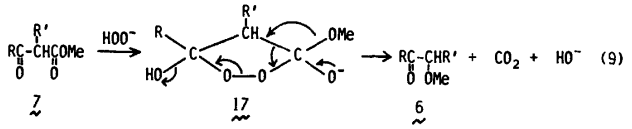

(9)

As a major pathway for the HOO^- oxidation of **1a**, carbanion **15a** is protonated to form olefinic hydroperoxide **15b**, which would be promptly decomposed into β-diketone **3** (or its enol **3'**).[28] The diketone **3** could be isolated in *ca.* 30% yield from the reaction mixture at an earlier stage. A possible scheme for the cleavage of **3** is probably *via* an epoxidation of enol **3'** (Eq. 10).[29]

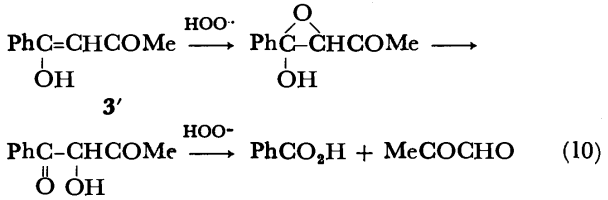

(10)

The facile cleavage of α-hydroxy ketones with HOO^- is reported previously.[30a] The involvement of pyruvaldehyde is in agreement with a fact that CO_2 yields from the aldehyde were in the same range (40—50%) with those from diketone **3'** when treated with a mixture of 1.2 M H_2O_2 and 0.2 M NaOH in 50% EtOH.[30b]

The HOO^- oxidation of **1b** would proceed similarly as Scheme 1. The formation of methyl benzoate seems to suggest a diepoxide pathway (Eq. 11). Since methoxyl group in **18** is probably of very low migratory aptitude, oxirene **18** is further oxidized to diepoxide and then to α-diketone. Ester formation from α-diketone and HOO^-/MeO^- is established.[31]

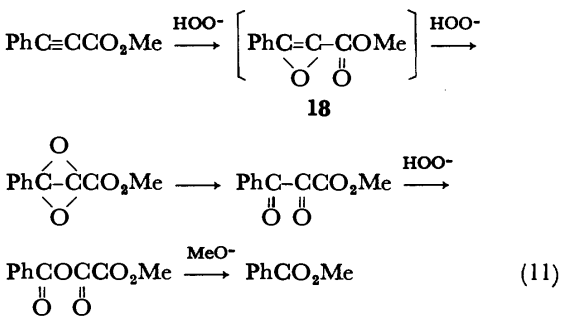

(11)

In conclusion, acetylenic ketone **1a** is cleaved efficiently by HOO^-, β-diketone **3** being a predominant intermediate. α-Keto oxirene is probably formed even as a minor pathway and affords rearranged products in a different way from the corresponding diazo ketone. β-Keto esters are found to be oxidized by HOO^- to α-alkoxy ketones *via* a novel oxidative substitution of ester group.

Experimental

IR and NMR spectra were recorded on a Parkin-Elmer 337 and a Hitachi R-24 spectrometer, respectively. GLC analysis was carried out by a Yanagimoto G-180 gas chromatograph using biphenyl as an internal standard and three columns: PEG 20M, 10% on Chromosorb WAW, 1 m; Silicon OV-17, 5% on Shimalite W, 1 m; Apiezone GE 15% and 5% H_3PO_4 on Celite 545, 1.5 m. GC-MS spectra were recorded on a JEOL JMS D300 mass spectrometer.

Materials. 4-Phenyl-3-butyn-2-one (**1a**),[32] methyl phenylpropiolate (**1b**),[33] and methyl α-benzoylpropionate (**7a**)[34] were prepared by the literature methods. Methyl α-acetylphenylacetate (**7c**) was prepared from α-phenylacetoacetonitrile.[35] α-Methoxypropiophenone (**6a**) and α-methoxy-α-phenylacetone (**8c**) were obtained by BF_3-catalyzed decomposition[36] of α-diazopropiophenone[37] and 1-diazo-1-phenyl-2-propanone.[38] 2-Diazo-1-phenyl-1,3-butanedione (**9**) was synthesized from benzoylacetone and tosyl azide.[39] Purities of these materials were checked by NMR and/or GLC analysis.

Oxidation of 4-Phenyl-3-butyn-2-one (1a) with HOO^-. In a 50-ml flask were added EtOH (6 ml), 4 M H_2O_2 (12 ml), **1a** in EtOH (1 M×2 ml), water (10 ml), 10^{-2} M EDTA (2 ml), and 1 M NaOH (8 ml). After 10 h at 25 °C, 1 M HCl (10 ml) was added and evolved CO_2 gas was determined by titration with aqueous $Ba(OH)_2$. Then the reaction mixture was

diluted with saturated NaCl and extracted three times with ether. Benzoic and acetic acids were determined by GLC after methylation with diazomethane.

In another run, benzoylacetone **3** could be isolated from 15 min reaction of 0.08 M **1a**, 0.17 M H_2O_2, and 0.17 M NaOH in 50% EtOH at 25 °C. After acidification with HCl, dilution with water, and extraction with ether, 30% of **3** was isolated by column chromatography using Mallinckrodt silica gel (100 mesh, pH 4) and petroleum ether–chloroform (2 : 1). Its NMR and IR spectra were identical with those of authentic sample.

The addition rate of HOO^- was followed by UV absorbance of **1a** at 277 nm in water. The reaction was conducted with 5×10^{-5} M **1a** and 2—10 mM H_2O_2 in buffered aqueous solution. The results are listed in Table 1.

Decomposition of 2-Diazo-1-phenyl-1,3-butanedione (9). Photolysis of **9** was conducted with a low pressure (254 nm) or medium pressure Hg lamp (>290 nm through Pyrex filter). Typically, a solution of 0.02 M **9** in alcohol was photolyzed for 4—8 h at room temperature. Thermolysis was carried out at 80 °C in MeOH or 90 °C in EtOH. The products were identified and determined by NMR, GLC and/or GC-MS analyses.

NMR and GC-MS Data. NMR data for products and authentic sample are as follows (δ, $CDCl_3$). Benzoylacetone (**3**): 2.17 (s, 3H), 6.15 (s, 1H), 7.4—8.0 (m, 5H); minor keto isomer: 2.27 (s, 3H), 4.07 (s, 2H). Methyl α-benzoylpropionate (**7a**): 1.50 (d, J=5.6 Hz, 3H), 3.68 (s, 3H), 4.41 (q, J=5.6 Hz, 1H), 7.4—7.6 (m, 3H), 7.9—8.1 (m, 2H). α-Methoxypropiophenone (**6a**): 1.43 (d, J=6.7 Hz, 3H), 3.29 (s, 3H), 4.42 (q, J=6.7 Hz, 1H), 7.4—7.6 (m, 3H), 7.9—8.2 (m, 2H). Methyl α-benzoylacetate (**7b**); keto isomer: 3.64 (s, 3H), 3.86 (s, 2H); enol isomer: 3.73 (s, 3H), 5.62 (s, 1H), 12.66 (s, 1H); 7.3—8.0 (m, 5H). Methyl α-acetylphenylacetate (**7c**): 2.06 (s, 3H), 3.65 (s, 3H), 4.52 (s, 1H), 7.23 (s, 5H). α-Methoxyacetophenone (**6b**): 3.40 (s, 3H), 4.50 (s, 2H), 7.4—7.6 (m, 3H), 7.85—8.04 (m, 2H). α-Methoxy-α-phenylacetone (**6c**): 2.11 (s, 3H), 3.89 (s, 3H), 4.67 (s, 1H), 7.39 (s, 5H); GC-MS, *m/e* (relative intensity), 43, 121 (100%), 164 (<1%).

2-Methoxy-1-phenyl-1,3-butanedione (**13**, R=Me): 2.24 (s, 3H), 3.30 (s, 3H), 7.2—7.6 (m, 5H), 14.95 (s, 1H); GC-MS, *m/e* (rel intensity), 105 (100), 118 (25), 150 (35), 160 (11), and 192 (3). 1-Methoxy-2-phenyl-1,3-butanedione (**14**, R=Me): 2.36 (s, 3H), 3.54 (s, 3H), 5.10 (s, 1H); GC-MS, *m/e* (rel intensity), 105 (18), 118 (60), 150 (100), 160 (27), and 192 (9). 2-Ethoxy-1-phenyl-1,3-butanedione (**13**, R=Et): 1.18 (t, J=5 Hz, 3H), 2.34 (s, 3H), 3.58 (q, J=5 Hz, 2H), 15.2 (s, 1H); GC-MS, *m/e* (rel intensity), 91 (4), 105 (100), 118 (21), 136 (11), 160 (14), 164 (36), and 206 (4). 1-Ethoxy-2-phenyl-1,3-butanedione (**14**, R=Et): 1.21 (t, J=5 Hz, 3H), 2.29 (s, 3H), 3.70 (q, J=5 Hz, 2H), 5.13 (s, 1H); GC-MS, *m/e* (rel intensity), 91 (9), 105 (17), 118 (49), 136 (30), 160 (34), 164 (100), 165 (11), and 206 (8).

References

1) Contribution No. 302.

2) D. Swern, "Organic Peroxides," ed by D. Swern, Wiley, New York, N. Y. (1971), Vol. 2, p. 476; B. Plesnicar, "Oxidation in Organic Chemistry," ed by W. S. Trahanovsky, Academic Press, New York (1978), Part C, p. 212.

3) R. N. McDonold and P. A. Schwab, *J. Am. Chem. Soc.*, **86**, 4866 (1964); J. Ciabattoni, P. A. Campbell, C. A. Renner, and P. W. Concannon, *J. Am. Chem. Soc.*, **92**, 3826 (1970); P. W. Cancannon and J. Ciabattoni, *ibid.*, **95**, 3284 (1973); Y. Ogata, Y. Sawaki, and H. Inoue, *J. Org. Chem.*, **38**, 1044 (1973); K. M. Ibne-Rasa, R. H. Pater, J. Ciabattoni, and J. O. Edwards, *J. Am. Chem. Soc.*, **95**, 7894 (1973).

4) a) W. M. Jones, "Rearrangements in Ground and Excited States," ed by P. de Mayo, Academic Press, New York, N. Y. (1980), Vol. 1, p. 119; b) A. Greenberg and J. F. Liebman, "Strained Organic Molecules," Academic Press, New York, N. Y. (1978), p. 312; c) R. Breslow, *Angew. Chem., Int. Ed., Engl.*, **7**, 565 (1968).

5) Y. Ogata, Y. Sawaki, and T. Ohno, *J. Am. Chem. Soc.*, **104**, 216 (1982).

6) J. I. Dickson and S. I. Miller, "The Chemistry of the Carbon-Carbon Triple Bonds," ed by S. Patai, Wiley, Chichester (1978), Part 2, p. 814.

7) H. O. House, "Modern Synthetic Reactions," 2nd ed, Benjamin, Calif. (1972), p. 306.

8) Parts of this work were taken from the Master Dissertation of H. Inoue, Nagoya University, 1973.

9) H. Kropf and R. Schroeder, *Justus Liebigs Ann. Chem.*, **1976**, 2325.

10) J. E. McIsaac, Jr., L. R. Subbaraman, J. Subbaraman, H. A. Mulhausen, and E. J. Behrman, *J. Org. Chem.*, **37**, 1037 (1972).

11) M. L. Bender, "Mechanism of Homogeneous Catalysis from Protons to Proteins," Wiley, New York, N. Y. (1971), p. 321.

12) T. C. Bruice, J. J. Bruno, and W. S. Chor, *J. Am. Chem. Soc.*, **85**, 1659 (1963).

13) W. P. Jencks and J. Carriuolo, *J. Am. Chem. Soc.*, **82**, 675 (1960); T. C. Bruice and S. J. Benkovic, *ibid.*, **86**, 418 (1964); F. M. Menger and J. H. Smith, *ibid.*, **94**, 3825 (1972).

14) N. J. Fina and J. O. Edwards, *Int. J. Chem. Kinet.*, **5**, 1 (1973); A. P. Grekov and V. Ya, *Russ. Chem. Rev.*, **47**, 661 (1978).

15) Y. Sawaki and Y. Ogata, *Bull. Chem. Soc. Jpn.*, **54**, 793 (1981).

16) S. Oae, Y. Kadoma, and Y. Yano, *Bull Chem. Soc. Jpn.*, **42**, 1110 (1969).

17) For example, J. O. Edwards and R. G. Pearson, *J. Am. Chem. Soc.*, **84**, 16 (1962); J. Gerstein and W. P. Jencks, *ibid.*, **86**, 4655 (1964); J. E. Dixon and T. C. Bruice, *ibid.*, **93**, 6592 (1971); J. L. Kice and L. F. Mullan, *ibid.*, **98**, 4259 (1976).

18) W. Kirmse, "Carbene Chemistry," 2nd ed, Academic Press, New York, N. Y. (1971), p. 475; H. Meier, K.-P. Zeller *Angew. Chem., Int. Ed., Engl.*, **14**, 32 (1975); W. M. Jones, Ref 4a, p. 95.

19) A significant wavelength effect has been reported in the photolysis of dibenzoyldiazomethane.[20] H-abstraction became predominant when irradiating at 254 nm in EtOH. We ascertained this tendency; the photolysis at 366 nm or thermolysis at 80 °C afforded in turn rearranged product predominantly.

20) N. Baumann, *Helv. Chim. Acta*, **55**, 2716 (1972).

21) K.-P. Zeller, H. Meier, and E. Müller, *Tetrahedron*, **28**, 5831 (1972).

22) M. J. S. Dewar and C. A. Ramsden, *J. Chem. Soc., Chem. Commun.*, **1973**, 688.

23) O. P. Strausz, R. K. Gosavi, A. S. Denes, and I. G. Csizmadia, *J. Am. Chem. Soc.*, **98**, 4784 (1976); K. Tanaka and M. Yoshimine, *ibid.*, **102**, 7655 (1980).

24) Of a similar situation is the addition of *t*-BuOO⁻ to α-vinyl ketones; N. C. Yang and R. A. Finnegan, *J. Am. Chem. Soc.*, **80**, 5845 (1958).

25) Strain energy for oxirene ring may be assumed to be *ca.* 55 kcal/mol; P. v. R. Schleyer, J. E. Williams, and K. R. Blanchard, *J. Am. Chem. Soc.*, **92**, 2377 (1970).

26) J. Hine, "Physical Organic Chemistry," McGraw-Hill,

New York, N. Y. (1956), p. 283.
27) G. B. Payne, *J. Org. Chem.*, **26**, 4793 (1961).
28) Hydroperoxy olefin such as **15b** where HOO group is directly attached to double bond carbon is unknown. Although details for the conversion of **15** into **3'** is ambiguous, we feel a homolytic path is possible.
29) Similar α-ketol formation is known in the peroxy acid oxidation of β-diketones; H. O. House and W. F. Gannon, *J. Org. Chem.*, **23**, 879 (1958).
30) a) Y. Ogata, Y. Sawaki, and M. Shiroyama, *J. Org. Chem.*, **42**, 4061 (1977); b) Under the same conditions, pyruvic acid afforded a quantitative yield of CO_2.
31) Y. Sawaki and C. S. Foote, *J. Am. Chem. Soc.*, **101**, 6292 (1979).
32) D. Nightingate and F. Wadsworth, *J. Am. Chem. Soc.*, **67**, 416 (1945).
33) T. W. Abbot, "Organic Syntheses," Wiley, New York, N. Y. (1943), Vol. 2, p. 515. The acid was methylated *via* the acid chloride.
34) E. E. Royals, *J. Am. Chem. Soc.*, **70**, 487 (1948).
35) R. H. Kimball, C. D. Jefferson, and A. B. Pike, *Org. Synch.*, Coll. Vol. II, 284 (1943); P. L. Julian, J. J. Oliver, R. H. Kimball, A. B. Pike, and G. D. Jefferson, *ibid.*, p. 487.
36) M. S. Newman and P. F. Beal, III, *J. Am. Chem. Soc.*, **72**, 5161 (1950).
37) A. L. Wilds and A. L. Meader, *J. Org. Chem.*, **13**, 763 (1948).
38) M. Regitz, *Chem. Ber.*, **98**, 1210 (1965).
39) M. Regitz, *Chem. Ber.*, **99**, 3128 (1966).

Bitter Limonoids from the Fruit of *Melia azedarach* L. *var. japonica* Makino[1)]

Yoshiyasu FUKUYAMA,† Iwao MIURA,† and Masamitsu OCHI*
Faculty of Science, Kochi University, Akebono-cho, Kochi 780
†*Laboratories of Natural Products Chemistry, Otsuka Pharmaceutical Co. Ltd., Kawauchi-cho, Tokushima 771-01*
(Received August 27, 1982)

Two new bitter limonoids, ohchinolal (**1**) and ohchinin (**2**), have been isolated from the fruit of *Melia azedarach* L. *var. japonica* Makino, and their structures have been established as **1** and **2** by spectroscopic and chemical methods. The complete assignments of the ^1H and ^{13}C NMR data are described.

Recent investigations of the plants of the family Meliaceae have resulted in the isolation of many limonoids of biological interest, such as those with potent cytotoxic activity[2)] and with insect antifeedant and insecticidal properties.[3,4)] Our continuing search for biologically active constituents of *Melia azedarach* L. *var. japonica* Makino has now led to the isolation of two new bitter limonoids, designated as ohchinolal and ohchinin, the latter as the natural precursor of ohchinin acetate (**3**).[5)] The present paper deals with the structural determination of these new compounds.

Ohchinolal (**1**), $C_{34}H_{44}O_{10}$, mp 163—164.5 °C, $[\alpha]_D^{23}$

TABLE 1. ^1H NMR SPECTRA AT 400 MHz OF OHCHINOLAL (**1**) AND OHCHININ (**2**)[a)]

		1		**2**
H_1		5.08 (dd, 3.2, 2.7)		5.09 (dd, 2.7, 2.7)
$H_{2\alpha}$		2.22 (ddd, 16.2, 3.5, 2.7)		2.31 (ddd, 13.8, 3.0, 2.7)
$H_{2\beta}$		2.02 (ddd, 16.2, 3.2, 2.7)		2.14 (ddd, 13.8, 3.0, 2.7)
H_3		3.75 (ddd, 9.2, 3.5, 2.7)		3.91 (ddd, 8.9, 3.0, 3.0)
H_5		3.66 (d, 12.2)		2.78 (d, 12.4)
H_6		5.26 (dd, 12.2, 2.7)		4.04 (dd, 12.4, 3.2)
H_7		4.03 (d, 2.7)		4.21 (d, 3.2)
H_9		2.84 (dd, 8.4, 3.2)		2.71 (dd, 9.5, 3.0)
H_{11}		2.24 (dd, 15.7,3.2)		2.19 (dd, 15.1, 3.0)
		2.32 (dd, 15.7, 8.4)		2.34 (dd, 15.1, 9.5)
H_{15}		5.49 (dddq, 7.8, 6.8, 1.8, 1.4)		5.48 (dddq, 8.4, 6.8, 1.9, 1.4)
$H_{16\alpha}$		2.27 (dd, 12.4, 6.8)		2.15 (dd, 12.2, 8.4)
$H_{16\beta}$		2.09 (ddd, 12.4, 9.2, 7.8)		2.24 (ddd, 12.2, 8.6, 6.8)
H_{17}		3.65 (dd, 9.2, 1.8)		3.61 (dd, 8.6, 1.9)
H_{21}		7.25 (dd, 1.9, 0.8)		7.14 (dd, 1.4, 1.0)
H_{22}		6.29 (dd, 1.6, 0.8)		6.18 (dd, 1.9, 1.0)
H_{23}		7.33 (dd, 1.9, 1.6)		7.13 (dd, 1.9, 1.4)
H_{28}		9.74 (s)		3.66 (d, 7.6)
				4.17 (d, 7.6)
Me_{18}		1.65 (d, 1.4)		1.65 (d, 1.4)
Me_{19}		1.08 (s)		0.98 (s)
Me_{29}		1.00 (s)		1.17 (s)
Me_{30}		1.41 (s)		1.32 (s)
CO_2Me		3.23 (s)		3.11 (s)
OAc		1.98 (s)		
OH		2.73 (d, 9.2)[b)]		2.46 (d, 8.9)[b)]
OTig[c)]	$H_{3'}$	6.94 (qq, 7.0, 1.6)		
	$Me_{4'}$	1.86 (dq, 7.0, 1.1)		
	$Me_{5'}$	1.94 (dq, 1.6, 1.1)		
Ocin[c)]			$H_{2'}$	6.50 (d, 15.9)
			$H_{3'}$	7.72 (d, 15.9)
			$H_{5'}$	7.57 (m)
			$H_{6'}$	7.41 (m)
			$H_{7'}$	7.41 (m)

a) The spectra were determined at 25 °C in $CDCl_3$ solutions, with TMS as the internal standard. The multiplicity and J values (in Hz) are in parentheses. b) These signals disappeared on addition of D_2O.

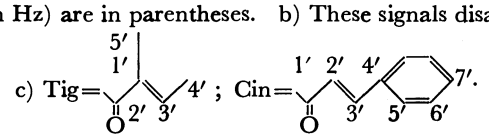

TABLE 2. ^{13}C CHEMICAL SHIFTS OF OHCHINOLAL (1) AND OHCHININ (2)[a)]

Carbon	1	2	Carbon	1	2
1	75.2 d	73.4 d	19	16.9 q	17.0 q
2	28.5 t	30.7 t	20	127.2 s	127.3 s
3	76.5 d	72.7 d	21	139.1 d	138.9 d
4	47.2 s	44.4 s	22	110.8 d	110.8 d
5	35.2 d	39.7 d	23	143.1 d	143.0 d
6	69.1 d	71.1 d	28	206.9 d	78.1 t
7	86 2 d	86.3 d	29	14.0 q	20.0 q
8	49.2 s	49.2 s	30	17.1 q	13.2 q
9	39.7 d	39.1 d	OCH_3	51.5 q	51.6 q
10	42.3 s	41.2 s	$OCO\underline{C}H_3$	20.8 q	
11	30.4 t	30.8 t	$O\underline{C}OCH_3$	170.4 s	
12	172.6 s	172.8 s	1′	166.4 s	165.7 s
13	135.7 s	134.6 s	2′	128.7 s	118.3 d
14	146.4 s	146.7 s	3′	143.1 d	145.6 d
15	87.7 d	88.2 d	4′	12.1 q	135.1 s
16	41.3 t	41.3 t	5′	14.5 q	128.4 d
17	49.8 d	49.7 d	6′		129.2 d
18	13.0 q	15.4 q	7′		130.7 d

a) The spectra were measured at 100.61 MHz in $CDCl_3$ solutions, and the shifts are given in ppm (δ) relative to the internal TMS. Assignments were made by means of off-resonance and selective proton-noise decoupling techniques.

$+52°$ (c 0.22, EtOH), was isolated from the methanol extract of the fruit as colorless prisms in a 0.013% yield by means of extensive column chromatography. It had IR absorptions attributable to a hydroxyl group (3475 cm^{-1}) and a β-substituted furan ring (3150, 1500, and 875 cm^{-1}). The 400 MHz ^1H NMR spectrum showed signals due to three tertiary methyl groups at $\delta=1.00$, 1.08, and 1.41, one vinylic methyl group at $\delta=1.65$ (d, $J=1.4$ Hz), one acetyl group at $\delta=1.98$, one secondary hydroxyl group at $\delta=2.73$ (d, $J=9.2$ Hz), one ester methyl group at $\delta=3.23$, and one formyl group at $\delta=9.74$ (s). The presence of a tigloyl group was also evident from the ^1H NMR signals at $\delta=1.86$ (3H, dq, $J=7.0$ and 1.1 Hz), 1.94 (3H, dq, $J=1.6$ and 1.1 Hz), and 6.94 (1H, qq, $J=7.0$ and 1.6 Hz), and the MS fragment at m/z 529 [$M^+-CH_3CH=C(CH_3)-C\equiv O^+$]. In addition, extensive ^1H NMDR studies, as summarized in Table 1, revealed the presence of four partial structures (**A**), (**B**), (**C**), and (**D**), the last one showing the following long-range couplings: $J_{H_{15},H_{17}}=1.8$ Hz, $J_{H_{15},H_{18}}=1.4$ Hz, and $J_{H_{17},H_{18}}\approx 0.1$ Hz. The ^{13}C NMR data for **1**, obtained with the assistance of off-resonance and selective proton-noise decoupling techniques, showed the presence of another ester-type carbonyl carbon atom at δ_C 172.6, along with three methylene groups, three methine groups, five oxygen-bearing methine groups, three quaternary carbon atoms, and one tetrasubstituted double bond.

The spectral data and the analogy with the congeners isolated from Melia species[5,6] suggested a close structural relationship between **1** and salannin (**4**).[7] The lack of the ^{13}C NMR signal characteristic for the C_{28} of salannin-type limonoids around δ_C 78 and the paramagnetic shift of the ^1H NMR signal due to H_6 indicate the absence of the C_6–O–C_{28} ether linkage which exists in **4**. The location of the formyl group at C_{28} was revealed by the observation of a nuclear Overhauser effect (NOE) on H_5 (13%) upon the irradiation of the

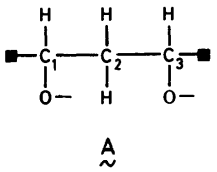

A

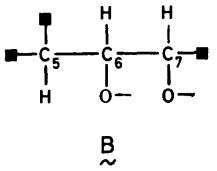

B

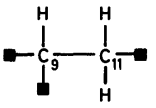

C

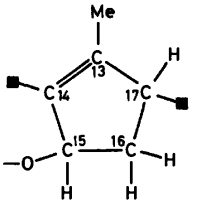

D

formyl proton. The positions of the secondary hydroxyl and tigloyloxyl groups were elucidated as follows. The oxidation of **1** with pyridinium chlorochromate, accompanied by the elimination of tiglic acid, gave an enone (**5**), $C_{29}H_{34}O_8$, as an oil. The ^1H NMR spectrum of **5** contained a typical AB quartet at $\delta=5.99$ and 6.99 ($J=10.3$ Hz, H_2 and H_1 respectively) indicative of an α,β-unsaturated ketone, while the irradiation of the methylene protons at C_{11} under NOE conditions produced a clear enhancement of the intensity of the latter signal (5.2%). This fact suggested the presence of a $-\underset{H}{C_1}=\underset{H}{C_2}-\underset{O}{C_3}-$ grouping in **5** and, hence, the location of the tigloyloxyl group at C_1 and the secondary hydroxyl group at C_3 in **1**. The appearance of the signal of H_6 in **1** at a lower field ($\delta=5.26$) as compared with that of **3** ($\delta=4.05$)[5] revealed the position of the remaining acetoxyl group at C_6.

The ^1H NMDR studies of **1** for the partial structure (**D**) elucidated the chemical shift and the coupling

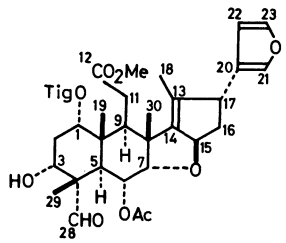

1

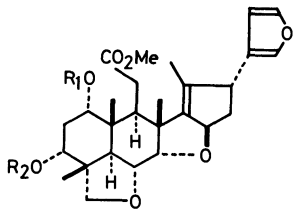

2 R_1 = Cin, R_2 = H
3 R_1 = Cin, R_2 = Ac
4 R_1 = Tig, R_2 = Ac

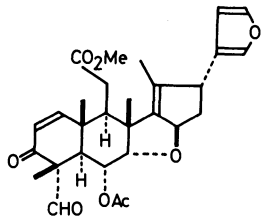

5

constant values, as summarized in Table 1. From the examination of the J values and the model, it is concluded that H_{15} and H_{17} face opposite sides. The α-configuration for C_{17}-furan is common to all the limonoids;[8] consequently, the C_{15}-ether linkage of **1** must be β-oriented. The α-configuration of the C–O linkages at C_1, C_3, C_6, and C_7 was evident from the J values of their α-protons.[3a,5] From the evidence outlined above, we proposed Structure **1** for ohchinolal.

The second compound (**2**), $C_{36}H_{42}O_8$, mp 184—185 °C, $[\alpha]_D^{23}$ +64° (*c* 0.17, EtOH), was isolated in a 0.020% yield as colorless needles from the more polar fraction; it displayed spectral data similar to those of ohchinin acetate (**3**).[5] The only significant difference in their IR and ^{1}H NMR data was the replacement of the acetoxyl group in **3** by the secondary hydroxyl group [ν_{max} 3450 cm^{-1}; δ=2.46 (d, J=8.9 Hz, OH) and 3.75 (ddd, J=8.9, 3.0, and 3.0 Hz, H_3)] in **2**. This relationship was verified by the acetylation of **2**, which gave the acetate (**3**). Thus, the name "Ohchinin," which we reserved for the natural precursor of **3** in the previous paper,[5] must be assigned to Compound **2**.

Experimental

All the mps were determined on a Mitamura micro-melting-point apparatus and are uncorrected. The IR and UV spectra were recorded on a JASCO model A-202 spectrophotometer and a Hitachi 340 spectrophotometer respectively. The ^{1}H and ^{13}C NMR spectra were taken on a Bruker WH-400 instrument in $CDCl_3$ solutions, with TMS as the internal standard. A JASCO apparatus, model DIP-140, was used for the measurement of the rotations. Column chromatography was performed using neutral alumina (Merck, activity III) and silicic acid (Wakogel C-200).

Isolation. The air-dried and milled fruit (2 kg) of *Melia azedarach* L. *var. japonica* Makino collected in Tokushima City in February, 1980, was extracted with methanol (6 l) at room temperature for two weeks. The methanol extract was then concentrated up to about 0.5 l, water (0.1 l) was added, and it was washed with petroleum ether The aqueous methanol layer was diluted with water (0.5 l) and then extracted with dichloromethane. The dichloromethane layer was washed with water, dried over $MgSO_4$, and evaporated to dryness. Then the residue (50 g) was subjected to chromatography over neutral alumina (1 kg), eluting with benzene–ethyl acetate mixtures, the ethyl acetate increasing from 10 to 70%. Elution with 30% ethyl acetate in benzene gave a fraction (20 g) which was rechromatographed over silicic acid (600 g), using 60% ethyl acetate in hexane as the eluent, to yield ohchinolal (**1**) (380 mg). Subsequent elution with 80% ethyl acetate in hexane afforded ohchinin (**2**) (485 mg).

Ohchinolal (1). The crude material was recrystallized from ether to give colorless prisms (250 mg); mp 163—164.5 °C, $[\alpha]_D^{23}$ +52° (*c* 0.22, EtOH); IR (KBr) 3475, 3150, 1730, 1710, 1690, 1645, 1500, 1250, 1040, 970, and 875 cm^{-1}; UV (EtOH) 215 nm (ε 15000); ^{1}H NMR (see Table 1); ^{13}C NMR (see Table 2); MS (70 eV) *m/z* (rel intensity) 612 (M^+, 22), 584 ($M^+ - CO$, 2), 552 ($M^+ - AcOH$, 6), 529 ($M^+ - C_5H_7O$, 12), 314 (13), 273 (39), 231 (69), 174 (38), 83 ($C_5H_7O^+$, 81), 55 (86), and 43 (100). Found: *m/z* 612.2955. Calcd for $C_{34}H_{44}O_{10}$: M, 612.2934.

Ohchinin (2). The crude substance was recrystallized from methanol to yield colorless needles (400 mg); mp 184—185 °C, $[\alpha]_D^{23}$ +64° (*c* 0.17, EtOH); IR (KBr) 3450, 3140, 1725, 1695, 1625, 1570, 1300, 1264, 1160, 865, 795, and 770 cm^{-1}; UV (EtOH) 215 and 276 nm (ε 22000 and 19000 respectively); ^{1}H NMR (see Table 1); ^{13}C NMR (see Table 2); MS (70 eV) *m/z* (rel intensity) 602 (M^+, 65), 587 ($M^+ - CH_3$, 3), 471 ($M^+ - C_9H_7O$, 12), 283 (73), 259 (20), 230 (16), and 131 ($C_9H_7O^+$, 100). Found: *m/z* 602.2906. Calcd for $C_{36}H_{42}O_8$: M, 602.2933.

The Oxidation of 1 with Pyridinium Chlorochromate. To a suspension of pyridinium chlorochromate (100 mg) in dichloromethane (2 ml) we added a solution of **1** (20 mg) in dichloromethane (0.4 ml). The mixture was stirred for 5 h at room temperature. After dilution with dichloromethane (10 ml), the solution was shaken with a 0.1 M (1 M=1 mol dm^{-3}) aqueous NaOH solution (10 ml) and then separated. The organic layer was washed with water, dried over $MgSO_4$, and evaporated to dryness. The product was chromatographed over silicic acid (3 g), with 50% ethyl acetate in hexane as the eluent, to yield an enone (**5**) as a viscous oil (8 mg); IR ($CHCl_3$) 1730, 1670, 1610, 1490, 1220, 1020, 900, and 865 cm^{-1}; UV (EtOH) 220 nm (ε 9800); ^{1}H NMR ($CDCl_3$) δ= 1.30, 1.31, and 1.42 (3H each, s, 29-, 19-, and 30-H_3), 1.72 (3H, d, J=1.4 Hz, 18-H_3), 1.99 (3H, s, Ac), 2.07 (1H, ddd, J= 12.2, 8.1, and 8.1 Hz, 16β-H), 2.23 (1H, dd, J=12.2 and 6.5 Hz, 16α-H), 2.49 (1H, dd, J=15.7 and 4.9 Hz, 11-H_a), 2.56 (1H, dd, J=4.9 and 4.9 Hz, 9-H), 2.63 (1H, dd, J=15.7 and 4.9 Hz, 11-H_b), 3.57 (3H, s, OCH_3), 3.58 (1H, d, J=12.2 Hz, 5-H), 3.67 (1H, br d, J=8.1 Hz, 17-H), 4.12 (1H, d, J=2.8 Hz, 7-H), 5.27 (1H, dd, J=12.2 and 2.8 Hz, 6-H), 5.49 (1H, m, 15-H), 5.99 (1H, d, J=10.3 Hz, 2-H), 6.99 (1H, d, J=10.3 Hz, 1-H), 6.22, 7.21, and 7.34 (1H each, br s, 22-, 21-, and 23-H), and 9.35 (1H, s, 28-H); MS (70 eV) *m/z* (rel intensity) 510 (M^+, 9), 482 ($M^+ - CO$,9), 422 ($M^+ - CO - AcOH$, 3), 259 (14), 247 (21), 231 (36), and 43 (100). Found: *m/z* 510.2326. Calcd for $C_{29}H_{34}O_8$: M, 510.2254. The combined aqueous solution was acidified with 3 M hydrochloric acid and extracted with ether. The ethereal solution was washed with saturated brine, dried over $MgSO_4$, and evaporated to dryness to give an acidic fraction (4 mg), which was found to contain tiglic acid by means of TLC and MS comparison with an authentic sample [MS (70 eV) *m/z* (rel intensity) 100 (M^+, 96) 85 ($M^+ - CH_3$, 34), 82 ($M^+ - H_2O$, 32), and 55 ($M^+ - COOH$, 100)].

Acetylation of **2**. A solution of **2** (8 mg) in acetic anhydride (0.1 ml) and pyridine (0.4 ml) was allowed to stand at room temperature overnight and then worked up in the usual way. The product was recrystallized from ether–dichloromethane to give an acetate as colorless prisms (7 mg); it was identified by mixed mp, IR, and ^{1}H NMR comparison with ohchinin acetate (**3**) [mp 223—226 °C; IR (KBr) 3160, 3060, 1735, 1695, 1640, 1585, 1500, and 875 cm^{-1}; ^{1}H NMR: see Ref. 5].

References

1) Part VI in the series of "Limonoids from *Melia azedarach* L. *var. japonica* Makino." Part V: see M. Ochi, H. Kotsuki, M. Ido, H. Nakai, M. Shiro, and T. Tokoroyama, *Chem. Lett.*, **1979**, 1137.

2) J. Polonsky, Z. Varon, B. Arnoux, C. Pascard, G. R. Pettit, J. M. Schmidt, and L. M. Lange, *J. Am. Chem. Soc.*, **100**, 2575 (1978); J. Polonsky, Z. Varon, B. Arnoux, C. Pascard, G. R. Pettit, and J. M. Schmidt, *ibid.*, **100**, 7731 (1978); J. Polonsky, Z. Varon, Ch. Marazona, B. Arnoux, G. R. Pettit, J. M. Schmidt, M. Ochi, and H. Kotsuki, *Experientia*, **35**, 987 (1979); S. D. Jolad, J. J. Hoffmann, K. H. Schram, J. R. Cole, M. S. Tempesta, and R. B. Bates, *J. Org. Chem.*, **46**, 641 (1981).

3) W. Kraus and R. Cramer, *Justus Liebigs Ann. Chem.*, **1981**, 181; M. Nakatani, J. C. James, and K. Nakanishi, *J. Am. Chem. Soc.*, **103**, 1228 (1981).

4) Professor I. Kubo, University of California, Berkeley, personal communication.

5) M. Ochi, H. Kotsuki, T. Kataoka, T. Tada, and T. Tokoroyama, *Chem. Lett.*, **1978**, 331.

6) W. Kraus and M. Bokel, *Chem. Ber.*, **114**, 267 (1981), and the references cited therein.

7) R. Henderson, R. McCrindle, A. Melera, and K. H. Overton, *Tetrahedron*, **24**, 1525 (1968).

8) V. P. Gullo, I. Miura, K. Nakanishi, A. F. Cameron, J.D. Connolly, F.D. Duncanson, A.E. Harding, R. McCrindle, and D. A. H. Taylor, *J. Chem. Soc., Chem. Comm.*, **1975**, 345, and the references cited therein.

 © 1983 The Chemical Society of Japan Bull. Chem. Soc. Jpn., 56, 1143—1148 (1983)

The Synthesis and Studies of Several [2.2.2]Ferrocenophane Derivatives[1)]

Akira KASAHARA,* Taeko IZUMI, Iwao SHIMIZU, Tadashi OIKAWA, Hirosni UMEZAWA, and Isao HOSHINO

Department of Applied Chemistry, Faculty of Engineering, Yamagata University, Yonezawa 992

(Received September 7, 1982)

Several ferrocenophanes, in which the two cyclopentadienyl rings are linked by acetylenic and olefinic bonds and aromatic rings, have been synthesized *via* the titanium-induced reductive coupling of the corresponding formyl compounds. The structures of these ferrocenophane compounds were determined by means of their IR and NMR spectra. The transannular π-electronic interactions between the two chromophores were examined on the basis of the electronic spectra.

Because of the topology and the mostly rigid molecular structure, a large number of layered compounds have been synthesized and their physical and chemical properties studied.[2)] Many ferrocenophanes of [*m*](1,1′)- or [*m.n*](1,1′)-type are known in which one or more intramolecular bridges link heteroannular positions with one or more ferrocene moieties; however, there have been only a few investigations of ferrocenophanes with interactions between the bridging elements. Tanner and Wennerstrom[3)] have recently reported the synthesis of [2.2.2.2]ferrocenophanetetraenes. Moreover, as a part of our studies of metallocenophane chemistry, we ourselves have reported the synthesis of [0]metacyclo-[2]metacyclo[0](1,1′)ferrocenophan-7-ene,[4)] in which substantial repulsive interactions exist between the two aromatic rings. These results have prompted us to study the synthesis of [2.2.2]ferrocenophane derivatives (**1**—**4**), in which the ferrocene moiety is linked by acetylenic and olefinic bonds and aromatic rings.

Results and Discussion

Although a number of synthetic methods have recently been developed for [2.2]cyclophane,[2)] the reductive coupling of carbonyl compounds with low-valent titanium reagents[5)] is still very convenient and advantageous for the synthesis of cyclophane because of the availability of the intermediary compounds.[3,4,6)]

In the present work, we applied the same method for the synthesis of [2.2.2]ferrocenophane derivatives; [2]paracyclo[2]paracyclo[2](1,1′)ferrocenophan-9-ene-1,17-diyne (**1**),[7)] [2]metacyclo[2]metacyclo[2](1,1′)ferrocenophan-9-ene-1,17-diyne (**2**), [2]orthocyclo[2]orthocyclo[2](1,1′)ferrocenophan-9-ene-1,17-diyne (**3**), and [2]paracyclo[2]paracyclo[2](1,1′)ferrocenophane-1,9,17 triene (**4**) were synthesized *via* the titanium-induced coupling of dialdehyde (**5a**—**d**). The syntheses of the intermediate dialdehydes; 1,1′-bis(*p*-formylphenylethynyl)ferrocene (**5a**), 1,1′-bis(*m*-formylphenylethynyl)ferrocene (**5b**), and 1,1′-bis(*o*-formylphenylethynyl)ferrocene (**5c**) were carried out by means of the palladium-catalyzed substitution[8)] of 1,1′-diiodoferrocene (**6**) with acetylenic compounds (**7a**—**c**), whereas another dialdehyde, 1,1′-bis(*p*-formylstyryl)ferrocene (**5d**), was prepared by the palladium-catalyzed substitution[9)] of **6** with *p*-formylstyrene (**7d**).

The reductive coupling reactions of dialdehyde (**5a**—**d**) with low-valent titanium reagents ($TiCl_4$–Zn[5a)] or $TiCl_3$–$LiAlH_4$[5b)]) using a high-dilution method led to the formation of ferrocenophanes (**1**—**4**), accompanied by the formation of the reduction products of **5a**—**d**. The structures of ferrocenophanes (**1**—**4**) were determined on the basis of the IR, NMR, and mass spectra and the elementary analyses.

The IR spectrum of **1** reveals the presence of triple and *cis* olefinic bonds, and the NMR spectrum includes the proposed structure. In the NMR spectrum of **1**, it is noteworthy that the vinylene protons (H_c), which can be easily assigned by means of their relative intensities, appear at a lower field than the aromatic protons, by analogy with the case of [2.2.2](1,3,5)cyclophane-1,9,17-triene (vinylene protons δ=7.37 ppm).[10)] In ferrocene, the distance between the two cyclopentadienyl rings is 3.32 Å.[11)] On the other hand, in **1** the molecule probably exists in the conformation illustrated by Structure 1, with the phenylethynyls approximately parallel to one another and approximately coplanar to the plane of the cyclopentadienyl ring. Thus, in **1**, substantial repulsive interactions must exist between the two phenylethynyl groups, which are bound together by a vinylene bridge at both ends. In the NMR spectrum of **1**, as expected, the aromatic protons (δ=6.47 and 6.82) appear at higher fields than the corresponding protons of the reference compounds, 1,1′-bis(*p*-tolylethynyl)ferrocene (**8a**) (δ=7.10 and 7.38). This phenomenon indicates that the two benzene rings in **1** are held face-to-face in close proximity by the vinylene bridge.

The NMR spectrum of **2** is also consistent with the proposed structure, and the stepped (*anti*) conformation is suggested by the large upfield shift ($\Delta\delta$, 0.59—0.76) for inner aryl protons (H_a) and the downfield shift of the outer aryl protons (H_b, H_c, and H_d) ($-\Delta\delta$, 0.08—0.13), compared with the corresponding signals of the reference compound, 1,1′-bis(*m*-tolylethynyl)ferrocene (**8b**).

On the other hand, in the NMR spectrum of **3**, the aromatic proton signals are observed at nearly the same positions as those of the reference compound, 1,1′-bis(*o*-tolylethynyl)ferrocene (**8c**). This suggests that the two aromatic rings in **3** are not held in a face-to-face conformation and that the *anti*-conformation for **3** is accommodated.

In the IR spectrum, Compound **4** showed the presence of *trans* and *cis* vinylene groups at 950 and 730 cm^{-1} respectively. Moreover, the NMR spectrum of **4** indicated the presence of the signals of two A_2X_2 patterns due to *p*-disubstituted aromatic (J=8 Hz) and

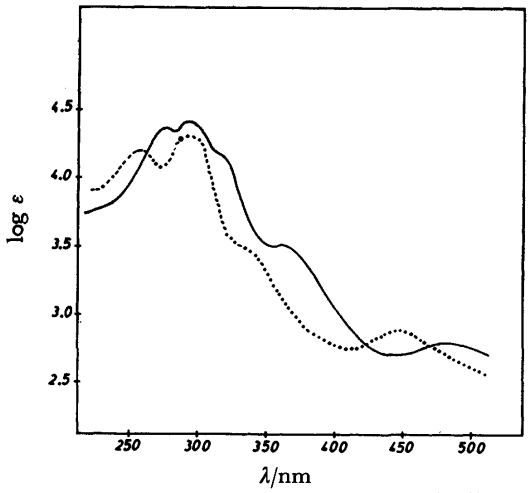

Fig. 1. Electronic spectra of **1** and **8a** in dioxane.
——: **1**, ------: **8a**.

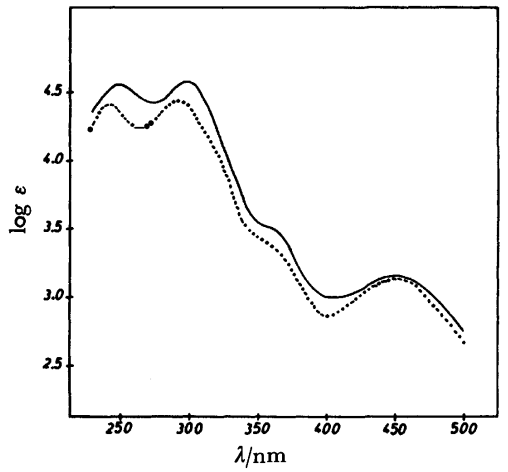

Fig. 2. Electronic spectra of **2** and **8b** in dioxane.
——: **2**, ------: **8b**.

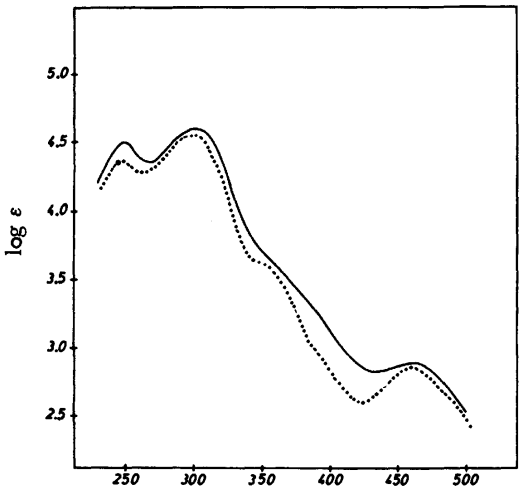

Fig. 3. Electronic spectra of **3** and **8c** in dioxane.
——: **3**, ------: **8c**.

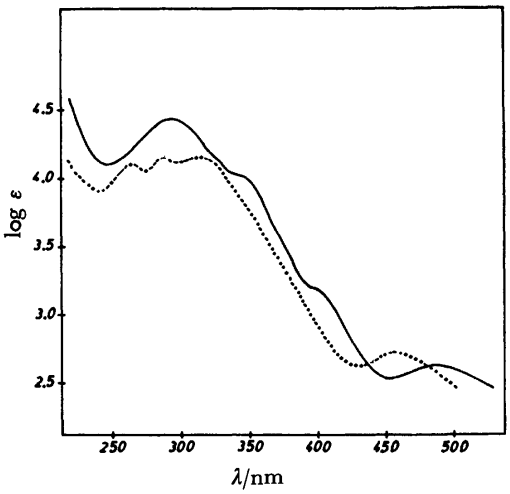

Fig. 4. Electronic spectra of **4** and **8d** in dioxane.
——: **4**, ------: **8d**.

trans vinylene protons (J=16 Hz), in addition to those attributable to 1,1′-disubstituted ferrocene and *cis* vinylene protons. These data are best explained by the parallel stacked configuration (**4**) rather than by the cross-stacked one (**4a**). The protons of aromatic and olefinic groups in **4** are shifted upfield by about 0.5 ppm compared with those of the reference compound, 1,1′-bis(*p*-methylstyryl)ferrocene (**8d**). This phenomenon may be caused by the diamagnetic shielding effect due to an overlapping of the two styryl groups.

The electronic spectra data of the cyclophane (**1**—**4**) and the reference compounds (**8a**—**d**) are summarized in Figs. 1—4. It is well known that the transannular electronic interaction in cyclophane results in the bathochromic and hyperchromic shifts of the absorption bands in its electronic spectrum and that the magnitude of these shifts can simply be utilized as a measure of the interaction.[2] Both phenylacetylene[12] and styrene[13] show no absorption in the long-wavelength region above 300 nm. The electronic spectra of **1**, **2**, and **4** show somewhat bathochromic and hyperchromic shifts and an unambiguous broadening in the range of 230—310 nm, especially as compared with those of the reference compounds, **8a**, **8b**, and **8d** respectively. This may be due to transannular π-electronic interactions between the two chromophores in **1**, **2**, and **4**. On the other hand, Compound **3** exhibits some hyperchromic shift in the 230—310 nm region; however the spectra are practically identical with those of the reference compound, **8c**. This indicates that the interaction between the two chromophores in **3** is relatively weak and that the *anti*-conformation for **3** is also accommodated.

On the other hand, the electronic spectrum of ferrocene has two main absorptions, 325 and 440 nm. In the case of the ring-tilted ferrocenophane, it has been found that the 440-nm band undergoes a bathochromic shift with a marked increase in intensity.[14] In the electronic spectra of **1** and **4**, the 440-nm band undergoes a bathochromic shift and increases in intensity, compared with those of **8a** and **8d** bearing a no-tilt ferrocene ring. This may be caused by a ferrocene ring-tilt distortion due to an interaction between the two phenylethynyl or styryl groups in **1** or **4**.

In Compounds **2** and **3**, the electronic spectra in the

Table 1. NMR spectra of the cyclophane and reference compounds

Compound	δ, in $CDCl_3$		
	Aromatic-ring protons	Ferrocene-ring protons	Other protons
1	6.47 (d, J=8 Hz, 4H, $\underline{H}_a$) 6.82 (d, J=8 Hz, 4H, $\underline{H}_b$)	4.24 (t, 4H, $\underline{H}_\beta$) 4.47 (t, 4H, $\underline{H}_\alpha$)	7.18 (s, 2H, $\underline{H}_c$)
8a	7.10 (d, J=8 Hz, 4H, $\underline{H}_a$) 7.38 (d, J=8 Hz, 4H, $\underline{H}_b$)	4.30 (t, 4H, $\underline{H}_\beta$) 4.52 (t, 4H, $\underline{H}_\alpha$)	2.31 (s, 6H, $-C\underline{H}_3$)
2	6.44 (s, 2H, $\underline{H}_a$) 7.11—7.33 (m, 6H, $\underline{H}_b + \underline{H}_c + \underline{H}_d$)	4.29 (t, 4H, $\underline{H}_\beta$) 4.44 (t, 4H, $\underline{H}_\alpha$)	8.18 (s, 2H, $-C\underline{H}=C\underline{H}-$)
8b	7.03—7.20 (m, 8H, Ar-$\underline{H}$)	4.27 (t, 4H, $\underline{H}_\beta$) 4.49 (t, 4H, $\underline{H}_\alpha$)	2.22 (s, 6H, $-C\underline{H}_3$)
3	6.98—7.28 (m, 8H, Ar-$\underline{H}$)	4.22 (m, 4H, $\underline{H}_\beta$) 4.51 (m, 4H, $\underline{H}_\alpha$)	7.31 (s, 2H, $-C\underline{H}=C\underline{H}-$)
8c	7.01—7.33 (m, 8H, Ar-$\underline{H}$)	4.29 (t, 4H, $\underline{H}_\beta$) 4.49 (t, 4H, $\underline{H}_\alpha$)	2.40 (s, 6H, $-C\underline{H}_3$)
4	6.49 (d, J=8 Hz, 4H, $\underline{H}_e$) 6.71 (d, J=8 Hz, 4H, $\underline{H}_d$)	4.24 (t, 4H, $\underline{H}_\beta$) 4.42 (t, 4H, $\underline{H}_\alpha$)	5.98 (d, J=16 Hz, 2H, $\underline{H}_a$) 6.29 (d, J=16 Hz, 2H, $\underline{H}_b$) 7.17 (s, 2H, $\underline{H}_c$)
8d	7.06 (d, J=8 Hz, 4H, $\underline{H}_d$) 7.18 (d, J=8 Hz, 4H, $\underline{H}_c$)	4.24 (t, 4H, $\underline{H}_\beta$) 4.39 (t, 4H, $\underline{H}_\alpha$)	2.30 (s, 6H, $-C\underline{H}_3$) 6.67 (b-s, 4H, $\underline{H}_a + \underline{H}_b$)

Table 2. IR spectra of the cyclophane and reference compounds

Compound	KBr, $\tilde{\nu}$/cm^{-1}
1	3100, 1400, 810 (1,1′-disubstituted ferrocene ring), 2200 (–C≡C–), 730 (*cis* –CH=CH–), 1600, 1580, 820 (*p*-disubstituted benzene ring), 710, and 690 (distorted benzene ring)
8a	3100, 1410, 805 (1,1′-disubstituted ferrocene ring), 2200 (–C≡C–), 1600, 1580, 1500, and 820 (*p*-disubstituted benzene ring)
2	3100, 1410, 810 (1,1′-disubstituted ferrocene ring), 2200 (–C≡C–), 1630, 720 (*cis* –CH=CH–), 1600, 1580, 1500, 845, and 765 (*m*-disubstituted benzene ring)
8b	3100, 1410, 810 (1,1′-disubstituted ferrocene ring), 2200 (–C≡C–), 1600, 1500, 850, and 770 (*m*-disubstituted benzene ring)
3	3100, 1410, 810 (1,1′-disubstituted ferrocene ring), 2200 (–C≡C–), 1640, 960 (*trans* –CH=CH–), 1600, 1500, and 740 (*o*-disubstituted benzene ring)
8c	3100, 1410, 810 (1,1′-disubstituted ferrocene ring), 2200 (–C≡C–), 1600, 1500, and 740 (*o*-disubstituted benzene ring)
4	3100, 1400, 805 (1,1′-disubstituted ferrocene ring), 1630, 950, (*trans* –CH=CH–), 730 (*cis* –CH=CH–), 1600, 1580, 1500, 820 (*p*-disubstituted benzene ring), 710, and 685 (distorted benzene ring)
8d	3100, 1400, 810 (1,1′disubstituted ferrocene ring), 1640, 960 (*trans* –CH=CH–), 1600, 1580, and 820 (*p*-disubstituted benzene ring)

330—450 nm region are closely similar to those of the reference compounds bearing a no-tilt ferrocene ring, **8b** and **8c**. This indicates that no ferrocene-ring distortion occurs in **2** and **3**.

The IR spectra of [2.2]paracyclophane system are known to reveal obvious features. One is the increase in the intensity of the band in the 1580—1600 cm^{-1} region, which is related to the increased double-bond character due to the distortion of the benzene rings.[15] The other is the appearance of a strong new maximum in the 710-cm^{-1} region. Longone and Warren[15b] reported that the strong maxima at 725 cm^{-1} in [2.2]-paracyclophane and at 710 cm^{-1} in 4,7,12,15-tetramethyl[2.2]paracyclophane might be characteristic bands associated with the distorted benzene ring in the [2.2]-paracyclophane system. Otsubo *et al.*[15c] reported the same phenomenon in the multilayered [2.2]paracyclophane system. Besides the strong peak around 1600 cm^{-1}, the ferrocenophanes, **1** and **4**, exhibit the characteristic strong new band around 710 cm^{-1}, whereas the reference compounds bearing strain-free benzene rings, **8a** and **8d**, exhibit no band in this region. This phenomenon may be due to the distortion of the benzene rings in **1** and **4**. On the other hand, near 710 cm^{-1}, the IR spectra of **2** and **3** are closely similar to those of the open-chain models, **8b** and **8c**. This may be due to the lack of distortion of the benzene rings in **2** and **3**. (see Table 2).

Experimental

Materials and Measurements. All the melting points are uncorrected. The 1,1′-diiodoferrocene (**6**),[16] *p*- (**7a**)[17] and *o*-ethynylbenzaldehyde diethyl acetal (**7c**),[18] and *p*-formylstyrene (**7c**)[19] were prepared as has been described in the literature. The *m*-ethynylbenzaldehyde diethyl acetal (**7b**) was prepared from (*m*-bromophenylethynyl)trimethylsilane[20]

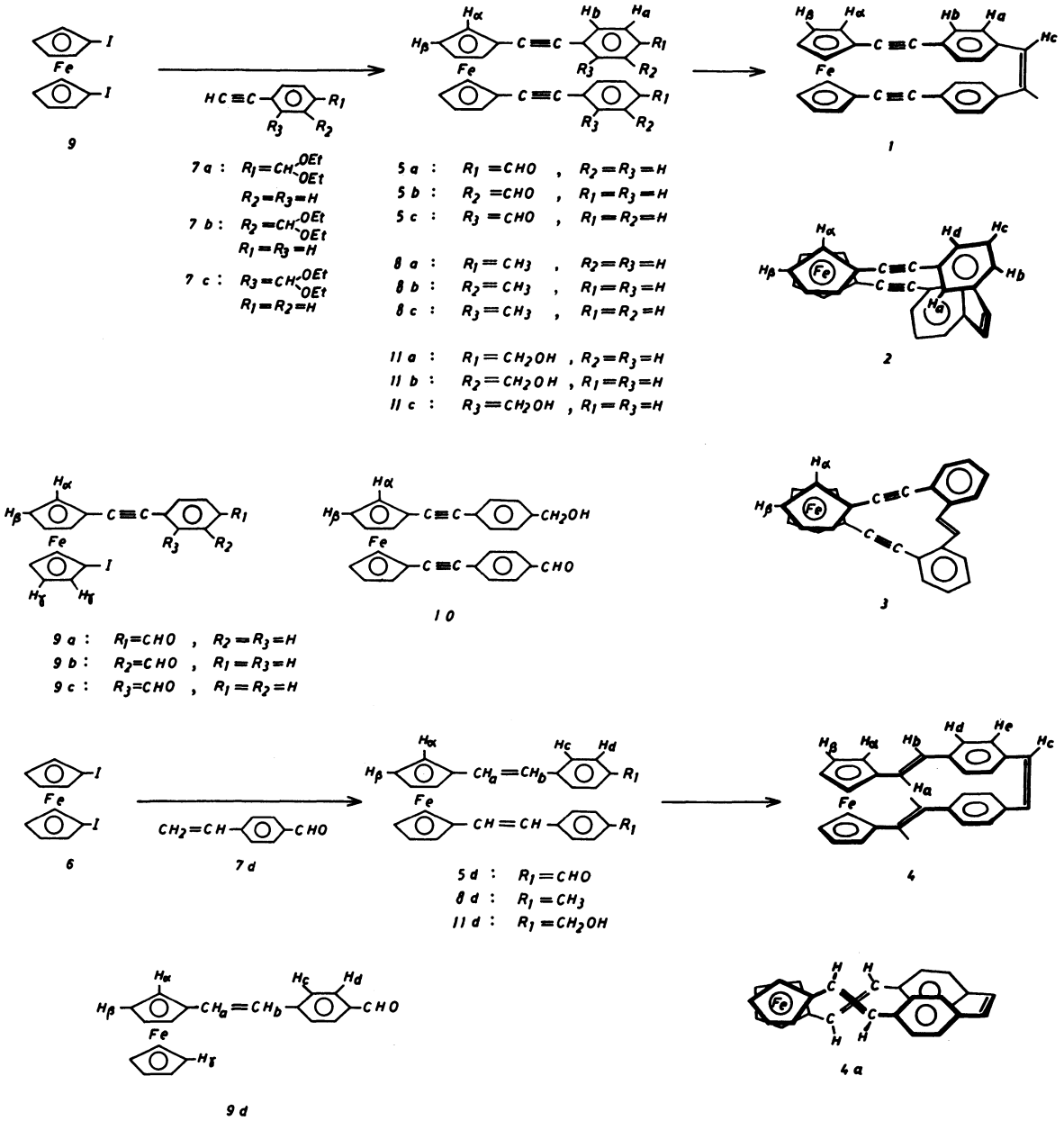

Scheme 1.

by a modification of the method in the literature.[17] The IR, NMR, mass, and electronic spectra were recorded with Hitachi 260-10, Hitachi R-22, Hitachi RMU-6M, and Hitachi 200-10 spectrometers respectively.

1,1'-Bis(p-formylphenylethynyl)ferrocene (5a). A mixture of **6** (4.37 g, 0.01 mol), **7a** (5.71 g, 0.28 mol), copper(I) iodide (0.19 g, 0.001 mol), dichlorobis(triphenylphosphine)palladium (II) (0.70 g, 0.001 mol), and diethylamine (80 cm^3) was heated under nitrogen in an autoclave at 80 °C for 8 h. After the removal of the diethylamine under reduced pressure, chloroform and water were added to the residue. The chloroform layer was separated and washed thoroughly with 10% hydrochloric acid to hydrolyze the acetal to aldehyde. The resulting chloroform layer was washed with a saturated sodium hydrogen carbonate solution and a saturated sodium chloride solution, dried over anhydrous magnesium sulfate, filtered, and concentrated. The residue was purified by silica-gel column chromatography.

The first fraction, eluted with hexane–benzene (1 : 1), gave 1-(*p*-formylphenylethynyl)-1'-iodoferrocene (**9a**) as reddish crystals (mp 139—141 °C) in a 45% yield based on **6** (1.98 g): IR (KBr): 2200 (–C≡C–), 1700 (–CHO), 1600, 1580, 820 (*p*-disubstituted benzene ring), 3100, and 805 cm^{-1} (1,1'-disubstituted ferrocene ring). NMR ($CDCl_3$): δ=4.22 (m, 6H, $\underline{H}_\beta$+$\underline{H}_\gamma$), 4.51 (m, 2H, $\underline{H}_\alpha$), 7.56 (d, J=8 Hz, 2H, Ar–$\underline{H}$), 7.80 (d, J=8 Hz, 2H, Ar–$\underline{H}$), and 9.96 (s, 1H, –C$\underline{H}$O). Found; C, 51.62; H, 2.81%; M^+, 440. Calcd for $C_{19}H_{13}FeIO$: C, 51.85; H, 2.97%; M, 440.

The second fraction, eluted with benzene–chloroform (1 : 1), gave **5a**, as deep red crystals (mp 210 °C (decomp)) in a 27% yield (1.19 g): IR (KBr): 2200 (–C≡C–), 1690 (–CHO), 1600, 1580, 820 (*p*-disubstituted benzene ring), 3100, and 805 cm^{-1} (1,1'-disubstituted ferrocene ring). NMR ($CDCl_3$): δ=4.37 (t, 4H, $\underline{H}_\beta$), 4.59 (t, 4H, $\underline{H}_\alpha$), 7.47 (d, 4H, $\underline{H}_a$), 7.71 (d, 4H, $\underline{H}_b$), and 9.98 (s, 2H, –C$\underline{H}$O). Found: C, 75.85; H, 3.96%; M^+, 442. Calcd for $C_{28}H_{18}FeO_2$: C, 76.03; H, 4.10%; M,

442.

1,1'-Bis(m-formylphenylethynyl)ferrocene (5b). In the presence of $(Ph_3P)_2PdCl_2$ and CuI, the palladium-catalyzed substituted of **6** with **7b** was carried out in the same way as has been described for **5a**; 1-(*m*-formylphenylethynyl)-1'-iodoferrocene (**9b**) (reddish crystals; mp 113—115 °C) and **5b** (reddish crystals; mp 164—165 °C) were thus obtained in 34 and 27% yields respectively.

9b: IR (KBr): 1700 (-CHO), 2200 (-C≡C-), 1600, 1580, 820, 780 (*m*-disubstituted benzene ring), 3100, and 805 cm^{-1} (1,1'-disubstituted ferrocene ring). NMR ($CDCl_3$): δ=4.20 (m, 6H, $\underline{H}_\beta+\underline{H}_\gamma$), 4.49 (m, 2H, $\underline{H}_\alpha$), 7.34—7.89 (m, 4H, Ar-$\underline{H}$), and 9.93 (s, 1H, -C$\underline{H}$O). Found: C, 51.73; H, 2.85%; M^+, 440. Calcd for $C_{19}H_{13}FeIO$: C, 51.85; H, 2.97%; M, 440.

5b: IR (KBr): 1700 (-CHO), 2200 (-C≡C-), 1600, 1580, 850, 770 (*m*-disubstituted benzene ring), 3100, and 805 cm^{-1} (1,1'-disubstituted ferrocene ring). NMR ($CDCl_3$): δ=4.31 (t, 4H, $\underline{H}_\beta$), 4.53 (t, 4H, $\underline{H}_\alpha$), 7.29—7.75 (m, 8H, Ar-$\underline{H}$), and 9.83 (s, 2H, -C$\underline{H}$O). Found: C, 75.78; H, 4.01%; M^+, 442. Calcd for $C_{28}H_{18}FeO_2$: C, 76.03; H, 4.10%; M, 442.

1,1'-Bis(o-formylphenylethynyl)ferrocene (5c). In the presence of $(Ph_3P)_2PdCl_2$ and CuI, the palladium-catalyzed substitution of **6** with **7c** was carried out in the same way as has been described for **5a**; 1-(*o*-formylphenylethynyl)-1'-iodoferrocene (**9c**) (reddish oil) and **5c** (reddish crystals; mp 178—179 °C) were thus obtained in 40 and 14% yields respectively.

9c: IR (neat): 1690 (-CHO), 2200 (-C≡C-), 1600, 1580, 740 (*o*-disubstituted benzene ring), 3100, and 810 cm^{-1} (1,1'-disubstituted ferrocene ring). NMR ($CDCl_3$): δ=4.34 (m, 6H, $\underline{H}_\beta+\underline{H}_\gamma$), 4.55 (m, 2H, $\underline{H}_\alpha$), 7.21—7.74 (m, 4H, Ar-$\underline{H}$), and 10.24 (s, 1H, -C$\underline{H}$O). Found: C, 51.77; H, 2.90%; M^+, 440. Calcd for $C_{19}H_{13}FeIO$: C, 51.85; H, 2.97%; M, 440.

5c: IR (KBr): 1690 (-CHO), 2200 (-C≡C-), 1600, 1580, 1500, 740 (*o*-disubstituted benzene ring), 3100, and 810 cm^{-1} (1,1'-disubstituted ferrocene ring). NMR ($CDCl_3$): δ=4.36 (t, 4H, $\underline{H}_\beta$), 4.58 (t, 4H, $\underline{H}_\alpha$), 7.29—7.74 (m, 8H, Ar-$\underline{H}$), and 10.47 (s, 2H, -C$\underline{H}$O). Found: C, 75.92; H, 3.98%; M^+, 442. Calcd for $C_{28}H_{18}FeO_2$: C, 76.03; H, 4.10%: M, 442.

1,1'-Bis(p-formylstyryl)ferrocene (5d). A mixture of **6** (4.37 g, 0.01 mol), **7a** (3.70 g, 0.28 mol), palladium(II) acetate (0.04 g, 0.002 mol), triphenylphosphine (0.10 g, 0.004 mol), and triethylamine (2.83 g. 0.28 mol) in acetonitrile (60 cm^3) was heated under nitrogen in an autoclave at 90 °C for 10 h. After the removal of the solvent under reduced pressure, the residue was extracted with chloroform. The chloroform extracts were washed with 10% hydrochloric acid, a saturated sodium hydrogencarbonate solution, and a saturated sodium chloride solution, dried over anhydrous magnesium sulfate, filtered, and concentrated. The residue was purified by column chromatography on silica gel.

The first fraction, eluted with benzene, gave (*p*-formylstyryl)-ferrocene (**9d**); yellowish red crystals; mp 145—147 °C, 1.10 g (35% yield based on **6**). IR (KBr): 1690 (-CHO), 1635, 965 (*trans* -CH=CH-), 1600, 1500, 820, (*p*-disubstituted benzene ring), 3100, and 805 (1,1'-disubstituted ferrocene ring). NMR ($CDCl_3$): δ=4.12 (s, 5H, $\underline{H}_\gamma$), 4.32 (t, 2H, $\underline{H}_\beta$), 4.48 (t, 2H, $\underline{H}_\alpha$), 6.67 (d, J=15 Hz, 1H, $\underline{H}_b$), 7.04 (d, J=15 Hz, 1H, $\underline{H}_a$), 7.49 (d, J=8 Hz, 2H, $\underline{H}_c$), 7.78 (d, J=8 Hz, 2H, $\underline{H}_d$), and 9.93 (s, 1H, -C$\underline{H}$O). Found: C, 72.06; H, 4.95%; M^+, 316. Calcd for $C_{19}H_{16}FeO$: C, 72.17; H, 5.10%; M, 316.

The second fraction, eluted with benzene-chloroform (1 : 1), gave **5d** as reddish crystals (mp 218 °C (decomp)) in a 54% yield (2.41 g). IR (KBr): 1695 (-CHO), 1630, 960 (*trans* -CH=CH-), 1600, 1500, 830 (*p*-disubstituted benzene ring), 3100, and 810 (1,1'-disubstituted ferrocene ring). NMR ($CDCl_3$): δ=4.33 (t, 4H, $\underline{H}_\beta$), 4.48 (t, 4H, $\underline{H}_\alpha$), 6.53 (d, J=16 Hz, 2H, $\underline{H}_b$), 6.82 (d, J=16 Hz, 2H, $\underline{H}_a$), 7.28 (d, J=8 Hz, 4H, Ar-$\underline{H}$), 7.63 (d, J=8 Hz, 4H, Ar-$\underline{H}$), and 9.89 (s, 2H, -C$\underline{H}$O). Found: C, 75.19; H, 4.77%; M^+, 446. Calcd for $C_{28}H_{22}FeO_2$: C, 75.35; H, 4.96%; M, 446.

The Reductive Coupling of 5a with $TiCl_4$-Zn. Under a nitrogen atmosphere, Zn dust (5.22 g, 0.08 mol) was added to a solution of $TiCl_4$ (7.58 g, 0.04 mol) in dry THF (150 cm^3) with cooling. The mixture was then refluxed for 1.5 h to give a deep black solution. To the metal complex solution thus obtained we added a solution of **5a** (3.53 g, 0.008 mol) and dry pyridine (0.60 g) in dry THF (550 cm^3) over 11 h under refluxing, followed by an additional 10-h period of reflux. The reaction mixture was then cooled to room temperature and quenched with a 20% aqueous K_2CO_3 solution. After filtration, the filtrate was extracted with chloroform. The chloroform extracts were washed with water and dried over anhydrous magnesium sulfate. After the removal of the solvents, the residue was dissolved in benzene and chromatographed on silica gel.

The first fraction, eluted with benzene, gave **8a** as reddish crystals (mp 193—194 °C) in a 3.5% yield. Compound **8a** is identical in all respects with 1,1'-bis(*p*-tolylethynyl)ferrocene, which was prepared by the palladium-catalyzed substitution of **6** with *p*-tolylacetylene in the same way as has been described for **5a**. Found: C, 81.08; H, 5.29%; M^+, 414. Calcd for $C_{28}H_{22}Fe$: C, 81.16; H, 5.35%; M, 414.

The second fraction, eluted with benzene, gave **1** as deep reddish crystals (mp 260 °C (decomp)) in a 15% yield. Found: C, 81.83; H, 4.31%; M^+, 410. Calcd for $C_{28}H_{18}Fe$: C, 81.96; H, 4.42%; M, 410.

The third fraction, eluted with chloroform, gave 1-(*p*-formylphenylethynyl)-1'-[*p*-(hydroxymethyl)phenylethynyl]-ferrocene (**10**) as reddish orange crystals (mp 190 °C (decomp)) in a 6% yield. IR (KBr): 3300 (-OH), 1700 (-CHO), 2200 (-C≡C-), 1600, 1500, 820 (*p*-disubstituted benzene ring), 3100, and 805 cm^{-1} (1,1'-disubstituted ferrocene ring). NMR (DMSO-d_6): δ=4.36 (t, 4H, $\underline{H}_\beta$), 4.56 (t, 4H, $\underline{H}_\alpha$), 4.72 (s, 2H, -C$\underline{H}_2$-), 5.78 (b-s, 1H, -O$\underline{H}$), 6.91 (d, 2H, Ar-$\underline{H}$), 7.34—7.52 (m, 6$\underline{H}$, Ar-$\underline{H}$) and 9.88 (s, 1H, -C$\underline{H}$O). Found: C, 75.60; H, 4.44%; M^+, 444. Calcd for $C_{28}H_{20}FeO_2$: C, 75.69; H, 4.53%; M, 444.

The fourth fraction, eluted with chloroform–ethanol (10 : 1) gave 1,1'-bis[*p*-hydroxymethyl)phenylethynyl]ferrocene (**11a**) as reddish orange crystals (mp 195 °C (decomp)) in a 3% yield. IR (KBr): 3300 (-OH), 2200 (-C≡C-), 1600, 1500, 840 (*p*-disubstituted benzene ring), 3100, and 815 cm^{-1} (1,1'-disubstituted ferrocene ring). NMR (DMSO-d_6): δ=4.00 (b-s, 2H, -O$\underline{H}$), 4.36 (t, 4H, $\underline{H}_\beta$), 4.56 (t, 4H, $\underline{H}_\alpha$), 4.76 (s, 4H, -C$\underline{H}_2$-), 6.97 (d, 4H, Ar-$\underline{H}$), and 7.33 (d, 4H, Ar-H). Found: C, 75.17; H, 4.85%; M^+, 446. Calcd for $C_{28}H_{22}FeO_2$: C, 75.35; H, 4.96%; M, 446.

The Reductive Coupling of 5b with $TiCl_4$-Zn. The reductive coupling of **5b** was carried out in the same way as has been described for the reaction of **5a** with $TiCl_4$-Zn, and the products were separated by chromatography on silica gel.

The first fraction, eluted with benzene, gave as reddish orange crystals (mp 114—115 °C) in a 7% yield. Compound **8b** was found to be identical with 1,1'-bis(*m*-tolylethynyl)-ferrocene, which has been prepared by the palladium-catalyzed substitution of **6** with *m*-tolylacetylene in the way described for **5a**. Found: C, 81.10; H, 5.28%; M^+, 414. Calcd for $C_{28}H_{22}Fe$: C, 81.16; H, 5.35%; M, 414.

The second fraction, eluted with benzene, gave **2** as reddish crystals (mp 215—216 °C) in a 22% yield. Found: C, 81.88; H, 4.36%; M^+, 410. Calcd for $C_{28}H_{18}Fe$: C, 81.96; H, 4.42%; M, 410.

The third fraction, eluted with chloroform, gave 1,1'-bis[*m*-

(hydroxymethyl)phenylethynyl]ferrocene (**11b**) as reddish orange crystals (mp 245 °C (decomp)) in a 12% yield. IR (KBr): 3300 (-OH), 2200 (-C≡C-), 1600, 1500, 870, 770 (*m*-disubstituted benzene ring), 3100, and 805 cm^{-1} (1,1'-disubstituted ferrocene ring). NMR (acetone-d_6): δ=2.15 (b-s, 2H, -OH), 4.29 (t, 4H, H_β). 4.51 (t, 4H, H_α). 4.72 (s, 4H, $-CH_2-$), and 7.28—7.58 (m, 8H, Ar-H). Found: C, 75.25; H, 4.90%; M^+, 446. Calcd for $C_{28}H_{22}FeO_2$: C, 75.35; H, 4.96%; M, 446.

The Reductive Coupling of 5c with $TiCl_4$-Zn. The reductive coupling for **5c** with $TiCl_4$-Zn was carried out in the same way as has been described for the reaction of **5a** with $TiCl_4$-Zn, and the products were separated by chromatography on silica gel.

The first fraction, eluted with benzene, gave **8c** as reddish orange crystals (mp 97—98 °C) in a 9% yield. Compound **8c** was found to be identical with 1,1'-bis(*o*-tolylethynyl)ferrocene, which has been prepared by the palladium-catalyzed substitution of **6** with *o*-tolylacetylene in the same way as has been described for **5a**. Found: C, 81.03; H, 5.19%; M^+, 414. Calcd for $C_{28}H_{22}Fe$: C, 81.16; H, 5.35%; M, 414.

The second fraction, eluted with benzene, gave **3** as reddish crystals (mp 216—217 °C) in a 26% yield. Found: C, 81.87; H, 4.33%; M^+, 410. Calcd for $C_{28}H_{18}Fe$: C, 81.96; H, 4.42%; M, 410.

The third fraction, eluted with chloroform, gave 1,1'-bis[*o*-(hydroxymethyl)phenylethynyl]ferrocene (**11c**) as reddish orange crystals (mp 201—203 °C) in a 5% yield. IR (KBr): 3400 (-OH), 2200 (-C≡C-), 1600, 1500, 740 (*o*-disubstituted benzene ring), 3100, and 810 cm^{-1} (1,1'-disubstituted ferrocene ring). NMR (acetone-d_6): δ=2.06 (b-s, 2H, -OH), 4.30 (t, 4H, H_β), 4.55 (t, 4H, H_α), 4.75 (s, 4H, $-CH_2-$), and 7.28—7.71 (m, 8H, Ar-H). Found: C, 75.19; H, 4.85%; M^+, 446. Calcd for $C_{28}H_{22}FeO_2$: C, 75.35; H, 4.96%; M, 446.

The Reductive Coupling of 5d with $TiCl_3$-$LiAlH_4$. Under a nitrogen atmosphere, $LiAlH_4$ (0.76 g, 0.02 mol) was added to a stirred slurry of $TiCl_3$ (6.47 g, 0.0042 mol) in dry THF (150 cm^3) at 0 °C. After the resulting black suspension has been stirred for 20 min, a solution of **5d** (3.79 g, 0.0085 mol) in dry THF (100 cm^3) was added drop by drop to this mixture for 6 h under refluxing, followed by an additional 7-h period of reflux. After cooling to room temperature, the reaction was worked up in the way described for **5a**; the crude products were chromatographed on silica gel.

The first fraction, eluted with hexane, gave **8d** as reddish crystals (mp 143—144 °C) in a 1.4% yield. Compound **8d** was found to be identical with 1,1'-bis(*p*-methylstyryl)ferrocene, which has been prepared by the palladium-catalyzed substitution of **6** with *p*-methylstyrene in the same way as has been described for **5d**. Found: C, 80.30; H, 6.14%; M^+, 418. Calcd for $C_{28}H_{26}Fe$: C, 80.38; H, 6.26%; M, 418.

The second fraction, eluted with benzene, gave **4** as reddish crystals (mp 230 °C (decomp)) in a 2.2% yield. Found: C, 81.03; H, 5.35%; M^+, 414. Calcd for $C_{28}H_{22}Fe$: C, 81.16; H, 5.35%; M, 414.

The third fraction, eluted with chloroform–ethanol (10 : 1), gave 1,1'-bis[*p*-(hydroxymethyl)styryl]ferrocene (**8d**) as reddish yellow crystals (mp 152—154 °C) in 3.2% yield. IR (KBr): 3400, (-OH), 1635, 955 (*trans* -CH=CH-), 1600, 1500, 830 (*p*-disubstituted benzene ring), 3100, and 805 cm^{-1} (1,1'-disubstituted ferrocene ring). NMR (DMSO-d_6): δ=2.65 (b-s, 2H, -OH), 4.28 (t, 4H, H_β), 4.49 (t, 4H, H_α), 4.78 (s, 4H, $-CH_2-$), 6.62 (d, J=16 Hz, 2H, -C=CH-Ar), 7.01 (d, J=16 Hz, 2H, -CH=C-Ar-), 7.43 (d, J=8 Hz, 4H, Ar-H), and 7.75 (d, J=8 Hz, 4H, Ar-H). Found: C, 74.56; H, 5.69%; M^+, 450. Calcd for $C_{28}H_{26}FeO_2$: C, 74.67; H, 5.81%; M, 450.

References

1) A preliminary report dealing with a part of this work has appeared: A. Kasahara, T. Izumi, and I. Shimizu, *Chem. Lett.*, **1979**, 1119.

2) S. Misumi, *Kagaku No Ryoiki*, **28**, 927 (1974); **32**, 651 (1978); Y. Sakata, *ibid.*, **28**, 947 (1974); *Yuki Gosei Kagaku Kyokai Shi*, **38**, 164 (1980); S. Misumi and T. Otsubo, *Acc. Chem. Res.*, **11**, 251 (1978).

3) D. Tanner and O. Wennerstrom, *Acta Chem. Scand., Ser. B*, **34**, 529 (1980).

4) A. Kasahara, T. Izumi, and H. Umezawa, *Chem. Lett.*, **1980**, 1039.

5) a) T. Mukaiyama, T. Sato, and J. Hanna, *Chem. Lett.*, **1973**, 1041; b) J. E. McMurry and M. P. Fleming, *J. Am. Chem. Soc.*, **96**, 4708 (1974); c) J. E. McMurry and L. R. Krepski, *J. Org. Chem.*, **41**, 3929 (1976); d) A. Ishida and T. Mukaiyama, *Chem. Lett.*, **1976**, 1127; e) J. E. McMurry, M. P. Fleming, K. L. Kees, and L. R. Krepski, *J. Org. Chem.*, **43**, 3255 (1978).

6) A. Kasahara and T. Izumi, *Chem. Lett.*, **1978**, 21.

7) The nomenclature system used is that proposed by B. H. Smith in "Bridged Aromatic Compounds," Academic Press, New York (1964).

8) K. Sonogashira, Y. Tohda, and N. Hagihara, *Tetrahedron Lett.*, **1975**, 4467.

9) R. F. Heck and J. P. Nolley, Jr., *J. Org. Chem.*, **37**, 2320 (1972).

10) V. Boekelheide and R. A. Hollins, *J. Am. Chem. Soc.*, **92**, 3512 (1970).

11) J. D. Dunitz, L. E. Orgel, and A. Rich, *Acta Crystallogr.*, **9**, 373 (1956).

12) R. A. Morton, A. Hassan, and T. C. Calloway, *J. Chem, Soc.*, **1934**, 883.

13) C. G. Overberger and D. Tanner, *J. Am. Chem. Soc.*, **77**, 369 (1955).

14) T. H. Barr and W. E. Watts, *J. Organomet. Chem.*, **15**, 177 (1968); A. G. Obsorne and R. H. Whiteley, *ibid.*, **193**, 345 (1980).

15) a) D. J. Cram and H. Steinberg, *J. Am. Chem. Soc.*, **73**, 5691 (1951); b) D. T. Longone and C. L. Warren, *ibid.*, **84**, 1507 (1962); c) T. Otsubo, S. Mizogami, I. Otsubo, Z. Tozuka, A. Sakagami, Y. Sakata, and S. Misumi, *Bull. Chem. Soc. Jpn.*, **46**, 3519 (1973).

16) R. W. Fish and M. Rosenblum, *J. Org. Chem.*, **30**, 1253 (1965).

17) A. Kasahara, T. Izumi, I. Shimizu, M. Satou, and T. Katou, *Bull. Chem. Soc. Jpn.*, **55**, 2434 (1982).

18) T. Ojima, T. Yokomachi, and A. Kimura, *Bull. Chem. Soc. Jpn.*, **49**, 2840 (1976).

19) R. H. Wiley and P. H. Hobson, *J. Am. Chem. Soc.*, **71**, 2429 (1949).

20) C. Eaborn, A. R. Thompson, and D. R. M. Walton, *J. Chem. Soc. C*, **1967**, 1364.

 © 1983 The Chemical Society of Japan Bull. Chem. Soc. Jpn., 56, 1149—1154 (1983)

Syntheses of 5-Deoxy-, 5,4′-Dideoxy-, 5-Deoxy-5-epichloro-, and 5,4′-Dideoxy-5,4′-diepichlorokanamycin A

Toshiaki Miyake,* Tsutomu Tsuchiya, Toshiyuki Nishi, and Sumio Umezawa
Institute of Bioorganic Chemistry, 1614 Ida, Nakahara-ku, Kawasaki 211
(Received September 8, 1982)

5,4′-Dideoxy-5,4′-diepichlorokanamycin A has been synthesized from 1,3,6′,3″-tetrakis(*N*-benzyloxycarbonyl)-4″,6″-*O*-cyclohexylidenekanamycin A by treatment with sulfuryl chloride, followed by deblocking. Similar treatment of 2′,3′,4′,2″-tetra-*O*-acetyl-1,3,6′,3″-tetrakis(*N*-benzyloxycarbonyl)-4″,6″-*O*-cyclohexylidenekanamycin A gave 5-deoxy-5-epichlorokanamycin A. 5,4′-Dideoxykanamycin A and 5-deoxykanamycin A were synthesized from the corresponding 5,4′-diepichloro and 5-epichloro derivatives by reductive dechlorination with sodium metal in liquid ammonia or tributylstannane. The structures of these derivatives were confirmed by the ^{1}H- and ^{13}C-NMR spectroscopy.

In previous papers[1,2] we reported the syntheses of 4′-deoxykanamycin A and B, which show activities against some kanamycin-resistant strains including *Pseudomonas aeruginosa*. This paper describes the preparation of some chloro and deoxy derivatives of kanamycin A modified at C-5 and C-4′ utilizing sulfuryl chloride.

Chlorination of sugars by sulfuryl chloride has been extensively studied.[3] In the case of methyl α-D-glucopyranoside (**1**), Helferich *et al.*[4] observed, in the beginning of the 1920's, the formation of 4,6-dichloro-4,6-dideoxy-α-D-hexoside 2,3-cyclic sulfate by treating **1** with sulfuryl chloride, the correct structure of the product being later determined[5] as a 4,6-dichlorogalactoside derivative formed by inversion of the configuration at C-4. This result indicates that chlorination does not occur at the 2- and 3-hydroxyl groups of a α-D-gluco-

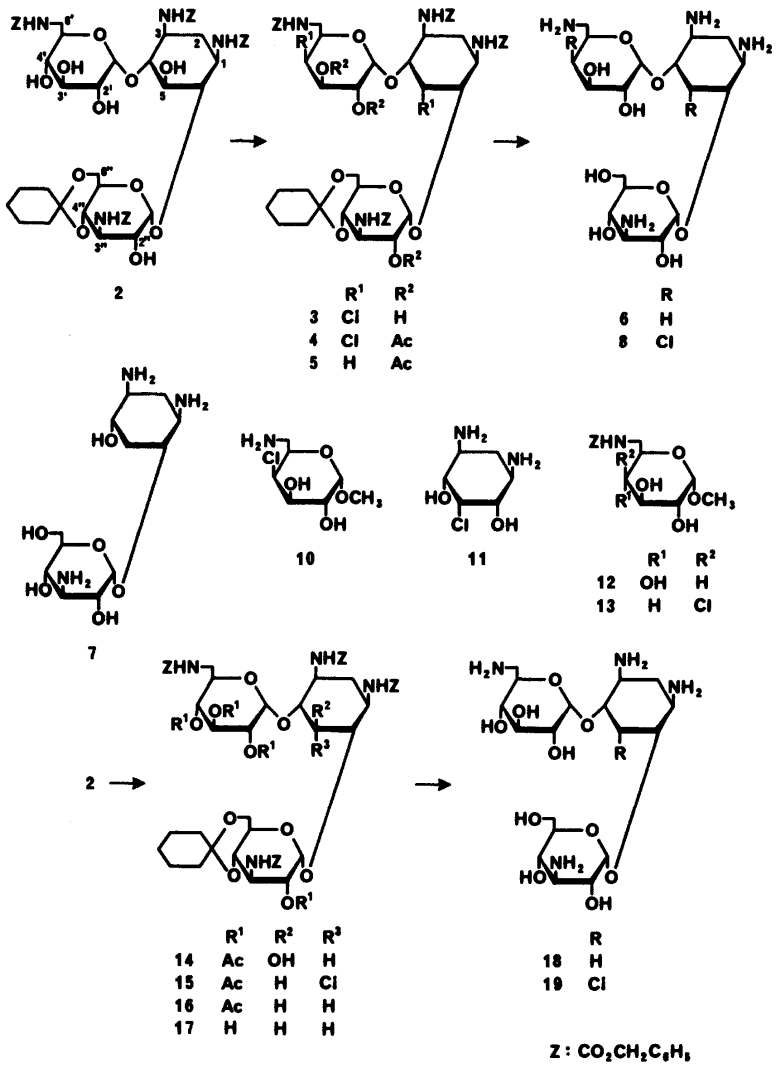

Scheme 1.

pyranoside derivative and, after desulfation (or dechlorosulfation[3]), they are regenerated. Regarding kanamycin A, there are four amino and seven hydroxyl groups in the molecule, and, even if the amino and 4″- and 6″-hydroxyl groups are protected, five reactive hydroxyl groups still remain; among them, the 2′-, 3′-, and 2″-hydroxyl groups are expected not to be replaced by chlorine atoms by treatment with sulfuryl chloride from the above point of view.

We were, therefore, interested in the selective chlorination of a kanamycin A derivative, 1,3,6′,3″-tetrakis(*N*-benzyloxycarbonyl)-4″,6″-*O*-cyclohexylidenekanamycin A[2] (**2**) with sulfuryl chloride. Treatment of **2** with the reagent in dichloromethane–pyridine gave the corresponding 5,4′-diepichloro derivative (**3**) in 45% yield. It should be noted that the 5-epichlorination simultaneously occurred in addition to the 4′-epichlorination, which was unexpected from the steric point of view, because the 5-hydroxyl group of kanamycin derivatives are known to be less reactive among the hydroxyl groups against benzoylation and sulfonylation[2,6,7] due to the bulkiness of the adjacent substituents attached at C-4 and 6. Recently, Suami *et al.*[8] also reported the 5-epichlorination of a protected kanamycin B derivative with sulfuryl chloride.

In order to prepare 5,4′-dideoxykanamycin A (**6**), **3** was treated with sodium metal in liquid ammonia, and the desired **6** was obtained in a low yield (19%) after decyclohexylidenation. As already reported,[9] in the case of methyl 3-chloro-4,6-*O*-cyclohexylidene-2,3-dideoxy-2-(*p*-toluenesulfonamido)-α-D-glucopyranoside,[9] reductive dechlorination smoothly occurred by the same treatment. Treatment of the 2′,3′,2″-tri-*O*-acetyl derivative (**4**) of **3** with sodium in liquid ammonia gave **6** in 27% yield together with 6-*O*-(3-amino-3-deoxy-α-D-glucopyranosyl)-2,5-dideoxystreptamine (**7**). The structure of the latter was confirmed by the paper-chromatography of the acidic hydrolyzates of **7**. Occurrence of the high-degree hydrolysis of a glycoside bond of **4** is somewhat surprising.

In order to improve the yield of **6**, **4** was treated in trial, with tributylstannane in the presence of α,α′-azobis(isobutyronitrile)[10] in 1,4-dioxane, affording 4′-deoxy derivative (**5**) in high yield. Successive deblocking of the acetyl, cyclohexylidene, and benzyloxycarbonyl groups of **5** gave **6** in 77% overall yield from **4**.

Next, to prepare a chloro derivative of kanamycin A, the protecting groups of **3** were removed to give 5,4′-dideoxy-5,4′-diepichlorokanamycin A (**8**). Its structure was determined by the ^{1}H-NMR spectra, which gave double doublets with small spacings (δ=5.10, J=4 and 1 Hz, H-4′) and a narrow triplet (δ=5.63, J=3 Hz, H-5) assignable to the protons attached to the carbon bearing chlorine atom; this indicates that both the chloro atoms are axially attached. The structure of **8** was further confirmed by methanolysis in the presence of Amberlite CG120 (H form) resin at a high temperature according to a reported procedure.[11] Methyl 3-amino-3-deoxy-α-D-glucopyranoside (**9**),[12,13] methyl 6-amino-4-chloro-4,6-dideoxy-α-D-galactopyranoside (**10**), and 2,5-dideoxy-5-epichlorostreptamine (**11**) were obtained after chromatography. The compound **10** was identical with that prepared by a different route. Methyl 6-amino-6-deoxy-α-D-glucopyranoside[14] was successively *N*-benzyloxycarbonylated (to give **12**), and 4′-epichlorinated by the method described for **3** (to give **13**), followed by removal of the *N*-protecting group to give **10**. Its ^{1}H-NMR spectrum showed double doublets assignable to equatorial H-4 (δ=4.98, J=3.2 and 1.0 Hz), the splitting pattern being comparable with that of the corresponding resonances of **8**.

5-Deoxy and 5-deoxy-5-epichloro derivatives of kanamycin A were further prepared as follows: The protected kanamycin A (**2**) was acetylated and the resulting 2′,3′,4′,2″-tetra-*O*-acetyl derivative (**14**) having a free hydroxyl group at C-5 was treated with sulfuryl chloride in a similar manner as described above to give the 5-deoxy-5-epichloro derivative (**15**). Treatment of **15** with sodium metal in liquid ammonia in a manner as described for **6** followed by deacetylation and decyclohexylidenation gave 5-deoxykanamycin A (**18**) in good yield (69%). The yield was somewhat surprising because **3** or **4** gave poor yields of **6** by the same treatment. The compound **18** was recently synthesized *via* glycosidation by Kavadias *et al.*,[15] or isolated from the fermentation broths of *S. kanamyceticus*.[16] Reduction of **15** with tributylstannane (to give **16**) followed by deprotection also gave **18**. Deprotection of **15** gave the desired 5-deoxy-5-epichlorokanamycin A (**19**).

The ^{13}C-chemical shifts of the final deoxy compounds (**6**, **8**) and kanamycin A are shown in Table 1. Expected downfield shift (2.3 ppm) based on the shift of kanamycin A[2] caused by the 4′-deoxygenation was observed at C-6′ of **6**, which was not observed in the spectrum of **18**. Upfield shifts (4.8 and 5.4 ppm) caused by the 5-deoxygenation were observed at the C-1′ in both **6** and **18**. Similar upfield shifts were reported for 5-

Table 1. The ^{13}C chemical shifts[a] of **6**, **18**, kanamycin A (KMA) measured in D_2O (at pD 9.5)

Carbon	6	18	KMA[e]
1′	95.6	95.0	100.4
2′	73.6	72.0	72.7
3′	68.7[b]	72.0	73.7
4′	36.2	71.8	71.9
5′	67.7[b]	73.5	73.7
6′	44.7	42.1	42.4
1	52.3	52.3	51.2
2	36.2	36.2	36.3
3	53.3	53.3	49.8
4	83.6[c]	83.7[d]	88.2
5	34.4	34.4	74.9
6	77.0[c]	77.3[d]	88.7
1″	101.1	101.1	100.8
2″	72.4	72.5	72.7
3″	55.0	54.9	55.1
4″	70.6	70.6	70.2
5″	73.1	73.1	73.0
6″	61.7	61.7	61.2

a) In ppm downfield from TMS calculated as $\delta^{TMS}=\delta^{dioxane}+67.4$ ppm. b)—d) The values may be reversed. e) Shift assignments were based on the shifts of kanamycin A (pH 9.6) reported.[19]

Table 2. The ^{13}C chemical shifts[a] of **8**, **19**, **10**, kanamycin A (KMA), and methyl 6-amino-6-deoxy-α-D-glucopyranoside (Me 6AG) measured in 20% ND_3 in D_2O

Carbon	**8**	**19**	KMA	**10**	Me 6AG
1′	95.2	94.8	101.0	100.8	100.5
2′	72.1	72.5	73.0	60.2	72.6
3′	69.5[b]	74.5[d]	74.4[f]	71.7[g]	74.2
4′	65.0	72.4	72.3	65.3	72.4
5′	69.0[b]	73.8[d]	74.1[f]	69.7[g]	73.3
6′	43.4	43.0	43.1	43.5	42.8
1	48.8	48.9	51.7		
2	37.0	37.1	36.8		
3	48.1	48.2	50.3		
4	85.2[c]	85.4[e]	88.9		
5	62.2	62.1	75.3		
6	77.9[c]	77.2[e]	89.0		
1″	102.4	102.6	101.2[h]		
2″	72.9	72.9	73.1		
3″	55.4	55.5	55.6		
4″	71.1	71.1	70.6		
5″	74.4	74.0	73.5		
6″	61.6	61.7	61.5		
OCH_3				56.4	56.2

a) In ppm downfield from external TMS. b)—g) The values may be reversed. h) Assigned by selective proton decoupling at H-1″.

deoxykanamycin B [4.3 (as the free base, pD 11)[8] and 4.2 ppm (as the sulfate, pD 7)[17]]. In Table 2, the ^{13}C-chemical shifts of the final chloro compounds (**8**, **19**), **10**, methyl 6-amino-6-deoxy-α-D-glucopyranoside, and kanamycin A are compared. Upfield shifts (7.3 and 7.1 ppm) caused by the 4′(or 4)-epichlorination were observed at C-4′ of **8** and C-4 of **10**, but no obvious difference as experienced in the 4′-deoxy derivatives was observed on the shifts of C-6′ (C-6 in the case of **10**) between the chloro compounds (**8**, **19**, **10**) and kanamycin A. Upfield shifts caused by 5-deoxy-5-epichlorination were observed at C-1′ by 5.8 (**8**) and 6.2 ppm (**19**). Recently a similar upfield shift[18] (4.5 ppm) at C-1′ was observed in 5-epikanamycin B compared with kanamycin B.

The antibacterial activities of the compounds **6**, **8**, **18**, **19**, and kanamycin A are shown in Table 3. It was concluded, by the comparison, that the 4′-epichlorination of kanamycin A caused lack of activity. The 5-deoxygenation of kanamycin A caused lowering of activity in accord with the report by Kavadias *et al.*[15]

Experimental

IR spectra were determined in KBr disks with a Hitachi 285 infrared spectrophotometer. ^1H-NMR spectra were recorded at 90 MHz with a Varian EM-390 spectrometer. ^{13}C-NMR spectra were recorded on a Varian XL-100 spectrometer with a Varian 620-L data processing system (25.2 MHz). Tetramethylsilane ($\delta=0$) was used as the internal standard (in organic solvents), or as the external standard (in deuterium oxide). Thin-layer chromatography (TLC) was carried out on E. Merck precoated silica gel 60 plates with the spray of sulfuric acid or 0.5% ninhydrin in pyridine for detection. Paper chromatography (PPC) was carried out on Toyo-Roshi paper No. 50 with 1-butanol–pyridine–water–acetic acid (6 : 4 : 3 : 1), descending for 7—8 d, unless otherwise stated, and spots were visualized by 0.5% ninhydrin in pyridine. For column chromatography, silica gel (Wakogel C-200) was used, unless otherwise stated.

*1,3,6′,3″-Tetrakis(*N*-benzyloxycarbonyl)-5,4′-dideoxy-5,4′-diepichloro-4″,6″-*O*-cyclohexylidenekanamycin A (**3**).* To a solution of **2**[2] (504 mg) in a mixture of dry dichloromethane (9 ml) and dry pyridine (3.5 ml), was added sulfuryl chloride (0.55 ml, 15 mol equivalents for **2**) gradually at −78 °C and the solution was kept at the temperature for 30 min, then at room temperature for 1.5 h. A solution of sodium iodide (750 mg) in aqueous pyridine (1 : 2, 7.5 ml) was added to the reaction mixture. The resulting solution showed, on TLC with chloroform–ethanol (10 : 1), spots at R_f 0.4 (**3**, major), 0.25 (**2**, slight), 0.07 (minor), and others. Concentration of the mixture gave a syrup, which was dissolved in chloroform. The solution was washed with water, dried ($MgSO_4$), and concentrated to give a brown solid (405 mg), which was chromatographed on a silica-gel column with chloroform–ethanol = 15 : 1 to give a colorless solid of **3**, 235 mg (45%), $[\alpha]_D^{25}$ +80° (*c* 0.5, *N*,*N*-dimethylformamide).

Found: C, 58.83; H, 5.80; N, 4.72; Cl, 6.41%. Calcd for $C_{56}H_{66}N_4O_{17}Cl_2$: C, 59.10; H, 5.85; N, 4.92; Cl, 6.23%.

*2′,3′,2″-Tri-*O*-acetyl-1,3,6′,3″-tetrakis(*N*-benzyloxycarbonyl)-4″,6″-*O*-cyclohexylidene-5,4′-dideoxy-5,4′-diepichlorokanamycin A (**4**).* To a solution of **3** (102 mg) in dry pyridine (2 ml) was added acetic anhydride (0.051 ml, 6 mol equivalents for **3**) and the solution was kept at room temperature overnight. After

Table 3. Antibacterial spectra of **6**, **8**, **18**, **19**, and kanamycin A (KMA)

Test Organisms[a]	Minimal inhibitory concentration/μg ml^{-1}				
	6	**8**	**18**	**19**	KMA
Staphylococcus aureus FDA 209P	6.25	>100	6.25	12.5	3.12
Sarcina lutea PCI 1001	25	—	25	100	12.5
Klebsiella pneumoniae PCI 602	12.5	>100	3.12	12.5	1.56
Salmonella typhi T-63	3.12	>100	1.56	6.25	1.56
Escherichia coli K-12	6.25	>100	3.12	12.5	3.12
Escherichia coli K-12 ML1629[b]	>100	>100	>100	>100	>100
Pseudomonas aeruginosa A3	3.12	>100	100	100	25
Pseudomonas aeruginosa No. 12	25	—	>100	>100	>100
Mycobacterium smegmatis ATCC 607[c]	6.25	—	3.12	6.25	1.56

a) Agar dilution streak method (nutrient agar, 37 °C, 18 h). b) This strain phosphorylates the 3′-hydroxyl groups of kanamycins. c) Measured after 48 h.

addition of acetic anhydride (0.025 ml), the solution was heated at 50 °C for 6 h. The solution showed, on TLC with chloroform–ethanol (10 : 1), a single spot at R_f 0.41. Addition of water (0.1 ml) followed by concentration gave a syrup. A chloroform (10 ml) solution of the syrup was washed successively with 5% aqueous sodium hydrogencarbonate solution, and water, dried ($MgSO_4$), and concentrated to give a pale brown solid (110 mg), which was purified by passing through a short column of silica gel with chloroform–2-butanone=3 : 1 to give a colorless solid of **4**, 98.7 mg (87%), $[\alpha]_D^{25}$ +86° (*c* 0.5, chloroform); ^{1}H-NMR ($CDCl_3$): δ=1.73, 2.13, 2.19 (each 3H s, $COCH_3$).

Found: C, 59.05; H, 5.71; N, 4.39; Cl, 5.87%. Calcd for $C_{62}H_{72}N_4O_{20}Cl_2$: C, 58.91; H, 5.74; N, 4.43; Cl, 5.61%.

2′,3′,2″-Tri-O-acetyl-1,3,6′,3″-tetrakis(N-benzyloxycarbonyl)-4″,6″-O-cyclohexylidene-5,4′-dideoxykanamycin A (**5**). To a solution of **4** (93.5 mg) in dry 1,4-dioxane (2 ml) were added tributylstannane (0.3 ml) and α,α′-azobis(isobutyronitrile) (10 mg) and the reaction mixture was heated at 80 °C for 2 h under the nitrogen atmosphere. The resulting solution showed, on TLC with chloroform–2-butanone (3 : 1), a single spot at R_f 0.11 (*cf.* **4**, R_f 0.26). The solution was concentrated under reduced pressure to give a solid, which was thoroughly washed with ether and chromatographed on a silica-gel column with chloroform–ethanol=15 : 1 to give a solid of **5**, 78.6 mg (89%), $[\alpha]_D^{25}$ +82° (*c* 0.5, *N,N*-dimethylformamide); ^{1}H-NMR (pyridine-d_5): δ=1.99 (6H) and 2.28 (3H) (each s, $COCH_3$); 1.0—2.8 (25H, C_6H_{10}, $3COCH_3$, CH_2 at C-2,5,4′).

Found: C, 62.07; H, 6.20; N, 4.91%. Calcd for $C_{62}H_{74}N_4O_{20}$: C, 62.30; H, 6.24; N, 4.69%.

5,4′-Dideoxykanamycin A (**6**). *A) From* **5**: To a suspension of **5** (46.2 mg) in dry 1,4-dioxane–methanol (4 : 1, 1 ml) was added 1 M sodium methoxide (1 M=1 mol dm^{-3}) in methanol (0.025 ml), and the mixture was stirred at room temperature for 15 min. The resulting clear solution was neutralized with Dowex 50W×8 resin (H form) pretreated with 1,4-dioxane, filtered, and the filtrate was concentrated to give a solid, 42.0 mg. The deacetyl product was suspended in 80% aqueous acetic acid, and the mixture was stirred at 80 °C for 20 min. The resulting clear solution containing the decyclohexylidenated product was hydrogenated with palladium black under atmospheric pressure of hydrogen for 40 min. The resulting product was purified by chromatography over CM-Sephadex C-25 (NH_4 form, 0→0.3 M aqueous ammonia) to give a solid of **6**, 18.6 mg (86% as the 1.7 carbonate), $[\alpha]_D^{25}$ +130° (*c* 0.5, water); PPC: $R_{f\ \text{kanamycin A}}$ 1.1; TLC (1-butanol–ethanol–chloroform–10 M aqueous ammonia=4 : 7 : 2 : 7): R_f 0.20 (*cf.* kanamycin A, R_f 0.17).

Found: C, 42.42; H, 7.10; N, 10.00%. Calcd for $C_{18}H_{36}N_4O_9\cdot 1.7\,H_2CO_3$: C, 42.41; H, 7.12; N, 10.04%.

Acidic hydrolysis of **6** (6 M HCl, 100 °C, 50 min) gave three products, on PPC (descending for 2 d), corresponding to 3-amino-3-deoxy-D-glucose ($R_{f\ \text{2-deoxystreptamine (DST)}}$ 2.5), 6-amino-4,6-dideoxy-D-*xylo*-hexose ($R_{f\ \text{DST}}$ 2.0) and 2,5-dideoxystreptamine ($R_{f\ \text{DST}}$ 1.6) (*cf.* 6 amino-6-deoxy-D-glucose, $R_{f\ \text{DST}}$ 1.6).

B) From **3**: To a solution of **3** (131 mg) in liquid ammonia (≈35 ml) at −60 °C was added sodium metal (≈260 mg) with stirring, and the resulting deep-blue solution was kept at −50 °C for 2 h. Addition of methanol (5 ml) followed by concentration gave a solid. An aqueous solution of the de(benzyloxycarbonyl)-5,4′-dideoxy intermediate was stirred with Dowex 50W×8 resin (H form, 30 ml), and the resin, after packed in a column and washing it with water, was treated with 1 M aqueous ammonia. The ninhydrin-positive fractions were collected and concentrated. The solid obtained was chromatographed over CM-Sephadex C-25 (NH_4 form, 00.3 M aqueous ammonia) to give a solid of **6**, 12.6 mg (19% as the dicarbonate).

C) From **4**: **4** (60.2 mg) was treated with sodium metal (≈140 mg) in liquid ammonia (≈20 ml) as described for B). Deacetylation of the resulting product was carried out by treating it with 1 M aqueous sodium hydroxide at 50 °C for 30 min. Purification in a manner as described above gave a solid of **6** (6.7 mg, 27% as the 1.2 carbonate) and that of **7** (10.1 mg, 60% as the 0.7 carbonate).

6: Found: C, 43.75; H, 7.18; N, 10.53%. Calcd for $C_{18}H_{36}N_4O_9\cdot 1.2H_2CO_3$: C, 43.76; H, 7.35; N, 10.63%.

7: $[\alpha]_D^{25}$ +72° (*c* 1, water); PPC: $R_{f\ \text{kanamycin A}}$ 2.3; TLC (1-butanol–ethanol–chloroform–10 M aqueous ammonia=4 : 7 : 2 : 7): R_f 0.28; ^{1}H-NMR (D_2O): δ=1.5—2.4 (2H m, H-2ax and 5ax), 2.4—3.2 (2H m, H-2eq and 5eq), 5.53 (1H d, *J* 4 Hz, H-1′).

Found: 43.52; H, 7.55; N, 11.78%. Calcd for $C_{12}H_{25}N_3O_6\cdot 0.7H_2CO_3$: C, 43.49; H, 7.59; N, 11.98%.

PPC of the acidic hydrolyzates of **7** (6 M HCl, 100 °C, 30 min; descending for 2 d): $R_{f\ \text{2-deoxystreptamine (DST)}}$ 2.6 (3-amino-3-deoxy-D-glucose) and 1.6 (2,5-dideoxystreptamine).

5,4′-Dideoxy-5,4′-diepichlorokanamycin A (**8**). A suspension of **3** (161 mg) in 80% aqueous acetic acid was stirred at 90 °C for 45 min. The resulting clear solution was hydrogentated with palladium black under atmospheric pressure of hydrogen at room temperature for 20 min. The crude product was chromatographed over CM-Sephadex C-25 (NH_4 form, 0→0.1 M aqueous ammonia) to give a solid of **8**, 71.5 mg (84% as the monocarbonate monohydrate), $[\alpha]_D^{25}$ +146° (*c* 1, water); PPC: $R_{f\ \text{kanamycin A}}$ 2.5; TLC (1-butanol–ethanol–chloroform–10 M aqueous ammonia=4 : 7 : 2 : 7): R_f 0.32 (*cf.* kanamycin A, R_f 0.18); ^{1}H-NMR (as the HCl salt, in D_2O): δ=5.10 (1H dd, $J_{3',4'}$ 4 Hz, $J_{4',5'}$ 1 Hz, H-4′), 5.63 (1H t, $J_{4,5}=J_{5,6}$ 3 Hz, H-5).

Found: C, 38.21; H, 6.19; N, 9.25; Cl, 12.05%. Calcd for $C_{18}H_{34}N_4O_9Cl_2\cdot H_2CO_3\cdot H_2O$: C, 37.94; H, 6.36; N, 9.32; Cl, 11.79%.

Methanolysis of **8**. To a suspension of **8** (56.8 mg, as the 0.8 carbonate) in dry methanol (4 ml) was added Amberlite CG120 resin (H form, 200—400 mesh, dried *in vacuo* at 60 °C), and the mixture was stirred in a sealed tube at 100 °C for 4.5 h. The mixture was filtered, and the solid was washed with 1 M aqueous ammonia. The filtrate and washings combined were concentrated to give a solid (46.7 mg). The solid showed, on TLC with 1-butanol–ethanol–chloroform–10 M ammonia (4 : 7 : 2 : 7), spots at R_f 0.60 (**10**), 0.58 (minor), 0.55 (**9**), and 0.42 (**11**). The solid was chromatographed over CM-Sephadex C-25 (NH_4 form, 0→0.1 M aqueous ammonia) to give solids of **9** (16.2 mg, 82% as the 0.1 carbonate), **10** (8.0 mg, 38% as the free base), and **11** (10.2 mg, 50% as the 0.3 carbonate) (cited in order of elution).

9: $[\alpha]_D^{25}$ +116° (*c* 1, water) (lit,[12] +144°, lit,[13] +136°); ^{1}H-NMR (20% ND_3 in D_2O): δ=3.93 (3H s, OCH_3), 5.25 (1H d, $J_{1,2}$ 3.8 Hz, H-1).

Found: C, 42.28; H, 7.44; N, 6.81%. Calcd for $C_7H_{15}NO_5\cdot 0.1H_2CO_3$: C, 42.75; H, 7.68; N, 7.06%.

10: $[\alpha]_D^{25}$ +208° (*c* 1, water); ^{1}H-NMR (20% ND_3 in D_2O): δ=4.98 (1H dd, $J_{3,4}$ 3.3 Hz, $J_{4,5}$ 1 Hz, H-4), 5.33 (1H d, $J_{1,2}$ 3.8 Hz, H-1).

Found: C, 39.54; H, 6.50; N, 6.34; Cl, 16.54%. Calcd for $C_7H_{14}NO_4Cl$: C, 39.72; H, 6.67; N, 6.62; Cl, 16.75%.

11: ^{1}H-NMR (20% ND_3 in D_2O): δ=5.03 (1H t, $J_{4,5}=J_{5,6}$ 3.3 Hz, H-5).

Found: C, 37.99; H, 6.63; N, 13.64%. Calcd for $C_6H_{13}N_2O_2Cl\cdot 0.3H_2CO_3$: C, 37.98; H, 6.88; N, 14.06%.

Methyl 6-Amino-4-chloro-4,6-dideoxy-α-D-galactopyranoside (**10**) *Obtained from* **13**. A solution of **13** (55.0 mg) in 1,4-dioxane–

methanol (2 : 1, 1 ml) was hydrogenated with palladium black in the usual manner to give a solid of **10**, 28.9 mg (86% as the base).

Methyl 6-Benzyloxycarbonylamino-6-deoxy-α-D-glucopyranoside (12). A mixture of methyl 6-amino-6-deoxy-α-D-glucopyranoside[14] (530 mg), benzyl chloroformate (0.46 ml) and anhydrous sodium carbonate (293 mg) in aqueous acetone (1 : 1, 10 ml) was stirred at room temperature for 45 min. Usual work-up gave a solid of **12**, 835 mg (93%), $[\alpha]_D^{25}$ +40° (*c* 0.5, chloroform); IR: 1700, 1560 cm^{-1}.

Found: C, 55.14; H, 6.41; N, 4.28%. Calcd for $C_{15}H_{21}NO_7$: C, 55.04; H, 6.47; N, 4.28%.

Methyl 6-Benzyloxycarbonylamino-4-chloro-4,6-dideoxy-α-D-galactopyranoside (13). To a solution of **12** (516 mg) in dry dichloromethane (15.5 ml)–dry pyridine (0.7 ml) was added sulfuryl chloride (0.47 ml, 4 mol equivalents for **12**) at −78 °C. Successive workup as described for **3** gave a syrup, which was recrystallized from ethanol to give needles of **13**, 329 mg (60%), mp 126—128 °C; $[\alpha]_D^{25}$ +129° (*c* 1, chloroform); TLC (chloroform–ethanol, 8 : 1): R_f 0.37 (*cf.* **12**, R_f 0.23); ^{1}H-NMR (pyridine-d_5–D_2O, 20 : 1): δ=4.90 (1H dd, *J* 1 and 3 Hz, H-4).

Found: C, 52.36; H, 5.89; N, 3.85; Cl, 10.34%. Calcd for $C_{15}H_{20}NO_6Cl$: C, 52.10; H, 5.83; N, 4.05; Cl, 10.25%.

2',3',4',2''-Tetra-O-acetyl-1,3,6',3''-tetrakis(N-benzyloxycarbonyl)-4'',6''-O-cyclohexylidenekanamycin A (14). To a solution of **2** (519 mg) in dry pyridine (10 ml) was added acetic anhydride (0.36 ml) and the solution was kept at room temperature overnight, then more acetic anhydride (0.36 ml) was added and the solution was heated at 50 °C for 4 h. The reaction mixture was then worked up as described for **4** to give a solid of **14**, 537 mg (90%), $[\alpha]_D^{25}$ +76° (*c* 0.5, chloroform); IR: 1240 cm^{-1}; ^{1}H-NMR ($CDCl_3$): δ=1.87 (3H), 2.02 (6H), and 2.07 (3H) (each s, $COCH_3$).

Found: C, 60.35; H, 5.99; N, 4.40%. Calcd for $C_{64}H_{76}N_4O_{23}$: C, 60.56; H, 6.04; N, 4.41%.

2',3',4',2''-Tetra-O-acetyl-1,3,6',3''-tetrakis(N-benzyloxycarbonyl)-4'',6''-O-cyclohexylidene-5-deoxy-5-epichlorokanamycin A (15). To a solution of **14** (201 mg) in dry dichloromethane (2 ml)–dry pyridine (0.4 ml) was added sulfuryl chloride (0.06 ml, 5 mol equivalents for **14**) at −78 °C, and the solution was kept at the temperature for 30 min, then at room temperature for 1.5 h. The solution showed, on TLC with chloroform–2-butanone (3 : 2), a single spot at R_f 0.45 (*cf.* **14**, R_f 0.31). The reaction mixture was then worked up as described for **3** omitting the treatment with sodium iodide to give a solid of **15**, 170 mg (83%), $[\alpha]_D^{25}$ +74° (*c* 0.5, *N,N*-dimethylformamide).

Found: C, 59.44; H, 5.87; N, 4.30; Cl, 3.01%. Calcd for $C_{64}H_{75}N_4O_{22}Cl$: C, 59.69; H, 5.87; N, 4.35; Cl, 2.75%.

2',3',4',2''-Tetra-O-acetyl-1,3,6',3''-tetrakis(N-benzyloxycarbonyl)-4'',6''-O-cyclohexylidene-5-deoxykanamycin A (16). Compound **15** (112 mg) was treated with tributylstannane similarly as described for **5** to give a solid of **16**, 96.8 mg (89%), $[\alpha]_D^{25}$ +84° (*c* 0.5, chloroform), ^{1}H-NMR ($CDCl_3$): δ=1.83, 2.00, 2.03, 2.13 (each 3H s, $COCH_3$), 1.0—2.4 (26H, C_6H_{10}, 4$COCH_3$, CH_2 at C-2,5).

Found: C, 61.53; H, 6.22; N, 4.52%. Calcd for $C_{64}H_{76}N_4O_{22}$: C, 61.33; H, 6.11; N, 4.47%.

1,3,6',3''-Tetrakis(N-benzyloxycarbonyl)-4'',6''-O-cyclohexylidene-5-deoxykanamycin A (17). Compound **16** (52.1 mg) was deacetylated as described for **6** (A) to give a solid of **17**, 42.2 mg (93%), $[\alpha]_D^{25}$ +66° (*c* 0.5, *N,N*-dimethylformamide).

Found: C, 60.93; H, 6.28; N, 4.93%, Calcd for $C_{56}H_{68}N_4O_{18}\cdot H_2O$: C, 60.97; H, 6.40; N, 5.08%.

5-Deoxykanamycin A (18). *A) From 17*: The protecting groups of **17** (98.5 mg) were removed as described for **6** (A) to give a solid of **18**, 21.5 mg (42% as the 1.5 carbonate), $[\alpha]_D^{25}$ +124° (*c* 0.5, water) [lit,[15] +101.8° (free base)]; PPC: $R_{f\ kanamycin\ A}$ 0.9; TLC (1-butanol–ethanol–chloroform–10 M aqueous ammonia=4 : 7 : 2 : 7): R_f 0.13; ^{1}H-NMR (D_2O): δ=1.6—3.4 (4H, CH_2 at C-2,5); 5.55 (1H d, *J* 4 Hz, H-1' or 1''), 5.65 (1H d, *J* 3 Hz, H-1'' or 1').

Found: C, 41.94; H, 7.03; N, 9.75%. Calcd for $C_{18}H_{36}N_4O_{10}\cdot 1.5H_2CO_3$: C, 41.71; H, 7.00; N, 9.98%.

PPC of the acidic hydrolyzates of **18** (6 M HCl, 100 °C, 50 min; descending for 2 d): $R_{f\ 2\text{-deoxystreptamine}}$ 2.5 (3-amino-3-deoxy-D-glucose) and 1.6 (6-amino-6-deoxy-D-glucose and 2,5-dideoxystreptamine).

B) From 15: **15** (54.6 mg) was treated with sodium metal in liquid ammonia as described for **6** (B) to give a solid of **18**, 16.0 mg (69% as the 1.3 carbonate).

Found: C, 42.22; H, 7.00; N, 10.26%. Calcd for $C_{18}H_{36}N_4O_{10}\cdot 1.3H_2CO_3$: C, 42.21; H, 7.09; N, 10.20%.

5-Deoxy-5-epichlorokanamycin A (19). Compound **15** (252 mg) was treated as described for **6** (A) to give a solid of **19**, 81.4 mg (75% as the 0.8 carbonate), $[\alpha]_D^{25}$ +128° (*c* 1, water); PPC: $R_{f\ kanamycin\ A}$ 1.0; ^{1}H-NMR (20% ND_3 in D_2O) δ=5.6 (3H m, H-5,1', 1'').

Found: C, 41.01; H, 6.96; N, 9.98; Cl, 6.32%. Calcd for $C_{18}H_{35}N_4O_{10}Cl\cdot 0.8H_2CO_3$: C, 40.86; H, 6.68; N, 10.14; Cl, 6.42%.

We are grateful to Professor Hamao Umezawa, Institute of Microbial Chemistry, for his suport and encouragement. We also thank Dr. Hiroshi Naganawa, Institute of Microbial Chemistry, for collaboration on ^{13}C-NMR spectral studies, and Mr. Saburo Nakada, Keio University, for carrying out elemental analyses.

References

1) S. Umezawa, Y. Nishimura, Y. Hata, T. Tsuchiya, M. Yagisawa, and H. Umezawa, *J. Antibiot.*, **27**, 722 (1974).
2) T. Miyake, T. Tsuchiya, S. Umezawa, and H. Umezawa, *Bull. Chem. Soc. Jpn.*, **50**, 2362 (1977).
3) E. Buncel, *Chem. Rev.*, **70**, 323 (1970).
4) B. Helferich, *Chem. Ber.* **54**, 1082 (1921).
5) P. D. Bragg, J. K. N. Jones, and J. C. Turner, *Can. J. Chem.*, **37**, 1412 (1959); J. K. N. Jones, M. B. Perry, and J. C. Turner, *ibid.*, **38**, 1122 (1960).
6) H. Umezawa, S. Umezawa, T. Tsuchiya, and Y. Okazaki, *J. Antibiot.*, **24**, 485 (1971); S. Umezawa, H. Umezawa, Y. Okazaki, and T. Tsuchiya, *Bull. Chem. Soc. Jpn.*, **45**, 3624 (1972).
7) Y. Takagi, T. Miyake, T. Tsuchiya, S. Umezawa, and H. Umezawa, *J. Antibiot.*, **26**, 403 (1973); *Bull. Chem. Soc. Jpn.*, **49**, 3649 (1976).
8) T. Suami, S. Nishiyama, Y. Ishikawa, and E. Umemura, *Bull. Chem. Soc. Jpn.*, **51**, 2354 (1978).
9) T. Miyake, T. Tsuchiya, Y. Takahashi, and S. Umezawa, *Carbohydr. Res.*, **89**, 255 (1981).
10) K. Hayashi, J. Iyoda, I. Shiihara, *J. Organomet. Chem.*, **10**, 81 (1967); H. Arita, Y. Matsushima, *J. Biochem.*, **70**, 795 (1971).
11) T. Tsuchiya, T. Usui, T. Kamiya, and S. Umezawa, *Carbohydr. Res.*, **77**, 267 (1979).
12) S. Peat and L. F. Wiggins, *J. Chem. Soc.*, **1938**, 1810.
13) H. Ogawa, T. Ito, S. Kondo, and S. Inoue, *Bull. Agric. Chem. Soc. Jpn.*, **23**, 289 (1959).
14) F. Cramer, H. Otterbach, and H. Springmann, *Chem. Ber.*, **92**, 384 (1959).
15) G. Kavadias, P. Dextraze, R. Masse, and B. Belleau,

Can. J. Chem., **56**, 2086 (1978).
16) H. Yasuda, T. Suami, T. Ishikawa, S. Umezawa, and H. Umezawa, Japan Kokai, 78-34988, Mar. 31, 1978.
17) T. Hayashi, T. Iwaoka, N. Takeda, and E. Ohki, *Chem. Pharm. Bull.*, **26**, 1786 (1978).
18) T. Suami and K. Nakamura, *Bull. Chem. Soc. Jpn.*, **52**, 955 (1979).
19) G. Kotowycz and R. U. Lemieux, *Chem. Rev.*, **73**, 669 (1973).

 © 1983 The Chemical Society of Japan Bull. Chem. Soc. Jpn., 56, 1155—1160 (1983)

Solution Conformation of Cyclic Dipeptides Having Aliphatic Side Chains

Masao TANIHARA, Tae HIZA, Yukio IMANISHI,* and Toshinobu HIGASHIMURA
Department of Polymer Chemistry, Faculty of Engineering, Kyoto University, Yoshida Honmachi, Sakyo-ku, Kyoto 606
(Received September 8, 1982)

Cyclic dipeptides having aliphatic side chains, *cyclo*(L-Val)$_2$, *cyclo*(L-Val–D-Val), *cyclo*(L-Leu)$_2$, and *cyclo*(L-Leu–D-Leu) were synthesized and their conformation in solution was investigated by circular dichroism (CD) and proton nuclear magnetic resonance (^{1}H NMR) spectroscopy. ^{1}H NMR spectra in $(CD_3)_2SO$ of *cyclo*(L-Val–D-Val) and *cyclo*(L-Leu–D-Leu) indicated that the diketopiperazine ring of these *trans* cyclic dipeptides takes a planar or a chair conformation and the molecules take a center-symmetric conformation. ^{1}H NMR spectra in $(CD_3)_2SO$ and CD spectra in CH_3OH and H_2O of *cyclo*(L-Val)$_2$ and *cyclo*(L-Leu)$_2$ indicated that the conformation of these *cis* cyclic dipeptides is planar-axial and flagpole-boat-type respectively. It is suggested that *cis* cyclic dipeptides having aliphatic side chains take such conformations in polar solvents because of the stabilization by attractive forces between aliphatic side chains.

It is well-known that the secondary structure of enzymes plays an important role in exerting their catalytic activities. Biologically active oligopeptides such as peptide antibiotics involve cyclic peptides containing unusual D-amino acids or *N*-substituted amino acids. These examples also show the importance of the secondary structure determined by these unusual amino acids on the biological activity. In order to investigate the structure/activity relationship of these polypeptides and oligopeptides, the use of synthetic cyclic peptides is very helpful.[1,2] In cyclic peptides side chain functional groups may be fixed in a specific arrangement owing to the rigid conformation of the ring moiety. The reduced freedom of conformation enables a detailed analysis of the conformation in solution to be made. The accumulation of information on the structure/activity relation will make possible the design of a molecule having a specific activity.

With this in mind we have synthesized *cyclo*(D-Leu–L-His) and *cyclo*(D-Val–L-His); these are cyclic dipeptides carrying a hydrophobic and a nucleophilic side chain, and we have investigated their hydrolytic activities toward carboxylic acid *p*-nitrophenyl esters. As consequence, these *trans* cyclic dipeptides proved to be effective catalysts for the hydrolyses of $CH_3(CH_2)_{10}COOC_6H_4NO_2(p\text{-})$ and $CH_3(CH_2)_8COOC_6H_4NO_2(p\text{-})$. On the other hand, the diastereomeric *cis* cyclic dipeptides were nearly inactive in the same reactions.[3,4] The conformation of these cyclic dipeptides in aqueous solution was investigated by nuclear magnetic resonance (NMR) and circular dichroism (CD) spectroscopy.[4,5] It was found that in these cyclic dipeptides the aromatic side chain of the histidine residue stacks over the diketopiperazine ring due to aromatic–amide interaction, and that in *trans* cyclic dipeptides the two side chains are situated on the opposite sides of the nearly planar diketopiperazine ring. Furthermore in *cis* cyclic dipeptides the two side chains compete for the space on the same side of the boat-type diketopiperazine ring. In the case of *cyclo*(L-Leu–L-His) the X-ray structural analysis of a single crystal revealed a conformation very similar to that observed in solution.[6]

In order to get some more general information about the conformational properties of cyclic dipeptides in solution, it is necessary to investigate the solution conformation of cyclic dipeptides having only aliphatic side chains, so that the aromatic–amide interaction is absent. It has been assumed[7] without firm experimental support that side chains of these cyclic dipeptides tend to take a pseudoequatorial position in a bowsprit-boat conformation of the diketopiperazine ring because of steric interactions between the side chains or between side chain and diketopiperazine ring. However, in some papers which have been published on the experimental studies of solution conformation before we started the present investigation, experimental evidence for a flagpole-boat conformation was presented. Hooker, Jr., *et al.*[8] carried out the CD investigation of *cyclo*(L-Ala)$_2$ and observed a flagpole-boat conformation in aqueous solution. Davies and Khaled[9] have measured ^{1}H NMR spectra of a number of *cyclo*(Gly–Xyz) and *cyclo*(Sar–Xyz) in $(CD_3)_2SO$ or D_2O and determined the superposition angle β of the ring from $^3J(H\text{–}C^\alpha\text{–}N\text{–}H)$ and $^5J(H\text{–}C^\alpha\text{–}C'\text{–}N\text{–}C^\alpha\text{–}H)$. They have found a boat-type conformation with many kinds of Xyz except of L-Pro and D-Abu.

We considered that the conformation of cyclic dipeptides consisting only of aliphatic α-amino acids in solution should be investigated in more detail. For this purpose, *cyclo*(L-Leu)$_2$, *cyclo*(L-Leu–D-Leu), *cyclo*(L-Val)$_2$, and *cyclo*(L-Val–D-Val) were synthesized and the relationship between the properties of aliphatic side chains and the solution conformation have been investigated.

Experimental

Cyclic Dipeptides. The *N*-terminal of an α-amino acid was blocked by benzyloxycarbonyl group and the *C*-terminal of the other α-amino acid was blocked by an ethyl ester group. Both were coupled with dicyclohexylcarbodiimide as a condensing agent to yield a linear dipeptide, both terminals of which were blocked. The benzyloxycarbonyl group was removed by catalytic hydrogenation, and the product was refluxed in CH_3OH to yield the cyclic dipeptides. Needle-like crystals were obtained by the recrystallization from CH_3OH/H_2O mixed solvent. The products subjected to thin layer chromatography with effluents $CHCl_3$(95)/CH_3OH(2)/AcOH(3) and *n*-BuOH(15)/AcOH(10)/H_2O(12)/pyridine(13) were ninhydrin-negative and colored with iodine (one spot). *cyclo*(L-Val)$_2$, mp 268 °C. Found: C, 60.33; H, 9.29; N, 13.86%.

Calcd for $C_{10}H_{18}N_2O_2$: C, 60.58; H, 9.15; N, 14.13%. *cyclo*-(L-Val-D-Val), mp 266—268 °C. Found: C, 60.14; H, 9.31; N, 14.12%. *cyclo*(L-Leu)$_2$, mp 276 °C. Found: C, 63.42; H, 9.98; N, 12.13%. Calcd for $C_{12}H_{22}N_2O_2$: C, 63.66; H, 9.82; N, 12.38%. *cyclo*(L-Leu-D-Leu), mp 275—278 °C. Found: C, 63.57; H, 9.69; N, 12.14%.

NMR Spectra. 100 MHz and 270 MHz ^{1}H NMR spectra were measured at room temperature with a Varian HA-100 and a Bruker WH-270 spectrometer, respectively. The solvent was $(CD_3)_2SO$ and the internal standard was $(CH_3)_4Si$. The sample concentration was 20 mg/0.4 cm^3 in 100 MHz measurement and 5 mg/0.4 cm^3 in 270 MHz NMR measurement, The NMR measurement in aqueous solution was impossible because of the extremely low solubility of cyclic dipeptides in water.

The NMR signals were assigned by the spin decoupling method in the 100 MHz or 270 MHz spectrum. The chemical shift and the coupling constant were determined from the 270 MHz NMR spectrum. The signal resolution was about $\pm$0.18 Hz.

CD Spectra. The CD spectra of the cyclic dipeptides in aqueous or methanolic solution were measured at room temperature using a JASCO J-20 spectropolarimeter. The concentration of the cyclic dipeptides was about 4×10^{-4} mol dm^{-3}, and quartz cells having optical path lengths 1 cm and 1 mm were used.

A Gaussian Cotton effect curve was assumed, and the spectra obtained were resolved into each Cotton effect component by a curve-fitting method. The molar elipticity $[\theta]$ was calculated by assuming the maximum wavelength, the half width, and the rotational strength, which were changed by $\pm$0.5, $\pm$0.5, and $\pm$0.1%, respectively. The FACOM M-190 system of Computer Center of Kyoto University was used for the computation. The computation was repeated until the standard deviation, which is the root-mean square of the difference between the calculated $[\theta]$ and the observed $[\theta]$ at each wavelength, became smaller than 10^3 deg cm^2 dmol^{-1}.

Results

NMR Spectra. cyclo*(L-Val)$_2$ and* cyclo*(L-Val-D-Val)*: 270 MHz NMR spectra of $(CD_3)_2SO$ solution of cyclic dipeptides consisting of two valyl residues were measured. Chemical shifts and coupling constants were determined on the basis of the NMR spectra and are shown in Table 1. In the NMR spectra, only one set of signals was observed for the amide protons, $C^\alpha H$, $C^\beta H$ and the $C^\gamma H_3$ for either cyclic dipeptide. This indicates that *cyclo*(L-Val)$_2$ assumes a C_2-symmetric conformation and *cyclo*(L-Leu-D-Leu) assumes a center-symmetric conformation.

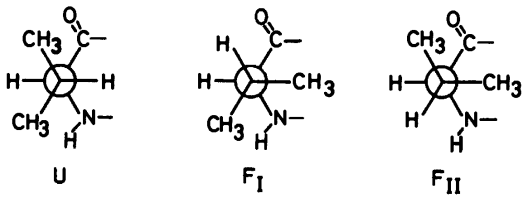

Fig. 1. Rotational isomers around C^α–C^β bond of valyl residue in cyclic dipeptide.

With regard to the side chain conformation of the valyl residues, three kinds of conformational states *U*, F_I, and F_{II} ($U + F_I + F_{II}=1$) corresponding to energy minima of internal rotation around C^α–C^β bond are available; these are illustrated in Fig. 1. The proportions of *U*, F_I, and F_{II} were calculated assuming the coupling constants between a pair of protons which are *gauche* and *trans* with regard to C^α–C^β bond to be 2.60 and 13.56 Hz, respectively.[10] On the above basis, $F_I + F_{II}$ values amount to 94% and 97% for *cyclo*(L-Val)$_2$ and *cyclo*(L-Val-D-Val), respectively. It is somewhat surprising that 94% of the available conformations of *cyclo*(L-Val)$_2$ are folded, because this type of conformation should suffer from steric crowding between side chains.

With regard to the conformation of diketopiperazine ring, information on the rotational angle ϕ of the ring can be obtained from $J_{H\text{-}C^\alpha\text{-}N\text{-}H}$. Since the diketopiperazine ring of the cyclic dipeptides are symmetric and if a planar *cis* peptide bond is assumed, the conformation of diketopiperazine ring is determined by ϕ. Karplus-type equations have been proposed[11-13] for the relationship between the H-C^α-N-H coupling constant and the dihederal angle θ [$\theta=|\phi-60|$]. However, the usual $J_{H\text{-}C^\alpha\text{-}N\text{-}H}$ values (2 Hz) of cyclic dipeptides give only scattered values of θ by the Karplus-type equations, and hence the determination of unequivocal θ value is in general difficult. In the 270 MHz NMR spectra of *cyclo*(L-Val)$_2$ and *cyclo*(L-Val-D-Val) the NH signal is a broad singlet. This makes the determination of $J_{H\text{-}C^\alpha\text{-}N\text{-}H}$ extremely difficult and inaccurate. $J_{H\text{-}C^\alpha\text{-}N\text{-}H}$ is about 1.5 Hz for either cyclic dipeptide as is seen in Table 1. Substitution of this value into the

Table 1. Chemical shifts[a] and coupling constants[b] in 270 MHz proton nuclear magnetic resonance spectra[c] of *cyclo*(L-Val)$_2$ and *cyclo*(L-Val-D-Val)

	δ_{NH}	$\delta_{C^\alpha H}$	$\delta_{C^\beta H}$	$J_{H\text{-}C^\alpha\text{-}N\text{-}H}$	$J_{H\text{-}C^\alpha\text{-}C^\beta\text{-}H}$
cyclo(L-Val)$_2$	7.91	3.68	2.18	$\approx$1.5	3.31
cyclo(L-Val-D-Val)	7.98	3.65	2.19	$\leq$1.5	2.94

a) δ in ppm below $(CH_3)_4Si$. b) J in Hz. c) In $(CD_3)_2SO$, $(CH_3)_4Si$ as internal standard.

Table 2. Chemical shifts[a] and coupling constants[b] in 270 MHz proton nuclear magnetic resonance spectra[c] of *cyclo*(L-Leu)$_2$ and *cyclo*(L-Leu-D-Leu)

	δ_{NH}	$\delta_{C^\alpha H}$	$\delta_{C^\beta H^1}$	$\delta_{C^\beta H^2}$	$J_{H\text{-}C^\alpha\text{-}N\text{-}H}$	$J_{H\text{-}C^\alpha\text{-}C^\beta\text{-}H^1}$	$J_{H\text{-}C^\alpha\text{-}C^\beta\text{-}H^2}$
cyclo(L-Leu)$_2$	8.15	3.71	1.45	1.59	$\approx$2.4	8.46	5.15
cyclo(L-Leu-D-Leu)	8.07	3.75	1.51	1.60	$\leq$1.5	7.35	5.15

a) δ in ppm below $(CH_3)_4Si$. b) J in Hz. c) In $(CD_3)_2SO$, $(CH_3)_4Si$ as internal standard.

Ramachandran equation[11] or the Bystrov equation[12] led to $\theta>60°$ ($\phi<0°$), while that into the Cung equation[13] gave $\theta\leq60°$ ($\phi\geq0°$). Therefore, the ring conformations are not very explicit but seem to be nearly planar.

The $C^{\alpha}H$ signals of *cyclo*(L-Val)$_2$ and *cyclo*(L-Val–D-Val) in 270 MHz NMR spectra are a broad doublet. The latter signal does not become much sharper when it is decoupled with NH. This observation as well as the broad singlet NH signals of *cyclo*(L-Val)$_2$ and *cyclo*(L-Val–D-Val) in 270 MHz NMR spectra could be interpreted if the symmetric ring conformations of *cyclo*(L-Val)$_2$ and *cyclo*(L-Val–D-Val) fluctuate around the C^{α}–N bond on the NMR time scale.

cyclo*(L-Leu)$_2$ and* cyclo*(L-Leu–D-Leu)*: 270 MHz NMR spectra of $(CD_3)_2SO$ solution of cyclic dipeptides consisting of two leucyl residues were measured. The chemical shifts and coupling constants were determined on the basis of the NMR spectra, and are shown in Table 2. Similarly to the case of cyclic dipeptides of valine, only one set of signals was observed for each proton. Therefore, it can be concluded that *cyclo*(L-Leu)$_2$ assumes a C_2-symmetric conformation and *cyclo*(L-Leu–D-Leu) assumes a center-symmetric conformation.

With regard to the side chain conformation of the leucyl residues, similarly to the case of the cyclic dipeptides of valine, three kinds of conformational states F, U_{I} and U_{II} ($F+U_{\mathrm{I}}+U_{\mathrm{II}}=1$) corresponding to energy minima of internal rotation around C^{α}–C^{β} bond are available, which are illustrated in Fig. 2. Similarly to the case of cyclic dipeptides of valine, the proportions of each conformer were calculated from $J_{\mathrm{H\text{-}C^{\alpha}\text{-}C^{\beta}\text{-}H}}$ values listed in Table 2 using the theoretical coupling constants of *trans* and *gauche* proton pairs. Consequently, F% were 23.5 and 33.6 for *cyclo*(L-Leu)$_2$ and *cyclo*(L-Leu–D-Leu), respectively. Since the conformation of *cyclo*(L-Leu)$_2$ and *cyclo*(L-Leu–D-Leu) is C_2-symmetric and center-symmetric, respectively, the proportions of F–F conformation are also 23.5 and 33.6%, respectively. When the C^{α} substituent changed from the isopropyl group of valine to the isobutyl group of leucine, the fraction of folded conformation decreased. However, still one quarter of the available conformations of *cyclo*(L-Leu)$_2$ are folded ones. These should be sterically crowded because of the two bulky side chains accommodated in the same side of diketopiperazine ring. Therefore, this observation suggests that in *cyclo*(L-Leu)$_2$ some kind of stabilization must occur between side chains or between a side chain and the diketopiperazine ring.

In the 270 MHz NMR spectra of *cyclo*(L-Leu)$_2$, the NH signal is a relatively sharp doublet, giving $J_{\mathrm{H\text{-}C^{\alpha}\text{-}N\text{-}H}}$ to be 2.4 Hz as seen in Table 2. This value leads to $\theta\leq60°$ ($\phi\geq0°$) through any of the three Karplus-type equations. It was therefore concluded that *cyclo*(L-Leu)$_2$ assumes a flagpole-boat conformation in which side chains occupy pseudoaxial positions. The $C^{\alpha}H$ signal of *cyclo*(L-Leu)$_2$ in 100 MHz NMR spectrum is a broad triplet, and it becomes a sharp quartet when it is decoupled with NH. These observations suggest that the C_2-symmetric conformation of *cyclo*(L-Leu)$_2$ is rigid on the NMR time scale.

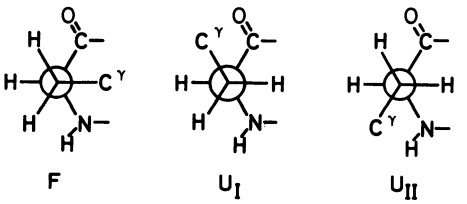

Fig. 2. Rotational isomers around C^{α}–C^{β} bond of leucyl residue in cyclic dipeptide.

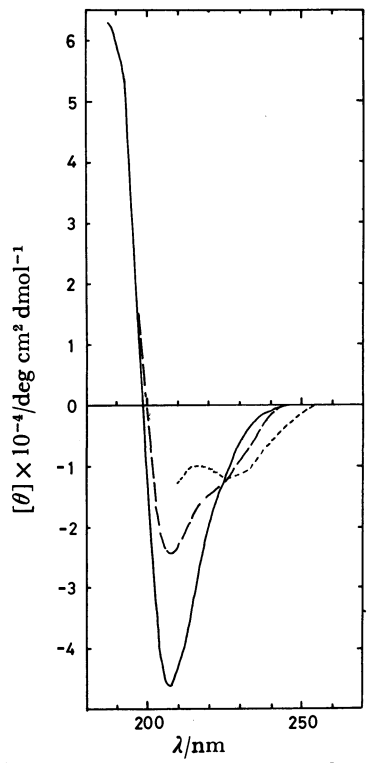

Fig. 3. Circular dichroism spectra of *cyclo*(L-Leu)$_2$. (——), in H_2O: (– – –), in CH_3OH: (------), in dioxane.

On the other hand, the NH signal of *cyclo*(L-Leu–D-Leu) in 270 NHz NMR spectra is a broad singlet, which makes the determination of $J_{\mathrm{H\text{-}C^{\alpha}\text{-}N\text{-}H}}$ extremely difficult and inaccurate. As seen in Table 2, $J_{\mathrm{H\text{-}C^{\alpha}\text{-}N\text{-}H}}$ of *cyclo*(L-Leu–D-Leu) is about 1.5 Hz, which leads to $\theta>60°$ ($\phi<0°$) by the Ramachandran equation[11] and the Bystrov equation[12] and $\theta\leq60°$ ($\phi\geq0°$) by the Cung equation.[13] Therefore, the ring conformation is not explicit but seems to be nearly planar. In 100 MHz NMR spectra of *cyclo*(L-Leu–D-Leu), the $C^{\alpha}H$ signal and the NH signal are a broad triplet and a broad singlet, respectively. The former signal becomes a sharp triplet by the decoupling with NH, and the latter signal becomes a sharp singlet by the decoupling with $C^{\alpha}H$. These observations suggest that the center-symmetric conformation of *cyclo*(L-Leu–D-Leu) is rigid on the NMR time scale.

CD Spectra. With NMR spectroscopy, except in the case of *cyclo*(L-Leu)$_2$, the coupling constant $J_{\mathrm{H\text{-}C^{\alpha}\text{-}N\text{-}H}}$ was not precisely determined and the dihedral angle θ was scattered according to the choice of Karplus-type equations. Consequently, the details of the symmetric

Table 3. Circular dichroism of *cyclo*(L-Leu)$_2$ in aqueous and methanol solution

Solvent	Amide π-π^* transition high energy lobe			Amide π-π^* transition low enenrgy lobe			Amide n-π^* transition		
	λ_{max} nm	Half width nm	Rotational strength[a]	λ_{max} nm	Half width nm	Rotational strength[a]	λ_{max} nm	Half width nm	Rotational strength[a]
H_2O	190	9	0.39	205	10	−0.28	218	12	−0.10
CH_3OH	195	10	0.35	202	10	−0.30	222	12	−0.09

a) In Debye-Bohr-magneton unit.

Table 4. Circular dichroism of *cyclo*(L-Val)$_2$ in aqueous and methanol solution

Solvent	Amide π-π^* transition			Amide n-π^* transition		
	λ_{max} nm	Half width nm	Rotational strength[a]	λ_{max} nm	Half width nm	Rotational strength[a]
H_2O	199	11	−0.41	222	11	0.12
CH_3OH	200	11	−0.47	224	13	0.13

a) In Debye-Bohr-magneton unit.

conformations of the diketopiperazine ring are often difficult to clarify. However, CD spectroscopy seems to be helpful to determine the ring conformation of cyclic dipeptides, as we succeeded in the conformational analysis of *cyclo*(L- or D-Leu–L-His).[5] The usefulness of CD spectroscopy is related with a result of computation that the Cotton effect due to the amide π-π^* transition changes the sign at $\theta=60°$.[8,14]

Figure 3 shows CD spectra of *cyclo*(L-Leu)$_2$ in aqueous solution and organic solvents. In aqueous solution, a positive maximum at 190 nm region and a negative minimum at 208 nm region are observed. In CH_3OH solution the negative minimum at 208 nm decreases in intensity and a shoulder appears at 225 nm region. In dioxane, which is less polar, a clear minimum exsists at 227 nm. The shoulder appearing in the 225 nm region has been observed in CD spectra of *cyclo*(L-Ala)$_2$ in CH_3OH and $(EtO)_3PO$ solutions by Hooker, Jr., *et al.*[8] They observed a week positive Cotton effect at 240 nm region in addition to the shoulder at 225 nm region, but they did not discuss the origin of the shoulder. With the present *cyclo*(L-Leu)$_2$ we did not observe any positive Cotton effect at 240 nm region. The same situation as in the case of *cyclo*(L-Leu)$_2$ was met in the CD spectrum of *cyclo*(Gly–L-Leu).[5] Therefore, we ascribe the negative minimum which shifts to the red in nonpolar solvents to the Cotton effect due to the amide π-π^* transition.[8] Furthermore, we ascribed the positive Cotton effect at 190 nm and the negative Cotton effect at 208 nm to a pair of Cotton effects due to the splitting of the amide π-π^* transition. According to this assignment, the CD spectra shown in Fig. 3 were resolved into the component Cotton effects, and are shown in Table 3. A pair of Cotton effects due to an exciton splitting should be opposite in sign and same in the absolute values of the rotational strength. In *cyclo*(L-Leu)$_2$ the couplet of lower wavelength is somewhat stronger than its pair, which should have been caused by the contribution from a Cotton effect at much lower wavelength. Since among two Cotton effects due to the exciton splitting of the amide π-π^* transition

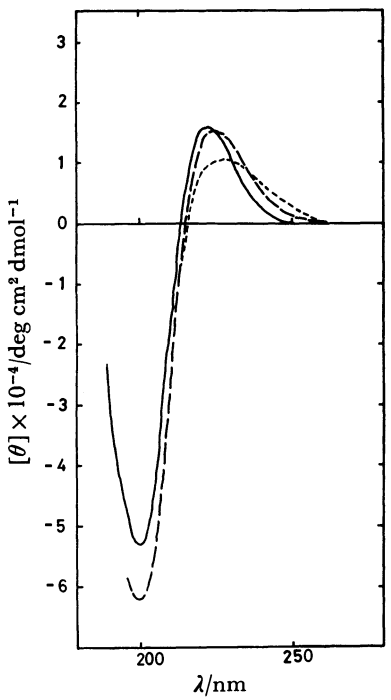

Fig. 4. Circular dichroism spectra of *cyclo*(L-Val)$_2$. (——), in H_2O: (----), in CH_3OH: (------), in dioxane.

the one at the longer wavelength is negative and the other at the shorter wavelength is positive, the rotational angle around N–C$^\alpha$ bond ϕ should be positive. This conclusion is supported by the computation of the CD spectrum of *cyclo*(L-Ala)$_2$ by Hooker, Jr., *et al.*[8] and that of a dipeptide having two substituted *cis* peptide bonds by Bayley, *et al.*[14] It is therefore concluded from CD spectra that the diketopiperazine ring of *cyclo*(L-Leu)$_2$ assumes a flagpole-boat conformation. This conclusion agrees with that obtained from the NMR spectra in $(CD_3)_2SO$ solution. The general conclusion is that *cyclo*(L-Leu)$_2$ assumes a flagpole-boat conformation in aqueous, CH_3OH and $(CD_3)_2SO$ solutions.

Figure 4 shows CD spectra of *cyclo*(L-Val)$_2$ in aqueous

solution and organic solvents. In aqueous solution two distinct Cotton effects were observed, one being negative at 200 nm and the other positive at 222 nm. On change of solvent from H_2O to CH_3OH and further to dioxane, the positive Cotton effect at 222 nm red shifted and a slight hypochromic effect was observed. The positive Cotton effect at 222 nm region is ascribed to the amide n-π^* transition allowing for its wavelength and intensity. On the other hand, the negative Cotton effect at 200 nm region is ascribed to the amide π-π^* transition allowing for its wavelength and intensity. In the present case no evidence for the splitting of the amide π-π^* transition was obtained. This has not been usual with many cyclic dipeptides. In fact, the curve-fitting method using various parameters was unable to realize a pair of Cotton effects having different sign in the 180—210 nm region. Therefore, it was considered that *cyclo*(L-Val)$_2$ shows the only Cotton effect without the splitting of the amide π-π^* transition. The results of spectral resolution by the curve-fitting method and the assignments of spectrum are shown in Table 4.

The methods of computation reported by Hooker, Jr., *et al.*[8] and Bayley, *et al.*,[14] which were applied to *cyclo*(L-Leu)$_2$, cannot be applied in the present case because of the absence of the splitting of the amide π-π^* transition. Taking into account the fact that the splitting of the π-π^* transition occurs with a nonplanar diketopiperazine ring, a planar ring (ϕ=0°) was considered for *cyclo*(L-Val)$_2$. Under such conditions the rotational strength of the amide π-π^* transition due to the exciton splitting is zero, and the observed Cotton effect of the amide π-π^* transition should have appeared due to an unclarified mechanism. No theoretical support can be provided for this explanation and a further investigation is necessary.

With *cyclo*(L-Val–D-Val) and *cyclo*(L-Leu–D-Leu) no optical activity was observed in 190—300 nm region. As was shown by NMR spectra in $(CD_3)_2SO$ solution, these cyclic dipeptides are considered to assume a symmetric conformation in aqueous solution on the time scale of the CD spectrum. In other words, their diketopiperazine ring should assume either a planar or a chair-like conformation rather than a boat-type conformation.

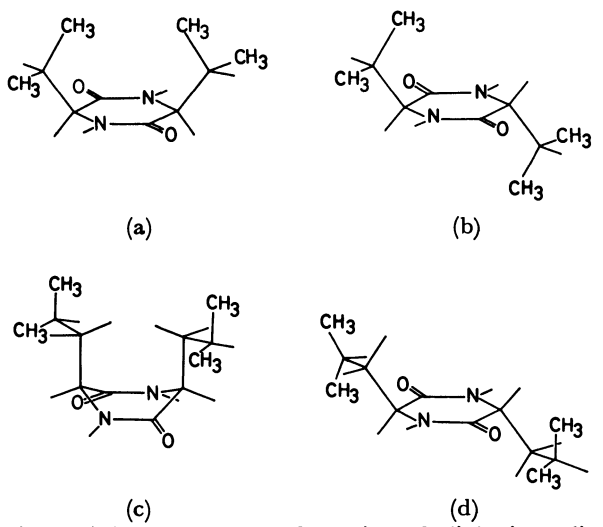

Fig. 5. Most probable conformation of aliphatic cyclic dipeptides in solution. (a), *cyclo*(L-Val)$_2$: (b), *cyclo*(L-Val–D-Val): (c), *cyclo*(L-Leu)$_2$: (d), *cyclo*(L-Leu–D-Leu).

Based on these experimental results, the most probable conformations of the four cyclic dipeptides were considered and are shown in Fig. 5.

Discussion

In the present investigation, conformations of different aliphatic cyclic dipeptides were investigated using ^1H NMR and CD spectroscopy. The same method has been used to determine the solution conformation of *cyclo*(L-Leu–L-His),[5] which was in a good agreement with the crystalline structure investigated by X-ray diffraction analysis.[6] This suggests the validity of the spectroscopy employed in the present investigation to determine the solution conformation of aliphatic cyclic dipeptides.

Vičar, *et al.*[15] investigated the side chain conformation of aliphatic cyclic dipeptide in $(CD_3)_2SO$ by ^{13}C NMR spectroscopy. According to them, *cyclo*(L-Val)$_2$ and *cyclo*(L-Val–D-Val) assume a folded conformation perfectly. On the other hand, the proportions of the folded and the unfolded form of C_2-symmetric *cyclo*(L-Leu)$_2$ were 55 and 45%, respectively. Those of C_2-symmetric *cyclo*(L-Leu–D-Leu) were 50 and 50%, respectively. A folded conformation is in general more important for their results than for the present results. However, both investigations agree in their general aspects.

Exner and Kostelnik[16] investigated the conformation of *cyclo*(L-Leu)$_2$ and *cyclo*(L-Leu–D-Leu) in $(CH_3)_2SO$ or CF_3CO_2H by ^{13}C NMR spectroscopy. They observed that two substituents of *cyclo*(L-Leu)$_2$ were magnetically equivalent and therefore the molecule took a symmetric conformation, which agrees with our conclusion reached by ^1H NMR spectroscopy. While they discussed their experimental results on the assumption that the diketopiperazine ring of *cyclo*(L-Leu)$_2$ takes a bowsprit-boat conformation, they had no experimental evidence to support the assumption. We believe that the conformation of the diketopiperazine ring of *cyclo*(L-Leu)$_2$ is flagpole-boat-type, which is supported by CD spectroscopy. Exner and Kostelnik reported the magnetic nonequivalence of two Leu residues in *cyclo*(L-Leu–D-Leu), which does not agree with our conclusion obtained by ^1H NMR spectroscopy. They synthesized *cyclo*(L-Leu–D-Leu) by the isomerization-cyclodimerization method in which L-leucine was heated at 200 °C in ethylene glycol. Under such drastic conditions, the isomerization of the cyclic dipeptide has been reported.[17,18] Since the isomerization should occur at random, their reaction product might have contained *cyclo*(L-Leu)$_2$ and *cyclo*(D-Leu)$_2$ as well as *cyclo*(L-Leu–D-Leu). This might be a reason for the magnetic nonequivalence observed by Exner and Kostelnik.

According to our experimental results, as shown in Fig. 5, *cyclo*(L-Leu)$_2$ and *cyclo*(L-Val)$_2$ take a flagpole-boat conformation and a planar-axial conformation, respectively. This conclusion differs from previous assumptions that aliphatic cyclic dipeptides in general

take bowsprit-boat conformation.[7] Furthermore, it is somewhat suprising that as far as the side chain conformation is concerned, an attractive force rather than a repulsive force operates between the aliphatic substituents.

The present experimental results can be explained on the basis that the isopropyl groups of *cyclo*(L-Val)$_2$ or the isobutyl groups of *cyclo*(L-Leu)$_2$ solubilized in polar solvents such as water, $(CH_3)_2SO$, and CH_3OH may be stabilized more by solvation of two substituents in a stacked state than by independent solvation of each substituent. In *cyclo*(L-Leu)$_2$ an attractive force between the side chains should be strong enough in polar solvents to confine the solution conformation in that characterized by $\phi > 0°$. This situation has led to a distinct H–C$^{\alpha}$–N–H coupling in NMR spectrum and a distinct splitting of the amide π-π^* transition in the CD spectrum. On the other hand, in *cyclo*(L-Val)$_2$ the conformation of the diketopiperazine ring seems to be planar-axial and to fluctuate around that conformation. This was implied by the facts that the NH signal in 270 MHz spectrum was a broad singlet, and that the splitting of the amide π-π^* transition in the CD spectrum seemed to be absent. However, the attractive force operating between the aliphatic side chains has not been explicitly observed, and a further investigation should be necessary to confirm it.

The present authors are very grateful to Prof. T. Miyazawa of the University of Tokyo for the measurement of 270 MHz NMR spectrum and the discussion of the experimental results.

References

1) Y. Imanishi, *Adv. Polym. Sci.*, **20**, 1 (1976).
2) C. M. Deber, V. Madison, and E. R. Blout, *Acc. Chem. Res.*, **9**, 106 (1976).
3) Y. Imanishi, M. Tanihara, T. Sugihara, and T. Higashimura, *Biopolymers*, **16**, 2203 (1977).
4) Y. Masuda, M. Tanihara, Y. Imanishi, and T. Higashimura, *Biopolymers* (submitted).
5) M. Tanihara, Y. Imanishi, and T. Higashimura, *Biopolymers*, **16**, 2217 (1977).
6) I. Tanaka, T. Iwata, N. Takahashi, T. Ashida, and M. Tanihara, *Acta Crystallogr.*, **33**, 3902 (1977).
7) "Peptides, Polypeptides, and Proteins," ed by E. R. Blout, F. A. Bovey, M. Goodman, and N. Lotan, John Wiley and Sons, New York (1974).
8) T. M. Hooker, Jr., P. M. Bayley, W. Radding, and J. A. Schellman, *Biopolymers*, **13**, 549 (1974).
9) D. B. Davies and Md. A. Khaled, *J. Chem. Soc., Perkin Trans. 2*, **1976**, 1238.
10) K. G. R. Pachler, *Spectrochim. Acta*, **20**, 581 (1964).
11) G. N. Ramachandran, R. Chandrasekaran, and K. D. Kopple, *Biopolymers*, **10**, 2113 (1971).
12) V. F. Bystrov, V. T. Ivanov, S. L. Portnova, T. A. Balashova, and Yu. A. Ovchinnikov, *Tetrahedron*, **29**, 873 (1973).
13) M. T. Cung, M. Marraud, and J. Neel, *Macromolecules*, **7**, 606 (1974).
14) P. M. Bayley, E. B. Nielsen, and J. A. Schellman, *J. Phys. Chem.*, **73**, 228 (1969).
15) J. Vicăr, F. Piriou, P. Fromageot, K. Bláha, and S. Fermandjian, *Collect. Czech. Chem. Commun.*, **45**, 482 (1980).
16) M. Exner, and R. J. Kostelnik, *Biopolymers*, **16**, 1387 (1977).
17) J. Dale and K. Titlestad, *J. Chem. Soc., Chem. Commun.*, **1972**, 255.
18) P. Gund and D. F. Veber, *J. Am. Chem. Soc.*, **101**, 1855 (1979).

Synthetic Studies on the Validamycins. IV. Synthesis of DL-Valienamine and Related Branched-chain Unsaturated Aminocyclitols[1]

Tatsushi Toyokuni, Seiichiro Ogawa, and Tetsuo Suami*
Department of Applied Chemistry, Faculty of Science and Technology, Keio University, Hiyoshi, Kohoku-ku, Yokohama 223
(Received September 13, 1982)

The first synthesis has been achieved of the racemates of valienamine and its related, branched-chain unsaturated aminocyclitols. Two synthetic routes for valienamine were developed, one of which is stereoselective and highly efficient. The key transformation is a stereospecific S_N2' attack (apofacial) by an azide ion on the allyl chloride, prepared by regioselective epoxidation of the conjugated diene followed by treatment with hydrochloric acid. Some information is described which is furnished from ^{13}C NMR spectra for the new branched-chain unsaturated aminocyclitols and cyclitols.

Microbial degradation of validamycin A (**1**)[2] by several soil bracteria such as *Pseudomonas denitrificans*[3] and *Flavobacterium saccharophilium*[4] gave validamine (**2**) and a branched-chain unsaturated aminocyclitol, valienamine (**3**), which is a common cardinal block of the antibiotic validamycins[5] and whose structure has been assigned as 1D-(1,3,6/2)-6-amino-4-hydroxymethyl-4-cyclohexene-1,2,3-triol by ^1H NMR spectroscopy.[3] The valienamine unit serves also as an essential block of several recently-discovered oligosaccharides, highly effective α-glucosidase inhibitors.[6] Furthermore, **3** itself has proved to exhibit an α-glucosidase inhibitory activity as well as an antibiotic activity against *Bacillus* species.[7] The above facts have in recent years stimulated considerable interest in synthetic studies of valienamine and its analogs.[8]

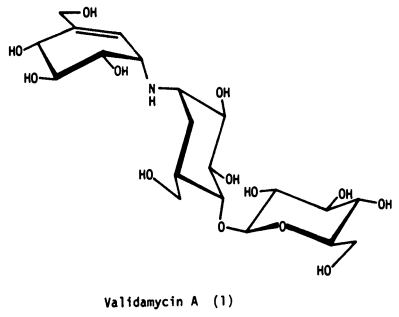
Validamycin A (1)

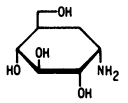
Validamine (2)

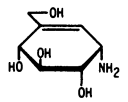
Valienamine (3)

In the present paper, as part of studies directed toward the total synthesis of validamycin A and related substances,[9] the first synthesis of DL-valienamine and related branched-chain unsaturated aminocyclitols is described. In addition, ^{13}C NMR spectra of peracetyl derivatives of aminocyclitols synthesized were measured and part of resonances were assigned by assuming the cyclohexene ring to be in a half-chair conformation.

Results and Discussion

Synthesis of Branched-chain Unsaturated Aminocyclitols Related to Valienamine. It was previously reported[9] that bromination of tri-*O*-acetyl-(1,3/2)-4-methylene-5-cyclohexene-1,2,3-triol (**4**)[10] gave two 1,4-addition products **5** and **6**, from which four monobromo derivatives **7**—**10** of the branched-chain unsaturated cyclitols were prepared. Azidolysis of these bromo compounds and successive reduction readily afforded several branched-chain unsaturated aminocyclitols including DL-valienamine in good yield.

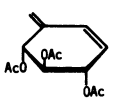
4

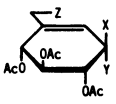

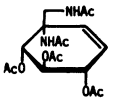
25

	X	Y	Z
5	H	Br	Br
6	Br	H	Br
7	OAc	H	Br
8	H	OAc	Br
9	H	Br	OAc
10	Br	H	OAc
11	N_3	H	N_3
12	NHAc	H	NHAc
13	H	N_3	N_3
14	H	NHAc	NHAc
15	OAc	H	N_3
16	OAc	H	NHAc
17	H	OAc	N_3
18	H	OAc	NHAc
19	N_3	H	OAc
20	NHAc	H	OAc
21	H	N_3	OAc
22	H	NHAc	OAc
23	OAc	H	OAc
24	H	OAc	OAc

When **5** was treated with sodium azide in *N,N*-dimethylformamide (DMF) at room temperature for 1 h,[11] the crystalline diazide **11** was exclusively obtained in 88% yield. Similar treatment of **6** with an azide ion gave the diazide **13** as a homogeneous syrup in 96% yield. The ^1H NMR spectrum of **13** revealed the olefinic proton (H-5) as a doublet (J=7.5 Hz) at δ=5.94, supporting the pseudoaxial conformation for the C-6 azido group of **13**.[12] However, in the ^1H NMR spectrum of **11**, the H-5 appeared as a poorly resolved multiplet overlapping with H-3. Configurational assignment of C-6 of **11** was, therefore, made by comparing the chemical shift of H-6 in **11** with that of **13**. The signal, observed at δ=4.38 in **13**, was shifted upfield in **11**, indicating that the H-6 is pseudoaxial,[13] that is, **11** is the C-6 epimer of **13**. In both cases, azidolysis proceeded *via* a direct S_N2 mechanism with inversion of the configuration at C-6.

Selective reduction of the azido group of **11** was readily achieved by treatment with hydrogen sulfide[14] in pyridine–water (1 : 1) at room temperature and, after

treatment with acetic anhydride in pyridine, the product was isolated as the crystalline bis(acetamide) **12** in 90% yield. On the other hand, reduction of **13** with sodium boronhydride in 2-propanol at the reflux temperature followed by a similar acetylation gave, after chromatography on silica gel, two crystalline bis(acetamide)s **14** and **25** in 43 and 18% yields, respectively. The structures of **12** and **14** were confirmed by observing the expected singlet at $\delta=5.43$[15] and doublet ($J=4.5$ Hz) at $\delta=5.65$ for the olefinic protons (H-5) of **12** and **14**, respectively. The spectrum of **25** exhibited two olefinic protons as a doublet of doublets ($J=1.5$ and 10.5 Hz) and a broad doublet ($J=10.5$ Hz) at $\delta=5.56$ and 6.21, in support of the proposed structure. The configuration at C-4 was tentatively assigned by assuming that the C-6 azido group would migrate to C-4 during the reduction through a boron-assisted allylic rearrangement (S_N2').[16]

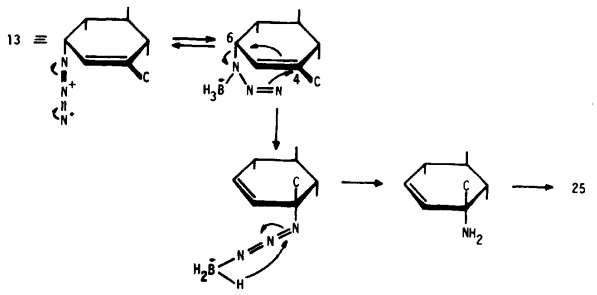

Similarly, the bromides **7** and **8** were converted into the monoazides **15** and **17** in 96 and 80% yields, respectively, which were in turn converted into the corresponding acetamides **16** and **18** in 91 and 87% yields, respectively, by reduction with hydrogen sulfide followed by acetylation.

Synthesis of DL-*Valienamine (22).* The synthesis of DL-valienamine starting from **6** was first worked out. The regioselective displacement reaction[9] at C-7 by an acetoxyl group was fairly improved by use of potassium acetate and 18-crown-6. Treatment of **6** with potassium acetate in DMF in the presence of 18-crown-6 at room temperature produced after 2.5 h a mixture of monobromides **9** and **10**, which, without further isolation, was subjected to azidolysis of the remaining secondary bromine atom, giving, after chromatography on silica gel, two azido compounds **19** (43%) and **21** (26%), together with a syrupy 3 : 1 mixture (9%) of **23** and **24**.[9] The structures of **19** and **21** were assigned, on the basis of a criterion similar to that used for the configurational assignment on C-6 of **11**, by use of the result that the pseudoaxial H-6 proton of **19** resonates at higher field ($\delta=4.12$—4.30) than does the pseudoequatorial H-6 proton of **21** ($\delta=4.41$). Further support was provided by the appearance of the doublet ($J=7.5$ Hz) at $\delta=5.96$ due to the olefinic proton (H-5) of **21**, indicating that the allylic proton (H-6) is pseudoequatorial. Starting from either **5** or **6** gave almost the same distributions of products **19** and **21**.

Reduction of **19** and **21** with hydrogen sulfide followed by acetylation afforded the acetamides **20** and **22** in 69 and 70% yields, respectively. The ^1H NMR spectra of **22** in $CDCl_3$ and in DMSO-d_6 were superimposable on those of an authentic sample of penta-*N*,*O*-acetyl-(+)-valienamine.[17] The structure of **20** was confirmed by an observation of the coupling constant ($J=8.5$ Hz) between H-1 and H-6, indicative of an axial-pseudoaxial relationship between these protons. Compounds **20** and **22** were also obtained by reduction of **19** and **21** with sodium boronhydride in 2-propanol in appropriate yields without any allylic rearrangements of the azido group.

Alternative Stereospecific Synthesis of **22**. Although the synthesis of DL-valienamine had been accomplished, the preparation of large quantities of **21** was very tedious because of nonselectiveness of the reaction. This, coupled with the difficulty of separating **21** from **19** purely, required us to develop an alternative stereoselective route for **21**. For this purpose the spiro epoxide **26** obtainable by regioselective epoxidation of **4**[18] was chosen as the starting material. If S_N2' attack of an azide ion on allylic halides, prepared by halogenation of spiro epoxide with hydrogen halides, would proceed stereospecifically, **19** or **21** could be obtained selectively.

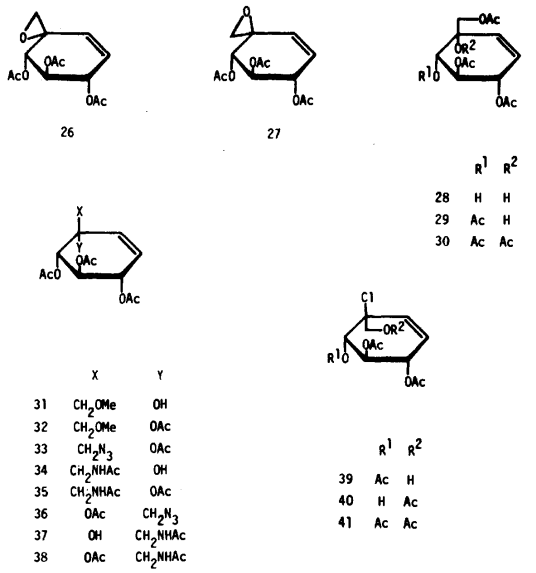

	X	Y
31	CH_2OMe	OH
32	CH_2OMe	OAc
33	CH_2N_3	OAc
34	CH_2NHAc	OH
35	CH_2NHAc	OAc
36	OAc	CH_2N_3
37	OH	CH_2NHAc
38	OAc	CH_2NHAc

	R^1	R^2
28	H	H
29	Ac	H
30	Ac	Ac

	R^1	R^2
39	Ac	H
40	H	Ac
41	Ac	Ac

Treatment of **4** with 1.2 molar equiv. of *m*-chloroperoxybenzoic acid in dichloromethane at room temperature yielded two crystalline spiro epoxides **26** (24%) and **27** (8%), together with a branched-chain cyclitol triacetate **28** (13%) and a mixture of slower-moving (on TLC) products from which pentaacetate **24**, after acetylation, was isolated (21% from **4**). TLC analysis indicated that **26** and **27** were both acid-labile and partly changed, under acidic conditions, into **24** and **28**, respectively. Therefore, the yield of **26** and especially of **27** were increased when the oxidation was carried out under buffered conditions (see experimental section).

In the ^1H NMR spectrum of **28**, a triplet ($J=8$ Hz) at $\delta=3.70$ due to H-2 changed to a doublet ($J=8$ Hz) on deuteration. The structure of **28** was finally confirmed by converting it into known **29** and **30**[9] by the usual acetylation. The structures of **26** and **27** were deduced from their behavior under acidic conditions (CH_2Cl_2, TsOH monohydrate, pH *ca.* 3). The pentaacetate **24** derived from **26** was considered to be formed through an S_Ni' mechanism by assistance of the C-4 acetoxyl

group at C-5, leading to the 4,5-cyclic acetoxonium ion that would be opened by a trace of water. On the other hand, the pentaacetate **28** derived from **27** might be formed through an S_N1 mechanism with the participation of C-2 acetoxyl group. For further confirmation, **26** was converted into known methyl ethers **31** and **32**[9] on treatment with methanolic sodium methoxide in methanol followed by acetylation.

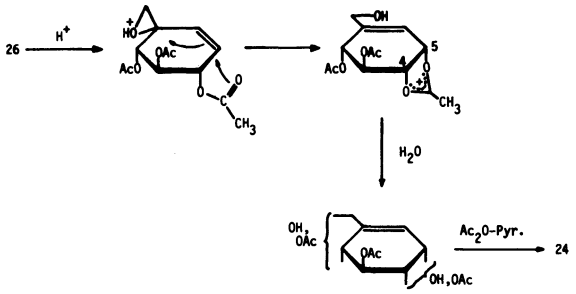

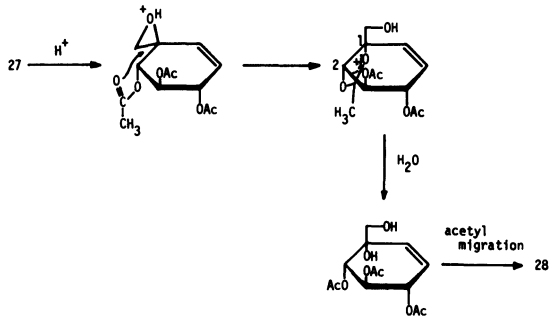

Azidolysis of **26** and **27** with sodium azide in DMF followed by acetylation gave the single azides **33** and **36** in 86 and 81% yields, respectively. They were converted, by reduction with hydrogen sulfide and successive acetylation, into the corresponding acetamides **34** and **35**, and **37** and **38**, respectively. Further acetylation of **34** and **37** yielded **35** and **38** quantitatively. Presumably the formation of **34** and **37** involved the acetyl group migration, during the reduction, from the tertiary hydroxyl to the amino group generated.

Epoxide ring opening of **26** with concd hydrochloric acid in tetrahydrofuran at 0 °C gave a sole crystalline chlorohydrin **39** quantitatively. An attempt to purify **39** with a silica-gel column resulted in the acetyl group migration giving rise to an isomer **40**. Acetylation of **39** and **40** under acidic conditions gave the same tetraacetate **41** in a quantitative yield. The ^{1}H NMR spectrum revealed the C-7 methylene protons as a singlet at δ=4.32, indicative of the presence of an acetoxymethyl group in support of the assigned structure.

Azidolysis of **41** with sodium azide in DMF at 60 °C gave only one azido product stereospecifically in 93% yield, which proved to be identical in all respects with **21**. The reaction seemed to involve an S_N2' mechanism (apofacial)[19] through an initial attack of an azide ion at C-6. When **41** was treated with sodium acetate, a complex mixture of **23**, **24**, **29**, and **30** was formed. The neighboring acetoxyl group participation was likely to predominate when a weak nucleophile was used.

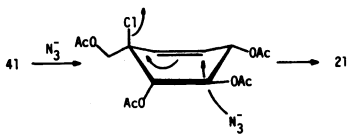

Preparation of Protected Valienamine. In order to prepare the building blocks for the synthesis of validoxylamines and related biologically-important secondary amines, diisopropylidene and benzylidene derivatives of DL-valienamine were synthesized.

De-*O*-acetylation of **21** with methanolic sodium methoxide gave the hydroxy azide **43**, which was successively treated with an excess of 2,2-dimethoxypropane in the presence of *p*-toluenesulfonic acid in DMF, giving the crystalline di-*O*-isopropylidene derivative **47** in 72% yield. Similarly, **44** was directly obtained, along with **47**, from the mixture of **19** and **21** prepared by azidolysis of **9**. In this case, attempted isolation of the hydroxy azides **42** and **43** failed because of their similar chromatographic mobilities.

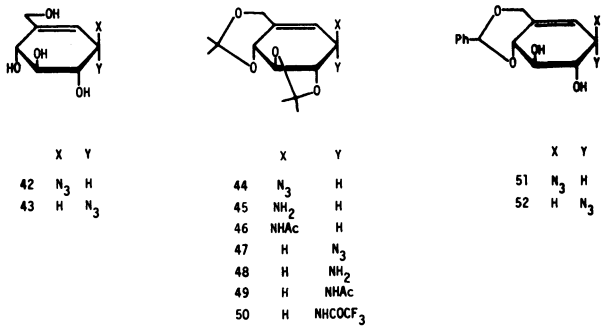

	X	Y
42	N_3	H
43	H	N_3

	X	Y
44	N_3	H
45	NH_2	H
46	NHAc	H
47	H	N_3
48	H	NH_2
49	H	NHAc
50	H	$NHCOCF_3$

	X	Y
51	N_3	H
52	H	N_3

On the other hand, benzylidenation of the mixture of the hydroxy azides **42** and **43** with 1.2 molar equiv. of α,α-dimethoxytoluene gave, after a silica-gel column chromatography, **51** and **52** in 43 and 18% yields, respectively. Their ^{1}H NMR spectra revealed the vinylic protons as a broad singlet at δ=5.41 for **51** and a doublet (J=5 Hz) at δ=5.69 for **52**, confirming the assigned structures.

Compounds **44** and **47** were reduced with hydrogen sulfide in 1 : 1 pyridine–water to give **45** and **48** in quantitative yields, respectively, which were converted into the corresponding acetamides **46** and **49**. Compound **48** was further converted into the trifluoroacetamide **50** on treatment with trifluoroacetic anhydride in pyridine. Di-*O*-isopropylidene derivative **48** thus obtained is a very versatile building block for the preparation of validoxylamines and related secondary amines. Recently the synthesis of DL-validoxylamine B using **48** was accomplished.[1b]

^{13}C NMR Spectra of Valienamine and Related Compounds. On the basis of the ^{13}C NMR data for 1-methylcyclohexene,[20] the chemical shift assignment on peracetyl derivatives of valienamine (**22**) and related aminocyclitols (**12**, **14**, **16**, **18**, and **20**) and cyclitols (**23** and **24**) could be made by assuming the cyclohexene ring to be in a half-chair conformation. The results are summarized in Table 1.

The chemical shift of the methyl carbon of acetyl group is nearly indifferent to their stereochemical

Table 1. ^{13}C Chemical shift data in ppm downfield from internal TMS[a)]

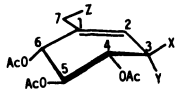

Compound[b)]				Carbon atom								
No.	X	Y	Z	C-1	C-2	C-3	C-4	C-5	C-6	C-7	CH_3	
											OAc	NHAc
12	NHAc	H	NHAc	132.84	125.71	48.65	70.95	70.56	72.35	38.80	20.36 20.22	22.36
14	H	NHAc	NHAc	135.35	122.9	43.84	69.36	67.86	69.85	39.26	20.34	22.30 22.23
16	OAc	H	NHAc	135.40	123.02	←	70.31,	71.41	→	38.96	20.57 20.41 20.25	22.39
18	H	OAc	NHAc	139.60	120.12	70.19[d)]	67.49	64.85	69.23[d)]	39.02	20.45 20.28	22.31
20	NHAc	H	OAc	130.39	129.61	48.70	70.08[d)]	69.81[d)]	71.92	61.99	20.22	22.38
22	H	NHAc	OAc	132.57	126.01	43.82	69.01	67.59	69.44	62.23	20.36	22.25
23[c)]	OAc	H	OAc	133.43	125.94	71.87[d)]	70.67[e)]	70.09[e)]	72.37[d)]	62.31	20.79 20.53	
24[c)]	H	OAc	OAc	137.35	123.29	70.26[d)]	67.99	65.19	69.78[d)]	62.47	20.79 20.62	

a) Unless otherwise noted, the ^{13}C NMR spectra were measured in dimethyl-d_6 sulfoxide. b) For convenience, the carbon atoms were numbered as for derivatives of 1-methylcyclohexene. c) Measured in $CDCl_3$. d), e) Assignments may be reversed.

environment. However, it is obvious that the methyl carbon of acetamido (NHAc) group appears at lower field by 1.44—2.17 ppm than that of acetoxyl (OAc) group.

The chemical shift of C-7 is influenced not only by the substituent (OAc, NHAc) attached thereto but also by the orientation of the substituent at C-3. When an OAc group is attached (Z=OAc), the C-7 appears in the range 61.99—62.47 ppm, whereas it appears at upper field (38.80—39.26 ppm) when an NHAc group is attached (Z=NHAc). In addition, a pseudoaxial OAc or NHAc group at C-3 causes a down-field shift of 0.06—0.46 ppm for C-7.

The sp^2 carbons appear in the range 130.39—139.60 ppm for a quarternary sp^2 carbon (C-1) and in the range 120.12—129.61 ppm for a tertiary sp^2 carbon (C-2). It is noteworthy that their chemical shifts depend on substituents (OAc, NAc) at the allylic positions (C-3 or C-7) and also on the configuration at C-3. Thus, the replacement of an OAc group by an NHAc group at each position causes a downfield shift for the β sp^2 carbon by 1.97—3.67 ppm and an upfield shift for the γ sp^2 carbon by 2.56—4.78 ppm. In addition, the pseudoaxial OAc or NHAc group at C-3 (Y=OAc, NHAc) causes an upfield shift of 2.65—3.60 ppm for the β carbon (C-2) and a downfield shift of 2.18—4.20 ppm for the γ carbon (C-1). The latter γ effect on sp^2 carbon[21)] is interesting because in cyclohexane rings the γ effect caused by an axial substituent is generally associated with upfield shifts.[22)] This effect is presumably due to some steric interaction.[23)]

Experimental

General. Melting points were determined on a Büchi 510 capillary melting point apparatus and are uncorrected. Unless otherwise noted, ^1H NMR spectra were taken on a Varian EM-390 (90 MHz) in chloroform-*d* ($CDCl_3$), dimethyl-d_6 sulfoxide (DMSO-d_6), or methanol-d_4 (CD_3OD) with reference to tetramethylsilane as an internal standard. The peak positions are given in terms of δ-values and values given for coupling constants are of first-order. ^{13}C NMR spectra were obtained on a Varian XL-100 spectrometer in $CDCl_3$ or DMSO-d_6 containing a drop of TMS as an internal standard with complete proton-decoupling. TLC was performed on a precoated silica gel 60 F-254 plaques (Merck, Darmstadt; 0.25 mm thickness), and the spots were visualized by heating above 150 °C after spraying with concd sulfuric acid. The silica gel used for a column chromatography was Wakogel C-300 (Wako Pure Chemical Industries, Ltd.). Solutions were dried over anhydrous sodium sulfate and evaporated under reduced pressure at 40—50 °C. Acetylation was conventionally carried out with acetic anhydride in anhydrous pyridine at room temperature overnight and the reaction mixture was evaporated to remove an excess of reagents. Crude syrupy products (acetates) were usually purified preliminarily by rapid passage through a short column of active alumina with chloroform.

DL-*Tri*-O-*acetyl*-(*1,3*/*2,6*)-*6*-*azido*-*4*-*azidomethyl*-*4*-*cyclohexene*-*1,2,3*-*triol* (***11***). A mixture of DL-tri-*O*-acetyl-(1,3,6/2)-6-bromo-4-bromomethyl-4-cyclohexene-1,2,3-triol (**5**)[9)] (0.16 g), sodium azide (0.1 g, 4 molar equiv.), and *N,N*-dimethylformamide (DMF) (6 ml) was stirred at room temperature for 1 h. The mixture was diluted with ethyl acetate (20 ml), and the organic layer was thoroughly washed with cold water (3× 10 ml) and then dried. Evaporation of the solvent left a

syrup which crystallized upon standing in a desiccator overnight. Recrystallization from ethanol gave **11** (0.12 g, 88%): mp 82—83 °C; ^{1}H NMR ($CDCl_3$) δ=2.03 (3H, s), 2.09 (3H, s), and 2.11 (3H, s) (OAc), 3.81 (2H, broad s, C$\underline{H}_2N_3$), 4.14—4.38 (1H, m, H-6), 5.14—5.50 (2H, m, H-1 and H-2), and 5.59—5.98 (2H, m, H-3 and H-5).

Found: C, 44.14; H, 4.60; N, 23.67%. Calcd for $C_{13}H_{16}N_6O_6$: C, 44.32; H, 4.58; N, 23.85%.

DL-*Tri*-O-*acetyl-(1,3,6/2)-6-azido-4-azidomethyl-4-cyclohexene-1,2,3-triol (13)*. A mixture of DL-tri-*O*-acetyl-(1,3/2,6)-6-bromo-4-bromomethyl-4-cyclohexene-1,2,3-triol (**6**)[9] (0.2 g), sodium azide (0.12 g, 4 molar equiv.), and DMF (10 ml) was treated similarly as described in the preparation of **11** for 0.5 h. The crude product was purified by passing through a short column of silica gel with chloroform to give **13** (0.16 g, 96%) as a homogeneous syrup: ^{1}H NMR (60 MHz,[24]) $CDCl_3$) δ= 2.03 (3H, s), 2.07 (3H, s), and 2.11 (3H, s) (OAc), 3.77 (2H, broad s, C$\underline{H}_2N_3$), 4.38 (1H, t, J=7.5 Hz, H-6), 4.95—5.80 (3H, m, H-1, H-2, and H-3), and 5.94 (1H, broad d, J=7.5 Hz, H-5).

Found: C, 44.10; H, 4.63; N, 23.55%. Calcd for $C_{13}H_{16}N_6O_6$: C, 44.32; H, 4.58; N, 23.85%.

DL-*Penta*-N,O-*acetyl-(1,3/2,6)-6-amino-4-aminomethyl-4-cyclohexene-1,2,3-triol (12)*. Into a stirred solution of **11** (94 mg) in 1 : 1 pyridine–water (5 ml) was bubbled hydrogen sulfide at room temperature for 1.5 h, during which insoluble sulfur appeared. The yellowish mixture was evaporated and the residue was acetylated in the usual way. The crude product was transferred to the top of a column of silica gel (3 g) and first eluted with benzene, giving sulfur as colorless needles, and then with 1 : 5 ethanol–benzene, giving colorless crystals. Recrystallization from ethanol gave **12** (92 mg, 90%) as feathers: mp 229.5—230.5 °C (sintering at 228 °C): ^{1}H NMR (DMSO-d_6) δ=1.80 (6H, s), 1.94 (6H, s), and 1.98 (3H, s) (OAc and NAc), 3.45 (1H, dd, J=4 and 16.5 Hz, changing to d with J=16.5 Hz on deuteration) and 3.82 (1H, dd, J=7 and 16.5 Hz, changing to d with J=16.5 Hz on deuteration) (C$\underline{H}_2$NHAc), 4.45—4.80 (1H, m, H-6, changing on deuteration), 4.87—5.33 (2H, m, H-1 and H-2), 5.43 (1H, broad s, H-5), 5.61 (1H, broad d, J=*ca.* 6 Hz, H-3), 7.85 (1H, dd, J= 4 and 7 Hz, C-7-N$\underline{H}$Ac, disappearing on deuteration), and 8.10 (1H, d, J=ɔ Hz, C-6-N$\underline{H}$Ac, disappearing on deuteration).

Found: C, 53.15; H, 6.30; N, 7.20%. Calcd for $C_{17}H_{24}N_2O_8$: C, 53.12; H, 6.29; N, 7.29%.

DL-*Penta*-N,O-*acetyl-(1,3,6/2)-6-amino-4-aminomethyl-4-cyclohexene-1,2,3-triol (14)* and DL-*Penta*-N,O-*acetyl-(1,3,4/2)-4-amino-4*-C-*aminomethyl-5-cyclohexene-1,2,3-triol (25)*. A suspension of **13** (144 mg), sodium boronhydride (93 mg), and 2-propanol (5 ml) was refluxed gently for 1 h. After cooling, the excess of hydride was decomposed by gradual addition of 6 M (1 M=1 mol dm^{-3}) acetic acid (*ca.* 2 ml), and then the mixture was evaporated to dryness. The resulting soild was acetylated in the usual way, and the product was chromatographed on a column of silca gel (5 g). Elution with 1 : 5 ethanol–benzene gave three fractions.

The first fraction gave a small amount of unresolved mixture, which was not further characterized.

The second fraction gave a colorless syrup, which crystallized on standing in a desiccator overnight. Recrystallization from ethanol gave **25** (29 mg, 18%): mp 178.5—181 °C (sintering at 170 °C); ^{1}H NMR ($CDCl_3$) δ=1.94 (3H, s), 1.99 (6H, s), 2.01 (3H, s), and 2.06 (3H, s) (OAc and NAc), 3.28 (1H, dd, J=6 and 13 Hz, changing to d with J=13 Hz on deuteration) and 3.81 (1H, dd, J=6.3 and 13 Hz, changing to d with J=13 Hz on deuteration) (C$\underline{H}_2$NHAc), 5.00 (1H, d, J=10.5 Hz, H-3), 5.15—5.70 (2H, m, H-1 and H-2), 5.56 (1H, dd, J=1.5 and 10.5 Hz, H-6), and 5.92—6.33 (3H, m, H-5 and 2×N$\underline{H}$Ac, changing to broad d with J=10.5 Hz at δ=6.21 on deuteration).

Found: C, 52.91; H, 6.07; N, 7.43%. Calcd for $C_{17}H_{24}N_2O_8$: C, 53.12; H, 6.29; N, 7.29%.

The third fraction gave colorless crystals, which were recrystallized from ethanol, giving **14** (67 mg, 43%) as columns: mp 253—255 °C; ^{1}H NMR (DMSO-d_6) δ=1.77 (3H, s), 1.84 (3H, s), 1.91 (3H, s), and 1.97 (6H, s) (OAc and NAc) 3.46 (1H, dd, J=5 and 15 Hz, changing to d with 15 Hz on deuteration) and (3.92 1H, dd, J=7.5 and 15 Hz, changing to d with J=15 Hz on deuteration) (C$\underline{H}_2$NHAc), 4.74 (1H, ddd, J=4.5, 5, and 9 Hz, H-6, changing to dd with J=4.5 and 5 Hz on deuteration), 4.95 (1H, dd, J=5 and 10.5 Hz, H-1), 5.34 (1H, dd, J=7.5 and 10.5 Hz, H-2), 5.55 (1H, d, J=7.5 Hz, H-3), 5.65 (1H, d, J=4.5 Hz, H-5), 7.84 (1H, dd, J=5 and 7.5 Hz, C-7-N$\underline{H}$Ac, disappearing on deuteration), and 8.11 (1H, d, J=9 Hz, C-6-N$\underline{H}$Ac, disappearing on deuteration).

Found: C, 52.84; H, 6.23; N, 6.99%. Calcd for $C_{17}H_{24}N_2O_8$: C, 53.12; H, 6.29; N, 7.29%.

DL-*Tetra*-O-*acetyl-(1,3/2,4)-5-azidomethyl-5-cyclohexene-1,2,3,-4-tetrol (15)*. A mixture of DL-tetra-*O*-acetyl-(1,3/2,4)-5-bromomethyl-5-cyclohexene-1,2,3,4-tetrol (**7**)[9] (0.15 g), sodium azide (47 mg, 2 molar equiv.), and DMF (6 ml) was stirred at room temperature overnight. The mixture was diluted with ethyl acetate (20 ml) and successively washed with cold water (3×10 ml), and then dried. Evaporation of the solvent gave **15** (0.13 g, 96%) as an analytically pure colorless syrup: ^{1}H NMR ($CDCl_3$) δ=1.98 (6H, s) and 2.02 (6H, s) (OAc), 3.78 (2H, s, C$\underline{H}_2N_3$), 5.21—5.45 (2H, m, H-2 and H-3), 5.45—5.65 (1H, m, H-1), and 5.65—5.88 (2H, broad s, H-4 and H-6).

Found: C, 48.51; H, 5.17; N, 11.12%. Calcd for $C_{15}H_{19}N_3O_8$: C, 48.78; H, 5.19; N, 11.38%.

DL-*Tetra*-O-*acetyl-(1,2,4/3)-5-azidomethyl-5-cyclohexene-1,2,3,-4-tetrol (17)*. A mixture of DL-tetra-*O*-acetyl-(1,2,4/3)-5-bromomethyl-5-cyclohexene-1,2,3,4-tetrol (**8**)[9] (0.15 g), sodium azide (47 mg, 2 molar equiv.), and DMF (5 ml) was treated similarly as described in the preparation of **15**. The crude product was purified by passing through a silica-gel column (5 g) with 1 : 5 2-butanone–toluene as an eluent to give **17** (108 mg, 80%) as a syrup: ^{1}H NMR ($CDCl_3$) δ=2.01 (3H, s), 2.04 (3H, s), and 2.11 (3H, s) (OAc), 3.84 (2H, s, C$\underline{H}_2N_3$), 5.15 (1H, dd, J=4 and 10.5 Hz, H-2), 5.29—5.76 (3H, m, H-1, H-3, and H-4), and 6.00 (1H, broad d, J=6 Hz, H-6).

Found: C, 48.96; H, 5.26; N, 11.25%. Calcd for $C_{15}H_{19}N_3O_8$: C, 48.78; H, 5.19; N, 11.38%.

DL-*Penta*-N,O-*acetyl-5-aminomethyl-5-cyclohexene-1,2,3,4-tetrol (16)*. Hydrogen sulfide was bubbled into a stirred solution of **15** (0.13 g) in 2 : 1 pyridine–water (9 ml) at room temperature for 1.5 h. The mixture was evaporated and the residue was acetylated in the usual way. The product was purified by passing through a short column of silica gel with 1 : 5 ethanol–benzene as an eluent to give colorless crystals. Recrystallization from ethanol gave **16** (0.12 g, 91%): mp 131.5—132.5 °C; ^{1}H NMR ($CDCl_3$) δ=1.98 (3H, s), 2.01 (6H, s), 2.04 (3H, s), and 2.07 (3H, s) (OAc and NAc), 3.71 (1H, dd, J=5 and 15 Hz, changing to d with J=15 Hz on deuteration) and 3.98 (1H, dd, J=7 and 15 Hz, changing to d with J=15 Hz on deuteration) (C$\underline{H}_2$NHAc), 5.15—5.43 (2H, m, H-2 and H-3), and 5.43—6.02 (4H, m, H-1, H-4, H-6, and N$\underline{H}$Ac, changing to relatively narrow m at δ=5.43—5.82 on d uteration).

Found: C, 52.68; H, 5.95; N, 3.52%. Calcd for $C_{17}H_{23}NO_9$: C, 52.98; H, 6.02; N, 3.63%.

DL-*Penta*-N,O-*acetyl-(1,2,4/3)-5-aminomethyl-5-cyclohexene-1,2,-3,4-tetrol (18)*. Reduction of **17** (69 mg) with hydrogen

sulfide in 2 : 1 pyridine–water (5 ml), followed by acetylation, was carried out in the same manner as in the preparation of **16**. The product was purified by passage through a silica-gel column (3 g) with 1 : 10 ethanol–benzene to give **18** (62 mg, 87%): mp 148.5—149.5 °C; ^{1}H NMR ($CDCl_3$) δ=1.97 (3H, s), 2.00 (3H, s), 2.02 (3H, s), and 2.08 (6H, s) (OAc and NAc), 3.75 (1H, dd, J=5.5 and 15 Hz, changing to d with J=15 Hz on deuteration) and 4.00 (1H, dd, J=7 and 15 Hz, changing to d with J=15 Hz on deuteration) ($C\underline{H}_2$NHAc), 5.08 (1H, ddd, J=0.8, 3.5, and 10 Hz, H-2), 5.50 (1H, dd, J=8 and 10 Hz, H-3), 5.52—5.73 (2H, m, H-1 and H-4), and 5.73—5.97 (2H, broad d, J=*ca.* 5 Hz, H-6 and N$\underline{H}$Ac, changing to dd with J=0.8 and 6.5 Hz at δ=5.87 on deuteration).

Found: C, 53.15; H, 5.93; N, 3.69%. Calcd for $C_{17}H_{23}NO_9$: C, 52.98; H, 6.02; N, 3.63%.

DL-*Tetra*-O-*acetyl*-*(1,3/2,6)*- ***(19)*** *and* -*(1,3,6/2)*-*6*-*azido*-*4*-*cyclohexene*-*1,2,3*-*triol* ***(21)***. A mixture of **6** (338 mg), potassium acetate (78 mg, 1 molar equiv.), 18-crown-6 (0.1 g), and DMF (10 ml) was stirred at room temperature for 2.5 h. The sodium azide (105 mg, 2 molar equiv.) was then added to the mixture and the stirring was continued for an additional 1 h. The mixture was then diluted with ethyl acetate (30 ml) and the solution was washed with cold water several times, and dried. TLC indicated the presence of three components, together with a trace of some other products. Evaporation of the solvent and chromatography of the residue on a silica-gel column (10 g) with 1 : 10 2-butanone–toluene as an eluent gave three fractions. The first fraction gave crystals, which were recrystallized from ethanol, giving **19** (125 mg, 43%) as tiny prisms: mp 68—68.5 °C; ^{1}H NMR ($CDCl_3$) δ=2.01 (3H, s), 2.03 (3H, s), 2.05 (3H, s), and 2.08 (3H, s) (OAc), 4.12—4.30 (1H, m, H-6), 4.38 and 4.70 (AB-quartet, J=15 Hz, $C\underline{H}_2$OAc), 5.14—5.43 (2H, m, H-1 and H-2), and 5.67—5.86 (2H, m, H-3 and H-5).

Found: C, 48.68; H, 5.21; N, 11.28%. Calcd for $C_{15}H_{19}N_3O_8$: C, 48.78; H, 5.19; N, 11.38%.

The second fraction gave **21** (76 mg, 26%) as a syrup: ^{1}H NMR ($CDCl_3$) δ=2.03 (3H, s), 2.05 (6H, s), and 2.12 (3H, s) (OAc), 4.41 (1H, dd, J=4.5 and 7.5 Hz, H-6), 4.40 and 4.70 (AB-quartet, J=13 Hz, $C\underline{H}_2$OAc), 5.15 (1H, dd, J=4.5 and 10 Hz, H-1), 5.49 (1H, dd, J=7 and 10 Hz, H-2), 5.68 (1H, broad d, J=7 Hz, H-3), and 5.96 (1H, broad d, J=7.5 Hz, H-5).

Found: C, 48.64; H, 5.19; N, 11.23%. Calcd for $C_{15}H_{19}N_3O_8$: C, 48.78; H, 5.19; N, 11.38%.

The third fraction gave a homogeneous syrupy mixture of DL-penta-*O*-acetyl-(1,3/2,4)- (**23**) and -(1,2,4/3)-5-hydroxymethyl-5-cyclohexene-1,2,3,4-tetrol (**24**), weighing 26 mg (9%). By comparing its ^{1}H NMR spectrum with those of authentic samples[9] the ratio of **23** and **24** was found to be *ca.* 3 : 1.

When **5** was used instead of **6**, a similar result was obtained.

DL-*Penta*-N,O-*acetyl*-*(1,3,6/2)*-*6*-*amino*-*4*-*hydroxymethyl*-*4*-*cyclohexene*-*1,2,3*-*triol (penta*-N,O-*acetyl*-DL-*valienamine)* ***(22)***.

a) Hydrogen sulfide was bubbled into a solution of **21** (57 mg) in 2 : 1 pyridine–water (3 ml) at room temperature for 1 h. The mixture was evaporated and the residue was acetylated in the usual way. Purification of the acetate by passage through a silica-gel column (2 g) with 1 : 10 ethanol–benzene gave crystals, which were recrystallized from ethanol to afford **22** (42 mg, 70%) as tiny prisms: mp 180—181 °C; ^{1}H NMR ($CDCl_3$) δ=2.03 (6H, s) and 2.06 (9H, s) (OAc and NAc), 4.36 and 4.66 (AB-quartet, J=14 Hz, $C\underline{H}_2$OAc), 4.89—5.23 (2H, m, H-1 and H-6), 5.69—6.00 (2H, m, H-5 and N$\underline{H}$Ac, changing to broad d with J=4.5 Hz at δ=5.90; ^{1}H NMR (100 MHz,[25] DMSO-d_6) δ=1.86 (3H, s), 1.93 (3H, s), and 2.20 (9H, s) (OAc and NAc), 4.42 and 4.67 (AB-quartet, J=14 Hz, $C\underline{H}_2$OAc), 4.81 (1H, td, J=4.5 and 9.0 Hz, H-6), 5.03 (1H, dd, J=4.5 and 9.5 Hz, H-1), 5.36 (1H, dd, J=7 and 9.5 Hz, H-2), 5.58 (1H, d, J=7 Hz, H-3), 5.87 (1H, broad d, J=4.5 Hz, H-5), and 8.15 (1H, d, J=9 Hz, N$\underline{H}$Ac, disappearing on deuteration). The spectra were superimposable on those of an authentic optically-active sample.[17]

b) A suspension of **21** (43 mg), sodium boronhydride (13 mg), and 2-propanol (3 ml) was refluxed for 3.5 h. After cooling, the excess of hydride was decomposed by gradual addition of 6 M acetic acid and the mixture was evaporated to dryness. The residue was acetylated in the usual way and the product was chromatographed on a silica-gel column (2 g) with 1 : 1 2-butanone–toluene as an eluent, giving **22** (26 mg, 65%): mp 178—179.5 °C, identical with the compound obtained above.

DL-*Penta*-N,O-*acetyl*-*(1,3/2,6)*-*6*-*amino*-*4*-*hydroxymethyl*-*4*-*cyclohexene*-*1,2,3*-*triol* ***(20)***. *a)* Compound **19** (195 mg) was similarly reduced by hydrogen sulfide to give **20** (140 mg, 69%): mp 120—121 °C; ^{1}H NMR ($CDCl_3$) δ=1.94 (3H, s), 2.00 (3H, s), and 2.03 (9H, s) (OAc and NAc), 4.35 and 4.68 (AB-quartet, J=13 Hz, $C\underline{H}_2$OAc), 4.84 (1H, dd, J=7.7 and 8.5 Hz, H-6, changing to d with J=8.5 Hz on deuteration), 5.10 (1H, dd, J=8.5 and 10.5 Hz, H-1), 5.37 (1H, dd, J=7.8 and 10.5 Hz, H-2), 5.74 (2H, broad s, H-3 and H-5), and 6.06 (1H, broad d, J=*ca.* 7.7 Hz, N$\underline{H}$Ac, disappearing on deuteration).

Found: C, 53.18; H, 6.04; N, 3.55%. Calcd for $C_{17}H_{23}NO_9$: C, 52.98; H, 6.02; N, 3.63%.

b) Compound **19** (134 mg) was treated with sodium boronhydride (41 mg) in a similar manner as in the preparation of **22** to give **20** (84 mg, 65%): mp 119—120 °C, identical with the compound obtained above.

Epoxidation of ***4***: *Synthesis of* DL-*2,3,4*-*Tri*-O-*acetyl*-*1,7*-*anhydro*-*(1,2,4/3)*- ***(26)*** *and* -*(1,3/2,4)*-*1*-C-*hydroxymethyl*-*5*-*cyclohexene*-*1,2,3,4*-*tetrol* ***(27)***. *a)* A mixture of DL-tri-*O*-acetyl-(1,3/2)-4-methylene-5-cyclohexene-1,2,3-triol (**4**)[18] (0.3 g), 70% *m*-chloroperoxybenzoic acid (*m*CPBA) (0.33 g, 1.2 molar equiv.), and dichloromethane (5 ml) was stirred at room temperature for 12 h. The progress of reaction was monitored by TLC (1 : 5 2-butanone–toluene). Two new components (R_f 0.42 and 0.36) appeared and then were gradually converted into slower-moving components before **4** was completely consumed. The reaction mixture was cooled in an ice-bath, and the precipitates (*m*-chlorobenzoic acid) were removed by filtration. The filtrate was washed successively with 10% aqueous sodium sulfite solution, saturated aqueous sodium hydrogencarbonate solution, and water, and then dried. Evaporation of the solvent and chromatography of the residue (0.23 g) on a silica-gel column (7 g) with 1 : 5 2-butanone–toluene gave, as the first fraction, **27** (25.4 mg, 8%) as plates: mp 124.5—125.5 °C; ^{1}H NMR ($CDCl_3$) δ=2.01 (6H, s) and 2.05 (3H, s) (OAc), 2.73 and 3.18 (AB-quartet, J=5 Hz, $C\underline{H}_2O$), 5.32—5.55 (3H, m, H-3, H-4, and H-5), 5.55—5.75 (1H, m, H-2), and 5.84 (1H, dd, J=1.5 and 10 Hz, H-6).

Found: C, 54.73; H, 5.65%. Calcd for $C_{13}H_{16}O_7$: C, 54.93; H, 5.67%.

The second fraction gave crystals, which were recrystallized from ethanol to give **26** (76 mg, 24%) as plates: mp 108.5—109 °C; ^{1}H NMR ($CDCl_3$) δ=2.02 (3H, s) and 2.06 (6H, s) (OAc), 2.88 (2H, s, $C\underline{H}_2O$), 5.29—5.60 (4H, m, H-2, H-3, H-4, and H-5), and 5.96 (1H, dd, J=2 and 10.5 Hz, H-6).

Found: C, 54.73; H, 5.69%. Calcd for $C_{13}H_{16}O_7$: C, 54.93; H, 5.67%.

The third fraction gave crystals, which were recrystallized from ethanol to give DL-3,4,7-tri-*O*-acetyl-(1,2,4/3)-1-*C*-hydroxymethyl-5-cyclohexene-1,2,3,4-tetrol (**28**) (44 mg, 13%): mp 100.5—102 °C; ^{1}H NMR ($CDCl_3$) δ=2.05 (3H, s), 2.07 (3H,

s), and 2.11 (3H, s) (OAc), 2.99 (1H, d, J=8 Hz, C-2-OH, disappearing on deuteration), 3.23 (1H, s, C-1-OH, disappearing on deuteration), 3.70 (1H, t, J=8 Hz, H-2, changing to d with J=8 Hz on deuteration), 4.07 and 4.25 (AB-quartet, J=12 Hz, C$\underline{H}_2$OAc), 5.28 (1H, t, J=8 Hz, H-3), 5.45 (1H, dd, J=1 and 12 Hz), and 5.69 (1H, dd, J=1 and 12 Hz) and 5.85 (1H, dd, J=1 and 12 Hz) (H-5 and H-6).

Further elution of the column gave an unresolved mixture (163 mg). After acetylation in the usual way, followed by fractionation on a silica-gel column (8 g) with 1 : 5 2-butanone–toluene, pentaacetate **24** was obtained in 91 mg (21% from **4**) as a syrup. The ^{1}H NMR spectrum was superimposable on that of an authentic sample.[9]

Acetylation of **28** (29 mg) with acetic anhydride (2 ml) and pyridine (2 ml) at room temperature for 4 d gave, after separation by a silica-gel column (3 g with) 1 : 5 2-butanone–toluene, DL-penta-*O*-acetyl- (**30**) and DL-2,3,4,7-tetra-*O*-acetyl-(1,2,4/3)-1-*C*-hydroxymethyl-5-cyclohexene-1,2,3,4-tetrol (**29**) in 19 mg (52%) and 8 mg (24%) as a syrup, respectively. These compounds were identical with the authentic samples.[9]

b) Compound **4** (0.3 g) was treated with 70% *m*CPBA (0.33 g, 1.2 molar equiv.) in dichloromethane (15 ml), buffered at pH 8 with phosphate buffer solution[26] (20 ml), with vigorous stirring at room temperature. After 20 min, an additional amount of *m*CPBA (0.28 g) was added to the reaction mixture and stirring was continued for further 40 min. The organic layer was then separated and washed similarly as described above. Evaporation of the solvent followed by fractionation of the residual products on a silica-gel column (10 g) gave **26** (124 mg, 31%) and **27** (86 mg, 27%).

c) The above reaction was carried out similarly by using saturated aqueous sodium hydrogencarbonate solution as an acid scavenger, instead of the phosphate buffer solution. Compounds **26** and **27** were obtained in 37 and 29% yields, respectively.

d) A similar epoxidation reaction was carried out in the presence of solid sodium hydrogencarbonate as an acid acceptor. Compounds **26** and **27** were isolated in 39 and 28% yields, respectively.

*Reaction of Spiro Epoxides **26** and **27** under Acidic Conditions.* Spiro epoxides **26** and **27** were each dissolved in dichloromethane containing a trace of *p*-toluenesulfonic acid monohydrate (pH *ca.* 3) and each solution was left at room temperature for 30 min. Examination on TLC revealed that **26** had been converted into slower-moving products, which were convertible into pentaacetate **24** by acetylation, whereas **27** led to triacetate **28**.

*Reaction of **26** with Sodium Methoxide.* To a solution of **26** (0.11 g) in methanol (5 ml) was added 1 M methanolic sodium methoxide (1.3 ml), and the mixture was left at room temperature overnight. After neutralization with Amberlite IR-120 (H^+), the solution was evaporated and the residue was acetylated in the usual way for 5 d. The products were fractionated on a silica-gel column (7 g) with 1 : 5 2-butanone–toluene as an eluent to give DL-tetra-*O*-acetyl-(1,2,4/3)-1-*C*-methoxymethyl-5-cyclohexene-1,2,3,4-tetrol (**32**) (76 mg, 55%), mp 130—131 °C, and the triacetate **31** (11 mg, 9%) as a syrup. They were identical with authentic samples[9] previously obtained from **5**.

DL-*Tetra*-O-*acetyl-(1,2,4/3)-1*-C-*azidomethyl-5-cyclohexene-1,2,-3,4-tetrol (**33**).* A mixture of **26** (125 mg), sodium azide (87 mg), ammonium chloride (24 mg), and DMF (2 ml) was stirred at room temperature for 20 h and then at 60 °C for 3 h. The mixture was evaporated to dryness and the residue was acetylated with acetic anhydride (2 ml) and pyridine (2 ml) at room temperature for 2 d and then at 40 °C overnight. The mixture was evaporated and the residue was purified by passage through a silica-gel column (10 g) with 1 : 8 2-butanone–toluene to give **33** (140 mg, 86%) as a syrup: ^{1}H NMR ($CDCl_3$) δ=2.00 (3H, s), 2.02 (3H, s), and 2.07 (6H, s) (OAc), 3.56 and 3.91 (AB-quartet, J=12.5 Hz, C$\underline{H}_2$N$_3$), 5.20 (1H, dd, J=1.5 and 10.5 Hz, H-2), 5.29—5.64 (2H, m, H-3 and H-4), and 5.73 (1H, dd, J=3 and 11 Hz) and 6.17 (1H, dd, J=1.5 and 11 Hz) (H-5 and H-6).

Found: C, 48.05; H, 5.21; N, 11.26%. Calcd for $C_{15}H_{19}N_3O_8$: C, 47.78; H, 5.19; N, 11.38%.

DL-*Tetra*-O-*acetyl-(1,3/2,4)-1*-C-*azidomethyl-5-cyclohexene-1,2,-3,4-tetrol (**36**).* A mixture of **27** (126 mg), sodium azide (87 mg), ammonium chloride (24 mg), and DMF (2 ml) was treated in a similar manner as in the preparation of **33**. The crude product was subsequently acetylated with acetic anhydride (2 ml) and pyridine (2 ml) at room temperature for 2 d. The mixture was evaporated and the residue was purified by passage through a short column of alumina with ethyl acetate to give crystals, which were recrystallized from ethanol, giving **36** (132 mg, 81%) as particles: mp 99—100 °C; ^{1}H NMR ($CDCl_3$) δ=2.00 (6H, s), 2.03 (3H, s), and 2.08 (3H, s) (OAc), 3.41 and 3.72 (AB-quartet, J=13 Hz, C$\underline{H}_2$N$_3$), 5.27—5.79 (3H, m, H-1, H-2, and H-3), and 5.79—6.03 (2H, m, H-5 and H-6).

Found: C, 47.84; H, 5.22; N, 11.35%. Calcd for $C_{15}H_{19}N_3O_8$: C, 47.78; H, 5.19; N, 11.38%.

DL-*Penta*-N,O-*acetyl-(1,2,4/3)-1*-C-*aminomethyl-5-cyclohexene-1,2,3,4-tetrol (**35**).* Into a stirred solution of **32** (135 mg) in 2 : 1 pyridine–water (3 ml) was bubbled hydrogen sulfide at room temperature for 5 d. The mixture was evaporated to dryness and the residue was acetylated in the usual way for 2 d. The crude products, which were shown to contain two components (R_f 0.27 and 0.39) by TLC analysis (1 : 5 ethanol–benzene), were placed on a column of silica gel (5 g) and first eluted with toluene, giving sulfur, and then with 1 : 5 ethanol-toluene, giving desired products. The fraction having R_f 0.4 yielded **35** (40 mg, 28%) as a syrup: ^{1}H NMR ($CDCl_3$) δ= 1.93 (3H, s), 2.00 (3H, s), 2.02 (3H, s), 2.05 (3H, s), and 2.09 (3H, s) (NAc and OAc), 3.04 (1H, dd, J=6 and 14 Hz, changing to d with J=14 Hz on deuteration) and 4.44 (1H, dd, J=7.5 and 14 Hz, changing to d with J=14 Hz on deuteration) (C$\underline{H}_2$NHAc), 5.08 (1H, d, J=10.5 Hz, H-2), 5.36—5.53 (1H, m, H-4), 5.59 (1H, dd, J=7.5 and 10.5 Hz, H-3), 5.72 (1H, dd, J=3 and 10 Hz, H-5), 6.11 (1H, broad t, J=*ca.* 7 Hz, N$\underline{H}$, disappearing on deuteration), and 6.43 (1H, dd, J=1.5 and 10 Hz, H-6).

Found: C, 53.17; H, 6.03; N, 3.37%. Calcd for $C_{17}H_{23}NO_9$: C, 52.98; H, 6.02; N, 3.63%.

The fraction having R_f 0.3 yielded DL-*N*-acetyl-2,3,4-tri-*O*-acetyl-(1,2,4/3)-1-*C*-aminomethyl-5-cyclohexene-1,2,3,4-tetrol (**34**) (83 mg, 66%) as a syrup: ^{1}H NMR ($CDCl_3$) δ=1.96 (3H, s), 2.00 (3H, s), 2.02 (3H, s), and 2.10 (3H, s) (OAc and NAc), 3.00 (1H, dd, J=6 and 14 Hz, changing to d with J=14 Hz on deuteration) and 3.62 (1H, dd, J=7 and 14 Hz, changing to d with J=14 Hz on deuteration) (C$\underline{H}_2$NHAc), 3.37—3.83 (1H, m, O$\underline{H}$, disappearing on deuteration), 5.01 (1H, d, J=10 Hz, H-2), 5.29—5.62 (2H, m, H-3 and H-4), 5.63 (1H, dd, J=1.5 and 10 Hz, H-5), 5.88 (1H, dd, J=1 and 10 Hz, H-6), and 6.36 (1H, broad t, J=*ca.* 7 Hz, N$\underline{H}$Ac, disappearing on deuteration).

Found: C, 52.72; H, 6.26; N, 3.97%. Calcd for $C_{15}H_{21}NO_8$: C, 52.47; H, 6.17; N, 4.08%.

Further acetylation of **34** at 50 °C for 2 d gave **35** quantitatively.

DL-*Penta*-N,O-*acetyl-(1,3/2,4)-1*-C-*aminomethyl-5-cyclohexene-1,2,3,4-tetrol (**38**).* Reduction of **36** (92 mg) with hydrogen sulfide and successive acetylation, were carried out in a similar way as in the preparation of **35**. Similar fractionation of the

acetylated products gave two fractions (R_f 0.25 and 0.32, 1 : 5 ethanol–benzene). The fraction having R_f 0.32 gave **38** (76 mg, 79%): mp 183—184 °C; ^{1}H NMR ($CDCl_3$) δ=1.97 (3H, s), 2.03 (9H, s), and 2.08 (3H, s) (OAc and NAc), 3.48 (1H, dd, J=5.5 and 14 Hz, changing to d with J=14 Hz on deuteration) and 3.88 (1H, dd, J=5 and 14 Hz, changing to d with J=14 Hz on deuteration) ($C\underline{H}_2NHAc$), 5.36—5.65 (2H, m, H-2 and H-3), and 5.68—6.11 (4H, m, H-4, H-5, H-6, and N$\underline{H}$Ac, changing on deuteration).

Found: C, 53.34; H, 6.14; N, 3.52%. Calcd for $C_{17}H_{23}NO_9$: C, 52.98; H, 6.02; N, 3.63%.

The fraction having R_f 0.25 gave DL-*N*-acetyl-2,3,4-tri-*O*-acetyl-(1,3/2,4)-1-*C*-aminomethyl-5-cyclohexene-1,2,3,4-tetrol (**37**) (11 mg, 13%) as a syrup: ^{1}H NMR ($CDCl_3$) δ=2.02 (9H, s) and 2.10 (3H, s) (OAc and NAc), 3.46 (1H, broad s, O$\underline{H}$, disappearing on deuteration), 3.57 (2H, d, J=6 Hz, $C\underline{H}_2$-NHAc, changing to s on deuteration), 5.13—5.53 (3H, m, H-2, H-3, and H-4), 5.62 (1H, broad d, J=*ca.* 10.5 Hz) and 5.80 (1$\underline{H}$, d, J=10.5 Hz) (H-5 and H-6), and 5.97—6.32 (1H, m, N$\underline{H}$, disappearing on deuteration).

Found: C, 52.86; H, 6.23; N, 3.88%. Calcd for $C_{15}H_{21}NO_8$: C, 52.47; H, 6.17; N, 4.08%.

Further acetylation of **37** at room temperature for 2 d yielded **38** quantitatively.

DL-*Tetra-O-acetyl-(1,3/2,4)-4-chloro-4-C-hydroxymethyl-5-cyclohexene-1,2,3-triol (**41**).* To a cooled, stirred solution of **26** (0.11 g) in tetrahydrofuran (4 ml) was added 12 M hydrochloric acid[27] (0.035 ml), and the mixture was allowed to stand at 0—5 °C for 1 h. The mixture was then neutralized by gradual addition of solid sodium hydrogencarbonate with ice-cooling. After precipitates had been removed by filtration, the filtrate was evaporated to give a syrup, which was crystallized from ethanol–water, affording **39** (124 mg, 100%) as particles: mp 125—126.6 °C; ^{1}H NMR ($CDCl_3$) δ=1.98 (3H, s), 2.02 (3H, s), and 2.10 (3H, s) (OAc), 2.78 (1H, broad s, O$\underline{H}$, disappearing on deuteration), 3.70 and 4.01 (AB-quartet, J=11.5 Hz, $C\underline{H}_2OH$), 5.25—5.67 (3H, m, H-1, H-2, and H-3), and 5.75 (2H, broad s, H-5 and H-6).

Found: C, 48.70; H, 5.40; Cl, 11.06%. Calcd for $C_{13}H_{17}ClO_7$: C, 48.68; H, 5.34; Cl, 11.05%.

Purification of **39** by chromatography on silica gel with 1 : 5 2-butanone–toluene induced an acetyl group migration, which led to partial transformation into syrupy 1,2,7-triacetate **40**: ^{1}H NMR ($CDCl_3$) δ=2.02 (3H, s), 2.08 (3H, s), and 2.10 (3H, s) (OAc), 2.99 (1H, d, J=6 Hz, O$\underline{H}$, disappearing on deuteration), 4.00—4.22 (1H, m, H-3, changing to dd with J=2 and 8 Hz at δ=4.11 on deuteration), 4.39 (2H, s, $C\underline{H}_2OAc$), 5.18—5.70 (2H, m, H-1 and H-2), and 5.57 (1H, d, J=10 Hz) and 5.75 (1H, broad d, J=10 Hz) (H-5 and H-6).

Found: C, 48.73; H, 5.46; Cl, 11.06%. Calcd for $C_{13}H_{17}ClO_7$: C, 48.68; H, 5.34; Cl, 11.05%.

Treatment of **39** and **40** with acetic anhydride containing a trace of sulfuric acid at room temperature overnight gave the tetraacetate **41** in a quantitative yield. Recrystallization from ethanol gave an analytical sample, thin plates: mp 90—91 °C; ^{1}H NMR ($CDCl_3$) δ=1.98 (3H, s), 2.01 (3H, s), 2.08 (3H, s), and 2.11 (3H, s) (OAc), 4.32 (2H, s, $C\underline{H}_2OAc$), 5.37—5.62 (3H, m, H-1, H-2, and H-3), and 5.62 (1H, d, J=10 Hz) and 5.78 (1H, d, J=10 Hz) (H-5 and H-6).

Found: C, 49.58; H, 5.13; Cl, 9.84%. Calcd for $C_{15}H_{19}ClO_8$: C, 49.66; H, 5.28; Cl, 9.77%.

*Azidolysis of **41** with Sodium Azide.* A mixture of **41** (90 mg), sodium azide (32 mg, 2 molar equiv.), and DMF (4 ml) was stirred at 60 °C for 15 h. TLC (1 : 5 2-butanone–toluene) indicated that **4** (R_f 0.47) was converted into a sole azide (R_f 0.41). The mixture was then diluted with ethyl acetate (10 ml) and the solution was washed with cold water thoroughly, and dried. Evaporation of the solvent gave **21** (85 mg, 93%) as a syrup, which was shown to be identical with the authentic sample by ^{1}H NMR analysis.

*Acetolysis of **41** with Sodium Acetate.* A mixture of **41** (53 mg), sodium acetate (48 mg, 4 molar equiv.), and DMF (2 ml) was stirred at 110 °C for 30 h. The mixture was then evaporated and the residue was acetylated in the usual way. TLC and ^{1}H NMR analyses indicated that the acetylated product contained **23**, **24**, **29**, and **30**. Further isolation was not attempted.

DL-*1,2 : 3,7-Di-O-isopropylidene-(1,3,6/2)-6-azido-4-hydroxymethyl-4-cyclohexene-1,2,3-triol (**47**).* To an ice-cooled, stirred solution of **21** (0.16 g) in methanol (3 ml) was added 1 M methanolic sodium methoxide (1 ml), and the mixture was left at 0—5 °C overnight. The reaction mixture was then treated with Amberlite IR-120 (H^+) and evaporated to give a syrup (97 mg). Without further purification, the syrup was dissolved in DMF (3 ml) and to the solution was added 2,2-dimetho ypropane (1 ml) and *p*-toluenesulfonic acid (8 mg). The mixture was stirred at room temperature overnight. After neutralization with solid sodium hydrogencarbonate, the mixture was diluted with ethyl acetate (30 ml), then washed with cold water (3×10 ml), and dried. Evaporation of the solvent left a syrup, which crystallized upon standing in a desiccator. Recrystallization from ethanol gave **47** (88 mg, 72% from **21**): mp 116.5—117.5 °C; ^{1}H NMR ($CDCl_3$) δ=1.40 (3H, s), 1.47 (6H, s), and 1.52 (3H, s) (isopropylidene $C\underline{H}_3$), 3.61 (1H, dd, J=4 and 9.5 Hz, H-1), 3.97 (1H, dd, J=7.5 and 9.5 Hz, H-1), 3.97 (1H, dd, J=7.5 and 9.5 Hz, H-2), 4.15—4.57 (4H, m, H-3, H-6, and $C\underline{H}_2O$), and 5.41 (1H, broad d, J=*ca.* 6 Hz, H-5).

Found: C, 55.37; H, 6.75; N, 14.67%. Calcd for $C_{13}H_{19}N_3O_4$: C, 55.51; H, 6.81; N, 14.94%.

DL-*1,2 : 3,7-Di-O-isopropylidene-(1,3/2,6)-6-azido-4-hydroxymethyl-4-cyclohexene-1,2,3-triol (**44**).* A mixture of DL-tetra-*O*-acetyl-(1,3,6/2)-6-bromo-4-hydroxymethyl-4-cyclohexene-1,2,3-triol (**9**)[9] (0.3 g), sodium azide (72 mg, 1.5 molar equiv.), and DMF (10 ml) was stirred at room temperature for 3 h. TLC showed the formation of two products **19** (major) and **21** (minor). The mixture was diluted with ethyl acetate (40 ml) and the solution was washed with cold water, and then dried. Evaporation of the solvent gave a syrupy mixture of **19** and **21** (0.29 g, 100%).

A 0.16 g portion of the mixture was then treated with 1 M methanolic sodium methoxide (3 ml) in methanol (3 ml) at 0—5 °C overnight. The mixture was neutralized with Amberlite IR-120 (H^+) and evaporated, giving a colorless syrup (68 mg), which was purified by a silica-gel column (3 g) with 1 : 3 2-butanone–toluene to give a syrupy mixture of DL-(1,3/2,6)- (**42**) and (1,3,6/2)-6-azido-4-hydroxymethyl-4-cyclohexene-1,2,3-triol (**43**) (59 mg, 66%). Isolation of **42** and **43** was not achieved, because their chromatographic mobilities on silica gel were identical.

Found: C, 41.97; H, 5.50; N, 20.60%. Calcd for $C_7H_{11}N_3O_4$: C, 41.79; H, 5.51; N, 20.89%.

The syrupy mixture (85 mg) was dissolved in DMF (3 ml) and treated with 2,2-dimethoxypropane (1 ml) in the presence of *p*-toluenesulfonic acid (8 mg) at room temperature for 24 h. After neutralization with solid sodium hydrogencarbonate, the mixture was worked up similarly as described in the preparation of **47**. The crude products were fractionated on a silica-gel column (6 g) with 1 : 15 2-butanone–toluene as an eluent to give two fractions. The first fraction gave **44** (75 mg, 42% from **9**): mp 79—80 °C; ^{1}H NMR ($CDCl_3$) δ=1.40 (3H, s), 1.46 (6H, s), and 1.54 (3H, s) (isopropylidene $C\underline{H}_3$), 3.50 (1H, dd, J=8 and 10 Hz) and 3.69 (1H, dd, J=7 and 10 Hz) (H-1 and H-2), 4.00—4.67 (4H, m, H-3, H-6, and $C\underline{H}_2O$), and

5.28 (1H, s, H-5).

Found: C, 55.37; H, 6.75; N, 14.67%. Calcd for $C_{13}H_{19}N_3O_4$: C, 55.51; H, 6.81; N, 14.94%.

The second fraction gave **47** (17 mg, 9% from **9**): mp 116—117 °C, identical with the compound obtained from **21** described above.

DL-*1,2: 3,7-Di-O-isopropylidene-(1,3,6/2)-6-acetamido-4-hydroxymethyl-4-cyclohexene-1,2,3-triol (49).* Hydrogen sulfide was bubbled into a solution of **47** (80 mg) in 1 : 1 pyridine–water (3 ml) at room temperature for 1 h. The pale yellow mixture with sulfur precipitated was evaporated and the syrup residue was placed on a short column of alumina. The first fraction eluted with toluene gave sulfur as needles and the second fraction, showing a positive test of ninhydrin, eluted with ethanol gave DL-1,2 : 3,7-di-*O*-isopropylidene-(1,3,6/2)-6-amino-4-hydroxymethyl-4-cyclohexene-1,2,3-triol (**48**) (72 mg, 100%) as a syrup.

Acetylation of **48** (30 mg), without further purification, in the usual way gave, after recrystallization from ethanol, **49** (35 mg, 98%) as particles: mp 241—242 °C; ^{1}H NMR ($CDCl_3$–D_2O) δ=1.41 (3H, s), 1.45 (6H, s), and 1.55 (3H, s) (isopropylidene C$\underline{H}_3$), 1.99 (3H, s, NAc), 3.50—3.86 (2H, m, H-1 and H-2), 4.13 and 4.47 (AB-quartet, J=15 Hz, C$\underline{H}_2$O), 4.50 (1H, broad d, J=*ca.* 5 Hz, H-3), 4.66—4.94 (1H, m, H-6), and 5.62 (1H, broad d, J=*ca.* 5 Hz, H-5).

Found: C, 60.85; H, 7.83; N, 4.61%. Calcd for $C_{15}H_{23}NO_5$: C, 60.59; H, 7.80; N, 4.71%.

DL-*1,2 : 3,7-Di-O-isopropylidene-(1,3,6/2)-6-trifluoroacetamido-4-hydroxymethyl-4-cyclohexene-1,2,3-triol (50).* To an ice-cooled solution of **48** (0.26 g) in pyridine (4 ml) was added dropwise trifluoroacetic anhydride (0.45 ml) and the mixture was left at room temperature overnight. Evaporation of the solvent followed by coevaporation with toluene several times gave a colorless syrup, which solidified upon standing in a desiccator to give **50** (0.34 g, 96%). It was analytically pure without further purification: ^{1}H NMR ($CDCl_3$) δ=1.41 (6H, s), 1.46 (3H, s), and 1.54 (3H, s) (isopropylidene C$\underline{H}_3$), 3.56—3.82 (2H, m, H-1 and H-2), 4.11 and 4.41 (AB-quartet, J=15 Hz, C$\underline{H}_2$O), 4.39—4.55 (1H, m, H-6, relatively sharpened on deuteration), and 5.61 (1H, broad d, J=*ca.* 5 Hz, H-5).

Found: C, 51.16; H, 5.77; N, 3.97%. Calcd for $C_{15}H_{20}NF_3O_5$: C, 51.28; H, 5.74; N, 3.99%.

DL-*1,2:3,7-Di-O-isopropylidene-(1,3/2,6)-6-acetamido-4-hydroxymethyl-4-cyclohexene-1,2,3-triol (46).* Compound **44** (190 mg) was reduced in a similar manner as described in the preparation of **48** to give DL-1,2 : 3,7-di-*O*-isopropylidene-(1,3/2,6)-6-amino-4-hydroxymethyl-4-cyclohexene-1,2,3-triol (**45**) (170 mg, quantitative) as a syrup, showing a positive test of ninhydrin.

Acetylation of **45** (30 mg) in the usual way gave **46** (33 mg, 92%) as a pale yellow syrup, which was crystallized from ether by scratching the flask to give **46** (22 mg, 62%): mp 178—179 °C; ^{1}H NMR ($CDCl_3$–D_2O) δ=1.39 (3H, s), 1.43 (6H, s), and 1.52 (3H, s) (isopropylidene C$\underline{H}_3$), 1.96 (3H, s) (NAc), 3.53 (1H, t, J=9 Hz, H-2), 3.78 (1H, dd, J=7.5 Hz, H-1), 4.12 and 4.46 (AB-quartet, J=12.5 Hz, C$\underline{H}_2$O), 4.57—4.81 (2H, m, H-3 and H-6), and 5.38 (1H, broad s, H-5).

Found: C, 60.69; H, 7.64; N, 4.81%. Calcd for $C_{15}H_{23}NO_5$: C, 60.59; H, 7.80; N, 4.71%.

DL-*3,7-O-Benzylidene-(1,3/2,6)- (51) and -(1,3,6/2)-6-azido-4-hydroxymethyl-4-cyclohexene-1,2,3-triol (52).* A syrupy mixture (247 mg) of **42** and **43** was dissolved in DMF (10 ml) and treated with α,α-dimethoxytoluene (0.228 ml, 1.2 molar equiv.) in the presence of *p*-toluenesulfonic acid (12 mg) at 60—65 °C under reduced pressure (22 mmHg) (1 mmHg=133.322 Pa) for 3.5 h. TLC (1 : 2 2-butanone–toluene) indicated the formation of two products (major, R_f 0.4; minor, R_f 0.3). After neutralization with Amberlite IRA-400 (OH^-), the solvent was removed by evaporation and the residue was fractionated on a silica-gel column (5 g) with 1 : 3 2-butanone–toluene as an eluent. The first fraction gave **51** (154 mg, 43%) as needles: mp 149—150 °C; ^{1}H NMR (CD_3OD) δ=3.45 (1H, dd, J=9 and 10.5 Hz, H-2), 3.67 (1H, dd, J=7.5 and 10.5 Hz, H-1), 3.98 (1H, broad d, J=*ca.* 7.5 Hz, H-6), 4.18—4.47 (3H, m, H-3 and C$\underline{H}_2$O), 5.41 (1H, s, H-5), 5.67 (1H, s, benzylic proton), and 7.29—7.64 (5H, m, phenyl).

Found: C, 57.96; H, 5.26; N, 14.48%. Calcd for $C_{14}H_{15}N_3O_4$: C, 58.13; H, 5.23; N, 14.53%.

The second fraction gave **52** (64 mg, 18%) as feathers: decomp at 180.5 °C; ^{1}H NMR (CD_3OD) δ=3.62—4.00 (2H, m, H-1 and H-2), 4.15—4.42 (2H, m, H-3 and H-6), 4.50 (2H, s, C$\underline{H}_2$O), 5.69 (1H, d, J=5 Hz, H-5), 5.70 (1H, s, benzylic proton), and 7.28—7.68 (5H, m, phenyl).

Found: C, 58.06; H, 5.34; N, 14.88%. Calcd for $C_{14}H_{15}N_3O_4$: C, 58.13; H, 5.23; N, 14.53%.

The authors express their sincere thanks to Dr. Shoji Omoto, Meiji Seika Kaisha, Ltd., for the ^{13}C NMR spectra, to Mr. Saburo Nakada for the elementary analyses, and to Mr. Yasuo Abe and Mr. Yoshikazu Iwasawa for assistance in preparative experiments. The present work was partially supported by a Grant-in-Aid for Scientific Research No. 56550617 from the Ministry of Education, Science and Culture.

References

1) Preliminary accounts of portions of this article have been presented previously: a) S. Ogawa, T. Toyokuni, and T. Suami, *Chem. Lett.*, **1980**, 713; b) S. Ogawa, T. Toyokuni, Y. Iwasawa, Y. Abe, and T. Suami, *Chem. Lett.*, **1982**, 279.

2) T. Suami, S. Ogawa, and N. Chida, *J. Antibiot.*, **33**, 98 (1980), and the references cited therein.

3) Y. Kameda and S. Horii, *J. Chem. Soc., Chem. Commun.*, **1972**, 746.

4) Y. Kameda, N. Asano, M. Teranishi, and K. Matsui, *J. Antibiot.*, **33**, 1573 (1980).

5) T. Iwasa, H. Yamamoto, and M. Shibata, *J. Antibiot.*, **23**, 595 (1970).

6) Review: E. Truscheit, W. Frommer, B. Junge, L. Müller, D. D. Schmidt, and W. Wingender, *Angew. Chem., Int. Ed. Engl.*, **20**, 744 (1981).

7) Y. Kameda, N. Asano, M. Yoshikawa, and K. Matsui, *J. Antibiot.*, **33**, 1575 (1980).

8) After our work on the synthesis of DL-valienamine and its related compounds had been completed,[18] Paulsen's group reported the synthesis of chiral valienamine starting from quebrachitol: H. Paulsen and F. R. Heiker, *Angew. Chem., Int. Ed. Engl.*, **19**, 904 (1980); see also *Carbohydr. Res.*, **102**, 83 (1982).

9) For the previous paper in this series: T. Toyokuni, Y. Abe, S. Ogawa, and T. Suami, *Bull. Chem. Soc. Jpn.*, **56**, 505 (1983).

10) All the compounds described in this paper are racemic. All the formulas depict one enantiomer of the respective racemates. The nomenclature is based on the IUPAC-IUB Tentative Cyclitol Nomenclature Rule [*J. Biol. Chem.*, **243**, 5809 (1968)].

11) The progress of the azidolysis is readily followed by TLC sprayed with concd sulfuric acid, whereupon the azido compounds formed are visualized brown. This is often observed in the azidolysis of the pseudo-sugar derivatives.

12) R. J. Abraham, H. Gottschalck, H. Paulsen, and W. A.

Thomas, *J. Chem. Soc.*, **1965**, 6268; A. A. Chalmers and R. H. Hall, *J. Chem. Soc., Perkin Trans. 2*, **1974**, 728.

13) L. M. Jackman and S. Sternhell, "Applications of Nuclear Magnetic Resonance Spectroscopy in Organic Chemistry," 2nd ed, Pergamon Press, New York (1969), pp. 83, 238.

14) T. Adachi, Y. Yamada, and I. Inoue, *Synthesis*, **1977**, 45.

15) One of the remarkable features in the ^{1}H NMR spectra of valienamine and its related aminocyclitols and cyclitols is the fact that a vicinal pseudoequatorial substituent (X=OAc, NHAc) causes the resonance of an olefinic proton (H_A) to move upfield (by *ca.* 0.12 ppm) relative to their pseudoaxial epimers.

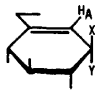

16) A similar allylic rearrangement was reported in the reduction of 4-*O*-benzoyl-2,3,6-trideoxy-β-L-*erythro*-hex-2-enopyranosyl azide with lithium aluminium hydride: J. Boivin, M. Pais, and C. Monneret, *Carbohydr. Res.*, **79**, 193 (1980).

17) An authentic sample was kindly provided by Dr. Satoshi Horii of Takeda Chemical Industries, Ltd. (Osaka).

18) S. Ogawa, T. Toyokuni, M. Omata, N. Chida, and T. Suami, *Bull. Chem. Soc. Jpn.*, **53**, 455 (1980).

19) M. E. Toromanoff, *C. R. Hebd Seances Acad. Sci., Ser. C*, **284**, 113 (1977).

20) E. Breitmaier and W. Voelter, "^{13}C NMR Spectroscopy," 2nd ed, Verlag Chemie, New York (1978), p. 76.

21) A similar effect is found in the literature where ^{13}C NMR data of methyl 3,4-dideoxy-DL-glyc-3-enopyranosides were presented: M. Chmielewski, A. Banaszek, and A. Zamojski, *Carbohydr. Res.*, **83**, 3 (1980).

22) R. J. Abraham and P. Loftus, "Proton and Carbon-13 NMR Spectroscopy," Heydens and Son Ltd., London (1980), p. 29.

23) E. Breitmaier and W. Voelter, "^{13}C NMR Spectroscopy," 2nd ed, Verlag Chemie, New York (1978), p. 74.

24) Taken on a Varian EM-360A (60 MHz) spectrometer.

25) Taken on a Varian HA 100D (100 MHz) spectrometer.

26) Phosphate buffer was prepared by adding sufficient aqueous 0.1 M Na_2HPO_4 to 0.1 M NaH_3PO_4 up to pH 8.

27) When 1 M hydrochloric acid was used, the reaction required a longer time (24 h) for completion and a formation of side-products (probably by de-*O*-acetylation) was observed

 © 1983 The Chemical Society of Japan Bull. Chem. Soc. Jpn., 56, 1171—1175 (1983)

Ditritylation of Methyl and Benzyl α-D-Gluco-, -Manno-, and -Galactopyranosides and Preparation of Their Partially Benzylated Derivatives[1)]

Shinkiti Koto,* Naohiko Morishima, Toyosaku Yoshida, Masaharu Uchino, and Shonosuke Zen

School of Pharmaceutical Sciences, Kitasato University, Shirokane, Minato-ku, Tokyo 108

(Received September 14, 1982)

The ditritylation of methyl and benzyl α-D-gluco-, -manno-, and -galactopyranosides with trityl chloride in pyridine at 70 °C proceeds in a regioselective manner to give the 2,6-ditrityl ethers of the glucosides, the 3,6-ones of the mannosides, and both 2,6- and 3,6-ones of the galactosides. The rearrangement of the trityl group from *O*-3 to *O*-2 of the mannosides at 100 °C causes the selective formation of the 2,6-ditrityl ethers. From the 2,6- and the 3,6-ditrityl ethers, the 3,4- and 2,4-dibenzyl ethers of the hexopyranosides are prepared.

Trityl group has been used for the selective protection of the primary hydroxyl group of carbohydrates;[2)] tritylation of the secondary one has also often been carried out.[2,3)] The continuing methodological study of oligosaccharide synthesis[4)] needs efficient synthetic routes to various kinds of partially benzylated monosaccharides. This has made us investigate the ditritylation of methyl and benzyl α-D-gluco-, -manno-, and -galactopyranosides in order to protect the primary hydroxyl group and one of the secondary ones temporarily. To our surprise, no practical synthesis of such ditrityl ethers has been reported.† They are useful precursors of partially benzylated sugars, some of which have been synthesized *via* partial stannylation by Ogawa *et al.*[5)]

Results and Discussion

The ditritylation of the methyl hexosides with three molar amounts of trityl chloride (TrCl) in pyridine (Py) proceeded smoothly at 50 and 70 °C (Table 1). The locations of trityl groups in the ditrityl ethers were determined by analyzing the ^{1}H NMR spectra of their acetates (Table 5). The structures of the ditrityl ethers were further confirmed by their conversion into the dibenzyl ethers through benzylation followed by detritylation as described below. The results of the reactions conducted at 50 and 70 °C in Table 1 indicate that the regioselectivity of the reaction depends on the steric disposition of the hydroxyl group involved. The starting materials were always exhausted and the primary hydroxyl group was completely tritylated. The second trityl group was introduced to *O*-2 of the glucoside, *O*-3 of the mannoside, and both *O*-2 and *O*-3 of the galactoside, preferentially. Small amounts of the 4,6-ditrityl ethers of the glucoside and the mannoside were also isolated, but that of the galactoside was not detected.

Table 1. Yields of ditrityl and monotrityl ethers of hexopyranosides

Starting material	Temp/°C	Time/h	Yield/% 2,6-Ditrityl ether		3,6-Ditrityl ether		4,6-Ditrityl ether		6-Monotrityl ether	
1	50	18	**7**	36	**8**	19	**9**	12	**1t**[a)]	32
	70	18		52		12		12		18
	100	18		34		2		6		39
2	50	18	**13**	3	**14**	62	**15**	9	**2t**[b)]	26
	70	18		6		56		7		16
	100	18		45		5		4		37
3	50	18	**19**	32	**20**	39			**3t**[c)]	27
	70	8[g)]		39		37				19
	100	6[g)]		35		16				41
4	70	18	**10**	53	**11**	4	**12**	7	**4t**[d)]	16
	100	18		43		3		4		38
5	70	18	**16**	4	**17**	46	**18**	6	**5t**[e)]	19
	100	18		28		12		3		38
6	70	8[g)]	**21**	37	**22**	31			**6t**[f)]	19
	100	5[g)]		36		14				42

a) B. Helferich and J. Becker, *Justus Liebigs Ann. Chem.*, **440**, 1 (1924). b) A. J. Watters, R. C. Hockett, and C. S. Hudson, *J. Am. Chem. Soc.*, **61**, 1528 (1939). c) H. H. Baer and S. A. Abbas, *Carbohydr. Res.*, **77**, 117 (1979). d) S. Koto, S. Inada, T. Yoshida, M. Toyama, and S. Zen, *Can. J. Chem.*, **59**, 255 (1981). e) $[\alpha]_D^{20}+16°$ (*c* 0.6, $CHCl_3$). Found: C, 74.56; H, 6.25%. Calcd for $C_{32}H_{32}O_6$: C, 74.98; H, 6.30%. f) Mp 84—87 °C, $[\alpha]_D^{20}+60°$ (*c* 1.0, $CHCl_3$). Found: C, 74.26; H, 6.40%. Calcd for $C_{32}H_{32}O_6$: C, 74.98; H, 6.30%. g) Longer reaction time caused serious coloration of the reaction mixture and significant depression of yields.

† Ogawa *et al.* have synthesized **7** *via* stannylation (Ref. 5d).

Table 2. Results of reaction of dityrityl ethers with pyridinium chloride

Starting material	Time/h	Yield/%			
		2,6-Dityrityl ether	3,6-Dityrityl ether	4,6-Dityrityl ether	6-Trityl ether
7	18	38	2	1	53
8	18	26	9	1	56
9	18	28	4	2	59
13	18	68	0	0	24
14	18	50	9	0	27
15	18	21	17	2	57
19	6	48	2	0	45
20	6	1	23	0	74

Thus, the orders of reactivity of the secondary hydroxyl group to TrCl in Py at 50 to 70 °C are: OH-2≫OH-3≥OH-4 for the glucoside, OH-3≫OH-4≥OH-2 for the mannoside, and OH-2≈OH-3≥OH-4 for the galactoside; in other words, the equatorial hydroxyl groups vicinal to the axial oxygenous substituent are reactive, whereas the axial ones are not.[2b,6] Highly selective introduction of the trityl group to OH-3 of methyl 6-deoxy-α-L-mannopyranoside and fairly high reactivity of not only OH-2 but OH-3 toward tritylation of methyl 6-deoxy-α-L-galactopyranoside were reported by Otake *et al.*[3b] Benzyl α-D-hexopyranosides also exhibited similar trends of the reactivity of secondary hydroxyl groups in the tritylation at 70 °C.

A remarkable change in the regioselectivity occurred in the tritylation of mannosides **2** and **5** at 100 °C. The formation of the 2,6-dityrityl ether **13** predominated and that of the 3,6-isomer **14** was much lower. The dityritylation of the glucosides and the galactosides also raised the selectivity for the 2,6-dityrityl ethers. The increase in the yield of the monotrityl ether in each case at 100 °C suggests that the trityl group at the secondary hydroxyl group is apt to undergo the reverse reaction with pyridinium chloride (Py·HCl) formed during tritylation in Py (Eq. 1).[7] Since Py·HCl always

$$=CHOH + TrCl + Py \rightleftharpoons =CHOTr + Py\cdot HCl \quad (1)$$

precipitated during the tritylation at 70 °C, while the reaction at 100 °C was homogeneous, greater solubility of the salt in Py at 100 °C may help the reverse reaction in Eq. 1. The time course of the reaction of **2** at 100 °C shows that the second trityl group enters into OH-3 and then rearranges to OH-2 (Fig. 1). It was further found that the 3,6-dityrityl ether **14** was converted into the 2,6-isomer **13** in the presence of Py·HCl in Py at 100 °C

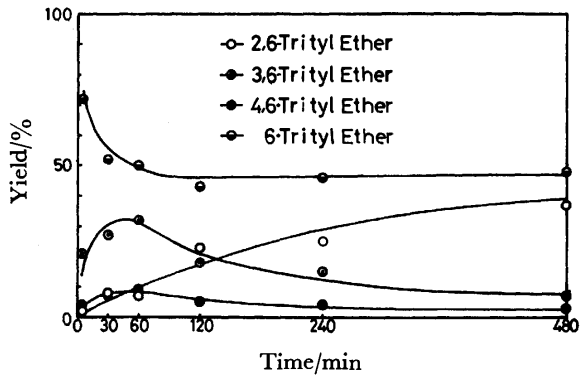

Fig. 1. Time course of tritylation of methyl α-D-mannopyranoside (**2**). Using three molar amount of trityl chloride in pyridine at 100 °C.

(Table 2). The 4,6-isomer **15** behaved in a similar manner. Contrary to these results, the 2,6-isomer **13** did not rearrange. The glucosides exhibited similar trends as shown in Table 2; the 3,6- and the 4,6-dityrityl ethers were converted into the 2,6-isomer but the 2,6-isomer did not change into the 3,6- and the 4,6-isomers. As for the galactosides, although the 3,6-isomer did not rearrange into the 2,6-isomer, the results in Table 2 show that the latter is more resistant to degradation into the monotrityl ether **3t** than the former. Thus, the tritylation of the hexopyranosides with TrCl in Py at 100 °C furnishes a quasi-equilibrium mixture in which the 2,6-dityrityl ether predominates.[8]

The 2,6- and the 3,6-dityrityl ethers thus obtained afforded the 3,4- and the 2,4-dibenzyl ethers, respectively, with ease through benzylation and subsequent

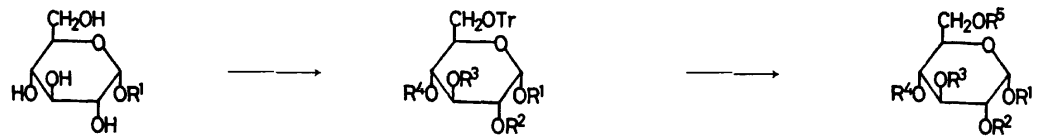

1(4) R^1=Me(Bn)

1t (4t) R^1=Me(Bn), R^2=R^3=R^4=H
7 (10) R^1=Me(Bn), R^2=Tr, R^3=R^4=H
8 (11) R^1=Me(Bn), R^3=Tr, R^2=R^4=H
9 (12) R^1=Me(Bn), R^4=Tr, R^2=R^3=H
7a (10a) R^1=Me(Bn), R^2=Tr, R^3=R^4=Ac
8a (11a) R^1=Me(Bn), R^3=Tr, R^2=R^4=Ac
9a (12a) R^1=Me(Bn), R^4=Tr, R^2=R^3=Ac

23 (25) R^1=Me(Bn), R^3=R^4=Bn, R^2=R^5=H
24 (26) R^1=Me(Bn), R^2=R^4=Bn, R^3=R^5=H
23a (25a) R^1=Me(Bn), R^3=R^4=Bn, R^2=R^5=Ac
24a (26a) R^1=Me(Bn), R^2=R^4=Bn, R^3=R^5=Ac

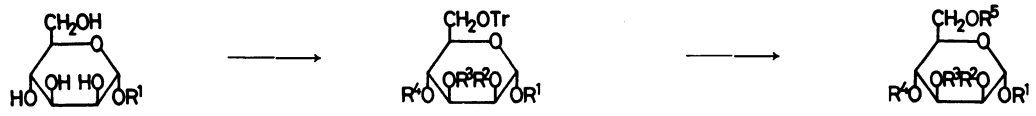

2 (**5**) R^1=Me(Bn) **2t** (**5t**) R^1=Me(Bn), R^2=R^3=R^4=H
13 (**16**) R^1=Me(Bn), R^2=Tr, R^3=R^4=H **27** (**29**) R^1=Me (Bn), R^3=R^4=Bn, R^2=R^5=H
14 (**17**) R^1=Me(Bn), R^3=Tr, R^2=R^4=H **28** (**30**) R^1=Me(Bn), R^2=R^4=Bn, R^3=R^5=H
15 (**18**) R^1=Me(Bn), R^4=Tr, R^2=R^3=H
13a (**16a**) R^1=Me(Bn), R^2=Tr, R^3=R^4=Ac **27a** (**29a**) R^1=Me(Bn), R^3=R^4=Bn, R^2=R^5=Ac
14a (**17a**) R^1=Me(Bn), R^3=Tr, R^2=R^4=Ac **28a** (**30a**) R^1=Me(Bn), R^2=R^4=Bn, R^3=R^5=Ac
15a (**18a**) R^1=Me(Bn), R^4=Tr, R^2=R^3=Ac

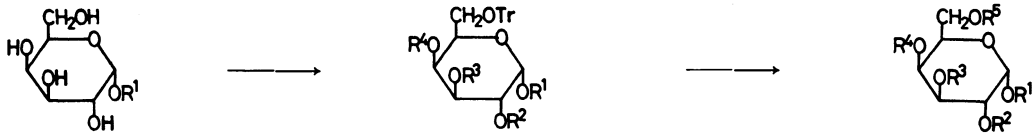

3 (**6**) R^1=Me(Bn) **3t** (**6t**) R^1=Me(Bn), R^2=R^3=R^4=H
19 (**21**) R^1=Me(Bn), R^2=Tr, R^3=R^4=H **31** (**33**) R^1=Me(Bn), R^3=R^4=Bn,R^2=R^5=H
20 (**22**) R^1=Me(Bn), R^3=Tr, R^2=R^4=H **32** (**34**) R^1=Me(Bn), R^2=R^4=Bn, R^3=R^5=H
19a (**21a**) R^1=Me(Bn), R^2=Tr, R^3=R^4=Ac **31a** (**33a**) R^1=Me(Bn), R^3=R^4=Bn, R^2=R^5=Ac
20a (**22a**) R^1=Me(Bn), R^3=Tr, R^2=R^4=Ac **32a** (**34a**) R^1=Me(Bn), R^2=R^4=Bn, R^3=R^5=Ac

Table 3. Physical and Analytical Data of Ditrity Ethers of Methyl and Benzyl α-D-Hexosides

Compound	Mp θ_m/°C	$[\alpha]_D^{20}$/°	(c, $CHCl_3$)	Formula	Calcd (%) C	Calcd (%) H	Found (%) C	Found (%) H	R_f[a] TB	R_f[a] HE	Lit
7	108—109	+36	(1.0)	$C_{45}H_{42}O_6$	79.62	6.24	79.49	6.20	0.26		b)
8	96—99	+49	(1.0)				79.64	6.50	0.54		
9	124—125	+53	(1.0)				79.57	6.48	0.10		
10	104—106	+48	(0.3)	$C_{51}H_{46}O_6$	81.14	6.14	81.02	6.21	0.40		
11	100—101	+40	(0.6)				81.36	6.10	0.70		
12	127—130	+59	(0.3)				80.88	6.13	0.13		
13	99—104	−8	(0.5)	$C_{45}H_{42}O_6$	79.62	6.24	79.58	6.49	0.35		
14	167	+30	(1.0)				78.38	6.55	0.66		
15	112—114	+16	(0.5)				79.48	6.47	0.22		
16	104—105	+12	(1.2)	$C_{51}H_{46}O_6$	81.14	6.14	80.75	6.12	0.42	0.40	
17	85—87	+27	(0.5)				81.10	6.52	0.69	0.64	
18	63—66	+34	(1.4)				80.56	6.10	0.42	0.35	
19	113—118	+36	(0.5)	$C_{45}H_{42}O_6$	79.62	6.24	79.50	6.26	0.63		
20	104	+63	(1.0)				79.61	6.61	0.34		
21	106—107	+30	(1.0)	$C_{51}H_{46}O_6$	81.14	6.14	80.75	6.33	0.62		
22	96—97	+45	(1.0)				81.00	6.09	0.48		

a) TM=Toluene: 2-butanone (10 : 1). HE=Hexane: ethyl acetate (3 : 1). b) Ref. 5d: $[\alpha]_D^{20}$+32.8° (c 0.90 , $CHCl_3$).

detritylation.[9] The structures of the dibenzyl ethers were readily determined through the examination of the ^1H NMR spectra of their acetates (Table 6) and are consistent with that of the starting ditrityl ethers.

Experimental

General. Methyl α-D-glucopyranoside (**1**, Tokyo Kasei) and methyl α-D-mannopyranoside (**2**, Sigma) were used directly. Methyl α-D-galactopyranoside monohydrate (**3**·H_2O, Pfanstiehl) was dehydrated *in vacuo* over P_2O_5 at 80 °C before use. Benzyl α-D-glucopyranoside (**4**) was prepared as before;[4a] benzyl α-D-manno- and -galactopyranoside (**5** and **6**) were synthesized from the respective hexoses in a similar manner. Trityl chloride (TrCl, Tokyo Kasei) was used directly and pyridinium chloride (Py·HCl, Tokyo Kasei) was dried over P_2O_5 *in vacuo* before use. Pyridine (Py) was distilled from BaO. For other items, see the preceeding reports.[4] Acetylation was carried out with excess acetic anhydride in Py at room temperature; chromatographycally pure acetates were obtained through column chromatography on silica gel (Kanto Kagaku) with the mixture of benzene and 2-butanone (gradient elution).

Procedure for Ditritylation. A mixture of a glycoside (2.0 mmol), TrCl (3.0 equiv.) and Py (5.0 ml/g of glycoside) was heated under anhydrous conditions with good stirring. Py·HCl soon precipitated in the reaction at 70 °C, but did not at 50 and 100 °C. After cooling and quenching with iced water, the mixture was extracted with $CHCl_3$. The organic

Table 4. Physical and analytical data of dibenzyl ethers of methyl and benzyl α-D-hexosides

Compound	Mp θ_m/°C	$[\alpha]_D^{20}$/°	(c, $CHCl_3$)	Formula	Calcd (%) C	Calcd (%) H	Found (%) C	Found (%) H	Lit
23	108—109	+106	(1.0)	$C_{21}H_{26}O_6$	67.36	7.00	67.21	7.07	a)
24[e]	74—75	+88	(0.6)				67.10	6.90	
25	—	+94	(2.4)	$C_{27}H_{30}O_6$	71.98	6.71	71.04	6.73	
26[f]	78—79	+123	(0.5)				71.42	6.70	b)
27	—	+14	(0.7)	$C_{21}H_{26}O_6$	67.36	7.00	66.54	7.27	c)
28	—	+31	(0.8)				66.93	7.31	d)
29	—	+35	(1.3)	$C_{27}H_{30}O_6$	71.98	6.71	71.37	6.68	
30	81—83	+34	(0.7)				72.22	6.69	
31	132—133	+98	(1.0)	$C_{21}H_{26}O_6$	67.36	7.00	67.14	6.98	
32	101—102	+59	(0.9)				67.30	7.11	
33	94—95	+66	(0.5)	$C_{27}H_{30}O_6$	71.98	6.71	71.52	6.74	
34	123—124	+94	(0.6)				71.88	6.81	

a) Ref. 5c, mp 105—106 °C, $[\alpha]_D^{20}$+101.3° (c 0.545, $CHCl_3$). b) Ref. 5e, mp 77—78 °C, $[\alpha]_D^{20}$+157.6° (c 1.3, $CHCl_3$). c) Ref. 5b, $[\alpha]_D^{20}$+50.0 (c 0.22, $CHCl_3$). d) Ref. 5a, $[\alpha]_D^{20}$+23.5° (c 0.77, $CHCl_3$). e) Identified with the product obtained from methyl 2,4-di-*O*-benzyl-6-*O*-trityl-α-D-glucopyranoside (Ref. 4a) *via* detritylation. f) Identified with the product obtained from benzyl 2,4-di-*O*-benzyl-α-D-glucopyranoside (Ref. 4a) *via* detritylation.

Table 5. ^1H NMR data of acetates of dityrityl ethers of methyl and benzyl α-D-hexosides[a]

Compound	Chemical shifts/ppm[b] H-1	H-2	H-3	H-4	H-5	OAc	OAc	OMe	Coupling constants/Hz J_{12}	J_{23}	J_{34}	J_{45}
7a	3.86	3.36	5.47	4.51	3.71	1.63	1.72	2.31	3.4	9.5	9.5	9.1
8a	4.81	4.89	3.42	4.97	3.54	1.21	1.34	3.31	3.9	10.4	10.4	9.3
9a	4.72	4.24	5.46	2.74	3.16	1.09	1.94	3.64	3.8	9.9	9.6	9.6
10a	4.01	3.45	5.46	4.53	3.82	1.60	1.69	—	3.5	9.9	9.5	9.5
11a	5.00	4.88	3.67	5.03	3.53	1.87	1.96	—	3.8	9.8	9.8	9.8
12a	4.88	4.31	5.54	2.78	4.38	1.11	1.91	—	4.0	9.8	9.8	9.8
13a	3.91	3.71	4.87	5.90	3.71	1.66	1.74	3.07	1.5	3.1	10.2	10.2
14a	4.46	4.05	3.78	5.27	3.46	1.43	2.16	3.23	1.8	3.0	9.9	9.9
15a	4.47	5.00	5.17	2.86	4.26	1.07	1.75	3.59	1.4	3.1	9.2	9.2
16a	4.16	3.84	4.99	5.98	3.85	1.69	1.78	—	1.5	3.6	10.5	10.5
17a	4.73	4.23	3.81	5.37	3.50	1.76	2.21	—	1.5	3.0	9.8	9.8
18a	4.59	5.88	5.28	2.91	4.38	1.09	1.72	—	1.5	3.3	9.3	9.3
19a	3.89	3.63	5.36	5.31	3.88	1.63	1.72	3.32	3.6	9.5	3.2	1.0
20a	4.76	5.13	3.89	4.46	3.28	1.74	1.98	3.18	3.8	10.4	3.1	1.0
21a	4.07	3.67	5.27	5.35	3.90	1.61	1.65	—	3.6	10.0	3.0	1.0
22a	4.90	5.10	3.98	4.63	3.35	1.60	2.01	—	3.6	10.2	3.0	1.0

a) At 90 MHz in CCl_4 with Me_4Si. b) Underlined values are of H–C–OAc

Table 6. ^1H NMR data of acetates of dibenzyl ethers of methyl and benzyl α-D-hexosides[a]

Compound	Chemical shifts/ppm[b] H-1	H-2	H-3	H-4	H-5	OAc	OAc	OMe	Coupling constants/Hz J_{12}	J_{23}	J_{34}	J_{45}
23a	4.76	4.65	3.87	3.38	3.64	1.83	1.95	3.32	4.0	10.0	10.0	8.6
24a	4.58	3.38	5.42	n	n	1.86	1.96	3.30	4.0	9.5	9.5	n
25a	4.92	4.63	3.91	3.39	n	1.85	1.93	—	3.9	9.8	9.0	9.5
26a	4.74	3.33	5.50	3.37	n	1.87	1.97	—	4.0	9.6	9.6	9.6
27a	4.52	5.23	3.82	n	n	1.94	2.07	3.31	1.5	3.0	8.6	n
28a	n	n	5.03	n	n	1.86	1.97	3.32	n	3.3	9.0	n
29a	4.78	5.29	3.90	n	n	1.97	2.06	—	1.5	3.3	8.7	n
30a	n	n	5.08	n	n	1.86	1.96	—	2.1	3.4	8.5	n
31a	4.84	5.14	3.81	n	n	1.90	1.99	3.29	3.5	11.0	2.9	n
32a	4.59	3.88	5.08	n	n	1.91	1.94	3.30	3.5	10.5	3.0	n
33a	5.05	5.17	n	n	n	1.93	1.96	—	3.5	10.0	n	n
34a	4.81	n	5.15	n	n	1.93	1.95	—	3.5	11.0	3.0	n

a) At 90 MHz in CCl_4 with Me_4Si. b) Underlined values are of H–C–OAc.

layer was washed with H_2O well, dried over Na_2SO_4, evaporated under reduced pressure at ≈50 °C, and chromatographed on silica gel (Kanto Kagaku, No. 37047, >100 mesh) with toluene–2-butanone system (gradient elution, 100 : 1→1 : 1). This gave the results as summarized in Table 1. Physical and analytical data of the dityrityl ethers are summarized in Table 3. The ^1H NMR data of the acetates of the dityrityl ethers are listed in Table 5.

Procedure for Rearrangement of Dityrityl Ethers. A mixture of dityrityl ether (50 mg, 0.074 mmol), Py·HCl (17 mg, 2.0 equiv.), and Py (0.25 ml) was heated at 100 °C under anhydrous conditions. After processing as above, chromatography gave the results in Table 2.

Procedure for Transformation of Dityrityl Ethers into Dibenzyl Ethers. A mixture of dityrityl ether (1.0 mmol), crushed KOH (7 g/g of dityrityl ether), and $PhCH_2Cl$ (20 ml/g of dityrityl ether) was heated at ≈110°C for 18 h under good stirring. After filtration and evaporation under reduced pressure on a boiling water bath, the resulting mixture was heated in a mixture (20 ml/g of dityrityl ether) of CF_3CO_2H, MeOH, and $CHCl_3$ (1 : 3 : 10, v/v/v) for 2—5 h. After neutralization with triethylamine and evaporation, the residue was chromatographed on silica gel using toluene–2-butanone system to give the dibenzyl ethers (60—75% yield). Physical and analytical data of the dibenzyl ethers are summarized in Table 4. The ^1H NMR spectral data of the acetates of the dibenzyl ethers are listed in Table 6.

References

1) Partly presented at the 44th National Meeting of the Chem. Soc. Jpn. Okayama, Oct. 1981.

2) a) B. Helferich, *Adv. Carbohydr. Chem.*, **3**, 79 (1948); b) A. H. Haines, *ibid.*, **33**, 11 (1976); c) C. B. Reese, "Protective Group in Organic Chemistry," ed by J. F. W. McOmie, Plenum Press, New York (1973), Chap. 3; T. W. Greene, "Protective Groups in Organic Synthesis," John Wiley and Sons, Inc. New York (1981), Chap. 2.

3) a) R. C. Hockett and C. S. Hudson, *J. Am. Chem. Soc.*, **56**, 945 (1934); E. L. Jackson, R. C. Hockett, and C. S. Hudson, *ibid.*, **56**, 947 (1934); R. C. Hockett, H. G. Fletcher, Jr., and J. B. Ames, *ibid.*, **63**, 2516 (1941); R. C. Hockett and D. F. Mowery, Jr., *ibid.*, **65**, 403 (1943); N. C. Yung and J. J. Fox, *ibid.*, **83**, 3060 (1961); A. F. Cook and J. G. Moffatt, *ibid.*, **89**, 2697 (1967); W. W. Zorbach, S. L. de Bernardo, and K. V. Baht, *Carbohydr. Res.*, **11**, 413 (1969); K. Koizumi and T. Utamura, *Chem. Pharm. Bull.*, **29**, 3118 (1981); b) T. Otake and T. Sonobe, *Bull. Chem. Soc. Jpn.*, **49**, 1050 (1978); T. Otake, T. Sonobe, and T. Suami, *ibid.*, **52**, 3109 (1979).

4) a) S. Koto, S. Inada, T. Yoshida, M. Toyama, and S. Zen, *Can. J. Chem.*, **59**, 255 (1981); b) S. Koto, N. Morishima, C. Kusuhara, S. Sekido, T. Yoshida, and S. Zen, *Bull. Chem. Soc. Jpn.*, **55**, 2995 (1982); N. Morishima, S. Koto, and S. Zen, *Chem. Lett.*, **1982**, 1039.

5) a) T. Ogawa and M. Matsui, *Carbohydr. Res.*, **62**, Cl (1978); b) T. Ogawa and K. Sasajima, *ibid.*, **93**, 67 (1981); c) T. Ogawa, Y. Takahashi, and M. Matsui, *ibid.*, **102**, 207 (1982); d) T. Ogawa, T. Nukada, and M. Matsui, *ibid.*, **102**, 263 (1982); e) T. Ogawa and T. Kaburagi, *ibid.*, **103**, 53 (1982).

6) J. M. Williams and A. C. Richardson, *Tetrahedron*, **23**, 1369 (1967).

7) B. Helferich, P. Speidel, and W. Toeldte, *Chem. Ber.*, **56**, 766 (1927); C. D. Hurd, C. O. Mack, E. M. Filachione, and J. C. Sowden, *J. Am. Chem. Soc.*, **59**, 1952 (1937); M. L. Wolfrom, W. J. Burke, and S. W. Waisbrot, *ibid.*, **61**, 1827 (1939).

8) The stability of the 2,6-dityrityl ethers might be, at least in part, attributable to the inductive effect of the anomeric center. The effect may slightly decrease the electronegativity of the oxygen at C-2 to depress effectively its affinity to the proton of the acid PyH^+ in the competing basic medium Py, as in the following equation:

$$\mathrm{ROTr} + \mathrm{PyH^+ \cdot Cl^-} \rightarrow [\overset{\mathrm{H}}{\mathrm{ROTr}}]^+\mathrm{Cl^-} + \mathrm{Py} \rightarrow \mathrm{ROH} + \mathrm{TrCl} + \mathrm{Py}$$

9) In the case of the glucosides, however, the monotrityl ether, **1t** and **4t**, are practically better precursors of the 2,4-dibenzyl ethers, **24** and **26**, respectively, because they are readily prepared through detritylation of methyl and benzyl-2,4-di-*O*-benzyl-6-*O*-trityl-α-D-glucopyranoside (Ref. 4a) prepared directly from **1t** and **4t**.

Synthesis and Enzymatic Carboxylation of a Biotin-containing Peptide Representing the Coenzyme Binding Site of *E. coli* Acetyl-CoA Carboxylase†

Hiroki KONDO,* Shingo UNO, Fumio MORIUCHI, Junzo SUNAMOTO, Susumu OGUSHI,†† and Daisuke TSURU††

Department of Industrial Chemistry, Faculty of Engineering, Nagasaki University, Nagasaki 852

††*Faculty of Pharmaceutical Sciences, Nagasaki University, Nagasaki 852*

(Received September 16, 1982)

A biotin-containing pentapeptide Boc–Glu–Ala–Met–Bct–Met (**1**) that corresponds to the coenzyme binding site of *E. coli* acetyl–CoA carboxylase has been prepared. Peptide **1** as well as free biotin served as a substrate for the carboxylation reaction catalyzed by the biotin carboxylase subunit dimer of *E. coli* acetyl–CoA carboxylase. The Michaelis constant, K_m, and the maximum velocity, V_{max}, for **1** were 18 mM and 2.8 μM min^{-1} (1 M=1 mol dm^{-3}), respectively. The corresponding values for biotin were 214 mM and 28 μM min^{-1}. Thus, the overall reactivity (V_{max}/K_m) of peptide **1** exceeded that of biotin by 20%.

The biotin (**2**)-dependent carboxylation reaction plays a pivotal role in the synthesis of long-chain fatty acids in biological systems.[1] It is firmly established that the enzymatic carboxylation proceeds *via* the *N*-carboxybiotin intermediate (**3**), which in turn transfers the

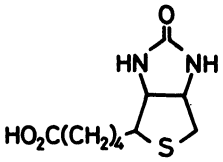

2

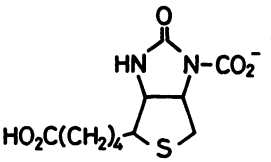

3

carboxyl group to an acceptor substrate such as acetyl–CoA. By some enzymes biotin itself can be carboxylated, though the Michaelis constant of biotin carboxylation is enormously high compared to that for the natural substrate BCCP, biotin carboxyl carrier protein.[2] It is, hence, clear that the protein attaching to the coenzyme plays an important part in the recognition and binding of biotin to the enzyme active site.[3] In our previous communication we have prepared several biotin-containing peptides such as **4** that corresponds to a local biotin-binding sequence of *E. coli* acetyl–CoA carboxylase BCCP subunit.[4] Unfortunately, however, all

Ac–Met–Bct–Met–Met–OMe

4

these peptides were sparingly soluble in most common solvents and were not feasible for kinetic studies of biotin carboxylation by the enzyme. To improve solubility the peptide sequence was extended towards the *N*-terminus to incorporate glutamic acid.[5] The presence of this extra carboxyl group as well as the *C*-terminal one should increase the solubility of the resulting peptide in neutral aqueous media. This proved to be the case as described below. Furthermore, this peptide (**1**) was found to be carboxylated by the biotin carboxylase subunit of *E. coli* acetyl–CoA carboxylase. The preliminary results on the kinetics of this enzymatic carboxylation are also presented in this article.

† The abbreviations used are: Ala, L-alanine; Glu, L-glutamic acid; Lys, L-lysine; Met, L-methionine; Bct, *N*'-biotinyl-L-lysine; Boc, *t*-butoxycarbonyl; Cbz, benzyloxycarbonyl; CbzCl, benzyloxycarbonyl chloride; DCC, dicyclohexylcarbodiimide; HOBt, 1-hydroxybenzotriazole; NEM, *N*-ethylmorpholine; ATP, adenosine 5'-triphosphate; NADH, nicotinamide adenine dinucleotide, reduced form; DEAE, diethylaminoethyl.

Results

Synthesis. It was envisioned that the liquid phase synthesis of target peptide **1** may be achieved by either one of the following routes. In one route biotin is incorporated at the early stage of peptide synthesis by coupling Boc–Bct and methionine methyl ester.[3] The peptide chain is then elongated step by step up to the *N*-terminal glutamic acid. In the other the biotin-free pentapeptide is prepared first and the coenzyme is incorporated subsequently.[4] The latter strategy was actually adopted in order to be free from possible side reactions on the biotin skeleton and/or interference of the biotin's urea moiety with a coupling reaction.[3] In addition, expensive biotin may be saved in the

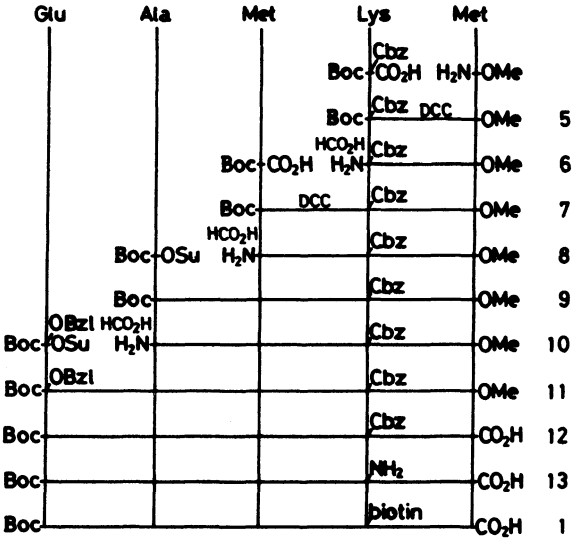

Fig. 1. Synthetic route to peptide **1**.

Table 1. Physical properties and analytical data of peptides

Compd	Yield %	Mp θ_m/°C	TLC, R_f[a]	$[\alpha]_D^{27}$/°	Formula	Calcd (%) C	H	N	Found (%) C	H	N
5	72	101.5—103	0.89(A)	−7.6(*c* 1, AcOEt)	$C_{25}H_{39}N_3O_7S$	57.12	7.48	7.99	56.74	7.58	8.06
7	44	137—138	0.81(B)	−14.5(*c* 1, AcOEt)	$C_{30}H_{48}N_4O_8S_2$	54.86	7.37	8.53	54.95	7.52	8.48
9	67	155—156.5	0.81(C)	−28.6(*c* 1, DMF)	$C_{33}G_{53}N_5O_9S_2\cdot H_2O$	53.13	7.43	9.39	53.24	7.30	9.45
11	57	153—154.5	0.88(D)	−17.0(*c* 1, MeOH)	$C_{45}H_{66}N_6O_{12}S_2\cdot H_2O$	56.00	7.10	8.70	55.96	7.06	9.02
12	80	167—169	0.77(E)	ND[b]	$C_{37}H_{58}N_6O_{12}S_2\cdot H_2O$	51.61	7.02	9.76	51.52	6.97	9.74

a) TLC solvents: A, AcOEt: pet. ether=5 : 1; B, AcOEt: pet. ether=1 : 1; C, MeOH: AcOEt: ether=1 : 1 : 7; D, MeOH: AcOEt=1 : 4; E, MeOH. b) ND: Not determined.

Table 2. Kinetic parameters for the carboxylation of biotin and derivatives by the biotin carboxylase subunit of *E. coli* acetyl-CoA carboxylase at 30.0 °C

Substrate	K_m/mM	V_{max}/μM min^{-1}	$(V_{max}/K_m)/10^5$ min^{-1}	Ref.
Biotin	214	28	13	This work
1	18	2.8	16	This work
BCCP	0.0004	—	9.4×10^5	12, 13

latter route. Thus, the parent pentapeptide was prepared according to the scheme illustrated in Fig. 1. The DCC coupling method was employed for the synthesis of di- and tripeptide. The third and fourth couplings were accomplished by the active ester method of *N*-hydroxysuccinimide. Each coupling proceeded smoothly and the products obtained were analytically pure (Table 1).

The carboxyl groups of Glu side chain and *C* terminal Met were deprotected by saponification. The final deprotection of the Lys amino moiety with Na/NH_3 was followed by coupling of the resulting peptide with *p*-nitrophenyl biotinate.[4] This led to the incorporation of coenzyme to the peptide, but in low yield (12%). The product was satisfactory by all criteria set forth previously for the purity and identity of biotin-containing peptides; TLC, ^1H NMR and a color test with *p*-dimethylaminocinnamaldehyde.[4] Peptide **1** is soluble considerably in neutral to alkaline aqueous solutions and feasible for kinetic studies on its enzymatic carboxylation.

Enzymatic Carboxylation. The carboxylation of peptide **1** and biotin mediated by the biotin carboxylase subunit dimer of *E. coli* acetyl-CoA carboxylase was carried out at 30 °C (Eq. 1).

$$\text{Biotin} + HCO_3^- + \text{ATP} \longrightarrow \text{Biotin-}CO_2^- + \text{ADP} + \text{Pi} \quad (1)$$

The reaction was followed either by the incorporation of radioactive hydrogencarbonate into biotin or the formation of ADP.[6] Both methods gave virtually identical results. Peptide **1** as well as biotin was carboxylated at a reasonable rate by ≈8 milli-units of enzyme in the presence of 1 mM ATP and 8 mM sodium hydrogencarbonate. The initial rate data obtained by the coupled assay were analyzed in terms of a Lineweaver-Burk plot (Fig. 2). The kinetic parameters are summarized in Table 2. The Michaelis constant K_m for biotin (214 mM) is close to the literature value (170 mM).[2] The corresponding value for peptide **1** (18 mM) indicates that the binding of **1** to the enzyme is about 12 times tighter than that of biotin. On the other hand, the maximum rate, V_{max}, is larger for biotin by a factor of ten than for peptide **1**. This makes the difference in the first-order rate constant (V_{max}/K_m) between the two substrates smaller, only 20% greater in favor of peptide **1**.

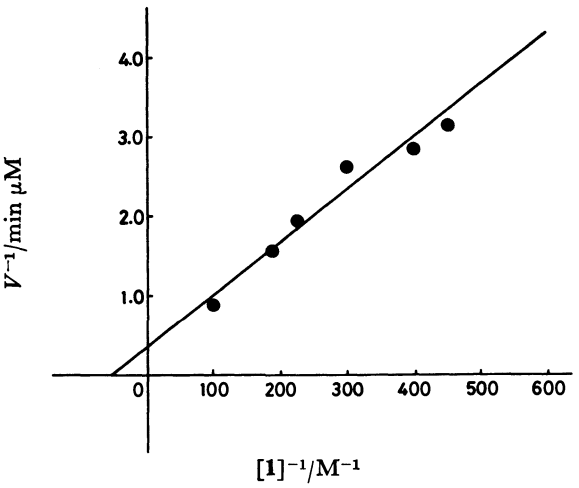

Fig. 2. Lineweaver-Burk plot for the carboxylation of peptide **1** catalyzed by the biotin carboxylase subunit of *E. coli* acetyl-CoA carboxylase in 100 mM triethanolamine buffer, pH 8.0 at 30.0 °C.

Discussion

Part of the primary structure adjacent to the coenzyme-binding site of several biotin-dependent enzymes has been elucidated.[5,7,8] These enzymes share a strikingly similar local sequence in the vicinity of biocytin, suggesting that these enzymes evolved from a common ancestor. An interesting feature of the amino acid sequence, as viewed from a chemical standpoint, is the fact that biocytin is flanked by methionines in all cases. In the case of *E. coli* acetyl-CoA carboxylase another methionine is placed at the *C*-terminal side of the sequence. Thus, the successive four amino acid residues contain a sulfide moiety each in their side chain. It seems likely that this sulfide cluster plays a certain

role in the carboxylation-transcarboxylation cycle of biotin catalysis. For example, the sulfide cluster might be required for the efficient binding of biotin to the enzyme active site during its carboxylation and subsequent carboxyl transfer reactions. In other words, the enzyme recognizes not only the coenzyme but also the neighboring amino acid residues. Also, the peptide sequence adjacent to biocytin could help biotin to assume a specific spatial orientation that may presumably be needed for biotin to bind to the enzyme active site tightly. A further possibility would be the protection by the acyclic sulfides of the biotin's cyclic sulfide from being oxidized. All these hypotheses could be proven only when model peptides representing the biotin binding site become available to test their interaction with the enzyme.[3,4] In this article we have prepared a pentapeptide that represents the coenzyme binding site of *E. coli* acetyl–CoA carboxylase. The synthetic strategy was basically the same as that adopted previously for the synthesis of tetrapeptides.[4] The target peptide (**1**) obtained gave correct analysis but the yield at the final biotinylation step was far from satisfactory (12%). This result is rather strange in veiw of the fact that biotinylation was successfully accomplished even with larger peptides such as glucagon and insulin by the same method.[9,10] In our hands, the active ester method gave the best results, and other coupling methods tested such as the mixed anhydride method with isobutyl chloroformate and the DCC coupling method gave even poorer yields. This poses a serious problem to the synthesis of larger biotin-containing peptides by this method. An alternative route is the incorporation of biotin at the early stage of peptide synthesis by, for example, coupling of Boc–Bct with a growing peptide chain.[3] In addition, the solid phase method may be worth a serious consideration to save time in accomplishing such a synthesis. Our preliminary attempt to prepare biotin-containing peptides by this method appears promising (unpublished results from this laboratory).

The biotin carboxylase subunit of *E. coli* acetyl–CoA carboxylase was capable of carboxylating the biotinyl moiety of peptide **1** as well as free biotin. In conformity with our expectation, peptide **1** was found to bind to the enzyme by one order of magnitude more tightly than biotin. This clearly indicates that the amino acid residues surrounding the coenzyme play an indispensable role in the interaction of biotin with the enzyme active site. All or at least two of the substrates involved in this carboxylation (Eq. 1) must encounter at some moment of the reaction in the enzyme active site. In light of the fact that magnesium(II) ion is the essential component of the reaction and that the metal ion is often found associated with ATP in many biochemical reactions involving ATP,[11] a ternary metal complex composed of magnesium(II), ATP and biotin or HCO_3^- may be the reactive species in this carboxylation reaction. We showed previously that amide groups of peptide **4** have potential to interact with magnesium ion.[4] This could increase the affinity of the biotinyl moiety for the metal ion, and eventually for the enzyme active site.

In contrast to the binding process, the subsequent catalytic process was less favorable for peptide **1** than for free biotin. This unfavorable catalysis offsets a large gain in binding, leading to an enhancement of the overall reactivity of **1** relative to biotin by a small margin (20%). Nevertheless, this figure is significant, since all synthetic derivatives of biotin reported to date such as *d*-biotin methyl ester and biocytin are poorer substrates than biotin for acetyl–CoA carboxylase.[2] The natural substrate of *E. coli* acetyl–CoA carboxylase (BCCP) shows not only tight binding but also high reactivity, but its overall reactivity is governed predominantly by the former term (Table 2).[12,13] In this sense, an improvement of the binding properties of biotin leads automatically to the development of a good substrate for the enzyme. Such a substrate and its analogues are of vital importance in studying and understanding the molecular basis of enzyme-substrate interaction in this carboxylase system. A further synthetic approach to this goal is now in progress in this laboratory.

Experimental

Apparatus. Melting points were determined on a Yanagimoto hot-stage apparatus and are uncorrected. IR spectra were taken on a JASCO A-100 spectrophotometer, while UV spectra were on a Hitachi 200-10 spectrophotometer. ^1H NMR spectra were recorded either on a JEOL JNM-MH-100 or a JEOL JNM-FX-90Q spectrometer. Optical rotations were determined on a Jasco DIP-4. Radioactivity was determined on an Aloka liquid scintillation counter LSC-703.

Materials. Amino acids, *O-t*-butyl *S*-4,6-dimethyl-2-pyrimidinyl thiocarbonate, CbzCl, DCC, and HOBt were obtained from Protein Research Foundation. *d*-Biotin, *p*-dimethylaminocinnamaldehyde, *N*-hydroxysuccinimide, and NEM were the products of Wako Pure Chemical Ind. Co. Scintillation cocktail ACS II and sodium [^{14}C] hydrogencarbonate (0.1 mCi/mmol, 1 Ci$=3.7\times10^{10}$ becquerels) were purchased from Amersham. DEAE-cellulose and phosphocellulose were the products of Brown Company. Lactate dehydrogenase and pyruvate kinase were obtained from Boehringer Mannheim, while bovine serum albumin (BSA), phosphoenol pyruvate (PEP), glutathione, NADH, and ATP were from Seikagaku Kogyo Co.

Enzyme Preparation and Assay. *Escherichia coli* B cells were grown in an enriched medium composed of 1 M potassium phosphate buffer (pH 7.4), yeast extracts and D-glucose. The harvested cells were broken on a French press. The cell-free extracts were subjected to enzyme purification according to the procedures of Guchhait *et al.*[6] Enzyme activity was determined by following either the incorporation of sodium [^{14}C] hydrogencarbonate into biotin or the formation of ADP by the "coupled assay".[6] In the former method, the assay mixture (0.50 ml) consisting of 1 mM ATP, 8 mM $MgCl_2$, 8 mM $NaH^{14}CO_3$ (0.1 mCi/mmol), 50 mM potassium *d*-biotinate, 3 mM glutathione, 0.6 mg/ml BSA, 10% ethanol and the enzyme in 100 mM triethanolamine buffer (pH 8.0) was incubated at 30 °C for a certain period of time. The reaction was initiated by the enzyme and was terminated by the addition of 2 drops of ice-cold 1-octanol. This was followed immediately by an introduction of gaseous carbon dioxide to the reaction mixture at 0 °C for 40 min. An aliquot (0.10 ml) of ice-cold 0.1 M NaOH was added and the resulting solution was transferred to a scintillation vial containing 6 ml of ACS II to determine radioactivity. In the latter method, the formation of ADP was coupled with the oxidation of NADH.

Thus, an assay mixture (1.0 ml) contained the same components as those described above except for unlabeled hydrogencarbonate, instead of radioactive one, plus 0.5 mM PEP, 5 units of lactate dehydrogenase, 3 units of pyruvate kinase and 0.2 mM NADH. The reaction was started by the addition of enzyme at 30 °C and the decrease of NADH absorption was determined at 340 nm. One unit of enzyme activity is defined by the amount of enzyme needed to form 1 μmol of 1-carboxybiotinate per min.

Boc-Lys(Cbz)-Met-OMe (5). To a solution of 21.5 g (55 mmol) of Boc-Lys(Cbz), 11.5 g (55 mmol) of Met-OMe·HCl and 6.3 g (55 mmol) of NEM in 180 ml DMF was added 11.3 g (55 mmol) of DCC at 0 °C. The whole mixture was stirred for 8 h at room temperature. The precipitated DCUrea was filtered off. Evaporation of the solvent left an oil, which was taken up in 180 ml of ethyl acetate. The solution was washed with the following solutions: 4% $NaHCO_3$, saturated NaCl, 10% citric acid, saturated NaCl, H_2O. The organic layer was dried over Na_2SO_4, concentrated to *ca.* 50 ml and kept in a freezer. The product was obtained in 72% yield (21.3 g).

Lys(Cbz)-Met-OMe·HCO_2H (6). A sample of **5** (21.3 g, 41 mmol) was allowed to react with 100 ml of 99% HCO_2H for 5 h at room temperature. Methanol was added and the solvents were evaporated *in vacuo*. The product was crystallized from methanol-ether in 90% yield (19.5 g). Mp 203—204 °C. Complete removal of the Boc group was confirmed by the disappearance of the 1.35 ppm signal.

Boc-Met-Lys(Cbz)-Met-OMe (7). This peptide was synthesized by reaction of **6** (21.1 g, 46 mmol) with Boc-Met (11.5 g, 46 mmol) in the presence of NEM (5.3 g, 46 mmol), HOBt (6.23 g, 46 mmol), and DCC (9.52 g, 46 mmol). The reaction mixture was worked up analogously to that for **5**. The product was recrystallized from ethyl acetate-petroleum ether.

Met-Lys(Cbz)-Met-OMe·HCO_2H (8). Reaction of **7** (10.0 g, 51 mmol) with 100 ml of 99% HCO_2H in the way identical with that described for **6** gave 7.8 g of **8** in 87% yield.

Boc-Ala-Met-Lys(Cbz)-Met-OMe (9). Boc-Ala-OSu (3.23 g, 11 mmol) was allowed to react with **8** in 50 ml of DMF containing 1.27 g (11 mmol) of NEM for 8 h at room temperature. The solvent was removed *in vacuo* and the residue was taken up in 400 ml of ethyl acetate. The organic solution was washed with the solvents used for **5**. After drying over Na_2SO_4, the solution was concentrated to a small volume to provide 5.5 g of the product in 67% yield.

Ala-Met-Lys(Cbz)-Met-OMe·HCO_2H (10). Treatment of 4.6 g (6.3 mmol) of **9** with 100 ml of 99% HCO_2H and the subsequent work-up yielded 4.9 g of the product (94%).

Boc-Glu(OBzl)-Ala-Met-Lys(Cbz)-Met-OMe (11). Reaction of 3.5 g (5.0 mmol) of **10** with 3.38 g (7.5 mmol) of Boc-Glu(OBzl)-OSu in 100 ml of DMF containing 0.60 g (5.0 mmol) of NEM gave 2.7 g of the product.

Boc-Glu-Ala-Met-Lys(Cbz)-Met (12). A sample of **11** (1.04 g, 1.1 mmol) was dissolved in 27 ml of methanol and 14 ml of dioxane. To this was added 2.3 ml of 1 M sodium hydroxide and the whole mixture was stirred for 7 h at room temperature. After adding 11 ml of water, the organic solvents were removed *in vacuo*. The remaining aqueous solution was washed with ether and then brought to pH 3 with 10% citric acid at 0 °C. The product obtained was further purified by recrystallization from methanol-ether. The NMR spectrum of this peptide revealed a complete removal of *O*-Bzl and *O*-Me protecting groups.

Boc-Glu-Ala-Met-Lys-Met (13). A sample of **12** (1.2 g, 1.4 mmol) was dissolved in 80 ml of liquid ammonia. Sodium was added in small portions with stirring. When the blue color of the solution was retained for a few minutes, the reaction was quenched by ammonium chloride. Ammonia was evaporated off. Methanol was added to the residue and the insoluble material was filtered off. The filtrate was concentrated to dryness and the solid left was taken up in 1% acetic acid. The insoluble starting material was removed by filtration. For desalting the filtrate was subjected to column chromatography on a Sephadex G-10 column (3.2×56 cm) with 1% acetic acid as an eluant. The peak fractions were pooled and lyophillized to yield 0.77 g (70%) of the product, mp 221—223 °C. TLC R_f 0.45 (E). Complete removal of the protecting group was ascertained on the basis of the lack of signals for the benzyloxycarbonyl group at 4.98 and 7.28 ppm in the NMR spectrum of this peptide.

Boc-Glu-Ala-Met-Bct-Met (1). A sample of **13** (0.26 g, 0.33 mmol) dissolved in 2 ml of water was mixed with *p*-nitrophenyl biotinate (0.14 g, 0.50 mmol)[14] in 10 ml of DMF containing 0.15 g (1.32 mmol) of NEM. The whole mixture was stirred for a day at room temperature. The solvents were removed *in vacuo* and methanol (40 ml) was added to the residue. The precipitates formed were collected by filtration, 47 mg (12%), mp 199—203 °C. TLC R_f 0.59 (E). This peptide is ninhydrin-negative but develops a pink color upon spraying of *p*-dimethylaminocinnamaldehyde, confirming the presence of a biotinyl moiety.[15] The characteristic ^1H NMR signals for the biotinyl protons are the following: (DMSO-d_6) 2.84 (d, J=14 Hz, 5-exo), 2.56 (d, J=14 Hz, 5-endo), 6.36 (s, NH) and 6.41 (s, NH).

The authors are grateful to Prof. K. Soda of Kyoto University for his kind donation of *E. coli* B cells. Thanks are also due to Professors T. Naito and M. Sugii of Nagasaki University for the use of their French press and scintillation counter, respectively. We are indebted to Professors M. Koida and T. Yoshimoto for helpful discussions. This work was supported by Grants-in-Aid for Special Project Research 521325 and 56109007 from the Ministry of Education, Science and Culture, and in part by the Eighteenth Bank Fund for Community Development and Promotion.

References

1) H. G. Wood and R. E. Barden, *Ann. Rev. Biochem.*, **46**, 385 (1977).
2) P. Dimroth, R. B. Guchhait, E. Stoll, and M. D. Lane, *Proc. Natl. Acad. Sci. U. S. A.*, **67**, 1353 (1970).
3) M. Bodansky and D. T. Fagan, *J. Am. Chem. Soc.*, **99**, 235 (1977).
4) H. Kondo, F. Moriuchi, and J. Sunamoto, *Bull. Chem. Soc. Jpn.*, **55**, 1579 (1982).
5) M. R. Sutton, R. R. Fall, A. M. Nervi, A. W. Alberts, P. R. Vagelos, and R. A. Bradshaw, *J. Biol. Chem.*, **252**, 3934 (1977).
6) R. B. Guchhait, S. E. Polakis, P. Dimroth, E. Stoll, J. Moss, and M. D. Lane, *J. Biol. Chem.*, **249**, 6633 (1974).
7) D. B. Rylatt, D. B. Keech, and J. C. Wallace, *Arch. Biochem. Biophys.*, **183**, 113 (1977).
8) W. L. Maloy, B. U. Bowien, G. K. Zwolinski, K. G. Kumar, H. G. Wood, L. H. Ericsson, and K. A. Walsh, *J. Biol. Chem.*, **254**, 11615 (1979).
9) K. C. Flanders, D. H. Mart, R. J. Folz, R. D. England, S. A. Codican, D. E. Harris, A. D. Floyd, and R. S. Gurd, *Biochemistry*, **21**, 4244 (1982).
10) K. Hofmann, F. M. Finn, H.-J. Friesen, C. Diaconescu, and H. Zahn, *Proc. Natl. Acad. Sci. U. S. A.*, **74**, 2697 (1977).

11) J. Moss and M. D. Lane, *Adv. Enzymol.*, **35**, 321 (1971).
12) A. M. Nervi, A. W. Alberts, and P. R. Vagelos, *Arch. Biochem. Biophys.*, **143**, 401 (1971).
13) S. E. Polakis, F. S. Guchhait, E. E. Zwergel, and M. D. Lane, *J. Biol. Chem.*, **249**, 6657 (1974).
14) E. A. Bayer and M. Wilchek, *Methods Enzymol.*, **46**, 613 (1977).
15) D. B. McCormick, *J. Heterocycl. Chem.*, **10**, 235 (1973).

 © 1983 The Chemical Society of Japan Bull. Chem. Soc. Jpn., 56, 1181—1186 (1983)

Solution Conformation of *cyclo*(-L-Cys(*S*-Acm)-D-Leu-L-His-L-Cys(*S*-Acm)-D-Leu-L-His-) and Interaction with Cu(II)

Masato KODAKA,*,† Toru SHIMIZU, and Masahiro HATANO
Chemical Research Institute of Non-aqueous Solutions, Tohoku University, Sendai 980
†*National Chemical Laboratory for Industry, Tsukuba 305*
(Received September 17, 1982)

Proton NMR spectra of a cyclic peptide, *cyclo*-(*S*-acetamidomethyl-L-cysteinyl)-D-leucyl-L-histidyl-(*S*-acetamidomethyl-L-cysteinyl)-D-leucyl-L-histidyl, were measured and analyzed in order to investigate its conformation and its interaction with Cu(II). A linear peptide, [*N*-(*t*-butoxycarbonyl)-*S*-acetamidomethyl-L-cysteinyl]-D-leucyl-L-histidyl-(*S*-acetamidomethyl-L-cysteinyl)-D-leucyl-L-histidine methyl ester, was also investigated for comparison. It was strongly suggested that the cyclic hexapeptide forms transannular hydrogen bonds between the cysteine residue peptide bonds and thus two β-turns exist in the D-leucyl-L-histidyl sequences. This finding is particularly noteworthy because the present cyclic peptide has no prolines which are frequently seen in β-turn structures of proteins, naturally occurring peptides or synthetic peptides and because the cyclic peptide we studied is composed of amino acids all bearing the large side chains which seemed likely to prevent β-turn formation due to their steric hindrance. The interactions of the cyclic peptide and the linear peptide with Cu(II) were also studied by observing ^{1}H NMR spectral changes on addition of $CuCl_2$. It was suggested that the imidazolyl groups in the peptides are directly coordinated to Cu(II).

Imidazolyl and carbamoyl groups of histidine and glutamine (or asparagine) residues or main-chain peptide bonds seem to play an important role for the coordination of proteins or naturally occurring peptides to metal cations. It seems particularly interesting to study the interaction of metal cation with the cyclic peptide having both imidazolyl groups and peptide bonds at the side chains. Few studies have been undertaken about the interaction of metal cations with imidazole and amide-containing cyclic peptide. Cyclic peptides are better ligands than linear peptides in the following respects: (i) In naturally occurring antibiotics or other biologically functional peptides, there are many cyclic peptides which have much higher activities than those of the corresponding linear peptides, such as gramicidin S.[1] Therefore, cyclic peptides are important from the biological point of view. (ii) Intramolecular rotations around the main-chain bonds are restricted by cyclization and thus overall conformations are relatively rigid. Contributions of the end groups to the metal ligations can be excluded for cyclic peptides. These features would make the NMR analyses much easier.

D-Leucine is incorporated into the cyclic peptide in order to place the imidazolyl and the acetamido groups on the same side of the cyclic molecular plane. This would make the imidazolyl and acetamido groups liable to coordinate to metal cations.

In this paper, the conformation of the cyclic peptide in the solution has been investigated in detail. We have also studied the effect of Cu(II) on the ^{1}H NMR spectra of the cyclic peptide.

Experimental

Materials. The syntheses of [*N*-(*t*-butoxycarbonyl)-*S*-acetamidomethyl-L-cysteinyl]-D-leucyl-L-histidyl-(*S*-acetamidomethyl-L-cysteinyl)-D-leucyl-L-histidine methyl ester (**1**) (Boc-L-Cys(*S*-Acm)-D-Leu-L-His-L-Cys(*S*-Acm)-D-Leu-L-His-OCH_3) and *cyclo*-(*S*-acetamidomethyl-L-cysteinyl)-D-leucyl-L-histidyl-(*S*-acetamidomethyl-L-cysteinyl)-D-leucyl-L-histidyl (**2**) (*cyclo*(-L-Cys(*S*-Acm)-D-Leu-L-His-L-Cys(*S*-Acm)-D-Leu-L-His-)) used in the present study have been described elsewhere.[2] $CuCl_2 \cdot 2H_2O$ was of reagent grade. D_2O was the product of Commissariat à L'Energie Atomique of France, and dimethyl-d_6 sulfoxide (DMSO-d_6) was obtained from E. Merck, Japan.

Methods. Proton NMR spectra were recorded on a Bruker CXP-300 FT NMR spectrometer operating in the pulsed Fourier transform mode at 300.07 MHz using a spinning 5 mm tube. Sodium 2,2-dimethyl-2-silapentane-5-sulfonate (DSS) was used as an internal reference (0.00 ppm) in D_2O solution, and partially deuterated dimethyl sulfoxide (2.49 ppm from DSS) was used as a reference in DMSO-d_6 solution. The pD values given are the actual pH meter readings and have not been corrected for the deuterium isotope effect at the glass electrode and pK_a* refers to the pK_a value determined from the chemical shifts of imidazolyl C-2 proton in D_2O. Adjustment of pD was made by adding either NaOD or DCl. Observed NMR signals were assigned to the individual amino acid residue by comparing the chemical shifts of the peptides with those of model compounds and by using the technique of homonuclear spin decoupling.

Results

^{1}H NMR Signals of Acm-Methylene Protons. Proton NMR spectra of the linear and the cyclic peptides in D_2O are shown in Fig. 1. The chemical shift difference between the two protons of the Acm-CH_2 in the cyclic peptide (**2**) (each resonance is further split into two by geminal protons spin-spin coupling) is greater than those in the linear peptide (**1**), indicating that the former methylene protons are located in environments considerably different from each other in D_2O solution. The motional fluctuation of the molecule may apparently reduce the environmental difference of the two protons of the Acm-CH_2 for the linear peptide. In DMSO solution, however, only one resonance split into two by the spin-spin coupling with the amide NH proton (not shown in a figure) was seen for the cyclic peptide, suggesting that the environments of the two protons of the Acm-CH_2 in the cyclic peptide are similar to each other in DMSO solution. For the linear peptide, the two resonances corresponding to the Acm-CH_2 observed

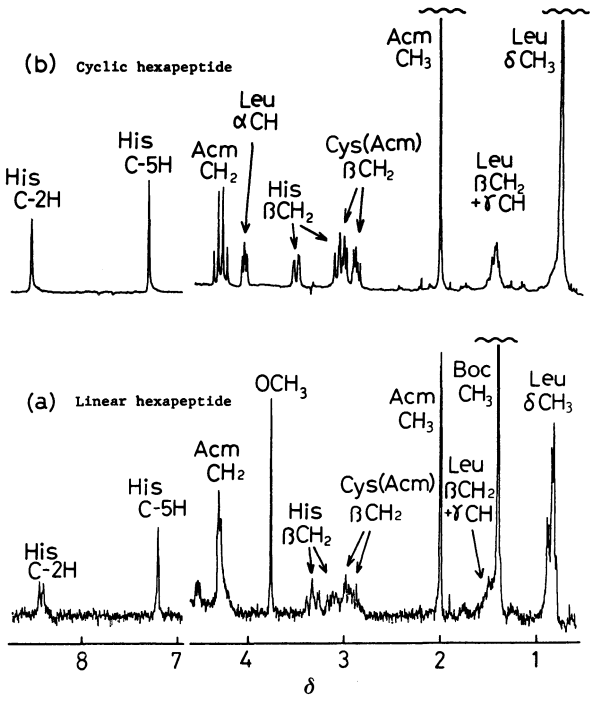

Fig. 1. The 300 MHz proton NMR spectra of linear or cyclic peptides in D_2O solution; peptide concentrations, 1.0×10^{-3} mol dm^{-3}; (a) Boc-L-Cys(*S*-Acm)-D-Leu-L-His-L-Cys(*S*-Acm)-D-Leu-L-His-OCH_3, (b) *cyclo*(-L-Cys(*S*-Acm)-D-Leu-L-His-L-Cys(*S*-Acm)-D-Leu-L-His-).

in D_2O solution do not appear to be split significantly in DMSO solution, too (not shown in a figure).

pK_a* *Values.* The changes of the chemical shifts of the histidyl C-2 and C-5 protons in both the the linear and the cyclic peptides and the change of the chemical shift of one of the histidyl β-CH_2 protons in the cyclic peptide were measured as a function of pD as shown in Figs. 2 and 3. The observed histidyl C-2 proton chemical shifts (δ_{obsd}) were fitted by a nonlinear least-squares method to the equation (1)

$$\delta_{obsd} = \delta_0 + [(\delta_+ - \delta_0)\times 10^{(pK_a^*-pD)}/\{1+10^{(pK_a^*-pD)}\}] \quad (1)$$

in which δ_+ is the chemical shift of the fully protonated histidine and δ_0 that of the neutral histidine. The theoretical curves with the pK_a* values fitted are drawn as shown in Figs. 2 and 3. The pK_a* values of the linear peptide are 6.40 and 6.25, corresponding to those of the two different histidine residues in the molecule, and the pK_a* value of the cyclic peptide is 6.18. The chemical shifts of the histidyl C-5 and β-CH_2 protons were also fitted for comparison. As a whole the values obtained from the C-2 proton chemical shifts agree well with those obtained from the C-5 proton chemical shifts (6.25 and 6.33 for the linear peptide, and 6.19 for the cyclic peptide) and that obtained from the histidyl β-CH_2 chemical shift (6.15 for the cyclic peptide). These values are as a whole a little smaller than those reported.[3)]

Conformation of Histidyl Side Chain in D_2O. The rotamer populations of the histidyl side chain of the cyclic peptide were estimated from the H-C^α-C^β-H protons coupling constant ($J_{\alpha\beta}$) at acidic and basic regions in D_2O solution. In simplified approximation,

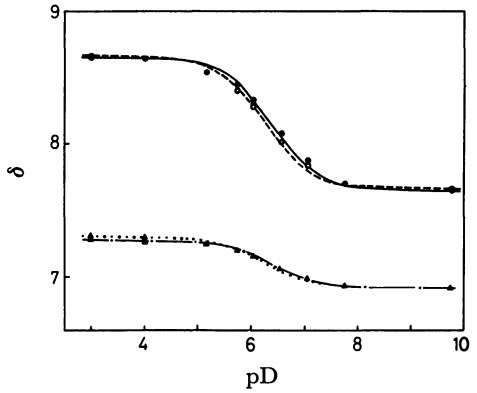

Fig. 2. Effects of pD on the chemical shifts of the histidyl C-2 and C-5 proton resonances of 1.0×10^{-3} mol dm^{-3} Boc-L-Cys(*S*-Acm)-D-Leu-L-His-L-Cys(*S*-Acm)-D-Leu-L-His-OCH_3. The symbols refer to C-2(●, ○) and C-5 (▲, △). The theoretical curves were fitted to the experimental data by a nonlinear least-squares analysis; pK_a*, 6.40 (——), 6.25 (------), 6.33 (·-·-·), 6.25 (·····).

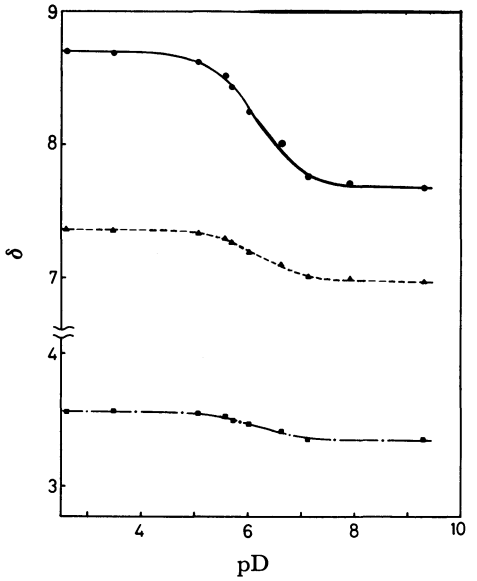

Fig. 3. Effects of pD on the chemical shifts of the histidyl C-2, C-5 and one of the histidyl β-CH_2 protons of 1.0×10^{-3} mol dm^{-3} *cyclo*(-L-Cys(*S*-Acm)-D-Leu-L-His-L-Cys(*S*-Acm)-D-Leu-L-His-). The symbols refer to C-2 (●), C-5 (▲) and low-field resonance of the β-CH_2 (■). The theoretical curves were fitted to the experimental data by a nonlinear least-squares analysis; pK_a*, 6.18 (——), 6.19 (------), 6.15 (-·-·).

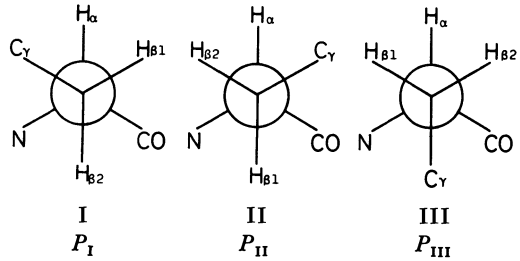

Fig. 4. Examples of rotamers possible for the histidine residue. P_I, P_{II}, and P_{III} denote the rotamer populations.

we have assumed that the $J_{\alpha\beta}$ values are weighted averages of different conformations in fast equilibrium and that a distribution is restricted to the three staggered rotamers in Fig. 4 and the two gauche coupling constants are equal. The $J_{\alpha\beta}$ values of the gauche and the trans rotamers were calculated as 3.2 Hz (J_g) and 12.4 Hz (J_t), respectively, from the Karplus-like equation (2) proposed by Kopple *et al.*,[4]

$$J_{\alpha\beta} = 11.0\cos^2\theta - 1.4\cos\theta + 1.6\sin^2\theta, \quad (2)$$

where θ denotes the dihedral angle of H–C$^\alpha$–C$^\beta$–H planes. Then, the following equations will hold.[5]

$$P_I = (J_{\alpha\beta 2}-J_g)/(J_t-J_g) = (J_{\alpha\beta 2}-3.2)/9.2 \quad (3)$$

$$P_{II} = (J_{\alpha\beta 1}-J_g)/(J_t-J_g) = (J_{\alpha\beta 1}-3.2)/9.2 \quad (4)$$

$$P_{III} = 1 - P_I - P_{II}, \quad (5)$$

where $J_{\alpha\beta 1}$ and $J_{\alpha\beta 2}$ signify the H–C$^\alpha$–C$^\beta$–H$_{\beta 1}$ and the H–C$^\alpha$–C$^\beta$–H$_{\beta 2}$ protons coupling constants, respectively, and P_I, P_{II}, and P_{III} denote the rotamer populations as shown in Fig. 4. P_I, P_{II}, and P_{III} were determined from Eqs. 3—5 by using the experimental values of $J_{\alpha\beta 1}$ and $J_{\alpha\beta 2}$, assuming that the resonance at higher field was that of H$_{\beta 2}$.[6] The observed coupling constants and the estimated rotamer populations are summarized in Table 1.

Temperature Dependence of Chemical Shifts in DMSO-d_6. The temperature coefficients ($-d\delta/dT$) of the main-chain amide and the side-chain Acm amide protons were measured in the temperature range 292—332 K in DMSO-d_6 solution as shown in Table 2, in order to know which protons were shielded from the solvent. One can recognize easily that only the cysteinyl peptide bond proton of the cyclic peptide has the fairly small temperature coefficient (0.0014 ppm deg^{-1}), as compared with the others (0.0028—0.0043 ppm deg^{-1}). In addition, the chemical shift of this proton at 292 K (7.43 ppm) is significantly smaller than that found in an ordinary random-coiled peptide (8.29 ppm for cystine).[7]

Conformation of Cyclic Peptide **2** *in DMSO.* As the cyclic peptide in this study is presumed to take a fairly rigid skeleton conformation, the observed H–N–C$^\alpha$–H protons coupling constant ($J_{HN\alpha}$) would be interpreted in terms of a single conformation. Therefore, the dihedral angle (θ') of H–N–C$^\alpha$–H planes can be estimated from the $J_{HN\alpha}$ value by using the following Karplus-like equation (6) proposed by Ramachandran *et al.*,[8]

$$J_{HN\alpha} = 7.9\cos^2\theta' - 1.5\cos\theta' + 1.3\sin^2\theta'. \quad (6)$$

The conventional ϕ values ($\theta'=|\phi-60°|$ for L-amino acid and $\theta'=|\phi+60°|$ for D-amino acid) can be obtained from the θ' values.[9] In general, two θ' values are possible for a given $J_{HN\alpha}$ value and two ϕ values are possible for a given θ' value, and thus at most four ϕ values are possible. Accordingly, one must estimate the θ' and ϕ values by building a model of the cyclic peptide consistent with the requirement of the Corey-Pauling-Koltun (CPK) molecular model, assuming that all the peptide bonds take the trans conformation ($\omega=+180°$[9]). Thus, the experimentally obtained $J_{HN\alpha}$ values are shown in Table 3.

Effect of Cu(II) on ^1H *NMR Spectra.* In the present study, the effect of Cu(II) addition has been also examined. As Cu(II) has an unpaired electron extremely fast longitudinal and transverse relaxations of the protons situated near Cu(II) will be expected. Accordingly, the signals which are broadened on addition of trace amounts of Cu(II) will be those of the protons located near Cu(II). Of course, the broadenings will be somewhat ascribed to the conformational changes of the molecules caused by the complexation with Cu(II) in the high concentration range of Cu(II). Figure 5 indicates ^{1}H NMR spectral change of the cyclic peptide caused by adding Cu(II) in D_2O solution. There is a tendency that the histidyl C-2, C-5 and β-CH_2 proton signals are markedly broadened on addition of Cu(II) while those of the Acm–CH_2 and Acm–CH_3

Table 1. Conformational parameter of histidyl side chain of *cyclo*(-L-Cys(*S*-Acm)-D-Leu-L-His-L-Cys(*S*-Acm)-D-Leu-L-His-) in D_2O

pD	$J_{\alpha\beta 1}$[a] / Hz	$J_{\alpha\beta 2}$[a] / Hz	P_I[b]	P_{II}[b]	P_{III}[b]
3.28	3.2	11.7	0.92	0.00	0.08
8.40	3.6	9.9	0.73	0.04	0.23

a) H–C$^\alpha$–C$^\beta$–H coupling constants. $\beta 1$ and $\beta 2$ denote H$_{\beta 1}$ and H$_{\beta 2}$ as shown in Fig. 4. b) Rotamer populations as shown in Fig. 4, assuming that histidyl imidazole is in fast equilibrium among three staggered rotamers.

Table 2. Main chain amide and side chain acetamido proton resonances of linear and cyclic pertides in dimethyl sulfoxide

	Linear peptide[a]			Cyclic peptide[a]	
	δ[b]	$-d\delta/dT$[c] / ppm deg^{-1}		δ[b]	$-d\delta/dT$[c] / ppm deg^{-1}
His_I	8.37	0.0040	His	8.65	0.0033
His_{II}, Cys_{II}	8.24	0.0040	Leu	8.43	0.0043
Leu_I, Leu_{II}	8.01	0.0028	Cys	7.43	0.0014
Cys_I	6.93	0.0035	Acm	8.53	0.0035
Acm_I, Acm_{II}	8.55	0.0035			

a) Linear and cyclic peptides are represented as Boc-L-Cys_I(*S*-Acm_I)-D-Leu_I-L-His_I-L-Cys_{II}(*S*-Acm_{II})-D-Leu_{II}-L-His_{II}-OCH_3 and *cyclo*(-L-Cys(*S*-Acm)-D-Leu-L-His-L-Cys-(*S*-Acm)-D-Leu-L-His-), respectively. b) Chemical shifts-referred to the partially deuterated dimethyl sulfoxide (2.49 ppm from DSS) at 292 K. c) Temperature coefficients in the temperature range 292—332 K.

Table 3. Conformational parameters of main chain of *cyclo*(-L-Cys(*S*-Acm)-D-Leu-L-His-L-Cys(*S*-Acm)-D-Leu-L-His-) in dimethyl sulfoxide

	$J_{HN\alpha}$[a] / Hz	θ'[b] / deg	ϕ[c] / deg
His	6.7	143	−83
Leu	4.3	125	+65
Cys	6.7	143	−157

a) H–N–C$^\alpha$–H coupling constant at 322 K. b) Dihedral angle of H–N–C$^\alpha$–H planes estimated from $J_{HN\alpha}$ value. c) Conventional angle obtained from θ' according to the IUPAC-IUB convention.[9]

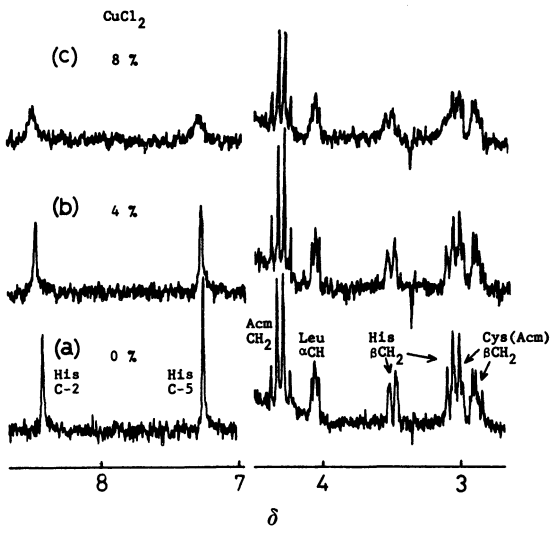

Fig. 5. Effect of $CuCl_2$ addition on the 300 MHz ^1H NMR spectrum of 1.0×10^{-3} mol dm^{-3} *cyclo*(-L-Cys(*S*-Acm)-D-Leu-L-His-L-Cys(*S*-Acm)-D-Leu-L-His-) in D_2O solution at pD 5.70. Contents of $CuCl_2$ (mol%) are (a) 0%, (b) 4%, and (c) 8%.

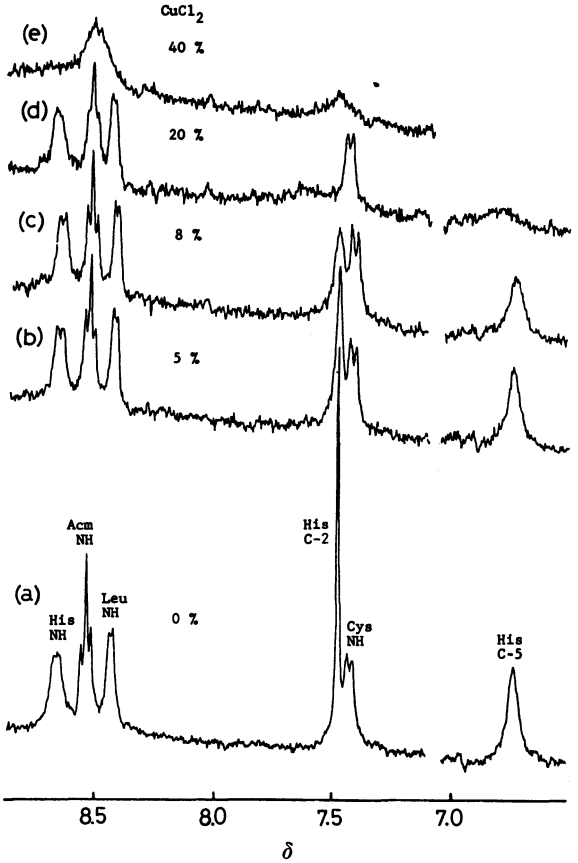

Fig. 6. Effect of $CuCl_2$ addition on the 300 MHz ^1H NMR spectrum of 2.4×10^{-3} mol dm^{-3} *cyclo*(-L-Cys(*S*-Acm)-D-Leu-L-His-L-Cys(*S*-Acm)-D-Leu-L-His-) in DMSO-d_6 solution. Contents of $CuCl_2$ (mol%) are (a) 0%, (b) 5%, (c) 8%, (d) 20%, and (e) 40%.

(not shown in Fig. 5) proton signals are not broadened significantly compared to the histidyl proton signals. Figure 6 shows the change of ^1H NMR spectrum on addition of Cu(II) in DMSO-d_6. The signals of the histidyl C-2 and C-5 protons are broadened or disappear, whereas those of the Acm amide proton and the Acm-CH_2 and the Acm-CH_3 protons (not shown in Fig. 6) are affected much less compared with those of the histidyl protons.

Discussion

The ^1H NMR spectrum of the cyclic hexapeptide (Fig. 1 (b)) clearly indicated that it takes a C_2 symmetric conformation on the NMR time scale, since the same kind of amino acid residues in the molecule shows the same chemical shift. In contrast to this, the spectrum of the linear peptide (Fig. 1 (a)) is more complex, because the two identical amino acid residues are situated in different environments in the molecule. The large difference of the chemical shifts between the two protons of the Acm-CH_2 in the cyclic peptide can be attributed to the environmental difference of these protons probably caused by the particular orientation of the Acm-group in D_2O. This is in striking contrast with the behavior of the Acm-CH_2 protons in DMSO-d_6 solution, where these protons appear to have the same chemical shift (not shown in a figure).

The difference of the pK_a* values of the histidyl imidazolyl groups between the linear (6.25 and 6.40) and the cyclic (6.18) peptides seems to be due to the conformational difference between these two peptides. The two pK_a* values, 6.25 and 6.40, in the linear peptide must reflect the environmental difference between the two histidyl imidazoles, one situated in the C-terminal and the other in the middle of the molecule. In the present study, however, it is impossible to determine which of the histidines corresponds to each of the pK_a* values. On the other hand, the cyclic peptide has only one pK_a* value, 6.18, indicating the identical environment of the two histidine residues.

We have estimated the rotamer populations of the histidyl side chain for the cyclic peptide from the H-C^α-C^β-H protons coupling constant, $J_{\alpha\beta}$. One can see readily from Table 1 that the population of the rotamer I is predominant in both acidic and basic solutions, which indicates that the histidyl imidazole is not folded on the cyclic molecular plane but extended outward. It is generally known that in cyclic dipeptides aromatic side chain is frequently folded but in larger cyclic peptides such folding is rare[10] and that histidyl imidazole has a tendency to orient itself toward the adjacent amide NH group of the peptide backbone.[6] These tendencies are consistent with the results in the present study. It has been also reported that in the case of histidyl side chain the torsion angle χ_2[9] is apt to be around 90°.[6] The CPK molecular model built according to all these results shows that the histidyl imidazolyl plane faces toward the adjacent leucyl side chain, and so the resonances of the leucyl side chain are expected to be shifted to higher field compared with those found in ordinary peptides owing to the imidazole ring current field effect. This inference is supported by the experimental results that the chemical shifts of the leucyl $\beta CH_2+\gamma CH$ (*ca.* 1.47 ppm) and δCH_3 (*ca.* 0.76

ppm) at pD 6.22 of the cyclic peptide are smaller than the chemical shifts (*ca.* 1.6 ppm and *ca.* 0.9 ppm, for the leucyl $\beta CH_2+\gamma CH$ and δCH_3, respectively) of random-coil proteins and peptides reported by McDonald *et al.*[11]

As mentioned in the Results section, the cysteinyl peptide bond proton of the main chain in the cyclic peptide has the temperature coefficient (0.0014 ppm deg^{-1}) strikingly lower than the others (0.0028—0.0043 ppm deg^{-1}) and the chemical shift of this proton (7.43 ppm) is located at the magnetic field much higher than that (8.29 ppm for cystine) of an ordinary peptide.[7] The abnormal chemical shifts of amide protons in a strong hydrogen-bonding solvent such as DMSO may be ascribed to the shielding of the amide protons from the solvent by intramolecular hydrogen bonds or other causes.[10,12-17] Some cyclic hexapeptides form transannular intramolecular hydrogen bonds,[10,12-17] and thus it seems very likely that the cyclic hexapeptide in the present study forms the similar transannular hydrogen bonds between the cysteinyl peptide bonds. This will suggest that two β-turns exist in the D-leucyl-L-histidy sequences. In proteins and naturally occurring or synthetic peptides, proline residues are frequently contributed to β-turn conformations.[18] The cyclic hexapeptide we studied has no proline residues. This finding is thus in contrast of our expectation and noteworthy. The cyclic peptide we studied is composed of the amino acid residues all having the large side chains, which seem to prevent β-turn formation owing to steric hindrance. The orientations of the side chains may happen to be favorable for β-turn formation in the D-leucyl-L-histidyl sequence.

Table 4. Chemical shift of leucyl side chain (δCH_3) in various environment[a]

	δ
Boc-D-Leu-OH	0.88
	0.86
	0.85
	0.82
F_3C-CO-Gly-Gly-L-Leu-L-Ala-OCH_3[b]	0.89
	0.85
Boc-D-Leu-L-His-OCH_3	0.83
	0.81
	0.80
	0.79
Boc-L-Cys(*S*-Acm)-D-Leu-L-His-L-Cys(*S*-Acm)-	0.81
D-Leu-L-His-OCH_3	0.79
	0.77
cyclo(-L-Cys(*S*-Acm)-D-Leu-L-His-L-	0.78
Cys(*S*-Acm)-D-Leu-L-His-)	0.76
	0.73
	0.71

a) Chemical shifts corresponding to all signals observed apparently are described here, except for the tetrapeptide. b) Random coiled tetrapeptide investigated by Bundi *et al.*[7]

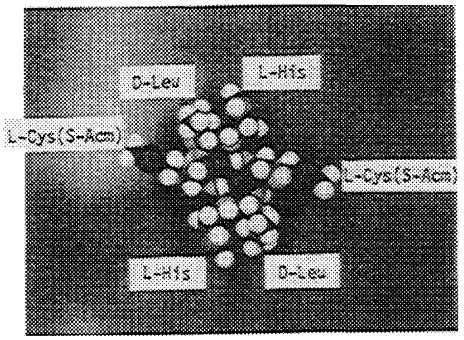

Fig. 7. Corey-Pauling-Koltun (CPK) model of the conformation proposed for *cyclo*(-L-Cys(*S*-Acm)-D-Leu-L-His-L-Cys(*S*-Acm)-D-Leu-L-His-) in DMSO.

The CPK molecular model of the cyclic peptide was built in view of the θ' values derived from the Eq. 6, the transannular hydrogen bonds between the two cysteinyl peptide bonds and the conformational maps proposed by Venkatachalam.[19] We have assumed here that all the peptide bonds take trans conformation ($\omega = +180°$[9]). This assumption seems to be reasonable for the present study, although some deviations from the standard planar trans conformation due to steric hindrance are possible. We have assumed further that the histidyl imidazolyl plane in DMSO solution is apt to be orientated toward the same direction as that in D_2O solution (Table 1). This assumption also seems to be reasonable, since the leucyl δCH_3 proton signals in DMSO-d_6 are shifted to higher field when the leucine residue is situated in D-leucyl-L-histidyl sequence as is shown in Table 4. It is considered that θ' obtained in this way represents an approximate value, since there is some uncertainty in the analysis of $J_{HN\alpha}$. Thus, the error in θ' seems to be about $\pm 10°$.[20,21] The conformation proposed in the present study is shown in Fig. 7, and the estimated θ' and ϕ values are summarized in Table 3.

As is indicated in the Results section, the histidyl imidazoles seem to be mainly coordinated to Cu(II). In order to investigate the complexation quantitatively we have further estimated the dissociation rate constant of the Cu(II)–peptide complex. Figure 8 shows the relation between the reciprocal of the transverse relaxation time ($1/T_{2A}$) of the histidyl C-2 and C-5 protons

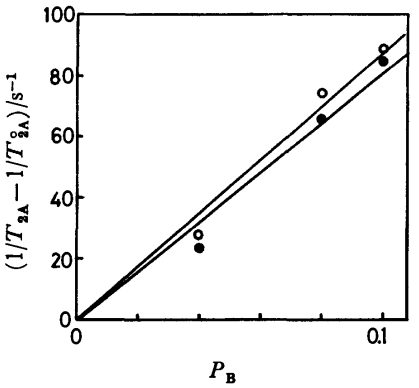

Fig. 8. Paramagnetic effect of Cu(II) on the transverse relaxation rates of the histidyl C-2 (—○—) and C-5 (—●—) proton resonances of *cyclo*(-L-Cys(*S*-Acm)-D-Leu-L-His-L-Cys(*S*-Acm)-D-Leu-L-His-). P_B denotes the mole fraction of the Cu(II)–peptide complex, and T_{2A} and T_{2A}° denote the transverse relaxation times in the presence and absence of Cu(II), respectively.

and the mole fraction of the complex (P_B) in D_2O solution at pD 5.7. $1/T_{2A}$ is obtained experimentally from the following equation (7),

$$1/T_{2A} = \pi\Delta\nu_{1/2}, \quad (7)$$

where $\Delta\nu_{1/2}$ denotes half-band-width of a signal. In the present experimental condition the following equation (8) holds approximately,[22]

$$1/T_{2A} - 1/T_{2A}^{\circ} = P_B/\tau_B, \quad (8)$$

where T_{2A} is the transverse relaxation time of the histidyl C-2 or C-5 proton in the presence of Cu(II), T_{2A}° is that in the absence of Cu(II), and τ_B is the lifetime of the complex. From Fig. 8 we can obtain the dissociation rate constant ($k_d=1/\tau_B$) of the Cu(II)–peptide complex as to be *ca.* 1×10^3 s^{-1}.

In conclusion, the findings we obtained are significantly noteworthy in that D-leucyl-L-histidyl sequence is liable to form β-turn in a cyclic hexapeptide, since this type of peptide sequence in β-turn has never been found. It was also found that Cu(II) interacts with histidyl imidazoles but not with Acm groups, perhaps owing to the conformational rigidity of the cyclic peptide. We are now continuing to investigate other cyclic hexapeptides having sequences such as X-D-leucyl-L-histidyl, X-glycyl-L-histidyl, *etc.* in order to confirm the formation of β-turn by D-leucyl-L-histidyl sequence.

References

1) S. Matsuura, M. Waki, T. Kato, and N. Izumiya, *Bull. Chem. Soc. Jpn.*, **46**, 977 (1973).
2) M. Kodaka, T. Shimizu, and M. Hatano, *Bull. Chem. Soc. Jpn.*, to be submitted.
3) M. Ptak, A. Heitz, and M. Dreux, *Biopolymers*, **17**, 1129 (1978).
4) K. D. Kopple, G. R. Wiley, and R. Tauke, *Biopolymers*, **12**, 627 (1973).
5) K. G. R. Pachler, *Spectrochim. Acta*, **20**, 581 (1964).
6) H. Jäckle and P. L. Luisi, *Biopolymers*, **20**, 65 (1981).
7) A. Bundi, C. Grathwohl, J. Hochmann, R. M. Keller, G. Wagner, and K. Wüthrich, *J. Magn. Reson.*, **18**, 191 (1975).
8) G. N. Ramachandran, R. Chandrasekaran, and K. D. Kopple, *Biopolymers*, **10**, 2113 (1971).
9) "IUPAC-IUB Commission on Biochemical Nomenclature," *Biochemistry*, **9**, 3471 (1970).
10) T. Sugihara, Y. Imanishi, T. Higashimura, and Y. Shimonishi, *J. Org. Chem.*, **41**, 2584 (1976).
11) C. C. McDonald and W. D. Phillips, *J. Am. Chem. Soc.*, **91**, 1513 (1969).
12) K. D. Kopple, M. Ohnishi, and A. Go, *J. Am. Chem. Soc.*, **91**, 4264 (1969).
13) K. D. Kopple, T. J. Schamper, and A. Go, *J. Am. Chem. Soc.*, **96**, 2597 (1974).
14) L. G. Pease, C. M. Deber, and E. R. Blout, *J. Am. Chem. Soc.*, **95**, 258 (1973).
15) K. D. Kopple, M. Ohnishi, and A. Go, *Biochemistry*, **8**, 4087 (1969).
16) R. Schwyzer, C. Grathwohl, J. P. Meraldi, A. Tun-Kyi, R. Vogel, and K. Wüthrich, *Helv. Chim. Acta*, **55**, 2545 (1972).
17) S. L. Portnova, V. V. Shilin, T. A. Balashova, J. Biernat, V. F. Bystrov, V. T. Ivanov, and Yu. A. Ovchinnikov, *Tetrahedron Lett.*, **1971**, 3085.
18) L. M. Gierasch, C. M. Deber, V. Madison, C.-H. Niu, and E. R. Blout, *Biochemistry*, **20**, 4730 (1981).
19) C. M. Venkatachalam, *Biopolymers*, **6**, 1425 (1968).
20) D. W. Hughes and C. M. Deber, *Biopolymers*, **21**, 169 (1982).
21) K. D. Kopple, *Biopolymers*, **10**, 1139 (1971).
22) T. J. Swift and B. E. Connick, *J. Chem. Phys.*, **37**, 307 (1962).

 © 1983 The Chemical Society of Japan Bull. Chem. Soc. Jpn., 56, 1187—1191 (1983)

Phosphinyl and Phosphinothioyl Amino Acids and Peptides. VII. The Use of the Dimethylphosphinothioyl Group as a Thiol-protecting Group of Cysteine

Masaaki Ueki* and Kozo Shinozaki

Department of Applied Chemistry, Science University of Tokyo, 1-3 Kagurazaka, Shinjuku-ku, Tokyo 162

(Received September 20, 1982)

The use of the dimethylphosphinothioyl (Mpt) group for the protection of the thiol function in the cysteine side-chain was studied. *N,S*-Bis(Mpt)-L-cysteine was obtained directly by means of a Schotten-Baumann-type reaction of Mpt–Cl with L-cysteine. The *S*–Mpt group was stable under acidic conditions, except for HBr in acetic acid, and it could be removed by treatment with $AgNO_3$ or $Hg(OAc)_2$ in an aqueous medium. Glutathione was synthesized by utilizing the new *S*-protecting group.

The selection of proper protecting groups for various kinds of functional groups of amino acids is very important in peptide synthesis. Some of the common amino acids with side-chain functional groups can be incorporated into a peptide chain without protecting these groups, but the thiol function of cysteine should be protected up to the last stage of the synthesis because of its high nucleophilicity and its lability to air oxidation.

Recently we reported the use of a series of phosphinothioyl groups for the protection of the α-amino functions of amino acids by taking advantage of the well-known acid lability of the P–N bonds.[1-4] These groups could also be utilized for the protection of the phenolic hydroxyl group of tyrosine.[5] Since the P–O bond was stable under the usual acidic conditions encountered during the peptide synthesis, a good orthogonal relationship between the *N*- and *O*-phosphinothioyl groups was established. Since it seems that a similar advantage can be expected for the *S*-phosphinothioyl groups, we tried to use these groups for the protection of the thiol function of cysteine.

In an earlier paper of this series we have already described the preparation and some reactions of *S*-diphenylphosphinothioyl(Ppt) derivatives of L-cysteine and its ester.[2] In these studies it was found that the thiol function was phosphinothioylated preferentially rather than the amino function and that it was regenerated by alkaline hydrolysis. However, *N,S*-Bis(Ppt)-L-cysteine, which would be a key compound to be used in peptide synthesis, could be successfully prepared in only a low yield. We also found that the dimethylphosphinothioyl(Mpt) group was more acid-labile than the Ppt group when used as an amino-protecting group.[3] We have now tried to prepare the Mpt derivatives of L-cysteine.

Results and Discussion

When the L-cysteine methyl ester was treated with dimethylphosphinothioyl chloride (Mpt–Cl)[3] in the presence of *N,N*-diisopropylethylamine (DIEA), the *N,S*-Bis(Mpt)-L-cysteine methyl ester (**1**) was obtained in a 79% yield as a chromatographically homogeneous oil. Because of the high reactivity of the Mpt–Cl, a Schotten-Baumann-type reaction of L-cysteine with the Mpt–Cl could also be performed without difficulty to afford *N,S*-Bis(Mpt)-L-cysteine (**2**) in a 50% yield as its dicyclohexylamine (DCHA) salt. From **1** and **2**, the *N*-Mpt group could be removed selectively by treatment with HCl reagents to give the *S*-Mpt-L-cysteine methyl ester hydrochloride (**3**) and *S*-Mpt-L-cysteine hydrochloride (**4**) in quantitative and 89% yields respectively:

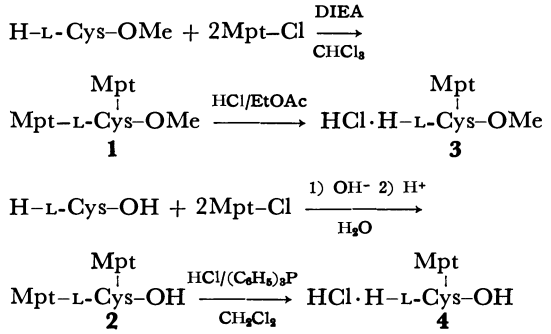

Table 1. Stability of the *S*-Mpt group

Compound	Reagent	Equiv.	Temp °C	Time h	Reaction[a]
Mpt-L-Cys(Mpt)-OMe	2 M† HCl/1 M Ph_3P/CH_2Cl_2	50	RT	24	None
	2 M HCl/EtOAc	50	RT	24	None
	1 M HCl/CH_3OH	50	RT	24	None
	2 M HCl/AcOH	50	RT	24	None
H-L-Cys(Mpt)-OH	1 M HCl/H_2O	100	RT	24	None[b]
	1 M HCl/H_2O	100	100	15 min	Partial
	6 M HCl/H_2O	120	110	20	Complete
	25% HBr/AcOH	100	RT	30 min	Partial
	TFA	100	RT	24	None

a) Detected by TLC. b) Determined by means of an amino-acid-analyzer. † 1 M=1 mol dm^{-3}.

Although these results thus already presented good proof of the acid stability of the *S*-Mpt group, it was further tested under various kinds of acidic conditions; the results are shown in Table 1.

The *S*-Mpt group is stable toward dry hydrogen chloride in organic solvents and trifluoroacetic acid (TFA), although the group is partly cleaved by HBr in acetic acid, probably because of the presence of small amounts of bromine molecules. Under the strongly acidic conditions used for the hydrolysis of peptides prior to amino-acid analysis (6 M HCl, 110 °C 20 h), the P–S bond was also hydrolyzed.

Under the conditions of alkaline hydrolysis, the *S*-Mpt group was removable, while the removal reaction was sometimes accompanied by β-elimination to give dehydroalanine (ΔAla) derivatives. For example, **4** was hydrolyzed completely within 2 h at room temperature by treatment with 4 molar equiv. of a 1 M NaOH solution to regenerate cysteine, but the *t*-butoxycarbonyl-(Boc)-L-alanyl-*S*-Mpt-L-cysteine methyl ester (**6**) gave a 2.5 : 1 mixture of Boc-L-alanyl-L-cysteine and Boc-L-alanyldehydroalanine:

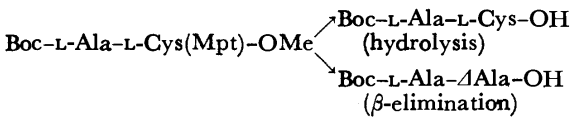

The elimination reaction was found to occur also by means of the action of a tertiary base. If this side reaction is such that it can not be avoided in the presence of any tertiary base, the *S*-Mpt-L-cysteine residue will lose its merit as a synthetic unit. Therefore, the dependence of the ΔAla formation upon the base strength was examined by using **6** as a model compound. The reaction was carried out in a sample tube for NMR spectroscopy measurements, and the yield of the Boc-L-alanyldehydroalanine methyl ester (**7**) produced was obtained from the intensity of the ester methyl signal of **7**. The

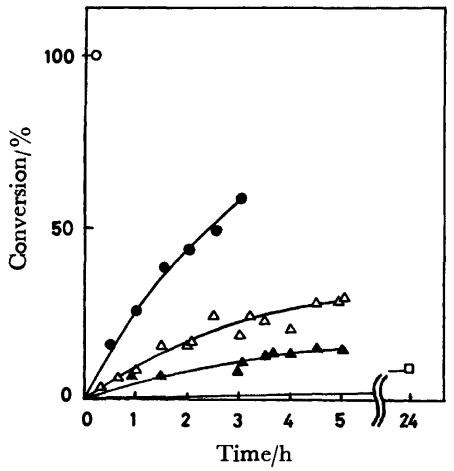

Fig. 1. Effects of the structure of tertiary amines on the dehydroalanine formation

Boc-L-Ala-L-Cys(Mpt)-OMe —Base, $CDCl_3$→ Boc-L-Ala-ΔAla-OMe

(○: DBU, ●: triethylamine, △: tributylamine, ▲: 1,2,2,6,6-pentamethylpiperidine, □: DIEA)

Table 2. Removal of the *S*-Mpt group from H-L-Cys-(Mpt)-OH by $AgNO_3$ or $Hg(OAc)_2$ at 0 °C in H_2O

Reagent	Equiv.	Time / h	Amino-acid ratio			
			Gly[a]	Cys	Cys(Mpt)	Unknown
$AgNO_3$	2	1	1	0.78	0	+
$AgNO_3$	3	1	1	0.95	0	+
$AgNO_3$	4	20 min	1	0.95	0	±
$AgNO_3$	4	30 min	1	1.10	0	−
$Hg(OAc)_2$	1	1	1	0.41	0.24	+
$Hg(OAc)_2$	2	1	1	0.77	0	+
$Hg(OAc)_2$	3	1	1	1.02	0	−

a) Internal standard.

results summarized in Fig. 1 show that the *S*-Mpt group is stable enough in the presence of such a bulky base as DIEA to allow the repeated treatments with this base which are necessary to neutralize acid salts of peptide amines containing the *S*-Mpt-L-cysteine residue during synthesis. It may also be noted that the *S*-Mpt-L-cysteine residue can be converted to the ΔAla residue so readily by the action of 1,8-diazabicyclo[5.4.0]-undec-7-ene (DBU) as to make *S*-Mpt-L-cysteine a new and easily available precursor of ΔAla.

The removal of the *S*-Mpt group without any accompanying ΔAla formation was accomplished by utilizing $AgNO_3$ or $Hg(OAc)_2$ as a catalyst for the hydrolysis. The removal conditions were studied by using **4** (neutralized by NH_4OH) as a substrate, since **4** was eluted from the standard amino-acid-analyzer column in the same position with glutamic acid and could be easily monitored. From these reactions it was found that an unexpected intermediate was produced. This intermediate, which could not be isolated, was also hydrolyzed by the use of the metallic reagents in excess, as is shown in Table 2. In order to elucidate the structure of the intermediate, the reaction was attempted by using a dipeptide model, which might produce a more stable intermediate and a dehydroalanine derivative. A starting dipeptide, H-L-Ala-L-Cys(Mpt)-OH (**9**), and the expected products, H-L-Ala-L-Cys-OH (**10**) and H-L-Ala-ΔAla-OH (**11**), were prepared according to the procedures illustrated in Fig. 2.

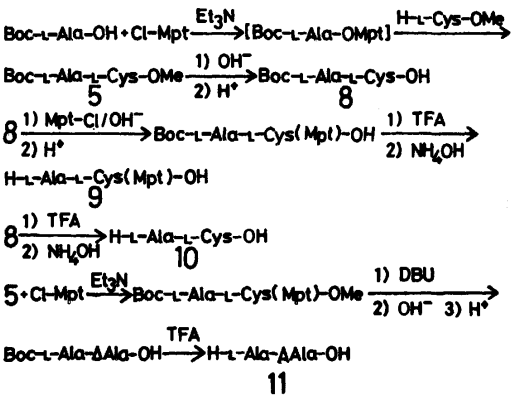

Fig. 2. Synthesis of model peptides.

Elution patterns from an amino-acid-analyzer column of a mixture of products from the reaction of **9** with $AgNO_3$ are shown in Fig. 3. Although the starting

material, **9** (elution volume=110 cm³), disappeared within 60 min at 0 °C upon the use of 2 molar equiv. of $AgNO_3$, the reaction was still incomplete, as was shown by the presence of an intermediate. When a 4 molar excess of the reagent was used, complete deprotection occurred to afford **10** (elution volume =115 cm³), without any accompanying dehydroalanine formation (elution volume of **11**=132 cm³). In order to elucidate the structure of the intermediate, it was isolated from a separate reaction mixture by ion-exchange chromatography to give a considerably pure solid material, which showed methyl-proton signals coupled with P, but different from those for the Mpt group. Based on this result, it was speculated that the structure of the compound was the *S*-dimethylphosphinyl (Dmp=$-P(O)(CH_3)_2$) derivative of **10**, H-L-Ala-L-Cys(Dmp)-OH (**12**), produced by the oxidative desulfurization of **9**:

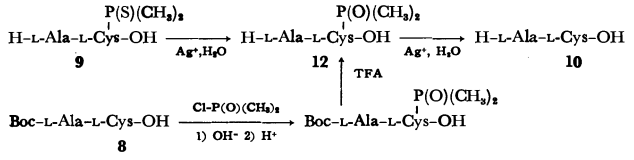

This speculation was confirmed by analyzing a product prepared by the reaction of **8** with dimethylphosphinyl chloride, followed by *N*-deprotection by TFA. As expected, a peak appeared at the same position as the unknown product described above. This result does not necessarily mean that the removal of the *S*-Mpt group by $AgNO_3$ proceeds only through the intermediate formation of the Dmp derivative, but the consumption of $AgNO_3$ being more than the expected amount would be explained by this extra oxidation.

As an application of the Mpt group as a thiol-protecting group, the synthesis of glutathione was attempted according to the scheme illustrated in Fig. 4.

The removal of the *S*-Mpt group was performed either at the final stage (Method A) or before the removal of the other protecting groups (Method B); the latter gave a better yield.

Further applications of the *S*-Mpt-L-cysteine derivatives for the synthesis of cysteine and dehydroalanine containing peptides are now in progress.

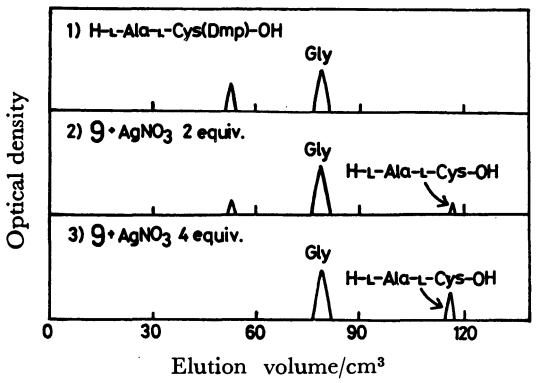

Fig. 3. Elution patterns of a model peptide, glycine (internal standard) and products from the deprotection reaction of H-L-Ala-L-Cys(Mpt)-OH by $AgNO_3$.

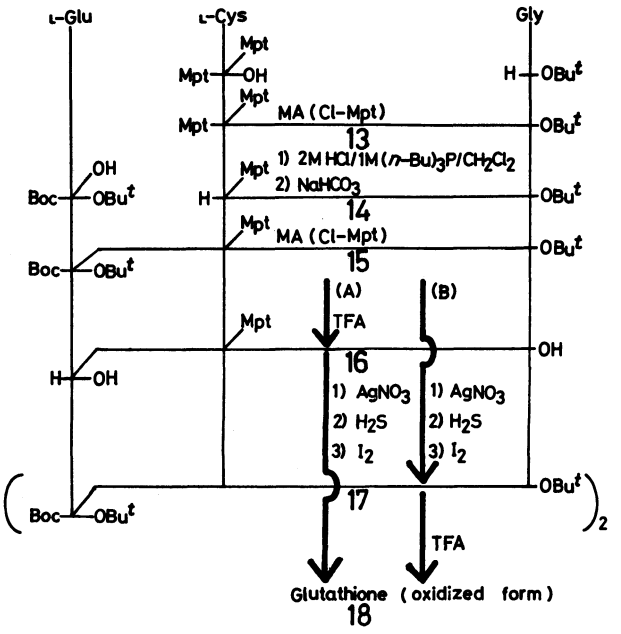

Fig. 4. Synthesis of glutathione.

Experimental

Thin-layer chromatography (TLC) was performed on silica gel plates (Merck $60F_{254}$) in the following solvent systems: dichloromethane (R_f^1), ether (R_f^2), ethyl acetate (R_f^3), chloroform–methanol–acetic acid (95 : 5 : 3, R_f^4), chloroform–methanol–acetic acid (85 : 25 : 20, R_f^5), chloroform–methanol–acetic acid–water (45 : 30 : 6 : 9, R_f^6), phenol–water (4 : 1 w/v, R_f^7), and 1-butanol–ethyl acetate–acetic acid–water (1 : 1 : 1 : 1, R_f^8). The products were detected on TLC plates using ultraviolet light, iodine vapor, ninhydrin, and the sodium nitroprusside reagent.

N,S-Bis(dimethylphosphinothioyl)-L-cysteine Methyl Ester (Mpt-L-Cys(Mpt)-OMe) (1). A solution of Mpt-Cl[3] (1.29 g, 10 mmol) in 10 cm³ of chloroform was added to a suspension of HCl·H-L-Cys-OMe (0.858 g, 5 mmol) in 10 cm³ of chloroform and 2.1 cm³ (15 mmol) of *N,N*-diisopropylethylamine at 0 °C. After having been stirred for 3 h at 0 °C, the solution was evaporated *in vacuo*. The residue was dissolved in ethyl acetate. The solution was washed successively with water, an ice-cold 5% citric acid solution, water, a 5% sodium hydrogencarbonate solution, water, and a saturated sodium chloride solution, dried over anhydrous sodium sulfate, and evaporated. The oily residue was dissolved in dichloromethane and placed in a silica-gel column (2×10 cm). Subsequent elution with dichloromethane gave **1** as colorless oil; 1.26 g (79%). $[\alpha]_D^{24}$ −13.0° (*c* 1, ethanol); R_f^1 0.60, R_f^2 0.76. Found: C, 29.91; H, 6.30; N, 4.36%. Calcd for $C_8H_{19}NO_2P_2S_3$: C, 30.09; H, 6.00; N, 4.39%.

N,S-Bis(dimethylphosphinothioyl)-L-cysteine Dicyclohexylamine Salt (Mpt-L-Cys(Mpt)-OH·DCHA) (2). L-Cys (2.24 g, 20 mmol) was dissolved in a 1 M sodium hydroxide solution (20 cm³), and then Mpt-Cl (5.65 g, 44 mmol) in ether (40 cm³) was added, drop by drop, at 0 °C. While the mixture was being stirred vigorously, the 1 M sodium hydroxide solution was added carefully, at a rate chosen so as to maintain the pH of the solution between 9.0 and 9.5, until no drop in the pH was observed. Then the solution was extracted twice with ethyl acetate. The aqueous layer was acidified (pH 3—4) with solid citric acid at 0 °C and then extracted with ethyl acetate several times. The organic layer was washed with

water, dried over anhydrous sodium sulfate, and evaporated *in vacuo*. The oily residue was dissolved in ethyl acetate and treated with DCHA (4 cm³, 20 mmol). DCHA salt was collected by filtration, washed with ethyl acetate and ether, and dried. Subsequent recrystallization from ethanol gave **2** as colorless crystals; 5.0 g (50%). mp 150—151 °C; $[\alpha]_D^{24}$ −6.2° (*c* 1, methanol); R_f^4 0.35, R_f^5 0.88. Found: C, 46.34; H, 8.14; N, 5.91; P, 11.97%. Calcd for $C_{19}H_{40}N_2O_2P_2S_3 \cdot 1/2\ H_2O$: C, 46.04, H, 8.34; N, 5.65; P, 12.49%.

S-*Dimethylphosphinothioyl*-L-*cysteine Methyl Ester Hydrochloride (H*–L-*Cys(Mpt)*–*OMe·HCl) (**3**).* Compound **1** (9.65 g, 30 mmol) was stirred with 2.2 M HCl in ethyl acetate at room temperature for 2.5 h. The solvent was then removed *in vacuo*, and the residue was dissolved in methanol. The solution was treated with Amberlyst A-21 resin to neutralize it and to remove a small amount of dimethylphosphinothioic acid (Mpt–OH), and then filtered. The filtrate was treated with an equimolar amount of HCl in methanol and evaporated to give a chromatographically homogeneous oil; 8.19 g (quantitative). R_f^4 0.14, R_f^5 0.58.

S-*Dimethylphosphinothioyl*-L-*cysteine Hydrochloride (H*–L-*Cys-(Mpt)*–*OH·HCl) (**4**).* Compound **2** (4.87 g, 10 mmol) was separated between a 5% citric acid solution and ethyl acetate. The ethyl acetate layer was washed with water, dried, and evaporated. The residue was dissolved in methanol (4 cm³) and dichloromethane (30 cm³), 2 M HCl/1 M Ph_3P/CH_2Cl_2[3] (15 cm³) was added at 0 °C, and the mixture was kept standing at room temperature for 3 h. The crystalline precipitate was then collected by filtration, washed with CH_2Cl_2, and dried over P_2O_5; 2.22 g (89%). An analytical sample was recrystallized from methanol–CH_2Cl_2–ether; mp 157—158 °C (decomp); $[\alpha]_D^{24}$ −18.4° (*c* 1, methanol); R_f^5 0.21. Found: C, 24.13; H, 5.54; N, 5.53; P, 12.61%. Calcd for $C_5H_{13}NO_2PS_2Cl$: C, 24.09; H, 5.26; N, 5.61; P, 12.40%.

N-(t-*Butoxycarbonyl*)-L-*alanyl*-L-*cysteine Methyl Ester (Boc*–L-*Ala*–L-*Cys*–*OMe) (**5**).* Mpt–Cl (2.57 g, 20 mmol) was added to an ice-cold, stirred solution of Boc–L-Ala–OH (3.78 g, 20 mmol) and triethylamine (2.80 cm³, 20 mmol) in 20 cm³ of chloroform, after which the mixture was stirred for 1 h.[6] To this solution, a mixture of HCl·H–L-Cys–OMe (3.43 g, 20 mmol) and triethylamine (5.6 cm³, 40 mmol) in 80 cm³ of chloroform was added in several portions at 0 °C. After having been kept stirring for 1 h at this temperature, the solution was washed in the usual way, dried, and evaporated *in vacuo*. The solidified residue was washed with ether and recrystallized from ethyl acetate–petroleum ether to give colorless crystals; 3.62 g (59%). mp 110—112 °C; $[\alpha]_D^{26}$ −35.0 °C (*c* 1, ethanol); R_f^2 0.16, R_f^3 0.62. Found: C, 46.74; H, 7.10; N, 9.29%. Calcd for $C_{12}H_{22}N_2O_5S$: C, 47.04; H, 7.24; N, 9.11%.

N-(t-*Butoxycarbonyl*)-L-*alanyl*-S-*dimethylphosphinothioyl*-L-*cysteine Methyl Ester (Boc*–L-*Ala*–L-*Cys(Mpt)*–*OMe) (**6**).* To an ice-cold solution of Boc–L-Ala–L-Cys–OMe (1.53 g, 5 mmol) and *N,N*-diisopropylethylamine (0.871 cm³, 5 mmol) in 5 cm³ of chloroform, Mpt–Cl (0.643 g, 5 mmol) was added, after which the mixture was stirred continuously for 1 h at 0 °C and for 3 h at room temperature. The solution was washed in the usual manner, dried over anhydrous sodium sulfate, and evaporated *in vacuo*. The solid residue was recrystallized from ethyl acetate–petroleum ether to give colorless crystals; 1.69 g (85%). mp 106—108 °C; $[\alpha]_D^{24}$ −28.5° (*c* 1, ethanol); R_f^2 0.38, R_f^3 0.72. Found: C, 42.04; H, 6.81; N, 7.18%. Calcd for $C_{14}H_{27}N_2O_5PS_2$: C, 42.20; H, 6.83; N, 7.03%.

N,S-*Bis(dimethylphosphinothioyl)*-L-*cysteinylglycine* t-*Butyl Ester (Mpt*–L-*Cys(Mpt)*–*Gly*–*OBu^t) (**13**).* Compound **2** (803 mg, 1.65 mmol) was dissolved in 4 cm³ of chloroform and treated with Mpt–Cl (212 mg, 1.65 mmol) at 0 °C. To this solution a solution of the glycine *t*-butyl ester (217 mg, 1.65 mmol) and *N,N*-diisopropylethylamine (0.29 cm³, 1.65 mmol) in 2 cm³ of chloroform was added, after which the solution was stirred for 2 h at 0 °C. After the solvent had been changed to ethyl acetate, the solution was washed with water, an ice-cold 5% citric acid solution, water, a 5% sodium hydrogencarbonate solution, water, and a saturated sodium chloride solution, and dried. After the removal of the solvent *in vacuo*, an oily residue was dissolved in dichloromethane and the solution was placed in a silica-gel column (1.7×20 cm). Subsequent elution by ether gave colorless crystals; 629 mg (91%). An analytical sample was recrystallized from ethyl acetate–petroleum ether; mp 110—112 °C; $[\alpha]_D^{20}$ −24° (*c* 1, methanol); R_f^2 0.17, R_f^3 0.54. Found: C, 37.03; H, 6.84; N, 6.45%. Calcd for $C_{13}H_{28}N_2O_3P_2S_3$: C, 37.31; H, 6.74; N, 6.69%.

S-*Dimethylphosphinothioyl*-L-*cysteinylglycine* t-*Butyl Ester (H*–L-*Cys(Mpt)*–*Gly*–*OBu^t) (**14**).* Compound **13** (1.88 g, 4.49 mmol) was treated with 2 M HCl in dichloromethane containing 1 M of tributylphosphine (13.45 cm³). After having been stirred at 0 °C for 2.5 h and at room temperature for 6.5 h, the solution was evaporated. The residue was separated between water and ethyl acetate. The aqueous layer was washed with ethyl acetate, the pH was adjusted to 9 by adding solid sodium hydrogencarbonate, and extracted several times with ethyl acetate. The combined extracts were washed with water, dried over anhydrous sodium sulfate, and evaporated. The oily residue was purified by passing its ethyl acetate solution through a short silica-gel column (3×12 cm) to give a chromatographically homogeneous oil; 1.45 g (99%). R_f^4 0.21, R_f^5 0.68.

N-(t-*Butoxycarbonyl*)-L-*γ-glutamyl*-S-*dimethylphosphinothioyl*-L-*cysteinylglycine Di*-t-*butyl Ester*

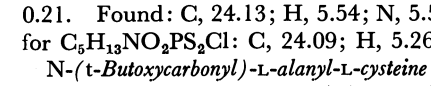

(**15**). To an ice-cold solution of Boc–L-Glu–OBu^t·DCHA (737 mg, 1.52 mmol) in 3 cm³ of chloroform, Mpt–Cl (195 mg, 1.52 mmol) was added in several portions, after which the solution was stirred at 0 °C for 1 h. To this solution a mixture of Compound **14** (547 mg, 1.68 mmol) and *N,N*-diisopropylethylamine (0.29 cm³, 1.68 mmol) in 10 cm³ of chloroform was added. After having been stirred at 0 °C for 2 h, the solution was washed in the usual manner, dried, and evaporated *in vacuo*. The residue was purified by silica-gel column chromatography. After the elution of a small amount of symmetric dimethylphosphinothioic anhydride (Mpt–O–Mpt), Compound **15** was obtained as an amorphous solid by eluting with CH_2Cl_2 and then with CH_2Cl_2–methanol (9/1, v/v); 840 mg (90%). $[\alpha]_D^{20}$ −40° (*c* 1, methanol); R_f^2 0.25, R_f^3 0.74. Found: C, 48.77; H, 7.70; N, 6.54%. Calcd for $C_{25}H_{46}O_8N_3S_2P \cdot 1/2\ CH_3OH$: C, 48.79; H, 7.71; N, 6.69%.

L-*γ-Glutamyl*-S-*dimethylphosphinothioyl*-L-*cysteinylglycine*

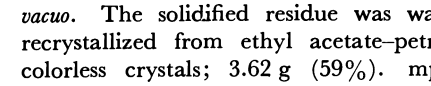

(**16**). Trifluoroacetic acid (16.55 cm³) was added to an ice-cold solution of Compound **15** (1.093 g, 1.79 mmol) in 9 cm³ of CH_2Cl_2 containing anisole (3.57 cm³). After having been kept standing at room temperature overnight, the solution was evaporated. The residue was separated between water and ether, and the organic layer was extracted several times with water. The combined aqueous layer and extracts were evaporated *in vacuo*. Then the solid residue was dissolved in water, and the solution was placed in a column (1.2×51 cm) of Dowex 1-X2 ion-exchange resin (acetate form). The column was eluted with 8% acetic acid. The desired fractions (172—277 cm³) were pooled and evaporated *in vacuo* to give **16** as colorless crystals; 0.629 g (85%). An analytical sample was recrystallized from hot

water; mp 202—203 °C; $[\alpha]_D^{20}$ −23° (*c* 1, H_2O); R_f^6 0.23, R_f^8 0.42. Found: C, 34.89; H, 5.42; N, 10.08%. Calcd for $C_{12}H_{22}O_6N_3PS_2 \cdot 2/3\ H_2O$: C, 35.03; H, 5.72; N, 10.21%.

N,N′-[*Bis*[N-(*t-butoxycarbonyl*)-L-*γ-glutamyl*]-L-*cystinyl*]*bis*-(*glycine*) *Tetra*-t-*butyl Ester* 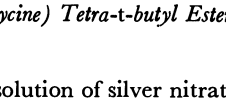 (**17**). A solution of silver nitrate (340 mg, 2 mmol) in water (5 cm³) was added to a solution of Compound **15** (306 mg, 0.5 mmol) in methanol (10 cm³) containing pyridine (0.16 cm³, 2 mmol) at 0 °C. The mixture was stirred at 0 °C for 1 h. H_2S gas was then bubbled through the solution at 0 °C for 1 h. The precipitate was removed by filtration, and the filtrate was evaporated *in vacuo*. The residue was dissolved in ethyl acetate, and the solution was washed with water, dried and evaporated. The residue was dissolved in CH_2Cl_2, and the solution was placed in a column (0.6×25 cm) of silica gel which was then eluted with ether. The eluates were combined and evaporated *in vacuo* to give a colorless oil; 261 mg (100%). R_f^2 0.31, R_f^3 0.76. This material was dissolved in methanol (5 cm³) containing pyridine (0.09 cm³, 1.1 mmol). To this a 0.1 M I_2–KI solution in 90% ethanol (2.63 cm³) was added at 0 °C. After this solution had been stirred for 1 h, the organic solvents were removed. The residue was dissolved in ethyl acetate, and the solution was washed with water and a sodium thiosulfate solution, dried, and evaporated. The residue was dissolved in CH_2Cl_2, and the solution was placed in a column (0.6×25 cm) of silica gel which was then eluted with CH_2Cl_2, followed by ether. The eluates were combined and evaporated *in vacuo* to give **17** as colorless crystals; 242 mg (93%). mp 102—107 °C; $[\alpha]_D^{20}$ −73° (*c* 1, methanol); R_f^2 0.42, R_f^3 0.84. Found: C, 53.12; H, 7.85; N, 8.05%. Calcd for $C_{46}H_{80}O_{16}N_6S_2$: C, 53.26; H, 7.77; N, 8.10%.

Glutathione (Oxidized Form) 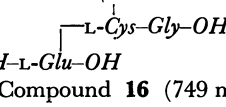 (**18**). *Method A*: To a solution of Compound **16** (749 mg, 1.63 mmol) in water (70 cm³) containing pyridine (0.58 cm³, 7.15 mmol), 7.15 cm³ of 1 M silver nitrate solution was added at 0 °C. The mixture was then stirred at 0 °C for 1 h. H_2S gas was bubbled through the solution at 0 °C for 1 h. The precipitate was removed by filtration, and the filtrate was evaporated *in vacuo*. The residue was dissolved in a small volume of water and methanol, after which the solution was adjusted to pH 7 with pyridine at 0 °C and treated with iodine (232 mg, 1.83 mmol) in methanol (10 cm³). After the removal of the methanol *in vacuo*, the solution was placed in a column (1.2×61 cm) of Dowex 1-X2 ion-exchange resin (acetate form). The column was eluted with water (200 cm³) and then 10 % acetic acid. The desired fractions were colcollected, evaporated *in vacuo*, and dried over P_2O_5 to give **18** as colorless crystals; 270 mg (52%).

Method B: To a solution of Compound **17** (1.017 g, 0.98 mmol) in CH_2Cl_2 (20 cm³) containing anisole (5.11 cm³), trifluoroacetic acid (36.23 cm³) was added at room temperature. After having been kept standing overnight, the solvent was evaporated *in vacuo*; the residue was dissolved in water and placed in a column of Dowex 1-X2 ion-exchange resin (acetate form). Elution as described in Method A gave colorless crystals; 602 mg (97%). An analytical sample was recrystallized from water–ethanol; mp 178—180 °C; $[\alpha]_D^{20}$ −105° (*c* 1, H_2O) (lit,[7] mp 175—195 °C; $[\alpha]_D^{27}$ −92.8° (*c* 1.2, H_2O), lit,[8] $[\alpha]_D$ −94° (*c* 1, H_2O)); R_f^7 0.03, R_f^8 0.13. Found: C, 37.89; H, 5.70; N, 13.03%. Calcd for $C_{20}H_{32}N_6O_{12}S_2 \cdot H_2O$: C, 38.09; H, 5.43; N, 13.33%.

References

1) M. Ueki and S. Ikeda, *Chem. Lett.*, **1976**, 827.

2) S. Ikeda, F. Tonegawa, E. Shikano, K. Shinozaki, and M. Ueki, *Bull. Chem. Soc. Jpn.*, **52**, 1431 (1979).

3) M. Ueki, T. Inazu, and S. Ikeda, *Bull. Chem. Soc. Jpn.*, **52**, 2424 (1979).

4) M. Ueki, S. Ikeda, and T. Handa, *Bull. Chem. Soc. Jpn.*, **54**, 3865 (1981).

5) M. Ueki and T. Inazu, *Bull. Chem. Soc. Jpn.*, **55**, 204 (1982).

6) M. Ueki and T. Inazu, *Chem. Lett.*, **1982**, 45.

7) C. Berse, R. Boucher, and L. Piche, *Can. J. Chem.*, **37**, 1733 (1959).

8) B. Marinier and M. Berube, *Can. J. Chem.*, **50**, 1633 (1972).

Bromination of Biphenylene Derivatives Having an Electron-releasing Substituent. A Preferential Formation of Benzocyclooctene Derivatives

Hiroto KIDOKORO, Yuko SAITO, Masaru SATO, Seiji EBINE,* Sadao SATO,†
Tadashi HATA,† and Chihiro TAMURA†
Department of Chemistry, Saitama University, Urawa, Saitama 338
†*Analytical and Metabolic Research Laboratories, Sankyo Co. Ltd., 1-2-58 Hiromachi, Shinagawa-ku, Tokyo 140*
(Received September 25, 1982)

3-Substituted 2-bromobiphenylenes were brominated to give benzocyclooctene or 7(8*H*)-benzocyclooctenone derivatives, but not biphenyl derivatives. The structure of 5,8,10-tribromo-7(8*H*)-benzocyclooctenone was determined by X-ray diffraction analysis.

Biphenylene itself prefers an addition reaction to a substitution reaction on treatment with bromine,[1] probably because biphenylene has a partial anti-aromaticity in the central four-membered ring. On the other hand, biphenylene derivatives having an electron-releasing substituent at the 2-position undergo a predominant bromine-substitution reaction at the 3-position.[1] Further bromination of monobrominated biphenylene derivatives was previously reported to give biphenyl derivatives,[2,3] but the reaction product on bromination of 2-bromo-3-methoxybiphenylene was later corrected by us to be benzocyclooctene derivatives.[4] We now report a reexamination of bromination of 2,6-diethyl-, 2-acetoxy-, and 2-acetamidobiphenylenes.[5]

It was reported that the bromination of 2-ethylbiphenylene gave an inseparable mixture of mono- and dibrominated products.[6] On the other hand, 2,6-diethylbiphenylene was brominated in dichloromethane to give 3,7-dibromo-2,6-diethylbiphenylene (**1**) in moderate yield, which was further brominated with an excess of bromine to give 3,5,8,10-tetrabromo-2,7-diethylbenzocyclooctene (**2**) in 70% yield. The structure of **2** was assigned by electronic and ^{1}H-NMR spectral analogy to 5,8,10-tribromo-7-methoxybenzocyclooctene (**3**).[4,5] Thus, **2** showed a ^{1}H-NMR spectrum having two olefinic multiplets at δ=6.58 and 6.74.

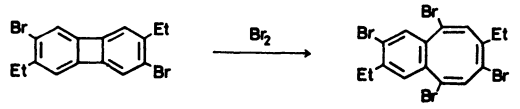

(**1**) (**2**)

2-Acetoxybiphenylene was treated with 2 equivalents of bromine at room temperature to give a small amount of the monobrominated product **4** and tribromo ketone **5** in 34% yield. The structure of **4** was assigned to 2-acetoxy-3-bromobiphenylene by its ^{1}H-NMR spectrum: δ=2.32 (s, 3H, $OCOCH_3$), 6.48 (s, 1H, H-1), and 6.5—7.0 (m, 5H, H-4 and Ar–H). Tribromo ketone **5** was the same product with that obtained on bromination of 2-methoxybiphenylene,[4] and was probably formed by the action of a trace of acid on intermediately formed 7-acetoxy-5,8,10-tribromobenzocyclooctene (**6**). The result suggests that bromination of **4** gives **6** easily.

Bromination of 2-acetamidobiphenylene was reported to give 2-acetamido-3-bromobiphenylene (**7**) in 65% yield, which was further brominated to give a biphenyl derivative.[3] We reexamined the reaction of 2-acetamidobiphenylene with an excess of bromine in acetic

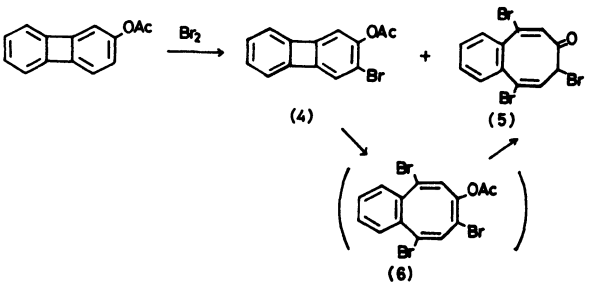

acid, and obtained 5,8,10-tribromo-7(8*H*)-benzocyclooctenone (**5**) although in low yield, in addition to a tribromo compound (**A**) (mp 156—157 °C). (**A**) was previously assigned as 3-acetamido-2′,4,6-tribromobiphenyl (**9**) by Baker *et al.*, but the above result suggests that (**A**) is a benzocyclooctene derivative which transforms easily to **5** on acid hydrolysis. (**A**) was alternatively obtained on bromination of **6** in dichloromethane at room temperature in high yield and was converted on treatment with 48% hydrobromic acid in boiling ethanol to **5** in 80% yield. We reprepared (**A**) according to Baker and co-workers' direction,[3] and found it to have a ^{1}H-NMR having two olefinic doublets at δ=6.73 and 6.94 (J=1.3 Hz) and an electronic spectrum closely similar to those of **2** and **3** (Fig. 1), proving that (**A**) is 7-acetamido-5,8,10-tribromobenzocyclooctene (**8**).

We prepared **9** in the following manner. The reaction of *m*-nitrobenzenediazonium tetrafluoroborate with bromobenzene in the presence of 18-crown-6 gave a

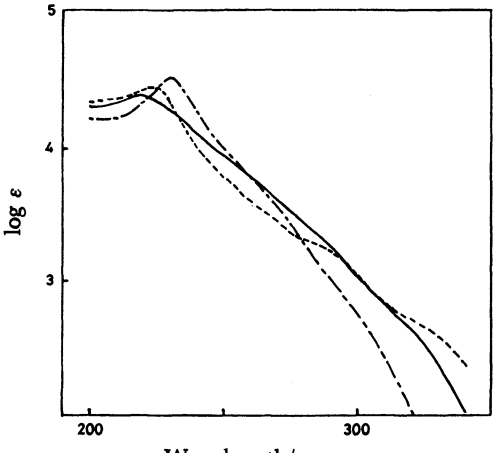

Fig. 1. Electronic spectra of **3** (------), **2** (·–·–·), and **8** (——).

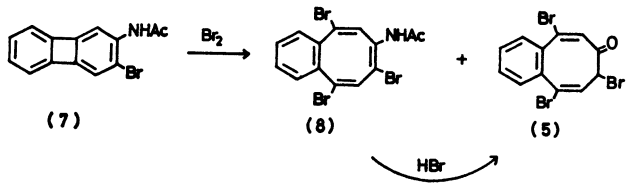

mixture of 2′-bromo- and 4′-bromo-3-nitrobiphenyl in good yield. The former product (separated in 13% yield) was converted by reduction and successive acetylation to 3-acetamido-2′-bromobiphenyl, which was brominated, according to the procedure described by Baker *et al.*, to give **9**, colorless needles, mp 117—118 °C. The ^{1}H-NMR of **9** showed the following signals: δ=2.26 (s, 3H, $COCH_3$), 7.15—7.55 (m, 4H, H-3′—H-6′), 7.70 (broad s, 1H, NH), 7.97 (s, 1H, H-2), and 8.45 (s, 1H, H-5). **9** gave an IR spectrum different from that of **8**. Thus, **8** was unequivocally proved not to be **9**. Ultimately, the structure of **5** was determined by an X-ray crystallographic analysis (see below).

There seems to be a common trend on bromination of biphenylene derivatives having an electron-releasing substituent at the C_2 position. In these derivatives, bromination gives exclusively 3-substituted 2-bromobiphenylenes.[1] Further bromination of the 2-substituted 3-bromobiphenylenes takes place at the C_{4a}-position, forming an intermediate biphenylenium ion, similarly to the bromination of biphenylene itself, because the C_3-position is already occupied by the bromo substituent and the electron-releasing ability of the 2-substituent is cancelled by the electron-withdrawing bromo substituent. Successive addition of a bromide ion on the intermediate biphenylenium ion formed occurs exclusively at the C_{8b}-position, not at the C_{4b}-position. The resulting dibromo adducts undergo a spontaneous ring-opening to give benzocyclooctene derivatives. The bromide ion attack on the biphenylenium ion at the C_{4b}-position and subsequent C_{4a}–C_{4b} bond fission to biphenyl derivatives do not take place. An exceptional example that bromine attacked the unsubstituted benzene ring of 2-substituted biphenylene was presented in bromination of 2-ethylbiphenylene to 3,6- and 3,7-dibromo-2-ethylbiphenylenes.[6]

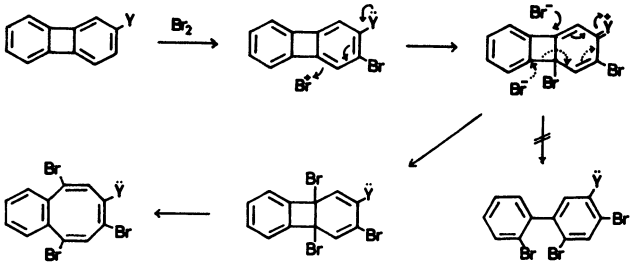

Table 1. Fractional atomic coordinates ($\times 10^4$), with estimated standard deviations in parentheses

Atom	x	y	z
C(1)	264(15)	1101(10)	4226(9)
C(2)	−672(14)	555(12)	3889(11)
C(3)	−269(16)	−143(11)	3517(11)
C(4)	1076(17)	−340(9)	3528(9)
C(5)	3570(16)	−106(8)	3916(9)
C(6)	4305(14)	195(9)	3682(10)
C(7)	5088(13)	972(8)	3268(7)
C(8)	3960(14)	1625(7)	3228(8)
C(9)	3611(15)	1899(8)	4053(8)
C(10)	2637(14)	1574(7)	4527(8)
C(4A)	2100(14)	195(7)	3858(8)
C(10A)	1660(13)	938(8)	4199(8)
O(7)	6302(10)	1087(8)	3031(7)
Br(5)	3636(2)	−1204(1)	4375(1)
Br(8)	4569(2)	2536(1)	2509(1)
Br(10)	2349(2)	1958(1)	5626(1)

Table 2. Bond lengths and angles with estimated standard deviations in parentheses

Bond length	l/Å		l/Å
C(1)–C(2)	1.378(23)	C(7)–C(8)	1.524(18)
C(1)–C(10A)	1.376(19)	C(7)–O(7)	1.248(16)
C(2)–C(3)	1.340(26)	C(8)–C(9)	1.430(18)
C(3)–C(4)	1.340(23)	C(8)–Br(8)	1.963(13)
C(4)–C(4A)	1.421(20)	C(9)–C(10)	1.318(19)
C(5)–C(6)	1.344(20)	C(10)–C(10A)	1.496(18)
C(5)–C(4A)	1.506(20)	C(10)–Br(10)	1.883(12)
C(5)–Br(5)	1.931(13)	C(4A)–C(10A)	1.391(18)
C(6)–C(7)	1.452(20)		
Bond angle	ϕ/°		ϕ/°
C(2)–C(1)–C(10A)	120.5(11)	C(7)–C(8)–Br(8)	109.6(7)
C(1)–C(2)–C(3)	121.9(16)	C(9)–C(8)–Br(8)	112.0(5)
C(2)–C(3)–C(4)	118.6(15)	C(8)–C(9)–C(10)	124.9(12)
C(3)–C(4)–C(4A)	122.3(11)	C(9)–C(10)–C(10A)	121.8(8)
C(6)–C(5)–C(4A)	134.6(11)	C(9)–C(10)–Br(10)	120.5(7)
C(6)–C(5)–Br(5)	114.5(8)	C(10A)–C(10)–Br(10)	117.5(7)
C(4A)–C(5)–Br(5)	110.9(7)	C(4)–C(4A)–C(5)	118.6(8)
C(5)–C(6)–C(7)	127.7(14)	C(5)–C(4A)–C(10A)	123.3(11)
C(6)–C(7)–C(8)	119.4(11)	C(4)–C(4A)–C(10A)	117.7(13)
C(6)–C(7)–O(7)	116.4(11)	C(1)–C(10A)–C(4A)	118.7(11)
C(8)–C(7)–O(7)	123.8(9)	C(1)–C(10A)–C(10)	118.4(8)
C(7)–C(8)–C(9)	110.3(7)	C(10)–C(10A)–C(4A)	122.9(14)

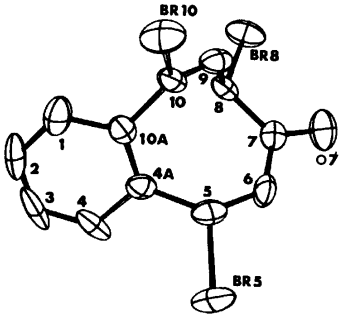

Fig. 2. Molecular conformation and atomic labelling.

TABLE 3. TORSION ANGLES OF THE EIGHT-MEMBERED RING

Torsion angle	ϕ/°	
	This study	Boat form of cyclooctane
C(4a)-C(5)-C(6)-C(7)	−0.2	0.0
C(5)-C(6)-C(7)-C(8)	13.6	73.5
C(6)-C(7)-C(8)-C(9)	63.6	0.0
C(7)-C(8)-C(9)-C(10)	−90.7	−73.5
C(8)-C(9)-C(10)-C(10a)	−7.8	0.0
C(9)-C(10)-C(4b)-C(4a)	57.6	73.5
C(10)-C(10a)-C(4a)-C(5)	10.6	0.0
C(10a)-C(4a)-C(5)-C(6)	−57.2	−73.5

Crystal and Molecular Structures of 5. The geometrical aspects of the molecule and the atomic numbering are shown in Fig. 2. Bond lengths and angles, and torsion angles are given in Tables 2 and 3, respectively.

The conformation of the eight-membered ring can be described as an approximation to the boat form, although there are some significant deviations. A comparison of the torsion angles found in this study with those calculated for the boat conformation of cyclooctane by Hendrickson,[9] shows that the major difference is at the C(7)–C(6) and C(7)–C(8) bonds attached to the carbonyl group. This may be due to the conjugating effect between the carbonyl group and adjacent double bonds, and these related four atoms, C(5), C(6), C(7), and O(7), are almost planar with a maximum deviation of 0.077 Å at C(6). Thus, the *endo*-cyclic bond angles of the eight-membered ring range from 134.6° (C(4a)–C(5)–C(6)) to 110.3° (C(7)–C(8)–C(9)), corresponding to regular octahedral and tetrahedral angles, respectively. The Br(8) atom is located at the equatrial position of the eight-membered ring.

Experimental

3,7-Dibromo-2,6-diethylbiphenylene (1). To a solution of 2,6-diethylbiphenylene[6] (0.20 g, 0.96 mmol) in dichloromethane (20 ml) was added a solution of bromine (19.7 ml of 0.5% v/v solution, 1.9 mmol) in dichloromethane under ice-cooling. The solution was stirred for 1 h at room temperature, then poured into water and extracted with dichloromethane. After drying over anhyd sodium sulfate the extract was evaporated. The crystalline residue was recrystallized from acetone-hexane. The title compound (128 mg, 36%) was obtained as yellow needles, mp 165—166 °C. Found: C, 52.72; H, 3.91%. Calcd for $C_{16}H_{14}Br_2$: C, 52.49; H, 3.85%. UV (EtOH): 210.2 (log ε 3.91), 252 (4.61), 261 (5.00), and 372 nm (3.82). IR (KBr): 2950, 1555, 1417, and 880 cm^{-1}. ^{1}H-NMR ($CDCl_3$): δ=1.15 (t, 6H, J=7.5 Hz, CH_3), 2.62 (q, 4H, J=8 Hz, CH_2), 6.58 (s, 2H, H-1 and H-5), and 6.84 (s, 2H, H-4 and H-8). MS (70 eV): *m/e* 364 (M^+, 84%), 349 (M^+ +2, 100%).

3,5,8,10-Tetrabromo-2,7-diethylbenzocyclooctene (2). To a solution of **1** (0.12 g, 0.33 mmol) in dry dichloromethane (10 ml) was added a solution of bromine (8.4 ml of 0.5% v/v solution, 0.81 mmol) in dichloromethane. The solution was stirred for 4 h at room temperature. The color of bromine did not disappear. The solution was washed with aq sodium hydrogencarbonate and dried over anhyd sodium sulfate. After evaporation, the crude crystalline residue was recrystallized from acetone-hexane. The title compound (116 mg, 70%) was obtained as pale yellow cubics, mp 133—135 °C. Found: C, 36.29; H, 2.39%. Calcd for $C_{16}H_{11}Br_4$: C, 36.54; H, 2.68%. UV (EtOH): 230 nm (log ε 4.62). IR (KBr): 2950, 1610, 1330, 950, and 640 cm^{-1}. ^{1}H-NMR ($CDCl_3$): δ=0.88 (t, 3H, J=8.0 Hz, CH_3), 1.26 (t, 3H, J=7.0 Hz, CH_3), 1.9—2.5 (m, 2H, CH_2), 2.77 (q, 2H, J=7.3 Hz, CH_2), 6.58 (m, 1H, H-4), 6.74 (m, 1H, H-7), 7.30 (s, 1H, H-6′), and 7.58 (s, 1H, H-3′). ^{13}C-NMR ($CDCl_3$): δ=11.4 (q), 13.7 (q), (29.0 (t), 29.1 (t), 115.5 (s), 119.2 (s), 121.9 (s), 125.1 (s), 129.7 (d), 132.8 (d), 134.8 (d), 135.8 (s), 136.4 (s), 142.4 (s), and 144.2 (s). MS (70 eV): *m/e* 522 (M^+, 0.01%), 442 (M^+ −Br, 5.4%), 362 (M^+ −2Br, 13.5%), and 29 (Et^+, 100%).

Bromination of 2-Acetoxybiphenylene. To a solution of 2-acetoxybiphenylene[7] (0.20 g, 0.95 mmol) in dichloromethane (20 ml) was added a solution of bromine (0.30 mg, 1.9 mmol) in dichloromethane (19.5 ml) under ice-cooling. The solution was stirred for 1.5 h, then washed with aq sodium hydrogencarbonate, and dried over anhyd sodium sulfate. After evaporation, the oily residue was subjected to TLC on silica gel by elution with benzene–ethyl acetate. 5,8,10-Tribromo-7(8*H*)-benzocyclooctenone (**5**) (132 mg, 35%)[4] was obtained, along with an oily mixture. The latter oil was treated three times with methanol to form a small amount of 2-acetoxy-3-bromobiphenylene as yellow needles, mp 125—126 °C. Found: C, 58.39; H, 3.04%. Calcd for $C_{14}H_9BrO_2$: C, 58.15; H. 3.13%. UV (EtOH): 245 (log ε 4.60), 254 (4.97), 345 (3.47), and 365 nm (3.67). IR (KBr): 1765, 1420, 1200, and 745 cm^{-1}. ^{1}H-NMR ($CDCl_3$): δ=2.32 (s, 3H, $COCH_3$), 6.48 (s, 1H, H-1), and 6.5—7.0 (m, 5H). MS (70 eV): *m/e* 288 (M^+, 2.3%), 246 (M^+ −CH_2CO, 34%), 139 (M^+−Br−CH_2CO−CO, 100%) and 138 (M^+ −Br−CH_3CO−CO).

Bromination of 2-Acetamidobiphenylene. To a solution of 2-acetamidobiphenylene[8] (0.33 g, 1.6 mmol) in acetic acid (30 ml) was added a solution of bromine (2 ml of 10% v/v solution, 3.8 mmol) in the same solvent. The solution was stirred for 2 h at 80 °C, then poured into water (150 ml), and extracted three times with ether. The extract was dried over anhyd magnesium sulfate. After evaporation, the residue was chromatographed on silica gel by elution with benzene–ethyl acetate. One of the products obtained was **5** (64 mg, 10%) (mp 138—139 °C).[4] The other was **8** (colorless crystals, mp 155—156 °C) (177 mg, 25%). Found: C, 37.54; H, 2.23; N, 3.03%. Calcd for $C_{14}H_{10}Br_3NO$: C, 37.54; H, 2.25; N, 3.13%. IR (KBr): 1655, 1620, 1292, and 940 cm^{-1}. ^{1}H-NMR ($CDCl_3$): δ=2.03 (s, 3H, $COCH_3$), 6.73 (d, 1H, J=1.3 Hz, H-4), 6.94 (d, 1H, J=1.3 Hz, H-7), 7.3 (broad s, 1H, NH), and 7.44 (s, 4H, Ar-H). ^{13}C-NMR ($CDCl_3$): δ=29.4 (q), 122.2 (s), 125.9 (s), 129.1 (d), 129.5 (d), 129.6 (d), 130.3 (d), 132.3 (d), 133.9 (s), 136.6 (s) 138.3 (s), 139.7 (s), and 145.2 (s), MS (70 eV): *m/e* 445 (M^+, 0.8%), 366 (M^+ −Br, 16%), 323 (M^+−Br−CH_3CO, 38%), and 246 (M^+−2Br−CH_2CO,

100%).

5,8,10-Tribromo-7(8H)-benzocyclooctenone (5). To a solution of 2-acetamido-3-bromobiphenylene (58 mg, 0.2 mmol) in dry dichloromethane (7 ml) was added a solution of bromine (4 ml of 0.5% v/v solution, 0.38 mmol) under ice-cooling. The solution was stirred for 2 h at room temperature. After the usual work-up, the residue obtained was purified by TLC on silica gel by elution with benzene–dichloromethane. The title compound (85 mg, 94%) was obtained.

A solution of **8** (53 mg, 0.12 mmol) in ethanol (2 ml) and 48% hydrobromic acid (0.5 ml) was refluxed for 2 h. After usual work-up, the product obtained was recrystallized from hexane–acetone to give the title compound (35 mg, 80%).

2'-Bromo- and 4'-Bromo-3-nitrobiphenyl. To a suspension of 3-nitrobenzenediazonium tetrafluoroborate, prepared from *m*-nitroaniline (6.7 g, 0.05 mol), in dry bromobenzene, were added 18-crown-6 (0.5 g) and potassium acetate (7.54 g, 0.077 mol). The mixture was stirred for 1.5 h under water-cooling and then filtered. The filtrate was washed with a saturated aq solution of sodium chloride, and dried over anhyd magnesium sulfate. After evaporation, the red oily residue was chromatographed on alumina using benzene–hexane as eluent to give a colorless oil (10.1 g), from which 2'-bromo-3-nitrobiphenyl (1.82 g, 13%) and 4'-bromo-3-nitrobiphenyl (1.1 g, 8%) were obtained by fractional recrystallization from ether. 2'-Bromo-3-nitrobiphenyl, colorless plates, mp 76—78 °C (lit,[3] 77—78 °C). IR (KBr): 1535, 1352, 763, 739, and 687 cm^{-1}. ^{1}H-NMR ($CDCl_3$): δ=7.1—7.6 (m, 3H), 7.6—8.1 (m, 3H), 8.2—8.5 (m, 2H). ^{13}C-NMR ($CDCl_3$): δ=122.1 (s), 122.4 (d), 124.3 (d), 127.6 (d), 128.8 (d), 129.6 (d), 130.9 (d), 133.2 (d), 135.4 (d), 139.9 (s), 142.3 (s), and 147.8 (s). 4'-Bromo-3-nitrobiphenyl, colorless crystals, mp 84—85 °C. IR (KBr): 1535, 1359, 877, 824, 796, 763, 738, and 675 cm^{-1}. ^{1}H-NMR ($CDCl_3$): δ=7.3—8.1 (m, 6H) and 8.15—8.6 (m, 2H).

3-Acetamido-2',6-dibromobiphenyl. According to the direction described by Baker *et al.*,[3] 3-acetamido-2'-bromobiphenyl, prepared by reduction and subsequent acetylation of 2'-bromo-3-nitrobiphenyl, was brominated to give the title compound in 72% yield, but 3-acetamido-2',4,6,-tribromobiphenyl was not isolated.

5-Acetamido-2',4,6-tribromobiphenyl. 2',6-Dibromobiphenyl (365 mg, 1 mmol) and anhydrous sodium acetate (621 mg) were dissolved in boiling acetic acid (9.5 ml) and acetic anhydride (0.8 ml). To the mixture was added a solution of bromine (0.50 g, 3.1 mmol) in acetic acid (5 ml). The solution was refluxed for 1 h and poured into ice-water. The crystals were collected by suction, then washed with water, and dried. The products were chromatographed on silica gel by elution with benzene–ethyl acetate to give a colorless oil (227 mg, 50.6%) and colorless crystals (156 mg, 42.7%). The latter was recovered starting material. Crystallization and recrystallization of the former oil from ether gave the title compound as colorless crystals, mp 117—118 °C.

X-Ray Crystallography of 5. A crystal of dimensions 0.4 $\times$0.4$\times$0.2 mm obtained from hexane–acetone, was used for the intensity measurements. Intensity data were obtained on a Rigaku four-circle automatic diffractometer, equipped with graphite-monochromated Cu *Kα* radiation, and using the θ-2θ scan technique ($2\theta \leq 127°$). 1554 independent reflecions ($F_o \geq 2.5\,\sigma F_o$) were corrected for Lorentz and polarization factors but not for absorption.

Crystal Data. $C_{12}H_7OBr_3$, orthorhombic, Pbca, z=8, a=9.667(2), b=16.261(3), c=15.957(3) Å, D_{calcd}=2.08 g/cm^3. The structure was solved by heavy atom methods. The positional and thermal parameters were refined by block diagonal least-squares methods. The positions of all hydrogen atoms were located from a difference Fourier synthesis. The final discrepancy index R is 0.079. The positional parameters for nonhydrogen atoms are listed in Table 1. Thermal parameters for nonhydrogen atoms, fractional coordinates and isotropic thermal hydrogen atoms, and observed and calculated structure factors are kept at the Chemical Society of Japan (Document No. 8313).

References

1) M. P. Cava and M. J. Mitchel, "*Cyclobutadiene and Related Compounds*," Academic Press, New York and London (1965), p. 255; J. W. Barton, "*Nonbenzenoid Aromatics*" ed by J. P. Snyder, Academic Press, New York and London, (1969), p. 32.

2) J. M. Blatchly, D. V. Gardner, J. F. W. McOmie, and M. L. Watts, *J. Chem. Soc., C*, **1968**, 1545.

3) W. Baker, J. F. W. McOmie, D. R. Preston, and V. Rogers, *J. Chem. Soc.*, **1958**, 414.

4) H. Kidokoro, M. Sato, and S. Ebine, *Bull. Chem. Soc. Jpn.*, **55**, 3204 (1982).

5) A part of this work was published in a preliminary report: H. Kidokoro, M. Sato, and S. Ebine, *Chem. Lett.*, **1981**, 1269.

6) D. V. Gardner and J. F. W. McOmie, *J. Chem. Soc., C*, **1968**, 2420.

7) J. M. Blatchly, D. V. Gardner, and J. F. W. McOmie, *J. Chem. Soc., C*, **1967**, 272.

8) W. Baker, J. F. W. McOmie, *J. Chem. Soc.*, **1958**, 2666.

9) J. B. Hendrickson, *J. Am. Chem. Soc.*, **89**, 7036 (1967).

Aryliminodimagnesium Reagents. VI. The Reactions with Conjugated Carbonyl Compounds. The Initial Coordination and the Electron-transfer in the Reactions of Organomagnesium Reagents

Masao Ōkubo,* Masatoshi Yoshida, Kotomi Horinouchi, Hiroshi Nishida, and Yoshinori Fukuyama

Department of Chemistry, Faculty of Science and Engineering, Saga University, Honjō-machi, Saga 840

(Received October 1, 1982)

The reactions of aryliminodimagnesium reagents ($ArN(MgBr)_2$) with benzylideneacetophenones, quinones, and benzils were examined. Among the product-distributions in the reactions with the enones and the α-diketones, some examples in which *p*-MeO-substituted substrates gave higher yields of condensation products were obtained. The results are in contrast with the product-distributions in the reaction of ArMgBr with Ar^1COAr^2 and that of $ArN(MgBr)_2$ with Ar^1NO_2: *p*-Cl-Substituted substrates are advantageous for the formation of addition and/or condensation products. These reactions of the two organomagnesium reagents were classified into "coordination controlled" and "electron-transfer controlled" ones on the basis of the combination of electron-donating ability of reagents with the electron-accepting ability of substrates. The classification was illustrated also on the basis of the relative difference of the energy levels of HOMO's and LUMO's of the reactants.

The sequence of the Grignard reaction of benzophenone is formulated as shown in Scheme 1. In

1) coordination:

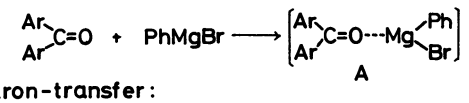

2) electron-transfer:

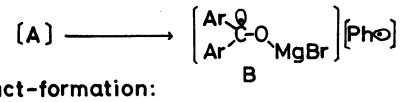

3) product-formation:

i) radical recombination:

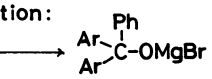

ii) radical-anion reaction:

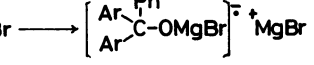

Scheme 1.

general, the initial coordination process is quite rapid and the subsequent electron-transfer process is rate-determining.[1-3] The two types of elementary reactions, i) and ii), are possible for the product-formation process: An evidence for the radical recombination was reported on the basis of product analysis,[4] while another evidence was obtained by ESR on the replacement of electronegative substituents.[2]

The rate-determining electron-transfer process of the reaction of Scheme 1 is accelerated by the electron-attracting *p*-halogeno substituents of the substrate and also by the electron-repelling *p*-methoxyl substituent of the reagent.[2,3] The similar type of the electronic effect of substituents was observed in the product-distribution obtained on the condensation of aryliminodimagnesium reagents ($ArN(MgBr)_2$, aryl-IDMg) with nitroarenes (Scheme 2): A high combined yield of unsymmetrical and symmetrical azoarenes was obtained when Ar^1 had *p*-MeO and Ar^2 had *p*-Cl substituents, while a high yield of azoxyarene was obtained when

$$Ar^1N(MgBr)_2 + Ar^2NO_2 \longrightarrow Ar^1\text{-}N{=}N(O)\text{-}Ar^2 + Ar^1\text{-}N{=}N{=}Ar^2 + Ar^1\text{-}N{=}N\text{-}Ar^1$$

Scheme 2.

the reactants were reversely substituted.[3,5] Though the detailed mechanism of the IDMg reaction remains to be studied, the similar type of the electronic effect of substituents found in the reactions of Schemes 1 and 2 will allow the present authors to compare the reactivities of the two organomagnesium reagents in the common elementary processes, *i.e.*, the initial coordination of the substrate to the Mg atom of the reagent and the subsequent electron-transfer.

A different type of substituent effect was reported previously on the condensation of aryl-IDMg with diaryl ketones (Scheme 3): even the least electron-accepting bis(*p*-dimethylamino)benzophenone gave a sufficient yield of the anil,[6,7] and a higher combined yield of products was obtained in the reaction with 1-methoxy-9-fluorenone than that with 1-halogeno-9-fluorenone.[8]

$$Ar^1N(MgBr)_2 + Ar^2COAr^3 \longrightarrow Ar^1\text{-}N{=}C(Ar^2)(Ar^3)$$

Scheme 3.

In order to find the reason for the apparent contradiction, the reaction of aryl-IDMg with some other types of carbonyl compounds was investigated. In this paper, the product-distribution obtained in the IDMg reaction with benzylideneacetophenones, quinones, and benzils will first be described, and compared with that obtained in the Grignard reaction with the same substrates, respectively. On the basis of the comparison, the role of the initial coordination in the IDMg reaction with carbonyl compounds, including diaryl ketones, will be emphasized. The types of the electronic substituent effects found in the reactions of the two organomagnesium reagents with nitro and carbonyl compounds will be classified and discussed in terms of the electron-accepting and -donating abilities of the reactants.[8]

Results and Discussion

IDMg Reaction with Benzylideneacetophenones. In the Grignard (ArMgBr) reaction of benzylideneaceto-

Table 1. Product-distribution in the IDMg reaction with benzylideneacetophenones (Scheme 4b)

Expt No.	Ar^1	Ar^2	Ar	[IDMg]/[Enone]	Product Type[b]	Product Yield/%
1	2,4,6-$Me_3C_6H_2$	C_6H_5	4-MeC_6H_4	1.2	**4**	42—64
2	2,4,6-$Me_3C_6H_2$	C_6H_5	4-$MeOC_6H_4$	1.2	**4**	43
3	4-ClC_6H_4	4-ClC_6H_4	4-$MeOC_6H_4$	1.2	**4**	20
4	4-ClC_6H_4	4-MeC_6H_4	4-$MeOC_6H_4$	1.2	**5**	7.5
5	4-$MeOC_6H_4$	C_6H_5	4-MeC_6H_4	1.2	**6a** **6b**	37 12
6	4-$MeOC_6H_4$	C_6H_5	4-MeC_6H_4	3.0	**6a**	74
7	4-$MeOC_6H_4$	DMB[a]	4-MeC_6H_4	1.2	**7**	10
8	4-$MeOC_6H_4$	DMB[a]	4-MeC_6H_4	5.0	**7**	59

a) DMB=2,6-Me_2-4-*t*-BuC_6H_2. b) Types of products are given in Scheme 4b.

phenones, **1**, the normal 1,2-addition product, **2**, and the conjugate 1,4-addition product, **3**, are obtained when an excessive molar equivalent of the reagent is used (Scheme 4a): The product **3** is obtained usually in yields higher than 90% almost independently of the electronic effect of substituents of the enones.[9] When a deficient equivalent of the reagent was used, a product due to the radical dimerization at the the β-position of the enone was isolated.[10] The high spin densities on the carbonyl and the β-positions were observed[11,12] and the electron-transfer mechanism for the 1,4-addition and the dimerization was proposed.[2]

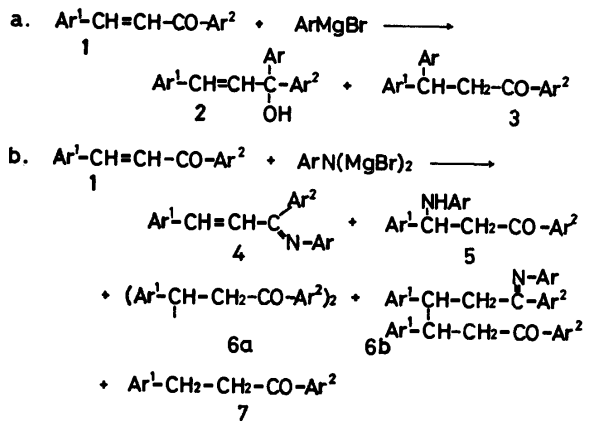

Scheme 4.

In contrast, the IDMg reaction with the same substrate gave an appreciably different product-distribution (Scheme 4b and Table 1): The types of products, **4**—**7**, and their yields were specified dramatically by the electronic and steric effect of the benzylidene and benzoyl moieties, Ar^1 and Ar^2, respectively.

The hindered Ar^1 and the unhindered Ar^2 lead to a moderate yield of the normal condensation product **4** (Expts 1 and 2): A low yield of **4** was obtained when both Ar^1 and Ar^2 had the electron-attracting *p*-Cl substituent (Expt 3). A low yield of the 1,4-addition product **5** was obtained only when Ar^1 had *p*-Cl substituent and Ar^2 had *p*-Me substituent (Expt 4). The reductive dimerization product **6a** and the condensation-dimerization product **6b**, both of which were indicative of the existence of the electron-transfer process, were obtained in fair yield when Ar^1 had *p*-MeO substituent (Expts 5 and 6): A high yield of **6a** was obtained when a larger excess of the reagent was used (Expt 6). The reduction product **7** was formed when the enone had hindered Ar^2 (Expts 7 and 8): The comparison of the results of Expts 5 and 6 with those of Expts 7 and 8 shows that the bulkiness of the substrate is in favor of hydrogen abstraction from the solvent molecule by the intermediate radicals but not of their dimerization. No product other than the unreacted enones and the products **4**—**7** were detected in Expts 1—8.

The notably different profiles of the reaction of Scheme 4b from those of Scheme 4a are explained in terms of the moderate reactivity[3,6]—electron-donating ability—of aryl–IDMg compared with that of ArMgBr and also in terms of the initial coordination of substrate to the Mg atom of the reagent. The first factor, the moderate reactivity of aryl–IDMg, is responsible for the unexpectedly enhanced selectivity observed in the reaction of Scheme 4b. The second factor, the effective initial coordination, is responsible for the high yields of the typical radical products in Expts 5—8 in comparison with the low yields of condensation or addition products in Expts 3 and 4: The *p*-MeO substituent of the substrate is advantageous for the coordination and facilitates the subsequent electron-transfer and the product-formation. The attempt to detect the intermediate radicals by ESR at room temperature was unsuccesful: No sufficient accumulation of them is due to the weakly electron-donating ability of the reagent. The role of the initial coordination will be discussed again in the final section.

IDMg Reaction with Quinones. The reaction of PhMgBr with quinones under the ordinary reaction conditions lead to the formation of hydroquinone and biphenyl,[13] their formation indicating the existence of the electron-transfer process. Some products due to radical substitution were also reported,[14] and the detection of the semiquinone radical by ESR was successful only by use of a fully diluted reaction mixture.[15]

The reactions of aryl–IDMg with 2-methyl- and 2-methoxy-1,4-naphthoquinones were clearly different from that with 9,10-anthraquinone. In the reactions with the naphthoquinones, complex mixtures containing large amounts of quinhydrone-like products and hardly soluble black materials were obtained: The normal

condensation products, quinone imines, were isolated only in low yields (10—20%). In the reaction with anthraquinone, in contrast, good yields of the quinone imines were obtained and no formation of unidentifiable products was observed. The results of the individual reactions will be described first, and a summary discussion will be given in terms of the electron-accepting ability of the quinones.

In the reactions of 2-methyl-1,4-naphthoquinone with 4—6 molar equiv. of *p*-Me– and *p*-MeO–C_6H_4–IDMg, a lower than 10% yield of dark red products—quinone mono- and diimines—was isolated from the complex mixture. The quinone imines show the ^{1}H-NMR spectra having more than two Me- and MeO-proton signals probably due to the geometrical isomerism around the >C=N– groups: The separation of the isomers was unsuccessful.

In the reaction of 2-methoxy-1,4-naphthoquinone, **8**, with *p*-Me–C_6H_4–IDMg (4 molar quiv., Scheme 5a), a dark red product which had more than two *p*-Me–C_6H_4 groups but no MeO group was isolated from the complex mixture. The ^{1}H-NMR spectrum has three or four signals at the range of δ=2.3—2.4: The splitt pattern, which indicates that the isolated product is a mixture, changes gradually, during the repeated treatment on silica gel, into another pattern consisting of two signals at δ=2.40 and 2.36. The final product, **10**, shows ν_{OH} absorption band at 3350 cm^{-1} (mp 136 °C). In the reaction with 1,2-naphthoquinone, **11** (Scheme 5b), the quinone diimine, **12** (mp 175 °C), isolated in 4% yield shows two Me-proton signals at δ=2.36 and 2.30: The splitt pattern resembles closely that of **10**. The structure of the primary product in the reaction of **8** is thus assigned to the condensation-replacement product, **9** (yield: 20%), which isomerizes into **10** during the quenching with aqueous NH_4Cl and the subsequent treatment with moist silica gel.

It should be noted here briefly that the formation of the oxidative coupling product, 4,4′-dimethylazobenzene, in the reaction of *p*-Me–C_6H_4–IDMg is associated with the structure of quinones. The azoarene was isolated in 8% yield in the reaction with **11**. The azoarene is the sole identifiable product (yield: 19%) in the reaction with 9,10-phenanthraquinone, which also gave large amounts of unidentifiable black materials and no condensation product. The formation of symmetrical azoarenes is unavoidable in the IDMg reaction with nitroarenes (Scheme 2).[3] The oxidative coupling of the IDMg molecules is thus ascribed to the structural resemblance of the *ortho*-quinones and nitroarenes, those having the similarly oriented two oxygen atoms.

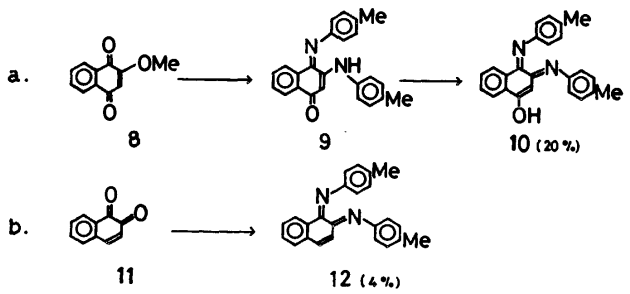

Scheme 5.

In contrast to the poor yields of the condensation products in the reactions of the naphthoquinones and phenanthraquinone, anthraquinone gave good yields of the quinone mono- and diimine depending clearly upon the electron-donating abilities of the reagents, *p*-Me– and *p*-MeO–C_6H_4–IDMg (Scheme 6 and Table 2). The less electron-donating former reagents gave the monoimine, **14** (R=Me), even by use of the reagent in a large excess, whereas the more electron-donating latter reagent gave the diimine, **15** (R=MeO).

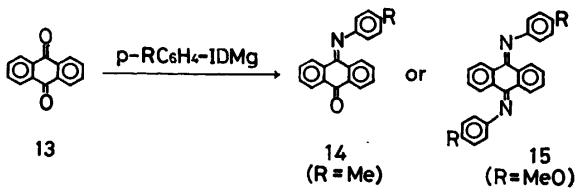

Scheme 6.

The inertness of **14** (R=Me) towards *p*-Me–C_6H_4–IDMg is understood by considering the intramolecular charge separation as depicted by the structure, **14a**, which is more favorable for the initial coordination to the reagent's Mg atom but is less favorable for the subsequent electron-transfer. In order to check the electron-repelling resonance effect, *N*-methylacridone, **16**, was treated with the same reagent (Scheme 7): The yield of the corresponding imine, **18**, was 28% by use of 1.2 molar equiv. of the reagent (recovery of **16**: 56%) but the yield was improved to 94% by use of four molar equivalents. The reaction of xanthone, **17**, with aryl–

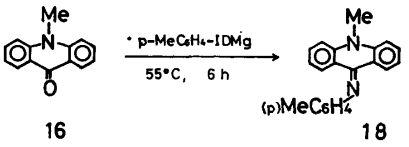

Scheme 7.

Table 2. Product-distribution in the IDMg reaction with anthraquinone (Scheme 6)

Expt No.	[IDMg][a] / [Substrate]	R	Amount of THF/ml	Reaction time at 55 °C / h	Yield/% 14	15	Azo	Recovered
9	4	Me	195	1	16	—	1.8	58
10	8	Me	100	6	68	—	1.3	Yes
11	16	Me	65	48	44	—	2.6	Yes
12	8	MeO	100	6	—	41	2.0	23

a) Sixteen millimols of IDMg reagents were used.

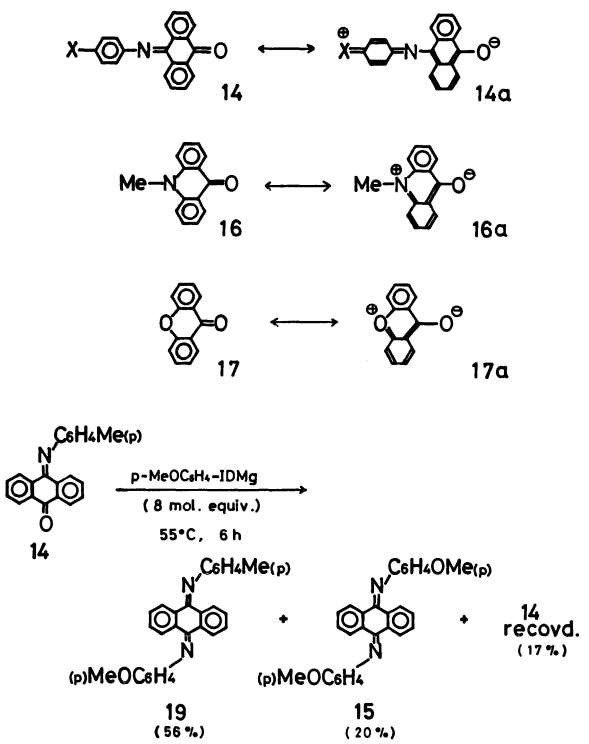

Scheme 8.

IDMg was reported.[5] On the basis of these results, **14** was treated with the more electron-donating *p*-MeO–C_6H_4–IDMg (8 molar equiv.): The expected mixed diimine, **19** and the exchange product, **15** (R=MeO), were obtained (Scheme 8).

The profiles of the IDMg reaction with the quinones described above can be understood by taking their reduction potentials (E_0/V)[16] into account: 1,2-Naphthoquinone (0.58)>1,4-naphthoquinone (0.48)> 9,10-phenanthraquinone (0.46)≫9,10-anthraquinone (0.15). The order of the values seems to be correlated to the following series of the yields of the condensation products: No formation of 9,10-phenanthraquinone imines, the poorest yield 1,2-naphthoquinone diimine (**12**), the 10% yield of 2-methyl-1,4-naphthoquinone imines, the 20% yield of the condensation-replacement product **9**, and the good yields of 9,10-anthraquinone imines (**14** and **15**). The fact that the IDMg reaction with the least electron-accepting (*i.e.*, oxidizing) quinone proceeds most smoothly is indicative of the important role of the combination of electron-donating and -accepting abilities of the reactants.

IDMg Reaction with Benzils. The reaction of benzil and its derivatives, **20**, with excessive amounts of ArMgBr was utilized for preparing substituted benzopinacols, **21**[17] (Scheme 9a): The by-products and the mechanism of the reaction have not been studied extensively, but the ESR evidence for the electron-transfer was reported very recently.[18]

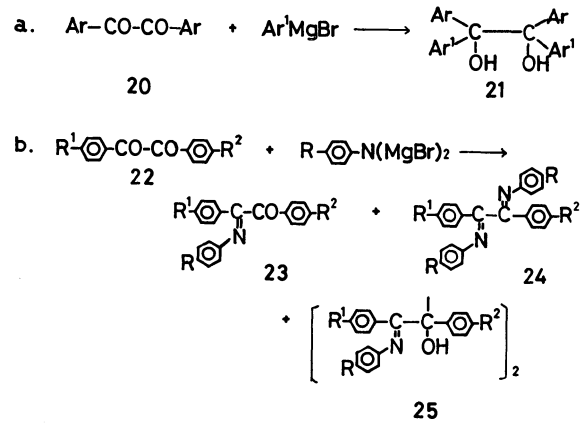

Scheme 9.

The reaction of *p*-substituted benzils with excessive equivalents of aryl–IDMg gave monoimine, **23**, diimine, **24**, and the condensation-dimerization product, **25**, in high combined yields (Scheme 9b and Table 3): The appreciable formation of **25** is reasonable since the higher electron-accepting ability of α-dicarbonyl compound[12] causes a rapid electron-transfer even from the moderately electron-donating reagent.

The distribution of the three types of products was varied but not so dramatically by the reaction conditions (Expts 13—15) and also by the substituents of both substrate and reagent (Expts 14, 16, and 17). The much smaller variation of product-distribution than that of the reaction of Scheme 4b is attributed to the higher electron-accepting ability of benzils: The electronic effect upon the product-distribution is not enhanced but reduced. The intermediate radical derived from 4,4′-dimethylbenzil, **22** (R^1=R^2=Me), observed easily at room temperature, gave the ESR spectrum indicating the symmetrical distribution of the free spin on the two *p*-methylbenzoyl moieties (a^H_{Me}=

Table 3. Product-distribution in the IDMg reaction with benzils (Scheme 9b)

Expt No.	Substrate		Reagent	[IDMg]	Yield/%[a]				
	R^1	R^2	R	[Substrate]	**23**	**24**	**25**	Azo	Recov.
13	Me	Me	OMe	2.5	32	16	32	Trace	4
14	Me	Me	OMe	5.0	21	24	40	—	—
15	Me	Me	OMe	5.0[b]	34	26	28	Trace	8
16	MeO	MeO	Me	5.0	17	28	38	Trace	—
17	Cl	Cl	Me	5.0	28	10	35	Trace	4
18	Cl	MeO	Me	1.5[c]	59[d]	4	25	Trace	10

a) Yields obtained after heating at 55 °C for 6 h. b) The addition was carried out in the "reverse" manner. c) For examining the difference between the reactivities of the two carbonyl groups, a small amount of the reagent was added in the "reverse" manner. d) The constitution of the two isomeric 1 : 1-product is given in the text.

1.2 G, a^{H}_{O-H}=2.1 G, 1 G=10^{-4} T).

Though the radical concentration observed in the reaction of 4,4'-dimethoxybenzil, **22** (R^1=R^2=MeO), was remarkably lower than that observed in the reaction of 4,4'-dimethylbenzil, the very similar distribution of the three types of products were obtained (Table 3, Expts 14 and 16). Both the effective electron-transfer from the reagent in Expt 14 and the effective coordination of the substrate to the reagent in Expt 16 are responsible for the closely similar results.

The examination of the reaction with an unsymmetrical benzil, **22** (R^1=Cl, R^2=MeO), gave an explicit evidence for the initial coordination as a governing factor for the product-distribution. In the reaction using one and a half molar equivalents of *p*-Me-C_6H_4-IDMg, a high yield of a mixture of the isomeric monoimines, **23a** and **23b**, was obtained (Expt 18). The

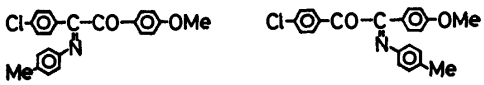

23a **23b**

chromatographic separation of the isomers was incomplete, but the comparison of the ^{1}H-NMR chemical shifts of the Me- and MeO-protons with those of the monoimines obtained in Expts. 16 and 17 showed that the mixture contained **23a** and **23b** in an approximate molar ratio of 1 : 2. Also the relative yields of mono- and diimines in Expts 16 and 17 reflect the advantage of the substrate's *p*-MeO group over the *p*-Cl group for the product-formation.

General Discussion. The significance of the combination of electron-donating ability of reagents with electron-accepting ability of substrates in the reactions of organomagnesium reagents (ArMgBr and ArN-$(MgBr)_2$) was pointed out very recently.[8] Since the new method for preparing unsymmetrical azoxy- and azoarenes by the IDMg reaction with the highly electron-accepting nitroarenes[19,20] owes its success to the moderately electron-donating ability of the reagent,[3,6] it is reasonable to classify the profiles of the reactions of the organomagnesium reagents from the same standpoint. The classification into three types will be given in the following.

The type A represents the "hardly controllable reactions" leading to the formation of large amounts of radical products due to much vigorous electron-transfer. The first example is the reaction of highly electron-donating ArMgBr with highly electron-accepting $PhNO_2$ (A-1). The formation of the three types of products, ArNHPh, ArOH, and Ar–Ar, in comparable yields (50—60%) was reported:[21] The high yield of the biphenyl is the result of efficient oxidative coupling of the reagent molecules. The second example is the reaction of the moderately electron-donating aryl–IDMg with the strongly electron-accepting naphthoquinones (A-2) described above.

The type B represents the "electron-transfer controlled reactions" which involve the moderate electron-transfer followed by efficient formation of normal products due to addition and/or condensation. The reactions of this type are accelerated by the electron-attracting *p*-F and *p*-Cl substituents of substrates and also by the electron-repelling *p*-MeO substituent of reagents. The first example is the well-studied reaction of ArMgBr with the moderately electron-accepting diaryl ketones (B-1; *cf.* Scheme 1). The second example is the IDMg reaction with nitroarenes (B-2; Scheme 2). The reactions B-1 and B-2 involve the rapid coordination followed by the rate-determining electron-transfer[1] and the subsequent product-formation. The more moderate reaction of imino compounds with ArMgBr (B-3) was reported.[8,22]

The type C represents the "coordination controlled reactions," the product-distributions of which are governed by the initial coordination of the substrates to the Mg atom of the reagent: The electron-repelling *p*-MeO substituent of both reactants is favorable for the product-formation. The examples are the IDMg reactions with diaryl ketones (C-1), benzylideneacetophenones (C-2), and benzils (C-3). Though the existence of the electron-transfer process in C-1 and C-2 reactions is indicated by the formation of diarylmethanols[7] and that of **6** respectively, the attempt to detect the ketyl-type radicals by ESR at room temperature is unsuccessful: This fact suggests that the process in these reactions takes place after the initial coordination has been completed. The favorable role of the *p*-MeO-substituted reagent in the type C reactions can be ascribed to the acceleration of the subsequent electron-transfer process. The reaction C-3 involves the most rapid electron-transfer among the three examples: This reaction has the type B character with regard to the substituent effect upon the concentration of radicals (*vide supra*). It is quite reasonable that, as the electron-donating and -accepting abilities of the reactants are lowered, the rate-determining step is shifted to the just initial coordination process (*cf.* Scheme 1).

The electron-accepting ability of substrates should be estimated by comparing the relative values of the reduction potentials:[16,20] The comparison of the published values in detail between the different types of substrates is not always possible at present because the conditions for the measurements have not been generalized.[20] With regard to the electron-donating ability of reagents, the situation is same because any standard method for determining the oxidation poten-

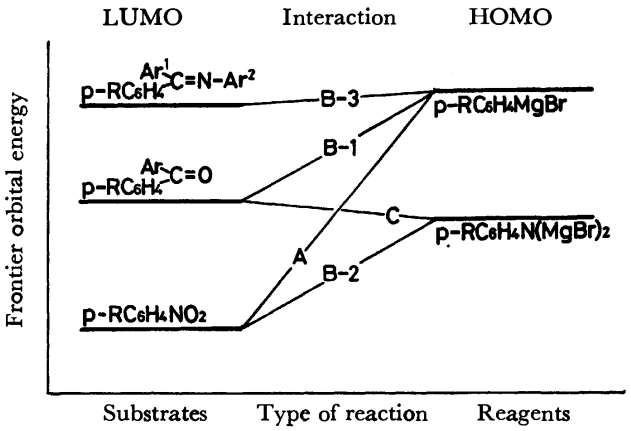

Fig. 1. An illustration diagram for the correlation of frontier orbital energies with reaction profiles.

TABLE 4. ANALYTICAL DATA AND PHYSICAL CONSTANTS OF PRODUCTS

Product No.	Mp θ_m/°C	Formula	Found (Calcd) (%) C	H	N	NMR data δ
14	86—87	$C_{25}H_{25}N$	88.65 (88.49)	7.22 (7.37)	4.14 (4.12)	CCl_4, 8.02—6.24 (13H, m), 2.28 and 2.24 (3H, two s lines), 2.16 (3H, s), 2.10 (3H, s)
24	119—120	$C_{25}H_{25}NO$	84.29 (84.50)	6.99 (7.04)	4.04 (3.94)	CCl_4, 8.16—6.46 (13H, m), 3.88 (3H, d), 2.40 (6H, s), 2.36 (3H, s)
34	179	$C_{22}H_{17}Cl_2NO$	69.02 (69.11)	4.57 (4.45)	3.73 (3.66)	$CDCl_3$, 8.00—6.00 (14H, m), 3.81 (3H, s)
45	116—117	$C_{23}H_{22}ClNO_2$	72.79 (72.72)	5.69 (5.79)	3.78 (3.69)	$CDCl_3$, 7.76—6.34 (12H, m), 4.76 (1H, t), 4.16 (1H, broad s), 3.60 (3H, s), 3.26 (2H, d), 2.36 (3H, s); IR: 3390 and 1670 cm^{-1}
56a	An oil	$C_{32}H_{30}O_4$	80.19 (80.33)	6.39 (6.27)		CCl_4, 8.12—6.50 (18H, m), 3.60 (6H, s), 2.90—2.80 (2H, m), 2.28—2.10 (4H, m); IR: 1680 cm^{-1}
56b	An oil	$C_{39}H_{37}NO_3$	82.42 (82.54)	6.72 (6.52)	2.39 (2.47)	CCl_4, 8.02—6.56 (22H, m), 3.65 (3H, s), 3.60 (3H, s), 2.90—2.60 (4H, m), 2.40—2.30 (2H, m), 2.12 (3H, s); IR: 1685 cm^{-1}
87	An oil	$C_{22}H_{28}O_2$	81.57 (81.48)	8.59 (8.64)		CCl_4, 7.16—6.66 (6H, m), 3.64 (3H, s), 2.88 (2H, t), 2.26 (2H, t), 2.16 (6H, s), 1.26 (9H, s); IR: 1695 cm^{-1}
10	135	$C_{24}H_{20}N_2O$	81.79 (81.82)	5.72 (5.68)	7.99 (7.95)	$CDCl_3$, 8.24—8.06 (2H, m), 7.80—7.16 (10H, m), 6.84—6.26 (2H, m), 2.40 (3H, s), 2.36 (3H, s)
12	175	$C_{24}H_{20}N_2$	85.78 (85.71)	5.87 (5.95)	8.35 (8.33)	$CDCl_3$, 8.62—8.20 (2H, m), 7.80—7.60 (2H, m), 7.36—6.70 (10H, m), 2.36 (3H, s), 2.30 (3H, s)
1014	165—168.5	$C_{21}H_{15}NO$	84.73 (84.85)	5.14 (5.05)	4.78 (4.71)	$CDCl_3$, 8.36—8.24 (2H, m), 7.70—7.36 (6H, m), 7.20 and 6.76 (4H, ABq), 2.40 (3H, s)
1315	183—186	$C_{28}H_{22}N_2O_2$	80.49 (80.38)	5.19 (5.26)	6.61 (6.69)	$CDCl_3$, 8.44—8.28 (2H, m), 7.70—6.90 (6H, m), 6.94 (8H, s), 3.82 (6H, s)
18	86—89	$C_{21}H_{18}N_2$	84.49 (84.56)	6.03 (6.04)	9.48 (9.39)	CCl_4, 7.30—6.64 (12H, m), 3.30 (3H, s), 2.29 (3H, s)
19	79—84	$C_{28}H_{22}N_2O$	84.01 (83.58)	5.39 (5.47)	7.07 (6.96)	CCl_4, 8.42—8.24 (2H, m), 7.56—6.72 (14H, m), 3.74 (3H, s), 2.34 (3H, s)
1423	An oil	$C_{23}H_{21}NO_2$	80.41 (80.47)	6.15 (6.12)	4.01 (4.08)	CCl_4, 7.90—7.64 (4H, m), 7.32—6.60 (8H, m), 3.63 (3H, s), 2.38 (3H, s), 2.30 (3H, s)
1424	160—163	$C_{30}H_{28}N_2O_2$	80.40 (80.35)	6.19 (6.25)	6.23 (6.25)	CCl_4, 7.82 and 7.18 (8H, ABq), 6.66 (8H, s), 3.68 (6H, s), 2.36 (6H, s)
1425	233—236	$C_{46}H_{42}N_2O_4$	80.51 (80.46)	6.02 (6.12)	4.16 (4.08)	$CDCl_3$, 8.04—7.92 (4H, m), 7.50—7.12 (16H, m), 6.90—6.76 (4H, m), 3.76 (6H, s), 2.36 (6H, s), 2.30 (6H, s)
1623	An oil	$C_{23}H_{21}NO_3$	76.95 (76.88)	5.79 (5.85)	3.93 (3.89)	$CDCl_3$, 7.92—7.58 (4H, m), 6.92—6.62 (8H, m), 3.78 (3H, s), 3.73 (3H, s), 2.17 (3H, s)
1624	195—197	$C_{30}H_{28}N_2O_2$	79.98 (80.35)	6.41 (6.25)	6.21 (6.25)	$CDCl_3$, 7.82 (4H, d), 6.86 (8H, d), 6.48 (4H, d), 3.78 (6H, s), 2.24 (6H, s)
1625	>250	$C_{46}H_{42}N_2O_6$	76.71 (76.88)	5.76 (5.84)	3.94 (3.89)	$CDCl_3$, 7.92 and 7.84 (4H, d), 7.34—7.10 (8H, m), 7.00—6.66 (12H, m), 4.08 (2H, broad s), 3.78 (6H, s), 3.74 (6H, s), 2.20 (6H, s)
1723	An oil	$C_{21}H_{15}Cl_2NO$	68.62 (68.48)	4.01 (4.07)	3.69 (3.80)	CCl_4, 7.84 and 7.42 (4H, ABq), 7.68 and 7.32 (4H, ABq), 6.86 and 6.76 (4H, ABq), 2.22 (3H, s)
1724	Not purified					$CDCl_3$, 7.84 and 7.40 (8H, ABq), 6.98 and 6.62 (8H, ABq), 2.27 (6H, s)
1725	>250 scarcely soluble					DMSO-d_6, 8.00—7.90 (4H, m), 7.46—6.90 (20H, m), 2.25 (6H, s)
1823a	An oil					CCl_4, 7.77 and 7.37 (4H, ABq), 7.66 (2H, d), 6.98—6.64 (6H, m), 3.83 (3H, s), 2.20 (3H, s)
1823b	An oil					CCl_4, 7.88 and 7.43 (4H, ABq), 7.72 (2H, d), 7.04—6.76 (6H, m), 3.78 (3H, s), 2.26 (3H, s)

tials of these reagents has not been established.[23] However, the classification of the reaction profiles given above enables us to make qualitative estimates of the reduction potentials of substrates, including nitroarenes and diaryl ketones,[20] and those of the oxidation potentials of the reagents.

Since the oxidation and reduction potentials are correlated to the energy levels of the frontier molecular orbitals of the electron-acceptors and -donors,[24-26] the classification given above can be illustrated in terms of the energy levels of the lowest unoccupied molecular orbitals (LUMO) of substrates and those of the highest occupied ones (HOMO) of reagents as shown in Fig. 1: Only the LUMO's of the typical substrates are designated for simplicity and their levels relative to those of the HOMO's of the reagents are given arbitrarily. The three types of the reaction profiles (A, B, and C) are also designated in the figure.

The discussion and the illustration given above are only qualitative at present, and detailed studies are needed especially for determining the precise mechanisms and the energy levels of the reactants. However, the classification of the reactions into "electron-transfer controlled" and "coordination controlled" ones will provide a clue for understanding the rather complicated profiles of the reactions of organomagnesium reagents.

Experimental

The melting points are uncorrected.

Materials and Procedures. The benzylideneacetophenones were prepared by condensation of the corresponding benzaldehydes and acetophenones in ethanol containing potassium hydroxide. The naphthoquinones, 9,10-anthraquinone, 9,10-phenanthraquinone, and *N*-methylacridone were commercially available. The symmetrical and unsymmetrical benzils were prepared by condensation of benzaldehydes followed by oxidation by copper(II) sulfate in pyridine.[27]

The procedures of the IDMg reaction were reported previously.[3,6,7] The ESR measurements were carried out according to the reported method.[2]

Products. The presence of the quinhydrone-like products in the black mixtures of products obtained in the IDMg reactions with the naphthoquinone and 9,10-phenanthraquinone was suggested from the fact that a part of the starting materials was recovered after the treatment of the mixture with aqueous sodium hydroxide: The black color characteristic to quinhydrones faded to some extent during the treatment.

The melting points, the results of elemental analyses, and the NMR data of the products of IDMg reactions are summarized in Table 4. The products are designated by the numbers given in the reaction schemes (gothic letters) as well as the experiment numbers given in the tables (super-prefixes). The chromatographic separations of the products, ^{17}**24**, ^{17}**25**, ^{18}**23a**, and ^{18}**23b** from the individual reaction mixtures were incomplete, and were not submitted to the elemental analyses: The contents of these products in the mixture (Table 3) were estimated by inspecting the NMR spectra of chromatographic fractions.

The support of this work by research grants from the Ministery of Education, Science and Culture (C-56540308) is gratefully acknowledged.

References

1) T. Holm and I. Crossland, *Acta Chem. Scand.*, **25**, 59 (1971); T. Holm, *ibid.*, **27**, 1552 (1973).
2) M. Ōkubo, *Bull. Chem. Soc. Jpn.*, **50**, 2379 (1977).
3) M. Ōkubo, T. Takahashi, and K. Koga, *Bull. Chem. Soc. Jpn.*, **56**, 199 (1983).
4) E. C. Ashby, J. Bowers, and R. Depriest, *Tetrahedron Lett.*, **1980**, 3541.
5) M. Okubo and K. Koga, *Bull. Chem. Soc. Jpn.*, **56**, 203 (1983).
6) M. Ōkubo and S. Ueda, *Bull. Chem. Soc. Jpn.*, **53**, 281 (1980).
7) M. Ōkubo, S. Hayashi, M. Matsunaga, and Y. Uematsu *Bull. Chem. Soc. Jpn.*, **54**, 2337 (1981).
8) M. Ōkubo and Y. Uematsu, *Bull. Chem. Soc. Jpn.*, **55**, 1121 (1982).
9) E. P. Kohler, *Am. Chem. J.*, **38**, 511 (1907); E. P. Kohler and W. D. Peterson, *J. Am. Chem. Soc.*, **55**, 1073 (1933).
10) R. A. Kretchmer, *J. Org. Chem.*, **37**, 2747 (1972).
11) K. W. Bowers, R. W. Griese, T. Grimshaw, H.O. House, K. Kronberger, and D. K. Roe, *J. Am. Chem. Soc.*, **92**, 2783 (1970).
12) G. A. Russell and G. R. Stevenson, *J. Am. Chem. Soc.*, **93**, 2432 (1971).
13) L. I. Smith and H. M. Crawford, *J. Am. Chem. Soc.*, **50**, 869 (1928).
14) P. W. Cameron and W. Meckel, *J. Chem. Soc., Chem. Commun.*, **1967**, 623.
15) C. Blomberg, H. H. Grootvehl, T. H. Gerner, and F. Bickelhaupt, *J. Organomet. Chem.*, **24**, 549 (1970).
16) G. E. K. Branch and M. Calvin, "The Theory of Organic Chemistry," Prentice-Hall Inc., New York (1941), Chap. 7.
17) W. E. Bachmann and J. W. Ferguson, *J. Am. Chem. Soc.*, **56**, 2081 (1934).
18) K. Maruyama, The 45th National Meeting of the Chemical Society of Japan, Tokyo, April 1982, Abstr., No. 4C-40.
19) K. Maruyama and T. Otsuki, *Bull. Chem. Soc. Jpn.*, **41**, 444 (1968).
20) P. Zuman, "Substituent Effects in Organic Polarography," Plenum Press, New York (1967), Chap. 3, p. 55.
21) D. N. Kursanov and P. A. Solodkov, *Chem. Abstr.*, **30**, 2181 (1936).
22) M. Ōkubo and S. Ueda, *Bull. Chem. Soc. Jpn.*, **52**, 3346 (1979).
23) T. Holm, *Acta Chem. Scand., Ser. B*, **28**, 809 (1974).
24) S. Nagakura and J. Tanaka, *Bull. Chem. Soc. Jpn.*, **32**, 734 (1959).
25) A. Streitwieser, Jr., "Molecular Orbital Theory for Organic Chemists," John Wiley and Sons, Inc., New York (1961), Chap. 7.
26) I. Fleming, "Frontier Orbitals in Organic Chemical Reactions," John Wiley and Sons, Inc., New York (1976), Chaps. 3 and 5.
27) H. T. Clarke and E. E. Dreger, *Org. Synth.*, Coll. Vol. I, 87 (1941).

 © 1983 The Chemical Society of Japan Bull. Chem. Soc. Jpn., 56, 1203—1205 (1983)

The Cycloaddition of *N,N*-Diethyl-1,3-butadienylamine with Some Diarylnitrilimines

Tatsuo OIDA,* Shigeo TANIMOTO,* Hideyuki IKEHIRA, and Masaya OKANO
Institute for Chemical Research, Kyoto University, Uji, Kyoto 611
(Received October 12, 1982)

The cycloaddition of *N,N*-diethyl-1,3-butadienylamine with some diarylnitrilimines was investigated. 1,3-diaryl-4-vinylpyrazoles, (1,3-diaryl-2-pyrazolin-5-yl)acetaldehydes, 1,3-diaryl-4-(1,3-diaryl-2-pyrazolin-5-yl)-pyrazoles, and 1,3-diarylpyrazoles were obtained.

The presence of conjugated double bonds in conjunction with a amino group makes 1,3-butadienylamines potentially useful intermediates for organic synthesis. For example, recent publications from our laboratory have described the Diels-Alder reactions[1,2] of *N,N*-diethyl-1,3-butadienylamine (**3**) with *trans*-diaroylethylenes and with acetylenecarboxylic acid esters and have illustrated the utility of this diene for the synthesis of 1,3-diarylisobenzofurans and aromatic carboxylic acid esters. In addition to these publications, many reports on the reaction of **3** with various dienophilic reagents such as fulvenes,[3] benzofurazan oxide,[4] and triafulvene,[5] as well as alkyl esters of atropic acid[6] have appeared. Similar experiments using benzonitrile oxide as an enophile were performed in 1970 by Caramella and Bianchessi,[7] who demonstrated that the reaction is applicable to the preparation of 4,5′-diisoxazole ring system. As nitrilimines bear a structural resemblance to nitrile oxides, it would be interesting to utilize the nitrilimines in the cycloaddition with **3**. To our knowledge, there has not been any information published concerning the cycloaddition of **3** with nitrilimines, although the corresponding reaction of 1,3-butadiene (with *C,N*-diphenylnitrilimine) to afford 1,3-diphenyl-5-vinyl-2-pyrazoline has already been elucidated by Huisgen and his co-workers.[8] In this paper we wish to report that the cycloaddition of **3** with several diarylnitrilimines (**2**) proceeds smoothly in benzene to afford the following four kinds of compounds or at least the latter two of them; 1,3-diaryl-4-vinylpyrazoles (**6**), (1,3-diaryl-2-pyrazolin-5-yl)acetaldehydes (**8**), 1,3-diaryl-4-(1,3-diaryl-2-pyrazolin-5-yl)pyrazoles (**9**), and 1,3-diarylpyrazoles (**10**). Among these compounds, only **10** was an unexpected product. In order to explain the formation of **10**, we anticipated that intermediate *trans*-1,3-diaryl-4-(1,3-diaryl-2-pyrazolin-5-yl)-5-diethylamino-2-pyrazolines (**7**) were initially formed; these underwent a deprotonation at the 4′-position (see formula **7**) and the simultaneous bond fission between 4-C and 5′-C, accompanied by a release of the diethylamino group at the 5-position.

Results and Discussion

First, the cycloaddition between **3** and *N*-(*p*-nitrophenyl)-*C*-phenylnitrilimine (**2a**) prepared *in situ* by the dehydrochlorination of *N*-(*p*-nitrophenyl)benzohydrazonoyl chloride (**1a**) was carried out in benzene at room temperature. The products isolated from the reaction mixture were shown to be 1-(*p*-nitrophenyl)-3-phenyl-4-vinylpyrazole (**6a**), [1-(*p*-nitrophenyl)-3-phenyl-2-pyrazolin-5-yl]acetaldehyde (**8a**), 1-(*p*-nitrophenyl)-4-[1-(*p*-nitrophenyl)-3-phenyl-2-pyrazolin-5-yl]-3-phenylpyrazole (**9a**), and 1-(*p*-nitrophenyl)-3-phenylpyrazole (**10a**). When the reaction was conducted at 80 °C, the products isolated from the reaction mixture were the latter two and neither of the former two was found. Similarly, the cycloaddition of **3** with *C,N*-diphenylnitrilimine (**2b**) in benzene at either room temperature or 80 °C gave two products; 1,3-diphenyl-4-(1,3-diphenyl-2-pyrazolin-5-yl)pyrazole (**9b**) and 1,3-diphenylpyrazole (**10b**). In the same manner, the cycloaddition reactions have also been achieved employing diarylnitrilimines derived from *N*-(*p*-chlorophenyl)benzohydrazonoyl chloride (**1c**) and *N*-phenyl-*p*-nitrobenzohydrazonoyl chloride (**1d**).

It is easy to understand the mechanism concerning the formations of **6a** and **8a**. The former should be

TABLE 1. REACTION OF SOME NITRILIMINES (**2**) WITH *N,N*-DIETHYL-1,3-BUTADIENYLAMINE (**3**)

Run	Hydrazonoyl chloride (**1**) used		Mole ratio **1/3**	Reaction conditions[a]		Yield/%[b] of			
	Ar	Ar′		Temp/°C	Time/h	**6**	**8**	**9**	**10**
1	C_6H_5	*p*-$NO_2C_6H_4$	1.5	rt,	20	31	36	12	17
2	C_6H_5	*p*-$NO_2C_6H_4$	2.3	rt,	20	21	48	14	10
3	C_6H_5	*p*-$NO_2C_6H_4$	2.3	−10[c]	6	0	0	4	7
4	C_6H_5	*p*-$NO_2C_6H_4$	2.9	80	8	0	0	40	42
5	C_6H_5	C_6H_5	1.0	rt,	20	0	0	17	15
6	C_6H_5	C_6H_5	2.1	rt,	20	0	0	42	23
7	C_6H_5	C_6H_5	2.6	80	8	0	0	51	39
8	C_6H_5	*p*-ClC_6H_4	2.8	80	8	0	0	53	24
9	*p*-$NO_2C_6H_4$	C_6H_5	2.5	80	8	0	0	20	18

a) Benzene was used as the solvent unless otherwise noted. b) Yield was based upon **3**, and was of the isolated product. c) The solvent here is 50 ml of toluene.

Table 2. Physical properties and analytical data of thf products

Product	Mp θ_m/°C	^{1}H-NMR spectra[a] (δ, in DMSO-d_6 or $CDCl_3$)	MS (70 eV) m/e (M^+)	Found (Calcd) (%) C	H	N
6a	163—165 (EtOH)	5.23 (dd, 1H), 5.55 (dd, 1H), 6.55 (dd, 1H), 8.07 (s, 1H), 7.1—8.4 (m, 9H)	291	70.07 (70.09)	4.42 (4.50)	14.65 (14.43)
8a	185—186 (EtOH)	2.8—3.3 (m, 2H), 3.53 (d, 2H), 4.7—5.3 (m, 1H), 7.0—8.4 (m, 9H), 9.9—10.0(broad s, 1H)	309	65.78 (66.01)	4.62 (4.89)	13.80 (13.59)
9a	>300 (DMF)	3.4—4.4 (m, 2H), 5.6—6.0 (m, 1H), 6.9—8.7 (m, 19H)	530	67.78 (67.91)	4.18 (4.18)	15.80 (15.84)
10a	170—171 (EtOH) (lit,[9] 169—169.5)	6.78 (d, 1H), 7.1—8.4 (m, 9H), 7.82 (d, 1H)	265	67.79 (67.91)	4.20 (4.18)	15.81 (15.84)
9b	208 (EtOH)	3.21 (dd, 1H), 3.85 (dd, 1H), 5.55 (dd, 1H), 6.7—8.1 (m, 21H)	440	81.73 (81.79)	5.49 (5.49)	12.68 (12.71)
10b	85—86 (EtOH) (lit,[10] 84—85)	6.77 (d, 1H), 7.1—8.2 (m, 11H)	220	82.06 (81.79)	5.37 (5.49)	13.00 (12.71)
9c	282—286 (EtOH)	3.2—4.0 (m, 2H), 5.61 (dd, 1H), 6.9—8.3 (m, 19H)	508	70.62 (70.73)	4.53 (4.35)	10.89 (11.00)
10c	132—133 (EtOH)	6.66 (d, 1H), 7.2—8.0 (m, 10H)	254	70.98 (70.73)	4.52 (4.35)	10.82 (11.00)
9d	274—278 (DMF)	3.3—4.2 (m, 2H), 5.6—5.8 (m, 1H), 6.8—8.8 (m, 19H)	530	68.25 (67.91)	4.24 (4.18)	15.59 (15.84)
10d	135—137 (EtOH) (lit,[11] 136)	6.74 (d, 1H), 7.1—7.9 (m, 5H), 7.90 (d,1H), 7.9—8.3 (m, 4H)	265	68.19 (67.91)	4.41 (4.18)	15.52 (15.84)

a) The ^{1}H-NMR spectra of **9a**, **9c**, and **9d** were measured in DMSO-d_6 and the other products in $CDCl_3$.

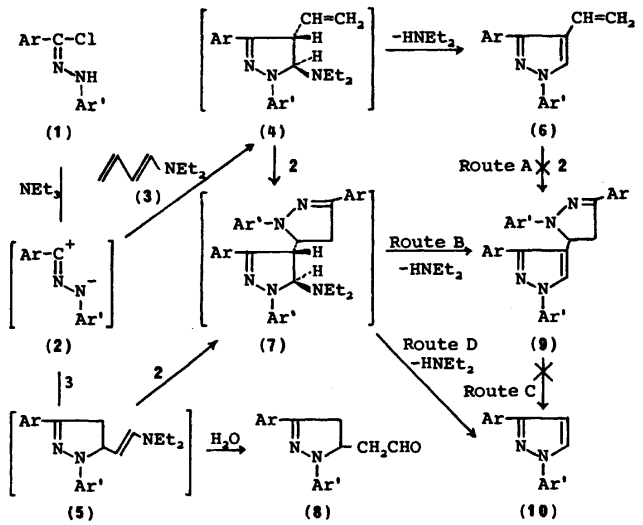

Scheme 1.

produced *via* a process which involves a regioselective addition of **2a** to the amino-substituted double bond of **3** and a subsequent releasing of the amino group from the intermediate *trans*-5-diethylamino-1-(*p*-nitrophenyl)-3-phenyl-4-vinyl-2-pyrazoline (**4a**). On the other hand, the formation of the latter is believed to be the result of a regioselective addition of **2a** to the terminal double bond of **3** to afford 5-(2-diethylaminovinyl)-1-(*p*-nitrophenyl)-3-phenyl-2-pyrazoline (**5a**), which is further converted to **8a** by hydrolysis. Regarding the formation of **9**, two routes are conceivable; these are represented as routes A and B in Scheme 1. If we assume that route A is operative for the formation of **9**, we are unable to find any substantial explanation of the fact that the cycloaddition of **3** with **2a** in toluene at −10 °C (Run 3 in Table 1) gave only **9a** and **10a**, and no **6a** wa detected. Presumably, **9** were produced by the deamination of the intermediate **7**.

All attempts to decompose **9** to **10** failed. For example, heating of **9** with triethylamine in benzene resulted in the recovery of the starting material together with a small amount of tarry matter, indicating that route C should be ruled out. Thus, we offer a feasible pathway (route D) as mentioned previously in this report. The

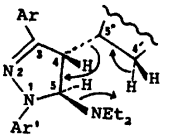

presumption that routes B and D are operative as mentioned above is in accord with the observation that the **9a** : **10a** mole ratio in the reaction products of **2a** with **3** was constant under the given reaction conditions and independent of the reaction time (see Experimental).

Because **10a** was an unexpected compound, we synthesized it by the reaction of **1a** with vinyl acetate in the presence of triethylamine, and confirmed that it is identical to that obtained by the cycloaddition of **2a** with **3** (see Experimental).

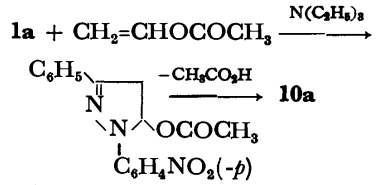

Experimental

The ^{1}H-NMR and mass spectra were recorded on Varian

EM-360 and JEOL-01SG spectrometers, respectively. The hydrazonoyl chlorides were prepared by the method of Huisgen and his co-workers.[1] Commercial organic materials were used and after distillation or recrystallization. Commercial inorganic materials were used without further purification.

*Reaction of a Hydrazonoyl Chloride (**1**) with* N,N-*Diethyl-1,3-butadienylamine (**3**) in the Presence of Triethylamine. General Procedure*: To a suspension of 0.30 g (2.4 mmol) of **3** and a hydrazonoyl chloride (the mole ratio of the hydrazonoyl chloride to **3** in each run is listed in Table 1) in 50 ml of benzene was added an excess of triethylamine. Exactly twice as much triethylamine as the hydrazonoyl chloride by molar quantity was used. The mixture was stirred under a nitrogen atmosphere in the manner described in Table 1, and poured into 50 ml of aqueous NH_4Cl. After the mixture was stirred thoroughly, the aqueous layer separated. The organic layer was dried ($MgSO_4$), and the volatile solvent was removed under reduced pressure leaving a residue, which was chromatographed (SiO_2, 20% chloroform–benzene).

*Determination of 1-(*p-*Nitrophenyl)-4-[1-(*p-*nitrophenyl)-3-phenyl-2-pyrazolin-5-yl]-3-phenylpyrazole (**9a**) : 1-(*p-*Nitrophenyl)-3-phenylpyrazole (**10a**) Mole Ratio in the Reaction Products of* N-*(p-Nitrophenyl)-*C-*phenylnitrilimine (**2a**) with* N,N-*Diethyl-1,3-butadienylamine (**3**)*. To a suspension of 0.26 g (2.1 mmol) of **3** and 1.5 g (5.4 mmol) of **1a** in 100 ml of benzene was added 1.0 g (10 mmol) of triethylamine. The mixture was heated at reflux temperature under a nitrogen atmosphere. After 2 h, an aliquot was taken of the homogeneous reaction mixture (0.25 ml). Similar aliquots were taken at 4, 8, and 20 h. From each of these aliquots, a mixture of **1a**, **9a**, and **10a** was isolated by preparative TLC (SiO_2, 40% chloroform-benzene as eluent) and **9a** : **10a** mole ratio was determined using a Waters Associates HPLC. The results are summarized in the following table:

Reaction time/h	Mole ratio(**9a**/**10a**)
2	0.33
4	0.34
8	0.33
20	0.35

*Synthesis of 1-(*p-*Nitrophenyl)-3-phenylpyrazole (**10a**) by the Reaction of* N-*(*p-*Nitrophenyl)benzohydrazonoyl Chloride (**1a**) with Vinyl Acetate in the Presence of Triethylamine.* To a mixture of 0.50 g (1.8 mmol) of **1a** and 4.7 g (55 mmol) of vinyl acetate was added 0.54 g (5.3 mmol) of triethylamine. The mixture was heated at reflux temperature for 8 h under a nitrogen atmosphere, after which the mixture was cooled and diluted with *ca.* 20 ml of benzene. The benzene solution was washed repeatedly with aqueous NH_4Cl, dried ($MgSO_4$), and the volatile solvent was removed under reduced pressure leaving a residue, which was slowly filtered through a SiO_2 column. The elution was carried out with 90% benzene–ether. The collected effluent was dried ($MgSO_4$) and evaporated, The resulting precipitate was collected and recrystallized from ethanol to afford 0.23 g of **10a**; mp 169—170 °C (yield, 48% based on **1a**).

References

1) T. Oida, S. Tanimoto, T. Sugimoto, and M, Okano, *Synthesis*, **1980**, 131.
2) S. Tanimoto, Y. Matsumura, T. Sugimoto, and M. Okano, *Tetrahedron Lett.*, **1977**, 2899.
3) L. C. Dunn and K. N. Houk, *Tetrahedron Lett.*, **1978**, 3411; Y. N. Grupta, S. R. Mani, and K. N. Houk, *ibid.*, **23**, 5773 (1982).
4) P. Devi, J. S. Sandhu, and G. Thyagarajan, *J. Chem. Soc., Chem. Comm.*, **1979**, 710.
5) J. Ciabattoni and S. C. Nathan, *J. Am. Chem. Soc.*, **89**, 3081 (1967).
6) G. Satzinger, *Justus Liebigs Ann. Chem.*, **728**, 64 (1969).
7) P. Caramella and P. Bianchessi, *Tetrahedron*, **26**, 5773 (1970).
8) R. Huisgen, M. Seidel, and G. Wallbillich, *Tetrahedron*, **17**, 3 (1962).
9) K. v. Auwers and H. Mauss, *Justus Liebigs Ann. Chem.*, **452**, 182 (1927).
10) K. v. Kuwers and W. Schmidt, *Ber.*, **58**, 528 (1925).
11) N. K. Kochetkov, E. D. Khomutova, O. B. Mikhailova, and A. N. Nesmeyanov, *Izv. Akad. Nauk SSSR, Otd., Khim. Nauk*, **1957**, 1118.

The Mechanism of the Reaction of 3,5-Dinitrobenzonitrile with Sodium Methoxide in Methanol

Takehiro Abe
College of General Education, Tohoku University, Kawauchi, Sendai 980
(Received October 14, 1982)

The reaction of 3,5-dinitrobenzonitrile in a methanolic solution containing a low sodium-methoxide concentration has been reinvestigated. The final product has been found to be methoxy(3,5-dinitrophenyl)methanimine, which is produced by a catalytic reaction. The reaction mechanism has been presented for the formation of the Meisenheimer complexes and the final product in the reaction system. The rate and thermodynamic stabilities for their formation have been discussed on the basis of the LUMO coefficients of 3,5-dinitrobenzonitrile and from the relative potential energies of their formation respectively, considering also the solvent effects.

Previously Fendler *et al.*[1] proposed Scheme 1 for the reaction of 3,5-dinitrobenzonitrile (**1**) with the methoxide ion in methanol. They considered that the product (**4**) was more likely formed through **3**. Moreover, they

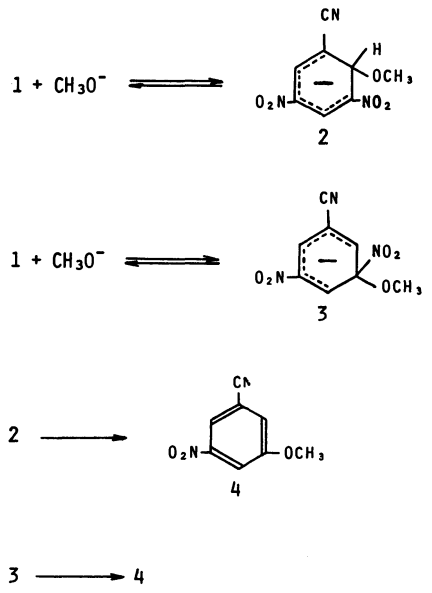

Scheme 1.

observed the presence of the 3,5-dinitrobenzonitrile anion radical in the reaction system. The present author has been interested in their observation of the radical in connection with our work[2] on anion-radical precursors in nucleophilic substitution. The author has, therefore, reinvestigated the reaction product and, surprisingly, obtained a product different from **4**. In this paper, this product will be reported. Moreover, the reaction mechanism for the formation of the Meisenheimer complexes and product in the reaction system will be qualitatively discussed by simple theoretical treatments, taking the solvent effects into account.

Results and Discussion

The Main Product Formed from 3,5-Dinitrobenzonitrile in a Methanolic Solution Containing a Low Sodium-methoxide Concentration. The addition of a solution of **1** (*ca.* 10^{-5} mol dm^{-3}) in methanol to a methanolic solution of sodium methoxide (10^{-4}—10^{-2} mol dm^{-3}) results in the immediate formation of a red color, which however, rapidly fades.[1] The colored species showing absorption bands at 490 and 390 nm is assigned by Fendler *et al.*[1] to 1-methoxy-2-cyano-4,6-dinitrocyclohexadienide (**2**). Here, the intensity of the 490-nm band is comparable with that of the 390-nm band. These bands could be observed by fast scanning (1200 nm/min) with a usual spectrophotometer at room temperature immediately after the preparation of a methanolic solution of **1** (2.91×10^{-4} mol dm^{-3}) and CH_3ONa (8.12×10^{-3} mol dm^{-3}). These bands completely disappeared within several minutes after the preparation. However, the methanolic solution of **1** (1.95×10^{-4} mol dm^{-3}) and CH_3ONa (0.341 mol dm^{-3}) showed weak but stable absorption bands at 480, 365, and 300 nm within 5 min after the preparation. The intensity of the 480-nm band was considerably weak compared with that of the 365-nm band. The observation of the stable bands suggests the resulting product, which is not **4** but **5** (see Experimental section), further reacts with the methoxide ion to give a Meisenheimer complex like **2**, for the 480- and 365-nm bands are characteristic of 2,4-dinitrocyclohexadienide.[3] Actually, as will be described below, the isolated product (**5**) shows these bands in the presence of CH_3ONa. The pure product (**5**) could be precipitated by allowing **1** to react with a catalytic quantity of CH_3ONa in methanol and by then adding water. The catalytic reaction is quite fast, because the pure product was obtained by adding water (25 cm^3) to a methanolic solution (several cm^3) of **1** (913.4 μmol) and CH_3ONa (51.2 μmol) *ca.* 7 min after the preparation of the solution. The isolated product was identified as **5** (see Experimental section). The methanolic solution of **5** at a relatively high CH_3ONa concentration gave

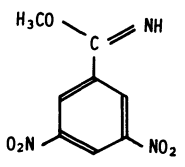

5

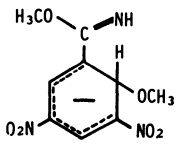

6

absorption bands at 480 and 378 nm, as is shown in Fig. 1. Their absorbances changed somewhat with the time. These bands are due probably to the formation of **6**, judging from their characteristic wavelengths and from the NMR spectrum of dimethyl sulfoxide (DMSO)-

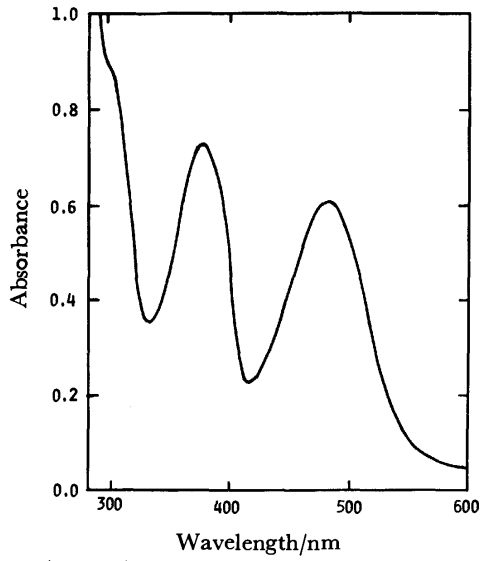

Fig. 1. Absorption spectrum of the methanolic solution of **5** (0.972 mmol dm^{-3}) and CH_3ONa (0.614 mol dm^{-3}).

d_6 solution of **5** and CH_3ONa.

The product of **5** is different from that of **4** reported by Fendler *et al.*[1] They poured the NMR sample of the isolated potassium salt of **2** (in methanol or DMSO-d_6) or of *in situ*-generated **2** (in DMSO-d_6) into water, acidified the resulting solution with HCl, and thus obtained the precipitates of **4**. If the solution diluted with water was alkaline enough, the resulting dinitrobenzene derivatives might further react in the solution, because dinitrobenzenes are apt to react in alkaline solutions. In this case, therefore, the acidification with HCl should be done before the dilution with water. In the present experiment, however, the acidification of the reddish-orange methanolic solution of **1** and CH_3ONa before the dilution with water gave a white precipitate of methyl 3,5-dinitrobenzoate. When the methanolic solution of only **5** was treated with HCl, the same precipitate was obtained. It is, therefore, obvious that the product of methyl 3,5-dinitrobenzoate obtained by the acidification of the reddish orange solution was given by the further reaction of the resulting product of **5** with HCl in methanol containing a little water. On the other hand, a similar acidification of the red solution of **1** and CH_3ONa in the DMSO containing a little methanol reproduced **1**. Thus, because of the presence of the protic solvent of methanol, **5** is produced as a stable product from the solution of **1** in the methanol containing a low CH_3ONa concentration.

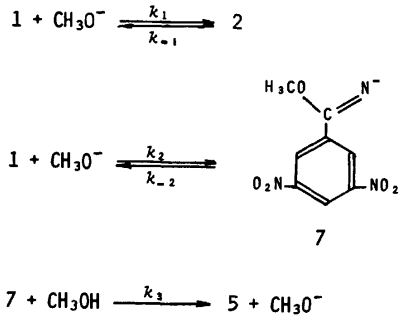

Scheme 2.

Mechanism of the Reactions of ***1*** *in the Methanol Containing a Low CH_3ONa Concentration.* In view of the experimental finding that the methoxide ion acts as a catalyst in the formation of **5**, Scheme 2 instead of Scheme 1 is poposed for the mechanism of the reactions of **1**. At a high CH_3ONa concentration, **5** further reacts with CH_3O^- to form **6**, as has been described above. The decomposition of the most typical Meisenheimer complex of sodium 1,1-dimethoxy-2,4,6-trinitrocyclohexadienide in methanol is considered to consist not of unimolecular, but of bimolecular reactions with proton and with methanol.[4] In the present alkaline reaction system, the reaction of **2** with H^+ may be neglected. The reverse reaction of **2** should, therefore, be written as $\mathbf{2}+CH_3OH \rightarrow \mathbf{1}+CH_3O^-+CH_3OH$. Therefore, k_{-1} contains the initial concentration of methanol, *i.e.*, $[CH_3OH]_0$, which is kept constant throughout the reaction. Similarly, the unimolecular decomposition of **7** may be written as $\mathbf{7}+CH_3OH \rightarrow \mathbf{1}+CH_3O^-+CH_3OH$, and k_{-2} may also contain $[CH_3OH]_0$.

Fendler *et al.*[1] have found that the formation of **2** in methanol attains equilibrium rapidly and that the observed pseudo-first order rate constant, k_{obsd}, for the subsequent decay of **2** is given by:

$$k_{obsd} = -\frac{d(\ln[\mathbf{2}])}{dt}. \quad (1)$$

Moreover, they have found that k_{obsd} is related to the initial methoxide concentration $[CH_3O^-]_0$ by means of the following equation:

$$k_{obsd} = \frac{\alpha[CH_3O^-]_0}{[CH_3O^-]_0+\beta}, \quad (2)$$

where α and β are constants. Their experimental conditions satisfy the requirements that the initial concentration of **1** (a_0) be much smaller than $[CH_3O^-]_0$ and that $[CH_3O^-]_0$ be much smaller than $[CH_3OH]_0$. Therefore, $[CH_3O^-]_0$ and $[CH_3OH]_0$ are regarded as being kept constant throughout the reaction. They obtained values of $1/\alpha$ and β/α by rearranging Eq. 2 into the expression of $[CH_3O^-]_0/k_{obsd}=\beta/\alpha+(1/\alpha)[CH_3O^-]_0$. Using their data[1] of k_{obsd} *vs.* $[CH_3O^-]_0$ at 25 °C, the present author recalculated and obtained $1/\alpha=(3.07\pm0.09)$ s and $\beta/\alpha=(1.60\pm0.02)$ mol dm^{-3} s, from which $\alpha=0.326\,s^{-1}$ and $\beta=0.521$ mol dm^{-3} were obtained.

Scheme 2 can account for Eq. 2 as follows. According to Fendler *et al.*,[1] let us assume a preliminary equilibrium for the formation of **2**, whose equilibrium constant, K_1, is written as:

$$K_1 = \frac{k_1}{k_{-2}} = \frac{[\mathbf{2}]}{[CH_3O^-]_0[\mathbf{1}]}. \quad (3)$$

At the initial time ($t=0$), therefore, a_0 is written as:

$$a_0 = [\mathbf{1}]_0 + [\mathbf{2}]_0. \quad (4)$$

Scheme 2 gives the following rate equations for the increases in the concentrations of **1** and **7**:

$$\frac{d[\mathbf{1}]}{dt} = -k_2[CH_3O^-]_0[\mathbf{1}] + k_{-2}[\mathbf{7}], \quad (5)$$

$$\frac{d[\mathbf{7}]}{dt} = k_2[CH_3O^-]_0[\mathbf{1}] - (k_{-2}+k_3[CH_3OH]_0)[\mathbf{7}], \quad (6)$$

where t denotes the time. Here let us assume the

following inequality:

$$F = \frac{k_2k_3[CH_3OH]_0[CH_3O^-]_0}{k_2[CH_3O^-]_0+k_{-2}+k_3[CH_3OH]_0} < 1\ s^{-1}. \quad (7)$$

The validity of Eq. 7 will be described below. By solving Eqs. 5 and 6 simultaneously, one finally obtains the following approximate expression for [**1**]:

$$[1] = \frac{(k_{-2}+k_3[CH_3OH]_0)[1]_0}{k_2[CH_3O^-]_0+k_{-2}+k_3[CH_3OH]_0} \times \exp\left(-\frac{k_2k_3[CH_3OH]_0[CH_3O^-]_0}{k_2[CH_3O^-]_0+k_{-2}+k_3[CH_3OH]_0} \times t\right). \quad (8)$$

The combination of Eqs. 1, 3, and 8 leads to:

$$k_{obsd} = \frac{k_3[CH_3OH]_0[CH_3O^-]_0}{[CH_3O^-]_0+(k_{-2}+k_3[CH_3OH]_0)/k_2}. \quad (9)$$

Equation 9 is equivalent to Eq. 2. Thus, the experimental relation of Eq. 2 can be accounted for according to Scheme 2. By comparing Eq. 9 with F in Eq. 7, one obtains the relation of $F=k_{obsd}$. The k_{obsd} values measured by Fendler *et al.*[1] are less than 0.16 s^{-1}. Therefore, the assumption of Eq. 7 is reasonable. By comparing the values of α and β with $k_3[CH_3OH]_0$ and $(k_{-2}+k_3[CH_3OH]_0)/k_2$ respectively in Eq. 9, one obtains $k_3=0.326\ s^{-1}/[CH_3OH]_0$ and $k_2=(k_{-2}+0.326\ s^{-1})/0.521$ mol dm^{-3}. From these relations for k_3 and k_2, one obtains $k_3=1.33\times10^{-2}$ mol^{-1} dm^3 s^{-1} at 25.0 °C ($[CH_3OH]_0=24.55$ mol dm^{-3}) and may say that k_2 is larger than either k_{-2} or k_3. If the steady-state treatment is applied to the concentration of **7**, one obtains finally an expression for k_{obsd} in which the denominator of Eq. 9 is replaced by $(k_{-2}+k_3[CH_3OH]_0)/k_2$. In this case, therefore, Eq. 2 cannot be accounted for.

Explanation of the Rates and Thermodynamic Stabilities of the Formations of **2**, **7**, *and* **8** *by Theoretical Treatments Taking the Solvent Effect into Account.* In the case of a DMSO solution containing a little methanol, not only **2**[1,5,6] but **8**[6] is observed by NMR spectroscopy. Crampton and Khan[7] reported that **8** shows an absorption band at 550 nm in the DMSO.

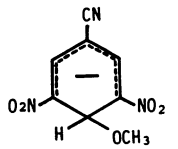

8

Indeed, the longer absorption band characteristic of the Meisenheimer complex,[3] like **8**, was distinctly observed at 560 nm with the usual spectrophotometer when a small quantity of solid CH_3ONa was added to a solution of **1** in DMSO. The formation of **8** is kinetically faster, but thermodynamically less stable, than that of **2** in the DMSO.[6,7] On the other hand, **8** has never been observed in a methanolic solution containing no DMSO. However, the following findings related to the present case seem to suggest the transient formation of **8** in methanol. Terrier *et al.*[3b,6] found that the equilibrium constant for the formation of 1-hydroxy-4-cyano-2,6-dinitrocyclohexadienide from **1** and OH^- in a mixture of water and DMSO decreases with a decrease in the amount of DMSO, while the rate constant for the decomposition of the complex increases reversely. By a temperature-jump method, Bernasconi[8] found that the formation of 1,3-dimethoxy-2,4,6-trinitrocyclohexadienide, corresponding to **8**, proceeds even in methanol, and that the equilibrium constant for the formation of the complex is exceedingly small compared with that for 1,1-dimethoxy-2,4,6-trinitrocyclohexadienide, corresponding to **2**, while the rate constant for the decomposition of the 1,3-dimethoxy complex is exceedingly large compared with that of the 1,1-dimethoxy complex. In view of the above findings, one may consider the transient formation of **8** in methanol on the assumptions that the equilibrium constant for the formation is very small and that the rate constant for the decomposition of **8** is quite large. Moreover, by analogy with the case of the DMSO solution, one may consider that, in methanol, the formation of **8** is kinetically faster and thermodynamically less stable than that of **2**. Thus, one may conclude as follows: The formation of **2** is kinetically slower and thermodynamically more stable than that of **8** in both methanol and DMSO. The formation of **5** is the slowest in methanol and is not produced in the DMSO containing a little methanol.

An attempt will now be made to account for the above conclusions by drawing the potential-energy profiles against a reaction coordinate for the formations of **2**, **7**, and **8** in methanol or DMSO. The rates of these formations may be lower in the order of the increase in the activation energies, because the frequency factors of the rate constants for these formations proceeding in the identical solution of **1** and CH_3O^- may be regarded as approximately the same. According to the frontier orbital theory[9] and the symmetry rules[10] for chemical reactions, CH_3O^- may attack the atomic positions of **1** more easily in the order of their increasing absolute values of the coefficients of the lowest unoccupied molecular orbital (LUMO) for **1** on the assumption that the initial slopes of the potential-energy curves for the formations of **2**, **7**, and **8** are proportional to their activation energies. The theory and the rules have been widely accepted. Accordingly, the rates of the formations of **2**, **7**, and **8** may be lower in the order of the decrease in the coefficients of the LUMO because the activation energies increase in the same order. On the other hand, the thermodynamic stabilities of **2**, **7**, and **8** in the solution increase in the order of their decreasing potential energies and will be discussed by considering their relative potential energies.

Let us consider a neutral solute molecule with a π-electron system and a dipole moment of $\boldsymbol{p}$ (in its free state). By the use of the Onsager reaction field, the rth coefficient (c_{Lr}) of the LUMO for the π-electron system containing n core atoms is given approximately, according to a previous paper,[11] as follows:

$$c_{Lr} = c^\circ_{Lr} + \frac{\varepsilon_r-1}{2\varepsilon_r+1} \times \frac{2e\boldsymbol{p}}{a^3}\sigma_{Lr}, \quad (10)$$

where:

$$\sigma_{Lr} = \sum_{k\neq L}^{all} \frac{\left(\sum_{p=1}^{n} c^\circ_L c^\circ_{kp} \boldsymbol{r}_p\right)}{\varepsilon^\circ_L - \varepsilon^\circ_k} c^\circ_{kr}. \quad (11)$$

Here, e is the charge of the proton, ε_r is a relative permittivity of the solvent, a is a cavity radius, ε°_k is an

energy level of the kth MO for the free solute molecule, c°_{kp} is the pth coefficient of the kth MO, and r_p is a position vector of the pth atom. The letter L denotes the LUMO. Equation 10 is written by neglecting the hydrogen-bonding effect due to a change ($\delta\alpha_p$) in the Coulomb integral of the pth atom, because it is convenient to evaluate the effect of $\delta\alpha_p$ resulting from the hydrogen bonding between the pth atom and the solvent molecule by directly solving a secular equation taking $\delta\alpha_p$ into account using a computer. In the present case, the Onsager reaction field is used for convenience instead of the better Block and Walker reaction field for the neutral molecule,[11] since the reaction field used below for an anion is the Onsager one. As has been described in the previous paper,[11] a dispersion effect is not considered in the above treatment. Consequently, the application of Eq. 10 to a solute molecule with no permanent dipole moment or only a small one is unfavorable. In the present treatment, however, the dispersion effect on all the coefficient of the LUMO is neglected on the assumption that the small dispersion effect of the identical solvent causes no considerable changes in any of the coefficients for the identical solute molecule.

All the molecules of **2**, **7**, and **8** are anions. One considers an anion consisting of N charged particles as a whole. The energy of the ground state, Ψ°_g, of the anion in its free state is denoted by E°_g. The charge and position vector of the jth particle of the N particles are denoted by e_j and r_j respectively. As will be given in the Appendix, the reaction potential (ϕ_R) and field ($\boldsymbol{R}$) of the anion at the center of the cavity are written, respectively, as:

$$\phi_R = \frac{1-\varepsilon_r}{\varepsilon_r} \times \frac{1}{a}\left(\sum_{j=1}^{N} e_j\right), \tag{12}$$

$$\boldsymbol{R} = \frac{\varepsilon_r - 1}{2\varepsilon_r + 1} \times \frac{2\boldsymbol{p}_g}{a^3}, \tag{13}$$

where $\boldsymbol{p}_g$ is the dipole moment of the free anion in its ground state. Here, $\sum e_j$ is $-e$ for the present anion. Both Eqs. 12 and 13 give potential energies twice the corresponding Helmholtz free energies.[12,13] According to the previous paper,[11] the perturbation for the anion in the solution can be written from Eqs. 12 and 13 as:

$$H' = \sum_{j=1}^{N} e_j(\phi_R - \boldsymbol{R}\cdot\boldsymbol{r}_j). \tag{14}$$

From the first-order perturbation theory, therefore, the energy, E_g, of the anion in the solution can easily be obtained as follows:

$$\begin{aligned} E_g &= E^{\circ}_g + (\Psi^{\circ *}_g|H'|\Psi^{\circ}_g) \\ &\quad + \sum_{m\neq g} \frac{(\Psi^{\circ *}_g|H'|\Psi^{\circ}_m)(\Psi^{\circ *}_m|H'|\Psi^{\circ}_g)}{E^{\circ}_g - E^{\circ}_m}, \\ &= E^{\circ}_g - \frac{\varepsilon_r - 1}{\varepsilon_r} \times \frac{e^2}{a} - \boldsymbol{R}\cdot\boldsymbol{p}_g - \frac{R^2\alpha_g}{2}, \end{aligned} \tag{15}$$

where E°_m is an energy of the mth excited state of the free anion and α_g is the isotropic polarizability of the free anion in the ground state. Here, one assumes that the differences among the E°_g values of **2**, **7**, and **8** are mainly due to their π-electronic energies of $2\sum^{occu}\varepsilon^{\circ}_k$, because their σ-bonds are approximately the same except for the bonds of CN, such as C≡N and C=N$^-$. The σ-electronic energy of **7** containing the C=N$^-$ bond is higher by roughly the energy (E_{C-N}) of a C–N bond than those of **2** and **8**, both containing the C≡N bonds. The magnitude of E_{C-N} is considered to be 291.6 kJ mol^{-1} of the C–N bond[14] for the relative potential energy of **7**. In the case of **2** and **8**, the energy (E_{OCH_3}) of the π-electron system of OCH_3 must be considered, because the methoxyl group of **7** participates in the π-electron system. Accordingly, from Eq. 15, the relative potential energy (E_r) being considered for the anion may be approximately written as:

$$\begin{aligned} E_r &= \Delta E + 2\sum_{k=1}^{occu}\varepsilon^{\circ}_k - \frac{\varepsilon_r - 1}{\varepsilon_r} \times \frac{e^2}{a} \\ &\quad - \frac{\varepsilon_r - 1}{2\varepsilon_r + 1} \times \frac{2p_g^2}{a^3} - \left(\frac{\varepsilon_r - 1}{2\varepsilon_r + 1}\right)^2 \times \frac{2p_g^2\alpha_g}{a^6} - \Delta E_H, \end{aligned} \tag{16}$$

Table 1. Atomic coordinates and molecular orbital parameters for π-electron systems of **1**, **2**, **7**, and **8**

Position	Atomic coordinates[a] x/Å	y/Å	Integrals[b]
1	0	1.38	$h_7=h_{10}=2$
2	1.20	0.69	$h_8=h_9=h_{11}$
3	1.20	−0.69	$=h_{12}=1.5$
4	0	−1.38	$h_{14}=0.5$
5	−1.20	−0.69	$h_{14'}=0$
6	−1.20	0.69	$h_{15'}=2$
7	2.47	−1.43	
8	3.67	−1.38	$k_{3,7}=k_{5,10}$
9	2.43	−2.62	$=k_{13,14}=k_{13,14'}$
10	−2.47	−1.43	$=k_{13,15'}=0.8$
11	−3.67	−1.38	$k_{7,8}=k_{7,9}$
12	−2.43	−2.62	$=k_{10,11}=k_{10,12}$
13	0	2.85	$=0.7$
14	0	4.01	
14′	1.14	3.50	
15′	−1.16	3.51	

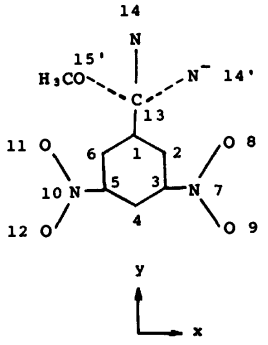

a) 1 Å=0.1 nm. b) Coulomb ($\alpha_r=\alpha_0+h_r\beta_0$) and resonance ($\beta_{rs}=k_{rs}\beta_0$) integrals for the rth atom and the r–s bond respectively.

Table 2. Values of α_r due to hydrogen bondings

Case	$\delta\alpha_8/\beta_0$	$\delta\alpha_9/\beta_0$	$\delta\alpha_{11}/\beta_0$	$\delta\alpha_{12}/\beta_0$	$\delta\alpha_{14}/\beta_0$
1	0	0	0	0	0
2	0	0	0	0	0.1
3	0.1	0	0	0	0.1
4	0.1	0	0.1	0	0
5	0.1	0	0.1	0	0.1
6	0.1	0.1	0.1	0.1	0
7	0.1	0.1	0.1	0.1	0.1

where $\Delta E=E_{C-N}+E_{OCH_3}$. Here, ΔE_H is the stabilization energy due to hydrogen bondings between the anion and protic solvent molecules.

The parameters used for the present Hückel MO calculations were taken, for the most part, from Ref. 15: They are shown in Table 1, together with the atomic coordinates based on the X-ray crystal analysis of *m*-dinitrobenzene.[16] The value of $h_{14'}$ is taken to be smaller than that (0.5) for Ṅ by 0.5, because the nitrogen atom of C=N⁻ may decrease its electronegativity compared with that of Ṅ because of the presence of the negative charge on the nitrogen. Here, α_0 and β_0 denote the Coulomb and resonance integrals respectively for the carbon atom bonded to a carbon atom, where $\beta_0=-3.00$ eV (1 eV$=9.648\times10^4$ J mol^{-1}) is assumed. The LUMO coefficients relating to the formations of **2**, **7**, and **8** are shown in the first row of Case 1 in Table 3. The row shows the relation of $c^0_{L4}>|c^0_{L2}|>c^0_{L13}$ in the case of the absence of the solvent. In order to apply Eq. 10 to **1** in methanol, the dipole moment (p) of **1** is necessary, but it can not be found. Therefore, p was estimated to be 0.07 D (1 D$=3.333\times10^{-30}$ C m) in the negative direction of the y axis from the vector sum of the dipole moments of benzonitrile (4.14 D[14]) and nitro groups (4.21 D[14]). The relative permittivities used for methanol and DMSO are 32.70 and 46.68[17] respectively at 25 °C. The relative permittivity of the solution was taken to be approximately equal to that of the solvent. The value of a was tentatively assumed to be the same value of 4.4 Å (1 Å=0.1 nm) as was assumed for a radius of the Meisenheimer complex of 1,3,5-trinitrobenzene with cyanide.[18] The results of calculations according to Eq. 10 are listed in the second row of Case 1 in Table 3. The row shows that the same relation of $c_{L4}>|c_{L2}|>c_{L13}$ holds for the case of the methanolic solution. This relation also holds for the case of DMSO, because the difference in the value of $(\varepsilon_r-1)/(2\varepsilon_r+1)$ between methanol and DMSO is very small. In a methanolic solution, however, the hydrogen bondings can be expected to be formed between **1** and methanol, because the formations of hydrogen bondings are found for the interactions of methanol with nitromethane and with acetonitrile.[19] The hydrogen bonding between methanol and acetonitrile is somewhat stronger than that between methanol and nitromethane.[19] According to the β-scale of the solvent hydrogen-bond acceptor basicities,[20] the hydrogen-acceptor ability of benzonitrile is somewhat stronger than that of nitrobenzene. In view of the above findings, Cases 2—7 in Table 2 have been selected in order to examine the effect of the hydrogen bondings. The most probable case may be either 5 or 7, because the concentration of methanol present as the solvent is extremely high. From the solvent effects on a hyperfine splitting constant in the ESR spectrum of the di-*t*-butyl nitroxide radical,[11] the value of $\delta\alpha_r$ due to the hydrogen bonding was estimated as follows: From the difference in the hyperfine splitting constants between the observed and calculated values for the solvent of methanol, the magnitude of 0.0556 mT was estimated to be due to the hydrogen bonding between methanol and the radical. The combination of the magnitude and the last term of Eq. 20 of Ref. 11 leads to $\delta\alpha_0=0.1\ \beta_0$, where the Hückel MO's used for the π-electron system of N=O were obtained by taking $\alpha_N=\alpha_0+0.5\,\beta_0$, $\alpha_O=\alpha_0+\beta_0$, and $\beta_{NO}=\beta_0$. For convenience, therefore, $\delta\alpha_r=0.1\ \beta_0$ was assumed for all the oxygen and nitrogen atoms of the nitro and cyano groups respectively in **1**, as is indicated in Table 2. The results of the calculations for Cases 2—7 in Table 2 are listed in Table 3. All the cases in Table 3 give the relation of $|c_{L4}|>|c_{L2}|>|c_{L13}|$. Thus, this relation may hold for the methanolic solution of **1**, even if **1** forms hydrogen bonds with the methanol molecules. As has been described above, the relation means that the activation energies of the formations of **2**, **7**, and **8** in

Table 3. Values of c^0_{Lr}, c_{Lr}, and σ_{Lr} (y) for **1** in methanol

Case[a]	(c^0_{L2}) c_{L2}	(c^0_{L4}) c_{L4}	(c^0_{L13}) c_{L13}	$\sigma_{L2}(y)/\text{Å}\beta_0^{-1}$	$\sigma_{L4}(y)/\text{Å}\beta_0^{-1}$	$\sigma_{L13}(y)/\text{Å}\beta_0^{-1}$
1	(−0.0730)	(0.4604)	(0.0343)	1.7347	−1.1255	−2.1220
	−0.0716	0.4595	0.0326			
2	(0.0540)	(−0.4493)	(−0.0034)	−1.3289	1.0521	1.4638
	0.0529	−0.4485	−0.0022			
3	(−0.0182)	(0.4549)	(0.0062)	1.6711	−1.0862	−1.5598
	−0.0169	0.4540	0.0049			
4	(0.0840)	(−0.4737)	(−0.0436)	−1.9362	1.0817	2.4030
	0.0825	−0.4728	−0.0417			
5	(0.0627)	(−0.4629)	(−0.0088)	−1.4940	1.0745	1.6617
	0.0616	−0.4620	−0.0075			
6	(0.0967)	(−0.4872)	(−0.0546)	−2.0962	0.9078	2.6695
	0.0951	−0.4865	−0.0526			
7	(−0.0730)	(0.4775)	(0.0156)	1.6430	−0.9999	−1.8705
	−0.0718	0.4767	0.0141			

a) Case numbers correspond to those of Table 2.

Table 4. Relative potential energies of **2**, **7**, and **8** in methanol

Anion	$(\Delta E+2\sum_{k=1}^{occu}\varepsilon_k^0)$	Coordinates of center of mass (x/Å, y/Å)	Dipole moment (Debye) obtained by setting the origin at the center of mass: Vector sum of moments of the bonds and groups x	y	Moment of the negative charge x	y	Total moment x	y	p_g	$-\frac{\varepsilon_r-1}{2\varepsilon_r+1}\cdot\frac{2p_g^2}{a^3}$	E_r
2	$18\alpha_0+31.762\beta_0$	(−0.17, 0.25)	−0.53	−0.12	7.68	16.51	−8.21	−16.63	18.55	$0.802\beta_0$	$18\alpha_0+32.564\beta_0$
8	$18\alpha_0+31.858\beta_0$	(0, −0.54)	0	0.79	0	17.00	0	−16.21	16.21	$0.613\beta_0$	$18\alpha_0+32.471\beta_0$
7	$18\alpha_0+31.732\beta_0$	(−0.09, 0.11)	1.95	−4.44	−5.91	−16.28	7.86	11.84	14.22	$0.472\beta_0$	$18\alpha_0+32.204\beta_0$

methanol may be higher in the order of **2**, **8**, and **7**.

When Eq. 16 is applied to the anions of **2**, **7**, and **8**, the third term in Eq. 16 is the same for all the anions, because their charges are the same. Here, one assumes that the values of a_g and ΔE_H are approximately the same for all the anions, because their constituent atoms are the same and because, in view of their structures, their abilities to form the hydrogen bonds seem not to differ considerably. Moreover, the fifth term of Eq. 16 is smaller than the fourth one. Accordingly, the difference in the E_r values among the anions are mainly due to the first, second, and fourth terms of Eq. 16. Here, therefore, only these terms are considered as the relative potential energies (E_r). Here, $E_{C-N}=-1.007\ \beta_0$ and $E_{OCH_3}=2\alpha_0+4\beta_0$ are dropped out for **2** and **8** and for **7** respectively. The sums of the first and second terms are shown in the second column of Table 4. The total dipole moments of each anion in the directions of the x and y axes were estimated from the vector sums of two moments; the vector sum of the moments of the constituent bonds and groups and the moment of the negative charge of the anion. The vector sums obtained by using the moments[14] of the bonds and groups are shown in Table 4. The dipole moment of the anion varies with the way of setting the origin of the coordinates; the center of the mass of the anion is usually set as its origin.[18] Therefore, the moments of the negative charges of **2**, **7**, and **8** were calculated by shifting the origins at their centers of masses, shown in Table 4. The negative charge of **7** is located in the nitrogen atom of $C{=}N^-$ and is immediately calculated from the nitrogen coordinates. The negative charges of **2** and **8** are distributed in their π-electron systems, and their moments are equal to the π-moments. The π-moments are given by multiplying the coordinates of the centers of the negative-charge distributions by $-e$. The coordinates of each center of the distribution were calculated by using the Hückel MO's which had been obtained with the use of the parameters and coordinates in Table 1. The moments of the negative charges and the total moments are shown in Table 4. Then, each moment of p_g was obtained from the vector sum of the total x- and y-moments, as is shown in Table 4. Here, 4.4 Å was assumed for all the a values. With the use of the p_g values, the fourth terms of Eq. 16 were calculated to be as shown in Table 4. Accordingly, the relative potential energies, calculated considering only the first, second, and fourth terms of Eq. 1, are shown in the last column of Table 4. The column shows that the relative potential energies of **2**, **7**, and **8** in methanol may be higher in the order of **2**, **8**, and **7**, since $\beta_0<0$.

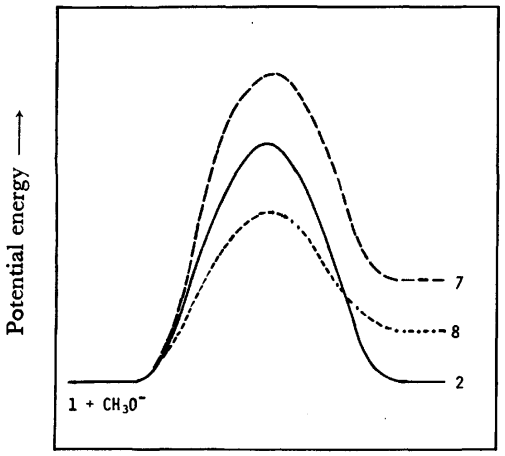

Fig. 2. Profile of potential energy curves for the formations of **2**, **7**, and **8** in methanol.

Thus, from the above discussions of the activation energies and the relative potential energies for the formations of **2**, **7**, and **8**, one may qualitatively draw the potential energy curves *vs.* an arbitrary reaction coordinate as is shown in Fig. 2. The fact that, in methanol, **5** is finally produced from **7** in spite of the activation and potential energies for **7** being highest can be explained by the irreversible reaction of **7** with methanol. Because of these energies for **7** being highest, the concentration of **7** may be small in a methanolic solution, and **5** may be irreversibly produced the most slowly. The relative permittivities of methanol and DMSO are both large. Their contributions to the activation and potential energies for the formations of **2**, **7**, and **8** do not differ considerably in the present treatments, since the contributions of the hydrogen bondings between the methanol molecules and the anions are assumed to be the same and are excluded. The potential energy curves of Fig. 2 can, therefore, probably be applied qualitatively to the case of the DMSO solvent. Thus, Fig. 2 can account for the conclusions that the formation of **2** is kinetically slower and thermodynamically more stable than that of **8**, both in methanol and in DMSO, and that the formation of **5** is the slowest in methanol and is not produced in DMSO. Bernasconi[21] found the enthalpy change of (4.2±6.7) kJ mol^{-1} for the formation of 1-methoxy-2,4,6-trinitrocyclohexadienide from 1,3,5-trinitrobenzene and the methoxide ion in methanol at 25 °C. Since the dipole moment of **1** has been estimated

to be very small, as has been described above, the relationship of the relative potential energies between **2** and the system of **1** and CH_3O^- probably resembles that for the case of 1,3,5-trinitrobenzene. Accordingly, the relative potential energy of **2** is probably near that of **1**+CH_3O^-. In the DMSO solution, a mixture of **2** and **8** (5%) is present at equilibrium.[6] This means that the relative potential energy of **8** is not so high as that of **2**.

Experimental

The melting points were measured by a Yanaco micro-melting apparatus and were uncorrected. The IR spectra were measured as KBr disks by means of a Hitachi grating infrared spectrophotometer 215. The ^{1}H-NMR spectra were measured, with tetramethylsilane as the internal standard, on a Hitachi high-resolution NMR spectrometer, R-22 (90 MHz). The UV spectra were recorded with a Hitachi autorecording spectrophotometer 340 at room temperature.

Material. 3,5-Dinitrobenzonitrile (Aldrich) was checked for purity by means of thin-layer chromatography and was used without further purification.

Reaction of 3,5-Dinitrobenzonitrile With Sodium Methoxide in Methanol. A): When 1.00 cm^3 of a CH_3ONa (1.02 mmol) solution in methanol was added to the solution prepared by dissolving 173.8 mg of **1** (0.900 mmol) in 15 cm^3 of methanol, a reddish-orange solution was immediately produced. This colored solution was acidified with an aqueous HCl solution *ca.* 2 min after the addition of CH_3ONa; a pale-orange solution was thus obtained. When the volume of the pale-orange solution was doubled with water, white crystals were precipitated; they were subsequently separated. The white crystals (mp 106.0—108.1 °C) were found to be pure by means of thin-layer chromatography. The IR spectrum of the white crystals exhibited absorption bands similar to those of the methyl ester (mp 106.0—108.0 °C) obtained by the esterification of 3,5-dinitrobenzoic acid (Kanto, G. R.). The white crystals, therefore, were identified as methyl 3,5-dinitrobenzoate; NMR(DMSO-d_6): δ=3.96 (3H, s), 8.90 (2H, d, J= 2 Hz), and 9.03 ppm (1H, t, J=2 Hz); IR: 1730 and 1305 cm^{-1}.

B): When 50 mm^3 of a CH_3ONa (51.2 μmol) solution in methanol was added to the solution prepared by dissolving 1.0008 g of **1** (5.1823 mmol) in 50 cm^3 of methanol, a reddish-orange solution was immediately formed. When the colored solution was left to stand in the dark at room temperature for two days, a pale yellowish-orange solution was obtained. When the volume of the pale-colored solution was doubled with water, crystals were precipitated. The crystals were filtered off, washed three times with water, and dried. The pale yellow crystals (0.6867 g) thus isolated were found to be pure by means of thin-layer chromatography. The crystals were identified as **5**; mp 109.1 °C; UV(CH_3OH): *ca.* 230 (sh, ε 2.03×10^4), *ca.* 298 (sh, 8.3×10^2), *ca.* 310 (sh, 6.7×10^2) and *ca.* 340 nm (sh, 2.0×10^2); NMR(DMSO-d_6): δ=3.28 (1H, somewhat broad), 3.89 (3H, s), and 8.90—8.95 ppm (3H, dd); IR: 3330 and 1650 cm^{-1}. Found: C, 42.84; H, 2.95; N, 18.73%. Calcd for $C_8H_7N_3O_5$: C, 42.68; H, 3.13; N, 18.66%.

An aqueous HCl solution was added to a solution of **5** in methanol. To the resulting solution water was then added in a large quantity. Then, white crystals were precipitated and subsequently separated. The IR spectrum of the white crystals exhibited absorption bands similar to those of methyl 3,5-dinitrobenzoate.

The NMR sample prepared by adding solid CH_3ONa to a solution of **5** in DMSO-d_6 showed a spectrum characteristic of a Meisenheimer complex, *i.e.*, δ=8.43 (1H, d, J=2 Hz), 7.68 (1H, d, J=2 Hz), and 5.55 ppm (1H, s), although the sample showed a changeable spectrum for several minutes after the addition of CH_3ONa.

C): A solution of CH_3ONa (3.071 mmol) in methanol was added to a solution prepared by dissolving 0.26936 g of **1** (1.3948 mmol) in as little methanol as possible. A red solution was thus immediately formed; it was left to stand overnight in a refrigerator. After the evaporation of some of the solvent by means of a suction at room temperature, crystals precipitated; they were susequently isolated. The IR spectrum of the pale greyish crystals exhibited mainly absorption bands similar to those of **5**, besides a few weak bands due to other substances.

Reproduction of 1 from a Red Solution of 1 and CH_3ONa in the DMSO Containing a Little Methanol. When 1.00 cm^3 of a solution of CH_3ONa (1.024 mmol) in methanol was added to a solution prepared by dissolving 116 mg of **1** (0.601 mmol) in 3.00 cm^3 of DMSO, a red solution was immediately produced. After being shaken, the red solution was left to stand in the dark at room temperature for *ca.* 15 min. Then, two drops of an aqueous dilute solution of HCl were added to the red solution; a yellow solution resulted. When a 25-cm^3 portion of water was added to the yellow solution, white crystals were precipitated. When these crystals were filtered off, washed three times with water, and dried, pale orange crystals (72 mg) were obtained. The IR spectrum of the crystals exhibited absorption bands similar to those of **1**. A similar experiment using DMSO containing 18-crown-6 (Nisso, 1.39 mmol) also gave a reproduction of **1**.

The author wishes to thank Dr. Kuninobu Kabuto of Tohoku University for the NMR measurements.

Appendix

Let us consider a solute molecule contained within a spherical cavity with a radius of a in an isotropic, continuous medium of a solvent with a relative permittivity of ε_r. The permittivity in the cavity is assumed to be unity. Let the origin be the center of the cavity, and let us use the polar coordinates of $\{r, \theta, \phi\}$ to express a position. Let the standard coordinate of θ be the direction of the dipole moment, $\boldsymbol{p}_g$, of the solute. One considers a collection ($\sum_{j=1}^{N} e_j$) of N point charges for the solute molecule, and $\boldsymbol{p}_g$ is written as $\sum_{j=1}^{N} e_j \boldsymbol{r}_j$.

According to Kirkwood's treatment,[12,13] the reaction potential (Φ_R) inside the cavity and the potential (Φ_O) outside the cavity can be written, respectively, as:

$$\Phi_R = \sum_{n=0}^{\infty} \frac{(n+1)(1-\varepsilon_r)}{(n+1)\varepsilon_r+n} \times \frac{1}{a^{2n+1}} \times \sum_{j=1}^{N} e_j r_j^n r^n P_n(\cos\theta_{jr}), \quad \text{(i)}$$

and:

$$\Phi_O = \sum_{n=0}^{\infty} \frac{(2n+1)}{(n+1)\varepsilon_r+n} \times \frac{1}{r^{n+1}} \times \sum_{j=1}^{N} e_j r_j^n P_n(\cos\theta_{jr}), \quad \text{(ii)}$$

where $P_n(\cos\theta_{jr})$ is a simple Legendre polynomial and θ_{jr} is the difference in θ between the positions of $\{r, \theta, \phi\}$ and $\{r_j, \theta_j, \phi_j\}$. Neglecting terms higher than n=1, one reduces Φ_R and Φ_O to:

$$\Phi_R(n=1) = \frac{(1-\varepsilon_r)}{\varepsilon_r} \times \frac{1}{a}\left(\sum_{j=1}^{N} e_j\right) + \frac{2(1-\varepsilon_r)}{2\varepsilon_r+1} \times \frac{1}{a^3}\sum_{j=1}^{N} e_j r_j \cos\theta_{jr}, \quad \text{(iii)}$$

and:

$$\Phi_0(n=1) = \frac{1}{\varepsilon_r} \times \frac{1}{r}\left(\sum_{j=1}^{N} e_j\right) + \frac{3}{2\varepsilon_r+1} \times \frac{1}{r^2}\sum_{j=1}^{N} e_j r_j \cos\theta_{jr}, \quad \text{(iv)}$$

respectively. From Eq. iii, one immediately obtains the reaction potential, $\Phi_R(0)$, at the origin as:

$$\Phi_R(0) = \frac{(1-\varepsilon_r)}{\varepsilon_r} \times \frac{1}{a}\left(\sum_{j=1}^{N} e_j\right). \quad \text{(v)}$$

The electric field, E_r, outside the cavity is obtained by $\boldsymbol{E}_r = -\partial\Phi_0\ (n=1)/\partial r$ in the direction of r. The polarization charge, P_a, induced per unit of area over the cavity is given by putting $r=a$ into the equation of $P_r = \{(\varepsilon_r-1)/4\pi\} \cdot |\boldsymbol{E}_r|$. The charge induced on the infinitesimal area of the cavity surface contained in the solid angle between θ_{jr} and $(\theta_{jr} + \mathrm{d}\theta_{jr})$ is given by $2\pi a^2 P_a \sin\theta_{jr}\,\mathrm{d}\theta_{jr}$, which produces an electric field of $2\pi P_a \sin\theta_{jr}\cos\theta_{jr}\,\mathrm{d}\theta_{jr}$ at the origin in the direction of $\boldsymbol{p}_g$. Then, the reaction field, $\boldsymbol{R}$, parallel to $\boldsymbol{p}_g$ at the point of origin is obtained as follows:

$$\begin{aligned}\boldsymbol{R} &= 2\pi\int_0^{\pi} P_a \sin\theta_{jr}\cos\theta_{jr}\,\mathrm{d}\theta_{jr} \\ &= \frac{(\varepsilon_r-1)}{2\varepsilon_r a^2} \times \left(\sum_{j=1}^{N} e_j\right)\int_0^{\pi} \sin\theta_{jr}\cos\theta_{jr}\,\mathrm{d}\theta_{jr}, \\ &+ \frac{3(\varepsilon_r-1)\boldsymbol{p}_g}{(2\varepsilon_r+1)a^3}\int_0^{\pi} \sin\theta_{jr}\cos^2\theta_{jr}\,\mathrm{d}\theta_{jr}, \\ &= \frac{\varepsilon_r-1}{2\varepsilon_r+1} \times \frac{2\boldsymbol{p}_g}{a^3}. \end{aligned} \quad \text{(vi)}$$

References

1) E. J. Fendler, J. H. Fendler, N. L. Arthur, and C. E. Griffin, *J. Org. Chem.*, **37**, 812 (1972).
2) T. Abe and Y. Ikegami, *Bull. Chem. Soc. Jpn.*, **49**, 3227 (1976); **51**, 196 (1978).
3) Almost all references concerning Meisenheimer complexes up to April, 1981, are cited in the following reviews: a) *M.* J. Strauss, *Chem. Rev.*, **70**, 667 (1970); b) F. Terrier, *ibid.*, **82**, 77 (1982).
4) T. Abe, *Bull. Chem. Soc. Jpn.*, **53**, 1399 (1980).
5) M. I. Foreman and R. Foster, *Can. J. Chem.*, **47**, 729 (1969).
6) F. Terrier, F. Millot, and M.-P. Simonnin, *Tetrahedron Lett.*, **1971**, 2933.
7) M. R. Crampton and H. A. Khan, *J. Chem. Soc., Perkin Trans. 2*, **1973**, 710.
8) C. F. Bernasconi, *J. Am. Chem. Soc.*, **93**, 6975 (1971).
9) K. Fukui and H. Fujimoto, *Bull. Chem. Soc. Jpn.*, **41**, 1989 (1968); **42**, 3399 (1969).
10) R. C. Pearson, *Acc. Chem. Res.*, **4**, 152 (1971).
11) T. Abe, S. Tero-Kubota, and Y. Ikegami, *J. Phys. Chem.*, **86**, 1358 (1982).
12) J. G. Kirkwood, *J. Chem. Phys.*, **1**, 351 (1934).
13) D. L. Beveridge and G. W. Schnuelle, *J. Phys. Chem.*, **79**, 2562 (1975).
14) "Kagaku Binran," ed by the Chemical Society of Japan, Maruzen Publishing Co., Tokyo (1975), Kisohen (Fundamental Part), II, pp. 975, 1404, 1406.
15) A. Streitwieser, Jr., "Molecular Orbital Theory for Organic Chemists," John Wiley and Sons, New York (1961), p. 135.
16) I. Trotter, *Acta Crystallogr.*, **14**, 244 (1961).
17) J. A. Riddick and W. B. Bunger, "Organic Solvents," Wiley-Interscience, New York (1970), pp. 145, 466.
18) T. Abe, *Bull. Chem. Soc. Jpn.*, **54**, 327 (1981).
19) E. Greinacher, W. Luttke, and R. Mecke, *Z. Elektrochem.*, **59**, 23 (1955).
20) M. J. Kamlet and R. W. Taft, *J. Am. Chem. Soc.*, **98**, 377 (1976).
21) C. F. Bernasconi, *J. Am. Chem. Soc.*, **92**, 4682 (1970).

3-Chloro-2-chloromethyl-4-(4-chlorophenoxy)-1-butene as a Functionalized Isoprene Unit. An Electrochemical Preparation and Some Reactions

Kenji UNEYAMA, Nobu HASEGAWA, Hiroyuki KAWAFUCHI, and Sigeru TORII*
Department of Industrial Chemistry, School of Engineering, Okayama University, Okayama 700
(Received October 20, 1982)

3-Chloro-2-chloromethyl-4-(4-chlorophenoxy)-1-butene (**1**) was prepared in 72% yield by electrooxidative double ene-type chlorination of 1-(4-chlorophenoxy)-3-methyl-2-butene. The electrolysis was conducted at room temperature in a two layer solvent system of dichloromethane and water in the presence of acids (HCl, H_2SO_4, H_3PO_4, *etc*). Either 3-chloro-2-methyl-4-(4-chlorophenoxy)-1-butene or **1** was selectively prepared, respectively after 4 or 10 F/mol of electricity were passed using platinum foils as electrodes in an undivided cell. The similar electrolysis of the related 3-methyl-2-butenyl derivatives **2b** and **2c** provided the ene-type products, 3-chloro-2-methyl-4-benzyloxy-1-butene and 4-chloro-1-ethynyl-1,5-dimethyl-5-hexenyl acetate, respectively. In contrast, 3-methyl-2-butenyl derivatives **2d**—**f** and 3-methyl-2-butenoic acid afforded a variety of products such as chlorohydrin, vinyl chloride, and sulfoxide other than ene-type products, suggesting that the functional group of R in **2** affects the reaction course. The elongation at 2-chloromethyl group and the subsequent dechlorophenoxylation convert **1** into 2-(phenylsulfonylmethyl)-1,3-butadiene and 2-(phenylthiomethyl)-1,3-butadiene.

Functionalization and subsequent elongation of isoprene derivatives are one of the effective approaches to the terpene synthesis.[1] Although there have been known various isoprene derivatives as a synthetic building block, 3-chloro-2-chloromethyl-4-(4-chlorophenoxy)-1-butene (**1**) has not been prepared. The compound **1** has two allylic chlorine atoms and can be elongated at the chloromethyl group and subsequently can be converted into a conjugated diene by reductive elimination of the another allylic chlorine atom. This paper describes an electrochemical preparation and some modifications of **1** along with the electrochemical chlorinative functionalization of the related isoprene derivatives **2a**—**g**.

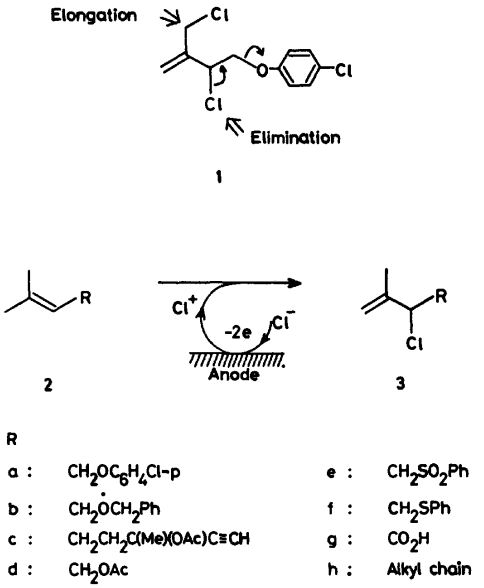

R
a : $CH_2OC_6H_4Cl$-p
b : CH_2OCH_2Ph
c : $CH_2CH_2C(Me)(OAc)C{\equiv}CH$
d : CH_2OAc
e : CH_2SO_2Ph
f : CH_2SPh
g : CO_2H
h : Alkyl chain

Scheme 1.

Results and Discussion

So far as the allylic chlorination of olefins is concerned, the selenium reagent-mediated NCS chlorination,[2] the action of hypochlorous acid[3] or calcium hypochlorite in dichloromethane[4] and the chlorination with *t*-butyl hypochlorite in the presence of silica gel[5] have been reported. Recently, we communicated an electrochemical chlorinative ene-type reaction of isoprenoids **2h** which offers a simple and highly regio- and chemoselective access to allylic chloride **3h**.[6] The electrolysis is conducted in a two layer solvent system where a chloronium ion or the corresponding active chlorinating reagent is electrooxidatively generated in an aqueous sodium chloride layer and the chlorination occurs subsequently in a dichloromethane layer.[6,7] The electrochemical chlorination, however, did not afford the doubly chlorinated products related to **1** presumably due to the deactivation of the double bond of **3h** by electronegative chlorine atom. On this basis, the acid-promoted activation of the electrochemically generated chlorinating reagent was devised to enable the double ene-type chlorination, and also the electrolysis of isoprene derivatives **2a**—**g** was examined in detail where substituents affect the reaction pathway markedly.

The electrolysis was conducted in a two layer solvent system of CH_2Cl_2–H_2O (2 : 1) using an undivided cell. Platinum electrodes were settled in an aqueous sodium chloride layer and a gentle stirring was preferable to avoid a complete mixing which induced chlorohydrination partially.[8] Upon no stirring the reaction solution, a current efficiency was extremely low. The complete mixing enhances the solubilization of the chlorinating reagent produced in a water layer into the dichloromethane layer to improve the current efficiency, meanwhile it induces chlorohydrination by the increased contact of the water layer with the organic layer. Thus, electrolysis of **2a** in the presence of a large excess amount of sodium chloride and hydrochloric acid in CH_2Cl_2–H_2O at room temperature afforded **3a** in 84% yield after 4 F/mol and **1** in 72% yield after 10 F/mol. Most of mineral acids (HCl, HNO_3, H_2SO_4, H_3PO_4) are effective for the double ene-type chlorination and likewise organic acids affect the reaction highly. However, formic acid is not effective since the current efficiency is unexpectedly low (Table 1). Although formic acid is known to activate *t*-butylhypochlorite for the chemical ene-type chlorination,[9] it is a reducing agent so that it would reduce the electrogenerated

chlorinating reagent. In fact, **1** was obtained in 63% yield by the reaction of **2a** with sodium hypochlorite in CH_2Cl_2–H_2O in the presence of hydrochloric acid. In contrast to this, none of **1** was detected in the presence of formic acid while only 7% of **3a** was isolated and 92% of **2a** was recovered.

The relation of the acid concentration and the yields is shown in Fig. 1. Excess use of hydrochloric acid accelerated dichlorination whereas in the absence of the acid, 57% of the starting substance **2a** was recovered, and 34% of **3a** was obtained but none of **1** was isolated even after 10 F/mol of electricity was passed. In fact, 40 F/mol of electricity was required in order to complete monochlorination of **2a** (89%) in the absence of acid.[10]

The yields of **1** and **3a** are dependent to electricity passed (F/mol) (Fig. 2). In the presence of excess amount of acid, the starting substance **2a** disappeared almost completely at around 4 F/mol where the yield of **3a** reached to an optimum, while the yield of **1** increased steadily in proportion to electricity. This result suggests that **2a** is more reactive toward the chlorinating reagent than **3a**.

The effect of the solvent is also noteworthy. The use of immiscible solvents in water such as dichloromethane, chloroform, 1,2-dichloroethane, and benzene all of which constitute a two-phase system leads to a selective formation of **1** and **3a**. In contrast, the use of miscible solvents such as methanol and acetonitrile induced predominantly chlorohydrination, chloromethoxylation, and chloroacetamidation, respectively. Ethyl acetate is immiscible but slightly soluble in water[11] so that it affected both ene-type chlorination and chlorohydrination. The transition state of the ene-type chlorination where chlorination to double bond and deprotonation from methyl group take place concertedly, is not cation-like,[12] and therefore it would be favored in less polar and water-immiscible solvents.

The mechanism of the acid-catalyzed ene-type chlorination is not clear yet at this stage. However, it is proposed that a protonated chlorinating reagent would be more reactive for the ene-type chlorination.[9] The electrochemically generated chlorinating reagent would be in equilibrium as shown in Eq. 1.[13]

$$2\,HOCl \rightleftharpoons Cl_2O + H_2O \quad (1)$$

Since chlorine monoxide (Cl_2O) is more soluble in

Table 1. Effect of acids on the electrochemical ene-type chlorination of **2a**[a] in dichloromethane–water.

Acid	Products (%) 4 F/mol			10 F/mol		
	2a	**3a**	**1**	**2a**	**3a**	**1**
HCl	0	84	4	0	0	72
H_2SO_4[c]	0	80	4	0	2	65
HNO_3	0	80	6	0	2	66
H_3PO_4[d]	0	75	4	0	1	63
AcOH	0	76	12	0	1	66
$CH_3(CH_2)_2CO_2H$	0	85	2	0	46	36
$C_{10}H_{16}O_4S$[b]	0	79	4	0	2	71
HCO_2H	73	19	0	49	42	0

a) CH_2Cl_2 (8 ml)–H_2O (4 ml)–3 mol dm^{-3} acid (1ml). b) *dl*-10-Camphorsulfonic acid. c) 1.5 mol dm^{-3} of H_2SO_4 (1 ml). d) 1 mol dm^{-3} of H_3PO_4 (1 ml).

Table 2. Effect of solvents on the electrochemical ene-type chlorination of **2a**[a]

Solvent[b]	Products (%) **2a**	**3a**	**1**	Others
CH_2Cl_2–H_2O	0	84	3	—
$CHCl_3$–H_2O	3	84	0	—
$ClCH_2CH_2Cl$–H_2O	13	75	0	—
C_6H_6–H_2O	11	79	0	—
AcOEt–H_2O	0	0[c]	51	**4a**(32), **4d**(15)
MeOH–H_2O	18	0	0	**4a**(41), **4b**(24)
MeCN–H_2O	0	0	0	**4a**(31), **4c**(60)
$(C_2H_5)_2O$–H_2O	47	40	1	**4a**(11)

a) A constant current (20 mA/cm^2, 4 F/mol) was applied. b) Organic solvent (8 ml)–water (4 ml)–3.2 mol dm^{-3} HCl (1 ml). c) At 3 F/mol, **3a** (36%) and **1** (21%) were obtained.

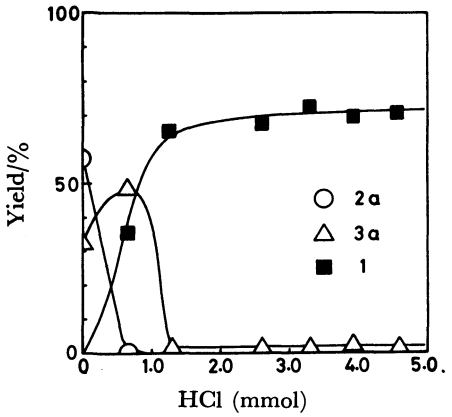

Fig. 1. The relation of the yields of **1** and **3a** with the concentration of HCl in the electrochemical ene-type chlorination of **2a** in CH_2Cl_2 (8 ml)–H_2O (4 ml) containing **2a** (50 mg, 0.25 mmol) and NaCl (500 mg, 8.6 mmol). The constant current (20 mA/cm^2, 10 F/mol) was applied at room temperature.

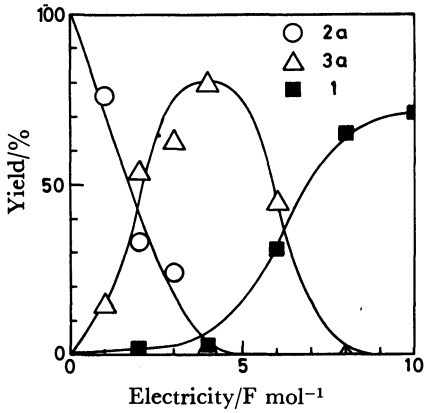

Fig. 2. The relation of the yields of **1** and **3a** with electricity (F/mol) in the electrochemical ene-type chlorination of **2a** in CH_2Cl_2 (8 ml)–H_2O (4 ml)–3.2 mol dm^{-3} HCl (1 ml) containing **2a** (50 mg) and NaCl (500 mg).

TABLE 3. THE ELECTROCHEMICAL ENE-TYPE CHLORINATION OF **2a**—**g** IN DICHLOROMETHANE–WATER[a)]

Substrate **2** R	F/mol[b)]	Product (%)		
		3	**5**	Others
2a $CH_2OC_6H_4Cl$-*p*	4.0	84	0	0
2b $CH_2OCH_2C_6H_5$	4.0	81	0	0
2c $CH_2CH_2C(OAc)(CH_3)C{\equiv}CH$	5.0	86	0	0
2d CH_2OAc[c)]	3.2	0	85	0
2e $CH_2SO_2C_6H_5$[e)]	4.0	23	0	**7**(68)
2f $CH_2SC_6H_5$[d,e)]	4.0	0	0	**8**(77)[f)]
2g CO_2H	4.0	0	55	0

a) CH_2Cl_2 (8 ml)–H_2O (4 ml)–3.2 mol dm^{-3} HCl (1 ml). b) Current density 20 mA/cm^2. c) 1,2-dichloroethane was employed as a solvent. d) Current density 7 mA/cm^2. e) 3.2 mol dm^{-3} (1.5 ml) was used. f) **2f** (7%) was recovered.

organic solvents than in water,[14)] the electrogenerated chlorinating reagent would preferentially migrate as chlorine monoxide into the organic phase where the acid-catalyzed ene-type chlorination proceeds. The fact that the use of organic acids (Table 1) highly facilitates the ene-type reaction suggests the hypothesis.

The electrolyses of **2b**—**g** were carried out in similar conditions and the result is shown in Table 3. The result suggests that the reaction pathways of **2** with the electrogenerated chlorinating reagent are extensively affected by the nature of the substituents on the prenyl moiety. The desired chlorination of **2a**, **2b**, and **2c**, proceeds smoothly to give **3a** (84%), **3b** (81%), and **3c** (86%), respectively. However, the electrolyses of **2d**, **2e**, **2f**, and **2g**, are quite dissimilar to the ene-type chlorination. Both **2d** and **2g** provided chlorohydrins **5a** and **5b**. The chlorohydrination of **2d** would proceed *via* intramolecular trapping of the carbocation **6** by acetoxyl group.[15)] Sulfone **2e** gave preferentially a vinyl chloride derivative **7** (68%) along with **3d** (23%). Deprotonation of H-2 would compete with the normal ene-type deprotonation because of the higher acidity

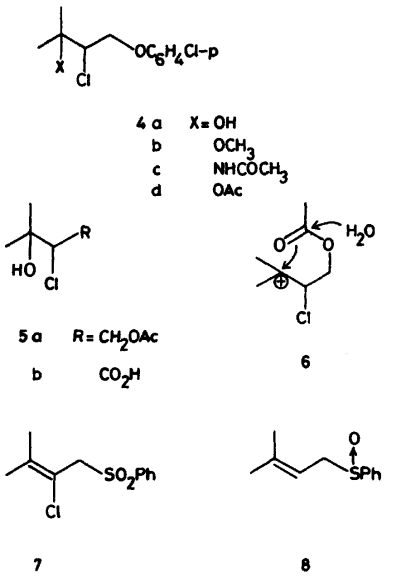

Scheme 2.

of H-2 than H-4 by the electron-withdrawing nature of benzenesulfonyl group. Sulfide **2f** is oxidized at the divalent sulfur atom to give sulfoxide **8**. The exclusive sulfoxidation can be rationalized by the fact that the divalent sulfur atom is more readily oxidized both by electrode process and by chemical reagents like NBS.[16)]

Substitution reaction of **1** with sodium benzenesulfinate in DMF proceeded smoothly at chloromethyl group providing **9a** in 72% yield. Likewise, reaction of **1** with sodium benzene thiolate in DMF at −20 °C yielded **9b** (92%). Dechlorophenoxylation of both **9a** and **9b** were performed in 87 and 74% yields, respectively by reduction with zinc in ethanol.[17)]

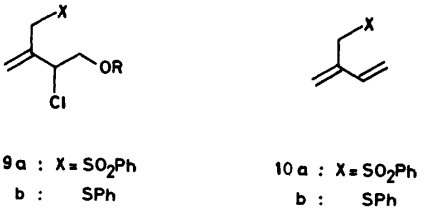

Scheme 3.

Experimental

All boiling and melting points are uncorrected. IR spectra were determined with a JASCO IRA-I infrared spectrometer. ^1H NMR spectra were obtained with a Hitachi R-24 (60 MHz) or a JEOL FX-100 (100 MHz) spectrometer and the chemical shifts are expressed in ppm (δ) downfield from TMS as an internal standard.

Electrolysis. Electrolysis was carried out in a beaker (3 cm in diameter and 10 cm in height) fitted with two platinum foil electrodes (1.5×2 cm^2) in 7—10 mm apart. A constant current (20 mA/cm^2) was applied by a regulated DC powder instrument (Metronix 543B). The electrodes were settled in a water layer and the reaction solution was gently stirred by a magnetic stirrer so that the water layer can well contact with the organic layer but drops of the water layer do not disperse into the organic layer.

Electrolysis of 2a; 3-Chloro-2-chloromethyl-4-(4-chlorophenoxy)-1-butene (1) and 3-chloro-2-methyl-4-(4-chlorophenoxy)-1-butene (3a). A mixture of **2a** (50 mg, 0.25 mmol, NaCl (500 mg, 8.5 mmol) and 3.2 mol dm^{-3} HCl (1 ml) in CH_2Cl_2 (8 ml) –H_2O (4 ml) was electrolyzed at room temperature for 27.3 min (4 F/mol). The mixture was neutralized with saturated $NaHCO_3$ and the organic substances were extracted with ether. The organic layer was washed two times with brine, dried (Na_2SO_4), and concentrated under reduced pressure. The residue was chromatographed over silica gel (Wako-gel C-200, *n*-hexane) to give a colorless oil (54 mg) whose HPLC analysis (μ-porasil, hexane–AcOEt=20 : 1) showed purity of **3a** was over 90%. Thus, yield of **3a** was 84%. Other products were **1** (3%), 3-chloro-2-methyl-4-(3,4-dichlorophenoxy)-1-butene (2—3%) and the unidentified product (2—3%) by HPLC analysis: **1**: Bp 118 °C/0.02 mmHg (1 mmHg≈133.322 Pa); IR: 1630, 1595, 1580, 1240 cm^{-1}; ^1H NMR ($CDCl_3$) δ=4.18 (s, 2H, CH_2Cl), 4.21 (d, J=7 Hz, 2H, CH_2), 4.80 (*t*, J=7 Hz, 1H, CHCl), 5.42 (br. s, 2H, CH_2=), 6.7—7.3 (m, 4H, ArH). Found: C, 49.92; H, 4.33%. Calcd for $C_{11}H_{11}Cl_3O$: C, 49.75; H, 4.15%. **3a**: Bp 105 °C/0.33 mmHg; IR: 1650 (C=C), 1595, 1580, 1240 cm^{-1}; ^1H NMR (CCl_4) δ=1.84 (s, 3H, CH_3), 4.08 (d, J=6 Hz, 2H, CH_2), 4.55 (dd, J_1=6 Hz, J_2=5 Hz, 1H, CHCl), 4.9—5.3 (m,

2H, CH_2=), 6.5—7.2 (m, 4H, ArH). Found: C, 57.36; H, 5.11%. Calcd for $C_{11}H_{12}Cl_2O$: C, 57.17; H, 5.20%.

*3-Chloro-2-methyl-4-benzyloxy-1-butene (**3b**)*: Bp 65 °C/0.03 mmHg; IR: 1645 (C=C), 1600, 1580, 1120 cm^{-1}; ^1H NMR (CCl_4) δ=1.75 (br. s, 3H, CH_3), 3.55 (d, J=7 Hz, 2H, CH_2), 4.42 (t, J=7 Hz, 1H, CHCl), 4.45 (s, 2H, CH_2), 4.8—5.1 (m, 2H, CH_2=), 7.20 (br. s, 5H, ArH). Found: C, 68.53; H, 7.35%. Calcd for $C_{12}H_{15}ClO$: C, 68.42; H, 7.13%.

*4-Chloro-1-ethynyl-1,5-dimethyl-5-hexenyl Acetate (**3c**)*: Bp 80 —82 °C/0.03 mmHg; IR: 3300 (≡CH), 2100 (C≡C), 1740 (AcO) cm^{-1}; ^1H NMR ($CDCl_3$) δ=5.13 (br. s, 1H, =CH_2), 5.00 (br. s, 1H, =CH_2), 4.46 (t, J=6.6 Hz, 1H, CHCl), 2.62 (s, 1H, ≡CH), 2.08 (s, 3H, Ac), 2.2—1.9 (m, 4H, CH_2), 1.86 (br. s, 3H, CH_3), 1.74 (s, 3H, CH_3). Found: C, 63.06; H, 7.55%. Calcd for $C_{12}H_{17}O_2Cl$: C, 63.01; H, 7.49%.

*3-Chloro-2-methyl-4-phenylsulfonyl-1-butene (**3e**)*: Bp 117 °C/ 0.02 mmHg; IR: 1640 (C=C), 1580, 1310 (SO_2), 1140 (SO_2) cm^{-1}; ^1H NMR (CCl_4) δ=1.75 (br. s, 3H, CH_3), 1.77 (s, 3H, CH_3), 3.55 (d, J=7 Hz, 2H, CH_2), 4.80 (t, J=7 Hz, 1H, CHCl), 4.92 (br. s, 1H, CH=), 5.10 (br. s, 1H, CH=), 7.3—8.0 (m, 5H, ArH). Found: C, 53.93; H, 5.32%. Calcd for $C_{11}H_{13}O_2ClS$: C, 54.00; H, 5.32%.

*3-Chloro-2-methyl-4-(4-chlorophenoxy)-2-butanol (**4a**)*: Bp 113 °C/0.02 mmHg; IR: 3400 (OH), 1590, 1580, 1250 cm^{-1}; ^1H NMR (CCl_4) δ=1.36 (s, 6H, CH_3), 2.4 (br. s, 1H, OH), 4.0—4.5 (m, 3H, $CHClCH_2O$), 6.7—7.4 (m, 4H, ArH). Found: C, 53.15; H, 5.85%. Calcd for $C_{11}H_{14}O_2Cl_2$: C, 53.03; H, 5.62%.

*2-Chloro-3-methyl-3-methoxybutyl 4-Chlorophenyl Ether (**4b**)*: Bp 91 °C/0.015 mmHg; IR: 2830, 1605, 1250 cm^{-1}; ^1H NMR (CCl_4) δ=1.27 (s, 3H, CH_3), 1.33 (s, 3H, CH_3), 3.23 (s, 3H, CH_3O), 3.9—4.6 (m, 3H, $CHClCH_2O$), 6.7—7.3 (m, 4H, ArH). Found: C, 54.63; H, 6.13%. Calcd for $C_{12}H_{16}O_2Cl_2$: C, 54.77; H, 6.09%.

N-[*2-Chloro-1,1-dimethyl-3-(4-chlorophenoxy)propyl*] *Acetamide (**4c**)*: Bp 110 °C/0.035 mmHg; IR: 3260 (NH), 1650 (C=O) cm^{-1}; ^1H NMR ($CDCl_3$) δ=1.49 (s, 6H, CH_3), 1.92 (s, 3H, CH_3), 4.0—4.4 (m, 2H, CH_2O), 4.94 (dd, J_1=6 Hz, J_2=4 Hz, 1H, CHCl), 6.31 (br. s, 1H, NH), 6.6—7.3 (m, 4H, ArH). Found: C, 53.74; H, 5.79%. Calcd for $C_{13}H_{17}O_2NCl_2$: C, 53.81; H, 5.86%.

*2-Chloro-1,1-dimethyl-3-(4-chlorophenoxy)propyl Acetate (**4d**)*: Bp 120 °C/0.03 mmHg; IR: 1740 (C=O), 1595, 1580, 1240 cm^{-1}; ^1H NMR ($CDCl_3$) δ=1.67 (s, 6H, CH_3), 2.06 (s, 3H, Ac), 4.14 (dd, J_1=7.2 Hz, J_2=10.5 Hz, 1H, CH_2O), 4.37 (dd, J_1=4.2 Hz, J_2=10.5 Hz, 1H, CH_2O), 4.80 (dd, J_1=4.2 Hz, J_2=7.2 Hz, CHCl), 6.80—7.44 (m, 4H, ArH). Found: C, 53.76; H, 5.59%. Calcd for $C_{13}H_{16}O_3Cl_2$: C, 53.62; H, 5.55%.

*2-Chloro-3-hydroxy-3-methylbutyl Acetate (**5a**)*: Bp 93 °C/0.03 mmHg; IR: 3440 (OH), 1740 (C=O), 1250 cm^{-1}; ^1H NMR ($CDCl_3$) δ=1.30 (s, 6H, CH_3), 2.05 (s, 3H, Ac), 2.73 (s, 1H, OH), 3.8—4.6 (m, 3H, $CHClCH_2O$). Found: C, 46.53; H, 7.26%. Calcd for $C_7H_{13}O_3Cl$: C, 46.55; H, 7.20%.

*2-Chloro-3-hydroxy-3-methylbutanoic Acid (**5b**)*: The carboxylic acid **5b** was esterified with diazomethane in ether and the analytical data were measured as its methyl ester. Bp 92 °C/ 0.02 mmHg; IR: 3460 (OH), 1740 (C=O), 1170 cm^{-1}; ^1H NMR (CCl_4) δ=1.34 (s, 6H, CH_3), 2.3—2.8 (m, 1H, OH), 3.79 (s, CH_3O), 4.16 (s, 1H, CHCl). Found: C, 43.32; H, 6.57%. Calcd for $C_6H_{11}O_3Cl$: C, 43.37; H, 6.63%.

*2-Chloro-3-methyl-1-phenylsulfonyl-2-butene (**7**)*: Bp 120 °C/ 0.02 mmHg; IR: 1640 (C=C), 1585, 1305 (SO_2), 1140 (SO_2) cm^{-1}; ^1H NMR (CCl_4) δ=1.65 (s, 3H, CH_3), 1.80 (s, 3H, CH_3), 4.08 (s, 2H, CH_2), 7.3—8.0 (m, 5H, ArH). Found: C, 54.17; H, 5.55%. Calcd for $C_{11}H_{13}O_2ClS$: C, 54.00; H, 5.32%.

*3-Methyl-2-butenylphenylsulfoxide (**8**)*: Bp 88 °C/0.03 mmHg; IR: 1665 (C=C), 1580, 1045 (SO) cm^{-1}; ^1H NMR ($CDCl_3$) δ=1.43 (s, 3H, CH_3), 1.73 (s, 3H, CH_3), 3.56 (d, J=8 Hz, 2H, CH_2), 5.12 (t, J=8 Hz, 1H, =CH), 7.31—7.90 (m, 5H, ArH), Found: C, 68.05; H, 7.29%. Calcd for $C_{11}H_{14}OS$: C, 67.99; H, 7.27%.

*3-Chloro-4-(4-chlorophenoxy)-2-(phenylsulfonylmethyl)-1-butene (**9a**)*: Mp: 49—51 °C; IR: 1640 (C=C), 1320 (SO_2), 1230. 1150 (SO_2) cm^{-1}; ^1H NMR ($CDCl_3$) δ=4.03 (s, 2H, CH_2SO_2), 4.26 (d, J=6.3 Hz, 2H, CH_2O), 4.91 (t, J=6.3 Hz, 1H, CHCl), 5.60 (s, 1H, CH=), 5.25 (s, 1H, CH=), 6.7—7.4 (m, 4H, ArH), 7.5—8.1 (m, 5H, ArH). Found: C, 55.06; H, 4.17%. Calcd for $C_{17}H_{16}O_3Cl_2S$: C, 55.00; H, 4.31%.

*3-Chloro-4-(4-chlorophenoxy)-2-(phenylthiomethyl)-1-butene(**9b**)*: Bp 136 °C/0.025 mmHg; IR: 1600, 1580, 1495, 1240 cm^{-1}; ^1H NMR ($CDCl_3$) δ=3.66 (s, 2H, CH_2S), 4.18 (d, J=6 Hz, 2H, CH_2O), 4.86 (t, J=6 Hz, 1H, CHCl), 5.15 (br. s, 1H, CH_2=), 5.22 (br. s, 1H, CH_2=), 6.5—7.4 (m, 9H, ArH). Found: C, 60.17; H, 4.69%. Calcd for $C_{17}H_{16}OSCl_2$: C, 60.19; H, 4.72%.

*2-(Phenylsulfonylmethyl)-1,3-butadiene (**10a**)*: Mp 41—42 °C IR: 1595, 1320 (SO_2), 1310, 1150 (SO_2) cm^{-1}; ^1H NMR ($CDCl_3$) δ=4.03 (s, 2H, CH_2), 5.04—5.37 (m, 4H, CH_2), 6.32 (dd, J_1=11 Hz, J_2=18 Hz, 1H, CH=), 7.5—8.0 (m, 5H, ArH). Found: C, 63.39; H, 5.64%. Calcd for $C_{11}H_{12}O_2S$: C, 63.46; H, 5.77%.

*2-(Phenylthiomethyl)-1,3-butadiene (**10a**)*: Bp 70 °C/0.03 mmHg; IR: 1630 (C=C), 1590 cm^{-1}; ^1H NMR ($CDCl_3$) δ= 3.75 (s, 2H, CH_2), 5.18 (s, 2H, CH_2=), 5.22 (d, J=11.5 Hz, 1H, CH_2=), 5.41 (d, J=17.5 Hz, 1H, CH_2=), 6.46 (dd, J_1= 11.5 Hz, J_2=17.5 Hz, 1H, CH=), 7.2—7.5 (m, 5H, ArH). Found: C, 74.89; H, 6.87%. Calcd for $C_{11}H_{12}S$: C, 75.00; H, 6.82%.

References

1) K. Takabe, T. Katagiri, J. Tanaka, *Koryo*, **108**, 27 (1974); Y. Fujita, Y. Ninagawa, T. Nishida, and K. Itoi, *Yuki Gosei Kagaku Kyokai Shi*, **37**, 244 (1979); S. Torii, K. Uneyama, and T. Inokuchi, *Koryo*, **125**, 47 (1979).

2) T. Hori and K. B. Sharpless, *J. Org. Chem.*, **44**, 4202, 4208 (1979).

3) S. Marmor and J. G. Maroski, *J. Org. Chem.*, **31**, 4278 (1966).

4) S. G. Hedge, M. K. Vogel, J. Saddler, T. Hrinyo, N. Rockwell, R. Haynes, M. Oliver, and J. Wolinski, *Tetrahedron Lett.*, **21**, 441 (1980); S. G. Hedge, and J. Wolinsky, *ibid.*, **22**, 5019 (1981).

5) W. Sato, N. Ikeda, and H. Yamamoto, *Chem. Lett.*, **1982**, 141.

6) S. Torii, K. Uneyama, T. Nakai, and T. Yasuda, *Tetrahedron Lett.*, **22**, 2291 (1981).

7) S. Torii, H. Tanaka, N. Saitoh, T. Siroi, M. Sasaoka, and J. Nokami, *Tetrahedron Lett.*, **22**, 3193 (1981).

8) Chlorohydrin **4a** (11%) was obtained as one of by-product.

9) R. D. G. Cooper, *Tetrahedron Lett.*, **21**, 781 (1980); L. A. Paquette, L. W. Hertel, R. Gleiter, M. C. Bohm, M. A. Beno, and G. G. Christoph, *J. Am. Chem. Soc.*, **103**, 7106 (1981).

10) **1** (6%) was obtained as a byproduct.

11) Solubility (g/100 g of water) of the solvents employed is as follows; CH_2Cl_2 (2), $CHCl_3$ (0.8), $ClCH_2CH_2Cl$ (0.9), C_6H_6 (0), AcOEt (7.9), MeOH (∞), MeCN (∞).

12) M. Yoshioka, T. Tsuji, S. Uyeo, S. Yamamoto, T. Aoki, Y. Nishitani, S. Mori, H. Satoh, Y. Hamada, H. Ishitobi, and W. Nagata, *Tetrahedron Lett.*, **21**, 351 (1980).

13) The chemistry of chlorine monoxide is reviewed. J. J.

Renard and H. I. Bolker, *Chem. Rev.*, **76**, 487 (1976).
14) S. Goldschmidt, *Chem. Ber.*, **52B**, 753 (1919).
15) S. Winstein, C. R. Lindegren, H. Marshall, and L. L, Ingraham, *J. Am. Chem. Soc.*, **75**, 147 (1953); The acetoxyl group participation toward selenirenium type cation has been proposed. K. Uneyama, K. Takano, and S. Torii, *Tetrahedron Lett.*, **23**, 1161 (1982).
16) S. Torii, K. Uneyama, K. Iida, and K. Sasaki, *Tetrahedron Lett.*, **1972**, 4513.
17) H. O. House and R. S. Ro, *J. Am. Chem. Soc.*, **80**, 182 (1958).

 © 1983 The Chemical Society of Japan Bull. Chem. Soc. Jpn., 56, 1219—1222 (1983)

Preparation of New Nitrogen-bridged Heterocycles. 6.[1] First Synthesis of 2-Aroylfuro[2,3-*b*]indolizine Derivatives

Akikazu KAKEHI,* Suketaka ITO, Tsuyoshi OHIZUMI, and Masayoshi ITO
Department of Industrial Chemistry, Faculty of Engineering, Shinshu University, Wakasato, Nagano 380
(Received November 8, 1982)

Alkaline treatment of 2-(aroylmethoxy)-3-(2,2-dicyanovinyl)indolizine derivatives, readily available from the step-by-step reactions of 1-(ethoxycarbonylmethyl)-2-picolinium salts with a base, (ethoxymethylene)malononitrile followed by some phenacyl bromides in ethanol, afforded smoothly the title compounds, 2-aroylfuro[2,3-*b*]-indolizine derivatives, in good yields. These furoindolizines could be also obtained directly from the pyridinium salts without the isolation of intermediate 3-vinylindolizines. Formation mechanisms and some physical properties of these furoindolizines are also discussed.

Recently, we have found a one-pot synthesis of 2-alkoxy- and 2-acyloxy-3-vinylindolizine derivatives using a single Michael addition of various vinylating agents onto 2(3*H*)-indolizinones generated in situ from the corresponding 1-(ethoxycarbonylmethyl)-2-picolinium salts.[1] Since effective functionalization of indolizine derivatives has been scarcely reported except the cyclization of 2-allylidenedihydropyridines[2] and 3-vinylation of 3-unsubstituted indolizines,[3] this route not only has high value from the stand of synthetic methodology, but also polyfunctionalized compounds, thus obtained, should be useful as a synthone for the transformations from them to fused heterocycles and other synthetic intermediates. In this paper we wish to report the syntheses of the indolizine molecules designed as both possessing an active methylene group and a 2,2-dicyanovinyl group as a masked carbonyl one and their successful transformations to furo[2,3-*b*]indolizine derivatives by an alkaline treatment.

Results and Discussion

Preparations of 2-(Aroylmethoxy)- and 2-(Benzyloxy)-3-(2,2-dicyanovinyl)indolizine Derivatives. The reasons for the selection of 2-(aroylmethoxy)-3-(2,2-di cyanovinyl)indolizines as a model compound in this paper are following: a) The molecules have both a nucleophilic reaction center in the 2-substituent and a vinyl moiety which serves as a potential carbonyl group, and b) the subsequent reaction using these functional groups may provide a useful path to furan-fused heterocycles. These 2-(aroylmethoxy)-3-(2,2-dicyanovinyl)-indolizines **9**—**20** were synthesized from the reactions of 1-(ethoxycarbonylmethyl)pyridinium salts **1**—**4** in ethanol with base and (ethoxymethylene)malononitrile **5**, followed by the alkylations with phenacyl bromides **6**—**8** according to the procedure developed by us.[1] On the other hand, 2-benzyloxy derivatives **22** and **23** were also prepared by similar reactions of salts **2** and **4** using benzyl bromide **21** as an alkylating agent in order to compare their reactivities with those of 2-(aroylmethoxy)indolizines **9**—**20** (Scheme 1).

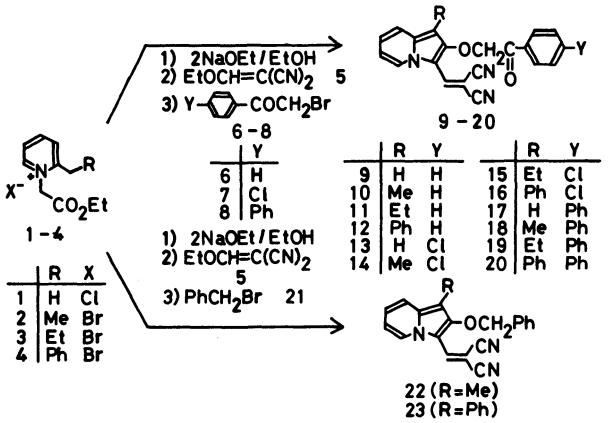

	R	X
1	H	Cl
2	Me	Br
3	Et	Br
4	Ph	Br

	Y
6	H
7	Cl
8	Ph

	R	Y
9	H	H
10	Me	H
11	Et	H
12	Ph	H
13	H	Cl
14	Me	Cl
15	Et	Cl
16	Ph	Cl
17	H	Ph
18	Me	Ph
19	Et	Ph
20	Ph	Ph

Scheme 1.

Structural elucidation of these indolizines **9**—**20**, **22**, and **23** were achieved by their elementary analyses and by their spectral comparisons with those of known 1- and 3-vinylindolizine derivatives.[1-3]

Facile Formation of Furo[2,3-b]indolizine Derivatives. When the retro-aldol reaction of the 2,2-dicyanovinyl group in indolizine **9** to a formyl group was examined in ethanol with an aqueous alkali,[4] the direct formation of 2-benzoylfuro[2,3-*b*]indolizine **25**, red prisms, mp 124—127 °C, was observed instead of initially expected 3-formylindolizines such as **24**. Similar treatment of 2-(aroylmethoxy)indolizines **10**—**20** afforded the corresponding 2-aroylfuro[2,3-*b*]indolizine derivatives **26**—**36** as red crystals in comparatively good yields. On the other hand, the reactions of 2-(benzyloxy)indolizines **22** and **23** with an aqueous alkali did not give furoindolizines such as **39** at all, but yielded 2-(benzyloxy)-3-formylindolizines **37** and **38** as colorless oil and crystals in 79 and 75% yields, respectively. Furthermore, our attempts to prepare 2-phenylfuro[2,3-*b*]indolizine derivatives such as **39** from these 3-formylindolizines **37** and **38** under various basic conditions were unsuccessful (Schemes 2 and 3). Next, we examined the possibility of one-pot synthesis from pyridinium salts **1**—**4** to **25**—**36**, since both formation reactions of 3-vinylindolizines **9**—**20** and furoindolizines **25**—**36** took place always in the same solvent such as ethanol. As might be expected, the same products **25**—**36** could be obtained directly in 10—57% yields by the successive reactions of salt **1**—**4** with sodium ethoxide, (ethoxymethylene)malononitrile **5**, bromides **6**—**8**, and aqueous alkali. Similar furoindolizines **41**—**44** were also formed from the reactions of salt **1**—**4** by using *p*-methylphenacyl bromide **40** as an alkylating agent (Scheme 4).

The structures of furoindolizines **25**—**36** and **41**—**44** were mainly determined by the physical and spectral

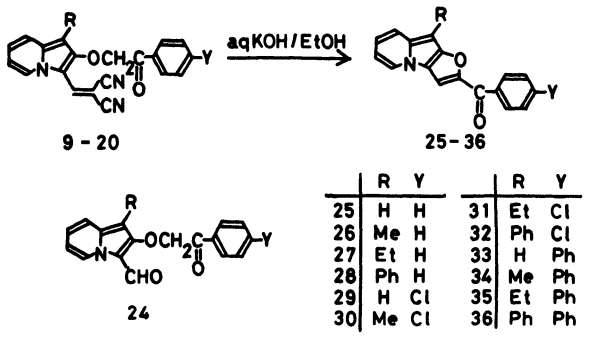

	R	Y		R	Y
25	H	H	31	Et	Cl
26	Me	H	32	Ph	Cl
27	Et	H	33	H	Ph
28	Ph	H	34	Me	Ph
29	H	Cl	35	Et	Ph
30	Me	Cl	36	Ph	Ph

Scheme 2.

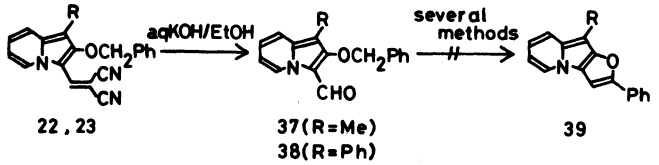

Scheme 3.

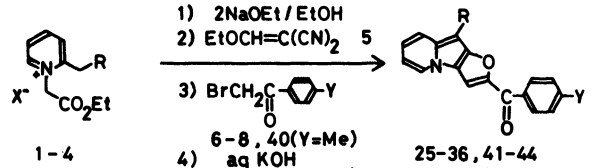

	R	Y		R	Y
25	H	H	33	H	Ph
26	Me	H	34	Me	Ph
27	Et	H	35	Et	Ph
28	Ph	H	36	Ph	Ph
29	H	Cl	41	H	Me
30	Me	Cl	42	Me	Me
31	Et	Cl	43	Et	Me
32	Ph	Cl	44	Ph	Me

Scheme 4.

means and by the mechanistic consideration of the reactions. In particular, the elementary analyses of **25**—**36** and **41**—**44** were in good accord with the proposed compositions but not with those of initially expected 3-formylindolizines **24** at all. This fact was also supported clearly by the molecular ions in the Mass spectra of 2-benzoylfuro[2,3-*b*]indolizine derivatives **25**—**28**. In the NMR spectra of **25**—**36** and **41**—**44**, all of the skeletal proton signals appeared in an aromatic region and any other signals due to the formyl and the methylene protons could not be detected. For example, the NMR spectrum of **25** exhibited proton signals at δ=6.33 (1H, s), 6.62 (1H, dd, J=7.0 and 1.5 Hz), 6.95 (1H, br t, J=9.0 and 7.0 Hz), 7.58 (1H, s), and 7.3—8.2 (7H, m) due to the 9-H, 6-H, 7-H, 3-H, and 5-, 8-, and phenyl-H, respectively. Similar signal patterns and chemical shifts supporting the furoindolizine structure were always observed in the NMR spectra of compounds **26**—**36** and **41**—**44** (See Table 1). Furthermore, the qualitative tests (Ehrlich, Shear, and Liebermann-Burchard reactions) for furan rings were positive in all cases. Interestingly, the carbonyl absorption bands in the IR spectra of these furoindolizines **25**—**36** and **41**—**44** appeared in extremely lowered region (1592—1618 cm^{-1}), suggesting maybe large contribution of delocalized structures **45** and/or **46** as shown in Scheme 5.

TABLE 1. NMR SPECTRA OF FURO[2,3-*b*] INDOLIZINE DERIVATIVES

Compd No[a]	C-3	C-6	C-7	C-9		C-5,8 and Phenyl-H	
25	7.58	6.62	6.95	6.33		7.3—8.2	
	s	dt	br t	s		m	
26	7.54	6.53	6.88	2.43		7.2—8.2	
	s	dt	br t	s		m	
27	7.57	6.54	6.86	1.40	2.94	7.3—8.2	
	s	dt	br t	t	q	m	
28	b)	6.65	7.02	7.3—8.2		7.3—8.2	
		dt	br t	m		m	
29	7.62	6.60	6.92	6.30		7.3—8.2	
	s	dt	br t	s		m	
30	7.56	6.57	6.92	2.44		7.3—8.3	
	s	dt	br t	s		m	
31	7.58	6.57	6.92	1.41	2.91	7.3—8.2	
	s	dt	br t	s	q	m	
32	b)	6.68	7.02	7.3—8.3		7.3—8.3	
		dt	br t	m		m	
33	7.67	6.59	6.90	6.33		7.3—8.3	
	s	dt	br t	s		m	
34	7.60	6.54	6.88	2.43		7.3—8.3	
	s	dt	br t	s		m	
35	7.62	6.50	6.83	1.39	2.88	7.3—8.3	
	s	dt	br t	s	q	m	
36	b)	6.65	7.00	7.3—8.3		7.3—8.3	
		dt	br t	m		m	
41	7.54	6.57	6.87	6.30		7.1—8.2	2.44[c]
	s	dt	br t	s		m	s
42	7.54	6.52	6.87	2.43		7.1—8.2	2.43[c]
	s	dt	br t	s		m	s
43	7.60	6.56	6.90	1.43	2.93	7.1—8.2	2.48[c]
	s	dt	br t	t	q	m	s
44	7.70	6.67	7.02	7.2—8.3		7.2—8.3	2.48[c]
	s	dt	br t	m		m	s

a) The coupling constants of these molecules were as follows; $J_{5,6}=J_{6,7}=7.0$ Hz, $J_{7,8}=9.0$ Hz, $J_{6,8}=1.5$ Hz, and $J_{Et}=7.0$ Hz. b) Overlapped with the phenyl signals. c) The methyl signal of the *p*-methylbenzoyl group.

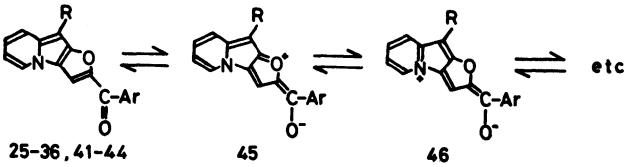

Scheme 5.

On the other hand, compounds **37** and **38** were determined to be 2-benzyloxy-3-formylindolizine derivatives, since their NMR spectra showed the presences of the formyl protons (δ=9.73 (**37**) and 9.79 (**38**)) and the methylene protons (δ=5.22 (**37**) and 4.88 (**38**)), and the elementary analysis of **38** were in accord with the suggested structure.

Mechanistically, the formation reaction of furoindolizines **25**—**36** and **41**—**44** can be explain reasonably by the intermediacy of 2-(aroylmethoxy)-3-formylindolizines such as **24** *via* the retro-aldol reaction of 2-(aroylmethoxy)-3-(2,2-dicyanovinyl)indolizine deriva-

tives and subsequent intramolecular aldol reaction between the 2- and 3-substituents in **24** (Scheme 6). Since 2-(benzyloxy)-3-fromylindolizines **37** and **38** from 3-vinylindolizines **22** and **23** were actually isolated and the utility of the 2,2-dicyanovinyl group as a masked carbonyl is extensively realized,[4] the former hypothesis seems to be undoubtful. The latter reaction is also one of the most important methods for the syntheses of fused furans.[5] The failure to obtain 2-phenylfuro[2,3-*b*]-indolizines such as **39** from 2-(benzyloxy)-3-formylindolizines **22** and **23** must be owing to low acidity of the methylene group of the 2-substituent in contrast with that of the 2-aroylmethoxy group in indolizine derivatives such as **9**—**20**.

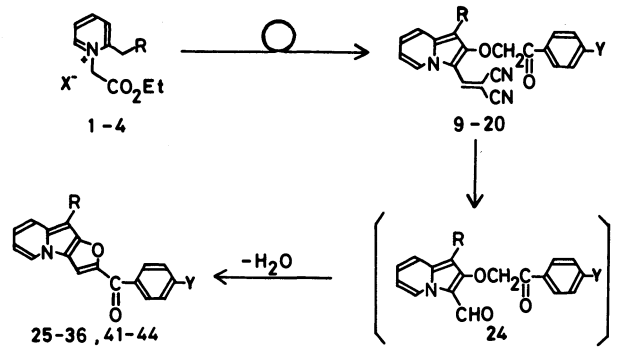

Scheme 6.

Experimental

Melting points were measured with a Yanagimoto MP-S3 micromelting point apparatus and are uncorrected. Microanalyses were carried out on a Perkin-Elmer 240 elemental analyzer. NMR spectra were determined with a Varian EM360A NMR spectrometer in deuteriochloroform with tetramethylsilan as an internal standard, chemical shifts expres-

Table 2. Some data of 3-vinylindolizinederivatives

Compd No.	Reactant	Yield %	Mp θ_m/°C	KBr $\nu_{C=O}$ cm^{-1}	KBr ν_{CN} cm^{-1}	Formula	Calcd (%) C	Calcd (%) H	Calcd (%) N	Found (%) C	Found (%) H	Found (%) N
9	**1 5 6**	19	211—213	1687	2200	$C_{20}H_{13}N_3O_2$	73.38	4.00	12.84	73.53	4.10	12.60
10	**2 5 6**	61	225—227	1690	2195	$C_{21}H_{15}N_3O_2$	73.89	4.43	12.31	73.81	4.37	12.44
11	**3 5 6**	49	203—207	1696	2200	$C_{22}H_{17}N_3O_2$	74.35	4.82	11.82	74.28	4.93	11.78
12	**4 5 6**	56	198—201	1688	2195	$C_{26}H_{17}N_3O_2$	77.41	4.25	10.42	77.37	4.19	10.51
13	**1 5 7**	3	243—245	1690	2200	$C_{20}H_{12}N_3O_2Cl$	66.40	3.34	11.61	66.29	3.48	11.58
14	**2 5 7**	39	217—219	1697	2201	$C_{21}H_{14}N_3O_2Cl$	67.12	3.76	11.18	66.89	3.84	11.32
15	**3 5 7**	32	202—204	1699	2207	$C_{22}H_{16}N_3O_2Cl$	67.78	4.14	10.78	67.89	4.17	10.70
16	**4 5 7**	53	182—184	1691	2199	$C_{26}H_{16}N_3O_2Cl$	71.32	3.68	9.60	71.48	3.72	9.56
17	**1 5 8**	2	240—243	1691	2210	$C_{26}H_{17}N_3O_2$	77.41	4.25	10.42	77.21	4.33	10.53
18	**2 5 8**	69	218—221	1689	2195	$C_{27}H_{19}N_3O_2$	77.68	4.59	10.07	77.72	4.63	9.99
19	**3 5 8**	57	199—202	1696	2210	$C_{28}H_{21}N_3O_2$	77.94	4.91	9.74	78.12	5.01	9.46
20	**4 5 8**	48	188—191	1698	2201	$C_{32}H_{21}N_3O_2$	80.15	4.41	8.76	79.94	4.57	8.93
22	**2 5 21**	65	140—142	—	2206	$C_{20}H_{15}N_3O$	76.66	4.83	13.41	76.73	4.95	13.21
23	**4 5 21**	68	170—172	—	2185	$C_{25}H_{17}N_3O$	79.98	4.56	11.19	79.86	4.70	11.17

Table 3. Some data of furo[2,3-*b*]indolizine derivatives

Compd No.	Reactant No. (No.)[a]	Yield % (%)[a]	Mp θ_m/°C	KBr $\nu_{C=O}$ cm^{-1}	Formula	Calcd (%) C	Calcd (%) H	Calcd (%) N	Found (%) C	Found (%) H	Found (%) N
25	**9 (1 5 6)**	97 (12)	124—127	1618	$C_{17}H_{11}NO_2$	78.15	4.24	5.36	77.90	4.27	5.57
26	**10 (2 5 6)**	95 (57)	119—121	1609	$C_{18}H_{13}NO_2$	78.52	4.75	5.08	78.36	4.83	5.17
27	**11 (3 5 6)**	82 (46)	117—119	1595	$C_{19}H_{15}NO_2$	78.87	5.22	4.84	78.68	5.36	4.88
28	**12 (4 5 6)**	99 (46)	186—188	1600	$C_{23}H_{15}NO_2$	81.88	4.48	4.15	81.75	4.65	4.11
29	**13 (1 5 7)**	73 (17)	185—187	1608	$C_{17}H_{10}NO_2Cl$	69.05	3.41	4.74	68.82	3.47	4.68
30	**14 (2 5 7)**	88 (39)	197—199	1602	$C_{18}H_{12}NO_2Cl$	69.80	3.91	4.52	69.71	3.87	4.61
31	**15 (3 5 7)**	84 (42)	188—190	1604	$C_{19}H_{14}NO_2Cl$	70.48	4.36	4.33	70.32	4.37	4.47
32	**16 (4 5 7)**	51 (31)	227—229	1595	$C_{23}H_{14}NO_2Cl$	74.30	3.80	3.77	74.04	3.89	3.87
33	**17 (1 5 8)**	60 (14)	171—173	1605	$C_{23}H_{15}NO_2$	81.88	4.48	4.15	81.86	4.59	4.07
34	**18 (2 5 8)**	76 (49)	200—203	1596	$C_{24}H_{17}NO_2$	82.03	4.88	3.99	81.93	4.89	4.07
35	**19 (3 5 8)**	65 (25)	154—156	1597	$C_{25}H_{19}NO_2$	82.17	5.24	3.83	82.08	5.30	3.87
36	**20 (4 5 8)**	50 (28)	208—210	1594	$C_{29}H_{19}NO_2$	84.24	4.63	3.39	84.01	4.62	3.18
41	**(1 5 40)**	(11)	154—156	1597	$C_{18}H_{13}NO_2$	78.53	4.76	5.09	78.53	4.80	5.04
42	**(2 5 40)**	(44)	135—137	1592	$C_{19}H_{15}NO_2$	78.87	5.22	4.84	78.68	5.24	4.86
43	**(3 5 40)**	(25)	153—155	1598	$C_{20}H_{17}NO_2$	79.19	5.65	4.62	79.40	5.63	4.42
44	**(4 5 40)**	(41)	212—213	1595	$C_{24}H_{17}NO_2$	82.03	4.88	3.99	82.09	4.89	3.92

a) One-pot synthesis.

sed in terms of δ, mass spectra done with a JEOL LMS-01SG-2 mass spectrometer with a JEC-6 spectrocomputer attached, and IR spectra taken with a Hitachi 260-10 Infrared spectrophotometer.

Preparations of 3-(2,2-Dicyanovinyl)indolizine Derivatives ***9—20, 22, and 23.*** *General Method*: To an ethanolic solution (70 ml) of 1-(ethoxycarbonylmethyl)-2-picolinium salt (3 mmol), an ethanolic sodium ethoxide (6 ml, 6 mmol), (ethoxymethylene)malononitrile **5** (3 mmol), and phenancyl bromide (3.5 mmol) were added step-by-step at intervals of 3 min at 60—70 °C. After kept for an hour at this temperature, the reaction mixture was chilled to room temperature. Because of the extremely low solubility of 3-(2,2-dicyanovinyl)indolizines **9—20**, **22**, and **23**,[6] their isolations were carried out by filtrating crude indolizines precipitated from the reaction solution or separated by pouring into water (200 ml). Recrystallizations of the crude compounds from ethanol or chloroform gave pure **9—20**, **22**, and **23** as yellow needles. These results and some properties are given in Table 2.

*Preparations of 2-Aroylfuro[2,3-*b*]indolizine Derivatives* ***25—36 and 41—44.*** *Method A*: To an ethanolic suspension (50 ml) of 2-(aroylmethoxy)-3-(2,2-dicyanovinyl)indolizine (1 mmol), aqueous potassium hydroxide (2 g in 5 ml of water) was added rapidly. After the suspended indolizine was completely disappeared and the resulting solution turned red (about 3—5 min), the reaction mixture was poured into 200 ml of water, neutralized carefully with diluted hydrochloric acid, and extracted twice with chloroform (100 ml). The combined extract was filtered through phase separating filter and the resulting filtrate concentrated at reduced pressure. Recrystallizations of crude products from ethanol or chloroform gave the corresponding 2-aroylfuro[2,3-*b*]indolizines **25—36** as red or dark red crystals. These results and some properties are shown in Tables 1 and 3.

Method B: To the reaction mixture described in the preparations of 3-vinylindolizines **9—20**, aqueous potassium hydroxide (2 g in 5 ml of water) was added and, after 5 min, the resulting reddish solution was poured into 200 ml of water. The aqueous solution was neutralized with diluted hydrochloric acid, extracted twice with chloroform (100 ml), and the combined solution was filtered through phase separating filter and then the filtrate concentrated at reduced pressure. The residue was separated by column chromatography (alumina) using ether and then chloroform as eluents. Recrystallizations from ethanol or chloroform gave the corresponding furoindolizines **25—36**. Similar treatment of the reaction mixtures using *p*-methylphenacyl bromide **40** as an alkylating agent gave furoindolizines **41—44**. These results and some properties are summarized in Tables 1 and 3.

Preparations of 2-(Benzyloxy)-3-formylindolizines ***37*** *and* ***38.*** These 3-formylindolizines were prepared according to the procedure (Method A) described above. Some data of compounds **37** and **38** are as follows: **37**: 79%, colorless oil, ν (Neat) 1620 cm^{-1} (C=O), $\delta(CDCl_3)=2.23$ (3H, s, 1-Me), 5.22 (2H, s, OCH_2), 6.7—7.6 (8H, m 6-, 7-, 8-, and phenyl-H), 9.61 (1H, d, $J=7.0$ Hz, 5-H), and 9.73 (1H, s, CHO). Because of its unstability, pure specimen for its elemental analysis could not be obtained.

38: 75%, colorless prisms, mp 106—107 °C, ν(KBr) 1668 cm^{-1} (C=O), $\delta(CDCl_3)=4.88$ (2H, s, OCH_2), 6.7—7.8 (13H, m, 6-, 7-, 8-, and two phenyl-H), 9.62 (1H, d, $J=7.0$ Hz, 5-H), and 9.79 (1H, s, CHO). Found: C, 80.72; H, 5.40; N, 4.18%. Calcd for $C_{22}H_{17}NO_2$: C, 80.71; H, 5.23; N, 4.28%.

Furthermore, our attempts to obtain 2-phenylfuroindolizines such as **39** from these compounds **37** and **38** under some alkaline conditions (ethanolic sodium ethoxide, potassium *t*-butoxide, and potassium acetate-acetic anhydride) were unsuccessful.

References

1) For part 5 of this series, see A. Kakehi, S. Ito, B. Wada, K. Watanabe, K. Nishimura, and A. Kumagai, *Bull. Chem. Soc. Jpn.*, **55**, 3590 (1982).

2) a) A. Kakehi, S. Ito, T. Maeda, R. Takeda, M. Nishimura, M. Tamashima, and T. Yamaguchi, *J. Org. Chem.*, **43**, 4837 (1978). b) A. Kakehi, S. Ito, T. Ohizumi, and T. Maeda, *J. Org. Chem.*, **47**, 369 (1982).

3) Y. Yamashita, D. Suzuki, and M. Masumura, *Heterocycles*, **16**, 1499 (1981).

4) J. B. Paine III, R. B. Woodward, and D. Dolphin, *J. Org. Chem.*, **41**, 2826 (1976).

5) A. Rössig, *Ber.*, **17**, 2988 (1884); R. Stoermer, *ibid.*, **30**, 1700 (1897); R. Stoermer and M. Schaffer, *ibid.*, **36**, 2863 (1903); P. C. Johnson and A. Robertson, *J. Chem. Soc.*, **1950**, 2381; C. P. Huttrer and E. Dale, *Chem. Rev.*, **48**, 543 (1951).

6) The NMR spectra of 2-(aroylmethoxy)-3-vinylindolizine derivatives **9—20** except 2-benzyloxy analogs **22** and **23** could not be measured from the same reason. The NMR spectra of **22** and **23** were as follows: **22**: $\delta(CDCl_3)=2.20$ (3H, s, 1-Me), 5.24 (2H, s, OCH_2), 6.7—7.6 (9H, m, 6-, 7-, 8-, vinyl-, and phenyl-H), and 8.30 (1H, br d, $J=7.0$ Hz, 5-H). **23**: $\delta(CDCl_3)=4.92$ (2H, s, OCH_2), 6.7—7.7 (14H, m, 6-, 7-, 8-, vinyl-, and two phenyl-H), and 8.30 (1H, br d, $J=7.0$ Hz, 5-H).

 © 1983 The Chemical Society of Japan Bull. Chem. Soc. Jpn., 56, 1223—1226 (1983)

Studies on Salt Hydrate for Latent Heat Storage, II. Eutectic Mixture of Pseudo-binary System $CH_3CO_2Na \cdot 3H_2O$–$CO(NH_2)_2$

Takahiro WADA,* Fumiko KIMURA, and Ryoichi YAMAMOTO

Material Research Laboratory, Matsushita Electric Industrial Co. Ltd., 1006 Kodama, Osaka 571

(Received July 5, 1982)

With a view of developing latent heat storage materials, mixtures of pseudo-binary system, $CH_3CO_2Na \cdot 3H_2O$–$CO(NH_2)_2$ (sodium acetate trihydrate–urea) were subjected to differentital scanning calorimetry, and the partial phase diagram for ternary system CH_3CO_2Na–$CO(NH_2)_2$–H_2O at ambient pressure was constructed. The eutectic mixture, containing 0.6 mass fraction of $CH_3CO_2Na \cdot 3H_2O$ and 0.4 mass fraction of $CO(NH_2)_2$, melts congruently at 31.5 °C with a heat of fusion of 226 J/g, which is larger than the heat of fusion of $CaCl_2 \cdot 6H_2O$, 180 *J/g*. Thus, mixtures of system $CH_3CO_2Na \cdot 3H_2O$–$CO(NH_2)_2$ are promising for solar energy storage.

Recently, some mixtures containing salt hydrate have been studied in order to develop latent heat storage materials. Böer *et al.*[1] used a eutectic mixture of system $Na_2SO_4 \cdot 10H_2O$–NH_4Cl–NaCl as a heat storage material for a solar house "solar one." Yoneda and Takanashi[2] studied on mixtures of system $Mg(NO_3)_2 \cdot 6H_2O$–$MgCl_2 \cdot 6H_2O$ and found that the eutectic mixture of this system melts at 59.1 °C and that its heat of fusion is 144 J/g.

In contrast, no mixtures of salt hydrate and organic compound have yet been studied. In this study, mixtures of pseudo-binary system $CH_3CO_2Na \cdot 3H_2O$–$CO(NH_2)_2$ were subjected to measurements using differential scanning calorimetry (DSC). From these measurements, the partial phase diagram for ternary system CH_3CO_2Na–$CO(NH_2)_2$–H_2O at ambient pressure was constructed and the heat of fusion of the eutectic mixture was determined. The linear velocity of the crystallization from pseudo-binary molten mixtures of system $CH_3CO_2Na \cdot 3H_2O$–$CO(NH_2)_2$ was measured and the microstructure of the mixtures was observed and photographed. From the experimental results, we conclude that the $CH_3CO_2Na \cdot 3H_2O$–$CO(NH_2)_2$ mixture is suitable for solar energy storage.

Experimental

Materials. $CH_3CO_2Na \cdot 3H_2O$, CH_3CO_2Na, $CO(NH_2)_2$, and $Na_4P_2O_7 \cdot 10H_2O$ were obtained commercially. $Na_4P_2O_7 \cdot 10H_2O$ was ground and passed through a 100 mesh sieve before use.

Differential Scanning Calorimetry. Differential scanning calorimetry (DSC) was performed with an SSC 560U DSC (Dainiseikosha Co.), a heat flux DSC. Weighed quantities of $CH_3CO_2Na \cdot 3H_2O$, $CO(NH_2)_2$, *etc.* were heated and mixed to a homogeneous melt. One drop of this melt was placed in a 15 μl silver crucible and was solidified. After the crucible was closed, the sample was heated at the rate of 0.5 °C/min from 10 °C to 90 °C. The melting temperature of the sample was obtained from the endothermic peak on the sample temperature curve. The heat of fusion was obtained from the endothermic peak area. This DSC system was calibrated by using ice (t_m: 0.0 °C; ΔH_m: 335 J/g), sodium sulfate decahydrate (t_m: 32.4 °C), and sodium acetate trihydrate (t_m: 58.4 °C) as standards.

Microscopic and Microphotographic Studies. For microscopic and microphotographic studies, slides were prepared and examined under a microscope. A very small drop of melt was placed on a slide and covered with a cover glass. Nucleation was started from one side.

Linear Velocity of Crystallization. The experimental technique for determining the linear velocity of crystallization was similar to that adopted by Dietz *et al.*[3] Measurement was made in a Pyrex glass tube, 500 mm in length, 1 mm in wall thickness, and 8 mm in inner diameter, provided with two right-angled bends. The tube was placed in a water bath thermostated to ±0.1 °C. The melt was seeded at one end and the time required for the crystal boundary to move a definite distance was measured by a stopwatch. The linear velocity of crystallization was determined for various degrees of supercooling in this manner.

Results and Discussion

The phase diagram for binary system CH_3CO_2Na–H_2O based on Greem's data[4] is shown in Fig. 1. In this figure, W_a shows the mass fraction of CH_3CO_2Na and W_b the mass fraction of H_2O. Therefore, the quantity on the abscissa, $100 \times W_a/(W_a+W_b)$, is the weight per cent of CH_3CO_2Na in the system. We see that $CH_3CO_2Na \cdot 3H_2O$ melts incongruently to an aqueous solution containing 58% CH_3CO_2Na by weight in equilibrium with the balance of CH_3CO_2Na as solid anhydrate, and that the balance of CH_3CO_2Na as solid anhydrate dissolves entirely in its water of crystallization at 78 °C.

DSC curves for some mixtures of pseudo-binary system

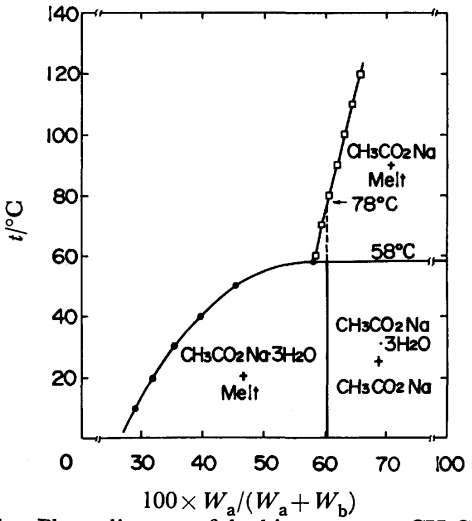

Fig. 1. Phase diagram of the binary system CH_3CO_2Na–H_2O. ●: Melting point of $CH_3CO_2Na \cdot 3H_2O$, □: melting point of CH_3CO_2Na.

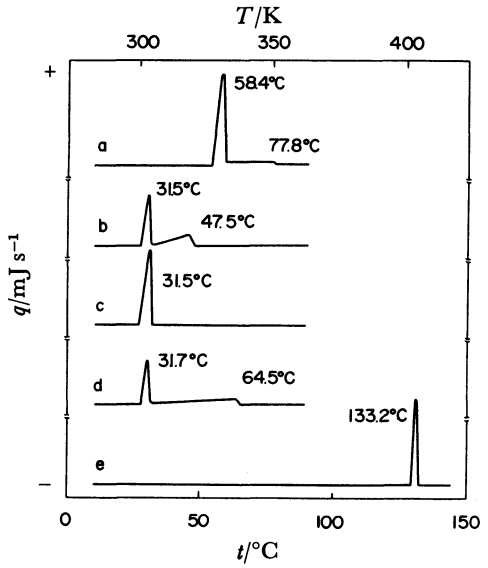

Fig. 2. DSC curves of mixtures of the pseudo-binary system $CH_3CO_2Na \cdot 3H_2O$–$CO(NH_2)_2$. a: $CH_3CO_2Na \cdot 3H_2O$, b: 0.2 mass fraction of $CO(NH_2)_2$, c: 0.4 mass fraction of $CO(NH_2)_2$, d: 0.6 mass fraction of $CO(NH_2)_2$, e: $CO(NH_2)_2$.

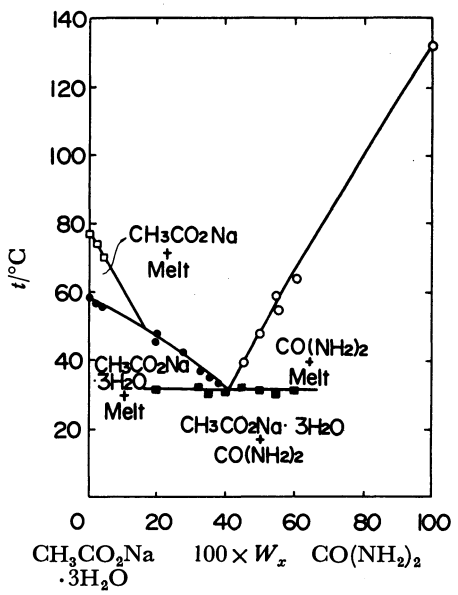

Fig. 3. Pseudo-binary section in a ternary system CH_3CO_2Na–$CO(NH_2)_2$–H_2O at ambient pressure. ●: Melting point of $CH_3CO_2Na \cdot 3H_2O$, ○: melting point of $CO(NH_2)_2$, □: melting point of CH_3CO_2Na, ■: eutectic point.

$CH_3CO_2Na \cdot 3H_2O$–$CO(NH_2)_2$ are illustrated in Fig. 2. Considering the phase diagram of the system $CH_3CO_2Na \cdot H_2O$ shownin Fig. 1, we understand that the peak at 58.4 °C on the DSC curve for $CH_3CO_2Na \cdot 3H_2O$ corresponds to the melting of $CH_3CO_2Na \cdot 3H_2O$ and that the change at 77.8 °C in the DSC curve for $CH_3CO_2Na \cdot 3H_2O$ corresponds to the entire dissolution of the CH_3CO_2Na as solid anhydrate in the water of crystallization.

The pseudo-binary section in ternary system CH_3CO_2Na–$CO(NH_2)_2$–H_2O at ambient pressure which is constructed from such DSC curves is shown in Fig. 3.

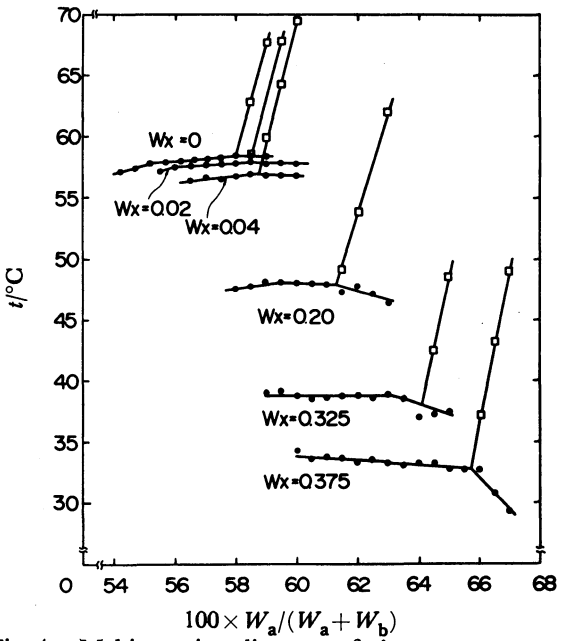

Fig. 4. Melting-point diagram of the ternary system, CH_3CO_2Na–$CO(NH_2)_2$–H_2O, at ambient pressure without $CO(NH_2)_2$ content. ●: Melting point of $CH_3CO_2Na \cdot 3H_2O$, □: melting point of CH_3CO_2Na.

This pseudo-binary section is confirmed by the cooling method adopted by Carlson *et al.*[5] In this figure, W_x shows the mass fraction of $CO(NH_2)_2$, so the quantity on the abscissa $100 \times W_x$ indicates the weight per cent of $CO(NH_2)_2$ in the system. From this figure, it is clear that pseudo-binary system $CH_3CO_2Na \cdot 3H_2O$–$CO(NH_2)_2$ forms a eutectic mixture without forming any new addition compounds. The eutectic mixture of this system, containing 0.6 mass fraction of $CH_3CO_2Na \cdot 3H_2O$ and 0.4 mass fraction of $CO(NH_2)_2$, melts congruently at 31.5 °C.

Melting-point diagrams at ambient pressure for system CH_3CO_2Na–$CO(NH_2)_2$–H_2O, in which the mass fraction of $CO(NH_2)_2$ is kept constant, are plotted in Fig. 4. In this figure, W_a shows the mass fraction of CH_3CO_2Na and W_b the mass fraction of H_2O. Therefore, the quantity on the abscissa, $100 \times W_a/(W_a+W_b)$, is the weight per cent of CH_3CO_2Na in the system with no $CO(NH_2)_2$ content. The melting-point diagram for system $CH_3CO_2Na \cdot H_2O$, which does not contain $CO(NH_2)_2$, is in good agreement with previous data.[4] It is apparent that as the mass fraction of $CO(NH_2)_2$, W_x, increases, the liquidus lines on the $CH_3CO_2Na \cdot 3H_2O$ side shift to lower temperatures and that the liquidus lines on the CH_3CO_2Na side shift to higher concentrations of CH_3CO_2Na.

A partial phase diagram of ternary system CH_3CO_2Na–$CO(NH_2)_2$–H_2O at ambient pressure is constructed by using the results of Figs. 1, 3, and 4 and shown in Fig. 5. From this figure, it is understandable that $CH_3CO_2Na \cdot 3H_2O$ comes to melt congruently when a sufficient quantity of $CO(NH_2)_2$ or H_2O is added to it. Moreover, the liquidus line on the $CH_3CO_2Na \cdot 3H_2O$ side is lowered by addition of $CO(NH_2)_2$ or H_2O. Thus, the effect of addition of

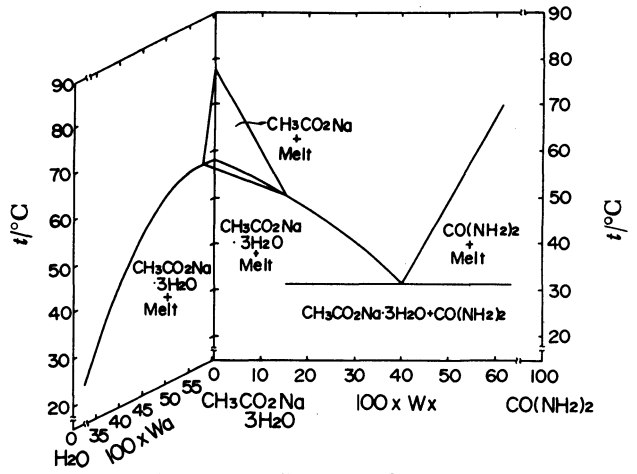

Fig. 5. Partial phase diagram of the ternary system CH_3CO_2Na–$CO(NH_2)_2$–H_2O at ambient pressure.

$CO(NH_2)_2$ to $CH_3CO_2Na \cdot 3H_2O$ is similar to that of addition of H_2O. But, the eutectic point of pseudo-binary system $CH_3CO_2Na \cdot 3H_2O$–$CO(NH_2)_2$ is 31.5 °C, which is suitable for solar energy storage, whereas the eutectic point of system $CH_3CO_2Na \cdot 3H_2O$–H_2O is −18 °C, which is too low. The reason why $CH_3CO_2Na \cdot 3H_2O$ is brought to the point of melting congruently by the addition of a sufficient quantity of $CO(NH_2)_2$ is that $CO(NH_2)_2$ acts not only as a solute in $CH_3CO_2Na \cdot 3H_2O$ melt but also as a solvent for CH_3CO_2Na like H_2O. That is to say, as an aqueous solution of $CO(NH_2)_2$ acts as a mixed solvent for CH_3CO_2Na, the solubility of CH_3CO_2Na for unit mass of H_2O is higher in the mixture of system $CH_3CO_2Na \cdot 3H_2O$–$CO(NH_2)_2$ melt than in the melt of $CH_3CO_2Na \cdot 3H_2O$ without any other substances.

The heat of fusion of the eutectic mixture of this pseudo-binary system is found to be 226 J/g by DSC. This value is larger than the heat of fusion of another latent heat storage material, $CaCl_2 \cdot 6H_2O$ (t_m: 29.5 °C), 180 J/g. The heat of fusion of a binary eutectic mixture ΔH_m^{eu} is calculated from the equation.[6]

$$\Delta H_m^{eu} = T_m^{eu}\left\{W^A\left(\frac{\Delta H_m{}^A}{T_m{}^A}\right) + W^B\left(\frac{\Delta H_m{}^B}{T_m{}^B}\right)\right\}, \quad (1)$$

where W^A and W^B are the mass fractions of components A and B, respectively, T_m^A, T_m^B, and T_m^{eu} are the melting points (in absolute temperature) of component A, component B, and eutectic mixture, respectively, and ΔH_m^A and ΔH_m^B are the heats of fusion of components A and B per unit mass, respectively. This equation is applicable to the eutectic mixture of pseudo-binary system $CH_3CO_2Na \cdot 3H_2O$–$CO(NH_2)_2$, by letting, A and B correspond to $CH_3CO_2Na \cdot 3H_2O$ and $CO(NH_2)_2$, respectively. $CH_3CO_2Na \cdot 3H_2O$ melts incongruently at 58.4 °C with a heat of fusion of 264 J/g,[7] and $CO(NH_2)_2$ melts at 133 °C with a heat of fusion of 251 J/g.[8] Accordingly we take T_m^A=332 K, T_m^B=406 K, T_m^{eu}=305 K, ΔH_m^A=264 J/g, ΔH_m^B=251 J/g, W^A=0.60, and W^B=0.40. Consequently, ΔH_m^{eu} is 221 J/g. This value is in good agreement with the experimental result, 226 J/g.

Microphotographs of mixtures of $CH_3CO_2Na \cdot 3H_2O$ and $CO(NH_2)_2$ are given in Figs. 6—8. The study with a microscope clearly proves that the solid immediately separating out from a eutectic melt is entirely different in appearance from other solids. Large prisms of $CH_3CO_2Na \cdot 3H_2O$ in the eutectic matrix are shown in Fig. 6. White needles of $CO(NH_2)_2$ in the eutectic matrix are shown in Fig. 7. An extremely regular pattern microphotographed for the solid eutectic matrix is shown in Fig. 8.

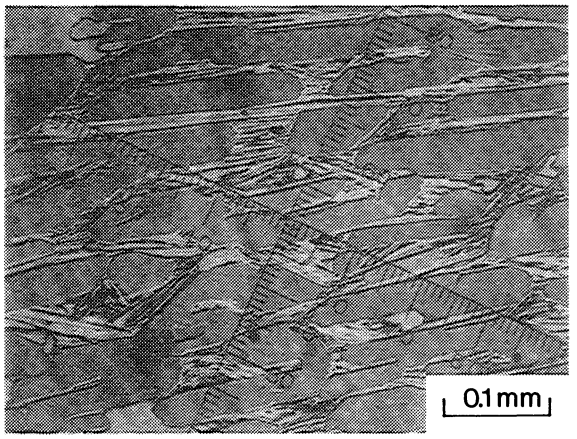

Fig. 6. Microstructure of mixture containing 0.2 mass fraction of $CO(NH_2)_2$.

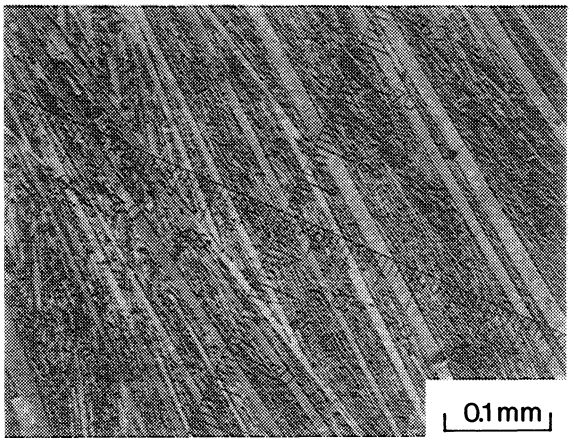

Fig. 7. Microstructure of mixture containing 0.6 mass fraction of $CO(NH_2)_2$.

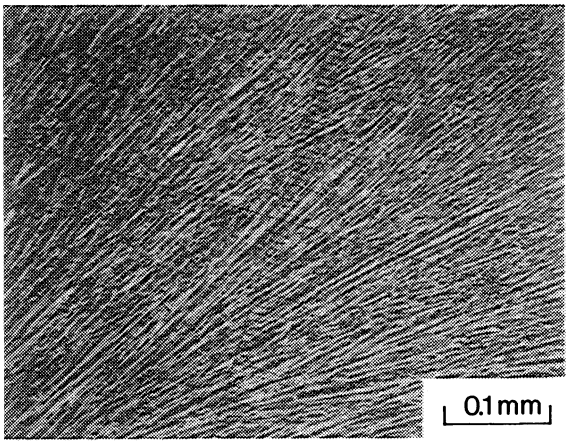

Fig. 8. Microstructure of eutectic mixture containing 0.4 mass fraction of $CO(NH_2)_2$.

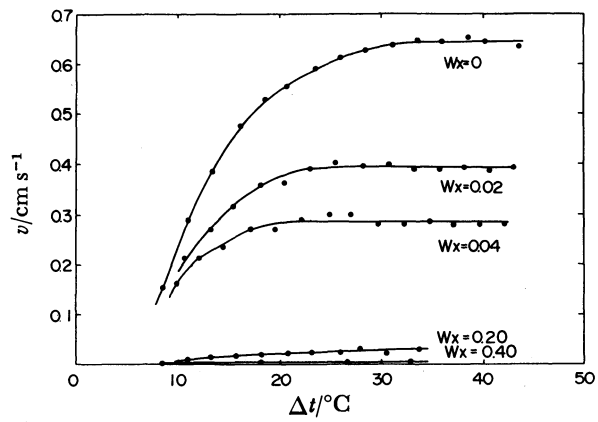

Fig. 9. Linear velocity of crystallization of various melts.

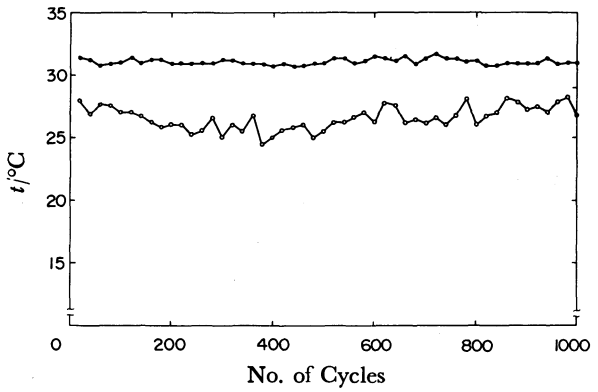

Fig. 10. Changes in melting point t_m and the temperature at which supercooling is broken t_l with cycling.
●: t_m, ○: t_l.

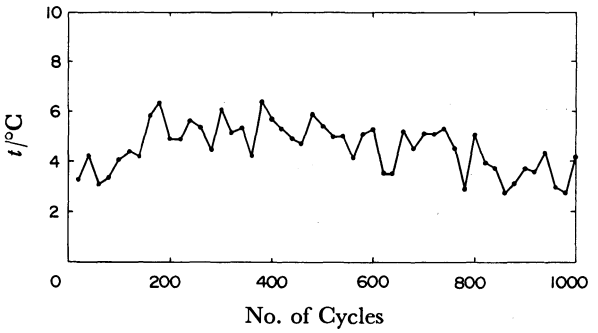

Fig. 11. Changes in supercooling Δt_l with cycling.

Linear velocities of crystallization of various melts are plotted against the supercooling Δt in Fig. 9. The linear velocity of crystallization of $CH_3CO_2Na \cdot 3H_2O$ ($W_x=0$) is in good agreement with the value determined by Dietz *et al.*[3] It is clear that the linear velocity of crystallization of the melt containing 0.04 mass fraction of $CO(NH_2)_2$ at $\Delta t=20$ °C falls to less than half the linear velocity of crystallization of $CH_3CO_2Na \cdot 3HO_2$ at $\Delta t=20$ °C. The linear velocity of crystallization of this eutectic melt at $\Delta t=20$ °C, 0.002 cm/s, is about 1/300 of the linear velocity of crystallization of $CH_3CO_2Na \cdot 3H_2O$ melt at $\Delta t=20$ °C.

To make sure that the mixture of system $CH_3CO_2Na \cdot 3H_2O$–$CO(NH_2)_2$ continuously repeats stable freezing, 30 g of the eutectic mixture of pseudo-binary system $CH_3CO_2Na \cdot 3H_2O$–$CO(NH_2)_2$, in the presence of 0.3 g of $Na_4P_2O_7 \cdot 10H_2O$ as the nucleation catalyst for $CH_3CO_2Na \cdot 3H_2O$, was subjected to cycles of linearly programmed consequtive heating and coolings between 5 and 45 °C in a manner similar to the one adopted previously.[9] Melting points t_m's and temperatures at which the supercooling is broken, t_i's as determined by 1000 continuous heating and cooling cycles, are shown in Fig. 10. The supercooling $\Delta t_i(=t_m-t_i)$ is calculated by using the results in Fig. 10 and plotted in Fig. 11. From these figures, it is apparent that the supercooling of this eutectic mixture Δt_i is almost 6 °C for all the cycles.

$CH_3CO_2Na \cdot 3H_2O$ starts to crystallize from the eutectic melt with the aid of $Na_4P_2O_7 \cdot 10H_2O$ crystals and soon $CO(NH_2)_2$ starts to crystallize. This eutectic mixture was observed not to separate into the components $CH_3CO_2Na \cdot 3H_2O$ and $CO(NH_2)_2$. After 1000 continuous heating and cooling cycles, the heat of fusion of this sample was measured by DSC. The value obtained is 222 J/g, which is in good agreement with the initial heat of fusion of this eutectic mixture, 226 J/g. Consequently, the mixtures of system $CH_3CO_2Na \cdot 3H_2O$–$CO(NH_2)_2$ are promising for solar energy storage.

The authors wish to express their thanks to Dr. Ryoichi Kiriyama for his helpful discussions and to Drs. Eiichi Hirota and Masanari Mikoda for their continuous encouragement. They are also grateful to Dr. Yoshihiro Matsuo for his discussions throughout this work.

References

1) K. W. Böer, J. H. Higgins, and J. K. O'Connor, IECEC '75 Record, 7 (1975).
2) N. Yoneda and S. Takanashi, *Solar Energy*, **21**, 61 (1978).
3) P. L. Dietz, Jr., J. S. Brukner, and C. A. Hollingsworth, *J. Phys. Chem.*, **61**, 944 (1957).
4) W. F. Green, *J. Phys. Chem.*, **12**, 655 (1908).
5) B. Carlsson, H. Stymne, and G. Wettermark, *Solar Energy*, **23**, 343 (1979).
6) M. Kaminoto, T. Tanaka, T. Tani, and T. Horigome, *Solar Energy*, **24**, 581 (1980).
7) M. Telkes, "Solar Materials Science," ed by L. E. Murr, Academic Press, New York (1980), Chap. 11.
8) T. Ozawa, M. Kamimoto, R. Sakamoto, Y. Takahashi, and K. Kanari, *Bull. Electrotech. Lab.* **43**, 19 (1979).
9) T. Wada and R. Yamamoto, *Bull. Chem. Soc. Jpn.*, **55**, 3603 (1982).

 © 1983 The Chemical Society of Japan Bull. Chem. Soc. Jpn., 56, 1227—1230 (1983)

Synthesis of the 1,2,4-Triazolo[4,3-*a*]quinazolin-5-ones and Related Compounds

H. A. El-Sherief,* A. E. Abdel-Rahman, G. M. El-Naggar, and A. M. Mahmoud
Chemistry Department, Faculty of Science, Assiut University, Assiut, Egypt
(Received June 16, 1982)

2-Hydrazino-3-phenyl-4(3*H*)-quinazolinone (**1**) underwent ring closure with aliphatic acid, aldehydes, and carbon disulfide to 1-alkyl-, 1-aryl-, and 1-mercapto-4-phenyl-1,2,4-triazolo[4,3-*a*]quinazolin-5(4*H*)-ones (**7**) for instance. The 1-alkylthio-3-phenyl-1,2,4-triazolo[4,3-*a*]quinazolin-5(4*H*)-ones were readily obtained from **7** and alkyl halides. Reaction of **1** with ethyl acetoacetate gave the corresponding hydrazone which was readily converted into 2-(3-methyl-5-oxo-2-pyrazolin-1-yl)-3-phenyl-4(3*H*)-quinazolinone.

The fusion of quinazoline ring with other biologically active nuclei has aroused considerable interest for synthetic organic chemists because many members of this family exhibit im potant biological activity.[1-3] Some tetrazolo[1,5-*a*]quinazolinones have been prepared,[4] as pesticides, from the corresponding 2-hydrazino-3-aryl-4(3*H*)-quinazolinones and nitrous acid. Tennant[5] first prepared 3-phenyl-1,2,3-triazolo[1,5-*a*]-quinazolin-5-one by condensation of *o*-azidobenzoic acid with phenylacetonitrile.

It has been observed in the present study that 2-hydrazino-3-phenyl-4(3*H*)-quinazolinone (**1**) reacted with acetyl chloride in the presence of potassium carbonate in dry chloroform gave 2-(2-acetylhydrazino)-3-phenyl-4(3*H*)-quinazolinone (**2**). Heating of **2** above its melting point for 10 min gave 1-methyl-4-phenyl-1,2,4-triazolo[4,3-*a*]quinazolin-5(4*H*)-one (**3a**), which also can be obtained *via* another route, by refluxing **1** or **2** in acetic acid. In a similar way, reaction of **1** with formic acid and propionic acid gave the corresponding 4-phenyl-1,2,4-triazolo[4,3-*a*]quinazolin-5(4*H*)-one (**3b**) and 1-ethyl-4-phenyl-1,2,4-triazolo-[4,3-*a*]quinazolin-5(4*H*)-one (**3c**) respectively as shown in the following scheme:

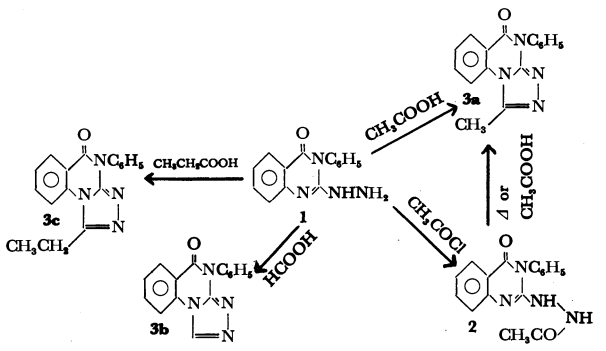

The NMR spectrum of **3a** (in $CDCl_3$) showed a singlet at 2.72 (3H, CH_3), a multiplet at 7.4—7.1 (5H, C_6H_5), and another multiplet at 8.2—7.8 (4H of quinazolinone ring), while the NMR spectrum of **3c** showed a triplet at 1.14 (3H, CH_3), a quartet at 3.23 (2H, CH_2), a multiplet at 7.4—7.0 (5H, C_6H_5) and a multiplet at 8.3—7.8 (4H of quinazolinone ring).

Although the isomerization of 1,2,4-triazolo[4,3-*c*]-quinazolines to 1,2,4-triazolo[1,5-*c*]quinazolines has been reported,[6] no such isomerization has been found in 4-phenyl-1,2,4-triazolo[4,3-*a*]quinazolin-5(4*H*)-one system. When **1** was treated with formic acid under milder conditions[7,8] than those used above, **3b** was obtained.

Fusion of **1** with benzaldehyde, for 3 min, gave benzaldehyde (4-oxo-3-phenyl-3,4-dihydro-2-quinazolinyl)hydrazone (**4a**), which was dehydrogenated to 1,4-diphenyl-1,2,4-triazolo[4,3-*a*]quinazolin-5(4*H*)-one (**5a**) when the reaction was continued for 2 h at 220—225 °C. The same result was also obtained by ring closure of 2-(2-benzoylhydrazino)-3-phenyl-4(3*H*)-quinazolinone (**6**) when heated over its melting point for 10 min. Similarly a series of the hydrazones (**4b—e**)

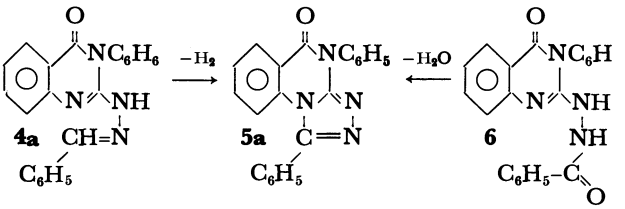

(Table 1) and 1-aryl-4-phenyl-1,2,4-triazolo[4,3-*a*]-quinazolin-5(4*H*)-ones (**5b—e**) (Table 2) were prepared from **1** and the appropriate aldehydes.

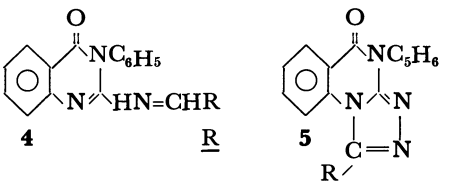

4 and **5a**; C_6H_5
b; C_6H_4Cl-*m*
c; C_6H_4Cl-*p*
d; $C_6H_4CH_3$-*p*
e; $C_6H_4OCH_3$-*p*

The IR spectra of **4a—e** showed bands at 1700—1685 and 3320—3260 cm^{-1} assignable to C=O and NH stretching frequencies, respectively. While the IR spectra of **5a—e** indicated the disappearance of the NH stretching frequency and revealed a characteristic band for C=O at 1690—1680 cm^{-1}.

Further, the reaction of **1** with one equivalent of carbon disulfide resulted in ring closure to 1-mercapto-4-phenyl-1,2,4-triazolo[4,3-*a*]quinazolin-5(4*H*)-one (**7**), which was readily converted into the corresponding alkylthio derivatives **8a—d** with alkyl halides in basic medium.

The NMR spectrum of **8b** (in $CDCl_3$) showed a triplet at 1.63 (3H, CH_3), a quartet at 3.5 (2H, S-CH_2) and a multiplet at 7.6—8.2 (9H, aromatic protons)

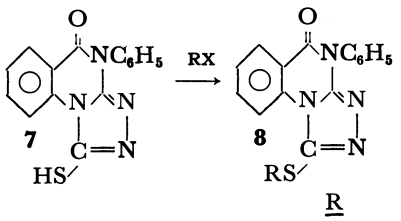

8a; CH_3
8b; C_2H_5
8c; CH_2CH
8d; $CH_2C_6H_5$
8e; $CH_2COOC_2H_5$
8f; CH_2COOH
8g; $CH_2CONHCH_2C_6H_5$

which is in agreement with its structure. Reaction of **7** with ethyl chloroacetate in dry acetone in the presence of potassium carbonate gave 1-ethoxycarbonylmethylthio-4-phenyl-1,2,4-triazolo[4,3-*a*]quinazolin-5(4*H*)-one (**8e**). The IR spectrum of **8e** showed two carbonyl bands one at 1690 cm^{-1} (due to quinazolinone nucleus) and the other at 1740 cm^{-1} (due to the ester group).

However, treatment of **8e** with aq potassium carbonate solution (5%) at 50 °C for 1 h gave 1-carboxymethylthio-4-phenyl-1,2,4-triazolo[4,3-*a*]quinazolin-5(4*H*)-one (**8f**), which was readily obtained by treatment of **7** with chloroacetic acid in the presence of potassium carbonate in dry acetone.

The IR spectrum of **8f** showed two carbonyl bands one at 1685 cm^{-1} (of quinazolinone nucleus) and the other at 1670 cm^{-1} (of the carboxyl group). Synthesis of 1-(benzylcarbamoylmethylthio)-4-phenyl-1,2,4-triazolo[4,3-*a*]quinazolin-5(4*H*)-one (**8g**) was achieved by reaction of **8e** with benzylamine in boiling ethanol. The IR spectrum of **8g** showed bands at 3180 cm^{-1} (NH), 1690 cm^{-1} (C=O of quinazolinone nucleus) and at 1665 cm^{-1} (C=O of amide).

On the other hand, treatment of **1** with ethyl acetoacetate in boiling ethanol produced the corresponding hydrazone **9**. Its IR spectrum exhibited two carbonyl bands one at 1685 cm^{-1} (due to quinazolinone ring) and the other at 1735 cm^{-1} (due to the ester group). When **9** was heated above its melting point for 5 min, the corresponding pyrazolinone **10** was obtained.

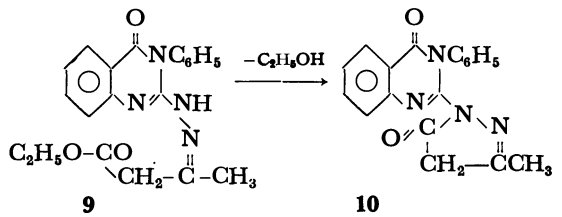

The IR spectrum of 2-(3-methyl-5-oxo-2-pyrazolin-1-yl)-3-phenyl-4(3*H*)-quinazolinone (**10**) showed in addition to the carbonyl band of quinazolinone nucleus at 1690 cm^{-1}, the amide band at 1665 cm^{-1}.

Refluxing of **1** with acetone gave the corresponding hydrazone **11a**. According to the literature,[9] attempted formation of **3a** by heating of **11a** at 220—225 °C for 2 h failed. However, **11a** was readily acetylated and sulfonylated using acetic anhydride and benzenesulfonyl chloride in pyridine to give the corresponding derivatives **11b** and **11c** respectively.

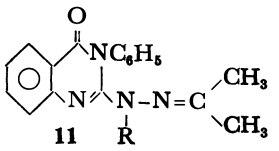

11a; H
b; $COCH_3$
c; $SO_2C_6H_5$

The IR spectrum of **11a** showed band at 1690 cm^{-1} (C=O of quinazolinone ring) and at 3320 cm^{-1} (NH group). While, the IR spectra of **11b** and **11c** revealed the disappearance of the NH stretching frequency.

Experimental

Melting points reported are uncorrected. IR spectra were recorded on a Beckman IR-20 spectrophotometer. ^1H NMR spectrum was recorded on a Varian EM-360 60 MHz using TMS as the internal standard.

2-(2-Acetylhydrazino)-3-phenyl-4(3H)-quinazolinone (2). To a solution of **1** (5 g, 0.02 mol) in dry chloroform (100 ml) containing anhyd potassium carbonate (0.5 g), acetyl chloride (0.01 mol) was added slowly. After the addition was complete, the reaction mixture was heated on a water bath for 1 h. The solvent was evaporated and the crude product was collected and crystallized from water as colorless needles, 2.3 g (80%), mp 142 °C. Found: C, 65.46; H, 4.91; N, 19.18%. Calcd for $C_{16}H_{14}N_4O_2$: C, 65.30; H, 4.76; N, 19.05%.

1-Methyl-4-phenyl-1,2,4-triazolo[4,3-a]quinazolin-5(4H)-one (3a). **2** (1 g) was heated above its melting point for 5 min and after cooling, recrystallized from ethanol as colorless needles, 0.6 g (60%), mp 313 °C. The same compound was also obtained by refluxing **2** (1 g) with acetic acid (10 ml) for 20 min. The separated product was crystallized from ethanol 0.7 g (70%), no depression of melting point occurred on admixture with the sample prepared by the above procedure.

3a was also obtained by refluxing **1** (2.5 g; 0.01 mol) with acetic acid for 2 h, as described above in 65% yield. Found: C, 69.67; H, 4.46; N, 20.31%. Calcd for $C_{16}H_{12}N_4O$: C, 69.57; H, 4.35; N, 20.29%.

4-Phenyl-1,2,4-triazolo[4,3-a]quinazolin-5(4H)-one (3b). A mixture of **1** (0.01 mol), 2.5 g and formic (20 ml) was refluxed for 2 h, then the excess acid was evaporated under reduced pressure and the residue was crystallized from ethanol to give colorless needles, 2.1 g (80%), mp 332—334 °C. Found: C, 68.74; H, 3.66; N, 21.45%. Calcd for $C_{15}H_{10}N_4O$: C, 68.70; H, 3.82; N, 21.37%.

The same product was obtained by heating the above mixture at 55 °C for 45 min. The excess acid was evaporated under reduced pressure at 50 °C and the crude product was crystallized from ethanol to give **3b**. There is no melting point depression and the infrared was superimposable with that of **3b** prepared according to above procedure.

1-Ethyl-4-phenyl-1,2,4-triazolo[4,3-a]quinazolin-5(4H)-one (3c). It was prepared by refluxing a mixture of **1** (2.5 g; 0.01 mol) and propionic acid (20 ml) as previously described in **3b**. The crude product was crystallized from ethanol–benzene mixture as colorless needles, 2 g (70%), mp 285—287 °C. Found: C, 70.46; H, 4.70; N, 19.61%. Calcd for $C_{17}H_{14}N_4O$: C, 70.34; H, 4.83; N, 19.31%.

Table 1. Physical data of hydrazones **4a—e**

Compd No.	Mp θ_m/°C	Formula	Calcd(Found) (%) C	H	N
4a	232	$C_{21}H_{16}N_4O$	74.12	4.71	16.47
			(74.36	4.65	16.61)
b	223	$C_{21}H_{15}N_4OCl$	67.37	4.01	14.97
			(67.28	4.26	14.66)
c	287	$C_{21}H_{15}N_4OCl$	67.37	4.01	14.97
			(67.35	4.16	14.85)
d	242	$C_{22}H_{18}N_4O$	74.57	5.08	15.82
			(74.36	5.18	15.63)
e	238	$C_{22}H_{18}N_4O_2$	71.35	4.86	15.14
			(71.58	4.78	15.41)

Table 2. 1-Aryl-4-phenyl-1,2,4-triazolo [4,3-*a*] quinazolin-5(4*H*)-ones (**5a—e**)

Compd No	Mp θ_m/°C	Formula	Calcd(Found) (%) C	H	N
5a	238	$C_{21}H_{14}N_4O$	74.56	4.14	16.57
			(74.46	4.08	16.28)
b	225	$C_{21}H_{13}N_4OCl$	67.74	3.49	15.05
			(67.65	3.51	15.14)
c	261	$C_{21}H_{13}N_4OCl$	67.74	3.49	15.05
			(67.65	3.31	15.21)
d	299	$C_{22}H_{16}N_4O$	75.00	4.55	15.91
			(75.21	4.46	15.81)
e	282	$C_{22}H_{16}N_4O_2$	71.74	4.35	15.22
			(71.65	4.52	15.41)

Table 3. 1-Alkylthio-4-phenyl-1,2,4-triazolo [4,3-*a*]quinazolin-5(4*H*)-ones (**8a—d**)

Compd No.	Mp θ_m/°C	Formula	Calcd(Found) (%) C	H	N	S
8a	213—215	$C_{16}H_{12}N_4OS$	62.33	3.89	18.18	10.39
			(62.46	3.71	18.09	10.56)
b	183	$C_{17}H_{14}N_4OS$	63.35	4.34	17.39	9.94
			(63.48	4.46	17.21	9.76)
c	186—187	$C_{18}H_{14}N_4OS$	64.67	4.19	16.76	9.58
			(64.92	4.36	16.81	9.77)
d	195	$C_{22}H_{16}N_4OS$	68.75	4.16	14.58	8.33
			(68.71	4.35	14.33	8.18)

*Reaction of 2-Hydrazino-3-phenyl-4(3H)-quinazolinone (**1**) with Aldehydes.* A mixture of appropriate aldehyde (0.011 mol) and **1** (0.01 mol) was heated for 3 min, and after cooling to room temperature, crystallized from ethanol–benzene mixture as colorless needles. The yield was about 85—90%.

*2-(2-Benzoylhydrazino)-3-phenyl-4(3H)-quinazolinone (**6**).* It was prepared from **1** (0.02 mol) and benzoyl chloride (0.02 mol) in chloroform solution containing potassium carbonate as previously described in **2**. The crude product was crystallized from ethanol as colorless needles, 2.4 g (69%), mp 149—151 °C. IR (KBr), 3340 (NH), 3230 (NH), 1665 (amide CO) cm^{-1}. Found: C, 70.56; H, 4.31; N, 15.62%. Calcd for $C_{21}H_{16}N_4O$: C, 70.79; H, 4.49; N, 15.73%.

*1-Aryl-4-phenyl-1,2,4-triazolo[4,3-a]quinazolin-5(4H)-ones (**5a—e**).* A mixture of appropriate aldehyde (0.015 mol) and **1** (0.01 mol) was heated at 210—225 °C for 2 h. The pyrolysis residue was cooled and triturated with ethanol. The crude product was crystallized from ethanol (charcoal) forming colorless needles of **5a—e**. The yield was about 55—65%. **5a** was also obtained by heating benzaldehyde (4-oxo-3-phenyl-3,4-dihydro-2-quinazolinyl)hydrazone (**4a**) for 1 h at 220—225 °C. The pyrolysis residue, treated as described above gave **5a** in yield 45%.

The same product **5a**, was also obtained in 70% yield by heating **6** (1 g) over its melting point for 10 min as described in **3a**.

*1-Mercapto-4-phenyl-1,2,4-triazolo[4,3-a]quinazolin-5(4H)-one (**7**).* **1** (2 g), methanol (100 ml), potassium hydroxide (0.7 g), and carbon disulfide (6 ml) were refluxed for 4 h. After removal of the methanol, dilute potassium hydroxide was added and the alkaline solution was filtered. After precipitation with dilute hydrochloric acid, the crude product was filtered and recrystallized from ethanol as colorless needles, 1.8 g (77%), mp 342—344 °C. Found: C, 61.41; H, 3.26; N, 19.18; S, 10.76%. Calcd for $C_{15}H_9N_4OS$: C, 61.22; H, 3.40; N, 19.05; S, 10.88%.

*Reaction of **7** with Alkyl Halides.* A solution of **7** (0.5 g; 0.002 mol) and sodium hydroxide (0.1 g) in water (10 ml) was stirred while the appropriate alkyl halide (0.004 mol) was added dropwise. The reaction mixture was stirred for 2 h, then the excess alkyl halide was evaporated and the residue recrystallized from benzene–pet. ether (60—80 °C) mixture, forming colorless needles of the products **8a—d**. The yield was about 65—70%.

*1-Ethoxycarbonylmethylthio-4-phenyl-1,2,4-triazolo[4,3-a]quinazolin-5(4H)-one (**8e**).* To a solution of **7** (1 g) in dry acetone (30 ml) containing anhyd potassium carbonate (0.5 g), ethyl chloroacetate (0.5 ml) was added slowly. The reaction mixture was refluxed on a steam bath for 30 min, then filtered, evaporated and the crude product was collected and crystallized from pet. ether (60—80°C) as colorless needles, 0.9 g (70%), mp 116 °C. Found: C, 60.15; H, 4.32; N, 14.95; S, 8.71%. Calcd for $C_{19}H_{16}N_4O_3S$: C, 60.00; H, 4.21; N, 14.73; S, 8.42%.

*1-Carboxymethylthio-4-phenyl-1,2,4-triazolo[4,3-a]quinazolin-5(4H)-one (**8f**).* A mixture of **8e** (0.5 g) and 20 ml sodium carbonate solution (5%) was stirred for 2 h at 50 °C. The reaction mixture was cooled and acidified, the solid separated was filtered off and crystallized from ethanol as colorless needles to give **8f**, mp 208 °C, 0.3 g (75%). Found: C, 57.81; H, 3.51; N, 15.71; S, 9.26%. Calcd for $C_{17}H_{12}N_4O_3S$: C, 57.95; H, 3.41; N, 15.91; S, 9.09%.

The same product was also obtained by reaction of **7** (0.5 g) and chloroacetic acid in the presence of potassium carbonate in acetone as described before in **8e**. Evaporation of the solvent after acidification gave **8f** in 45% yield.

*1-(Benzylcarbamoylmethylthio)-4-phenyl-1,2,4-triazolo[4,3-a]-quinazolin-5(4H)-one (**8g**).* A mixture of **8e** (0.5 g) and benzylamine (0.3 g) in ethanol (15 ml) was refluxed for 2 h. The reaction mixture was reduced to its half volume and cooled. The separated product was collected and recrystallized from the same solvent as colorless needles, mp 254 °C, (0.3 g; 50%). Found: C, 65.41; H, 4.51; N, 15.90; S, 7.51%. Calcd for $C_{24}H_{19}N_5O_2S$: C, 65.30; H, 4.30; N, 15.87; S, 7.26%.

*2-(3-Methyl-5-oxo-2-pyrazolin-1-yl)-3-phenyl-4(3H)-quinazolinone (**10**).* *a)*: A mixture of **1** (0.002 mol) and ethyl acetoacetate (0.0025 mol) in ethanol (30 ml) was refluxed for 3 h. The reaction mixture was concentrated and cooled. The separated colorless product was crystallized from the same solvent to give the corresponding hydrazone (**9**) mp 142 °C, 5.9 g (82%). Found: C, 65.71; H, 5.58; N, 15.61%. Calcd for $C_{20}H_{20}N_4O_3$: C, 65.93; H, 5.49; N, 15.38%.

b): The hydrazone **9** (0.5 g) was heated over its melting

point for 10 min, the residue was cooled and crystallized from pyridine–methanol mixture as colorless needles (**10**), mp 360 °C, 0.3 g (75%). Found: C, 67.86; H, 4.52; N, 17.81%. Calcd for $C_{18}H_{14}NO_2$: C, 67.79; H, 4.40; N, 17.61%.

*Acetone (4-Oxo-3-phenyl-3,4-dihydro-2-quinazolinyl) hydrazone (**11a**).* A mixture of **1** (1 g) and acetone (15 ml) was refluxed for 2 h. The solvent was evaporated the residue was crystallized from ethanol as colorless needles, mp 185 °C, 0.9 g (81%). Found: C, 69.76; H, 5.58; N, 19.36%. Calcd for $C_{17}H_{16}N_4O$: C, 69.86; H, 5.47; N, 19.17%.

*Acetylation of **11a**.* A mixture of **11a** (0.2 g), acetic anhydride (1 ml) and pyridine (1 ml) was heated on a steam bath for 30 min. The yellow crystalline product was separated, collected and crystallized from ethanol to give **11b**, mp 278 °C, 0.2 g (93%). Found: C, 71.78; H, 5.76; N, 17.80%. Calcd for $C_{19}H_{18}N_4O$: C, 71.69; H, 5.66; N, 17.61%.

*Sulfonylation of **11a**.* A mixture of **11a** (0.2 g), benzenesulfonyl chloride (0.2 ml) and pyridine (2 ml) was heated on a steam bath for 30 min. The reaction mixture was cooled and poured into cold water. The brown solid product was collected and crystallized from methanol to give **11c** as brown crystals, mp 194—195 °C, 0.1 g (45%). Found: C, 63.76; H, 4.51; N, 12.80; S, 7.42%. Calcd for $C_{23}H_{20}N_4O_3S$: C, 63.88; H, 4.62; N, 12.96; S, 7.40%.

References

1) M. Lempert-Sreter, K. Lempert, P. Bruck, and G. Toth, *Acta Chim. Acad. Sci. Hung.*, **94**, 391 (1977).

2) H. K. Gakhar, A. Jain, and N. Kumar, *J. Indian Chem. Soc.*, **1981**, 166.

3) S. Naqui and V. R. Srinivasan, *Tetrahedron Lett.*, **1962**, 25, 1193.

4) R. Bowie, J.M. Cox, G.M. Farrell, and M.C. Shephard, Ger. Offen. 2 539 396 (Cl. CO7D, AO1N); 18 Mar 1976, Brit. Appl. 38, 796 174, 05 Sep. 1974; p. 79; *Chem. Abstr.*, **85**, 5681 n (1976).

5) G. Tennant, *J. Chem. Soc., C*, **1966**, 2290.

6) K. T. Potts and E. G. Brugel, *J. Org. Chem.*, **35**, 3448 (1970).

7) G. A. Reynolds, J. A. Van Allen, J. F. Tinker, C. F. H. Allen, H. R. Beifuss, and D. M. J. Burness, *J. Org. Chem.*, **24**, 779, 787, 793, 796, 1205, 1478 (1959).

8) M. Ogata, H. Kano, Y. Makisumi, and S. Takahashi, *Chem. Pharm. Bull.*, **7**, 903 (1959).

9) D. Shiho and S. Tagami, *J. Am. Chem. Soc.*, **82**, 4044 (1960).

The Disproportionation Constants of Mercurry(I) in Dilute Solutions. II[1)]

Isao SANEMASA,* Toyohisa KOBAYASHI, Toshio DEGUCHI, and Hideo NAGAI
Department of Chemistry, Faculty of Science, Kumamoto University, Kurokami 2-39-1, Kumamoto 860
(Received August 9, 1982)

Synopsis. The equilibrium constants, K_d, of mercury-(I) disproportionation have been measured by passing air containing mercury(0) vapor through mercury(I) solutions. At 15, 20, 25, 30, and 35 °C, the values of K_d were 1.3, 2.9, 5.2, 8.8, and 11×10^{-9} mol dm^{-3} respectively at $\mu=0.1$ ($NaClO_4$).

In the preceding paper we have reported the equilibrium constants, K_d, for this reaction:[1)]

$$Hg_2^{2+} \rightleftharpoons Hg(aq) + Hg^{2+}. \quad (1)$$

The values of K_d we estimated are, however, considerably larger than those which have more recently been reported.[2)] Our previous method of determining K_d may have caused some uncertainty in the absolute accuracy, so we have decided to reevaluate K_d by a modification of this earlier method.

The disproportionation occurs according to Reaction 1 by letting air flow through a solution containing Hg_2^{2+}, until finally only Hg^{2+} ions remain in the solution. Now, let us consider special conditions where the air introduced into the mercury(I) solution contains vapor of metallic mercury. Under such circumstances, the equilibrium of Reaction 1 will be attained depending on the dissolved Hg(aq) concentration. The K_d can be straightforwardly calculated by means of this equation:

$$K_d = [Hg(aq)][Hg^{2+}]/[Hg_2^{2+}]$$
$$= [Hg(aq)]\{[Hg^{2+}]_0 + [Hg_2^{2+}]_0 - [Hg_2^{2+}]\}/[Hg_2^{2+}], \quad (2)$$

where the subscript 0 denotes the initial concentration.

The apparatus used is shown in Fig. 1. Air flowed by means of an air-pump P at a constant rate of 100 cm^3 min^{-1} through a cylindrical tube A, which was packed with silica gel, and a condenser B. The dried air was introduced into a flask C in which a few drops of metallic mercury had been put, and then bubbled successively into three flasks, D, E, and F. Finally, the air was released out of a cylindrical tube G in which a 1 mol dm^{-3} nitric acid solution had been placed in order to split off the contaminated mercury vapor. The flask C was maintained at a constant temperature below 10 °C by circulating thermostated water through a jacket outside the flask. The flasks, D, E, and F, were

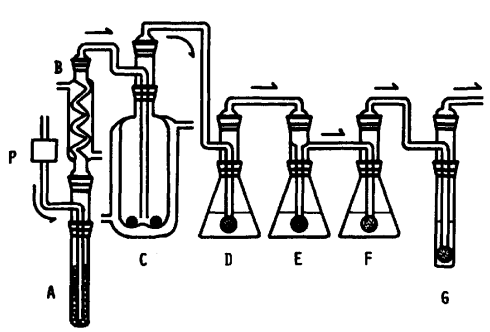

Fig. 1. Apparatus.

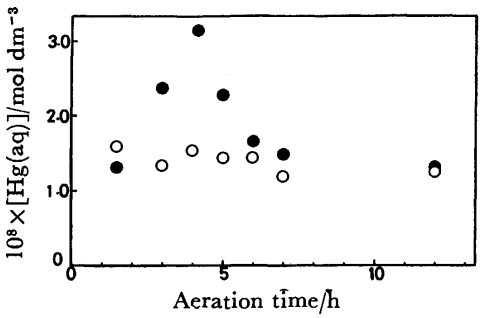

Fig. 2. Concentrations of Hg(aq) dissolved in D and F flasks as a function of aeration time. ○: D Flask, ●: F Flask. Temperature: 25.0 °C.

immersed in another thermostat controlled within 0.05 °C. In the E flask we placed a 100 cm^3 mercury(I) solution in 0.05 mol dm^{-3} perchloric acid, the ionic strength of which had been adjusted to 0.1 with sodium perchlorate. The same volumes of 0.05 mol dm^{-3} $HClO_4$ ($\mu=0.1$, $NaClO_4$) solutions in the absence of mercury(I) were placed in the D and F flasks, which were utilized to estimate the [Hg(aq)] in the E flask. The dissolved Hg(aq) concentrations in the D and F flaks were determined by an atomic-absorption method, and the remaining Hg_2^{2+} concentrations in the E flask were measured spectrophotometrically at 236.5 nm; $[Hg_2^{2+}]_0 = 1.02 \times 10^{-5}$ mol dm^{-3} in all the runs.

As will be seen in Fig. 2, the Hg(aq) concentrations in the D flask were almost constant, irrespective of the aeration time, while those in the F flask increased at first to attain a maximum and then decreased to approach those in the D flask. The initial increase in [Hg(aq)] in the postponed flask is due to the liberation of Hg^0 from mercury(I) in the E flask. We presumed that, when the [Hg(aq)] in the F flask was the same as that in the D flask, the [Hg(aq)] must be the same as in the E flask as well, and that, under such circumstances, the disproportionation equilibrium of mercury-(I) in the E flask should be reached. After a 6-hour aeration, the amount of $[Hg_2^{2+}]$ remaining in the E flask and the mean values of [Hg(aq)] in the D and F flasks were used to calculate K_d by means of Eq. 2. The calculations were made by the successive approximation. That is, $[Hg^{2+}]_0$ was neglected as a first approximation, then, by using the approximate K_d value, $[Hg^{2+}]_0$ was estimated. It corresponded in most cases to *ca.* 10% of $\{[Hg_2^{2+}]_0 - [Hg_2^{2+}]\}$. Next, by using the $[Hg^{2+}]_0$ estimated, the second K_d value was calculated; it was no longer changed by further successive calculations.

The summary of the experimental results and the estimated disproportionation constants are listed in Table 1. The present result, 5.2×10^{-9} mol dm^{-3} at 25 °C, is in good agreement with that of the literature:

Table 1. Summary of experimental results and disproportionation constants estimated

Temp °C	$10^8 \times$ [Hg(aq)] mol dm^{-3}		$10^6 \times [Hg_2^{2+}]^{c)}$ mol dm^{-3}	$10^9 \times K_d$ mol dm^{-3}	
	Flask D	Flask F		a)	b)
15.0	0.686	0.686	8.8	1.1	1.2
	0.933	0.909	8.9	1.3	1.4
				Average	1.3
20.0	1.19	1.24	8.6	2.3	2.6
	1.45	1.61	8.7	2.6	3.0
	1.52	1.52	8.7	2.6	3.0
				Average	2.9
25.0	1.24	1.31	7.4	4.8	5.2
	1.09	1.09	7.1	4.8	5.1
				Average	5.2
30.0	1.43	1.65	6.5	8.8	9.5
	1.37	1.55	6.5	8.3	8.9
	1.28	1.34	6.5	7.5	8.1
				Average	8.8
35.0	1.48	1.64	6.3	9.7	10
	1.54	1.61	5.8	12	13
	0.92	1.05	5.1	9.9	10
				Average	11

a) First approximation by neglecting $[Hg^{2+}]_0$. b) The corrected K_d. c) $[Hg_2^{2+}]_0 = 1.02 \times 10^{-5}$ mol dm^{-3} in all runs.

3.0[2] and 5.3[3] $\times 10^{-9}$ mol dm^{-3} at 25 °C. Our previous results, which are two to four times larger than those obtained in the present work, are considered to be less reliable. In the previous method, we estimated K_d by combining two rate constants determined by separate experiments; one was concerned with Hg^0 transfer from the aqueous to the gaseous phase, and the other, with the disproportionation of mercury(I).[1] The additional errors of the two rate constants may be responsible for the lesser reliability.

In general, the reliability of the method of determining K_d depends on how accurately it can determine the concentration of Hg(aq), which is in equilibrium with Hg_2^{2+} and Hg^{2+} ions. In this respect, several attempts that make use of the characteristic distribution of Hg^0 between aqueous and non-aqueous phases[3] or between aqueous and gaseous phases[2] have been made. We assume in the present method that the solubilities of Hg^0 in aqueous solutions in the presence of Hg_2^{2+} and Hg^{2+} ions are identical with those in their absence under the same vapor pressure of metallic mercury. It should be noticed that the concentration of Hg(aq) in each run is not a saturated solubility, but a so-called steady-state solubility. That is, mercury vapor continuously supplies Hg^0 to an aqueous phase, while the air stream bubbled out of the solution removes the dissolved Hg(aq) at a certain rate.

The total mercury concentrations in the D and F flasks, which can be measured by the atomic-absorption technique by using a tin(II) reductant, did not increase after more than a 10-hour aeration. We concluded, therefore, that the air-oxidation of the dissolved Hg^0 in 0.05 mol dm^{-3} $HClO_4$ solutions did not occur during the aeration. This is why we used air instead of nitrogen gas.

From the temperature dependence of K_d, the ΔH and ΔS values for Reaction 1 were found to be 79 kJ mol^{-1} and 108 J mol^{-1}K^{-1} at 25 °C.

References

1) Preceding paper: I. Sanemasa and T. Hirata, *Bull. Chem. Soc. Jpn.*, **50**, 3255 (1977).

2) S. Okouchi and S. Sasaki, *Nippon Kagaku Kaishi*, **1980**, 1291.

3) H. C. Moser and A. F. Voigt, *J. Am. Chem. Soc.*, **79**, 1937 (1957).

ESR Studies of Unstable Six-coordinated Cobalt(II) Complexes Produced by γ-Radiolysis of Glassy Solutions at 77 K

Mikio HOSHINO,* Shiro KONISHI, Masao NAKAJIMA, and Masashi IMAMURA
The Institute of Physical and Chemical Research, Wako, Saitama 351

(Received August 12, 1982)

Synopsis. ESR spectra of γ-irradiated glassy solutions of cobalt(II) chelates of *N,N'*-bis(1-methyl-3-oxobutylidene)-ethylenediamine (acacen) having two NH_3 in the axial positions at 77 K show the formation of a metastable cobalt(II) complex in which two NH_3 are forced to be confined in the axial positions.

Fundamental researches on intra- and intermolecular electron transfer mechanisms of metal complexes are of great importance in relation to understanding of the redox reactions occurring in biological systems.[1-4] Numerous kinetics studies for the outer-sphere electron transfer between metal complexes have revealed that the complexes reorganize the ligand molecules with receiving or releasing electrons.[5-7]

Recently, unstable complexes having an anion in the axial position were reported to be formed by the radiation-chemical reduction of the metal complexes in rigid solutions at 77 K.[8-11] These complexes release the anions on warming the solution. In the present paper we wish to report the formation of an unstable six-coordinated complex, Co(II)(acacen)$(NH_3)_2$, having two neutral NH_3 molecules in the axial positions. The complex is considered to be an intermediate in the following reaction,

$$[\text{Co(III)(acacen)}(NH_3)_2]^+ + e^- \longrightarrow \text{Co(II)(acacen)} + 2NH_3, \quad (1)$$

where Co(II)(acacen) and Co(III)(acacen)$(NH_3)_2$ are represented, respectively, as

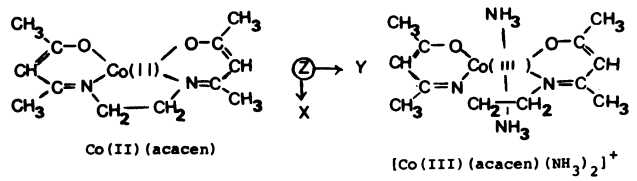

Experimental

$[Co(III)(acacen)(NH_3)_2]^+[X^-]$ (X=Cl and Br) was prepared according to the method reported by Costa *et al.*[12] Water was purified three times by distillation and ethylene glycol was used as supplied.

Radiolysis was performed with γ-rays from 1.2 kCi ^{60}Co source at 77 K at a dose rate of 57000 rad min^{-1}. ESR spectra were measured on a JEOL JES-FE-3AX X-band spectrometer.

Results and Discussion

When a 1 : 1 mixture of ethylene glycol and water containing 10^{-3} M $[Co(III)(acacen)(NH_3)_2]^+[X^-]$ was irradiated with γ-rays at room temperature, Co(II)-(acacen) was produced. As shown in reaction 1, this result indicates that $[Co(III)(acacen)(NH_3)_2]^+$ is reduced with electrons ejected from solvent molecules (S) upon γ-irradiation

$$S \longrightarrow S^{+\cdot} + e. \quad (2)$$

The use of a mixture of ethylene glycol and water in radiolysis has been applied to the selective formation of one-electron reduced species of solutes.[13]

The ESR spectrum *a* of Fig. 1 was observed for the γ-irradiated solution of $[Co(III)(acacen)(NH_3)_2]^+[Br^-]$ at 77 K. Beside the intense signal from solvent radicals around 3250 gauss, four of the eight hyperfine lines due to the interaction of an unpaired electron and the cobalt nucleus ($I=7/2$) are clearly observed. The spectrum dramatically changed to *b* of Fig. 1 after warming the irradiated solution to room temperature and recooling it to 77 K. Since an authentic Co(II)-(acacen) solution shows an ESR signal identical with *b* of Fig. 1, it is evident that the reduced species giving the spectrum *a* of Fig. 1 produces Co(II)(acacen) at higher temperatures. The most probable structure of the species is Co(II)(acacen)$(NH_3)_2$ in which two NH_3 molecules are forced to be confined in the axial positions owing to the solvent rigidity at 77 K. The γ-radiolysis of a $[Co(III)(acacen)(NH_3)_2]^+[Cl^-]$ solution gives the same ESR spectrum as *a* of Fig. 1. This result indicates that the anions, Cl^- and Br^-, do not exert strong effect to the cobalt atom contrary to the case of constrained complexes.[8-10] Presumably, the anions are located far from the cobalt atom.

For preparing the solution of Co(II)(acacen)$(NH_3)_2$ using the reaction

$$\text{Co(II)(acacen)} + 2NH^3 \longrightarrow \text{Co(II)(acacen)}(NH_3)_2$$

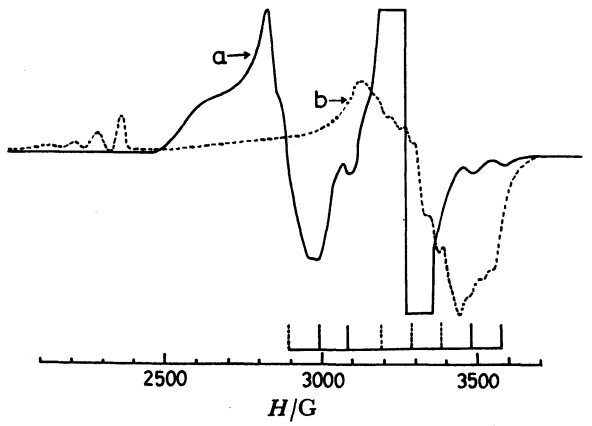

Fig. 1. ESR spectra of Co(II)(acacen) and Co(II)-(acacen)$(NH_3)_2$ in a 1 : 1 mixture of ethylene glycole and water at 77 K. a: ESR spectrum of Co(II)-(acacen)$(NH_3)_2$ obtained with γ-irradiating the solution of $[Co(III)(acacen)(NH_3)_2]^+[Br^-]$ for 45 min at 77 K; b: ESR spectrum observed after warming the irradiated solution to room temperature and recooling it to 77 K.

Table 1. ESR parameters of Co(II)(acacen) and Co(II)(acacen)$(NH_3)_2$ in a 1 : 1 mixture of ethylene glycol and water at 77 K

	g_x [a]	g_y [a]	g_z	A_x^{Co} [b]	A_y^{Co} [b]	A_z^{Co} [b]
Co(II)(acacen)	3.157[c]	1.930[c]	2.006[c]	110±5	36±2	36±2
Co(II)(acacen)$(NH_3)_2$	2.3—2.5[d]	2.3—2.5[d]	2.023[c]	d)	d)	90±4

a) x and y directions are arbitrary. b) Values are in units of 10^{-4} cm^{-1}. c) Experimental errors are 0.002. d) Values were not determined with precision because of poor resolution of the ESR spectrum.

Co(II)(acacen) was dissolved in ethanol saturated with NH_3 gass. However, the decomposition of Co(II)-(acacen) took place by dissolution and no formation of Co(II)(acacen)$(NH_3)_2$ was detected by ESR measurement. It is likely that the formation constant of Co(II)(acacen)$(NH_3)_2$ is very small.

In Table 1 are listed the ESR parameters of Co(II)-(acacen) and Co(II)(acacen)$(NH_3)_2$. The unpaired electron of Co(II)(acacen) has been established to be located in the d_{z^2} orbital of the cobalt atom.[14-16] The **g** tensors are related to the excited state energies, $\Delta E(d_{yz} \rightarrow d_{z^2})$ and $\Delta E(d_{xz} \rightarrow d_{z^2})$, by equations[17]

$$g_x = 2.002 - 6\,k_x^2\lambda/\Delta E(d_{yz} \rightarrow d_{z^2}), \quad \text{(i)}$$

$$g_y = 2.002 - 6\,k_y^2\lambda/\Delta E(d_{xz} \rightarrow d_{z^2}), \quad \text{(ii)}$$

$$g_z = 2.002, \quad \text{(iii)}$$

where λ is the spin-orbit coupling constant and k_x and k_y, the orbital reduction parameters. The large in-plane g anisotropy ($g_x \simeq 3$ and $g_y \simeq g_z \simeq 2$) of Co(II)(acacen) has been interpreted by assuming that the d_{yz} lies closely below the d_{z^2} and d_{xz}, far below.[14]

In contrast to Co(II)(acacen), the ESR spectrum of Co(II)(acacen)$(NH_3)_2$ indicates a nearly axial symmetry about the cobalt atom. The d_{z^2} orbital probably interacts with the nonbonding orbitals of two NH_3 molecules in the axial positions. This interaction increases the d_{z^2} orbital energy, resulting in a substantial decrease in the in-plane g anisotropy as is predicted by equations i and ii. The reduction of out-of-plane puckering due to two NH_3 molecules would also has an effect on the decrease in the anisotropy as suggested in the case of Co(II)(acacen)(Py) (Py : pyridine).[14] Strict theories,[18,19] however, should be applied for complete understanding of the ESR spectrum of Co(II)(acacen)$(NH_3)_2$.

The present study shows that the unstable six-coordinated cobalt(II) complex produced after one-electron reduction undergoes reorganization and ejection of ligand molecules in the axial positions. This kind of unstable complexes should play an important role in the outer-sphere electron transfer of metal complexes as a reaction intermediate.

References

1) J. Rawling, S. Wherland, and H. B. Gray, *J. Am. Chem. Soc.*, **98**, 2177 (1976).
2) C. Creutz and N. Sutin, *J. Biol. Chem.*, **249**, 6788 (1974).
3) D. Dolphin and R. H. Felton, *Acc. Chem. Res.*, **7**, 26 (1974).
4) L. E. Bennet, *Prog. Inorg. Chem.*, **18**, 1 (1973).
5) N. Sutin, *Ann. Rev. Nucl. Sci.*, **12**, 285 (1962).
6) M. Chou, C. Creutz, and N. Sutin, *J. Am. Chem. Soc.*, **99**, 5615 (1977).
7) N. Sutin, *J. Photochem.*, **10**, 19 (1979).
8) S. Konishi, M. Hoshino, K. Yamamoto, and M. Imamura, *Chem. Phys. Lett.*, **72**, 459 (1980).
9) S. Konishi, M. Hoshino, and M. Imamura, *J. Phys. Chem.*, **84**, 3437 (1980).
10) M. Hoshino, S. Konishi, Y. Terai, and M. Imamura, *Inorg. Chem.*, **21**, 89 (1982).
11) S. Konishi, M. Hoshino, and M. Imamura, *J. Phys, Chem.*, **86**, 1412 (1982).
12) G. Costa, G. Mestroni, G. Tauzher, and L. Stefani, *J. Organomet. Chem.*, **6**, 181 (1966).
13) M. Nakamura and S. Fujiwara, *J. Coord. Chem.*, **1**, 221 (1971).
14) B. M. Hoffman, F. Bassolo, and D. L. Diemente, *J. Am. Chem. Soc.*, **95**, 6497 (1973).
15) F. L. Urbach, R. D. Bereman, J. A. Topich, M. Hariharan, and B. J. Kalbacher, *J. Am. Chem. Soc.*, **95**, 6497 (1973).
16) B. M. Hoffman, D. L. Diemente, and F. Bassolo, *J. Am. Chem. Soc.*, **96**, 5063 (1974).
17) A. H. Maki, E. Edelstein, A. Davidson, and R. H. Holm, *J. Am. Chem. Soc.*, **86**, 4580 (1964).
18) C. Busetto, F. Cariati, A. Fusi, M. Gulloti, F. Morazzoni A. Pasini, R. Ugo, and V. Valenti, *J. Chem. Soc., Dalton Trans.*, **1973**, 754.
19) B. R. McGarvy, *Can. J. Chem.*, **53**, 2498 (1975).

Growth Morphology of Alumina Whiskers

Takashi HAYASHI,* Masatoshi IWATA, and Hajime SAITO
Department of Applied Chemistry, Faculty of Engineering, Nagoya University, Furo-cho, Chikusa-ku, Nagoya 464
(Received September 10, 1982)

Synopsis. Alumina whiskers were grown on a substrate by hydrolysis of aluminium fluoride vapor. The present paper describes some observations concerning the growth and morphology of alumina whiskers. The most frequently observed types in this work were A_2-whiskers and C-whiskers.

The growth of alumina whiskers by vapor phase reaction has been accomplished by several investigators.[1-4] The growth of alumina whiskers occurs with the main crystallographic direction, and the corresponding crystals are sometimes referred to as A_1, A_2, A/C and C-type whiskers. C-whiskers grow in the c direction, [0001], of the hexagonal system, and A_1- and A_2-whiskers grow in the c plane in a [10$\bar{1}$0] direction and in a [11$\bar{2}$0] direction, respectively, and A/C-whiskers grow by approximately equal alteration of the growth direction in the A and C direction.

The size, morphology and crystallographic orientation of whiskers depend strongly on the experimental growth conditions. In the preceding paper,[5] we reported the growth of alumina whiskers by the hydrolysis of aluminium fluoride vapor. The present paper describes some observations concerning the growth and morphology of alumina whiskers.

The apparatus has been previously described in detail.[5] The graphite tube, which was used as a reactor, consisted of a region for vaporization of AlF_3 and a region for growth of Al_2O_3. AlF_3, which was evaporated in a furnace at a given temperature ranging from 710 to 1070 °C, was introduced into the reaction chamber with a carrier gas (Ar gas) and reacted with H_2O vapor, introduced through another inlet with a carrier gas, on a polycrystalline Al_2O_3 substrate. The desired vapor pressure of H_2O was obtained by bubbling the carrier gas through water at 0 °C and diluting the moist carrier gas with the appropriate flow of dry carrier gas. The experimental conditions were as follows: Growth temp: 1400 °C, Growth time: 3 h, AlF_3 vapor pressure: 10^{-4}—10 Torr,† H_2O vapor pressure: 10^{-3}—20 Torr, Ar gas flow rate: 100—200 ml/min. The morphology of the crystals formed was examined by optical microscopy.

Influence of AlF_3 vapor pressure, P_{AlF_3}, and H_2O vapor pressure, P_{H_2O}, on the morphology of the crystals was investigated and the relation between P_{AlF_3} and P_{H_2O} is shown in Fig. 1. Alumina crystals which had various morphology, *viz.* fine powder, bulk crystals, platelet crystals and whiskers, were formed on the substrate, depending on the growth conditions. With the simultaneous decrease of AlF_3 and H_2O vapor pressure, the crystals changed their forms from powder to bulky or platelet crystals and finally to whiskers. Adequate vapor pressures of AlF_3 and H_2O for both needle crystal and whisker growths were found to be below about 5 Torr. Whiskers only were formed under the lower vapor pressures, *i.e.* $P_{AlF_3}<1$ Torr, $P_{H_2O}<1$ Torr. The morphology of the crystals formed depended also on the growth region on the substrate. In the narrow region at which direct impingement of reactant gases occurred, the formation of fine powder or coarse polycrystalline deposits tended to occur, while whiskers tended to grow in the regions which ran along the flow of mixture gases towards the outlet.

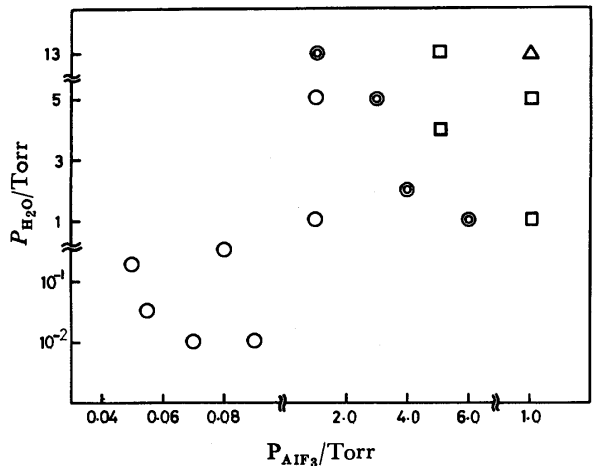

Fig. 1. Influence of P_{AlF_3} and P_{H_2O} on the morphology of grown crystals. Ar(AlF_3): 150 ml/min, Ar(H_2O): 200 ml/min. △: Powdery polycrystal, □: bulk crystal, ◎: needle crystal, ○: whisker.

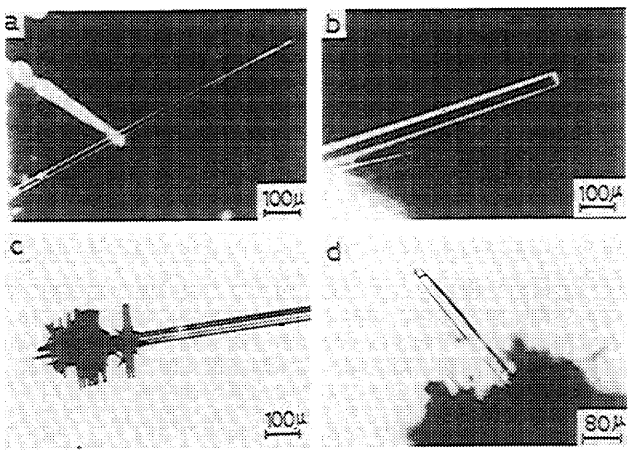

Fig. 2. Optical micrographs of whiskers. (a): Tapered whisker, (b): thin ribbon-like whisker, (c): branched whisker, (d): whisker having a droplet at its tips.

Many whiskers grew straight and grew up to the length of several mm (maximum 7—8 mm) with diameters up to 50 μm. Typical optical micrographs of alumina whiskers are shown in Fig. 2. The most frequently observed types were A_2- and C-whiskers. As expected from its morphology their cross sections showed rectangular and hexagonal shapes, respectively. In the whiskers formed in the present work, both platelet

† 1 Torr=133.322 Pa.

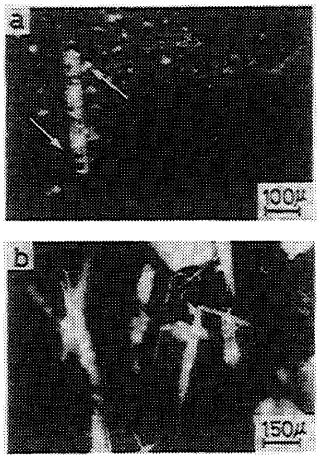

Fig. 3. Optical micrographs of kinked whisker. (a): 90° growth kinks, (b): 60° growth kinks.

and hexagonal forms were observed. Two types exist in the former: pillar and needle-like whiskers. On the other hand, the C-whiskers having many branches on the lateral surfaces near the whisker tip were occasionally observed in the latter. These branched whiskers, inclined at right angles and at about 45° to the crystal axes, were considered to be A-whisker and A/C-whiskers,[6] respectively. These branching tended to occur easily near the whisker tip when the C-whisker reached a certain length. Such secondary whisker growth is similar to the results reported by Sears[6] in which A-type whiskers grow predominantly at the thickened tip of C-whiskers. In some cases, although very rare, a whisker which had a small globule at its tip was observed. It is thought that they grew according to the VLS mechanism in the presence of impurities.

Besides the straight whiskers, kinked whiskers having 60°, 90°, and 120° angles were sometimes observed, as shown in Fig. 3. The possible angle between A_1 growth direction and A_2 growth direction are 30°, 90°, and 150°. It was considered by optical technique that 90° growth kink (Fig. 3,a) occurred by changing the growth direction such as A_1-A_2-A_1 direction or A_2-A_1-A_2 direction, but not such as A-C-A direction. That is, in the case of an A_1 or A_2-whisker which is bounded by both {0001} and {1120} or {1010} types of columnar surfaces two-dimensional nucleation should occur on the {1120} or {1010} surfaces at a lower supersaturation than on the {0001} surfaces, because the surface energy is least for the most closely packed surface {0001}.[6] Also, A-type whiskers would change growth direction by 60°,[6] as shown in Fig. 3,b, because the possible angles between one A growth direction and another A growth direction are 60° and 120°.

References

1) R. C. DeVries and G. W. Sears, *J. Chem. Phys.*, **31**, 1256 (1959).
2) W. W. Webb and W. D. Forgang, *J. App. Phy.*, **28**, 1449 (1957).
3) H. G. Wiedemann and E. Sturzenegger, *Naturwissenschaften*, **61**, 65 (1974).
4) W. B. Campbell, *Chem. Eng. Prog*, **62**, 68 (1966).
5) I. Yamai and H. Saito, *J. Cryst. Growth*, **45**, 511 (1978).
6) G. W. Sears and R. C. DeVries, *J. Chem. Phys.*, **39**, 2837 (1963).

Syntheses and Characterization of Lanthanoid(III) Propoxyacetate

Satoshi KONDO,* Kiyofumi NAGAI, and Akira OUCHI
Department of Chemistry, College of General Education, The University of Tokyo, Komaba 3-8-1, Meguro-ku, Tokyo 153

(Received September 30, 1982)

Synopsis. New lanthanoid(III) complexes with the formula of $ML_3 \cdot H_2O$, where M=La, Ce, Pr, Nd, Eu, Dy, or Er, and HL=propoxyacetic acid, have been synthesized; they are isostructural with each other. From the shift direction of the ^{1}H-NMR peaks of L^- in an aqueous solution upon adding Eu(III) or Pr(III) salt, the ligand is likely to be coordinated to the metal by both the ether and carboxyl oxygen atoms.

The interesting structures of some lanthanoid(III) carboxylate complexes in their crystals have already been revealed by the single crystal X-ray diffraction technique.[1-5] The structure of lanthanoid(III) alkylthioacetates has also been elucidated, and it has been found that the ligand is coordinated to the metal only by the carboxylate oxygen atoms, not by the sulfide sulfur atom.[6] On the other hand, in the case of tris-(diglycolato)lanthanoid(III) complexes, the ligand acts as a terdentate where the central metal is coordinated to both the ether and carboxylate oxygen atoms.[7] Therefore, it was thought to be interesting to synthesize the lanthanoid(III) alkoxyacetates and to check whether or not the ether oxygen atom of the ligand in them is coordinated to the metal. The complexes obtained were found to be stable to moisture, even in open air.

Experimental

Synthesis of Lanthanum(III) Propoxyacetate Monohydrate, $La(C_3H_7OCH_2CO_2)_3 \cdot H_2O$. The ligand, propoxyacetic acid, was obtained by Rule's method.[8] Propoxyacetic acid (2.13 g, 18 mmol) and sodium hydrogencarbonate (1.43 g, 17 mmol) were dissolved in about 7 cm^3 of water, and lanthanum(III) chloride heptahydrate (1.86 g, 5 mmol) dissolved in 3 cm^3 of water was added to the former solution. The mixture was then stirred and heated, and the complex was precipitated. It was filtered off, dissolved in about 40 cm^3 of hot water, concentrated by means of a rotary vacuum evaporator to about 10 cm^3, and left standing at room temperature overnight. The crystals thus obtained were filtered off, washed with a little water, and dried in open air. Although the yield of the first crop obtained was only 21%, crystals of almost the same purity were also obtained when the filtrate in a beaker was kept longer in a silica-gel desiccator; the total yield was about 66%.

The propoxyacetates of Ce, Pr, Nd, Eu, and Dy were obtained in almost the same way, and their yields were comparable. In the case of the Er complex, the product appeared as an oily layer when the starting materials were mixed and heated: it gradually turned into a solid precipitate within a few minutes while it was being stirred and cooled.

These complexes have the formula of $M(C_3H_7OCH_2CO_2)_3 \cdot H_2O$. Analyses (Calcd values were obtained from the formula of $C_{15}H_{29}O_{10}M$): M=La, Found: La, 27.16; C, 35.35; H, 5.76%. Calcd: La, 27.33; C, 35.45; H, 5.75%. M=Ce, Found: Ce, 27.61; C, 35.42; H, 5.74%. Calcd: Ce, 27.50; C, 35.36; H, 5.74%. M=Pr, Found: Pr, 27.49; C, 35.25; H, 5.88%. Calcd: Pr, 27.61; C, 35.31; H, 5.73%. M=Nd, Found: Nd, 27.94; C, 35.13; H, 5.71%. Calcd: Nd, 28.08;; C, 35.08; H, 5.69%. M=Eu, Found: Eu, 29.18; C, 34.52 H, 5.74%. Calcd: Eu, 29.15; C, 34.56; H, 5.61%. M=Dy, Found: Dy, 30.58; C, 33.73; H, 5.63%. Calcd: Dy, 30.55; C, 33.87; H, 5.50%. M=Er, Found: Er, 31.14; C, 33.48; H, 5.60%. Calcd: Er, 31.17; C, 33.57; H, 5.45%.

Magnetic Moments, X-Ray, Infrared Spectra, and ^{1}H-NMR Measurements. Their X-ray powder patterns were obtained by the use of a diffractometer, model DX-GO-F JEOL, using Cu $K\alpha$ radiation from 3 to 60° in 2θ.

The infrared spectra of the samples were obtained by means of a JASCO A202 infrared spectrophotometer, using Nujol and hexachloro-1,3-butadiene mull. The ^{1}H-NMR was measured by means of a Varian EM-390 spectrometer, using D_2O as the solvent and sodium 3-(trimethylsilyl)-1-propanesulfonate (DSS) as the internal standard.

The magnetic moments of the complexes at room tempeature were measured by the use of a Gouy balance.

Results and Discussion

From the analyses and from their X-ray powder patterns, all of these seven complexes are isostructural. Their single crystals have a layer structure, consisting of mica-like thin films. As there is a tendency found extreme cleavage, the single-crystal diffraction study has not yet been completed. The magnetic moments of $ML_3 \cdot H_2O$, where HL=propoxyacetic acid are; M=La, diamagnetic; M=Ce, 2.4_9; M=Pr, 3.5_0; M=Nd, 3.5_3; M=Eu, 3.2_8; M=Dy, 10.6_8; M=Er, 9.6_1 BM,** respectively. They mean that no significant metal-metal interaction exists.[9]

Both the ν_{as}(COO) and ν_s(COO) absorptions of the IR spectra split into several peaks. The main ν_{as}(COO) peak of each complex appears between 1596 (La complex) and 1608 (Er complex) cm^{-1}, and the wave number increases depending on the atomic number of the central metal. The wave number of the maximum of the ν_{as}(COO) peak is higher than that of the corresponding lanthanoid(III) alkylthioacetates (about 1590—1580 and 1540 cm^{-1}).[6]

In Fig. 1 are shown the shifts of ^{1}H-NMR peaks of sodium butyrate, propylthioacetate, and propoxyacetate in a D_2O solution upon the addition of europium(III) chloride or of praseodymium(III) chloride. In all cases, the shift direction of the peaks upon the addition of Eu(III) is the opposite of that upon the addition of Pr(III): the ratio of the two shifts is about 1 : 2 for the same proton of the same acid salt. This means that the shifts occur mainly because of the dipole effect.[10] In the case of butyrate, where the central metal atom is coordinated only to the carboxyl oxygen atoms, all the proton peaks shift in the same direction—downfield by Pr(III) and upfield by Eu(III). Also, in the case of propylthioacetate, where the lanthanoid metal atom is coordinated only to the carboxyl oxygen atoms,[6] the shift direction of all the proton signals is the same as

** 1 BM=9.274078(36)·10^{-24} J T^{-1}.

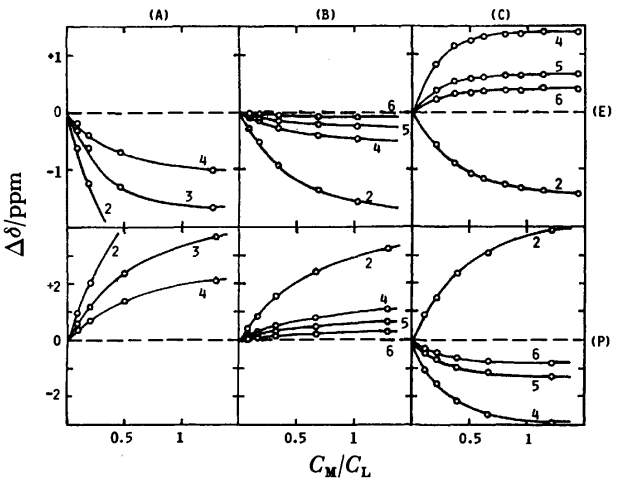

Fig. 1. The shifts of ^{1}H-NMR peaks by the addition of europium(III) chloride (E: the upper ones), or praseodymium(III) chloride (P: the lower ones), in D_2O solution. C_M/C_L=mol/mol. C_M: Concentration of Eu(III) or Pr(III). C_L: Concentration of propoxyacetate. Downfield $\Delta\delta$ was shown positive. Original chemical shifts for (A) CH_3(4)-CH_2(3)-CH_2(2)-CO_2Na, (B) CH_3(6)-CH_2(5)-CH_2(4)-S-CH_2(2)-CO_2Na, (C) CH_3-(6)-CH_2(5)-CH_2(4)-O-CH_2(2)-CO_2Na: (A) (4) 0.87-(t), (3) 1.53(m), (2) 2.15(t); (B) (6) 0.94(t), (5) 1.58(m), (4) 2.52 (t), (2) 3.15(s); (C) (6) 0.88(t), (5) 1.59(m), (4) 3.46(t), (2) 3.88(s) ppm (in δ, DSS=0; s: singlet, t: triplet, and m: multiplet). The concentration of the original sodium salts are, (A) 0.069; (B) 0.068; (C) 0.20 mol dm^{-3} for (E)s, and (A) 0.067; (B) 0.068; (C) 0.19 mol dm^{-3} for (P)s. Used $EuCl_3$ or $PrCl_3$ solutions: (A), (B), 0.13 mol dm^{-3}; (C) 0.37 mol dm^{-3} containing 0.19 mol dm^{-3} of sodium propoxyacetate.

that of butyrate. Thus, all the ligand protons of butyrate or of propylthioacetate can be expected to be out of the axial cone of the central lanthanoid atom.

On the other hand, in the case of propoxyacetate, as is shown in Fig. 1, only the signal of the protons of the methylene group which is next to the carboxyl group shifts in the same direction as those of the butyrate or of propylthioacetate. The signals of propoxyl protons, on the contrary, shift in the opposite direction, and the shift decreases rapidly depending on the increase in the distance between the proton and the ether oxygen atom.[11] This seems to be because the ether oxygen atom moves in the axial direction, while the propoxyl group shifts into the axial cone. Therefore, from this ^{1}H-NMR result, the propoxyacetate ion is found to be coordinated to the lanthanoid(III) metal atom by both carboxyl and ether oxygen atoms.

The authors are greatly obliged to the Shin-Etsu Chemical Co., Ltd., for aiding this study by presenting the highly pure lanthanoid(III) oxides.

References

1) G. G. Sadikov, G. A. Kukina, and M. A. Porai-Koshits, *Zh. Strukt. Khim.*, **8**, 492 (1967).
2) A. S.Antsyshkina and M. A. Porai-Koshits, *Koord. Khim.*, **2**, 565 (1976).
3) E. Hansson, *Acta Chem. Scand.*, **27**, 2441, 2813 (1973).
4) G. G. Sadikov, G. A. Kukina, and M. A. Porai-Koshits, *Zh. Strukt. Khim.*, **8**, 551 (1967).
5) J. W. Bats, R. Kalus, and H. Fuess, *Acta Crystallogr., Sect. B*, **35**, 1225 (1979).
6) S. Kondo, M. Shimoi, A. Ouchi, and T. Takeuchi, *Bull. Chem. Soc. Jpn.*, **55**, 2840 (1982).
7) J. Albertsson, *Acta Chem. Scand.*, **22**, 1563 (1968); **24**, 3527 (1970).
8) H. G. Rule, W. Hay, and J. Paul, *J. Chem. Soc.*, **1928**, 1347.
9) T. Moeller, "Comprehensive Inorganic Chemistry," Pergamon Press, Oxford, U. K. (1973), Vol. 4, p. 10.
10) B. Bleaney, C. M. Dobson, B. A. Levine, R. B. Martin, R. J. P.Williams, and A. V. Xavier, *J. Chem. Soc., Chem. Commun.*, **1972**, 791.
11) H. M. McConnell and K. E. Robertson, *J. Chem. Phys.*, **29**, 136 (1958).

The Isotope Effects in the Reactions of Phenylcarbene with Alcoholic Matrices

Hideo Tomioka,* Yasuji Ozaki, and Yasuji Izawa
Department of Industrial Chemistry, Faculty of Engineering, Mie University, Tsu, Mie 514
(Received May 12, 1982)

Synopsis. Product analysis studies on the reaction of phenylcarbene in deuterated alcoholic matrices at 77 K revealed that isotope effect on O–H (D) insertion is very small while substantial isotope effect was observed for C–H (D) insertion.

Recent reports from this[1-4] and other[5-8] laboratories have shown that the reactivity of arylcarbenes dramatically changes in rigid matrix at low temperature. The C–H insertion products increased drastically at lower temperature at the expense of characteristic singlet products (*vide infra*) and are believed to be derived from triplet arylcarbene *via* hydrogen atom abstraction and radical recombination. For example, we have found[1-4] in the reaction of arylcarbene with alcohol that the C–H insertion products increase dramatically at lower temperature at the expense of the OH insertion product. Recent kinetic studies of Platz[9,10] and Gasper[11] have demonstrated that the hydrogen atom abstraction from matrix is not a classical process but quantum mechanical tunneling in nature. There is little doubt that tunneling is often involved in hydrogen atom and proton transfer. It has been indicated[12] in the hydrogen atom abstraction by radicals that one of the characteristic phenomena for tunneling reaction is a very large kinetic isotope effect. For example, Ingold *et al.*[12] have observed k_H/k_D for the intramolecular hydrogen atom tunneling of 2,4,6-tri-*t*-butylphenyl radical is 1.3×10^4 at 123 K, while the maximum possible value for k_H/k_D for the simple rupture of a C–H/C–D bond is estimated to be 260 at 123 K. Similarly, Williams *et al.*[13] have reported that k_H/k_D is larger than 1.3×10^3 for intermolecular hydrogen atom abstraction by $CH_3\cdot$ from matrix at 110 K. Thus in order to obtain more precise insight into the mechanism of carbene reaction in matrix, it is quite important to investigate isotope effect on the product distribution. We wish to report here the product analysis studies on the reaction of phenylcarbene in deuterated alcoholic matrices at 77 K.

Results and Discussion

Degassed solutions of phenyldiazomethane (**1**) in methanol and its deuterated modifications were photolyzed at 77 K until all of **1** was destroyed. The product distributions were determined by GC and reported in Table 1. It is evident that isotope effect on O–H (D) insertion is very small but that there is a substantial isotope effect on C–H (D) insertion.

$$\underset{\mathbf{1}}{PhCH{=}N_2} \xrightarrow[-N_2]{h\nu} \underset{77\ K}{[PhCH{:}]} \xrightarrow[MeOH]{} \underset{\mathbf{3}}{PhCH_2OMe} + \underset{\mathbf{4}}{PhCH_2CH_2OH} \quad (1)$$

Accepting the assumption that the relative yields of products are directly proportional to their relative rates of formation, k_H/k_D for O–H and C–H insertion can be calculated to be 1.2 and 5.6, respectively. A more instructive result is provided in a study of a series of isotopically labelled 2-propanols (see Table 2). Thus,

$$\underset{\mathbf{1}}{} \xrightarrow[-N_2]{77\ K,\ Pr^iOH} PhCH_2OPr^i + \underset{\mathbf{5}}{PhCH_2\text{–}\overset{CH_3}{\overset{|}{C}}\text{–}OH} \quad \underset{\mathbf{6}}{\overset{CH_3}{\overset{|}{C}}H_3} + PhCH_2CH_2\overset{CH_3}{\overset{|}{C}}HOH \quad (2)$$

$$\underset{\mathbf{7}}{}$$

Table 1. Isotope effects in the reaction of phenylcarbene with isotopically labelled methanol at 77 K

Matrix	Yield/%[a]	
	3	**4**
CH_3OH	40.8	26.2
CH_3OD	39.1	31.1
CD_3OD	64.6	9.1

a) Other minor products (≈5%) detected in each run were toluene, bibenzyl, stilbenes, and aldehyde azine. Yield of these minor products was not altered by matrix.

Table 2. Isotope effects in the reaction of phenylcarbene with isotopically labelled 2-propanol at 77 K

Matrix	Yield/%[a]		
	5	**6**	**7**
$(CH_3)_2CHOH$	15.3	52.7	11.9
$(CH_3)_2CDOH$	15.7	17.2	48.7
$(CD_3)_2CHOH$	20.4	50.5	7.3

a) See footnote a in Table 1.

β-C–H insertion product (**7**) increased dramatically in 2-propan-2-*d*-ol matrix while α-C–H insertion (**6**) became dominant in 2-propan-1,1,1,3,3,3-d_6-ol matrix. Thus, k_H/k_D for α-C–H and β-C–H insertion can be similarly calculated to be 3.1 and 2.2, respectively.

The lack of isotope effect on O–H (D) insertion along with the kinetic observation[9,10,17] that retardation of the decay rate of triplet arylcarbene is not significant in alcohol-*hydroxyl-d* matrix indicates that abstraction of hydrogen from an O–H bond of alcohol by triplet carbene hardly occurs in matrix. This is quite reasonable in light of the large O–H bond dissociation energy (103 kcal/mol).[14] Most of ethers are then derived from singlet carbene even in rigid matrix.

Considerable isotope effect on C–H insertion supports the idea that C–H insertion products are arising from

triplet carbene, presumably *via* the abstraction-recombination mechanism. It is somewhat surprising, however, to note that the observed C–H isotope effect is not so large as to prevent the formation of C–D insertion products. In their studies of isotope effect on H atom tunneling, Williams *et al.*[13] have shown that main decay pathways of $CH_3\cdot$ radicals change from H atom abstraction to recombination with other $CH_3\cdot$ radicals in going from CH_3NC to CD_3NC matrix because of large kinetic isotope effect. No appreciable increase in such recombination products as azine and stilbene even in CD_3OD matrix indicates that decay pathways of triplet phenylcarbene are primarily D atom abstraction even in the perdeutrated solvent. The result is consistent with the kinetic observation that isotope effects with arylcarbenes are much more modest (*vide infra*).[9,10] This is partly attributable to a matrix-site problem. The rate of a hydrogen atom tunneling process is dependent upon not only the barrier height but also width: the barrier height is the classical activation energy but the barrier width is the distance that the hydrogen atom must tunnel from matrix molecule to the arylcarbene. The kinetic studies[9–11] show that decay of triplet carbene does not follow the simple pseudo first order kinetics. Such nonexponential decay has been attributed to the effects of different matrix sites offering various degrees of freedom for reaction. The findings[15] that arylcarbene generated in rigid isobutane matrix results in dramatic increase in primary C–H insertion over tertiary have been interpreted in terms of such effects of different matrix sites. In the early stages of the reaction, the reactive sites are quickly depleted while the remaining carbenes are in less reactive sites. The matrix isotope effects are found[9] to vary with matrix sites. Thus, for diphenylcarbene in toluene-d_8, matrix rate constants $k_H/k_D=6.92$ at 77 K, but initial rate constants (10% decay) $k_H/k_D=23$ at 77 K. The bulk chemistry of low temperature samples must reflect sum of those carbenes located in various sites.[16]

Experimental

Materials. Phenyldiazomethane was prepared as described in the literature[17] immediately before use. All deuterated methanols were purchased from E. Merck and used without purification. 2-Propan-2-*d*-ol was prepared by $LiAlD_4$ (E. Merck) reduction of CH_3COCH_3 and 2-propan-1,1,1,3,3,3-d_6-ol was prepared $LiAlH_4$ reduction of CD_3COCD_3 (E. Merck) according to literature procedures.[18] The undeuterated solvents were distilled over anhydrous $CaSO_4$ prior to use. Authentic samples of phenylcarbene adducts with alcohols (**3**—**7**) were synthesized as described in the literature.[19]

Low Temperature Irradiations and Product Analyses. All irradiations were carried out with a Halos 300-W high-pressure mercury lamp with a water-cooled jacket. In a typical procedure, 0.005 mmol of the freshly prepared diazomethane was added to a 2.0 ml of alcohol in Pyrex tubes. Sample tubes were sealed under vacuum after three freezethaw cycles, immersed in a trasparent Dewar filled with liquid nitrogen, and irradiated until all of the diazomethane was destroyed. Product identifications were established by GC or GC-MS comparisons using authentic samples. Product distributions were conveniently determined on 2.0 m 5% OV-17 column at 120 °C.

References

1) H. Tomioka, T. Inagaki, and Y. Izawa, *J. Chem. Soc., Chem. Commun.*, **1976**, 1023; H. Tomioka, T. Inagaki, S. Nakamura, and Y. Izawa, *J. Chem. Soc., Perkin Trans. 1*, **1979**, 130.
2) H. Tomioka and Y. Izawa, *J. Am. Chem. Soc.*, **99**, 6128 (1977).
3) H. Tomioka, S. Suzuki, and Y. Izawa, *Chem. Lett.*, **1980**, 293.
4) H. Tomioka, H. Okuno, and Y. Izawa, *J. Chem. Soc., Perkin Trans. 2*, **1980**, 1636.
5) R. A. Moss and U.-H. Dolling, *J. Am. Chem. Soc.*, **93**, 954 (1971).
6) R. A. Moss and M. A. Joyce, *J. Am. Chem. Soc.*, **99**, 1262 (1977).
7) R. A. Moss and J. K. Huselton, *J. Am. Chem. Soc.*, **100**, 1314 (1978).
8) R. A. Moss and M. A. Joyce, *J. Am. Chem. Soc.*, **100**, 4475 (1978).
9) V. P. Senthilnathan and M. S. Platz, *J. Am. Chem. Soc.*, **102**, 7637 (1980).
10) V. P. Senthilnathan and M. S. Platz, *J. Am. Chem. Soc.*, **103**, 5503 (1981).
11) C.-T. Lin and P. P. Gasper, *Tetrahedron Lett.*, **21**, 3553 (1980).
12) G. Brunton, D. Griller, L. R. C. Barclay, and K. U. Ingold, *J. Am. Chem. Soc.*, **98**, 6803 (1976).
13) J.-T. Wong and F. Williams, *J. Am. Chem. Soc.*, **94**, 2930 (1972).
14) J. G. Calvert and J. N. Pittz, Jr., "Photochemistry," John Wiley and Sons, New York (1967).
15) H. Tomioka, *J. Am. Chem. Soc.*, **101**, 256 (1979).
16) These results parallel those of Platz *et al*, who report more extensive studies of chemical and kinetic isotope effects and the results of tunneling calculations; M. S. Platz, V. P. Senthilnathan, B. B. Wright, and C. W. McCurdy, Jr., submitted for publication. We thank Professor Platz for a prepublication copy of their manuscript.
17) X. Creary, *J. Am. Chem. Soc.*, **102**, 1611 (1980).
18) L. Kaplan, *J. Am. Chem. Soc.*, **77**, 5469 (1955).
19) H. Tomioka, S. Suzuki, and Y. Izawa, *J. Am. Chem. Soc.*, **104**, 1047 (1982).

Reaction Mechanism of 2-(Trimethylsilylmethyl)pyridine with Benzonitrile[1)†]

Takeo KONAKAHARA* and Kenji SATO

Department of Industrial and Engineering Chemistry, Faculty of Science and Technology, Science University of Tokyo, Noda, Chiba 278

(Received July 10, 1982)

Synopsis. The mechanism of the reaction of lithiated 2-(trimethylsilylmethyl)pyridine with benzonitrile is discussed. The reaction proceeds through (*E*)- and (*Z*)-1-phenyl-2-(2-pyridyl)-1-(trimethylsilylamino)ethene, which are quantitatively converted to 2-phenacylpyridine by acidic hydrolysis.

Reaction of a nitrile with a Grignard or organolithium reagent has been extensively investigated by many workers.[2,3)] It is a good synthetic method of ketimines which give ketones by hydrolysis. It is difficult to find a reaction of an α-silyl carbanion with a nitrile, although its reaction with a carbonyl compound has been discussed as the Peterson reaction.[4)] In the course of our investigation of α-silyl carbanion with carbonyl compound or their analogs, we previously reported that *p*-substituted benzonitriles gave the corresponding 2-phenacylpyridine derivatives in high yield when the nitriles were treated with lithiated 2-(trimethylsilylmethyl)pyridine.[1)]

In this paper, we wish to report a mechanism of the reaction of lithiated 2-(trimethylsilylmethyl)pyridine (**1**) with benzonitrile (**2**). The reaction was found to proceed through (*E*)- and (*Z*)-1-phenyl-2-(2-pyridyl)-1-(trimethylsilylamino)ethene, (**4**) and (**5**), which were isolated in good yield, and converted to 2-phenacylpyridine (**3**) quantitatively by acidic hydrolysis.

Results and Discussion

In order to study the behavior of the trimethylsilyl group throughout the reaction, the following three quenching experiments were performed (Table 1). Firstly, the reaction mixture of **1** with **2** was quenched with water at 0 °C (instead of aq ammonium chloride which was used in preparation of **3**[1)]) after stirring for 1 h at −75 °C and for 2 h at room temperature (method A). The organic extract did not contain any **3**, but did contain (*E*)-1-phenyl-2-(2-pyridyl)-1-(trimethylsilylamino)ethene (**4**) and its *Z*-isomer (**5**) (**4** : **5**=10 : 90, by GLC) with a small amount of the unreacted **1** (Scheme 1). A mixture of **4** and **5** was isolated in good yield (74%) by distillation under reduced pressure (**4** : **5**=20 : 80, by GLC; 43 : 57, by ^{1}H-NMR[5)]). Both **4** and **5** were quantitatively converted to **3** by hydrochloric acid, but they did not change to **3** by sodium hydroxide. On the other hand, quenching with *aq.* THF at −75 °C after 5 min (method B) gave a different ratio (**4** : **5**=70 : 30, by GLC under the same conditions as method A). This fact suggests that the formation of **4** is kinetically controlled, while that of **5** is thermodynamically controlled.

The structures of **4** and **5** were determined by their spectroscopic properties. The MS of the distillate obtained by method A, showed a molecular ion (M^+) peak at *m/z* 268 (molecular weight of **4** and **5**: $C_{16}H_{20}N_2Si$=268.43), and the ^{1}H-NMR spectrum of the same

Table 1. Quenching experiment in the reaction of **1** with **2**[a)]

Method	Reaction θ/°C	Reaction t/min	Quenching Quencher	Quenching θ/°C	Ratio of **4**: **5**[b)]
A	−75	60	H_2O	0	10 : 90[c)]
	r.t.	120			(25 : 75)[d)]
B[c)]	−75	5	H_2O/THF	−75	70 : 30
C[c)]	−75	30	AcOH/THF[e)]	−75	100 : ≈0

a) Molar ratio **1** : **2** : LDA = 1 : 1 : 1; spectra were measured after drying, followed by evaporation of the solvent. b) Determined by GLC (10% Silicone GE SE-30, 80 → 200 °C, 8 °C/min, Rt/min=21 and 22.5, respectively). c) Analyzed wtihout purification; includes the unreacted **1**. d) Estimated by GLC and ^{1}H-NMR data of the distillate; **4** : **5**=20 : 80 by GLC, 43 : 57 by ^{1}H-NMR. e) Excess acetic acid was removed *in vacuo*, followed by washing with sodium hydroxide.

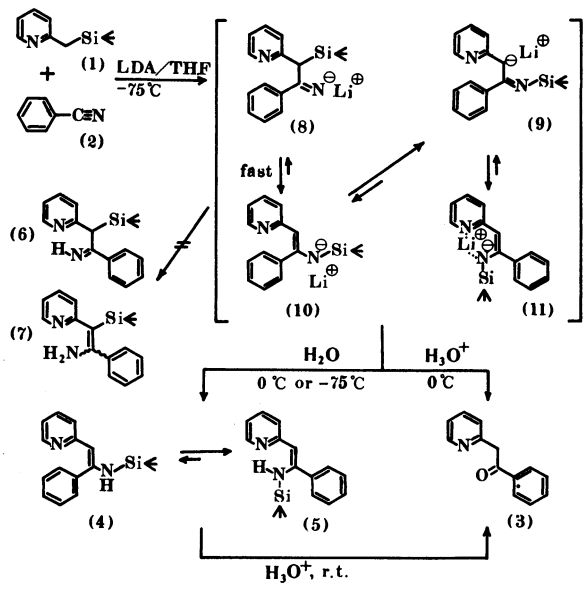

Scheme 1.

sample consists of two kinds of trimethylsilyl groups (δ=0.04 for **5** and 0.12 for **4**), two kinds of alkenyl protons (δ=5.23 for **5** and 5.46 for **4** as singlet respectively), and two kinds of N–H protons (δ=9.62 for **5** and 7.85 for **4**), together with the ABCX system for the pyridine protons complicated with multiplet phenyl protons. The IR spectrum suggested the presence of the enamine system (ν_{NH} 3470 cm^{-1} and $\nu_{C=C\text{-}trans}$ 1620 cm^{-1} for **5** and $\nu_{C=C\text{-}cis}$ 1630 cm^{-1} for **4**) together with the trimethylsilyl group (δ_{sCH_3} 1253 cm^{-1} and 840 cm^{-1}). No absorption of C=N bond was observed. The absorption band at 930 cm^{-1} was assigned to $\nu_{asSi\text{-}N}$.[6)] Enamines **4** and **5** easily lost the trimethylsilyl group under acidic medium (Scheme 1), although a trimethylsilyl group attached to a *secondary* carbon is less reactive.[4c)] This does not indicate the presence of the Si–C bond, but the presence of the Si–N bond.[7)] It is

† A preliminary report of this work was presented at the 45th National Meeting of the Chemical Society of Japan, Tokyo, April 1982, Abstr. No. 1G46.

consistent with the result from the IR spectrum; therefore, an imino compound (**6**) and its enamine tautomer (**7**) derived from (**8**) are not stable intermediates. Moreover, *N*-trimethylsilyl imine derived from **9** by C-protonation was not observed.[8]

Finally, the reaction mixture of **2** was quenched with glacial acetic acid in THF at −75 °C after stirring at −75 °C for 30 min (method C). Only **4** was included in the reaction mixture (Table 1 and Experimental).

In conclusion, the lithiated **1** reacts with **2** to give the imino compound **8**, which was immediately converted to the (*E*)-enamide **10** by 1,3-migration of the trimethylsilyl group from C to N (Scheme 1).[7] Through the corresponding imine tautomer **9**, **10** is isomerized to the (*Z*)-enamide **11**, which is thermodynamically more stable. These anions are resonance-stabilized by the electron-attracting 2-pyridyl group and trimethylsilyl group adjacent to the negatively charged nitrogen atom. The anion which would be an intermediate in the reaction of **1** with aldimines[9] would not become stabilized in this way.

Experimental

The melting points and boiling points were uncorrected. The IR spectra were recorded on a Hitachi Model 260-10 spectrophotometer, and the ^{1}H-NMR spectra with a JEOL SNM-FX 100 spectrometer for solutions in $CDCl_3$. The chemical shift are reported in δ (internal TMS). The mass spectra were recorded with a Hitachi RMU-7M double-focusing mass spectrometer at 70 eV. The analytical GLC determination was carried out with a Shimadzu GC-4CPF apparatus equipped with a 10% Silicone GE SE-30 column (4 mm × 2 m) and operated in programmed-temperature mode (80→200 °C, 8 °C/min).

Materials. 2-(Trimethylsilylmethyl)pyridine **1** was prepared by a method reported previously.[1]

Preparation of 2-Phenacylpyridine **3**. A method has been reported in Ref. 1.

Quenching the Reaction of **1** *with* **2**. The reaction was performed in the same way as the preparation of **3**, and the reaction mixture was quenched by the following three methods, before being analyzed by means of IR, GLC, and ^{1}H-NMR (without purification, except for method A). The results are summarized in Table 1.

Method A: A solution of butyllithium (8.6 g, 0.02 mol) in hexane was added to a solution of diisopropylamine (2.0 g, 0.02 mol) in THF (54 ml) at −75 °C with stirring under nitrogen. To the solution, 0.02 mol of **1** was added slowly and stirred for an additional 10 min. The mixture was treated with a THF solution of **2** (0.02 mol), and stirred for 1 h at −75 °C and for 2 h at room temperature. The reaction mixture was quenched with 50 ml of water at 0 °C. The crude product thus obtained was distilled under reduced pressure. Yield, 74% (the mixture of (*E*)-1-phenyl-2-(2-pyridyl)-1-(trimethylsilylamino)ethene **4** and the *Z*-isomer **5**, **4** : **5** = 10 : 80 by GLC and 43 : 57 by ^{1}H-NMR), bp 125.2—130 °C/1.0 mmHg (1 mmHg≈133.322 Pa). An attempt to separate **5** from **4** by column chromatography on Al_2O_3 (neutral) resulted in failure because of hydrolysis of **4** and **5** during the operation. IR (neat) 3470 (ν_{NH}), 1630 ($\nu_{C=C}$ of **4**), 1620 ($\nu_{C=C}$ of **5**), 1253 (δ_{SiCH_3}), and 930 (ν_{Si-N}) cm^{-1}; MS (70 eV) *m/z* (rel intensity) 270 (M+2, 1.0), 269 (M+1, 4.1), 268 (M$^+$, 14.9), 267 (M−1, 8.2), 256 (1.0), 255 (6.2), 254 (24.0), 253 (M−CH_3, 100), 197 (2.3), 196 (15.9), 195 (M−Si$(CH_3)_3$, 35.1), 150 (9.7), 132 (8.4), and 73 (28.1); ^{1}H-NMR δ 0.04 (5.14H, s, Si$(CH_3)_3$ of **5**), 0.12 (3.86H, s, Si$(CH_3)_3$ of **4**), 5.23 (0.57H, s, CH= of **5**), 5.46 (0.43H, s, CH= of **4**), 6.6—8.35 (9H, ABCX system for 2-Py-H and m for Ph-H), 7.85 (0.43H, b, NH of **4**) and 9.62 (0.57H, b, NH of **5**). Found: C, 72.32; H, 7.50; N, 10.45%; *m/z* 268.1385. Calcd for $C_{16}H_{20}N_2Si$: C, 71.59; H, 7.51; N, 10.44%; M$^+$, *m/z* 268.1393.

Method B: The reaction was performed on a smaller scale than in method A (**1**, 3 mmol). After stirring for 5 min at −75 °C, the reaction mixture was quenched with aq THF (H_2O : THF = 1 : 2 v/v, 10 ml) at −75 °C. The crude product contained the unreacted **1** and **2**. IR (neat) 1632 ($\nu_{C=C}$ of **4**), 1620 ($\nu_{C=C}$ of **5**), 1255 (δ_{SiCH_3}), and 930 (ν_{Si-N}) cm^{-1}; ^{1}H-NMR δ 0.14 (s, Si$(CH_3)_3$ of **4**), 5.21 (s, CH= of **5**), and 5.43 (s, CH= of **4**), 6.6—8.4 (ABCX system for 2-Py-H and m for Ph-H), 7.8 (b, NH of **4**), and 9.6 (b, NH of **5**).

Method C: The reaction was performed on the same scale as in method B. After stirring for 30 min at −75 °C, the reaction mixture was quenched with 2 ml of glacial acetic acid in THF (7 ml) and stirred for 1 h at −75 °C. The resultant white precipitate (CH_3COOLi) was removed by filtration under nitrogen atmosphere. The filtrate was concentrated, and excess acetic acid and volatile products were removed under reduced pressure below 40 °C. All these operations were performed under nitrogen atmosphere to prevent the product from undergoing acidic hydrolysis. The residue was washed with 2 M NaOH to remove any trace of acetic acid (it was found that the product **4** did not change during the washing). IR (neat) 1635 ($\nu_{C=C}$ of **4**), 1240 (δ_{SiCH_3}), and 930 (ν_{Si-N}) cm^{-1}; ^{1}H-NMR δ 0.11 (s, Si$(CH_3)_3$ of **4**) and 5.48 (s, CH= of **4**), 6.6—8.4 (ABCX system for 2-Py-H and singlet-like Ph-H), and 7.9 (b, NH of **4**).

Acidic Hydrolysis of **4** *and* **5**. The mixture of **4** and **5** (167 mg) was dissolved in ether (30 ml), and shaken with 2 M HCl (13 ml) for 10 min at room temperature. After washing with ether, the aq. phase was made alkaline (pH 13) with Na_2CO_3, and completely extracted with ether. Both the enamines **4** and **5** were quantitatively converted to **3**.

The present work was partially supported by a Grant-in-Aid for Scientific Research (No. 56750604) from the Ministry of Education, Science and Culture and by the Saneyoshi Foundation.

References

1) Preliminary report: T. Konakahara and Y. Takagi, *Heterocycles*, **14**, 393 (1980).

2) For reviews: M. S. Kharasch and O. Reinmuth, "Grignard Reactions of Non-Metallic Substances," Prentice-Hall, New York (1954), Chap. 10; F. C. Schaffer, "The Chemistry of the Cyano Group," ed by Z. Rappoport and S. Patai, Interscience Pub., p. 276.

3) W. B. Edwards, III, *J. Heterocycl. Chem.*, **12**, 413 (1975); J.-M. Vierfond, Y. Mittery, L. Mascrier-Demagny, and M. Miocqe, *Tetrahedron Lett.*, **22**, 1219 (1981).

4) a) D. J. Peterson, *J. Org. Chem.*, **33**, 780 (1968); b) K. Shimoji, H. Taguchi, K. Ojima, H. Yamamoto, and H. Nozaki, *J. Am. Chem. Soc.*, **96**, 1620(1974); c) T. Konakahara and Y. Takagi, *Synthesis*, **1979**, 192, and references cited therein.

5) A difference between the ratio of **4** : **5** by GLC and that by ^{1}H-NMR is explained on the basis of a thermal *cis-trans* isomerization of **4** to **5** by imine–enamine tautomerization during the GLC operation.

6) K. S. Mazdiyasni and C. M. Cooke, *J. Am. Chem. Soc.*, **56**, 628 (1973).

7) A trimethylsilyl group has a stronger affinity for N than for C and easily transfers from C to N (for example, K. Itoh, N. Kato, and Y. Ishii, *J. Organomet. Chem.*, **22**, 49 (1970)).

8) *s*-Enamines derived from metalated imines by *N*-protonation have been reported to be metastable and to rearrange to the starting imines (R. Knorr and P. Low, *J. Am. Chem. Soc.*, **102**, 3241 (1980)).

9) T. Konakahara and Y. Takagi, *Tetrahedron Lett.*, **21**, 2073 (1980).

Selective Oxidation of Sulfides to Sulfoxides by a Polymeric Reagent Electrochemically Generated and Recycled *in Situ*

Jun-ichi Yoshida, Hiroshi Sofuku, and Nariyoshi Kawabata*

Department of Chemistry, Faculty of Polytechnic Science, Kyoto Institute of Technology, Matsugasaki, Sakyo-ku, Kyoto 606

(Received August 11, 1982)

Synopsis. A polymeric reagent electrochemically generated from crosslinked poly(4-vinylpyridine) hydrobromide was found to oxidize sulfides to give sulfoxides in high yields. The exhausted polymeric reagent was regenerated by continuous electrochemical oxidation *in situ*.

Recently we have reported a facile oxidation of alcohols by a polymeric reagent electrochemically generated from crosslinked poly(4-vinylpyridine) hydrobromide (PVP·HBr).[1,2] Since the exhausted polymeric reagent is regenerated by continuous electrochemical oxidation in situ, the method does not consume any chemical oxidant and does not produce any contaminating reduced product. Based on this methodology, we have begun a program to study the selective oxidation of a variety of functional groups. In this note, we wish to report that the polymeric reagent electrochemically generated from PVP·HBr acts as an effective reagent for the selective oxidation of sulfides to sulfoxides.

$$RSR' + H_2O \xrightarrow[PVP\cdot HBr/CH_3CN]{\text{electric current}} R\overset{O}{\overset{\|}{S}}R' + H_2 \quad (1)$$

In the case of alcohol oxidation, the substrate undergoes a net oxidative dehydrogenation (Eq. 2). The present reaction of sulfides provides another application of the method in which water acts as the primary oxidant in the net sense (Eq. 3).

$$(\text{substrate})H_2 \xrightarrow[PVP\cdot HBr]{\text{electric current}} (\text{substrte}) + H_2 \quad (2)$$

$$(\text{substrate}) + H_2O \xrightarrow[PVP\cdot HBr]{\text{electric current}} (\text{substrate})O + H_2 \quad (3)$$

The sulfide oxidation reaction can be carried out by either the ex-cell method or the in-cell method. In the case of the ex-cell method, the polymeric oxidizing reagent was prepared by passing the electric current (4.5 mF) through PVP·HBr beads (3.00 wet g, containing 5.10 mmol of HBr) in acetonitrile as reported previously.[1] The polymeric reagent was separated by filtration and allowed to react with dibutyl sulfide (2.30 mmol) in acetonitrile at room temperature to afford dibutyl sulfoxide (0.64 mmol).

The in-cell method is more convenient. The electric current was passed through a mixture of a catalytic amount of PVP·HBr, (3.00 wet g) containing 4.94 mmol of HBr, dibutyl sulfide (20.0 mmol) and acetonitrile (3.0 ml) in an undivided cell at 30 °C. After 2.4 F/mol of electricity (based on the sulfide) was passed, GLC analysis of the reaction mixture showed the formation of dibutyl sulfoxide in a quantitative yield. During the course of the reaction hydrogen gas evolved in a quantitative yield, indiacting that water acts as a primary oxidant. The result indicates the efficient electrochemical regeneration of the exhausted polymeric reagent *in situ*. After removal of the resin beads by filtration, the product was isolated by bulb-to-bulb distillation (95% yield). The oxidation of other sulfides also proceeded smoothly under the similar conditions to provide the corresponding sulfoxides in good to excellent yields as

Table 1. Oxidation of sulfides by a polymeric reagent electrochemically generated and recycled *in situ*[a]

Sulfide	Sulfide/Br$^-$ [b]	Electricity F/mol [c]	Product	Yield[d] %
n-$C_4H_9SC_4H_9$-n	4.38	2.24	n-$C_4H_9S(O)C_4H_9$-n	95
	4.04	2.40		(100)
		2.38		(100)[e]
		2.40		(100)[f]
	5.17[g]	2.40		(83)[h]
n-$C_8H_{17}SCH_3$	4.08	2.02	n-$C_8H_{17}S(O)CH_3$	72
	4.27	2.40		(78)
	3.63	2.04		83
	4.27	2.40		(95)
$PhSCH_3$	4.07	2.40	$PhS(O)CH_3$	86
	4.14	2.20		(96)

a) Reactions were carried out with 20.0 mmol of sulfides and 3.00 wet g of PVP·HBr beads in 3.0 ml of acetonitrile at 30°C. b) The molar ratio of sulfide to the bromide ion contained in PVP·HBr. c) Based on the sulfide. d) Isolated yield, based on the sulfide. Yields determined by GLC analysis are given in parentheses. e) The second use of the resin. f) The third use of the resin. g) PVP·HCl was used instead of PVP·HBr. h) Significant amount of dibutyl sulfone was produced as a by-product.

shown in Table 1.

The resin beads are reusable in the electrochemical oxidation. In this case the resin beads were separated from the reaction mixture by filtration, washed with organic solvents, soaked in water, filtered to remove excess water, and used for the electrochemical oxidation of sulfide. The activity of the resin beads did not decrease after the second use.

It is noteworthy that when crosslinked poly(4-vinylpyridine) hydrochloride (PVP·HCl) was used instead of PVP·HBr, the yield of the sulfoxide was lower and significant amount of the sulfone was produced. Thus, the polymeric reagent electrochemically generated from PVP·HCl has higher oxidizing ability than that from PVP·HBr. This is probably due to the higher oxidation potential of the chloride ion than that of the bromide ion.

Although there are several known procedures for the selective oxidation of sulfides to sulfoxides[3] involving either supported reagents[4] or electrochemical methods,[5] the present method is a useful alternative to the conventional methods due to the following features and advantages. (1) The reaction is highly selective and sulfides essentially free from sulfone are obtained in high yields. (2) The procedure is quite simple and the product can be isolated by filtration followed by simple distillation. (3) The resin beads are reusable. (4) Only the electricity and water are consumed during the reaction.

The mechanism of this reaction will be discussed elsewhere.

Experimental

General. A Trio Model PR-653 regulated DC power supply or Kikusui Model PAB-32-0.5 regulated DC power supply was used as a source of electric current. ^{1}H NMR spectra were recorded on a Varian T-60A spectrometer in carbon tetrachloride using tetramethylsilane as an internal standard. IR spectra were recorded on a Hitachi Model 215 grating spectrophotometer. GLC analysis were performed on a Shimadzu GC-4B or GC-4C gas chromatograph.

Materials. Crosslinked poly(4-vinylpyridine) hydrobromide (PVP·HBr) and crosslinked poly(4-vinylpyridine) hydrochloride (PVP·HCl) were prepared as reported previously.[1] Other chemicals were used as obtained commercially.

Electrochemical Oxidation of Sulfides. The reactions were carried out in an undivided cell equipped with two platinum electrodes ($10\times10\times0.5$ mm^3) parallel to each other with about 10 mm of space between them. A sulfide (20 mmol) and PVP·HBr (3.0 g, wet) were allowed to react in 3.0 ml of acetonitrile with a constant electric current (50 mA) at 30 °C under slow stirring. The crude reaction mixture was analyzed by GLC. The mixture was filtered and the filtrate was dried over Na_2SO_4. After evaporation of the solvent, bulb-to-bulb distillation of the residue yielded the products, which were identified by comparison of their IR and ^{1}H NMR spectra with those of authentic materials.

We thank Koei Chemical Co., Ltd, for gifts of 4-vinylpyridine and divinylbenzene. We are also grateful to the Ministry of Education, Science and Culture for a Grant-in-Aid for Scientific Research No. 56750598 for partial support of this work.

References

1) J. Yoshida, R. Nakai, and N. Kawabata, *J. Org. Chem.*, **45**, 5269 (1980).

2) Indirect electrochemical oxidation reactions using the bromide ion as mediator have been reported. For example, T. Shono, Y. Matsumura, S. Yamane, and S. Kashimura, *Chem. Lett.*, **1982**, 565; S. Torii, K. Uneyama, H. Tanaka, T. Yamanaka, T. Yasuda, M. Ono, and Y. Kohmoto, *J. Org. Chem.*, **46**, 3312 (1981); S. Torii, K. Uneyama, M. Ono, H. Tazawa, and S. Matsunami, *Tetrahedron Lett.*, **1979**, 4661.

3) S. R. Sandler and W. Karo, "Organic Functional Group Preparation," Academic Press (1968), Chap. 19.

4) K. T. Liu and Y-C. Tong, *J. Org. Chem.*, **43**, 2717 (1978).

5) P. T. Cottrell and C. K. Mann, *J. Electrochem. Soc.*, **116**, 1499 (1969); K. Uneyama and S. Torii, *Tetrahedron Lett.*, **1971**, 329; B. E. Firth and L. L. Miller, *J. Am. Chem. Soc.*, **98**, 8272 (1976).

Cyclic Peptides. XV. Synthesis of [4-α-Hydroxyalanine]AM-toxin II

Kosaku NODA,* Junko NAKASHIMA, Sannamu LEE,† and Nobuo IZUMIYA†
Laboratory of Biochemistry, Fukuoka Women's University, Kasumigaoka, Higashi-ku, Fukuoka 813
†*Laboratory of Biochemistry, Faculty of Science, Kyushu University, 33, Hakozaki, Higashi-ku, Fukuoka 812*
(Received August 12, 1982)

Synopsis. An AM-toxin II analog, *cyclo*(–L-Ala[1]–L-Hmb[2]–L-App[3]–Hyala[4]–), with an α-hydroxyalanine (Hyala) residue in place of dehydroalanine in position 4 was synthesized from pyruvoyl–L-Ala–L-Hmb–L-App–amide (Hmb, 2-hydroxy-3-methylbutanoic acid; App, 2-amino-5-phenylpentanoic acid) by intramolecular condensation between the pyruvoyl and carbamoyl groups. The synthetic peptide did not show the toxic activity of AM-toxin II.

The cyclotetradepsipeptide AM-toxins are phytotoxic metabolites of *Alternalia mali* causing necrosis on apple leaves. The structure of AM-toxin II[1] was shown to be *cyclo*(–L-Ala[1]–L-Hmb[2]–L-App[3]–ΔAla[4]–).[2] Previously, we attempted the synthesis of their analogs with L-Phe or L-Tyr residue replacing the uncommon aromatic amino acid in position 3 by the intramolecular condensation of pyruvoyl–L-Ala–L-Hmb–L-Phe–NH_2 (**1b**) or –L-Tyr–NH_2 (**1c**).[3] The product was, however, identified to be cyclotetrapeptide **2b** or **2c** containing a Hyala residue instead of ΔAla expected (Fig. 1), and did not show the activity of AM-toxins. The inactivity of **2b** or **2c** is not attributed to the replacement of ΔAla by Hyala, because [L-Phe[3]]AM-toxin[4] and [L-Tyr-(Me)[3]]AM-toxin[5] were also almost inactive.

In order to examine the influence of substitution of ΔAla by Hyala in position 4 on the activity, we have synthesized [Hyala[4]]AM-toxin II (**2a**). The Hyala residue was expected to contribute toward the toxic activity, because it might be a possible precursor of

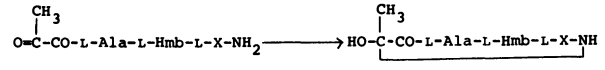

1a, X=App **2a**, X=App
1b, X=Phe **2b**, X=Phe
1c, X=Tyr **2c**, X=Tyr

Fig. 1. Intramolecular condensation of pyruvoyl-tripeptide amides.

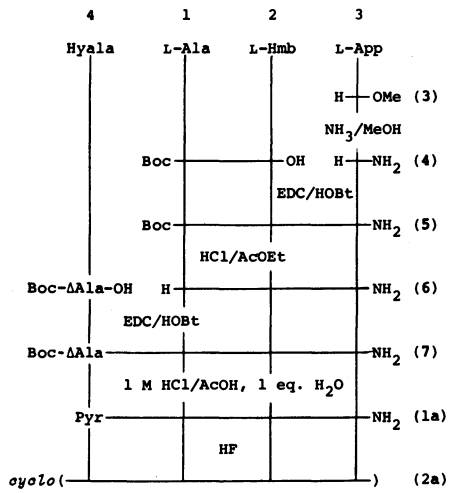

Fig. 2. Synthetic route for [Hyala[4]]AM-toxin II (**1a**).

ΔAla, and an AM-toxin I analog with L-Ser[4], the structural isomer of Hyala, possessed a recognizable activity.[6]

Figure 2 shows the reaction route for the synthesis. The tripeptide, Boc–L-Ala–L-Hmb–L-App–NH_2 (**5**), was prepared by coupling of Boc–L-Ala–L-Hmb–OH and L-App amide (**4**) by the EDC method.[7] Removal of the Boc group of **5** followed by coupling with Boc–ΔAla–OH afforded tetrapeptide amide **7**, which was converted to pyruvoyl-tripeptide amide **1a** by the treatment with HCl in AcOH in the presence of an equivalent amount of water. Treatment of **1a** with HF cyclized the peptide intramolecularly with the formation of Hyala residue to give the desired peptide **2a**. Dimer and polymer formation was not observed in this reaction. After purification by chromatography with silicic acid, the homogeneity and identity of the product were established by thin-layer chromatography, mass spectroscopy and ^{1}H-NMR spectroscopy. The singlet peak assingned for the α-OH of Hyala residue in the NMR data suggests that the Hyala is of a single optical configuration of either L or D.

Bioassay showed that, even at high concentration, **2a** did not show the toxic activity for the induction of necrosis on apple leaves. Thus, replacement of the ΔAla residue by Hyala eliminated the biological activity. The possible conversion of serine residue to ΔAla in the biological system was suggested from the previous results that [L-Ala[4]]AM-toxin I was inactive[4] while [L-Ser[4]]analog was active.[6] The present data indicates that there is no possibility of such a conversion of the Hyala residue to ΔAla in the biological system. The chemical conversion of the Hyala residue to ΔAla is under investigation.

Experimental

Thin layer chromatography was carried out on silica gel G (Merck) with the following solvent systems: R_f^1, $CHCl_3$–MeOH (9 : 1); R_f^2, $CHCl_3$–MeOH–AcOH (85 : 10 : 5); R_f^3, *n*-BuOH–AcOH– pyridine–H_2O (4 : 1 : 1 : 2). Optical rotations were measured with a Union polarimeter PM-201, Mass spectra were taken on a Hitachi RMS-4 mass spectrometer and NMR spectra on a JEOL LNM PS-100 spectrometer.

H–L-App–OMe·HCl (3·HCl). This compound was obtained by the treatment of H–L-App–OH[8] with MeOH and $SOCl_2$ according to the procedure described in the literature;[9] yield, 96%; mp 115 °C;$[\alpha]_D^{25}$ +21.5° (*c* 2, EtOH); R_f^1 0.23; R_f^2 0.54.

Found: C, 59.08; H, 7.39; N, 5.83%. Calcd for $C_{12}H_{18}N_2O_2Cl$: C, 59.13; H, 7.44; N, 5.75%.

H–L-App–NH_2·HCl (4·HCl). This compound was prepared from **3**·HCl by the treatment with saturated NH_3 in MeOH according to the literature;[10] yield, 82%; mp 200 °C; $[\alpha]_D^{25}$ +17.0° (*c* 1, EtOH); R_f^2 0.05; R_f^3 0.67.

Found: C, 57.70; H, 7.55; N, 12.28%. Calcd for $C_{11}H_{17}N_2OCl$: C, 57.76; H, 7.49; N, 12.25%.

Boc-L-Ala-L-Hmb-L-App-NH_2 (5). Boc-L-Ala-L-Hmb-OH[6] (1.45 g, 5 mmol), **4·HCl** (1.14 g, 5 mmol), HOBt (1.35 g, 10 mmol) and NEt_3 (0.70 ml, 5 mmol) was dissolved in DMF (10 ml). To the solution, EDC·HCl (1.15 g, 6 mmol) was added at 0 °C. The mixture was stirred for 1 h at 0 °C and overnight at room temperature, and evaporated *in vacuo*. The residue was treated with a mixture of water and AcOEt. The organic layer was washed with 4% $NaHCO_3$ and 10% citric acid, dried (Na_2SO_4), and evaporated. The product was recrystallized from AcOEt–ether–petroleum ether; yield, 1.67 g (72%); mp 94—95 °C; $[\alpha]_D^{25}$ −40.0° (*c* 1, EtOH); R_f^1 0.40; R_f^2 0.63.

Found: C, 62.33; H, 8.16; N, 9.17%. Calcd for $C_{24}H_{37}N_3O_6$: C, 62.18; H, 8.05; N, 9.07%.

Boc-ΔAla-L-Ala-L-Hmb-L-App-NH_2 (7). Compound **5** (963 mg, 2.1 mmol) was treated with 2 M HCl in AcOEt (25 ml) for 1 h at room temperature, and the mixture was concentrated *in vacuo*, the concentration being repeated twice after addition of AcOEt. The solid residue was washed with ether by means of decantation, and dried in a desiccator. The hydrochloride of H-L-Ala-L-Hmb-L-App-NH_2 (**6·HCl**) was obtained as a powder. To the solution of **6·HCl**, Boc-ΔAla-OH[3] (374 mg, 2 mmol), HOBt (338 mg, 2.5 mmol) and NEt_3 (0.28 ml, 2 mmol) in DMF (10 ml) was added EDC·HCl (383 mg, 2 mmol). The mixture was stirred for 1 h at 0 °C and overnight at room temperature, and evaporated. The residue was treated with a mixture of 20% NaCl and AcOEt. The organic layer was washed with 4% $NaHCO_3$ and saturated NaCl, dried (Na_2SO_4), and evaporated. The product was recrystallized from MeOH–ether–petroleum ether; yield, 643 mg (60%); mp 95—97 °C; $[\alpha]_D^{25}$ −21.0° (*c* 1, EtOH); R_f^1 0.41; R_f^2 0.64.

Found: C, 60.68; H, 7.62; N, 10.47%. Calcd for $C_{27}H_{40}N_4O_7$: C, 60.88; H, 7.57; N, 10.52%.

Pyr-L-Ala-L-Hmb-L-App-NH_2 (1a). Compound **7** (533 mg, 1 mmol) was dissolved in 1 M HCl in AcOH (5 ml) containing an equivalent of water (18 μl). After being kept for 10 min at 60 °C, the solution was evaporated. The residual solid was collected with the aid of ether; yield, 422 mg (96%). This compound was used in the cyclization reaction without further purification.

cyclo(-L-Ala-L-Hmb-L-App-Hyala-) (2a). A solution of **1a** (217 mg, 0.5 mmol) in anhydrous HF (5 ml) was stirred for 1 h at 0 °C. After HF was evaporated, the residual solid was dissolved in $CHCl_3$ and the solution chromatographed on silicic acid (Mallinckrodt, 100 mesh) using a column (1.2 cm × 10 cm) and a solvent system of $CHCl_3$–AcOEt (1 : 1). The main fractions (6—16 ml) were collected and evaporated. The residue was collected with the aid of ether; yield, 160 mg (74%); mp 124—126 °C; $[\alpha]_D^{25}$ −44.0° (*c* 1, DMF); R_f^1 0.39; R_f^2 0.47. NMR (signals arising only from Hyala residue are given) (DMSO-d_6) δ=2.38 (3H, s, HyalaCH$_3$), 7.04 (1H, s, HyalaOH), 7.35 (1H, s, HyalaNH).

Found: C, 60.77; H, 7.31; N, 9.63%; *m/e* 433. Calcd for $C_{22}H_{31}N_3O_6$: C, 60.95; H, 7.21; N, 9.69; M^+, 433.

Biological Assay. Biological assays on apple leaves (susceptible cultivar, Indo) were carried out as described previously.[6] Product **2a** did not show the toxicity at concentration up to 100 μg/ml, whereas synthetic or natural AM-toxin II showed at 0.02 μg/ml.

References

1) T. Ueno, T. Nakashima, Y. Hayashi, and H. Fukami, *Agric. Biol. Chem.*, **39**, 2081 (1975).

2) Abbreviations given by the IUPAC-IUB Commission, *J. Biol. Chem.*, **247**, 977 (1972), have been used throughout. Additional abbreviations: ΔAla, dehydroalanine; App, 2-amino-5-phenylpentanoic acid; EDC, 1-ethyl-3-(3-dimethylaminopropyl)carbodiimide; Hmb, 2-hydroxy-3-methylbutanoic acid; HOBt, 1-hydroxybenzotriazole; Hyala, α-hydroxyalanine; Pyr, pyruvoyl; Tyr(Me), *O*-methyltyrosine.

3) K. Noda, Y. Shibata, E. Gross, Y. Shimohigashi, and N. Izumiya, *Int. J. Pept. Protein Res.*, **18**, 423 (1981).

4) Y. Shimohigashi, S. Lee, T. Kato, and N. Izumiya, *Bull. Chem. Soc. Jpn.*, **51**, 584 (1978).

5) Y. Shimohigashi, S. Lee, H. Aoyagi, T. Kato, and N. Izumiya, *Int. J. Pept. Protein Res.*, **10**, 197 (1977).

6) Y. Shimohigashi, S. Lee, H. Aoyagi, T. Kato, and N. Izumiya, *Int. J. Pept. Protein Res.*, **10**, 232 (1977).

7) J. C. Sheehan, J. Preston, and P. A. Cruickshank, *J. Am. Chem. Soc.*, **87**, 2492 (1965).

8) Y. Shimohigashi, S. Lee, and N. Izumiya, *Bull. Chem. Soc. Jpn.*, **49**, 3280 (1976).

9) M. Brenner and W. Huber, *Helv. Chim. Acta*, **36**, 1109 (1953).

10) J. P. Greenstein and M. Winitz, "Chemistry of the Amino Acids," John Wiley and Sons, Inc., New York (1961), Vol. 2, p. 1188.

The Synthesis of Cyclohepta[4,5]pyrrolo[2,3-*d*] thiazoles

Kunihide FUJIMORI,* Nobuhiro HIRAKO, and Kameji YAMANE*
Department of Chemistry, Faculty of Science, Shinshu University, Asahi, Matsumoto 390
(Received August 20, 1982)

Synopsis. Cyclohepta[4,5]pyrrolo[2,3-*d*]thiazole and its amino derivatives were obtained in a few steps by starting with 2-amino-1-azaazulene.

1-Azaazulenes(cyclohepta[*b*]pyrroles) are important and interesting compounds not only as non-benzenoid analogues of indoles and isomers of quinolines, but also as azulenoid heterocyclic compounds. Several azulenoid heterocyclic compounds which consist of the 1-aza-azulene ring condensed with heterocyclic aromatics are known.[1] In a previous paper,[2] the preparation of cyclohepta[*b*]thieno[3,2-*d*]pyrrole was reported.

We now wish to report the synthesis of cyclohept[4,5]-pyrrolo[2,3-*d*]thiazole and its amino derivatives. 2-Amino-1-azaazulene (**1**),[3] on treatment with thiocyanogen bromide prepared by adding bromine to a solution of potassium thiocyanate in acetic acid and filtering off the potassium bromide, gave 2-amino-3-thiocyanato-1-azaazulene (**2**). When this compound (**2**) was cyclized by the action of acetic anhydride at the boiling point, 2-acetylaminocyclohepta[4,5]pyrrolo[2,3-*d*]thiazole (**3**) was obtained in a 78% yield. Compound (**3**), when boiled with dilute hydrochloric acid, was converted to 2-aminocyclohepta[4,5]pyrrolo[2,3-*d*]thiazole (**4**). On treatment with acetic anhydride, **4** afforded **3**. On the other hand, in the case of the treatment of **2** with concentrated hydrochloric acid in ethanol, disulfide (**5**) was obtained in an 84% yield. The structure of **5** was established on the basis of the spectral data and the results of elemental analysis (see Experimental). The mass spectrum of **5** is similar to that of 2-amino-1-azaazulene (**1**) in its fragmentation pattern below *m/e* 144. Compound **4** was diazotized with a concentrated aqueous sodium nitrite solution in 85% phosphoric acid, followed by treatment with phosphinic acid to give cyclohepta[4,5]pyrrolo[2,3-*d*]thiazole (**6**) as reddish purple prisms in a 41% yield.

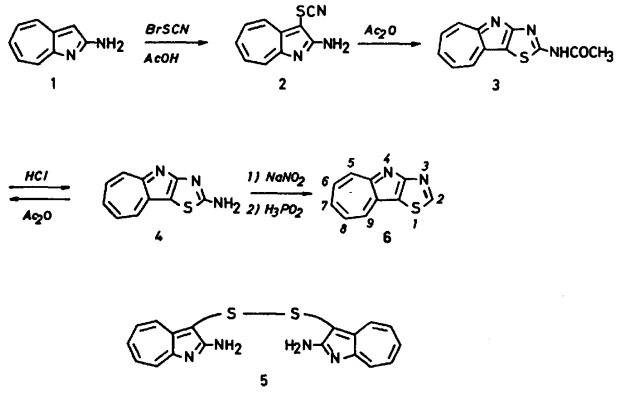

1 2 3 4 6 5

Experimental

All the melting points are uncorrected.

2-Amino-1-azaazulene (1). A solution of 2-chloro-1-azaazulene (6.18 g) in dry ethanol (130 ml) was saturated with ammonia and heated at 170 °C in a sealed tube for 64 h. After cooling, the reaction mixture was concentrated, diluted with water, neutralized with a 10% sodium hydroxide solution, and extracted with chloroform. The extract was dried, the solvent was removed, and the residue was chromatographed on a silica-gel column. From the methanol effluent, **1** was obtained as golden leaves (4.08 g, 75%); mp 177—178 °C (lit. 3 mp 171—172 °C); ^{1}H NMR (100 MHz, in $CDCl_3$) δ=5.54 (2H, bs, NH_2), 6.54 (1H, s, H-3), 7.29—7.74 (3H, m, H-5,6,7), and 7.88—8.12 (2H, m, H-4,8); MS *m/e* 144 (M^+), 117, 89, and 58.5. (Found: C, 75.25; H, 5.72; N, 19.42%).

2-Amino-3-thiocyanato-1-azaazulene (2). To a stirred solution of **1** (1.00 g) in acetic acid (25 ml), thiocyanogen bromide prepared from potassium thiocyanate (1.01 g) and bromine (1.45 g) in acetic acid (35 ml) was added, drop by drop. After stirring for 2.5 h, the reaction mixture was diluted with water and neutralized with a sodium carbonate solution. The resulting precipitate was filtered off and recrystallized from ethanol to give **2** as yellow prisms (1.17 g, 84%); mp 164 °C (decomp); IR (KBr) 3464, 3304, 2162, 1644, 1513, and 1500 cm^{-1}; UV(CH_3OH) 213 (log ε 4.19), 239 (4.07), 285 (4.54), 361 (3.86), and 426 nm (3.58). Found: C, 59.78; H, 3.41; N, 21.07; S, 16.05%. Calcd for $C_{10}H_7N_3S$: C, 59.68; H, 3.51; N, 20.88; S, 15.93%.

*2-Acetylaminocyclohepta[4,5]pyrrolo[2,3-*d*]thiazole (3).* *(a)*: A mixture of **2** (400 mg) and acetic anhydride (2.50 g) was refluxed for 3 h. After cooling, the reaction mixture was poured into water and neutralized with a sodium hydrogencarbonate solution. The resulting precipitate was filtered off, dried, and recrystallized from *N,N*-dimethylformamide to give **3** as purple micro needles (380 mg, 78%); mp 285 °C (decomp); IR (KBr) 3304, 3157, 2912, 1695, 1515, and 1501 cm^{-1}; UV (CH_3OH) 217 (log ε 3.78), 244 (3.64), 303 (4.36), 325 (4.16), 352 (3.60), and 368 nm (3.63). Found: C, 59.48; H, 3.74; N, 17.52; S, 13.26%; M^+, 243. Calcd for $C_{12}H_9ON_3S$: C, 59.24; H, 3.73; N, 17.27; S, 13.18%; M, 243.

(b): A mixture of **4** (100 mg) and acetic anhydride (1.0 ml) was refluxed for 30 min. The reaction mixture was then treated by a method similar to that used for (*a*). Recrystallization from *N,N*-dimethylformamide yielded purple micro needles (80 mg, 66%) of **3** (mp 285 °C), which was identified by a mixed-melting-point determination and by a comparison of its infrared spectrum with that of the sample prepared by means of Method (*a*).

*2-Aminocyclohepta[4,5]pyrrolo[2,3-*d*]thiazole (4).* A mixture of **3** (280 mg) and 6 mol dm^{-3} hydrochloric acid (14 ml) in ethanol was heated at 110 °C for 3 h. After the removal of the solvent, water (50 ml) was added to the residue. When the solution was made slightly basic with a 10% sodium hydroxide aqueous solution, a precipitate separated out. The precipitate was collected by filtration, washed with water, and recrystallized from ethanol to give purple prisms (220 mg, 93%); mp 231 °C (decomp); IR(KBr) 3389, 3272, 3059, 1498, 1469, 1428, and 1407 cm^{-1}; UV(CH_3OH) 216 (log ε 4.63), 237 (4.45), 298 (5.09), 327 (4.98), 361 (4.21), 378 (4.10), and 493 nm (3.85). Found: C, 59.45; H, 3.40; N, 20.73; S, 15.97%. Calcd for $C_{10}H_7N_3S$: C, 59.68; H, 3.51; N, 20.88; S, 15.94%.

2,2'-Diamino-3,3'-dithiodi(1-azaazulene) (5). To a suspension of **2** (260 mg) in ethanol (26 ml), concentrated hydro-

chloric acid (2.6 ml) was added, after which the mixture was refluxed for 10 h. The reaction mixture was evaporated *in vacuo*, and the residue was diluted with water. The solution was then neutralized with a sodium carbonate aqueous solution. The resulting precipitate was filtered off, dried, and recrystallized from *N,N*-dimethylformamide to give red micro needles (190 mg, 84%); mp 255 °C (decomp); IR(KBr) 3457, 3382, 3288, 1640, and 1500 cm^{-1}; UV(CH_3OH) 216 (log ε 4.48), 280 (4.75), and 426 nm (3.92); MS *m/e* 350 M^+, 175, 144, 117, 89, and 58.5. Found: C, 61.55; H, 4.04; N, 15.94; S, 18.16%. Calcd for $C_{18}H_{14}N_4S_2$: C, 61.69; H, 4.03; N, 15.99; S, 18.30%.

*Cyclohepta[4,5]pyrrolo[2,3-d]thiazole (**6**).* A solution of **4** (1.00 g) in 85% phosphoric acid was cooled to −10 °C, after which a concentrated aqueous solution of sodium nitrite (857 mg) was slowly stirred in below the surface at such a rate as to maintain the temperature below −5 °C. To the resulting solution, prechilled (0 °C) 50% phosphinic acid was vigorously stirred in, drop by drop. The reaction mixture was then allowed to warm to room temperature with continued stirring for 1 h and then diluted with water. The resulting solution was made alkaline by adding a potassium carbonate aqueous solution, and extracted with benzene. The benzene layer was dried over anhydrous sodium sulfate and evaporated under reduced pressure. The residue was chromatographed on a silica-gel column with benzene–ethyl acetate (3 : 7). The reddish purple effluent was freed from the solvent to give **6** (374 mg, 41%) as reddish purple prisms; mp 142.5—143.5 °C; IR(KBr) 3050, 1585, 1487, 1463, and 1435 cm^{-1}; UV(cyclohexane 252 (log ε 3.96), 296 (4.80), 312 (4.10), 343 (3.80), 359 (3.86), 525 (2.90), 546 (2.85), 563 (2.84), 588 (2.61), 608 nm (2.58); ^1H NMR (90 MHz, in $CDCl_3$) δ=7.6—8.0 (3H, m, H-6,7,8), 8.64 (1H, dm, J=8.8 Hz, H-9), 8.8—8.9 (1H, m, H-5), and 9.39 (1H, s, H-2); ^{13}C NMR (22.5 MHz, in $CDCl_3$) δ=179.6(C-3a), 163.2(C-2), 161.9(C-4a), 137.9(C-5), 137.7(C-9a), 137.5(C-7), 133.8(C-9), 130.1(C-6), 128.5(C-8), and 115.9(C-9b). Found: C, 64.44; H, 3.25; N, 15.13; S, 17.15%; M^+, 186. Calcd for $C_{10}H_6SN_2$: C, 64.49; H, 3.25; N, 15.05; S, 17.22%; M, 186.

The authors wish to express their thanks to Professor Yasuo Iwanami of Keio University and Dr. Takeshi Inagaki of the Nitto Chemical Industry Co., Ltd., for their measurements and analyses of the mass spectra. We are also grateful to the Sankyo Co., Ltd., for doing the elemental analyses.

This work was partially supported by a Grant-in-Aid for Scientific Research No. 00547021 from the Ministry of Education, Science and Culture.

References

1) A. Sato, Doctoral Thesis, Tohoku University, Sendai 1962; T. Nozoe, S. Seto, and T. Toda, *Bull. Chem. Soc. Jpn.* **41**, 208 (1968); There is a survey of azaazulenes: T. Nishiwaki and N. Abe, *Heterocycles*, **15**, 547 (1981).

2) K. Yamane, K. Fujimori, and T. Takeuchi, *Chem. Lett.*, **1981**, 293.

3) T. Nozoe, S. Seto, S. Matsumura, and T. Terasawa, *Chem. Ind.*, **1954**, 1357.

Preparation of Alkanesulfenamides by Selective Elimination of *t*-Butyl Group in *S*-Alkyl-*S*-*t*-butylsulfilimines

Tamotsu YAMAMOTO,* Masa-aki KAKIMOTO,† Takeshi MAEJIMA, and Makoto OKAWARA†

Department of Industrial Chemistry, Faculty of Engineering, Kanto Gakuin University, Mutsuura, Kanazawa-ku, Yokohama 236

†*Research Laboratory of Resources Utilization, Tokyo Institute of Technology, Nagatsuta-cho, Midori-ku, Yokohama 227*

(Received August 21, 1982)

Synopsis. *N*-Tosylalkanesulfenamides have been prepared *via* the reactions of alkyl halides with 2-methyl-2-propanethiolate followed by *S*-imination with chloramine T and the thermolysis. This method comprises the use of selective elimination of *t*-butyl group in *S*-alkyl-*S*-*t*-butylsulfilimines.

Sulfenamides are useful compounds as synthetic intermediates, sulfenating agents, and as industrial additives such as accelerators in rubber vulcanization, pesticides, fungicides, and radioprotective agents.

Up to the present various kinds of sulfenamides have been prepared. Among them, only a few examples of alkanesulfenamides[1] have been synthesized because of their instability and unavailability of the corresponding sulfenyl source.

On the other hand, the thermolysis of the sulfilimines which have one or more hydrogens at β-carbon has been known to give an effective, preparative route to olefins[2] and vinyl monomers.[3] Since the thermolysis gives arenesulfenamides in good yields at the same time, it seems to be an effective route to alkanesulfenamides. No active attempt to prepare labile alkanesulfenamides, however, has been made. Thus, to prepare alkanesulfenamides by the thermolysis under mild conditions, the use of *t*-butyl group being liable to eliminate as isobutylene has been undertaken.

For this purpose *S*-alkyl-*S*-*t*-butyl-*N*-tosylsulfilimines were prepared and thermolyzed as follows. First alkyl *t*-butyl sulfides were prepared by the reaction of alkyl halides (**1**) with 2-methyl-2-propanethiol in a phase transfer system. Subsequently sulfides (**2**) were allowed to react with chloramine T (CT) to give *S*-alkyl-*S*-*t*-butyl-*N*-tosylsulfilimines (**3**) in high yields. The structures of sulfilimines **3** were confirmed by IR and NMR spectra and elemental analyses. The results obtained are given in Table 1.

$$\underset{\mathbf{1}}{RX} + t\text{-BuSH} \xrightarrow{NaOH/H_2O\text{-}PTC} \underset{\mathbf{2}}{RS\text{-}t\text{-}Bu} \xrightarrow{CT} \underset{\mathbf{3}}{\overset{R}{\underset{t\text{-}Bu}{\diagdown}}\!\!>S{=}NTs}$$

The thermolysis of **3** was carried out in methanol (at 40 °C or 60 °C), benzene (under refluxing) or without solvent (at 10 °C above mp of **3**). The thermolysis in refluxing benzene gave the best result, affording *N*-tosylalkanesulfenamide (**4**) accompanied with *N*-tosyl-2-methyl-2-propanesulfenamide (**5**) in some cases.

$$\underset{\mathbf{3}}{\overset{R}{\underset{t\text{-}Bu}{\diagdown}}\!\!>S{=}NTs} \xrightarrow{\Delta} \underset{\mathbf{4}}{RS\text{-}NHTs} \text{ or (and) } \underset{\mathbf{5}}{t\text{-}BuS\text{-}NHTs}$$

Thus *S*-*t*-butyl-*S*-ethyl-*N*-tosylsulfilimine (**3a**) was thermolyzed in refluxing benzene for 4 h to give *N*-tosylethanesulfenamide (**4a**) quantitatively. Similarly the other sulfilimines, *S*-*t*-butyl-*S*-propyl-, *S*-butyl-*S*-*t*-butyl-, and *S*-*t*-butyl-*S*-hexyl-*N*-tosylsulfilimines (**3b**, **3c**, and **3d**), were thermolyzed to give the corresponding *N*-tosylalkanesulfenamides, *N*-tosyl-1-propane-, -2-butane-, and -1-hexanesulfenamides (**4b**, **4c**, and **4d**) in quantitative yields, respectively. These sulfenamides were almost pure as shown by their sharp mp's and spectral data without purification. These are so stable as to be stored in sealed bottles at room temperature or preferably at lower temperature in an ice box. With *S*-*t*-butyl-*S*-isopropyl-*N*-tosylsulfilimine (**3e**), two kinds of sulfenamides, *N*-tosyl-2-propane- and 2-methyl-2-propanesulfenamides (**4e** and **5**), were obtained as a mixture with the molar ratio (**4e** to **5**) of about 5, which was determined by NMR and mass spectroscopies. These results are given in Tables 2 and 3. As shown in Table 2, the selectivity of eliminating either *t*-butyl or alkyl group is remarkably exclusive for the former.

TABLE 1. THE RESULTS OF THE PREPARATION OF **3**

R	Mp θ_m/°C	Yield/%	IR $\tilde{\nu}$/cm^{-1} $\nu_{S=N}$	IR $\tilde{\nu}$/cm^{-1} ν_{SO_2}	NMR δ in $CDCl_3$	Found(Calcd)(%) C	H	N
a C_2H_5	108—109	78	960	1280 1130	1.10 (t, 3H) 1.28 (s, 9H) 2.40 (s, 3H) 2.72 (q, 2H) 7.24 (d, 2H) 7.80 (d, 2H)	54.03 (54.31)	7.31 (7.38)	4.81 (4.87)
b C_3H_7	83—84	79	970	1279 1134	0.89 (t, 3H) 1.28 (s, 9H) 1.1—1.8(m, 2H) 2.40 (s, 3H) 2.4—2.8(t, 2H) 7.20 (d, 2H) 7.72 (d, 2H)	55.53 (55.77)	7.90 (7.70)	4.82 (4.65)
c C_4H_9	102—103	77	969	1280 1132	0.76 (t, 3H) 1.28 (s, 9H) 1.1—2.0(m, 4H), 2.40 (s, 3H) 2.64 (m, 2H) 7.20 (d, 2H) 7.76 (d, 2H)	56.85 (57.09)	8.30 (8.00)	4.65 (4.44)
d C_6H_{13}	103—104	98	960	1280 1135	0.88 (t, 3H) 1.32 (s, 9H) 1.0—2.1 (m, 8H) 2.44 (s, 3H) 2.68 (m, 2H) 7.24 (d, 2H) 7.80 (d, 2H)	59.27 (59.42)	8.48 (8.52)	4.20 (4.08)
e *i*-C_3H_7	96—97	87	990	1283 1127	1.20 (d, 6H) 1.28 (s, 9H) 2.44 (s, 3H) 3.22 (m, 1H) 7.20 (d, 2H) 7.78 (d,2H)	55.68 (55.77)	8.00 (7.70)	4.55 (4.65)

Table 2. The results of thermolyses of 3's in refluxing benzene for 4 h

3 R-S(t-Bu)=NTs R	Mp θ_m/°C	4 Yield %	Mass (M^+) (m/e)	Composition(%) 4	5
a C_2H_5	64—65	≃100	231	≃100	≃0
b C_3H_7	59—60	≃100	245	≃100	≃0
c C_4H_9	38—38.5	≃100	259	≃100	≃0
d C_6H_{13}	34—35	≃100	287	≃100	≃0
e i-C_3H_7	79—80	83	245	83	17

Table 3. NMR spectra of 4

	NMR ($CDCl_3$) δ
4a	1.26 (t, 3H) 2.46 (s, 3H) 2.80 (q, 2H) 6.26 (s, 1H) 7.30 (d, 2H) 7.80 (d, 2H)
4b	0.97 (t, 3H) 1.4—2.2 (m, 2H) 2.45 (s, 3H) 2.72 (t, 2H) 6.27 (s, 1H) 7.37 (d, 2H) 7.90 (d, 2H)
4c	0.88 (t, 3H) 1.1—1.9 (m, 4H) 2.44 (s, 3H) 2.74 (t, 2H) 6.26 (s, 1H) 7.29 (d, 2H) 7.80 (d, 2H)
4d	0.88 (t, 3H) 1.0—1.8 (m, 8H) 2.44 (s, 3H) 2.72 (t, 2H) 6.20 (s, 1H) 7.26 (d, 2H) 7.78 (d, 2H)
4e	1.24 (d, 6H) 2.46 (s, 3H) 3.28 (m, 1H) 6.33 (s, 1H) 7.28 (d, 2H) 7.78 (d, 2H)

The procedure mentioned above may be an effective method, starting from alkyl halides, to prepare alkanesulfenamides *via* alkyl *t*-butyl sulfides and then sulfilimines, in good yields, and further a convenient route to other *N*-substituted alkanesulfenamides by the exchange reaction with amines.[4]

Experimental

Preparation of 3. *General Procedure*: To a stirring solution of chloramine T (11 mmol) in 30 ml of MeOH was added 10 mmol of **2**, which was prepared from the corresponding halide **1**, 2-methyl-2-propanethiol and NaOH in water containing tetrabutylammonium bromide (1%), keeping the temperature below 20 °C (0 °C for **3e**). After 3—4 h stirring the resulting mixture was evaporated to dryness *in vacuo*. The organic part in the residue obtained was dissolved in 30 ml of $CHCl_3$, and the solution was washed with water and dried over anhydrous Na_2SO_4. After the dried solution was evaporated to dryness *in vacuo*, the resulting viscous residue was triturated with ether until the white solid of **3** was deposited. Crude **3** was collected by filtration and purified by reprecipitation from CH_2Cl_2 and ether.

Thermolysis of 3. *General Procedure*: To 20 ml of dried benzene was added 2 mmol of **3**. The resulting mixture was heated under refluxing in a stream of nitrogen. After 4 h the solution obtained was evaporated to dryness under reduced pressure to give white solid of **4**. Sulfenamide **4** obtained in such a manner was almost pure without purification. For the purification of crude **4**, reprecipitation using dried ether and hexane was taken.

References

1) For example: N. E. Heiner and L. Field, *J. Org. Chem.*, **35**, 3012 (1970); F. A. Davis, A. J. Friedman, E. W. Kluger, E. B. Skibo, E. R. Fretz, A. P. Milica, and W. C. LeMasters, *ibid.*, **42**, 967 (1977).

2) S. Oae, K. Tsujihara, and N. Furukawa, *Tetrahedron Lett.*, **1970**, 2663.

3) T. Yamamoto and M. Okawara, *Chem. Lett.*, **1975**, 581.

4) T. Yamamoto, M. Imaura, and M. Okawara, *Kobunshi Ronbunshu*, **31**, 171 (1974).

A Convenient Synthesis of 2-Phenylbenzo[*b*]thiopyrylium Perchlorates

Hiroyuki NAKAZUMI,* Tamio UEYAMA, Takashi ENDO, and Teijiro KITAO
Department of Applied Chemistry, College of Engineering, University of Osaka Prefecture, Sakai, Osaka 591
(Received August 26, 1982)

Synopsis. 2-Phenylbenzo[*b*]thiopyrylium perchlorates were conveniently prepared in good yields by reduction of 2-phenyl-4*H*-benzo[*b*]thiopyran-4-ones (thioflavones) with aluminium hydride, followed by treatment with acid in the presence of 2,3-dichloro-5,6-dicyano-*p*-benzoquinone.

Flavonoid derivatives are well known to be pharmacologically active compounds. It has been reported that 2-phenylbenzo[*b*]pyrylium salts which are an important group of naturally occurring coloring matters, termed anthocyanins,[1] are significantly active in tumour-inhibiting tests.[2] 2-Phenylbenzo[*b*]thiopyrylium salts (**4a—d**) are the interesting thio analogs of anthocyanins, and a new group of pharmacologically active compounds. There are only a few known examples of synthesis of the title compounds.[3,4] For example, compound **4a** has been prepared in low yield by reduction of 2-phenylthiochroman-4-one (**3**) in a several stage process from benzenethiol.[3] In this paper, we report a convenient method for the preparation of the title compounds (**4a—d**) from 2-phenyl-4*H*-benzo-[*b*]thiopyran-4-ones (thioflavones) (**1a—d**) which can be easily prepared from benzenethiols and ethyl benzoylacetates.[5]

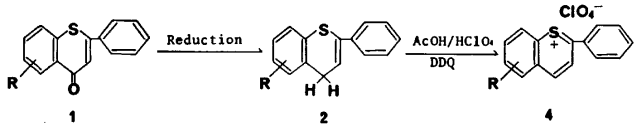

1 2 4

1a, 2a, 4a: R=H
1b, 2b, 4b: R=5-OCH_3
1c, 2c, 4c: R=6-OCH_3
1d, 2d, 4d: R=7-OCH_3 Scheme 1.

We investigated the reduction of **1a** with various reagents to prepare the title compound (**4a**). The results are summarized in Table 1. We now found that reduction of **1a** with $LiAlH_4$ and $AlCl_3$ (1/1) gave quantitatively 2-phenyl-4*H*-benzo[*b*]thiopyran **2a** which was identified by means of its NMR spectrum. The use of only $LiAlH_4$ gave compound **2a** in low yield together with other products as 2-phenylthiochroman-4-one **3** (entries 3—5, Table 1). When $NaBH_4$ is used, no reduction product was obtained (entry 6). From these results, it was shown that in the reduction of thioflavone (**1a**) with $LiAlH_4$–$AlCl_3$ a carbonyl group at the 4-position was not converted to a hydroxyl group, but to a methylene group.

Table 1. Reduction of **1** (R=H) at 25 °C

Entry	Reagent	Solvent	Reaction time/min	Yield of **2a**[a] %
1	$LiAlH_4/AlCl_3$(1/1)	THF	100	95
2	$LiAlH_4/AlCl_3$(1.5/1)	THF	100	57[b]
3	$LiAlH_4$	THF	100	2[c]
4	$LiAlH_4$	Et_2O	60	24[c]
5	$LiAlH_4$	Pyridine	200	6[d]
6	$NaBH_4$	*i*-C_3H_7OH	900	No reaction

a) Isolated Yields. b) **1a** recovered (34%). c) Structures of other products are not assigned (a number of spots on TLC were observed). d) **1a**; 29% and **3**; 22%.

Treatment of a solution of **2a** in glacial acetic acid with 60% perchloric acid for 24 h at room temperature gave 2-phenylbenzo[*b*]thiopyrylium perchlorate **4a** and 2-phenylthiochroman **5** in 45% yield, respectively. In the presence of 2,3-dichloro-5,6-dicyano-*p*-benzoquinone (DDQ), compound **4a** could be obtained selectively in 68% yield by treatment of **2a** with the same acid for 1 h at room temperature. In this reaction, it seems likely that compound **4a** is formed by elimination of a hydride ion from compound **2a**. Other new 2-phenylbenzo[*b*]-thiopyrylium salts (**4b—d**) could be obtained in high yield (81—89%) from thioflavones (**1b—d**) by the same reduction (entry 1), followed by treatment with acid in the presence of DDQ. The present method may be extended to the general synthesis of 2-phenylbenzo[*b*]-thiopyrylium perchlorates.

Thioflavones (**1a—d**) and the title compounds (**4a—d**) are currently being tested for antimicrobial activity.

Experimental

All the melting points are uncorrected. Proton NMR spectra were taken on a JEOL JNM-MH-100 spectrometer with tetramethylsilane as an internal standard. Elemental analyses were recorded on a Yanaco CHN recorder MT-2. Mass spectra were recorded on a Hitachi RMU-6E mass spectrometer operating at 80 eV.

2-Phenyl-4H-benzo[b]*thiopyran-4-ones (1a—d).* Compounds **1a** and **1c** were generally prepared by Bossert's method. **1a**: mp 125—127 °C (lit,[5] 124—127 °C), **1c**: mp 155—157 °C (lit,[5] 157 °C). Compounds **1b** (R=5-MeO) and **1d** (R=7-MeO) were obtained as follows; Reaction mixture which was prepared by Bossert's method (starting materials: *m*-methoxybenzenethiol and ethyl benzoylacetate) was chromatographed on silica gel using benzene/acetone (20/1) as an eluent to give **1b** (18%) and **1d** (33%). **1b**: mp 204—205 °C, ^{1}H-NMR($CDCl_3$): δ 3.97 (s, 3H), 6.90 (d, J=8 Hz, 1H), 7.08—7.23 (m, 2H), 7.38—7.68 (m, 6H), *m/e* (rel intensity): 268 (M^+, 100), 267 (37), 240 (29), 222 (52), 210 (26), Found: C, 71.62; H, 4.51%. Calcd for $C_{16}H_{12}O_2S$: C, 71.82; H, 4.34%. **1d**: mp 137—139 °C (lit,[5] 150 °C).

2-Phenyl-4H-benzo[b]*thiopyrans (2a—d).* To a stirred suspension at 25 °C of $LiAlH_4$ (0.19 g, 5 mmol) and $AlCl_3$ (0.66 g, 5 mmol) in THF (30 ml) was added dropwise **1a** (1.2 g, 5 mmol) in THF (15 ml). The reaction mixture was stirred for 100 min at 25 °C, and then water (1.0 ml) and concd H_2SO_4 (2.5 ml) were added. After filtration, the filtrate was extracted with ether to give compound **2a** in 95% yield; mp 61—63 °C (lit,[3] 63—65 °C). Other compounds (**2b—d**) were similarly prepared and recrystallized from methanol. The mp, NMR, mass spectra, and results of elemental analysis of these compounds are summarized in Table 2.

Table 2. 2-Phenyl-4*H*-benzo[*b*]thiopyrans

Compd	Mp θ_m/°C	^{1}H-NMR in $CDCl_3$ δ	*m/e* (rel intensity)	Calcd (Found) (%) C	H
2b	58—59	3.89 (s, OCH_3), 3.65 (d, J=5 Hz, 2H) 6.32 (t, J=5 Hz, 1H), 6.86 (d, J=8 Hz, 1H) 7.10—7.81 (m, 7H)	254 (100), 253 (60) 239 (28), 223 (21) 221 (9), 177 (47)	75.56 (75.90)	5.55 (5.24)
2c	105—107	3.89 (s, OCH_3), 3.61 (d, J=5 Hz, 2H) 6.41 (t, J=5 Hz, 1H), 6.92—7.04 (m, 2H) 7.46—7.89 (m, 6H)	254 (100), 253 (75) 239 (12), 221 (11) 210 (18), 177 (45)	(75.80)	(5.37)
2d	83—84	3.90 (s, OCH_3), 3.59 (d, J=5 Hz, 2H) 6.44 (t, J=5 Hz, 1H), 6.95 (d, d, J=2 and 8 Hz, 1H), 7.15 (d, J=2 Hz, 1H), 7.31 (d, J=8 Hz, 1H), 7.49—7.90 (m, 5H)	254 (100), 253 (73) 239 (10), 221 (9) 210 (9), 177 (29)	(75.37)	(5.47)

Table 3. 2-Phenylbenzo[*b*]thiopyrylium perchlorates

Compd	Mp θ_m/°C	Yield %	^{1}H-NMR in CF_3COOH δ	Calcd (Found) (%) C	H
4b	190—192	81	4.22 (s, OCH_3), 7.50—8.25 (m, 8H) 8.67 (d, J=10 Hz, 1H), (d, J=10 Hz, 1H)	54.47 (54.10)	3.71 (3.69)
4c	231—233	82	4.27 (s, OCH_3), 7.81—8.35 (m, 7H) 8.68 (d, J=10 Hz, 1H), 9.01 (d, J=10 Hz, 1H) 9.49 (d, J=10 Hz, 1H)	(54.18)	(3.62)
4d	180—182	89	4.32 (s, OCH_3), 7.78—8.22 (m, 7H) 8.56 (d, J=9 Hz, 1H), 8.71 (d, J=9 Hz, 1H) 9.25 (d, J=9 Hz, 1H)	(54.63)	(3.67)

2-Phenylthiochroman-4-one (3). A solution of $LiAlH_4$ (0.2 g) in dry pyridine (20 ml) was added to a solution of **1a** (1.0 g) in pyridine (15 ml) at 25 °C. The mixture was stirred for 200 min at 25 °C, and then methanol (2.0 ml) and dilute hydrochloric acid (50 ml) were added. After extraction with ether, the extracts were washed with dilute HCl and evaporated. The residue was chromatographed on silica gel using benzene as an eluent to give **3** (22%), **1a** (29%) and **2a** (6%).

2-Phenylbenzo[b]*thiopyrylium Perchlorates (4a—d). Method A*: Compound **2a** (1.1 g) was dissolved in glacial acetic acid (6 ml), and then 60% perchloric acid (3.3 g) was added. After 1 d at room temperature, ether was added, and the resulting solid was separated and recrystallized from glacial acetic acid containing a small amount of perchloric acid to give **4a** (0.72 g). Compound **5** was isolated in 45% yield when the filtrate was extracted with ether, and recrystallized from methanol. **5**: mp 52—54 °C; *m/e* 226 (M^+, 86), 135 (100), 92 (52), 91 (42); ^{1}H-NMR ($CDCl_3$): δ 2.25—2.40 (m, 2H), 2.84—3.04 (m, 2H), 4.46 (d, d, J=9 and 3 Hz, 1H), 7.01—7.54 (m, 9H). Found: C, 79.15; H, 6.09%. Calcd for $C_{15}H_{14}S$: C, 79.60; H, 6.23%.

Method B: A solution of DDQ (1.37 g) in glacial acetic acid (20 ml) was added to a solution of **2a** (1.07 g) in glacial acetic acid (6 ml) under the stirring. After 30 min, 60% perchloric acid (3.3 g) was added, and the mixture was stirred for 30 min. The resulting solid was separated, and ether was added to the filtrate. The resulting solid was again separated. The collected solid was recrystallized from glacial acetic acid to give **4a** (1.0 g) in 65% yield. The other compounds **4b—d** were similarly prepared. The yields, mp's, NMR spectra, and results of elemental analysis of these compounds are summarized in Table 3.

References

1) J. Griffiths, "Colour and Constitution of Organic Molecules," Academic Press, London (1976), p. 260.
2) O. K. Kabiev and S. M. Vermenichev, *Vop. Onkol.*, **60** (1970); *Chem. Abstr.*, **73**, 108115n (1970).
3) A. Lüttringhaus, N. Engelhard, and A. Kolb, *Justus Liebigs Ann. Chem.*, **654**, 189 (1962).
4) N. Engelhard and A. Kolb, *Justus Liebigs Ann. Chem.*, **673**, 136 (1964).
5) F. Bossert, *Justus Liebigs Ann. Chem.*, **680**, 40 (1964).

Tosylation Reaction of D-Glucuronolactone

Hiroshi ITOH* and Kiyohiko TAJIMA
The Noguchi Institute, 1-8-1 Kaga, Itabashi-ku, Tokyo 173
(Received September 13, 1982)

Synopsis. The tosylation reaction of D-glucuronolactone with tosyl chloride in pyridine gave directly 5-*O*-tosyl-D-glucuronolactone and 2,5-di-*O*-tosyl-D-glucuronolactone.

The selective acylation for hydroxyl groups in carbohydrate is important in the synthesis of carbohydrate derivatives. The formation of the quarternary pyridinium salts or chlorination at anomeric carbon take place in the tosylation of carbohydrates having a free glycosidic hydroxyl group with tosyl chloride in pyridine.[1] For example, 2,3,6-tri-*O*-methyl-4-*O*-tosyl-D-glucose or 6-*O*-tosyl-D-glucose was not directly obtained from 2,3,6-tri-*O*-methyl-D-glucose or D-glucose, respectively.[2,3] In continuing the studies about reactions of D-glucuronolactone (**1**), however, 5-*O*-tosyl-D-glucuronolactone (**2**) or 2,5-di-*O*-tosyl-D-glucuronolactone (**3**) was obtained by the direct tosylation of **1** in pyridine with tosyl chloride.

At first, equimolar tosyl chloride was used to afford **2** in 49% yield with a trace of **3**. Compound **2** was also tosylated under the same conditions to give **3** in 39% yield. And then tosylation of **1** with bimolar tosyl chloride gave **2** and **3** in 30 and 31% yields, respectively. The structure of **2** was confirmed by elemental analysis, IR, and ^{1}H-NMR spectra, and by converting it into the isopropylidene derivative, 1,2-*O*-isopropylidene-5-*O*-tosyl-D-glucuronolactone (**4**).[4] The structure of **3** was confirmed by elemental analysis, IR, and ^{1}H-NMR spectra, and by converting it into the acetate, 1-*O*-acetyl-2,5-di-*O*-tosyl-D-glucuronolactone (**5**). The chemical shifts of the ^{1}H-NMR spectra for compounds **1**, **2**, and **3** are listed in the Table. These show the characteristic deshielding effect of the sulfonyl group, the signals of H-2 or H-5 being shifted to lower field. And compound **2** was further methylated and acetylated to give methyl 2-*O*-acetyl-5-*O*-tosyl-D-glucurosiduronolactone (**6**). Compound **6** was also synthesized from methyl D-glucurosiduronolactone by tosylation with equimolar tosyl chloride followed by acetylation. These results indicate a selectivity of the hydroxyl groups in **1** towards tosylation. The order of reactivity HO-5> HO-2 agree well with the result that the degree of hydrogen bonding of HO-5 is higher than that of HO-2.[5]

TABLE 1. CHEMICAL SHIFTS OF ^{1}H-NMR (DMSO-d_6) FOR COMPOUNDS **1**, **2**, AND **3**

Compound	H-1	H-2	H-3	H-4	H-5 (δ)
1	5.17	3.77	← 4.20—4.90 →		
2	5.23	4.03	← 4.50—4.90 →		5.55
3	5.31	4.67	← 4.60—5.06 →		5.56

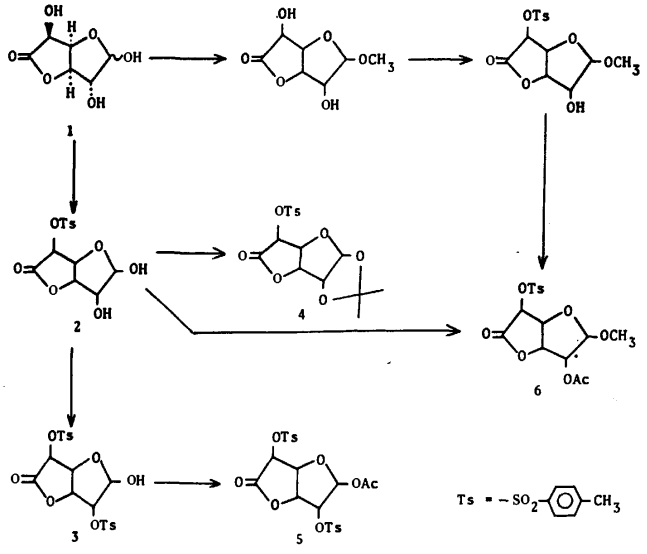

Experimental

Melting points are uncorrected. The infrared spectra and ^{1}H-NMR spectra were recorded on a JASCO A-102 spectrometer and a JNM-PMX 60 spectrometer, respectively, under standard conditions.

5-O-Tosyl-D-glucuronolactone (2). To a solution of D-glucuronolactone (**1**) (1.8 g) in pyridine (10 ml) was added dropwise a solution of tosyl chloride (1.9 g) in pyridine (10 ml) within 15 min at 0 °C. The mixture was stirred for 16 h at room temperature, after which time pyridine was evaporated under reduced pressure. The residue was extracted with ethyl acetate–5% HCl solution and the ethyl acetate solution was washed with $NaHCO_3$ aq and water. After evaporation of ethyl acetate, the residue was recrystallized from acetone–petroleum ether to give **2** (1.6 g, 49%) as white needles: mp 183—184 °C. ^{1}H-NMR (DMSO-d_6) δ=2.43 (3H, s), 4.03 (1H, s), 4.50—4.90 (2H, m), 5.23 (1H, d, J=3.6 Hz), 5.46—5.80 (2H, m), 6.75 (1H, d, J=3.6 Hz), 7.68 (4H, m). IR (KBr) 3500, 3420, 1780, 1580, 1175 cm^{-1}. Found: C, 47.20; H, 4.09; S, 9.73%. Calcd for $C_{13}H_{14}O_8S$: C, 47.27; H, 4.27; S, 9.71%.

2,5-Di-O-tosyl-D-glucuronolactone (3). Compound **3** was prepared for 64 h in a similar manner to that described above, using 1.8 g of **1** and 3.8 g of tosyl chloride. After evaporation of ethyl acetate, the residue was extracted with benzene. The insoluble material was **2** (1.0 g, 30%). The soluble material was **3**; it was recrystallized from benzene–petroleum ether twice (1.4 g, 31%) and was further recrystallized from acetone–petroleum ether to give **3** as white curdy crystals having a constant mp of 173—175 °C. ^{1}H-NMR (DMSO-d_6) δ=2.43 (6H, s), 4.60—5.06 (3H, s), 5.31 (1H, d, J=3.2 Hz), 5.56 (1H, d, J=6.4 Hz), 7.37—8.06 (9H, m). IR (KBr) 3460, 1800, 1580 cm^{-1}. Found: C, 49.47; H, 4.07; S, 13.21%. Calcd for $C_{20}H_{20}O_{10}S_2$: C, 49.58; H, 4.16; S, 13.24%.

1,2-O-Isopropylidene-5-O-tosyl-D-glucuronolactone (4). The solution of **2** (0.48 g) in acetone (5 ml) and trifluoroacetic acid (0.5 ml) was refluxed for 20 h. After evaporation of the excess reagent under reduced pressure, the residue was recrystallized from benzene–petroleum ether to give **4** (0.48 g, 90%): mp 187—188 °C (lit,[4] 189—194 °C).

1-O-Acetyl-2,5-di-O-tosyl-D-glucuronolactone (5). Compound **3** was acetylated with acetic anhydride–trifluoroacetic acid (55 °C, 15 h). The obtained **5** was a mixture of α and β

anomers (1 : 4.7).

*Methyl 2-O-acetyl-5-O-tosyl-D-glucurosiduronolactone (**6**).* Compound **2** was methylated with methanol–Dowex 50WX2 (R. T. 2 h) and acetylated with acetic anhydride–pyridine (R. T. 2 h) and **6** was recrystallized from acetone–petroleum ether; white needles: mp 121—122.5 °C. ^{1}H-NMR ($CDCl_3$) δ=2.11 (3H, s), 2.48 (3H, s), 3.33 (3H, s), 4.86—5.33 (5H, m), 7.66 (4H, m). IR (KBr) 2920, 1800, 1750, 1590 cm^{-1}.

References

1) R. S. Tipson, *Adv. Carbohydr. Chem.*, **8**, 107 (1953).
2) K. Hess and F. Neumann, *Ber.*, **68**, 1360 (1935).
3) F. Hardegger and R. M. Montavon, *Helv. Chim. Acta*, **29**, 1199 (1946).
4) J. K. N. Jones, *Can. J. Chem.*, **34**, 310 (1956).
5) K. Dax and H. Weidman, *Adv. Carbohydr. Chem. Biochem.*, **33**, 189 (1976).

An Improved Method for Preparation of *N*-Alkyl-2(3*H*)-benzothiazolone Analogs

Yoo TANABE,* Takayuki OKABE, Akiko KAKIMIZU, Nobuo OHNO and Hirosuke YOSHIOKA
Pesticide Research Department, Sumitomo Chemical Co. Ltd., 4-2-1 Takatsukasa, Takarazuka, Hyogo 665
(Received September 17, 1982)

Synopsis. A number of *N*-alkyl-2(3*H*)-benzothiazolone analogs could be prepared from *N*-monosubstituted aniline and chlorocarbonylsulfenyl chloride. The new method consists of carbamoylation of aniline and successive Friedel-Crafts type ring closure of an intermediate carbamoylsulfenyl chloride in the presence of suitable Lewis or protic acid catalyst.

N-Alkyl-2(3*H*)-benzothiazolone derivatives (**3**) are well known as useful biologically active substances, *i.e.*, herbicides,[1] fungicides[2] and antiallergic drugs.[3] Therefore, synthesis of 2(3*H*)-benzothiazolone has been studied extensively, and the following two methods[4] which start from aniline are typical ones. According to the first method, *N*-alkyl-2(3*H*)-benzothiazolones (**3**) are prepared by the following series of reactions: 1) Condensation of aniline with thiocyanate ion to give phenylthiourea, 2) oxidative (*e.g.* Br_2 or SO_2Cl_2) cyclization to 2-aminobenzothiazole, 3) transformation of the 2-amino derivative to 2(3*H*)-benzothiazolone by diazotization and subsequent acid hydrolysis of the 2-chlorobenzothiazole, 4) *N*-alkylation to **3**. In the other method, a substituted aniline and carbon disulfide are coupled to give the corresponding 2-mercaptobenzothiazole, which is then converted to **3** by H_2O_2-oxidation followed by alkylation. The former method is general one to prepare *N*-alkyl-2(3*H*)-benzothiazolone, but requires several steps. The latter is of limited applicability, since the coupling reaction often requires drastic reaction conditions (high temperature (up to 150 °C) and pressure (≈3 atm)), and generally give low yields with certain exceptions such as 2-mercaptobenzothiazole.

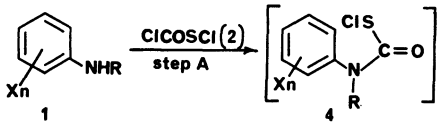

1 **4**

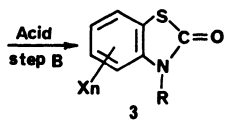

3

Scheme 1.

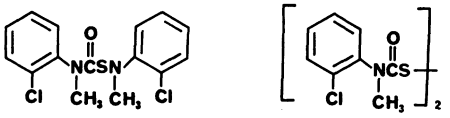

6 **5**

In contrast, Zumach *et al.* reported[5] a remarkable method for preparation of *N*-methyl-2(3*H*)-benzothiazolone (**3**) by condensation of *N*-methylaniline (**1**) and chlorocarbonylsulfenyl chloride (CCSC) (**2**), an effective "bifunctional" reagent,[7] and they described that the reaction proceeds stepwise as shown in Scheme 1: step A, carbamoylation of *N*-alkylaniline (**1**) with CCSC (**2**) and step B, ring-closure by way of Friedel-Crafts type C–S bond formation. When X_n on **1** is hydrogen atom or an electron donating group, the second step occurs spontaneously. However, when X_n is an electron-withdrawing group, such as halogen or cyano group, step B did not proceed and even a trace amount of benzothiazole (**3**) was not obtained, but the disulfide (**5**, Table 1,(c)) was found. The failure in the cyclization step seems to result from low reactivity of the benzene ring of the aniline (**1**) on the Friedel Crafts cyclization by an electron-withdrawing groups X_n.

In order to overcome the problem, we have extensively attempted a variety of Friedel-Crafts catalysts for the cyclization step B, and found that 1.5 mol of Lewis acid ($AlCl_3$, $FeCl_3$) or a large excess of protic acid (H_2SO_4,[8] CF_3CO_2H) gave *N*-alkyl-2(3*H*)-benzothiazolone (**3**) in

Table 1. Preparation of 4-chloro-*N*-methyl-2(3*H*)-benzothiazolone (**3a**)

Base/step A (equiv. *vs.* **1a**)	Acid/step B (equiv. *vs* **1a**)	Solvent	Yield/%
N,*N*-Dimethylaniline(1.1)	None	Toluene[a)]	–[c)]
N,*N*-Dimethylaniline(1.1)	$AlCl_3$(1.5)	Toluene[a)]	78.2
N,*N*-Dimethylaniline(1.1)	$FeCl_3$(1.5)	Toluene[b)]	48.4
N,*N*-Dimethylaniline(1.1)	BF_3·Et_2O(1.5)	Toluene[a)]	Trace
N,*N*-Dimethylaniline(1.1)	CF_3CO_2H(5.0)	Toluene[a)]	20.0
N,*N*-Dimethylaniline(1.1)	Conc H_2SO_4(10)	Toluene[b)]	76.1
N,*N*-Diethylaniline(1.1)	Conc H_2SO_4(10)	Toluene[b)]	76.5
Pyridine(1.1)	Conc H_2SO_4(10)	Toluene[b)]	42.8
Triethylamine(1.1)	Conc H_2SO_4(10)	Toluene[b)]	5.5
N,*N*-Dimethylaniline(1.1)	Conc H_2SO_4(10)	CH_2Cl_2[b)]	15.0
N,*N*-Dimethylaniline(1.1)	Conc H_2SO_4(10)	CCl_4[b)]	69.4
N,*N*-Dimethylaniline(1.1)	Conc H_2SO_4(10)	Hexane[b)]	Trace
N,*N*-Dimethylaniline(1.1)	Conc H_2SO_4(20)	Toluene[b)]	66.0
N,*N*-Dimethylaniline(1.1)	Conc H_2SO_4(5.0)	Toluene[b)]	18.0
2-Chloro-*N*-methylaniline(1.1)	Conc H_2SO_4(10)	Toluene[b)]	52.5

a) Refluxed for 3 h on step B. b) 0—5 °C for 1 h and r.t. for 8 h. c) Bis(*N*-(2-chlorophenyl) methylcarbamoyl) sulfide (**5**) was obtained in 30% yield as a main product.

Table 2. Preparation of *N*-alkyl-2(3*H*)-benzothiazolone (**3**) in concd H_2SO_4

Product[c)]	R	X_n	Yield/%
3a	CH_3	4-Cl	76.1
3b	CH_3CH_2	4-Cl	72.5
3c	$CH_2CO_2CH_2CH_3$	4-Cl	61.0
3d	CH_3	4-Cl, 6-Cl	57.8
3e	CH_3	6-Cl	78.2
3f	CH_3	6-CN	62.0
3g	CH_3	5-Cl, 7-Cl	59.5
3h	CH_3	4-Br	75.5
3i	CH_3	5-Cl[b)]	71.5

a) 10 mol equiv. *vs.* *N*-alkylaniline (**1**) was used. b) Containing a 10% of 7-chloro-*N*-methyl-2(3*H*)-benzothiazolone originated by the cyclization toward C-2 position of 3-chloroaniline. c) These physical and analitical data are given in experimental tail.

good yield. It is noteworthy that C–S bond formation between the aromatic carbon and the sulfenyl halide was successfully conducted in a protic acid media such as conc H_2SO_4.

Various types of amines were tried as acid scavenger in the step A. For example, in case of *N*-methyl-2-chloroaniline, *N,N*-dialkylaniline gave favorable yield of 4-chloro-*N*-methyl-2(3*H*)-benzothiazolone (**3a**), while pyridine and triethylamine gave poor yield. *N*-Methyl-2-chloro-aniline could also behave as an acid scavenger and gave 53% yield of (**3a**) and *N*-(2-chlorophenyl)-methylcarbamoyl 2-chloro-*N*-methylanilino sulfide (**6**) in 11% yield as a major by-product (Table 1). It was found that the reaction was very sensitive to solvents and bases. It seemed that solvents such as toluene, carbon tetrachloride, and certain tertiary amines such as *N,N*-dimethylaniline are favorable for the step A.

The results were shown in Tables 1 and 2.

Experimental

Materials. CCSC (**2**) was prepared from CCl_3SCl and 95%-H_2SO_4.[6]

Analyses of the Products. Purity of *N*-Alkyl-2(3*H*)-benzothiazolone (**3**) were analyzed by GLC on a 1.5 m×3 mm XE-60 (5 wt%) column at 200 °C.

4-Chloro-N-methyl-2(3H)-benzothiazolone (3a). CCSC (**2**, 5.08 g, 3.83×10^{-2} mol) was added to a solution of 2-chloro-*N*-methylaniline (**1a**, 5.00 g, 3.53×10^{-2} mol) and *N,N*-dimethylaniline (4.73 g, 3.83×10^{-2} mol) in toluene (70 ml) at 0 °C and the solution was stirred at 0 °C for 1 h. After removal of *N,N*-dimethylaniline hydrochloride salt by filtration, the filtrate which contained sulfenyl halide intermediate (**4a**, was added to a suspension of $AlCl_3$ (7.66 g, 5.75×10^{-2} mol) in toluene (50 ml) at room temperature during 30 min, and heated under reflux for 3 h. Then the reaction mixture was poured into water (100 ml) and extracted with toluene. The organic layer was washed with sat. $NaHCO_3$ solution (100 ml) and dried with $MgSO_4$. The solvent was removed *in vacuo*, and the resultant crude crystals were recrystallized from EtOH to give **3a** (4.45 g, 78.2%). (Table 1). In the same manner, the intermediate sulfenyl halide (**4a**, X=2-Cl, R=CH_3) in toluene was added to conc H_2SO_4 (37 g, 0.38 mol) at 0—5 °C, and kept under stirring at room temperature for 5 h. The reaction mixture was worked up with ice (50 g) to give **3a** (4.43 g, 76.1%). (Tables 1 and 2): mp 124—128 °C (lit,[8] mp 130 °C); IR (Nujol) 2950, 1750 (C=O), 1440, 1210, 1160, 1100 and 1060 cm^{-1}; ^{1}H-NMR ($CDCl_3$) δ=6.08—7.50 (m, 3H, arom.) and 3.80 (s, 3H); ^{13}C-NMR ($CDCl_3$) δ=169.93 (s, C=O), 133.91, 129.09, 124.82, 123.43, 121.15, 117.30 and 33.05 (s, N-$\underline{C}H_3$).

4-Chloro-N-ethyl-2(3H)-benzothiazolone (3b): Mp 97.4 °C (lit,[2] mp 98—99 °C). *4-Chloro-N-(ethoxycarbonylmethyl)-2(3H)-benzothiazolone (3c)*: Mp 78.5 °C (lit,[1] mp 77 °C). *6-Chloro-N-methyl-2(3H)-benzothiazolone (3e)*: Mp 109.5—112.9 °C (lit,[2] mp 109 °C). *4-Bromo-N-methyl-2(3H)-benzothiazolone (3h)*: Mp 141.5 °C (lit,[2] mp 139—140 °C). *5-Chloro-N-methyl-2(3H)-benzothiazolone (3i)*: Mp 102 °C (lit,[9] mp 105—106 °C).

4,6-Dichloro-N-methyl-2(3H)-benzothiazolone (3d): Mp 144—146 °C; ^{1}H-NMR ($CDCl_3$) δ=3.85 (s, 3H) and 7.05—7.55 (m, 2H); Found: C, 41.24; H, 2.11; N, 5.87; S, 13.95 Cl, 30.55%. Calcd for $C_8H_5NOSCl_2$: C, 41.05; H, 2.15; N, 5.99; S, 13.70; Cl, 30.29%.

6-Cyano-N-methyl-2(3H)-benzothiazolone (3f): Mp 141 °C; ^{1}H-NMR ($CDCl_3$) δ=3.80 (s, 3H) and 7.05—7.65 (m, 3H); Found: C, 56.98; H, 3.15; N, 14.55; S, 16.86%. Calcd for $C_9H_6N_2OS$: C, 57.25; H, 3.18; N, 14.73; S, 16.86%.

5,7-Dichloro-N-methyl-2(3H)-benzothiazolone (3g): Mp 97—100 °C; ^{1}H-NMR ($CDCl_3$) δ=3.85 (s, 3H) and 7.20—7.60 (m, 2H); Found C, 41.16; H, 2.16; N, 5.96; S, 13.10; Cl, 30.82%. Calcd for $C_8H_5NOSCl_2$: C, 41.05; H, 2.15, N, 5.99; S, 13.70; Cl, 30.29%.

Bis(N-(2-chlorophenyl)methylcarbamoyl) Sulfide (5): A solution of the sulfenyl halide intermediate (**4a**, X=2-Cl, R=CH_3) in toluene (20 ml) prepared from 2-chloro-*N*-methylaniline (2.00 g, 1.41×10^{-2} mol) in the same manner to those described for **3a**, was heated under reflux for 3 h. Then the solvent was removed in vacuo and the residue was poured into water (40 ml) and extracted with $CHCl_3$ (40 ml×2). The organic layer was washed with aqueous 10% HCl (50 ml×2), sat. $NaHCO_3$ solution (50 ml) and dried with $MgSO_4$. The solvent was removed *in vacuo*, and the resultant product were subjected to column chromatography (silica gel using $CHCl_3$ as an eluent) to give **5** (1.25 g, 30%), mp 172—174 °C; IR (Nujol) 2720, 1680 (C=O), 1465, 1260, 850, and 720 cm^{-1}; ^{1}H-NMR ($CDCl_3$) δ=6.50—7.80 (m, 8H, arom) and 3.30 (s, 6H); ^{13}C-NMR ($CDCl_3$) δ=164.57 (s, C=O), 137.91, 134.64, 134.52, 131.79, 131.06, 128.32 and 37.90 (s, N-CH_3); Found: C, 47.67; H, 3.50; N, 6.91; S, 15.50; Cl, 17.61%; Calcd for $C_{16}H_{14}Cl_2N_2O_2S_2$: C, 47.89; H, 3.52; N, 6.98; S, 15.98; Cl, 17.67%.

M-(2-Chlorophenyl)methylcarbamoyl (2-Chloro-N-methylanilino Sulfide (6). CCSC (**2**, 5.08 g, 3.83×10^{-2} mol) was added to a solution of 2-chloro-*N*-methylaniline (**1a**, 10.0 g, 7.06×10^{-2} mol) in toluene (70 ml) at 0 °C and the solution was stirred at 0 °C for 1 h. After removal of 2-chloro-*N*-methylaniline hydrochloride by filteration, the filtrate was treated by the same procedure employed in the preparation of **3a**. 6.50 g of crude material was obtained after work up. The crude material was purified by column chromatography (silica gel using $CHCl_3$ as an eluent) to give **3a** (4.16 g, 59%) and **6** (0.66 g, 11%). oil; IR (film) 2920, 1740 (C=O), 1660, 1580, 1480, 1340, 1280 and 1120 cm^{-1}; ^{1}H-NMR ($CDCl_3$), δ=6.55—7.80 (m, 8H, arom.), 3.35 (s, 3H), and 3.17 (s, 3H); MS: (70 ev, DI) *m/e* (rel intensity)=340 (M^+, 40), 168 (100), 140 (68), and 77 (24).

References

1) For example, Benazoline® (4-chloro-*N*-(carboxymethyl)-2(3*H*)-benzothiazolone), British Patent 862226 (The Boots Co. Ltd., 1965).

2) T. Uematsu, Japan Patent 90261 (Sumitomo Chemical Co. Ltd., 1978).

3) I. Ueda, Japan Patent 92952 (Fujisawa Pharmaceutical Co. Ltd., 1979).

4) R. C. Elderfield, "Heterocyclic Compounds," John Wiley and Sons, New York (1957), p. 484.

5) V. G. Zumach and E. Kühle, *Angew. Chem., Int. Ed. Engl.*, **82**, 63 (1970).

6) CCSC (**2**) is also commercially available from Fulka Chemical Corp.

7) For example, see K. Pilgram and R. D. Skiler, *J. Org. Chem.*, **38**, 1575 (1973).

8) As indicated in Table 2, the yield of **3** decreased significantly when 5.0 equiv. of concd H_2SO_4 was used in the step B.

9) E. Hoggarth. *J. Chem. Soc.*, **1949**, 3315.

Dimethyl and Diethyl 2-Oxo-1,3-propanedisulfonates as Practical Alkylating Reagents

Fumio OGURA,* Hachiro YAMAGUCHI,† Tetsuo OTSUBO, Takao NAKANO, and Takahiro SAITO

Department of Applied Chemistry, Faculty of Engineering, Hiroshima University, Shitami, Saijo, Higashi-Hiroshima 724

(Received October 9, 1982)

Synopsis. The title sulfonates, easily accessible from acetone, were found to be effective and practical alkylating agents.

2-Oxo-1,3-propanedisulfonic acid (**1**), *sym*-disulfonic acid of acetone, was readily prepared by sulfonation with fuming sulfuric acid as a highly hygroscopic crystalline solid.[1,2] The sulfonic acid (**1**) was converted to the dichloride (**2**) with $SOCl_2$ containing a small amount of nitromethane, and **2** was reacted with methanol and ethanol to yield methyl and ethyl esters (**3** and **4**) respectively.

$$CH_3COCH_3 \longrightarrow \underset{\mathbf{1}}{O{=}C(CH_2SO_3H)_2} \xrightarrow{SOCl_2} \underset{\mathbf{2}}{O{=}C(CH_2SO_2Cl)_2} \xrightarrow{ROH} O{=}C(CH_2SO_3R)_2$$

3: R=CH_3, **4**: R=C_2H_5

With the purpose of utilizing these disulfonates as practical alkylating reagents, we studied the alkylation of phenol with them. Thus, phenol was alkylated with **3** or **4** in aq NaOH, and the reaction products were submitted to quantitative gas-chromatographic analysis. For comparison, the alkylation of phenol with conventional reagents was carried out under the same reaction conditions, and the products were analyzed similarly. The combined results are shown in Table 1. From the results obtained, it can be concluded that **3** and **4** react as effectively as dialkyl sulfates in the alkylation.[3] Furthermore, they have several advantages over the sulfates worthy of comment: 1. In **3** and **4** both alkyl groups could be used for the alkylation quite smoothly. 2. No severe toxicity such as that of the dialkyl sulfates was observed. 3. The sulfonates were stable compounds and had a good crystallinity in spite of their low melting points. Therefore, they were easy to handle and showed good reactivities, even in the aq-phase reactions. At present we have not yet tried these sulfonates on many kinds of substrates. However, considering the above results, they seem to be highly promising reagents. For example, sodium *S*-methyl thiosulfate (Bunte salt) was prepared in a good yield by the reaction of sodium thiosulfate on **3**.

Table 1. Comparison of alkylating reagents in the alkylation of phenol

Alkylating agent[a]	Reaction conditions[b] Temp/°C	Time/h	Yield/%
		1	76.0
		2	89.8
3	40	3	89.8
		4	95.4
		6	97.2
		1	81.5
		2	82.7
$(CH_3O)_2SO_2$[c]	40	3	84.0
		4	83.8
		6	83.1
$CH_3SO_3CH_3$	40	6	92.6
CH_3-C$_6$H$_4$-SO_3CH_3	40	4	68.4
CH_3I	40	4	16.9
		2	70.8
4	30	3	79.9
		6	82.5
		2	65.1
$(C_2H_5O)_2SO_2$[c]	30	3	71.2
		5.5	84.5
CH_3-C$_6$H$_4$-$SO_3C_2H_5$	30	6	33.5
$H_2C(CH_2SO_3C_2H_5)_2$	30	2	80.6
C_2H_5Br	30	6	7.5
C_2H_5I	30	6	2.5

a) The molar ratios of alkylating agents to phenol were 1 : 2 for the three disulfonates and 1 : 1 for all the other cases. b) As a base, 12 M aq NaOH was used in 1.5 times and twice the molar quantity of phenol for methylation and ethylaiton respectively. c) Only one alkyl group could be used for the alkylation under these conditions.

Experimental

The melting points were not corrected. The solvents were of a reagent grade. All the known compounds were confirmed by a comparison of the melting points, spectroscopic data, and retention times with those of the authentic samples or the reported data. The ^{1}H-NMR spectra were recorded on a JEOL PMX-60 spectrometer, and the shifts were given in δ units from internal TMS. The gas-chromatographic analysis was performed on a Yanagimoto GCG-550T gas chromatograph equipped with a TCD, using helium as a carrier gas.

2-Oxo-1,3-propanedisulfonyl Dichloride (2): 2-Oxo-1,3-propanedisulfonic acid (**1**, 221.7 g, 1.02 mol)[1] was mixed with $SOCl_2$ (850 g, 7.14 mol) containing nitromethane (31 g, 0.51 mol),[4] and the mixture was refluxed for 6 h to obtain a clear solution. Crystals deposited on cooling were collected by means of suction filtration and washed with cold abs benzene. The chloride (169.3 g, 65%) could be used directly for a further reaction. Recrystallized crystals (from abs benzene) showed a mp of 106—107 °C. ^{1}H-NMR(CD_3COCD_3): 5.17 (s, CH_2). Found: S, 25.30%. Calcd for $C_3H_4O_5Cl_2S_2$: S, 25.10%.

Dimethyl 2-Oxo-1,3-propanedisulfonate (3): To a chilled and stirred methanol (13 g, 0.41 mol), **2** (5.0 g, 0.02 mol) was added, portion by portion, to keep the temperature of the reaction mixture below −10 °C. The mixture was concen-

† Present address: Faculty of Pharmaceutical Sciences, Fukuyama University, Fukuyama 729-02.

trated under reduced pressure immediately after the addition was complete, and ice-cold water was added to the residue. The crystals thus precipitated were collected by means of suction filtration was washed with cold water. Colorless crystals (4.21 g, mp 69—69.5 °C, 87.8%) were thus obtained. ^{1}H-NMR ($CDCl_3$): 2.98 (s, CH_3, 6H), 4.47 (s, CH_2, 4H). Found: C, 24.63; H, 4.15%. Calcd for $C_5H_{10}O_7S_2$: C, 24.39; H, 4.09%.

Diethyl 2-Oxo-1,3-propanedisulfonate (4): By the same procedure, **4** was prepared from **2** and EtOH as colorless crystals (mp 45.5—46.5 °C) in an 80.1% yield. ^{1}H-NMR ($CDCl_3$): 1.43 (t, CH_3, 3H), 4.38 (q, CH_2, 2H), 4.43 (s, CH_2, 2H). Found: C, 30.50; H, 5.10%. Calcd for $C_7H_{10}O_7S_2$: c, 30.65; H, 5.14%.

Alkylation of Phenol and the Quantitative Product Analysis by Gas Chromatography: As an example, the methylation with **3** will be described below. Phenol (0.423 g, 4.49 mmol) was dissolved in 12 M aq NaOH (0.56 ml, 6.72 mmol). To the stirred solution, **3** (0.556 g, 2.25 mmol) and octane (an internal standard, 0.336 g, 2.94 mmol) were added, and the mixture was reacted at 40 °C for a definite time (Table 1). The reaction mixture was then diluted with ice-cold water and extracted with ether. The extract was washed with 1 M aq NaOH, dried, and subjected to gas-chromatographic analysis with the following column: $3\phi \times 200$ mm packed with Apiezon grease L. (15%) on Uniport B (80—100 mesh).[5]

Sodium S-Methyl Thiosulfate: To an aq solution of $Na_2S_2O_3$ (30.50 g, 192.9 mmol in 52 ml H_2O), **3** (15.19 g, 61.75 mmol) was added, and the mixture was stirred at room temp for 17 h. The mixture was then concentrated to dryness under reduced pressure, and the residual solid was extracted with EtOH. Ether was added to the extracts to precipitate the Bunte salt as colorless crystals of monohydrate (15.07 g, 72.63%); mp 156—157 °C (decomp). ^{1}H-NMR (DMSO-d_6): 2.33 (s, CH_3, 3H), 3.33 (s, 2H, H_2O): In D_2O, a singlet methyl peak was observed at a filed 2.57 δ lower from internal DSS. Found: C, 7.14; H, 2.80%. Calcd for $CH_3O_3S_2Na \cdot H_2O$: C, 7.14; H, 3.00%.

Diethyl 1,3-Propanedisulfonate: To a stirred ethanol solution of sodium ethoxide, prepared from sodium (1.91 g, 83 mmol) and ethanol (40 g), 1,3-propanedisulfonyl dichloride[6] (10 g, 41 mmol) was added at −5 °C. After stirring for 1 h at 26 °C, the mixture was concentrated under reduced pressure, poured into cold water, and extracted with ether. Before extraction, the pH of the mixture was adjusted to 4 with HCl. The combined extracts were dried (Na_2SO_4) and concentrated under reduced pressure to yield the sulfonate as a light yellow oil (8.0 g, 74.1%), which solidified in a freezer. ^{1}H-NMR ($CDCl_3$): 1.40 (t, CH_3, 6H), 2.32 (quin, CH_2, 2H), 3.33 (t, CH_2, 4H), 4.30 (q, CH_2, 4H).

References

1) W. G. Grot, *J. Org. Chem.*, **30**, 515 (1965); H. Yamaguchi and K. Monden, *Bulletin of the Faculty of Engineering, Hiroshima University*, **24**, 13 (1975).

2) The diammonium salt of **1** is obtained as a by-product of the industrial process of manufacturing methyl methacrylate. G. Schroeder, H. Fink, and G. Goth, Japan Patent 45-29170 (1970).

3) Diethyl 1,3-propanedisulfonate was also a good ethylating reagent, and both ethyl groups could be used easily. However, this reagent was not so easily accessible as **4** and was rather unstable. Methyl methanesulfonate was also a good methylating agent, but it was rather unstable and expensive.

4) Nitromethane was essential for the smooth reaction, and without it a poor reproducibility was often observed.

5) The thermal-response factors necessary for the analysis were determined in separate experiments. Nonane was used as an internal standard for the ethylation.

6) W. Autenrieth and E. Bölli, *Ber.*, **58**, 2144 (1925); P. W. Clutterbuck and J. B. Cohen, *J. Chem. Soc.*, **121**, 125 (1922).

Bromination of 4*H*-Cyclopenta[*def*]phenanthrenamines

Masaaki Yoshida, Masahiro Minabe,* Wataru Ookawa,† and Kazuo Suzuki††
Department of Industrial Chemistry, Faculty of Engineering, Utsunomiya University, Ishiicho, Utsunomiya 321
(Received October 18, 1982)

Synopsis. Bromination of 4*H*-cyclopenta[*def*]phenanthren-1-amine, -2-amine, -3-amine, or -8-amine with bromine in chloroform took place at the 2-, 1-, 8-, or 9-position, respectively. The second bromine was introduced at the 8-, 3-, 2-, or 3-position. Similar regioselectivity was observed in the system of bromine in acetic acid–48% hydrobromic acid and of hydrobromic acid in dimethyl sulfoxide. The corresponding acetylamino compound was brominated at the same position as that of the parent amine.

The electrophilic bromination of 4*H*-cyclopenta[*def*]-phenanthrene has been reported to give 1-bromide accompanied by 3- and 8-bromo isomers.[1] When the 1-, 2-, or 3-position of 4*H*-cyclopenta[*def*]phenanthrene was already occupied by an electron-withdrawing group such as a nitro, bromo, or acetyl substituent, the second substituent entered the 5- or 7-position upon nitration or acetylation.[2]

The present paper deals with the bromination of 4*H*-cyclopenta[*def*]phenanthrene having an electron-donating amino group.

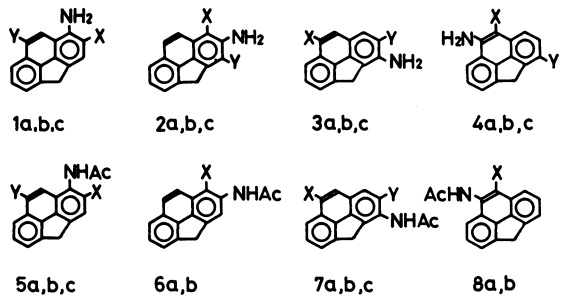

(a: X=Y=H, b: X=Br, Y=H, c: X=Y=Br)
Scheme 1.

Table 1. Bromination of 4*H*-cyclopenta[*def*]-phenanthrenamines

Reactant	Procedure[a]	Bromide (%) Mono-	Bromide (%) Di-	Recovered reactant %
1a	I	89(**1b**)	trace(**1c**)	trace
1a	II	31(**1b**)		65
5a	III	15(**5b**)		85
2a	I	80(**2b**)	12(**2c**)	trace
2a	II	16(**2b**)		71
6a	III	99(**6b**)		
3a	I	20(**3b**)	34(**3c**)	26
3a	II	15(**3b**)		29
7a	III	61(**7b**)		33
4a	I	45(**4b**)	31(**4c**)	13
4a	II	52(**4b**)		47
8a	III	84(**8b**)		trace

a) See Experimental.

Brominations of 4*H*-cyclopenta[*def*]phenanthren-1-amine (**1a**),[3] -2-amine (**2a**), -3-amine (**3a**), and -8-amine (**4a**) were carried out to afford the monobromides (**1b, 2b, 3b, 4b**) and dibromides (**1c, 2c, 3c, 4c**). The substitution with bromine in the acetamides (**5a, 6a, 7a, 8a**) took place at the same position as that of the parent amines to give the monobromides (**5b, 6b, 7b,** and **8b**) (Scheme 1). Table 1 shows the results obtained by gas-chromatographic analyses.

The structural proof of these monobromo amines was established by deamination which gave the known bromo-4*H*-cyclopenta[*def*]phenanthrenes.[1] The configuration of the dibromo amines was estimated by the IR, NMR, and UV spectral data. These physical properties are summarized in Table 2.

In each bromination, no other monobromo isomers were detected by methods of NMR, gas chromatography (Silicone DC-QF 1 or Dexsil 300 GC), and high performance liquid chromatography. The reaction of the amines with bromine in carbon tetrachloride or carbon disulfide gave results similar to those in chloroform. The same regioselectivity was observed in the bromination using a solvent system of acetic acid–48% hydrobromic acid (4 : 1 by volume) in which it had been expected the amines would convert easily to the corresponding conjugated acids.[4] No dibromo amine could be detected by the reaction with hydrobromic acid (48%) in dimethyl sulfoxide, which is similar to the reaction of fluorenamine.[5]

The reaction of **4a** proceeds with regioselectivity analogous to that of 9-phenanthrenamine.[6] The 9-position of **4a** corresponds to the highly reactive 1-position of 2-methoxynaphthalene.[7] A second bromine may be introduced at the 3-position of **4b**, and reactions of **2a** and **3a** can be explained by similar considerations. The bromination of **1a** took place at the 2-position, which corresponds to the reactive 2-position of 1-methoxynaphthalene.[7]

In the acetamide series, the yield of **5b** was only 50% after 60 min of reaction; on the other hand, 98% of **6b** was obtained after 1 min. The low reactivity of **5a** may be interpreted by the fact that the 2-position of the parent hydrocarbon is less reactive than the other positions. The 1-acetylamino group is less electron-donating than the 1-amino group and controls the regioselectivity to be effective at the 2-position, but does not enhance the reactivity significantly.

Experimental

All the melting points are uncorrected. The IR and UV data were recorded with IR-G spectrophotometer (JASCO) as KBr pellets, and using model UV-180 apparatus (Shimadzu) as cyclohexane solutions, respectively. The ^{1}H NMR spectra were obtained with JNM-C-60HL instrument (JEOL) using

† Present address: Kao Soap Co. Ltd., Bunka-2, Sumida-ku, Tokyo 131.
†† Present address: Akita Technical College, Iijima-bunkyocho, Akita 011.

Table 2. Physical properties of bromo-4*H*-cyclopenta[*def*]phenanthrenamines

Compd	Mp(decomp) θ_m/°C	IR $\tilde{\nu}$/cm^{-1}	NMR δ	UV λ_{max}/nm (log ε)	Retention time/s
1b	169.0—169.5	3320, 3420	4.17 (2H, s), 4.61 (2H, s, NH_2), 7.50—7.74(6H, m)	236 (4.62), 282 (4.45), 310 (3.93), 356 (3.68), 373 (3.74)	330
2b	170.5—171.0	3280, 3400	4.16 (2H, s), 4.37 (2H, s, NH_2), 7.11 (1H, s, H-3), 7.39—7.83 (5H, m)	243 (4.38), 268 (4.84), 289 (4.24), 309 (3.98), 364 (3.49), 373 (3.49), 380 (3.51)	380
3b	123.5—124.5	3310, 3400	4.03 (2H, s, NH_2), 4.09 (2H, s), 6.94 (1H, d, J=8.4 Hz, H-2), 7.48—7.95 (5H, m)	252 (4.64), 290 (4.01), 329 (4.12), 363 (3.67)	460
4b	153.0—154.0	3340, 3440	4.26 (2H, s), 4.76 (2H, s, NH_2), 7.47—7.85 (6H, m)	229 (4.49), 254 (4.66), 323 (4.05), 364 (3.45)	360
1c	164.0—165.0	3360, 3470	4.19 (2H, s), 4.53(2H, s, NH_2), 7.51—7.91 (5H, m)	238 (4.60), 254 (4.40), 290 (4.53), 319 (3.93), 366 (3.70), 383 (3.72)	830
2c	215.0—215.5	3300, 3460	4.20 (2H, s), 4.76(2H, s, NH_2), 7.44—7.86 (5H, m)	269 (4.86), 291 (4.27), 313 (4.14), 363 (3.65), 380 (3.70)	810
3c	175.0—175.5	3370, 3460	4.03 (2H, s), 4.40(2H, s, NH_2), 7.54—7.83 (5H, m)	228 (4.49), 257 (4.70), 292 (4.05), 330 (4.13), 348 (3.95), 365 (3.89)	980
4c	162.0—163.0	3360, 3460	4.13 (2H, s), 4.80(2H, s, NH_2), 7.55—7.69 (5H, m)	231 (4.52), 257 (4.65), 325 (4.12), 370 (3.49)	810
5b	236.0—237.0	1658, 3240	2.21 (3H, s), 4.33(2H, s), 7.44—7.91 (6H, m), 9.79 (1H, s, NH)	218 (4.44), 262 (4.71), 297 (4.08), 308 (4.10), 337 (3.16), 354 (3.07)	870
6b	220.0—220.5	1652, 3260	2.15 (3H, s), 4.35(2H, s), 7.72—8.20 (6H, m), 9.63 (1H, s, NH)	241 (4.17), 273 (4.80), 309 (3.95), 330 (3.05), 346 (3.24), 364 (3.33)	810
7b	251.5—252.0	1660, 3250	2.16 (3H, s), 4.35(2H, s), 7.71—7.80 (5H, m), 8.10 (1H, s, H-9), 9.98 (1H, s, NH)	222 (4.26), 259 (4.56), 311 (4.16), 355 (3.10)	1390
8b	227.0—228.0	1654, 3240	2.24 (3H, s), 4.41(2H, s), 7.64—7.98(6H, m), 10.02 (1H, s, NH)	238 (4.48), 257 (4.69), 302 (4.09), 313 (4.09), 335 (3.23), 353 (3.15)	820
5c	255.0—257.0	1658, 3240	2.23 (3H, s), 4.39(2H, s), 7.70—8.04 (5H, m), 9.96 (1H, s, NH)	235 (4.36), 263 (4.75), 301 (4.12), 313 (4.13), 341 (3.50), 358 (3.50)	
7c	314.0—315.0	1662, 3250	2.18 (3H, s), 4.30(2H, s), 7.77—7.87 (3H, m), 8.16—8.21 (2H, m), 9.87 (1H, s, NH)	230 (4.42), 264 (4.80), 311 (4.15), 339 (3.37), 357 (3.37)	

$CDCl_3$ (**1**—**4**) or DMSO-d_6 (**5**—**8**) as the solvent. The agreement between the calculated and found values in the elemental analysis of the new compounds is within ±0.3% of variation.

The yield of each bromination is estimated from the average value of three or more runs. The components of the reaction mixtures were separated by gas chromatography (Shimadzu GC-6AM) using a column (1 m) containing 3% Dexsil 300 GC on Chromosorb WAW at 250 °C using FID detector. The amount of each peak was calculated by comparison with octacosane or dotriacontane which has been added as the internal reference to the substrate before the reaction. Retention time of each product is tabulated in Table 2.

The reactants were synthesized by the method similar to that described elsewhere.[3] Chloroform was percolated through an alumina column before use and the other solvents were distilled.

Bromination of 4H-Cyclopenta[def]*phenanthren-1-amine (**1a**).*

Typical Procedure I: Amine **1a** (103.2 mg, 0.5035 mmol) and dotriacontane (21.10 mg) were dissolved in $CHCl_3$ (50 ml), and cooled at 0 °C in the dark. A solution of Br_2 (1.2 mol equivalent to **1a**) in $CHCl_3$ (*ca.* 10 ml) was added all at once to the mixture, and the resulting mixture was stirred for 1 min. Aqueous $NaHSO_3$ (1%, 50 ml) was added to quench the reaction; the organic layer was neutralized by aqueous ammonia (28%) and dried over anhydrous Na_2SO_4, and the solution was submitted to gas chromatography.

Upon evaporation of the solvent, the residue was chromatographed on a silica-gel column (1.8 cm ϕ, 60 cm) with benzene. The lower band of the column was extracted with benzene to give a trace amount of **1c**, mp 164.0—165.0 °C (decomp). The middle band yielded 82 mg (58%) of **1b**, mp 169.0—169.5 °C (decomp) by recrystallization from a mixture of benzene–hexane (*ca.* 1 : 1). The upper band of the column gave a trace amount of **1a**, mp 128—129 °C.

Procedure II: The amine (0.5 mmol) was treated with HBr (48%, 0.6 mmol) in DMSO (60 ml) at 80 °C for 60 min. After addition of aqueous $NaHSO_3$ and neutralization by aqueous ammonia, the mixture was extracted with benzene (50 ml) and analyzed by means of gas chromatography.

The reaction of **3a** gave, in addition to **3b**, a significant amount of dark tar materials from a silica-gel column; these were not studied further.

Procedure III: The acetamide (0.5 mmol) was allowed to react with Br_2 (0.6 mmol) in $CHCl_3$ (85 ml) at 0 °C for 5 min. The resulting solution was treated by a method similar to that described above.

*Deamination of **1b**.* Bromo amine **1b** (134.6 mg, 0.47 mmol) was dissolved in a mixture of THF (2 ml), concd HCl (5 ml), and H_2O (5 ml) and the resulting amine hydrochloride was diazotized with aqueous $NaNO_2$ (5%, 1 ml) at 0—5 °C according to the literature.[8] The reaction mixture was stirred with H_3PO_2 (*ca.* 50%, 3.5 ml) for 17 h at room temperature. The precipitate was extracted with benzene and the benzene solution was chromatographed on a silica gel to yield 2-bromo-4*H*-cyclopenta[*def*]phenanthrene (30.4 mg, 24%), mp 91—92 °C, identical in all respects with an authentic sample.[1]

Also, **2b** afforded the 1-bromide (50% yield, mp 85—86 °C), **3b** gave 8-bromide (42%, mp 94.5—95.5 °C), and **4b** yielded 8-bromide (66%), respectively, by a treatment similar to those described above.

*Acetylation of **1b**.* Bromo amine **1b** (142 mg, 0.50 mmol) was treated with Ac_2O (10 ml) in dry benzene (50 ml) at reflux for 30 min to give **5b** (160 mg, 98%), mp 236—237 °C (decomp), which was identical in all respects with the product obtained by bromination of **5a**.

References

1) M. Yoshida, M. Minabe, and K. Suzuki, *J. Org. Chem.*, **44**, 3029 (1979).

2) M. Yoshida, H. Hirota, M. Minabe, and K. Suzuki, *J. Chem. Eng. Data*, **26**, 220 (1981).

3) M. Yoshida, S. Nagayama, M. Minabe, and K. Suzuki, *J. Org. Chem.*, **44**, 1915 (1979).

4) In our analogous experiment, the reaction of 8,9-dihydro-4*H*-cyclopenta[*def*]phenthren-2-amine with Br_2 in HOAc–HBr showed regioselectivity different from that in $CHCl_3$.

5) T. L. Fletcher, M. J. Namkung, and H.-L. Pan, *Chem. Ind. (London)*, **1957**, 660.

6) R. De Ridder and R. H. Martin, *Bull. Soc. Chim. Belg.*, **69**, 534 (1960); *Chem. Abstr.*, **55**, 14408 (1961).

7) C. Eaborn, P. Golborn, R. E. Spillett, and R. Taylor, *J. Chem. Soc., B*, **1968**, 1112.

8) H.-L. Pan and T. L. Fletcher, *Synthesis*, **1973**, 610.

The Generation of the Ethenethiolate Anion and Its Reaction with Several Chloromethyl Alkyl Ethers and Sulfides

Shigeo TANIMOTO,* Hideyuki IKEHIRA, Tatsuo OIDA, and Toshio KOKUBO
Institute for Chemical Research, Kyoto University, Uji, Kyoto 611

(Received October 18, 1982)

Synopsis. 2-Ethoxy-1,3-oxathiolane was deprotonated at the 4-position, followed by the cycloelimination of the resultant anion, leading to ethyl formate and the ethenethiolate anion. The anion was trapped by several chloromethyl alkyl ethers and sulfides to afford alkoxy(vinylthio)methanes and alkylthio(vinylthio)methanes respectively.

In a previous article[1] it was shown that 2-ethoxy-1,3-oxathiolane (**1**) undergoes ring cleavage on treatment with an excess of butyllithium in hexane, giving 5-nonanol together with 5-butyl-5-nonanol. By a similar treatment, 2-ethoxy-1,3-dithiolane (**2**) was also opened to produce 5-nonanethiol, along with 5-butyl-5-nonanethiol. Although the correct mechanism of these reactions is even now in doubt, it may involve three steps. The first step is the deprotonation at the 4-position of **1** or **2**. The second one is the cycloelimination of the resultant anion, leading to ethyl formate or *O*-ethyl thioformate, along with the ethenethiolate anion. The last step is the nucleophilic attack of 2 mol of butyllithium on the intermediate ethyl formate or *O*-ethyl thioformate to afford 5-nonanol or 5-nonanethiol.

Deprotonation at the 4-position of the 1,3-dithiolane ring by a strong base was initially confirmed by Wilson and his co-workers,[2] who reported that the reaction of 2-hexyl-1,3-dithiolane with an excess of butyllithium in ether gives 5-undecanethiol and 5-(butylthio)-undecane. More recently, we ourselves have found[3] that several 2-alkyl-2-aryl- and 2,2-diaryl-1,3-dithiolanes undergo predominant fragmentation by lithium diisopropylamide (LDA) in tetrahydrofuran, a process which is initiated by proton abstraction from C-4. Thus, it is conceivable that the reaction of **2** with butyllithium proceeds by a mechanism involving deprotonation at the 4-position in the first step. On the other hand, no description of deprotonation at the 4-position of the 1,3-oxathiolane ring by any one of the strong bases is available, although it is already well known that a few 1,3-oxathiolane derivatives are capable of proton abstraction from their C-2.[4] In order to verify the deprotonation at C-4 of the 1,3-oxathiolane ring by a strong base, we submitted **1** to a deprotonation-fragmentation sequence using LDA, since a hydrogen at C-4 seems to be more labile than that at C-2 in **1**. When **1** was treated with an excess of LDA in tetrahydrofuran at −78 °C, followed by the addition of an appropriate chloromethyl alkyl ether or sulfide, a series of alkoxy(vinylthio)methanes (**5**) or alkylthio(vinylthio)methanes (**6**) were obtained in moderate yields, suggesting the intermediary presence of the ethenethiolate anion (**4**) in the course of the reaction. The formation of the intermediate **4** is best explained by assuming that the initial deprotonation by LDA occurred not at the 2-position, but at the 4-position of **1**, and that it is followed by the fragmentation. On that occasion, there is no reaction between the less nucleophilic LDA and the ethyl formate which has been produced simultaneously.

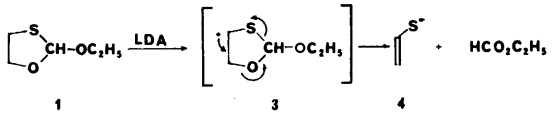

1 3 4

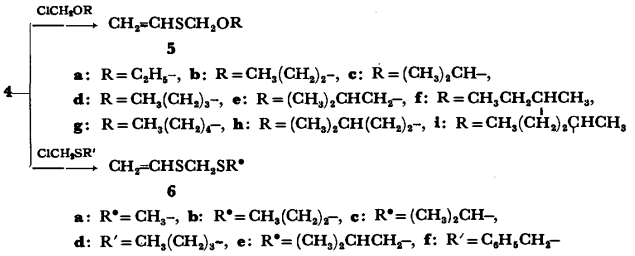

TABLE 1. REACTION PRODUCTS IN THE REACTION OF THE ETHENETHIOLATE ANION (**4**) WITH CHLOROMETHYL ALKYL ETHERS

R in chloromethyl alkyl ether used	**5** Abbr.	Yield/%[a]	Bp θ_b/°C (Torr)[b]	Found (Calcd)(%) C	H	^{1}H-NMR (δ, in $CDCl_3$)
C_2H_5–	**5a**	47	55—58(30) [lit[5], 41(17)]	51.08 (50.81)	8.61 (8.53)	1.19 (t, 3H), 3.54 (q, 2H), 4.77 (s, 2H), 5.19 (d, 1H), 5.30 (d, 1H), 6.40 (dd, 1H)
$CH_3(CH_2)_2$–	**5b**	39	64—70(27) [lit[5], 52(11)]	54.26 (54.50)	8.99 (9.15)	0.91 (t, 3H), 1.3—1.8 (m, 2H), 3.42 (t, 2H), 4.78 (s, 2H), 5.18 (d, 1H), 5.28 (d, 1H), 6.42 (dd, 1H)
$(CH_3)_2CH$–	**5c**	47	52—57(25.5) [lit[5], 47(15)]	54.33 (54.50)	9.04 (9.15)	1.15 (d, 6H), 3.6—4.2 (m, 1H), 4.78 (s, 2H), 5.20 (d, 1H), 5.31 (d, 1H), 6.42 (dd, 1H)
$CH_3(CH_2)_3$–	**5d**	58	71—75(23)	57.28 (57.49)	9.61 (9.65)	0.90 (t, 3H), 1.2—1.8 (m, 4H), 3.46 (t, 2H), 4.76 (s, 2H), 5.16 (d, 1H), 5.27 (d, 1H), 6.37 (dd, 1H)
$(CH_3)_2CHCH_2$–	**5e**	51	66—70(25)	57.31 (57.49)	9.40 (9.65)	0.90 (d, 6H), 1.5—2.2 (m, 1H), 3.22 (d, 2H), 4.71 (s, 2H), 5.11 (d, 1H), 5.22 (d, 1H), 6.31 (dd, 1H)
$CH_3CH_2CHCH_3$ |	**5f**	50	64—68(23.5)	57.19 (57.49)	9.46 (9.65)	0.89 (t, 3H), 1.12 (d, 3H), 1.1—1.7 (m, 2H), 3.3—3.9 (m, 1H), 4.75 (s, 2H), 5.19(d, 1H), 5.29 (d, 1H), 6.40 (dd, 1H)
$CH_3(CH_2)_4$–	**5g**	60	91—97(22.5)	59.77 (59.95)	9.95 (10.06)	0.89 (t, 3H), 1.1—1.8 (m, 6H), 3.47 (t, 2H), 4.76 (s, 2H), 5.20 (d, 1H), 5.31 (d, 1H), 6.39 (dd, 1H)
$(CH_3)_2CH(CH_2)_2$–	**5h**	58	85—91(23)	60.04 (59.95)	10.09 (10.06)	0.90 (d, 6H), 1.2—1.9 (m, 3H), 3.50 (t, 2H), 4.77 (s, 2H), 5.20 (d, 1H), 5.28 (d, 1H), 6.40 (dd, 1H)
$CH_3(CH_2)_2CHCH_3$ |	**5i**	56	79—85(22.5)	59.82 (59.95)	10.06 (10.06)	0.90 (t, 3H), 1.19 (d, 3H), 1.2—1.8 (m, 4H), 3.4—3.9 (m, 1H), 4.80 (s, 2H), 5.20 (d, 1H), 5.28 (d, 1H), 6.41 (dd, 1H)

a) Isolated yield (based on 1). b) 1 Torr=133.322 Pa.

Table 2. Reaction products in the reaction of the ethenethiolate anion (**4**) with chloromethyl alkyl sulfides

R′ in chloromethyl alkyl sulfide used	**6** Abbr.	Yield/%[a]	Bp θ_b/°C (Torr)[b]	Found (Calcd)(%) C	H	^{1}H-NMR (δ, in $CDCl_3$)
CH_3–	**6a**	67	60—66 (26.5) [lit,[6] 48(7)]	40.26 (39.96)	6.75 (6.71)	2.10 (s, 3H), 3.75 (s, 2H), 5.16 (d, 1H), 5.20 (d, 1H), 6.39 (dd, 1H)
$CH_3(CH_2)_2$–	**6b**	62	94—99 (21.5) [lit,[6] 79—80(7)]	48.72 (48.60)	8.20 (8.16)	0.98 (t, 3H), 1.3—1.9 (m, 2H), 2.61 (t, 2H), 3.77 (s, 2H), 5.10 (d, 1H), 5.19 (d, 1H), 6.42 (dd, 1H)
$(CH_3)_2CH$–	**6c**	58	66—69 (9.5) [lit,[6] 67(7)]	48.77 (48.60)	8.09 (8.16)	1.30 (d, 6H), 2.8—3.3 (m, 1H), 3.79 (s, 2H), 5.07 (d, 1H), 5.18 (d, 1H), 6.38 (dd, 1H)
$CH_3(CH_2)_3$–	**6d**	56	96—102 (5)	51.88 (51.80)	8.61 (8.69)	0.91 (t, 3H), 1.1—1.8 (m, 4H), 2.64 (t, 2H), 3.76 (s, 2H), 5.20 (d, 1H),5.24 (d, 1H), 6.26 (dd, 1H)
$(CH_3)_2CHCH_2$–	**6e**	63	83—88 (4.5)	52.03 (51.80)	8.74 (8.69)	0.98 (d, 6H), 1.5—2.2 (m, 1H), 2.50 (d, 2H), 3.76 (s, 2H), 5.20 (d, 1H), 5.23 (d, 1H), 6.40 (dd, 1H)
$C_6H_5CH_2$–	**6f**	32	135—142 (4)	61.09 (61.18)	6.08 (6.16)	3.55 (s, 2H), 3.76 (s, 2H), 5.19 (d, 1H), 5.24 (d, 1H), 6.37 (dd, 1H), 7.0—7.6 (m, 5H)

a) Isolated yield (based on **1**). b) 1 Torr=133.322 Pa.

The products obtained in this procedure are summarized in Tables 1 and 2, together with their physical properties. Some of these products have been already synthesized by other chemists *via* another route; therefore, our procedure provides an alternative method for the preparation of these acetals.

Experimental

The starting compound **1** was prepared as previously reported.[1] The chloromethyl ethyl ether and chloromethyl methyl sulfide were commercially available and were distilled just before use. The other chloromethyl alkyl ethers and sulfides were made according to one of the published procedures.[7]

*Generation of Ethenethiolate Anion (**4**) from 2-Ethoxy-1,3-oxathiolane (**1**) with LDA and Trapping of **4** by Chloromethyl Alkyl Ethers and Sulfides. General Procedure*: A solution of diisopropylamine (5.0 g, 49.4 mmol) in tetrahydrofuran (40 ml) was cooled to −10—−5 °C under nitrogen, treated with a 1.56 molar solution (31 ml, 48.4 mmol) of butyllithium in hexane, and then stirred at the same temperature for 30 min. The solution of LDA thus prepared was cooled to −78 °C, and a solution of **1** (2.7 g, 20.1 mmol) in tetrahydrofuran (3 ml) was added. After an additional 30 min stirring at −78 °C, 40.8 mmol of a chloromethyl alkyl ether or a sulfide was stirred in. The stirring was continued for 30 min at −78 °C and then for a further 1—2 h at room temperature, after which the mixture was quenched with 60 ml of saturated aqueous NH_4Cl and then extracted with ether (3×50 ml). The combined organic layer was washed repeatedly with a 10% aqueou NaOH solution saturated with Na_2SO_4 and once with saturated aqueous Na_2SO_4. The layer was dried over anhydrous $MgSO_4$, filtered, and concentrated *in vacuo* to give a residue, which was then distilled. The distillate was further chromatographed on silica gel to provide a pure product. Five% ether–hexane was used as the eluent for **5**, and hexane, for **6**.

References

1) S. Tanimoto, T. Miyake, and M. Okano, *Bull. Inst. Chem. Res., Kyoto Univ.*, **55**, 276 (1977).

2) S. R. Wilson, G. M. Georiadis, H. N. Khatri, and J. E. Bartmess, *J. Am. Chem. Soc.*, **102**, 3577 (1980); S. R. Wilson, P. Caldera, and M. A. Jester, *J. Org. Chem.*, **47**, 3319 (1982).

3) H. Ikehira, S. Tanimoto, T. Oida, and M. Okano, *J. Org. Chem.*, in press.

4) For example, M. Jones, P. Temple, E. J. Thomas, and G. H. Whitham, *J. Chem. Soc., Perkin Trans. 1*, **1974**, 433.

5) R. Kroker and H. Ringsdorf, *Makromol. Chem.*, **121**, 240 (1969).

6) K. D. Gollmer, F. H. Mueller, and H. Ringsdorf, *Makromol. Chem.*, **92**, 122 (1966).

7) H. R. Henze, V. B. Duff, W. H. Matthews, J. W. Melton, and E. O. Forman, *J. Am. Chem. Soc.*, **64**, 1222 (1942); H. Böhme, H. Fischer, and R. Frank, *Justus Liebigs Ann. Chem.*, **563**, 54 (1949); A. J. Hill and D. T. Keach, *J. Am. Chem. Soc.*, **48**, 257 (1926); J. W. Farren, H. R. Fife, F. E. Clark, and C. E. Garland, *ibid.*, **47**, 2419 (1925).

A Revised Absolute Configuration of 2-Hydroxy-1,1'-binaphthyl

Kuninobu KABUTO,* Fujiko YASUHARA, and Shozo YAMAGUCHI
Department of Chemistry, College of General Education, Tohoku University, Kawauchi, Sendai 980
(Received October 29, 1982)

Synopsis. The absolute configuration of 2-hydroxy-1,1'-binaphthyl (**3**) has been revised to (*R*)-(+) in THF by a reexamination of the previously reported chemical correlation between **3** and 2,2'-diamino-1,1'-binaphthyl. This revised configuration agreed with that obtained from the assignment by means of the MTPA/LSR method.

In the course of the ^{1}H NMR study aimed at determining the absolute configuration of axially chiral biaryls using α-methoxy-α-trifluoromethylphenylacetic acid (MTPA, Mosher's reagent) derivatives (esters and amides) and achiral lanthanoide shift reagents (MTPA/LSR method),[1] we have found that the (*R*)-MTPA esters (amides) of a series of binaphthyls with the configuration indicated in Fig. 1A have larger lanthanoid-induced shifts of the signals due to MeO groups in the MTPA moieties (LIS_{OMe}) than the alternate derivatives of the binaphthyls with the opposite configuration (Fig. 1B). These results can reasonably be interpreted[1] by considering the preferred coordination of the shift reagent to the diastereomeric MTPA derivatives. We faced, however, an exceptional case in correlating the relative magnitudes of LIS_{OMe} to the absolute configurations of the binaphthyls of this type; the regurality described above did not hold for a fundamental binaphthol **3** if the reported configuration of **3** is correct.

There have been two reports on the absolute configuration of **3**. In the first report, (*R*) configuration was tentatively assigned to (+)-isomer in methanol from the result of Prelog's atrolactic acid synthesis.[2] In the second, (−)-**3** was correlated chemically to (−)-2,2'-diamino-1,1'-binaphthyl (**1**), whose configuration had been known to be (*S*), thus establishing the absolute configuration as (*R*)-(−) in THF, as is shown in Scheme 1.[3,4] Although this result seems to contradict that obtained from the Prelog rule, it must be noticed that the optical rotation in each study was taken in a different solvent. We have found that the sign of the optical rotation of **3** in methanol is the opposite of that in THF. The results from these two independent studies, therefore, eventually agree and contradict the result obtained by the use of the MTPA/LSR method. This discrepancy needs to be investigated further, and so we have reexamined the reported chemical correlation between **3** and **1**.

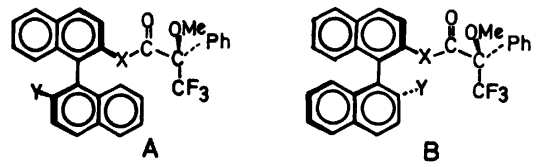

X=O; Y=OMe, (*R*)-MTPA ester
X=NH; Y=H, (*R*)-MTPA amide
Fig. 1.

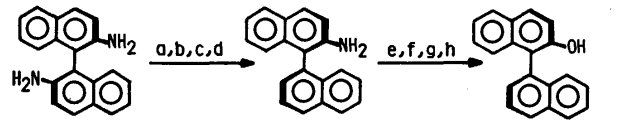

(S)-1	(R)-2	(R)-3
$[\alpha]_D^{30}$ (benzene)	$[\alpha]_D^{25}$ (THF)	$[\alpha]_D^{20}$ (THF)
-87.5°, c 1.57	-26.9°, c 1.13	+4.77°, c 0.86
Ref. 3, -95.5°(25°C)	-51.4°, c 1.0	-2.9°, c 1.0

Scheme 1. Configurational correlation between **1** and **3**. a: 1 equiv. Ac_2O, b: HNO_2, c: 48% H_3PO_2, d: concd HCl, e: HNO_2, f: 42% HBF_4, g: 100 °C/AcOH, h: 5% KOH/MeOH.

In the reexamination of the correlation, (*S*)-(−)-**1** was correlated to (−)-**2**, in agreement with the reported result, while (−)-**2** was converted to (+)-**3**, contrary to the previous result. In order to confirm this result, the same correlation was carried out using (*R*)-(+)-**1**, and (−)-**3** was obtained by way of (+)-**2**. In addition, the CD spectra of (−)-**3** and (+)-**2** (Fig. 2) showed the same sign of the Cotton effect, indicating that the configurations of these two were the same.[5] From these new facts, the absolute configurfftion of **3** must be revised to (*R*)-(+) in THF and (*R*)-(−) in methanol.[6] Thus, it is clear that the MTPA/LSR method affords the correct assignment of the configuration of **3**.

Although it has been widely accepted that the Prelog rule can be extended to axially chiral biaryls[7,8] on the basis of Berson's correlation model,[9] it is now clear that the model leads to a wrong configurational assignment for **3**. Therefore, the general applicability of Berson's model must be reconsidered.

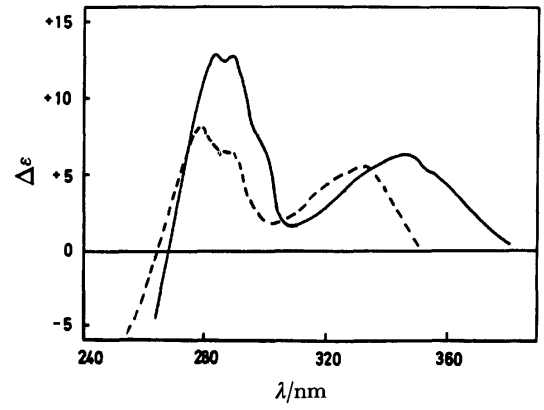

Fig. 2. CD spectra of **2** and **3** in methanol.
——: **2**, ------: **3**; The spectra were determined on the partially active **2** [$[\alpha]_D^{25}$ +24.7° (*c* 0.96, THF), 38% e.e., based on the maximum rotation (+65.2°) estimated by NMR[13]] and **3** [$[\alpha]_D^{20}$ −12.6° (*c* 1.45, THF), 98% e.e.] and corrected for enantiomeric purities.

Experimental

Instruments. The ^{1}H NMR spectra were determined on a Hitachi R-22, 90 MHz spectrometer. The optical rotations were taken on a Perkin-Elmer 241 electronic polarimeter using a 1-dm thermostated microcell. The CD spectra were taken on a JASCO J-20 spectropolarimeter using a 1-cm cell.

(±)-2-Hydroxy-1,1′-binaphthyl (3). A mixture of 2-methoxy-1,1′-binaphthyl (1.42 g, 5 mmol, mp 113—114 °C, lit,[2] 110—111 °C) and lithium iodide (1.34 g, 10 mmol, dried at 300 °C under nitrogen) in collidine (8 ml) was refluxed for 10 h. After cooling, the mixture was poured into ice-water (60 ml) and extracted with benzene. The extract was washed with 2 M HCl, saturated $NaHCO_3$, water, and dried (Na_2SO_4), and then concentrated to give colorless crystals, which were subsequently recrystallized from methanol; 0.97 g (72%), mp 93—95 °C,[10] M$^+$ 270. Found: C, 88.99; H, 5.38%. Calcd for $C_{20}H_{14}O$: C, 88.86; H, 5.22%. ^{1}H NMR ($CDCl_3$) 4.89 (s, OH), 6.9—8.0 (m, aromatic H); IR ($CHCl_3$) 3540, 3050, 3000, 1615, 1595, 1380, 1190 cm^{-1}.

Resolution of 3. The racemic **3** (81 mg, 0.3 mmol) was esterified with acid chloride of (*R*)-MTPA [88 μl, $[\alpha]_D^{24}$ +134.5° (*c* 5.6, CCl_4)] in pyridine (1 ml) in the presence of 4-dimethylaminopyridine (24 mg, 2 mmol) overnight at room temperature. After a usual work-up, the crude product was purified by column chromatography (silica gel, 7% AcOEt in hexane); the resulting diastereomeric mixture of (*R*)-(+)-MTPA esters (105 mg, 72%) was subsequently resolved by HPLC; Lichrospher SI 100 (Merk) 7.8 mm × 30 cm, 3% diisopropyl ether in hexane, Flow rate, 4 ml/min, α=1.15. Less polar (*R*)-MTPA ester; 53 mg, ^{1}H NMR ($CDCl_3$) 2.72 (s, OMe), 6.9—8.0 (m, aromatic H), IR ($CHCl_3$) 1772 cm^{-1}. More polar (*R*)-MTPA ester; 39 mg, ^{1}H NMR ($CDCl_3$) 2.82 (s, OMe), 6.9—8.0 (m, aromatic H), IR ($CHCl_3$) 1772 cm^{-1}.

A solution of less polar (*R*)-MTPA ester (50 mg) in 5% methanolic KOH (1 ml) was refluxed for 1/2 h. After acidification with 2 M HCl, the mixture was extracted with benzene, and the extract was washed with saturated $NaHCO_3$ and water, and then dried (Na_2SO_4). The solvent was removed, and the residue was purified by TLC (silica gel, 20% AcOEt in hexane) to give 23.5 mg of **3**; mp 160—163 °C (recrystallized from MeOH), $[\alpha]_D^{30}$ +1.9°, $[\alpha]_D^{20}$ +5.6° (*c* 1.0, MeOH), $[\alpha]_D^{20}$ −12.9° (*c* 1.34, THF); M$^+$ 270. Found: C, 88.96; H, 5.26%. Calcd for $C_{20}H_{14}O$: C, 88.86, H, 5.22%.

By the same procedure, the more polar (*R*)-MTPA ester (39 mg) afforded 18.3 mg of **3**; mp 161—164 °C[11] (recrystallized from MeOH); $[\alpha]_D^{30}$ −1.8°,[11] $[\alpha]_D^{20}$ −5.2° (*c* 1.03, MeOH); $[\alpha]_D^{20}$ +13.0°[11] (*c* 1.12, THF).

Configurational Assignment of 3 by the (R)-MTPA/LSR Method. A ^{1}H NMR shift study was conducted on a carbon tetrachloride solution of the diastereomeric mixture of (*R*)-MTPA esters (49 mg) prepared from a partially active **3** ($[\alpha]_D^{20}$ −6.83° (*c* 1.61, THF)) and acid chloride of (*R*)-MTPA. The lanthanoid-induced shifts of the signals due to MeO groups in the MTPA moieties (LIS_{OMe}) were determined by the successive addition of Eu(fod)$_3$ (0.1—0.5 equivalent). The smaller MeO signal initially located at 2.82 ppm showed a larger induced shift (LIS_{OMe}=5.8) than the larger one at 2.72 ppm (LIS_{OMe}=5.1). From the consideration of the preferred coordination of the shift reagent with the diastereomeric MTPA esters,[1] (*R*) configuration was assigned to (+)-isomer in THF.

Chemical Correlation between the Absolute Configurations of 3 and 1. By the previously reported procedure,[3] a partially active (*S*)-(−)-**1**[12] ($[\alpha]_D^{30}$ −87.5° (*c* 1.57, benzene)) was transformed to (*R*)-(−)-**2**; $[\alpha]_D^{25}$ −26.9° (*c* 1.13, THF); M$^+$ 269. Found: C, 89.35; H, 5.78; N, 5.21%. Calcd for $C_{12}H_{15}N$: C, 89.18; H, 5.61; N, 5.20%.

This (−)-**2** (128 mg) was further converted to crude **3** (60 mg, $[\alpha]_D^{25}$ +1.30° (*c* 1.08, THF)) by the procedure previously described in the literature (diazotization, thermal decomposition of diazonium salt in acetic acid, and hydrolysis, successively). The crude **3** was purified by HPLC (Lichrospher SI 100 (Merk) 7.8 mm × 30 cm, 6% AcOEt in hexane) to give colorless crystals; 42.8 mg, M$^+$ 270, $[\alpha]_D^{20}$ +4.77° (*c* 0.86, THF). The IR ($CHCl_3$) and ^{1}H NMR ($CDCl_3$) spectra of this product agreed with those of authentic racemic and optically active **3**.

By the same procedure, (R)-(+)-**1**[12] ($[\alpha]_D^{30}$ +77.6° (*c* 1.64, benzene)) was correlated to (*S*)-(+)-**2** ($[\alpha]_D^{25}$ +24.7° (*c* 0.96, THF)), which was successively correlated to (*S*)-(−)-**3**, M$^+$ 270; $[\alpha]_D^{20}$ −2.43° (*c* 1.48, THF).

We are grateful to Dr. T. M. Suzuki of the Government Industrial Research Institute for the CD measurement.

References

1) K. Kabuto, F. Yasuhara, and S. Yamaguchi, *Tetrahedron Lett.*, **22**, 659 (1981).

2) J. A. Berson and M. A. Greenbaum, *J. Am. Chem. Soc.*, **80**, 653 (1958).

3) H. Akimoto and S. Yamada, *Tetrahedron*, **27**, 5999 (1971).

4) In Ref. 3, the authors stated that (*S*)-(−)-**3** and (*S*)-(−)-**2** were obtained from (*S*)-(−)-**1**. According to Cahn-Ingold-Prelog sequence rule, however, the configuration of **2** and **3** should be (*R*).

5) These CD spectra showed the same sign as, and a pattern similar to, those of (*R*)-2,2′-disubstituted 1,1′-binaphthyls, whose configurations correspond to (*S*)-**2** and (*S*)-**3**; K. Mislow, E. Bunnenberg, R. Records, K. Wellman, and C. Djerassi, *J. Am. Chem. Soc.*, **85**, 1342 (1963).

6) Very recently, this observation has been confirmed by Meyers and Cram. a) A. I. Meyers and K. A. Lutomski, *J. Am. Chem. Soc.*, **104**, 879 (1982); b) J. M. Willson and D. J. Cram, *ibid.*, **104**, 881 (1982).

7) J. D. Morrison and H. S. Mosher, "Asymmetric Organic Reactions," Prentice-Hall, New Jersey (1971), p. 63.

8) J. C. Fiaud, "Stereochemistry," ed by H. B. Kagan, Georg Thieme, Stuttgart (1977), Vol. 3, p. 31.

9) J. A. Berson and M. A. Greenbaum, *J. Am. Chem. Soc.*, **80**, 445 (1958).

10) The mp does not agree with the previously reported value (188—189 °C, Ref. 2).

11) The mp and optical rotation are different from the values reported in Ref. 2 (mp 199—199.5 °C, $[\alpha]_D^{30}$ +21.7° in MeOH). However, these values are close to those recently reported by Meyers (mp 159—161°C, $[\alpha]_D$+13.8° in THF, Ref. 6a).

12) The mistypings [(*R*)-(−) and (*S*)-(+)-**5**] in our previous communication[1] should be corrected to (*R*)-(+) and (*S*)-(−).

13) K. Kabuto, F. Yasuhara, and S. Yamaguchi, *Tetrahedron Lett.*, **21**, 307 (1980).

Sesquiterpenoids in Cultured Cells of Liverwort, *Calypogeia granulata* INOUE

Reiji TAKEDA* and Kenji KATOH

Suntory Institute for Bioorganic Research, Wakayama-dai, Shimamoto-cho, Mishima-gun, Osaka 618

(Received October 30, 1982)

Synopsis. Three new sesquiterpenoids, trinoranastreptene, 2-acetoxy-3-hydroxybicyclogermacrene and 3-acetoxy-2-hydroxybicyclogermacrene, were isolated from cultured cells of *Calypogeia granulata* INOUE. Their structures have been established by spectroscopic analysis.

Recentry, we reported the production of volatile sesquiterpenoids by cultured cells from liverwort of *Calypogeia granulata* INOUE.[1] The result was that the production of essential oil in cultured cells, intact plants and redifferentiated plants was similar. Furthermore, we reported the isolation and structural determination of two new trinor-sesquiterpenoids, 3,10-dihydro-1,4-dimethylazulene and 3,7-dimethylindene-6-carbaldehyde, and biosynthetic studies of trinor-sesquiterpenoids, 1,4-dimethylazulene and 3,7-dimethylindene-6-carbaldehyde, using cultured cells instead of intact plants.[2] The isolation of three new sesquiterpenoids and the identification of eight sesquiterpenoids from the same cultured cells are reported.

The fresh cultured cells for 20 d were steam-distilled to obtain the essential oil (0.3% of fresh weight) as blue oil. The essential oil was subjected to SiO_2 column chromatography using hexane, $CHCl_3$ and Et_2O to give three fractions, I, II, and III. Sesquiterpene hydrocarbons from Fr. I were identified as β-elemene, bicycloelemene, eremophilene, ledene, alloaromadendrene and anastreptene[3] by IR, MS, and GC-retention time of authentic samples. 3-Acetoxy- and 3-hydroxybicyclogermacrene were isolated from Fr. II and identified with authentic data.[4] Three new sesquiterpenoids, trinoranastreptene (**1**), 2-acetoxy-3-hydroxybicyclogermacrene (**2**), and 3-acetoxy-2-hydroxybicyclogermacrene (**3**) were isolated from Fr. I and III, and their structures are described below.

Trinoranastreptene (**1**) was isolated from Fr. I by preparative GC. The molecular formula $C_{12}H_{16}$ of **1** was determined by the appearence of a molecular ion peak at m/z 160 in its mass spectrum. The 360 MHz ^{1}H NMR spectrum indicated signals due to a tertiary methyl at δ 0.93, olefinic methyl at δ 1.73, allylic CH_2 at δ 1.95 and 2.42, and three olefinic protons at δ 5.17, 5.49, and 6.12. In the decoupling experiments of **1**, irradiation of 4-CH_3 collapsed signals of 3-H and 2-H_A to sharp peaks and a multiplet of 2-H_B to a broad double doublet. Also, irradiation of 2-H_B converted two broad doublets of 3-H and 2-H_A into two broad singlets. Further, irradiation of the signal due to 6-H collapsed a double double doublet of 7-H to double doublet. In the NOE experiment of **1**, a 5% NOE was observed on 6-H upon irradiation of 4-CH_3. These results indicate that trinoranastreptene has a partial structure **1a**. The comparison of the 360 MHz NMR of **1** and **4** was quite similar except for the signals of two olefinic protons in **1** and two methyl groups and two protons on the cyclopropane ring in **4**. Also, 1-H of **1** appeared at low field of δ 1.98 relative to 1-H of **4** at δ 1.40. It was represented that 1-H of **4** shifted to high field by anisotropic effect of cyclopropane moiety. These results, together with biogentic consideration showed that the new trinor-sesquiterpene is most favourably represented by formula **1**.

2-Acetoxy-3-hydroxybicyclogermacrene (**2**) and 3-acetoxy-2-hydroxybicyclogermacrene (**3**) were isolated from fraction III by flash chromatography on SiO_2 eluted with hexane–EtOAc (3 : 1). Their molecular weight by high resolution mass spectra indicated the molecular formula to be $C_{17}H_{26}O_3$. Their IR spectra showed a hydroxyl absorption band (**2**: 3450; **3**: 3450 cm^{-1}) an ester absorption band (**2**: 1725; **3**: 1720 cm^{-1}) and a trisubstituted double bond absorption band (**2** and **3**: 1660 and 840 cm^{-1}). The ^{1}H NMR spectra of **2** and **3** indicated signals of two protons on the cyclopropane ring (**2**: δ 0.73 and 1.34; **3**: 0.73 and 1.34), *gem*-dimethyl group (**2**: δ 1.09 and 1.12; **3**: 1.05 and 1.10), two olefinic methyl groups (**2**: δ 1.66 and 1.72; **3**: 1.58 and 1.75), acetoxy methyl group (**2**: δ 2.13; **3**: 2.11) two methine protons (**2**: δ 4.45 and 5.42; **3**: 4.49 and 5.08) adjacent to oxygen and two olefinic protons (**2**: δ 5.10 and 5.23; **3**: 4.90 and 5.08). Acetylation of **2** and **3**, respectively yielded the same diacetate **5** identical in IR and ^{1}H NMR spectra. The ^{1}H NMR spectral signals of **3** closely resembled the corresponding signals in the spectrum of 3-acetoxybicyclogermacrene (**6**) isolated from the same cultured cells, with exception of signal of one proton on a carbon bearing a hydroxyl group at C-2, showing that this compound possessed the same bicyclogermacrene-type sesquiterpene skeleton. The location of acetoxyl and hydroxyl groups in **2** was suggested to be at C-2 and C-3 by spin decoupling experiments. When the proton attached to acetoxyl group at δ 5.42 was irradiated, proton on carbon bearing hydroxyl group (3-H) at δ 4.45 and olefinic proton (1-H) at δ 5.23 collapsed to

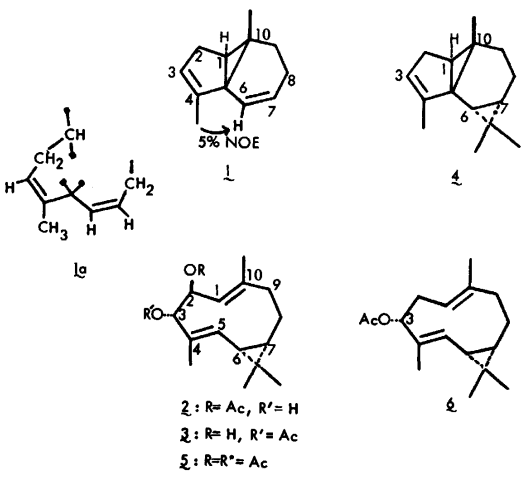

broad singlet, respectively. From the above results, the structures of two new sesquiterpenes were established to be **2** and **3**.

The relative stereostructure was determined by the following way. In the NOE experiments of **2**, a 12% NOE was observed on 6-H upon irradiation of 4-CH_3. Also, an 11% NOE was observed on 3-H upon irradiation of 4-CH_3. This result indicates that the hydroxyl group at C-3 and cyclopropane ring have a *cis* relation. The fact that 2-H is coupled to 3-H and 1-H with $J_{2,3}=3.0$ and $J_{1,2}=8.5$ Hz indicates that 2-H and 3-H have a *trans* relation based on inspection of Dreiding models.[5]

Experimental

IR spectra were measured with a Hitachi EPI-G2 spectrometer, ^{1}H NMR spectra with a JEOL FX-100 (100 MHz) or a Nicolet NT-360 (360 MHz) spectrometer in deuteriochloroform solution containing tetramethylsilane as an internal standard, low resolution mass spectra with a Hitachi RMU-6 and high resolution mass spectra with a JEOL 01SG-2, with direct inlet system operating at 70 eV. An analytical GC was performed with a Hitachi 163 type apparatus equipped with a Thermon 600 T glass capillary column, and preparative GC with a Varians model 920 fitted with an aluminum column (10 ft × 3/8 in) packed with 5% Thermon 1000 on Chromosorb W. The gas chromatograph was operated at a bath temperature of 180 °C, He gas was used as the carrier gas. Kieselgel 60 (E. Merck, Darmstadt) was used for column chromatography. Thin-layer chromatography (TLC) was carried out on Kieselgel GF_{254} (E. Merck, Darmstadt) in 0.25 mm thickness.

Isolation. The gametophyte cells developed from spores were cultured for 20 d in twenty 500 ml culture flasks, and the filtered cells (500 g) were steam-distilled to give 1.5 g of a blue oil (2—3.3% of dry weight). The essential oil was subjected to column chromatography on SiO_2. Elution with hexane gave sesquiterpene hydrocarbons (F-I) and 1,4-dimethylazulene. Elution with $CHCl_3$ yielded 3-acetoxybicyclogermacrene and 3-hydroxybicyclogermacrene (F-II). Elution with Et_2O yielded crude 2-acetoxy-3-hydroxybicyclogermacrene and 3-acetoxy-2-hydroxybicyclogermacrene (F-III).

Trinoranastreptene (**1**) was isolated from F-1 by preparative GC, as a colorless oil, ^{1}H NMR δ 0.93 (3H, s, 10-CH_3), 1.73 (3H, br. s, 4-CH_3), 2.00 (1H, br. dd, J=6.4 and 8.5 Hz, 1-H), 1.94 (1H, br. dd, J=6.4 and 17.2 Hz, 2-H_A), 2.42 (1H, m, 2-H_B), 5.16 (1H, br. s, 3-H), 5.49 (1H, ddd, J=2.5, 6.4 and 9.3 Hz, 7-H), and 6.12 (1H, d, J=9.3 Hz, 6-H); MS *m/z* (%) 160 (42, M^+, $C_{12}H_{16}$), 145 [100, $(M-CH_3)^+$], 130 (21).

2-Acetoxy-3-hydroxybicyclogermacrene (2) and 3-Acetoxy-2-hydroxybicyclogermacrene (3). The crude fraction (F-III) was purified by column chromatography on SiO_2. Elution with hexane–EtOAc (3 : 1) gave **2** (60 mg), colorless viscous oil, $[\alpha]_D^{22}$ −10.3° (*c* 0.8, $CHCl_3$); IR (film) 3450, 1725, 1660, and 840 cm^{-1}; ^{1}H NMR δ 0.73 (1H, ddd, J=3.0, 9.0, and 12.5 Hz, 7-H), 1.09 and 1.12 (3H each, s, *gem*-dimethyl), 1.34 (1H, dd, J=8.5 and 12.5Hz, 6-H), 1.66 and 1.72 (3H each, br. s, 4-CH_3 and 10-CH_3), 2.48 (1H, m, 9-H_A), 4.45 (1H, d, J=3.0 Hz, 3-H), 5.10 (1H, br. d, J=8.5 Hz, 5-H), 5.23 (1H, br. d, J=8.5 Hz, 1-H), and 5.42 (1H, dd, J=3.0 and 8.5 Hz, 2-H); MS *m/z* (%) 278 (trace, M^+), 218 [21, $(M-60)^+$], 137 (51), and 109 (100). Found: *m/z* 278.1908. Calcd for $C_{17}H_{26}O_3$: M, 278.1925.

Successive elution with the same solvent yielded **3** (45 mg), as a colorless viscous oil, $[\alpha]_D^{22}$ +63.2° (*c* 1.2, $CHCl_3$); IR (film) 3450, 1720, 1660, and 840 cm^{-1}; ^{1}H NMR δ 0.73 (1H, ddd, J=3.0, 9.0, and 12.5 Hz, 7-H), 1.05 and 1.10 (3H each,s, *gem*-dimethyl), 1.34 (1H, dd, J=8.5 and 12.5 Hz, 6-H), 1.58 and 1.75 (3H each, br. s, 4-CH_3 and 10-CH_3), 2.49 (1H, m, 9-H_A), 4.49 (1H, dd, J=3.0 and 8.5 Hz, 2-H), 4.90 (1H, br. d, J=8.5 Hz, 1-H), 5.08 (1H, br. d, J=8.5 Hz, 5-H), and 5.26 (1H, d, J=3.0 Hz, 3-H); MS *m/z* (%) 278 (trace, M^+), 218 [35, $(M-60)^+$], 152 (100), 109 (95). Found: *m/z* 278.1903. Calcd for $C_{17}H_{26}O_3$: M, 278.1925.

Acetylation of 2-Acetoxy-3-hydroxybicyclogermacrene (2). A solution of **2** (10 mg) in dry pyridine (1 ml) and Ac_2O (0.5 ml) was kept at room temperature for 1 d. The reaction mixture was treated in the usual way to give a residue, which was chromatographed on SiO_2. Elution with hexane–EtOAc (10 : 1) gave diacetate **5** (10 mg).

Acetylation of 3-Acetoxy-2-hydroxybicyclogermacrene (3). This compound (5 mg) was treated with Ac_2O (0.5 ml) and dry pyridine (1 ml) at room temperature for 1 d and then worked up in the usual way. The resulting residue was chromatographed on SiO_2 using hexane–EtOAc (10 : 1) to give diacetate **5** (6 mg), colorless viscous oil, IR (film) 1735, 1645 and 850 cm^{-1}; ^{1}H NMR δ 1.06 and 1.27 (3H each, s, *gem*-dimethyl), 1.66 and 1.77 (3H each, br. s, 4-CH_3 and 10-CH_3), 2.05 and 2.09 (3H each, s, -$COCH_3$), 4.96 (1H, br. d, J=8.5 Hz, 5-H), 5.09 (1H, br. d, J=8.5 Hz, 1-H), 5.39 (1H, d, J=3.0 Hz, 3-H), and 5.52 (1H, dd, J=3.0 and 8.5 Hz, 2-H); MS *m/z* (%) 320 (1, M^+, $C_{19}H_{28}O_4$), 278 [7, $(M-42)^+$], 218 [24, $(M-60)^+$], 152 (57), 109 (50), and 43 (100).

References

1) R. Takeda and K. Katoh, *Planta*, **151**, 525 (1981).
2) R. Takeda and K. Katoh, *J. Am. Chem. Soc.*, submitted.
3) N. H. Anderson, P. Bissonette, C. B. Liu, B. Shunk, Y. Ohta, C. W. Tseng, A. Moore, and S. Huneck, *Phytochemistry*, **16**, 1731 (1977).
4) Y. Asakawa, M. Toyota, and T. Takemoto, *Phytochemistry*, **19**, 2141, (1980).
5) K. Nishimura, I. Horibe, and K. Tori, *Tetrahedron*, **29**, 271, (1973).

Synthesis of 2,2-Dimethyl-2*H*-pyran-fused Flavonols Using the Modified Algar-Flynn-Oyamada Reaction

A. C. Jain,* S. M. Gupta, and Anita Sharma
Department of Chemistry, University of Delhi, Delhi-110007, India

(Received July 10, 1982)

Synopisis. 6-Acetyl-2,2-dimethylchromenes when separately condensed with *p*-anisaldehyde in the presence of ethanolic NaOH and subsequently oxidized with alkaline hydrogen peroxide without isolating the intermediate chalcones afforded the corresponding 2,2-dimethyl-2*H*-pyran-fused flavonols respectively in good yields. Thus, flavonols having free 3-hydroxyl and fused with 2,2-dimethyl-2*H*-pyran can be synthesized easily.

A number of naturally occurring flavonols possess 2,2-dimethyl-2*H*-pyran ring fused either linearly or angularly with the ring A. For example, sericetin (**1**) was isolated from *Mundulea vericea*[1] in 1960. The synthesis of this natural compound was itself achieved by Jain *et al.*[2] using galangin as the starting flavonol and introducing 2,2-dimethyl-2*H*-pyran ring system later. Similarly, kaempferol derivatives were synthesized by Jain *et al.*[3] An alternative approach for the same synthesis could be to carry out the flavonol synthesis starting from acetophenones having already condensed 2,2-dimethyl-2*H*-pyran ring. Since flavonols are best synthesized[4] by reactions using either Allan-Robinson condensation or Algar-Flynn-Oyamada (AFO) reaction and the former reaction is a high temperature reaction, we attempted preparation of 2,2-dimethyl-2*H*-pyran-fused flavonols by the latter reaction. The normal practice of carrying out the AFO reaction is to subject polyhydroxychalcones, completely protected except for the 2′-hydroxyl group, to oxidation with alkaline hydrogen peroxide.[5] Thus, a large number of flavonols including natural ones have been synthesized by this method.[4] In literature, Ozawa *et al.*[6] have also carried out the above reaction on the reaction mixture of the corresponding ketones and aldehydes without isolating the chalcones. Later, the same modified AFO reaction was also used for the synthesis of a few more flavonols by Smith *et al.*[7] We have now used this modified method for the synthesis of 2,2-dimethyl-2*H*-pyran-fused flavonols.

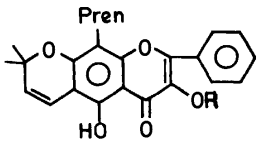

1

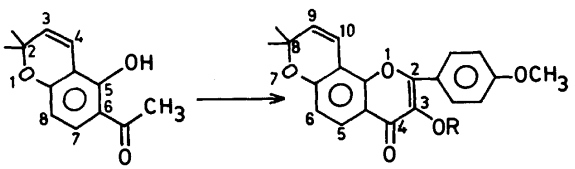

2 **3**. R = H; **4**. R = CH_3; **5**. R = $COCH_3$

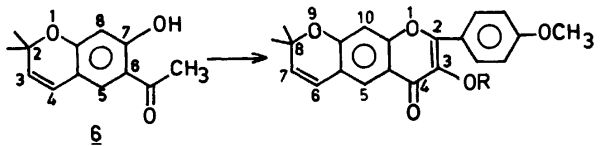

6 **7**. R = H; **8**. R = CH_3

As model cases, we have chosen 6-acetyl-2,2-dimethyl-5-hydroxychromene (**2**) and the corresponding 7-hydroxy isomer (**6**) as ketones and *p*-anisaldehyde as an aldehyde. The former chromene when condensed with *p*-anisaldehyde at a room-temperature in the presence of alkali and subsequently treated after 24 h with alkaline H_2O_2 in cold (below 15 °C) without isolating the intermediate chalcone, gave a flavonol derivative. It was identified as 3-hydroxy-2-(4-methoxyphenyl)-8,8-dimethyl-4*H*,8*H*-benzo[1,2-*b* : 5,6-*b*′]-dipyran-4-one (**3**) on the basis of its UV and ^{1}H NMR studies, which ruled out the possibility of alternate formation of the corresponding aurone, aurone hydrate or benzofuran derivatives, which are sometimes reported to form in the AFO reaction.[4] The UV spectrum (see Experimental) was typically of a flavonol derivative and the presence of hydroxyl group was indicated by positive iron(III) chloride reaction and by ^{1}H NMR signal at δ 13.86 and confirmed by the formation of its methyl ether (two methoxyls resonating at δ 3.72 and 3.78) and monoacetate (resonance signal of $-OCOC\underline{H}_3$ at δ 2.26). Further, the ^{1}H NMR spectra of the parent flavonol and its two derivatives showed the resonance signals of all the expected aromatic protons and 2,2-dimethyl-2*H*-pyran ring protons (see Experimental).

A parallel series of experiments with the isomeric chromene (**6**) and *p*-anisaldehyde gave 3-hydroxy-2-(4-methoxyphenyl)-8,8-dimethyl-4*H*,8*H*-benzo[1,2-*b* : 5,4-*b*′]dipyran-4-one (**7**) in very good yields. Again, the structure was established by UV and NMR spectra of the product itself and its methyl ether. From the above results, it appears that the modified AFO reaction can make 2,2-dimethyl-2*H*-pyran-fused flavonols easily accessible. This method has an additional advantage that the pyranoflavonols with a free hydroxyl group in position 3 can be obtained directly.

Experimental

All the mp reported are uncorrected. Unless stated otherwise, UV spectra were recorded on DU-2 spectrophotometer in methanol; the absorption values in parentheses represent log ε values; ^{1}H NMR spectra were recorded on Perkin-Elmer

R-32 (90 MHz) spectrometer in $CDCl_3$; chemical shifts are expressed in ppm downfield from TMS used as an internal reference compound; R_f values recorded refer to TLC plates for which the solvent system was one of the following: (A) chloroform, (B) benzene: petroleum ether (2 : 1) and (C) benzene : petroleum ether (2 : 3); new compounds (**3**, **5**, and **7**) reported showed satisfactory C and H percentages in elemental estimations.

*3-Hydroxy-2-(4-methoxyphenyl)-8,8-dimethyl-4*H,*8*H-*benzo*[*1*,*2*-b : *5*,*6*-b']*dipyran-4-one (3)*. A solution of 6-acetyl-5-hydroxy-2,2-dimethylchloromene[8] (**2**) (0.8 g, 3.68 mmol) and *p*-anisaldehyde (0.45 ml, 3.68 mmol) in ethanol (5 ml) was mixed with vigorous stirring with aq NaOH (0.5 g) at a room-temperature, when a heavy precipitate formed at once, presumably due to the salt formation. The mixture was allowed to stand overnight at a room-temperature and then dissolved in aq NaOH (1.25 g/7.5 ml). After cooling below 15 °C, H_2O_2 (0.42 ml, 30%, 3.68 mmol) was added quickly with stirring. As the oxidation mixture stood, the temperature rose between 38—40 °C. The mixture was cooled after 30 min and solidified with dil sulfuric acid, when the pyranoflavonol and inorganic sulfate precipitated out. The inorganic sulfate was dissolved by pouring the mixture in large amount of water. After standing for some time, the solid was filtered and crystallized from methanol when **3** formed as light yellow needles (600 mg), mp 137—138 °C; light brown color with ethanolic iron (III) chloride; R_f 0.58 (solvent B); Found: C, 71.7; H, 5.4%. Calcd for $C_{21}H_{18}O_5$: C, 72.0; H, 5.1%; UV: λ_{max} 360—368 (4.25), 273—281 (3.87) and 230 nm (4.12); IR: ν_{max} 3470 and 1625 cm^{-1}; ^1H NMR: δ 1.36 (s, 6H, $(C\underline{H}_3)_2C$<), 3.81 (s, 3H, $-OC\underline{H}_3$), 5.51 (d, 1H, J=9 Hz, $\underline{H}_9$), 6.31 (d, 1H, J=9 Hz, $\underline{H}_{10}$), 6.70 (d, 1H, J=10.5 Hz, $\underline{H}_6$), 6.85 (d, 2H, J=9 Hz, $\underline{H}_{3',5'}$), 7.51 (d, 2H, J=9 Hz, $\underline{H}_{2',6'}$), 7.62 (d, 1H, J=10.5 Hz, $\underline{H}_5$) and 13.86 (s, 1H, $-O\underline{H}$ at position 3).

The acetate prepared by the acetic anhydride-pyridine method was obtained as an yellow solid, mp 88—90 °C; R_f 0.32 (solvent B); Found: C, 70.3; H, 5.0%. Calcd for $C_{23}H_{20}O_6$: C, 70.4; H, 5.1%; ^1H NMR: δ 1.42 (s, 6H, $(C\underline{H}_3)_2C$<), 2.26 (s, 3H, $-OCOC\underline{H}_3$), 3.77 (s, 3H, $-OC\underline{H}_3$), 5.64 (d, 1H, J=9.5 Hz, $\underline{H}_9$), 6.34 (d, 1H, J=9.5 Hz, $\underline{H}_{10}$), 6.68 (d, 1H, J=10 Hz, $\underline{H}_6$), 6.82 (d, 2H, J=9 Hz, $\underline{H}_{3',5'}$), 7.47 (d, 2H, J=9 Hz, $\underline{H}_{2',6'}$), and 7.52 (d, 1H, J=10 Hz, $\underline{H}_5$).

*3-Methoxy-2-(4-methoxyphenyl)-8,8-dimethyl-4*H,*8*H-*benzo*[*1*,*2*-b : *3*,*4*-b']*dipyran-4-one (4)*. A solution of the above flavonol (**3**, 100 mg) in dry acetone (5 ml) was refluxed with dimethyl sulfate (0.15 ml) and K_2CO_3 (0.5 g) on water bath for 1 h. The product gave **4** as light yellow oil (80 mg), light red color with ethanolic iron (III) chloride R_f 0.29 (solvent B); ^1H NMR: δ 1.42 (s, 6H, $(C\underline{H}_3)_2C$<), 3.72, 3.78 (2s, 6H, 2-$OC\underline{H}_3$), 5.60 (s, 1H, J=9.5 Hz, $\underline{H}_9$), 6.51 (d, 1H, J=9.5 Hz, $\underline{H}_{10}$), 6.63 (d, 1H, J=10 Hz, $\underline{H}_6$), 6.85 (d, 2H, J=9 Hz, $\underline{H}_{3',5'}$), 7.43 (d, 2H, J=9 Hz, $\underline{H}_{2',6'}$), and 7.48 (d, 1H, J=10 Hz, $\underline{H}_5$).

*3-Hydroxy-2-(4-methoxyphenyl)-8,8-dimethyl-4*H,*8*H-*benzo*[*1*,*2*-b : *5*,*4*-b']dipyran-4-one *(7)*. A solution of 6-acetyl-7-hydroxy-2,2-dimethylchromene[9,10] (**6**) (0.92 mmol, 0.2 g) and an equivalent amount of *p*-anisaldehyde (0.11 ml) in ethanol (2 ml) was mixed with aq NaOH (0.12 g in 2.5 ml water). After 24 h at a room-temperature, the resulting solution was mixed in aq NaOH (0.32 g in 1.5 ml), cooled below 15 °C and treated with hydrogen peroxide (0.1 ml, 30%). The product was worked up and crystallized from methanol when **7** was obtained as light yellow needles (0.15 g), mp 157—158 °C; light brown color with ethanolic iron (III) chloride; R_f 0.74 (solvent C); Found: C, 72.3; H, 5.3%. Calcd for $C_{21}H_{18}O_5$: C, 72.0; H, 5.1%; UV: λ_{max} 366—381 (4.04), 272 (3.99), and 228 nm (4.15); IR: ν_{max} 3475 and 1625 cm^{-1}; ^1H NMR: δ 1.37 (s, 6H, $(C\underline{H}_3)_2C$<), 3.85 (s, 3H, $-OC\underline{H}_3$), 5.52 (d, 1H, J=9 Hz, $\underline{H}_7$), 6.27 (d, 1H, J=9 Hz, $\underline{H}_6$), 6.33 (s, 1H, $\underline{H}_{10}$), 6.85 (d, 2H, J=9 Hz, $\underline{H}_{3',5'}$), 7.43 (d, 2H, J=9 Hz, $\underline{H}_{2',6'}$), 7.62 (s, 1H, $\underline{H}_5$) and 13.54 (s, 1H, $-O\underline{H}$ at position 3).

*3-Methoxy-2-(4-methoxyphenyl)-8,8-dimethyl-4*H,*8*H-*benzo*[*1*,*2*-b : *5*,*4*-b']*dipyran-4-one (8)*. A solution of the above flavonol (**7**, 100 mg) in acetone (5 ml) was refluxed with dimethyl sulfate (0.15 ml) and K_2CO_3 (0.5 g) for 1 h and the reaction mixture was worked up as usual when **8** was obtained as a light yellow oil (70 mg); R_f 0.35 (solvent C); ^1H NMR: δ 1.42 (s, 6H, $(C\underline{H}_3)_2C$<), 3.80, 3.85 (2s, 6H, 2-$OC\underline{H}_3$), 5.46 (d, 1H, J=9.5 Hz, $\underline{H}_7$), 6.26 (d, 1H, J=9.5 Hz, $\underline{H}_6$), 6.36 (s, 1H, H_{10}) 6.85 (d, 2H, J=9 Hz, $\underline{H}_{3',5'}$), 7.40 (s, 1H, $\underline{H}_5$) and 7.49 (d, 2H, J=9 Hz, $\underline{H}_{2',6'}$).

The authors thank the CSIR for awarding SRF and JRF to SMG and AS respectively.

References

1) B. F. Burrows, W. D. Ollis, and L. M. Jackman, *Proc. Chem. Soc.*, **1960**, 177.
2) A. C. Jain and M. K. Zutshi, *Tetrahedron*, **29**, 3347 (1973).
3) A. C. Jain and R. K. Gupta, *Aust. J. Chem.*, **28**, 607 (1975).
4) H. Wagner and L. Farkas, "The Flavonoids," ed by J. B. Harborne, T. J. Mabry, and H. Mabry, Chapman and Hall, London (1975), p. 127.
5) L. Farkas, L. Hörhammer, H. Wagner, H. Rosler, and R. Gurniak, *Chem. Ber.*, **97**, 610 (1964).
6) H. Ozawa, T. Okuda, and S. Matsumoto, *J. Pharm. Soc. Jpn.*, **71**, 1178 (1958).
7) M. A. Smith, R. M. Neumann, and B. A. Webb, *J. Hetrocyclic Chem.*, **5**, 425 (1968).
8) A. C. Jain, P. Lal, and T. R. Seshadri, *Indian J. Chem.*, **7**, 1072 (1969).
9) B. S. Bajwa, P. Lal, and T. R. Seshadri, *Indian J. Chem.*, **9**, 17 (1971).
10) T. Anthonsen, *Acta Chem. Scand.*, **23**, 3605 (1969).

On the Sorption Behaviour of Some Cations on Cobalt Hexacyanoferrate(III) Exchanger. Binary Separations of Rb^+ and Cs^+ on Columns

Ajay K. JAIN,* Rajpal SINGH, and Chand BALA
Department of Chemistry, University of Roorkee, Roorkee 247672, India
(Received March 3, 1982)

Synopsis. Sorption behaviour of Ag, Cs, Rb, Co(II), Zn(II), and Fe(III) ions at low concentration (0.2 mmol) is studied in different concentrations of nitric acid and ammonium nitrate on cobalt hexacyanoferrate(III) exchanger. log K_d *vs.* log concentration plots show that the sorption of these ions is not followed through ion exchange mechanism, only. In case of Rb^+ and Cs^+, a very low K_d is observed at high concentration of nitric acid (>5 mol dm^{-3}) thereby showing the possibility of their elution on columns. For various other ions, such as Ba, Sr, Mn, Hg(II), Mg, Cd, Ca, Pb, Ni, La, and Th, the K_d values are almost zero. Thus the binary separation of Rb^+ and Cs^+ from a number of ions on the columns of this exchanger has been carried out.

During the last two decades a number of inorganic sorbents[1-6] have been prepared and their ion exchange behaviour studied. Although a number of hexacyanoferrates(III)[7-9] are insoluble, they have been little studied, with regard to their sorption behaviour. Recently we have reported on the sorption properties of chromium hexacyanoferrate(III).[10] This sorbent was found to be chemically more stable and showed better selectivity in sorption behaviour as compared to corresponding chromium hexacyanoferrate(II).[11] In view of better stability and selectivity of this hexacyanoferrate(III) exchanger, we have thought it desirable to investigate the exchange properties of other metal hexacyanoferrates(III). In a recent preliminary communication,[12] we have reported on the use of cobalt hexacyanoferrate(III)(CoFic) as Cu(II) selective exchanger. This exchanger is highly stable in salt solution and mineral acids and possesses potentiality for important separations. Further, sorption studies on this exchanger have now been undertaken.

Experimental

Cobalt(II) chloride (B. D. H.) and potassium hexacyanoferrate(III) (Sarabhai merck) both analytical reagent grade were used in the preparation of the exchanger without further purification. All other salts and acids were also of analytical grade. Radioisotopes of ^{134}Cs, ^{86}Rb, ^{110m}Ag, $^{85}Sr+^{89}Sr$, ^{133}Ba, ^{54}Mn, ^{58}Co, ^{65}Zn, ^{203}Hg, and $^{55}Fe+^{59}Fe$ were obtained from Bhabha Atomic Research Centre, Bombay.

Apparatus. pH measurements were made with ELICO pH meter model LI 10. Bausch and Lomb spectronic 20 was used for spectrophotometric determination of ions. Gamma counting of ^{110m}Ag, ^{134}Cs, ^{86}Rb, $^{85+89}Sr$, ^{54}Mn, ^{58}Co, ^{65}Zn, ^{203}Hg, and $^{55}Fe+^{59}Fe$ was done on a Scintillation counter (ECIL, Hyderabad) employing a well type NaI (Tl) crystal.

Preparation of Exchanger. Cobalt(II) potassium hexacyanoferrate(III) ($KCoFe(CN)_6 \cdot 5H_2O$) as reported earlier,[12] was obtained by the gradual addition of cobalt(II) chloride (0.12 mol dm^{-3}) to potassium hexacyanoferrate(III) (0.06 mol dm^{-3}) in a thermostat at 80 °C. The precipitate thus obtained was digested for ≈35 h and finally was washed with distilled water by centrifugation and dried in an oven at 80 °C. The precipitate was equilibrated with 1 mol dm^{-3} HNO_3 for 48 h, the acid being intermittently replaced. All further studies were carried out with exchanger pretreated with HNO_3.

Determination of Ions. Mg, Ca, Ni, Cu(II), Pb, Cd, Al, and Bi were determined by EDTA titrations and radiometric method was used for the determination of radio isotopes.

Determination of Distribution Coefficient. The distribution coefficients were determined by the batch equilibration method by shaking the exchanger (0.1 gm) with 10 cm^3 of 2×10^{-4} mol dm^{-3} metal ion solution in different concentrations of nitric acid or ammonium nitrate.

Determination of Sorption Capacity for Cs^+ and Rb^+ and Column Operation. Studies on the maximum uptake of Cs^+ and Rb^+ on cobalt hexacyanoferrate(III) were carried out by shaking 50 mg of the exchanger with 20 cm^3 solution of Rb^+ or Cs^+ (10^{-6} to 10^{-1} mol dm^{-3}). For column operations, a column of i.d. 0.5 cm containing 0.5 g exchanger was used. Column capacity was determined from breakthrough experiment using Rb^+ or Cs^+ solution (0.1 mol dm^{-3}) at 4 drops (≈0.2 cm^3) per minute and found to be 0.4 mequiv. g^{-1} both for Cs^+ and Rb^+. For separation studies, the column was loaded with a mixture of the metal ions pair to be separated and the elution was started after 15 min at a flow rate of 4 drops (≈0.2 cm^3) per minute.

Results and Discussion

The extent of static sorption of Rb^+ and Cs^+ at different concentrations is given in Table 1. It is seen that in dilute solutions (10^{-4}—10^{-6} mol dm^{-3}) the sorption of Rb^+ and Cs^+ is almost cent percent and it attains a constant value at concentration of 10^{-1} mol dm^{-3} The maximum sorption capacity is found to be 1.68 mequiv. g^{-1} for Cs^+ and 3.4 mequiv. g^{-1} for Rb^+ ions. This high sorption capacity indicates that K^+ is substituted by Rb^+ or Cs^+, the theoretical exchange capacity on the basis of K^+ being liberated is 2.5 mequiv. g^{-1}. The release of K^+ was detected experimentally. The excess sorption capacity of Rb^+ ions may be due to molecular adsorption of Rb^+.

Sorption behaviour of Rb^+, Cs^+, Ag^+, Co^{2+}, Zn^{2+}, and Fe^{3+} For the efficient use of this exchanger in the separation and isolation, it is necessary to have information about their sorption behaviour in presence of acids and salt solutions. Therefore, in order to work out the conditions for the elution of these ions from the column, the variation of their K_d values at 2×10^{-4} mol dm^{-3} concentration was investigated as a function of NH_4NO_3 and HNO_3 concentration. As usual these results in terms of log K_d *vs.* log concentration of NH_4NO_3 and HNO_3 are shown in Figs. 1 and 2, respectively. Perusal of

TABLE 1. SORPTION OF Cs^+ AND Rb^+ IONS ON COBALT HEXACYANOFERRATE(III) AS A FUNCTION OF $CsNO_3$ OR RbCl CONCENTRATION

Concentration of $CsNO_3$ or RbCl mol dm^{-3}	mequiv. of Cs sorbed g^{-1} of the exchanger	mequiv. of Rb sorbed g^{-1} of the exchanger
5×10^{-1}	1.68	3.4
3×10^{-1}	1.68	3.4
1×10^{-1}	1.68	3.4
1×10^{-2}	0.76	1.66
8×10^{-3}	0.62	1.48
5×10^{-3}	0.50	1.41
2×10^{-3}	0.32	0.68
1×10^{-3}	0.31	0.38
1×10^{-4}	0.04	0.04
1×10^{-5}	0.004	0.004
1×10^{-6}	0.0004	0.0004

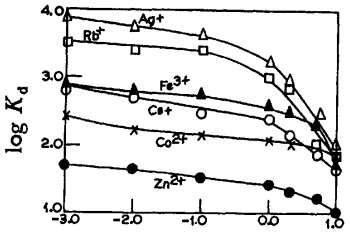

Fig. 1. Variation of log K_d of Cs^+, Rb^+, Ag^+, Co^{2+}, Zn^{2+}, and Fe^{3+} ions with log NH_4NO_3 concentration.

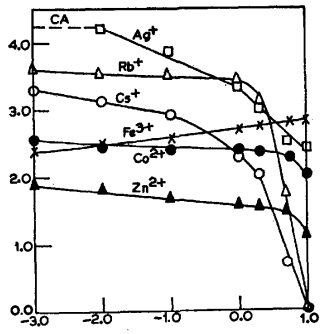

Fig. 2. Variation of log K_d of Cs^+, Rb^+, Ag^+, Co^{2+}, Zn^{2+}, and Fe^{3+} ions with log HNO_3 concentration.

these plots (Fig. 1) shows that the sorption of Ag^+, Rb^+, and Cs^+ ions is little affected upto NH_4NO_3 concentration of 1 mol dm^{-3} and the slope of the plots (−1.3; −1.0, −0.7 for Ag^+, Rb^+, and Cs^+) in the range 1 mol dm^{-3} to 10 mol dm^{-3} approximate to −1 indicating that sorption of these ions may be proceeding through ion exchange mechanism. In the lower concentration range, 10^{-3} to 1 mol dm^{-3}, the exchanger does not get saturated with the NH_4^+ ions and the slope of ≈−1.0 is not thus obtained. The effect of HNO_3 on K_d (Fig. 2) is different in that the K_d of Cs^+ and Rb^+ falls approximately to zero value at 10 mol dm^{-3} HNO_3 and slope of −1 is obtained only for Ag^+ in higher concentration range.

The effect of HNO_3 or NH_4NO_3 concentration on Co^{2+}, Zn^{2+}, and Fe^{3+} is significantly different from that of Cs^+, Rb^+, and Ag^+. The K_d values of these ions remains almost unchanged even in higher concentration of the acid and salt. These ions thus appear to be irreversibly sorbed on the exchanger. This irreversible sorption may be due to the formation of a mixed phase involving the substitution of potassium and cobalt(II) ions. The K_d values of Fe^{3+} surprisingly increases at higher acidity, which possibly indicates the formation of more stable new phase. Similar behaviour was observed for the adsorption of number of bivalent ions on zinc hexacyanoferrate(II) and hexacyanoferrate(III).[7]

Separations of Cs^+ and Rb^+. It is seen from K_d values (Table 2) that the exchanger can be used to separate Cs^+ and Rb^+ from a number of metal ions. 10 mol dm^{-3} HNO_3 was used to elute Cs^+ or Rb^+ from the columns as the K_d of these ions is decreased to appeoximately zero value (Fig. 2) in higher acid concentration. Although, the exchanger has high affinity for Ag^+, but it cannot be used for its recovery because its elution from the columns is very difficult. Further Cs^+ and Rb^+ can also not be separated from Co^{2+}, Zn^{2+}, and Fe^{3+} as they can not be eluted even at high HNO_3 or NH_4NO_3 concentration. The low K_d values (≈0 to 43) of the metal ions, such as Ba(II), Sr(II), Mn(II), Hg(II), Cd(II), Ca(II), Pb(II), Ni(II), Al(III), La(III), Bi(III), and Th(IV), were obtained in their 0.002 mol dm^{-3} solution in 0.01 mol dm^{-3} corresponding acid. Thus the separation of Cs^+ and Rb^+ from these metal ions, which can be eluted with 0.01 mol dm^{-3} HNO_3 is possible and a number of binary separations (Table 2) of analytical importance have been carried out. The recovery of other ions is sharp and quantitative whereas

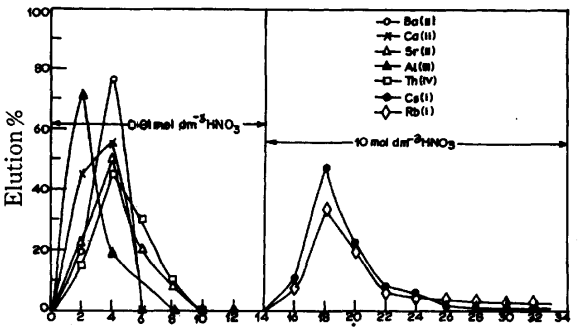

Fig. 3. Separation of Cs^+ or Rb^+ from other cations on cobalt hexacyanoferarte(III)

Table 2. Binary separations of Cs^+ (K_d=200) and Rb^+ (K_d=2401) from various cations on cobalt hexacyanoferrate(III) columns

Sample No.	Other cation	Amount taken/μg				Recovery of Cs^+	Recovery of Rb^+
		K_d a) $cm^3\ g^{-1}$	Cs^+	Rb^+	Other cations	%	%
1	Ba(II)	1	531.64	342	549.44	96.0	90.5
2	Sr(II)	12	531.64	342	350.54	96.2	90.5
3	Mn(II)	4	531.64	342	219.76	95.0	91.0
4	Hg(II)	1	531.64	342	802.44	95.9	91.0
5	Mg(II)	0	531.64	342	97.28	96.0	90.8
6	Cd(II)	0	531.64	342	449.64	95.8	90.6
7	Ca(II)	0	531.64	342	160.32	96.0	90.6
8	Pb(II)	5	531.64	342	828.84	95.2	90.6
9	Ni(II)	0	531.64	342	234.84	95.9	90.5
10	Al(III)	11	531.64	342	107.92	96.0	90.7
11	La(III)	0	531.64	342	555.68	96.0	90.9
12	Bi(III)	43	531.64	342	836.00	95.2	90.2
13	Th(IV)	0	531.64	342	928.40	96.0	90.6

Recovery of all other cations is almost 100%. a) K_d values of Cs^+, Rb^+, and other metal ions are determined at 0.002 mol dm^{-3} concentration of the metal salt solution in 0.01 mol dm^{-3} corresponding acid.

more than 90 percent of Rb^+ and Cs^+ could be eluted with 18 cm^3 of 10 mol dm^{-3} HNO_3. With larger amounts of HNO_3, almost complete recovery of Cs^+ and Rb^+ is possible. Few typical separations are shown in Fig. 3.

Thus this exchanger is useful for many important separation of Cs^+ and Rb^+ from large number of metal ions and is superior to nickel and cobalt hexacyanoferrate(II)[13] exchangers where the elution of Cs^+ from the column is difficult.

One of the authors (Chand Bala) is thankful to CSIR for financial assistance.

References

1) C. B. Amphlett, "Inorganic Ion Exchangers," Elsevier Publishing Company, Amsterdam (1964).
2) J. A. Marinsky and Y. Marcus, "Ion Exchange and Solvent Extraction," Marcel Dekker, New York (1973).
3) V. Vesely and V. Pekarek, *Talanta*, **19**, 219 (1972).
4) V. Pekarek and V. Vesely, *Talanta*, **19**, 1245 (1972).
5) H. F. Walton, *Anal. Chem.*, **50**, 36R (1978).
6) S. C. Churms and S. African, *Ind. Chem.* **19**, 148 (1965).
7) M. T. Ganzerli-Valentini, U. Pisani, S. Meloni, and V. Maxia *J. Inorg. Nucl. Chem.*, **37**, 1269 (1975).
8) M. Cola, M. T. Ganzerli-Valentini, and P. A. Borroni, *J. Inorg. Nucl. Chem.*, **40**, 1041 (1978).
9) J. B. Ayers and W. H. Waggoner, *J. Inorg. Nucl. Chem.*, **33**, 721 (1971).
10) A. K. Jain, S. Agrawal, and R. P. Singh, *J. Radioanal. Chem.*, **60**, 111 (1980).
11) W. U. Malik, S. K. Srivastava, R. P. Singh, and S. Kumar, *J. Radioanal. Chem.*, **36**, 469 (1977).
12) A. K. Jain, R. P. Singh, and C. Bala, *Analyst* **107**, 770 (1982)
13) W. E. Prout, E. R. Russell, and H. J. Groh, *J. Inorg. Nucl. Chem.*, **27**, 473 (1965).

Concentration of Organic Pollutants in Water by Evaporation at Reduced Pressure

Kohei URANO,* Seok Ching YAP, and Koji HAYASHI
Department of Safety and Environmental Engineering, Yokohama National University, 156 Tokiwadai, Hodogaya-ku, Yokohama 240
(Received June 18, 1982)

Synopsis. The relative volatilities α of various organic compounds were obtained as a parameter to determine the recovery for the concentration at reduced pressure and room temperature. The evaporation technique is an efficient method for concentrating large molecular weight compounds and ionizing compounds, if ionization is promoted by adjusting the pH of water.

While the research on water pollution and water treatment was conducting, it was sometimes necessary to determine organic pollutants of sub-ppm levels. The authors[1-4] studied various chromatographic methods such as steam carrier gas chromatography (SCGC), gel chromatography (Gel C), and high performance liquid chromatography (HPLC) for direct analyses of organic pollutants in water. However, development of a feasible concentration method is neccesary for these analytical techniques, since direct injection into SCGC, Gel C, or HPLC and analyses by other methods provide only a limited success at ppm levels. In the analysis of drinking water, Cathorne *et al.*[5] used the evaporation technique with a rotary evaporator and the extraction by methanol. These methods are applicable to only small sample sizes and no experiments has been done to ascertain the recovery efficiency. Loy[6] and Kuo *et al.*[7] used the distillation technique to concentrate volatile organics in the distillate. These methods required elevated temperatures, and are considered to be unsuitable for organic compounds that hydrolyse or decompose at elevated temperatures. Cathorne *et al.*[5] obtained large sample sizes by using a freeze-dryer. However, there has been no report on its efficiency for various organic compounds. The purpose of this study is to investigate the recovery efficiency of concentration method at room temperature using the freeze-dryer as a simple and efficient apparatus for concentrating organic pollutants in water for subsequent analytical techniques.

Experimental

The aqueous solutions ranging from 2 to 20 mg/L of organic compounds shown in Table 1 were used in this study. The sample number for each compound as shown in the table is used in Figs. 2 and 3.

The apparatus used in this study consisted of a Yamato freeze-dryer model D-35. It was connected to a vacuum pump, with evacuation rate of 300 L/min, as shown in Fig. 1. The inner container of the freeze-dryer was cooled by a Neslob Cooler to a temperature of −35 to −45 °C. Kjeldahl flasks were filled with 50 mL (V_o) of the sample solutions whose initial concentrations were C_o, cooled in another freezer to form a layer of ice, and then attached to the trap by means of flask joints. The cooling of the samples before evaporation prevented a loss of liquid due to scattering at a sudden decrease in pressure. If the temperature was not controlled during the evaporation, the liquid would freeze, and the concentration process would become time-consuming. Therefore, during the evaporation process, the flasks were partially immersed in a water bath maintained at a temperature of 35 °C so that the solutions in the flasks were kept at a temperature of about

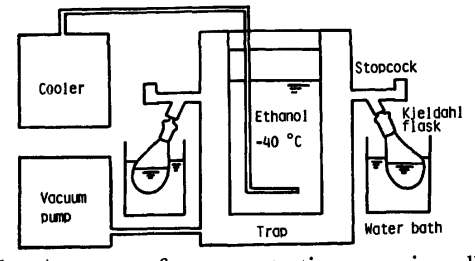

Fig. 1. Apparatus for concentrating organic pollutants by evaporation.

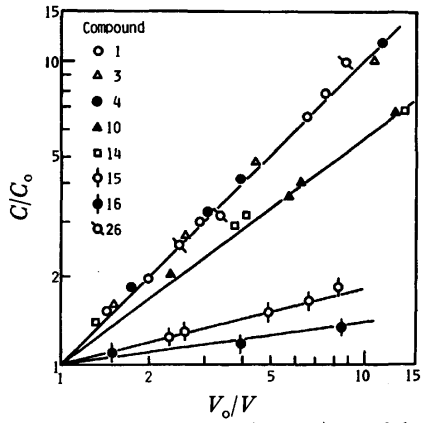

Fig. 2. Relationship between log V_o/V and log C/C_o of solutions of organic compounds.

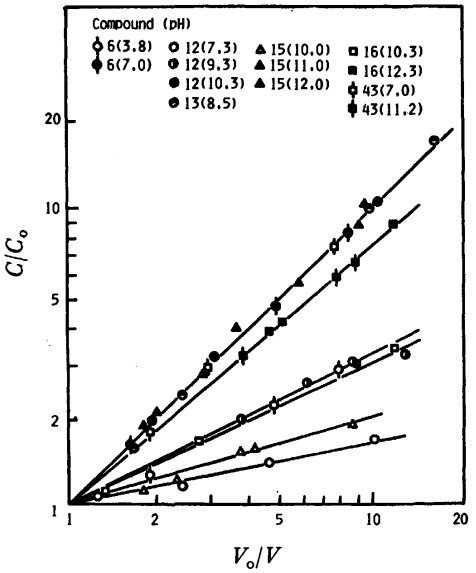

Fig. 3. Relationship between log V_o/V and log C/C_o at different pH values. (Numbers in parenthesis show pH values.)

Table 1. Experimental values of relative volatility α of organic compounds tested

Compound No.	Name	α	$\frac{P_{org}}{P_{H_2O}}$	Compound No.	Name	α	$\frac{P_{org}}{P_{H_2O}}$
1	Sodium benzenesulfonate	0.0	0.0	27	Methyl acetate	5.0	9.1
2	Sodium *p*-methylbenzenesulfonate	0.0	0.0	28	Ethyl propionate	1.4	1.6
				29	Ethyl butyrate	0.9	0.7
3	Sodium 1-butanesulfonate	0.0	0.0	30	Butyl acetate	2.1	—
4	1-Nonanesulfonic acid	0.0	0.0	31	Acetaldehyde	3.1	42.8
5	Sodium *p*-ethylbenzenesulfonate	0.0	0.0	32	Propionaldehyde	0.5	14.7
				33	Isobutyraldehyde	1.0	—
6	*m*-Chlorobenzoic acid	0.2	—	34	Butyraldehyde	0.6	5.1
7	Benzoic acid	0.2	0.0	35	Hexanal	0.8	—
8	*p*-Hydroxybenzoic acid	0.0	—	36	Benzaldehyde	1.6	0.0
9	*m*-Hydroxybenzoic acid	0.0	0.0	37	Isobutyl methyl ketone	1.2	—
10	*m*-Toluic acid	0.3	—	38	Diethyl ketone	1.7	1.5
11	*m*-Nitrobenzoic acid	0.1	—	39	Acetone	1.4	10.8
12	*o*-Nitrophenol	1.3	0.0	40	Methylamine	1.0	127.7
13	*o*-Chlorophenol	1.6	0.1	41	Ethylamine	0.5	49.8
14	Resorcinol	0.3	0.0	42	Propylamine	0.6	13.7
15	Phenol	0.8	0.0	43	Butylamine	0.3	—
16	*o*-Cresol	0.9	0.0	44	Aniline	1.3	0.0
17	Formic acid	0.7	1.9	45	*p*-Nitroaniline	1.6	0.0
18	Acetic acid	0.7	0.7	46	1,6-Hexanediamine	0.0	—
19	Butyric acid	0.7	0.0	47	*o*-Aminobenzoic acid	0.1	—
20	Hexanoic acid	0.6	0.0	48	Isobutyl alcohol	1.6	—
21	Heptanoic acid	0.6	0.0	49	Pentyl alcohol	2.1	—
22	Lacic acid	0.0	—	50	Isopentyl alcohol	1.4	—
23	Malic acid	0.0	—	51	Octyl alcohol	1.4	0.0
24	Malonic acid	0.0	—	52	Benzyl alcohol	0.7	0.0
25	Sodium oxalate	0.0	—	53	Polyethylene glycol	0.0	0.0
26	Adipic acid	0.0	—	54	Humic acid	0.0	0.0

20 °C. At fixed intervals of time, each flask was removed in turn and the weight of the residual solution was measured to obtain the solution volume V. The solution volume V was found to decrease linearly with time at a rate of about 1 mL/min in this method. The concentration C of the residual solution was measured using TOC analyser, TOD analyser, or UV spectrometer. In this way, the volume ratio V_0/V and concentration factor C/C_0 were obtained.

Results and Discussion

If the relative volatility α, which is defined as the ratio of concentration ratio of two components in vapor phase to that in the liquid phase, equals 1.0, no separation takes place. If α is less than 1.0, concentration is possible by the evaporation method. If α is greater than 1.0, concentration is impossible by the evaporation method, but the concentration will be possible by trapping the vapor. The following equations were obtained by considering mass balance; $(C-\mathrm{d}C)\times(V-\mathrm{d}V)=CV-\alpha C\mathrm{d}V$ or $(\alpha-1)C\mathrm{d}V=V\mathrm{d}C-\mathrm{d}C\mathrm{d}V\simeq V\mathrm{d}C$, where $\mathrm{d}V$ is the change in volume of solution and $\mathrm{d}C$ is the change in concentration of solution within a short time. Integrating the above equation between C_0 and C, and V_0 and V, we obtain $(1-\alpha)\log V_0/V=\log C/C_0$. Thus, a plot of $\log C/C_0$ against $\log V_0/V$ will give a straight line with slope $(1-\alpha)$. Therefore, if the value of α for the organic compound in aqueous solution is known, the recovery for the concentration method by evaporation can be predicted from the values of $(1-\alpha)$.

When the sample solution is assumed to be ideal and to obey Raoult's Law, the equilibrium partial pressure p equals the product of its vapor pressure P for pure compound and its mole fraction x in the liquid, and the total pressure P_T is obtained as $P_T=p_{org}+p_{H_2O}=P_{org}x+P_{H_2O}(1-x)$. Thus, the mole fraction of the organic compound in the vapor phase is $y=p_{org}/P_T=P_{org}x/P_T$, and that of water is $1-y=p_{H_2O}/P_T=P_{H_2O}(1-x)/P_T$. Consequently, the value of α can be given as $\alpha=y(1-x)/x(1-y)=P_{org}/P_{H_2O}$ for the ideal solution. However, actual water samples containing organic compounds which require concentration are not necessarily ideal, and the values of α for various organic compounds have not been reported so far.

Examples of the plot of $\log C/C_0$ against $\log V_0/V$ are shown in Fig. 2. For almost all the compounds, the plots could be represented approximately by straight lines, although some volatile compounds in the initial unsteady period deviated from the lines. The values of α for the various organic compounds were computed, and the results are shown in Table 1 together with the values of P_{org}/P_{H_2O} at 20 °C. It was found that the values of α for large molecular weight compounds such as humic acid and polyethylene glycol, sulfonic acids, and dicarboxylic acids were approximately 0, and these compounds could be concentrated with 100% recovery, while the values of α for benzaldehyde and aliphatic esters, alcohols, and ketones were larger than 1, and no concentration was expected. There are many compounds whose values of α were not equal to the calculated values of P_{org}/P_{H_2O}. Furthermore, the values of α for ionizing compounds like acids and amines increased with increasing concentrations, while those of non-ionizing compounds such as propionaldehyde and benzyl alcohol did not show any distinctive change. The experiments were repeated by adjusting the pH of solutions to 7 and 10—12 for acids and amines, and phenolic compounds, respectively. The representative results are shown in Fig. 3. All the tested compounds, except *o*-nitrophenol, can be concentrated with approximately 100% recovery at the pH values where 99% to 99.9% ionization of the compounds were secured, For *o*-nitrophenol, which has a large α value in the unionized form, approximately 100% recovery was obtained at 99.99% ionization.

This concentration method was applied to preconcentrate anionic surfactants in river water and biologically treated sewage before analyses with HPLC. The recovery of nearly 70% by means of TOC was obtained after $V_0/V=10$ was attained. Since anionic surfactants are mainly sulfonates or sulfates, it can be assumed that the recovery of the surfactants was 100%. In the analyses of phenolic compounds and sulfonates in treated wastewater from an oil refinery, preconcentration was necessary, and the recovery of approximately 90% was obtained by means of TOC after V_0/V reached 10.

References

1) K. Urano, K. Katagiri, and K. Kawamoto, *Water Res* **14**, 741 (1980).

2) K. Urano, K. Ogura, and H. Wada, *Water Res.*, **15**, 225 (1981).

3) K. Urano, H. Maeda, K. Ogura and H. Wada, *Water Res.*, **16**, 323 (1982).

4) K. Urano, H. Furuune, and K. Hayashi, *Bull. Chem. Soc Jpn.*, **55**, 2248 (1982).

5) B. Cathorne, C. D. Watts, and M. Fielding, *J. Chromatogr.*, **185**, 671 (1979).

6) E. W. Loy, Jr., Report of Chem. Services Br., Region IV, 1973, US EPA.

7) P. P. K. Kuo, E. S. K. Chian, and F. B. Dewalle, *Water Res.*, **11**, 1005 (1977).

 © 1983 The Chemical Society of Japan Bull. Chem. Soc. Jpn., 56, 1273—1278 (1983)

X-Ray Diffraction Study of Mixing States in the Carbon Tetrachloride Solutions of Methanol and Pentane

Masami TANAKA,† Keiko NISHIKAWA,*,†† Kazuyuki TOHJI,††
and (the late) Tsunetake FUJIYAMA†††

† *Department of Chemistry, Faculty of Science, Tokyo Metropolitan University, Setagaya-ku, Tokyo 158*
†† *Department of Chemistry, Faculty of Science, Gakushuin University, Toshima-ku, Tokyo 171*
††† *Institute for Molecular Science, Myodaiji, Okazaki 444*

(Received July 10, 1981)

A simple method has been proposed for estimating the state of mixing in a binary solution directly from the radial distribution function. The method has been applied to the estimation of the size of the cluster or aggregate in a binary solution of methanol and carbon tetrachloride. Pure liquid carbon tetrachloride and a binary solution of pentane and carbon tetrachloride have also been studied as reference systems. The number of methanol molecules which form a cluster in the solution at the volume ratio of 8.5(CCl_4):1.5(CH_3OH) has been estimated to be about 18, which is in good agreement with an estimate by light scattering.

Many X-ray diffraction studies have been carried out to investigate molecular arrangements in liquids. However, the structure analysis for a molecular liquid, even if it is a pure liquid, is rather difficult. A structure cannot be uniquely determined by diffraction methods, since the packing of polyatomic molecules in the liquid is three-dimensional while the information on molecular geometry obtainable from a diffraction pattern is limited to only one dimension. Usually a structure model is constructed by comparing an intensity or radial distribution function calculated for a model with the experimental one. However, it is often difficult to find a model which can sufficiently explain the experimental facts. Even if a model which yields a calculated intensity in good agreement with the experimental one is obtained, there is no assurance that this model is unique. It is often the case that models which are different from one another in the sense of a three-dimensional arrangement give very similar scattering intensities.

For a multi-component organic solution, it becomes still more difficult to make a structure analysis, and very few studies have been carried out. One example is the work by Narten on a CCl_4–$C(CH_3)_4$ system.[1] He observed a radial distribution function only up to 10 Å and interpreted the radial distribution function of the mixture only as a superposition of the radial distribution functions corresponding to the components, CCl_4 and $C(CH_3)_4$. Therefore, his interpretation is only valid for those peaks due to intramolecular interferences or due to intermolecular interferences for the first nearest neighbors concerned. In the case of a mixture of molecular liquids, one should carefully consider the state of mixing, that is, how one component is mixed with the other components, or how molecules of one component are dispersed in molecules of the other components. As will be described in this paper, the information from the radial distribution function up to large distance is important for considering the state of mixing.

In this report we present a simple method by which we estimate the state of mixing in binary mixtures with carbon tetrachloride solvent directly from a radial distribution function. The existence of a long-range correlation in the observed radial distribution function for pure liquid CCl_4 has been well established.

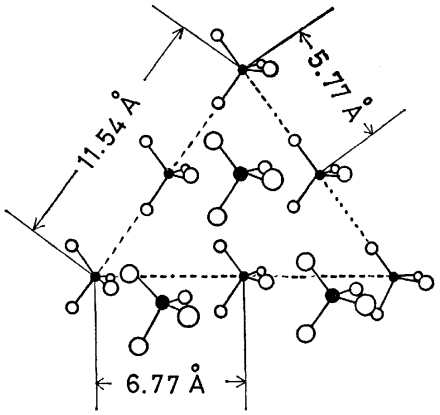

Fig. 1. Packing model for pure liquid CCl_4 (see Ref. 2).
Packing of adjacent molecules is head-tail head-tail with the molecular distance of 5.77 Å. We call this model a "bcc cluster model," because the three-dimensional packing results in a bcc lattice.

The structure of pure liquid CCl_4 has been investigated in detail and a reasonable local structural model has been proposed,[2,3] as shown in Fig. 1. The scattering intensity curve can supply suitable information for the destruction of this long-range structure of liquid CCl_4 by the addition of the other components.

In order to obtain information about the state of mixing, we carried out an X-ray diffraction experiment. Two kinds of carbon tetrachloride solutions, CCl_4–CH_3OH and CCl_4–n-C_5H_{12} systems, were chosen for the samples. In a CCl_4–CH_3OH system, methanol molecules are expected to form clusters through strong hydrogen-bonding. This expectation has been supported by the observed entropy change on mixing,[4] the magnitude of the concentration fluctuation observed by a light scattering experiment, and by theoretical interpretations.[5–7] For a CCl_4–n-C_5H_{12} system, on the other hand, a state of random mixing is believed to be realized.[8,9] It has been reported for the binary solution of methanol and carbon tetrachloride that the fluctuation of concentration has a maximum value at the molar ratio of 7.0(CCl_4):3.0(CH_3OH). It is expected that the aggregate number of methanol molecules becomes maximum at this concentration. Therefore, we observed the diffraction in-

tensity at the corresponding volume ratio of 8.5(CCl_4): 1.5(solute) for the CCl_4–CH_3OH and CCl_4–n-C_5H_{12} systems.

In these systems, it is important that the scattering intensities of the X-rays for the solute molecules, methanol and pentane, are negligibly weak in comparison with that for the solvent molecule, carbon tetrachloride.

Experimental

The scattering intensities of X-rays from liquid samples were measured at 25 °C. An energy-dispersive diffractometer with a vertical goniometer (θ-2θ scanning system) was used.[10] A fine-focus X-ray tube with a tungsten target was used at 45 kV and 20 mA. The scattering intensity was recorded by a multi-channel pulse-height analyzer connected with a Si(Li)-detector. The scattering intensity was measured by the transmission method at scattering angles, 2θ, of 2.5, 4.0, 7.0, 12.0, 20.0, and 35.0°.

The sample holder was the same as that used previously.[11] In the present study, windows of Mylar film (20 μm) were used. The specimens used in this experiment were of commercially available reagent grade. Carbon tetrachloride and pentane were used without further purification. Methanol was further purified by a single distillation.

Data Analysis

The observed scattering intensity was smoothed and was corrected for the scattering from the windows. The scattering intensity curve, thus obtained, was normalized to the energy-distribution curve of the incident beam. The absorption correction was also made by the use of calculated absorption coefficients.[12] The corrected intensity curve was then converted to an absolute scale (in the electron unit) by fitting the experimental intensity to the theoretical one at large s-values. For a pure liquid, the theoretical intensity may be estimated from the intensity calculated for one free molecule. In the case of a binary mixture, the theoretical intensity is a superposition of the scattering intensities from the two components. However, as the scattering intensities from CH_3OH and n-C_5H_{12} are negligibly weak in comparison with that from CCl_4, the theoretical intensity at large s-values may be obtained from the intensity calculated for carbon tetrachloride only. This corresponds to the treatment in which a CCl_4 molecule is fixed as a central molecule and the radial distribution function is regarded as the distribution of other molecules (CCl_4 molecules or solute molecules) around the central molecule. This treatment excludes the case in which a solute molecule occupies the position of the central molecule in the radial distribution function. In the calculation of the scattering intensity for a free CCl_4 molecule, the internuclear distances and the mean-square amplitudes of vabration for CCl_4 obtained by gas electron diffraction[13] were used. The Compton scattering intensity calculated by Cromer was subtracted.[14] The total coherent intensity thus obtained is

$$I_{co}(s) = \sum_n f_n(s)^2 + i_1(s) + i_2(s), \qquad (1)$$

where $f_n(s)$ is the atomic scattering factor, $i_1(s)$ is the coherent intensity from atomic pairs belonging to a

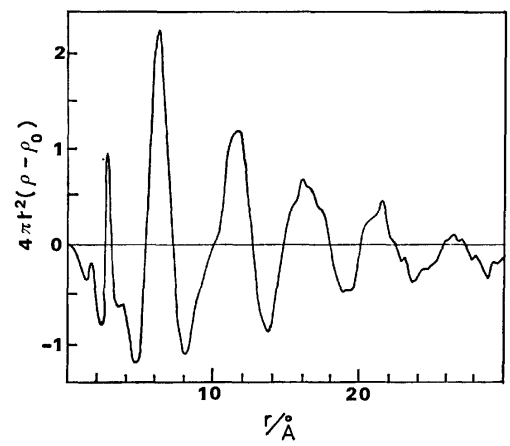

Fig. 2. Radial distribution function observed for liquid CCl_4 at room temperature.

CCl_4 molecule, $i_2(s)$ is the coherent intensity from atomic pairs belonging to different CCl_4 molecules.

The electron radial distribution function from which the bulk density was subtracted, $4\pi r^2(\rho(r)-\rho_0)$, was obtained by the Fourier transformation of $si(s)$ which is defined by $si(s)=s(i_1(s)+i_2(s))$,

$$4\pi r^2(\rho(r)-\rho_0) = \{2r/(\pi \sum_n Z_n^2)\} \sum si(s)\cdot\sin(sr)\Delta s, \qquad (2)$$

where ρ_0 is the bulk liquid density of CCl_4 in the mixture and Z_n is the atomic number of the n-th atom of a CCl_4 molecule.

In the energy-dispersive method, the scattering intensity is scarcely influenced by the fluctuation in the incident beam intensity. Therefore, the accuracy of the observed intensity is mainly limited to the statistical random error, which is estimated to be about 0.5% of the total intensity. The error of scaling due to the neglect of the scattering intensity of the solute molecule is less than 1% in the s-region used for the scaling.

Results and Discussion

The electronic radial distribution functions observed for pure liquid CCl_4,[10] CCl_4–n-C_5H_{12}, and CCl_4–CH_3OH are shown in Figs. 2, 3, and 4, respectively. It can be seen from these figures that, in the case of the CCl_4–CH_3OH system, the peaks occuring at r-values larger than 18 Å are smeared out. On the other hand, there exists clear structure correlation in the mixture of CCl_4–n-C_5H_{12} up to values as large as those observed in the pure liquid CCl_4.

Radial Distribution Function of a Solution with "Vacancies." As described in the introduction, the scattering power of X-rays from solute molecules, methanol or pentane, is negligibly weak in comparison with that from carbon tetrachloride. Therefore, in the first approximation the scattering from these binary systems can be analyzed as though the CCl_4 liquid had "vacancies" whose volumes are equal to those of solute molecules or clusters of the solute molecules. This "vacancy" does not mean that a real void exists in the liquid, but that the scattering power of X-rays by a solute molecule or a cluster can be disregarded.

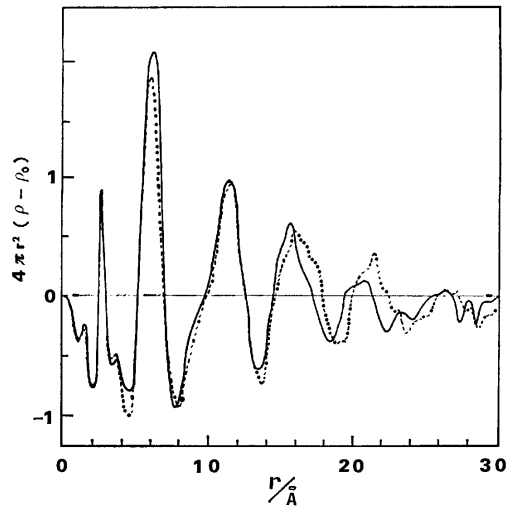

Fig. 3. Radial distribution functions for a binary solution of CCl_4 and n-C_5H_{12}. (——): Observed, (·····): calculated for "ideal mixing."

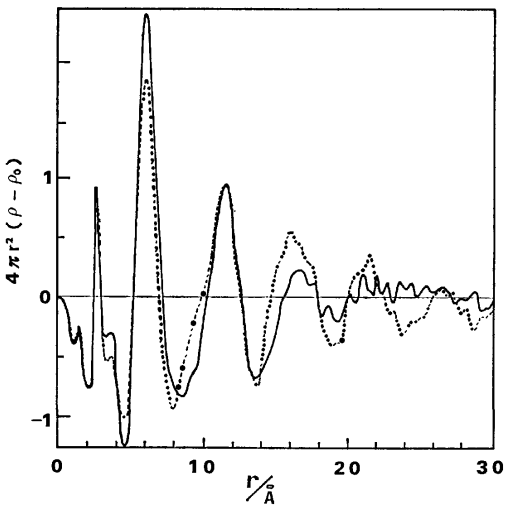

Fig. 4. Radial distribution functions for a binary solution of CCl_4 and CH_3OH. (——): Observed, (·····): calculated for "ideal mixing."

Hereafter in this paper, the term "vacancy" is used in this sense. The analysis of the radial distribution function observed in the binary solutions can be replaced by the analysis of the "vacancy" distribution in liquid CCl_4. In the analysis of the mixing state of such solutions, the following assumptions were made:

(a) It is possible to neglect the scattering intensity of X-rays from solute molecules.

(b) On passing from a pure liquid to the solution, the structure of the solvent is not influenced by the solute molecules.

The error caused by the assumption (a) is estimated to be 5% in the radial distribution function. Namely, the radial distribution functions with "vacancies" in place of the solute molecules are estimated to be 5% smaller in amplitude than the real radial distributions shown by the solid curves in Figs. 3 and 4 containing the contribution of scattering power of solute molecules. This situation, however, does not affect the following discussion. The assumption (b) means that an integral number of sites or CCl_4 molecules is replaced by non-scattering solute molecules ("vacancy") without distortion of the distribution of the sites, namely, the positions which would be occupied by CCl_4 molecules if the system were pure CCl_4 liquid. So the volume of the "vacancy" is assumed to be an integral multiple of the volume of a CCl_4 molecule. Under those assumptions, we will consider the relation between the state of mixing in a binary solution and the radial distribution function.

The radial distribution curve of liquid CCl_4 shows several peaks up to $r \simeq 28$ Å (Fig. 2). By looking at these peaks we may say that a certain number of molecules are located around a representative central molecule at a certain distance from it, if we ignore complications arising from the fact that the molecules are polyatomic and have structure and orientation. In other words, if we sat on the representative central molecule and looked around, we would see several sites that are occupied by other molecules. As is described in the analysis, the data are scaled in such a way that the central molecule is always a CCl_4 molecule and never a "vacancy."

The peak height of the radial distribution curve at a distance r is proportional to the time-averaged number of molecules which occupy the sites at a distance r from the central molecule. Because of the isotropy of the liquid, it is only necessary to consider one representative site instead of all the sites which are located at a given distance from the central molecule.

In the case of the binary solutions discussed in the present paper, the site is not always occupied by another molecule, but is sometimes occupied by a "vacancy." As a result, the peak-height of the radial distribution function decreases in comparison with that of a pure liquid.

If we denote the maximum length between two points within the "vacancy" by $2R$, (which is equal to the diameter in the case of a spherical "vacancy"), it is shown in Appendix that

(i) For $r \geq 2R$, the peak-height decreases to $(1-\alpha)$ times that of the pure liquid where α is the volume fraction of the "vacancies."

(ii) For $r < 2R$, the extent of decrease is less than that for $r \geq 2R$.

Figures 2, 3, and 4 show the quantity $4\pi r^2(\rho(r)-\rho_0)$ instead of the radial distribution function, where ρ_0 is the value of $\rho(r)$ in the limiting case of $r \to \infty$. The term $-\rho_0$ appears because the Fourier transform of the interference term of the coherent intensity is computed without the central scattering (the scattering intensity at $2\theta=0°$).[15] The value of ρ_0 for a binary solution is evidently $(1-\alpha)$ times that of the pure liquid. Thus the above statements (i) and (ii) are valid also for the curve of $4\pi r^2(\rho(r)-\rho_0)$.

Now, let us consider the distribution function of the binary solutions of carbon tetrachloride for two model cases.

1) The case where the size of a "vacancy" is nearly equal to that of CCl_4 molecule.

In this case, the size of the "vacancy" $2R$ is equal to the diameter of a CCl_4 molecule. Therefore, the

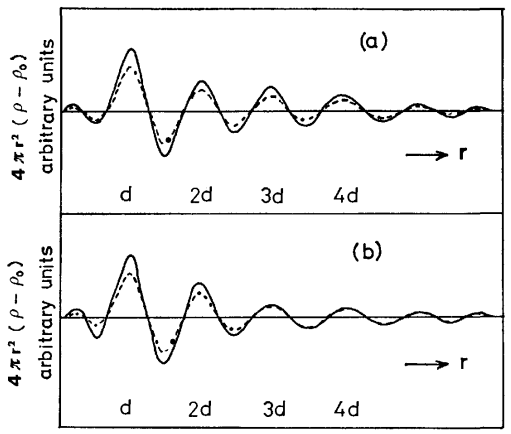

Fig. 5. Radial distribution functions expected for various mixing states for a model case of $\alpha \simeq 0.25$.
(a) The case that the "vacancy" size is equal to that of a CCl_4 molecule. (——): Pure CCl_4, (----): ideal mixing. (b) The case that the "vacancy" size is three times as large as that of CCl_4 molecule. (——): Solution, (----) ideal mixing.

above statements (i) and (ii) predict that the distribution function in this case is reduced by a factor of $(1-\alpha)$ from that of the pure liquid for all the r-values exceeding the diameter of a CCl_4 molecule. In other words, all the peaks beyond that of the first nearest neighbors are reduced to $(1-\alpha)$ times those of the pure liquid. Hereafter, we call this case "ideal mixing." The distribution function in this case is schematically shown in Fig. 5(a), where α is tentatively assumed to be 0.25.

2) The case where the size of the "vacancy" is larger than that of a CCl_4 molecule.

As an example, we consider the case where the "vacancy" size $2R$ is three times as large as the diameter of CCl_4 molecule. The peak-heights of the distribution function, in this case, are considerably stronger than those of the "ideal mixing" case for peaks corresponding to $r<2R$, *i.e.*, the first and second nearest neighbors. For the peaks corresponding to larger r, the distribution function has essentially the same magnitude as that of the "ideal mixing" case, that is, $(1-\alpha)$ times those of the pure liquid. This situation is schematically visualized in Fig. 5(b).

We reach the conclusion that we can estimate the "vacancy" size directly from the observed distribution function. That is to say, the observed radial distribution function becomes equal to that of the "ideal mixing" case at $2R$, which corresponds to the maximum length of the "vacancy." The distribution curve of the "ideal mixing" case can be obtained as $(1-\alpha)$ times that for pure liquid CCl_4.

States of Mixing in CCl_4–n-C_5H_{12} System. The experimental radial distribution function, $4\pi r^2(\rho(r)-\rho_0)$, is shown in Fig. 3 (see the solid curve). A correlation as clear as that for pure liquid CCl_4 (see Fig. 2) is observed up to 27—28 Å. It is also seen that the peak heights of the distribution function are similar to those expected from "ideal mixing," *i.e.*, those obtained by multiplying the distribution function of pure liquid CCl_4 of Fig. 2 by $(1-\alpha)$. The important feature of the distribution curve for CCl_4–n-C_5H_{12} is that the intensity reduction, $(1-\alpha)$, on passing from pure liquid to the solution is nearly equal at any distance r, which corresponds to the situation drawn in Fig. 5(a). This suggests that the state of mixing in the CCl_4–n-C_5H_{12} is "ideal." Since the sizes of the solute and solvent molecules are almost the same, n-C_5H_{12} molecules are randomly dispersed in CCl_4 liquid without forming clusters.

States of Mixing in CCl_4–CH_3OH System. The experimental radial distribution function is shown in Fig. 4 by the solid line, while the distribution function expected for "ideal mixing" is illustrated by a broken line. The magnitude of the former curve is larger than that of the latter at the first peak at 6.3 Å, and these two curves are nearly equal at 12 Å. The peak at 6.3 Å observed for pure liquid CCl_4 has been assigned to the superposition of the first nearest correlations at 5.77 and 6.77 Å (see Fig. 1). The peak at about 12 Å corresponds mainly to the interference at (2×5.77) Å, although it is superimposed on other interferences. On the whole, the behavior of the observed distribution function relative to the "ideal mixing" is similar to that of Fig. 5(b).

The fact that the height of the two curves coincide at 12 Å indicates that the diameter of the methanol cluster is about 12 Å, if the form of the cluster is assumed to be nearly spherical. Since the diameter of a CCl_4 molecule is about 6 Å, the cluster volume is estimated to be about eight times as large as that of a CCl_4 molecule. As the molecular volumes of carbon tetrachloride and methanol at room temperature are 153 and 66.4 Å^3 respectively, the number of methanol molecules which form a cluster is estimated to be $153\times8/66.4\simeq18$. This conclusion is in good agreement with that from the light scattering experiment,[6] which found that the cluster formed in the CCl_4–CH_3OH system at 0.3 mole fraction was composed of about 17 molecules.

In the experimental radial distribution curve shown in Fig. 4, the observed peaks at larger r-values become broader and weaker in comparison with those of "ideal mixing." This deviation of the observed distribution function from that of the "ideal mixing" case at r-values longer than 16 Å may be ascribed to the modification of the long-range structure of liquid CCl_4 caused by the existence of the solute molecules. A detailed analysis of this effect is left for a future problem.

In summary, the distribution functions observed for CCl_4 solutions can be explained by the use of a simple model. This result, in turn, supports the validity and the usefulness of the model for the elucidation of the state of mixing in a binary solution. The present study demonstrates that X-ray diffraction can be used to study the state of mixing in solution without recourse to small-angle-scattering, when the solution contains two kinds of molecules and one component has a much larger scattering power than that of the other component.

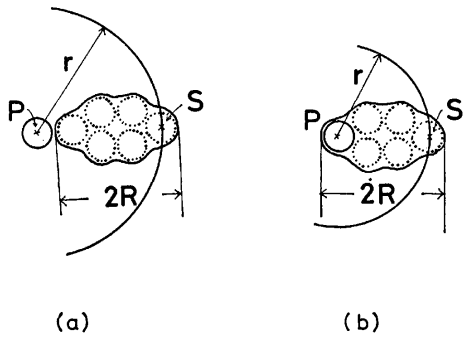

Fig. 6. Particular arrangements of a representative central molecule and a "vacancy". Small circle is a central molecule. The dotted circles are the sites replaced by a "vacancy." (a) The case of $r \geq 2R$ and (b) the case of $r < 2R$. See Appendix for details.

Appendix

Derivation of Statements (i) and (ii) in the Text about the Peak Heights of the Radial Distribution Curve of Binary Solutions.

In the following discussion, it is assumed that an integral number of sites or CCl_4 molecules are replaced by "vacanices" and that the structure or the distribution of the sites are not distorted even if some of the sites are occupied by "vacancies." The radial distribution function shows the time-averaged number of molecules which occupy the site at a distance r from a molecule, which is defined as a representative central molecule. In Fig. 6 are shown a representative central molecule P in a binary solution, a site S located at a distance r from P, and a "vacancy" in a particular orientation. In the treatment of this paper (see Data Analysis), the central site P is always occupied by a CCl_4 molecule.

(A) As long as the distance between S and P is equal to or larger than the effective size of the "vacancy" $2R$, any dotted circle in the vacancy can occupy the site S and all possible orientations of the "vacancy" are permitted. Even if the "vacancy" is orientated in such a way as shown in Fig. 6(a), where the "vacancy" is in contact with the central molecule P, this orientation is still permissible. Therefore, the fraction that the site is occupied by a "vacancy" is simply the volume fraction α, and the time-averaged number of CCl_4 molecules which occupy the site S is $(1-\alpha)$ times that of pure liquid CCl_4. This factor leads to the factor $(1-\alpha)$ for the decreasing factor of the peak height in the case $r \geq 2R$.

(B) If the site S is located at r which is less than $2R$, it happens that some of the orientations of a "vacancy" which occupies the site S should be excluded in counting the fraction that the site is occupied by a "vacancy." In Fig. 6(b), one such orientation is shown. This arrangement should be excluded, because in this orientation the central molecule has also to be replaced by the "vacancy," in contradiction to the initial assumption. Accordingly, the fraction that the site S is occupied by a "vacancy" is less, and the fraction that the site S is occupied by a CCl_4 molecule is more, than that of the case in (A). So the peak height is larger than that of the case in (A).

As is described above, the peak height of the radial distribution curve at a distance r is proportional to the time-averaged number of molecules which occupy the sites at a distance r from a representative central molecule. On the other hand, we may also say that the peak height of the radial distribution curve is proportional to the space-averaged number of molecules which can find a site at a distance r from them occupied by another molecule. This is a space-averaged picture of the problem in contrast to the time-averaged picture mentioned in the preceding. In the following, the statements (i) and (ii) described in the text will be derived on the basis of the space-averaged picture of the problem.

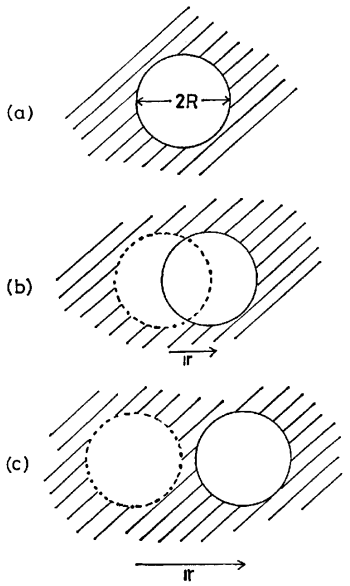

Fig. 7. The space-averaged picture.
(a) A part of the binary solution. A vacant space is a solute molecule or a cluster of them. The diameter of the space is $2R$. (b) The solid circle is the "vacancy." The dotted circle is the "image" obtained by shifting by $\boldsymbol{r}$, in the case of $r < 2R$. (c) In the case of $r \geq 2R$.

According to the assumption of the present work, the radial distribution function is that of pure liquid CCl_4 multiplied by the probability that a site at a distance r from molecule of carbon tetrachloride is found outside the "vacancy," in other words, within the portion of the solution that is occupied by carbon tetrachloride. This probability is given by a characteristic function or a shape function of a figure[16] and can be evaluated as follows.

In Fig. 7(a) is depicted a part of the solution where a vacant space shows a solute molecule and the shaded portion is occupied by solvent molecules. Although there only one vacant space is shown in Fig. 7(a), the figure should extend almost infinitely containing an enormous number of vacant spaces, keeping their volume fraction equal to that of the solute molecules denoted by α.

We then draw an "image" of the figure by shifting the whole figure by a vector $\boldsymbol{r}$ as shown in Fig. 7(b). It is evident that only those molecules that are in the shaded region of Fig. 7(b) can find a site outside the vacant spaces at the position defined by the vector $\boldsymbol{r}$ from themselves. The ratio of the volume of the shaded region of Fig. 7(b) to that of Fig. 7(a) gives the probability that a site at a distance r from a solvent molecule and in a particular direction defined by the vector $\boldsymbol{r}$ is found outside the vacant spaces.

The ratio gradually decreases as r becomes larger, but it remains constant for any orientaion of the "vacancy" if r exceeds $2R$, the maximum length between any two points in the "vacancy" (see Fig. 7(c)). The constant value of the ratio is $(1-2\alpha)/(1-\alpha) \simeq 1-\alpha$.

Because of the isotropy of the liquid, the foregoing argument is valid in any direction of the vector. Thus the probability that a site at a distance r from a solvent molecule is found outside the solute molecules decreases gradually from unity to $(1-\alpha)$ as r increases from 0 to $2R$, and remains constant, $(1-\alpha)$, in the region of r beyond $2R$.

In the present qualitative discussion, such a complication as overlapping of the image of a vacant space with another vacant space is ignored, since this effect should only modify the probability on the order of α^2.

The authors wish to express their thanks to Professor Takao Iijima, Gakushuin University, for his helpful suggestions and discussion.

References

1) A. H. Narten, ORNL Rept. ORNL-4203 (1967).
2) K. Nishikawa and Y. Murata, *Bull. Chem. Soc. Jpn.*, **52**, 233 (1979).
3) K. Nishikawa, K. Tohji, M. Shima, and Y. Murata, *Chem. Phys. Lett.*, **64**, 154 (1979).
4) G. Scatchard and L. B. Tickner, *J. Am. Chem. Soc.*, **74**, 3274 (1952).
5) T. Fujiyama and M. Tanaka, *Bull. Chem. Soc. Jpn.*, **51**, 1655 (1978).
6) T. Kato, T. Nakanishi, and T. Fujiyama, *Bull. Chem. Soc. Jpn.*, **53**, 2173 (1980).
7) T. Kato, N. Ito, and T. Fujiyama, *Bull. Chem. Soc. Jpn.*, **53**, 2167 (1980).
8) D. V. S. Jain, *Indian J. Chem.*, **8**, 815 (1970).
9) D. V. S. Jain, *Indian J. Chem.*, **9**, 465 (1971).
10) Y. Murata and K. Nishikawa, *Bull. Chem. Soc. Jpn.*, **51**, 411 (1978).
11) K. Nishikawa and N. Kitagawa, *Bull. Chem. Soc. Jpn.*, **53**, 2804 (1980).
12) "International Tables for X-Ray Crystallography," Kynoch Press, Birmingham (1962), Vol. III.
13) Y. Morino, Y. Nakamura, and T. Iijima, *J. Chem. Phys.*, **32**, 643 (1960).
14) D. T. Cromer, *J. Chem. Phys.*, **50**, 4857 (1969).
15) S. Miyake, "X-Sen No Kaisetsu," Asakura, Tokyo (1969).
16) A. Guinier and G. Fournet, "Small-Angle Scattering of X-Rays," John Wiley & Sons, London (1955).

 © 1983 The Chemical Society of Japan Bull. Chem. Soc. Jpn., 56, 1279—1283 (1983)

The Conversion of CH_3OH into Olefins over Al_2O_3–Cr_2O_3 Treated with CF_3Cl

Akito Kurosaki and Susumu Okazaki*

Department of Industrial Chemistry, Faculty of Engineering, Ibaraki University, Hitachi, Ibaraki 316

(Received April 15, 1982)

A mixed oxide of Al and Cr having an atomic ratio(Al/Cr) of around 9 showed catalytic activity for the conversion of CH_3OH into olefins and aromatic compounds after treatment with CF_3Cl at 450 °C. The mixed oxide treated with CF_3Cl adsorbed a considerable amount of NH_3, even at temperatures as high as 500 °C. Analyses of the compositions on the surface layer by using XPS showed that the F component was predominantly bound to Al, not to Cr. Strong acid sites related to the less crystallized AlF_3 seemed to be able to promote the conversion of CH_3OH.

Hydrocarbon production from methanol has become an important process for obtaining materials such as ethylene and propylene from coal, instead of petroleum. The catalytic activity of metal oxides in the conversion of CH_3OH into olefins have, however been little reported on, work having been limited to certain zeolites[1-2] such as ZSM-5 (Mobil Oil Company),[3] heteropolyacids and/or their salts,[4-5] and aluminum dihydrogenphosphate.[6] Sufficiently strong acid sites seem to be essential for the promotion of the reaction.

It has been previously found that Al_2O_3–Cr_2O_3 promotes the disproportionation of CF_3Cl into CF_4 and CF_2Cl_2 at temperatures higher than 400 °C.[7] The scission of the strong C–F bond in the CF_3 group[8] is essential for the disproportionation, and the surface of Al_2O_3–Cr_2O_3 should be first fluorinated when the mixed oxide is used as a disproportionation catalyst. Accordingly, the Al_2O_3–Cr_2O_3 surface treated with CF_3Cl, is considered to have strong acid sites and may be expected to promote the conversion of CH_3OH into olefins. Consequently, the catalytic activities of treated Al_2O_3–Cr_2O_3, with various Al/Cr atomic ratios, were examined and compared to those of unfluorinated Al_2O_3–Cr_2O_3, Al_2O_3, and Cr_2O_3. The effects of CF_3Cl treatment on the surface activation were compared with those of treatment with other chlorofluoromethanes and CCl_4. The surface compositions and properties of treated single and mixed oxides were investigated in connection with the catalytic activities.

Experimental

Materials. Various oxides were prepared from their nitrates through the respective hydroxides. The mixed hydroxides were prepared from aqueous solutions of nitrates by coprecipitation with 28% aqueous ammonia, the final pH being adjusted to 8.0—9.0. The precipitates of the mixed hydroxides were thoroughly washed with deionized water and separated by decantation. After drying at 120 °C for 12 h, the mixed hydroxides were heat-treated in air at 600 °C for 3 h; they were then converted to the mixed oxides. Just before their use as catalysts, the oxides were compressed to 30—40 mesh granules under pressure; they were then submitted to surface treatments with a flow of halogen-substituted methane diluted with He at 450 °C for 30 min in a flow reactor. Although mainly CF_3Cl was used as the surface-treatment agent, other chlorofluoromethanes (CF_2Cl_2 and $CFCl_3$) and CCl_4 were also used for comparison with CF_3Cl. All the chlorofluoromethanes (supplied by the Mitsui Fluorochemical Co.) were of purities higher than 99.9%.

Reaction Procedure. The conversion of CH_3OH was carried out in a pulse reactor connected with a modified gaschromatographic analyzer at 400 °C, using He as the diluent. The pulse size was 1 μl; the weight of the catalyst and the velocity of the diluent were kept constant at 30 mg and 35 ml/min respectively.

The product gas, including CO and CH_4, was first condensed at about −196 °C in a 3-m column packed with Tenax GC. Then the condensed products were allowed to evaporate by removing the liquid nitrogen trap; the column was subsequently heat-treated up to about 150 °C. The evaporated gas flowed through TCD, and the composition of the product was analyzed.

Also, the conversion of the dimethyl ether to olefins was carried out in the same reactor by an operation similar to that described above. In these operations, the low-boiling components, such as CO and CH_4, were almost entirely recovered in a column immersed in the liquid-nitrogen trap. The material balances for the conversions of CH_3OH and CH_3OCH_3 were more than 70% and about 85% respectively.

Determinations of Surface Compositions and Properties. The compositions in the surface layer were determined by XPS using a Shimadzu ESCA-750 apparatus. The spectra were measured with Mg $K\alpha$ radiation. The base pressure of the spectrometer was usually below 10^{-7} Torr (1 Torr ≈133.322 Pa) during the experiments. The compositions were calculated from the area of the peaks (*i.e.*, the maxima in the counting rate) in the spectra on the basis of photoionization cross-sections at 1254 eV in units of the C ls cross-section of 22200 barns.[9] The errors inherent in such a determination are generally 10—30% of the observed value.

The surface areas were determined by applying the BET method to the adsorption isotherm of N_2 at −196 °C. The structures of Al_2O_3 and Al_2O_3–Cr_2O_3 were determined from the powder-diffraction patterns obtained with a Rigaku Denki Gigerflex X-ray diffractometer using filtered Cu $K\alpha$ radiation. The surface acidities were measured by means of the amounts of NH_3 adsorbed at different temperature.

Results and Discussion

Effects of Atomic Ratio (Al/Cr). Table 1 shows the effect of the mixed oxide atomic ratio on the catalytic activity before and after treatment with CF_3Cl. For comparison, SiO_2–Al_2O_3 (N-631, Nikki Chemical Co.), which is a typical strong solid acid, was also used. Except for SiO_2–Al_2O_3, which caused the formation of a slight amount of olefin, none of the single and mixed oxides promoted any olefin formation. On the other hand, except for Cr_2O_3, when the oxides were pretreated with CF_3Cl at 450 °C and then used as catalysts, considerable amounts of ethylene and propene were formed from CH_3OH. The catalytic

TABLE 1. DECOMPOSITION OF CH_3OH OVER VARIOUS CATALYSTS AT 400 °C

Catalyst	Product distribution (mol%)							
	CO	CO_2	CH_4	C=C	C=C-C	C_{6-7}[b]	DME	CH_3OH
Al_2O_3	6.2	0	20.4	0	0	0	53.8	19.0
Cr_2O_3	51.0	32.4	3.5	0	0	0	0	14.1
SiO_2-Al_2O(N-631)	0	0	0	Trace	Trace	0	76.1	23.9
Al/Cr:9.5/0.5[a]	15.1	41.4	6.0	0	0	0	0	37.8
9/1	20.4	44.3	7.4	0	0	0	0	27.9
8.5/1.5	16.7	39.6	6.7	0	0	0	0	37.0
8/2	14.4	38.9	5.7	0	0	0	0	41.0
Al_2O_3-F	0	0	0	3.6	7.9	Trace	55.4	32.9
Cr_2O_3-F	7.9	8.7	0.8	0	0	Trace	0	79.6
N-631-F	0	0	0	5.1	11.4	0	66.8	16.7
Al/Cr:9.5/0.5-F	0	0.6	0	7.3	10.9	1.4	60.2	19.6
9/1-F	0	1.2	0	7.1	12.9	1.8	55.4	21.6
8.5/1.5-F	0	1.0	0	7.0	6.8	1.8	55.9	27.5
8/2-F	0	1.1	0	5.6	9.6	1.6	50.5	31.6

a) Al/Cr denotes the Al_2O_3-Cr_2O_3 mixed oxide catalyst; -F denotes the catalyst treated with CF_3Cl. b) C_{6-7} denote benzene and/or toluene.

TABLE 2. DECOMPOSITION OF CH_3OH OVER Al_2O_3-Cr_2O_3 (Al/Cr=9/1) TREATED WITH VARIOUS CHLOROFLUOROMETHANE OR CCl_4

Treatment species	Product distribution(mol%)							
	CO	CO_2	CH_4	C=C	C=C-C	C_{6-7}	DME	CH_3OH
No treatment	20.4	44.3	7.4	0	0	0	0	27.9
CCl_4	2.6	2.1	3.6	29.5	0	0	62.2	0
$CFCl_3$	2.2	1.8	4.0	13.1	0	0.3	75.7	2.8
CF_2Cl_2	0	1.2	Trace	12.5	Trace	1.1	63.7	21.5
CF_3Cl	0	1.2	0	7.1	12.9	1.8	55.4	21.6

TABLE 3. EFFECT OF CF_3Cl-TREATMENT TEMPERATURE ON CATALYTIC ACTIVITY

Temperature/°C	Product distribution(mol%)[a]						Conversion of disproportionation of CF_3Cl/%[4]
	CO_2	C=C	C=C-C	C_{6-7}	DME	CH_3OH	
400	2.6	7.0	0.9	1.8	66.2	21.5	26.5
450	1.2	7.1	12.9	1.8	55.4	21.6	30.8
500	1.0	3.5	6.9	1.8	32.8	54.0	19.5

a) CO and CH_4 were not observed in the product gases for any of the runs.

activity of Cr_2O_3 for the formations of CO and CO_2 decreased remarkably with the pretreatment, suggesting that the active O atoms on the Cr_2O_3 surface may be removed by the reaction with CF_3Cl.

A maximal conversion of CH_3OH into olefins was obtained with the mixed oxide having the atomic ratio of Al/Cr=9/1. The same atomic ratio also gave a maximum disproportionation for CF_3Cl.[7] Since the disproportionation can be promoted only by the strong acid,[7] the strong acid sites must be formed most abundantly on Al_2O_3-Cr_2O_3 (9/1) after treatment with CF_3Cl.

Comparison of Treatment Using CF_3Cl with Those Using Other Chlorofluoromethanes or CCl_4. The catalytic activities of Al_2O_3-Cr_2O_3 treated with different chlorofluoromethanes or CCl_4 are shown in Table 2 for the CH_3OH conversion. The Al_2O_3-Cr_2O_3 treated with CCl_4 showed the highest activity at the first pulse of the reactant. However, large amount of deposits, which seemed to be aluminum chloride and/or chromium chloride, were formed on the reactor walls and finally clogged the reactor outlet. The deposited amounts decreased with an increase in the number of F atoms in the chlorofluoromethane molecule used for the surface treatment. Thus, when CF_3Cl was used for the treatment, there were hardly any deposits found during the reaction.

When the mixed oxide treated with CCl_4, $CFCl_3$, or CF_2Cl_2 was used as a catalyst, ethylene was obtained as the main olefinic product. On the other hand, a good deal of propene was produced, together with ethylene, when the mixed oxide was treated with CF_3Cl.

Effect of CF_3Cl-treatment Temperature on Catalytic Activity. The effect of the treatment temperature with CF_3Cl on the catalytic activity for the conversion

Table 4. Surface composition of treated component or mixed oxide

Oxide	Composition(atom%)					Atomic ratio	
	O	F	Cl	Cr	Al	Cr/Al	F/Al
Al/Cr:9/1	69.9	0	0	3.1	27.0	0.11	—
-treated with CCl_4	57.7	0	5.8	2.9	33.6	0.09	—
-$CFCl_3$	46.2	20.5	1.7	3.5	28.1	0.12	0.7
-CF_2Cl_2	36.8	21.6	1.8	3.5	36.3	0.10	0.6
-CF_3Cl	31.2	37.7	0	3.7	27.4	0.13	1.4
Al_2O_3	63.7	0	0	0	36.3	—	—
-treated with CF_3Cl	44.3	23.2	0	0	32.5	—	0.7
Cr_2O_3	67.3	0	0	32.7	0	—	—
-treated with CF_3Cl	65.3	0	0	34.7	0	—	—

Table 5. Conversion of DME over oxides before and after treatment with CF_3Cl

Oxide[a]	Product distribution(mol%)						
	CO	CO_2	CH_4	C=C	C=C–C	C_{6-7}	DME
Al_2O_3	18.4	0.5	55.0	0	0	0	26.1
Cr_2O_3	7.6	3.2	2.6	0	0	0	86.6
Al/Cr:9/1	7.2	84.6	8.2	0	0	0	0
Al_2O_3-F[b]	0	0	0	6.7	0.6	0	92.7
Cr_2O_3-F	7.1	2.6	3.7	0.6	0	0	86.0
Al/Cr:9/1-F	0	1.7	1.7	2.4	5.6	0	88.6

a) All the oxides were heat-treated at 600 °C for 3 h before the treatment with CF_3Cl or use as a catalyst. b) -F denotes a catalyst treated with CF_3Cl similarly to that shown in Table 1. The treatment conditions with CF_3Cl were the same as for the conversion of CH_3OH.

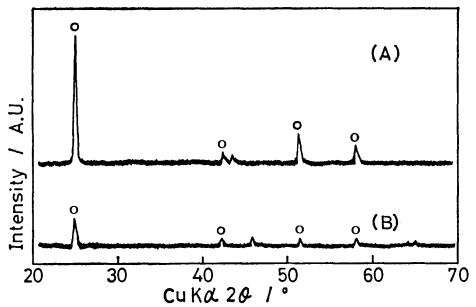

Fig. 1. X-Ray diffraction patterns.
(A): Al_2O_3 treated with CF_3Cl, (B): Al_2O_3–Cr_2O_3 treated with CF_3Cl. (○): Peaks due to α-AlF_3.

of CH_3OH is shown in Table 3. The CF_3Cl treatment was most effectively carried out at 450 °C to give an increase in the catalytic activity for the CH_3OH conversion similar to that for the CF_3Cl disproportionation.

Effect of H_2-treatment before the Treatment with CF_3Cl. To know the effect of reduction on the catalytic activity, Al_2O_3–Cr_2O_3 (9/1) was treated with H_2 at 450 and 600 °C before the treatment with CF_3Cl at 450 °C. The catalytic activity for the formation of olefins was remarkably decreased by the pretreatment with H_2 at 450 °C. Particularly, the formation of propene was not observed when the mixed oxide was pretreated with H_2, although the amount of dimethyl ether formed increased with the pretreatment. The catalytic activity of the mixed oxide treated with CF_3Cl remained for the formation of dimethyl ether, even when the mixed oxide was pretreated at as high a temperature as 650 °C.

Surface Composition and Degree of Crystallization of the Oxide after Treatments. The surface compositions determined by XPS, after treatment with chlorofluoromethanes or CCl_4, are shown in Table 4. In the mixed oxides treated with $CFCl_3$ or CF_2Cl_2, only a small amount of the Cl component was found, together with a much larger amount of the F component. Furthermore, the Cl component was not detected in the mixed oxide treated with CF_3Cl. The F component in the mixed oxide (Al/Cr=9/1) increased with an increase in the number of F atoms in the molecule used for the surface treatment. As is shown in the last line in Table 4, Cr_2O_3 did not bind the F component at all during the treatment with CF_3Cl. In contrast to Cr_2O_3, Al_2O_3 bound a good deal of the F component, as is shown in the seventh line of Table 4. This fact suggests that the F atoms in the mixed oxide may combine with Al, not Cr, atoms.

The X-ray diffraction analysis of Al_2O_3 and Al_2O_3–Cr_2O_3 after treatment with CF_3Cl (Fig. 1) showed that α-AlF_3 formed on both oxides and that the degree of crystallization of the aluminum fluoride on the treated mixed oxide was far less than that on the treated Al_2O_3. The X-ray diffraction patterns ascribable to

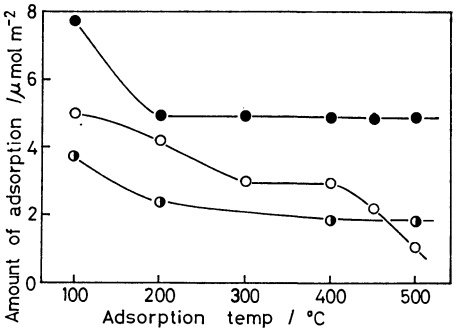

Fig. 2. Adsorption of NH_3 at various temperatures. ◑: SiO_2–Al_2O_3 (N-631), ○: Al_2O_3–Cr_2O_3(9/1), ●: Al_2O_3–Cr_2O_3 treated with CF_3Cl.

metal chlorides and the chromium compound was not observed at all. The absence of the Cl component in the most active oxide, *i.e.*, Al_2O_3–Cr_2O_3 (Al/Cr= 9/1) treated with CF_3Cl, has also been shown by the results obtained by using XPS (Table 4). Thus, the high catalytic activity of the treated mixed oxide may be due not to aluminum chloride, but to the less crystallized, and so active, aluminum fluoride formed on the surface by the treatment.

Conversion of DME over Oxides before and after Treatment with CF_3Cl. As Table 5 shows, Al_2O_3, Cr_2O_3, and Al_2O_3–Cr_2O_3 (Al/Cr=9/1) promote only the conversion of dimethyl ether to CO, CO_2, and CH_4 before treatment with CF_3Cl. After such a treatment, Al_2O_3 and Al_2O_3–Cr_2O_3 showed activities for the conversion of dimethyl ether into olefins. In particular, the Al_2O_3–Cr_2O_3 promoted a formation of propene similar to that observed in the conversion of CH_3OH.

For the conversion of CH_3OH catalyzed by ZSM-5 or other zeolites, it is generally accepted that the formation of hydrocarbons proceeds according to the pathway shown below:[1,5,6]

$$CH_3OH \rightleftharpoons CH_3OCH_3 \longrightarrow C_2H_4,\ C_3H_6,$$
$$\text{and } C_4H_8 \textit{ etc.} \begin{cases} \nearrow \text{Paraffins} \\ \searrow \text{Aromatics.} \end{cases}$$

The fact that dimethyl ether gives a similar or essentially the same product distribution as methanol (shown in Table 1) shows that the pathway described above may be acceptable also for the conversion catalyzed by the treated Al_2O_3–Cr_2O_3 or the treated Al_2O_3. The strong acid sites formed by treatment with CF_3Cl should promote the slowest step in the reaction sequence.

Surface Properties and Formation of Active Sites. The specific surface areas of the mixed oxides before and after treatment with CF_3Cl were almost completely independent of the atomic ratio in the Al/Cr range from 1/0 to 8/2. Hence, the specific surface area does not seemed to be a factor determining the mixed oxide catalytic activity, which is maximal when the atomic ratio of Al/Cr equals 9/1.

As is shown in Fig. 2, the amount of NH_3 adsorbed on treated Al_2O_3–Cr_2O_3 (9/1) at temperatures higher than 450 °C was much more than that on SiO_2–Al_2O_3 or untreated Al_2O_3–Cr_2O_3 (9/1). This fact shows that fair amounts of strong acid sites should be formed

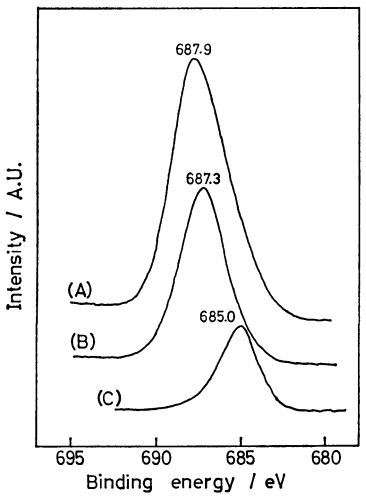

Fig. 3. F 1S peaks in XPS.
(A): Al_2O_3–Cr_2O_3 treated with CF_3Cl, (B): AlF_3, (C): CrF_3.

on the mixed oxides treated with CF_3Cl at 450 °C.

Figure 3 shows that the position of the F is peak (687.9 eV) in the spectrum of Al_2O_3–Cr_2O_3 (9/1) treated with CF_3Cl is close to those of AlF_3 (687.3 eV) or Al_2O_3 treated with CF_3Cl (687.1 eV), while it is far from that of CrF_3. Thus, it is elucidated that the active sites should be related to aluminum fluoride or to Al atoms (or ions) bonded to F atoms (or ions) on the surface.

Because AlF_3 has the highest positive partial charge (0.72) among the typical strong electron-acceptors, such as BF_3 (0.56), $AlCl_3$ (0.57), BCl_3 (0.41), and $GaCl_3$ (0.32),[10] it should be an extremely strong solid acid. However, it tends to form stable crystals due to the very small radius of the F ion and its large electronegativity and, further, the large ion potential, *i.e.*, the ratio of the ionic valence to the ionic radius, of the Al ion. Consequently, it is desirable to prevent the crystallization for aluminum fluoride to fully function as a strong solid-acid catalyst.

By considering also that Cr_2O_3 itself did not catalyze the formation of olefins at all, even after treatment with CF_3Cl (Table 1), and that no F component was found in Cr_2O_3 treated with CF_3Cl (Table 4), the major effect of Cr_2O_3 in the treated mixed oxide seems to be only structural. That is, the crystal structure of Cr_2O_3 is a corundum type in which O atoms are appeared in an approximately hexagonal close-packed arrangement and Al^{3+} ions are situated in two-thirds of the octahedral holes;[11] furthermore, the ionic radius (0.63 Å[12]) is comparatively close to that of Al^{3+} (0.51 Å[12]). Hence, small amounts of Cr^{3+} ions added to Al_2O_3 may be thoroughly mixed with Al^{3+} and may thus suppress the crystallization of AlF_3 by intervening between Al^{3+} ions. However, Cr_2O_3 itself is catalytically far less active for the formation of olefins from CH_3OH, even after treatment with chlorofluoromethanes. Accordingly, the addition of Cr^{3+} in a larger amount was not beneficial for the enhancement of the catalytic activity because an excess Cr_2O_3 component hinders the formation and the function of active aluminum fluoride on the surface. Thus, an optimal

amount of Cr constituent was observed at around 10 atom% in the CF_3Cl-treated mixed oxide.

References

1) K. Fujimoto, T. Shikada, and H. Tomonaga, *Nippon Kagaku Kaishi*, **1982**, 229.
2) T. Inui, T. Ishihara, N. Morinaga, G. Takeuchi, E. Araki, T. Kanie, and Y. Takegami, *Nippon Kagaku Kaishi*, **1982**, 221.
3) C. D. Chang and A. J. Silvestri, *J. Catal.*, 47, 249 (1977).
4) Y. Ono, T. Baba, and T. Keii, *J. Chem. Soc., Chem. Commun.*, **1981**, 400.
5) A. Kasai, T. Okuhara, M. Misono, and Y. Yoneda, *Chem. Lett.*, **1981**, 449.
6) S. Kikkawa, Y. Shimizu, and S. Higuchi, *Chem. Lett.*, **1979**, 849.
7) S. Okazaki and H. Eriguchi, *Chem. Lett.*, **1980**, 891.
8) W. A. Sheppard and C. M. Sharts, "Organic Fluorine Chemistry," W. A. Benjamin, New York (1969), p. 3.
9) J. H. Scofield, *J. Electron Spectros. Relat. Phenom.*, **8**, 129 (1976).
10) R. T. Sanderson, "Inorganic Chemistry," translated by S. Fujiwara *et al.*, Hirokawa Shoten, Tokyo (1975), p. 167.
11) A. F. Wells, "Structural Inorganic Chemistry," Clarendon Press, Oxford (1975), p. 450.
12) "CRC Handbook of Chemistry and Physics," ed by R. C. Wheast, CRC Press, West Palm Beach (Florida) (1978—1979), p. F-213.

Catalytic Activity of Sn-Mo Oxides for Propene Oxidation

Takehiko ONO,* Tetsuo IKEHATA, and Yutaka KUBOKAWA*

Department of Applied Chemistry, University of Osaka Prefecture, Sakai, Osaka 591

(Received April 30, 1982)

Sn-Mo oxides were subjected to experimental studies with reference to their catalytic C_3H_6 oxidation and their own reduction by C_3H_6. In the oxidation Sn–Mo oxides are 30—40 times more active than MoO_3 but only 4—5 times than SnO_2. With Sn-Mo oxides as well as SnO_2, the oxidation is zero order in C_3H_6 and about half order in O_2, in contrast to those with MoO_3. It is proposed that the oxidation proceeds via a redox mechanism with the reduction step proceeding very rapidly. ^{18}O tracer experiments show that the mobility of lattice oxygen in Sn-Mo oxides is lower than that in MoO_3 but similar to that in SnO_2. From these results together with those of structural studies, it is concluded that the active phase of Sn-Mo oxides is characterized by the MoO_3 highly dispersed on SnO_2 or Mo ions dissolved in SnO_2, and that their high reducibility possibly originates from the existence of SnO_2 itself in them.

Partial oxidation of alcohols on Sn-Mo oxides has been investigated by several workers, *e.g.*, Niwa *et al.*[1] and Okamoto *et al.*,[2] who investigated the mechanism of the oxidation and the correlation between activity and surface structure for these systems, respectively, by using various techniques such as ESR and XPS. As regards the oxidation of alkenes on Sn–Mo oxides, Morooka *et al.*,[3] Butein,[4] and Ai[5] investigated oxidation at lower temperatures in the presence of water vapor and emphasized the importance of acid-base properties of the oxides in the oxidation. Although the alkene oxidation at higher temperatures has been invesigated by several workers,[6,7] no detailed kinetic studies on the oxidation have been reported. Margolis[6] investigated the propene oxidation by Mössbauer spectroscopy and concluded that adsorbed oxygen plays a significant role in the oxidation. There seems to be no unambiguous evidence supporting their conclusion.

In a previous work we carried out studies on the rate of oxidation of alkenes on V–Sn[8,9] and V–Mo[9] oxides and on their reduction with alkenes, together with ^{18}O tracer studies. These studies, together with structural ones using ESR and X-ray Diffraction, *etc.*, have allowed us to discuss the promoter effect for these systems. In the present work, similar studies have been extended to the oxidation of C_3H_6 on Sn–Mo oxides.

Experimental

Material. Sn–Mo catalysts were prepared as follows. Tin hydroxide precipitates obtained from solutions of tin(II) chloride and ammonia were added to a solution containing a required quantity of ammonium heptamolybdate. The resulting slurry was evaporated with constant stirring, dried, and heated in air at 450 °C. SnO_2 was prepared in a similar manner from a tin hydroxide obtained as described above. MoO_3 was prepared by heating ammonium heptamolybdate in air at 450 °C.

Sn–Mo–M catalysts were prepared by mixing MoO_3 with SnO_2 in a desired ratio and heating the mixture in air at 600 °C for 0.5 h. $^{18}O_2$ (99.1%) was obtained from B.O.C. Limited (U. K.).

Surface areas of catalysts as determined by the BET method were as follows: MoO_3, 1.3—2.0; Sn-Mo(75)(containing Mo in 75 mol%), 18; Sn-Mo(50), 19.5; Sn-Mo(10), 33; SnO_2, 6.8; Sn-Mo(50)-M, 5.1 m^2/g. Prior to measurement, all catalysts were subjected to pretreatment with oxygen at 450 °C.

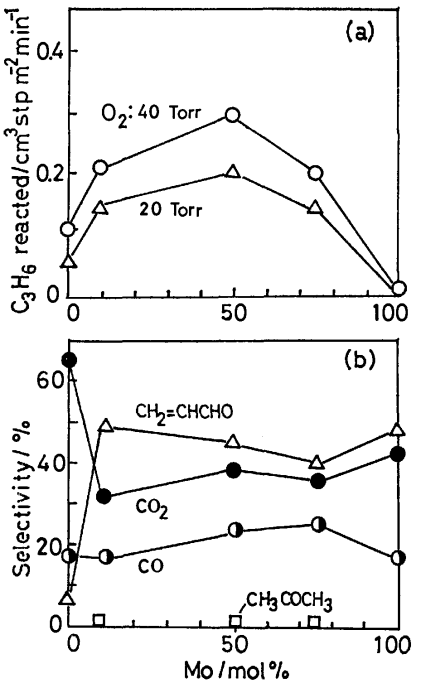

Fig. 1. Rates(a) and product selectivities(b) of C_3H_6 oxidation over Sn–Mo catalysts at 400 °C. $P_{C_3H_6}$= 23 Torr(1 Torr=133.3 N m^{-2}). The product selectivities scarcely changed with oxygen pressure.

Apparatus and Procedure. The catalytic oxidation and the reduction of oxides were carried out in a closed circulation system (320 cm^3). In order to obtain initial rates, conversions were kept below *ca.* 5%. Reaction products such as CH_2=CHCHO, CH_3COCH_3, CO_2, and CO were detected by gas chromatography. The ^{18}O% for a reaction product was determined with a Hitachi RMU-6E mass spectrometer at the following ionization voltages: 80 V for CO and CO_2 and 15 V for CH_2=CHCHO. X-Ray diffraction patterns for catalysts were obtained on a Rigaku-Denki D-3F X-ray diffractometer using Cu $K\alpha$ radiation with a Ni filter. IR spectra of catalysts were recorded on a Hitachi G2 spectrometer, samples being prepared by the KBr pellet technique.

Results and Discussion

C_3H_6 Oxidation over Sn–Mo Oxides and Their Reduction with C_3H_6. Figure 1 shows the rate of oxidation of C_3H_6 and the selectivity for oxidations as a

TABLE 1. C_3H_6 OXIDATION OVER Sn-Mo CATALYSTS

Catalyst (Mo%)	Reaction order		Rate[a] C_3H_6 reacted	Selectivity CH_2=CHCHO
	C_3H_6	O_2	cm^3 stp m^{-2} min^{-1}	%
MoO_3[b]	1.0	0	0.005	50
Sn-Mo(75)	0.1	0.3	0.13	40
Sn-Mo(50)	0	0.4	0.23	40
Sn-Mo(10)	0	0.4	0.15	50
SnO_2	0	0.4	0.09	5

a) $P_{C_3H_6}$=23 Torr, P_{O_2}=20 Torr, and temp 400 °C. b) See Ref. 10.

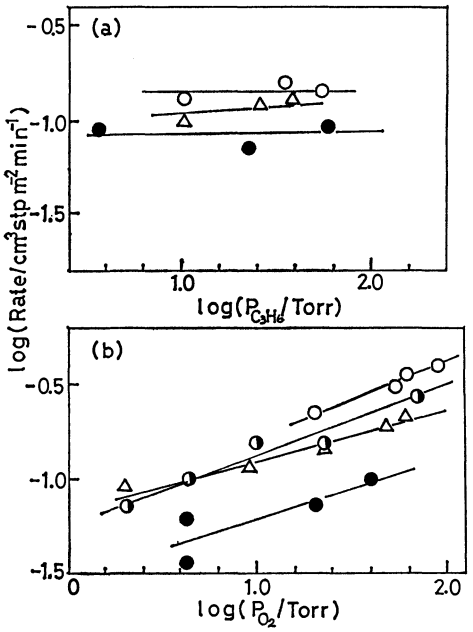

Fig. 2. Dependence of the rate of C_3H_6 oxidation upon C_3H_6 and O_2 pressures over Sn–Mo catalysts at 400 °C. (a) P_{O_2}=20 Torr. (b) $P_{C_3H_6}$=23 Torr. △: Sn-Mo(75), ○: Sn-Mo(50), ◑: Sn-Mo(10), ●: SnO_2.

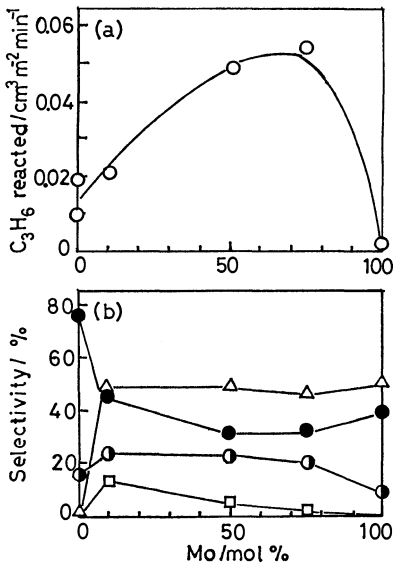

Fig. 3. Reduction of Sn–Mo catalyst with C_3H_6 at 400 °C.
(a) Amount of C_3H_6 reacted. (b) Product selectivities. $P_{C_3H_6}$=23 Torr. Symbols in (b) are the same as those in Fig. 1b.

function of MoO_3 content. The rate of oxidation passes through a maximum, though not pronounced, at Sn–Mo (50). The distribution of products is essentially the same for all the Sn–Mo oxides. The selectivity toward CH_2=CHCHO formation is about 40—50%, the remainder being for CO and CO_2. With SnO_2, the CH_2=CHCHO formation is markedly reduced, while the CO_2 formation is increased. With all the Sn–Mo oxides, formation of CH_3COCH_3 takes place with ratios of CH_3COCH_3 to CH_2=CHCHO less than 0.1 above 400 °C.

Figure 2 shows the dependence of the rate of C_3H_6 oxidation upon O_2 and C_3H_6 pressures, from which reaction orders for the oxidation were determined as shown in Table 1. With MoO_3, the reaction is first order in C_3H_6 and zero order in O_2. It is apparent that the orders for Sn–Mo oxides are similar to those for SnO_2.

Rates of the reduction of Sn–Mo oxides with C_3H_6 were determined in the reaction time range 0.5—3.0 min. Amounts of CO, CO_2, and CH_3COCH_3 formed increase linearly with increasing reaction time, while the CH_2=CHCHO formation takes place practically only in the initial measurement (0.5—1 min), scarcely proceeding any more in later periods. By assuming the initial value to approximate the rate of CH_2=CHCHO formation, yields and distributions were determined as a function of MoO_3 content (Fig. 3). A comparison of the rates of oxidation in the presence and absence of oxygen (Figs. 1 and 3) indicates that there is no marked difference between both the rates of oxidation. Furthermore, essentially the same product distributions are obtained with both the oxidations in the presence and absence of oxygen. This suggests that no adsorbed oxygen plays a significant role in the C_3H_6 oxidation over Sn–Mo oxides. It is therefore concluded that the oxidation proceeds via a redox mechanism, *i.e.*, the repetition of the reduction of oxides with C_3H_6 and their reoxidation with gaseous oxygen. The fact that the oxidation is zero order in C_3H_6 and about half order in O_2, suggests that the reduction of oxides with C_3H_6 is very rapid, the rate-determining step in the oxidation being their reoxidation by gaseous oxygen.

With the Sn–Mo (50) catalyst, initial rates of reduction were determined as a function of C_3H_6 pressure. As shown in Fig. 4, the rate of formation of CH_3COCH_3 increases linearly with increasing pressure of C_3H_6,

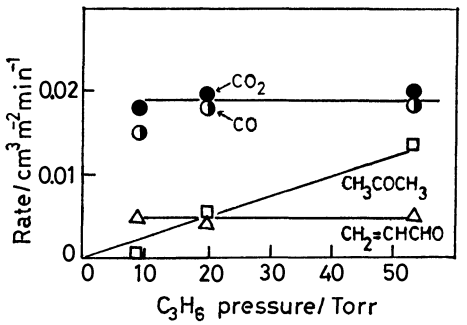

Fig. 4. Variation in the rate of reduction of Sn–Mo(50) with C_3H_6 pressure at 350 °C.

while the rates of formation of CO, CO_2, and CH_2=CHCHO are almost independent of C_3H_6 pressure. These results, together with the fact that the CH_2=CHCHO formation is observed only in the initial measurement, suggest that a very small fraction of the surface is responsible for the reduction, *i.e.*, that the rate for the active part is very large. Such a high rate of reduction is in agreement with the kinetics of the oxidation, *i.e.*, zero order in C_3H_6 and about half order in O_2. Furthermore, it should be noted that essentially the same behavior was observed with the reduction of SnO_2, where reduction products consist of only CO and CO_2.

Structure of Sn–Mo Oxides. According to X-ray diffraction studies, Sn–Mo (10) and Sn–Mo (75) show diffraction lines due only to SnO_2 and MoO_3, respectively. With Sn–Mo (50), lines attributable to SnO_2 as well as MoO_3 appear. No lines indicating any formation of new compounds between SnO_2 and MoO_3 appear, in agreement with results by previous workers.[2,11] The sizes of SnO_2 and MoO_3, as determined from the broadening of diffraction lines,[12] are 15—20 nm and >200 nm, respectively. Intensities of the diffraction lines of MoO_3 in Sn–Mo oxide catalysts were compared with those of mechanical mixtures of MoO_3 and SnO_2. The results indicate that 40—50 mol% of MoO_3 in Sn–Mo (50) and (75) is missing.

In a manner similar to that adopted in a previous work[8] on V–Sn oxides, the intensity of the band due to Mo=O stretching vibration for Sn–Mo oxides was determined as a function of the concentration of Mo ions in KBr pellets. The results are compared with those of similar experiments for MoO_3 (Fig. 5). About 40—50% of MoO_3 in Sn–Mo (50) and (75) exhibits no IR absorption. These results suggest presence of an amorphous material in Sn–Mo (50) and (75) oxides. Although the nature of the amorphous material is unclear, the disappearance of the Mo=O band seems to result from a strong interaction between MoO_3 and SnO_2. No new bands due to the amorphous material are observed to appear. The new bands might be masked by the bands due to SnO_2 or MoO_3. The disappearance of Mo=O band observed with Sn–Mo (10) is attributable to dissolution of Mo ions in SnO_2, as in the case with V–Sn oxides.[8] Okamoto *et al.*[2] have also concluded that the decrease in the crystallinity of MoO_3 in Sn–Mo oxides is attributable to the dissolution of Mo ions in SnO_2 as well as to the

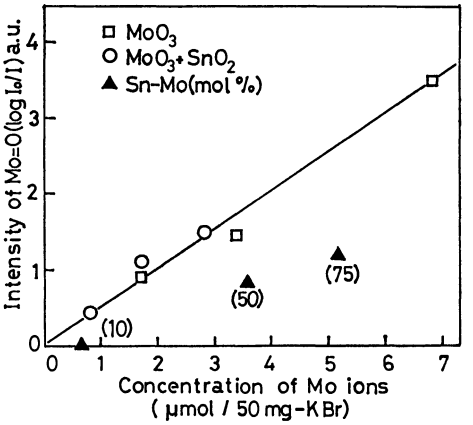

Fig. 5. Estimation of MoO_3 concentration in Sn–Mo oxides.
1 wt% of Sn–Mo oxide in KBr. ○: Mechanical mixture of MoO_3 and SnO_2 at room temperature.

formation of an amorphous material between MoO_3 and SnO_2.

After a heat treatment up to 750 °C the surface area of Sn–Mo (10) decreased from 33 to 25 m^2/g, suggesting a slight increase in the crystal size of SnO_2; no new diffraction lines appeared. With Sn–Mo(50), the intensity of the diffraction lines due to SnO_2 increases by a factor of 1.5, while the MoO_3 crystals grow markedly in the direction perpendicular to the b-axis. Its surface area increases from 19 to 27 m^2/g. In the case of Sn–Mo(75), new diffraction lines due to SnO_2 appear, its surface area increasing from 18 to 29 m^2/g. Such behavior seems explicable in terms of the idea that the amorphous material in Sn–Mo(50) and (75) is decomposed to form SnO_2 and MoO_3, the former crystal being very fine because of its very high melting point. Thus, the presence of amorphous material is confirmed. The lack of any new compounds in Sn–Mo oxides suggests that their promoter effect is attributable to the existence of both Mo ions dissolved in SnO_2 and the amorphous material or of either one.

Catalytic Oxidation of C_3H_6 Using $^{18}O_2$ Tracer. Participation of lattice oxygen in the C_3H_6 oxidation on Sn–Mo oxides was examined by using $^{18}O_2$ as an oxidant instead of ordinary oxygen. No change in the ^{18}O content in oxygen occurred during the reaction, *i.e.*, no formation of $^{18}O^{16}O$ proceeded, which suggests that the exchange of oxygen with the catalyst oxygen is negligible under the present experimental conditions.

As shown in Table 2, with SnO_2 as well as Sn–Mo oxides there is little or no difference between the ^{18}O contents of oxidation products such as CO, CO_2, and CH_2=CHCHO, while with MoO_3 the ^{18}O content of CH_2=CHCHO is larger than those of CO and CO_2. By assuming that the ^{18}O content of H_2O is the average of those of CO, CO_2, and CH_2=CHCHO, for all the oxidation products the ^{18}O content can be determined with each catalyst (Table 2 and Fig. 6).

As previously shown,[9] the feature of the increase in the ^{18}O content of oxidation products with the pro-

TABLE 2. ^{18}O CONTENT IN THE PRODUCTS OF C_3H_6 OXIDATION OVER Sn-Mo OXIDES
$P_{C_3H_6}=23$ Torr (1 Torr = 133.3 N m^{-2}), $P(^{18}O_2)=8$ Torr, and temp 400 °C

Catalyst	Reaction time / min	Yield/μmol m^{-2} of each product and its ^{18}O content/%[a]			Total yield[b] / μmol-oxygen atoms m^{-2}	Average[c] ^{18}O%	Lattice oxygen[d] participation / μmol m^{-2} (layers)
		CO_2	CO	CH_2=CHCHO			
SnO_2	1	3.0 (40)	0.9 (38)	—	11	40	30 (1—2)
	2.3	7.1 (50)	1.3 (38)	—	24	47	
Sn-Mo(50)	1	4.2 (31)	3.8 (33)	1.8 (35)	24	32	70 (3—4)
	2	9.2 (43)	7.6 (48)	4.5 (48)	51	45	
MoO_3	5.5	2.9 (19)	4.2 (21)	0.8 (33)	19	20	90—150 (4—7)
	15	12.7 (34)	12.7 (39)	3.0 (50)	70	37	

a) Values in parentheses. b) This value was nearly the same as that obtained from the amount of $^{18}O_2$ consumed in the oxidation. c) (Total amount of ^{18}O/total amount of oxygen) × 100. d) See Ref. 13.

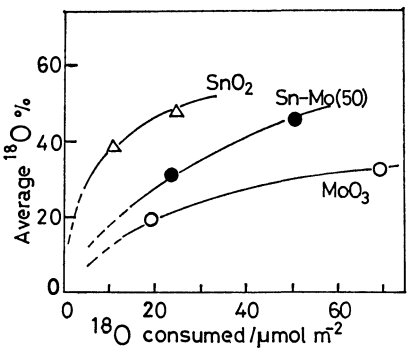

Fig. 6. Average ^{18}O%[a] in the products *vs.* amount oxygen consumed[b] in the oxidation at 400 °C. a),b) See Table 2.

gress of reaction provides information on to what extent lattice oxygen participates in the oxidation. The number of sublayers of the oxide participating in the oxidation was calculated (Table 2), as has been done by Keulks *et al.*[13] The extent of participation of lattice oxygen increases in the order SnO_2<Sn–Mo(50)<MoO_3, while the rate of oxidation on Sn–Mo oxides is about 30 times larger than that on MoO_3. Such features are in contrast to those for Bi–Mo oxides, where the extent of participation of lattice oxygen is in parallel with the rate of oxidation.[13] As regards the nature of such different features, it should be noted that the extent of participation of lattice oxygen for the present system is much smaller than those for Bi–Mo[13] and V–Mo oxides.[9] Furthermore, rate-determining steps for the oxidation differ between Sn–Mo oxides and MoO_3 or Bi–Mo oxides, *etc.*, the reoxidation for the former and the reduction for the latter being the rate-determining step. Accordingly, it appears inappropriate to correlate the catalytic activity solely with the extent of participation of lattice oxygen.

Reduction of ^{18}O Substituted Sn–Mo Oxide and Comparison of Sn–Mo(50) with Sn–Mo(50)–M. Studies of reduction of ^{18}O substituted Sn–Mo oxides with C_3H_6 also are expected to give information on to what extent oxide layers are associated with the reduction of oxides and their reoxidation. Sn–Mo(50), Sn–Mo(50)–M, SnO_2, and MoO_3 were reduced with CO at 400—500 °C, 20—40% of the surface lattice oxygen being removed as CO_2. Then, the reduced oxides were reoxidized with $^{18}O_2$ around 300 °C. The period of reoxidation was 10 h for MoO_3, 2 h for SnO_2, and 2—4 h for Sn–Mo oxides. The amounts of ^{18}O incorporated were nearly the same as those removed by the reduction. As shown in Table 3, the ^{18}O content in products for MoO_3 is much smaller than that for SnO_2, the corresponding values for Sn–Mo oxides being similar to those for SnO_2. These facts indicate that the mobility of lattice oxygen in Sn–Mo oxides as well as in SnO_2 is lower than that in MoO_3.

Table 3 also includes results of similar experiments for Sn–Mo(50)–M, where the ^{18}O content in products is larger than the corresponding values for Sn–Mo(50). Furthermore, the IR band due to the Mo=O vibration for Sn–Mo(50)–M decreased in intensity by about 20% in comparison with 40—50% for Sn–Mo(50). Such behavior would be expected from the difference in preparation procedures between both the Sn–Mo(50) oxides. However, there is little or no difference between the distributions of products of C_3H_6 oxidation for both the oxides, although the rate of oxidation for Sn–Mo(50) is about 1.5 times higher than for Sn–Mo(50)–M. Accordingly, it appears that essentially the same active phase as that for Sn–Mo(50) may be formed for Sn–Mo(50)–M, for example by the heat treatment of a mechanical mixture of SnO_2 and MoO_3 at 600 °C.

The Nature of the Active Phase of Sn–Mo Oxides. As described above, the reduction of Sn–Mo oxides with C_3H_6 proceeds very rapidly as compared to their reoxidation. The results obtained in the present work as well as by Seiyama *et al.*[14] suggest that essentially the same situation is expected for SnO_2. Accordingly, it seems likely that such a high reducibility of Sn–Mo oxides arises from the existence of SnO_2 itself in Sn–Mo oxides. As described above, the active phase of

Table 3. ^{18}O content in the products of the reduction of ^{18}O substituted oxides with C_3H_6. $P_{C_3H_6}=23$ Torr

Catalyst		MoO_3	SnO_2	Sn-Mo(50)-M		Sn-Mo(50)	
Amount of ^{18}O substituted/ μmol m^{-2}		4.9	6.6	6.3	8.0	5.5	5.5
Reduction temp/°C		400	400	350	430	350	430
Reduction time/min		10	5	5	0.5	2	1
Amount of product/ μmol m^{-2}	CO_2	0.10	2.36	0.62	0.62	1.4	2.0
		(<0.5)	(20)	(12)	(7)	(7)	(3)
(^{18}O content/%)	CO	0.062	0.27	0.85	0.80	1.2	1.6
		(<0.5)	(—)	(16)	(11)	(8)	(4)
	CH_2=CHCHO	0.17		0.62	0.84	0.40	0.58
		(<0.5)		(—)	(15)	(13)	(6)
Total amount of lattice oxygen reacted/μmol m^{-2}		0.80	7.6	5.1	5.2	4.0	10.4

Sn–Mo oxides consist of both or either of Mo ions dissolved in SnO_2 and the amorphous material formed from interaction of molybdenum oxide with tin oxide. The results of the reduction of ^{18}O substituted Sn–Mo(50) oxides show that so far as the features of the reduction are concerned, Sn–Mo oxides resemble SnO_2 rather than MoO_3. This suggests that the amorphous material in Sn–Mo oxides can be approximated to some extent by the MoO_3 highly dispersed on SnO_2, where the crystallinity of MoO_3 disappears.

Although the situation is unclear for Sn–Mo(75) which exhibits no diffraction lines due to SnO_2, it is to be noted that there is no marked difference between the rates of oxidation for all the Sn–Mo oxides. In addition, the selectivity for oxidation is essentially the same for all Sn–Mo oxides. This suggests that for Sn–Mo(75) it seems unnecessary to assume the existence of active phases other than the amorphous material (the MoO_3 highly dispersed on SnO_2). Although the active phase of Sn–Mo(10) consists of Mo ions dissolved in SnO_2, there is no marked difference in the surface structures associated with the oxidation between the Mo ions dissolved in SnO_2 and the MoO_3 highly dispersed on SnO_2, since no special features of the C_3H_6 oxidation are observed with Sn–Mo(10).

Such features are out of accord with results of oxidation of alcohols on Sn–Mo oxides described by Okamoto *et al.*[2] who found that the active phase responsible for the oxidation varies according as the composition becomes rich or poor in Mo. According to the work of Niwa *et al.*,[1] however, the rate of oxidation of alcohol on Sn–Mo oxides is independent of the catalyst composition.

Seiyama *et al.*,[14] have shown that there is little or no doubt that on SnO_2 the oxidative dehydrogenation of C_3H_6 to π-allyl species proceeds very easily, whereas the formation of CH_2=CHCHO from the π-allyl hardly takes place. Accordingly, it appears unlikely that the oxygen necessary for the formation of CH_2=CHCHO on Sn–Mo oxides originates from SnO_2; the source of this oxygen seems to be the MoO_3 adjacent to SnO_2. Such a reaction sequence is essentially the same as the model proposed by Haber,[15] who claimed that the formation of π-allyl from C_3H_6 and that of CH_2=CHCHO from π-allyl occur on SnO_2 and MoO_3, respectively. Of course, in the case of Sn–Mo oxides the reactivity of SnO_2 as well as MoO_3 will be enhanced by their mutual contact. In fact the rate of oxidation of C_3H_6 over Sn–Mo oxides is higher than that over SnO_2 as well as MoO_3. Furthermore, the fact that Sn–Mo oxides are 30—40 times more active than MoO_3 but only 4—5 times than SnO_2, is in agreement with what would be expected from the reaction sequence proposed above.

The authors wish to thank Mr. Masafumi Yoshioka for carrying out part of the experiments.

References

1) M. Niwa, M. Mizutani, M. Takahashi, and Y. Murakami, *J. Catal.*, **70**, 14 (1981).
2) Y. Okamoto, K. Oh-hiraki, T. Imanaka, and S. Teranishi, *J. Catal.*, **71**, 99 (1981).
3) Y. Morooka, Y. Takita, and A. Ozaki, *J. Catal.*, **23**, 183 (1971); S. Tan, Y. Morooka, and A. Ozaki, *ibid.*, **17**, 132 (1970); Y. Takita, Y. Morooka, and A. Ozaki, *ibid.*, **52**, 95 (1978).
4) J. Butein, *J. Catal.*, **10**, 188 (1968); **13**, 373 (1969).
5) M. Ai, *J. Catal.*, **40**, 327 (1975).
6) L. Ya. Margolis, *J. Catal.*, **21**, 93 (1971).
7) V. I. Lazukin, M. Ya. Rubanik, Ya. V. Zhigailo, A. A. Kurganov, and Zh. F. Buteiko, *Katal. Katal., Akad. Nauk. Ukr. SSR Respub. Mezhvedom.* Sb. **2**, 50 (1966) (Russ.); *Chem Abstr*, **66**, 75620y (1967); V. I. Lazukin, V. M. Belousov, and M. Ya. Rubanik, *Ukr. Khim. Zh.* (Russ. Ed.), **32**, 321 (1966); *Chem. Abstr.*, **65**, 2111g (1966).
8) T. Ono, Y. Nakagawa, and Y. Kubokawa, *Bull. Chem. Soc. Jpn.*, **54**, 343 (1981).
9) T. Ono and Y. Kubokawa, *Bull. Chem. Soc. Jpn.*, **55**, 1748 (1982).
10) E.g., Y. Morooka, S. Tan, and A. Ozaki, *J. Catal.*, **17**, 125 (1970).
11) M. Araki, T. Nishimura, T. Hayakawa, and T. Ishikawa, *Sekiyu Gakkai Shi*, **17**, 666 (1974).
12) "X-sen Kessho-Gaku," ed by I. Nitta, Maruzen, Tokyo (1961).
13) G. W. Keulks and L. D. Krenzke, Proc. 6th Int. Cong. Catal., London, 1976, Vol. 2, p. 806; L. D. Krenzke and G. W. Keulks, *J. Catal.*, **61**, 316 (1980).
14) T. Seiyama, N. Yamazoe, and M. Egashira, Proc. 5th Int. Cong. Catal., Maiami, 1972, Vol. 2, p. 997.
15) J. Haber, *Int. Chem. Eng.*, **15**, 21 (1975).

 © 1983 The Chemical Society of Japan Bull. Chem. Soc. Jpn., 56, 1289—1300 (1983)

Fluorescence Spectrum and Its Intensity of Europium Tris(ethyl sulfate) Enneahydrate

Tomoyuki OHOKA and Yoshifumi KATO*

Department of Chemistry, Faculty of Science, Kobe University Nada-ku, Kobe 657

(Received June 24, 1982)

The polarized fluorescence spectrum of the europium tris(ethyl sulfate) enneahydrate crystal was measured at 95 K by using excitation lines of an Ar^+ laser. The multipole character of transitions and the energies and crystal quantum numbers for the crystal field components of the $^7F_J(J=0, 1,\cdots,6)$ and $^5D_{0,1}$ terms were determined from the spectral analysis. It was ascertained that most of the transitions were due to forced electric dipole transitions but some of them due to magnetic dipole transitions, in which nine strong lines appeared as magnetic dipole radiations satisfying the selection rule for ion levels, while three weak lines were magnetic dipole radiations forbidden in ions. The relative intensities of both the forbidden electric dipole transitions and the magnetic dipole transitions were calculated by the crystal field wavefunctions obtained to reproduce the experimental data. From the comparison of the calculated intensities with the observed ones, the ratio of the populations of the $^5D_0$ term to the $^5D_1$ term in fluorescent process was estimated to be about 20, although the $^5D_0$ term was 1750 cm^{-1} lower than the $^5D_1$ term. The result suggested that the configuration mixing due to *g*-orbitals was significant to allow electric dipole transitions.

It has been already well known[1] that the trivalent europium ion of $4f^6$ configuration has a regular ^7F_J multiplet followed by a ^5D_J multiplet and is the only one with a nondegenerate ground state $^7F_0$ among trivalent rare earth metal ions. For the europium tris(ethyl sulfate) enneahydrate, $Eu(C_2H_5SO_4)_3\cdot 9H_2O$ (Eu(ES)), Sayre and Freed[2] determined most of the crystal field components of $^7F_J(J=0,1,\cdots,6)$ terms from the polarized fluorescence spectrum and partially analysed the ultraviolet absorption spectrum. They also pointed out that some of fluorescence lines with $\Delta J=\pm 1$ in the $^5D_{0,1}\rightarrow{}^7F_{0,1,2}$ transitions were due to magnetic dipole (MD) radiation and not due to electric dipole (ED) radiation from the polarization measurements, although the transition probability due to MD transitions is, in general, extremely smaller than that due to ED transitions for parity-allowed transitions (see Appendix A). Similar MD transitions were also observed in the fluorescence spectra of Eu^{3+} and Tb^{3+} in $LaCl_3$ by Dieke *et al.*,[3,4] where only MD transitions satisfying the selection rule for ions ($\Delta J=0, \pm 1$) were observed in the crystals. Hellwege *et al.*[5,6] separately determined the energies and quantum numbers of the crystal field components of the $^7F_{0,1}$, $^5D_{0,1,2}$, and several electronic terms in the ultraviolet region from the absorption spectrum of Eu(ES) and its Zeeman effect.

The present paper deals with a further investigation of the crystal field components of the ^7F_J terms in Eu(ES) from the polarization properties of the laser-excited fluorescence spectrum at the liquid nitrogen temperature. The laser-excited technique is anticipated to give detailed information for the energy levels of a crystal, because of powerful capacity of laser as a light source and the facility of selective excitation to a specific ion level in crystals. Then the fluorescence transition probabilities for both the forbidden ED transitions and the allowed MD transitions are calculated from the wavefunctions which have been determined to reproduce the observed crystal field levels by using the tensor-operator method.[7] Some discussions are presented by comparing calculated relative intensities with observed ones.

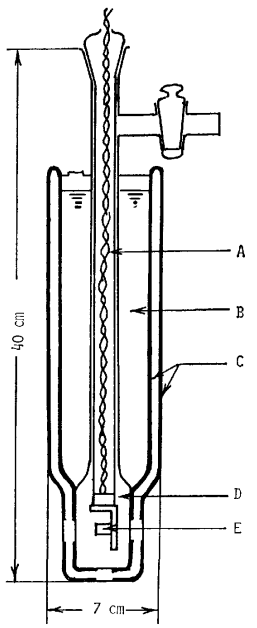

Fig. 1. Glass Dewar vessel for fluorescence measurements at liquid nitrogen temperature. A: Thermocouple, B: liquid nitrogen, C: silver plating, D: nitrogen gas, E: crystal.

Experimental

Preparation of the compound and the crystal growth were described in a previous paper.[8] A crystal was cut into a square rod of $3\times 3\times 8$ mm^3 with the largest side along the principal axis of the crystal. A single crystal was attached to a copper block in a special glass Dewar vessel (Fig. 1), which was filled with nitrogen gas at atomospheric pressure to prevent dehydration of crystalline water under vacuum. Since a crystal was cooled by heat conduction through nitrogen gas, the temperature of the crystal measured by a thermocouple was 95 K under incident Ar^+ laser beam at the liquid nitrogen temperature. The fluorescence spectrum was measured under a 90° scattering geometry by a Spex 14018 double spectrometer equipped with a cooled RCA C31034 photomultiplier and a Coherent Radiation model CR-4 Ar^+ laser. The exciting lines of 457.9 nm (21837

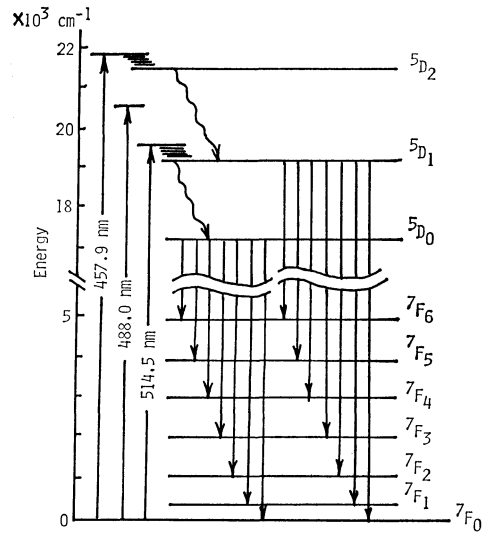

Fig. 2. Energy level diagram and observed fluorescence process of $Eu(C_2H_5SO_4)_3 \cdot 9H_2O$.

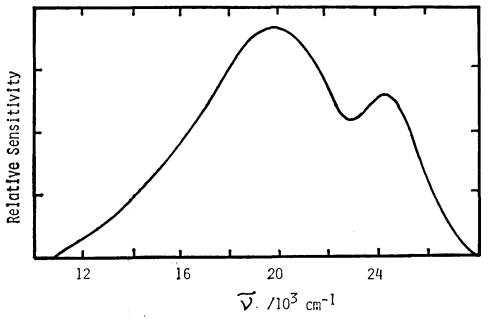

Fig. 3. Intensity response curve of the apparatus. The ordinate is in an arbitrary unit.

cm^{-1}) and 514.5 nm (19435 cm^{-1}) produced fairly intensive fluorescence and the fluorescence by the former was about 100 times as strong as that by the latter, while the exciting line of 488.0 nm (20492 cm^{-1}) scarcely produced fluorescence lines. This fact might easily be seen from the energy level diagram of the Eu^{3+} ion in Fig. 2. Almost all the electrons at 95 K occupy the lowest $^7F_0$ level and not the next $^7F_1$ level being about 380 cm^{-1} higher than the former. Thus, it is possible to produce directly the $^7F_0 \rightarrow {}^5D_2$ and $^7F_0 \rightarrow {}^5D_1$ excitations by the 457.9 and 514.5 nm exciting lines, respectively, and furthermore the former involves an ED transition allowed by the selection rule for crystal field levels, but the latter does not. Since such a condition is not satisfied by the 488.0 nm excitation, the 457.9 nm excitation yields the most intensive fluorescence. The measurement was carried out with the incident laser power of about 200 mW at the position of the crystal and the spectral slit-width was 4—10 cm^{-1} because most of fluorescence lines had intrinsically broad line-width even at 95 K. Wavenumbers were calibrated by already-known lines of neon, krypton, and argon discharge lamps. The accuracy of wavenumbers was within 1 cm^{-1}. The correction of the intensity response for the spectrometer-detector system as a function of wavenumber was performed by the calibration with a standardized tungsten source (Ushio No. 701038). The curve of the intensity response had the maximum at about 20000 cm^{-1} with gradual decrease toward low-wavenumber side and the relative intensity at 12000 cm^{-1} was about one-tenth of that at 20000 cm^{-1} (Fig. 3). The reproducibility of intensities did not vary seriously over all the lines. The average accuracy of intensities was estimated to be within 15% except those for the very weak $^5D_{0,1} \rightarrow {}^7F_{5,6}$ transitions. However, the intensity of very weak transitions was considered to have a fairly large amount of error.

Table 1. Crystal quantum number classification for C_{3h} symmetry

J	M_J $\mu=0$	$\mu=\pm1$	$\mu=\pm2$	$\mu=3$	No. levels
0	0				1
1	0	±1			2
2	0	±1	±2		3
3	0	±1	±2	−3, +3	5
4	0	±1	±2, ∓4	−3, +3	6
5	0	±1, ∓5	±2, ∓4	−3, +3	7
6	−6, 0, +6	±1, ∓5	±2, ∓4	−3, +3	9

Table 2. Selection rules for C_{3h} symmetry in case of even number of electrons

	For electric dipole					For magnetic dipole			
μ'	μ 0	±1	±2	3	μ'	μ 0	±1	±2	3
0			σ	π	0	σ	π		
±1		σ	π	σ	±1	π	σ	π	
±2	σ	π	σ		±2		π	σ	π
3	π	σ			3			π	σ

Fluorescence Spectra and Wavefunctions

According to the analysis of the crystal structure of rare earth metal tris(ethyl sulfate) enneahydrates,[9,10] the space group is $P6_3/m$ (C_{6h}^2) and the site symmetry around a rare earth metal ion is C_{3h}. A rare earth metal ion has nine water molecules as nearest neighbors, where the water oxygen atoms are at a distance of about 2.4 A from the metal ion. An ion level $|JM)$ under a crystal field splits into several crystal field levels which are designated by the crystal quantum number μ originally introduced by Hellwege[11] and thereafter partially extended by others.[1] The classification of levels split by C_{3h} symmetry of a given J term is tabulated in Table 1, where the level with double signs is twofold degenerate. The selection rules for ED and MD transitions in C_{3h} symmetry are shown for an even number of electrons in Table 2.[12] The fluorescence spectra of Eu(ES) excited by the 457.9 and 514.5 nm lines of an Ar^+ laser at 95 K are shown in the range from about 19000 to 14000 cm^{-1} in Figs. 4 and 5, where σ- (Fig. 4) and π-polarized (Fig. 5) spectra stand for the radiation emitted in directions perpendicular and parallel to the principal axis of a crystal, respectively. In these figures, all the lines except V, V(O–H), V(C–H), and Vib Raman are due to the fluorescence. The distinction between fluorescence lines and vibrational Raman lines could easily be made when the polarized spectra excited by the 457.9 and 514.5 nm lines are compared with

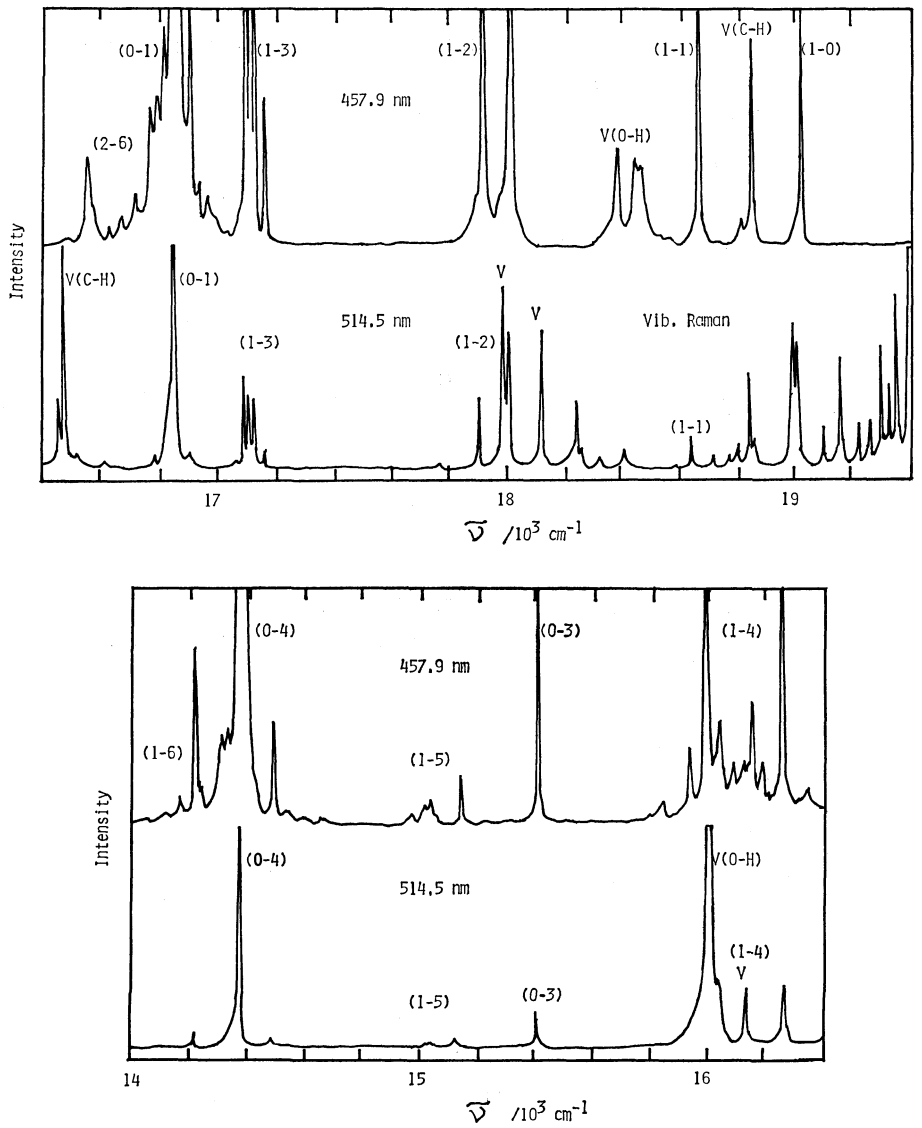

Fig. 4. σ-polarized fluorescence spectra of $Eu(C_2H_5SO_4)_3 \cdot 9H_2O$ at 95 K by the exciting lines of 457.9 nm (21837 cm^{-1}) and 514.5 nm (19435 cm^{-1}) of Ar^+ ion laser. Fluorescence lines between ^5D_J and $^7F_{J'}$ are shown by the notations of (J-J'). Notations of V, V(C–H),V(O–H), and Vib Raman indicate the vibrational Raman lines.

those by the 488.0 nm line or the polarized spectra of La(ES) without f electrons. In the latter spectra there were no fluorescence lines. Observed vibrational frequencies of polarized Raman spectra of Eu(ES) and La(ES) at 95 K are given in Table 3, where ZX- and ZZ-polarizations correspond to σ- and π-polarizations for fluorescences, and also to A_g and E_{1g} irreducible representations for vibrations, respectively. Although the fluorescence lines by the 457.9 nm excitation partially overlap with weak lines from the $^5D_2$ manifold, the latter lines could readily be distinguished from the $^5D_{0,1} \rightarrow {}^7F_J$ lines by comparing with the spectra of the 514.5 nm excitation. Thus the fluorescence lines were reasonably assigned to the transitions between crystal field levels. The nature of radiations was also clarified from the polarization properties following the selection rules and the result of calculated transition probabilities (see later section). The result obtained is given in Table 4, together with observed relative intensities. It can be seen in Table 4 that nine strong MD transitions are observed in the $^5D_{0,1} \rightarrow {}^7F_{0,1,2}$ transitions (the case of $\Delta J = \pm 1$ allowed for ions), and furthermore three very weak MD transitions are also observed in the $^5D_0 \rightarrow {}^7F_{3,4,5}$ transitions (the case of $|\Delta J| > 1$ forbidden for ion), where ΔJ is the difference of J between ion levels regarding a transition. The former MD transitions are those presented already by Sayre and Freed,[2] and the latter MD transitions in case of $|\Delta J| > 1$ have not yet been reported for any rare earth crystals so far as we know. Such transitions should be allowed to occur when there exist considerable interactions between crystal field components belonging to ion levels with different J (J-mixing), in addition to strong spin-orbit interactions (see Appendix A). Since the terms $^5D_{0,1}$ consist of only the crystal field levels with $\mu = 0$ and ± 1, the levels with $\mu = 0$ in the lower terms ^7F_J are able to be determined only by MD

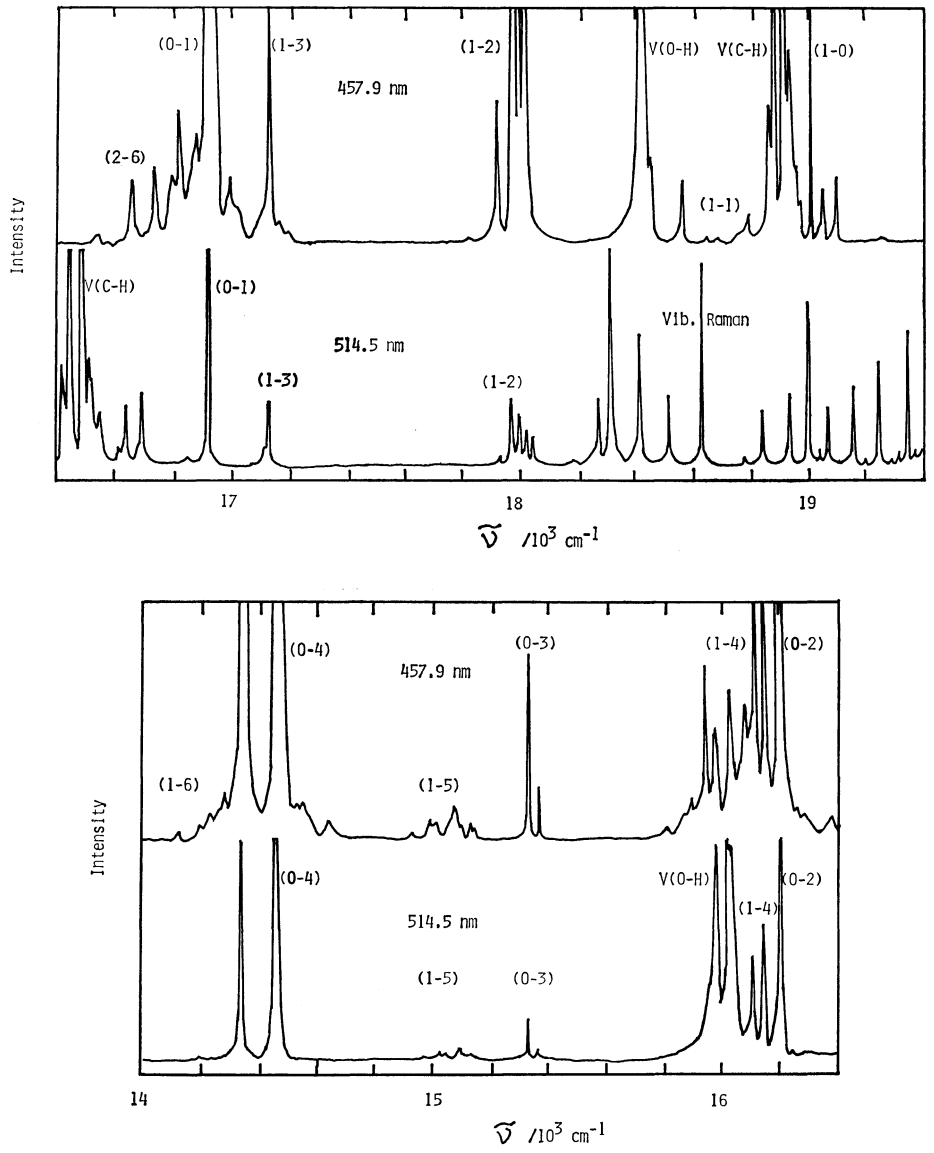

Fig. 5. π-polarized fluorescence spectra of $Eu(C_2H_5SO_4)_3 \cdot 9H_2O$ at 95 K by the exciting lines of 457.9 nm (21837 cm^{-1}) and 514.5 nm (19435 cm^{-1}) of Ar^+ ion laser. Notations are the same as in Fig. 4.

transitions and not by ED transitions as can be seen in the selection rules (Table 2). Observed energies and quantum numbers of crystal field levels are compared with those by Sayre and Freed[2] as given in Table 5. In both the results, there are few discrepancies between them regarding the wavenumbers and the crystal quantum numbers, but the $\mu=0$ levels in the $^7F_{3,4,5}$ terms are first acertained by the present analysis, and the present energy values are more accurate.

Wavefunctions. In order to calculate theoretically the transition probability between crystal field levels, it is necessary to have reliable wavefunctions in a crystal. Under intermediate coupling the wavefunctions of a rare earth metal ion are expressed by

$$|\phi_n) = \sum_n c_n |f^N : qSLJ), \quad (1)$$

where q is additional quantum numbers specifying a state except S, L, and J. When such an ion is placed in a crystal field, crystal field wavefunctions are given as

$$|\phi_a) = \sum_i a_i |f^N : qSLJM). \quad (2)$$

The Hamiltonian in crystals can be written as

$$H = H_{ion} + H_{cry}, \quad (3)$$

where H_{ion} and H_{cry} are the ion and crystal-field parts of interactions, respectively. The H_{ion} part consisting of the Coulomb and spin-orbit interactions can be expressed by a linear combination of the terms with the Slater radial integrals F_n (n=2,4,6) and the spin-orbit coupling constant ζ_{4f}. We further take account of scalar two-body electrostatic interactions arising from the second-order perturbation energies. These contribute to the H_{ion} as the terms with three configuration interaction (CI) parameters α, β, and γ.[14,15] Here we approximate that the site symmetry at a rare earth metal ion is D_{3h} instead of C_{3h} as adopt-

Table 3. Observed frequencies of polarized vibrational spectra of lanthanum and europium tris(ethyl sulfate) enneahydrate crystals at 95 K

$A_g(ZZ)$ Raman shift ν/cm^{-1}		$E_{1g}(ZX)$ Raman shift ν/cm^{-1}		Assignment[b]
La(ES)[a]	Eu(ES)[a]	La(ES)	Eu(ES)	
	40 vw	32 s	38 s	lattice mode
49 m	56 m			
63 m	72 s	60 vs	68 s	
88 m	99 m	82 m	93 m	
113 m	125 w	104 m	116 m	
		122 m	140 m	
160 s	177 s			
185 vw		190 w	197 w	
		236 s	246 vw	
258 s	265 m	252 m	259 s	
340 m	370 m	305 m	321 m	δ(CCO)
424 vs	424 vs	418 m	419 m	$\rho_r(SO_3)$
		430 s	432 s	
575 m	574 sh	538 w	540 w	$\delta(SO_3)$
	579 m	575 m	576 m	
619 w	625 w	610 w	662 w	
		628 w	655 w	
			704 vw	
809 vs	810 vs			$\rho_r(CH_2)$
934 m	933 m			ν(C-C)
1009 s	1011 s			ν(S-O)
1072 s	1073 vs			ν(C-O)
1110 m	1111 m	1155 vw	1155 vw	ν(S-O)
1215 w	1213 w	1200 m	1201 m	
		1291 m	1292 m	$\rho_w(CH_2)$
1367 w	1367 w			$\delta(CH_3)$
1392 w	1393 w			
1459 sh	1460 sh	1446 s	1447 s	$\delta(CH_2)$
1465 s	1466 m			
2727 m	2725 m			comb
	2778 m			
2788 sh	2790 vw			
2866 m	2868 m			ν(C-H)
2895 sh	2894 sh			
2921 s	2920 s			
2946 vs	2944 vs			
2978 vs	2977 vs	2984 s	2986 s	
2994 s	2993 s			
3031 w	3031 w	3006 w	3007 w	
3375 w	3373 m	3374 m	3375 m	ν(O-H)
3397 w	3395 w	3390 m	3389 m	
3442 vs	3440 vs	3445 m	3446 m	

a) vs: Very strong, s: strong, m: medium, w: weak, vw: very weak, sh: shoulder. b) ν: Stretching, δ: bending, ρ_r: rocking, ρ_w: wagging, comb: combination. The assignment is based on the analysis of the internal modes of $La(C_2H_5SO_4)_3 \cdot 9H_2O$ and $La(C_2H_5SO_4)_3 \cdot 9D_2O$ at room temperature in a previous work (see Ref. 13).

ed by most of authors. The adequacy of this assumption has already been discussed by Margolis.[16] In practice, the site symmetry is D_{3h} as far as nine oxygen atoms of the crystalline waters as nearest neighbors are concerned, and the contributions of six ES ions as next nearest neighbors to the crystal field is considered to be very small. Then the crystal field potential of D_{3h} may be expanded by the irreducible tensor $C_n^{(k)}$ [12] as

$$H_{cry}(D_{3h}) = B_0^2 C_0^{(2)} + B_0^4 C_0^{(4)} + B_0^6 C_0^{(6)} + B_6^6 [C_6^{(6)} + C_{-6}^{(6)}], \quad (4)$$

in which B_n^k is the crystal field parameter to be determined from experimental data. The matrix element of the Hamiltonian is reduced by the tensor-operator technique.[12,17] Since we are interested in the crystal field levels of the $^5D_{0,1}$ and ^7F_J terms only, a set of limited electronic terms interacting strongly with these terms is considered, *i.e.*, ^7F, $^5D1$, $^5D2$, $^5D3$, ^5L, $^5G1$, $^5G2$, $^5G3$, $^3P1$, $^3P3$, and $^3P6$ terms, where a final index of terms is an additional index following the table of Nielson-Koster,[18] which corresponds to q in Eq. 1. The procedure of the parameter determination is described in a previous paper.[17] At first, the diagonalization of the H_{ion} part with F_2, F_4, F_6, ζ_{4f}, α, β, and γ as adjustable parameters was performed by fitting calculated values to the centers of gravity of J-manifolds (*i.e.*, the "ion level" in crystals) derived from the experiments. Secondly the crystal field parameters were determined from the deviations of crystal field levels regarding individual "ion level". Finally a minor readjustment of all the parameters was made by the least-squares method by diagonalizing the entire Hamiltonian. Thus the eigenvectors for the "ion levels" (the c_n in Eq. 1) and the crystal field levels (the a_i in Eq. 2) have been determined separately. The final parameters are given in Table 6. The wavefunctions determined are considered to be fairly reliable from the root mean square (rms) deviations evaluated for both ion levels and crystal field levels (Table 6).

Fluorescence Intensity

Judd[19] and Ofelt[20] independently derived the theory for the line strength of induced electric dipole transitions observed between states of rare earth metal ions within the $4f^N$ configuration imbedded in crystalline solids and solutions. Here the basic theory for ED transitions being known as the Judd-Ofelt theory and then the theory for MD transitions are outlined. The fluorescence intensity I in erg per sec of spontaneous emission between ψ_a and ψ_b states is given as

$$I(\psi_a:\psi_b) = g(\psi_a)N(\psi_a)hc\sigma A(\psi_a:\psi_b), \quad (5)$$

where $g(\psi_a)$ and $N(\psi_a)$ are respectively the degeneracy and the number of ions in the initial state ψ_a, σ is the transition frequency in cm^{-1}, and $A(\psi_a:\psi_b)$ is the spontaneous transition probability. The transition probability due to dipole radiations can be written as

$$A(\psi_a:\psi_b) = 64\pi^4\sigma^3[\chi_e|\langle\psi_a|\boldsymbol{D}_e|\psi_b\rangle|^2 + \chi_m|\langle\psi_a|\boldsymbol{D}_m|\psi_b\rangle|^2]/[3h(2J+1)], \quad (6)$$

TABLE 4. FLUORESCENCE SPECTRUM OF $Eu(C_2H_5SO_4)_3 \cdot 9H_2O$

Lower level	Upper level: $^5D_0(0)$[a] Wavenumber[b] $\tilde{\nu}$/cm^{-1}	Int.[c]	Energy[d]	$^5D_1(\pm1)$[a] Wavenumber $\tilde{\nu}$/cm^{-1}	Int.	Energy	$^5D_1(0)$[a] Wavenumber $\tilde{\nu}$/cm^{-1}	Int.	Energy	Average energy[d]
$^7F_0(0)$				19020.3π	1.28*	0.0	19024.5σ	1.00*	0.0	0.0
$^7F_1(\pm1)$	16902.2π	141.*	358.8	18661.8σ	2.19	358.4	(18663.7π	0.03*	360.7)[e]	358.6
(0)	16863.1σ	123.*	397.9	(18623.0π	0.02*	397.2)[e]				397.9
$^7F_2(\pm1)$				18003.8σ	13.4*	1016.2	18007.7π	6.83*	1016.5	1016.4
(±2)	16227.1σ	28.8	1033.7	17985.6π	13.3*	1034.4				1034.1
(0)				17913.3π	1.73*	1106.7	17917.7σ	7.40*	1106.5	1106.6
$^7F_3(3)$	15403.2π	2.13	1857.4	17162.8σ	0.87	1857.0	17165.9π	0.14	1858.1	1857.5
(0)	15380.6σ	0.41*	1880.0							1880.0
(±2)	15357.1σ	2.85	1903.5	17115.7π	10.1	1904.1	17120.7σ	6.36	1903.3	1903.6
(3′)				17106.6σ	2.85	1913.2	17110.5π	2.38	1913.5	1913.4
(±1)				17091.6σ	9.77	1928.2				1928.2
$^7F_4(\pm2)$	14476.8σ	161.	2783.6	16235.7π	10.0	2783.8	(16240.0σ	0.25	2783.7)[e]	2783.7
(±1)				16176.6σ	6.38	2842.9	16181.2	4.60	2842.8	2842.9
(3)	14370.9π	159.	2889.4	16130.2σ	f)	2889.3				2889.4
(0)	(14369.2σ	0.50*	2892.0)[e]							2892.0
($\pm2'$)	14367.1σ	130.	2893.2	16125.8π	0.82	2893.7	16130.2σ	f)	2893.5	2893.5
(3′)	14202.9π	3.70	3057.4	15962.5σ	1.94	3057.0	15966.2π	7.84	3057.5	3057.3
$^7F_5(\pm1)$				15161.6σ	0.26	3857.6				3857.6
(±2)	13383.3σ	0.32	3876.8	15142.1π	0.75	3877.1	15146.4σ	0.47	3877.0	3877.0
($\pm1'$)				15111.1σ	0.25	3908.1				3908.1
(3)	13228.3π	1.43	3931.7	15088.2σ	1.10	3931.0				3931.4
($\pm2'$)	13264.7σ	0.34	3995.3	15024.1π	0.67	3995.1	15028.2σ	0.90	3995.2	3995.2
(0)	13242.8σ	0.38*	4017.2	15002.0π	0.46	4017.2	15006.6σ	0.91	4016.8	4017.1
(3′)				14954.6σ	0.60	4064.6	14959.8π	0.77	4063.6	4064.1
$^7F_6(3)$	12322.7π	0.50	4937.1	14083.2σ	0.18	4935.7				4936.4
(±2)	12307.2σ	1.26	4952.5							4952.5
(3′)	12288.0π	1.18	4971.7	14046.0σ	0.16	4972.9	14050.1π	0.05	4973.0	4972.5
($\pm2'$)	12273.8σ	4.09	4985.9	14032.8π	0.32	4986.1	14036.9σ	0.08	4986.2	4986.1
(±1)				14025.2σ	0.24	4993.7				4993.7
($\pm1'$)				14001.8σ	0.11	5017.1				5017.1

a) The calculated energy of the $^5D_0(0)$ level is 17256.3 cm^{-1} in vacuum. The observed energies of the $^5D_1(\pm1)$ and $^5D_1(0)$ levels are 19015.0 and 19019.2 cm^{-1} in vacuum, respectively. The lines with asterisk are due to MD transition. b) Wavenumbers in cm^{-1} observed in air. c) Relative intensity in case that the intensity of the $^5D_1(0) \rightarrow {}^7F_0(0)$ transition is taken as 1.00. d) Energies in vacuum. Units in cm^{-1}. e) Values in parentheses are less reliable. f) The sum of the intensities of the $^5D_1(\pm1) \rightarrow {}^7F_4(3)$ and $^5D_1(0) \rightarrow {}^7F_4(\pm2')$ transitions is 5.21.

where $\boldsymbol{D}_e$ and $\boldsymbol{D}_m$ are ED and MD operators, respectively, while χ_e and χ_m are the correction factors of the medium related to the refractive index of the medium. When assumed that the surrounding medium around a rare earth metal ion is optically isotropic, the two correction factors might be taken to be equal approximately.[21] After eliminating the frequency dependence of σ^4 and making the correction of the intensity response for observed intensities, a relative intensity may be written as

$$I_r(\psi_a:\psi_b) = g(\psi_a)N(\psi_a)[|(\psi_a|\boldsymbol{D}_e|\psi_b)|^2 + |(\psi_a|\boldsymbol{D}_m|\psi_b)|^2]/(2J+1). \quad (7)$$

The matrix elements in Eq. 7 can be evaluated theoretically if the crystal-field wavefunctions are available.

Matrix Element of Electric Dipole Operator. ED operator $\boldsymbol{D}_e$ is given as

$$\boldsymbol{D}_e = -e\sum_i \boldsymbol{r}_i(\mathbf{C}_\rho^{(1)})_i = -e\boldsymbol{D}'_e, \quad (8)$$

where $\mathbf{C}_\rho^{(1)}$ is the irreducible tensor of rank 1 and $\rho=0$ gives the z-component corresponding to π-polarized radiation, while $\rho=\pm1$ gives the $(x\pm iy)$-components corresponding to σ-polarized radiation. An ED transition between states within the $4f^N$ configuration is parity-forbidden. According to the Judd-Ofelt theory, we consider that the admixing of $nl^{N-1}n'l'$ configurations of opposite parity to nl^N configuration arises from the addition of a static crystal field with odd parity to the Hamiltonian. Then a perturbed state $\psi_{a'}$ and perturbing odd potential V_{odd} are shown by

$$|\psi_{a'}) = |\psi_a) - \sum_\eta [(nl^{N-1}n'l':\eta|V_{odd}|\psi_a)/\Delta E(\eta)] \times |nl^{N-1}n'l':\eta), \quad (9a)$$

$$\Delta E(\eta) = E(nl^{N-1}n'l':\eta) - E(\psi_a) \simeq \Delta E(n'l'), \quad (9b)$$

Table 5. Crystal field energy levels of $Eu(C_2H_5SO_4)_3 \cdot 9H_2O$

Term	Present		Sayre-Freed[a]	
	Crystal Q.N.	Energy/cm^{-1}	Crystal Q.N.	Energy/cm^{-1}
$^7F_0$	0	0.0	0	0.0
$^7F_1$	±1	358.6	±1	356.
	0	397.9	0	398.
$^7F_2$	±1	1016.4	0	1015.
	±2	1034.1	±2	1031.
	0	1106.6	±1	1106.
$^7F_3$	3	1857.5	3	1856.
	0	1880.0		
	±2	1903.6	±2	1903.
	3′	1913.4	3′	1913.
	±1	1928.2	±1	1929.
$^7F_4$	±2	2783.7	±2	2782.
	±1	2842.9	±1	2841.
	3	2889.4	3	2890.
	0	2892.0		
	±2′	2893.5	±2′	2893.
	3′	3057.3	3′	3056.
$^7F_5$	±1	3857.6	±1	3858.
	±2	3877.0	±2	3880.
	±1′	3908.1		
	3	3931.4	3	3937.
			±1′	3955.
	±2′	3995.2	3′	3997.
	0	4017.1	±2	4021.
	3′	4064.1		
$^7F_6$			±1	4915.
	3	4936.4	3	4937.
	±2	4952.5	±2	4958.
	3′	4972.5	3′	4976.
	±2′	4986.1	±2	4992.
	±1	4993.7	±1′	4996.
	±1′	5017.1		
$^5D_0$	0	17256.3	0	17257.
$^5D_1$	±1	19015.0	±1	19015.
	0	19019.2	0	19020.

a) See Ref. 2.

and

$$V_{\text{odd}} = \sum_i \sum_{t,p} A_{tp} r_i^t (\mathbf{C}_p^{(t)})_i, \tag{10}$$

where $|nl^{N-1}n'l':\eta)$ is a mixing state and the unperturbed state $|\psi_a)$ is given in Eq. 2. From the perturbation theory, the final expression for the matrix element of $\boldsymbol{D}'_e$ is written in tensor-operator technique as

$$\begin{aligned}(\psi_{a'}|\boldsymbol{D}'_e|\psi_{b'}) = &\sum_{i,j}\sum_{\lambda}\sum_{t,p} a_i^* b_j (-1)^{2J+S+L'+\lambda-M+p+\rho} \\ &\times \delta(S,S')(2\lambda+1)[(2J+1)(2J'+1)]^{1/2} \\ &\times \begin{pmatrix} l & \lambda & t \\ \rho & -p-\rho & p \end{pmatrix}\begin{pmatrix} J & \lambda & J' \\ -M & p+\rho & M' \end{pmatrix} \\ &\times \begin{Bmatrix} J & J' & \lambda \\ L' & L & S \end{Bmatrix} T(t,\lambda)(qSL\|\boldsymbol{U}^{(\lambda)}\|q'SL'),\end{aligned} \tag{11}$$

Table 6. Parameters and root mean square deviations of $Eu(C_2H_5SO_4)_3 \cdot 9H_2O$

	For 10 ion levels		For 32 crystal levels	
Parameter/cm^{-1}	F_2	393.8	B_0^2	167.8
	F_4	54.29	B_0^4	−504.7
	F_6	5.947	B_0^6	−615.3
	ζ_{4f}	1277.5	B_6^6	524.5
	α	48.5		
	β	−690.5		
	γ	990.5		
rms deviation/cm^{-1}		71.3		6.0

$$\begin{aligned}T(t,\lambda) = &A_{tp}\sum_{l'}(-1)^{l+l'}2(2l+1)(2l'+1) \\ &\times \begin{pmatrix} l & 1 & l' \\ 0 & 0 & 0 \end{pmatrix}\begin{pmatrix} l & t & l' \\ 0 & 0 & 0 \end{pmatrix}\begin{Bmatrix} 1 & \lambda & t \\ l & l' & l \end{Bmatrix} \\ &\times (R_{nl}|r|R_{n'l'})(R_{n'l'}|r^t|R_{nl})/\Delta E(\eta).\end{aligned} \tag{12}$$

Under the site symmetry of D_{3h}, the odd potential can be written as[20]

$$V_{\text{odd}}(D_{3h}) = \sum_i \sum_t A_{t3} r_i^t (\mathbf{C}_3^{(t)} - \mathbf{C}_{-3}^{(t)})_i. \tag{13}$$

From the triangular condition for the n-j symbols in Eqs. 11 and 12 in case of $l=3$, the following relations can be shown,

$$\lambda = 2, 4, 6, \quad t = \lambda \pm 1, \quad l' = 2, 4. \tag{14}$$

Since the parameters $T(t,\lambda)$ contain perturbing crystal field parameters A_{tp}, and radial integrals and energies regarding mixing states $|nl^{N-1}n'l':\eta)$, it is difficult to estimate the $T(t,\lambda)$ theoretically without introducing several drastic assumptions. In order to study the oscillator strength of a group of lines corresponding to the transitions between the components of a pair of J-manifolds, Judd[19] carried out an ingenious simplification for the basic expression by supposing the energy differences in Eq. 12 as being independent of mixing states and by making the sum over M, M', and ρ. Then the resultant expression with a single set of three adjustable parameters could be directly related to the oscillator strength derived from lanthanide solution spectra and it satisfactorily reproduced the experimental results. However, we have followed an alternate parametrization proposed by Axe,[21] which is appropriate to describe the relative intensity of the transitions between crystal field levels by taking the $T(t,\lambda)$ themselves as adjustable parameters. Following the Judd-Axe treatment, a line strength between J-manifolds $S(\varphi_n J:\varphi_m J')$ defined in crystals is given as

$$\begin{aligned}S(\varphi_n J:\varphi_m J') = &\sum_t \sum_\lambda (2\lambda+1)T(t,\lambda)^2 \\ &\times |(\varphi_n J|\boldsymbol{U}^{(\lambda)}|\varphi_m J')|^2/(2t+1).\end{aligned} \tag{15}$$

The matrix elements of the unit tensor of rank λ can be calculated by the eigenvectors of the "ion levels" given in Eq. 1 as

$$\begin{aligned}(\varphi_n J|\boldsymbol{U}^{(\lambda)}|\varphi_m J') = &\sum_{n,m} c_n^* c_m \delta(S,S')(-1)^{S+L'+J-\lambda} \\ &\times [(2J+1)(2J'+1)]^{1/2}\begin{Bmatrix} J & J' & \lambda \\ L' & L & S \end{Bmatrix} \\ &\times (f^N:qSL\|\boldsymbol{U}^{(\lambda)}\|f^N:q'SL').\end{aligned} \tag{16}$$

Consequently, the parameters $T(t,\lambda)$ may be evaluated

TABLE 7. OBSERVED AND THEORETICAL RELATIVE LINE STRENGTHS IN $Eu(C_2H_5SO_4)_3 \cdot 9H_2O$

Lower level	Upper level					
	S_{obsd}		S_{theo}			
	$^5D_0$	$^5D_1$	$^5D_0$		$^5D_1$	
			ED	MD	ED	MD
$^7F_0$		3.56				0.0243
$^7F_1$	405.	4.48		0.0938	$0.00551T(3,2)^2$	0.000037
$^7F_2$	57.6	64.5	$0.00747T(3,2)^2$		$0.00174T(3,2)^2$	0.208
$^7F_3$	8.24	52.3			$0.00987T(3,2)^2 + 0.00826[T(3,4)^2+T(5,4)^2]$	
$^7F_4$	745.	55.4	$0.0106[T(3,4)^2+T(5,4)^2]$		$0.0121[T(3,4)^2+T(5,4)^2]$	
$^7F_5$	3.13	11.6			$0.00499[T(3,4)^2+T(5,4)^2] + 0.000396[T(5,6)^2+T(7,6)^2]$	
$^7F_6$	12.4	1.89	$0.00167[T(5,6)^2+T(7,6)^2]$		$0.00255[T(5,6)^2+T(7,6)^2]$	

by the line strengths derived from experiments and the calculated values of $(\varphi_n J|U^{(\lambda)}|\varphi_m J')$. Now the number of $T(t,\lambda)$ to be evaluated is five from the restriction in Eq. 14; $T(3,2)$, $T(3,4)$, $T(5,4)$, $T(5,6)$, and $T(7,6)$.

Matrix Element of Magnetic Dipole Operator. MD operator $\boldsymbol{D}_m$ is given as

$$\boldsymbol{D}_m = -\beta(2\boldsymbol{S}+\boldsymbol{L}) = -\beta\boldsymbol{D}'_m, \quad \beta = -eh/(4\pi mc). \tag{17}$$

As MD operator is of even parity, MD transitions are allowed between states within the $4f^N$ configuration. The matrix element of MD transitions in crystals is reduced as

$$(\psi_a|(\boldsymbol{D}'_m)_\rho|\psi_b) = \sum_{i,j} a_i^* b_j (-1)^{J-M} \begin{pmatrix} J & 1 & J' \\ -M & \rho & M' \end{pmatrix} \times (f^N:qSLJ\|\boldsymbol{D}'_m\|f^N:q'S'L'J'), \tag{18}$$

where $\rho=0$ and ±1 correspond respectively to σ- and π-polarized radiations contrary to ED transitions. Following the results of Condon and Shortley,[22] the nonzero matrix elements must be diagonal in the quantum numbers q, S, and L, and furthermore the MD transitions are restricted by the selection rule on J ($\Delta J=0, \pm1$) to the following three cases:

1) $J'=J$,

$$(qSLJ\|\boldsymbol{D}'_m\|qSLJ') = g[J(J+1)(2J+1)]^{1/2}, \tag{19}$$

where

$$g = 1 + [J(J+1)+S(S+1)-L(L+1)]/[2J+1)].$$

2) $J'=J-1$,

$$(qSLJ\|\boldsymbol{D}'_m\|qSLJ') = \left[\frac{(S+L+J+1)(S+L+1-J)(J+S-L)(J+L-S)}{4J}\right]^{1/2}. \tag{20}$$

3) $J'=J+1$,

$$(qSLJ\|\boldsymbol{D}'_m\|qSLJ') = \left[\frac{(S+L+J+2)(S+J+1-L)(L+J+1-S)(S+L-J)}{4(J+1)}\right]^{1/2}. \tag{21}$$

After all, MD transition probability is able to be evaluated straightforwardly by using Eq. 1 for ion levels and Eq. 2 for crystal field levels, respectively.

Comparison of Observed and Calculated Intensities.

Populations of $^5D_{0,1}$ Terms: The observed relative line strengths S_{obsd} and theoretical ones S_{theo} from Eq. 15 for ED transitions and from the ion wavefunctions of Eq. 1 for MD transitions are tabulated in Table 7. Here, nonzero elements involving $T(t,\lambda)$ parameters for ED transitions are restricted by the triangular condition of the 6-j symbol in Eq. 16, whereas those for MD transitions are also limited by the selection rule of ion levels ($\Delta J=0, \pm1$). The S_{obsd} has been derived from the observed intensities by adding appropriate weights regarding the degeneracy of levels concerned and polarization measurements (see Appendix B). For the $^5D_0 \rightarrow {}^7F_{3,5}$ transitions, the S_{obsd} has been obtained from the experiments although these are very small, while there are no corresponding S_{theo} values for both ED and MD transitions. This fact solely results from the approximation adopted in the theory and may be explicable on the basis of the J-mixing effect of the crystal field interactions. The S_{obsd} values are still the quantity involving the populations of initial levels, while the S_{theo} values are independent of such population as be obvious from the definition. Thus, it is possible to estimate the population of initial levels. The fluorescent transitions originate from three crystal field levels; *i.e.*, the $^5D_0(0)$, $^5D_1(\pm1)$, and $^5D_1(0)$ levels. The $^5D_0(0)$ level is about 1750 cm^{-1} below the upper pair of nondegenerate $^5D_1(0)$ and doubly degenerate $^5D_1(\pm1)$ levels, and the two components of the $^5D_1$ term are separated by only 4.2 cm^{-1}. When we assume that three crystal field levels belonging to the $^5D_1$ term are populated identically by electrons, the ratio of the population of the $^5D_0$ to that of the $^5D_1$ is expressed as

$$\frac{N(^5D_0)}{N(^5D_1)} = \frac{S_{obsd}(^5D_0:{}^7F_J)/S_{theo}(^5D_0:{}^7F_J)}{S_{obsd}(^5D_1:{}^7F_{J'})/S_{theo}(^5D_1:{}^7F_{J'})} = R(^5D_0 \rightarrow {}^7F_J:{}^5D_1 \rightarrow {}^7F_{J'}), \tag{22}$$

here $N(^{2S+1}L_J)$ stands for the sum of populations over all the components of a J-manifold. Although the S_{obsd} of the $^5D_1 \rightarrow {}^7F_{1,2}$ transitions can arise from both ED and MD transitions, it will be supposed undoubtedly from the comparison of the order of magnitudes for the S_{obsd} and S_{theo} regarding the $^5D_1 \rightarrow {}^7F_{0,1,2}$ transitions that the $^5D_1 \rightarrow {}^7F_1$ transition is dominantly due to ED transition, while the $^5D_1 \rightarrow {}^7F_2$ transition is

Table 8. Ratios of parameters $T(t,\lambda)$

	$T(3,4)/T(3,2)$	$T(5,4)/T(3,2)$	$T(5,6)/T(3,2)$	$T(7,6)/T(3,2)$
Present	0.0130	3.01	−0.593	−0.712
Axe[a)]	0.000	−3.52	—	—

a) Data from Ref. 21.

Table 9. Comparison of observed and calculated relative transition probabilities

Lower level	Upper level: $^5D_0(0)$ Calcd ED	$^5D_0(0)$ Calcd MD	$^5D_0(0)$ Obsd	$^5D_1(\pm1)$ Calcd ED	$^5D_1(\pm1)$ Calcd MD	$^5D_1(\pm1)$ Obsd	$^5D_1(0)$ Calcd ED	$^5D_1(0)$ Calcd MD	$^5D_1(0)$ Obsd
$^7F_0(0)$					3.07	1.28		2.59	1.00
$^7F_1(\pm1)$		6.95	6.95	1.84	0.007	2.19		0.003	0.03
(0)		6.96	6.06		0.0	0.01			
$^7F_2(\pm1)$		0.004		0.50	12.0	13.4		5.91	6.83
(±2)	1.42		1.42	0.013	12.1	13.4	0.31		0.0
(0)					1.83	1.73		8.19	7.40
$^7F_3(3)$	0.044		0.10	0.68		0.87	0.0		0.14
(0)		0.015	0.02						
(±2)	0.061		0.14	9.82	0.002	10.1	3.01		6.38
(3′)				3.70		2.85	3.25		2.38
(±1)				7.96	0.045	9.77		0.033	0.0
$^7F_4(\pm2)$	5.55		7.93	9.31	0.0	10.1	0.49		0.25[a)]
(±1)		0.005	0.0	6.40	0.002	6.38	3.96	3.96	4.60
(3)	8.58		7.83	3.66		b)			
(0)		0.033	0.03						
$(\pm2′)$	2.33		6.40	0.79	0.003	0.82	2.34		b)
(3′)	0.0		0.18	1.50		1.94	6.76		7.84
$^7F_5(\pm1)$				0.11	0.0	0.26			
(±2)	0.0082		0.02	1.21	0.0	0.75	0.39		0.47
(±1)				0.085	0.004	0.25			
(3)	0.075		0.07	0.78		1.10			
$(\pm2′)$	0.023		0.02	1.71	0.014	0.67	1.46		0.90
(0)		0.016	0.02						
(3′)				0.73		0.60	1.68		0.77
$^7F_6(3)$	0.032		0.02	0.14		0.18			
(±2)	0.11		0.06	0.071	0.003	0.0			
(3′)	0.0		0.06	0.033		0.16	0.030		0.05
$(\pm2′)$	0.031		0.20	0.016	0.0	0.32	0.085		0.08
(±1)		0.003	0.0	0.14	0.0	0.24			
$(\pm1′)$				0.0	0.004	0.11		0.002	0.0

a) Less accurate value for the overlap due to the $^5D_0(0) \rightarrow {}^7F_2(\pm2)$ transition. b) The sum of the relative transition probabililities for the $^5D_1(\pm1) \rightarrow {}^7F_4(3)$ and $^5D_1(0) \rightarrow {}^7F_4(\pm2′)$ transitions is 5.21.

mainly due to MD transition. Then, by substituting the values given in Table 7 into Eq. 22, the population ratios can be evaluated from several possible pairs of transitions as

$$R(^5D_0 \rightarrow {}^7F_1 : {}^5D_1 \rightarrow {}^7F_2) = 17.9 \quad \text{(MD character)} \qquad (23a)$$

$$R(^5D_0 \rightarrow {}^7F_2 : {}^5D_1 \rightarrow {}^7F_1) = 16.9 \quad \text{(ED character)} \qquad (23b)$$

$$R(^5D_0 \rightarrow {}^7F_4 : {}^5D_1 \rightarrow {}^7F_4) = 29.6 \quad \text{(ED character)} \qquad (23c)$$

$$R(^5D_0 \rightarrow {}^7F_6 : {}^5D_1 \rightarrow {}^7F_6) = 16.9 \quad \text{(ED character)}. \qquad (23d)$$

The average value of the ratios becomes 20.3 and agrees well with Axe's estimate[21] (=19) which was estimated from only a set of MD transitions corresponding to Eq. 23a by similar analysis. Since the population ratio of the $^5D_0$ term to one crystal field component of the $^5D_1$ term is only seven, it will be seen that the electron population on upper levels in fluorescent process extremely deviates from the Boltzmann distribution as be expected. Strictly speaking, as the fluorescence intensity must be proportional to the population difference between two levels concerned and not to the population of only the upper level, the population ratio should be estimated from

the intensities of transitions terminating to the same level. Therefore, the fact that the ratios from both Eqs. 23a and 23b are nearly equal to those from Eqs. 23c and 23d may be interpreted as follows: The population of the $^7F_2$ term is almost equal to that of the $^7F_1$ term or small populations of these terms are neglected when compared with large populations on the upper terms $^5D_0$ and $^5D_1$. However, $R(^5D_0\rightarrow{}^7F_1:{}^5D_1\rightarrow{}^7F_0)$ is 47.4 which is over twice as large as the ratio determined. This will probably result from the fact that there exists considerable intensity decrease due to self-absorption for the $^5D_1\rightarrow{}^7F_0$ transition as will be seen later, or the electron population of the lowest ground $^7F_0(0)$ level is not always neglected when compared with the populations of the upper $^5D_0$ and $^5D_1$ terms.

Parameters $T(t,\lambda)$ and Relative Transition Probabilities: When both observed relative intensities I_r and line strengths S_{obsd} for all the transitions from only the $^5D_0$ term are divided by 20.3, resultant observed quantities are independent of the populations of initial levels and correspond to the relative transition probabilities obtained by experiments. Thus, the $T(t,\lambda)^2$ values can be evaluated by a least-squares method from the comparison of the S_{theo} and observed line strengths not involving the population for ED transitions. Furthermore, the determination of the sign of $T(t,\lambda)$ and a minor refinement are made to reproduce the experimental intensities between crystal field levels ascertained as ED transition. The final values of $T(t,\lambda)$ are given as the ratios to $T(3,2)$ in Table 8, together with Axe's estimate. The present values are in good agreement in magnitude with Axe's values, but the sign of $T(5,4)/T(3,2)$ differs from that of Axe. This fact will probably arise from the difference of both cases with respect to the method to reproduce the experimental results. In the present estimate, the final adjustment of the five $T(t,\lambda)$ values is performed for the $^5D_{0,1}\rightarrow{}^7F_J(J=0,1,\cdots6)$ transitions by using the crystal field wavefunctions including complete J-mixing in Eq. 11, while Axe determined three parameters; $T(3,2)$, $T(3,4)$, and $T(5,4)$, for the $^5D_{0,1}\rightarrow{}^7F_J(J=0,1,\cdots4)$ transitions to reproduce both the observed line strengths and the ratio of intensities between the Stark components only within individual J-manifolds by the wavefunctions without J-mixing determined from symmetry consideration alone. The comparison of observed transition probabilities between crystal field levels with calculated ones is given in Table 9, where the values are described as relative values by putting the calculated transition probability of the $^5D_0(0)\rightarrow{}^7F_1(\pm1)$ for ED transitions and that of the $^5D_0(0)\rightarrow{}^7F_2(\pm2)$ for MD transitions to be equal to the corresponding observed values, respectively. The agreement is considered to be satisfactory in view of the approximation used in calculations and the accuracy on experiments. Especially, the nature of radiations from the $^5D_1(\pm1)$ level to degenerate levels $\mu=\pm1$, and $\mu=\pm2$ of the ^7F_J terms, which cannot be distinguished only from polarization measurements as be seen from the selection rules, is determined clearly from the calculated results. In Table 9, the calculated transition probabilities for

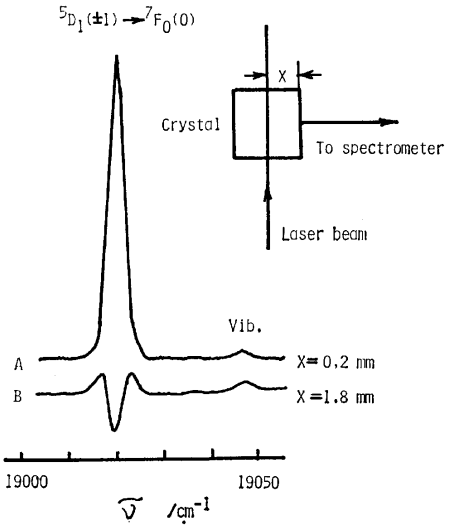

Fig. 6. π-polarized spectrum of the $^5D_1(\pm1)\rightarrow{}^7F_0(0)$ transition of $Eu(C_2H_5SO_4)_3\cdot9H_2O$ at 95 K, showing self-absorption.

two MD transitions from the $^5D_1(0)$ and $^5D_1(\pm1)$ levels to the lowest ground $^7F_0(0)$ level are considerably larger than the corresponding observed values. In practice, these MD transitions only showed heavily self-reserved line-shape in all the observed fluorescence lines when a laser beam passed through the middle of a crystal, as be seen in the case (B) of Fig. 6. Since self-absorption can occur when the absorbers and emitters are specially separated, we always attempted to pass an incident beam as close as possible to the crystal plane facing to a spectrometer (case (A) of Fig. 6). Such a fact that some of fluorescence lines to the lowest ground manifold only exhibit self-absorption at liquid nitrogen temperature has already been reported in other rare earth crystals.[23,24] Thus it does not seem to be an unjustifiable deduction to conclude that there still exists considerable intensity decrease for the above-mentioned MD transitions, although these line-shape did not show typical double humps even in a careful measurement. This phenomenon occurs in a 90° scattering measurement, but should be eliminated by 180° scattering.

Mixing Orbitals for Forbidden ED Transitions: Since the $T(t,\lambda)$ values are related to the radial wavefunctions $R_{n'l'}$ of mixing states, we introduce a parameter Γ following Axe[21] as

$$\Gamma=\sum_{n'}\Omega(n'g)/[\sum_{n'}\Omega(n'g)+\sum_{n'}\Omega(n'd)], \tag{24}$$

where

$$\Omega(n'l')=(R_{4f}|r|R_{n'l'})(R_{n'l'}|r^t|R_{4f})/\Delta E(n'l'). \tag{25}$$

Then the parameter Γ may be considered as a kind of measure on the contribution of admixing orbital $n'l'$ to allow ED transitions: $\Gamma=0$ means the contribution from d orbitals only, while $\Gamma=1$ is the contribution from g orbitals only. Appropriate ratios between $T(t,\lambda)$ values given in Eq. 12 are shown easily as a function of Γ as

$$\frac{T(3,4)}{T(3,2)}=\frac{1.95-1.42\Gamma}{1.0+1.50\Gamma}, \tag{26}$$

$$\frac{T(5,6)}{T(5,4)} = \frac{6.71-6.19\Gamma}{1.0+5.00\Gamma}. \quad (27)$$

Eq. 26 gives a maximum ratio of 1.95 for $\Gamma=0$ (pure d orbitals) and a minimum ratio of 0.212 for $\Gamma=1$ (pure g orbitals), whereas Eq. 27 gives a maximum ratio of 6.71 for $\Gamma=0$ and a minimum ratio of 0.081 for $\Gamma=1$. From the $T(t,\lambda)$ values of Table 8,

$$|T(3,4)/T(3,2)| = 0.0130, \quad |T(5,6)/T(5,4)| = 0.197. \quad (28)$$

Consequently, an unexpected conclusion that $n'g$ orbitals play a predominant role as configuration mixing for ED transitions is derived from both the cases. Dieke *et al.*[25] pointed out that the $4f^{N-1}5d$ configuration gave prominent contribution to emission spectra of the doubly and triply ionized rare earth metal ions. The present result, however, might not be somewhat surprising presumption when recognized that an $n'g$ orbital energy is not so higher than an $n'd$ orbital energy.

Appendix

(A) For an ED allowed transition in ions the oscillator strength f is of the order of magnitude one. An ED transition probability A^{E}_{ion} is related to the oscillator strength as[1]

$$A^{E}_{ion} = \frac{8\pi^2 e^2 \nu^2}{3mc^3} f = 2.68\times 10^9 (\sigma/Ry)^2 f, \quad (A1)$$

where σ is the wavenumber of transition and Ry is the Rydberg constant. Therefore, an ED allowed transition probability for a rare earth metal ion in crystals may be $10^8\ s^{-1}$ with a permissible factor of $10^{\pm 2}$ in the visible or near ultraviolet region. Since the ratio of an allowed MD transition probability, A^{M}_{ion}, to A^{E}_{ion} is expressed by $|[eh/4\pi mc]/e\langle r\rangle|^2$, A^{M}_{ion} becomes $10^2\ s^{-1}$. For the ED transition between the levels of the $4f^N$ configuration, the wavefunction must contain the terms of the configurations with odd parity. Thus the wavefunction is expanded by the perturbation theory as

$$\begin{aligned}|\psi_{a'}) = {} & |4f^N\psi_a : qSL) \\ & - \sum_k [(\varphi_k|H_{SO}|\psi_a)/\Delta E(4f)]\,|4f^N\varphi_k : qSLJ) \\ & - \sum_l [(\varphi_l|V_{even}|\psi_a)/\Delta E(4f)]\,|4f^N\varphi_l : qSLJM) \\ & - \sum_m [(\varphi_m|V_{odd}|\psi_a)/\Delta E(n'l')]\,|4f^{N-1}n'l'\varphi_m : qSLJM),\end{aligned} \quad (A2)$$

where the first term is unperturbed SL basis, and the second, third, and fourth terms are mixing states by the spin-orbit interaction, even- and odd-potential due to the crystal field, respectively. Here, $(\varphi_k|H_{SO}|\psi_a)$, $(\varphi_l|V_{even}|\psi_a)$, $(\varphi_m|V_{odd}|\psi_a)$, $\Delta E(4f)$, $\Delta E(n'l')$ may be the order of 10^2—10^3, 10^2, 10^2, 10^3—10^4, and 10^4—$10^5\ cm^{-1}$, respectively. Thus the transition probability responsible for crystal spectra is able to be expressed in terms of A^{E}_{ion} or A^{M}_{ion} as follows:

(I) for ED transition,

$$A^{E}_{cry} \simeq A^{E}_{ion}[(\varphi_k|H_{SO}|\psi_a)/\Delta E(4f)]^2 \times [(\varphi_m|V_{odd}|\psi_a)/\Delta E(n'l')]^2 = 10\ s^{-1}, \quad (A3)$$

(II) for MD transition ($\Delta J=0,\pm 1$),

$$A^{M}_{cry} \simeq A^{M}_{ion}[(\varphi_k|H_{SO}|\psi_a)/\Delta E(4f)]^2 = 1\ s^{-1}, \quad (A4)$$

(III) for MD transition ($|\Delta J|>1$),

$$A^{M}_{cry} \simeq A^{M}_{ion}[(\varphi_k|H_{SO}|\psi_a)/\Delta E(4f)]^2 \times [(\varphi_l|V_{even}|\psi_a)/\Delta E(4f)]^2 = 10^{-3}\ s^{-1}. \quad (A5)$$

Consequently, for the transitions within the $4f^N$ configuration the MD transition probability can be comparable to the ED forbidden one on some occasions. Especially, the $^5D_J \rightarrow {}^7F_{J'}$ transitions in a crystal are considered to be a further favorable case to yield MD transition, because these transitions also satisfy the selection rules for ion levels: $\Delta S=0,\pm 1$, $\Delta L=0,\pm 1$, and $\Delta J=0,\pm 1$. However, it will be easily found that even in the range of 20000 to 10000 cm^{-1} there are several fluorescence transitions of other triply ionized rare earth ions to satisfy the same conditions as the $^5D_J \rightarrow {}^7F_{J'}$ transitions of Eu^{3+} do; *e.g.*, $Nd^{3+}(^2H_{9/2}\rightarrow {}^4I_{9/2,11/2})$, $Sm^{3+}(^4G_{5/2}\rightarrow {}^6H_{5/2,7/2})$, $Tb^{3+}(^5D_4\rightarrow {}^7F_{3,4,5})$, $Er^{3+}(^2H_{11/2}\rightarrow {}^4I_{11/2,13/2})$, and $Tm^{3+}(^1G_4\rightarrow {}^3H_{4,5})$.

(B) The average intensity scattered from an ion or atom is associated with the intensities by polarization measurements,

$$I = \frac{1}{3}(I_X+I_Y+I_Z) \propto \frac{1}{3}(|\langle \boldsymbol{D}_X\rangle|^2+|\langle \boldsymbol{D}_Y\rangle|^2+|\langle \boldsymbol{D}_Z\rangle|^2), \quad (B1)$$

where I_X, I_Y, and I_Z are polarized intensities along X, Y, and Z axes in the space-fixed Cartesian coordinate, respectively, and $\langle \boldsymbol{D}\rangle$ is the matrix element of either the electric $\boldsymbol{D}_e$ or magnetic dipole moment $\boldsymbol{D}_m$. For an uniaxial crystal as rare earth tris(ethyl sulfate) enneahydrates, I_X must be equal to I_Y. One can estimate $I_X(|\langle(\boldsymbol{D}_e)_X\rangle|^2)$ and $I_Z(|\langle(\boldsymbol{D}_e)_Z\rangle|^2)$ from the intensities corresponding to σ- and π-polarized radiations for ED transitions respectively, whereas $I_X(|\langle(\boldsymbol{D}_m)_X\rangle|^2)$ and $I_Z(|\langle(\boldsymbol{D}_m)_Z\rangle|^2)$ or MD transitions are obtained inversely from π- and σ-polarization measurements. Consequently the average intensities are given as

$$\begin{aligned} I_e &= \frac{1}{3}(I_\pi+2I_\sigma) \quad \text{for ED transition,} \\ I_m &= \frac{1}{3}(I_\sigma+2I_\pi) \quad \text{for MD transition.}\end{aligned} \quad (B2)$$

This fact also may be verified analytically from direct estimate of the matrix elements of dipole moment operators in terms of $|JM)$ basis. In the evaluation of the line strength S_{obsd} (Table 7) from observed polarized intensities (Table 4), S_{obsd} is given as relative value by omitting the coefficient of 1/3 in Eq. B2.

This work was partially supported by a Grant-in-Aid for Scientific Research to Y. K. from the Ministry of Education, Science and Culture (No. 435045).

References

1) G. H. Dieke, "Spectra and Energy Levels of Rare Earth Ions in Crystals," Interscience Publ., New York (1968).
2) E. V. Sayre and S. Freed, *J. Chem. Phys.*, **24**, 1213 (1956).
3) L. G. DeShazer and G. H. Dieke, *J. Chem. Phys.*, **38**, 2190 (1963).
4) K. S. Thomas, S. Singh, and G. H. Dieke, *J. Chem. Phys.*, **38**, 2180 (1963).
5) K. H. Hellwege, U. Johnsen, H. G. Kahle, and G. Schaack, *Z. Phys.*, **148**, 112 (1957). The energies of the crystal field levels of the $^7F_1$ and $^5D_{0,1,2}$ terms given in this article are those at 294 K. Since the energy in crystals, in general, increases with the temperature rise, then the energies obtained at 95 K were several cm^{-1} less than those

by this article.
6) K. H. Hellwege, S. Hüfner, and A. Pöcker, *Z. Phys.*, **172**, 453 (1963).
7) G. Racah, *Phys. Rev.*, **62**, 438 (1942); **63**, 367 (1942); **76**, 1352 (1949).
8) Y. Kato, T. Nagai, and T. Nakaya, *Chem. Phys. Lett.*, **39**, 183 (1976).
9) D. R. Fitzwater and R. E. Rundle, *Z. Kristallogr.*, **112**, 362 (1959).
10) C. R. Hubbard, C. O. Quicksall, and R. A. Jacobson, *Acta Crystallogr., Sect. B*, **30**, 2613 (1974).
11) K. H. Hellwege, *Ann. Physik*, **4**, 95 (1949).
12) B. G. Wybourne, "Spectroscopic Properties of Rare Earths," Interscience Publ., New York (1965).
13) Y. Kato, T. Kurimoto, and T. Takenaka, *Spectrochim. Acta*, Part A, **33**, 1033 (1977).
14) K. Rajnak and B. G. Wybourne, *Phys. Rev.*, **132**, 280 (1963).
15) B. R. Judd, "Operator Techniques in Atomic Spectroscopy," McGraw-Hill, New York (1963).
16) J. S. Margolis, *J. Chem. Phys.*, **35**, 1367 (1967).
17) Y. Kato, T. Nagai, and A. Saika, *Bull. Chem. Soc. Jpn.*, **50**, 862 (1977).
18) C. W. Nielson and G. F. Koster, "Spectroscopic Coefficients for the p^n, d^n, and f^n Configurations," M. I. T. Press, Cambridge, Mass. (1963).
19) B. R. Judd, *Phys. Rev.*, **127**, 750 (1962).
20) G. S. Ofelt, *J. Chem. Phys.*, **37**, 511 (1962).
21) J. D. Axe, Jr., *J. Chem. Phys.*, **39**, 1154 (1963).
22) E. U. Condon and G. H. Shortley, "The Theory of Atomic Spectra," Cambridge Univ. Press, Cambridge, England (1957).
23) U. V. Kumar, D. R. Rao, and P. Venkateswarlu, *J. Chem. Phys.*, **67**, 3448 (1977).
24) Y. Kato, K. Okada, S. Hayashi, and T. Takenaka, *Chem. Phys. Lett.*, **61**, 266 (1979).
25) G. H. Dieke, H. M. Crosswhite, and B. Dunn, *J. Opt. Soc. Am.*, **51**, 820 (1961).

Effect of Adsorption of Potassium Iodide on Catalytic Activity of Plate-type Raney Nickel

Tomio Yoshino* and Tuneyo Abe

Faculty of Pharmaceutical Science, Tokushima University of Arts and Science, Yamashiro-cho, Tokushima 770

(Received June 25, 1982)

An experimental investigation was made of the adsorptive activity of Raney nickel catalyst toward potassium iodide over a wide KI concentration range and of the change with KI adsorption of hydrogenating activity toward unsaturated alcohol and ketone. Adsorbed amounts of K^+ and I^- ions were determined by potentiometry and radioactivity measurement. The adsorptive activity *vs.* I^- concentration relation yields a definitive break at equilibrium concentration 5.5×10^{-5} mol dm^{-3} (surface coverage 26%), the adsorption features in the lower and higher ranges relative to the break point being approximately represented by Freundlich's and BET equations, respectively. Adsorption sites effective for I^- ion in the Freundlich region disappear almost completely when the catalyst is preheated at 600 °C. The surface coverage causing the hydrogenation activity to decrease by 50% is 3% for allyl alcohol and 0.3% for 2-butanone. With allyl alcohol, however, even such a catalyst as has preadsorbed *ca.* 5-monolayer amount of I^- ions possesses a 33% residual activity, though catalyst coverages over 26% result in only a little decrease in activity. These results suggest that the adsorption sites in the Freundlich region may function as strong catalytically active centers for the hydrogenation, which are unstable to heating.

Many reports have dealt with the relation between adsorption of halogen compounds on Raney nickel and catalysis by Raney nickel with preadsorbed halogen compounds. Pattison and Degering[1] reported that the rate of catalytic reduction of styrene was remarkably decreased when the concentration of chloride ion to be preadsorbed exceeded 4.2×10^{-4} mol/g RNi. On reduction of carbonyl groups in unsaturated ketones by Raney nickel, Hoshiai *et al.*[2,3] reported that a complete loss of the hydrogenation activity of catalyst occurred when Raney nickel had preadsorbed more than 4.1×10^{-4} mol of iodide ion per gram of Raney nickel. Sokol'skii and Zakumbaeva[4] reported that catalytic reduction of *p*-nitrophenol and similar compounds was decelerated in the coexistence of alkali halides.

Recent reports[5,6] indicate that preadsorption of NaBr on a modified Raney nickel for asymmetric hydrogenation results in a marked increase in yield owing to enantioface-differentiating hydrogenation and that this increase is caused by selective adsorption of NaBr at active centers involving aluminium compounds[7-9] lacking asymmetric selectivity. Little has yet been clarified of the relation between the adsorption on catalyst surface and the change in catalytic activity.

The present paper deals with the relation between the adsorptive activity of Raney nickel for KI and the catalytic activity of KI-preadsorbed Raney nickel for hydrogenation of unsaturated alcohols or ketones, with particular reference to the nature of surfaces of such catalyst preparations.

Experimental

Materials. Raney alloy was prepared by placing a nickel plate, 0.05 mm thick and 99.96% pure, between aluminium plates, 0.1 mm thick and 99.995% pure, and subjecting the sandwich heated at 630 °C in a nitrogen stream to hot-rolling with a dental roller. A plate-type Raney nickel catalyst,[10,11] suited for the present experiment, was prepared by treating the Raney alloy with a solution of 20 wt% sodium hydroxide at 50 °C for 1 h. The catalyst, thus obtained or further preannealed in a hydrogen atmosphere at 30—600 °C for 1 h, was used to determine the adsorption and hydrogenation activities; the catalyst was divided before use into portions of 16 cm^2 in apparent area (BET specific surface area 4.2×10^2 cm^2/cm^2).

Allyl alcohol, 2-butanone, and mesityl oxide (4-methyl-3-penten-2-one) were of special grade and used without further purification. Solutions of potassium iodide (special grade) were prepared by use of distilled water.

Procedures. The adsorption experiment was carried out by shaking the catalyst, in 100 ml aqueous solution of initial concentration 10^{-7}—10^{-2} mol dm^{-3} of KI labeled with 0.3 μCi of ^{131}I, in an atmosphere of nitrogen at 20—30 °C for 1 h. The catalyst was washed twice with 10 ml ethanol and then twice with 10 ml of a reactant before being used for reduction experiments. Adsorbed and desorbed amounts of iodide ion were determined with a well-type scintillation counter (Fuji Electric Model NHS 2) by measuring radioactivities on 1 ml portions taken from the adsorbate solution and the liquid employed for desorption experiment, respectively. Potentiometric measurement with a microprocessor ionalyzer (Orion Research Model 901) was employed to determine the amount of potassium ion adsorbed from aqueous solution.

The activity of catalysts was determined by use of liquid-phase hydrogenation on 3 ml allyl alcohol, 2-butanone, or mesityl oxide at 1 atm and 70 °C. Products were analyzed with a gas chromatograph (Yanagimoto Model G 180).

Results

Adsorbed Amount and Adsorption Isotherm. Both the time required for saturation adsorption to be reached and the adsorbed amount of I^- ion depend on temperature; with initial concentration 10^{-4} mol dm^{-3}, these values are about 60 min and 4.5×10^{-10} mol/BET cm^2 at 20 °C and about 30 min and 3.1×10^{-10} mol/BET cm^2 at 30 °C. It is noticed that the adsorbed amount may be estimated with a relative error less than about 10% under the same experimental conditions.

Figure 1 illustrates the effect of equilibrium concentration, C, on adsorbed amounts, v, of K^+ and

Table 1. Desorption of iodide ion from the catalyst in ethanol and reactant

Reactant	Initial [KI] mol/dm³	Adsorbed I⁻ mol/BET cm²	Desorbed fraction/% of I⁻			
			Ethanol	Reactant	Reaction	Total
Allyl alcohol	10^{-6}	5.70×10^{-12}	0.82	8.06	1.95	10.83
	10^{-3}	8.14×10^{-10}	1.35	4.63	1.61	7.59
2-Butanone	10^{-6}	5.70×10^{-12}	0.92	3.16	3.20	7.22
	10^{-3}	8.14×10^{-10}	1.19	2.80	0.80	4.79
4-Methyl-3-penten-2-one	10^{-6}	5.70×10^{-12}	0.84	4.27	0.70	5.77
	10^{-3}	8.14×10^{-10}	1.18	2.47	0.53	4.18

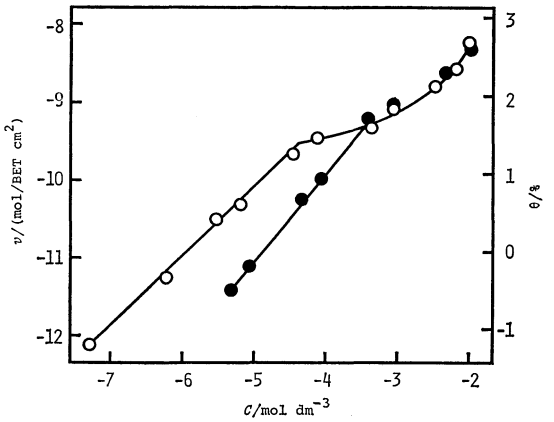

Fig. 1. Adsorption isotherm by the plot of the logarithm of the equilibrium concentration (C) on the logarithm of the adsorbed amount (v) (●: K^+ ion, ○: I^- ion) and surface coverage (θ) of I^- ion at 30 °C.

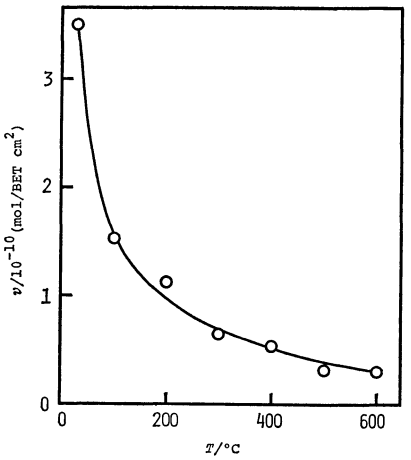

Fig. 2. Variation of I^- adsorptivity at 30 °C of the catalyst preheated for 1 h in H_2. The initial concentration of the adsorbate was 10^{-4} mol dm^{-3}.

I^- ions. Surface coverage, θ, of I^- ion was obtained by a calculation using the value of 2.06 Å as the ionic radius of the ion adsorbed on the surface of Raney nickel. The adsorbed amount of I^- ion, as shown in Fig. 1, yields a break at equilibrium concentration about 5.5×10^{-5} mol dm^{-3} ($v=3.2\times10^{-10}$ mol/BET cm²; $\theta=26\%$). Below the break point, the adsorbed amount is given by Freundlich's equation[12]

$$\log v = a + \frac{1}{n}\log C,$$

where a is a constant, evaluated to be 1.2 from Fig. 1. Beyond the break point, the equilibrium data approximately obey a BET equation, suggesting a multilayer adsorption of I^- ions. In fact, the 100% coverage is obtained at $C=2.1\times10^{-3}$ mol dm^{-3} and $v=1.2\times10^{-9}$ mol/BET cm², and the highest coverage, so far obtained, is 475%.

The isosteric differential heat of adsorption of I^- ion, as obtained by processing the above results according to Clausius-Clapeyron's equation,[13] decreases exponentially with increasing surface coverage of I^- ions in the Freundlich region, and is estimated to be 6.3×10^3 and 3.8×10^3 J/mol at coverages 3 and 25%, respectively.

The adsorbed amount of K^+ ion, as with the adsorption of I^- ion, yields a break at equilibrium concentration about 4.3×10^{-4} mol dm^{-3} (adsorbed amount, 5.4×10^{-10} mol/BET cm²; surface coverage of I^- ion, 43%). Below the break point, the adsorbed amount is much less than that of I^- ion. Beyond the point, however, both the adsorbates, K^+ and I^- ions, give equimolar adsorbed amounts.

Adsorption on Preheated Catalyst. Figure 2 illustrates the variation of the I^- adsorption activity of catalyst caused by application of sintering at 30—600 °C in a hydrogen atmosphere. The adsorptive activity of 3.5×10^{-10} mol/BET cm² ($\theta=28.1\%$) of the catalyst obtained by pretreatment at 30 °C was decreased by a 100 °C sintering to 1.5×10^{-10} mol/BET cm² (12.3%) corresponding to about 56% decrease and by a 600 °C sintering to 0.3×10^{-10} mol/BET cm² (2.4%) corresponding to about 91% decrease. These results suggest that many of the active centers for halogen adsorption are easily caused to disappear even by preheating at low temperature.

Desorption of the Adsorbate. The I^- preadsorbed catalyst was used for the reduction experiment after being successively washed with ethanol and the reactant for the reduction. Table 1 indicates fractions of I^- ions desorbed due to the washing with ethanol (the 4th col.), the washing with the reactant (the 5th col.), and the reduction (the 6th col.), the sum of these fractions being given in the 7th column. The desorption of I^- ion, as seen from Table 1, obviously depends on the initial concentration, giving higher fractions at 10^{-6} mol dm^{-3} than at 10^{-3} mol dm^{-3}; most of the adsorbate is desorbed with allyl alcohol in contrast with 2-butanone and mesityl oxide, the desorptive capacity being in the decreasing order:

Table 2. Change in activity of the preadsorbed catalyst for hydrogenation

Adsorbed I^- mol/BET cm^2	Coverage %	Rate of hydrogenation[a] mmol/h			
		Allyl alcohol	2-Butanone	4-Methyl-3-penten-2-one	
0	—	2.85	0.21	1.12[b]	0.37[c]
7.69×10^{-13}	0.06	2.13	0.17	0.57	0.32
5.70×10^{-12}	0.46	1.93	0.10	0.28	0.24
5.33×10^{-11}	4.28	1.27	0.08	0.22	0.15
3.11×10^{-10}	24.96	1.23	0.06	0.17	0.11
8.14×10^{-10}	65.41	1.21	0.04	—	—
5.92×10^{-9}	475.1	0.93	0.02	—	—

a) In the liquid phase at 1 atm and 70 °C. b) This column refers to product 4-methyl-2-pentanone produced from 4-methyl-3-penten-2-one. c) This column refers to product 4-methyl-2-pentanol.

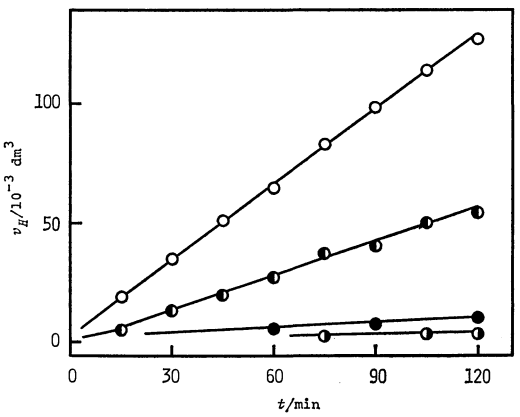

Fig. 3. Time dependences of hydrogen absorption (v_H) by allyl alcohol (○,◐) and by 2-butanone (●,◑) through the catalyst with (◐,◑) or without (○,●) preadsorption of KI. The initial concentration of the adsorbate was 10^{-5} mol dm^{-3}.

allyl alcohol>2-butanone>mesityl oxide.

Hydrogenation Activity of Preadsorbed Catalyst. Figure 3 illustrates the time dependence of the hydrogen adsorption by allyl alcohol or 2-butanone when the substrate is hydrogenated by catalysts with or without preadsorbed potassium iodide (adsorbed amount, 5.3×10^{-11} mol/BET cm^2; coverage, 4.3%). At 70 °C and 1 atm, the hydrogenation activity of catalyst remains constant over a period of 120 min, and is in general higher for the unsaturated alcohol than for the ketone. The hydrogenation activity is lowered by the preadsorption to 42.5% for the alcohol and 38.8% for the ketone.

Table 2 shows rates of hydrogenation of allyl alcohol, 2-butanone, and mesityl oxide on KI preadsorbed catalysts. The hydrogenation of the alcohol or the ketone yielded only 1-propanol or 2-butanol, respectively, but mesityl oxide gave both 4-methyl-2-pentanone and 4-methyl-2-pentanol. As seen from Table 2, the rate of hydrogenation of these compounds is highest for allyl alcohol regardless of the extent of preadsorption, and the rate for the alcohol by such a catalyst as has preadsorbed *ca.* 5-monolayer amount of adsorbate is 33% of that by the catalyst without preadsorption. It turns out that the rate of formation of 4-methyl-2-pentanone and 4-methyl-2-pentanol is remarkably decreased with increasing amount of preadsorbed I^- ions in the low adsorption phase; hydrogenation yields for the catalyst with 4.3% coverage are 71 and 29% for the carbon double bond and carbonyl group of mesityl oxide, respectively.

Discussion

As revealed from Fig. 1, the mode of adsorption of I^- ion is changed according as the adsorbate concentration falls in the lower or higher range relative to the definitive break. In the lower range, the Freundlich region, the isosteric heat of adsorption decreases exponentially with increasing adsorbed amount, and the surface coverage is so low (below 26%) that the surface interaction between adsorbate ions may be neglected and therefore the adsorbate ions may be considered to occupy heterogeneous adsorption sites successively with preference from higher to lower adsorption-activity sites. The number of ionic bonds of the K^+ with I^- ions adsorbed on the catalyst surface, in this region, seems to be smaller for the adsorbed amount than for that of adsorbed I^- ions, because a portion of the I^- ions may be stabilized electrostatically through the specific adsorption or may combine with H^+ instead of K^+ ion.[14]

On the contrary, in the higher concentration range than the break point where the BET equation holds, the change in the mode of adsorption seems to be caused by strong ionic interaction between the adsorbates on the catalyst, as well as by capillary condensation on the porous surface. In addition, multilayer adsorption may be considered to take place at the catalytic surface with equimolar adsorption of counterionic adsorbates to form an ionic double layer at the solid/liquid interface.

As seen from Table 1, the greater portion of the amount of I^- desorbed from the catalyst surface is involved in the course of washing at room temperature, though the absolute fraction desorbed varies with the initial iodide and reactant concentrations and the desorption is made to proceed a little further during the following reduction run at 70 °C. These results suggest that capillary condensation is more important than the Langmuir type adsorption for the understanding of the mechanism of desorption.

As shown in Fig. 2, adsorption sites effective for halogen ions in the Freundlich region are so unstable to heating as to disappear to a considerable extent even at relatively low temperatures and almost completely at 600 °C. In a previous work,[15] it was reported that the catalytic activity of plate-type Raney nickel is decreased by thermal pretreatment, *e.g.*, a catalyst annealed at 600 °C has an activity as low as 16% of that of a 100 °C-annealed one for reduction of acetone and 29% of that of a 150 °C-annealed one for reduction of benzene. These facts indicate that both the adsorption sites and the active sites for hydrogenation are caused easily to disappear by preheating the catalyst.

The hydrogenation activity of catalyst lowers with increasing amount of I^- ions preadsorbed in the Freundlich region, this tendency being more pronounced in the lower adsorption phase, as seen from Table 2. Thus, the surface coverage at the 50% lowering is about 3% for allyl alcohol and about 0.3% for 2-butanone. For the latter compound, the relative catalytic activity lowers to 0.36 at surface coverage 3%; the activity for the reduction of carbonyl group in ketone is remarkably decreased by the preadsorption of I^- ion. Similarly, in the case of mesityl oxide, the hydrogenation of carbon double bond proceeds much more rapidly than that of carbonyl group on catalysts of the same coverage. These results suggest that the preadsorbed I^- ions preferentially occupy many of the strong adsorption sites at or near the active centers effective mainly for the reduction of carbonyl group.

In the case of the adsorption in the range beyond the Freundlich region, the hydrogenation activity of catalyst depends negligibly on surface coverage as seen from Table 2. The residual activity displayed at more than 100% coverage implies wide distribution of preadsorbed I^- ions over the heterogeneous surface of catalyst and partial desorption from the surface of those ions upon attack by the reactant.

The above results agree with previous results,[1-3] though no direct, quantitative comparision can be made for differences in adsorbate properties or adsorption conditions.

Hofer and Hintermann[16] examined properties of the active center of Raney nickel by X-Ray diffraction line broadening analysis and reported that annealed Raney nickel catalysts with much lowered activity had lost many of their surface structural defects. Pearce and Leuis,[17] using the same method, reported that a highly active Raney nickel catalyst was unstable for heating and possessed much more structural defects, microstrains, and stacking faults than an inactive catalyst. As mentioned above, we[15] also reported that active sites of Raney nickel are associated with lattice defects, vacancies and dislocations because the hydrogenation activity of preannealed catalyst was decreased in a temperature range where defects vanish.

It is concluded from the present results that the adsorption sites for I^- ions in the Freundlich region and the greater portion of the active sites for hydrogenation are the same sites on catalyst surface or are located very close to each other, and that they are related to heterogeneous lattice defects.

The authors wish to thank Professor Emeritus Jiro Yasumura (Tokushima University) for his helpful discussion.

References

1) J. N. Pattison and E. F. Degering, *J. Am. Chem. Soc.*, **73**, 611 (1951).
2) K. Hoshiai and J. Miyata, *Kogyo Kagaku Zasshi*, **60**, 253 (1957).
3) K. Hoshiai and I. Iwasawa, *Kogyo Kagaku Zasshi*, **61**, 846 (1958).
4) D. V. Sokol'skii and G. D. Zakumbaeva, *Tr. Inst. Khim. Nauk, Akad. Nauk Kaz. SSR*, **5**, 3 (1959).
5) T. Harada and Y. Izumi, *Chem. Lett.*, **1978**, 1195.
6) T. Harada, A. Tai, M. Yamamoto, H. Ozaki, and Y. Izumi, Proc. 7th Int. Congr. Catal. Part A, Tokyo (1980), pp. 364—375.
7) Y. Orito, S. Niwa, and S. Imai, *Yuki Gosei Kagaku Kyokai Shi*, **34**, 236 (1976).
8) T. Harada, S. Onaka, A. Tai, and Y. Izumi, *Chem. Lett.*, **1977**, 1131.
9) A. Hoek and W. M. H. Sachtler, *J. Catal.*, **58**, 276 (1979).
10) J. Yasumura, T. Yoshino, and S. Abe, *Ind. Eng. Chem., Pro. Res. Dev.*, **7**, 252 (1968).
11) T. Yoshino, H. Yagi, and Y. Tegawa, *Nippon Kagaku Kaishi*, **1980**, 16.
12) P. Fejes, "Contact Catalysis," ed by Z. G. Szabó and D. Kalló, Elsevier Scientific Publishing Co., Amsterdam (1976), Vol. 1, pp. 153—161.
13) T. Keii, "Kyuchaku," Kyoritsu Shuppan, Tokyo (1965), Chap. 2.
14) A. Kitahara and A. Watanabe, "Kaimen Denki Gensho," Kyoritsu Shuppan, Tokyo (1972), Chap. 2.
15) T. Yoshino, *Nippon Kagaku Zasshi*, **87**, 558 (1968).
16) E. M. Hofer and H. E. Hintermann, *Trans. Faraday Soc.*, **60**, 1457 (1964).
17) C. E. Pearce and D. Leuis, *J. Catal.*, **26**, 318 (1972)

Suppression of Electroreductive Dimerization of Benzaldehyde by Addition of α-Cyclodextrin

Tomokazu MATSUE, Chikako TASAKI, Masamichi FUJIHIRA, and Tetsuo OSA*

Pharmaceutical Institute, Tohoku University, Aobayama, Sendai 980

(Received July 12, 1982)

The effect of α-cyclodextrin (α-CD) on the electroreduction of benzaldehyde was investigated. The reduction in aqueous system produces benzyl alcohol and 1,2-diphenyl-1,2-ethanediol (hydrobenzoin, dimerization product). The addition of α-CD caused the decrease in the yield of hydrobenzoin. This suppression effect was observed both in the controlled potential and controlled current electrolyses. This is accounted for by the retardation of the dimerization rate between the neutral radicals, since inclusion of substrate provides severe steric hindrance around the reaction site. The addition had only a small influence on the stereochemistry of hydrobenzoin formed by the dimerization.

Electrochemical reduction of carbonyl compounds to the corresponding alcohols is an important subject in organic electrochemistry. However, the reduction accompanies the concurrent formation of dimerization products.[1] In order to suppress the dimerization the following conditions are usually employed;[2] (i) low concentration of starting material, (ii) high current density, (iii) low pH, *etc.* We intend to suppress the dimerization from a quite different standpoint, *i.e.*, steric control at "molecular-level" by addition of cyclodextrin (CD).[3] This compound, constructed from cyclic glucose oligomers, has an ability to include a variety of organic substrates in their hydrophobic interior. Taking advantage of this unique property, we have carried out the selective electrosyntheses; the regioselective chlorination of benzene derivatives[4] and the selective reduction of *o*-nitrophenol in the presence of the *p*-isomer.[5] Recently, Smith and Utley demonstrated that CD acts as a proton source in nonaqueous media.[6] Although complexation is observed in polar aprotic media such as dimethyl sulfoxide and *N,N*-dimethylformamide, the binding ability of CD is much smaller than that in aqueous media.[3] Therefore, aqueous system should be used in order to draw the ability effectively.

We report herein the suppression of electroreductive dimerization of benzaldehyde by addition of α-CD in aqueous solution. The electrochemical reduction of benzaldehyde have been extensively investigated,[1,2] but the reduction mechanism is not clearly identified.[7] The generally accepted mechanism in neutral aqueous media is as follows:[2]

$$\mathrm{ArCHO} + \mathrm{e} \rightleftharpoons \mathrm{ArCHO^{-\cdot}} \quad (1)$$

$$\mathrm{ArCHO^{-\cdot}} + \mathrm{H^+} \longrightarrow \mathrm{ArCHOH\cdot} \quad (2)$$

$$2\mathrm{ArCHOH\cdot} \longrightarrow \mathrm{ArCH(OH)CH(OH)Ar} \quad (3)$$

(1,2-diphenyl-1,2-etnanediol, hydrobenzoin)

$$\mathrm{ArCHOH\cdot} + \mathrm{e} \longrightarrow \mathrm{ArCHOH^-} \quad (4)$$

$$\mathrm{ArCHOH^-} + \mathrm{H^+} \longrightarrow \mathrm{ArCH_2OH} \text{ (benzyl alcohol).} \quad (5)$$

In the above mechanism benzyl alcohol is produced *via* ECEC process. However, it can also be formed *via* regeneration mechanism[8] (or disproportionation mechanism) followed by protonation.

$$\mathrm{ArCHO^{-\cdot}} + \mathrm{ArCHOH\cdot} \rightleftharpoons \mathrm{ArCHO} + \mathrm{ArCHOH^-} \quad (6)$$

With α-CD, complexation of benzaldehyde is anticipated to reduce the dimerization rate since covering by α-CD produces severe steric hindrance around the reaction site, resulting in suppression of formation of 1,2-diphenyl-1,2-ethanediol (hydrobenzoin). If the dimerization between included molecules is permissible, the addition of α-CD may also affect the stereochemistry of hydrobenzoin[9] since inclusion makes the phenyl group more bulky, so that upon dimerization the approaching of each phenyl group would be sterically hindered.

Experimental

All controlled potential and controlled current electrolyses were carried out with a Yanaco VE-8 electrolyzer at room temperature. The cell was a divided H-type with a mercury pool cathode (area 6 cm^2) and a graphite or Pt gauze anode. The catholyte consisted of 25 ml phosphate buffers (pHs 4.6, 7.0, and 9.1) containing 25 mmol dm^{-3} benzaldehyde. In the controlled potential electrolysis, the potentials were referenced to a saturated calomel electrode (SCE) and the cathode potential was set at −1.3 V (at pH 4.6) and at −1.4 V *vs.* SCE (at pHs 7.0 and 9.1).

After the electrolysis, the catholyte was extracted with ether and the extract was analyzed by gas chromatography. Gas chromatographic analysis was carried out using a Shimadzu GC-4CM machine equipped with hydrogen flame ionization detector. The column used in the analyses of benzyl alcohol and unreacted benzaldehyde was 200 mm × 3 mm ϕ SUS packed with 10% Carbowax 20 M on Chromosorb W, and the column temperature was kept at 170 °C. Nitrogen was used as the carrier gas. Hydrobenzoin and its stereochemistry (*dl*/*meso* ratio) were determined by the reported method.[9]

Cyclic voltammetric experiments were carried out using a conventional instruments with a hanging mercury drop electrode (HMDE) in a phosphate buffer and the potentials were measured with respect to an SCE.

The dissociation constant for α-CD-benzaldehyde complex were determined by spectroscopic methods.[10] The analysis showed that the dissociation constant for the complex is $(4.3\pm0.9)\times10^{-3}$ mol dm^{-3}.

Results and Discussion

For mechanistic study, polarography is more appropriate and more accurate,[5,7] but cyclic voltammetry was carried out to see the effect of α-CD on the reduction of benzaldehyde in the present study due to

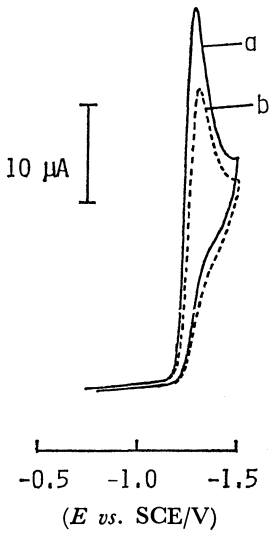

Fig. 1. Cyclic voltammograms of 2.0 mmol dm^{-3} benzaldehyde in the absence (a) and presence (b) of 10 mmol dm^{-3} α-CD at pH 7.0.
Electrode: HMDE, scan rate: 80 mV s^{-1}.

its convenience. Figure 1 shows the cyclic voltammograms of 2 mmol dm^{-3} benzaldehyde in the absence (curve (a)) and presence (curve (b)) of 10 mmol dm^{-3} α-CD in aqueous phosphate buffer (pH 7.0). Curve (a) shows an irreversible reduction peak at −1.30 V *vs.* SCE. As shown in curve (b), upon addition of α-CD to the electrolyte solution, the peak current becomes lower and the peak potential shifts slightly (*ca.* 20 mV) in the cathodic direction. The decrease in peak current is accounted for by the decrease in the effective diffusion coefficient due to the complex formation of benzaldehyde with large α-CD molecule.[5] As described below, the addition of α-CD results in suppression of electroreductive dimerization of benzaldehyde and consequently in the increase in the number of electrons, *n*, consumed for the reduction of one molecule of benzaldehyde. The decrease of the diffusion coefficient is therefore more than that would be expected without change in *n*. The shift in peak potential is probably caused by the "micro-solvent effect"[3] of α-CD; the similar effect has been also observed in the electroreduction of *p*-nitrophenol in the presence of α-CD.[5] In the present conditions concentrations of benzaldehyde and α-CD are 2 and 10 mmol dm^{-3}, respectively), *ca.* 70% of benzaldehyde exists as the complexed form.

Figure 2 depicts the relationship between the ratio of hydrobenzoin to benzyl alcohol, [HB]/[BA], and the conversion of benzaldehyde in the controlled potential electrolysis at −1.3 V *vs.* SCE. The [HB]/[BA] ratio is high at low conversions but decreases with increasing conversion (*i.e.*, decreasing the concentration of unreacted benzaldehyde). This indicates that the hydrobenzoin formation is predominated over the benzyl alcohol formation at beginning of the electrolysis. The tendency is quite consistent with that reported by Aoki and Sekine[7] in which they explained this phenomenon by the concentration effect.

The [HB]/[BA] ratios observed in the presence of

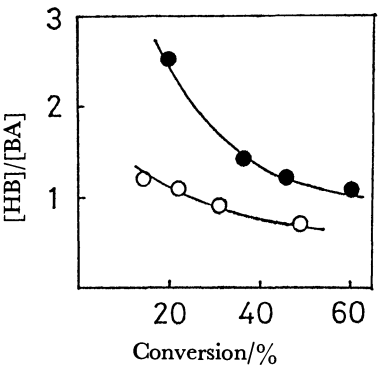

Fig. 2. Relationship between [HB]/[BA] ratio and conversion observed in the controlled potential electrolysis at −1.3 V *vs.* SCE (pH 4.6).
●: Without CD, ○: with α-CD (40 mmol dm^{-3}), initial concentration of benzaldehyde: 25 mmol dm^{-3}.

TABLE 1. THE [HB]/[BA] RATIO OBSERVED IN THE CONTROLLED POTENTIAL ELECTROLYSIS UNDER DIFFERENT pH CONDITIONS[a]

pH	Without CD	With α-CD (40 mmol dm^{-3})
4.6	1.2±0.2	0.5±0.2
7.0	2.2±0.4	0.7±0.2
9.1	2.8±0.5	1.0±0.3

a) Cathode potential: −1.3 V *vs.* SCE (at pH 4.6), −1.4 V *vs.* SCE (at pHs 7.0 and 9.1). Initial concentration of benzaldehyde: 25 mmol dm^{-3}. Conversion: 40—60%.

α-CD are lower than those in the absence of α-CD. This clearly suggests that α-CD suppresses the hydrobenzoin formation, *i.e.*, dimerization reaction. Under the initial conditions (concentrations of benzaldehyde and α-CD are 25 and 40 mmol dm^{-3}, respectively), *ca.* 80% of benzaldehyde in the electrolyte solution is included in α-CD's cavity since the dissociation constant for the complex is $(4.3\pm0.9)\times10^{-3}$ mol dm^{-3}. Even if the reduction products, benzyl alcohol and hydrobenzoin, can be trapped strongly by α-CD, the inclusion ratio of benzaldehyde is maintained above 75% through electrolysis. In spite of the fact that such high complex formation is maintained, the suppression effect of α-CD on the dimerization becomes small as the electrolysis proceeds as shown in Fig. 2. At relatively high conversions, benzyl alcohol formation takes precedence over the hydrobenzoin formation, therefore, α-CD cannot exhibit its ability effectively under such conditions.

Table 1 shows the [HB]/[BA] ratios observed in the controlled potential electrolyses under different pH conditions. In all cases the addition of α-CD resulted in decreases in the ratio, indicating that α-CD suppresses the dimerization. From Table 1 it can be seen that the ratio is dependent on the pH of the electrolyte. However, the trend cannot be attributed mainly to the pH effect since the cathode potentials in the present cases are not sufficiently negative with respect to the half-wave potentials.[7] We selected the relatively mild potentials since sufficiently negative potentials (*i.e.*, high current densities) favored

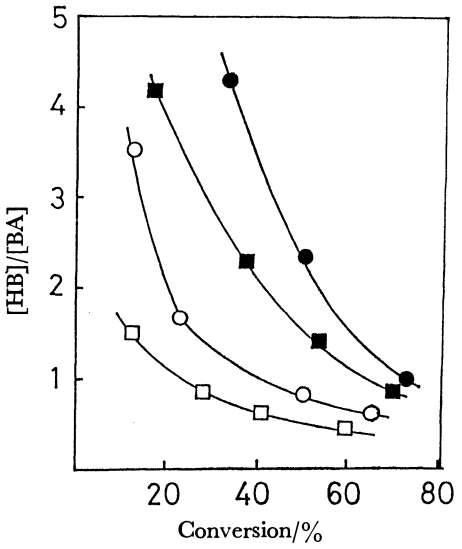

Fig. 3. Relationship between [HB]/[BA] ratio and conversion observed in the controlled current electrolysis at pH 4.6.
●: 0.33 A dm^{-2}, without CD, ○: 0.33 A dm^{-2} with α-CD (40 mmol dm^{-3}), ■: 0.50 A dm^{-2}, without CD, □: 0.50 A dm^{-2}, with α-CD (40 mmol dm^{-3}), initial concentration of benzaldehyde: 25 mmol dm^{-3}.

benzyl alcohol formation;[2] such conditions are not suitable for demonstrating the effect of α-CD.

The current density has a large influence on the product ratio.[2] Then, we carried out the controlled current electrolysis of benzaldehyde in the presence of α-CD. Figure 3 depicts the relationship between the [HB]/[BA] ratio and conversion of benzaldehyde in the controlled current electrolyses at 0.33 and 0.50 A dm^{-2}. Benzyl alcohol formation is favored at high current density in agreement with previous results.[2] In this case, the addition of α-CD also led to decrease in the [HB]/[BA] ratio.

As described above, α-CD can suppress the dimerization reaction both in the controlled potential and in the controlled current electrolyses. It seems possible that the dimerization rate in Eq. 3 is suppressed by the steric hindrance caused by the bulky α-CD molecule since benzaldehyde is included in the interior of α-CD. The anion radical and neutral radical of benzaldehyde must be included in α-CD judging from the results by Smith and Utley;[6] however, the determination of dissociation constants of the inclusion complexes is impossible since these radicals undergo following-up chemical reactions which are complicated. The suppression effect of α-CD may also explained by some influences of α-CD on other elementary reactions. However, the exact mechanism for the electroreduction of benzaldehyde is still unclear,[7] therefore, further discussion is beyound this paper. The current efficiencies of the electrolyses were higher than 70% and the addition of α-CD did not affect the current efficiency.

Finally we investigated the effect of α-CD on the stereochemistry of hydrobenzoin formed by the dimerization reaction. The *dl/meso* ratios[9] of hydrobenzoin are listed in Table 2. The effect of α-CD is quite small, though the addition of α-CD results in a slight increase in the *dl/meso* ratio. This result indicates that dimerization between molecules included in α-CD hardly takes place due to the steric hindrance. The dimerization would occur between free molecules; in the presence of α-CD *ca.* 20% of benzaldehyde exists in the free form at any instance. Therefore, the addition of α-CD cannot largely affect the stereochemistry of hydrobenzoin. The above argument also suggest that α-CD suppresses the dimerization rate (Eq. 3).

Table 2. Diastereomeric ratio (*dl/meso* ratio) of hydrobenzoin formed by the controlled potential electrolysis[a]

pH	Without CD	With α-CD (40 mmol dm^{-3})
7.0	0.96	1.11
9.1	0.85	0.97

a) Cathode potential: −1.4 V *vs.* SCE. Initial concentration of benzaldehyde: 25 mmol dm^{-3}.

In conclusion, the addition of α-CD to the electrolyte solution results in suppression of electroreductive dimerization of benzaldehyde (hydrobenzoin formation). This is probably attained by reducing the dimerization rate between the intermediate radicals, since inclusion of substrate in α-CD provides a severe steric hindrance around reaction sites. The addition has a small influence on the stereochemistry of hydrobenzoin formed in the present electrolysis. This also supports the suppression effect of α-CD on the dimerization rate.

References

1) L. G. Feoktitov and H. Lund, "Organic Electrochemistry," ed by M. M. Baizer, Mercel Dekker, New York (1973), Chap. VIII.
2) M. D. Birkett and A. T. Kuhn, *Electrochim. Acta*, **25**, 273 (1980) and references therein.
3) W. Saenger, *Angew. Chem., Int. Ed. Engl.*, **19**, 344 (1980).
4) T. Matsue, M. Fujihira, and T. Osa, *J. Electrochem. Soc.*, **126**, 500 (1979); **128**, 1478 (1981); *Bull. Chem. Soc. Jpn.*, **52**, 3692 (1979).
5) T. Osa, T. Matsue, and M. Fujihira, *Heterocycles*, **6**, 1833 (1977); T. Matsue, M. Fujihira, and T. Osa, *Anal. Chem.*, **53**, 722 (1981); *J. Electrochem. Soc.*, **129**, 1681 (1982).
6) C. Z. Smith and J. H. P. Utley, *J. Chem. Soc., Chem. Commun.*, **1981**, 492, 792.
7) S. Aoki, F. Mizutani, Y. Tanaka, and T. Sekine, *Denki Kagaku*, **47**, 679 (1979); S. Aoki, K. Machida, F. Mizutani, and T. Sekine, *ibid.*, **48**, 304 (1980); S. Aoki and T. Sekine, *ibid.*, **49**, 169 (1981).
8) L. Nadjo and J. M. Saveant, *J. Electroanal. Chem.*, **33**, 419 (1971).
9) J. H. Stocker and R. M. Jenevin, *J. Org. Chem.*, **33**, 2145 (1968); V. J. Puglisi, G. L. Clapper, and D. H. Evans, *Anal. Chem.*, **41**, 279 (1969).
10) F. Cramer, W. Saenger, and H.-Ch. Spatz, *J. Am. Chem. Soc.*, **89**, 14 (1967).

 © 1983 The Chemical Society of Japan Bull. Chem. Soc. Jpn., 56, 1308—1313 (1983) [Vol. 56, No. 5

Excimer Fluorescence of 1,2-Di(9-anthryl)ethane, 1,3-Di(9-anthryl)propane, and 9,9′-Bianthryl at High Pressures

Kimihiko HARA,* Yoshikazu KATOU, and Jiro OSUGI

Department of Chemistry, Faculty of Science, Kyoto University, Sakyo-ku, Kyoto 606

(Received July 22, 1982)

Fluorescence spectra of 1,2-di(9-anthryl)ethane (**1**), 1,3-di(9-anthryl)propane (**2**), and 9,9′-bianthryl (**3**) have been studied at high pressures up to 50 kbar both in crystalline state and in PMMA matrix. In the case of **1** and **2** in crystalline state, the excimer emissions appear reversibly at high pressures accompanied by the reversible red shifts. While in PMMA the fluorescence spectra assigned as locally excited state are observed, whose peak shifts are quite analogous to that of anthracene in the same matrix. As for **3**, a new band also appears at high pressure which is similar to the intramolecular charge-transfer band. Possible interpretations of the pressure effects are discussed.

Since the first discovery by Förster and Kasper[1] concerning the complexes between excited and ground state aromatic hydrocarbons which were named "excimer," numerous aromatic hydrocarbons have been found to exhibit excimer fluorescence and the results have been summarized in some reviews.[2] Their prominent feature is the broad and structureless fluorescence band which is shifted 4000—6000 cm^{-1} to lower frequencies relative to the normal molecular fluorescence. This fluorescence has been observed both in fluid solutions and in solid state at atmospheric pressure, if the structure allows a close overlap of molecular planes.

Recently the presence of the so-called "second excimer"[3] with a smaller overlap between the two anthracene moieties as compared with the sandwich arrangement has been suggested for 1,2-di(9-anthryl)-ethane in solution by Hayashi *et al.*[4] Dianthrylalkanes, where a pair of anthracene molecules are linked with methylene groups, have a possibility of the formation of intramolecular excimers.

The primary effect of pressure is to decrease interatomic distances and to increase overlap between adjacent electronic orbitals. Thus, the excimer formation in the solid state is expected to be highly pressure dependent if the crystal structures or molecular conformations are appropriate to allow a sandwich conformation. In the crystals such as anthracene, which has not a dimer structure, the excimer formation has been reported by the application of high pressure,[5] although the crystals with dimer structure such as perylene, pyrene, and 9-methylanthracene are known to exhibit excimer fluorescence at atmospheric pressure.

In this paper we report our studies of the pressure dependence of the excimer formation in 1,2-di(9-anthryl)ethane (**1**), 1,3-di(9-anthryl)propane (**2**), and 9,9′-bianthryl (**3**) [*i.e.*, (anthracene)-$(CH_2)_n$-(anthracene) for n=2, 3, and 0, respectively] up to 50 kbar both in the crystalline state and in the plastic media. Previously we published a preliminary results of **1**.[6] This paper presents the results of a more complete analysis where some points are corrected. In addition, since the high pressure cell, the emission apparatus, and the operation employed for this work have not been previously described, some details are also given here.

Experimental

Materials. The samples of **1**, **2**, and **3** used in this studies were prepared according to the literature procedure.[7-9] **1** was recrystallized from toluene and purified further by sublimation under vacuum. **2** and **3** were purified by successive recrystallizations from benzene and acetic anhydride, respectively. No impurity was detectable in TLC analysis, elementary analysis, and spectroscopic analysis of the purified samples.

The measurements were carried out for the crystals diffused in the NaCl crystal which was used as pressure transmitting medium, and for the poly(methyl methacrylate) (PMMA) film. Methyl methacrylate monomer was purified by the ordinary method[10] and thermally polymerized in bulk. The PMMA was purified by reprecipitations from benzene solution with methanol as precipitant. The compound and the PMMA were dissolved in dichloromethane at a concentration of less than 1%, forming approximately 0.07 mm thick films after evaporating the solvent under nitrogen atmosphere and at reduced pressure. The salt pellet is usually 0.5 mm thick. Two half cylinders of NaCl single crystal are cut to fit the sample hole of the high pressure cell and the pellet or film is inserted in between.

High Pressure Cell. The high pressure cell used for emission measurements is similar to Drickamer's type 1 cell[11] except for some modifications. It has two windows at 90° and uses NaCl as a pressure transmitting fluid, as well as NaCl windows. The outer steel jacket is SNCM hardened to HRC: 45—50. The inner cell is made from maraging steel YAG 300 hardened to HRC: 60. The carboloy pistons are jacketed with SNCM.

The pressure calibration was based on the shift of the R_1 fluorescence line of ruby at 694.2 nm as determined at the NBS (0.75 cm^{-1}/kbar)†. This cell can be used up to 50 kbar with no trouble in pistons as well as in windows.

Emission Apparatus. A block diagram of the emission spectrometer apparatus is shown in Fig. 1. The 27300 cm^{-1} band of a Hanovia 200 W Hg-Xe arc lamp is used as the excitation light source, which is mounted in an LH 150 lamp housing of Schoeffel LPS 271 power supply. The exciting light is dispersed through an ISA Jobin-Yvon H20 monochromator. Quartz lenses focus the excitation light into the high pressure cell. The emitted light is observed by the front surface illumination at 90° to the excitation light. Quartz lenses then collect the emitted light from the sample and focus it onto the entrance slit of the emission monochromator, an ISA Jobin-Yvon HRS 600 mm monochromator with a 1200 grooves/mm grating. For detection

† 1 bar=10^5 Pa.

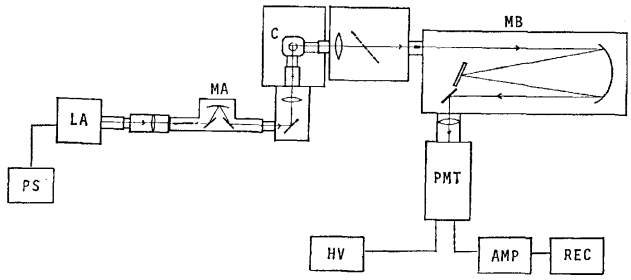

Fig. 1. Schematic diagram of apparatus for measuring the pressure effect on fluorescence.
C: High pressure cell, LA: excitation lamp, MA: excitation monochromator, MB: emission monochromator, PMT: cooled photomultiplier, PS: power supply, HV: high voltage power supply, AMP: amplifier, REC: recorder.

of the emitted light, the photomultiplier tube used is a Hamamatsu R562 which is operated at a cathode voltage of −1000 V by Fluke 415B, and cooled to −70 °C by a Hamamatsu C659 cooling apparatus. The amplified signal is displayed on a recorder.

The spectrometer can also be employed to measure excitation spectra, where the broad spectrum of a Hanovia 150 W Xe arc lamp and the wavelength drive of the excitation monochromator are required. The spectral corrections were made by quinine sulfate in 0.05 M H_2SO_4 (1 M= 1 mol dm^{-3}) as a reference standard.

Results

Fluorescence Spectra of **1**. Figure 2(a) summarizes the fluorescence spectra of **1** in different matrices at atmospheric pressure, which are normalized at each peak maximum. The spectrum of the crystal exhibits the normal fluorescence, which corresponds to that from ^1L_a state of anthracene. By forming into NaCl pellet with the compression of less than 7 kbar, this band decreases and a new broad structureless band appears at the energy of about 20000 cm^{-1}, although it is relatively weak in intensity. The corresponding change is not observed in the fluorescence excitation spectra. The new band decreases by the thermal annealing and reverts to the original crystalline spectra for 2 h at 100 °C. Thermal annealing removes the irreversible effects.

In PMMA, on the other hand, the main band at around 24000—25000 cm^{-1} are also assigned as the locally excited band, although the vibrational structure disappears. As a reference standard the fluorescence spectra of anthracene at atmospheric pressure in both matrices are shown in Fig. 2(b), where the concentration is about twice of that in **1**. The loss of vibrational structures in **1** may come from some intramolecular interactions accompanied by the substitution at the 9 position of anthracene since the transition moment of ^1L_a state is along the short molecular axis of anthracene. But it has appeared in **2** with larger separation between the two anthracene parts.

Figures 3 and 4 illustrate the effect of pressure on the fluorescence spectra of **1** in crystalline state and in PMMA matrix, respectively. They are normalized

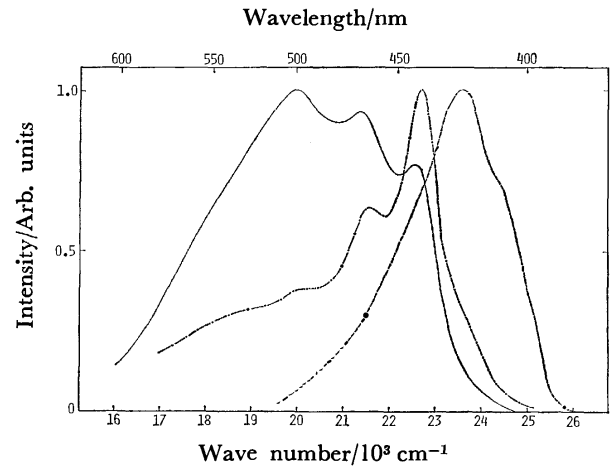

Fig. 2(a). Fluorescence spectra of **1** in different matrices at atmospheric pressure.
——: Crystals in NaCl pellet, —·—·: crystals, — — —: in PMMA matrix. (They are normalized at the wavenumber corresponding to the maximum intensity.)

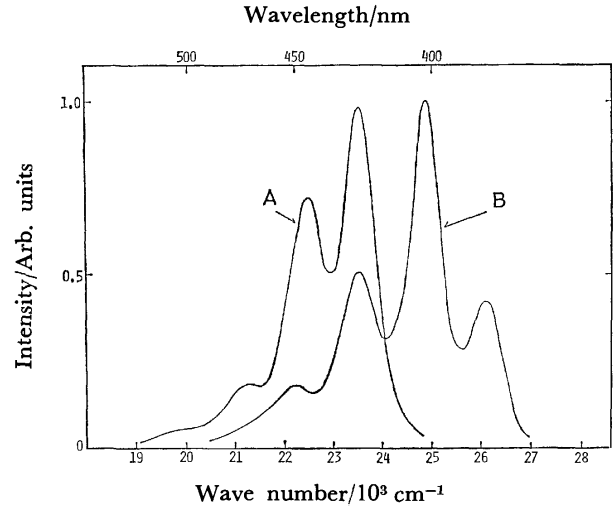

Fig. 2(b). Fluorescence spectra of anthracene.
A: Crystals in NaCl pellet, B: in PMMA

at their peak maxima. In crystals the new broad band grows in intensity at the expence of the normal emission with increasing pressure. These effects are reversible with pressure. The intensity of the normal emission returns to the spectrum obtained before compression, which indicates that no photochemical process is occuring at high pressures.

In PMMA, the band at 20000 cm^{-1} is not observed, but a new shoulder at 22000—23000 cm^{-1} appears as the pressure is applied. It is also reversible with pressure. The fluorescence excitation spectra do not show any new bands at high pressures and the behavior on the spectra are also reversible with pressure.

Fluorescence Spectra of **2**. Figure 5 shows the fluorescence spectra of the crystal at various pressures. A broad structuresless band is observed even at atmospheric pressure as a dominant band. The normal fluorescence appears as a small shoulder which disappears with increasing pressure.

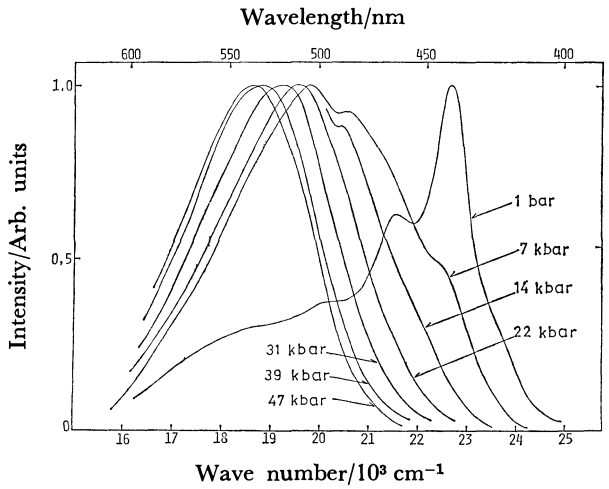

Fig. 3. Fluorescence spectra of **1** in crystals at various pressures.

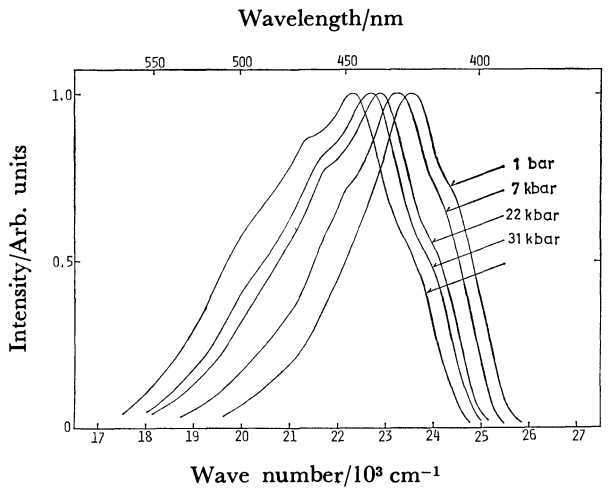

Fig. 4. Fluorescence spectra of **1** in PMMA matrix at various pressures.

Figure 6 shows the fluorescence spectra of **2** in PMMA. The spectrum at atmospheric pressure agrees with that in methanol–ethanol reported by Kobayashi *et al.*[13], except that there exists a shoulder at around 22000 cm^{-1}. It corresponds to that of anthracene monomer. In all cases the fluorescence excitation spectra shows no corresponding change with pressure except for the peak shift.

Fluorescence Spectra of ***3***. Figure 7 illustrates the fluorescence spectra of the crystal at various pressures. The spectrum of **3** at atmospheric pressure exhibits a broad emission at 22200 cm^{-1}. As the pressure is applied, this band decreases relatively with accompanying a red shift and a new band appears at around 20000 cm^{-1} at a pressure of 14 kbar. At the higher pressure the intensity of this peak increases and shifts toward red.

The effect of pressure in PMMA matrix are shown in Fig. 8. The spectrum at atmospheric pressure agrees with that in MCH–IP (1:3) reported by Schneider *et al.*[14] As the pressure is applied, it seems that the broad band of the lower energy grows up relatively, and at the pressure higher than about 14 kbar only

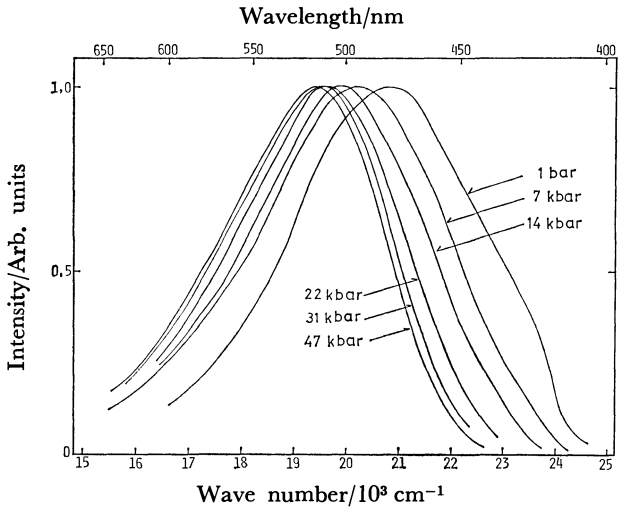

Fig. 5. Fluorescence spectra of **2** in crystals at various pressures.

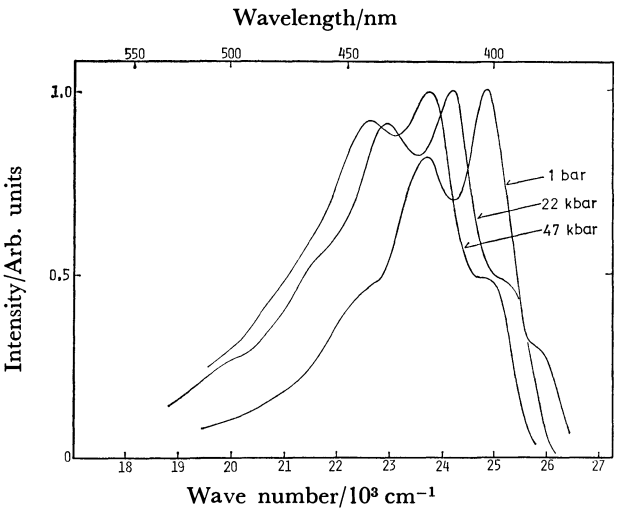

Fig. 6. Fluorescence spectra of **2** in PMMA matrix at various pressures.

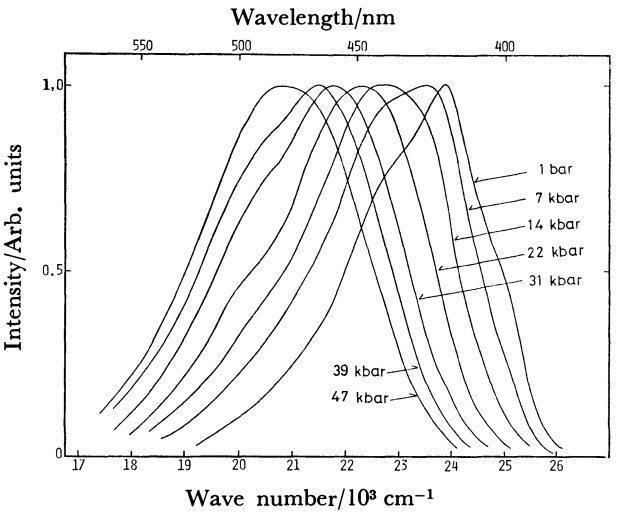

Fig. 7. Fluorescence spectra of **3** in crystals at various pressures.

Table 1. Emission peak maximum of **1**, **2**, **3**, and anthracene

Pressure	Peak maximum/10^3 cm^{-1}							
	1		**2**		**3**		Anthracene	
	Crystal	In PMMA	Crystal	In PMMA	Crystal	In PMMA	Crystal	In PMMA
1 bar	—	23.5	20.9	24.8	22.2	23.8	—	24.9
7 kbar	19.8	23.3	20.3	24.7	21.7	23.5	21.0	24.6
14	19.8	23.2	20.0	24.4	21.1	22.7	20.1	24.4
22	19.5	22.9	19.7	24.2	20.0	22.3	19.8	24.1
31	19.2	22.7	19.7	23.9	19.4	21.7	19.3	23.9
39	18.8	22.5	19.6	23.8	18.7	21.3	18.5	23.7
47	18.6	22.3	19.5	23.7	18.1	20.7	17.8	23.6

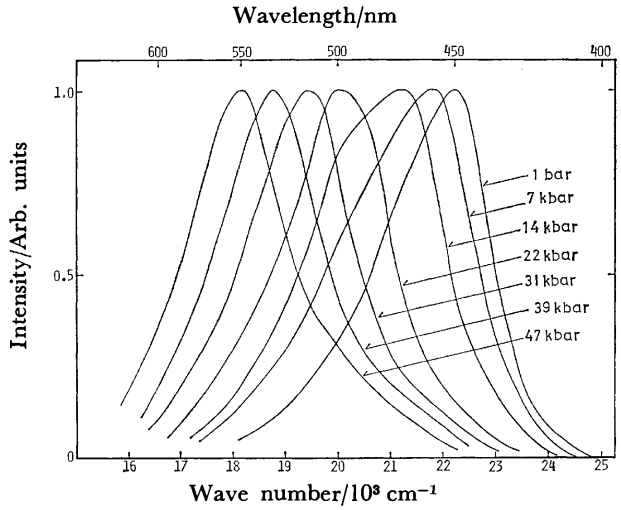

Fig. 8. Fluorescence spectra of **3** in PMMA matrix at various pressures.

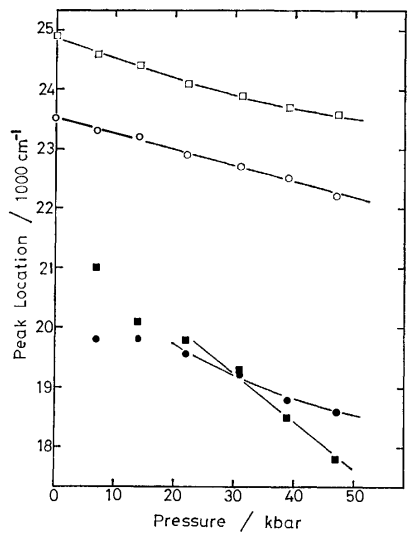

Fig. 9. Peak shift of **1** and anthracene.
○: **1** in PMMA, ●: **1** in crystals, □: anthracene in PMMA, ■: anthracene in crystals.

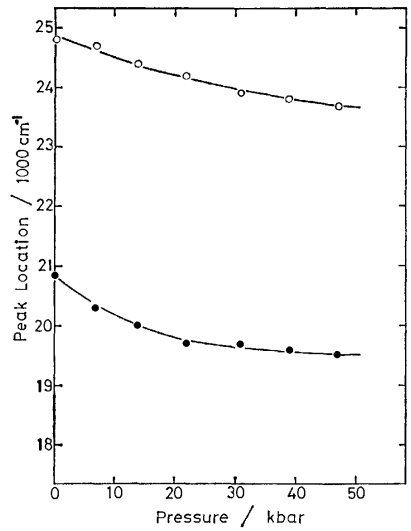

Fig. 10. Peak shift of **2** in crystals (●) and in PMMA (○).

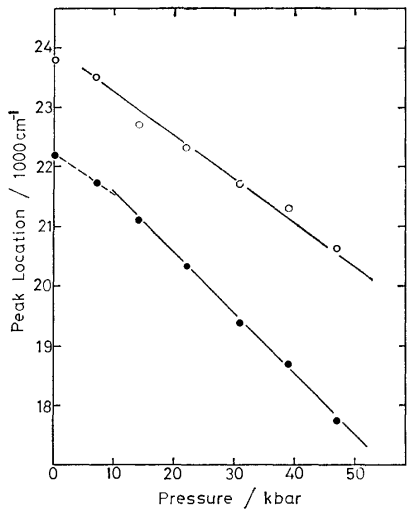

Fig. 11. Peak shift of **3** in crystals (●) and in PMMA (○).

this peak remains. In both cases no change is observed in the fluorescence excitation spectra. These effects are completely reversible with pressure.

Spectral Shifts with Pressure. As expected, there is a red shifts with pressure in all the fluorescence bands. The effects of pressure on the peak locations of **1**, **2**, and **3** both in crystalline state and in PMMA matrices are given in Table 1 and Figs. 9—11. Maxima were carefully read from the corrected curves. The peak shift of anthracene that is measured also

in this work for the sake of comparison is included in Table 1 and in Fig. 9. The amounts of the peak shift of **1** and **2** in PMMA with pressure agree with that of anthracene in the same matrix. The result confirms that the emissions in PMMA for these compounds are originated from the locally excited state in anthracene parts and that these are not the excimer like band with special interactions between the two anthracene chromophores. On the other hand, the excimer emission exhibits a larger shift as compared with that of the locally excited state in PMMA. The lower pressure region of **1** in crystal is the band for the locally excited state.

Careful examination of the results of **3** in crystal indicates that there might be two types of pressure sensitivity. So long as seeing in the peak shift, no nonlinear behavior with pressure is detected in PMMA matrix.

Discussion

The application of high pressure to crystals may create structural defects which are supposed to be crystallographic imperfections with excimer structure and act as a trap to capture singlet excitons. The effect of the creation of such defects is to be observed as irreversible pressure effects.[5] The irreversible behavior for **1** in the formation of sample pellet is likely to be originated from this effect. Thus, all the completely reversible pressure effects at the pressure higher than the residual pressure indicate the intrinsic effects on the excimer conformations. The residual pressure is less than 7 kbar.

The fluorescence spectra of **1** exhibits the vibrational structure from anthracene chromophores at atmospheric pressure. It looks like the type A crystals as classified by Stevens,[15] which fluoresce only normal emissions such as anthracene, naphthalene, and phenanthrene. For the crystal of **1** in NaCl matrix resembling to anthracene, the new broad band which appears at a lower energy region than the normal fluorescence by about 3000 cm^{-1} as the pressure is applied can be assigned as the excimer existing only in the excited state, since no change is observed in the excitation spectra except for the peak shift.

Ferguson *et al.*[16,17] developed an ingenious technique for producing the excimers of **1**. They prepared in single crystals of photocycloadduct of **1** by photocleavage so that a complete parallel conformation for **1** are kept by the constraint in the rigid matrix. By this method they observed three types of excimer emissions for **1**. Based on its energy value, our high-pressure induced excimer emission for **1** with a maximum at 19800 cm^{-1} at 14 kbar seems to correspond to the species B excimer by Ferguson *et al.*[16] with a maximum at 19600 cm^{-1} at 6 K. They proposed to its molecular conformation a partially overlapped sandwich structure with parallel molecular planes. Thus, if the high-pressure induced excimer is intramolecular, it will be the type of species B. If it is intermolecular, it is not a type of completely overlapped sandwich type excimer. The fact that the corresponding band is not observed in PMMA and the analogous behavior to anthracene suggest that this excimer is formed intermolecularly. However, the shoulder appeared in PMMA matrix at around 21000 cm^{-1} under pressure may indicate a formation of intramolecular one, whose peak maximum is close to that observed by Hayashi *et al.*[4] in solution.

The excimer fluorescence observed for **2** in crystals resembles that of type B crystals in which the molecules are arranged pair-wise. The fact that such type B structure is easily achieved suggests that this excimer is formed intramolecularly. This explanation is also based on the results that in PMMA matrix there exists a shoulder band besides the main band of the locally excited state as seen in Fig. 6, and that the relative intensity increases at lower energy region, and this behavior does not change with concentration. Its band maximum lies in the higher wave number as compared with 9-methylanthracene which has a pair-wise structure in the crystal. The amount of the peak shift, however, is similar to that of 9-methylanthracene. This may indicate that the excimer formed has not a complete sandwich arrangement, but has a structure with different mutual orientations such as the species B or C by Ferguson *et al.*, and also the type II by Hayashi *et al.* that have been reported for **1**. The proposed molecular conformations of the excimers for **1** by Ferguson *et al.* are visually shown as follows;

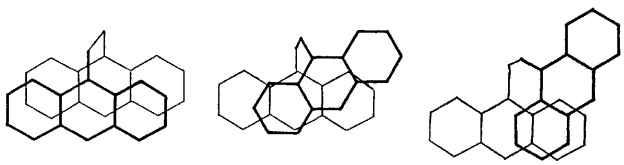

(A) (B) (C)

where (A) is the species A with a complete overlapped sandwich structure, while (B) and (C) are the species B and C, respectively with a smaller overlapped structure. The structure (B) corresponds to type II by Hayashi *et al.*

The excimer peak shifts of **1** and **2** under pressure saturate at the higher pressure region in comparison with that of anthracene. In the case of **2**, it shows only a little change with pressure at higher than 30 kbar, as seen in Fig. 10. While in anthracene it shows a linear pressure dependence of -73 ± 7 cm^{-1}/kbar, which agrees with the reported result[5] within the error limits of the experiments. The difference in peak shifts among these compounds reflects that the more bulky molecule is the more difficult in the molecular motion to stabilize the excimer conformation.

As for **3**, it is impossible to achieve the intramolecular sandwich arrangement. The interesting properties have been reported by Schneider *et al.*[14] that the interaction between the two chromophores shows characteristics of the charge-transfer interactions in the excited state under the influence of solvent perturbations, which accompanies a small conformational change. The fluorescence in polar solvent shows a broad featureless band which is caused by the intramolecular charge transfer resulted from the conformational change in the excited state.

The band maximum of the fluorescence spectra of **3** in crystals at atmospheric pressure is 22200 cm^{-1} as seen in Fig. 7. This cannot be assigned to the charge-transfer band, but to the locally excited fluorescence band from anthracene moiety. In some solvents the corresponding band has been observed at atmospheric pressure, and it has been confirmed that π-electron systems of two anthracene chromophores are scarecely interact with each other, not only by the measurements of absorption and fluorescence spectra,[14] but also by the measurements of polarizability,[18] dipole moment,[18] half reduction potential,[19] molecular refraction,[20] and conbustion energy.[21] Hexane is one of such solvents in which only the locally excited fluorescence band appears. The measurement of pressure effects in hexane up to 6 kbar showed *ca.* -50 cm^{-1}/kbar,[22] which is analogous to that observed in PMMA matrix and in the lower pressure region in the crystal.

On the other hand, the new band observed at the higher pressure than about 15 kbar in crystal can be assigned as the charge-transfer band. It has a peak shift of -77 ± 13 cm^{-1}/kbar. Such a larger peak shift corresponds to that in polar solvents as methanol in which only the charge-transfer band is observed.[22] The high sensitivity with pressure indicates the characteristics of the charge-transfer state. The charge-transfer state shows also a high sensitivity with the solvent polarity change. Thus, the increase in pressure has the same effect as the increase in solvent polarity.

It has been calculated by Schneider *et al.*[23] that the twisted angle between the two anthracene chromophores in **3** is 90° in the ground state, while in the excited state it changes by $\pm12°$. The results of the pressure-induced new band and its larger red shift with pressure are considered to be correlated with the analogous intramolecular conformational change at high pressures. Namely, the change of the twisted angle is to be achieved with increasing pressure, and as the result, the charge transfer state is more stabilized. Further details of the research will be reported in a subsequent paper.

This research was supported in part by a Grant-in-Aid for Scientific Research No. 447007 from the Ministry of Education, Science and Culture, and in part by Grants for Joint Research in Fundamental Chemistry of Japan Society for the Promotion of Science.

References

1) Th. Förster and Kasper, *Z. Phys. Chem. NF.*, **1**, 275 (1954).
2) Th. Förster, *Angew. Chem.*, **81**, 364 (1969); J. B. Birks, "Photophysics of Aromatic Molecules," Wiley-Interscience, London (1970), Chap. 7; W. Klöpffer, "Organic Molecular Photophysics," ed by J. B. Birks, Wiley-Interscience, London (1973), Vol. 1, Chap. 7.
3) G. E. Johnson, *J. Chem. Phys.*, **62**, 4967 (1975).
4) T. Hayashi, T. Suzuki, N. Mataga, Y. Sakata, and S. Misumi, *Chem. Phys. Lett.*, **38**, 599 (1976); T. Hayashi, N. Mataga, Y. Sakata, S. Misumi, M. Morita, and J. Tanaka, *J. Am. Chem. Soc.*, **98**, 5910 (1976).
5) P. F. Jones, *J. Chem. Phys.*, **48**, 5448 (1968); P. F. Jones and M. Nicol, *ibid.*, **48**, 5440 (1968).
6) K. Hara, Y. Katou, and J. Osugi, *Chem. Phys. Lett.*, **81**, 357 (1981).
7) F. H. C. Stewart, *Aust. J. Chem.*, **14**, 177 (1961); **21**, 1107 (1968).
8) E. A. Chandross and C. J. Dempster, *J. Am. Chem. Soc.*, **92**, 3586 (1970).
9) A. Magnus, H. Hartmann, and F. Becker, *Z. Phys. Chem.*, **197**, 75 (1951).
10) B. A. Baldwin and H. W. Offen, *J. Chem. Phys.*, **46**, 4509 (1967).
11) H. G. Drickamer and A. S. Balchan, "Modern Very High Pressure Techniques," ed by G. H. Wentorf, Butterworths, London (1962), p. 25; R. A. Fitch, T. E. Slykhouse, and H. G. Drickamer, *J. Opt. Soc. Am.*, **47**, 1015 (1957).
12) R. A. Forman, G. Piermarini, J. D. Barnett, and S. Block, *Science*, **176**, 284 (1972); J. D. Barnett, S. Block, and G. J. Piermarini, *Rev. Sci. Instr.*, **44**, 1 (1973); G. J. Piermarini, S. Block, J. D. Barnett, and R. A. Forman, *J. Appl. Phys.*, **46**, 2774 (1975).
13) T. Kobayashi, S. Nagakura, and M. Szwarc, *Chem. Phys.*, **39**, 105 (1979).
14) V. F. Schneider and E. Lippert, *Ber. Bunsenges. Phys. Chem.*, **72**, 1155 (1968).
15) B. Stevens, *Spectrochim. Acta*, **18**, 439 (1962).
16) J. Ferguson, M. Morita, and M. Puza, *Chem. Phys. Lett.*, **42**, 288 (1976).
17) B. F. Anderson, J. Ferguson, M. Morita, and G. B. Robertson, *J. Am. Chem. Soc.*, **101**, 1832 (1979).
18) W. Liptay, G. Walz, W. Baumann, H. Schlosser, H. Deckers, and N. Detzer, *Z. Naturforsch., A*, **26**, 2020 (1971).
19) G. J. Hojitink, *Recl. Trav. Chim. Pays-Bas*, **74**, 1525 (1955).
20) J. A. Bigot and D. W. Van Krevelen, *Trans. Faraday Soc.*, **56**, 322 (1960).
21) A Magnus, H. Hartmann, and F. Becker, *Z. Phys. Chem.*, **197**, 75 (1951).
22) K. Hara, T. Arase, and J. Osugi, unpublished data.
23) V. F. Schneider and Lippert, *Ber. Bunsenges. Phys. Chem.*, **74**, 624 (1970).

Kinetics of the Formation of the Intermediate Complex in the Aromatic Nucleophilic Substitution of Methyl 4-Methoxy-3,5-dinitrobenzoate with Piperidine in Dimethyl Sulfoxide

Yoshinori HASEGAWA

College of General Education, Tohoku University, Kawauchi, Sendai 980

(Received August 13, 1982)

The intermediate complex in the aromatic nucleophilic substitution of methyl 4-methoxy-3,5-dinitrobenzoate with piperidine in dimethyl sulfoxide was confirmed by visible absorption spectroscopy. Kinetics of the formation of the intermediate were studied by a stopped-flow spectrophotometer, and rate and equilibrium constants were determined. The observable intermediate (Z^-) was the conjugate base of the initial zwitterionic complex (ZH). Proton transfer between ZH and Z^- was rate limiting and the intermediate formation was base catalyzed.

Bunnett and coworkers have confirmed the existence of the intermediate complex in the aromatic nucleophilic substitution of 1-ethoxy-2,4-dinitronaphthalene with primary and cyclic secondary amines in dimethyl sulfoxide (DMSO) and presented the mechanism for the formation and decomposition of the intermediate.[1,2] As regard to the formation of the intermediate, proton transfer between XH and X^- is rapid and therefore the formation of the intermediate is not base catalyzed.

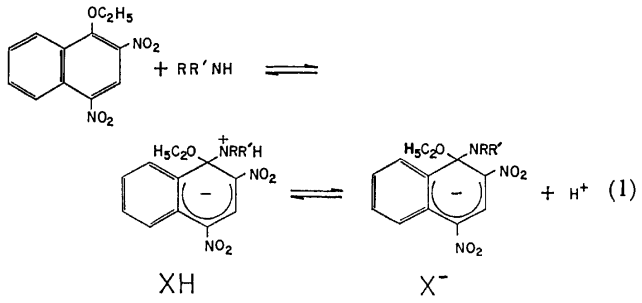

XH X^-

Contrary, kinetic studies on the formation of the anionic σ-complexes[3-5] of trinitrobenzene with primary and secondary amines have shown that proton transfer between YH and Y^- is rate limitting under certain conditions.[5-9]

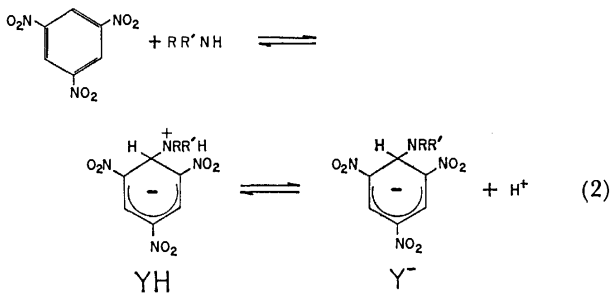

YH Y^-

Crampton and Gibson have demonstrated from kinetics of the formation of the σ-complex from trinitrobenzene and piperidine in DMSO that proton transfer is rate limiting over the entire range of piperidine concentrations used.[9]

We have observed the visible absorption spectrum of the intermediate complex of methyl 4-methoxy-3,5-dinitrobenzoate (MDNB) with piperidine in DMSO and studied on kinetics of the formation of the intermediate.

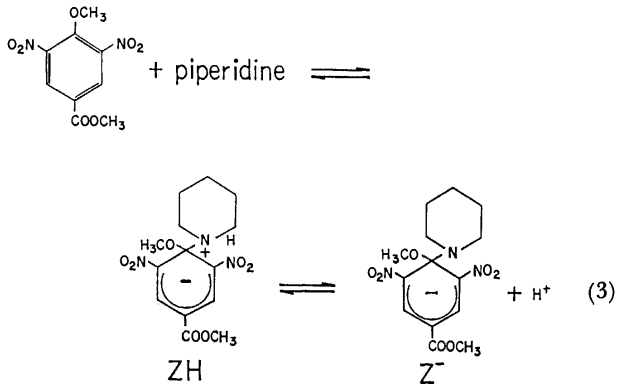

ZH Z^-

Experimental

Materials. MDNB was prepared by esterification of 4-chloro-3,5-dinitrobenzoic acid followed by nucleophilic substitution of chlorine by sodium methoxide. The compd was recrystallized from methanol. NMR (DMSO-d_6); δ=8.63 (aromatic protons), 3.99 (OCH_3), 3.92 ($COOCH_3$). Methyl 3,5-dinitro-4-piperidinobenzoate was prepared by substitution of the methyl ester of 4-chloro-3,5-dinitrobenzoic acid with piperidine. The compd was recrystallized from methanol. NMR (DMSO-d_6); δ=8.39 (ring protons), 3.87 ($COOCH_3$), 3.00 (CH_2NCH_2), 1.56 ($CH_2CH_2CH_2$). Piperidine was refluxed over sodium and distilled. Piperidine hydrochloride was prepared from piperidine and concentrated hydrochloric acid in methanol and recrystallized from methanol. S. G. DMSO, tetrapropylammonium iodide, and 1,4-diazabicyclo-[2.2.2]octane (DABCO) were used as supplied.

Measurements. Piperidine (2.8×10^{-4} mol) was injected into a NMR tube containing a DMSO-d_6 solution (0.4 cm^3) of MDNB (2.0×10^{-4} mol) and NMR spectra were recorded on a Hitachi R-22 Spectrometer. Visible absorption spectra were recorded using a Hitachi RSP-2 Rapid Scan Spectrophotometer and a Hitachi 340 Spectrophotometer. Kinetic measurements were carried out using a thermostatted stopped-flow spectrophotometer (Union Giken RA-401).

Results

NMR Spectroscopy. After addition of piperidine to a solution of MDNB, the resonance peaks at δ= 8.63, 3.99, and 3.92 gradually disappeared and completely vanished 1 h after addition at 34 °C. At the expense of the peaks of MDNB, new resonance peaks appeared at δ=8.25, 3.77, 3.06, and 1.58. The new

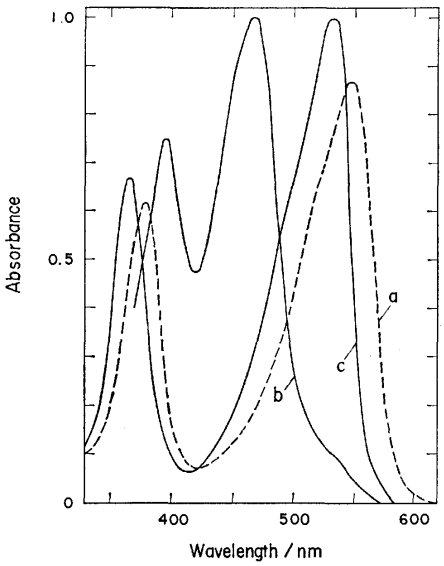

Fig. 1. The visible absorption spectrum observed immediately after mixing of MDNB (4.9×10^{-5} M, 1 M=1 mol dm^{-3}) with piperidine (0.32 M) in DMSO, a; the spectra observed with the DMSO solution containing MDNB (4.9×10^{-5} M), potassium methoxide (8.0×10^{-3} M), and methanol (0.8% by volume); b and c, *ca.* 1/3 s and 5 min after mixing respectively.

peaks are attributed to methyl 3,5-dinitro-4-piperidinobenzoate; δ=8.25 (aromatic protons), 3.77 ($COOCH_3$), 3.06 (CH_2NCH_2), 1.58 ($CH_2CH_2CH_2$). No evidence for formation of an anionic σ-complex was obtained from NMR spectroscopy.

Visible Absorption Spectroscopy. The spectrum observed immediately after mixing of MDNB with piperidine in DMSO is a in Fig. 1. The absorption bands at 378 and 545 nm slowly decreased in intensity and disappeared several hours after mixing at room temperature.

For comparison, we tried to observe the visible absorption spectra of MDNB with potassium methoxide in DMSO. The spectra observed *ca.* 1/3 s and 5 min after mixing are b and c in Fig. 1, respectively. The absorption bands at 395 and 465 nm appeared at the initial stage are attributed to the 1,3-complex.[10,11] The spectrum c with absorption maxima at 367 and 532 nm is due to the 1,1-complex.[10-12]

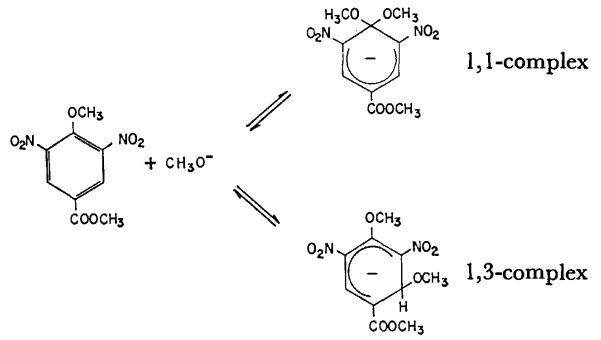

The similarity of the spectrum a to c leads to the conclusion that the spectrum c is due to the intermediate complex ZH or/and Z$^-$. The formation of the intermediate is too fast to be measured by conventional means but can be measured by a stopped-flow spectrophotometer.

Table 1. Equilibrium absorbance of MDNB with piperidine and piperidine hydrochloride in DMSO[a]

[Piperidine] / M	A_{545}[b] 20 °C	25 °C	30 °C
0.040	0.041	0.030	
0.051		0.048	0.026
0.061	0.084	0.068	
0.071	0.115		0.053
0.081	0.138	0.116	0.066
0.12	0.26	0.24	0.136
0.16		0.33	0.21
0.24	0.53		0.35
0.32[c]		1.16	

a) $[MDNB]_0$ 6.0×10^{-5} M; [piperidine hydrochloride] 5.0×10^{-3} M; [tetrapropylammonium iodide] 5.0×10^{-3} M. b) Absorbance at 545 nm. c) In the absence of piperidine hydrochloride and tetrapropylammonium iodide. Conversion of MDNB to Z$^-$ is virtually complete. ε_{545} 19300 M^{-1} cm^{-1}.

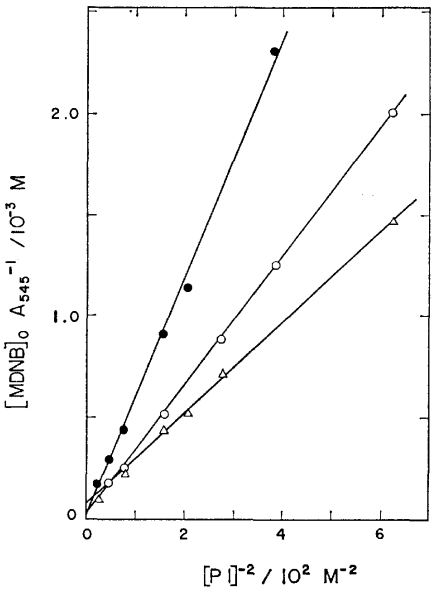

Fig. 2. Plots of $[MDNB]_0$ A_{545}^{-1} *vs.* $[Pi]^{-2}$.

Equilibria. Let us rewrite Eq. 3 as Eq. 4.

$$MDNB \underset{k_{-1}}{\overset{k_1[Pi]}{\rightleftharpoons}} ZH \underset{k_{PiH^+}[PiH^+]}{\overset{k_{Pi}[Pi]}{\rightleftharpoons}} Z^- \quad (4)$$

An equilibrium constant K for the over all conversion of MDNB into Z$^-$ is defined by Eq. 5.

$$K = \frac{[Z^-][PiH^+]}{[MDNB][Pi]^2} \quad (5)$$

And then

$$K = \frac{k_1 k_{Pi}}{k_{-1} k_{PiH^+}}. \quad (6)$$

Assuming that k_{Pi} is much larger than k_{PiH^+},[13] Eq. 5 is rearranged as follows:

$$\frac{[MDNB]_0}{A} = \frac{[PiH^+]}{K\varepsilon[Pi]^2} + \frac{1}{\varepsilon}, \quad (7)$$

Table 2. Rate date in the presence of piperidine in large excess of MDNB at 25 °C[a)]

[Piperidine] M	[DABCO] M	k_{f1} s^{-1}	$k_{f1}/[Piperidine]^2$ $s^{-1}M^{-2}$
0.016		0.0068	27
0.020		0.0113	28
0.030		0.024	27
0.040		0.048	30
0.061		0.105	28
0.081		0.20	30
0.12		0.38	26
0.16		0.63	25
0.20		0.95	24
0.24		1.12	19.4
0.081	0.038	0.20	
0.081	0.076	0.22	
0.081	0.16	0.27	
0.081	0.23	0.28	
0.030[b)]		0.024	
0.12[b)]		0.36	
0.24[b)]		1.02	
0.12[c)]		0.38	

a) $[MDNB]_0$ 6.0×10^{-5} M. b) In the presence of salt; [tetrapropylammonium iodide] 1.00×10^{-2} M. c) In the presence of water; $[H_2O]$ 0.22 M.

where $[MDNB]_0$, A and ε are the stoicheiometric MDNB concentration, equilibrium absorbance, and the molar extinction coefficient, respectively.

In the presence of piperidine and piperidine hydrochloride in large excess of MDNB, equilibrium absorbance at 545 nm measured with a stopped-flow spectrophotometer is presented in Table 1. Measurements were carried out at μ 0.01 M using tetrapropylammonium iodide. Plots of $[MDNB]_0 A_{545}^{-1}$ *vs.* $[Pi]^{-2}$ in Fig. 2 give straight lines. K 0.117, 0.083, and 0.045 M^{-1} at 20, 25, and 30 °C respectively were obtained.

Kinetic Analysis. Kinetic runs were carried out in the presence of piperidine in large excess of MDNB and in the absence of piperidine hydrochloride. Under these conditions, we may write as follows:

$$MDNB \underset{k_{r2}}{\overset{k_{f1}}{\rightleftharpoons}} Z^- + AH^+, \tag{8}$$

where AH^+ is the species formed from deprotonatin of ZH by piperidine and is equall in concentration to Z^-, and k_{f1} and k_{r2} are the pseudo-first-order rate constant for the forward reaction and the second-order reverse rate constant, respectively. The solution for Eq. 8 is presented by Eq. 9.[14)]

$$\ln\left(\frac{[MDNB]_0[Z^-]_e+[Z^-]([MDNB]_0-[Z^-]_e)}{[MDNB]_0([Z^-]_e-[Z^-])}\right)= \left(\frac{2[MDNB]_0-[Z^-]_e}{[Z^-]_e}\right)k_{f1}t, \tag{9}$$

where $[Z^-]$ and $[Z^-]_e$ are concentrations of Z^- during the reaction and at equilibrium respectively.

Making use of the steady-state approximation with respect to ZH, k_{f1} is given by Eq. 10. The second-order rate constant k_{f2} for the forward reaction is given by Eq. 11.

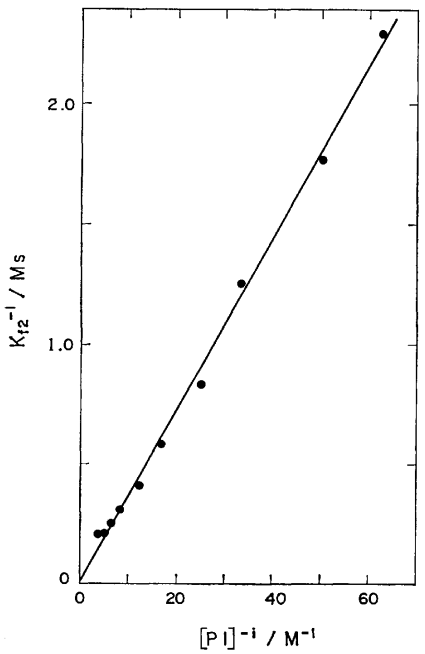

Fig. 3. A plot of k_{f2}^{-1} *vs.* $[Pi]^{-1}$.

$$k_{f1} = \frac{k_1[Pi]k_{PI}[Pi]}{k_{-1}+k_{PI}[Pi]} \tag{10}$$

$$k_{f2} = k_{f1}/[Pi]. \tag{11}$$

Rate date are presented in Table 2. When concentrations of piperidine are smaller than 0.12 M values of $k_{f1}/[Pi]^2$ are substantially constant. This fact implies that k_{-1} is much larger than $k_{PI}[Pi]$ and deprotonation of ZH is rate limiting in the forward direction.

Equation 10 is rearranged as Eq. 12.

$$\frac{1}{k_{f2}} = \frac{1}{k_1} + \frac{k_{-1}}{k_1k_{PI}[Pi]} \tag{12}$$

A plot of k_{f2}^{-1} *vs.* $[Pi]^{-1}$ in Fig. 3 gives straight line. k_1k_{PI}/k_{-1} 28 $s^{-1}M^{-2}$ and k_1 100 $s^{-1}M^{-1}$ were obtained from the inversion of the slope and of the intercept, respectively. And then k_{PI}/k_{-1} 0.28 M^{-1}. From K 0.083 M^{-1}, k_{PIH^+} 340 $s^{-1}M^{-1}$.

Kinetic runs were made with piperidine and DABCO in large excess of MDNB. Under these conditions, k_{f1} is given by Eq. 13.

$$k_{f1} = \frac{k_1[Pi](k_{PI}[Pi]+k_{DABCO}[DABCO])}{k_{-1}+k_{PI}[Pi]+k_{DABCO}[DABCO]}, \tag{13}$$

where k_{DABCO} is the rate constant for deprotonation of ZH by DABCO. As shown in Table 2, k_{f1} increases with DABCO concentration. The intermediate formation is catalyzed by DABCO. At a given concentration of DABCO, k_{DABCO}/k_{-1} can be calculated from Eq. 13 using k_{PI}/k_{-1} 0.28 M^{-1} and k_1 100 $s^{-1}M^{-1}$. The mean value of k_{DABCO}/k_{-1} obtained was 0.067 M^{-1}.

Kinetics were studied in the presence of both piperidine and piperidine hydrochloride in large excess of MDNB. Under these pseudo-first-order conditions, both forward and reverse reactions are pseudo-first-order and so observed rate constant k_{obsd} is the sum

Table 3. Rate date in the presence of piperidine and piperidine hydrochloride in large excess of MDNB at 25 °C[a)]

[Piperidine] / M	[Piperidine hydrochloride] / 10^{-3} M	[Tetrapropylammonium iodide] / 10^{-3} M	k_{obsd} / s^{-1}	k_{calcd} / s^{-1}
0.040	5.0	5.0	1.75	1.72
0.051	5.0	5.0	1.73	1.75
0.071	5.0	5.0	1.78	1.82
0.081	5.0	5.0	1.88	1.84
0.12	5.0	5.0	2.1	2.0
0.16	5.0	5.0	2.6	2.3
0.24	5.0	5.0	3.2	3.1
0.081	6.5	3.5	2.5	2.3
0.081	8.5	1.5	3.0	3.0
0.081	10.0		3.3	3.5
0.081[b)]	6.5	3.5	2.6	
0.081[b)]	8.5	1.5	3.1	

a) $[MDNB]_0$ 6.0×10^{-5} M. b) $[H_2O]$ 0.22 M.

Table 4. Summary of rate and equilibrium constants[a)]

	20 °C	25 °C	30 °C
k_1k_{Pi}/k_{-1} / $s^{-1}M^{-2}$		28±2	
k_{Pi}/k_{-1} / M^{-1}		0.28±0.16	
k_1 / $s^{-1}M^{-1}$		100±50	
k_{PiH^+} / $s^{-1}M^{-1}$		340±70	
k_{DABCO}/k_{-1} / M^{-1}		0.067±0.073	
K / M^{-1}	0.117±0.012	0.083±0.008	0.045±0.005
ΔG^0 / kcal mol^{-1}		1.47±0.10	
ΔH^0 / kcal mol^{-1}		−16.7±0.3	
ΔS^0 / kcal del^{-1} mol^{-1}		−0.061±0.013	

a) 1 cal=4.184 J.

of the forward and reverse component.

$$MDNB \underset{k_{r1}}{\overset{k_{f1}}{\rightleftharpoons}} Z^{-1} \quad (14)$$

$$k_{obsd} = k_{f1} + k_{r1} \quad (15)$$

Making use of the steady-state approximation with respect to ZH, k_{obsd} is given by Eq. 16.

$$k_{obsd} = \frac{k_1[Pi]k_{Pi}[Pi] + k_{-1}k_{PiH^+}[PiH^+]}{k_{-1} + k_{Pi}[Pi]} \quad (16)$$

Rate date are presented in Table 3. k_{calcd} was calculated from Eq. 16 using k_1 100 $s^{-1}M^{-1}$, k_{PiH^+} 340 $s^{-1}M^{-1}$ and k_{Pi}/k_{-1} 0.28 M^{-1}.

In some cases, kinetic date were obtained in the presence of tetrapropylammonium iodide or water and are presented in Tables 2 and 3.

Rate and equilibrium constants are summarized in Table 4.

Discussion

Intermediate Complex. The similarity of the spectrum a in Fig. 1 to c of the Meisemheimer complex of similar structure affords an evidence for the formation of the intermediate complex.

NMR spectroscopy failed to detect an evidence for intermediate formation. Owing to its insufficient stability (K 0.045 M^{-1} at 30 °C), the intermediate is too small in concentration to be detected by NMR.

Plots of $[MDNB]_0$ A_{545}^{-1} *vs.* $[Pi]^{-2}$ give straight lines. This indicate that the intermediate exists predominantly as its conjugate base rather than the zwitterionic form.

Rate Limiting Proton Transfer. The most striking feature in the formation of the intermediate is that the deprotonation of ZH is rate limiting in the forward direction. The intermediate formation is base catalyzed.

Our results are k_1 100 $s^{-1}M^{-1}$ and k_{Pi}/k_{-1} 0.28 M^{-1}. As the intercept of a plot of k_{f2}^{-1} *vs.* $[Pi]^{-1}$ is small, the value of k_1 obtained from the inversion of the intercept may have high uncertainity. Using our results, under [Pi] 0.06, 0.12, and 0.24 M, $k_{Pi}[Pi]$ are 0.017 k_{-1}, 0.034 k_{-1}, and 0.068 k_{-1}, respectively. These mean that under high piperidine concentrations a process from ZH to Z^- is not negligible. Thus, the depature from constant values of $k_{f1}/[Pi]^2$ under high piperidine concentrations in Table 2 will be appropriately explained by use of our results. As shown in Table 3, k_{calcd} values are in accordance with observed rate constants.

Bunnett *et al.* demonstrated that proton transfer is rapid and so not rate limiting in the formation of the intermediate complex from 1-ethoxy-2,4-dinitronaphthalene and piperidine in DMSO.[2)] The intermediate ZH of MDNB has two nitro groups which will prevent for piperidine to attack on ZH. The steric circumstance of the intermediate of 1-ethoxy-2,4-dinitronaphthalene is different from that of ZH. The difference of the steric circumstance will cause the difference of a rate limiting process.

Effect of Salt and Water. Rates are unaffected by the presence of tetrapropylammonium iodide (0.01 M). Furthermore, rates remain almost constant in the presence of water (0.22 M).

We are grateful to Mrs. H. Yasuhara and Dr. K. Kabuto for obtaining NMR spectra and their helpful discussions.

References

1) J. A. Orvik and J. F. Bunnett, *J. Am. Chem. Soc.*, **92**, 2417 (1970).
2) J. F. Bunnett, S. Sekiguchi, and L. A. Smith, *J. Am. Chem. Soc.*, **103**, 4865 (1981).
3) M. J. Strauss, *Chem. Rev.*, **70**, 667 (1970).
4) S. Sekiguchi, *Yuki Gosei Kagaku Kyokai Shi*, **36**, 633

(1978).
5) F. Terrier, *Chem. Rev.*, **82**, 77 (1982).
6) E. Buncel and W. Eggimann, *J. Am. Chem. Soc.*, **99**, 5958 (1977).
7) C. F. Bernasconi, M. C. Muller, and P. Schmid, *J. Org. Chem.*, **44**, 3189 (1979).
8) T. O. Bamkole, J. Hirst, and I. Onyido, *J. Chem. Soc., Perkin Trans. 2*, **1981**, 1201.
9) M. R. Crampton and B. Gibson, *J. Chem. Soc., Perkin Trans. 2*, **1981**, 533.
10) M. R. Crampton, M. A. El Ghariani, and H. A. Khan, *J. Chem. Soc., Chem. Commun.*, **1971**, 834.
11) M. R. Crampton, M. A. El Ghariani, and H. A. Khan, *Tetrahedron*, **28**, 3299 (1972).
12) M. R. Crampton and H. A. Khan, *J. Chem. Soc., Perkin Trans. 2*, **1972**, 1173.
13) It is known that the amine complex exists predominantly as its conjugate base rather than the zwitterionic form.[1,2,9]
14) See, for example, K. J. Laidler, "Chemical Kinetics," McGraw-Hill, New York (1965), p. 21.

 © 1983 The Chemical Society of Japan Bull. Chem. Soc. Jpn., 56, 1319—1321 (1983)

The Molecular Structure of Bromo(ethyl)[(−)-sparteine]magnesium(II),† a Catalyst for the Asymmetric-selective Polymerization of Racemic Methacrylates

Hiroyuki KAGEYAMA, Kunio MIKI, Nobuo TANAKA,†† Nobutami KASAI,*
Yoshio OKAMOTO,** and Heimei YUKI**,†††

Department of Applied Chemistry, Faculty of Engineering, Osaka University, Yamadaoka, Suita, Osaka 565

***Department of Chemistry, Faculty of Engineering Science, Osaka University, Machikaneyama, Toyonaka, Osaka 560*

(Received September 18, 1982)

The molecular structure of EtMgBr-(−)-sparteine, which initiates asymmetric (enantiomer) selective polymerization of racemic methacrylates, has been determined by means of X-ray diffraction. The crystal is orthorhombic, space group $P2_12_12_1$, $a=11.278(2)$, $b=14.112(3)$, $c=11.746(2)$ Å, $Z=4$. The structure was established by the heavy atom method and refined by the block-diagonal least-squares procedure: $R=0.100$ for 1272 non-zero reflections. The Mg atom is tetrahedrally coordinated by the Et group, Br and two N atoms of the (−)-sparteine.

Recently, Okamoto, Yuki, and their co-workers have studied the asymmetric-selective (enantiomer selective) polymerization of racemic methacrylates, especially that of the (*RS*)-α-methylbenzyl methacrylate ((*RS*)-MBMA).[1-5]

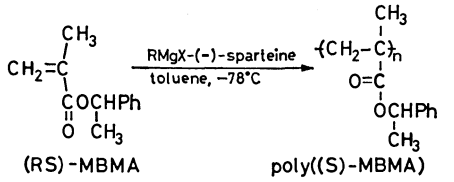

In this reaction, in toluene at −78 °C, the (*S*)-monomer polymerizes preferentially over the (*R*)-monomer by the presence of a complex between a primary or secondary Grignard reagent and a chiral bidentate ligand, (−)-sparteine†††† or its derivative. The activity and selectivity of the catalysts were discussed[6] on the basis of the molecular structures determined by means of X-ray diffraction. This study deals with the molecular structure of the EtMgBr-(−)-sparteine complex which has a high catalytic activity on the asymmetric-selective polymerization of the MBMA. Interests on the structure and the reactivity of the present complex and also on the conformation of the (−)-sparteine ligand, either one-boat or all-chair form, promoted this study.

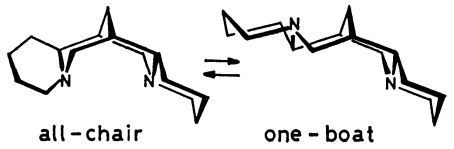

Experimental

Crystals used were obtained from a toluene solution. A crystal with approximate dimensions of $0.50\times0.50\times0.38$ mm, sealed in a thin-walled glass capillary tube under nitrogen atmosphere, was mounted on a Rigaku automated, four-circle X-ray diffractometer. The unit-cell dimensions were precisely determined by the least-squares fit using 2θ values of 25 strong reflections.

Crystal Data. $C_{17}H_{31}N_2MgBr$, M 367.7, orthorhombic space group $P2_12_12_1$, $a=11.278(2)$, $b=14.112(3)$, $c=11.746(2)$ Å, $V=1869.5(5)$ Å^3, $D_C=1.306$ g cm^{-3} for $Z=4$, μ(Mo $K\alpha$) = 23.62 cm^{-1}.

Reflection intensities were measured on the diffractometer with Zr-filtered Mo $K\alpha$ radiation by the θ-2θ scan technique ($2\theta\leqq50.5°$). The 2θ scan rate was 4° min^{-1} and the scan width $\Delta2\theta=(2.0+0.7\tan\theta)°$ Backgrounds were counted for 7.5 s at both ends of a scan. Four standard reflections measured after every 27 reflections showed less than 3% intensity fluctuations during the data collection. However the peak profiles of reflections were not so sharp, reflection intensities were rather low, and high order reflections were scarcely observed to have non-zero intensity. Of the 1937 reflections measured only 1272 had non-zero intensities. Usual Lorentz and polarization corrections were applied but absorption and extinction corrections were ignored.

Structure Solution and Refinement

The heavy atom method was applied to solve the structure. The position of the Br atom was determined from the three-dimensional Patterson function. The Mg, N, and C atoms except the C(16) were located by the subsequent Fourier synthesis. The structure was refined isotropically by the block-diagonal least-squares procedure (*HBLS* V).[7] The remaining C(16) atom could be located on the difference Fourier synthesis. Further refinement was carried out anisotropically for non-hydrogen atoms except for the C(10), C(16), and C(17) atoms, because thermal parameters of these atoms could not be refined anisotropically. Hydrogen atoms could not be located on the difference Fourier synthesis. At the final stage of the refinement the anomalous dispersion of the Br and Mg atoms[8] was considered; the R value became 0.100 for non-zero reflections ($R_w=0.103$). The final atomic positional parameters and equivalent[9] (or isotropic) tem-

† Abbreviated as EtMgBr-(−)-sparteine

†† Present address: Institute for Protein Research, Osaka University, Yamadaoka, Suita, Osaka 565.

††† Present address: Tezukayama-Gakuin Women's Junior College, Tezukayama, Sumiyoshi-ku, Osaka 558.

†††† Dodecahydro-7,14-methano-2*H*,6*H*-dipyrido[1,2-*a*:1′, 2′-*e*][1,5] diazocine.

TABLE 1. FINAL ATOMIC POSITIONAL PARAMETERS WITH THEIR ESTIMATED STANDARD DEVIATIONS IN PARENTHESES

Atom	x	y	z	B_{eq} or B/Å^2
Br	−0.04812(24)	0.56688(15)	0.41953(20)	5.4
Mg	−0.0501(7)	0.4081(5)	0.3286(6)	4.0
N(1)	0.0901(15)	0.4029(12)	0.2064(14)	4.6
N(2)	−0.1614(15)	0.4283(14)	0.1809(14)	5.1
C(1)	−0.0411(25)	0.2853(12)	0.4496(15)	5.4
C(2)	−0.2901(17)	0.4467(17)	0.2202(25)	7.0
C(3)	−0.3317(21)	0.3648(16)	0.2854(22)	6.5
C(4)	−0.3363(21)	0.2767(22)	0.2133(29)	8.5
C(5)	−0.1980(22)	0.2609(17)	0.1639(24)	6.4
C(6)	−0.1616(24)	0.3464(15)	0.1005(20)	6.3
C(7)	−0.0331(20)	0.3328(15)	0.0494(17)	5.0
C(8)	−0.0112(21)	0.4176(17)	−0.0244(18)	5.8
C(9)	−0.0044(26)	0.5053(16)	0.0568(21)	7.1
C(10)[a]	−0.1262(19)	0.5196(15)	0.1198(19)	4.8(5)
C(11)	0.0998(21)	0.4937(18)	0.1386(23)	6.3
C(12)	0.2212(26)	0.5081(20)	0.0796(23)	7.5
C(13)	0.3263(26)	0.4947(23)	0.1667(26)	8.7
C(14)	0.3194(17)	0.3991(21)	0.2177(23)	7.1
C(15)	0.1976(20)	0.3885(18)	0.2811(23)	6.2
C(16)[a]	−0.0802(37)	0.2959(27)	0.5428(32)	12.7(13)
C(17)[a]	0.0693(19)	0.3194(13)	0.1310(16)	4.2(5)

a) Refined isotropically.

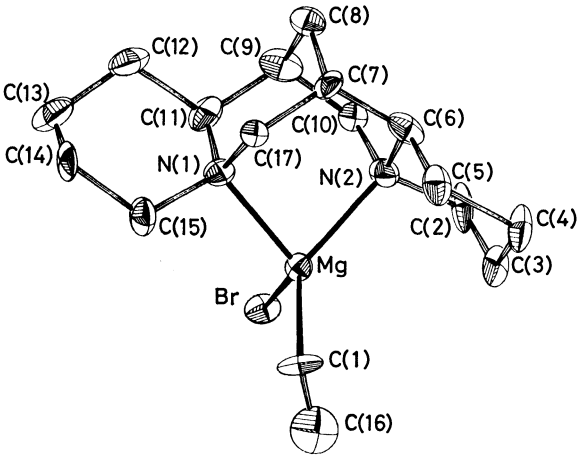

Fig. 1. A perspective view of the EtMgBr-(−)-sparteine molecule with the numbering scheme of atoms. Non-hydrogen atoms are drawn as thermal ellipsoids with 20% probability level.[11]

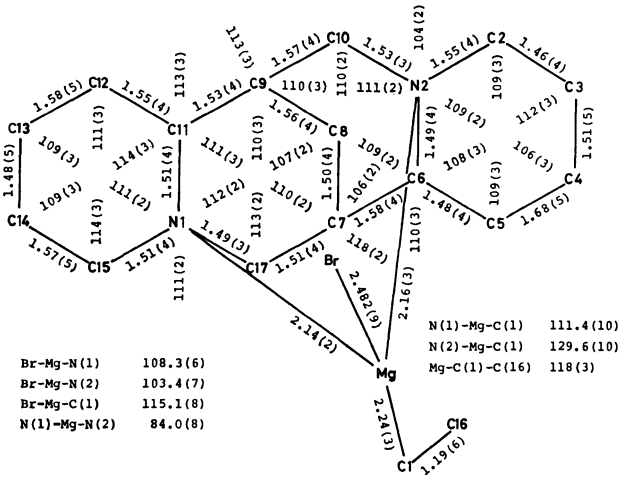

Fig. 2. Selected bond lengths (l/Å) and bond angles (ϕ/°) in the EtMgBr-(−)-sparteine molecule.

perature factors are listed in Table 1.†††††

The neutral atomic scattering factors were taken from the International Tables for X-Ray Crystallography.[10] All the computations were done on an ACOS 700 or 900 computer at the Computation Center, Osaka University.

Results and Discussion

Molecular Structure. A perspective view (*ORTEP II*)[11] of the EtMgBr-(−)-sparteine complex with the numbering scheme of atoms is presented in Fig. 1. Selected bond lengths and bond angles are listed in Fig.2.

The Mg atom is tetrahedrally coordinated by the two N atoms of the (−)-sparteine, the C atom of the Et group, and the Br atom. The N(1)–Mg–N(2) angle [84.0(8)°] is equal to that observed in EtMgBr-(−)-α-isosparteine[12] but is smaller than the corresponding angles in dichloro[(−)-sparteine] cobalt(II) [90.4(3)°],[13] dichloro[(−)-α-isosparteine] cobalt(II) [89.0(2)°],[14] and dichloro[β-isosparteine] copper(II) [90.6(2)°].[15] This can be attributed to the fact that two N atoms of the (−)-sparteine ligand are spatially fixed, and hence the longer the coordination bonds between N atoms and the central metal atom((Mg–N)$_{av}$=2.15††††††, (Co–N)$_{av}$=2.05[13], Co–N=2.07[14], and

††††† Tables of observed and calculated structure factors and anisotropic temperature factors are kept at the Chemical Society of Japan, Document No. 8321.

†††††† Present study.

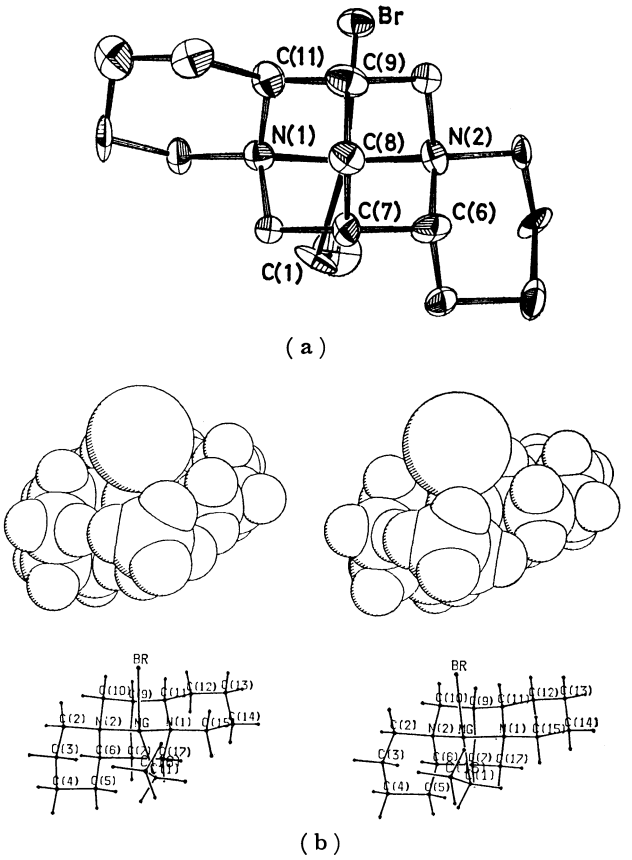

Fig. 3. (a) Molecular structure projected down along the bisector of the N(1)–Mg–N(2) angle. Non-hydrogen atoms are drawn as thermal ellipsoids with 20% probability level.[11] (b) Space-filling model of the molecule viewed up along the bisector.[17]

$(Cu–N)_{av}=1.99$[15]) is the smaller the N–Metal–N angle is expected to be. The C(1)–Mg–Br angle [115.1(8)°] in the present complex is slightly larger than the tetrahedral angle. The N(2)–Mg–C(1) [129.6(10)°] and N(2)–Mg–Br [103.4(7)°] angles largely deviated from the tetrahedral angle, whereas the N(1)–Mg–C(1) [111.4(10)°] and N(1)–Mg–Br [108.3(6)°] angles are similar to it.

Of the two possible conformations, the (−)-sparteine ligand takes the all-chair form. In addition to the bulky Br and ethyl group of the EtMgBr, the coordination of the (−)-sparteine to the Mg atom makes the space small around the N(1) atom but not the neighborhood of the N(2) as can be seen in Fig. 3. This fact may favor the selective coordination of the (*S*)-monomer to the Mg atom of the EtMgBr–(−)-sparteine at the initial stage of polymerization of the methacrylate, which is favorable to the subsequent (*S*)-monomer selection.

Crystal Structure. The packing of EtMgBr–(−)-sparteine molecules in a unit-cell is shown in Fig. 4. The dimeric association of molecules, observed in the crystal structures of Grignard reagents, $[EtMgBr, Et_3N]_2$[17] and $[EtMgBr, (i\text{-}Pr)_2O]_2$[18] is not observed. The closest intermolecular atomic contact is C(17) $(x, y, z)\cdots Br(-x, -1/2+y, 1/2-z)$ (3.62(3) Å).

A part of the cost of this study was defrayed by the Grant-in-Aid (No. 434024) for Scientific Research from the Ministry of Education, Science and Culture.

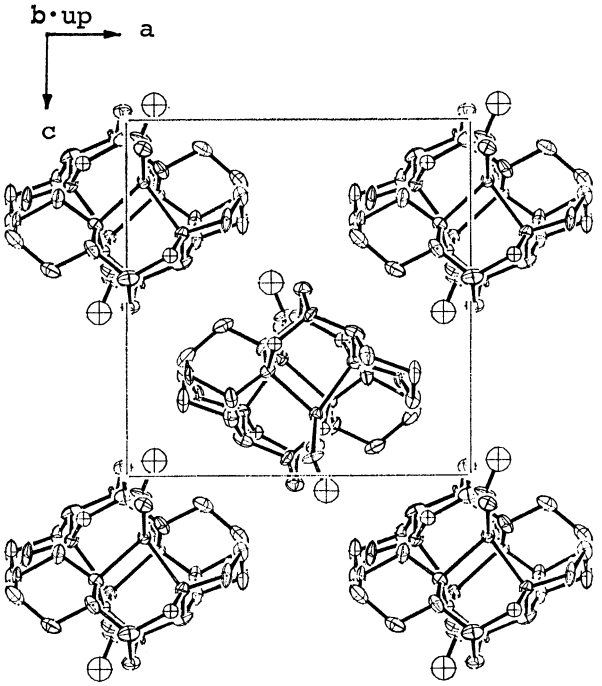

Fig. 4. The crystal structure of EtMgBr-(−)-sparteine.[11]

References

1) Y. Okamoto, K. Ohta, and H. Yuki, *Chem. Lett.*, **1977**, 617.
2) Y. Okamoto, K. Urakawa, K. Ohta, and H. Yuki, *Macromolecules*, **11**, 719 (1978).
3) Y. Okamoto, K. Ohta, and H. Yuki, *Macromolecules*, **11**, 724 (1978).
4) Y. Okamoto, K. Suzuki, K. Ohta, and H. Yuki, *J. Polym. Sci., Polym. Lett. Ed.*, **17**, 293 (1979).
5) Y. Okamoto, H. Gamaike, and H. Yuki, *Makromol. Chem.*, **179**, 1341 (1978).
6) Y. Okamoto, K. Suzuki, T. Kitayama, H. Yuki, H. Kageyama, K. Miki, N. Tanaka, and N. Kasai, *J. Am. Chem. Soc.*, **104**, 4618 (1982).
7) T. Ashida, *HBLS* V, The Universal Crystallographic Computing System-Osaka The Computation Center, Osaka Univ., (1973), p. 55.
8) "International Tables for X-Ray Crystallography," The Kynoch Press, Birmingham (1974), Vol. IV, p. 148.
9) W. C. Hamilton, *Acta Crystallogr.*, **12**, 609 (1959).
10) "International Tables for X-Ray Crystallography," The Kynoch Press, Birmingham (1974), Vol. IV, p. 71.
11) C. K. Johnson, *ORTEP* II, ORNL-5138, Oak Ridge National Laboratory, Tennessee (1976).
12) H. Kageyama, K. Miki, Y. Kai, N. Kasai, Y. Okamoto, and H. Yuki, *Acta Crystallogr., Sect. B*, **38**, 2264 (1982).
13) R. Kuroda and S. F. Mason, *J. Chem. Soc., Dalton Trans.*, **1977**, 371.
14) R. Kuroda and S. F. Mason, *J. Chem. Soc., Dalton Trans.*, **1979**, 727.
15) L. S. Childers, K. Folting, L. L. Merritt, Jr., and W. E. Streib, *Acta Crystallogr., Sect. B*, **31**, 924 (1975).
16) S. Motherwell, *PLUTO*, Cambridge Crystallographic Files User Mannual (1976).
17) J. Toney and G. D. Stucky, *J. Chem. Soc., Chem. Commun.*, **1967**, 1168.
18) A. L. Spek, P. Voorbergen, G. Schat, C. Blomberg, and F. Bickelhaupt, *J. Organomet. Chem.*, **77**, 147 (1974).

Polarizability and Electrocapillary Measurements of the Nitrobenzene-Water Interface

Takashi KAKIUCHI and Mitsugi SENDA*

Department of Agricultural Chemistry, Faculty of Agriculture, Kyoto University, Sakyo-ku, Kyoto 606

(Received September 27, 1982)

Electrocapillary curves have been measured of the interface between nitrobenzene solution of tetrabutylammonium tetraphenylborate and aqueous solution of lithium chloride using a dropping electrolyte solution electrode under the precise control of the electrical potential difference and of the ion transfer current across the interface. The nitrobenzene-water interface could be electrically polarized over the voltage span of 300 mV. The residual current was explained as due to both the transfer of tetrabutylammonium ion and tetraphenylborate ion through the interface and the charging current at the interface. The electrocapillary curve was parabolic in shape. The surface charge *vs.* potential curve derived from the electrocapillary curve agreed with that obtained from the differential capacity *vs.* potential curve of the interface. The results indicate that the interface can virtually be treated as an ideal polarized interface over a certain potential range.

This paper describes the measurements of electrocapillary curves at the polarizable interface between aqueous solution of lithium chloride and nitrobenzene solution of tetrabutylammonium tetraphenylborate by the drop time method using a dropping electrolyte solution electrode. Guastalla[1] was the first to show that an electric field across the interface between two immiscible solutions containing ions and ionic surfactants produces changes in the interfacial tension and he called his finding "electroadsorption." Since then, such phenomena have been studied mainly by Blank and Feig,[2] Blank,[3] Watanabe *et al.*,[4,5] Dupeyrat and Michel,[6] Gavach *et al.*,[7-10] Joos,[11,12] and Dupeyrat and Nakache.[13] Watanabe considered it to be electrocapillarity, while Blank and Feig and also Dupeyrat and Nakache made a distinction between electroadsorption and electrocapillarity. In most of these works, except the recent ones by Gavach *et al*,[9,10] however, the electrical potential and the current across the interface were neither controlled nor measured precisely enough to define the electrical state of the interface.

Recently, polarizability of the interface between two immiscible electrolyte solutions has been discussed on the basis of the transfer free energies of ions from one solvent to the other by Koryta *et al.*,[14] who have showed that one can endow the liquid–liquid interface with electrical polarization in a certain range of the potential difference across the interface by choosing suitable ions to be dissolved in the two phases, *e.g.*, lithium chloride in water and tetrabutylammonium tetraphenylborate (TBATPB) in nitrobenzene. Such polarizable interfaces have been extensively used in electrochemical studies[15,16] of ion transfer and electron transfer at the interface.

An interface of two immiscible electrolyte solutions, which behaves practically as an ideal polarized interface, if realized, can be a subject of rigorous thermodynamic theory of an ideal polarized interface and, hence, the electric double layer structure of the interface can be elucidated on the basis of electrocapillary measurements. The purpose of this study is to demonstrate experimentally the existence of such polarized interfaces where there is only negligible ion transfer current through the interface and to establish an experimental method for electrocapillary measurements under the precise control of the potential difference across the interface.

Experimental

A dropping electrolyte solution electrode[14] (DESE) was used to record current-potential curves and to determine electrocapillary curves at a polarized nitrobenzene-water interface. Figure 1 shows the cell configuration used in this study. An aqueous solution, 1, was dropped upward into a nitrobenzene solution, 2, from the tip of a poly(tetrafluoro-

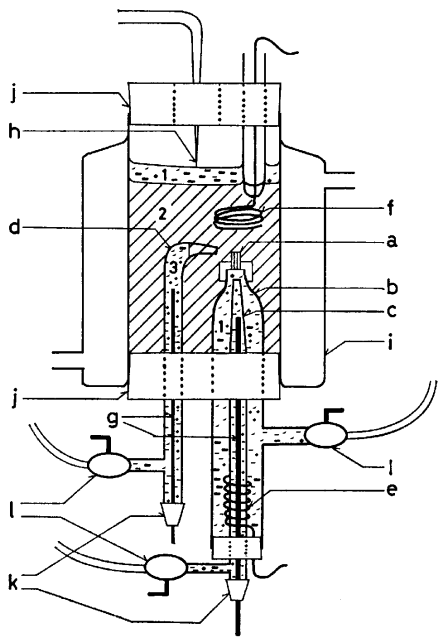

Fig. 1. Electrochemical cell with dropping electrolyte solution electrode for measuring current-potential curves and electrocapillary curves at nitrobenzene-water interface.
(1) 0.1 mol dm^{-3} LiCl aqueous solution; (2) 0.1 mol dm^{-3} TBATPB nitrobenzene solution; (3) 0.1 mol dm^{-3} TBACl aqueous solution; (a) dropping electrolyte solution electrode tip; (b) glass tube; (c and d) reference electrodes with Luggin capillaries; (e and f) auxiliary electrodes; (g) Ag/AgCl electrodes; (h) fine glass capillary; (i) water-jaketted cell; (j) silicon rubber stopper; (k) silicone rubber cap; (l) stop cock.

ethylene) (PTFE) capillary, a, whose inner diameter and length were 0.5 and 4 mm, respectively. The PTFE capillary was fitted on the top opening of a glass tube, b. By using a PTFE capillary, which neither water nor nitrobenzene wets the surface of, very reproducible drop time was achieved. The cell had four electrodes, *i.e.*, two reference electrodes (c and d) and two auxiliary electrodes(e and f) to meet with a four-electrode potentiostat[17,18] for precise control of the potential drop across the interface. The reference electrodes were Ag/AgCl electrodes, g, immersed in 0.1 mol dm^{-3} LiCl aqueous solution, 1, and in 0.1 mol dm^{-3} tetrabutylammonium chloride (TBACl) aqueous solution, 3. Luggin capillaries sensed the potential of the aqueous and nitrobenzene phases, respectively, in close proximity to the DESE. The auxiliary electrodes were coiled platinum wires. A fine glass capillary, h, was connected to an aspirator to suck off excess aqueous solution flowing out of the DESE, so that the hydrostatic pressure above the tip of the DESE was kept constant during each measurement. The cell assembly was mounted on a heavy molding board which was placed on four cushions made of rubber damper plates and soft rubber balls. This table effectively eliminated most of ambient vibration and resulted in good reproducibility of the drop time of the DESE. The cell was water-jacketed (i in Fig. 1) to maintain the temperature of the cell at 25.00±0.05 °C.

The DESE was connected to an electrolyte solution reservoir of a 200 ml seperatory funnel through a PTFE tubing of 2 mm inner diameter. In the middle of this PTFE tubing a PTFE capillary of 0.25 mm inner diameter and 6 m length was inserted to regulate the flow rate of aqueous electrolyte solution. The flow rate, v, was typically 3×10^{-4} cm^3 s^{-1} when the height of the solution reservoir, H, was 75 cm. The PTFE capillary regulator was immersed in a water bath controlled at 25.00±0.05 °C to regulate precisely the flow resistance, $\alpha=v/H$, of the PTFE capillary regulator. The flow rate was determined to the precision of 0.01×10^{-4} cm^3 s^{-1} using a 1 ml serological pipet and the α-value of the DESE was determined to be 4.63×10^{-6} cm^2 s^{-1} for 0.1 mol dm^{-3} LiCl at 25.00±0.05 °C.

For converting the drop time, t_d, to the interfacial tension, γ, we used the following two equations,[19,20] which have been derived by assuming a spherical drop:

$$\frac{\alpha t_d}{3} = \sigma^3 \ln\left(\frac{x_0(1-x)}{x(1-x_0)}\right) + \sigma^2\left(\frac{1}{x}-\frac{1}{x_0}\right) + \frac{\sigma}{2}\left(\frac{1}{x^2}-\frac{1}{x_0^2}\right) + \frac{1}{3}\left(\frac{1}{x^3}-\frac{1}{x_0^3}\right) \quad (1)$$

$$\Delta\rho g/x^3 = 2\pi r\gamma[1-r(4\pi/3)^{1/3}x] \quad (2)$$

with $\sigma=2\gamma(4\pi/3)^{1/3}/P$, $x=(3/4\pi)^{1/3}/R$ and $x_0=(3/2\pi)^{1/3}/r$, where R is the radius of a drop, r the radius of the orifice of the DESE tip, P the effective hydrostatic pressure, $\Delta\rho$ the difference between the densities of the nitrobenzene and the aqueous solution phases, and g is the accelaration of gravity. By solving these two simultaneous equations numerically, we obtain γ as a function of t_d for given values of α, r, P, and $\Delta\rho$. The density of the aqueous solution and nitrobenzene solution was determined using a Lipkin-Davison pycnometer. The r value was calibrated as 0.240 mm by using mutually saturated nitrobenzene and water at 25.0 °C, the value of 25.1 mN m^{-1} being used for the interfacial tension.[21] The drop time, typically 50 s at $H=75$ cm, was measured to the precision of 0.01 s with an electronic stopwatch. The relative standard deviation of the drop time of the DESE was 0.2% for several consecutive drops.

Since the potential difference across the interface was controlled with respect to the two reference electrodes, the electrochemical cell studied can be represented by

$$\begin{array}{ccccccc} \text{I} & \text{II} & & \text{III} & & & \\ \text{Ag} & \text{AgCl} & \text{0.1 mol dm}^{-3}\ \text{TBACl} & & & & \\ & & \text{(water)} & & & & \\ & & \text{IV} & & & & \\ & & \text{0.1 mol dm}^{-3}\ \text{TBATPB} & & & & \\ & & \text{(nitrobenzene)} & & & & \\ & & \text{V} & & \text{VI} & \text{VII} & \\ & & \text{0.1 mol dm}^{-3}\ \text{LiCl} & & \text{AgCl} & \text{Ag.} & \\ & & \text{(water)} & & & & \end{array} \quad (A)$$

The interface between the phases III and IV is a non-polarizable one and the potential drop across the interface is determined by the activities of TBA^+ ion in the two phases.[18,22,23] Therefore, the left-hand-side half cell, Ag/AgCl/III(W)/IV(NB), virtually functions as a reference electrode reversible to TBA^+ ion in the nitrobenzene phase IV. The interface III/IV was made just inside the Luggin capillary in nitrobenzene phase. The right-hand-side half cell V(W)/AgCl/Ag is reversible to Cl^- ion in the phase V. The potential applied to the cell(A), $E=E^{W-}_{O+}$, is defined by the potential of the right-hand-side reference electrode, E_{right}, with respect to that of the left, E_{left}; $E^{W-}_{O+}=E_{right}-E_{left}$, where the superscript W− and subscript O+ indicate that the reference electrodes in aqueous and nitrobenzene phases are reversible to an anion and a cation, respectively.

When one applies a potential difference across the interface between the phases IV and V by using the four electrode potentiostat, the uncompensated solution resistance between the tips of the two Luggin capillaries mostly resides in the solution thread in the PTFE capillary tip of the DESE, whose resistance was calculated to be 21 kΩ for 0.1 mol dm^{-3} LiCl at 25 °C. Since the residual current flowing through the interface was usually less than 0.2 μA in the polarization potential range (see Fig. 2 below), the iR drop across the uncompensated solution resistance should be less than 4 mV. The error in the potential control due to this iR drop was further minimized to less than 0.1 mV by using the positive feedback circuit equipped in the four-electrode potentiostat.[18]

Lithium chloride monohydrate(a Merk's spurapur grade product) was dissolved into twice distilled water to prepare the stock solution of LiCl. The concentration of LiCl was determined by potentiometric titration with a standard silver nitrate solution. A 0.1 mol dm^{-3} LiCl aqueous solution was prepared from this stock solution. TBATPB was prepared as described previously.[24] TBACl was first recrystallized from aceton–ether mixture. Then, trace impurities of iodide ion were removed from aqueous TBACl solution by metathesis with silver chloride. Nitrobenzene was distilled under reduced pressure and the middle 60% of the distillate was collected and shaken with active alumina overnight. The last treatment was important to reduce the residual current to a low level. After filtration, nitrobenzene was washed and equilibrated with twice distilled water at 25 °C. Nitrobenzene solution of TBATPB was prepared in dark immediately before use.

Results and Discussion

Current-potential Curve. Figure 2 shows a current-potential curve (d.c.polarogram) obtained with the DESE in the dark for the interface between 0.1 mol dm^{-3} LiCl aqueous solution and 0.1 mol dm^{-3} TBATPB

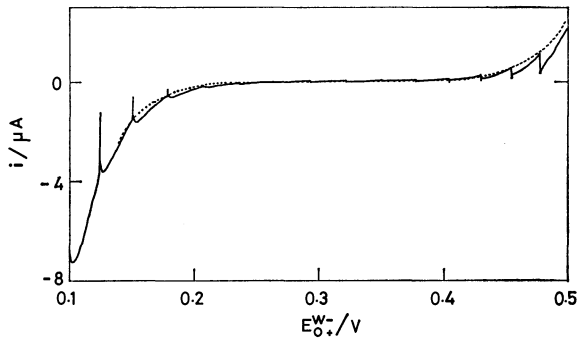

Fig. 2. Current-potential curve for the interface between 0.1 mol dm^{-3} LiCl aqueous solution and 0.1 mol dm^{-3} TBATPB nitrobenzene solution at 25 °C. (——): Experimental. The potential was scanned from 0.1 to 0.5 V with the scan rate of 0.5 mV s^{-1}. (----): calculated by Eq. 3.

nitrobenzene solution. The transfer of a positive charge from the aqueous to the nitrobenzene phase was taken as the positive direction of the current. This polarogram indicates that the current across the interface is negligible except for a trace residual current (less than 0.6 μA cm^{-2}) in the potential range between 0.22 and 0.42 V and that the interface can be polarized over a voltage span of almost 300 mV.

The standard ion transfer potentials of j ion across the water(W)–nitrobenzene(NB) interface, $\Delta^{W}_{NB}\phi^{0}_{j}$, are −0.248, 0.395, 0.372, and −0.324[25,26] for j=TBA$^+$, Li$^+$, TPB$^-$, and Cl$^-$, respectively. Since $\Delta^{W}_{NB}\phi^{0}_{TBA}$ is less negative than $\Delta^{W}_{NB}\phi^{0}_{Cl}$ and $\Delta^{W}_{NB}\phi^{0}_{TPB}$ is less positive than $\Delta^{W}_{NB}\phi^{0}_{Li}$, TBA$^+$ and TPB$^-$ ions are most easily transferable through the interface among the four ions. Accordingly, the "residual" current in the polarization potential range should be attributed to the transfer of TBA$^+$ or TPB$^-$ ion or both. Then the current increase in the positive direction at the positive extreme of the applied potential in Fig. 2 should be mainly due to the transfer of TPB$^-$ ion and the current increase in the negative direction at the negative extreme to that of TBA$^+$ ion from the nitrobenzene to the aqueous phase. The transfer of Li$^+$ and Cl$^-$ ions may be negligible compared with that of TBA$^+$ and TPB$^-$ ions in the potential range considered. It can be shown that the current-potential relationship for the transfer of TBA$^+$ and TPB$^-$ ions from the nitrobenzene to the aqueous phase, where LiCl serves as the supporting electrolyte for the mass transfer of TBA$^+$ and TPB$^-$ ions in the aqueous phase, can be expressed, in analogy to the electrolytic current at a dropping mercury electrode in the absence of supporting electrolyte,[27,28] by

$$i = 4.168Fv^{2/3}t_d^{1/6}c_sA \tag{3}$$

with

$$A = \frac{(D^{W}_{TPB})^{1/2}/q-(D^{W}_{TBA})^{1/2}/p}{1+\frac{(1-t^{NB}_{TBA})}{p}\left(\frac{D^{W}_{TBA}}{D^{NB}_{s}}\right)^{1/2}+\frac{t^{NB}_{TBA}}{q}\left(\frac{D^{W}_{TPB}}{D^{NB}_{s}}\right)^{1/2}},$$

where i is the current, v the flow rate of an aqueous solution, c_s the concentration of TBATPB in the nitrobenzene phase, t_d the drop time, t^{NB}_{TBA} the transport number of TBA$^+$ ion in the nitrobenzene phase, D_j the diffusion coefficient of j ion (j=TBA$^+$ or TPB$^-$) in the aqueous(W) and nitrobenzene(NB) phases, and p, q and D^{NB}_{s} are given by

$$p = \exp\left[\frac{F}{RT}(\Delta\phi-\Delta^{W}_{NB}\phi^{0}_{TBA})\right]$$

$$q = \exp\left[-\frac{F}{RT}(\Delta\phi-\Delta^{W}_{NB}\phi^{0}_{TPB})\right]$$

and

$$D^{NB}_{s} = \frac{2D^{NB}_{TBA}D^{NB}_{TPB}}{D^{NB}_{TBA}+D^{NB}_{TPB}},$$

where F, R, and T are used in the usual meaning. $\Delta\phi$ is the potential difference across the interface and is related to the applied potential by

$$E = E^{W-}_{O+} = \Delta\phi + E_{ref} \tag{4}$$

where E_{ref} is the constant which depends only on the reference electrode system. In deriving Eq. 3 we assumed that the surface concentrations of TBA$^+$ and TPB$^-$ ions in the two phases, $c^{W,0}_{TBA}$, $c^{NB,0}_{TBA}$, $c^{W,0}_{TPB}$, and $c^{NB,0}_{TPB}$ are related by Nernst equations:

$$\Delta\phi = \Delta^{W}_{NB}\phi^{0}_{TBA} + \frac{RT}{F}\ln\frac{c^{NB,0}_{TBA}}{c^{W,0}_{TBA}}$$

and

$$\Delta\phi = -\Delta^{W}_{NB}\phi^{0}_{TPB} - \frac{RT}{F}\ln\frac{c^{NB,0}_{TPB}}{c^{W,0}_{TPB}}$$

and that the transfer of Li$^+$ and Cl$^-$ ions across the interface is negligibly small compared with that of TBA$^+$ and TPB$^-$.

In Fig. 2 the dashed line is a theoretical polarogram which was calculated from Eq. 3 with c_s=0.1 mol dm^{-3}, t_d=50 s, v=0.00036 cm^3 s^{-1}, $D^{W}_{TBA}=D^{W}_{TPB}=5.1\times10^{-6}$ cm^2 s^{-1}, $D^{NB}_{TBA}=D^{NB}_{TPB}=2.6\times10^{-6}$ cm^2 s^{-1},[17] and E_{ref}=0.25 V. For the sake of simplicity, the diffusion potential which may exist in the vicinity of the interface was not taken into account. Agreement between the experimental curve and the theoretical one is good, indicating that the "residual" current in the polarization potential range is largely due to the transfer across the interface of the most easily transferable ions in the two phases.

From Eq. 3 we can expect that the ion transfer current becomes zero at

$$E_{i=0} = \frac{RT}{2F}\ln(D^{W}_{TBA}/D^{W}_{TPB})^{1/2} + \frac{1}{2}(\Delta^{W}_{NB}\phi^{0}_{TBA}+\Delta^{W}_{NB}\phi^{0}_{TPB}) + E_{ref}. \tag{5}$$

In the present case $E_{i=0}$ was calculated to be 0.32 V when E_{ref}=0.25 V. Thus the residual current at and in the vicinity of this potential is due to the charging current of the polarized nitrobenzene–water interface. Figure 3 shows a representative current-time curve at E=0.31 V. The current increases suddenly at the moment of a drop's birth(indicated by an arrow in Fig. 3), then decays subsequently with time. This behavior is quite similar to that of the charging current usually observed at an ideal polarized dropping mercury electrode. Since E=0.31 V is 45 mV more positive than the potential of zero charge of the interface (see below), a positive-going current is observed at

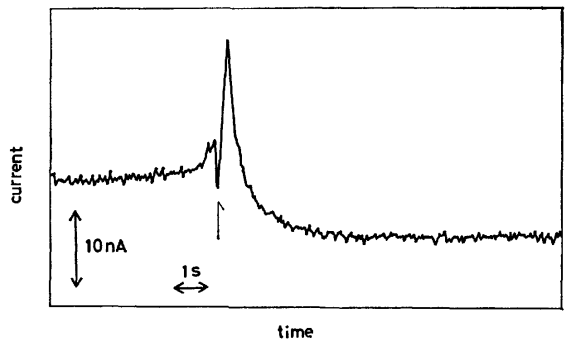

Fig. 3. Current *vs.* time curve at 0.31 V for the interface between 0.1 mol dm^{-3} LiCl aqueous solution and 0.1 mol dm^{-3} TBATPB nitrobenzene solution. The arrow indicates the instant of a drop's birth.

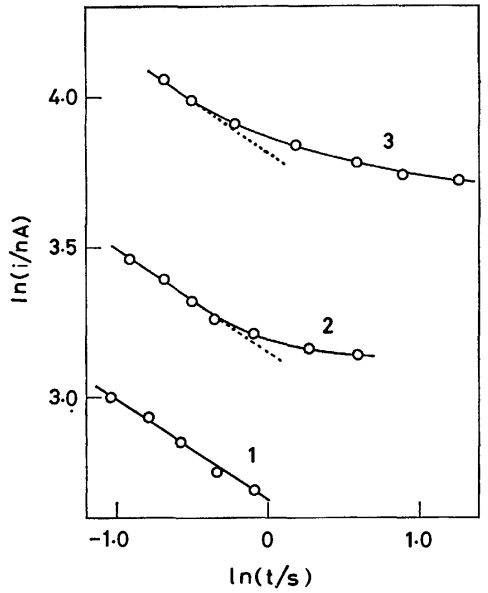

Fig. 4. log i *vs.* log t plot at 0.310(1), 0.330(2), and 0.370 V(3). Dashed lines by the curves are drawn to indicate the slope of $-1/3$.

this potential. As the drop grows and approaches to its maximum stage the residual current increases to an appreciable value, which may be attributable to residual impurities. The decaying part of the current in the current-time curves recorded at three different applied potentials are plotted in logarithmic scales in Fig. 4. At E=0.31 V the plot gives a straight line with the slope of $-1/3$, which is equal to the theoretical value for the charging current.[29] As the applied potential shifts to more positive value the slope of log i *vs.* log t curves deviates from $-1/3$ at large t, indicating that the contribution of ion transfer current (here the transfer of TPB^- ion) becomes appreciable with the increase of the applied potential.

Electrocapillary Curve. Figure 5 shows an electrocapillary curve for the interface between 0.1 mol dm^{-3} TBATPB nitrobenzene solution and 0.1 mol dm^{-3} LiCl aqueous solution. The vertical bars on the curve indicate the standard deviation for the thrice-repeated measurements. The pooled standard deviation was 0.16 mN m^{-1} in the potential range between 0.2 and 0.4 V.

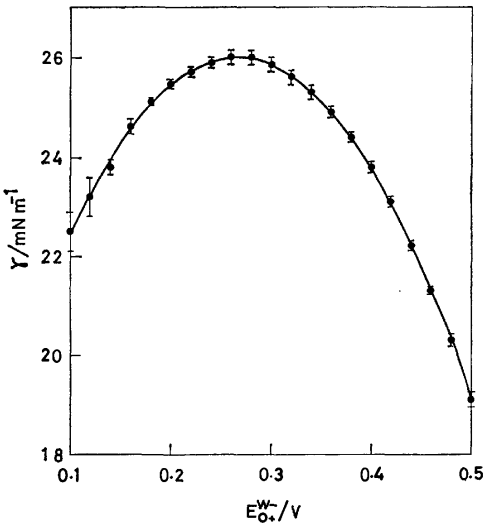

Fig. 5. Electrocapillary curve for the interface between 0.1 mol dm^{-3} LiCl aqueous solution and 0.1 mol dm^{-3} TBATPB nitrobenzene solution at 25 °C. Vertical bars indicate the standard deviation for triplicate measurements.

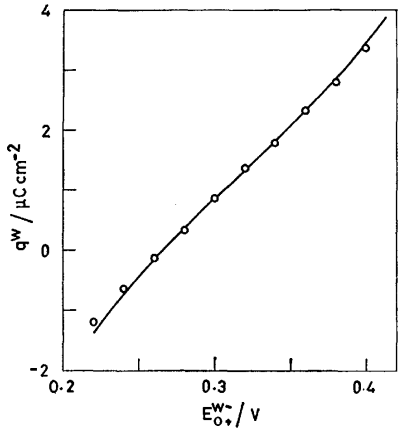

Fig. 6. Comparison of surface charge densities in aqueous solution side obtained from the differentiation of the electrocapillary curve (○) and from the integration of differential capacity curve (—) for the interface between 0.1 mol dm^{-3} LiCl aqueous solution and 0.1 mol dm^{-3} TBATPB nitrobenzene solution.

Thermodynamic theory of ideal polarized interface between two immiscible[30] or partially miscible[31] electrolyte solutions gives

$$-\left(\frac{\partial\gamma}{\partial E^{W-}_{O+}}\right)_{T,P,\mu} = q^W = -q^{NB}$$
$$= F(\Gamma^W_{Li}-\Gamma^W_{Cl}) = F(\Gamma^{NB}_{TPB}-\Gamma^{NB}_{TBA})$$

and

$$-\left(\frac{\partial^2\gamma}{\partial E^{W-2}_{O+}}\right)_{T,P,\mu} = \left(\frac{\partial q^W}{\partial E^{W-}_{O+}}\right)_{T,P,\mu} = C_d,$$

where q^W and q^{NB} are the surface charge densities in the aqueous and the nitrobenzene solution side, respectively, Γ^α_j the surface concentration of j ion in the aqueous(α=W) or the nitrobenzene(α=NB) solution side, C_d the differential capacity of the interface.

The electrocapillary curve was numerically differentiated using the moving quadratic fitting method.[32] The resultant q^{W} *vs.* E^{W}_{O+} curve is shown in Fig. 6, giving the potential of the electrocapillary maximum or the potential of zero charge, $E_{pzc}=0.265$ V. Also plotted in Fig. 6 are the surface charge density data calculated from the differential capacity *vs.* potential curve obtained for the same interface using an a.c. polarographic method.[33] Agreement between the two results is excellent. These results indicate that the interface virtually behaves as an ideal polarized interface.

The present study experimentally demonstrates that the interface between two immiscible electrolyte solutions can be electrically polarized in a certain potential range by choosing suitable electrolytes in the two phases. The residual current can be explained as due to the minute ion transfer across the interface of the most easily transferable ion or ions present in the two phases as well as the charging current of the interface. The present study also shows that the thermodynamic theory of ideal polarized interface can be applied to the interface for elucidating its equilibrium properties in a certain potential range, that is, the potential range where disturbance in the double layer structure caused by the transfer of ion or ions across the interface appears to be not appreciable. Subsequent papers will describe some detailed structure of the electrical double layer at the nitrobenzene–water interface that has been elucidated on the basis of electrocapillarity measurements.

This work was supported by Grant-in-Aid for Scientific Research No. 56104004 from the Ministry of Education, Science and Culture of Japan.

References

1) J. Guastalla, "Proc. Second International Congress of Surface Activity III," Butterworths, London (1957), p. 112.
2) M. Blank and S. Feig, *Science*, **141**, 1173 (1963).
3) M. Blank, *J. Colloid Interface Sci.*, **22**, 51 (1966).
4) A. Watanabe, M. Matsumoto, H. Tamai, and R. Gotoh, *Kolloid Z. Z. Polym.*, **220**, 152 (1967).
5) A. Watanabe and H. Tamai, *Hyomen*, **13**, 67 (1975).
6) M. Dupeyrat and J. Michel, *J. Colloid Interface Sci.*, **29**, 605 (1969).
7) C. Gavach, *Experimentia Suppl.*, **18**, 321 (1971).
8) B. d'Epenoux and C. Gavach, *J. Colloid Interface Sci.*, **56**, 138 (1976).
9) C. Gavach, P. Seta, and B. d'Epenoux, *J. Electroanal. Chem. Interfacial Electrochem.*, **83**, 225 (1977).
10) M. Gros, S. Grom, and C. Gavach, *J. Electroanal. Chem. Interfacial Electrochem.*, **89**, 29 (1978).
11) P. Joos and M. Van Bockstacle, *J. Phys. Chem.*, **80**, 1573 (1976).
12) Y. Verburgh and P. Joos, *J. Colloid Interface Sci.*, **74**, 384 (1980).
13) M. Dupeyrat and E. Nakache, *J. Colloid Interface Sci.*, **73**, 332 (1980).
14) J. Koryta, P. Vanýsek, and M. Březina, *J. Electroanal. Chem. Interfacial Electrochem.*, **75**, 211 (1977).
15) Z. Samec, V. Mareček, and J. Weber, *J. Electroanal. Chem. Interfacial Electrochem.*, **100**, 841 (1979).
16) Z. Samec, V. Mareček, and J. Weber, *J. Electroanal. Chem. Interfacial Electrochem.*, **103**, 11 (1979).
17) Z. Samec, V. Mareček, J. Koryta, and M. W. Khail, *J. Electroanal. Chem. Interfacial Electrochem.*, **83**, 393 (1977).
18) M. Senda, T. Kakutani, and T. Osakai, *Denki Kagaku*, **49**, 322 (1981).
19) J. M. Los and D. W. Murray, "Adv. in Polarography," ed by I. S. Longmuir, Pergamon, London (1960), Vol. 2, p. 425.
20) G. S. Smith, *Trans. Faraday Soc.*, **47**, 63 (1961).
21) D. S. Donachue and F. E. Bartell, *J. Phys. Chem.*, **56**, 480 (1952).
22) Le Quoc Hung, *J. Electroanal. Chem. Interfacial Electrochem.*, **115**, 159 (1980).
23) T. Kakiuchi and M. Senda, in preparation.
24) T. Kakutani, T. Osakai, and M. Senda, *Bull. Chem. Soc. Jpn.*, **56**, 991 (1983).
25) J. Rais, *Collect. Czech. Chem. Commun.*, **36**, 3253 (1971).
26) J. Rais, P. Selucký, M. Kyrš, *J. Inorg. Nucl. Chem.*, **38**, 1376 (1976).
27) D. MacGillavry, *Recl. Trav. Chim. Pays-Bas*, **56**, 1039 (1937).
28) I. Tachi and M. Senda, *Denki Kagaku*, **21**, 575 (1953).
29) D. Ilkovič, *Collect. Czech. Chem. Commun.*, **8**, 170 (1936).
30) M. Senda and T. Kakiuchi, paper presented at the 27th Annual Meeting on Polarography, Oct. 1981 (Yokohama), abstract: *Rev. Polargr. (Kyoto)*, **27**, 49 (1981).
31) T. Kakiuchi and M. Senda, in preparation.
32) P. R. Mohilner and D. M. Mohilner, "Computers in Chemistry and Instrumentation," ed by J. S. Mattson, H. B. Mark, Jr., and H. C. MacDonald, Jr., Marcel Dekker, New York (1972), Vol. 2, p. 3.
33) T. Osakai, T. Kakutani, T. Kakiuchi, and M. Senda, paper presented at the 27th Annual Meeting on Polarography, Oct. 1981 (Yokohama), abstract: *Rev. Polarogr. (Kyoto)*, **27**, 51 (1981).

 © 1983 The Chemical Society of Japan Bull. Chem. Soc. Jpn., 56, 1327—1336 (1983)

Polarized Raman and Infrared Spectra of Tetramethyl- and 2,6-Dimethylpyrazines

Yoshimi Ishibashi, Fumiko Arakawa, Hiroko Shimada,* and Ryoichi Shimada†

Department of Chemistry, Faculty of Science, Fukuoka University, Nanakuma, Jonan-ku, Fukuoka 814

† *Department of Chemistry, Faculty of Science, Kyushu University 33, Hakozaki, Higashi-ku, Fukuoka 812*

(Received September 27, 1982)

The polarized Raman and infrared spectra of tetramethyl- and 2,6-dimethylpyrazines were studied. Relative intensities of the non-totally symmetric Raman bands for the tetramethylpyrazine crystal were calculated assuming the oriented gas model. Assignments of the fundamental vibrations for tetramethyl- and 2,6-dimethylpyrazines were made through the expected and observed polarization behaviors of the Raman and infrared bands and also through the normal coordinate calculation.

Although the Raman and infrared spectra of pyrazine were studied by many workers,[1-7] only a few investigations were made on the vibrational spectra of methyl-substituted pyrazines. Oertel and Myhre[8] and Bus *et al.*[9] discussed qualitative frequency shifts of the Raman and infrared bands caused by methyl substitution. Watanabe *et al.*[10] studied very recently the normal vibrations of 2-methylpyrazine based on the polarization behaviors of the Raman and infrared bands and on the normal coordinate calculation. Niimori *et al.*,[11] Lim *et al.*,[12] and Hirota *et al.*[13] investigated the natures of the lowest triplet states of tetramethyl- and 2,6-dimethylpyrazines through the kinetic and vibrational analyses of the phosphorescence emissions. They made tentative assignments of the normal vibrations without studies of the vibrational spectra.

In this work, the Raman and infrared spectra of tetramethyl- and 2,6-dimethylpyrazines were investigated and assignments of the normal vibrations were made.

Experimental

Material. The samples, tetramethyl- and 2,6-dimethylpyrazines, obtained from Aldrich Chemical Co. were purified by zone-refining of about 100 passages followed by sublimation under reduced pressure.

Optical Measurement. The polarization behavior of the Raman spectrum was observed in molten and single crystal phases with a JEOL 400 T Laser Raman Spectrophotometer. The sample was excited with the 514.5 nm line from an Ar^+ ion laser. A well-grown single crystal of tetramethylpyrazine obtained by the Bridgman method was cut along the cleavage ab plane, and the a and b crystal axes were determined by observation of the birefringence. Then the crystal was cut along the ac and bc planes and a cubic sample of about $(7\text{ mm})^3$ was obtained. As tetramethylpyrazine sublimates very quickly, Canada balsam was spread over the whole surface of the crystal sample. The method of measurement of the polarized Raman spectrum was exactly the same as that described previously.[14] Since the crystal structure of 2,6-dimethylpyrazine has not been studied yet and the crystal melts by irradiation of the laser beam at room temperature, the polarized Raman spectrum was measured in the following way. The signle crystal grown in a glass tube of about 3 mm in diameter by the Bridgman method was held in a capillary cell system of JEOL Model RS-VTC 41 in such a way that the direction of the crystal growth orients parallel to the polarization direction of the excitation laser beam. The temperature of the cell was kept at 0 °C. The Raman scattering was observed at right angles with the excitation light beam. The Raman spectrum polarized parallel to the crystal growth direction is referred to as // spectrum and the spectrum polarized perpendicular to as $\perp$ spectrum. The polarized Raman spectrum was measured for two crystal orientations. In the first orientation a sharp band at 1534 cm^{-1}, which is strong and depolarized in molten phase, appears strongly in the // spectrum and in the second orientation the 1534 cm^{-1} band appears strongly in the $\perp$ spectrum.

The infrared spectrum was observed in single crystal, liquid, vapor, and CCl_4 or CS_2 solution with a Hitachi Infrared Spectrophotometer Model 345 over the range of 4000 to 200 cm^{-1}. The single crystal was prepared in the following way. The sample was melted on a KRS-5 plate and covered with another hot KRS-5 plate. Then the two plates were put on a heated brass block and allowed to cool gradually. The crystal formed between two plates was held between two sheets of polaroid films whose polarization directions were set at right angles to each other and a single crystal portion was selected. The rest portion of the crystal was masked with a sheet of black paper. The polarized infrared spectrum was measured with the incident lights polarized parallel and perpendicular to the crystal growth direction. The first spectrum is referred to as // and the second to as $\perp$ spectrum.

Normal Coordinate Calculation

A normal coordinate calculation was performed through the standard ***GF*** matrix method with a FACOM M-200 computer at the Computer Center of Kyushu University. The structural parameter of the tetramethylpyrazine molecule was taken from the data given by Braam *et al.*[15] Since the molecular structure of 2,6-dimethylpyrazine has not been studied yet, the structural parameters of the pyrazine ring and methyl group were assumed to be the same as the data given by Wheatley[16] and by Keidel and Bauer,[17] respectively.

The ***F*** matrix elements for the in-plane vibrations were evaluated with the potential field of an improved modification of the Urey-Bradley force field.[14,18] The potential field is given by

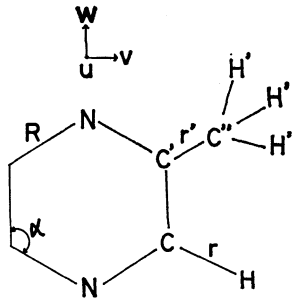

Fig. 1. Symbols for the atoms and internal coordinates.

$$V = V_{UB} + \rho[\overset{6}{\Sigma}(\Delta R,\ \Delta R)_o - \overset{6}{\Sigma}(\Delta R,\ \Delta R)_m + \overset{3}{\Sigma}(\Delta R,\ \Delta R)_p] + \Sigma k^o(\Delta r,\ \Delta r) + \Sigma k^m(\Delta r,\ \Delta r) + \Sigma h^m(\Delta R,\ \Delta\alpha) + \Sigma f^o(\Delta\alpha,\ \Delta\alpha),$$

where the symbols such as V_{UB} are the same as those used in the previous paper.[14,18] The symbols given for atoms and internal coordinates are shown in Fig. 1. For the out-of-plane vibrations the valence force field and ϕ type torsional coordinates were used. The notations of the force constants Q, q, P, p, and t are the same as those given by Whiffen.[19] In the case of the out-of-plane vibration, R and r' refer to the torsional coordinates constructing the ring and side bond, respectively. Procedure of the calculation was exactly the same as described in the previous paper.[14,18]

Calculation of Derived Polarizability Tensors

Tetramethylpyrazine crystallizes in the orthorhombic space group D_{2h}^{15} with four molecules in the unit cell, each molecule being located at the site of symmetry C_i.[15,20] The projection of the crystal structure on the ab plane is shown in Fig. 2. No factor group splitting was observed for the bands due to molecular vibrations and thus, the relationship between the derived polarizability tensors for the free molecule and crystal was derived on the basis of the simple oriented gas model. Evaluation of the matrix elements of the derived polarizability tensors of tetramethylpyrazine was made following the procedure applied for the naphthalene and anthracene crystals by Ito *et al.*[21] The derived polarizability tensor of a free molecule i with respect to the crystal-fixed coordinates is given by

$$\alpha'_{m_i}(Q_\lambda) = \boldsymbol{T}_i\, \alpha'_m(Q_\lambda)\, \tilde{\boldsymbol{T}}_i,$$
$$i = 1,2,3,4,$$

where $\alpha'_m(Q_\lambda)$ is the derived polarizability tensor of a free molecule with respect to a normal vibration Q_λ, and $\boldsymbol{T}$ the transformation matrix between the molecule-fixed u, v, w and crystal-fixed a, b, c coordinates. Using the assumption of the oriented gas model and symmetry coordinates S_{Ag}, S_{B1g}, S_{B2g}, and S_{B3g} appropriate to the four molecule unit cell, the derived polarizability tensors with respect to the unit cell vibrations are given for each symmetry species by

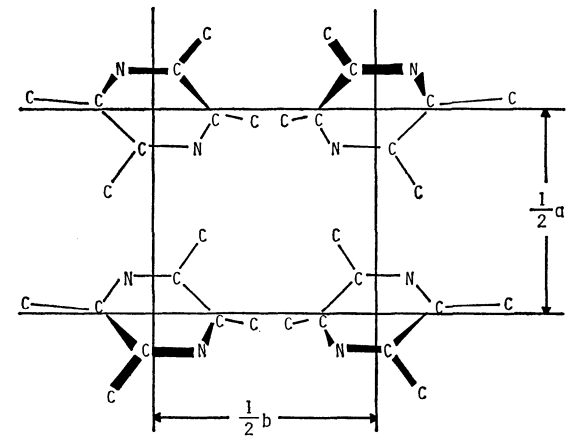

Fig. 2. Projection of the tetramethylpyrazine crystal on the ab plane.

$$\alpha'_u(S_{Ag}) = \begin{vmatrix} A_{aa} & 0 & 0 \\ 0 & A_{bb} & 0 \\ 0 & 0 & A_{cc} \end{vmatrix},$$

$$\alpha'_u(S_{B_{1g}}) = \begin{vmatrix} 0 & A_{ab} & 0 \\ A_{ba} & 0 & 0 \\ 0 & 0 & 0 \end{vmatrix},$$

$$\alpha'_u(S_{B_{2g}}) = \begin{vmatrix} 0 & 0 & A_{ac} \\ 0 & 0 & 0 \\ A_{ca} & 0 & 0 \end{vmatrix},$$

$$\alpha'_u(S_{B_{3g}}) = \begin{vmatrix} 0 & 0 & 0 \\ 0 & 0 & A_{bc} \\ 0 & A_{cb} & 0 \end{vmatrix},$$

where A's are functions of the direction cosines and the elements of the derived polarizability tensors of a free molecule.

According to the character table and selection rules for the D_{2h} molecule, we derived simple analytical expressions of A's for the vibrations belonging to different species of the molecule. These results are given in Table 1.

Results and Discussion

The force constants finally obtained after several iterative calculations for the in-plane and out-of-plane vibrations of tetramethyl- and 2,6-dimethylpyrazines are given in Table 2. The calculated vibrational frequencies and modes are given in Table 3, together with the experimental results. The molecular structures of tetramethyl- and 2,6-dimethylpyrazines were assumed to belong to the point groups D_{2h} and C_{2v}, respectively. The u axis is taken perpendicular to the molecular plane and the v and w axes in the plane with the w axis passing through the nitrogen atoms. The moments of inertia calculated from the molecular structures and the expected rotational envelopes for the infrared bands in vapor phase are given in Table 4. The depolarization measurements of the Raman spectra observed in molten phase and polarized Raman

TABLE 1. ELEMENTS OF THE DERIVED POLARIZABILITY TENSORS OF TETRAMETHYLPYRAZINE

	b_{1g}	b_{2g}	b_{3g}
A_{aa}	$2a_u^{\dagger}a_v\alpha'_{uv}$	$2a_ua_w\alpha'_{uw}$	$2a_va_w\alpha'_{vw}$
A_{bb}	$2b_ub_v\alpha'_{uv}$	$2b_ub_w\alpha'_{uw}$	$2b_vb_w\alpha'_{vw}$
A_{cc}	$2c_uc_v\alpha'_{uv}$	$2c_uc_w\alpha'_{uw}$	$2c_vc_w\alpha'_{vw}$
A_{ab}	$(a_ub_v+a_vb_u)\alpha'_{uv}$	$(a_ub_w+a_wb_u)\alpha'_{uw}$	$(a_vb_w+a_wb_v)\alpha'_{vw}$
A_{ac}	$(a_uc_v+a_vc_u)\alpha'_{uv}$	$(a_uc_w+a_wc_u)\alpha'_{uw}$	$(a_vc_w+a_wc_v)\alpha'_{vw}$
A_{bc}	$(b_uc_v+b_vc_u)\alpha'_{uv}$	$(b_uc_w+b_wc_u)\alpha'_{uw}$	$(b_vc_w+b_wc_v)\alpha'_{vw}$
	a_g		
A_{aa}	$a_u^2\alpha'_{uu}+a_v^2\alpha'_{vv}+a_w^2\alpha'_{ww}$		
A_{bb}	$b_u^2\alpha'_{uu}+b_v^2\alpha'_{vv}+b_w^2\alpha'_{ww}$		
A_{cc}	$c_u^2\alpha'_{uu}+c_v^2\alpha'_{vv}+c_w^2\alpha'_{ww}$		
A_{ab}	$a_ub_u\alpha'_{uu}+a_vb_v\alpha'_{vv}+a_wb_w\alpha'_{ww}$		
A_{ac}	$a_uc_u\alpha'_{uu}+a_vc_v\alpha'_{vv}+a_wc_w\alpha'_{ww}$		
A_{bc}	$b_uc_u\alpha'_{uu}+b_vc_v\alpha'_{vv}+b_wc_w\alpha'_{ww}$		

† a_u, a_v,$\cdots c_w$ are the direction cosines of the a and u, a and v,$\cdots$c and w axes, respectively.

TABLE 2. FORCE CONSTANTS FOR THE IN-PLANE AND OUT-OF-PLANE VIBRATIONS OF TETRAMETHYL- AND 2,6-DIMETHYLPYRAZINES

K_{N-C}	5.6 J/dm^2	H_{N-C-H}	0.24 J/dm^2	ρ	0.24 J/dm^2	P_H	0.31 aJ/rad^2
$K_{N-C'}$	5.4	$H_{C'-C''-H'}$	0.29	$k^o_{r',r'}$	0.20	$q^o_{R,R}$	−0.01
$K_{C-C'}$	5.0	$H_{H'-C''-H'}$	0.53	$k^o_{r',r}$	0.07	$q^o_{r',r'}$	0.03
$K_{C'-C''}$	3.0	$F_{C'\cdots C'}$	0.90	$k^m_{r',r'}$	0.20	$q^m_{R,R}$	−0.01
K_{C-H}	4.5	$F_{N\cdots C}$	0.55	$k^m_{r',r}$	0.06	$p^o_{C'',C''}$	0.05
$K_{C''-H'}$	4.74	$F_{C'\cdots N}$	0.70	$h^m_{R,\alpha}$	−0.12 pJ/dm rad	$p^o_{C'',H}$	0.055
$H_{C'-N-C'}$	0.30	$F_{C\cdots C}$	0.90	$f^o_{\alpha,\alpha}$	0.10 aJ/rad^2	$p^m_{C'',C''}$	−0.05
$H_{N-C'-C}$	0.55	$F_{N\cdots C''}$	0.90	$Q_{N-C'}$	0.16	$p^m_{H,H}$	−0.055
H_{C-N-C}	0.30	$F_{C\cdots C''}$	0.48	$Q_{C'-C'}$	0.22	$t^o_{R,C''}$	−0.04
$H_{N-C-C'}$	0.45	$F_{C'\cdots H}$	0.50	$Q_{C-C'}$	0.22	$t^m_{R,C''}$	−0.05
$H_{N-C'-C''}$	0.25	$F_{N\cdots H}$	0.41	Q_{N-C}	0.20	$t^o_{R,H}$	−0.02
$H_{C-C'-C''}$	0.22	$F_{C'\cdots H'}$	0.20	$Q_{C'-C''}$	0.11	$t^m_{R,H}$	−0.02
$H_{C'-C-H}$	0.25	$F_{H'\cdots H'}$	−0.20	$P_{C''}$	0.28		

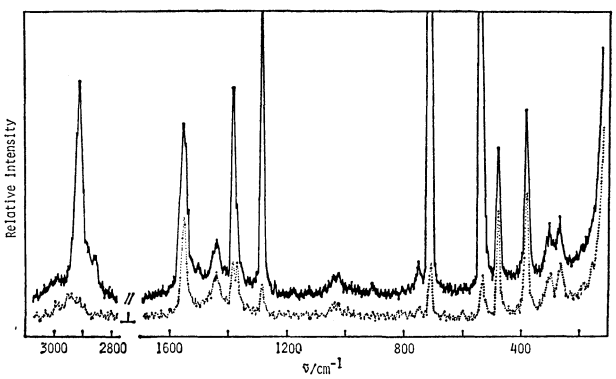

Fig. 3. Depolarization measurement of the Raman spectrum of tetramethylpyrazine.

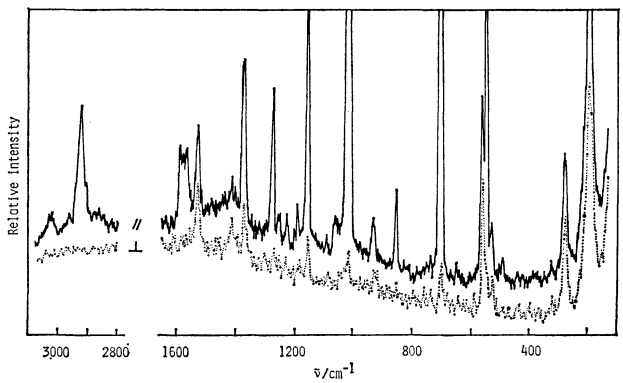

Fig. 4. Depolarization measurement of the Raman spectrum of 2,6-dimethylpyrazine.

spectra observed in single crystals of tetramethyl- and 2,6-dimethylpyrazines are shown in Figs. 3, 4, 5, and 6, respectively. The polarized Raman spectrum of tetramethylpyrazine was denoted with two symbols such as ab as used in the previous paper.[14] The first letter refers to the direction of polarization of the excitation light and the second to that of the scattering light.

The polarized Raman spectra of 2,6-dimethylpyrazine observed for the two different orientations of the crystal described in the experimental section are shown in Figs. 6 (A) and (B). We denote type α for the band whose intensity is stronger in the // spectrum than in the $\perp$ spectrum and type β for the band whose intensity is *vice versa*. The polarization behavior of a Raman band is represented by two symbols such as $\alpha\beta$, where the first and second letters refer to the polarization behaviors observed in the first and second crystal orientations and shown in Figs. 6 (A) and (B), respectively. For example, the polarization behavior

Table 3. Normal vibrations of 2,6-dimethyl- and tetramethylpyrazines

Symmetry species		Mode	2,6-Dimethylpyrazine		Tetramethylpyrazine	
C_{2v}	D_{2h}		Obsd $\tilde{\nu}$/cm^{-1}	Calcd $\tilde{\nu}$/cm^{-1}	Obsd $\tilde{\nu}$/cm^{-1}	Calcd $\tilde{\nu}$/cm^{-1}
a_1	a_g	ν_{8a} Ring	1587	1583	1547	1543
		ν_2 ϕ-CH_3 str.	1197	1210	1283	1277
		ν_1 Ring	709	706	715	734
		ν_{6a} Ring	556	548	530	531
		ν_{9a} CH_3 bend.[a]	1159	1147	296	279
	b_{1u}	ν_{19a} Ring	1450	1460	1440	1439
		ν_{12} Ring	1020	1028	1220	1207
		ν_{13} ϕ-CH_3 str.[a]	3030	3034	680	666
		ν_{18a} CH_3 bend.	420	425	310	328
b_2	b_{3g}	ν_{8b} Ring	1534	1540	1510	1522
		ν_{7b} ϕ-CH_3 str.[a]	2975	2983	1050	1069
		ν_3 CH_3 bend.[a]	1254	1240	600	580
		ν_{6b} Ring	568	559	478	465
	b_{2u}	ν_{19b} Ring	1417	1415	1410	1404
		ν_{14} Ring	1305	1304	1330	1322
		ν_{20b} ϕ-CH_3 str.	935	940	810	830
		ν_{15} CH_3 bend.	285	289	270	282
b_1	b_{2g}	ν_4 Ring	675	673	750	749
		ν_5 CH_3 wag.[a]	747	752	275	263
		ϕ-CH_3 tor.				91
	b_{3u}	ν_{16b} Ring	445	453	457	471
		ν_{11} CH_3 wag.	198	196		191
		ϕ-CH_3 tor.		160		130
a_2	b_{1g}	ν_{10a} CH_3 wag.	220	224	380	381
		ϕ-CH_3 tor.	190	171		214
	a_u	ν_{16a} Ring	415	410	550	545
		ν_{17a} CH_3 wag.[a]	955	940		268
		ϕ-CH_3 tor.				79
		Characteristic vibrations of CH_3 group				
a_1	a_g	Antisym. C–H str.			2990	2968
		Antisym. C–H str.			2930	2940
		Sym. C–H str.	2926	2921	2725	2725
		CH_3 degen. def.			1440	1441
		CH_3 sym. def.	1378	1379	1383	1375
		CH_3 rock.	856	847	920	938
	b_{1u}	Antisym. C–H str.			2985	2968
		CH_3 sym. def.			1360	1363
b_2	b_{3g}	CH_3 degen. def.			1430	1442
		CH_3 sym. def.			1367	1357
	b_{2u}	Antisym. C–H str.	2860	2863	2950	2968
		Antisym. C–H str.			2925	2940
		Sym. C–H str.	2915	2921		
		CH_3 degen. def.	1486	1486	1460	1452
		CH_3 sym. def.	1350	1362	1378	1364
		CH_3 rock.			990	970
b_1		CH_3 degen. def.	1480	1484		
		CH_3 rock.	880	884		
	b_{1g}	CH_3 degen. def.			1450	1443

a) CH_3 is replaced by H in the case of 2,6-dimethylpyrazine.

TABLE 4. POLARIZATION BEHAVIORS OF THE RAMAN AND INFRARED BANDS OF TETRAMETHYL- AND 2,6-DIMETHYLPYRAZINES

		Tetramethylpyrazine								2,6-Dimethylpyrazine			
Moment of inertia 10^{-45} kg m^2						I_w 7.61	I_v 3.80	I_u 11.2	I_w 4.32		I_u 6.49	I_v 2.27	
Symmetry species of vibration		a_g	b_{1g}	b_{2g}	b_{3g}	a_u	b_{1u}	b_{2u}	b_{3u}	a_1	a_2	b_1	b_2
Infrared	Vapor (Rotational band type)						B	A	C	B		C	A
	Crystal						I[a]	II[a]	III[a]	II[a]		III[a]	I[a]
Raman	Liquid	p	dp	dp	dp					p	dp	dp	dp
	Crystal		cc ab	aa cc	bb cc					$\alpha\alpha$[a]	$\beta\beta$[a]	$\alpha\beta$[a]	

a) These polarization behaviors were experimentally determined by comparison with the band envelope in the infrared vapor spectrum.

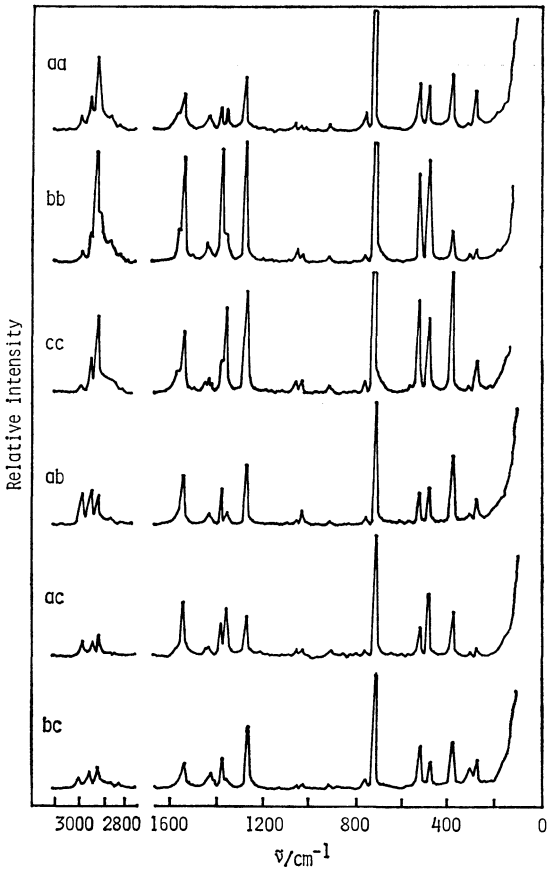

Fig. 5. Polarized Raman spectrum of the tetramethylpyrazine single crystal.

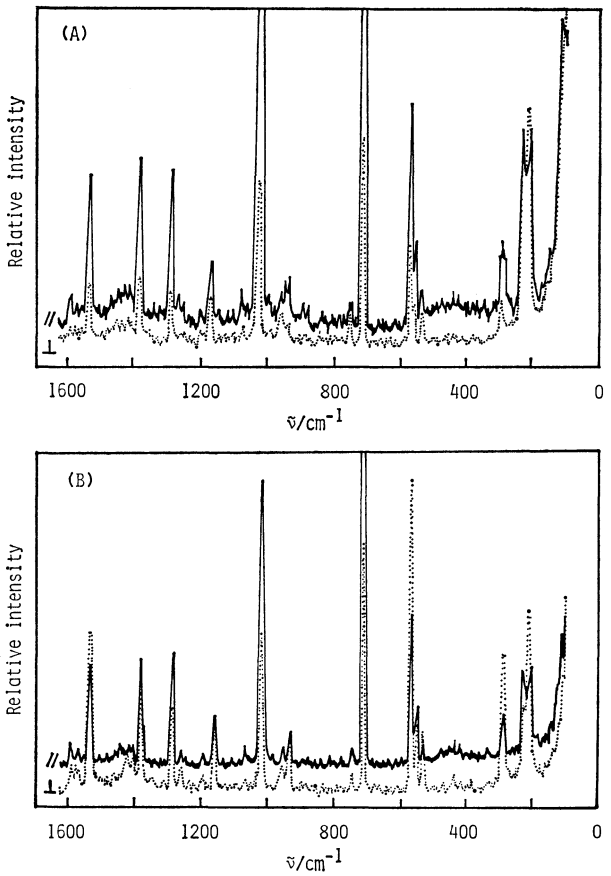

Fig. 6. Polarized Raman spectrum of the 2,6-dimethylpyrazine single crystal. For the polarization behaviors of the (A) and (B), see text.

of the 1534 cm^{-1} band is represented by $\alpha\beta$. The observed polarization behaviors of the non-totally symmetric Raman bands can be classified into three types $\alpha\alpha$, $\beta\beta$, and $\alpha\beta$ through which each Raman band can be experimentally assigned to a certain symmetry species.

The polarized infrared spectra of tetramethyl- and 2,6-dimethylpyrazines are shown in Figs. 7 and 8, respectively. The infrared crystal bands can be classified into three types I, II, and III based on their polarization behaviors. In the first type, the intensities of the // and $\perp$ components of the bands are nearly equal to each other. In the second type, the intensity of the // component is stronger than that of the $\perp$ one, and in the third type, the intensity of the $\perp$ component is much stronger than that of the // one.

Tetramethylpyrazine. The direction cosines between the crystal and molecular axes were calculated using the X-ray diffraction data given by Braam *et al.*[15] and the matrix elements of the derived polarizability tensor listed in Table 1 were evaluated. Squares of the calculated elements of the derived polarizability tensors, which are proportional to the Raman intensities, are given in Table 5 for the non-totally g symmetric vibrations. In this calculation,

Table 5. Squared values of the elements of the derived polarizability tensors for tetramethylpyrazine

	b_{1g}	b_{2g}	b_{3g}
$(A_{aa})^2$	0.19	0.76	0.10
$(A_{bb})^2$	0.08	0.06	0.91
$(A_{cc})^2$	0.53	0.39	0.41
$(A_{ab})^2$	0.40	0.15	0.05
$(A_{ac})^2$	0.10	0.01	0.24
$(A_{bc})^2$	0.10	0.23	0.00

values of the derived polarizability tensors of the free molecule, α'_{uv}, α'_{uw}, and α'_{vw}, are taken to be 1 in order to discuss the relative intensities of the Raman bands belonging to a certain symmetry species. It is expected from Table 5 that the b_{1g} vibrations appear strongly in the cc and ab spectra, the b_{2g} vibrations in the aa and cc spectra and the b_{3g} vibrations in the bb and cc spectra. These expected polarization behaviors of the Raman bands are given in Table 4.

a_g Species: Strongly polarized Raman bands observed at 1547, 1383, 1283, 715, and 530 cm^{-1} in the depolarization measurements were directly ascribed to the a_g vibrations and assigned to the ν_{8a}, ν_{CH_3} symmetric deformation, ν_2(ϕ-CH_3 stretching), ν_1, and ν_{6a} vibrations, respectively based on the calculation. A very broad and almost depolarized Raman band observed around 300 cm^{-1} in liquid phase splits into two bands at 305 and 296 cm^{-1} in the single crystal Raman spectrum. The polarization behavior of the 305 cm^{-1} band corresponds to the b_{3g} vibration, while that of the 296 cm^{-1} band does not correspond to any non-totally symmetric vibrations. Therefore, the 296 cm^{-1} band was assigned to the totally symmetric ν_{9a}(CH_3 bending) vibration.

b_{3g} Species: A Raman band observed at 478 cm^{-1} has strong intensity in the bb spectrum and medium intensity in the cc spectrum. Raman bands observed at 1510 and 1050 cm^{-1} have rather weak intensities in the bb and cc spectra and extremely weak intensities in all other spectra. Table 4 indicates that the polarization behaviors of these bands are consistent with the b_{3g} vibration. Therefore, the 1510, 1050, and 478 cm^{-1} bands were assigned to the ν_{8b}, ν_{7b} (ϕ-CH_3 stretching), and ν_{6b} vibrations of b_{3g} species, respectively. A very weak Raman band at 600 cm^{-1} was observed only in the bb spectrum and thus this band was assigned to the ν_3(CH_3 bending) vibration.

b_{1g} Species: A Raman band observed at 380 cm^{-1} has strong intensity in the cc spectrum and medium intensity in the ab and aa spectra. These polarization behaviors are consistent with the b_{1g} vibration. Thus the 380 cm^{-1} band was assigned to the ν_{10a} (CH_3 wagging) vibration.

b_{2g} Species: A Raman band observed at 275 cm^{-1} has stronger intensity in the aa and cc spectra compared with those in other spectra. A Raman band observed at 750 cm^{-1} decreases its intensity in the order of aa>cc>bc≈ab>bb≈ac spectra. These polarization behaviors definitely indicate that the 275 and 750 cm^{-1} bands have to be assigned to the b_{2g} vibration and hence assigned to the ν_5 (CH_3 wagging) and ν_4 vibrations, respectively.

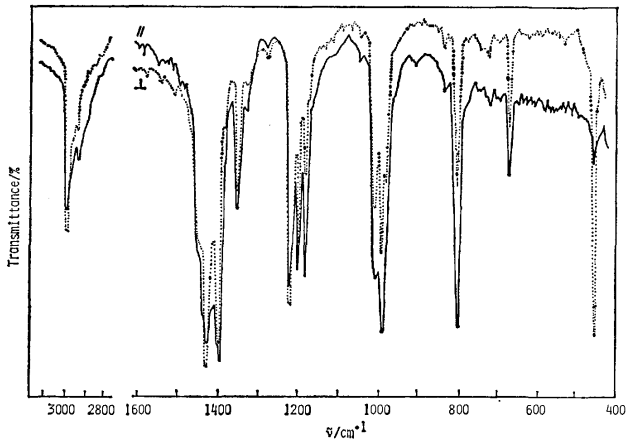

Fig. 7. Polarized infrared spectrum of the tetramethylpyrazine single crystal.

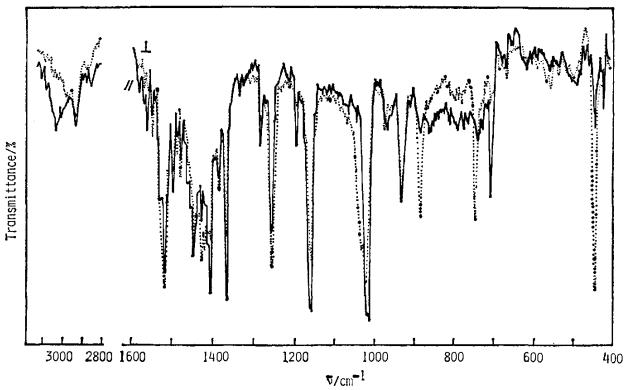

Fig. 8. Polarized infrared spectrum of the 2,6-dimethylpyrazine single crystal.

The assignment of a Raman band observed at 1367 cm^{-1} is rather difficult. This band is depolarized in the molten Raman spectrum, while its polarization behavior in the crystal Raman spectra does not correspond to any non-totally symmetric vibrations. Therefore, this band was tentatively assigned to the superposition of the CH_3 symmetric deformation vibration of b_{3g} species and the overtone vibration of the ν_{13}(ϕ-CH_3 stretching) vibration.

b_{1u} Species: According to Table 4, the infrared b_{1u} band is expected to show the B type band envelope in vapor. Infrared bands observed at 1360 and 1220 cm^{-1} showed the B band type in vapor and the type I polarization behavior in crystal. Since the band envelope and polarization behavior of the infrared band directly depend on the direction of the transition moment, it is expected that the infrared bands showing the type I polarization behavior in crystal should be assigned to the b_{1u} vibration. Strong infrared bands observed at 1440 and 1220 cm^{-1}, a medium intense band at 1360 cm^{-1} and a weak band at 680 cm^{-1} show the type I behavior in crystal and thus these bands were assigned to the ν_{19a}, ν_{12}, ν_{CH_3} symmetric deformation, and ν_{13}(ϕ-CH_3 stretching) vibrations of

TABLE 6. VIBRATIONAL ANALYSES OF THE RAMAN AND INFRARED SPECTRA OF TETRAMETHYLPYRAZINE

Raman				Infrared				Assignment
Liquid			Crystal Pol.	Solution		Crystal Pol.	Vapor type	
$\tilde{\nu}$/cm^{-1}	Int.	Pol.		$\tilde{\nu}$/cm^{-1}	Int.			
2990	m	p						antisym. C–H str. (a_g)
				2985	w	I		antisym. C–H str. (b_{1u})
				2950	m	II		antisym. C–H str. (b_{2u})
2935	sh	dp	cc,ab					$2\nu_2+\nu_{10a}$ (b_{1g})
2930	s	p						antisym. C–H str. (a_g)
				2925	m	II		antisym. C–H str. (b_{2u})
2868	vw	p						$2\nu_2+\nu_{9a}$ (a_g)
2820	vw	p						$\nu_2+\nu_{8a}$ (a_g)
2760	vw	p						$2CH_3$ sym. def. (a_g)
2725	vw	p						sym. C–H str. (a_g)
2580	vw	p						$2\nu_2$ (a_g)
1555	m	dp	aa,cc					$\nu_2+\nu_5$ (b_{2g})
1547	s	p						ν_{8a} (a_g)
1510	vw	dp	bb,cc					ν_{8b} (b_{3g})
				1460	sh	II		CH_3 degen. def. (b_{2u})
1450	m		cc,ab					CH_3 degen. def. (b_{1g})
1440	m	p						CH_3 degen. def. (a_g)
				1440	s	I		ν_{19a} (b_{1u})
1430	m		bb,cc					CH_3 degen. def. (b_{3g})
				1410	vs	II		ν_{19b} (b_{2u})
				1403	s	I		$\nu_{20b}+\nu_3$ (b_{1u})
1383	s	p						CH_3 sym. def. (a_g)
				1378	sh	II		CH_3 sym. def. (b_{2u})
1367	m	dp						CH_3 sym. def. (b_{3g}) $2\nu_{13}$ (a_g)
				1360	m	I	B	CH_3 sym. def. (b_{1u})
				1330	vw	II		ν_{14} (b_{2u})
1283	s	p						ν_2 (ϕ-CH_3 str.) (a_g)
				1280	vw	I		$\nu_{6b}+\nu_{20b}$ (b_{2u})
				1220	s	I	B	ν_{12} (b_{1u})
				1200	m	I		$\nu_{6a}+\nu_{13}$ (b_{1u})
				1180	m	II		CH_3 rock.$+\nu_{15}$ (b_{2u})
1050	w	dp	bb,cc					ν_{7b} (ϕ-CH_3 str.) (b_{3g})
1030	w	p						$\nu_4+\nu_5$ (a_g)
				1015	m	I		$\nu_1+\nu_{18a}$ (b_{1u})
				990	s	II		CH_3 rock. (b_{2u})
				970	sh	I		$\nu_{9a}+\nu_{13}$ (b_{1u})
920	vw	p						CH_3 rock. (a_g)
				835	vw	I		$\nu_{6a}+\nu_{18a}$ (b_{1u})
				810	m	II	A	ν_{20b} (ϕ-CH_3 str.) (b_{2u})
750	w	dp	aa,cc					ν_4 (b_{2g})
				730	w	I		$\nu_5+\nu_{16b}$ (b_{1u})
715	vs	p						ν_1 (a_g)
				680	w	I		ν_{13} (ϕ-CH_3 str.) (b_{1u})
600	vw	dp	bb					ν_3 (CH_3 bend.) (b_{3g})
550[a]	vw			545[a]	vw			ν_{16a} (a_u)
530	s	p						ν_{6a} (a_g)
478	s	dp	bb,cc					ν_{6b} (b_{3g})
				457	m	III	C	ν_{16b} (b_{3u})
380	s	dp	cc,ab					ν_{10a} (CH_3 wag.) (b_{1g})
				310[b]	w			ν_{18a} (CH_3 bend.) (b_{1u})
305	vw	dp	bb,cc					tor.+tor'. (b_{3g})
296	vw	p?						ν_{9a} (CH_3 bend.) (a_g)
275	m	dp	aa,cc					ν_5 (CH_3 wag.) (b_{2g})
				270[b]	vw			ν_{15} (CH_3 bend.) (b_{2u})

a) Observed in crystal phase. b) Observed in liquid phase.

Table 7. Vibrational analyses of the Raman and infrared spectra of 2,6-dimethylpyrazine

Raman				Infrared				
Liquid			Crystal Pol.	Liquid		Crystal Pol.	Vapor type	Assignment
$\tilde{\nu}$/cm^{-1}	Int.	Pol.		$\tilde{\nu}$/cm^{-1}	Int.			
3030	w	p		3030	s	II		ν_{13} (a_1)
2975	vw	dp		2965	m		A	ν_{7b} (b_2)
2926	m	p						sym. C-H str. (in CH_3) (a_1)
2915	vw			2920	m	I		sym. C-H str. (in CH_3) (b_2)
2860	vw	dp		2855	vw	I		antisym. C-H str. (in CH_3) (b_2)
1587	m	p		1584	vw	II		ν_{8a} (a_1)
1575	w	p		1563	vw	II		$\nu_{12}+\nu_{6a}$ (a_1)
				1550	w	I		$\nu_3+\nu_{18a}$ (b_2)
1534	m	dp	$\alpha\beta$	1535	s	I	A	ν_{8b} (b_2)
				1486	w	I		CH_3 degen. def. (b_2)
				1480	w	III		CH_3 degen. def. (b_1)
1450	vw	p		1452	w	II		ν_{19a} (a_1)
1417	w	dp	$\alpha\beta$	1420	m	I	A	ν_{19b} (b_2)
				1418[a]	w	III		$\nu_{6a}+CH_3$ rock. (b_1)
1405[a]				1410	m	II		$2\nu_1$ (a_1)
				1383	w	III		$\nu_{9a}+CH_3$ wag. (b_1)
1378	m	p		1367	m	II	B	CH_3 sym. def. (a_1)
1350	vw		$\alpha\beta$	1359	w	I		CH_3 sym. def. (b_2)
1305	vw	dp		1305[b]	vw			ν_{14} (b_2)
1278	m	p		1280	w	II		$\nu_1+\nu_{6a}$ (a_1)
1254	w	dp	$\alpha\beta$	1255	vs	I	A	ν_3 (b_2)
1197	w	p		1197	vw	II		ν_2 (ϕ-CH_3 str.) (a_1)
1159	m	p		1159	vs	II	B	ν_{9a} (a_1)
1070	w		$\alpha\alpha$	1060[b]	vw			$\nu_{10a}+CH_3$ rock. (a_2)
				1020	m	III		$\nu_{18a}+\nu_5$ (b_1)
1020	s	p		1016	vs	II	B	ν_{12} (a_1)
				970	w	I		$\nu_5+\nu_{10a}$ (b_2)
955	w	dp	$\alpha\alpha$					ν_{17a} (a_2)
935	w	dp	$\alpha\beta$	932	m	I	A	ν_{20b} (ϕ-CH_3 str.) (b_2)
890	w							$2\nu_{16b}$ (a_1)
880	w		$\beta\beta$	870	s	III	C	CH_3 rock. (b_1)
856	m	p						CH_3 rock. (a_1)
747	w	dp	$\beta\beta$	745	m	III		ν_5 (b_1)
709	vs	p		707	w	II		ν_1 (a_1)
675	w	dp						ν_4 (b_1)
568	m	dp	$\alpha\beta$	570[b]	w			ν_{6b} (b_2)
556	s	p						ν_{6a} (a_1)
535	w	dp	$\beta\beta$					(b_1)
500	vw	dp						$\nu_{18a}+\nu_{10a}$ (a_2)
445	vw	dp		444	vs	III	C	ν_{16b} (b_1)
420	vw			420[b]	w			ν_{18a} (CH_3 bend.) (a_1)
415	vw	dp						ν_{16a} (a_2)
325	vw	dp						
285	m	dp	$\alpha\beta$	280[b]	w			ν_{15} (CH_3 bend.) (b_2)
220	m	dp	$\alpha\alpha$	225[b]	w			ν_{10a} (CH_3 wag.) (a_2)
198	s	dp	$\beta\beta$					ν_{11} (CH_3 wag.) (b_1)
190	sh	dp	$\alpha\alpha$					ϕ-CH_3 tor. (a_2)

a) Observed in crystal phase. b) Observed in liquid phase.

b_{1u} species, respectively. A weak infrared band found at 310 cm^{-1} in liquid was tentatively assigned to the ν_{18a} (CH_3 bending) vibration based on the calculation.

b_{2u} Species: A medium intense infrared band observed at 810 cm^{-1} showed the A band type in vapor. From Table 4, this band was ascribed to the b_{2u} vibration. This band showed the type II polarization behavior in crystal. Therefore, the infrared bands at 1410, 1330, and 810 cm^{-1} showing the type II character in crystal were assigned to the ν_{19b}, ν_{14}, and ν_{20b}

(ϕ-CH_3 stretching) vibrations of b_{2u} species, respectively. A weak band observed at 270 cm^{-1} in liquid was assigned to the ν_{15} (CH_3 bending) vibration based on the calculation.

b_{3u} Species: As a medium intense bands observed at 457 cm^{-1} showed the typical C band type in vapor, this band was definitely ascribed to the b_{3u} vibration and assigned to the ν_{16b} vibration. The CH_3 wagging and ϕ-CH_3 torsional vibrations belonging to b_{3u} species were not detected in the infrared spectrum because of their low frequencies.

a_u Species: Extremely weak infrared and Raman bands observed at 545 and 550 cm^{-1}, respectively, in crystal might be assigned to the ν_{16a} vibration of a_u species. These bands are considered to appear in the spectra by the crystal force distorsion.

2,6-Dimethylpyrazine. *a_1 Species*: Strong and polarized Raman bands observed at 3030, 1587, 1450, 1197, 1159, 1020, 709, and 556 cm^{-1} in molten phase were straightforwardly assigned to the totally symmetric ν_{13}, ν_{8a}, ν_{19a}, ν_2(ϕ-CH_3 stretching), ν_{9a}, ν_{12}, ν_1, and ν_{6a} vibrations, respectively. The corresponding infrared bands showed the type II polarization in crystal and the B band type in vapor. A very weak Raman band at 420 cm^{-1} was assigned to the totally symmetric ν_{18a}(CH_3 bending) vibration based on the calculation.

b_1 Species: A very strong infrared band at 444 cm^{-1} showed the typical C band type in vapor and the type III polarization behavior in crystal. An infrared band at 745 cm^{-1} showed the type III behavior and a depolarized Raman band at 747 cm^{-1} showed the $\beta\beta$ polarization behavior in crystal. According to Table 4, the 444 and 745 cm^{-1} bands should be assigned to the b_1 vibrations and thus assigned to the ν_{16b} and ν_5 vibrations, respectively. A Raman band at 198 cm^{-1} showed the $\beta\beta$ character in crystal and thus this band was assigned to the ν_{11}(CH_3 wagging) vibration of b_1 species. Depolarized Raman band at 675 cm^{-1} was assigned to the ν_4 vibration based on the calculation.

b_2 Species: The infrared bands having the A band envelope in vapor showed the type I polarization behavior in crystal and the corresponding Raman band showed the $\alpha\beta$ polarization character in crystal. According to Table 4, the band showing these polarization behaviors could be assinged to the b_2 vibration. Infrared bands observed at 2965, 1535, 1420, 1255, and 932 cm^{-1} showing the A band type in vapor were assigned to the ν_{7b}, ν_{8b}, ν_{19b}, ν_3, and ν_{20b}(ϕ-CH_3 stretching) vibrations, respectively. Raman bands at 568 and 285 cm^{-1} showed the $\alpha\beta$ polarization character in crystal and assigned to the ν_{6b} and ν_{15}(CH_3 bending) vibrations, respectively. A weak and depolarized Raman band at 1305 cm^{-1} was assigned to the ν_{14} vibration based on the calculation.

a_2 Species: Depolarized Raman bands observed at 955, 220, and 190 cm^{-1} showed the $\alpha\alpha$ polarization character in crystal. These bands were assigned to the ν_{17a}, ν_{10a}(CH_3 wagging), and ϕ-CH_3 torsional vibrations of a_2 species, respectively, because the Raman bands showing the $\beta\beta$ and $\alpha\beta$ polarization behaviors in crystal were already assigned to the b_1 and b_2 vibrations, respectively. A weak and depolarized Raman band at 415 cm^{-1} was assigned to the ν_{16a} vibration based on the calculation.

The characteristic vibrations for CH_3 group of tetramethyl- and 2,6-dimethylpyrazines were determined based on the observed polarization behaviors of the Raman and infrared bands as well as the normal coordinate calculation. Detailed vibrational analyses of the Raman and infrared spectra are given in Tables 6 and 7, and the normal vibrations are summarized in Table 3.

The normal coordinate calculation made for tetramethylpyrazine suggests that the ν_1, ν_{12}, ν_{6b}, ν_{14}, and ν_{16a} vibrations in this molecule couple with the ϕ-CH_3 stretching (ν_2), ϕ-CH_3 stretching (ν_{13}), CH_3 bending (ν_3), ϕ-CH_3 stretching (ν_{20b}), and CH_3 wagging (ν_{17a}) vibrations, respectively. Observed vibrational frequencies of the ν_1 and ν_{6b} vibrations are lower and the frequencies of the ν_{12}, ν_{14}, and ν_{16a} vibrations are higher than those of the corresponding vibrations of pyrazine. These observation are consistent with the calculated results mentioned above. In 2,6-dimethylpyrazine the CH_3 group concerned with the ϕ-CH_3 stretching (ν_{13}), CH_3 bending (ν_3), and CH_3 wagging (ν_{17a}) vibrations is replaced with the H atom and these vibrations do not couple with the ν_{12}, ν_{6b}, and ν_{16a} vibrations, respectively. Therefore, the observed vibrational frequencies of ν_{12}, ν_{6b}, and ν_{16a} vibrations are nearly the same as those of pyrazine, while the frequency of the ν_1 vibration is lower and that of the ν_{14} vibration is higher than those of pyrazine.

We believe that the assignment of the normal vibrations given for tetramethyl- and 2,6-dimethylpyrazines are reliable and quite useful in the reasonable vibrational analyses of the phosphorescence spectra of these molecules.

References

1) R. C. Lord, A. J. Marson, and F. A. Miller, *Spectrochim. Acta*, **9**, 113 (1957).

2) J. D. Simmons, K. K. Innes, and G. M. Begun, *J. Mol. Spectrosc.*, **14**, 190 (1964).

3) S. Califano, G. Adembri, and G. Sbrana, *Spectrochim. Acta*, **20**, 385 (1964).

4) K. K. Innes, J. P. Byrne, and I. G. Ross, *J. Mol. Spectrosc.*, **22**, 125 (1967).

5) G. Sbrana, V. Schettino, and R. Righini, *J. Chem. Phys.*, **59**, 2441 (1973).

6) J. Zarembowitch and L. Bokobza-Sebagh, *Spectrochim. Acta, Part A*, **32**, 605 (1976).

7) I. Suzuki, Y. Udagawa, and M. Ito, *Chem. Phys. Lett.*, **64**, 333 (1979).

8) R. P. Oertel and D. V. Myhre, *Anal. Chem.*, **44**, 1589 (1972).

9) J. Bus, Th. J. Liefkens, and W. Schwaiger, *Recl. Trav. Chim. Pays-Bas*, **92**, 123 (1973).

10) T. Watanabe, H. Shimada, and R. Shimada, *Bull. Chem. Soc. Jpn.*, **55**, 2564 (1982).

11) K. Niimori, K. Fukuda, N. Nishi, and M. Kinoshita, Symposium on the Molecular Structure and Molecular Electronic Structure, Tokyo, October 1974, Abstr. No. 20A10.

12) S. L. Madej, G. D. Gillispie, and E. C. Lim, *Chem. Phys.*, **32**, 1 (1978).

13) K. Miyake, S. Yamauchi, and N. Hirota, Symposium

on the Molecular Structure and Molecular Electronic Structure, Fukuoka, October 1980, Abstr. No. 4B19.
14) Y. Ishibashi, R. Shimada, and H. Shimada, *Bull. Chem. Soc. Jpn.*, **55**, 2765 (1982).
15) A. W. M. Braam, A. Eshuis, and A. Vos, *Acta Crystallogr., Sect. B*, **37**, 730 (1981).
16) P. J. Wheatley, *Acta Crystallogr.*, **10**, 182 (1957).
17) F. A. Keidel and S. H. Bauer, *J. Chem. Phys.*, **25**, 1218 (1956).
18) S. Kizuki, Y. Ishibashi, H. Shimada, and R. Shimada, *Mem. Fac. Sci. Kyushu Univ., Ser. C*, **13**, 7 (1981).
19) D. H. Whiffen, *Philos. Trans. R. Soc. London, Ser. A*, **248**, 131 (1955).
20) D. T. Cromer, A. J. Ihde, and H. L. Ritter, *J. Am. Chem. Soc.*, **73**, 5587 (1951).
21) M. Suzuki, T. Yokoyama, and M. Ito, *Spectrochim. Acta, Part A*, **24**, 1091 (1968).

 © 1983 The Chemical Society of Japan Bull. Chem. Soc. Jpn., 56, 1337—1340 (1983)

Temperature Programmed Reduction of Copper–Silica Catalysts Prepared by Ion Exchange Method[1)]

Masahide Shimokawabe,* Nobutsune Takezawa, and Haruo Kobayashi

Department of Chemical Process Engineering, Faculty of Engineering, Hokkaido University, Sapporo 060

(Received September 27, 1982)

Temperature programmed reduction (TPR) has been used to study copper–silica catalysts which were prepared by ion exchange method and the effects of preparation of catalysts upon their reducibilities were elucidated. Three peaks appeared with maxima at 265—300 °C (α), 400 °C (β), and 650—800 °C (γ) over the catalysts calcined at 500 °C. Highly dispersed cupric oxide clusters were reduced to metallic copper, giving α peak. Isolated copper(II) ions which were strongly interacted with silica surface were reduced stepwise to metallic copper through copper(I) ion species, giving α and γ peaks. However, isolated copper(II) ions which were weakly interacted with the support gave α and β peaks. When the catalysts were precalcined above 800 °C, the fourth peak (α') appeared at 330—350 °C and α, β, and γ peaks diminished. This was assigned to the reduction of bulk CuO which was crystallized from species described above. The reducibility of copper–silica catalyst was found to depend strongly upon the conditions of preparation.

Characterization of catalysts is one of the important initial steps for catalyst design.[2)] In our previous work,[3)] copper–silica catalysts prepared by ion exchange method were characterized by means of a variety of analytical methods such as DTA, TG, UV, XPS, AES, and XRD and it was shown that the precursor states of the catalysts depended sensitively upon copper loading and the calcination temperature. The activity and selectivity of methanol steam reforming $CH_3OH+H_2O=CO_2+3H_2$ were found to be strongly influenced by the preparation of the catalysts[4–6)] and metallic copper formed in the course of the reaction was suggested to be active sites for the reaction. The reducibility of the catalyst was also closely associated with the preparation conditions of the catalyst.[7)] Recently, TPR method has been successfully applied for the characterization of supported metal catalysts[8,9)] and TPR peaks obtained are found to reflect sensitively the states of the catalysts such as valence of active species and metal-support interaction. In these connections, the copper-silica catalysts were reduced by hydrogen under temperature programmed conditions and their reducibilities were extensively studied in relation to the states of the precursor species.

Experimental

Catalysts. The catalysts were prepared in a manner similar to that employed in the previous work.[3)] Hydroxyl protons on silica gel (Nihon Chromato. Co., 60—80 mesh in granules) were exchanged at a pH=11—12 overnight with tetrammine copper(II) cations which had been prepared from copper(II) nitrate (Wako Pure Chemicals, extra pure grade) and an aqueous ammonia solution. The ion exchange silica gel was filtered, washed with distilled water and dried at 110 °C for 12 h, and were further calcined in air under various conditions covering temperature range of 500—900 °C and calcination time of 3 min to 3 h. Copper loading in catalyst was estimated from the concentrations of the mother solution and of the filtrate. These were determined by titration with EDTA solution of known concentration by use of PAN as an indicator. Copper loading thus determined varied in the range of 0.5—13.0 wt% copper. As previously stated,[3,5)] no nitrate anion was held on the surface as revealed by XPS of the catalysts and chemical analysis of the solution.

Temperature Programmed Reduction (TPR). A hydrogen–nitrogen mixture (4% hydrogen) was passed over the catalyst at a total flow rate of 50 ml/min. TPR runs were carried out at a heating rate of 10 °C/min with a programming temperature controller (Muto HM 53) and hydrogen consumption was monitored by thermal conductivity cell attached to a gas chromatograph (Ohkura Electric Co. Model 701). The reactor was made of quartz tubing of 12 mm in diameter and the catalyst sample of 0.5—3.0 g was mount ed on loosely packed quartz wool. The temperature was simultaneously recorded with hydrogen concentration on a multipen recorder (Hitachi 056) using a chromel-alumel thermocouple.

Results and Discussion

Copper Loading and TPR Spectra. Figure 1 illustrates TPR spectra obtained over the catalysts which had been prepared by calcination at 500 °C for 3 h in air. Three peaks are seen with maxima at 265—300 °C (referred to as α-peak), 440 °C (β-peak) and 665—800 °C (γ-peak), and these peak areas depend markedly upon copper loading. On the catalysts with high copper loading (10.4 and 13.0 wt% copper), α peak appears predominantly with a small β peak on its shoulder. Three peaks α, β, and γ are seen separately on the catalysts with medium loading (5 wt% copper), while only α and γ peaks are perceptible on the catalyst with copper loading below 2 wt%. The amounts of hydrogen consumed were estimated from the peak area and were plotted against copper loading in Fig. 2. The total amount of hydrogen consumed was found to be practically equal to that of hydrogen required for complete reduction of cupric oxide to metallic copper. α-Peak increases monotonically with the increase of copper loading while β and γ peaks attain to the maximum and decrease as the loading is increased. In Fig. 3, peak area ratio α/γ is plotted against copper loading. It is seen that α/γ decreases and tends to approach unity as the loading is lowered.

In our previous work,[3)] the precursor states of copper–silca catalyst which was prepared by ion exchange method were characterized with the help of a variety of analytical methods and it was shown that when copper(II) ions were held no silica gel support, various states of the precursors appeared. Relative amounts

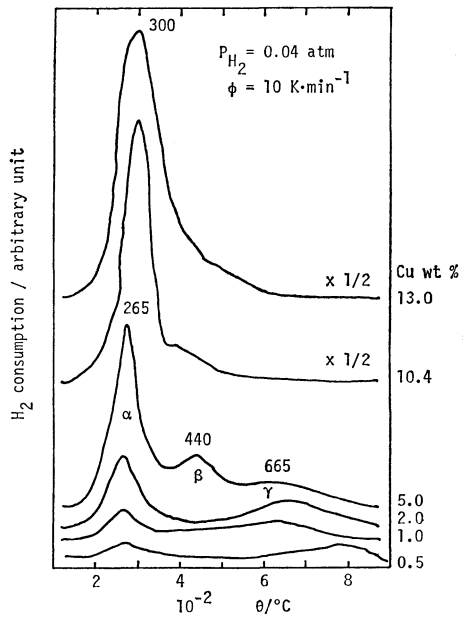

Fig. 1. TPR spectra of Cu/SiO_2 catalysts calcined at 500 °C for 3 h.

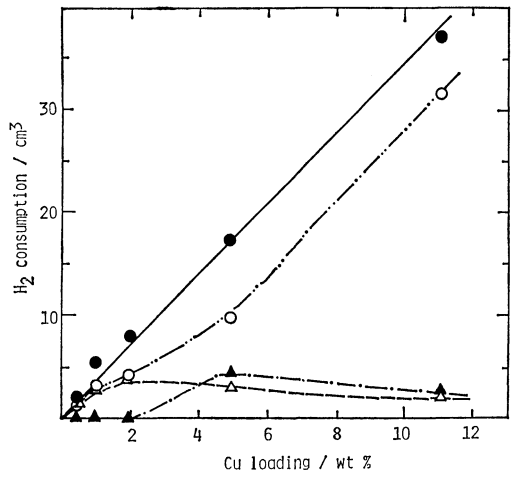

Fig. 2. Cu-loading and the amounts of consumed hydrogen in the course of TPR runs.
(—●—), Total amount of consumed hydrogen. (—○—), Amount of consumed hydrogen which gave α-peak. (—▲—), Amount of consumed hydrogen which gave β-peak. (—△—), Amount of consumed hydrogen which gave γ-peak.

of these species were found to be sensitively affected by copper loading and calcination temperature. On the catalyst with copper loading below 0.5—1 wt%, the precursor which was calcined in the temperature range 300—720 °C existed as isolated copper(II) ions, while with higher copper loadings it existed as small clusters of CuO. When the catalyst was calcined above 720 °C, the latter species were crystallized into bulk CuO, while the former species were partly clustered but in part still remained as isolated copper(II) ions.

In the present work, a variety of TPR peaks were observed. α and β Peaks appeared with the same intensity at lower copper loading (below 2 wt%), while at higher copper loading (10.4 and 13.0 wt%), the

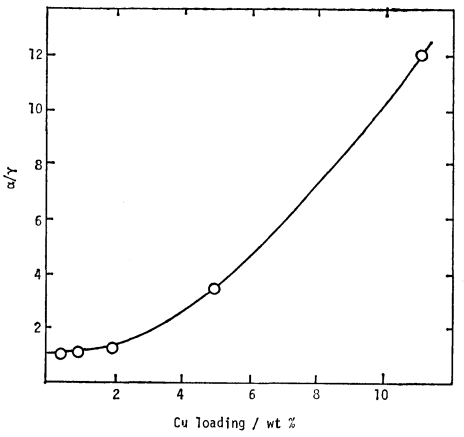

Fig. 3. The ratio of TPR peak areas α/γ against Cu-loading.

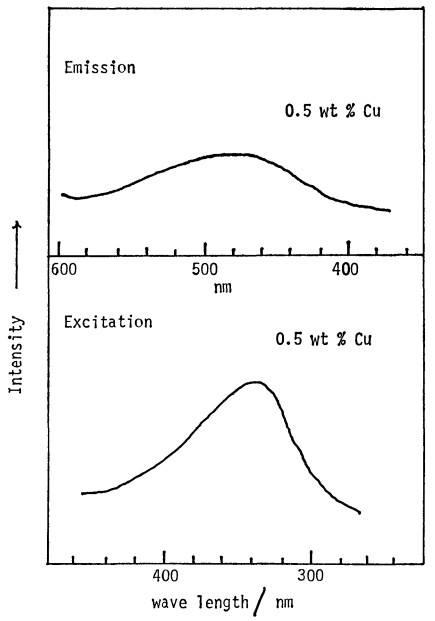

Fig. 4. Phosphorescence spectra of Cu/SiO_2 catalysts which were employed for TPR run to 400 °C.

former peak was exceedingly large compared to other TPR peaks. On the basis of the previous results as to the characterization of the catalyst,[3] it is very likely that α-peak obtained on the catalyst with high copper loading is ascribed to the reduction of small clusters of CuO. These species were transformed to metallic copper as evidenced by the amount of the hydrogen consumption. On the catalyst with 0.5 wt% copper loading the phosphorescence spectra were obtained after a TPR run was carried out to 400 °C where α-peak was completed (Fig. 4). In both the emission and the excitation modes, the peaks due to copper(I) ions are seen at 340 and 490 nm, respectively. α-Peak obtained for the catalysts with low copper loading is, therefore, ascribable to the reduction of isolated copper(II) ions to copper(I) ions. In these respects, γ-peak is ascribed to the reduction of the formed copper(I) ions to metallic copper, so that the ratio of peak area α/γ approaches unity as the loading is lowered. Both isolated copper(II) ions and copper(I)

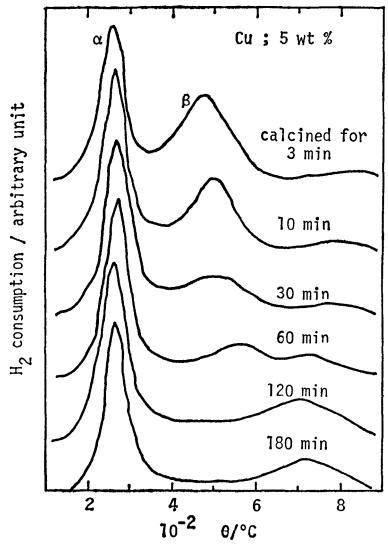

Fig. 5. TPR spectra of Cu/SiO_2 (5.0 wt% copper) catalyst calcined at 500 °C.

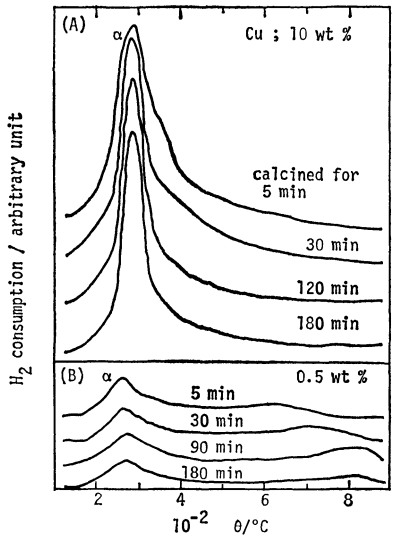

Fig. 6. TPR spectra of Cu/SiO_2 (10.0 wt% and 0.5 wt% copper) catalysts calcined at 500 °C.

ions formed were presumably interacted strongly with silica and stabilized on the support. The copper(II) ions were, therefore, reduced stepwise to metallic copper through the copper(I) ions. On the other hand, the results obtained at medium copper loading appeared to be puzzling in which β-peak was seen. It was tentatively concluded that copper(II) ions which were weakly interacted with silica were also reduced to copper(I) ions, giving α peak, and the formed copper(I) ions were then reduced to metallic copper at the temperature where β peak appeared.

Figure 5 illustrates TPR spectra of Cu/SiO_2 (5.0 wt%) catalysts which were calcined at 500 °C for different length of time. As the calcination time becomes longer, β-peak decreases but γ-peak increases. However, the intensity of α-peak remains practically unchanged. The interaction between copper(II) ions and silica was suggested to be strengthened during the course of calcination. Figure 6 illustrates TPR spectra which were obtained for the catalysts (10 and 0.5 wt% copper) calcined at 500 °C for different length of time. On the catalyst with 10 wt% copper small β-peak on α-peak diminishes with time and only α-peak is observed after 180 min. On the catalyst with 0.5 wt% copper the peaks are initially observed at 260 and 650 °C but γ-peak shifts to higher temperature when the calcination time is increased. This also indicates that the mutual interaction between isolated copper(II) ion and silica support is enhanced with the calcination time.

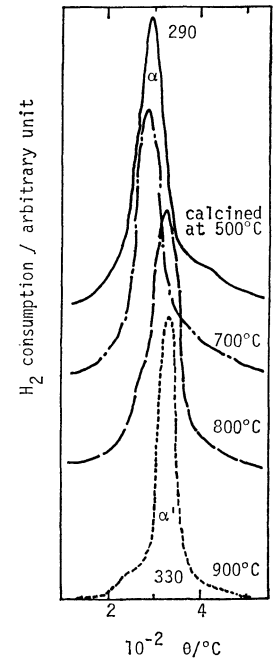

Fig. 7. TPR spectra of Cu/SiO_2 (10.4 wt% copper) catalysts and calcination temperature.

Calcination Temperature and TPR Spectra. Figure 7 illustrates TPR spectra obtained over Cu/SiO_2 catalyst (10 wt%) which was calcined at different temperatures for 3 h in air. α-Peak predominates on the catalyst calcined below 700 °C, but when the catalysts is calcined at 800 or 900 °C, this peak decreases to a considerable extent and a new peak (referred to as α'-peak) appears at 330 °C. As previously examined[3] by XRD, no CuO patterns were observed on the catalyst precalcined below 720 °C, but they grew when the catalyst was precalcined above this temperature. α'-Peak is, therefore, ascribed to the reduction of the bulk CuO. In fact, support-free CuO gave a peak at 340 °C.

Figure 8 shows TPR spectra obtained for the catalysts with lower copper loadings (2.0 and 0.5 wt% copper) which were calcined at various temperatures. The spectra are somewhat complicated compared to those obtained on the catalysts with higher copper loadings. When the cataylsts with 2 wt% copper is calcined at 900 °C, α' peak grows evidently at the expense of α and γ peaks. On the catalyst with 0.5 wt% copper, however, α' peak is also observed while α peak grows slightly but γ peak decreases. This indicates that isolated copper(II) ion precursors transform into CuO clusters and the latter species further transform into

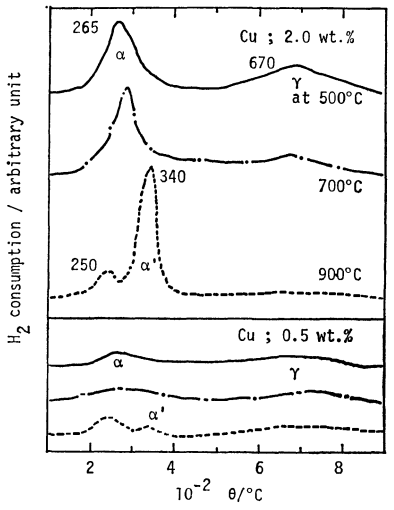

Fig. 8. TPR spectra of Cu/SiO_2 (2.0 and 0.5 wt% copper) catalysts and calcination temperature.

bulk CuO when the catalyst is precalcined at 900 °C. This substantially coincided with the previous results obtained by UV diffuse reflectance spectroscopy in which it was shown that the isolated species became partially clustered but in part still retained its orginal state.

Conclusion

TPR technique has been used to study copper–silica catalysts with varying copper loading and calcination. Four peaks were observed with maxima at 265—300 °C (α), 400 °C (β), 650—800 °C (γ), and 330—350 °C (α'). Relative peak intensities of these peaks depended upon copper loading and calcination temperature. It was concluded that α peak was ascribed to the reduction of highly dispersed CuO clusters and isolated copper(II) ions which were either strongly or weakly held on the support. The CuO clusters were easily reduced to metallic copper, while the isolated species were merely reduced to copper(I) ions when α peak was completed. These isolated copper(II) ions were concluded to be reduced stepwise to metallic copper and consequently β and γ peaks were ascribed to the reduction of intermediate copper(I) ions to metallic copper. When the catalyst was calcined at 900 °C, CuO clusters transformed into bulk CuO to a considerable extent and gave α' peak in TPR runs. On the other hand, the copper ions in the catalyst with lower copper loading are only partly transformed into bulk CuO clusters even after calcination at 900 °C.

The present research has been partially supported by the Grant-in-Aid for Scientific Researches of the Ministry of Education, Science and Culture to which the authors are greatly acknowledged.

Added in Note: After the present work was presented at the Chemical Society of Japan Meeting, April 3, 1981 and at Catalysis Society Meeting, October 15, 1981, Okayama, the TPR work [S. J. Gentry and P. T. Walsh, *J. Chem. Soc., Faraday Trans. 1*, **78**, 1515 (1982)] was recently published for copper catalysts which were prepared by impregnation on silica and alumina. The results shown are practically in accord with those obtained in the present work in which the TPR peaks obtained are reported to be greatly affected by calcination temperature and copper loading.

References

1) Present work was presented at the Chemical Society of Japan Meeting, April 3, 1981 and Catalysis Society Meeting, October 15, 1981, Okayama.
2) "Characterization of Catalysts," ed by J. M. Thomas and R. M. Lambert, John Wilely & Sons, Chichester (1980).
3) M. Shimokawabe, N. Takezawa, and H. Kobayashi, *Appl. Catal.*, **2**, 379 (1982).
4) H. Kobayashi, N. Takezawa, C. Minochi, and K. Takahashi, *Chem. Lett.*, **1980**, 1197.
5) H. Kobayashi, N. Takezawa, and C. Minochi, *J. Catal.*, **69**, 487 (1981).
6) N. Takezawa, H. Kobayashi, A. Hirose, M. Shimokawabe, and K. Takahashi, *Appl. Catal.*, **4**, 127 (1982).
7) N. Takezawa, H. Kobayashi, Y. Kamegai, and M. Shimokawabe, *Appl. Catal.*, **3**, 381 (1982).
8) J. W. Jenking, B. D. McNicol, and S. D. Robertson, *Chem. Tech.*, **316** (1977).
9) H. C. Yao, M. Sieg, and H. K. Plummer, Jr., *J. Catal.*, **59**, 306 (1979).

 © 1983 The Chemical Society of Japan Bull. Chem. Soc. Jpn., 56, 1341—1345 (1983)

Pressure Effects on the Hydrolysis of 3-Nitro-4-acyloxybenzoic Acids Catalyzed by Hexadecyltrimethylammonium Bromide Micelle[1)]

Syoichi Makimoto, Keizo Suzuki, and Yoshihiro Taniguchi*

Department of Chemistry, Faculty of Science and Engineering, Ritsumeikan University, Kita-ku, Kyoto 603

(Received October 22, 1982)

The rates of the hydrolysis of 3-nitro-4-acetoxybenzoic acid (NABA), 3-nitro-4-propionyloxybenzoic acid (NPBA), 3-nitro-4-butyryloxybenzoic acid (NBBA), and 3-nitro-4-valeryloxybenzoic acid (NVBA), catalyzed by the hexadecyltrimethylammonium bromide (HTAB) micelle, were measured at pressures up to 2 kbar at 25 °C in Tris buffer solution (0.01 M,† pH 8.7). The ester binding constant K increased and the rate constant of the hydrolysis catalyzed by micelle k_m decreased with longer alkyl chains of esters at 1 bar. The k_m values were separated into the contribution of k_{OH} (hydroxide ion catalyzed hydrolysis) and k_T (Tris catalyzed hydrolysis), which increased monotonically up to 2 kbar. On the other hand, the K values decreased and then inversed with minima at about 1.5 kbar except for that of NABA. From the pressure dependence of log K, the volume changes, ΔV, accompanying the ester binding to the HTAB micelle at 1 bar were estimated to be in the range of 11 ± 2 cm³/mol for NABA to 23 ± 2 cm³/mol for NVBA. The activation volumes for the hydrolysis catalyzed by micelle, were measured as -6 ± 2 cm³/mol for $\Delta V^{\ddagger}_{OH}$ and -16 ± 2 cm³/mol for $\Delta V^{\ddagger}_{T}$ for each ester. The activation volumes for the spontaneous hydrolysis were measured as -5 ± 2 cm³/mol for $\Delta V^{\ddagger}_{OH}$ and -16 ± 2 cm³/mol for $\Delta V^{\ddagger}_{T}$ for each ester. The reaction mechanism was discussed in terms of ΔV and ΔV^{*}.

Hydrolysis of esters catalyzed by micelles as the enzyme-model is recognized to be markedly accelerated above the critical micelle concentration (cmc) and to follow the kinetics of Michaelis-Menten type.[2,3)] Such an accelerating effect is explained by the incorporation of esters into the micellar phase, which is caused by the driving force of the electrostatic and hydrophobic interactions between esters and micelles. In fact, the cooperative effect of electrostatic and hydrophobic interactions on the substrate binding is important for some kinds of protease.

In the previous report,[4)] we have studied about the HTAB micelle-system concerning the hydrophobic interaction as the driving force of the incorporation of neutral esters into the micellar phase. The volume change ΔV accompanying the ester binding to the micellar system at 1 bar was in the range of 0 cm³/mol for *p*-nitrophenyl acetate (PNPA) to 18 cm³/mol for *p*-nitrophenyl hexanoate (PNPH), which means the increment of the positive volume of 2.4 cm³/mol for methyl or methylene group of esters for the transfer of ester molecules from an aqueous environment to the micellar phase. While, ΔV at the formation of the electrostatic interaction (charge neutralization) for 1:1 electrolytes is believed to be around 10 cm³/mol.[5)] So, we can expect that the pressure effects on the electrostatic interactions are larger than hydrophobic effects, especially for an ionic ester molecule containing only a short alkyl chain. The study about the system containing both interactions above as a driving force of the incorporation of ester into the micellar phase is meaningful to clearify the more detail mechanism of protease.

In the present work, the hydrolysis rate of anionic esters of 3-nitro-4-acyloxybenzoic acids catalyzed by a cationic HTAB micelle was measured at the pressures up to 2 kbar at 25 °C to obtain the pressure dependences of the substrate bindings and the micelle-catalyzed hydrolysis. The reaction mechanism is discussed in terms of the volume change for the formation of the micelle–ester complex and the activation volumes for the hydrolysis catalyzed by micelle, being compared with the previous date.[4)]

† 1 M=1 mol dm⁻³.

Experimental

Materials. NABA, NPBA, NBBA, and NVBA synthesized[6)] and HTAB were purified by previous method,[4)] except NABA and NPBA to be recrystallized 5 times from benzene–diisopropyl ether. NABA: mp 156—158 °C (lit,[7)] mp 156—158 °C); MS (75 eV), Found: *m/e* 225.02745. Calcd for $C_9H_7N_1O_6$: M, 225.02734. NPBA: mp 143.5—145.5 °C. Found: *m/e* 239.04252. Calcd for $C_{10}H_9N_1O_6$: M, 239.04300.

Apparatus and Procedure. The measurement of the hydrolysis reaction up to 2 kbar is described in previous report.[4)] The rate was determined by observing the change in the optical density at $\lambda_{max}=410$ nm of 3-nitro-4-hydroxybenzoate anion at pH 8.7 in 0.01 M Tris buffer solution up to 2 kbar at 25 °C±0.5 °C. The cmc of HTAB at pH 8.7 in 0.01 M Tris buffer solution up to 2 kbar was determined by the measurement of the absorption spectra of salicylic acid ($\lambda_{max}=295$ nm) as a probe at 25 °C.

Results and Discussion

The apparent rate constant, k_{app}, of the hydrolysis at 1 bar increases suddenly above cmc of HTAB as shown in Fig. 1. Assuming that one ester molecule is incorporated into a micelle and that the aggregation number, N, of the micelle is independent of ester incorporation, Bunton *et al.*[8)] showed that the scheme of the enzyme-catalyzed reaction in Eq. 1 is applicable to the present kinetic behavior,

$$M + S \overset{K}{\rightleftharpoons} MS \xrightarrow{k_m} M + P, \quad S \xrightarrow{k_s} P. \qquad (1)$$

Here M, S, MS, P, K, k_m, and k_s denote the micelle, esters the micelle–ester complex, products the binding constant between esters and micelles, the rate constants of hydrolysis catalyzed by micelle, and that of the spontaneous hydrolysis, respectively. The concentration of micelle is given by Eq. 2,

$$[M] = (C_D - \text{cmc})/N. \qquad (2)$$

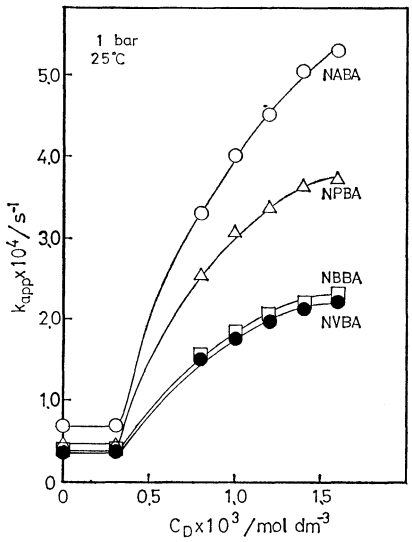

Fig. 1. Hydrolysis of anionic esters in HTAB micelle at 1 bar, pH 8.7 (0.01 M Tris buffer) and 25 °C. Each ester concn is 2.0×10^{-4} M.

TABLE 1. CMC AND AGGREGATION NUMBERS OF HTAB MICELLE AT VARIOUS PRESSURES AND 25 °C

P/kbar	0.001	0.5	1.0	1.5	2.0
10^{-4}(cmc)/M	2.9	3.4	3.7	3.5	3.4
$N^{p,a)}$	95	60	52	60	76

a) Ref. 4.

Here C_D is the total concentration of HTAB. The cmc values of HTAB in our experimental conditions at each pressure are shown in Table 1 with values of the aggregation numbers, N, of HTAB micelle. The values of K and k_m determined by Lineweaver-Burk plots[4] in Fig. 2 for anionic esters at 1 bar and Fig. 3 for NBBA up to 2 kbar, are shown in Table 2 with the values of k_s at various pressure.

Ester Binding. From NMR studies[9,10] of benzoate and alkyl phenol (C_nH_{2n+1}-⟨○⟩-OH, n=1, 2, 3) in micellar solutions, benzoate ions exist near the micellar surface, in which the aromatic ring is located between quaternary ammonium head groups of HTAB molecules. Alkyl phenol molecules penetrate more into the micelle with increasing alkyl chains. Therefore, NABA is expected to be incorporated near the micellar surface and the other anionic esters with longer alkyl chains of acyl groups penetrate more into the hydrocarbon core of the micelle. The results mean the difference of the site of solubilization into the micelle between NABA and longer alkyl chains of esters. So that the inversion phenomena at plots of log K *vs.* pressure as shown in Fig. 4 correspond to the appearence of a maximum of the cmc of HTAB at 1 kbar in Table 1. The linear decrease of log K of NABA with increasing pressure was also observed in the systems of PNPA–HTAB[4] and methyl acetate–dodecyl hydrogensulfate micelle.[11] The change of volume ΔV being accompanied by the formation of MS complex at 1 bar in Table 3 is determined from the initial slope of plots of log K *vs.* pressure.

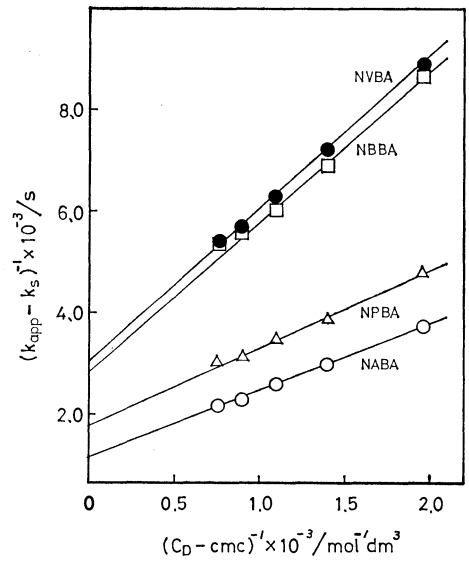

Fig. 2. Lineweaver-Burk plots for anionic esters in HTAB micelle at 1 bar, pH 8.7 (0.01 M Tris buffer) and 25 °C. Each ester concn is 2.0×10^{-4} M.

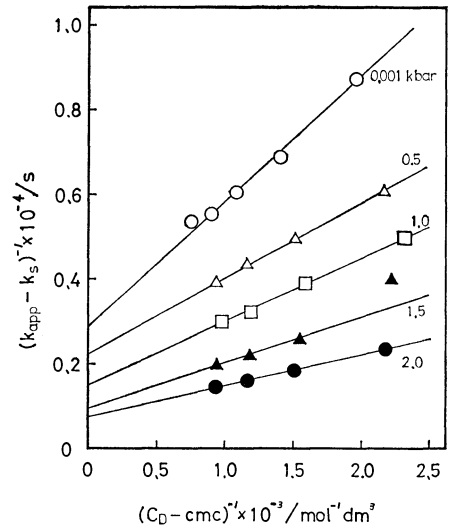

Fig. 3. Lineweaver-Burk plots for NBBA in HTAB micelle under five pressures, pH 8.7 (0.01 M Tris buffer) and 25 °C. Each ester concn is 2.0×10^{-4} M.

The K value increases with increasing alkyl chain of acyl groups of esters, and it is larger than that of neutral ester[4] at 1 bar and 25 °C except NVBA. The fact means that the electrostatic interaction in addition to the hydrophobic interaction plays an important role in the driving force of the incorporation of anionic esters with micelles. If the driving force for the ester incorporation is a sum of the electrostatic and hydrophobic interactions, the volume change ΔV is given by Eq. 3,

$$\Delta V = \Delta V_{ele} + \Delta V_{H\phi}. \quad (3)$$

Here ΔV_{ele} and $\Delta V_{H\phi}$ denote the volume changes of dehydration being accompanied by electrostatic and hydrophobic interactions between a ester molecule and a HTAB micelle, respectively. If an anionic charge of esters is neutralized completely by the electrostatic

Table 2. Kinetic parameters of the basic hydrolysis of anionic esters catalyzed by HTAB micelle and spontaneous hydrolysis at various pressures and 25 °C

P/kbar	$K\times10^{-4}/M^{-1}$				$k_m\times10^4/s^{-1}$				$k_s\times10^4/s^{-1}$			
	NABA	NPBA	NBBA	NVBA	NABA	NPBA	NBBA	NVBA	NABA	NPBA	NBBA	NVBA
0.001	7.34	11.3	11.7	13.5	9.83	5.95	3.48	3.13	0.647	0.457	0.390	0.367
0.5	6.11	8.42	7.88	8.10	16.9	11.2	5.00	4.95	0.931	0.670	0.584	0.538
1.0	4.28	6.98	5.37	5.36	21.2	14.4	7.65	8.96	1.52	1.12	0.997	0.900
1.5	3.88	5.63	5.34	4.78	33.9	22.7	12.5	13.8	2.25	1.67	1.53	1.36
2.0	3.09	6.26	5.43	4.87	55.1	40.4	20.2	21.6	3.39	2.57	2.41	2.09

Table 3. Volume changes accompanying the formation of MS complex (ΔV), the activation volumes of the hydrolysis for tris- and hydroxide ion-catalyzed hydrolysis (ΔV_T^* and ΔV_{OH}^*) in micellar and nonmicellar systems at 1 bar and 25 °C

Substrates R 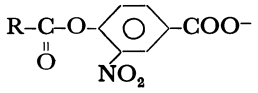	Volume changes[a]/cm³ mol⁻¹				
	ΔV	$(\Delta V_T^*)_{micelle}$	$(\Delta V_{OH}^*)_{micelle}$	ΔV_T^*	ΔV_{OH}^*
CH_3-	11				
C_2H_5-	13	−16	−6	−16	−5
n-C_3H_7-	18				
n-C_4H_9-	23				
p-Nitrophenyl esters[b]					
CH_3-	0				
C_2H_5-	4	−19	−6	−18	−3
n-C_3H_7-	9				
n-C_4H_9-	14				

a) ±2 cm³/mol. b) From Ref. 4.

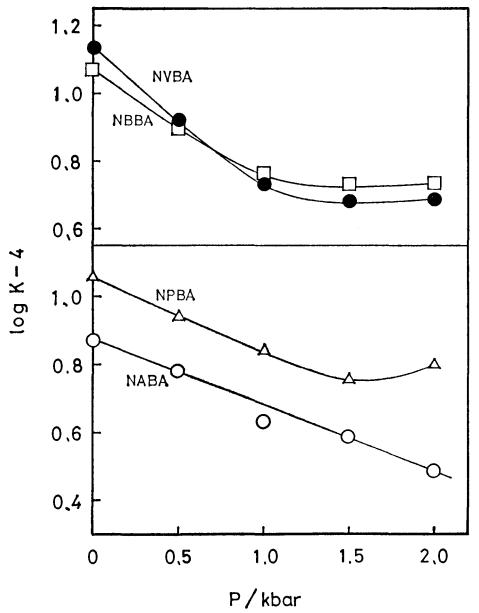

Fig. 4. Log K *vs.* P at 25 °C.

interaction on the transfer of esters from the aqueous environment to that of the polycationic micelle, we can estimate about 11 cm³/mol as ΔV_{ele} for the release of the electrostriction around ionic esters as 1:1 electrolyte from the neutralization process such as $CH_3COO^- + H^+ \longrightarrow CH_3COOH$.[12] On the base of $\Delta V_{ele}=11$ cm³/mol, the calculated $\Delta V_{H\phi}$ values for anionic esters are 0 cm³/mol for NABA, 3 cm³/mol for NPBA, 7 cm³/mol for NBBA, and 12 cm³/mol for NVBA. They are in good agreement with $\Delta V_{H\phi}$ values for series of neutral p-nitrophenyl esters[4] with the hydrophobic interaction alone on the incorporation process. Therefore, ΔV values of anionic esters may be explained by the dehydration through both electrostatic and hydrophobic interactions between ester molecules and HTAB micelle.

Hydrolysis in Micelle. The rate constant k_s of spontaneous hydrolysis of anionic esters in Tris buffer solution can separate into the contributions of hydroxide ion and free-amine Tris catalysis as given by Eq. 4,

$$k_s = k_{OH}[OH] + k_T[Tris]. \quad (4)$$

Table 4 shows the k_{OH} and k_T values of NABA, determined by the same method of Neuman *et al.*[13] In the micellar catalyst,[4] the hydroxide ion concentration is higher near the HTAB micellar cations, while the distribution of neutral free-amine Tris would not be influenced by the micelle. Therefore, the pseudo-first-order rate constants for the hydroxide ion catalyst in micelle, $(k_{OH})_{micelle}$, are given by Eq. 5,

$$(k_{OH})_{micelle} = k_{OH}/\langle OH\rangle_{micelle}. \quad (5)$$

Here $\langle OH\rangle_{micelle}$ is the average concentration of the hydroxide ions near the micellar phase determined by using the previous date.[4] The $(k_T)_{micelle}$ values were also determined from Eq. 6 with the known $(k_{OH})_{micelle}$ values. The values of ΔV_{OH}^* and ΔV_T^* of NABA

$$k_m^{\prime} = \sum_i (k_{OH})_{micelle}\langle OH\rangle_{micelle}^{\prime} + \sum_i (k_T)_{micelle}[Tris] \quad (6)$$

Table 4. Rate constants for hydrolysis of NABA at various pressures and 25 °C[a]

P/kbar	k_{OH}/M^{-1} s^{-1},[b]	$k_T \times 10^3$/M^{-1} s^{-1},[c]
0.001	7.35	2.73
0.5	8.07	3.22
0.75	8.33	4.42
1.0	9.43	4.95
1.25	8.45	6.46
1.5	9.63	7.77
1.75	11.5	8.00
2.0	11.2	10.7

a) Ester concn *ca.* 5.0×10^{-5} M. b) Calcd from the Eq. $k = k_{OH}[OH] + k_T[Tris]$ using date from experiments at both 0.01 and 0.05 M total buffer concns. c) Calcd for total buffer concn.

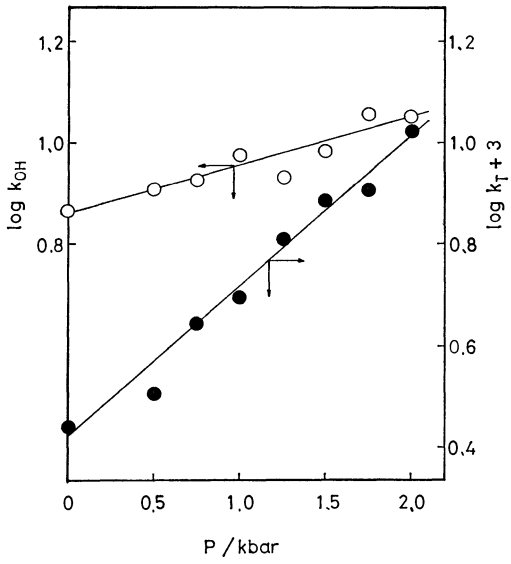

Fig. 5. Log k_{OH} and log k_T *vs.* P for NABA in nonmicellar system at 25 °C.

for the spontaneous and micellar hydrolysis in Table 3 were obtained by the linear relation of logarithms of k_{OH} and k_T in each system (Figs. 5 and 6).

In nonmicellar systems, the value of ΔV_{OH}^* of -5 cm³/mol for anionic esters is slightly more negative value than that of -3 cm³/mol for nonionic esters. The ΔV_{OH}^* value should be given by a balance between the negative volume change for the bimolecular reaction and the positive volume change for the difference of the solvation effect between reactants and the activation complex. The former is expected to have a negative value of *ca.* -10 cm³/mol for the formation of one covalent bond,[14] for both anionic and nonionic esters. In latter case, it may be expected that there is a difference between anionic and nonionic esters in the solvation effect accompanying the formation of the tetrahedral intermediate. When a ester molecule reacts with a hydroxide ion, the charge dispersion of the activation complex takes place accompanying the formation of the tetrahedral intermediate in the transition state. The partial desolvation effect of hydroxide ions at the initial state with the formation

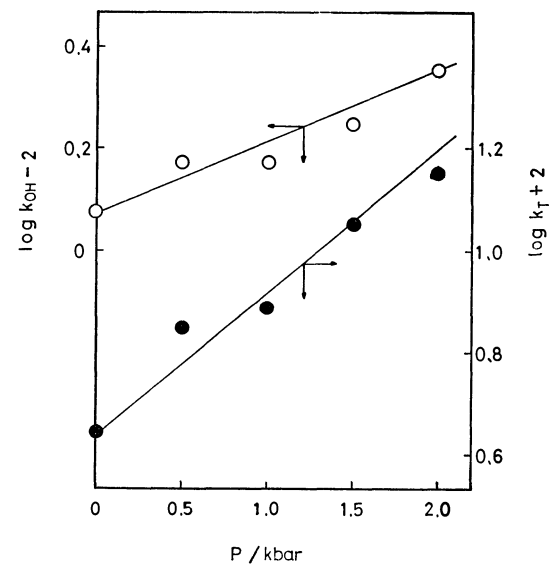

Fig. 6. Log k_{OH} and log k_T *vs.* P for NABA in micellar system at 25 °C.

of the tetrahedral intermediate contributions to the positive volume change. Therefore, the difference of ΔV_{OH}^* between -3 cm³/mol for PNPA and -5 cm³/mol for NABA is correspond to the difference of the desolvation effect on the base hydrolysis between anionic and nonionic esters.

In the micellar system, the solvation effect of water molecules both on the reactants and on the activated complex may be negligible due to the incorporation into the hydrophobic atmosphere and polyions of HTAB micelle. Therefore, the value of $(\Delta V_{OH}^*)_{micelle}$ for NABA is in good agreement with that of PNPA, which has been explained by the only contribution of the formation of one covalent bond without solvation effect.

We are grateful acknowledged to Mr. Hideo Hisatomi and Mr. Syoichi Tanamachi of Ritsumeikan University for the synthesis of esters, and Miss Kayoko Saeki of Kobe Women's College of Pharmacy for the measurement of the purity of the esters by a mass spectrometer.

References

1) a) Studies of Polymer Effects under Pressure. Part 6; b) This article was also presented as part of an invited lecture at the 8th AIRAPT Conference in Uppsala, Sweden, 1981.

2) J. H. Fendler and E. J. Fendler, "Catalysis in Micellar and Macromolecular systems," Academic Press, New York (1975).

3) J. Baumrucker, M. Calzadilla, and E. H. Cordes in "Reaction Kinetics in Micelles," ed by E. H. Cordes, Plenum Press, New York (1973), p. 25.

4) Y. Taniguchi, S. Makimoto, and K. Suzuki, *J. Phys. Chem.*, **85**, 2218 (1981).

5) T. Asano and W. J. le Noble, *Chem Rev.*, **78**, 407 (1978).

6) Y. Taniguchi, K. Simokawa, H. Hisatomi, S. Tanamachi, and K. Suzuki, *Macromolecules*, **11**, 829 (1978).

7) C. G. Overberger, T. St. Pierr, N. Vorchheimer, J. Lee, and S. Yaroslavshy, *J. Am. Chem. Soc.*, **87**, 296 (1965).

8) C. A. Bunton, E. J. Fender, L. Sepulveda, and K. U. Yang, *J. Am. Chem. Soc.*, **90**, 5512 (1968).
9) C. A. Bunton and M. J. Minch, *J. Phys. Chem.*, **78**, 1490 (1974).
10) F. Tokiwa and K. Aigami, *Kolloid Z. Z. Polym.*, **246**, 688 (1971).
11) Y. Taniguchi, O. Inoue, and K. Suzuki, *Bull. Chem. Soc. Jpn.*, **52**, 1327 (1979).
12) K. Suzuki, Y. Taniguchi, and T. Watanabe, *J. Phys. Chem.*, **77**, 1918 (1973).
13) R. C. Neuman, Jr., W. Kauzmann, and A, Zipp, *J. Phys. Chem.*, **77**, 2628 (1973).
14) W. J. le Noble, *Prog. Phys. Org. Chem.*, **5**, 207 (1967).

Study of Ion Transport across Amphoteric Ion Exchange Membrane. II. Transport of Symmetric Tetraalkylammonium Chlorides

Kozue KAIBARA,* Hideaki SONODA, Yoshihiko NAGATA, and Hideo KIMIZUKA

Department of Chemistry, Faculty of Science, Kyushu University, Hakozaki, Higashi-ku, Fukuoka 812, Japan

(Received December 6, 1982)

Transport characteristics of NH_4Cl, $(CH_3)_4NCl$ (TMA–Cl), $(C_2H_5)_4NCl$ (TEA–Cl), $(n\text{-}C_3H_7)_4NCl$ (TPA–Cl), and $(n\text{-}C_4H_9)_4NCl$ (TBA–Cl) across homogeneous type amphoteric ion exchange membrane (1.0-PA-29, Kanegafuchi Chem. Ind.) were studied. Membrane potentials and conductances of the concentration cell systems were measured to calculate the membrane permeabilities which represent a measure of ionic permselectivity. Membrane potential changed considerably with cationic species and the membrane tended to behave more anionic selectively with increasing bulkiness of cations. The cationic permeabilities calculated from electrochemical data were $P_{NH_4}>P_{TMA}>P_{TEA}>P_{TPA}>P_{TBA}$. Membrane permeabilities to chloride ions, P_{Cl}, were greater than those to cations in all the systems studied and it was interesting that P_{Cl} values and their dependencies on external electrolyte concentration were almost unchanged irrespective of the difference in cationic species. The present experiment was designed in order to examine the effects of ionic size on the transport processes across homogeneous type amphoteric ion exchange membrane. The obtained results indicated that the hydrated radius of permeant ion is an important factor to control the ionic transport processes and to reveal the potentiometric selectivity in these systems. It was suggested that the ion transport across homogeneous type amphoteric ion exchange membrane is strongly affected by hydrodynamic properties of permeant ion, but scarcely influenced by ionic charges of which effects are well known to be exclusive in the uniform cation and anion exchange membranes.

It has been well known that the charge-mosaic and layered type ion exchange membrane systems exhibit unique transport characteristics unexpected for the uniform ion exchange membrane system, such as piezodialysis, circulating electric current, and rectifying phenomena.[1–4] Including these interesting phenomena, the study of fundamental transport characteristics of homogeneous type amphoteric ion exchange membrane has not been systematically carried out yet.

As reported in the preceding paper, our preliminary experiments illustrated the unique transport characteristics of a 1.0-PA-29 amphoteric ion exchange membrane having a homogeneous structure (Kanegafuchi Chemical Industry Co., Ltd.).[5] A 1.0-PA-29 membrane demonstrated the permselectivity in response to ionic size of permeant electrolyte and, therefore, it seems to be possible that the membrane permselectivity is improved by introducing the amphoteric properties into the polymeric membrane structure. It was also suggested in the preceding paper that electrolyte permeation through the 1.0-PA-29 membrane does not depend upon the coupling flow mechanisms and, accordingly, the charge-mosaic membrane model is not suitable to analyse the transport processes across homogeneous type amphoteric ion exchange membrane.[5,6]

The present experiment was carried out to illustrate more clearly the potentiometric selectivity to ions and to confirm the fact that the ionic size of permeant is a dominant factor controlling the ionic transport processes across homogeneous type amphoteric ion exchange membrane. For this purpose, the transport characteristics of ammonium chloride and of a series of symmetric tetraalkylammonium chlorides, such as tetramethyl-, tetraethyl-, tetrapropyl-, and tetrabutylammonium chlorides, were examined, since a series of tetraalkylammonium ions has similar physicochemical properties except ionic bulkiness. In case of the usual uniform cation exchange membrane (Neosepta CL-25T, Tokuyama Soda Industry Co., Ltd.), membrane potential data for these tetraalkylammonium ions showed the almost ideal Nernstian slope against the logarithmic external electrolyte activity changes irrespectively of the difference in ionic sizes.[7] On the contrary, as shown later the membrane potential data of tetraalkylammonium chloride systems with a 1.0-PA-29 amphoteric ion exchange membrane changed considerably with the hydrated ionic size so as to reveal the potentiometric selectivity. In the present paper, we also discuss to some extent distinctive ion transport characteristics across amphoteric and uniform ion exchange membranes.

Experimental

A 1.0-PA-29 amphoteric ion exchange membrane was kindly supplied by the Central Research Laboratory of Kanegafuchi Chemical Industry Co., Ltd. and the membrane preparation processes were described elsewhere.[6] Ion exchange groups of this membrane are sulfonic acid and trimethylamine types attached to the cross-linked polystyrene skeleton supported by poly(vinyl chloride) network. Basic physicochemical properties are as follows (see also Ref. 5): Cationic and anionic exchange capacity, 1 mequiv./g-wt membrane; cationic/anionic capacity ratio, 1.0 ± 0.2; membrane thickness, 0.1 mm. The closest distance between cationic and anionic exchange sites can be roughly estimated to be *ca.* 0.75 nm when the total ion exchange capacity is 2 mequiv. and the degree of swelling is 0.5; in these situations, it seems to be hard to realize the ion transport mechanisms described with the charge-mosaic model system.[6] Experimental setup and methods were the same as those reported in the previous experiments.[5,8,9]

Electrochemical data, such as the membrane potential and conductance, were measured to estimate the electroconductive membrane permeability. Measurements were carried out on the systems where solution phases I and II were divided by membrane phase; electrolyte concentrations of phase I were varied from 10^{-1} to 10^{-3} mol dm^{-3} and

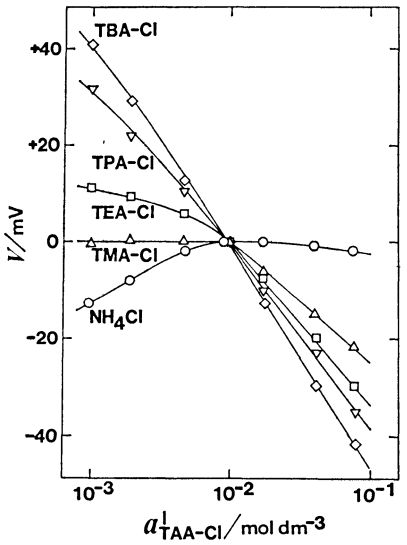

Fig. 1. Membrane potential data as a function of the mean electrolyte activity of phase I.
○: NH_4Cl, △: TMA–Cl, □: TEA–Cl, ▽: TPA–Cl, ◇: TBA–Cl.

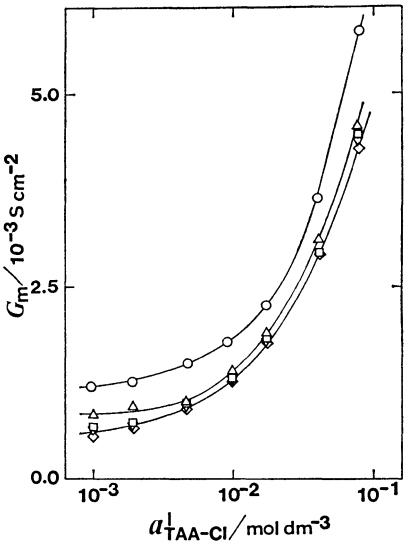

Fig. 2. Membrane conductance data as a function of the mean electrolyte activity of phase I. Symbols are the same as in Fig. 1.

those of phase II were kept constant at 10^{-2} mol dm^{-3}. Electrolyte solutions were prepared from extra pure chemicals (Nakarai Chemicals Ltd.) with conductivity water; ammonium chloride and symmetric tetraalkylammonium chlorides having methyl, ethyl, propyl, and butyl groups were used. All the experiments were carried out under the regulated room temperature, 25±1 °C.

Results and Discussion

Membrane potentials and conductances for the concentration cell systems of NH_4Cl, $(CH_3)_4NCl$ (TMA–Cl), $(C_2H_5)_4NCl$ (TEA–Cl), $(n\text{-}C_3H_7)_4NCl$ (TPA–Cl), and $(n\text{-}C_4H_9)_4NCl$ (TBA–Cl) were measured to estimate the membrane permeabilities. Figures 1 and 2 illustrate the membrane potential and conductance data as a function of mean electrolyte activity of phase I. As can be seen in Fig. 1, each system exhibits different slope of the membrane potential *vs.* logarithmic electrolyte activity plot; the negative slopes indicate that a 1.0-PA-29 amphoteric ion exchange membrane is more permselective to chloride ion than alkylammonium ions in the present situations. Figure 1 also shows that the permeability to chloride ions in general increases under conditions of higher external electrolyte concentrations. These negative slopes of membrane potential plots in Fig. 1 indicating the anionic selectivity decrease with decreasing bulkiness of respective cations from TBA^+ to TMA^+ and, in case of the NH_4Cl system, the potential plots tend to turn positive slope indicating the cationic selectivity of the membrane.

It is the most remarkable feature of the 1.0-PA-29 amphoteric membrane that the potentiometrically selective responses are observed even for ions of the same number of electric charge, as also discussed in the preceding paper.[5] In case of the system with usual uniform cation exchange membranes (*e.g.*, Neosepta CL-25T, Tokuyama Soda Co., Ltd.), similar membrane potential responses indicating the ideal Nernstian characteristics were observed to a series of cations from NH_4^+ to TBA^+; therefore, these membranes developed mainly for the desalination processes are ideally permselective to all the univalent cations and the characteristic potential responses specific to each cation were not observed.[7] Situations are the same in the uniform anion exchange membrane; membrane potential data for bulky surfactant anions were almost the same as those for simple anions.[10,11]

Membrane conductance data are summarized in Fig. 2. Membrane conductance values were not so distinctive to each system as membrane potential values but slightly dependent upon the cationic size. By the way, there is a striking difference between the conductance values of amphoteric ion exchange membrane and those of uniform cation exchange membrane. In case of the usual cation exchange membrane composed of various types of synthetic polymer, such as ACI (Asahi Chemical Industry Co., Ltd.), AMF C-103 (American Machine and Foundry Co., Ltd.), or CL-25T, the membrane conductance values of NH_4Cl amount to over hundred times as those of TBA–Cl system.[6,12]

On the basis of these electrochemical data, electroconductive membrane permeabilities to cation and chloride ion were estimated for each system; electroconductive permeabilities are defined and introduced to describe transport processes related to ionic mobility on the basis of nonequilibrium thermodynamics.[5,9,13] Electrochemical quantities are expressed as a function of membrane permeabilities to tetraalkylammonium ion (or ammonium ion) and chloride ion, P_{TAA} and P_{Cl}:

$$\begin{aligned} V_0 &= t_{TAA}V_{TAA} + t_{Cl}V_{Cl} \\ &= (g_{TAA}/G_m)V_{TAA} + (g_{Cl}/G_m)V_{Cl} \\ &= -(RT/F)\ln[(P_{TAA}a^{II}_{TAA}+P_{Cl}a^{I}_{Cl})/(P_{TAA}a^{I}_{TAA}+P_{Cl}a^{II}_{Cl})] \end{aligned} \quad (1)$$

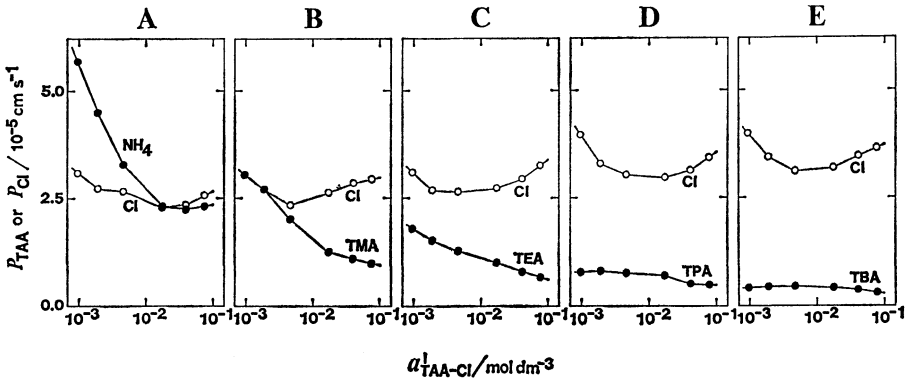

Fig. 3. Electroconductive membrane permeabilities as a function of the mean electrolyte activity of phase I. Closed and open circles indicate membrane permeabilities to cation and chloride ion, P_{TAA} and P_{Cl}, respectively.
A: NH_4Cl, B: TMA–Cl, C: TEA–Cl, D: TPA–Cl, E: TBA–Cl.

$$G_m = g_{TAA} + g_{Cl} = \frac{F^2}{RT}\left\{(a^{I}_{TAA}a^{II}_{TAA})^{1/2}P_{TAA}\frac{\sinh[F(V_0-V_{TAA})/2RT]}{F(V_0-V_{TAA})/2RT} + (a^{I}_{Cl}a^{II}_{Cl})^{1/2}P_{Cl}\frac{\sinh[F(V_0-V_{Cl})/2RT]}{F(V_0-V_{Cl})/2RT}\right\}, \quad (2)$$

where V_0 is the membrane potential in the absence of electric current, G_m is the membrane conductance, a is the activity, t is the transport number, and g is the ionic membrane conductance; V_{TAA} and V_{Cl} are the Nernst equilibrium membrane potentials to tetraalkylammonium ion (or ammonium ion) and chloride ion; F, R, and T indicate usual physical meanings; the subscripts TAA and Cl refer to tetraalkylammonium ion (or ammonium ion) and chloride ion; the superscripts I and II refer to solution phases I and II divided by membrane phase, respectively. Electroconductive membrane permeabilities, P_{TAA} and P_{Cl}, represent the membrane permselectivities to respective ions by indicating the order of electrical migration speed across membrane phase.

Membrane permeability values calculated by Eqs. 1 and 2 with electrochemical data are summarized in Fig. 3. As illustrated in this figure, the values of permeability to chloride ions show only a small change independently of difference in paired cationic species, while those to cations decrease with increasing bulkiness of respective cations as: $P_{NH_4} > P_{TMA} > P_{TEA} > P_{TPA} > P_{TBA}$. It can be also seen that the membrane permeability to smaller cations increases with decreasing external electrolyte concentrations of phase I, but for larger cations, this tendency is reduced and the permeability values are depressed to almost constant low level as shown by P_{TPA} and P_{TBA} values.

The membrane permeability ratios, P_{NH_4}/P_{Cl}, P_{TMA}/P_{Cl}, P_{TEA}/P_{Cl}, P_{TPA}/P_{Cl}, and P_{TBA}/P_{Cl}, are plotted as a function of mean electrolyte activity of phase I in Fig. 4. As expected from the respective permeability values, the permeability ratios decrease with increasing cationic bulkiness. Also in a uniform cation exchange membrane such as a Neosepta CL-25T, P_{TAA} values decrease with increasing cationic bulkiness in the same manner as the present experiment; however, P_{TAA}/P_{Cl} values are more than 100 and constant independently

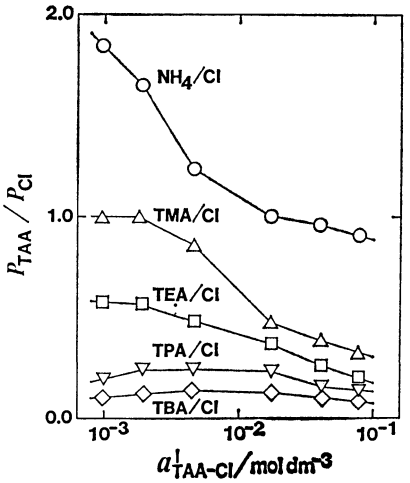

Fig. 4. Membrane permeability ratios as a function of the mean electrolyte activity of phase I.
○: P_{NH_4}/P_{Cl}, △: P_{TMA}/P_{Cl}, □: P_{TEA}/P_{Cl}, ▽: P_{TPA}/P_{Cl}, ◇: P_{TBA}/P_{Cl}.

of cationic bulkiness.[7] These are reasonable results as expected from Eq. 1, since the almost ideal Nernst membrane potentials were observed for the CL-25T membrane system and, accordingly, P_{TAA}/P_{Cl} ratios should be constant and approach to infinitely large values.

The present results suggest that the possible origin of the potentiometric selectivity of 1.0-PA-29 amphoteric ion exchange membrane is a sieve effect on permeant ions as also discussed in the preceding paper.[5] To examine further correlations between the membrane permeability and ionic size, the permeability values and permeability ratios are plotted against the values of hydrated radii of permeant ions, r_H,[14,15] in Figs. 5 and 6, respectively. These figures illustrate the reasonable correlation of hydrated ionic radius to both the permeability and the permeability ratio. The hydrated radii of tetraalkylammonium ions are almost the same as the crystal ionic radii owing to poor hydration. These results suggest that the transport process across amphoteric ion exchange membrane is strongly affected by the hydrated radius of permeant

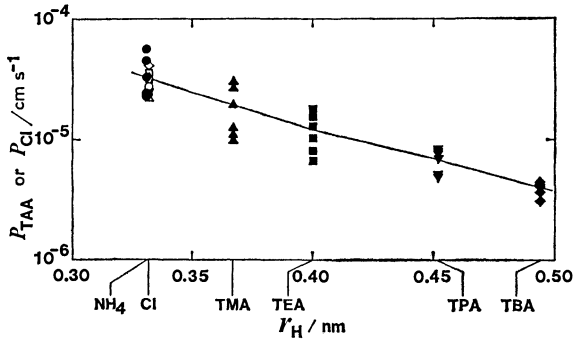

Fig. 5. Electroconductive membrane permeability *vs.* hydrated ionic radius plots.
●: P_{NH_4}, ▲: P_{TMA}, ■: P_{TEA}, ▼: P_{TPA}, ◆: P_{TBA}. P_{Cl}'s are indicated by corresponding open symbols. Solid line traces the average values of respective ions.

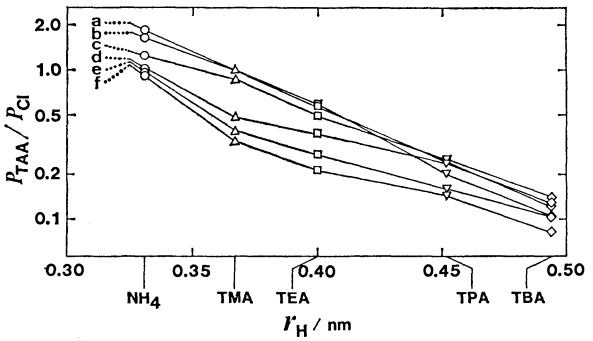

Fig. 6. Membrane permeability ratio *vs.* hydrated ionic radius plots. Symbols are the same as in Fig. 4. a, b, c, d, e, and f refer to the systems in which the electrolyte concentrations of phase I are 1×10^{-3}, 2×10^{-3}, 5×10^{-3}, 2×10^{-2}, 5×10^{-2}, and 1×10^{-1} mol dm^{-3}, respectively.

ion. Since the electroconductive membrane permeability is a function of the ionic mobility within membrane phase,[9,13,16] it is likely that the permeability values are inversely proportional to ionic size, although the mobility of permeant ion within membrane phase is not always the same as that in free solution phase and the ion movement through polymeric substance having charged sites is rather deviated from the movement in free media due to various effects.

As mentioned earlier, differences in electrochemical properties of tetraalkylammonium systems between the usual highly selective ion exchange membrane and the homogeneous type amphoteric ion exchange membrane are as follows: In the former membrane system, the membrane potential responses depend upon strictly the number of ionic charges so as to show the almost ideal Nernst potential for all the systems, but the membrane conductances are spread over wide range of values. In case of the latter membrane system as shown in the present results, the potentiometric selectivity to univalent cations of different ionic sizes is revealed, but the membrane conductances stay at similar values for all the systems. These experimental facts and estimated permeability values suggest some differences in possible ion transport mechanisms of uniform and amphoteric ion exchange membranes. It is generally realized that the ion transport process across uniformly charged membrane is controlled by the co-ion permeation.[16] Only the extremely small electrolyte fluxes are observed in the uniform ion exchange membrane under the steady conditions without membrane electric current, since the co-ion penetrations into membrane phase from external phase are prevented by high electric potential barrier. On the contrary, relatively large salt fluxes were observed in the homogeneous amphoteric membranes irrespectively of the low electrical membrane conductance.[17] It is especially interesting that the membrane permeability to chloride ion is maintained at nearly constant level for all the electrolyte systems having different size of cations as can be seen in Fig. 3. These results suggest that both the cations and anions independently migrate through the membrane phase with the interaction to electric fields built up by positively and negatively charged sites. Three dimensional array of the positive and negative charge, in which each site is adjacent at about 0.75 nm distance to oppositely charged sites, could effectively function rather as a sieve to select the size of permeant ions than as an electrical barrier. Under these situations, the ion transport across homogeneous type amphoteric ion exchange membrane seems to resemble preferably to that in free aqueous electrolyte solution, and consequently the large salt flux is expected.

As a matter of course, the ion permeability of 1.0-PA-29 membrane depends not only upon the hydrated ionic radius but also upon factors such as specific interactions of ions to exchange groups and to matrix polymer of membrane. It is, however, conceivable as shown in the present results that the effects of hydrated ionic size play an important role in the transport process of ions across the amphoteric ion exchange membrane with a homogeneous binary charged structure. On the contrary, the ionic size effects are almost concealed with the ionic charge effects in the uniform ion exchange membrane, and accordingly the potentiometric selectivity to univalent cations is not exposed. The most noticeable property of the 1.0-PA-29 membrane system with ammonium and tetraalkylammonium chlorides is that the slope of membrane potential *vs.* logarithmic electrolyte activity curve is changed stepwise in relation to the cationic hydrated radius as an indication of the appreciable variation in the relative membrane permeability with the constant chloride permeability. The present results suggest that the transport processes of ions across amphoteric ion exchange membrane explicitly reflect the hydrodynamic properties of permeant ions, while the ionic charge effects are dominant in the uniform ion exchange membrane.

We thank members of Central Research Laboratory of Kanegafuchi Chemical Industry Co., Ltd., especially Dr. Tamiyuki Eguchi, for preparing and supplying the amphoteric membrane, 1.0-PA-29, used in this work. This work was supported in part by a Grant-in-Aid for Scientific Research from the Ministry of Education, Science and Culture.

References

1) R. Neihof and K. Sollner, *J. Gen. Physiol.*, **38**, 613 (1955).
2) O. Kedem and A. Katchalsky, *Trans. Faraday Soc.*, **59**, 1918 (1963).
3) J. N. Weinstein, B. M. Misra, D. Kalif, and S. R. Caplan, *Desalination*, **12**, 1 (1973).
4) A. A. Sonin and G. Grossman, *J. Phys. Chem.*, **76**, 3996 (1972).
5) A. Yamauchi, S. Tsuruyama, H. Masumori, Y. Nagata, K. Kaibara, and H. Kimizuka, *Bull. Chem. Soc. Jpn.*, **55**, 3297 (1982).
6) T. Eguchi, S. Mori, and M. Shimokawa, *Membrane*, **3**, 289 (1978).
7) K. Inenaga, A. Yamauchi, and H. Kimizuka, *Bull. Chem. Soc. Jpn.*, **50**, 2584 (1977).
8) K. Kaibara, H. Ito, N. Inoue, and H. Kimizuka, *Mem. Fac. Sci., Kyushu Univ. Ser. C*, **12**, 125 (1980).
9) K. Kaibara and H. Kimizuka, *Bull. Chem. Soc. Jpn.*, **55**, 1743 (1982).
10) K. Kaibara, T. Nakahara, I. Satake, and R. Matuura, *Mem. Fac. Sci., Kyushu Univ. Ser. C*, **7**, 1 (1970).
11) K. Shirahama, *Kolloid Z. Z. Polym.*, **250**, 620 (1972).
12) H. Kawabe, H. Jacobson, I. Miller, and H. P. Gregor, *J. Colloid Interface Sci.*, **21**, 79 (1966).
13) H. Kimizuka and K. Kaibara, *J. Colloid Interface Sci.*, **52**, 516 (1975).
14) R. A. Robinson and R. H. Stokes, "Electrolyte Solutions," Butterworths & Co., London (1959).
15) E. R. Nightingale, Jr., *J. Phys. Chem.*, **63**, 1381 (1959).
16) H. Kimizuka, K. Kaibara, E. Kumamoto, and M. Shirōzu, *J. Memb. Sci.*, **4**, 81 (1978).
17) H. Kimizuka, K. Kaibara, and Y. Nagata, 7th International Biophysics Congress, Mexico City, August 1981, Abstr. 348.

 © 1983 The Chemical Society of Japan Bull. Chem. Soc. Jpn., 56, 1351—1356 (1983)

The Precipitation of Human Fibrinogen by Zinc Chloride

Hiroshi MAEDA,* Takaaki KISHI, and Shoichi IKEDA

Department of Chemistry, Faculty of Science, Nagoya University, Chikusa-ku, Nagoya 464

(Received December 8, 1982)

The precipitation of human fibrinogen by $ZnCl_2$ was studied by measuring the turbidity and the protein concentration in the supernatant (referred as solubility). Different kinetic patterns, either fast or slow, were observed in both solubility and turbidity depending on whether $ZnCl_2$ concentration (C_M) was larger or smaller than the critical concentration. In the slow pattern, the increase of the turbidity and the decrease of the solubility both occurred slowly and almost linearly with time. In the fast pattern, these changes occurred rapidly and stationary values were reached within 30 min for the turbidity and 2 h for the solubility. These two stationary values were found to be linearly related to each other. The stationary solubility decreased as C_M increased, while it increased with the total amount of the protein. The dissolution of the precipitates was very slow resulting in a practically irreversible precipitation. A gelation model was proposed to account for these characteristic features, according to which fibrinogen molecules were linked to each other through the 'bond' mediated by a zinc atom.

The interaction of zinc ions with human plasma proteins was studied by Cohn *et al.* in relation to their system for the separation of the components of human blood.[1] Complete flocculation of human γ-globulin occurred under the presence of $ZnSO_4$.[2] The binding constant of zinc ions to human serum albumin was shown to be close to that to imidazole.[3] Recently, gelation of bovine fibrinogen was found when various metal ions including Zn^{2+} were added.[4]

Recently, we have also found that the precipitation of human fibrinogen occurs on addition of various divalent metal chlorides.[5] Among them $ZnCl_2$ and $CuCl_2$ were most effective. The interaction of fibrinogen with $ZnCl_2$ or $CuCl_2$ was studied by circular dichroism and fluorescence. However, the mechanism of the precipitation was not clear at all.

In the present study, the precipitation of human fibrinogen by $ZnCl_2$ was examined at a fixed pH of 7.4 in 0.15 M NaCl (1 M=1 mol dm^{-3}), by the measurement of the solubility and by the kinetics of precipitation. The interaction of $CuCl_2$ with tris(hydroxymethyl)aminomethane (Tris) buffer, found previously,[5] prevents us from the measurement of the solubility in the $CuCl_2$–fibrinogen system. Consequently, the present study was carried out on the $ZnCl_2$–fibrinogen system.

The results on the solubility and the kinetics of precipitation obtained in the present study were rather unusual from the standpoint of a phase equilibrium or a coagulation of hydrophobic colloids. Therefore, a considerable amount of efforts is made in the present study to find a reasonable and simple model for a possible mechanism of the present precipitation.

Experimental

Fibrinogen (Kabi, grade L) was dissolved into 0.15 M NaCl and dialyzed against 0.15 M NaCl for 24—36 h and then freeze-dried. Tris and $ZnCl_2$ were purchased from Nakarai chemicals Co. Ltd. (Kyoto). The freeze-dried material was dissolved into the solvent [Tris–HCl 1.0×10^{-2} M (pH 7.4)+NaCl 0.15 M]. Final NaCl concentrations were not larger than 0.17 M even at the highest protein concentration. The protein concentration (g dm^{-3}) was calculated from the absorbance at 280 nm for 1 cm light path, Abs, as Abs/1.60. $ZnCl_2$ concentration (C_M) was expressed in M (mol dm^{-3}).

The protein concentration of the solution phase under phase separation was determined as follows. A given amount (0.01—0.1 cm^3) of $ZnCl_2$ solution was added to a protein solution (4 cm^3, 0.22—0.23 g dm^{-3}) in a glass tube. After a planned incubation period, the glass tube was put into a rotor and centrifuged at ca 1000 g for 20 min. Temperature was kept at 22±2 °C. Then, the absorbance of the supernatant was measured and the concentration was evaluated. The value was assigned to the time when the centrifugation was *started*. Identical results were obtained under different conditions: 500 g for 20 min or 1000 g for 50 min.

In the kinetics of the precipitation, the change of the turbidity was recorded automatically after the complete mixing was established within 1 or 2 s. The details of the mixing procedure will be described in the accompanying paper.[6]

Absorption spectra and turbidity were measured with a Shimadzu UV-200 S spectrophotometer using a cell of 1 cm light path.

Results

The Protein Concentration in Solution Phase. The protein concentration in the solution phase was measured by absorption at 280 nm after centrifugation at 1000 *g* for 20 min. Throughout the present study, the supernatant concentration is conventionally called as 'solubility', though it does not represent a solubility as defined by the phase rule as shown later. The total protein concentration, was 0.22—0.23 g dm^{-3}. The time course of the protein concentration in the solution phase was followed by applying the above procedure at different times after the addition of $ZnCl_2$. Two distinct patterns were found as shown in Fig. 1 depending on the $ZnCl_2$ concentration C_M. At $C_M=1.9\times10^{-5}$ M or lower, the protein concentration decreased slowly with time. This behavior is typical to the slow coagulation phase of hydrophobic colloids. At $C_M=4.5\times10^{-5}$ M or higher, the protein concentration decreased rapidly and reached a stationary value after about 2 h. This behavior also resembles the fast coagulation of hydrophobic colloids. However, the stationary concentrations were different for different 'coagulant' concentration C_M, as shown in Fig. 1, which cannot be properly explained based on the picture of the coagulation of hydrophobic colloids.

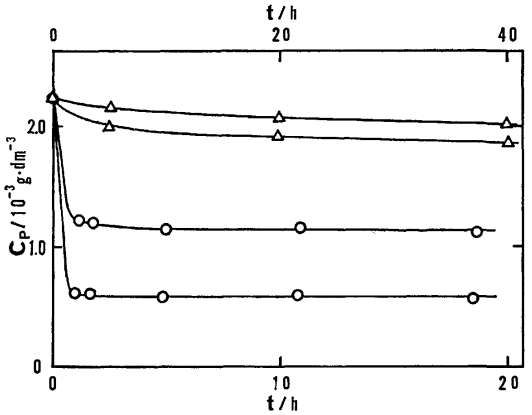

Fig. 1. Time course of the solubility.
$ZnCl_2$ concentrations(mol dm^{-3}) (from top to bottom): 9.02×10^{-6}, 1.80×10^{-5}, 4.49×10^{-5}, and 1.00×10^{-4}. Triangles refer to the upside abscissa.

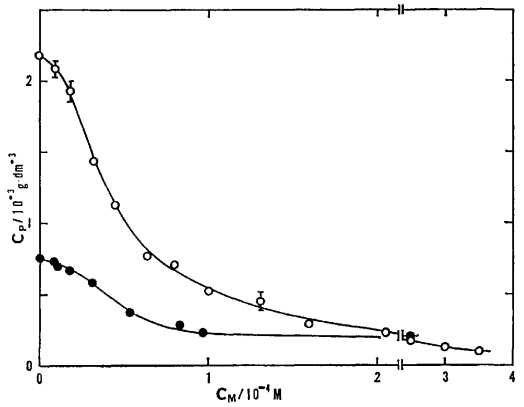

Fig. 2. Dependence of the stationary solubilities on $ZnCl_2$ concentration C_M.
The total protein concentrations (g dm^{-3}): 0.22 (○) and 0.077 (●).

The results in Fig. 1 suggest the presence of a kind of critical concentration in the range $(2—4)\times10^{-5}$ M. The rate of the concentration change of fibrinogen differed markedly depending on whether C_M was larger or smaller than the critical concentration.

In Fig. 2, the stationary values of the 'solubility' are plotted as functions of $ZnCl_2$ concentration C_M for two different total protein concentrations. The values at about 20 h were taken in place of the stationary values in the case of the low total protein concentration, at which the time course of the 'solubility' was not examined. The same approximate procedure was used for small values of C_M at which the protein concentration decreased slowly without exhibiting a stationary state. There are two characteristic features about the present precipitation as clearly shown in Fig. 2. The stationary values depend on $ZnCl_2$ concentration, as already noticed in Fig. 1. This dependence suggests that the chemical potential of $ZnCl_2$ plays an important role in the precipitation. It is likely, therefore, that the interaction of fibrinogen with Zn^{2+} ions leading to the precipitation is rather reversible. The other feature is that the stationary protein concentration depends not only on C_M but

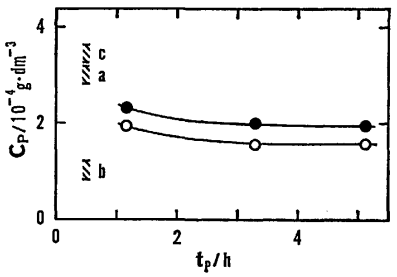

Fig. 3. Dependence of the solubility after dilution on the incubation time for precipitation t_p.
Measuring time of the solubility after dilution: 8 (○) and 20 (●) h. About three levels a, b, and c, see text.

also on the total amount of the protein. A simple phase equilibrium is hence ruled out, while phase equilibria of a multicomponent system can account for this dependence. In a study of bovine fibrinogen, the protein did not behave as a single component as defined by the phase rule.[7]

Irreversible Nature of the Precipitation. The following two kinds of experiments were carried out to examine the reversibility of the precipitation of fibrinogen by the addition of $ZnCl_2$.

Experiment A: A solution of $ZnCl_2$ was added to a protein solution (4 cm^3, 0.22 g dm^{-3}) to give a metal concentration of 1.70×10^{-4} M. Identical solutions were prepared in multiplicate. About one hour after the addition of $ZnCl_2$, one of the members was subject to centrifugation and the 'solubility' was determined as 0.030 g dm^{-3} (level a in Fig. 3), which was consistent with that given in Fig. 2. The other members of the solutions, which were not centrifuged, were diluted with 8 cm^3 of the solvent (containing no $ZnCl_2$) at the time about 70 or 200 or 310 min after the addition of $ZnCl_2$.

The 'solubilities' of these diluted solutions were measured at about 8 and 20 h after the dilution was made. If the precipitation is reversible, the expected 'solubility' can be read from the 'solubility curve' in Fig. 2 corresponding to the low total protein concentration (defined by filled circles) at $C_M=5.66\times10^{-5}$ M, which is about 0.035 g dm^{-3} (level c in Fig. 3). At about 8 h after the dilution (open circles), the 'solubility' was significantly larger than what would be expected for the completely irreversible situation (level b in Fig. 3). Undoubtedly, the precipitates can dissolve, even though slowly. The results as well as these expected values for the completely reversible and irreversible situations are indicated in Fig. 3. At about 20 h after the dilution (filled circles), the 'solubility' increased appreciably from that found at 8 h after the dilution (open circles). The increment of the 'solubility' was nearly independent of the *incubation time for the precipitation*. However, if compared at the same *incubation time for the dissolution*, the 'solubility' is larger if the *incubation time for the precipitation* is shorter. The dependence on the *incubation time for the precipitation* disappeared when it was longer than about 3 h. This dependence is closely related to the time course of the 'solubility' shown in Fig. 1.

In Fig. 3, the 'solubility' never reaches the value expected for the reversible situation (level c) even at 20 h after the dilution. Consequently, the present precipitation is rather irreversible in the sense that the rate of dissolution is very slow.

Experiment B: A small volume of $ZnCl_2$ solution was added to a protein solution (4 cm^3) of a concentration of 0.22 g dm^{-3} to make the metal concentration C_M to be 1.29×10^{-4} M. The 'solubility' was measured at about 5 h after the addition of $ZnCl_2$ to confirm the stationary value. The measured 'solubility' was 0.039 g dm^{-3}, consistent with the results in Fig. 2. Then 2 cm^3 of a protein solution (0.22 g dm^{-3}) containing no $ZnCl_2$ was added and kept for 8 and 20 h. The final metal concentration was the two thirds of the initial value, *i.e.*, 8.57×10^{-5} M. The 'solubilities' measured at 8 and 20 hours were nearly the same and 0.056 g dm^{-3}.

Consider the situation immediately after the above mixing. The protein concentration in the solution phase is 0.1 g dm^{-3} $(0.039\times2/3+0.22\times1/3)$. The 'solubility' expected at $C_M=1.29\times10^{-4}$ M for this total protein concentration is between the two 'solubility' curves in Fig. 2. If the solubility is assumed to be proportional to the total protein concentration, then the 'solubility' is 0.031 g dm^{-3}. On the other hand, the 'solubility' expected for a completely reversible situation is 0.063 g dm^{-3}: the 'solubility' at $C_M=8.57\times10^{-5}$ M for the total protein concentration of 0.22 g cm^{-3}. Since the observed 'solubility' (0.056 g dm^{-3}) was close to 0.063 g dm^{-3} rather than 0.031 g dm^{-3}, it is likely that the precipitation of newly added protein occurred under the control of the amount of the precipitates present in advance to the mixing.

In this experiment, the amount of the precipitates increased after mixing the two solutions. The time dependence of the 'solubility' was not found, therefore, between 8 and 20 h, in contrast to the case shown in Fig. 3, where the dissolution of the precipitates was followed.

A conclusion derived from Experiment A is an extremely slow rate of dissolution of the precipitates. On the other hand, Experiment B suggests that the 'solubility' is controlled by the amount of the precipitates, indicating a microscopic reversibility between the precipitates and the solution phase. The idea of the phase equilibria of a multicomponent system cannot reconcile one of these two results with the other.

Kinetics of Precipitation. The time courses of the turbidity are shown in Figs. 4(A) and (B) for the protein concentration of 0.22—0.23 g dm^{-3}: the same concentration as used in the study of solubility. At $C_M=2.97\times10^{-5}$ M, the turbidity increased linearly but only slightly. However, at $C_M=3.95\times10^{-5}$ M, a sigmoidal increase began to appear. Typical sigmoidal patterns were obtained at $C_M=4.92\times10^{-5}$ M[Fig. 4 (A)], 5.88 and 6.84×10^{-5} M[Fig. 4(B)]. At $C_M\approx(9.7—9.8)\times10^{-4}$ M, a sigmoidal shape could not be recognized any more, probably because the lag time was too short to be detected in the time scale of the present experiment.

The present kinetics can be summarized in the following two points. First, there is a critical $ZnCl_2$ concentration C_M*, below which the turbidity increases linearly but very slowly (slow phase) and above which it increases rapidly in a sigmoidal way (fast phase). The critical concentration was $(3—4)\times10^{-5}$ M for the protein concentration of 0.23 g dm^{-3}. In the second place, the turbidity reaches a stationary value after 25—30 min in the present kinetics as shown by horizontal bars in Fig. 4(A) if $C_M\geq C_M$*. The similar kinetic behavior was recently observed in the gelation of bovine fibrinogen by metal ions, where a stationary turbidity was reached after 2—3 min.[4] This kind of behavior has been rarely observed in the studies on the coagulation of colloids. Since the details of the kinetics of the present precipitation will be described in the following paper,[6] it is sufficient in the present study to point out the close relationship between the 'solubility' and the turbidity as shown below.

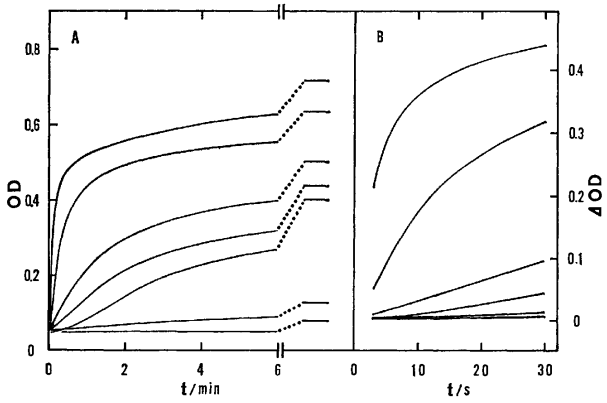

Fig. 4. Time courses of the turbidity at 350 nm. Protein concentration: 0.22—0.23 g dm^{-3}. $ZnCl_2$ concentrations(mol dm^{-3}) (from top to bottom): 1.88×10^{-4}, 9.68×10^{-5}, 6.84×10^{-5}, 5.88×10^{-5}, 4.92×10^{-5}, 3.95×10^{-5}, and 2.97×10^{-5}. In (B) $\Delta OD=OD(t)—OD(t=0)$ is given.

When the kinetic results shown in Figs. 4(A) and (B) are compared with the time course of the 'solubility' in Fig. 1, a good correspondence is found. At first, the critical $ZnCl_2$ concentration found in Fig. 1 lies between 2 and 4×10^{-5} M, which coincides with C_M* ($(3—4)\times10^{-5}$ M) found in the kinetics. When $C_M<C_M$*, both turbidity and 'solubility' change slowly with time in an approximately linear way. When $C_M\geq C_M$*, the turbidity increases and reaches a stationary value, as the 'solubility' decreases and reaches a stationary value. Accordingly, we can conclude that these two kinds of experiments are observing the same process but in terms of different quantities in different time ranges. We can reasonably assume that the change of the protein concentration occurred mostly within about 30 min if $C_M\geq C_M$*, as judged from the kinetic data.

To examine the correlation between the stationary turbidity and the stationary 'solubility', they are plotted against each other in Fig. 5. To construct this plot, the 'solubilities' at the $ZnCl_2$ concentrations where the kinetic measurements were carried out were read from a curve shown in Fig. 2. A good correlation is found between the two quantities as shown in Fig. 5. In other words, the turbidity in the present study

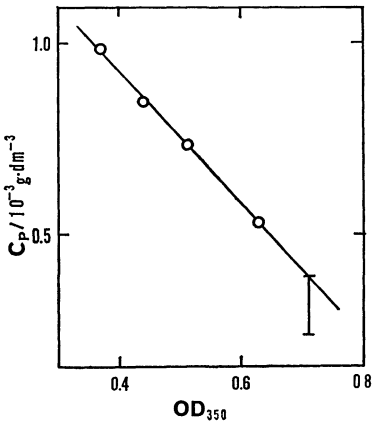

Fig. 5. Correlation between the stationary solubility C_p and the stationary turbidity at 350 nm.
The total protein concentration: 0.22—0.23 g dm^{-3}.

is approximately linearly related to the 'solubility'.

Summary of the Present Results. The 'solubility' behavior examined in the present study is considerably complex. It is pertinent, therefore, to summarize main results concerning a process characterizing the fast kinetic pattern. As to the slow pattern, we cannot make any discussion at present. The main results can be summarized into the four points.

(1) A critical $ZnCl_2$ concentration C_M* exists which defines different time courses of the 'solubility'.

(2) Stationary values of the 'solubility' exist and they decrease as $ZnCl_2$ concentration C_M increases.

(3) The 'solubility' increases with the total amount of the protein.

(4) The precipitates dissolve very slowly, so the precipitation is irreversible to a considerable extent.

The results (1)—(4) cannot be understood consistently by a phase equilibrium even the polydispersity is taken into account, since it fails to explain the irreversible nature. The coagulation of colloids cannot explain the dependence on the 'coagulant' concentration [result (2)], even though it is assumed that a thermodynamically stable fibrinogen solution is converted to a colloidal dispersion of kinetic stability by the addition of $ZnCl_2$.

If we regard the present precipitation as a kind of gelation, on the other hand, these results seem to be understood rather reasonably. The critical concentration is related to the gel point. The dependence of the solubility (proportional to the amount of the sol) on the total amount is consistent with gelation. Irreversible bond formation is also rather frequently encountered in gelation. On the other hand, it is difficult to explain the existence of a finite solubility still after the gelation is completed. However, the 'bond' between fibrinogen molecules is mediated by a zinc atom in the present case. Therefore, there is a room for models describing the coupling between the reversible binding of Zn^{2+} ions and the highly irreversible precipitation. An attempt will be given in the next section.

A Simplified Model. Gelation of Trifunctional Units: We will present a model with some assumptions, which can account for all the results (1)—(4) and for several

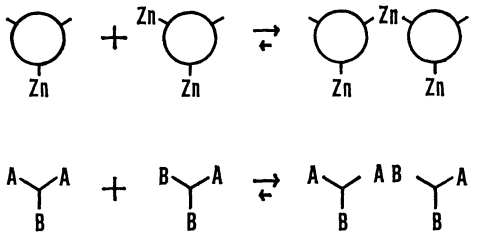

Fig. 6. Schematic representation of the model for gelation.
Free and bound sites on a fibrinogen molecule (represented as a circle) are denoted as A and B, respectively. The bond between two fibrinogen molecules is mediated by a zinc atom. In the model the bond is formed as a reaction between two 'functional groups' A and B.

kinetic results as well, although qualitatively.

Each fibrinogen molecule consists of a pair of three chains, $(A\alpha)_2(B\beta)_2\gamma_2$[8] and presumably carries a number of binding sites for Zn^{2+} ions of different affinities. The number of binding sites should be an even number because of the symmetric structure. However, a simple model of three equivalent binding sites is assumed here, hoping that the essential features of more realistic but more complicated models are fully retained in it (Assumption 1).

The binding equilibrium can be written in terms of free and occupied sites A and B (Assumption 2).

$$A + Zn^{2+} \overset{K}{\rightleftharpoons} B. \quad (1)$$

The association constant K is written in terms of site concentrations [A] and [B].

$$[B]/[A] = KC_M. \quad (2)$$

Here and throughout, free Zn^{2+} ion concentration is approximated to the total metal concentration C_M. At a given protein concentration, relative populations of four possible species A_3, A_2B, AB_2, and B_3 are 1: $2KC_M$: $2(KC_M)^2$: $(KC_M)^3$. As discussed later, values of KC_M in the present study are considered to be much smaller than unity. The contribution from species B_3 is therefore neglected in the following analysis. The binding equilibrium described by Eq. 1 is established instantly compared with the time scale of the present precipitation.

It is assumed that the reaction between site A and site B occurs after the binding equilibrium is established (Assumption 3). An example of the reaction leading to aggregation is schematically depicted in Fig. 6. For species A_2B or AB_2, this kind of association occurs with any other species as well as with themselves, while species A_3 or B_3 cannot associate with themselves. Flory has shown that the self-association of species A_2B or AB_2 cannot produce a gel, though three-dimensional branched polymers are formed.[9] Accordingly, any one of the four species alone cannot produce a gel.

Next, we examine the reactions in binary mixtures of A_3+A_2B or A_2B+AB_2. At low $ZnCl_2$ concentrations, the system can be well approximated to a binary mixture A_3+A_2B. In this mixture, association occurs between A_3 and A_2B as well as between two A_2B mole-

cules. However, gelation does not occur in this mixture. At larger $ZnCl_2$ concentrations where the population of AB_2 is significant, a ternary mixture has to be considered. Since an essential reaction leading to gelation occurs between A_2B and AB_2, we will examine, for simplicity, a binary mixture of A_2B and AB_2. We introduce the extent of reaction p_A (p_B) for a 'functional group' A(B), after the standard theory of gelation.[10] As shown in Appendix, a critical extent of reaction for gelation exists in this mixture. The range of gelation is given as follows.

$$\begin{aligned} &2(2-X_1)/(4+X_1) \ll P_A \ll 1, \text{ for } X_1 \leqq 0.5. \\ &2(1+X_1)/(5-X_1) \ll p_B \ll 1, \text{ for } X_1 \geqq 0.5. \end{aligned} \quad (3)$$

Here X_1 denotes the mole fraction of A_2B. Since $A_2B:AB_2 \simeq 1:KC_M$, and since KC_M is considered to be much smaller than unity, X_1 is supposed to be much larger than 0.5.

In Flory's model, the extent of reaction goes to unity as gelation is completed, since crosslinkings are allowed in gels (but not in soluble aggregates).[10,11] In this extreme case, no free B groups are present any more in gels, while free A groups are still present in gels since p_A is smaller than unity ($p_A=(2-X_1)/(1+X_1)<1$). In this situation, the 'solubility' is expected to be negligibly small.

According to Stockmayer's model, on the other hand, the extent of reaction does not exceed a certain limit, since no crosslinkings are allowed even in gels.[11] A finite solubility can be expected in this case. The limiting value of p_B is calculated in Appendix for the binary mixture A_2B+AB_2 and given as $(2-X_1)^{-1}$. This value is nearly equal to but always smaller than $2(1+X_1)/(5-X_1)$, the critical extent of reaction for $X_1 \geqq 0.5$. Since X_1 is expected to be much larger than 0.5, gelation cannot occur in the binary mixture A_2B+AB_2 if crosslinkings are forbidden in gels.

It is likely that the actual situation lies between these two extreme cases; the limiting value of p_B, $p_B(\infty)$, lies between $(2-X_1)^{-1}$ and unity. Consequently, we can expect that there are not a few free A and B groups in gels even when the gelation is completed ($t \to \infty$). Returning to the original ternary mixture, $A_3+A_2B+AB_2$, we find that a certain amount of soluble substances can exist in equilibrium with these free A and B groups in gels. In soluble fraction, these free A and B groups are present in species A_3, A_2B, and possibly in soluble aggregates. The 'solubility' is hence guaranteed if both free A and B groups are present in gels to a considerable amount even when the gelation is completed. In the above argument, we have to assume that the participation of species A_3 into gelation does not alter the essential features of the gelation of the binary mixture A_2B+AB_2 (Assumption 4).

The suggested 'solubility' is larger when $ZnCl_2$ concentration C_M is lower, if compared at the same protein content, as a consequence of the assumed mass action law:Eq. 2. Since the concentration of species A_3 increases with the total amount of the protein, the 'solubility' also increases with the latter. The critical concentration C_M^* can be identified with the gel point. From these considerations, it is clear that the present model can account for the results (1)—(3). One obvious way to account for result(4), the slow rate of dissolution of the precipitates, is to assume that the rate of dissolution is greatly reduced if crosslinkings occur in gels (Assumption 5). It is to be noted that the validity of the above arguments on the existence of the solubility and its dependence on C_M does not depend on the rate of dissolution of the precipitates.

In this way, the present model can explain the four main results by identifying the present precipitation with a gelation. Also, the time course of the turbidity can be understood based on the present model. Since the turbidity does not develop until the extent of reaction reaches a critical value for the gelation, a lag time will be observed in the kinetics.

Discussion

In the last section, we present a model to account for the present results on the precipitation of human fibrinogen with $ZnCl_2$. It is frequently inferred in deriving various properties of the model that the occupied fraction of binding sites for Zn^{2+} ions is very small. This point is discussed here.

As a rough estimation of the value of the association constant K defined as Eq. 2, we can take $1\times10^3\ M^{-1}$, since the association constant of imidazole with Zn^{2+} ions was about $6\times10^2\ M^{-1}$.[12] The range of KC_M in the present study is then below 0.2 (corresponding to $C_M=2\times10^{-4}$ M) or smaller. When KC_M is 0.1, the fractions of various species are 0.82(A_3), 0.16(A_2B), and 0.016(AB_2) and species B_3 can be safely neglected as assumed. Since X_1 can be roughly equated to the ratio $A_2B/(A_2B+AB_2)$, it is about 0.91. At $C_M=C_M^*$ ($\approx3\times10^{-5}$ M), $KC_M^*\approx3\times10^{-2}$ and $X_1\approx0.97$. Practically, gelation does not occur below C_M^*, for X_1 is nearly unity. It is found that the conditions used in the preceding section, $X_1 \gg 0.5$ and $KC_M \ll 1$, are reasonable.

It has been reported that fibrinogen is a heterogeneous mixture.[7,13-16] However, this point is not taken into account in developing the present model for the sake of simplicity. The introduction of the heterogeneity into the model does not violate its validity, since it only makes the model more versatile.

The most important feature of the present model resides in the respect that it can account for the finite solubility (dependent on $ZnCl_2$ concentration) in the situation that gelation is completed and is highly irreversible. However, the problem is treated only approximately in the present study. Moreover, the treatment is based on the classical theory of gelation, according to which the most probable distribution is considered for an infinitely large system and the mean field approximation is often used. Although the mean field approximation is criticized from the standpoint of the scaling theory,[17] and although the ensemble averages should be used in place of the most probable distribution as was recently carried out by computer simulation,[18,19] it is hoped that the present simple treatment gives an essentially correct picture of the present results.

Appendix

Gelation of a binary mixture of trifunctional units, A_2B and AB_2, is considered here based on the most probable distribution for an infinitely large system.

The mole fractions of A_2B and AB_2 are denoted as X_1 and X_2, respectively: $X_1+X_2=1$.

The extents of reaction of A and B groups are denoted as p_A and p_B. They are related to each other by Eq. A1.

$$p_A(1+X_1) = p_B(1+X_2). \tag{A1}$$

The expected number of units(irrespective of A_2B and AB_2) bound to A_2B is $2p_A+p_B$. Similarly, $2p_B+p_A$ is the expected number of units bound to AB_2. Gelation occurs when the expected numbers of units bound to both kinds of unit are equal to or larger than 2, *i.e.*,

$$2p_A + p_B \geqq 2, \tag{A2}$$

and

$$2p_B + p_A \geqq 2. \tag{A3}$$

Other obvious restrictions on p_A and p_B are

$$p_A \leqq 1 \text{ and } p_B \leqq 1. \tag{A4}$$

When these conditions are rearranged and coupled, we find that gelation occurs if the following conditions are satisfied.

$$\begin{aligned} &2(1+X_1)/(4+X_1) \leqq p_B \leqq (1+X_1)/(2-X_1) \text{ for } X_1 \leqq 0.5. \\ &2(1+X_1)/(5-X_1) \leqq p_B \leqq 1 \text{ for } X_1 \geqq 0.5. \end{aligned} \tag{A5}$$

Inequalities (A5) are given in the text as inequalities (3). For pure species, either $X_1=1$ (pure A_2B) or $X_1=0$ (pure AB_2), gelation occurs only at the end of reaction, either $p_B=1$ or $p_A=1$ ($p_B=0.5$) depending on whether X_1 is larger or smaller than 0.5. This is Flory's result.[9]

Next, the limiting extents of reaction of A and B groups when the gelation is completed are evaluated according to Stockmayer's model, in which no crosslinkings are allowed not only in soluble aggregates (as in most theories) but also in gels (contrary to Flory's model).[10,11] As a first step ($n=1$), only one unit, either A_2B or AB_2, is chosen. The number of unreacted A or B groups, $A_f(1)$ or $B_f(1)$, is given on the average as $A_f(1)=2X_1+X_2$ or $B_f(1)=2X_2+X_1$. The number of reacted groups, $A_b(1)$ or $B_b(1)$, is zero. As the second step ($n=2$), all three groups of a unit chosen in the first step are reacted to make a tetramer [$N(2)=4$]. As the third step ($n=3$), all the unreacted groups on the tetramer are reacted and an aggregate consisting of 10 units [$N(3)=10$] is produced. We define in this way $A_f(n)$, $B_f(n)$, $A_b(n)$, $B_b(n)$, and $N(n)$ as the numbers of A and B groups unreacted, reacted and the total number of units when the n-th step is finished.

The following recurrence formulas are obtained for $A_f(n)$ and $B_f(n)$.

$$\begin{aligned} A_f(n) &= (1+X_1)A_f(n-1) + X_1B_f(n-1), \\ B_f(n) &= (1+X_2)B_f(n-1) + X_2A_f(n-1). \end{aligned} \tag{A6}$$

$A_b(n)$, $B_b(n)$, and $N(n)$ are given as follows.

$$A_b(n) = B_b(n) = \sum_{i=1}^{n-1} [A_f(i)+B_f(i)] = 3(2^{n-1}-1). \tag{A7}$$

$$N(n) = 1 + 3(2^{n-1}-1). \tag{A8}$$

From these results, we obtain

$$\begin{aligned} p_A(n) &= 3(2^{n-1}-1)/[1+X_1+3(1+X_1)(2^{n-1}-1)]. \\ p_B(n) &= 3(2^{n-1}-1)/[1+X_2+3(1+X_2)(2^{n-1}-1)]. \end{aligned} \tag{A9}$$

In the limit that n goes to infinity,

$$p_A(\infty) = (1+X_1)^{-1} \text{ and } p_B(\infty) = (1+X_2)^{-1}. \tag{A10}$$

This result is given in the text.

References

1) E. J. Cohn *et al.*, *J. Am. Chem. Soc.*, **72**, 465 (1950).
2) N. H. Martin and D. J. Perkins, *Discuss. Faraday Soc.*, **18**, 361 (1955).
3) F. R. N. Gurd and D. S. Goodman, *J. Am. Chem. Soc.*, **74**, 670 (1952).
4) F. S. Stevens, M. M. Griffin, B. S. Brown, and T. P. Hulley, *Int. J. Biol. Macromol.*, **4**, 367 (1982).
5) H. Maeda, T. Kishi, S. Ikeda, S. Sasaki, and K. Kito, *Int. J. Biol. Macromol.*, (1983) in press.
6) T. Kishi, H. Maeda, and S. Ikeda, *Bull. Chem. Soc. Jpn.*, **56**, 1365 (1983).
7) R. W. Hartley, Jr., and D. F. Waugh, *J. Am. Chem. Soc.*, **82**, 978 (1960).
8) R. F. Doolittle, *Adv. Protein Chem.*, **27**, 2 (1973).
9) P. J. Flory, "Principles of Polymer Chemistry," Cornell University Press, New York (1953), Chap. IX, 2a.
10) P. J. Flory, "Principles of Polymer Chemistry," Cornell University Press, New York (1953), Chap. IX.
11) W. H. Stockmayer, *J. Chem. Phys.*, **11**, 45 (1943).
12) J. T. Edsall, G. Felsenfeld, D. S. Goodman, and F. R. N. Gurd, *J. Am. Chem. Soc.*, **76**, 3054 (1954).
13) D. F. Mosher and E. R. Blout, *J. Biol. Chem.*, **248**, 6986 (1973).
14) M. W. Mosesson, J. S. Finlayson, R. A. Umfleet, and D. Galanakis, *J. Biol. Chem.*, **247**, 5210 (1972).
15) J. S. Finlayson, M. W. Mosesson, T. J. Bronzert, and J. J. Pisano, *J. Biol. Chem.*, **247**, 5220 (1972).
16) M. W. Mosesson, J. S. Finlayson, and R. A. Umfleet, *J. Biol. Chem.*, **247**, 5223 (1972).
17) P.-G. de Gennes, "Scaling Concepts in Polymer Physics," Cornell University Press, New York (1979), Chap. V.
18) E. Donoghue and J. H. Gibbs, *J. Polymer Sci., Polymer Symp.*, **63**, 131 (1978).
19) E. Donoghue and J. H. Gibbs, *J. Chem. Phys.*, **70**, 2346 (1973).

 © 1983 The Chemical Society of Japan Bull. Chem. Soc. Jpn., 56, 1357—1361 (1983)

Kinetics of the Precipitation of Human Fibrinogen by $ZnCl_2$ and $CuCl_2$

Takaaki KISHI, Hiroshi MAEDA,* and Shoichi IKEDA

Department of Chemistry, Faculty of Science, Nagoya University, Chikusa-ku, Nagoya 464

(Received December 8, 1982)

Kinetics of the precipitation of human fibrinogen by the addition of $ZnCl_2$ was followed by the turbidity at 350 or 500 nm. Fast or slow precipitation occurred depending on whether the metal concentration (C_M) was higher or lower than its critical value. In fast precipitations, the turbidity reached the stationary value within about 30 min. From the stationary values of the turbidity the critical concentration could be determined. A sigmoidal increase of the turbidity was often observed at low protein concentrations (C_P); the lag time decreased with both C_M and C_P. At the final stage of the precipitation, the turbidity reached the stationary value exponentially; the characteristic time constant was almost independent of both C_M and C_P. These kinetic behaviors were consistent with the gelation model proposed to the present precipitation. When $CuCl_2$ was used in place of $ZnCl_2$, similar kinetic behaviors were obtained in many respects, suggesting the similar mechanism of precipitation for both $ZnCl_2$ and $CuCl_2$. Changes from slow to fast precipitation were observed when ionic strength was lowered.

In the preceding paper,[1] the precipitation of human fibrinogen was examined and the process was shown to be best understood as a kind of gelation where the extent of reaction did not exceed a limit even when gelation was completed. Also an interesting result was obtained in the study that the turbidity was linearly related to the 'solubility' of the protein.[1] Here and throughout the present study, the term solubility does not refer to a thermodynamic phase equilibrium but only represents the protein concentration in the supernatant. The time course of the turbidity can be interpreted as the time course of the solubility in the precipitation of human fibrinogen by $ZnCl_2$. This situation is different from that frequently encountered in the kinetics of coagulation of colloids, where the turbidity is a complex quantity and only its initial changes are used to extract information on the coagulation. In the present study, kinetics of precipitation of human fibrinogen was followed by the turbidity at different protein concentrations and at various $ZnCl_2$ or $CuCl_2$ concentrations.

The interaction of fibrinogen with $CuCl_2$ could not be studied in the previous study,[1] because the measurement of the solubility was hampered by the interaction of $CuCl_2$ with Tris buffer.[2] Since the absorbance at 350 or 500 nm is little affected by the interaction of $CuCl_2$ with Tris buffer, the effect of $CuCl_2$ on the precipitation of human fibrinogen can be studied in the present study by following the time course of the turbidity.

Experimental

Fibrinogen, $ZnCl_2$, $CuCl_2$, and Tris were the same as used in the previous studies.[1,2]

In the kinetics of precipitation, the mixing of $ZnCl_2$ (or $CuCl_2$) solutions was carried out by pushing down a plunger until it reached the bottom of a cell followed by pulling it up. The cell was placed in the light path of a spectrophotometer. In this way, 0.01 to 0.1 cm^3 of metal chloride solution in a basket attached to the end of a plunger could be mixed with a protein solution (3—4 cm^3) contained in a cell. The change of the absorbance (turbidity) was automatically recorded on a recorder (chart speed 0.2 cm/s). It took less than one second for this single down and up manual motion. The extent of uniform mixing was checked using a dye solution. It was found that about 99% of the final absorbance was obtained by a single down-up motion. It took less than 2 s for two successive motions, which gave a practically complete mixing. Absorption spectra and the turbidity were both measured with a Shimadzu UV-200 S spectrophotometer using a cell of 1 cm light path.

The protein concentration (g dm^{-3}) was determined as described in the preceding paper.[1] $ZnCl_2$ or $CuCl_2$ concentration was denoted as C_M and expressed in M (mol dm^{-3}).

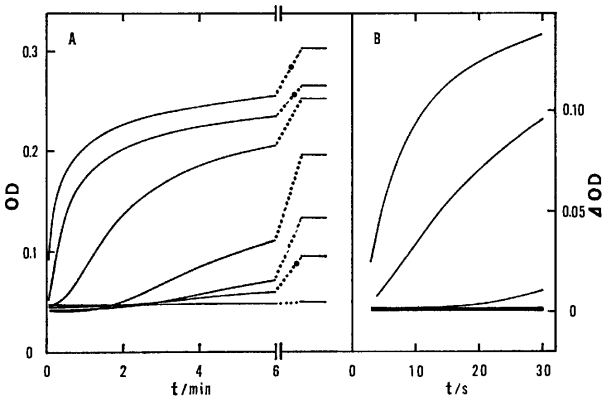

Fig. 1. Time courses of the turbidity at 350 nm at the protein concentration of 0.078 g dm^{-3}. $ZnCl_2$ concentrations (mol dm^{-3}) (from top to bottom): 3.75×10^{-4}, 1.88×10^{-4}, 9.68×10^{-5}, 7.79×10^{-5}, 6.84×10^{-5}, 4.92×10^{-5}, and 2.97×10^{-5}. In (B), ΔOD represents a change from the original level ($t=0$) at each $ZnCl_2$ concentration. Stationary values obtained at 25—30 min are indicated with horizontal bars in (A).

Results

I. $ZnCl_2$. Time Course of the Turbidity: The time course of the turbidity was followed at two protein concentrations, 0.078 and 0.93—0.94 g dm^{-3}. The data obtained at an intermediate concentration (0.23 g dm^{-3}) were given in the preceding paper.[1]

Characteristic time courses were most evident at the lowest protein concentration (0.078 g dm^{-3}) as shown in Figs. 1 (A) and (B). At a $ZnCl_2$ concentration (C_M) of 3.0×10^{-5} M, the turbidity increased slightly and linearly with time. At $C_M=4.9\times10^{-5}$ M, how-

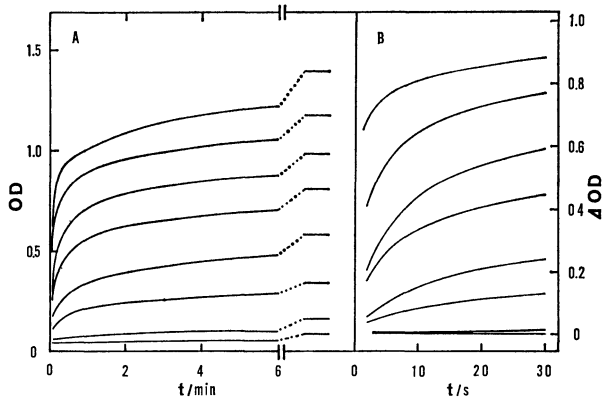

Fig. 2. Time courses of the turbidity at 500 nm at the protein concentration of 0.93—0.94 g dm^{-3}.
$ZnCl_2$ concentrations (mol dm^{-3}) (from top to bottom): 1.88×10^{-4}, 9.68×10^{-5}, 7.79×10^{-5}, 6.84×10^{-5}, 5.88×10^{-5}, 4.92×10^{-5}, 2.97×10^{-5} and 1.99×10^{-5}. In (B), ΔOD represents a change from the original level ($t=0$) at each $ZnCl_2$ concentration. Stationary values obtained at 25—30 min are indicated with horizontal bars in (A).

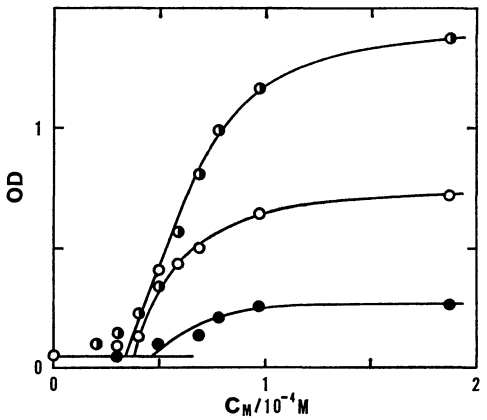

Fig. 3. Stationary turbidities as functions of $ZnCl_2$ concentration C_M.
Protein concentrations (g dm^{-3}): 0.93—0.94 (◑), 0.22—0.23 (○), and 0.078 (●). Wavelength: 350 nm (○,●) and 500 nm (◑).

ever, a sigmoidal shape began to appear; after a lag time the turbidity began to increase and reached a stationary value after 25—30 min.

Typical sigmoidal patterns were clearly observed for a range of $(6.8—9.7)\times10^{-5}$ M. At $ZnCl_2$ concentrations larger than 1.9×10^{-4} M, a sigmoidal shape could not be recognized any more in Fig. 1(A). However, when initial stages were closely examined, as shown in Fig. 1(B), then the presence of a lag time was noticed up to 3.8×10^{-4} M, since initial slopes at these concentrations (1.88 to 3.75×10^{-4} M) could not be extrapolated to zero time. Accordingly, the time course can be characterized by a sigmoidal increase when C_M is larger than about 5×10^{-5} M. In this concentration range, the lag time became shorter and the turbidity in the second phase became larger as C_M increased.

At the intermediate protein concentration (0.23 g dm^{-3}), essentially the same kinetic behavior was observed, which was already reported in the preceding paper.[1]

At the largest protein concentration (0.93—0.94 g dm^{-3}), the turbidity at 500 nm was followed. Sigmoidal changes were not observed except at $C_M=2.97\times10^{-5}$ M, as shown in Figs. 2(A) and (B). However, we assume that the kinetics follow the sigmoidal pattern and that the lag time is only too short to be detected in the time scale of the present experiment. It is to be noted in Fig. 2(A) that the turbidity increases only slightly but rather linearly with time at $C_M=1.99\times10^{-5}$ M. A slow phase was thus present even at this high protein concentration. This clearly indicates that the slow phase is not identical to the first step of the sigmoidal pattern but it is a different process other than the fast phase.

*The Critical $ZnCl_2$ Concentration C_M**: As shown in Figs. 1 and 2 and as suggested in the preceding paper, a critical $ZnCl_2$ concentration C_M* can be defined from kinetics, above which the turbidity increases rapidly but in a sigmoidal shape and reaches a stationary value. To evaluate the critical concentration more accurately, the stationary values of the turbidity are plotted against C_M for three protein concentrations in Fig. 3. The data at the intermediate concentration were taken from the preceding paper.[1] When the stationary turbidities obtained from the fast phase are extrapolated to the original level (protein solution in the absence of $ZnCl_2$), the value of abscissa corresponds to C_M*. The values are $(4—5)\times10^{-5}$ M ($(3—5)\times10^{-5}$ M), $(3.5—4.0)\times10^{-5}$ M ($(3—4)\times10^{-5}$ M), and $(2.5—3.5)\times10^{-5}$ M ($(2—3)\times10^{-5}$ M), for the protein concentrations of 0.078, 0.23 and 0.92—0.94 g dm^{-3}, respectively. The values in parentheses are those estimated from a change of the kinetic patterns (from a slow to a fast pattern).

In a previous study, critical concentrations were determined by turbidimetric titrations.[2] At a protein concentration of about 1.1 g dm^{-3}, C_M* was reported as about 4×10^{-5} M for $ZnCl_2$ at pH 7.4,[2] which approximately coincides with C_M* determined in the present study for the concentration of 0.94 g dm^{-3}. Accordingly, it is shown that the critical concentrations were adequately assessed in the previous study.[2]

Lag Times for the Turbidity: In Fig. 4, lag times obtained at different protein concentrations are shown in a logarithmic scale against $ZnCl_2$ concentration C_M. The kinetic data exhibiting no sigmoidal pattern were interpreted as having lag times smaller than 1 s, and represented on a horizontal line below 1 s in Fig. 4.

At the protein concentration of 0.078 g dm^{-3}, lag times could be determined directly from the kinetic patterns if $C_M<1\times10^{-4}$ M. For $C_M>1\times10^{-4}$ M, the lag times were determined as follows. The kinetic data given in Fig. 1(A) were plotted according to the first-order kinetics. A good linearity resulted between log(amplitude) and the time not only at a later stage of the reaction, which will be discussed in a later section, but also at some initial stage. Here the amplitude of the reaction is defined as [OD(∞)—OD(t)]. However, when the linear relation at the

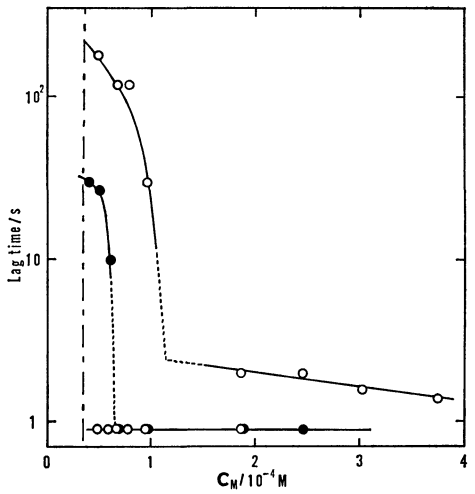

Fig. 4. Dependence of the lag time for the turbidity on $ZnCl_2$ concentration C_M.
Protein concentrations (g dm^{-3}): 0.93—0.94(○, on the lowest horizontal line), 0.22—0.23 (●), 0.078 (○). The points on the lowest horizontal line only represent that lag times are less than 1 second. A vertical chain line indicates the approximate location of the critical $ZnCl_2$ concentration C_M* (for details see text).

initial stage was extrapolated up to the total amplitude [OD(∞)−OD(0)], the time at the intersection was larger than zero and it was taken as the lag time.

The lag time decreases with an increasing C_M at a given protein concentration; fairly sharply at low $ZnCl_2$ concentrations and afterwards it becomes almost independent on C_M. The 'transition range' of C_M undoubtedly decreases as the protein concentration decreases. At a protein concentration of 0.93—0.94 g dm^{-3}, the range is probably lower than the critical concentration C_M*; the precipitation switches from the slow to the fast phase when C_M exceeds C_M*, nevertheless lag times are not observed since they are too short to be measured. The dependence of lag times on C_M will be discussed later, where another interpretation of the dependence will be presented. According to the interpretation, the lag times decrease with C_M rather continuously instead of changing in a sharp 'transition' manner.

Initial Rates of the Precipitation: Generally, initial rates of the coagulation of colloids are plotted against the coagulant concentration in a double logarithmic way to find a critical concentration, at which a slow coagulation changes into a fast one. The same procedure is applied to the present kinetic data. When sigmoidal patterns appeared, initial rates were obtained from the slope of the second step.[3] For the concentrations lower than C_M*, initial rates were evaluated as [OD(t)−OD(0)]/t, where t was taken as 20—30 min.

In Fig. 5, these initial rates are plotted against C_M for three protein concentrations in a double logarithmic way. Unexpectedly, similar results are seen as found in the coagulation of colloids. At each protein concentration, the logarithm of the initial rate linearly increases with log C_M and then reaches a constant level, thus defining a break. It may be argued that the concentration at the break would represent a critical concentration between a slow and a fast coagulation. However, the critical concentration in this sense is given by C_M* in the present case. It is to be noted that there is no break around C_M* in Fig. 5. At the lowest protein concentration (curve c), another break occurs around log $C_M \approx -4$. At the concentration lower than this point, typical patterns were observed as shown in Figs. 1(A) and (B).

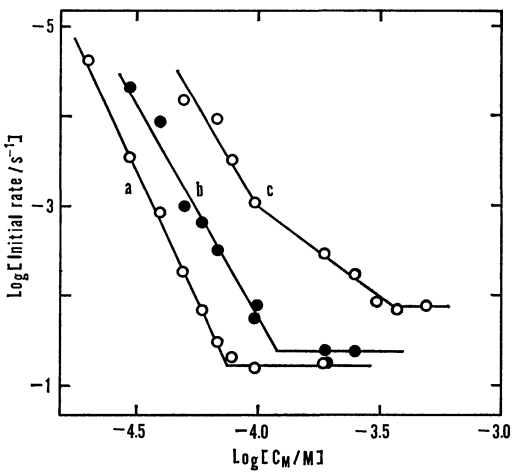

Fig. 5. Log $[dOD/dt]_{t=0}$ against log C_M for the precipitation of fibrinogen with $ZnCl_2$.
Protein concentrations (g dm^{-3}): (a) 0.93—0.94, (b) 0.22—0.23, (c) 0.078. Optical density: 350 nm (b and c) and 500 nm (a).

It is not fully understood, at present, why the initial rates of the present precipitation formally resemble those of the coagulation of colloids. This point will be discussed later.

Final Stage of the Precipitation: It is stressed in the introduction part that the kinetics of the present precipitation is closely related to that of the solubility. Therefore, the whole time course of the turbidity can, potentially, provide useful information of the present precipitation. However, it is too complicated to be analyzed properly, at present. In the preceding two sections, the initial stage of the kinetics is examined; the lag times and the initial rates.

It was found that the final stage of the present kinetics, shown in Figs. 1 and 2, could be described in terms of a single exponential function of time. Therefore, the amplitude $A(t)$, which is equal to [OD(∞)−OD(t)], can be expressed as Eq. 1.

$$A(t) = A_0(t) + A_1 \exp(-t/\tau) \quad (1)$$

The contribution from the term $A_0(t)$ generally becomes negligible about 3—4 and 6—8 min after the addition of $ZnCl_2$, at low and high $ZnCl_2$ concentrations. Consequently, a fraction larger than 3/4 of the entire time region can be described in terms of a single exponential at all C_M (if $C_M > C_M$*) and protein concentrations examined. The relative contribution from the exponential term, A_1/A_t, is shown in Fig. 6(A) as functions of C_M at three protein concentrations. The total amplitude A_t is defined as $A_0(0)+A_1$.

At a low protein concentration of 0.08 g dm^{-3}, the

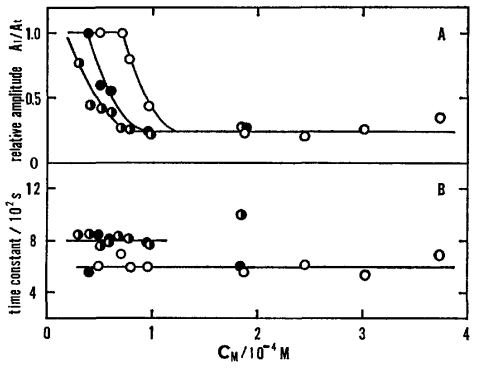

Fig. 6. Relative kinetic amplitude (A_1/A_t) (A) and the characteristic time constant (B) of the final stage of the precipitation as functions of $ZnCl_2$ concentration C_M.
Protein concentrations (g dm^{-3}): 0.93—0.94 (◑), 0.22—0.23 (●), and 0.078 (○).

ratio A_1/A_t is unity if $C_M \lesssim 7\times10^{-5}$ M. Under this condition, the entire time course can be represented by Eq. 2 using a lag time t_o,

$$A(t) = A_1 \exp(-(t-t_o)/\tau) \quad (t \geqq t_o). \tag{2}$$

When C_M becomes larger than 7×10^{-5} M, the relative contribution of the exponential term A_1/A_t becomes smaller than unity and decreases further as C_M increases and reaches as low as 0.2 at large C_M values. In other words, the contribution from other fast processes is dominant for C_M larger than 1×10^{-4} M. As the protein concentration increases, the contribution from the fast processes becomes significant even at lower C_M values as shown in Fig. 6(A).

The time constant τ characterizing the final exponential change is independent of C_M and only slightly dependent on the protein concentration as shown in Fig. 6(B). At the final stage of precipitation, it is likely that the growth of gel occurs as a unimolecular reaction with respect to a monomer protein (P) in solution.

$$\text{P} + \text{gel}(n\text{-mer}) \xrightarrow{k} \text{gel}[(n+1)\text{-mer}]$$
$$\text{d(P)/d}t = -k\text{(P)}, \quad \text{(P)} = \text{(P)}_o \exp(-kt). \tag{3}$$

It is quite reasonable, then, that this rate constant k, which is the reciprocal of τ, is independent of both C_M and protein concentration under the present condition of excess Zn^{2+} ions.

II. $CuCl_2$. The time courses of the turbidity were also measured in the case of $CuCl_2$ at three protein concentrations: about 0.045, 0.23—0.26, and 0.94 g dm^{-3}. Two different kinetic patterns, fast and slow, were also found in the case of $CuCl_2$ depending on whether $CuCl_2$ concentration (C_M) was larger or smaller than the critical value C_M*. Generally, kinetic behavior was similar to that found in the case of $ZnCl_2$. These results suggest that the essential mechanism for the fast precipitation is also common to both cases, $ZnCl_2$ and $CuCl_2$.

The critical concentrations obtained from the kinetic studies were: $(3—3.5)\times10^{-4}$ M ($(3—3.9)\times10^{-4}$ M), $(1.8—2.0)\times10^{-4}$ M ($(1.3—1.8)\times10^{-4}$ M), and $(1—1.5)\times10^{-4}$ M ($(1—2)\times10^{-4}$ M) for the protein concentrations of 0.045, 0.23, and 0.94 g dm^{-3}, respectively. The values in parentheses were estimated from the change of kinetic patterns.

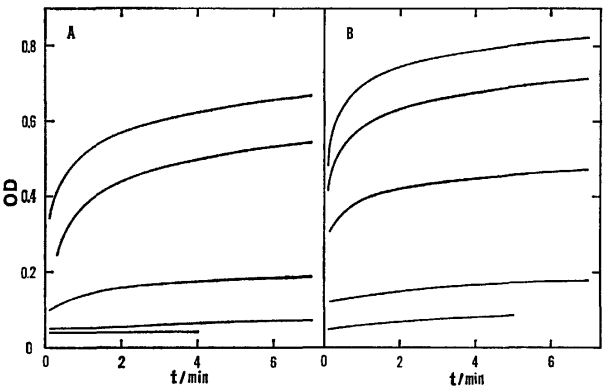

Fig. 7. Effects of ionic strength on the kinetics of precipitation in the case of $CuCl_2$.
NaCl concentrations (mol dm^{-3}): 0.15 (A) and 0.015 (B). Protein concentrations (g dm^{-3}): 0.23 (A) and 0.26 (B). $CuCl_2$ concentrations (mol dm^{-3}) (from top to bottom): (A) 3.87×10^{-4}, 3.78×10^{-4}, 2.76×10^{-4}, 1.82×10^{-4}, and 1.25×10^{-4}. (B) 2.86×10^{-4}, 2.35×10^{-4}, 1.82×10^{-4}, 1.25×10^{-4}, 6.45×10^{-5}.

In the case of $CuCl_2$, the effect of ionic strength was also examined at the protein concentration of about 0.23—0.26 g dm^{-3}.

The kinetic data obtained at 0.15 and 0.015 M NaCl are presented in Figs. 7 (A) and (B), respectively. At 0.015 M NaCl, a fast pattern was already observed even at $C_M = 6.5\times10^{-5}$ M. The critical concentration was thus reduced considerably as ionic strength decreased. This result is consistent with the previous finding[2]. The critical concentration at 0.015 M NaCl was estimated as about $(0.5—1.0)\times10^{-4}$ M from the stationary values of the turbidity.

Discussion

Lag Time for the Turbidity. In the preceding paper, a gelation model was proposed to account for the characteristic features of the present precipitation. The validity of the proposed model is further confirmed in the present kinetic study, since sigmoidal increase of the turbidity is best understood as representing a gelling process. The lag time for the turbidity is no more than the time interval before the extent of reaction reaches the gel point.

According to the classical kinetics of gelation,[4-6] the lag time t_o is given by Eq. 4[4] for the gelation of N units having f identical functional groups ('homogelation').

$$t_o = [f(f-2)Nk]^{-1}. \tag{4}$$

Here k denotes the association rate constant, which is not necessarily identical to the rate constant introduced in Eq. 3.

In the present model, gelation among various species has to be considered, such as A_x, $A_{x-1}B$, $A_{x-2}B_2$, and so on. Here x denotes the total number of binding sites per fibrinogen, which was tentatively assumed as three in the preceding paper.[1] The interconversion

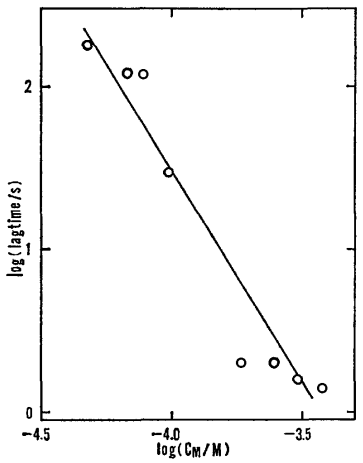

Fig. 8. A double lagarithmic plot of the dependence of the lag time on $ZnCl_2$ concentration C_M. Protein concentration: 0.078 g dm^{-3}.

among these species occurs through the binding equilibria with Zn^{2+} ions. Moreover, the 'bond' is formed only between A and B groups. Therefore, Eq. 4 cannot be applied to the present model in a strict sense. Instead of following the exact kinetic equations relevant to the present model, only a brief discussion is presented here to help understanding the obtained results on the lag time.

The number of units N in Eq. 4 may be approximately equated to the number of various species other than A_x (no zinc ions are bound to it), which is given as

$$N \approx N_p KC_M(1-KC_M)^{-1}. \quad (5)$$

Here N_p denotes the total number of fibrinogen molecules in solution. If species A_x considerably contributes to the aggregation, then we have to set $N \approx N_p$. Generally, we may write $N \approx N_p(KC_M)^{a'}$, where a' varies between 0 and 1. Since KC_M is much smaller than unity as examined in the preceding paper[1], the number of B groups is much smaller than that of A groups. Consequently, the number of 'functional groups' f in Eq. 4 is roughly proportional to KC_M x. Because $KC_M \ll 1$, the term $(f-2)$ in Eq. 4 exhibits a complex dependence on C_M. However, for the moment, we are allowed to write as follows with another parameter a.

$$t_0 \approx N_p^{-1}(KC_M)^{-(2+a)} \quad (0 \leqq a \leqq 1). \quad (6)$$

At a constant protein concentration, *i. e.*, at a constant N_p, Eq. 6 predicts that log(lag time) varies linearly with log C_M with a slope between -2 and -3. The data at the lowest protein concentration (0.08 g dm^{-3}) shown in Fig. 4 are replotted in a double logarithmic way in Fig. 8. An approximately linear relation holds with a slope of about -2.6, consistent with Eq. 6. Unfortunately, the validity of Eq. 6 at higher protein concentrations cannot be examined, since lag times could not be obtained for a wide range of C_M.

Initial Rates of the Precipitation. It is suggested in the preceding paper that the present precipitation is a kind of gelation.[1] Nevertheless, the initial rates of the present precipitation apparently exhibit typical dependence on the 'coagulant' concentration C_M. Although the implication of this unexpected result is not fully understood, the following consideration provides an interpretation of the result.

When Figs. 3 and 5 are compared, it is found that both concentration dependences are very similar. A close relation between the initial rate and the kinetic amplitude (the stationary turbidity) can be shown in the simplest manner, if the turbidity $A(t)$ can be expressed in a single exponential form.

$$A(t) = A_0 \exp(-t/\tau) \quad (7)$$

Then the initial rate $[-(dA/dt)_{t=0}]$ is given as A_0/τ. In this assumed situation, the logarithm of the initial rate is related to log A_0 and log τ. Accordingly, it can happen that the dependence of the initial rates on C_M is totally ascribed to the dependence of the kinetic amplitude A_0 on C_M. Consequently, if the initial stages of the present precipitation can be described by Eq. 7, with a proper τ, then the results shown in Fig. 5 can be understood as essentially identical to those given in Fig. 3.

We thank Professor M. Tagawa, Nara Women's University, for her kind advice in the construction of the mixing device.

References

1) H. Maeda, T. Kishi, and S. Ikeda, *Bull. Chem. Soc. Jpn.*, **56**, 290 (1983).
2) H. Maeda, T. Kishi, S. Ikeda, S. Sasaki, and K. Kito, *Int. J. Biol. Macromol.*, in press (1983).
3) R. H. Ottewill and A. Watanabe, *Kolloid-Z.*, **170**, 38 (1960).
4) W. H. Stockmayer, *J. Chem. Phys.*, **11**, 45 (1943).
5) R. M. Ziff, *J. Stat. Phys.*, **23**, 241 (1980).
6) R. M. Ziff and G. Stel, *J. Chem. Phys.*, **73**, 3492 (1980).

The Low Lying Electronic States of Dichloromaleic Anhydride

Yoshimi Ishibashi, Ryoichi Shimada,† and Hiroko Shimada*

Department of Chemistry, Faculty of Science, Fukuoka University, Nanakuma, Jonan-ku, Fukuoka 814

† *Department of Chemistry, Faculty of Science, Kyushu University 33, Hakozaki, Higashi-ku, Fukuoka 812*

(Received December 18, 1982)

The polarized Raman and infrared spectra of dichloromaleic anhydride were studied and the assignments of the normal vibrations were reinvestigated based on the polarization behaviors of the spectral bands and on the normal coordinate calculation. Using the assignments the vibrational structure of the phosphorescence spectrum was analyzed and the phosphorescence lifetime was also measured. These results indicate that the lowest triplet state of this molecule is a $^3(\pi, \pi^*)$ state perturbed by closely located $^3(n, \pi^*)$ states. The near ultraviolet absorption and phosphorescence excitation spectra were measured and four absorption bands due to $^3(n, \pi^*)\leftarrow {}^1A_1$, $^1A_2(n, \pi^*)\leftarrow {}^1A_1$, $^1B_1(n, \pi^*)\leftarrow {}^1A_1$, and $^1A_1(\pi, \pi^*)\leftarrow {}^1A_1$ transitions were found. The polarization experiment made on the $^1A_2(n, \pi^*)\leftarrow {}^1A_1$ absorption suggests that this transition borrows the intensity from the $^1A_1(\pi, \pi^*)\leftarrow {}^1A_1$ transition.

The assignments of the normal vibrations of dichloromaleic anhydride were first made by Rogstad *et al.*[1] based on the infrared vapor contours, the depolarization measurement of the Raman bands and the normal coordinate calculation. Their assignments given for the non-totally symmetric vibrations seem to be unreliable because the assignments were not made based on the enough experimental evidences and the reasonable vibrational analysis of the phosphorescence spectrum could not be made using their assignments.

The near ultraviolet absorption spectra and phosphorescence lifetimes of maleic anhydride and its halo derivatives were first studied by Scharf and Leismann.[2] They suggested that the lowest singlet and triplet states of dichloromaleic anhydride are to be a $^1(n, \pi^*)$ and a mixed state of $^3(n, \pi^*)$ and $^3(\pi, \pi^*)$ configurations, respectively. Detailed studies for the electronic states of these molecules have not been made yet.

In this work, the assignments of the normal vibrations of dichloromaleic anhydride are reexamined on the basis of the polarization behaviors of the Raman and infrared spectra and the assignments given for several bands by previous workers are corrected. The low lying excited singlet and triplet states of this molecule are studied in detail through the vibrational analyses of the phosphorescence and phosphorescence excitation spectra and also the polarized near ultraviolet absorption spectrum.

Experimental

Material. Dichloromaleic anhydride obtained from Aldrich Company was purified by zone-refining of about 100 passages followed by sublimation under reduced pressure. Cyclohexane of Dotite Spectrosol grade was purified by passing through the activated silica gel and alumina columns.

Optical Measurement. The Raman spectrum was observed in the liquid and single crystal phases with a JEOL 400 T Laser Raman Spectrophotometer. The sample was excited with the 514.5 nm beam from an Ar^+ ion laser. The single crystal was obtained in the following way. The sample was sealed in a evacuated closed glass tube. Temperature of one side of the tube, where the sample was placed, was kept a little higher than the other side. Crystals grown in the tube were collected. The well grown and approximately rectangular shaped single crystal was selected with a polarization microscope and used for the observation of the polarized Raman spectrum. Although the crystal structure of dichloromaleic anhydride was not determined yet, the directions of the crystal growth and the two-fold symmetry axis of the crystal were found to be the crystal axes by observation of the birefringence under the polarization microscope. These axes were tentatively taken to be the c and b axes, respectively. The a axis was taken to be perpendicular to both the b and c axes. The method of the measurement of the polarized Raman spectrum was exactly the same as that described previously.[3]

The infrared spectrum was observed with a Hitachi Infrared Spectrophotometer Model 345 over the range of 4000—250 cm^{-1} in the vapor and single crystal phases. The vapor spectrum was observed at 50 °C with a gas cell of 10 cm in optical path. The polarized infrared spectrum of a single crystal grown between two KRS-5 plates was measured with an AgBr wire-grid polarizer by the method described in the previous paper.[4] The infrared spectrum of the thin film obtained by sublimation was also observed.

The phosphorescence lifetime and the time resolved phosphorescence spectrum were measured in cyclohexane at 1.4 K using the optical setup described in the previous paper.[5] The short lifetime phosphorescence was observed in the following way. The sample was excited for 40 ms and the excitation was cut off. 1 ms after ceasing the excitation, the phosphorescence was sampled for 40 ms. The longer lifetime phosphorescence was observed with the exciting, waiting and sampling times of 120, 360, and 120 ms, respectively.

The excitation spectrum was observed in cyclohexane at 77 K monitoring the intensity of the phosphorescence 0-0 band with the excitation light source of a 500 W Xenon arc lamp of Ushio UXL-500D. The near ultraviolet absorption spectrum was observed in cyclohexane and in the thin film at room temperature and at 77 K with a Hitachi Ultraviolet Spectrophotometer Model 323 over the range of 500—210 nm. The polarized ultraviolet absorption spectrum was also measured with the single crystal grown between two quartz plates over the range of 350—315 nm.

Normal Coordinate Calculation

A normal coordinate calculation was performed through the standard GF matrix method with FACOM M-200 computer at the computer center of Kyushu University. Hilderbrandt *et al.*[6] showed that the mo-

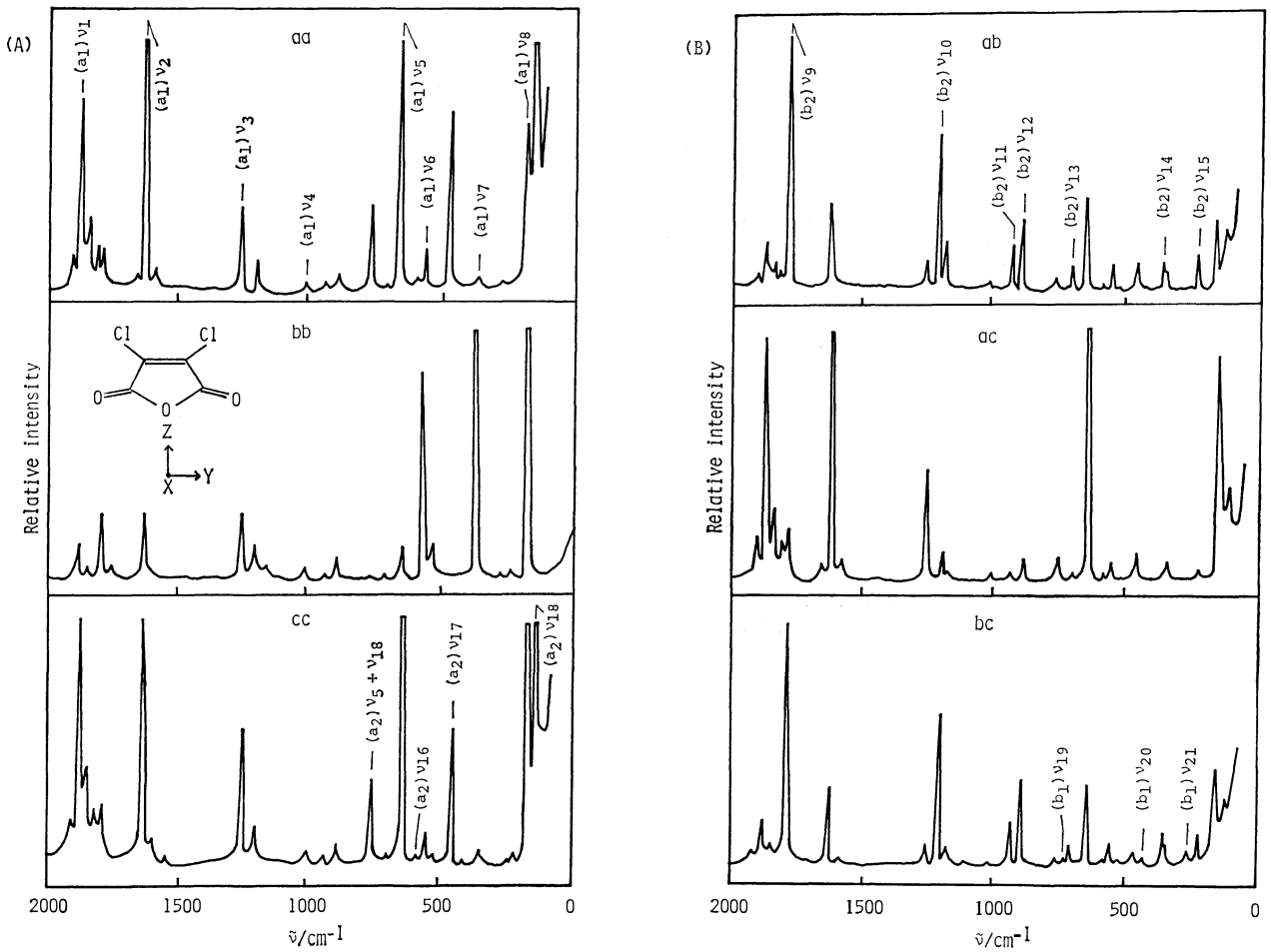

Fig. 1. Polarized Raman spectrum of the dichloromaleic anhydride single crystal. (A): aa, bb, and cc spectra, (B): ab, ac, and bc spectra.

Table 1. Force constants for the in-plane vibrations of dichloromaleic anhydride

$K_{C'=C'}$	8.15	$F_{C'\cdots Cl}$	0.65
$K_{C'-C}$	3.52	$F_{C\cdots Cl}$	0.63
$K_{C-O'}$	2.60	$F_{C'\cdots O}$	0.30
$K_{C'-Cl}$	3.20	$F_{O'\cdots O}$	0.54
$K_{C=O}$	10.83	$k^{\circ}_{r_{Cl},r_{Cl}}$	0.08
$H_{C'-C'-C}$	0.03	$k^{\circ}_{r_{Cl},r_{O}}$	0.03
$H_{C'-C-O'}$	0.49	$k^{m}_{r_{O},r_{O}}$	0.08
$H_{C-O'-C}$	0.50	$k^{m}_{R,R}$	−0.02
$H_{C'-C'-Cl}$	0.07	h^{m}_{R,α_O}	0.03
$H_{C-C'-Cl}$	0.10	h^{m}_{R,α_C}	0.01
$H_{C'-C=O}$	0.28	h^{m}_{R,β_O}	−0.02
$H_{O'-C=O}$	0.65	$h^{m}_{R,\beta_{Cl}}$	−0.01
$F_{C\cdots C'}$	0.60	$f^{\circ}_{\alpha,\alpha}$	0.03
$F_{C'\cdots O'}$	0.74	$f^{\circ}_{\beta_{Cl},\beta_O}$	0.05
$F_{C\cdots C}$	0.96	$f^{\circ}_{\beta_{Cl},\beta_{Cl}}$	0.01

Force constants denoted by K, H, F, and k are given in J/dm² (=mdyn/Å) units, and those denoted by h and f are in pJ/dm rad (=mdyn/rad) and aJ/rad² (=mdyn Å/rad²) units, respectively. C′ is the carbon atom bonded to Cl. O′ is the oxygen atom in the ring.

Table 2. Force constants for the out-of-plane vibrations of dichloromaleic anhydride

$Q_{C=C}$	0.35	$p^{\circ}_{Cl,Cl}$	0.04
Q_{C-C}	0.70	$p^{\circ}_{Cl,O}$	0.03
Q_{C-O}	0.80	$p^{m}_{O,O}$	0.03
$q^{\circ}_{C=C,C-C}$	−0.05	$p^{m}_{Cl,O}$	0.01
$q^{\circ}_{C-C,C-O}$	−0.08	$t^{\circ}_{C=C,Cl}$	−0.12
$q^{\circ}_{C-O,C-O}$	−0.03	$t^{\circ}_{C-O,O}$	−0.10
q^{m}	0.02	$t^{\circ}_{C-C,O}$	−0.06
P_{Cl}	0.36	$t^{\circ}_{C-C,Cl}$	−0.04
P_O	0.34		

Force constants are given in aJ/rad² (=mdyn Å/rad²) units.

lecular structure of maleic anhydride belongs to the point group C_{2v} and gave the geometric parameters for the molecular structure. We assumed that the molecular geometry of dichloromaleic anhydride was the same as that of maleic anhydride except for the C–Cl bond, whose distance was assumed to be 0.177 nm.

The F matrix elements for the in-plane and out-of-plane vibrations were evaluated with the potential fields of an improved modification of the Urey-Bradley force field and the valence force field, respectively, as used for the calculation made on maleic anhydride.[3]

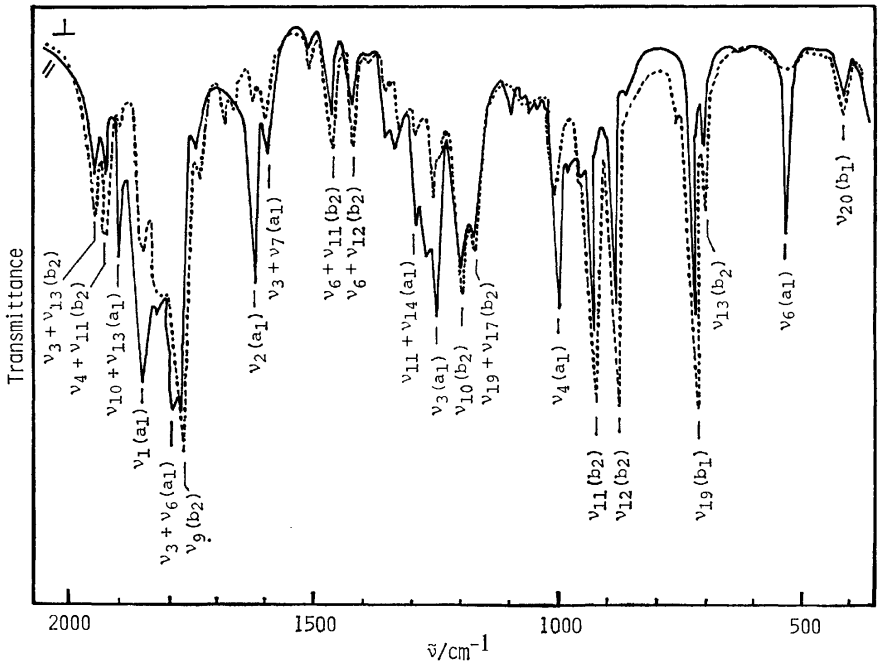

Fig. 2. Polarized infrared spectrum of the dichloromaleic anhydride single crystal.

The notations of the force constants are exactly the same as those given in the previous calculation.[3]

Results and Discussion

Normal Vibration. The force constants finally obtained after several iterative normal coordinate calculations for the in-plane and out-of-plane vibrations are given in Tables 1 and 2, respectively. The calculated frequencies and vibrational modes are given in Table 3, together with the experimentally assigned vibrational frequencies.

The polarized Raman spectrum is shown in Fig. 1. The spectrum was denoted by two symbols such as ab. The first letter refers to the direction of the polarization of the excitation light and the second to that of the scattering light. The non-totally symmetric Raman bands were divided into three types of polarization behavior according to the relative intensities of the bands in the polarized spectrum. The intensities of the bands belonging to the first type are much stronger in the ab and bc spectra than those in other spectra. The intensities of the second type bands are much stronger in the aa and cc spectra than those in other spectra, and the third type bands can be observed only in the bc spectrum with appreciable intensity.

The polarized infrared spectrum observed in the single crystal is shown in Fig. 2. The spectra measured with the incident lights polarized parallel and perpendicular to the crystal growth direction are referred to as // and ⊥ spectra and drawn with the solid and dotted lines, respectively. The polarized infrared bands can be divided into two types according to their polarization behaviors. The bands belonging to the first type appear strongly in the // spectrum and extremely weakly in the ⊥ spectrum. The bands belonging to the second type appear strongly in the ⊥ spectrum and weakly in the // spectrum. These two types of the bands are denoted as types I and II, respectively. Rogstad *et al.*[1] indicated that the infrared vapor bands belonging to the a_1, b_1, and b_2 symmetry species show the B, C, and A band envelopes, respectively, from the calculated values of the moments of inertia, where the z axis was taken to be along the C_2 symmetry axis and the x axis to be perpendicular to the molecular plane.

The assignments of the normal vibrations belonging to each symmetry species were made based on the following observations.

a_1 Species: The polarized bands in the depolarization measurement of the Raman spectrum can be definitely assigned to the a_1 vibrations. The infrared crystal bands showing the type I polarization behavior are also to be assigned to the a_1 bands, since the corresponding infrared vapor bands showed the B band envelope and the frequencies coincide with those of the Raman a_1 bands.

b_2 Species: The b_2 bands showing the A band envelope in the infrared vapor spectrum showed the type II polarization behavior in the infrared crystal spectrum. The corresponding Raman bands were observed strongly in the ab and bc polarized Raman spectra.

b_1 Species: The b_1 bands showing the C band envelope in the infrared vapor spectrum showed the type II polarization behavior in the infrared crystal spectrum. The corresponding Raman bands were observed only in the bc polarized Raman spectrum with appreciable intensity.

a_2 Species: The crystal Raman bands showing the aa and cc polarization behavior should be assigned to the a_2 vibration, because other two polarization behaviors of the Raman bands were already ascribed

Table 3. Normal vibrations of dichloromaleic anhydride

Sym. species	Vibrational mode	Raman			Infrared			Calcd $\tilde{\nu}$/cm^{-1}	Obsd Rogstad *et al.* $\tilde{\nu}$/cm^{-1}
		Liquid		Crystal Pol.	Crystal		Vapor type		
		$\tilde{\nu}$/cm^{-1}	Pol.		$\tilde{\nu}$/cm^{-1}	Pol.			
a_1	ν_1 C=O str.	1868	p		1858	I		1869	1870
	ν_2 C=C str.	1616	p		1613	I	B	1619	1623
	ν_3 C-O str.	1245	p		1245	I	B	1246	1244
	ν_4 C-C str.	1003	p		1007	I	B	1006	1003
	ν_5 Ring def.	640	p					642	637
	ν_6 C-Cl str.	545	p		542	I	B	538	540
	ν_7 C=O bend.	351	p					352	350
	ν_8 Cl bend.	175	p?					153	188
b_2	ν_9 C=O str.	1792	dp	ab, bc	1780	II	A	1793	1799
	ν_{10} C-C str.	1203	dp	ab, bc	1200	II	A	1206	1201
	ν_{11} C-O str.	932	dp	ab, bc	916	II	A	934	926
	ν_{12} C-Cl str.	884	dp	ab, bc	872	II	A	886	884
	ν_{13} C=O bend.	697	dp	ab, bc	697	II	A	698	697
	ν_{14} Ring def.	356	dp	ab, bc				356	419
	ν_{15} Cl bend.	237	dp	ab, bc				239	174
a_2	ν_{16} Ring def.	585	dp	aa, cc				585	760
	ν_{17} C=O wag.	463	dp	aa, cc				468	462
	ν_{18} Cl wag.	123	dp	aa, cc				132	127
b_1	ν_{19} Ring def.	723		bc	718	II	C	719	723
	ν_{20} C=O wag.	421	dp	bc	419	II	C	420	258
	ν_{21} Cl wag.	255		bc				238	236

to the b_2 and b_1 vibrations, and no corresponding bands were observed in the infrared spectrum.

The normal vibration thus determined are given in Table 3 and also shown in Figs. 1 and 2. The assignments for the a_1 vibrations given in this work exactly agree with those given by Rogstad *et al.*[1] This is quite natural because the a_1 vibrations were straightforwardly determined based on the depolarization measurement of the Raman bands. On the other hand, our assignments given for the non-totally symmetric vibrations were somewhat different from those given by them as can be seen in Table 3. Rogstad *et al.*[1] gave the assignments based on the band envelope in the infrared vapor spectrum, where only four band envelopes could be observed. In our work, the assignments were made based on the polarization behaviors of the Raman and infrared bands and also on the band envelope in the infrared vapor spectrum, where eleven band envelopes were observed. Therefore, we believe that our assignments are to be more reliable than those given by Rogstad *et al.*

Phosphorescence Spectrum. Dichloromaleic anhydride emits a weak yellow phosphorescence in cyclohexane matrix. Scharf and Leismann[2] measured the phosphorescence lifetime in mixed solvents of methylcyclohexane and isopentane, and of ethanol and isopentane at 77 K and got the lifetimes of 13.9 and 75 ms, respectively. We analyzed the phosphorescence decays observed in cyclohexane at 1.4 K with changing the exciting, waiting and sampling times of the phosphorescence and obtained the lifetimes of 62 and about 300 ms. The third lifetime component could not be precisely measured due to its extremely weak intensity. The decay analysis showed that the third lifetime is longer than 1500 ms. These values of the lifetime would be reasonable because the lifetime observed in cyclohexane at 77 K was 150 ms. We also traced the measurement made by Scharf and Leismann, but we could not reproduce their results.

The time resolved phosphorescence spectrum is shown in Fig. 3. The vibrational analysis of the short lifetime phosphorescence spectrum will be discussed first. The strongest and shortest wavelength band observed at 477.88 nm was taken as the 0-0 band. Very strong bands separated by 639 and 1621 cm^{-1} from the 0-0 band were assigned to the ring deformation (ν_5) and C=C stretching (ν_2) vibrations, respectively. These bands constitute the main progressions. Medium intense bands separated by 180, 1008, 1245, and 1881 cm^{-1} from the 0-0 band were assigned to the Cl bending (ν_8), C–C stretching (ν_4), and C–O stretching (ν_3), and C=O stretching (ν_1) vibrations, respectively. These bands belong to the totally symmetric species. A medium intense band separated by 420 cm^{-1} from the 0-0 band was assigned to the C=O wagging (ν_{20}) vibration of the b_1 symmetry species. Medium intense bands separated by 453 and 585 cm^{-1} were assigned to the C=O wagging (ν_{17}) and ring deformation (ν_{16}) vibrations of the a_2 species, respectively. Detailed vibrational analysis is given in Fig. 3.

The middle lifetime phosphorescence spectrum could not be successfully measured because of its very weak intensity. The intensity ratio of the 0-0 bands of the middle and short lifetime phosphorescence spectra was

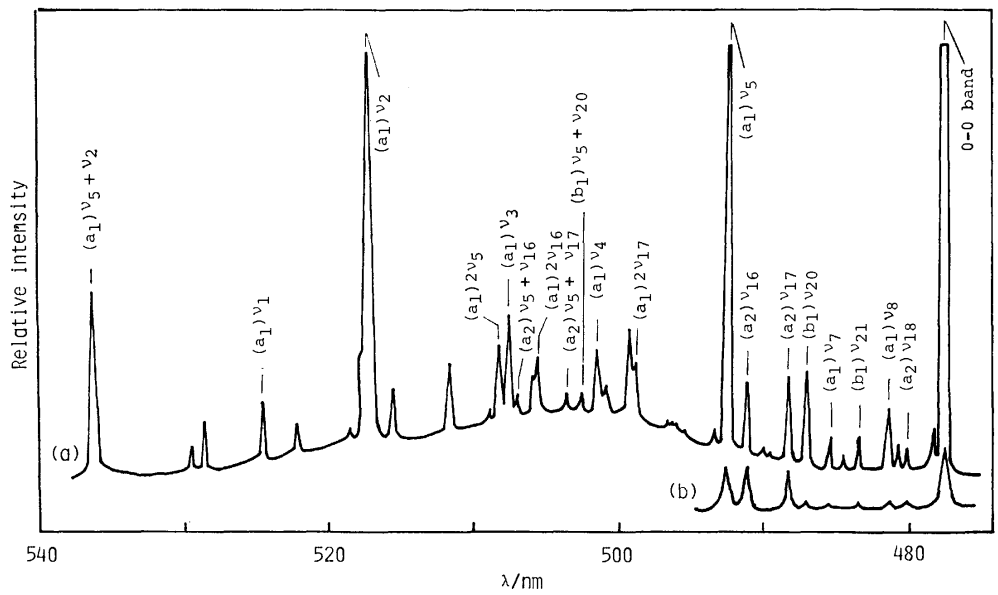

Fig. 3. Phosphorescence spectrum of dichloromaleic anhydride in cyclohexane at 1.4 K. The exciting, waiting, and sampling times of the phosphorescence are (a): 40, 1, 40 ms, (b): 120, 360, and 120 ms, respectively.

measured to be less than 1/100. The most characteristic spectral feature of the middle lifetime phosphorescence is that the relative intensities of the bands assigned to the Cl wagging (ν_{18}), C=O wagging (ν_{17}), and ring deformation (ν_{16}) vibrations of the a_2 species to the intensity of the 0-0 band remarkably increased compared with those of the short lifetime phosphorescence.

A weak phosphorescence excitation spectrum was observed in the 450 nm region in cyclohexane at 77 K, but no spectrum could be observed in the 470 nm region. A extremely weak absorption spectrum was also observed in the 450 nm region with the f-value of about 1×10^{-7} in cyclohexane at room temperature as shown in Fig. 4. The observed band is separated by about 1000 cm^{-1} from the 0-0 band of the phosphorescence spectrum. These observations suggest that the lowest triplet state of this molecule is a $^3(\pi, \pi^*)$ state and a $^3(n, \pi^*)$ state is located about 1000 cm^{-1} above the phosphorescent $^3(\pi, \pi^*)$ state. These assignments of the states are consistent with the relatively short $\pi\leftarrow\pi^*$ phosphorescence lifetime and the complicated vibronic structure of the phosphorescence spectrum. The strong intensities of the 0-0 and totally symmetric ν_5 and ν_2 bands in the short lifetime phosphorescence spectrum indicate that the lowest $^3(\pi, \pi^*)$ state is strongly coupled with the $^1B_1(n, \pi^*)$ state through the first order spin-orbit interaction. This means that the short lifetime phosphorescence arises from the B_1 triplet sublevel. Observations of the out-of-plane b_1 and a_2 bands with medium intensity in the short lifetime phosphorescence and the remarkable intensification of the a_2 vibronic bands relative to the intensity of the 0-0 band in the middle lifetime phosphorescence indicate that the phosphorescent $^3(\pi, \pi^*)$ state is vibronically coupled with the closely located $^3(n, \pi^*)$ states as suggested by Scharf and Leismann.[2]

Near Ultraviolet Absorption Spectrum. The near ultraviolet absorption spectra observed in cyclohexane and the thin film prepared by sublimation at room temperature and 77 K, respectively, are shown in Fig. 4. The absorption observed in the 290—230 nm region with $\varepsilon\approx7000$ in cyclohexane looses the intensity in the thin film spectrum. We observed the infrared spectrum of the thin film sample with the unpolarized light. The b_2 and b_1 vibrational bands were observed with strong intensity, while the a_1 band with very weak intensity. This observation clearly indicates that the 290—230 nm absorption should be ascribed to the $^1A_1(\pi, \pi^*)\leftarrow{}^1A_1$ transition.

The absorption observed in the 350—300 nm region with $\varepsilon\approx25$ in cyclohexane, which was ascribed to the $n\rightarrow\pi^*$ transition by Scharf and Leismann,[2] shifts toward the blue side in the thin film. Generally the absorption observed in the solid at low temperature shows the red shift and hence two absorption systems are expected to locate in this region. We observed the polarized near ultraviolet absorption spectrum of the single crystal grown between two quartz plates and the result is shown in Fig. 4. The notations of the // and $\perp$ spectra are the same as those given in the polarized infrared spectrum of the single crystal grown between two KRS-5 plates. The observation indicates that the polarization of the 350—325 nm absorption is clearly different from that of the 325—300 nm absorption. By analogy with the polarization behaviors of the infrared bands, the former absorption could be ascribed to the forbidden $^1A_2(n, \pi^*)\leftarrow{}^1A_1$ transition perturbed by the $^1A_1(\pi, \pi^*)\leftarrow{}^1A_1$ transition and the latter to the $^1B_1(n, \pi^*)\leftarrow{}^1A_1$ transition.

The phosphorescence excitation spectrum observed in cyclohexane at 77 K gives well resolved vibrational structure as shown in Fig. 4. The longest wavelength and very weak band at 355.0 nm was taken as the 0-0 band of the $^1A_2(n, \pi^*)\leftarrow{}^1A_1$ absorption, which may appears in the spectrum by the crystal field dis-

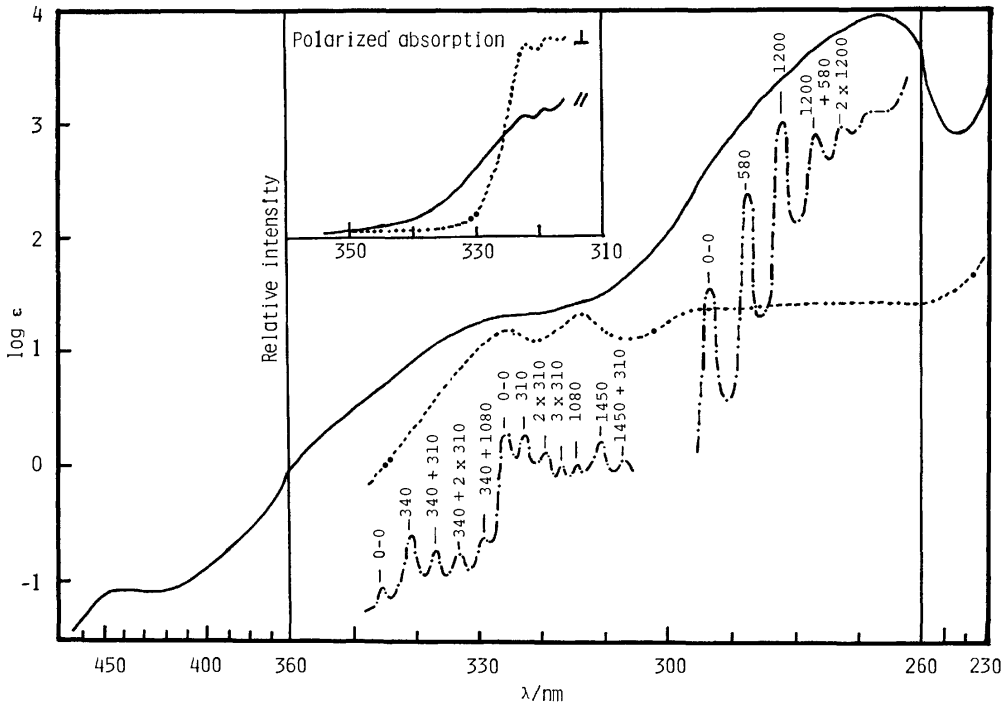

Fig. 4. Near ultraviolet absorption and phosphorescence excitation spectra of dichloromaleic anhydride. ——: Absorption spectrum in cyclohexane at room temperature, ----: absorption spectrum in the thin film at 77 K, -·-·-: phosphorescence excitation spectrum in cyclohexane at 77 K. Polarization behavior of the 350—315 nm absorption region is shown in the upper part of the figure. The absorption spectrum in cyclohexane was plotted against log ε, while the other spectra were against relative intensity.

tortion. A strong band separated by 340 cm^{-1} from the 0-0 band was ascribed to the perturbing vibration of the a_2 species. The frequency of 340 cm^{-1} was assigned to the upper state frequency of the C=O wagging (ν_{17}) vibration. This assignment would be reasonable because the C=O wagging vibration could be expected to be most effective for the vibronic coupling between the (n, π^*) and (π, π^*) states. Band intervals of 310 and 1080 cm^{-1} were observed and these were assigned to the upper state frequencies of the C=O bending (ν_7) and C–O stretching (ν_3) vibrations of the a_1 species, respectively.

A strong band at 325.7 nm was taken as the 0-0 band of the $^1B_1(n, \pi^*) \leftarrow {}^1A_1$ absorption. The upper state frequencies of the ν_7 and ν_3 vibrations were also observed in this absorption. A strong band separated by 1450 cm^{-1} from the 0-0 band was ascribed to the upper state C=O stretching (ν_1) vibration of the a_1 species.

A strong band at 293.2 nm was taken as the 0-0 band of the $^1A_1(\pi, \pi^*) \leftarrow {}^1A_1$ absorption. Band separations of 580 and 1200 cm^{-1} were observed and these were assigned to the upper state frequencies of the ring deformation (ν_5) and C=C stretching (ν_2) vibrations of the a_1 species, respectively. These vibrations were observed quite strongly in the $^3(\pi, \pi^*) \rightarrow {}^1A_1$ phosphorescence spectrum as described above.

The CNDO-MO calculation suggests that the two n orbitals on the O atoms of the C=O bonds couple with each other through the C–O bonds and hence the $n \rightarrow \pi^*$ transition gives rise to changes of the C=O and also C–O bond characters. Therefore, the observations of the C=O bending, C–O stretching, and C=O stretching vibrations in the $^1A_2(n, \pi^*) \leftarrow {}^1A_1$ and $^1B_1(n, \pi^*) \leftarrow {}^1A_1$ excitation spectra could be reasonably understood.

References

1) A. Rogstad, P. Klaboe, B. N. Cyvin, S. J. Cyvin, and D. H. Christensen, *Spectrochim. Acta, Part A*, **28**, 111 (1972).

2) H.-D. Scharf and H. Leismann, *Z. Naturforsch., B*, **28**, 662 (1973).

3) Y. Ishibashi, R. Shimada, and H. Shimada, *Bull. Chem. Soc. Jpn.*, **55**, 2765 (1982).

4) S. Kizuki, Y. Ishibashi, H. Shimada, and R. Shimada, *Mem. Fac. Sci. Kyushu Univ. Ser. C*, **13**, 7 (1981).

5) Y. Urabe, T. Watanabe, Y. Ishibashi, H. Shimada, and R. Shimada, *Mem. Fac. Sci. Kyushu Univ. Ser. C*, **13**, 1 (1981).

6) R. L. Hilderbrandt and E. M. A. Peixoto, *J. Mol. Struct.*, **12**, 31 (1972).

Mono-complex Formation Kinetics of 2-Thenoyltrifluoroacetone with Nickel(II) and Copper(II) Ions in Aqueous Solution

Isao Ando,* Kiyomi Yoshizumi, Kazuhisa Ito, Kikujiro Ujimoto, and Hirondo Kurihara

Department of Chemistry, Faculty of Science, Fukuoka University, Nanakuma, Jonan-ku, Fukuoka 814-01

(Received July 29, 1982)

The mono-complex formation of 2-thenoyltrifluoroacetone (HTTA) with nickel(II) and copper(II) ions was studied in aqueous solution at 25.0 °C and an ionic strength of 0.20 mol dm^{-3} by means of a stopped-flow method. The rate-[H$^+$] profiles for the formation of these mono-complexes revealed that the rate-determining step of the complex formation interchanges depending upon hydrogen-ion concentration, as in the case of the Ni(II)–bpy complex. The rate constants of the mono-complex formation with TTA$^-$, k_f, and that with HTTA, k_{fh}, were determined from the rate-[H$^+$] profile in the region of the high hydrogen-ion concentration, where the pseudo-equilibrium of acid dissociation of the ligand was maintained during the complex formation; $k_f=(9.2\pm3.0)\times10^2$, $k_{fh}=(1.3\pm0.3)\times10^{-1}$ mol^{-1} dm^3 s^{-1} for the Ni(II)–TTA complex and $k_f=(2.0\pm1.2)\times10^3$, $k_{fh}=(5.0\pm0.9)\times10^{-1}$ mol^{-1} dm^3 s^{-1} for the Cu(II)–TTA complex. The deprotonation-rate constants of HTTA could be evaluated from the apparent rate constants of the complex formation in low hydrogen-ion concentration. The values thus obtained agreed well with that determined independently by a pH jump method.

Many complex formations with the ligands which have both acidic and basic conjugated forms in aqueous solution have been investigated kinetically for various metal ions, especially nickel(II) ion.[1-6] In those studies the concentration ratio at protolytic equilibrium (the pseudo-equilibrium of acid dissociation) of the ligand has been taken as constant throughout the course of the complex formation. However, the pseudo-equilibrium may fail in a complex formation with the ligand undergoing a slow proton-transfer reaction. Recently we found the first such example, so far as we know, in the mono-complex formation of Ni(II)–bpy at low hydrogen-ion concentration.[7] The kinetic measurements under such conditions lead to erroneous rate constants because of the failure of the pseudo-equilibrium of the ligand. It is, therefore, essential in the kinetic study of the complex formation with such a ligand to make sure the maintenance of the acid-base pseudo-equilibrium of the ligand during the complex formation.

β-Diketones undergo a slow proton-transfer reaction[8-11] and also form the complexes with various metal ions.[10-16] Hence, further results are expected to prove that the proton-transfer process of β-diketones is the rate-determining step of the complex formation in some experimental conditions, especially in low hydrogen-ion concentration. In this study we investigated fully the rate-[H$^+$] profiles for the complex formation of nickel(II) and copper(II) ions with 2-thenoyltrifluoroacetone (HTTA) as an available β-diketone. The results showed that the deprotonation process of HTTA could be the rate-determining step of these complex formations under some given conditions.

This phenomenon provided a new method of the estimation of the deprotonation-rate constant of the ligand, by measuring the complex-formation rate.

Experimental

Materials and Sample Solutions. Nickel(II) and copper(II) sulfates were purchased from Wako Pure Chemical Industries and were purified by recrystalization from water before use. 2-Thenoyltrifluoroacetone (Dotite TTA) was purchased from Dojindo Laboratories and used without further purification. All other chemicals were of guaranteed reagent grade and used without further purification, unless otherwise noted.

The stock solution of nickel(II) or copper(II) ion was prepared by dissolving the corresponding sulfate in water acidified faintly with sulfuric acid, and the metal-ion concentration of the solution was determined by edta titration. The stock solution of HTTA was prepared by dissolving a desired amount of it in water. Deionized-distilled water was used for all preparations of the solution.

These stock solutions were appropriately diluted for kinetic measurements. The ionic strength of the resulting solution was adjusted to 0.20 mol dm^{-3} with sodium sulfate, and the sample solution contained no buffer.

For the measurement of the acid dissociation constant of HTTA, the ionic strength of the sample solutions was adjusted to 0.20 mol dm^{-3} with sodium chloride, and the pH of them was adjusted with the following buffers: acetate buffer at pH 4—6.5, phosphate buffer at pH 5.5—8. Each buffer was added at the concentration smaller than 0.05 mol dm^{-3}.

Kinetic Measurement of Proton Transfer. The rates of proton-transfer of the ligand were measured at 25.0 °C by the pH jump technique[17,18] according to the following procedure. The solution of HTTA in dilute sulfuric acid (pH 4—4.5) was rapidly mixed with a dilute sodium hydroxide solution at the same ionic strength in a Union RA-1300 stopped-flow spectrophotometer. The increase of TTA$^-$ concentration caused by pH jumping was followed as the increase in absorbance at 339 nm, the wavelength of maximum absorption of TTA$^-$. The apparent first-order rate constant for the deprotonation of HTTA at reaction time zero, k_{dpo}, was evaluated according to a previous method.[17,18] Each k_{dpo} value was obtained from fifteen kinetic runs.

Kinetic Measurement of Complex Formation. The complex formation was followed at 349 nm and 25.0 °C by means of a Union RA-1300 stopped-flow spectrophotometer, as reported previously.[7] The concentration of metal ion was always kept in large excess (400 or more times that of HTTA) in order to ensure only the mono-complex formation. The complex formation obeyed first-order kinetics within the 50% conversion. Each pseudo first-order rate constant, k_{obsd}, was obtained from ten kinetic runs.

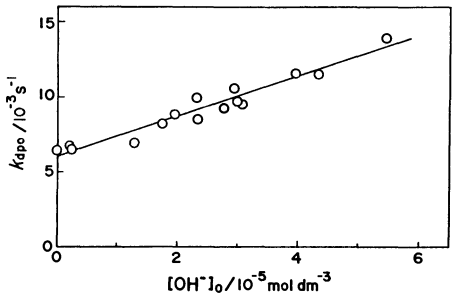

Fig. 1. Plot of k_{dpo} against $[OH^-]_0$ for 2-thenoyltrifluoroacetone.
The solid line is the linear regression line for the plot.

Measurement of Acid Dissociation Constant. Absorption spectra of HTTA in aqueous solution were recorded on a Hitachi 323 recording spectrophotometer. The acid dissociation constant, K_a, of HTTA was measured by the spectrophotometric titration at 339 nm and 25.0 °C by means of a JASCO Uvidec-2 digital spectrophotometer equipped with a thermostated cell holder.

Results and Discussion

Deprotonation Reaction of HTTA. The absorbance of HTTA at 339 nm remarkably increases with increasing pH. A spectrophotometric titration over the pH range of 2 to 8 at this wavelength yielded the number of transferred protons of 1.03±0.01 and the pK_a value of 6.35±0.01, indicating that the spectral change should be ascribed to the acid dissociation of HTTA to TTA^-. This pK_a value is in good agreement with the literature value.[19] The same spectral change was also observed on the heels of a pH jump in the stopped-flow apparatus by a rapid scanning technique. Consequently the apparent first-order rate constants for the deprotonation reaction of HTTA, k_{dpo}, can be determined by the stopped-flow pH jump technique.

The proton transfer of HTTA presumably proceeds through the following two simultaneous reaction paths, as in the cases of phen, pyridine and its derivatives:[17,18]

$$HTTA \underset{k_p}{\overset{k_{dp}}{\rightleftharpoons}} TTA^- + H^+, \quad (1)$$

$$HTTA + OH^- \underset{k_{H_2O}}{\overset{k_{OH}}{\rightleftharpoons}} TTA^- + H_2O, \quad (2)$$

where k_{dp}, k_p, k_{OH}, and k_{H_2O} are the rate constants in Reactions 1 and 2, respectively. Since the decreasing rate of HTTA concentration is expressed by

$$-d[HTTA]/dt = (k_{dp}+k_{OH}[OH^-])[HTTA] - (k_p+k_{H_2O}[H_2O]/[H^+])[TTA^-][H^+], \quad (3)$$

at reaction time zero k_{dpo} can be expressed as a function of hydroxide-ion concentration at reaction time zero, $[OH^-]_0$;

$$k_{dpo} = k_{dp} + k_{OH}[OH^-]_0. \quad (4)$$

The plot of k_{dpo} against $[OH^-]_0$ gave a straight line, as shown in Fig. 1. The values of k_{dp} and k_{OH} given in Table 1 were obtained from the intercept and the slope of the linear regression line in Fig. 1. The k_{dp} value was in good agreement with the rate constant of the enolation of keto tautomer of HTTA, $(8.4\pm0.3)\times10^{-3}$ s^{-1} obtained by the bromination method.[11] According to Jaffe and co-workers,[11] the concentration ratio of enol to keto tautomer in aqueous HTTA solution is 4.4×10^{-3} and the rate-determining step of the enolation is the deprotonation of keto tautomer. Therefore, k_{dp} in this study corresponds to the enolation-rate constant of keto form. This k_{dp} value is also comparable to that of other β-diketones.[20]

Table 1. Rate constants for the mono-complex formation and the proton-transfer reaction of 2-thenoyltrifluoroacetone at 25.0 °C and 0.20 mol dm^{-3} ionic strength

Rate constant	Ni-TTA	Cu-TTA
k_f/mol^{-1} dm^3 s^{-1}	$(9.2\pm3.0)\times10^2$	$(2.0\pm1.2)\times10^3$
k_{fh}/mol^{-1} dm^3 s^{-1}	$(1.3\pm0.3)\times10^{-1}$	$(5.0\pm0.9)\times10^{-1}$
k_{dp}/s^{-1}	$(7.2\pm1.1)\times10^{-3}$ a)	$(2.8\pm1.0)\times10^{-3}$ a)
	$(6.0\pm0.6)\times10^{-3}$ b)	
k_{OH}/mol^{-1} dm^3 s^{-1}	$(1.3\pm0.2)\times10^2$ b)	

a) The values were obtained from the data of the complex formation rates. b) The value was obtained by the pH jump method.

Complex Formation Kinetics. The mono-complex formation of nickel(II) and copper(II) ions with HTTA is thought to proceed through the following two concurrent reaction paths:

$$M^{2+} + TTA^- \xrightarrow{k_f} MTTA^+, \quad (5)$$

$$M^{2+} + HTTA \xrightarrow{k_{fh}} MTTA^+ + H^+, \quad (6)$$

where k_f and k_{fh} are the second-order rate constants in Reactions 5 and 6, respectively. As long as the pseudo-equilibrium of the acid dissociation of HTTA holds throughout the complex formation, the rate of the complex formation is expressed by

$$d[MTTA^+]/dt = (k_f[TTA^-] + k_{fh}[HTTA])[M^{2+}] = \{(k_f+k_{fh}[H^+]/K_a)/(1+[H^+]/K_a)\} \times [M^{2+}][TTA'], \quad (7)$$

where [TTA′] denotes the analytical concentration of HTTA, in the early stage of the complex formation, in which the dissociation of the complex can be ignored. Therefore, the pseudo first-order rate constant, k_{obsd}, is correlated with k_f and k_{fh} by

$$k_{obsd}(1+[H^+]/K_a)/[M^{2+}] = k_f + k_{fh}[H^+]/K_a. \quad (8)$$

Figure 2 shows the plots of k_{obsd} values against $[H^+]$ according to Eq. 8 for the formation of the mono-complexes of Ni(II)- and Cu(II)-TTA. In both cases, the plots in the $[H^+]$-region higher than around 2×10^{-3} mol dm^{-3} yield linear relationships, while the data at lower $[H^+]$ deviate below the straight lines extrapolated from the high $[H^+]$-region. This suggests that the pseudo-equilibrium of the acid dissociation of HTTA holds only in the high $[H^+]$-region, on the analogy of the mono-complex formation of Ni(II)-bpy.[7] Hence, the k_f and k_{fh} values given in Table 1 were obtained from the intercept and the slope of the straight lines in the high $[H^+]$-region where the pseudo-equilibrium seems to hold.

In order to verify the establishment of the pseudo-

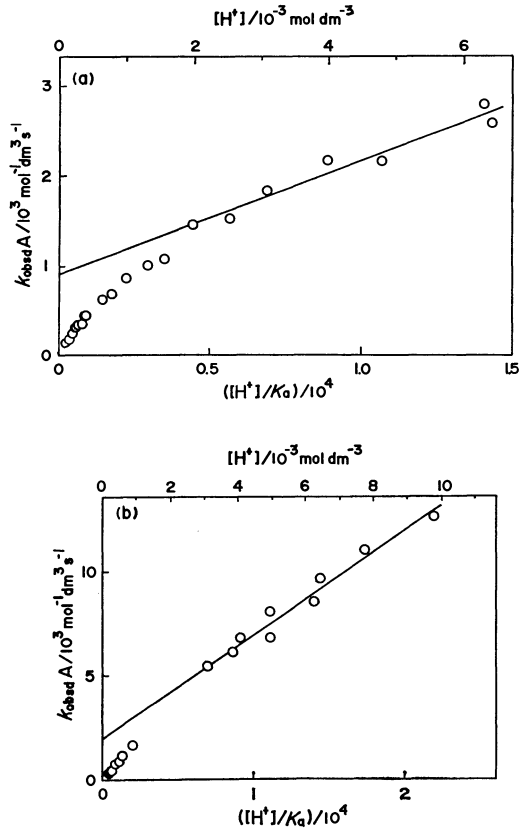

Fig. 2. Plots of $k_{obsd}A$ against $[H^+]/K_a$.
$A=(1+[H^+]/K_a)/[M^{2+}]$. (a) Ni(II)–TTA complex; $[Ni^{2+}]=2.00\times10^{-2}$ mol dm^{-3}, $[HTTA]=5.00\times10^{-5}$ mol dm^{-3}. (b) Cu(II)–TTA complex; $[Cu^{2+}]=1.02\times10^{-2}$ mol dm^{-3}, $[HTTA]=1.04\times10^{-5}$ mol dm^{-3}.

equilibrium of the acid dissociation of HTTA in the $[H^+]$-region where the k_f and k_{fh} values evaluated, the initial rates of the processes concerned were compared with each other. Figure 3 illustrates the initial rates for the Ni(II)–TTA system as a function of pH, where (rate f), (rate fh), (rate dp), and (rate p) are the rates of the complex formation in Reactions 5 and 6, and those of the deprotonation of HTTA and the protonation of TTA^- through Reaction 1, respectively. The subscript 0 denotes the values at reaction time zero. The deprotonation rate in Reaction 2 was ignored because of its negligible contribution to (rate dp) in acidic solution. These initial rates were calculated using the k_f, k_{fh}, and k_{dp} values obtained and the initial concentrations of the species participating in the reactions. As the equilibrium of the acid dissociation of HTTA holds at reaction time zero, $(\text{rate p})_0$ must be equal to $(\text{rate dp})_0$. As can be seen in Fig. 3, with the Ni(II)–TTA system the pseudo-equilibrium mentioned above proved to hold over the pH range where the k_f and k_{fh} values were evaluated, because at pH below 3 $(\text{rate dp})_0$ is larger than $(\text{rate f})_0$, and $(\text{rate p})_0$ is larger than $(\text{rate fh})_0$. With Cu(II)–TTA system, the establishment of the pseudo-equilibrium was also confirmed in the high $[H^+]$-region.

In order to establish the mechanism assumed in this study, the k_{dp} value of HTTA was evaluated from

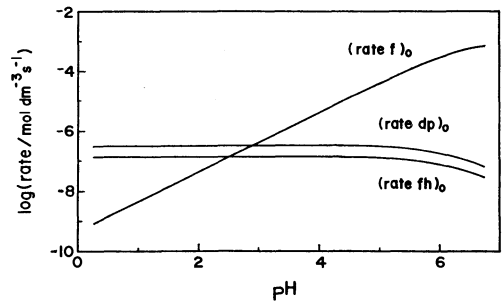

Fig. 3. Relationship between initial rates and pH for the Ni(II)–TTA complex at 25.0 °C.

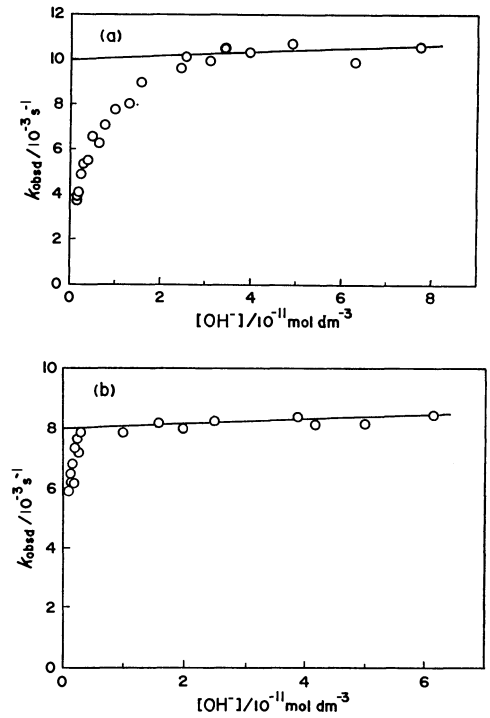

Fig. 4. Plots of k_{obsd} against $[OH^-]$ for (a) Ni(II)–TTA and (b) Cu(II)–TTA complex.
Data were taken from Fig. 2.

the data of the complex formation in the pH range where the rate was controlled by the deprotonation rate, and was compared to that obtained by the pH jump method. At the pH beyond 3, $(\text{rate dp})_0$ is less than $(\text{rate f})_0$ and comparable to $(\text{rate fh})_0$, as shown in Fig. 3. Therefore, the rate of the complex formation should be controlled by (rate dp) and (rate fh), after having been stationary with respect to $[TTA^-]$. Under such conditions, the rate of the complex formation is expressed by

$$d[MTTA^+]/dt = (k_{dp}+k_{OH}[OH^-]+k_{fh}[M^{2+}])[HTTA]. \quad (9)$$

Accordingly,

$$k_{obsd} = k_{OH}[OH^-] + (k_{dp}+k_{fh}[M^{2+}]). \quad (10)$$

Figure 4 shows the plots of k_{obsd} against $[OH^-]$ for the Ni(II)- and Cu(II)–TTA systems. The k_{obsd} values were evaluated from the absorbance change after the reaction became stationary. The k_{dp} values of HTTA in both systems were evaluated from the

intercepts of these straight lines at relatively high [OH^-], using [M^{2+}] and k_{fh} values. Although the k_{OH} values were also evaluated from their slopes, no significant value was obtained because of the experimental error due to the extremely low hydroxide-ion concentration. The k_{dp} values are summarized in Table 1 together with the k_{dp} and k_{OH} values obtained by the pH jump method. The average value of k_{dp} obtained by the complex-formation experiments is in excellent agreement with that by the pH jump method. This fact strongly supports the conclusion that the proton-transfer reaction of the ligand can be the rate-determining step of the complex formation depending upon the hydrogen-ion concentration. Additionally, it should be noted that the k_{dp} value of the ligand could be evaluated from the data of the complex-formation kinetics.

Jaffe and co-workers studied the same systems on the assumption that keto form of HTTA does not react directly with metal ion.[11] According to their description, the present k_f corresponds to the complex-formation rate constant of enolate ion, k_{fh} to the complex-formation rate constant of enol tautomer or to the enolation-rate constant of keto tautomer, and k_{dp} to the enolation-rate constant. Our values of k_f and k_{fh} for the Ni(II)–TTA system differ from their corresponding values, 1.0×10^4 and 2.3 $mol^{-1}\,dm^3\,s^{-1}$, respectively. For the Cu(II)–TTA system, the k_f value in this study is remarkably different from their's, $\geqq 3\times10^6$ $mol^{-1}\,dm^3\,s^{-1}$. Since k_{fh} is the overall rate constant, irrespective of keto or enol form of HTTA, the small value of k_{fh} may be partly ascribed to the unreactivity of the keto form. M. R. Jaffe *et al.* assumed that the equilibrium between enol tautomer and enolate ion of HTTA is always maintained throughout the reaction. This assumption seems to be reasonable only just after the reaction occurred. However, the direct deprotonation and/or the deprotonation *via* enol from keto form of HTTA become significant during the progress of the reaction. Comparing the initial rates of the complex-formation processes and the proton-transfer process, (rate f) and/or (rate fh) are larger than (rate dp) in both Ni(II)– and Cu(II)–TTA systems under their experimental conditions. This suggests that the pseudo-equilibrium for the acid dissociation or the enolation of the ligand failed in the course of the complex formation. This presumably explains the discrepancies of the rate constants between Jaffe's and our study. The fact that the rate constants in this study are not characteristic for metal ions should support the conclusion that in the complex formation forming the six-membered chelate ring the closure of the chelate ring is the rate-determining step.[15]

In conclusion, we obtained further evidence that the proton-transfer reaction of the ligand became the rate-determining step of the complex formation depending on the hydrogen-ion concentration, as in the case of the Ni(II)–bpy complex. Under such conditions, the deprotonation-rate constant of the ligand could be determined from the complex-formation rate, as well as by the pH jump method.

The authors wish to thank Professor S. Kida and Professor T. Taketatsu of Kyushu University for valuable discussions and encouragement. The present work was partially supported by a grant from the Central Research Institute of Fukuoka University.

References

1) K. Kustin and J. Swinehart, *Prog. Inorg. Chem.*, **13**, 107 (1970).
2) D. J. Hewkin and R. H. Prince, *Coord. Chem. Rev.*, **5**, 45 (1970).
3) J. C. Cassatt and R. G. Wilkins, *J. Am. Chem. Soc.*, **90**, 6045 (1968).
4) J. E. Letter, Jr., and R. B. Jordan, *Inorg. Chem.*, **10**, 2692 (1971).
5) J. C. Cassatt, W. A. Johnson, L. M. Smith, and R. G. Wilkins, *J. Am. Chem. Soc.*, **94**, 8399 (1972).
6) R. W. Taylor, H. K. Stepien, and D. B. Rorabacher, *Inorg. Chem.*, **13**, 1282 (1974).
7) I. Ando, S. Nishijima, K. Ujimoto, and H. Kurihara, *Bull. Chem. Soc. Jpn.*, **55**, 2881 (1982).
8) F. Hibbert, "Comprehensive Chemical Kinetics," ed by C. H. Bamford and C. H. F. Tipper, Elsevier, Amsterdam (1977), Vol. 8, Chap. 2.
9) J. C. Reid and M. Calbin, *J. Am. Chem. Soc.*, **72**, 2948 (1950).
10) R. W. Taft, Jr., and E. H. Cook, *J. Am. Chem. Soc.*, **81**, 46 (1959).
11) M. R. Jaffe, P. Fay, M. Cefola, and N. Sutin, *J. Am. Chem. Soc.*, **93**, 2878 (1971).
12) A. V. Celiano, M. Cefola, and P. S. Gentile, *J. Phys. Chem.*, **65**, 2194 (1961).
13) A. V. Celiano, M. Cefola, and P. S. Gentile, *J. Phys. Chem.*, **66**, 1132 (1962).
14) W. K. Ong and R. H. Prince, *J. Chem. Soc., A*, **1966**, 458.
15) R. G. Pearson and O. P. Anderson, *Inorg. Chem.*, **9**, 39 (1970).
16) A. Adin and L. Newman, *J. Inorg. Nucl. Chem.*, **32**, 3321 (1970).
17) I. Ando, J. Saito, K. Ujimoto, and H. Kurihara, *Fukuoka Univ. Sci. Reports*, **11**, 47 (1981).
18) I. Ando, K. Ujimoto, and H. Kurihara, *Bull. Chem. Soc. Jpn.*, **55**, 713 (1982).
19) V. M. Peshkova and P. Ang, *Russ. J. Inorg. Chem.*, **7**, 765 (1962).
20) J. R. Jones, *Prog. Phys. Org. Chem.*, **9**, 241 (1972).

The Reaction of *cyclo*-Triphosphate with Ethylenediamine

Mitsutomo Tsuhako,* Akiko Nakahama, Shigeru Ohashi,† Hiroyuki Nariai,†† and Itaru Motooka††

Kobe Women's College of Pharmacy, Kitamachi, Motoyama, Higashinada-ku, Kobe 658

† *Department of Chemistry, Faculty of Science, Kyushu University 33, Hakozaki, Higashi-ku, Fukuoka 812*

†† *Department of Chemistry, Faculty of General Education, Kobe University, Tsurukabuto, Nada-ku, Kobe 657*

(Received September 17, 1982)

The reaction of sodium *cyclo*-triphosphate (P_{3m}) with ethylenediamine (en) was studied with special attention paid to the kinds and amounts of products under various conditions and to its reaction mechanism. 1) The reaction of P_{3m} with ethylenediamine in the pH range of 8—12 gave six new compounds; three of them were identified as *N,N*-bis(2-aminoethyl)phosphorodiamidate (P_1-en_2), *N*-(2-aminoethyl)amidodiphosphate (P_2-en), and *N*-(2-aminoethyl)-*P*-amidotriphosphate (P_3-en). 2) The formation of P_3-en and P_2-en was most favored at a pH near 10(about 32 and 9% respectively), while that of P_1-en_2 proceeded extensively at pH 10—12(about 12%). 3) The amounts of products varied greatly depending on the mixing ratio of P_{3m} and ethylenediamine. P_1-en_2 was the predominant product at $en/P_{3m} > 1$, while P_3-en was at $en/P_{3m} \leqq 1$. 4) At a pH value below 10, tetra-(P_4) and pentaphosphate (P_5) were formed in addition to the above products. The reaction between P_{3m} and ethylenediamine scarcely proceeded under acidic conditions. 5) Ortho-(P_1), pyro-(P_2), and triphosphate (P_3) did not react with ethylenediamine at all. 6) The reaction mechanism between P_{3m} and ethylenediamine was discussed.

Linear condensed phosphates have found wide practical applications as food and drug additives, detergents, and fertilizers,[1–3] but little is known about the applications of cyclic condensed phosphates.[4] It was first reported by Quimby and Flautt[5] in 1959 that cyclo-triphosphate (P_{3m}), a six-membered cyclic phosphate, readily undergoes a ring-opening reaction in the presence of ammonia to give amidotriphosphate. After that, it was reported that P_{3m} reacts with amines, such as alkylamine,[6,7] 1,6-hexandiamine[8] and amino acids,[9–12] to yield new compounds with a P–N bond in their molecules. Recently, it was found that P_{3m} also reacts with other organic compounds, such as alcohols,[13] sugar,[13] and nucleoside,[14–19] and that it is effective for the stabilization of vitamin C.[20] As a result, extensive attention has been paid to the potential commercial applications of P_{3m}. However, the details of the reaction of P_{3m} with these organic compounds still remain unclear. In the present study, therefore, P_{3m} was allowed to react with ethylenediamine, the simplest member of the diamine family, under various conditions, and the kinds and amounts of the products as well as the reaction mechanism were investigated by using anion-exchange chromatography, chemical analysis for phosphorus and ethylenediamine, and IR spectroscopy.

Experimental

Chemicals. The sodium *cyclo*-triphosphate, $Na_3P_3O_9 \cdot 6H_2O$, was prepared by the procedure described in a previous paper[21] and recrystallized five times from an aqueous solution. Unless otherwise stated, guaranteed reagents from Wako Chemical Industries, Ltd., were used without further purification.

Reaction between cyclo-*Triphosphate and Ethylenediamine.* A 0.5 mol dm^{-3} portion of the sodium *cyclo*-triphosphate (P_{3m}) solution was mixed with a 0.5 or 5 mol dm^{-3} ethylenediamine (en) solution (molar ratio; P_{3m}:en=1:1 and 1:10), the mixed solution was controlled to the prescribed pH by adding a 6 mol dm^{-3} hydrochloric acid or sodium hydroxide solution(pH:12, 10, and uncontrolled), and the reaction was allowed to proceed at room temperature. Since the pH of the mixed solutions lowered as the reaction progresses, it was held at the prescribed pH, when required, by adding a sodium hydroxide solution.

Anion-exchange chromatography, the determination of phosphorus, and IR spectroscopy were carried out by the methods described in a previous paper.[21]

A Yanagimoto Micro Elemental Analyzer, MT-2 type, was used for the determination of ethylenediamine in the reaction products.

Results and Discussion

Reaction of cyclo-*Triphosphate with Ethylenediamine.* The initial pH of the mixed solution of P_{3m} and ethylenediamine at a molar ratio of 1:1 was above 14, but it was lowered sharply with the progress of the reaction, reaching about 12 after 2 h and going down to about 8.7 after 3 d. This indicates that P_{3m} reacted with water or ethylenediamine to afford chain-phosphates or their derivatives. To prove this, we attempted to separate and determine the reaction products by means of anion-exchange chromatography. An example of the results obtained is given in Fig. 1, which shows the elution patterns for the reaction products after 1 and 7 d. Then, the pH values of the solution were about 9.2 and 8.3 respectively. As can be seen, elution peaks of P_1, P_2, and P_3 appeared after 1 d. In addition, a large peak of an unknown compound(designated as Compound D) was observed between the peaks of P_1 and P_2, and two other peaks of unknown compounds(Compounds A and B) were noticed before the peak of P_1. Furthermore, peaks of tetra-(P_4) and pentaphosphate(P_5) were also observed after 39 d, though they are not shown in Fig. 1.

Figure 2 shows the changes in the amounts of P_1, P_2, P_3, P_4, and P_5, as well as in Compounds A, B, and

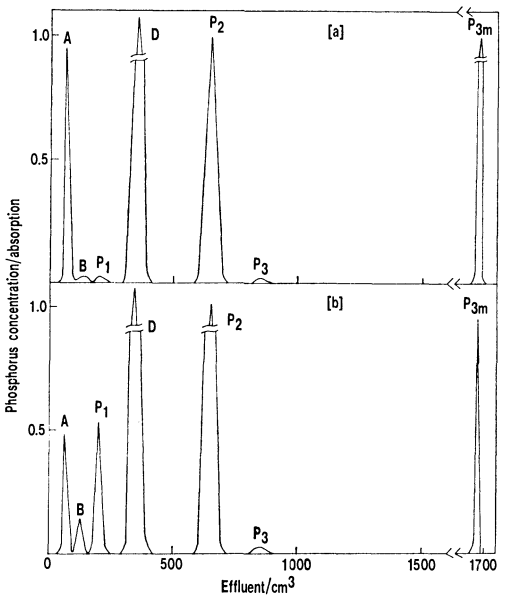

Fig. 1. Elution patterns for the reaction products of P_{3m} with ethylenediamine.
[a]: After 1 d(pH 9.2), [b]: after 7 d(pH 8.3).

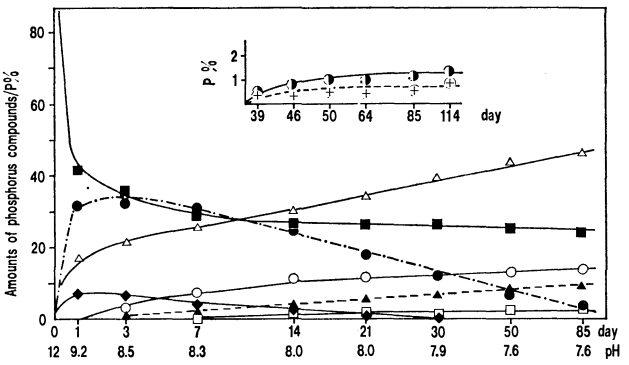

Fig. 2. Change of the amounts of phosphorus compounds in the reaction of P_{3m} with ethylenediamine.
—○—: P_1, —△—: P_2, —□—: P_3, --⊕--: P_4, —◑—: P_5, —◆—: Compound A, --▲--: B, —·—●—·—: D, —■—: P_{3m}.

D, with the passage of time or with the decrease in the pH. It is apparent from the figure that Compound D began to be formed immediately after the reaction, and that its amount reached a maximum level of 32.4% after 3 d, followed by a gradual decrease with the reaction time or with a decrease in the pH. A similar tendency was observed in Compound A. Compound B, on the other hand, was first observed after 3 d, and its amount increased with the time, reaching about 8.7% after 114 d. The amounts of P_1 and P_2 also showed a gradual increase with the time, reaching about 13.8 and 48.2% respectively after 114 d. The formation of P_2 was particularly marked. These results indicate that the formation of Compounds A and D is favored by a high pH. To provide further evidence for this, the reaction of P_{3m} with ethylenediamine was carried out at the controlled pH values of 12 and 10 at a mixing ratio of 1:1.

Figure 3 shows the elution patterns for the reaction

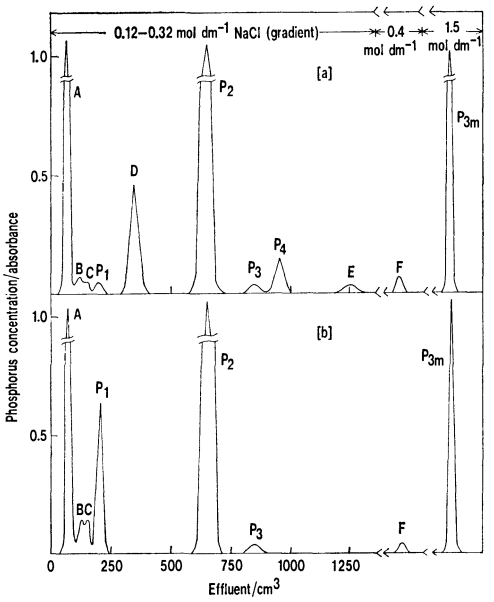

Fig. 3. Elution patterns for the reaction products of P_{3m} with ethylenediamine at pH 12.
[a]: After 1 d, [b]: 17 d.

mixture after 1 and 17 d at pH 12. In this experiment, the gradient elution technique with a 0.12—0.32 mol dm^{-3} sodium chloride solution was used for the eluant up to 1600 cm^3, while the step-wise elution method with 0.4 and 1.5 mol dm^{-3} sodium chloride solutions was used for the elution of an unknown compound F and P_{3m}, respectively. Compared with the reaction of P_{3m} with ethylenediamine at an uncontrolled pH, we observed remarkable differences in the kinds and amounts of products at pH 12. That is, a small peak of an unknown compound(Compound C) was observed between the elution peaks of P_1 and Compound B. In addition, a peak of an unknown compound(Compound E) was also found at an eluant of 1250 cm^3, and another one of an unknown compound (Compound F) when the mixture was eluted with a 0.4 mol dm^{-3} sodium chloride solution. In short, six unknown compounds(Compounds A, B, C, D, E, and F) were formed by the reaction of P_{3m} with ethylenediamine at pH 12. Sodium pyrophosphate decahydrate, $Na_4P_2O_7 \cdot 10H_2O$, began to precipitate after 3 d, and its amount increased with the time. P_4 was formed in significant quantities(about 9.8%) in the initial stage of the reaction(up to 5 d), but its amount decreased after that with the lapse of time. Figure 4 shows the changes in the amounts of P_1, P_2, P_3, and P_4, as well as in Compounds A through F, with the time. As can be seen from Fig. 3, the elution peaks of Compounds B and C were too close together to be determined. Also, all attempts to separate Compounds B and C by changing the elution conditions failed. The sum of the amounts of Compounds B and C is, therefore, shown in Fig. 4. A comparison of Fig. 4 with Fig. 2 indicates a marked difference between the reactions carried out at pH 12 and those carried out with no control of the pH. Particularly, when the pH of the solution was not controlled, the formation of Compound D was apparently favored under mildly

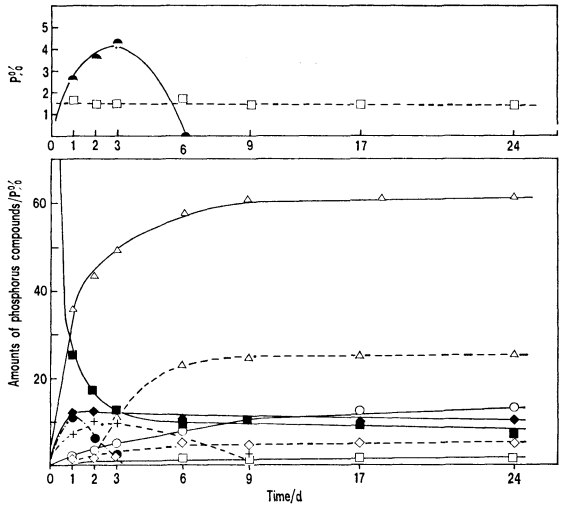

Fig. 4. Change of the amounts of phosphorus compounds in the reaction of P_{3m} with ethylenediamine at pH 12.
—○—: P_1, —△—: P_2(total), --△--: P_2(precipitated)
—□—: P_3, --⊕--: P_4, —◆—: A, --◇--: B+C,
—·—●—·—: D, —◓—: E, --□--: F, —■—: P_{3m}.

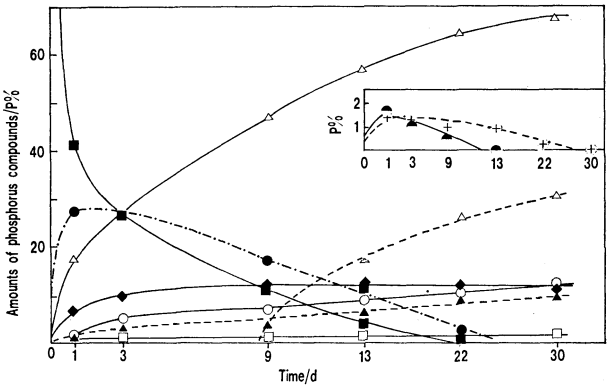

Fig. 5. Change of the amounts of phosphorus compounds in the reaction of P_{3m} with ethylenediamine at pH 10.
—○—: P_1, —△—: P_2(total), --△--: P_2(precipitated)
—□—: P_3, --⊕--: P_4, —◆—: A, —▲—: B,
—·—●—·—: D, —◓—: E, —■—: P_{3m}.

alkaline conditions(pH 10—8.5). Compound A, on the contrary, was produced more readily in highly alkaline regions(pH 12). Compounds C, E, and F were also formed in high pH regions, but their amounts were rather small. Compound E was produced in significant quantities in the initial stage of the reaction (up to 3 d), but disappeared completely after 6 d. In addition, the precipitation of $Na_4P_2O_7 \cdot 10H_2O$ was observed after 3 d at pH 12. The same phenomenon has been experienced by the present authors in the reaction of P_{3m} with L-valine[21] or glycine.[22]

In contrast, the products obtained by the reaction of P_{3m} with ethylenediamine at pH 10 were very similar to those in the reaction at an uncontrolled pH; the products obtained at pH 10 were Compounds A, B, D, and E, but Compounds C and F were not formed at all. The only difference between the two reactions was that Compound E was produced at pH 10, while

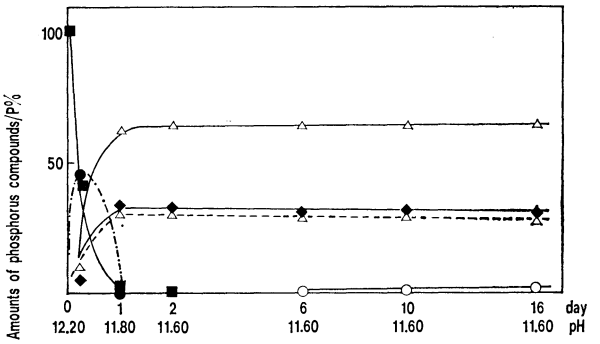

Fig. 6. Change of the amounts of phosphorus compounds in the reaction of P_{3m} with ethylenediamine.
—○—: P_1, —△—: P_2(total), --△--: P_2(precipitated)
—◆—: A, —·—●—·—: D —■—: P_{3m}.

P_5 was produced at an uncontrolled pH.

Figure 5 shows the changes in the amounts of products (Compounds A, B, D, and E), as well as P_1, P_2, P_3, P_4, and P_{3m}, with the lapse of time at pH 10. It is apparent from Fig. 5 that Compound D was formed in considerable quantities in the initial stage, its amount reaching a maximum level of about 28.6% after 1 d and then decreasing with time. The amount of Compound A, on the other hand, gradually increased for the first week and after that was almost constant(about 11.5%).

Figures 2, 4, and 5 show that Compound A is stable at a pH of 10 or higher. The amounts of P_4 and Compound E were very small, about 1.5% for both.

The formation of the products(Compounds A, B, C, D, E, and F) in the reaction between P_{3m} and ethylenediamine at a molar ratio of 1:1 under various pH conditions may be summarized as follows: 1) Compound D was rapidly formed in the initial stage of the reaction(1—3 d) at pH 10—8.5, its amount reaching about 32%. 2) Compound A was formed in significant quantities at pH 10—12, its amount reaching about 12%. This compound was stable within this pH region for a long time(30 d). 3) Compound B was formed at pH 10 over a long period(30 d), its amount reaching about 9.2%. However, it was found only in minute quantities at pH 12, and the rate of its formation was also very low at a pH of 8.5 or lower. 4) Compound C was produced only in a high pH region(12 or higher) and in small quantities(about 2%). 5) Compound E was formed in the initial stage of the reaction (1—3 d) at a pH of 10 or higher, but it was decomposed almost completely after two weeks. Its amount was about 4.5% at pH 12. 6) Compound F was formed at a pH of 12 or higher, but its amount was as small as about 1.7%. Besides these compounds, the formation of P_4 and P_5 was also observed at a pH of 10 or lower; their amounts tended to increase slightly as the pH was lowered to near neutral. The mechanism of the formation of P_4 and P_5 will be presented in detail later.

No reaction of P_{3m} with ethylenediamine took place under acidic conditions. This is probably ascribable to the formation of inactive $H_3N^+CH_2CH_2NH_2$ or $H_3N^+CH_2CH_2N^+H_3$.

Next, the effect of the mixing ratio of P_{3m} and ethyl-

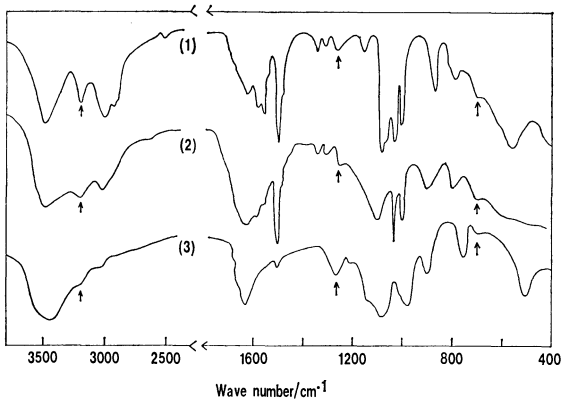

Fig. 7. IR spectra of the compounds A, B, and D. (1): Compound A, (2): B, (3): D. Arrow(↑): absorption due to the P–N bond.

enediamine on the kinds and amounts of reaction products was studied. Figure 6 shows the changes in the amounts of various phosphates with the time at a molar ratio of P_{3m}:en=1:10. As can be seen, the reaction proceeded at a higher rate in the presence of a large excess of ethylenediamine. The products obtained in the reaction were P_1, P_2, P_3, and Compounds A, D, and E. However, the date for P_3 and Compound E are omitted in Fig. 6, because their amounts are very small. In response to the consumption of P_{3m}, Compound D began to be formed immediately after the reaction, its amount reaching about 47% after 5 h; thereafter, it decreased rapidly. On the contrary, Compound A began to be formed after 5 h, its amount reaching about 37% after 1 d. P_2 was also formed concurrently with the formation of Compound A, its amount reaching about 64%. Precipitates of $Na_4P_2O_7 \cdot 10H_2O$ were observed about 3 h after the reaction. As may be apparent from Fig. 6, the reaction of P_{3m} with ethylenediamine at a molar ratio of 1:10 afforded Compound A and P_2 as the main products; the amount of the former(about 32% as phosphorus concentration) is just half that of the latter (about 64%). This suggests that Compound A is an orthophosphate derivative of ethylenediamine.

The results obtained by the reactions in the mixing-ratio range from P_{3m}:en=1:0.1 to 1:10 may be summarized as follows: the formation of Compound A was predominant at $P_{3m}/en<1$, and that of Compound D, at $P_{3m}/en \geqq 1$.

Molecular Structures of the Three Unknown Compounds, A, B, and D. Compounds A, B, and D were isolated by anion-exchange chromatography according to the method described in the previous paper;[21] the structure of each compound was then investigated by means of chemical analysis for phosphorus and ethylenediamine and by means of IR spectroscopy, as well as by means of its structural change with the pH.

Chemical analysis revealed that the P/en ratios are 1:2, 2:1, and 3:1 for Compounds A, B, and D respectively. This indicates that Compound A may be a P_1-derivative of ethylenediamine containing P_1 and ethylenediamine in the molar ratio of 1:2, Compound B, a P_2-derivative of ethylenediamine(P_2:en=1:1), and Compound D, a P_3-derivative of ethylenediamine(P_3:en=1:1).

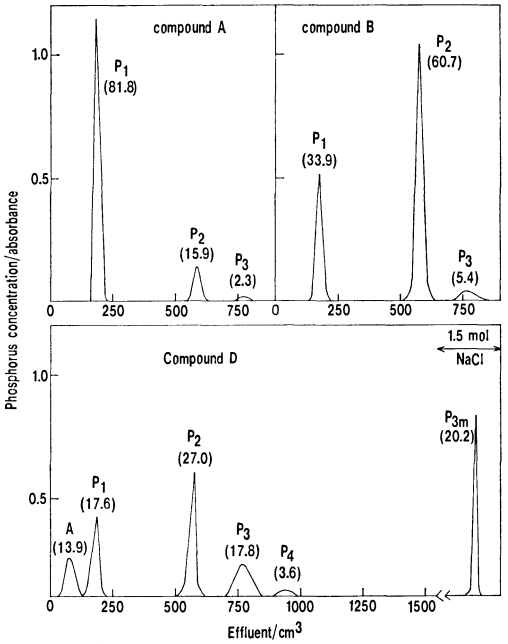

Fig. 8. Decomposition of the compounds A, B, and D at pH 3.

Figure 7 shows the IR spectra of Compounds A, B, and D as measured by means of a KBr tablet. For Compound A, characteristic absorptions due to the P–N bond were observed at about 3330—3150, 1270, 875, and 700 cm^{-1},[23-25] while those attributable to the P–O bond were noticed at about 1160 and 970—1050 cm^{-1}.[26,27] Absorptions that can be assigned to the $-CH_2-$ group were also observed at 2925, 2850, and 1470 cm^{-1},[28] while characteristic absorptions due to the $-NH_2$ were present at about 3500 and 1065 cm^{-1}.[28] For Compound B, absorptions ascribable to the P–N bond were noticed at about 3330—3150, 1260, and 700 cm^{-1}, but the absorption due to the P–N bond near 875 cm^{-1} was uncertain because of overlapping with the strong absorption due to the P–O–P bond near 900 cm^{-1}. A peak that can be assigned to the P–O bond was also observed at 970—1050 cm^{-1}.

Compound D, as in the case of Compound B, showed characteristic absorptions due to the P–N, P–O–P, and P–O bonds. Also, there were characteristic bands[29] of the vibrations of the triphosphate anion at about 1230(ν_{as} PO_2), 1160(ν_{as} PO_3), 1000(ν_s PO_3), 735($\delta_s PO_2$), and 510 cm^{-1} in Compound D.

These results of chemical analysis and IR spectroscopy indicate that Compounds A, B, and D are phosphate derivatives of ethylenediamine containing the P–N bond in their molecules. Compounds B and D, which showed absorption due to both the P–N and P–O–P bonds, can be considered as pyro- and triphosphates derivatives of ethylenediamine. Compound A, on the other hand, has no P–O–P bond in the molecule, and so it may be regarded as an orthophosphate derivative of ethylenediamine.

To provide further evidence for the above, Compounds A, B, and D were dissolved in distilled water,

allowed to stand for 15 min. at a pH controlled to 3 by adding dilute hydrochloric acid, and then analyzed by anion-exchange chromatography. The results are shown in Fig. 8, the numerals in which are the amounts of products represented in P%. It is apparent from Fig. 8 that Compound A, upon acidification (to pH 3), was decomposed to give P_1 in about an 80% yield. P_2 and P_3 were also formed at the same time, though in small amounts. This clearly indicates that Compound A is a P_1-derivative of ethylenediamine(P_1-en_2), in which two molecules of ethylenediamine are combined with P_1. On the other hand, Quimby[5] and also Feldmann and Thilo[6] reported that, when amidophosphates having the P–N bond were acidified, the condensation of phosphate took place and amidotriphosphate was recyclized to P_{3m}.

The formation of P_2 and P_3 by the hydrolysis of P_1-en_2 under the acidic conditions in the present study may be explained by the mechanism described by Quimby[5] and by Feldmann and Thilo:[6]

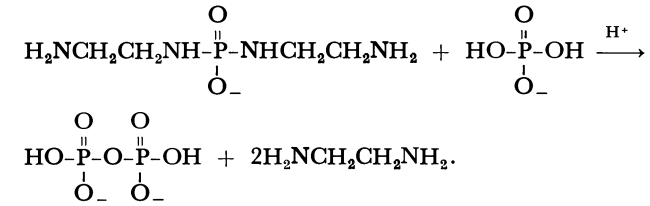

That is, the P_1 formed by the hydrolysis of P_1-en_2 reacts with undecomposed P_1-en_2 or partially hydrolyzed $H_2NCH_2CH_2NH\text{-}\overset{\overset{O}{\|}}{P}\text{-}OH$ (P_1-en) to form P_2, which in turn reacts with P_1-en_2 or P_1-en to give P_3.

Compound B, when acidified, affords about 61% in P_2, 34% in P_1, and 5% in P_3. This indicates that this compound is $^{-}O\text{-}\overset{\overset{O}{\|}}{P}\text{-}O\text{-}\overset{\overset{O}{\|}}{P}\text{-}NHCH_2CH_2NH_2$ (P_2-en), in which one molecule of ethylenediamine is attached to P_2. The large amount of P_1 observed may be ascribed to the hydrolysis of the P_2 once formed.

It is apparent from Fig. 8 that, under acidic conditions, Compound D is changed into P_1, P_2, P_3, P_4, and Compound A, and that about 20% of it is recyclized to P_{3m}. This shows clearly that Compound D is a triphosphate derivative of ethylenediamine.

It was demonstrated that Compound A is *N,N'*-bis(2-aminoethyl)phosphorodiamidate $H_2NCH_2CH_2\text{-}\overset{\overset{O}{\|}}{P}\text{-}NHCH_2CH_2NH_2$, Compound B, *N*-(2-aminoethyl)amidodiphosphate $^{-}O\text{-}\overset{\overset{O}{\|}}{P}\text{-}O\text{-}\overset{\overset{O}{\|}}{P}\text{-}NHCH_2CH_2NH_2$, and Compound D, *N*-(2-aminoethyl)-*P*-amidotriphosphate $^{-}O\text{-}\overset{\overset{O}{\|}}{P}\text{-}O\text{-}\overset{\overset{O}{\|}}{P}\text{-}O\text{-}\overset{\overset{O}{\|}}{P}\text{-}NHCH_2CH_2NH_2$, from the results of the chemical analysis for phosphorus and ethylenediamine and from the results of IR spectroscopy, as well as from the results of the hydrolysis of these compounds under acidic conditions.

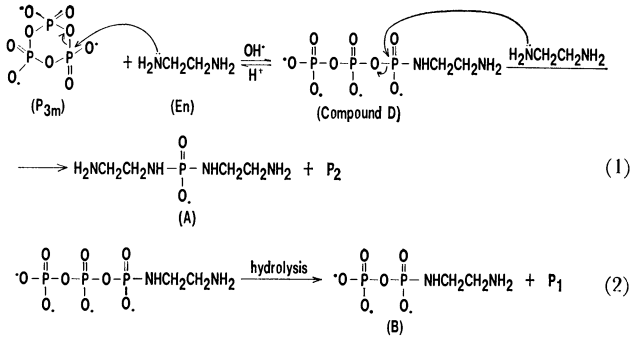

Fig. 9. Mechanism of the reaction of P_{3m} with en.

The structures of Compounds C, E, and F have not yet been characterized because they were formed in only minute amounts and could not be isolated in a pure form.

Reaction of Short-chain Phosphates with Ethylenediamine. A solution of trisodium orthophosphate (P_1), tetrasodium pyrophosphate (P_2), or pentasodium triphosphate (P_3) was mixed with an ethylenediamine solution in a molar ratio of 1:1, and then the mixed solution was adjusted with a hydrochloric acid or sodium hydroxide solution to pH 12 and allowed to react at room temperature. No reaction products were observed at all in the reaction of ethylenediamine with P_1, P_2, or P_3.

Reaction Mechanism of P_{3m} and Ethylenediamine. The mechanism of the reaction between P_{3m} and ethylenediamine at pH 10—12 is summarized in Fig. 9. Probably, the first step of the reaction is the nucleophilic attack of the lone pair of the nitrogen atom in ethylenediamine on the phosphorus atom in P_{3m} to cause a ring opening of *cyclo*-triphosphate, forming P_3-en. The P_3-en once formed is then attacked by free ethylenediamine or undergoes hydrolysis to give P_1-en_2 or P_2-en.

This reaction mechanism can reasonably explain the fact that P_3-en, formed predominantly in the initial stage of the reaction at pH 10—12, was gradually converted into P_1-en_2, P_2-en, and other phosphates with the passage of time. In the presence of a large excess of ethylenediamine(P_{3m}:en=1:5—1:10), it was found that P_3-en, which was formed in large quantities immediately after the reaction, completely disappeared after 1 d, leaving only P_1-en_2 and P_2. This fact also supports the above mechanism in which the reaction of P_3-en with free ethylenediamine affords P_1-en_2.

References

1) Van Wazer, "Phosphorus and Its Compounds," John Wiley and Sons, New York (1961), Vol. II, p. 1462.

2) E. Kobayashi, "Chemistry of Phosphates and Their Applications," ed by S. Hori, Kagaku Kogyo-sha, Tokyo (1969), p. 183.

3) S. Ueda, "Mukikagaku Zensho, Phosphorus," ed by S. Ohashi, Maruzen, Tokyo (1965), p. 343.

4) S. Y. Kalliney, in J. Griffith and M. Grayson(editors),

"Topics in Phosphorus Chemistry," John Wiley and Sons, New York (1972), Vol. 7, p. 299.
5) O. T. Quimby and T. J. Flautt, *Z. Anorg. Allg. Chem.*, **296**, 220 (1958).
6) W. Feldmann and E. Thilo, *Z. Anorg. Allg. Chem.*, **327**, 159 (1964).
7) W. Feldmann, *Z. Chem.*, **1**, 26 (1965).
8) N. M. Dombrovskii and A. I. Dorosh, Russ. *J. Inorg. Chem.*, **17**, 981 (1972).
9) W. Feldmann, *Z. Chem.*, **4**, 154 (1969).
10) J. Rabinowitz, *Helv. Chim. Acta*, **52**, 2663 (1969); **53**, 1350 (1970); **54**, 1483 (1971).
11) J. Rabinowitz, *Nature*, **224**, 795 (1969).
12) N. M. Chung, R. Lohrmann, L. E. Orgel, and J. Rabinowitz, *Tetrahedron*, **27**, 1205 (1971).
13) W. Feldmann, *Chem. Ber.*, **100**, 3850 (1967).
14) A. W. Schwartz, *Chem. Commun.*, **1969**, 1393.
15) M. J. Bishop, R. Lohrmann, and L. E. Orgel, *Nature*, **237**, 162 (1972).
16) A. M. Schoffstall, *Origins Life*, **7**, 399 (1976).
17) A. W. Schwartz and C. Ponnamperuma, *Nature*, **218**, 443 (1968).
18) R. Saffhill, *J. Org. Chem.*, **35**, 2881 (1970).
19) M. Tsuhako, M. Fujimoto, and S. Ohashi, *Chem. Lett.*, **1981**, 849.
20) M. Tsuhako, T. Matsuo, H. Nariai, I. Motooka, and M. Kobayashi, *Yakugaku Zasshi*, **101**, 404 (1981).
21) M. Tsuhako, N. Fujita, A. Nakahama, T. Matsuo, M. Kobayashi, and S. Ohashi, *Bull. Chem. Soc. Jpn.*, **53**, 1968 (1980).
22) M. Tsuhako, S. Ohashi, H. Nariai, and I. Motooka, *Chem. Pharm. Bull.*, **30**, 3882 (1982).
23) E. Steger, *Z. Anorg. Allg. Chem.*, **309**, 305 (1961).
24) E. Steger and G. Mildner, *Z. Anorg. Allg. Chem.*, **332**, 314 (1964).
25) E. Kobayashi, *Nippon Kagaku Kaishi*, **1972**, 38; **1973**, 1437.
26) D. E. C. Corbridge and E. J. Lowe, *J. Chem. Soc.*, **1954**, 493.
27) D. E. C. Corbridge, *J. Appl. Chem.*, **6**, 456 (1956).
28) K. Nakanishi, "Infrared Absorption Spectra," Nankodo, Tokyo (1970), pp. 26, 44.
29) V. A. Lyutsko, N. F. Ermolenko, and L. I. Prodan, *Russ. J. Inorg. Chem.*, **20**, 792 (1975).

Pyrolytic Sulfurization Gas Chromatography. XIV. Simultaneous Determination of the Absolute Contents of C, H, O, and N in an Organic Compound by Means of a Calibration Method

Tadashi HARA* and Fujio OKUI

Department of Chemical Engineering, Faculty of Engineering, Doshisha University, Karasuma Imadegawa, Kamigyo-ku, Kyoto 602

(Received September 17, 1982)

The absolute content of C, H, O, and N in an organic compund including a metal organic chelate was satisfactorily determined on the basis of pyrolytic sulfurization gas chromatography. A 1.0—1.3 mg sample was weighed on a microbalance, and was subjected to pyrolytic sulfurization. The gases evolved by the reaction were estimated by gas-chromatography. By using both the analytical result of each product and its calibration factor previously obtained by analyzing cyanoguanidine, 8-quinolinol, and sucrose as standard samples, the absolute content of C, H, O, and N was calculated satisfactorily for each substance.

Pyrolytic sulfurization gas chromatography (PSGC) was originated[1] and has been reported[2-13] by the authors for the purpose of establishing a new method of elemental analysis by which several elements in an organic compound can be simultaneously determined. By using PSGC, the atomic ratio between C, H, O, and N in a usual organic compound,[1] a metal organic chelate compound,[3,13] a polymer,[5] and an organic halogen compound[7,9] have been successfully and simultaneously determined.

In PSGC, a 0.3—0.5 mg sample is subjected to pyrolytic sulfurization with 5 mg of high purity sulfur[4] in a sealed quartz tube. The gaseous products from this reaction, carbon dioxide (CO_2), carbonyl sulfide (COS), carbon disulfide (CS_2), hydrogen sulfide (H_2S), and nitrogen molecule(N_2), are estimated by gas-chromatography, followed by the calculation of the atomic ratio between C, H, O, and N. Organic elemental analysis by PSGC is mainly characterized by the followings: 1) The atomic ratio between C, H, O, and N can be simultaneously determined within an absolute error of about $\pm 0.2\%$;[12] 2) no weighing is necessary for sampling and thus a microbalance is not necessary; 3) no additional combustion is required for a less combustible compound; 4) this method is applicable to various compounds such as metal organic chelates, thermosetting polymers, and organic halogen compounds; 5) the atomic ratio between C, H, O, N, Cl, Br, and I in an organic halogen compound can be determined[9] in a single analysis; and 6) the measurement is inexpensive because with a slight modification commercial apparatus is available. However, PSGC is not yet as satisfactory as conventional organic elemental analysis based on an oxygen combustion technique in the following respects; 1) the absolute amount of each element in a sample cannot be determined; as in PSGC only the atomic ratio between C, H, O, and N in a sample is calculated from the analytical data of the gaseous products. 2) Compounds which contain elements additional to C, H, O, and N cannot be analyzed. These problems must be solved by further improvement of PSGC, to establish a method by which each absolute content of C, H, O, and N in a sample can be determined. Therefore, the present study has been carried out with this objective in mind. Since the reaction products obtained by pyrolytic sulfurization of a common organic compound sample is restricted to CO_2, COS, CS_2, H_2S, and N_2, calibration curves of these products were easily obtained by analyzing three standard samples which were previously weighed. By using such calibration curves, various samples could be analyzed and the absolute content of C, H, O, and N in a sample was successfully and simultaneously determined.

Experimental

Apparatus and Reagents. The apparatus used in this study was the same as that previously reported.[11] A definite amount of sample was measured on a Shimadzu microbalance MDP-5.

The organic compounds used as analytical samples were of reagent grade for elemental analysis except for cyanoguanidine, which was of reagent grade for melting-point standard.

Procedure. A sample in the range of 1.0 to 1.3 mg was weighed exactly in a quartz tube, which was closed at one end, and about 10 mg of S was also added. The air inside the quartz tube containing the sample and S was next displaced with He for 10 min, after which the other end of the tube was sealed. The ampule was next heated for 1 min in a high-frequency induction furnace as described in the previous study.[10] The gaseous products evolved in the reaction between a sample and S were analyzed by gas-chromatography under the same conditions as those previously reported.[11] From the analytical data, the absolute contents of C, H, O, and N in a sample were separately calculated by use of calibration curves of the products which had been previously obtained by analyzing three standard samples, such as cyanoguanidine, 8-quinolinol, and sucrose.

Results and Discussion

Sample Amount. According to the conventional PSGC, 0.3—0.5 mg of sample has been subjected to pyrolytic sulfurization. Since a sample had to be weighed, in the present study, to four significant figures with the microbalance which could weigh to a precision of 1 μg, a sample more than 1 mg was used for an analysis. Therefore, the following examinations were undertaken to confirm whether PSGC could be applied or not to the analysis using about 1 mg of sample. 1) Approximately 0.5—1.3 mg of alanine as a standard sample and 10 mg of S (5 mg of S was

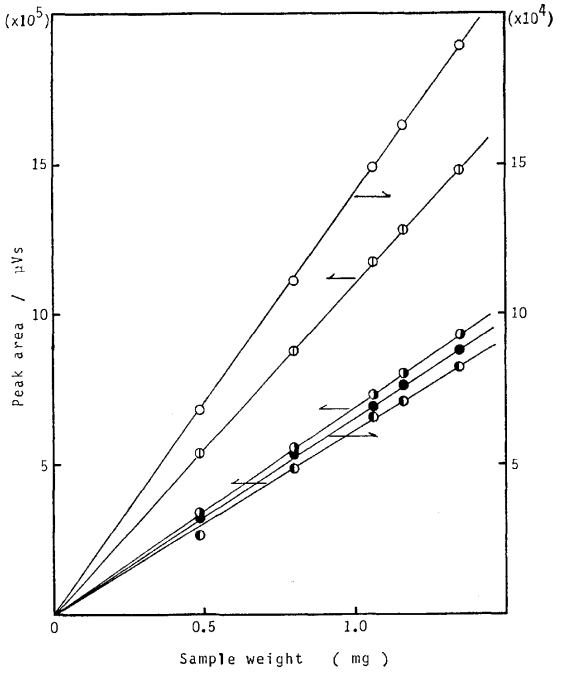

Fig. 1. Relationship between sample weight and peak area of each product. ○: N_2, ●: CO_2, ⦶: H_2S, ◑: COS, and ◐: CS_2.

used in the conventional PSGC) were subjected to PSGC analysis, and the relationship between the sample weight and the peak area of each product was determined. Figure 1 shows that a plot of peak area of each product *vs.* sample weight gives a straight line. 2) In order to examine the reproducibility of the analytical value under the present conditions, the present PSGC analysis was repeated 10 times using 1 mg of alanine and 10 mg of S. The same procedure was repeated 10 times with 0.5 mg of alanine and 5 mg of S. By using these analytical data, the analytical values under the present conditions were compared with those under the previous ones by estimating the coefficient of variation (CV) of the peak area ratio of each product to their sum (Table 1). These examinations indicate that PSGC analysis is also feasible for use with 1 mg samples though the reproducibility of the analytical values under the present conditions is slightly inferior to those under the conventional ones, as is inferred from Table 1.

Calculation Method of C, H, O, and N Content. The individual absolute content of C, H, O, and N in a sample can be calculated theoretically by the following equations.

$$\mathrm{C(wt\%)} = \frac{W_A(\mathrm{C})[f_C(\mathrm{CO_2})N(\mathrm{CO_2}) + f_C(\mathrm{COS})N(\mathrm{COS}) + f_C(\mathrm{CS_2})N(\mathrm{CS_2})]}{w} \times 100 \quad (1)$$

$$\mathrm{H(wt\%)} = \frac{W_A(\mathrm{H})f_H(\mathrm{H_2S})N(\mathrm{H_2S})}{w} \times 100 \quad (2)$$

$$\mathrm{O(wt\%)} = \frac{W_A(\mathrm{O})[f_O(\mathrm{CO_2})N(\mathrm{CO_2}) + f_O(\mathrm{COS})N(\mathrm{COS})]}{w} \times 100, \quad (3)$$

Table 1. Reproducibility of the peak area ratio of each procuct to their sum

Sample weight (mg)	CV/%[a]				
	N_2	CO_2	H_2S	COS	CS_2
1	0.850	1.84	0.385	0.508	1.29
0.5	0.451	0.942	0.230	0.484	1.06

a) Calculated from 10 runs for alanine.

Table 2. Products from each standard sample

Standard sample	Products
Cyanoguanidine	N_2, H_2S, CS_2
8-Quinolinol	N_2, H_2S, COS, CS_2
Sucrose	CO_2, H_2S, COS, CS_2

$$\mathrm{N(wt\%)} = \frac{W_A(\mathrm{N})f_N(\mathrm{N_2})N(\mathrm{N_2})}{w} \times 100, \quad (4)$$

where $W_A(\alpha)$ is the atomic weight of α(α=C, H, O, and N), $N(\beta)$ is the mole number(mol) of β(β=CO_2, COS, CS_2, H_2S, and N_2), w is the sample weight(mg), and $f_\alpha(\beta)$ is the number of element α in a reaction product β. Then the following equation is defined in the case of gas-chromatographic analysis.

$$A(\beta) = F(\beta)N(\beta), \quad (5)$$

where $A(\beta)$: peak area(μV s) of β and $F(\beta)$: proportional constant (μV s/mol), which is called calibration factor. Moreover, $f_\alpha(\beta)$ are offered by the following values.

$$f_C(\mathrm{CO_2}) = f_C(\mathrm{COS}) = f_C(\mathrm{CS_2}) = f_O(\mathrm{COS}) = 1 \quad (6)$$

$$f_H(\mathrm{H_2S}) = f_O(\mathrm{CO_2}) = f_N(\mathrm{N_2}) = 2 \quad (7)$$

Therefore, by introducing Eqs. 5—7 into Eqs. 1—4, Eqs. 1—4 are rewritten as follows.

$$\mathrm{C(wt\%)} = W_A(\mathrm{C})\left[\frac{A(\mathrm{CO_2})}{F(\mathrm{CO_2})} + \frac{A(\mathrm{COS})}{F(\mathrm{COS})} + \frac{A(\mathrm{CS_2})}{F(\mathrm{CS_2})}\right] \times \frac{1}{w} \times 100 \quad (8)$$

$$\mathrm{H(wt\%)} = W_A(\mathrm{H}) \times \frac{2A(\mathrm{H_2S})}{F(\mathrm{H_2S})} \times \frac{1}{w} \times 100 \quad (9)$$

$$\mathrm{O(wt\%)} = W_A(\mathrm{O}) \times \left[\frac{2A(\mathrm{CO_2})}{F(\mathrm{CO_2})} + \frac{A(\mathrm{COS})}{F(\mathrm{COS})}\right] \times \frac{1}{w} \times 100 \quad (10)$$

$$\mathrm{N(wt\%)} = W_A(\mathrm{N}) \times \frac{2A(\mathrm{N_2})}{F(\mathrm{N_2})} \times \frac{1}{w} \times 100 \quad (11)$$

Each absolute content of C, H, O, and N in a sample can be calculated by use of Eqs. 8—11 from the analytical data of a sample if the values of $F(\beta)$ have been determined by Eqs. 8—11 from the analytical data of standard samples.

Determination of Calibration Factors. According to the PSGC method, the carbon in a sample is converted to CO_2(its amount is negligibly small when the value of C/O exceeds about 8), COS, and CS_2, hydrogen is converted to H_2S, oxygen to CO_2 and COS, and nitrogen to N_2 by the pyrolytic sulfurization. Therefore, in order to determine $F(\beta)$ of the products, the

TABLE 3. CALIBRATION FACTOR

Standard sample	Calibration factor/μV s mol^{-1}[a)]				
	$F(N_2)$	$F(CO_2)$	$F(H_2S)$	$F(COS)$	$F(CS_2)$
Cyanoguanidine	269.5		297.4		473.4
8-Quinolinol	268.2		302.6	401.3	
Sucrose		300.1	296.4		
Average	268.9	300.1	298.8	401.3	473.4

a) Average of 3 runs for each standard sample.

TABLE 4. ANALYTICAL RESULTS OF VARIOUS ORGANIC COMPOUNDS

Sample	C (wt%)			H (wt%)			O (wt%)			N (wt%)		
	Calcd	Found	Error	Calcd	Found	Error	Calcd	Found	Error	Calcd	Found	Error
Acetoanilide	71.09	71.28	+0.19	6.71	6.78	+0.07	11.84	12.02	+0.18	10.36	10.26	−0.10
Acetone 2,4-dinitrophenylhydrazone	45.38	45.67	+0.29	4.23	4.20	−0.03	26.87	27.01	+0.14	23.52	23.22	−0.30
Anthracene	94.34	94.06	−0.28	5.66	5.66	0.00						
Anthraquinone	80.76	80.49	−0.27	3.87	3.86	−0.01	15.37	15.48	+0.11			
Benzoic acid	68.85	68.97	+0.12	4.95	4.98	+0.03	26.20	26.26	+0.06			
Benzoin	79.22	79.34	+0.12	5.70	5.65	−0.05	15.08	15.37	+0.29			
2,2-Bis(ethylsulfonyl)-propane	36.82	37.00	+0.18	7.06	7.08	+0.02	28.03	28.20	+0.17			
Bis(2,4-pentanedionato)-magnesium(II)	46.45	46.14	−0.31	7.02	7.08	+0.06	37.13	37.09	−0.04			
Caffeine	49.48	49.23	−0.25	5.19	5.21	+0.03	16.48	16.18	−0.30	28.85	28.79	−0.06
Cholesterol	83.87	83.39	−0.48	11.99	11.87	−0.12	4.14	4.30	−0.16			
Cyclohexanone 2,4-dinitrophenylhydrazone	51.80	51.88	+0.08	5.07	5.18	+0.11	23.00	23.19	+0.19	20.13	20.25	+0.12
Cyclohexanone oxime	63.68	63.53	−0.15	9.80	9.75	−0.05	14.14	14.15	+0.01	12.38	12.28	−0.10
Cyclohexanone semicarbazone	54.14	54.57	+0.43	8.44	8.49	+0.05	10.31	10.57	+0.26	27.07	27.00	−0.07
N,N'-Diphenylthiourea	68.39	68.35	−0.04	5.30	5.33	+0.03				12.27	12.33	+0.06
Ethyl *p*-aminobenzoate	65.44	65.26	−0.18	6.71	6.79	+0.08	19.37	19.65	+0.28	8.48	8.48	0.00
Guaiacol carbonate	65.69	65.71	+0.02	5.15	5.07	−0.08	29.17	29.14	−0.03			
Hippuric acid	60.33	60.07	−0.26	5.06	5.08	+0.02	26.79	26.78	−0.01	7.82	7.83	+0.01
α-Methyl D-glucoside	43.30	43.54	+0.24	7.27	7.29	+0.02	49.44	49.46	+0.02			
Nicotinic acid	58.54	58.52	−0.02	4.09	4.13	+0.04	25.99	26.15	+0.16	11.38	11.25	−0.13
p-Nitroaniline	52.17	52.27	+0.10	4.38	4.42	+0.04	23.17	23.24	+0.07	20.28	20.32	+0.04
Phenacetin	67.02	67.19	+0.17	7.31	7.18	−0.13	17.85	17.83	−0.02	7.82	7.77	−0.05
Phenylmercury(II) acetate	28.53	28.55	+0.02	2.39	2.40	+0.01	9.50	9.59	+0.09			
Succinic acid	40.68	40.43	−0.25	5.12	5.12	0.00	54.19	54.03	−0.16			
Sulfathiazole	42.34	42.48	+0.14	3.55	3.57	+0.02	12.53	12.52	−0.01	16.46	16.38	−0.08
Thiourea	15.78	15.61	−0.17	5.30	5.34	+0.04				36.80	36.59	−0.21
p-Toluenesulfonamide	49.11	48.92	−0.19	5.30	5.30	0.00	8.18	8.00	−0.18			
Triphenylphosphine	82.43	82.33	−0.10	5.76	5.80	+0.04						
Tris(2,4-pentanedionato)iron(III)	51.01	50.79	−0.22	5.99	5.98	−0.01	27.18	27.18	0.00			
Vanillin	63.15	63.49	+0.34	5.30	5.31	+0.01	31.55	31.34	−0.21			

compounds which satisfy the following requirements must be selected as the standard samples; 1) N-containing compound, 2) H-containing compound, 3) C-containing and O-free compound, 4) C-containing and O-rich compound from which CO_2 is produced, and 5) C-containing and O-poor compound from which CO_2 is produced in small amounts. In the present study, cyanoguanidine will satisfy the requirements of 1), 2), and 3), sucrose will satisfy that of 4), and 8-quinolinol will satisfy that of 5). Accordingly there substances were selected as the standard samples for the determination of $F(\beta)$. The reaction products from each standard sample on pyrolytic sulfurization are shown in Table 2. As can be seen from Table 2, $F(N_2)$ can be calculated by Eq. 11 from the analytical results for cyanoguanidine and 8-quinolinol; $F(H_2S)$ by Eq. 9 from that of cyanoguanidine, 8-quinolinol, and sucrose; $F(COS)$ by Eq. 10 from that of 8-quinolinol; and $F(CS_2)$ by Eq. 8 from that of cyanoguanidine. $F(CO_2)$ can also be calculated by Eq. 10 from both $F(COS)$ and the analytical result of sucrose. The calibration factor of each product was shown in Table 3. All of the calibration factors (Table 3) were used for the calibration of each absolute content of C, H, O, and N in a sample.

Analysis of Various Organic Compounds. Various organic compounds including metal organic chelates were analyzed by the present procedure; the results are shown in Table 4. Table 4 indicates that each absolute content of C, H, O, and N in an organic compound can be successfully and simultaneously determined by the present method.

Comparison of the Present Method with the Conventional PSGC. The present method was compared with the conventional PSGC in the following manner. An analysis using about 1 mg of sample is repeated 10 times by use of alanine as a standard sample, and both the absolute content of C, H, O, and N in alanine and the atomic ratio between C, H, O, and N were calculated by the present method and by the conventional PSGC, respectively. Moreover, fluctuation of analytical data by the present method and the conventional PSGC, respectively, was also calculated and the value of CV for each value of C, H, O, and N was compared (Table 5). Table 5 indicates that the present method is superior to the conventional PSGC with regard to the value of H but inferior for C and O.

Table 5. Comparison of the present method with the conventional PSGC

Method	CV/%[a]			
	C	H	O	N
Present	0.820	0.217	0.562	0.646
Conventional PSGC	0.351	0.685	0.357	0.654

a) Calculated from 10 runs for alanine.

From the results obtained by the present study, it can be concluded that the absolute content of C, H, O, and N in an organic compound can also be determined, if necessary, by PSGC. This makes possible the simultaneous determination of the atomic ratio between C, H, O, and N in an organic compound without weighing a sample. This will make PSGC a more valuable method in organic elemental analysis.

References

1) K. Tsuji, K. Fujinaga, and T. Hara, *Bull. Chem. Soc. Jpn.*, **50**, 2292 (1977).
2) T. Hara, K. Fujinaga, and K. Tsuji, *Bull. Chem. Soc. Jpn.*, **51**, 1110 (1978).
3) T. Hara, K. Fujinaga, and K. Tsuji, *Bull. Chem. Soc. Jpn.*, **51**, 2951 (1978).
4) T. Hara, K. Fujinaga, K. Tsuji, and F. Okui, *Bull. Chem. Soc. Jpn.*, **51**, 3079 (1978).
5) T. Hara, K. Fujinaga, F. Okui, and K. Negayama, *Sci. Eng. Rev. Doshisha Univ.*, **21**, 241 (1981).
6) T. Hara, K. Fujinaga, and F. Okui, *Bull. Chem. Soc. Jpn.*, **53**, 951 (1980).
7) T. Hara, K. Fujinaga, and F. Okui, *Bull. Chem. Soc. Jpn.*, **53**, 1308 (1980).
8) T. Hara, K. Fujinaga, and F. Okui, 3rd World Chromatography Conference, Zürich, July 1980, Abstr. p 7.
9) T. Hara, K. Fujinaga, and F. Okui, *Bull. Chem. Soc. Jpn.*, **54**, 2956 (1981).
10) T. Hara and F. Okui, *Bull. Chem. Soc. Jpn.*, **55**, 329 (1982).
11) T. Hara and F. Okui, *Bull. Chem. Soc. Jpn.*, **55**, 2127 (1982).
12) T. Hara and F. Okui, *Bull. Chem. Soc. Jpn.*, **55**, 3450 (1982).
13) T. Hara, K. Fujinaga, and F. Okui, *Bull. Chem. Soc. Jpn.*, **55**, 3800 (1982).

Determination of a Small Amount of Biological Constituent by Use of Chemiluminescence. I. The Flow-injection Analysis of Protein

Tadashi HARA,* Motohiro TORIYAMA, and Kazuhiko TSUKAGOSHI

Department of Chemical Engineering, Faculty of Engineering, Doshisha University, Karasuma Imadegawa, Kamigyo-ku, Kyoto 602

(Received October 14, 1982)

A new method in which luminol-hydrogen peroxide luminescent system is used has been proposed for the determination of the presence of protein. Since the catalytic activity of copper(II) for the chemiluminescent reaction between luminol and hydrogen peroxide decreased when copper(II) interacted with polypeptide linkage, this phenomenon was applied to the determination of protein. Determination of protein was carried out by a flow-injection method. The effects of reagent concentration, flow-rate, and reaction time on the analytical value were examined and the conditions for the determination of protein were established. Similar calibration curves were obtained for human serum albumin, bovine serum albumin, bovine serum α-globulin, and bovine serum γ-globulin. According to the present flow-injection method using chemiluminescent reaction, a small amount of protein could be conveniently and economically determined over a wide range of concentration, 7×10^{-4}—7×10^{-2} g dm^{-3}, with the detection limit of 0.2 μg and at the rate of about 30 samples per hour. The present method was applicable to the determination of protein in serum.

It is well known that the chemiluminescence (CL) emitted by 5-amino-2,3-dihydro-1,4-phthalazinedione (luminol) in the presence of hydrogen peroxide(H_2O_2) is remarkably enhanced by a catalyst such as Co(II), Co(III), Cr(III), Cu(II), Fe(II), Fe(III), Hg(II), Mn(II), Ni(II), Os(IV), Os(VIII), and their complex compounds.[1] This has been used for the determination of a small amount of H_2O_2 or metal ion.[2-4] Since the catalytic activity of copper(II) for the CL reaction between luminol and H_2O_2 was found to decrease with the amount of coexisting protein, a new method for the determination of protein based on this phenomenon was examined. Judging from the facts that the catalytic activity of a copper(II) complex is maximum when two of the four coordination sites are occupied by a ligand, while it is not observed when all four coordination sites are occupied by a ligand,[5] and that copper(II) in the biuret reaction reacts with four nitrogen atoms of a polypeptide chain to form a violet complex,[6] the decrease of the catalytic activity of a copper(II) complex in the present study seems to be attributed to the formation of a copper(II)–polypeptide complex, that is, the occupation of four coordination sites by a protein molecule.

Various methods such as a Kjeldahl method, a biuret method, a UV method, a Lowry method, a dyestuff combination method, and a fluorometric(thiamine) method have been reported for the determination of protein.[7] Though both a Kjeldahl method and a biuret method are known as standard methods, the former is difficult to operate and the latter is less sensitive. A UV method and a Lowry method are sensitive but they are unsuitable for the determination of protein in a unknown sample because the analytical values obtained by them vary by the kind of protein. A dyestuff combination method is also unsuitable for the determination of protein having different origins because the reaction between dyestuff and protein is too complicated. These methods can estimate protein amounts more than 1 μg, whereas a thiamine method based on fluorescence can estimate 0.1—1.0 μg protein.[8] However the fluorometric method requires a complicated procedure and has to be applied under rigid conditions. The CL method for the determination of protein is characterized by the following: 1) Highly sensitive, 2) determinable over a wide range of protein concentration, 3) easy to operate, 4) inexpensive apparatus and reagent, and 5) it is easy to set up the flow-injection system. This will make the CL method available for the determination of a trace amount of protein in various samples.

Experimental

Reagent. A luminol solution was prepared as 1.0×10^{-3} mol dm^{-3} by dissolving luminol in the buffer solution (pH 10.15) containing 0.1 mol of potassium hydroxide and of boric acid in 1 dm^{-3}. A H_2O_2 solution was prepared (2.5×10^{-3} mol dm^{-3}) by diluting a 0.3 wt% H_2O_2 solution with water.

A copper(II) solution was prepared as a 2.0×10^{-2} mol dm^{-3} concentration by dissolving copper(II) sulfate pentahydrate 5.0 g, potassium sodium tartrate 45.0 g, sodium hydroxide 8.0 g, and potassium iodide 5.0 g in that order and by bringing the mixture to 1 dm^{-3} with water.[9] Each catalyst solution, which contained copper(II), hematin(ICN Pharmaceuticals, Inc.), hexacyanoferrate(III), or osmium(VIII) oxide, was prepared by diluting with the above-mentioned buffer solution. The reagents used were of commercially available special grade. Human serum albumin and bovine serum α-globulin from ICN Pharmaceuticals, Inc., and bovine serum albumin(BSA) and bovine serum γ-globulin from SIGMA CHEMICAL Co., and control serum(Q-PAK-Chemistry Control Serum II) from HYLAND were used.

Ion exchange water was distilled for use.

Apparatus and Procedure. Both a luminol solution which had been left standing overnight in a dark place and a buffer solution were degassed by stirring under reduced pressure and were then used. The schematic diagram of the apparatus which was set up for flow-injection analysis is shown in Fig. 1. A Teflon tube(1 mm i.d.) and a connector were used. A buffer solution(a), a H_2O_2 solution(b), and a luminol solution(c) were delivered at the flow rate of 2.5 cm^3 min^{-1} with the corresponding pumps: (p_1), (p_2), (p_3)-(PERISTA MINI PUMP SJ-1211). A buffer solution and

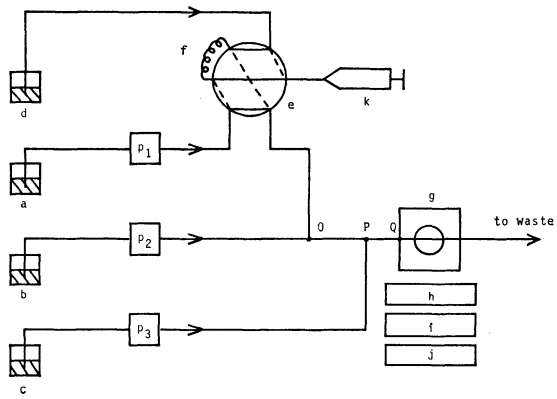

Fig. 1. Flow-injection system.
a: Buffer solution, b: hydrogen peroxide solution, c: luminol solution, d: sample solution, e: six-way cook, f: sampling loop, g: flow cell, h: photomultiplier, i: amplifier, j: recorder, k: cylinge, and P_1, P_2, P_3: pump.

a H_2O_2 solution were first mixed and the resulting mixture was combined with a luminol solution; the distances between P and O or Q were 35 and 10 cm, respectively. A sample solution containing protein was diluted with a buffer solution and to it a copper(II) solution was added so as to become 5.0×10^{-6} mol dm^{-3}; it was held at 30 °C for 50 min. A definite amount(0.4 cm^3) of the sample solution thus obtained was injected into the line of a buffer solution. If the catalytic activity of a metal salt catalyst had to be examined, the catalyst solution alone was injected into the line of a buffer solution instead of the above-mentioned sample solution. A poly(vinyl chloride) tube(45 cm$\times$0.8 mm i.d.) was spirally wound and was then used as the cell (g). The CL intensity of the solution passing through the cell was measured by a photomultiplier(h) (Hamamatsu TV Co. Ltd., R928), amplified with a amplifier(i)(Horiba Ltd., OPE-402), and recorded on a recorder(j)(Yokogawa Electric Works, Ltd., 3046). The net CL intensity of a sample solution was obtained by subtracting the background (the CL intensity of the solution containing no sample) from the observed intensity. The ratio of CL intensity of a protein sample solution to that of a 5.0×10^{-6} mol dm^{-3} copper(II) solution was used for the presentation of data. According to the present apparatus, measurement could be done at the rate of about 30 samples per hour.

Results and Discussion

Determination of Analysis Conditions. The effect of H_2O_2 concentration and of luminol concentration on the CL intensity are shown in Figs. 2 and 3, respectively. As can be seen from Fig. 2, the CL intensity increased with an increasing concentration of H_2O_2 and was accompanied by increasing noise. The CL intensity in Fig. 3 was found to be maximum when the luminol concentration was the same (1.0×10^{-3} mol dm^{-3}) as the H_2O_2 concentration. Therefore 1.0×10^{-3} mol dm^{-3} luminol and 2.5×10^{-3} mol dm^{-3} H_2O_2 were chosen as their optimum concentrations in the following experiment.

Though the CL intensity increased with an increasing flow rate, all the flow rates were set at 2.5 cm^3 min^{-1} because of the capacity of the pumps. The high sensitivity was attained by adding a H_2O_2 solution to a buffer solution, followed by mixing the mixed solution with a luminol solution.

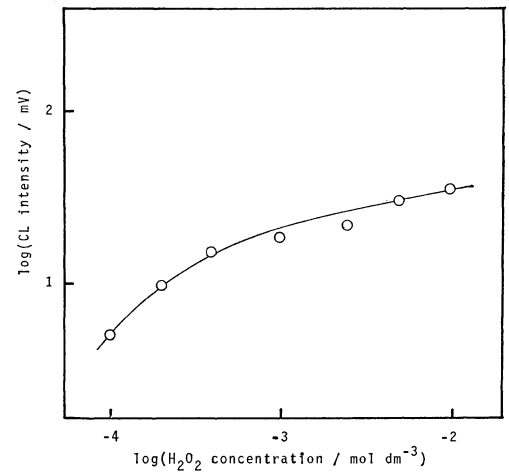

Fig. 2. Effect of H_2O_2 concentration on CL intensity. Conditions: 1.0×10^{-4} mol dm^{-3} luminol and 1.0×10^{-5} mol dm^{-3} $K_3[Fe(CN)_6]$.

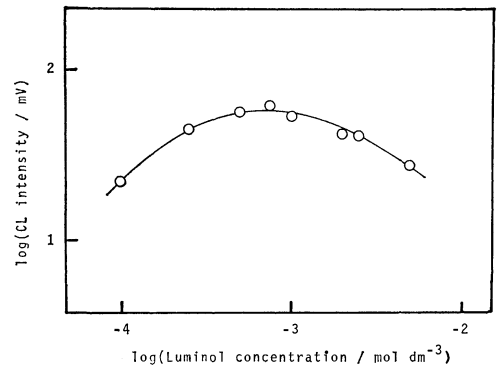

Fig. 3. Effect of luminol concentration on CL intensity. Conditions: 1.0×10^{-3} mol dm^{-3} H_2O_2 and 1.0×10^{-5} mol dm^{-3} $K_3[Fe(CN)_6]$.

Selection of Chemiluminescent Catalyst. We examined the catalytic activity of copper(II) sulfate, and of osmium(VIII) oxide and hematin, which are compounds of Os and Fe belonging to the eighth group transition elements in the periodic table and had been known to show high catalytic activity for the CL reaction.[10] The relationship between catalyst concentration and CL intensity was obtained by means of the apparatus shown in Fig. 1 (Fig. 4). Chemiluminescent response was observed for 1×10^{-7}—5×10^{-5} mol dm^{-3} copper(II) sulfate, 2×10^{-9}—2×10^{-6} mol dm^{-3} osmium(VIII) oxide, and 5×10^{-10}—5×10^{-6} mol dm^{-3} hematin, respectively.

By using a definite amount of 5.0×10^{-6} mol dm^{-3} copper(II) sulfate, 7.9×10^{-7} mol dm^{-3} osmium(VIII) oxide, and 4.0×10^{-7} mol dm^{-3} hematin solutions, which were slightly higher concentrations than those at each middle point in the above-mentioned catalyst concentrations, three calibration curves were obtained for BSA (Fig. 5). When a hematin solution or copper(II) sulfate solution was added to a protein solution, their catalytic activities or CL intensity decreased with time and finally stabilized after 2 h at room tem-

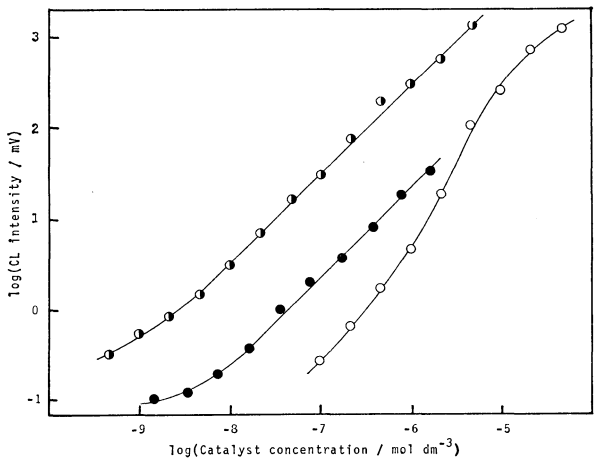

Fig. 4. Relationship between catalyst concentration and CL intensity.
○: $CuSO_4$, ●: OsO_4, and ◑: hematin. Conditions: 1.0×10^{-3} mol dm^{-3} luminol and 2.5×10^{-3} mol dm^{-3} H_2O_2.

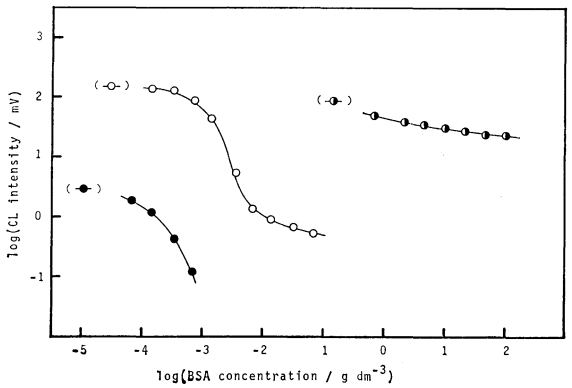

Fig. 5. Calibration curve of BSA for each catalyst.
○: $CuSO_4$, ●: OsO_4, ◑: hematin, and (○): BSA free. Conditions: 5.0×10^{-6} mol dm^{-3} $CuSO_4$, 7.9×10^{-7} mol dm^{-3} OsO_4, 4.0×10^{-7} mol dm^{-3} hematin, 1.0×10^{-3} mol dm^{-3} luminol, and 2.5×10^{-3} mol dm^{-3} H_2O_2.

perature. In a similar experiment using osmium(VIII) oxide, the catalytic activity or CL intensity did not stabilize until after about 24 h. Judging from the detection limit of protein, concentration range suitable for the determination of protein, lowering of CL intensity by a definite amount of protein, and time necessary for the stabilization of CL intensity, copper(II) sulfate was most recommendable as a chemiluminescent catalyst for the present study.

The CL intensities in the presence of copper(II) sulfate alone or of copper(II) sulfate-tartaric acid are shown in Fig. 6. The catalytic activity of the former was a little smaller than that of the latter and its difference was remarkable at high concentration of copper(II), 1×10^{-5}—5×10^{-5} mol dm^{-3}, where the formation of copper(II) hydroxide was observed after allowing the copper(II) solution to stand alone for several hours. Therefore, the above difference seems to be related to the formation of copper(II) hydroxide. The catalytic activity of copper(II) solution was ob-

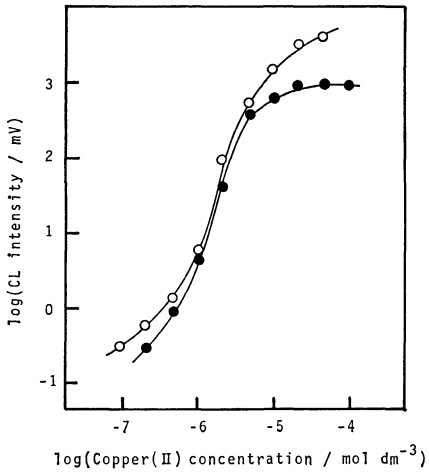

Fig. 6. Effect of tartaric acid on the CL intensity in the presence of copper(II) catalyst.
○: Copper(II)+tartaric acid and ●: copper(II) alone. Conditions: 1.0×10^{-3} mol dm^{-3} luminol and 2.5×10^{-3} mol dm^{-3} H_2O_2.

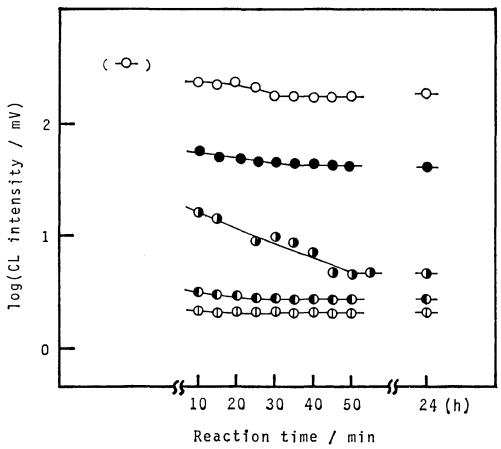

Fig. 7. Relationship between reaction time and CL intensity.
○: 1.4×10^{-3} g dm^{-3}-, ●: 3.5×10^{-3} g dm^{-3}-, ◑: 7.0×10^{-3} g dm^{-3}-, ◐: 1.4×10^{-2} g dm^{-3}-, ⓘ: 3.5×10^{-2} g dm^{-3}- BSA, and (○): BSA free. Conditions: 1.0×10^{-3} mol dm^{-3} luminol and 2.5×10^{-3} mol dm^{-3} H_2O_2.

tained with good reproducibility in the presence of tartaric acid without producing the copper(II) hydroxide. A small amount of potassium iodide was also added to the copper(II) solution to prevent it from undergoing autoreduction.[11] The calibration curve for copper(II) sulfate-tartaric acid was not linear but sigmoidal. The reason for this remains unclear.

Determination of Protein. The relationship between CL intensity and elapsed time after mixing of copper(II) with each BSA solution of 1.4×10^{-3}, 3.5×10^{-3}, 7.0×10^{-3}, 1.4×10^{-2}, and 3.5×10^{-2} g dm^{-3} was examined at 30 °C; the result was shown in Fig. 7. CL intensity decreased with time after mixing, but no lowing of CL intensity was observed in 50 min—24 h after mixing. It was, therefore, necessary for the determination of protein to hold the mixed solution

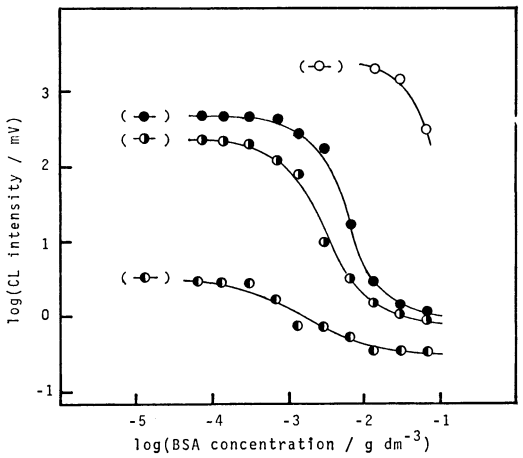

Fig. 8. Effect of copper(II) concentration on the calibration curve of BSA.
○: 5.0×10^{-5} mol dm^{-3}-, ●: 1.0×10^{-5} mol dm^{-3}-, ◑: 5.0×10^{-6} mol dm^{-3}-, ◐: 1.0×10^{-6} mol dm^{-3}-copper-(II), and (○): BSA free.
Conditions: 1.0×10^{-3} mol dm^{-3} luminol and 2.5×10^{-3} mol dm^{-3} H_2O_2.

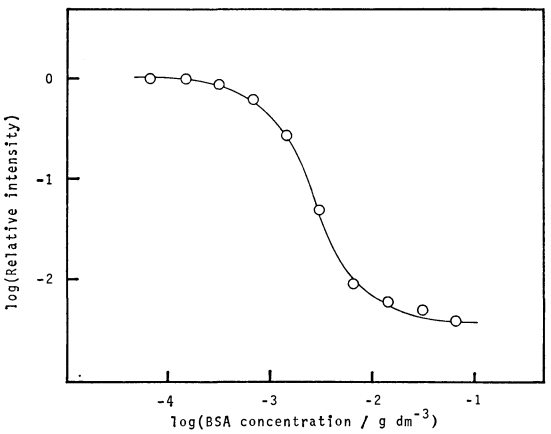

Fig. 9. Calibration curve of BSA by the present method.
Conditions: 1.0×10^{-3} mol dm^{-3} luminol and 2.5×10^{-3} mol dm^{-3} H_2O_2.

of copper(II) and protein at 30 °C for 50 min.

Figure 8 showed calibration curves of BSA which were obtained by use of 1.0×10^{-6}, 5.0×10^{-6}, 1.0×10^{-5}, and 5.0×10^{-5} mol dm^{-3} of copper(II) sulfate. The detection limit of protein concentration and the decrease of CL intensity for a definite amount of protein suggested that a 5.0×10^{-6} mol dm^{-3} copper(II) sulfate solution be used in the present study.

The calibration curve for BSA was obtained under the same conditions as specified above (Fig. 9), and it was usable for the determination of protein in the concentration range of 7×10^{-4}—7×10^{-2} g dm^{-3}. The decrease of CL intensity in the presence of protein is attributed to the lowing of the catalytic activity of copper(II) based on the formation of a copper(II)–polypeptide complex. This is understandable from the following facts: 1) The catalytic activity of a copper-(II) complex is maximum when two of the four coordination sites are occupied by a ligand, while it is

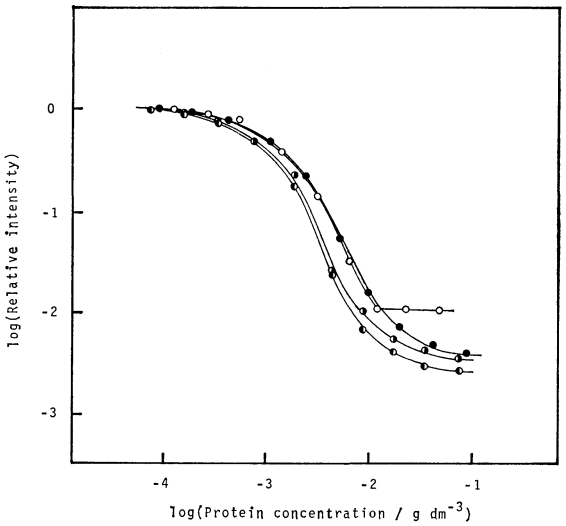

Fig. 10. Calibration curves of various proteins.
○: Bovine serum α-globulin, ●: human serum albumin, ◑: bovine serum albumin, and ◑: bovine serum γ-globulin.
Conditions: 1.0×10^{-3} mol dm^{-3} luminol and 2.5×10^{-3} mol dm^{-3} H_2O_2.

not observed when all four coordination sites are occupied by a ligand,[5] 2) copper(II) in the biuret reaction reacts with four nitrogen atoms of a polypeptide chain to form a violet complex.[6] The present method makes use of the formation of copper(II)–polypeptide complex and estimates the amount of protein indirectly by measuring the catalytic activity of copper(II) for CL; it will be suitable for the determination of protein in a biological fluid sample in which no constituent except protein shows biuret reaction.[12]

The calibration curves for human serum albumin, bovine serum α-globulin, and bovine serum γ-globulin were prepared in a way similar to that for BSA; they are compared in Fig. 10. The constant CL intensity in the concentration range of 1.2×10^{-2}—6.0×10^{-2} g dm^{-3} bovine serum α-globulin may be attributed to insolubility of protein because suspended substances were observed at protein concentrations above 1.0×10^{-1} g dm^{-3}. Furthermore there were some differences between CL intensities of individual proteins. Assuming that the decrease of CL intensity is based on the decrease of catalytic activity by the formation of copper(II)–polypeptide complex, the differences between CL intensities of individual proteins will markedly depend on the total amount of the peptide linkage in a definite weight of protein.

According to the present method, 7×10^{-4}—7×10^{-2} g dm^{-3} protein could be determined with a detection limit of 0.2 μg. The present method is shown in Table 1 together with some typical conventional methods and with their determinable amounts of protein. The present method was 10—100 times as sensitive as in the conventional methods, except for a thiamine(fluorometric) method, and was applicable to the determination of a wide concentration range of protein. Furthermore the present method is characterized by easy operation based on a flow-injection system and by

TABLE 1. RANGE OF PROTEIN DETERMINABLE BY VARIOUS METHODS

Method	Determinable range (μg)	Ref.
Present	0.2—20	
Micro biuret	26—530	13
Kjeldahl	30—100	14
UV	20—100	15
Lowry	5—100	16
Dyestuff combination	1—10	17
Thiamine	0.1—1.0	8

TABLE 2. REPRODUCIBILITY OF THE PRESENT METHOD

BSA concentration/g dm^{-3}	CV value/%
0	7.7
7.0×10^{-4}	7.9
7.0×10^{-3}	6.5
7.0×10^{-2}	3.7

inexpensive reagent and apparatus. According to a thiamine(fluorometric) method, 0.1—1.0 μg of protein can be determined but it requires a complicated procedure and has to be applied under rigid conditions.

As can be seen from Fig. 10, the difference in analytical data based on the difference of CL intensity was about 50% for the two kinds of protein in which the difference was maximum. This value seems reasonable if we take the corresponding values of a dyestuff combination method(about 200%) and of a Lowry method(about 20%) into consideration.

The coefficient of variation (CV) of the present method for the determination of protein is shown in Table 2. The CV values increased with a decreasing concentration of protein. Since the fluctuating flow offered by a pump seriously affected the precision of the present determination, an improvement of the apparatus was still necessary for the minimization of this CV value.

Application to Serum Analysis. In order to determine the amount of protein in serum by the present method, a serum sample is diluted to 10^3—10^5 times its volume. The effect of iron salt, chloride, and urea contained in the serum on the CL intensity was examined by use of iron(III) chloride hexahydrate, potassium chloride, and urea. Fe(III) 2.0×10^{-8} mol dm^{-3}, Cl^- 1.0×10^{-4} mol dm^{-3}, and $(NH_2)_2CO$ 1.0×10^{-5} mol dm^{-3} corresponding to the concentration at 10^3 times' dilution of a serum sample did not influence the CL intensity at all.

Then different amounts of BSA were added to a definite amount of control serum(final concentration 1.2×10^{-3} g dm^{-3}), and the total amount of protein was estimated by use of the calibration curve of BSA (Fig. 11). The analytical value of the ordinate indicated the protein content in a sample solution, which was expressed as BSA. The difference between straight lines I and II just corresponded to the added amount of control serum. This result showed that the present method was applicable to the determination of protein in a serum sample without being interfered with by

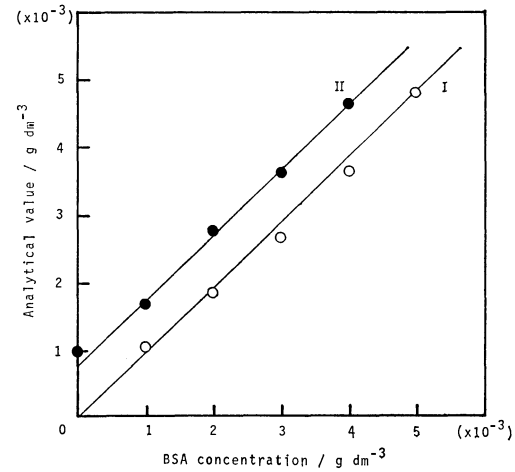

Fig. 11. Relationship between BSA concentration and analytical value.
○: BSA and ●: BSA+control serum.
Conditions: 1.2×10^{-3} g dm^{-3} control serum, 1.0×10^{-3} mol dm^{-3} luminol, and 2.5×10^{-3} mol dm^{-3} H_2O_2.

coexisting constituents. Here 0.01 μl of control serum was diluted to 10^5 times volume and analyzed.

On the basis of the above-mentioned investigation, a method for the determination of a small amount of protein was newly established. The present method by means of a flow-injection system is characterized by the following: 1) Protein amounts are determinable in the protein concentration range of 7×10^{-4}—7×10^{-2} g dm^{-3} with detection limit of 0.2 μg; 2) the method is 10—100 times more sensitive than the conventional methods except the fluorometric one; 3) it is easy to operate; 4) it is inexpensive in the apparatus and the reagent; 5) about 30 samples per hour can be measured. The present method is applicable to the determination of protein in a serum sample and is expected to promote the field of highly sensitive detection of protein amounts.

The authors wish to thank Mr. Masakatsu Imaki (Horiba Ltd.,) for providing the apparatus necessary for the present study.

References

1) A. P. Golovina, V. K. Runov, and N. B. Zorv, "Ferrites Transition Elements Luminescence," Springer-Verlag, Berlin (1981), p. 95.
2) W. R. Seitz, W. W. Suydam, and D. M. Hercules, *Anal. Chem.*, **44**, 957 (1972).
3) D. T. Bostick and D. M. Hercules, *Anal. Chem.*, **47**, 7 (1975).
4) J. L. Burguera, A. Townshend, and S. Greenfield, *Anal. Chim. Acta*, **114**, 209 (1980).
5) H. Ojima, *Nippon Kagaku Zasshi*, **79**, 1076 (1958).
6) K. Sano, "Bunseki-library 3 Rinshō Kagaku Bunseki II," ed by the Japan Society for Analytical Chemistry, Tokyo Kagaku Dōjin, Tokyo (1979), Chap. 5, pp. 140—143.
7) K. Sugawara and M. Soejima, "Seibutsu Kagaku Jikken-hō 7 Tanpakushitsu No Teiryō-hō," Japan Scientific

Societies Press, Tokyo (1981), Chap. 2.
8) T. Kinoshita, F. Iinuma, K. Astumi, and A. Tsuji, *Anal. Biochem.*, **77**, 471 (1977).
9) C. T. E. Weichselbaum, *Am. J. Clin. Pathol.*, **16**, 40 (1946).
10) M. Yamada and S. Suzuki, *Bunseki*, **1980**, 549.
11) K. Sano, "Bunseki-library 3 Rinshō Kagaku Bunseki II," ed by the Japan Society for Analytical Chemistry, Tokyo Kagaku Dōjin, Tokyo (1979), Chap. 5, pp. 125—132.
12) K. Sugawara and M. Soejima, "Seibutsu Kagaku Jikken-hō 7 Tanpakushitsu No Teiryō-hō," Japan Scientific Societies Press, Tokyo (1981), Chap. 4.
13) R. F. Itzhaki and D. M. Gill, *Anal. Biochem.*, **9**, 401 (1964).
14) L. Hambr Æ us, E. Forsum, L. Abrahamsson, and B. Lönnerdal, *Anal. Biochem.*, **72**, 78 (1976).
15) G. C. Webster, *Biochim. Biophys. Acta*, **207**, 371 (1970).
16) O. H. Lowry, N. J. Rosebrough, A. L. Farr, and R. J. Randall, *J. Biol. Chem.*, **193**, 265 (1951).
17) J. A. Johnson and J. A. Lott, *Chin. Chem.*, **24**, 1931 (1978).
18) K. Kanamoli and K. Sano, *Rinshō Byōri*, **28**, 235 (1980).

 © 1983 The Chemical Society of Japan Bull. Chem. Soc. Jpn., 56, 1388—1392 (1983) [Vol. 56, No. 5

Magnetic Property and Crystal Structure of Alkoxo-bridged Bi- and Tetranuclear Copper(II) Complexes with Condensation Products of 3-Ethoxymethylene-2,4-pentanedione and Amino Alcohols

Naohide Matsumoto,* Toshihiro Tsutsumi, Akira Ohyoshi, and Hisashi Ōkawa†

Department of Industrial Chemistry, Faculty of Engineering, Kumamoto University, Kurokami 2-39-1, Kumamoto 860

† *Department of Chemistry, Faculty of Science, Kyushu University, Hakozaki, Higashi-ku, Fukuoka 812*

(Received September 24, 1982)

Alkoxo-bridged polynuclear copper(II) complexes with condensation products of 3-ethoxymethylene-2,4-pentanedione and each of three amino alcohols, 2-aminoethanol, 3-amino-1-propanol, and 1-amino-2-propanol, were prepared and characterized by elemental analyses, infrared spectra, electronic spectra, molecular weight measurements, magnetic susceptibility measurements, and crystal structure analysis, the complexes being abbreviated as Cu(L-2), Cu(L-3), and Cu(L-2m), respectively. Cu(L-3) is a dimer, but Cu(L-2m) and Cu(L-2) are tetramers. The magnetic susceptibility of violet Cu(L-3), whose electronic spectrum exhibits a d-d band maximum at 17.7×10^3 cm^{-1}, is in conformity to the Bleaney-Bowers equation with exchange integral $-2J=$ 920 cm^{-1}. Cu(L-3) consists of alkoxo-bridged centrosymmetric binuclear units, where the geometries around the copper ion and bridged oxygen atom are planar and the angle of Cu–O–Cu is 103.6(1)°. The magnetisms of blue complexes Cu(L-2) and Cu(L-2m) exhibiting a d-d band maximum at 15.7×10^3 cm^{-1} obey the Curie-Weiss law with positive Weiss constants 17 and 20 K, respectively, and are in accord with the Heisenberg model based on a tetranuclear cubane-like structure.

A great number of hydroxo- or alkoxo-bridged polynuclear copper(II) complexes have been studied in order to clarify the mechanism of magnetic interactions operating between copper(II) ions.[1-4] Hatfield *et al.*[1,2] found that the $2J$ value representing the copper(II)–copper(II) magnetic interaction correlates linearly with the angle of Cu–O–Cu, and emphasized the importance of the angle for the spin-exchange interaction. Kida and coworkers[3-9] investigated extensively the polynuclear copper(II) complexes with linear aliphatic amino alcohols such as $R_2N(CH_2)_nOH$, $R_2N(CH_2)_mX(CH_2)_nOH$, and $RS(CH_2)_mNH(CH_2)_nOH$ (R=alkyl; m,n=2 or 3; X=S, NH). Their conclusion with respect to the relationship between structure and magnetic property can be summarized as follows: (1) The planarity around the bridging oxygen atom is essentially important for the spin-exchange interaction rather than the angle of Cu–O–Cu; (2) the axial coordination accompanies deviation from the planarity around the oxygen atom and decreases the magnetic interaction; (3) the ring size of the chelate ring consisting of amino alcohol and copper ion is important in determining not only the planarity around the bridging oxygen atom, *i.e.*, the magnetic interaction, but also which the complex prefers to be, dimeric, trimeric, or tetrameric species. Two copper(II) complexes with each of ligands derived from 2,4-pentanedione and 2-aminoethanol or 3-amino-1-propanol (to be abbreviated as Cu(eia) and Cu(pia), respectively), may supply a set of typical examples for this point, since the complex Cu(pia) is a dimer with 0.41 BM. at room temperature, while the complex Cu(eia) is a cubane-like tetramer with 1.87 BM. at room temperature.[10]

In this study, polynuclear copper(II) complexes with Schiff base ligands derived from 3-ethoxymethylene-2,4-pentanedione and each of three amino alcohols, 2-aminoethanol, 3-amino-1-propanol, and 1-amino-2-propanol, have been prepared in order to examine their conclusion, (these complexes to be abbreviated as Cu(L-2), Cu(L-3), and Cu(L-2m), respectively). The complexes were characterized by elemental analyses, molecular weights, infrared spectra, electronic spectra, magnetic susceptibility measurements, and single-crystal X-ray analysis. Properties have been discussed in relation to the size of the chelate ring involving the amino alcohol and copper ion.

Experimental

Syntheses. 3-Ethoxymethylene-2,4-pentanedione was prepared from 2,4-pentanedione, acetic anhydride, and triethyl orthoformate according to the procedure of Riley and Busch.[11]

H_2L-2: To 50 cm^3 of 98% ethanolic solution of 0.05 mol of freshly prepared 3-ethoxymethylene-2,4-pentanedione was slowly added 0.05 mol of 2-aminoethanol in 30 cm^3 of ethanol at room temperature. After the reaction mixture had been allowed to stand for several hours in a refrigerator, white crystals which precipitated were collected and dried *in vacuo*. Found: C, 50.63; H, 8.02; N, 7.62%. Calcd for $C_8H_{13}NO_3\cdot H_2O$: C, 50.79; H, 7.93; N, 7.40%. IR: 3260 (ν_{OH}) and 1613 ($\nu_{C=N}$) cm^{-1}.

Cu(L-2): Ligand (H_2L-2), copper(II) acetate monohydrate, and sodium hydroxide in a mole ratio of 1:1:2 were mixed in ethanol and the mixture was refluxed for 1 h. The ethanol was removed by evaporation to dryness and dichloromethane was added. The resultant slurry was filtered and during the volume reduction of solution, crystalline Cu(L-2) was precipitated. It was recrystallized from a mixture of dichloromethane and methanol as dark blue crystals. Found: C, 40.97; H, 4.87; N, 6.01%. Calcd for $C_8H_{11}NO_3$-Cu: C, 41.28; H, 4.76; N, 6.01%.

Cu(L-2m) and Cu(L-3): Copper(II) complexes Cu(L-2m) and Cu(L-3) were prepared by mixing copper(II) acetate monohydrate, 3-ethoxymethylene-2,4-pentanedione, the corresponding amino alcohol, and sodium hydroxide in a mole ratio of 1:1:1:2 in ethanol. The mixture was refluxed

for 1 h and the ethanol was removed to dryness by evaporation. The resultant solid was dissolved in dichloromethane and the solution was filtered, and during the volume reduction of solution, crystalline materials were precipitated. Complexes Cu(L-2m) and Cu(L-3) were recrystallized from a mixture of dichloromethane and methanol as dark blue rhombic and violet plate crystals, respectively. Found for Cu(L-2m): C, 43.39; H, 5.49; N, 5.25%. Calcd for $C_9H_{13}NO_3Cu$: C, 43.81; H, 5.31; N, 5.68%. Found for Cu(L-3): C, 43.68; H, 5.43; N, 5.69%. Calcd for $C_9H_{13}NO_3Cu$: C, 43.81; H, 5.31; N, 5.68%.

Physical Measurements. Infrared spectra were measured with Nujol mulls on a Shimadzu IR-410 spectrophotometer. Electronic spectra were recorded on a Hitachi 323 spectrophotometer in dichloromethane. Molecular weights were determined in benzene at 40 °C on a Corona vapor pressure osmometer Model 117. Magnetic susceptibilities were measured by the Faraday method in the temperature range from the liquid nitrogen temperature to room temperature. The apparatus was calibrated by use of $[Ni(en)_3]S_2O_3$.[12] The susceptibility was corrected for the diamagnetism of component atoms by use of Pascal's constants.[13] Effective magnetic moment was calculated from the equation $\mu_{eff}=2.828\sqrt{(\chi_A-N\alpha)T}$, where χ_A is the magnetic susceptibility per copper atom and $N\alpha$ is the temperature independent paramagnetism.

X-Ray Analysis of Cu(L-3). Violet plate-like crystals of Cu(L-3) were obtained by slow precipitation from a dichloromethane and methanol solution at room temperature. A crystal with approximate dimensions of $0.4\times0.5\times0.5$ mm^3 was cut out from a large crystal and used for X-ray diffraction study. Unit-cell parameter and intensity data were obtained on a Rigaku Denki AFC-5 automated four-circle diffractometer with a monochromatized Mo $K\alpha$ radiation ($\lambda=0.71069$ Å) at 24 ± 1 °C. Unit-cell parameters were determined by the least-squares refinement based on 20 reflections in the range $15°<2\theta<41°$. Crystal data: $C_{18}H_{26}N_2O_6Cu_2$, F.W.=493.5, monoclinic, space group=$P2_1/c$, $a=5.700(1)$, $b=8.654(3)$, $c=20.270(5)$ Å, $\beta=95.05(2)°$, $V=996.1(5)$ Å^3, $D_x=1.645$ ($Z=2$), $D_m=1.61$ g cm^{-3} (by the flotation method in aqueous KI solution), μ(Mo $K\alpha$)=13.4 cm^{-1}.

Intensity data were collected by the θ-2θ scan technique with a scan rate of 8° min^{-1} in 2θ. For weak reflections the peak scan was repeated two or three times depending on their intensities. Three standard reflections were monitored every 100 reflections throughout the set to confirm no occurrence of decay in intensity. A total of 1756 reflections with $2.5°<2\theta<50°$ were collected, of which independent 1514 reflections with $|F_o|>3\sigma(|F_o|)$ were considered as "observed" and used for structural analysis. Intensity data were corrected for the Lorentz and polarization effects but not for absorption because of the small crystal size and low absorption coefficient.

The structure was solved by the conventional heavy-atom method and refined by the block-diagonal least-squares method. In the least-squares calculation, the function minimized was $\sum w(|F_o|-k|F_c|)^2$ where $w=1/\sigma(|F_o|)^2$. The neutral atomic scattering factors for H, C_{cov}, N, O, and Cu were taken from International Tables for X-Ray Crystallography, Vol. IV.[14] Anomalous dispersion corrections $\Delta f'$ and $\Delta f''$ for all the component atoms were also taken from the literature.[14] All calculations were carried out on a FACOM M-200 computer at the Computer Center of Kyushu University by use of the UNICS II Crystallographic Computing System.[15,16] The coordinates of the copper atom were easily obtained by an interpretation of Harker's peaks on the Patterson map. A Fourier synthesis based on the copper position revealed all the nonhydrogen atoms. Least-squares refinement with isotropic thermal parameters and then with anisotropic ones reduced the disagreement factors $R=\sum(|F_o|-|F_c|)/\sum|F_o|$ and $R_w=[\sum w(|F_o|-|F_c|)^2/\sum w|F_o|^2]^{1/2}$ to 6.00 and 7.55%, respectively. At this stage, a difference Fourier synthesis was calculated and located all the hydrogen atoms at chemically reasonable positions. Further refinement with anisotropic thermal parameters for nonhydrogen atoms and isotropic temperature factors for hydrogen atoms gave final values of 4.20 and 4.39% for R and R_w, respectively. The final difference Fourier synthesis showed no significant features.

Final positional parameters with estimated standard deviations are given in Table 1. Lists of structure factors (F_o and F_c) and anisotropic thermal parameters have been deposited as the supplementary data at the Chemical Society of Japan as Document No. 8312.

Table 1. Final atomic parameters for Cu(L-3)

A. Nonhydrogen atoms[a]

Atom	x	y	z	B_{eq}/Å^2
Cu	−285.2(10)	1392.1(6)	424.2(3)	2.4
O1	−1338(6)	−679(3)	303(2)	3.3
O2	1313(6)	3320(3)	463(2)	3.2
O3	1567(7)	6518(4)	1990(2)	5.0
N	−2189(6)	1937(4)	1116(2)	2.5
C1	−3072(9)	−1463(5)	628(2)	3.3
C2	−3361(9)	−757(6)	1302(2)	3.7
C3	−4097(9)	901(6)	1275(3)	3.8
C4	−1850(8)	3178(5)	1472(2)	2.6
C5	−186(8)	4371(5)	1417(2)	2.5
C6	1277(8)	4394(5)	893(2)	2.6
C7	2866(9)	5717(6)	765(3)	3.5
C8	−39(9)	5576(5)	1926(2)	3.2
C9	−1894(10)	5697(6)	2401(3)	3.9

B. Hydrogen atoms[a]

Atom	x	y	z	B/Å^2
H1A	−259(7)	−254(4)	70(2)	2.0(0.9)
H1B	−457(8)	−143(5)	35(2)	3.9(1.1)
H2A	−442(8)	−130(5)	151(2)	3.4(1.0)
H2B	−180(9)	−85(6)	161(2)	5.8(1.3)
H3A	−465(8)	123(5)	164(2)	3.6(1.1)
H3B	−524(8)	99(5)	93(2)	3.7(1.1)
H4	−290(7)	326(4)	181(2)	2.1(0.9)
H7A	210(7)	663(5)	77(2)	2.8(1.0)
H7B	423(8)	554(5)	101(2)	4.3(1.1)
H7C	338(7)	565(5)	38(2)	3.3(1.0)
H9A	−341(8)	575(5)	223(2)	3.5(1.0)
H9B	−167(9)	655(5)	268(2)	5.3(1.3)
H9C	−192(8)	489(5)	263(2)	4.2(1.1)

a) Atomic coordinates for nonhydrogen and hydrogen atoms have been multiplied by 10^4 and 10^3, respectively. The hydrogen atoms are labeled for identification by reference to the atoms to which they are attached.

Results and Discussion

Infrared Spectra. The OH stretching vibration at 3260 cm^{-1} observed for the free ligand H_2L-2 is

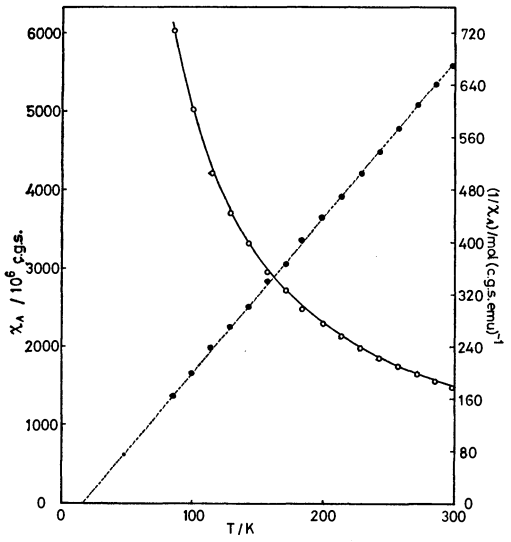

Fig. 1. Temperature dependence of magnetic susceptibility of Cu(L-2). Solid line of magnetic susceptibility represents the theoretical curve based on the equation (2) with the parameters of $J=40\ \mathrm{cm^{-1}}$, $J'=4\ \mathrm{cm^{-1}}$, $g=2.05$, $N\alpha=60\times10^{-6}$ c.g.s. emu/mol.

absent in complex Cu(L-2), indicating that alcoholic proton is lost upon the complexation.

Electronic Spectra. Visible and ultraviolet spectra of the complexes were obtained in dichloromethane and the band maxima are given in Table 2. Electronic spectra of the complexes consist of a broad band in the visible region assignable to the d-d transition with an extinction coefficient of the order of *ca.* 150 $\mathrm{mol^{-1}\,dm^{3}\,cm^{-1}}$ and several bands in the ultraviolet region assignable to charge-transfer bands. The spectrum of complex Cu(L-3) exhibits a d-d transition band maximum at $17.7\times10^{3}\ \mathrm{cm^{-1}}$, while the spectra of complexes Cu(L-2) and Cu(L-2m) exhibit a band maximum at $15.5\times10^{3}\ \mathrm{cm^{-1}}$. This indicates that the coordination environment might be different between the two groups. The bands at *ca.* $(27\text{—}28)\times10^{3}\ \mathrm{cm^{-1}}$ is characteristic of alkoxo-bridged copper(II) complexes and is assignable to the $p_{\pi}(O)\rightarrow d(Cu)$ charge-transfer transition.[3]

Molecular Weights. Molecular weights were estimated by vapor pressure osmometry. The results were as follows: Found for Cu(L-3): 440; calcd for $C_{18}H_{26}N_2O_6Cu_2$ as dimer:496. Found for Cu(L-2): 920; calcd for $C_{32}H_{44}N_4O_{12}Cu_4$ as tetramer: 931. Found for Cu(L-2m): 925; calcd for $C_{36}H_{52}N_4O_{12}Cu_4$ as tetramer: 987. It is apparent that complexes Cu (L-2) and Cu(L-2m) with a five-membered chelate ring involving an amino alcohol and copper ion are tetramer, whereas complex Cu(L-3) with a six-membered chelate ring is dimer.

Magnetic Properties. The magnetic moment of complex Cu(L-3) is 0.35 BM. at room temperature, indicating the operation of a strong antiferromagnetic spin-exchange interaction between the copper(II) ions. The temperature dependence of the magnetic susceptibilities can be interpreted in terms of the following Bleaney-Bowers equation[17] with a paramagnetic impurity term[18] for the isotropic exchange interaction

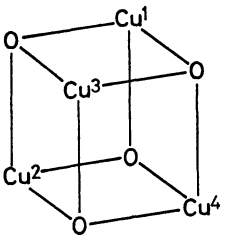

Fig. 2. Structure of tetranuclear cubane-like copper-(II) complex.

TABLE 2. ELECTRONIC SPECTRAL DATA MEASURED IN DICHLOROMETHANE

Complex	Band maxima $\tilde{\nu}/10^{3}\ \mathrm{cm^{-1}}$ (log ε)[a]			
Cu(L-3)	17.7(2.18)	27.7(3.85)	32.2(4.15)	37.3(4.45)
Cu(L-2)	15.7(2.16)	27.0(2.72)*	32.4(4.14)*	36.7(4.45)
Cn(L-m)	15.7(2.21)	27.3(2.72)	32.8(3.96)*	36.4(4.06)*

a) Symbol * means shoulder.

in a copper(II) dimer:

$$\chi_A=\frac{Ng^2\beta^2}{3kT}\left[1+\frac{1}{3}\exp(-2J/kT)\right]^{-1}(1-p)+\frac{0.45p}{T}+N\alpha, \quad (1)$$

where χ_A is the magnetic susceptibility per copper ion, p is the ratio of mononuclear copper(II) ions to total copper(II) ions, and N, g, J, β, and $N\alpha$ have the usual meanings. The experimental data fit Eq. 1 with magnetic parameters $-2J=920\ \mathrm{cm^{-1}}$, $g=2.10$, $p=0.01$, and $N\alpha=60\times10^{-6}$ c.g.s. emu/mol.

The magnetic moments of complexes Cu(L-2) and Cu(L-2m) are 1.88 and 1.86 BM. at room temperature, respectively. As shown in Fig. 1, the magnetisms of complexes Cu(L-2) and Cu(L-2m) obey the Curie-Weiss law with positive Weiss constants 17 and 20 K, respectively, indicating that a ferromagnetic interaction is operative in these complexes. For complexes with this kind of magnetic properties, the tetranuclear cubane-like structure shown in Fig. 2 has been assumed and the temperature dependence of their magnetic properties has been interpreted on the basis of the Heisenberg model.[6,15] The Hamiltonian for the spin-exchange interaction of a tetranuclear structure may be written as $H=-2J_{12}S_1S_2-2J_{13}S_1S_3-2J_{14}S_1S_4-2J_{23}S_2S_3-2J_{24}S_2S_4-2J_{34}S_3S_4$, where the numbering of copper ions are given in Fig. 2. On assuming $J=J_{13}=J_{24}$ and $J'=J_{12}=J_{23}=J_{34}=J_{14}$, magnetic susceptibilities are given by

$$\begin{aligned}\chi_A=3g^2\{&10\exp[(J+2J')/kT]+4\exp(-J/kT)\\&+2\exp[(J-2J')/kT\}/32T\{4\exp[(J+2J')/kT]\\&+5\exp(-J/kT)+\exp(-Q(11)/kT)\\&+\exp(-Q(22)/kT)+\exp(-Q(33)/kT)\\&+\exp(-Q(44)/kT)+3\exp[(J-2J')/kT]\}+N\alpha, \quad (2)\end{aligned}$$

where $Q(11)$, $Q(22)$, $Q(33)$, and $Q(44)$ have the same meanings as those used by Hatfield and Inman.[19] The exchange integral (J, J'), g, and $N\alpha$ were evaluated from the best-fit of experimental data to Eq. 2. The evaluated values for Cu(L-2) are $J=40\ \mathrm{cm^{-1}}$,

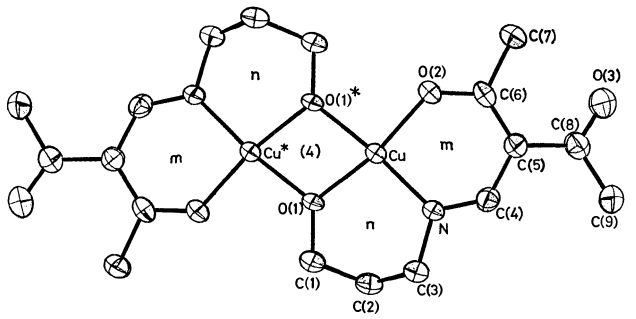

Fig. 3. Molecular structure of Cu(L-3) with the atom numbering scheme.

$J'=4$ cm^{-1}, $g=2.05$, and $N\alpha=60\times10^{-6}$ c.g.s. emu/mol, and those for Cu(L-2m) are $J=40$ cm^{-1}, $J'=5$ cm^{-1}, $g=2.10$, and $N\alpha=60\times10^{-6}$ c.g.s. emu/mol. It is found that the magnetic behavior of complexes Cu(L-2) and Cu(L-2m) can be interpreted in terms of Eq. 2 formulated on the basis of the tetranuclear cubane-like structure and the assumption that both J and J' are positive.

Molecular Structure of Cu(L-3). The molecular structure of complex Cu(L-3) consists of discrete alkoxo-bridged centrosymmetric binuclear units, as deduced on the molecular weight measurement and magnetic behavior. An ORTEP plot of the perspective molecule is shown in Fig. 3, with the atom numbering scheme. Bond lengths and angles with estimated standard deviations are given in Table 3.

The coordination geometry around the copper ion is a square planar within ±0.01 Å for deviations of the component atoms. The geometries of Cu(O)(O)Cu and around the bridging oxygen atom are perfectly planar. Such a structural feature is similar with the related copper(II) complex Cu(pia) containing the ligand derived from 2,4-pentanedione and 3-amino-1-propanol,[10] and has been observed for binuclear copper(II) complexes associated with strong antiferromagnetic interaction.[4] The Cu–O–Cu angle 103.6(1)° is smaller than that of Cu(pia) (106°).[10] The saturated six-membered chelate ring containing amino alcohol has a chair conformation, and atoms Cu and C(2) are displaced by −0.13 and 0.70 Å, respectively, from the plane through O(1), C(1), C(3), and N. The acetyl group is tilted to the unsaturated six-membered chelate ring by 12.5° due to the steric hindrance between the acetyl and methyl groups attached to the unsaturated chelate ring. This steric hindrance is also found in the deviations of O(3) and C(7) by 0.21 and −0.16 Å, respectively, from the plane through atoms C(5), C(6), and C(8).

Based on the above-described results, it has been established that complexes Cu(L-2) and Cu(L-2m) with a five-membered chelate ring consisting of amino alcohol and copper ion are of tetranuclear cubane-like structure associated with ferromagnetic interaction, whereas complex Cu(L-3) with a six-membered chelete ring is a dimer associated with strong antiferromagnetic interaction. Mikuriya *et al.*[20] examined a number of molecular structures of alkoxo-bridged polynuclear copper(II) complexes and pointed out that for the formation of binuclear copper(II) complexes the favorable chelate ring system is the 6-6-(4)-6-6 and 5-6-(4)-6-5 fused chelate ring systems, and that the 6-5-(4)-5-6 system often forms a stable tetranuclear species, where the fused chelate ring system is represented by m-n-(4)-n-m according to their notation (Fig. 3). The complexes prepared in this study supply good examples to support their suggestions. The planarity around the bridging oxygen atom should be mainly attributable to the conformation of the chelate ring involving amino alcohol and copper ion. It can be considered that in the case of complex Cu(L-3) the chair conformation of the six-membered chelate ring allows a planar geometry around the bridging oxygen atom and that the complex prefers to be a dimer associated with strong antiferromagnetic interaction. On the other hand, for complexes Cu(L-2) and Cu(L-2m) with a five-membered chelate ring, it can be considered that the deviation from the planar geometry around the bridging oxygen atom should occur and that the oxygen atom can coordinate to another copper ion to form a tetranuclear copper(II) complex, since a five-membered chelate ring takes a gauche or envelope conformation.

Table 3. Bond distances and angles with estimated standard deviations in parentheses, for Cu(L-3)[a]

Bond distance	l/Å		l/Å
Cu···Cu*	2.994(1)	N-C(4)	1.299(5)
Cu-O(1)	1.899(3)	C(4)-C(5)	1.412(6)
Cu-O(1)*	1.910(3)	C(5)-C(6)	1.407(6)
Cu-N	1.905(3)	C(5)-C(8)	1.463(6)
Cu-O(2)	1.899(3)	O(2)-C(6)	1.275(5)
O(1)-C(1)	1.408(6)	C(6)-C(7)	1.496(6)
C(1)-C(2)	1.517(6)	C(8)-O(3)	1.224(6)
C(2)-C(3)	1.494(7)	C(8)-C(9)	1.494(7)
N-C(3)	1.467(6)		
Bond angle	**ϕ/°**		**ϕ/°**
Cu-O(1)-Cu*	103.6(1)	Cu-N-C(4)	123.1(3)
Cu-O(1)-C(1)	128.3(2)	C(3)-N-C(4)	117.3(3)
Cu*-O(1)-C(1)	127.7(2)	N-C(4)-C(5)	128.9(4)
O(1)-Cu-O(1)*	76.3(1)	C(4)-C(5)-C(6)	121.0(3)
O(1)-Cu-N	97.7(1)	C(4)-C(5)-C(8)	117.5(4)
N-Cu-O(2)	93.0(1)	C(6)-C(5)-C(8)	121.3(4)
O(1)*-Cu-O(2)	93.0(1)	C(5)-C(6)-O(2)	123.4(4)
O(1)-Cu-O(2)	168.3(1)	C(5)-C(6)-C(7)	123.3(3)
O(1)*-Cu-N	173.2(1)	O(2)-C(6)-C(7)	113.1(4)
O(1)-C(1)-C(2)	111.2(3)	Cu-O(2)-C(6)	129.2(3)
C(1)-C(2)-C(3)	113.9(4)	C(5)-C(8)-O(3)	123.1(4)
C(2)-C(3)-N	112.5(4)	C(5)-C(8)-C(9)	120.1(4)
Cu-N-C(3)	119.4(2)	O(3)-C(8)-C(9)	116.7(4)

a) Symbol * means $-x$, $-y$, $-z$.

We would like to thank Professor Sigeo Kida, Faculty of Science, Kyushu University for allowing us to use the X-ray diffractometer. Thanks are also due to Mr. Toshiaki Kanao of Kumamoto University for the molecular weight measurement.

References

1) E. D. Estes, W. E. Hatfield, and D. J. Hodgson, *Inorg. Chem.*, **13**, 1654 (1974).
2) D. L. Lewis, K. T. McGregor, W. E. Hatfield, and D. J. Hodgson, *Inorg. Chem.*, **13**, 1013 (1974).
3) M. Mikuriya, M. Nakamura, H. Ōkawa, and S. Kida, *Chem. Lett.*, **1982**, 839.
4) M. Mikuriya, H. Ōkawa, and S. Kida, *Bull. Chem. Soc. Jpn.*, **55**, 1086 (1982).
5) Y. Nishida and S. Kida, *J. Inorg. Nucl. Chem.*, **38**, 451 (1976).
6) Y. Nishida and S. Kida, *Chem. Lett.*, **1974**, 339.
7) M. Mikuriya, H. Ōkawa, and S. Kida, *Bull. Chem. Soc. Jpn.*, **54**, 2943 (1981).
8) N. Matsumoto, Y. Nishida, S. Kida, and I. Ueda, *Bull. Chem. Soc. Jpn.*, **49**, 177 (1976).
9) N. Matsumoto, Y. Nishida, I. Ueda, and S. Kida, *Bull. Chem. Soc. Jpn.*, **49**, 1308 (1976).
10) J. A. Bertland and J. A. Kelley, *Inorg. Chim. Acta.* **4**, 203 (1970).
11) D. P. Riley and D. H. Busch, *Inorg. Synth.*, Coll. Vol. XVIII, 37 (1978).
12) N. F. Curtis, *J. Chem. Soc.*, **1961**, 3147.
13) P. W. Selwood, "Magnetochemistry," Interscience Publishers, New York (1956).
14) "International Tables for X-Ray Crystallography," Kynoch Press, Birmingham (1974), Vol. IV.
15) T. Sakurai, H. Iwasaki, Y. Watanabe, K. Kobayashi, Y. Bando, and Y. Nakamichi, *Rikagaku Kenkyusho Hokoku* (in Japanese), **50**, 75 (1972).
16) S. Kawano, *Rep. Comp. Cent. Kyushu Univ.*, **13**, 39 (1980).
17) B. Bleaney and K. D. Bowers, *Proc. R. Soc. London, Ser. A*, **214**, 451 (1952).
18) K. E. Hyde, G. Gordon, and G. F. Kokoszka, *J. Inorg. Nucl. Chem.*, **30**, 2155 (1968).
19) W. E. Hatfield and G. W. Inman, Jr., *Inorg. Chem.*, **8**, 1376 (1969).
20) M. Mikuriya, H. Ōkawa, and S. Kida, *Bull. Chem. Soc. Jpn.*, **53**, 2871 (1980) and references therein.

 © 1983 The Chemical Society of Japan Bull. Chem. Soc. Jpn., 56, 1393—1400 (1983)

Mixed-ligand Palladium(II) Complexes Containing *O,O'*-Chelated β-Diketonate and η^3-Carbon-bonded Ethyl 3-Oxobutanoate Anions. Preparation and Reactions with Some Lewis Bases**

Kurumi YAMADA, Shigeru BABA,† Yukio NAKAMURA,* and Shinichi KAWAGUCHI

Department of Chemistry, Faculty of Science, Osaka City University, Sumiyoshi-ku, Osaka 558

(Received October 20, 1982)

Novel palladium(II) complexes [Pd(β-dik)(η^3-etac)] (**5**), in which anions of a β-diketone and ethyl 3-oxobutanoate coordinate to the central metal atom by the *O,O'*-chelation and the η^3 carbon bonding, respectively, were prepared by the reactions of a dinuclear complex [PdCl(η^3-etac)]$_2$ with thallium(I) β-diketonates in benzene or acetone at room temperature. Reactions of **5** with Lewis bases (L) such as triphenylphosphine, diethylamine, propylamine and benzylamine were investigated. In almost all reactions, only the η^3-carbon-bonded ester ligand in **5** was converted into a terminal-carbon-bonded one to afford complexes [Pd(β-dik)(etac-C^4)L]. The bonding modes for the ligands in these products as well as in **5** were determined by means of IR and ^{1}H and ^{13}C NMR spectroscopy.

Four kinds of coordination modes for the monoanion of ethyl 3-oxobutanoate have been observed so far in palladium(II) complexes: *O,O'*-chelation (**1**, **3**),[1] η^3 carbon bonding (**2**),[2] central carbon bonding (**3**),[1] and terminal carbon bonding (**4**).[3]

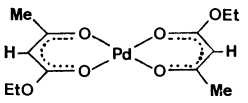

1

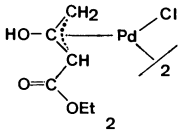

2

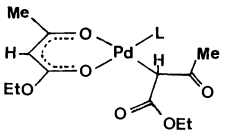

3

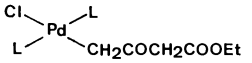

4

Of these complexes, **3** and **4** were derived from **1** and **2** by the reactions with Lewis bases, respectively. Similarly, all these bonding modes described above[4–6] as well as *O*-unidentate bonding[7,8a,b] have also been established for 2,4-pentanedione and other β-diketones in palladium(II) and platinum(II) complexes. Comprehensive studies on the interconversion among these bonding modes of β-diketonate anions have recently been performed.[8]

As the continuation of this line of studies, we intended to prepare novel complexes of palladium(II) which involve two kinds of coordination modes for β-diketonate monoanions and to examine relative stability of each bonding mode. In this paper, preparation and characterization of complexes **5a**—**c** and their reactions with some Lewis bases to show which bonding mode is less stable are described.

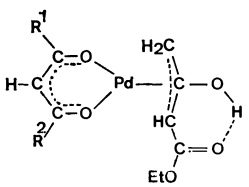

	R^1	R^2
5a	CH_3	CH_3
5b	$CH_3(CF_3)$	$CF_3(CH_3)$
5c	CF_3	CF_3

† Present address: Toyo Polymer Co., Ltd., Minamikaneden, Suita 564.

Results and Discussion

Preparation and Characterization of Complexes **5**. The η^3 complex of ethyl 3-oxobutanoate anion with palladium(II), [PdCl(η^3-etac)]$_2$ (**2**), which was first prepared by Tezuka *et al.*,[2a] was used as a starting material for preparation of complexes **5**. The bridge-splitting and concurrent chloride-abstracting reactions of **2** with twice molar amounts of thallium(I) β-diketonates yielded mononuclear complexes **5a**, **5b**, and **5c** in high yields, whose analytical data are given in Table 1.

The ^{1}H NMR data for complexes **5** in $CDCl_3$ are listed in Table 2 and compared with those for **2** which were previously reported[9] and reasonably interpreted on the basis of the η^3 structure confirmed by X-ray analysis.[2b] Complex **5c** shows five signals due to the etac ligand, together with a singlet at 6.12 ppm attributable to the methine proton of the *O,O'*-chelated hfac ligand.[4] These five signals from etac appear as a singlet at 3.74 ppm, two doublets at 2.80 and 3.87 ppm, a triplet at 1.36 ppm and a multiplet centered at 4.3 ppm, with relative intensities of 1:1:1:3:2. The first three signals can be assigned to the H^a, H^b, and H^c protons of the allylic moiety and the others to methyl and methylene protons of the ethyl groups by comparison with those of **2**. The spectral pattern similar to that of the starting complex **2** confirms that the η^3 structure of the etac ligand in **2** is maintained intact in the reaction product **5c**, although the H^d signal observed for **2** can not be detected for **5c**. This conclusion is firmly supported by the ^{13}C NMR for **5c** and **2** listed in Table 3. Both spectral data are in fairly good agreement with each other, although three additional signals from hfac appear in the spectrum of **5c**. The three signals resonate at 90.1, 175.4, and 117.8 ppm from internal Me_4Si and each couples to ^{19}F nuclei appearing as a multiplet, a quartet and a quartet, respectively, the coupling constants increasing in this order. These signal frequencies and

** In this paper β-dik represents a monoanion of β-diketones such as 2,4-pentanedione (acacH), 1,1,1-trifluoro-2,4-pentanedione (tfacH), and 1,1,1,5,5,5-hexafluoro-2,4-pentanedione (hfacH), etac denoting that of ethyl 3-oxobutanoate.

TABLE 1. ANALYTICAL DATA FOR THE NEWLY PREPARED COMPLEXES

No.	Complex	Found(Calcd)(%) C	H	N	Mol wt[a)]
5a	[Pd(acac)(η^3-etac)]	39.56(39.48)	4.68(4.81)		
5b	[Pd(tfac)(η^3-etac)]	33.65(33.97)	3.33(3.37)		
5c	[Pd(hfac)(η^3-etac)]	29.66(29.85)	2.28(2.28)		
6a	[Pd(acac)(etac-C^4)(PPh_3)]	57.68(58.35)	5.24(5.23)		596(597)
6b	[Pd(tfac)(etac-C^4)(PPh_3)]	53.69(53.61)	4.25(4.34)		654(651)
6c	[Pd(hfac)(etac-C^4)(PPh_3)]	50.63(49.42)	3.61(3.58)		715(705)
6d	[Pd(acac)(etac-C^4)(Et_2NH)]	43.96(44.18)	6.56(6.67)	3.36(3.43)	402(418)
6e	[Pd(tfac)(etac-C^4)(*n*-$PrNH_2$)]	38.21(37.56)	5.04(4.95)	3.24(3.13)	477(478)
7	[Pd(etac-C^4)($PhCH_2NH_2$)$_3$](hfac)	50.31(50.31)	4.87(4.88)	5.54(5.50)	

a) In CH_2Cl_2 at 28 °C.

TABLE 2. ^{1}H NMR DATA FOR COMPLEXES **5** IN $CDCl_3$[a)]

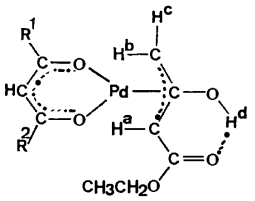

5

Complex	R^1	R^2	β-dik CH_3	β-dik CH	η^3-etac[b)] CH_3-CH_2	H^c	H^b	H^a	H^d	Coupling constants in Hz
2					1.31 t	4.29m	3.74 d	2.59 dd	3.59	10.46 d	J(bc)=3.4, J(bd)=1.2, $J(CH_3-CH_2)$=7.2
5a	CH_3	CH_3	1.94, 1.98	5.35	1.37 t	4.3m	3.58 d	2.58 d	3.48		J(bc)=4.0, $J(CH_3-CH_2)$=8.0
5b	CH_3,CF_3		2.09 2.12	5.73	1.36 t 1.38 t	4.3m	3.69 d	2.68 d	3.59		J(bc)=3.0, $J(CH_3-CH_2)$=6.8
5c	CF_3	CF_3		6.12	1.36 t	4.3m	3.87 d	2.80 d	3.74		J(bc)=4.0, $J(CH_3-CH_2)$=8.0

a) Chemical shifts in ppm from internal Me_4Si at 33 °C. d: Doublet, dd: doublet of doublets, t: triplet, m: multiplet. b) H^d proton signals for **5** are not observable.

coupling constants are compatible with those for the *O,O'*-chelate of hfac.[4)]

As is seen in Table 2, the similarity of the ^{1}H NMR data for **5b** to those for **5c**, except the additional methyl signal from tfac in **5b**, shows that the coordination structures of the β-dik and etac ligands around palladium are the same in these complexes. Owing to the unsymmetrical nature of tfac, two geometrical isomers, *cis*(CH_3,CH_2) and *trans*(CH_3,CH_2), coexist in the case of **5b**.

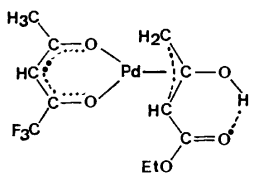

cis(CH_3,CH_2)

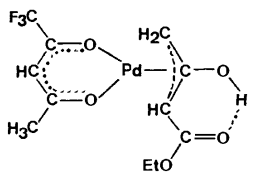

trans(CH_3CH_2)

Although the very slight splitting is recognized in the methyl signals from the tfac and ester ligands, other signals do not discriminate these two isomers. On the other hand, the ^{13}C NMR spectrum (Table 3) of **5b** clearly exhibits the presence of *cis*(CH_3,CH_2) and *trans*(CH_3,CH_2) isomers in $CDCl_3$, two sets of signals attributable to the trifluoromethyl-substituted carbonyl carbon and the methyl and methylene carbons of ethyl group appearing at 167.8, 14.0, 62.0 and at 168.3, 14.5, 62.2 ppm, respectively. Each set of signals can be assigned only arbitrarily to the cis or trans isomer.

Complexes **5** including the acac complex **5a** are soluble in most organic solvents such as haloalkanes, ketones, ethers, aromatic hydrocarbons, and even in hexane. Although **5b** and **5c** are stable in these organic solvents, **5a** is rather unstable and a less soluble substance precipitates from its solution in chloroform on addition of hexane, which is not isolated in a pure form (see Experimental section). The ^{1}H NMR spectrum of **5a** in $CDCl_3$, therefore, includes some signals other than those assignable to [Pd(acac)-(η^3-etac)], even immediately after dissolution. Only the latter signals are listed in Table 2. In this case, two methyl signals from acac are observed at 1.94 and 1.98 ppm and such different environments of the

TABLE 3. ^{13}C NMR DATA FOR COMPLEXES **5b** AND **5c** IN $CDCl_3$[a]

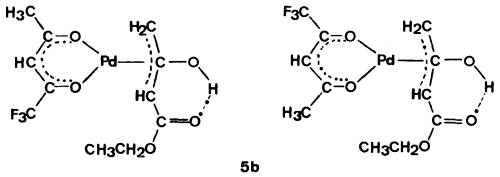

5b

cis(CH_3,CH_2) *trans*(CH_3,CH_2)

tfac					η^3-etac			
CH_3	CH	CF_3	$CF_3\underline{C}O$	$CH_3\underline{C}O$	CH_3-CH_2	CH_2	CH	C-OH
28.8	95.2	118.8q (285)	167.8q, 168.3q (33)	194.5	14.0, 14.5 / 62.0, 62.2	41.2	42.1	154.8

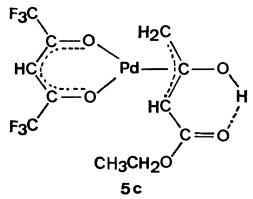

5c

	hfac			η^3-etac					
	CH	CF_3	$CF_3\underline{C}O$	CH_3-CH_2		CH_2	CH	C-OH	C=O
2				14.5	62.3	46.4	47.7	152.0	175.4
5c	90.1m (2)	117.8q (285)	175.4q (34)	13.9	62.5	42.4	43.2	156.0	175.7

a) Chemical shifts in ppm from internal Me_4Si. Figures in parentheses give $J(^{19}F-C)$ in Hz. q: Quartet, m: multiplet.

TABLE 4. CHARACTERISTIC IR BANDS IN NUJOL[a]

Complex	β-dik	etac		
	$\nu(C{\cdots}O)+\nu(C{\cdots}C)$ / cm^{-1}	$\nu(OH)/cm^{-1}$	$\nu(C{=}O)/cm^{-1}$ Ester	Ketone	$\delta(CCC)$ or $\nu(Pd-C)/cm^{-1}$
2[b]		3200m	1675 vs		548 s
5a	1577 vs, 1520 vs	3200w	1673 s		548w
5b	1610 vs, 1523 m	3200w	1670 s		545w
5c	1627 vs, 1605 s, 1557 m, 1532 m	3200w	1675 s		543w
6a	1580 vs, 1515 vs		1743 s	1661 s	c)
6b	1620 vs, 1520 m		1741 s,	1665 s	c)
6c	1625 vs, 1540 m		1745 vs	1670 s	c)
6d	1568 vs, 1525 vs		1745 vs	1640 s	540m
6e	1615 vs, 1517 m		1725 vs	1630 s, sh	d)
7	1661 vs		1698 s	1645 vs	525 s

a) vs: Very strong, s: strong, m: medum, w: weak, sh: shoulder. b) Ref. 3a. c) Not assignable due to overlapping with the ligand bands of triphenylphosphine. d) Not detectable.

methyl hydrogens are caused by unsymmetric coordination of the ester ligand in **5a**.

Table 4 lists the characteristic IR bands of complexes **5** and products of their reactions with Lewis bases. The bonding modes of the β-dik and etac ligands are easily diagnosed on the basis of the spectral pattern in the 1500—1700-cm^{-1} region. Two or four bands observed in the 1520—1627-cm^{-1} region for **5** are assigned to the $\nu(C{\cdots}O)+\nu(C{\cdots}C)$ vibrations of the *O,O'*-chelates of β-dik,[4] while a band in the 1670—1675-cm^{-1} region is assigned to the $\nu(C{=}O)$(ester) of the η^3-carbon-bonded etac ligand.[2a] Weak bands around 545 and 3200 cm^{-1} are attributed to the δ(CCC) and ν(OH) vibrations, respectively, characteristic of the η^3 carbon bonding of etac by reference to the data for complex **2**.[2a]

TABLE 5. ^{1}H NMR DATA FOR COMPLEXES **6** AND **7** IN $CDCl_3$[a]

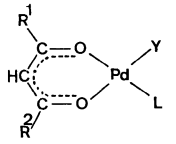

6

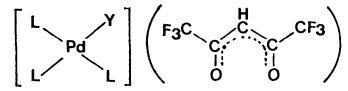

7

(Pd-Y = Pd-$CH_2COCH_2COOCH_2CH_3$)

Complex		R^1	R^2	L	β-dik		etac-C^4			
					CH_3	CH	CH_3-CH_2		CH_2	CH_2-Pd
6a		CH_3	CH_3	PPh_3	1.58, 2.00	5.27	1.19 t	4.09 q	3.54	2.26 d {4}
6b[b]	*cis*(CH_3,P)	CH_3	CF_3	PPh_3	1.74	5.72	1.18 t	4.12 q	3.56	2.31 d {3}
	trans(CH_3,P)	CF_3	CH_3		2.18				3.62	2.40 d {3}
6c		CF_3	CF_3	PPh_3		6.30	1.23 t	4.26 q	3.64	2.59 d {2}
6d[c]		CH_3	CH_3	Et_2NH	1.90	5.27	1.27 t	4.19 q	3.56	2.67
6e[c]		CH_3,	CF_3	*n*-$PrNH_2$	2.10	5.71	1.30 t	4.22 q	3.55	2.72
						5.73				2.76
7[c]		CF_3	CF_3	$PhCH_2NH_2$		5.62	1.22 t	4.15 q	3.64	2.30

a) Same as footnote a) for Table 2. Figures in braces give $^3J(^{31}P\text{-}H)$ in Hz. b) Data for the low-temperature limitting spectrum at −29 °C are given. c) Chemical shifts for L. Et: 2.7 m, 1.42 t (for **6d**). *n*-Pr: 2.7 m, 1.7 m, 0.99 t (for **6e**). CH_2: 3.49 (for **7**).

Reactions of **5** *with Lewis Bases Producing Terminal-carbon-bonded Complexes of etac.* Although the reactions of complexes **5** with triphenylphosphine and a variety of nitrogen bases such as propylamine, diethylamine, *t*-butylamine, benzylamine, pyridine, and piperidine were tried, only five complexes of the type **6** and complex **7** listed in Table 1 could be isolated as reaction products in pure forms. Quite high solubilities of these products in most organic solvents described earlier make those isolation difficult. When complexes **5** were allowed to react with an equimolar amount of triphenylphosphine in benzene or chloroform, the η^3 carbon bonding of the etac ligand in **5** was converted into the terminal carbon bonding to afford neutral complexes **6a**, **6b**, and **6c**.

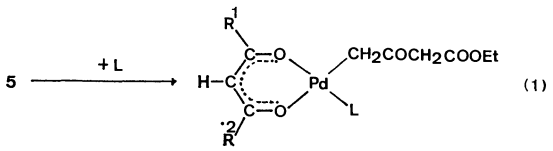

(1)

	R^1	R^2	L
6a	CH_3	CH_3	PPh_3
6b	CH_3(CF_3)	CF_3(CH_3)	PPh_3
6c	CF_3	CF_3	PPh_3
6d	CH_3	CH_3	Et_2NH
6e	CH_3(CF_3)	CF_3(CH_3)	*n*-$PrNH_2$

Similarly, diethylamine and propylamine reacted with **5a** and **5b** to produce **6d** and **6e**, respectively. In contrast with these bases, benzylamine reacted with **5c** to give solely the cationic complex **7**, irrespective of the reactant mole ratio, which has hfac as a counter anion in the outer sphere.

$$\mathbf{5c} \xrightarrow{+3L} [Pd(CH_2COCH_2COOEt)L_3](CF_3COCHCOCF_3) \quad \mathbf{7}\ (L=PhCH_2NH_2) \qquad (2)$$

The analytical and molecular weight data for these complexes isolated are also included in Table 1.

The ^{1}H NMR data for complexes **6** and **7** are collected in Table 5. The H^a, H^b, and H^c signals observed for **5** are lost in **6a**—**c** and instead two signals appeared at 3.54—3.64 and 2.26—2.59 ppm as a singlet and a doublet with relative intensity of 1:1, each signal corresponding to 2H protons. Such a spectral change indicates that the η^3-carbon-bonded etac ligand in **5** was converted into the terminal-carbon-bonded one in **6a**—**c** as shown by Eq. 1. Thus, the singlet and the doublet are assigned to protons of the central methylene and the terminal methylene coordinated to palladium, respectively, by reference to the spectral data of **4** (L=py or 1/2·bipy).[3a] The latter methylene protons couple to ^{31}P cis to them to give a doublet with $^3J(P\text{-}H)=2\text{—}4$ Hz.

As Fig. 1a shows, the ^{1}H NMR spectrum of **6a** in the methyl and methylene proton regions exhibits two methyl signals from acac at 1.58 and 2.00 ppm. The lower-field signal is assigned to the methyl protons trans to P, while the higher-field one to the methyl cis to P because such an appreciable upfield shift is caused by the anisotropic shielding effect of triphenylphosphine at the cis position.[6a]

Figure 1b shows the variable-temperature ^{1}H NMR spectra of **6b** in the same regions as in Fig. 1a. The spectrum at room temperature (33 °C) is composed of a broad singlet (3.56 ppm), a broad doublet (2.37 ppm), and two collapsed signals (*ca.* 1.7 and 2.2 ppm). With increasing temperature, the first two signals sharpen, while the other two give a coalesced signal. On the other hand, as the temperature is lowered, the first two signals become broader and split, and then sharpen to give two sets of signals each composed of a singlet and a doublet at −29 °C. Similarly, other two signals gradually sharpen with decreasing temperature finally giving two sharp singlets at 1.74 and 2.18 ppm, which correspond to resonances of the meth-

Table 6. ^{13}C NMR data for complex **6c** in $CDCl_3$[a)]

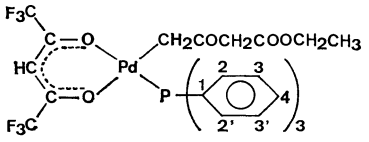

6c

hfac			etac-C^4					
CH	CF_3	$CF_3\underline{C}O$	CH_3–CH_2		CH_2–Pd	CH_2	C=O(O)	C=O
89.9	117.4 q, 117.7 q (285) (285)	174.9 q (35)	14.1	60.7	26.9 d [5.1]	50.4	168.3	205.6

a) Same as footnote for Table 3. Figures in parentheses and brackets give $J(^{19}F\text{-}C)$ and $J(^{31}P\text{-}C)$, respectively. Chemical shifts for PPh_3: C^1, 127.6 d[55.7]; C^2, 134.4 d[11.1]; C^3, 128.6 d[11.1]; C^4, 131.3 d[2.6].

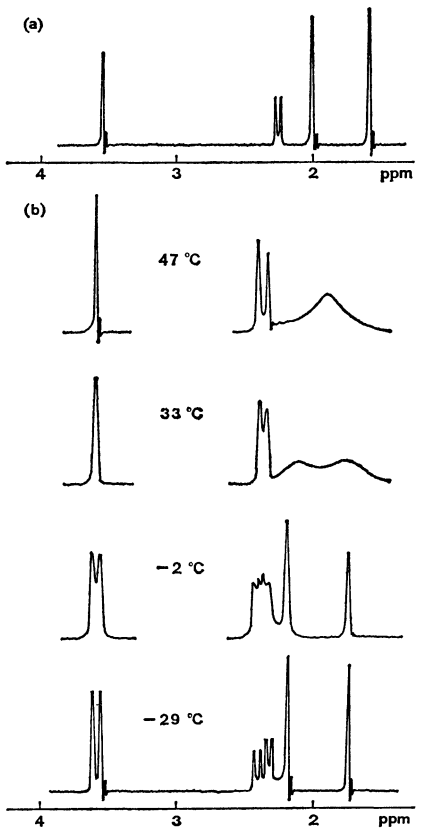

Fig. 1. ^1H NMR spectra at 100 MHz of (a) [Pd(acac)(etac-C^4)(PPh_3)], **6a** ($CDCl_3$; 33 °C) and (b) [Pd(tfac)(etac-C^4)(PPh_3)], **6b** ($CDCl_3$; −29, −2, 33, and 47 °C) in the methyl and methylene proton regions.

yl groups cis and trans to P (compare Figs. 1a and 1b). These results imply that complex **6b** exists as a mixture of two geometrical isomers, *cis*(CH_3, P) and *trans*(CH_3, P) (in the mole ratio of 1:1.3), in $CDCl_3$ at −29 °C and these isomers are readily interconvertible at 33 °C and above. In Table 5, the low-temperature limitting spectral data for these isomers are given.

Table 6 denotes the ^{13}C NMR data for **6c** as a representative of **6** which gives the most simple spectrum. Two trifluoromethyl signals appear at 117.4 and 117.7 ppm as quartets with $^1J(C\text{–}F)=285$ Hz, thus reflecting the slight difference in environments caused by the trans ligands, etac and triphenylphosphine and also showing stereochemical rigidity of this complex in $CDCl_3$ at room temperature.

Much attention has recently been given to the mechanisms of geometrical isomerization of the square-planar metal complexes.[10)] In the case of the present complex **6b**, coupling of the terminal methylene protons of etac to ^{31}P is maintained during the isomerization (see Fig. 1b), showing inapplicability of the dissociative mechanism involving the Pd–P bond rupture. Thus the transformation, as depicted below, of a five-coordinate intermediate **A**, in which the fifth coordination site of palladium is occupied by the ester carbonyl oxygen atom, may be the most probable mechanism to be proposed:

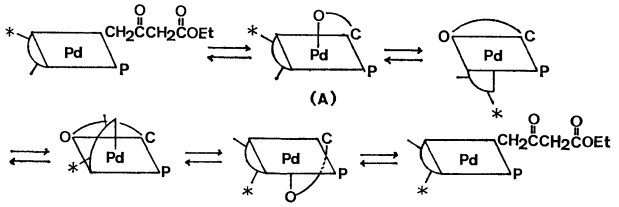

The *C,O*-chelation of tfac as in **A** has been found as a stable bonding mode for the tfac dianion in a series of [Pd(tfac(2-)-*C,O*)LL']-type complexes[11)] and the Pt(II) analogues.[12)] An intermolecularly associated complex, in which the metal atom of a reacting species is coordinated by the ester carbonyl oxygen of a neighboring molecule, is also conceivable as an alternative intermediate for the coordination-site exchange. Such an example that another molecule of the same species acts as a catalyst was found for the σ-pyridyl complex, [Pd(acac)(σ-pyridyl)PPh_3], and the effect was termed "self catalysis" by Tanaka *et al.*[13)] Similar phenomenon was also observed for [Pd(acac)(CH_2CN)PPh_3].[14)] As described above, complexes **6a** and **6c** are stereochemically rigid in $CDCl_3$ at room temperature, while **6b** shows fluxional motion under the same conditions. However, it is not rationalized why only complex **6b** having the unsymmetric tfac ligand brings about the coordination-site exchange.

As is seen in Table 5, reaction products with nitrogen bases, both **6d** and **6e**, show only a single methyl

signal from β-dik in their ^{1}H NMR spectra. Two possibilities are conceivable: 1) Accidental coincidence of the two methyl signals; 2) coalescence to a single peak by coordination-site exchange of the β-dik ligand. In the present case, the second possibility to occur will probably be excluded because the acac complex **6a** does not cause such a reaction and **6e** shows two methine and CH_2–Pd proton signals corresponding to the *cis*(CH_3,N) and *trans*(CH_3,N) isomers.

The product complex, **7**, from the reaction of **5c** with benzylamine gave satisfactory analysis as Pd(etac)(hfac)$(PhCH_2NH_2)_3$ which differs from other products, **6**, in composition. However, the coordination mode of etac to palladium is the same as that in **6** on the basis of the similarity of ^{1}H NMR data (Table 5). On the other hand, the methine proton from hfac in **7** resonates at higher field (5.62 ppm) than that (6.30 ppm) in **6c**. Such an upfield shift of the methine proton signal is generally observed for the outer-sphere complexes of the type $[PdL_4](hfac)_2$ compared with the *O,O'*-chelate because of the higher charge density on noncoordinating anion: the methine protons of $[Pd(hfac)_2]$,[4] $[Pd(n\text{-}PrNH_2)_4](hfac)_2$,[8a] $[Pd(py)_4](hfac)_2$,[8b] and $[Pd(PMe_2Ph)_4](hfac)_2$[8b] resonate at 6.42, 5.92, 6.00, and 5.67 ppm in $CDCl_3$, respectively.

When the IR spectral data (Table 4) of **5** and **6** are compared with each other, a considerable difference is noticed only in the absorption bands characteristic of the etac ligand. Thus complexes **5** have the ν(OH) and ν(C=O)(ester) bands at around 3200 and 1670 cm^{-1}, respectively, while complexes **6** show no absorption bands around 3200 cm^{-1}, but exhibits two strong ν(C=O) vibrations in the 1725—1745 and 1630—1670-cm^{-1} regions. This confirms the above-mentioned conclusion that the η^3-carbon-bonded enolate anion of 3-oxobutanoate was converted into the terminal-carbon-bonding of the keto tautomer. These carbonyl bands assignable to the ν(C=O)(ester) and ν(C=O)(keto) vibrations are also found for complexes of the type **4** as follows: [PdCl(etac-*C*^{4})$(py)_2$] 1740vs, 1650vs; [PdCl(etac-*C*^{4})(bipy)] 1730vs, 1640vs.[3a]

The IR spectrum of complex **7** has four bands of strong to medium intensities in the 1600—1700-cm^{-1} region. Of these, a medium band observed at 1619 cm^{-1} is assigned to the $\delta(NH_2)$ vibration of the coordinated benzylamine and hence omitted in Table 4. Although two strong bands at 1698 and 1645 cm^{-1} are slightly closer mutually than those for **6**, they can be assigned to the ν(C=O) vibrations of the terminal-carbon-bonded etac ligand. On the other hand, no band shows in the region attributable to the ν(C≡O) + ν(C≡C) vibrations of the *O,O'*-chelated β-dik ligand, but instead a strong band appears at 1661 cm^{-1}. The frequency of this band is close to that for potassium 1,1,1,5,5,5-hexafluoro-2,4-pentanedionate, thus conforming to the cationic formulation [Pd(etac-*C*^{4})$(PhCH_2NH_2)_3$](hfac) which was deduced from the ^{1}H NMR spectral data.

Consideration on Bonding Nature of the β-dik and etac Ligands in **5**. As described before, complexes **5b** and **5c** are stable in solution, but **5a** is rather unstable in most organic solvents and decomposes to give an uncharacterized crude substance. The stability difference among these complexes may be brought about by the substituent effect for the methyl groups of acac. The more basic acac ligand can coordinate more tightly to palladium than tfac and hfac do and destabilize the η^3-carbon-bonding of etac to the metal as a result. The conversion of the η^3-carbon-bonded etac ligand in **5a** into the terminal-carbon-bonded one without any free ligand in solution could produce a less soluble substance in which presumably the vacant site of palladium is coordinated by a free carbonyl oxygen of another molecule.

In all the reactions of **5** with Lewis bases except that of **5c** with benzylamine, it was found that the O,O'-chelate of the β-dik ligand in **5** is more stable than the η^3 carbon bonding of etac and the latter was converted into the terminal-carbon-bonding. Powell *et al.* have studied insertion reactions of olefins,[15] 1,2-dienes,[16] and 1,3-dienes[17] (L') into the allylic palladium bonds of the η^3-allylic complexes (η^3-allyl)Pd(X) (X=hfac, acac, or chloride). In either case of the bidentate ligands (hfac and acac), the η^1-allylic complex (η^1-allyl)(L')Pd(X) was conceivable as

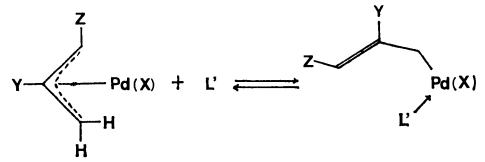

an intermediate on the basis of *syn-anti* proton exchange on the NMR time scale, whereupon the less substituted terminal carbon of the allylic moiety invariably linked with the metal atom. These results are also in accord with the present case to give **6** but not the central-carbon-bonded etac complexes as follows:

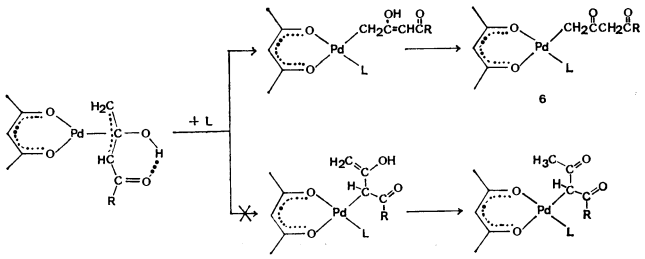

However, similar palladium(II) complexes, **3**, containing the central-carbon-bonded etac ligand have been prepared so far by the reactions of bis-*O,O'*-chelate, **1**, with L (L=a variety of nitrogen bases).[1]

Experimental

Preparation of Complexes **5**. The starting dinuclear η^3 complex, $[PdCl(\eta^3\text{-etac})]_2$ (**2**) was prepared according to the Yanase's modification[9] of the method originally proposed by Tezuka.[2a]

[Pd(acac)(η³-etac)] (**5a**): Complex **2** (225 mg, 0.415 mmol) was dissolved in benzene (30 cm^3) on heating and then the solution was cooled to room temperature. Thallium(I) 2,4-pentanedionate (277 mg, 0.913 mmol) was added to the solution and the mixture was stirred for 2 h at room temperature. After standing for further 2—3 h, the mixture was filtered to remove thallium(I) chloride precipitated

and the filtrate was concentrated to 5 cm³ under reduced pressure. On addition of hexane, a crude decomposition product was deposited and again removed by filtration. The filtrate was evaporated to dryness to obtain a yellow solid (214 mg) in a 71% yield.

The crude substance shows no IR band at 3200 cm^{-1}, which is assigned to the ν(OH) vibration of the η^3-carbon-bonded etac, but instead shows a new strong IR absorption at 1620 cm^{-1}. The substance has not been further characterized because of its poor solubility in most organic solvents.

[Pd(tfac)(η³-etac)] (5b): Thallium(I) 1,1,1-trifluoro-2,4-pentanedionate (326 mg, 0.913 mmol) was added to a suspension of **2** (225 mg, 0.415 mmol) in acetone (20 cm³). After being stirred for 30 min at room temperature, the mixture was allowed to stand for further 2—3 h to precipitate thallium(I) chloride, which was filtered and the filtrate was then concentrated to 2—3 cm³ under reduced pressure. On addition of hexane to the concentrate, a pale yellow solid (246 mg) was obtained in a 76% yield.

[Pd(hfac)(η³-etac)] (5c): To a suspension of **2** (225 mg, 0.415 mmol) in acetone (20 cm³) was added thallium(I) 1,1,1,5,5,5-hexafluoro-2,4-pentanedionate (376 mg, 0.913 mmol). After being stirred for 30 min at room temperature, the mixture was allowed to stand for additional 2—3 h and then filtered to give a transparent solution, which was evaporated to dryness under reduced pressure. The residue was redissolved in hexane and filtered again to remove a small amount of insoluble substance. The filtrate was evaporated to dryness under reduced pressure, affording a pale yellow solid (302 mg) in an 82% yield.

Reactions of [Pd(β-dik)(η³-etac)] (5) with Lewis Bases. 5a with Triphenylphosphine: Triphenylphosphine (156 mg, 0.598 mmol) was added to a benzene (15 cm³) solution of **5a** (200 mg, 0.598 mmol) and the mixture was stirred for 20 min at room temperature. The solvent was then evaporated to 2—3 cm³ under reduced pressure before adding hexane to deposit a yellow powder of [Pd(acac)(etac-C^4)(PPh_3)] (**6a**). Scratching the flask was necessary to deposit **6a** effectively. Recrystallization from benzene–hexane gave a yellow crystalline solid (303 mg) in an 85% yield.

5b with Triphenylphosphine: Complex **5b** (100 mg, 0.257 mmol) was also allowed to react with triphenylphosphine (68 mg, 0.26 mmol) in benzene (10 cm³) at room temperature. After being stirred for 30 min, the solution was concentrated to 2—3 cm³ under reduced pressure and hexane was added to the concentrate. A yellow crystalline solid of [Pd(tfac)(etac-C^4)(PPh_3)] (**6b**), deposited from the solution on standing at room temperature. The yield was 139 mg (81%).

5c with Triphenylphosphine: Chloroform (10 cm³) was used as a solvent for the reaction of **5c** (100 mg, 0.226 mmol) with triphenylphosphine (59 mg, 0.23 mmol). When the reaction mixture was stirred for 20 min at room temperature and then concentrated under reduced pressure, an oily substance was obtained, which was extracted with petroleum ether and the extract was left at −20 °C to give an orange crystalline solid of [Pd(hfac)(etac-C^4)(PPh_3)] (**6c**). The yield was 76 mg (48%).

5a with Diethylamine: Diethylamine (0.07 cm³, 0.677 mmol) was added to a benzene (15 cm³) solution of **5a** (200 mg, 0.598 mmol) and the mixture was stirred for 1 h at room temperature before the solvent was evaporated to 2—3 cm³ under reduced pressure. A pale yellow powder of [Pd(acac)(etac-C^4)(Et_2NH)] (**6d**), was deposited by scratching the flask after the addition of hexane. Recrystallization from benzene–hexane gave a crystalline solid in a 53% yield (132 mg).

5b with Propylamine: Propylamine (0.03 cm³, 0.364 mmol) was added to a benzene (10 cm³) solution of **5b** (140 mg, 0.360 mmol) and the mixture was stirred for 20 min at room temperature. Evaporation of the solvent under reduced pressure left an oily residue, which was extracted with hexane. A yellow powder of [Pd(tfac)(etac-C^4)(*n*-$PrNH_2$)] (**6e**), precipitated from the extract on standing overnight at −20 °C. The yield was 103 mg (60%).

5c with Benzylamine: A three times molar amount of benzylamine (0.10 cm³, 0.914 mmol) was allowed to react with **5c** (130 mg, 0.294 mg) in benzene (10 cm³) for 30 min with stirring at room temperature. Evaporation of the solvent under reduced pressure left an oily substance. The substance was redissolved in a small amount of acetone, hexane was added to the solution, and then the solution was kept for a week at −20 °C, from which a pale yellow powder of [Pd(etac-C^4)($PhCH_2NH_2$)$_3$](hfac) (**7**), was precipitated. The yield was 130 mg (59%). Even when an equimolar amount of benzylamine was used, the same complex **7** was produced in a low yield.

Measurements. Infrared spectra were obtained in Nujol mull with a JASCO DS 701G infrared spectrophotometer. NMR spectra were recorded on JNM-MH100 (in the case of ^1H) and FX60Q (for ^{13}C) instruments. Molecular weight was determined in dichloromethane at 28 °C with a vapor pressure osmometer manufactured by Knauer, West Berlin, West Germany.

References

1) S. Okeya and S. Kawaguchi, *Inorg. Chem.*, **16**, 1730 (1977).

2) a) Y. Tezuka, T. Ogura, and S. Kawaguchi, *Bull. Chem. Soc. Jpn.*, **42**, 443 (1969); b) K. Oda, N. Yasuoka, T. Ueki, N. Kasai, and M. Kakudo, *ibid.*, **43**, 362 (1970).

3) a) S. Baba, T. Sobata, T. Ogura, and S. Kawaguchi, *Bull. Chem. Soc. Jpn.*, **47**, 2792 (1974); b) M. Horike, Y. Kai, N. Yasuoka, and N. Kasai, *J. Organomet. Chem.*, **86**, 269 (1975).

4) For *O,O'*-chelation: S. Okeya, S. Ooi, K. Matsumoto, Y. Nakamura, and S. Kawaguchi, *Bull. Chem. Soc. Jpn.*, **54**, 1085 (1981).

5) For η^3 carbon bonding and terminal carbon bonding: a) Z. Kanda, Y. Nakamura, and S. Kawaguchi, *Inorg. Chem.*, **17**, 910 (1978); b) S. Okeya, Y. Nakamura, S. Kawaguchi, and T. Hinomoto, *Bull. Chem. Soc. Jpn.*, **55**, 477 (1982).

6) For central carbon bonding: a) S. Baba, T. Ogura, and S. Kawaguchi, *Bull. Chem. Soc. Jpn.*, **47**, 665 (1974); b) M. Horike, Y. Kai, N. Yasuoka, and N. Kasai, *J. Organomet. Chem.*, **72**, 441 (1974); c) T. Ito, T. Kiriyama, and A. Yamamoto, *Bull. Chem. Soc. Jpn.*, **49**, 3250 (1976); d) T. Ito, T. Kiriyama, Y. Nakamura, and A. Yamamoto, *ibid.*, **49**, 3257 (1976).

7) For *O*-unidentate bonding: a) T. Ito, T. Kiriyama, and A Yamamoto, *Chem. Lett.*, **1976**, 835; b) S. Okeya, F. Egawa, Y. Nakamura, and S. Kawaguchi, *Inorg. Chim. Acta*, **30**, L319 (1978); c) S. Ooi, T. Matsushita, K. Nishimoto, Y. Nakamura, and S. Kawaguchi, *Inorg. Chim. Acta*, in press.

8) a) S. Okeya, H. Sazaki, M. Ogita, T. Takemoto, Y. Onuki, Y. Nakamura, B. K. Mohapatra, and S. Kawaguchi, *Bull. Chem. Soc. Jpn.*, **54**, 1978 (1981); b) S. Okeya, Y. Nakamura, and S. Kawaguchi, *ibid.*, **54**, 3396 (1981); c) S. Okeya, Y. Nakamura, and S. Kawaguchi, *ibid.*, **55**, 1460 (1982).

9) N. Yanase, Y. Nakamura, and S. Kawaguchi, *Inorg. Chem.*, **19**, 1575 (1980).

10) G. K. Anderson and R. J. Cross, *Chem. Soc. Rev.*, **9**, 185 (1980).
11) S. Okeya, Y. Kawakita, S. Matsumoto, Y. Nakamura, S. Kawaguchi, N. Kanehisa, K. Miki, and N. Kasai, *Bull. Chem. Soc. Jpn.*, **55**, 2134 (1982).
12) S. Okeya, Y. Nakamura, S. Kawaguchi, and T. Hinomoto, *Inorg. Chem.*, **20**, 1576 (1981).
13) H. Tanaka, K. Isobe, and S. Kawaguchi, *Chem. Lett.*, **1981**, 769.
14) Y. Nakamura, 32nd Symposium on Coordination Chemistry, Nagasaki, October 1982, Abstr. No. 2C03.
15) R. P. Hughes and J. Powell, *J. Organomet. Chem.*, **60**, 387 (1973).
16) R. P. Hughes and J. Powell, *J. Organomet. Chem.*, **60**, 409 (1973).
17) R. P. Hughes and J. Powell, *J. Am. Chem. Soc.*, **94**, 7723 (1972).

Solvent Effects on the Extraction of Gallium(III) with Decanoic Acid

Hiromichi YAMADA,* Shozo IMAI, and Eiichi TAKEUCHI
Faculty of Engineering, Gifu University, 1-1, Yanagido, Gifu 501-11

(Received November 5, 1982)

Extraction of gallium(III) with decanoic acid (HA) in several solvents was carried out at 25 °C and at an aqueous ionic strength of 0.1 mol/dm³($NaClO_4$). Organic solvents used are toluene, chlorobenzene, 1,2-dichloroethane, and 1-octanol. Extracted species differs from solvent to solvent: $Ga_6A_{18}(H_2O)_w$ for toluene, Ga_3A_9 for chlorobenzene, GaA_3 and Ga_3A_9 for 1,2-dichloroethane and $GaA_2(OH)$, $Ga_2A_4(OH)_2$ and Ga_2A_6 for 1-octanol. The less polar the solvent, the more extensive is the polymerization of the extracted species.

Polymeric metal carboxylates are known to be extracted into the organic phase with carboxylic acids. In particular, aluminium(III),[1] gallium(III),[2] indium(III),[3] and scandium(III)[4] are characterized to be extracted into benzene as hexameric species.

In the previous paper,[5] it has been shown that copper(II) is extracted with decanoic acid in various inert solvents as dimeric copper(II) decanoate, $Cu_2A_4(HA)_2$, and that the solvent effect on the extraction constants was interpreted in terms of the regular solution theory.

The present paper describes the results on the extraction of gallium(III) with decanoic acid in several organic solvents. The more polar the solvent, the less polymerized are the extracted decanoates.

Experimental

Reagents. *Gallium(III) Perchlorate Solution*: Metallic gallium (99.99%) was dissolved in a small excess of concentrated perchloric acid. The solution was diluted as required and standardized complexiметrically with the Cu–EDTA–TAR system as an indicator.[6] 8-Quinolinol was used for the determination of lower concentration of gallium in the organic phase.

Sodium Perchlorate: The reagent grade sodium perchlorate was recrystallized from distilled water after removal of the impurities (heavy metal ions) as hydroxides at pH≃8.

Decanoic Acid: Chemically pure grade decanoic acid was purified by distillation.

Solvents: Toluene and chlorobenzene of reagent grade were washed successively with concentrated sulfuric acid, with dilute sodium hydroxide solution and then with distilled water. Reagent grade 1,2-dichloroethane was washed with dilute potassium hydroxide solution and then with distilled water. Reagent grade 1-octanol was washed successively with dilute potassium hydroxide solution, with dilute perchloric acid solution and with distilled water.

All other reagents were reagent grade and used as purchased.

Procedure. Partition was carried out in a thermostat at 25±0.2 °C using a 50 cm³ centrifuge tube in which 15 cm³ each of the aqueous and organic phases were contacted. Shaking for overnight was found sufficient for complete equilibration in each solvent system used. Ionic strength in the aqueous phase was adjusted to 0.1 mol/dm³ with sodium perchlorate. Total concentration of gallium was 5×10^{-3} mol/dm³. Hydrogen ion concentration in the aqueous phase was measured without any phase separation with 1.00×10^{-2} mol/dm³ perchloric acid solution (ionic strength 0.1 mol/dm³) as a standard. Then the measured pH values were corrected for the apparent liquid junction potential.[3]

Apparatus. For mechanical shaking in a thermostat, TAIYO incubator, M-1 (Taiyokagaku-Kogyo Co., Tokyo) was used. The pH measurements were carried out with a Beckman research pH Meter Model 101900 (Beckman Instruments, Inc., Fullerton, California, U.S.A.) and Orion research microprocessor Ionalyzer 901 (Orion Research Inc., U.S.A.). The temperature of a sample solution was kept constant in a Coolnics Circulator Model CTE-1B (Komatsu Solidate Co., Komatsu, Japan). Colorimetric determination of gallium in the organic phase was carried out on a Shimadzu double-beam type UV-210A spectrophotometer (Shimadzu Seisakusho Ltd., Kyoto, Japan).

Results and Discussion

When a j-merized gallium(III) decanoate of the composition $Ga_jA_aH_h$ ($3j=a-h$) is responsible for the extraction of gallium ion with decanoic acid, the extraction equilibria for toluene, chlorobenzene and 1,2-dichloroethane are written as:

$$jGa^{3+} + \frac{a}{2}(HA)_{2,o} \overset{K_{ex(jah)}}{\rightleftharpoons} (Ga_jA_aH_h)_o + 3jH^+$$

$$\text{with} \quad K_{ex(jah)} = \frac{[Ga_jA_aH_h]_o[H^+]^{3j}}{[Ga^{3+}]^j[(HA)_2]_o^{a/2}}, \tag{1}$$

where the subscript o refers to the organic phase and $(HA)_{2,o}$ denotes the dimeric decanoic acid in the organic phase.

On the other hand, the dimerization of decanoic acid does not occur to any appreciable extent in 1-octanol. The extraction equilibrium for 1-octanol is then expressed as follows:

$$jGa^{3+} + a(HA)_o \overset{K_{ex(jah)}}{\rightleftharpoons} (Ga_jA_aH_h)_o + 3jH^+$$

with the extraction constant:

$$K_{ex(jah)} = \frac{[Ga_jA_aH_h]_o[H^+]^{3j}}{[Ga^{3+}]^j[HA]_o^a}. \tag{2}$$

Total concentration of gallium in the organic phase, $C_{Ga,o}$ is given by the following equations corresponding to Eqs. 1 and 2, respectively:

$$C_{Ga,o} = \sum_j\sum_a j[Ga_jA_aH_h]_o$$

$$= \sum_j\sum_a jK_{ex(jah)}([Ga^{3+}][H^+]^{-3})^j[(HA)_2]_o^{a/2} \tag{3}$$

and

$$C_{Ga,o} = \sum_j\sum_a jK_{ex(jah)}([Ga^{3+}][H^+]^{-3})^j[HA]_o^a. \tag{4}$$

Under the present experimental conditions, the hydrolysis and complexation of gallium ion not being appreciable in the aqueous phase, the total concentration of gallium in the aqueous phase, $C_{Ga,w}$ may be regarded as $[Ga^{3+}]$.

Suppose that only $Ga_jA_aH_h$ is responsible for the

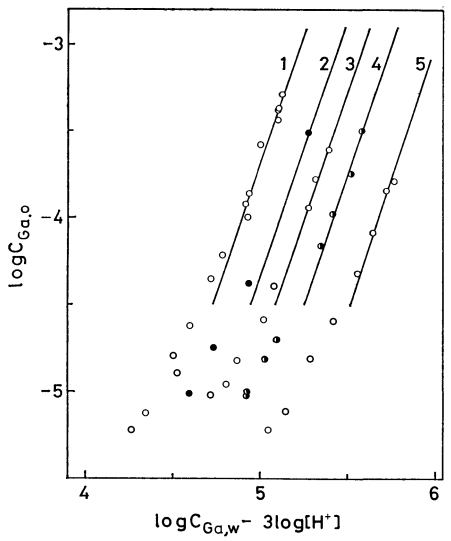

Fig. 1. Determination of the degree of polymerization of Ga(III) decanoate in 1,2-dichloroethane.
Solid lines are the straight lines with a slope of 3.0. C_{HA}; No. 1: 2.0, No. 2: 1.5, No. 3: 1.25, No. 4: 1.0, No. 5: 0.7 mol/dm^3.

extraction. Equations 5 and 6 can then be derived from Eqs. 3 and 4, respectively:

$$C_{Ga,o} = jK_{ex(jah)}(C_{Ga,w}[H^+]^{-3})^j[(HA)_2]_o^{a/2} \quad (5)$$

and

$$C_{Ga,o} = jK_{ex(jah)}(C_{Ga,w}[H^+]^{-3})^j[HA]_o^a \quad (6)$$

which are rewritten as a logarithmic form:

$$\log C_{Ga,o} = j(\log C_{Ga,w} - 3\log[H^+]) + \frac{a}{2}\log[(HA)_2]_o + \log j + \log K_{ex(jah)} \quad (7)$$

and

$$\log C_{Ga,o} = j(\log C_{Ga,w} - 3\log[H^+]) + a\log[HA]_o + \log j + \log K_{ex(jah)}. \quad (8)$$

These expressions provide a basis for the determination of the degree of polymerization of Ga(III) decanoates and the number of decanoic acid molecules involved in the extracted species. The degree of polymerization of the extracted species can be determined from the slope of the plot of $\log C_{Ga,o}$ against $(\log C_{Ga,w} - 3\log[H^+])$ at constant $[(HA)_2]_o$ (or $[HA]_o$ in the case of 1-octanol). The plot for toluene fitting well the straight line with a slope of six, the hexameric Ga(III) decanoate is extracted into toluene. And in the lower concentration of gallium in the organic phase the plot deviates slightly upward from the straight line with a slope of 6.0. This suggests that there would be at least another extracted species less polymerized than the main hexameric species. The plot for chlorobenzene fitting well the straight line with a slope of 3.0, the trimeric Ga(III) decanoate is responsible for the extraction. In the case of 1,2-dichloroethane, as evident from Fig. 1, the degree of polymerization of extracted species depends on the concentration of gallium in the organic phase. The plot deviates upward from the straight line with a slope of three with decreasing concentration of gallium in the 1,2-dichloroethane phase. Therefore, another extracted species less polymerized than 3.0 is responsible for the extraction together with the main trimeric species. If the other extracted species is $Ga_{j'}A_{a'}H_{h'}$, the concentration of gallium in the organic phase is written as follows:

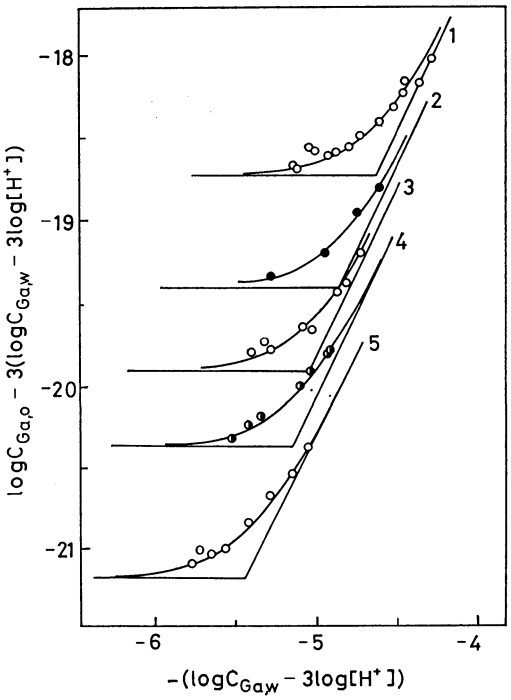

Fig. 2. Determination of the degree of polymerization of Ga(III) decanoate in 1,2-dichloroethane by the curve fitting method.
Solid curves are the normalized curves, $\log(1+X^2)$ *vs.* $\log X$. Solid lines are the asymptotes of the normalized curves. Numbers are the same as in Fig. 1.

$$C_{Ga,o} = 3[Ga_3A_aH_h]_0 + j'[Ga_{j'}A_{a'}H_{h'}]_o, \quad (9)$$

where $j'<3$. And we have the following expression from Eq. 9:

$$\frac{C_{Ga,o}}{(C_{Ga,w}[H^+]^{-3})^3} = 3K_{ex(3ah)}[(HA)_2]_o^{a/2} \times \left\{1 + \frac{j'K_{ex(j'a'h')}}{3K_{ex(3ah)}}[(HA)_2]_o^{(a'-a)/2} \times (C_{Ga,w}[H^+]^{-3})^{(j'-3)}\right\}, \quad (10)$$

where $K_{ex(3ah)}$ and $K_{ex(j'a'h')}$ represent the extraction constants of the trimer, $Ga_3A_aH_h$ and j'-mer, $Ga_{j'}A_{a'}H_{h'}$, respectively. According to Eq. 10, comparing the plot of $\{\log C_{Ga,o} - 3(\log C_{Ga,w} - 3\log[H^+])\}$ against $-(\log C_{Ga,w} - 3\log[H^+])$ at constant $[(HA)_2]_o$ with the normalized curves, $\log(1+X^n)$ *vs.* $\log X$, we find the degree of polymerization of the other extracted species, $Ga_{j'}A_{a'}H_{h'}$. The results are shown in Fig. 2. The plot fits well the normalized curve with $n=2$, that is, $-(j'-3)=2$ or $j'=1$.

Figure 3 depicts the results for 1-octanol. As shown in Fig. 3, the slope of the plot according to Eq. 8 is close to two at higher concentration of gallium in the organic phase. The plot, however, deviates grad-

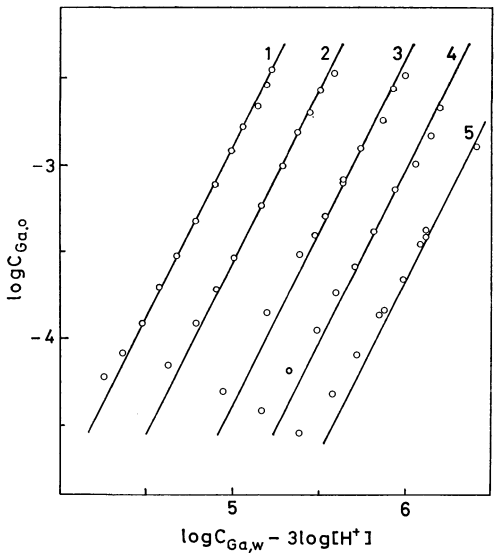

Fig. 3. Determination of the degree of polymerization of Ga(III) decanoate in 1-octanol.
Solid lines are the straight lines with a slope of 2.0. C_{HA}; No. 1: 2.0, No. 2: 1.5, No. 3: 1.0, No. 4: 0.7, No. 5: 0.5 mol/dm^3.

ually upward from the straight line with a slope of two with decreasing gallium concentration in the organic phase. Therefore, the monomer and dimer may be involved in the extraction for 1-octanol. Now suppose a monomer GaA_aH_h and a dimer $Ga_2A_{a'}H_{h'}$ are responsible for the extraction, the following expression can be derived from Eq. 4:

$$\log C_{Ga,o} - (\log C_{Ga,w} - 3\log[H^+]) = \log K_{ex(1ah)} + a\log[HA]_o$$
$$\log\left\{1+\frac{2K_{ex(2a'h')}}{K_{ex(1ah)}}[HA]_o^{(a'-a)}C_{Ga,w}[H^+]\right\}, \quad (11)$$

where $K_{ex(1ah)}$ and $K_{ex(2a'h')}$ represent the extraction constants of the monomer GaA_aH_h and the dimer $Ga_2A_{a'}H_{h'}$, respectively. According to Eq. 11, fitting the plot of $\{\log C_{Ga,o} - (\log C_{Ga,w} - 3\log[H^+])\}$ against $(\log C_{Ga,w} - 3\log[H^+])$ at constant $[HA]_o$ with the normalized curve, $\log(1+X)$ *vs.* $\log X$, we can confirm the degree of polymerization of the extracted species. The results are depicted in Fig. 4. The obtained curves fitting well the normalized curve, $\log(1+X)$ *vs.* $\log X$, the monomeric and dimeric gallium decanoates are involved in the extraction in 1-octanol.

Thus, the degree of polymerization of the extracted species is determined as follows: Hexamer for toluene, trimer for chlorobenzene, monomer and trimer for 1,2-dichloroethane and monomer and dimer for 1-octanol.

Subsequently, the number of decanoic acid molecules involved in the extracted species was determined. In the region where the j-mer prevails, the following equation is derived from Eq. 3:

$$\frac{1}{j}\log C_{Ga,o} - (\log C_{Ga,w} - 3\log[H^+]) = \frac{1}{j}\log\sum_a (K_{ex(jah)}[(HA)_2]_o^{a/2}) + \frac{1}{j}\log j. \quad (12)$$

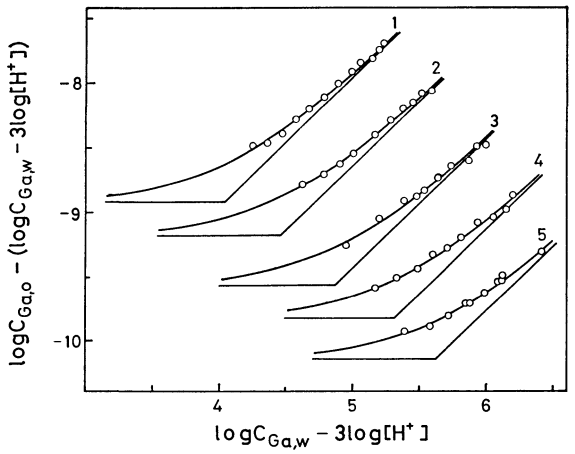

Fig. 4. Determination of the degree of polymerization of Ga(III) decanoate in 1-octanol by the curve fitting method.
Solid curves are the normalized curves, $\log(1+X)$ *vs.* $\log X$. Solid lines are the asymptotes of the normalized curves. Numbers are the same as in Fig. 3.

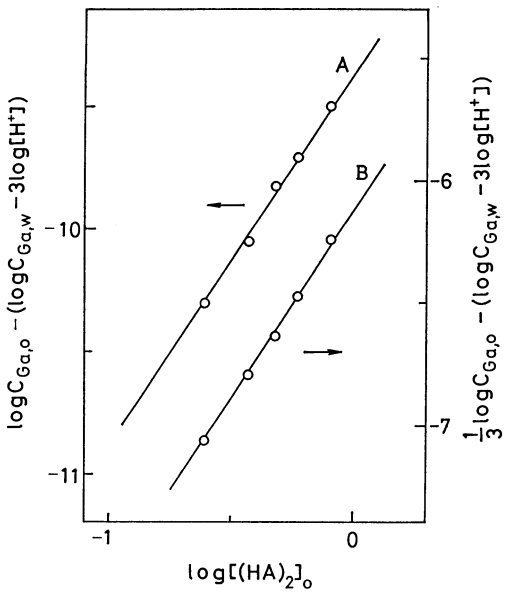

Fig. 5. Determination of the number of decanoic acid involved in Ga(III) decanoates in 1,2-dichloroethane. Solid lines are the straight lines with a slope of 1.5. A: Monomeric Ga(III) decanoate. B: Trimeric Ga(III) decanoate.

This is corresponding to toluene, chlorobenzene and 1,2-dichloroethane. On the basis of Eq. 12, the total number of decanoic acid molecules involved in the j-mer can be determined from the slope of the plot of $\{(1/j)\log C_{Ga,o} - (\log C_{Ga,w} - 3\log[H^+])\}$ against $\log[(HA)_2]_o$. Both plots for toluene and chlorobenzene fit the straight line with a slope of 1.5, that is, $a=18$ and $a=9$, respectively. In addition, by the coulometric titration using the Karl-Fischer reagent, it was proved that more than one water molecule per atom of gallium was involved in the hexameric Ga(III) decanoate in the toluene phase. Consequently, we conclude that the extracted species involved in the

TABLE 1. EXTRACTED SPECIES AND EXTRACTION CONSTANTS

Solvent	ε[a)]	δ[b)]	Extracted species	Extraction constants $\log K_{ex(jah)}$
Benzene[2)]	2.3	9.15	$Ga_6A_{12}(OH)_6$	-35.8 ± 0.1
			$Ga_6A_{18}(H_2O)_6$	-34.3 ± 0.1
			$Ga_jA_aH_h$:($j<6$)	
Toluene	2.4	8.9	$Ga_6A_{18}(H_2O)_w$:($w>6$)	-33.21 ± 0.05
			$Ga_jA_aH_h$:($j<6$)	
Chlorobenzene	5.5	9.5	Ga_3A_9	-19.14 ± 0.03
1,2-Dichloroethane	10.4	9.9	GaA_3	-9.42 ± 0.03
			Ga_3A_9	$-18.9\ \pm0.1$
1-Octanol	10.3	10.3	$GaA_2(OH)$	-9.54 ± 0.02
			$Ga_2A_4(OH)_2$	-14.92 ± 0.02
			Ga_2A_6	-15.26 ± 0.02

a) Dielectric constant. b) Solubility parameter.

toluene phase are $Ga_6A_{18}(H_2O)_w(w>6)$ and $Ga_jA_aH_h$ ($j<6$). While, only Ga_3A_9 is extracted into the chlorobenzene phase. Figure 5 shows the number of decanoic acid involved in the monomeric and trimeric Ga(III) decanoates which are extracted into the 1,2-dichloroethane solution. The straight lines with a slope of 1.5 are obtained in both the monomer and trimer, that is, $a/2=1.5$ and $a/6=1.5$, respectively. Thus, the monomer GaA_3 and trimer Ga_3A_9 are responsible for the extraction with decanoic acid in 1,2-dichloroethane.

And further, from the intercepts of the plots of the left hand side of Eq. 12 against $\log[(HA)_2]_o$, we can determine the extraction constants for each extracted species. The results obtained for each extracted species are summarized in Table 1.

On the other hand, for 1-octanol the following relation is set up in place of Eq. 12:

$$\frac{1}{j}\log C_{Ga,o} - (\log C_{Ga,w} - 3\log[H^+]) = \frac{1}{j}\log\sum_a (K_{ex(jah)}[HA]_o^a) + \frac{1}{j}\log j. \quad (13)$$

The plot of the left hand side of Eq. 13 against $\log[HA]_o$ (Fig. 6) illustrates the number of decanoic acid molecules involved in the monomer and dimer which are extracted into 1-octanol. As evident from Fig. 6, the number of molecules of decanoic acid involved in the monomer is equal to 2 and then h is equal to -1. Therefore, from the electroneutrality of the extracted species, one hydroxide ion should be involved in the extracted monomer, since no perchlorate ion was found in the extracted species. The extraction constant $K_{ex(12-1)}$ for $GaA_2(OH)$ was determined from the intercept of the plot in Fig. 6. Decanoic acid molecules involved in the dimer depends on the concentration of decanoic acid in the organic phase. At lower concentration of decanoic acid in the organic phase, the plot falls on the straight line with a slope of 4.0, that is, $a=4$, and then $h=-2$. In analogy with the monomer described above, two hydroxide ions should be involved in the dimeric extracted species. But at higher concentration of $[HA]_o$, the slope tends to be steeper. This result suggests the presence of another dimeric species in which is involved more than four

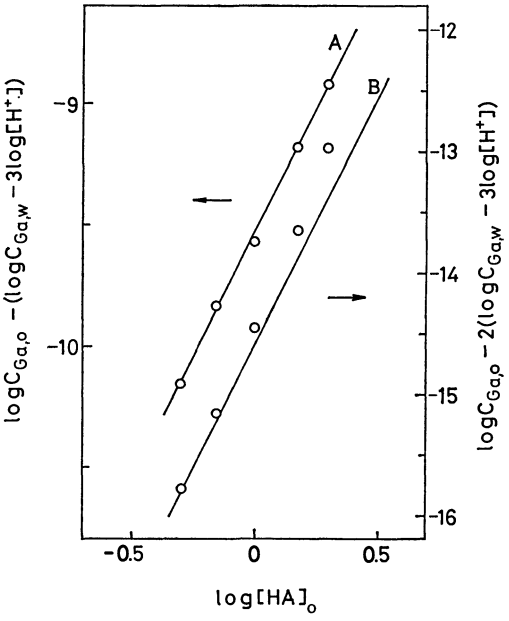

Fig. 6. Determination of the number of decanoic acid involved in Ga(III) decanoates in 1-octanol. Solid lines, A and B are the straight lines with a slope of 2.0 and 4.0, respectively. A: Monomeric Ga(III) decanoate. B: Dimeric Ga(III) decanoate.

decanoic acid molecules. Now, suppose the two dimeric species $Ga_2A_4(OH)_2$ and $Ga_2A_aH_h(a>4)$ are both responsible for the extraction. In this case, the total concentration of gallium in the organic phase can be expressed as follows:

$$C_{Ga,o} = 2[Ga_2A_4(OH)_2]_o + 2[Ga_2A_aH_h]_o. \quad (14)$$

And with the aid of the extraction constants $K_{ex(24-2)}$ and $K_{ex(2ah)}$, Eq. 14 can be rewritten as:

$$\log C_{Ga,o} - 2(\log C_{Ga,w} - 3\log[H^+]) - 4\log[HA]_o = \log\left\{1+\frac{K_{ex(2ah)}}{K_{ex(24-2)}}[HA]_o^{(a-4)}\right\} + \log 2 + \log K_{ex(24-2)}. \quad (15)$$

Then the values of $\{\log C_{Ga,o} - 2(\log C_{Ga,w} - 3\log[H^+]) - 4\log[HA]_o\}$ are plotted against $\log[HA]_o$. According to the curve-fitting method, in which the plot is compared with the normalized curves, $\log(1+X^n)$

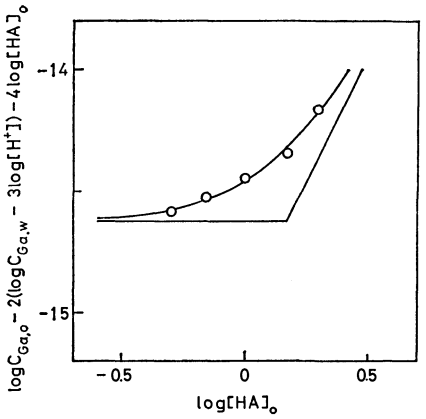

Fig. 7. Determination of the number of decanoic acid involved in dimeric Ga(III) decanoates in 1-octanol by the curve fitting method.
Solid curve is the normalized curve, $\log(1+X^2)$ *vs.* $\log X$. Solid lines are the asymptotes of the normalized curve.

vs. $\log X$, the number of decanoic acid molecules in another dimeric species can be determined together with the extraction constants of the two dimeric Ga(III) decanoates. The results are shown in Fig. 7. As shown in Fig. 7, the plot fits well with the normalized curve, $\log(1+X^2)$ *vs.* $\log X$, that is, $n=a-4=2$, or $a=6$. The extraction constants $K_{ex(24-2)}$ and $K_{ex(260)}$ determined by the curve-fitting method are given in Table 1. Consequently, $GaA_2(OH)$, $Ga_2A_4(OH)_2$, and Ga_2A_6 are extracted in the 1-octanol phase.

Then, the extraction equilibria for different solvents are described as follows:
toluene:

$$6Ga^{3+} + 9(HA)_{2,o} + wH_2O \overset{K_{ex(6180)}}{\rightleftharpoons} (Ga_6A_{18}(H_2O)_w)_o + 18H^+$$

chlorobenzene:

$$3Ga^{3+} + \frac{9}{2}(HA)_{2,o} \overset{K_{ex(390)}}{\rightleftharpoons} (Ga_3A_9)_o + 9H^+$$

1,2-dichloroethane:

$$Ga^{3+} + \frac{3}{2}(HA)_{2,o} \overset{K_{ex(130)}}{\rightleftharpoons} (GaA_3)_o + 3H^+$$

$$3Ga^{3+} + \frac{9}{2}(HA)_{2,o} \overset{K_{ex(390)}}{\rightleftharpoons} (Ga_3A_9)_o + 9H^+$$

1-octanol:

$$Ga^{3+} + 2(HA)_o + H_2O \overset{K_{ex(12-1)}}{\rightleftharpoons} (GaA_2(OH))_o + 3H^+$$

$$2Ga^{3+} + 4(HA)_o + 2H_2O \overset{K_{ex(24-2)}}{\rightleftharpoons} (Ga_2A_4(OH)_2)_o + 6H^+$$

$$2Ga^{3+} + 6(HA)_o \overset{K_{ex(260)}}{\rightleftharpoons} (Ga_2A_6)_o + 6H^+.$$

In the 1,2-dichloroethane and 1-octanol phases, the trimerization and dimerization of Ga(III) decanoates are written as follows, respectively:
1,2-dichloroethane phase:

$$3GaA_3 \overset{K_{trim}}{\rightleftharpoons} Ga_3A_9$$

1-octanol phase:

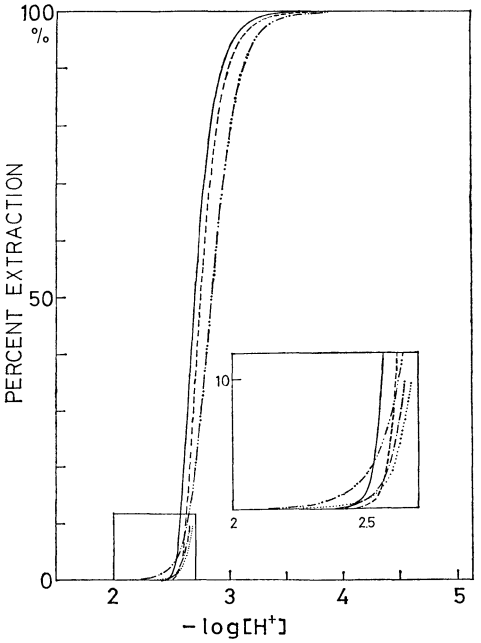

Fig. 8. The calculated extraction curves based on the results obtained in this study.
——: Toluene, ---: benzene, —·—: 1-octanol, ···: 1,2-dichloroethane, —·—: chlorobenzene. $C_{Ga,tot}=5\times10^{-3}$ mol/dm^3, $C_{HA}=1.0$ mol/dm^3.

$$2GA_2(OH) \overset{K_{dim-1}}{\rightleftharpoons} Ga_2A_4(OH)_2.$$

$$2GaA_2(OH) + 2HA \overset{K_{dim-2}}{\rightleftharpoons} Ga_2A_6 + 2H_2O$$

with the following trimerization and dimerization constants calculated from the respective extraction constants: $\log K_{trim}=9.4\pm0.2$, $\log K_{dim-1}=4.16\pm0.06$ and $\log K_{dim-2}=3.82\pm0.06$ (where the deviation of each polymerization constant originates in the uncertainties in the respective extraction constants).

Figure 8 shows the calculated extraction curves based on the results obtained in this investigation. The extracted species and the extraction constants are summarized in Table 1 together with the dielectric constants and the solubility parameters of solvents. The uncertainties in the respective extraction constants represent the probable deviations of the experimental data from the best fit curve or straight line. The previous results for benzene are also included in Fig. 8 and Table 1 for comparison.

The extraction of Ga(III) differs from that of copper(II): We observe the same extracted species with the similar extraction constant for the extraction of copper(II) decanoate in different inert solvents(hexane, cyclohexane, carbon tetrachloride, toluene, benzene, chlorobenzene and 1,2-dichloroethane).[5] The main extracted species are the hexameric Ga(III) decanoate for benzene and toluene, the trimer for chlorobenzene and the monomer and trimer for 1,2-dichloroethane, respectively. The less polar the solvent, the more extensive is the polymerization of the extracted species. In chlorobenzene and 1,2-dichloroethane the emulsion was observed in the region where the percent extraction of gallium exceeds 10%. This low extractability of gallium in these nonsolvating polar solvents

results from the formation of some hydrated less polymerized species.

As was expected from the similarity of the physical properties of the two solvents, the same hexameric species with the similar extraction constant is extracted for both benzene and toluene, and the same trimer with the similar extraction constant is found for both chlorobenzene and 1,2-dichloroethane.

On the other hand, it was found that the quite different species from those in nonsolvating solvents were extracted into 1-octanol. As we have already reported, also in the extraction of copper(II) there was a remarkable difference in the extracted species between 1-octanol[7] and nonsolvating solvents.[5] Though the less polymerized species are responsible for the extraction of gallium(III) with decanoic acid in 1-octanol, no emulsion appeared, which was the feature different from chlorobenzene and 1,2-dichloroethane. Then, the formation of some solvated, less polymerized species would contribute to a good extractability. Therefore, it can be assumed that Ga(III) decanoate in 1-octanol is polymerized through a mechanism different from that in nonsolvating solvents such as benzene and toluene *etc.*

Consequently, the results obtained in this paper suggest that the solvent used plays an important part in the extraction of metals with carboxylic acids.

The authors wish to thank Professor Motoharu Tanaka of Nagoya University for his valuable discussions and Dr. Yukio Fujii of Gifu University for his interest in this work. The present work was partially supported by Grant-in-Aid for Scientific Research (No. 57540326) from the Ministry of Education, Science and Culture.

References

1) M. Tanaka, N. Nakasuka, and H. Yamada, *J. Inorg. Nucl. Chem.*, **32**, 2791 (1970).
2) H. Yamada and M. Tanaka, *J. Inorg. Nucl. Chem.*, **35**, 3307 (1973).
3) M. Tanaka, N. Nakasuka, and H. Yamada, *J. Inorg. Nucl. Chem.*, **32**, 2759 (1970).
4) H. Yamada, K. Tanaka, and M. Tanaka, *J. Inorg. Nucl. Chem.*, **37**, 2016 (1975).
5) H. Yamada and M. Tanaka, *J. Inorg. Nucl. Chem.*, **38**, 1501 (1976).
6) H. Yamada, I. Kojima, and M. Tanaka, *Anal. Chim. Acta*, **52**, 35 (1970).
7) H. Yamada, S. Suzuki, and M. Tanaka, *J. Inorg. Nucl. Chem.*, **43**, 1873 (1981).

 © 1983 The Chemical Society of Japan Bull. Chem. Soc. Jpn., 56, 1407—1409 (1983)

Inversion of the Retention Volume Order of Enantiomers Caused by the Concentration of Eluent[1)]

Ushio SAKAGUCHI, Ippei YAMAMOTO, Shinji IZUMOTO, and Hayami YONEDA*

Department of Chemistry, Faculty of Science, Hiroshima University, Hiroshima 730

(Received November 12, 1982)

The retention volumes of enantiomers of several complex anions on the IEX 220 anion-exchange resin, when eluted by an aqueous solution of Δ-$[Co(en)_3]^{3+}$, Δ-$[Co(sep)]^{3+}$, or Δ-$[Co(l\text{-chxn})_3]^{3+}$, have been measured as a function of the eluent concentration, where en=ethylenediamine, sep=1,3,6,8,10,13,16,19-octaazabicyclo-[6.6.6]eicosane, and *l*-chxn=(−)-*trans*-1,2-cyclohexanediamine. The order of retention volumes of enantiomers of some complex anions has been found to be inverted by the concentration of the eluents. The mechanism of the inversion has been discussed.

Optical resolution of metal complex ions has been effected frequently by ion-exchange chromatography.[2)] Usually, the complex ion is adsorbed on an achiral ion-exchange resin and eluted by an aqueous solution of some optically active substance (resolving agent). In this type of experiment, it would appear rather reasonable to assume that the faster-eluted enantiomer should be the one which forms the favorable diastereomeric pair with the resolving agent in the eluent. Though such is often the case indeed, such an assumption does not necessarily hold true because of the two fundamental processes involved in the chromatographic separation; adsorption of complex ions to the resin in the stationary phase and ion-pairing of complex ions with the resolving agent in the mobile phase. Thus, critical examination is needed to establish which of these two processes governs the chromatographic optical resolution.

In this work, we have measured the retention volumes of enantiomers of several complex anions when eluted by an aqueous solution of Δ-$[Co(en)_3]^{3+}$, Δ-$[Co(sep)]^{3+}$, or Δ-$[Co(l\text{-chxn})_3]^{3+}$, as a function of the eluent concentration, where en=ethylenediamine, sep=1,3,6,8,10,13,16,19-octaazabicyclo[6.6.6]eicosane, and *l*-chxn=(−)-*trans*-1,2-cyclohexanediamine. It has been found that the order of retention volumes of enantiomers of some complex anions is inverted by the concentration of the eluents. The implications of this result have been discussed from the viewpoints of the above two processes and the mode of chiral discrimination between complex ions.

Experimental

All the metal complexes used in this work were available from previous works.[3,4)]

The resin used was the IEX 220 (Toyo Soda Manufacturing Co., Ltd.), which is based on a styrene-divinylbenzene copolymer and carries the tetraalkylammonium group as the functional group. A column (50×4 mm) of the IEX 220 anion-exchange resin was equilibrated with an eluent, which was an aqueous solution of an optically active cationic complex. An aqueous solution containing one enantiomer of an anionic complex and bis(glycinato)copper(II), which was used as a marker for void volume measurement, was injected by a syringe on top of the column and eluted at an elution rate of 0.3 cm³/min. The concentration of the cationic complex in eluents was varied from 4×10^{-3} to 60×10^{-3} mol dm^{-3}. The adjusted retention volumes were obtained from the elution curves as in the previous studies.[3,4)] The retention volumes were found to be reproducible to within 0.05%.

Results

In this work, one enantiomer of an anionic complex was adsorbed on an anion-exchange resin and eluted by an aqueous solution containing a Δ complex cation. The adjusted retention volumes obtained in this way are summarized in Table 1. The most noteworthy feature in Table 1 is the inversion of the order of retention volumes of some enantiomers caused by the concentration of the eluents. For example, in the combination of Δ-$[Co(sep)]Cl_3$···$[Co(mal)_2(en)]^-$ (mal=malonate dianion), the faster-eluted enantiomer at lower eluent concentrations is Λ, whereas it is Δ at an eluent concentration higher than 15×10^{-3} mol dm^{-3}. Likewise, Δ-$[Co(edta)]^-$ (edta=ethylenediaminetetraacetate) is eluted faster by the 4×10^{-3} mol dm^{-3} solution of Δ-$[Co(sep)]Cl_3$, while Λ-$[Co(edta)]^-$ is eluted faster by the eluent of higher concentrations or by an eluent containing Δ-$[Co(sep)]Br_3$. A similar inversion takes place for other combinations. Further, the bromide salts are more effective in inverting the retention volume orders than the chloride salts, in that lower concentrations of bromides yielded similar results obtained for higher concentrations of chlorides.

Discussion

Recently, we have studied the mode of chiral discrimination between optically active complex ions in solution.[3)] It was proposed there that (i) chiral discrimination is effected along the C_2 axis of Δ-$[Co(en)_3]^{3+}$ and Δ-$[Co(sep)]^{3+}$, while it is effected along the C_3 axis of Δ-$[Co(l\text{-chxn})_3]^{3+}$, (ii) the chirality of $[Co(edta)]^-$ or $[Co(tdta)]^-$ (tdta=1,4-butanediamine-*N*,*N*,*N*′,*N*′-tetraacetate) is recognized by a complex cation along their pseudo C_3 axes, whereas the chirality of $[Co(mal)_2(en)]^-$ or $[Co(ox)_2(en)]^-$ (ox=oxalate) is recognized along their C_2 axes, and (iii) favorable ion pairs are formed in the combinations for which the handedness of chelate rings of both ions, when oriented along the above axes, is the same.[3)] The handedness of a Δ complex ion can be specified as either P(C_3) (right-handed propeller) when viewed along the C_3 axis, or M(C_2) (left-handed propeller) when viewed along the C_2 axis.[5)] For example, the

TABLE 1. THE ADJUSTED RETENTION VOLUMES (cm^3) OBTAINED ON A COLUMN (50×4 mm) OF THE IEX 220 RESIN(ANION-EXCHANGER)
The elution rate was 0.3 cm^3/min.

Eluent	Concn[a]	Sample							
		K[Co(edta)]		K[Co(tdta)]		Na[Co(ox)$_2$(en)]		Na[Co(mal)$_2$(en)]	
		Δ	Λ	Δ	Λ	Δ	Λ	Δ	Λ
Δ-[Co(en)$_3$]Cl$_3$	4	19.33	18.60	16.70	16.31	11.78	11.89	2.952	2.871
	15	4.436	4.380	3.879	3.625	3.213	3.270	0.903	0.922
Δ-[Co(sep)]Cl$_3$	4	17.29	17.81	16.58	19.66	11.02	10.82	3.230	3.131
	8	9.234	8.952	8.043	8.367	6.450	6.447	1.945	1.802
	15	4.565	4.391	4.353	3.936	3.461	3.335	0.979	0.999
Δ-[Co(sep)]Br$_3$	4	9.834	9.675	9.768	9.711	6.898	6.612	2.121	2.143
	8	5.400	5.280	5.940	5.580	3.115	3.120	1.590	1.680
Δ-[Co(*l*-chxn)$_3$]Cl$_3$	4	13.89	14.66	8.769	10.24	10.97	11.22	3.038	3.014
	15	3.321	3.941	1.724	2.117	3.088	3.461	1.020	0.980
	30					1.920	2.130		
	60					1.200	1.200		
Δ-[Co(*l*-chxn)$_3$]Br$_3$	4	9.480	10.470	6.750	7.830	6.750	6.330	3.030	2.880

a) The eluent concentration is in 10^{-3} mol dm^{-3}.

favorable pair is M(C_2)–M(pseudo C_3) for Δ-[Co(sep)]$^{3+}$···Λ-[Co(edta)]$^-$, where the former chirality notation refers to the cation and the latter one to the anion. Likewise, the favorable pairs are P(C_3)–P(pseudo C_3) for Δ-[Co(*l*-chxn)$_3$]$^{3+}$···Λ-[Co(edta)]$^-$, M(C_2)–M(C_2) for Δ-[Co(sep)]$^{3+}$···Λ-[Co(ox)$_2$(en)]$^-$, and P(C_3)–P(C_2) for Δ-[Co(*l*-chxn)$_3$]$^{3+}$···Λ-[Co(ox)$_2$(en)]$^-$. The ions [Co(en)$_3$]$^{3+}$, [Co(tdta)]$^-$, and [Co(mal)$_2$(en)]$^-$ can be considered in the same way as for [Co(sep)]$^{3+}$, [Co(edta)]$^-$, and [Co(ox)$_2$(en)]$^-$, respectively.

The inversion of the retention volume order of enantiomers obtained in this work may be explained by combining the above ideas with the two fundamental processes in ion-exchange chromatographic experiments. The origin of the inversion of the combination Δ-[Co(sep)]$^{3+}$···[Co(mal)$_2$(en)]$^-$ will be considered as an example. In this work, one enantiomer of an anionic complex was adsorbed on the anion-exchange resin and eluted by an aqueous solution containing a Δ complex cation. The [Co(mal)$_2$(en)]$^-$ ion will be adsorbed to the resin functional group along its C_2 axis *via* two oxygen atoms of coordinated malonates. At higher eluent concentrations, the elution is governed by ion-pairing in the mobile phase rather than in the stationary phase. This is because the chloride or bromide ions in the eluent replace the [Co(mal)$_2$(en)]$^-$ ions adsorbed on the resin and the concentration of [Co(mal)$_2$(en)]$^-$ in the mobile phase is thus enhanced. As a result, the enantiomer that associates more favorably with Δ-[Co(sep)]$^{3+}$ in the mobile phase is eluted faster and shows a smaller retention volume than its enantiomorph. The favorable combination is therefore Δ–Δ or M(C_2)–M(C_2), as stated previously, and this situation is illustrated in Fig. 1(a).

At lower eluent concentrations, the elution is governed by adsorption of a complex anion to the resin functional group, which means that chiral discrimination is effected through ion-pairing of the Δ cation with the [Co(mal)$_2$(en)]$^-$ ion adsorbed to the resin, *i.e.*, chiral discrimination is effected in the stationary phase. Recall that the [Co(mal)$_2$(en)]$^-$ anion is bound to the resin along its C_2 axis, leaving only the pseudo C_3 axis for the ion-pairing direction for the Δ cation. Thus, the Δ-[Co(sep)]$^{3+}$ cation will be forced to associate with [Co(mal)$_2$(en)]$^-$ along the anion's pseudo C_3 axis. This situation is illustrated in Fig. 1(b). It should be noted here that the handedness of chelate rings of the complex anion is inverted depending upon the direction of watching the anion;[5] Δ-[Co(mal)$_2$(en)]$^-$ is left-handed or M(pseudo C_3) when watched along the pseudo C_3 axis, while it is right-handed or P(C_2) when watched along the C_2 axis. Since Δ-[Co(sep)]$^{3+}$ has the M(C_2) chirality and is discriminated along its C_2 axis, and since the enan-

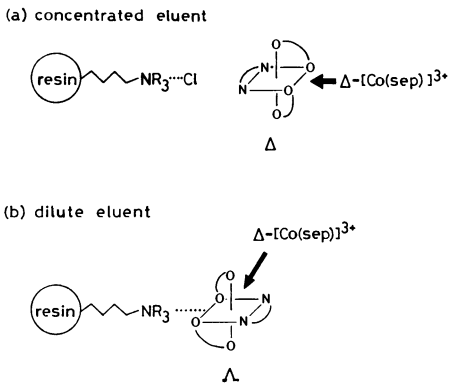

Fig. 1. An illustration of the ion-pairing equilibrium in stationary and mobile phases. The enantiomer depicted for [Co(mal)$_2$(en)]$^-$ is the one which forms the favorable pair with Δ-[Co(sep)]$^{3+}$. The cation discriminates the chirality of the anion along (a) the anion's C_2 axis and (b) the anion's pseudo C_3 axis.

tiomer of the anion that associates more favorably with the M(C_2) cation should have the same M chirality, the preferred enantiomer is either M(C_2) or M(pseudo C_3). As depicted in Fig. 1(b), the [Co(mal)$_2$(en)]$^-$ anion is now assumed to be discriminated along its pseudo C_3 axis. Thus, the M(pseudo C_3) enantiomer (the Λ enantiomer) is preferred and the favorable pair at lower eluent concentration is Δ-[Co(sep)]$^{3+}$···Λ-[Co(mal)$_2$(en)]$^-$. Namely, at higher eluent concentrations, the anion is discriminated along its C_2 axis in the mobile phase, whereas at lower eluent concentrations, the anion has to be discriminated along its pseudo C_3 axis in the stationary phase. This may be responsible for the observed inversion. The results for the other combinations may be explained similarly.

The above reasoning seems to gain some support from the results obtained by using the bromide salts instead of the chloride salts. The bromide anion is known to be adsorbed to anion-exchange resins more strongly or selectively than the chloride ion.[6] Thus, compared with the chloride ion, the bromide ion will enhance the effective concentration of a complex anion in the mobile phase, which will in turn enhance the ion-pairing with a Δ cation in the mobile phase. This will make the situation similar to that depicted in Fig. 1(a). Namely, the bromide ion is more effective in driving the dynamic equilibrium to the side of elution-governing. This may be the reason for the bromides being more effective in inverting the retention volume orders.

In Table 1, it is also noted that [Co(mal)$_2$(en)]$^-$ shows much smaller retention volumes than the other anions for all the eluents. This suggests either that this complex anion associates very strongly with the Δ cations in the mobile phase, or that [Co(mal)$_2$(en)]$^-$ is adsorbed very weakly to the resin. But the former possibility seems to be unlikely, because even at lower Δ-[Co(sep)]Cl$_3$ concentrations, where the elution is adsorption-governed as explained above, this anion exhibits much smaller retention volumes than the other complex anions. Thus, [Co(mal)$_2$(en)]$^-$ may be adsorbed to the resin more weakly than [Co(edta)]$^-$, [Co(tdta)]$^-$, and [Co(ox)$_2$(en)]$^-$ owing possibly to greater hydration of [Co(mal)$_2$(en)]$^-$. An indication that [Co(mal)$_2$(en)]$^-$ is hydrated to a greater extent than [Co(edta)]$^-$ has been obtained recently by conductance measurements.[7]

Conclusion

The inversion of the retention volume orders of enantiomers reflects that ion-pairing is highly directional both in mobile and stationary phases and a cation recognizes an inverted chirality of an anion when the cation approaches the anion along different directions.

Acknowledgement is made to Dr. S. Yamazaki, Toyo Soda Manufacturing Co., Ltd. (Tokyo), for the gift of the IEX 220 resin.

References

1) Part 4 of "Chiral Recognition in Solution." Part 3; U. Sakaguchi, A. Tsuge, and H. Yoneda, *Inorg. Chem.*, in press.

2) L. Druding and G. B. Kauffman, *Coord. Chem. Rev.*, **3**, 409 (1968); Y. Yoshikawa and K. Yamasaki, *ibid.*, **28**, 205 (1979); H. Yoneda, *J. Liq. Chromatogr.*, **2**, 1157 (1979); H. Yoneda, S. Yamazaki, and T. Yukimoto, in "Stereochemistry of Optically Active Transition Metal Compounds," ed by B. E. Douglas and Y. Saito, ACS Symposium Series No. 119, American Chemical Society (1980), p. 315.

3) U. Sakaguchi, I. Yamamoto, S. Izumoto, and H. Yoneda, *Bull. Chem. Soc. Jpn.*, **56**, 153 (1983).

4) U. Sakaguchi, A. Tsuge, and H. Yoneda, *Inorg. Chem.*, in press.

5) A. J. McCaffery, S. F. Mason, and B. J. Norman, *J. Chem. Soc., A*, **1965**, 5094.

6) See, *e.g.*; R. Kunin, in "Technique of Inorganic Chemistry," ed by H. B. Jonassen and A. Weissberger, Interscience Publishers, New York (1965), Vol. IV, pp. 1—30.

7) H. Yokoyama and M. Nishimura, Proc. IVth International Symposium on Solute-Solute-Solvent Interactions, July 4—10, 1982, Osaka, 1P-20.

Reactions of Chloro[4-[2-(methylthio)anilino]-3-penten-2-onato-*O,N,S*]-palladium(II) with Carbanions and Pyridine Derivatives

Katsuma Hiraki,* Masayoshi Onishi, Minoru Hayashida, and Kyogo Kurita

Department of Industrial Chemistry, Faculty of Engineering, Nagasaki University, Bunkyo-machi, Nagasaki 852

(Received November 19, 1982)

A Schiff base, 4-[2-(methylthio)anilino]-3-penten-2-one (Hmtap), prepared from acetylacetone and 2-(methylthio)aniline, reacted with $Na_2[PdCl_4]$ in the presence of sodium ethoxide to give [PdCl(mtap-*O,N,S*)] (**1**). Complex **1** was treated with carbanions formed from dimethyl malonate, methyl cyanoacetate, and malononitrile in the presence of sodium methoxide to afford the corresponding (disubstituted methyl)palladium(II) complexes, [Pd(CHYY')(mtap-*O,N,S*)] (Y,Y'=COOMe and/or CN). On the other hand, **1** reacted with Tl(acac) to yield an *O,O'*-chelating complex, [Pd(mtap-*N,O*)(acac)], in which the mtap moiety served as a bidentate ligand. Moreover, **1** reacted with 2,2'-bipyridine (bpy) and 4-(dimethylamino)pyridine (dmapy) in the presence of $NaClO_4 \cdot H_2O$ to give [Pd(mtap-*N,O*)(bpy)]ClO_4 and [Pd(mtap-*O,N,S*)(dmapy)]ClO_4, respectively. These complexes are characterized by means of elemental analysis and IR and NMR spectroscopy.

The previous papers from our laboratory revealed that Schiff bases, 4-(α-picolylamino)- and 4-[2-(diphenylphosphino)ethylamino]-3-penten-2-ones (Hpap and Hdpeap, respectively) reacted with $Na_2[PdCl_4]$ in the presence of base to yield [PdCl(pap-*N,N,O*)][1] and [PdCl(dpeap-*O,N,P*)],[2] respectively. In these square planar palladium(II) complexes, the Schiff bases served as a monoanionic tridentate ligand. Carbanions formed from active methylene compounds displaced the remaining chloro ligand at the fourth coordination site in the complexes to give (disubstituted methyl) palladium(II) complexes retaining the NNO- or ONP-typed tridentate chelate.[1,2]

It is interesting to investigate both the coordinating ability of sulfur atom in an ONS-typed chelate and the stabilizing effect of the chelate for the carbon-palladium σ-bond. In this paper, we present some palladium(II) complexes derived from reactions of chloro[4-[2-(methylthio)anilino]-3-penten-2-onato-*O,N,S*]palladium(II) [PdCl(mtap-*O,N,S*)] [mtap=4-[2-(methylthio)anilino]-3-penten-2-onato] with the carbanions or a few pyridine derivatives. Furthermore, the coordination ability of the sulfur atom in the mtap chelate and the stabilizing effect of the chelate for the C–Pd σ-bond were compared with the respective ones of the pap and dpeap chelates.

Results and Discussion

*Preparation of Hmtap and [PdCl(mtap-*O,N,S*)].* A mixture of 2-(methylthio)aniline and an excess amount of acetylacetone was refluxed to give colorless crystals of Hmtap in 84% yield. The spectroscopic data of Hmtap were quite consistent with its structure. Furthermore, it was possibly associated with the hydrogen-bonded keto-enamine form, by analogy with the cases of Hpap[1] and other related Schiff bases.[3]

After treating an ethanol solution of $Na_2[PdCl_4]$ with Hmtap in the presence of an equimolar amount of sodium ethoxide, the resulting red microcrystals were collected and assignable to [PdCl(mtap-*O,N,S*)] (**1**) (*vide infra*). In the ^{1}H-NMR spectrum of **1** in $CDCl_3$, methyl group on sulfur showed a downfield shift by 0.42 ppm due to the coordination to palladium.

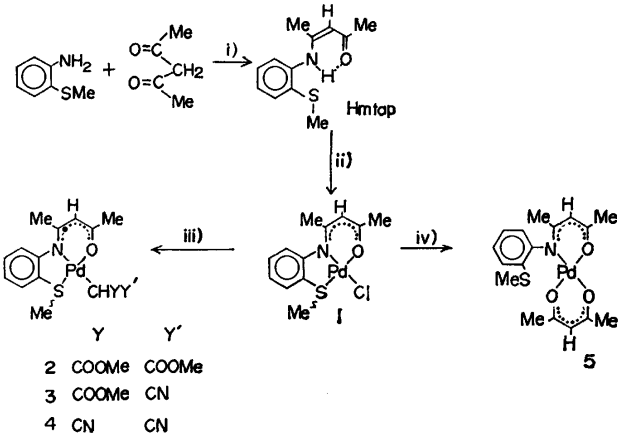

Scheme 1. i) Reflux, ii) $Na_2[PdCl_4]+NaOC_2H_5$, iii) $CH_2YY'+NaOCH_3$, iv) Tl(acac).

Mass spectrum of **1** exhibited a parent-ion pattern centered at *m/e* 362, corresponding to [^{106}Pd^{35}Cl(mtap-*O,N,S*)]. In the far-infrared spectrum, there were two bands at 325 and 338 cm^{-1} for ν(Pd–^{37}Cl) and ν(Pd–^{35}Cl), respectively.

*Reactions of **1** with Carbanions Derived from Active Methylene Compounds.* Reactions of **1** with carbanions, formed from dimethyl malonate, methyl cyanoacetate, and malononitrile, were carried out in THF at room temperature to yield complexes, [Pd{$CH(CO_2CH_3)_2$}(mtap-*O,N,S*)] (**2**), [Pd{$CHCN(CO_2CH_3)$}(mtap-*O,N,S*)] (**3**), and [Pd{$CH(CN)_2$}(mtap-*O,N,S*)] (**4**), respectively, as shown in Scheme 1. No reaction occurred between **1** and a carbanion formed from ethyl nitroacetate, in analogy with the case of [PdCl(pap)] system.[1] The complexes obtained in this study are considerably stable in the solid state in air. Yields, microanalytical data, and spectroscopic properties are summarized in Tables 1—3.

The IR spectra of **1**—**4**, as well as **5**—**8**,[4] showed three bands near 1560, 1515, and 1380 cm^{-1}, characteristic of 4-amino-3-penten-2-onato-*N,O* moiety. The ^{1}H-NMR spectra of **1**—**8** exhibited three singlets in the range of δ 1.35—2.9, ascribable to 1-, 5-, and sulfur-bonded methyl groups of the mtap moiety (Table

Table 1. Yields and properties of the palladium(II) complexes

Compound		Yield[a] %	Mp[c] θ_m/°C	Found(Calcd)(%) H	C	N	Λ_M[d]
[PdCl(mtap-*O*,*N*,*S*)]	**1**	75[b]	160—163	3.87(3.90)	39.50(39.80)	3.87(3.87)	—
[Pd{CH(CO_2Me)$_2$}(mtap-*O*,*N*,*S*)]	**2**	48	191—192	4.60(4.62)	44.09(44.60)	3.00(3.06)	—
[Pd{CHCN(CO_2Me)}(mtap-*O*,*N*,*S*)]	**3**	68	179	4.35(4.27)	45.01(45.24)	6.48(6.59)	—
[Pd{CH(CN)$_2$}(mtap-*O*,*N*,*S*)]	**4**	37	175—178	3.85(3.86)	45.47(45.99)	10.83(10.73)	—
[Pd(mtap-*N*,*O*)(acac)]	**5**	17	155—157	5.07(4.97)	47.68(47.95)	3.04(3.29)	—
[Pd(mtap-*N*,*O*)(bpy)]ClO_4	**6**	70	196—198	3.84(3.81)	45.03(45.37)	7.08(7.22)	126
PdCl(mtap)(dmapy)	**7**	82	148	5.04(4.99)	46.90(47.12)	8.63(8.68)	59.5
[Pd(mtap-*O*,*N*,*S*)(dmapy)]ClO_4	**8**	77	102—115	4.65(4.41)	41.68(41.62)	7.78(7.66)	108

a) Based on **1**, unless noted elsewhere. b) Based on $Na_2[PdCl_4]$. c) With decomposition. d) Molar conductivity, Ω^{-1} cm^2 mol^{-1}, at 10^{-3} mol/l in acetonitrile solution at 25 °C.

Table 2. ^{1}H-NMR spectra and selected IR bands

Complex	^{1}H-NMR Data[a] mtap[b] 1-CH_3	5-CH_3	*S*-CH_3	CH	Others[c]	IR Data $\tilde{\nu}$/cm^{-1} [i]
1	2.32	2.12	2.80	5.28	—	—
2	2.24	2.08	2.75	5.16	3.65(Me), 3.69(CH)	1718 ν(C=O), 1122 ν(C-O)
3[d]	2.28	2.08	2.81[e]	5.19	3.30(CH)[e], 3.68(Me)	2207 ν(C≡N), 1698 ν(C=O)
4	2.32	2.09	2.84	5.22	2.84(CH)	2222 s, 2170 w ν(C≡N)
5	2.00[f]	1.35	2.43	5.09[f]	1.73(Me), 2.09(Me)[f], 5.17(CH)[f]	1560 ν(C⋯O)
6	2.24	1.85	2.30	5.33	8.30d(bpy-H^6, H$^{6'}$)[g,h]	1608 ν(C=N)[j], 1093 (ClO_4)
7a	2.34	2.14	2.81	5.25	3.02(NMe_2), 6.43d(H$^\beta$)[g], 7.68d(H$^\alpha$)[g]	1618, 1573 ν(C=N)[j]
7b	2.06	1.69	2.40	5.22	2.87(NMe_2), 6.16d(H$^\beta$)[g], 7.60d(H$^\alpha$)[g]	1078, 1023 ν(C-N)
8	2.37	2.13	2.72	5.38	3.10(NMe_2), 6.66d(H$^\beta$)[g], 7.98d(H$^\alpha$)[g]	1617 ν(C=N)[j], 1091[k] ν(ClO_4)

a) δ Value (ppm) from TMS, in $CDCl_3$. Most of the signals, expect for ones noted elsewhere, appear as a singlet. b) Phenylene protons are omitted. c) Assignment is given in parentheses. d) Measured at 27 °C. See the text about the signals at −5 °C. e) A broad signal. f) Assigned tentatively because of similarity of the chemical shifts. g) Doublet [^3J(HH) = 7—8 Hz]. h) The other proton signals were observed at δ = 7.1—8.3 as multiplets. i) In $CHCl_3$ solution, except for **8**. See the text about the IR bands of the mtap moiety. j) Due to pyridine ring. k) In KBr disk.

Table 3. ^{1}H-decoupled ^{13}C-NMR data of the palladium complexes[a]

Complex	mtap[b] 1-$\underline{C}H_3$	5-$\underline{C}H_3$	S$\underline{C}H_3$	$\underline{C}$H	$\underline{C}$⋯N	$\underline{C}$⋯O	Pd-CHYY′ $\underline{C}$H	$\underline{C}$=O	O$\underline{C}H_3$	$\underline{C}$≡N
2	25.9	24.3	27.5	104.4	163.4	180.9	32.3	174.2	50.9	—
3	25.7	24.4	27.8	104.6	163.7	180.7	12.2	174.3	51.9	122.4
4[c]	25.7	24.7	28.0	104.9	164.8	180.7	−10.6	—	—	119.8

a) δ value (ppm) from TMS. In $CDCl_3$, except for **4**. b) Phenylene carbon resonances are omitted. c) In CD_2Cl_2.

2). Among them, two resonances at the highest and an intermediate fields were assigned to 5- and 1-methyl protons of the 3-penten-2-onato-*N*,*O* moiety, respectively, on the basis of both analogy with the data for [Pd(CHYY′)(pap)] (Y,Y′ = CO_2CH_3 and/or CN)[1] and the difference of electronegativities of the nearly-located coordinating atoms, nitrogen and oxygen. This assignment was also supported by the {^{1}H}-^{13}C-NMR data of C⋯N and C⋯O groups (Table 3). The remaining resonance at the lowest field was unambiguously associated with the sulfur-bonded methyl group.

The ^{1}H-NMR spectra of **2**—**4** exhibited a singlet in the range of δ 2.8—3.7, assignable to a palladium-bonded methine proton (Table 2). As for **2**, there was a singlet at δ 3.65 for two esteric methyl groups with a satisfactory intensity implying their spectroscopic equivalence. In addition, its IR spectrum in chloroform showed only one ν(C=O) band at 1718 cm^{-1}, and the wave number was indicative of retention of esteric carbonyl groups without bonding of oxygen to hydrogen or palladium in an enol fashion. The IR spectrum of **4** exhibited a strong ν_{as}(C≡N) band at 2222 cm^{-1} together with a very weak ν_s(C≡N) one at 2170 cm^{-1}, attributable to a *C*-bonded dicyanomethyl group, Pd–CH(CN)$_2$ rather than an *N*-bonded 2-cyanoetheniminato one, Pd–N=C=CH–CN.[5] On the

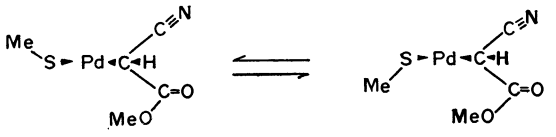

Fig. 1. Two configurational isomers of **3**. The 4-anilino-3-penten-2-onato-*O,N* moiety is deleted for simplification.

basis of these facts, **2**—**4** were concluded to have the structure with the carbon-palladium σ-bond, as shown in Scheme 1. The ^{1}H-decoupled ^{13}C-NMR data are fully consistent with the *C*-bonded structure (Table 3). The methine carbons bonded to palladium appeared as a singlet at δ 32.3 for **2**, at δ 12.2 for **3**, and at δ −10.6 for **4**. It is noteworthy that the higher-field resonances of the methine carbons in **3** and **4** are reasonably correlated to the smaller deshielding effect of the cyano group as compared with that of ester group,[6] together with the shielding effect by palladium through the σ-bond. A similar high-field shift was observed in the case of [Pd{CH(CO$_2$R)Z}-(pap)] (Z=CO$_2$C$_2$H$_5$ or CN).[1] As for three methyl carbon resonances in the range of δ 24—28, two singlets near δ 24.5 and 25.8 were attributable to 5- and 1-methyl carbons of the 3-penten-2-onato-*N,O* moiety on the analogy of their chemical shifts to the coorresponding data of [Pd{CH(CO$_2$R)Z}(pap)].[1] Especially, the singlet near δ 25.8 was associated with the 1-methyl carbon on the basis of both the actual coincidence of the chemical shift with the corresponding value for [Pd{CH(CO$_2$R)Z}(pap)][1] and the difference of the electronegativities of the nearly-located coordinating atoms (*vide ante*). The third singlet near δ 27.8 was ascribed to sulfur-bonded methyl carbon.

The configuration of **3** is diastereotopic leading to two configurational isomers, because of the sp^3 sulfur atom and the asymmetric carbon bonded to palladium. It is notable that **3** showed temperature-dependent ^{1}H-NMR spectra. At 27 °C, **3** showed two slightly broad signals at δ 2.81 (3H, SC$\underline{H}_3$) and 3.30 (1H, Pd–C$\underline{H}$) and a sharp singlet at δ 2.08 (3H, 5-C$\underline{H}_3$), as seen in Table 2. Each of these three signals separated into two considerably sharp singlets at −5 °C; SC$\underline{H}_3$ at δ 2.85 (2.4 H) and 2.68 (0.6H); Pd–C$\underline{H}$ at δ 3.32 (0.8H) and 3.22 (0.2H); and 5-C$\underline{H}_3$ at δ 2.09 (2.4H) and 2.07 (0.6H).[7] These data indicate that inversion of the sulfur-bonded methyl group in **3** took place rapidly on the NMR time scale above room temperature and that the two configurational isomers, as shown in Fig. 1, were fixed in the population ratio of about 4:1 at −5 °C, owing to the quenching of the inversion. Similar configurational change at sulfur atom has been observed as regards (dialkyl sulfide)-palladium(II) complexes.[8-10]

In sharp contrast to the cases of carbanions derived from dimethyl malonate, methyl cyanoacetate and malononitrile, **1** reacted with Tl(acac) to give an *O,O'*-chelated acetylacetonato complex, **5**. This structure was confirmed by the lack of ν(C=O) band of free carbonyl groups and by a singlet resonance at δ 5.09 characteristic of the methine proton of the *O,O'*-chelated acetylacetonato moiety. Dissociation of sulfur

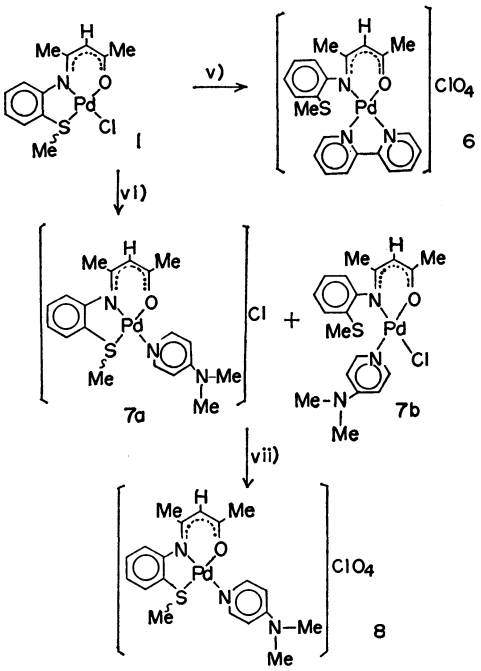

Scheme 2. v) 2,2'-Bipyridine+NaClO$_4$, vi) dmapy, vii) NaClO$_4$·H$_2$O.

donor in the mtap moiety from palladium by the incoming acac chelate was shown by the upfield shift of the *S*-methyl proton resonance by *ca.* 0.4 ppm. In addition, 5-methyl protons of **5** resonated at a higher field by *ca.* 0.6 ppm than those of **1**—**4**. This upfield shift was attributed to the anisotropic effect due to the phenylene ring, lying actually perpendicular to the coordination plane. The dpeap complex, [PdCl-(dpeap-*O,N,P*)] reacted easily with Tl(acac) in CH$_2$Cl$_2$ at room temperature to yield a (diacetylmethyl)palladium(II) complex involving a palladium-carbon σ-bond stabilized by the phosphine.[2] It has been reported that triphenylphosphine and pyridine also stabilized the diacetylmethyl-palladium(II) bond.[11,12] On the other hand, our present mtap system could not furnish a stabilizing field enough to produce the (diacetylmethyl)palladium(II) complex, and labile coordination property of the sulfur donor helped the formation of the *O,O'*-chelated structure. In our previous research,[1] Tl(acac) did not react with [PdCl-(pap)] under THF reflux, owing to rigid coordinate bonds to palladium.

Reactions of **1** *with Pyridine Derivatives.* Dissociation of the *S*-donor from palladium in **5** led us to undergo the reactions of **1** with some pyridine derivatives in order to elucidate the coordination behavior of the *S*-donor to palladium. When **1** was treated with excess 4-picoline in THF at room temperature, no 4-picoline adduct to **1** was isolated. On the other hand, the ^{1}H-NMR spectrum of a mixture of **1** and 2,2'-bipyridine (bpy) (1:1) exhibited signals corresponding to two species of [PdCl(mtap-*O,N,S*)] and [Pd(mtap-*N,O*)(bpy)]Cl in a ratio of 73:27, indicating the following equilibrium.

$$[PdCl(mtap\text{-}ON,S)] + bpy \rightleftharpoons [Pd(mtap\text{-}N,O)(bpy)]Cl$$

Preference of 2,2'-bipyridine to bidentate coordination brought about the equilibrium leading to [Pd(mtap-

N,O)(bpy)]Cl with the dissociation of the *S*-donor. The dissociation of the *S*-donor in [Pd(mtap-*N,O*)-(bpy)]Cl was determined easily by the chemical shift of the *S*-methyl proton resonance. The mixture of the two species was converted quantitatively to [Pd(mtap-*N,O*)(bpy)]ClO_4 (**6**) by treatment with $NaClO_4 \cdot H_2O$ in THF at room temperature (Scheme 2).

Complex **1** was also treated with a slight excess of 4-(dimethylamino)pyridine (dmapy), a well-known strong base, in THF at room temperature to give a pale yellow powder (**7**), which was suggested as a 1:1 adduct of **1** with dmapy by its elemental analysis. Moreover, the ^{1}H-NMR spectrum of **7** in $CDCl_3$ revealed the coexistence of two isomers, which are [Pd(mtap-*O,N,S*)(dmapy)]Cl (**7a**) and [PdCl(mtap-*N,O*)(dmapy)] (**7b**) in a ratio of 55:45. *S*-Methyl proton resonances unambiguously indicated the retention of the *S*-donor coordination to palladium in **7a** and dissociation of the *S*-donor in **7b**. An ionic complex, [Pd(mtap-*O,N,S*)(dmapy)]ClO_4 (**8**), was obtained quantitatively from the mixture of **7a** and **7b** and $NaClO_4 \cdot H_2O$. Transformation of **7b** to **8** proceeded reasonably through **7a**. These results indicate that the *S*-donor in **1** is relatively labile and can be displaced by the strong nucleophile or the multidentate ligand. In the case of 4-picoline, nucleophilicity is not enough, together with its non-chelate structure.

Experimental

Materials and General Proceduces. 2-(Methylthio)aniline[13] and thallium(I) acetylacetonate[14] were prepared by the respective literature methods. Solvents were dried by the standard methods and distilled. Preparative operations were performed under nitrogen. ^{13}C-NMR spectra were recorded on JEOL FX-90-Q, using tetramethylsilane as an internal standard. Mass spectra were obtained with a Nichiden-Varian TE-600 gas chromatograph-mass spectrometer. IR and ^{1}H-NMR spectra, melting points, and molar conductivities were measured according to the methods described in the previous paper.[1] The temperature of the NMR samples was determined with methanol or 1,3-propanediol.

Preparation of 4-[2-(Methylthio)anilino]-3-penten-2-one (Hmtap). A mixture of 2-(methylthio)aniline (0.13 mol) and acetylacetone (0.33 mol) was refluxed for 3 h with removal of liberated water. Unreacted starting materials were removed under *ca.* 0.5 mmHg (1 mmHg≈133.322 Pa) at *ca.* 100 °C, and the residue was recrystallized from dichloromethane and hexane to yield colorless crystals of Hmtap: Found: C, 65.18; H, 6.96; N, 6.33%; M^+, 221. Calcd for $C_{12}H_{15}NOS$: C, 65.12; H, 6.83; N, 6.33%; M, 221.32. Mp 58 °C: IR ($CHCl_3$) 3375 (NH), 1616, 1566, and 1518 cm^{-1} (α,β-unsaturated β-amino ketone); ^{1}H-NMR ($CDCl_3$) δ= 1.85 (3H, s, CH_3), 2.10 (3H, s, CH_3), 2.38 (3H, s, SCH_3), 5.22 (1H, s, CH), 7.0—7.4 (4H, m, aromatic CH), and 12.20 (1H, broad, NH).

Preparation of [PdCl(mtap-O,N,S)] 1. An ethanol solution of sodium ethoxide (6.1 mmol) was added slowly to a mixture of $Na_2[PdCl_4]$ (6.1 mmol) and Hmtap (6.8 mmol) in ethanol (150 ml). After stirring at room temperature for 16 h, the solvent was removed under vacuum. Recrystallization of the residue from dichloromethane and hexane gave red microcrystals of **1**.

Reactions of 1 with Carbanions Formed from Active Methylene Compounds. Dimethyl malonate (0.80 mmol) in THF was treated with sodium methoxide (0.96 mmol), followed by slow addition of **1** (0.80 mmol) in THF. The mixture was stirred for 27 h at room temperature, and the solvent was removed under vacuum. The residue was recrystallized from dichloromethane and hexane to yield brown microcrystals of [Pd{$CH(COOCH_3)_2$}(mtap-*O,N,S*)] (**2**). Complex **1** reacted similarly with methyl cyanoacetate and malononitrile to afford reddish orange microcrystals of [Pd{$CHCN(CO_2CH_3)$}(mtap-*O,N,S*)] (**3**) and orange ones of [Pd{$CH(CN)_2$}(mtap-*O,N,S*)] (**4**), respectively.

Reaction of 1 with Thallium Acetylacetonate. Thallium(I) acetylacetonate (1.0 mmol) was added in portions to a dichloromethane solution (10 ml) of **1** (0.8 mmol) and the mixture was stirred for 30 h under reflux. After the solvent was evaporated *in vacuo*, the residue was recrystallized from benzene and hexane, yielding light-brown microcrystals of [Pd(mtap-*N,O*)(acac)] (**5**).

Reaction of 1 with 2,2′-Bipyridine. Sodium perchlorate–water(1/1) (0.69 mmol) was added to a THF suspension of **1** (0.69 mmol) and 2,2′-bipyridine (0.89 mmol), and the mixture was stirred for 20 h at room temperature. The solvent was removed under vacuum, and the recrystallization of the residue from dichloromethane and hexane gave a pale yellow powder of [Pd(mtap-*N,O*)(bpy)]ClO_4 (**6**).

Reaction of 1 with 4-(Dimethylamino)pyridine. 4-(Dimethylamino)pyridine (1 mmol) was added to a THF (20 ml) suspension of **1** (0.83 mmol) and the color turned into orange-yellow. After stirring for 20 h at room temperature, a pale yellow precipitate was collected and washed with diethyl ether and hexane to give PdCl(mtap)(dmapy) (**7**).

A THF (20 ml) suspension of **7** was treated with sodium perchlorate–water(1/1) in a molar ratio of 1:1.2, followed by stirring at room temperature for several hours. After filtration and removal of the solvent from the filtrate, the residue was recrystallized from dichloromethane and diethyl ether, and [Pd(mtap-*O,N,S*)(dmapy)]ClO_4 (**8**) was isolated as red microcrystals.

The authors thank Mrs. Hisako Mazume and Miss Yumi Kojima, Nagasaki University, for their technical assistance.

References

1) K. Hiraki, M. Onishi, and H. Matsuo, *J. Organomet. Chem.*, **185**, 111 (1980).
2) K. Hiraki, T. Masumoto, Y. Fuchita, and Y. Zegi, *Bull. Chem. Soc. Jpn.*, **54**, 1044 (1981).
3) G. O. Dudek and R. H. Holm, *J. Am. Chem. Soc.*, **83**, 2099 (1961).
4) As for **5**—**8**, reaction products of **1** with pyridine derivatives, see the latter section.
5) W. H. Baddley and P. Choudhury, *J. Organomet. Chem.*, **60**, C74 (1973).
6) J. B. Stothers, "Carbon-13 NMR Spectroscopy," Academic Press, New York (1972), Chap. 5.
7) The other signals did not change actually.
8) R. J. Cross, T. H. Green, and R. Keat, *J. Chem. Soc., Dalton Trans.*, **1976**, 1150.
9) E. W. Abel, G. W. Farrow, K. G. Orrell, and V. Šik, *J. Chem. Soc., Dalton Trans.*, **1977**, 42.
10) Y. Fuchita, K. Hiraki, Y. Yamaguchi, and T. Maruta, *J. Chem. Soc., Dalton Trans.*, **1981**, 2405.
11) S. Baba, T. Ogura, and S. Kawaguchi, *Bull. Chem. Soc. Jpn.*, **47**, 665 (1974).
12) M. Horike, Y. Kai, N. Yasuoka, and N. Kasai, *J. Organomet. Chem.*, **72**, 441 (1974).
13) D. W. Meek, G. Dyer, and O. Workman, *Inorg. Synth.*, **16**, 169 (1976).
14) W. H. Nelson, W. J. Randall, and D. F. Martin, *Inorg. Synth.*, **9**, 53 (1971).

Stereochemical Investigation on Asymmetrically Modified Raney Nickel Catalyst. Mode of Interaction between Modifying Reagent and Substrate in the Enantioface-differentiating Process

Akira TAI,* Tadao HARADA, Yuji HIRAKI, and Sigeki MURAKAMI
Institute for Protein Research, Osaka University, Yamada-oka, Suita, Osaka 565

(Received May 27, 1982)

The mode of enantioface-differentiating hydrogenation with asymmetrically modified Raney nickel (MRNi) was investigated by using various sorts of modifying reagents and substrates. The optical yields (O.Y.) of the hydrogenation of methyl acetoacetate over MRNi for different modifying reagents occured in the following order: $HO_2CCH(OH)CH(OH)CO_2H$ (O.Y. 85%) > $HO_2CCH(OX)CH(OH)CO_2H$, (X = CH_3–, and PhCO–) ≈ $HO_2CCH_2CH(OH)CO_2H$ (O.Y. 61—65%) ≫ $HO_2CCH(OX)CH(OX)CO_2H$ (X = CH_3–, and PhCO) ≈ $CH_3CH(OH)CH(OH)CO_2H$ (O.Y. 1—8%). The hydrogenation of various substrates of the structure, R–C(Y)–CH_2–C(=O)–R′, over tartaric acid-modified Raney nickel (TA-MRNi), gave high optical yields only when the substituent –Y functioned as a good hydrogen bond acceptor like a carbonyl group, and two pairs of hydrogen bondings between substrate and two hydroxyl groups of tartaric acid were available. As for the stereochemistry of the reaction in such a case, (*R,R*)-TA-MRNi always gave (*R*)-product in excess. Based on the stereochemistry of the reaction and the role of hydrogen bonds between modifying reagent and substrate, a stereochemical model is proposed to elucidate the mode of enantioface-differentiating hydrogenation of prochiral ketones over TA-MRNi.

It has been reported that the asymmetric modification of Raney nickel (RNi) with an aqueous solution of tartaric acid (TA) and NaBr gave an excellent catalyst (TA–NaBr–MRNi) for the enantioface-differentiating hydrogenation. The hydrogenation of methyl acetoacetate (MAA) over this catalyst gave methyl 3-hydroxybutyrate (MHB) in a quantitative chemical yield and almost 90% of optical yield. Studies on the development of the above-mentioned catalyst have made it clear that the enantioface-differentiating ability of the catalyst is governed by two major factors. The first one is the proportion of the number of enantioface-differentiating reaction sites (where the enantioface-differentiating hydrogenation of substrate takes place by the aid of modifying reagent) to the number of non-enantioface-differentiating sites (where the racemic product is produced because of the absence of the modifying reagent on the catalyst). Our recent study has shown that NaBr on the catalyst is specifically adsorbed on the non-enantioface-differentiating reaction sites, inhibiting the hydrogenation activity of these sites.[1] Thus, the hydrogenation of MAA over TA–NaBr–MRNi proceeded overwhelmingly at the enantioface-differentiating reaction sites in giving the product with a high optical purity. The second factor is the degree of the intrinsic enantioface-differentiating ability of the modifying reagent, which depends not only on the structural features but also on the mode of adsorption on the catalyst surface. Arguing from the structural features of TA and MAA, and the stereochemistry of the hydrogenation product, we have proposed a mode of interaction between TA and MAA at the enantioface-differentiating step of the hydrogenation.[2] In this paper, we wish to report the details on the mode of enantioface-differentiation process and the validity of the proposed stereochemical model, based on the following two series of investigations: 1) The hydrogenation of MAA over RNi modified with NaBr and the compound whose structure is analogous to TA, and 2) the hydrogenation of various prochiral ketones over TA–NaBr–MRNi.

Results

Hydrogenations of MAA over Various Sorts of MRNi. Several analogs of TA were prepared and their enantioface-differentiating abilities (e.d.a.) were evaluated from the optical yield of the hydrogenation of MAA over the MRNi prepared from TA-analogs and NaBr. The results are summarized in Table 1.

Among the compounds examined, only TA and 2-methyl-TA gave rise to more than 70% of e.d.a. (Entries 1 and 2). When one of the hydroxyl groups of TA was replaced by H–, benzoyloxyl or methoxyl group, appreciable decreases of e.d.a. were observed (Entries 3, 4, and 5). The e.d.a.'s of this type of compounds were around 65%. The replacement of one of the carboxyl groups of TA by a methyl group resulted in a complete loss of e.d.a. (Entry 6), even if vicinal hydroxyl groups existed. A drastic decrease in e.d.a. was also observed when both hydroxyl groups of TA were acylated or alkylated (Entries 7 and 8). These results clearly show that two hydroxyl groups and two carboxyl groups in TA were absolutely necessary functional groups for the effective enantioface-differentiation of MAA.

Hydrogenations of Prochiral Ketones over TA–NaBr–MRNi. In Table 2, the results of the hydrogenation of various prochiral ketones over TA-NaBr–MRNi are summarized.

In the series of the hydrogenations of methyl esters of α-, β-, γ-, and δ-keto acids (**1a**—**4a**) over TA–NaBr–MRNi, the excellent optical yield was obtained only with β-keto ester (Entry 2). Furthermore, the hydrogenation rate of **2a** was much faster than those of **1a**, **3a**, and **4a**. Although γ-keto ester (**3a**) was

Table 1. Degree of enantioface differentiaitng ability(e.d.a.) of TA and its analogues determined by hydrogenation of MAA[a)]

No.	Modifying reagent	e.d.a. of MRNi[b)] %	Configuration of product
1	(*R,R*)-TA(I)	83	*R*
2	(*2R,3R*) 2-Methyl-TA(II)	74	*R*
3	(*2R,3R*) *O*-Benzoyl-TA(III)	65	*R*
4	(*2R,3R*) *O*-Methyl-TA(IV)	68	*R*
5	(*S*) Malic acid(V)	61	*S*
6	(*2S,3R*) 2,3-Dihydroxybutyric acid(VI)	1.2	*S*
7	(*2R,3R*) *O,O'*-Dibenzoyl-TA(VII)	8	*R*
8	(*2R,3R*) *O,O'*-Dimethyl-TA(VIII)	0.2	*R*

a) MAA(100 mmol) in methyl propionate(23 ml) and acetic acid(0.2 ml) was subjected to hydrogenation over MRNi prepared from 1.6 g of Raney alloy at initial hydrogen pressure of 100 kg/cm^2 at 100 °C. b) Degree of e.d.a. was evaluated by the optical yield(%) of the reaction of MAA to MHB.

hydrogenated to **3b** in 40% optical yield, the hydrogenations of α- and δ-keto ester gave only racemic **1b** and **4b**, respectively (Entries 1 and 4).

It is interesting that the hydrogenations of simple ketone (**5a**) and γ-keto ester (**3a**) proceeded with almost the same optical yields but in opposite directions of enantioface-differentiation; that is, **3a** gave (*R*)-**3b** in excess, while **5a** gave (*S*)-**5b** in excess (Entries 3 and 5).

In the preceding paper, which dealt with the hydrogenation of **1a**—**4a** with various amino acid–MRNi's it was shown that the geometrical fitness of functional groups in the modifying reagent and substrate was an essential factor for giving high optical yield.[3)] It is thus expected that **2a** can enter a well-fitting interaction with TA, whereas other substrates (**1a**, **3a**, **4a**, and **5a**) cannot.

Two types of homologues of **2a**, that is, alkyl acetoacetates (**6a**—**9a**) and methyl alkanoylacetates (**10a**—**12a**) were found to be smoothly hydrogenated over TA–NaBr–MRNi in uniformly excellent optical yields (Entries 6—12).

Acetylacetone (**13a**), in which one of the carbonyl groups takes the place of the ester carbonyl group of **2a**, was also found to be a good substrate.[4)] In this case, TA–NaBr–MRNi differentiates not only the enantioface of carbonyl group but also the one out of two carbonyl groups in **13a**. When the hydrogenation of **13a** is discontinued at 1.1 molar equivalent of hydrogen uptake, a mixture of **13b** and 2,4-pentanediol in a ratio of 91 to 9 was obtained. The optical yield of **13b** was 74%. (Entry 13). The complete hydrogenation of **13a** gave (*2R,4R*)-2,4-pentanediol of high optical purity.[5)]

The compounds, in which the ester group of **2a** was substituted with some other polar functional group such as $-SO_2CH_3$ (**14a**, **15a**),[6)] $-CH_2OH$ (**16a**),[7)] and $-CH_2OCH_3$ (**17a**) were found to be favorable substrates for the enantioface-differentiating hydrogenation with TA–NaBr–MRNi. As shown in Table 2 (Entries 14—17), the hydrogenation of these substrates over (*R,R*)-TA–NaBr–MRNi proceeded in reasonable optical yields in giving (*R*)-isomer in excess.

From the results mentioned above, it becomes evident that the essential factor for a good substrate is the presence of an oxygen atom bound to the β-carbon from the prochiral carbonyl group (to be hydrogenated as shown below).

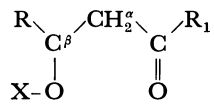

Discussion

The rigorous enantioface-differentiating reaction over MRNi should be attained when the preadsorbed modifying reagent is well settled on the nickel surface and offers uniform chiral binding sites for the prochiral substrate approaching the nickel surface. The adsorbed substrates are uniformly orientated on the nickel surface with one side of enantiofaces by the aid of the well-fitting interaction between binding sites of modifying reagent and substrate.

According to the physicochemical studies[8)] on the mode of adsorption of modifying reagent on the nickel surface, a 2-hydroxyl carboxylic acid is coordinated to a surface nickel atom only through its carboxyl group dissociated as a carboxylate ion, while its hydroxyl group is essentially free from the surface metal.

In order to implant a modifying reagent and make it stationary on the surface of a catalyst, interactions may be required between modifying reagent and catalyst surface at more than two points. Thus, the presence of two carboxyl groups is expected to be one of the necessary conditions for a good modifying reagent. This consideration is compatible with the experimental results that the modifying reagent of high e.d.a. are limited to α-hydroxyl and α,β-dihydroxyl dicarboxylic acid.

The poor e.d.a.'s of *O,O'*-dibenzoyl- and *O,O'*-dimethyl-TA indicate that no effective interactions leading to the efficient enantioface-differentiation take place between modifying reagent and MAA, as a result of the absence of free hydroxyl groups in the modifying reagent. Although α-hydroxyl dicarboxylic acids (malic acid, *O*-benzoyl-TA, and *O*-methyl-TA) gave moderate e.d.a.'s, high e.d.a.'s (more than 70%) were exhibited only by using α,β-dihydroxyl dicarboxylic acid. Thus it is evident that two hydroxyl groups in a modi-

Table 2. Enantioface differentiating hydrogenation of various prochiral ketones with TA-NaBr-MRNi

No.	Substrate	Reaction conditions[a]				Product(Configuration)	Chemical yield/%	Optical yield/%
		Substrate (mmol)	Solvent	Temp °C	Time h			
1	Methyl pyruvate(**1a**)	110	MP[b]	100	36	Methyl lactate(**1b**) (*S*)	95	2
2	Methyl acetoacetate(**2a**)	100	MP	100	5	Methyl 3-hydroxybutyrate(**2b**) (*R*)	98	86
3	Methyl 4-oxopentanoate(**3a**)	88	MP	100	48	Methyl 4-hydroxypenanoate(**3b**) (*R*)		
						4-Pentanolide(**3c**) (*R*)	78[c]	38
4	Methyl 5-oxohexanoate(**4a**)	80	MP	100	48	Methyl-5-hydroxyhexanoate(**4b**)		
						5-Hexanolide(**4c**) (*R*/*S*)	74[c]	0
5	2-Hexanone(**5a**)	101	THF	100	48	2-Hexanol(**5b**) (*S*)	82	28
6	Ethyl acetoacetate(**6a**)	88	THF	85	5	Ethyl 2-hydroxybutyrate(**6b**) (*R*)	97	87
7	Isopropyl acetoacetate(**7a**)	80	THF	100	5	Isopropyl 3-hydroxybutyric acid(**7b**) (*R*)	95	88
8	Isobutyl acetoacetate(**8a**)	72	THF	100	5	Isobutyl 3-hydroxybutyrate(**8b**) (*R*)	95	88
9	Hexyl acetoacetate(**9a**)	62	THF	100	5	Hexyl 3-hydroxybutyrate(**9b**) (*R*)	96	88
10	Methyl 3-oxopentanoate(**10a**)	88	MP	100	5	Methyl 3-hydroxypentanoate(**10b**) (*R*)[g]	75	87
11	Methyl 4-methyl-3-oxopentanoate(**11a**)	80	MP	100	5	Methyl 3-hydroxy-4-methylpenatanoate(**11b**) (*R*)[g]	80	87
12	Methyl 3-oxotetradecanoate(**12a**)	39	MP	100	5	Methyl 3-hydroxytetradecanoate(**12b**) (*R*)	(79)[d]	86[17]
13	Acetylacetone(**13a**)	105	THF	100	—	4-Hydroxy-2-pentanone(**13b**) (*R*)	—	74[4]
14	1-Methylsulfonyl-2-butanone(**14a**)	56	THF	100	15	Methyl 2-hydroxybutyl sulfone(**14b**) (*R*)	96[e]	68[6]
15	1-Methylsulfonyl-2-heptanone(**15a**)	46	THF	100	15	Methyl 2-hydroxyheptyl sulfone(**15b**) (*R*)	93[e]	69[6]
16	4-Hydroxy-2-butanone(**16a**)	120	THF	85	14	1,3-Butanediol(**16b**) (*R*)	88	69[7]
17	4-Methoxy-2-butanone(**17a**)	102	THF	85	14	4-Methoxy-2-butanol(**17b**) (*R*)[f]	90	68

a) Substrate(amount listed in table) in solvent(23 ml) and AcOH(0.2 ml) was subjected to hydrogenation at initial hydrogen pressure of 100—120 kg/cm^2. b) Methyl propionate, c) Isoated yields of **3c** and **4c**, d) Isolated yield of 3-hydroxytetradecanoic acid obtained by the saponification of hydrogenation product. e) Evaluated from the weight of crude crystals obtained after the removal of solvent. f) The optical rotation of the sample was the same sign as that of 4-methoxy-2-butanol obtained by the reaction of (*R*)-1,3-butanediol with CH_3I and Ag_2O. g) The absolute configuration of (−)-**10b** and (−)-**11b** was estimated to be *R*, on the fact that all known (−)-methyl 3-hydroxyalkanoates have *R*-configuration.

Table 3. Analytical data of synthesized modifying reagent

No.	Compound	Configuration	Mp θ_m/°C	$[\alpha]_D^{20}$/°		Found(%)		Calcd(%)		Ref.
				In this work	Literature	C	H	C	H	
1	2,3-Dihydroxy-2-methylbutanedioic acid	*2R,3R*	161	−5.61(*c* 3.2, H_2O)	−5.60	36.52	5.03	36.50	4.91	9
2	*O*-Benzoyltartaric acid	*R,R*	203	−6.4(*c* 1.16, EtOH)	−4.4	52.8	3.94	51.97	3.97	10
3	*O*-Methyltartaric acid	*R,R*	176	+47.2(*c* 2.5, H_2O)	+45.4(*c* 2, H_2O)	36.39	4.93	36.59	4.91	11
4	2,3-Dihydroxybutyric acid	*2S,3R*	109	−12.3(*c* 5, 1 M HCl)	−17.75(*c* 1, H_2O)	33.80	4.96	32.76	4.99	12
5	*O,O'*-Dibenzoyltartaric acid	*R,R*	84—87	−109.0(*c* 1.15, EtOH)	−125(*c* 1.13, EtOH)	57.61	4.15	57.45	4.29	13
6	*O,O'*-Dimethyltartaric acid	*R,R*	153—155	+74.3(*c* 8.8, H_2O)	+74.7(*c* 8.9, H_2O)	39.86	5.56	40.45	5.68	14

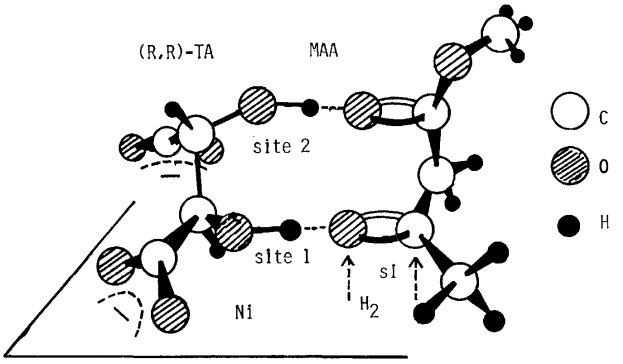

Fig. 1. Schematic representation of the interaction between (*R*,*R*)-TA and MAA on the MRNi.

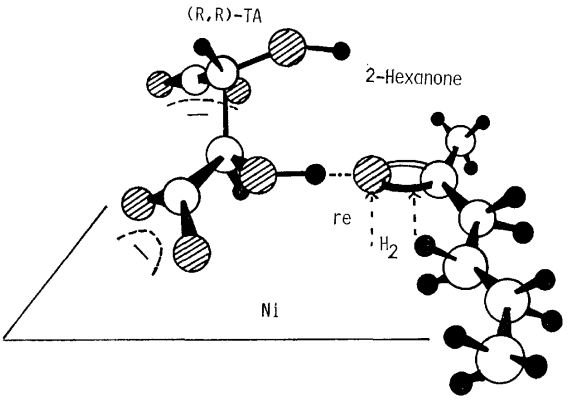

Fig. 2. Schematic representation of the interaction between (*R*,*R*)-TA and 2-hexanone on the MRNi.

fying reagent play an indispensable role in the enantioface-differentiation of MAA and analogs. Based on the hydrogen-bonding capacity between two hydroxyl groups in TA and two carbonyl groups in MAA, we have proposed the modes of co-adsorbed MAA and TA on the catalyst (Fig. 1).[5] When the mode of interaction is examined by a CPK model, it is expected that one of the hydroxyl groups of TA will come close to the catalyst surface (site 1), whereas the second hydroxyl group is somewhat remote from the surface (site 2).

If the adsorption of MAA takes place as shown in Fig. 1, the carbonyl group of MAA to be hydrogenated is fixed with site 1 and comes close to the surface of catalyst with its *si*-face facing to the catalyst. The MAA thus adsorbed is ready to be hydrogenated by the supply of activated hydrogen from the surface (*si*-face attack).

Thus, the hydrogenation of MAA over (*R*,*R*)-TA–NaBr–MRNi was expected to proceed predominantly by *si*-face attack.

As may be found in Fig. 1, the two hydroxyl groups of TA are arranged at a separation of around 2.5 Å and function as donors of the hydrogen bondings. Thus, it is predicted that not only MAA but also the compounds having two hydrogen bond acceptors arranged at a distance of around 2.5 Å, should be hydrogenated over TA–NaBr–MRNi in high optical yields. The good predictability of our stereochemical model is proved by the results summarized in Table 2. That is, all compounds satisfying the structural requirement shown in Fig. 1 were hydrogenated in high optical yields.

α-Keto ester (**1a**), which mostly exists in anti conformation, cannot make the interaction with TA through two hydrogen bonds. Even when it takes syn conformation its structure does not easily allow a well-fitting interaction with TA. Thus, the hydrogenation of **1a** was slow and gave an extremely poor optical yield.

In the case of γ-keto ester (**3a**), the distance between two carbonyl groups is a little longer than that between hydroxyl groups in TA. Therefore, a well fitting interaction leading to a high optical yield is not expected. However, the flexible nature enables the substrate to make some two-point interactions with TA. Thus, the hydrogenation of **3a** over (*R*,*R*)-TA–NaBr–MRNi gave (*R*)-**3b** in excess with a moderate optical yield.

A flexible $CH_3OCCH_2CH_2CH_2-$ group in δ-keto
O
ester (**4a**) behaves either as an acceptor of hydrogen bonding with its ester carbonyl, or as a simple hydrophobic alkyl chain. The almost negligible optical yield in the reaction of **4a** would be caused by the exsistence of the two opposite modes of adsorptions. One is the same adsorption mode as in **2a** or **3a** and gives the product of *si*-face attack. The other mode is caused by the repulsion of hydrophobic chain with the hydroxyl group of TA, as will be discussed shortly.

In the case of simple ketone (**5a**), the adsorption mode is determined only by the hydrophobic alkyl group. The proximity of the hydroxyl groups of TA on the catalyst is expected to form a highly hydrophilic region. When the carbonyl group of **5a** interacts with one of the hydroxy groups of TA (site 1), the other hydroxyl group of TA (site 2) should expel the large hydrophobic hydrocarbon residue of the substrate to the other side. Consequently, the mode of adsorption shown in Fig. 2, leading to the *re*-face attack in giving (*S*)-isomer in excess, is expected to be preferable for **5a**. Since this sort of differentiation originates from the repulsive force and the only one-point interaction between substrate and modifying reagent, the reaction rate and optical yield are expected to be less than those of β-keto ester. Thus, the stereochemistry and the slow rate of hydrogenation of **5a** were explained by the partial modification of the above-mentioned stereochemical model.

The data listed in Table 2 show that the substrate being hydrogenated at the higher rate gives always the higher optical yield. The result clearly shows that the some attractive force between modifying reagent and substrate leading to the rigorous stereocontrol also functions to increase the concentration of the substrate at the reaction site. That is, the enhancements of both optical yield and rate in the hydrogenation of β-keto esters over TA–MRNi must originate from the hydrogen bondings between the modifying reagent and the substrate on the catalyst surface.

Table 4. Hydrogenation products of various substrates over TA-NaBr-MNi

Substrate		Isolated product		Method for the determination of optical purity	Optically pure compound	
		Bp θ_b/°C(mmHg)	$[\alpha]_D^{20}$/°		$[\alpha]_D^{20}$/°	Configuration
1a	**1b**	60—61(35)	−0.16(neat)	A	−8.25(neat)	*S*[20]
2a	**2b**	70—71(20)	−19.0(neat)	A	−22.95(neat)	*R*
3a	**3c**	88—90(15)	+13.3(*c* 4, dioxane)	A	−35.1(*c* 4, dioxane)	*S*[21]
4a	**4c**	100—101(15)	0 (neat)	A	—	
5a	**5b**	134—136(760)	+3.24(neat)	A	+11.57(neat)	*S*[22]
6a	**6b**	80—81(20)	−13.8(*c* 10, ethanol)	B	—	
7a	**7b**	78—79(21)	−11.5(*c* 10, ethanol)	B	—	
8a	**8b**	101—103(20)	−10.9(*c* 10, ethanol)	B	—	
9a	**9b**	128—130(10)	−9.3(*c* 10, ethanol)	B	—	
10a	**10b**	80—82(17)	−12.6(*c* 5, ethanol)	C	—	
11a	**11b**	88—89(16)	−23.5(*c* 5, ethanol)	C	—	
17a	**17b**	52—53(15)	−20.6(*c* 10, ethanol)	C	—	

Experimental

The ^{1}H-NMR and IR spectra were taken with a JEOL-FX-100 spectrometer and a Shimadzu IR 27G spectrometer, respectively.

The optical rotation was measured with a Perkin Elmer 241 polarimeter. The GLC was carried out with a Shimadzu 6A-PF Gas Chromatography, using 3 m—5 mm o.d. glass column packed with 2% Silicone OV-17 on Chromosorb W. (OV-17), 5% Tween 80 on Shimalite W (TW 80), or 5% neopentyl glycol succinate on Chromosorb W (NPGS), at the stated temperature.

All chemicals except those described below were obtained from commercial sources and were used without further purification.

Modifying Reagent. All modifying reagents employed in this study were synthesized by the reported methods. The physical and analytical data are listed in Table 3.

Substrate. Methyl pyruvate (**1a**):[3] bp 61—63 °C/13 mmHg (1 mmHg≈133.322 Pa), methyl 4-oxopentanoate (**3a**):[3] bp 76—78 °C/12 mmHg, methyl 5-oxohexanoate (**4a**):[3] bp 95—97 °C/15 mmHg, isopropyl acetoacetate (**7a**):[15] bp 82—84 °C/13 mmHg, isobutyl acetoacetate (**8a**):[15] bp 88—90 °C/19 mmHg, hexyl acetoacetate (**9a**):[15] bp 133—134 °C/24 mmHg, methyl 3-oxopentanoate (**10a**):[16] bp 68—71 °C/13 mmHg, methyl 4-methyl-3-oxopentanoate (**11a**):[16] bp 85—87 °C/22 mmHg, methyl 3-oxotetradecanoate (**12a**):[17] mp 30 °C, methyl 2-oxobutylsulfone (**14a**):[18] mp 44.0—44.5 °C, methyl 2-oxoheptylsulfone (**15a**):[18] mp 37—38 °C, 4-hydroxy-2-butanone (**16a**):[7] bp 56—58 °C, and 4-methoxy-2-butanone (**17a**):[19] bp 48—49 °C/20 mmHg were prepared by the reported methods.

MRNi. The modifying solution was prepared by dissolving 0.67 mol equivalent of modifying reagent and 10 g of NaBr in 100 ml of deionized water.

The solution was adjusted to pH 3.2 with 1 mol dm^{-3} NaOH. The Raney nickel prepared from 1.9 g of alloy (Kawaken Fine Chemical Co. Ni/Al=42/58) was subjected to modification at 100 °C by the method reported before.[1]

Hydrogenation. The hydrogenation was carried out in a 100 ml autoclave under 90—120 kg/cm^2 of initial hydrogen pressure at the conditions specified in Table 1 or 2 in the text.

Data listed in Entries 12, 13, 14, 15, and 16 in Table 2 are taken from our published papers. The details of isolation and determination of optical purity of each reaction product are described in the paper cited in Table 2.

The hydrogenation products of **1a**, **2a**, **5a** to **11a**, and **17a** in Table 2 were purified by fractional distillation. The hydrogenation products of **3a** and **4a**, mixture of ester of hydroxy acid and lactone, were converted to the corresponding lactone by refluxing in benzene with Amberlyst 15 for 3 h.[3] The resulting lactone was purified by fractional distillation.

The isolated hydrogenation products are listed in Table 4.

The optical purity of the reaction products was determined by three different methods, referred to as A, B, and C in Table 4.

(A) The optical purity was directly determined by polarimetry based on the published value of $[\alpha]_D^{20}$ for optically pure material.

(B) The optical purity of the hydrogenation product was evaluated from the optical purity of MHB derived from the hydrogenation product via saponification and the following esterification with CH_2N_2.

(C) The optical purity was determined by ^{1}H-NMR in the presence of Eu(hfmc)$_3$. In the case of **10b**, and **11b**, the difference of chemical shift for methyl proton of $-\overset{\overset{O}{\|}}{C}-O-CH_3$ (singlet) of (*S*) and (*R*)-isomers was 5.5 Hz when the spectra were measured with solution of **10b** or **11b** (10 mg) and Eu(hfmc)$_3$ (25 mg) in 400 μl of $CDCl_3$.

In the case of **17b**, the difference for methyl proton of (*R*) and (*S*)-isomer was 8 Hz in the spectra taken with a solution of **17b** (10 mg) and Eu(hfmc)$_3$ (5 mg) in 400 μl of $CDCl_3$.

The results are listed in Table 2.

The authors wish to express their thanks to Professor Yoshiharu Izumi and Dr. Hiroshi Ozaki, Institute for Protein Research, Osaka University, for helpful suggestions.

This work was partially supported by Grant-in-Aid for Scientific Research No. 56540304 from the Ministry of Education, Science and Culture.

References

1) T. Harada, A. Tai, Y. Yamamoto, H. Ozaki, and Y. Izumi, Proc. 7th Int. Congr. Catal. Tokyo, 364 (1980).

2) A. Tai, H. Watanabe, and T. Harada, *Bull. Chem. Soc. Jpn.*, **52**, 1468 (1979).

3) S. Okamoto, T. Harada, and A. Tai, *Bull. Chem.*

Soc. Jpn., **52**, 2670 (1979).
4) A. Tai, K. Ito, and T. Harada, *Bull. Chem. Soc. Jpn.*, **54**, 223 (1981).
5) K. Ito, T. Harada, and A. Tai, *Bull. Chem. Soc. Jpn.*, **53**, 1179 (1980).
6) Y. Hiraki, K. Ito, T. Harada, and A. Tai, *Chem. Lett.*, **1981**, 131.
7) S. Murakami, T. Harada, and A. Tai, *Bull. Chem. Soc. Jpn.*, **53**, 1356 (1980).
8) A. Hatta and W. Suetaka, *Bull. Chem. Soc. Jpn.*, **48**, 2428 (1975).
9) S. Tatsumi, Y. Izumi, M. Imaida, and Y. Fukuda, *Bull. Chem. Soc. Jpn.*, **39**, 602 (1966).
10) W. Langenbeck and O. Herbst, *Chem. Ber.*, **86**, 1524 (1953).
11) W. N. Haworth, *J. Chem. Soc.*, **105**, 8 (1915).
12) F. W. Bachelor and G. A. Miana, *Can. J. Chem.*, **47**, 4089 (1969).
13) C. L. Butler and L. H. Cretcher, *J. Am. Chem. Soc.*, **55**, 2605 (1933).
14) T. Purdie and J. C. Irvine, *J. Chem. Soc.*, **79**, 962 (1902).
15) S. O. Lawessor, S. Gronwall, and R. Sandberg, *Org. Syn.*, Coll. Vol. V, p. 155 (1973).
16) B. Riegel and W. M. Lilienfeld, *J. Am. Chem. Soc.*, **67**, 1273 (1945).
17) N. Nakahata, M. Imaida, H. Ozaki, T. Harada, and A. Tai, *Bull. Chem. Soc. Jpn.*, **55**, 2186 (1982).
18) H. O. House and J. K. Larson, *J. Org. Chem.*, **33**, 61 (1968).
19) R. C. Elderfield, *J. Am. Chem. Soc.*, **72**, 1334 (1950).
20) T. Purdie and J. C. Irvine, *J. Chem. Soc.*, **75**, 484 (1899).
21) H. Minato, *Chem. Pharam. Bull.*, **9**, 625 (1961).
22) R. H. Pickard and J. Kenyon, *J. Chem. Soc. Trans.*, **99**, 1/3 44 (1911).

Aryl Rearrangement on the Photolysis of 2-Aryl-2-ethoxy-2-phenylethyl Cobaloxime

Masaru TADA,* Kunimi INOUE, and Masami OKABE

Department of Chemistry, School of Science and Engineering, Waseda University, Shinjuku-ku, Tokyo 160

(Received June 7, 1982)

The photolysis of 2-aryl-2-ethoxy-2-phenylethyl cobaloxime followed by hydrolysis gave two kinds of substituted 1,2-diphenylethanones arising *via* phenyl or substituted-phenyl migration. The substituent effect on the aryl rearrangement is similar to that on the reported neophyl rearrangement, and the rearrangement takes place by a radical mechanism without the deep involvement of cobaloxime(II).

Organo-bis(dimethylglyoximato)(pyridine)cobalt(III), hereafter organo-cobaloxime(III) or R–(Co), has been often used as a model compound of coenzyme B_{12}, organo-cobalamin(III).[1] The photolysis of the Co–C bond of an organo-cobaloxime(III) gives organic radical and cobaloxime(II), (Co^{II}), pair[2] which reasonably mimics the substrate radical and cobalamin(II) in an enzymatic system.[3] In studies on the photolyses of β-acylalkyl cobaloximes, we have demonstrated that the migration of the β-acyl group takes place in a radical state.[1b] However, we have not ruled out the possibility that the rearrangement takes place under the influence of the paramagnetic cobaloxime(II). Some interactions between cobaloxime(II) and the organic radical can be envisaged; one is a charge transfer, and another is a orbital interaction.

It has been established that the neophyl rearrangement has a slightly polar character as depicted in Eq. 1 in an exaggerated manner.[4] These situations

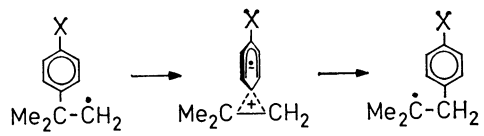

(1)

prompted us to investigate the substituent effect in the aryl rearrangement on the photolysis of 2-aryl-2-ethoxy-2-phenylethyl cobaloxime(III) (**1**). The same substituent effect as the reported neophyl rearrangement should be observed if the rearrangement is not influenced by cobaloxime(II).

Results

Preparation of 2-Aryl-2-ethoxy-2-phenylethyl Cobaloxime (1). The route of synthesizing the organo-cobaloxime is shown in Eq. 2. 1-Aryl-1-phenylethene

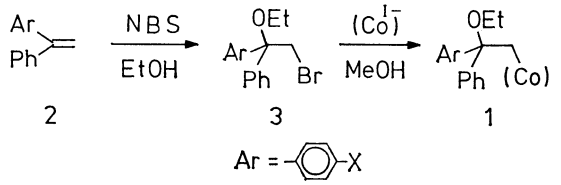

(2)

(**2**) was obtained by the reaction of (*p*-substituted phenyl)magnesium bromide with acetophenone or the reaction of phenylmagnesium bromide with *p*-substituted acetophenone followed by dehydration. The olefin **2** was then treated with *N*-bromosuccinimide in ethanol to give 2-aryl-2-ethoxy-2-phenylethyl bromide (**3**). The organo-cobaloxime **1** was prepared by the reaction of the bromide **3** with cobaloxime(I) anion.[5] The structure of the organo-cobaloxime **1** was ascertained by elemental analysis and spectral data (see the Experimental part).

Photolysis of Organo-cobaloxime 1 in Benzene. Anaerobic photolysis followed by acid treatment of 2,2-diphenyl-2-ethoxyethyl cobaloxime (**1a**) gave 1,2-diphenylethanone (**5a**), which formed by the hydrolysis of the primary products, *cis*- and *trans*-enol ethers **4**[6] (Eq. 3). The photolyses of the organo-cobaloximes

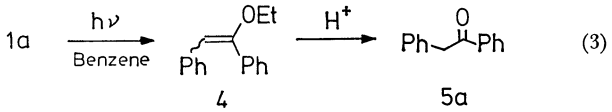

(3)

1b—e followed by hydrolyses gave two kinds of substituted 1,2-diphenylethanones arising *via* phenyl group migration (**5b—d**) or *via* substituted phenyl group migration (**6b—e**) (Table 1). The residual organo-cobaloximes decomposed into olefins **2** on chromatography of the products on Florisil in the workup step. This property is common to 2-alkoxy-2,2-diarylethyl cobaloximes.[7] The material balance before and after the reaction is well maintained in all photolyses.

When the *p*-substituent X was an electron-withdrawing group, the substituted phenyl group migrated in preference to the phenyl group. When the substituent was cyano group (X=CN), no migration of phenyl group was observed. When the substituent was an electron-releasing group (X=Me), the phenyl group migrated preferentially.

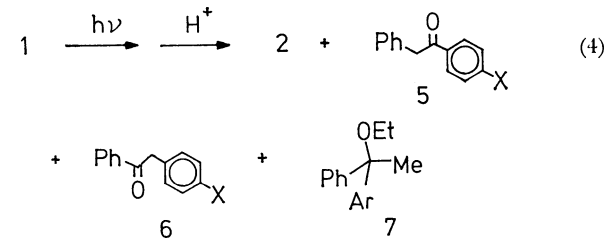

(4)

Photolysis of Organo-cobaloxime 1 in Chloroform or Acetonitrile. The anaerobic photolysis of **1** in chloroform gave the ketones **5** and **6** together with 1-aryl-1-ethoxy-1-phenylethane (**7**) (Table 2).[8] The latter product is expected to be generated by the hydrogen abstraction of the radical intermediate from chloroform. The photolysis in chloroform is faster than in benzene and no starting material was left under similar

Table 1. Photolysis of organo-cobaloxime 1 in benzene

Substrate	Substituent X	Product composition (%) 5	6	Ratio 6/5	k_{rel}[a]	Total yield/% 5+6
1a	H	50[b]	50[b]	1.00	1.00	62
1b	Me	60	40	0.67	0.72	73
1c	Cl	24	76	3.17	1.76	78
1d	Br	21	79	3.76	1.91	93
1e	CN	0	100	—	35.0	75

a) Relative rate of the migration of *p*-substituted phenyl group to that of the phenyl group; the values were determined by the thermal decomposition of the ester of 3-aryl-3-methylperoxybutanoic acid (C. Rüchardt and R. Hecht).[4] b) In the case of **1a** the product was divided equally been **5** and **6**.

Table 2. Photolysis of organo-cobaloxime 1 in chloroform or acetonitrile

Substrate	Substituent X	Solvent	Product composition (%) 5	6	7	Product ratio 6/5	7/5	Total yield/% 5+6+7
1a	H	$CHCl_3$	27[a]	27[a]	46	1.00	1.69	82
1b	Me	$CHCl_3$	28	16	56	0.57	2.00	70
1c	Cl	$CHCl_3$	17	50	33	2.94	1.92	82
1e	CN	$CHCl_3$	0	100	0	—	—	72
1b	Me	MeCN	59	41	Trace	0.69	*ca.* 0	58
1c	Cl	MeCN	21	79	0	3.76	0	80
1e	CN	MeCN	0	100	0	—	—	73

a) In the case of **1a** the migrated product was divided equally between **5** and **6**.

conditions to the photolysis in benzene. The photolyses of the cobaloxime in chloroform or chloroform itself is expected to produce hydrogen chloride in trace amount, and the acid hydrolysis of the enol ethers seem to take place under the photolysing conditions.

The ratios of **6/5** in chloroform are similar to those in benzene. The ratio of hydrogen abstraction to phenyl rearrangement (**7/5**) does not vary much with the substituent X on the non-rearranged aryl group.

The photolysis of organo-cobaloxime **1** in acetonitrile, a polar solvent, gave similar results as in benzene except for the formation of **7b** in trace amount from **1b** (Table 2).

Discussion

In the present study we found that the order of the aryl groups in migration-ability is similar to the order in the neophyl rearrangement by a radical mechanism.[4] This finding indicates that the aryl migration on the photolysis of organo-cobaloxime **1** involves a radical mechanism. The substituent effect observed in the present study and the reported neophyl rearrangement is interpreted in terms of the slightly polar transition state (**9** or **10**). The polarization can be ascribed to the electron-releasing character of the

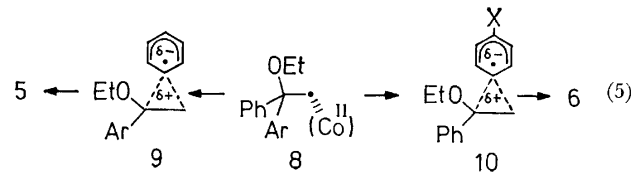

cyclopropane ring.[9] When the substituent X is an electron-withdrawing group, the transition state **10** is more stabilized and the migration of the *p*-substituted phenyl group becomes more favorable (Eq. 5).

The ratio of **6/5** is not much affected by the polarity of the solvent; this indicates that the charge transfer or electron transfer between (Co^{II}) and the radical species is not an important factor in driving the rearrangement. Furthermore the charge separation in the transition states (**9** and **10**) is not so extensive that the stabilization of the transition states does not depend strongly on the polarity of the solvent. From the limitation of the present study we can not discuss the absolute formation rate of **5** and **6**, and the discussion must be limited to the relative rate of phenyl or aryl migration. The present findings are explained by the assumption that both transition states **9** and **10** are stabilized to a similar extent by a polar solvent. The solvent dependence of the formation of **7** can be understood as a consequence of the hydrogen donating ability of the solvent.[10] It can be assumed that the rates of hydrogen abstraction and phenyl migration are independent of the substituent X on the non-rearranged aryl group. Therefore the variation in the formation of **5** and **7** depending on X in chloroform can be explained in terms of the difference in the rate of the migration of the substituted phenyl group.

The organo-cobaloxime **1e** (X=CN) did not give the hydrogen-abstracted product **7** even in chloroform, a strong hydrogen donor. On the other hand, the decomposition of the ester of 3-(*p*-cyanophenyl)-3-methylperoxybutanoic acid gives a small amount of the hydrogen-abstracted product even in tetralin,[4] which is a weaker hydrogen donor than chloroform.[10] It

is considered that cobaloxime(II) in the radical pair **8** may promote the rearrangement by weak orbital interaction.

In conclusion the photolysis of organo-cobaloxime **1** causes the homolytic cleavage of Co–C bond, and the resulting radical pair does not cause the charge transfer or electron transfer between cobaloxime(II) and the organic radical. The intervention of ionic species in the rearrangement is thus ruled out, though the weak orbital interaction in the radical pair may promote the rearrangement. The explanation of the insensitivity of the formation ratio **6**/**5** to solvent polarity must await more ellaborate studies.

Experimental

Preparation of 1-Aryl-1-phenylethene (2). The preparations of 1,1-diphenylethene (**2a**),[11] 1-(*p*-methylphenyl)-1-phenylethene (**2b**),[12] 1-(*p*-chlorophenyl)-1-phenylethene (**2c**),[13] and 1-(*p*-bromophenyl)-1-phenylethene (**2d**),[14] are described in the literature. 1-(*p*-Cyanophenyl)-1-phenylethene (**2e**) is prepared as described below.

To a solution of *p*-cyanoacetophenone (7.25 g, 50 mmol) in dry ether (100 cm^3) a solution of phenylmagnesium bromide (50 mmol) in dry ether (20 cm^3) was added dropwise at 0 °C. After stirring for 30 min at room temperature, saturated ammonium chloride solution (10 cm^3) was added dropwise at 0 °C. The ethereal solution was decanted and evaporated to give crude 1-(*p*-cyanophenyl)-1-phenylethanol. A mixture of the crude material and powdered potassium hydrogensulfate (8 g) in toluene (50 cm^3) was refluxed for 10 h. After the addition of water (50 cm^3), the mixture was extracted with ether (2×50 cm^3). The combined ethereal extracts were dried over anhydrous sodium sulfate. Distillation gave 5.06 g (49%) of pure **2e**, bp 116 °C/93 Pa. Found: C, 87.52; H, 5.58; N, 6.49%. Calcd for $C_{15}H_{11}N$: C, 87.77; H, 5.40; N, 6.82%. IR (CCl_4) 2225, 901, and 698 cm^{-1}; NMR (CCl_4) δ=5.51 (d, 1H, J=1 Hz), 5.57 (d, 1H, J=1 Hz), 7.22—7.45 (m, 5H), 7.47 (d, 2H, J=8 Hz), and 7.63 (d, 2H, J=8 Hz).

Preparation of 2-Aryl-2-ethoxy-2-phenylethyl Bromide (3). 2,2-Diphenyl-2-ethoxyethyl bromide (**3a**) was prepared from **2a** by the reported method.[15] The general procedure for the preparations of 2-ethoxy-2-(*p*-methylphenyl)-2-phenylethyl bromide (**3b**), 2-(*p*-chlorophenyl)-2-ethoxy-2-phenylethyl bromide (**3c**), 2-(*p*-bromophenyl)-2-ethoxy-2-phenylethyl bromide (**3d**), and 2-(*p*-cyanophenyl)-2-ethoxy-2-phenylethyl bromide (**3e**) is described below.

To a suspension of *N*-bromosuccinimide (2 g, 11.2 mmol) in dry ethanol (20 cm^3) a solution of **2** (10 mmol) in dry ethanol (10 cm^3) was added dropwise at −10 °C. After stirring for 2 h at −10 °C and for 4 h at room temperature, the resulting succinimide was filtered off and the filtrate was evaporated. The residue was placed on a silica gel column and eluted with benzene to give the bromide **3** (53—77%). **3b**—**e** were converted directly to the organo-cobaloximes **1b**—**e** without further purification.

3b, oil; NMR (CCl_4) δ=1.18 (t, 3H, J=7 Hz), 2.25 (s, 3H), 3.23 (q, 2H, J=7 Hz), 4.13 (s, 2H), and 6.95—7.48 (m, 9H).

3c, oil; NMR (CCl_4) δ=1.23 (t, 3H, J=7 Hz), 3.23 (q, 1H, J=7 Hz), 3.27 (q, 1H, J=7 Hz), 4.05 (d, 1H, J=12 Hz), 4.13 (d, 1H, J=12 Hz), and 7.08—7.43 (m, 9H).

3d, oil; NMR (CCl_4) δ=1.20 (t, 3H, J=7 Hz), 3.18 (q, 1H, J=7 Hz), 3.23 (q, 1H, J=7 Hz), 4.07 (d, 1H, J=12 Hz), 4.13 (d, 1H, J=12 Hz), and 7.06—7.58 (m, 9H).

3e, mp 97—99 °C; IR (CCl_4) 2225 and 697 cm^{-1}; NMR (CCl_4) δ=1.20 (t, 3H, J=7 Hz), 3.18 (q, 1H, J=7 Hz), 3.31 (q, 1H, J=7 Hz), 4.12 (d, 1H, J=10 Hz), 4.23 (d, 1H, J=10 Hz), 7.12—7.40 (m, 5H), and 7.45 (bs, 4H).

Preparation of 2-Aryl-2-ethoxy-2-phenylethyl Cobaloxime (1). The organo-cobaloxime **1** was prepared from the bromide **3** (5 mmol) and cobaloxime(I) (6 mmol) in methanol (15 cm^3) in the conventional manner.[7] Chromatography on aluminum oxide containing 10% (w/w) of water using benzene–chloroform as an eluent and recrystallization from acetonitrile yielded pure **1** (44—65%).

The strong infrared absorption bands due to the cobaloxime(III) moiety are common to all **1**: 1560, 1450, 1240—1200, and 1100—960 cm^{-1}.

1a, mp 142 °C (decomp). Found: C, 58.29; H, 5.96; N, 11.99%. Calcd for $C_{29}H_{36}N_5O_5Co$: C, 58.68; H, 6.11; N, 11.80%. NMR ($CDCl_3$) δ=1.22 (t, 3H, J=7 Hz), 1.83 (s, 12H), 2.56 (s, 2H), 3.00 (q, 2H, J=7 Hz), 6.85—7.30 (m, 12H), 7.45—7.63 (m, 1H), and 8.35—8.47 (m, 2H).

1b, mp 146 °C (decomp). Found: C, 59.30; H, 6.51; N, 11.68%. Calcd for $C_{30}H_{38}N_5O_5Co$: C, 59.30; H, 6.30; N, 11.53%. NMR ($CDCl_3$) δ=1.29 (t, 3H, J=7 Hz), 1.81 (s, 12H), 2.15 (s, 3H), 2.45 (d, 1H, J=10 Hz), 2.65 (d, 1H, J=10 Hz), 2.97 (q, 2H, J=7 Hz), 6.73—7.27 (m, 11H), 7.39—7.60 (m, 1H), and 8.32—8.45 (m, 2H).

1c, mp 156 °C (decomp). Found: C, 55.73; H, 5.75; N, 11.26%. Calcd for $C_{29}H_{35}N_5O_5ClCo$: C, 55.46; H, 5.62; N, 11.15%. NMR ($CDCl_3$) δ=1.20 (t, 3H, J=7 Hz), 1.82 (s, 12H), 2.36 (d, 1H, J=10 Hz), 2.56 (d, 1H, J=10 Hz), 2.96 (q, 1H, J=7 Hz), 2.99 (q, 1H, J=7 Hz), 6.78—7.37 (m, 11H), 7.43—7.56 (m, 1H), and 8.36—8.55 (m, 2H).

1d, mp 158 °C (decomp). Found: C, 52.10; H, 5.16; N, 10.08%. Calcd for $C_{29}H_{35}N_5O_5BrCo$: C, 51.80; H, 5.25; N, 10.41%. NMR ($CDCl_3$) δ=1.24 (t, 3H, J=7 Hz), 1.85 (s, 12H), 2.35 (d, 1H, J=10 Hz), 2.64 (d, 1H, J=10 Hz), 2.97 (q, 1H, J=7 Hz), 3.03 (q, 1H, J=7 Hz), 6.94—7.38 (m, 11H), 7.51—7.71 (m, 1H), and 8.46—8.56 (m, 2H).

1e, mp 154 °C (decomp). Found: C, 58.03; H, 5.78; N, 13.80%. Calcd for $C_{30}H_{35}N_6O_5Co$: C, 58.25; H, 5.70; N, 13.59%. NMR ($CDCl_3$) δ=1.22 (t, 3H, J=7 Hz), 1.87 (s, 6H), 1.91 (s, 6H), 2.43 (d, 1H, J=10 Hz), 2.63 (d, 1H, J=10 Hz), 3.03 (q, 1H, J=7 Hz), 3.10 (q, 1H, J=7 Hz), 6.98—7.87 (m, 12H), and 8.43—8.62 (m, 2H). IR ($CHCl_3$) 2230 cm^{-1}.

Photolysis of Organo-cobaloxime 1. A Typical Procedure for 1a in Benzene: A solution of the organo-cobaloxime **1a** (1.25×10^{-3} mol dm^{-3}) in benzene (15 cm^3) was placed in a Pyrex tube, dipped in an ultrasonic bath, and bubbled with argon from a syringe needle for 30 min. The solution was irradiated externally for 12 h with a 450-W high-pressure Hg lamp mounted in a rotary irradiation apparatus (Rikosha RH-400), the distance between the lamp and the reaction tube being *ca.* 5 cm. The reaction solution was evaporated *in vacuo* and the residue was chromatographed on Florisil, using chloroform as an eluent, to give the mixture of *cis*- and *trans*-enol ethers **4**[16] containing a small amount of **2a**. A solution of the enol ethers **4** in ether/ methanol/ aqueous hydrogen chloride (6 mol dm^{-3}) (5:3:1) was stirred overnight. After the addition of saturated aqueous sodium hydrogencarbonate, the mixture was extracted several times with ether. The combined ethereal extracts were washed with water and dried over anhydrous sodium sulfate. Evaporation of the solvent gave 1,2-diphenylethanone (**5a**) and **2a**.

Photolyses of ***1b—e*** *in Benzene*: The photolyses of **1b—e** were carried out by the procedure described above. A similar workup gave the mixture of olefin **2** and enol ethers containing a small amount of hydrolysis products **5** and **6**. Acid treatment of the mixture gave the products **2**, **5**, and **6**, which were identified by comparison with authentic samples synthesized by reported methods.[16-22] The results are summarized in Table 1. The physical data of the products are as follows.

5b,[16] mp 106—108 °C. IR ($CHCl_3$) 1677 cm^{-1}; NMR ($CDCl_3$) δ=2.38 (s, 3H), 4.23 (s, 2H), 7.03—7.43 (m, 7H), and 7.91 (d, 2H, J=8 Hz).

6b,[17] mp 92—94 °C. IR ($CHCl_3$) 1675 cm^{-1}; NMR ($CDCl_3$) δ=2.28 (s, 3H), 4.22 (s, 2H), 7.14 (s, 4H), 7.37—7.60 (m, 3H), and 7.87—8.17 (m, 2H).

5c,[18] mp 106—108 °C. IR ($CHCl_3$) 1680 cm^{-1}; NMR ($CDCl_3$) δ=4.22 (s, 2H), 7.22 (bs, 5H), 7.34 (d, 2H, J=8 Hz), and 7.90 (d, 2H, J=8 Hz).

6c,[19] mp 132—133 °C. IR ($CHCl_3$) 1681 cm^{-1}; NMR ($CDCl_3$) δ=4.22 (s, 2H), 7.03—7.62 (m, 7H), and 7.82—8.07 (m, 2H).

5d,[20] mp 110—111 °C. IR ($CHCl_3$) 1680 cm^{-1}; NMR ($CDCl_3$) δ=4.18 (s, 2H), 7.20 (bs, 5H), 7.48 (d, 2H, J=9 Hz), and 7.76 (d, 2H, J=9 Hz).

6d,[21] mp 145—147 °C. IR ($CHCl_3$) 1681 cm^{-1}; NMR ($CDCl_3$) δ=4.20 (s, 2H), 7.08 (d, 2H, J=9 Hz), 7.30—7.64 (m, 5H), and 7.88—8.01 (m, 2H).

6e,[22] mp 112—114 °C. IR ($CHCl_3$) 2240 and 1686 cm^{-1}; NMR ($CDCl_3$) δ=4.33 (s, 2H), 7.20—7.69 (m, 7H), and 7.84—8.12 (m, 2H).

Photolysis of ***1a*** *in Chloroform*: The same procedure for the photolysis in benzene was employed but the acid treatment was not required. The products thus obtained are **5a** and 1,1-diphenyl-1-ethoxyethane (**7a**) (see Table 2).

7a, oil. IR (CCl_4) 702 cm^{-1}; NMR (CCl_4) δ=1.27 (t, 3H, J=7 Hz), 1.78 (s, 3H), 3.20 (q, 2H, J=7 Hz), and 6.90—7.38 (m, 10H). The structure of **7a** was determined by an unequivocal synthesis from 1,1-diphenylethanol,[11] diethyl sulfate, and sodium hydride in THF.

Photolyses of ***1b***, ***1c***, *and* ***1e*** *in Chloroform*: The photolyses of **1b**, **1c**, and **1e** were carried out by using the same procedure as for the photolysis of **1a** in chloroform, and the results are summarized in Table 2.

7b, oil. IR (CCl_4) 701 cm^{-1}; NMR (CCl_4) δ=1.15 (t, 3H, J=7 Hz), 1.74 (s, 3H), 2.23 (s, 3H), 3.18 (q, 2H, J=7 Hz), and 6.79—7.28 (m, 9H). The structure of **7b** was determined by an unequivocal synthesis from 1-(*p*-methylphenyl)-1-phenylethanol,[12] diethyl sulfate, and sodium hydride in THF.

7c, oil. IR (CCl_4) 701 cm^{-1}; NMR (CCl_4) δ=1.16 (t, 3H, J=7 Hz), 1.74 (s, 3H), 3.18 (q, 2H, J=7 Hz), and 6.97—7.29 (m, 9H). The structure of **7c** was determined by an unequivocal synthesis from 1-(*p*-chlorophenyl)-1-phenylethanol,[13] diethyl sulfate, and sodium hydride in THF.

Photolyses of ***1b***, ***1c***, *and* ***1e*** *in Acetonitrile*: The same procedure described for the photolysis of **1a** in benzene was employed and the results are summarized in Table 2.

References

1) a) G. N. Schrauzer and R. J. Windgassen, *J. Am. Chem. Soc.*, **89**, 143 (1967); J. N. Lowe and L. L. Ingraham, *ibid.*, **93**, 3801 (1971); R. B. Silverman and D. Dolphin, *ibid.*, **98**, 4626 (1976); B. T. Golding, T. J. Kemp, C. S. Sell, P. J. Sellars, and W. P. Watson, *J. Chem. Soc. Perkin Trans. 2*, **1978**, 839; H. Flohr, W. Pannhorst, and J. Retey, *Helv. Chim. Acta*, **61**, 1565 (1978); M. P. Atkins, B. T. Golding, A. Bury, M. D. Johnson, and P. J. Sellars, *J. Am. Chem. Soc.*, **102**, 3630 (1980). b) M. Tada, K. Miura, M. Okabe, S. Seki, and H. Mizukami, *Chem. Lett.*, **1981**, 33; M. Okabe, T. Osawa, and M. Tada, *Tetrahedron Lett.*, **22**, 1899 (1981).

2) M. Tada, M. Okabe, and K. Miura, *Chem. Lett.*, **1978**, 1135; B. T. Golding, T. J. Kemp, P. J. Sellars, and E. Nocchi, *J. Chem. Soc., Dalton Trans.*, **1977**, 1266.

3) B. M. Babior, *Acc. Chem. Res.*, **8**, 376 (1975).

4) C. Ruchardt and R. Hecht, *Chem. Ber.*, **98**, 2471 (1965).

5) G. N. Schrauzer, *Inorg. Synth.*, **11**, 65 (1968).

6) The spectral data of the mixture of *cis*- and *trans*-enol ethers **4** were reported and coincide with the present data except for the relative intensity of each absorption band. W. Grell and H. Machleidt, *Justus Liebigs Ann. Chem.*, **699**, 53 (1966).

7) M. Okabe and M. Tada, *Bull. Chem. Soc. Jpn.*, **55**, 1498 (1982).

8) The photolysis of **1d** in chloroform gave **5a** besides **5d**, **6d**, and **7d**. **5a** must be a secondary product since those ketones **5d** and **6d** gave **5a** under the reaction conditions, and therefore the result of the photolysis of **1d** is omitted from Table 2.

9) K. Komatsu, I. Tomioka, and K. Okamoto, *Tetrahedron Lett.*, **21**, 947 (1980).

10) J. K. Kochi, "Free Radicals," John-wiley and Sons, New York (1973), Vol. 1, pp. 299 and 303.

11) C. F. H. Allen and S. Converse, *Org. Synth.*, Coll. Vol. I, 226 (1956).

12) C. D. Hurd and C. N. Webb, *J. Am. Chem. Soc.*, **49**, 546 (1927).

13) E. Bergmann and A. Bondi, *Chem. Ber.*, **64**, 1468 (1931).

14) A. G. Evans, P. M. S. Jones, and J. H. Thomas, *J. Chem. Soc.*, **1958**, 4563.

15) P. Lipp, *Chem. Ber.*, **56**, 567 (1923).

16) F. Brown and F. G. Mann, *J. Chem. Soc.*, **1948**, 858.

17) A. Mckenzie, A. K. Mill, and J. R. Myles, *Chem. Ber.*, **63**, 904 (1930).

18) K. B. Wiberg and O. Aniline, *J. Org. Chem.*, **37**, 3229 (1972).

19) A. Fischer, B. A. Grigor, J. Packer, and J. Vaughan, *J. Am. Chem. Soc.*, **83**, 4208 (1961).

20) E. P. Kohler and W. D. Peterson, *J. Am. Chem. Soc.*, **55**, 1073 (1933).

21) R. Hüttel and K. Franke, *Chem. Ber.*, **93**, 1433 (1960).

22) A. Padwa, T. Brookhart, D. Dehm, and G. Wubbels, *J. Am. Chem. Soc.*, **100**, 8247 (1978).

A Convenient Method for the Synthesis of Adenylyl-(2′—5′)-adenylyl-(2′—5′)-adenosine Using 3′-*O*-Benzoyladenosine Derivatives

Hiroshi TAKAKU* and Souichi UEDA

Laboratory of Organic Chemistry, Chiba Institute of Technology, Tsudanuma, Narashino, Chiba 275

(Received July 5, 1982)

N^6,3′-*O*-Dibenzoyladenosine was prepared by treating 2′,3′-*O*-(dibutylstannylene)-N^6-benzoyladenosine with benzoyl chloride in methanol. The trimeric adenylyl-(2′—5′)-adenylyl-(2′—5′)-adenosine was synthesized in a good yield using N^6,3′-*O*-dibenzoyladenosine as the starting material *via* the phosphotriester approach.

It has recently been reported[1] that 5′-*O*-triphosphoryl-adenylyl-(2′—5′)-adenylyl-(2′—5′)-adenosine (pppA$^{2'}$p$^{5'}$A$^{2'}$p$^{5'}$A) is isolated from interferon-treated cells and is acting as an inhibitor of cell-free protein synthesis. The pppA$^{2'}$p$^{5'}$A$^{2'}$p$^{5'}$A is synthesized from rabbit reticulocytes with double-stranded RNA and ATP. The core A$^{2'}$p$^{5'}$A$^{2'}$p$^{5'}$A has also been found to be an inhibitor of Concanavalin A-stimulated DNA synthesis.[2] Consequently, several groups have recently described the chemical synthesis of various structurally modified 2′—5′ linked triadenylates.[3]

In this paper, we report a convenient method for the synthesis of adenylyl-(2′—5′)-adenylyl-(2′—5′)-adenosine (2—5 core) by using N^6,3′-*O*-dibenzoyladenosine as the starting material.

Preparation of N^6,3′-O-*Dibenzoyladenosine.* Moffatt and his co-workers have recently reported[4] that when 2′,3′-*O*-stannylene nucleosides were treated with benzoyl chloride and triethylamine in dry methanol, 3′-*O*-benzoylnucleoside derivatives were obtained in good yields. This method may serve for the preparation of 3′-*O*-protected adenosine derivative as a key intermediate for the synthesis of 2′—5′ adenylate trimers.

We examined the preparation of N^6,3′-*O*-dibenzoyladenosione **3** by a modification of the procedure of Moffatt and his co-workers[4]. 2′,3′-*O*-(Dibutylstannylene)-N^6-benzoyladenosine (**2**) was easily obtained as a crystalline product in 56% yield by the reaction of N^6-benzoyladenosine (**1**) with dibutyltin oxide in dry methanol, and by subsequent crystallization of the product from ethanol–acetone. In this reaction, a very small ammount of debenzoylated product can be detected on TLC. However, the by-product could be separated from **2** since it was removed by crystallization from ethanol–acetone.

Nucleoside derivative **2** thus obtained (1.0 molar equiv.) was treated with benzoyl chloride (5.0 molar equiv.) in the presence of triethylamine (5.0 molar equiv.) in dry methanol at room temperature. After 15 min, the reaction mixture was worked up and purified to give N^6,3′-*O*-dibenzoyladenosine (**3**) in 48% yield. Product **3** was characterized by elemental analysis and NMR spectroscopy. ^{1}H-NMR spectra of **3** showed the characteristic downfield of the H-1′ and H-3′ signals, and the presence of signals due to the $C_{2'}$–OH and $C_{5'}$–OH groups. For H-1′ of **3**, the data were consistent with the rules developed by Reese and his co-workers;[5] namely 3′-substituted compounds had larger $J_{1',2'}$ coupling constants, and their H-1′ signal showed high field shifts compared to that of the 2′-isomar.

The reaction of **3** with dimethoxytrityl chloride in dry pyridine gave corresponding 5′-*O*-dimethoxytrityl-N^6-dibenzoyladenosine (**4**) in 86% yield.

When **3** was treated with methanolic ammonia for 16 h at 25 °C, the corresponding adenosine was obtained in 97% yield.

Synthesis of Adenylyl-(2′—5′)-adenylyl-(2′—5′)-adenosine (Core). The synthesis of 2′—5′ linked triadenylates (2—5 core) **8** by using **4** is as follows: The nucleoside derivative **4** was phosphorylated with 5-chloro-8-quinolyl phosphate[6] in the presence of 8-quinolylsulfonyl chloride (QS)[7] in dry pyridine for 2 h to give correspondong phosphodiester **5** in almost quantitative yield. The ^{31}P NMR spectrum of **5** (pyridine) consists of one resonance signal at δ +4.68.

Phosphodiester intermediate **5** thus obtained (1.5 molar equiv.) was now allowed to react together with N^6, 2′,3′-*O*-tribenzoyladenosine (1.0 molar equiv.) and 1-(8-quinolylsulfonyl)-1*H*-tetrazole (QS-te)[8] After 1 h, no starting material, N^6,2′,3′-*O*-tribenzoyladenosine

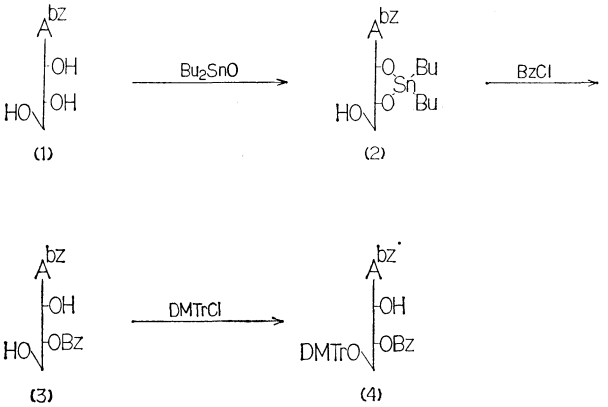

Scheme 1.

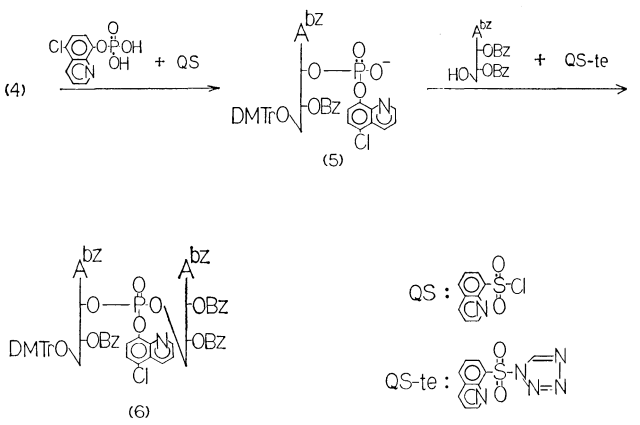

Scheme 2.

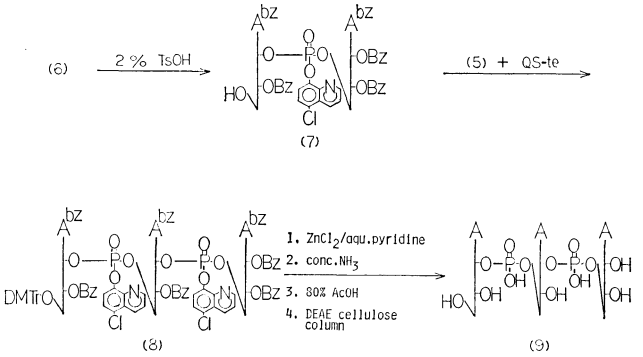

Scheme 3.

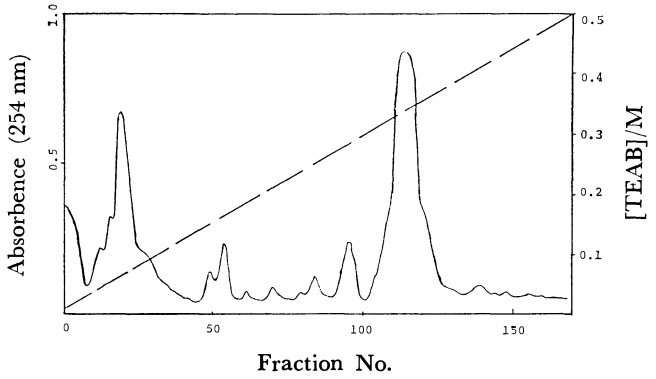

Fig. 1. Chromatography of the trinucleotide on a column (1.0×55 cm) of DEAE cellulose DE-52 equilibrated with 0.01 M TEAB. Elution was performed with a linear gradient of TEAB (0.01—0.5 M, total 550 ml). Fractions of 3 ml were collected every 10 min. The main peak contained the product $A^{2'}p^{5'}A^{2'}p^{5'}A$.

can be detected on TLC in the reaction mixture. Work-up and purification by short silica-gel column chromatography afforded the required dinucleotide **6** in 92% yield. Fully protected dinucleotide **6** was treated with 2% *p*-toluenesulfonic acid solution in a mixture of dichloromethan and methanol (7:3 v/v) for 15 min at 0 °C.[6] The reaction mixture was neutralized with phosphate buffer (pH 8) solution and the mixture was worked up and precipitated with hexane and ether (95:5 v/v) to give partially protected dinucleotide **7** in 92% yield. Compound **7** was used for the next coupling reaction without further purification. Phosphodiester intermediate **5** (1.5 molar equiv.) was condensed with **7** (1.0 molar equiv.) in the presence of QS-te (4.5 molar equiv.) in dry pyridine. After 1 h, the reaction was nearly completed as judged by TLC, and the reaction mixture was worked up and chromatograph to give the fully protected trinucleotide ($A^{2'}p^{5'}A^{2}p^{5'}A$) (core) **8** in 93% yield.

In the above reaction, 1-(8-quinolylsulfonyl)-1*H*-tetrazole (QS-te) can be effectively used as the coupling agent for the synthesis of internucleotidic bonds.

The protecting groups of **8** was removed in the following order to obtain **9**. Treatment of **9** with zinc chloride (25 parts) in aqueous pyridine for 24 h at room temperature removed completely 5-chloro-8-quinolyl protective groups. The resulting compound which contains soley phosphodiester bonds was then treated with concentrated aqueous ammonia for 5 h at 50 °C to cleave the benzoyl groups. Finally, the treatment with 80% acetic acid solution for 5 min removed the dimethoxytrityl group. $A^{2'}p^{5'}A^{2'}p^{5'}A$ (core) **9** thus obtained was then purified through a DEAE cellulose DE-52 column with a linear gradient of 0.01—0.5 M† triethylammonium hydrogencarbonate (TEAB, pH 7.5) (Fig. 1), and the yield was *ca.* 73%.

The purity of **9** was checked by TLC, paper chromatography, and paper electrophoresis. The presence of only 2′—5′ internucleotidic bonds in the completely deblocked product thus obtained was established by complete digestion of **9** with snake venom phosphodiesterase to the expected products in the correct ratio, and it was insensitive to nuclease P1 which cleaves only 3′—5′ linkage.

Experimental

UV absorption spectra were measured with a Shimadzu Model UV-200 spectrophotometer. Proton nuclear magnetic resonance spectra at 100 MHz were taken with JEOL JNMPS 100 spectrometer; the shifts are given in ppm (δ) relative to tetramethylsilane as an internal standard. Merck silica gel $60F_{254}$ plates were usually developed in solvents A [CH_2Cl_2–MeOH (9:1 v/v)], and B [C_6H_6–$(CH_3)_2CO$ (1:1 v/v)]. DC-Alufolien cellulose F sheets were used for TLC. Paper chromatography was performed by using the descending technique on Toyo Roshi No. 51A. The solvent systems employed were the following: solvent C [2-propanol–concentrated aqueous ammonia–water (7:1:2 v/v)], solvent D [1-propanol–concentrated aqueous ammonia–water (55:35:10 v/v)], and solvent E [1-butanol–acetic acid–water (5:2:3 v/v)]. Paper electrophoresis was carried out on Toyo Roshi No. 51A paper in 0.05 M triethylammonium hydrogencarbonate (pH 7.5) at 1100 V/40 cm. Kanto Chemical silica gel was used for short column chromatography. Anion exchange chromatography on DEAE cellulose DE-52 was carried out with a linear gradient of triethylammonium hydrogencarbonate (pH 7.5). Compounds containing the dimethoxytrityl group were detected on TLC by spraying the samples with 10% sulfonic acid solution and drying them in a stream of warm air.

8-Quinolylsulfonyl chloride and tetrazole were purchased from the Dojin Chemical Co.

Enzymatic hydrolyses were done as described previously.[8,9]

2′,3′-O-(Dibutylstannylene)-N⁶-benzoyladenosine (2). A suspension of N^6-benzoyladenosine[10] **1** (4.58 g, 12.3 mmol) and dibutyltin oxide (3.07 g, 12.3 mmol) in dry methanol (300 ml) was heated under reflux. After 30 min the solution was evaporated to dryness and the residue was crystallized from ethanol–acetone (1:1 v/v), giving 4.15 g (56%) of **2**: Mp 167—169 °C; UV (MeOH) λ_{max} 278 nm, λ_{min} 247 nm; R_f 0.1 (solvent A); Calcd for $C_{25}H_{21}N_5O_5$: C, 51.94; H, 6.97; N, 12.11%. Found: C, 51.81; H, 7.06; N, 12.17%.

N⁶,3′-O-Dibenzoyladenosine (3). Nucleoside derivative **2** (7.50 g, 12.45 mmol) was co-evaporated with dry methanol (2×15 ml) and dissolved in dry methanol (156 ml). To the solution was added benzoyl chloride (7.7 ml, 62.30 mmol) and triethylamine (8.7 ml, 62.30 mmol). After being kept at room temperature for 15 min, the solution was concentrated and the residue was triturated with ether (3×

† 1 M=1 mol dm^{-3}.

150 ml) and water (3×150 ml), and then dried *in vacuo*. The residue was recrystallized from ethanol to give 2.89 g (48%) of **3**: Mp 195—198 °C; R_f 0.50 (solvent A); UV (MeOH) λ_{max} 278, 228 nm, λ_{min} 248 nm; NMR (DMSO-d_6) δ=3.91 (brs, 2H, H-5′), 4.50 (brd, 1H, $J_{3',4'}$=2 Hz, H-4′), 5.22 (dd, 1H, $J_{1',2'}$=7.5 Hz, $J_{2',3'}$=5.5 Hz, H-2′), 5.59 (t, 1H, C_5'-OH), 5.73 (d, 1H, H-3′), 6.18 (d, 1H, C_2'-OH), 6.30 (d, 1H, $J_{1',2'}$=7.5 Hz, H-1′), 7.65 and 8.12 (m, total 10H, Ar), 8.91 (s, 2H, C_2-H and C_8-H), (The signals at δ=5.59 and 6.18 disappeared on addition of D_2O); Calcd for $C_{24}H_{21}N_5O_6$: C, 60.63; H, 4.45; N, 14.73%. Found: C, 60.40; H, 4.59; N, 14.81%.

5′-O-Dimethoxytrityl-N⁶-3′-O-dibenzoyladenosine (4). N^6-3′-*O*-Dibenzoyladenosine (**3**) (1.35 g, 2.83 mmol) was co-evaporated with dry pyridine and treated with dimethoxytrityl chloride (1.05 g, 3.10 mmol) in dry pyridine (14 ml) at room temperature. After 3 h, an aliquot was analyzed by TLC to confirm the starting material [R_f 0.50 (solvent A)] tritylated [R_f 0.55 (solvent A)]. The mixture was poured into ice-water (30 ml), extracted with CH_2Cl_2 (3× 30 ml), and the extract was washed with water (3 times). The solution was evaporated after being dried over Na_2SO_4 and the residue was co-evaporated with toluene (3 times). The residue was redissolved in CH_2Cl_2 (10 ml) and the solution was poured into hexane (500 ml). The precipitate was collected and dried in a dessicator over P_2O_5 to give **4** (1.67 g, 76%): UV (MeOH) λ_{max} 278, 231 nm, λ_{min} 256 nm; R_f 0.55 (solvent A); NMR ($CDCl_3$) δ=3.79 (s, 6H, OCH_3), 6.27 (d, 1H, $J_{1',2'}$=6.5 Hz, H-1′), 6.65—8.11 (m, 23H, Ar).

5′-O-Dimethoxytrityl-N⁶-3′-O-dibenzoyladenosine 3′-(5-Chloro-8-quinolyl) Phosphate (5). Nucleoside **4** (2.40 g, 3.09 mmol) and 5-chloro-8-quinolyl phosphate (1.20 g, 4.65 mmol) were co-evaporated with dry pyridine, and then treated with 8-quinolinesulfonyl chloride (QS) (2.13 g, 9.27 mmol) in dry pyridine (30 ml) for 2 h at room temperature. The phosphodiester product was detected by TLC [R_f 0.05 (solvent A)] and the mixture was quenched with ice-water. The product was extracted with CH_2Cl_2 (3×30 ml), and the extract was washed with 0.1 M triethylammonium hydrog ncarbonate (pH 7.5) (3×30 ml), then with water (3× 30 ml), and dried over Na_2SO_4. The CH_2Cl_2 layer was concentrated to 15 ml, and poured into hexane–ether (9:1 v/v) (400 ml). The precipitate was collected and dried in a dessicator over P_2O_5 *in vacuo* to give the triethylammonium salt of **5** (3.17 g, 98%); UV (MeOH) λ_{max} 280, 236 nm, λ_{min} 256 nm; R_f 0.05 (solvent A); ^{31}P NMR (pyridine, 85% H_3PO_4) δ+4.68.

Preparation of Fully Protected Dinucleotide (6). Phosphodiester **6** (1.08 g, 1.03 mmol) and N^6,2′,3′-*O*-tribenzoyladenosine (0.39 g, 0.68 mmol) were co-evaporated with dry pyridine, and then treated with 1-(8-quinolylsulfonyl)-1*H*-tetrazole (QS-te) (0.68 g, 2.60 mmol) in dry pyridine (5 ml) for 1 h at room temperature. The reaction mixture was quenched with ice-water, and then extracted with CH_2Cl_2 (3×15 ml). The combined organic extracts were washed with 0.1 M triethylammonium hydrogencarbonate (pH 7.5) (2×20 ml), then with water (2×20 ml), and was dried over Na_2SO_4 and concentrated. The residue was co-evaporated with toluene (3 times), dissolved in CH_2Cl_2, and the solution was applied on a short column of silica gel. Elution was performed with a stepwise gradient of methanol (0—5%) in CH_2Cl_2, and the product was precipitated with hexane–ether (95:5 v/v) (150 ml). The precipitate was collected and dried in a dessicator over P_2O_5 *in vacuo* to give fully protected dinucleotide **6** (1.02 g, 92%): *R* 0.53 (solvent A), 0.81 (solvent B); UV (MeOH) λ_{max} 278, 230 nm, λ_{min} 255 nm.

Detritylation of Fully Protected Dinucleotide (6). Fully protected dinucleotide **6** (0.79 g, 0.49 mmol) was dissolved in CH_2Cl_2–MeOH (7:3 v/v) (17 ml) containing 2% *p*-toluenesulfonic acid and the solution was kept for 15 min at 0 °C. The detritylated product was detected by TLC [R_f 0.48 (solvent A)] and the reaction mixture was washed with phosphate buffer (pH 8), and then with water (3× 20 ml). The CH_2Cl_2 layer was dried over Na_2SO_4 and evaporated *in vacuo*. The residue was dissolved in CH_2Cl_2 and the solution was poured into hexane–ether (95:5 v/v) (80 ml). The precipitate was collected and dried in a dessicator over P_2O_5 *in vacuo* to give the 5′-hydroxyl dinucleotide **7** (0.59 g, 92%): R_f 0.48 (solvent A), R_f 0.62 (solvent B); UV (MeOH) λ_{max} 278, 232 nm, λ_{min} 255 nm.

Preparation of Fully Protected Trinucleotide (8). Phosphodiester derivative **5** (0.76 g, 0.72 mmol) and 5′-hydroxyl dinucleotide **7** (0.60 g, 0.40 mmol) were co-evaporated with dry pyridine, and then treated with QS-te (0.47 g, 1.80 mmol) in dry pyridine (4 ml) for 1 h at room temperature. After usual work-up as described in the preparation of **6**, the product was applied on a short column of silica gel. Elution was performed with a stepwise gradient of methanol (0—5%) in CH_2Cl_2 and the desired fully protected trinucleotide was precipitated with hexane–ether (95:5 v/v) (50 ml). The precipitate was collected and dried in a dessicator over P_2O_5 *in vacuo* to give fully protected trinucleotide **8** (0.99 g, 93%): R_f 0.50 (solvent A), R_f 0.75 (solvent B); UV (MeOH) λ_{max} 278, 230 nm, λ_{min} 256 nm.

Unblocking of Fully Protected Trinucleotide (8). A solution of fully protected trinucleotide **8** (23 mg, 0.01 mmol) and $ZnCl_2$ (1.02 g, 5.0 mmol) in aqueous pyridine (10%) (20 ml) was stirred at room temperature. After 24 h the reaction mixture was treated with Dowex 50W-X2 (pyridinium form), filtered, and the filtrate was concentrated to gum. The gum was redissolved in concentrated aqueous ammonia (20 ml) at 50 °C. After 5 h the solution was evaporated under reduced pressure. The residue was treated with 80% acetic acid (15 ml) for 15 min. The acetic acid was removed by repeated co-evaporation with 1-butanol. The residue was dissolved in 0.01 M triethylammonium hydrogencarbonate (pH 7.5) (50 ml) and the solution was washed with CH_2Cl_2 (2×20 ml). The solution was applied on a column of DEAE cellulose DE-52 (hydrogencarbonate form). The elution profile and conditions are shown in Fig. 1. The appropriate fractions were combined and lyophilized to give the corresponding trinucleotide **9** (252 OD, 73%). The purity of **9** was checked by TLC, paper chromatography, and paper electrophoresis as well as complete hydrolysis by snake venom phosphodiesterase to adenosine (A_{260}=8.44) and adenosine 5′-phosphate (A_{260}=16.80). Ratio of adenosine and adenosine 5′-phosphate was 1.00: 1.94. On the other hand, when it was incubated with nuclease Pl, $A^{2'}p^{5'}A^{2'}p^{5'}A$, **9** was recovered in 99.2% yield: R_f 0.21 (solvent D), $R_{f_{pA}}$ 0.71 (solvent D); $R_{f_{pA}}$ 0.78 (0.05 M triethylammonium hydrogencarbonate, pH 7.5); UV (H_2O, pH 7.0) λ_{max} 257 nm.

We thank Professor Tsujiaki Hata of Tokyo Institute of Technology for discussion throughout the investigation.

References

1) B. R. G. Williams, and I. M. Kerr, *Nature*, **276**, 88 (1978); I. M. Kerr and R. E. Brown, *Proc. Natl. Acad. Sci. U.S.A.*, **75**, 256 (1976); A. Schimt, A. Zilverstein, L. Shulman,

P. Federman, H. Berissi, and M. Revel, *FEBS Lett.*, **95**, 276 (1978); A. G. Hovanessian and I. M. Kerr, *Eur. J. Biochem.*, **84**, 149 (1978).

2) A. Kimchi, H. Schure, and M. Ravel, *Nature*, **282**, 849 (1979).

3) M. Ikehara, K. Ohie, and E. Ohtsuka, *Tetrahedron Lett.*, **1979**, 3677; H. Sawai, T. Shibata, and M. Ohono, *ibid.*, **1979**, 4573; S. S. Jones and C. B. Reese, *J. Am. Chem. Soc.*, **101**, 7399 (1979); K. K. Ogilvie and N. Y. Theriault, *Tetrahedron Lett.*, **1979**, 2111; J. A. J. Den Hertog, J. Doornbos, R. Crea, and J. H. van Boom, *Recl. Trav. Chim. Pays-Bas*, **98**, 469 (1979); J. Ehgers and U. Krahmar, *Angew. Chem.*, **91**, 1007 (1979); A. K. Markham, R. A. Poter, M. J. Gait, R. C. Sheppard, and I. M. Kerr, *Nucleic Acids Res.*, **6**, 2569 (1979); R. Charubala and W. Pfleiderer, *Tetrahedron Lett.*, **1980**, 1933; J. B. Chattopadhaya, *ibid.*, **1980**, 4113; C. Gioeli, M. Kwiatkowski, B. Oberg, and J. B. Chattopadhaya, *ibid.*, **1981**, 1741; J. Imai and P. F. Torrence, *J. Org. Chem.*, **46**, 4015 (1981); E. Ohtsuka, A. Yamane, and M. Ikehara, *Chem. Pharm. Bull.*, **30**, 376 (1982).

4) D. Wagner, J. P. H. Verheyden, and J. G. Moffatt, *J. Org. Chem.*, **39**, 24 (1974).

5) H. P. M. Fromageot, B. E. Griffin, C. B. Reese, J. E. Sulston, and D. R. Trenthan, *Tetrahedron*, **22**, 705 (1966).

6) H. Takaku, R. Yamaguchi, T. Nomoto, and T. Hata, *Tetrahedron Lett.*, **1979**, 3857; H. Takaku, T. Nomoto, Y. Sakamoto, and T. Hata, *Chem. Lett.*, **1979**, 1225.

7) H. Takaku, M. Kato, M. Yoshida, and T. Hata, *Nucleic Acids Res. Spec. Publ.*, **5**, 345 (1978); *Chem. Lett.*, **1979**, 811; H. Takaku, M. Kato, and S. Ishikawa, *J. Org. Chem.*, **46**, 4062 (1981).

8) H. Takaku and M. Yoshida, *J. Org. Chem.*, **46**, 598 (1981); H. Takaku, T. Nomoto, and K. Kamaike, *Chem. Lett.*, **1981**, 543; H. Takaku, K. Kamaike, and K. Kasuga, *ibid.*, **1982**, 197.

9) H. Takaku, M. Kato, M. Yoshida, and R. Yamaguchi, *J. Org. Chem.*, **45**, 3347 (1980).

10) R. H. Hall, *Biochemistry*, **3**, 769 (1964).

Oxygen Promoted Addition of 1,3-Dioxolane to Electron-deficient Alkenes

Yoshihisa WATANABE,* Yasushi TSUJI, and Ryo TAKEUCHI

Department of Hydrocarbon Chemistry, Faculty of Engineering, Kyoto University, Sakyo-ku, Kyoto 606

(Received July 27, 1982)

1,3-Dioxolane reacted with electron-deficient alkenes, such as diethyl maleate, maleic anhydride, diethyl fumarate and fumaronitrile, under an oxygen atmosphere or in air to give 1:1 adducts in good to excellent yields. The presence of oxygen promoted the reaction. The reaction appears to be characteristic of 1,3-dioxolane. Methylal and ethylal did not react with diethyl maleate under the same conditions.

Recently, great attention has been paid to C_1 chemistry, in which carbon monoxide and methanol are key materials as starting C_1 compounds.[1] However, only a little attention has been paid to the chemistry of other C_1 compounds, such as formic acid and formaldehyde. We have recently shown that formic acid, a C_1 derivative from carbon monoxide, could be used as a hydrogen source for catalytic reduction of ketones and aldehydes.[2]

On the other hand, 1,3-dioxolane, formaldehyde ethylene acetal, is known to react with several alkenes by UV irradiation, or in the presence of radical initiators.[3] The reactions have been considered to proceed in radical mechanisms. The present work describes the reaction of 1,3-dioxolane with electron-deficient alkenes under an air or an oxygen atmosphere to give 1:1 adducts. The reaction is simple and convenient, since the reaction is carried out without irradiation or radical initiators.

Results and Discussion

1,3-Dioxolane reacted with such electron-deficient alkenes as diethyl maleate, maleic anhydride, diethyl fumarate, and fumaronitrile in air at 120 °C for 6 h to give 1:1 adducts (Scheme 1). The results are listed in Table 1. These alkenes reacted with 1,3-dioxolane only at the 2-position. On the other hand, simple alkenes such as 1-octene reacted at the 4-position as well as at the 2-position of 1,3-dioxolane to give 1:1 adducts in low yields by initiators.[4] In the present study, diethyl maleate reacted with 1,3-dioxolane in air or under oxygen atmosphere to give 1:1 adducts in 73 and 83% yields, respectively (Runs 1 and 2).

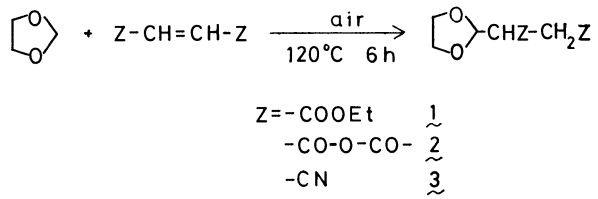

Scheme 1.

The higher yield under the latter conditions suggests that the oxygen atmosphere may be more favorable than air for the formation of the 1:1 adducts. No 1:1 adduct was obtained under an argon atmosphere. These results showed that the presence of oxygen was essential for the reaction. Conversion of diethyl maleate and yield of the 1:1 adduct decreased at a lower reaction temperature (80 °C) and a shorter reaction time (3 h) (Runs 3 and 4). Radical initiators such as di-*t*-butyl peroxide (DTBP) or azobisisobutyronitrile (AIBN) could also initiate the reaction under an inert atmosphere (Runs 5 and 6). As a radical initiator, DTBP was more effective than AIBN. The decomposition of DTBP has a half-life of about 20 h at 120 °C and of about 1 h at 150 °C, whereas AIBN decomposes into 1-cyano-1-methylethyl radicals under mild conditions (40 °C). AIBN is useful as a initiator in the range from 40 °C to 80 °C.[5] The radical species from AIBN would not work efficiently at such a high reaction temperature (120 °C). Oxygen atmosphere appears to be more favorable to the reaction than the addition of initiators.

The effect of molar ratio, 1,3-dioxolane/alkene, on the product yield was examined in detail by employing diethyl maleate. The results are shown in Table 2.

TABLE 1. THE 1:1 ADDITION OF 1,3-DIOXOLANE TO ALKENES[a]

Run	Alkene	Conversion[b] %	Atmosphere	Product	Yield[b] %
1	Diethyl maleate	93	Air	**1**	73
2	Diethyl maleate	100	Oxygen	**1**	83
3[c]	Diethyl maleate	39	Air	**1**	16
4[d]	Diethyl maleate	50	Air	**1**	24
5[e]	Diethyl maleate	100	Argon	**1**	69
6[f]	Diethyl maleate	40	Argon	**1**	18
7	Maleic anhydride	98	Air	**2**	89
8	Diethyl fumarate	100	Air	**1**	38
9	Fumaronitrile	54	Air	**3**	23

a) A mixture of 1,3-dioxolane (60 mmol) and alkene (6.0 mmol) was stirred at 120 °C for 6 h. b) Determined by GLC based on the amount of alkene used. c) Reaction temperature: 80 °C for 6 h. d) Reaction time: 3 h at 120 °C. e) DTBP was used as a radical initiator. f) AIBN was used as a radical initiator.

Table 2. The 1:1 addition of 1,3-dioxolane to diethyl maleate: effect of molar ratio

Run	Molar ratio[b]	Conversion/%[c]	Product yield/%[c]
10	1:1	57	4
11	5:1	85	52
12	10:1	93	73
13	20:1	100	88

a) At 120 °C, for 6 h, under air. b) 1,3-Dioxolane/Maleate. c) Product **1**: Determined by GLC based on the amount of diethyl maleate.

The yield of 1:1 adduct decreased dramatically with a decrease in the molar ratio. In runs 10 and 11, the product mixture contained a considerable amount of oligomers, whose molecular weights were less than 800 according to gel-permeation chromatography.

With maleic anhydride, the 1:1 adduct was obtained in excellent yield (Run 7). However, the alkenes with (*E*)-configuration gave the product in poor yields. Diethyl fumarate and fumaronitrile gave the 1:1 adducts in 38 and 23% yields respectively (Runs 8 and 9).

For this reaction, only the alkene having two electron-withdrawing groups appears to react with 1,3-dioxolane under the conditions used. Methyl acrylate and acrylonitrile gave no 1:1 adducts even at a more elevated temperature, 180 °C. 1-Hexene was also inactive for the present reaction.

The reactions is considered to proceed in radical mechanisms (Scheme 2), since the 1:1 adduct was

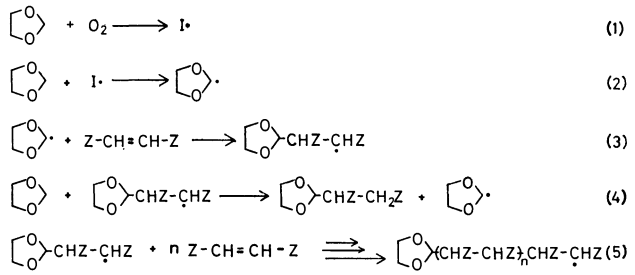

Scheme 2.

obtained with radical initiators (Runs 5 and 6) and the reaction was inhibited completely with a radical scavenger such as 2,6-di-*t*-butyl-4-methylphenol. A peroxide species is generated by the reaction of 1,3-dioxolane with oxygen (Step 1), and this presumably initiates the chain reaction leading to the 1:1 adducts (Step 2—4). In the reaction between 2-phenyl-1,3-dioxolane and oxygen, a peroxide species has been isolated.[6] In runs 10 and 11, the yields of 1:1 adduct drastically decreased. In these runs, step 5 would predominate and many oligomers of the alkene were produced.

The present reaction is characteristic of 1,3-dioxolane. Methylal and ethylal, formaldehyde dimethyl acetal and diethyl acetal, did not react with diethyl maleate under the same reaction coditions as run 1 (Scheme 3). This difference occurs because peroxide species are liable to be generated with the more strained cyclic ether.[7]

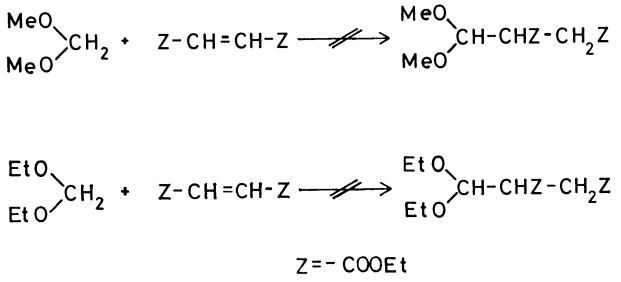

Scheme 3.

The present reaction is considered to be a modified hydroformylation reaction since the ethylene acetal moiety is easily hydrolyzed into carbonyl groups. Hydroformylation of internal conjugated alkenes such as diethyl maleate and maleic anhydride is known to be rather difficult and requires severe conditions.[8] Therefore, the present reaction offers an alternative route to the hydroformylation of these alkenes with a simple precedure under rather mild conditions.

Experimental

1,3-Dixolane and other reagents were carefully purified by distillation over suitable drying reagents before use. The boiling points are uncorrected. IR spectra were measured on a Hitachi model 215 grating spectrophotometer. ^{1}H-NMR spectra (300 MHz) were recorded on a Nicolet NTC-300 spectrometer equipped with 1180E computer system. ^{13}C-NMR spectra (25.05 MHz) were obtained using a JEOL JNM FX-100 pulsed Fourier Transform spectrometer. The chemical shift values were expressed in ppm relative to Me_4Si as an internal standard. Gel-permeation chromatograms were recorded on a Waters ALC/GPC 244 equipped with four columns ($10^5+10^4+10^3+500$ Å). The molecular weight was estimated according to calibration curves obtained with standard polystyrenes.

General Reaction Procedure. A 50 ml stainless steel autoclave equipped with a glass liner was charged with an alkene (6 mmol, 1.0 ml) and 1,3-dioxolane (60 mmol, 4.2 ml) under an air or an oxygen atmosphere. The autoclave was set in an oil bath and the temperature was raised to 120 °C in 20 min. The mixture was stirred magnetically at 120 °C for 6 h. The products were isolated by distillation under reduced pressures and submitted to analysis (IR, NMR, and MS). The GLC analysis of the reaction products was made using a column (3 mmϕ × 3 m) packed with Silicone OV-17 on Uniport HP 60—80 mesh. The yields of products were determined by GLC.

The Reaction of Diethyl Maleate or Fumarate with 1,3-Dioxolane gave ***1***. **1**: Colorless oil, bp 116—119 °C/0.9 Torr (1 Torr≈133.322 Pa). ^{13}C-NMR ($CDCl_3$): δ=14.1 (q, $-COOCH_2\underline{C}H_3$), 30.4(t, $-CH-\underline{C}H_2-$), 45.9 (d, $-\underline{C}H-CH_2-$), 60.7(t, $-C\underline{O}OCH_2CH_3$), 61.6(t, $-COO\underline{C}H_2CH_3$), 65.3(t, $-\underline{C}H_2CH_2-$), 102.9 (d, $-O-\underline{C}H-O-$), 170.8 (s, C=O), and 171.8 (s, C=O). ^{1}H-NMR ($CDCl_3$): δ=1.25 (3H, t, J=6.9 Hz, $-COOCH_2C\underline{H}_3$), 1.27 (3H, t, J=6.9 Hz $-COOCH_2C\underline{H}_3$), 2.59(1H, d of d, J=16.8, 4.6 Hz, $-CH-CH_2-$), 2.76(1H, d of d, J=16.8, 9.2 Hz, $-CH-C\underline{H}_2-$), 3.20(1H, d of d of d, J=9.2, 4.6, 4.6 Hz, $-C\underline{H}-CH_2-$), 3.84—4.01(4H, m, $-O-C\underline{H}_2-C\underline{H}_2-O-$), 4.13(2H, q, J=6.9 Hz, $-COOC\underline{H}_2CH_3$), 4.19(2H, q, J=6.9 Hz, $-COOC\underline{H}_2-CH_3$), and 4.19 (1H, d, J=4.6 Hz, $-O-C\underline{H}-O-$). IR (neat): 1735 cm^{-1} (ν C=O) and 1030 cm^{-1} (ν C-O-C). MS(*m/e*): 246(M^+), and 201 (M^+-OEt). Found: C, 53.95;

H, 7.60; O 38.74%. Calcd for $C_{11}H_{18}O_6$: C, 53.65; H, 7.37; O, 38.98%.

The Reaction of Maleic Anhydride with 1,3-Dioxolane Gave **2**. **2**: Colorless oil, bp 128—138 °C/1.2 Torr. ^{13}C-NMR ($CDCl_3$): δ=28.5 (t, -CH-$\underline{C}H_2$-), 44.8(d, -$\underline{C}$H-CH_2-), 65.7(t, -O-$\underline{C}H_2$-$\underline{C}H_2$-O-), 100.7(d, -O-$\underline{C}$H-O-), and 169.6 (s, C=O). ^{1}H-NMR ($CDCl_3$): δ=2.958 (1H, d, J=8.4 Hz, -CH-C$\underline{H}_2$-), 2.961(1H, d, J=6.6 Hz, -CH-C$\underline{H}_2$-), 3.54(1H, d of d of d, J=8.4, 6.6, 2.4 Hz, -C$\underline{H}$-CH_2-), 3.84—4.17(4H, m, -C$\underline{H}_2$-C$\underline{H}_2$-), and 5.29 (1H, d, J=2.4 Hz, -O-C$\underline{H}$-O-). IR (neat): 1785 cm^{-1} (ν C=O), and 1860 cm^{-1} (ν C=O).

The Reaction of Fumaronitrile with 1,3-Dioxolane Gave **3**. **3**: Colorless oil, bp 111—114 °C/4 Torr. The ^{13}C-NMR spectra of the isolated product gave a similar pattern to those of **1** and **2**. ^{13}C-NMR ($CDCl_3$): δ=16.3 (t, -CH-C$\underline{H}_2$-), 33.9 (d, -$\underline{C}$H-CH_2-), 66.1 (t, -O-$\underline{C}H_2$-$\underline{C}H_2$-O-), 100.6 (d, -O-$\underline{C}$H-O-), 115.5 (s, -CN), and 119.1 (s, -CN).

The 1:1 Addition in the Presence of Radical Initiator. The 50 ml autoclave was charged with diethyl maleate (6.0 mmol, 1.0 ml), 1,3-dioxolane (60 mmol, 4.2 ml), and a radical initiator, DTBP (0.6 mmol, 87.7 mg) or AIBN (0.6 mmol, 81.7 mg), and then the mixture was stirred at 120 °C for 6 h under an argon atmosphere.

The Reaction in the Presence of Radical Scavenger. The 50 ml autoclave was charged with diethyl maleate (6.0 mmol, 1.0 ml), 1,3-dioxolane (60 mmol, 4.2 ml), and 2,6-di-*t*-butyl-4-methylphenol (15 mmol, 3.31 g) under air. The mixture was stirred at 120 °C for 6 h.

References

1) J. Falbe, "New Syntheses with Carbon Monoxide," Springer-Verlag, Berlin, Heidelberg (1980); I. Wender and P. Pino, "Organic Syntheses via Metal Carbonyls," Interscience New York, (1977), Vol 2.

2) Y. Watanabe, T. Ohta, and Y. Tsuji, *Bull. Chem. Soc. Jpn.*, **55**, 2441 (1982).

3) I. Rosenthal and D. Elad, *J. Org. Chem.*, **29**, 2220 (1964).

4) R. Laland, B. Millard, and M. Cazaux, *Tetrahedron Lett.*, **1969**, 745.

5) C. Walling and E. S. Huyser, *Org. React.*, **13**, 115 (1963).

6) A. Reiche, E. Schmitz, and E. Beyer, *Chem. Ber.*, **91**, 1935 (1958).

7) R. R. Legault and D. C. Leweis, *J. Am. Chem. Soc.*, **64**, 1354 (1942).

8) Ref. 1, pp. 116—123.

Synthetic Studies on Methyl α-Trioxacarcinoside B

Tetsuo SUAMI,* Katsumi NAKAMURA, and Tamio HARA

Department of Applied Chemistry, Faculty of Science and Technology, Keio University, Hiyoshi, Kohoku-ku, Yokohama, 223

(Received August 14, 1982)

Trioxacarcinose B is a unique carbohydrate which has been discovered in antibiotic trioxacarcin A as a component. As a step of total synthesis of the antibiotic, methyl α-trioxacarcinoside B has been synthesized from methyl 2,3-anhydro-6-deoxy-α-L-*allo*-hexopyranoside by a 7 steps reaction in a yield of 4.3%. The product has been identified by comparison with the authentic sample which was prepared by methanolysis of the antibiotic.

Trioxacarcinose A and B are unique carbohydrates which are components of antitumor antibiotic trioxacarcin A produced by *Streptomyces ochraceus*.[1,2,3]

Methanolysis of the antibiotic afforded a mixture of two methyl glycosides: methyl trioxacarcinoside A and B.

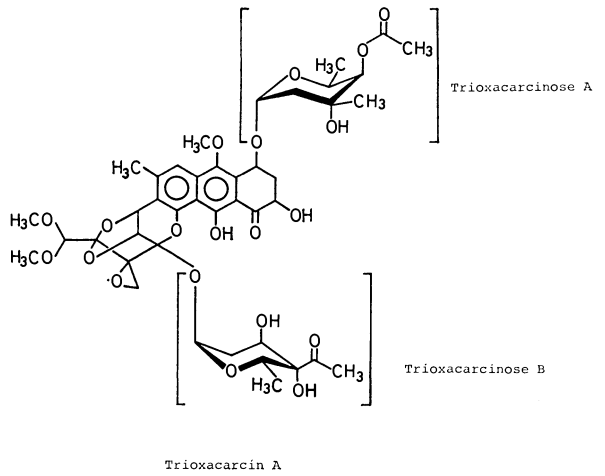

Trioxacarcin A

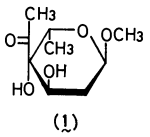

(1)

Trioxacarcinose A is a known sugar and its de-*O*-acetyl derivative is named axenose, which has been synthesized by Garegg and Norberg.[4] Trioxacarcinose B has been known as a component of naturally occurring isoquinocycline B[5] but its synthesis has never been described; a closely related compound, methyl 2,6-dideoxy-4-*C*-(L-glycero-4[1]-hydroxyethyl)-α-L-*xylo*-hexopyranoside, was synthesized by Paulsen and Sinnwell.[6]

We have attempted to synthesize methyl α-trioxacarcinoside B (**1**) from the readily accessible methyl 2,3-anhydro-6-deoxy-α-L-*ribo*-hexopyranosid-4-ulose (**2**).[6]

Treatment of **2** with 2-methyl-1,3-dithiane[7] in the presence of butyllithium in tetrahydrofuran (THF) yielded two products: methyl 2,3-anhydro-6-deoxy-4-*C*-(2-methyl-1,3-dithiolan-2-yl)-α-L-*allo*-hexopyranoside (**3**) and the corresponding L-*galacto* derivative (**4**) in 26 and 7% yields, respectively.

Reduction of **3** with $LiAlH_4$ in THF afforded methyl 2,6-dideoxy-4-*C*-(2-methyl-1,3-dithiolan-2-yl)-α-L-*ribo*-hexopyranoside (**5**) in a quantitative yield.

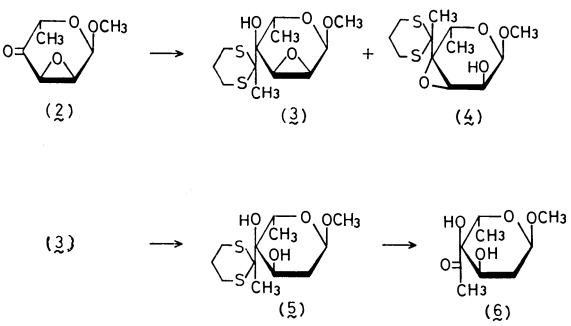

(2) (3) (4) (3) (5) (6)

Scheme 1.

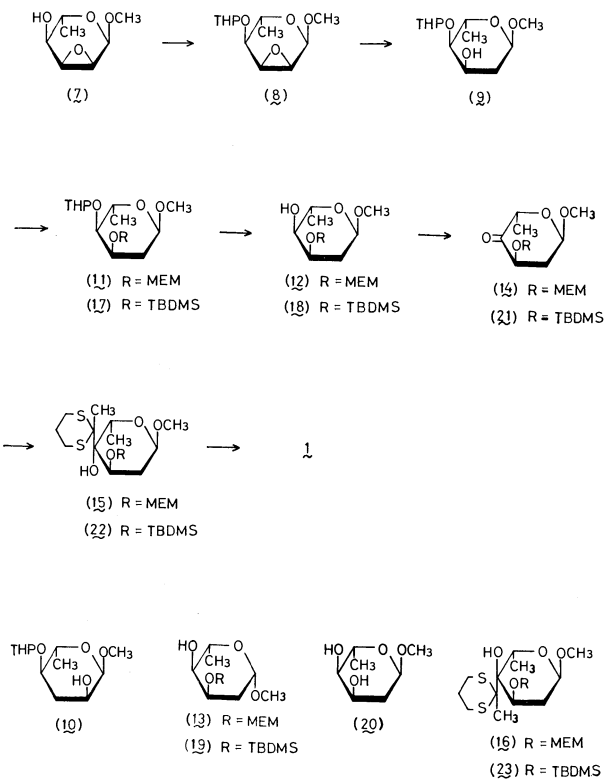

(7) (8) (9) (11) R = MEM (17) R = TBDMS (12) R = MEM (18) R = TBDMS (14) R = MEM (21) R = TBDMS (15) R = MEM (22) R = TBDMS 1

Scheme 2.

Deprotection of **5** with mercury(II) chloride and mercury(II) oxide in aq methanol gave crystalline methyl 4-*C*-acetyl-2,6-dideoxy-α-L-*ribo*-hexopyranoside (**6**) in 38% yield, which was found to be the 4-epimer of **1** by ^1H NMR spectroscopy.

To avoid the formation of **4**, an alternative route has been attempted. Protection of the hydroxyl group on C-4 of methyl 2,3-anhydro-6-deoxy-α-L-*allo*-hexo-

pyranoside[6] (**7**) with 3,4-dihydro-2*H*-pyran and successive hydrogenation of the 2,3-oxirane ring with $LiAlH_4$ afforded two products: the 2-deoxy derivative (**9**) and the 3-deoxy derivative (**10**) in 80 and 19% yields, respectively.

Protection of another hydroxyl group on C-3 in **9** with a 2-methoxyethoxymethyl group (MEM) gave the fully protected compound (**11**) as a syrup. Selective deprotection of the tetrahydropyranyl group in **11** with pyridinium *p*-toluenesulfonate in methanol[8] gave the anomers (**12**) and (**13**) in 71 and 23% yields, respectively.

Oxidation of **12** with ruthenium tetraoxide gave methyl 2,6-dideoxy-3-*O*-(2-methoxyethoxymethyl)-α-L-*erythro*-hexopyranosid-4-ulose (**14**) in a yield of 86%. When **14** reacted with 2-methyl-1,3-dithiane[7] in the presence of butyllithium, methyl 2,6-dideoxy-3-*O*-(2-methoxyethoxymethyl)-4-*C*-(2-methyl-1,3-dithiolan-2-yl)-α-L-*xylo*-hexopyranoside (**15**) was obtained in 54% yield, together with a small amount of the corresponding 4-epimer (**16**). Deprotection of **15** in methanolic hydrogen chloride gave **1** in 23% yield.

In this reaction process (**11**→**12**→**14**→**15**→**1**), another protective group, *t*-butyldimethylsilyl group (TBDMS), was used analogously to result in the process (**17**→**18**→**21**→**22**→**1**).

Experimental

General Methods. Melting points were determined on a Büchi 510 capillary melting point apparatus and are uncorrected. Solutions were concentrated under reduced pressure below 50 °C. Optical rotation was measured on a Japan Spectroscopic Co. DIPL-SL polarimeter. ^1H NMR spectra were taken on a Varian EM-390 (90 MHz) spectrometer in deuteriochloroform with reference to tetramethylsilane as an internal standard. Chemical shifts are given in δ-values, and the *J*-values given are of first-order. TLC was performed on precoated Wakogel B-5F plates (Wako Pure Chemical Co., Ltd.), and silica gel (Wakogel C-200) was employed for column chromatography.

*Methyl 2,3-Anhydro-6-deoxy-4-C-(2-methyl-1,3-dithiolan-2-yl)-α-L-allo-hexopyranoside (**3**) and Methyl 3,4-Anhydro-6-deoxy-4-C-(2-methyl-1,3-dithiolan-2-yl)-α-L-galacto-hexopyranoside (**4**).* To a stirred solution of 2-methyl-1,3-dithiane (342 mg, 2.5 mmol) in THF (3.0 ml), a 1.8 ml portion of 1.6 M (1 M = 1 mol dm^{-3}) butyllithium hexane solution (2.9 mmol) was added with acetone–Dry Ice cooling (−30 °C) in an argon atmosphere. After 1.5 h, the mixture was cooled at −70 °C and a solution of methyl 2,3-anhydro-6-deoxy-α-L-*ribo*-hexopyranosid-4-ulose (**2**, 400 mg, 2.5 mmol) in THF (3.0 ml) was added to the mixture. After stirring for 10 min, a 0.6 ml portion of acetic acid was added to the reaction mixture. The mixture was concentrated and the residue was dissolved in chloroform. The chloroform solution was washed with H_2O, dried over anhydrous Na_2SO_4 and concentrated. The residue was recrystallized from ethyl acetate–hexane to give 189 mg (26%) of **3**: mp 140—141 °C; $[\alpha]_D^{23}$ −65.5° (*c* 0.84, $CHCl_3$). The ^1H NMR spectrum of **3** was superimposable on that of the corresponding D-diastereomer.[7]

Found: C, 49.17; H, 6.69; S, 21.75%. Calcd for $C_{12}H_{20}S_2O_4$: C, 49.29; H, 6.81; S, 21.93%.

The mother liquor was concentrated and the residue was purified on a silica-gel column with 1:8 (v/v) ethyl acetate–toluene as an eluant. Fractions homogeneous on TLC (R_f 0.59) in 1:1 (v/v) ethyl acetate–toluene were combined and concentrated. The residue was recrystallized from ether to give 54 mg (7%) of **4**: mp 127—128 °C; $[\alpha]_D^{23}$ −115.9° (*c* 2.67, CH_3OH). The ^1H NMR spectrum of **4** was superimposable on that of the corresponding D-diastereomer.[7]

Found: C, 49.46; H, 6.81; S, 21.72%. Calcd for $C_{12}H_{20}S_2O_4$: C, 49.29; H, 6.81; S, 21.93%.

*Methyl 2,6-Dideoxy-4-C-(2-methyl-1,3-dithiolan-2-yl)-α-L-ribo-hexopyranoside (**5**).* To a suspension of $LiAlH_4$ (83 mg, 2.2 mmol) in THF (8.0 ml), a solution of **3** (245 mg, 0.8 mmol) in THF (8.0 ml) was added. After refluxing for 1 h, the reaction mixture was quenched in ice-cooled water (10 ml). The precipitates were filtered off and the filtrate was concentrated. The residue was purified on a silica-gel column with 1:9 (v/v) ethyl acetate–toluene. Fractions homogeneous on TLC (R_f 0.48) in 1:3 (v/v) ethyl acetate–toluene were combined and concentrated to give 239 mg (97%) of **5** as a syrup: $[\alpha]_D^{23}$ −67.1° (*c* 2.16, CH_3OH). The ^1H NMR spectrum of **5** was identical with that of the corresponding D-diastereomer.[7]

Found: C, 48.73; H, 7.43; S, 21.52%. Calcd for $C_{12}H_{22}S_2O_4$: C, 48.95; H, 7.53; S, 21.78%.

*Methyl 4-C-Acetyl-2,6-dideoxy-α-L-ribo-hexopyranoside (**6**).* To a stirred solution of **5** (207 mg, 0.7 mmol) in 80% aq methanol (16.0 ml), mercury(II) chloride (344 mg, 1.3 mmol), and mercury(II) oxide (365 mg, 1.7 mmol) were added. After 1 h, the mixture was filtered and the filtrate was concentrated. The residue was dissolved in chloroform and the solution was washed with 1 M KI solution and cold water, dried over anhydrous Na_2SO_4 and concentrated. The residue was purified on a silica-gel column with 5:1 (v/v) cyclohexane–ethyl acetate. Fractions homogeneous on TLC (R_f 0.50) in 30:1 (v/v) chloroform–methanol were combined and concentrated to give 55 mg (38%) of **6**: mp 35—39 °C; $[\alpha]_D^{23}$ −183.2° (*c* 0.61, $CHCl_3$); ^1H NMR δ = 1.18 (3H, d, $J_{5,6}$ = 7.0 Hz, H-6), 2.01 (1H, ddd, $J_{1,2ax.}$ = 3.0 Hz, $J_{2ax.,2eq.}$ = 15.0 Hz, $J_{2ax.,3}$ = 4.5 Hz, H-2ax.), 2.30 (3H, s, CH_3), 2.44 (1H, ddd, $J_{1,2eq.}$ = 4.0 Hz, $J_{2eq.,2ax.}$ = 15.0 Hz, $J_{2eq.,3}$ = 3.5 Hz, H-2eq.), 3.38 (3H, s, OCH_3), 3.85 (1H, q, $J_{5,6}$ = 7.0 Hz, H-5) and 4.84 (1H, dd, $J_{1,2ax.}$ = 3.0 Hz, $J_{1,2eq.}$ = 3.5 Hz, H-1).

Found: C, 52.12; H, 7.54%. Calcd for $C_9H_{16}O_5$: C, 52.93; H, 7.90%.

*Methyl 2,6-Anhydro-6-deoxy-4-O-tetrahydropyranyl-α-L-allo-hexopyranoside (**8**).* To a stirred mixture of 3,4-dihydro-2*H*-pyran (896 mg, 10.6 mmol) and pyridinium *p*-toluenesulfonate (234 mg, 0.9 mmol) in CH_2Cl_2 (60.0 ml), methyl 2,3-anhydro-6-deoxy-α-L-*allo*-hexopyranoside[6] (**7**, 1.50 g, 9.4 mmol) was added. After 22 h, the reaction mixture was diluted with CH_2Cl_2, washed with cold water, dried over anhydrous Na_2SO_4 and concentrated. The residue was purified on a silica-gel column with 1:12 (v/v) ethyl acetate–toluene. Fractions homogeneous on TLC (R_f 0.29) in 1:3 (v/v) ethyl acetate–toluene were combined and concentrated to give 2.19 g (96%) of **8** as a syrup: ^1H NMR δ = 1.17 (d, $J_{5,6}$ = 6.5 Hz) and 1.25 (d, $J_{5,6}$ = 6.5 Hz) (3H, H-6), 3.41 (3H, s, OCH_3), 4.77 (3/2 H, d, *J* = 3.0 Hz, H-1 and THP's H-1) and 5.00 (1/2 H, bs, THP's H-1).

Found: C, 59.29; H, 8.14%. Calcd for $C_{12}H_{20}O_5$: C, 59.00: H, 8.25%.

*Methyl 2,6-Dideoxy-4-O-tetrahydropyranyl-α-L-ribo-hexopyranoside (**9**) and Methyl 3,6-Dideoxy-4-O-tetrahydropyranyl-α-L-ribo-hexopyranoside (**10**).* To a mixture of $LiAlH_4$ (0.4 g, 10.5 mmol) and THF (50 ml), a solution of **8** (2.36 g, 9.7 mmol) in THF (10 ml) was added. After the mixture was heated under reflux for 1 h, water (60 ml) was added to the mixture. The mixture was filtered and the filtrate

was concentrated. The residue was purified on a silica-gel column with 1:12 (v/v) acetone–hexane. Fractions homogeneous (R_f 0.40) on TLC in 1:3 (v/v) acetone–hexane were combined and concentrated to give 1.91 g (80%) of **9** as a syrup.

Found: C, 58.75; H, 8.80%. Calcd for $C_{12}H_{22}O_5$: C, 58.52; H, 9.00%.

Fractions homogeneous (R_f 0.30) on TLC in the same solvent system were combined and concentrated to give 0.45 g (19%) of **10** as a syrup.

Found: C, 58.59; H, 8.76%. Calcd for $C_{12}H_{22}O_5$: C, 58.52; H, 9.00%.

*Methyl 2,6-Dideoxy-3-*O*-(2-methoxyethoxymethyl)-4-*O*-tetrahydropyranyl-α-*L*-ribo-hexopyranoside (**11**).* To a stirred solution of **9** (0.68 g, 2.8 mmol) in CH_2Cl_2 (4.0 ml), 2-methoxyethoxymethyl chloride (0.68 g, 2.8 mmol) and *N,N*-diisopropylethylamine (0.72 g, 5.5 mmol) were added. After 1 h, the mixture was diluted with CH_2Cl_2, washed with water, dried over anhydrous Na_2SO_4 and concentrated. The residue was purified on a silica-gel column with 1:8 (v/v) ethyl acetate–toluene. Fractions homogeneous (R_f 0.22) on TLC in 1:1 (v/v) ethyl acetate–toluene were combined and concentrated to give 0.68 g (74%) of **11** as a syrup: ^{1}H NMR δ=1.19 (d, $J_{5,6}$=6.5 Hz) and 1.28 (d, $J_{5,6}$=6.5 Hz) (3H, H-6), 3.30 (3H, s, OCH_3), 3.36 (3H, s, OCH_3) and 4.57—4.95 (4H, m, H-1, THP's H-1 and $-OCH_2O-$ of MEM).

Found: C, 57.57; H, 8.83%. Calcd for $C_{16}H_{30}O_7$: C, 57.47; H, 9.04%.

*Methyl 2,6-Dideoxy-3-*O*-(2-methoxyethoxymethyl)-α-*L*-ribo-hexopyranoside (**12**) and Methyl 2,6-Dideoxy-3-*O*-(2-methoxyethoxymethyl)-β-*L*-ribo-hexopyranoside (**13**).* A mixture of **11** (0.68 g, 2.0 mmol) and pyridinium *p*-toluenesulfonate (51 mg, 0.2 mmol) in methanol (30 ml) was heated at 50 °C for 1 h. The mixture was concentrated and the residue was purified on a silica-gel column with 1:1 (v/v) ethyl acetate–toluene. Fractions homogeneous (R_f 0.10) on TLC in the same solvent were combined and concentrated to give 0.36 g (71%) of **12** as a syrup: $[\alpha]_D^{23}$ −184.4° (*c* 1.28, $CHCl_3$); ^{1}H NMR δ=1.25 (3H, d, $J_{5,6}$=6.5 Hz, H-6), 1.84 (1H, ddd, $J_{1,2ax.}$=4.5 Hz, $J_{2ax.,2eq.}$=15.0 Hz, $J_{2ax.,3}$=3.5 Hz, H-2eq.), 3.32 (3H, s, OCH_3), 4.64 (1H, dd, $J_{1,2ax.}$=4.5 Hz, $J_{1,2eq.}$=1.5 Hz, H-1) and 4.80 (2H, s, $-OCH_2O-$ of MEM).

Found: C, 53.02; H, 8.60%. Calcd for $C_{11}H_{22}O_6$: C, 52.79; H, 8.86%.

Fractions homogeneous (R_f 0.16) on TLC were concentrated to give 0.12 g (23%) of **13** as a syrup: $[\alpha]_D^{24}$ −36.5° (*c* 1.24, $CHCl_3$); ^{1}H NMR δ=1.28 (3H, d, $J_{5,6}$=6.5 Hz, H-6), 1.61 (1H, ddd, $J_{1,2ax.}$=9.5 Hz, $J_{2ax.,2eq.}$=14.0 Hz, $J_{2ax.,3}$=3.0 Hz, H-2ax.), 2.11 (1H, ddd, $J_{1,2eq.}$=2.5 Hz, $J_{2ax.,2eq.}$=14.0 Hz, $J_{2,3}$=4.0 Hz, H-2eq.), 3.35 (3H, s, OCH_3), 3.44 (3H, s, OCH_3), 4.60 (1H, dd, $J_{1,2ax.}$=9.5 Hz, $J_{1,2eq.}$=2.5 Hz, H-1) and 4.77 (2H, s, $-OCH_2O-$ of MEM).

Found: C, 53.04; H, 8.68%. Calcd for $C_{11}H_{22}O_6$: H, 52.79; H, 8.86%.

*Methyl 2,6-Dideoxy-3-*O*-(2-methoxyethoxymethyl)-α-*L*-erythro-hexopyranosid-4-ulose (**14**).* To a stirred mixture of **12** (0.34 g, 1.3 mmol), K_2CO_3 (56 mg, 0.5 mmol), RuO_2 (8.9 mg), and chloroform (4 ml), a solution of $NaIO_4$ (0.48 g, 2.3 mmol) in water (5 ml) was added. After 5 h, 2-propanol was added to the reaction mixture. The mixture was filtered, and the filtrate was diluted with chloroform, washed with water, dried over anhydrous Na_2SO_4 and concentrated. The residue was purified on a silica-gel column with 1:2 (v/v) ethyl acetate–toluene. Fractions homogeneous (R_f 0.36) on TLC in 1:1 (v/v) ethyl acetate–toluene were combined and concentrated to give 0.29 g (86%) of **14** as a syrup: $[\alpha]_D^{22}$ −127.7° (*c* 5.68, $CHCl_3$); ^{1}H NMR δ=1.29 (3H, d, $J_{5,6}$=6.5 Hz, H-6), 1.86 (1H, ddd, $J_{1,2}$=6.0 Hz, $J_{2,2'}$=13.5 Hz, $J_{2,3}$=13.0 Hz, H-2), 2.63 (1H, dt, $J_{1,2'}$=7.0 Hz, $J_{2,2'}$=13.5 Hz, $J_{2',3}$=7.0 Hz, H-2'), 3.36 (3H, s, OCH_3), 3.37 (3H, s, OCH_3), 4.31 (1H, q, $J_{5,6}$=6.5 Hz, H-5), 4.51 (1H, dd, $J_{2,3}$=13.0 Hz, $J_{2',3}$=7.0 Hz, H-3), 4.80 (2H, s, $-CH_2O-$ of MEM) and 4.97 (1H, dd, $J_{1,2}$=6.0 Hz, $J_{1,2'}$=7.0 Hz, H-1).

Found: C, 53.40; H, 8.05%. Calcd for $C_{11}H_{20}O_6$: C, 53.22; H, 8.12%.

*Methyl 2,6-Dideoxy-3-*O*-(2-methoxyethoxymethyl)-4-*C*-(2-methyl-1,3-dithiolan-2-yl)-α-*L*-xylo-hexopyranoside (**15**) and Methyl 2,6-Dideoxy-3-*O*-(2-methoxyethoxymethyl)-4-*C*-(2-methyl-1,3-dithiolan-2-yl)-α-*L*-ribo-hexopyranoside (**16**).* A mixture of 2-methyl-1,3-dithiane (0.16 g, 1.2 mmol), 1.6 M hexane solution of butyllithium (0.82 ml, 1.3 mmol), and THF (2.0 ml) was stirred for 1.5 h at −30 °C in an argon atmosphere. To the mixture, a solution of **14** (0.29 g, 1.2 mmol) in THF (2.0 ml) was added at −70 °C. After 20 min, the reaction mixture was mixed with acetic acid (0.3 ml) and concentrated. The residue was dissolved in chloroform and the solution was washed with water, dried over anhydrous Na_2SO_4 and concentrated. The residue was purified on the column with 1:5 (v/v) ethyl acetate–toluene. Fractions homogeneous (R_f 0.49) on TLC in the same solvent were combined and concentrated to give 0.24 g (54%) of **15** as a syrup: $[\alpha]_D^{24}$ −82.8° (*c* 1.69, $CHCl_3$); ^{1}H NMR δ=1.35 (3H, d, $J_{5,6}$=6.5 Hz, H-6), 1.75 (3H, s, CH_3), 2.92 (1H, s, OH), 3.31 (3H, s, OCH_3), 3.36 (3H, s, OCH_3), 4.30 (1H, t, J=3.0 Hz, H-3), 4.36 (1H, q, $J_{5,6}$=6.5 Hz, H-5), 4.64 (1H, t, J=2.5 Hz, H-1), 4.84 (1H, d, J=13.5 Hz, $-OCH(H')O-$ of MEM) and 4.92 (1H, d, J=13.5 Hz, $-OCH(H')O-$ of MEM).

Found: C, 50.49; H, 7.71; S, 16.52%. Calcd for $C_{16}H_{30}S_2O_6$: C, 50.24; H, 7.90; S, 16.76%.

Fractions homogeneous (R_f 0.36) gave 94 mg (22%) of **16** as a syrup. The structure of **16** was established by converting **5** into **16** as follows.

To a stirred solution of **5** (56 mg, 0.2 mmol) in CH_2Cl_2 (2 ml), 2-methoxyethoxymethyl chloride (47 mg, 0.4 mmol), and *N,N*-diisopropylethylamine (49 mg, 0.4 mmol) were added. The mixture was worked up as described in the preparation of **16** to give 20 mg (28%) of **16**.

*Methyl 3-*O*-(t-Butyldimethylsilyl)-2,6-dideoxy-4-*O*-tetrahydropyranyl-α-*L*-ribo-hexopyranoside (**17**).* To a stirred solution of **9** (1.86 g, 7.6 mmol) in DMF (5.0 ml), imidazole (1.28 g, 18.8 mmol) and *t*-butyldimethylsilyl chloride (1.59 g, 10.6 mmol) were added. After 20 h, the mixture was concentrated and the residue was purified on a column with 1:20 (v/v) ethyl acetate–hexane were concentrated to give 2.67 g (97%) of **17** as a syrup: ^{1}H NMR δ=0.87 and 0.89 (9H, s×2, $-SiC(CH_3)_3$), 1.17 (d, $J_{5,6}$=6.5 Hz) and 1.26 (d, $J_{5,6}$=6.5 Hz) (3H, H-6), 3.25 and 3.27 (3H, s×2, OCH_3), 4.56—4.68 (3/2 H, m, H-1 and THP's H-1) and 4.80 (1/2 H, bs, THP's H-1).

Found: C, 59.68; H, 9.75%. Calcd for $C_{18}H_{36}O_5Si$: C, 59.96; H, 10.06%.

*Methyl 3-*O*-(t-Butyldimethylsilyl)-2,6-dideoxy-α-*L*-ribo-hexopyranoside (**18**), Methyl 3-*O*-(t-Butyldimethylsilyl)-2,6-dideoxy-β-*L*-ribo-hexopyranoside (**19**), and Methyl 2,6-Dideoxy-α-*L*-ribo-hexopyranoside (**20**).* To a stirred solution of **17** (0.53 g, 1.5 mmol) in methanol (20 ml), pyridinium *p*-toluenesulfonate (37 mg) was added at 40 °C. After 1.5 h, the mixture was concentrated and the residue was purified on a column with 1:20 (v/v) ethyl acetate–hexane. Fractions homogeneous (R_f 0.58) on TLC in the same solvent were concen-

trated to give 0.16 g (40%) of **18** as a syrup: $[\alpha]_D^{22}$ −134.5° (*c* 1.12, $CHCl_3$); ^1H NMR δ=0.09 (3H, s, -SiC$(CH_3)_3$), 0.11 (3H, s, -SiCH_3), 0.91 (9H, s, -SiC$(CH_3)_3$), 1.25 (3H, d, $J_{5,6}$=6.5 Hz, H-6), 1.77 (1H, dt, $J_{1,2ax.}$=4.0 Hz, $J_{2ax.,2eq.}$=15.0 Hz, $J_{2ax.,3}$=4.0 Hz, H-2ax.), 2.00 (1H, ddd, $J_{1,2eq}$=2.0 Hz, $J_{2ax.,2eq.}$=15.0 Hz, $J_{2eq.,3}$=4.0 Hz, H-2eq.), 2.18 (1H, d, $J_{4,4-OH}$=10.0 Hz, 4-OH), 3.25 (3H, s, OCH_3), 3.83 (1H, dq, $J_{4,5}$=9.0 Hz, $J_{5,6}$=6.5 Hz, H-5), 4.03 (1H, q, $J_{2ax.,3}$=4.0 Hz, $J_{2eq.,3}$=4.0 Hz, $J_{3,4}$=4.0 Hz, H-3) and 4.63 (1H, dd, $J_{1,2ax.}$=4.0 Hz, $J_{1,2eq.}$=2.0 Hz, H-1).

Found: C, 56.84; H, 9.79%. Calcd for $C_{13}H_{28}O_4Si$: C, 56.48; H, 10.21%.

Fractions homogeneous (R_f 0.44) on TLC gave 0.10 g (25%) of **19** as a syrup: $[\alpha]_D^{22}$ −11.6° (*c* 1.22, $CHCl_3$); ^1H NMR δ=0.12 (6H, s, -Si$(CH_3)_2$), 0.94 (9H, s, -SiC$(CH_3)_3$), 1.28 (3H, d, $J_{5,6}$=6.0 Hz, H-6), 1.57 (1H, ddd, $J_{1,2ax.}$=9.0 Hz, $J_{2ax.,2eq.}$=13.5 Hz, $J_{2ax.,3}$=3.0 Hz, H-2ax.), 1.84 (1H, d, $J_{4,4-OH}$=10.0 Hz, 4-OH), 1.97 (1H, ddd, $J_{1,2eq.}$=2.5 Hz, $J_{2ax.,eq.}$=13.5 Hz, $J_{2eq.,3}$=3.5 Hz, H-2eq.), 3.13 (1H, ddd, $J_{3,4}$=3.5 Hz, $J_{4,4-OH}$=10.0 Hz, $J_{4,5}$=9.0 Hz, H-4), 3.55 (3H, s, OCH_3), 3.71 (1H, dq, $J_{4,5}$=9.0 Hz, $J_{5,6}$=6.0 Hz, H-5), 4.11 (1H, dt, $J_{3,4}$=3.5 Hz, $J_{2ax.,3}$=3.0 Hz, $J_{2eq.,3}$=3.5 Hz, H-3) and 4.62 (1H, dd, $J_{1,2ax.}$=9.0 Hz, $J_{1,2eq.}$=2.5 Hz, H-1).

Found: C, 56.66; H, 9.93%. Calcd for $C_{13}H_{28}O_4Si$: C, 56.48; H, 10.21%.

Fractions homogeneous (R_f 0.05) on TLC gave 44 mg (12%) of **20** as a syrup: $[\alpha]_D^{23}$ −165.4° (*c* 1.08, $CHCl_3$); ^1H NMR δ=1.31 (3H, d, $J_{5,6}$=6.0 Hz, H-6), 1.87 (1H, dt, $J_{1,2ax.}$=3.5 Hz, $J_{ax.,2eq.}$=15.0 Hz, $J_{2eq.,3}$=3.0 Hz, H-2eq.), 3.10 (1H, dd, $J_{3,4}$=3.0 Hz, $J_{4,5}$=10.0 Hz, H-4), 3.36 (3H, s, OCH_3), 3.70 (1H, dq, $J_{4,5}$=10.0 Hz, $J_{5,6}$=6.0 Hz, H-5) and 4.76 (1H, dd, $J_{1,2ax.}$=3.5 Hz, $J_{1,2eq.}$=1.5 Hz, H-1).

Found: C, 51.79; H, 8.55%. Calcd for $C_7H_{14}O_4$: C, 51.84; H, 8.70%.

*Methyl 3-O-(t-Butyldimethylsilyl)-2,6-dideoxy-α-*L*-erythro-hexopyranosid-4-ulose (21).* Compound **18** (0.16 g, 0.6 mmol) was oxidized with ruthenium tetraoxide in a chloroform solution and the reaction mixture was worked up analogously as described in the preparation of **14** to give 82 mg (52%) of **21** as a homogeneous syrup: R_f 0.76 on TLC in 1:4 (v/v) ethyl acetate-hexane; $[\alpha]_D^{22}$ −173.9° (*c* 3.86, $CHCl_3$); ^1H NMR δ=0.05 (3H, s, SiCH_3), 0.13 (3H, s, SiCH_3), 0.90 (9H, s, SiC$(CH_3)_3$), 1.30 (3H, d, $J_{5,6}$=6.5 Hz, H-6), 1.89 (1H, ddd, $J_{1,2}$=7.0 Hz, $J_{2,2'}$=14.0 Hz, $J_{2,3}$=13.0 Hz, H-2), 2.55 (1H, dt, $J_{1,2'}$=7.0 Hz, $J_{2,2'}$=14.0 Hz, $J_{2',3}$=7.0 Hz, H-2'), 3.39 (3H, s, OCH_3), 4.29 (1H, q, $J_{5,6}$=7.0 Hz, H-5), 4.46 (1H, dd, $J_{2,3}$=13.0 Hz, $J_{2',3}$=7.0 Hz, H-3), 4.91 (1H, t, $J_{1,2}$=7.0 Hz, $J_{1,2'}$=7.0 Hz, H-1).

Found: C, 57.16; H, 9.28%. Calcd for $C_{13}H_{26}O_4Si$: C, 56.90; H, 9.55%.

*Methyl 3-O-(t-Butyldimethylsilyl)-2,6-dideoxy-4-C-(2-methyl-1,3-dithiolan-2-yl)-α-*L*-xylo-hexopyranoside (22) and Methyl 3-O-(t-Butyldimethylsilyl)-2,6-dideoxy-4-C-(2-methyl-1,3-dithiolan-2-yl)-α-*L*-ribo-hexopyranoside (23).* Compound **21** (0.13 g, 0.5 mmol) was treated with 2-methyl-1,3-dithiane in THF as described in the preparation of **15** to give 87 mg (44%) of **22** as a syrup: R_f 0.63 on TLC in 1:4 (v/v) ethyl acetate-hexane; $[\alpha]_D^{22}$ −121.6° (*c* 1.96, $CHCl_3$); ^1H NMR δ=0.11 (3H, s, SiCH_3), 0.13 (3H, s, SiCH_3), 0.91 (9H, s, SiC$(CH_3)_3$), 1.37 (3H, d, $J_{5,6}$=6.5 Hz, H-6), 1.79 (3H, s, CH_3), 3.29 (3H, s, OCH_3), 4.42 (1H, q, $J_{5,6}$=6.5 Hz, H-5) and 4.65 (1H, d, J=4.5 Hz, H-1).

Found: C, 52.00; H, 8.40; S, 15.15%. Calcd for $C_{18}H_{36}S_2O_4Si$: C, 52.90; H, 8.88; S, 15.69%.

Fractions (R_f 0.72 on TLC in the same solvent) gave 6.1 mg (3%) of **23** as a syrup: ^1H NMR δ=0.17 (6H, s, Si$(CH_3)_2$), 0.91 (9H, s, SiC$(CH_3)_3$), 1.55 (3H, d, $J_{5,6}$=7.0 Hz, H-6), 1.96 (3H, s, CH_3), 2.26 (1H, dt, $J_{1,2eq.}$=5.0 Hz, $J_{2ax.,2eq.}$=14.5 Hz, $J_{2eq.,3}$=5.0 Hz, H-2eq.), 3.30 (3H, s, OCH_3), 3.57 (1H, s, 4-OH), 4.11 (1H, q, $J_{5,6}$=7.0 Hz, H-5), 4.55 (1H, dd, $J_{2ax.,3}$=8.0 Hz, $J_{2eq.,3}$=5.0 Hz, H-3) and 4.65 (1H, t, $J_{1,2ax}$=5.0 Hz, $J_{1,2eq.}$=5.0 Hz, H-1).

The structure of **23** was elucidated by converting **5** to **23** as follows. To a stirred solution of **5** (33 mg, 0.1 mmol) in DMF (0.5 ml), imidazole (19 mg, 0.3 mmol) and *t*-butyldimethylsilyl chloride (20 mg, 0.1 mmol) were added. The mixture was worked up as described in the preparation of **17** to give 26 mg (57%) of **23**.

Methyl α-Trioxacarcinoside B (1). *(a)*: To a stirred solution of **15** (0.12 g, 0.6 mmol) in methanol (2.0 ml), methanol (2.0 ml) containing 20% HCl was added. After 20 h, the mixture was concentrated and the residue was purified on a silica-gel column with 1:7 (v/v) ethyl acetate-toluene. Fractions homogeneous (R_f 0.70) on TLC in 30:1 (v/v) chloroform-methanol were combined and concentrated. The residue was recrystallized from isopropyl ether to give 15 mg (23%) of **1**: mp 111—112 °C; $[\alpha]_D^{24}$ −154.2° (*c* 0.34, $CHCl_3$). The product was identical with an authentic sample[3,5] in all respects.

(b): An 87 mg portion of **22** was treated with methanolic HCl analogously as described in *(a)* above to give 3.5 mg (8%) of **1**.

The authors wish to express their thanks to Dr. Kunikatsu Shirahata for his helpful advice and to Kyowa Hakko Co. for providing an authentic sample of **1**. Also, they thank Mr. Saburo Nakada for his elemental analysis.

References

1) F. Tomita, T. Tamaoki, S. Morimoto, and K. Fujimoto, 225th Meeting of Japan Antibiot. Res. Assoc., Sept. 25, 1981, Tokyo.

2) T. Tamaoki, T. Iida, K. Shirahata, and F. Tomita, 225th Meeting of Japan Antibiot. Res. Assoc., Sept. 25, 1981, Tokyo.

3) K. Shirahata, T. Iida, and N. Hirayama, 24th Symposium on the Chemistry of Natural Products, Osaka, Oct. 14, 1981, Abstr. pp. 199—206.

4) P. J. Garegg and T. Norberg, *Acta Chem. Scand., Ser. B*, **29**, 507 (1972).

5) Matern and H. Griesebach, *Eur. J. Biochem.*, **29**, 5 (1972).

6) H. Paulsen and V. Sinnwell, *Chem. Ber.*, **111**, 869 (1978).

7) H. Paulsen and V. Sinnwell, *Chem. Ber.*, **111**, 879 (1978).

8) M. Miyashita, A. Yoshikoshi and P. A. Grieco, *J. Org. Chem.*, **42**, 3772 (1977).

 © 1983 The Chemical Society of Japan Bull. Chem. Soc. Jpn., 56, 1435—1440 (1983)

Synthesis of Potential Antineoplastic Anthracenedione Derivatives. I. Sugar Derivatives

Katsumi NAKAMURA, Tomoyuki ASAI, Tamio HARA, Naoki MINORIKAWA, and Tetsuo SUAMI*

Department of Applied Chemistry, Faculty of Science and Technology, Keio University, Hiyoshi, Kohoku-ku, Yokohama, 223

(Received November 22, 1982)

Seven 1-*O*-glycosyl derivatives of 4-[2-(2-hydroxyethylamino)ethylamino]-9,10-anthracenedione have been prepared as potential antineoplastic agents.

Doxorubicin (adriamycin)[1] and daunorubicin (daunomycin)[2] are well known as the clinically useful, antineoplastic agents and members of anthracycline antibiotics, together with carminomycin,[3] dihydrodaunomycin,[4] rhodomycin B,[5] pyrromycin,[6] and cinerubin.[7] Their cytotoxic effects are primarily due to their ability to intercalate their molecules between the base pairs of the DNA double helix.

The utilization of doxorubicin and daunorubicin is, however, limited by undesirable side effects, such as irreversible cardiotoxicity. To avoid the side effect and to improve antineoplastic activity, a series of anthracenedione derivatives having one or two aminoalkyl side chains, as model compounds of intercalating agents, have been studied by Double and Brown.[8]

Among these model compounds, bis(substituted aminoalkylamino)anthracenediones[9] and 1-hydroxy-4-[2-(2-hydroxyethylamino)ethylamino]-9,10-anthracenedione[10] (**1**) have exhibited good antineoplastic activities.[11]

Also, it has been well known that significant cytotoxic activity is always associated with aminoglycosides of the parent nucleus of anthracycline antibiotics.[12] This seems to be due to an electrostatic interaction between the phosphate group of the DNA molecules and the amino groups of a sugar moiety in the antibiotics.

While, in a series of anthracenedione derivatives, it has never been established that whether a glycosidation of the nucleus does improve its cytotoxic activity or not. To clarify this interesting problem, seven glycosides of **1** have been prepared, and their preliminary antineoplastic activity has been determined against leukemia L1210 in mice.

Results and Discussion

Preferential mono-*N*-acetylation of **1** with acetic anhydride in methanol gave 4-[2-(*N*-acetyl-2-hydroxyethylamino)ethylamino]-1-hydroxy-9,10-anthracenedione (**2**) in 74% yield. Protection of the primary hydroxyl group of **2** with trityl chloride in pyridine afforded the compound (**3**) in 90% yield. Successive acetylation of **3** with acetic anhydride in pyridine gave the two compound (**4**) and (**5**) in 59 and 33% yield, respectively. Selective *O*-deacetylation of **4** gave the aglycon (**6**) in 94% yield.

Condensation of **6** with acetobromoglucose in the presence of silver carbonate and quinoline afforded the product (**7**) in 84% yield. Detritylation of **7** with aqueous acetic acid and successive *O*-deacetylation in methanolic ammonia gave the compound (**9**). An attempt was made to remove *N*-acetyl groups on the side chain by alkaline hydrolysis, but it was failed, owing to a cleavage of the glycosidic linkage.[13]

An alternative protective group was used, instead of the acetyl group, to cleave *N*-acetyl bond under more mild conditions. Treatment of **1** with di-*t*-butyl dicarbonate resulted in a formation of 4-[2-(*N*-*t*-butoxycarbonyl-2-hydroxyethylamino) ethylamino]-1-hydroxy-9,10-anthracenedione (**10**) in 80% yield.

Tritylation of **10** gave the compound (**11**) in 77% yield. Acetylation of **11** in an appropriate conditions yielded preferentially *O*-acetyl derivative (**12**) in 95% yield. Treatment of **12** with trifluoroacetic anhydride in pyridine gave the compound (**13**) in 68% yield by causing a scission of the *O*-acetyl bond.

Direct *N*-acylation of **11** with trifluoroacetic anhydride in pyridine yielded a complex mixture which could not be able to isolate **13** in a good yield.

Condensation of **13** with acetobromoglucose in the presence of silver carbonate and quinoline afforded the product (**14**) in 80% yield.

Complete deprotection of **14** gave the aimed 1-(β-D-glucopyranosyloxy)-4-[2-(2-hydroxyethylamino)-ethylamino]-9,10-anthracenedione (**16**) in 48% yield. The structure of **16** was confirmed by converting **16** into hepta-*N*,*O*-acetyl derivative (**17**) which was determined by ^{1}H NMR spectroscopy.

Using the same aglycon **13** and the analogous condensation procedure, six 1-*O*-glycosyl analogs have been synthesized. The sugar moieties used are β-D-galactopyranosyl, 6-deoxy-β-D-glucopyranosyl, α-L-rhamnopyranosyl, 2-acetamido-2-deoxy-β-D-glucopyranosyl, 3-acetamido-3-deoxy-β-D-glucopyranosyl and β-cellobiosyl residues.

The preliminary determination of antineoplastic activity against leukemia L1210 in mice revealed that the glycosidation of the 1-*O*-hydroxyl group in **1** was

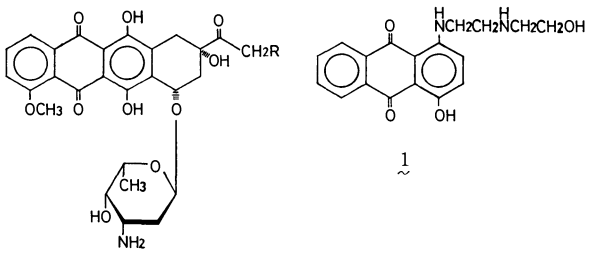

Doxorubicin R=OH
Daunorubicin R=H

1

Scheme 1.

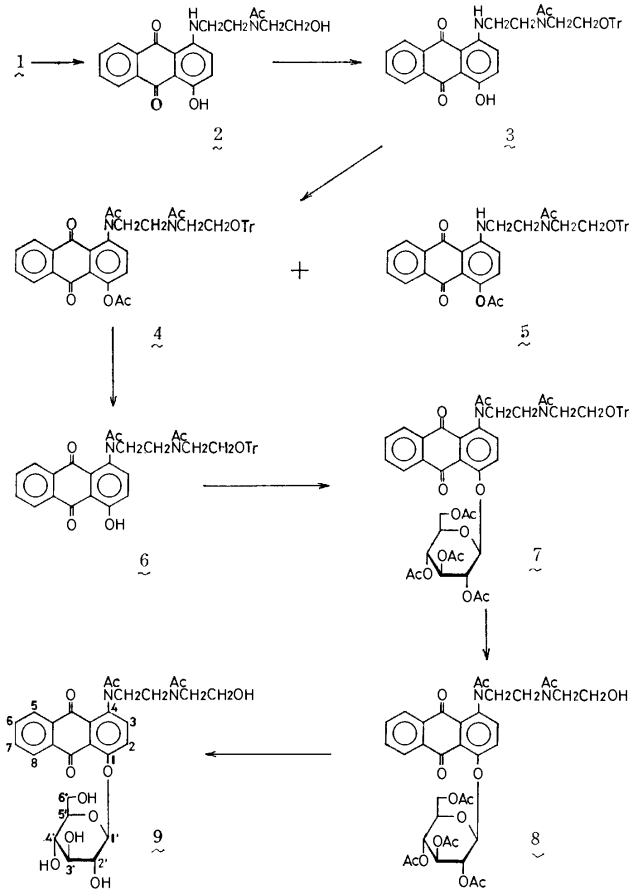

Scheme 2.

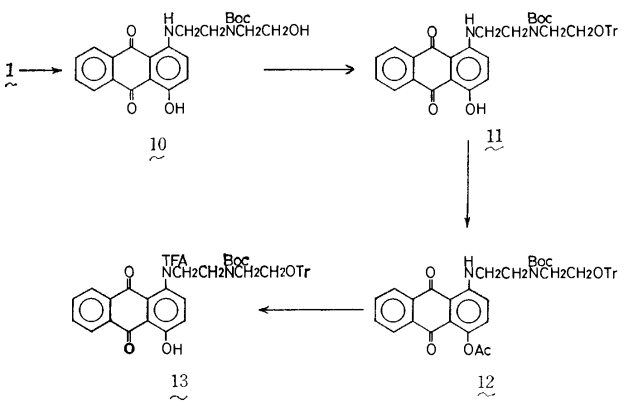

Scheme 3.

not hopeful in the production of large increase of life span in the leukemia L1210 transplanted mice. Details of the determination of antineoplastic activity will be reported elsewhere.

Experimental

General Methods. Melting points were determined on a Büchi 510 capillary melting point apparatus and are uncorrected. Solutions were concentrated under reduced pressure below 50 °C. The optical rotation were measured on a Japan Spectroscopic DIPL-SL polarimeter. The IR spectra were recorded with a Hitachi 225 spectrophotometer and expressed in reciprocal centimeters. The UV spectra were measured with a Japan Spectroscopic UVIDEC-1

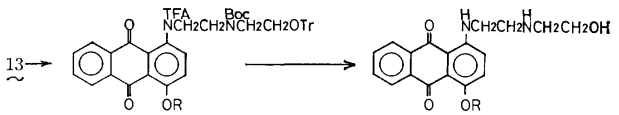

14	2,3,4,6-tetra-*O*-acetyl-*β*-D-glucopyranosyl	**16**	*β*-D-glucopyranosyl
18	2,3,4,6-tetra-*O*-acetyl-*β*-D-galactopyranosyl	**24**	*β*-D-galactopyranosyl
19	2,3,4-tri-*O*-acetyl-6-deoxy-*β*-D-glucopyranosyl	**25**	6-deoxy-*β*-D-glucopyranosyl
20	2,3,4-tri-*O*-acetyl-*α*-L-rhamnopyranosyl	**26**	*α*-L-rhamnopyranosyl
21	2,2′,3,3′4′,6,6′-hepta-*O*-acetyl*β*-cellobiosyl	**27**	*β*-cellobiosyl
22	2-acetamide-3,4,6-tri-*O*-acetyl-2-deoxy-*β*-D-glucopyranosyl	**28**	2-acetamide-2-deoxy-*β*-D-glucopyranosyl
23	3-acetamide-2,4,6-*O*-acetyl-3-deoxy-*β*-D-glucopyranosyl	**29**	3-aceiamide-3-deoxy-*β*-C-glucopyranosyl

Scheme 4.

spectrophotometer. ^{1}H NMR spectra were taken on a Varian EM-390 (90 MHz) spectrometer in chloroform-*d* with reference to tetramethylsilane as an internal standard. The chemical shifts are given in *δ*-values and *J*-values given are of first-order. TLC was performed on precoated silica gel 60 F-254 plaques (Merk, Darmstadt; 0.25 mm thickness). The silica gel used for a column chromatography was Wakogel C-200 (Wako Pure Chemical Co. Ltd.).

4-[2-(N-Acetyl-2-hydroxyethylamino)ethylamino]-1-hydroxy-9,10-anthracenedione (2). To a stirred solution of **1** (100 mg) in methanol (6 ml), acetic anhydride (0.3 ml) was added at room temperature. After 45 min, the solution was stand at 0—5 °C overnight. The products were collected by filtration and recrystallized from ethanol to give 84 mg (74%) of **2**, mp 149—150 °C; UV ($CHCl_3$) 253 (log *ε*, 4.56), 287 (3.89), 555 (4.09), 593 nm (4.04). ^{1}H NMR (pyridine-d_5): *δ*=2.27 (3H, s, NAc), 7.21 (1H, s, H-3), 7.32 (1H, s, H-2), 7.53—7.78 (2H, m, H-6 and 7), 8.18—8.43 (2H, m, H-5 and 8), 10.45 (1H, bs, aromatic NH).

Found: C, 63.92; H, 5.44; N, 7.15%. Calcd for $C_{20}H_{20}N_2O_5 \cdot 1/2\,H_2O$: C, 63.65; H, 5.61; N, 7.42%.

4-[2-[N-Acetyl-2-(trityloxy)ethylamino]ethylamino]-1-hydroxy-9,10-anthracenedione (3). To a stirred solution of **2** (1.00 g) in pyridine (90 ml), trityl chloride (4.53 g) was added at 50 °C. After 65 h, the mixture was concentrated, and the residue was dissolved in chloroform. The chloroform solution was washed with water, dried over anhydrous Na_2SO_4 and concentrated. The residue was purified on a column using 1:3 (v/v) ethyl acetate–toluene. Fractions homogeneous (R_f 0.36) on TLC in the same solvent were combined and concentrated. The residue was recrystallized from chloroform–petroleum ether to give 1.49 g (90%) of **3**, mp 238—240 °C; UV ($CHCl_3$) 556 (log *ε*, 4.24), 594 nm (4.21). ^{1}H NMR: *δ*=2.13 (3H, s, NAc), 3.20—3.73 (8H, m, CH_2 of side chain), 7.13—7.43 (17H, m, H-2,3 and $C(C_6\underline{H}_5)_3$), 7.65—7.83 (2H, m, H-6 and 7), 8.23—8.40 (2H, m, H-5 and 8), 10.28 (1H, bs, aromatic NH), 13.68 (1H, s, 1-OH).

Found: C, 74.83; H, 5.66; N, 4.42%. Calcd for $C_{39}H_{34}N_2O_5 \cdot H_2O$: C, 74.50, H, 5.77; N, 4.46%.

1-Acetoxy-4-[N-acetyl-2-[N-acetyl-2-(trityloxy)ethylamino]ethylamino]-9,10-anthracenedione (4) and 1-Acetoxy-4-[2-[N-acetyl-2-(trityloxy)ethylamino]ethylamino]-9,10-anthracenedione (5). To a solution of **3** (300 mg) in pyridine (10 ml), acetic anhy-

dride (8 ml) was added. After 24 h at 100 °C, the mixture was concentrated, and the residue was dissolved in ethyl acetate. The solution was washed with sat. $NaHCO_3$ solution, H_2O dried over anhydrous Na_2SO_4 and concentrated. The residue was purified on the column using 15:1 (v/v) benzene–ethyl acetate. Fractions homogeneous (R_f 0.22) on TLC in 3:1 (v/v) benzene–ethyl acetate were concentrated and recrystallized from methanol to give 203 mg (59%) of **4**, mp 168—170 °C; UV ($CHCl_3$) 320 (log ε, 3.97), 348 (4.04), 408 nm (3.73); IR (KBr) 1765 (phenolic Ac), 1710 (aromatic NAc), 1655 (quinone), 1625 cm^{-1} (NAc). ^1H NMR; δ=2.20 (3H, s, NAc), 2.48 (3H, s, phenolic Ac), 2.62 (3H, s, aromatic NAc), 3.22—3.67 (6H, m, NAc-$CH_2C\underline{H}_2NAcC\underline{H}_2C\underline{H}_2OTr$), 4.25—4.55 (2H, m, NAc-$C\underline{H}_2CH_2NAc$), 7.09—7.48 (16H, m, aromatic protonand $C(C_6\underline{H}_5)_3$), 7.53—7.73 (2H, m, aromatic protons), 7.82—8.00 (1H, m, aromatic proton), 8.23—8.48 (2H, m, H-5 and 8).

Found: C, 74.06; H, 5.34; N, 3.78%. Calcd for $C_{43}H_{38}N_2O_7$: C, 74.34; H, 5.51; N, 4.03%.

Fractions homogeneous (R_f 0.38) on TLC in 3:1 (v/v) benzene–ethyl acetate were concentrated and the residue was recrystallized from methanol to give 106 mg (33%) of **5**, mp 146—148 °C; UV ($CHCl_3$) 249 (log ε, 4.52), 277 (3.99), 321 (3.77), 508 nm (3.83); IR (KBr) 1775 (phenolic Ac), 1670 (quinone), 1635 cm^{-1} (quinone and NAc). ^1H NMR: δ=2.12 (3H, s, NAc), 2.39 (3H, s, phenolic Ac), 3.18—3.52 (8H, CH_2 of side chain), 7.09—7.42 (17H, m, H-2,3 and $C(C_6\underline{H}_5)_3$), 7.52—7.73 (2H, m, H-6 and 7), 8.00—8.22 (2H, m, H-5 and 8), 9.95 (1H, bs, aromatic NH).

Found: C, 73.79; H, 5.79; N, 4.04%. Calcd for $C_{41}H_{36}N_2O_6\cdot H_2O$: C, 73.42; H, 5.71; N, 4.18%.

4-[N-Acetyl-2-[N-acetyl-2-(trityloxy)ethylamino]ethylamino]-1-hydroxy-9,10-anthracenedione (6). To a stirred solution of **4** (150 mg) in ethanol (10 ml), 1 M NaOH (1 M=1 mol dm^{-3}) solution (8 ml) was added. After 24 h, 1 M HCl solution (8 ml) was added to the mixture. Pecipitated solids were collected, washed with water, and dissolved in chloroform. After drying over anhydrous Na_2SO_4, the solution was concentrated, and the residue was purified on a column using 10:1 (v/v) benzene–ethyl acetate. Fractions homogeneous (R_f 0.20) in 3:1 (v/v) benzene–ethyl acetate were combined and concentrated. The residue was recrystallized from ethanol to give 132 mg (94%) of **6**, mp 257—258 °C; UV ($CHCl_3$) 313 (log ε, 4.36), 348 (4.42), 503 nm (4.23); IR (KBr) 1710 cm^{-1} (aromatic NAc), 1650 (quinone), 1625 (quinone and NAc). ^1H NMR: δ=2.18 (3H, s, NAc), 2.70 (3H, s, aromatic NAc), 3.20—3.67 (6H, m, $NAcCH_2C\underline{H}_2$-$NAcC\underline{H}_2CH_2OTr$), 4.27—4.53 (2H, m, $NAcC\underline{H}_2CH_2NAc$), 7.10—7.47 (16H, m, aromatic proton and $C(C_6H_5)_3$), 7.57—7.77 (2H, m, aromatic protons), 7.92—8.07 (1H, m, aromatic proton), 8.30—8.57 (2H, m, H-5 and 8).

Found: C, 75.57; H, 5.62; N, 4.04%. Calcd for $C_{41}H_{36}N_2O_6$: C, 75.44; H, 5.56; N, 4.29%.

1-(2,3,4,6-Tetra-O-acetyl-β-D-glucopyranosyloxy)-4-[N-acetyl-2-[N-acetyl-2-(trityloxy)ethylamino]ethylamino]-9,10-anthracenedione (7). To a solution of **6** (100 mg) in quinoline (3 ml) and benzene (3 ml), acetobromoglucose (202 mg) and silver carbonate (218 mg) were added in the dark. The mixture was stirred for 47 h at room temperature, the insoluble materials were removed by filtration, and then the filtrate was diluted with benzene. The solution was washed with 5% H_2SO_4, sat. $NaHCO_3$ solution and water. After drying over anhydrous Na_2SO_4, the solution was concentrated, and the residue was purified on a column using 3:1 (v/v) benzene–ethyl acetate. Fractions homogeneous (R_f 0.28) on TLC in 1:1 (v/v) benzene–ethyl acetate were concentrated and the residue was resolidified with benzene–hexane to give 127 mg (84%) of **7**, mp 123—129 °C; $[\alpha]_D^{22}$ −17.1° (*c* 0.55, $CHCl_3$); UV (EtOH) 325 (log ε, 4.24), 348 (4.28), 430 nm (4.04). ^1H NMR: δ=2.03 (6H, s, Ac×2), 2.08 (3H, s, Ac), 2.18 (6H, s, Ac×2), 2.62 (3H, s, aromatic NAc), 3.19—3.63 (6H, m, $NAcCH_2C\underline{H}_2NAcC\underline{H}_2C\underline{H}_2$-OTr), 3.83 (1H, m, H-5′), 4.13—4.47 (4H, m, $NAcC\underline{H}_2$-CH_2NAc and H-6′), 5.03—5.47 (4H, m, H-1′, 2′, 3′, and 4′), 7.06—7.40 (16H, m, aromatic proton and $C(C_6\underline{H}_5)_3$), 7.50—7.70 (2H, m, aromatic protons), 7.77—7.90 (1H, m, aromatic proton), 8.30—8.43 (2H, m, H-5 and 8).

Found: C, 66.94; H, 5.60; N, 2.67%. Calcd for $C_{55}H_{54}N_2O_{15}$: C, 67.20; H, 5.54; N, 2.85%.

1-(2,3,4,6-Tetra-O-acetyl-β-D-glucopyranosyloxy)-4-[N-acetyl-2-(N-acetyl-2-hydroxyethylamino)ethylamino]-9,10-anthracenedione (8). A solution of **7** (600 mg) in 80% aqueous acetic acid (10 ml) was heated for 40 min at 100 °C. The solution was concentrated and the residue was purified on a column using 1:10 (v/v) ethanol–toluene. Fractions homogeneous (R_f 0.20) on TLC in 1:5 (v/v) ethanol–toluene were combined and concentrated. The residue was resolidified with benzene–hexane to give 367 mg (81%) of **8**. ^1H NMR: δ=2.03 (6H, s, Ac×2), 2.10 (3H, s, Ac), 2.15 (3H, s, Ac), 2.18 (3H, s, Ac), 2.58 (3H, s, aromatic NAc), 3.42—3.95 (7H, m, H-5′ and $NAcCH_2C\underline{H}_2NAcC\underline{H}_2C\underline{H}_2OTr$), 4.12—4.60 (4H, m, H-6′ and $NAcC\underline{H}_2CH_2NAc$), 5.00—5.47 (4H, m, H-1′, 2′, 3′, and 4′), 7.47—7.90 (4H, m, H-2,3,6, and 7), 8.17—8.38 (2H, m, H-5 and 8).

4-[N-Acetyl-2-(N-acetyl-2-hydroxyethylamino)ethylamino]-1-(β-D-glucopyranosyloxy)-9,10-anthracenedione (9). A solution of **8** (300 mg) in methanolic ammonia (5 ml) was stirred for 24 h at 0—5 °C. The solution was concentrated and the residue was washed with hot methanol to give 203 mg (88%) of **9** as yellow solid, mp 218—220 °C; UV (H_2O) 225 (log ε, 4.65), 314 (4.01), 352 (4.07), 427 nm (3.88). ^1H NMR (pyridine-d_5): δ=2.20 (3H, s, NAc), 2.77 (3H, s, aromatic NAc), 5.33 (1H, d, J=7.5 Hz, H-1′), 7.40—7.55 (2H, m, H-2 and 3), 7.87—8.05 (2H, m, H-6 and 7), 8.22—8.43 (2H, m, H-5 and 8).

Found: C, 58.88; H, 5.45; N, 4.64%. Calcd for $C_{28}H_{32}N_2O_{11}$: C, 58.74; H, 5.63; N, 4.89%.

4-[2-[N-(t-Butoxycarbonyl)-2-hydroxyethylamino]ethylamino]-1-hydroxy-9,10-anthracenedione (10). To a stirred solution of **1** (1.00 g) in 1 M NaOH solution (8 ml) and dioxane (12 ml), di-*t*-butyl dicarbonate (2.00 g) was added. After 1 h, 1 M HCl solution (8 ml) was added to the mixture and the solution was extracted with ethyl acetate. The Organic layer was washed with water, dried over anhydrous Na_2SO_4, and concentrated. The residue was purified on a column using 2:1 (v/v) benzene–ethyl acetate. Fractions homogeneous (R_f 0.26) on TLC in 1:1 (v/v) benzene–ethyl acetate were concentrated to give 1.04 g (80%) of **10** as amorphous solid; UV ($CHCl_3$) 253 (log ε, 4.58), 291 (3.88), 558 (4.11), 608 nm (4.07). ^1H NMR: δ=1.47 (9H, s, Boc), 2.57 (1H, bs, $CH_2CH_2O\underline{H}$), 3.28—3.55 (6H, m, $NHC\underline{H}_2$-$C\underline{H}_2N(Boc)C\underline{H}_2CH_2OH$), 3.73 (2H, t, J=4.5 Hz, $CH_2C\underline{H}_2$-OH), 7.10 (2H, d, J=3.0 Hz, H-2 and 3), 7.52—7.72 (2H, m, H-6 and 7), 8.05—8.22 (2H, m, H-5 and 8), 10.13 (1H, bs, aromatic NH), 13.47 (1H, s, 1-OH).

Found: C, 64.93; H, 6.13; N, 6.32%. Calcd for $C_{23}H_{26}N_2O_6$: C, 64.93; H, 5.92; N, 6.58%.

4-[2-[N-(t-Butoxycarbonyl)-2-(trityloxy)ethylamino]ethylamino]-1-hydroxy-9,10-anthracenedione (11). To a stirred solution of **10** (966 mg) in pyridine (30 ml), trityl chloride (1.89 g) was added. After 24 h at 50 °C, the mixture was poured into ice-cooled water, and the precipitates were collected. The product was purified on a column using 1:3 (v/v) ethyl

acetate–hexane. Fractions homogeneous (R_f 0.56) on TLC in the same solvent were concentrated, and the residue was recrystallized from hexane to give 1.16 g (77%) of **11**, mp 151—152 °C; UV ($CHCl_3$) 254 (log ε, 4.45), 294 (3.65), 559 (3.68), 601 nm (3.64). ^1H NMR: δ=1.30—1.56 (9H, m, Boc), 3.03—3.56 (8H, m, CH_2 of side chain), 7.00—7.40 (17H, m, H-2,3 and $C(C_6\underline{H}_5)_3$), 7.50—7.70 (2H, m, H-6 and 7), 8.10—8.27 (2H, m, H-5 and 8), 10.18 (1H, bs, aromatic NH), 13.47 (1H, s, 1-OH).

Found: C, 75.40; H, 6.32; N, 4.13%. Calcd for $C_{42}H_{40}N_2O_6$: C, 75.42; H, 6.03; N, 4.19%.

1-Acetoxy-4-[2-[N-(t-butoxycarbonyl)-2-(trityloxy)ethylamino]-ethylamino]-9,10-anthracenedione (12). Compound **11** (100 mg) was acetylated with acetic anhydride (3 ml) and pyridine (6 ml) for 20 h. The mixture was concentrated and the residue was purified on a column using 1:3 (v/v) ethyl acetate–hexane. Fractions homogeneous (R_f 0.25) on TLC in the same solvent were concentrated and the residue was recrystallized from hexane to give 101 mg (95%) of **12**, mp 85—88 °C; UV ($CHCl_3$) 250 (log ε, 4.66), 278 (4.19), 319 (4.03), 511 nm (4.01); IR (KBr) 1765 cm^{-1} (phenolic Ac), 1690 (NBoc), 1655 (quinone), 1630 (quinone). ^1H NMR: δ=1.27—1.48 (9H, m, Boc), 2.40 (3H, s, phenolic Ac), 3.03—3.63 (8H, m, CH_2 of side chain), 7.00—7.47 (17H, m, H-2,3 and $C(C_6\underline{H}_5)_3$), 7.52—7.77 (2H, m, H-6 and 7), 8.00—8.28 (2H, m, H-5 and 8), 10.00 (1H, bs, aromatic NH).

Found: C, 74.34; H, 6.22; N, 3.84%. Calcd for $C_{44}H_{42}N_2O_7$: C, 74.35; H, 5.96; N, 3.94%.

4-[2-[N-(t-Butoxycarbonyl)-2-(trityloxy)ethylamino]-N-(trifluoroacetyl)ethylamino]-1-hydroxy-9,10-anthracenedione (13). To a ice-cooled solution of **12** (300 mg) in pyridine (10 ml), trifluoroacetic anhydride (0.6 ml) was added with stirring, and the mixture was stirred for 21 h at room temperature. The mixture was poured into ice cold water, and the precipitates were filtered off. The product was purified on a column using 1:8 (v/v) ethyl acetate–hexane. Fractions homogeneous (R_f 0.45) on TLC in 1:3 (v/v) ethyl acetate–hexane were concentrated and solidified with hexane to give 276 mg (86%) of **13** as amorphous solid; UV ($CHCl_3$) 257 (log ε, 4.59), 338 (3.60), 402 nm (3.82); IR (KBr) 1700 (C=O, broad), 1640 (quinone). ^1H NMR: δ=1.30 (9H, s, Boc), 7.03—7.52 (17H, m, H-2,3 and $C(C_6\underline{H}_5)_3$), 7.63—7.83 (2H, m, H-6 and 7), 8.07—8.30 (2H, m, H-5 and 8), 13.10 (1H, s, 1-OH).

Found: C, 68.83; H, 5.42; N, 3.44%. Calcd for $C_{44}H_{39}N_2F_3O_7$: C, 69.10; H, 5.14; N, 3.66%.

1-(2,3,4,6-Tetra-O-acetyl-β-D-glucopyranosyloxy)-4-[2-[N-(t-butoxycarbonyl)-2-(trityloxy)ethylamino]-N-(trifluoroacetyl)ethylamino]-9,10-anthracenedione (14). To a stirred solution of **13** (1.35 g) in quinoline (5 ml) and benzene (5 ml), acetobromoglucose (2.18 g) and silver carbonate (916 mg) were added. After 54 h in the dark, the reaction mixture was filtered and the filtrate was diluted with benzene. The solution was washed with 5% H_2SO_4 solution, H_2O, sat. $NaHCO_3$ solution, H_2O, dried over anhydrous Na_2SO_4, and concentrated. The residue was purified on the column using 7:1 (v/v) benzene–ethyl acetate and 1:3 (v/v) ethyl acetate–hexane. Fractions homogeneous (R_f 0.52) on TLC in 1:1 (v/v) ethyl acetate–hexane were concentrated and recrystallized from cyclohexane to give 1.55 g (80%) of **14**, mp 113—118 °C; $[\alpha]_D^{22}$ −28.7° (*c* 0.53, $CHCl_3$); UV (EtOH) 255 (log ε, 4.55), 347 nm (3.68). ^1H NMR: δ=1.30 (9H, s, Boc), 2.02 (9H, s, Ac×3), 2.15 (3H, s, Ac), 4.98 (4H, m, H-1′2′,3′, and 4′), 7.07—7.43 (17H, m, H-2,3 and $C(C_6\underline{H}_5)_3$), 7.56—7.73 (2H, m, H-6 and 7), 7.93—8.12 (2H, m, H-5 and 8).

Found: C, 63.85; H, 5.45; N, 2.38%. Calcd for $C_{58}H_{57}N_2F_3O_{16}$: C, 63.61; H, 5.25; N, 2.56%.

1-(β-D-Glucopyranosyloxy)-4-[2-(2-hydroxyethylamino)ethylamino]-9,10-anthracenedione (16). Compound **14** (241 mg) was dissolved in trifluoroacetic acid (1 ml) under ice cooling and stirred at room temperature. The mixture was concentrated and the residue was purified on a column using 5:1 (v/v) benzene–ethanol. Fractions homogeneous (R_f 0.34) on TLC in 1:3 (v/v) benzene–ethanol were concentrated to give 116 mg of **15** as amorphous solid. The solid was dissolved in methanolic ammonia (5 ml) and the solution was stirred overnight at 0—5 °C. Precipitated solids were collected and washed with ethyl acetate–methanol to give 52 mg (48% from **14**) of **16**, mp 211—218 °C; UV (MeOH) 248 (log ε, 4.56), 280 (3.93), 526 nm (3.87); IR (KBr) 1640 cm^{-1}, 1630 (quinone).

Found: C, 58.42; H, 5.78; N, 5.52%. Calcd for $C_{24}H_{28}N_2O_9 \cdot 1/4\,H_2O$: C, 58.47; H, 5.83; N, 5.68%.

2-(2,3,4,6-Tetra-O-acetyl-β-D-glucopyranosyloxy)-4-[N-acetyl-2-(N-acetyl-2-aceloxyethylamino)ethylamino]-9,10-anthracenedione (17). Compound **16** (10 mg) was acetylated with acetic anhydride (1.5 ml) and pyridine (1.5 ml) at 100 °C. The mixture was diluted with ethyl acetate, washed with water, dried over anhydrous Na_2SO_4, and concentrated. The residue was solidified with benzene–hexane to give 13 mg (81%) of **17**, mp 102—112 °C; $[\alpha]_D^{23}$ −19.0° (*c* 0.62, $CHCl_3$); UV (EtOH) 208 (log ε, 4.91), 230 (4.92), 311 (4.31), 346 (4.34), 421 nm (4.12). ^1H NMR: δ=2.03 (3H, s, Ac), 2.05 (6H, s, Ac×2), 2.10 (3H, s, Ac), 2.17 (6H, s, Ac×2), 2.63 (3H, s, aromatic NAc), 3.45—3.91 (5H, m, $NAcCH_2C\underline{H}_2$-$NAcC\underline{H}_2CH_2OAc$ and H-5′), 4.10—4.66 (6H, m, $NHAc$-$C\underline{H}_2CH_2NAcCH_2C\underline{H}_2OAc$ and H-6′), 5.01—5.44 (4H, m, H-1′,2′,3′, and 4′), 7.49—7.93 (4H, m, H-2,3,6, and 7), 8.20—8.43 (2H, m, H-5 and 8).

Found: C, 58.44; H, 5.18; N, 3.27%. Calcd for $C_{38}H_{42}N_2O_{16}$: C, 58.31; H, 5.41; N, 3.85%.

Condensation of 13 with Halogen Sugars. Halogen sugars of galactose,[14] 6-deoxyglucose,[15] L-rhamnose,[16] cellobiose,[17] 2-acetamido-2-deoxyglucose,[18] 3-acetamido-3-deoxyglucose,[19] were prepared according to the authentic methods. The reaction procedure was analogous as described in the preparation of **14**.

1-(2,3,4,6-Tetra-O-acetyl-β-D-galactopyranosyloxy)-4-[2-[N-(t-butoxycarbonyl)-2-(trityloxy)ethylamino]-N-(trifluoroacetyl)ethylamino]-9,10-anthracenedione (18). Compound **18** was obtaine in 93% yield from **13** and showed a spot at R_f 0.45 on TLC in 1:1 (v/v) ethyl acetate–hexane; mp 118—125 °C; $[\alpha]_D^{20}$ −5.9° (*c* 1.05, $CHCl_3$); UV (EtOH) 225 (log ε, 4.83), 258 (4.75), 350 nm (3.80). ^1H NMR: δ=1.31 (9H, s, Boc), 2.02 (6H, s, Ac×2), 2.17 (6H, s, Ac×2), 7.07—7.43 (17H, m, H-2,3 and $C(C_6\underline{H}_5)_3$), 7.48—7.75 (2H, m, H-6 and 7), 7.83—8.20 (2H, m, H-5 and 8).

Found: C, 63.57; H, 5.43; N, 2.41%. Calcd for $C_{58}H_{57}N_2F_3O_{16}$: C, 63.61; H, 5.25; N, 2.56%.

1-(2,3,4-Tri-O-acetyl-6-deoxy-β-D-glucopyranosyloxy)-4-[2-[N-(t-butoxycarbonyl)-2-(trityloxy)ethylamino]-N-(trifluoroacetyl)-ethylamino]-9,10-anthracenedione (19). Compound **19** was obtained in 91% yield from **13** and showed a spot at R_f 0.42 on TLC in 1:3 (v/v) ethyl acetate–toluene; mp 146—148 °C; $[\alpha]_D^{24}$ −24.8° (*c* 1.16, $CHCl_3$); UV ($CHCl_3$) 256 (log ε, 4.62), 350 nm (3.71). ^1H NMR: δ=1.30 (12H, bs, Boc and H-6′), 2.00 (6H, s, Ac×2), 2.10 (3H, s, Ac), 4.67—5.47 (4H, m, H-1′,2′,3′, and 4′), 6.90—7.80 (19H, m, H-2,3,6,7 and $C(C_6\underline{H}_5)_3$), 7.80—8.23 (2H, m, H-5 and 8).

Found: C, 65.05; H, 5.54; N, 2.53%. Calcd for $C_{56}H_{55}N_2F_3O_{14}$: C, 64.86; H, 5.35; N, 2.70%.

1-(2,3,4-Tri-O-acetyl-α-L-rhamnopyranosyloxy)-4-[2-[N-(t-

butoxycarbonyl)-2-(trityloxy)ethylamino]-N-(trifluoroacetyl)ethylamino]-9,10-anthracenedione (20). Compound **20** was obtained in 42% yield from **13** and showed a spot at R_f 0.47 on TLC in 1:3 (v/v) ethyl acetate–toluene; mp 115—119 °C; $[\alpha]_D^{24}$ −24.6° (*c* 1.00, $CHCl_3$); UV ($CHCl_3$) 256 (log ε, 4.67), 354 nm (3.75). ^{1}H NMR δ=1.21 (3H, d, $J_{5',6'}$= 6.0 Hz, H-6'), 1.31 (9H, s, Boc), 2.03 (6H, (6H, s, Ac×2), 2.16 (3H, s, Ac), 6.97—7.77 (19H, m, H-2,3,6,7, and C(C$_6$H$_5$)$_3$), 7.80—8.27 (2H, m, H-5 and 8).

Found: C, 64.68; H, 5.35; N, 2.76%. Calcd for $C_{56}H_{55}N_2F_3O_{14}$: C, 64.86; H, 5.35; N, 2.70%.

1-(2,2',3,3',4',6,6'-Hepta-O-acetyl-β-cellobiosyloxy)-4-[2-[N-(t-butoxycarbonyl)-2-(trityloxy)ethylamino]-N-(trifluoroacetyl)-ethylamino]-9,10-anthracenedione (21). Compound **21** was obtained in 66% yield from **13** and showed a spot at R_f 0.45 on TLC in 1:3 (v/v) ethyl acetate–toluene; mp 131—139 °C; $[\alpha]_D^{27}$ −31.1° (*c* 0.52, $CHCl_3$); UV (EtOH) 214 (log ε, 4.61), 254 (4.51), 341 nm (3.70). ^{1}H NMR: δ= 1.30 (9H, s, Boc), 1.93 (3H, s, Ac), 1.97 (3H, s, Ac), 2.00 (3H, s, Ac), 2.07 (9H, s, Ac×3), 2.13 (3H, s, Ac), 6.91—7.43 (17H, m, H-2,3 and C(C$_6$H$_5$)$_3$), 7.53—7.79 (2H, m, H-6 and 7), 7.87—8.13 (2H, m, H-5 and 8).

Found: C, 60.51; H, 5.45; N, 1.95%. Calcd for $C_{70}H_{73}N_2F_3O_{24}$: C, 60.78; H, 5.31; N, 2.03%.

1-(2-Acetamido-3,4,6-tri-O-acetyl-2-deoxy-β-D-glucopyranosyloxy)-4-[2-[N-(t-butoxycarbonyl)-2-(trityloxy)ethylamino]-N-(trifluoroacetyl)ethylamino]-9,10-anthracenedione (22). Compound **22** was obtaine in 82% yield from **13** and showed a spot at R_f 0.32 on TLC in 1:3 (v/v) ethyl acetate–chloroform; mp 148—150 °C; $[\alpha]_D^{21}$ +29.2° (*c* 1.06, $CHCl_3$); UV ($CHCl_3$) 256 (log ε, 4.64), 345 nm (3.71). ^{1}H NMR: δ= 1.32 (9H, s, Boc), 2.00 (3H, s, Ac), 2.03 (6H, s, Ac×2), 2.07 (3H, s, Ac), 6.43 (1H, d, *J*=9.0 Hz, NHAc), 7.07—7.47 (17H, m, H-2,3 and C(C$_6$H$_5$)$_3$), 7.50—7.85 (2H, m, H-6 and 7), 7.90—8.20 (2H, m, H-5 and 8).

Found: C, 63.44; H, 5.44; N, 3.85%. Calcd for $C_{58}H_{58}N_3F_3O_{15}$: C, 63.67; H, 5.34; N, 3.84%.

1-(3-Acetamido-2,4,6-tri-O-acetyl-3-deoxy-β-D-glucopyranosyloxy)-4-[2-[N-(t-butoxycarbonyl)-2-(trityloxy)ethylamino]-N-(trifluoroacetyl)ethylamino]-9,10-anthracenedione (23). Compound **23** was obtained in 62% yield from **13** and showed a spot at R_f 0.24 on TLC in 1:1 (v/v) ethyl acetate–chloroform; mp 182—186 °C; $[\alpha]_D^{21}$ +10.8° (*c* 1.01, $CHCl_3$); UV (EtOH) 211 (log ε, 4.61), 254 (4.52), 346 nm (3.63). ^{1}H NMR: δ=1.34 (9H, s, Boc), 1.85 (3H, s, Ac), 2.07 (3H, s, Ac), 2.19 (6H, s, Ac×2), 7.10—7.52 (17H, m, H-2,3 and C(C$_6$H$_5$)$_3$), 7.56—7.96 (2H, m, H-6 and 7), 8.01—8.32 (2H, m, H-5 and 8).

Found: C, 63.75; H, 5.50; N, 3.72%. Calcd for $C_{58}H_{58}N_3F_3O_{15}$: C, 63.67; H, 5.34; N, 3.84%.

Deprotection of **18**, **19**, **20**, **21**, **22**, *and* **23**. Deprotection was worked up with trifluoroacetic acid and methanolic ammonia analogously as described in the preparation of **16**.

1-(β-D-Galactopyranosyloxy)-4-[2-(2-hydroxyethylamino)ethylamino]-9,10-anthracenedione (24). Compound **24** was obtained in 52% yield from **18**; mp 202—205 °C; IR (KBr) 1655 cm^{-1} and 1630 (quinone).

Found: C, 58.02; H, 5.73; N, 5.44%. Calcd for $C_{24}H_{28}N_2O_9\cdot 1/2\,H_2O$: C, 57.94; H, 5.88; N, 5.63%.

1-(6-Deoxy-β-D-glucopyranosyloxy)-4-[2-(2-hydroxyethylamino)-ethylamino]-9,10-anthracenedione (25). Compound **25** was obtained in 26% yield from 19; mp 175—180 °C; IR (KBr) 1655 cm^{-1} and 1630 (quinone).

Found: C, 58.50; H, 5.84; N, 5.38%. Calcd for $C_{24}H_{28}N_2O_8\cdot H_2O$: C, 58.76; H, 6.17; N, 5.71%.

4-[2-(2-Hydroxyethylamino)ethylamino]-1-(α-L-rhamnopyranosyloxy)-9,10-anthracenedione (26). Compound **26** was obtained in 39% yield from 20; mp 162—164 °C; IR (KBr) 1655 cm^{-1} and 1630 (quinone).

Found: C, 58.69; H, 5.94; N, 5.79%. Calcd for $C_{24}H_{28}N_2O_8\cdot H_2O$: C, 58.76; H, 6.17; N, 5.71%.

4-[2-(2-Hydroxyethylamino)ethylamino]-1-(β-cellobiosyloxy)-9,10-anthracenedione (27). Compound **27** was obtained in 43% yield from **21**; mp 198—206 °C; IR (KBr) 1645 cm^{-1} and 1620 (quinone).

Found: C, 53.79; H, 5.80; N, 4.26%. Calcd for $C_{30}H_{38}N_2O_{14}\cdot H_2O$: C, 53.88; H, 6.03; N, 4.19%.

1-(2-Acetamido-2-deoxy-β-D-glucopyranosyloxy)-4-[2-(2-hydroxyethylamino)ethylamino]-9,10-anthracenedione (28). Compound **28** was obtained in 53% yield from **22**; mp 186—189 °C; IR (KBr) 1650 cm^{-1} and 1625 (quinone).

Found: C, 57.24; H, 5.83; N, 7.31%. Calcd for $C_{26}H_{31}N_3O_9\cdot H_2O$: C, 57.03; H, 6.08; N, 7.67%.

1-(3-Acetamido-3-deoxy-β-D-glucopyranosyloxy)-4-[2-(2-hydroxyethylamino)ethylamino]-9,10-anthracenedione (29). Compound **29** was obtained in 40% yield from **23**; mp 118—121 °C; IR (KBr) 1650 cm^{-1} and 1625 (quinone).

Found: C, 58.18; H, 5.88; N, 7.30%. Calcd for $C_{26}H_{31}N_3O_9\cdot 1/2\,H_2O$: C, 57.99; H, 5.99; N, 7.80%.

Acetylation of **24**, **25**, **26**, **27**, **28**, *and* **29**. Acetylation was worked up with acetic anhydride and pyridine at room temperature.

1-(2,3,4,6-Tetra-O-acetyl-β-D-galactopyranosyloxy)-4-[2-(N-acetyl-2-acetoxyethylamino)ethylamino]-9,10-anthracenedione (30). Compound **30** was obtained in 81% yield from **24** and showed a spot at R_f 0.54 on TLC in 1:1 (v/v) acetone–toluene; mp 85—98 °C; UV (EtOH) 206 (log ε, 4.43), 247 (4.61), 316 (3.74), 511 nm (3.89). ^{1}H NMR: δ=1.99 (6H, s, Ac× 2), 2.01 (3H, s, Ac), 2.15 (3H, s, Ac), 2.19 (3H, s, Ac), 7.09—7.29 (2H, m, H-2 and 3), 7.37—7.74 (2H, m, H-6 and 7), 7.94—8.23 (2H, m, H-5 and 8).

Found: C, 58.05; H, 5.53; N, 3.62%. Calcd for $C_{36}H_{40}N_2O_{15}$: C, 58.38; H, 5.44; N, 3.62%.

1-(2,3,4-Tri-O-acetyl-6-deoxy-β-D-glucopyranosyloxy)-4-[2-(N-acetyl-2-acetoxyethylamino)ethylamino]-9,10-anthracenedione (31). Compound **31** was obtained in 66% yield from **25** and showed a spot at R_f 0.53 on TLC in 1:5 (v/v) ethanol–toluene; mp 101—103 °C; UV ($CHCl_3$) 250 (log ε, 4.53), 276 (4.00), 320 (3.72), 516 nm (3.85). ^{1}H NMR: δ=1.22 (3H, d, $J_{5',6'}$=3.0 Hz, H-6'), 2.00 (6H, s, Ac×2), 2.02 (3H, s, Ac), 2.10 (3H, s, Ac), 2.15 (3H, s, Ac), 4.70—5.37 (4H, m, H-1',2',3', and 4'), 7.30 (1H, d, *J*=9.0 Hz, aromatic proton), 7.52 (1H, d, *J*=9.0 Hz, aromatic proton), 7.60—7.83 (2H, m, H-6 and 7), 7.97—8.30 (2H, m, H-5 and 8), 10.11 (1H, bs, aromatic NH).

Found: C, 60.07; H, 5.62; N, 3.89%. Calcd for $C_{34}H_{38}N_2O_{13}$: C, 59.82; H, 5.61; N, 4.10%.

1-(2,3,4-Tri-O-acetyl-α-L-rhamnopyranosyloxy)-4-[2-(N-acetyl-2-acetoxyethylamino)ethylamino]-9,10-anthracenedione (32). Compound **32** was obtained in 97% yield from **26** and showed a spot at R_f 0.49 on TLC in 1:5 (v/v) ethanol–toluene; mp 192—194 °C; UV ($CHCl_3$) 249 (log ε, 4.71), 276 (4.18), 320 (3.88), 514 nm (4.04). ^{1}H NMR: δ=1.20 (3H, d, $J_{5',6'}$=6.0 Hz, H-6'), 2.03 (3H, s, Ac), 2.06 (6H, s, Ac× 2), 2.12 (3H, s, Ac), 2.18 (3H, s, Ac), 4.93—6.00 (4H, m, H-1',2',3', and 4'), 7.13—7.50 (2H, m, H-2 and 3), 7.56—7.98 (2H, m, H-6 and 7), 8.03—8.43 (2H, m, H-5 and 8), 10.10 (1H, bs, aromatic NH).

Found: C, 59.81; H, 5.66; N, 3.87%. Calcd for $C_{34}H_{38}N_2O_{13}$: C, 59.82; H, 5.61; N, 4.10%.

1-(2,2',3,3',4',6,6'-Hepta-O-acetyl-β-cellobiosyloxy)-4-[2-(N-acetyl-2-acetoxyethylamino)ethylamino]-9,10-anthracenedione (33). Compound **33** was obtained in 86% yield from **27** and showed

a spot at R_f 0.53 on TLC in 1:3 (v/v) ethanol–toluene; mp 162—164 °C; UV (EtOH) 247 (log ε, 4.64), 271 (3.99), 316 (3.72), 509 nm (3.95). ^{1}H NMR: δ=1.97 (3H, s, Ac), 1.98 (3H, s, Ac), 1.99 (3H, s, Ac), 2.01 (3H, s, Ac), 2.07 (3H, s, Ac), 2.08 (3H, s, Ac), 2.09 (3H, s, Ac), 2.14 (3H, s, Ac), 2.17 (3H, s, Ac), 7.30 (1H, d, J=6.5 Hz, aromatic proton), 7.50 (1H, d, J=6.5 Hz, aromatic proton), 7.60—7.78 (2H, m, H-6 and 7), 8.13—8.33 (2H, m, H-5 and 8), 10.11 (1H, bs, aromatic NH).

Found: C, 55.94; H, 5.58; N, 2.58%. Calcd for $C_{48}H_{56}N_2O_{23}$: C, 56.03; H, 5.49; N, 2.72%.

*1-(2-Acetamido-3,4,6-tri-O-acetyl-2-deoxy-β-D-glucopyranosyloxy)-4-[2-(N-acetyl-2-acetoxyethylamino)ethylamino]-9,10-anthracenedione (**34**).* Compound **34** was obtained in 70% yield from **28** and showed a spot at R_f 0.26 on TLC in 1:2 (v/v) acetone–chloroform; mp 179—182 °C; UV ($CHCl_3$) 250 (log ε, 4.70), 280 (4.17), 319 (3.96), 514 nm (4.00). ^{1}H NMR: δ=1.99 (3H, s, Ac), 2.03 (3H, s, Ac), 2.05 (9H, s, Ac×3), 2.13 (3H, s, Ac), 3.33—3.80 (6H, m, NHC$\underline{H}_2$-C$\underline{H}_2$N(Ac)C$\underline{H}_2$CH_2OAc), 3.87—4.47 (6H, m, H-2′,5′,6′, and CH_2C$\underline{H}_2$OAc), 4.87—5.33 (3H, m, H-1′,3′,4′), 7.03 (1H, bd, J=6.0 Hz, N$\underline{H}$Ac), 7.22 (1H, d, J=9.0 Hz, aromatic proton), 7.41 (1H, d, J=9.0 Hz, aromatic proton), 7.53—7.83 (2H, m, H-6 and 7), 7.90—8.30 (2H, m, H-5 and 8), 9.93—10.20 (1H, bs, aromatic NH).

Found: C, 58.25; H, 5.60; N, 5.49%. Calcd for $C_{36}H_{41}N_3O_{14}$: C, 58.45; H, 5.59; N, 5.68%.

*1-(3-Acetamido-2,4,6-tri-O-acetyl-3-deoxy-β-D-glucopyranosyloxy)-4-[2-(N-acetyl-2-acetoxyethylamino)ethylamino]-9,10-anthracenedione (**35**).* Compound **35** was obtained in 93% yield from **29** and showed a spot at R_f 0.52 on TLC in 1:3 (v/v) ethanol–toluene; mp 96—106 °C; UV (EtOH) 205 (log ε, 4.51), 247 (4.61), 514 nm (3.91). ^{1}H NMR: δ=1.81 (3H, s, Ac), 2.05 (6H, s, Ac×2), 2.15 (3H, s, Ac), 2.18 (6H, s, Ac×2), 3.43—3.76 (6H, m, NHC$\underline{H}_2$C$\underline{H}_2$N(Ac)-CH_2CH_2OAc), 4.01—4.69 (6H, m, H-3′,5′,6′ and CH_2C$\underline{H}_2$-OAc), 5.06—5.60 (3H, m, H-1′,2′, and 4′), 7.37—7.82 (3H, m, aromatic protons), 8.00—8.32 (3H, m, aromatic protons), 10.06 (1H, bs, aromatic NH).

Found: C, 58.30; H, 5.68; N, 5.80%. Calcd for $C_{36}H_{41}N_3O_{14}$: C, 58.45; H, 5.59; N, 5.68%.

The authors wish to express their thanks to Dr. Iwao Umezawa for his evaluation of the antineoplastic activity and to Mr. Saburo Nakada for his elementary analysis.

References

1) A. DiMarco, M. Gaetani, and B. Scarpinato, *Cancer Chemother. Rept.*, **55**, 33 (1969).

2) A. DiMarco, M, Gaetani, P. Orezzi, B. Scarpinato, R. Silverstein, M. Soldati, T. Dasdia, and L. Valentini, *Nature*, **201**, 706 (1964); A. DiMarco, M. Gaetani, P. Orezzi, and M. Soldati, 3rd. Int. Congr. of Chemistry, Stuttgart (1963); F. Arcamone, G. Franceschi, P. Orezzi, C. Cassinelli, W. Barbieri, and R. Mondelli, *J. Am. Chem. Soc.*, **86**, 5334 (1964).

3) G. R. Pettit, J. J. Einck, C. L. Herald, R. H. Ode, R. B. Von Dreele, P. Brown, M. L. Branshnikova, and G. F. Ganse, *J. Am. Chem. Soc.*, **97**, 7387 (1975).

4) J. Lunel, J. Prend'homme, Ger. Offen. 1,911,240; *Chem. Abstr.*, **72**, 20603 (1970); F. Arcamone, A. Cassinelli, S. Penco, and L. Tognoli, Ger. Offen. 1,923,885; *Chem. Abstr.*, **72** 131086 (1970).

5) H. Brockmann and K. Bauer, *Naturwissenschaften*, **37**, 492 (1950); H. Brockmann, *Fortschr. Chem. Org. Naturstoffe.*, **21**, 127 (1963).

6) Z. Vanek, J. Tax, I. Komersova, P. Sedmura, and J. Vokoun, *Folia Microbiol.*, **22**, 139 (1977).

7) L. Ettkinger, E. Gäumann, R. Hutter, W. Keller-Schierlein, F. Kradolfer, L. Neipp, V. Prelog, P. Reusser, and H. Zahner, *Chem. Ber.*, **92**, 1867 (1959).

8) J. C. Double and J. R. Brown, *J. Pharm. Pharmacol.*, **27**, 502 (1975).

9) R. K.-Y. Zee-Cheng and C. C. Cheng, *J. Med. Chem.*, **21**, 291 (1978).

10) R. K.-Y. Zee-Cheng, E. G. Podrebarac, C. C. Menon, and C. C. Cheng, *J. Med. Chem.*, **22**, 501 (1979).

11) R. K. Johnson, R. K.-Y. Zee-Cheng, W. W. Lee, E. M. Acton, D. W. Henry, and C. C. Cheng, *Cancer Treat. Rep.*, **63**, 425 (1979).

12) D. W. Henry, "Cancer Chemotherapy," ed by A. C. Sartorelli, ACS Symp. Ser., 30, (1976), p. 15.

13) C. E. Ballou, *Adv. Carbohydr. Chem.*, **9**, 59 (1954); L. Hough and A. C. Richardson, "Rodd's Chemistry of Carbon Compounds," ed by S. Coffey, Elsevier, Amsterdam, London, New York (1967), Vol. 1, Part F, p. 338.

14) R. G. Hansen, W. J. Rutter and P. Krichevsky, *Biochem. Prepar.*, **4**, 1 (1955).

15) J. Compton, *J. Am. Chem. Soc.*, **60**, 395 (1938).

16) G. M. Bebault, G. G. S. Dutton, and C. K. Warfield, *Carbohydr. Res.*, **34**, 174 (1974).

17) E. Fischer and Zemplen, *Ber.*, **43**, 2536 (1910).

18) D. H. Leaback and P. G. Walker, *J. Chem. Soc.*, **1957** 4754.

19) H. Paulsen and C.-P. Herold, *Chem. Ber.*, **104**, 1311 (1971). And 3-acetamido-1,2,4,6-tetra-*O*-acetyl-3-deoxy-β-D-glucopyranoside was treated with hydrogen chloride and acetyl chloride in dioxane.

 © 1983 The Chemical Society of Japan Bull. Chem. Soc. Jpn., 56, 1441—1445 (1983)

Pseudo-sugars. VIII. Synthesis of DL-1-Epivalidamine and Related Compounds[1,2]

Seiichiro OGAWA, Masayuki OYA, Tatsushi TOYOKUNI, Noritaka CHIDA, and Tetsuo SUAMI*

Department of Applied Chemistry, Faculty of Science and Technology, Keio University, Hiyoshi, Kohoku-ku, Yokohama 223

(Received November 11, 1982)

DL-1-Epivalidamine has been synthesized starting from the dianhydro compound derived from DL-1,2,3-tri-*O*-acetyl-(1,3/2,4,6)-4-bromo-6-bromomethyl-1,2,3-cyclohexanetriol. DL-7-Amino-7-deoxy-1-epivalidamine, which is considered to be a homolog of 2-deoxystreptamine, has also been prepared.

In connection with the previous paper of this series,[3] the 1-epimer of validamine and its derivatives have been synthesized regioselectively from the dianhydro derivative of (hydroxymethyl)cyclohexanetetrol.

It was described that the nucleophilic substitution reaction of DL-1,2,3-tri-*O*-acetyl-(1,3/2,4,6)-4-bromo-6-bromomethyl-1,2,3-cyclohexanetriol (**1**)[3] with an azide ion proceeded specifically through an S_N2 mechanism to give the diazido compound with an inversion of the configuration at C-4.[3] On the other hand, attempted introduction of an azido function at C-4 with retention of the configuration have been made *via* an intermediate cyclic 3,4-acetoxonium ion or a 3,4-epoxide,[4] but all failed probably due to a steric hindrance of a bulky substituent at C-6 and/or a ready anchimeric assistance of the C-2 acetoxyl group at C-3. Therefore, in order to control the course of a nucleophilic attack at the oxirane ring, the 2,7-anhydro ring was introduced to protect the C-2 hydroxyl group and to restrict a conformational flexibility. Thus, treatment of **1** with an excess of methanolic sodium methoxide at reflux for 2 h gave selectively the dianhydro compound **2** in 65% yield. The structure of **2** was confirmed on the basis of analytical data and ^{1}H NMR spectroscopy. In the ^{1}H NMR spectrum, the signal due to the C-7 endo proton appeared as a doublet (J_{gem}=9 Hz) at δ 3.75, which would correspond to the dihedral angle $\Phi_{5,7endo}$ (90°) ($J_{5,7endo}$= *ca.* 0 Hz) derived from a Dreiding model.

A nucleophilic substitution reaction of **2** with a methoxide ion or azide ion occurred regiospecifically at C-1 to give, after successive acetylation, the methyl ether **3** (87%) or the azide **4** (81%). An attack of an anion at C-2 seemed to be hindered by the ring oxygen atom. The structures were established by the ^{1}H NMR spectra. In the spectrum of **3**, the signal for the C-7 endo proton was remarkably deshielded (*ca.* 0.25 ppm) by a close proximity of the endo methoxyl group. Compound **4** was hydrogenated in ethanol in the presence of Raney nickel followed by acetylation to give the amine acetate **5** in 40% yield, which was alternatively prepared in 74% yield by ammonolysis of **2** in methanol followed by acetylation. *O*-Deacetylation of **5** with methanolic sodium methoxide followed by the conventional tosylation gave the ditosylate **6** in 45% overall yield. Opening of the anhydro ring of **3** was effected by heating in acetic acid–acetic anhydride (1:1) in a sealed tube at 85 °C for 20 h to give DL-2,3,4-tri-*O*-acetyl-1-*O*-methyl-(1,3,5/2,4)-5-acetoxymethyl-1,2,3,4-cyclohexanetetrol (**7**) in 39% yield.

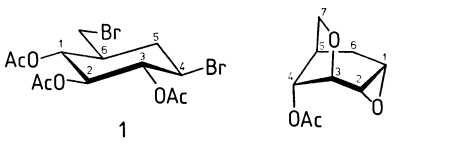

	X
3	OMe
4	N_3
5	NHAc

Scheme 1.

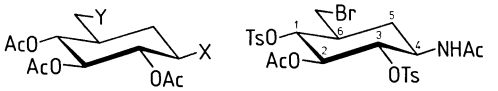

	X	Y
7	OMe	OAc
8	NHAc	Br
9	NHAc	OAc
10	NHAc	N_3
11	NHAc	NHAc

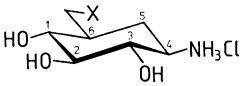

	X
13	OH
14	NH_3Cl

Scheme 2.

The anhydro ring of **5** was cleaved readily by the influence of 30% hydrobromic acid in acetic acid in a sealed tube at 75 °C for 23 h to give DL-1,2,3-tri-*O*-acetyl-(1,3/2,4,6)-4-acetamido-6-bromomethyl-1,2,3-cyclohexanetriol (**8**, 67%). Similarly, the corresponding bromo ditosylate **12** was obtained from **6** in 45% yield. The ^{1}H NMR spectrum of **12** was in fully accord with the assigned structure, establishing the ring structure of **4**.

The C-7 bromine atom of **8** was easily displaced by an acetate ion or an azide ion in the usual way to produce a peracetyl 1-epivalidamine (**9**, 61%) or the azido compound (**10**, 90%). Compound **10** was reduced with Raney nickel and successively acetylated to give the diamine diacetate **11** in 92% yield. Acid hydrolysis of **9** and **11** with 6 M hydrochloric acid

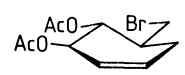

15

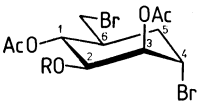

R	
16	H
17	Ac

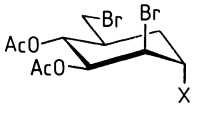

X	
18	Br
19	OAc
20	OH

21

Scheme 3.

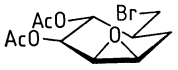

22

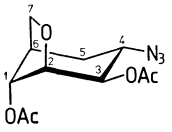

23

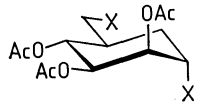

X	
24	N_3
25	NHAc

Scheme 4.

(1 M=1 mol dm^{-3}) at reflux for 2 h gave the hydrochloride **13** and the dihydrochloride **14** in quantitatively yields, respectively.

Compound **13** was pseudo-β-DL-glucopyranosylamine, and **14** was considered to be a homolog of 2-deoxystreptamine, a common constituent of clinically important aminocyclitol containing antibiotics.[5] Therefore, biological activities of antibiotics being replaced the 2-deoxystreptamine moiety with this homolog may be of considerable interest.

Interest in a reactivity of the stereoisomer **21** of **2** stimulated us to prepare it from (bromomethyl)cyclohexenediol diacetate **15**.[1] Treatment of **15** with bromine in aqueous acetic acid at room temperature afforded, after chromatography on silica gel, three dibromides **16** (34%), **19** (1.4%), and **20** (16%), and one tribromide **18** (0.7%). The ^{1}H NMR spectrum of triacetate **17** derived from **16** was interpreted by a first-order method, confirming the assigned structure. Mechanistically, an intermediate α-bromonium ion was opened by the adjacent trans acetoxyl group followed by acetyl group migration to give **16**, whereas, a β-bromonium ion was attacked from the rear side by nucleophiles present.[6] A similar treatment of **16** with an excess of methanolic sodium methoxide gave **21** in 84% yield. The ^{1}H NMR spectrum of **21** showed the signal for the C-7 endo proton as a doublet (J_{gem}=9.3 Hz) at δ 3.87 somewhat higher-field as compared with that of the *exo*-epoxide **2**.

In contrast with the case of **2**, a nucleophilic substitution reaction of **21** with an azide ion was shown to be very slow and give a complex mixture of products after a prolonged reaction time. The C-4 endo acetoxyl group seemed to interfere the attack of a nucleophile at C-1 or C-2. Therefore, the epoxide **22** was prepared by treatment of **15** with *m*-chloroperoxybenzoic acid in 1,2-dichloroethane in 23% yield.[7] Reaction of **22** with sodium azide and ammonium chloride in aqueous *N*,*N*-dimethylformamide gave selectively the diazide **24** in 65% yield. When the similar reaction was carried out in the absence of ammonium chloride, the monoazide **23** was obtained in 25% yield, together with **24** (48%). The epoxide ring seemed to be first opened by an azide ion and then the C-3 hydroxyl group, formed by an acetyl group migration under the basic conditions, competed with an azide ion to attack the C-6 bromomethyl group. Compound **24** was similarly converted into the diamine diacetate **25** in 41% yield. The ^{1}H NMR spectra of **24** and **25** supported their assigned structures.

Experimental[8]

DL-*4*-O-*Acetyl-1,2*:*3,7*-dianhydro-*(1,2,4/3,5)-5-hydroxymethyl-1,2,3,4-cyclohexanetetrol* (syn-*9-Acetoxy*-trans-*3,8-dioxatricyclo*[*4.2.1.0*^{2,4}]*nonane) (2).* A mixture of DL-tri-*O*-acetyl-(1,3/2,4,6)-4-bromo-6-bromomethyl-1,2,3-cyclohexanetriol (**1**)[3] (10 g) in methanol (140 ml) containing sodium (2.33 g) was refluxed for 2 h. After having been cooled, the reaction mixture was treated with 1 M hydrochloric acid for neutralization and then evaporated to dryness. The residue was treated with acetic anhydride (20 ml) and pyridine (30 ml) at room temperature overnight. The reaction mixture was concentrated and the residue was dissolved in ethyl acetate and the solution was passed through a short column of alumina. The filtrate was evaporated and the residue was recrystallized from ligroin to give 2.8 g (65%) of **2** as needles: mp 64.5—65.5 °C. ^{1}H NMR ($CDCl_3$) δ=2.03 (3H, s, OAc), 3.03—3.20 (2H, br s, H-1 and H-2), 3.75 (1H, d, J_{gem}=9 Hz, H-7endo), 4.10 (1H, ddd, $J_{5,7exo}$=7.5 Hz, $J_{6exo,7exo}$=2 Hz, H-7exo), 4.78—4.83 (2H, m, H-3 and H-4).

Found: C, 58.68; H, 6.57%. Calcd for $C_9H_{12}O_4$: C, 58.38; H, 6.57%.

DL-*2,4-Di*-O-*acetyl-3,7-anhydro-1*-O-*methyl-(1,3,5/2,4)-5-hydroxymethyl-1,2,3,4-cyclohexanetetrol (3).* A mixture of **2** (0.20 g) and 5 M methanolic sodium methoxide (8 ml) was refluxed for 1 h. The reaction mixture was processed similarly as described for the preparation of **2** and the product was acetylated in the usual way to give, after crystallization from ethanol, 0.24 g (87%) of **3** as plates: mp 75—76.5 °C. ^{1}H NMR ($CDCl_3$) δ=2.00 (3H, s) and 2.08 (3H, s) (OAc), 3.35 (3H, s, OMe), 3.81 (1H, ddd, $J_{5,7exo}$=4.5 Hz, $J_{6exo,7exo}$=1.5 Hz, J_{gem}=7.5 Hz, H-7exo), 4.00 (1H, d, H-7endo), 4.26 (1H, t, $J_{2,3}$=$J_{3,4}$=4.5 Hz, H-3), 4.85 (2H, t, $J_{1,2}$=$J_{4,5}$=4.5 Hz, H-2 and H-4).

Found: C, 55.76; H, 6.92%. Calcd for $C_{12}H_{18}O_6$: C, 55.80; H, 7.04%.

DL-*1,3-Di*-O-*acetyl-2,7-anhydro-(1,3/2,4,6)-4-azido-6-hydroxymethyl-1,2,3-cyclohexanetriol (4).* A mixture of **2** (0.30 g), sodium azide (0.37 g), and 90% aqueous 2-methoxy-

ethanol (6 ml) was heated at 110 °C for 1 h. The reaction mixture was evaporated to dryness and the residue was treated with acetic anhydride and pyridine at 60 °C for 2 h. The product was crystallized from ethanol–ether to give 0.36 g (81%) of **4** as prisms: mp 62.5—63.5 °C. ^{1}H NMR ($CDCl_3$) δ=2.00 (3H, s) and 2.08 (3H, s) (OAc), 3.67—4.07 (2H, m, H-7 and H-7′), 4.25 (1H, dd, $J_{1,2}$=3 Hz, $J_{2,3}$=5 Hz, H-2), 4.76—5.03 (2H, m, H-1 and H-3).

Found: C, 49.14; H, 5.73; N, 15.59%. Calcd for $C_{11}H_{16}N_3O_5$: C, 48.88; H, 5.98; N, 15.55%.

DL-*1,3-Di*-O-*acetyl-2,7-anhydro-(1,3/2,4,6)*-4-*acetamido*-6-*hydroxymethyl-1,2,3-cyclohexanetetrol (5)*. *a)*: A solution of **4** (0.20 g) in ethanol (10 ml) was hydrogenated in the presence of Raney nickel T-4[9] (one spatula) at room temperature overnight. The catalyst was removed by filtration and the filtrate was evaporated to dryness. The residue was treated with acetic anhydride and pyridine in the usual way. The product was crystallized from ethanol–ether to give 85 mg (40%) of **5** as needles: mp 108.5—109.5 °C. ^{1}H NMR ($CDCl_3$) δ=1.95 (3H, s), 2.00 (3H, s), and 2.14 (3H, s) (NAc and OAc), 3.88 (2H, br s, H-7 and H-7′), 4.00—4.27 (1H, m, H-4), 4.14 (1H, dd, $J_{1,2}$=6 Hz, $J_{2,3}$=3 Hz, H-2), 4.74 (1H, t, $J_{3,4}$=3 Hz, H-3), 4.90 (1H, t, $J_{1,6}$=6 Hz, H-1), 6.19 (1H, br d, J=9 Hz, NH).

Found: C, 54.98; H, 6.67; N, 5.16%. Calcd for $C_{13}H_{19}NO_6$: C, 54.72; H, 6.73; N, 4.91%.

b): A mixture of **2** (2.8 g) and methanolic ammonia (150 ml, saturated at 5 °C) was heated in a sealed tube at 105 °C for 30 h. After having been cooled, the reaction mixture was concentrated and the residue was treated with acetic anhydride and pyridine in the usual way. The product was recrystallized from ethanol–ether to give 3.2 g (74%) of **5**, identical with the compound obtained from **4**.

DL-*2,7-Anhydro-1,3-di*-O-p-*tolylsulfonyl*-*(1,3/2,4,6)*-*4*-*acetamido*-*6*-*hydroxymethyl*-*1,2,3*-*cyclohexanetriol (6)*. Compound **5** (0.26 g) was dissolved in 1 M methanolic sodium methoxide (5 ml) and the mixture was allowed to stand at room temperature overnight. The reaction mixture was neutralized with Amberlite IR-120 (H^+) and concentrated to an oil, which was treated with *p*-toluenesulfonyl chloride (1.1 g) in pyridine (7 ml) at room temperature for 2 d. The reaction mixture was poured into ice-water and extracted with chloroform (10 ml×3). The extracts were washed with aqueous sodium hydrogencarbonate and water, and dried. Evaporation of the solvent gave an oil (0.38 g), which was crystallized from ethanol to give 0.21 g (45%) of **6** as prisms: mp 156—157 °C. ^{1}H NMR ($CDCl_3$) δ=1.77 (3H, s, NAc), 2.40 (6H, s, tosyl methyl), 3.68—4.10 (4H, m, H-2 ,H-4, H-7, and H-7′), 4.41 (1H, dd, $J_{2,3}$=4.5 Hz, $J_{3,4}$=3 Hz, H-3), 4.72 (1H, t, $J_{1,2}$=$J_{1,6}$=4.5 Hz, H-1), 5.83 (1H, br d, J=7.5 Hz, NH), 7.23 (2H, d) and 7.67 (2H, d) and 7.26 (2H, d), and 7.76 (2H, d) (J=9 Hz, phenyl).

Found: C, 53.93; H, 5.32; N, 2.62; S. 12.31%. Calcd for $C_{23}H_{27}NO_8S_2$: C, 54.21; H, 5.35; N, 2.75; S, 12.58%.

DL-*2,3,4-Tri*-O-*acetyl-1*-O-*methyl-(1,3,5/2,4)*-*5*-*acetoxymethyl-1,2,3,4-cyclohexanetetrol (7)*. A mixture of **3** (0.2 g), acetic acid (2 ml), and acetic anhydride (2 ml) was heated in a sealed tube at 85 °C for 20 h. After having been cooled, the mixture was poured into ice water (20 ml) and then neutralized with sodium hydrogencarbonate and extracted with ethyl acetate (20 ml). The extract was washed with aqueous sodium hydrogencarbonate and water, dried, and concentrated to dryness. The product was crystallized from ethanol–ether to give 0.11 g (39%) of **7** as needles: mp 74.5—75.5 °C. ^{1}H NMR ($CDCl_3$) δ=1.97 (3H, s), 2.00 (3H, s), and 2.03 (6H, s) (OAc), 3.33 (3H, s, OCH_3), 3.16—3.57 (1H, m, H-1), 3.90—4.17 (2H, m, H-7 and H-7′), 4.73—5.37 (3H, m, H-2, H-3, and H-4).

Found C, 53.56; H, 6.66%. Calcd for $C_{16}H_{24}O_9$: C, 53.32; H, 6.73%.

DL-*1,2,3-Tri*-O-*acetyl-(1,3/2,4,6)*-*4*-*acetamido*-*6*-*bromomethyl-1,2,3-cyclohexanetriol (8)*. A mixture of **5** (2.0 g) and 30% hydrogen bromide–acetic acid (4 ml) was heated in a sealed tube at 75 °C for 23 h. After having been cooled, the mixture was poured into ice-water and the solution was processed similarly as described for preparation of **7**. The product was crystallized from ethanol to give 1.9 g (67%) of **8** as prisms: mp 184—184.5 °C. ^{1}H NMR ($CDCl_3$) δ=1.92 (3H, s), 1.98 (3H, s), and 2.03 (6H, s) (NAc and OAc), 3.34 (2H, br d, $J_{6,7}$=$J_{6,7'}$=3 Hz, H-7 and H-7′). 3.83—4.37 (1H, m, H-4), 4.83 (1H, t) and 5.11 (1H, t) ($J_{1,2}$=$J_{2,3}$=9 Hz, H-2 and H-3), 4.91 (1H, t, $J_{1,6}$=9 Hz, H-1), 5.82 (1H, br d, J=7.5 Hz, NH).

Found: C, 44.06; H, 5.29; N, 3.55; Br, 19.31%. Calcd for $C_{15}H_{22}O_7BrN$: C, 44.12; H, 5.44; N, 3.43; Br, 19.57%

DL-*2*-O-*Acetyl-1,3-di*-O-p-*tolylsulfonyl-(1,3/2,4,6)*-*4*-*acetamido*-*6*-*bromomethyl-1,2,3-cyclohexanetriol (12)*. A mixture of **6** (0.15 g) and 15% hydrogen bromide in acetic acid (2 ml) was heated in a sealed tube at 85 °C for 22 h. The reaction mixture was poured into ice-water (30 ml) and, after, neutralization with sodium hydrogencarbonate, extracted with chloroform (45 ml). The extract was processed similarly as described for preparation of **7**. The product was crystallized from acetone to give 0.17 g (45%) of **12** as prisms: mp 207—209 °C. ^{1}H NMR (DMSO-d_6) δ=1.49 (3H, s) and 1.73 (3H, s) (NAc and OAc), 2.88—3.62 (2H, m, H-7 and H-7′), 3.80—4.30 (1H, m, H-4), 4.56 (1H, dd) and 4.67 (1H, dd) ($J_{1,2}$=$J_{2,3}$=10.5 Hz, $J_{1,6}$=$J_{3,4}$=7.5 Hz, H-1 and H-3), 5.19 (1H, t, H-2), 7.33 (2H, d) and 7.59 (2H, d), and 7.38 (2H, d) and 7.68 (2H, d) (J=9 Hz, phenyl).

Found: C, 47.28; H, 4.77; N, 2.08%. Calcd for $C_{25}H_{30}O_9BrNS_2$: C, 47.46; H, 4.79; N, 2.21%.

DL-*1,2,3-Tri*-O-*acetyl-(1,3/2,4,6)*-*4*-*acetamido*-*6*-*acetoxymethyl-1,2,3-cyclohexanetriol (9)*. A mixture of **8** (0.2 g), anhydrous sodium acetate (0.24 g), and 90% aqueous 2-methoxyethanol (5 ml) was heated at 85 °C for 23 h. The reaction mixture was evaporated and the residue was acetylated in the usual way. The product was recrystallized from ethanol–ether to give 0.12 g (61%) of **9** as prisms: mp 109—110 °C. ^{1}H NMR δ=1.89 (3H, s), 1.96 (3H, s), 1.98 (3H, s), and 2.00 (6H, s) (NAc and OAc), 3.82—4.27 (3H, m, H-4, H-7, and H-7′), 4.78 (1H, t) and 5.08 (1H, t) ($J_{1,2}$=$J_{2,3}$=$J_{3,4}$=9 Hz, H-2 and H-3), 4.96 (1H, t, $J_{1,6}$=9 Hz, H-1), 5.73 (1H, br d, J=7.5 Hz, NH).

Found: C, 52.61; H, 6.38; N, 3.59%. Calcd for $C_{17}H_{25}NO_9$: C, 52.70; H, 6.52; N, 3.62%.

DL-*1,2,3-Tri*-O-*acetyl-(1,3/2,4,6)*-*4*-*acetamido*-*6*-*azidomethyl-1,2,3-cyclohexanetriol (10)*. A mixture of **8** (0.20 g), sodium azide (0.1 g), and 90% aqueous 2-methoxyethanol (4 ml) was heated at 85 °C for 3 h. The reaction mixture was evaporated and the residue was acetylated in the usual way. The product was recrystallized from ethanol to give 0.16 g (90%) of **10** as prisms: mp 152.5—154 °C. ^{1}H NMR ($CDCl_3$) δ=1.91 (3H, s), 1.97 (3H, s), 2.02 (3H, s), and 2.03 (3H, s) (NAc and OAc), 3.18 (1H, dd, $J_{6,7}$=4.5 Hz, J_{gem}=12 Hz, H-7), 3.36 (1H, dd, $J_{6,7'}$=4.5 Hz, H-7′), 3.87—4.27 (1H, m, H-4), 4.79 (1H, t) and 5.08 (1H, t) ($J_{1,2}$=$J_{2,3}$=$J_{3,4}$=9 Hz, H-2 and H-3), 4.84 (1H, t, $J_{1,6}$=9 Hz, H-1), 5.85 (1H, br d, J=7.5 Hz, NH).

Found: C, 48.78; H, 5.97; N, 14.84%. Calcd for $C_{15}H_{22}N_4O_7$: C, 48.63; H, 6.00; N, 15.13%.

DL-*1,2,3-Tri*-O-*acetyl*-*(1,3/2,4,6)*-*4*-*acetamido*-*6*-*acetamido*-

*methyl-1,2,3-cyclohexanetriol (**11**).* A mixture of **10** (0.10 g) in ethanol (10 ml) was hydrogenated in the presence of Raney nickel T-4 (one spatula) in a Parr shaker apparatus at room temperature overnight. The mixture was processed as described for the preparation of **5**. The product was crystallized from ethanol to give 0.10 g (92%) of **11**: mp 56—57.5 °C. ^{1}H NMR ($CDCl_3$) δ=1.87 (3H, s), 1.97 (6H, s), 2.00 (3H, s), and 2.05 (3H, s) (NAc and OAc), 2.83 (1H, dd, $J_{6,7}$=5 Hz, J_{gem}=7.5 Hz, H-7), 3.55 (1H, dd, $J_{6,7'}$=3 Hz, H-7'), 3.90—4.28 (1H, m, H-4), 4.71 (1H, dd) and 4.74 (1H, dd) ($J_{1,2}=J_{2,3}$=9 Hz, $J_{1,6}$=10 Hz, $J_{3,4}$=10.5 Hz, H-1 and H-3), 5.09 (1H, t, H-2), 5.75 (1H, br d, J=5 Hz, 4-NH), 6.01 (1H, m, 7-NH).

Found: C, 52.98; H, 6.73; N, 6.91%. Calcd for $C_{17}H_{26}N_2O_8$: C, 52.82; H, 6.79; N, 7.25%.

DL-*(1,3/2,4,6)-4-Amino-6-hydroxymethyl-1,2,3-cyclohexanetriol Hydrochloride (**13**).* A mixture of **9** (0.20 g) and 6 M hydrochloric acid (10 ml) was refluxed for 90 min, and then evaporated to dryness. The residue was crystallized from ethanol–water to give 0.11 g (100%) of **13** as prisms: mp 195—196 °C. TLC (cellulose): R_f 0.37, 1-butanol–ethanol–water–17% aqueous ammonia (4:5:2:4).[10]

Found: C, 39.59; H, 7.63; N, 6.31; Cl, 16.80%. Calcd for $C_7H_{16}NO_4Cl$: C, 39.34; H, 7.56; N, 6.56; Cl, 16.59%.

DL-*(1,3/2,4,6)-4-Amino-6-aminomethyl-1,2,3-cyclohexanetriol Dihydrochloride (**14**).* A mixture of **11** (0.61 g) and 6 M hydrochloric acid (25 ml) was refluxed for 2 h, and then evaporated to dryness. The residue was crystallized from ethanol–water to give 0.39 g (100%) of **14** as prisms: mp 194 °C, decomposed at 200—228 °C. TLC (cellulose): R_f 0.22, 1-butanol–ethanol–water–17% aqueous ammonia (4:5:2:4).[10]

Found: C, 33.54; H, 7.04; N, 11.00; Cl, 28.59%. Calcd for $C_7H_{18}N_2O_3Cl_2$: C, 33.74; H, 7.30; N, 11.25; Cl, 28.45%.

Bromination of DL-*1,2-Di-O-acetyl-(1,3/2)-3-bromomethyl-5-cyclohexene-1,2-diol (**15**).*[11] Compound **15**[1] (2.0 g) was dissolved in acetic acid (30 ml) and then water (15 ml) was added. To the stirred solution was added bromine water (40 ml) containing 0.67 ml of bromine dropwise during 20 min at room temperature. After the reaction mixture was allowed to stand in a refrigerator overnight, the precipitates were collected by filtration and washed thoroughly with water to give a crystalline mixture (1.65 g) of products, which contained one major (R_f 0.20) together with two minor components [R_f 0.33 and 0.75 in 2-butanone–toluene (1:6)]. Recrystallization of the mixture from ethanol gave DL-1,3-di-*O*-acetyl-(1,4/2,3,6)-4-bromo-6-bromomethyl-1,2,3-cyclohexanetriol (**16**, 0.92 g, 34%) as needles: mp 176—178 °C. ^{1}H NMR ($CDCl_3$) δ=2.11 (6H, s, OAc), 3.36 (2H, d, J=4.5 Hz, H-7 and H-7'), 4.12 (1H, br dd, $J_{1,2}$=9.5 Hz, $J_{2,3}$=3 Hz, H-2, on deuteration), 4.20—4.35 (1H, m, H-4), 4.90 (1H, t, $J_{1,6}$=9.5 Hz, H-1), 5.12 (1H, br t, $J_{3,4}$=3 Hz, H-3).

Found: C, 34.14; H, 4.17; Br, 40.96%. Calcd for $C_{11}H_{16}O_5Br_2$: C, 34.05; H, 4.16; Br, 41.18%.

Compound **16** (0.82 g) was acetylated with acetic anhydride in pyridine in the usual way and the product was recrystallized from ethanol to give 0.41 g (45%) of the triacetate **17** as prisms: mp 96.5—97 °C. ^{1}H NMR ($CDCl_3$, 60 MHz) δ=2.00 (3H, s), 2.09 (3H, s), and 2.17 (3H, s) (OAc), 3.34 (2H, d, J=4.5 Hz, H-7 and H-7'), 4.33 (1H, q, $J_{3,4}=J_{4,5ax}=J_{4,5eq}$=3 Hz, H-4), 5.29 (1H, t, $J_{1,2}=J_{1,6}$=9.5 Hz, H-1), 5.63 (1H, dd, $J_{2,3}$=3 Hz, H-2).

Found: C, 36.40; H, 4.22; Br, 37.35%. Calcd for $C_{13}H_{18}O_6Br_2$: C, 36.30; H, 4.42; Br, 37.16%.

The mother liquor of the crystalline mixture was neutralized with sodium hydrogencarbonate and extracted with ethyl acetate (150 ml). The extracts were concentrated and the residual oil was chromatographed on a silica gel column (50 g) with 2-butanone–toluene (1:15) as an eluent. The first fraction gave DL-1,2-di-*O*-acetyl-(1,4/2,3,6)-3,4-dibromo-6-bromomethyl-1,2-cyclohexanediol (**18**, 22 mg, 0.7%) as prisms: mp 94—95 °C. ^{1}H NMR ($CDCl_3$) δ=1.99 (6H, s, OAc), 3.19—3.35 (2H, m, H-7 and H-7'), 5.12—5.34 (2H, m, H-1 and H-2).

Found: C, 29.55; H, 3.51; Br, 52.95%. Calcd for $C_9H_{10}O_4Br_3$: C, 29.30; H, 3.35; Br, 53.16%.

The second fraction gave (R_f 0.54) gave DL-1,3,4-tri-*O*-acetyl-(1,4/2,3,5)-2-bromo-5-bromomethyl-1,3,4-cyclohexanetriol (**19**, 40 mg, 1.4%) as an oil. ^{1}H NMR ($CDCl_3$) δ=2.00 (6H, s) and 2.04 (3H, s) (OAc), 3.10—3.42 (2H, m, H-7 and H-7'), 4.29 (1H, dd, $J_{1,2}$=3 Hz, $J_{2,3}$=3.5 Hz, H-2), 4.90 (1H, dd, $J_{3,4}$=9 Hz, H-3), 5.02—5.32 (2H, m, H-1 and H-4).

Found: C, 36.64; H, 4.20; Br, 37.17%. Calcd for $C_{13}H_{18}O_6Br_2$: C, 36.30; H, 4.23; Br, 37.15%.

The third fraction (R_f 0.33) gave DL-3,4-di-*O*-acetyl-(1,4/2,3,5)-2-bromo-5-bromomethyl-1,3,4-cyclohexanetriol (**20**, 0.44 g, 16%) as prisms: mp 109—110 °C. ^{1}H NMR ($CDCl_3$) δ=2.00 (6H, s, OAc), 3.12—3.46 (2H, m, H-7 and H-7'), 4.06—4.25 (1H, m, H-1), 4.25—4.40 (1H, m, H-2), 4.95—5.30 (2H, m, H-3 and H-4).

Found: C, 34.27; H, 4.29; Br, 40.97%. Calcd for $C_{11}H_{16}O_5Br_2$: C, 34.05; H, 4.16; Br, 41.18%.

The fourth fraction gave an additional amount of **16** (37 mg, total yield, 35.5%).

DL-*4-O-Acetyl-1,2:3,7-dianhydro-(1,2,3,5/4)-5-hydroxymethyl-1,2,3,4-cyclohexanetetrol (**21**).* A mixture of **16** (0.40 g) and 1 M methanolic sodium methoxide (6.4 ml) was heated at 60 °C for 3.5 h. TLC [2-butanone–toluene (1:2)] indicated that **16** (R_f 0.44) disappeared immediately with a formation of an intermediate compound (R_f 0.08) which was then converted into a single compound (R_f 0.31). The reaction mixture was neutralized with 1 M hydrochloric acid and concentrated. The residue was treated with acetic anhydride and pyridine at room temperature overnight. The product was purified by chromatography on silica gel with 2 butanone–toluene (1:5) as an eluent to give 0.16 g (84%) of **21** as an oil. TLC: R_f 0.38 [2-butanone–toluene (1:4)]. ^{1}H NMR ($CDCl_3$) δ=2.14 (3H, s, OAc), 2.47—2.82 (1H, m, H-5), 3.87 (1H, d, J_{gem}=9.3 Hz, H-7endo), 4.08 (1H, dd, $J_{5,7exo}$=4.7 Hz, H-7exo), 4.22—4.47 (1H, m, H-1 or H-2), 4.47—4.69 (2H, m, H-3 and H-1 or H-2), 5.13 (1H, t, $J_{3,4}=J_{4,5}$=4.8 Hz, H-4).

Found: C, 58.40; H, 6.50%. Calcd for $C_9H_{12}O_4$: C, 58.69; H, 6.57%.

DL-*3,4-Di-O-acetyl-1,2-anhydro-(1,2,3,5/4)-5-bromomethyl-1,2,3,4-cyclohexanetetrol (**22**).* A mixture of **15** (1.5 g), *m*-chloroperoxybenzoic acid (1.52 g, *ca.* purity 70%), and dry 1,2-dichloroethane (40 ml) was refluxed for 3 h. The reaction mixture was washed with successively with 10% aqueous sodium sulfite (40 ml×3), saturated aqueous sodium hydrogencarbonate (40 ml×3), and water (40 ml×2), and dried over anhydrous sodium sulfate. Evaporation of the solvent gave an oil, which was crystallized from ethanol. Recrystallization from ethanol–ether gave 0.44 g (23%) of **22**: mp 112.5—114 °C. ^{1}H NMR ($CDCl_3$) δ=2.02 (3H, s) and 2.05 (3H, s) (OAc), 3.08—3.45 (4H, H-1, H-2, H-7, and H-7'), 5.01 (1H, dd, $J_{3,4}$=8.5 Hz, $J_{4,5}$=9.5 Hz, H-4), 5.19 (1H, dd, $J_{2,3}$=1.5 Hz, H-3).

Found: C, 43.10; H, 4.85; Br, 25.76%. Calcd for $C_{11}H_{15}O_5Br$: C, 43.01; H, 4.92; Br, 26.02%.

*Reaction of **22** with Sodium Azide.* *a) In the Presence of Ammonium Chloride*: A mixture of **22** (63 mg), sodium

azide (67 mg, 5 molar equiv.), ammonium chloride (110 mg, 10 molar equiv.), and 90% aqueous *N,N*-dimethylformamide (DMF) (5 ml) was stirred at 80—85 °C for 3 h. The mixture was concentrated and the residue was treated with acetic anhydride (5 ml) and pyridine (5 ml) at room temperature overnight. Evaporation of the excess reagent gave a crude product which was purified by chromatography on silica gel (3 g) with 2-butanone–toluene (1:10) as an eluent to give 48 mg (67%) of DL-1,2,3-tri-*O*-acetyl-(1,4/2,3,6)-4-azido-6-azidomethyl-1,2,3-cyclohexanetriol (**24**) as an oil. TLC: R_f 0.52 [2-butanone–toluene (1:5)]. ^{1}H NMR ($CDCl_3$) δ=1.98 (3H, s), 2.04 (3H, s), and 2.11 (3H, s) (OAc), 3.24 (1H, dd, $J_{6,7}$=6 Hz, J_{gem}=12 Hz, H-7), 3.41 (1H, dd, $J_{6,7'}$=4 Hz, H-7'), 3.87 (1H, br q, J=*ca.* 4 Hz, H-4), 5.01—5.32 (3H, m, H-1, H-2, and H-3).

Found: C, 44.34; H, 5.36; N, 23.48%. Calcd for $C_{13}H_{18}N_6O_6$: C, 44.07; H, 5.12; N, 23.72%.

b) In the Absence of Ammonium Chloride: A mixture of **22** (0.10 g), sodium azide (0.11 g, 5 molar equiv.), and 90% aqueous DMF (5 ml) was stirred at 80—85 °C for 3 h. The mixture was concentrated and the residue was treated with acetic anhydride and pyridine in the usual way. TLC indicated the formation of two major products [R_f 0.52 and 0.45, 2-butanone–toluene (1:5)]. Evaporation of the excess reagent and the products were fractionated by a silica-gel column (5 g) with 2-butanone–toluene (1:10) as an eluent. The first fraction (R_f 0.52) gave 55 mg (48%) of **24** as an oil. The second fraction (R_f 0.45) gave DL-1,3-di-*O*-acetyl-2,7-anhydro-(1,4/2,3,6)-4-azido-6-hydroxymethyl-1,2,3-cyclohexanetriol (**23**, 22 mg, 25%) as an oil. ^{1}H NMR ($CDCl_3$) δ=2.12 (3H, s) and 2.15 (3H, s) (OAc), 2.65 (1H, quintet, J=3.3 Hz, H-6), 3.65—4.12 (3H, m, H-4 and CH_2O), 4.19 (1H, br d, J=*ca.* 6 Hz, H-2), 4.90—5.19 (2H, m, H-1 and H-3).

Found: C, 48.89; H, 5.54; N, 15.92%. Calcd for $C_{11}H_{15}N_3O_5$: C, 49.07; H, 5.62; N, 15.61%.

*DL-1,2,3-Tri-O-acetyl-(1,4/2,3,6)-4-acetamido-6-acetamidomethyl-1,2,3-cyclohexanetriol (**25**).* A solution of **24** (0.54 g) in ethanol (10 ml) containing acetic anhydride (0.9 ml) was hydrogenated in the presence of Raney nickel T-4 for 28 h. The reaction mixture was filtered and the filtrate was concentrated. The residue was taken up in chloroform (50 ml) and passed through a short column of alumina. The filtrate was concentrated and the residue was crystallized from ethanol to give 0.24 g (41%) of **25** as prisms: mp 197—199 °C. ^{1}H NMR ($CDCl_3$, 60 MHz) δ=2.00 (9H, s), 2.07 (3H, s), and 2.11 (3H, s) (NAc and OAc), 3.30—4.30 (2H, br m, H-7 and H-7'), 4.90—5.45 (4H, m, H-1, H-2, H-3, and H-4), 6.30 (1H, br t, J=6 Hz, C_7–NHAc), 6.70 (1H, br d, J=7 Hz, C_4–NHAc).

Found: C, 52.98; H, 6.78; N, 7.12%. Calcd for $C_{17}H_{26}N_2O_8$: C, 52.84; H, 6.78; N, 7.25%.

The authors express their sincere thanks to Mr. Saburo Nakada for the elementary analyses.

References

1) The preceding paper of this series: S. Ogawa, T. Toyokuni, T. Kondoh, Y. Hattori, S. Iwasaki, M. Suetsugu, and T. Suami, *Bull. Chem. Soc. Jpn.*, **54**, 2739 (1981).

2) The nomenclature and numbering of cyclitols used in this paper follow IUPAC and IUB tentative rules for cyclitol nomenclature [*J. Biol. Chem.*, **243**, 5809 (1968)]. All compounds described in this paper are racemic and the formulas depict only one of the respective enantiomers.

3) S. Ogawa, K. Nakamoto, M. Takahara, Y. Tanno, N. Chida, and T. Suami, *Bull. Chem. Soc. Jpn.*, **52**, 1174 (1979).

4) Unpublished results.

5) S. Umezawa, *Adv. Carbohydr. Chem. Biochem.*, **30**, 111 (1974); T. Suami, "Modification of Aminocyclitol Antibiotics," in "Aminocyclitol Antibiotics," ed by K. L. Rinehart, Jr., and T. Suami, American Chemical Society (1980), Chap. 3, pp. 43—73.

6) The structures of **18**, **19**, and **20** were tentatively assigned on the basis of analytical data and ^{1}H NMR spectra.

7) The isomeric epoxide expected to be formed as a major product seemed to be decomposed by an anchimeric reaction of the adjacent acetoxyl group under these conditions.

8) Melting points were determined on a Büchi 510 capillary melting point apparatus and are uncorrected. Unless otherwise noted, ^{1}H NMR spectra were taken on a Varian EM-390 (90 MHz) spectrometer with reference to tetramethylsilane as an internal standard. The 60 MHz spectra were similarly taken on a Varian EM-360 spectrometer. The peak positions are given in terms of δ-values and values given for coupling constants are of first-order. TLC was performed on precoated silica gel 60 F-254 plates (Merck, Darmstadt; 0.25 mm thickness). The silica gel used for a column chromatography was Wakogel C-300 (Wako Pure Chemical Industries, Ltd.). Organic solutions were concentrated below 50 °C under reduced pressure.

9) S. Nishimura, *Bull. Chem. Soc. Jpn.*, **32**, 61 (1959).

10) TLC was performed on precoated cellulose F-254 plates (Merck, Darmstadt; 0.10 mm thickness).

11) This experiment was carried out by assistance of Mr. Kenji Kato, to whom our thanks are due.

Regio-controlled Prenylation and Geranylation of 3-Furylmethylmagnesium Bromide. Selective Syntheses of 3-Substituted Furanoid and 2-Substituted 3-Methylfuranoid Terpenes

Shuki Araki and Yasuo Butsugan*

Department of Synthetic Chemistry, Nagoya Institute of Technology, Gokiso-cho, Showa-ku, Nagoya 466

(Received October 27, 1982)

Coupling reactions of 3-furylmethylmagnesium bromide with prenyl and geranyl diethyl phosphates gave 2-substituted 3-methylfurans, rosefuran and sesquirosefuran, as the main products. When the reactions were carried out in the presence of a catalytic amount of copper(I) iodide, normal coupling occurred and 3-substituted furans, perillene and dendrolasin, were formed in good yields. The related naturally occurring 3-substituted thiophene, 3-(4-methyl-3-pentenyl)thiophene, was also synthesized from 3-thienylmethylmagnesium bromide and prenyl diethy phosphate.

3-Substituted furans and 2-substituted 3-methylfurans are widely distributed in nature.[1] Dendrolasin (**1**)[2] and sesquirosefuran (**2**),[3] and their monoterpene homologs, perillene (**3**)[4] and rosefuran (**4**),[5] are examples of such furanoid terpenes. We have previously described[6] that **1** and **2** were selectively synthesized by the regio-controlled geranylation of 3-furylmethylmagnesium bromide (**7**) with geranyl diethyl phosphate (**8**) using copper(I) iodide as a catalyst. In this article, full experimental details of the above reactions as well as the selective syntheses of **3** and **4** by the same methodology are described. A convenient synthesis of the thiophene analog (**5**), a constituent of the essential oil of hop,[7] is also reported.

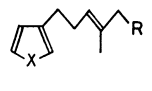

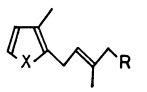

1 X=O, R= $CH_2CH=C(CH_3)_2$ 2 X=O, R= $CH_2CH=C(CH_3)_2$

3 X=O, R=H 4 X=O, R=H

5 X=S, R=H 6 X=S, R=H

Results and Discussion

Reaction of 3-Furylmethylmagnesium Bromide with Geranyl Diethyl Phosphate. The Grignard reagent, 3-furylmethylmagnesium bromide (**7**), was prepared in the conventional manner from the known 3-furylmethyl bromide[8] in tetrahydrofuran. Geranyl diethyl phosphate (**8**) was added to a solution of the Grignard reagent **7** at −78 °C and the mixture was left overnight at room temperature. Workup followed by vacuum distillation gave a colorless oil. GLPC analysis revealed that the oil consisted of three components (**A**, **B**, and **C**) in the ratio of 7:77:16. They were separated by preparative GLPC and the structures were assigned on the basis of the spectroscopic data. Compound **A**, having the shortest retention time, showed characteristic signals of a terminal vinyl group in addition to a methylene singlet adjacent to the furan ring in its ^1H NMR spectrum. This compound was assigned as 3-(2,6-dimethyl-2-vinyl-5-heptenyl)furan (**9**). IR and ^1H NMR data of the main product **B** and the third component **C** were in good agreement with the literature values of sesquirosefuran (**2**) and dendrolasin (**1**), respectively.

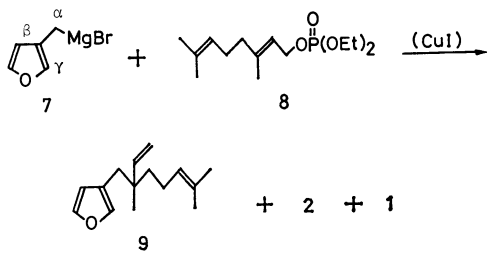

Table 1. Grignard reaction of **7** with geranyl phosphate **8** and geranyl bromide

Geranyl compound	CuI	Product ratio **9** : **2** : **1**	Total yield %
Phosphate **8**	Absence	7 : 77 : 16	83
	Presence	21 : 0 : 79	81
Bromide	Absence	32 : 45 : 22	82
	Presence	25 : 6 : 68	83

The results show that the Grignard reagent **7** was electrophilically attacked mainly at the γ-position (C-2 ring carbon) by the geranyl phosphate **8**. This observation is consistent with the facts that 3-furylmethylmagnesium chloride reacts at the γ-position with hard electrophiles such as carbon dioxide and formaldehyde leading to 3-methyl-2-furoic acid and 3-methylfurfuryl alcohol, respectively.[9] When geranyl bromide, a softer electrophile than the phosphate **8**, was employed as a geranylation reagent, the γ-regioselectivity decreased from 77% to 45% (Table 1).

When the reaction of **7** and **8** was conducted in the presence of a catalytic amount (10 mol% of **7**) of copper(I) iodide, normal coupling at the α-position exclusively took place;[10] dendrolasin(**1**) was formed in 79% selectivity accompanied by 21% of the regioisomer **9**. In this case, reaction at the γ-position (formation of **2**) was negligible. Preference for the α-coupling was also observed in the copper(I)-catalyzed reaction of **7** with geranyl bromide, though the selectivity was lower.[11] Results are summarized in Table 1.

Reaction of 3-Furylmethylmagnesium Bromide with Prenyl Diethyl Phosphate. When prenyl diethyl phosphate (**10**) was employed in place of **8**, a mixture of prenylated 3-methylfurans was obtained in 78% combined yield. GLPC of the mixture showed four peaks (**D**,

E, **F**, and **G**) in the ratio of 2:7:72:19. Although compound **D** could not be isolated because of its small quantity, the remaining three components were isolated by preparative GLPC, and characterized. Peak **E** was a new compound and the structure was deduced to be 3-(2,2-dimethyl-3-butenyl)furan (**12**), by means of MS and ^{1}H NMR spectra. Peaks **F** and **G** were found to be identical with rosefuran **4** and perillene **3**, respectively, on the basis of IR, Mass, and ^{1}H NMR spectral comparisons with those in literatures.[4,5] Peak **D** could be, therefore, tentatively assigned as 2-(1,1-dimethyl-2-propenyl)-3-methylfuran (**11**). As expected, the copper(I)-catalyzed reaction of **7** with **10** gave **12** and **3** in the ratio of 2:98 in 83% yield. Again, in this catalytic reaction the coupling at the γ-position was not observed.

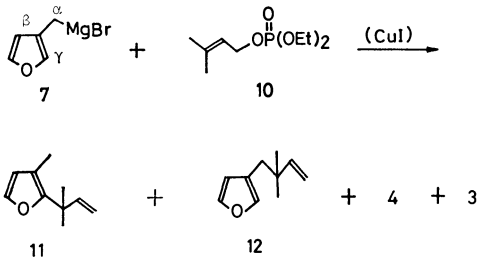

Reaction of 3-Thienylmethylmagnesium Bromide with Prenyl Diethyl Phosphate. As described, geranyl (**8**) and prenyl diethyl phosphates(**10**) attacked prefentially the harder γ-position (adjacent position to the hard oxygen atom) of 3-furylmethylmagnesium bromide **7** rather than the α-position. The γ-position of 3-thienylmethylmagnesium bromide (**13**), in which the oxygen atom of **7** is replaced by soft sulfur atom, must be softer than the α-position and therefore the phosphates should attack the α-position. This proved to be the case. The reaction of **13** with **10** gave 3-(4-methyl-3-pentenyl)thiophene (**5**) in 71% yield accompanied with a trace amount (1%) of 3-(2,2-dimethyl-3-butenyl)-thiophene (**14**). No trace of γ-substituted products such as **6** was observed in this reaction. The thiophene derivative **5** is a constituent of a hop oil,[7] and although synthesized by the photo-induced reaction between myrcene and elemental sulfur in a trace yield,[12] this is the first practical synthesis so far reported. By the addition of copper(I) iodide, the product ratio (**14**:**5**) changed from 1:99 to 18:82. γ-Substitution was not observed in this catalytic reaction.

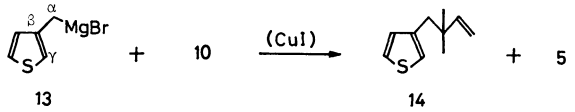

Experimental

General. Infrared spectra were recorded on a JASCO IRA-1 spectrometer. ^{1}H NMR spectra were determined with a Hitachi R-24A (60 MHz) spectrometer, or with a JEOL JNM-FX-100 (100 MHz) spectrometer in CCl_4 or in $CDCl_3$. Chemical shifts (δ) are recorded in ppm downfield from Me_4Si. Mass spectra were measured on a Hitachi M-52 mass spectrometer, operating with an ionization energy of 20 eV. GLPC analyses and preparative GLPC were performed on a Yanaco G1800 gas chromatograph, equipped with columns (1 m, 2 m, or 3 m × 3 mm) packed with Apiezon grease L on Uniport B (15%). Elemental analyses were performed at the Elemental Analysis Center of Kyoto University. For Kugelrohr distillation, a Shibata GTO-250R glass tube oven was used.

Material. Geranyl (**8**) and prenyl diethyl phosphates (**10**) were prepared according to the method for the corresponding diphenyl phosphates.[13] 3-Furylmethyl bromide[8] and 3-thienylmethyl bromide[14] were prepared by the methods described in the literatures. Copper(I) iodide, obtained from Nakarai Chemicals, LTD., was used as received.

Reaction of 3-Furylmethylmagnesium Bromide (7) with Geranyl Diethyl Phosphate (8). (a) In the Absence of Copper(I) Iodide: 3-Furylmethyl bromide (403 mg, 2.5 mmol) in THF (4 ml) was added dropwise to magnesium turnings (120 mg, 5 mmol) in THF (1 ml) cooled in an ice-salt bath. After the addition was complete, the mixture was gradually warmed to room temperature and further stirred at that temperature for 1 h. To remove the excess magnesium, the resulting Grignard solution was transferred by a syringe to the second flask and cooled to −78 °C. To this was added a solution of geranyl diethyl phosphate (**8**) (435 mg, 1.5 mmol) in THF (3 ml), the mixture was gradually warmed to room temperature and left overnight. Saturated aqueous ammonium chloride was added and the products were extracted with ether. The extracts were washed with brine, dried over anhydrous sodium sulfate and concentrated. The residue was distilled (bp 130 °C/3 Torr, 1 Torr ≈133.322 Pa) to give a colorless oil (272 mg, 83% yield). GLPC analysis using the 1 m column (temperature 160 °C, He 90 ml/min) showed three peaks of **9** (t_R=12 min), **2** (14.5), and **1** (16.5) in the ratio of 7:77:16. They were isolated by preparative GLPC.

3-(2,6-Dimethyl-2-vinyl-5-hepenyl)furan (9): IR (neat) 2930, 1640, 1520, 1454, 1416, 1376, 1168, 1069, 1028, 1002, 912, 872, 786, and 732 cm^{-1}; ^{1}H NMR (CCl_4) δ=7.20 (m, 1H, furan), 7.08 (s, 1H, furan), 6.13 (m, 1H, furan), 5.73 (dd, J=17, 11 Hz, 1H, CH_2=C<u>H</u>–), 5.2—4.5 (m, 3H, olefin), 2.31 (s, 2H, CH_2), 2.2—1.0 (m, 4H, CH_2), 1.60 (s, 3H, CH_3), 1.51 (s, 3H, CH_3), 0.91 (s, 3H, CH_3); MS *m/z* (rel intensity) 218 (M^+; 22), 137 (22), 123 (36), 95 (59), 81 (86), and 69 (100); Found: C, 82.71; H, 10.00%. Calcd for $C_{15}H_{22}O$: C, 82.51; H, 10.16%.

Sesquirosefuran (2): IR (neat) 2930, 1665, 1514, 1448, 1380, 1150, 1085, 890, and 724 cm^{-1}; ^{1}H NMR ($CDCl_3$) δ=7.21 (d, J=1.6 Hz, 1H, furan), 6.15 (d, J=1.6 Hz, 1H, furan), 5.26 (t, J=7 Hz, 1H, olefin), 5.08 (br, 1H, olefin), 3.28 (d, J=7 Hz, 2H, CH_2), 2.02 (m, 4H, CH_2), 1.96 (s, 3H, ring-CH_3), 1.70 (s, 3H, CH_3), 1.67 (s, 3H, CH_3), 1.59 (s, 3H, CH_3); MS *m/z* (rel intensity) 218 (M^+; 68), 175 (45), 149 (43), 131 (43), 123 (100), 95 (45), and 69 (67).

Dendrolasin (1): IR (neat) 2930, 1670, 1562, 1505, 1444, 1382, 1164, 1064, 1025, 874, and 778 cm^{-1}; ^{1}H NMR (CCl_4) 7.19 (m, 1H, furan), 7.08 (m, 1H, furan), 6.13 (m, 1H, furan), 5.05 (m, 2H, olefin), 2.31 (m, 4H, CH_2), 1.96 (m, 4H, CH_2), 1.63 (s, 3H, CH_3), 1.55 (s, 6H, CH_3); MS *m/z* (rel intensity) 218 (M^+; 7), 203 (17), 175 (18), 136 (17), 123 (10), 95 (12), 82 (17), 81 (56), and 69 (100).

(b) In the Presence of Copper(I) Iodide: The Grignard reagent **7** prepared as above was added to a suspension of copper(I) iodide (47 mg, 0.25 mmol) in THF (1 ml) at −5 °C and stirred for 15 min. To this mixture was added the phosphate **8** (435 mg, 1.5 mmol) in THF (3 ml) at −78 °C. The mixture was treated as described. Distillation (bp 130 °C/3 Torr) gave a mixture of **9** and **1** (265 mg, 81%

yield) in the ratio of 21:79 (by GLPC).

The reactions of **7** with geranyl bromide were carried out in the same procedure. The results are summarized in Table 1.

Reaction of 3-Furylmethylmagnesium Bromide (7) with Prenyl Diethyl Phosphate (10). (a) In the Absence of Copper(I) Iodide: To the Grignard solution **7**, prepared from magnesium (240 mg, 10 mmol) and the bromide (805 mg, 5 mmol) in THF (10 ml), was added a solution of prenyl diethyl phosphate (**10**) (666 mg, 3 mmol) in THF (5 ml) at −78 °C. The mixture was treated as described. Distillation (bp 115 °C/35 Torr) afforded a colorless oil (350 mg, 78% yield). GLPC analysis using the 3 m column (temperature 135 °C, He 32 ml/min) showed four peaks of **11** (t_R=16 min), **12** (18), **4** (27), and **3** (29) in the ratio of 2:7:72:19. Products **12**, **4**, and **3** could be isolated by preparative GLPC.

3-(2,2-Dimethyl-3-butenyl)furan (12): ^{1}H NMR ($CDCl_3$) δ=7.31 (m, 1H, furan), 7.18 (m, 1H, furan), 6.24 (m, 1H, furan), 5.86 (dd, J=18, 10 Hz, 1H, CH_2=C<u>H</u>–), 5.0—4.7 (m, 2H, C<u>H$_2$</u>=CH–), 2.38 (s, 2H, CH_2), 1.00 (s, 6H, CH_3); MS *m/z* (rel intensity) 150 (M^+; 62), 135 (27), 82 (59), 81 (47), 69 (100), and 41 (24). IR and elemental analysis could not be performed because of the small quantity of this sample.

Rosefuran (4): IR (neat) 2950, 1680, 1514, 1448, 1376, 1150, 1082, 1024, 892, and 726 cm^{-1}; ^{1}H NMR (CCl_4) δ=7.03 (d, J=1.6 Hz, 1H, furan), 5.95 (d, J=1.6 Hz, 1H, furan), 5.15 (t, J=7 Hz, 1H, olefin), 3.10 (d, J=7 Hz, 2H, CH_2), 1.83 (s, 3H, ring-CH_3), 1.63 (s, 6H, CH_3); MS *m/z* (rel intensity) 150 (M^+; 100), 135 (43), 111 (46), 95 (27), 71 (33), and 69 (54).

Perillene (3). IR (neat) 2950, 1680, 1508, 1446, 1380, 1168, 1068, 1030, 878, and 782 cm^{-1}; ^{1}H NMR (CCl_4) δ=7.20 (m, 1H, furan), 7.09 (m, 1H, furan), 6.13 (m, 1H, furan), 5.04 (t, J=7 Hz, 1H, olefin), 2.30 (m, 4H, CH_2), 1.63 (s, 3H, CH_3), 1.53 (s, 3H, CH_3); MS *m/z* (rel intensity) 150 (M^+; 83), 135 (27), 82 (30), 81 (47), 69 (100), and 41 (33).

(b) In the Presence of Copper(I) Iodide: The Grignard reagent **7**, prepared from magnesium (120 mg, 5 mmol) and the bromide (403 mg, 2.5 mmol) in THF (5 ml), was added to a suspension of copper(I) iodide (47 mg, 0.25 mmol) in THF (1 ml) at −5 °C and stirred for 20 min. To this mixture was added the phosphate **10** (333 mg, 1.5 mmol) in THF (3 ml) at −78 °C. The mixture was treated as described. Distillation (bp 110 °C/25 Torr) gave a mixture of **12** and **3** (187 mg, 83% yield) in the ratio of 2:98 (by GLPC).

Reaction of 3-Thienylmethylmagnesium Bromide (13) with Prenyl Diethyl Phosphate (10). (a) In the Absence of Copper(I) Iodide: 3-Thienylmethyl bromide (885 mg, 5 mmol) in THF (8 ml) was added dropwise to magnesium turnings (240 mg, 10 mmol) in THF (2 ml) cooled in an ice-salt bath. After the addition was complete, the mixture was gradually warmed to room temperature and stirred at that temperature for 1 h. The solution of the Grignard reagent thus prepared was transferred by the aid of a syringe into the second flask and cooled to −78 °C. To this was added a solution of prenyl diethyl phosphate (**10**) (666 mg, 3 mmol) in THF (5 ml) and the mixture was left overnight at room temperature. Workup followed by distillation (bp 155 °C/37 Torr) gave a colorless oil (352 mg, 71% yield). GLPC analysis using the 2 m column (tempetature 170 °C, He 76 ml/min) showed two peaks of **14** (t_R=11 min) and **5** (16) in the ratio of 1:99. They were isolated by preparative GLPC.

3-(2,2-Dimethyl-3-butenyl)thiophene (14): IR (neat) 3100, 2980, 2940, 1642, 1466, 1416, 1380, 1362, 1004, 914, 854, 836, and 784 cm^{-1}; ^{1}H NMR (CCl_4) δ=7.05 (m, 1H, thiophene), 6.77 (m, 2H, thiophene), 5.80 (dd, J=17, 8 Hz, 1H, CH_2=C<u>H</u>–), 5.05—4.65 (m, 2H, C<u>H$_2$</u>=CH–), 2.55 (s, 2H, CH_2), 0.95 (s, 6H, CH_3); MS *m/z* (rel intensity) 166 (M^+; 38), 110 (22), 98 (41), 97 (100), and 69 (75); Found: C, 72.02; H, 8.78%. Calcd for $C_{10}H_{14}S$: C, 72.23; H, 8.49%.

3-(4-Methyl-3-pentenyl)thiophene (5): IR (neat) 3110, 2980, 2935, 2860, 1675, 1442, 1378, 1240, 1104, 1079, 839, and 775 cm^{-1}; ^{1}H NMR (CCl_4) δ=7.10 (m, 1H, thiophene), 6.80 (m, 2H, thiophene), 5.05 (t, J=7 Hz, 1H, olefin), 2.85—2.15 (m, 4H, CH_2), 1.62 (s, 3H, CH_3), 1.50 (s, 3H, CH_3); MS *m/z* (rel intensity) 166 (M^+; 56), 151 (16), 110 (65). 98 (38), 97 (100), and 69 (60); Found: C, 71.97; H, 8.57%. Calcd for $C_{10}H_{14}S$: C, 72.23; H, 8.49%.

(b) In the Presence of Copper(I) Iodide: The Grignard reagent **13** prepared from magnesium (240 mg, 10 mmol) and the bromide (885 mg, 5 mmol) in THF (10 ml) was added to a suspension of copper(I) iodide (94 mg, 0.5 mmol) in THF (2 ml) at −5 °C and stirred for 15 min. To the mixture was added the phosphate **10** (666 mg, 3 mmol) in THF (5 ml) and the whole was treated as described above. Distillation (bp 160 °C/40 Torr) gave an oil (387 mg, 78% yield). GLPC showed that the oil was a mixture of **14** and **5** in the ratio of 18:82.

We wish to thank the Instrumental Center, the Institute for Molecular Science, for assistance in obtaining the ^{1}H NMR spectra (100 MHz).

References

1) "Chemistry of Terpenes and Terpenoids," ed by A. A. Newman, Academic Press, London, New York (1972); "Terpenoids and Steroids" ed by K. H. Overton, The Chemical Society, London, Specialist Periodical Reports, (1971—1976), Vol. 1—6; ed by J. R. Hanson, *ibid.*, (1977—1979, 1981), Vol. 7—10.

2) Isolation: A. Quilico, F. Piozzi, and M. Pavan, *Tetrahedron*, **1**, 177 (1957); T. Sakai, K. Nishimura, and Y. Hirose, *Tetrahedron Lett.*, **1963**, 1171; *Bull. Chem. Soc. Jpn.*, **38**, 381 (1965); Y. Hirose, M. Abu, and Y. Sekiya, *Nippon Kagaku Zasshi*, **82**, 725 (1961). Synthesis: Y. Nakahara, M. Matsui, and K. Mori, *Agric. Biol. Chem.*, **38**, 2243 (1974); S. Takahashi, *Synth. Commun.*, **6**, 331 (1976); W. C. Still, *J. Am. Chem. Soc.*, **100**, 1481 (1978), and references cited therein; K. Inomata, S. Aoyama, and H. Kotake, *Bull. Chem. Soc. Jpn.*, **51**, 930 (1978); S. Katsumura, A. Ohsuka, and M. Kotake, *Heterocycles*, **10**, 87 (1978); Y. Kojima, S. Wakita, and N. Kato, *Tetrahedron Lett.*, **20**, 4577 (1979); J. Nokami, T. Sudo, H. Nose, and S. Wakabayashi, *ibid.*, **22**, 4489 (1981).

3) Isolation: a) N. Hayashi, H. Komae, S. Eguchi, M. Nakayama, S. Hayashi, and T. Sakao, *Chem. Ind. (London)*, **1972**, 572. Synthesis: b) D. R. Gedge and G. Pattenden, *Tetrahedron Lett.*, **1977**, 4443 and references cited therein; c) A. Takeda, K. Shinhama, and S. Tsuboi, *Bull. Chem. Soc. Jpn.*, **50**, 1903 (1977); d) H. Kotake, K. Inomata, H. Kinoshita, S. Aoyama, and Y. Sakamoto, *Heterocycles*, **10**, 105 (1978).

4) Isolation: H. Suzuki, *Yakugaku Zasshi*, **56**, 841 (1936); R. Bernardi, C. Cardani, D. Ghiringhelli, A. Selva, A. Baggini, and M. Pavan, *Tetrahedron Lett.*, **1967**, 3893. Synthesis: P. Gosselin, S. Masson, and A. Thuillier, *J. Org. Chem.*, **44**, 2807 (1979); A. Hoppmann and P. Weyerstahl, *Tetrahedron*, **34**, 1723 (1978); J. E. McMurry and S. F. Donovan, *Tetrahedron Lett.*, **1977**, 2869, and references cited

therein.

5) Isolation: G. Büchi, E. Kovats, P. Euggist, and G. Uhde, *J. Org. Chem.*, **33**, 1227 (1968). Synthesis: Ref. 3b and 3c.

6) S. Araki and Y. Butsugan, *Chem. Lett.*, **1982**, 177.

7) A. Suggett, M. Moir, and J. C. Seaton, *Proc. European Brewery Conv. Congress, Berlin (West)*, **1979**, 91.

8) K. A. Parker and W. S. Johnson, *Tetrahedron Lett.*, **1969**, 1329.

9) E. Sherman and E. D. Amstutz, *J. Am. Chem. Soc.*, **72**, 2195 (1950).

10) Very recently, Li_2CuCl_4-catalyzed coupling of 3-furylmethylmagnesium chloride with organic halides has been reported: S. P. Tanis, *Tetrahedron Lett.*, **23**, 3115 (1982).

11) Copper(I)-catalyzed reaction of 3-furylmethylmagnesium chloride with geranyl chloride has been described: D. Nasipuri and G. Das, *J. Chem. Soc., Perkin Trans. 1*, **1979**, 2776.

12) T. L. Peppard and J. A. Elvidge, *Chem. Ind. (London)*, **1979**, 552; J. A. Elvidge, S. P. Jones, and T. L. Peppard, *J. Chem. Soc., Perkin Trans. 1*, **1982**, 1089.

13) J. A. Miller and H. C. S. Wood, *J. Chem. Soc., C*, **1968**, 1837.

14) E. Campaigne and B. F. Tuldar, *Org. Synth.*, Coll. Vol. IV, 921 (1963).

The Identification of 3-Amino-9*H*-pyrido[3,4-*b*]indole Derivatives in L-Tryptophan Pyrolysates

Masao TADA,* Hisaaki SAEKI, and Atsushi OIKAWA

Research Institute for Tuberculosis and Cancer, Tohoku University, Seiryomachi 4-1, Sendai 980

(Received August 16, 1982)

The compounds, 3-amino-9*H*-pyrido[3,4-*b*]indole and 3-amino-1-methyl-9*H*-pyrido[3,4-*b*]indole, which are effectors in induction of sister chromatid exchanges in human cells, were isolated from pyrolysis products of L-tryptophan and characterized by HPLC and UV techniques.

A number of heterocyclic amines in pyrolysates of amino acids, proteins, and proteinaceous foods were found to be highly mutagenic to *Salmonella typhimurium*.[1] Sugimura *et al.*[2,3] reported that the main mutagenic components of pyrolysates of L-tryptophan were 3-amino-1,4-dimethyl- (**1**) and 3-amino-1-methyl-5*H*-pyrido[4,3-*b*]indole (**2**). Compounds **1** and **2** have been synthesized from 2-indolecarboxylic acid and 2,5-lutidine, respectively.[4] The isolation of 2-amino- (**3**) and 2-amino-3-methyl-9*H*-pyrido[2,3-*b*]indole (**4**) as mutagens from the pyrolysis product of tryptophan was also reported.[5] 9*H*-Pyrido[3,4-*b*]indole (**5**, norharman) and its 1-methyl derivative (**6**, harman) were also found in the pyrolysates.[3] Compounds **1** and **2** are carcinogenic to rodents[6] and active in inducing sister chromatid exchanges (SCEs) in human cells.[7]

In a previous paper,[8] we reported that 3-amino-9*H*-pyrido[3,4-*b*]indole (**7**) and 3-amino-1-methyl compound (**8**) were relatively weak SCE inducers, and inhibited SCE induction by other stronger SCE inducers. Thus, it is quite interesting to examine whether those compounds **7** and **8** are present in pyrolysates of amino acids and proteins or not. This paper describes the identification of **7** and **8** in L-tryptophan pyrolysates.

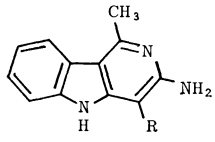

1, R=CH_3
2, R=H

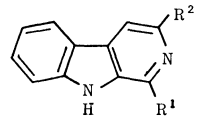

5, R^1=R^2=H
6, R^1=CH_3, R^2=H
7, R^1=H, R^2=NH_2
8, R^1=CH_3, R^2=NH_2
9, R^1=NH_2, R^2=H

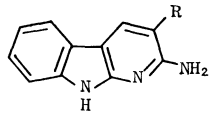

3, R=H
4, R=CH_3

Results and Discussion

Pyrolysis of L-*Tryptophan and Analyses of Products.* A one hundred gram sample of L-tryptophan was pyrolyzed and dry-distilled by a direct flame at 400 to 500 °C for 1 h to give a tar (61 g). The tar was separated into acidic, basic, and neutral fractions by the ordinary method to afford 22 g of basic mixture. The mixture was fractionated by a silica-gel column using dichloromethane and a mixture of dichloromethane and ethanol as elution solvents. The fraction expected to contain the title derivatives was further fractionated on a column of silica gel into four subfractions by eluting with a mixture of dichloromethane and ethanol. The material at each step of purification was checked by thin-layer chromatography. Each of the resulting subfractions was subjected to preparative thin-layer chromatography on a silica-gel plate with an appropriate solvent system. The bands corresponding to **2**, **3**, **5**—**8**, and 1-amino-9*H*-pyrido[3,4-*b*]indole (**9**) were made visible under UV light, scraped off, and extracted with methanol. This isolation protocol is summarized in Fig. 1. Each of the methanol extracts was then applied to high performance liquid chromatography (HPLC) to analyze the target compounds, **2**, **3**, **5**—**8**, and **9**, qualitatively and quantitatively.

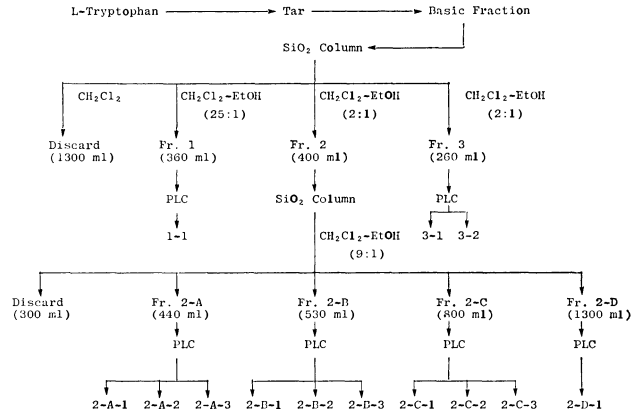

Fig. 1. Protocol for isolation of the target compounds from the pyrolysate.

Typical examples of analytical HPLC of fractions containing the target compounds are shown in Fig. 2. Satisfactory coincidence of retention times of the target bases with those of the authentic specimens was observed. The retention times of the title compounds, **7** and **8**, under various chromatographic conditions were in agreement with the bases of the pyrolysates (Table 1).

Analytical HPLC of Fraction 2-C-2 under the chromatographic condition No. 2 (Table 1) is shown in Fig. 3. Retention times of Peaks I and II coincided with those of **7** and **8**, respectively. Peaks I and II fractions were pooled separately from several identical runs of HPLC. As shown in Fig. 4, the absorption curves in UV of these two peak substances were completely identical to those of synthetic **7** and **8**, respectively. These facts confirm that peaks I and II are

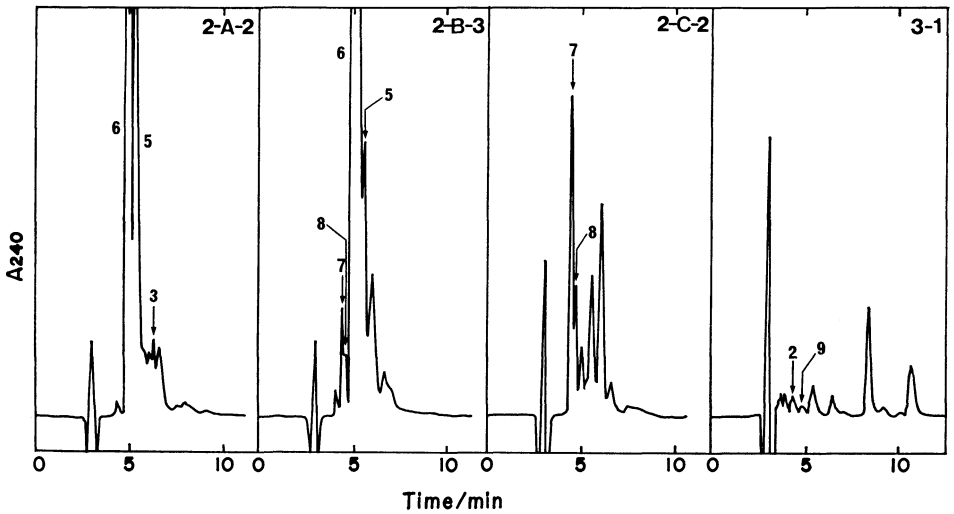

Fig. 2. Analytical HPLC of typical fractions containing the target compounds. The chromatographic conditions are shown as No. 1 in Table 1.

Table 1. Retention times of the target compounds in various HPLC systems

No.	Column	Solvent system	Time/min						
			2	**3**	**5**	**6**	**7**	**8**	**9**
1	μBondapak C_{18}[a]	CH_3CN/0.02 M[b] KH_2PO_4 (45/55)	4.1	6.3	5.0	4.9	4.2	4.4	4.5
2	LS-410 ODS SIL[c]	MeOH/H_2O/NH_4OH (60/40/1)	12.0	9.4	14.2	18.6	6.1	7.2	16.9
3	LS-470 OH SIL[c]	MeOH/H_2O (8/2)					9.3	13.6	
4	LS-410 ODS SIL	CH_3CN/0.02 M KH_2PO_4 (45/55)					6.1	5.9	
5	LS-470 OH SIL	CH_3CN/0.02 M KH_2PO_4 (45/55)					4.0	3.8	

Column size: 4×300 mm. Flow rate: 1.0 ml/min. Detector: UV 240 nm.
a) Waters associate. b) 1 M=1 mol dm^{-3}. c) Toyo Soda Manuf. Co., Ltd.

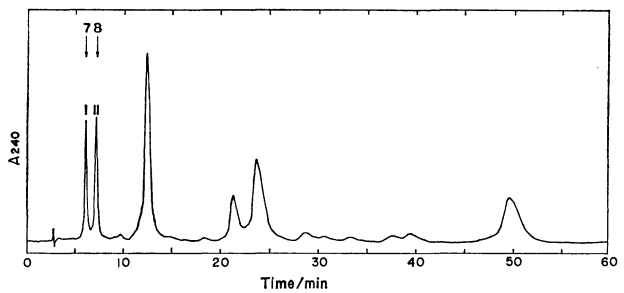

Fig. 3. HPLC of Fraction 2-C-2. Arrows indicate the retention times of **7** and **8**. The chromatographic conditions are shown as No. 2 in Table 1.

of **7** and **8**, respectively. Both **7** and **8** were also detected in fr. 2-B-2. Analyses of other bases of the pyrolysates were worked up in a similar manner to that given above. Compounds **3**, **5**, and **6** were mainly detected in both fr. 2-A-1 and fr. 2-A-2. Compounds **2** and **9** were found in fr. 2-D-1, fr. 3-1, and fr. 3-2. The contents of the target compounds were estimated from HPLC data, ignoring their decomposition and loss during separation, and are shown in Table 2.

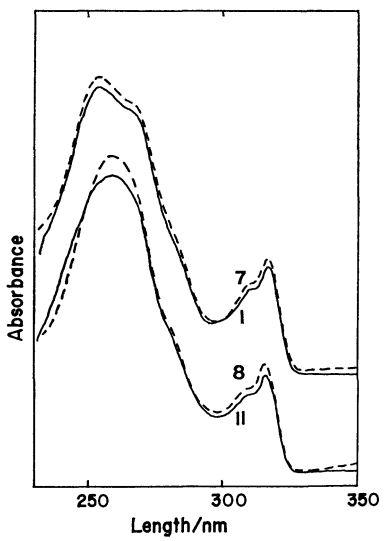

Fig. 4. UV spectra of Peaks I and II (——) and compounds **7** and **8** (----).

Compounds **7** and **8**, in methanol solution were stable at room temperature in the dark, but were considerably photosensitive. At a distance of 20 cm

TABLE 2. PYROLYSATES OF L-TRYPTOPHAN (100 g)

Compound	Content/mg
6	1140—1040
5	852—846
3	249—101
7	12.7—11.9
8	4.7—3.1
9	4.9—0.11
2	2.6—0.28

from a 20 W-fluorescent tube the half-life times of **7** and **8** were *ca.* 25 h and *ca.* 12.5 h in methanol, respectively (Fig. 5). From these facts it seems that the original contents of **7** and **8** in the fresh pyrolysates did not differ so much from each other as those seen in Table 2. Compound **2** was stable under these conditions.

The present work shows that the combined use of column and preparative thin-layer chromatography, HPLC, and UV is highly effective for analysis of pyrolysis products.

The identification of the title derivatives in pyrolysates of natural substances are currently under investigation.

Synthesis of 9H-Pyrido[3,4-b]indole Derivatives. 1,2,3,4-Tetrahydro-9*H*-pyrido[3,4-*b*]indole-3-carboxylic acid (**10**)[9] was treated with methanol and ethanol to afford methyl and ethyl esters (**11** and **12**), respectively. The methyl ester (**11**) was dehydrogened with sulfur to give methyl 9*H*-pyrido[3,4-*b*]indole-3-carboxylate (**13**). Treatment of the ethyl ester (**12**) under similar conditions resulted in dehydrogenation to afford ethyl carboxylate (**14**). When lead(IV) acetate was used, compounds **11** and **12** were also converted into **13** and **14**, respectively, but the yields were poor. Treatment of **13** and **14** with acid yielded the carboxylic acid (**15**) in a quantitative yield. The acid (**15**) was treated with methanol and ethanol in the presence of acid to afford the esters **13** and **14** in quantitative yields, respectively.

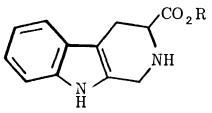

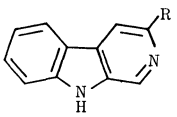

10, R=H
11, R=CH_3
12, R=CH_2CH_3

13, R=CO_2CH_3
14, R=$CO_2CH_2CH_3$
15, R=CO_2H
16, R=$CONHNH_2$
17, R=CON_3
18, R=$NHCO_2CH_2C_6H_5$.

The carboxylic acid (**15**) was submitted to Curtius rearrangement by the diphenylphosphinic azide method[10] to yield the desired 3-amino derivative (**7**), which was confirmed to be exactly identical with the product obtained by the modified Snyder's method.[11] In this method, either **13** or **14** was converted to the hydrazide (**16**), which was then treated with nitrous acid to afford the corresponding azide (**17**). The treatment of the azide (**17**) with benzyl alcohol in toluene gave the benzyl carbamate (**18**), which was further submitted to the acidic or alkaline hydrolysis to yield the amino compound (**7**). In comparison with the overall yields of **7** from **13**, this modified method was better than the diphenylphosphinic azide method. Recently, Agarwal *et al.*[12] reported that **7** could be synthesized starting from methyl DL-1,2,3,4-tetrahydro-9*H*-pyrido-[3,4-*b*]indole-3-carboxylate *via* a Curtius reaction. Their method is essentially the same as our modified method.

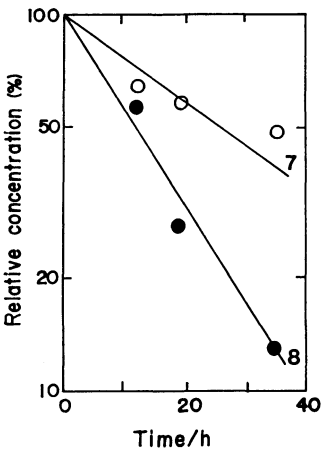

Fig. 5. Time course of degradation of **7** and **8**.

Experimental

Column chromatography was carried out over silica gel (Merck, Kieselgel 60). Merck pre-coated silica gel 60 F-254 TLC plates (5×20 cm²) and PLC plates (20×20 cm²) were used for the TLC and preparative TLC, respectively. Unless otherwise noted, the developing solvent system was a CH_2Cl_2–ethanol (9:1, v/v) mixture, and visualization was effected by the use of a Pan UV lamp. The homogeneity of each compound was always checked by TLC on silica gel. HPLC was made with a Toyo Soda Model HLC-803A equipped with an appropriate analytical column. Retention times of HPLC under various conditions are shown in Table 1. Absorption spectra were recorded with a Hitachi Model EPI-S_2 IR spectrophotometer and a Hitachi Model 124 spectrophotometer. Mass spectra were run with a Shimadzu LKB-9000 spectrometer, operating at an electron beam energy of 70 eV and with direct inlet. All melting points were taken on a hot-stage apparatus and are uncorrected.

Pyrolysis of L-Tryptophan. A hundred grams of L-tryptophan dried with P_2O_5 was pyrolyzed and dry-distilled by a direct flame at 400—500 °C for 1 h to give a tar (61 g). The tar was dissolved in ether (1 L) and the solution was extracted with 20% HCl (400 ml×5). The extracts were combined, cooled, and made alkaline with NaOH. The alkaline mixture was then extracted with ether (250 ml×6). The ethereal extract was washed (H_2O), dried (Na_2SO_4), and concentrated, giving 22.6 g of basic substances. The substances were dissolved in CH_2Cl_2 and fractionated by a silica-gel column (3×20 cm) using CH_2Cl_2 and CH_2Cl_2–EtOH (25:1 and 2:1, v/v) mixtures as elution solvents, giving three fractions (lst fr., 0.49 g; 2nd fr., 3.72 g; 3rd fr., 1.36 g). The second fraction was expected to contain 3-amino compounds, **7** and **8**, and was further fractionated on a column (5×20 cm) of silica gel into four subfractions by a CH_2Cl_2–EtOH (9:1, v/v) mixture to afford fractions, 2-

A-2-D. These procedures of fractionations are shown in Fig. 1. Each fraction was then subjected to preparative TLC to develop multiple times. In the cases of the lst fraction, fraction 2-C, and 3rd fraction, the number of times of development was three, and in the cases of fractions 2-A and 2-B it was two. In the case of 3rd fraction, the developing solvent system was a CH_2Cl_2–EtOH (4:1, v/v) mixture. A plate charged with fraction 2-D was developed six times.

The bands corresponding to **2**, **3**, **5**—**8**, and **9** were visualized under UV light. As shown in Fig. 1, band 1—1 was obtained from fr. 1, bands 3—1 and 3—2 from fr. 3, and band 2-D-1 from fr. D, respectively. Fractions 2-A, 2-B, and 2-C were each divided by similar chromatography into three bands. Each band was then scraped off, added to methanol, and mixed well. Each methanol mixture was centrifugalized and the resulting supernatant was then applied to HPLC to analyze the contents of the target compounds. These results are shown in Table 2.

*3-Amino-1-methyl-5*H*-pyrido[4,3-*b*]indole (**2**).* Compound **2** was supplied under the Research Resources Program (No. 57010022) for Cancer Research, the Ministry of Education, Science, and Culture: TLC R_f 0.01; UV (MeOH) 241 (log ε 4.61), 263 (4.87), 303 (4.00), and 315 nm (4.00).

*2-Amino-9*H*-pyrido[2,3-*b*]indole (**3**).* Compound **3** was also supplied under the same program as described above: TLC R_f 0.47; UV (MeOH) 231 (log ε 4.10), 260 (3.66), and 337 nm (3.76).

*9*H*-Pyrido[3,4-*b*]indole (**5**).* Compound **5** was prepared by a procedure similar to that reported[13] and purified with column chromatography, giving needles (from dil MeOH): mp 199—200 °C; TLC R_f 0.30; UV (MeOH) 233 (log ε 4.61), 248 (sh, 4.37), 281 (sh, 4.09), 288 (4.29), 366 (3.67), and 349 nm (3.68); IR (KBr) 3260 and 1630 cm^{-1}.

*1-Methyl-9*H*-pyrido[3,4-*b*]indole (**6**).* Compound **6** was prepared as reported[14] and purified with the chromatography, giving needles (from dil MeOH): mp 229—230 °C; TLC R_f 0.22; UV (MeOH) 234 (log ε 4.63), 238 (sh, 4.62), 248 (4.43), 281 (sh, 4.07), 287 (4.29), 333 (3.75), and 347 nm (3.76); IR (KBr) 3210 and 1622 cm^{-1}.

*Compounds **11** and **12**.* To a suspension of **10** (8.8 g) in MeOH (200 ml), conc. H_2SO_4 (10 ml) was added. The mixture was refluxed for 8 h, concentrated, poured into ice, and made neutral with K_2CO_3. The resulting mixture was extracted with CH_2Cl_2 and the extract was then washed (H_2O), dried ($MgSO_4$), and concentrated, giving 7.6 g (81%) of the methyl ester (**11**): TLC R_f 0.69.

A mixture of **10** (13 g) in EtOH (200 ml) and conc. H_2SO_4 (12 ml) was treated as above to afford 7.78 g (54%) of the ethyl ester (**12**): TLC R_f 0.76.

*The Esters **13** and **14**.* *i) With Sulfur*: A suspension of **11** (2.6 g) and powdered sulfur (1 g) in xylene (40 ml) was refluxed for 6 h and cooled. The crystals which then formed were purified by column chromatography to yield 2.05 g (80%) of **13**. Recrystallization from EtOH gave needles: mp 255—257 °C (decomp); TLC R_f 0.48; UV (MeOH) 216, 232, 269, 301 sh, 330, 345 nm; IR (KBr) 3250, 1723, and 1710 cm^{-1}.

Found: C, 68.78; H, 4.35; N, 12.10%. Calcd for $C_{13}H_{10}N_2O_2$: C, 69.01; H, 4.46; N, 12.38%.

The ethyl ester (**14**) was prepared from **12** in a 68% yield under similar conditions to those described above: Needles (from C_6H_6–EtOH); mp 207—208 °C; TLC R_f 0.53; IR (KBr) 3250 and 1725 cm^{-1}.

Found: N, 11.35%. Calcd for $C_{14}H_{12}N_2O_2$: N, 11.66%.

The esters **13** and **14** were obtained in quantitative yield by the treatment of the acid (**15**) with MeOH and EtOH in the presence of H_2SO_4, respectively.

ii) With Lead(IV) Acetate: To a solution of **11** (2.3 g) in acetic acid (35 ml), lead(IV) acetate (9.3 g) freshly prepared from Pb_3O_4 was added, and the mixture was allowed to stand at room temperature for 30 min. After addition of ethylene glycol (1 ml), the mixture was poured into ice-water and made alkaline with dil. aqueous ammonia to yield 565 mg (25%) of **13**.

The ester **14** was obtained in a 28% yield by the same treatment of **12** with lead(IV) acetate.

*The Carboxylic Acid (**15**).* *i) From **13***: A suspension of **13** (1.0 g) in 5% aq NaOH solution (20 ml) was heated on a water bath for 8 h to give a clear solution. Acetic acid was added to the solution to make it acidic. The precipitate thereby formed was collected, washed (MeOH), and dried, giving the carboxylic acid (**15**) in a quantitative yield: mp 318—320 °C (decomp).

*ii) From **14***: Treatment of **14** under similar conditions gave **15** in a quantitative yield.

*3-Amino-9*H*-pyrido[3,4-*b*]indole (**7**).* *i) By Modified Snyder's Method*: To a suspension of methyl ester **13** (5 g) in 1-pentanol (50 ml) and ethanol (15 ml), 100% hydrazine hydrate (20 ml) was added. The mixture was refluxed for 5 h, cooled, and filtered, giving 4.92 g (98%) of the hydrazide (**16**): TLC R_f 0.06; IR (KBr) 3320, 3240 (broad), and 1650 cm^{-1}. To a solution of **16** (2.26 g, 10 mmol) in conc. HCl (1.5 ml) and water (100 ml), a solution of $NaNO_2$ (828 mg, 12 mmol) in water (5 ml) was added under cooling with ice-water. The resulting mixture was allowed to stand in the cold with stirring for 30 min and then neutralized with saturated $NaHCO_3$ solution to give 2.27 g (96%) of the azide (**17**): TLC R_f 0.55. A mixture of **17** (2.27 g) in xylene (25 ml; dried with "Dry Soda") and benzyl alcohol (2.2 ml; dried with molecular sieve 3A) was heated at 110—120 °C for 20 min and then allowed to stand in a refrigerator overnight to afford 2.81 g (92%) of the benzyl carbamate (**18**): mp 208—212 °C (decomp), TLC R_f 0.53. To a suspension of **18** (2.8 g) in ethylene glycol (30 ml) and water (3 ml), KOH (3 g) was added. The mixture was stirred and heated at 150—160 °C for 30 min to yield 1.40 g (86%) of the amine (**7**). The overall yield of **7** from **13** is 74%: Bright yellow scales (from aq DMF); mp 286—288 °C (blacken) and 290—291 °C (decomp); TLC R_f 0.11, R_f 0.14 with CH_2Cl_2–EtOH (4:1, v/v); UV (MeOH) 236 (log ε 4.53), 248 (sh, 4.49), 292 (sh, 4.00), and 299 nm (4.10); IR (KBr) 3460, 3420, 3300, and 1625 cm^{-1}.

Found: C, 72.05; H, 4.90; N, 22.71%; M^+ 183. Calcd for $C_{11}H_9N_3$: C, 72.11; H, 4.95; N, 22.94%; M 183.

The acidic hydrolysis of the carbamate (**18**) was made as follows: A suspension of **18** (159 mg, 5 mmol) in 10% HCl (10 ml) was refluxed for 5 h and then made alkaline with diluted KOH aq solution, giving 64 mg (70%) of **7**.

The ethyl ester **14** was converted into the hydrazide **16** in an 85% yield under similar conditions.

ii) By Diphenylphosphinic Azide Method: To a mixture of **15** (850 mg) in triethylamine (1 ml), diphenylphosphinic azide (1.20 g) was added. The resulting mixture was heated at 80 °C for 1 h. Benzyl alcohol (1 ml) was added to the mixture, which was further heated at 120 °C for 10 h. After purification with column chromatography, 150 mg (12%) of the carbamate **18** was obtained and the alkaline hydrolysis of **18** gave **7**. The overall yield of **7** from **15** is 10%.

*3-Amino-1-methyl-9*H*-pyrido[3,4-*b*]indole (**8**).* Compound **8** was prepared from the methyl ester by a procedure

of the method of Snyder *et al.*,[11] giving needles (from MeOH) (Found: C, 73.01; H, 5.59; N, 21.45%): mp 228—229 °C; TLC R_f 0.11; R_f 0.15 with CH_2Cl_2–EtOH (4:1, v/v); UV (MeOH) 240 (log ε 4.56), 291 (sh, 4.00), and 297 nm (4.09); IR (KBr) 3380, 3170 (broad), and 1632 cm^{-1}. MS M^+ 197.

*1-Amino-9H-pyrido[3,4-b]indole (**9**).* According to the method reported by Snyder *et al.*,[15] **9** was prepared by the reaction of **5** and $NaNH_2$ in liquid NH_3, giving needles (from dil EtOH) in a 95% yield: mp 203—204 °C (decomp), TLC R_f 0.03; R_f 0.19 with CH_2Cl_2–EtOH (4:1, v/v); UV (MeOH) 240 (log ε 4.70), 278 (3.90), 288 (4.00), 299 (3.47), 326 (3.73), 337 (3.85), and 350 nm (3.78); IR (KBr) 3420, 3370, 3310, and 1632 cm^{-1}.

We thank Professor Kyozo Ogura, Tohoku University, for his helpful discussion. The present work was partially supported by Grants-in Aid for Cancer Research No. 57010079 from the Ministry of Education, Science and Culture, No. 55-04 from the Ministry of Health and Welfare, and from the Association for the Advancement of Cancer Research of Japan.

References

1) T. Sugimura, "A View of a Cancer Researcher on Environmental Mutagens," in "Environment Mutagens and Carcinogens," eds by T. Sugimura, S. Kondo, and H. Takebe, University of Tokyo Press, Tokyo, and Alan R. Liss, Inc., New York (1982), pp. 3—20, and references cited therein.

2) T. Sugimura, T. Kawachi, M. Nagao, T. Yahagi, Y. Seino, T. Okamoto, K. Shudo, T. Kosuge, K. Tsuji, K. Wakabayashi, Y. Iitaka, and A. Itai, *Proc. Jpn. Acad.*, **53**, 58 (1977).

3) T. Kosuge, K. Tsuji, K. Wakabayashi, T. Okamoto, K. Shudo, Y. Iitaka, A. Itai, T. Sugimura, T. Kawachi, M. Nagao, T. Yahagi, and Y. Seino, *Chem. Pharm. Bull.*, **26**, 611 (1978).

4) H. Akimoto, A. Kawai, H. Nomura, M. Nagao, T. Kawachi, and T. Sugimura, *Chem. Lett.*, **1977**, 1061.

5) D. Yoshida and T. Matsumoto, *Agric. Biol. Chem.*, **43**, 1155 (1979).

6) N. Matsukura, T. Kawachi, K. Morino, H. Ohgaki, T. Sugimura, and S. Takayama, *Science*, **213**, 346 (1981).

7) H. Tohda, A. Oikawa, T. Kawachi, and T. Sugimura, *Mutat. Res.*, **77**, 65 (1980).

8) H. Tohda, M. Tada, R. Sugawara, and A. Oikawa, *Mutat. Res.*, **116**, 137 (1983).

9) A. Brossi, A. Focella, and S. Teitel, *J. Med. Chem.*, **16**, 418 (1973).

10) K. Ninomiya, T. Shioiri, and S. Yamada, *Chem. Pharm. Bull.*, **22**, 1398 (1974).

11) H. R. Snyder, S. M. Parmerter, and H. G. Walker, *J. Am. Chem. Soc.*, **70**, 237 (1948).

12) S. K. Agarwal, A. K. Saxena, and P. C. Jain, *Indian J. Chem.*, **19B**, 45 (1980).

13) D. G. Harvey, E. J. Miller, and W. Robson, *J. Chem. Soc.*, **1941**, 153.

14) D. G. Harvey and W. Robson, *J. Chem. Soc.*, **1938**, 97.

15) H. R. Snyder, H. G. Walker, and F. S. Werber, *J. Am. Chem. Soc.*, **71**, 527 (1949).

Syntheses of Acyclic Polyethers Containing a Ferrocene Nucleus and Its Extraction Ability

Sadatoshi Akabori,* Michiko Ohtomi, Masaru Sato,† and Seiji Ebine††

Department of Chemistry, Toho University, Funabashi, Chiba 274

† *Chemical Analysis Center, Saitama University, Urawa, Saitama 338*

†† *Department of Chemistry, Faculty of Science, Saitama University, Urawa, Saitama 338*

(Received September 13, 1982)

Acyclic polyethers (**7**) (containing a ferrocene nucleus in both terminal sites) were synthesized by a one-pot reaction of 1,1′-diacetoxyferrocene with halide. Also, ferrocene derivatives (**11**) having polyethylene glycols were synthesized by the reaction of potassium salt of hydroxyferrocene with dihalide in DMF. On the addition of alkali metal thiocyanate in methanol, a hypsochromic shift and an increasing intensity of the absorption band at 438 nm were observed in ferrocene-containing polyethers **7**, suggesting the complexing of **7** with cations. However, a similar spectral change could not be observed in **11**. **7a** extracts silver and thallium ions most effectively, the extraction efficiency of several metal cations being in this order: $Ag^+ > Tl^+ > Cs^+ > K^+ > Li^+ > Na^+$.

While the investigations of macrocyclic polyether complexes[1] have been steadily gaining popularity during the past several years, it seems that most attention has so far been focused on the syntheses of new types of ligands. During the course of our investigation of polyoxa[*n*]ferrocenophanes **1**, **2**, and **3**,[2-4] we observed

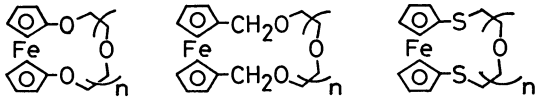

1 2 3

1a n=4 n=2~4 n=1~4
1b n=3

that the incorporation of a ferrocene nucleus into the framework of a crown-ether ring increases the extraction efficiency toward a transition-metal cation. For example, **1** showed a high extraction percentage with the thallium cation, although it showed little or no extractability with alkali-metal cations. Furthermore, **2** similarly showed a high complexing ability with thallium and silver cations, although **1** decomposed rapidly when the silver cation was present. Those results suggest that the distance between the iron atom of the ferrocene nucleus and the incorporated silver cation controls the oxidation of the ferrocene nucleus.[3] In this connection, we wish now to report the syntheses of acyclic polyethers (**7**)(containing a ferrocene nucleus in both terminal sites) and ferrocene derivatives (**11**) having polyethylene glycols and the complexing ability of **7** and **11** with alkali and transition metal cations.

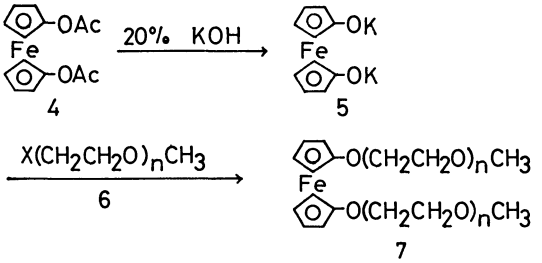

6a n=3 X=Cl 7a n=3
6b n=2 X=Br 7b n=2
6c n=1 X=Br 7c n=1
6d n=0 X=I 7d n=0

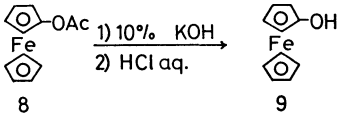

8 9

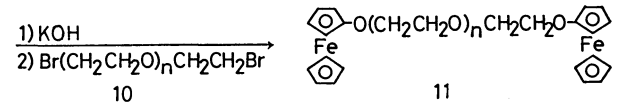

10 11

10a n=4 11a n=4
10b n=3 11b n=3
10c n=2 11c n=2

Syntheses. The syntheses of **7a—d** were carried out by the following method. The hydrolysis of 1,1′-diacetoxyferrocene (**4**) was carried out under an atmosphere of nitrogen by the usual method. To the resulting alkali solution of the potassium salt of 1,1′-dihydroxyferrocene (**5**) we added at once a solution of halide (**6**) in 60% ethanol at the reflux temperature. Then the mixture was refluxed for 3.5 h. After a usual work-up, the products were chromatographed on silica gel. From the main fraction, pure **7a—d** were obtained in moderate to good yields. It is noteworthy that this one-pot preparation of **7** starting directly from **4** avoids the isolation of very air-sensitive 1,1′-dihydroxyferrocene.[5] Compounds **11a—c** (containing a ferrocene nucleus in both terminal sites) were prepared by the reaction of hydroxyferrocene (**9**), which had itself been obtained by the hydrolysis of acetoxyferrocene (**8**), with appropriate dihalide (**10**) in DMF in the presence of potassium hydroxide. The molecular formula of **7a** was deduced to be $C_{24}H_{38}O_8Fe$ by means of mass spectroscopy (M^+, *m/e* 510) and the elemental analysis. In the ^{1}H-NMR spectrum of **7a**, the resonance for the α- and β-ring protons of the ferrocene nucleus appeared as the A_2B_2 pattern at δ=4.10 (4H, t, J=2.0 Hz) and 3.84 (4H, t, J=2.0 Hz) respectively, in addition to the signal of methylene protons as a multiplet at δ=3.45—3.90 (m, 24H) and the signal of the methyl group as a singlet at

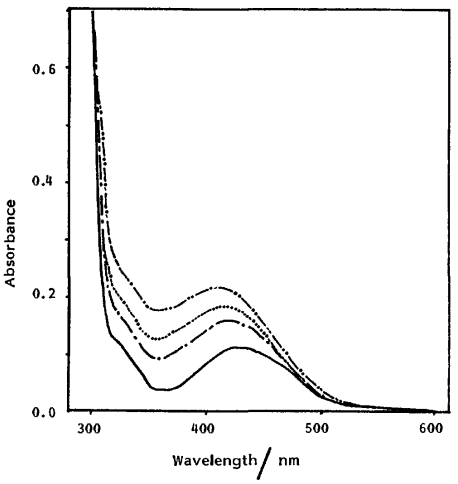

Fig. 1. Spectral change of **7a** by the addition of KSCN. Time: —— 0, ——— 1 h, ---- 2 h, —··— 3 h. Concentration: [**7a**]=1×10^{-3} M, [KSCN]=2.0×10^{-2} M.

δ=3.35 (s, 6H). The IR spectrum of **7a** showed ferrocene ring C–H absorption and ether-linkage absorption near 1480 and 1125 cm^{-1} respectively, but no absorption attributable to hydroxyl and carbonyl groups. The molecular formula of **11a** was deduced to be $C_{30}H_{38}O_6Fe_2$ by means of mass spectroscopy (M^+, *m/e* 608) and elemental analysis. The ^{1}H-NMR spectrum of **11a** showed the signal of unsubstituted ferrocene-ring protons as a singlet at δ=4.14 and the substituted ring protons as the A_2B_2 pattern at δ=4.06 (t, J=2.0 Hz, 4H, H_α) and 3.80 (t, J=2.0 Hz, 4H, H_β), in addition to the signal of the methylene protons at δ=3.72—3.94 (m, 8H) and 3.64 (s, 12H). The IR spectrum of **11** displayed absorptions of the ferrocene ring and ether linkage at 1470 and 1100 cm^{-1} respectively, but the absence of any bands arising from the hydroxyl group. The electronic spectra of **7** and **11** (λ_{max} 434 nm in MeOH) suggest the presence of a ferrocene nucleus. The structures of other new compounds were also determined by a method similar to that described above.

Additive Effect of Metal Salt. At first we examined the electronic spectral change in the ferrocenyl derivatives upon the addition of metal thiocyanate in order to determine the cation complexing ability qualitatively. It is well known[6] that the spectral shapes in the curves for the complexing polyethers are altered by the addition of complexable salts. A typical spectral change in **7a** on the addition of potassium thiocyanate in methanol is shown in Fig. 1. All compounds containing a ferrocene nucleus in the middle of the polyethylene glycol chain show a characteristic absorption maximum at 434 nm in methanol. Upon the addition of potassium thiocyanate, the curve of **7a** shows a remarkable change. Its hypsochromic shift and increase in absorbance suggest the complex formation between **7a** and potassium thiocyanate. These results are listed in Table 1. On the other hand, Compounds **11a—c**, which contain a ferrocene nucleus in both terminals, showed no spectral change upon the addition of any given alkali metal salt. In these compounds, no conformational change imposed on complexing with the metal cation takes place, probably because of the steric repulsion between the two ferrocenyl groups. Therefore, **11** could have no complexing ability with the metal cation.

Table 1. Electronic absorption spectral data and their metal complexes in methanol[a]

Compound	Additive salt λ/nm (ε)			
	None	LiSCN	NaSCN	KSCN
7a	431(112)	434(137)	431(134)	417(159)
7b	434(108)	434(124)	434(122)	432(110)
7c	434(92)	434(112)	434(105)	434(92)
7d	434(142)	434(137)	434(124)	434(112)

a) Measured in the presence of about a 50-fold molar excess of alkali metal thiocyanate at 20 °C.

Extractability. The extraction efficiency of **7** with alkali, alkaline earth, and transition-metal cations was measured according to Pedersen's method;[7] the results are listed in Table 2, together with those for **1a** and **1b**, which were synthesized previously.[2] It was observed that **7** showed only a little complexing ability with alkali and alkaline earth-metal cations, although they showed a relatively high complexing ability with transition metal cations. For the silver cation, Compounds **7a—d** have an excellently high complexing ability, as shown in Table 2. When the concentration of **7** was 7×10^{-4} M (1 M=1 mol dm^{-3}), the extractability could not be obtained because a rapid oxidative decomposition of the ferrocene nucleus by the complxed silver cation took place. However, this interaction may be weaker than that of polyoxa-[*n*]ferrocenophanes (**1**) with a closed oxyethylene chain, because, according to a consideration of its molecular model, the complexed silver ion in **7** is situated in a position apart from the iron atom of ferrocene because

Table 2. Extraction of metal picrates from aqueous to organic phase (%)[a,b]

Compound	Li^+	Na^+	K^+	Cs^+	Ag^+	Tl^+	Ca^{2+}	Ba^{2+}	Cd^{2+}
7a	4.4	4.2	7.7	8.8	51[c]	25	4.3	2.5	5.6
7b	3.6	3.4	2.9	3.2	40[c]	5.8	6.0	3.2	7.2
7c	1.9	1.5	1.1	1.9	33[c]	2.0	2.9	—	4.2
7d	2.5	1.6	1.7	1.3	20[c]	0.8	2.9	—	3.3
1a	—	1.6	22.7	18.4	28.3[c]	79.7	—	—	—
1b	—	1.5	4.5	5.6	18.8[c]	25.2	—	—	—

a) Solvents: Water and dichloromethane (equal volumes). b) Ferrocenyl ether=7.0×10^{-4} M. Picric acid=7.0×10^{-5} M. Metal nitrate=0.1 M. c) Ferrocenyl ether=7.0×10^{-5} M.

of the flexibility of the polyether chain. The extractability of the metal cations by **7a** was in this order: $Na^+ < Li^+ < K^+ < Cs^+ < Tl^+ < Ag^+$.

These phenomena can be explained by the HSAB rule;[8] that is, the incorporation of the iron atom of ferrocene (a soft acid) into the framework of acyclic polyethers decreases the affinity to a hard cation (alkali and alkaline-earth metal ions) and increases the affinity to a soft transition-metal cation. Furthermore, the extraction efficiency of **7** for the several alkali metal cations examined here was in this order: **7a**>**7b**>**7c**≈**7d**. These results suggest that the extraction efficiency of these cations is dependent on the length of the oxyethylene unit of acyclic polyethers (**7**). The above results suggest that there is an appreciable interaction between the incorporated metal ion and the iron atom of the ferrocene nucleus. It is also surprising that **7a** and **7b**, containing many oxygen atoms, showed some extraction efficiency with the lithium ion, although **1a** and **1b** showed no extraction efficiency with the lithium ion. According to a consideration of their molecular models, this was probably because of the nonfitness between the guest ion and the hole size of the host molecule. The extraction efficiency of the lithium ion with **7a** and **7b** suggests that the lithium ion becomes incorporated into the cavity formed by one of the two acyclic polyether arms, while the uptake of the lithium ion into the cavity made by the two side oxyethylene arms seems to be unfavorable because the ion radius of the lithium cation is too small for fitting with the hole size of the host molecule. It is also interesting to note that **7a** and **7b** showed only a little extraction efficiency with alkaline earth-metal ions, although alkaline earth metal ions were not extracted by any of the compounds **1**.

Experimental

The melting points are uncorrected. The mass spectra were taken by using a JEOL-OlSG-2 spectrometer. The ^{1}H-NMR spectra were obtained on a Hitachi R-90 spectrometer, TMS being chosen as the internal standard. The optical spectra were obtained on a Hitachi Model 200-10 spectrometer.

Materials. 1,1′-Diacetoxyferrocene (**4**)[2,5] and acetoxyferrocene (**8**)[5,9] were prepared according to the previously reported method. The other reagents employed were commercial materials or were prepared by the usual methods.

Syntheses of 7a—d. *General Procedure*: **4** (2.14 mmol) was added to a 20% aq potassium hydroxide solution (17 ml) under nitrogen, and the mixture was stirred at 100 °C. After 30 min, a solution of halide (**6**) (4 ml) in ethanol was added all at once, and then the mixture was stirred for 3.5 h at 120 °C. After the solution had been cooled to room temperature, 30 ml of water was added to the reaction mixture. The ether extracts were combined, washed with water, dried over anhydrous magnesium sulfate, and concentrated to give a residue. The residual oil was chromatographed on a silica-gel column, using acetone as the solvent. The crude **7** thus obtained was rechromatographed on a column of silica gel. Elution with chloroform gave pure **7** as a yellow oil.

1,1′-Bis(1,4,7,10-tetraoxaundecyl)ferrocene (7a). Yellow oil, 53% yield. Found: C, 56.20; H, 7.58%. Calcd for $C_{24}H_{38}O_8Fe$: C, 56.47; H, 7.45%. MS (75 eV): *m/e* 510 (M^+, 81.7%) and 218 ($Fc(OH)_2$, 7.2%). ^{1}H-NMR ($CDCl_3$): δ=4.10 (t, 4H, J=2.0 Hz, H_α), 3.84 (t, 4H, J=2.0 Hz, H_β), 3.45—3.90 (m, 24H, OCH_2CH_2O), 3.35 (s, 6H, OCH_3).

1,1′-Bis(1,4,7-trioxaoctyl)ferrocene (7b). Yellow oil, 67% yield. Found: C, 57.13; H, 7.29%. Calcd for $C_{20}H_{30}O_6Fe$. C, 56.87; H, 7.11%. MS (75 eV): *m/e* 422 (M^+, 100%) and 218 ($Fc(OH)_2$). ^{1}H-NMR ($CDCl_3$): δ=4.16 (t, 4H, J=2.0 Hz, H_α), 3.93 (t, 4H, J=2.0 Hz, H_β), 3.60—4.01 (m, 16H, OCH_2CH_2O), and 3.43 (s, 6H, OCH_3).

1,1′-Bis(1,4-dioxapentyl)ferrocene (7c). Yellow oil, 85% yield. Found: C, 57.70; H, 6.87%. Calcd for $C_{16}H_{22}O_4Fe$: C, 57.49; H, 6.59%. MS (75 eV): *m/e* 334 (M^+, 100%) and 218 ($Fc(OH)_2$). ^{1}H-NMR ($CDCl_3$): δ=4.17 (t, 4H, J=2.0 Hz, H_α), 3.92 (t, 4H, J=2.0 Hz, H_β), 3.60—3.90 (m, 8H, OCH_2CH_2O), and 3.40 (s, 6H, OCH_3).

1,1′-Dimethoxyferrocene. Orange crystals, mp 36—37 °C (lit,[5] 35—36 °C), 78% yield. Found: C, 58.32; H, 5.81%. Calcd for $C_{12}H_{14}O_2Fe$: C, 58.54; H, 5.69%. MS (75 eV): *m/e* 246 (M^+, 100%) and 218 ($Fc(OH)_2$, 72.8%). ^{1}H-NMR ($CDCl_3$): δ=4.12 (t, 4H, J=2.0 Hz, H_α), 3.91 (t, 4H, J=2.0 Hz, H_β), and 3.58 (s, 6H, OCH_3).

Syntheses of 11a—c. *General Procedure*: **8** (3.2 mmol) was added to ethanol (16 ml) containing 10% aq potassium hydroxide. The mixture was stirred for 1 h at 100 °C under nitrogen and then evaporated in a vacuum. After the residue had been cooled to room temperature, dilute sulfuric acid (10 ml) was added to the residue, and the resulting yellow precipitates were collected by filtration. The yellow solid was dissolved in *N,N*-dimethylformamide (50 ml). To the solution was added potassium hydroxide (1.0 g), and the resulting solution was stirred at room temperature. After 20 min, dibromide (**10**) (0.98 mmol) was added all at once, and the mixture was stirred for 7 h at 80—100 °C. After the solution had been cooled to room temperature, water (200 ml) was added to the reaction mixture. The solution was extracted with four 100 ml-portions of ether. The ether extracts were combined, washed with water, dried, and concentrated to give dark yellow oil. The residue was chromatographed on a silica-gel column. Elution with chloroform gave yellow crystals except for **11a**.

Pentaethylene Glycol Diferrocenyl Ether (11a). Yellow oil, 68% yield. Found: C, 59.15; H, 6.48%. Calcd for $C_{30}H_{38}O_6Fe$: C, 59.41; H, 6.27%. MS (75 eV): *m/e* 608 (M^+, 87.8%) and 202 (FcOH, 100%), and 121 ($C_5H_5Fe^+$, 65.4%). ^{1}H-NMR ($CDCl_3$): δ=4.15 (s, 10H, Fc–H), 4.06 (t, 4H, J=2.0 Hz, H_α), 3.80 (t, 4H, J=2.0 Hz, H_β), 3.72—3.94 (m, 8H, OCH_2CH_2O), 3.64 (s, 12H, OCH_2CH_2O).

Tetraethylene Glycol Diferrocenyl Ether (11b). Yellow crystals, mp 49—51 °C, 86% yield. Found: C, 59.60; H, 6.30%. Calcd for $C_{28}H_{34}O_5Fe$: C, 59.79; H, 6.05%. MS (75 eV): *m/e* 562 (M^+, 100%), 202 (FcOH, 78.2%), and 121 ($C_5H_5Fe^+$, 60.9%). ^{1}H-NMR ($CDCl_3$): δ=4.14 (s, 10H, Fc–H), 4.05 (t, 4H, J=2.0 Hz, H_α), 3.78 (t, 4H, J=2.0 Hz, H_β), 3.72—3.92 (m, 8H, OCH_2CH_2O), and 3.67 (s, 8H, OCH_2CH_2O).

Triethylene Glycol Diferrocenyl Ether (11c). Yellow crystals, mp 87—89 °C, 68% yield. Found: C, 60.35; H, 5.98%. Calcd for $C_{26}H_{30}O_4Fe$: C, 60.28; H, 5.79%. MS (75 eV): *m/e* 518 (M^+, 100%), 202 (FcOH, 46.9%), 121 ($C_5H_5Fe^+$, 57.7%). ^{1}H-NMR ($CDCl_3$): δ=4.16 (s, 10H, Fc–H), 4.06 (t, 4H, J=2.0 Hz, H_α), 3.80 (t, 4H, J=2.0 Hz, H_β), 3.72—3.95 (m, 8H, OCH_2CH_2), and 3.61 (s, 4H, OCH_2CH_2).

Method of Solvent Extraction. Solvent extraction was carried out by the method described by Pedersen.[7] Equal volumes (5 ml) of dichloromethane containing 7×10^{-4} (or 7×10^{-5}) M of **7** and an aq solution containing 1×10^{-1} M MNO_3 (M: metal cations) and 7×10^{-5} M picric acid were agitated throughly at 25 °C. The solution was then

equilibrated at 25 °C, the aliquot of the upper aq solution was withdrawn, and its electronic spectrum was recorded. A similar extraction was performed with pure dichloromethane. The extractability was determined by means of the difference between two absorbances of picrate in the aq solution and by calculating using by the following equation:

$$\text{Extractability} = \frac{A_0 - A}{A_0} \times 100.$$

A_0 is the absorbance in the absence of MNO_3. A is the absorbance in the presence of MNO_3.

The authors wish to acknowledge the assistance given in the experimental work by Mr. Yoichi Habata and Miss Hiroko Ohteki in the experimental work.

References

1) R. E. Izatt and J. J. Christensen, "Synthetic Multidentate Macrocyclic Compounds," Academic Press, New York (1978).
2) S. Akabori, Y. Habata, Y. Sakamoto, M. Sato, and S. Ebine, *Bull. Chem. Soc. Jpn.*, **56**, 537 (1983).
3) S. Akabori, H. Fukuda, Y. Habata, M. Sato, and S. Ebine, *Chem. Lett.*, **1982**, 1393.
4) M. Sato, M. Kubo, S. Ebine, and S. Akabori, *Tetrahedron Lett.*, **23**, 185 (1982).
5) A. N. Nesmeyanov, V. A. Sazonova, and V. N. Drozd, *Chem. Ber.*, **93**, 2717 (1960).
6) C. J. Pedersen, *J. Am. Chem. Soc.*, **89**, 7017 (1967).
7) C. J. Pedersen, *Fed. Proc.*, **27**, 1305 (1968).
8) T.-L. Ho, "Hard and Soft Acids and Bases Principles in Organic Chemistry," Academic Press, New York and London (1977), p. 162.
9) S. Akabori, M. Sato, and S. Ebine, *Synthesis*, **1981**, 278.

Syntheses of Polyoxathia[*n*]ferrocenophanes and Its Extraction Ability with Metal Cations

Sadatoshi AKABORI,* Yoichi HABATA, Masaru SATO,† and Seiji EBINE††

Department of Chemistry, Faculty of Science, Toho University, Funabashi, Chiba 274

† *Chemical Analysis Center, Saitama University, Urawa, Saitama 338*

†† *Department of Chemistry, Faculty of Science, Saitama University, Urawa, Saitama 338*

(Received November 10, 1982)

Mononuclear polyoxathia[*n*]ferrocenophanes (**8a—d**) and binuclear polyoxadithia[*n,n*]ferrocenophanes were synthesized by the reaction of 1,1′-bis(ω-chloropolyethyleneoxy)ferrocene with sodium sulfide in *N,N*-dimethylformamide and the complexing ability of **8a—d** with alkali and transition metal cations was measured by an extraction method. Compound **8d** extracts a thallium ion specifically, the extraction efficiency of several ions being in the order: $Tl^+ \gg Rb^+ > K^+ > Cs^+ > Na^+ > Li^+$.

During the past decade, several papers[1] have described the remarkable interactions between alkali metal ions and crown ethers containing oxygen and heteroatoms. However papers concerned with the complexing ability of transition metal ions by crown ethers are rare.[2] Recently the syntheses of highly functionalized crown ethers have been reported, and in this connection several research groups[3-6] have described the preparation of new-type crown ethers containing a ferrocene unit as a ring member, in which the iron atom may play a role of coordinatable heteroatom. We have previously reported that polyoxa[*n*]ferrocenophanes (**1** and **2**)[7,8] and polyoxathia-[*n*]ferrocenophanes (**3**)[9] exhibit considerably enhanced transition metal cation binding, compared with the corresponding ring-membered crown ethers. In this paper we discuss the syntheses of polyoxathia[*n*]ferrocenophanes (**8**) and polyoxadithia[*n,n*]ferrocenophanes (**9**) and the complexing behavior of **8a—d** with alkali and transition metal picrates.

Syntheses of 8 and 9. It has been reported[7] that the potassium salt of 1,1′-dihydroxyferrocene (**5**), which is obtained from 1,1′-diacetoxyferrocene (**4**), reacts with the dihalide of polyethylene glycol (**6**) to give polyoxa[*n*]ferrocenophane (**1**). This method has been applied to the syntheses of **7**. We first attempted the reaction of ten molar equivalent of **6** with **5** which was obtained by the hydrolysis of **4**. The product, however, was an intractable mixture of unwanted materials and the yield of the desired **7** was very low. Subsequently, we examined the reaction of **4** with **6** in the presence of 18-crown-6 as phase transfer catalyst[10] (Scheme 1) and obtained the corresponding **7** in 26—54% yields together with small amounts of **1** which was formed by the reaction of an equivalent molar quantity of **6** with **4**. The structures of **1a—d** were also determined by the spectral data and admixture with authentic samples.[7] The molecular formula of **7a** was, for example, deduced to be $C_{14}H_{16}Cl_2O_2Fe$ by mass spectroscopy (M^+, *m/e* 342, 344) and elemental analysis. In the ^{1}H-NMR spectrum of **8a**, the resonances for the α- and β-ring protons of ferrocene nucleus appeared as an A_2B_2 pattern at δ=4.05 (t, J=2.0 Hz), and 3.65 (t, J=2.0 Hz), respectively, in addition to the signal of the methylene protons as a multiplet at δ=3.65—4.05 (m, 8H). The IR spectrum of **7** showed ferrocene ring C–H absorption and ether linkage absorption near 1470 and 1110 cm^{-1}, respectively, but no absorption attributable to hydroxy and carbonyl groups. A new series of polyoxathia[*n*]ferrocenophanes (**8**) and polyoxadithia[*n,n*]ferrocenophanes (**9**) were synthesized by the reaction of an equimolar amount of sodium sulfide with dichloride (**7**) in several solvents. Best results were achieved when *N,N*-dimethylformamide (DMF) was used as solvent at refluxing temperature. For example, the reaction of **7b** with sodium sulfide in DMF gave a mixture of mononuclear 1,4,10,13-tetraoxa-7-thia[13]ferrocenophane (**8b**) and binuclear 1,4,10,13,24,27,33,36-octaoxa-7,30-dithia[13,13]ferrocenophane (**9b**) in 22% and less than 1% yields, respectively. However, from the reactions of **7a** and **7d** with sodium sulfide the binuclear **9a** and **9d** could not be isolated. Furthermore, the yields of the products were very low when *t*-butyl alcohol or *t*-butyl alcohol–water (1:1) was used as solvent, although the products were similar. The structures of the products **8a—d**, **9b**, and **9c** were established by their spectral data and elemental analyses. The structures of **8b** and **9b** were confirmed as follows. The molecular formula of **8b** was deduced to be $C_{18}H_{24}O_4SFe$ by elemental analysis and mass spectroscopy (M^+, *m/e* 392). In the ^{1}H-NMR spectrum of **8b**, the resonance for the methylene protons attached to the sulfur atom appeared as a triplet (4H, J=10 Hz) at δ=2.85, in addition to a multiplet (12H, $-CH_2CH_2OCH_2CH_2S-$) at δ=3.65—4.00 and a pair of triplets (each 4H, J=2.0 Hz, Fc–H_α, Fc–H_β) at δ=4.10 and 3.82. The molecular formula of **9b** was also deduced to be $C_{36}H_{48}O_8S_2Fe$ by mass spectroscopy (M^+, *m/e* 748) and elemental analysis. In the ^{1}H-NMR spectrum of **9b**, the resonance for methylene protons attached

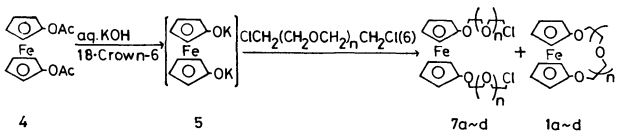

4 5 7a~d 1a~d

a; n=0, b; n=1, c; n=2, d; n=3

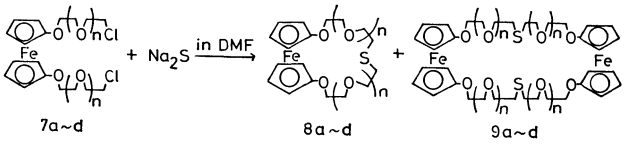

7a~d 8a~d 9a~d

a; n=0, b; n=1, c; n=2, d; n=3

Table 1. Extraction of metal picrates from aqueous to organic phase (%)[a,b]

Compd	Li^+	Na^+	K^+	Rb^+	Cs^+	Tl^+	Ag^+
8a	0.7	0.7	0.5	0.8	0.5	0.8	Decomp
8b	1.2	1.2	1.4	0.8	1.5	8.3	Decomp
8c	0.7	1.4	1.2	3.8	5.1	37.4	Decomp
8d	0.9	2.0	22.5	25.4	20.6	82.1	Decomp
1a	—	1.5	4.5	4.6	5.6	25.2	Decomp
B15C5	1.2	23.9	50.1	27.5	12.8	56.0	33.6

a) Solvents: Water and dichloromethane (equal volumes). b) Ferrocenophane $=7.0\times10^{-4}$ M (1 M = 1 mol dm^{-3}). Picric acid $=7.0\times10^{-5}$ M. Metal nitrate = 0.1 M.

to the sulfur atom appeared as triplet (4H, $J=11$ Hz) at $\delta=2.80$, in addition to a multiplet (24H, $-OCH_2CH_2OCH_2CH_2S-$) at $\delta=3.61$—4.00, a pair of triplets (each 8H, $J=2.0$ Hz, Fc–H_α, Fc–H_β) at $\delta=$ 4.09 and 3.84. The structures of the other new compounds were also determined by similar methods.

Extraction Efficiency of 8a—d. Compounds **8a—d** were tested for extractability with metal ions by the Pedersen method.[11] The data are summarized in Table 1, along with those of **1a** and benzo-15-crown-5. Compounds **8** (except **8d**) showed poor extraction efficiency with alkali metal ions. Furthermore, **8b** showed less extraction efficiency than those of the corresponding ring membered polyoxaferrocenophane (**1a**) with all alkali metal cations except lithium. This is not surprising for the ferrocenophanes since Pedersen[12] has shown that the complexing power of crown ethers for alkali metal ions is largely destroyed by substituting –S– for –O– in the macrocyclic polyether ring. From the HSAB rule[13] it is expected that the incorporation of a sulfur atom (a soft atom) into the macrocycle has a strong influence on the complexing ability with transition metal ions (a soft atom). Indeed, the extraction efficiency of **8** toward thallium ion was remarkably higher than those toward alkali metal ions, although the benzo-crown ether showed a similar extraction efficiency toward any of the cations described above. However, it was shown that the extraction efficiency of **8b** with thallium ion is weaker than that of **1a** which has the same ring member. For silver cation, the extraction efficiency of **8**, especially **8d**, could not be measured because of a rapid decomposition in which the iron atom of ferrocene nucleus might be oxidized by the incorporated silver cation. These results are similar to those of the extraction efficiency of **1** with silver ion.[7] Finally, it is noteworthy that **8d** showed high preference toward transition metal ions and the relationship between the hole size of the host molecule and the size of the guest ions was the second factor. The results seem to be reasonable when considering that the macrocyclic polyethers complex with cations within their very larger rings by wrapping themselves completely arround the cation. These results are similar to those of the complexing ability of macrocyclic antibiotics such as nonactin with metal cations.[14]

Experimental

All melting points are not corrected. ^{1}H-NMR spectra were determined in the indicated solvent on a Hitachi R-90 spectrometer. Chemical shifts are expressed in parts par million downfield from an internal tetramethylsilane. Mass spectra were recorded on a JEOL-OlSG-2 spectrometer and Hitachi M-80 spectrometer at 75 and 70 eV, respectively. Optical spectra were obtained on an Hitachi Model 100-10 spectrometer.

Materials. All solvents and reagents were used as purchased unless otherwise specified. 1,1′-diacetoxyferrocene (**4**) was prepared according to the previously reported method. 1,11-dichloro-3,6,9-trioxaundecane (**6c**) and 1,14-dichloro-3,6,9,12-tetraoxatetradecane (**6d**) were prepared according to the usual method. Silica gel for thin layer chromatography utilized Wakogel B-5F.

1,1′-Bis(3-chloro-1-oxapropyl)ferrocene (7a). 1,1′-Diacetoxyferrocene (**4**) (0.8 g, 2.6 mmol) was added to 10% aq potassium hydroxide solution (10 ml) containing 18-crown-6 (0.2 g, 0.075 mmol) under nitrogen and the mixture was stirred under refluxing. After 20 min a large excess of 1,2-dichloroethane (12 g, 80 mmol) was added at once and the mixture was stirred for 6 h at 80 °C. After the solution was cooled to room temperature, the mixture was extracted with three 20 ml portions of ether. The extracts were combined, washed with water, and concentrated *in vacuo*. The residual oil was chromatographed on a silica gel TLC (acetone–hexane 1:9 as eluent). The first band was extracted with acetone at room temperature, followed by filtration and evaporation of the solvent, to give a yellow oil which solidified on standing. The crude material was recrystallized from hexane to give 1,4-dioxa[4]ferrocenophane (**1a**) in 9% yield; mp 129—131 °C (lit,[7] 129—131 °C). The second band was extracted with acetone at room temperature, followed by filtration and evaporation of the solvent, to give yellow crystals. Recrystallization of the crude material from hexane gave **7a**, mp 58—59.5 °C, in 54% yield. ^{1}H-NMR ($CDCl_3$): $\delta=4.05$ (t, $J=2.0$ Hz, 4H, Fc–H_α), 3.65 (t, $J=2.0$ Hz, 4H, Fc–H_β), 3.65—4.05 (m, 8H, $-OCH_2-CH_2Cl$). MS (75 eV): *m/e* 342 and 344 (M^+). Found: C, 48.98; H, 4.66%. Calcd for $C_{14}H_{16}Cl_2O_2Fe$: C, 49.27; H, 4.66%.

1,1′-Bis(7-chloro-1,4-dioxahexyl)ferrocene (7b). Reaction of **4** (0.8 g, 2.6 mmol) with **6b** (12 g, 75 mmol) by the method described above gave **1b** (2%) and **7b** (53%). **1b**, mp 120—121 °C (lit,[7] 120—121 °C). **7b**, oil, ^{1}H-NMR ($CDCl_3$): $\delta=4.20$ (t, $J=2.0$ Hz, 4H, Fc–H_α), 3.80 (t, $J=$ 2.0 Hz, 4H, Fc–H_β), 3.65—4.07 (m, 16H, $-OCH_2CH_2-OCH_2CH_2Cl$). MS (75 eV): *m/e* 430 and 432 (M^+). Found: C, 49.93; H, 5.89%. Calcd for $C_{18}H_{24}Cl_2O_4Fe$: C, 50.15; H, 5.61%.

1,1′-Bis(9-chloro-1,4,7-trioxanonyl)ferrocene (7c). Reaction of **4** (0.8 g, 2.6 mmol) with **6c** (12 g, 60 mmol) gave **1c** (0.5%) and **7c** (26%). **1c**, mp 58—59 °C. **7c**, oil, ^{1}H-NMR ($CDCl_3$): $\delta=4.12$ (t, $J=2.0$ Hz, 4H, Fc–H_α), 3.89 (t, $J=2.0$, 4H, Fc–H_β), 3.76 (s, 12H, $-OCH_2CH_2O-$), 3.70—3.98 (m, 12H, $-OCH_2CH_2OCH_2CH_2Cl$). MS (75

eV): *m/e* 518 and 520 (M^+). Found: C, 50.63; H, 6.41%. Calcd for $C_{22}H_{32}Cl_2O_6Fe$: C, 50.89; H, 6.21%.

*1,1'-Bis(12-chloro-1,4,7,10-tetraoxadodecyl)ferrocene (**7d**).* Reaction of **4** (0.8 g, 2.0 mmol) with **6d** (12 g, 49 mmol) gave **1d** (0.7%) and **7d** (26%). **1d**, mp 60—61 °C (lit,[7] 60—61 °C). **7d**, oil, ^{1}H-NMR ($CDCl_3$): δ=4.13 (t, J=2.0 Hz, 4H, Fc-H_α), 3.87 (t, J=2.0 Hz, 4H, Fc-H_β), 3.75 (s, 16H, $-OCH_2CH_2O-$), 3.71—4.00 (m, 16H, $-OCH_2CH_2OCH_2CH_2Cl$). MS (75 eV): *m/e* 606 and 608 (M^+). Found: C, 51.57; H, 6.70%. Calcd for $C_{26}H_{40}Cl_2O_8Fe$: C, 51.42; H, 6.64%.

*Reaction of **7a** with Sodium Sulfide in DMF.* To a solution of $Na_2S\cdot 9H_2O$ (0.864 g, 3.6 mmol) in 200 ml of DMF at refluxing temperature was added a solution of **7a** (1.03 g, 3.00 mmol) in 40 ml of DMF under nitrogen. Stirring was continued at refluxing temperature for 20 h, and the reaction mixture was then cooled to room temperature. After evaporation of the solvent, the residue was diluted with water and extracted three times with ether. The combined extracts were washed with water, dried over anhydrous magnesium sulfate, and concentrated. The residual oil was chromatographed on silica gel TLC (dichloromethane: tetrachloromethane 4:1 as eluent). The first band was extracted with acetone at room temperature, followed by filtration and evaporation of the solvent, to give a yellow oil which solidified on standing. The crude material was recrystallized from hexane to give **8a**, mp 104—106 °C, in 66% yield. ^{1}H-NMR ($CDCl_3$): δ=4.20 (t, J=2.0 Hz, 4H, Fc-H_α), 4.14 (t, J=10.0 Hz, 4H, $-SCH_2CH_2O-$), 3.79 (t, J=2.0 Hz, 4H, Fc-H_β), 2.92 (t, J=10 Hz, $-OCH_2CH_2S-$). MS (75 eV): *m/e* 304 (M^+). Found: C, 55.61; H, 5.65%. Calcd for $C_{14}H_{16}O_2SFe$: C, 55.28; H, 5.31%. The second band was extracted with acetone at room temperature, followed by filtration and evaporation of the solvent, to give yellow crystals. Recrystallization of the crude material from hexane gave the starting material, mp 58.5—59.5 °C.

*Reaction of **7b** with Sodium Sulfide in DMF.* Reaction of **7b** (1.29 g, 3.00 mmol) with $Na_2S\cdot 9H_2O$ (0.864 g, 3.60 mmol) in 240 ml of DMF gave a mixture of **1b**, the starting material, and **9b**. After usual work-up, the reaction mixture was chromatographed on silica gel TLC (hexane: acetone 4:1). The first fraction was extracted with acetone, followed by filtration and evaporation of the solvent, to give yellow crystals. Recrystallization of the crude material from hexane gave **8b** as yellow crystals, mp 93—95 °C, in 21% yields. ^{1}H-NMR ($CDCl_3$): δ=4.10 (t, J=2.0 Hz, 4H, Fc-H_α), 3.82 (t, J=2.0 Hz, 4H, Fc-H_β), 3.65—4.00 (m, 12H, $-OCH_2CH_2O-$), and 2.85 (t, J=11 Hz, $-CH_2SCH_2-$, 4H). MS (75 eV): *m/e* 392 (M^+). Found: C, 55.13; H, 6.36%. Calcd for $C_{18}H_{24}O_4SFe$: C, 55.11; H, 6.17%. The second band gave the starting material, oil (8%). The third fraction was extracted with acetone. Evaporation of the solvent gave yellow oil. Crystallization of the crude material from hexane give pure **9b**, mp 108—109 °C, in 0.8% yield. ^{1}H-NMR ($CDCl_3$): δ=4.09 (t, J=2.0 Hz, 8H, Fc-H_α), 3.84 (t, J=2.0 Hz, 8H, Fc-H_β), 3.61—4.00 (m, 24H, $-OCH_2CH_2O-$), 2.80 (t, J=11 Hz, 8H, $-SCH_2CH_2O-$). MS (75 eV): *m/e* 784 (M^+). Found: C, 55.35; H, 6.24%. Calcd for $C_{36}H_{48}O_8S_2Fe$: C, 55.11; H, 6.17%.

*Reaction of **7c** with Sodium Sulfide in DMF.* Reaction of **7c** (1.55 g, 3.00 mmol) with $Na_2S\cdot 9H_2O$ (0.864 g, 3.60 mmol) in 240 ml of DMF gave a mixture of **8c**, **9c**, and the starting material. **8c**, mp 52—53.5 °C, in 30% yield, ^{1}H-NMR ($CDCl_3$): δ=4.09(t, J=2.0 Hz, 4H, Fc-H_α), 3.82 (t, J=2.0 Hz, 4H, Fc-H_β), 3.66 (s, 8H, $-OCH_2CH_2O-$), 3.60—3.95 (m, 12H, $-OCH_2CH_2OCH_2CH_2O-$), 2.79 (t, J=11 Hz, 4H, $-SCH_2CH_2O-$). MS(75 eV): *m/e* 480 (M^+). Found: C, 55.28; H, 6.93%. Calcd for $C_{22}H_{32}O_6SFe$: C, 55.00; H, 6.71%. **9c**, oil, a trace yield, ^{1}H-NMR ($CDCl_3$): δ=4.01 (t, J=2.0 Hz, 8H, Fc-H_α), 3.80 (t, J=2.0 Hz, 8H, Fc-H_β), 3.58 (s, 16H, $-OCH_2CH_2O-$), 3.47—3.80 (m, 24H, $-OCH_2CH_2OCH_2CH_2Cl$), 2.67 (t, J=11 Hz, 8H, $-SCH_2CH_2O-$). MS (75 eV): *m/e* 961 (M^+). Found: C, 55.26; H, 6.90%. Calcd for $C_{44}H_{64}O_{12}S_2Fe$: C, 55.00, H, 6.71%.

*Reaction of **7d** with Sodium Sulfide in DMF.* Reaction of **7d** (1.82 g, 3.00 mmol) with $Na_2S\cdot 9H_2O$ (0.864 g, 3.60 mmol) in 240 ml of DMF gave a mixture of **8d** and the starting material. **8d**, mp 47—48 °C, 38% yield, ^{1}H-NMR ($CDCl_3$): δ=4.10 (t, J=2.0 Hz, 4H, Fc-H_α), 3.83 (t, J=2.0 Hz, 4H, Fc-H_β), 3.69 (s, 16H, $-OCH_2CH_2O-$), 3.56—4.05 (m, 12H, $-OCH_2CH_2O-$), and 2.67 (t, J=11 Hz, 4H, $-SCH_2CH_2O-$). MS (75 eV): *m/e* 568 (M^+). Found: C, 55.23; H, 7.01%. Calcd for $C_{26}H_{40}O_8SFe$: C, 54.94; H, 7.09%.

Extraction Ability. Extraction ability of **8** with metal cations was examined by the method described in the previous paper.[7]

The authors wish to acknowlege the assistance given by Mr. Ribun Turuoka and Sumio Shibahara in the experimental work.

References

1) "Host Guest Complex Chemistry I," ed by F. Vögtle, Springer-Verlag, Perlin, Heidelberg, New York (1981); R. E. Izatt and J. J. Christensen, "Synthetic Multidentate Macrocyclic Compounds," Academic Press, New York (1978).

2) P. B. Chock, *Proc. Natl. Acad. Sci. U.S.A.*, **69**, 1939 (1972). G. W. Liesegang, M. M. Farrow, F. A. Vazguez, N. Purdie, and E. M. Eyring, *J. Am. Chem. Soc.*, **99**, 3240 (1977).

3) G. Oepen and F. Vögtle, *Liebigs Ann. Chem.*, **1979**, 1094.

4) A. P. Bell and C. D. Hall, *J. Chem. Soc., Chem. Commun.*, **1980**, 193.

5) J. F. Biernat and T. Wilczewski, *Tetrahedron*, **36**, 2521 (1980).

6) B. Czech and A. Ratajczak, *Pol. J. Chem.*, **54**, 767 (1980).

7) S. Akabori, Y. Habata, Y. Sakamoto, M. Sato, and S. Ebine, *Bull. Chem. Soc. Jpn.*, **56**, 537 (1983).

8) S. Akabori, H. Fukuda, Y. Habata, M. Sato, and S. Ebine, *Chem. Lett.*, **1982**, 1393.

9) M. Sato, M. Kubo, S. Ebine, and S. Akabori, *Tetrahedron Lett.*, **23**, 2717 (1982).

10) S. Akabori, M. Sato, and S. Ebine, *Synthesis*, **1981**, 178.

11) C. J. Pedersen, *Fed. Proc.*, **27**, 1305 (1968).

12) C. J. Pedersen, *J. Org. Chem.*, **36**, 254 (1971).

13) T.-L. Ho, "Hard and Soft Acids and Bases Principles in Organic Chemistry," Academic Press, New York and London (1977), p. 162.

14) J. H. Prestegard and S. I. Chan, *Biochemistry*, **8**, 3921 (1969); *J. Am. Chem. Soc.*, **92**, 4440 (1970).

Hydroxymethylation and Alkoxymethylation of Methacryloguanamine

Toshihiro SEO,* Kenji ABE, and Toshio KAKURAI

Department of High Polymer Technology, Tokyo Institute of Technology, Ookayama, Meguro-ku, Tokyo 152

(Received October 7, 1982)

The reaction of 2-amino-4-(substituted amino)-6-isopropenyl-1,3,5-triazines (methacryloguanamine) with formaldehyde gave several new monomers having hydroxymethyl groups in satisfactory yields. These monomers were easily converted into the corresponding alkyl ethers with methanol. Their melting points and solubilities were affected considerably by the species and the number of substituted groups. Especially, tetrakis(hydroxymethyl)methacryloguanamine and its methoxymethyl derivative were readily soluble in water and nonpolar solvents, respectively. The former was polymerized and crosslinked smoothly to yield a insoluble polymer. Copolymerization of the latter with methyl methacrylate, however, gave soluble polymers, formed flexible and tough films. Similarly, the reactive polymers were prepared from polymers containing guanamine structure by hydroxymethylation followed by etherification.

Poymers containing amino-1,3,5-triazinyl groups have been investigated as industrial materials and heat-stable polymers. Furthermore, the polymers with aminotriazine units in the side or main chain are expected to have a variety of other properties, such as rigidity, intermolecular interaction, thermal stability and basicity.[1-3]

Recently, 2-amino-4-(substituted amino)-6-isopropenyl-1,3,5-triazines (methacryloguanamine) were readily prepared from methacrylic active esters and biguanides.[4] The syntheses and properties of copolymers of these monomers with styrene, unsaturated carboxylic acid, and their alkyl esters have been studied previously:[1,5] Softening and glass transition temperature rose, specific gravity increased, and solubilities markedly changed with the content of triazine units; copolymers with methacrylic acid were ampholytes.

This paper describes the syntheses of new reactive monomers with hydroxymethyl and methoxymethyl groups, starting from *N*-substituted methacryloguanamines by hydroxymethylation followed by etherification as given below; their polymerization and some properties of both the monomers and the polymers further were investigated. Similarly, the preparation of polymers having pendant highly reactive groups by polymer side reaction will be reported.

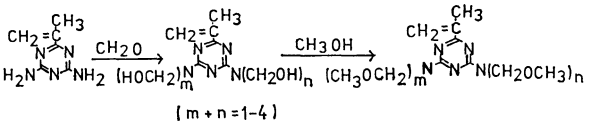

Experimental

Materials. Biguanides were prepared by the method of Kono and Odo[6] or Cohn[7] from dicyanodiamide and the corresponding amines. Formalin (*ca.* 37 wt%), paraformaldehyde, benzoyl peroxide, and DMSO-d_6 were commercial materials. All other reagents and solvents were commercially available and were used after purification if necessary. 2,4-Diamino-(AIPT), 2-amino-4-dimethylamino-(DMAIPT)-, and 2-amino-4-anilino-6-isopropenyl-1,3,5-triazine (AAIPT) were prepared from phenyl methacrylate and biguanides by the procedure described previously.[4]

Procedure. Hydroxymethylation and etherification of *N*-substituted methacryloguanamine were as described below.

2,4-Bis[bis(hydroxymethyl)amino]-6-isopropenyl-1,3,5-triazine (4F-AIPT): A mixture of 2.79 g (18.5 mmol) of AIPT and 12 cm³ of formalin which was adjusted to pH 9.0 with aqueous sodium hydroxide solution, was stirred at 50 °C. This mixture became homogeneous after 2 h and was stirred for another hour. The solution was allowed to stand at room temperature, and concentrated at 5—10 °C using evaporator. To the resulting solution was added 100 cm³ of ether, and colorless crystals (mp 122—124 °C) was obtained in 67.8% yield.

Found: C, 44.07; H, 6.29; N, 26.08%. Calcd for $C_{10}H_{17}N_5O_4$: C, 44.28; H, 6.27; N, 25.83%.

2,4-Bis[bis(methoxymethyl)amino]-6-isopropenyl-1,3,5-triazine (4M-AIPT): A mixture of 2.57 g of 4F-AIPT and 1 cm³ of concd HCl (*ca.* 35 wt%) in 30 cm³ of methanol was stirred at room temperature for 30 min and became clear. After the solution had been neutralized with a methanol solution of potassium hydroxide, and it was concentrated under reduced pressure at 10—20 °C. To the remaining product was added 75 cm³ of water, and the crude product obtained were recrystallized from ether to afford collorless needles (mp 46—47 °C) in 80.0% yield.

Found: C, 50.93; H, 7.89; N, 21.75%. Calcd for $C_{14}H_{25}O_4$: C, 51.38; H, 7.65; N, 21.41%.

Polymerization was carried out in vacuum-sealed ampoules. Methanol or methanol-water solution was used as a precipitant. The composition of compounds were evaluated from the carbon and nitrogen contents.

Measurement. IR, UV, and ^{1}H-NMR spectra were recorded on a Hitachi 285 spectrometer, a Hitachi 139 spectrometer, and a Hitachi R-24B (60 MHz) spectrometer, respectively. DTA experiments were carried out on a Shimadzu thermal analyzer DT-20. Softening temperature was measured with a Shimadzu MM-2 micro-softening apparatus.

Results and Discussion

Hydroxymethylation and Alkoxymethylation of Methacryloguanamines. As shown in Table 1, the reaction of 2,4-diamino-6-isopropenyl-1,3,5-triazine(AIPT) with formaldehyde was carried out at 50 °C for 3 h in the presence of basic catalyst. The observed molar ratio of hydroxymethyl group to AIPT increased with increasing initial molar ratio. Especially, for the molar ratio of 3.0 and 8.0, di- and tetrakis(hydroxymethyl) derivatives were obtained in adequate purity and satisfactory yield, respectively. Moreover, these monomers were easily converted into the corresponding derivatives with a large excess of methanol at room

Table 1. Hydroxymethylation[a] and alkoxymethylation[b] of 2,4-diamino-6-isopropenyl-1,3,5-triazine (AIPT)

Monomer No.	Formalin (cm^3)	Solvent (cm^3)	Ratio F/AIPT	Yield %	Observed[c] F or M / AIPT ratio	N (%)[d] Found (Calcd)
F-AIPT	3.0	Water (6)	2.0	83.4	1.3	36.63
2F-AIPT	4.5	Water (5)	3.0	85.6	2.0	32.40 (33.18)
3F-AIPT	6.0	—	4.0	73.1	3.3	27.40
4F-AIPT	12.0	—	8.0	67.8	4.0	26.08 (25.83)
2M-AIPT	—	Methanol (30)	—	55.6	2.0	29.10 (29.29)
4M-AIPT	—	Methanol (30)	—	80.0	4.0	21.75 (21.41)

a) Conditions; AIPT: 2.79 g (18.5 mmol), at pH 9.0, at 50 °C, for 3 h, F: formaldehyde or hydroxymethyl group. b) Conditions; 2F-AIPT or 4F-AIPT: 9.5 mmol, concd HCl: 1.0 cm^3, at room temp, for 30 min, M: methoxymethyl group. c) Calculated from the carbon and the nitrogen content. d) Calcd % of N are for pure bis- and tetrakis(hydroymethyl), and its methoxy derivatives.

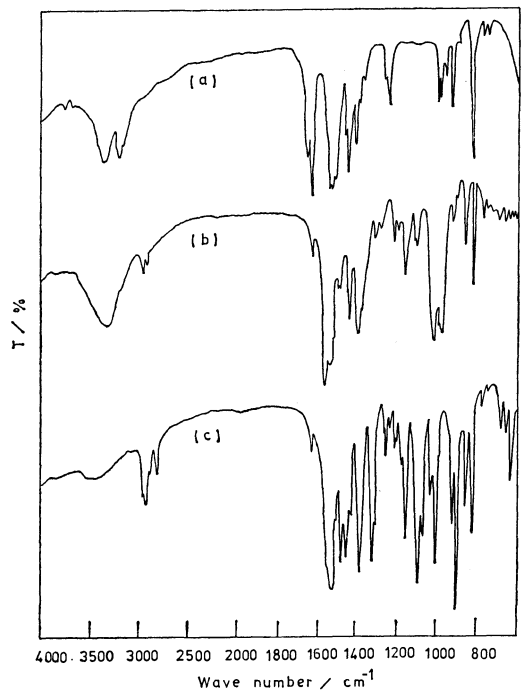

Fig. 1. IR spectra of (a) 2,4-diamino-6-isopropenyl-1,3,5-triazine (AIPT), (b) the tetrakis(hydroxymethyl) derivative (4F-AIPT), and (c) the tetrakis(methoxymethyl) derivative (4F-AIPT).

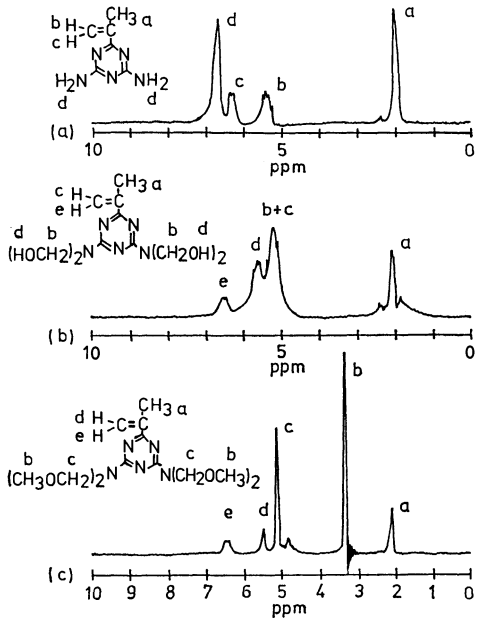

Fig. 2. ^{1}H-NMR spectra of (a) 2,4-diamino-6-isopropenyl-1,3,5-triazine (AIPT) in DMSO-d_6, and (b) the tetrakis(hydroxymethyl) derivative (4F-AIPT) in DMSO-d_6, and (c) the tetrakis(methoxymethyl) derivative (4M-AIPT) in CCl_4.

temperature in the presence of acid catalyst.

The new monomers were identified by elemental analyses, IR, ^{1}H-NMR, and UV spectra. For example, the IR spectra of tetrakis(hydroxymethyl) and tetramethoxy derivatives are shown in Fig. 1. The characteristic bands of isopropenyl-1,3,5-triazine were observed at 830 (the triazine ring), 1640 (the C=C stretching), and 930 cm^{-1} (the C–H bending), whereas the absorption near 1640—1660 cm^{-1} due to the N–H scissoring was rarely detected. In Fig. 1(b) the absorption at 1000 cm^{-1} due to C–O stretching indicates the presence of hydroxymethyl group;[8] the strong absorptions near 2950 and 1110 cm^{-1} are assigned to the C–H stretching and the C–O–C stretching of methoxymethyl group, respectively.

In the NMR spectrum given in Fig. 2(b), the signal at 6.68 ppm due to the protons of NH_2 group is rarely observed, and the appearance of the absorption in the region of 5.1 to 5.5 ppm may be attributed to the methylene protons and the hydroxyl group protons on $N(CH_2OH)_2$; in Fig. 2(c) the singlet signals at 3.35 and 5.16 ppm are due to the absorptions for the methoxyl and methylene protons on $N(CH_2OCH_3)_2$,[8] and the characteristic signals of isopropenyl group are also found at 2.11(CH_3), 5.49 and 6.49 ppm (CH_2=C). The ratio of the absorption intensities of the signals is recognized to be in agreement with the calculated one for pure hydroxymethyl or methoxymethyl derivative.

Table 2 shows that the solubilities of the reactive monomers obtained increased generally with the reduction of melting point (T_m). T_m of the hydroxymethyl derivatives rose 90 to 124 °C with the number of substituents, but became much lower than that of

Table 2. Properties of hydroxymethyl and methoxymethyl derivatives of 2,4-diamino-6-isopropenyl-1,3,5-triazine (AIPT)

Monomer No.	Observed[a] F or M / AIPT ratio	Mp θ_m/°C (Lit)[5]	Solubilities[b] δ 7.4 Hex	7.7 Et_2O	9.1 Bz	9.3 MEK	9.7 DOX	14.5 MeOH	23.4 H_2O	UV (MeOH) λ_{max}/nm ($\varepsilon \times 10^{-3}$)
4M-AIPT	4.0	46—47	++	++	++	++	++	++	+	277 (3.54)
2F-AIPT	2.0	87—90	−	−	+	++	++	++	+	275 (3.05)
F-AIPT	1.3	91—93	−	−	+	++	++	++	+	274 (2.94)
3F-AIPT	3.3	107—108	−	−	±	++	++	++	++	277 (3.18)
4F-AIPT	4.0	122—124	−	−	−	++	++	++	++	278 (3.40)
2M-AIPT	2.0	223—226	−	−	−	−	++	+	−	276 (3.20)
AIPT	—	247—248 (247—248)	−	−	−	−	+	+	±	271 (2.58)

a) F: Hydroxymethyl group, M: methoxymethyl group. b) ++: Readily soluble, +: soluble, ±: soluble at heating, −: insoluble, Hex: hexane, Et_2O: diethyl ether, Bz: benzene, MEK: ethyl methyl ketone, DOX: dioxane, MeOH: methanol, δ: solubility parameter.

Table 3. Hydroxymethylation[b] and alkoxylation[c] of 2-amino-4-(substituted amino)-6-isopropenyl-1,3,5-triazines

Monomer[a] No.	Ratio F/Triazine	Solvent (cm^3)	Yield/%	Observed[d] F or M / Triazine ratio	N (%)[e] Found (Calcd)
F-DMAIPT	8	Water (5)	88.2	1.0	33.17 (33.65)
M-DMAIPT	—	Methanol (30)	98.0	1.0	30.91 (31.53)
F-AAIPT	8	Water (20) / Dioxane (30)	85.1	1.4	26.12
M-AAIPT	—	Methanol (30)	63.0	1.4	24.31

a) Substituent; DMAIPT: 4-dimethylamino, AAIPT: 4-anilino. b) Conditions; DMAIPT or AAIPT: 15.0 mmol, at pH 9.0, at 50 °C, for 8 h, F: formaldehyde or hydroxymethyl group. c) Conditions; F-DMAIPT or F-AAIPT: 12.0 mmol, concd HCl: 1.0 cm^3, at room temp, for 30 min, M: methoxymethyl group. d) Calculated from the carbon and the nitrogen content. e) Calcd % of N are for pure mono(hydroxymethyl) and mono(methoxymethyl) derivatives.

AIPT (248 °C). Then, these derivatives became more soluble in MEK, alcohols and water compared to AIPT; these properties could be related to not only the decrease of intermolecular interaction between aminotriazine rings, but also the increase of intra- and intermolecular hydrogen bonding of hydroxymethyl group to nitrogen atom on the triazine ring.

On the other hand, upon introducing methoxyl groups into the bis(hydroxymethyl) derivative, T_m rose markedly and the solubilities decreased; this may be due to the increase of modelately strong interaction between triazine rings with NH groups.

The tetramethoxy derivative, however, showed noticeable properties: This monomer melts at a very low temperature (47 °C), soluble not only in alchols and water, but also readily soluble in nonpolar solvents such as hexane, benzene, and carbon tetrachloride; this suggests that introduction of four methoxyl groups to AIPT reduces the rigidity of the triazine ring, decreases extremely its intra- and intermolecular interaction,[5] and increases the hydrophobicity as well as the hydrophilicity.

In addition, in the UV spectra, the electron-releasing effect of hydroxymethyl and methoxymethyl groups resulted in a bathochromic shift compared with AIPT; ε values also increased.

Subsequently, as shown Table 3, the reaction of *N*-dimethylamino- (DMAIPT) or *N*-phenylmethacryloguanamine (AAIPT) with excess formaldehyde was performed at 50 °C for 8 h; the molar number of the combined formaldehyde to guanamine, however, was 1.0 and 1.4, respectively. Then, the almost complete conversion of these monomers to their methoxy derivatives occurred during a rapid lapse of time.

Table 4 shows that the reduction of T_m occurred remarkably with hydroxymethylation, and T_m rises significantly again with etherification. The mono(hydroxymethyl) derivative of DMAIPT as well as the tetramethoxy derivative of AIPT exhibited high solubilities in water and nonpolar solvents, in which the corresponding methoxy derivative was insoluble. The hydroxymethyl derivative of AAIPT was more readily soluble in benzene and alcohols than the methoxy derivative, but insoluble in water.

As a result, new reactive monomers were readily prepared from *N*-substituted methacryloguanamine, by hydroxymethylation followed by methoxymethylation; then these monomers differ in the melting points and the solubilities, which are affected markedly by the species and the number of substituents attached to triazine ring.[4]

Table 4. Properties of hydroxymethyl and methoxymethyl derivatives of 2-amino-4-(substituted amino)-6-isopropenyl-1,3,5-triazines

Monomer[a] No.	Observed[b] F or M / Triazine ratio	Mp θ_m/°C (Lit)[5]	Solubilities[c] δ 7.4 Hex	7.7 Et_2O	9.1 Bz	9.3 MEK	9.7 DOX	14.5 MeOH	23.4 H_2O	UV (MeOH) λ_{max}/nm ($\varepsilon \times 10^{-3}$)
F-DMAIPT	1.0	118—119	+	++	++	++	++	++	+	287 (3.07)
M-DMAIPT	1.0	149—151	−	−	−	−	−	++	+	280 (3.19)
DMAIPT	—	191—192 (191—192)	−	+	++	+	++	++	±	288 (2.74)
F-AAIPT	1.4	63— 68	−	−	++	−	++	++	−	252 (18.3)
M-AAIPT	1.4	184—186	−	−	−	−	−	++	−	251 (17.1)
AAIPT	—	174—175 (174—174.5)	−	+	++	+	++	++	−	252 (22.7)

a) Substituent; DMAIPT: 4-dimethylamino, AAIPT: 4-anilino. b) F: Hydroxymethyl group, M: methoxymethyl group. c) ++: Readily soluble, +: soluble, ±: soluble at heating, −: insoluble, δ: solubility parameter.

Table 5. Copolymerization[a] of 2,4-bis[bis(methoxymethyl)amino]-6-isopropenyl-1,3,5-triazine (4M-AIPT) with methyl methacrylate (MMA)

Polymer	4M-AIPT or AIPT in monomer (mol%)	Conversion wt%	4M-AIPT or AIPT in copolymer (mol%)	η_{sp}/C[c] dl g^{-1}	Solubilities[e] δ 9.0 IPA	Bz	10.0 DOX	MCS	12.0 AcA	DMSO	14.5 MeOH	Softening temperature °C
P(4M-AIPT -MMA)	10.4	39.5	24.7	0.48	+	++	++	++	++	++	+	92—97
	20.0	37.8	50.3	0.51	+	++	++	++	++	++	+	118—123
P(AIPT-[b] -MMA)	18.9	48.1	26.7	1.21[d]	−	−	−	±	+	++	−	255—265
	58.3	43.0	52.6	—	−	−	−	−	+	±	−	>300
Poly(MMA)	—	50.2	—	0.63	+	++	++	+	++	+	−	145—155

a) Conditions; [4M-AIPT]+[MMA]=0.40 mol dm^{-3}, [*N*,*N*-dimethylaniline]=[BPO]=2×10^{-3} mol dm^{-3}, in dioxane at 30 °C, for 24 h. b) AIPT: 2,4-Diamino-6-isopropenyl-1,3,5-triazine. c) C=0.30 g/dl, in benzene at 30 °C. d) C=0.30 g/dl, in DMSO at 30 °C. e) ++: Readily soluble, +: soluble, ±: soluble at heating, −: insoluble, IPA: isopropyl alcohol, MCS: Methyl cellosolve, DMSO: dimethyl sulfoxide, δ: solubility parameter.

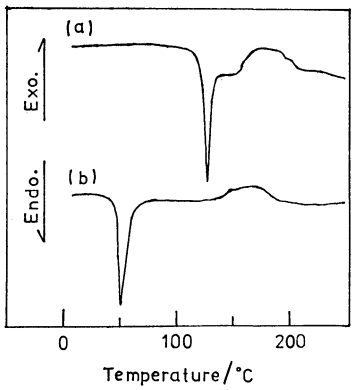

Fig. 3. DTA curves of (a) the tetrakis(hydroxymethyl) derivative (4F-AIPT) and (b) the tetrakis(methoxymethyl) derivative (4M-AIPT), derived from 2,4-diamino-6-isopropenyl-1,3,5-triazine (AIPT) at heating rate of 10 °C/min.

Preparation of Polymers Containing Hydroxymethylguanamines and/or Their Alkyl Ethers. As given in Fig. 3, the tetrakis(hydroxymethyl) derivative (4F-AIPT) melts at 125 °C and exhibited a broad peak near 130—180 °C, which probably corresponds to reaction (condensation and polymerization). Thus, by hot melt at 80—100 °C in aqueous solution, 4F-AIPT was polymerized and crosslinked smoothly to yield an insoluble polymer, having softening temperature (T_s) of over 300 °C; similarly, copolymerizations of 4F-AIPT with methyl methacrylate (MMA), using redox initiator at 30 °C, formed insoluble polymer films, which did not softened up to 300 °C.

On the other hand, the tetramethoxy derivative (4M-AIPT) was relatively stable below 100 °C, but polymerized at 140—160 °C to give a benzene-soluble polymer which softened at 150—155 °C. Moreover, as shown in Table 5, the redox copolymerizations of 4M-AIPT with MMA gave polymers having much lower softening temperature (90—120 °C) than both T_s of the polymer containing AIPT (over 250 °C) and T_s of poly(MMA) (145—155 °C); these polymers showed fair solubilities in not only benzene and dioxane, but also in alcohols and DMSO, and gave a more flexible, tough, and transparent film, compared with the polymer containing AIPT.

Finally, as shown in Table 6, AIPT–MMA copolymer (AIPT content 10.2 mol%) reacted with paraformaldehyde in DMF at 80 °C over basic catalyst to give a crosslinked insoluble polymer with hydroxymethyl groups, having T_s of over 300 °C. Subsequently, hydroxymethylation was carried out at pH 9 using a large excess of paraformaldehyde and butanol at 60 °C, followed by hydroxymethylation at pH 3 with maleic anhydride as acid catalyst. Then, the IR spectra of the product shows the strong absorptions

Table 6. Hydroxymethylation and alkoxymethylation of copolymer of 2,4-diamino-6-isopropenyl-1,3,5-triazine (AIPT) with methyl methacrylate (MMA)

Starting[a] polymer (g)	Paraform-aldehyde (g)	DMF/Butyl alcohol (cm^3/cm^3)	Temp/pH/Time °C / h	Yield g	IR[d] $\tilde{\nu}/cm^{-1}$	Softening temperature °C	Solubilites
1.05	0.30	50/20	80/8/3[b]	1.14	1000, s	>300	Insoluble
1.13	1.70	20/20	60/9/9[b] 60/3/9[c]	1.32	1000, m (CH_2OH) 1100, s (CH_2OBu)	108—113	Readily soluble: IPA, Bz, MEK, DOX, MCS, DMSO
1.80	1.90	50/40	60/9/18[b] 60/3/18[c]	2.05	1000, m 1100, m	105—110	Soluble: DMSO, Acetic acid

a) AIPT-MMA copolymer (triazine content 10.2 mol%); softening temperature: 177—187 °C, soluble: DOX, MCS, DMSO, Acetic acid, Insoluble: IPA, Bz, MEK. b) Hydroxymethylation. c) Butoxymethylation using maleic anhydride as acid catalyst. d) s: Strong intensity, m: medium intensity.

near 1110 cm^{-1} (CH_2OBu) and 1000 cm^{-1} (CH_2OH), and the C(%)/N(%) value (10.4) became much larger than that of starting polymer (8.6); the polymer probably contains 10 mol% of triazine rings having two butoxymethyl groups and one hydroxymethyl group as pendants. The properties of this polymer, therefore, are very similar to that of the above-mentioned copolymers containing more than 25 mol% of triazine rings with four methoxyl groups; the polymer obtained, which softened at 108—113 °C, dissolved freely in 2-propanol, benzene, and MEK, whereas the starting polymer, having T_s of 177—187 °C, was insoluble in these solvents. A longer reaction period gave a flexible polymer, film, soluble only in DMSO or organic acid, maybe due to the intramolecular crosslinking reaction.

In conclusion, the reactive polymers containing hydroxymethyl and/or alkoxymethylguanamines were readily prepared both by polymerization of the suitable monomers and by polymer side reaction. Their properties were greatly affected by the species of substituents and the composition of the polymer;[5] these effects can be based upon not only the rigidity of triazine rings and the flexibility of substituents, but also their intra- and/or intermolecular interactions and reactivities.

In addition, these polymers are thermally crosslinkable with or without acid catalyst. Therefore, the above monomers and polymers having highly reactive groups may be utilized as a crosslinking agent for thermosetting resin or an adhesive as well as a modifier for improved properties of various polymers.

The authors wish to thank Mr. T. Saito of Tokyo Institute of Technology for his elementary analysis.

References

1) Y. Yuki, H. Mutsujika, and K. Kito, *Kobunshi Ronbunshu*, **36**, 385 (1979); T. Seo, T. Kanai, and T. Kakurai, *Nippon Kagaku Kaishi*, **1981**, 1013; T. Seo, T. Hoga, and T. Kakurai, *ibid.*, **1982**, 485.

2) T. Seo, H. Ishiwata, and T. Kakurai, *Nippon Kagaku Kaishi*, **1980**, 87.

3) T. Seo, H. Ishiwata, and T. Kakurai, *Nippon Kagaku Kaishi*, **1974**, 2419; T. Seo, H. Okamoto, and T. Kakurai, *ibid.*, **1975**, 165.

4) T. Seo, Y. Aoki, and T. Kakurai, *Nippon Kagaku Kaishi*, **1980**, 342.

5) Y. Yuki, T. Kakurai, and T. Noguchi, *Bull. Chem. Soc. Jpn.*, **43**, 2123 (1970); T. Seo and T. Kakurai, *ibid.*, **55**, 2942 (1982).

6) K. Kono and K. Odo, *Yuki Gosei Kagaku Kyokai Shi*, **20**, 649 (1962).

7) G. Cohn, *J. Prakt. Chem.*, **84**, 394 (1911).

8) T. Uragami and M. Oiwa, *Bull. Chem. Soc. Jpn.*, **42**, 2426 (1969).

 © 1983 The Chemical Society of Japan Bull. Chem. Soc. Jpn., 56, 1467—1475 (1983)

The Synthesis of Tetrakisdehydrotetraazaannulenes. Tetramethyl[36]-, -[48]annulene, and Their Benzoannelated Derivatives

Jūro Ojima,* Mitsuru Kirita, Yoshiko Murosawa, and Tetsuya Nakada

Department of Chemistry, Faculty of Science, Toyama University, Gofuku, Toyama 930

(Received October 13, 1982)

The conjugated mono-, di-, tri-, and tetraene, containing a terminal acetylene group were converted into a variety of symmetrical and unsymmetrical conjugated azines on treatment with aqueous hydrazine in ethanol. Oxidative couplings of these azines were attempted using anhydrous copper(II) acetate in pyridine and ether. Each of unsymmetrical azines, 3,16-dimethyl-8,9-diaza-3,5,7,9,11,13,15-octadecaheptaene-1,17-diyne and 1,10-bis(*o*-ethynylphenyl)-4,5-diaza-1,3,5,7,9-decapentaene, gave the corresponding two isomeric cyclic dimers: The former gave 7,12,25,30-tetramethyl-8,10,26,28-tetrakisdehydro-1,2,17,18-tetraaza[36]annulene and 7,12,25,30-tetramethyl-8,10,26,28-tetrakisdehydro-1,2,19,20-tetraaza[36]annulene, and the latter gave 6,7:12,13:24,25:30,31-tetrabenzo-8,10,26,28-tetrakisdehydro-1,2,17,18-tetraaza[36]annulene and 6,7:12,13:24,25:30,31-tetrabenzo-8,10,26,28-tetrakisdehydro-1,2,19,20-tetraaza[36]annulene, although only in poor yields. Coupling of symmetrical azines, 3,22-dimethyl-12,13-diaza-3,5,7,9,11,13,15,17,19,21-tetraeicosadecaene-1,23-diyne and 1,16-bis(*o*-ethynylphenyl)-8,9-diaza-1,3,5,7,9,11,13,15-hexadecaoctaene, furnished cyclic dimers, 11,16,35,40-tetramethyl-12,14,36,38-tetrakisdehydro-1,2,25,26-tetraaza[48]annulene and 10,11:16,17:34,35:40,41-tetrabenzo-12,14,36,38-tetrakisdehydro-1,2,25,26-tetraaza[48]annulene, respectively, in moderate yields. Examination of ^{1}H NMR spectra indicates that these tetraazaannulenes are atropic.

In 1974, Yamamoto and Sondheimer attempted oxidative couplings of conjugated azines **1a—c** using copper(II) acetate monohydrate in pyridine and ether under relatively dilute conditions in order to obtain the corresponding monomeric and/or dimeric cyclic compounds, which are macrocyclic analogs of pyridazine (**2**) and 1,2,4,5-tetrazine (**3**), respectively.[1] They obtained cyclic dimer **4**, a higher analog of **3**, only from azine **1b**. Subsequently, Darby *et al.* found that oxidative coupling of terminal diacetylenes to macrocyclic 1,3-diacetylenes usually proceeds in good yield when anhydrous copper(II) acetate instead of the monohydrate is employed.[2] We used advantageously the conditions for oxidative couplings of symmetrical conjugated, methylated azines **12**, **14**, **16** and their benzoannelated azines **24**, **26**, **28**. In practice, cyclic dimers **5** and **6** were obtained from azines **14** and **26**, respectively, as similarly as **4** formed from azine **1b**, and further we could also obtain cyclic dimer **7** from azine **16**.[3] However, we could not obtain monomeric cyclic compounds corresponding to higher analogs of pyridazine (**2**) from these azines even under the conditions reported by Darby *et al.*,[2] as well as under several different conditions. Thus, the failure of attempts to obtain monomeric compounds from these azines led us to consider the following.

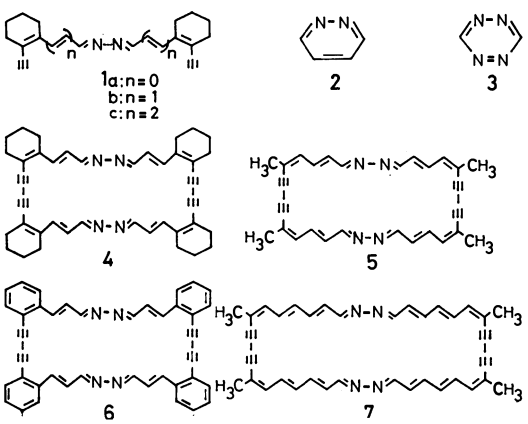

Firstly, oxidative couplings should be attempted under high dilution conditions in order to obtain monomers from azines. Secondly, if symmetrical azines would be converted into the corresponding monomers, preparation of unsymmetrical azines available from aldehydes **8—11** and **20—23** is worthwhile, since we had it in mind that the unsymmetrical azines (**13**, **17**, **18**, **25**, **29**, **30**) make formally a potentially aromatic $(4n+2)\pi$-electron system on their intramolecular cyclization, in contrast that the symmetrical azines (**12**, **14**, **16**, **19**, **24**, **26**, **28**, **31**) do a nonaromatic $4n\pi$-system. This paper is concerned with synthesis and properties of title compounds together with attempts of oxidative couplings of symmetrical and unsymmetrical azines **12—19** and **24—31**, prepared from aldehydes **8—11** and **20—23**.

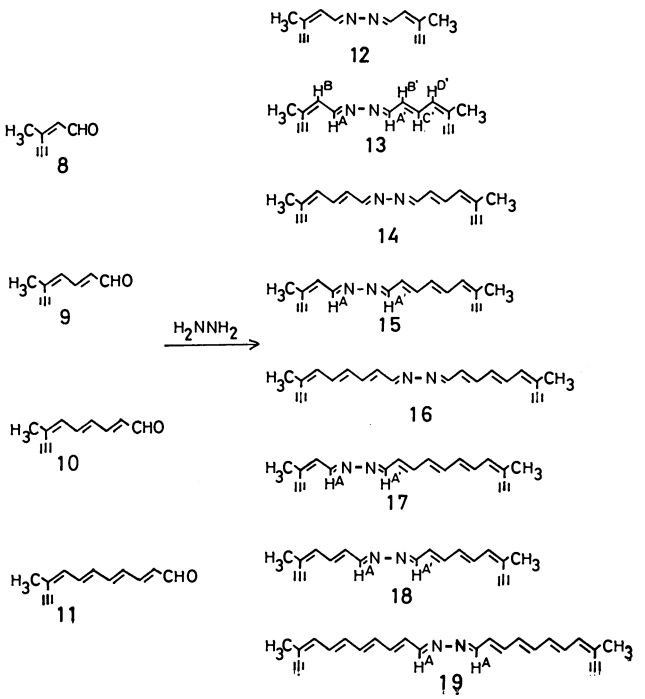

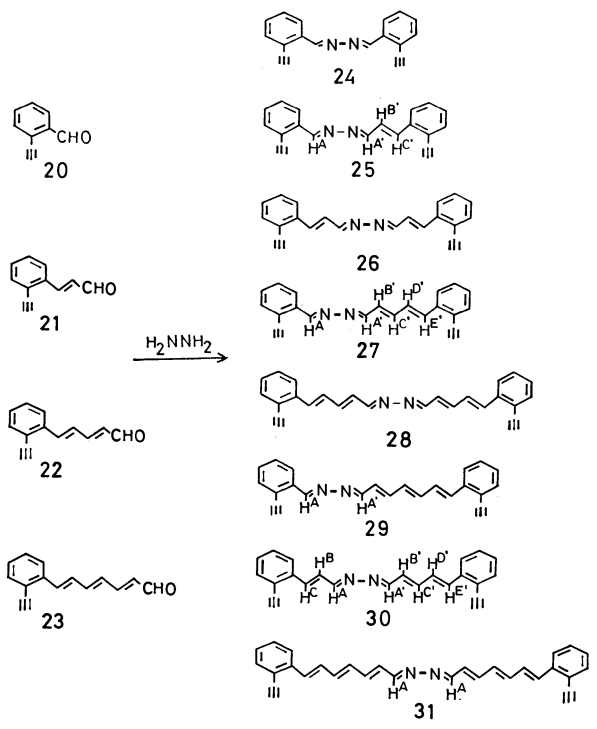

Results and Discussion

For preparation of azines **12**—**19**, a large amount of aldehydes **8**—**11** were required. Therefore, reported procedures[3,4] of preparation of aldehydes **9** and **10** were reexamined, since yields were variable (20—80% in different experiments on **8** and 15—55% in those on **9**). The starting material was (*Z*)-3-methyl-2-penten-4-ynal (**8**), which was prepared by acid treatment of 1-chloro-3-methyl-1-penten-4-yn-3-ol.[5] A homologation of **8** to (2*E*,4*Z*)-5-methyl-2,4-heptadien-6-ynal (**9**)[4] as well as a further homologation of **9** to (2*E*,4*E*,6*Z*)-7-methyl-2,4,6-nonatrien-8-ynal (**10**)[3] was modified, according to the procedure of that of (*Z*)-3-*t*-butyl-2-penten-4-ynal reported by Iyoda *et al.*[6] Isolation of diethyl acetal of **8**, condensation of the acetal with ethyl vinyl ether in the presence of boron trifluoride etherate, and then hydrolysis of the condensate with aqueous acetic acid containing sodium acetate gave the dienyne aldehyde **9** in 64% yield. The aldehyde **9** was then homologated to the trienyne aldehyde **10** in 70% yield in a similar manner to that of **8** to **9**, except without isolation of diethyl acetal of **9** (Experimental). Thus, modification of a reported procedure could be adapted to preparation of a large amount of aldehydes **9** and **10**.

For preparation of benzoannelated azines **24**—**31**, the starting material was *o*-ethynylbenzaldehyde (**20**), which was prepared as reported.[8] A homologation of **20** to **21**,[9] and subsequent homologations of **21**[10] to **22**[11] were carried out by Wittig condensation with [(1,3-dioxolan-2-yl)methyl]triphenylphosphonium bromide and lithium ethoxide, followed by hydrolysis, as reported previously.

Treatment of aldehydes **8**—**11** and **20**—**23** in ethanol with aqueous hydrazine yielded the corresponding symmetrical azines **12**, **14**, **16**, **19**, **24**, **26**, **28**, **31**, respectively, as described previously.[3] Similarly, combination of two different aldehydes in each group of **8**—**11** and **20**—**23** in place of only one yielded a variety of unsymmetrical azines **13**, **15**, **17**, **18**, **25**, **27**, **29**, **30**. As expected in formation of unsymmetrical azines, the product was admixed with two different symmetrical azines: For formation of **13**, **12**, and **14** were also formed. Careful chromatography on alumina resulted in an almost complete separation of three azines. The yields and melting points of these unsymmetrical azines are summarized in Table 1, altogether with those of symmetrical azines **19** and **31**.

Table 1. Yields and melting points of azines

Compd	Yield %	Mp θ_m/°C
13	23	137—138 (decomp)
15	19	132—133 (decomp)
17	22	100—101 (decomp)
18	46	172—173 (decomp)
19	39	238—240 (decomp)
25	41	136—137
27	30	141—142
29	43	143—144
30	23	136—137
31	54	278—279 (decomp)

Oxidative couplings of these azines were attempted. At first, in order to obtain monomeric cyclic compounds from symmetrical azines **12**, **14**, **16**, an attempt was made under high dilution conditions. Thus, very slow addition of **12** was done to a stirred solution of anhydrous copper(II) acetate in a large volume of pyridine, ether, and methanol (*ca.* 2000 ml, 500 ml, 500 ml). After careful work up of the reaction mixture, the product was chromatographed on alumina. However, no monomeric and dimeric compounds were obtained. Oxidative couplings of azines **14** and **16** under high dilution conditions were carried out similarly to that of azine **12**. Neither azines **14** nor **16** gave monomers, but the respective dimers **5** and **7** in lower yields than in those under the conditions reported previously.[3]

These results led us to consider it impossible to obtain monomeric cyclic compounds from the other azines even if high dilution conditions would be used. Therefore, we turned out to investigate thereafter oxidation of azines, summarized in Table 1, using anhydrous copper(II) acetate in pyridine and ether at 50 °C under relatively dilute conditions as reported by Darby *et al.*[2]

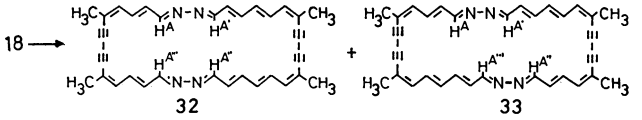

Among the unsymmetrical methylated azines, none of **13**, **15**, and **17** gave monomeric and dimeric cyclic compounds in attempted oxidative couplings. On the other hand, an oxidative coupling of azine **18** resulted in a mixture of cyclic dimers in a yield of 3.5%, which,

upon chromatography on alumina, yielded a high melting isomer and a low melting isomer in a ratio of *ca.* 3:1. As the isomerism can reasonably be attributed to positional isomers due to two azine groups in tetrakisdehydro[36]annulene system, we tentatively assigned a high melting isomer to 7,12,25,30-tetramethyl-8,10,26,28-tetrakisdehydro-1,2,17,18-tetraaza-[36]annulene (**32**) and a low melting isomer to 7,12,25,30-tetramethyl-8,10,26,28-tetrakisdehydro-1,2,19,20-tetraaza[36]annulene (**33**). Both **32** and **33** were obtained as microcrystalline purple powders, and decomposed on exposure to diffused light and air within 1—2 d, and did at 144 °C and 112 °C, respectively, on attempted melting point determination. The gross structure of **32** and **33** was supported by mass spectra, which showed molecular ion peaks at *m/e* 520. The infrared spectra of **32** and **33** exhibited maxima at 2180 and 2190 (–C≡C–), 1615 and 1620 (C=N), respectively, and 995 cm^{-1} (*trans* C=C), but no maxima at −3300 cm^{-1} due to a terminal acetylene. The electronic spectra of both **32** and **33** in tetrahydrofuran, illustrated in Fig. 1, altogether with those of tetramethyl[32]- **5** and -[40]annulene **7**, showed main maxima at the same wavelength, 367 nm, which is middle

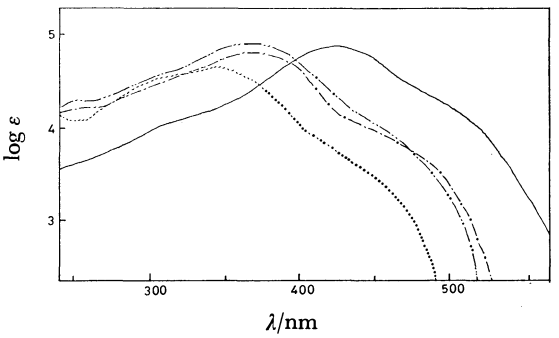

Fig. 1. Electronic spectra of tetraazatetrakisdehydroannulenes **5** (----), **32** (————), **33** (————————), and **7** (——) in THF.

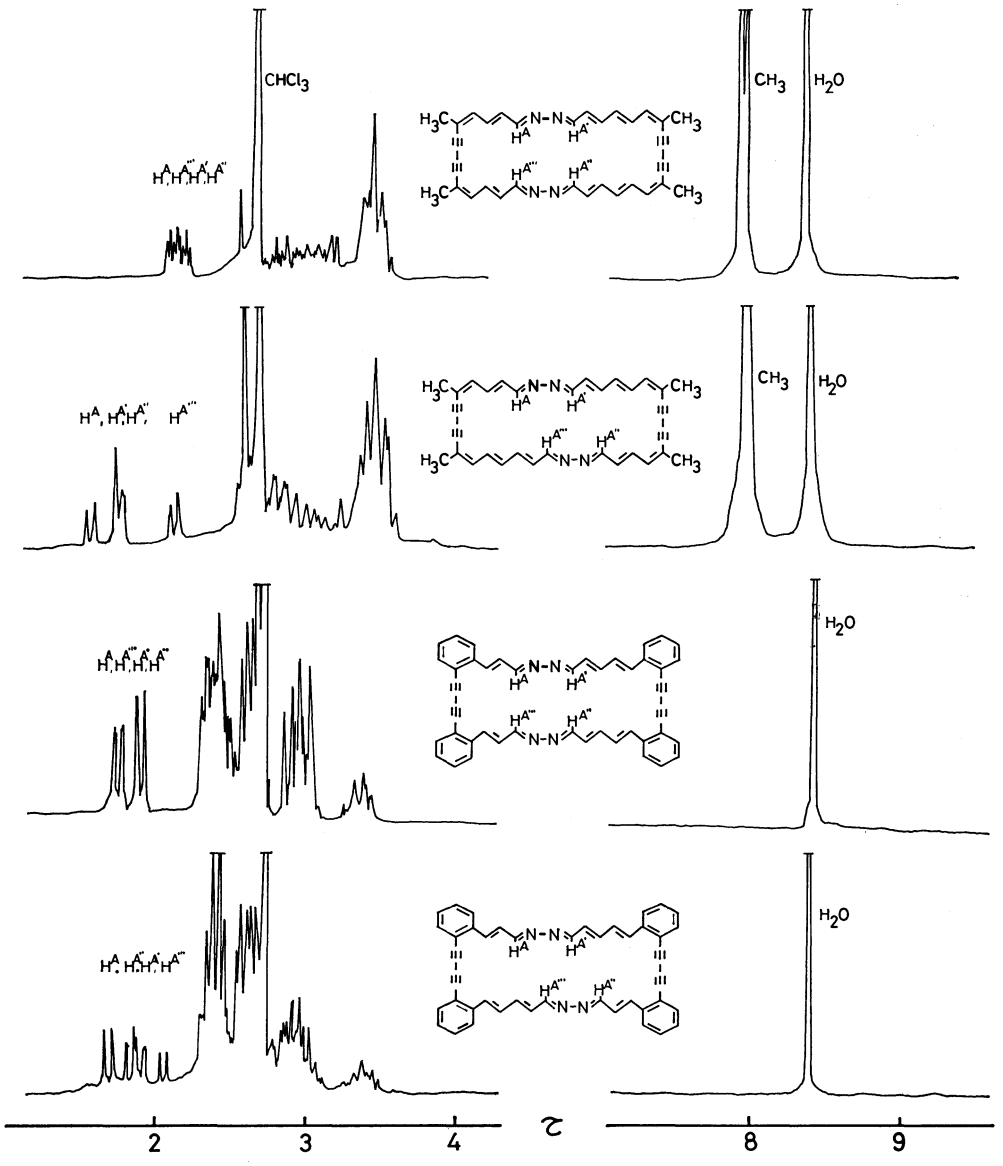

Fig. 2. The ^1H NMR FT spectra of **32**, **33**, **38**, and **39** in $CDCl_3$ at 200 MHz (internal standard, TMS).

one of the main maxima observed in **5** (339 nm) and **7** (381 nm), reflecting the number of double bonds in the cyclic conjugated system.

The ^{1}H NMR spectra were taken in $CDCl_3$ at 200 MHz, and are reproduced in Fig. 2. In these ^{1}H NMR spectra of cyclic tetraazaannulene system, it has been found that only protons adjacent to nitrogen atom resonate at relatively low field among olefinic protons. In annulenes **5** and **7** the protons (H^A) resonate at τ 2.30 and 2.03, respectively.[3] The spectrum of **32** consists of signals of τ 2.14 (1H, d, J=9 Hz, H^A), 2.16 (1H, d, J=9.5 Hz, $H^{A'''}$), 2.23 (1H, d, J=9.5 Hz, $H^{A'}$), 2.26 (1H, d, J=9 Hz, $H^{A''}$), *ca.* 2.6—3.6 (m, olefinic H), 7.98 (6H, s, Me), and 8.01 (6H, s, Me). On the other hand, the spectrum of **33** showed signals at τ 1.59 (1H, d, J=9.5 Hz, H^A), 1.77 (1H, d, J=9.5 Hz, $H^{A''}$), 1.78 (1H, d, J=10 Hz, $H^{A'}$), 2.14 (1H, d, J=10 Hz, $H^{A'''}$), *ca.* 2.6—3.6 (m, olefinic H), 8.00 (3H, s, Me), and 8.03 (3H, s, Me). Thus, the spectrum of **32** exhibits four doublets due to olefinic protons adjacent to nitrogen in narrow region and in high field as compared with those of the corresponding protons of **33**, although we have no explanation for these observations.

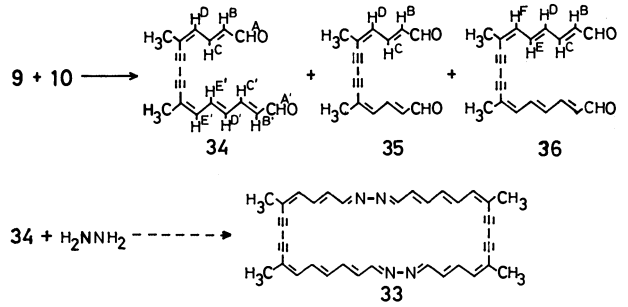

We attempted the following chemical means to determine which isomer should be assigned to the structure **33**. If the reaction similar to that of preparation of azines, between hydrazine and dialdehyde **34** would occur, an expected cyclic product have the structure **33** which is identical to that of one of the two isomers from azine **18**, eliminating the structure **32**. For this aim we prepared the pentaenediynedial **34**. The dialdehyde **34** was obtained in 25% yield from **9** and **10** by oxidative coupling, admixed with tetraenediynedial **35** and hexaenediynedial **36**. The dialdehyde **34** thus obtained was subjected to a reaction with aqueous hydrazine in ethanol. However, no evidence for the presence of the same product as that obtained from azine **18** was detected. Thus, although we could not elucidate the exact structual assignment between **32** and **33**, we believe that the isomer which shows four doublets at very narrow region (τ 2.14—2.26) in its ^{1}H NMR spectrum, has the structure of **32** as described above, from comparison with ^{1}H NMR spectra of annulenes **5** and **7**.

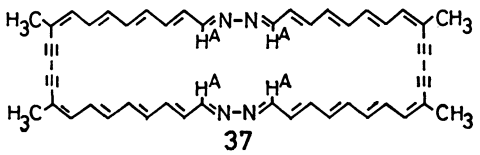

The azine **19** gave cyclic dimer, 11,16,35,40-tetramethyl-12,14,36,38-tetrakisdehydro-1,2,25,26-tetraaza-[40]annulene (**37**), on oxidation in 20% yield. The dimeric structure **37** was established by mass spectrum. The mass spectral measurement of **37** using direct inlet system was not satisfactory owing to decomposition during measurement. However, the spectrum by a field desorption technique was satisfactory one, revealing a molecular ion peak at *m/e* 676 (mol wt, 676). The electronic spectrum of **37** showed main maximum at 420 nm, exhibiting a bathochromic shift by 39 nm as compared with that of [40]annulene **7**. The ^{1}H NMR spectrum of **37** showed only one doublet at τ 1.98 due to olefinic protons (H^A) adjacent to nitrogen, revealing a symmetrical structure of **37**, a multiplet at τ 2.2—3.5 due to other olefinic protons, and a singlet at τ 8.04 due to methyl protons.

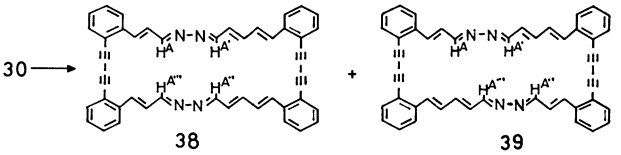

We carried out oxidative couplings of benzoannelated unsymmetrical azines **25**, **27**, **29**, **30** and symmetrical azine **31** under the same conditions as those for methylated azines. When these were done, we expected a stabilizing effect due to fused benzene rings on products of these reactions. However, we could not also obtain cyclic dimers from azines **25**, **27**, **29**, similarly to the cases of the corresponding methylated azines **13**, **15**, **17**. On the other hand, as in the case of the corresponding methylated azine **18**, azine **30** gave two cyclic dimers **38** and **39** in better yield (17%) than in that of **32** and **33** from azine **18**. The molecular weight of both **38** and **39** could not be determined by mass spectra owing to their low volatility. The structual assignment of **38** and **39** follows from examination of their IR, ^{1}H NMR, and electronic spectra, given in Experimental section. Both **38** and **39** showed main maxima at the same wavelength (355 nm) in tetrahydrofuran, as similarly to those observed in both **32** and **33**. The ^{1}H NMR spectra of **38** and **39**, illustrated in Fig. 2, resembled those of **32** and **33**, and the chemical shifts of H^A, $H^{A'}$, $H^{A''}$, $H^{A'''}$ protons are closer between **38** and **39** than between **32** and **33**.

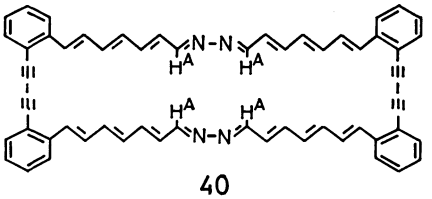

Azine **31** afforded cyclic dimer **40**. The very low solubility and involatility of compound **40** prevented a complete characterization, but UV and ^{1}H NMR spectral data supported the structure **40**.

The chemical shifts of olefinic and methyl protons of the annulenes **32**, **33**, **37**, **38**, **39**, **40** indicates that these annulenes are atropic molecules.

In conclusion, oxidative couplings of conjugated azines **12**—**19** and **24**—**31** did not furnish cyclic monomers, but cyclic dimers in some cases. It was found that a possibility to obtain cyclic dimers is high from symmetrical azines than from unsymmetrical ones.

Experimental

All boiling and melting points are uncorrected. IR spectra were measured on Hitachi 260-50 spectrophotometer as KBr disk unless otherwise stated; only significant maxima are reported. Electronic spectra on Hitachi 124 or Hitachi 220 A spectrophotometer were recorded in nm, in tetrahydrofuran solution. The ε-values are given in parentheses, the shoulder being denoted by sh. Mass spectra were measured with JEOL JMS-200 spectrometer at 75 eV using a direct inlet system or JMS-D spectrometer equipped with field desorption system. ^{1}H NMR spectra were taken on Varian EM-390 (90 MHz) or Varian XL-200 (200 MHz) spectrometer, and refer to solution in $CDCl_3$, in τ-values with TMS as an internal standard. The coupling constants (J) are given in Hz. The individual assignments are made on the basis of multiplicities and coupling constants. Alumina (II—III) was used for column chromatography. Progress of most reactions was followed by TLC using Merck precoated alumina. Preparative TLC was carried out on 20×20 cm alumina plates (Merck, 0.5 or 2 mm thick). Evaporation of solvents was performed at water aspirator pressure, and sodium sulfate was used as drying agent unless otherwise specified.

Diethyl Acetal of (2Z)-3-Methyl-2-penten-4-ynal (8). This compound was prepared by a slight modification of the reported procedure.[5b] A mixture of 3-methyl-2-penten-4-ynal (**8**)[5] (37.8 g, 0.40 mol), ammonium nitrate (3.0 g), and triethyl orthoformate (50.0 g, 0.38 mol) in abs ethanol (105 ml) was heated under reflux for 2 min. Then the mixture was poured onto dilute aq ammonia and extracted with benzene. The extracts were washed with dilute aq ammonia, and passed through Hyflo Super-Cel. The filtrate was concentrated to one-fourth its original volume and the concentrate was mixed with saturated aq sodium hydrogensulfite soln (440 ml). The mixture was stirred for 30 min at room temp. Then the mixture was passed through Hyflo Super-Cel and the precipitates formed were washed with benzene. The filtrate was washed with aq sodium chloride soln and dried over potassium carbonate. After removal of solvent, the residual dark red liquid was distilled, giving diethyl acetal of **8** (42.9 g, 69%) as a colorless liquid; bp 81 °C/19 mmHg** (lit,[5b] 59%, 77 °C/12 mmHg), MS *m/e* 168 (M^+, 37%) and 123 (100); mol wt 168.2; IR (neat) 3300 (-C≡CH), 2100 (-C≡C-), 1135, and 1060 cm^{-1} (C-O-C); ^{1}H NMR (90 MHz) τ=4.18 (d, 8, 1H, olefinic H), 4.70 (d, 8, 1H, $-C\underline{H}(OCH_2CH_3)_2$), *ca.* 6.2—6.5 (m, 4H, $-C\underline{H}_2CH_3$), 6.80 (-C≡CH), 8.07 (s, 3H, CH_3), and 8.78 (t, 7, 6H, $-CH_2C\underline{H}_3$).

(2E,4Z)-5-Methyl-2,4-heptadien-6-ynal (9). This compound was prepared with a modification of the previously described method.[4] To a soln of diethyl acetal of **8** (33.1 g, 0.20 mol) in dry benzene (244 ml) was added a soln of boron trifluoride etherate (243 mg) in dry benzene (12 ml) at 37 °C with stirring, and then a soln of ethyl vinyl ether (17.2 g, 0.24 mol) in dry benzene (63 ml) was added slowly dropwise during 1.5 h at 38—40 °C with stirring. After the mixture had been stirred at the same temp for 2 h, finely powdered potassium carbonate (22.5 g) was added. The inorganic material was removed by filtration and washed with ether. Then the filtrate was added to a mixture of sodium acetate trihydrate (104 g), water (66 ml), and acetic acid (1420 ml), and the soln was stirred under reflux for 3 h. After cooling, the reaction mixture was poured onto water and extracted with benzene. The combined extracts were washed with water, aq sodium hydrogencarbonate, and aq sodium chloride soln successively, and dried. After removal of solvent, the residual red liquid was chromatographed on alumina (200 g). The fractions eluted with hexane gave the aldehyde **9** (21.7 g, 92%, 64% based on **8**) as a red liquid. For spectral properties of **9**, see Ref. 4.

(2E,4E,6Z)-7-Methyl-2,4,6-nonatrien-8-ynal (10). This compound was prepared with a modification of the previously described method.[3] To a mixture of the dienyne aldehyde **9** (10.0 g, 83.2 mmol) and triethyl orthoformate (150 g, 0.91 mol) was added a soln of *p*-toluenesulfonic acid monohydrate (2.0 g) in abs ethanol (20 ml). After being stirred at room temp overnight, the reaction mixture was poured onto aq sodium hydrogencarbonate soln, and extracted with benzene. The extracts were washed with aq sodium hydrogencarbonate and sodium chloride soln, and dried over potassium carbonate. Evaporation of solvent yielded a crude diethyl acetal of **9** as a red liquid. The liquid was dissolved in dry benzene (100 ml) and warmed to 35 °C in a flask equipped with a dropping funnel, a condenser, and a magnetic stirrer. A soln of boron trifluoride etherate (238 mg) in dry benzene (7.5 ml) was added, and then a soln of ethyl vinyl ether (7.0 g, 97 mmol) in dry benzene (25 ml) was added during 3 h with stirring at 35—37 °C. After the mixture had been stirred for a further 1.5 h at the same temp, finely powdered potassium carbonate (22.0 g) was added. The inorganic material was removed by filtration and washed with ether. Then a mixture of the filtrate, sodium acetate trihydrate (33.0 g), acetic acid (493 ml), and water (23 ml) was heated under reflux with stirring at 79—80 °C for 3 h, and then allowed to cool to room temp. The mixture was poured onto aq sodium chloride soln and extracted with benzene. The extracts were washed successively with aq sodium hydrogencarbonate and aq sodium chloride soln, and dried. The residue obtained on evaporation of solvent was chromatographed on alumina (120 g). The fractions eluted with 10% ether in hexane yielded the trienyne aldehyde **10** (8.50 g, 70%, lit,[3] 50%) as an unstable red solid. For spectral and physical properties, see Ref. 3.

(2E,4E,6E,8Z)-9-Methyl-2,4,6,8-undecatetraen-10-ynal (11). This compound was prepared from **10** by Wittig condensation with [(1,3-dioxolan-2-yl)methyl]triphenylphosphonium bromide and lithium ethoxide, followed by hydrolysis with dilute hydrochloric acid, as reported previously.[7]

3,12-Dimethyl-6,7-diaza-3,5,7,9,11-tetradecapentaene-1,13-diyne (13). A soln of **8** (3.1 g, 33 mmol) and **9** (4.0 g, 33 mmol) in ethanol (98 ml) was added dropwise during 1.5 h to a stirred soln of hydrazine sulfate (5.0 g), sodium carbonate (6.1 g), and water (105 ml) at 12—19 °C. The mixture was stirred for a further 40 min at 17—18 °C. Then the mixture was poured onto aq sodium hydrogencarbonate soln and extracted with benzene. The extracts were washed with aq sodium hydrogencarbonate soln and dried over potassium carbonate. The residual dark red liquid, after solvent removal, was chromatographed on alumina (150 g). The early fractions eluted with hexane–ether (4:1—3:2) gave azine **12**[3] (1.58 g, 26%). The following fractions eluted with hexane–ether (2:3) gave azine **13** (1.59 g, 23%) as a solid. Recrystallization from hexane–benzene afforded yellow leaflets: mp 137—138 °C (decomp); MS *m/e* 210 (M^+, 80%) and 195 (100); mol wt 210.3; IR 3200 (-C≡CH),

**1 mm Hg≈133.322 Pa.

2150 (-C≡C-), 1615 (C=N), 1585 (C=C), 980, and 960 cm^{-1} (*trans* C=C); UV_{max} 273 (2860), 308 sh (9880), 326 sh (20000), 338 (23800), 353 (24800), and 370 nm (16200); ^1H NMR (90 MHz) τ=1.37 (d, 10, 1H, H^A), 1.73 (d, 10, 1H, $H^{A'}$), 2.78 (dd, 15, 11, 1H, $H^{C'}$), 3.37 (d, 11, 1H, H^B), 3.47 (d, 11, 1H, $H^{D'}$), 3.48 (dd, 15, 11, 1H, $H^{B'}$), 6.53 (s, 2H, -C≡CH), 7.88 (s, 3H, CH_3), and 7.95 (s, 3H, CH_3).

Found: C, 79.94; H, 6.70; N, 13.27%. Calcd for $C_{14}H_{14}N_2$: C, 79.96; H, 6.71; N, 13.32%.

The later fractions eluted with hexane–ether (1:1) gave azine **14**[3] (937 mg, 12%).

*3,14-Dimethyl-6,7-diaza-3,5,7,9,11,13-hexadecahexaene-1,15-diyne (**15**).* A soln of **8** (1.60 g, 17 mmol) and **10** (2.50 g, 17 mmol) in ethanol (50 ml) was added dropwise during 1.5 h to a stirred soln of hydrazine sulfate (2.6 g), sodium carbonate (3.1 g), and water (54 ml) at 17—21 °C. The mixture was stirred for a further 30 min at 20—21 °C. Then the mixture was worked up as in the preparation of **13**. The residual red liquid, after solvent removal, was chromatographed on alumina (200 g). The early fractions eluted with hexane–ether (2:3) gave azine **14** (887 mg, 29%). The following fractions eluted with hexane–ether (2:3—1:4) gave azine **15** (748 mg, 19%) as a solid. Recrystallization from chloroform–ethanol afforded orange needles: mp 132—133 °C (decomp); MS *m/e* 236 (M^+, 40%) and 39 (100); mol wt 236.3; IR 3200 (-C≡CH), 2100 (-C≡C-), 1620 (C=N), 1595 (C=C), and 990 cm^{-1} (*trans* C=C); UV_{max} 233 (13500), 277 (8410), 289 (8870), 342 sh (46100), 359 (64400), 377 (69400), and 395 nm (50300); ^1H NMR (90 MHz) τ=1.33 (d, 10, 1H, H^A), 1.75 (d, 10, 1H, $H^{A'}$), 2.88—3.70 (m, 6H, olefinic H), 6.52 (s, 1H, -C≡CH), 6.57 (s, 1H, -C≡CH), 7.87 (s, 3H, CH_3), and 7.97 (s, 3H, CH_3).

Found: C, 81.21; H, 6.87; N, 11.74%. Calcd for $C_{16}H_{16}N_2$: C, 81.32; H, 6.83; N, 11.86%.

The later fractions eluted with ether gave azine **16**[3] (440 mg, 8.9%).

*3,16-Dimethyl-6,7-diaza-3,5,7,9,11,13,15-octadecaheptaene-1,17-diyne (**17**).* A soln of **8** (1.70 g, 18 mmol) and **11** (3.10 g, 18 mmol) in ethanol (53 ml) was added dropwise during 1 h to a stirred soln of hydrazine sulfate (2.70 g), sodium carbonate (3.30 g), and water (57 ml) at 23 °C. The mixture was stirred for a further 2 h at the same temp. After the mixture was worked up as in the preparation of **13**, the residual brown liquid was chromatographed on alumina (17×4 cm). The early fractions eluted with hexane–ether (3:7) gave azine **12**[3] (1.71 g, 52%). The following fractions eluted with hexane–ether (2:3) gave azine **17** (1.04 g, 22%) as a solid. Recrystallization from hexane–benzene afforded brown needles: mp 100—101 °C (decomp); MS *m/e* 262 (M^+, 35%) and 78 (100); mol wt 262.3; IR 3200 (-C≡CH), 2100 (-C≡C-), 1620 (C=N), 1570 (C=C), and 1000 cm^{-1} (*trans* C=C); UV_{max} 248 (11000), 293 (6940), 305 (7770), 359 sh (38300), 381 sh (58300), 397 (66400), and 417 nm sh (51500); ^1H NMR (90 MHz) τ=1.33 (d, 10, 1H, H^A), 1.75 (d, 10, 1H, $H^{A'}$), *ca.* 2.9—3.8 (m, 8H, olefinic H), 6.52 (s, 1H, -C≡CH), 6.58 (s, 1H, -C≡CH), 7.88 (s, 3H, CH_3), and 7.98 (s, 3H, CH_3).

Found: C, 82.04; H, 7.13; N, 10.98%. Calcd for $C_{18}H_{18}N_2$: C, 82.40; H, 6.92; N, 10.68%.

The later fractions eluted with benzene–chloroform gave azine **19** (405 mg, 6.6%). Azine **19** was also prepared from aldehyde **11** (*vide infra*).

*3,16-Dimethyl-8,9-diaza-3,5,7,9,11,13,15-octadecaheptaene-1,17-diyne (**18**).* A soln of **9** (2.00 g, 17 mmol) and **10** (2.40 g, 17 mmol) in ethanol (49 ml) was added dropwise during 1.5 h to a stirred soln of hydrazine sulfate (2.50 g), sodium carbonate (3.00 g), and water (32 ml) at 14—21 °C. The mixture was stirred for a further 30 min at 20 °C. After the mixture was worked up as in the preparation of **13**, the residual dark brown liquid was chromatographed on alumina (130 g). The early fractions eluted with hexane–ether (1:1) gave azine **14** (501 mg, 13%). The following fractions eluted with hexane–ether (3:7) gave azine **18** (1.99 g, 46%) as a solid. Recrystallization from chloroform–ethanol afforded yellow needles: mp 172—173 °C (decomp); MS *m/e* 262 (M^+, 33%) and 115 (100); mol wt 262.3; IR 3280 (-C≡CH), 2100 (-C≡C-), 1620 (C=N), 1575 (C=C), and 980 cm^{-1} (*trans* C=C); UV_{max} 246 (15000), 253 sh (14300), 262 sh (11900), 298 sh (13700), 310 sh (16000), 362 sh (62600), 377 (80500), 394 (85000), and 414 nm (59000); ^1H NMR (90 MHz) τ=1.72 (d, 10, 1H, H^A), 1.75 (d, 10, 1H, $H^{A'}$), *ca.* 2.6—3.7 (m, 8H, olefinic H), 6.54 (s, 1H, -C≡CH), 6.58 (s, 1H, -C≡CH), 7.95 (s, 3H, CH_3), and 7.97 (s, 3H, CH_3).

Found: C, 82.09; H, 7.01; N, 10.63%. Calcd for $C_{18}H_{18}N_2$: C, 82.40; H, 6.92; N, 10.68%.

The later fractions eluted with ether gave azine **16** (465 mg, 9.7%).

*3,22-Dimethyl-12,13-diaza-3,5,7,9,11,13,15,17,19,21-tetraeicosadecaene-1,23-diyne (**19**).* A soln of **11** (0.70 g, 4.1 mmol) in ethanol (39 ml) was added dropwise during 1.5 h to a stirred soln of hydrazine sulfate (2.8 g), sodium carbonate (3.8 g), and water (30 ml) at 27 °C. The mixture was stirred for a further 1 h at the same temp and worked up as in the preparation of **13**. The residual dark red liquid was chromatographed on alumina (4×12 cm). The fractions eluted with chloroform gave azine **19** (698 mg, 39%) as a partly crystallized liquid. Crystallization from a variety of solvents were unsuccessful in our hands owing to low solubility and instability of **19**. Repeated layer chromatography (0.5 mm thick) gave brown microcrystals: mp 238—240 °C (decomp); MS (field desorption method) *m/e* 340 (M^+); mol wt 340.4; IR 3300 (-C≡CH), 2090 (-C≡C-), 1620 (C=N), 1570 (C=C), and 1010 cm^{-1} (*trans* C=C); UV_{max} 293 (32200), 303 (31800), 402 sh (59900), 418 (73600), 437 (72500), and 468 nm sh (43500); ^1H NMR (200 MHz) τ=1.75 (d, 10, 2H, H^A), *ca.* 2.6—3.6 (m, 14H, olefinic H), 6.58 (s, 2H, -C≡CH), and 8.01 (s, 6H, CH_3).

*1,6-Bis(o-ethynylphenyl)-2,3-diaza-1,3,5-hexatriene (**25**).* A soln of **20** (3.0 g, 23 mmol) and **21** (3.6 g, 23 mmol) in ethanol (70 ml) was added dropwise during 1.5 h to a stirred soln of hydrazine sulfate (3.2 g), sodium carbonate (3.8 g), and water (32 ml) at 18 °C. The mixture was stirred for a further 2 h at the same temp. Then the mixture was worked up as in the preparation of **13**. The residual light yellow solid was chromatographed on alumina (250 g). The early fractions eluted with hexane–ether (17:3) gave azine **24**[3] (0.67 g, 10%). The following fractions eluted with hexane–ether (7:3) gave azine **25** (2.67 g, 41%) as a solid. Recrystallization from hexane–benzene afforded yellow needles: mp 136—137 °C; MS *m/e* 282 (M^+, 16%) and 139 (100); mol wt 282.3; IR 3280 (-C≡CH), 2105 (-C≡C-), 1630 (C=N), 1610 (C=C), 990, and 970 cm^{-1} (*trans* C=C); UV_{max} 236 (18700), 246 (16300), 253 sh (15700), 265 sh (10500), 322 sh (26700), 336 (30000), 348 sh (28400), and 360 nm sh (19000); ^1H NMR (90 MHz) τ=0.83 (s, 1H, H^A), 1.42 (d, 10, 1H, $H^{A'}$), 1.70—1.80 (m, 1H, benzenoid H), 2.19—2.93 (m, 9H, $H^{B'}$, $H^{C'}$, and benzenoid H), and 6.46 (s, 2H, -C≡CH).

Found: C, 85.25; H, 4.96; N, 9.94%. Calcd for $C_{20}H_{14}N_2$: C, 85.08; H, 5.00; N, 9.92%.

The later fractions eluted with hexane–ether (2:3) gave azine **26**[3] (1.68 g, 27%).

*1,8-Bis(o-ethynylphenyl)-2,3-diaza-1,3,5,7-octatetraene (**27**),*

A soln of **20** (4.3 g, 33 mmol) and **22** (6.0 g, 33 mmol) in ethanol (86 ml) was added dropwise during 2 h to a stirred soln of hydrazine sulfate (4.6 g), sodium carbonate (5.5 g), and water (46 ml) at 18 °C. The mixture was stirred for a further 2 h at the same temp, and worked up as in the preparation of **13**. The residual dark red solid was chromatographed on alumina (4×13 cm). The early fractions eluted with hexane–ether (9:1) gave azine **24** (3.0 g, 35%). The following fractions eluted with hexane–ether (4:1–3:2) gave azine **27** (3.0 g, 30%) as a solid. Recrystallization from hexane–benzene afforded yellow needles: mp 141—142 °C; MS *m/e* 308 (M^+, 100%); mol wt 308.3; IR 3325, 3290 (–C≡CH), 2110 (–C≡C–), 1610 (C=N), 1005, and 975 cm^{-1} (*trans* C=C); UV_{max} 235 (17200), 254 sh (14200), 288 (6340), 341 sh (33900), 357 (44200), 370 (44500), and 390 nm sh (28900); ^1H NMR (200 MHz) τ=0.88 (s, 1H, H^A), 1.59 (d, 10, 1H, $H^{A'}$), 1.76—1.83 (m, 1H, benzenoid H), 2.30—2.78 (m, 7H, benzenoid H), 2.94 (dd, 14, 11, 1H, $H^{C'}$), 2.96 (d, 16, 1H, $H^{E'}$), 2.97 (dd, 16, 11, 1H, $H^{D'}$), 3.30 (dd, 14, 11, 1H, $H^{B'}$), and 6.61 (s, 2H, –C≡CH).

Found: C, 85.90; H, 5.34; N, 9.02%. Calcd for $C_{22}H_{16}N_2$: C, 85.69; H, 5.23; N, 9.09%.

The later fractions eluted with ether gave azine **28**[3] (3.8 g, 32%).

1,10-Bis(o-ethynylphenyl)-2,3-diaza-1,3,5,7,9-decapentaene (29). A soln of **20** (3.4 g, 26 mmol) and **23** (5.4 g, 26 mmol) in ethanol (68 ml) was added dropwise during 1.5 h to a stirred soln of hydrazine sulfate (3.6 g), sodium carbonate (4.3 g), and water (36 ml) at 19 °C. The mixture was stirred for a further 3 h at the same temp. Then the mixture was poured onto aq sodium hydrogencarbonate soln and extracted with chloroform. The extracts were washed with aq sodium hydrogencarbonate soln and dried. The residual dark red liquid obtained after solvent removal was chromatographed on alumina (4×15 cm). The early fractions eluted with hexane–ether (9:1) gave azine **24**[3] (2.2 g, 32%). The following fractions eluted with hexane–ether (4:1–1:1) gave azine **29** (3.7 g, 43%) as a solid. Recrystallization from hexane–benzene afforded yellow needles: mp 143—144 °C; MS *m/e* 334 (M^+, 25%) and 129 (100); mol wt 334.4; IR 3280 (–C≡CH), 2100 (–C≡C–), 1620 (C=N), 1600, 1590 (C=C), and 1005 cm^{-1} (*trans* C=C); UV_{max} 227 (27900), 260 sh (14800), 267 sh (13400), 277 sh (10400), 292 (8130), 307 sh (9180), 380 sh (56300), 392 (59100), and 410 nm sh (46000); ^1H NMR (200 MHz) τ=0.89 (s, 1H, H^A), 1.60 (d, 10, 1H, $H^{A'}$), 1.78—1.84 (m, 1H, benzenoid H), 2.33—2.80 (m, 7H, benzenoid H), 2.94—3.46 (m, 6H, olefinic H), and 6.61 (s, 2H, –C≡CH).

Found: C, 86.32; H, 5.33; N, 8.35%. Calcd for $C_{24}H_{18}N_2$: C, 86.20; H, 5.43; N, 8.38%.

The later fractions eluted with chloroform gave azine **31** (2.8 g, 26%). Azine **31** was also prepared from aldehyde **23** (*vide infra*).

1,10-Bis(o-ethynylphenyl)-4,5-diaza-1,3,5,7,9-decapentaene (30). A soln of **21** (5.2 g, 33 mmol) and **22** (6.0 g, 33 mmol) in ethanol (86 ml) was added dropwise during 2.5 h to a stirred soln of hydrazine sulfate (4.6 g), sodium carbonate (5.5 g), and water (46 ml) at 15 °C. The mixture was stirred for a further 3 h at the same temp. Then the mixture was worked up as in the preparation of **13**, the residual brown liquid was chromatographed on alumina (4×13 cm). The early fractions eluted with hexane–ether (4:1) gave azine **26**[3] (2.9 g, 29%). The following fractions eluted with hexane–ether (3:2) gave azine **30** (2.6 g, 23%) as a solid. Recrystallization from hexane–benzene afforded yellow needles: mp 136—137 °C; MS *m/e* 334 (M^+, 30%) and 180 (100); mol wt 334.4; IR 3310, 3280 (–C≡CH), 2110 (–C≡C–), 1630 (C=N), 1610, 1600 (C=C), 1010, and 990 cm^{-1} (*trans* C=C); UV_{max} 227 (27900), 257 (17500), 296 sh (8100), 360 sh (51400), 372 (57100), 387 (54500), and 410 nm sh (52000); ^1H NMR (200 MHz) τ=1.57 (d, 10, 1H, H^A), 1.67 (d, 10, 1H, $H^{A'}$), 2.26—3.06 (m, 13H, H^B, H^C, $H^{C'}$, $H^{D'}$, $H^{E'}$, and benzenoid H), 3.52 (dd, 14, 11, 1H, $H^{B'}$), 6.58 (s, 1H, –C≡CH), and 6.60 (s, 1H, –C≡CH).

Found: C, 86.10; H, 5.15; N, 8.60%. Calcd for $C_{24}H_{18}N_2$: C, 86.20; H, 5.43; N, 8.38%.

The later fractions eluted with ether gave azine **28** (4.2 g, 35%).

1,16-Bis(o-ethynylphenyl)-8,9-diaza-1,3,5,7,9,11,13,15-hexadecaoctaene (31). A soln of **23** (0.50 g, 2.4 mmol) in ethanol (5.7 ml) was added dropwise during 30 min to a stirred soln of hydrazine sulfate (0.31 g), sodium carbonate (0.37 g), and water (3.1 ml) at 15 °C. The mixture was stirred for a further 2 h at the same temp. Then the mixture was worked up as in the preparation of **29**, the residual red solid was chromatographed on alumina (3×10 cm). The fractions eluted with chloroform gave azine **31** (268 mg, 54%) as a solid. Recrystallization from chloroform–ethanol afforded red needles: mp 278—279 °C (decomp); MS *m/e* 412 (M^+, 25%) and 178 (100); mol wt 412.5; IR 3280 (–C≡CH), 2100 (–C≡C–), 1620 (C=N), 1600, 1580 (C=C), and 1005 cm^{-1} (*trans* C=C); UV_{max} 230 (16700), 268 (11700), 295 sh (9110), 357 sh (17700), 418 (62600), 437 (62300), and 459 nm sh (41700); ^1H NMR (200 MHz) τ=1.73 (d, 10, 2H, H^A), 2.34—2.80 (m, 8H, benzenoid H), 2.95—3.49 (m, 12H, olefinic H), and 6.62 (s, 2H, –C≡CH).

Found: C, 87.34; H, 5.79; N, 6.85%. Calcd for $C_{30}H_{24}N_2$: C, 87.34; H, 5.87; N, 6.79%.

Oxidative Coupling of 18 to Two Isomeric Tetramethyl[36]annulenes 32 and 33. A soln of azine **18** (2.68 g, 10.2 mmol) in pyridine (160 ml) and dry ether (53 ml) was added dropwise during 4 h to a stirred soln of anhyd copper(II) acetate (13.0 g) in pyridine (355 ml) and dry ether (120 ml) kept at 50 °C; the mixture was stirred for a further 1 h at the same temp. Then the mixture was chilled and filtered through Hyflo Super-Cel. After the precipitates formed were washed with benzene, the filtrate was poured onto water. The organic layer combined with the benzene extracts from aq layer was washed with water fifteen times to remove pyridine, and dried over potassium carbonate. The residual dark red liquid, after solvent removal, was passed through a short column of alumina. The red liquid thus obtained was chromatographed on alumina (4×10 cm). The fractions eluted with hexane–ether (3:7–2:3) gave a slightly crude **32** (132 mg, 2.5%) as a crystalline liquid. Repeated thin layer chromatography gave a solid. Recrystallization from chloroform–ethanol afforded purple microcrystals: mp 144 °C (decomp); MS *m/e* 520 (M^+, 25%) and 115 (100); mol wt 520.6; IR 2190 (–C≡C–), 1620 (C=N), and 1000 cm^{-1} (*trans* C=C); UV_{max} 252 (17200) and 367 nm (62800), and see Fig. 1; ^1H NMR (200 MHz) τ=2.14 (d, 9, 1H, H^A), 2.16 (d, 9.5, 1H, $H^{A'''}$), 2.23 (d, 9.5, 1H, $H^{A'}$), 2.26 (d, 9, 1H, $H^{A''}$), *ca.* 2.6—3.6 (m, 16H, olefinic H), 7.98 (s, 6H, CH_3), and 8.01 (s, 6H, CH_3), and see Fig. 2. Compound **32** formed crystals containing 1 mol of chloroform.

Found: C, 69.59; H, 5.39; N, 8.89%. Calcd for $C_{36}H_{32}N_2 \cdot CHCl_3$: C, 69.43; H, 5.21; N, 8.76%.

The following fractions eluted with hexane–ether (2:3) gave a slightly crude **33** (50 mg, 0.90%) as a partly crystallized liquid. Thin layer chromatography gave a solid. Recrystallization from chloroform–ethanol afforded purple microcrystals: mp 112 °C (decomp); MS *m/e* 520 (M^+, 7%) and 18 (100); mol wt 520.6; IR 2180 (–C≡C–), 1615 (C=N),

and 1000 cm^{-1} (*trans* C=C); UV_{max} 251 (16000) and 367 nm (58400), and see Fig. 1; ^1H NMR (200 MHz) τ=1.59 (d, 9.5 1H, H^A), 1.77 (d, 9, 1H, $H^{A''}$), 1.78 (d, 10, 1H, $H^{A'}$), 2.14 (d, 10, 1H, $H^{A''}$), *ca.* 2.6—3.6 (m, 16H, olefinic H), 8.00 (s, 6H, CH_3), and 8.03 (s, 6H, CH_3), and see Fig. 2.

*5,10-Dimethyl-2,4,10,12,14-hexadecapentaene-6,8-diynedial (**34**).* A soln of **9** (3.30 g, 27.5 mmol) and **10** (4.00 g, 27.4 mmol) in pyridine (74 ml) and methanol (74 ml) was added dropwise during 1 h to a stirred soln of copper(II) acetate monohydrate (37.0 g) in pyridine (298 ml) and methanol (298 ml) at 20 °C. After being stirred at room temp overnight, the reaction mixture was poured onto aq sodium chloride soln and extracted with benzene. The extracts were washed with 3 M† hydrochloric acid until it turned acidic, and then with aq sodium hydrogencarbonate soln, and dried. The residual red liquid, after solvent removal, was chromatographed on alumina (4×10 cm). The early fractions eluted with hexane–ether (3:2) gave the tetraenediynedial **35** (840 mg, 13%) (*vide infra*). The following fractions eluted with hexane–ether (1:1) gave the desired pentaenediynedial **34** (1.79 g, 25%) as a solid. Recrystallization from benzene afforded orange needles: mp 48—49 °C; MS *m/e* 264 (M^+, 10%) and 78 (100); mol wt 264.3; IR 2190 (–C≡C–), 1670 (CHO), 1610 (C=C), 1010, 990, and 980 cm^{-1} (*trans* C=C); UV_{max} 257 sh (10100), 268 (10800), 318 (23800), 340 sh (23800), 375 (27400), and 405 nm sh (19800); ^1H NMR (90 MHz) τ=0.27 (d, 8, 1H, CH^AO), 0.33 (d, 8, 1H, $CH^{A'}O$), 2.42 (dd, 16, 11, 1H, H^C), 2.60 (s, 6H, benzene), 2.74 (dd, 16, 12, 1H, $H^{E'}$), 2.83 (dd, 16, 11, 1H, $H^{C'}$), 3.33 (d, 12, 1H, H^D), 3.43 (d, 12, 1H, $H^{F'}$), 3.45 (dd, 16, 12, $H^{D'}$), 3.78 (dd, 16, 8, 2H, H^B and $H^{B'}$), 7.90 (s, 3H, CH_3), and 7.95 (s, 3H, CH_3).

Found: C, 83.92; H, 6.39%. Calcd for $C_{18}H_{16}O_2 \cdot C_6H_6$: C, 84.17; H, 6.47%.

Compound **34** formed crystals containing 1 mol of benzene.

The later fractions eluted with hexane–ether (3:2) gave the hexaenediynedial **36** (607 mg, 7.6%) (*vide infra*).

The teraenediynedial **35** and the hexaenediynedial **36** were also prepared from **9** and **10**, respectively, in higher yields than in those described above.

*5,10-Dimethyl-2,4,10,12-tetradecatetraene-6,8-diynedial (**35**).* A soln of **9** (3.00 g, 25 mmol) in pyridine (35 ml) and methanol (35 ml) was added dropwise during 30 min to a stirred soln of copper(II) acetate monohydrate (18.0 g) in pyridine (138 ml) and methanol (138 ml) at 20 °C. After being stirred at room temp overnight, the reaction mixture was worked up as in the preparation of **34**. The residual red liquid obtained after solvent removal was chromatographed on alumina (4×10 cm). The fraction eluted with hexane–ether (3:2) gave the teraenediynedial **35** (1.65 g, 54%) as a crystalline liquid. Crystallization from hexane–benzene afforded yellow needles: mp 160—161 °C; MS *m/e* 238 (M^+, 4%) and 165 (100); mol wt 238.2; IR 2200 (–C≡C–), 1675 (CHO), 1610 (C=C), 1000, and 980 cm^{-1} (*trans* C=C); UV_{max} 245 sh (13200), 254 (17200), 293 (23900), 339 (25700), 62 (25200), and 387 nm (20600); ^1H NMR (90 MHz) τ=0.25 (d, 8, 2H, CHO), 2.43 (dd, 15, 12, 2H, H^C), 3.31 d, 12, 2H, H^D), 3.78 (dd, 15, 11, 2H, H^B), and 7.87 (s, H, CH_3).

Found: C, 80.94; H, 5.99%. Calcd for $C_{16}H_{14}O_2$: C, 0.64; H, 5.92%.

*7,12-Dimethyl-2,4,6,12,14,16-octadecahexaene-8,10-diynedial (**36**).* A soln of the aldehyde **10** (6.00 g, 43 mmol) in pyridine (59 ml) and methanol (59 ml) was added dropwise during 1 h to a stirred soln of copper(II) acetate monohydrate (30.0 g) in pyridine (235 ml) and methanol (235 ml) at 19 °C. After being stirred at room temp overnight, the reaction mixture was worked up as in the preparation of **34**. The residual red liquid obtained after solvent removal was chromatographed on alumina (4×15 cm). The hexaenediynedial **36** (2.50 g, 40%) was obtained from the fractions eluted with hexane–ether (2:3). Recrystallization from hexane–benzene afforded orange needles: mp 130—131 °C; MS *m/e* 290 (M^+, 18%) and 203 (100); mol wt 290.3; IR 2200 (–C≡C–), 1680 (CHO), 1610, 1590 (C=C), 1010, and 985 cm^{-1} (*trans* C=C); UV_{max} 239 (18300), 283 (17600), 321 sh (31600), 334 (35400), 377 (32500), 391 sh (31300), and 423 nm (21900); ^1H NMR (90 MHz) τ=0.32 (d, 8, 2H, CHO), 2.72 (dd, 15, 12, 2H, H^E), 2.85 (dd, 15, 12, 2H, H^C), 3.43 (dd, 16, 12, 2H, H^D), 3.45 (d, 12, 2H, H^F), 3.76 (dd, 15, 8, 2H, H^B), and 7.93 (s, 6H, CH_3).

Found: C, 82.70; H, 6.32%. Calcd for $C_{20}H_{18}O_2$: C, 82.73; H, 6.25%.

*The Reaction of **34** with Hydrazine Sulfate.* A soln of pentaenediynedial **34** (1.15 g, 4.36 mmol) in ethanol (26 ml) was added dropwise during 1.5 h to a stirred soln of hydrazine sulfate (0.66 g) and sodium carbonate (0.80 g) in water (19 ml) at room temp. The mixture was stirred for a further 1 h at the same temp. Then the mixture was worked up as in the preparation of **13**. The residual red liquid obtained after solvent removal was chromatographed on alumina. However, we could not detect the fractions containing cyclic products corresponding to **33**.

*Oxidative Coupling of **19** to Tetramethyl[48]annulene **37**.* A soln of **19** (3.30 g, 9.69 mmol) in pyridine (152 ml) and dry ether (51 ml) was added dropwise during 1 h to a stirred soln of anhyd copper(II) acetate (12.0 g) in pyridine (337 ml) and dry ether (113 ml) kept at 45 °C; the mixture was stirred for a further 30 min at the same temp. Then the mixture was chilled and filtered through Hyflo Super-Cel. The precipitates formed were washed with chloroform, and the filtrate was poured onto water. The organic layer combined with the chloroform extracts from aq layer was washed with water ten times to remove pyridine and dried. The residual brown liquid obtained after solvent removal was chromatographed on alumina (4×12 cm). The early fractions contained pyridine. The following fractions eluted with chloroform contained the desired **37**. The dark red liquid obtained was again chromatographed on alumina (4×9 cm). The fractions eluted with benzene–chloroform (1:1) gave **37** (618 mg, 19%) as a crystalline liquid. Although crystallization was unsuccessful in our hands due to low solubility of **37**, thin layer chromatography (0.5 mm thick) afforded purple microcrystals: mp 175—176 °C (decomp); MS (field desorption method) *m/e* 676 (M^+); mol wt 676.8; IR 2180 (–C≡C–), 1620 (C=N), 1595 (C=C), and 1000 cm^{-1} (*trans* C=C); UV_{max} 300 sh (10300) and 420 nm (73200); ^1H NMR (200 MHz) τ=1.98 (d, 10, 1H, H^A), *ca.* 2.4—3.5 (m, 20H, olefinic H), and 8.04 (s, 12H, CH_3).

*Oxidative Coupling of **30** to Two Isomeric Tetrabenzo[36]annulenes **38** and **39**.* A soln of azine **30** (1.2 g, 36 mmol) in pyridine (66 ml) and dry ether (22 ml) was added dropwise during 2.5 h to a stirred soln of anhyd copper(II) acetate (4.5 g) in pyridine (125 ml) and dry ether (42 ml) kept at 50 °C; the mixture was stirred for a further 2 h at the same temp and chilled. After work up as in the preparation of **37**, the residual red liquid obtained by solvent removal was chromatographed on alumina (3×8 cm). The fractions eluted with ether–benzene (1:4) gave a mixture of **38** and **39** as a brown liquid. The liquid was again chromatographed on alumina (4×15 cm). The early fractions eluted

† 1 M=1 mol dm^{-3}.

with benzene–chloroform gave **38** (118 mg, 9.8%) as a solid. Recrystallization from chloroform–ethanol afforded yellow microcrystals: mp 182 °C (decomp); IR 2200, 2150 (–C≡C–), 1620 (C=N), 1605, 1600 (C=C), 1000, and 980 cm^{-1} (*trans* C=C); UV_{max} 238 (68100), 263 (52200), 307 sh (59000), and 355 nm (95100); ^1H NMR (200 MHz) τ= 1.76 (d, 9.5, 1H, H^A), 1.77 (d, 9.5, 1H, $H^{A'''}$), 1.90 (d, 10, 1H, $H^{A'}$), 1.91 (d, 10, 1H, $H^{A''}$), and *ca.* 2.3—3.8 (m, 28H, olefinic and benzenoid H), and see Fig. 2. The following fractions eluted with benzene–chloroform gave **39** (86 mg, 7.0%) as a solid. Recrystallization from chloroform–ethanol afforded yellow microcrystals: mp 234 °C (decomp); IR 2220, 2150 (–C≡C–), 1630 (C=N), 1610, 1600 (C=C), 1000, and 980 cm^{-1} (*trans* C=C); UV_{max} 267 sh (39200), 282 (50400), 355 (90700), 410 sh (31100), and 435 nm sh (17100); ^1H NMR (200 MHz) τ=1.70 (d, 9.5, 1H, H^A), 1.85 (d, 9.5, 1H, $H^{A''}$), 1.89 (d, 9.5, 1H, $H^{A'}$), 2.06 (d, 9.5, 1H, $H^{A'''}$), and *ca.* 2.3—3.7 (m, 37H, olefinic and benzenoid H), and see Fig. 2.

*Oxidative Coupling of **31** to Tetrabenzo*[48]*annulene **40**.* A soln of azine **31** (2.80 g, 6.79 mmol) in pyridine (124 ml) and dry ether (41 ml) was added dropwise during 1 h to a stirred soln of anhyd copper(II) acetate (8.50 g) in pyridine (236 ml) and dry ether (79 ml) kept at 50 °C; the mixture was stirred for a further 30 min at the same temp. After work up as in the preparation of **37**, the residual dark red liquid obtained by solvent removal was chromatographed on alumina (4×10 cm). The early fractions contained pyridine. The later fractions eluted with chloroform gave **40** (414 mg, 15%) as a dark red gum, which resisted attempted crystallization and did not run from the base line on preparative layer chromatography. Precipitates formed from chloroform solution afforded purple powders: mp 235—240 °C (decomp ; IR 2200, 2140 (–C≡C– , 1620 (C=N), 1590, 1580 (C=C), and 1000 cm^{-1} (*trans* C=C); UV_{max} 290 (27300), 416 (92200), and 470 nm sh (44700); ^1H NMR τ=1.99 (d, 9, 4H, H^A), and *ca.* 2.3—3.6 (m, 40H, olefinic and benzenoid H).

*Oxidative Couplings of Azines **13**, **15**, **17**, **25**, **27**, **29**.* These oxidative couplings were carried out under almost the same conditions as those described for azines **18** and **30**. However, in attempted runs, no monomeric and dimeric cyclic compounds were obtained.

*Oxidative Coupling of **14** to Tetramethyl*[32]*annulene **5**[3] under High Dilution Conditions.* A soln of azine **14** (2.1 g, 8.9 mmol) in ether (77 ml), methanol (77 ml), and pyridine (309 ml) was added dropwise during 8 h to a stirred soln of anhyd copper(II) acetate (16.2 g) in pyridine (2100 ml), ether (525 ml), and methanol (525 ml) kept at 68—70 °C. After being refluxed for a further 2 h at the same temp, the mixture was allowed to stand overnight at room temp. Then the mixture was concentrated to 150 ml *in vacuo* on a water bath kept below 45 °C. The concentrate was chilled, diluted with benzene (200 ml), and filtered through Hyflo Super-Cel. The precipitates formed were washed with benzene, and the filtrate was poured onto water. The organic layer combined with benzene extracts from aq layer was washed with water ten times to remove pyridine and dried over potassium carbonate. After removal of solvent, the residual red liquid was chromatographed on alumina (150 g). The fractions eluted with ether–benzene (7:3) gave the corresponding cyclic dimer **5** (116 mg, 2.8%). No monomeric product could be obtained.

*Oxidative Coupling of **16** to Tetramethyl*[40]*annulene **7**[3] under High Dilution Conditions.* A soln of azine **16** (3.40 g, 11.8 mmol) in ether (102 ml), methanol (102 ml), and pyridine (410 ml) was added dropwise during 7 h to a stirred and refluxing soln of anhyd copper(II) acetate (18.0 g) in pyridine (2141 ml), ether (410 ml), and methanol (410 ml) kept at 72—74 °C. After being stirred for a further 1.5 h, the mixture was worked up as in the isolation of **5**, as described above. The residual red liquid obtained after solvent removal was chromatographed on alumina (180 g). The fractions eluted with benzene–chloroform gave the corresponding cyclic dimer **7** (330 mg, 9.8%).

*Oxidative Coupling of Azine **12**.* This was carried out in almost the same scale as that for azine **14** described above. However, no desired cyclic products could be obtained.

The present work was partially supported by a Grant-in-Aid from the Itō Science Foundation.

References

1) K. Yamamoto and F. Sondheimer, *Tetrahedron*, **30**, 4229 (1974).
2) N. Darby, T. M. Cresp, and F. Sondheimer, *J. Org. Chem.*, **42**, 1960 (1977).
3) J, Ojima, Y. Shiroishi, and M. Fujiyoshi, *Bull. Chem. Soc. Jpn.*, **51**, 2112 (1978).
4) J. Ojima, M. Ishiyama, and A. Kimura, *Bull. Chem. Soc. Jpn.*, **50**, 1584 (1977).
5) a) E. R. H. Jones and B. C. L. Weedon, *J. Chem. Soc.*, **1946**, 937; b) I. Heilbron, E. R. H. Jones, and M. Julia, *ibid.*, **1949**, 1430; c) J. Ojima, T. Katakami, G. Nakaminami, and M. Nakagawa, *Bull. Chem. Soc. Jpn.*, **49**, 292 (1976).
6) a) M. Iyoda, M. Miyazaki, and M. Nakagawa, *Bull. Chem. Soc. Jpn.*, **49**, 2306 (1976); b) M. Iyoda and M. Nakagawa, *ibid.*, **51**, 3363 (1978).
7) J. Ojima, K. Wada, and M. Terasaki, *Tetrahedron Lett.*, **1981**, 457; *J. Chem. Soc., Perkin Trans. 1*, **1982**, 51.
8) J. Ojima, T. Yokomachi, and A. Kimura, *Bull. Chem. Soc. Jpn.*, **49**, 2840 (1976).
9) J. Ojima, A. Kimura, Y. Yokoyama, and T. Yokoyama, *Bull. Chem. Soc. Jpn.*, **48**, 367 (1975).
10) J. Ojima, M. Ishiyama, A. Kimura, and Y. Yokoyama, *Tetrahedron Lett.*, **1975**, 1909, and see Ref. 11.
11) J. Ojima, M. Enkaku, and M. Ishiyama, *J. Chem. Soc., Perkin Trans. 1*, **1977**, 1548.

Persistent Nitrogen-centered Free Radicals, *N*-(Arylthio)-3,5-di-*t*-butylphenylaminyls. The Reactions with Phenols[1)]

Yozo MIURA,* Akifumi YAMAMOTO, and Masayoshi KINOSHITA

Department of Applied Chemistry, Faculty of Engineering, Osaka City University, Sumiyoshi-ku, Osaka 558

(Received October 23, 1982)

The reactions of *N*-(4-chlorophenylthio)-3,5-di-*t*-butylphenylaminyl (**1**) with phenols were examined. The reaction with 2,6-dimethyl- and di-*t*-butylphenols gave 2,6-dimethyl- and di-*t*-butyl-*p*-benzoquinone 3,5-di-*t*-butylphenylimines, respectively, in excellent yields. In the reaction with unsubstituted phenol, 2,6-bis[*N*-(4-chlorophenylthio)-3,5-di-*t*-butylphenylamino]-*p*-benzoquinone 3,5-di-*t*-butylphenylimine was obtained in 32—56% yields. On the other hand, the reactions with *p*-substituted phenols such as *p*-cresol, *p*-*t*-butylphenol, and 2,4-di-*t*-butylphenol, gave phenols which were substituted by **1** at the *ortho*-positions to the OH group. Furthermore, the reactions with *o*-cresol, 2,6-di-*t*-butyl-*p*-cresol, and 1-naphthol were examined. On the basis of these results, plausible mechanisms for the reactions are presented.

Reactions of phenols with nitroxide radicals have been widely studied from the synthetic viewpoint. For example, the reaction of potassium nitrosodisulfonate (Fremy's salt) with phenols, well-known as the Teuber reaction,[2)] gave a variety of quinones, usually in excellent yields. Similarly, the reactions using organic nitroxides afforded quinones in relatively good yields.[3,4)]

In contrast to the widely studied reactions of nitroxide radicals with phenols, the reactions with nitrogencentered free radicals have rarely been investigated. Rieker *et al.* reported that phenylamino radicals reacted with phenols to give quinone imines in 5—40% yields.[5)] On the other hand, the reactions reported by Barton *et al.* of bis(arylthio)aminyl radical with phenols gave quinone *N*-thioimines in fair to good yields.[6)]

In a continuous study on *N*-thioaminyl radicals ($R_1\dot{N}SR_2$),[1)] we have found that *N*-(arylthio)-3,5-di-*t*-butylphenylaminyls persist in solution, even in the presence of oxygen and can be isolated as crystalline dimers which dissociate, upon dissolution, into the original radicals with relatively large equilibrium constants.[7)]

In order to examine the properties of this new class of nitrogen-centered free radicals, we carried out the reactions of *N*-(4-chlorophenylthio)-3,5-di-*t*-butylphenylaminyl (**1**) with a variety of phenols. In this paper we wish to report the results.

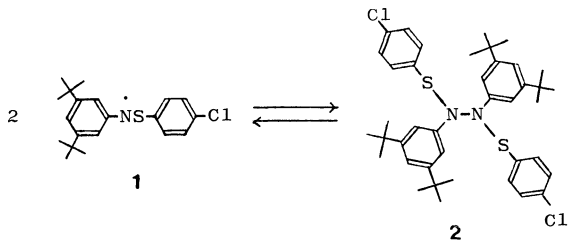

Results and Discussion

The reactions of **1** with phenols were carried out at room temperature under a nitrogen atmosphere. The completion of the reactions was indicated by discharge of the dark blue color attributable to **1**. The results of the reactions are summarized in Table 1.

Table 1. Results of the reactions of **1** with phenols[a)]

Phenol	Molar ratio of **1**/Phenol	Products (Yield/%)[b)]
2,6-Me_2	3.0	**3**(96)
2,6-*t*-Bu_2	3.0	**7**(92)
Unsubstituted	3.0	**11**(32)
Unsubstituted	5.4	**11**(56)
2-Me	1.0	**15**(13)
2-Me	3.0	**15**(57)
1-Naphthol	1.0	**17**(26), **18**(trace)
1-Naphthol	3.0	**17**(39), **18**(22)
4-Me	4.0	**19**(≧86)[c)]
4-*t*-Bu	1.0	**22**(22), **24**(9.8)
4-*t*-Bu	2.0	**22**(29), **24**(30)
4-*t*-Bu	3.8	**22**(trace), **24**(82)
2,4-*t*-Bu_2	2.0	**26**(90)
2,6-*t*-Bu_2-4-Me	2.0	**27**(61)

a) In benzene at room temperature. b) Iolated yields based on starting phenol. c) Based on the isolated yield (86%) of **21**.

The reaction of 2,6-dimethylphenol with 3 equiv. (1.5 equiv. of **2**) of **1** was complete in 1 min on addition of the phenol, and the resulting orange-red reaction mixture gave 2,6-dimethyl-*p*-benzoquinone 3,5-di-*t*-butylphenylimine (**3**) almost quantitatively. The other products from the reaction were *N*-(4-chlorophenylthio)-3,5-di-*t*-butylaniline (**4**), and small amounts of bis(p-chlorophenyl) disulfide (**5**) and *N*,*N*-bis(4-chlorophenylthio)-3,5-di-*t*-butylaniline (**6**). Based on these products, this reaction mechanism can be reasonably described as in Scheme 1.

Similarly, 2,6-di-*t*-butylphenol reacted rapidly with 3 equiv. of **1** to give 2,6-di-*t*-butyl-*p*-benzoquinone 3,5-di-*t*-butylphenylimine (**7**) in 92%. This imine is probably produced by the same mechanism as above.

The reaction of unsubstituted phenol with 5.4 equiv. of **1** gave only **11** as quinone imine in 56% yield, and other quinone imines such as **12** and **13** were not found among the products. Quinone imine **11** was relatively unstable, being decomposed slowly in hydrocarbon solvents, and rapidly in methanol to **14** and bis(*p*-chlorophenyl) disulfide (Scheme 3). A plausible mechanism for the formation of **11** is represented

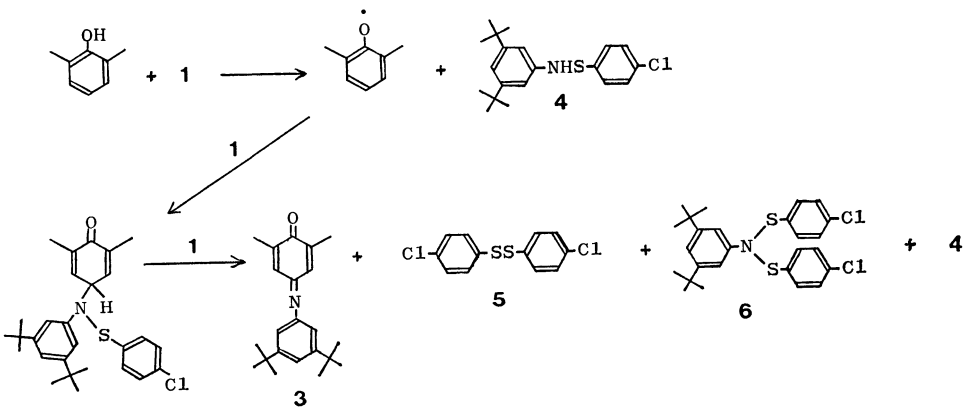

Scheme 1.

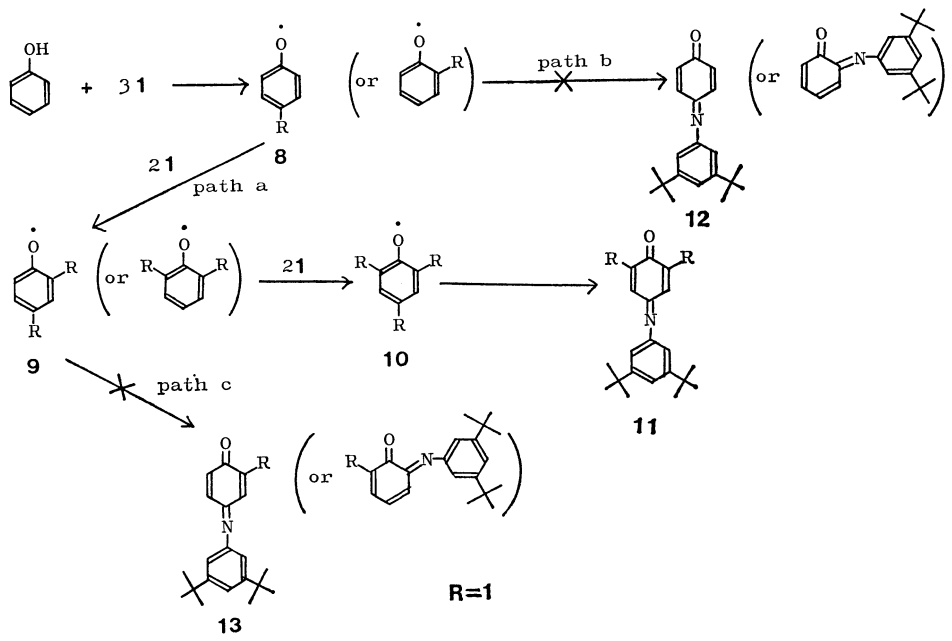

Scheme 2.

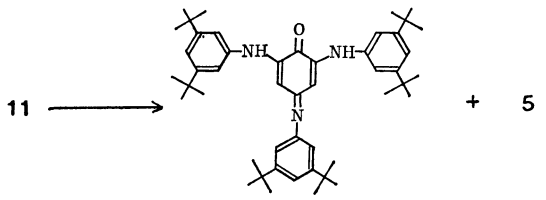

Scheme 3.

in Scheme 2. This reaction requires 7 equiv. of **1**, provided that the phenol is converted exclusively into **11**. However, even when the ratio of **1** to the phenol was 3, the quinone imine formed was only **11**. This interesting observation suggests that addition (path a) of **1** to the intermediate phenoxyl radicals **8** and **9**, giving **11** as the final product, is much faster than elimination (paths b and c) of a *p*-chlorophenylthiyl radical from the phenoxyl radicals, giving **12** and **13**.

In the previously reported reactions of phenols with free radicals,[2-6] unsubstituted phenol was converted into the unsubstituted quinone or quinone imine, and monosubstituted phenols were usually converted into the monosubstituted quinones or quinone imines. Thus, the formation of the polysubstituted quinone imine such as **11** in the reaction with unsubstituted phenol is different from the previous results.

The reaction of *o*-cresol with 1—3 equiv. of **1** gave similarly only one quinone imine (**15**) in 13—57% yields. This quinone imine seems to be produced *via* **16**, by assumption of the above reaction.

In contrast to the above reactions, the reactions of 1-naphthol with **1** gave two kinds of quinone imines (**17** and **18**). For example, a 1:3 equimolar mixture

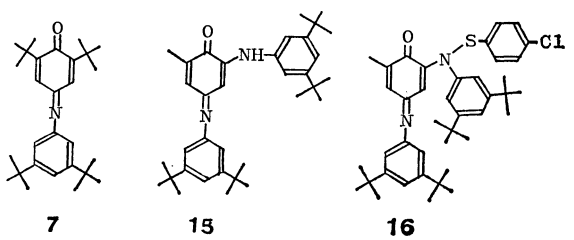

of 1-naphthol and **1** afforded **17** and **18** in 39 and 22% yields, respectively. However, a 1:1 mixture of the naphthol and **1** gave only **17** in 26% yield (**18** was shown to be present in trace amounts by TLC inspection of the reaction mixture). In order to examine whether **18** was produced *via* **17** or not, a 1:2 equimolar mixture of **17** and **1** was stirred in benzene at room temperature for 2 h. TLC inspection showed no reaction occurred.

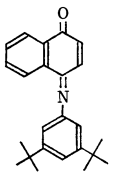

17

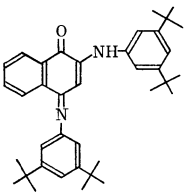

18

The reactions of **1** with *p*-substituted phenols such as *p*-cresol, *p*-*t*-butylphenol, and 2,4-di-*t*-butylphenol gave *ortho*-substituted phenols and no quinone imine was found among the products. For example, the reaction of *p*-cresol with 4 equiv. of **1** gave phenol **19** in good yield (≧86%). This phenol was not stable enough to be isolated. In order to confirm its structure, **19** was converted into a thermally stable benzoic ester **20** by treatment with benzoyl chloride. The phenol was decomposed slowly in benzene solution at room temperature (1 d for complete decomposition), and rapidly on reflux (30 min) to give dark yellow-blue crystals of **21** in 27% yield. The structure of this unexpected product was confirmed by IR, and ^{1}H and ^{13}C NMR spectroscopy, and the molecular weight (determined by vapor pressure osmometry).[5] The IR spectrum showed absorptions of NH at 3350 cm^{-1} and C=O at 1620 cm^{-1}, and in the ^{13}C NMR spectrum eight singlet peaks due to the aromatic, quinonoid, and carbonyl carbons and five doublet peaks due to the aromatic and quinonoid carbons were found. The observed molecular weight (807) was in good agreement with that calculated (798). Furthermore, the ^{1}H NMR spectrum and elemental analysis gave satisfactory results. On the basis of these instrumental analyses, we identified the crystal as **21**.

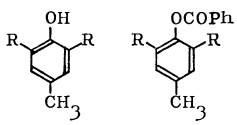

19 20

R=1

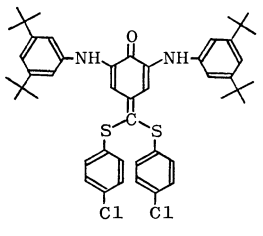

21

In the case of 4-*t*-butylphenol, 1:1 and 1:2 equimolar mixtures of the phenol and **1** gave two kinds of phenols, **22** and **24**, in 22—29 and 9.8—30%, respectively. However, a 1 3.8 equimolar mixture of the phenol and **1** afforded only **24** in 82% yield. On the other hand, the reaction of 2,4-di-*t*-butylphenol with 2 equiv. of **1** gave phenol **26** in 90% yield. These phenols, as well as **19**, were very unstable and could not be obtained as pure crystals. To confirm their structures, **22** and **24** were converted into the benzoic esters **23** and **25** by the same procedure as for **19**. In the case of **26**, however, the corresponding benzoic ester could not be obtained in the same manner, probably because of steric hindrance due to the bulky *o*-*t*-butyl group in **26**.

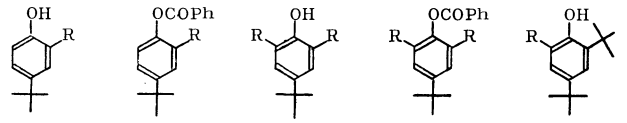

22 23 24 25 26

R=1

The previously reported reactions of *p*-substituted phenols with nitroxide or bis(phenylthio)aminyl radicals gave *o*-quinones or *o*-quinone imines.[2-6] On the other hand, the reactions of **1** with *p*-substituted phenols afforded polysubstituted phenols such as **19** and **22**, but never *o*-quinone imines. This unusual result is worthy of note.

The reaction of 2,6-di-*t*-butyl-*p*-cresol with 2 equiv. of **1** yielded **27** in 61% yield. However, the careful TLC inspection of the reaction mixture revealed that **27** was not the product formed at the completion of the reaction. When the reaction mixture, which was light blue at the completion of the reaction, was allowed to stand at room temperature for 1 d, the color of the reaction mixture changed from light blue to light orange; TLC inspection revealed the complete decomposition of the initially formed product and the appearance of **27**. It seems that the initially formed product is **28**, which is a coupling product of **1** and 2,6-di-*t*-butyl-*p*-methylphenoxyl radical, and that **27** was produced through the coupling of **1** and quinone methide **29**. A similar reaction occured between 2,4,6-trimethylphenol and benzoyl *t*-butyl nitroxide radical.[4] An attempt to isolate **28** was unsuccessful.

Finally, the reaction of **1** with 2,4,6-tri-*t*-butylphenol

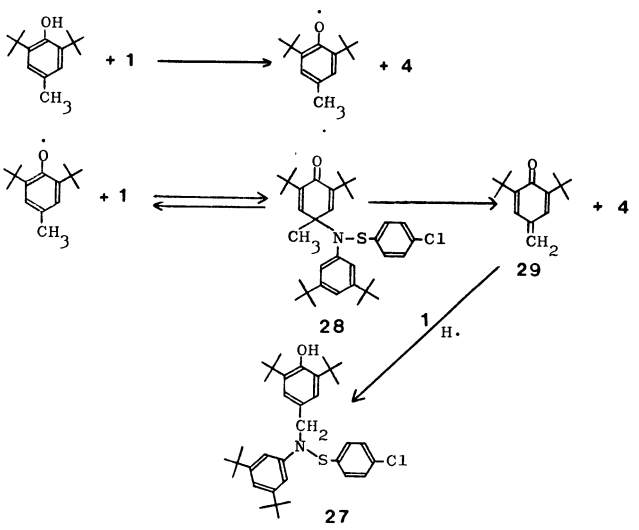

Scheme 4.

was examined. However, the mixture of **1** and the phenol gave no coupling product.

Experimental

All melting points were taken on a Yanaco micro melting-point apparatus and are uncorrected. IR spectra were run on a JASCO Model IR-G spectrometer, and UV and visible spectra were recorded with a Hitachi 220 spectrophotometer. Mass spectra were taken with a Hitachi M-52 spectrometer. ^{1}H NMR spectra were recorded with a Hitachi Perkin Elmer R-20 (60 MHz) or JEOL PS-100 (100 MHz) spectrometer with tetramethylsilane as internal standard, and ^{13}C NMR spectra were taken on a JEOL FX-100 (25 MHz) spectrometer.

The phenols were commercially available and were purified by distillation or recrystallization from the appropriate solvents. Dimer **2** was prepared by our previous method.[7]

General Procedure for the Reactions of 2 with Phenols. Dimer **2** in benzene (30 ml) was stirred at room temperature until the dimer was completely dissolved in the solution (*ca.* 1 h). After nitrogen was bubbled through the stirred dimer solution for 30 min, a benzene solution (2 ml) of the phenol was added in one portion to the dimer solution, and the resulting reaction mixture was stirred for 10—120 min with continuous bubbling of nitrogen. After the solvent was removed by either evaporation or freeze-drying, the residue was chromatographed on alumina (Merck Art 1097; column size 3×40 cm) or silica gel (Wako gel C-200; column size 3×40 cm) with the appropriate solvents. The results are shown in Table 1.

Reaction with 2,6-Dimethylphenol. To a benzene solution of **2** (400 mg, 0.577 mmol) a benzene solution of 2,6-dimethylphenol (47 mg, 0.39 mmol) was added and the resulting red reaction mixture was stirred for 10 min, evaporated, and the residue chromatographed on alumina. Elution with benzene–hexane (1:5) gave a mixture of bis(*p*-chlorophenyl) disulfide (**5**) and *N*,*N*-bis(4-chlorophenylthio)-3,5-di-*t*-butylaniline (**6**); subsequent elution with benzene–hexane (1:2) gave *N*-(4-chlorophenylthio)-3,5-di-*t*-butylaniline (**4**) (227 mg, 0.653 mmol) and 2,6-dimethyl-*p*-benzoquinone 3,5-di-*t*-butylphenylimine (**3**) (120 mg, 0.371 mmol). The quinone imine was recrystallized from methanol to give red needles; mp 118—120 °C; IR (KBr): 1640 cm^{-1} (C=O); UV and vis (hexane): 451 (ε 3600), 291 (16500), and 270 (19800) nm; MS (70 eV): *m/e* (rel intensity), 325 (M^++2, 29), 324 (M^++1, 32), 323 (M^+, 100), 309 (23), 308 (74), 252 (32), 91 (21), and 57 (64); ^{1}H NMR (CCl_4): δ=1.33 (s, *t*-Bu, 18H), 1.86 and 2.02 (d, J=1.6 Hz, *syn*- and *anti*-CH_3, 6H), and 6.42—7.02 (m, aromatic and quinonoid, 5H). Found: C, 81.40; H, 9.04; N, 4.38%. Calcd for $C_{22}H_{29}NO$: C, 81.69; H, 9.04; N, 4.33%.

The mixture of **5** and **6** was treated on a preparative silica-gel TLC (Merck, Art 7730; 20×20 cm, 30 g) with benzene–hexane (1:20) as eluant to give 33 mg (0.12 mmol) of **5** and 28 mg (0.057 mmol) of **6**. The products **4**, **5**, and **6** were identified by comparison (mps and IR spectra) with authentic samples.[7,9]

Reaction with 2,6-Di-t-butylphenol. To a benzene solution of **2** (350 mg, 0.505 mmol) a benzene solution of 2,6-di-*t*-butylphenol (69 mg, 0.33 mmol) was added. The resulting red reaction mixture was stirred for 10 min, evaporated, and the residue chromatographed on alumina with benzene–hexane (1:5) to give 125 mg (0.307 mmol) of **7** which was recrystallized from methanol to afford red prisms; mp 75—77 °C; IR (KBr): 1640 cm^{-1} (C=O); UV and vis (hexane): 445 (ε 4040), 295 (16800), and 272 (17200) nm; MS (70 eV): *m/e* (rel intensity), 409 (M^++2, 19), 408 (M^++1, 31), 407 (M^+, 100), 392 (18), and 57 (45); ^{1}H NMR (CCl_4): δ=1.19 and 1.32 (s, *syn*- and *anti*-*t*-Bu, 18H), 1.32 (s, *t*-Bu, 18H), and 6.54—7.09 (m, aromatic and quinonoid, 5H). Found: C, 82.30; H, 10.22; N, 3.51%. Calcd for $C_{28}H_{41}NO$: C, 82.50; H, 10.14; N, 3.44%.

Reaction with Phenol. To a benzene solution of **2** (400 mg, 0.577 mmol) a benzene solution of phenol (36 mg, 0.38 mmol) was added and the resulting red reaction mixture was stirred for 10 min. The solvent was removed by freeze-drying and the resultant red powdery residue was chromatographed on silica gel with benzene–hexane (3:1), using a column cooled by circulating ice-water. The fractions of the red zone were collected and concentrated to *ca.* 30 ml below 10 °C under reduced pressure. The residual solvent (benzene) was then removed by freeze-drying to give red powdery crystals of **11** (120 mg, 0.122 mmol) (TLC one spot). Since this product was thermally unstable, recrystallization was unsuccessful. The results of instrumental and elemental analyses for the powdery **11** are as follows: IR (KBr): 1660 cm^{-1} (C=O); ^{1}H NMR (CCl_4)[10]: δ=1.18 (s, *t*-Bu, 18H), 1.25 (s, *t*-Bu, 36H), and 6.52—7.15 (m, aromatic and quinonoid, 19H). Found: C, 73.57; H, 7.59; N, 3.86%. Calcd for $C_{60}H_{73}Cl_2N_3OS_2$: C, 72.99; H, 7.45; N, 4.26%.

Similarly, the reaction of 400 mg (0.577 mmol) of **2** with 20 mg (0.21 mmol) of phenol gave 118 mg (0.120 mmol) of **11**.

Conversion of 11 into 14. Quinone imine **11** (95 mg, 0.096 mmol) in 20 ml of methanol was stirred for 20 min at room temperature. After complete removal of the solvent in vacuum, the residue was chromatographed on alumina (column size 3×20 cm) with benzene–hexane (1:1) as eluant, giving 23 mg (0.080 mmol, 83%) of bis(*p*-chlorophenyl) disulfide and 62 mg (0.088 mmol, 92%) of quinone imine **14**. This quinone imine was recrystallized from methanol to give dark red prisms; mp 133—136 °C; IR (KBr): 3370 (NH) and 1630 cm^{-1} (C=O); UV and vis (hexane): 495 ε 8300), 414 (7300), and 271 (36800) nm; MS (70 eV): *m/e* (rel intensity), 703 (M^++2, 27), 702 (M^++1, 55), 701 (M^+, 100), and 57 (50); ^{1}H NMR (CCl_4): δ=1.12 (s, *t*-Bu, 18H), 1.19 (s, *t*-Bu, 18H), 1.36 (s, *t*-Bu, 18H), 6.46—7.01 (m, aromatic and quinonoid, 11H), and 6.82 (s, NH, 2H, exchanged by D_2O). Found: C, 81.80; H, 9.73; N, 5.84%. Calcd for $C_{48}H_{67}N_3O$: C, 82.12; H, 9.62; N, 5.98%.

The bis(*p*-chlorophenyl) disulfide isolated was identified by its IR spectrum.

Direct Preparation of 14. 1) A reaction mixture, obtained from 400 mg (0.577 mmol) of **2** and 36 mg (0.38 mmol) of phenol, was evaporated and the residue was dissolved in 20 ml of methanol. The solution was stirred for 20 min at room temperature and the solvent was completely removed in vacuum, the residue was chromatographed on alumina. Elution with benzene–hexane (1:2) gave bis(*p*-chlorophenyl) disulfide and **4**, and subsequent elution with benzene–hexane (2:1) gave 95 mg (0.14 mmol, 37%) of **14**. 2) The reaction mixture, obtained from 400 mg (0.577 mmol) of **2** and 36 mg (0.38 mmol) of phenol, was refluxed in benzene for 30 min and evaporated. The resulting residue was chromatographed on alumina in the same manner as described above to give 90 mg (0.13 mmol, 33%) of **14**.

Reaction with o-*Cresol.* To a benzene solution of **2** (400 mg, 0.577 mmol) was added a benzene solution of *o*-cresol (41 mg, 0.38 mmol) and the resulting red reaction mixture was stirred for 10 min. The mixture was evaporated and the residue chromatographed on alumina, using a column

cooled by circulating ice-water. Elution with benzene–hexane (1:1) gave bis(*p*-chlorophenyl) disulfide, **4**, and **6**, and subsequent elution with benzene–hexane (2:1) gave 112 mg (0.22 mmol) of **15**. This quinone imine was dissolved in a small amount (2 ml) of benzene, 10 ml of hexane was added to the solution and cooled to 5 °C, giving dark red needles (this quinone imine was immediately decomposed in methanol and slowly in benzene and hexane at reflux); mp 175—176 °C; IR (KBr): 3330 (NH) and 1640 cm^{-1} (C=O); UV and vis (hexane): 486 (ε 6050) and 275 (22600) nm; MS (70 eV): *m/e* (rel intensity), 514 (M^++2, 48), 513 (M^++1, 93), 512 (M^+, 100), 455 (15), and 57 (74); ^1H NMR (CCl_4)[11]: δ=1.10, 1.18, 1.32, and 1.34 (s, *t*-Bu, 36H), 1.96 and 2.08 (d, J=1.4 Hz, *syn*- and *anti*-CH_3, 3H), and 6.24—6.88 (m, aromatic, quinonoid, and NH, 9H). Found: C, 81.59; H, 9.84; N, 5.15%. Calcd for $C_{35}H_{48}N_2O$: C, 81.98; H, 9.44; N, 5.46%.

Similarly, the reaction of 130 mg (0.188 mmol) of **2** with 41 mg (0.38 mmol) of *o*-cresol gave 26 mg (0.051 mmol) of **15**.

Reaction with 1-Naphthol. To a benzene solution of **2** (409 mg, 0.590 mmol) a benzene solution of 1-naphthol (56 mg, 0.39 mmol) was added. The resulting red reaction mixture was stirred for 120 min, evaporated, and the residue chromatographed on alumina with benzene–hexane (2:3). The fractions of the red zone (mixture of quinone imines **17** and **18**) were collected, concentrated, and the residue was run on a preparative alumina TLC (Merck, Art 1064; 20×40 cm, 80 g) to afford 52 mg (0.15 mmol) of **17** and 46 mg (0.084 mmol) of **18**. The quinone imines were recrystallized from methanol; **17**: red prisms; mp 148—150 °C; IR (KBr): 1650 cm^{-1} (C=O); UV and vis (hexane): 454 (ε 3460), 435 (sh, 3120), and 255 (22000) nm; MS (70 eV): *m/e* (rel intensity), 346 (M^++1, 47), 345 (M^+, 100), 330 (35), 274 (22), 140 (21), and 57 (52); ^1H NMR (CCl_4): δ=1.37 (s, *t*-Bu, 18H) and 6.56—8.52 (m, aromatic and quinonoid, 9H). Found: C, 83.03; H, 7.97; N, 4.02%. Calcd for $C_{24}H_{27}NO$: C, 83.44; H, 7.88; N, 4.05%.

Quinone imine **18**: red prisms; mp 200—202 °C; IR (KBr): 3350 (NH) and 1650 cm^{-1} (C=O); UV and vis (hexane): 468 (ε 6770), 277 (25500), 248 (sh, 21000), and 235 (sh, 23200) nm; MS (70 eV): *m/e* (rel intensity), 550 (M^++2, 20), 549(M^++1, 57), 548 (M^+, 100), and 57 (28); ^1H NMR (CCl_4): δ=1.17 (s, *t*-Bu, 18H), 1.24 (s, *t*-Bu, 18H), 7.26 (s, NH, 1H, exchanged by D_2O), and 6.56—8.60 (m, aromatic and quinonoid, 11H). Found: C, 82.85; H, 8.96; N, 5.33%. Calcd for $C_{38}H_{48}N_2O$: C, 83.16; H, 8.82; N, 5.11%.

On the other hand, the reaction of 136 mg (0.196 mmol) of **2** with 56 mg (0.39 mmol) of 1-naphthol gave only 35 mg (0.10 mmol) of **17** (**18**: trace amounts from TLC inspection of the reaction mixture).

Reaction with p-*Cresol.* To a benzene solution of **2** (400 mg, 0.577 mmol) a benzene solution of *p*-cresol (31 mg, 0.29 mmol) was added and the resulting mixture stirred for 15 min, turning light greenish yellow. After the solvent was removed by freeze-drying, the residue was dissolved in 20 ml of dry benzene and cooled to 5 °C in an ice-water bath. To the solution was added 0.58 g (5.7 mmol) of triethylamine and 0.48 g (3.4 mmol) of benzoyl chloride with stirring, and the mixture was stirred for 20 min at 5 °C and for 3 h at room temperature. The mixture was washed with K_2CO_3 aq solution, then with water, and dried over anhyd $MgSO_4$. After filtration and concentration, the residue was chromatographed on alumina (Merck, Art 1097) with benzene–hexane (1:2) to give 218 mg (0.250 mmol, 86%) of **20**, which was recrystallized from methanol–benzene; colorless prisms; mp 167—168.5 °C; IR (KBr): 1745 cm^{-1} (C=O); ^1H NMR (CCl_4): δ=1.12 (s, *t*-Bu, 36H), 2.29 (s, CH_3, 3H), and 6.76—7.25 (m, aromatic, 21H). Found: C, 74.15; H, 6.70; N, 3.05%. Calcd for $C_{54}H_{60}Cl_2N_2O_2S_2$: C, 74.37; H, 6.94; N, 3.21%.

The reaction mixture, obtained from 400 mg (0.577 mmol) of **2** and 31 mg (0.29 mmol) of *p*-cresol, was refluxed for 30 min, turning dark red. After the mixture was evaporated, the residue was chromatographed on alumina. Elution with benzene–hexane (2:3) gave a mixture of **4** and **5**. Subsequent elution with benzene gave 63 mg (0.079 mmol, 27%) of **21**, which was recrystallized from methanol; dark yellow-blue needles; mp 138—140 °C; IR (KBr): 3350 (NH) and 1620 cm^{-1}; ^1H NMR (CCl_4): δ=1.29 (s, *t*-Bu, 36H) and 6.91—7.68 (m, aromatic, quinonoid, and NH, 18H). ^{13}C NMR ($CDCl_3$): δ=177.5 (s), 152.2 (s), 139.7 (s), 138.9 (s), 138.7 (s), 136.0 (s), 134.0 (s), 132.9 (d), 132.7 (s), 129.0 (d), 117.0 (d), 114.6 (d), 103.2 (d), 35.2 (s), and 31.6 (q); molecular weight determined by vapor pressure osmometry (Knauer; benzene, 45 °C): 807 (calcd: 798). Found: C, 70.46; H, 6.94; N, 3.38%. Calcd for $C_{47}H_{54}Cl_2OS_2$: C, 70.74; H, 6.82; N, 3.51%.

Reaction with p-t-*Butylphenol.* To a benzene solution of **2** (400 mg, 0.577 mmol) a benzene solution of *p-t*-butylphenol (87 mg, 0.58 mmol) was added and the reaction mixture stirred for 30 min, turning colorless or wine-red. The solvent was removed by freeze-drying and the residue was chromatographed on silica gel, using a column cooled by circulating ice-water. Elution with benzene–hexane (2:3) gave 177 mg (0.509 mmol) of **4** and 145 mg (0.172 mmol) of **24**, and subsequent elution with benzene–hexane (2:1) gave 84 mg (0.17 mmol) of **22**. Isolation of **22** and **24** was performed by the same procedure as for **11**. Since these isolated phenols contained small amounts of impurities, they were recrystallized. However, this caused further decomposition of the phenols. In order to confirm their structures, the phenols were converted into stable benzoic esters **23** and **25** by treating them with benzoyl chloride. Phenol **22**: IR (KBr): 3420 cm^{-1} (OH); ^1H NMR (benzene-d_6): δ=1.07 (s, *t*-Bu, 9H), 1.23 (s, *t*-Bu, 18H), 5.06 (s, OH, 1H), and 6.70—7.28 (m, aromatic, 10H).

Phenol **24**: IR (KBr): 3480 cm^{-1} (OH); ^1H NMR (benzene-d_6): δ=1.00 (s, *t*-Bu, 9H), 1.26 (s, *t*-Bu, 36H), 5.36 (s, OH, 1H), and 6.77—7.30 (m, aromatic, 16H).

The reaction of 400 mg (0.577 mmol) of **2** with 175 mg (1.17 mmol) of *p-t*-butylphenol gave 126 mg (0.254 mmol) of **22** and 96 mg (0.11 mmol) of **24**. On the other hand, the reaction of 400 mg (0.577 mmol) of **2** with 46 mg (0.31 mmol) of the phenol gave only 211 mg (0.251 mmol) of **24** (**22**: trace amounts from TLC inspection).

Conversion of 22 into Benzoic Ester 23. To a stirred solution of **22** (142 mg, 0.286 mmol) and triethylamine (0.58 g, 5.7 mmol) in dry benzene (10 ml), 0.24 g (1.7 mmol) of benzoyl chloride was added at 5 °C. After being stirred for 2 h at room temperature, the reaction mixture was passed through a short column (4×10 cm) packed with alumina (Merck, Art 1097; eluant benzene) to remove unreacted benzoyl chloride. After concentration of the eluate, methanol–water was added to the residue to give 168 mg (0.280 mmol, 98%) of a light yellow powder (TLC one spot), which was recrystallized from methanol–water: colorless prisms; mp 134—136 °C; 141 mg (0.235 mmol, 82%); IR (KBr): 1745 cm^{-1} (C=O); ^1H NMR (CCl_4): δ=1.15 (s, *t*-Bu, 18H), 1.32 (s, *t*-Bu, 9H), and 6.78—7.68 (m, aromatic, 15H). Found: C, 73.72; H, 6.94; N, 2.28%. Calcd for $C_{37}H_{42}ClNO_2S$: C, 74.04; H, 7.05; N, 2.33%.

Conversion of 24 into Benzoic Ester 25. The conversion

was carried out by the same procedure as that for **22**. To a stirred solution of **24**(125 mg, 0.148 mmol) and triethylamine (0.58 g, 5.7 mmol) in dry benzene (10 ml) was added 0.24 g (1.7 mmol) of benzoyl chloride at 5 °C. The reaction mixture was stirred for 2 h at room temperature and passed through a short column packed with alumina. After concentration of the eluate, methanol–water was added to the residue to give 132 mg (0.140 mmol, 95%) of colorless crystals (TLC one spot), which were recrystallized from methanol–benzene: colorless needles; mp 176—177 °C; 111 mg (0.117 mmol, 79%); IR (KBr): 1750 cm^{-1} (C=O); ^1H NMR (CCl_4): δ=1.16 (s, *t*-Bu, 36H), 1.24 (s, *t*-Bu, 9H), and 6.79—7.35 (m, aromatic, 21H). Found: C, 72.36; H, 7.01; N, 2.85%. Calcd for $C_{57}H_{66}Cl_2N_2O_2S_2$: C, 72.36; H, 7.03; N, 2.96%.

*Reaction with 2,4-Di-*t*-butylphenol.* To a benzene solution of **2** (200 mg, 0.289 mmol) a benzene solution of 2,4-di-*t*-butylphenol (60 mg, 0.29 mmol) was added and the resulting reaction mixture was stirred for 20 min, turning colorless or wine-red. The solvent was removed by freeze-drying and the residue was chromatographed on silica gel, using a column cooled by circulating ice-water. Elution with benzene–hexane (1:3) gave 143 mg (0.259 mmol) of powdery **26**, which was isolated from the eluate by the same procedure as for **11**. Since the phenol isolated was contaminated with trace amounts of bis(*p*-chlorophenyl) disulfide, it was recrystallized. However, this resulted in further decomposition of the phenol. IR (KBr): 3500 cm^{-1} (OH); ^1H NMR (benzene-d_6): δ=1.14 (s, *t*-Bu, 9H), 1.24 (s, *t*-Bu, 18H), 1.53 (s, *t*-Bu, 9H), 5.53 (s, OH, 1H), and 6.70—7.35(m, aromatic, 9H).

*Reaction with 2,6-Di-*t*-butyl-*p*-cresol.* To a benzene solution of **2** (400 mg, 0.577 mmol) a benzene solution of 2,6-di-*t*-butyl-*p*-cresol (125 mg, 0.567 mmol) was added and the reaction mixture was stirred for 10 min, turning light blue. After standing for 1 d at room temperature, the resulting yellow reaction mixture was evaporated and the residue chromatographed on alumina with benzene–hexane (1:2) to give 196 mg (0.346 mmol) of **27** as a yellow oil, which was recrystallized from methanol–water (20:1): light orange prisms: mp 130—131 °C; IR (KBr): 3580 cm^{-1} (OH); MS (70 eV): *m/e* (rel intensity), 565 (M^+, 4), 422 (16), 346 (83), 219 (100), 204 (30), and 57 (44); ^1H NMR (CCl_4): δ= 1.22 (s, *t*-Bu, 18H), 1.35 (s, *t*-Bu, 18H), 4.73 (s, CH_2, 2H), 4.92 (s, OH, 1H), and 6.76—7.17 (m, aromatic, 9H). Found: C, 74.50; H, 8.51; N, 2.22%. Calcd for $C_{35}H_{48}ClNOS$: C, 74.24; H, 8.54; N, 2.47%.

References

1) Part 18 in the series "ESR Studies of Nitrogen-Centered Free Radicals." For Part 17, see: Y. Miura, A. Yamamoto, Y. Katsura, M. Kinoshita, S. Sato, and C. Tamura, *J. Org. Chem.*, **47**, 2618 (1982).

2) H. Zimmer, D. C. Lankin, and S. W. Horgan, *Chem. Rev.*, **71**, 229 (1971).

3) A. R. Forrester and R. H. Thomson, *J. Chem. Soc., C*, **1966**, 1844.

4) S. A. Hussain, T. C. Jenkins, and M. J. Perkins, *J. Chem. Soc., Perkin Trans. 1*, **1979**, 2809.

5) A. Rieker and H. Kessler, *Z. Naturforsch., B*, **21**, 939 (1966).

6) D. H. R. Barton, I. A. Blair, P. D. Magnus, and R. K. Norris, *J. Chem. Soc., Perkin Trans. 1*, **1973**, 1031.

7) Y. Miura, A. Yamamoto, Y. Katsura, and M. Kinoshita, *J. Org. Chem.*, **45**, 3875 (1980).

8) The mass spectrum of **21** showed no peak, probably due to the decomposition of the compound to polymeric products.

9) Y. Miura, A. Yamamoto, and M. Kinoshita, *Bull. Chem. Soc. Jpn.*, **54**, 3215 (1981).

10) Quinone imine **11** was gradually decomposed during the NMR measurement.

11) The ratio of *syn*:*anti* isomers is 1:5 (or 5:1) from the NMR spectrum.

A New Synthesis of Triphenodithiazines and Triphenodithiazinequinoes

Hisao Nishi,* Yuichi Hatada, and Kiyoshi Kitahara
Department of Applied Chemistry, Faculty of Engineering, Saitama University, Shimo-Okubo, Urawa 338
(Received November 4, 1982)

A new class of 6,13-bis(arylamino)triphenodithiazines has been synthesized by condensing chloranil with arylamines followed by the reaction of the resulting 2,5-bis(arylamino)-3,6-dichloro-1,4-benzoquinones with zinc 2-aminobenzenthiolates (**4**) in the presence of a base in Methyl Cellosolve. On the other hand, the reaction of 2,5-dianilino-3,6-dichloro-1,4-benzoquinone (**3a**) with **4** in DMF proceeded unexpectedly to give 7,14-dihydro-6,13-triphenodithiazinequinones by eliminating the anilino groups of **3a**.

Few triphenodithiazine ([1,4]benzothiazino[2,3-*b*]-phenothiazine) derivatives have been studied in comparison with triphenodioxazine derivatives, which are useful dyes and pigments.[1] Recently, however, Mital and Jain *et al.* have reported[2,3] the synthesis of 6,13-dichlorotriphenodithiazine and its derivatives. In a previous paper, we ourselves studied[4,5] the dechlorination of some 6,13-dichlorotriphenodithiazine (**Ia**) and -dioxazine (**Ib**) with tin powder in polyphosphoric acid (PPA), as is shown in Scheme 1. Then, it was

Table 1. 2,5-Bis(arylamino)-3,6-dichloro-1,4-benzoquinone derivatives **3**

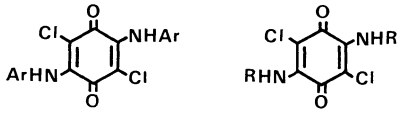

Compd No.	Substituent Ar or R	Yield %	Mp θ_m/°C	Appearance	N-Anal. Found (Calcd) (%)	Cl Br-Anal. Found (Calcd) (%)
3a		88	312—313	Black plates	7.88 (7.80)	20.5 (19.7)
3b	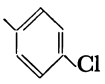	76	305—308	Black plates	6.65 (6.54)	34.6 (33.1)
3c	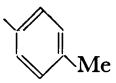	84	312—315	Black plates	7.34 (7.24)	19.4 (18.3)
3d	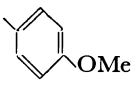	88	300—302	Dark green plates	6.85 (6.68)	17.0 (16.9)
3e		76	324—326	Brown needles	5.61 (5.42)	—
3f	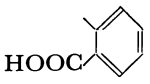	48	365 (decomp)	Brown needles	6.35 (6.24)	16.1 (15.9)
3g	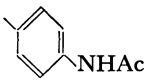	80	350 (decomp)	Greenish brown needles	12.1 (11.8)	15.4 (15.0)
3h		73	310 (decomp)	Dark brown needles	9.41 (9.38)	11.8 (11.9)
3i	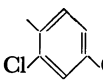	32	304—306	Brown needles	5.68 (5.63)	— (42.8)
3j	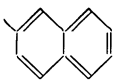	80	288 (decomp)	Black plates	6.32 (6.10)	16.7 (15.4)
3k		66	240—241	Reddish purple needles	7.86 (7.55)	18.7 (19.1)
3l	$-C_4H_9$	87	199—200	Reddish purple needles	8.91 (8.78)	22.0 (22.3)

clarified that the replacement of two chlorine atoms at the 6 and 13 positions by hydrogen atoms brought about a decrease in the melting point and a strong hypsochromic shift in the electronic spectrum.

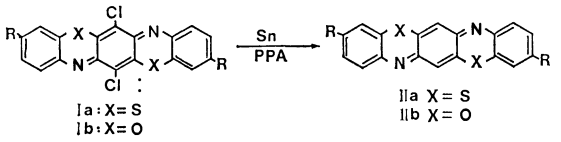

Scheme 1.

Furthermore, it will be interesting to ascertain the effects on the physical properties of the introduced bulky substituents at these positions. We wish here to report the synthesis and several properties of the new triphenodithiazines (**5**) and 7,14-dihydro-6,13-triphenodithiazinequinones (**6**). We have established these novel synthetic routes to be as is shown in Scheme 2. These compounds may be suited for new organic pigments.

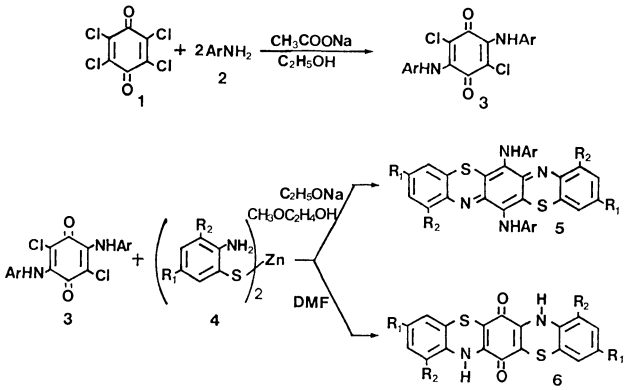

Scheme 2.

Results and Discussion

The condensation of chloranil **1** (1:2 molar ratio) with amines **2** in ethanol containing sodium acetates gave 2,5-bis(arylamino)-3,6-dichloro-1,4-benzoquinones (**3**) in good yields by using Mital's method.[2] These findings are summarized in Table 1.

Zinc 2-aminobenzenethiolate (**4a**) was prepared from commercial 2-aminobenzenethiol by Nodiff's method.[6] Zinc 2-aminobenzenethiolate derivatives **4b—h** were synthesized by improving Mital's method.[2] The basic hydrolysis of substituted 2-aminobenzothiazoles with 50% aqueous potassium hydroxide afforded the corresponding potassium 2-aminobenzenethiolates in the solution. These salts were converted to zinc 2-aminobenzenethiolates **4b—h** by the following treatment. That is, the potassium-salt solution was adjusted with acetic acid to pH 8 and filtered; then, methanol and zinc chloride in a 15% acetic acid solution were added to this filtrate. Some examples of these results are summarized in Table 2. The use of Compound **4** was necessary to cause the following reaction to proceed smoothly without forming a tarry product.

In the presence of sodium ethoxide, Compound **3** reacted with Compound **4** in 2-methoxyethanol (Methyl Cellosolve) to give 6,13-bis(arylamino)triphenodithiazine derivatives **5** as a new class of heterocycles. The

Table 2. Zinc 2-aminobenzenethiolate derivatives

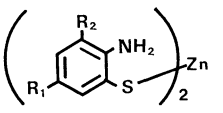

Compd No.	Substituent R_1	Substituent R_2	Yield %	Mp[a] θ_m/°C (decomp)	N-Anal. Found (Calcd) (%)	Mass M+ (mol wt)
4a	H	H	87	282	9.05 (8.93)	312 (313.76)
4b	Cl	H	86	274	7.40 (7.32)	380 (382.64)
4c	Me	H	87	300	8.44 (8.20)	340 (341.82)
4d	OMe	H	89	280	7.80 (7.50)	372 (373.82)
4e	Br	H	83	262	6.12 (5.94)	— (469.74)
4f	5,6-Benzo	H	53	244	6.93 (6.77)	412 (413.88)
4g	Cl	Cl	70	272	6.21 (6.20)	448 (451.52)
4h	Me	Me	54	248	7.64 (7.58)	368 (369.88)

a) These results were obtained by DTA.

synthetic results of Compound **5** are listed in Table 3. When the molar ratio of sodium ethoxide: Compound **3a** (Ar=phenyl) were equal to 1, 2, 4, and 8, Compound **5a** was obtained in yields of 26, 40, 42, and 29% respectively. The best yield of Compound **5a** was afforded by using a 1.5-fold excess of **4a** in relation to the **3a** in Methyl Cellosolve.

The decomposition point of Compound **5**, as examined by DTA, was observed to be as high as the other triphenodithiazines previously reported by us.[4,5] Especially, the replacement of two chlorine atoms at the 6 and 13 positions in Compound **Ia** to phenyl groups caused a rise in the decomposition point. Compound **5** was easily soluble in organic solvents. However, by the introduction of *p*-(benzamido)anilino groups at the 6 and 13 positions Compound **5** became sparingly soluble as compared with that of other arylamino groups.

The UV and visible absorption spectra showed 320—358 nm in H_2SO_4 and 555—621 nm in dioxane respectively. When the R_1 and R_2 substituents were hydrogen atoms, the UV and visible spectra of Compound **5** were found in the narrow regions of 320—328 nm and 555—560 nm respectively. These values were nearly the same as those of 6,13-dichlorotriphenodithazine[5] (**Ia**) (UV: λ_{max} 332 nm, visible: λ_{max} 560 nm) and triphenodithiazine[5] (**IIa**) (UV:λ_{max}(H_2SO_4) 321 nm, visible: λ_{max}(dioxane) 560 nm). It was suggested that the spectral change caused by conjugation effect was very little, for 6,13-disubstituted arylamino groups could not be coplanar with the triphenodithiazine ring.

The bathochromic effect was observed by introducing the substituents, R_1 and/or R_2. Especially, the annelation compound **5n** showed a remarkable shift in both UV and visible spectra. The streak colors of

TABLE 3. 6,13-BIS(ARYLAMINO)TRIPHENODITHIAZINE DERIVATIVES **5**

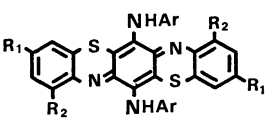

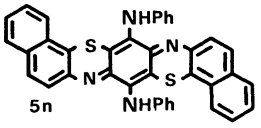

Compd No.	Substituent Ar	R_1	R_2	Yield %	Mp[a] θ_m/°C (decomp)	Appearance (Streak color)	N-Anal. Found (Calcd) (%)	Cl Br-Anal Found (Calcd) (%)	Visible[b] λ_{max}/nm ($\varepsilon \times 10^{-4}$)	UV[c] λ_{max}/nm ($\varepsilon \times 10^{-4}$)
5a		H	H	50	500	Green needles (Purple)	11.6 (11.2)	—	555 (5.0)	328 (5.9)
5b	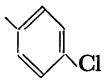	H	H	60	455	Green needles (Purple)	9.93 (9.84)	12.8 (12.5)	555 (4.3)	323 (4.4)
5c	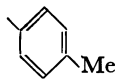	H	H	42	460	Green needles (Purple)	10.8 (10.6)	—	557 (4.0)	320 (4.3)
5d	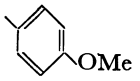	H	H	14	463	Brown needles (Purple)	10.2 (9.99)	—	559 (5.2)	324 (5.3)
5e	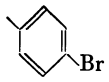	H	H	48	480	Brown needles (Purple)	8.54 (8.51)	25.1 (24.2)	555 (4.4)	323 (4.8)
5f	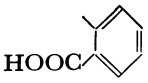	H	H	24	432	Blue needles (Purple)	9.38 (9.52)	—	558 (4.0)	330 (5.1)
5g	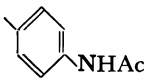	H	H	29	428	Brown needles (Purple)	13.9 (13.7)	—	560 (—)	328 (6.1)
5h		H	H	25	450	Purple powder (Purple)	11.5 (11.4)	—	560 (—)	326 (3.6)
5i	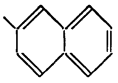	H	H	34	450	Brown needles (Purple)	9.36 (9.33)	—	557 (3.4)	326 (3.5)
5j		Cl	H	19	465	Brown needles (Violet)	9.85 (9.84)	12.7 (12.5)	579 (4.2)	337 (4.2)
5k		Me	H	20	495	Dark blue powder (Violet)	10.7 (10.6)	—	591 (5.2)	352 (5.1)
5l		OMe	H	16	460	Green needles (Violet)	10.2 (9.99)	—	578 (4.6)	336 (4.3)
5m		Br	H	25	390	Violet powder (Violet)	8.73 (8.51)	23.8 (24.2)	591 (3.6)	339 (3.5)
5n		3,4-Benzo	H	26	500	Brown needles (Blue)	9.37 (9.33)	—	621 (4.2)	358 (4.7)
5o	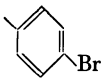	Br	H	28	500	Violet powder (Violet)	7.05 (6.87)	— (39.2)	586 (3.7)	336 (3.2)
5p	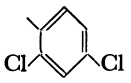	Cl	Cl	26	443	Violet powder (Violet)	7.29 (7.22)	— (36.6)	599 (3.5)	345 (3.0)
5q		Cl	H	32	390	Violet powder (Violet)	10.6 (10.4)	8.81 (8.78)	590 (3.9)	337 (4.3)

a) These results were obtained by DTA. b) In dioxane. c) In H_2SO_4.

TABLE 4. 6,13-TRIPHENODITHIAZINEQUINONE DERIVATIVES **6**

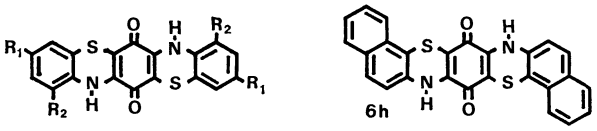

Compd No.	Substituent R_1	Substituent R_2	Yield %	Mp[a] θ_m/°C (decomp)	Appearance (Streak color)	N-Anal. Found (Calcd) (%)	Cl Br-Anal. Found (Calcd) (%)	Visible[b] λ_{max}/nm ($\varepsilon \times 10^{-4}$)	UV[b] λ_{max}/nm ($\varepsilon \times 10^{-4}$)	IR ν_{N-H} cm^{-1}	IR $\nu_{C=O}$ cm^{-1}
6a	H	H	73	393	Blue powder (Blue)	7.91 (8.00)	—	723 (5.6)	334 (6.2)	3240	1635
6b	Cl	H	68	414	Blue powder (Blue)	6.65 (6.68)	17.1 (17.9)	733 (6.8)	337 (6.3)	3240	1630
6c	Me	H	66	357	Blue powder (Blue)	7.45 (7.40)	—	749 (6.4)	335 (6.2)	3250	1635
6d	OMe	H	64	342	Blue powder (Greenish blue)	6.89 (6.83)	—	773 (5.2)	331 (6.4)	3200	1630
6e	Br	H	55	417	Dark blue powder (Greenish blue)	5.63 (5.51)	30.6 (31.4)	749 (5.6)	340 (5.2)	3250	1635
6f	Cl	Cl	15	417	Green powder (Greenish blue)	5.81 (5.74)	28.9 (29.1)	748 (6.7)	348 (6.8)	3240	1640
6g	Me	Me	34	372	Dark blue powder (Blue)	6.94 (6.89)	—	750 (6.8)	342 (6.7)	3250	1640
6h	3,4-Benzo	H	57	420	Green powder (Green)	6.32 (6.22)	—	860 (5.7)	362 (6.6)	3250	1620

a) These results were obtained by DTA. b) In H_2SO_4.

Compound **5** were from purple to blue.

The IR absorption spectra in KBr showed the N–H stretching band (around 3300 cm^{-1}) and the disappearance of the C=O stretching band (around 1660 cm^{-1}) of Compound **3**.

On the other hand, the reaction of Compound **3a** (Ar=phenyl) with Compound **4** in *N*,*N*-dimethyformamide (DMF), in the absence of a base, afforded 7,14-dihydro-6,13-triphenodithiazinequinone derivatives **6** by eliminating the anilino groups of Compound **3a**.[7] The synthetic results of Compound **6** are listed in Table 4. Some of the triphenodithiazinequinones have already been synthesized by another synthetic route.[8] A good yield of Compound **6a** (unsubstituted) was obtained only when the molar ratio of **3a**:**4a** was 1:2 in DMF. This reaction was tested in various solvents: chlorobenzene, nitrobenzene, anisole, acetic acid, cyclohexanol, Methyl Cellosolve, DMF, *etc.* Consequently, DMF was found to be the best solvent for dissolving **3** together with **4**.

Several **3** compounds as well as **3a** reacted with **4a** to give the same compound, **6a**, in 60—68% yields. When **3k** (R=cyclohexyl) or **3l** (R=butyl) was used as the starting material, however, Compound **6a** was obtained in a low yield.

The **6** compounds decomposed at 342—420 °C, and the streak colors were from blue to green. Because the **6** compounds were sparingly soluble in the usual solvents, then UV and visible absorption spectra were measured as 331—362 nm and 723—860 nm respectively in H_2SO_4. Accordingly, the visible spectra were actually observed in the near-infrared region. The bathochromic effect of Compound **6** was observed as well as that of Compound **5**.

The IR absorption spectra in KBr showed a N–H stretching band (around 3250 cm^{-1}) and a C=O stretching band (around 1630 cm^{-1}).

It may be assumed that the reaction mechanisms are based on Pearson's HSAB (Hard and Soft Acids and Bases) principle[9], as is shown in Schemes 3a and 3b. The mechanisms in the residual side of the intermediate can also be similarly.

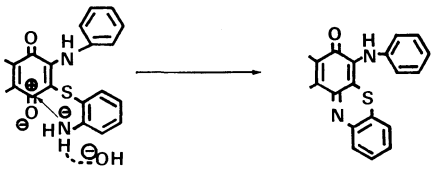

Scheme 3a. Hard acid and hard base type.

Scheme 3b. Soft acid and soft base type.

Experimental

The melting points are uncorrected. The DTA was measured on Rigaku Denki YGHD. The IR spectra were taken with a JASCO IRA-2 apparatus. The UV and visible spectra were recorded with a Hitachi EPS-3T apparatus.

Condensation of Chloranil ***1*** *with Amines* ***2***. To a stirred

suspension of **1** (0.025 mol) and sodium acetate (0.061 mol in ethanol (50 ml), we added arylamine **2** (0.10 mol). The mixture was then heated under reflux for 3—5 h and filtered while still hot. The residue was washed with ethanol, hot water, and water, and dried. Recrystallization from the appropriate solvents gave 2,5-bis(arylamino)-3,6-dichloro-1,4-benzoquinones (**3**) in a good yield. The yield and properties of **3** are listed in Table 1.

Preparation of 6,13-Dianilino-type ***5***. A mixture of **3** (0.0025 mol), zinc salt of substituted 2-aminobenzenethiol **4** (0.0025 mol), and sodium ethoxide (0.0075 mol) was refluxed for 6—8 h in Methyl Cellosolve (150 ml) and then cooled overnight. The precipitated solid was collected, washed with Methyl Cellosolve, ethanol, hot 3 M HCl (1 M=1 mol dm^{-3}), and water, and dried. Recrystallization from *o*-dichlorobenzene produced 6,13-bis(arylamino)triphenodithiazines (**5**). The yield and properties of **5** are listed in Table 3.

Preparation of 6,13-Quinone-type ***6***. A mixture of **3** (0.0025 mol) and **4** (0.0050 mol) in DMF (50 ml) was refluxed for 12 h and filtered while still hot. The residue was washed with hot DMF until the filtrate was almost colorless, washed with ethanol, and dried. Further, the solid was washed with hot 3 M HCl for a long time and then with water, and dried. Sublimation *in vacuo* gave 7,14-dihydro-6,13-triphenodithiazinequinones (**6**). The yield and properties of **6** are listed in Table 4.

References

1) H. Nishi and M. Kubo, *Senryo To Yakuhin*, **21**, 177 (1976).
2) R. L. Mital and S. K. Jain, *J. Chem. Soc., C*, **1971**, 1875.
3) N. K. Goswami, R. R. Gupta, and S. K. Jain, *Indian J. Chem., Sect. B*, **19**, 4 (1980).
4) H. Nishi, M. Kubo, S. Tokita, A. Ejima, and M. Murayama, *Nippon Kagaku Kaishi*, **1977**, 588.
5) H. Nishi and M. Murayama, *Nippon Kagaku Kaishi*, **1979**, 432.
6) E. D. Nodiff and M. Hausman, *J. Org. Chem.*, **31**, 625 (1966).
7) H. Nishi, U. Hatada, K. Kitahara, and K. Muroi, *Nippon Kagaku Kaishi*, **1982**, 1579.
8) R. Shibata, *Kogyo Kagaku Zasshi*, **30**, 438 (1928).
9) T.-L. Ho, "Hard and Soft Acids and Bases Principle in Organic Chemistry," Academic Press, New York (1977).

 © 1983 The Chemical Society of Japan Bull. Chem. Soc. Jpn., 56, 1487—1489 (1983)

Conformations and Restricted Rotation about Amide C–N Bonds of 2,2-Dichloro-1′-formyl-3′,4′-dihydrospiro[cyclopropane-1,2′(1′*H*)-quinoline] and Related Compounds

Hiroko Suezawa (née Endo), Minoru Hirota,* Michiharu Sugiura,† and Yoshiki Hamada†

Department of Applied Chemistry, Faculty of Engineering, Yokohama National University, Hodogaya-ku, Yokohama 240

† *Faculty of Pharmacy, Meijo University, Tempaku-ku, Nagoya 468*

(Received November 5, 1982)

Conformational preference and rotational barriers of 1′,1′,2,2-tetrachloro-3′-formyl-1′a,7′b-dihydrospiro-[cyclopropane-1,2′(3′*H*)-cyclopropa[*c*]quinolines] (**1**) and related *N*-formyl heterocyclic compounds were determined by ^{1}H- and ^{13}C-NMR spectroscopy. The *sp*-conformer is usually more preferable in **1** and their rotational barriers about amide C–N bond are within a relatively narrow range from 70.7 to 72.8 kJ mol^{-1}. Infrared carbonyl absorptions of these compounds also support the preferred conformation from the NMR data. The results were discussed from the view point of N–C=O conjugation.

In the course of investigations on mono- and diazanaphthalenes and related heterocycles, a new synthesis of cyclopropa[*c*]quinolines,[1] 2,2-dichloro-1′-formylspiro-[cyclopropane-1,2′(1′*H*)-quinoline] and related heterocyclic amides[2,3] have been reported by the present authors. Steric effect on the conformations and dynamic behaviors of these amides are very interesting, since they have sterically hindered *N*-formyl groups. The rotational barriers of amides have been studied very extensively, and a great deal of investigations have been reported.[4] One of the present authors has also studied the effect of intramolecular hydrogen bonding on the rotational barrier of *N*,*N*-dimethylbenzamide.[5] In this connection, the conformational preference and rotational barriers of 1′,1′,2,2-tetrachloro-3′-formyl-1′a,7′b-dihydrospiro[cyclopropane-1,2′(3*H*)-cyclopropa[*c*]quinolines] (**1**), 2,2-dichloro-5′-formylspiro[cyclopropane-1,6′(5′*H*)-phenanthridine] (**2**), and related compounds were determined and discussed from the view of the ring-conformation and steric hindrance on the amide group in this paper.

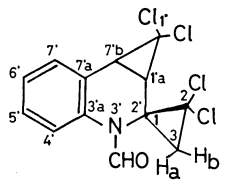

1

a: Unsubstituted
b: 6′-CH_3 d: 7′-CH_3
c: 6′-C_2H_5O e: 7′b-CH_3

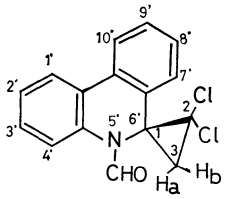

2

a: Unsubstituted
b: 3-CH_3

Experimental

Preparation and identification of the materials were reported previously.[1-3,6] Commercially available spectro grade solvents were used without further purification. Temperature-dependent ^{1}H-NMR spectra were recorded on a JEOL JNM C-60H spectrometer. The exchange rates between the two sites (usually unequivalent) were evaluated by use of total line shape analysis program. NOE measurements were carried out with a JEOL JMN FX-90Q spectrometer. Infrared spectra were measured on carbon tetrachloride solutions using a Hitachi 225 infrared spectrophotometer.

Results and Discussion

Rotational Barriers about the C–N Bonds of N-*Formyl Groups and Conformational Preference.* In order to examine steric and electronic effects on the rotational barrier of **1**, ^{1}H dynamic NMR measurements were carried out on the following compounds in addition to **1** and **2**.

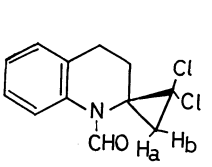

3

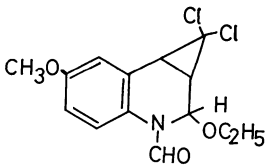

4

a: Unsubstituted
b: 3′-Br-4′-OCH_3

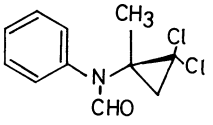

5

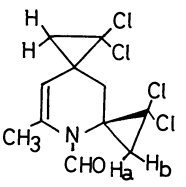

6

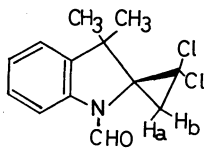

7

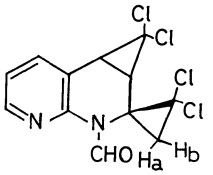

8

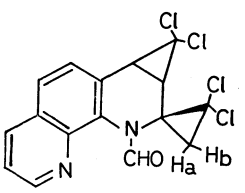

9

Table 1. ^{1}H-DNMR results (in $CDCl_3$) and infrared C=O absorptions (in CCl_4) of the heterocyclic amides **1**—**9**

Compd	CHO Chemical shift (Relative intensity)		T_c	ΔG^{*} a)	$\nu_{C=O}$	
	sp	*ap*	K	kJ mol^{-1}	cm^{-1}	
1a	8.43(66)	8.30(34)	321.2	72.4	1709	1700 sh
1b	8.32(70)	8.21(30)	321	72.0	1708	1701 sh
1c	8.31(66)	8.23(34)	320	72.8	1706	1700 sh
1d	8.33(70)	**8.20**(30)	321	72.0	1709	1700 sh
1e	8.32(73)	8.20(27)	310	70.7	1709	1700 sh
2a	8.50(75)	8.45(25)	307.3	72.8	1702	1696 sh
2b	8.53(20)	8.41(80)	312.2	69.0	1697	1702 sh
3a	8.56(66)	8.45(34)	306	68.2	1696	1702 sh
3b	8.80(45)	**8.46**(55)	288.0	61.9	1708	1701 sh
4 b)	8.45(38)	8.65(62) c)	363.2	80.8	1695	1701 sh
5	8.53(20)	8.44(80)	312	69.9	1700	1707 sh
6	**8.10**(35) d)	**8.45**(65) d)	324.8	70.7	1700	1707 sh
7	8.83(30)	**8.30**(70)	304.7	63.2	1687	1700 sh
8	9.05(100) e)					
9	8.90(100) e)					

a) ΔG^{*} values are always given with respect to the more stable conformer (at 298.2 K). b) In DMSO-d_6. c) Synperiplanar to ethoxyl group. d) With reference to vicinal CH_3 group. e) A sharp singlet at −60 °C.

The DNMR data including free energies of activation of these *N*-formyl azaheterocycles are given in Table 1, together with the chemical shift and intensity data at the temperatures below coalescence temperatures (T_c). Coalescence of the two formyl signals usually occurs near room temperature.

Since amide group has a tendency to take a planar conformation, the two different planar (or nearly planar) conformers ((A) and (B) in Fig. 1) are possible in these heterocyclic amide, each of which giving a separate formyl proton signal below T_c. With the compounds **1**—**6**, the signal at the lower field was assigned to the formyl proton *syn* to aromatic ring and the one at the higher field to the *anti* formyl proton. The assignment was ascertained by the nuclear Overhauser enhancement of *anti*-formyl proton by irradiation of 3-hydrogen atom (H_a) on the spirocyclopropane ring in some typical instances. Two formyl signals in **6** were assigned unambiguously by NOE

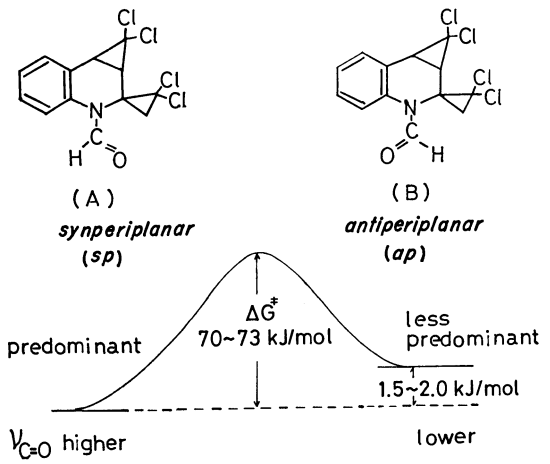

Fig. 1.

experiments irradiating both cyclopropyl methylene (H_a) and vicinal methyl groups (Chemical shifts given by bold letters in Table 1 were assigned by NOE.). The compound **1a** is expected to have a nearly planar and rather rigid tetrahydropyridine ring, because it has a fused cyclopropane ring on the 3 and 4 positions (1′a and 7′a positions of the new ring system). Thus the spirocyclopropane ring lies nearly perpendicular to the heterocyclic ring and facing to the formyl group. The *sp*-conformation is generally more stable than the *ap*-conformation in **1a**—**d**, the free energy difference between the two conformers being 1.5—2.0 kJ mol^{-1}. Since several evidence concerning the steric hindrance of *peri*(8)-hydrogen atom towards the planarity of 1-carbonyl group on the naphthalene nucleus have been reported,[8] the destabilizing effect due to *peri*-hydrogen might be the reason for the preference of *sp*-conformer in **1a**—**d**. Introduction of electron-donating substituent *para* to the formamide moiety on the aromatic ring is expected to lessen the resonance contribution by the aromatic ring and to increase the rotational barrier of the C–N bond. . However, the ΔG^{*} values of **1b**—**d** agree with that of **1a**, showing no indication of substituent effect. Methyl substituent on 7′a-position in **1e** again does not affect the rotational barrier considerably. The ΔG^{*} and the conformational ratios of **2** are also very close to those of **1**. This can be another evidence for the nearly planar ring conformation of **1**.

^{13}C-NMR data of **1** and **2** are given in Table 2. These compounds have two separate signals in the carbonyl region. Since the formyl carbon atom is not expected to be displaced considerably by rotating the formyl group around the C–N bond, through-space field and anisotropy effect is assumed to be nearly identical on the carbonyl carbon atoms of the both conformers. Therefore, the difference in chemi-

Table 2. ^{13}C-Chemical shifts

Orientation of C=O group	*sp*-Conformer Towards dichloro-cyclopropropyl	*ap*-Conformer Towards aromatic ring
1b	164.5	160.9
1c	164.5	160.9
1e	164.9	160.9
2a	162.7	160.4
2b	162.4	160.4
3a	163.5	160.9
9	167.7	—

cal shifts should arise from the change in conjugation effect through C–N bond. This can be another evidence for the steric hindrance in different degrees to the planarity of conformers of **1** and **2**.

The rotational barriers of **3a**, **5**, and **6** (68.2, 69.2, and 70.7 kJ mol^{-1}, respectively) are almost similar to those of **1** and **2**, suggesting the similarity in conformations around the formyl groups of these compounds. Dispiro[cyclopropane-1,2′(1′*H*)-pyridine-4′,(3′*H*) 1″-cyclopropane] (**6**) is void of fused aromatic ring. However, it is reasonable that its ΔG^* value is almost identical with those of **1**, since the steric effect by *ortho*-methyl group is nearly equivalent to that of *peri*-hydrogen atom as evidenced by other experiments of the authors.[9] *N*-(2,2-Dichloro-1-methylcyclopropyl)formanilide also supposed to take a nearly planar conformation to keep the cross-conjugated amide system including cyclopropyl moiety. 1′-Formyl-3′,3′-dimethylspiro[cyclopropane-1,2′-indoline] (**7**) has a considerably low rotational barrier about the amide C–N bond. It is quite unexpected since the steric hindrance to the planarity seems less in this five-membered analog **7**. The rotational barrier about the similar bond of *N*-formylindoline has however been reported to be 64.8 kJ mol^{-1},[10] which is very close to the ΔG^* of **7**.

As a model for a formanilide in which aryl–nitrogen conjugation is forbidden perfectly by steric hindrance, the rotational barrier of *N*,2′,6′-trimethylformanilide (**10**) was determined to be 77.0 kJ mol^{-1}. The barrier is considerably high. This fact can be interpreted that the steric inhibition of Ar–N conjugation enhances the effect of N–C=O conjugation, resulting higher $C_{carbonyl}$–N bond order. The barriers of **1** and **2** are considerably lower than that of **10**. This implies the persistence of conjugative effect by aromatic system in **1** and other compounds of similar ΔG^* values, in spite of considerable deviation from the planarity and cross-conjugative effect by the carbonyl group.

The Infrared Carbonyl Frequency and Conjugative Effect. Frequencies (in cm^{-1}) of the carbonyl stretching absorption bands of **1**—**9** are given in Table 1. Carbonyl stretching frequency of amide is affected most remarkably by the amount of resonance contribution of mesomeric structure D. The contribution of D is suppressed both by the loss of the planarity of N–C=O system and the neighbor electronegative group repelling the negative charge on the carbonyl oxygen atom. In the case of the heterocyclic amide carrying spiro(dichlorocyclopropane)moiety (**1**, **3**, **5**, and **6**), the carbonyl group *syn* to the cyclopropane moiety absorbs at 1707—1709 cm^{-1}, considerably higher frequency than normal formanilide (for example, 1686 cm^{-1} for $C_6H_5NMeCHO$ (**11**)). The high frequency shift can be attributed to the neighbor electronegative group effect, in a through space manner, by the dichlorocyclopropane moiety. The carbonyl group opposing to *peri*-hydrogen atom generally absorbs at 1700—1701 cm^{-1}. The frequency is also considerably higher than that of **11**, suggesting the deviation from the planarity in this conformer. Intensities of the two carbonyl bands (in Table 1) agree qualitatively with the abundances of the two conformers which are estimated from the intensities of their ^{1}H signals at low temperatures (Table 1). Both carbonyl bands of the phenanthridine derivatives **2** shifts to *ca.* 5 cm^{-1} lower frequencies than the corresponding bands of **1**. Low frequency shifts are also observed with the carbonyl bands of **4** which is void of dichlorocyclopropane moiety. *N*-Formyltetrahydro-1,8-naphthyridine derivative **8** shows a single formyl signal at a very low field (9.05 ppm) in ^{1}H-NMR and also a symmetrical carbonyl band at 1712 cm^{-1}. This behavior is best explained by assuming that the *sp*-conformer is extremely stable, probably because of the electrostatic repulsive force between the lone pair electrons on heteroaromatic nitrogen and on carbonyl oxygen. Weak hydrogen bond-like attractive interaction between formyl hydrogen and lone pair electrons on heteroaromatic nitrogen is also possible.

The authors are grateful to Dr. Kazuhisa Abe for his kind advice and assistance throughout this work. This research was supported in part by the Grant-in-Aid for Special Project Research from the Ministry of Education, Science and Culture.

References

1) M. Sugiura, Y. Hamada, and M. Hirota, *Chem. Pharm. Bull.*, **27**, 1518 (1979).
2) Y. Hamada and M. Sugiura, *Yakugaku Zasshi*, **100**, 168 (1980).
3) Y. Hamada, M. Sugiura, and M. Hirota, *Tetrahedron Lett.*, **22**, 2893 (1981).
4) For review, see L. M. Jackman, "Dynamic Nuclear Magnetic Resonance Spectroscopy," ed by L. M. Jackman and F. A. Cotton, Academic Press, New York (1975), pp. 204—215.
5) M. Hirota and K. Todokoro, *Chem. Lett.*, **1974**, 777.
6) Y. Hamada and M. Sugiura, Preprint of the Tokai Regional Meeting of the Pharmaceutical Society of Japan, Nagoya, Oct. 1981, p. 108.
7) The conformations A and B (in Fig. 1) was named synperiplanar (*sp*) and antiperiplanar (*ap*), respectivily, with reference to the orientation of carbonyl oxygen to spirodichloropropane ring.
8) M. Ōki, M. Hirota, and S. Hirofuji, *Spectrochem. Acta*, **22**, 1537 (1966) and cited therein. On the steric effect of similar type in carbonium ions, see H. C. Brown, "Steric Effects in Conjugated System," ed by G. W. Gray Butterworths Publ. Ltd., London(1958), p. 103.
9) Y. Nagawa, M. Ono, M. Hirota, Y. Hamada, and I. Takeuchi, *Bull. Chem. Soc. Jpn.*, **49**, 1322 (1976); T. Kogane, R. Hirota, K. Abe, and M. Hirota, *J. Chem. Soc., Perkin Trans. 2*, **1981**, 652.
10) O. Buchardt, P. L. Kumler, and C. Lohse, *Acta Chem. Scand.*, **23**, 1155 (1969).

Photoinduced Alcoholysis of α,α,α-Tribromoacetophenone to Benzoylformate

Yasuji IZAWA, Katsuhiro ISHIGURO, and Hideo TOMIOKA*

Department of Industrial Chemistry, Faculty of Engineering, Mie University, Tsu, Mie 514

(Received November 8, 1982)

Irradiation of *p*-substituted α,α,α-tribromoacetophenones (**1**) in O_2-saturated alcohols (MeOH, prim. and sec. alcohols) afforded a new alcoholysis product, benzoylformate (**2**), in good yield (75—85%) along with benzoate and radical (reduction) products. Sensitization experiments showed that **2** was derived from the triplet excited **1**. Formation of **2** as well as the decomposition rate of **1** were greatly accelerated by oxygen, presumably as a result of the involvement of the normally forbidden $S_0 \rightarrow T_1$ transition of **1** due to the oxygen-**1** charge transfer complex. Independent synthesis and reaction of possible intermediates in the photoalcoholysis of **1** leading to **2** suggested that **2** was formed from spontaneous (dark) reactions of initial photoalcoholysis product, α,α-dibromo-α-alkoxyacetophenone.

Since photoinduced solvolysis reactions of nitrophenyl phosphates were first discovered by Havinga *et al.*,[1] related reactions were found to occur with other aromatic esters, ethers, halides, *etc.*, reacting with a variety of nucleophiles.[2] Interest has increased in this new domain of chemistry, not only from the stand-point of the reaction mechanism but also from a synthetic viewpoint. These reactions often proceed to a high degree of conversion—resulting in good yields of products which are sometimes difficult to prepare by other reactions. Although the investigations in this field had been mainly focussed on the aromatic photosubstitutions, since the report[3] by Zimmerman and Sandel on the photosolvolysis of benzyl acetate in aqueous dioxane to form benzyl alcohol, a considerable amount of work has been reported[4-9] on the photochemistry of benzyl compounds, mainly benzyl halides, in nucleophilic solvents. It has been reported that products resulting from both heterolysis and homolysis of the benzyl-heteroatom are formed either upon direct irradiation or upon photosensitization. Apart from work with benzyl halides there has been increasing interest paid recently to photolysis of alkyl and cycloalkyl halides.[10,11] Contrary to the earlier belief that only radical intermediates are involved, it becomes clear that cationic, as well as free radical, intermediates may also play an important role in the solution-phase photochemistry of simple alkyl halides. Competing ionic and radical photobehavior has also been observed[12-14] for haloalkenes. However, there are only a few reports on the study of photochemical behavior of α-halo carbonyl compounds. Although the intervention of an α-keto carbonium ion has been suggested in the photoelimination[15] and photorearrangement[16] of some α-halo ketones, few attempts have been made to trap α-keto carbonium ions intermolecularly with nucleophiles. We have already shown that the intermediate generated photolytically from α-halo esters can be trapped by phosphite[17] and electron-rich aromatic nuclei.[18] As an extension of this study, we examined the photolysis of α,α,α-trichloroacetophenone in alcohols and found[19] that a new photoalcoholysis product benzoylformate was formed, albeit in low yield (≈10%), along with other radical products. The formate clearly arose from nucleophilic trapping of ionic species. Since thermal (dark) nucleophilic attack of alcohol on trihaloacetophenone is known to occur exclusively at the carbonyl function to give benzoate (haloform reaction), the formation of formate in the present photoalcoholysis reaction is quite significant and in sharp contrast with the other photosolvolysis reactions in which the type of photoproducts is mostly similar to that obtained in the dark reaction. Thus, it is of obvious interest to get deeper insight into the nature of this novel photoalcoholysis. We wish to report here that tribromoacetophenone undergoes the photoalcoholysis much more efficiently than the trichloro analog, forming benzoylformate in much higher yield (75—85%). The present study also reveals the important role of oxygen, the excited state intermediates leading to photoalcoholysis, and the chemical intermediates leading to benzoylformate.

Results and Discussion

Irradiation of an oxygen-saturated solution of α,α,α-tribromoacetophenone (**1a**) in MeOH for 2 h resulted in the formation of methyl benzoylformate (**2a**, R=Me, 76%) as the main product along with small amounts of methyl benzoate (**3**, R=Me, ≈1%), di- (**4**), and monobromoacetophenones (**5**) (<5%). The identity of these products was confirmed by comparison with authentic samples. Control experiments showed that there was no reaction under identical conditions in the absence of light. Plots of the product yields determined by GC as a function of irradiation time in MeOH (Fig. 1) suggest that esters (**2** and **3**) and the dibromide (**4**) are the primary photoproducts of tribromoacetophenone, but that monobromide (**5**) is apparently derived from **4**. Control experiments also showed that irradiation of **4** in MeOH gave **5**

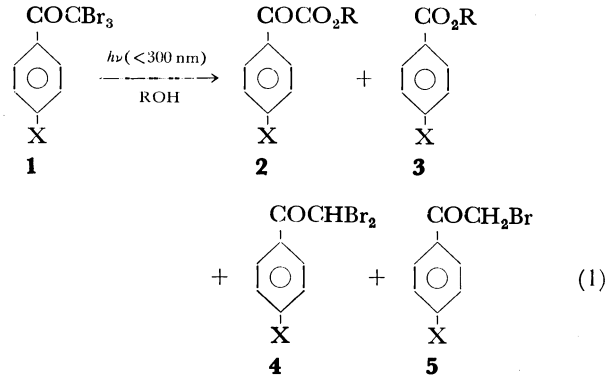

(1)

a: X=H, **b**: X=MeO, **c**: X=Br, **d**: X=CN.

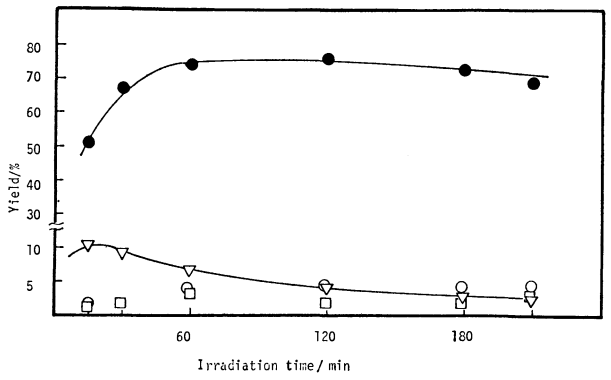

Fig. 1. Yields of **2a** (●), **3a** (□), **4a** (▽), and **5a** (○) during irradiation of **1a** in non-degassed methanol.

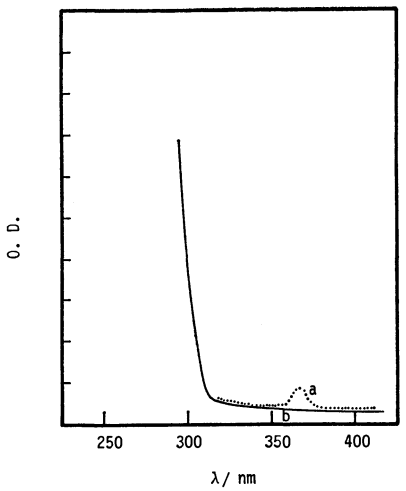

Fig. 2. Absorption bands induced by saturation with oxygen; a) saturated with oxygen, b) after degassing by bubbling argon.

along with small amounts of the esters (**2** and **3**). The latter two acetophenones apparently arise at least principally *via* radicals. On the other hand, the major photoproduct **2** clearly arises from nucleophilic trapping of ionic species. This alcoholysis is applicable to a wide variety of alcohols as summarized in Table 1. Yields of formate **2** were generally good (75—85%) for MeOH and the primary and secondary alcohols, but decreased rather sharply with tertiary alcohol-concomitant with formation of several by-products, *e.g.*, benzaldehyde. This is in a marked contrast with the similar photolysis[19] of trichloroacetophenone in an alcohol, where the yields of formate are generally low (≈10%) and the main products are radical products, *e.g.*, dichloroacetophenone. Photolysis of trifluoroacetophenone in alcohol gave neither the alcoholysis product nor radical products.

Effects of Oxygen. Since oxygen has been shown[10] to have a marked effect on some photosolvolytic processes, we next examined the effect of oxygen on the present photoalcoholysis reaction. The results summarized in Table 2 indicate that oxygen has a marked effect on the product ratio. When the solution was purged with oxygen for 30 min before irradiation, the formation of the formate (**2**) as well as the rate of decomposition of **1** were substantially increased. But when the solution was deoxygenated by bubbling argon, both the formation of **2** and the decomposition rate were suppressed, concomitant with appreciable increase in the dibromide (**4**). In connection with the acceleration of the reaction by oxygen, we have examined the UV absorption spectra of **1** in the presence and absence of oxygen. Oxygen-saturated tribromoacetophenone shows a contact charge transfer spectrum with oxygen at around 363 nm, which disappears on bubbling with argon (Fig. 2). The involvement of the charge-transfer (CT) complex in the photoalcoholysis reaction was shown by irradiating the CT band selectively with monochromatic light. Thus, when the irradiation of the monochromatic light of 363 nm was carried out in the presence of oxygen, the yield of the formate was about three

Table 1. Yields of **2**—**5** from irradiations of **1** in ROH[a]

Tribromo-acetophenone	ROH	Irradiation time/h	Yield/%[b]			
			2	**3**	**4**	**5**
1a	MeOH	2.0	76.4(76.0)	5.5	4.3	1.2
	EtOH	1.0	81.5(76.6)	1.9	3.6	1.5
	n-PrOH	2.0	73.3(69.0)	≈1	5.0	2.3
	i-PrOH	2.0	76.4(70.3)	≈1	4.2	≈1
	n-BuOH	2.0	76.4	≈1	3.2	1.3
	i-BuOH	3.5	86.8	≈1	2.5	1.0
	s-BuOH	2.0	75.5	≈1	3.2	≈1
	t-BuOH[c]	3.5	4.9	3.6	2.3	≈1
1b	MeOH	2.0	61.9	4.4	5.8	≈1
1c	MeOH	2.0	86.2	7.8	3.2	≈1
1d	MeOH	2.0	59.0	3.5	5.4	≈1

a) Irradiations were performed on a 40 mM (1 M = 1 mol dm^{-3}) solution of **1** in Pyrex tubes at 10 °C. The solution was purged with oxygen before irradiation. b) Determined by GC. The maximum yields of **2** from time-conversion curves (See Fig. 1) were indicated. Yields in parentheses refered to isolated product based upon **1** used. c) PhCHO was formed in ≈40% yield.

Table 2. Effect of oxygen on photoreaction **1a** in MeOH[a]

Conditions[b]	λ/nm	Irradiation time/min	Conversion %	Yield/%[c]			
				2a	**3a**	**4a**	**5a**
O_2	Hg[d]	15	65.6	51.0	2.0	10.4	1.2
	Hg[d]	30	91.4	67.5	2.0	8.6	2.0
	363[e]	70	—	32.0	<1	≈1	<1
	265[e]	70	—	9.8	<1	5.4	2.0
Ar	Hg[d]	15	51.2	18.0	1.7	20.3	1.3
	Hg[d]	30	84.5	25.7	3.9	19.9	1.4
	363[e]	70	—	11.2	<1	≈1	<1
	265[e]	70	—	12.4	<1	6.5	1.5

a) Irradiations were performed on a 40 mM solution of **1a** in Pyrex tubes at 10 °C. b) The solution was purged with oxygen (O_2) or argon (Ar) for 30 min before irradiation. c) Determined by GC. d) 300W high pressure mercury lamp. e) Monochromatic light from 250W Xenon lamp.

Table 3. Effect of sensitizer and quencher on photoreaction of **1a** in MeOH[a]

Additive	Yield/%[b]			
	2a	**3a**	**4a**	**5a**
None	51.0	2.0	10.4	1.2
Ph_2CO[c]	66.3	1.3	2.3	<1
1,3-Pentadiene[d]	30.8	<1	13.8	3.5
Cyclohexene[d]	35.7	<1	16.9	4.2
Hydroquinone[d]	32.5	<1	15·8	5.2

a) Irradiations were preformed on a 40 mM solution of **1a** in oxygen-saturated MeOH in Pyrex tubes at 10 °C for 15 min. b) Determined by GC. c) About 5-fold excess of Ph_2CO was added as a triplet sensitizer. Irradiated with monochromatic light of 366 nm. d) 0.5 mM.

times that obtained in the similar irradiation in the absence of oxygen. The yield of **2** was not appreciably altered by oxygen when the absorption maximum of **1** (265 nm) was irradiated. It should be noted that the product distributions exhibited a wavelength dependence. That is, the yield of radical products was higher at 265 nm than at 363 nm.

Sensitization and Quenching Studies. When the irradiation was carried out in the presence of benzophenone as a triplet sensitizer with monochromatic light of 366 nm, where >98% of the incident light was absorbed by the sensitizer, the yield of **2** was essentially unaltered with its rate of formation being accelerated (Table 3). This indicates that **2** is essentially derived from the triplet excited state of **1**. Addition of 1,3-pentadiene as a triplet quencher in the reaction caused a marked decrease in the formate formation (Table 3). However, the examination of the product distributions as a function of the concentration of 1,3-pentadiene showed that the formation of dibromide, as well as the decomposition rate of **1**, increased as the concentration of the quencher was increased. The data are presented graphically in Fig. 3 in the usual form of a Stern-Volmer plot. A possible explanation is that 1,3-pentadiene is not acting as a triplet quencher, but as a hydrogen-atom donor. This was easily confirmed by the findings that the Stern-

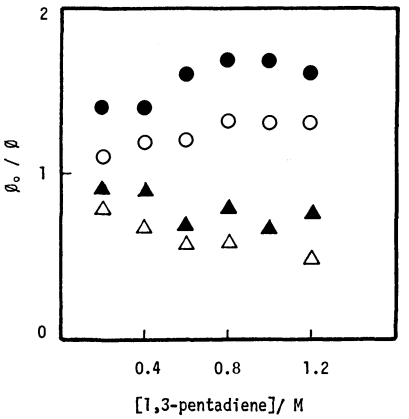

Fig. 3. Effect of 1,3-pentadiene on the quantum yield for formation of **2a** (●), **3a** (○), and **4a** (▲) from **1a** (△) in methanol.

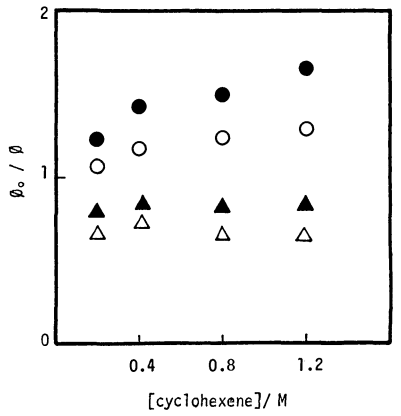

Fig. 4. Effect of cyclohexene on the quantum yield.

Volmer plot using cyclohexene, a good hydrogen donor, also resulted in similar dependence of product distributions (Fig. 4). These results can be interpreted as indicating that there is a delicate balance between ionic (photoalcoholysis) and radical (photoreduction) pathways.

Effects of Solvent. The present photoalcoholysis can be similarly carried out in a mixture of MeOH and solvent (1:10 v/v), instead of absolute MeOH. As summarized in Table 4, however, the product

Table 4. Effect of solvent on photoreaction of **1a** in MeOH[a)]

Solvent	Yield/%[b)]			
	2a	**3a**	**4a**	**5a**
MeCN	38.1	<1	15.9	2.9
Et_2O	23.4	2.4	19.9	6.1
EtOAc	23.5	<1	16.8	4.2
$CHCl_3$	27.7	1.4	15.7	3.5
PhH	52.5	3.2	3.2	<1
CCl_4	64.1	1.0	<1	<1
None[c)]	51.0	2.0	10.4	1.2

a) Irradiations were performed on a 40 mM solution of **1a** in oxygen-saturated mixtures of MeOH and solvent (1:10 v/v) in Pyrex tubes for 15 min. b) Determined by GC. c) Absolute MeOH was used as solvent.

distributions were somewhat sensitive to the nature of solvent employed. Notably, the significant increase in the yield of **2** was observed in CCl_4 and benzene, while the yield was decreased concomitant with the appreciable increase in **4** and **5** in other solvents. Apparently, the difference reflects in part the hydrogen donor ability of solvents. A good hydrogen donor like ether favors the radical pathway by trapping radicals to give **4** and **5** in competition with ionic process leading to **2** and **3**. The heavy-atom effect in the case of CCl_4 facilitates the intersystem crossing of the excited singlet state to the triplet. CCl_4 is therefore the best co-solvent for the photoalcoholysis.

Effects of Substituents. A number of *p*-substituted tribromoacetophenones were irradiated in an attempt to learn whether there might be any effect of ring substituents on the photoalcoholysis. The results summarized in Table 1 indicate that, just as with tribromoacetophenone itself, the principal products of the substituted tribromoacetophenones were the corresponding benzoylformates, with small amounts of benzoates and dibromoacetophenones also being formed. Thus, neither strong electron-donating nor -withdrawing substituents caused much change in the yield of **2**. This is to be noted in connection with the facts that many photosolvolytic reactions of aryl compounds have been shown[2,20)] to be dramatically affected by ring substituents. For example, Grinter *et al.*[21)] have shown in the photohydrolysis of monosubstituted benzylidyne trifluorides that *m*-chlorobenzylidyne trifluoride shows hardly any reactivity under the conditions where the *m*-hydroxy derivative undergoes photohydrolysis. Such a marked sensitivity to ring substituents often limits the photosolvolytic method as a general synthetic procedure, although its mechanistic implications are very important. The fact that the present photoalcoholysis can be applicable, regardless of the aryl substituents, opens a route to the benzoylformates from the readily available tribromoacetophenones.

Reaction Mechanism. From the above results it is seen that tribromoacetophenones afford new photosolvolytic products, benzoylformates, which are most easily rationalized as resulting from nucleophilic trapping of a cationic intermediate. The corresponding free radical (reduction) products are also observed in lower yield. These results pose two main questions as to the reaction mechanism. (1) Are the excited state intermediates leading to photoalcoholysis the same as those leading to homolysis? That is, where does branching occur in the photoreaction scheme? (2) What are the possible chemical intermediates in the formation of benzoylformate **2**?

(1) Previous works in this field have examined the effect of sensitizer on the competing ionic and radical photobehavior of halides. It has been indicated[9)] in the photolysis of benzyl halides in nucleophilic solvents that, in general, the triplet states produced by sensitization favor heterolysis, whereas the excited states produced as a result of direct light absorption disfavor heterolysis compared with homolysis. The present results (effects of benzophenone photosensitizer and solvent) also indicate that the benzoylformate comes from a triplet excited state of **1**. In their interesting work on photosolvolysis of alkyl iodide, Kropp and his coworkers have proposed[10)] that ionic intermediates are not produced directly from the photoexcited state, but that the photoexcited state decays by homolysis to a radical pair, which may undergo radical reactions or may undergo electron transfer to afford an ion pair, which would then undergo carbocation reactions.

$$R\text{-}X \xrightarrow{h\nu} [R\cdot X\cdot] \xrightarrow[\text{transfer}]{\text{electron}} [R^+X^-] \qquad (2)$$

This is mainly based on the observation that irradiation of alkyl halide in an alcohol saturated with oxygen resulted in simultaneous quenching of the formation of the free radical product and the ionic product, suggesting trapping of the radical by oxygen in competition with the electron transfer process. The reductive work-up of the resulting mixture affords alcohol arising from peroxide. In the present photoalcoholysis, presence of oxygen also caused quenching of the formation of the radical product (**4**, **5**), but it increased the formation of alcoholysis product. Similar marked acceleration of photoalcoholysis by oxygen has been observed[22)] in the irradiation of α,α,α-trichlorotoluene in alcohol and explained in terms of the involvement of the normally forbidden $S_0 \rightarrow T_1$ transition of trichlorotoluene due to the trichlorotoluene–oxygen charge-transfer (CT) complex. Moreover, such complexes of organic compounds with oxygen have been frequently observed[23)] and are responsible for some photochemical reactions[24)] in the presence of oxygen. Since the present photoalcoholysis product is derived from the triplet excited state of **1**, the effect of oxygen is attributable to the CT complex which facilitates the intersystem crossing. However, we cannot eliminate the possibility that some of the formate may arise from the reaction of oxygen with an initially formed radical *via* homolytic C–Br cleavage. A possible test of this, involving an $^{18}O_2$ tracer experiment, is in progress and will be reported later. The effects of hydrogen donor on the product distributions are more intriguing in this respect. Thus, the addition of a hydrogen donor, *e.g.*, 1,3-pentadiene, cyclohexene, and hydroquinone, always resulted in a marked in-

crease in the reduction product at the expense of the formate. This is most conveniently explained in terms of the idea that radical and ionic photoproducts from **1** are coupled, as shown in Eq. 2, through the common intermediacy of the radical pair. Appreciable increase in the apparent decomposition rate of **1** in the presence of a hydrogen donor suggests that there is substantial recombination within the radical pair to regenerate the starting bromide **1**. The origin of the solvent effect, in which the use of poor hydrogen donor solvent affords increased yields of ionic product, is also thought to be at least in part due to decreased opportunity for the common radical pair to abstract hydrogen from the solvent. The markedly increased ionic behavior of bromides as compared with their chloro analog also reflects that chlorine atoms abstract hydrogen from the solvent cage (in competition with the electron transfer process) more readily than bromine atoms do.

The mechanism of a route from triplet substrates to solvolysis products is very important. Recently, McKenna and his coworkers have studied the photosolvolysis of benzyl halides and suggested[6] that the formation of photosolvolysis product from triplet substrates must include interconversion of loose singlet and triplet radical pairs, followed by electron transfer in the singlet pair to give a solvent-separated ion pair (see Scheme 1). The present results can be

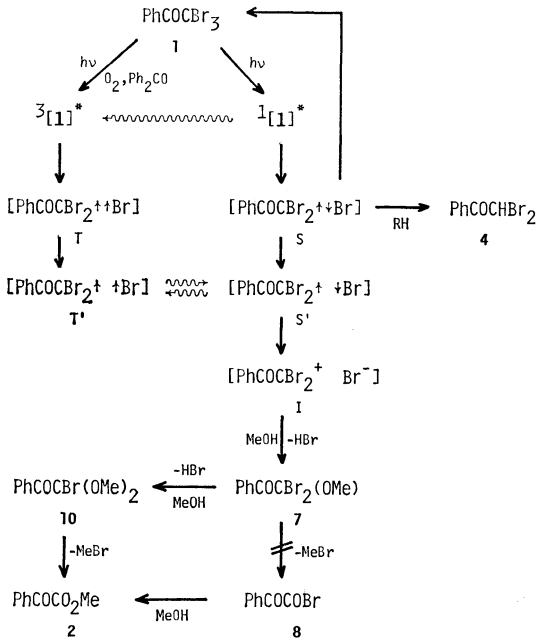

Scheme 1.

equally well explained by this suggestion. Presumably, singlet radical pairs (S) are very reactive and might either undergo recombination to **1** or abstract hydrogen from the solvent to give dibromoacetophenone (**4**), before they form loose radical pairs (S'). Triplet radical pairs (T), on the other hand, are less reactive and have enough lifetime to shift to loose radical pairs (T') where the partners are already adequately separated to form a solvent-separated ion pair (I).

(2) There are *a priori* several intermediates for the formation of **2** from the photoalcoholysis of **1**. In the photohydrolysis of monosubstituted benzylidyne trifluoride, Grinter and his coworkers[21] have isolated benzoyl fluoride as an intermediate. Sugimori and his coworkers[22] have also suggested that ethyl chloride and intermediary benzoyl chloride are generated from α-ethoxy-α,α-dichlorotoluene in the photoethanolysis of α,α,α-trichlorotoluene. α-Methoxy-α,α-dibromoacetophenone (**7**), a possible initial photoalcoholysis product, was easily prepared by bromination of α-methoxyacetophenone (**6**) in CCl_4. **7** was, however, stable in non-hydroxylic solvent either upon standing in dark or upon prolonged irradiation. When dissolved in MeOH at room temperature, **7** reacted instantaneously to give methyl benzoylformate (**2**) almost quantitatively. More conveniently, when bromination of **6** was carried out in MeOH, **2** was obtained in quantitative yield. Bromination of α,α-dimethoxyacetophenone (**9**) in CCl_4 resulted in a 1:1 mixture of α-bromo-α,α-dimethoxyacetophenone (**10**) and methyl benzoylformate. The former was gradually changed to the formate upon standing at room temperature. These facts indicate that benzoylformyl bromide (**8**) is not generated in the present photoalcoholysis and that the initial photoalcoholysis product **7** reacted spontaneously with MeOH to give **2** probably *via* dimethoxybromoacetophenone (**10**).

Experimental

Instrumentation. UV spectra were recorded on a Hitachi 220-S spectrophotometer. IR spectra were measured on a JASCO IR-G recording spectrometer, and ^1H NMR spectra were determined with a JEOL JNM-MH-100 NMR spectrometer in $CDCl_3$ with Me_4Si as an internal reference. GC analyses were performed on a Yanagimoto Model G-180 instrument with flame ionization detector using a 2.0 m×4.0 mm column packed with (A) 5% PEG 6000 and (B) 5% OV-17 on 60—80 mesh Diasolid L.

Materials. Mono- (**5a—d**),[25] di- (**4a—d**),[26] and tribromoacetophenones (**1a—d**)[26] were prepared by bromination of corresponding acetophenones. Trifluoroacetophenone was prepared[27] by the Friedel-Crafts reaction.

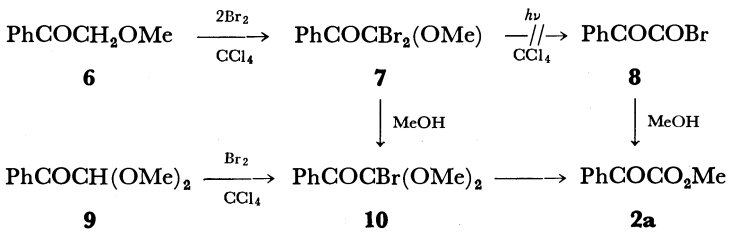

Scheme 2.

Authentic benzoylformates (**2a**—**d**) were prepared[28] from the corresponding dichloroacetophenone followed by esterification. All alcohols were dried and distilled before use.

Irradiation for Product Isolation. In a typical run, a solution of tribromoacetophenone (300 mg) in MeOH (30 ml) was placed in a Pyrex tube. The solution was purged with oxygen at 0 °C for 20—30 min before irradiation. The tube was then septum-sealed and irradiated with a high-pressure, 300W, Hg lamp with a water-cooled jacket. The progress of the reaction was monitored by GC. After irradiation for 2 h, the mixtures were concentrated on a rotary evaporator and chromatographed on 2.0×30 cm^2 silica gel (Woelm, activity III) column with $CHCl_3$ as eluent to give methyl benzoate ($\approx$2 mg, $\approx$1%), methyl benzoylformate (110 mg, 80%), and a mixture of mono- and dibromoacetophenone, all of which showed the same NMR spectra and GC retention times as authentic samples.

Irradiation for Analytical Purposes. Irradiations outlined in Tables 1—4 were carried out on 40 mM solution of **1** in alcohol in a Pyrex tube of 5.0 ml capacity. The progress of the reaction was monitored by GC analysis of aliquots removed periodically from the irradiation mixture in order to obtain time-conversion curves for each product. The identity of the products was confirmed either by GC comparison with authentic samples prepared as above or by separation of each of the components by column chromatography, followed by spectroscopic identification. A purge of the samples with the gas (O_2 or Ar) was carried out at 0 °C with vigorous stirring by a magnetic stirring bar.

Sensitized irradiations were conducted by using a Ritsu MC-20 radiating monochromator (250-W Xenon arc lamp) so as to assure absorption of most of incident light by the photosensitizer; when sensitized irradiation was carried out in Pyrex tubes containing 131 mM benzophenone ($\varepsilon\approx70$ at 366 nm) and 25 mM **1a** ($\varepsilon\approx1.0$ at 366 nm) with light of 366 nm wavelength from the monochromator, more than 98% of the incident light was absorbed by the sensitizer.

For quenching studies, a stock solution of **1** in MeOH was prepared, and 3 ml portions were added to Pyrex tubes containing varying amounts of quenchers. The tubes were then septumsealed and placed in the "merry-go-round" for irradiation. The irradiation was generally interrupted at about 30% completion in order to minimize error associated with product decomposition.

Bromination of α-Methoxyacetophenone. *(A) In CCl_4*: To a stirred solution of α-methoxyacetophenone[29] **6** (0.45 g, 3.0 mmol) in CCl_4 (20 ml) was added dropwise a solution of Br_2 (0.49 g, 3.0 mmol) in the same solvent (2.0 ml) at room temperature, and the mixture was further stirred for an additional 1 h. Evaporation of the solvent *in vacuo* gave crude α-methoxy-α-bromoacetophenone as a yellow oil: 0.63 g, 92%; ^{1}H NMR 3.62 (s, 3H), 6.37 (s, 1H), 7.20—8.10 (m, 5H).

To a refluxing solution of crude α-methoxy-α-bromoacetophenone (0.63 g, 2.7 mmol) in CCl_4 (20 ml) was added dropwise a solution of Br_2 (0.46 g, 2.8 mmol) in the same solvent, and the mixture was refluxed for an additional 1 h. Evaporation of the solvent *in vacuo* gave crude α-methoxy-α,α-dibromoacetophenone **7** as a yellow oil: 0.67 g, 80%; ^{1}H NMR 3.79 (s, 3H), 7.00—8.10 (m, 5H).

7 (0.67 g, 2.2 mmol) was dissolved in MeOH 10 ml) and left for 30 min at room temperature. Evaporation of the solvent gave methyl benzoylformate (**2a**) almost quantitatively.

(B) In MeOH: A solution of Br_2 (1.0 g, 6.3 mmol) in MeOH (4 ml) was added dropwise to a refluxing solution of **6** (0.46 g, 3.1 mmol) in the same solvent (20 ml), and the mixture was further boiled for an additional 1 h. Evaporation of the solvent *in vacuo* gave crude **2a** (0.47 g, 92%).

Bromination of α,α-Dimethoxyacetophenone (9). When **9**[30] was reacted with equivalent bromine in refluxing CCl_4, the crude product after evaporation of the solvent was shown to be 1:1 mixture of **10** and **2a** by NMR analysis, which also revealed that **2a** was increased at the expense of **10** upon standing at room temperature and that **2a** was the exclusive product after standing overnight.

References

1) E. Havinga, R. O. de Jongh, and W. Dorst, *Recl. Trav. Chim. Pays-Bas*, **75**, 378 (1956).

2) For review, see E. Havinga and J. Cornelisse, *Pure. Appl. Chem.*, **47**, 1 (1976).

3) H. E. Zimmerman and V. R. Sandel, *J. Am. Chem. Soc.*, **85**, 915 (1963).

4) A. L. Maycock and G. A. Berchtold, *J. Org. Chem.*, **35**, 2532 (1970).

5) M. A. Ratcliff, Jr. and J. K. Kochi, *J. Org. Chem.*, **36**, 3112 (1971).

6) D. C. Appleton, D. C. Bull, R. S. Givens, V. Lillis, J. McKenna, J. M. McKenna, and A. R. Walley, *J. Chem. Soc., Chem. Commun.*, **1974**, 473; V. Lills, J. McKenna, J. M. McKenna, I. H. Williams, *ibid.*, **1974**, 474; J. McKenna, J. M. McKenna, M. J. Smith, P. S. Taylor, B. Brocklehurst, D. C. Appleton, S. Thackeray, and A. R. Walley, *ibid.*, **1977**, 108; D. C. Appleton, D. C. Bull, R. S. Givens, V. Lillis, J. McKenna, J. M. McKenna, S. Thackeray, and A. R. Walley, *J. Chem. Soc., Perkin Trans. 2*, **1980**, 77; V. Lillis, J. McKenna, J. M. McKenna, M. J. Smith, P. S. Taylor, and I. H. Williams, *ibid.*, **1980**, 83; D. C. Appleton, B. Brocklehurst, J. McKenna, J. M. McKenna, S. Thackeray, A. R. Walley, *ibid.*, **1980**, 87.

7) D. A. Jaeger, *J. Am. Chem. Soc.*, **97**, 902 (1975).

8) C. E. Griffin and M. L. Kaufman, *Tetrahedron Lett.*, **1965**, 773.

9) S. J. Cristol and B. E. Greenwald, *Tetrahedron Lett.*, **1976**, 2105; S. J. Cristol and T. H. Bindel, *J. Org. Chem.*, **45**, 951 (1980); S. J. Cristol and T. H. Bindel, *J. Am. Chem. Soc.*, **103**, 7287 (1981).

10) P. J. Kropp, T. H. Jones, and G. S. Poindexter, *J. Am. Chem. Soc.*, **95**, 5420 (1973); G. S. Poindexter and P. J. Kropp, *ibid.*, **96**, 7142 (1974); P. J. Kropp, G. S. Poindexter, N. J. Pienta, and D. C. Hamilton, *ibid.*, **98**, 8135 (1976); P. J. Kropp, J. R. Gibson, J. J. Snyder, and G. S. Poindexter, *Tetrahedron Lett.*, **1978**, 207; N. J. Pienta and P. J. Kropp, *J. Am. Chem. Soc.*, **100**, 655 (1978).

11) R. R. Perkins and R. E. Pincock, *Tetrahedron Lett.*, **1975**, 943.

12) S. A. McNeely and P. J. Kropp, *J. Am. Chem. Soc.*, **98**, 4319 (1976).

13) T. Suzuki, T. Sonoda, S. Kobayashi, and H. Taniguchi, *J. Chem. Soc., Chem. Commun.*, **1976**, 180; T. Kitamura and S. Kobayashi, *Tetrahedron Lett.*, **1979**, 1619.

14) B. Sket and M. Zupan, *J. Chem., Soc., Perkin Trans. 1*, **1979**, 752.

15) P. C. Purohit H. R. Sonawane, *Tetrahedron*, **37**, 873 (1980), and references cited therein.

16) B. E. Kaplan and A. L. Hartwig, *Tetrahedron Lett.*, **1970**, 4855.

17) H. Tomioka, Y. Izawa, and Y. Ogata, *Tetrahedron*, **24**, 5739 (1968).
18) Y. Izawa, H. Tomioka, M. Kutsuna, and Y. Toyama, *Bull. Chem. Soc. Jpn.*, **52**, 3465 (1979).
19) Y. Izawa, H. Tomioka, M. Natsume, S. Beppu, and H. Tsujii, *J. Org. Chem.* **45**, 4835 (1980).
20) H. E. Zimmerman, *Adv. Photochem.*, **1**, 183 (1963).
21) R. Grinter, E. Heilbronner, T. Petrzilka, and P. Seiler, *Tetrahedron Lett.*, **1968**, 3845.
22) T. Ishigami, Y. Kinoshita, and A. Sugimori, *Chem. Lett.*, **1974**, 149.
23) H. Tsubomura and R. S. Mulliken, *J. Am. Chem. Soc.*, **82**, 5966 (1960); H. Ishida, H. Takahashi, H. Sato, and H. Tsubomura, *ibid.*, **92**, 275 (1970).
24) K. S. Wei and A. H. Adelamn, *Tetrahedron Lett.*, **1969**, 3297; C. von Sonntag, K. Neuwald, H.-P. Schuchmann, F. Weeke, and E. Janssen, *J. Chem. Soc., Perkin Trans. 2*, **1975**, 171.
25) R. M. Cowper, and L. H. Davidson, *Org. Synth.*, Coll. Vol. II, 480 (1950).
26) J. G. Aston, J. D. Newkirk, J. Dorsky, and D. M. Jenkins, *J. Am. Chem. Soc.*, **64**, 1413 (1942).
27) S. G. Cohen, H. T. Wolosinski, and P. J. Scheuer, *J. Am. Chem. Soc.*, **71**, 3440 (1949).
28) B. B. Corson, R. A. Dodge, S. A. Harris, and R. K. *Org. Synth.*, Coll. Vol. I, 241, (1932).
29) R. B. Moffett and R. L. Shviner, *Org. Synth.*, Coll. Vol. II, 509, (1950).
30) H. A. Riley nad A. R. Gray, *Org. Synth.*, Coll. Vol. II, 509, (1950).

Preparation and Characterization of Poly(thienylene)s

Takakazu YAMAMOTO,* Ken-ichi SANECHIKA, and Akio YAMAMOTO
Research Laboratory of Resources Utilization, Tokyo Institute of Technology, 4259 Nagatsuta, Midori-ku, Yokohama 227

(Received November 20, 1982)

Nickel compounds ($NiCl_2$ and $NiCl_2$(2,2′-bipyridine)) catalyze polycondensation of dihalothiophenes (2,5-dihalothiophenes, 2,4-dibromothiophene, and 3-methyl-2,5-dibromothiophene) by dehalogenation with magnesium to give the corresponding poly(thienylene) type polymers (poly(2,5-thienylene), poly(2,4-thienylene), and poly(3-methyl-2,5-thienylene)). Copolymerization of 2,5-dibromothiophene and 2,4-dibromothiophene affords copolymers formulated as $\{2,5\text{-}C_4H_2S\}_m\{2,4\text{-}C_4H_2S\}_n$. About 15 wt% of poly(2,5-thienylene) prepared in THF at 66 °C is soluble in $CHCl_3$ at room temperature and the $CHCl_3$-soluble fraction has a molecular weight of 1370. The remaining fraction is considered to have a higher molecular weight as judged from its physical properties. IR and ^{1}H-NMR spectra of the polymers are consistent with the structures described above. The electronic spectra of poly(2,5-thienylene) and poly(3-methyl-2,5-thienylene) show large bathochromic shifts of the π-π^* absorption bands from those of thiophene and 3-methylthiophene, respectively, indicating that π-electrons in these polymers are extensively delocalized along the polymer chains. In contrast to the electronic spectra of these polymers, that of poly(2,4-thienylene) shows only a minor shift of the π-π^* absorption band from that of thiophene reflecting the less extensive π-electron delocalization along the polymer chain in the poly(2,4-thienylene). All the polymers are nonsensitive to air and have high thermal stabilities.

Preparation of polymers having π-conjugation systems along the polymer chains is a subject of recent interest in connection with their potential utility as polymer conductors or semiconductors.[1] A previous paper[2] from our group revealed that the transition metal catalyzed C–C coupling reaction between RMgX and R′X[3] was applicable to the preparation of poly(phenylene) type polymers from dihaloaromatic compounds, X–Ar–X,

$$n\,X\text{-}Ar\text{-}X + n\,Mg \longrightarrow [X\text{-}Ar\text{-}MgX] \xrightarrow{[M]} \{Ar\}_n \quad (1)$$

M = Ni, Pd, etc.

We have applied this transition metal-catalyzed dehalogenative polycondensation to the preparation of poly(2,5-thienylene) from 2,5-dihalothiophene,

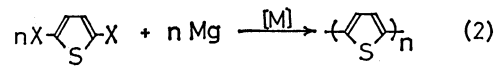

(2)

The polymer has a π-conjugation system similar to that of poly(acetylene) which shows high electric conductivities when doped with electron acceptors such as I_2 and AsF_5 or electron donors such as Li and Na,[1]

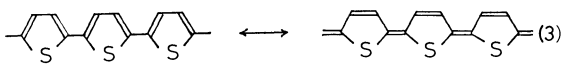

(3)

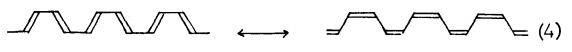

(4)

This paper deals with the preparation and characterization of poly(2,5-thienylene) and its related polymers including its methylated analogue (poly(3-methyl-2,5-thienylene)), its isomer (poly(2,4-thienylene)), and copolymers of 2,5-dibromothiophene and 2,4-dibromothiophene,

Part of the results were briefly reported in communication form.[4] After publication of our first communication, Lin and Dudek[5] also reported preparation of

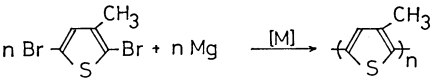

(5)

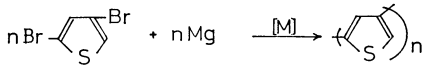

(6)

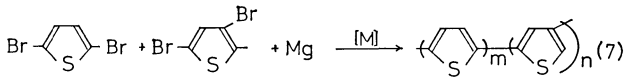

(7)

poly(2,5-thienylene) using a similar technique, and more recently preparation of polymers having similar π-conjugation systems to that of poly(2,5-thienylene), poly(2,5-pyrrolylene) derivatives[6] and poly(2,5-selenienylene),[7] by using the dehalogenative polycondensation technique has been reported. Electrochemical polymerization of thiophene in an $[N(Et)_4][BF_4]$ solution was also reported.[8]

Results and Discussion

Preparation of Polymers. Poly(2,5-thienylene): Table 1 shows results of the dehalogenative polycondensation of dihalothiophenes. As shown in Table 1, 2,5-dibromothiophene and 2,5-dichlorothiophene are polymerized at reflux temperature of THF (66 °C) to give poly(2,5-thienylene) according to Eq. 2. 2,5-Dibromothiophene and 2,5-dichlorothiophene seem to have almost the same reactivities in the polymerization.

Gas chromatographic analysis of compounds obtained by hydrolysis of the reaction product of 2,5-dibromothiophene and magnesium (1:1) before addition of the catalyst revealed that the 1:1 reaction of 2,5-dibromothiophene and magnesium afforded a mixture containing 2,5-C_4H_2S(MgBr)Br and 2,5-$C_4H_2S(MgBr)_2$ as well as intact 2,5-dibromothiophene in about 2:1:1 ratio. Thus, the polymerization is considered to proceed through the C–C coupling between these compounds,

TABLE 1. PREPARATION OF POLY(THIENYLENE)S

Expt	Monomer[a]	Catalyst[b]	Solvent[c]	Temp °C	Time h	Yield %	$CHCl_3$-extractable[d] fraction / $CHCl_3$-unextractable fraction
1	2,5-$C_4H_2SBr_2$	None	THF	66	5	0	
2	2,5-$C_4H_2SBr_2$	$NiCl_2$(bpy)	THF	66	3	61	22/78
3	2,5-$C_4H_2SBr_2$	$NiCl_2$(bpy)	THF	66	5	78	Not measured
4	2,5-$C_4H_2SBr_2$	$NiCl_2$(bpy)	THF	25	21	7	37/63
5	2,5-$C_4H_2SBr_2$	$NiCl_2$	THF	66	5	54	Not measured
6	2,5-$C_4H_2SBr_2$	$NiCl_2$(bpy)	THF+n-Bu_2O	110	1	48	2/98
7	2,5-$C_4H_2SBr_2$	$NiCl_2$(bpy)	Et_2O	35	4	8	70/30
8	2,5-$C_4H_2SBr_2$	$NiCl_2$(dppp)	THF	66	3	49	Not measured
9	2,5-$C_4H_2SBr_2$	$PdCl_2$(bpy)	THF	66	5	0	
10	2,5-$C_4H_2SBr_2$	$FeCl_3$	THF	66	5	14	Not measured
11	2,5-$C_4H_2SBr_2$	Fe(acac)$_3$	THF	66	5	12	Not measured
12	2,5-$C_4H_2SBr_2$	$CoCl_2$	THF	66	5	5	Not measured
13	2,5-$C_4H_2SCl_2$	$NiCl_2$(bpy)	THF	66	4	40	27/73
14	2,4-$C_4H_2SBr_2$	$NiCl_2$(bpy)	THF	66	5	17	69/31
15	2,4-$C_4H_2SBr_2$	$NiCl_2$(bpy)	THF+n-Bu_2O	110	5	58	29/71
16	3-Me-2,5-C_4HSBr_2	$NiCl_2$(bpy)	THF	66	3	55	83/17
17	3-Me-2,5-C_4HSBr_2	$NiCl_2$(bpy)	THF+n-Br_2O	110	3	40	95/5

a) $C_4H_2SX_2$=Dihalothiophene. 3-Me-C_4HSBr_2=3-Methyl-2,5-dibromothiophene. b) bpy=2,2′-Bipyridine. dppp=1,3-Bis(diphenylphosphino)propane. 0.003 mol% of the catalyst per monomer was added. c) THF+n-Bu_2O=1:4 mixture of THF and dibutyl ether. d) See text.

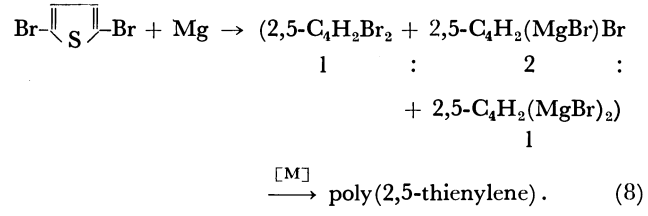

$$\text{Br-(2,5-thienylene)-Br} + \text{Mg} \rightarrow (\underset{1}{\text{2,5-}C_4H_2Br_2} + \underset{2}{\text{2,5-}C_4H_2(MgBr)Br} + \underset{1}{\text{2,5-}C_4H_2(MgBr)_2}) \xrightarrow{[M]} \text{poly(2,5-thienylene)}. \quad (8)$$

It is seen in Table 1 that nickel catalysts are effective for the polymerization, whereas $PdCl_2$(bpy), which has high activities in the preparation of the poly(phenylene) type polymers, is not. $FeCl_3$, Fe(2,4-pentanedionato)$_3$, and $CoCl_2$ showed feeble catalytic activities. When the polymerization was carried out at lower temperatures (Expts 4 and 7), the yield of the polymer as well as the proportion of the $CHCl_3$-unextractable fraction (*vide infra*) decreased. The polymerization at 110 °C by using a 1:4 mixture of THF and dibutyl ether (Expt 6) proceeded smoothly and most of the polymer obtained was not extractable by hot $CHCl_3$.

When the ratio of Mg to 2,5-dibromothiophene deviates from unity, yield of the polymer and the proportion of the $CHCl_3$-unextractable fraction considerably decrease in accord with the theory of polycondensation. Addition of a monofunctional compound, 2-bromothiophene, also causes decrease in the yield and the proportion of the $CHCl_3$-unextractable fraction.

Poly(2,4-thienylene) and Poly(3-methyl-2,5-thienylene): Polymerization of 2,4-dibromothiophene and 3-methyl-2,5-dibromothiophene can be carried out analogously. However, as for the polymerization of 2,4-dibromothiophene, polymerization at the reflux temperature of THF did not give a satisfactory yield and the polymerization at higher temperature by using a 1:4 mixture of THF and dibutyl ether (Expt 15) was required to get a reasonably high yield.

Copolymers: Table 2 summarizes results of copolymerization of 2,5-dibromothiophene and 2,4-dibromothiophene according to Eq. 7. In Table 2 the ratio of the 2,5- and 2,4-thienylene units in the polymer was calculated from relative intensities of absorption bands in IR spectra characteristic of 2,5-thienylene and 2,4-thienylene units (*vide infra*). The calibration line for the calculation was obtained by taking IR spectra of samples containing pure poly(2,5-thienylene) and poly(2,4-thienylene) in various ratios.

It is seen from Table 2 that the ratio between 2,5- and 2,4-thienylene units in the copolymers is almost the same as the ratio of the two monomers employed for the copolymerization (Runs 4 and 5). This indicates that both monomers have almost the same reactivities in the copolymerization (2,4-dibromothiophene seems to have a slightly higher reactivity), and consequently the polymer is considered to have a random sequence with respect to the two thienylene units. The compositions of the copolymers obtained in Runs 2 and 3 could not be determined from their IR spectra, since the proportions of 2,4-thienylene units were too small. The data obtained in Runs 4 and 5, however, suggest that the copolymers obtained in Runs 2 and 3 contain *ca.* 6 and 13% of 2,4-thienylene units, respectively.

Properties of Polymers: Poly(2,5-thienylene) prepared in Expt 2 in Table 1 was fractionated into two parts by extraction with hot $CHCl_3$. The brown $CHCl_3$-extract (22 wt%) softens at 116 °C. About 2/3 of the $CHCl_3$-extract (about 14 wt% of the crude polymer) was soluble in $CHCl_3$ at room temperature and had number-average molecular weight of 1370 as de-

Table 2. Copolymerization of 2,5-dibromothiophene and 2,4-dibromothiophene[a)]

Run	Monomer ratio		Time	Yield[b)]	Ratio of monomer unit in the polymer	
	2,5-Dibromo-thiophene	2,4-Dibromo-thiophene	h	%	2,5-Thienylene	2,4-Thienylene
1	100	0	3	81	100	0
2[c)]	94	6	3	61	d)	
3	87	13	2	54	d)	
4	65	35	3	65	62	38
5	48	52	2	42	44	56
6	0	100	5	58	0	100

a) Catalyst: $NiCl_2$(bpy) (0.003 mol/monomer). Solvent: THF for Runs 1 and 2, and an 1:4 mixture of THF and $(n\text{-Bu})_2O$ for Runs 3—6. b) Calculated from the weight and carbon content of the crude polymer. c) Data from Ref. 2a using commercially available (from Merck Co. Ltd.) 2,5-dibromothiophene without purification. d) The proportion of 2,4-thienylene is too small to be determined from IR.

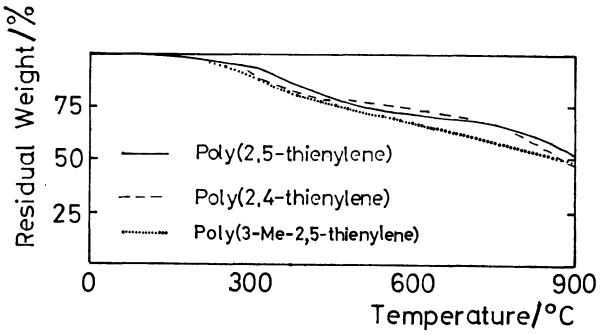

Fig. 1. Thermogravimetric analyses of poly(thienylene)s.

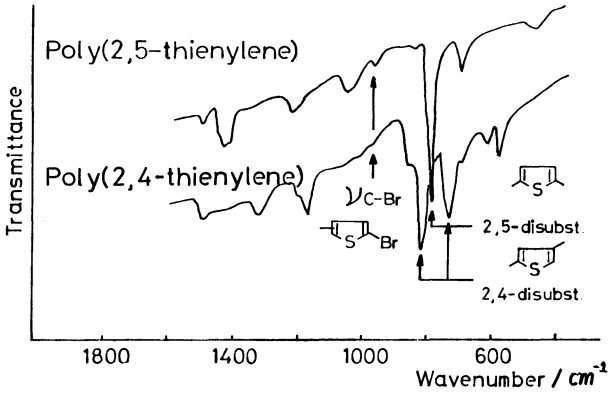

Fig. 2. IR spectrum of poly(2,5-thienylene) and poly(2,4-thienylene).

termined by VPO. The molecular weight corresponds to a formula of $Br\{C_4H_2S\}_{14.8}Br$ and analytical data roughly agrees with the formulation (Found: C, 51.6; H, 2.8. Calcd: C, 51.7; H, 2.8). The remaining $CHCl_3$-unextractable polymer (78 wt%) is insoluble in most organic solvents and seems to have a higher molecular weight than the $CHCl_3$-soluble fraction as judged from its higher thermal stability, lower solubility, and analytical data which show higher carbon content (C, 53.7; H, 2.7).[9)]

Thermogravimetric analyses of poly(2,5-thienylene) and related polymers are shown in Fig. 1. Poly(2,5-thienylene)s prepared in experiments other than Expt 2 were also separated into the $CHCl_3$-extractable and -unextractable fractions and the fractions were found to have similar properties described above.

Poly(2,4-thienylene) and the copolymers of 2,5- and 2,4-dibromothiophenes have similar thermal stabilities to that of poly(2,5-thienylene), but there is a trend that both the proportion and molecular weight of the $CHCl_3$-soluble fraction extracted at room temperature increase with increase in the proportion of the 2,4-thienylene unit in the polymer chain. In the case of pure poly(2,4-thienylene) 23 wt% of the crude polymer was soluble in $CHCl_3$ at room temperature, and the $CHCl_3$-soluble fraction had a number average molecular weight of 2100, which corresponds to a formula of $Br\{C_4H_2S\}_{23.7}Br$.

A larger part of poly(3-methyl-2,5-thienylene) is extractable by hot $CHCl_3$ and a fraction soluble in $CHCl_3$ at room temperature had a higher molecular weight (M_w=2300) than poly(2,5-thienylene) prepared under similar conditions, indicating that solubility of poly(2,5-thienylene) is enhanced by substitution of the 3-hydrogen of the thienylene ring with the CH_3 group. Poly(3-methyl-2,5-thienylene) has similar thermal stability to that of poly(2,5-thienylene) as shown in Fig. 1. Poly(2,5-thienylene), poly(2,4-thienylene), and the copolymers have apparent specific gravities of 1.3—1.4 as measured by weighing pellets of the polymers obtained by pressing them at 600 kg/cm^2. Poly(3-methyl-2,5-thienylene) had a somewhat smaller apparent specific gravity, 1.2.

IR and NMR Spectra. The IR spectra of the polymers are consistent with the structures of the polymers shown in Eqs. 2, 5, 6, and 7. Figure 2 shows the IR spectra of poly(2,5-thienylene) and poly(2,4-thienylene). The IR spectrum of poly(2,5-thienylene) shows one sharp out-of-plane δ(C–H) vibration band characteristic of 2,5-disubstituted thienylene[10)] at 788 cm^{-1}, whereas that of poly(2,4-thienylene) shows two out-of-plane δ(C–H) vibration bands at 730 and 820 cm^{-1}. The out-of-plane δ(C–H) vibration band of poly(3-methyl-2,5-thienylene) appears at 810 cm^{-1}. The IR spectra of the copolymers show both bands assignable to the 2,5-thienylene and 2,4-thienylene units and the composition of the copolymers were determined from their relative intensities as described before.

ν(C–Br) and ν(C–Cl) bands of the terminal halo-

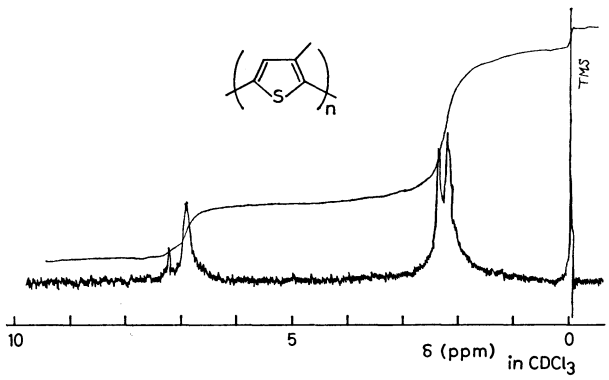

Fig. 3. ^{1}H-NMR spectrum of Poly(3-methyl-2,5-thienylene) in $CDCl_3$. 100 MHz.

thienyl groups are sometimes observable at 980 and 1000 cm^{-1}, respectively, but the intensities of the bands were very weak.

The ^{1}H-NMR spectra of the $CHCl_3$-soluble poly(2,5-thienylene) and poly(2,4-thienylene) show complex bands in a range of δ 6.5—7.5 assignable to hydrogens of the thienylene unit, whereas that of the $CHCl_3$-soluble poly(3-methyl-2,5-thienylene) (Figure 3) shows two absorption bands at δ 2.0—2.5 and δ 6.5—7.1 in an intensity ratio of 3:1, the former being assignable to the CH_3 protons and the latter to hydrogen directly attached to the thienylene ring. The separation of the CH_3 band into two peaks seems to be due to the presence of both *s-trans* and *s-cis* configuration and/or head-to-tail and head-to-head units in the polymer chain,

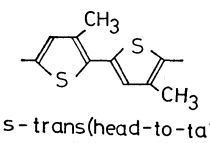
s-trans(head-to-tail)

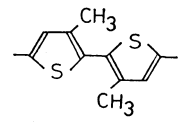
s-trans(head-to-head)

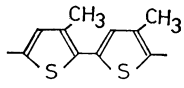
s-cis(head-to-tail)

It is known[11] that 2,2′-bithiophene derivatives exist as mixtures of *s-trans* and *s-cis* isomers in solution.

Optical Properties. The extent of π-conjugation in the polythienylenes is reflected in their colors and electronic spectra. Poly(2,5-thienylene) and poly(3-methyl-2,5-thienylene) are dark reddish brown, whereas poly(2,4-thienylene) is light brown. The electronic spectrum of the $CHCl_3$-soluble poly(2,5-thienylene) shows a large bathochromic shift of the π-π^* absorption band from the λ_{max} of thiophene at 230 nm to 418 nm (Fig. 4), but that of the $CHCl_3$-soluble poly(2,4-thienylene) shows only a small shift. When exposed to UV-light (365 or 253.7 nm) poly(2,5-thienylene) fluorecses a light green color, whereas poly(2,4-thienylene) does not show the fluorescence. These results indicate that the π-electrons in poly(2,5-thienylene) are extensively delocalized along the polymer chain

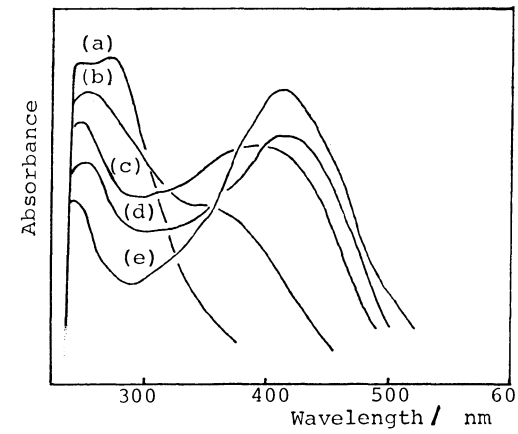

Fig. 4. Electronic spectra of $CHCl_3$-soluble (a) poly(2,4-thienylene) (M_w=2100), (b) copolymer obtained in Run 5 in Table 2, (c) copolymer obtained in Run 4 in Table 2, (d) copolymer obtained in Run 3 in Table 2, and (e) poly(2,5-thienylene) (M_w=1370). $\varepsilon_{max}/C_4H_2S$=about 5000 for all polymers.

(Eq. 3), whereas those in poly(2,4-thienylene) are not.

If a simplified molecular orbital theory proposed by Hückel[12] for conjugated polyens can be applied to other π-conjugated polymers $H\{A\}_nH$ (A=π-electron-system containing unit such as *p*-phenylene and 2,5-thienylene), the energies of the orbitals of the polymer are given by the following equation,

$$E_i = \alpha + 2\beta \cos\frac{i\pi}{n+1} \quad (i=1,2,\cdots, n), \tag{9}$$

where α and β represent energy of an orbital of isolated unit, A, and exchange integral between the two orbitals in the adjacent two A's, respectively. Application of this equation to HOMO of A gives the following energies of the polymer $H\{A\}_nH$

$$E_i(\text{occupied}) = \alpha_1 + 2\beta_1 \cos\frac{i\pi}{n+1} \quad (i=1,2,\cdots, n), \tag{10}$$

where α_1 and β_1 represent the energy of HOMO of A and exchange integral between the HOMO's in the adjacent two A's, respectively. Application to LUMO gives an analogous equation,

$$E_i(\text{unoccupied}) = \alpha_2 + 2\beta_2 \cos\frac{i\pi}{n+1} \quad (i=1,2,\cdots, n), \tag{11}$$

E_i(occupied) and E_i(unoccupied) given by Eqs. 10 and 11 are depicted in Fig. 5.

Equations 10 and 11 afford the following highest occupied energy ε_1 and the lowest π-π^* transition energy $\Delta\varepsilon$

$$\varepsilon_1 = \alpha_1 - 2\beta_1 \cos\frac{\pi}{n+1} \tag{12}$$

$$\Delta\varepsilon = (\alpha_2-\alpha_1) + 2(\beta_1+\beta_2) \cos\frac{\pi}{n+1} \tag{13}$$

and cosequently a plot of ε_1 against $\Delta\varepsilon$ is expected to give a linear line with a slope of $-2\beta_1/2(\beta_1+\beta_2)$. By using data of peak anode potential which corresponds to $-\varepsilon_1$ and the lowest π-π^* transition energy which

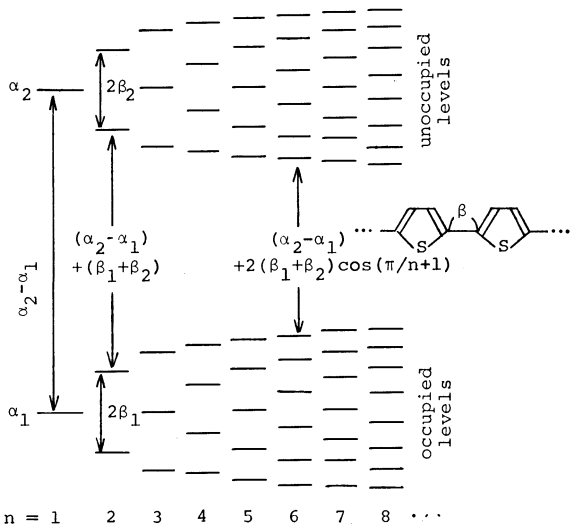

Fig. 5. Energy levels in $H\{A\}_nH$.

corresponds to $\Delta\varepsilon$, Diaz and his coworkers showed[1g] that the plot of $-\varepsilon_1$ against $\Delta\varepsilon$ actually gives straight lines with a slope of *ca.* 0.5 for oligo(*p*-phenylene), oligo(2,5-thienylene), and oligo(2,5-pyrrolylene). The value of the slope indicates that β_1 and β_2 equal to each other in these oligomers. The β_1 (or β_2 estimated using the data of Diaz is -0.63 eV for oligo(2,5-thienylene) and -0.58 eV for oligo(*p*-penylene).

Since poly(*p*-phenylene) is known to be converted into a good electric conductor with an electric conductivity of 10^4 S cm^{-1} when doped with AsF_5,[1c] the present result that the absolute value of β in oligo(2,5-thienylene) is larger than that in oligo(*p*-phenylene) implies a possibility that poly(2,5-thienylene) can be converted into similar or better electric conductors when doped with suitable acceptors. The observed values of $\Delta\varepsilon$ of oligo- or poly(2,5-thienylene), $H\{2,5\text{-}C_4H_2S\}_n$ (n=3, 4, ∞), agree well with values calculated by using Eq. 13 and the $(\alpha_2-\alpha_1)$ and $(\beta_1+\beta_2)$ values estimated from the λ_{max}'s of thiophene and 2,2'-bithiophene.

Figure 4 indicates the electronic spectra of the copolymers. It is seen that the λ_{max} shifts to longer wavelength with increase in the content of the 2,5-thienylene unit reaching 418 nm where the pure poly-(2,5-thienylene) shows the absorption peak. This indicates that the π-electrons in the sequence composed of 2,5-thienylene units are delocalized along the polymer chain, whereas the delocalization is broken by intervention of the 2,4-thienylene unit. These results clearly indicate that the polymer obtained in the copolymerization is not a mixture of the two homopolymers but it contains both the 2,5- and 2,4-thienylene units in a polymer chain.

The electronic spectrum of poly(3-methyl-2,5-thienylene) also shows a large bathochromic shift of the π-π^* absorption band from λ_{max} of 3-methylthiophene at 230 nm to 420 nm, the magnitude of the bathochromic shift (190 nm) being almost the same as that observed for nonsubstituted poly(2,5-thienylene). This indicates that π-electrons in poly(3-methyl-2,5-thienylene) are also extensively delocalized along the polymer chain, similarly to those in poly(2,5-thienylene). It is reported[13] that optical properties of substituted poly(acetylene)s, $\{CH{=}CR\}_n$, are much different from $\{CH{=}CH\}_n$ because of difficulties in forming a planar π-electron-conjugated polymer chain due to the steric repulsion between R and H or two R's. The finding obtained with poly(3-methyl-2,5-thienylene) is in contrast to the finding obtained with $\{CH{=}CR\}_n$, and the examination with the CPK molecular model indicates that there exists no special steric repulsion in forming a planar, conjugated polymer chain in the case of poly(3-methyl-2,5-thienylene) composed of recurring 5-membered rings.

As revealed by the electronic spectra of the polymers, the degree of delocalization of π-electrons along the polymer chain is affected by the mode of joining the thienylene units as well as by the composition of the two kinds of thienylene units in the copolymer. The degree of delocalization of π-electrons determines reactivities and electric conducting properties of the polymers as will be reported in the succeeding paper.

Stability in Air. All the poly(thienylene)s described above have high stabilitities in air in contrast to the sensitivity of poly(acetylene) against oxygen in air. The IR spectra of poly(thienylene)s showed no change after exposure of the polymer to air more than 1 year. Their high stabilities in air provide a great advantage in using them in various possible application.

Comparison with Electrochemically Prepared Poly(thiophene). Recently it has been reported that electrochemical oxidation of thiophene gives an electric conducting polymer film[8] and it has been proposed that the polymer has a structure similar to above-mentioned poly(2,5-thienylene).[8b] However, the IR spectrum of the electrochemically prepared polymer[8b] is somewhat different from that of poly(2,5-thienylene) prepared in the present study. Particularly notable in the IR spectrum of the polymer prepared by the electrochemical method is that the characteristic band of the 2,5-thienylene unit around 788 cm^{-1} due to the δ(C–H) absorption is considerably weaker in the IR spectrum.[18] It may be argued that the electrochemically prepared polymer of thiophene has a structure somewhat different from that of poly(2,5-thienylene).

Experimental

Materials. Commercially available 2,5-dibromothiophene was recrystallized from hexane. 2,4-Dibromothiophene,[14] 3-methyl-2,5-dibromothiophene,[15] $NiCl_2$(bpy),[16] and $NiCl_2$(dppp)[17] were prepared according to methods in literature. Solvents for polymerization were dried over Na, distilled under dry N_2, and stored under dry N_2. Granular magnesium was activated by stirring under N_2 for 1 d.

Preparation of Polymers. Expt 2 in Table 1: 2,5-Dibomothiophene (22.7 g, 94.0 mmol) was added dropwisely into a vessel containing 2.29 g (94.0 mmol) of Mg and dry THF (60 ml). After consumption of all magnesium (1—2 h) at room temperature a small amount of the solution taken by a micro syringe was hydrolyzed with water, and gas chromatography indicated the hydrolyzed product contained thiophene, 2-bromothiophene, and 2,5-dibromo-

thiophene in a 1:2:1 ratio. When $NiCl_2$(bpy) (90 mg, 3.1×10^{-1} mmol) was added to the remaining THF solution of the product of the reaction of 2,5-dibromothiophene and magnesium, a smooth polymerization started. After carrying out the reaction for 5 h under reflux, the polymerization solution was poured into an HCl-acidic methanol mixture to obtain a dark brown precipitate. From the methanol solution a yellow solid (0.10 g, low-molecular weight poly(2,5-thienylene)) was recovered. The dark brown precipitate was collected over a glass filter, washed with methanol repeatedly, and dried in vacuum to yield 7.0 g (78%) of crude poly(2,5-thienylene), which was fractionated into $CHCl_3$-extractable (78 wt%) and $CHCl_3$-unextractable (22 wt%) fractions by extracting it with $CHCl_3$ by using a Soxhlet extractor. About 2/3 of the $CHCl_3$-extract was soluble in $CHCl_3$ at room temperature. The other polymerization in THF or diethyl ether was carried out analogously.

Expt 6 in Table 1: A similar reaction between 2,5-dibromothiophene and magnesium (1:1) was carried out in dry THF (10 cm^3). After completion of the reaction, dibutyl ether (40 cm^3) and $NiCl_2$(bpy) were added. After carrying out the polymerization for 1 h under reflux (100 °C), the reaction mixture was poured into the HCl-acidic methanol and polymer obtained was treated as in the case of Expt 2 described above. The other polymerizations in the mixture of THF and dibutyl ether were carried out analogously.

Analysis and Measurements. Microanalysis of C and H was performed by Mr. T. Saito of our laboratory by using Yanagimoto CHN Autocorder Type MT-2. IR and ^{1}H-NMR spectra were recorded on a Hitachi Model 295 spectrometer and a Japan Electron Optics Laboratory PS-100 NMR spectrometer, respectively. Thermogravimetric analysis was performed with a Shimadzu thermoanalyzer TGA-30. Glc analysis was carried out with a Shimadzu GC-6A or GC-3BT gas chromatograph. Molecular weight was determined by a Corona 117 vapor pressure osmometer.

Reference

1) For example, a) H. Shirakawa, E. J. Louis, A. G. MacDiarmid, C. K. Ciang, and A. J. Heeger, *J. Chem. Soc., Chem. Commun.*, **1977**, 578; b) Y. W. Park, A. J. Heeger, M. A. Druy, and A. G. MacDiarmid, *J. Chem. Phys.*, **73**, 946 (1980); c) L. W. Shacklett, H. Eckhardt, R. R. Chance, G. G. Miller, D. M. Inory, and R. H. Baughman, *ibid.*, **73**, 4098 (1980); d) H. Shirakawa and T. Yamabe, "Synthetic Metal", Kagaku Zokan, **87** (1980); e) G. Wegner, *Angew. Chem., Int. Ed. Engl.*, **20**, 361 (1981); f) K. K. Kanazawa, A. F. Diaz, W. D. Gill, P. M. Grant, G. B. Street, G. P. Gardini, and J. F. Kwak, *Synth. Metals*, **1**, 329 (1979/90); g) A. F. Diaz, J. Crowley, J. Bargon, G. P. Gardini, and J. B. Torrance, *J. Electroanal. Chem.*, **121**, 355 (1981).

2) a) T. Yamamoto and A. Yamamoto, *Chem. Lett.*, **1977**, 353; b) T. Yamamoto, Y. Hayashi, and A. Yamamoto, *Bull. Chem. Soc. Jpn.*, **51**, 2091 (1978).

3) K. Tamao, K. Sumitani, Y. Kiso, M. Zembayashi, A. Fujioka, S. Kodama, I. Nakajima, A. Minato, and M. Kumada, *Bull. Chem. Soc. Jpn.*, **49**, 1958 (1976); A. Sekiya and N. Ishikawa, *J. Organomet. Chem.*, **118**, 349 (1976); M. Uchino, A. Yamamoto, and S. Ikeda, *ibid.*, **24**, C63 (1970).

4) T. Yamamoto, K. Sanechika, and A. Yamamoto, *J. Polym. Sci., Polym. Lett. Ed.*, **18**, 9 (1980); *Chem. Lett.*, **1981**, 1079; K. Sanechika, T. Yamamoto, and A. Yamamoto, *J. Polym. Sci., Polym. Lett. Ed.*, **20**, 365 (1982).

5) J. W-P. Lin and L. P. Dudek, *J. Polym. Sci., Polym. Chem., Ed.*, **18**, 2869 (1980).

6) I. Khoury, P. Kovacic, and H. M. Gilow, *J. Polym. Sci., Polym. Lett. Ed.*, **19**, 395 (1981).

7) M. Bezoari, P. Kovacic, S. Gronowitz, and A-B. Hörnfieldt, *J. Polym. Sci., Polym. Lett. Ed.*, **19**, 347 (1981).

8) a) V. L. Afanas'ev, I. B. Nazarova, M. L. Khidekel, *Izv. Akad. Nauk SSSR, Ser. Khim.*, 1687 (1980); b) G. Tourilon and F. Garniew, *J. Electroanal. Chem.*, **135**, 173 (1982).

9) Although the $CHCl_3$-extractable fraction did not contain magnesium, the $CHCl_3$-unextractable fraction contained magnesium (2.5—3.0 wt%) as proved by macroanalysis. $MgBr_2$ captured by poly(2,5-thienylene) through coordination to sulfur may be the origin of the magnesium component. For this reason, the true carbon content of the $CHCl_3$-unextractable poly(2,5-thienylene) is regarded to be higher than the found value. It was difficult to remove magnesium from the $CHCl_3$-unextractable fraction.

10) C. J. Pouchert, "The Aldrich Library of Infrared Spectra", Aldrich, Milwaukee (1975).

11) P. Bucci, M. Longeri, C. A. Veracini, and L. Lunazzi, *J. Am. Chem. Soc.*, **96**, 1305 (1974).

12) E. Hückel, *Z. Phys.* **76**, 628 (1932).

13) *E. g.*, T. Matsuda, Y. Okano, Y. Kuwane, and T. Higashimura, *Polym. J.*, **12**, 907 (1981).

14) S. O. Lawessen, *Ark. Kemi.*, **11**, 317 (1957).

15) W. Steinkopf and H. Jacob, *Justus Liebigs Ann. Chem.*, **515**, 273 (1935).

16) J. A. Broomhead and F. P. Dwyer, *Aust. J. Chem.*, **14**, 250 (1961).

17) G. R. van Hecke and W. D. Horrocks, Jr., *Inorg. Chem.*, **5**, 1968 (1966).

18) A recent paper (M. Aizawa, S. Watanabe, H. Shinohara, and H. Shirakawa, 47th National Meeting of the Chem. Soc. of Jpn., Kyoto (1983) 4Q47) published after submitting this paper also reported the electrochemical preparation of poly(thienylene), and we were informed that the IR spectrum of the poly(thienylene) showed a strong absorption band at about 780 cm^{-1} when the polymer did not contain much dopant (M. Aizawa, private communication).

Formation of Adducts of Poly(thienylene)s with Electron Acceptors and Electric Conductivities of the Adducts

Takakazu YAMAMOTO,* Ken-ichi SANECHIKA, and Akio YAMAMOTO

Research Laboratory of Resources Utilization, Tokyo Institute of Technology, 4259 Nagatsuta, Midori-ku, Yokohama 227

(Received November 20, 1982)

Affinities of poly(thienylene) type polymers toward electron acceptors (iodine and SO_3) and electric conductivities of the polymer-electron acceptor adducts have been investigated. π-Conjugated poly(2,5-thienylene) has a high affinity toward iodine to absorb 60 wt% of iodine per the polymer. Poly(3-methyl-2,5-thienylene) has a higher affinity toward iodine and absorbs 136 wt% of iodine per the polymer. In the case of copolymer composed of 2,5- and 2,4-thienylene units the affinity against iodine increases with increase in the proportion of the 2,5-thienylene unit in the copolymer. The poly(2,5-thienylene)–iodine and poly(3-methyl-2,5-thienylene)–iodine adducts show electric conductivities of 5×10^{-2} S cm^{-1} and 4×10^{-1} S cm^{-1}, respectively, at room temperature. The activation energies of the electric conduction are 10 kJ/mol and 7.6 kJ/mol for the poly(2,5-thienylene)–iodine adduct (wt% of iodine=60) and poly(3-methyl-2,5-thienylene)–iodine adduct (wt% of iodine=136), respectively. The electric conductivity of the copolymer–iodine adduct sharply decreases on introduction of the 2,4-thienylene unit into the copolymer. The electric conductivity of the iodine adduct of the copolymer containing only 6% of 2,4-thienylene unit drops to *ca.* 1/100 of that of the iodine adduct of pure poly-(2,5-thienylene). The activation energy of the electric conduction of the polymer-iodine adducts decreases with increase in the content of the 2,5-thienylene unit as well as with the increase in the amount of iodine absorbed. Every poly(thienylene) type polymer has a high affinity toward SO_3, a stronger electron acceptor than iodine, to absorb about 70 wt% of SO_3 per the polymer. The SO_3–polymer adducts have electric conductivities of *ca.* 10^{-4} S cm^{-1}.

Synthesizing electric conducting π-conjugated polymers and revealing the mechanism of the electric conduction are subjects of recent interest. Several polymers including poly(acetylene),[1] poly(*p*-phenylene),[2] poly(pyrrolylene),[3] and poly(phenylene sulfide)[4] have been found to have high electric conductivities when they form adducts with electron acceptors or electron donors.

In the preceding paper[5] we reported preparation of poly(2,5-thienylene) having conjugated thiophene

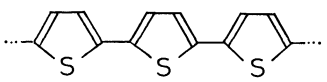

rings and compared its properties with those of poly-(2,4-thienylene). It was revealed that the π-electrons in poly(2,5-thienylene) are extensively delocalized whereas the conjugation in poly(2,4-thienylene) is very limited. The difference in the electron delocalization is expected to be reflected in the chemical reactivities of these polymers toward electron acceptors and hence in their development of electric conductivities. In the present paper we wish to report on the reactions of these polymers with electron acceptors such as iodine and SO_3 and on the enhancement of electric conductivities on their adduct formation. Since the polymers employed in the present study are structurally better defined than electrochemically prepared polymers having similar π-conjugation systems (poly(pyrrole),[3] poly(thiophene),[6] and poly(furan)[6]), one can investigate effects of the structure of the polymers (*e.g.*, effect of the bonding between the thienylene units in the polymer chain, effect of the CH_3-substituent, and effect of the composition of the copolymer) on the affinity toward electron acceptors and electric conductivities of the adducts. This is taken as one of advantages of the present study.

Results and Discussion

Formation of Adducts with Electron Acceptors. As described in the preceding paper, poly(2,5-thienylene) is colored dark reddish brown with its λ_{max} in $CHCl_3$ at 418 nm. When exposed to the vapor of I_2, the color of poly(2,5-thienylene) changes from deep brown to black, indicating the formation of an adduct between the polymer and iodine. Figure 1 shows time course of the absorption of iodine by $CHCl_3$-unextractable poly(2,5-thienylene), and copolymers composed of 2,5- and 2,4-thienylene units on exposure to the vapor of I_2 at room temperature (29—31 °C). Pure poly(2,5-thienylene) has a high affinity toward iodine and it absorbs about 60 wt% of iodine on its prolonged exposure to the iodine vapor. Most of the iodine once absorbed by poly(2,5-thienylene) are not removed by evacuation at room temperature. A copolymer composed of 94% of 2,5-thienylene and 6% of 2,4-thienylene units has almost the same affinity toward iodine as the 2,5-thienylene homopolymer, whereas further increase in the fraction of 2,4-thienylene unit in the copolymer strongly decreases the affinity toward iodine. Thus, the final amount of iodine absorbed by a copolymer containing 13% of 2,4-thienylene unit ((3) in Fig. 1) decreases to about 30 wt%.

The delocalization of π-electrons along the recurring 2,5-thienylene units is expected to raise the energy level of HOMO as shown in Fig. 5 of our preceding paper[5] and this makes poly(2,5-thienylene) strongly interact with an electron acceptor, iodine in this case. On the other hand such delocalization is absent in poly(2,4-thienylene) as we observed in the electronic spectra. Thus, intervention of the 2,4-thienylene unit into the 2,5-thienylene polymer will break the delocalization and the interaction between the polymer and iodine then decreases in accord with the data

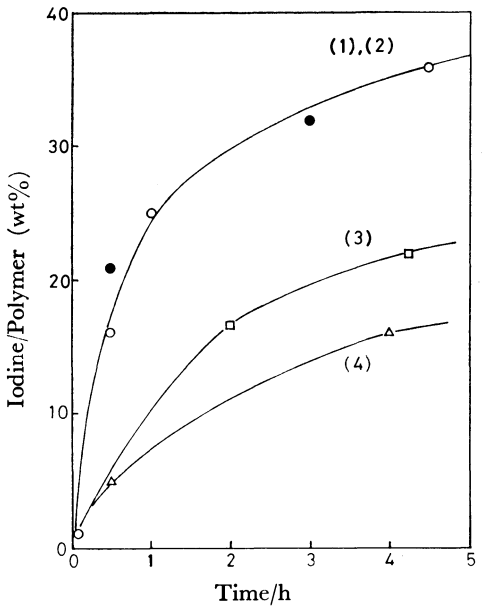

Fig. 1. Time course of absorption of iodine by poly-(2,5-thienylene) and copolymers composed of 2,5- and 2,4-thienylene units. Exposed to vapor of I_2 in a vacuum line at room temperature. 2,5-Thienylene: 2,4-thienylene=100:0 (○, (1)); 94:6 (●, (2)); 87:13 (□, (3)); 62:38 (△, (4)). In Figs. 1, 3, 4, and 5 the number attached to a curve or line corresponds to the number of Run in Table 2 of our preceding paper.[5]

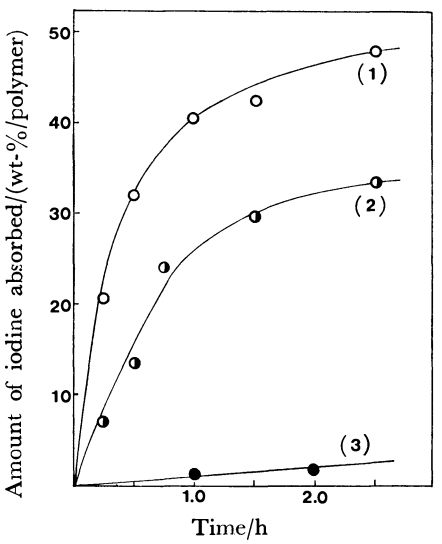

Fig. 2. Time course of absorption of iodine by poly-(2,5-thienylene). ○: $CHCl_3$-unextractable fraction, ◑: $CHCl_3$-soluble fraction (M_w=1370), ●: CH_3OH-soluble fraction (M_w=600).

shown in Fig. 1.

Although the $CHCl_3$-unextractable poly(2,5-thienylene) has a strong affinity toward iodine, $CHCl_3$-soluble (M_w=1370) and methanol-soluble (M_w=600) fractions have considerably weaker affinities (especially in the case of the methanol-soluble fraction) toward iodine (Fig. 2), indicating that the extent of delocalization in the polymers is not sufficient to lend the polymer strong affinity toward iodine.

The methyl-substituted polymer, poly(3-methyl-2,5-thienylene), has a higher affinity toward iodine than poly(2,5-thienylene). Thus, $CHCl_3$-soluble and $CHCl_3$-unextractable poly(3-methyl-2,5-thienylene) absorb 116 and 136 wt% of iodine, respectively, after exposure to the vapor of iodine for 10 h, the amounts being more than twice of the amounts of iodine absorbed by the $CHCl_3$-soluble and $CHCl_3$-unextractable unsubstituted poly(2,5-thienylene), respectively. Enhancement of electron-donating ability of poly(2,5-thienylene) by the methyl substitution accounts for the higher affinity of poly(3-methyl-2,5-thienylene) toward iodine. The iodine adducts of the poly(thienylene) type polymers have high stabilities in air, which provide an advantage in using the iodine adducts as semiconductors or positive electrodes in galvanic cells.[7]

In IR spectra of the polymers, the absorption bands are generally broadened on the complex formation with iodine. The IR spectra of the adducts generally show four major peaks in a region of 1000—1400 cm^{-1} which are assignable to skeletal deformation vibration of the thienylene group. The poly(2,5-thienylene)–iodine adduct has an apparent specific gravity of 2.2. An ESR spectrum of the adduct shows an absorption signal at g=2.008.

When the polymers are exposed to a vapor of SO_3, a stronger electron acceptor, every poly(thienylene) type polymer absorbs about 50—60 wt% of SO_3. Since thiophene itself has donor properties, such a strong acceptor as SO_3 seems to be able to interact even with nonconjugated poly(2,4-thienylene). The $CHCl_3$-soluble poly(2,5-thienylene) is soluble in concd H_2SO_4 and the fluorescing blue solution gives rise to an absorption band at 850 nm ($\varepsilon_{max}=6\times10^3$) which may be assigned to a CT band.

In contrast to the facile formation of adducts with iodine and SO_3, poly(2,5-thienylene) and its related polymer did not form adducts with tetracyanoquinodimethan, a typical organic electron acceptor. Since it is known that tetracyanoquinodimethan forms a stable 1:1 adduct with thiophene,[8] the low affinity of the polymers against tetracyanoquinodimethan seems to be due to difficulty in entry of the electron acceptor into microcrystals of the polymers or due to sterical non-fitting of tetracyanoquinodimethan with the polymers. Kossmehl and Chatzitheodorou reported formation of adducts of poly(2,5-thienylene) prepared by our method with AsF_5, one of the strongest electron acceptors, and electric conductivity of the adducts.[9]

When poly(2,5-thienylene) was dipped into a THF solution of potassium naphthalenide, color of the polymer changed from deep reddish brown to black, suggesting formation of an adduct of the polymer with potassium similar to the reported adduct of poly(acetylene) with alkali metals.[1,10] However, characterization of the adduct was not feasible due to the high air-sensitivity of the adduct (explosive in air).

Electric Conductivity. Iodine Adduct: All the poly(thienylene) type polymers are insulators having electric conductivity of 10^{-14}—10^{-11} S cm^{-1}. The electric conductivity, however, increases markedly on the ad-

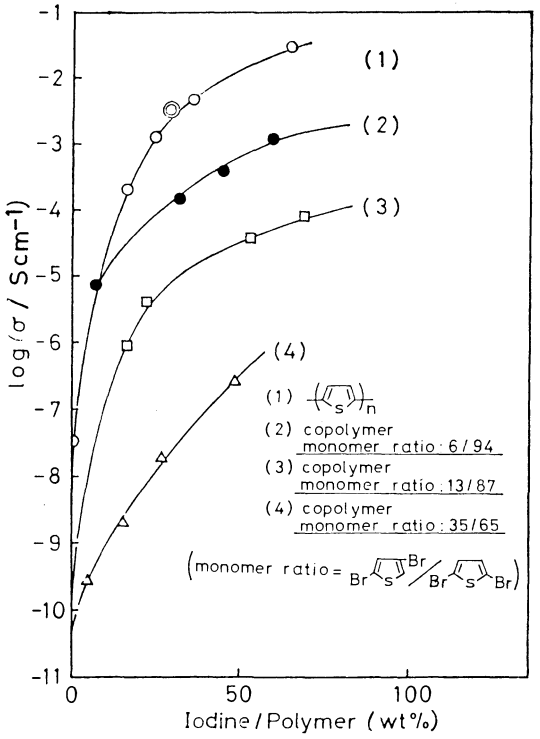

Fig. 3. Electric conductivities of the iodine adducts of poly(2,5-thienylene) and the copolymers *vs.* amount of iodine absorbed. The numbering of the curve corresponds to that in Fig. 1.

duct formation with the electron acceptors as observed in the other π-conjugated polymers such as poly(acetylene)[1] and poly(*p*-phenylene).[2] Figure 3 shows the increase of the electric conductivities of poly(2,5-thienylene) and the copolymers on interaction with iodine.

The following observations are made from experiments related to Fig. 3.

(1) The electric conductivity, σ, increases with increase in the amount of iodine absorbed. The electric conductivity of the poly(2,5-thienylene)–iodine adduct is comparable to those of commercially used inorganic semiconductors such as doped Si and Ge ($\sigma = 10^{-4}$—10^{1} S cm^{-1}).

(2) The composition of the copolymer strongly influences the electric conductivity, incorporation of only 6% of 2,4-thienylene unit causes decrease in the electric conductivity by a factor of 10^2 ((2) in Fig. 3), although the incorporation of only 6% of 2,4-thienylene unit does not affect the electronic spectrum[5] and the affinity of the polymer toward iodine. The steep decrease in the electric conductivity by the contamination with only a small amount of 2,4-thienylene unit indicates that the electric conductivity is strongly influenced by the extent of the delocalization of π-electrons along the polymer chain. However, it is inferred from these results that the random incorporation of considerable proportion of insulating 2,4-thienylene unit, roughly one part per two parts of the 2,5-thienylene units, still leaves appreciable conductivity in the polymer ((4) in Fig. 3).

(3) A 1:1 mixture of poly(2,5-thienylene) and poly(2,4-thienylene) on treatment with iodine shows much

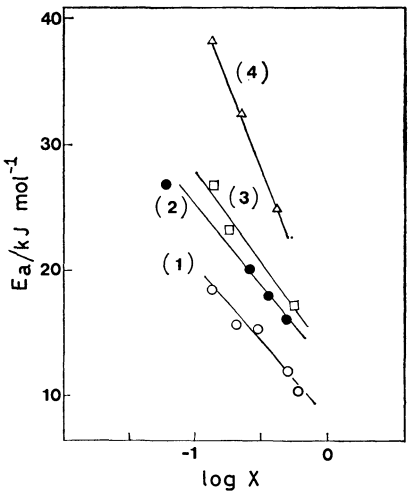

Fig. 4. Activation energy of the electric conduction of the iodine adducts of poly(2,5-thienylene) and copolymers *vs.* logarism of the amount of iodine absorbed (X= mass of iodine/mass of polymer). For numbering of the line, see a caption of Fig. 1.

higher electric conductivity (see a double circle in Fig. 3) than the copolymer containing 2,5- and 2,4-thienylene units in about 1:1 ratio. Although the electronic spectral data reported in our preceding paper have afforded evidence that the polymer obtained by the dehalogenative polycondensation of a mixture of 2,5- and 2,4-dibromothiophene is not a mixture of two homopolymers, the present result renders additional evidence for the formation of the copolymer. In the absorption of iodine by the 1:1 mixture of pure poly(2,5-thienylene) and poly(2,4-thienylene), iodine is absorbed only by poly(2,5-thienylene). Therefore, the 1:1:0.27 mixture of poly(2,5-thienylene), poly(2,4-thienylene), and iodine shown by the double circle in Fig. 3 is considered to be a mixture of poly(2,5-thienylene) absorbing 54 wt% of iodine and pure poly(2,4-thienylene). On this basis it may be concluded that electric conductivity of 2×10^{-2} S cm^{-1} of poly(2,5-thienylene) containing 54 wt% of iodine has decreased to 4×10^{-3} S cm^{-1} (datum shown by the double circle) by mixing with the insulating poly(2,4-thienylene).

Poly(3-methyl-2,5-thienylene)–iodine adducts show somewhat higher electric conductivities than the poly(2,5-thienylene)–iodine adducts: for example, poly(3-methyl-2,5-thienylene) absorbing 136 wt% of iodine has an electric conductivity of 4×10^{-1} S cm^{-1}.

The electric conductivities, σ, of the iodine-adducts varies with temperature according to the following equation,

$$\sigma = \sigma_0 \exp(-E_a/RT). \quad (1)$$

Figure 4 shows plots of the activation energy, E_a, of the electric conduction against logarithm of the amount iodine absorbed, log X. As shown in Fig. 4 a linear correlation holds between E_a and log X for each polymer. A similar linear correlation between E_a and log X has been observed concerning the electric conduction of poly(acetylene) absorbing moderate amounts of iodine (3—30 wt% per poly(acetylene)). This de-

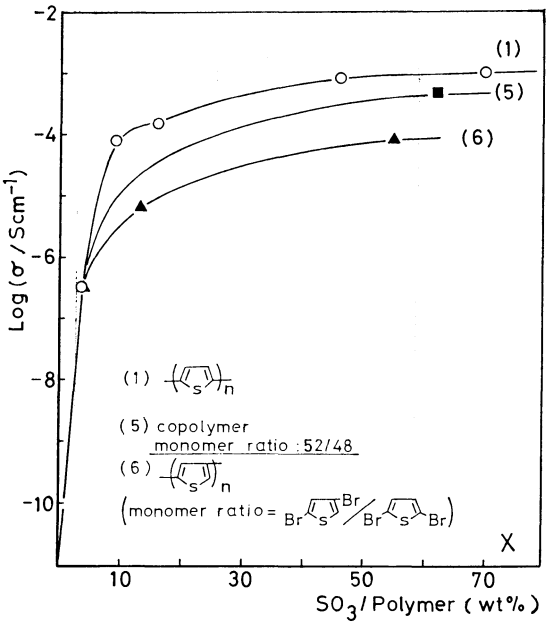

Fig. 5. Electric conductivities of the SO_3 adducts of poly(2,5-thienylene) (1), poly(2,4-thienylene) (6), and a copolymer composed of 52% of 2,5-thienylene and 48% of 2,4-thienylene units (5).

crease in E_a with the increase in the amount of iodine absorbed by poly(acetylene) is called "semiconductor-metal transition" since further increase in the amount of iodine absorbed gives the poly(acetylene)–iodine adduct a metallic conductivity ($\sigma > 10^3$ S cm^{-1}) with small E_a.[1b,d] However, in cases of poly(2,5-thienylene) and the copolymers the iodine adducts still show appreciable activation energies even at a high concentration of iodine and metal-like conductivity has not been attained, although a recent paper reported that electrochemically prepared poly(thienylene-0.25BF_4) have electric conductivity of 10^1—10^2 S cm^{-1}.[6b]

E_a increases with increase in the proportion of 2,4-thienylene unit in the copolymer. The iodine adduct of the $CHCl_3$-unextractable poly(3-methyl-2,5-thienylene) (iodine=136 wt%) shows somewhat lower activation energy of the electric conduction (E_a=7.6 kJ/mol) than the iodine adduct of poly(2,5-thienylene).

SO_3 Adduct: Figure 5 shows the electric conductivities of the SO_3 adducts of poly(2,5-thienylene), poly(2,4-thienylene), and a copolymer containing 2,5- and 2,4-thienylene units in about 1:1 ratio. Although π-conjugated poly(2,5-thienylene), among the polymers, shows the highest electric conductivity on the adduct formation with SO_3, the structure of the polymer affects the electric conductivity to a much less extent, compared with the iodine adducts of the polymers. The activation energy for the electric conduction of the SO_3 adducts decreases with increase in the amount of SO_3 absorbed (Fig. 6), but such a linear correlation observed for the iodine adducts (Fig. 5) is not observed for the SO_3 adducts. An ESR spectrum of the SO_3–poly(2,5-thienylene) shows an absorption signal at g=1.962.

Mechanism of the Electric Conduction. It is known

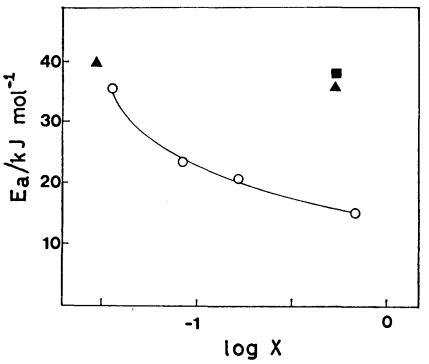

Fig. 6. Activation energy of the electric conduction of the SO_3 adducts of poly(2,5-thienylene) (○), poly(2,4-thienylene) (▲), and a copolymer composed of 52% of 2,5-thienylene and 48% of 2,4-thienylene units (■). X=mass of SO_3/mass of polymer.

that a part of iodine absorbed by poly(acetylene) exists in the form of I_3^- and it is generally accepted that the counter cation (hole) formed in poly(acetylene) participates in the electric conduction.[1b-c] Since poly(thiophene) reportedly has ionization potential of 0.7 V[6c] comparable to that of poly(acetylene) (0.7 V), it will be reasonable to assume that iodine can abstract an electron from poly(2,5-thienylene) to form an ion pair and the electron conduction originates from the migration of the cation center along the π-conjugated chain.[11] If the 2,4-thienylene unit is incorporated into the polymer chain, the migration of the cation center will stop at the 2,4-thienylene unit and thus the electric conduction will be hindered in accord with the results described above.

The electric conductivity of the SO_3–poly(2,4-thienylene) adduct, however, is not explained by such a simple mechanism and thinking of special mechanisms of the electric conduction (for example, SO_3^- assisted migration of the cationic center or tunnel effect) seems to be necessary.

Experimental

Materials. Poly(thienylene) type polymers were prepared according to methods described in our preceding paper.[5] Commercially available I_2 and SO_3 were used without purification. Tetracyanoquinodimethan was purified by recrystallization before use. The THF solution of potassium naphthalenide was prepared by a reaction of naphthalene (2.0 g, 16 mmol) and potassium metal (1.5 g, 38 mmol) in THF (15 cm^3) for 21 h at room temperature. Remaining potassium was filtered off.

Absorption of Electron Acceptors. Powdery poly(thienylene) type polymer placed in a glass vessel was exposed to vapor of iodine at room temperature by using a vacuum line. The amount of iodine absorbed was measured by weighing the polymer-iodine adduct and halogen analysis of the adduct. Both data coincided within an experimental error. The reactions of the polymers with SO_3 (vapor) were carried out analogously. When a pellet prepared by pressing the powdery polymer at 600 kg/cm^2 was used, the rate of absorption of iodine was considerably slower.

Measurement of the Electric Conductivity. The powdery polymer-electron acceptor adduct was molded into a pellet

(diameter = 1.3 cm) by pressing it at 600 kg/cm². From the pellet a bar was obtained by cutting off other parts of the pellet, and the electric conductivity was measured with the bar using the four-point method. A Takeda Riken TR-8651 electrometer was used to measure the electric conductivity.

Measurement of Spectra. Electronic and IR spectra were recorded on Hitachi model 200-20 and Hitachi model 295 spectrometers, respectively.

References

1) a) H. Shirakawa, E. J. Louis, A. G. MacDiarmid, C. K. Chiang, and A. J. Heeger, *J. Chem. Soc., Chem. Commun.*, **1977**, 578; b) Y. W. Park, A. J. Heeger, M. A. Druy, and A. G. MacDiarmid, *J. Chem. Phys.*, **73**, 946 (1980); c) W. P. Su, J. R. Schrieffer, and A. J. Heeger, *Phys. Rev. Lett.*, **42**, 1698 (1979); d) H. Shirakawa and T. Yamabe, "Synthetic Metal", Kagaku-Dojin, Kyoto (1980) and references therein; e) Y. Furukawa, I. Harada, M. Tasumi, H. Shirakawa, and S. Ikeda, *Chem. Lett.*, **1981**, 1489; f) J. C. W. Chien, *J. Polym. Sci., Polym. Lett. Ed.*, **19**, 249 (1981).

2) D. M. Ivory, G. G. Miller, J. M. Sowa, L. W. Shacklette, R. R. Chance, and R. H. Baughmann, *J. Chem. Phys.*, **71**, 1506 (1979); L. W. Shacklette, R. R. Chance, D. M. Ivory, G. G. Miller, and R. H. Baughman, *Synth. Metals.*, **1**, 307 (1979); M. Tanaka, A. Watanabe, H. Fujimoto, and J. Tanaka, *Chem. Lett.*, **1980**, 907.

3) A. F. Diaz, K. K. Kanazawa, and G. P. Gardini, *J. Chem. Soc., Chem. Commun.*, **1979**, 635; K. K. Kanazawa, A. F. Diaz, W. D. Gill, P. M. Grant, G. B. Street, G. P. Gardini, and J. F. Kwak, *Synth. Metals*, **1**, 329 (1979/80); A. F. Diaz and J. I. Castillo, *J. Chem. Soc., Chem. Commun.*, **1980**, 397.

4) J. F. Rabolt, T. C. Clarke, K. K. Kanazawa, J. R. Reynolds, and G. B. Street, *J. Chem. Soc., Chem. Commun.*, **1980**, 347; R. R. Chance, L. W. Schacklette, G. G. Miller, D. M. Ivory, J. M. Sowa, R. L. Elsenbaumer, and R. H. Baughmann, *ibid.*, **1980**, 348.

5) T. Yamamoto, K. Sanechika, and A. Yamamoto, *Bull. Chem. Soc. Jpn.*, **56**, 1497 (1983).

6) a) V. L. Afanas'ev, I. B. Nazarova, and M. L. Khidekel, *Izv. Akad. Nauk SSSR, Ser, Khim.*, **1980**, 1687; b) Tourillon and F. Garnier, *J. Electroanal. Chem.*, **135**, 173 (1982); c) A. F. Diaz, J. Crowley, J. Bargon, G. P. Gardini, and J. B. Torrance, *ibid.*, **121**, 355 (1981).

7) T. Yamamoto, *J. Chem. Soc., Chem. Commun.*, **1981**, 187; D. MacInnes, Jr., M. A. Druy, P. J. Nigrey, D. P. Nairns, A. G. MacDirmid, and A. J. Heeger, *ibid.*, **1981**, 317; Japan Kokai, 56-136469 (1981).

8) B. P. Bespalov, A. A. Pankratov, and V. V. Titov, *Zh. Org. Khim.*, **10**, 134 (1974).

9) G. Kossmehl and G. Chatzitheodorou, *Makromol. Chem. Rapid Commun.*, **2**, 551 (1981).

10) C. K. Chiang, M. A. Druy, S. C. Gau, A. J. Heeger, E. J. Louis, A. G. MacDiarmid, Y. W. Park, and H. Shirakawa, *J. Am. Chem. Soc.*, **100**, 1013 (1978).

11) This explains chemical concept of the electric conduction. Physical treatment of the electric conduction of poly(acetylene)-acceptor (or donor) adducts have revealed that positive (or negative) solitons play important roles in the electric conduction (Refs. 1c and 1d as well as H. Takayama, Y. R. Lin-Lin, and K. Maki, *Phys. Rev. B*, **21**, 21 (1980)).

Alkylation of the Sulfur- and Nitrogen-containing Compounds Analogous to Thiazoline Systems

Yoshio OHARA, Kin-ya AKIBA,† and Naoki INAMOTO*

Department of Chemistry, Faculty of Science, The University of Tokyo, Hongo, Bunkyo-ku, Tokyo 113

(Received November 26, 1982)

N,N-Dimethyl-2-(alkylthio)ethylamines and 3-methylthiazolidines underwent *N*-methylation both with trimethyloxonium tetrafluoroborate (**3a**) and with methyl iodide. In the methylation of *N,N*-dimethyl-*o*-(methylthio)aniline, the main reaction was *S*-methylation. On the other hand, in the *o*-ethylthio derivative, *S*-methylated product was major with methyl iodide, while *N*-methylated product was major with **3a**. In the *N*-ethyl or *N*-benzyl derivative, only *S*-methylation occurred with both reagents. 3-Methyl-2, 2-diphenyl-2,3-dihydrobenzothiazole gave *S*-methylated product with **3a**, suggesting that *S*-methylation becomes major when the 2-substituent is bulkier. 4-Methyl-3,4-dihydro-2*H*-benzo[*b*][1,4]thiazine was methylated on the nitrogen with **3a**, while it gave *S*-methylated product with methyl iodide. Phenothiazines and 1-dialkylamino-8-(methylthio)-naphthalenes gave only *S*-methylated products. The selective *S*-methylation in the case of *N*-methylation was carried out through protonation on the nitrogen atom followed by methylation with **3a**. Possibility of intramolecular interaction between sulfonio and amino groups has been discussed based on their NMR data.

In the alkylation of a compound containing both sulfur and nitrogen atoms, the position of alkylation depends on the structure of the compound and the kind of alkylating reagent.[1] We previously reported that 3-alkyl-2,3-dihydrobenzothiazoles were selectively alkylated on the nitrogen with Meerwein reagents.[1]

Therefore, our work on alkylation was extended to the compounds containing both sulfur and nitrogen atoms analogous to thiazoline systems, in order to obtain an information on the relation between the structure of the compound and the alkylated position.

Results and Discussion

Methylation of N,N-*Dimethyl-2-(alkylthio)ethylamines (**1**) and 3-Methylthiazolidines (**7**).* *N,N*-Dimethyl-2-(methylthio)ethylamine (**1a**) reacted with methyl iodide to give trimethyl(2-methylthioethyl)ammonium iodide (**2a**(I^-)), while with trimethyloxonium tetrafluoroborate (**3a**) it gave a mixture of *N*-methylated (**2a**(BF_4^-)) and *N,S*-dimethylated salts (**4a**). These structures could be assigned by NMR.

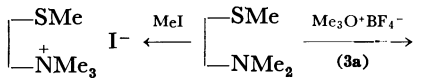

2a(I^-) **1a**

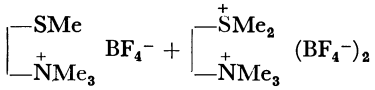

2a(BF_4^-) **4a**

Accordingly, **1a** is methylated on nitrogen to give **2a** both with methyl iodide and with **3a**, but with a stronger alkylating reagent such as **3a**, **2a** is further methylated on the sulfur to give **4a**.

Based on the above result, we succeeded in preparation of the sulfonium salt (**6**) from **1**. The nitrogen atom in **1** was first protonated with tetrafluoroboric acid and then the ammonium salt was methylated with **3a** to give [2-(dialkylsulfonio)ethyl]dimethylammonium salt (**5**) which was deprotonated to give **6**.

† Present address: Department of Chemistry, Faculty of Science, Hiroshima University, Higashisenda-machi, Hiroshima 730.

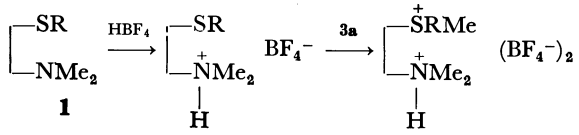

1 **5**

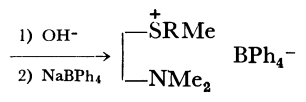

6

a: R=Me
b: R=Et

3-Methylthiazolidines (**7**) were methylated with **3a** to give cyclic ammonium salts (**8**) analogously to that of **1**. The NMR spectra of **8** were analogous to those of 3,3-dimethylbenzothiazolinium salts,[1] confirming the structure (**8**).

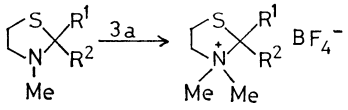

7 **8**

a: R^1=Ph, R^2=H
b: R^1=R^2=Me

Thus it is concluded that aliphatic or alicyclic compounds containing sulfur and nitrogen atoms are selectively alkylated on nitrogen both with methyl iodide and with **3a**.

Methylation of o-*(Alkylthio)aniline Derivatives (**9**).* Methylation of *N,N*-dimethyl-*o*-(methylthio)aniline (**9a**) with methyl iodide–silver perchlorate system gave a mixture of the sulfonium (**10a**(ClO_4^-)) and the ammonium salts (**11a**(ClO_4^-)) in a ratio of *ca.* 4:1 (by NMR), while methylation with **3a** gave a mixture of **10a**(BF_4^-) and **11a**(BF_4^-) in a ratio of *ca.* 1.5:1. The salts **10a** and **11a** were isolated in pure form by repeated recrystallization from ethanol.

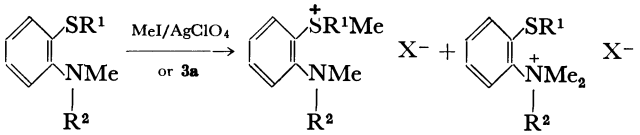

9 **10**(X^-) **11**(X^-)

a: R^1=R^2=Me; **b**: R^1=Et, R^2=Me: **c**: R^1=Me, R^2=Et; **d**: R^1=Me, R^2=$PhCH_2$. X=ClO_4, BF_4.

The results are consistent with that methyl iodide is regarded as a soft reagent possessing a considerable affinity to sulfur atom and **3a** as a hard one possessing a considerable affinity to nitrogen.

Methylation of **9b** with methyl iodide–silver perchlorate gave a mixture of **10b**(ClO_4^-) and **11b**(ClO_4^-) in a ratio of 2:1, while that with **3a** gave a mixture of **10b** (BF_4^-) and **11b**(BF_4^-) in a ratio of 1:2, indicating to be more selective than in the case of **9a**. In the former, the ratio did not change after single recrystallization, but in the latter, only **11b** was isolated after single recrystallization. Both **9c** and **9d** gave only *S*-methylated products (**10c** and **10d**) with both reagents.

These results are attributed to the considerable decrease of the nucleophilicity of nitrogen atom due to conjugation with benzene ring as compared with that of sulfur atom, and suggest that a congestion around sulfur atom moderately decreases the *S*-methylation, while a congestion around the nitrogen drastically decreases *N*-methylation with **3a**.

*Methylation of 3-Methyl-2,2-diphenyl-2,3-dihydrobenzothiazole (**12c**) and 4-Methyl-3,4-dihydro-2H-benzo[b][1,4]-thiazine (**16**).*

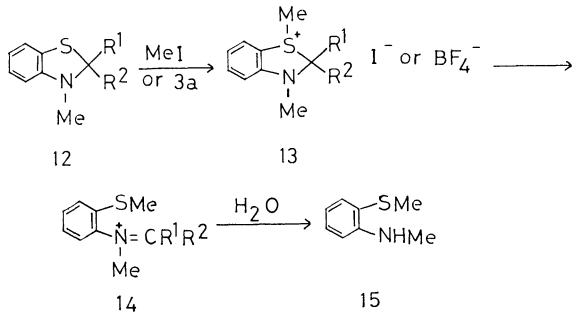

a: $R^1=R^2=Me$; **b**: $R^1=H$, $R^2=Ph$; **c**: $R^1=R^2=Ph$; **d**: $R^1=H$, $R^2=t$-Bu.

3-Methyl-2,3-dihydrobenzothiazoles (**12**) are methylated on the nitrogen atom.[1] However, considering the above results, it is expected that **12** would be methylated rather on the sulfur atom, if a bulky group exists at the 2-position, because of steric congestion around the nitrogen due to shorter C–N bond than C–S bond.

In fact, Hori *et al.*[2] have reported that methylation of 2,2,3-trimethyl-2,3-dihydrobenzothiazole (**12a**) with methyl iodide gave ring-opening immonium salt (**14a**) *via* *S*-methylated compound (**13a**). We also found that methylation of 3-methyl-2-phenyl-2,3-dihydrobenzothiazole (**12b**) with **3a** gave *N*-methyl-*o*-(methylthio)aniline (**15**) as by-product,[1] which is decomposition product of *S*-methylated product (**13b**).[2]

Therefore, **12c** was methylated with **3a** to expect *S*-methylation. Actually, the reaction gave *S*-methylated **13c** in 31% yield. Very recently, Hori *et al.*[3] have reported that methylation of **12d** with **3a** gave **15** through unstable **13d**.

On the other hand, methylation of **16** with **3a** selectively gave ammonium salt (**17**), while methylation with methyl iodide–silver perchlorate gave sulfonium salt (**18**).

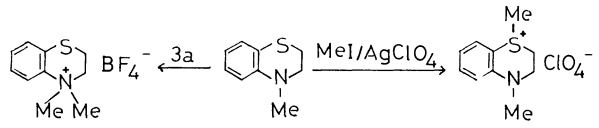

The difference in **12** and **16** may be ascribable to an effect of five-membered ring fused with benzene ring in **12**. Namely, it is considered that thiazoline ring makes the delocalization of the lone pair electrons of nitrogen conformationally unfavorable, while sulfur atom can resonate with benzene ring under such circumstances.[4] Thus the reactivity towards **3a** becomes larger on nitrogen than on sulfur analogously to the aliphatic systems.

*Alkylation of Phenothiazines (**19**).* 10-Methylphenothiazine (**19a**) was methylated on sulfur even with **3a** to give sulfonium salt (**20a**). The ethylated salt (**20a'**) from **19a** with triethyloxonium tetrafluoroborate (**3b**) was different from the methylated salt (**20b**) from **19b** with **3a**, indicating that these salts were sulfonium salts. Phenothiazine (**19c**) was also methylated on sulfur with methyl iodide–silver perchlorate to give sulfonium salt (**20c**).

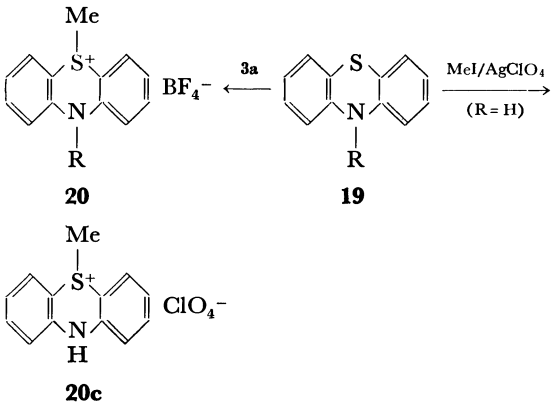

a: R=Me; **b**: R=Et; **c**: R=H

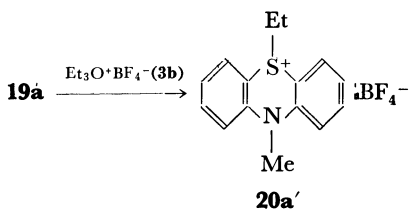

These facts indicate that the reactivity on the nitrogen atom extremely decreases because of the large delocalization of lone pair electrons over two benzene rings. It may also be attributed to not only the steric hindrance due to two benzene rings but also the steric hindrance due to two *peri*-hydrogen atoms.

*Methylation of 1-Dialkylamino-8-(methylthio)naphthalenes (**24**).* 1-Dialkylamino-8-(methylthio)naphthalenes (**24**) were prepared from the reported hexachlorostannate (**21**)[5] as Scheme 1.

Methylation of **24** with methyl iodide–silver perchlorate gave sulfonium salt (**25**), while with **3a** it gave a mixture of *S*-methylated **25a** and ammonium tetrafluoroborate (**26a**) from **24a** and only **26b** from **24b**.

Table 1. Chemical shifts[a] of *N*- or *S*-methyl protons in parent compounds and the methylated salts (δ, at 34 °C)

Parent		In $CDCl_3$[b]	Salt	In DMSO-d_6[b]	
1a	SMe	2.12	**6a**(BPh_4^-)	$\overset{+}{S}$Me	2.48(2.68)
	NMe	2.27		NMe	2.16(2.71)
1b	SMe	—	**6b**(BPh_4^-)	$\overset{+}{S}$Me	2.31(2.58)
	NMe	2.28		NMe	2.15(2.65)
9a	SMe	2.41(2.59)	**10a**(ClO_4^-)	$\overset{+}{S}$Me	3.21(3.56)
	NMe	2.74(3.46)		NMe	2.79(3.45)
9b	SMe	—	**10b**(ClO_4^-)	$\overset{+}{S}$Me	3.23(3.62)
	NMe	2.72		NMe	2.80(3.51)
9c	SMe	2.39	**10c**(ClO_4^-)	$\overset{+}{S}$Me	3.21
	NMe	2.70		NMe	2.77
24a	SMe	2.40	**25a**(ClO_4^-)	$\overset{+}{S}$Me	3.23(3.41)
	NMe	2.69		NMe	2.82(3.34)
24b	SMe	2.40	**25b**(ClO_4^-)	$\overset{+}{S}$Me	3.21(3.33)
					3.27(3.37)
	NMe	2.67		NMe	2.84(3.24)
29	PhSMe	2.48	**30**(ClO_4^-)	$\overset{+}{S}$Me	3.33(3.28)
31	$PhNMe_2$	2.90	**32**(ClO_4^-)	$\overset{+}{N}$Me	3.69(3.68)
33	o-$C_6H_4(NMe_2)_2$	2.77	**34**(BF_4^-)	$\overset{+}{N}$Me	3.82(3.88)
				NMe	2.72(3.09)
35	1-NaPh-SMe[c]	2.53	**36**(ClO_4^-)	$\overset{+}{S}$Me	3.43
37	1-Naph-NEt-Me[c]	2.83	**38**(BF_4^-)	$\overset{+}{N}$Me	3.91

a) Accuracy is within ±0.02 ppm. b) Values in parenthesis are those in CF_3COOH. c) Naph denotes naphthalene ring.

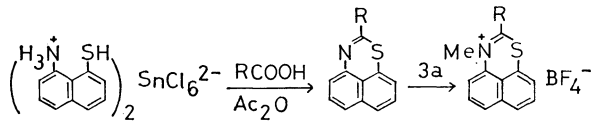

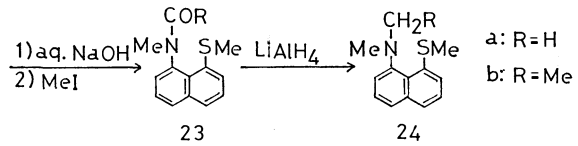

Scheme 1.

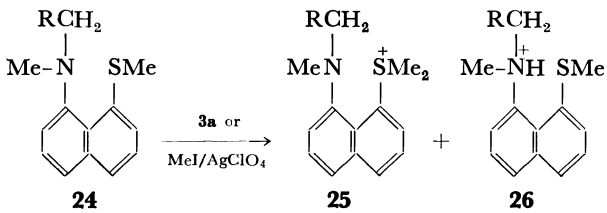

a: R=H; **b**: R=Me

Apparently **26** is derived from the protonation of **24** in the course of the decomposition of **3a** by ethanol. Methylation on the nitrogen atom did not take place even with Meerwein reagent, because of an extremely large steric congestion around the nitrogen atom.

Possibility of Intramolecular Interaction Between Sulfonio and Amino Groups. It would be expected that the sulfonium salts (**27**) containing amino group such as **6**, **10**, and **25** may be in an equilibrium with ammonio-sulfuranes (**28**) or exist in the form of **28**, which have both an ammonium part and a σ-sulfurane part (hypervalent I-type[6]).

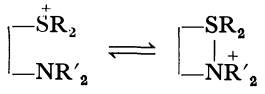

27 **28**

Although many stable σ-sulfuranes have recently been synthesized by Martin *et al.*,[7] there is no example of the σ-sulfurane such as **28**, which has alkyl groups on sulfur atom. Therefore, it is quite interesting to examine whether there is any possibility of contribution of **28** in **27**.

In order to characterize the structures of **6**, **10**, and **25**, several reference compounds and their methylated compounds were prepared. In Table 1 were shown chemical shifts of methyl protons in both parent and their methylated compounds. The accuracy for these data was estimated to be ±0.01 ppm for the solvent effect (checked by changing the ratio of DMSO-d_6 to $CDCl_3$), −0.02 ppm for S^+-Me, +0.02 ppm for *N*-Me in methanol-d_4 *vs.* DMSO-d_6, and the concentration effect was essentially negligible.

The *N*-methyl protons in **6** (δ 2.15) are in rather higher field than those in parent compound (**1**) (δ

2.28), probably because of anisotropy effect due to tetraphenylborate anion (*cf.* **10d**(BPh_4^-): δ 2.61 (NMe), 2.91 (SMe) *vs.* **10d**(BF_4^-): δ 2.63 (NMe), 3.12 (SMe)).

Both in **10** and **25**, the *N*-methyl protons are in lower field than those in parent compounds (**9** and **24**). The *S*-methyl protons in **10** and **25** are not so low as for those of reference compounds (**30** and **36**). This may be attributed to **28**. It is considered that **28** is decomposed by protonation in trifluoroacetic acid, so that the *S*-methyl chemical shifts in **10** and **25** are in lower field by the release of lone pair electrons on nitrogen. However, these phenomena can be interpreted as the inductive effect due to additional cationic center by protonation of the amino group.

In **34**, the methyl protons of dimethylamino group are in rather higher field than those in parent **33**, while that in **10** is rather lower than that in parent **9**. This phenomenon may be interpreted by the contribution of **28**. However, the inductive effect by the sulfonio group is slightly stronger than that by the ammonio group.[8] Therefore, the above fact can also be attributed to the difference of inductive effect.

From the above discussion based on NMR, no definite conclusion to support the structure **28** could be obtained. However, since the amino and sulfonio groups in **25a** are fixed closely (0.22—0.25 nm) in the peri position, there may be a possibility of strong interaction between nitrogen and sulfur atoms. The related works are in progress.

Experimental

All the boiling and melting points are not corrected. ^{1}H NMR spectra were measured with Hitachi R-24B and R-20B spectrometers using TMS as an internal standard.

Materials. *N,N*-Dimethyl-2-(methylthio)ethylamine (**1a**),[9,10] 3-methyl-2,2-diphenyl-2,3-dihydrobenzothiazole (**12c**),[11] 4-methyl-3,4-dihydro-2*H*-benzo[*b*][1,4]thiazine (**16**),[12] *N*-methyl- (**19a**) and *N*-ethylphenothiazines (**19b**),[13] and *N,N,N',N'*-tetramethyl-*o*-phenylenediamine (**33**)[14] were prepared by the reported methods. *N,N*-Dimethyl-2-(ethylthio)ethylamine (**1b**) was prepared by a similar method to that of **1a**, bp 90 °C/60 mmHg (1 mmHg≈133.322 Pa) (lit,[15] 61 °C/16 mmHg). 3-Methyl-2-phenyl- (**7a**)[16] and 2,2,3-trimethylthiazolidines (**7b**)[16] were prepared by the reported method.[17]

N,N-*Dimethyl-o-(methylthio)aniline (9a).* *o*-(Methylthio)aniline (5.05 g, 36.3 mmol) was methylated with Me_2SO_4 (8.9 ml, 94 mmol) and K_2CO_3 (7 g) in C_6H_6 (20 ml) to give **9a** (4.18 g, 69%), bp 92 °C/0.2 mmHg (lit,[18] 130 °C/20 mmHg).

N,N-*Dimethyl-o-(ethylthio)aniline (9b).* This compd was prepared by a similar methylation of *o*-(ethylthio)-aniline in 56% yield, bp 95 °C/0.3 mmHg; ^{1}H NMR ($CDCl_3$): δ=1.32 (t, J=7 Hz, 3H), 2.72 (s, 6H), 2.90 (q, J=7 Hz, 2H), and 7.0—7.2 (br s, 4H). Found: C, 66.02; H, 8.49; N, 7.95%. Calcd for $C_{10}H_{15}NS$: C, 66.25; H, 8.34; N, 7.73%.

N-*Ethyl*-N-*methyl*-o-*(methylthio)aniline (9c).* Bis[*o*-(ethylamino)phenyl] disulfide,[19] prepared from 3-ethylbenzothiazolium iodide (9.62 g, 33.0 mmol), was methylated with **3a** (3.16 g, 21.4 mmol) in CH_2Cl_2 (20 ml) and then treated with aq NaOH. After dry column chromatography (DCC) (SiO_2, CCl_4) the methylated product was reduced with sodium (0.5 g, 22 mmol) in liq NH_3 (50 ml) and ether (20 ml). To the residue, after evaporation, were added EtOH (20 ml) and MeI (1.5 ml). Extraction with ether after addition of water and distillation gave **9c** (1.19 g, 20%), bp 80 °C/0.3 mmHg; ^{1}H NMR ($CDCl_3$): δ=1.10 (t, J=7 Hz, 3H), 2.39 (s, 3H), 2.70 (s, 3H), 2.97 (q, J=7 Hz, 2H), and 7.04 (br s, 4H). Found: C, 66.05; H, 8.51; N, 7.56%. Calcd for $C_{10}H_{15}NS$: C, 66.25; H, 8.34; N, 7.73%.

N-*Benzyl*-N-*methyl*-o-*(methylthio)aniline (9d).* To a mixture of *o*-(methylthio)aniline (17.3 g, 124 mmol), benzaldehyde (60 g, 590 mmol), NaOAc (20 g, 240 mmol), and AcOH (100 ml) in EtOH (250 ml) was added $NaBH_4$ (25 g, 660 mmol) portionwise. After stirring for 4 h and usual work-up, distillation gave *N*-benzyl-*o*-(methylthio)aniline (21.4 g, 75%), bp 142 °C/0.25 mmHg. The aniline (16.1 g, 70 mmol) was treated with the Me_2SO_4 (8.0 ml, 85 mmol) and Na_2CO_3 (8 g, 76 mmol) in C_6H_6 (60 ml) to give **9d** (6.44 g, 38%), bp 142 °C/0.2 mmHg; ^{1}H NMR ($CDCl_3$): δ=2.41 (s, 3H), 2.60 (s, 3H), 4.07 (s, 2H), and 7.0—7.6 (m, 9H). Found: C, 74.00; H, 7.15; N, 5.89%. Calcd for $C_{15}H_{17}NS$: C, 74.03; H, 7.04; N, 5.76%.

Preparation of 24. *1) 24a*: Naphtho[1,8-*de*][1,3]-thiazine (**22a**) was prepared by a modified method of preparation of **22b**.[5b] To anhyd NaOAc (19 g) in boiling HCOOH (160 ml) were added tin (8.0 g, 68 mmol) and **21** (18.9 g, 30.5 mmol) under nitrogen. To this soln was added Ac_2O (26 ml) portionwise, and the mixture was neutralized with aq NH_3. From the ethereal extract of the resulting ppt, **22a** was isolated by DCC (SiO_2, CH_2Cl_2–CCl_4 (1:2)), 4.73 (42%), mp 95—110 °C; ^{1}H NMR ($CDCl_3$): δ=6.6—7.4 (m, 6H) and 7.97 (s, 1H). Found: C, 71.61; H, 3.63; N, 7.60; S, 17.20%. Calcd for $C_{17}H_7NS$: C, 71.32; H, 3.81; N, 7.56; S, 17.31%.

22a (2.16 g, 11.7 mmol) was methylated with **3a** (3.09 g, 20.9 mmol) in refluxing CH_2Cl_2 (70 ml) for 1.5 h. After addition of ether, the resulting ppt was suspended in EtOH (60 ml), aq NaOH (6 g, 70 ml H_2O) was added under nitrogen, and refluxing was kept for 1 h. MeI (3.5 ml, 56 mmol) was added, and the mixture was heated for 0.5 h. After usual work-up, DCC (Al_2O_3, CH_2Cl_2) gave **23a** (1.29 g, 48%), bp 165 °C/0.5 mmHg; ^{1}H NMR ($CDCl_3$): δ=2.40 (s, 3H), 3.23 (s, 3H), 6.9—7.8 (m, 6H), and 8.00 (s, 1H). Found: C, 67.35; H, 5.60; N, 5.92%. Calcd for $C_{13}H_{13}NOS$: C, 67.50; H, 5.66; N, 6.06%.

To **23a** (1.29 g, 5.6 mmol) in ether (30 ml) at 0 °C was added dropwise $LiAlH_4$ (450 mg, 12 mmol) in ether (40 ml), and the mixture was stirred for 1 h. After usual work-up, distillation gave **24a** (1.03 g, 85%), bp 110 °C/0.15 mmHg; ^{1}H NMR ($CDCl_3$): δ=2.40 (s, 3H), 2.69 (s, 6H), and 7.0—7.7 (m, 6H). Found: C, 71.61; H, 7.09; N, 6.57; S, 14.27%. Calcd for $C_{13}H_{15}NS$: C, 71.84; H, 6.96; N, 6.44; S, 14.75%.

2) 24b: **23b** was prepared in the same manner as that of **23a** from **22b**[5b] in 52% yield; ^{1}H NMR ($CDCl_3$): δ= 1.71 (s, 3H), 2.45 (s, 3H), 3.19 (s, 3H), and 6.9—7.9 (m, 6H).

24b was prepared in the same manner as that of **24a** in 57% yield, bp 125 °C/0.25 mmHg; ^{1}H NMR ($CDCl_3$): δ=1.07 (t, J=7 Hz, 3H), 2.40 (s, 3H), 2.67 (s, 3H), 3.04 (dq, J=7 Hz and 2 Hz, 2H), and 7.0—7.8 (m, 6H). Found: C, 72.44; H, 7.42; N, 5.97; S, 13.51%. Calcd for $C_{14}H_{17}NS$: C, 72.68; H, 7.41; N, 6.05; S, 13.86%.

Methyl 1-Naphthyl Sulfide (35). 1-Naphthalenethiol was prepared from 1-naphthalenesulfonyl chloride (6.05 g, 26.7 mmol) and zinc (12.2 g, 186 mmol) in concd H_2SO_4 (13 ml) by a similar method to Org. Synth.,[20] and methylated with MeI (3 ml) and NaOH (2 g) in EtOH (30 ml). Usual work-up gave **35** (1.20 g, 26%), bp 90 °C/0.25

mmHg (lit,[21] 104 °C/1 mmHg).

N-Ethyl-N-methyl-1-naphthylamine (37). 1-Naphthylamine (6.83 g, 47.7 mmol) was treated with triethyl orthoformate (10.6 g, 71.2 mmol) and concd H_2SO_4 (0.3 g) by a similar method to Org. Synth.[22] to give *N*-ethyl-*N*-naphthylformamide (71.4 g, 78%), bp 153 °C/0.1 mmHg. This amide (4.19 g, 21.0 mmol) was reduced with $LiAlH_4$ (600 mg, 16 mmol) in ether (90 ml). After usual work-up, DCC (Al_2O_3, hexane) gave **37** (2.85 g, 73%), bp 90 °C/0.3 mmHg; ^1H NMR ($CDCl_3$): $\delta=1.19$ (t, $J=7$ Hz, 3H), 2.83 (s. 3H), 3.13 (q, $J=7$ Hz, 2H), and 6.9—8.4 (m, 7H). Found: C, 84.43; H, 8.21; N, 7.43%. Calcd for $C_{13}H_{15}N$: C, 84.28; H, 8.16; N, 7.56%.

General Procedure of Alkylation. *1) With 3 (Method I):* A mixture of a compd (5 mmol) and **3a** or **3b** (5.5—7 mmol) in CH_2Cl_2 (10—15 ml) was stirred at room temp for several hours. The soln was evaporated to a few ml, to which abs ether was added. The resulting ppt was washed with ether followed by addition of a few ml of EtOH to decompose **3**, washed with ether, and dried *in vacuo*. NMR spectrum of a portion of the crude ppt in DMSO-d_6 was measured to determine the ratio of sulfonium and ammonium salts. The yield was determined after recrystallization.

2) With Methyl Iodide in the Presence of Silver Perchlorate (Method II): To a compd (5 mmol) and MeI (5.5—7.5 mmol) in CH_2Cl_2 (10—20 ml) was added $AgClO_4$ (5 mmol) with $MeNO_2$ (5 ml). The mixture was stirred at room temp for several hours. The filtrate was treated by the same method as in Method I.

2a(I^-): 94% yield (Method II but without $AgClO_4$), mp 226—227.5 °C (decomp) (from EtOH); ^1H NMR: $\delta=2.17$ (s, 3H), 2.6—2.9 (m, 4H), and 3.22 (s, 9H).

2a(BF_4^-): 28% yield from filtrate by Method I, mp 166—170 °C (from MeOH-Et_2O): ^1H NMR: $\delta=2.18$ (s, 3H), 2.6—3.8 (m, 4H), and 3.14 (s, 9H). Found: C, 32.76; H, 7.38; N, 6.45%. Calcd for $C_6H_{15}BF_4NS$: C, 32.60; H, 7.30; N, 6.34%.

4a: 25% yield from ppt by Method I, mp 239—242 °C (from MeOH-MeCN); ^1H NMR: $\delta=2.99$ (s, 6H), 3.17 (s, 9H), and 3.81 (br s, 4H). Found: C, 25.76; H, 5.72; N, 4.20%. Calcd for $C_7H_{19}B_2F_8NS$: C, 26.04; H, 5.93; N, 4.34%.

8a(BF_4^-): not crystallize; 60% yield (Method I); ^1H NMR: $\delta=2.93$ (s, 3H), 3.21 (s, 3H), 3.3—4.5 (m, 4H), 6.20 (s, 1H), and 7.4—8.0 (m, 5H). Found: C, 47.13; H, 5.62; N, 4.79%. Calcd for $C_{11}H_{16}BF_4NS$: C, 47.00; H, 5.74; N, 4.98%.

8b(BF_4^-): 50% yield (Method I), mp 190—192 °C (decomp) (from EtOH-Et_2O); ^1H NMR: $\delta=1.80$ (s, 6H), 3.21 (s, 6H), 3.25 (br t, $J=6$ Hz, 2H), and 4.08 (br t, $J=6$ Hz, 2H). Found: C, 35.78; H, 7.15; N, 5.75%. Calcd for $C_7H_{16}BF_4NS$: C, 36.07; H, 6.92; N, 6.01%.

10a(ClO_4^-): 65% yield (Method II), mp 143—145 °C (from EtOH); ^1H NMR: $\delta=2.79$ (s, 6H), 3.21 (s, 6H), and 7.3—8.1 (m, 4H). Found: C, 42.78; H, 5.86; N, 5.04%. Calcd for $C_{10}H_{16}ClNO_4S$: C, 42.63; H, 5.72; N, 4.97%. The ^1H NMR spectrum of the crude salt showed methyl peaks of **11a**(ClO_4^-) at $\delta=2.69$ (SMe) and 3.87 (Me_3N^+), indicating formation of a mixture of **10a** and **11a** in a ratio of *ca.* 4:1.

Mixture of **10a**(BF_4^-) and **11a**(BF_4^-): *ca.* 1.5:1 in crude (Method I); 81% yield after recrystd from EtOH. **10a** (BF_4^-): from soluble part to CH_2Cl_2; mp 127—128 °C (from EtOH-Et_2O); ^1H NMR: $\delta=2.81$ (s, 6H), 3.21 (s, 6H), and 7.3—8.0 (m, 4H). Found: C, 44.62; H, 6.22; N, 5.22%. Calcd for $C_{10}H_{16}BF_4NS$: C, 44.63; H, 5.99; N, 5.20%. **11a**(BF_4^-): from the insoluble part; mp 186—186.5 °C (from EtOH); ^1H NMR: $\delta=2.67$ (s, 3H), 3.83 (s, 9H), and 7.2—8.0 (m, 4H). Found: C, 44.49; H, 6.03; N, 5.20%. Calcd for $C_{10}H_{16}BF_4NS$: C, 44.63; H, 5.99; N, 5.20%.

Crude mixture of **10b**(ClO_4^-) and **11b**(ClO_4^-): *ca.* 2:1 (Method II); 99% yield. Recrystallization from EtOH gave the mixture of the same ratio, 69% yield, mp 100—101 °C. **10b**(ClO_4^-): ^1H NMR: $\delta=1.30$ (t, $J=7$ Hz, 3H), 2.80 (s, 6H), 3.23 (s, 3H), *ca.* 3.6 (q, $J=7$ Hz, 2H), and 7.1—7.9 (m, 4H). **11b**(ClO_4^-): ^1H NMR: $\delta=1.38$ (t, $J=7$ Hz, 3H), *ca.* 3.2 (q, $J=7$ Hz, 2H), 3.89 (s, 9H), and 7.1—7.9 (m, 4H). Found (mixture): C, 44.59; H, 6.27; N, 5.03%. Calcd for $C_{11}H_{18}ClNO_4S$: C, 44.67; H, 6.13; N, 4.74%.

Crude mixture of **10b**(BF_4^-) and **11b**(BF_4^-): *ca.* 1:2 (Method I), 96% yield. Pure **11b**(BF_4^-): 46% yield; ^1H NMR: $\delta=1.32$ (t, $J=7$ Hz, 3H), 3.16 (q, $J=7$ Hz, 2H), 3.81 (s, 9H), and 7.2—7.9 (m, 4H). **10b**(BF_4^-): ^1H NMR: $\delta=1.21$ (t, $J=7$ Hz, 3H), 2.78 (s, 3H), 3.19 (s, 3H), *ca.* 3.6 (t, $J=7$ Hz, 2H), and 7.2—7.9 (m, 4H).

Crude mixture of **10c**(ClO_4^-) and **11c**(ClO_4^-) ($\delta=3.69$, *N*-Me): >10:1 (Method II), 89% yield. Pure **10c**(ClO_4^-): 33% yield, mp 107—108 °C (from EtOH); ^1H NMR: $\delta=1.14$ (t, $J=7$ Hz, 3H), 2.77 (s, 3H), 3.06 (q, $J=7$ Hz, 2H), 3.21 (s, 6H), and 7.3—8.0 (m, 4H). Found: C, 44.59; H, 6.08; N, 4.85%. Calcd for $C_{11}H_{18}ClNO_4S$: C, 44.67; H, 6.13; N, 4.74%.

Crude mixture of **10c**(BF_4^-) and **11c**(BF_4^-): >10:1 (Method I), *ca.* 100% yield. Pure **10c**(BF_4^-): 42% yield, mp 95—96 °C (from EtOH); ^1H NMR: $\delta=1.11$ (t, $J=7$ Hz, 3H), 2.73 (s, 3H), 3.03 (q, $J=7$ Hz, 2H), 3.17 (s, 6H), and 7.3—8.0 (m, 4H). Found: C, 46.71; H, 6.50; N, 4.82%. Calcd for $C_{11}H_{18}BF_4NS$: C, 46.66; H, 6.41; N, 4.95%.

10d(ClO_4^-): 99% yield (Method II), mp 104—105 °C (from EtOH-Et_2O); ^1H NMR: $\delta=2.67$ (s, 3H), 3.19 (s, 6H), 4.16 (s, 2H), and 7.3—8.1 (m, 9H). Found: C, 53.40; H, 5.73; N, 3.86%. Calcd for $C_{16}H_{20}ClNO_4S$: C, 53.70; H, 5.63; N, 3.91%.

10d(BF_4^-): by Method I; ^1H NMR: $\delta=2.63$ (s, 3H), 3.12 (s, 6H), 4.09 (s, 2H), and 7.0—8.0 (m, 9H). Because of difficulty of purification, BF_4^- was exchanged with Ph_4B^- to give **10d**(BPh_4^-): 37% yield, mp 135—136.5 °C; ^1H-NMR: $\delta=2.61$ (s, 3H), 2.91 (s, 6H), 4.05 (s, 2H), and 6.6—7.8 (m, 29H). Found: C, 83.33; H, 6.77; N, 2.36%. Calcd for $C_{40}H_{40}BNS$: C, 83.17; H, 6.98; N, 2.42%.

13c(BF_4^-): 31% yield (Method I), mp 178.5—179.5 °C (from EtOH); ^1H NMR: $\delta=2.36$ (s, 3H), 2.88 (s, 3H), and 6.6—7.9 (m, 14H). Found: C, 62.10; H, 5.05; N, 3.60%. Calcd for $C_{21}H_{20}BF_4NS$: C, 62.24; H, 4.97; N, 3.46%.

17: 38% yield (Method I), mp 90—93 °C (from EtOH-Et_2O); ^1H NMR: $\delta=3.60$ (s, 6H), 3.3—3.8 (m, 2H), 4.0—4.3 (m, 2H), and 6.5—8.0 (m, 4H). Found: C, 45.06; H, 5.49; N, 5.34%. Calcd for $C_{10}H_{14}BF_4NS$: C, 44.97; H, 5.28; N, 5.24%.

18(BPh_4^-): 43% yield by Method II followed by anion exchange, mp 226—227.5 °C (decomp); ^1H NMR: $\delta=2.96$ (s, 3H), 3.49 (s, 3H), 3.62 (br s, 4H), and 6.5—7.5 (m, 24H). Found: C, 81.90; H, 7.05; N, 2.89%. Calcd for $C_{34}H_{34}BNS$: C, 81.75; H, 6.86; N, 2.80%.

20a: 79% yield (Method I), mp 264.5—265.5 °C (decomp) (from EtOH); ^1H NMR: $\delta=2.92$ (s, 3H), 3.72 (s, 3H), and 7.1—8.0 (m, 8H). Found: C, 53.15; H, 4.52; N, 4.73%. Calcd for $C_{14}H_{14}BF_4NS$: C, 53.36; H, 4.48; N, 4.44.

20a': 82% yield (Method I), mp 158.5—160 °C (from EtOH); ^{1}H NMR: δ=1.08 (t, J=7 Hz, 3H), 3.33 (q, J=7 Hz, 2H), 3.69 (s, 3H), and 7.1—8.0 (m, 8H). Found: C, 54.67; H, 5.04; N, 4.56%. Calcd for $C_{15}H_{16}BF_4NS$: C, 54.73; H, 4.90; N, 4.26%.

20b: 81% yield (Method I), mp 241—242.5 °C (decomp) (from EtOH); ^{1}H NMR: δ=1.47 (t, J=7 Hz, 3H), 2.89 (s, 3H), 4.33 (q, J=7 Hz, 2H), and 7.1—8.1 (m, 8H). Found: C, 54.59; H, 4.86; N, 4.31%. Calcd for $C_{15}H_{16}BF_4NS$: C, 54.73; H, 4.90; N, 4.26%.

20c: 59% yield (Method II), mp 184.5—187 °C (decomp) (from EtOH); ^{1}H NMR: δ=2.88 (s, 3H), 7.0—8.0 (m, 8H), and 11.1 (br s, 1H); IR (KBr): 3300 cm^{-1} (NH). Found: C, 49.96; H, 3.98; N, 4.70%. Calcd for $C_{13}H_{12}ClNO_4S$: C, 49.77; H, 3.86; N, 4.46%.

25a(ClO_4^-): 85% yield (Method II), mp 196—197.5 °C (from EtOH); ^{1}H NMR: δ=2.82 (s, 6H), 3.23 (s, 6H), and 7.5—8.4 (m, 6H). Found: C, 50.80; H, 5.38; N, 4.46%. Calcd for $C_{14}H_{18}ClNO_4S$: C, 50.68; H, 5.47; N, 4.22%.

Crude mixture of **25a**(BF_4^-) and **26a**(BF_4^-): 2:3 (Method I); 93% yield; ^{1}H NMR: **25a**, δ=2.79 (s, 6H) and 3.19 (s, 6H); **26a**, δ=2.48 (s, 3H) and 2.98 (s, 6H).

25b(ClO_4^-): 36% yield (Method II), mp 107.5—109 °C; ^{1}H NMR: δ=1.17 (t, J=7 Hz, 3H), 2.84 (s, 3H), 3.24 (d, J=3.6 Hz, 6H), 3.3—3.8 (m, 2H), and 7.6—8.4 (m, 6H). Found: C, 52.21; H, 5.92; N, 3.81%. Calcd for $C_{15}H_{20}ClNO_4S$: C, 52.09; H, 5.83; N, 4.05%.

26b(BF_4^-): 87% yield (Method I), mp 148—150 °C (from EtOH); ^{1}H NMR: δ=1.09 (t, J=7 Hz, 3H), 2.50 (s, 3H), 3.00 (br s, 6H), 3.40 (br q, J=7 Hz, 2H), and 7.3—8.1 (m, 6H). Found: C, 53.20; H, 5.84; N, 5.04%. Calcd for $C_{14}H_{18}BF_4NS$: C, 52.68; H, 5.68; N, 4.39%.

30: 57% yield (Method II), mp 162—163 °C (from EtOH); ^{1}H NMR: δ=3.33 (s, 6H) and 7.6—8.2 (m, 5H).

32: 93% yield (Method II), mp 183—186 °C (from EtOH); ^{1}H NMR: δ=3.69 (s, 9H) and 7.5—8.1 (m, 5H).

34: 78% yield (Method I), mp 142—143 °C (from EtOH); ^{1}H NMR: δ=2.72 (s, 6H), 3.82 (s, 9H), and 7.3—8.0 (m, 4H).

36: 97% yield (Method II), mp 157—158 °C (from EtOH); ^{1}H NMR: δ=3.43 (s, 6H) and 7.7—8.6 (m, 7H).

38: 48% yield (Method I), mp 165—166 °C (from EtOH); ^{1}H NMR: δ=0.99 (t, J=7 Hz, 3H), 3.91 (s, 6H), 4.45 (q, J=7 Hz, 2H), and 7.5—8.7 (m, 7H).

Preparation of ***6***. *1)* ***6a***: **1a** (222 mg, 1.87 mmol) was protonated with 42% aq HBF_4 (2 ml) in CH_2Cl_2 (8 ml). The resulting material was dissolved in CH_2Cl_2 (10 ml), to which was added **3a** (431 mg, 2.91 mmol). After usual work-up, recrystallization from EtOH-MeCN gave **5a** (487 mg, 85%). A suspension of **5a** (342 mg, 1.11 mmol) in CH_2Cl_2 (15 ml) was deprotonated with aq NaOH and the aqueous layer was separated, to which was added aq $NaBPh_4$. The resulting ppt was recrystd from EtOH-MeCN to give colorless crystals of **6a**, 297 mg (59% yield based on **5a**), mp 160 °C (decomp); ^{1}H NMR (DMSO-d_6): δ=2.16 (s, 6H), 2.48 (s, 6H), 2.3—2.6 (br t, J=6 Hz, 2H), 3.16 (br t, J=6 Hz, 2H), and 6.6—7.5 (m, 20H). Found: C, 79.72; H, 8.25; N, 3.09%. Calcd for $C_{30}H_{36}BNS$: C, 79.46; H, 8.00; N, 3.09%.

2) ***6b***: **5b** was prepared from **1b** by the same method as that of **5a**, *ca.* 100% yield; ^{1}H NMR (DMSO-d_6): δ=1.39 (t, J=7 Hz, 3H), 2.86 (s, 6H), 2.93 (s, 3H), 3.40 (q, J=7 Hz, 2H), and 3.58 (br s, 4H). Similarly **6b** was obtained in 64% yield, mp 143—147 °C (decomp) (from EtOH-Me_2CO); ^{1}H NMR (DMSO-d_6): δ=1.12 (t, J=7 Hz, 3H), 2.15 (s, 6H), 2.31 (s, 3H), 2.4—3.2 (m, 6H), and 6.7—7.6 (m, 20H). Found: C, 79.81; H, 8.44; N, 3.25%. Calcd for $C_{31}H_{38}BNS$: C, 79.64; H, 8.19; N, 3.00%.

References

1) K. Akiba, Y. Ohara, and N. Inamoto, *Bull. Chem. Soc. Jpn.*, **55**, 2976 (1982), and references cited therein.

2) M. Hori, T. Kataoka, H. Shimizu, and Y. Imai, *Chem. Pharm. Bull. (Tokyo)*, **25**, 1482 (1977).

3) M. Hori, T. Kataoka, H. Shimizu, and N. Ueda, *Tetrahedron Lett.*, **22**, 3071 (1981).

4) S. Oae, "Yuki Iou Kagobutsu No Kagaku," Kagaku Dojin, Kyoto (1968), No. I, p. 8.

5) a) M. T. Bogert and J. H. Bartlett, *J. Am. Chem. Soc.*, **53**, 4046 (1931); b) H. van B. Joy and M. T. Bogert, *J. Org. Chem.*, **1**, 236 (1936).

6) J. I. Musher, *Angew. Chem., Int. Ed. Engl.*, **8**, 54 (1969); S. Tamagaki and S. Oae, *Kagaku No Ryoiki*, **31**, 117, 218 (1977).

7) E. F. Perozzi, J. C. Martin, and I. C. Paul, *J. Am. Chem. Soc.*, **96**, 6735 (1974); L. J. Adzima and J. C. Martin, *J. Org. Chem.*, **42**, 4001 (1977); L. J. Adzima, C. C. Chiang, I. C. Paul, and J. C. Martin, *J. Am. Chem. Soc.*, **100**, 953 (1978); P. H. W. Lau and J. C. Martin, *ibid.*, **100**, 7077 (1978).

8) O. Exner, in "Advances in Linear Free Energy Relationships," ed by N. B. Chapman and J. Shorter, Plenum, New York (1972), pp. 28, 29, 32.

9) R. J. H. Clark and J. McAless, *Inorg. Chem.*, **11**, 342 (1972).

10) M. L. Moore, *Org. React.*, **5**, 323 (1949).

11) K. Akiba, T. Kawamura, M. Hisaoka, and N. Inamoto, *Bull. Chem. Soc. Jpn.*, **48**, 3262 (1975).

12) R. N. Prasad and K. Tietje, *Can. J. Chem.*, **44**, 1247 (1966).

13) K. Fujii, *Yakugaku Zasshi*, **77**, 3 (1957).

14) G. Friedmann, M. Brini, P. Ederle, J. Gasser, P.-J. Holderith, M. Vernois, and J.-M. Widmaier, *Bull. Soc. Chim. Fr.*, **1970**, 706.

15) G. Tsatsas, C. Sandris, and D. Kontonassias, *Bull. Soc. Chim. Fr.*, **1963**, 2160.

16) E. D. Bergmann, and A. Kaluszyner, *Recl. Trav. Chim. Pays-Bas*, **78**, 289 (1959).

17) R. Kuhn and F. Drawert, *Justus Liebigs Ann. Chem.*, **590**, 55 (1954).

18) T. Zincke and S. Siebert, *Ber.*, **48**, 1242 (1915).

19) A. I. Kiprianov and Z. N. Pazenko, *J. Allg. Chem. (Russ.)*, **19**, 1523 (1949); *Chem. Abstr.*, **44**, 3487 (1950).

20) K. Adams and C. S. Marvel, *Org. Synth.*, Coll. Vol. I, 504 (1941).

21) P. H. Lumbroso and C. Marschalk, *J. Chim. Phys.*, **48**, 123 (1951).

22) R. M. Roberts and D. J. Vogt, *Org. Synth.*, Coll. Vol. IV, 420 (1963).

The Reaction of Benzonitrile Oxides with *S,S*-Dimethyl-*N*-(2,4,6-trihalophenyl)sulfimides. The Formation of Benzoxazole Derivatives

Shinsaku SHIRAISHI,* Tohru HAYAKAWA, and Tadashi SHIGEMOTO

Institute of Industrial Science, The University of Tokyo, Roppongi, Minato-ku, Tokyo 106

(Received November 27, 1982)

The reactions of nitrile oxides with *S,S*-dimethyl-*N*-(2,4,6-trihalophenyl)sulfimides gave unusual products, which structure was determined to be 2-aryl-4,6-dihalobenzoxazoles from their elementary analyses and spectral data. While the reactions with *S,S*-dimethyl-*N*-(2-bromophenyl)- or *S,S*-dimethyl-*N*-(2,4-dibromophenyl)-sulfimide gave 1,2,4-benzoxadiazine derivatives. A plausible reaction mechanism for the unusual formation of benzoxazoles was proposed.

Nitrile oxides are typical 1,3-dipoles and are known to react with various unsaturated bonds, not only with carbon-carbon unsaturated bonds but also with hetero unsaturated ones. Many studies have also been reported on the reaction with ylides.[1,2] We reported before that benzimidazole 3-oxides and/or benzoxadiazines were obtained in the reactions of aromatic nitrile oxides with *N*-aryl-*S,S*-dialkylsulfimides, and suggested that the reaction proceed *via* nitroso intermediacy as shown in Scheme 1.[3] Gilchrist *et al.* reported the formation of 1,2,4-benzoxadiazines in the reaction of nitrile oxides with *N*-aryl-*S,S*-dimethylsulfimides.[4] As a support of nitroso intermadiacy, though it is in an indirect manner, dibenzyl sulfide was isolated in the reaction with *N*-aryl-*S,S*-dibenzylsulfimides.[5]

During the course of the study, we attempted the reactions of nitrile oxides with *S,S*-dimethyl-*N*-(2,4,6-trihalophenyl)sulfimides, in expectation to isolate or detect the nitroso intermediate. In the reactions, however, unusual reaction products were isolated against the expectation, as reported in the previous communication.[6] We describe here the result of the further investigation of the reactions with *S,S*-dimethyl-*N*-(2,4,6-trihalophenyl)sulfimides together with the reactions with *S,S*-dimethyl-*N*-(2-halophenyl)sulfimides.

Results and Discussion

We tried the reactions of benzonitrile oxide (**1a**) and *p*-chloro- (**1b**) and *p*-bromobenzonitrile oxide (**1c**) with *S,S*-dimethyl-*N*-(2,4,6-tribromophenyl) sulfimide (**2a**) and *S,S*-dimethyl-*N*-(2,4,6-trichlorophenyl)sulfimide (**2b**). The results of the reactions and the analytical data of the reaction products are shown in Table 1. High resolution mass spectra of the products gave the molecular formulae of $C_{13}H_6NOXY_2$ (X= H,Cl,Br; Y=Br,Cl), which were consistent with the analytical data. The molecular formulae shows the loss of dimethyl sulfide, one halogen and one nitrogen atoms from the sum of the two starting components.

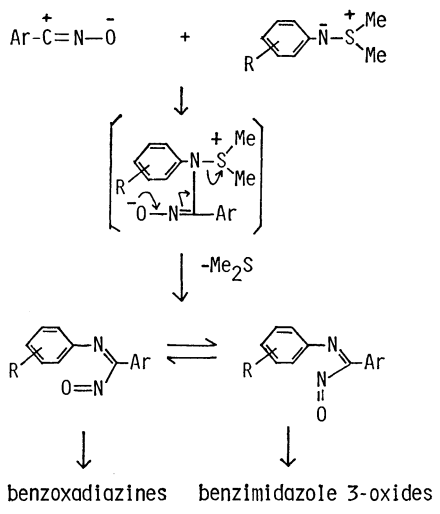

Scheme 1.

Mass fragmentation pattern of the product **3a** is shown in Scheme 2. Elimination of CO and benzonitrile from the molecular ion is observed to occur independently. The fragmentation pattern is common to the other reaction products and is very similar to those of benzoxazole and 1,2-benzisoxazole derivatives.[7] The unusual reaction products are suggested to have benzoxazole or 1,2-benzisoxazole structure.

In order to determine the structure of the product, we compared the UV and ^{13}C NMR spectra of them with those of 2-phenylbenzoxazole (**4**) and 3-phenyl-1,2-benzisoxazole (**5**), which were synthesized by methods of Somayajulu[8] and of Minisci,[9] respectively. UV spectra of the products **3a**—**f** and the reference compounds **4** and **5** are listed in Table 2. Absorption maxima of **3a**—**f** are at 305—316 nm with ε_{max} of $(2.6—3.8)\times10^4$. The spectral pattern of the products resembles to that of **4** more closely than that of **5**. ^{13}C NMR spectral data are listed in Table 3. The signals due to C-2, C-3a and C-7a of 2-phenylbenzoxazole (**4**) are at 162.1, 141.5, and 150.1 ppm.[10] On the other hand, the signals due to C-3, C-3a, and C-7a of 3-phenyl-1,2-benzisoxazole (**5**) are at 157.2, 120.4, and 163.8 ppm. The signals at 162—164 ppm of the reaction products **3a**—**f** can be assigned to be C-2

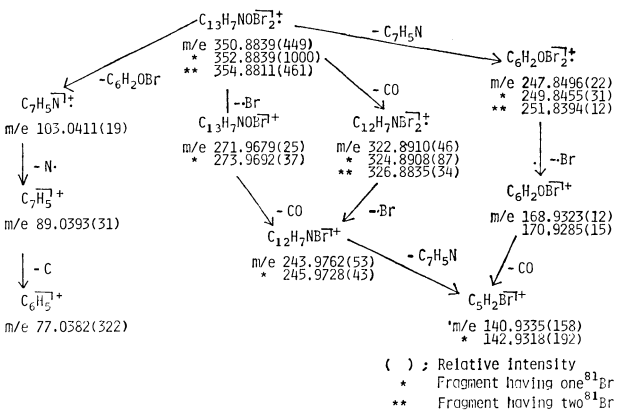

Scheme 2. Mass fragmentation of **3a**.

Table 1. Yields and analytical data of 2-aryl-4,6-dihalobenzoxazoles (**3a—f**)

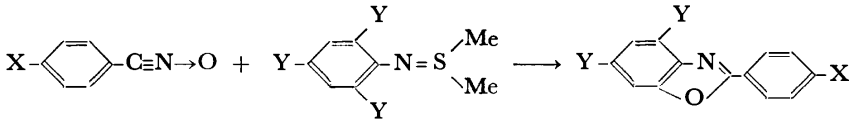

1a—c **2a—b** **3a—f**

Compd	X	Y	Yield/%	Mp θ_m/°C		Anal. (%) Found	Anal. (%) Calcd	MS (M^+) Found	MS (M^+) Calcd
3a	H	Br	37	148—149	C	44.02	44.23	350.8839	350.8894
					H	1.83	2.00		
					N	3.74	3.97		
3b	Cl	Br	50	182—183	C	40.96	40.30	384.8505	384.8505
					H	1.36	1.56		
					N	3.71	3.62		
3c	Br	Br	51	181—183	C	36.08	36.15	428.8038	428.7999
					H	1.35	1.40		
					N	3.19	3.24		
3d	H	Cl	46	143—144.5	C	58.87	59.09	262.9870	262.9906
					H	2.76	2.65		
					N	5.11	5.30		
3e	Cl	Cl	43	190—191	C	52.22	52.26	296.9391	296.9517
					H	2.25	2.01		
					N	4.77	4.69		
3f	Br	Cl	57	196—197	C	45.45	45.48	340.8936	340.9011
					H	1.89	1.75		
					N	4.16	4.18		

Table 2. UV and visible spectra of 2-aryl-4,6-dihalobenzoxazoles

Compd	λ_{max}/nm	$\varepsilon_{max} \times 10^{-4}$
3a	310	2.90
3b	316	3.21
3c	315	3.76
3d	305	2.57
3e	310	3.17
3f	311	3.34
4	299	2.14
5	287	0.71

carbon atom of benzoxazole structure. Assignment of the other signals is shown in the Table.

^{1}H NMR spectral data are shown in Table 4. The signals due to H-5 and H-7 of **3a—c** happened to appear at the same chemical shift in $CDCl_3$, but became separated in D_2SO_4. For example, the signals of **3a** at 7.64 ppm in $CDCl_3$ comes to appear at 8.58 and 8.50 separetedly in D_2SO_4. The recovered samples from the D_2SO_4 solutions were confirmed to be unchanged from the orginal ones. In the case of **3d—f**, the signals due to H-5 and H-7 were observed at different positions even in $CDCl_3$. The data are well consistent with the proposed 2-arylbenzoxazole structure.

The data mentioned above, however, cannot definitely rule out the isomeric structure of 2-aryl-5,7-dihalobenzoxazoles. But the melting point of **3a** is 148—149 °C (See Table 1) and much different from that of 5,7-dibromo-2-phenylbenzoxazole which was reported to melt at 175—176 °C.[11]

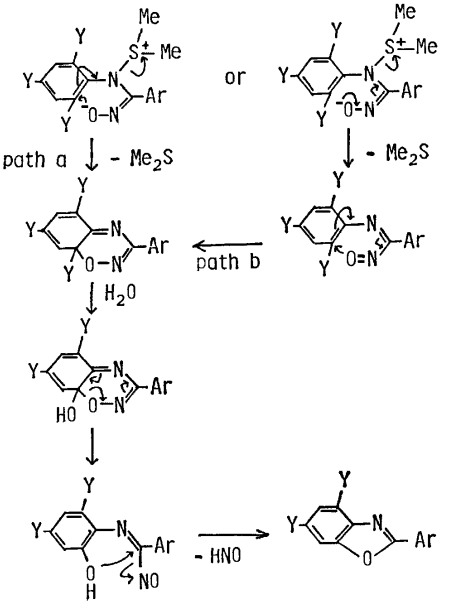

Scheme 3. Reaction route to the 2-arylbenzoxazole.

Thus the structure of the reaction products was determined to be 2-aryl-4,6-dihalobenzoxazole.

This structure determination was further confirmed by an independent synthesis of the authentic sample of 2-phenyl-4,6-dichlorobenzoxazole by the condensation of benzaldehyde with 3,5-dichloro-2-aminophenol. Infrared, ^{1}H NMR, and mass spectra of the authentic sample were the same as those of the compound **3d**. Also the melting point and R_f-value of thin layer chromatography were the same.

Table 3. ^{13}C NMR Spectra of 2-aryl-4,6-dihalobenzoxazoles (**3a**—**f**), 2-phenylbenzoxazole (**4**), and 3-phenyl-1,2-benzisoxazole (**5**)

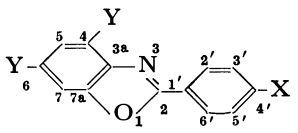

3a—f

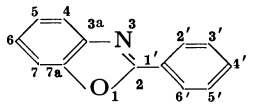

4

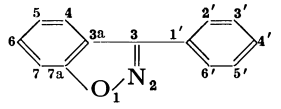

5

Compd	C-2	C-3a	C-4	C-5	C-6	C-7	C-7a	C-1′	C-2′,6′	C-3′,5′	C-4′
3a	163.8	141.0	117.8	130.5	126.0	113.2	150.8	—	127.9	128.8	132.1
3b	163.0	141.1	118.2	130.8	124.6	113.2	—	—	129.3	129.3	138.6
3c	162·3	141.5	118.2	130.8	124.4	113.3	150.1	—	129.3	129.3	138.6
3d	163.6	138.6	125.7	124.9	130.2	109.6	150.6	129.5	127.5	128.5	131.7
3e	162.2	138.2	124.3	125.1	130.5	109.7	150.7	—	128.8	129.0	131.9
3f	162.6	138.5	126.7	125.1	131.2	109.7	150.6	130.5	128.9	131.9	133.3
4	162.1	141.5	119.6	125.1	124.4	110.5	150.1	130.6	127.0	128.8	131.4
5	157.2*	120.4	123.8	122.1	130.2	110.1	163.8	134.3	128.0	129.1	129.7

* C-3.

Table 4. ^{1}H NMR spectra of 2-aryl-4,6-dihalobenzoxazoles

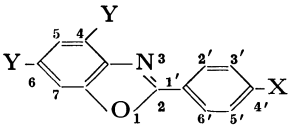

Compd	X	Y	In $CDCl_3$ δ	In D_2SO_4 δ*	Assignment
3a	H	Br	7.64(s, 2H)	8.59 and 8.50	H-5 and 7
			7.46(m, 1H)	8.43	H-4′
			7.52(m, 2H)	8.33	H-3′ and 5′
			8.20(m, 2H)	8.91	H-2′ and 6′
3b	Cl	Br	7.58(s, 2H)	8.56 and 8.50	H-5 and 7
			7.46(d, 2H)	8.23	H-3′ and 5′
			8.08(d, 2H)	8.78	H-2′ and 6′
3c	Br	Br	7.61(s, 2H)	8.52 and 8.46	H-5 and 7
			7.60(d, 2H)	8.36	H-3′ and 5′
			8.06(d, 2H)	8.67	H-2′ and 6′
3d	H	Cl	7.31(d, 1H)		H-7
			7.42(d, 1H)		H-5
			7.45(m, 1H)		H-4′
			7.49(m, 2H)		H-3′ and 5′
			8.18(m, 2H)		H-2′ and 6′
3e	Cl	Cl	7.37(d, 1H)		H-7
			7.49(d, 1H)		H-5
			7.50(d, 2H)		H-3′ and 5′
			8.18(d, 2H)		H-2′ and 6′
3f	Br	Cl	7.37(d, 1H)		H-7
			7.47(d, 1H)		H-5
			7.63(d, 2H)		H-3′ and 5′
			8.07(d, 2H)		H-2′ and 6′

* ppm from external TMS.

In order to see the scope and limitation of this unusual formation of 2-arylbenzoxazole derivatives, we tried the reaction of nitrile oxide (**1a**—**c**) with only one ortho-substituted *N*-arylsulfmides, such as *S,S*-dimethyl-*N*-(2-bromophenyl)sulfmide (**2c**) and *S,S*-dimethyl-*N*-(2,4-dibromophenyl)sulfimide (**2d**). The reaction products in the reactions were benzoxadiazine derivatives and no benzoxazole derivatives nor benzimidazole 3-oxide were formed. The yields of the 1,2,4-benzoxadiazines were very high as seen in Table 5. The result that no benzimidazole 3-oxide was formed is consistent with the mechanistic consideration previously reported.[3]

The reaction mechanism leading to benzoxazole formation is not obvious yet, but may be considered to be the same as that for the 1,2,4-benzoxadiazine formation at the initial stage of the reaction. The subsequent stages may be such as illustrated in Scheme 3. In this reaction, the intervention of a nitroso intermediate can neither be regarded nor disregarded at present, but by taking its intervention into consideration, the reactions of nitrile oxides with *N*-phenyl-

TABLE 5. YIELDS AND ANALYTICAL DATA OF 3-ARYL-4*H*-1,2,4-BENZOXADIAZINES (**6a—f**)

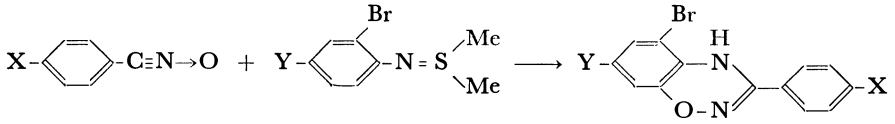

1a—c **2c—d** **6a—f**

Compd	X	Y	Yield/%	Mp θ_m/°C		Anal. (%) Found	Calcd
6a	H	H	86	111—112	C	54.12	54.00
					H	2.84	3.14
					N	9.81	9.69
6b	Cl	H	92	95— 96	C	48.79	48.26
					H	2.29	2.49
					N	8.68	8.66
6c	Br	H	85	106—107	C	42.18	42.43
					H	1.92	2.19
					N	7.26	7.61
6d	H	Br	80	113—115	C	42.86	42.43
					H	2.22	2.19
					N	7.08	7.61
6e	Cl	Br	91	147—149	C	38.80	38.80
					H	2.01	1.75
					N	7.03	6.96
6f	Br	Br	80	142—143	C	34.96	34.94
					H	1.28	1.58
					N	5.97	6.27

sulfimide, *N*-(2,6-dihalophenyl)sulfmides, and *N*-(2-azaaryl)sulfimides can be interpreted in terms of the same type of the intermediacy. The reaction of *N*-(2-pyridyl)sulfimide with a nitrile oxide, for example, have been reported to give a 1,2,4-triazolo[1,5-*a*]pyridine derivative *via* nitroso intermediate.[12] In the reaction forming benzoxazole derivatives presented here, the cyclized intermediate from the nitroso intermediate has a halogen substituent at the angular carbon atom which is linked with oxygen atom. This type of C–Cl bond is considered to be highly susceptible to hydrolysis. Therefore, the intermediate hydrolyzed with moisture in the reaction mixture, then once ring opened and recyclized to the benzoxazole with loss of the nitroso group. This mechanistic speculation is based on an assumption of the participation of water in the reaction. A further investigation as to the effect of some nucleophiles as well as water is now under progress and will be presented elsewhere.

Experimental

Melting points were measured using a micro-melting-point measuring apparatus (Yazawa Co., Ltd.) and are uncorrected. IR spectra were recorded with a JASCO IRA-1 spectrophotometer. Mass spectra were recorded with a Hitachi RMU-7L high-resolution mass spectrometer. UV spectra were recorded with a JASCO UVIDEC-505 spectrophotometer. ^{1}H NMR and ^{13}C NMR spectra were measured in $CDCl_3$ with JEOL JMN-MH 100 and FX-60 spectrometers respectively, and chemical shifts were reported in ppm from internal tetramethylsilane, unless otherwise cited. Column chromatography was conducted on silica gel (Wakogel C-200) with chloroform as an eluent.

Materials. Benzonitrile oxide and *p*-substituted benzonitrile oxides were generated at low temperature from the corresponding benzhydroxamoyl chlorides, which were synthesized by the usual methods.[13] *N*-aryl-*S*,*S*-dimethylsulfimides were prepared from dimethyl sulfoxide, substituted anilines, and trifluoroacetic anhydride.[14]

Reaction of Sulfimides with Nitrile Oxides. A General Procedure: A solution of hydroxamoyl chloride (1 mmol) in 10 ml of tetrahydrofuran (THF) was cooled below −10 °C. An equimolar amount of triethylamine was added to the solution through microsyringe. The solution became turbid due to the precipitation of triethylammonium chloride. Then an equimolar amount of sulfmide in 10 ml of THF was added dropwise to the mixture, during which the reaction mixture was kept below −10 °C. After the mixture was allowed to stand at ambient temperature overnight, triethylammonium chloride was separeted by filtration and the solvent was removed by evaporation under reduced pressure. The residue was worked up with column chromatography on silica gel (Wakogel C-200) with chloroform as an eluent to give a 2-arylbenzoxazole, which was recrystallized from methanol. Some typical examples follow.

*Reaction of Benzonitrile Oxide (**1a**) with* S,S-*Dimethyl*-N-*(2,4,6-tribromophenyl)sulfimide (**2a**)*: Into a cooled solution of 0.65 g (1 mmol) of benzhydroxamoyl chloride in 10 ml of THF was added 140 µl (1 mmol) of triethylamine at a temperature below −10 °C. A white precipitate of triethylammonium chloride deposited. Then 0.391 g (1 mmol) of **2a** in 5 ml of THF was added dropwise to the mixture kept below −10 °C, through a dropping funnel, which was washed with 5 ml of THF. The mixture was allowed to stand at ambient temperature overnight. Triethylammonium chloride was separeted by filtration and the filtrate was evaporated. The residue was worked up with column chromatography. 2-Phenyl-4,6-dibromobenzoxazole (**3a**) was isolated and weighed 0.13 g (37%). It was purified

by recrystallization from methanol.

Reaction of p-*Bromobenzonitrile Oxide (**1c**) with* S,S-*Dimethyl*-N-*(2-bromophenyl)sulfimide (**2c**)*: A solution of 0.236 g (1 mmol) of *p*-bromobenzhydroxamoyl chloride in 10 ml of THF was cooled below −10 °C by an ice-salt bath. Triethylamine 140 μl (1 mmol) was added into the solution through microsyringe, depositing a white precipitate of triethylammonium chloride. Then 0.235 g (1 mmol) of **2c** in 5 ml of THF solution was added dropwise through a dropping funnel to the mixture, during which the reaction mixture was kept below −10 °C. The dropping funnel was washed with 5 ml of THF. The solution was allowed to stand at ambient temperature overnight. Triethylammonium chloride was removed by filtration and the solvent was evaporated. The residue was worked up with column chromatography. 3-(*p*-Bromophenyl)-5-bromo-4*H*-1,2,4-benzoxadiazine (**6c**) 0.310 g (85%) was isolated and recrystallized from ether–petroleum ether.

Independent Synthesis of 2-Phenyl-4,6-dichlorobenzoxazole: 3,6-Dichloro-2-aminophenol was synthesized by method of Hodgson and Wignall.[15] The condensation reaction was carried out according to the method of Osman and Bassiouni[16] with a slight modification. A mixture of the 2-aminophenol 1.6 g (9 mmol) and benzaldehyde 3.8 g (36 mmol) was heated to reflux for 10 h. The reaction mixture was then cooled to room temperature and poured into methanol to give a precipitate, which was collected by filtration and dried. 2-Phenyl-4,6-dichlorobenzoxazole 1.4 g (60%) was isolated and recrystallized from methanol.

References

1) R. Huisgen and J. Wuff, *Chem. Ber.*, **102**, 1833, 1848 (1969).
2) C. Grundmann and P. Grunanger, "The Nitrile Oxides," Springer-Verlag, Berlin (1971), pp. 62, 134.
3) S. Shiraishi, T. Shigemoto, and S. Ogawa, *Bull. Chem. Soc. Jpn.*, **51**, 563 (1978).
4) T. L. Gilchrist, C. J. Harris, and C. W. Ress, *J. Chem. Soc., Chem. Commun.*, **1974**, 485; T. L. Gilchrist, C. J. Harris, F. D. King, M. E. Peek, and C. W. Ress, *J. Chem. Soc., Perkin Trans. 1*, **1976**, 2161.
5) S. Shiraishi, T. Shigemoto, S. Katsuta, and S. Ogawa, *Nippon Kagaku Kaishi*, **1981**, 989.
6) T. Shigemoto, K. Imamura, T. Hayakawa, S. Ogawa, K. Matsumoto, and S. Shiraishi, *Chem. Lett.*, **1981**, 843.
7) A. Maquestiau, Y. V. Haverbeke, R. Flammang, and J. Pierard, *Bull. Soc. Chim. Belg.*, **84**, 207 (1975).
8) V. V. Somayajulu and N. V. Subba Rao, *Proc. Indian Acad. Sci., Sect. A*, **59**, 396, (1964).
9) F. Minisci and A. Quilico, *Chim. Ind. (Milan).*, **46**, 428 (1964).
10) J. Llinares, J. P. Galy, R. Faure, E. J. Vincent, and J. Elguero, *Can. J. Chem.*, **57**, 937 (1977).
11) A. H. Blatt, *J. Org. Chem.*, **20**, 591 (1955).
12) T. L. Gilchrist, C. J. Harris, D. G. Hawkins, C. J. Moody, and C. W. Ress, *J. Chem. Soc., Perkin Trans. 1*, **1976**, 2166.
13) M. H. Benn, *Can. J. Chem.*, **42**, 2393 (1964); P. Rajagopalan, B. G. Advani, and C. N. Talaty, *Org. Synth.*, Coll. Vol. V, 504 (1973).
14) A. K. Sharma, T. Ku, A. D. Dawson, and D. Swern, *J. Org. Chem.*, **40**, 2758 (1975).
15) H. H. Hodgson and J. S. Wignall, *J. Chem. Soc.*, **1927**, 2216.
16) A. M. Osman and I. Bassiouni, *J. Org. Chem.*, **27**, 558 (1962).

 © 1983 The Chemical Society of Japan Bull. Chem. Soc. Jpn., 56, 1519—1521 (1983)

Base-induced Oxygenation and Chemiluminescence of 10-Methylacridinium and 1-Methylquinolinium Salts in Dimethyl Sulfoxide[1]

Nobutaka Suzuki,* Yoshihiko Kazui, Toshio Tsukamoto,
Masahiro Kato, and Yasuji Izawa
Department of Industrial Chemistry, Faculty of Engineering, Mie University, Tsu, Mie 514
(Received December 9, 1982)

10-Methylacridinium methyl sulfate and the 1-methylquinolinium salt gave strong light emission, when oxidized with ground state oxygen in the presence of *t*-BuOK in DMSO, owing to the fluorescence of 10-methyl-9(10*H*)-acridinone and 1-methyl-1(4*H*)-quinolinone excited to their S_1 state.

Lucigenin[2] is one of the most powerful chemiluminescent compound (quantum yield of CL: Φ_{CL} 3.0×10^{-3})[3] and has the most complex mechanism known so far, for the chemiluminescence reactions.[4]

In the course of the studies on chemiluminescence (CL) of 9,10-substituted acridine compounds,[5] a new chemiluminescent reaction of 10-methylacridinium salts (**1**), which resembles to lucigenin apparently, was found when oxidized by molecular oxygen under basic conditions. We describe here the bright blue chemiluminescent reactions of 10-methylacridinium methyl sulfate (**1a**) owing to the fluorescence of 10-methyl-9(10*H*)-acridinone (**2**) excited to the S_1 state, when oxidized with ground state oxygen in the presence of t-BuOK in dimethyl sulfoxide (DMSO) (scheme 1). The similar CL reaction of 1-quinolinum methyl sulfate (**3**) is also described. Happ *et al.* reported a weak CL of a similar chemiluminescent system, 10-methylacridinium chloride (**1b**) *via* addition of $^-$CN anion to 9-carbon, catal zed by excess KCN, instead of *t*-BuOK, in DMSO/H_2O (9:1).[6] Under the similar conditions, **1a** yielded reduced amounts of CL (less than 1/3 of that by *t*-BuOK).

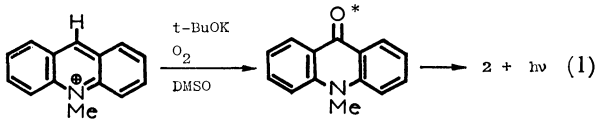

(1)

1a: X=OSO_3Me
1b: X=Cl

2*

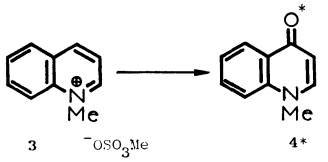

(2)

3 $^-OSO_3Me$ **4***

CL spectrum of **1** was identical with the fluorescence (FL) spectrum of **2** (420 and 435 nm) under the similar basic conditions (*t*-BuOK/DMSO/O_2 or KCN/DMSO–H_2O/O_2). These results suggest that the emitter in the CL reactions is the ketone **2** generated during the reactions quantitatively. When treated first by the base *in vacuo* (freeze-thaw cycle: 10^{-4} mmHg** $\times$3 times)[7] and then by oxygen, **1a** also gave CL. The compound **3** showed the similar behavior under the similar conditions above.

The behavior of **1a** in the present reactions shows that the reaction pathway is different both from that of the Happ's[6] and also that for the 9-substituted compounds shown by Kamiya and Sugimoto.[8]

Contamination of **1** with acridine (**5**) or its *N*-protonated salt was suspected to be responsible for the strong CL emission. In fact, acridine itself showed CL, although it was very weak, to give 9(10*H*)-acridinone under the similar conditions (scheme 3).

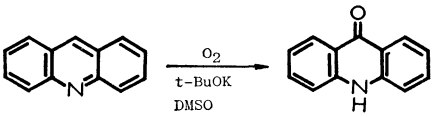

(3)

5 **6**

Rosenthal and Bercovici[9] found that the final product, **2**, gave CL in DMSO when treated with KO_2. The CL spectrum exhibits a broad emission band with three peaks, maxima at 470, 494, and 532 nm of the relative intensities 3:5:2, respectively, owing to the fluorescence of radical anion of **2**. The comparison of CL spectra shows that the present CL reactions do not result from the Rosenthal's mechanism (scheme 4).

$$2 + O_2^{\cdot-} \longrightarrow (2^{\cdot-})^* + O_2$$
$$(2^{\cdot-})^* \longrightarrow 2^{\cdot-} + h\nu \qquad (4)^{9)}$$

The degradation energy of 67.3 kcal/mol***, at least, is required for exciting **2** to the lowest singlet excited state.[5] (i) If one O_2 molecule oxidizes one molecule of **1** to give one molecule of **2** and 1/2 molecule of H_2O_2,[6,10] the balance of the heat of reaction (ΔH) would be $\Delta H = +5.6$ kcal/mol (scheme 5), which is not sufficient to excite **2**. (ii) If one O_2 molecule oxidizes two molecules of **1** to give two molecules of **2** and H–OR, ΔH would be -113.5 kcal/mol, which is sufficient for exciting **2** to its S_1 state (scheme 6) (Table 2). Thus, we prefer the latter mechanism (scheme 6) for the explanation of the present effective chemiluminescent reaction of **1a**.

Kamiya and Sugimoto[8] have investigated the similar chemiluminescent systems, 9-alkyl- and 9-benzyl-10-methyl-acridinium methyl sulfates (**7**) in the presence of *t*-BuOK and O_2 in DMSO solution (Φ_{CL} 10^{-2}—10^{-4}) and suggested the reaction mechanism initiating from a deprotonation reaction of the alkyl side chain of **7**. The emitter is probably the anhydrobase excited by the ketones **2*** produced primarily as the excited state(s). After mixing with *t*-BuOK in the

** 1 mmHg $\approx$ 133.322 Pa.
*** 1 kcal $\approx 4.184\times10^3$ J.

Table 1. Chemiluminescence of the acridinium compounds

	[Substrate] mmol/l	[*t*-BuOK] mmol/l	[KCN] mmol/l	Yield of **2**/%	Φ_{CL}/(einstein/mol × 10^3)[a]
1a	1.01	10	—	97	0.69
	1.01	—	10	99	0.20
1b	1.00	10	—	93	0.56
	1.00	—	10	39	0.063
3	1.00	10	—	+	0.014
	1.00	—	10	—[b]	—[b]
5	1.00	10	—	44	0.015
	1.00	—	10	—[b]	—[b]

a) Standard: luminol in aqueous solution (Ref. 11). b) Not detected.

Table 2. Balance sheets of bond energy[a,b]

	Energy spent kcal/mol		Energy gained kcal/mol		Balance kcal/mol
(i)	C-H	98.7	C=O	181	
	C=C	145.8	C-C	83	
	O=O	119.1	arom	43	
			1/2 HOOH	51[c]	
	Total	363.6	Total	358	$\Delta H = +5.6$
(ii)	2C-H	197.4	2C=O	362	
	2C=C	291.6	2C-C	166	
	O=O	119.1	2H-OR	221.2	
			2arom	86	
	Total	608.1/2	Total	835.2/2	$\Delta H = -113.5$

a) J. D. Roberts and M. C. Casterio, "Basic Principles of Org. Chem.," Benjamin, New York, N. Y. (1964). b) See T. Wilson and A. P. Schaap, *J. Am. Chem. Soc.*, **93**, 4126 (1971). c) J. G. Calvert and J. N. Pitts, Jr., "Photochemistry," Wiley, New York, N. Y. (1966), p. 824.

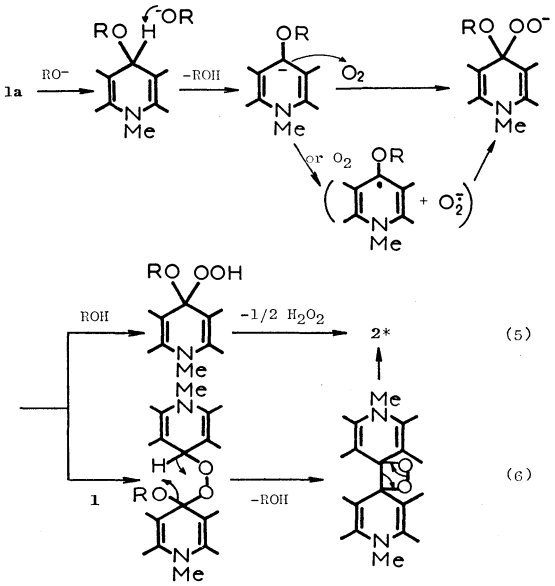

absence of O_2, the solution of **7** did not give CL on exposure to O_2 gas. The mechanism seems to be similar to the CL of lucigenin.[3]

Experimental

Instrumentation. All mps were uncorrected. Following spectrophotometers were used for spectral measurements: IR: JASCO IR-G and A-100; UV: Hitachi 220S Spectrophotometer; NMR: JEOL JNM-MH-100 (100 MHz) and FX-100 (99 MHz for ^1H and 25.05 MHz for ^{13}C); MS: JEOL JMS-D-100; Fluorescence: Hitachi MPF-2A. The spectral data are presented as follovs: IR in cm^{-1}; UV: λ_{max} in nm (ε given in parentheses); NMR: δ in ppm from int. TMS and J in Hz (accuracy±0.5 Hz); MS in m/z; fluorescence; λ_{max} in nm. GLC were carried out by Yanagimoto Yanaco G-1800F. GLC Conditions: Yanagimoto Yanaco G-1800F (FID); 10% Silicone GE-SE-30 on Diasolid L in 0.93×ϕ 4 mm stainless steel column; col. temperature 240 °C, inj. temperature 280 °C, carrier gas (N_2) 42.0 ml/min. TLC Conditions: Silica gel 60 PF_{254}-gipshaltig (Merck, #7749), thickness: 0.25 mm, $CHCl_3$.

Photometric determinations were made by measuring the output of R106 photomultiplier-photometers (Hitachi MPF-2A Fluorescence/Phosphorescence Photometer) exposed to the reacting solution. The values obtained were corrected for phototube spectral response. Quantum yields (Φ_{CL}) are relative to luminol.[11]

Materials. Acridine, quinoline, and 9(10*H*)-acridinone (**6**) were purchased. 10-Methylacridinium chloride (**1b**),[12] 10-methyl-9(10*H*)-acridinone (**2**),[13] and 1-methyl-1(4*H*)-quinolinone (**4**)[14] were prepared according to literatures.

1b: mp 180—187 °C (decomp) [lit,[12] mp 183 °C (decomp)]; ν_{max} (KBr) 1620, 1230, 1010, 730 cm^{-1}; δ (DMSO-d_6) 3.40 (4H, br), 4.80 (3H, s), 7.9—8.9 (8H, m), 10.30 (1H, s).

2: mp 207—209 °C (lit,[13] 203.5 °C); ν_{max} (KBr) 1630, 1590, 1490, 1180 cm^{-1}; δ ($CDCl_3$) 3.82 (3H, s), 7.46 (6H, m), 8.52 (2H, d).

4: mp 143—151 °C (lit,[14] 152 °C); ν_{max} (KBr) 1620 cm^{-1}; δ ($CDCl_3$) 3.80 (3H, s), 6.20 (1H, m), 7.50 (4H, m), 8.40 (1H, m).

*10-Methylacridinium Methyl Sulfate (**1a**)*: A solution of acridine (Nakarai Chem. Co) (5 g; 27.9 mmol) and dimethyl sulfate (bp 189 °C) (2.9 ml; 30.5 mmol) in benzene (50 ml) was stirred at 30—40 °C overnight with excluding moisture. Resulted precipitates were filtered and washed with ether. Into the mother liquor was added 1 ml of dimethyl sulfate. After strring, resulted ppt was collected with filtration. Yellow granules, mp >300 °C. Yields 7.14 g (23.4 mmol; 83%). Found C, 59.28; H, 5.15%. Calcd for $C_{15}H_{15}NO_4S$: C, 59.00; H, 4.952%; m/z 194 (cation part) ν_{max}

(KBr) 3000, 1390, 1220, 1170 cm^{-1}; δ (DMSO-d_6) 3.40 (3H, s), 4.88 (3H, s), 8.04 (2H, m), 8.60 (4H, m), 10.20 (1H, br, s).

1-Methylquinolinium Methyl Sulfate (3): A solution of quinoline (TCI) (3.0 ml: 3.27 g; 25.3 mmol) and dimethyl sulfate (10 ml: 13.3 g; 105 mmol) in benzene (30 ml) was stirred at 30—40 °C for 20 h and, then, cooled in an ice bath. Resulted precipitate was filtered and crystallized from acetone. Colorless needles, mp 98.0—99.0 °C (lit,[15] 100 °C), yields 5.04 g (19.7 mmol; 77.9%); ν_{max} (KBr) 1620, 1210, 1020, 760 cm^{-1}; δ (DMSO-d_6) 3.40 (3H, s), 4.64 (3H, s), 8.42 (2H, m), 9.35 (2H, m).

Chemiluminescent Reaction of 1 and 3: Each solution (2 ml) of **1a**, **1b**,[15] and **3** (1 mmol/l) in DMSO (dried over and distilled from CaH_2 and saturated by O_2 before use) was treated with DMSO solution (2 ml) of *t*-BuOK (Merck, 10 mmol/l) or KCN (Wako, 10 mmol/l) at room temperature. The mixture was flushed by O_2 gas for 10 min before and during the oxygenation reaction. Fast light emission was observed.[11] After neutralization of the resulted mixture with Dry Ice, solvents were evaporated *in vacuo* and the residue was extracted with ether, from which the final product **2**[13] and **4** were characterized by IR, NMR, and mp and identified on GLC and TLC with the authentic samples. The results are shown in Table 1. CL spectra were recorded and compared with their fluorescence spectra measured under the similar conditions.

Base Catalyzed Oxygenation of 5. The CL reactions of **5** (1.00 mmol/l) were observed under the similar conditions and the spectra and products were analysed as described above (Table 1). Products were also determined by UV spectra.

We thank Dr. T. Kondo and Professor T. Goto, Nagoya University, for taking MS; Professor I. Kamiya and Dr. T. Sugimoto for valued discussions, and the Ministry of Education, Science and Culture of Japan for the financial support (Grant-in-Aid).

References

1) Preliminary communication: N. Suzuki, Y. Kazui, M. Kato, and Y. Izawa, *Heterocycles*, **16**, 2121 (1981).
2) K. Gleu and W. Petsch, *Angew. Chem.*, **48**, 57 (1935).
3) J. R. Totter, *Photochem. Photobiol.*, **3**, 231 (1964).
4) For a list of relevant references, see E. H. White, "Light and Life," Johns Hopkins Press, Baltimore, MD. (1961), p. 195; F. McCapra, "Acridines," 2nd ed in "The Chemistry of Heterocyclic Compounds," ed by R. M. Acheson, Wiley, New York, N. Y. (1973), Vol. 9, pp. 615—630; K.-D. Gundermann, *Topics Curr. Chem.*, **46**, 61 (1974); I. Kamiya, "Chemiluminescence," 2nd ed, Kodansha, Tokyo (1976), p. 77—94 (in Japanese).
5) E. H. White, N. Suzuki, and W. H. Hendrickson, *Chem. Lett.*, **1979**, 1491.
6) J. W. Happ, E. G. Janzen, and B. C. Rudy, *J. Org. Chem.*, **35**, 3382 (1970); J. W. Happ and E. G. Janzen, *ibid.*, **35**, 96 (1970). There was no description on the quantum yield of CL.
7) For the vacuum apparatus used, see N. Suzuki and T. Goto, *Kagaku Kyoiku, (Chem. Education, Japan)*, **25**, 338 (1977).
8) I. Kamiya and T. Sugimoto, Abstr. Symp. on Photochemistry, held at Tsu, Mie, Japan, Oct. 1980, p. 312 and Sapporo, Japan, Oct. 1981, p. 107.
9) I. Rosenthal and T. Bercovici, *J. Chem. Soc., Chem. Commun.*, **1973**, 200.
10) E. G. Janzen, J. B. Pickett, J. W. Happ, and W. deAngelis, *J. Org. Chem.*, **35**, 88 (1970).
11) J. Lee and H. H. Seliger, *Photochem. Photobiol.*, **4**, 1015 (1965); **15**, 225 (1972).
12) A. Albert, "The Acridines," St. Martin's Press, New York, N. Y. (1966), p. 343.
13) K.-W. Lee, L. A. Singer, and K. D. Legg, *J. Org. Chem.*, **41**, 2685 (1976).
14) G. F. Tucker and J. L. Iroin, *J. Am. Chem. Soc.*, **73**, 1923 (1951).
15) A. Kaufmann, *Ber.*, **42**, 3779 (1909).

Synthesis of 5″-Deoxy-5″-fluorolividomycin B

Takahiro Torii, Tsutomu Tsuchiya,* Sumio Umezawa, and Hamao Umezawa†

Institute of Bioorganic Chemistry, 1614 Nakahara-ku, Kawasaki 211

† *Institute of Microbial Chemistry, Kamiosaki, Shinagawa-ku, Tokyo 141*

(Received December 13, 1982)

A masked lividomycin B derivative in which only the C-5″ hydroxyl group remains free has been prepared and treated with diethylaminosulfur trifluoride as the key step to give the title compound. A macrocyclic compound, that is, 2′,5″-carbamate was also obtained by the above reaction, and the structure was determined chemically and by the NMR-spectrum of its deblocked derivative.

Lividomycin B[1] is an amino glycoside antibiotic produced by *Streptomyces lividus* nov. sp. This antibiotic has strong activity[2] in inhibiting the growth of resistant strains producing 3′-phosphotransferase II which transfers the phosphate of ATP to the 3′-hydroxyl group of paromomycin I (which is synonymous with 3′-hydroxylividomycin B). However, lividomycin B is inactivated[2] by the other resistant strains producing 3′-phosphotransferase I, which transfers the phosphate to the 5″-hydroxyl group.[3] To overcome the inactivation by this enzyme, 5″-deoxylividomycin B[2] had been prepared; however, the derivative had only weak antibacterial activity, suggesting the importance of the role of the 5″-hydroxyl group in the antibacterial action. Recently we prepared several fluoro derivatives[4] of amino glycoside antibiotics in the purpose of developing useful antibacterial amino glycosides. This paper describes the preparation of 5″-deoxy-5″-fluorolividomycin B, to investigate the effect of strongly electronegative fluorine atom instead of the electronegative 5″-hydroxyl group.

First attempts to fluorinate the *N*,*O*-protected 5″-*O*-tosyl derivative[2] (**10**) with cesium fluoride or tetrabutylammonium fluoride, both of which are commonly used for fluorination, were unsuccessful, to give several unidentified products. Therefore, direct fluorination of a 5″-hydroxyl derivative (**6**) with diethylaminosulfur trifluoride[5] (DAST reagent) was attempted. Pentakis (*N*-benzyloxycarbonyl)lividomycin B[2] (**1**) reported earlier was treated with chlorotriphenylmethane in the presence of 2 molar equivalents of phenylboronic acid. Then, 5″-*O*- (**2**, 72%) and 6′-*O*-triphenylmethyl (**3**, 2%) derivatives were produced together with 6′,5″-bis(*O*-triphenylmethyl) derivative (**4**, 8%). Reaction without addition of phenylboronic acid gave **3** as the major product, suggesting that, in the presence of phenylboronic acid, a phenylboronic ester was tentatively formed between the 4′- and 6′-hydroxyl groups.[6] This facilitated the selective 5″-*O*-triphenylmethylation. Acetylation of **2** (to give **5**) followed by acidic hydrolysis of the triphenylmethyl group gave **6** carrying the free 5″-hydroxyl group. The structure of **6** was confirmed by the fact that tosylation of **6** gave the product identical with the derivative (**12**) obtained by debenzylidenation (to give **11**) of an authentic **10**[2] followed by acetylation.

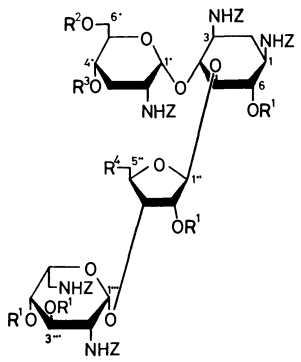

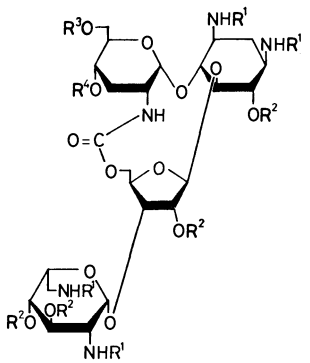

	R^1	R^2	R^3	R^4
1	H	H	H	OH
2	H	H	H	OTr
3	H	Tr	H	OH
4	H	Tr	H	OTr
5	Ac	Ac	Ac	OTr
6	Ac	Ac	Ac	OH
7	Ac	Ac	Ac	F
10	H	$C_6H_5CH=$		OTs
11	H	H	H	OTs
12	Ac	Ac	Ac	OTs
13	H	$C_6H_5CH=$		Cl
14	H	H	H	Cl
19	H	$C_5H_{10}C=$		OH
20	H	$C_5H_{10}C=$		OTr

	R^1	R^2	R^3	R^4
8	Z	Ac	Ac	Ac
16	H	H	H	H
17	H	H	H	H
18	Z	$C_5H_{10}C=$		H

Tr: $C(C_6H_5)_3$,
Ts: $O_2SC_6H_4CH_3(p)$,
Z: $CO_2CH_2C_6H_5$

Reaction of **6** with diethylaminosulfur trifluoride proceeded smoothly to give two products, the minor one being the desired 5″-deoxy-5″-fluoro derivative (**7**, 28%) and the major, 2′-*N*:5″-*O*-carbonyl macrocyclic compound (**8**, 61%). Deacetylation of **7** followed by catalytic debenzyloxycarbonylation gave the desired 5″-deoxy-5″-fluorolividomycin B (**9**).

The structure of **9** is evident from the synthetic pathway, but further confirmed by NMR spectral study. In ^{1}H-NMR spectrum, presence of $-CH_2F$ was clarified from the splitting pattern having large $^2J_{H,F}$ (47 Hz) values (see Experimental section). In (proton decoupled) ^{13}C-NMR spectrum, signals of C-5″,-4″, and -3″ appeared as a doublet with a spacing of 168.5 ($=^1J_{C,F}$), 17.7 ($=^2J_{C,F}$), and 6.7 Hz ($=^3J_{C,F}$), respectively (see Table 1), supporting the presence of above fragment.

As a reference compound, 5″-chloro-5″-deoxylividomycin B (**15**) was prepared. A *N*-protected 4′,6′-*O*-benzylidene-5″-chloro-5″-deoxy derivative (**13**) was prepared from **10**[2] according to the method of Watanabe,[7] and it was led to **15** by debenzylidenation (to give **14**) followed by catalytic debenzyloxycarbonylation. One-step deblocking of **13** by the catalytic hydrogenolysis required long reaction-period giving 5″-deoxylividomycin B[2] (**21**). The 5″-chloro structure of **15** was confirmed by the resonance of C-5″ appeared

at high-field (45.8 ppm) in ^{13}C-NMR spectrum, the value being typical for that of the terminal chloromethyl carbon of carbohydrates reported.[8]

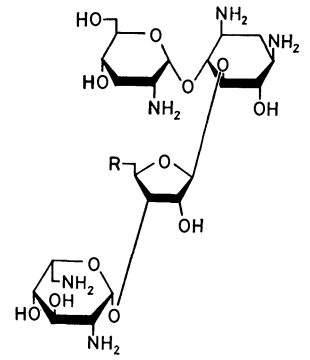

Lividomycin B	R=OH
9	R=F
15	R=Cl
21	R=H

The structure of 2′-*N*:5″-*O*-carbonyl compound (**8**) was determined as follows: Deacetylation of **8** with methanolic aqueous ammonia (to give **16**) followed by catalytic hydrogenolysis gave the 2′-*N*:5″-*O*-carbonyl compound (**17**). The presence of one carbonyl carbon was evidenced by the resonance at down-field (157.8 ppm) in ^{13}C-NMR spectrum. Bridging the 2′-amino and 5″-hydroxyl groups with a carbonyl was verified by the ^{1}H-NMR spectral study. The HC(2′)NH– proton resonances, which should appear at rather down-field ($\delta \approx 3.6$, see Experimental section), were not in the usual methine region (δ=2.5—3.1) of HCNH$_2$ (measured in 20% ND_3 in D_2O as the free base). Furthermore, one of the proton resonances of C(5″)H_AH_BO–, which appeared separately at δ= 4.10 and 5.15, lay beyond the usual region of methylene protons carrying a hydroxyl group. These results led to the conclusion that bridging the 2′-amino and 5″-hydroxyl groups with a carbonyl group occurred to give **8**.

A similar kind of cyclic carbamate formation as that of **8** was also observed[9] on fluorination of tetrakis-(*N*-benzyloxycarbonyl)sporaricin B with the DAST reagent. The tendency to form the carbamates in these cases will be ascribed[9] to the basic nature of fluoride ion liberated during the reactions.

Furthermore, the above conclusion was chemically confirmed. A *N*-protected derivative (**16**, *loc. cit.*) of **17** was treated with 1,1-dimethoxycyclohexane in a usual manner[10] to give the 4′,6′-*O*-cyclohexylidene derivative (**18**), which could not be triphenylmethylated by reaction with chlorotriphenylmethane (in pyridine, 50 °C, 2 d). On the other hand, 4′,6′-*O*-cyclohexylidene derivative (**19**) of **1** gave a mono-*O*-triphenylmethyl (5″-*O*-triphenylmethyl) derivative (**20**) by the same treatment. This result clearly shows that the 5″-hydroxyl group of **17** is blocked. Another structural confirmation was given from the alkaline hydrolysis (2 M aqueous NaOH,** 80 °C, 2 h) of **17**, when lividomycin B was obtained almost quantitatively.

** 1 M=1 mol dm^{-3}.

Table 1. The ^{13}C chemical shifts[a] of **9**, **15**, and lividomycin B (all as free bases) dissolved in 20% ND_3 in D_2O

Carbon	Lividomycin	**15**	**9**	$J_{C,F}$ of **9**
1′	99.7	99.5	99.6	
2′	50.3	50.2	50.2	
3′	35.8	35.3	35.3	
4′	65.4	65.5	65.5	
5′	74.5	74.4	74.4	
6′	61.5	61.6	61.6	
1	51.3[c]	51.2[d]	51.2	
2	36.7	36.7	36.7	
3	51.2[c]	51.1[d]	51.2	
4	84.2	84.0	84.1	
5	85.1	86.2	86.0	
6	78.4	78.5	78.6	
1″	109.3	110.5	110.5	
2″	74.1	74.1	73.9	
3″	77.1	77.6	75.4	$J_{C-3'',F}$=6.7 Hz
4″	82.4	80.7	80.1	$J_{C-4'',F}$=17.7 Hz
5″	62.2	45.8	83.1	$J_{C-5'',F}$=168.5 Hz
1‴	100.3	100.1	100.1	
2‴	53.8	53.6	53.6	
3‴	71.4	71.4	71.4	
4‴	69.4	69.3	69.3	
5‴	77.0	76.9	77.0	
6‴	42.2	42.0	42.0	

a) In ppm downfield from TMS calculated as $\delta^{TMS}=\delta^{dioxane}+67.4$ ppm. b) Assignments were made based on the data of lividomycin B reported,[6] and also on selective proton decoupling on the following cases (H-4, δ=3.44; H-5: 3.6—3.7, H-6: 3.23, H-1′: 5.21, H-1″: 5.33, H-3″: 4.40, H-1‴: 4.93, H-3‴: 4.00, H-5‴: $\approx$3.85). c,d) Figures indicated by the same character may be interconvertible.

Antibacterial spectra of **9** and **15** were shown in Table 2 in comparison with those of lividomycin B and 5″-deoxylividomycin B[2] (**21**). The substitutions of the 5″-hydroxyl group with halogens were shown to diminish the antibacterial activity as in the case of 5″-deoxygenation, although the fluoro compound (**9**) showed the best activity among them (**9**, **15**, **21**). The macrocyclic compound **17** was devoid of antibacterial action.

Experimental

General. ^{1}H-NMR spectra were recorded at 250 MHz at 30 °C (unless otherwise stated) in the FT mode with a Bruker WM 250 spectrometer. ^{13}C-NMR spectra were recorded at 30 °C (unless otherwise stated) in the FT mode with a Bruker WM 250 spectrometer operating at 62.5 MHz. Mass spectrum (field desorption) was recorded with a Hitachi M-80H spectrometer. Thin-layer chromatography (TLC) was performed on precoated Kieselgel 60, Merck. For column chromatography, silica-gel (Wakogel C-200) was used.

*1,3,2′,2‴,6‴-Pentakis(*N*-benzyloxycarbonyl)-5″-O-triphenylmethyllividomycin B (2).* A mixture of **1**[2] (5.0 g) and phenylboronic acid (0.94 g, 2 mol equiv. for **1**) in dry pyridine

Table 2. Minimal inhibitory concentration(μg/ml) of **9**, **15**, **21**, and lividomycin B

	Lividomycin B	**9**	**15**	**21**
Staphylococcus aureus FDA 209P	0.78	6.25	12.5	6.25
Staphylococcus aureus AP01	>100	>100	>100	>100
Micrococcus luteus PCI 1001	1.56	6.25	12.5	6.25
Bacillus subtilis NRRL B-558	0.39	3.12	6.25	3.12
Escherichia coli K-12	0.78	12.5	12.5	50
Escherichia coli K-12 ML1629	>100	50	50	100
Escherichia coli W677	1.56	12.5	25	25
Salmonella typhi T-63	0.39	6.25	6.25	25
Pseudomonas aeruginosa A3	0.78	12.5	50	25

(50 ml) was kept for 2 h at room temperature. Chlorotriphenylmethane (5.5 g) was added, and after standing the solution overnight at room temperature, another chlorotriphenylmethane (5.5 g) was added, and the solution was kept overnight at 37 °C. Addition of methanol (15 ml) and 1,3-propanediol (1 ml) followed by concentration gave a residue, which was extracted with chloroform. The chloroform-soluble products were separated by silica-gel column chromatography with chloroform-methanol (30: 1→25: 1→20: 1→10: 1, gradually changed) to give a solid each of **4**, 548 mg (8%), **3**, 136 mg (2%), **2**, 4.30 g (72%), and the starting material (**1**) recovered, 293 mg (6%).

Compound **2**: $[\alpha]_D^{20}+37°$ (*c* 1, chloroform); Found: C, 64.91; H, 5.87; N, 4.48%. Calcd for $C_{82}H_{89}N_5O_{23}$: C, 65.11; H, 5.93; N, 4.63%.

Compound **3**: $[\alpha]_D^{20}+23°$ (*c* 1, chloroform); Found: C, 64.89; H, 5.97; N, 4.63%. Calcd for $C_{82}H_{89}N_5O_{23}$: C, 65.11; H, 5.93; N, 4.63%.

Compound **4**: $[\alpha]_D^{20}+15°$ (*c* 1, chloroform); Found: C, 69.34; H, 5.92; N, 3.87%. Calcd for $C_{101}H_{103}N_5O_{23}$: C, 69.12; H, 5.92; N, 3.99%.

*6,4′,6′,2″,3‴,4‴-Hexa-*O*-acetyl-1,3,2′,2‴,6‴-pentakis(*N*-benzyloxycarbonyl)-5″-*O*-triphenylmethyllividomycin B (**5**).* A mixture of **2** (3.9 g), acetic anhydride (20 ml) and pyridine (40 ml) was kept at room temperature overnight. Another acetic anhydride (10 ml) was added and the mixture was kept further overnight. Concentraction gave a syrup, which was dissolved in chloroform. The organic solution was washed with 0.4 M aqueous potassium hydrogensulfate solution, then aqueous sodium hydrogencarbonate solution (saturated), dried over sodium sulfate, and concentrated. The residue was reprecipitated from hexane-chloroform to give a solid of **5**, 4.22 g (93%), $[\alpha]_D^{20}+31°$ (*c* 1, chloroform); ^{1}H-NMR ($CDCl_3$): $\delta=1.83$, 1.97, 2.00, 2.07, 2.08, and 2.17 (each 3H s, Ac).

Found: C, 63.72; H, 5.86; N, 3.88%. Calcd for $C_{94}H_{101}N_5O_{29}$: C, 63.97; H, 5.77; N, 3.97%.

*6,4′,6′,2″,3‴,4‴-Hexa-*O*-acetyl-1,3,2′,2‴,6‴-pentakis(*N*-benzyloxycarbonyl) lividomycin B(**6**).* A solution of **5** (4.22 g) in a mixture of acetic acid-acetone-water (2: 1: 1, 120 ml) was heated at 60 °C for 6 h. Concentration gave a syrup, which was dissolved in chloroform, and the organic solution was washed with aqueous sodium hydrogencarbonate (saturated). The product obtained by concentration was purified by silica-gel column chromatography with benzene-ethyl acetate (1: 1→2: 3) to give a solid of **6**, 3.52 g (97%), $[\alpha]_D^{20}+25°$ (*c* 1, chloroform); ^{1}H-NMR ($CDCl_3$): $\delta=1.93$ (3H), 2.00(6H), 2.05(3H), 2.08(3H), and 2.16(3H) (each s, Ac).

Found: C, 59.30; H, 5.75; N, 4.50%. Calcd for $C_{75}H_{87}N_5O_{29}$: C, 59.17; H, 5.76; N, 4.60%.

*6,4′,6′,2″,3‴,4‴′-Hexa-*O*-acetyl-1,3,2′,2‴,6‴-pentakis(*N*-benzyloxycarbonyl)-5″-deoxy-5″-fluorolividomycin B (**7**) and 6,4′,-6′,2″,3‴,4‴-Hexa-*O*-acetyl-1,3,2‴,6‴-tetrakis(*N*-benzyloxycarbonyl)-2′-*N*: 5′-*O*-carbonyllividomycin B (**8**).* To a cold (−15 °C) solution of **6** (300 mg) in dichloromethane (3.5 ml), was added diethylaminosulfur trifluoride (0.1 ml) and the solution was kept at the temperature for 15 min, then at room temperature for 30 min. After addition of water (0.1 ml) followed by standing for 30 min, chloroform (30 ml) was added, and the solution was washed with aqueous sodium hydrogencarbonate (saturated) and water, dried (sodium sulfate), and concentrated to give a syrup. On checking by TLC with benzene-ethyl acetate(1: 1), the syrup showed two spots at R_f 0.2 (**8**) and 0.5 (**7**) (*cf.* **6**: R_f 0.3). Separation of the products by silica-gel column chromatography with benzene-ethyl acetate (3: 2→2: 3) gave a solid each of **7**, 83 mg (28%) and **8**, 171 mg (61%).

Compound **7**: $[\alpha]_D^{20}+28°$ (*c* 1, chloroform); ^{1}H-NMR ($CDCl_3$): $\delta=1.77$, 1.92, 2.00, 2.06, 2.09, and 2.18 (each 3H s, Ac), 7.35 (25H s, $NHCO_2CH_2C_6\underline{H}_5$); Found: C, 58.87; H, 5.91; N, 4.49; F, 1.39%. Calcd for $C_{75}H_{86}FN_5O_{28}$: C, 59.09; H, 5.67; N, 4.59; F, 1.25%.

Compound **8**: $[\alpha]_D^{20}+43°$ (*c* 1, chloroform); ^{1}H-NMR ($CDCl_3$): $\delta=1.88$ (3H), 1.97 (6H), 2.06 (6H), and 2.13 (3H) (each s, Ac), 7.35 (20H s, $NHCO_2CH_2C_6\underline{H}_5$); Found: C, 57.46; H, 5.62; N, 4.87%. Calcd for $C_{68}H_{79}N_5O_{28}$: C, 57.74; H, 5.63; N, 4.95%.

*5″-Deoxy-5″-fluorolividomycin B (**9**).* A solution of **7** (80 mg) in a mixture of methanol (8 ml) and 28% aqueous ammonia (9 ml) was kept at room temperature overnight. Concentration gave a syrup (de-*O*-acetyl product), which was dissolved in 0.2 M methanolic hydrochloric acid (4 ml), and the solution was hydrogenated under atmospheric pressure of hydrogen in the presence of palladium catalyst for 2 h. The resulting crude product was purified by chromatography first on a column of Dowex 50 W (NH_4^+ form) (the charged column was washed with water, then 1 M aqueous ammonia was used as the developer), and then on a column of CM-Sephadex C-25 (0→0.1→0.3 M aqueous ammonia was used as the developer) to give pure **9** as the carbonate, 29 mg (83%), $[\alpha]_D^{20}+48°$ (*c* 1, water); ^{1}H-NMR (20% ND_3 in D_2O): $\delta=1.18$ (1H q, $J=12.5$ Hz H-2ax), 1.59 (1H q, $J=11.5$ Hz, H-3′ ax), 1.95 (1H dt, $J=12.5$, ≈4.5, ≈4.5 Hz, H-2eq), 2.01 (1H dt, $J=11.5$, ≈4.5 ≈4.5 Hz, H-3′eq) 4.95 (1H d, $J_{1''',2'''}\approx1.3$ Hz, H-1‴), 5.22 (1H d, $J_{1',2'}=3.5$ Hz, H-1′), 5.34 (1H d, $J_{1'',2''}\approx1.7$ Hz, H-1″). The signals for the AB part of an ABX system (A,B=H-5″a, −5″b; X=H-4″) were divided into two groups (each octet) centered at $\delta=4.62$ and 4.81, respectively. The upper quartet of each group was constituted from couplings of 11.5 ($=J_{5''a,5''b}$) and 4 Hz ($=J_{5''a,4''}$), and the lower quartet, from couplings of 11.5 and 2.5 Hz ($=J_{5''b,4''}$) (each 1H in total). These two groups were separated by 47 Hz ($=J_{5''a,F}=J_{5''b,F}$).

Found: C, 43.93; H, 7.17; N, 10.89; F, 2.58%. Calcd for $C_{23}H_{44}FN_5O_{12}\cdot H_2CO_3$: C, 43.43; H, 6.99; N, 10.55; F,

2.87%.

6,4′,6′,2″,3‴,4‴-Hexa-O-acetyl-1,3,2′,2‴,6‴-pentakis(N-benzyloxycarbonyl)-5″-O-tosylliuidomycin B (12). *From* **10**[2]: A solution of **10** (282 mg) in a mixture of acetic acid–acetone–water (2: 1: 1, 6 ml) was heated for 3 h at 60 °C. Concentration gave a syrup, which was dissolved in chloroform and the solution was washed with aqueous sodium hydrogencarbonate (saturated). Silica-gel column chromatography of the crude product with chloroform, then with chloroform–methanol (10: 1) gave a solid of **11**, 242 mg (91%), $[\alpha]_D^{20}+29°$ (*c* 1, chloroform); ^{1}H-NMR ($CDCl_3$): $\delta=2.32$ (3H s, Ts).

A mixture of **11** (136 mg) and acetic anhydride (2 ml) in dry pyridine (4 ml) was kept overnight at room temperature. Concentration gave a syrup, which was purified by silica-gel column chromatography with benzene–ethyl acetate (3: 1) to give a solid of **12**, 144 mg (90%), $[\alpha]_D^{20}+27°$ (*c* 1, chloroform); ^{1}H-NMR ($CDCl_3$): $\delta=1.80$, 1.87, 2.00, 2.06, 2.08, 2.21 (each 3H s, Ac); 2.42 (3H s, CH_3 of Ts).

Found; C, 58.45; H, 5.56; N, 4.13; S, 1.87%. Cacld for $C_{82}H_{93}N_5O_{31}S$: C, 58.74; H, 559; N, 4.18; S, 1.91%.

From **6**: A mixture of **6** (72 mg) and *p*-toluenesulfonyl chloride (105 mg) in pyridine (3.5 ml) was kept overnight at 37 °C. Concentration gave a syrup, which was purified as described above for **12** to give a solid of **12**, 72 mg (91%).

4′,6′-O-Benzylidene-1,3,2′,2‴,6‴-pentakis(N-benzyloxycarbonyl)-5″-chloro-5″-deoxylividomycin B (13). Prepared from **10**[2] (500 mg) with lithium chloride (580 mg) in *N,N*-dimethylformamide (95 °C, overnight) in the presence of calcium sulfate (Drierite), according to Watanabe[6]; a solid, 422 mg (93%), $[\alpha]_D^{20}+59°$ (*c* 1, chlornform).

1,3,2′,2‴,6‴-Pentakis(N-benzyloxycarbonyl)-5″-chloro-5″-deoxylividomycin B (14). A solution of **13** (300 mg) in a mixture of acetone–water–acetic acid (1: 1: 2, 6 ml) was heated at 60 °C for 3 h. Concentration gave a syrup, which was purified by silica-gel column chromatography first with chloroform, then with chloroform–methanol (10: 1) as the developers to give a solid of **14**, 261 mg (92%), $[\alpha]_D^{20}+35°$ (*c* 1, chloroform).

Found: C, 57.74; H, 5.76; N, 5.15; Cl, 2.95%. Calcd for $C_{63}H_{74}ClN_5O_{22}\cdot H_2O$: C, 57.90; H, 5.71; N, 5.36; Cl, 2.71%.

5″-Chloro-5″-deoxylividomycin B (15). A solution of **14** (monohydrate, 102 mg) in 0.2 M methanolic hydrochloric acid (10 ml) was hydrogenated in the presence of palladium black under atmospheric pressure of hydrogen for 2 h and the product was purified as described for **9** to give a solid of **15** as the carbonate, 48 mg (88%), $[\alpha]_D^{20}+51°$ (*c* 1, water); ^{1}H-NMR (20% ND_3 in D_2O): $\delta=1.18$ (1H q, $J=12.5$ Hz, H-2ax), 1.59 (1H q, $J=11.5$ Hz, H-3′ax), 1.94 (1H dt, $J=12.5$, ≈4.5, ≈4.5 Hz, H-2eq), 2.00 (1H dt, $J=11.5$, ≈4.5, ≈4.5 Hz, H-3′eq), 4.93 (1H d, $J_{1'',2''}\approx2$ Hz, H-1‴), 5.25 (1H d, $J_{1',2'}=3.5$ Hz, H-1′), 5.32 (1H d, $J_{1'',2''}\approx2$ Hz, H-1″).

Found: C, 41.69; H, 6.77; N, 9.79; Cl, 5.35%. Calcd for $C_{23}H_{44}ClN_5O_{12}\cdot H_2CO_3\cdot H_2O$: C, 41.29; H, 6.93; N, 10.03; Cl 5.07%.

1,3,2‴,6‴-Tetrakis(N-benzyloxycarbonyl)-2′-N:5″-O-carbonyllividomycin B (16). A solution of **8** (103 mg) in a mixture of methanol–28% aqueous ammonia (1: 1, 10 ml) was kept at room temperature overnight. The solid precipitated was filtered, washed with aqueous methanol (1: 1), and dired to give a solid of **16**, 78 mg (92%), $[\alpha]_D^{20}+41°$ (*c* 1, dimethyl sulfoxide).

Found: C, 57.57; H, 5.73; N, 5.85%. Calcd for $C_{56}H_{67}N_5O_{22}$: C, 57.87; H, 5.81; N, 6.03%.

2′-N:5″-O-Carbonyllividomycin B (17). A suspended mixture of **16** (70 mg) in 70% aqueous oxolane (10 ml) containing 0.1 ml of 2 M aqueous hydrochloric acid was hydrogenated in the presence of palladium black under atmospheric pressure of hydrogen at room temperature for 3 h with occasional additions of 0.1 M aqueous hydrochloric acid (2 ml×2). Filtration of the reaction mixture followed by concentration of the filtrate gave a residue, which was chromatographed on CM-Sephadex C-25 column with water, then with 0.3 M aqueous ammonia to give a ninhydrin-positive solid of **17**, 33 mg (71%), $[\alpha]_D^{20}+86°$ (*c* 1, water); ν_{max}^{KBr} 1700 cm^{-1}; *m/z* 626 (M^+), 600, 466 ($M^+-C_6H_{12}N_2O_3$), 440 ($600^+-C_6H_{12}N_2O_3$). ^{1}H-NMR (20% ND_3 in D_2O measured at 4 °C): $\delta=1.19$ (1H q, H-2a), 1.74 (1H q, H-3′a), 1.95 (1H apparent dt, H-2e), 2.09 (1H m, H-3′e), 2.6—3.05 (5H, H-1, 3, 2‴, 6‴a, 6‴b), 3.29 (1H t, H-6), 3.47 (1H t, H-4), 4.01 (1H t, H-3‴), 4.10 (1H d, H-5″a), 4.14 (1H dd, H-4″), 4.31 (1H d, H-2″), 4.51 (1H dd, H-3″; broad HOD signal at $\delta=4.2$—4.6 was suppressed by homogated decoupling), 4.97 (1H apparent s, H-1‴), 5.15 (1H dd, with small splittings, H-5″b), 5.96 (1H s, H-1″), 6.08 (1H d, H-1′); $J_{1,2a}=J_{2a,2e}=J_{2a,3}\approx12$, $J_{1,2e}=J_{2e,3}\approx4$, $J_{3,4}=J_{4,5}=J_{5,6}=J_{6,1}\approx9.5$, $J_{1'2'}=3.5$, $J_{2',3'a}=J_{3'a,3'e}=J_{3'a,4'}\approx12$, $J_{1'',2''}=0$, $J_{2'',3''}=4$, $J_{3'',4''}=9$, $J_{4'',5''a}=0$, $J_{4'',5''b}\approx4$, $J_{5''a,5''b}=13$, $J_{1'',2''}\approx1$, $J_{2'',3''}=J_{3'',4''}\approx3$ Hz. Irradiation of H-3″ caused H-2″ d to s, and H-4″ dd to a narrow-space d; irr. of H-5″ b caused H-4″ dd→a large-space d, and H-5″ a d →s; irr. at $\delta=2.7$ (H-3) caused H-2a q→t, H-2e dt→dd, and H-4 t→d; irr. at $\delta=2.87$ (H-1) caused H-2a q→t, H-2e dt→dd, and H-6 t→d; irr. at $\delta=2.95$ (H-2‴) caused H-3‴ t→d; irr. at $\delta=3.63$ (H-2′, 4′, 4‴) caused H-3‴ t→d, H-1′ d→s, H-3′a q→d, and H-3′e q→d, the latter two doublets forming an AB quartet.

^{13}C-NMR (20% ND_3 in D_2O, measured at 4 °C): 31.7 (C-3′), 36.1 (C-2), 42.2 (C-6‴), 50.3, 50.6, 51.3, 53.6 (C-2‴), 60.2, 61.4 (C-6′), 64.7, 69.1 (C-4‴), 71.4 (C-3‴), 72.8, 73.6, 74.5, 76.4, 77.0 (C-5‴), 78.1, 80.3, 81.4, 92.8, 98.9, 107.2, 157.8 (C=0) ppm.

Found: C, 40.42; H, 6.56; N, 9.21%. Calcd for $C_{24}H_{43}N_5O_{14}\cdot 2H_2CO_3\cdot H_2O$: C, 40.68; H, 6.43; N, 9.12%.

1,3,2‴,6‴-Tetrakis(N-benzyloxycarbonyl)-2′-N:5″-O-carbonyl-4′,6′-O-cyclohexylidenelividomycin B (18). To a solution of **16** (50 mg) in *N,N*-dimethylformamide (10 ml) were added 1,1-dimethoxycyclohexane (0.5 ml) and anhydrous *p*-toluenesulfonic acid (10 mg) and the mixture was heated at 30 °C under reduced pressure (10—15 Torr, 1 Torr≈133.322 Pa) for 6 h. Addition of aqueous sodium hydrogencarbonate (saturated, 0.5 ml) followed by evaporation gave a residue, which was washed with water. The water-insoluble product was washed with ether to give a solid, 51 mg (94%), $[\alpha]_D^{20}+38°$ (*c* 1, dimethyl sulfoxide).

Found: C. 59.33; H, 6.03; N, 5.12%. Calcd for $C_{62}H_{75}N_5O_{22}\cdot H_2O$: C, 59.08; H, 6.16; N, 5.56%.

1,3,2′,2‴,6‴-Pentakis(N-benzyloxycarbonyl)-4′,6′-O-cyclohexylidenelividomycin B (19). Compound **1** was treated with 1,1-dimethoxycyclohexane as described for **18** to give a solid of **19** in 90% yield, $[\alpha]_D^{20}+46°$ (*c* 1, chloroform).

Found: C, 60.96; H, 6.12; N, 5.01%. Calcd for $C_{69}H_{83}N_5O_{23}\cdot 1/2\,H_2O$: C, 60.96; H, 6.23; N, 5.15%.

1,3,2′,2‴,6‴-Pentakis(N-benzyloxycarbonyl)-4′,6′-O-cyclohexylidene-5″-O-triphenylmethyllividomycin B (20). Compound **19** (202 mg) was treated with chlorotriphenylmehtane (200 mg) in pyridine (4 ml) at 50 °C for 2 d. After usual work-up, the product was chromatographed on a silica-gel column with chloroform–methanol (30: 1) to give a solid of **20**, 158 mg (66%), $[\alpha]_D^{20}+28°$ (*c* 1, chloroform).

Found: C, 65.93; H, 6.20; N, 4.09%. Cacld for $C_{88}H_{97}N_5O_{23}\cdot H_2O$: C, 65.62; H, 6.20; N, 4.35%.

The authors wish to thank Mr. Saburo Nakada of Keio University for the microanalysis, Dr. Hiroshi Naganawa of Institute of Microbial Chemistry for measurement of a mass spectrum, and Miss Yukiko Suzuki of our Institute for measurements of NMR spectra. Thanks are also due Miss Junko Yamamoto of our Institute for preparation of the manuscript.

References

1) T. Mori, Y. Kyotani, I. Watanabe, and T. Oda, *J. Antbiot.*, **25**, 149 (1972).

2) S. Umezawa, I. Watanabe, T. Tsuchiya, H. Umezawa, and M. Hamada, *J. Antbiot.*, **25**, 617 (1972).

3) S. Kondo, H. Yamamoto, H. Naganawa, H. Umezawa, and S. Mitsuhashi, *J. Antbiot.*, **25**, 483 (1972).

4) T. Tsuchiya, T. Torii, S. Umezawa, and H. Umezawa, *J. Antbiot.*, **35**, 1245 (1982).

5) L. N. Markovskij, V. E. Pashinnik, and A. V. Kirsanov, *Synthesis*, 787 (1973); W. J. Middleton, *J. Org. Chem.*, **40**, 575 (1975).

6) T. Torri, T. Tsuchiya, I. Watanabe, and S. Umezawa *Bull., Chem. Soc. Jpn.*, **55**, 1178 (1982).

7) I. Watanabe, Thesis, Keio University "Synthetic Studies on Lividomycin and Butirosin Derivatives," 1979.

8) W. A. Szarek, D. M. Vyas, S. D. Gero, and G. Lukacs, *Can. J. Chem.*, **52**, 3394 (1974).

9) T. Torii, T. Tsuchiya, and S. Umezawa, *Carbohydr. Res.*, under Submission.

10) For example see: T. Jikihara, T. Tsuchiya, H. Umezawa, and S. Umezawa, *Carbohydr. Res.*, **89**, 91 (1981).

Studies on the β-Turn of Peptides. II.[1] Syntheses and Conformational Properties of *N*-(2,4-Dinitrophenyl)tetrapeptide *p*-Nitroanilides Related to the β-Turn Part of Gramicidin S

Kazuki SATO,* Masao KAWAI, and Ukon NAGAI

Mitsubishi-Kasei Institute of Life Sciences, 11 Minamiooya, Machida, Tokyo 194

(Received December 24, 1982)

N-(2,4-Dinitrophenyl)tetrapeptide *p*-nitroanilides related to the β-turn part of gramicidin S were synthesized and subjected to CD measurements. The β-turn preference of the tetrapeptide derivatives had correlation with the antibiotic activities of the gramicidin S analogs containing similar tetrapeptide sequences at their β-turn part. So, conformational preference of partial sequences of gramicidin S analogs seem to play a significant role for determining their biological activities.

Gramicidin S (GS) is a cyclic decapeptide antibiotic with the primary structure *cyclo*(–L-Val[1]–L-Orn[2]–L-Leu[3]–D-Phe[4]–L-Pro[5]–L-Val[1']–L-Orn[2']–L-Leu[3']–D-Phe[4']–L-Pro[5']–). Conformation of GS consists of the intramolecular antiparallel β-form with four hydrogen bonds between L-Val and L-Leu residues and two β-turns (type II') around the D-Phe–L-Pro sequences (Fig. 1).[2] The characteristic feature of the conformation is the orientation of side chains in which the charged L-Orn side chains are on one side and the hydrophobic L-Val and L-Leu side chains on the other side of the molecule. The conformation of GS is considered to be stabilized not only by the four intramolecular hydrogen bonds but also by the stable β-turn formed by D-Phe–L-Pro sequence. Izumiya *et al.* summarized the antibacterial activities of many GS analogs.[3] The activities of GS analogs were correlated to their conformations.[4] For example, the activity and the population of GS-type β-sheet conformer were in the order of GS≈[D-Ala[4,4']]-GS> [Gly[4,4']]-GS≫[L-Ala[4,4']]-GS≈0.[5] It is of interest to study β-turn preference of the amino acid sequences at the corner positions of GS analogs.

In the previous paper, we gave an outline of a new method to study the β-turn conformation of linear tetrapeptides.[1] *N*-(2,4-Dinitrophenyl)tetrapeptide *p*-nitroanilides (Dnp–tetrapeptide–pNA's)[6] exhibited characteristic CD spectra above 300 nm when they took β-turn conformations (Fig. 2). The Cotton effects were considered to be due to the interaction of the two terminal chromophores and the magnitude of the Cotton effects were shown to reflect the β-turn preference of the peptides.

This paper deals with the details of synthesis and conformational properties of Dnp–tetrapeptide–pNA's related to the β-turn part of GS and with the relation between the activity of GS analogs and the β-turn preference of their partial peptide sequences.

To study the effect of amino acid residues at 4,4'- and 5,5'-positions of GS on β-turn preference, we synthesized tetrapeptide derivatives having a general structure of Dnp–L-Leu–X–Y–L-Val–pNA (**7a—o**) for all the combinations of X=D-Ala, Gly, or L-Ala and Y=L-Pro, L-Leu, Gly, Sar, or D-Leu (Fig. 3). Boc–L-Pro–L-Val–pNA (**1a**) was prepared by EDC coupling of Boc–L-Pro–OH and H–L-Val–pNA, and deprotected with hydrogen chloride in formic acid, to afford H–L-Pro–L-Val–pNA·HCl (**2a**·HCl). Mixed anhydride coupling of Boc–L-Leu–OH and H–D-Ala–OEt afforded Boc–L-Leu–D-Ala–OEt (**3a**), which was converted into Boc–L-Leu–D-Ala–N_2H_3 (**4a**) with hydrazine hydrate. Compounds **2a** and **4a** were coupled by azide method to afford Boc–L-Leu–D-Ala–L-Pro–L-Val–pNA (**5a**), which was converted into the Dnp derivative, Dnp–L-Leu–D-Ala–L-Pro–L-Val–pNA (**7a**), by deprotection and subsequent treatment with 1-fluoro-2,4-dinitrobenzene. Homogeneities of the synthetic peptides were confirmed by thin-layer chromatography and elemental

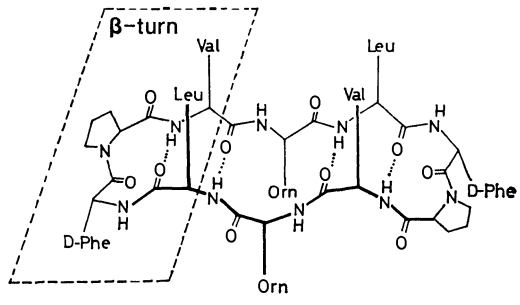

Fig. 1. β-Sheet conformation of gramicidin S.

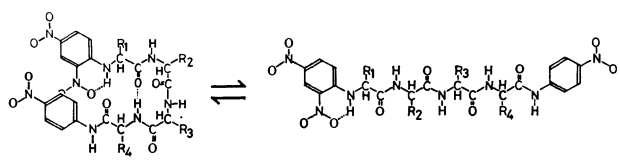

Fig. 2. Models of folded (β-turn) and non-folded conformers of a Dnp–tetrapeptide–pNA.

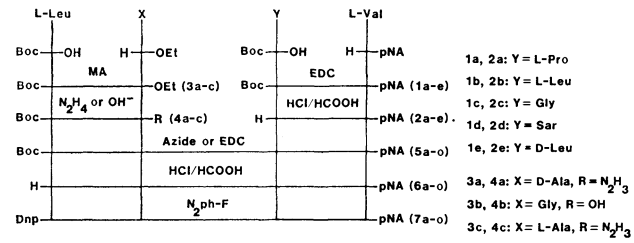

Fig. 3. Syntheses of Dnp–tetrapeptide–pNA's (**7a—o**).

analysis. Compounds **7b—o** were prepared by a similar manner as described for the synthesis of **7a** except for the steps of saponification of **3b** to **4b** and EDC coupling of **4b** and **2a—e** to afford **5f—j**.

Figures 4, 5, and 6 show CD spectra of synthetic peptides with a general structure of Dnp-L-Leu-D-Ala-Y-L-Val-pNA (**7a—e**), Dnp-L-Leu-Gly-Y-L-Val-pNA (**7f—j**), and Dnp-L-Leu-L-Ala-Y-L-Val-pNA (**7k—o**), respectively. From these figures it can be seen that the highest Cotton effects were observed

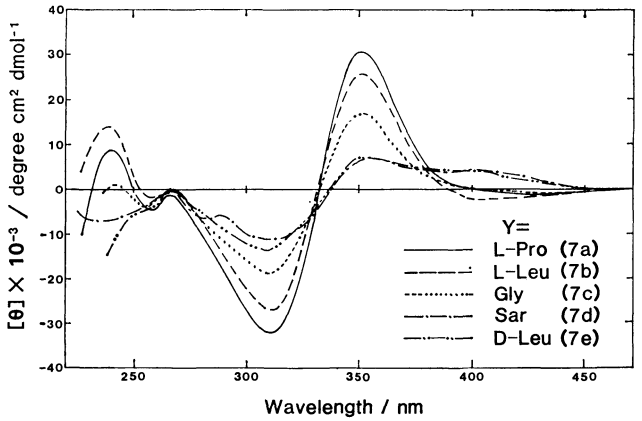

Fig. 4. CD spectra of Dnp-L-Leu-D-Ala-Y-L-Val-pNA's (**7a—e**) in MeOH.

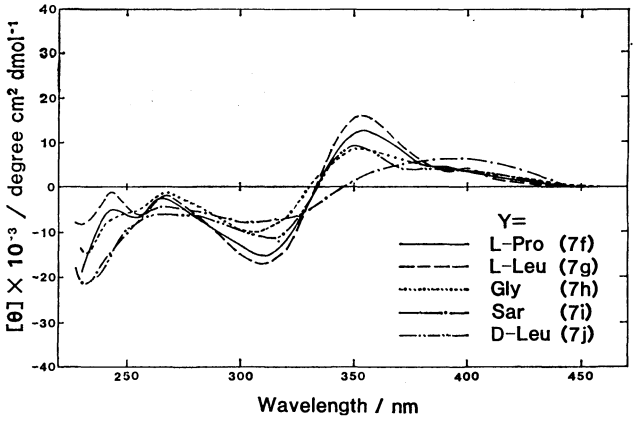

Fig. 5. CD spectra of Dnp-L-Leu-Gly-Y-L-Val-pNA's (**7f—j**) in MeOH.

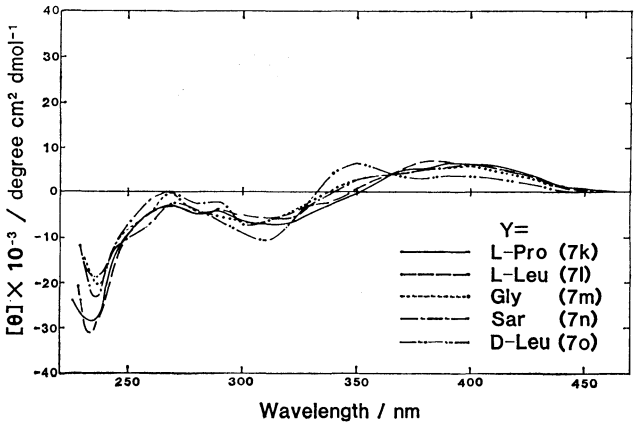

Fig. 6. CD spectra of Dnp-L-Leu-L-Ala-Y-L-Val-pNA's (**7k—o**) in MeOH.

in the case of X-Y=D-Ala-L-Pro or D-Ala-L-Leu. When Y is fixed to L-Pro or L-Leu, D-Ala at X position gives the highest CD band indicating strong β-turn preference of the sequence, Gly at X position gives weaker bands, and L-Ala gives negligibly small $[\theta]_{350}$-values suggesting their random conformations. The tendency is also kept though at a lower level when Y is fixed to Gly. Antibiotic activities of the GS analogs containing the tetrapeptide sequences with L-Pro at the Y position have good correlation with their β-turn preference described above. Though the synthesis of [D-Ala$^{4,4'}$, L-Leu$^{5,5'}$]-, [Gly$^{4,4'}$, L-Leu$^{5,5'}$]-, and [L-Ala$^{4,4'}$, L-Leu$^{5,5'}$]-GS have not been reported, we can predict that they would have the similar tendency of their conformations and antibiotic activities to that of [D-Ala$^{4,4'}$]-, [Gly$^{4,4'}$]-, and [L-Ala$^{4,4'}$]-GS.[5]

In the series of compounds with D-Ala at X position, both **7b** and **7c** with D-Ala-L-Leu and D-Ala-Gly sequences, respectively, also showed large Cotton effects as well as **7a**, but **7d** and **7e** showed very weak Cotton effects (Fig. 4). The L-Pro residue at 5,5'-positions of GS can be replaced by a variety of amino acids (Gly, L-Leu, L-Phe, Sar) without loss of activity.[3] So, high activities of [L-Leu$^{5,5'}$]-GS[7] and [Gly$^{5,5'}$]-GS[8] can be explained by the β-turn preference of their amino acid sequences at the corner positions. When Sar was at Y position, an exception was observed. Compounds **7d** with D-Ala-Sar sequence showed weak Cotton effects, though [Sar$^{5,5'}$]-GS was as active as GS.[9] The β-turn conformer in linear tetrapeptide **7d** would be decreased because of *cis-trans* isomerism of D-Ala-Sar bond. There has been no report about GS analogs having D-amino acid at 5,5'-positions, but D-D sequences at 4-5- and 4'-5'-positions are considered not to prefer the β-turn conformation and the analogs not to show any antibiotic activity since weak Cotton effects were observed in **7e** with D-Ala-D-Leu sequence. When the second residue X was L-Ala, all the derivatives (**7k—o**) showed weak Cotton effects (Fig. 6). This afford the reason why L-amino acid is not suitable for 4,4'-positions of GS, regardless of the configurations of the amino acid residues at 5,5'-positions. All the compounds with Gly at X position (**7f—j**) showed intermediate Cotton effects between the corresponding D-Ala (**7a—e**) and L-Ala (**7k—o**) compounds, respectively (Fig. 5), and the similar effect of substitution at the Y position on the CD spectra was observed.

Next, in order to study the contribution of L-Val$^{1,1'}$ and L-Leu$^{3,3'}$ residues of GS to the β-turn conformation, we synthesized Dnp-Gly-D-Ala-L-Pro-Gly-pNA (**12**), in which both of L-Leu and L-Val residues of **7a** were replaced with Gly residues. Figures 7 and 8 show the synthetic scheme and CD spectrum of **12**, respectively. Cotton effect of **12** was as strong as that of **7a**, indicating that **12** took the β-turn conformation to a high extent. The result agreed well with the fact that both L-Leu and L-Val residues had no significant role for stabilizing the conformation of GS but contributed to the activity of GS with the hidrophobic side chains.[3] For example, [L-Ala$^{1,1',3,3'}$]-GS had similar conformation to that of

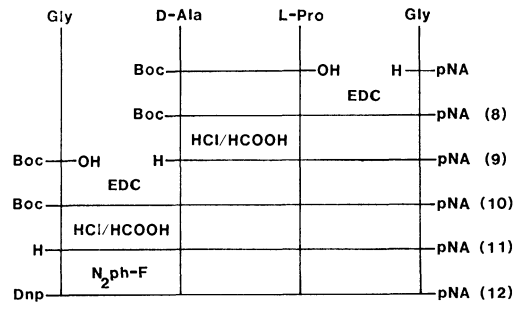

Fig. 7. Synthesis of Dnp–Gly–D-Ala–L-Pro–Gly–pNA (**12**).

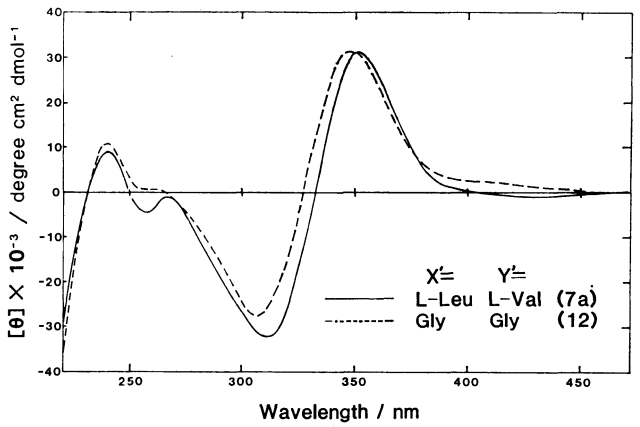

Fig. 8. CD spectra of Dnp–X'–D-Ala–L-Pro–Y'–pNA's (**7a** and **12**) in MeOH.

GS but had no antibiotic activity.[10]

Conformational properties of a number of tetrapeptides related to the corner position sequence of GS analogs were analyzed by means of CD spectra of their Dnp-pNA derivatives. From the results, following conclusion can be drawn: (i) D-Amino acids are suitable choice for the 4,4'-position residues. They can be replaced by Gly, but L-amino acids are not allowed for β-turn conformation at the corner. (ii) L-Pro seems the best choice of the 5,5'-residues for β-turn. It can be replaced by other L-amino acid, but D-amino acids are not allowed. (iii) The terminal L-Leu and L-Val residues of the tetrapeptide sequence seem to have no significant effect for stabilizing β-turn in the series of compounds. As a whole, structure-activity relationship of GS analogs concerning the 4,4'- and 5,5'-positions can be explained largely on the basis of β-turn preference of the tetrapeptide sequences at the corner positions.

Experimental

Synthesis of Peptides. All the melting points were measured on a Yanagimoto micro melting point apparatus and uncorrected. TLC's were carried out on Merck silica gel 60 F_{254} plates with the following solvent systems: R_f^1, $CHCl_3$-MeOH (5:1, v/v); R_f^2, $CHCl_3$-MeOH-AcOH (95:5:1, v/v); R_f^3, *n*-BuOH-AcOH-pyridine-H_2O (4:1:1:2, v/v). Optical rotations were measured on an Union automatic polarimeter PM-201. Yields, physical constants, and the results of elemental analyses of the synthetic peptides are summarized in Table 1.

*Boc-L-Pro-L-Val-pNA (**1a**).* To a chilled solution of Boc-L-Pro-OH (1.08 g, 5 mmol) and H-L-Val-pNA (1.19 g, 5 mmol) in DMF (20 ml) was added EDC·HCl (0.96 g, 5 mmol) at 0 °C. The mixture was stirred at 0 °C for 1 h and at room temperature overnight, evaporated *in vacuo*, and the residue was dissolved in EtOAc. The solution was washed successively with 10% citric acid, 4% $NaHCO_3$, and water, dried (Na_2SO_4), and evaporated. The residue was solidified by addition of ether and petroleum ether, and the product was recrystallized from EtOH-ether-petroleum ether; yield, 1.76 g (81%).

Compounds **1b**—**e** were prepared by a similar manner to that described for **1a**.

*H-L-Pro-L-Val-pNA·HCl (**2a**·HCl).* Compound **1a** (434 mg, 1 mmol) was dissolved in 0.1 M (1 M = 1 mol dm^{-3}) hydrogen chloride in formic acid (15 ml). The solution was allowed to stand at room temperature for 30 min and evaporated *in vacuo* to leave an oil which was crystallized by addition of ether; yield, 345 mg (93%).

Compounds **2b**—**e** were prepared by a similar manner to that described for **2a**.

*Boc-L-Leu-D-Ala-OEt (**3a**).* To a chilled solution of Boc-L-Leu-OH (2.31 g, 10 mmol) and TEA (1.4 ml, 10 mmol) in THF (20 ml) was added isobutyl chloroformate (1.31 ml, 10 mmol) at −15 °C. After 10 min, a chilled solution of H-D-Ala-OEt·HCl (1.54 g, 10 mmol) and TEA (1.4 ml, 10 mmol) in $CHCl_3$ (20 ml) was added. The reaction mixture was treated by a similar manner to that described for the preparation of **1a**; yield, 2.58 g (78%).

Boc-L-Leu-Gly-OEt (**3b**)[11] and Boc-L-Leu-L-Ala-OEt (**3c**)[11] were prepared as described for **3a**; yield, 85 and 81%, respectively.

*Boc-L-Leu-D-Ala-N_2H_3 (**4a**).* A solution of **3a** (1.65 g, 5 mmol) and hydrazine hydrate (4.85 ml, 100 mmol) in DMF (10 ml) was allowed to stand at room temperature for 3 d. The solution was evaporated and the residue was dissolved in $CHCl_3$ (100 ml). The solution was washed with water, dried (Na_2SO_4), and evaporated. The residue was solidified by addition of ether, and recrystallized from MeOH-ether; yield, 1.33 g (84%).

*Boc-L-Leu-Gly-OH (**4b**).* A solution of **3b** (1.58 g, 5 mmol) in a mixture of MeOH (20 ml) and 1 M NaOH (6 ml) was allowed to stand at room temperature for 1 h. After the addition of water (50 ml), the solution was concentrated at low temperature and acidified with 10% citric acid. The oily product was extracted with EtOAc and the solution was washed with H_2O, dried (Na_2SO_4), and evaporated. The residue was solidified by addition of ether and petroleum ether, and recrystallized from MeOH-ether-petroleum ether; yield, 1.38 g (96%).

Compound **4c** was prepared as described for **4a**.

*Boc-L-Leu-D-Ala-L-Pro-L-Val-pNA (**5a**).* To a solution of **4a** (158 mg, 0.5 mmol) in DMF (2 ml) were added 2 M hydrogen chloride in EtOAc (0.75 ml) and isopentyl nitrite (0.071 ml, 0.5 mmol) at −60 °C. After being left to stand at −20 °C for 20 min, the solution was cooled again to −60 °C and neutralized with TEA (0.21 ml, 1.5 mmol). To the mixture was added a chilled solution of **2a**·HCl (196 mg, 0.5 mmol) and TEA (0.07 ml, 0.5 mmol) in DMF (2 ml). The reaction mixture was stirred at 0 °C for 4 d and then evaporated. The residue was dissolved in EtOAc and the solution was washed successively with 10% citric acid, 4% $NaHCO_3$, and water, dried (Na_2SO_4), and evaporated. The residue was solidified by addition of ether and petroleum ether. The crude product (287 mg, 93%) dissolved in MeOH (2 ml) was applied to a column (3×170 cm) of Sephadex LH-20 and eluted with MeOH.

TABLE 1. YIELDS AND ANALYTICAL DATA OF SYNTHETIC PEPTIDES

Compound	Yield %	Mp θ_m/°C	$[\alpha]_D^{22}$ a) °	Found(%) C	Found(%) H	Found(%) N	Calcd(%) C	Calcd(%) H	Calcd(%) N	R_f^1	R_f^2	R_f^3
1a	81	94—96	−113.2	58.22	6.66	12.72	58.05	6.96	12.90	0.91	0.52	
1b	73	88—90	−61.6	58.66	7.13	12.30	58.65	7.61	12.44	0.94	0.54	
1c	75	175—177	−45.8	55.01	6.55	14.15	54.80	6.60	14.21	0.81	0.41	
1d	76	83—86	−81.1	55.45	7.29	14.09	55.87	6.91	13.72	0.96	0.57	
1e	68	168—170	−44.8	58.92	7.28	12.00	58.65	7.61	12.44	0.89	0.51	
2a·HCl	93	138—139	−60.4	50.33	6.08	14.42	50.59b)	6.37b)	14.75b)	0.49	0	0.76
2b·HCl	97	168—169	−1.6	51.50	6.92	13.83	51.57b)	7.13b)	14.16b)	0.65	0	0.84
2c·HCl	100	155—156	+14.0	47.29	5.55	16.73	47.21	5.79	16.94	0.03	0	0.61
2d·HCl	88	135—136	−32.8	47.84	5.86	15.60	47.52b)	6.27b)	15.83b)	0.35	0	0.72
2e·HCl	88	157—158	−48.8	51.92	6.99	14.59	52.17c)	7.08c)	14.32c)	0.62	0	0.85
3a	78	82—84	+4.2	58.62	9.42	8.62	58.16	9.15	8.48	0.96	0.78	
4a	84	96—98	+5.0	53.43	8.91	17.54	53.13	8.92	17.71	0.52	0.11	
4b	96	121—122	−26.3	54.36	7.97	9.63	54.15	8.39	9.72	0.17	0.11	
4c	80	171—172	−46.6	53.15	9.01	17.71	53.13	8.92	17.71	0.52	0.11	
5a	80	102—103	−55.5	58.15	7.77	13.28	58.23	7.49	13.58	0.83	0.42	
5b	75	218—219	−38.5	58.84	7.84	12.84	58.65	7.94	13.24	0.77	0.34	
5c	67	206—207	−31.4	55.78	7.32	14.43	56.04	7.32	14.53	0.77	0.31	
5d	78	118—120	−52.3	56.50	7.55	13.85	56.74	7.48	14.18	0.73	0.26	
5e	90	243—245	−20.4	57.07	8.37	12.67	57.03d)	8.03d)	12.88d)	0.81	0.52	
5f	67	124—126	−74.6	57.40	7.34	13.77	57.60	7.33	13.90	0.75	0.42	
5g	67	222—234	−64.8	58.17	7.77	13.34	58.04	7.79	13.54	0.75	0.28	
5h	61	142—143	−47.0	55.41	6.88	14.91	55.31	7.14	14.88	0.81	0.31	
5i	70	126—127	−77.4	55.77	7.49	14.33	56.04	7.32	14.53	0.65	0.30	
5j	63	187—188	−52.8	57.91	7.87	13.51	58.05	7.79	13.54	0.77	0.53	
5k	40	123—125	−134.8	58.09	6.93	13.37	58.23	7.49	13.58	0.77	0.32	
5l	63	241—242	−32.2e)	58.82	8.04	12.99	58.65	7.94	13.24	0.87	0.52	
5m	56	191—192	−52.0	55.95	7.32	14.58	56.04	7.32	14.53	0.72	0.24	
5n	68	123—125	−69.9	56.52	7.64	14.08	56.74	7.48	14.18	0.83	0.30	
5o	66	220—222	−43.8	58.93	7.94	13.25	58.65	7.94	13.24	0.77	0.41	
7a	67	126—128	+17.4	54.54	5.67	16.12	54.37	5.89	16.39	0.91	0.35	
7b	78	292—293	−57.1	55.32	6.10	15.94	54.87	6.33	15.99	0.91	0.33	
7c	87	215—216	+2.8e)	51.45	5.44	17.14	51.44b)	5.70b)	17.14b)	0.64	0.22	
7d	78	205—207	+18.6	52.59	5.61	16.72	52.89	5.82	17.02	0.89	0.28	
7e	70	283—284	+2.4e)	54.57	6.11	15.83	54.87	6.33	15.99	0.88	0.35	
7f	76	233—235	−2.2e)	52.95	5.63	16.43	53.01b)	5.78b)	16.49b)	0.79	0.36	
7g	90	284—285	+23.4e)	54.17	6.15	16.25	54.22	6.16	16.32	0.87	0.36	
7h	84	260—262	+12.4e)	51.41	5.34	17.72	51.43	5.43	17.77	0.68	0.14	
7i	80	223—225	+13.0e)	51.07	5.77	16.92	50.74d)	5.78d)	16.91d)	0.63	0.31	
7j	82	137—140	−7.8	54.34	6.22	16.12	54.22	6.16	16.32	0.84	0.40	
7k	76	135—136	−42.5	54.24	5.68	16.21	54.37	5.89	16.39	0.94	0.35	
7l	80	>300	+10.9	55.00	6.01	15.99	54.87	6.33	15.99	0.92	0.30	
7m	93	>300	+21.8e)	52.27	5.68	17.29	52.16	5.63	17.39	0.64	0.22	
7n	58	127—129	+8.0	53.01	5.59	16.82	52.89	5.82	17.02	0.90	0.30	
7o	66	251—253	+5.6e)	54.72	6.34	15.87	54.87	6.33	15.99	0.89	0.34	
8	77	231—233	+79.8	54.63	6.08	15.14	54.42	6.31	15.11	0.79	0.46	
9·HCl	73	203—206	−20.8	48.03	5.28	17.54	48.06	5.55	17.52	0.12	0	0.59
10	67	125—126	+37.0	52.76	6.03	15.81	53.07	6.20	16.14	0.69	0.25	
12	72	276—278	+51.8e)	48.98	4.43	18.83	49.15	4.47	19.10	0.56	0.13	

a) *c* 1, MeOH, unless otherwise stated. b) ½ H_2O. c) ¼ H_2O. d) H_2O. e) *c* 1, DMF.

The fractions with the desired product detected by UV absorption and TLC were collected and evaporated, and the oily residue was solidified by addition of ether and petroleum ether and recrystallized from MeOH-ether-petrolum ether; yield, 248 mg (80%).

Compounds **5b**—**e** and **5k**—**o** were prepared as described for **5a**.

Boc-L-*Leu*-*Gly*-L-*Pro*-L-*Val*-*pNA* (**5f**). This compound was prepared from **4b** (144 mg, 0.5 mmol) and **2a** (167 mg, 0.5 mmol) as described for **1a**; yield, 202 mg

(67%).

Compounds **5g**—**j** were prepared as described for **5f**.

H-L-Leu-D-Ala-L-Pro-L-Val-pNA·HCl (6a·HCl). Compound **5a** (118 mg, 0.2 mmol) was dissolved in 0.1 M hydrogen chloride in formic acid (3 ml). The solution was allowed to stand at room temperature for 30 min and evaporated to leave an oil. The product was used for the next reaction without further treatment; yield was quantitative.

Compounds **6b**—**o** were prepared as described for **6a**.

Dnp-L-Leu-D-Ala-L-Pro-L-Val-pNA (7a). To a solution of **6a**·HCl (106 mg, 0.2 mmol) and TEA (0.084 ml, 0.6 mmol) in DMF (2 ml) was added N_2ph-F (74 mg, 0.4 mmol). The reaction mixture was stirred at room temperature for 3 h and evaporated *in vacuo*. The residue dissolved in $CHCl_3$ (5 ml) was applied to a column (1.8×20 cm) of silica gel 60 (Merck) and the column was washed with $CHCl_3$. The desired product was eluted with a mixture of $CHCl_3$ and MeOH (5: 1, v/v). The fractions containing the desired product were evaporated to leave an oil, which was crystallized by addition of ether and recrystallized from MeOH-ether; yield, 91 mg (67%).

Compounds **7b**—**o** were prepared as described for **7a**.

Boc-D-Ala-L-Pro-Gly-pNA (8). This was prepared from Boc-D-Ala-L-Pro-OH[5] (573 mg, 2 mmol) and H-Gly-pNA (390 mg, 2 mmol) as described for **1a**; yield, 713 mg (77%).

H-D-Ala-L-Pro-Gly-pNA·HCl (9·HCl). This was prepared from **8** (463 mg, 1 mmol) as described for **2a**; yield, 292 mg (73%).

Boc-Gly-D-Ala-L-Pro-Gly-pNA (10). This was prepared from Boc-Gly-OH (88 mg, 0.5 mmol) and **9**·HCl (200 mg, 0.5 mmol) as described for **1a**; yield, 174 mg (67%).

H-Gly-D-Ala-L-Pro-Gly-pNA·HCl (11·HCl). This was prepared from **10** (104 mg, 0.2 mmol) as described for **6a**·HCl; yield was quantitative; R_f^1 0.12, R_f^3 0.68.

Dnp-Gly-D-Ala-L-Pro-Gly-pNA (12). This was prepared from **11**·HCl (91 mg, 0.2 mmol) as described for **7a**; yield, 84 mg (72%).

CD Measurements. CD spectra were recorded on a JASCO spectropolarimeter model J-20 or J-40 in a 0.5 mM MeOH solution at room temperature (23±2 °C) unless otherwise stated.

The authors wish to express their thanks to Professor Tatsuo Miyazawa and to Dr. Tsutomu Higashijima of The University of Tokyo for helpful discussion. Thanks are also due to the members of Analytical Department of System Engineering Laboratory, Mitsubishi-Kasei Industries Ltd., for elemental analyses.

References

1) Part I of this series: K. Sato, M. Kawai, and U. Nagai, *Biopolymers*, **20**, 1921 (1981).

2) A. Stern, W. A. Gibbons, L. C. Craig, *Proc. Natl. Acad. Sci. U. S. A.*, **61**, 734 (1968); R. Schwyzer and U. Ludescher, *Biochemistry*, **7**, 2591 (1968).

3) N. Izumiya, T. Kato, H. Aoyagi, M. Waki, and M. Kondo, "Synthetic Aspects of Biologically Active Cyclic Peptides—Gramicidin S and Tyrocidines," Kodansha, Tokyo, and Halsted Press, New York (1979), p. 58.

4) N. Izumiya, T. Kato, H. Aoyagi, M. Waki, and M. Kondo, "Synthetic Aspects of Biologically Active Cyclic Peptides—Gramicidin S and Tyrocidines," Kodansha, Tokyo, and Halsted Press, New York (1979), p. 78.

5) M. Kawai and U. Nagai, *Biopolymers*, **17**, 1549 (1978); T. Higashijima, M. Tasumi, T. Miyazawa, M. Kawai, and U. Nagai, "Peptide Chemistry 1977; Proceedings of the 15th Symposium on Peptide Chemistry," ed by T. Shiba, Protein Research Foundation, Osaka (1978), p. 97.

6) The abbreviations used in this paper are those recommended by IUPAC-IUB: *J. Biol. Chem.*, **247**, 977 (1972). Additional abbreviations: Boc, *t*-butoxycarbonyl; Dnp, 2,4-dinitrophenyl; pNA, *p*-nitroanilide; EDC, 1-ethyl-3-(3-dimethylaminopropyl)carbodiimide; N_2ph-F, 1-fluoro-2,4-dinitrobenzene; TEA, triethylamine; MA, mixed anhydride; TLC, thin-layer chromatography; GS, gramicidin S.

7) O. Abe, Y. Utsumi, and N. Izumiya, *Bull. Chem. Soc. Jpn.*, **50**, 2341 (1977).

8) H. Aoyagi, M. Kondo, T. Kato, S. Makisumi, and N. Izumiya, *Bull. Chem. Soc. Jpn.*, **40**, 1685 (1967).

9) H. Aoyagi, and N. Izumiya, *Bull. Chem. Soc., Jpn.*, **39**, 1747 (1966).

10) H. Takiguchi, H. Nishikawa, S. Ando, and N. Izumiya, *Bull. Chem. Soc. Jpn.*, **51**, 297 (1978).

11) D. S. Demp, S-L. H. Choong, and J. Pekaar, *J. Org. Chem.*, **39**, 3841 (1974).

Kinetics of Ion-exchange on Sodium-, Calcium-, and Magnesium Saturated Kaolinites

Om Prakash BANSAL

Chemical Laboratories, Dharam Samaj College, Aligarh-202001, India

(Received December 1, 1981)

The kinetics of Na^+, Ca^{2+}, Mg^{2+}, and Ni^{2+} ion-exchange reactions on kaolinite have been studied at four temperatures 16, 26, 36, and 46 °C. The mechanism of ion-exchange is a film diffusion as shown by interruption and ϕ tests. Kinetics parameters *e.g.* diffusion coefficients, half time of exchange, energies of activation have also been calculated and were used to predict the theoretical behaviour (mechanism) of Ni^{2+} exchange on the kaolinite surface.

The replacement of cations is one of the most important phenomenon which controls the storage capacity of a soil for plant nutrient elements. Thermodynamics is a powerful tool to study conditions at equilibrium but kinetics have an important role in the study of the mechanism of ion-exchange. A relatively little consideration has been given to the kinetics of ion-exchange. Various studies of the kinetics of ion-exchange on zeolites,[1] synthetic ion-exchangers[2-6] have been reported. Information in regard to kinetics of exchange in clays and soils is meagre.[7,8]

Nickel is an important trace element in plant nutrition and its formulation as $NiCl_2$ are often used as fungicide in soils. Kaolinite mineral is a 1:1 layer silicate, and occurs commonly in soils. It is a dioctahedral mineral with triclinic symmetry. The structure of the mineral involves hydrogen bonding between adjacent layers, which prevents the expansion of kaolinite beyond its basal spacing. Clay minerals constitute the most important reactive surface of soil providing reactive sites at the edges, corners, interlayer, and interlattice positions.[9-11] In the present report I have summarized my studies on the kinetics of exchange between Ni(II) and Na-, Ca-, Mg-kaolinites.

Experimental

Kaolinite used in these studies was a monomineralic standard from Bath, South Carolina. Less than 2 μm clay fraction was purified by sedimentation and centrifugation. It was converted into chloride free Na-kaolinite and then into Ca- and Mg-saturated kaolinites by ion exchange technique. The concentration of the mineral suspension ranged from 11.0 to 12.2 g dm^{-3}. The base exchange capacity (BEC) of the Na-kaolinite was 135 μequiv. g^{-1} clay, determined by Ganguli's method.[12] For the determination of the BEC of Ca- and Mg-kaolinite[13] a known volume of suspension was treated with a mixture consisting of 1 mol dm^{-3} $NiCl_2$ in 0.0001 mol dm^{-3} HCl (keeping in contact for 24 h) and the amount of calcium and magnesium released was estimated by titration with EDTA, giving the value 110 and 118 μequiv. g^{-1} clay respectively.

The ion-exchange reaction between Na-, Ca-, and Mg-kaolinites and Ni^{2+} can be represented as

$$2\overline{Na}^{+} + Ni^{2+} \rightleftharpoons \overline{Ni}^{2+} + 2Na^{+}, \quad (1)$$

$$\overline{M}^{2+} + Ni^{2+} \rightleftharpoons \overline{Ni}^{2+} + M^{2+}, \quad (2)$$

(where $M^{2+}=Ca^{2+}$ or Mg^{2+}).

Kinetic Measurement. Rates of exchange were measured by limited bath technique, for it, 10 cm^3 of appropriate clay suspensions were treated with 15 cm^3 of 0.002 mol dm^{-3} nickel solution. The solutions were kept in contact for appropriate time intervals (2—60 min) of time. The contents were then centrifuged and the concentration changes in the suspensions were determined by EDTA titrations in case of Ni^{2+}, Ca^{2+}, and Mg^{2+} ions and flame photometry in Na^+. The values of fractional attainment of equilibrium (F) at 16, 26, 36, and 46 °C were calculated using the expression:

$$F = \frac{\text{The amount of } Ni^{2+} \text{ exchange at time } t}{\text{The amount of exchange at infinite time (equilibrium)}}. \quad (3)$$

To perform the interruption test above procedure was applied for another set at two concentrations of Ni^{2+} and after a specified time intervals (10 and 30 min) the clay particles were removed and quickly separated from adhering solution by centrifugation. After 5 min they were re-immersed in their solutions and the experiment continued (Fig. 1). The concentration of Ni^{2+} at different time intervals at 16, 26, 36, and 46 °C was estimated before and after interruption.

The nature of the rate determining step was confirmed by calculating the value of function ϕ[14] as the values of are $\gg 1$ for film diffusion control and $\ll 1$ for particle diffusion. The values of ϕ are given by the following relation

$$\phi = \frac{X\bar{D}\delta}{CDr_o}(5+2\alpha_B^A), \quad (4)$$

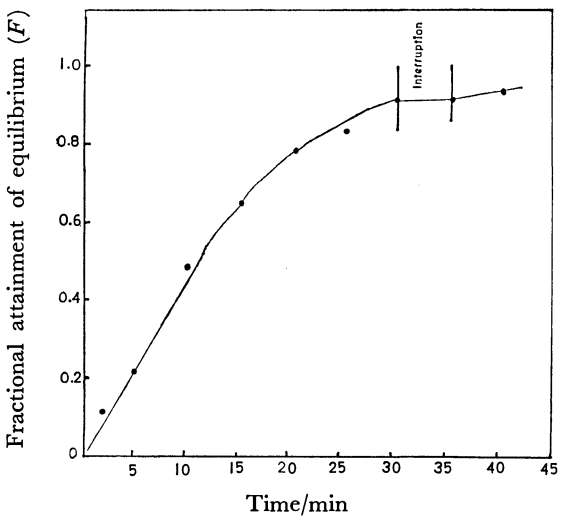

Fig. 1. The effect of interruption test on the rate of Ni^{2+} ion-exchange on Na-kaolinite at 16 °C after 30 min.

where X=concentration of fixed ionic groups taken as equivalent to a maximum exchange, C=concentration of counter ions in solution mequiv. cm^{-3}, $\overline{D}$=interdiffusion coefficient in the ion-exchanger, D=interdiffusion coefficient in the film, r_0=radius of clay particle (10^{-4} cm), δ=film thickness (10^{-2} cm in unstirred solution) and α_B^A the separation factor.

The separation factor α_B^A was calculated from the equivalent ionic fractions, using the equation

$$\alpha_{Na}^{Ni^{2+}} = \overline{X}_{Ni}(X_{Na})^2/X_{Ni}(\overline{X}_{Na})^2, \quad (5)$$

$$\alpha_{M^{2+}}^{Ni^{2+}} = \overline{X}_{Ni}X_M/\overline{X}_M X_{Ni}, \quad (6)$$

where $\overline{X}$=equivalent ionic fraction in clay phase and X= mole fraction in solution phase.

The values of $\overline{D}_i$ (effective diffusion coefficient in the clay phase) were calculated from the relationship:

$$\overline{D}_i = Br_0^2/\pi^2. \quad (7)$$

The value of B was obtained from the plots of Bt *vs.* t (Fig. 2), the Bt values have been obtained from the suitable values of 'F' as tabulated by Reichenberg.[15] The values of D_i were calculated by Wheeler's[16] relation $\overline{D}_i = D_{i_\varepsilon}/2$ which has a resemblance (within $\pm 15\%$ error) with the values obtained by Mackie and Meares[17] relation $\overline{D}_i = D_i[\varepsilon/(2-\varepsilon)]^2$, where ε is pore volume of clay. The fractional pore volume of Na-, Ca-, and Mg-kaolinites were determined from bulk and particle densities.

The half time of exchanges ($t_{1/2}$) were calculated from the expression

$$t_{1/2} = 0.23\delta r_0 X/DC. \quad (8)$$

Since temperature effect has been very useful in providing an insight into the theory of all rate processes, the energetics of Ni^{2+} ion-exchange on clay were examined by temperature studies. The diffusion coefficient (D_i) can be related to temperature by the following expression[18]

$$D_i = D_0 \exp(-E_a/RT). \quad (9)$$

The activation energy (E_a) was calculated by the linear relationships of $\log D_i$ *vs.* $1/T$ and D_0 by extrapolation (Fig. 3). The values are given in Table 2.

The enthalpy (ΔH_a), entropy (ΔS_a) and free energy (ΔG_a) of activation were calculated using the expressions[19]

$$\Delta H_a = E_a - RT, \quad (10)$$

$$D_0 = 2.72d^2kT/h \exp(\Delta S_a/R), \quad (11)$$

$$\Delta G_a = \Delta H_a - T\Delta S_a,$$

where d=ionic jump distance (5×10^{-8} cm), k=Boltzmann constant, h=Planck constant, R=gas constant and T=ab-

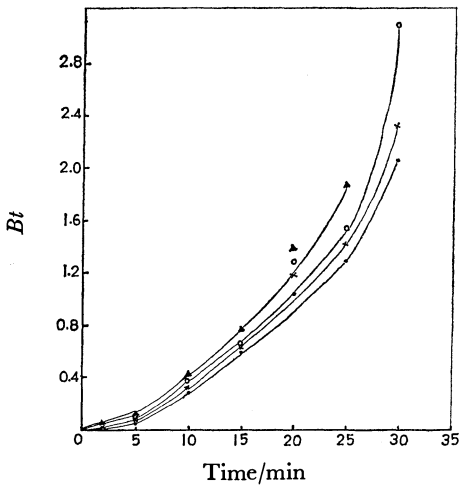

Fig. 2. A plot of Bt *vs.* t for Ni^{2+} ion-exchange on Na-kaolinites at 16 (●), 26 (×), 36 (○), and 46 °C (▲).

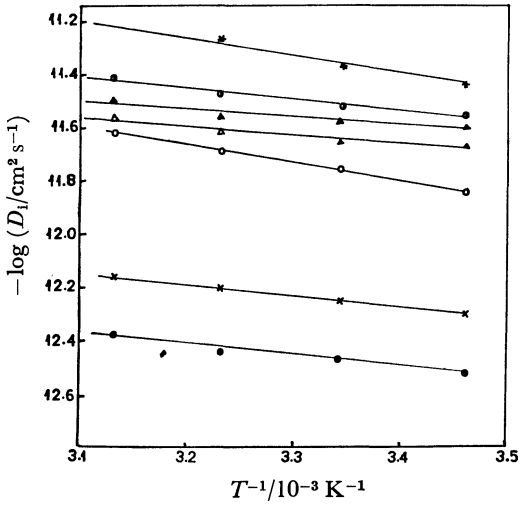

Fig. 3. A plot of $\log D_i$ *vs.* $1/T$ for Ni^{2+} ion-exchange on Na-kaolinite at 2 (●), 5 (×), 10 (○), 15 (△), 20 (▲), 25 (◑), and 30 (*) min time interval.

Table 1. Diffusion coefficients and ϕ values at different temperatures and time for Ni^{2+} ion-exchange on Na-, Ca-, and Mg-kaolinites

Temp K	Time min	Na-kaolinite					Ca-kaolinite					Mg-kaolinite				
		F	$\overline{D}_i\times10^{13}$ $cm^2\,s^{-1}$	$D_i\times10^{12}$ $cm^2\,s^{-1}$	ϕ	$t_{1/2}$ h	F	$\overline{D}_i\times10^{13}$ $cm^2\,s^{-1}$	$D_i\times10^{12}$ $cm^2\,s^{-1}$	ϕ	$t_{1/2}$ h	F	$\overline{D}_i\times10^{13}$ $cm^2\,s^{-1}$	$D_i\times10^{12}$ $cm^2\,s^{-1}$	ϕ	$t_{1/2}$ h
289	2	0.108	0.93	0.30	153	41.7	0.094	0.71	0.23	148	42.1	0.080	0.52	0.17	141	43.1
	5	0.216	1.54	0.50	177	28.3	0.190	1.20	0.39	171	28.9	0.161	0.88	0.29	163	29.3
	10	0.487	4.78	1.54	199	14.2	0.450	3.95	1.30	193	14.6	0.440	3.77	1.26	186	15.4
	15	0.649	6.69	2.16	217	9.0	0.609	5.61	1.84	214	10.1	0.577	4.70	1.57	204	10.1
	20	0.781	7.94	2.56	239	7.5	0.750	6.51	2.14	230	7.8	0.645	5.08	1.70	226	8.0
	25	0.830	8.69	2.80	261	5.8	0.792	7.30	2.40	251	6.2	0.766	6.50	2.17	240	6.4
	30	0.922	11.44	3.70	277	4.1	0.872	8.75	2.87	263	4.4	0.861	8.30	2.77	250	4·9
319	2	0.129	1.29	0.42	130	34.7	0.116	1.10	0.36	126	37.0	0.100	0.77	0.26	120	38.2
	5	0.257	2.12	0.68	144	21.6	0.233	1.90	0.62	139	23.0	0.200	1.29	0.43	135	24.2
	10	0.582	7.43	2.40	162	9.0	0.514	5.55	1.82	158	10.0	0.540	5.69	1.90	150	10.7
	15	0.711	8.60	2.78	177	5.9	0.636	7.27	2.38	175	6.9	0.633	6.52	2.17	168	8.0
	20	0.849	10.48	3.38	190	4.7	0.812	8.75	2.87	186	6.2	0.766	7.61	2.54	179	6.4
	25	0.906	12.50	4.03	208	3.8	0.865	10.41	3.41	207	4.4	0.862	9.46	3.15	201	5.0
	30	1.000	—	—	—	—	0.960	15.60	5.11	216	3.0	0.933	12.40	4.13	209	3·5

TABLE 2. ENERGY PARAMETERS FOR Ni^{2+} ION-EXCHANGE ON Na-, Ca-, AND Mg-KAOLINITES AT DIFFERENT TEMPERATURES (Time 2—30 min)

Nature of clay	Temp / K	E_a/kJ mol^{-1}	ΔH_a/kJ mol^{-1}	ΔS_a/J mol^{-1} deg^{-1}	ΔG_a/kJ mol^{-1}
Na-kaolinite	289	7.66 to 11.00	5.26 to 8.60	−210.2 to −187.8	59.5 to 69.3
	299		5.18 to 8.51	−210.6 to −188.2	61.5 to 71.5
	309		5.09 to 8.43	−211.0 to −188.6	63.4 to 73.6
	319		5.01 to 8.35	−211.4 to −189.0	65.3 to 75.8
Ca-kaolinite	289	8.61 to 12.92	6.20 to 10.52	−212.6 to −189.7	61.0 to 72.0
	299		6.13 to 10.43	−213.0 to −190.1	63.0 to 74.1
	309		6.04 to 10.35	−213.4 to −190.6	64.9 to 76.3
	319		5.96 to 10.27	−213.8 to −191.0	66.9 to 78.5
Mg-kaolinite	289	9.09 to 13.40	6.69 to 11.00	−214.9 to −191.3	62.0 to 73.1
	299		6.60 to 10.91	−215.4 to −191.8	63.9 to 75.3
	309		6.52 to 10.83	−215.8 to −192.2	65.9 to 77.5
	319		6.44 to 10.75	−216.3 to −192.7	67.9 to 79.7

solute temperature. The values obtained are recorded in Table 2.

Results and Discussion

To study the mechanism of ion-exchange both experimental and theoretical approach were used. The interruption test was applied as an experimental test to decide whether the kinetics are controlled by film diffusion or particle diffusion.[20] The results are presented in Fig. 1. These results showed no change in rate of exchange after 5 min interruption, indicate that the rate determining step is governed by film diffusion at all four temperatures studied. This is because that no concentration gradient was found to exist in the clay and the rate depended on the concentration differences across the film.

The values of ϕ calculated for the Na–Ni, Ca–Ni, and Mg–Ni exchanges at all four experimental temperatures were more than unity indicating that rate is controlled by film diffusion ($\phi \gg 1$) in all the case studied.[14] Table 1 also showed that order of exchange is Na->Ca->Mg-kaolinites as of ϕ values.

A plot of F (fractional attainment) *vs.* t (see Fig. 4) showed that Ni^{2+} exchange on Na-, Ca-, and Mg-kaolinites was characterized by a rapid initial exchange followed by subsequent falling in the rate as the concentration gradient diminished in the film. Rate of exchange also increases with rise in temperature from 16 to 46 °C, which may be due to the fact that mobility of Ni^{2+} increased with increase in temperature.

The values of half time of exchange ($t_{1/2}$) (Table 1) are in the order Mg>Ca>Na, and decreased with increase in time of contact, indicating that the rates of exchange as characterized by half time increased with time of contact (as half time decreases rate of exchange increases). With rise in temperature the $t_{1/2}$ values decreased, confirming the earlier inference.

An observation of Table 1 revealed that the rate of diffusion in the aqueous phase was much faster than in the clay phase at the all four temperatures in all the three exchanges studied and the order was Na->Ca->Mg-kaolinites. The diffusion coefficients increased with rise in temperature as well as with passage of time *i.e.* the rate of exchange of Ni^{2+} ion on Na-, Ca-, and Mg-kaolinites increased with time

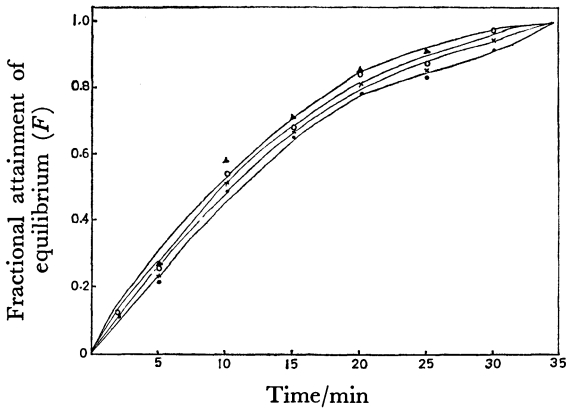

Fig. 4. A plot of fractional attainment of equilibrium (F) *vs.* t for Ni^{2+} ion-exchange on Na-kaolinite at 16 (●), 26 (×), 36 (○), and 46 °C (▲).

and temperature and the order of exchange was Na->Ca->Mg-kaolinite.

An examination of Table 2 showed an E_a range from 7.66 to 13.40 kJ/mol, and were in order Mg>Ca->Na-kaolinites. The magnitude of E_a showed that Ni^{2+} exchange is a film diffusion controlled process without steric hindrance.[21,22] The values of activation energies also confirm that order of exchange is Na->Ca->Mg-kaolinites. The low values of ΔH_a, support the physical type of adsorption involving ion-exchange process. The values of ΔH_a (see Table 2) decreased with rise in temperature or the rate of exchange of the Ni^{2+} increases as temperature of reaction went up, an inference in accordance with earlier conclusions. The negative values of ΔS_a (Table 2) pointed to a greater order produced during the activation process.[6,23] It may be due to formation of activated complex between Ni^{2+}, and Na-, Ca-, or Mg-kaolinites, resulting in a more orderly structure of Ni^{2+} ions on clay surface due to association or fixation and immobilisation of Ni^{2+} ions with consequent loss in the degrees of freedom of the system during the process. The free energy of activation (ΔG_a) (Table 2) for the exchange reaction had a tendency to increase with rise in temperature and were in order Na-<Ca-<Mg-kaolinites, indicating that the activated complexes of Ni^{2+} ions with Na-, Ca-, or Mg-kaolinites

were not very stable and probability of formation of activated complex further decreased with rise in temperature.[24] The increase in rate of exchange of Ni^{2+} with rise in temperature was due to large number of ions passing into an activated state with a less stable configuration.[23]

The author is thankful to Dr. S. S. Gupta, Principal, D. S. College, Aligarh (India) for necessary facilities and encouragement and to U. G. C., New Delhi for financial assistance.

References

1) G. E. Boyd, A. W. Adamson, and L. S. Myers, *J. Am. Chem. Soc.*, **69**, 2836 (1947).
2) S. J. Harvie and G. H. Nancollas, *J. Inorg. Nucl. Chem.*, **30**, 273 (1968).
3) A. Dyer and F. T. Ocon, *J. Inorg. Nucl. Chem.*, **33**, 3153 (1971).
4) A. Dyer and J. S. Gill, *J. Inorg. Nucl. Chem.*, **39**, 665 (1977).
5) J. P. Rawat and P. S. Thind, *J. Phys. Chem.*, **80**, 1384 (1976).
6) R. Turse and W. Reiman, *J. Phys. Chem.*, **65**, 111 (1961).
7) K. Bunzl, *J. Soil Sci.*, **25**, 517 (1974).
8) K. Bunzl, *J. Inorg. Nucl. Chem.*, **39**, 1049 (1977).
9) S. Khan and J. P. Singhal, *Soil Sci.*, **104**, 427 (1967).
10) D. H. Solomon, *Clays and Clay Minerals*, **16**, 31 (1968).
11) A. R. Swoboda and G. W. Kunze, *Soil Sci. Soc. Am. Proc.*, **32**, 806 (1968).
12) A. K. Ganguli, *J. Phys. Coll. Chem.*, **55**, 1417 (1951).
13) M. L. Jackson, "Soil Chemical Analysis," Prentice-Hall, Englewood, Inc., N. J. (1958).
14) F. Helfferich, "Ion Exchange," McGraw-Hill, New York (1962), Chap. 6.
15) D. Reichenberg, *J. Am. Chem. Soc.*, **75**, 589 (1953).
16) A. Wheeler, *Adv. Catal.*, **3**, 249 (1951).
17) J. S. Mackie and P. Meares, *Proc. R. Soc. London, Ser. A*, **232**, 510 (1955).
18) C. B. Amphlett, "Inorganic Ion Exchangers," Elsevier, Amsterdam (1964).
19) K. J. Laidler, "Chemical Kinetics," McGraw-Hill, New York (1965), Chap. I.
20) T. R. E. Kressman and J. A. Kitchner, *Discuss. Faraday Soc.*, **7**, 90 (1949).
21) B. A. Soldano and G. E. Boyd, *J. Am. Chem. Soc.*, **75**, 6099 (1953).
22) F. Helfferich, "Ion Exchanges," McGraw-Hill, New York (1962), Chap. 2.
23) S. Glasstone, "Text Book of Physical Chemistry," MacMillan, London (1960), Chap. XIII.
24) J. P. Singhal, S. U. Khan, and O. P. Bansal, *Indian J. Chem.*, **16**, 945 (1978).

Studies on Synthetic Inorganic Ion Exchangers. VI. Synthesis and Characterization of Iron(III) Molybdate as an Ion Exchanger

Pritam Singh THIND,* Harbans SINGH, and (Miss) PARVEEN
Department of Chemistry, Guru Nanak Dev University, Amritsar(Pb.), India

(Received September 16, 1981)

Six preparations of iron(III) molybdate were obtained at various pH values under different conditions. They all possess cation exchange properties. The preparation, obtained by reaction of iron(III) nitrate with ammonium molybdate at pH 1 with 24 h refluxing, is the stablest and has an ion exchange capacity of 1.39 mequiv. g^{-1}. The mole ratio of Fe: Mo is 1: 3. Distribution coefficients for many metal ions were determined on this preparation. On the basis of pH titrations, chemical and thermal analyses, and infrared and Mössbauer spectra, a tentative structure of iron(III) molybdate is proposed.

Since the classical work of Amphlett[1] numerous inorganic ion exchangers have been prepared and used for several possible applications.[2-5] Recently, some studies on iron-based exchangers have been reported.[6-8] A search of literature showed that no studies have so far been reported on iron(III) molybdate. In the present report we summarize synthesis and ion-exchange and physicochemical properties of iron(III) molybdate as a new ion exchanger.

Experimental

Reagents. Iron(III) nitrate (B. D. H.) and ammonium molybdate (Reanal, Hungary) were used for the synthesis. All other materials used were of analytical grade.

Apparatus. A thermostated oven, digital pH meter, TGA instrument (Fertilizer Corp. of India, Sindhri), Spectrochem 2000 (Hungary), Specol Spectrophotometer, MBS-35 (ECIL) Mössbauer apparatus were used for drying samples, pH measurements, thermal analysis, infrared and visible spectrophotometric measurements, and Mössbauer studies, respectively.

Synthesis. Six samples of iron(III) molybdate were prepared by mixing 0.05 mol dm^{-3} solution of iron(III) nitrate with 0.05 mol dm^{-3} solution of ammonium molybdate under the conditions given in Table 1. The pH of the mixed solution was adjusted by adding either acid or alkali solution. The precipitate obtained was filtered and washed with demineralized water. The gel was dried at 40 °C. The dried product broke down into granules when immersed in water. The material was converted into the hydrogen form by treating with 0.1 mol dm^{-3} nitric acid for 24 h with occasional shaking and intermittent supply of the acid. The material was then washed free of acid with demineralized water and was finally dried at 40 °C.

Ion-exchange Capacity. The ion-exchange capacity of a sample of iron(III) molybdate was determined by taking 1.0 g of the H-form exchanger in a glass column having a glass wool support. The column after being washed with demineralized water was eluted with 1.0 mol dm^{-3} sodium nitrate solution. A 400 cm^3 portion of the effluent was collected at a rate of 15—20 drops/min. The H^+ concentration of the effluent was determined by titration with a standard sodium hydroxide solution.

Ion-exchange capacity for some uni- and bivalent cations on sample 6 (Table 1) was also determined.

Chemical Analysis. One-half gram of sample was treated with 5 cm^3 of each of nitric and hydrochloric acids until it was dissolved, and diluted with water. Iron(III) was precipitated as iron(III) hydroxide and estimated. The molybdenum in the filtrate was precipitated by 8-quinolinol and determined as $MoO_2(C_9H_6ON)_2$.

Chemical Stability. Exchanger samples (0.2 g) were kept separately for 24 h in 20 cm^3 of each of various solvents, such as nitric, oxalic, hydrochloric, and acetic acids, dimethylformamide, and dioxane, and then filtered. The iron and molybdenum in the filtrate were determined spectrophotometrically by the 1,10-phenanthroline and thiocyanate methods, respectively.

pH Titration. pH titration on 0.2 g of iron(III) molybdate was performed by using 0.1 mol dm^{-3} standard solutions of lithium, sodium, and potassium hydroxides, aqueous ammonia, and their respective salts according to the method of Topp and Pepper.[9] The volume ratio of alkali to its salt solution was selected in such a way that the total volume of 20 cm^3 was to be maintained in each conical flask.

Sorption Studies. Distribution Coefficients of nineteen metal ions were determined on iron(III) molybdate in 50% ethanol. The loading of metal ions for the system was less than 3% of the working ion-exchange capacity of sample after 24 h of equilibrating period. The equation used for the calculation is,

TABLE 1. CONDITIONS OF PREPARATION AND PROPERTIES OF IRON(III) MOLYBDATES

Sample	Conditions of synthesis				Properties					
	Molarity of reagents mixed		Mixing ratio	pH	Refluxing time/h	Color in H-form	Ion exchange capacity for Na^+/mequiv. g^{-1}	Composition	Solubility in water/μg in 20 cm^{-3}	
	Fe	Mo	Fe:Me					Fe:Mo	Fe	Mo
1	0.05	0.05	2:1	1.0	—	Yellow	3.80	1:3.5	320	500
2	0.05	0.05	2:1	2.0	—	Brown	1.56	1:4.0	280	850
3	0.05	0.05	3:1	1.0	—	Yellow	3.43	1:3.8	420	600
4	0.05	0.05	2:1	1.0	8	Yellow	1.55	1:3.2	220	720
5	0.05	0.05	2:1	1.0	12	Yellow	1.52	1:3.1	240	520
6	0.05	0.05	2:1	1.0	24	Yellow	1.39	1:3.0	150	360

Table 2. Ion exchange capacity of iron(III) molybdate sample 6

Metal ion	Salt used	Solution	Hydrated radii/Å	pH	Ion exchange capacity/mequiv. g^{-1}
Li^+	$LiNO_3$	(1.0 mol dm^{-3})	3.40	6.05	1.34
Na^+	NaCl	(1.0 mol dm^{-3})	2.76	5.50	1.39
K^+	KNO_3	(1.0 mol dm^{-3})	2.32	6.90	1.47
Mg^{2+}	$Mg(NO_3)_2$	(0.5 mol dm^{-3})	7.00	6.00	1.80
Ca^{2+}	$Ca(NO_3)_2$	(0.5 mol dm^{-3})	6.30	6.40	1.86
Sr^{2+}	$Sr(NO_3)_2$	(0.5 mol dm^{-3})	—	6.50	1.92

$$K_d/cm^3\,g^{-1} = \frac{I-F}{F} \times \frac{20}{0.2},$$

where I and F are the volumes of the 0.025 mol dm^{-3} EDTA solutions required for titration before and after the equilibration, respectively. The total volume of the equilibrating solution was 20 cm^3 and the amount of exchanger taken was 0.2 g.

Structural Studies. Infrared absorption spectra of iron(III) molybdate in an H-form exchanger dried at 40, 100, 200, 600, or 700 °C were obtained in KBr media.

Thermogravimetric analysis of iron(III) molybdate in H-form exchanger was performed at a heating rate of 10 °C min^{-1}.

Mössbauer spectra of iron(III) molybdate in H-form exchanger dried at 40, 200, or 500 °C were obtained by using a ^{57}Co source at a constant acceleration. Sodium pentacyanonitrosyl ferrate(III) was used as the reference for the value of isomer shift to be reported.

Results and Discussion

Ion-exchange capacities of various samples prepared by refluxing are comparatively low. This is associated with the fact that stabler materials were obtained by refluxing the mother liquor. In order to investigate the working capacity of the exchanger, capacities for some uni- and bivalent cations were determined (Table 2). In general, exchange capacities for uni- and bivalent ions are found to be in the orders: $K^+ > Na^+ > Li^+$ and $Sr^{2+} > Ca^{2+} > Mg^{2+}$. These results show that ion exchange capacity depends upon hydrated radii of metal ions of the same group. We used the equilibrium in the solution phase where hydrated radii play an important role, so that the ion exchange capacity in the same group is found to decrease as the (hydrated) radii of ingoing cations increase.

A Chemical analysis of various samples (Table 1) revealed that Fe:Mo is 1:3. The results in Table 1 show that sample 6 is the stablest among the six samples. Its solubility in most of the common solvents is quite low as seen from Table 3. It is also observed that the chemical stability increases with increasing refluxing time. The pH titrations performed (Fig. 1) show that iron(III) molybdate behaves as a weak bifunctional cation exchanger.

Results of Mössbauer studies are given in Table 4. Originally, it was thought that one of the fundamental requirements of the Mössbauer effect expected to become actually applicable would be that Mössbauer atoms should be bound in a crystal lattice. It was, however, shown in an earlier paper[10] that there is a high possibility of observing the effect in amorphous substances (or in solid solution).

Table 3. Solubility of ion(III) molybdate sample 6 in various solvents

Solvent		Solubility/μg in 20 cm^3	
		Fe	Mo
HNO_3	(1.0 mol dm^{-3})	460	288
$H_2C_2O_4$	(1.0 mol dm^{-3})	1540	1220
HCl	(1.0 mol dm^{-3})	720	284
CH_3COOH	(1.0 mol dm^{-3})	1500	450
DMF		0	60
Dioxane		0	40

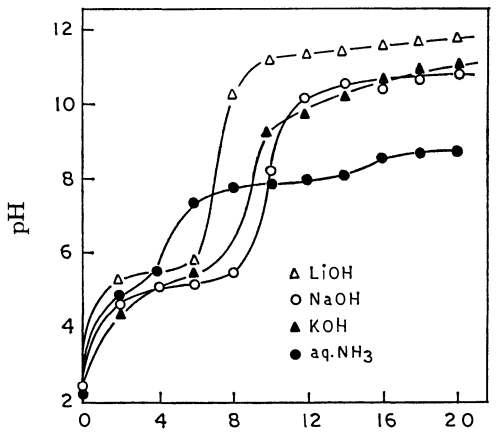

Volume of alkali solution added/cm^3

Fig. 1. pH titrations of iron (III) molybdate by added salt method.

Table 4. Isomer shift and quardrupole splitting of various inorganic iron compounds

Compound	Drying temp/°C	δ/mm s^{-1}	ε/mm s^{-1}
Iron(III) molybdate	R.T.[a)]	0.68	0.48
Iron(III) molybdate	200	0.61	0.59
Iron(III) molybdate	500	0.64	0.00
α-FeOOH	R.T.	0.53	0.00
β-FeOOH	R.T.	0.43	0.62
γ-FeOOH	R.T.	0.48	0.54
δ-FeOOH	R.T.	0.45	0.00

a) R.T.: Room temperature.

The Mössbauer spectrum of iron(III) molybdate in the H-form exchanger dried at 40 °C consists of a sharp and well defined doublet with δ=0.68 mm/s and

$\varepsilon=0.48$ mm/s at room temperature. These parameters characterize an iron atom in the "high spin tetravalent" state incorporated in the distorted octahedral site in the gel structure. The room temperature spectrum of the iron(III) molybdate dried at 200 °C shows a doublet which indicates a more covalent bonding and less distorted sites. Further, raising the drying temperature to 500 °C gives an unresolved single broad peak indicating a motional narrowing magnetic spectrum at room temperature. Further heat treatment results in growth of small particles in large crystallites as indicated by the isomer shift.

The results given in Table 4 allow a comparison of Mössbauer parameters of iron(III) molybdate dried at 40 °C with those of α,β,γ, and δ-FeOOH, which rules out the existence of α- and δ-FeOOH in the condensed phase with molybdate on the basis of quadrupole splitting. The value of quadrupole splitting for iron(III) molybdate which is close to that for γ-FeOOH, indicates the presence of the latter in the former. The product dried at 200 °C contains β-FeOOH, whereas the product dried at 500 °C contains iron in the form of α-Fe_2O_3.

The infrared spectra of the samples dried at 100, 200, 600, and 700 °C show that, as the drying temperature is raised, intensities of the bands at 3300 and 1625 cm^{-1} are decreased and ultimately caused to disappear at 600 °C due to complete removal of the water and OH groups present in the ion exchanger. Hence the product dried at 700 °C is simply a mixed oxide of iron and molybdenum, as confirmed by a single infrared band at 850 cm^{-1} due to the metal-oxygen bond.

In the light of the above discussion, chemical analysis, pH titrations, thermal analysis, Mössbauer spectra, and infrared absorption studies, a tentative structure of iron(III) molybdate can be worked out.

Results of the chemical analysis show that the ratio Fe:Mo in sample 6 iron(III) molybdate is 1:3. The thermogravimetric analysis shows that the loss in weight due to water molecules amounts to an extent of 20%. Since on heating oxides of iron and molybdenum are formed in the same ratio, the empirical formula for the mixed oxide should be $Fe_2O_3 \cdot 6MoO_3$ with a formula weight 1023.

If n is the number of moles of water per mole of mixed oxide, then

$$\frac{1800n}{(1023+18n)} = 20 \text{ or } n=24,$$

and the formula weight is 1275.

Thus, the structure of iron(III) molybdate may be

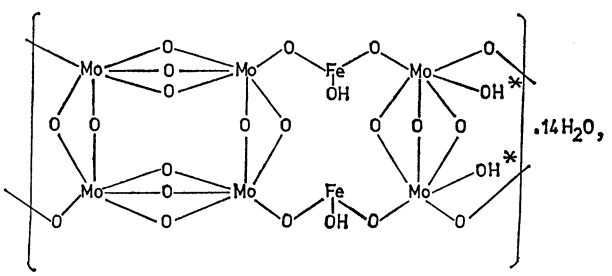

where the asterisked hydrogens are exchangeable protons.

Table 5. Distribution coefficients (K_d) for cations on iron(III) molybdate

Cation	K_d/cm^3 g^{-1}	Cation	K_d/cm^3 g^{-1}
Mg^{2+}	21	Ni^{2+}	17
Zn^{2+}	21	Cd^{2+}	20
Ba^{2+}	50	Bi^{3+}	400
Sr^{2+}	316	Al^{3+}	45
Ca^{2+}	80	La^{3+}	12
Pb^{2+}	650	Nd^{3+}	29
Cu^{2+}	15	Th^{4+}	80
Mn^{2+}	9	V^{5+}	121
Hg^{2+}	155	Ce^{4+}	54
Co^{2+}	239		

Table 6. Separation factors of some pairs of cations on iron-based synthetic inorganic ion exchanges

Separaction factor	Iron(III) molybdate	Iron(III) antimonate	Iron(III) phosphate
α_{Pb}^{Zn}	30.4	8.2	10.5
α_{Pb}^{Ba}	13.0	2.0	6.3
α_{Pb}^{La}	56.6	0.0	—
α_{Pb}^{Cu}	42.2	0.0	7.8
α_{Pb}^{Ni}	36.9	1.2	5.7
α_{Sr}^{Hg}	15.3	1.4	—
α_{Sr}^{Mn}	33.6	2.9	1.9
α_{Sr}^{Cd}	15.8	0.6	—

Iron(III) molybdate acts selectively for Pb^{2+}, Co^{2+}, Sr^{2+}, Hg^{2+}, and Bi^{3+}. For many other cations K_d values are quite low, as shown in Table 5. This makes it possible to separate the above cations from a number of other cations.

The order of selectivity for various cations is found to be: $Pb^{2+}>Bi^{3+}>Sr^{2+}>Co^{2+}>Hg^{2+}>V^{5+}>Th^{4+}=Ca^{2+}>Ce^{4+}>Ba^{2+}>Al^{3+}>Nd^{3+}>Zn^{2+}=Mg^{2+}=Cd^{2+}>Ni^{2+}>Cu^{2+}=La^{3+}>Mn^{2+}$.

On the basis of the selectivity sequence, separation factors were calculated (Table 6), and in all the cases separation factors on iron(III) molybdate are found to be greater than the other iron-based ion exchangers.

Thanks are due to Professor Harjit Singh and Dr. Ajaib Singh Brar for providing the research facilities and performing Mössbauer studies, respectively.

References

1) C. B. Amphlett, "Inorganic Ion Exchangers," Elsevier, Amsterdam (1964).
2) H. F. Walton, *Anal. Chem.*, **44**, 256R (1972).
3) H. F. Walton, *Anal. Chem.*, **46**, 398R (1974).
4) H. F. Walton, *Anal. Chem.*, **48**, 52R (1976).
5) H. F. Walton, *Anal. Chem.*, **50**, 36R (1978).
6) J. P. Rawat and P. S. Thind, *Can. J. Chem.*, **54**, 1982 (1976).
7) J. P. Rawat and J. P. Singh, *Can. J. Chem.*, **54**, 2534 (1976).
8) J. P. Rawat and D. K. Singh, *Anal. Chim. Acta*, **87**, 157 (1976).
9) H. E. Topp and K. W. Pepper, *J. Chem. Soc.*, **1949**, 3299.
10) V. A. Bryukhanov, V. I. Gol' danskii, N. N. Delyagin, and L. A. Kerytko, *Sov. Phys., JETP*, **16**, 321 (1963).

© 1983 The Chemical Society of Japan

NOTES

Bull. Chem. Soc. Jpn., 56, 1539—1540 (1983)

The Catalytic Isomerization of Butenes over a Sulfuric Acid-Graphite Intercalation Compound

Susumu Tsuchiya,* Masao Hara, and Hayao Imamura

Department of Industrial Chemistry, Faculty of Engineering, Yamaguchi University, Ube, Yamaguchi 755

(Received August 23, 1982)

Synopsis. The relative rate constants and the activation energies of the isomerization of butenes over sulfuric acid-graphite intercalation compound have been measured. *cis*-2-Butene is more reactive than 1-butene. The reaction profile shown on the triangular graph is of the *trans*-convex type.

Much attention has been paid to all the characteristic properties of graphite intercalation compounds, and the catalytic properties of the compounds have been extensively investigated in various reaction systems.[1-2] In this study, the interest has centered on the catalytic characteristics of the sulfuric acid–graphite intercalation compound (H_2SO_4–GIC), the isomerization of butenes being employed as a model reaction.

Experimental

A usual flow-type system with a by-pass at atmospheric pressure was employed to follow the reaction, nitrogen being used as the diluent. The H_2SO_4-GIC, the catalyst, prepared beforehand in a vacuum system similar to that described previously,[3] was fixed in the system.

The nitrogen stream with butene as a reactant was flowing only through the by-pass in the meantime; then it was diverted to flow through the reactor. The flowing rate of the nitrogen was *ca.* 40 cm³/min, the amount of catalyst used being 0.10 g for each run. The reaction mixtures were analyzed by means of gas chromatography with a column packing of 2,4-dimethylsulfolane on Uniport C.

The butenes were obtained from the Tokyo Kasei Kogyo Co., Ltd.; their purity was confirmed by gas chromatography to be more than 99%. Before each run, the catalyst was treated with a nitrogen stream at 373 K for 2 h, and the experimental results were well reproducible.

Results and Discussion

The double-bond migration and the *cis-trans* isomerization of butenes took place over H_2SO_4–GIC. The graphite does not show any catalytic activity for the reaction under the same experimental conditions. The skeletal isomerization could not be observed, as was reported previously.[3] No gaseous hydrocarbon other than butenes could be detected in the reaction mixtures under the present experimental conditions.

The rate of the isomerization of butenes was almost proportional to the pressure of the reactant. From the rates of reaction and the selectivity ratios, all six of the relative rate constants and the activation energies of reaction were determined in a manner similar to that described previously.[4] The results are shown in Fig. 1. It is of much interest that *cis*-2-butene is more reactive than 1-butene.

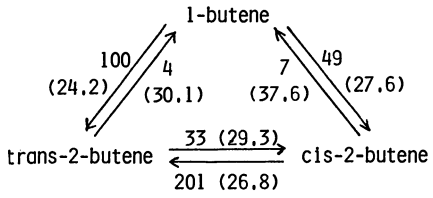

Fig. 1. Relative rate constants at 300 K and activation energies (kJ/mol) bracketed.

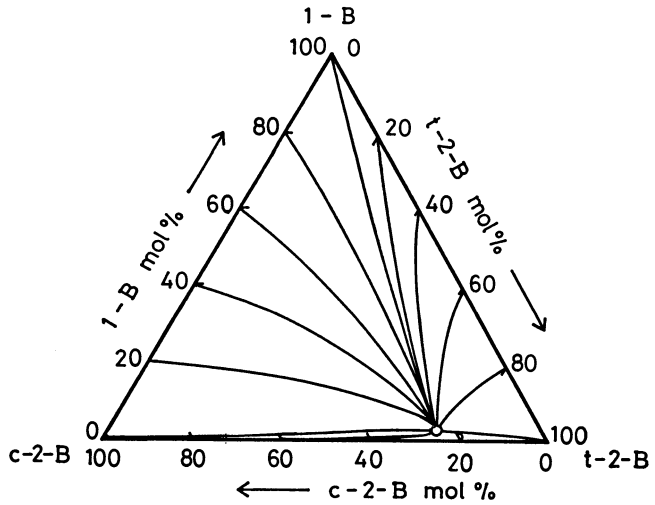

Fig. 2. Reaction profile of isomerization of butenes over H_2SO_4-GIC at 300 K.

Figure 2 shows the reaction paths calculated at 300 K. The triangular graph thus represents one of the catalytic characteristics of H_2SO_4–GIC for the isomerization of butenes. Since the rate equations employed are expressed on the basis of the sum of the forwards and backwards reactions, and since the time variable, t, is eliminated in the graph, the compositions of butenes can be shown from the initial to the equilibrium state. The curves, which originate from the left side of the triangle, bend convexly to the right. The profile may be named the "*trans*-convex type," which is entirely different from that obtained in the isomerization over KC_8.[4]

The following mechanisms for the isomerization of butenes have been proposed for different catalytic systems.[5] (1) A hydride-addition mechanism for metals, (2) a carbenium-ion mechanism for acid catalysts, and (3) an allylic mechanism for basic catalysts. When the isomerization takes place with a carbenium-ion mechanism, the selectivity ratio, *cis*/*trans*, is about unity, while 1/*cis* and 1/*trans* are less than 3.0,

usually less than 1.0. The selectivity ratios obtained in the present may be in agreement with a carbenium-ion mechanism.

The observed order of the relative rate constants of isomerization, *cis*-2-butene>1-butene>*trans*-2-butene, however, does not agree with what would be expected from a carbenium-ion mechanism. Accordingly, it can not necessarily be concluded that the active sites of H_2SO_4–GIC have same kind of acidic properties as hitherto reported.[6] The further discussion on the points will have to await new results, which may clarify the reaction mechanism.

This work was supported by a Grant-in-Aid for Scientific Research from the Ministry of Education, Science and Culture for which the authors' thanks are due.

References

1) M. A. M. Boersma, "Catal. Rev.-Sci. Eng.," ed by H. Heinemann and J. J. Carberry, Marcel Dekker, New York (1974), Vol. 10, p. 243.

2) M. A. M. Boersma, "Advanced Materials in Catalysis," ed by J. J. Burton and R. L. Garten, Academic Press, New York (1977), p. 67.

3) H. Imamura and S. Tsuchiya, *Z. Phys. Chem. N. F.*, **125**, 251 (1981).

4) S. Tsuchiya, T. Misumi, N. Ohuye, and H. Imamura, *Bull. Chem. Soc. Jpn.*, **55**, 3089 (1982).

5) J. Goldwasser and W. K. Hall, *J. Catal.*, **71**, 53 (1981).

6) *E. g.*, K. Tanabe, "Solid Acids and Bases-Their Catalytic Properties," Kodansha, Tokyo (1970), pp. 62, 118, 122, 123, 129, 146.

The Crystal and Molecular Structure of 3,4-Dichloronitrobenzene

Shigekazu KUMAKURA* and Yoshinobu KUROISHI

Department of Chemistry, Saitama University, 255 Shimo-okubo, Urawa 338

(Received October 5, 1982)

Synopsis. $C_6H_3Cl_2NO_2$, F. W. = 192.0, tetragonal, $I4_1/a$, $a=28.094(12)$, $c=3.838(6)$ Å, $V=3030$ Å^3, $Z=16$, $D_x=1.68$ Mg m^{-3}, μ(Mo $K\alpha$) = 0.8 mm^{-1}. Refinement with 1093 diffractometer data gave a final R value of 0.07. The molecule is practically planar except for the nitro group, the plane of which is inclined at 8.8° to the benzene plane. The two C–Cl bond distances are approximately equal to each other. The intermolecular Cl(2)···O(2^{11}) contact of 3.095 Å is remarkably short.

Our previous NQR study showed the equivalent character of the two C–Cl bonds in the title compound (abbreviated hereafter as DCNB), which are not equivalent with respect to the nitro substituent.[1] The crystal-structure analysis and a CNDO/2 calculation of DCNB have been carried out in order to clarify the C–Cl bond character in this compound.

Experimental

Commercial material was purified by recrystallization from a benzene solution. The crystals of DCNB are colorless needles. A crystal with dimensions of $0.3\times0.3\times0.4$ mm^3, obtained by cutting off a part of the specimen used for the NQR measurement and sealed in a Lindemann glass capillary, was used for the intensity measurement. The intensities of 1183 independent reflections were measured on a Rigaku automated four-circle diffractometer in $\omega/2\theta$ scan mode, using Mo $K\alpha$ radiation monochromated by a graphite crystal. Three standard reflections, monitored every 50 reflections, showed a steady decline in intensity; at the end of the data collection, the maximum reduction reached 13%. The intensity data were then put on a common scale with reference to the standard reflections. 1093 reflections with $|F_o|\geq3\sigma(|F_o|)$ were used for the analysis. No correction was made for absorption or extinction.

The positions of the Cl atoms were located from a sharpened Patterson map, and the remaining non-H atoms, by Fourier methods. A block-diagonal least-squares refinement using anisotropic temperature factors reduced the R value to 0.09. At this stage, a difference synthesis revealed all the hydrogen atoms in plausible positions. Further refinement was carried out including the isotropic H atoms. The final R value was 0.07 for 1093 observed reflections. A weighting scheme of $w=1$ if $|F_o|\geq5.5$ and $w=0.3$ otherwise was employed. The final atomic parameters and their standard deviations are listed in Table 1.[2] The atomic scattering factors were taken from the *International Tables for X-Ray Crystallography*.[3] The calculations were carried out on HITAC 5020E and 8800/8700 computers at the Computer Center of the University of Tokyo and on TOSBAC 3400 and HITAC 8250 computers at Saitama University.

TABLE 1. FRACTIONAL ATOMIC COORDINATES ($\times10^4$) AND EQUIVALENT THERMAL PARAMETERS (B_{eq}) FOR THE NON-HYDROGEN ATOMS, WITH e.s.d.'s IN PARENTHESES

Atom	x	y	z	B_{eq}/Å^2
O(1)	1748(2)	398(2)	4162(19)	8.27
O(2)	1098(2)	627(2)	6619(16)	6.88
N	1463(2)	697(2)	4933(17)	5.21
Cl(1)	833(1)	2397(1)	3572(6)	5.72
Cl(2)	1822(1)	2668(1)	186(6)	5.48
C(1)	1543(2)	1192(2)	3707(16)	3.82
C(2)	1192(2)	1517(2)	4159(16)	3.85
C(3)	1276(2)	1978(2)	3036(17)	4.04
C(4)	1712(2)	2091(2)	1623(15)	3.63
C(5)	2058(2)	1756(2)	1141(17)	4.17
C(6)	1976(2)	1292(2)	2234(18)	4.17

Results and Discussion

The bond lengths and angles of DCNB are shown in Fig. 1, together with the atomic numbering scheme. All the atoms of DCNB are practically coplanar except for those of the nitro group, the plane of which is inclined at 8.8° to the benzene plane. The geometry of the nitro group in DCNB seems to be normal as compared with those of unhindered nitro groups in other aromatic nitro compounds.[4–6] The C(2)–C(1)–C(6) bond angle is 124.1(5)°. Such an increase in the internal angle at the nitro-substituted carbon is commonly observed for other aromatic nitro compounds.[5,6] The C–C bond distances in the benzene ring vary from 1.358 Å to 1.390 Å. The C–Cl bond distances are 1.728(6) Å and 1.739(6) Å. A CNDO/2 calculation based upon the molecular geometry observed was carried out in order to gain a better understanding of the ground-state electronic distribution of the π orbitals.[7] The π characters of the C–C bonds in the benzene ring are essentially equivalent; those of the two C–Cl bonds are also equivalent (4%). These results reveal that the nitro group in DCNB exerts no influence on the electronic distribution of the π orbitals of the C–Cl bonds and are consistent with the conclusion derived from the NQR data.

The crystal structure viewed along the c axis is

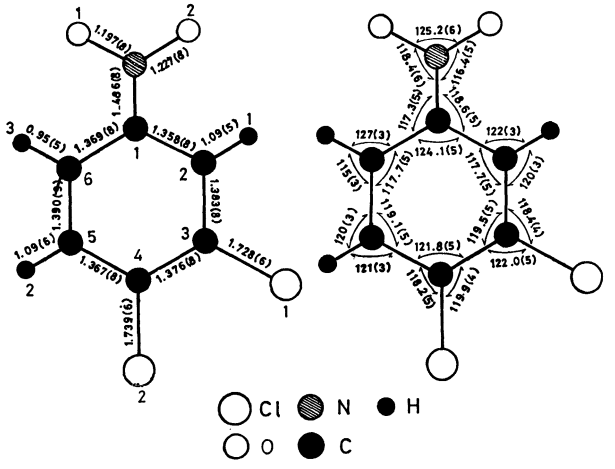

Fig. 1. Bond lengths (l/Å) and angles (ϕ/°) with their e.s.d.'s in parentheses.

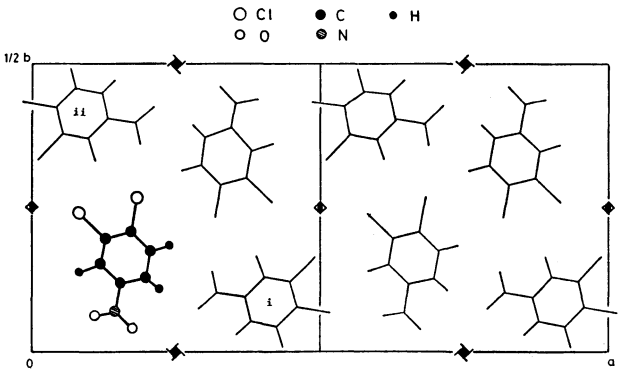

Fig. 2. A projection of the crystal structure along the c axis.

Table 2. Short C-Cl···O intermolecular distances

	C-Cl···O angle ϕ/°	Cl···O distance l/Å
2,5-Dichloro-1,4-benzoquinone	164	3.10
2,3-Dichloro-1,4-benzoquinone	164	3.01
2,3-Dichloro-1,4-naphthoquinone	164	3.10
3,4-Dichloronitrobenzene	164.8	3.095

presented in Fig. 2. The DCNB molecules are stacked in infinite columns along the c axis, with the mean interplanar distance of 3.601 Å. The intermolecular contacts between molecular stacks are normal except for Cl(2)···O(2^{ii}) (3.095 Å) and H(2)···O(2^{i}) (2.43 Å), which are shorter than the usually quoted van der Waals distances. The C(4)–Cl(2)···O(2^{ii}) angle is 164.8°. Similar short intermolecular contacts were observed in the crystals of some benzoquinone and naphthoquinone derivatives, which are listed in Table 2.[8] Gaultier, Hauw, and Schvoerer observed a red shift of the absorption maxima of the C=O stretching bands of these compounds in their crystalline and solution states, and proposed that the unusual contacts are attributable to charge-transfer interaction between the Cl atom and the carbonyl oxygen.[8] The absorption maxima of the symmetric and antisymmetric NO_2 stretching bands in the crystalline DCNB were observed at 1347.7 cm^{-1} and 1538.2 cm^{-1} respectively, and those in a CCl_4 solution, at 1345.2 cm^{-1} and 1534.6 cm^{-1}. Seemingly, these deviations are too small to be significant.

The authors are grateful to Professor Yoshihiko Saito for the use of the Rigaku four-circle diffractometer at the Institute of Solid State Physics, the University of Tokyo. Thanks are also due to Professor Takashi Shimozawa, Saitama University, for his keen interest and valuable discussion.

References

1) S. Kumakura, Y. Kuroishi, and T. Shimozawa, 23 rd National Meeting of the Chemical Society of Japan, Sapporo, August 1970, Abstr. p. 39. An analysis of the NQR data of DCNB was carried out again on the basis of its crystal structure as determined by the present study; the estimated values of the asymmetric parameters (η) are 0.13 and 0.15 for the meta and para Cl atoms respectively. The π characters of the two C–Cl bonds based on the η values are approximately equivalent with the mean value of 6% (R. Benson, *J. Chem. Phys.*, **22**, 2078 (1954); B. P. Dailey and C. H. Townes, *ibid.*, **23**, 118 (1955)).

2) The atomic parameters for the H atoms, the temperature factors for the non-H atoms, and the list of observed and calculated structure factors are kept at Document No. 8315 at the Chemical Society of Japan.

3) "International Tables for X-Ray Crystallography," The Kynoch Press, Birmingham (1968), Vol. III.

4) J. R. Holden and C. Dickinson, *J. Phys. Chem.*, **73**, 1199 (1969).

5) O. L. Carter, A. T. McPhail, and G. A. Sim, *J. Chem. Soc., A*, 822 (1966).

6) A. Domenicano, A. Vaciago, and C. A. Coulson, *Acta Crystallogr., Sect. B*, **31**, 221 (1975).

7) S. Kumakura and T. Kodama, *Bull. Chem. Soc. Jpn.*, **48**, 2339 (1975).

8) J. Gaultier, C. Hauw, and M. Schvoerer, *Acta Crystallogr., Sect. B*, **27**, 2199 (1971).

Structure of a Potent Antithyroid Drug, 6-Propyl-2-thiouracil

Nobuo OKABE,* Takaji FUJIWARA, Yuriko YAMAGATA, and Ken-ici TOMITA

Faculty of Pharmaceutical Sciences, Osaka University, Yamadaoka 1-6, Suita, Osaka 565

(Received October 8, 1982)

Synopsis. The crystal strure of 6-propyl-2-thiouracil (PTU), an antithyroid drug, has been determined as a 2:1 complex with 1,4-dioxane [$(C_7H_{10}N_2OS)_2(C_4H_8O_2)$]. The crystals are monoclinic, space group $P2_1/a$, with $a=8.983(5)$, $b=23.706(12)$, $c=4.942(2)$ Å, $\beta=95.79(3)°$, $V=1047.1(9)$ Å^3, $Z=4$, $D_x=1.36$ Mg m^{-3}, $D_m=1.35$ Mg m^{-3}, MW=214.29, λ(Cu $K\alpha$)=1.5418 Å. Final $R=0.098$ for 1575 reflexions.

6-Propyl-2-thiouracil (PTU) is a potent antithyroid drug as well as 2-thiouracil (TU) and 6-methyl-2-thiouracil (MTU). These compounds inhibit the biosynthesis of thyroid hormones and have been used for the treatment of hypothyroidism.[1-3] PTU is also known as a strong inhibitor of monoiodination of thyroid hormones in some tissues, such as liver, kidney or brain.[4,5] Although it appears that PTU inhibits the thyroid peroxidase in the thyroid gland or the deiodinase in some tissues, little is known about the actual mechanisms of these inhibitory effects. In this study, the molecular conformation of PTU is determined by X-ray analysis as a first step for elucidation of these inhibitory mechanisms.

Experimental

PTU and 1,4-dioxane were purchased from Nakarai Chemicals Ltd. Kyoto, Japan. PTU was crystallized from 2%(v/v) 1,4-dioxane aqueous solution by slow evaporation of the solvent at room temperature, and it was found that PTU crystallized as a 2:1 complex with 1,4-dioxane. A brittle needle crystal with the dimensions $0.30\times0.30\times0.15$ mm^3 was sealed in a capillary with mother liquor for X-ray analysis. Intensity data were collected on a Rigaku four-circle diffractometer AFC-5 with graphite-monochromated Cu $K\alpha$ radiation (45 kV, 25 mA) yielding 1809 independent reflexions with $2\theta\leq125°$. The intensities were corrected for Lorenz and polarization factors, but not for absorption. The structure was solved by MULTAN.[6] The positions of 14 non-hydrogen atoms were correctly determined and 14H atoms were located from a difference Fourier map. Refinement was performed by a block-diagonal least squares method up to $R=0.098$. The atomic scattering factors for C, N, O, and S were taken from International Tables for X-Ray Crystallography.[7]

Results and Discussion

The molecular shape of PTU complex with dioxane (2:1) is illustrated in Fig. 1. The final atomic parameters are listed in Table 1. The bond lengths and angles of PTU and dioxane are summarized in Table 2. These values are in good agreement with those of uracil[8] and its related derivatives, 2-thiouracil,[9] 1-methyluracil,[10] 1-ethyl-5-bromouracil,[11] and the dioxane complexes with oxalyl dichloride and oxalyl dibromide,[12] with iodoform[13] and with 1,7-diacetoxy-2,4,6-trinitro-2,4,6-triazaheptane,[14] except C(2)–S bond length of PTU, 1.647(5) Å, which is somewhat shorter than that of TU, 1.67 Å.[9] The propyl group attached to C(6) position forms an extended planar trans conformation. The uracil plane is nearly coplanar with the propyl one and the dihedral angle between the planes is 10.4(5)°. Bond lengths of the propyl group, C(6)–C(7), 1.500(8) Å, C(7)–C(8), 1.516 (8) Å, and C(8)–C(9), 1.532(8) Å are a little shorter in this order than that of the ideal C–C single bond

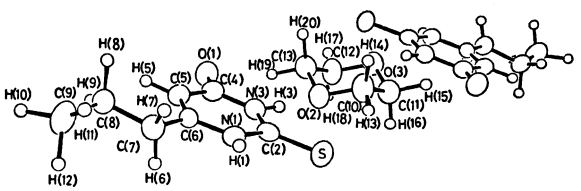

Fig. 1. A view of PTU complex with dioxane and the atomic numbering.

TABLE 1. FINAL ATOMIC PARAMETERS (POSITIONAL $\times10^4$, FOR H $\times10^3$) WITH e.s.d.'s IN PARENTHESES AND EQUIVALENT ISOTROPIC TEMPERATURE FACTORS (ISOTROPIC H)

$$B_{eq}=\frac{4}{3}\Sigma_i\Sigma_j\beta_{ij}a_ia_j.$$

Atom	x	y	z	$B_{eq}(B_{iso})$/Å^2
S	2654(2)	6413(1)	3654(3)	3.89(4)
O(1)	6342(4)	6934(1)	11236(7)	4.39(20)
O(2)	5012(4)	5536(1)	8839(6)	4.15(21)
N(1)	3384(5)	7451(2)	5262(7)	3.01(20)
N(3)	4594(5)	6741(2)	7684(8)	3.24(20)
C(2)	3581(6)	6887(2)	5596(9)	2.83(23)
C(4)	5396(6)	7126(2)	9410(9)	3.21(24)
C(5)	5120(6)	7705(2)	8932(9)	3.13(24)
C(6)	4126(5)	7855(2)	6866(9)	2.73(23)
C(7)	3718(6)	8450(2)	6066(9)	3.78(26)
C(8)	4412(6)	8893(2)	8014(10)	3.87(26)
C(9)	4062(7)	9485(2)	6883(10)	5.64(32)
C(10)	3714(6)	5195(2)	8455(10)	4.55(28)
C(13)	5828(6)	5413(2)	11436(10)	4.30(27)
H(1)	260(5)	761(2)	424(7)	2.6 (1.2)
H(3)	470(5)	632(2)	792(9)	4.9 (1.5)
H(5)	568(5)	802(2)	1020(8)	4.6 (1.4)
H(6)	383(5)	846(2)	415(8)	4.4 (1.4)
H(7)	240(5)	857(2)	609(8)	4.6 (1.3)
H(8)	551(5)	884(1)	887(8)	2.4 (1.2)
H(9)	409(4)	884(1)	1013(8)	2.5 (1.2)
H(10)	300(5)	941(2)	657(9)	5.1 (1.5)
H(11)	407(6)	961(2)	444(10)	9.5 (2.0)
H(12)	495(5)	983(2)	792(7)	4.3 (1.4)
H(13)	276(5)	535(2)	949(8)	4.5 (1.4)
H(14)	316(5)	537(2)	662(7)	2.3 (1.2)
H(19)	700(5)	567(2)	1181(8)	3.4 (1.3)
H(20)	514(6)	558(2)	1312(8)	5.4 (1.5)

Table 2. Intermolecular bond length and bond angles with e.s.d.'s in parentheses

Bond length	l/Å	Bond length	l/Å
S-C(2)	1.647(5)	C(7)-C(8)	1.516(8)
N(1)-C(2)	1.357(6)	C(8)-C(9)	1.532(8)
C(2)-C(3)	1.351(6)	O(2)-C(10)	1.416(6)
N(3)-C(4)	1.398(7)	O(2)-C(13)	1.442(7)
C(4)-C(5)	1.412(7)	C(10)-C(11)	1.499(8)
O(1)-C(4)	1.260(6)	O(3)-C(11)	1.442(7)
C(5)-C(6)	1.335(7)	O(3)-C(12)	1.416(6)
C(6)-C(7)	1.500(8)	C(12)-C(13)	1.499(8)
N(1)-C(6)	1.373(6)		
Bond angle	ϕ/°	Bond angle	ϕ/°
S-C(2)-N(1)	123.3(4)	N(1)-C(6)-C(7)	114.3(4)
S-C(2)-N(3)	122.2(4)	C(6)-C(7)-C(8)	114.2(4)
N(1)-C(2)-N(3)	114.5(4)	C(7)-C(8)-C(9)	110.3(5)
C(2)-N(3)-C(4)	124.4(5)	C(10)-O(2)-C(13)	109.9(4)
O(1)-C(4)-N(3)	118.0(4)	C(11)-O(3)-C(12)	109.9(4)
O(1)-C(4)-C(5)	124.4(5)	O(2)-C(10)-C(11)	109.0(4)
N(3)-C(4)-C(5)	117.5(5)	C(10)-C(11)-O(3)	109.8(4)
C(4)-C(5)-C(6)	118.7(5)	O(3)-C(12)-C(13)	109.0(4)
C(5)-C(6)-N(1)	120.3(5)	C(12)-C(13)-O(2)	109.8(4)
C(5)-C(6)-C(7)	125.3(5)		

known as 1.54 Å. The shortening of the C–C bonds occurs markedly close to the pyrimidine ring. This suggests the resonance effect between the pyrimidine ring and the propyl group, which may explain the extended planar conformation of the propyl group. No disordering of the propyl group was observed. This indicates that the observed trans conformation of the propyl group might be a most stable one in the crystal. The dioxane molecule takes a chair conformation which has been found in the crystals as a stable form.[12-14] The molecular packing of PTU and dioxane in the crystal is shown in Fig. 2. Two PTU and one dioxane molecules are joined together in pairs by the hydrogen bond formation, N(3)–H(3)···O(2) (or O(3)), 2.929(6) Å. A PTU molecule is also connected with adjacent molecules to form endless chains by the hydrogen bond, N(1)–H(1)··· O(1), 2.952(5) Å. The sulfur atom at C(2) position does not participate in the hydrogen bond network, while in the crystals structure of TU, the N–H···S hydrogen bond with the length of 3.32 Å was formed.[9] This may explain the reason why the bond length, C(2)–S of PTU is a little shorter than that of TU. No stacking interaction between uracil bases was observed.

The relative antithyroid activity of PTU is 75 and that of MTU is 100 assuming TU as 100.[1] Supposing that the extended planar trans conformation of PTU found in the crystal is dominant as the antithyroid active form, lower antithyroid activity of PTU as compared with MTU or TU may be interpreted by the conformational feature of PTU. The planarity of PTU with the extended planar propyl group may have some negative effects for binding ability of it at the active center of the enzyme by steric hindrance. When thyroid hormones bind to carrier proteins, the 4'-OH group of these participates in a hydrogen bond

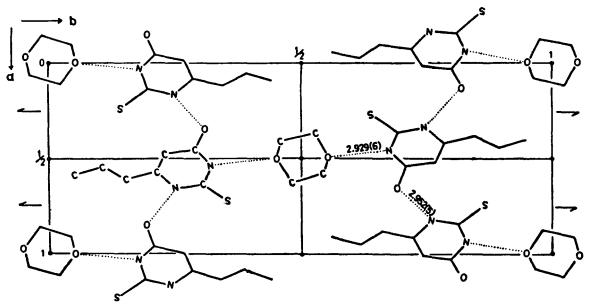

Fig. 2. Packing of the molecules viewed down c. The H atoms are excluded for clarity. The dotted lines represent the hydrogen bonds. Distances are in Å.

formation.[15] The hydrogen bond between PTU and dioxane may be concerned with the role of the 4'-OH group of the thyroid hormones at the active center of the enzyme. The three hydrogen bonds found in this crystal may be indispensable for fixing PTU on the binding site of the enzyme and for the following inhibitory action against the function of peroxidase or deiodinase resulted in the sulfur atom at C(2) position. Unfortunately, no physicochemical data on the interaction between PTU and relative enzymes is available. For this result, systematic studies concerning the effects of PTU on the endocrinal homeostasis may also be desirable.

References

1) A. Goth, "Medical Pharmacology," 9th ed, The C. V. Mosby Company, Saint Louis (1978), p. 494.
2) J. Crooks, "Meyer's Side Effects of Drug," ed by M. N. G. Dukes, American Elsevier Publishing Co. Inc., New York (1975), Vol. 8, p. 896.
3) G. W. Anderson, I. F. Halverstadt, W. H. Miller, and R. O. Roblin, Jr., *J. Am. Chem. Soc.*, **67**, 2197 (1945).
4) I. J. Chopra, D. H. Solomon, U. Chopra, S. Y. Wu, D. A. Fisher, and Y. Nakamura, "Recent Progress in Hormone Research," ed by R. O. Greep, Academic Press, New York (1978), Vol. 34, p. 521.
5) T. J. Visser, J. L. Leonard, M. M. Kaplan, and P. R. Larsen, *Biochem. Biophys. Res. Commun.*, **101**, 1297 (1981).
6) P. Main, S. E. Hull, L. Lessinger, G. Germain, J. P. Declerco, and M. M. Woolfson, "**MULTAN** 78. A System of Computer Programs for the Automatic Solution of Crystal Structures from X-Ray Diffraction Data," Univ. of York, England, and Louvain, Belgium (1978).
7) "International Tables for X-Ray Crystallography," Birmingham, Kynoch Press (1974), Vol. IV, pp. 72, 149.
8) G. S. Parry, *Acta Crystallogr.*, **7**, 313 (1954).
9) D. Tsernoglou, *Dissert. Abstr.*, (**B**)**27**, 2603 (1967).
10) D. W. Green, F. S. Mathews, and A. Rich, *J. Biol. Chem.*, **237**, 3573 (1962).
11) H. Mizuno, T. Fujiwara, and K. Tomita, *Bull. Chem. Soc. Jpn.*, **45**, 905 (1972).
12) E. Damm, O. Hassel, and C. Romming, *Acta Chem. Scand.*, **19**, 1159 (1965).
13) T. Bjorvatten, *Acta Chem. Scand.*, **23**, 1109 (1969).
14) R. E. Cobbledick and R. W. H. Small, *Acta Crystallogr., Sect. B*, **29**, 2585 (1973).
15) V. Cody, *Endocr. Rev.*, **1**, 140 (1980).

The X-Ray Structure of 2-Aminocyclohexanone Oxime Hydrochloride

Yukishige KITANO,* Yoshihisa MATSUKUMA,† Shinzo IMAMURA,†
Ryo TAKAGI,†† and Tamaichi ASHIDA††

Toray Research Center, Inc., Sonoyama, Ohtsu 520

† *Chemicals Research Laboratory, Basic Research Laboratories, Toray Industries, Inc., 9-1, Ooe, Minato, Nagoya 455-91*

†† *Faculty of Engineering, Nagoya University, Chikusa-ku, Nagoya 464*

(Received October 26, 1982)

Synopsis. The crystal structure of the title compound was determined by the X-ray method. The space group is $P\bar{1}$, with $a=8.537(1)$, $b=5.223(3)$, $c=9.505(1)$ Å, $\alpha=91.04(2)$, $\beta=80.58(1)$, $\gamma=99.16(3)°$, and $Z=2$. The hydroxyl group of the oxime takes the *anti* conformation to the amino group in the solid state. The molecules, linked together by NH···Cl and OH···Cl hydrogen bridges, form columns in the crystal.

2-Aminocyclohexanone oxime is easily converted into α-amino-ε-caprolactam by means of the Beckmann rearrangement reaction, which is well-known to be highly stereospecific in that the group *anti* to the hydroxyl group migrates in an acid-catalyst solution. In the solid state, however, it is anticipated that, because of the steric hindrance, the hydroxyl group of the oxime can not take the *syn* conformation to the amino group. In order to elucidate the stable conformation in the crystalline state, an X-ray structural analysis of two salts, hydrochloride and sulfate, was undertaken; the results show that hydroxyl groups take the *anti* conformation in both molecules, as might be expected.

The crystal data for both molecules are summarized in Table 1. The sulfate recrystallized from aqueous and ethanol solutions showed a disordered structure, with the sulfate ion disordered statistically about the two-fold crystallographic axis of the space group C2 and with several improbable bond dimensions being observed. Therefore, in this paper we will report only on the crystal structure of hydrochloride.

Experimental

The title compound was recrystallized from an aqueous solution as colorless plates elongated in the b direction. The unit-cell parameters were refined by the least-squares fit of 14 reflections as measured on a Hilger & Watts automatic four-circle diffractometer. The density was measured by flotation in a carbon tetrachloride-hexane mixture. A crystal with dimensions of $0.25\times0.35\times0.5$ mm³ was used for the data collection. The intensities of 1074 reflections with $2\theta\leq114°$ were measured by the $2\theta-\omega$ step-scan technique with Ni-filtered Cu $K\alpha$ radiation. No significant changes were observed in the intensities of the standard reflections measured periodically throughout the data collection. The measured intensities were corrected for Lorentz-polarization factors, but no absorption correction was applied. 895 reflections with $F\geq2\sigma(F)$ were used in the refinement of the structure.

Structure Determination and Refinement

The structure was solved by the usual Patterson and Fourier methods and refined by the block-diagonal least-squares procedure, using the HBLS VI program[1] with anisotropic temperature factors for all the non-hydrogen atoms and isotropic ones for the hydrogen atoms. In the refinement, the function minimized was $\Sigma w(|F_o|-|F_c|)^2$, with the weighting scheme of $w=[\sigma^2(F_o)+a|F_o|+b|F_o|^2]^{-1}$, where $\sigma(F_o)$ is the standard deviation based on the counting statistics. The final refinement ($a=0.0652$, $b=-0.0006$) led to the R value of 0.070. All the scattering factors were taken from the International Tables for X-Ray Crystallography.[2] The final atomic parameters are shown in Table 2.[3]

Table 1. Crystal data

	$C_6H_9(=NOH)$-$NH_3^+Cl^-$	$2C_6H_9(=NOH)$-$NH_3^+\cdot SO_4^{2-}$
Chemical formula	$C_6H_{13}N_2OCl$	$C_{12}H_{26}N_4O_6S$
Formula weight	164.5	352.4
Crystal system	Triclinic	Monoclinic
Space group	$P\bar{1}$	C2
a/Å	8.537(1)	9.673(8)
b/Å	5.223(3)	7.053(2)
c/Å	9.505(1)	12.936(4)
α/°	91.04(2)	—
β/°	80.58(1)	103.16(4)
γ/°	99.16(3)	—
V/Å³	410.7	859.4
D_{obsd}/g cm⁻³	1.32	1.35
D_{calcd}/g cm⁻³	1.328	1.362
Z	2	4

Results and Discussion

The bond lengths and angles of the atoms, excluding the hydrogen atoms, are shown in Fig. 1, together with the atomic numbering system. The estimated standard deviations of the bond lengths are 0.005—0.010 Å, while those of the bond angles are 0.4—0.5°. X-Ray structural analysis shows that the hydroxyl group of the oxime takes the *anti* conformation to the amino group in the crystalline state. The cyclohexane ring takes a chair form, and the ring C-C bond lengths and angles are in essential agreement with the values obtained in 3,3,5,5-tetramethylcyclohexanone oxime,[4] 3,3,5-trimethyl-5-phenylcyclohexanone oxime,[5] and 1,4-cyclohexane-dihydroxyimine.[6] The distance of the C(1)–N(1) bond (1.294 Å) suggests its double-bond character; the coplanarity of the C(1), C(2), C(6), N(1), and O atoms is due to this double-bond character(Table 3). The N(1)–O bond distance (1.404 Å) is also within the expected range of values.[7]

Table 2. Positional ($\times 10^4$, for H $\times 10^3$) and thermal parameters (B_{eq} for non-H $\times 10$, B_{iso} for H $\times 10$), with their estimated standard deviations in parentheses

Atom	x	y	z	B_{eq}(or B_{iso})/Å^2 a)
Cl	2488(2)	11190(3)	6166(1)	35(0.7)
O	5640(5)	1259(8)	1810(4)	39(2)
N(1)	4914(5)	3101(9)	2669(5)	32(3)
N(2)	3557(6)	6546(9)	4322(5)	36(3)
C(1)	3797(6)	3945(11)	2124(6)	31(3)
C(2)	2964(7)	5940(11)	2907(6)	31(3)
C(3)	1141(7)	5150(12)	3187(7)	40(4)
C(4)	578(7)	4413(12)	1753(7)	44(4)
C(5)	1386(8)	2287(12)	1050(7)	44(4)
C(6)	3213(7)	3057(12)	739(7)	41(4)
H(O)	617(7)	60(11)	230(7)	39(17)
H1(N2)	472(7)	708(10)	407(6)	27(15)
H2(N2)	307(8)	488(11)	494(7)	45(18)
H3(N2)	303(8)	842(11)	498(7)	44(18)
H(C2)	326(6)	819(10)	230(6)	25(14)
H1(C3)	48(8)	654(11)	386(7)	47(18)
H2(C3)	96(6)	345(9)	383(5)	11(12)
H1(C4)	67(8)	608(12)	126(7)	47(18)
H2(C4)	−61(8)	341(12)	206(7)	50(19)
H1(C5)	97(8)	183(11)	18(7)	53(20)
H2(C5)	105(7)	25(10)	172(6)	29(15)
H1(C6)	360(6)	484(11)	6(7)	34(17)
H2(C6)	359(9)	100(14)	23(9)	81(25)

a) The equivalent isotropic temperature factor defined by W. C. Hamilton (*Acta Crystallogr.*, **12**, 609 (1959)).

Table 3. Deviations of the atoms(l/Å) from the least-squares plane

C(1)	−0.001(14)	C(2)	−0.011(14)	C(6)	0.007(15)
N(1)	0.015(14)	O	−0.009(14)	N(2)a)	0.080(14)

a) Atom not included in the calculation of the plane.

Table 4. Hydrogen-bond system

Donor	Acceptor	Distance l/Å			Angle ϕ/°
D-H	A	D-H	H···A	D···A	D-H···A
N(2)-H1(N2)	Cl(i)	0.98(6)	2.39(6)	3.354(5)	170(5)
N(2)-H2(N2)	Cl(ii)	1.05(7)	2.22(7)	3.252(5)	170(5)
N(2)-H3(N2)	Cl(iii)	1.25(7)	1.89(7)	3.133(5)	170(5)
O-H(O)	Cl(iv)	0.81(6)	2.29(6)	3.104(4)	175(6)

Symmetry code: (i) $1-x, 2-y, 1-z$; (ii) $x, y-1, z$; (iii) x, y, z; (iv) $1-x, 1-y, 1-z$.

The C–N bond length, 1.524(8) Å, to the positively charged quaternary nitrogen atom N(2) is very near the values of 1.509 and 1.510 Å found in 1,2-cyclohexanediamine hydrobromide.[8]

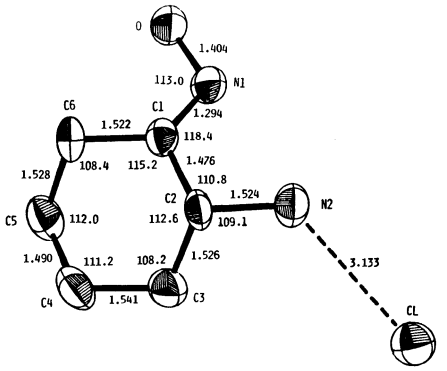

Fig. 1. ORTEP drawing of the molecule with atomic numbering, bond distances(l/Å) and bond angles(ϕ/°). The ellipsoids are drawn to enclose 50% probability.

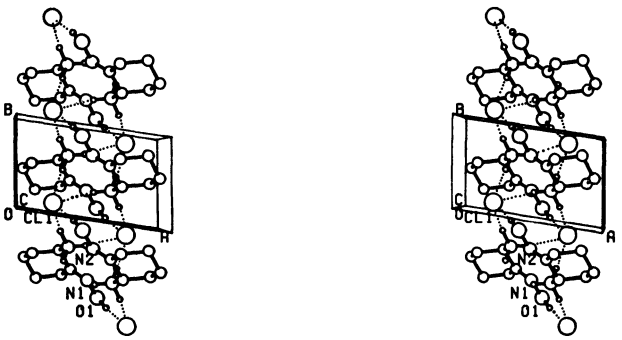

Fig. 2. A stereoview of the packing of the molecule in the unit cell. The hydrogen bonds are shown by dotted lines. For H-atoms only the atoms contributed to the hydrogen bonds are drawn for clarity.

The packing of the molecules in the crystal is shown in Fig. 2. The molecules, linked together by NH···Cl and OH···Cl hydrogen bridges, form columns parallel to the b axis. This column structure reasonably explains the pronounced cleavage parallel to (010). The dimensions of the hydrogen bonds are given in Table 4.

References

1) T. Ashida, "The Universal Crystallographic Computing System-Nagoya," The Computation Center, Nagoya Univ. (1981).

2) "International Tables for X-Ray Crystallography," Kynoch Press, Birmingham (1974), Vol. IV.

3) The lists of structure factors and anisotropic thermal parameters for the non-hydrogen atoms are deposited at the office of this Bulletin as Document No. 8316.

4) P. S. Toure, J. Lapasset, B. Boyer, and G. Lamaty, *Acta Crystallogr., Sect. B*, **36**, 2168 (1980).

5) P. S. Toure, J. Lapasset, B. Boyer, and G. Lamaty, *Acta Crystallogr., Sect. B*, **35**, 2790 (1979).

6) P. Groth, *Acta Chem. Scand.*, **22**, 128 (1968).

7) V. Bertolasi, G. Gilli, and A. C. Veronese, *Acta Crystallogr., Sect. B*, **38**, 502(1982), and the references cited therein.

8) M. D. Morse and J. P. Chesick, *Acta Crystallogr., Sect. B*, **32**, 954 (1976).

Contribution of Quadruply Degenerate π-Electron Orbitals to London Susceptibility

Tsuyoshi HORIKAWA and Jun-ichi AIHARA*

Department of Chemistry, Faculty of Science, Shizuoka University, Oya, Shizuoka 422

(Received November 24, 1982)

Synopsis. A graph-theoretical formula was derived to evaluate the contribution of quadruply degenerate π-electron orbitals to London diamagnetism. This formula enables us to calculate London susceptibilities of such compounds as *p*-terphenyl and perylene without factorization of their secular determinants.

In 1952 Berthier *et al.*[1] elaborately derived analytical formulas for London (or ring-currents) susceptibility[2,3] of a polycyclic conjugated system with nondegenerate and/or doubly and/or triply degenerate π-electron orbitals. However, there have been no such formulas for systems with quadruply degenerate orbitals. Secular equations of *p*-terphenyl (**1**) and perylene (**2**) were factored into algebraic equations of lower degree,[1] because they have quadruply degenerate orbitals. We have been developing graph theory of cyclic conjugated systems to elucidate their magnetic properties.[4-9] In this note we present a graph-theoretical formula of London susceptibility applicable to quadruply degenerate orbitals of a cyclic conjugated system.

Let a polycyclic conjugated system G be placed perpendicularly to the external magnetic field H, and its characteristic polynomial is denoted by $P_G(X,H)$. If there are quadruply degenerate π-electron orbitals in G, $P_G(X,0)$ can be written as

$$P_G(X, 0) = (X-X_0)^4 U(X), \tag{1}$$

where X_0 is the energy of quadruply degenerate orbitals.[10] $P_G(X,H)$ is expressible in the form:[5]

$$P_G(X, H) = P_G(X, 0) + H^2 \sum_i^G P_{G-r_i}(X, 0)\theta_i^2 + H^4 A(X) + \cdots. \tag{2}$$

Here, r_i is the ith π-electron ring in G;[11] G-r_i is a subsystem of G, obtained by deleting from G the ith π-electron ring and all π bonds incident to it; i runs over all π-electron rings in G, defined in Sachs' sense;[11] $\theta_i = eS_i/c\hbar$, where S_i is an area of the ith π-electron ring, and e, c, and $\hbar$ are the standard constants with these symbols; and $A(X)$ is a term proportional to H^4, which is not specified here.

Since the magnetic field can be treated as a small perturbation, field-dependent energies of the four orbitals which are degenerate in energy at $H=0$ are given by solving the following equation:[5]

$$P_G(X, H) = P_G(X, 0) + H^2 \sum_i^G P_{G-r_i}(X, 0)\theta_i^2 + H^4 A(X) = 0. \tag{3}$$

This equation is written as

$$(X-X_0)^4 = -H^2 S(X) - H^4 T(X), \tag{4}$$

where

$$S(X) = \frac{1}{U(X)} \sum_i^G P_{G-r_i}(X, 0)\theta_i^2 \tag{5}$$

and

$$T(X) = \frac{A(X)}{U(X)}. \tag{6}$$

Since $|X-X_0| \ll 1$ for the four orbitals, Eq. 4 can be expanded into

$$(X-X_0)^4 = -H^2\left\{S(X_0) + S^{(1)}(X_0)(X-X_0) + \frac{1}{2}S^{(2)}(X_0)(X-X_0)^2 + \frac{1}{6}S^{(3)}(X_0)(X-X_0)^3\right\} - H^4\{T(X_0) + T^{(1)}(X_0)(X-X_0)\}, \tag{7}$$

where

$$S^{(k)}(X_0) = \left[\frac{d^k}{dX^k}S(X)\right]_{X=X_0}, \tag{8}$$

and

$$T^{(1)}(X_0) = \left[\frac{d}{dX}T(X)\right]_{X=X_0}. \tag{9}$$

Higher-order terms missing on the right-hand side of Eq. 7 are obviously negligible.

Since Eq. 4 is an eigen-equation derived from an Hermitian matrix, all roots of Eq. 7 must be real for an arbitrary small value of H. Necessary conditions for the existence of four real roots are

$$S(X_0) = 0, \tag{10}$$

$$S^{(1)}(X_0) = 0, \tag{11}$$

and

$$S^{(2)}(X_0) < 0. \tag{12}$$

Otherwise, Eq. 7 would not always have four real roots. This can easily be proved by drawing graphs of the following two functions found in Eq. 7:

$$Y = (X-X_0)^4, \tag{13}$$

and

$$Y = -H^2\left\{S(X_0) + S^{(1)}(X_0)(X-X_0) + \frac{1}{2}S^{(2)}(X_0)(X-X_0)^2 + \frac{1}{6}S^{(3)}(X_0)(X-X_0)^3\right\}. \tag{14}$$

For an arbitrary small H value, Eqs. 10—12 are necessary for the two graphs to intersect fully with each other. In fact, secular equations of **1** and **2** satisfy these conditions. Then, Eq. 7 becomes

$$(X-X_0)^4 + \frac{H^2}{6}S^{(3)}(X_0)(X-X_0)^3 + \frac{H^2}{2}S^{(2)}(X_0)(X-X_0)^2 + H^4 T^{(1)}(X_0)(X-X_0) + H^4 T(X_0) = 0. \tag{15}$$

This is an algebraic equation in $(X-X_0)$ of degree 4.

Let the degenerate orbital energy X_0 split into X_1, X_2, X_3, and X_4, and the following expression is deduced straightforwardly from the coefficient of $(X-X_0)^3$ in Eq. 15:

$$\sum_{j=1}^{4}(X_j - X_0) = -\frac{H^2}{6}S^{(3)}(X_0). \quad (16)$$

Consequently, the sum of the energies of eight π electrons in these four orbitals is

$$\varepsilon(H) = 2\sum_{j=1}^{4}X_j = 8X_0 - \frac{H^2}{3}S^{(3)}(X_0). \quad (17)$$

It is to be noted that $\varepsilon(H)$ is independent of $T(X)$. More explicitly, $\varepsilon(H)$ is expressed as

$$\varepsilon(H) = 8X_0 + \frac{3U^{(1)}(X_0)V^{(2)}(X_0) - U(X_0)V^{(3)}(X_0)}{3U(X_0)^2}H^2, \quad (18)$$

where

$$U^{(1)}(X_0) = \left[\frac{d}{dX}U(X)\right]_{X=X_0} \quad (19)$$

and

$$V^{(k)}(X_0) = \left[\frac{d^k}{dX^k}P_{G-r_i}(X, 0)\theta_i^2\right]_{X=X_0}. \quad (20)$$

Finally, we obtain the following formula for a susceptibility contribution from eight π electrons in quadruply degenerate orbitals:

$$\Delta\chi_G = \left[\frac{d^2}{dH^2}\varepsilon(H)\right]_{H=0} = \frac{2}{3}\frac{3U^{(1)}(X_0)V^{(2)}(X_0) - U(X_0)V^{(3)}(X_0)}{U(X_0)^2}. \quad (21)$$

Susceptibility contributions from nondegenerate and doubly degenerate orbitals can be estimated using formulas published by Berthier *et al.*[1] or by us.[5] London susceptibilities of compounds **1** and **2** can now be calculated easily without factorization of their field-dependent secular determinants. They are 2.730 χ_0 and 4.120χ_0 for **1** and **2**, respectively, where χ_0 is London susceptibility of the benzene conjugated system. These values are identical with those reported by Berthier *et al.*[1,3]

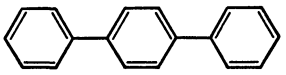

1

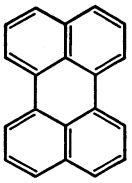

2

The following relationships are derived from Eqs. 10 and 11:

$$V(X_0) = \sum_{i}^{G}P_{G-r_i}(X_0, 0)\theta_i^2 = 0, \quad (22)$$

and

$$V^{(1)}(X_0) = \left[\frac{d}{dX}\sum_{i}^{G}P_{G-r_i}(X_0, 0)\theta_i^2\right]_{X=X_0} = 0. \quad (23)$$

These characterize quadruply degenerate orbitals.

A susceptibility contribution from six π electrons in triply degenerate orbitals can be formulated graph-theoretically in a similar way. It is given as

$$\Delta\chi_G = \frac{4U^{(1)}(X_0)V^{(1)}(X_0) - 2U(X_0)V^{(2)}(X_0)}{U(X_0)^2}, \quad (24)$$

where $U(X)$ is defined by

$$P_G(X, 0) = (X - X_0)^3U(X). \quad (25)$$

This is mathematically identical with the formula derived by Berthier *et al.*[1]

References

1) G. Berthier, M. Mayot, A. Pullman, and B. Pullman, *J. Phys. Radium*, **13**, 15 (1952).
2) F. London, *J. Phys. Radium*, **8**, 397 (1937).
3) B. Pullman and A. Pullman, "Les Théories Electroniques de la Chimie," Masson et Cie, Paris (1952), Chap. 9.
4) J. Aihara, *J. Am. Chem. Soc.*, **101**, 558 (1979).
5) J. Aihara, *J. Am. Chem. Soc.*, **101**, 5913 (1979).
6) J. Aihara, *Bull. Chem. Soc. Jpn.*, **53**, 1163 (1980).
7) J. Aihara, *Bull. Chem. Soc. Jpn.*, **54**, 1245 (1981).
8) J. Aihara, *J. Am. Chem. Soc.*, **103**, 5704 (1981).
9) J. Aihara, *Pure Appl. Chem.*, **54**, 1115 (1982).
10) In this note, all orbital energies are given (in units of β) relative to the carbon Coulomb integral.
11) H. Sachs, *Publ. Math. (Debrecen)*, **11**, 119 (1964); A. Graovac, I. Gutman, N. Trinajstić, and T. Živković *Theor. Chim. Acta*, **26**, 67 (1972).

Dimeric Copper(II) Acetate Complexes of Thiazoles and Oxazoles

Tadashi Tokii and Yoneichiro Muto*

Department of Chemistry, Faculty of Science and Engineering, Saga University, Saga 840

(Received October 18, 1982)

Synopsis. Copper(II) acetate monoadducts, $Cu(CH_3COO)_2 \cdot L$ (L=thiazole, benzothiazole, benzoxazole, 2-methylbenzothiazole, 2-methylbenzoxazole, 2,4-dimethylthiazole, or 2,4,5-trimethylthiazole) were prepared, and they all show antiferromangnetism ($-2J=318$—$344\ cm^{-1}$) of copper(II) dimer type. The variation in magnetic interaction with the steric nature of the ligand, L, is discussed.

The recent X-ray studies on dimeric copper(II) carboxylate adducts with pyridine analogues have demonstrated that ortho-substituents in the pyridine ring of the ligands make copper atoms displace out of the plane of the four carboxylate-oxygen atoms toward the nitrogen atom by the mutual repulsion between the substituents and the oxygen atoms.[1,2] Under such conditions the steric effect is expected to enhance the metal–metal distance; in fact, the Cu–Cu distance in dimeric copper(II) acetate adducts with pyridine (py), quinoline (quin), and 2-picoline (2-pic) increases in the order, py (2.630 Å)[3]<quin (2.652 Å)[1]<2-pic (2.671 Å),[4] as expected from the effectiveness of the steric effect. However, no significant correlation has been observed between the Cu–Cu distance and the magnitude of the singlet-triplet separation ($-2J$) in these adducts. In this work we prepared seven copper(II) acetate adducts, $Cu(CH_3COO)_2 \cdot L$, where L= thiazole (tz), benzothiazole (btz), benzoxazole (boz), 2-methylbenzothiazole (2-mbtz), 2-methylbenzoxazole (2-mboz), 2,4-dimethylthiazole (2,4-dmtz) or 2,4,5-trimethyloxazole (2,4,5-tmoz), and measured their magnetic susceptibilities as a function of temperature in order to obtain information on the effect of the ortho-substituents in L upon the magnetic interaction.

Experimental

Synthesis. A typical synthetic method is as follows. A solution of the ligand L (5 mmol) in ethanol (5 ml) was added to a solution of $Cu(CH_3COO)_2 \cdot H_2O$ (5 mmol) in ethanol (30 ml). After keeping the solution overnight at *ca.* 5 °C in a freezer, the separated green crystals were collected, washed with ethanol and dried at *ca.* 60 °C. **1.** $Cu(CH_3COO)_2 \cdot (tz)$. Found: C, 31.66; H, 3.57; N, 5.05; Cu, 23.69%. Calcd for $C_7H_9NO_4SCu$: C, 31.52; H, 3.40; N, 5.25; Cu, 23.82%. **2.** $Cu(CH_3COO)_2 \cdot (btz)$. Found: C, 41.66; H, 3.70; N, 4.34; Cu, 20.01%. Calcd for $C_{11}H_{11}NO_4SCu$: C, 41.70; H, 3.50; N, 4.42; Cu, 20.06%. **3.** $Cu(CH_3COO)_2 \cdot (boz)$. Found: C, 43.80; H, 3.84; N, 4.45; Cu, 21.03%. Calcd for $C_{11}H_{11}NO_5Cu$: C, 43.93; H, 3.69; N, 4.66; Cu, 21.13%. **4.** $Cu(CH_3COO)_2 \cdot (2\text{-mbtz})$. Found: C, 43.43; H, 3.95; N, 4.16; Cu, 19.22%. Calcd for $C_{12}H_{13}NO_4SCu$: C, 43.57; H, 3.96; N, 4.23; Cu, 19.21%. **5.** $Cu(CH_3COO)_2 \cdot (2\text{-mboz})$. Found: C, 45.65; H, 4.12; N, 4.46; Cu, 20.26%. Calcd for $C_{12}H_{13}NO_5Cu$: C, 45.79; H, 4.16; N, 4.45; Cu, 20.19%. **6.** $Cu(CH_3COO)_2 \cdot (2,4\text{-dmtz})$. Found: C, 36.87; H, 4.50; N, 4.67; Cu, 21.71%. Calcd for $C_9H_{13}NO_4SCu$: C, 36.67; H, 4.44; N, 4.75; Cu, 21.55%. **7.** $Cu(CH_3COO)_2 \cdot (2,4,5\text{-tmoz})$. Found: C, 40.90; H, 5.10; N, 4.73; Cu, 21.65%. Calcd for $C_{10}H_{15}NO_5Cu$: C, 41.02; H, 5.16; N, 4.78; Cu, 21.70%.

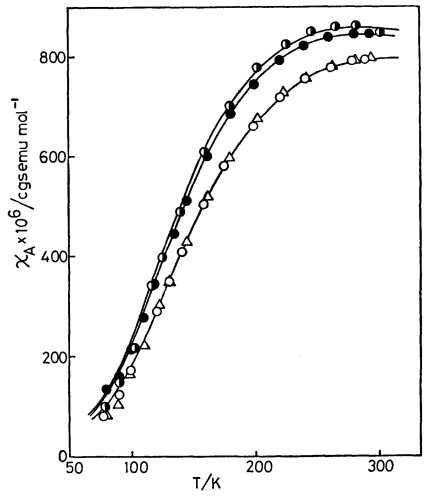

Fig. 1. Variation of magnetic susceptibilities with temperature.
△: $Cu(CH_3COO)_2 \cdot (tz)$, ○: $Cu(CH_3COO)_2 \cdot (btz)$, ◑: $Cu(CH_3COO)_2 \cdot (2\text{-mbtz})$, ●: $Cu(CH_3COO)_2 \cdot (2,4\text{-dmtz})$.
The solid curves were obtained as described in the text.

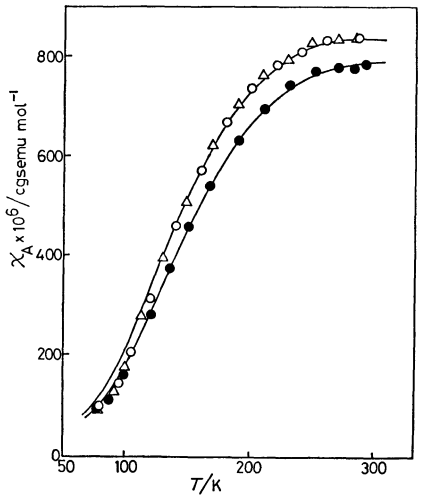

Fig. 2. Variation of magnetic susceptibilities with temperature.
●: $Cu(CH_3COO)_2 \cdot (boz)$, ○: $Cu(CH_3COO)_2 \cdot (2\text{-mboz})$, △: $Cu(CH_3COO)_2 \cdot (2,4,5\text{-tmoz})$.
The solid curves were obtained as described in the text.

Physical Measurement. Magnetic susceptibilities in the temperature range of 80—300 K were determined by the Gouy method. The correction for diamagnetic contributions was made by the use of Pascal's constant.[5] The cryomagnetic data are shown in Figs. 1 and 2 as plots of

Table 1. Magnetic data

	Complex	g	$-2J$/cm^{-1}
1	$Cu(CH_3COO)_2\cdot$(tz)	2.20	344
2	$Cu(CH_3COO)_2\cdot$(btz)	2.20	344
3	$Cu(CH_3COO)_2\cdot$(boz)	2.19	344
4	$Cu(CH_3COO)_2\cdot$(2-mbtz)	2.20	318
5	$Cu(CH_3COO)_2\cdot$(2-mboz)	2.20	327
6	$Cu(CH_3COO)_2\cdot$(2,4-dmtz)	2.20	322
7	$Cu(CH_3COO)_2\cdot$(2,4,5-tmoz)	2.20	327

the corrected molar magnetic susceptibility (χ_A) *vs.* the temperature (T).

Results and Discussion

Complexes **1**—**7** were readily isolated by the reaction of $Cu(CH_3COO)_2\cdot H_2O$ with the ligand in ethanol. However, under the similar conditions no adduct formation was observed between copper(II) acetate and benzo[*b*]thiophene or benzofuran. This finding indicates that the nitrogen atom in the ligand L is most probably the donor atom.

The variable-temperature magnetic susceptibility data were analyzed by the Bleaney-Bowers equation,

$$\chi_A = \frac{Ng^2\beta^2}{3kT}\left[1+\frac{1}{3}\exp\left(\frac{-2J}{kT}\right)\right]^{-1} + N\alpha. \quad (1)$$

where each symbol has the usual meaning. As can be seen in Figs. 1 and 2, the thermal magnetic data are well represented by Eq. 1. The g and $-2J$ values listed in Table 1 were evaluated from the best-fit of the experimental data to Eq. 1, assuming $N\alpha=60\times 10^{-6}$ cgs emu mol^{-1} (1 cgs emu mol$^{-1}=4\pi\times 10^{-6}$ m^3 mol^{-1}). On the basis of the magnetic behavior, a dimeric structure similar to that found in copper(II) acetate monohydrate can be assigned for the present acetate complexes.

Coordination of thiazole, benzothiazole or benzoxazole to the dimeric copper(II) acetate units will cause an increase in antiferromagnetic interaction as is seen in the $-2J$ value of the adducts, 344 cm^{-1}, a value somewhat larger than those reported for the well-characterized dimeric copper(II) acetate adducts (284—325 cm^{-1}).[6] It is also noted that the $-2J$ value of complex **2** is just the same as that of complex **1**; this suggests that the steric nature of the adjacent benzo group in benzothiazole does not exert any appreciable effect upon the magnitude of $-2J$. This observation is in accord with the fact that the $-2J$ of 320 cm^{-1} determined for $[Cu(CH_3COO)_2\cdot quin]_2$ is practically identical with that of 325 cm^{-1} found for $[Cu(CH_3COO)_2\cdot py]_2$.[6] On the other hand, the $-2J$ values for complexes **4**—**7** were found to fall in a rather low range of 318—327 cm^{-1}. For the mechanism of the magnetic interaction in dimeric copper(II) carboxylates, two models have been proposed: Cu–Cu direct exchange interaction, and superexchange interaction through the bridging carboxylato groups. The predominance of the latter mechanism has been recognized by some experimental evidence,[6-9] but it has also been suggested that the effect of the former interaction is not entirely negligible.[10] The direct interaction would be expected to decrease with increasing Cu–Cu separation, whereas the superexchange interaction may be affected by such structural features as the distances and angles within the Cu–O–C–O–Cu bridge and the geometry around the metal atom. In the present adducts, $Cu(CH_3COO)_2\cdot L$, the presence of methyl group at the 2-position of thiazole- or oxazole-ring will make the Cu–Cu distance increase with the displacement of the copper atom from its basal coordination plane toward the nitrogen atom in L, and will reduce both the direct and superexchange interactions. Thus, this steric effect seems to be the main factor for the decrease in the $-2J$ values of complexes **4**—**7** by 17—26 cm^{-1} as compared with those of complexes **1**—**3**.

Finally, it should be noted that the $-2J$ of complex **1** (344 cm^{-1}) is higher than that of $[Cu(CH_3COO)_2\cdot py]_2$ (325 cm^{-1}).[6] The pK_a of the terminal ligand of the former complex (2.44)[11] is lower than that of the latter (5.32).[12] We have also evaluated the $-2J$ of 341 cm^{-1} for dimeric copper(II) acetate adduct with 3,5-dichloropyridine (pK_a=0.67).[13] These facts are not in accord with the observation that, in the pyridine and picoline adducts of copper(II) propionate, the value of $-2J$ decreases as the pK_a of the terminal ligand decreases.[14] Thus, these magnetic data suggest that the $-2J$ in dimeric copper(II) carboxylate adducts is not a simple function of the base strength of the terminal ligand.

Refereaces

1) Yu. A. Simonov, V. I. Ivanov, A. V. Ablov, L. N. Mikova, and T. I. Malinovskii, *J. Struct. Chem.* (Engl. Transl.), **17**, 444 (1977).
2) J. A. Moreland and R. J. Doedens, *Inorg. Chem.*, **17**, 674 (1978).
3) G. A. Barclay and C. H. L. Kennard, *J. Chem. Soc.*, **1961**, 5244.
4) F. Pavelcik and F. Hanic, *J. Cryst. Mol. Struct.*, **8**, 59 (1978).
5) P. W. Selwood, "Magnetochemistry," Interscience Publishers, New York (1956), pp. 78 and 91.
6) R. J. Doedens, *Prog. Inorg. Chem.*, **21**, 209 (1976).
7) D. M. L. Goodgame, N. J. Hill, D. F. Marsham, A. C. Skapski, M. L. Smart, and P. G. H. Troughton, *J. Chem. Soc., Chem. Commun.*, **1969**, 629.
8) R. A. Zelonka and M. C. Baird, *Inorg. Chem.*, **11**, 134 (1972).
9) R. L. Beddoes, J. A. Connor, D. Dubowski, A. C. Jones, O. S. Mills, and R. Price, *J. Chem. Soc., Dalton Trans.*, **1979**, 781.
10) T. Asakawa, M. Inoue, K. Hara, and M. Kubo, *Bull. Chem. Soc. Jpn.*, **45**, 1054 (1972).
11) A. Albert, R. Goldacre, and J. Phillips, *J. Chem. Soc.*, **1948**, 2240.
12) G. J. Hawkins and D. D. Perrin, *J. Chem. Soc.*, **1962**, 1351.
13) T. Tokii and Y. Muto, unpublished data.
14) W. E. Marsh, G. O. Carlisle, and M. V. Hanson, *J. Inorg. Nucl. Chem.*, **39**, 1839 (1977).

Preparation and Molecular Structure of *cis*-β,*trans*(*sec*-*N*,*P*)-{(2-Aminoethyl)dimethylphosphine}(3,7-diazanonane-1,9-diamine)cobalt(III) Bromide Dihydrate

Tomoji Ohishi, Kazuo Kashiwabara, Haruko Ito,† Tasuku Ito,† and Junnosuke Fujita*

Department of Chemistry, Faculty of Science, Nagoya University, Chikusa-ku, Nagoya 464

† *Division of Applied Molecular Science, Institute for Molecular Science, Okazaki 444*

(Received November 27, 1982)

Synopsis. The reaction of *trans*-[$CoCl_2$(2,3,2-tet)]$^+$ (2,3,2-tet: 3,7-diazanonane-1,9-diamine) with (2-aminoethyl)-dimethylphosphine (edmp) afforded only one geometrical isomer of [Co(edmp)(2,3,2-tet)]$^{3+}$, the structure of which was determined by X-ray analysis to have the *cis*-β,*trans*-(*sec*-*N*,*P*) configuration.

Formation of cobalt(III)–phosphine complexes is often specific or selective concerning geometrical isomerism.[1,2] This note reports preparation and X-ray structure analysis of [Co(edmp)(2,3,2-tet)]$^{3+}$ (edmp: (2-aminoethyl)dimethylphosphine, 2,3,2-tet: 3,7-diazanonane-1,9-diamine) which is only one geometrical isomer formed by the reaction of *trans*-[$CoCl_2$(2,3,2-tet)]$^+$ with edmp.

Experimental

Preparation of the Complex. To an oxygen-free dimethyl sulfoxide solution (100 cm^3) of *trans*-[$CoCl_2$(2,3,2-tet)]-ClO_4[3] (340 mg, 0.84 mmol) was added an oxygen-free methanol solution (5 cm^3) of edmp[1] (91 mg, 0.87 mmol) with stirring under nitrogen atmosphere. After stirring for 2 h, the resulting orange solution was mixed with water (400 cm^3) and diethyl ether (100 cm^3) to extract unreacted edmp. The orange aqueous-dimethyl sulfoxide solution was diluted to 1 dm^3 with water and poured on a column (ϕ2.5×150 cm^2) of SP-Sephadex C-25. The product adsorbed was eluted with 0.2 mol dm^{-3} NaCl, giving two bands. The first yellow eluate was *fac*-[Co(edmp)$_3$]$^{3+}$.[1] The second orange eluate was evaporated to dryness under reduced pressure. The residue was extracted with methanol (200 cm^3). The extract was diluted with water (1 dm^3) and the solution was poured on a column (ϕ2.5×15 cm^2) of SP-Sephadex C-25. The complex adsorbed was eluted with 1 mol dm^{-3} KBr. The eluate was concentrated in a vacuum desiccator over P_4O_{10} to yield red-orange crystals, which were recrystallized from water and dried in air. Yield: *ca.* 50%. Found: C, 22.39; H, 5.93; N, 12.11%. Calcd for [Co(edmp)(2,3,2-tet)]$Br_3\cdot 2H_2O = C_{11}H_{36}N_5Br_3CoO_2P$: C, 22.02; H, 6.05; N, 11.67%. The complex in aqueous solution shows two d-d absorption bands at 21980 cm^{-1} (log ε=2.37) and 28740 cm^{-1} (log ε=2.41).

X-Ray Analysis. Crystal data: monoclinic, $P2_1/a$, a=17.719(2), b=8.776(1), c=14.966(1) Å, β=108.01(1)°, V=2213.2(4) Å^3, Z=4, D_m=1.803, D_x=1.801 g cm^{-1}, μ(Mo $K\alpha$)=6.63 mm^{-1}. A specimen with dimensions 0.32×0.34×0.37 mm^3 was used for the X-ray work. Diffraction data were collected on a Rigaku AFC-5 diffractometer with graphite monochromatized Mo $K\alpha$ radiation. Within the range $2\theta<60°$, 3687 independent reflections with $F_o>3\sigma(F_o)$ were obtained. Intensities were corrected for Lorentz and polarization factors, and for absorption.

The structure was solved by the direct method (MULTAN). The method used in the solution and refinement of the structure were standard and have been described previously.[4] Hydrogen atoms except for those bonded to one of water molecules of crystallization were located by the difference syntheses, and were included in the final refinement with the isotropic temperature factors. The final R indices were R=0.044 and R_w=0.043. Table 1 lists the atomic parameters.[5] The F_o-F_c data, final thermal parameters, and hydrogen atomic coordinates are preserved by the Chemical Society of Japan (Document No. 8322).

Table 1. Fractional coordinates (×10^5) with B_{eq}

Atom	x	y	z	B_{eq}/Å^2
Br(1)	40675(3)	18613(7)	44140(4)	4.1
Br(2)	14171(4)	2287(6)	28560(5)	4.2
Br(3)	34800(3)	85424(8)	5943(4)	3.9
Co	22676(3)	49733(7)	24400(4)	1.5
P	9522(7)	53602(13)	19744(8)	2.0
N(1)	21091(22)	29983(43)	17679(26)	2.4
N(2)	34350(21)	44867(44)	26961(24)	2.2
N(3)	24885(20)	68967(40)	31936(24)	1.9
N(4)	22829(20)	39577(40)	36157(24)	2.0
N(5)	22264(20)	60836(44)	12609(24)	2.2
C(1)	28715(31)	22073(58)	18669(37)	3.3
C(2)	34954(29)	33893(63)	19620(36)	3.2
C(3)	40523(27)	56984(65)	28415(35)	3.1
C(4)	39689(28)	68929(63)	35329(35)	3.2
C(5)	32094(29)	77763(54)	32107(33)	2.7
C(6)	24608(26)	65486(54)	41709(29)	2.3
C(7)	26902(27)	49339(55)	44270(29)	2.4
C(8)	15748(30)	72228(55)	9203(33)	2.8
C(9)	8059(27)	64172(62)	8816(33)	3.1
C(10)	3328(29)	36911(61)	16604(39)	3.6
C(11)	4932(28)	64326(64)	26840(35)	3.2
O(1)	-9162(24)	63131(63)	-43288(32)	6.4
O(2)	-3070(49)	334(90)	7625(53)	13.9

Table 2. Bond lengths (l/Å) and angles (ϕ/°) and their estimated standard deviations

Co	-P	2.243(1)		N(2)	-C(3)	1.492(7)	
Co	-N(1)	1.980(4)		N(3)	-C(5)	1.486(6)	
Co	-N(2)	2.029(4)		N(3)	-C(6)	1.510(6)	
Co	-N(3)	2.000(4)		N(4)	-C(7)	1.479(6)	
Co	-N(4)	1.965(4)		N(5)	-C(8)	1.493(7)	
Co	-N(5)	1.997(4)		C(1)	-C(2)	1.490(8)	
P	-C(9)	1.828(6)		C(3)	-C(4)	1.512(8)	
P	-C(10)	1.803(6)		C(4)	-C(5)	1.498(8)	
P	-C(11)	1.791(6)		C(6)	-C(7)	1.491(7)	
N(1)	-C(1)	1.495(7)		C(8)	-C(9)	1.520(8)	
N(2)	-C(2)	1.490(7)					
P	-Co -N(1)	90.2(1)		Co	-P -C(10)	116.6(2)	
P	-Co -N(4)	94.1(1)		Co	-N(5) -C(8)	116.2(3)	
P	-Co -N(2)	172.5(1)		Co	-N(2) -C(3)	122.4(3)	
P	-Co -N(3)	92.9(1)		Co	-N(3) -C(6)	108.4(3)	
P	-Co -N(5)	84.3(1)		C(9)	-P -C(10)	105.8(3)	
N(1)	-Co -N(3)	175.9(2)		C(9)	-P -C(11)	107.4(3)	
N(2)	-Co -N(3)	93.5(2)		C(10)	-P -C(11)	103.3(3)	
N(3)	-Co -N(4)	86.1(2)		P	-C(9) -C(8)	108.9(4)	
N(1)	-Co -N(4)	91.1(2)		C(2)	-N(2) -C(3)	110.6(4)	
N(2)	-Co -N(4)	90.3(2)		C(5)	-N(3) -C(6)	111.9(4)	
N(3)	-Co -N(5)	91.9(2)		N(1)	-C(1) -C(2)	108.0(4)	
N(1)	-Co -N(2)	83.6(2)		N(2)	-C(2) -C(1)	107.5(4)	
N(1)	-Co -N(5)	91.0(2)		N(2)	-C(3) -C(4)	111.8(4)	
N(2)	-Co -N(5)	91.5(2)		C(3)	-C(4) -C(5)	114.0(5)	
N(4)	-Co -N(5)	177.4(2)		N(3)	-C(5) -C(4)	114.8(4)	
Co	-P -C(9)	101.6(2)		N(3)	-C(6) -C(7)	110.7(4)	
Co	-N(1) -C(1)	112.1(3)		N(4)	-C(7) -C(6)	108.3(4)	
Co	-N(2) -C(2)	107.4(3)		N(5)	-C(8) -C(9)	106.9(4)	
Co	-N(3) -C(5)	117.7(3)		Co	-N(4) -C(7)	109.9(3)	
Co	-P -C(11)	120.9(2)					

Results and Discussion

Figure 1 shows a perspective view of the complex ion. The 2,3,2-tet ligand coordinates to the cobalt(III) ion with the four nitrogen atoms to form *cis*-β

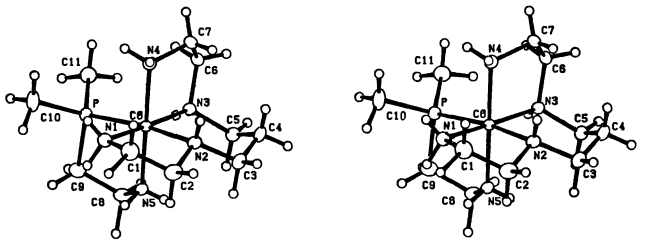

Fig. 1. A stereo view of $[Co(edmp)(2,3,2\text{-tet})]^{3+}$.

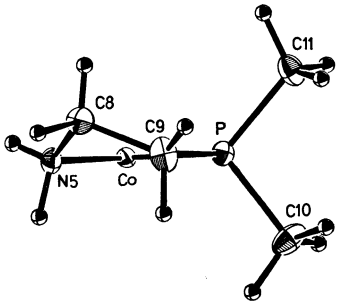

Fig. 2. Conformation of the edmp chelate ring.

configuration, and the phosphorus atom of edmp takes the position *trans* to the secondary amine (N2) of 2,3,2-tet. The bond distances and angles are listed in Table 2. The Co–N(2) distance of 2.029(4) Å is the longest among those reported for analogous 2,3,2-tet complexes, $(+)_{470}$-*Λ-cis-β*-$[Co(NO_2)_2\{(R)\text{-}NH_2CH_2CH_2NHCH(CH_3)CH_2CH_2NHCH_2CH_2NH_2\}]Br$ (2.004(4) Å)[6] and $(-)_{546}$-*Λ-cis-β*-$[Co(C_2O_4)\{(R,R)\text{-}NH_2CH_2CH_2NHCH(CH_3)CH_2CH(CH_3)NHCH_2CH_2NH_2\}]ClO_4$ (1.99(1) Å).[7] The elongation of the Co–N(2) bond can be attributed to trans influence of the phosphorus atom of edmp. Similar elongations of Co–N bonds have been observed in $(+)_{589}$-*Λ-fac*-$[Co(edmp)_3]Br_3\cdot 3H_2O$ (2.041 Å)[1] and $(+)_{589}$-*Λ*-$[Co(en)_2\{(CH_3)_2PCH_2CH_2P(CH_3)_2\}]Br_3\cdot 1.5H_2O$ (2.032 Å).[8] The Co–P distance of 2.243 Å is similar to 2.237(5)[1] and 2.256(3) Å[8] in the complexes given above.

The chelate rings of 2,3,2-tet and edmp in the *Λ*-complex adopt (*δ*-gauche)(chair)(*δ*-gauche) and pseudo *δ*-gauche conformations, respectively (Figs. 1 and 2). Bond angles around the phosphorus atom deviate argely from the normal tetrahedral angle; Co–P–C(11):120.9(2)°, Co–P–C(10):116.6(2)°, Co–P–C(9):101.6(2)°, and C(10)–P–C(11):103.3(3)°. These deviations seem to come from a crowded structure around the phosphorus atom.

The other *cis-β,cis(sec-N,P)* isomer was not formed. Molecular models indicate that this isomer has big steric hindrance among one methyl group and axial hydrogen atoms on C(3) and C(5). Attempts to prepare $[Co\{(CH_3)_2PCH_2CH_2P(CH_3)_2\}(2,3,2\text{-tet})]^{3+}$, which has the $-P(CH_3)_2$ group at the *cis(sec-N,P)* position, were unsuccessful, no reaction taking place between *trans*-$[CoCl_2(2,3,2\text{-tet})]^+$ and the diphosphine ligand. No *cis-α* isomer of a 2,3,2-tet complex has been reported probably because of strong preference of the chair conformation of the six-membered chelate ring. Thus the $[Co(edmp)(2,3,2\text{-tet})]^{3+}$ complex forms only one geometrical isomer of the *cis-β,trans(sec-N,P)* configuration.

This work was supported by the research grant of the Takeda Science Foundation.

References

1) I. Kinoshita, K. Kashiwabara, J. Fujita, K. Matsumoto, and S. Ooi, *Bull. Chem. Soc. Jpn.*, **54**, 2683 (1981).
2) K. Kashiwabara, K. Katoh, T. Ohishi, J. Fujita, and M. Shibata, *Bull. Chem. Soc. Jpn.*, **55**, 149 (1982).
3) B. Bosnich, R. D. Gillard, E. D. McKenzie, and G. A. Webb, *J. Chem. Soc., A*, **1966**, 1311; H. G. Hamilton, Jr., and M. D. Alexander, *Inorg. Chem.*, **5**, 2060 (1966).
4) T. Ito, K. Toriumi, and H. Ito, *Bull. Chem. Soc. Jpn.*, **54**, 1096 (1981).
5) The value of B_{eq} for O(2) of water of crystallization is relatively large. When the occupancy factor of O(2) was assumed to be 0.5 in the least-squares calculation, a normal thermal parameter ($B_{eq}=6.0$ Å^2) was obtained. The values observed in elemental analysis are closer to the values calculated as the sesqui hydrate (C, 22.35; H, 5.97; N, 11.85%) rather than those for the dihydrate (see text). These facts indicate that about 25% of water of crystallization are lost randomly from the crystal lattice.
6) P. W. R. Corfield, J. C. Dabrowiak, and E. S. Gore, *Inorg. Chem.*, **12**, 1734 (1973).
7) S. Yano, A. Fujioka, M. Yamaguchi, and S. Yoshikawa, *Inorg. Chem.*, **17**, 14 (1978).
8) S. Ohba, Y. Saito, T. Ohishi, K. Kashiwabara, and J. Fujita, *Acta Crystallogr., Sect. C*, **39**, 49 (1983).

Preparation and Characterization of Cobalt(III)–Phosphine Complexes of the Type [Co(CN)$_2$(acetylacetonate)(L)] (L: Tertiary 2-Aminoethylphosphines, and 1,2- and 1,3-Diphosphines)

Tomoji Ohishi, Kazuo Kashiwabara, and Junnosuke Fujita*

Department of Chemistry, Faculty of Science, Nagoya University, Chikusa-ku, Nagoya 464

(Received November 29, 1982)

Synopsis. Four new cobalt(III)-phosphine complexes of the type [Co(CN)$_2$(acetylacetonate)(L)] (L= $NH_2CH_2CH_2P(C_6H_5)_2$, $NH_2CH_2CH_2P(CH_3)_2$, $(C_6H_5)_2PCH{=}CHP(C_6H_5)_2$, and $(C_6H_5)_2PCH_2CH_2CH_2P(C_6H_5)_2$) were prepared. The geometrical structures of the 2-aminoethylphosphine, and 1,2- and 1,3-diphosphine complexes were assigned to have *trans(C,N)* and *cis* configurations, respectively on the basis of the ^{1}H and ^{13}C NMR spectra.

In previous papers,[1,2] we reported usefulness of ^{1}H and ^{13}C NMR spectra for assigning geometrical structures of mixed cobalt(III)–phosphine complexes. In order to extent such studies, we have prepared mixed cobalt(III)–phosphine complexes of the type [Co(CN)$_2$(acac)(L)], where acac denotes an acetylacetonate ion, and L is $NH_2CH_2CH_2P(C_6H_5)_2$(edpp), $NH_2CH_2CH_2P(CH_3)_2$(edmp), $(C_6H_5)_2PCH{=}CHP(C_6H_5)_2$(dpee), $(C_6H_5)_2PCH_2CH_2P(C_6H_5)_2$(dppe), or $(C_6H_5)_2PCH_2CH_2CH_2P(C_6H_5)_2$(dppp), and assigned their geometrical structures by means of ^{1}H and ^{13}C NMR techniques.

Experimental

The edpp[2] and edmp[3] ligands were prepared by the methods reported and handled under nitrogen atmosphere until they formed the cobalt(III) complexes. The dpee, dppe, and dppp ligands were purchased from Strem Chemicals Inc. Absorption, and ^{1}H and ^{13}C NMR spectra were recorded on a Hitachi 323 spectrophotometer, and JEOL JNM-PMX 60 and JNM-FX 100 spectrometers, respectively.

[Co(CN)$_2$(acac)(edpp)]·H$_2$O. A solution of K[Co(CN)$_2$(acac)$_2$][4] (638 mg, 1.8 mmol) and edpp (282 mg, 1.2 mmol) in oxygen-free methanol (100 cm^3) was stirred for 4 h at 50 °C. Water (400 cm^3) and diethyl ether (100 cm^3) were added to the solution to extract the unreacted edpp. The aqueous solution was passed through columns of SP-Sephadex C-25 and DEAE Sephadex A-25 ion exchangers successively to remove charged species. The effluent was evaporated to dryness under reduced pressure, and the residue was extracted with a small amount of methanol. The extract was chromatographed with an alumina column (ϕ1 cm×30 cm) and an eluent of benzene-ethanol (10:1), giving three orange bands. The complexes in the first and last bands were too small in the amount and not isolated. The eluate of the main second band was concentrated under reduced pressure to yield orange crystals of the complex. Yield: *ca.* 10%. Found: C, 54.69; H, 5.31; N, 8.98%. Calcd for $C_{21}H_{25}N_3CoO_3P$: C, 55.15; H, 5.51; N, 9.19%. The complex is hardly soluble in water, but soluble in common organic solvents.

[Co(CN)$_2$(acac)(edmp)]·1/2 H$_2$O. A solution of K[Co(CN)$_2$(acac)$_2$] (656 mg 1.9 mmol) and edmp (198 mg, 0.86 mmol) in oxygen-free methanol (80 cm^3) was stirred for 10 h at room temperature. The unreacted edmp and charged species in the resulting solution were removed by the procedures described above. The methanol extract containing only noncharged species was chromatographed with a column (ϕ2 cm×40 cm) of LH-20 Sephadex and an eluent of benzene-ethanol (10:1), yielding only one yellow-orange band. The complex was very soluble in water and common organic solvents, so that it was obtained as powder by evaporating the eluate to dryness. Yield: *ca.* 10%. Found: C, 40.89; H, 6.62; N, 12.54%. Calcd for $C_{11}H_{20}N_3CoO_{2.5}P$: C, 40.75; H, 6.22; N, 12.96%.

In the preparation of these edpp and edmp complexes, use of an equimolar amount of the aminoalkylphosphine ligand decreases the yield of the desired complex, affording dicyanobis(aminoalkylphosphine) complexes. No such reactions take place between [Co(CN)$_2$(acac)$_2$]$^-$ and diphosphine ligands as described below.

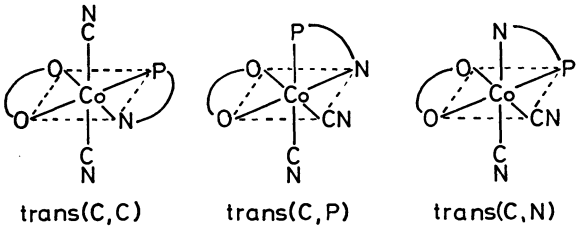

Fig. 1. Geometrical isomers of [Co(CN)$_2$(acac)(edpp or edmp)].

[Co(CN)$_2$(acac)(dpee)]·CHCl$_3$. This complex was prepared by a method similar to that for [Co(CN)$_2$(acac)(dppe)],[1] using K[Co(CN)$_2$(acac)$_2$] (348 mg, 1 mmol) and dpee (396 mg, 1 mmol), and recrystallized from chloroform. Yield: *ca.* 40%. Found: C, 56.31; H, 3.63; N, 3.58%. Calcd for $C_{34}H_{30}N_2CoCl_3O_2P_2$: C, 56.26; H, 4.16; N, 3.68%. The complex is insoluble in water but soluble in common organic solvents.

[Co(CN)$_2$(acac)(dppp)]·C$_6$H$_6$. A mixture of K[Co(CN)$_2$(acac)$_2$] (303 mg, 0.87 mmol), dppp (359 mg, 0.87 mmol), and a small amount of active charcoal in oxygen-free methanol (100 cm^3) was stirred for 10 h at 50 °C, and filtered. The filtrate was evaporated to dryness under reduced pressure. The residue was extracted with hot benzene (50 cm^3). On standing at room temperature the extract gave orange crystals of the complex. Yield: *ca.* 10%. Found: C, 68.10; H, 5.34; N, 3.98%. Calcd for $C_{40}H_{39}N_2CoO_2P_2$: C, 68.57; H, 5.61; N, 4.00%. The complex is insoluble in water but soluble in common organic solvents.

[Co(CN)$_2$(acac)(dppe)] was prepared by the method reported.[1]

Results and Discussion

The [Co(CN)$_2$(acac)(edpp or edmp)] complex can have three geometrical isomers (Fig. 1). In this study, each of the edpp and edmp complexes formed only one isomer. The isomers were resolved partially by the chromatographic method of Norden[5] using an alumina–(+)-lactose column. In the ^{13}C NMR spectra, the edpp and edmp complexes show signals due to two kinds of the phenyl and methyl (on P) groups, respectively, the two substituents on the phosphorus atom being diastereomeric. Thus both isomers are chiral and have either the *trans(C,P)* or the *trans(C,N)* structure. Of these two structures, the edpp complex

Table 1. ^{1}H and ^{13}C NMR spectral data for $[Co(CN)_2(acac)(L)]$, chemical shifts (δ/ppm) and ^{13}C-^{31}P coupling constants (J/Hz) in parentheses[a)]

	^{1}H NMR		^{13}C NMR					
	acac		acac			L		
L	CH_3	CH	CH_3	CH	CO	P-CH_2- or P-CH=	N-CH_3	P-CH_3
edpp[b)]	1.50	5.41	26.5	99.9	186.5	30.3(d, 28.1)	40.2	
	2.04		27.6(d, 5.0)		190.1(d, 2.4)			
edmp	1.97	5.67	27.4	99.9	191.0	33.3(d, 26.9)	41.9	8.4(d, 33.0)
	2.15		27.8(d, 6.1)		191.5(b)			13.7(d, 39.1)
dpee	0.82	4.90	26.2	99.5	187.5	146.1(61.6)[c)]		
	1.99		27.7(d, 6.1)		190.0(d, 2.6)	148.0(69.6)[c)]		
dppe	1.11	4.96	26.7	99.5	187.5	23.3(36.6)[c)]		
	1.93		27.7(d, 6.1)		190.0(d, 2.4)	27.5(46.6)[c)]		
dppp	1.47	5.16	26.9	99.6	186.2	26.5(80.5)[c)]		
	1.57		27.2(d, 6.1)		189.5(d, 2.4)	27.3(120.9)[c)]		

a) Solvent: $CDCl_3$ except for the edmp complex (CD_3OD), internal reference: TMS, d: doublet, b: broad. b) For the phenyl part,[2)] P-C_1: 126.5(d, 48.8), 127.9(d, 57.3), o-C: 131.1(d, 8.6), 131.7(d, 8.6), m-C: 128.3(d, 10.8), 128.8(d, 11.0), p-C: 132.5(d, 3.7), 133.1(d, 3.7). c) J represents $|J_{AX}+J_{BX}|$ of an ABX system.

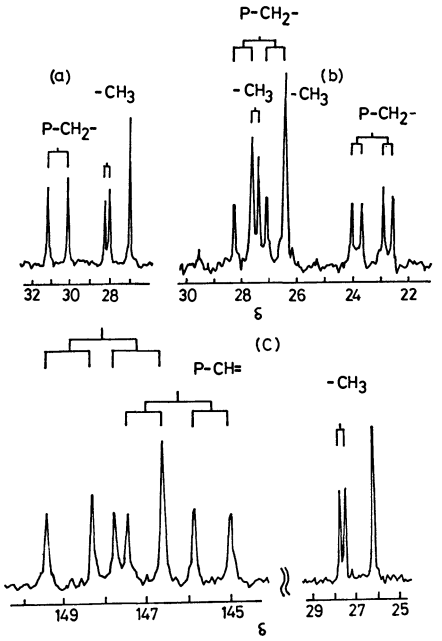

Fig. 2. ^{13}C NMR spectra of $[Co(CN)_2(acac)(L)]$. L: edpp(a), dppe(b), and dpee(c).

can be assigned to the *trans(C,N)* isomer from the ^{1}H NMR spectrum (Table 1). The methine proton of acac in this complex is observed at a fairly lower field than those of the corresponding diphosphine complexes and one methine proton of $[Co(acac)_2(edpp)]^+$ (4.93 ppm).[2)] One phenyl group of edpp in $[Co(acac)_2(edpp)]^+$ is disposed over one acac ring and its methine proton is shielded by this phenyl group to resonate at a high field. Thus $[Co(CN)_2(acac)(edpp)]$ has no phenyl group over the acac ring, and is assigned to the *trans(C,N)* isomer. This assignment is supported by the ^{13}C NMR spectrum. Each one of the two carbonyl and two methyl carbons of acac in this complex shows a doublet signal due to the three-bond and four-bond ^{13}C-^{31}P couplings, respectively (Fig. 2(a)). Such couplings have been observed only when C and P atoms are situated in *trans* positions to each other through central Co(III).[2)] The edmp complex shows similar patterns in the carbonyl and methyl regions of acac. Thus it is concluded that both edpp and edmp complexes have the *trans(C,N)* structure in which the phosphino group takes the position *trans* to one of the oxygen donor atoms of acac.

The structures of the diphosphine complexes can be assigned in a similar manner to *cis* configuration from the ^{1}H and ^{13}C NMR spectra. The ^{13}C NMR spectra of the complexes show two kinds of signal due to the methyl group and doublet signals due to one carbonyl and one methyl carbons. Furthermore, the methylene and methine carbons bonded to the P atom become a quartet, the two P atoms of the diphosphine ligand being non-equivalent. All these features support conclusively *cis* configuration for the diphosphine complexes.

The data for the first absorption bands of the complexes are as follows (cm^{-1} (log ε)); edpp: 23250(2.65), edmp: 24170(2.80), dpee: 23420(3.07), dppe: 23360 (3.12), dppp:23250(3.03). Thus the spectrochemical series of the ligands is edpp, dppp<dppe<dpee< edmp.

This work was supported by the research grant of the Takeda Science Foundation.

References

1) K. Kashiwabara, K. Katoh, T. Ohishi, J. Fujita, and M. Shibata, *Bull. Chem. Soc. Jpn.*, **55**, 149 (1982).

2) K. Kashiwabara, I. Kinoshita, T. Ito, and J. Fujita, *Bull. Chem. Soc. Jpn.*, **54**, 725 (1981).

3) I. Kinoshita, K. Kashiwabara, J. Fujita, K. Matsumoto, and S. Ooi, *Bull. Chem. Soc. Jpn.*, **54**, 2683 (1981).

4) H. Nishikawa, K. Konya, and M. Shibata, *Bull. Chem. Soc. Jpn.*, **41**, 1492 (1968).

5) B. Norden, *Inorg. Nucl. Chem. Lett*, **4**, 387 (1975).

Catalytic Hydrogenolysis of 1,1-Difluoro-2-phenyl- and 1,1-Difluoro-3-methyl-2-phenylcyclopropane

Koji Isogai,* Naomi Nishizawa, Tetsuji Saito, and Jun-ichi Sakai

Department of Applied Chemistry, Faculty of Engineering, Niigata University, Ikarashi, Niigata 950-21

(Received August 19, 1982)

Synopsis. The title compounds were hydrogenolyzd over PdO or Raney nickel. The C_2–C_3 bond of the cyclopropane ring underwent cleavage exclusively over the both catalysts. The contribution of the fluorine substituent to the lengthening and weakening the C_2–C_3 bond of the cyclopropane ring seems to become a dominant factor in the regioselectivity.

In a previous paper[1] we reported that the palladium oxide (PdO)-catalyzed hydrogenolysis of 1,1-dichloro-3-methyl-2-phenylcyclopropane caused exclusive cleavage of the C_2–C_3 bond, whereas both the C_1–C_2 and C_2–C_3 bonds were cleaved competitively using Raney nickel (R-Ni) as a catalyst.

In this paper, we wish to report that the regioselective cyclopropane ring cleavage occurs in the catalytic hydrogenolysis of 1,1-difluoro-2-phenylcyclopropane(**1**) and its 3-methyl derivative(**2**) by the use of PdO and R-Ni. The products arising from the C_2–C_3 bond cleavage of the cyclopropane ring were obtained exclusively.

The results are given in Tables 1 and 2. PdO-catalyzed hydrogenolysis of **1** gave propylbenzene(**1a**), 2-fluoro-1-phenylpropane(**1b**), and 2,2-difluoro-1-phenylpropane(**1c**). The addition of a large amount of potassium hydroxide reduced the rate of hydrogenolysis of **1** and gave a substantial amount of (*Z*)-2-fluoro-1-phenylpropene(**1d**). **1d** was hydrogenated readily to give **1a** and **1b** in the absence of the additive. Hence **1d** seems to be a precursor of **1a** and **1b**. Using R-Ni as a catalyst, **1** gave mainly **1a** accompanied by **1b** and **1c** in the absence and the presence of a base such as triethylamine (TEA). The addition of ethylenediamine (EDA), however, inhibited effectively the hydrogenolysis of **1**.

The catalytic hydrogenolysis of **2** was slower than that of **1** and gave butylbenzene(**2a**), 2-fluoro-1-phenylbutane(**2b**), (*Z*)-2-fluoro-1-phenyl-1-butene(**2d**), and (*Z*)-2-fluoro-1-phenyl-2-butene(**2e**). 2,2-Difluoro-1-phenylbutane(**2c**) was detected only in the case of the PdO-catalyzed hydrogenolysis in the absence of the additive, although **2c** was identified only by use of GC-MS (H^+=170) because of the difficulty to isolate **2c** by VPC preparatively. The products show more clearly that the cyclopropane ring cleavage occurs selectively at the C_2–C_3 bond, and the olefins are the important intermediates as the precursors of the final products.

Table 1. Hydrogenolysis of **1**

Catalyst		Additive	Time	Composition of products(%)				
	(mg)	(mmol)	min	**1**	**1a**	**1b**	**1c**	**1d**
PdO	2	—	90	1.8	14.6	40.1	43.5	—
PdO	10	KOH 1.5	45	25.0	53.0	—	5.3	16.7
R-Ni	15	—	180	—	68.6	14.5	16.9	—
R-Ni	15	TEA 0.4	120	—	92.5	6.0	1.5	—
R-Ni	15	EDA 0.4	600	99.4	0.6	—	—	—

31 mg (0.2 mmol) of **1** was used for each hydrogenolysis.

Table 2. Hydrogenolysis of **2**

Catalyst		Additive	Time	Composition of products(%)				
	(mg)	(mmol)	min	**2**	**2a**	**2b**	**2d**	**2e**
PdO	10	—	60	33.7	22.9	38.8	—	4.6
PdO	10	KOH 1.5	60	20.0	46.7	19.9	3.2	10.2
R-Ni	15	—	60	45.7	48.6	5.7	—	—
R-Ni	15	TEA 0.6	60	8.3	89.1	2.6	—	—
R-Ni	15	EDA 0.6	60	100	—	—	—	—

168 mg (1 mmol) of **2** was used for each PdO-catalyzed hydrogenolysis. 34 mg (0.2 mmol) of **2** was used for each R-Ni-catalyzed hydrogenolysis.

According to Hoffmann's proposal,[2] using the Walsh model as a basis, the π-electron donating groups raise the electron density of antibonding LUMO to cause weakening of ring bonds together with an increase in their length. The available data of ring bond lengths (Å) for C_1–C_2 and C_2–$C_{2'}$ bonds in cyclopropane,[3] dichloro-,[4] fluoro-,[5] and difluorocyclopropanes[6] are reported, respectively, as follows; 1.514, 1.514; 1.532, 1.534; 1.494, 1.527; 1.464, 1.553. Analogous deformation of the cyclopropane ring is expected for **1** and **2**. Therefore, the affinity of fluorine to the catalysts seems to become a minor factor even when R-Ni is used, and the cleavage of the cyclopropane ring of **1** and **2** occurs at the weakened C_2–C_3 bond exclusively.

A plausible pathway of hydrogenolysis of **2** is shown in Scheme 1. From species (B), the elimination of fluoride ion (or fluorine atom) is caused by the electron transfer from C_2– or C_3–metal bond to give (C) and (D). In competition with the elimination, unlike dichloro derivatives, the combination of *s*-type adsorbed hydrogen[7] at the C_2– and C_3–metal bonds occurs to give **2c** *via* (E). As the adsorption of EDA to the nickel catalyst is more stronger than that of monoamines, the adsorption by C_1–C_2 or C_2–C_3 bond of cyclopropane ring seems to be not strong enough to promote the hydrogenolysis.

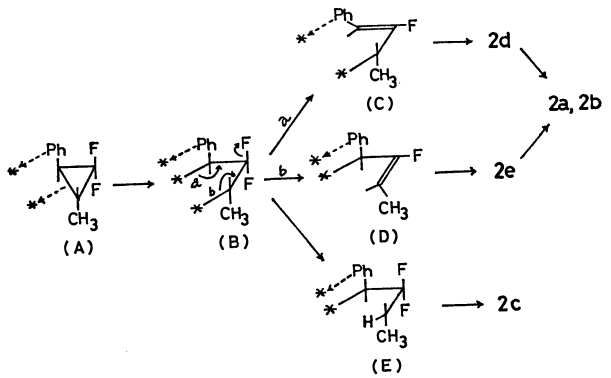

Scheme 1.

Experimental

*1,1-Difluoro-2-phenylcyclopropane (**1**).* **1** was prepared according to the method described in the literature.[8] The fraction, bp 55—65 °C/25 mmHg (1 mmHg=133.322 Pa) was purified preparatively by VPC. MS *m/e*: 154(M^+) ^{1}H NMR(CCl_4): δ=1.70 (2H, m, C(H)—C(H)—H), 2.67 (1H, m, C_6H_5-C(H)—C), 7.17 (5H, s, C_6H_5-). Found: C, 70.17; H, 5.31%. Calcd for $C_9H_8F_2$: C, 70.12; H, 5.23%.

*1,1-Difluoro-3-methyl-2-phenylcyclopropane (**2**).* **2** was prepared in a similar manner as **1** and the fraction, bp 45—50 °C/19 mmHg, was purified preparatively by VPC. MS *m/e*: 168(M^+), ^{1}H NMR(CCl_4): δ=1.36 (3H, m, CH_3-), 1.76 (1H, m, C(H)—C-CH_3), 2.16 (1H, m, C_6H_5-C(H)—C), 7.16 (5H, s, C_6H_5-). Found: C, 71.54; H, 6.05%. Calcd for $C_{10}H_{10}F_2$: C, 71.42; H, 5.99%.

General Procedure of Catalytic Hydrogenolysis. Substrates were hydrogenated over prescribed amount of PdO (Nippon Engelhard Co.) or R-Ni (alloy NDH, Kawaken Fine Chemical Co., was treated according to the W-5 method[9] and washed with water until free from the alkaline solution) catalyst in the presence or absence of additives, such as potassium hydroxide or amines, in methanol at room temperature under atmospheric pressure. The composition of products was determined by VPC (DOS, 2 m, 100 and 130 °C) at appropreate time intervals.

Identification of Products. After the hydrogenolysis proceeded appropriately, the reaction mixture was subjected to measurement of GC-MS. For measurement of NMR and elementary analysis, each component of the products was separated preparatively by VPC.

*Propylbenzene (**1a**)*: MS *m/e*: 120(M^+), which was identical with that of an authentic sample.

*2-Fluoro-1-phenylpropane (**1b**)*: MS *m/e*: 138(M^+), ^{1}H NMR (CCl_4): δ=1.24 (3H, dd, -CH_3, $J(CH_3$-H)=6.0 Hz, $J(CH_3$-F)=23 Hz), 2.65 (1H, dd, C_6H_5-C(H_a)—C(H_c)-, H_b, F, $J(H_a$-H_c)=6.0 Hz, $J(H_a$-F)=6.0 Hz), 2.98 (1H, dd, C_6H_5-C(H_b)—C(H_c)-, F, $J(H_b$-H_c)=6.0 Hz, $J(H_b$-F)=2.5 Hz), 4.73 (1H, mm, H_c-C(F)-CH_3, $J(H_c$-F)=48 Hz), 7.15 (5H, s, C_6H_5). Found: C, 77.68; H, 7.98%. Calcd for $C_9H_{11}F$: C, 78.23; H, 8.02%.

*2,2-Difluoro-1-phenylpropane (**1c**)*: MS *m/e*: 156(M^+), ^{1}H NMR(CCl_4): δ=1.46 (3H, t, -CF_2-CH_3, $J(CH_3$-F)=18 Hz), 3.08 (2H, t, C_6H_5-CH_2-CF_2-, $J(CH_2$-F)=15 Hz), 7.20 (5H, s, C_6H_5). Found: C, 69.12; H, 6.57%. Calcd for $C_9H_{10}F_2$: C, 69.21; H, 6.45%.

(Z)-*2-Fluoro-1-phenylpropene (**1d**)*: MS *m/e*: 136(M^+), ^{1}H NMR(CCl_4): δ=2.05 (3H, d, C(F)=C(H_3)-, $J(CH_3$-F)=15 Hz), 5.35 (1H, d, C_6H_5-C(F)=C(H)-, J(H-F)=36.5 Hz), 7.24 (5H, m, C_6H_5), IR(CCl_4): 1695 cm^{-1} (C=C). Found: C, 79.27; H, 6.98%. Calcd for C_9H_9F: C, 79.38; H, 6.66%.

*Butylbenzene (**2a**)*: MS *m/e*: 134(M^+), which was identical with that of an authentic sample.

*2-Fluoro-1-phenylbutane (**2b**)*: MS *m/e*: 152(M^+), ^{1}H NMR (CCl_4): δ=0.97 (3H, t, -CH_3), 1.15—1.94 (2H, m, -CHF-CH_2-CH_3), 2.67 (1H, dd, C_6H_5-C(H_a)—C(H_c)-, H_b, F, $J(H_a$-H_c)=6.0 Hz, $J(H_a$-F)=3.0 Hz), 3.01 (1H, ss, C_6H_5-C(H_a)—C(H_c)-, H_b, F, $J(H_b$-H_c)=6.0 Hz, $J(H_b$-F)=0 Hz), 4.50 (1H, mm, H_c-C(F)-F, $J(H_c$-F)=52 Hz), 7.15 (5H, s, C_6H_5). Found: C, 78.30; H, 8.49%. Calcd for $C_{10}H_{13}F$: C, 78.91; H, 8.61%.

(Z)-*2-Fluoro-1-phenyl-1-butene (**2d**)*: MS *m/e*: 150(M^+), ^{1}H NMR(CCl_4): δ=1.15 (3H, t, -CH_2-CH_3), 2.28 (2H, m, C=CF-CH_2-, J(H-F)=14 Hz), 5.30 (1H, ss, C_6H_5-C(H)=C-, F, J(H-F)=37 Hz), 7.27 (5H, m, C_6H_5), IR(CCl_4): 1685 cm^{-1} (C=C). Found: C, 79.86; H, 7.48%. Calcd for $C_{10}H_{11}F$: C, 79.79; H, 7.38%.

(Z)-*2-Fluoro-1-phenyl-2-butene (**2e**)*: MS *m/e*: 150(M^+), ^{1}H NMR(CCl_4): δ=1.60 (3H, mm, -CF=CH-CH_3, $J(CH_3$-H)=7.0 Hz), 3.42 (2H, ss, C_6H_5-CH_2-CF=C, H, J(H-F)=15 Hz), 4.48 (1H, mm, -C(F)=C(H)-CH_3, J(H-F)=35 Hz), 7.18 (1H, s, C_6H_5), IR(CCl_4): 1700 cm^{-1} (C=C). Found: C, 79.82; H, 7.47%. Calcd for $C_{10}H_{11}F$: C, 79.97; H, 7.38%.

The authors are grateful to the Japan Association of Chemistry for financial support. We also thank Mr. Masakazu Okumiya, Osaka University, for elementary analyses.

References

1) K. Isogai and S. Hirabayashi, *Bull. Chem. Soc. Jpn.*, **52**, 3757 (1979).
2) R. Hoffmann, *Tetrahedron Lett.*, **1970**, 2907.
3) W. J. Jones and B. P. Stoicheff, *Can. J. Phys.*, **42**, 2259 (1964).
4) W. Flygare, A. Narath, and W. Gwinn, *J. Chem. Phys.*, **36**, 200 (1962).
5) S. Durmaz and H. Kollmar, *J. Am. Chem. Soc.*, **102**, 6942 (1980).
6) A. T. Perretta and V. W. Laurie, *J. Chem. Phys.*, **62**, 2469 (1975).
7) T. Toya, *J. Res. Inst. Catal. Hokkaido Univ.*, **6**, 308 (1958); **8**, 209 (1961); *Kinzoku Butsuri*, **10**, 147 (1964).
8) K. Kamel, W. Kimpenhaus, and J. Buddrus, *Chem. Ber.*, **109**, 2351 (1976).
9) H. Adkins and H. R. Billica, *J. Am. Chem. Soc.*, **70**, 695 (1948).

Kinetic Study of Aqueous Decompositions of *N*-(2-Haloethyl)-*N'*-cyclohexyl-*N*-nitrosoureas. Effect of Haloethyl Group on the Preference in Decomposition Pathways

Kitaro YOSHIDA* and Kazuyuki YANO

Department of Chemistry, Saitama Medical School, 981 Kawakado, Moroyama, Iruma-gun, Saitama 350-04

(Received September 20, 1982)

Synopsis. The aqueous decompositions of the title nitrosoureas under various pH conditions were studied kinetically to generalize their hydrolytic mechanisms. The relative decomposition rates of these analogs were in order of the leaving ability of the halogen moiety, which also affected on the preference in their reaction pathways.

Extensive studies[1] on the mechanism of action of antitumor agent *N*-(2-chloroethyl)-*N'*-cyclohexyl-*N*-nitrosourea (CCNU, **1-Cl**) under chemical hydrolytic conditions have established at least three competitive reaction pathways (A, B, and C, Scheme 1). Pathway A provides cyclohexyl isocyanate and 1-chloro-(2-hydroxyazo)-ethane **3** (X=Cl) with the latter intermediate becoming 2-chloroethyl cation which attacks certain nucleotides *in vivo*. Pathway B proceeds *via* an unstable nitrosooxazolidine **4** which breaks down to give acetaldehyde as a volatile product. Both processes are necessarily attended with proton elimination from N' as an initial step and are kinetically indistinguishable. The third pathway C, however, takes place by nucleophilic attack to C-2 by nitroso oxygen to liberate the chloride ion and affords oxadiazoline intermediate **5**. Although relative contributions of each competing pathways are varied depending on pH, solvent polarity, and nature of buffering medium, the propensity of **1-Cl** to provide a significant quantity of 2-chloroethyl cation through pathway A is a mainstay of its antitumor activity. Incidentally, little has been investigated for the chemical reactivities of other halogenated analogs, **1-F** and **1-Br**.[2] This note describes and compares a few kinetic results of aqueous decompositions of **1** in various buffer solutions.

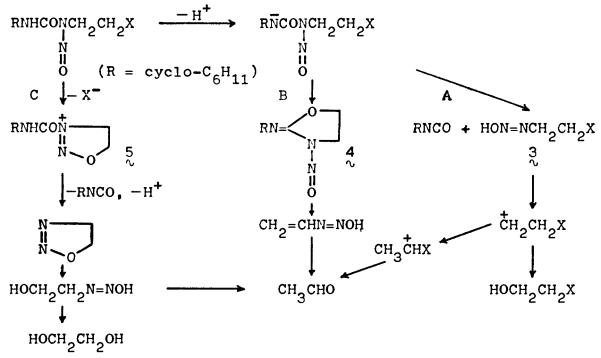

Scheme 1.

cyclo-$C_6H_{11}NHCON(CH_2)_nX$ (N, O)

	n	X
1-F:	2	F
1-Cl:	2	Cl
1-Br:	2	Br
2:	3	Br

Results and Discussion

The decomposition rates were measured by following the decrease of UV absorption of the substrates (230 nm). For each nitrosourea pseudo-first-order rate constant (k/s^{-1}) was observed and the kinetic data under various pH conditions are drawn in Fig. 1. As shown in Fig. 1, the rate of hydrolysis of **1-F** becomes larger with increasing hydroxide ion concentrations and is clearly dependent on pH over the whole range studied. A similar kinetic result was also observed for **1-Cl** within the range of pH 7—8. The decomposition rate of **1-Cl** is reduced at lower pH's, but the extent of the rate reduction becomes rather small. This trend is still more obvious in the case of bromine analog, **1-Br**. It is apparently shown that the reactivity of **1-Br** is higher than those of **1-F** and **1-Cl**. It decomposes at a rate 6 times faster than does **1-Cl** and is about 10 times more reactive than **1-F** at pH 7.1. Moreover, there is a broad pH range over which the decomposition rate is irrespective of acid or base.

Degradation study appears to be agreed with the above observations. When **1-Cl** was decomposed at pH 7.2, 2-chloroethanol was produced in 28% yield based on parent nitrosourea (Table 1), which must imply the occurence of elimination pathway A. Similarly, **1-Br** could afford the corresponding 2-haloethanol. Thus it would appear that the hydroxide ion catalyses are valid under the neutral conditions. However, as the pH is lowered, the contribution of the

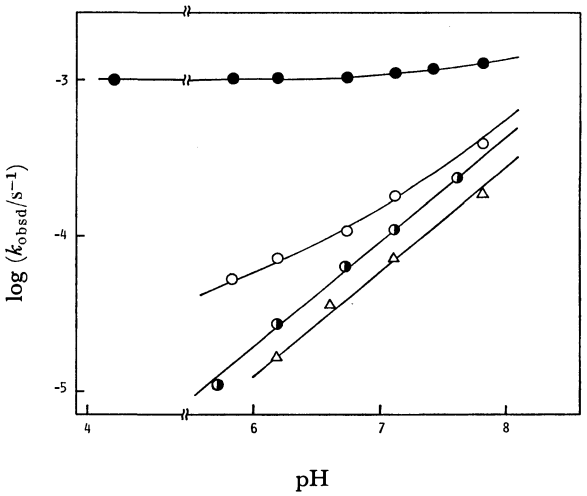

Fig. 1. Plots of $\log k_{obsd}$ *vs.* pH.
Nitrosourea, 1×10^{-4} M; 0.1 M buffer [acetate (pH—5), phosphate (5.8≤pH)]; μ=0.5 (NaCl); 36.9 °C.
○: **1-Cl**, ●: **1-Br**, ◑: **1-F**, △: **2**.

Table 1. The yields of 2-haloethanols from **1** in 0.1 M buffer at 36.9 °C

Nitrosourea	pH	
	4.30[a] Yield/%	7.20[b] Yield/%
1-Cl	13.3	28.2
1-Br	0	21.5

a) Acetate. b) Phosphate.

catalysis tends to decrease. At pH 4.3, the amount of 2-chloroethanol from **1-Cl** reduced to 13% yield. Most obviously, none of the formation of 2-bromoethanol from **1-Br** was looked under the same conditions.

The results suggest that at higher pH values, the abstraction of the ureido proton is substantial, while as the pH is decreased, the nitroso oxygen assisted mechanism (pathway C) becomes increasingly more important. In the case of **1-F**, a poor leaving group attached to C-2 may resist to such an intramolecular process.[3] Further consistent evidence with the favored formation of the oxadiazoline intermediate from **1-Br** was also available. We synthesized the next higher homolog with three methylene units **2**, since it has already been reported that an introducing of the third methylene group into methyl-(2-tosyloxyethyl)-*N*-nitrosamine [$CH_3N(NO)CH_2CH_2OTs$] causes to prohibit its intramolecular process in such a way as to retard its decomposition rate.[4] As would be expected, **2** was quite modest under the present conditions. It is less reactive than **1-Br** by a factor of 15 at pH 7.1. Also, the kinetic feature of **2** is distinctly separated from that of **1-Br** and is closely parallel to **1-F**. The remarkable difference between two reactivities of **1-Br** and **2** must be due to a conformational restriction whereby the cyclic oxadiazoline from **2** with six membered ring is much less favorable than that from **1-Br** with five membered one. Probably, **2** decomposes by ordinary mechanisms (A or B).

The present study shows that an alteration of haloethyl moiety of the title nitrosoureas causes significant influences not only on their relative decomposition rates but on the preference in particular reaction pathways. Such the variations are related to the leaving properties of the C-2 substituent.

Experimental

Materials. *N*-(2-Haloethyl)-*N'*-cyclohexyl-*N*-nitrosoureas (**1**) were prepared by the method of Johnston.[2] *N*-(3-Bromopropyl)-*N'*-cyclohexyl-*N*-nitrosourea (**2**) was prepared from condensation of 3-bromopropylamine with cyclohexyl isocyanate, followed by nitrosation by sodium nitrite (63% overall yield): mp 42—44 °C; IR (KBr) 3280 (NH), 1690 (C=O), 1520 (C-NH), and 1470 cm^{-1} (N=O); ^1H NMR ($CDCl_3$) δ=0.91—2.26 (12H, m), 3.28 (2H, t, J=6 Hz, $CH_2CH_2C\underline{H}_2Br$), 3.94 (2H, t, J=6 Hz, $C\underline{H}_2CH_2CH_2Br$), 3.96 (1H, m, methine), and 6.81 (1H, m, NH). Found: C, 40.86; H, 6.16; N, 14.35; Br, 27.03%. Calcd for $C_{10}H_{18}N_3O_2Br$: C, 41.11; H, 6.21; N, 14.38; Br, 27.35%.

Kinetics were performed with a Shimadzu UV 200 spectrophotometer according to our previous method.[5] The pH of the buffer solution was measured with a Toa-denpa pH meter (HM-5A).

Product Analysis. Nitrosourea **1-Cl** (70 mg) in acetonitrile (3 ml) was added to 300 ml of 0.1 M (1 M=1 mol dm^{-3}) phosphate buffer solution (pH 7.2, μ=0.5). After the solution was stirred at 36.9 °C for 23 h, 2-bromoethanol (18 mg) was added as an internal standard. The cooled solution was saturated by sodium chloride, extracted with three portions of ether (450 ml), dried and evaporated. The GLPC analysis of the crude product showed the formation of 2-chloroethanol in 28% yield. The yield of 2-bromoethanol from **1-Br** was also determined by using 2-chloroethanol as an internal standard. The results are summarized in Table 1. Control experiments indicated that both of the 2-haloethanols did not hydrolyzed at pH 7.2. Owing to its insolubility in ether, attempts to trap ethylene glycol were unsuccessful.

This paper is dedicated to Professor Kazuo Nagamatsu in our laboratory on the 60th anniversary of his birth.

References

1) Recent article, for example; J. W. Lown and S. M. S. Chauhan, *J. Org. Chem.*, **46**, 5309 (1981).

2) The screening data indicated that **1-F** was effective against certain leukemic cells, while **1-Br** was inactive; T. P. Johnston, G. S. McCaleb, P. S. Opliger, and J. A. Montgomery, *J. Med. Chem.*, **9**, 892 (1966).

3) The pH dependency of the decomposition rate of **1-F** was the same as that of *N*-ethyl-*N'*-cyclohexyl-*N*-nitrosourea, where the substitution on C-2 can be ruled out.

4) S. R. Koepke, R. Kupper, and C. J. Michejda, *J. Org. Chem.*, **44**, 2718 (1979).

5) K. Yoshida and K. Yano, *Bull. Chem. Soc. Jpn.*, **55**, 2200 (1982).

An Improved Synthesis of *threo*-3-Methyl-D-cysteine

Tateaki WAKAMIYA, Koichi FUKASE, Kuniaki SHIMBO, and Tetsuo SHIBA*

Department of Chemistry, Faculty of Science, Osaka University, Toyonaka, Osaka 560

(Received October 18, 1982)

Synopsis. Synthesis of *threo*-3-methyl-D-cysteine, a moiety of β-methyllanthionine as a component of the peptide antibiotics nisin and subtilin, was achieved *via* (2*R*,3*R*)-1-*t*-butoxycarbonyl-3-methyl-2-aziridinecarboxamide derived from D-threonine. An addition of thioacetic acid or thiobenzoic acid to the aziridinecarboxamide gave *S*-acyl-β-mercapto-α-amino acid amide derivatives which were hydrolyzed directly or after the preformation of disulfide bond to afford the desired amino acid.

In our previous paper,[1] we reported the preparation of *threo*-3-methyl-D-cysteine (**1**), *i.e.*, (2*S*,3*S*)-2-amino-3-mercaptobutanoic acid[2] which corresponds to a moiety of β-methyllanthionine (**2**)[3] in the peptide antibiotics

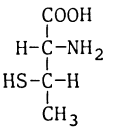

1

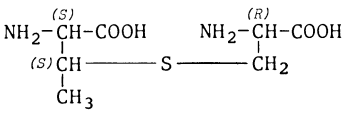

2

nisin[4] and subtilin,[5] *via* (2*R*,3*R*)-1-benzyloxycarbonyl-3-methyl-2-aziridinecarboxylic acid methyl ester (Z-3-MeAzyOMe) derived from D-threonine.[1] According to this procedure, the addition of thiobenzoic acid to the aziridinecarboxylic ester in the presence of $BF_3 \cdot Et_2O$ gave *threo*-*S*-benzoyl-*N*-benzyloxycarbonyl-3-methyl-D-cysteine methyl ester in less than 60% yield, which was caused by the formation of *N*-benzyloxycarbonyl-*O*-thiobenzoyl-D-threonine methyl ester as a by-product. Certainly, an equilibrium between thiobenzoic *S*-acid (C_6H_5COSH) and *O*-acid (C_6H_5CSOH) resulted in such undesirable side reaction. On the other hand, it was found that the reaction of thiobenzoic acid with 3-methyl-2-aziridinylcarbonyl peptides produced solely *S*-benzoyl-3-methylcysteinyl peptides without the addition of Lewis acid which seemed to enhance the reactivity of *O*-acid relatively.

Based on the above observation and consideration, we attempted to improve the synthetic procedure of **1** by use of aziridinecarboxamide in place of the ester derivative. Furthermore, *t*-butoxycarbonyl (Boc) group was adopted as *N*-protecting group rather than benzyloxycarbonyl (Z) group to prevent an attack of benzyl cation formed during acid hydrolysis to free mercapto group. Thus, (2*R*,3*R*)-1-*t*-butoxycarbonyl-3-methyl-2-aziridinecarboxamide [(2*R*,3*R*)-Boc-3-MeAzyNH$_2$] (**4**) was prepared in the usual way. The addition of thiobenzoic acid to **4** took place smoothly with the sole formation of *S*-benzoyl-*N*-Boc-*threo*-3-methyl-D-cysteinamide (**5a**) as we expected. An overall yield in the introduction of mercapto moiety was now considerably increased, even though the modified procedure required an extra step for the amidation. In addition, the easy precipitation of the product from the reaction mixture made the procedure so simple that we could avoid the tedious extraction step to separate the product from ill-smelling thiocarboxylic acid and also the column chromatographic purification as in the case of ester derivative.

However, although the introduction of mercapto moiety was able to be achieved successfully, acid hydrolysis of **5a** resulted in the unexpected formation of quite stable 5-methyl-2-phenyl-2-thiazoline-4-carboxylic acid (**6**)[6] which gave racemic amino acid conceivably through a tautomerism between **6** and **6′**

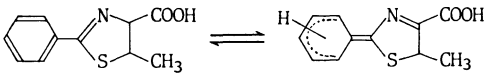

6 **6′**

under prolonged heating. Therefore, in order to avoid such an undesirable formation of thiazoline compound, *S*-benzoyl group was first removed to afford a disulfide derivative **7** which was then satisfactorily hydrolyzed to an optically pure *threo*-3,3′-dimethyl-D-cystine (**8**).[7]

Another or even better solution of the problem was arisen from the following consideration. Since the formation of stable thiazoline ring may be due to the stabilization of the molecule by phenyl group, suitable choice of the *S*-acyl moiety seemed to make the hydrolysis easy. Based on such an assumption, use of *S*-acetyl-*N*-Boc-*threo*-3-methyl-D-cysteinamide (**5b**) for this reaction was attempted. The compound **5b** was prepared in a similar manner as in the preparation of **5a**. Indeed, the acid hydrolysis of **5b** under the usual conditions proceeded readily *via* a labile thiazoline **9** as a plausible intermediate to produce an optically pure *threo*-3-methyl-D-cysteine (**1**) in a satisfactory yield. Thus, we succeeded to establish an improved preparative method of **1** which can be utilized as an important component for the syntheses of rings B, C, D, and E in nisin.

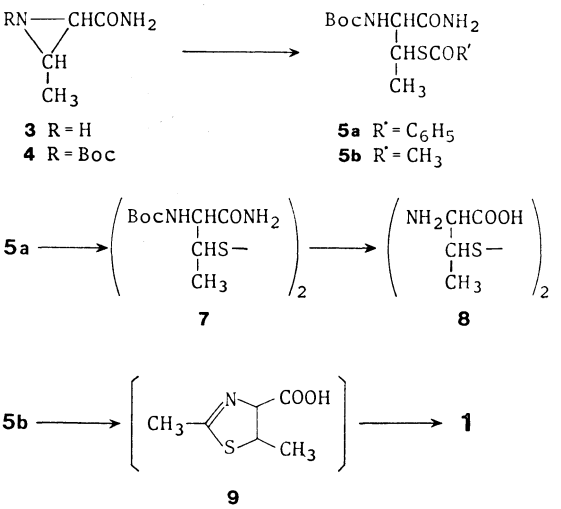

3 R = H, **4** R = Boc

5a R′ = C_6H_5, **5b** R′ = CH_3

7 **8**

9

Experimental

(2R,3R)-3-Methyl-2-aziridinecarboxamide [(2R,3R)-3-MeAzyNH$_2$] (3). A solution of (2*R*,3*R*)-3-MeAzyOMe prepared from (2*R*,3*R*)-trityl-3-MeAzyOMe (2.80 g, 7.84 mmol) according to the usual manner[8] in 45 ml of methanol was saturated with liquid ammonia under cooling in an ice-salt bath. The reaction mixture was kept in a pressure bottle at 25 °C for 4 d. Evaporation of the solvent and excess ammonia gave crystalline product in a yield of 740 mg (94%). A crop of the product was recrystallized from methanol and ether: mp 132—133.5 °C; $[\alpha]_D^{18}$ +103° (*c* 0.900, DMF).

Found: C, 48.00; H, 8.01; N, 27.54%. Calcd for $C_4H_8ON_2$: C, 47.99; H, 8.05; N, 27.98%.

(2R,3R)-Boc-3-MeAzyNH$_2$ (4). To a solution of (2*R*,3*R*)-3-MeAzyNH$_2$ (**3**) (7.20 g, 72.0 mmol) in 100 ml of methanol was added di-*t*-butyl dicarbonate (17.3 g, 79.0 mmol). The reaction mixture was concentrated *in vacuo* to afford crystalline product which was recrystallized from ethyl acetate and hexane: yield 12.3 g (85.3%); mp 118—119 °C; $[\alpha]_D^{18}$ +116° (*c* 1.06, $CHCl_3$).

Found: C, 53.96; H, 8.05; N, 13.89%. Calcd for $C_9H_{16}O_3N_2$: C, 53.99; H, 8.05; N, 13.99%.

S-*Benzoyl*-N-t-*butoxycarbonyl*-threo-*3-methyl*-D-*cysteinamide (5a).* Thiobenzoic acid (8.28 g, 60.0 mmol) was added to a solution of **4** (6.00 g, 30.0 mmol) in 60 ml of dichloromethane. A part of the crystalline product precipitated after stirring at room temperature overnight and hexane was added to complete the precipitation, yield 9.62 g (94.8%). An analytical sample was obtained by recrystallization from ethanol and hexane: mp 165.5—167 °C; $[\alpha]_D^{18}$ −41.7° (*c* 0.700, MeOH).

Found: C, 57.01; H, 6.64; N, 8.13; S, 9.37%. Calcd for $C_{16}H_{22}N_2O_4S$: C, 56.79; H, 6.55; N, 8.28; S, 9.47%.

S-*Acetyl*-N-t-*butoxycarbonyl*-threo-*3-methyl*-D-*cysteinamide (5b).* The reaction of thioacetic acid (6.36 g, 84.0 mmol) and **4** (6.00 g, 30.0 mmol) in dichloromethane (60 ml) was carried out in a similar manner as the preparation of **5a** and crystalline product **5b** was obtained in a yield of 7.86 g (94.9%). An analytical sample was prepared by recrystallization from ethyl acetate and hexane: mp 104—104.5 °C; $[\alpha]_D^{30}$ −35.5° (*c* 1.17, MeOH).

Found: C, 48.00; H, 7.29; N, 10.15; S, 11.68%. Calcd for $C_{11}H_{20}N_2O_4S$: C, 47.81; H, 7.29; N, 10.14; S, 11.60%.

N,N′-*Bis (t-butoxycarbonyl)*-threo-*3,3′-dimethyl*-D-*cystinediamide (7).* To a solution of **5a** (7.00 g, 20.7 mmol) in 200 ml of methanol was added dropwise 1 M† methylamine in methanol (20.7 ml, 20.7 mmol) for 8 h. After stirring overnight, 0.5 M iodine in methanol was added until the completion of the oxidation. The reaction mixture neutralized with methylamine was concentrated *in vacuo* to about 100 ml. The residue was cooled in an ice bath and the precipitate was filtered. The product was washed with hexane, suspended in water, and again filtered to afford pure material: yield 3.71 g (77.0%); mp 224—226 °C; $[\alpha]_D^{18}$ +82.1° (*c* 0.610, DMF).

Found: C, 46.22; H, 7.32; N, 11.91; S, 13.81%. Calcd for $C_{18}H_{34}N_4O_6S_2$: C, 46.33; H, 7.34; N, 12.01; S, 13.74%.

threo-*3,3′-Dimethyl*-D-*cystine (8).* A suspension of **7** (3.60 g, 7.72 mol) in 70 ml of 6 M HCl was refluxed for 10 h at 110 °C. The hydrolyzate concentrated *in vacuo* was suspended in 80 ml of ethanol to remove insoluble NH_4Cl and the filtrate was concentrated again. A solution of the residue in 25 ml of water and 30 ml of ethanol was neutralized with pyridine and then kept in refrigerator overnight. Crystalline precipitate was filtered, washed with ethanol, and recrystallized from water and ethanol: yield 1.96 g (94.7%); mp 190—196 °C (decomp); $[\alpha]_D^{27}$ −419° (*c* 0.540, 1 M HCl) [lit,[2d]) $[\alpha]_D^{19}$ −414° (*c* 1, 1 M HCl)].

Found: C, 34.65; H, 6.12; N, 10.06; S, 23.51%. Calcd for $C_8H_{16}O_4N_2S_2 \cdot 0.4H_2O$; C, 34.87; H. 6.15; N, 10.17; S, 23.27.

threo-*3-Methyl*-D-*cysteine (1).* A suspension of **5b** (1.00 g, 3.62 mmol) in 20 ml of 6 M HCl was refluxed for 10 h at 110 °C under argon atmosphere. The same work-up as mentioned for the preparation of **8** gave colorless crystalline product: yield 0.40 g (82%); mp 199.5—200 °C; $[\alpha]_D^{23}$ +16.9° (*c* 1.24, 1 M HCl) [lit,[2c]) $[\alpha]_D^{25}$ +17.5° (*c* 1, 1 M HCl)].

Found: C, 35.41; H, 6.82; N, 10.28; S, 23.03%. Calcd for $C_4H_9O_2NS \cdot 0.1H_2O$; C, 35.05; H, 6.77; N, 10.23; S, 23.41%.

† 1 M = 1 mol dm^{-3}.

References

1) T. Wakamiya, K. Shimbo, T. Shiba, K. Nakajima, M. Neya, and K. Okawa, *Bull. Chem. Soc. Jpn.*, **55**, 3878 (1982).

2) a) H. E. Carter, C. M. Stevens, and L. F. Ney, *J. Biol. Chem.*, **139**, 247(1941); b) H. R. V. Arnstein, *Biochem. J.*, **68**, 333 (1958); c) J. Hoogmartens, P. H. Claes, and H. Vanderhaeghe, *J. Org. Chem.*, **39**, 425 (1974); d) J. L. Morell, P. Fleckenstein, and E. Gross, *J. Org. Chem.*, **42**, 355 (1977).

3) P. Downey and S. Black, *J. Biol. Chem.*, **228**, 171 (1957).

4) E. Gross and J. Morell, *J. Am. Chem. Soc.*, **93**, 4634 (1971).

5) E. Gross, H. H. Kiltz, *Hoppe-Seyler's Z. Physiol. Chem.*, **354**, 310 (1973).

6) When the acid hydrolysis was stopped within 1—2 h, optically pure **6** was isolated: Yield 81%; mp 154—155.5 °C; $[\alpha]_D^{18}$ −114° (*c* 0.910, MeOH).

7) Dimethylamide derivative corresponding to **7** showed also an extreme resistance against the hydrolysis. A refluxing for a long time caused racemization of the product.

8) K. Nakajima and K. Okawa, *Biopolymers*, **20**, 1811 (1981).

Pyridinium-1-thioacylaminides

Hiroshi YOSHIDA,* Kiyomi URUSHIBATA, and Tsuyoshi OGATA
Department of Applied Chemistry, Faculty of Engineering, Shizuoka University, Hamamatsu 432
(Received November 1, 1982)

Synopsis. Pyridinium-, 2-methylpyridinium-, and 2,6-dimethylpyridinium-1-thioacylaminides (**5**—**7**) were prepared from the corresponding unsubstituted pyridinium-1-aminides and methyl dithiocarboxylates in fairly good yields. The alkylation reaction of **5**—**7** took place exclusively on the thiocarbonyl sulfur, yielding pyridinium salts in quantitative yields. The NMR spectroscopic studies indicated that *E* and *Z* forms existed for these pyridinium salts. The thermal decomposition of **5**—**7** yielded the corresponding pyridine, nitrile, and sulfur in good yields.

Recently a number of heterocyclic aminides have been prepared, and their physical and chemical properties have been clarified.[1-4] In a continuation of our previous studies of the *P*- and *S*-ylides and aminides[5] with C=S or C=N groups as substituents such as **1**, we have become interested in the chemistry of pyridinium-1-thioacylaminides **5**, **6**, and **7**:

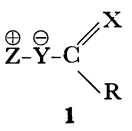

1

Z=Ph_3P, Ph_2S, Me_2S, Me_2SO
Y=CH, N
X=NR′, S
R=Ar, R′O,

Some pyridinium-1-aminides with thioacyl groups as substituents have been previously prepared. 2,4,6-Triphenylpyridinium perchlorate reacts with thioacylhydrazine to give the rather unstable 1-thioamidotriphenylpyridinium perchlorate, which then decomposes on attempted deprotonation.[2] Isothiocyanate reacts with free pyridinium-1-aminides **2**—**4** to yield thiourea derivatives.[3] 2-Methylpyridinium-1-[(methylthio)-thiocarbonylaminide](**6c**) has been prepared from free aminide **3**, carbon disulfide, and an alkylating reagent in a 59% yield.[4]

The action of methyl dithiocarboxylates to **2**, **3**, or **4**, generated from the corresponding 1-aminopyridinium mesitylene-sulfonates[6] and potassium carbonate in ethanol, yielded the expected pyridinium-1-thioacylaminides **5**, **6**, or **7** in good yields, as are listed in Table 1. The structure of the products was elucidated on the basis of their elemental analyses, ^{1}H-NMR spectra, alkylation reaction, and thermal-decomposition reaction.

The alkylation of the oxygen analogues of **5**, **6**, or **7** takes place on the aminide nitrogen, not on the acyl oxygen.[1b] In contrast, the alkylation of **5**, **6**, and **7** with various alkylating reagents (R′X) takes place exclusively on the sulfur, very easily at room temperature, to give the corresponding pyridinium salts **5**, **6**, and **7**(R′X) in fairly good yields.

Pyridinium 1-methoxythiocarbonylaminides **5d**, **6b**, and **7b** reacted with methyl iodide to give the corresponding (methylthio)carbonylaminides **8**, **9**, and **10** as final products in quantitative yields. The reaction with methyl benzenesulfonate yielded the expected salts **5d**, **6b**, and **7b**($MeOSO_2Ph$).

The stereochemistry of the salts was assigned on the basis of the fact that the R′ groups cis to the pyridine ring are shielded by the ring and that they appear at the higher field than the R′ trans to the ring.[7]

Alkylation and isomerization reaction of **5**—**7** were studied by means of NMR spectroscopy. On heating at 70 °C for 2 h in $CDCl_3$ **5**$(R'X)_Z$ and **6**$(R'X)_Z$ were easily isomerized to give equilibrium mixtures; in contrast, **7**$(R'X)_Z$ showed no isomerization on heating for 10—20 h, indicating the retardation of rotation around the C=N bond due to the steric hindrance.

The stereochemistry of the C=N bond with alkyl, aryl, alkoxy, alkylthio, or amino groups as substituents has been widely studied.[8] A number of factors seem to govern the *E*—*Z* equilibrium ratios for this system.[8] Table 2 seems to indicate that *E*-forms are furnished for the **5**(R′X) and **6**(R′X) salts, in this order with respect to the substituent R′:phenyl, alkylthio, and alkoxy. The steric effect seems to be a dominant factor for the salts with alkylthio groups as substituents **5f**(EtI, $PhCH_2Br$, $PhCOCH_2Br$), while interorbital repulsion[9] seems to control the stereochemistry of the salts with alkoxyl groups [**5d**, **5e**, and **7b**($MeOSO_2Ph$)].

The conformations of the initial alkylation products **5**, **6**, and **7**$(R'X)_Z$ seem to show that the starting aminides **5**—**7** were of the *Z*-form, indicating the importance of the delocalization of the aminide electrons through the thiocarbonyl groups of **5**—**7**, as is shown in Scheme 1.

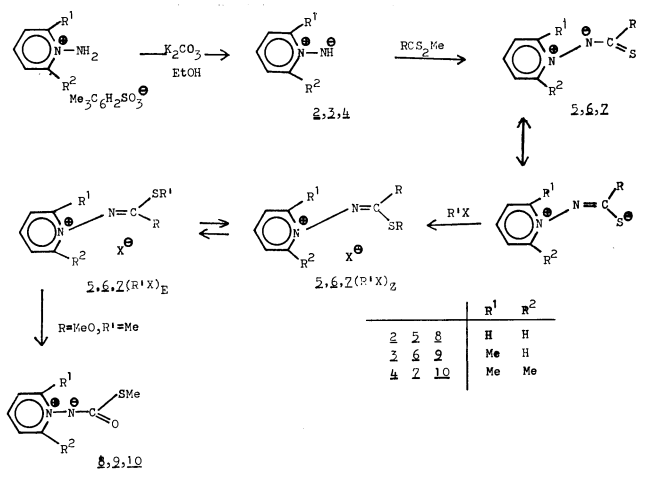

Scheme 1.

Although **5**—**7** were stable in a refrigerator, on heating at 80—120 °C in a solvent(benzene or toluene) a smooth decomposition was observed, yielding nitrile, pyridine, and sulfur in good yields.

Trapping experiments to find an intermediate, nitrile sulfide,[5b] for the thermolysis of **5**—**7** failed. On heating, a mixture of **5**, **6**, or **7** and dimethyl acetylenedicarboxylate in tarry mass, from which no crystalline compound was isolated.

Experimental

Preparation of 5—7. A mixture of 1-amino-, 1-amino-2-methyl-, or 1-amino-2,6-dimethylpyridinium mesitylenesulfonate[6] (1.1 mmol), potassium carbonate (3 mmol), and methyl dithiocarboxylate (1 mmol) in ethanol (25 cm³) was stirred for 2.5 h at room temperature. The solvent was then removed *in vacuo* at room temperature; the subsequent separation of the chloroform-soluble product yielded crystalline pyridinium-1-thioacylaminides **5—7**. The physical properties are collected in Table 1.

Alkylation of 5—7. To a solution of **5**, **6**, or **7** in benzene we added a 2-fold excess amount of an alkylation reagent (R'X) at room temperature. The reaction was checked by TLC (silica gel) until the starting material was reacted completely. The precipitated salt **5**, **6**, or **7**(R'X) was washed with dry benzene and dried *in vacuo* (Table 2). The isomerization and the determination of the equilibrium ratios in $CDCl_3$ were studied by means of NMR spectroscopy.

The Reaction of 5d, 6b, and 7b with Methyl Iodide. To a solution of **5d**, **6b**, or **7b**(1 mmol) in chloroform (5 cm³) we added methyl iodide (2 mmol) in one portion. The solution was then kept standing at room temperature for 12 h. The evaporation of the solvent and recrystallization from benzene gave **8**, **9**, or **10** in a quantitative yield. The NMR spectroscopic studies in $CDCl_3$ indicated that the initially formed salts showed the same spectra as those from the reaction with methyl benzenesulfonate. **8**: mp 131—132 °C; NMR($CDCl_3$) δ=2.33(SMe) and 7.6—8.8 (m, Ar). Found: C, 49.88; H, 4.73; N, 16.59%. Calcd for $C_7H_8N_2OS$: C, 49.98; H, 4.79; N, 16.65%. **9**: mp 116 °C; NMR($CDCl_3$) δ=2.35 (SMe), 2.71 (2-Me), and 7.6—8.8 (m, Ar). Found: C, 52.41; H, 5.64; N, 15.11%. Calcd for $C_8H_{10}N_2OS$: C, 52.73; H, 5.53; N, 15.37%. **10**: mp 142—143 °C; NMR($CDCl_3$) δ=2.34 (SMe), 2.67 (2,6-Me), and 7.7—8.8 (m, Ar). Found: C, 55.43; H, 6.02; N, 14.13%. Calcd for $C_9H_{12}N_2OS$: C, 55.08; H, 6.16; N, 14.27%.

Thermal Decomposition of 5—7. A solution of **5**, **6**, or **7** in benzene or toluene (100 mg in 3 cm³) was heated until the starting material had reacted completely. The prducts were confirmed by comparisons of their NMR spectra or VPC with those of authentic samples.

Table 1. The preparation of pyridinium-1-aminides, **5—7**

	R	Yield %	Mp θ_m/°C	NMR (δ in $CDCl_3$)[a]	Found(Calcd) (%) C	H	N
5a	4-MeC$_6$H$_4$	75	170—173	2.40(Me)	68.52 (68.39)	5.11 (5.30)	12.55 (12.27)
5b	Ph	88	167—169		67.01 (67.26)	4.63 (4.70)	13.24 (13.07)
5c	4-MeOC$_6$H$_4$	74	162—164	3.88(OMe)	63.92 (63.91)	5.02 (4.95)	11.81 (11.47)
5d	MeO	73	130—131	4.40(OMe)	49.63 (49.98)	4.67 (4.79)	16.80 (16.65)
5e	EtO	85	130—131	1.40(t, J=7 Hz, Me), 4.50(q, CH_2)	52.90 (52.73)	5.48 (5.53)	15.19 (15.37)
5f	MeS	81	124—126	2.53(SMe)	45.29 (45.63)	4.36 (4.38)	15.37 (15.20)
5g	EtS	89	127	1.38(t, J=7 Hz, Me), 3.20(q, CH_2)	48.30 (48.46)	5.14 (5.08)	14.45 (14.13)
6a	Ph	79	133—135	2.61(2-Me)	48.22 (48.39)	5.77 (5.30)	12.48 (12.27)
6b	MeO	83	108—109	2.67(2-Me), 4.05(OMe)	53.02 (52.73)	5.50 (5.53)	15.16 (15.37)
6c[b]	MeS	80	141—143	2.58(SMe), 2.65(2-Me)	48.25 (48.46)	5.22 (5.08)	14.04 (14.13)
7a	4-MeOC$_6$H$_4$	89	156	2.65(2,6-Me$_2$), 3.88(OMe)	65.92 (66.16)	5.87 (5.92)	10.63 (10.29)
7b	MeO	84	139—141	2.68(2,6-Me$_2$), 4.06(OMe)	55.21 (55.08)	6.03 (6.16)	14.61 (14.27)
7c	EtO	93	114—116	1.41(t, J=7 Hz), 2.68(2,6-Me$_2$), 4.51(q, CH_2)	56.83 (57.12)	6.64 (6.71)	13.72 (13.32)
7d	MeS	81	152—153	2.60(SMe), 2.68(2,6-Me$_2$)	51.08 (50.91)	5.89 (5.70)	13.01 (13.19)
7e	EtS	87	140—141	1.40(t, J=7 Hz, Me), 2.67(2,6-Me$_2$), 3.18(q, CH_2)	53.17 (53.06)	6.01 (6.23)	12.04 (12.38)

a) Aryl protons were observed at δ 7.4—8.2. b) Lit,[4] mp 128—129 °C; NMR ($CDCl_3$) δ=2.57(SMe) and 2.64(2-Me).

Table 2. properties of pyridinium salts **5—7**(R'X)

5—7(R'X)		Mp θ_m/°C	NMR(δ in $CDCl_3$) SMe **5—7**(R'X)$_Z$	**5—7**(R"X)$_E$	Z/E
5b	(MeI)	Oil	2.34	2.78	36 : 64
5c	(MeI)	136—138	2.37	2.75	30 : 70
5d	(MeOSO$_2$Ph)	Oil	2.43	2.60	83 : 17
5e	(MeBr)	115—117	2.39	2.63	83 : 17
5f	(MeI)	Oil	2.68, 2.75		—
	(EtI)	137—139	2.73	2.65	47 : 53
	(PhCH$_2$Br)	130—132	2.74	2.57	45 : 55
	(PhCOCH$_2$Br)	Oil	2.70	2.73	31 : 69
5g	(MeI)	135—137	2.65	2.73	53 : 47
6b	(MeOSO$_2$Ph)	Oil	2.46	2.64	80 : 20
6c	(MeI)	150	2.73, 2.82		
	(EtI)	97—99		2.69	45 : 55
7a	(MeI)	179—181	2.46		
7b	(MeOSO$_2$Ph)	Oil	2.59		
7c	(MeOSO$_2$Ph)	Oil	2.47		
7d	(MeI)	180—183	2.75, 2.85		
	(EtI)	142—144	2.85		
7e	(MeI)	157—159	2.74		

References

1) a) H. Timpe, "Advances in Heterocyclic Chemistry," Academic Press, New York (1974), Vol. 17, p. 213; b) W. J. McKillip, E. A. Sedor, B. M. Culbertison, and S. Wawzonek, *Chem. Rev.*, **73**, 255 (1973); c) Y. Tamura, *Yakugaku Zasshi*, **100**, 1 (1980).

2) A. R. Katrizky, J. Lewis, and P. L. Nie, *J. Chem. Soc., Perkin Trans. 1*, **1979**, 446.

3) R. Krishke, R. Grashey, and R. Huisgen, *Justus Liebigs Ann. Chem.*, **1977**, 498.

4) A. Kakehi, S. Ito, and K. Watanabe, *Bull. Chem. Soc. Jpn.*, **53**, 1775 (1980).

5) a) H. Yoshida, T. Ogata, and S. Inokawa, *Bull. Chem. Soc. Jpn.*, **53**, 1541 (1979); b) H. Yoshida, H. Taketani, T. Ogata, and S. Inokawa, *ibid.*, **49**, 3124 (1976).

6) Y. Tamura, J. Minamikawa, and M. Ikeda, *Synthesis*, **1977**, 1.

7) A. H. Gawer and B. P. Daily, *J. Chem. Phys.*, **42**, 2658 (1965).

8) a) C. G. McCarty, "The Chemistry of the Carbon-Nitrogen Double Bond," ed by S. Patai, Interscience Pub., London (1970), p. 363; b) G. Fodor and B. A. Phillips, "The Chemistry of Amidines and Imidates," ed by S. Patai, Interscience Pub., London (1975), p. 85.

9) E. Yeh, R. M. Moriarty, C. Yeh, and K. C. Ramey, *Tetrahedron Lett.*, **1972**, 2655.

Pseudo-sugars. IX. Synthesis of Three (Hydroxymethyl)-cyclohexanepentols[1)]

Seiichiro OGAWA, Toshinobu NAKAMURA, Noritaka CHIDA, and Tetsuo SUAMI*

Department of Applied Chemistry, Faculty of Science and Technology, Keio University, Hiyoshi, Kohoku-ku, Yokohama 223

(Received November 11, 1982)

Synopsis. Three new DL-(hydroxymethyl)cyclohexanepentols, of which configurations are related to biologically important *chiro*- and *myo*-inositols, have been synthesized as hexaacetates from DL-tri-*O*-acetyl-(1,3/2,4)-4-benzoyloxymethyl-5-cyclohexene-1,2,3-triol by osmium tetraoxide-oxidation or peroxy acid-oxidation followed by acid hydrolysis, and their structures have been established by ^{1}H NMR spectroscopy.

During the course of synthetic studies of hydroxyvalidamine and valienamine,[2)] three new (hydroxymethyl)cyclohexanepentols have been prepared and characterized as hexaacetates. These branched-chain cyclitols are useful not only as reference compounds for structural elucidation of new cyclitols by ^{1}H NMR spectroscopy, but also as biologically interesting inositol analogs with *chiro*- and *myo*-configurations.

Treatment of DL-tri-*O*-acetyl-(1,3/2,4)-4-benzoyloxymethyl-5-cyclohexene-1,2,3-triol (**1**)[2)] with osmium tetraoxide in aqueous *t*-butyl alcohol containing 3% hydrogen peroxide at 40 °C for 120 h, followed by conventional acetylation, gave, after chromatography on silica gel, two peracyl (hydroxymethyl)cyclohexanepentols **2** and **3** in 24 and 24% yields, respectively. The assigned structures were established on the basis of their ^{1}H NMR spectra. Thus, in the spectrum of **2**, the signals for H-1, H-2, H-3, H-4, and H-5 appear as a triplet (δ=5.67, J=3 Hz), a doublet of doublets (δ=4.95, J=3 and 10.2 Hz), a triplet (δ=5.43, J=10.2 Hz), a doublet of doublets (δ=5.22, J=9 and 10.2 Hz), and a doublet of doublets (δ=5.34, J=10.2 and 10.5 Hz), respectively, indicating equatorial-axial-axial-axial-axial conformations for H-1, H-2, H-3, H-4, and H-5. The spectrum of **3** exhibits the signal for H-4 as a triplet (J=10 Hz) at δ=5.42, which seems deshielded by 0.2 ppm relative to that of **2** by the C-2 acetoxyl group in the 1,3-diaxial disposition. *O*-Deacylation of **2** and **3** with methanolic sodium methoxide in methanol followed by acetylation gave crystalline hexaacetates **4** and **5** in 43 and 59% yields, respectively.

On the other hand, the epoxide **7** prepared specifically by peroxy acid-oxidation of the tetrahydroxy compound **6** derived from **1**[2)] was hydrolyzed by refluxing in aqueous 2-methoxyethanol containing 0.7% sulfuric acid for 2 h. The product was successively acetylated to give a single crystalline hexol hexaacetate **8** in 70% yield. The structure was assigned as shown in the scheme by ^{1}H NMR spectroscopy. The spectrum indicated the signals for two acetoxyl groups to be as a 6-proton singlet in the regions characteristic of axial groups (δ=2.13),[3)] supporting that the reaction involves trans-diaxial opening of the oxirane ring.

Experimental

Melting points were determined on a Mitamura Riken micro hot stage and are uncorrected. ^{1}H NMR spectra were taken on a Varian EM-390 (90 MHz) spectrometer in chloroform-*d* with reference to tetramethylsilane as an internal standard. TLC was performed on precoated silica gel 60 F-254 plates (Merck, Darmstadt; 0.25 mm thickness). The silica gel used for column chromatography was Wakogel C-300 (Wako Pure Chemical Industries, Ltd.).

Oxidation of DL-*Tri*-O-*acetyl-(1,3/2,4)-4-benzoyloxymethyl-5-cyclohexene-1,2,3-triol (1) with Osmium Tetraoxide.* To a solution of **1** (0.20 g) in aqueous *t*-butyl alcohol (3 ml) containing 3% hydrogen peroxide was added osmium tetraoxide (5 mg) in *t*-butyl alcohol (1 ml), and the mixture was stirred at 40 °C for 120 h. The reaction mixture was concentrated and the residue was treated with acetic anhydride (1 ml) and pyridine (1 ml) at room temperature overnight. Evaporation of the excess reagent gave crude

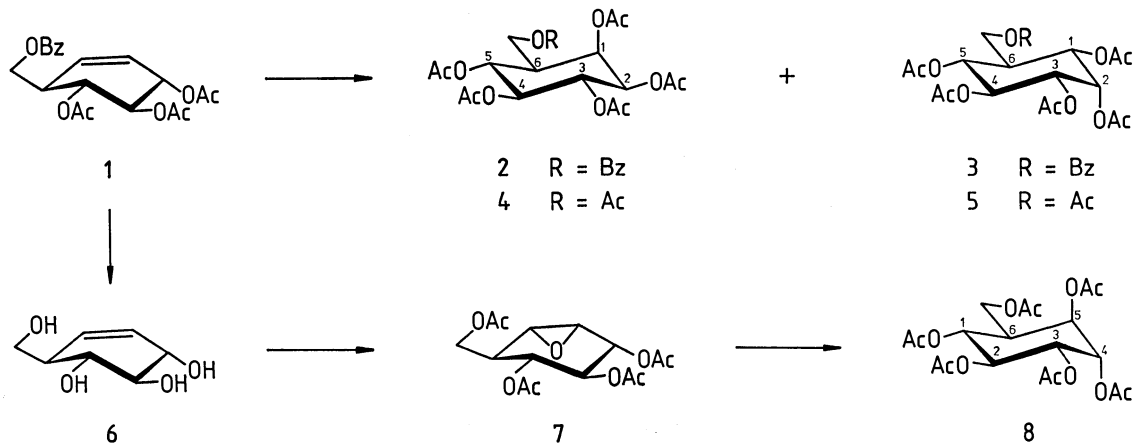

Scheme 1.

products, which were fractionated on a silica-gel column (8.5 g) with 2-butanone–toluene (1: 12) as an eluent. The first fraction [R_f 0.45, 2-butanone–toluene (1: 5)] gave an oil (61 mg, 24%), which was crystallized from ethanol to give 15 mg of DL-1,2,3,4,5-penta-*O*-acetyl-7-*O*-benzoyl-(1,2,4,6/3,5)-6-hydroxymethyl-1,2,3,4,5-cyclohexanepentol (**2**) as prisms: mp 156—158 °C; ^{1}H NMR ($CDCl_3$) δ=1.95 (3H, s), 1.99 (6H, s), 2.01 (3H, s), and 2.10 (3H, s) (OAc), 2.45 (1H, m, H-6), 4.08 (1H, dd, $J_{6,7}$=9 Hz, J_{gem}=11 Hz) and 4.35 (1H, dd, $J_{6,7'}$=4.5 Hz) ($C\underline{H}_2OBz$), and 7.33—8.03 (5H, m, phenyl).

Found: C, 56.85; H, 5.30%. Calcd for $C_{24}H_{28}O_{12}$: C, 56.69; H, 5.55%.

Compound **2** (160 mg) was treated with 0.3 M (1 M= 1 mol dm^{-3}) methanolic sodium methoxide (3 ml) at room temperature for 1 h, and the reaction mixture was neutralized by 1 M hydrochloric acid and concentrated. The residual product was acetylated in the usual way and the product was crystallized from ethanol to give 68 mg (43%) of the hexaacetate **4** as prisms: mp 158—159 °C; ^{1}H NMR ($CDCl_3$) δ=1.96 (3H, s), 1.98 (3H, s), 2.00 (6H, s), 2.01 (3H, s), and 2.12 (3H, s) (OAc), 3.85 (1H, dd, $J_{6,7}$=4.5 Hz, J_{gem}=10.8 Hz) and 4.04 (1H, dd, $J_{6,7'}$=9 Hz) ($C\underline{H}_2OAc$), 4.87 (1H, dd, $J_{1,2}$=3 Hz, $J_{2,3}$=10.2 Hz, H-2), and 5.51 (1H, dd, $J_{1,6}$=2.3 Hz, H-1).

Found: C, 51.11; H, 5.80%. Calcd for $C_{19}H_{26}O_{12}$: C, 51.12; H, 5.87%.

The second fraction (R_f 0.40) gave an oil (63 mg, 24%), which was crystallized from ethanol to give 18 mg of DL-1,2,3,4,5-penta-*O*-acetyl-7-*O*-benzoyl-(1,2,3,5/4,6)-6-hydroxymethyl-1,2,3,4,5-cyclohexanepentol (**3**) as prisms: mp 146—148 °C; ^{1}H NMR ($CDCl_3$) δ=1.97 (6H, s), 2.01 (3H, s), 2.06 (3H, s), and 2.16 (3H, s) (OAc), 2.60 (1H, br t, $J_{1,6}$ =$J_{5,6}$=10 Hz, H-6), 4.28 (2H, br s, $C\underline{H}_2OBz$), 5.18 (1H, t, $J_{4,5}$=10 Hz, H-5), 5.42 (1H, t, $J_{3,4}$=10 Hz, H-4), 5.57 (1H, t, $J_{1,2}$=$J_{2,3}$=2.5 Hz, H-2), and 7.25—8.07 (5H, m, phenyl).

Found: C, 56.56; H, 5.57%. Calcd for $C_{24}H_{28}O_{12}$: C, 56.69; H, 5.55%.

Compound **3** (230 mg) was *O*-deacylated similarly as described above and acetylated to give a crystalline product, which was recrystallized from ethanol to give 135 mg (59%) of the hexaacetate **5** as prisms: mp 180—182 °C; ^{1}H NMR ($CDCl_3$) δ=1.99 (6H, s), 2.01 (3H, s), 2.04 (6H, s), and 2.16 (3H, s) (OAc), 4.00 (2H, br d, J=2 Hz, $C\underline{H}_2OBz$), 5.37 (1H, t, $J_{3,4}$=$J_{4,5}$=10.5 Hz, H-4), and 5.87 (1H, t, $J_{1,2}$=$J_{2,3}$=3 Hz, H-2).

Found: C, 51.10; H, 5.78%. Calcd for $C_{19}H_{26}O_{12}$: C, 51.12; H, 5.87%.

DL-*Hexa-O-acetyl-(1,3,4/2,5,6)-6-hydroxymethyl-1,2,3,4,5-cyclohexanepentol (**8**).* A mixture of DL-tetra-*O*-acetyl-1,2-anhydro-(1,2,3,5/4,6)-6-hydroxymethyl-1,2,3,4,5-cyclohexanepentol (**7**)[2] (83 mg) in 2-methoxyethanol (2 ml) and 1% sulfuric acid (5 ml) was refluxed for 1.5 h. The reaction mixture was neutralized with sodium hydrogencarbonate and concentrated. The residue was acetylated and the product was purified by passage through a short column of alumina with chloroform. The crystalline product was recrystallized from ethyl acetate–hexane to give 75 mg (70%) of **8** as prisms: mp 102—105 °C; ^{1}H NMR ($CDCl_3$) δ=1.96 (3H, s), 2.00 (3H, s), 2.01 (3H, s), and 2.13 (6H, s) (OAc), 2.52 (1H, m, H-6), 3.93 (1H, dd, $J_{6,7}$=4.5 Hz, J_{gem}=11.3 Hz) and 4.19 (1H, dd, $J_{6,7'}$=8.3 Hz) ($C\underline{H}_2OAc$), 5.16 (1H, dd, $J_{2,3}$=9 Hz, $J_{3,4}$=3.2 Hz, H-3), 5.28 (1H, t, $J_{1,2}$=$J_{1,6}$=9 Hz, H-1), 5.38 (1H, t, $J_{4,5}$=3.2 Hz, H-4), and 5.41 (1H, t, H-2).

Found: C, 51.35; H, 5.88%. Calcd for $C_{19}H_{26}O_{12}$: C, 51.12; H, 5.88%.

The authors wish to express their thanks to Mr. Saburo Nakada for elemental analyses.

References

1) The preceding paper of this series: S. Ogawa, M. Oya, T. Toyokuni, N. Chida, and T. Suami, *Bull. Chem. Soc. Jpn.*, **56**, 1441 (1983). The nomenclature and numbering of cyclitols used in this paper follow the IUPAC and IUB Tentative Rules for Cyclitol Nomenclature [*J. Biol. Chem.*, **243**, 5809 (1968)]. All compounds described in this paper are racemic and the formulas depict only one of the respective enantiomers.

2) S. Ogawa, N. Chida, and T. Suami, *J. Org. Chem.*, in press.

3) F. W. Lichtenthaler and P. Emig, *Carbohydr. Res.*, **7**, 121 (1968); F. W. Lichtenthaler, G. Bambach, and P. Emig, *Chem. Ber.*, **102**, 994 (1969).

Studies on 2-Aziridinecarboxylic Acid. X.[1] Simple Stereospecific Synthesis of Optically Active Cystine and *threo*-3,3'-Dimethylcystine

Kiichiro NAKAJIMA* and Kenji OKAWA

Department of Chemistry, Faculty of Science, Kwansei Gakuin University, Nishinomiya 662

(Received November 20, 1982)

Synopsis. The reaction of (2*S*)-Z-Azy-OBzl, (2*S*, 3*S*)-Z-3-MeAzy-OBzl, and their enantiomers with H_2S gave the optically active cysteine and *threo*-3-methylcysteine derivatives *via* the stereospecific ring-opening reaction of aziridine, and subsequent oxidation and deblocking procedure gave the titled compounds in good yields.

Photaki[2] have reported the preparation of DL-*S*-tritylcysteine from L-serine *via* the β-elimination reaction of its *O*-tosylated derivative. Carter *et al.*[3] and Hoogmartens *et al.*[4] prepared 3-methylcystine *via* addition of thiol to 2-phenyl-4-ethylidene-5(4*H*)-oxazoline. Morell *et al.*[5] have reported that the displacement reaction of the *O*-tosyl-*allo*-threonine derivative with potassium thioacetate gave the *threo*-*S*-acetyl-3-methylcysteine, which was converted into *threo*-3,3'-dimethylcystine by hydrolysis and oxidation procedure. But these methods involved some technical trouble in obtaining the optically pure cystine or 3,3'-dimethylcystine, that is, the Carter-Hoogmartens's procedure requires a complex optical resolution procedure to get the optically pure product, and the Morell's procedure requires *allo*-threonine as a starting material to prepare *threo*-3-methylcysteine. More recently, Wakamiya *et al.*[6] reported the synthesis of *threo*-3,3'-dimethylcystine *via* ring-opening reaction of aziridine with thiobenzoic acid, this reaction still remained the problem concerning to the product, that is, two products of *S*-benzoyl and *O*-thiobenzoyl derivatives were prepared by this reaction procedure, due to the possible equilibrium in thiobenzoic acid, *e.g.* $C_6H_5COSH \rightleftharpoons C_6H_5CSOH$.

In this study, we employed a more simple stereospecific synthesis of optically active cystine and *threo*-3,3'-dimethylcystine. The synthetic route is shown in Scheme 1.

The aziridine derivatives used were benzyl (2*S*)-1-benzyloxycarbonyl-2-aziridinecarboxylate [(2*S*)-Z-Azy-OBzl] (**1a**), benzyl (2*S*,3*S*)-1-benzyloxycarbonyl-3-methyl-2-aziridinecarboxylate [(2*S*,3*S*)-Z-3-MeAzy-OBzl] (**2a**), and their enantiomers(**1b** and **2b**), which were prepared by *N*-benzyloxycarbonylation of (2*S*)-H-Azy-OBzl, (2*S*,3*S*)-H-3-MeAzy-OBzl, and their enantiomers with benzyloxycarbonyl chloride as described in our previous paper.[1] The ring-opening reaction of **1a**, **1b**, **2a**, and **2b** were carried out in dichloromethane saturated with H_2S in the presence of boron trifluoride etherate at room temperature for 3 h, and the corresponding cysteine derivatives obtained were oxidized with iodine in methanol solution to give the cystine(**3a**, **3b**) and 3,3'-dimethylcystine(**4a**, **4b**) derivatives. The deblocking procedure of benzyloxycarbonyl and benzyl ester was carried out in acetic acid saturated with HBr for 12 h at room temperature, and the crude cystine(**5a**, **5b**) and 3,3'-dimethylcystine (**6a**, **6b**) were purified by isoelectric point precipitation at pH 5 and recrystallized from hot water or water–ethanol to give the optically pure **5a**, **5b**, **6a**, and **6b**.

The above results show that, compared with conventional methods, synthesis of cysteine and 3-methylcysteine by the stereospecific ring-opening reaction of aziridine with H_2S is very convenient for transforming the serine or threonine into optically pure cystine or *threo*-3,3'-dimethylcystine.

Experimental

Uncorrected melting points are reported. The homogeneity of the products was checked by thin-layer chromatography on silica-gel plates. The optical rotations were determined at the D line on a Perkin-Elmer 141 polarimeter. The NMR spectra were obtained with Hitachi R 20 B high-resolution NMR spectrometer, the chemical shifts being obtained using TMS as the internal reference.

N,N'-*Bis*(*benzyloxycarbonyl*)-L-*cystine Dibenzyl Ester* (**3a**). Dry H_2S gas was bubbled through a solution of (2*S*-Z-Azy-OBzl (**1a**, 320 mg, 1.03 mmol) in dry CH_2Cl_2 (30 ml) until saturation at room temperature and $BF_3 \cdot OEt_2$ (5 drops) was added. Then H_2S gas was bubbled for additional 15 min. After the reaction mixture was stood at room temperature for 3 h, the solvent was removed *in vacuo*. The residual syrup was dissorved in MeOH (30 ml) at 0 °C and

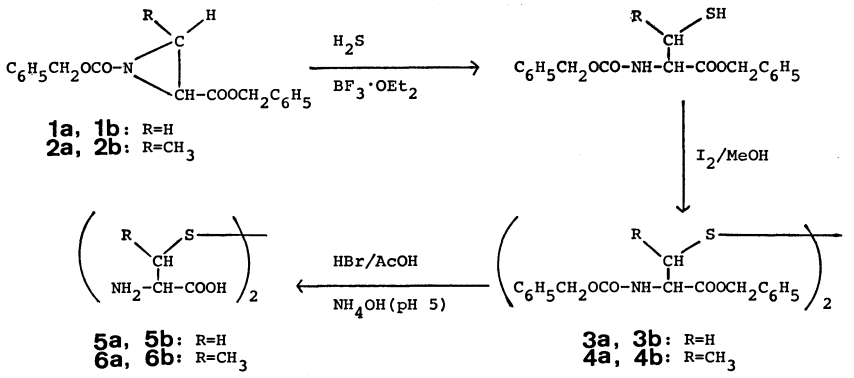

Scheme 1.

a 0.2 M (1 M=1 mol dm^{-1}) solution of I_2 in MeOH (13 ml) was added dropwise for 45 min with stirring, and additionaly stirred for 45 min at room temperature. And then, 10% sodium thiosulfate was added until the brown color has disappeared. After the reaction mixture was concentrated *in vacuo* to 10 ml, the product was extracted by ethyl acetate and the extract was washed with water, dried over Na_2SO_4, and concentrated *in vacuo*. The crude product was purified by silica-gel column chromatography($CHCl_3$). Crystallization from MeOH-ether-hexane gave **3a** (250 mg, 70%) 85.5—87.0 °C, $[\alpha]_D^{23}$ +38.0° (*c* 1.0, $CHCl_3$). NMR ($CDCl_3$) δ: 3.01 (4H d, CH_2), 5.08, 5.16 (8H 2s, CH_2), 4.62 (2H m, CH), 5.70 (2H bd, NH), 7.31 (20H s, C_6H_5).

Found: C, 62.68; H, 5.31; N, 4.12; S, 9.26%. Calcd for $C_{36}H_{36}N_2O_8S_2$: C, 62.77; H, 5.27; N, 4.07; S, 9.31%.

N,N′-*Bis(benzyloxycarbonyl)*-D-*cystine Dibenzyl Ester* (**3b**). The reaction of (2*R*-Z-Azy-OBzl (**1b**, 320 mg, 1.03 mmol) with H_2S was carried out as described above to give **3b** (285 mg, 80.3%) after recrystallization from MeOH-ether-hexane, mp 86—87 °C, $[\alpha]_D^{23}$ −39.8° (*c* 1.1, $CHCl_3$). NMR ($CDCl_3$) δ: 3.04 (4H d, CH_2), 4.63 (2H m, CH), 5.05, 5.10 (8H 2s, CH_2), 5.79 (2H bd, NH), 7.36 (20H s, C_6H_5).

Found: C, 62.72; H, 5.43; N, 4.22; S, 9.37%. Calcd for $C_{36}H_{36}N_2O_8S_2$: C, 62.77; H, 5.27; N, 4.07; S, 9.31%.

N,N′-*Bis(benzyloxycarbonyl)*-threo-3,3′-*dimethyl*-L-*cystine Dibenzyl Ester* (**4a**). The reaction of (2*S*,3*S*)-Z-3-MeAzy-OBzl (**2a**, 340 mg, 1.05 mmol) with H_2S was carried out as described above to give **4a** (280 mg, 74%) as a syrup, $[\alpha]_D^{23}$ +42.3° (*c* 1.0, MeOH). NMR ($CDCl_3$) δ: 1.02 (6H d, CH_3), 3.43 (2H dd, CH), 4.60 (2H dd, CH), 5.05, 5.10 (8H 2s, CH_2), 5.80 (2H bd, NH), 7.25 (20H s, C_6H_5).

Found: C, 63.71; H, 5.65; N, 4.10; S, 9.01%. Calcd for $C_{38}H_{40}N_2O_8S_2$: C, 63.68; H, 5.62; N, 3.91; S, 8.94%.

N,N′-*Bis(benzyloxycarbonyl)*-threo-3,3′-*dimethyl*-D-*systine Dibenzyl Ester* (**4b**). The reaction of (2*R*,3*R*)-Z-3-MeAzy-OBzl (**2b**, 340 mg, 1.05 mmol) with H_2S was carried out as described above to give **4b** (295 mg, 78%) as a syrup, $[\alpha]_D^{23}$ −42.5° (*c* 1.0, MeOH). NMR ($CDCl_3$) δ: 1.23 (6H d, CH_3), 3.44 (2H dd, CH), 4.60 (2H dd, CH), 5.07, 5.11 (8H 2s, CH_2), 5.68 (2H bd, NH), 7.28 (20H s, C_6H_5).

Found: C, 63.75; H, 5.73; N, 4.12; S, 9.11%. Calcd for $C_{38}H_{40}N_2O_8S_2$: C, 63.68; H, 5.62; N, 3.91; S, 8.94%.

L-*Cystine* (**5a**). **3a** (200 mg) was dissolved in acetic acid saturated with HBr (5 ml) at room temperature. After 12 h, the reaction mixture was concentrated *in vacuo*. The residue was triturated with anhydrous ether and was dissolved in small amount of water, and was adjusted to pH 5 with 5 M NH_4OH and ethanol was added. The precipitates were filtered off and recrystallized from hot water to give **5a** (57.8 mg, 78%), mp 204 °C (decomp), $[\alpha]_D^{23}$ −213° (*c* 1.1, 1 M HCl).

Found: C, 30.16; H, 4.92; N, 11.98; S, 26.42%. Calcd for $C_6H_{12}N_2O_4S_2$: C, 29.99; H, 5.03; N, 11.66; S, 26.68%.

D-*Cystine* (**5b**). **3b** (200 mg) was dissolved in acetic acid saturated with HBr (5 ml) at room temperature. After 12 h, the reaction mixture was worked up as described above to give **5b** (55.8 mg, 75.3%), which recrystallized from hot water, mp 206 °C (decomp), $[\alpha]_D^{23}$ +213° (*c* 1.0, 1 M HCl).

Found: C, 30.22; H, 5.12; N, 11.75; S, 26.58%. Calcd for $C_6H_{12}N_2O_4S_2$: C, 29.99; H, 5.03; N, 11.66; S, 26.68%.

L-threo-3,3′-*Dimethylcystine* (**6a**). **4a** (117 mg) was dissolved in acetic acid saturated with HBr (5 ml) at room temperature. After 12 h, the reaction mixture was worked up as described above to give **6a** (55 mg, 83%), was recrystallized from water-ethanol, mp 177.5—178 C (decomp), $[\alpha]_D^{23}$ +412.9° (*c* 0.6, 1 M HCl).

Found: C, 34.63; H, 6.22; N, 10.09; S, 23.32%. Calcd for $C_8H_{16}N_2O_4S_2 \cdot 1/2\,H_2O$: C, 34.64; H, 6.18; N, 10.10; S, 23.12%.

D-threo-3,3′-*Dimethylcystine* (**6b**). **4b** (141 mg) was dissolved in acetic acid saturated with HBr (5 ml) at temperature. After 12 h, the reaction mixture was worked up as described above to give **6b** (40 mg, 75.8%), which was recrystallized from water-ethanol, mp 175 °C (decom), $[\alpha]_D^{23}$ −414° (*c* 1.0, 1 M HCl). [lit,[6] $[\alpha]_D^{19}$ −416° (*c* 0.50, 1 M HCl), lit,[5] $[\alpha]_D^{13}$ −414° (*c* 1.0, 1 M HCl)].

Found: C, 34.65; H, 6.20; N, 10.12; S, 23.25%. Calcd for $C_8H_{16}N_2O_4S_2 \cdot 1/2\,H_2O$: C, 34.64; H, 6.18; N, 10.10; S, 23.12%.

References

1) Part IX: K. Nakajima, H. Oda, and K. Okawa, *Bull. Chem. Soc. Jpn.*, **56**, 520 (1983). The abbreviations of the IUPAC-IUB commision (*J. Biol. Chem.*, **247**, 977 (1972) are used. Z: benzyloxycarbonyl, Bzl: benzyl, "Azyline" is used as the name of 2-aziridinecarboxylic acid, "Azy" being its abbreviation. 3-MeAzy: 3-methyl-2-aziridinecarboxylic abid.

2) I. Photaki, *J. Am. Chem. Soc.*, **85**, 1123 (1963).

3) H. E. Carter, C. M. Stevens, and L. F. Ney, *J. Biol. Chem.*, **139**, 247 (1941).

4) J. Hoogmartens, P. J. Claes, and H. Vanderhaeghe, *J. Org. Chem.*, **39**, 425 (1974).

5) J. L. Morell, P. Fleckenstein, and E. Gross, *J. Org. Chem.*, **42**, 355 (1977).

6) T. Wakamiya, K. Shinbo, T. Shiba, K. Nakajima, M. Neya, and K. Okawa, *Bull. Chem. Soc. Jpn.*, **55**, 3878 (1982).

Penicillin-Cephalosporin Conversion. VII. An Improved Synthesis of 3-Methylenecephams

Shigeru Torii,* Hideo Tanaka, Takashi Siroi, Tomoyuki Madono, Norio Saitoh, Michio Sasaoka, and Junzo Nokami†

Department of Industrial Chemistry, School of Engineering, Okayama University, Okayama 700

† *Okayama University of Science, Ridai, Okayama 700*

(Received December 2, 1982)

Synopsis. Efficient conversion of 2-(7-oxo-2,6-diaza-4-thiabicyclo[3.2.0]hept-2-en-6-yl)-3-chloromethyl-3-butenoates (**4**), derived from natural penicillins, into 3-methylenecephams (**1**) has been performed by a simple two-step operation, which comprises replacement of the allylic chlorine atom of **4** with iodine and subsequent acid-catalyzed hydrolysis, leading to **1** in 70—54% overall yields. In the latter step, the ring opening of the thiazoline moiety and the intramolecular substitution of the iodide with the thiol group proceed simultaneously.

3-Methylenecephams **1** are important intermediates for the synthesis of useful cephalosporin antibiotics **2**, bearing an electronegative substituent, *e.g.*, halogen atom and methoxyl group, directly attached to the C-3 position.[1] These have been prepared by either reductive elimination of the acetoxyl group of 3-acetoxymethylcephalosporins[2] or chemical conversion of penicillins.[3] In connection with the current interest in the penicillin-cephalosporin conversion,[4] considerable efforts have been made to develop a significant route to **1** from natural penicillins.

In the preceding communication,[5] we disclosed electrolytic ene-type chlorination of thiazoline-azetidinones **3** derived from penicillins, providing 2-(7-oxo-2,6-diaza-4-thiabicyclo[3.2.0]hept-2-en-6-yl)-3-chloromethyl-3-butenoates **4**, which can be expected to be a good precursor of the 3-methylenecephams **1**. In fact, the conversion of **4** to **1** has been carried out by treatment with $AgClO_4$ in dioxane,[3a] although the yields are not satisfactory.[6] The insufficient yields in a practical sense and use of a stoichiometric amount of the expensive silver salt prompted us to find out a new and more efficient method for this purpose. We now report a convenient two-step conversion of **4** to **1** which comprises replacement of chlorine atom of **4** with iodine and subsequent acid-catalyzed hydrolysis of the thiazoline ring of **5**, leading to the desired 3-methylenecephams **1** via the intermediate **8** (Scheme 2).

It has been demonstrated that the hydrolysis of the thiazoline ring of **3** in aqueous acidic media affords thiol **6** in high yields.[7] Thus, the hydrolysis of **4** to the thiol **7** followed by the ring closure by the intramolecular nucleophilic substitution of the allylic chlorine atom with the mercapto group seemed to be a straightforward route to **1**. At first, we investigated this possibility since no such conversion has yet been realized. Hydrolysis of **4a** ($R^1=PhCH_2$; $R^2=CH_3$) in aqueous 30% $HClO_4$–acetone–CH_2Cl_2 (0.2:1:1) proceeded smoothly to afford the thiol **7a** ($R^1=PhCH_2$; $R^2=CH_3$). The ring closure of **7a** was attempted with base, *e.g.*, NaH, Na_2CO_3, pyridine, and 1,8-diazabicyclo[5.4.0]undec-7-ene (DBU) under various conditions. But all attempts brought about a complex mixture of the decomposition products of **7a** and

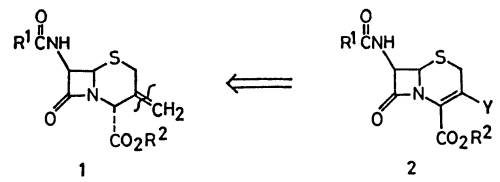

Scheme 1.

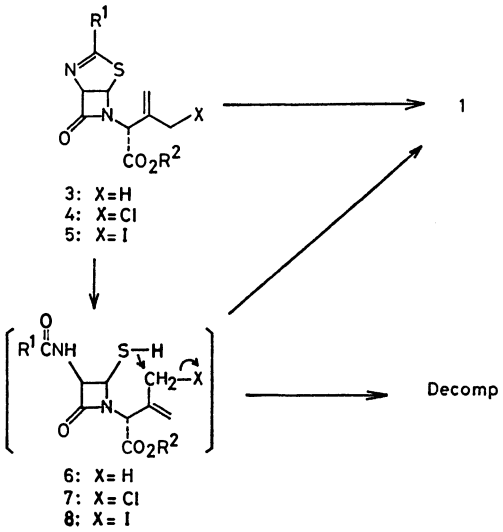

Scheme 2.

failed in obtaining the desired product **1**.

These failure made us believe that the allylic chloride is not reactive enough for this cyclization. Consequently, we tried to use iodide **5** in place of chloride **4**. The iodide **5a** ($R^1=PhCH_2$; $R^2=CH_3$) was readily prepared from **4a** by heating with NaI in acetone. Then, hydrolysis of **5a** in methanol–CH_2Cl_2 (3/1) containing aqueous 5% HCl at room temperature afforded the desired 3-methylenecepham **1a** (70% yield). Although thiol **8a** ($R^1=PhCH_2$; $R^2=CH_3$) could not be detected in the reaction mixture, the ring closure would proceed via **8a** at room temperature without using any base due to the high reactivity of the iodide **8a**. With regard to the acid hydrolysis (**5a**→**1a**), an aqueous 5% HCl–methanol–CH_2Cl_2 system was found to be most effective among the following systems (yields of **1a**): aqueous 5% HCl–methanol (60%); aqueous 30% $HClO_4$–methanol (43%), aqueous 10% H_2SO_4–methanol (43%); aqueous 5% HCl–acetone (39%).

The conversion of **4** to **1** could be also performed by one-pot reaction without isolation of the intermediates **5**. Thus, after iodization of **4** with NaI in refluxing acetone, the reaction mixture was concentrated and the residue was treated with aqueous 5% HCl–methanol–CH_2Cl_2, affording **1** in 57—70% yields.

Experimental

IR spectra were determined on a JASCO IRA-I grating infrared spectrometer. ^{1}H NMR spectra were recorded at 60 M Hz with a Hitachi R-24 spectrometer and chemical shifts are reported in parts per million (δ) relative to $(CH_3)_4Si$ ($\delta=0.0$ ppm) as an internal standard. 2-(7-oxo-2,6-diaza-4-thiabicyclo[3.2.0]hept-2-en-6-yl)-3-chloromethyl-3-butenoates **4** were prepared by the electrolytic ene-type chlorination[5] of thiazoline-azetidinones **3**. Authentic samples of 3-methylenecephams **1** were obtained by the reported procedure.[3]

Hydrolysis of ***4a*** *($R^1=PhCH_2$; $R^2=CH_3$)* A mixture of **4a** (59 mg, 0.16 mmol) in acetone (1 ml) and CH_2Cl_2 (1 ml) containing aqueous 30% $HClO_4$ (0.2 ml) was stirred at room temperature for 1 h. The mixture was diluted with CH_2Cl_2 washed with brine, dried (Na_2SO_4), and concentrated *in vacuo*, affording forms **7a** ($R^1=PhCH_2$; $R^2=CH_3$, 61 mg),[8] essentially homogeneous on TLC analysis: $R_f=0.05$ (SiO_2; benzene/AcOEt, 4/1). Without further purification,[9] the crude products were treated with DBU (5 μl) in *N,N*-dimethylformamide (1 ml) at -30 °C for 5 h. Usual work-up gave a complex mixture and any detectable amount of 3-methylenecepham **1a** ($R^1=PhCH_2$; $R^2=CH_3$) could not be observed on TLC analysis.

Conversion of ***4*** *to* ***1****.* *Procedure A*: A mixture of **4a** ($R^1=PhCH_2$; $R^2=CH_3$, 376 mg, 1.03 mmol) and NaI (230 mg, 1.53 mmol) in acetone (10 ml) was heated to reflux for 3 h. The mixture was diluted with water (5 ml) and extracted with AcOEt. Usual work-up followed by column chromatography (SiO_2, hexane/AcOEt, 4/1) afforded iodide **5a** ($R^1=PhCH_2$; $R^2=CH_3$, 425 mg, 90%): ^{1}H NMR ($CDCl_3$) δ 3.62 (2H, s, CH_2I), 3.74 (3H, s, CH_3O), 3.87 (2H, s, CH_2Ph), 5.04 (1H, s), 5.45 (1H, s), 5.91 (2H, br s), 7.27 (5H, s). Immediately after isolation of the product,[10] **5a** (59 mg, 0.13 mmol) was dissolved in methanol (0.5 ml) and CH_2Cl_2 (0.5 ml) containing aqueous 5% HCl (0.2 ml). After stirring for 15 h, usual work-up followed by column chromatography (SiO_2), benzene/AcOEt, 5/1) gave **1a** ($R=PhCH_2$; $R^2=CH_3$, 31 mg, 70%), which was identical in all respects with the authentic sample;[3c] IR ($CHCl_3$) 3385, 1770, 1744, 1678, 1506 cm^{-1}; ^{1}H NMR ($CDCl_3$) δ 3.17, 3.61, (2H, AB q, $J=14$ Hz, CH_2S), 3.60 (2H, s, CH_2CO), 3.74 (3H, s, CH_3O), 5.05 (1H, s), 5.18 (2H, br s), 5.35 (1H, d, $J=4$ Hz, CH(6)), 5.62 (1H, dd, $J=4$ and 10 Hz, CH(7)), 6.43 (1H, d, $J=10$ Hz, NH), 7.28 (5H, s).

Procedure B: A mixture of **4a** (82 mg, 0.22 mmol) and NaI (39 mg, 0.26 mmol) in acetone (1 ml) was heated to reflux for 3 h. After removal of the solvent *in vacuo*, the residue was dissolved in methanol (1.5 ml) and CH_2Cl_2 (0.5 ml) containing aqueous 5% HCl (0.4 ml). After being stirred at room temperature for 8 h, usual work-up gave **1a** ($R^1=PhCH_2$; $R^2=CH_3$, 55 mg) in 70% yield after column chromatography (SiO_2, benzene/AcOEt, 5/1). The IR and ^{1}H NMR spectra were fully identical with those of the sample **1a** prepared above.

In a similar manner as described above, benzyl 7-phenoxyacetamido-3-methylenecepham-4-carboxylate (**1b**) ($R^1=PhOCH_2$; $R^2=PhCH_2$) was obtained from **4b** ($R^1=PhOCH_2$; $R^2=PhCH_2$) in 57% overall yield, which was identical in all respects with the authentic sample; IR ($CHCl_3$) 3385, 1770, 1738, 1689, 1596 cm^{-1}; ^{1}H NMR ($CDCl_3$) δ 3.18, 3.58 (2H, AB q, $J=14$ Hz, CH_2S), 4.50 (2H, s, OCH_2CO), 5.15 (4H, br s), 5.23 (1H, s), 5.39 (1H, d, $J=4.5$ Hz, HC(6)), 5.70 (1H, dd, $J=4.5$ Hz and 9.5 Hz, HC(7)), 6.7 $-$7.5 (6H, m), 7.31 (5H, s).

References

1) a) Y. Hamashima, T. Kubota, K. Ishikura, K. Minami, K. Tokura, and W. Nagata, *Heterocycles*, **5**, 419 (1976); b) R. R. Chauvette and P. A. Pennington, *J. Am. Chem. Soc.*, **96**, 4986 (1974); c) S. Kukolja, M. R. Gleissner, A. I. Ellis, D. E. Dorman, and J. W. Paschal, *J. Org. Chem.*, **41**, 2276 (1976).

2) D. A. Hall, D. M. Berry, and J. C. Schneider, *J. Electroanal Chem.*, **30**, 155 (1977); M. Ochiai, O. Aki, A. Morimoto, T. Okada, and K. Morita, *Tetrahedron*, **31**, 115 (1975); M. Ochiai, O. Aki, A. Morimoto, T. Okada, K. Shinozaki, and Y. Asahi, *Tetrahedron Lett.*, **1972**, 2341, and see also Ref. 4a, p. 159.

3) a) S. Uyeo, T. Aoki, H. Itani, T. Tsuji, and W. Nagata, *Heterocycles*, **10**, 99 (1978); b) J. R. Corfield and C. G. Taylor, *Tetrahedron Lett.*, **1978**, 2915; c) Y. Maki and M. Sako, *J. Am. Chem. Soc.*, **99**, 5091 (1977); d) E. M. Gordon and C. M. Cimarusti, *Tetrahedron Lett.*, **1977**, 3425; e) S. Kukolja, S. R. Lammert, M. R. B. Gleissner, and A. I. Ellis, *J. Am. Chem. Soc.*, **98**, 5040 (1976), and see also Refs. 1 c and 4 a, p. 159.

4) a) "Topics in Antibiotic Chemistry," ed by P. G. Sammes, Ellis Horwood, Chichester (1980), Vol. 4; b) "Recent Advances in the Chemistry of β-Lactam Antibiotics," ed by J. Elks, The Chemical Society, Berlington House, London (1977).

5) S. Torii, H. Tanaka, N. Saitoh, T. Siroi, M. Sasaoka, and J. Nokami, *Tetrahedron Lett.*, **22**, 3193 (1981).

6) Treatment of **4a** ($R^1=PhCH_2$; $R^2=CH_3$) with $AgClO_4$ (1—1.2 equiv.) in dioxane provided 5—30% yields of **1a**.

7) M. Narisada, H. Onoue, M. Ohtani, F. Watanabe, T. Okada, and W. Nagata, *Tetrahedron Lett.*, **1978**, 1755.

8) Tentatively assigned based on the spectral data: IR ($CHCl_3$) 3380, 1775, 1745, 1680, 1510 cm^{-1}; ^{1}H NMR ($CDCl_3$) δ 1.90 (1H, br s), 3.63 (2H, s), 3.76 (3H, s), 4.18 (2H, s), 5.0—5.6 (5H, m), 7.28 (6H, br s).

9) Upon chromatography on a SiO_2 column, **7a** was decomposed even on a neutral SiO_2 (Mallinckrodt CC-7).

10) Iodide **5a** was unstable and gradually decomposed under standing in atmosphere.

Lewis Acid Mediated Reaction of Trimethylstyrylsilanes with Thioacetal Derivatives

Toshikazu HIRAO,* Shuichiro KOHNO, Yoshiki OHSHIRO, and Toshio AGAWA

Department of Applied Chemistry, Faculty of Engineering, Osaka University, Yamada-oka, Suita, Osaka 565

(Received December 6, 1982)

Synopsis. Treatment of trimethylstyrylsilanes with 1-ethoxy-1-(phenylthio)ethane or 2-ethoxy-1,3-dithiolane in the presence of Lewis acid gives the corresponding (*E*)-allyl sulfide or (*E*)-2-styryl-1,3-dithiolane, respectively. In both cases, a carbon-oxygen bond of thioacetal derivatives is cleaved selectively.

Electrophilic substitution reaction of vinylsilanes provides a versatile method for stereospecific and regioselective carbon–carbon bond formation.[1] However, electrophiles are limited to acid chloride,[2,3a] and α-chloro ether.[3] We previously found that acetal acts as an electrophile in the presence of Lewis acid, especially $MoCl_5$.[4] This methodology was used in the intramolecular reaction by Tius[5] and dithioacetal has been shown to be an electrophile in the cyclization reaction.[6] Now, we wish to report the Lewis acid mediated reaction of trimethylstyrylsilanes with monothioacetal.

Treatment of (*E*)-trimethylstyrylsilane (**1a**) with 1-ethoxy-1-(phenylthio)ethane in the presence of $MoCl_5$ at up to −20 °C gave the 1:1 adduct, (*E*)-1-phenyl-3-phenylthio-1-butene (**2**), in 42% yield exclusively.

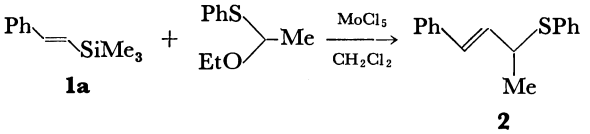

1a **2**

The reaction at −78 °C decreased the yield of **2**, as shown in Table 1. $TiCl_4$ was less effective than $MoCl_5$, as observed in the reaction with acetal.[4] A fission of a carbon-oxygen bond occurred selectively, and the product derived from the attack of $EtOC^+HMe$ was not detected. This finding exhibits a contrast to the reaction of trimethylstyrylsilanes with benzaldehyde diethyl acetal. In the latter case, both ethoxyl groups participate in the reaction to produce the 1,4-pentadiene derivatives selectively.

(*Z*)-Trimethylstyrylsilane (**1b**) was also allowed to react with 1-ethoxy-1-(phenylthio)ethane in the presence of $MoCl_5$ to yield the same allyl sulfide **2** (53%)

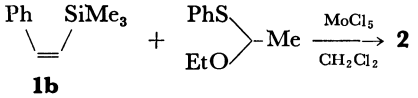

1b

exclusively. The stereochemistry of **1b** is not retained, which might be due to the Lewis acid catalyzed isomerization of the (*Z*)-allyl sulfide into the stable *E*-isomer as reported in the reaction of dichloromethyl methyl ether.[3d] This result strikingly contrasts with the stereospecific reaction of trimethylstyrylsilanes with acetal.

2-Ethoxy-1,3-dithiolane was subjected to the substitution reaction with trimethylstyrylsilanes in the presence of $BF_3 \cdot OEt_2$ to give the 1:1 adduct, (*E*)-2-styryl-1,3-dithiolane (**3**), though the yield was not high. Lewis acid such as $MoCl_5$ or $TiCl_4$ appeared to decompose 2-ethoxy-1,3-dithiolane giving none of the adduct. A carbon-oxygen bond of 2-ethoxy-1,3-dithiolane was cleaved selectively and the *E* product **3** was

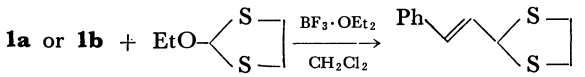

3, 20% from **1a**
22% from **1b**

formed regardless the configuration of the starting vinylsilanes **1**, as mentioned in the reaction with monothioacetal.

We showed a new carbon–carbon bond formation with trimethylstyrylsilanes, but it is disappointing to find that the other vinylsilanes such as 1-trimethylsilyl-1-hexene and -cyclohexene were not so reactive as trimethylstyrylsilanes.

Table 1. Reaction of (*E*)-trimethylstyrylsilane (**1a**) with 1-ethoxy-1-(phenylthio)ethane[a]

Lewis acid	Reaction temp/°C	Isolated yield/% of **2**
$MoCl_5$	−78	28
	−78→−20	42
$TiCl_4$	−78	10
	−78→−20	24

a) Reaction time, 4 h.

Experimental

^1H NMR and ^{13}C NMR spectra were obtained on a JEOL JNM-PMX 60 or JNM-FX 90Q with tetramethylsilane as an internal standard, respectively. IR spectra were recorded with a JASCO IRA-I spectrometer. The mass spectra were taken with a Hitachi RMU-6E spectrometer. Commercially available reagents were used unless otherwise noted. (*Z*)- and (*E*)-Trimethylstyrylsilanes,[7] 1-ethoxy-1-(phenylthio)ethane,[8] and 2-ethoxy-1,3-dithiolane[9] were prepared by the reported methods.

Reaction of 1a with 1-Ethoxy-1-(phenylthio)ethane. To a suspension of $MoCl_5$ (0.273 g, 1.0 mmol) in dichloromethane (4 ml) was added (*E*)-trimethylstyrylsilane (**1a**; 0.176 g, 1.0 mmol) and 1-ethoxy-1-(phenylthio)ethane (0.182 g, 1.0 mmol) in dichloromethane (4 ml) at −78 °C under nitrogen. The mixture was stirred at −78 °C for 2.5 h, and then warmed to −20 °C. At this temperature, the mixture was stirred for 1.5 h, and quenched with 50% aqueous methanol. The resultant mixture was warmed to 0 °C, and poured into saturated aqueous Na_2CO_3 solution (5 ml), which was extracted with ether (3×10 ml). The combined organic layers were dried over $MgSO_4$ and concentrated *in vacuo*. The residue was chromatographed on

a silica-gel column to give 0.101 g (42%) of (*E*)-1-phenyl-3-phenylthio-1-butene (**2**) and 0.0541 g of 1,1-bis(phenylthio)ethane. **2**: ^{1}H NMR ($CDCl_3$) δ 1.44 (d, 3H, J=7.1 Hz), 3.85 (qdd, 1H, J=7.1, 6.6, 0.2 Hz), 6.11 (dd, 1H, J=15.7, 6.6 Hz), 6.17 (dd, 1H, J=15.7, 0.2 Hz), 6.8—7.6 (m, 10H); ^{13}C NMR ($CDCl_3$) δ 20.7, 46.4, 126.3, 127.2, 127.3, 128.4, 128.6, 129.9, 131.6, 133.2, 134.7, 136.9; IR (neat) 1575, 960 cm^{-1}; MS *m/e* 240 (M^+).

Reaction of ***1b*** *with 1-Ethoxy-1-(phenylthio)ethane.* The reaction was carried out in the same way as mentioned above. The allyl sulfide **2** was produced in 53% yield.

Reaction of ***1a*** *with 2-Ethoxy-1,3-dithiolane.* To a solution of $BF_3 \cdot OEt_2$ (0.13 ml, 1.0 mmol) in dichloromethane (2 ml) was added (*E*)-trimethylstyrylsilane (**1a**; 0.176 g, 1.0 mmol) in dichloromethane (1 ml) at 0 °C under nitrogen. Then, 2-ethoxy-1,3-dithiolane (0.150 g, 1.0 mmol) in dichloromethane (2 ml) was added dropwise to the mixture at 0 °C for 30 min. The resultant solution was stirred at room temperature for 5 h. Saturated aqueous Na_2CO_3 solution (5 ml) was added to the mixture, which was extracted with ether (3×10 ml). The combined organic layers were dried over $MgSO_4$ and concentrated *in vacuo*. The residue was chromatographed on a silica-gel column to give 0.0416 g (20%) of (*E*)-2-styryl-1,3-dithiolane (**3**). Mp 67 °C (uncorrected); ^{1}H NMR ($CDCl_3$) δ 3.25 (broad s, 4H), 5.18 (d, 1H, J=7.6 Hz), 6.12 (dd, 1H, J=15.4, 7.6 Hz), 6.50 (d, 1H, J=15.4 Hz), 7.1—7.5 (m, 5H); IR ($CHCl_3$) 950 cm^{-1}; MS *m/e* 208 (M^+).

Reaction of ***1b*** *with 2-Ethoxy-1,3-dithiolane.* The reaction was carried out in the same way as mentioned above. (*E*)-2-Styryl-1,3-dithiolane (**3**) was produced in 22% yield.

References

1) T. H. Chan and I. Fleming, *Synthesis*, **1979**, 761.
2) I. Fleming and A. Pearce, *J. Chem. Soc., Chem. Commun.*, **1975**, 633.
3) a) J. P. Pillot, J. Dunogues, and R. Calas, *Bull. Soc. Chim. Fr.*, **1975**, 2143; b) T. H. Chan, P. W. K. Lau, and W. Mychajlowskij, *Tetrahedron Lett.*, **1977**, 3317; c) K. Yamamoto, O. Nunokawa, and J. Tsuji, *Synthesis*, **1977**, 721; d) K. Yamamoto, J. Yoshitake, N. T. Qui, and J. Tsuji, *Chem. Lett.*, **1978**, 859.
4) T. Hirao, S. Kohno, J. Enda, Y. Ohshiro, and T. Agawa, *Tetrahedron Lett.*, **22**, 3633 (1981).
5) M. A. Tius, *Tetrahedron Lett.*, **22**, 3335 (1981); M. A. Tius and S. Ali, *J. Org. Chem.*, **47**, 3163 (1982).
6) B. M. Trost and E. Murayama, *J. Am. Chem. Soc.*, **103**, 6529 (1981).
7) D. Seyferth, L. G. Vaughan, and R. Suzuki§, *J. Organomet. Chem.*, **1**, 437 (1964); F. Sato, H. Ishikawa, and M. Sato, *Tetrahedron Lett.*, **22**, 85 (1981).
8) M. F. Shostakovskiĭ, E. N. Prilezhaeva, and E. S. Shapiro, *Izv. Akad. Nauk SSSR, Otd. Khim. Nauk*, **1953**, 357; *Chem. Abstr.*, **48**, 9311 (1954).
9) K. Hatanaka, S. Tanimoto, T. Sugimoto, and M. Okano, *Tetrahedron Lett.*, **22**, 3243 (1981).

The Reaction of Organoboranes with Lithium Salts of Trisylhydrazones of Cycloalkanones Followed by Treatment with Iodine

Tsutomu BABA, Kamlakar AVASTHI, and Akira SUZUKI*

Department of Applied Chemistry, Faculty of Engineering, Hokkaido University, Sapporo 060

(Received December 15, 1982)

Synopsis. The titled reaction proceeds smoothly under mild conditions to give corresponding 1-alkylcycloalkenes in excellent yields. The overall reaction provides a convenient synthetic procedure of cycloalkenes for cycloalkanones, with various alkyl substituents readily available by means of hydrobortation.

Recently, organoborates have been recognized as important intermediates in the formation of carbon–carbon bonds.[1] On the other hand, there are various methods to convert ketones to alkenes,[2] one of which is the conversion through their tosylhydrazones (Bamford-Stevens reaction and the related reactions, Eq. 1).[3] Although such methods are established as

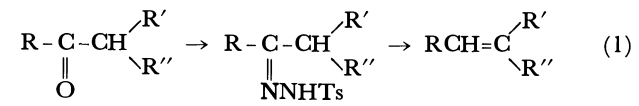

(1)

useful synthetic routes to alkenes with a wide variety of structures, they have unavoidable limitation that only alkenes with the skeltons of the parent ketones are obtained as shown in Eq. 1. Previously, we reported that the reaction of iodine with 1-alkenyltrialkylborates derived from trialkylboranes and 2,4,6-triisopropylphenylsulfonylhydrazones (trisylhydrazones) of methyl ketones provides a novel synthesis of 1,1-dialkylethylenes.[4] However, that procedure did not give satisfactory results for trisylhydrazones of cycloalkanones.

In this paper, we wish to report that the modified procedure by using THF as a solvent gives excellent results for cycloalkanone derivatives. Representative results are summarized in Table 1.

The reaction is considered to proceed through the vinylic anion[5] derived from a trisylhydrazone as reported previously.[4] More interesting examples involve unsymmetrical ketones, which can give rise to geometrically isomeric vinyllithium reagents. As an example of such a type, the derivative (**1**) formed from 2-methylcyclohexanone gives good yields of 1-alkyl-6-methylcyclohexenes (**2**).

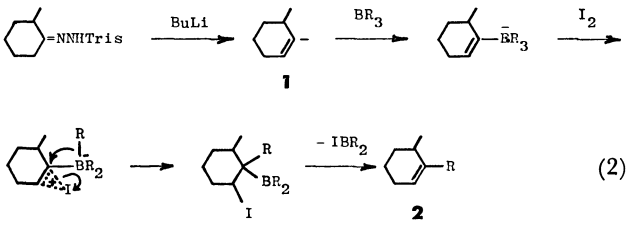

(2)

Experimental

Materials. Commercial alkenes and butyllithium were used. THF was purified by distillation from $LiAlH_4$ before use. Trialkylboranes were prepared by the hydroboration of corresponding alkenes with borane in THF.[6] Trisylhydrazones of cycloalkanones were prepared by the reported method[5] from ketones and 2,4,6-triisopropylphenylsulfonylhydrazide.[7]

Table 1. Synthesis of 1-alkylcycloalkenes from cycloalkanones

Cycloalkanone (Mp θ_m/°C of trisylhydrazone)	Organoborane R_3B, R =	Yield/%[a] of product[b]
(124 decomp)	Propyl	82
	Butyl	77
	s-Butyl	96
	Isobutyl	67
	Cyclopentyl	79
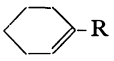		
(109 decomp)	Propyl	93
	Butyl	92
	s-Butyl	94
	Isobutyl	96
	Cyclopentyl	87
	Hexyl	92
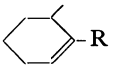		
(134 decomp)	Butyl	95
	s-Butyl	93
	Isobutyl	90
	Cyclopentyl	98
	Hexyl	96

a) Based on the organoborane used. b) Satisfactory spectral data and elemental analyses were obtained for all products.

The IR and NMR spectra were taken on a Hitachi-Perkin Elmer Model 125 spectrophotometer and a Hitach R-22 spectrometer at 90 MHz using tetramethylsilane as an internal standard, respectively.

General Procedure. The following procedure for the preparation of 1-propyl-6-methylcyclohexene is representative. A dry 50 ml-flask equipped with a magnetic stirring bar, a septum inlet, and a reflux condenser was flushed with dry nitrogen. The flask was charged under nitrogen with 0.784 g (2.04 mmol) of 2-methylcyclohexanone trisylhydrazone, mp 109 °C (decomp) and 10 ml of a 10% TMEDA solution in THF under stirring. The mixture was cooled to −78 °C, and 2.59 ml (5.03 mmol) of a 1.97 M (1 M = 1 mol dm^{-3}) solution of butyllithium in ether was added dropwise. The solution was stirred at the temperature for 30 min, and then allowed to warm to 0 °C. The flask was held at the temperature for additional 15 min to ensure the completion of nitrogen evolution. To the mixture again cooled to −78 °C, 0.65 ml (1.43 mmol) of a 2.2 M solution of tripropylborane in THF was added carefully. The mixture was stirred at −78 °C for 60 min followed by 60 min stirring at room temperature. The flask was again cooled to −60 °C and 0.40 g (1.57 mmol) of iodine in 4 ml of THF was added dropwise. The reaction mixture was stirred around −60 °C for 30 min followed by 60 min stirring at room temperature, and a few drops of aqueous sodium thiosulfate solution was added to remove an excess

of iodine. After the usual alkaline hydrogen peroxide oxidation, the solution was saturated with potasium carbonate. The VPC analysis of the separated organic layer indicated formation of 1-propyl-6-methylcyclohexene in a 93% yield.

Identification of the Products. In all cases analytically pure samples were obtained by preparative VPC with Varian autoprep Model-2800 and characterized by NMR, IR, and mass spectra, and elemental analyses.

Cyclohexanone Trisylhydrazone: Mp 125 °C (decomp). Found: C, 66.66; H, 9.04; N, 7.38; S, 8.42%. Calcd for $C_{21}H_{34}O_2N_2S$: C, 66.75; H, 9.01; N, 7.42; S, 8.49%. ^{1}H-NMR (CCl_4): δ 1.20 (d, 18H), 1.56 (s, 6H), 2.28 (s, 4H), 2.90 (m, 1H), 4.25 (m, 2H), 7.15 (s, 3H).

2-Methylcyclohexanone Trisylhydrazone: Mp 108 °C (decomp). Found: C, 67.49; H, 9.25; N, 7.01; S, 7.99%, Calcd for $C_{22}H_{36}O_2N_2S$: C, 67.48; H, 9.20; N, 7.15; S, 8.19%. ^{1}H-NMR (CCl_4): δ 0.94 (d, 3H), 1.22 (d, 18H), 1.60—2.15 (m, 10H), 2.85 (m, 1H), 4.25 (m, 2H), 7.06 (s, 2H).

Cyclopentanone Trisylhydrazone: Mp 133—134 °C (decomp). Found: C, 65.85; H, 8.85; N, 7.68; S, 8.80%. Calcd for $C_{20}H_{32}O_2N_2S$: C, 65.91: H, 8.92; N, 7.63; S, 8.60%. ^{1}H-NMR (CCl_4): δ 1.25 (d, 18H), 1.80 (s, 4H), 2.32 (d, 4H), 2.95 (m, 1H), 4.30 (m, 3H), 7.10 (s, 2H).

1-Propylcyclohexene: Found: C, 86.98; H, 13.02%. Calcd for C_9H_{16}: C, 87.02; H, 12.98%. Mass: $m/e=124$ (M+). IR (neat): 820, 1665 cm^{-1}. ^{1}H-NMR (CCl_4): δ 0.90 (t, 3H), 1.62 (m, 2H), 1.72—2.10 (m, 8H), 3.65 (t, 2H), 5.34 (s, H).

1-Butylcyclohexene: Found: C, 86.90; H, 13.10%. Calcd for $C_{10}H_{18}$: C, 86.88; H, 13.12%. Mass: $m/e=138$ (M+). IR (neat): 820, 1665 cm^{-1}. ^{1}H-NMR (CCl_4): δ 0.90 (t, 3H), 1.32 (m, 2H), 1.58 (m, 2H), 1.75—2.05 (m, 8H), 3.64 (t, 2H), 5.35 (s, H).

1-(s-Butyl)cyclohexene: Found: C, 86.80; H, 13.23%. Calcd for $C_{10}H_{18}$: C, 86.88; H, 13.12%. Mass: *m/e* 138 (M+). IR (neat): 810, 1660 cm^{-1}. ^{1}H-NMR (CCl_4): δ 0.84 (t, 3H), 0.95 (d, 3H), 1.62 (m, 2H). 1.72—2.05 (m, 8H). 3.68 (t, H), 5.40 (s, H).

1-Isobutylcyclohexene: Found: C, 86.72; H, 13.01%. Calcd for $C_{10}H_{18}$: C, 86.88; H, 13.12%. Mass; $m/e=138$ (M+). IR (neat): 820, 1660 cm^{-1}. ^{1}H-NMR (CCl_4): δ 0.86 (d, 6H), 1.54—2.05 (m, 9H), 3.68 (t, 2H), 5.35 (s, H).

1-Cyclopentylcyclohexene: Found: C, 87.89; H, 12.11%. Calcd for $C_{11}H_{18}$: C, 87.92; H, 12.08%. Mass: $m/e=150$ (M+). IR (neat): 820, 1665 cm^{-1}. ^{1}H-NMR (CCl_4): δ 1.50—2.30 (m, 17H), 5.40 (m,H).

1-Propyl-6-methylcyclohexene: Found: C, 86.66; H, 12.95%. Calcd for $C_{10}H_{18}$: C 86.88; H, 13.12%. Mass: $m/e=138$ (M+). IR (neat): 805, 1670 cm^{-1}. ^{1}H-NMR (CCl_4): δ 0.89 (t, 3H), 1.02 (d, 3H), 1.20—1.66 (m, 7H), 1.90—2.05 (m, 4H), 5.33 (s, H).

1-Butyl-6-methylcyclohexene: Found: C, 86.36; H, 13.01%. Calcd for $C_{11}H_{20}$: C, 86.76; H, 13.24%. Mass: $m/e=152$ (M+). IR (neat): 810, 1670 cm^{-1}. ^{1}H-NMR (CCl_4): δ 0.89 (t, 3H), 0.96 (d, 3H), 1.15—1.55 (m, 7H), 1.76—2.10 (m, 6H), 5.30 (s, H).

1-(s-Butyl)-6-methylcyclohexene: Found: C, 86.65; H, 13.35%. Calcd for $C_{11}H_{20}$: C, 86.76; H, 13.24%. Mass: $m/e=152$ (M+). IR (neat): 800, 1660 cm^{-1}. ^{1}H-NMR (CCl_4): δ 0.86 (d, 6H), 1.00 (d, 3H), 1.30—1.66 (m, 6H), 1.80—2.15 (m, 4H), 5.33 (s, H).

1-Isobuty-6-methylcyclohexene: Found: C, 86.80; H, 13.19%. Calcd for $C_{11}H_{20}$: C, 86.76; H, 13.24%. Mass: $m/e=152$ (M+). IR (neat): 790, 1660 cm^{-1}. ^{1}H-NMR (CCl_4): δ 0.88 (t, 6H), 1.02 (d, 3H), 1.18—1.30 (m, 4H), 1.45—1.65 (m, 4H), 1.95 (m, 2H), 5.32 (s, H).

1-Cyclopentyl-6-methylcyclohexene: Found: C, 87.69; C, 12.23%. Calcd for $C_{12}H_{20}$: C, 87.73; H. 12.27%. Mass: $m/e=164$ (M+). IR (neat): 800, 1650 cm^{-1}. ^{1}H-MNR (CCl_4): δ 1.02 (d, 3H), 1.20—2.00 (m, 15H), 2.20 (m, H), 5.38 (s, H).

1-Hexyl-6-methylcyclohexene: Found: C, 86.50; H, 13.38%. Calcd for $C_{13}H_{24}$: C, 86.58; H, 13.42%. Mass: $m/e=180$ (M+). IR (neat): 810, 1660 cm^{-1}. ^{1}H-NMR (CCl_3): δ 0.88 (t, 3H), 0.98 (d, 3H), 1.15—1.58 (m, 11H), 1.75—2.05 (m, 6H), 5.32 (s, H).

1-Butylcyclopentene: Found: C, 86.98: H, 12.89%. Calcd for C_9H_{16}: C, 87.02; H, 12.98%. Mass: $m/e=124$ (M+). IR (neat): 810, 1650 cm^{-1}. ^{1}H-NMR (CCl_4): δ 0.92 (t, 3H), 1.40 (m, 4H), 1.75—2.30 (m, 8H), 5.29 (s, H).

1-(s-Butyl)cyclopentene: Found: C, 87.21; H, 12.85%. Calcd for C_9H_{16}: C, 87.02; H, 12.98%. Mass; $m/e=124$ (M+). IR (neat): 790, 1660 cm^{-1}. ^{1}H-NMR (CCl_4): δ 0.88 (t, 3H), 0.92 (d, 3H), 1.48—2.22 (m, 9H), 5.28 (s, H).

1-Isobutylcyclopentene: Found: C, 86.94; H, 12.93%. Calcd for C_9H_{16}: C, 87.02; H, 12.98%. Mass: $m/e=124$ (M+). IR (neat): 800, 1660 cm^{-1}. ^{1}H-NMR (CCl_4): δ 0.90 (t, 6H), 1.50—2.25 (m, 9H), 5.30 (s, H).

1-Cyclopentylcyclopentene: Found: C, 88.12; H, 11.82%. Calcd for $C_{10}H_{16}$: C, 88.16; H, 11.84%. Mass: $m/e=136$ (M+). IR (neat): 800, 1650 cm^{-1}. ^{1}H-MNR (CCl_4): δ 1.30—1.93 (m, 9H), 2.05—2.35 (m, 6H), 5.30 (s, H).

1-Hexylcyclopentene: Found: C, 86.75; H, 13.24%. Calcd for $C_{11}H_{20}$: C, 86.76; H, 13.04%. Mass: $m/e=152$ (M+). IR (neat): 810, 1650 cm^{-1}. ^{1}H-NMR (CCl_4): δ 0.88 (t, 3H), 1.28 (m, 10H), 1.75—2.30 (m, 6H), 5.28 (s, H).

References

1) A. Suzuki, *Acc. Chem. Res.*, **15**, 178 (1982).

2) J. Barluenga, M. Yus, and P. Bernad, *J. Chem. Soc., Chem. Commun.*, **1978**, 847; R. Amouroux and T. H. Chan, *Tetrahedron Lett.*, **1978**, 4453.

3) R. H. Shapiro, *Org. React.*, **23**, 405 (1975); E. Vedejs, J. M. Dolphin, and W. T. Stolle, *J. Am. Chem. Soc.*, **101**, 249 (1979).

4) K. Avasthi, T. Baba, and A. Suzuki, *Tetrahedron Lett.*, **21**, 945 (1980).

5) A. R. Chamberlin, J. E. Stemke, and F. T. Bond, *J. Org. Chem.*, **43**, 147 (1978).

6) H. C. Brown, "Organic Syntheses *via* Boranes," Wiley, New York (1975), p. 18.

7) N. J. Cusack, C. B. Reese, A. C. Risius, and B. Roozpeikar, *Tetrahedron*, **32**, 2157 (1976).

A New Glycoside, Kusaginin Isolated from *Clerodendron trichotomum*

Atsushi SAKURAI* and Takahiko KATO†

Department of Chemistry, Faculty of Science, Shizuoka University, Ohya, Shizuoka 422

(Received December 22, 1982)

Synopsis. A new glycoside, kusaginin was isolated from *Clerodendron trichotomum* Thunb. and 2-(3,4-dihydroxyphenyl)ethyl 3-*O*-α-L-rhamnopyranosyl-4-*O*-(3,4-dihydroxycinnamoyl)-β-D-glucopyranoside was assigned to this substance from studies on the hydrolysis products and from analyses of the ^{1}H NMR and ^{13}C NMR spectra.

From the leaves of *Clerodendron trichotomum* Thunb. (Kusagi in Japanese) a flavonoid glycoside, acacetin 7-*O*-2-β-D-glucopyranuronosyl-β-D-glucopyranuronoside[1] and a bitter principle, clerodendrin A,[2] and from the fruits of the plant two blue pigments, trichotomin and trichotomin G_1,[3] have been isolated.

During our studies on the constituents of this plant we isolated a new glycoside and named it kusaginin (**1**). In this paper we wish to report the isolation and structure of **1**.

The methanol extract of the fresh leaves of the plant was triturated with water and ethyl acetate and the aqueous layer was subjected to chromatography on a column of Sephadex LH-20 eluting with methanol. The last effluent gave **1** as colorless crystals, mp 154—156 °C in 0.3% yield from wet plant. Compound **1** is optically active, $[\alpha]_D$ −104° and from its elemental analyses was suggested the formula $C_{29}H_{36}O_{15}$. The IR spectrum of **1** shows absorption bands indicative of the existence of a conjugated ester group at 1716 and 1278 cm^{-1} and the UV spectrum of **1** in ethanol shows absorption maxima characteristic of an ester of 3-(3,4-dihydroxyphenyl)-2-propenoic acid[4] at 202, 219, 245, 290, and 332 nm. From the IR spectrum coupled with ^{1}H NMR spectrum of **1** which has complex signals corresponding to the protons on oxygenated carbon atoms at δ 3.0—4.0, it is considered that **1** has sugar portions.

The ^{1}H NMR spectrum of **1** in DMSO-d_6 shows the signals attributed to the protons attached to two 1,3,4-trisubstituted benzene rings at δ 6.58 (1H, dd, J=1.5 and 8 Hz), 6.69 (1H, d, J=8 Hz), 6.71 (1H, d, J=1.5 Hz), 6.80 (1H, d, J=7.5 Hz), 6.95 (1H, dd, J=2 and 7.5 Hz), and 7.07 (1H, d, J=2 Hz), two *trans* olefinic protons at δ 6.28 (1H, d, J=16 Hz) and 7.58 (1H, d, J=16 Hz), two anomeric protons of sugar portions at δ 4.35 (1H, d, J=8 Hz) and 5.00 (1H, d, J=2 Hz), a proton attached to a carbon atom bearing an ester group at δ 4.67 (1H, t, J=9 Hz), methylene protons of a benzyl group at δ 2.67 (2H, t, J=7.5 Hz), and methyl protons at δ 0.98 (3H, d, J=6 Hz), besides them.

Acetylation of **1** with acetic anhydride and pyridine gave a nonaacetate of **1** as colorless crystals, mp 92—96 °C and its ^{1}H NMR spectrum shows the signals ascribed to the methyl protons of acetoxyl groups at δ 1.89 (3H, s), 1.97 (3H, s), 2.02 (3H, s), 2.08 (3H, s), 2.10 (3H, s), 2.26 (3H, s, aromatic acetoxyl), 2.28 (3H, s, aromatic acetoxyl), and 2.29 (6H, s, aromatic acetoxyl).

† Present address: Kuramoto Sangyo Co. Ltd., 1-4-1 Minamidai, Kawagoe, Saitama 350.

Treatment of **1** with 10% hydrogen chloride in methanol gave 2-(3,4-dihydroxyphenyl)ethanol (**2**),[5] methyl caffeate (**3**),[4] a substance **4**, methyl α-L-rhamnoside (**5**), methyl α-D-glucoside (**6**), and small amounts of methyl β-L-rhamnoside (**7**) and methyl β-D-glucoside (**8**). Since **4** gives **2**, **6**, and **8** by further treatment with hydrogen chloride in methanol and the ^{1}H NMR spectrum of **4** in CD_3OD shows a sharp doublet of 1′-proton of the D-glucose at δ 4.27 (J=7.5 Hz, axial/axial coupling indicative of β-D-glucoside), D-glucose and **2** should be linked by a β-glycoside bond. In the ^{13}C NMR spectra of **2**, **4**, methyl α-D-glucopyranoside (**6**), and methyl β-D-glucopyranoside (**8**) as shown in Table 1, the 8-carbon in **4** appears at a field lower by 7.5 ppm than that of **2** and the 7-carbon in **4** also appears at a field higher by 3.1 ppm than that of **2**. These results[6] indicate that the D-glucose in **4** might be linked by a β-glycoside bond to the C-8 of **2**.

Hydrolysis of **1** with sodium hydroxide in aqueous methanol gave caffeic acid (**9**)[5b,7] and a substance **10**. Since **10** gives **2**, **4**, **5**, and **6** by further treatment with hydrogen chloride in methanol and the ^{1}H NMR spectrum of **10** in CD_3OD shows a sharp doublet of 1″-proton of the L-rhamnose at δ 5.13 (J=1.8 Hz, equatorial/equatorial coupling indicative of α-L-rhamnoside), L-rhamnose and **4** should be linked by an α-glycoside bond. In the ^{13}C NMR spectra of **4**, methyl α-L-rhamnopyranoside (**5**), methyl β-L-rhamnopyranoside (**7**), and **10** as shown in Table 1, the 3′-carbon of the glucose in **10** appears at a field lower by 6.3 ppm than that of **4** and the 4′-carbon of the glucose in **10** also appears at a field higher by 1.5 ppm than that of **4**. These results indicate that the L-rhamnose in **10** might be linked by an α-glycoside bond to the C-3′ of **4**.

TABLE 1. CARBON-13 NMR CHEMICAL SHIFTS OF **1**, **2**, **3**, **4**, **5**, **6**, **7**, **8**, AND **10** IN CD_3OD

Compound		1	10	4	3	2	6	8	5	7
2-(3,4-Dihydroxy-	1	131.4	131.4	131.4		131.7	—	—	—	—
phenyl)ethanol	2	116.3*	116.3*	116.3*	—	116.2*	—	—	—	—
	3	145.8**	145.9**	145.9**	—	145.9**	—	—	—	—
	4	144.4**	144.4**	144.5**	—	144.4**	—	—	—	—
	5	117.0*	117.0*	117.0*	—	117.0*	—	—	—	—
	6	121.3	121.2	121.3	—	121.2	—	—	—	—
	7	36.4	36.3	36.4	—	39.5	—	—	—	—
	8	72.1	72.0	72.0	—	64.5	—	—	—	—
D-Glucose	1	103.9	103.9	104.2	—	—	101.1	105.1	—	—
	2	75.9	75.4	75.0	—	—	73.5	74.8	—	—
	3	81.6	84.2	77.9	—	—	75.1	77.7	—	—
	4	70.4	70.0	71.5	—	—	71.7	71.3	—	—
	5	75.9	77.5	77.9	—	—	73.5	77.7	—	—
	6	62.2	62.3	62.6	—	—	62.6	62.5	—	—
L-Rhamnose	1	102.8	102.5	—	—	—	—	—	102.6	102.7
	2	72.1	72.0	—	—	—	—	—	72.3	72.3
	3	72.1	72.0	—	—	—	—	—	72.0	74.9
	4	73.7	73.8	—	—	—	—	—	73.8	73.9*
	5	70.4	70.0	—	—	—	—	—	69.5	73.5*
	6	18.4	17.9	—	—	—	—	—	18.0	17.9
Caffeic acid	1	127.5	—	—	127.5	—	—	—	—	—
	2	114.5***	—	—	114.7*	—	—	—	—	—
	3	149.5	—	—	149.2	—	—	—	—	—
	4	146.5	—	—	146.5	—	—	—	—	—
	5	115.2***	—	—	115.1*	—	—	—	—	—
	6	123.2	—	—	122.9	—	—	—	—	—
	7	148.0	—	—	148.0	—	—	—	—	—
	8	116.3***	—	—	116.3*	—	—	—	—	—
	9	168.2	—	—	169.6	—	—	—	—	—
	CH_3	—	—	—	51.9	—	55.5	57.4	55.1	57.0

In parts per million downfield from tetramethylsilane. Asterisks indicate that assignments are unambigous.

Methanolysis and base catalyzed hydrolysis of **1** gave methyl caffeate (**3**) and caffeic acid (**9**) respectively as described above, which indicates that caffeic acid and **10** might be linked by an ester bond. In the in-beam electron impact mass spectrum[8,9] of an acetate of **1** could not be observed the molecular ion peak, however the spectrum exhibits a fragment ion peak corresponding to the ion structure **11** shown in Figure at m/z 273 as base peak, which indicates that caffeic acid should not be linked to the L-rhamnose in **1**. In the ^{1}H NMR spectrum of **1** irradiation of the proton on a carbon atom bearing the ester group at δ 4.67 shows no change in the spectral pattern of the anomeric proton of glucose at δ 4.35 and *vice versa*, which indicates that caffeic acid should not be linked to the 2-position of glucose in **1**.

In the ^{13}C NMR spectra of **1**, **3**, and **10**, the 9'''-carbonyl carbon in **1** appears at a field higher by 1.4 ppm than that of **3** and both 3'- and 5'-carbons in **1** also appear at fields higher by 2.6 and 1.6 ppm respectively than those of **10**. This fact is the consequence of steric compression[10] between the C-9 of caffeic acid and the C-3 or C-5 of D-glucose. These results indicate that caffeic acid might be linked by an ester bond to the C-4' of **10**.

These ^{1}H NMR and ^{13}C NMR spectroscopic data and all experimental results described above support the structure of kusaginin (**1**) to be 2-(3,4-dihydroxyphenyl)ethyl 3-*O*-α-L-rhamnopyranosyl-4-*O*-(3,4-dihydroxycinnamoyl)-β-D-glucopyranoside.

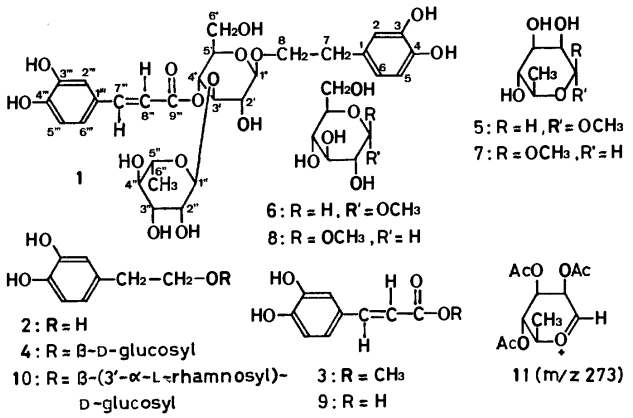

Experimental

All melting points are uncorrected. The ^{1}H NMR spectra were measured with a Varian EM-390 90 MHz NMR spectrometer. The ^{13}C NMR spectra were measured with a JEOL JNM-PFT-60 NMR spectrometer at 15.04 MHz. Chemical shifts were obtained by δ value (ppm) from tetramethylsilane as internal standard.

Isolation of Kusaginin (1). The fresh leaves of the plant (1.5 kg)[11] were extracted with methanol. The extract was condensed to a syrup under reduced pressure and the syrup was triturated with water (300 cm^3) and ethyl acetate (500 cm^3). The aqueous layer was condensed to a syrup under reduced pressure and the syrup was dissolved in methanol (150 cm^3). Each 50 cm^3 of the methanol solution was subjected to chromatography on a column of Sephadex LH-20 (3.5 × 120 cm) eluting with methanol. The last effluents gave **1** as colorless crystals after recrystallization from a mixture of methanol and chloroform: mp 154—156 °C; yield, 4.5 g (0.3% from wet plant); $[\alpha]_D^{20}$ −104° (*c* 1.0, MeOH); UV (EtOH) 202 (ε 41000), 219 (19300), 237 (sh 12500), 245 (11200), 290 (13200), 300 (sh 13600), and 332 nm (13600); IR (KBr) 3535, 3400—3100, 1716, 1640, 1606, 1598, 1523, 1445, 1390, 1310, and 1278 cm^{-1}. Found: C, 55.38; H, 5.79%. Calcd for $C_{29}H_{36}O_{15}$: C, 55.77; H, 5.81%.

Acetylation of **1** with acetic anhydride and pyridine at room temperature gave a nonaacetate of **1** as colorless crystals: mp 92—96 °C. Found: C, 56.23; H, 5.40%. Calcd for $C_{47}H_{54}O_{24}$: C, 56.29; H, 5.43%.

Methanolysis of 1. Compound **1** (500 mg) was dissolved in dry methanol containing 10 wt% of hydrogen chloride (30 cm^3), which was allowed to stand at room temperature for 20 h under nitrogen atmosphere. The mixture was concentrated to dryness under reduced pressure. The residue was subjected to chromatography on a column of Sephadex LH-20 in the same manner as described above and gave **2** (colorless crystals, mp 80—82 °C; yield, 85 mg), **3** (colorless crystals, mp 151—152 °C; yield, 135 mg), **4** (colorless oil; yield, 120 mg), and a mixture of sugars.

Acetylation of **4** with acetic anhydride and pyridine gave a hexaacetate of **4** as colorless crystals: mp 40.5—42 °C. Found: C, 54.82; H, 5.71%. Calcd for $C_{26}H_{32}O_{14}$: C, 54.93; H, 5.67%.

The sugar fraction was subjected to thin layer chromatography and the sugars were proved to be identical with authentic **5**, **6**, **7**, and **8**.

Hydrolysis of 1 with Sodium Hydroxide. Compound **1** (325 mg) was dissolved in a mixture of methanol (4 cm^3) and 1 M (1 M = 1 mol dm^{-3}) aqueous sodium hydroxide (4 cm^3), which was allowed to stand at room temperature for 4 h under nitrogen atmosphere. After being acidified with hydrochloric acid, the mixture was concentrated to dryness under reduced pressure. The residue was subjected to chromatography on a column of Sephadex LH-20 and gave **9** (colorless crystals, mp 207—208 °C; yield, 51 mg) and **10** (colorless oil; yield, 195 mg).

Acetylation of **10** with acetic anhydride and pyridine gave an octaacetate of **10** as colorless crystals: mp 71—73 °C. Found: C, 54.04; H, 5.64%. Calcd for $C_{36}H_{46}O_{20}$: C, 54.13; H, 5.80%.

References

1) M. Okigawa, H. Hatanaka, N. Kawano, I. Matsunaga, and Z. Tamura, *Tetrahedron Lett.*, **1970**, 2935.
2) N. Kato, M. Shibayama, and K. Munakata, *J. Chem. Soc., Perkin Trans. 1*, **1973**, 712.
3) S. Iwadare, Y. Shizuri, K. Sasaki, and Y. Hirata, *Tetrahedron*, **30**, 4105 (1974).
4) H. J. Klosterman and R. Z. Muggli, *J. Am. Chem. Soc.*, **81**, 2188 (1959).
5) a) C. Shöpf, G. Göttman, E. M. Meisel, and L. Neuroth, *Justus Liebigs Ann. Chem.*, **563**, 86 (1949); b) A. Stoll, J. Renz, and A. Brack, *Helv. Chim. Acta*, **33**, 1877 (1950).
6) J. B. Stothers, "Carbon-13 NMR Spectroscopy," Vol. 24 of "Organic Chemistry, a Series of Monographs," ed by A. T. Blomquist, H. Wasserman, Academic Press, New York, London (1972), Chap. 5, p. 144.
7) R. Krasemann, *Arch. Pharm.*, **293**, 712 (1960).
8) A. Dell, D. H. Williams, H. R. Morris, G. A. Smith, J. Feeney, and G. C. Roberts, *J. Am. Chem. Soc.*, **97**, 2497 (1975).
9) M. Ohashi, K. Tsujimoto, and A. Yasuda, *Chem. Lett.*, **1976**, 439.
10) G. C. Levy and G. L. Nelson, "Carbon-13 Nuclear Magnetic Resonance for Organic Chemists," Wiley-Interscience, New York, London, Sydney, Toronto (1972), Chap. 2, p. 24.
11) The plant was collected at Mt. Udo of Shizuoka City in the autumn of 1981.

Studies on Salt Hydrate for Latent Heat Storage. III. Pseudo-binary System, $CH_3CO_2Na \cdot 3H_2O$–$HCONH_2$

Takahiro WADA,* Fumiko KIMURA, and Ryoichi YAMAMOTO

Material Research Laboratory, Matsushita Electric Industrial Co. Ltd., Kadoma, Osaka 571

(Received July 29, 1982)

Synopsis. A pseudo-binary system $CH_3CO_2Na \cdot 3H_2O$–$HCONH_2$ has been studied by differential scanning calorimetry. In this system, a one to one addition compound $CH_3CO_2Na \cdot HCONH_2 \cdot 3H_2O$ is formed. This addition compound melts congruently at 40.5 °C and its heat of fusion is 255 J/g. So, it is hopeful for solar energy storage.

Salt hydrates have received attention recently, because of their large heat of fusion.[1] A few salt hydrates were used for solar energy storage.[2,3] Materials with melting points within the range 40—45 °C are suitable for solar energy storage.

In order to develop a latent heat storage material with melting point within the range 40—45 °C, the pseudo-binary system $CH_3CO_2Na \cdot 3H_2O$–$HCONH_2$ was studied by differential scanning calorimetry (DSC). From this measurement, the partial phase-diagram of the ternary system CH_3CO_2Na–$HCONH_2$–H_2O at ambient pressure was constructed. In this system, a one to one addition compound of the two components, $CH_3CO_2Na \cdot 3H_2O$ and $HCONH_2$ was formed. The heat of fusion of this addition compound was determined.

Experimental

$CH_3CO_2Na \cdot 3H_2O$, CH_3CO_2Na, and $HCONH_2$ were of guaranteed grade reagent supplied from Wako Pure Chemical Industries Ltd.

Differential scanning calorimetry (DSC) was performed using SSC 56OU DSC (DAINISEIKOSHA CO. Ltd.), which was heat-flux DSC. Weighed quantities of $CH_3CO_2Na \cdot 3H_2O$, $HCONH_2$, and other chemicals were heated and mixed to form a homogeneous melt. One drop of this melt was placed in a 15 μl silver crucible and was solidified. After the crucible was closed, the sample was heated at the rate of 0.5 °C/min from 10 °C to 90 °C. The melting temperature of the sample was obtained from the sample temperature curve at time corresponding to endothermal peak. This DSC system was calibrated by using ice (t_m: 0.0 °C, ΔH_m: 335 J/g), sodium sulfate decahydrate (t_m: 32.4 °C) and sodium acetate trihydrate (t_m: 58.4 °C) as standards.

Results and Discussion

The phase diagram of the binary system CH_3CO_2Na–H_2O based on W. F. Greem's data[4] is shown in Fig. 1. In this figure, W_a shows mass fraction of CH_3CO_2Na and W_b shows mass fraction of H_2O. We see that $CH_3CO_2Na \cdot 3H_2O$ melts incongruently to an aqueous solution containing 58 percent CH_3CO_2Na by weight in equilibrium with the balance of CH_3CO_2Na and that the balance of CH_3CO_2Na dissolves entirely in its water of crystallization at 78 °C.

The DSC curves of some mixtures of the pseudo-binary system $CH_3CO_2Na \cdot 3H_2O$–$HCONH_2$ are illus-

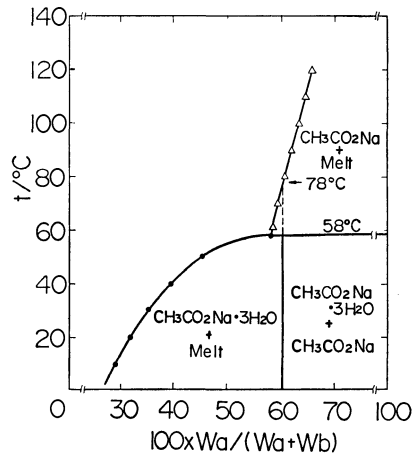

Fig. 1. Phase diagram of the binary system CH_3CO_2Na–H_2O.
●: Melting point of $CH_3CO_2Na \cdot 3H_2O$, △: melting point of CH_3CO_2Na.

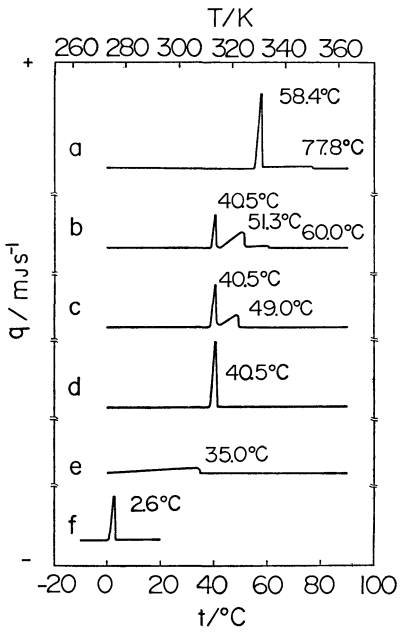

Fig. 2. DSC curves of mixtures of the pseudo-binary system $CH_3CO_2Na \cdot 3H_2O$–$HCONH_2$. a: $CH_3CO_2Na \cdot 3H_2O$, b: 0.10 mass fraction of $HCONH_2$, c: 0.15 mass fraction of $HCONH_2$, d: 0.25 mass fraction of $HCONH_2$, e: 0.50 mass fraction of $HCONH_2$, f: $HCONH_2$.

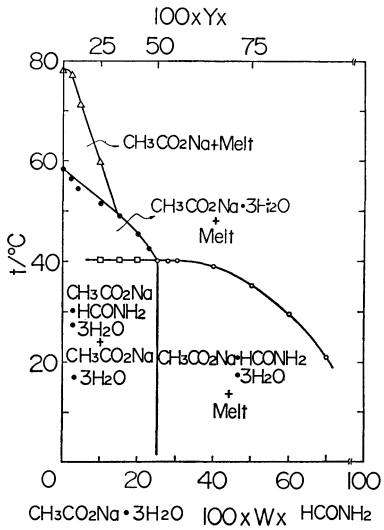

Fig. 3. Pseudo-binary section in the ternary system CH_3CO_2Na–$HCONH_2$–H_2O at ambient pressure.
●: Melting point of $CH_3CO_2Na \cdot 3H_2O$, ○: melting point of $CH_3CO_2Na \cdot HCONH_2 \cdot 3H_2O$, △: melting point of CH_3CO_2Na, □: eutectic point.

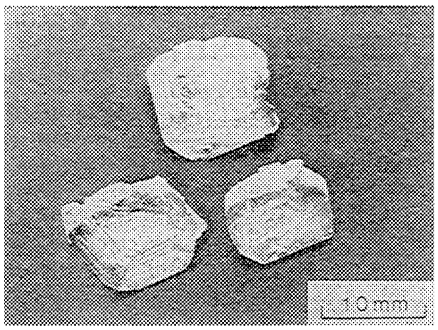

Fig. 4. Photograph of crystals of the addition compound, $CH_3CO_2Na \cdot HCONH_2 \cdot 3H_2O$.

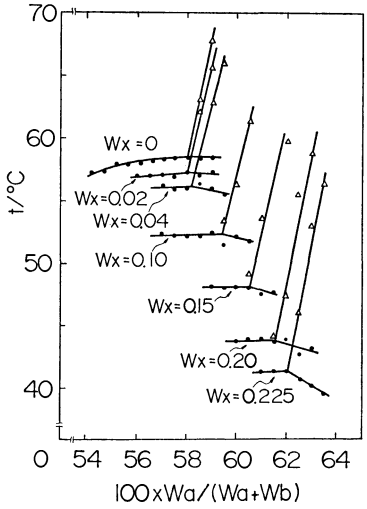

Fig. 5. Melting-point diagram of the ternary system CH_3CO_2Na–$HCONH_2$–H_2O, at ambient pressure in which the mass fraction of $HCONH_2$ is kept constant in each system. ●: Melting point of $CH_3CO_2Na \cdot 3H_2O$, △: melting point of CH_3CO_2Na.

trated in Fig. 2. In this figure, the numbers on the ordinate, q indicates heat flux. The heat absorption accompanying the dissolving of CH_3CO_2Na in its water of crystallization is much smaller than that accompanying the melting of $CH_3CO_2Na \cdot 3H_2O$ but it is illustrated in magnified scale. Considering the phase diagram of the system CH_3CO_2Na–H_2O shown in Fig. 1, we understand that the peak at 58.4 °C of DSC curve of $CH_3CO_2Na \cdot 3H_2O$ corresponds to the melting of $CH_3CO_2Na \cdot 3H_2O$ and the change at 77.8 °C corresponds to the entire dissolution of CH_3CO_2Na in its water of crystallization.

The pseudo-binary section in a ternary system CH_3CO_2Na–$HCONH_2$–H_2O at ambient pressure, which is constructed from such DSC curves, is shown in Fig. 3. In this figure, W_x shows mass fraction of $HCONH_2$, while Y_x shows mole fraction of $HCONH_2$. From this figure, it is clear that in the pseudo-binary system $CH_3CO_2Na \cdot 3H_2O$–$HCONH_2$, a one to one addition compound of the two components forms, and this addition compound $CH_3CO_2Na \cdot HCONH_2 \cdot 3H_2O$ melts congruently at 40.5 °C. The photograph of crystals of this addition compound is shown in Fig. 4. These crystals are colorless and transparent. The specific gravity of this crystal at room temperature is

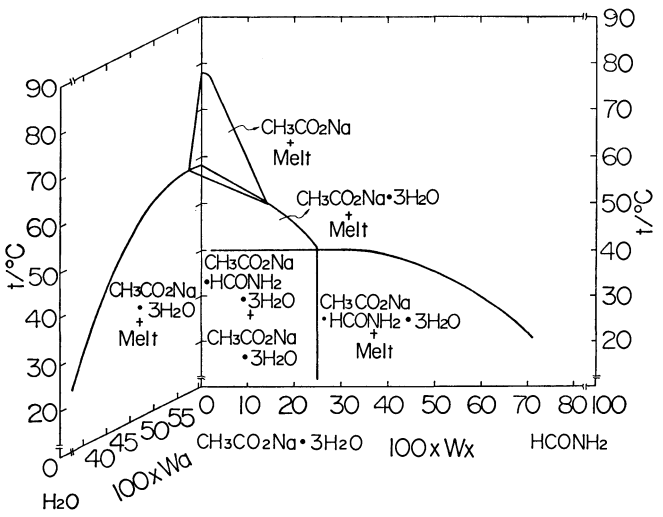

Fig. 6. Partial phase diagram of the ternary system CH_3CO_2Na–$HCONH_2$–H_2O at ambient pressure.

1.404 g/cm³.

The melting-point diagrams for the system CH_3CO_2Na–$HCONH_2$–H_2O at ambient pressure, in which the mass fraction of $HCONH_2$ is kept constant in each system are plotted in Fig. 5 by using DSC caves such as the curve (c) in Fig. 2. In this figure, the numbers on the abscissa, $100 \times W_a/(W_a+W_b)$ is weight percent of CH_3CO_2Na in the system without $HCONH_2$ content. The melting-point diagram for the system CH_3CO_2Na–H_2O which does not contain $HCONH_2$ is in good agreement with reported data.[4] It is apparent that as mass fraction of $HCONH_2$, W_x increases, the liquidus line on $CH_3CO_2Na \cdot 3H_2O$ side shifts to lower temperature and the liquidus line on CH_3CO_2Na side shifts to higher concentration of CH_3CO_2Na.

The partial phase diagram of the ternary system CH_3CO_2Na–$HCONH_2$–H_2O at ambient pressure is constructed by using the results of Figs. 1, 3, 5, and it is shown in Fig. 6.

The heat of fusion of the addition compound $CH_3CO_2Na \cdot HCONH_2 \cdot 3H_2O$ is found to be 255 J/g by DSC. This value is much larger than the heat of fusion of $Ca(NO_3)_2 \cdot 4H_2O$ (t_m: 43 °C), 142 J/g.

The melting point of this addition compound, 40.5 °C is suitable for solar energy storage and its heat of fusion is very large. So, this addition compound $CH_3CO_2Na \cdot HCONH_2 \cdot 3H_2O$ is, hopeful for solar energy storate use.

The authors wish to express their thanks to Dr. Ryoichi Kiriyama for his many helpful discussions and to Dr. Eiichi Hirota and Dr. Masanari Mikoda for their continuous encouragement. They are also grateful to Dr. Yoshihiro Matsuo for his discussions throughout this work.

References

1) M. Telkes, "Solar Materials Science," ed by L. E. Murr, Academic Press (1980), Chap. 11.
2) K. W. Böer, J. H. Higgins, and J. K. O'connor, *IECEC '75 Record*, **1975**, 7.
3) R. Stepler, *Popular Science*, **1980-3**, 49.
4) W. F. Green, *J. Phys. Chem.*, **12**, 655 (1908).

The Crystal and Molecular Structure of Daphnin Dihydrate: 7-(β-D-Glucopyranosyloxy)-8-hydroxycoumarin Dihydrate

Katsuhiko Ueno,* Mitsuhiko Sato,† and Norio Saito††

Research Institute for Polymers and Textiles, Yatabe-Higashi 1-1-4, Tsukuba, Ibaraki 305

†*Department of Biology, Faculty of Science, Tokyo Metropolitan University, Setagaya-ku, Tokyo 154*

††*Chemical Laboratory, Meiji-gakuin University, Minato-ku, Tokyo 108*

(Received March 13, 1982)

The title compound, $C_{15}H_{16}O_9 \cdot 2H_2O$, crystallizes in orthorhombic space group $P2_12_12_1$ with $a=7.082(2)$, $b=34.789(5)$, $c=6.867(2)$ Å, and $Z=4$. The structure was solved by direct method and refined by least-squares to a final R of 0.038 based on 1841 observed reflections measured on a four-circle diffractometer. The coumarin ring is approximately planar and the torsion angle around the glucosidic C–O bond is 13.5°; this is much smaller than the corresponding value in 8-glucosyloxy-7-hydroxycoumarin, and causes considerable intramolecular repulsion around the glucosidic linkage. The valence angle of the oxygen atom linking the coumarin and glucose moieties is quite large, 118.5°. The glucopyranose portion is in a C_1 chair conformation. Glucosidation at the 7-hydroxyl group brings about considerable decrease of the resonance system of the 7-hydroxylated coumarin moiety. Such an effect seems to play an important role in the transglucosidation of dihydroxycoumarin glucosides.

In the course of investigation on the biosyntheses of hydroxylated coumarins and their glucosides, some characteristic transglucosidases were isolated from *Daphne odora* and *Cicholium intybus*.[1] In *D. odora*, it is considered that 7-(β-D-glucosyloxy)-8-hydroxycoumarin (or daphnetin 7-glucoside: **D7G**) is formed from *p*-glucosyloxycinnamic acid and that this is changed into 8-(β-D-glucosyloxy)-7-hydroxycoumarin (or daphnetin 8-glucoside: **D8G**) by the action of transglucosidase. This reaction proceeds *via* two steps: *i.e.*, hydrolysis of **D7G** to 7,8-dihydroxycoumarin (or daphnetin: **D**) and glucose, and glucosidation of **D**, as shown in Fig. 1.[2] The back reaction, the formation of **D7G** from **D8G**, could not be detected. In order to elucidate the structural significance of these substrates for the interconversion reactions, the crystal structures of **D**[3] and **D8G**[4] have been determined. In **D8G** the glucosidation at 8-hydroxyl group of **D** caused little effect on the coumarin structure and the glucosyl moiety takes a conformation so as to minimize the intramolecular repulsion. This paper deals with the crystal structure of **D7G** to determine the effect of glucosidation at 7-hydroxyl group of **D**.

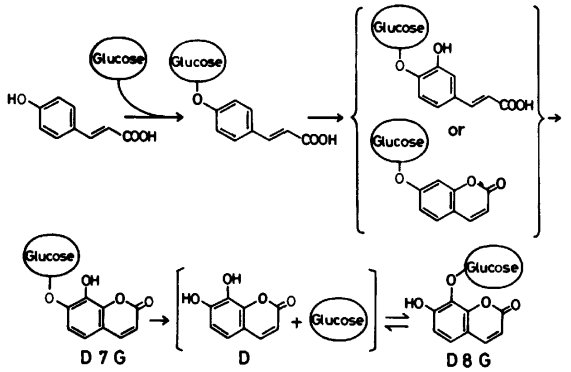

Fig. 1. Biosynthesis of **D7G** and conversion into **D8G**.

Experimental

Single crystals were prepared by slow evapolation from aqueous ethanol solution. They are colorless prisms elongated along the c axis. The space group was determined to be $P2_12_12_1$ from photographs. The density was measured by flotation method in a mixture of carbon tetrachloride and hexane. The lattice constants and intensity data were obtained on a Rigaku four-circle diffractometer with graphite monochromated Cu $K\alpha$ radiation. Of 1940 independent reflections measured within $2\theta<153°$, 1842 had intensities greater than 3σ ($|F_o|$) and these were used for the structure analysis. No correction was made for absorption. The crystallographic data are: $C_{15}H_{16}O_9 \cdot 2H_2O$, F.W.=376.3. Orthorhombic $P2_12_12_1$, $a=7.082(2)$, $b=34.789(5)$, $c=6.867(2)$ Å, $Z=4$, $D_x=1.48$ g cm^{-3}, $D_m=1.48$ g cm^{-3}, μ(Cu $K\alpha$)=12.7 cm^{-1}.

Structure Determination

The structure was solved by the direct method[5] and the structural parameters were refined by block-diagonal least-squares method. All the hydrogen atoms were located on a difference electron density map and their positional and isotropic thermal parameters were included in the refinement. In the later stage of refinement the 012 reflection seemed to be extinct and was given zero weight. The weighting scheme for the other reflections was $w=(10.0/|F_o|)$ if $|F_o|\geq 10.0$, $w=1.0$ if $10.0\geq|F_o|>3.0$, and $w=(|F_o|/3.0)$ if $|F_o|<3.0$. The final R value was 0.038 for 1841 observed reflections. Atomic scattering factors were taken from Ref. 6. The final atomic parameters are shown in Table 1 with equivalent isotropic temperature factors.[7]

Results

Bond Lengths and Angles. The perspective drawing of the molecule with the numbering system is shown in Fig. 2. The daphnetin moiety is nearly planar.[7] The bond lengths and angles are given in Fig. 3. The bond length of carbonyl C=O, 1.226 Å, is larger than those values in coumarin (1.203 Å),[8] gnidicoumarin (1.204 Å),[9] amyrolin (1.210 Å),[10] and xanthotoxin (1.198 Å),[11] and this is close to those of 7-hydroxylated coumarins such as **D** (1.219 Å), **D8G** (1.222 Å), and esculetin (1.227 Å).[12] In the benzene ring, the C(5)–C(6) and C(8)–C(9) bonds are somewhat shorter than the other four C–C bonds. In the 7-hydroxylated

TABLE. 1. FINAL POSITIONAL AND THERMAL PARAMETERS WITH STANDARD DEVIATIONS IN PARENTHESES

Atom	x	y	z	B_{eq}/Å^2
O(1)	0.9588(3)	0.46956(4)	0.6373(3)	2.36
C(2)	0.9211(4)	0.43149(6)	0.6367(3)	2.50
C(3)	0.7293(5)	0.41895(6)	0.6555(4)	2.90
C(4)	0.5871(4)	0.44451(7)	0.6610(4)	2.58
C(5)	0.4862(4)	0.51350(7)	0.6526(4)	2.41
C(6)	0.5355(3)	0.55198(6)	0.6457(4)	2.26
C(7)	0.7259(3)	0.56240(6)	0.6422(4)	1.86
C(8)	0.8685(4)	0.53467(6)	0.6406(4)	1.96
C(9)	0.8148(3)	0.49651(6)	0.6439(4)	1.94
C(10)	0.6258(4)	0.48515(6)	0.6512(4)	2.06
O(2)	1.0578(3)	0.41018(5)	0.6181(3)	3.46
O(8)	1.0547(2)	0.54355(5)	0.6322(4)	3.06
C(1′)	0.6645(3)	0.62976(6)	0.6751(4)	1.94
C(2′)	0.7813(4)	0.66600(6)	0.7045(4)	2.08
C(3′)	0.6495(4)	0.70052(6)	0.7261(4)	1.94
C(4′)	0.5086(4)	0.70284(6)	0.5606(4)	2.07
C(5′)	0.4087(4)	0.66413(6)	0.5406(4)	2.10
C(6′)	0.2741(4)	0.66150(7)	0.3703(5)	2.95
O(1′)	0.7913(2)	0.59970(4)	0.6341(3)	2.11
O(2′)	0.8932(3)	0.66158(5)	0.8749(3	2.99
O(3′)	0.7648(3)	0.73416(4)	0.7336(3)	2.49
O(4′)	0.3737(3)	0.73202(5)	0.6095(3)	2.94
O(5′)	0.5474(3)	0.63445(4)	0.5103(3)	2.09
O(6′)	0.3679(3)	0.66581(5)	0.1877(3)	3.21
O(W1)	1.1749(3)	0.71713(5)	0.9644(3)	3.02
O(W2)	1.1732(3)	0.60535(5)	0.8236(3)	3.20

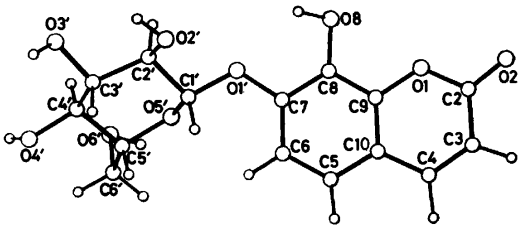

Fig. 2. Perspective drawing of the molecule with the numbering system used.

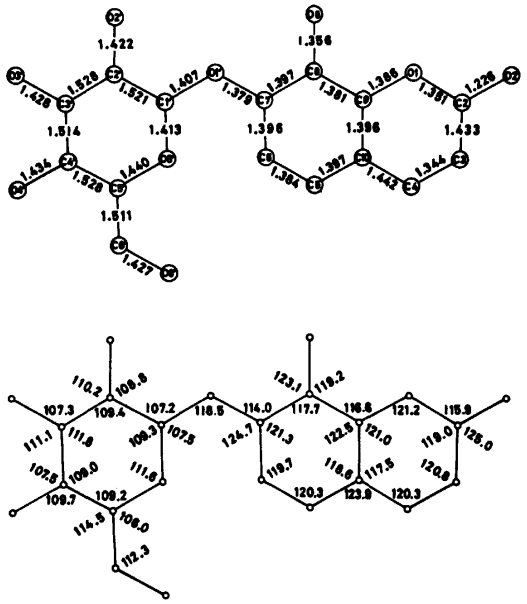

Fig. 3. Bond lengths (l/Å) and angles (ϕ/°). The e.s.d.s are 0.003—0.004 Å for lengths and 0.2—0.3° for angles.

coumarins so far determined by X-rays, the differences in length between C(5)–C(6) and C(6)–C(7) are significantly large. They are 0.024, 0.036, 0.039, and 0.032 Å for **D**, **D8G**, esculetin, and 4-methylumbelliferone,[13] respectively. However, the difference in this molecule, 0.012 Å, is rather small.

The glucopyranose ring is in the usual C_1 chair conformation; the endo- and exocyclic torsion angles are similar to those of **D8G** (Table 2). The anomeric effect in the bond lengths of the sequence C(5′)–O(5′)–C(1′)–O(1′) is unusual: C(5′)–O(5′)>O(5′)–C(1′)≃C(1′)–O(1′), which is similar to the case in **D8G**, whereas in usual β-glucosides C(5′)–O(5′)≃O(5′)–C(1′)>C(1′)–O(1′).[14]

Conformation of the Glucosyl Linkage. The anomeric C(1′)–O(1′) bond is twisted only by 13.8° against the daphnetin plane with the valence angle at O(1′) of 118.5°. The corresponding values in **D8G** are 101.8° and 114.4°, respectively, as shown in Fig. 4. While the glucosyl moiety in **D8G** takes the conformation so as to minimize intramolecular repulsion, the small torsion angle of glucosidic bond in **D7G** results in unusually short intramolecular distances between C(1′)···C(6) (2.863 Å) and C(1′)···H(C6) (2.59 Å). A great difference between the bond angles of C(6)–C(7)–O(1′) and C(8)–C(7)–O(1′), 10.7°, also indicates steric hindrance, while the corresponding values in **D** and **D8G** are only 6.0° and 6.3°, respectively. The angle at the glucosyl oxygen in **D7G** is definitely larger than that in **D8G** and is approximately the same as the value of the sp^2 angle. The geometries of the glycosyl linkage in the aromatic β-glycopyranosides so far determined are listed in Table 3. All of them, except for **D8G**, are similar to the

TABLE 2. ENDO- AND EXOCYCLIC TORSION ANGLES. ONLY FOR EXOCYCLIC ANGLES IS THE ENTIRE SEQUENCE OF ATOMS GIVEN

Endocyclic	ϕ/°		Exocyclic	ϕ/°	
	D7G	**D8G**		**D7G**	**D8G**
C(1′)C(2′)	57.3(2)	54.3(2)	O(1′)C(1′)C(2′)O(2′)	−66.1(2)	−69.3(2)
C(2′)C(3′)	−52.2(2)	−48.2(2)	O(2′)C(2′)C(3′)O(3′)	66.1(2)	69.4(2)
C(3′)C(4′)	52.1(2)	50.0(2)	O(3′)C(3′)C(4′)O(4′)	−69.2(2)	−69.7(2)
C(4′)C(5′)	−57.0(2)	−58.0(2)	O(4′)C(4′)C(5′)C(6′)	66.9(2)	62.5(3)
C(5′)O(5′)	65.6(2)	66.0(2)	C(4′)C(5′)C(6′)O(6′)	62.6(3)	69.4(3)
O(5′)C(1′)	−65.6(2)	−63.9(2)	O(5′)C(5′)C(6′)O(6′)	57.8(3)	−49.9(3)

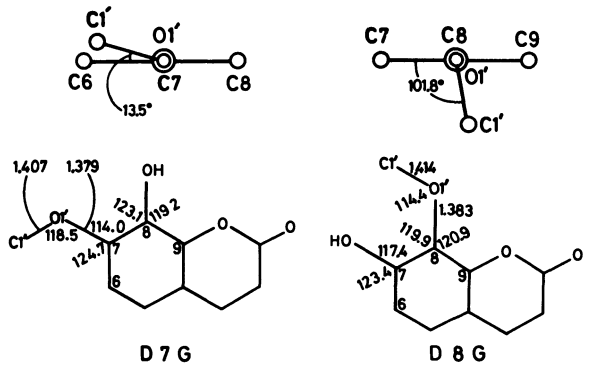

Fig. 4. Comparison of the glucosyl linkage in **D7G** and **D8G**.

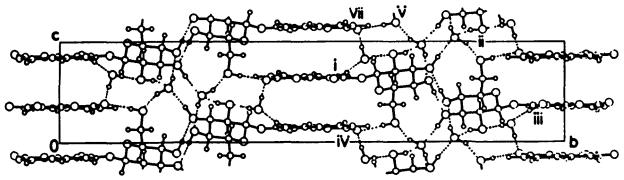

Fig. 5. Crystal structure viewed down the a axis. Hydrogen bonds are indicated by broken lines.

Table 3. Geometry of glycosidic linkage in aromatic β-glycopyranoside

	θ/° a)	ϕ/°b)	δ/°c)	Ref.
D7G	13.8	118.5	10.7	This work
D8G	78.2	114.4	6.0	4
p-Nitrophenyl β-*N*-acetylglucosaminide	16.0	120.0	9.7	17
p-Nitrophenyl β-D-xylopyranoside	23.6	118.5	9.3	18
p-Br-2-naphtyl β-D-glucoside	0.7	117.5	15.5	19
D	—	—	6.3	3

a) Torsion angle of glycosidic bond and aromatic plane. b) Valence angle at the bridge oxygen atom. c) Difference of the valence angles between each side of the glycosidic bond connecting to aromatic ring (between C(8)–C(7)–O(1′) and C(6)–C (7)–O(1′) in **D7G** and corresponding values in the others).

Table 4. Hydrogen bond distances and angles

Donor	Acceptor	Distance l/Å		Angle ϕ/°
(D)	(A)	D···A	H···A	D–H–A
O(8)H	O(W2)^{i}	2.656(3)	1.71(4)	157(4)
O(2′)H	O(W1)^{i}	2.845(3)	2.04(4)	146(4)
O(3′)H	O(W1)^{ii}	2.752(3)	1.79(4)	172(4)
O(4′)H	O(3′)^{iii}	2.744(3)	1.83(4)	179(4)
O(6′)H	O(2)^{iv}	2.738(3)	1.96(4)	154(4)
O(W1)Ha	O(6′)^{v}	2.721(3)	1.80(4)	160(4)
O(W1)Hb	O(4′)^{vi}	2.862(3)	2.04(4)	168(4)
O(W2)Ha	O(2)^{vii}	2.830(3)	1.94(4)	156(4)
O(W2)Hb	O(2′)^{i}	2.808(3)	2.08(4)	164(4)

Symmetry codes: (i) x, y, z; (ii) $-1/2+x, 3/2-y, 2-z$; (iii) $-1/2+x, 3/2-y, 1-z$; (iv) $3/2-x, 1-y, -1/2+z$; (v) $1+x, y, 1+z$; (vi) $1+x, y, z$; (vii) $5/2-x, 1-y, 1/2+z$.

structure in **D7G**. It is thus plausible that the glycosyl bond of aromatic β-glycopyranoside usually takes a conformation with small torsion angle of θ. π Electrons of the oxygen atom of glycosyl linkage may take part in the resonance of the aromatic ring and stabilize the molecular structure in spite of the large intramolecular repulsion; this will be explained in the discussion.

Crystal Structure. Figure 5 shows the crystal structure viewed along the a axis. The coumarin moieties are stacked along the c axis and a three-dimensional network of hydrogen bonding connects the molecules. The hydrogen bonds O(3′)–H···O(W1)–H···O(4′) form infinite arrays along the c axis and O(4′)–H···O(3′) connects the glucose moieties related by 2_1 axis along the a axis. The remaining six hydrogen bonds link the three molecules at i, v, and vii. The hydrogen bond parameters are listed in Table 4.

Discussion

It has been found that the structure of **D** can be well explained by the following resonance:

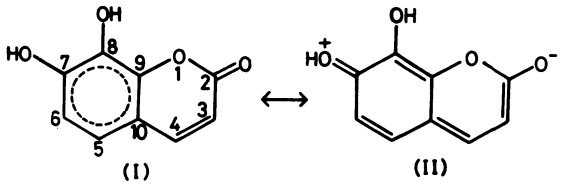

The contribution from the limiting structure(II) is also apparent in the related structures: esculetin, which has a hydroxyl group at the 6 position instead of 8, and 4-methylumbelliferone, which contains a methyl group bonded to C(4) instead of the 8-hydroxyl group. Such a conjugation effect has been postulated to account for the characteristic nature of the spectral[15] and chemical[16] properties in 7-hydroxylated coumarins.

The structure of **D8G** reveals that the glucosidation at 8-hydroxyl group of **D** causes little effect on the resonance of daphnetin moiety. The C(5)–C(6) bond is significantly shorter than C(6)–C(7) and the C(2)–O(2) bond is longer than the corresponding one of coumarin.

In the present **D7G** molecule, however, the contribution from the structure(II) is expected to be less as a result of the glucosidation at the 7-hydroxyl group. The difference between C(5)–C(6) and C(6)–C(7) is significantly smaller than that in **D8G**. Although a slight contribution from the structure(II) is observed for **D7G**, most of the resonance energy may be compensated by the intramolecular repulsion between the coumarin ring and the glucose moiety. These results clearly indicate that **D8G** is more stable energetically than **D7G**.

Action of transglucosidase for dihydroxycoumarin glucosides has already been shown in Fig. 1. Although the structure of the active site of the enzyme is still unknown, the structures of substrate and product can explain the reaction mechanism. At the intermediate stationary state of the enzymatic reaction, both **D7G** and **D8G** may be formed from **D** and glucose; however the formation of **D8G** is considered to be far more favorable in terms of the stability of the molecule, so

that glucose is transferred from **D7G** to **D8G**.

The authors are grateful to Professor Yoshio Sasada and Dr. Yuji Ohashi of Tokyo Institute of Technology for their valuable discussions and encouragement.

References

1) M. Sato and M. Hasegawa, *Phytochemistry*, **10**, 2367 (1971); **11**, 3149 (1972).
2) M. Sato and M. Hasegawa, *Phytochemistry*, **11**, 657 (1972).
3) K. Ueno and N. Saito, *Acta Crystallogr., Sect. B*, **32**, 946 (1976).
4) K. Ueno, N. Saito, and M. Sato, *Bull. Chem. Soc. Jpn.*, **51**, 3170 (1978).
5) J. Karle and H. Hauptman, *Acta Crystallogr.*, **9**, 635 (1956); J. Karle and I. L. Karle, *ibid.*, **21**, 849 (1966); G. Germaine and M. M. Woolfson, *ibid., Sect. B*, **24**, 91 (1968).
6) "International Tables for X-Ray Crystallography," Kynoch Press, Birmingham (1974), Vol. IV, pp. 72—73.
7) Lists of structure factors, anisotropic thermal parameters, atomic parameters for hydrogen atoms and the equation of least-squares plane have been deposited as Document No. 8319 at the Office of the Chemical Society of Japan.
8) E. Gavuzzo, F. Mazza, and E. Giglio, *Acta Crystallogr., Sect. B*, **30**, 1351 (1974).
9) M. S. Shen and R. F. Bryan, *Acta Crystallogr., Sect. B*, **31**, 2907 (1975).
10) K. Kato, *Acta Crystallogr., Sect. B*, **26**, 2022 (1970).
11) N. R. Stemple and W. H. Watson, *Acta Crystallogr., Sect. B*, **28**, 2485 (1972).
12) K. Ueno and N. Saito, *Acta Crystallogr., Sect. B*, **33**, 283 (1977).
13) S. Shimizu, S. Kashino, and M. Haisa, *Acta Crystallogr., Sect. B*, **31**, 1287 (1975).
14) M. Sundaralingam, *Biopolymers*, **6**, 189 (1968); S. Arnott and W. E. Scott, *J. Chem. Soc., Perkin Trans. 2*, **1972**, 324.
15) W. E. Sherman and E. Robins, *Anal. Chem.*, **40**, 803 (1968); G. Y. Yakatan, R. J. Juneau, and S. G. Schulman, *ibid.*, **44**, 1044 (1972); G. S. Beddard, S. Carlin, and R. S. Davidson, *J. Chem. Soc., Perkin Trans. 2*, **1977**, 262.
16) F. M. Dean, "Naturally Occurring Oxygen Ring Compounds," Butterworths, London (1973), Chap. 6, pp. 177—180.
17) L. Brehm and J. Moult, *Proc. R. Soc. London, Ser. B*, **188**, 425 (1975).
18) K. Harata, *Acta Crystallogr., Sect. B*, **32**, 1932 (1975).
19) K. Harata, private communication.

 © 1983 The Chemical Society of Japan Bull. Chem. Soc. Jpn., 56, 1581—1584 (1983)

Dispersibility of Magnetic and Nonmagnetic Iron(III) Oxides in 2-Butanone

Kazuhiko KANDORI,* Ayao KITAHARA, and Kijiro KON-NO
Department of Industrial Chemistry, Science University of Tokyo, Kagurazaka, Shinjuku-ku, Tokyo 162
(Received June 25, 1982)

The dispersion stability of needlelike and octahedral iron(III) oxides of magnetic or nonmagnetic particles in 2-butanone was studied. Two kinds of copolymers of poly(vinyl acetate-vinyl chloride-maleic acid) (VAVCCOOH) and poly(vinyl acetate-vinyl chloride-vinyl alcohol) (VAVCOH) were used as dispersants. The sedimentation of dispersions, the adsorption of copolymer dispersants on the particles and zeta potentials were measured. By polymer adsorption, the dispersion of nonmagnetic needlelike iron(III) oxide was stabilized and the dispersions of magnetic needlelike iron(III) oxides were somewhat stabilized, but the dispersions of magnetic octahedral iron(III) oxides were only slightly stabilized. This characteristic behavior of the sedimentation experiment was discussed in relation to the amount of polymer adsorption and zeta potential and was correlated with the observations by an electron microscope. The magnetic attractive force operating between the two magnetic particles was calculated to illustrate the dispersibility of magnetic oxides. It was suggested from the calculation that the strength of the magnetization and the volume of a particle are the main factors affecting the flocculation of the magnetic particles.

The dispersions of the magnetic particles in polar organic media have been used as a paint for magnetic tapes. Good dispersibility is necessary to improve the properties of the magnetic tapes. However, the fundamental studies on dispersibility are very few, though some rheological studies have been done.[1-3]

Many data on the stability of colloidal dispersions in nonpolar organic media as well as in water have been accumulated. The stability of colloidal dispersions in water has been discussed by the well-known DLVO theory,[4] and this theory has been extended to that in nonpolar organic media.[5-9] Recently, synthetic polymers have drawn attention as dispersants and the effect of adsorbed polymer layers on the stability of pigment dispersions has been reported.[10-16] The double layer interaction between the particles indicated by the DLVO theory and the steric stabilization by the adsorbed polymers must both be considered in order to illustrate the stabilization of pigment dispersions in nonpolar organic media.[17]

However, few studies on the stability in polar organic media such as alcohols and ketones have been done.[18]

In this paper, as fundamental study of magnetic paints, the dispersions of needlelike and octahedral iron(III) oxides of the magnetic or nonmagnetic particles were prepared in 2-butanone. The sedimentation of dispersed particles, the adsorption of copolymer dispersants on the particles and zeta potentials were measured. The characteristic behavior of the sedimentation experiment is compared with the observation by an electron microscope.

Experimental

Material. Five kinds of iron(III) oxides were prepared according to the references.[19-21] Each property of these iron(III) oxides is shown in Table 1. They were washed with 2-butanone in a Soxhlet apparatus for 16 h and then with hot distilled water in order to remove inorganic salts. This procedure was followed by drying in vacuum for 16 h at 100 °C; the materials were stored in a desiccator before use.

Two kinds of copolymers of poly(vinyl acetate-vinyl chloride-maleic acid) (abbreviated as VAVCCOOH) and poly (vinyl acetate-vinyl chloride-vinyl alcohol) (VAVCOH) were prepared[22-24] and used as dispersants. Their molecular weights and chemical compositions, determined by the gel permeation chromatographic method (GPC), are shown in Table 2. These copolymers were extracted with methanol in a Soxhlet apparatus for 16 h and dried in vacuum for 16 h at 60 °C.

The 2-butanone used as a solvent was purified as follows: It was shaken four times with saturated potassium carbonate solutions and kept over potassium carbonate anhydride for a day. It was then distilled and dried with Molecular Sieve 4A to remove any trace of water.

Preparation of Dispersions. The dispersion of the particle content of 0.2 wt% and fixed concentration of a dispersant** (VAVCCOOH or VAVCOH) was prepared by mixing the particles and the solution under irradiation with an ultrasonic apparatus (Kaijo Denki Co. Model TA-4015, Power Supply 150 W, 20 kHz) for 5 mins. No precipitation was observed

TABLE 1. PROPERTIES OF IRON (III) OXIDES

Particle No.	Shape	Class	Specific surface area / $m^2\ g^{-1}$	Saturation magnetization / emu g^{-1}	Size / Å	Density / g cm^{-3}
1	Needle	γ-Fe_2O_3	37.6	68	1470×160	4.3
2	Needle	α-Fe_2O_3	108	1	1610×142	3.9
3	Needle	α-Fe_2O_3	33.1	33[a]	1400×178	4.0
4	Octahedron	γ-Fe_2O_3	9.3	62	1820	4.5
5	Octahedron	α-Fe_2O_3	8.6	29[a]	1820	4.6

a) α-Fe_2O_3 keeps its magnetization.

** The viscosity of the dispersant solution was approximately equal to that of the solvent.

TABLE 2. GPC MOLECULAR WEIGHT DATA OF DISPERSANTS[a)]

Sample	$M_n \times 10^4$	$M_w \times 10^4$	M_w/M_n	Chemical component
VAVCCOOH	2.54	6.19	2.44	VA : VC : COOH=13 : 86 : 1
VAVCOH	3.29	6.95	2.11	VA : VC : OH=3 : 91.5 : 5.5

a) Apparatus: Water associates GPC-244, column: TSK-GEL, solvent: THF 2.0 ml/min 25 °C, sample: 0.5 w/v% 500 μl. Molecular weights were computed from the polystyrene calibration curve.

immediately after this procedure.

Estimation of Dispersion Stability. The stability of dispersion was estimated by the sedimentation experiment. The dispersion prepared by the above method was again shaken in a flask for 16 h at 30 °C and then transferred in a sedimentation tube. The dispersion had a height of 30 cm in each tube. The movement of the sharp boundary between supernatant and sediment was recorded with time after the material was introduced the tube and shaken at 30±0.1 °C.

A state of flocs of particles which formed in the medium after 24 h was directly observed by an electron microscope (JEM-100B). The sample was prepared as follows: Collodion solution was evaporated to obtain cellulose trinitrate. A small quantity of this cellulose trinitrate was dissolved (1.5 wt%) in the dispersion used for the sedimentation experiment. A small amount of the dispersion was dropped on the water (30 °C) and the film formed was stretched on the mesh used for an electron microscope.

The electron microscope observation showed that the states of flocs of particles were similar in all of the meshes for the same dispersion. No effect of collodion addition on the dispersibility was observed.

Adsorption and Zeta Potential Measurement. The amount of the polymer adsorbed on iron(III) oxides was determined as follows: The polymer solution of the known concentration involving a fixed amount of an iron(III) oxide (4 wt%) was shaken for a given period of time at 30±0.1 °C until adsorption equilibrium was reached. The adsorption equilibrium was reached after about 16 h for each system. The iron(III) oxides was then separated by centrifugation and a known amount of the supernatant was taken to determine the equilibrium polymer concentration. The quantity of polymer adsorbed was determined by direct weighting of the polymer which had been dried up by evacuated evaporation of the solvent from the supernatant.

Electrophoretic mobility was measured by microelectrophoresis with Laser Zee TM Model 500 (PEN KEM CO.) to which was attached externally a constant voltage power supply (BIO SCIENCE MODEL PS-30); here a rectangular quartz cell was used to prevent the leakage of electric current along the wall. Particles were illuminated by He-Ne laser (2 mW, 6328 Å). Zeta potential was calculated with use of the Hückel equation. The dispersion used for the microelectrophoresis was about 0.01 wt% diluent of the supernatant in the sedimentation experiment.

Results and Discussion

Effect of Polymer Concentration. All of the particles, especially the needlelike ones, were stabilized by the addition of polymer, as exemplified in Fig. 1. In order to examine the effect of the polymer concentration on the dispersibility and zeta potential, the sedimentation experiment and zeta potential measurement were carried out for the nonmagnetic needlelike particle (No. 2). The dependence of the height of the boundary in the sedimentation tube at 24 h after the shaking and zeta potential on the polymer concentration is indicated

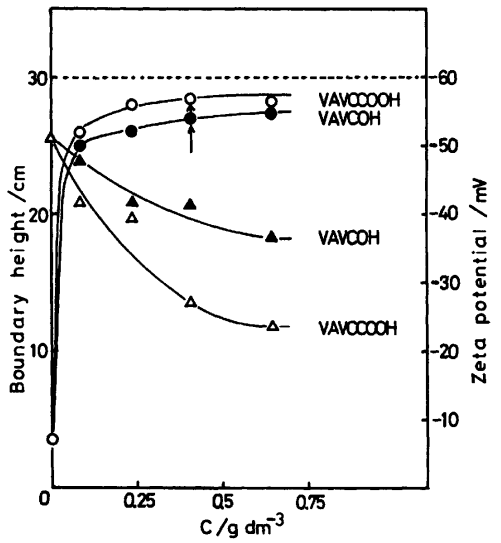

Fig. 1. Relation of the boundary height and ζ-potential with polymer concentration for No. 2 sample. Particle concentration=0.2 wt%. ○, ●: Boundary height, △, ▲: zeta potential.

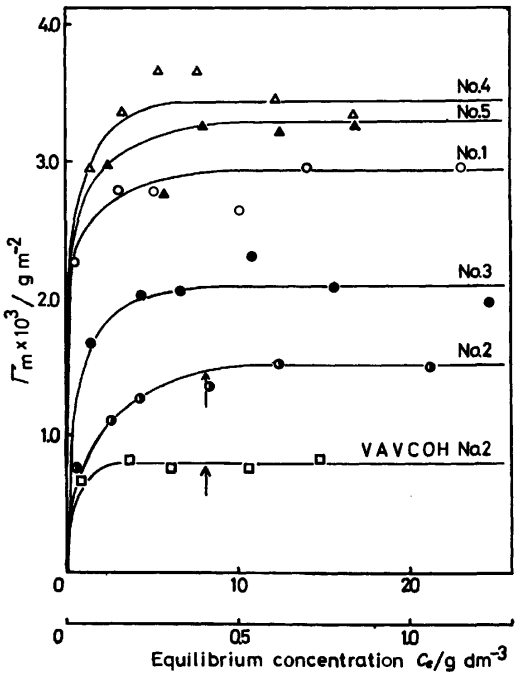

Fig. 2. Adsorption Isotherms. Particle concentration=4 wt%. The lower scale correspond to the particle concentration of 0.2 wt%. Arrows correspond with the arrows in Fig. 1.

in Fig. 1. The dispersion stability was markedly improved by addition of a small amount of both kinds of polymers and the zeta potential decreased gradually

Table 3. Results of each measurement for VAVCCOOH and VAVCOH systems

Particle No.	VAVCCOOH			VAVCOH	
	Initial velocity / mm min^{-1}	ζ-Potential / mV	$\Gamma_m \times 10^3$ / g m^{-2}	ζ-Potential / mV	$\Gamma_m \times 10^3$ / g m^{-2}
1	0.65	−46.9	2.95	−32.4	1.54
2	0.014	−29.2	1.57	−41.4	0.84
3	0.017	−32.2	2.00	−35.4	0.86
4	10	−24.9	3.40	−24.9	1.59
5	7.5	−23.8	3.37	−48.7	0.85

with increase of the polymer concentration. The decrease would be due to the shift of the slipping plane from the particle surface caused by the polymer adsorption.[15] The fact that the zeta potential of the VAVCOH system is higher than that of the VAVCCOOH system results from the difference of the adsorbed amount of polymer; this assertion will be depicted in Fig. 2.

The measurement of polymer adsorption was done in order to investigate the effect of polymer. The adsorption isotherms of VAVCCOOH for five kinds of iron(III) oxides (4 wt%) in 2-butanone are shown in Fig. 2. All isotherms were of the Langmuir type. Their Langmuir plots, $C/\Gamma \approx C$ curves, were linear in all cases. This same relationship was also obtained for the VAVCOH systems. One of them (No. 2) is shown in Fig. 2. The saturation values of adsorption (Γ_m) for the VAVCCOOH and VAVCOH were obtained from these Langmuir plots. The results are listed in Table 3. The saturation values of the adsorption for the VAVCCOOH system are larger than that for the VAVCOH system, as seen in Table 3. Such results would be due to the effect of functional groups in the interaction of the polymers with iron(III) oxides. It is known that carboxyl group interacts more strongly with oxide surfaces than does the hydroxyl group.[25-27]

The dispersibility was improved by addition of polymer, as pointed out in Fig. 1 of the sedimentation experiment. The polymer concentration shown by the arrow in Fig. 2, where the adsorption reaches approximately the saturation, coincides roughly with the concentration of the attainment of the stabilization shown by the arrows in Fig. 1. The effect of adsorbed polymer on the dispersibility of the nonmagnetic No. 2 sample can be illustrated from this correspondence.

Comparison of the Dispersibility of Five Kinds of Iron(III) Oxides. The sedimentation experiment was carried out for each sample to compare the dispersibilities of five kinds of iron(III) oxides. The change of the boundary height in the tube is shown as a function of time for five samples in Fig. 3. Here VAVCCOOH of 25 wt% per particles was used as a dispersant and the particle concentration was 0.2 wt%. The effect of the polymer on the stabilization of dispersions was marked in the system of the needlelike nonmagnetic iron(III) oxide (No. 2), as shown in Figs. 1 and 3. The dispersibility of No. 3, the needlelike magnetic iron(III) oxides, was considerably improved by the addition of the polymer, as shown in Fig. 3, though that of No. 1, needlelike and highly magnetic iron(III) oxide, was not much improved compared with Nos. 2 and 3. On the other hand, the dispersibility of the octahedral magnetic iron(III) oxides (Nos. 4 and 5) was scarcely improved at all. The improvement of the dispersibility of the five samples by VAVCOH was similar to that in the VAVCCOOH systems.

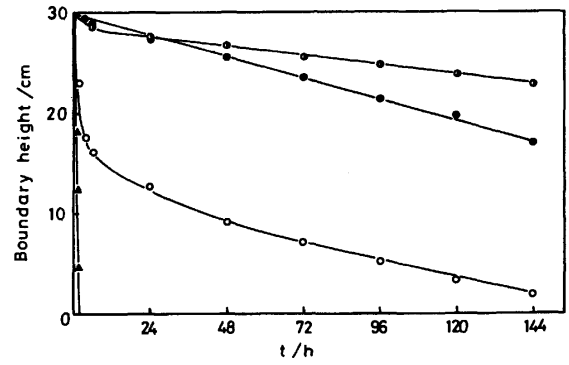

Fig. 3. Plots of boundary height *vs.* time.
○: No. 1, ●: No. 2, ◑: No. 3, ▲: No. 4, 5. [VAVCCOOH]=25 wt% per particles constant.

The initial velocity of the sedimentation curves, that is, the initial slope of the curves in Fig. 2, is listed in Table 3 to allow us to estimate the dispersibility. Table 3 shows that the order of the magnitude of sedimentation velocity is as follows:

$$\text{No. 4} \gtrsim \text{No. 5} \gg \text{No. 1} > \text{No. 3} > \text{No. 2.} \quad \text{(A)}$$

The electron microscope photographs of typical states of the flocs for each particle are shown in Fig. 4. These electron microscope observations show that the state of the flocs of particles is similar in all of the meshes for each particle. Figure 4 shows that the order of the size of the flocs is approximately as follows:

$$\text{No. 4} > \text{No. 1} > \text{No. 5} > \text{No. 3} > \text{No. 2.} \quad \text{(B)}$$

The particles of No. 2 do not form the flocs. The result of (B) agrees with the result of (A) except for the ordering between Nos. 1 and 5. The difference in (A) and (B) appearing between Nos. 1 and 5 can probably be ascribed to the difference in the density of the flocs.

Table 3 shows that there are no great differences among the zeta potentials of each particle, and the values do not agree with the flocs' size or with the sedimentation velocity. Moreover, the order of the saturation amount of adsorbed polymer (Γ_m) does not agree with that of the flocs' size.

The electric repulsion and the steric repulsion of the adsorbed polymer layer, therefore, are not the determinative factors of the formation of the flocs and the

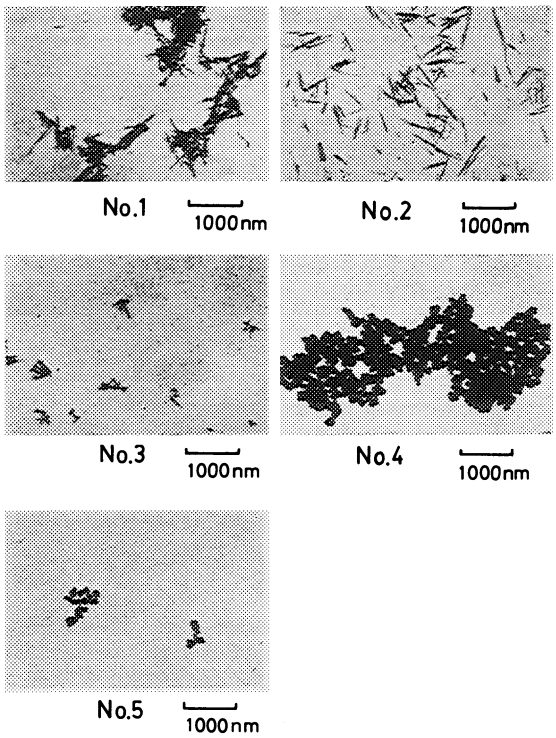

Fig. 4. Photographs of the electron microscope for each particle. Magnification: ×15000.

dispersibility of the five kinds of particles.

Here the magnetic attractive force has to be considered. The magnetic potential energy between two magnetic particles is expressed as follows:[28]

$$V_A^M = -K\left(\frac{M}{4\pi}\right)^2 \frac{V^2}{r^3},$$

where M is the strength of the saturation magnetization (Gauss), V is the volume of a particle, r is the distance between two particles and K is a constant ($K=2$ for the octahedral particles and head-tail interaction of the needlelike particles and $K=1$ for parallel interaction of the needlelike particles). The calculated values of V_A^M, at a constant distance r using the values of M in Table 1, are listed in Table 4. The order of the magnitudes of V_A^M agreed qualitatively with the results of (A) and (B).

Table 4. MAGNETIC ATTRACTIVE FORCE OF EACH PARTICLE

Particle No.	V_A^M/J
1	-8.0×10^{19}k[a]
2	-8.9×10^{15}k
3	-2.3×10^{19}k
4	-7.7×10^{23}k
5	-1.8×10^{23}k

a, $k=K/r^3$ (unit : m^{-3}).

The strength of the magnetization and the volume of a particle are, therefore, the main factors which control flocculation of the magnetic particles and the size of the flocs.

References

1) J. Seto, *Nippon Rheology Gakkaishi*, **5**, 156 (1977).
2) W. Nagashiro and T. Tsunoda, *J. Appl. Polym. Sci.*, **25**, 2961 (1980).
3) Th. L. Smith and C. A. Bruce, *J. Colloid Interface Sci.*, **72**, 13 (1979).
4) E. J. W. Verwey and J. Th. G. Overbeek, "Theory of Stability of Lyophobic Colloid," Elsevier, Amsterdam (1948).
5) J. L. Van der Minne and P. H. J. Hermanie, *J. Colloid Sci.*, **7**, 600 (1952).
6) H. Koelmans and J. Th. G. Overbeek, *Faraday Discuss. Chem. Soc.*, **18**, 52 (1954).
7) J. L. Van der Minne and P. H. J. Hermanie, *J. Colloid Sci.*, **8**, 38 (1953).
8) D. N. L. McGown and G. D. Parfitt, *Kolloid Z. Z. Polym.*, **220**, 56 (1967).
9) A. Kitahara, T. Tamura, and K. Kon-no, *Chem. Lett.*, **1979**, 1127.
10) T. Sato, *Yukagaku*, **30**, 203 (1981).
11) E. L. Mackor, *J. Colloid Sci.*, **6**, 492 (1961).
12) T. Sato, *Shikizai Kyokai Shi*, **47**, 385, 465 (1974); **48**, 341 (1975).
13) D. H. Napper, *Trans. Faraday Soc.*, **64**, 1701 (1968). D. H. Napper, *J. Colloid Interface Sci.*, **29**, 168 (1969).
14) E. J. Clayfield and E. C. Lumb, *J. Colloid Interface Sci.*, **49**, 489 (1974).
15) D. J. Meier, *J. Phys. Chem.*, **71**, 1861 (1967).
16) T. Sato and R. Ruch, "Stabilization of Colloidal Dispersions by Polymer Adsorption," Marcel Dekker, New York (1980), p. 69
17) J. Lyklema, *Adv. Colloid Interface Sci.*, **2**, 65 (1968).
18) N. D. Rooy, P. D. Bruyn, and J. Th. G. Overbeek, *J. Colloid Interface Sci.*, **75**, 542 (1980).
19) M. Kiyama, *Funtai Oyobi Funmatsu Yakin*, **23**, 77 (1976).
20) M. Camras, U. S. Patent 2694656 (1954).
21) M. Camras, Kokai Tokkyo Koho, 26-7776 (1951).
22) George R. Penn, Jr., U. S. Patent 2512726 (1950).
23) T. Saito, Kokai Tokkyo Koho, 28-1296 (1953).
24) D. Banks, Kokai Tokkyo Koho, 34-7244 (1959).
25) T. Matsumoto, K. Nonaka, and K. Nakamae, *Kobunshi Ronbun Shu*, **31**, 7 (1974).
26) T. Matsumoto, K. Nakamae, K. Nonaka, and S. Miyoshi, *Kobunshi Ronbum Shu*, **31**, 522 (1974).
27) S. Toya, K. Sumiya, H. Hashiyama, and T. Matsumoto, *Kobunshi Ronbun Shu*, **35**, 565 (1978).
28) R. E. Rosensweig, J. W. Netor, and R. M. Timmins, *AIChE Symp. Ser.*, **5**, 104 (1965).

 © 1983 The Chemical Society of Japan Bull. Chem. Soc. Jpn., 56, 1585—1587 (1983)

The Temperature Dependence of the Ultrasonic Relaxation Process Due to Interaction between Water and Allyl Cellosolve

Sadakatsu NISHIKAWA* and Tatsuro YAMAGUCHI
Department of Chemistry, Faculty of Science and Engineering, Saga University, Saga 840
(Received July 1, 1982)

Ultrasonic absorption and velocity measurements have been performed in aqueous solutions of Allyl Cellosolve (ethylene glycol monoallyl ether) as functions of the concentration and the temperature. Only a single relaxational absorption has been observed in the frequency range from 15 to 220 MHz and, it has been attributed to the perturbation of the equilibrium expressed as $AB \rightleftarrows A+B$, where A and B are the solute and the solvent molecule respectively. The rate constants at various temperatures have been determined from the concentration dependence of the relaxation frequency, and the thermodynamic parameters associated with the reaction have been calculated. The enthalpy change has also been estimated from the concentration dependence of the maximum excess absorption per wavelength. From these results, it has been concluded that Allyl Cellosolve molecules act as water structure promoters and that the interaction between the solute and the solvent is due to hydrogen bonding. Furthermore, the rate and the thermodynamic properties obtained are compared with those for aqueous solutions of other ethers.

It has been recognized that the interaction between water and biological compounds play important roles in living systems. However, the dynamical properties of the interactions have not been well interpreted because the rates are too fast and the complex reactions proceed at the same time. The ultrasonic absorption method has been used to investigate the dynamical properties in solutions. The present authors have also reported some ultrasonic results for aqueous solutions of alcohols and ethers.[1-5] In these solutions, we have found that the excess absorption associated with the interaction between the solute and the solvent is observed in the MHz frequency range, and have predicted from the concentration dependence of the absorption that the interaction may be due to hydrogen bonding. In order to confirm the origin of the interaction, an investigation of the temperature dependence of the absorption is required; it may provide useful information about the rate and the thermodynamic properties. For this purpose, Allyl Cellosolve (ethylene glycol monoallyl ether) has been chosen as a solute; in this report the results are compared with those of other ethers.

This kind of fundamental informations seems to be very important for the understanding of more complex interactions.

Experimental

The Allyl Cellosolve was purchased from the Tokyo Kasei Co., Ltd. and was distilled once under reduced pressure. The purity was confirmed to be more than 99.8% by means of the gas-chromatographic method. The sample solutions were prepared using doubly distilled water by weighing.

The ultrasonic absorption coefficients, α, were measured by a pulse method. The 5 MHz x-cut crystal was used in the frequency range from 15 to 95 MHz and the 20 MHz crystal, in the range from 60 to 220 MHz. An ultrasonic interferometer was used to measure the sound velocity, c, at 2.5 MHz. All the measurement cells were immersed in a water bath which was maintained within ± 0.005 °C. The measurements were carried out at 20, 25, and 30 °C.

Results and Discussion

Figure 1 shows an illustrative example of the ultrasonic absorption spectra for aqueous solutions of Allyl Cellosolve at 25 °C. They are all characteristic of a single relaxation process and are well described by the following equation.

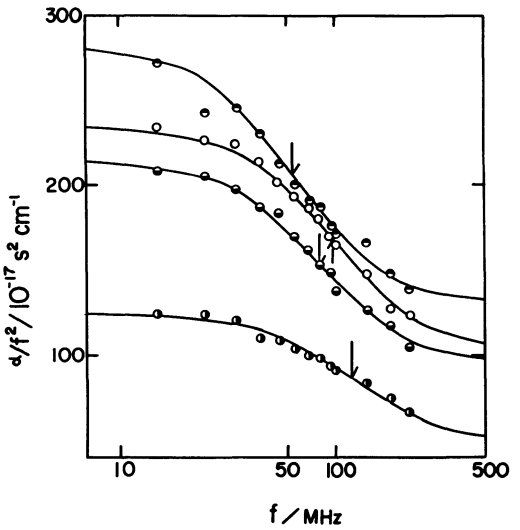

Fig. 1. Ultrasonic absorption spectra in aqueous solution of Allyl Cellosolve at 25 °C. Arrows show the positions of the relaxation frequency. ◑; 3.01 M, ◒; 3.50 M, ◓; 4.00 M, and ○; 4.50 M.

$$\alpha/f^2 = A/[1+(f/f_r)^2] + B, \quad (1)$$

where f is the frequency; f_r the relaxation frequency, and A and B, constants. These ultrasonic parameters, f_r, A, and B, were determined so as to obtain the best fit of the experimental data to Eq. 1, using a nonlinear least-meansquare method.[3] They are listed in Table 1 as a function of the analytical concentration of Allyl Cellosolve, C_e. The sound velocity shows a maximum at 2.5 M, 1 M=1 mol dm^{-3}, above which the excess absorption appears. The value of A which is the relaxation amplitude also shows a maximum at around 4.0 M though it is dependent on the temperature. These concentration dependences of ultrasonic properties are characteristic of aqueous solutions of nonelectrolytes, and we predict that the same mechanism as that proposed previously[1-5] is associated with the excess absorption in the aqueous solution of Allyl Cellosolve.

Table 1. Ultrasonic parameters for aqueous solution of Allyl Cellosolve at 25 °C

C_e / M[a]	f_r / MHz	A	B	r.m.s.[b]	c	ρ
		10^{-17} s^2 cm^{-1}			m s^{-1}	g cm^{-3}
3.01	118	75.3	49.3	2.75	1606	1.000
3.10	118	76.5	60.6	4.85	1603	1.000
3.27	89.8	120	95.9	4.41	1594	0.9999
3.50	84.6	119	94.7	3.19	1593	0.9987
3.75	65.0	140	116	4.51	1584	0.9979
4.00	63.5	150	131	4.60	1576	0.9960
4.23	88.9	140	116	3.55	1566	0.9950
4.51	96.7	130	103	2.78	1564	0.9942
4.77	102	115	105	3.25	1557	0.9937

a) 1 M=1 mol dm^{-3}. b) *r.m.s.* is defined as $\sum[[(\alpha/f^2)_{\text{calcd } i}-(\alpha/f^2)_{\text{exptl } i}]^2/N]^{1/2}$; the details of the procedure of the analysis are described in Ref. 3.

The model is as follosw:

$$\mathrm{AB} \underset{k_b}{\overset{k_f}{\rightleftharpoons}} \mathrm{A}+\mathrm{B}, \qquad (2)$$

$$C_1 \qquad C_2 \quad C_3$$

where AB stands for the complex; A, the Allyl Cellosolve and B, the water which has ability of hydrogen-bonding. The C_i's indicate the equilibrium concentrations of the individual components. It is assumed that the liquid water consists of two states, that is, the hydrogen-bonded water and the nonhydrogen-bonded water, and that the rates between these states are too fast to be observed in our frequency range. Only nonhydrogen-bonded water may participate in the reaction considered here. The relation between the relaxation frequency and the concentrations is derived as follows:

$$2\pi f_r = k_b[(C_e-\beta C_w+K)^2+4\beta C_w K]^{1/2}, \qquad (3)$$

where β is the mole fraction of the nonhydrogen-bonded water and C_w the analytical concentration of water, and where K is defined as $K=k_f/k_b$. The parameters, k_b, β, and K in Eq. 3 could be determined so as to get a reasonable curve which satisfied the experimental data to the relaxation frequency. The detail of the method for the determination have been shown elsewhere.[4] Similar experiments and calculations were performed at 20 and 30 °C. Figure 2 shows the concentration dependence of the relaxation frequency at various temperatures. The solid lines were calculated using the obtained parameters. The minimum position of the relaxation frequency shifts to a higher concentration with an increase in the temperature. This means that the fraction of the nonhydrogen-bonded water increases with the temperature. This is also clear from the temperature dependence of the β value. The obtained rate and the thermodynamic constants are listed in Table 2.

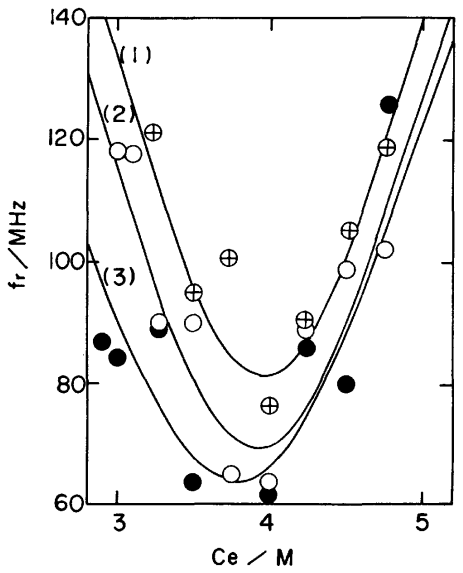

Fig. 2. Concentration dependence of the relaxation frequencies at various temperature. ⊕; 30 °C, ○; 25 °C, and ●; 20 °C.

Table 2. Rate and thermodynamic constants for interaction between water and Allyl Cellosolve

T / °C	β	$10^{-}k_b$ / M^{-1} s^{-1}	10^2K / M
20	0.113±0.002	3.3±0.3	8.9±0.8
25	0.121±0.001	3.7±0.2	9.0±0.7
30	0.123±0.002	4.0±0.2	10.0±0.6

Now, it is possible to estimate the activation enthalpy for the backward reaction, $\Delta H_b^{\ddagger}$, from the plots of $\ln(k_b)$ *vs.* $1/T$, and the enthalpy change of the reaction, ΔH, from those of $\ln(K)$ *vs.* $1/T$. Using the most probable values of the rate and equilibrium constants, they are calculated to be $\Delta H_b^{\ddagger}=14\pm3$ kJ mol^{-1} and $\Delta H=8\pm2$ kJ mol^{-1}. The forward rate constants in Table 3 are obtained from the relation of $K=k_f/k_b$. The forward activation enthalpy, $\Delta H_f^{\ddagger}$ is found to be 22 ± 4 kJ mol^{-1} from the relation of $\Delta H=\Delta H_f^{\ddagger}-\Delta H_b^{\ddagger}$. The entropy change of the reaction, ΔS, is also estimated to be approximately 13 J mol^{-1} deg^{-1} from $\Delta G=\Delta H-T\Delta S$, where ΔG is defined as $-\Delta G=RT\ln(K)$.

Another parameter which is obtained from the ultrasonic experiments is the maximum excess absorption per wave length, $\mu_{\max}$, which is expressed by this equation:

$$\mu_{\max} = Af_r c/2 = (\pi c^2\rho\Gamma/2RT)(\Delta V-\Delta H\alpha_p/\rho C_p)^2, \qquad (4)$$

where ρ is the solution density; ΔV, the volume change of the reaction; C_p, the specific heat, and α_p the thermal expansion coefficient. The term Γ is derived as $\Gamma=[1/C_1+1/C_2+1/C_3-1/(C_1+C_2+C_3)]^{-1}$ for the reaction considered here.[1] In order to determine accurately the enthalpy and volume changes of the reaction from Eq. 4, the values of α_p and C_p as the each concentration are necessary. Many thermodynamic parameters, including α_p and C_p in aqueous solutions of nonelectrolytes may show anomalous characters at around or less than the concentration where the sound velocity exhibits the maximum. The concentration range where the sound excess absorption appears is more than that concentration and so we may expect that these thermodynamic parameters change gradually with the concentration. Therefore, it is assumed that the α_p and C_p for the Allyl Cellosolve solution are expressed as linear functions of the mole fraction of the solute, n, in our

Table 3. Comparison of the rate and thermodynamic constants for three ethers at 25 °C

Solute	β	$10^{-7}k_f$ / s^{-1}	10^2K / M	Reference
Allyl Cellosolve	0.121	3.0	9.0	This work
Propyl Cellosolve	0.100	9.6	74	4
Butyl Cellosolve	0.029	4.2	25	3

limited concentration range. The values of α_p and C_p for Propyl Cellosolve are used for the estimation because the data for Allyl Cellosolve are unfortunately not available. They are $C_{p,\mathrm{soln}}=1.7n+4.2(1-n)$ [J g^{-1}] and $\alpha_{p,\mathrm{soln}}=1.1\times10^{-3}n+2.6\times10^{-4}(1-n)$ [deg^{-1}]. The obtained enthalpy and volume change are $\Delta H=8\pm4$ kJ mol^{-1} and $\Delta V=0.6\pm0.4$ cm^3 mol^{-1}. It should be noticed that a serious error may be contained in both the determinations of the enthalpy change of the reaction; these two values seem to be almost the same in the experimental error also because of the uncorrect values of the thermal expansion coefficient and the specific heat for Allyl Cellosolve. The obtained enthalpy change is still quite small; this might be because the reaction sites are surrounded by extremely polar water molecules.[6]

From these results in the present study, the following conclusions are derived. First, there are some aspects estimating the effects of solutes on the water structure.[7-10] The β parameter is also useful for the estimation because it is the fraction of nonhydrogen-bonded water molecule. As may be seen in Table 3, Allyl Cellosolve acts as a water structure promoter when the β value is compared with that in pure water.[10] However, its activity is not so much as that of the ether with a larger hydrophobic group. This dependence of the β parameter on the solute structure may reflect the effect of the hydrophobic group of the solute molecules or the hydrophobicity. With increasing the hydrophobicity, the fraction of the nonhydrogen-bonded water decreases.

Second, there might be various interactions between the solute and the solvent. The hydrogen bonding of water with the allyloxy group might also be possible. However, a similar concentration dependence of the ultrasonic absorption has been observed in alcohol solutions,[1,2,11] and even if such interaction exists, the time range may be different from ours. It might be considered in quite low frequency range because the water molecules around the alkyl group may be tightly bound by themselves.

Finally, other reaction mechanisms, for example, the association reactions between ethers by hydrogen-bonding, are possible causes of the excess absorption. However, the concentration dependence of the relaxation frequency can not be interpreted in terms of such reaction mechanisms. The background absorption, B, is still high than those expected from the classical aboorptions. Other relaxational absorptions may also exist in the higher frequency range. Therefore, we may confirm that the excess absorption solution is due to the interaction between water and the hydroxyl group of the ether.

References

1) S. Nishikawa, M. Mashima, and T. Yasunaga, *Bull. Chem. Soc. Jpn.*, **48**, 661 (1975).
2) S. Nishikawa, M. Mashima, M. Maekawa, and T. Yasunaga, *Bull. Chem. Soc. Jpn.*, **48**, 2353 (1975).
3) S. Nihikawa, M. Tanaka, and M. Mashima, *J. Phys. Chem.*, **85**, 686 (1981).
4) S. Nishikawa, Y. Yamashita, and M. Mashima, *Bull. Chem. Soc. Jpn.*, **55**, 1 (1982).
5) S. Nishikawa and T. Uchida, to be published.
6) M. Davies, "Hydrogen Bonding," ed by D. Dadzi, Pergamon Press, London (1956).
7) F. Franks, "Hydrogen Bonded Solvent Systems," ed by A. K. Convington and P. Jones, Taylor and Francis Press, London (1968).
8) G. D'Arrigo, G. Maisano, F. Mallamace, P. Migliardo, and F. Wanderlingh, *J. Chem. Phys.*, **75**, 4264 (1981).
9) J. L. Neal, and D. A. I. Goring, *J. Phys. Chem.*, **74**, 658 (1970).
10) C. M. Davis, Jr., and J. Jarzynski, *Adv. Mol. Relax. Proc.*, **1**, 155 (1968).
11) S. Nishikawa, M. Mashima, and T. Yasunaga, *Bull. Chem. Soc. Jpn.*, **49**, 1413 (1976).

General Relations between Bond Orders and Imaginary Bond-Bond Polarizabilities

Noriyuki MIZOGUCHI
Department of Physics, Meiji College of Pharmacy, Nozawa, Setagaya-ku, Tokyo 154
(Received August 3, 1982)

The imaginary bond-bond polarizability has been studied. Several general relations exist between the bond order and the imaginary bond-bond polarizability and between imaginary bond-bond polarizabilities.

Benzenoid hydrocarbons are known to have large magnetic anisotropies. A semiclassical theory by Pauling[1] showed that this arises from the Larmor precession of pi-electrons around the carbocyclic framework (ring current). In 1937 London[2,3] formulated this picture in simple quantum-mechanical terms. His method involves the use of gauge invariant atomic orbitals as a basis for the LCAO scheme. McWeeny[4,5] modified London's theory and represented the energy change due to the effect of the external magnetic field in terms of the imaginary bond-bond polarizability. When applied to a series of aromatic hydrocarbons, McWeeny's method gives a good agreement with experimental values of the ratio $\Delta\chi/\Delta\chi$ (benzene) and of NMR chemical shifts.[6-10] Here $\Delta\chi$ stands for the magnetic anisotropy of a conjugated system.

On the basis of McWeeny's method and with Gayoso-Boucekkine's unitary transformation,[11] Mallion[12] gave an explicit expression for the ring current in individual rings of polycyclic hydrocarbons. He emphasized, from the graph theoretical view point, that the concepts of "spanning tree"[13] and "circuit"[13] play impotant roles in the theory of the ring current. And many authers have discussed the concept of the ring current from the view point of the aromatic character of conjugated compounds.[14-19]

Imaginary bond-bond polarizability has been widely used to calculate the ring currents of conjugated systems. Nevertheless, the properties of the imaginary bond-bond polarizability have never been discussed. Only in Haddon's paper[20] is found a relation between the bond order and the imaginary bond-bond polarizability. But this is a special case of relations given in this paper.

Here the property of the imaginary bond-bond polarizability in a conjugated molecule will be discussed. And it will be shown that several general relations exist between bond orders and imaginary bond-bond polarizabilities.

The Imaginary Bond-Bond Polarizability

In order to understand the meaning of the imaginary bond-bond polarizability, the London-McWeeny theory, which is an extension of the simple HMO method, will be briefly outlined in this section. And each term of the expression for the magnetic susceptibility will be evaluated.

With London's approximations,[2] the resonance integrals in the presence of an external, uniform, magnetic field H normal to the plane of the molecule are given as[4-5]

$$\beta_{rs} = \beta \exp[2\pi i(e/hc)S_{rs}H] = \beta \exp(i\,\theta_{rs}),$$

where e, h, and c are the usual fundamental constants, S_{rs} the signed area of the triangle formed by an arbitrary origin and the bond r-s, counted positive if r-s is right-handed about the normal to the plane of the molecule, and β is the resonance integral in the absence of the magnetic field, which is assumed to be equal for all bonds.

With respect to the zero-field atomic orbital AO, the matrix elements of the perturbation due to the field are

$$\Delta_{rs} = \beta_{rs} - \beta = \beta\left(i\theta_{rs} - \frac{1}{2}\theta_{rs}^2 + \cdots\right).$$

The usual perturbation method gives the first- and second energy changes in the J-th molecular orbital MO (which is supposed to be nondegenerate):

$$\delta E_J^{(1)} = \sum_{rs} P_{J,sr}\Delta_{rs},$$

and

$$\delta E_J^{(2)} = \sum_{rs}\sum_{tu} \pi_{J,rs,tu}\Delta_{rs}\Delta_{tu}.$$

Here $P_{J,rs}$ is the partial bond order of the bond r-s[21] and is given by

$$P_{J,rs} = C_{rJ}C_{sJ},$$

and

$$\pi_{J,rs,tu} = \sum_{K(\neq J)} \frac{C_{rJ}C_{sK}C_{tK}C_{uJ}}{E_J - E_K},$$

where C_{rJ} and E_J are the coefficients of the r-th AO and the orbital energy of the J-th MO in the absence of the magnetic field. In this article, for simplicity, all the coefficients of AO are supposed to be real, since the wave function can always be written in real form in the absence of the magnetic field.

If we keep the first two terms in the series expansion of the perterbation and let X_{rs} and Y_{rs} be the real and imaginary parts of Δ_{rs} respectively, then

$$X_{rs} = -\frac{\beta}{2}\theta_{rs}^2 = X_{sr},$$

and

$$Y_{rs} = \beta\,\theta_{rs} = -Y_{sr}.$$

Considering the above equations, the first- and second energy changes in the J-th MO can be written as follows:

$$\delta E_J^{(1)} = 2\sum_{(rs)} P_{J,rs}X_{rs},$$

and

$$\delta E_J^{(2)} = -\sum_{(rs)}\sum_{(tu)} \bar{\pi}_{J,(rs)(tu)} Y_{rs} Y_{tu},$$

where (rs) indicates a sum over bonds, not a double sum over atomic centers and we have written

$$\bar{\pi}_{J,(rs)(tu)} = \pi_{J,rs,tu} - \pi_{J,rs,ut} + \pi_{J,sr,ut} - \pi_{J,sr,tu}$$
$$= \sum_{K(\neq J)} \frac{(C_{rJ}C_{sK} - C_{sJ}C_{rK})(C_{tK}C_{uJ} - C_{uK}C_{tJ})}{E_J - E_K}. \quad (1)$$

Term $\bar{\pi}_{J,(rs)(tu)}$ is the partial imaginary bond-bond poplarizability between bonds r-s and t-u.[22]

Thus the energy change in the J-th MO is

$$\delta E_J = -\beta\left(\frac{2\pi e}{hc}\right)^2 \{\sum_{(rs)} P_{J,rs} S_{rs}^2 + \sum_{(rs)}\sum_{(tu)} \beta\bar{\pi}_{J,(rs)(tu)} S_{rs} S_{tu}\} H^2.$$

Moreover the total pi-electron energy change of a conjugated molecule is given by

$$\delta E = \sum_J \lambda_J \delta E_J = -\beta\left(\frac{2\pi e}{hc}\right)^2 \{\sum_{(rs)} P_{rs} S_{rs}^2 + \sum_{(rs)}\sum_{(tu)} \beta\,\bar{\pi}_{(rs)(tu)} S_{rs} S_{tu}\} H^2, \quad (2)$$

where λ_J is the occupation number of the J-th MO,

$$P_{rs} = \sum_J \lambda_J P_{J,rs},$$

and

$$\bar{\pi}_{(rs)(tu)} = \sum_J \lambda_J \bar{\pi}_{J,(rs)(tu)}$$
$$= \sum_J \lambda_J \sum_{K(\neq J)} \frac{(C_{rJ}C_{sK} - C_{sJ}C_{rK})(C_{tK}C_{uJ} - C_{uK}C_{tJ})}{E_J - E_K}. \quad (3)$$

Term P_{rs} is the Coulson bond order of bond r-s,[23] and the term $\bar{\pi}_{(rs)(tu)}$ is what McWeeny defined as the imaginary bond-bond polarizability between bonds r-s and t-u.[4-5] The magnetic susceptibility of a conjugated molecule is defined as the second derivative of the total pi-electron energy with respect to H, *i.e.*,

$$\chi = -\frac{\partial^2}{\partial H^2}[(E^0 + \delta E)]_{H=0}$$
$$= 2\beta\left(\frac{2\pi e}{hc}\right)^2 \{\sum_{(rs)} P_{rs} S_{rs}^2 + \sum_{(rs)}\sum_{(tu)} \beta\bar{\pi}_{(rs)(tu)} S_{rs} S_{tu}\}$$
$$= \sum_J \lambda_J \chi_J, \quad (4)$$

where E^0 is the zero-field total pi-electron energy of a conjugated molecule and χ_J is the partial magnetic susceptibility for the J-th MO, as defined in the last equation.[22]

From Eq. 3 it can easily be shown that the mutual imaginary bond-bound polarizability $\bar{\pi}_{(rs)(tu)}$ is antisymmetric with respect to rs and tu, *i.e.*,

$$\bar{\pi}_{(rs)(tu)} = -\bar{\pi}_{(rs)(ut)} = -\bar{\pi}_{(sr)(tu)}.$$

Since the sum in Eq. 3 is antisymmetric in J and K, for molecules in which all the pi-electrons are paired, the imaginary bond-bond polarizability can be written as follows:

$$\bar{\pi}_{(rs)(tu)} = 2\sum_J^{\text{occ}}\sum_K^{\text{unocc}} \frac{(C_{rJ}C_{sK} - C_{sJ}C_{rK})(C_{tK}C_{uJ} - C_{uK}C_{tJ})}{(x_J - x_K)\beta}, \quad (5)$$

where $\sum^{\text{occ}}$ and $\sum^{\text{unocc}}$ run over occupied and unoccupied MO's respectively, and, as in the usual HMO method, it has been assumed that the orbital energy E_J can be written as follows:

$$E_J = \alpha + \beta x_J.$$

Here α is the coulomb integral.

From Eq. 5, it can be shown that the self imaginary bond-bond polarizabilities of any bonds are positive, *i.e.*,

$$\bar{\pi}_{(rs)(rs)} > 0, \quad (6)$$

where β is assumed to be negative.

From Eq. 6 we can say that the terms associated with the self imaginary bond-bond polarizability in Eq. 4 correspond to the paramagnetic terms of the magnetic susceptibility. Since the bond order P_{rs} of the bond r-s is positive,[24] the first terms in Eq. 4 correspond to the diamagnetic terms of the magnetic susceptibility. But the other terms associated with the mutual imaginary bond-bond polarizabilities do not have definite effects on the magnetic susceptibility because these polarizabilities do not have a definite sign.

General Relations between Bond Orders and Imaginary Bond-Bond Polarizabilities

The property of the imaginary bond-bond polarizability in a conjugated molecule will be dependent on the topological nature of the carbon skeleton, *i.e.*, the mode of branching. But the degree of vertices (atoms) in the Hückel molecular graph does not exceed 3.[25] It is therefore enough to consider only two subgraphs G1 and G2 as shown in Figs. 1 and 2.

Let first consider subgraph G1. This is a sequence of vertices a_j $(j=1,2,\cdots,n)$ whose degrees are all two. Then we have the following equalities for these edges (bonds):

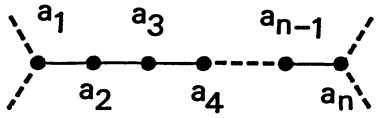

Fig. 1. Subgraph G1.

$$\bar{\pi}_{J,(rs)(a_i a_{i+1})} = \bar{\pi}_{J,(rs)(a_j a_{j+1})}, \quad (A')$$
$$\bar{\pi}_{(rs)(a_i a_{i+1})} = \bar{\pi}_{(rs)(a_j a_{j+1})}, \quad (A)$$
$$P_{J,a_i a_{i+1}} + \beta\bar{\pi}_{J,(a_i a_{i+1})(a_i a_{i+1})} = P_{J,a_j a_{j+1}} + \beta\bar{\pi}_{J,(a_j a_{j+1})(a_j a_{j+1})}, \quad (B')$$
$$P_{a_i a_{i+1}} + \beta\bar{\pi}_{(a_i a_{i+1})(a_i a_{i+1})} = P_{a_j a_{j+1}} + \beta\bar{\pi}_{(a_j a_{j+1})(a_j a_{j+1})}, \quad (B)$$
$$P_{J,a_i a_{i+1}} = \beta\bar{\pi}_{J,(a_i a_{i+1})(a_j a_{j+1})} - \beta\bar{\pi}_{J,(a_i a_{i+1})(a_i a_{i+1})}, \quad (C')$$
$$P_{a_i a_{i+1}} = \beta\bar{\pi}_{(a_i a_{i+1})(a_j a_{j+1})} - \beta\bar{\pi}_{(a_i a_{i+1})(a_i a_{i+1})}, \quad (C)$$

where $i, j = 1,2,\cdots,n$ and $i \neq j$.

Relations A' and A hold as far as a given edge r-s is not equal to edges a_i-a_{i+1} or a_j-a_{j+1}, *i.e.*, as far as the imaginary bond-bond polarizabilities under consideration are mutual ones. Relations B', B, C', and C hold even when the vertex a_1 is jointed to the vertex a_n, *i.e.*, even when the sequence of a_j $(j=1,2,\cdots,n)$ forms a ring.

Proof of Relations A' and A. We first consider Relation A' for $i=i$ and $j=i+1$. By substituting Eq. 1 into Relation A' and with some manipulations, the following equation is derived:

$$\beta(\bar{\pi}_{J,(rs)(a_ia_{i+1})} - \bar{\pi}_{J,(rs)(a_{i+1}a_{i+2})}) = \sum_{K(\neq J)} \frac{1}{x_J - x_K}(C_{rJ}C_{sK} - C_{sJ}C_{rK}) \times \{C_{a_{i+1}J}(C_{a_iK} + C_{a_{i+2}K}) - C_{a_{i+1}K}(C_{a_iJ} + C_{a_{i+2}J})\}. \quad (7)$$

Making use of the variational constraint for the vertex a_{i+1}

$$-x_JC_{a_{i+1}J} + C_{a_iJ} + C_{a_{i+2}J} = 0, \quad (8)$$

and with some manipulations, Eq. 7 can now be written as follows:

$$\beta(\bar{\pi}_{J,(rs)(a_ia_{i+1})} - \bar{\pi}_{J,(rs)(a_{i+1}a_{i+2})}) = \sum_K C_{a_{i+1}J}C_{a_{i+1}K}(C_{rJ}C_{sK} - C_{sJ}C_{rK}), \quad (9)$$

where the sum $\sum_{K(\neq J)}$ in Eq. 7 is changed to the sum $\sum_K$ since this change has no effect. Since, from the orthonormal property of the molecular orbitals, we have

$$\sum_J C_{rJ}C_{sJ} = \begin{cases} 1 & \text{if } r = s \\ 0 & \text{otherwise,} \end{cases} \quad (10)$$

it can be seen that the right hand side of Eq. 7 is equal to zero. Therefore it follows that

$$\bar{\pi}_{J,(rs)(a_ia_{i+1})} = \bar{\pi}_{J,(rs)(a_{i+1}a_{i+2})}. \quad (11)$$

After the repeated use of Eq. 11 for other edges Relation A′ is finally obtained. And Relation A can be obtained from Eq. 3 and Relation A′.

Proof of Relations B′ and B. After some manipulations similar to those in the proof of Relation A, the following equation can be derived:

$$\beta(\bar{\pi}_{J,(a_ia_{i+1})(a_ia_{i+1})} - \bar{\pi}_{J,(a_{i+1}a_{i+2})(a_{i+1}a_{i+2})}) = \sum_K C_{a_{i+1}J}C_{a_{i+1}K}\{C_{a_{i+1}J}(C_{a_iK} - C_{a_{i+2}K}) - C_{a_{i+1}K}(C_{a_iJ} - C_{a_{i+2}J})\}. \quad (12)$$

Because of Eq. 10, both the first and second terms of the right hand side of Eq. 12 are equal to zero. The third term of Eq. 12 is $-P_{J,a_ia_{i+1}}$ and the fourth term is equal to $P_{J,a_{i+1}a_{i+2}}$. Therefore we have

$$P_{J,a_ia_{i+1}} + \beta\bar{\pi}_{J,(a_ia_{i+1})(a_ia_{i+1})} = P_{J,a_{i+1}a_{i+2}} + \beta\bar{\pi}_{J,(a_{i+1}a_{i+2})(a_{i+1}a_{i+2})}. \quad (13)$$

After the repeated use of Eq. 13 for other edges we can obtain Relation B′ and thus Relation B.

Proof of Relations C′ and C. Making use of Eq. 8 for the vertex a_{i+1} and with some manipulations, we can obtain the following equation:

$$\beta\bar{\pi}_{J,(a_ia_{i+1})(a_{i+1}a_{i+2})} = \sum_K C_{a_{i+1}J}C_{a_{i+1}K}(C_{a_iJ}C_{a_{i+1}K} - C_{a_iK}C_{a_{i+1}J}) + \sum_{K(\neq J)}(C_{a_iJ}C_{a_{i+1}K} - C_{a_{i+1}J}C_{a_iK}) \times (C_{a_{i+1}J}C_{a_iK} - C_{a_{i+1}K}C_{a_iJ})\frac{1}{x_J - x_K}. \quad (14)$$

Since Eq. 10 holds, the first and second terms in the first sum of the right hand side of Eq. 14 are equal to $P_{J,a_ia_{i+1}}$ and to zero, respectively. The second sum is equal to $\beta\bar{\pi}_{J,(a_ia_{i+1})(a_ia_{i+1})}$. Therefore, the following equation is obtained:

$$\beta\bar{\pi}_{J,(a_ia_{i+1})(a_{i+1}a_{i+2})} = P_{J,a_ia_{i+1}} + \beta\bar{\pi}_{J,(a_ia_{i+1})(a_ia_{i+1})}. \quad (15)$$

After the repeated use of Eq. 15 for other edges, we can obtain Relation C′ and thus Relation C.

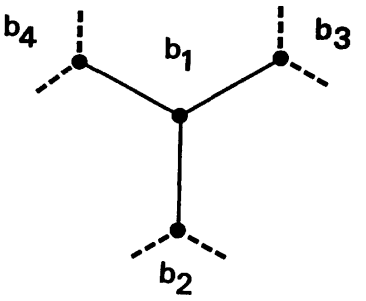

Fig. 2. Subgraph G2.

Next we consider subgraph G2 as shown in Fig. 2, in which the degrees of vertices b_2—b_4 are arbitrary and the vertex b_1 is jointed to vertices b_2—b_4. Then we have

$$\bar{\pi}_{J,(rs)(b_2b_1)} = \bar{\pi}_{J,(rs)(b_1b_3)} + \bar{\pi}_{J,(rs)(b_1b_4)}, \quad (D′)$$

$$\bar{\pi}_{(rs)(b_2b_1)} = \bar{\pi}_{(rs)(b_1b_3)} + \bar{\pi}_{(rs)(b_1b_4)}, \quad (D)$$

$$P_{J,b_1b_2} = \beta\bar{\pi}_{J,(b_1b_2)(b_3b_1)} + \beta\bar{\pi}_{J,(b_1b_2)(b_4b_1)} - \beta\bar{\pi}_{J,(b_1b_2)(b_1b_2)}, \quad (E′)$$

$$P_{b_1b_2} = \beta\bar{\pi}_{(b_1b_2)(b_3b_1)} + \beta\bar{\pi}_{(b_1b_2)(b_4b_1)} - \beta\bar{\pi}_{(b_1b_2)(b_1b_2)}. \quad (E)$$

Relations D′ and D hold even when a given edge r-s may be jointed to vertices b_2—b_4.

Proof of Relations D′ and D. Making use of the variational constraint for the vertex b_1,

$$-x_JC_{b_1J} + C_{b_2J} + C_{b_3J} + C_{b_4J} = 0,$$

and with some manipulations similar to those in the proof of Relation A, the following equation is derived:

$$\beta(\bar{\pi}_{J,(rs)(b_2b_1)} - \bar{\pi}_{J,(rs)(b_1b_3)}) = \sum_K C_{b_1J}C_{b_1K}(C_{sJ}C_{rK} - C_{rJ}C_{sK}) + \sum_{(K\neq J)}\frac{1}{x_J - x_K}(C_{rJ}C_{sK} - C_{sJ}C_{rK}) \times (C_{b_4J}C_{b_1K} - C_{b_1J}C_{b_4K}). \quad (16)$$

Note that in the first term of the right hand side of Eq. 16 the sum $\sum_{K(\neq J)}$ changes to the sum $\sum_K$. The first term of Eq. 16 is equal to zero since Eq. 10 holds. The second term of Eq. 16 is equal to $\beta\bar{\pi}_{J,(rs)(b_1b_4)}$. Therefore Relation D′ is obtained. Thus Relation D can be obtained from Eq. 3 and Relation D′.

Since the proofs of Relations E′ and E can be performed by the same way, they are omitted.

Discussion

The degeneracy of energy levels has not yet been considered. The derived relations between the partial bond order and the partial imaginary bond-bond polarizability, *i.e.*, Relations A′—E′, do not hold for degenerate energy levels. A slight modification is necessary for these energy levels. But it can be readily shown that Relations A—E hold also for molecules with degenerate energy levels as far as degenerate levels are not singly occupied. In such case we must, however, use the imaginary bond-bond polarizability in the form of Eq. 5.

Here $(4n+2)$-annulenes will be considered as examples. These molecules consist only of segments such as Subgraph G1. Therefore we consider only Relations A—C. Since these molecules have degenerate energy levels, we must, as dicussed above, use the imaginary

bond-bond polarizability in the form of Eq. 5. For annulenes, analylitical solutions of the secular equation have been reported. Therefore the sum in Eq. 5 can be performed and the following equations can be obtained:[20]

$$\bar{\pi}_{(rs)(tu)} = \frac{2}{N^2 \beta \sin(\pi/N)}, \quad (17)$$

$$\bar{\pi}_{(rs)(rs)} = \frac{2(1-N)}{N^2 \beta \sin(\pi/N)}, \quad (18)$$

$$P_{rs} = \frac{2}{N \sin(\pi/N)}, \quad (19)$$

where $N=4n+2$, and r-s and t-u are arbitrary two edges (bonds) in the annulene under consideration. Equation 17 is just Relation A for $(4n+2)$-annulenes. It should be noticed that Relation B can be obtained from their symmetry alone. Moreover from Eqs. 17 and 19 it follows that

$$\bar{\pi}_{(rs)(tu)} = \frac{P_{rs}}{N\beta}.$$

The above equation shows that all the mutual imaginary bond-bond polarizabilities in $(4n+2)$-annulenes are directly related to the bond order P_{rs} and equal to $P_{rs}/\beta N$. From Eqs. 17—19 we can obtain

$$P_{rs} + \beta\bar{\pi}_{(rs)(rs)} = \beta\bar{\pi}_{(rs)(tu)},$$

which is Relation C for $(4n+2)$-annulenes.

By use of a suitable unitary transformation[11-12] McWeeny[4] has shown that the sums in Eqs. 2 and 4, which runs over all bonds in a molecule, can be reduced to sums over one bond in each closed ring. We can show that the result of McWeeny's unitary transformation can be obtained by virtue of Relations A—E.[26] Moreover it is noteworthy that Relations A and D are very similar to Kirchhoff's law in the electro-magnetic theory. By virtue of Relations A—E, it can be shown that in the London-McWeeny theory the ring currents[12] are conserved.[26] The applications of Relations A—E to other problems will be discussed elsewhere.

We wish to thank Professor Haruo Hosoya, Ochanomizu University, and Professor Chuya Inoue, Meiji College of Pharmacy, for their helpful discussions.

References

1) L. Pauling, *J. Chem. Phys.*, **4**, 673 (1936).
2) F. London, *J. Phys. Radium*, **8**, 397 (1937).
3) L. Salem, "Molecular-Orbital Theory of Conjugated Systems," W. A. Benjamin, New York (1966), Chap. 4.
4) R. McWeeny, *Mol. Phys.*, **1**, 311 (1958).
5) J. D. Memory, "Quantum Theory of Magnetic Resonance Parameters," McGraw-Hill, New York (1968), Chap. 6.
6) I. J. Maddox and R. McWeeny, *J. Chem. Phys.*, **36**, 2353 (1962).
7) J. D. Memory, G. W. Parker, and J. C. Halsey, *J. Chem. Phys.*, **45**, 3567 (1966).
8) T. B. Cobb and J. D. Memory, *J. Chem. Phys.*, **47**, 2020 (1967).
9) C. W. Haigh and R. B. Mallion, *Mol. Phys.*, **22**, 955 (1971).
10) C. A. Coulson, J. A. N. F. Gomes, and R. B. Mallion, *Mol. Phys.*, **30**, 713 (1975).
11) J. Gayoso and A. Boucekkine, *C. R. Acad. Sci. Paris, Ser. C*, **272**, 184 (1971).
12) R. B. Mallion, *Proc. R. Soc. London, Ser. A*, **341**, 429 (1975).
13) R. J. Wilson, "Introduction to Graph Theory," Longman, London (1979), Chap. 4.
14) J. A. Elvidge and L. M. Jackman, *J. Chem. Soc.*, **1961**, 859.
15) H. J. Dauben, Jr., J. D. Wilson, and J. L. Laity, *J. Am. Chem. Soc.*, **91**, 1991 (1969); "Nonbenzenoid Aromatics," ed by J. P. Snyder, Academic Press, New York (1971), Vol. 2, Chap. 3.
16) G. M. Badger, "Aromatic Character and Aromaticity," Cambridge University Press, Cambridge (1969), Chap. 2.
17) J. Aihara, *J. Am. Chem. Soc.*, **101**, 5913 (1979).
18) R. B. Mallion, *Pure Appl. Chem.*, **52**, 1541 (1980).
19) J. Aihara, *J. Am. Chem. Soc.*, **103**, 5704 (1981); *Pure Appl. Chem.*, **54**, 1115 (1982).
20) R. C. Haddon, *J. Am. Chem. Soc.*, **101**, 1722 (1979).
21) Y. Ooshika, *J. Phys. Soc. Jpn.*, **12**, 1296 (1957).
22) T. Nakajima and S. Kohda, *Bull. Chem. Soc. Jpn.*, **39**, 804 (1966).
23) C. A. Coulson and H. C. Longuet-Higgins, *Proc. R. Soc. London, Ser. A*, **191**, 39 (1947); **192**, 16 (1947).
24) Strictly speaking, this is not correct. Certainly in conjugated molecules, the bond orders of almost bonds are positive. But a bond whose bond order is equal to zero is found, for example, in butalene. Moreover in a very unstable system there exists a bond whose bond order is negative. This subject will be discussed in detail elsewhere.
25) A. Graovac, I. Gutman, and N. Trinajstic, "Topological approach to the chemistry of conjugated molecules," Springer Verlag, Berlin (1977), Chap. 2.
26) N. Mizoguchi, to be published.

Cyclopropanation of Dimethyl Fumarate and Maleate with *gem*-Dihalides Catalyzed by Co(0)- or Ni(0)-Complex and Zinc

Hiroyoshi KANAI,* Yoshimasa NISHIGUCHI, and Hideki MATSUDA
Department of Hydrocarbon Chemistry, Faculty of Engineering, Kyoto University, Sakyo-ku, Kyoto 606
(Received September 22, 1982)

The reaction of bis(acetonitrile)bis(diethyl fumarate)cobalt(0) with dibromomethane gave diethyl *trans*-1,2-cyclopropanedicarboxylate in a 67% yield based on the cobalt complex. Dimethyl *cis*-1,2-cyclopropanedicarboxylate was obtained in a 52% yield from the reaction of dimethyl maleate with dibromomethane in the presence of acetonitrilebis(dimethyl maleate)nickel(0) accompanied by the formation of the *trans*-isomer in a 14% yield. The addition of zinc gave cyclopropanes in over 100% yields based on cobalt or nickel. 3-Methyl- and 3,3-dimethyl-1,2-cyclopropanedicarboxylic acid esters were produced by the reaction of dimethyl fumarate or maleate with 1,1-dibromoethane and 2,2-dibromopropane. The yield in the cobalt catalyst system decreases with an increase of substituents of *gem*-dibromides, while that in the nickel catalyst system does not vary appreciably. A small amount of dimethyl isopropenylsuccinate was formed as a by-product in the reaction of 2,2-dibromopropane. A mechanism is briefly discussed which involves metallacyclobutane as an intermediate.

In the previous paper,[1] we reported the cyclopropane synthesis in which electron-deficient olefins were allowed to react with dibromomethane by the catalysis of Ni(0)-complexes and zinc. We have found that the best catalytic species are those coordinated by olefin and solvent molecules without additional ligands. Their candidates are bis(acetonitrile)bis(dialkyl fumarate)-cobalt(0) and acetonitrilebis(dialkyl maleate)nickel-(0). The treatment of the complexes with dibromomethane gave cyclopropane derivatives in the absence of Lewis acids or sodium iodide.[1b]

1,2-Cyclopropanedicarboxylic acid esters are produced from base-catalyzed reactions of α-substituted acrylic esters with α-halo esters,[2] or from reactions of α-halo esters with acrylic esters or of polyhalo compounds with α,β-unsaturated diesters by copper–isonitrile complexes.[3] The cyclopropanation of dialkyl fumarate and maleate with *gem*-dihalides in the presence of Co(0)- or Ni(0)-complex and zinc serves as a method of the synthesis of 3-alkyl-1,2-cyclopropanedicarboxylic acid esters. We have studied the effects of several variables on the yield and on the stereochemistry.

Results and Discussion

Cyclopropanation of Dimethyl Fumarate with Dihalomethanes Catalyzed by Bis(acetonitrile)bis(dimethyl fumarate)cobalt(0) (1) and Zinc. The stoichiometric reaction of bis-(acetonitrile)bis(diethyl fumarate)cobalt(0) with dibromomethane in acetonitrile gave diethyl *trans*-1,2-cyclopropanedicarboxylate in a 67% yield based on cobalt (Eq. 1). The cyclopropanation needs neither Lewis

$$Co(E\text{-}H_5C_2O_2CCH{=}CHCO_2C_2H_5)_2(CH_3CN)_2 + CH_2Br_2 \longrightarrow \begin{matrix} H_5C_2O_2C & & H \\ & \diagdown\diagup & \\ H & & CO_2C_2H_5 \end{matrix} + CoBr_2 \quad (1)$$

acids nor sodium iodide nor zinc, differing from that of monosubstituted olefins with electron-withdrawing groups.[1] As the data in Table 1 indicate, the addition of zinc increases the yield based on cobalt to over 100%. Zinc reduces cobalt bromide formed in Eq. 1 to regenerate a catalytic species in the presence of dimethyl fumarate (Eq. 2). A small amount of reduction product

$$CoBr_2 + \begin{matrix} H & & CO_2CH_3 \\ \diagdown & & \diagup \\ & C{=}C & \\ \diagup & & \diagdown \\ H_3CO_2C & & H \end{matrix} + Zn \xrightarrow{CH_3CN} Co(E\text{-}H_3CO_2CCH{=}CHCO_2CH_3)_2(CH_3CN)_2 + ZnBr_2 \quad (2)$$

1

was formed by the zinc bromide–zinc system.[4] The reduction is suppressed by the addition of sodium iodide which does not affect the yield of cyclopropane.

The cyclopropanation proceeded slowly as shown in Fig. 1. An increase in the amount of zinc results in an increase in the yield and reduction in the reaction time. Excess cobalt compound rather decreased the yield. When cobalt halides with water of crystallization were used, the yield decreased due to the production of a considerable amounts of succinate. Manganese can be substituted for zinc as a reductant although it takes a long time to prepare Co(0)-complex.

The best yield based on dibromomethane is obtained when a 1:1 fumarate:dibromomethane mole ratio is used. A slight excess of dibromethane is necessary for the reaction of fumarate to proceed to completion. The

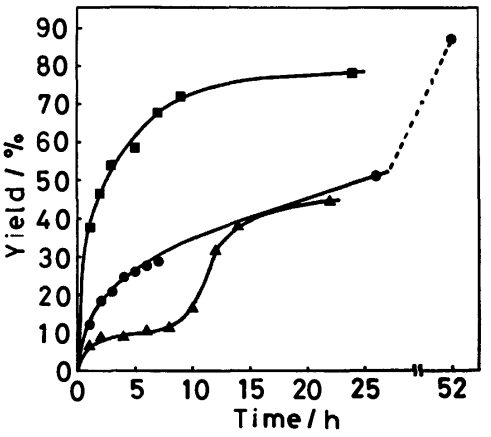

Fig. 1. Time dependence of the yields of cyclopropane derivatives in the reaction of dimethyl fumarate and maleate with dibromomethane catalyzed by the following systems. ●: (Fumarate) [Co] 1 mmol, NaI 2.5 mmol, Zn 15 mmol; ▲: (maleate) [Ni] 1 mmol, NaI 5 mmol, Zn 5 mmol; ■: (maleate) [Ni] 5 mmol, NaI 5 mmol, Zn 15 mmol.

Table 1. Cyclopropanation of dimethyl fumarate with dibromomethane catalyzed by Co(0)-complex and zinc[a)]

Catalytic system				CH_2Br_2 (mmol)	Time h	Conv.[b)] %	Yield[c)]/%	
X in CoX_2	(mmol)	NaI (mmol)	Zn (mmol)				Cyclopropane[d)]	Succinate
Cl	1	0	5	5	136	76	56	5.8
		0	8	6	63	98	64	3.4
		2.6	5	5	68	64	55	1.2
		2.5	8	5	91	100	76	1.4
		2.5	8	6	44	100	89	2.6
		5.0	8	6	44	97	85	1.6
		5.0	8	10	42	100	91	0.8
		2.5	30	6	3	91	83	7.7
		2.5	Mn 7	6	69	85	71	0.4
		LiI 3.0	5	5	117	69	48	tr
		KI 3.0	5	5	66	67	47	tr
	5	2.5	15	6	65	98	44	8.8
Br[e)]	1	2.5	8	6	47	91	58	13
I[f)]	1	2.5	8	6	65	86	55	14
Cl[g)]	1	2.5	8	6	114	77	15	0.6
Cl[h)]	1	2.5	5	5	89	94	57[i)] (8 : 92)	tr
Cl	1	0	8	CH_2Cl_2 15	280	100	8.0	80
		2.5	8	CH_2BrCl 6	70	94	91	6.4
		2.5	8	CH_2ClI 6	0.25	(100)[j)]	23	0
		2.5	8	CH_2I_2 5	52	100	32	7.6

a) To the Co(0)-fumarate complex prepared *in situ* from CoX_2, dimethyl fumarate (5 mmol), NaI, and zinc in CH_3CN (10 ml) was added dibromomethane and the mixture was stirred at room temperature for a given period of time. b) Conversion of dimethyl fumarate. c) Yield based on dimethyl fumarate. d) Dimethyl *trans*-1,2-cyclopropanedicarboxylate. e) $CoBr_2 \cdot 6H_2O$. f) $CoI_2 \cdot 4H_2O$. g) THF(10 ml) was used as solvent. h) Dimethyl maleate (5 mmol) was used in the place of fumarate. i) Total yield of dimethyl *cis*- and *trans*-1,2-cyclopropanedicarboxylate. The number in parenthesis is the ratio of *cis* to *trans*. j) Conversion of chloroiodomethane.

yield in the reaction of dimethyl fumarate with dihalomethanes is in the order: $CH_2BrCl > CH_2Br_2 > CH_2I_2 > CH_2ClI \gg CH_2Cl_2$. This contrasts with the observation that some modifications are needed to use dibromomethane as a reactant in the Simmons-Smith reaction.[5)]

Lithium and potassium iodides are less effective than sodium iodide and bring about a decrease in the yield. Acetonitrile is superior to THF as a solvent because the former causes stabilization of the cobalt(0)-complex.

When dimethyl maleate was allowed to react with cobalt chloride in the presence of zinc, a red-brown solution was obtained in the same manner as for dimethyl fumarate. The treatment of the solution with dibromomethane gave a large amount of dimethyl *trans*-1,2-cyclopropanedicarboxylate and very little of the *cis*-isomer. The red-brown solution containing Co(0)-complex was decomposed in air and analysis of the residual substrate gave almost pure dimethyl fumarate. The isomerization of dimethyl maleate occurred neither in the presence of **1** nor in the zinc bromide–zinc system. It may be assumed that the active catalyst for the isomerization of maleate is a cobalt(I) species which is formed in the course of the reduction.

*Cyclopropanation of Dimethyl Maleate with Dihalomethanes Catalyzed by Acetonitrilebis(dimethyl maleate)nickel(0) (**2**) and Zinc.* Three-coordinate acetonitrilebis(olefin)-nickel(0) (olefin=dimethyl maleate and fumarate) is prepared from nickel bromide, an olefin, and zinc in acetonitrile.[6)] Maleate is not isomerized during the preparation of the Ni(0)-complex in contrast to the case of the cobalt complex. The reaction of dimethyl maleate with dibromomethane in the presence of **2** gave dimethyl *cis*-1,2-cyclopropanedicarboxylate in a 52% yield based

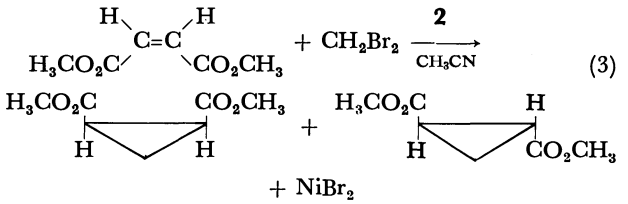

(3)

on nickel and the *trans*-isomer in a 14% yield (Eq. 3). Analysis of residual olefins shows a 90:10 dimethyl maleate: fumarate mole ratio. The addition of zinc increased the yield based on nickel in the same manner as in the cyclopropanation of the cobalt catalyst system (Table 2). Total yields of cyclopropane derivatives increased with an increase in the amounts of zinc and

TABLE 2. CYCLOPROPANATION OF DIMETHYL MALEATE AND FUMARATE WITH DIBROMOMETHANE CATALYZED BY Ni(0)-COMPLEX AND ZINC[a)]

Catalytic system			CH_2Br_2	Time	Conv.[b)]	Yield[b)]/%	
Ni (mmol)	NaI (mmol)	Zn (mmol)	(mmol)	h	%	Cyclopropane[c)] (*cis* : *trans*)	Succinate
Dimethyl maleate							
1	0	5	5	24	37	33 (81 : 19)	4.2
	5	5	5	24	42	31 (90 : 10)	0.4
	5	7	5	24	78	46 (83 : 17)	1.0
	5	10	5	24	94	56 (77 : 23)	2.0
	7	10	5	24	93	54 (70 : 30)	0.8
	5	13	5	24	100	63 (79 : 21)	1.8
	5	10	7	48	99	69 (75 : 25)	1.0
	5	Mn 10	5	24	100	64 (78 : 22)	2.0
1[d)]	5	5	5	48	56	16 (92 : 8)	1.2
3	7	15	5	8	97	53 (88 : 12)	1.6
5	5	15	5	24	95	78 (91 : 9)	3.0
1	5	5	CH_2Cl_2 5	24	8	0	4.0
	5	5	CH_2BrCl 5	24	43	37 (94 : 6)	4.8
	5	10	CH_2BrCl 5	48	90	73 (86 : 14)	9.6
	5	5	CH_2ClI 5	24	37	17 (90 : 10)	tr
	5	5	CH_2I_2 5	24	46	22 (83 : 17)	tr
Dimethyl fumarate							
1	5	5	5	48	34	34 (0 : 100)	0
	5	10	5	25	74	50 (0 : 100)	0.2
5	5	15	5	40	89	59 (0 : 100)	1.9
5	5	15	10	41	99	78 (0 : 100)	0.8

a) To the *in situ* prepared Ni(0)-complex from $NiBr_2$, dimethyl maleate (5 mmol) or fumarate (5 mmol), NaI, and zinc in CH_3CN (10 ml) was added dibromomethane and the mixture was stirred at room temperature for a given period of time. b) Based on olefin. c) Dimethyl *cis*- and *trans*-1,2-cyclopropanedicarboxylate. d) THF (10 ml) was used as solvent.

nickel compounds. In the presence of a small amount of zinc, cyclopropanation started under the catalysis of Ni(0)-complex prepared beforehand, followed by a slow reaction step, until the fast reaction set in (Fig. 1). A large excess of zinc suppressed the slow step to make the whole reaction proceed smoothly.

Selectivity for the *cis*-isomer formation decreases slightly with an increase in the amount of zinc. Appreciable retention of stereochemistry in the maleate can be explained if isomerization of maleate rarely occurs and no isomerization of dimethyl *cis*-1,2-cyclopropanedicarboxylate takes place, unlike cyclopropanation by the copper–isonitrile system.[3b)] No isomerization of dimethyl maleate occurred in the presence of **2**. It may be assumed, as in the reaction with cobalt catalyst system, that the isomerization catalyst is a nickel(I) species. Bromo(dimethyl maleate)nickel(I) is inert to the isomerization.[7)] Nickel(I) species responsible for the isomerization of maleate are presumed to be bromobis(dimethyl maleate)nickel(I) and bis(dimethylmaleate)-nickel(I) tribromozincate on the assumption that dimerization of terminal olefins is catalyzed by (π-C_3H_5)-NiBr and (π-C_3H_5)Ni($AlCl_4$).[8)]

A concomitant formation of the *trans*-isomer is originated from the cyclopropanation of fumarate. The initial rate for the formation of dimethyl *cis*-1,2-cyclopropanedicarboxylate from **2** and dibromomethane was 2.8×10^{-3} mol^{-1} min^{-1}, while that for the formation of the *trans*-isomer from acetonitrilebis(dimethyl fumarate)-nickel(0) (**3**) and dibromomethane was 1.4×10^{-4} mol l^{-1} min^{-1}. However, the cyclopropanation of the mixture of equal moles of maleate and fumarate gave the *trans*-isomer in a six-fold ratio to the *cis*-isomer, indicating that the coordinating strength of fumarate is greater than that of maleate. Dimethyl fumarate which is once formed inhibits the cyclopropanation of dimethyl maleate.

Manganese can be substituted for zinc as a reductant. The order of effectiveness of dihalomethanes is the same as that in the cyclopropanation of dimethyl fumarate by the cobalt catalyst system.

The cyclopropanation of dimethyl fumarate gave the corresponding cyclopropane derivative in yields similar to those in the reaction of dimethyl maleate. The cobalt catalyst system for the cyclopropanation of dimethyl fumarate is superior to the nickel one although it takes a longer reaction time.

Cyclopropanation of Dimethyl Fumarate and Maleate with gem-Dihalides. The cyclopropanation of dimethyl fumarate and maleate with *gem*-dihaloalkanes gave

TABLE 3. CYCLOPROPANATION OF DIMETHYL FUMARATE AND MALEATE WITH *gem*-DIHALIDES CATALYZED BY Co(0)- OR Ni(0)-COMPLEX AND ZINC[a)]

gem-Dihalide (mmol)	Catalyst	(mmol)	Olefin	Time h	Yield of product[b)] %	
CH_3CHBr_2 6	Co[c,d)]	1	Fumarate	47	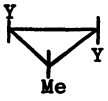	68 (3.1, —)
5	Ni	5	Fumarate	27	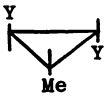	58 (2.4, —)
5	Ni	5	Maleate	27	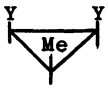	7
					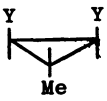	40 (5.2, —)
					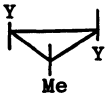	23
$(CH_3)_2CCl_2$ 6	Co[c)]	5	Fumarate	64	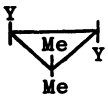	22 (36, 3.4)
$(CH_3)_2CBr_2$ 5	Co[c,d)]	5	Fumarate	48	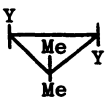	20 (28, 1.3)
$(CH_3)_2CBr_2$ 5	Co[c,d,e)]	5	Fumarate	70	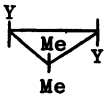	10 (35, 36)
5	Ni[d)]	5	Fumarate	27	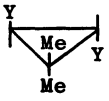	44 (3.4,3.0)
5	Ni[d)]	5	Maleate	27	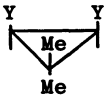	34 (10, 2.6)
					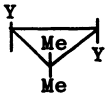	5
CH_5CHCl_2 5	Co	1	Fumarate	144	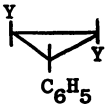	19

a) To the Co(0)- or Ni(0)-complex prepared *in situ* from $CoCl_2$ or $NiBr_2$, an olefin (5 mmol), NaI (5 mmol), and zinc (8 mmol) in CH_3CN (10 ml) was added *gem*-dihalide and the mixture was stirred at room temperature for a given period of time. b) Yield based on olefin. Y=CO_2CH_3. The numbers in parentheses are yields of dimethyl succinate and isopropenyl succinate. c) NaI (2.5 mmol). d) Zn (15 mmol). e) H_2O (0.1 ml) was added.

dimethyl 3-substituted *trans*- and *cis*-1,2-cyclopropanedicarboxylates under the catalysis of Co(0)- or Ni(0)-complex–zinc system (Table 3). The yield decreases with an increase of substituents of *gem*-dihaloalkanes in the cobalt system. A 1 : 1 cobalt : dimethyl fumarate mole ratio gave the best yield in the cyclopropanation with 2,2-dibromopropane. There is little difference in yields between the reactions of 2,2-dichloro- and 2,2-dibromopropane.

The reaction of dimethyl maleate with 1,1-dibromoethane catalyzed by the nickel catalyst system gave cyclopropane derivatives in a 70% yield: the ratio of *cis*-dicarboxylate to the *trans*-isomer is 67: 33 which is somewhat less than that produced in the reaction with dibromomethane. The ratio of the *cis*-methyl isomer to the *trans*-isomer in *cis*-dicarboxylates is 15: 85. It has been proposed that cyclopropanation proceeds *via* metallacyclobutane as an intermediate.[1] If the reductive elimination of a nickelacyclobutane intermediate takes place with retention of configuration, the configuration of the nickelacyclobutane would be that in which the methyl group is predominantly *trans* to both methoxy carbonyl groups by 1,2- and 1,3-steric repulsion. This leads to the *trans*-isomer (Eq. 4). In the reaction of

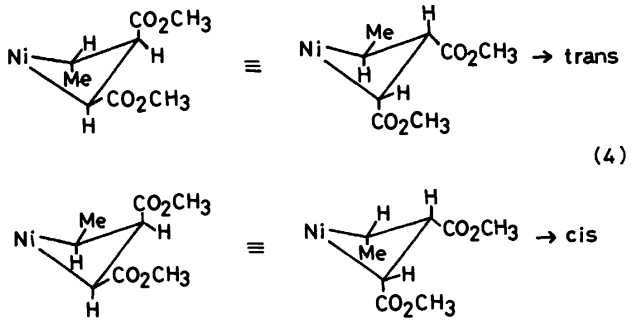

(4)

dimethyl maleate with 2,2-dibromopropane, dimethyl 3,3-dimethyl-1,2-cyclopropanedicarboxylate (*cis* : *trans*= 87 : 13) was obtained in a 39% yield.

Dimethyl isopropenylsuccinate was concomitantly produced in the reaction of dimethyl fumarate and maleate with 2,2-dibromopropane in both cobalt and nickel systems. Two mechanisms have been proposed for the olefin formation from platinacyclobutanes which involves splitting of α-C–H bond[9] and that of β-C–H bond.[10] The postulated intermediate has seven hydrogen atoms bonded to β-carbons and one hydrogen atom bonded to α-carbons (Eq. 5). If dimethyl isopropenylsuccinate is produced from metallacyclobutane,[11] its formation must be originated from splitting of β-C–H_a bond in methyl groups not of β-C–H_b bond in the methine group. The hydrogen of a methyl group is more easily split off than that of the methine group in platinacyclobutane.[9a,b] The addition of water promotes

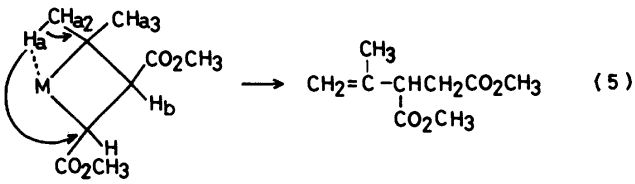

(5)

the olefin production in the reaction of dimethyl fumarate with 2,2-dibromopropane catalyzed by the cobalt catalyst system. Photolysis of platinacyclobutane gives mainly propylene in solvents of low dielectric constant (*e.g.* CH_2Cl_2), but mainly cyclopropane in solvents of high dielectric constant (*e.g.* CH_3CN, Me_2SO):[12] ionization of the platinacyclobutane precedes the formation of cyclopropane. Water, which has a high dielectric constant, should favor the formation of the ionized species. However, the effect of the solvent on the reaction of fumarate with 2,2-dibromopropane is opposite to that on the reaction of platinacyclobutane.

Mechanism. We have proposed a mechanism which involves metallacyclobutane as an intermediate. The cyclopropanation of electron-deficient monosubstituted olefins needs Lewis acids or sodium iodide and zinc as promotors in most cases.[1] Both components are not necessary for the cyclopropanation of dimethyl fumarate and maleate with *gem*-dihalides catalyzed by cobalt(0)- or Ni(0)-complex. Only the cyclopropane derivative of dimethyl fumarate was obtained in the competitive reaction between dimethyl fumarate and methyl acrylate, indicating that the coordinating strength of the former is greater than that of the latter. It may be concluded that the cyclopropanation of olefins coordinated strongly to the metal center does not need promotors such as Lewis acids nor sodium iodide. We added sodium iodide to prevent reduction of olefins by the zinc bromide–zinc system.[4]

Acetonitrile is the most suitable solvent among several examined. It is required for stabilization of Co(0)- and Ni(0)-olefin complexes. Tetrahydrofuran is preferable to acetonitrile for the cyclopropanation of monosubstituted olefins[1] in which Lewis acids or sodium iodide in combination with tetrahydrofuran may promote the catalysis of the nickel complex catalyst.

Metal–carbene complexes are generated by the reaction of Co(0)- or Ni(0)-complex with *gem*-dihalides.[13] Cobalta- and nickelacyclobutanes are produced from the reaction of metal–carbene complexes with olefins in a similar manner as titana- and tungstenacyclobutanes.[14] Reductive elimination of metallacyclobutanes gives exclusively cyclopropane derivatives unless R=R′=CH_3. It is not known at present whether too many hydrogens bonded to β-carbons facilitate their splitting, or whether the metallacyclobutane is distorted due to the bulkiness of two alkyl groups to accelerate access of hydrogens of β-carbons to the active center.

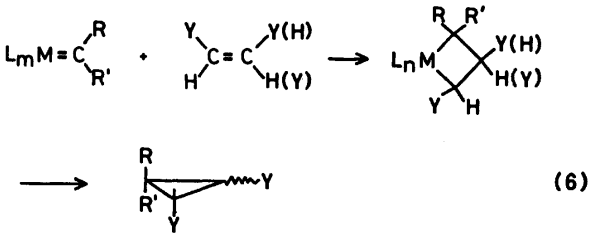

(6)

M = Co, Ni ; R, R′ = H, CH_3, C_6H_5 ; Y = CO_2CH_3 .

Experimental

All operations were done under an atmosphere of nitrogen. Chloroiodomethane was prepared by treating dichloromethane with sodium iodide in *N,N*-dimethylformamide.[15] Other chemicals were analytical grade commercial materials and used without further purification. Bis(acetonitrile)bis(diethyl fumarate)cobalt(0) was prepared from the reaction of cobalt chloride with diethyl fumarate in the presence of zinc in acetonitrile according to the method of Agnes *et al.*[16] Acetonitrilebis(dimethyl maleate)nickel(0) (**2**) was prepared according to the literature method.[6] ^{1}H NMR spectra were measured on a JEOL PM-60 spectrometer and ^{13}C NMR spectra on a JEOL FX-100 spectrometer. GLC analysis and preparative purification were performed on a Shimadzu GC-6A gas chromatograph equipped with FID and 3 mm×4 m (PEG 20M 20% on Celite 545) and 5 mm×3 m (silicon SE-30 20% on Celite 545) columns were used.

Reaction of Bis(acetonitrile)bis(diethyl fumarate)cobalt(0) with Dibromomethane. To a solution of bis(acetonitrile)bis(diethyl fumarate)cobalt(0) (1 mmol) in acetonitrile (5 ml) was added dibromomethane (2 mmol) and the reaction mixture was stirred for 7 h. Diethyl *trans*-1,2-cyclopropanedicarboxylate was obtained in a 67% yield based on cobalt.

*Reaction of **2** with Dibromomethane.* To a solution of **2** (1 mmol) in acetonitrile (10 ml) were added dimethyl maleate (3 mmol) and dibromomethane (5 mmol) and the reaction mixture was stirred for 24 h. Dimethyl *cis*-1,2-cyclopropanedicarboxylate and the *trans*-isomer were obtained in 52 and 14% yields based on nickel, respectively.

General Procedures for the Reaction of Dimethyl Fumarate or Maleate with gem*-Dihalides Catalyzed by* in Situ *Prepared Co(0)- or Ni(0)-complex and Zinc.* A 100-ml two-necked flask was charged with anhydrous cobalt chloride (1 mmol) or nickel bromide (1 mmol), sodium iodide, and zinc powder (8 mmol). Acetonitrile (10 ml) was introduced and the mixture was stirred magnetically for 20—30 min at room temperature to form the red-brown catalyst solution. *gem*-Dihalide (5 mmol) was then added and reacted at room temperature for the specified time.

The reactions between dimethyl fumarate or maleate and *gem*-dihalides are summarized in Tables 1, 2, and 3. Spectral and elemental analyses of some cyclopropane derivatives are given below.

Dimethyl c-*3-Methyl*-r-*1*, t-*2-Cyclopropanedicarboxylate*: ^{1}H NMR ($CDCl_3$) δ=1.24 (d, 3H), 1.6—2.5 (m, 3H), 3.68 (s, 6H). ^{13}C NMR ($CDCl_3$) δ=11.2 (HC–$\underline{C}H_3$), 23.8 (H$\underline{C}$–CH_3), 27.9 (*r*-1-$\underline{C}HCO_2CH_3$), 28.3 (*t*-2-$\underline{C}HCO_2CH_3$), 51.8 (*r*-1-$CO_2\underline{C}H_3$), 52.0 (*t*-2-$CO_2\underline{C}H_3$), 170.4 (*r*-1-$\underline{C}O_2CH_3$), 172.3 (*t*-2-$\underline{C}O_2CH_3$). Found: C, 55.94; H, 7.27%. Calcd for $C_8H_{12}O_4$: C, 55.80, H, 7.02%.

Dimethyl c-*3-Methyl*-r-*1*, c-*2-Cyclopropanedicarboxylate*: ^{13}C NMR ($CDCl_3$) δ=8.5 ($CH\underline{C}H_3$), 19.0 ($\underline{C}HCH_3$), 24.1 ($\underline{C}HCO_2CH_3$), 51.7 ($CO_2\underline{C}H_3$), 169.5 ($\underline{C}O_2CH_3$). Found (mixture of dimethyl *c*-3- and *t*-3-methyl-*r*-1,-*c*-2-cyclopropanedicarboxylate): C, 55.50; H, 7.10%. Calcd for $C_8H_{12}O_4$: C, 55.80; H, 7.02%.

Dimethyl t-*3-Methyl*-r-*1*, c-*2-Cyclopropanedicarboxylate*: ^{13}C NMR ($CDCl_3$) δ=16.8 ($CH\underline{C}H_3$), 20.6 ($\underline{C}HCH_3$), 29.2 ($\underline{C}HCO_2CH_3$), 52.0 ($CO_2\underline{C}H_3$), 170.2 ($\underline{C}O_2CH_3$).

Dimethyl trans-*3,3-Dimethyl-1,2-Cyclopropanedicarboxylate*: ^{1}H NMR ($CDCl_3$) δ=1.29 (s, 6H), 2.21 (s, 2H), 3.65 (s, 6H). ^{13}C NMR ($CDCl_3$) δ=20.4 (($\underline{C}H_3)_2C$), 30.4 ($(CH_3)_2\underline{C}$), 33.6 ($\underline{C}HCO_2CH_3$), 51.8 ($CO_2\underline{C}H_3$), 170.8 ($\underline{C}O_2CH_3$).

Dimethyl cis-*3,3-Dimethyl-1,2-Cyclopropanedicarboxylate*: ^{1}H NMR ($CDCl_3$) δ=1.21 (s, 3H), 1.39 (s, 3H), 1.87 (s, 2H), 3.64 (s, 6H). ^{13}C NMR ($CDCl_3$) δ=15.5 (*cis*-$\underline{C}H_3$), 26.0 (($CH_3)_2$-$\underline{C}$), 27.9 (*trans*-$\underline{C}H_3$), 31.8 ($\underline{C}HCO_2CH_3$), 51.6 ($CO_2\underline{C}H_3$), 169.4 ($\underline{C}O_2CH_3$).

Dimethyl c-*3-Phenyl*-r-*1*, t-*2-Cyclopropanedicarboxylate*: ^{1}H NMR ($CDCl_3$) δ=2.38—3.11 (m, 3H), 3.43 (s, 3H), 3.71 (s, 3H), 7.16 (s, br, 5H). ^{13}C NMR ($CDCl_3$) δ=25.8 (*cis*-$\underline{C}HCO_2CH_3$), 29.8 (*trans*-$\underline{C}HCO_2CH_3$), 32.8 ($\underline{C}HC_6H_5$), 51.8 (*cis*-$CO_2\underline{C}H_3$), 52.3 (*trans*-$CO_2\underline{C}H_3$), 168.7 (*cis*-$\underline{C}O_2CH_3$), 171.9 (*trans*-$\underline{C}O_2CH_3$). Found: C, 66.76; H, 6.15%. Calcd for $C_{13}H_{14}O_4$: C, 66.65; H, 6.02%.

Dimethyl Isopropenylsuccinate: ^{1}H NMR ($CDCl_3$) δ=1.76 (s, 3H), 2.36—2.88 (m, 3H), 3.64 (s, 3H), 3.68 (s, 3H), 4.86 (s, 2H). ^{13}C NMR ($CDCl_3$) δ=20.7 (CH_3), 35.1 (CH_2), 48.5 (CH), 51.8 ($CH_2CO_2\underline{C}H_3$), 52.2 ($CHCO_2\underline{C}H_3$), 114.3 (H_2C=), 141.3 (=$\underline{C}CH_3$), 172.1 ($CH_2\underline{C}O_2CH_3$), 172.9 ($CH\underline{C}O_2CH_3$).

The authors wish to express their thanks to Professor Kozo Tanabe of Hokkaido University for helpful discussions.

References

1) a) H. Kanai and N. Hiraki, *Chem. Lett.*, **1979**, 761; b) H. Kanai, N. Hiraki, and S. Iida, *Bull. Chem. Soc. Jpn.*, **56**, 1025 (1983).

2) a) L. L. McCoy, *J. Am. Chem. Soc.*, **82**, 6416 (1960); b) *J. Org. Chem.*, **25**, 2078 (1960); c) *J. Am. Chem. Soc.*, **84**, 2246 (1962).

3) a) T. Saegusa, K. Yonezawa, and Y. Ito, *Synth. Commun.*, **2**, 431 (1972); b) T. Saegusa, K. Yonezawa, I. Murase, T. Konoike, S. Tomita, and Y. Ito, *J. Org. Chem.*, **38**, 2319 (1973); c) Y. Ito, K. Yonezawa, and T. Saegusa, *ibid.*, **39**, 1763 (1974); d) Y. Ito, K. Yonezawa, and T. Saegusa, *ibid.*, **39**, 2769 (1974).

4) F. Toda and K. Iida, *Chem. Lett.*, **1976**, 695.

5) a) E. Legoff, *J. Org. Chem.*, **29**, 2048 (1964); b) R. D. Rieke, P. Tsu-Jung Li, T. P. Burns, and S. T. Uhm, *ibid.*, **46**, 4323 (1981).

6) F. Guerrieri and G. Salerno, *J. Organomet. Chem.*, **114**, 339 (1976).

7) M. Dubini and F. Montino, *Chim. Ind. (Milan)*, **49**, 1283 (1967).

8) a) B. Bogdanovic, B. Henc, H.-G. Karmann, H.-G. Nussel, D. Walter, and G. Wilke, *Ind. Eng. Chem.*, **62**, 34 (1970); b) B. Bogdanovic and G. Wilke, *Brennstoff-Chem.*, **49**, 323 (1968).

9) S. S. M. Ling and R. J. Puddephatt, *J. Chem. Soc., Chem. Commun.*, **1982**, 412.

10) a) T. H. Johnson and E. C. Hefty, *J. Org. Chem.*, **44**, 4896 (1979); b) T. H. Johnson and S.-S. Cheng, *J. Am. Chem. Soc.*, **101**, 5277 (1979); c) T. H. Johnson and E. C. Hefty, *J. Organomet. Chem.*, **212**, 23 (1981).

11) It can not be considered that isopropenylsuccinate is produced from free carbene insertion into fumarate and maleate because there is no other olefinic product than isopropenylsuccinate.

12) D. C. L. Perkins, R. J. Puddephatt, and C. F. H. Tipper, *J. Organomet. Chem.*, **186**, 419 (1980).

13) S. Takahashi, Y. Suzuki, K. Sonogashira, and H. Hagihara, *Chem. Lett.*, **1976**, 515.

14) a) P. G. Gassman and T. H. Johnson, *J. Am. Chem. Soc.*, **98**, 6057 (1976); b) F. N. Tebbe, G. W. Parshall, and G. S. Reddy, *ibid.*, **100**, 3611 (1978).

15) S. Miyano and H. Hashimoto, *Bull. Chem. Soc. Jpn.*, **44**, 2864 (1971).

16) G. Agnes, I. W. Bassi, C. Benedicento, R. Intrito, M. Caleaterra, and C. Santini, *J. Organomet. Chem.*, **129**, 401 (1977).

Association of Chlorophyll with Amides on Plasticized Polyethylene Particles. II. The Isomeric *N*-Pyridylmyristamides

Yoshihumi Kusumoto,*,† Gilbert R. Seely, and Velu Senthilathipan
Charles F. Kettering Research Laboratory, Yellow Springs, Ohio 45387 U.S.A.
(Received October 12, 1982)

When chlorophyll, together with certain other amphiphilic substances, is adsorbed to particles of polyethylene plasticized by incorporation of tetradecane, it is maintained in monomeric or oligomeric forms with characteristic absorption and fluorescence spectra. The present work describes the properties of chlorophyll a on such particles in the presence of the three isomeric *N*-pyridylmyristamides, and of the similarly shaped but not basic compound myristanilide, in an effort to ascertain the structural factors governing associations of these species. Absorption and fluorescence spectra at room temperature are resolved into minimal sets of Gaussian components, and relations between the component sets are proposed. The positions of the component bands and their relative abundance are characteristic of the amide used. The 3- and 4-pyridyl isomers bind more strongly to chlorophyll, probably by ligation of the pyridine nitrogen to Mg of the pigment. The 2-pyridyl isomer and myristanilide bind more weakly, probably through the amide carbonyl group. The association of chlorophyll into species with characteristic absorption and fluorescence bands is promoted more strongly by the 3- and 4-isomers than by the 2-isomer and myristanilide, and probably involves hydrogen bonding to chlorophyll carbonyl groups. A possible manner of association of chlorophyll in the presence of *N,N*-dimethylmyristamide is also presented. By way of comparison, chlorophyll adsorbed with *N*-dodecylpyridinium bromide, which lacks a nucleophilic function, is mainly in the microcrystalline hydrate form absorbing near 740 nm.

Preliminary accounts of this subject have reported the association of chlorophyll a with a number of amphiphilic amides when both are adsorbed to polyethylene particles swollen by absorption of a hydrocarbon diluent such as undecane.[1] The previous paper in this series (I) presented in some detail the evidence for interaction of chlorophyll with *N,N*-dimethylmyristamide (DMMA) adsorbed to swollen polyethylene.[2a] In the presence of sufficient DMMA, chlorophyll is maintained in monomeric and associated species with characteristic absorption and fluorescence spectral bands. The associated as well as the monomeric species were apparently capable of strong fluorescence even at chlorophyll densities corresponding to monolayer coverage, and photochemical activity was demonstrated.

We have also examined the interaction of chlorophyll with the closely related amphiphile *N*-methylmyristamide, and found quite different sorts of chlorophyll association.[2b] In this paper we report the association of chlorophyll with certain other *N*-monosubstituted amphiphilic amides, specifically the three isomeric *N*-pyridylmyristamides (NPMA's). These substances were chosen principally for two reasons. First, since the pyridine nitrogen function, like the amide carbonyl, is known to bind to the Mg of chlorophyll, we might find evidence for association of chlorophyll through either or both functions, depending on the isomer. Second, the pyridine chromophore provides a convenient means of accurately estimating the amphiphile concentration in the particle preparations, which is lacking for entirely aliphatic amides. We further include for comparison preparations with myristanilide (MAn), which resembles the NPMA's in shape but lacks pyridine nitrogen, and with *N*-dodecylpyridinium bromide (DPB), a surfactant made from pyridine which has no Lewis base function capable of binding to chlorophyll.

† Present address: Chemical Institute, College of Liberal Arts, Kagoshima University, Korimoto, Kagoshima 890.

Experimental

Materials. The isomeric *N*-pyridylmyristamides were prepared by reaction of the corresponding aminopyridines with myristoyl chloride in acetone or *N,N*-dimethylformamide, similarly to the procedure of Deady and Stillman,[3] and were purified by reprecipitation from methanol–aqueous ammonia. Myristanilide was prepared by reaction of myristoyl chloride with aniline in toluene containing triethylamine, and recrystallized finally from ethanol. *N*-Dodecylpyridinium bromide was prepared by refluxing pyridine with 1-bromododecane in toluene.

N-*(2-Pyridyl)myristamide*: IR (KBr): 3355 (N–H), 1698 (amide I), 1538 (amide II), 1590, 1447, and 778 cm^{-1} (pyridyl). UV_{max} (1-propanol): 276 (ε, 5670) and 236 nm (10360). Found: C, 74.70; H, 10.93; N, 8.84%. Calcd for $C_{19}H_{32}N_2O$: C, 74.95; H, 10.59; N, 9.20%.

N-*(3-Pyridyl)myristamide*: Mp 80.5—82 °C. IR (KBr): 3331, 1676, 1543, 1597, 1423, 802, and 707 cm^{-1}. UV_{max} (1-propanol): 279 (4400) and 241 nm (16450). Found: C, 75.48; H, 11.40; N, 9.07%.

N-*(4-Pyridyl)myristamide*: Mp 75—77 °C. IR (KBr): 3428, 1686, 1534, 1615, 1427, and 834 cm^{-1}. UV_{max} (1-propanol): 246.5 nm (17790). Found: C, 73.28; H, 10.79; N, 8.62%.

Myristanilide: Mp 84.5—85 °C. IR: 3312, 1670, 1549 (amide), and 1612, 1454, 759, 696 (phenyl). UV_{max} (1-propanol): 243 nm (16310).

N-*Dodecylpyridinium Bromide*: IR: 1650, 1497, 782, and 691 cm^{-1} (pyridinium). UV_{max}: 260 nm (4660).

Methods. The polyethylene particles swollen with tetradecane were prepared as described.[2] Tetradecane was used as diluent instead of undecane, as in (I), primarily because of its lower solubility in aqueous methanol. The swollen particles contained about 75% tetradecane. The adsorption of chlorophyll and amide from aqueous methanol was performed as described in (I), but because of their low solubility in 60% methanol, the amides were present only in the initial 90% methanol solution, along with chlorophyll. Chlorophyll and amphiphile contents of the recovered particles were estimated spectrophotometrically on a 1-propanol extract of a sample of particles. The uptake of amide by the particles is linear

with concentration at low values thereof, and their concentrations on the particles, $[NPMA]_p$, are related to their concentrations in 75% methanol solution ([NPMA]) by Eqs. 1—4.

$$[4\text{-NPMA}]_p/\mu\text{mol g}^{-1} = 0.84([4\text{-NPMA}]/\text{mM}),^{\dagger\dagger} \quad (1)$$

$$[3\text{-NPMA}]_p = 0.93[3\text{-NPMA}], \quad (2)$$

$$[2\text{-NPMA}]_p = 11.9[2\text{-NPMA}], \quad (3)$$

$$[\text{MAn}]_p = 48[\text{MAn}]. \quad (4)$$

Above 2.5 mM [3-NPMA] and about 1.5 mM [2-NPMA] or [MAn], the amount of amide bound to the particles exceeded that predicted by the equations, because of precipitation out of 75% methanol or multilayer adsorption. The proportionality constants suggest that 3-NPMA and 4-NPMA are adsorbed only to the particle surface, while MAn and 2-NPMA are dissolved in the particles to some extent. The solubility of 2-NPMA is perhaps owing to the formation of a cylic dimer, like that of 2-aminopyridine in CCl_4 solution.[4]

Absorption Spectroscopy. Absorption spectra were recorded on a Perkin-Elmer Hitachi 557 spectrophotometer, of mixtures not exceeding 2% (wt) of green particles with a densely scattering white paste. At these concentrations, the absorbance is proportional to the relative absorptivity, and the expected optical path enhancement by multiple scattering is observed.[5]

The pastes usually consist of three components: (1) a fluid, normally a non-solvent for chlorophyll such as water or glycerol; (2) a thickener, often a polysaccharide, to keep the particles in suspension; (3) an inert scattering material such as cellulose (Sigmacell, 20 μm particles). Two pastes that have proved useful in absorption spectroscopy are water (43.3%), Ficoll 400 (Pharmacia) (28.9%), cellulose (27.8%), and water (25.8%), sucrose (51.7%), cellulose (22.5%). For fluorescence spectroscopy a paste (CGW) of Carbowax PEG-1000 : glycerol : water (10 : 11 : 1 in wt/v/v) was used, so that the sample could be cooled to 77 K. A paste (OCC) which extracts chlorophyll from the particles was compounded out of 1-octanol (42.4%), Carbowax PEG 1500 (18.3%) and cellulose (39.3%). For recording spectra, the pastes were spread in an even layer 0.10 cm deep in a demountable silica cell. Second derivative absorption spectra were also recorded.

Fluorescence Spectroscopy. Most fluorescence spectra discussed here were recorded from the front surface of a thin layer of particles mixed with CGW paste, first at room temperature then after quickly cooling with liquid nitrogen.

Exciting light was provided by a Sylvania 250-W Q/CL/DC tungsten-halogen lamp and dispersed by a Beckman DU monochromator. It was focused on the sample surface at an angle of about 15° to the normal. The fluorescence was dispersed by a Spex 0.5 m Czerny-Turner monochromator, with 64×64 mm grating, 1200 grooves/mm, blazed for 750nm, and turned by a Minidrive stepping motor. The rated dispersion was 1.6 nm/mm, and it was usually operated with 1 mm slits.

The fluorescence was detected with a Hamamatsu R666 GaAs photomultiplier at 1000 V; the signal was amplified by a Keithley 610 B Electrometer and recorded on a Kipp and Zonen BD 12 Intergrating Recorder. The apparatus was calibrated for variation of sensitivity with wavelength by means of a tungsten lamp operated at different color temperatures.

Analysis of Spectra. Absorption spectra, and fluorescence spectra corrected for variation of sensitivity with wavelength, were resolved into Gaussian component bands with the aid of an IBM 5100 portable computer. Two programs were used. For absorption spectra, where the band positions (λ) are close together and there was little direct evidence for the value of the component bandwidths (B) at half peak height, all trial bandwidths were assumed to have the same value. This program found the trial band heights and the value of B which simultaneously fitted the spectrum at the N band positions, and minimized the sum of deviations at $N+1$ other points on the spectrum. The calculated spectrum was compared with the observed at about 30 points spaced 2 nm apart, and trial band positions were adjusted to remove any systematic deviations. If no further adjustment could return a satisfactory fit, one more band was added and the process was repeated.

For all fluorescence spectra and some absorption spectra the assumption of identical B was plainly invalid. The program in these cases assumed trial values of λ and B for each band, and calculated band heights to match the observed spectrum at the N band positions. Band positions and widths were varied individually, and bands added if necessary, until acceptable fit was obtained to the observed spectrum.

So far as possible, only bands identified as peaks or shoulders in the absorbance or fluorescence spectrum, or as troughs or shoulders in the second derivative spectrum, were included as trial bands in the analysis. A minimal number of other components were introduced only when resolution based on identified bands was unsatisfactory. Furthermore, the bandwidth of components located at $\lambda<720$ nm was not allowed to exceed 24 nm, approximately the maximum value observed under any circumstances for monomeric chlorophyll.[6]

An inherent limit to the precision of spectral reconstruction is the non-Gaussian shape of the chlorophyll band itself. However, the absorption spectrum of chlorophyll in acetone could be fitted by one Gaussian ($\lambda=661.7$ nm, $B=20.6$ nm) within 1% of peak height from 652 to 680 nm, and within 2% to 710 nm. Similar precision was accepted as evidence of satisfactory fit for the particle sample spectra. As a further test of acceptability, a single set of bands (λ, B within ±1 nm) should fit the spectra of all particles prepared with chlorophyll and a given surfactant. To a surprising extent these criteria have been met in the systems under discussion. In practice, the reconstructed spectrum proved sensitive to variations of $\pm(0.5—1)$nm in component band position and width, so that we have reasonable confidence in our representations.

Results

Chl in OCC. When green particles are mixed with this paste, chlorophyll is dissolved from them by the 1-octanol component. Absorption and fluorescence spectra (Fig. 1) are therefore of monomeric chlorophyll in a highly scattering solution and serve as a standard for comparison with chlorophyll adsorbed to particles in a highly scattering suspension. The absorption band can be represented well enough by one Gaussian component at 665.8 nm, with bandwidth $B=24$ nm. The fluorescence at room temperature is well represented by three components, at 680 nm ($B=23$ nm) 57.3%, 702 nm (20 nm) 9.0%, and 732 nm (40 nm) 33.8%, where the percentages represent the fraction of the integrated fluorescence intensity contributed by the component. The last two components are separated from the first by 450 and 1040 cm^{-1}, which perhaps correspond to pyrrole ring deformation and pulsation frequencies. At 77 K the same three components are present, with slightly altered contributions: 680(20)

†† 1 M=1 mol dm^{-3} and 1 mM=1×10^{-3} mol dm^{-3} in this paper.

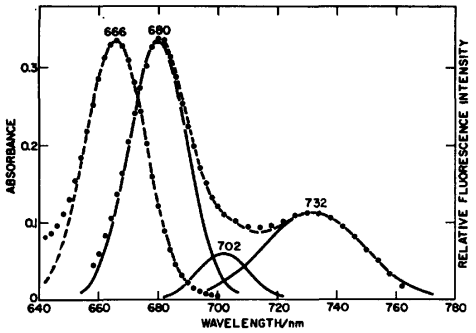

Fig. 1. Absorption and fluorescence spectra (the latter normalized at the 680-nm peak to match the absorption band) of chlorophyll-containing particles ($[Chl]_p$= 1.046 μmol g^{-1}) suspended in a paste of 1-octanol (42.4%), Carbowax 1500 (18.3%), and cellulose (39.3%) (OCC), in which chlorophyll is soluble. The particles were prepared with a concentration of 3-NPMA so low (0.625×10^{-3} M) that most of the chlorophyll was in the form of the microcrystalline hydrate absorbing around 740 nm (see Fig. 2). The disappearance of that band shows that the chlorophyll has dissolved in the OCC paste. For the absorption spectrum, 0.0109 g of green particles was blended with 0.721 g of OCC paste; for the fluorescence spectrum, 0.1235 g of particles with 0.300 g OCC paste. The red band of the absorption spectrum is represented adequately by one Gaussian component (dashed curve), the fluorescence spectrum by three. The fluorescence components are shown as solid traces, their sum as a dashed trace. Observed absorption and fluorescence intensities, the latter corrected for variation of instrumental sensitivity with wavelength, are plotted as open circles.

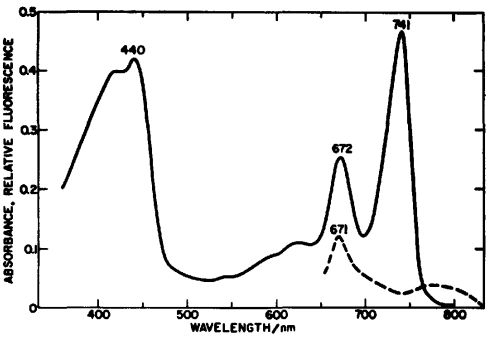

Fig. 2. Visible absorption and fluorescence spectra of particles containing chlorophyll (1.36 μmol g^{-1}) and DPB (2.66 μmol g^{-1}), the latter adsorbed from a 5 mM solution, initial concentration. For absorption spectral measurement, 0.0141 g of yellow-green particles was mixed with 0.578 g of a paste of Ficoll (39%), cellulose (Sigmacell, 15%), and water (46%). The paste scattering background has been subtracted. For fluorescence (dashed trace), 0.0585 g of particles was mixed with 0.255 g of the paste, and excited at 616 nm. There is indication of reabsorption by the strong 741 nm absorption band. The weak fluorescence was not corrected for variation of apparatus sensitivity to wavelength, because of uncertainty in the location of the baseline.

48.1%, 702(20) 9.4%, and 734(40) 42.6%.

Although there is little reason to doubt that chlorophyll is monomeric in this system, the Stokes shift (14 nm), and the 732 nm fluorescence vibronic component, are large in comparison with those of other spectra we have recorded, *i.e.*, chlorophyll in acetone, or in undecane solution with DMMA.[2] The absorption bandwidth (24 nm) is larger than twice the half-bandwidths in any of the solvents reported previously by Seely and Jensen.[6] The broadening and red-shifting are perhaps consequences of strong hydrogen-bonding between octanol and chlorophyll carbonyls in the ground and excited states.[7] The mirror-image relation between absorption and fluorescence bands is obvious, which incidentally demonstrates that reabsorption of fluorescence is not a domineering phenomenon in our systems.

N-*Dodecylpyridinium Bromide.* This surfactant is not basic and therefore does not bind to functional groups of chlorophyll. In sharp contrast to the foregoing spectra, the spectrum of chlorophyll (1.359 μmol g^{-1}) with DPB (2.66 μmol g^{-1}, from 5 mM DPB in solution initially) in Fig. 2 show mainly the microcrystalline hydrate form of the pigment (741 nm). The same form appears when chlorophyll is adsorbed to the particles in the absence of an amphiphile[2] and in many other systems where water is present.[8] The fluorescence is weak; the most prominent band in its spectrum (671 nm) probably corresponds to a small amount of monomeric chlorophyll absorbing around 662 nm. No attempt was made to resolve these spectra into components.

The presence of DPB does not prevent chlorophyll from associating with 3-NPMA on the same particle. Particles prepared with [DPB] and [3-NPMA], both 10 mM initially, and having the composition $[Chl]_p$= 1.212, $[DPB]_p$=1.55, and $[3\text{-NPMA}]_p$=5.32 μmol g^{-1}, had the same absorption and fluorescence spectra as chlorophyll in the presence of 3-NPMA alone (see below).

N-*(2-Pyridyl)myristamide.* As increasing amounts of an amphiphile such as 2-NPMA are present in solution to be adsorbed along with chlorophyll, the amount of chlorophyll in the 741 nm hydrated form decreases, and the amount in forms absorbing at shorter wavelengths increases. At sufficiently high amphiphile concentration, the 741 nm form of chlorophyll disappears altogether from the green particles. In Figs. 3—5, spectra of adsorbed chlorophyll with the three isomeric NPMA's are compared at $[Chl]_p$ around 1 μmol g^{-1}, and at a high enough NPMA concentration to eliminate the 741 nm species. In the absorption spectra, only the longest-wave, "red" band is shown and analysed; the remainder of the visible spectrum superficially resembles that of normal monomeric chlorophyll in a non-hydroxylic solvent. Differences seen at other chlorophyll and NPMA concentrations will be noted. Second derivative spectra generally show a sharper and more complex band system throughout the visible than is seen in the spectrum of chlorophyll in acetone, for example.

Spectra with 2-NPMA appear the easiest to interpret. At high amphiphile concentration the red absorption

band is resolved into two components, both relatively broad (Fig. 3a). The major one (666 nm) falls in the wavelength range expected for a monomeric chlorophyll species, but the minor one (684 nm) must represent some associated species, probably dimeric in chlorophyll. The fluorescence spectrum (Fig. 3b) is resolved into five components. Comparison with Fig. 1 suggests that the 693 nm component represents fluorescence from the 684 nm species in the absorption spectrum; the 1132 cm^{-1} interval between the 693 and 752 nm components, and their relative strength, suggest that the 752 nm component is a vibrational satellite of the other. Apart from these two bands, the fluorescence spectrum resembles that of monomeric chlorophyll in Fig. 1 (with a $\approx$6 nm blue shift), but the 726.5 nm component is distinctly stronger in the 2-NPMA spectrum.

At lower chlorophyll concentration ($[Chl]_p$=0.23 μmol g^{-1}), the spectra were quite similar to the foregoing,

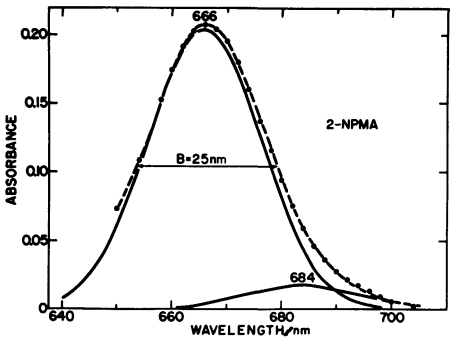

Fig. 3a. Absorption spectrum of particles containing chlorophyll (1.029 μmol g^{-1}) and 2-NPMA (68 μmol g^{-1}) in Ficoll–cellulose paste (0.0063 g green particles mixed with 0.603 g paste). The red band is most simply represented as the sum of two Gaussian components (solid traces), both 24 nm in bandwidth. Observed absorbances are plotted as open circles.

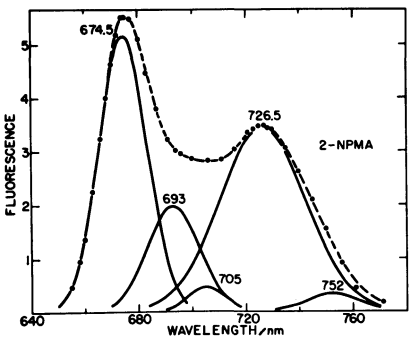

Fig. 3b. Fluorescence spectrum at room temperature of particles of Fig. 3a., 0.0794 g mixed with 0.191 g of CGW paste, under excitation at 600 nm. The spectrum is resolved into five components (solid traces): 674.5 nm (B=21 nm) 36.1%, 693(23) 15.2%, 705(16) 2.4%, 726.5(38) 43.7%, and 752(24) 2.5%. The sum of these is represented as a dashed trace, and observed fluorescence intensities are plotted as open circles. Compared to Fig. 1, there is more evidence of emission in longer-wavelength bands, indicating the presence of associated chlorophyll species.

but the monomer (674.5 nm) fluorescence component was greater (47.4%), and the 693 and 726 nm component contributions were smaller.

At 2-NPMA concentrations of 28 μmol g^{-1} or less, some of the chlorophyll remains in the 741 nm form. Now, a third component at 673.5 nm must be included to resolve the red band; *e.g.*, for $[Chl]_p$=1.10 and $[2\text{-NPMA}]_p$=28 μmol g^{-1}, the band was resolved into components at 666 nm (B=24 nm) 68.5%, 673.5(22) 29.2%, and 684(20) 2.3%. The fluorescence spectrum was not much different from that of Fig. 3b, and contained no component clearly corresponding to the 673.5 nm absorption component. This component may therefore represent the same species as the 672 nm band in Fig. 2. At 77 K the monomer fluorescence band at 674 nm was suppressed and replaced by a band in the 683—687 nm region. This band may reflect the 673.5 nm absorption component, or it may arise from a species formed on cooling the particles.

Myristanilide. This amphiphile resembles the NPMA's in shape but lacks the pyridine base function. Even more than 2-NPMA, it is soluble in the plasticized polyethylene particles and a fairly high concentration is needed to suppress the 741 nm chlorophyll species. Not many preparations have been examined with this amphiphile, but those that have show relatively simple absorption and fluorescence spectra, resembling those with 2-NPMA. The red absorption band of a preparation with $[Chl]_p$=0.974 and $[MAn]_p$=66.6 μmol g^{-1} in Ficoll–glycerol–cellulose paste is simple, but too broad (29 nm) to be represented by one Gaussian with $\leq$24 nm bandwidth. It was resolved satisfactorily into three components, at 658 nm (19.6%), 671 (64.7%), and 680.5 (15.7%), all with B=24 nm. However, the band is rather smooth and there are few clues to guide the selection of trial component wavelengths. The shape of the second derivative suggests that there may be four components in the red band region, and resolution into 655 nm (11.5%), 665 (34.8%), 674 (37.5%), and 682.5 (16.2%), all with B=20 nm, was also satisfactory. The fluorescence spectrum of the same preparation in CGW paste was resolved into four components, at 676 nm (B=24 nm) 52.1%, 697.5(20) 9.4%, 723.5(40) 33.3%, and 765(32) 5.2%. Except for the last component, the spectrum closely resembles that of monomeric chlorophyll in OCC, but displaced a few nm to the blue. At 77 K, the leading fluorescence band appears at 685 nm.

N-*(4-Pyridyl)myristamide.* The absorption spectrum resembles that with 2-NPMA but the red band, now at 668 nm, is broader. Two of three preparations showed a distinct shoulder in the second derivative spectrum around 684 nm, identifying a component there. The red band could not be resolved into two or even three bands of acceptable bandwidth as was done with the 2-NPMA preparations; a satisfactory resolution into four principal bands and a fifth, small band at 697.5 nm is presented in Fig. 4a. It was necessary to include a component (656 nm) at a shorter wavelength than the presumed monomer component band (666 nm), to represent the broadened short-wave side of the absorption band. The spectrum of a preparation with $[Chl]_p$=

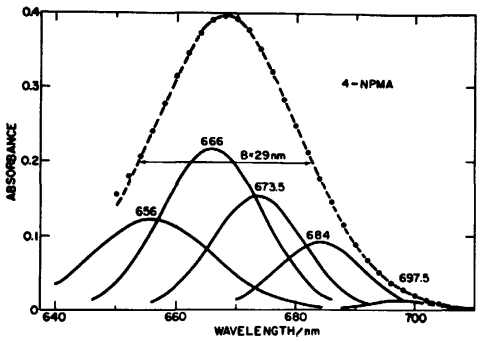

Fig. 4a. Absorption of particles containing chlorophyll (1.142 μmol g^{-1}) and 4-NPMA (4.18 μmol g^{-1}), 0.0082 g of green particles mixed with 0.608 g of Ficoll-cellulose paste. The broad red band is resolved into five components (solid traces): 656 nm (B=24 nm) 24.8%, 666(20) 37.0%, 673.5(18) 23.6%, 684(17) 13.2%, and 697.5(13) 1.4%. Their sum is shown as a dashed line, and observed absorbances are plotted as open circles.

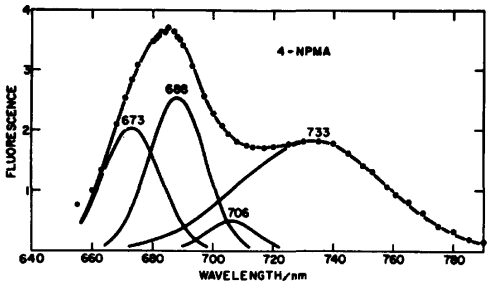

Fig. 4b. Fluorescence spectrum at room temperature of the particles of Fig. 4a, 0.0504 g mixed with 0.203 g of CGW paste, and excited at 600 nm. The fluorescence is resolved into four components (solid traces): 673 nm (B=23 nm) 21.4%, 688(22) 25.7%, 706(20) 4.6%, and 733(58) 48.3%. Their sum is shown as a dashed trace, and observed intensities as open circles. On cooling to 77 K, the strongest band is at 688 nm.

2.40 μmol g^{-1} and $[4\text{-NPMA}]_p$=3.50 μmol g^{-1} was similarly resolved, but the composition (656 nm (24 nm) 32.4%, 665.5(20) 24.2%, 673.5(18) 25.8%, 685(17) 15.3%, 697.5(13) 2.4%) indicates less monomeric component and more of all the others.

The fluorescence spectra of these preparations are markedly broadened and red-shifted, even at room temperature, compared to those with 2-NPMA (Fig. 3b). A resolution into four bands is presented in Fig. 4b. In

TABLE 1. ANALYSIS OF ABSORPTION AND FLUORESCENCE SPECTRA OF CHLOROPHYLL a WITH 3-NPMA ON POLYETHYLENE–TETRADECANE PARTICLES

$[Chl]_p$[a] μmol g^{-1}	$[3\text{-NPMA}]_p$ μmol g^{-1}	$\frac{[3\text{-NPMA}]_p}{[Chl]_p}$	λ/nm (B/nm)	%	λ/nm (B/nm)	%	λ/nm (B/nm)	%	λ/nm (B/nm)	%	λ/nm (B/nm)	%	λ/nm (B/nm)	%
Absorption spectra														
0.146	1.09	7.47	653 (18)	22.2	664.5 (16)	36.3	674 (16)	29.4	683 (14)	8.9	692 (13)	2.9	703 (8)	0.3
0.252	1.31	5.19	653 (18)	21.0	664.5 (16)	37.2	674 (16)	29.5	683 (14)	9.1	692 (13)	3.0	703 (8)	0.2
0.875	>8	>9	653 (18)	19.3	664.5 (16)	36.0	674 (16)	29.7	682.5 (14)	10.4	692 (13)	4.0	703 (8)	0.6
0.983	2.25	2.29	653 (18)	18.5	664.5 (16)	34.7	674 (16)	29.7	682.5 (14)	12.5	691.5 (11)	3.8	703 (8)	0.7
1.47	2.84	1.93	653 (18)	19.7	664.5 (16)	31.3	674 (16)	31.1	682.5 (14)	13.6	692 (11)	3.9	703 (8)	0.4
2.245	5.93	2.64	653 (18)	18.8	664.5 (16)	28.6	674 (16)	30.8	682.5 (14)	15.0	691.5 (13)	6.2	703 (8)	0.7
2.38	7.14	3.00	653 (18)	18.8	664.5 (16)	28.1	674 (16)	30.6	682.5 (14)	15.0	691.5 (13)	6.6	703 (8)	0.9
Fluorescence spectra														
0.146	1.09	7.47	670.7 (19)	46.9	687.5 (16)	11.3	700.5 (16)	8.7	710 (10)	0.9	724 (30)	26.1	748 (24)	6.1
0.405	6.60	16.3	670.5 (17)	45.3	686 (15)	13.6	700 (18)	7.9	—		727 (40)	33.2	b)	
0.875	>8	>9	671 (21)	34.3	688 (15)	11.9	700.5 (16)	8.4	710 (10)	0.3	724.5 (38)	39.9	756 (30)	5.2
2.245	5.93	2.64	671 (18)	28.5	688 (15)	20.4	700.5 (16)	10.8	711 (10)	0.4	722.5 (36)	33.6	766 (26)	6.2
2.38	7.14	3.00	670.5 (17)	32.0	687.5 (13)	14.8	699.5 (16)	13.5	711 (10)	0.5	722 (34)	39.2	b)	

a) The columns list the chlorophyll and 3-NPMA contents of the particles, the ratio of these quantities, and data for the component bands into which each spectrum was analyzed. These data are the peak wavelength (λ) and bandwidth (B) at half peak height, and the percent of the total integrated absorption or fluorescence occupied by the component band. Sometimes a small component at 741nm was present in the absorption spectrum; this was omitted from the analysis. b) A small component around 760 nm was omitted from the calculation because of excessively noisy trace in this region.

the red region, the component at 688 nm is stronger than the presumed monomer component at 673 nm. The broad band centered at 733 nm is probably complex, and contains vibrational satellites of the 673 and 688 nm bands, but appears too strong to be accounted for entirely this way.

On cooling the sample of Fig. 4b to 77 K, the 673 nm fluorescence is suppressed and the 688 nm component remains as the leading band in the spectrum. In the more concentrated sample with $[Chl]_p=2.40$ μmol g^{-1}, the leading band peak at 77 K is at 691 nm.

N-*(3-Pyridyl)myristamide.* Spectra with this isomer were the most complex of the three. A total of 15 preparations were examined ranging in chlorophyll content from $[Chl]_p=0.146$ to 2.38 μmol g^{-1}, and in initial 3-NPMA concentration (in 90% methanol) from 0.625 to 20 mM. Above 10 mM initial concentration the solubility limit of 3-NPMA in 75% methanol was exceeded, and crystals of the amide were to some extent collected with the particles, a circumstance that seems to have had no effect whatever on the visible spectrum of adsorbed chlorophyll. The red band is broadened, as it is in spectra with 4-NPMA, and the peak position varies with $[Chl]_p$ in the range 665—670 nm. The second derivative spectra were rather complex. Especially in relatively concentrated suspensions most preparations showed a trough or shoulder near 684 nm; several of these, particularly those with a low $[3\text{-NPMA}]_p/[Chl]_p$ ratio, also showed a sharp trough near 692 nm. Only when the initial 3-NPMA concentration was less than 2.5 mM, or $[3\text{-NPMA}]_p/[Chl]_p<2$, was there a significant amount of the 741 nm chlorophyll species in the particles.

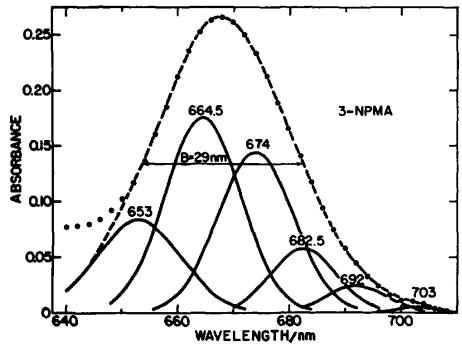

Fig. 5a. Absorption spectrum of particles containing chlorophyll (0.875 μmol g^{-1}) and at least 8 μmol g^{-1} 3-NPMA (see Table 1), 0.0085 g mixed with 0.577 g sucrose–cellulose paste. The broad red band is resolved into six components: 653 nm ($B=18$ nm) 19.3%, 664.5 (16) 36.0%, 674(16) 29.7%, 682.5(14) 10.4%, 692(13) 4.0%, and 703(8) 0.6%. The last three components are identified in numerous second derivative spectra, but the small 703 nm component may belong to the paste background. The sum of the components is shown as a dashed trace, and observed absorbances as open circles.

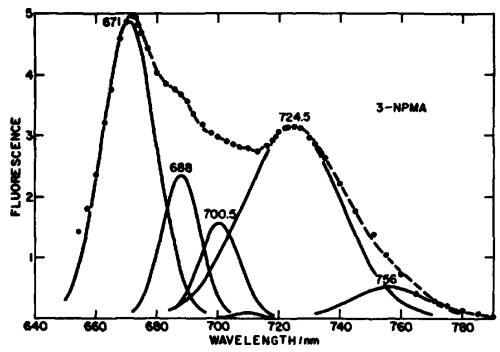

Fig. 5b. Fluorescence spectrum at room temperature of the particles of Fig. 5a, mixed with CGW paste, and excited at 600 nm. The spectrum is resolved into six components (solid traces): 671 nm ($B=21$ nm) 34.3%, 688(15) 11.9%, 700.5(16) 8.4%, 710(10) 0.3%, 724.5 (38) 39.0%, and 756(30) 5.2%. Their sum is shown as a dashed trace, and observed intensities as open circles. For fluorescence resolutions at other chlorophyll and 3-NPMA concentrations, see Table 1.

Acceptable resolution of absorption spectra was obtained with six components of almost invariable position and bandwidth at 653, 664.5, 674, 682.5, 692, and 703 nm. The 682.5 and 692 nm components were located approximately by second derivative spectroscopy, as just mentioned. The first three components were required to represent the broadening of the main part of the red band, as in the resolution of spectra with 4-NPMA. The 703 nm component is always small and may belong to the paste background. Results for several of the samples are compiled in Table 1, and one of the resolutions is illustrated in Fig. 5a. The resolution is really rather similar over the concentration ranges covered. However, the 682.5 and 692 nm component contributions increase by a factor of about 2 as $[Chl]_p$ increases, largely at the expense of the presumed monomeric component at 664.5 nm.

Fluorescence spectra were consistently resolved into six bands, near 671, 688, 700, 710, and 724 nm, and one in the range 748—766 nm. The 710 nm component is insignificant. Some resolutions are compiled in Table 1, and the one corresponding to the absorption spectrum of Fig. 5a is shown in Fig. 5b. The strongest fluorescence component at low $[Chl]_p$ is the 671 nm band, which evidently belongs to monomeric chlorophyll. The 688 nm component, which appears as a shoulder in Fig. 5b, appears as a peak in the $[Chl]_p=2.245$ μmol g^{-1} preparation, higher than the 671 nm peak and clearly set apart from it. The 700 and 724 nm bands also tend to increase somewhat with $[Chl]_p$, at the expense of monomer fluorescence.

On quickly cooling the preparation with smallest $[Chl]_p$ to 77 K, the main fluorescence band peak appeared at 685 nm; in the other preparations, the band appeared in the range 693—700 nm, generally near 695 nm.

Discussion

It has thus been possible to resolve both the absorption and fluorescence spectra of adsorbed chlorophyll into minimal, consistent sets of Gaussian components characteristic of the amphiphile adsorbed with it. The next step in comparison of amphiphiles is to determine, if possible, correspondences between absorption and fluorescence components (Table 2). This process is

TABLE 2. CORRELATION OF ABSORPTION AND FLUORESCENCE SPECTRA OF CHLOROPHYLL a ADSORBED TO POLYETHYLENE–TETRADECANE PARTICLES WITH VARIOUS AMIDE-CONTAINING AMPHIPHILES

Amphiphile[a]	Absorption components[b]			Fluorescence[c] by Eq. 5	Fluorescence components[b]			
	λ/nm	(*B*/nm)	%[d]	λ/nm	λ/nm	(*B*/nm)		%[d]
OCC	665.8	(24)	100	677	680	(23)		57.3
					702	(20)		8.9
					732	(40)		33.8
2-NPMA	666	(24)	92.5[e]	677	674.5	(21)		36.1
	673.5		0	685 ?	683—7		(77K)	
	684	(24)	7.5	695	693	(23)		15.2
					705	(16)		2.4
					726.5	(38)		43.7
					752	(24)		2.5
MAn	655	(20)	11.5[f]					
	665	(20)	34.8	673	676	(24)		52.1
	674	(20)	37.5	682 ?	686		(77K)	
	682.5	(20)	16.2	690	697.5	(20)		9.4
					723.5	(40)		33.3
					765	(32)		5.2
4-NPMA	656	(24)	24.8					
	666	(20)	37.0	674	673	(23)		21.4
	673.5	(18)	23.6	680				
	684	(17)	13.2	690	688	(22)		25.7
	697.5	(13)	1.4	701	706	(20)		4.6
					733	(58)		48.3
3-NPMA	653	(18)	19.3					
	664.5	(16)	36.0	669.5	671	(21)		34.3
	674	(16)	29.7	679				
	682.5	(14)	10.4	686.5	688	(15)		11.9
	692	(13)	4.0	694.5	695		(77K)	
	703	(8)	0.6		700.5	(16)		8.4
					710	(10)		0.3
					724.5	(38)		39.9
					756	(30)		5.2
DMMA[g]	661.5	(20)	43.9	669.5	670			
	674	(20)	37.9	682	681			
	683	(20)	1.4	—				
	689	(20)	16.8	697	695—700		(77K)	
					705		(77K)	
					725			

a) Abbreviations: OCC: Chlorophyll particles mixed with 1-octanol–Carbowax–cellulose paste; MAn: myristanilide; NPMA: *N*-pyridylmyristamide; DMMA: *N*,*N*-dimethylmyristamide. b) Absorption spectra of Figs. 1, 3a—5a and of MAn in a paste of 6 : 10 : 3 Ficoll : glycerol : cellulose. All fluorescence spectra were recorded on samples in CGW paste. The composition of the paste has little effect on the spectral properties of the particles. Components marked (77K) have been identified with certainty only at a low temperature usually as the leading band of the fluorescence spectra. c) Calculated from the Stepanov theory of spectral band shape.[9,10] Dashed lines connect calculated band positions with most probably corresponding observed positions. d) Percentages given for typical spectra of Figs. 1, 3—5 or as noted; $[Chl]_p$ *ca.* 1 μmol g^{-1} and 741 nm species absent. e) An alternative analysis gave: 656 nm (17.2%), 665.5 (53.9%), 674.5 (24.3%), 690 (4.6%), all with B=20 nm. This analysis accommodates the presence of a 673.5 nm band at low $[2\text{-NPMA}]_p$ and perhaps the strength of the fluorescence band at 726.5 nm (see Discussion). f) A resolution into three bands: 658 nm (19.6%), 671 (64.7%), and 680.5 (15.7%) all with B=24 nm gave an acceptable fit but does not correlate well with the fluorescence spectrum. g) Spectra recorded and analyzed as reported in (I); a slightly better resolution might have been achieved with an additional band near 653 nm. The 683 nm absorption component is sensitive to the value of B chosen and is not present with certainty within the accuracy of the analysis. The 705 nm component in fluorescence, and at 77 K, which is strong only in preparations with low $[DMMA]_p/[Chl]_p$ is unique to this amphiphile.

assisted by a relation derived from Stepanov theory between the frequencies ν_M^{abs} and ν_M^{flu} of corresponding absorption and fluorescence band maxima, Eq. 5,[9]

$$\nu_M^{abs} - \nu_M^{flu} = B^2/8(\ln 2)kT, \quad (5)$$

which has been shown to be valid for chlorophyll in solution.[10] The relation will be accurate unless there is substantial rearrangement in the excited state before emission, or variations in the molecular environment

which give rise to heterogeneous band broadening are preserved during the lifetime of the excited state. Fluorescence band positions were calculated for several of the absorption band components by Eq. 5 and are liested next to them in Table 2. These predicted positions are connected by dashed lines to observed bands to which they most likely correspond.

The absorption and fluorescence components belonging to monomeric chlorophyll bound to the NPMA's and MAn are located in the ranges 664.5—666 nm and 671—676 nm; agreement between positions predicted by Eq. 5 and assigned fluorescence bands is satisfactory. The three NPMA isomers also have absorption band components at 682.5 nm (3-NPMA) or 684 nm (2- and 4-NPMA) which are evidently related to fluorescence components at 688 nm (3- and 4-NPMA) or 693 nm (2-NPMA). The agreement between predicted and observed positions is again quite good. An analogous pair of bands for MAn was not obvious.

Acceptable resolution of absorption spectra of 3- and 4-NPMA, probably of MAn, and perhaps of 2-NPMA, required a pair of components on either side of the monomer component, *e.g.*, at 656 and 673.5 nm for 4-NPMA. Their positions suggest that they could be the result of exciton interaction in dimers similar to that of the cofacial covalently-linked pyrochlorophyllide dimer described by Bucks and Boxer.[11] Alternatively, they might represent heterogeneous broadening of the monomeric chlorophyll band, but if so, the broadening is not reflected in the fluorescence spectrum. We could not identify a fluorescence component, with the aid of Eq. 5, corresponding to either of these absorption components at room temperature in spectra with any of these four amphiphiles.

On the other hand, the fluorescence spectra with the NPMA's all contain a broad farred component at 726.5 nm (2-NPMA), 724.5 nm (3-NPMA), and 733 nm (4-NPMA) which is stronger than can be accounted for as vibrational satellites of shorter-wave fluorescence components, as assumed for chlorophyll in OCC. Indeed, chlorophyll in many other model systems shows a fluorescence band in this region.[2] Fluorescence in this region is usually ascribed to an absorption band in the 695—700 nm region, as in the example described by Hindman *et al.*[12] In none of our spectra have we been able to resolve an absorption band in this region broad enough to account for the farred emission. As was discussed in the case of DMMA, where a 725 nm emission band is prominent, a very weak but broad absorption band could escape detection, but it is also conceivable that the farred fluorescence is a kind of excimer emission, associated with absorption bands at much shorter wavelengths. It is tempting to associate the farred emission bands, which have no observed corresponding absorption bands, with the above-mentioned pair of absorption bands (*e.g.*, 656 and 673.5 nm), which have no corresponding fluorescence. The validity of such an assignment must be established by further experimentation.

Data for the DMMA system[2] are also transcribed in Table 2; it is evident that there is very good agreement between observed fluorescence band positions and those calculated from the absorption bands by Eq. 5.

However desirable it may be to assign structures to the associated chlorophyll species detected in these studies, it is rarely possible to do so on the basis of electronic spectra alone. Nevertheless, the nature of the system imposes some limitations on the kinds of association that can be imagined to exist. A discussion of structures reasonably proceeds from the following assumptions. (1) The chlorophyll molecules tend to float at or near the particle surface, with the phytyl groups directed toward the particle interior, and the porphyrin planes making an angle of about 50° to the surface, as they have been found to do in lecithin layers.[13] (2) The amphiphile will be similarly oriented at the particle surface, and will therefore bind primarily to the Mg from the underside of the porphyrin plane. (3) The *N*-substituent of the monosubstituted amides will be directed mainly *trans* to the myristoyl group.[14] (4) Because water is present in abundance during adsorption, the Mg and C(9) or ring carbonyl of chlorophyll will be bound to water (or possibly methanol) unless it is displaced by a stronger nucleophile or H-bond donor respectively.[7,15] (5) Established structures of chlorophyll hydrate species[16] and anhydrous chlorophyll oligomers[17] are valid models for chlorophyll association and its spectral manifestations.

It is clear, through earlier work with DMMA and other amphiphilic amides, that these compounds act as nucleophiles toward the Mg of chlorophyll, and thus keep most of the pigment in a monomeric state.[1,2] The amphiphiles used in the present work (except DPB) are also potentially capable of ligating Mg through their amide carbonyl groups. The monosubstituted amides (but not DMMA) can also form hydrogen bonds with carbonyl groups of chlorophyll. The NPMA's, but not MAn, are potentially able to bind to Mg through the pyridine function as well as through the carbonyl. Finally, since all of these functional groups are normally bound to water in aqueous systems, water may serve as an intermediate link in any of these connections.

The results of Table 2, taken as a whole, suggest that MAn and 2-NPMA behave somewhat differently from 3- and 4-NPMA. In spite of their greater solubility in the particles (or perhaps because of it), MAn and 2-NPMA interact rather weakly with chlorophyll, give absorption spectra which are somewhat broadened but not clearly structured, and show fluorescence in which monomer emission predominates. In contrast, 3- and 4-NPMA appear confined to the particle surface, where they interact strongly with chlorophyll, produce absorption bands which are distinctly structured and broadened, especially on the long-wavelength side, and show fluorescence spectra with important contributions from associated species. Models of these amides suggest that direct ligation of the carbonyl group to Mg of chlorophyll is somewhat hindered by the aromatic substituent, except perhaps in 3-NPMA. However, direct ligation of the pyridine nitrogen to Mg is unhindered in 3- and 4-NPMA, whereas it is almost impossible in 2-NPMA. It therefore seems likely that 3- and 4-NPMA are bound to the underside of the porphyrin plane through pyridine nitrogen, whereas 2-

NPMA and MAn are bound through the amide carbonyl, directly or perhaps through water. The binding of amide carbonyl in DMMA to Mg does not appear to be hindered.

According to Table 2, the three NPMA's and perhaps MAn give absorption spectral components in the range 682.5—684 nm, which are associated with fluorescence components in the range 688—693 nm. Particles with DMMA lack these components, within the sensitivity of the analysis. Since only the monosubstituted amides could form hydrogen bonds directly to chlorophyll carbonyls, it is possible that the associated species responsible for these bands are linked by ligation of the amide carbonyl or pyridine group to the Mg of one chlorophyll, and by a hydrogen bond from the amide nitrogen to the ring carbonyl of another. The monosubstituted amide thus acts as a bifunctional linking agent between two chlorophylls, much as simpler compounds such as alcohols do in solution at low temperature.[7] 3- and 4-NPMA form the strongest associations of this type. In this sort of association, the angle between the chlorophyll porphyrin planes is not well defined but tends to be rather large.

When a molecule of DMMA is bound through the amide carbonyl to the underside of one chlorophyll molecule, there is no functionality remaining by which it can link to another. However, chlorophyll adsorbed at high density to particles with DMMA does show bands of definite associated species at 674 and 689 nm. Construction of models, subject to the considerations outlined above, shows that the most likely way to link two chlorophyll molecules together is through a third DMMA molecule, bound to hydrated Mg on the upper side of one chlorophyll molecule and to the hydrated ring carbonyl group of the other. In this structure, the amide carbonyl is hydrogen-bonded to two waters at once, which is plausible because in the presence of water, amide carbonyls tend to be bound to two water molecules anyway.[18] The chlorophyll planes tend to be intermediate between parallel and perpendicular in this construction. If two chlorophyll molecules so connected produce the 674 nm absorption band component, three or more connected in series might give rise to the 689 nm component.

The four monosubstituted amides could link chlorophylls together in the same way, with one change: the amides could form hydrogen bonds directly from NH to chlorophyll carbonyl. The inequivalence of the linked chlorophyll molecules could be conductive to charge separation, as proposed by Yuen *et al.*,[19] and thus account for the farred band of fluorescence for which a charge-transfer excimer nature has been suggested.

The structures described above must be considered tentative until they can be supported by evidence bearing more directly on the nature of the linkages, such as resonance Raman spectroscopy. More important than the exact structures is that in these systems with closely related amphiphiles, the nature of chlorophyll association is conditioned by the structure of the amphiphile, and that the associated species are for the most part fluorescent.

This work was supported in part by Grant No. DE-FG01-80 ER10563 from the U. S. Department of Energy. We thank Dr. John W. McDonald for the C-H-N analyses, and Mr. Elwood R. Shaw for the synthesis of myristanilide. This is Contribution No. 802 from the Charles F. Kettering Research Laboratory.

References

1) G. R. Seely, "Chlorophyll Organization and Energy Transfer in Photosynthesis," Ciba Foundation Symposium 61 (new series), Excerpta Medica, Amsterdam (1979), pp. 41—59; *Biotechnol. Bioeng. Symp.* No. 8, 473—481 (1978); G. R. Seely and A. M. Rutkoski, "Photosynthesis I. Photophysical Processes-Membrane Energization," ed by G. Akoyunoglou, Balaban Int. Sci. Serv., Philadelphia (1981), pp. 213—221.

2) a) G. R. Seely, A. M. Rutkoski, Y. Kusumoto, V. Senthilathipan, and E. R. Shaw, *Photochem. Photobiol.*, **36**, 633 (1982); b) Y. Kusumoto, V. Senthilathipan, and G. R. Seely, *Photochem. Photobiol.*, in press (1983).

3) L. W. Deady and D. C. Stillman, *Aust. J. Chem.*, **32**, 381 (1979).

4) H. Sugeta, *Bull. Chem. Soc. Jpn.*, **54**, 3706 (1981).

5) W. L. Butler, *J. Opt. Soc. Am.*, **52**, 292 (1962).

6) G. R. Seely and R. G. Jensen, *Spectrochim. Acta*, **21**, 1835 (1965).

7) T. M. Cotton, P. A. Loach, J. J. Katz, and K. Ballschmiter, *Photochem. Photobiol.*, **27**, 735 (1978).

8) F. K. Fong, M. Kusunoki, L. Galloway, J. G. Matthews, F. E. Lytle, A. J. Hoff, and F. A. Brinkmann, *J. Am. Chem. Soc.*, **104**, 2759 (1982); V. Karg, P. Kis, and G. Nauer, *Bioelectrochem. Bioenerg.*, **8**, 691 (1981); K. Uehara, Y. Nakajima, M. Yonezawa, and M. Tanaka, *Chem. Lett.*, **1981**, 1643; I. Inamura K. Toki, T. Araki, and H. Ochiai, *ibid.*, **1980**, 1481; other references cited in Ref. 2a.

9) L. P. Kazachenko, *Opt. Spectrosc.*, **18**, 397 (1965).

10) F. F. Litvin and I. N. Stadnichuk, *Biofizika*, **24**, 651 (1979) (*Biophysics*, p. 671).

11) R. R. Bucks and S. G. Boxer, *J. Am. Chem. Soc.*, **104**, 340 (1982).

12) J. C. Hindman, R. Kugel, M. R. Wasielewski, and J. J. Katz, *Proc. Natl. Acad. Sci. U.S.A.*, **75**, 2076 (1978).

13) R. J. Cherry, K. Hsu, and D. Chapman, *Biochim. Biophys. Acta*, **267**, 512 (1972); A. J. Hoff, *Photochem. Photobiol.* **19**, 51 (1974); F. Podo, J. E. Cain, and J. K. Blasie, *Biochim. Biophys. Acta*, **419**, 19 (1976).

14) L. A. LaPlanche and M. T. Rogers, *J. Am. Chem. Soc.*, **86**, 337 (1964).

15) K. Ballschmiter and J. J. Katz, *J. Am. Chem. Soc.*, **91**, 2661 (1969).

16) L. L. Shipman and J. J. Katz, *J. Phys. Chem.*, **81**, 577 (1977); C. Kratky and J. D. Dunitz, *J. Mol. Biol.*, **113**, 431 (1977).

17) L. L. Shipman, T. M. Cotton, J. R. Norris, and J. J. Katz, *J. Am. Chem. Soc.*, **98**, 8222 (1976).

18) J. N. Spencer, S. K. Berger, C. R. Powell, B. D. Henning, G. S. Furman, W. M. Loffredo, E. M. Rydberg, R. A. Neubert, C. E. Shoop, and D.N. Blauch, *J. Phys. Chem.*, **85**, 1236 (1981).

19) M. J. Yuen, L. L. Shipman, J. J. Katz, and J. C. Hindmann, *Photochem. Photobiol.*, **32**, 281 (1980).

 © 1983 The Chemical Society of Japan Bull. Chem. Soc. Jpn., 56, 1607—1611 (1983)

Penetration of Lysine Hydrochloride into Lecithin Monolayers from Underlying Aqueous Solutions

Masayuki NAKAGAKI and Emiko OKAMURA*

Faculty of Pharmaceutical Sciences, Kyoto University, Yoshida-Shimoadachicho, Sakyo-ku, Kyoto 606

(Received October 23, 1982)

The surface pressure of the monolayers of dimyristoyl phosphatidylcholine (DMPC) on lysine mono- and dihydrochloride solutions was measured and the amount of positively charged lysine which had penetrated into a DMPC monolayer was calculated by successive approximation. The amount of penetration was smaller for lysine monohydrochloride than for the dihydrochloride. Moreover, both were smaller than that of uncharged lysine because mono- and dihydrochloride are more hydrophilic than uncharged lysine. The average area per molecule in the monolayer consisting of lysine and DMPC, A_{23}, was obtained. In the case of charged lysine, A_{23} increased with the mole fraction of lysine in a monolayer, X_2, in contrast it decreased with X_2 in the case of uncharged lysine. The partial molecular area of positively charged lysine was considerably larger than that of uncharged lysine. This indicates that the remarkable expansion of a monolayer is caused by the penetration of positively charged lysine because of electrostatic repulsion in the monolayer. The effect of sodium chloride on the adsorption of lysine was also investigated, but the amount adsorbed was independent of the presence of 0.5 mol dm^{-3} sodium chloride.

It has been widely accepted, according to the fluid mosaic model of Singer and Nicolson,[1] that biomembranes consist essentially of bimolecular lipid layers in which some proteins are dissolved. Many investigations of the interaction between lipids and proteins at the interfaces, have been made in order to elucidate the structure and the functions of the biomembranes.[2-7] From this point of view, the interaction between lecithin monolayers as a model of lipid membranes and lysine,[8] leucine and norleucine[9] as the components of proteins at the air/water interface was discussed in our previous papers.

Three typical patterns of the effects of different proteins on the properties of lipid bilayers and monolayers have been proposed by Papahadjopoulos *et al.*[10] 1) Simple adsorption, 2) adsorption and deformation, and 3) penetration. Which of the above three patterns is preferable depends on the kind of lipids or proteins that interact with each other, but, even for the same substances, the pattern or the intensity of interaction depends on the state and conditions of their existence. In the case of a basic amino acid, such as lysine, which was used in our previous work, the interaction with a lecithin monolayer should change with the pH of the solution, since the dissociation states of the amino and carboxyl groups of the amino acid changes. For lysine the pK values are: pK_1(COOH)=2.18, pK_2(α-NH_3^+)=8.95, and pK_3(ε-NH_3^+)=10.53,[11] and the possible charged forms of lysine, *i.e.*, free base (Lys), lysine monohydrochloride (Lys·HCl), and lysine dihydrochloride (Lys·2HCl) are (a), (b), and (c), in Fig. 1, respectively. The net charge is 0, +1, +2, in order of (a), (b), (c). Some appreciable changes in the interaction with lipids are expected to be caused by the difference between the charged forms. In this paper, Lys·HCl and Lys·2HCl were used, the amounts adsorbed onto lecithin monolayers were obtained, and discussed in comparison with the case of Lys.[8] Moreover, sodium chloride (NaCl) was used as an added electrolyte, and the effect of chloride ion (Cl^-) and that of the ionic strength were also investigated.

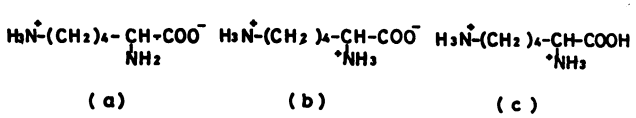

Fig. 1. Three forms of uncharged and charged lysine. (a) L-Lysine(free base) [Lys], (b) L-lysine monohydrochloride [Lys·HCl], and (c) L-lysine dihydrochloride [Lys·2HCl].

Experimental

Materials. Lys·HCl and Lys·2HCl, purchased from Wako Chemical Industries, Ltd, were dissolved in redistilled water. L-α-Dimyristoyl phosphatidylcholine (DMPC) from Sigma Company was used as lecithin, dissolved in distilled chloroform and preserved in a refrigerator until use. The stock solution was prepared every few days in order to avoid disintegration. NaCl from Merck and Co., Inc. was used without further purification.

Surface-tension Measurement. The surface tension of lysine hydrochloride solution, γ_{lys}, was measured by the capillary-height method, and the surface pressure of lysine hydrochloride, F_{lys}, was obtained by Eq. 1:

$$F_{lys} = \gamma_0 - \gamma_{lys}, \quad (1)$$

where γ_0 is the surface tension of pure water. The solution temperature was kept at 25±0.5 °C.

Surface-pressure Measurement. The surface pressure of the DMPC monolayer was measured by Wilhelmy's plate method. The details of this method were the same as described before.[8] The experimental error of the measurement was within ±0.1 mN m^{-1}. The temperature of the solution was kept at 25±0.5 °C.

Results

Surface Tension of Lysine Hydrochloride Solution. Figure 2 shows the surface tension of Lys·HCl or Lys·2HCl solution. The surface tension of Lys solution as already reported in Fig. 1 of Ref. 8 is also shown by open circles(○) in Fig. 2. It is seen that the surface tension decreases slightly with the increase in the concentration of solution, C_2, and the extent of the decrease is almost independent of the charged forms of the lysine.

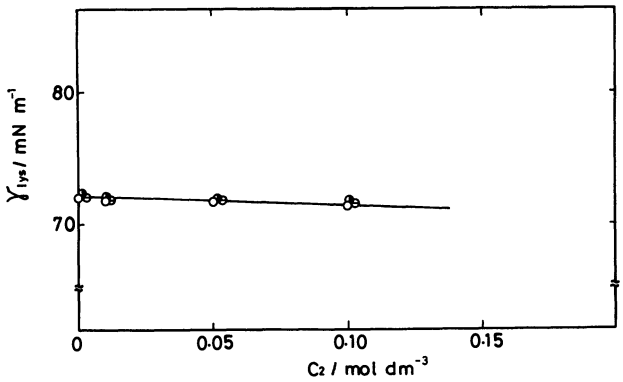

Fig. 2. The relation of surface tension, γ_{lys}, and the concentration of solution, C_2. ◑ Lys·HCl, ⊖Lys·2HCl. Symbols (○) designate the values in the case of Lys.

Surface Pressure-Area Curves of the DMPC Monolayers. The surface pressure-area curves of the DMPC monolayers spread on Lys·HCl and Lys·2HCl solutions are shown in Figs. 3(a) and (b), respectively. Although the curve shifted to the higher surface pressure region with the increase in concentration of lysine, C_2, in both cases, the extent of the shifts was larger in the case of Lys·2HCl than that of Lys·HCl.

The Amount Adsorbed onto a DMPC Monolayer. The relation between the surface pressure, F, and the concentration, C_2, at various constant areas per molecule of lecithin, A_3, was obtained from Figs. 3(a) and (b) and the amount of lysine adsorbed onto a DMPC monolayer was calculated, as described before,[8] by the following equation:

$$\Gamma_2 = \frac{1}{iRT}\left(1-\frac{\bar{A}_3}{A_3}\right)\left(\frac{\partial F}{\partial \ln C_2}\right)_{A_3}, \qquad (2)$$

where Γ_2 is the adsorbed amount of solute, R is the gas constant, T is the absolute temperature, and $\bar{A}_3$ is the partial molecular area of DMPC. $\bar{A}_3$ was approximated by the molecular area of DMPC on pure water, $A_3°$, by Pethica.[12] Hereafter, this will be called the first approximation. The values of the coefficient, i, to be discussed later in detail, are $i=2$ and 3 for Lys·HCl and Lys·2HCl, respectively, since no added electrolytes coexist in this case. Values of Γ_2 thus calculated in the first approximation are shown in Fig. 4. The values of Γ_2 in the case of Lys[8] are also shown in this figure. Besides the fact that the amount adsorbed Γ_2 increases with the concentration, C_2, it is seen from Fig. 4 that the value of Γ_2 is smaller for Lys·HCl(b) and Lys·2HCl(c) than for Lys(a). This indicates that the positively charged lysine(Lys·HCl or Lys·2HCl) is less adsorbed onto an interface than the uncharged lysine (Lys) because the hydrophobicity of the former two is stronger than that of the latter.

The Effect of Added Electrolytes. As an electrolyte, 0.5 mol dm^{-3} NaCl was added into the lysine solution and the effect of the ionic strength on the adsorption of lysine was investigated. The $\gamma_{lys}-C_2$ curves for Lys·HCl and Lys·2HCl are shown in Figs. 5(a) and (b), respectively. It was found that, in both cases, the surface tension decreased slightly with the increase in C_2, irrespective of whether or not a NaCl was added. The surface pressure-area curves of the DMPC monolayers spread on Lys·HCl and Lys·2HCl solutions with 0.5 mol dm^{-3} NaCl are shown in Figs. 6(a) and (b), respectively. The calculation of the amount of lysine adsorbed in the presence of added electrolytes is discussed later in detail.

Discussion

The Mixed Monolayers of DMPC and Lysine. It

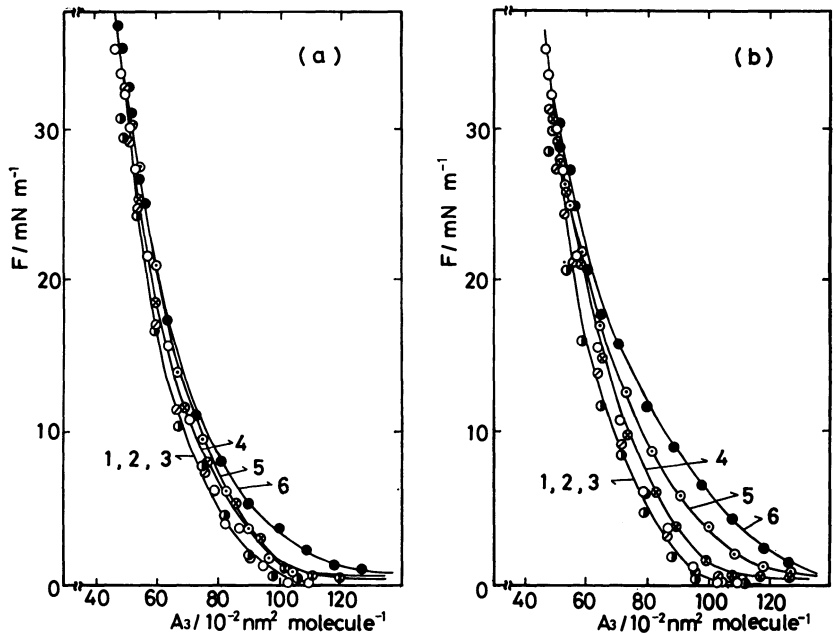

Fig. 3. The surface pressure, F, *vs.* the molecular area of lecithin, A_3, on (a)Lys·HCl solutions and (b) Lys·2HCl solutions.
C_2/mol dm^{-3}: 1. (○) 0, 2. (◑) 0.01, 3. (⊘) 0.02, 4. (⊗) 0.05, 5. (⊙) 0.07, 6. (●) 0.10.

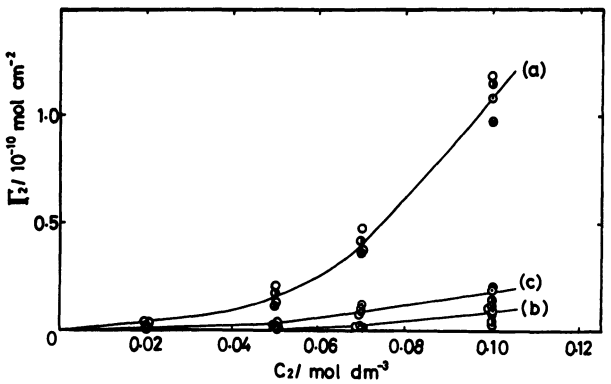

Fig. 4. The amounts of three differently charged lysine adsorbed onto DMPC monolayer, Γ_2, *vs.* C_2. (a) Lys, (b) Lys·HCl, (c) Lys·2HCl.
$A_3/10^{-2}$ nm^2 molecule^{-1}: ⊗ 100, ⊙ 90, ◑ 80, ○ 75.

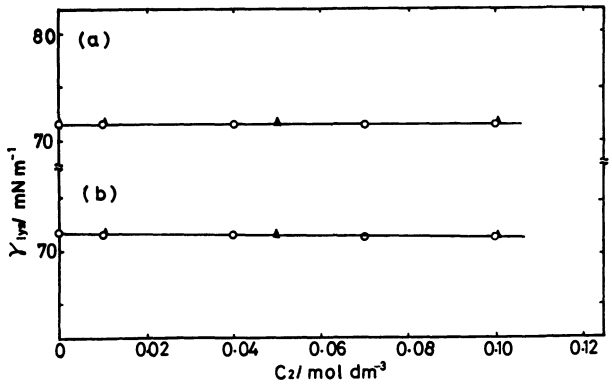

Fig. 5. Surface tension of various lysine solutions. (a) Lys·HCl, (b) Lys·2HCl. ▲ In salt-free water, ○ with 0.5 mol dm^{-3} NaCl.

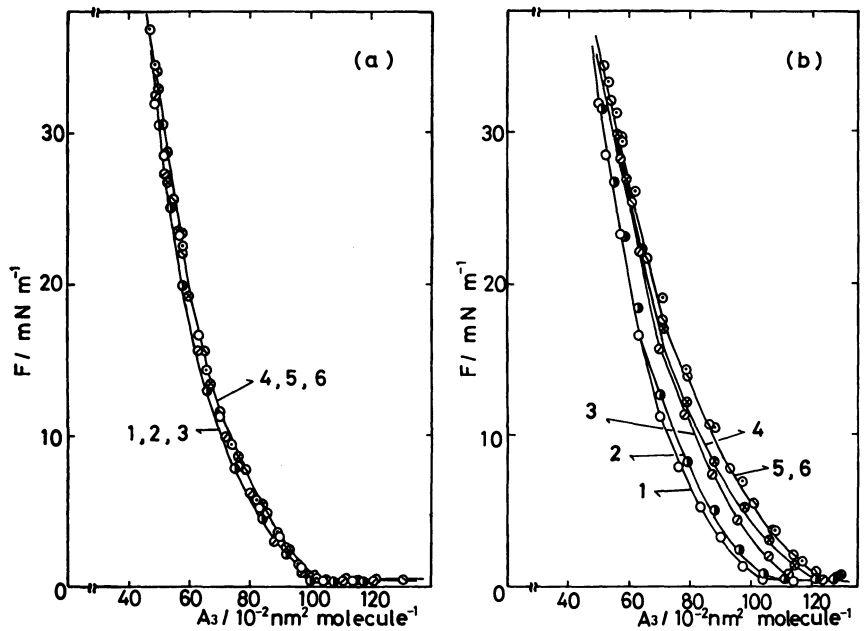

Fig. 6. F–A_3 curves of the DMPC monolayers in the presence of 0.5 mol dm^{-3} NaCl. (a) On Lys·HCl solutions, (b) on Lys·2HCl solutions.
C_2/mol dm^{-3}: 1. (○) 0, 2. (◑) 0.01, 3. (⊘) 0.02, 4. (⊗) 0.05, 5. (⊙) 0.07, 6. (⊘) 0.10.

may be considered that at an interface, a mixed monolayer of DMPC and lysine is formed as the result of the penetration of lysine into a DMPC monolayer. The mole fraction of lysine, in this mixed monolayer, X_2, and the average area per molecule of the monolayer, A_{23}, are given by:

$$X_2 = \frac{\Gamma_2}{\Gamma_2+\Gamma_3}, \tag{4}$$

and

$$A_{23} = \frac{1}{(\Gamma_2+\Gamma_3)N_A}, \tag{5}$$

respectively, where Γ_3 is the moles of DMPC per unit area ($=1/(A_3 \cdot N_A)$), and N_A is the Avogadro number. The relation between X_2 and A_{23} at a given surface pressure is shown in Figs. 7(a) and (b) in the cases of Lys·HCl and Lys·2HCl, respectively. It was found that, in each case, the value of A_{23} increased with the increase in the mole fraction of lysine, X_2. Because of the relatively small amount of penetration, the value of X_2 was smaller than 0.1 or 0.15 in the case of Lys·HCl or Lys·2HCl, respectively, even at a low pressure region, in spite of that the concentration of lysine solution, C_2, was as high as 0.1 mol dm^{-3}.

It can be seen in Fig. 7 that the partial molecular area of DMPC on the solution, $\bar{A}_3$, is almost constant in the region other than at very small X_2-value, but the value of $\bar{A}_3$ is not equal to that on pure water ($X_2=0$), $A_3°$. The amount of lysine hydrochloride adsorbed onto a DMPC monolayer, Γ_2, was therefore, recalculated by substituting in Eq. 2 the value of $\bar{A}_3$ obtained from Fig. 7, instead of $A_3°$, as described in the previous paper.[8] This will be called the second approximation. The successive approximation was allowed to proceeded three times by which the value of Γ_2 had converged to a defined value. The values, thus obtained, are shown in

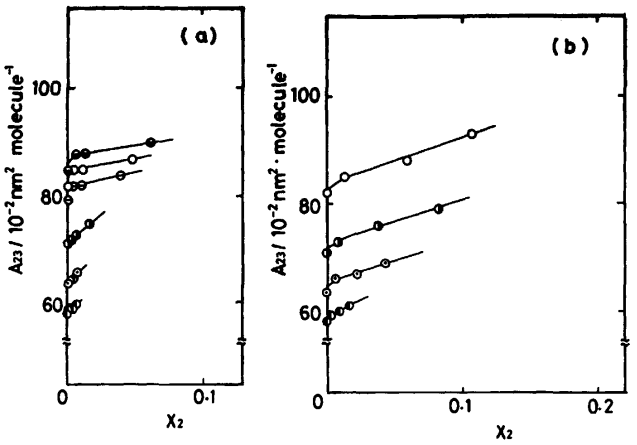

Fig. 7. The relation of the average area per molecule of a lysine-DMPC mixed monolayer, A_{23}, and the mole fraction of lysine, X_2. (a) Lys·HCl, (b) Lys·2HCl. F/mN m^{-1}: ◒ 4, ○ 5, ⊖ 6, ◑ 10, ⊙ 15, ○ 20.

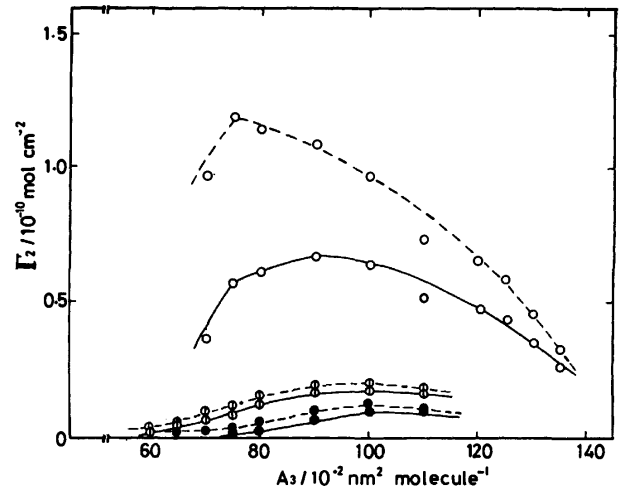

Fig. 8. The converged values of the amount of lysine adsorbed onto DMPC monolayer, when the concentration of solution, C_2, is 0.10 mol dm^{-3}. ● Lys·HCl, ⓘ Lys·2HCl. Broken lines show the values obtained on the assumption that $\bar{A}_3=A_3°$. Symbols (○) designate the values in the case of Lys.[8]

Fig. 8 by solid lines for example where the concentration of each lysine solution, C_2, is 0.10 mol dm^{-3}. Broken lines show the values calculated on the assumption that $\bar{A}_3=A_3°$. The data of lysine (free base)[8] is also shown in open circles(○). Although the converged values are smaller than the values obtained on the assumption that $\bar{A}_3=A_3°$, the sequence of the larger adsorbed amount was not changed, *i.e.*, it was Lys>Lys·2HCl> Lys·HCl, in each approximation, and this sequence was independent of the value of C_2. This order also coincided with the extent of shifts in surface pressure-area curves (Fig. 3). The result that Lys$^+$ has three units of electric charge (two + and one −) and is more hydrophilic than Lys^{2+} which has only two units of electric charges. Positive and negative charges in Lys$^+$ can interact with water molecules separately, in contrast to the case of macromolecules, such as proteins at the isoelectric point. In the latter case, the effect of the positive and negative

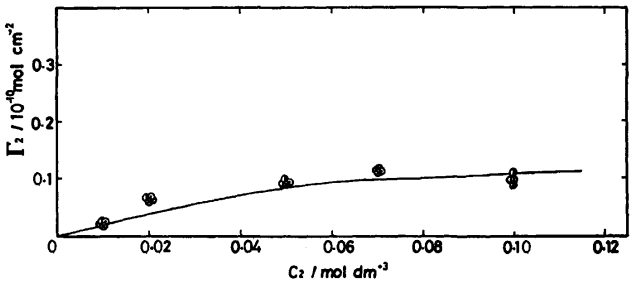

Fig. 9. The converged values of the amount of Lys·2HCl adsorbed onto DMPC monolayer, Γ_2, *vs.* C_2, in the presence of 0.5 mol dm^{-3} NaCl. A_3/10^{-2} nm^2 molecule^{-1}: ⊗ 100, ⊙ 90, ◑ 80, ○75.

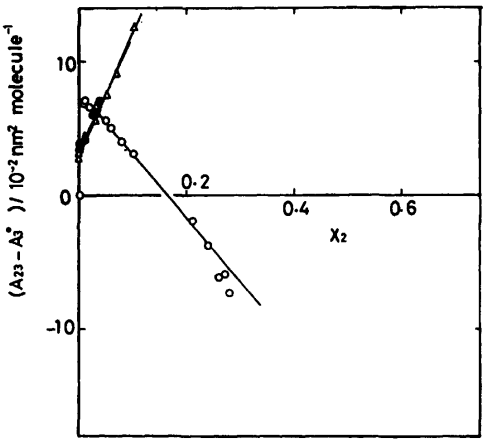

Fig. 10. $(A_{23}-A_3°)$ *vs.* X_2, obtained by the last approximation. ● Lys·HCl, △ Lys·2HCl. Symbols (○) designate the values in the case of Lys.[8]

electric charges would fairly compensate with each other since the distance to the water molecule at the surface of the macromolecule may be larger than the distance between the positive and negative charges.

The Effect of Added Electrolytes. The adsorbed amount of lysine, Γ_2, in the presence of electrolytes was calculated from Figs. 6(a) and (b), by using Eq. 2. When lysine hydrochloride $[(Lys^{+z+})(Cl^-)_{\nu_-}]$ (its concentration, C_2) and NaCl(C_3) are contained in the solution, the coefficient, i, in Eq. 2 is given by

$$i = 1 + \nu_- \frac{\nu_- C_2}{\nu_- C_2 + C_3}. \quad (3)$$

In this experiment, ν_- is equal to 1 or 2 in the case of Lys·HCl or Lys·2HCl, respectively, C_2 is 0—0.1 mol dm^{-3}, and C_3 is 0.5 mol dm^{-3}. Figure 9 shows the results thus obtained in the case of Lys·2HCl. The converged Γ_2-values are shown in this figure. It is seen that the values of Γ_2 in the presence of 0.5 mol dm^{-3} NaCl did not differ much from those in the absence of NaCl shown in Fig. 8. The same was also seen for Lys·HCl, though it is not shown in the figure. These facts indicate that the adsorption of lysine is not appreciably affected by the added NaCl electrolyte.

The Interaction between Charged Lysine and DMPC. The relation between the mole fraction of lysine, X_2, and the average area per molecule of the mixed monolayer, A_{23}, was obtained again, by using recalculated

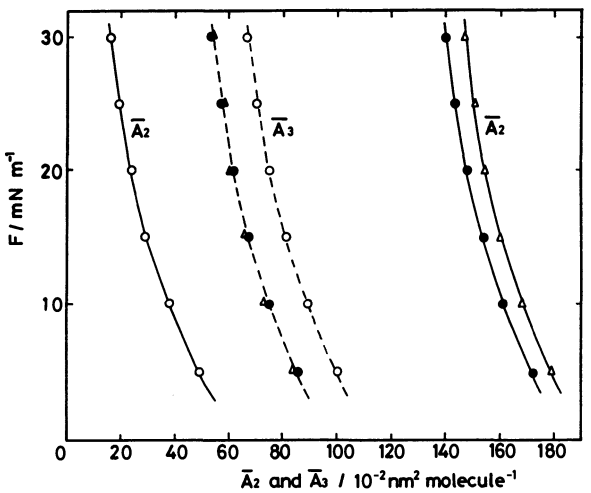

Fig. 11. The relation of the surface pressure, F, and the partial molecular areas of lysine, $\bar{A}_2$, and DMPC, $\bar{A}_3$. Solid lines show the values of $\bar{A}_2$, and broken lines show those of $\bar{A}_3$. ● Lys·HCl, △ Lys·2HCl. Symbols (○) designate the values in the case of Lys.[8]

values of Γ_2, in the case of lysine hydrochloride, and the values of $(A_{23}-A_3^\circ)$ were plotted against X_2 in Fig. 10. The open circles designate in the case of Lys. As the result of subtracting A_0^3 from A_{23}, the values of $(A_{23}-A_3^\circ)$ came on to one curve, independent of the surface pressure, F. It has also been found that $(A_{23}-A_3^\circ)$ increased with X_2 in the case of Lys·HCl of Lys·2HCl, on the contrary to the decrease in the case of Lys. This indicates that the positively charged lysine molecule which had penetrated into a DMPC monolayer occupied a larger area than lecithin. From Fig. 10, the relation between X_2 and A_{23} was obtained by the least-square method, and described in the cases of Lys·HCl and Lys·2HCl as follows:

$$A_{23} = A_3^\circ + 3.4 + 86.3X_2 \quad \text{(for Lys·HCl)} \tag{6}$$

$$A_{23} = A_3^\circ + 3.2 + 93.6X_2 \quad \text{(for Lys·2HCl),} \tag{7}$$

where Eq. 6 is, for the X_2 value smaller than 0.1, and Eq. 7 is for X_2 smaller than 0.15. The experimental errors of the constant in Eqs. 6 and 7 are 3.4 ± 0.5, 86.3 ∓ 3.5, 3.2 ± 0.5, and 93.6 ∓ 3.0, respectively. From these equations, the partial molecular area of lysine, $\bar{A}_2$, and that of DMPC, $\bar{A}_3$, are calculated respectively as follows:

$$\begin{cases} \bar{A}_2 = A_3^\circ + 89.7(\pm3.0) \\ \bar{A}_3 = A_3^\circ + 3.4(\mp0.5) \end{cases} \quad \text{(for Lys HCl)} \tag{6a}$$

$$\begin{cases} \bar{A}_2 = A_3^\circ + 96.8(\pm2.5) \\ \bar{A}_3 = A_3^\circ + 3.2(\mp0.5) \end{cases} \quad \text{(for Lys·2HCl)} \tag{7a}$$

These are shown in Fig. 11. The values of A_2 and $\bar{A}_3$ in the case of Lys are also shown with open circles. Solid lines and broken lines show the values of $\bar{A}_2$ and $\bar{A}_3$, respectively. The partial molecular area of DMPC, $\bar{A}_3$, was almost the same for both Lys·HCl and Lys·2HCl, although it was a little smaller than for Lys. On the other hand, the partial molecular area of lysine, $\bar{A}_2$, for Lys·HCl and Lys·2HCl, was remarkably larger than that for Lys, and the value of Lys·2HCl, which has Lys^{2+}, was a little larger than that of Lys·HCl, which has Lys^+. From this experiment on lysine hydrochloride, the following conclusions were deduced: 1) the amount of positively charged lysine adsorbed onto a DMPC monolayer is small because of its stronger hydrophilicity, and 2) the remarkable expansion of a monolayer is caused by electrostatic repulsion in the monolayer, at the time as the penetration of the charged lysine.

References

1) S. J. Singer and G. L. Nicolson, *Science*, **175**, 720 (1972).
2) P. T. Shafer, *Biochim. Biophys. Acta*, **373**, 425 (1074).
3) P. Chatelain, C. Berliner, J.-M. Ruysschaert, and J. Jaffe, *J. Colloid Interface Sci.*, **51**, 239 (1975).
4) H. J. Pownall, J. B. Massey, S. K. Kusserow, and A. M. Gotto, Jr., *Biochemistry*, **18**, 574 (1979).
5) R. A. Demel, Y. London, W. S. M. Geurts van Kessel, F. G. A. Vossenberg, and L. L. M. van Deenen, *Biochim. Biophys. Acta*, **311**, 507 (1973).
6) D. Hammermeister and G. Barnett, *Biochim. Biophys. Acta*, **332**, 125 (1974).
7) I. R. Miller and D. Bach, *Chem. Phys. Lipids*, **13**, 453 (1974).
8) M. Nakagaki and E. Okamura, *Bull. Chem. Soc. Jpn.*, **55**, 1352 (1982).
9) M. Nakagaki and E. Okamura, *Bull. Chem. Soc. Jpn.*, **55**, 3381 (1982).
10) D. Papahadjopoulos, M. Moscarello, E. H. Eylar, and T. Isac, *Biochim. Biophys. Acta*, **401**, 317 (1975).
11) Tanpakushitsu Kagaku, ed by S. Mizushima and S. Akabori, Kyōritsu Shuppan, Tokyo (1954), Chap. 2, p. 223.
12) B. A. Pethica, *Trans. Faraday Soc.*, **51**, 1402 (1955).

NMR Studies of Picolyl-type Carbanions. VI.[1,2] Anions Produced by Reactions of Methyl-substituted Quinolines and Isoquinolines with Butyllithium

Kazuyori KONISHI* and Kensuke TAKAHASHI†

The Industrial Technology Center of Mie Prefecture, Takajayakomori-cho, Tsu 514

†*Department of Industrial Chemistry, Nagoya Institute of Technology, Gokiso-cho, Showa-ku, Nagoya 466*

(Received October 29, 1982)

The ^{13}C and ^{1}H NMR spectra have been observed for the title anions with lithium as a counter ion in polar solvents. Two kinds of anions are formed by lithium-proton exchange and addition of butyllithium. The charge distributions in the anions are discussed in terms of the σ-included ω-HMO method. The former anions can be regarded as picolyl-type carbanions, but the latter ones are ionic species having two of three basic characteristics on picolyl-type carbanions.

In our previous papers, the ^{1}H, ^{7}Li, and ^{13}C NMR spectra were observed for charge-delocalized anions, I and II1 (shown below).[1,3,4] The studies have now been extended to the anions produced by reactions of methyl-substituted quinolines and isoquinolines with butyllithium. The present paper deals with charge distributions in the anions in terms of their ^{13}C chemical shifts and total ($\sigma+\pi$) electron densities. The anions prepared are numbered as follows:

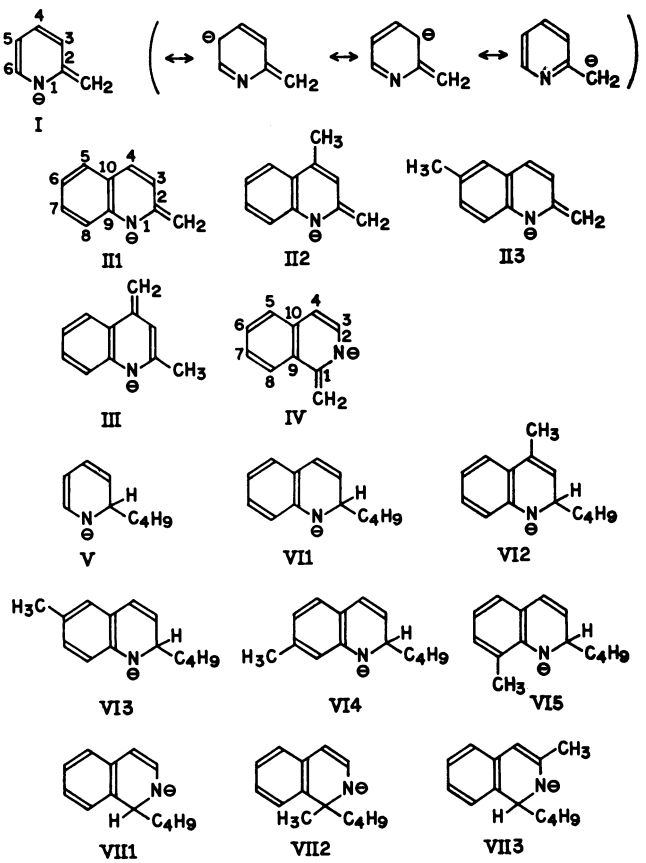

Experimental

The method of preparation of the anions is similar to that described previously.[3]

The ^{13}C spectra were measured at 22.6 and 25.0 MHz on a Hitachi R-42FT and a JEOL JNM-FX100 spectrometers respectively. The chemical shifts were evaluated with the solvent peaks used as an internal reference and then converted to δ_c values from TMS by taking 26.4 and 37.0 ppm for tetrahydrofuran (THF) and hexamethylphosphoric triamide (HMPA) respectively.

Theoretical Calculation

The total electron densities on the atoms were calculated for the anions by the σ-included ω-HMO method.[5] In this study, the fourth and the fifth terms in Eq. 1 (shown below), called through space effects, were introduced into the calculation of the π-electron density. The Coulomb integral associated with the π-AO of the λ-th atom, α_λ^π, is, therefore, given by

$$\alpha_\lambda^\pi = \alpha + \delta_\lambda^\pi\beta + \omega^\pi\Delta Q_\lambda^T\beta + \sum_\mu \omega'^\pi \Delta q_\mu^\pi \beta + \sum_\nu \omega''^\pi \Delta q_\nu^\pi \beta, \quad (1)$$

where

$$\Delta Q_\lambda^T = \Delta Q_\lambda^\sigma + \Delta q_\lambda^\pi, \quad (2)$$

ΔQ_λ^T, ΔQ_λ^σ, and Δq_λ^π are the net total, σ-, and π-electron densities on the atom λ respectively. The atom μ is adjacent to the atom λ and, further, the ν is adjacent to the μ. The values of ω'^π and ω''^π are assumed to be $\omega^\pi/1.5$ and $\omega^\pi/6.0$ respectively.[6] The resonance integral for the $\lambda-\mu$ bond, $\beta_{\lambda\mu}^\pi$, is given by

$$\beta_{\lambda\mu}^\pi = k_{\lambda\mu}^\pi\beta. \quad (3)$$

The parameters associated with π- and σ-AO's, used in the calculation, δ_λ^π, $k_{\lambda\mu}^\pi$, ω^π, δ_λ^σ, $k_{\lambda\mu}^\sigma$, and ω^σ, were taken from the paper of Miyajima *et al.*[5] This MO calculation was carried out using the Okitac-4300C computer system.

Results and Discussion

Typical spectra of the anions are shown in Figs. 1 and 2. The ^{1}H and ^{13}C chemical-shift data are given in Tables 1 and 2 respectively.

Reactions of Methyl-substituted Quinolines and Isoquinolines with Butyllithium. In methyl-substituted quinolines, 2-methyl-, 2,4-, and 2,6-dimethylquinolines, having a 2-methyl group, underwent metal-proton exchange to give charge-delocalized anions, II(III—III3),[4] but 4-, 6-, 7-, and 8-methylquinolines, having no 2-methyl group, did addition of butyllithium to give anionic σ-complexes, VI2—VI5. In the case of 2,4-dimethylquinoline, as well as 2,4-dimethyl- and 2,4,6-trimethyl-

Table 1. The proton chemical shifts of the anions, in THF at 60 MHz, in ppm[a)]

Anion	Assignment 2-H	3-H	4-H	5-H	6-H	7-H	8-H	CH_2		CH_3	
II1[b)]		5.92	6.19	6.46	6.06	6.60	6.25	2.88	3.09		
II2[b)]		5.88		6.75	6.03	6.62	6.31	2.88	3.07	c)	
II3[b)]		5.96	6.24	6.37		6.52	6.28	2.87	3.09	2.07	
III[d)]		5.29		7.36	6.41	6.79	6.70	3.36	3.76	c)	
VI1	4.10	5.21	6.17	6.45	5.76	6.57	6.08	1.37[e)]			0.93
VI2	c)	5.11		6.71	5.79	6.59	6.08	c)		c)	0.91
VI3	4.10	5.32	6.20	6.39		6.49	6.10	1.38[e)]		2.08	0.94
VI4	4.11	5.25	6.18	6.41	5.71		6.00	1.39[e)]		2.10	0.93
VI5	4.08	5.13	6.13	6.34	5.62	6.46		1.38[e)]		2.05	0.91

a) Errors are estimated to be within ± 0.03 ppm. b) These values should be adopted, though they are partly different from the corresponding values in Table 1 of Ref. 4. c) Chemical shifts are not available because of overlapping of the large solvent peak. d) Measured at 200 MHz. e) Center peak of complex multiplet.

Table 2. The carbon chemical shifts of the anions, in ppm[a)]

Anion	Solvent	Assignment 1-C	2-C	3-C	4-C	5-C	6-C	7-C	8-C	9-C	10-C	CH_2			CH_3	
I[b)]	THF		164.2	116.1	131.6	97.3	148.7					57.0				
	HMPA		161.3	113.6	129.8	92.2	149.8					62.6				
III[b)]	THF		159.0	126.0	128.6	126.3	111.8	128.2	117.7	155.8	122.7	70.2				
	HMPA		159.0	125.0	127.9	125.5	108.7	127.7	119.0	156.5	121.9	70.7				
II3	THF		159.5	125.9	128.9	126.7	120.3	129.5	118.1	153.4	122.4	68.2			20.9	
III	THF		149.5	103.1	152.7	123.9	116.5	126.7	123.1	145.5	124.2	72.5			24.8	
IV	THF	158.0		146.6	93.3	120.9	127.2	123.2	124.3	130.4	140.2	68.7				
V	THF		57.2	97.9	126.4	90.8	150.2					34.7	28.5	24.4		15.0
	HMPA		58.0	92.3	127.0	85.2	151.4					35.8	28.5	24.1		15.0
VI1	THF		57.7	120.5	127.9	127.8	107.6	128.6	115.0	159.5	122.0	42.6	27.7	24.4		14.9
	HMPA		58.7	117.8	127.6	126.7	101.8	128.1	116.8	159.9	118.5	43.0	27.5	24.1		14.9
VI2	THF		57.5	119.0	131.2	124.1	107.4	128.3	114.7	159.3	122.9	42.5	27.8	24.3	19.6	14.8
VI3	THF		57.4	121.2	127.5	128.4	116.3	129.4	114.5	157.1	122.3	42.3	27.8	24.3	20.8	14.9
VI4	THF		57.6	120.2	127.7	127.3	109.6	137.2	114.7	159.1	120.0	42.6	27.8	24.4	22.2	14.9
VI5	THF		58.1	118.8	127.7	125.8	105.3	128.9	122.6	158.3	120.7	41.4	28.1	24.3	20.0	15.0
VII1	THF	62.7		151.7	88.2	118.0	125.7	118.4	126.3	126.9	139.9	34.5	29.5	24.2		14.9
VII2	THF	59.0		150.6	85.6	117.1	124.4	117.8	125.1	127.5	141.2	41.8	29.9	24.8	28.2	15.0
VII3	THF	63.3		157.7	85.5	116.0	125.3	117.3	125.6	126.3	141.3	35.2	29.5	24.3	25.1	15.0
	HMPA	62.7		157.8	83.0	113.7	124.7	115.7	125.0	125.8	142.5	35.1	28.9	23.9	25.2	14.9

a) Errors are estimated to be within ± 0.3 ppm. b) From the data in Table 2 of Ref. 1.

pyridines,[3)] the exchange reaction occurred at the 2-methyl group, and the anion formed, II2, isomerized to III. Similar isomerizations were reported previously.[3)] Next, 1-methylisoquinoline underwent both exchange and addition to give IV and VII2 simultaneously, but 3-methylisoquinoline did only addition at the 1-position to give VII3. These reaction sites were confirmed by ^1H and ^{13}C chemical-shift considerations.

As can be seen from these results, two kinds of anionic species are formed by exchange and addition. In the case of quinoline and isoquinoline, having no methyl group, the addition reaction can be expected to occur at a specific position. In fact, quinoline, isoquinoline, and, furthermore, pyridine react with butyllithium to give anionic σ-complexes, VI1, VIII, and V.

Charge Distributions and Characteristics on the Anions. Typical ^1H NMR spectra of III and VI1 are shown in Figs. 1(a) and 1(b). The signals in the region of aromatic protons of both anions are present in higher fields than those of their starting materials. This upfield shift is ascribed to the excess-charge delocalization into the aromatic ring.[7)] Further, the 4-, 5-, and 7-proton signals of both anions appear at comparable fields, but the 3-, 6-, and 8-signals of VI1 do at a higher field than those of III respectively. This may arise from an increase of the negative charge in the aromatic ring except for the 2-position. The same tendencies are observed in the spectra of II2 and VI2, and II3 and VI3. Next, a typical spectrum of a mixture of IV and VII2 formed simultaneously is shown in Fig. 1(c). The signals, appearing as doublets, at δ 4.49 and 5.01 are attributable to the 4-protons of VII2 and IV respectively. The ratio of the two peak areas is about 1 : 1, indicating that IV and VII2 are present in this ratio. The signals at δ 3.28 and 3.68 are attributable to each of the methylene protons of IV. In III, the signals at δ 3.36 and 3.76 are also attributable to the methylene protons. The two protons of each anion, as well as those of II,[4)] show magnetic nonequivalence at room temperature. This nonequivalence is explained by the inhibited rotation around the bond between the ring and the methylene carbon, caused by the resonance stabilization in a molecular plane. Therefore, the methylene carbons of III—IV, as well as I—II, are virtually sp^2-hybridized.

The charge distributions in I, III, IV, V, VI1, and VIII are discussed on the basis of the relationship between the carbon(^{13}C) chemical shifts and the total electron densities. In Fig. 3, the total electron densities calculated by the method described before are plotted

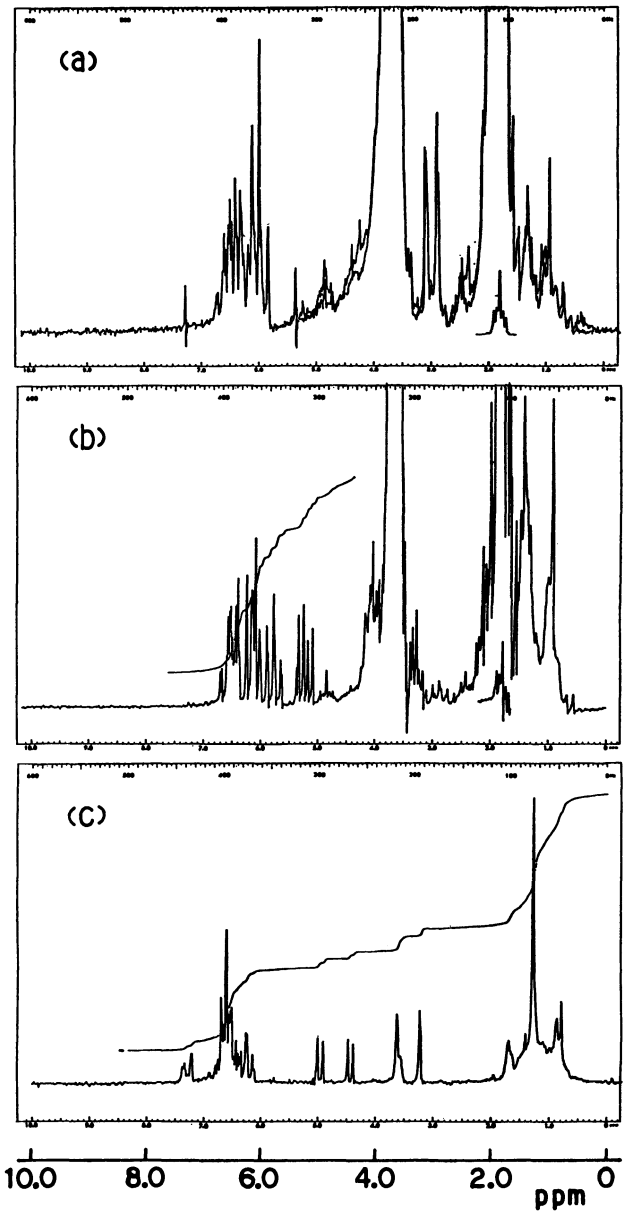

Fig. 1. ^{1}H spectra of the anions in THF at 60 MHz; (a) III, (b) VII, and (c) IV and VII2.

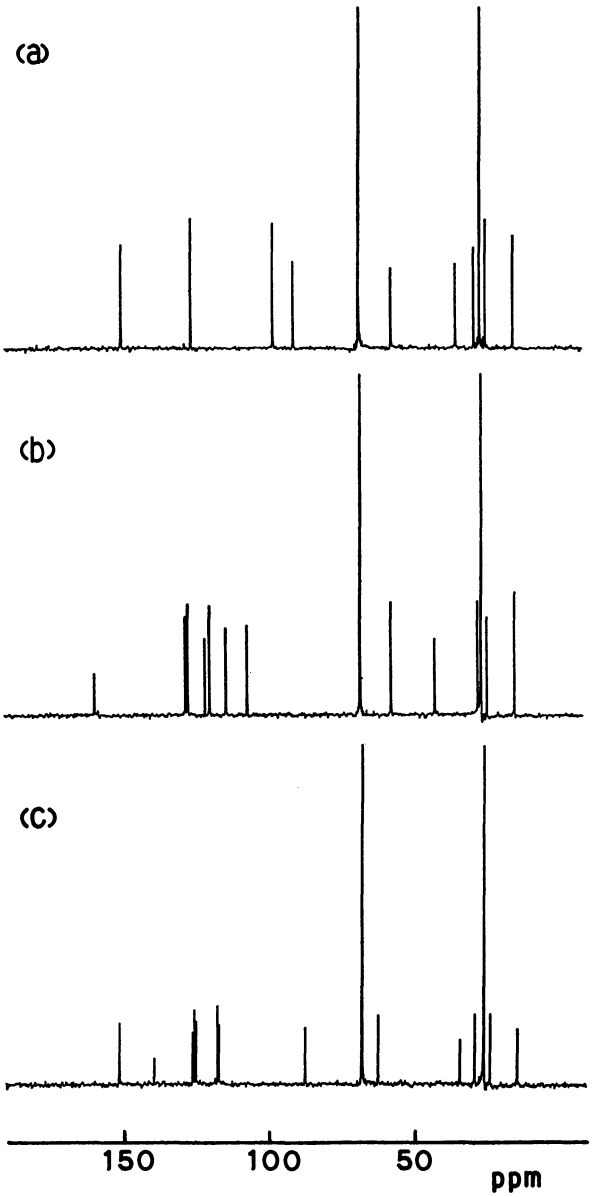

Fig. 2. ^{13}C spectra of the anions in THF at 25 MHz; (a) V, (b) VII, and (c) VIII.

against the carbon chemical shifts, except for the 2-carbons of V and VII, the 1-carbon of VIII, and the butyl carbons, having no π-electron. A good correlation exists between them, with a correlation coefficient of -0.981. Thus, these chemical shifts are linearly related to the total electron densities at the carbons in question, with a slope of -149 ppm electron^{-1}. This relationship implies that the total electron densities on the carbons of six different anions can be estimated from the observed carbon chemical shifts with an identical scale. The δ_c values of the aromatic carbons of I and V increase in the order 5-, 3-, 4-, and 6-carbons, showing that the total electron densities decrease in the same order. The δ_c values for III and VII, and for IV and VIII also increase in almost the same order respectively. In the aromatic rings of two kinds of anions, I, III, and IV, and the corresponding V, VII, and VIII, the

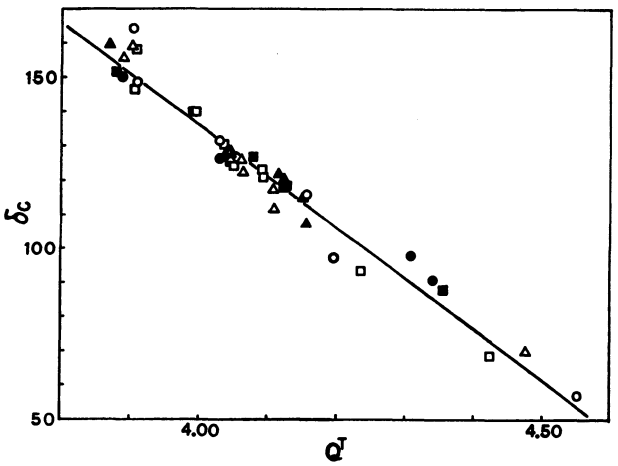

Fig. 3. ^{13}C chemical shifts *vs.* total electron densities. ○: I, △: III, □: IV, ●: V, ▲: VII, and ■: VIII in THF.

TABLE 3. THE TOTAL ($\sigma+\pi$) ELECTRON DENSITIES CALCULATED BY THE σ-INCLUDED ω-HMO METHOD (ω''-METHOD) FOR THE ANIONS

Anion Atom	I	III	V	VII	Atom	IV	VIII
1-N	5.486	5.568	5.681	5.775	1-C	3.908	
2-C	3.903	3.902			2-N	5.524	5.690
3-C	4.156	4.060	4.308	4.123	3-C	3.906	3.879
4-C	4.028	4.044	4.029	4.044	4-C	4.235	4.354
5-C	4.196	4.044	4.341	4.043	5-C	4.093	4.122
6-C	3.909	4.108	3.888	4.155	6-C	4.043	4.044
7-C		4.037		4.041	7-C	4.092	4.127
8-C		4.107		4.150	8-C	4.049	4.044
9-C		3.889		3.870	9-C	4.036	4.077
10-C		4.063		4.115	10-C	3.994	3.989
2-CH_2	4.552	4.476			1-CH_2	4.424	

charge-distribution patterns are clearly analogous respectively.

The carbon chemical shifts of I, III, V, VII, and VIII3 in THF and HMPA are given in Table 2. In the aromatic carbon shifts, the effect of a change in solvent from THF to HMPA, that is, the upfield shift induced by a change to a more polar solvent, is large on the 5-carbons of I and V, the 6-carbons of III and VII, and the 4-carbon of VIII3. The variation in the shift of V is similar to that of I, and those of VII and VIII3 are larger than and similar to that of III respectively. In addition, the ^{7}Li resonances for V, VII, and VIII3 in THF and HMPA are found in a range (0—$\pm$0.5 ppm) similar to those for I and III.[1] Therefore, two kinds of anions with lithium as a counter ion have essentially the same ion-pair structure, that is, V—VII, as well as I—II,[1] are present in THF as tight ion pairs in which the anion-cation interaction takes place mainly at the ring nitrogen and so are III—IV. In the case of V—VII, it is reasonable to regard the ring nitrogen as the site where the anion-cation interaction takes place mainly in view of the process of formation.

In conclusion, a series of anions, termed picolyl-type carbanions, with lithium as a counter ion in THF have basically three characteristics as follows: (1) This ionic species is formed by metal-proton exchange at a specific methyl group of the starting material and its methylene carbon is virtually sp^2-hybridized; (2) this ionic species is a charge-delocalized one and the total electron densities on the carbons can be estimated from the ^{13}C chemical shifts, that is, the observed chemical shifts are linearly related to the calculated electron densities; and (3) this ionic species is present as a tight ion pair in which the anion-cation interaction takes place mainly at the ring nitrogen. In view of these characteristics, I—IV can be regarded as picolyl-type carbanions, but V—VII are ionic species having the second and the third terms of the characteristics on picolyl-type carbanions.

The authors wish to thank Professor Y. Sasaki (Osaka University, Suita) for his kindness in giving opportunities to use the NMR facilities, and Mr. A. Yoshino (Nagoya Institute of Technology, Nagoya) for his help in measuring the 25 MHz spectra.

References

1) Part V in this series: K. Konishi, A. Yoshino, M. Katoh, K. Takahashi, Y. Kawada, T. Sugawara, and H. Iwamura, *Bull. Chem. Soc. Jpn.*, **54**, 3117 (1981).

2) K. Konishi and K. Takahashi, Preprint presented at the 42nd National Meeting of the Chemical Society of Japan, Sendai, September 1980, 4E06.

3) K. Takahashi, K. Konishi, M. Ushio, M. Takaki, and R. Asami, *J. Organomet. Chem.*, **50**, 1 (1973).

4) K. Konishi, Y. Onari, S. Goto, and K. Takahashi, *Chem. Lett.*, **1975**, 717.

5) G. Miyajima, H. Akiyama, and K. Nishimoto, *Org. Magn. Reson.*, **4**, 811 (1972).

6) H. Kuhn, *Tetrahedron*, **19**, Supplement 2, 437 (1963).

7) V. R. Sandel and H. H. Freedman, *J. Am. Chem. Soc.*, **85**, 2328 (1963).

Mössbauer Spectroscopic Study of $FeCl_3$-doped Polyacetylene

Hiroshi SAKAI,* Yutaka MAEDA, Taka-aki KOBAYASHI†, and Hideki SHIRAKAWA†

Research Reactor Institute, Kyoto University, Kumatori-cho, Sennan-gun, Osaka 590-04

†*Institute of Materials Science, University of Tsukuba, Sakura-mura, Niihari-gun, Ibaraki 305*

(Received November 1, 1982)

Mössbauer spectra of $FeCl_3$-doped polyacetylenes $[CH(FeCl_3)_y]_x$ (y=0.074, 0.087, and 0.13), which exhibit high electrical conductivities of ≈800, ≈800, and ≈100 S/cm at room temperature, have been measured at the temperatures of 290, 196, 78, and 5 K, respectively. The spectra consist of a superposition of two quadrupole-split doublets, described as doublet (A) and doublet (B), at 290, 196, and 78 K. At 5 K the doublet (A) splits into six lines arising from the magnetic hyperfine interaction, whereas the doublet (B) still remains paramagnetic. The doublet (B) increases remarkably in the Mössbauer absorption with decreasing temperature and is predominant. The values of the isomer shift, the quadrupole splitting, and the internal magnetic field, indicate that the iron compounds corresponding to the doublet (A) and (B) are $FeCl_2 \cdot nH_2O$ (n=1 and/or 2) and $FeCl_4^-$, respectively. These results established that the mechanism of the $FeCl_3$-doping process in polyacetylene is as follows:

$$2FeCl_3 + e^- \longrightarrow FeCl_4^- + FeCl_2,$$
$$FeCl_2 + nH_2O \longrightarrow FeCl_2 \cdot nH_2O (n=1 \text{ and/or } 2).$$

Polyacetylene, $(CH)_x$, has attracted much interest in recent years because this polymer exhibits dramatic increases in electrical conductivity on doping with electron acceptor molecules such as AsF_5, SbF_5, Br_2, and I_2, or electron donors such as Na and K metals. From analogy with graphite intercalation compounds, it is expected that metal halides can also be doped and act as acceptor dopants in polyacetylene. Recently Proń *et al.*[1] have found that $FeCl_3$-doped polyacetylene, $[CH(FeCl_3)_{0.10}]_x$, exhibits very high electrical conductivity of 780 S/cm at room temperature. This value is comparable to those of AsF_5- and I_2-doped polyacetylenes.[2] From the ^{57}Fe Mössbauer spectra at room temperature, they concluded that an Fe(II) compound formed by reduction of $FeCl_3$ existed as the dopant anion in the polymer. However, they carried out no Mössbauer effect measurement at any low temperature. In these circumstances, one might overlook the other iron compounds having the lower Debye temperatures.

We have investigated in more detail $FeCl_3$-doped polyacetylenes, $[CH(FeCl_3)_{0.074}]_x$, $[CH(FeCl_3)_{0.087}]_x$, and $[CH(FeCl_3)_{0.13}]_x$, by ^{57}Fe Mössbauer spectroscopy at 290, 196, 78, and 5 K, respectively, in order to reveal the chemical form of the active iron compound and the nature of the doping process. We find from the low temperature Mössbauer spectra that two distinct iron species, *i.e.*, $FeCl_4^-$ and $FeCl_2 \cdot nH_2O$ (n=1 and/or 2), exist in the polymers. In this paper we report the mechanism of the $FeCl_3$-doping process in polyacetylene from ^{57}Fe Mössbauer effect measurements at low temperatures.

Experimental

cis-Polyacetylene films were synthesized using the method described previously.[3] The $FeCl_3$-doping was carried out by immersing the *cis*-$(CH)_x$ film in a saturated solution of $FeCl_3$ in dry nitromethane. After doping the film was washed with dry nitromethane and vacuum-dried. The dopant content was controlled by the immersion time and determined by elemental analysis. The average Fe : Cl ratio was found to be 1 : 3.9, which was larger than that of the sample of Pron *et al.* (1 : 3.65).[1]

The d.c. electrical conductivity was measured at room temperature in an inert atmosphere by the standard four-probe technique. The Mössbauer effect measurements were made with the absorbers at temperatures of 290, 196, 78, and 5 K, respectively. The thicknesses of the absorber samples were about 20 mg natural iron/cm^2. The spectra obtained were analyzed by the least square method and the velocity scale was calibrated with the magnetic hyperfine six lines of an α-Fe metallic foil, so that values of the isomer shift are given with respect to α-Fe.

Results and Discussion

The Mössbauer spectra of the $[CH(FeCl_3)_{0.087}]_x$ sample at temperatures of 290, 196, 78 K are shown in Fig. 1. This sample exhibits a room temperature conductivity (σ_{RT}) of 800 S/cm. The spectra of the other systems, $[CH(FeCl_3)_{0.074}]_x$ (σ_{RT}≈800 S/cm) and $[CH(FeCl_3)_{0.13}]_x$ (σ_{RT}≈100 S/cm), are similar to those of the $[CH(FeCl_3)_{0.087}]_x$ system. In this temperature range, the spectra consist of a superposition of two quadrupole-split doublets ((A) and (B)), as indicated by the dashed lines. The Mössbauer spectrum at 5 K of the $[CH(FeCl_3)_{0.074}]_x$ system, which has the lowest dopant content of our specimens, is shown in Fig. 2. At 5 K the doublet (A) splits into six well-resolved lines arising from the magnetic hyperfine interaction, whereas the doublet (B) still remains paramagnetic with the small quadrupole splitting. The solid lines in Figs. 1 and 2 represent the best superimposed Lorentzian curves fitted by the least square method. The Mössbauer data obtained for the $[CH(FeCl_3)_{0.087}]_x$ sample are summarized in Table 1 together with the result of Proń *et al.*[1] The data for the other systems were in good agreement with those for this system within the experimental error.

From the values of the quadrupole splitting (ΔE_Q) and the isomer shift (δ), the species possessing the large quadrupole doublet (A) is identified as a typical high spin (S=2) Fe(II) compound whereas that of the small doublet (B) is a high spin (S=5/2) Fe(III) compound. The Mössbauer absorption of the doublet (B) increases remarkably with lowering of the temperature from 290 to 5 K. This phenomenon is characteristic of compounds having a low Debye temperature. The values of ΔE_Q

Table 1. Mössbauer parameters of the $[CH(FeCl_3)_{0.087}]_x$ system

T / K	Fe(II) species				Fe(III) species			
	ΔE_Q / mm s^{-1}	δ[a] / mm s^{-1}	H_{int} / kOe	2Γ / mm s^{-1}	ΔE_Q / mm s^{-1}	δ[a] / mm s^{-1}	H_{int} / kOe	2Γ / mm s^{-1}
290	2.35±0.03	1.16±0.03	—	0.35±0.02	0.24±0.06	0.23±0.06	—	0 40±0.04
196	2.56±0.03	1.23±0.03	—	0.38±0.02	0.26±0.03	0.29±0.03	—	0.48±0.02
78	2.61±0.03	1.28±0.03	—	0.35±0.02	0.30±0.03	0.33±0.03	—	0.55±0.02
5	2.52±0.03	1.26±0.03	250±10	0.35±0.02	0.31±0.03	0.31±0.03	—	0.57±0.02
RT[b]	2.38±0.10	1.15±0.10						

a) With respect to the center of an α-Fe metallic foil at room temperature. b) Data from Ref. 1.

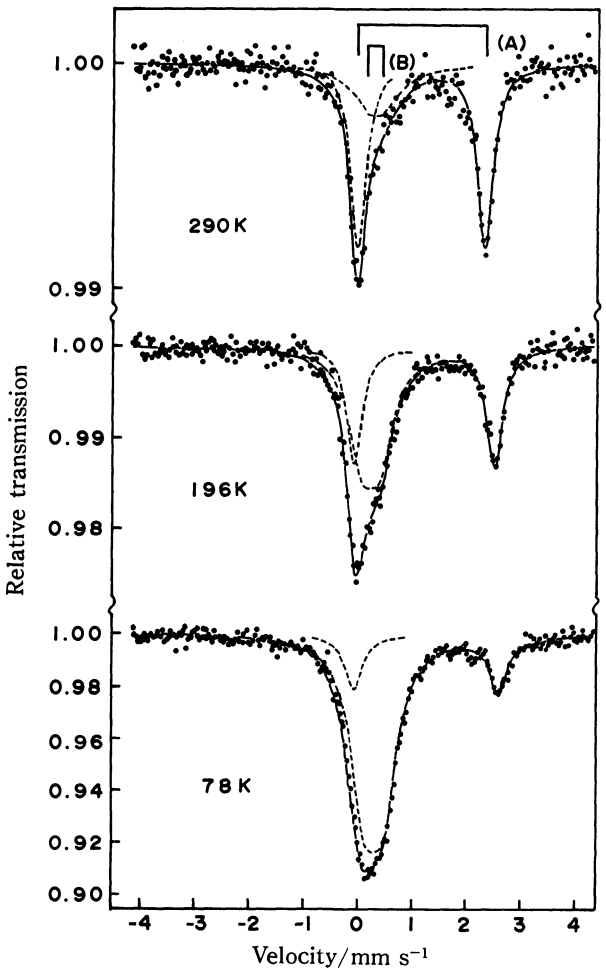

Fig. 1. Mössbauer spectra of the $[CH(FeCl_3)_{0.087}]_x$ system at 290 K, 196 K, and 78 K.

and δ for the doublet (A) at room temperature are in good agreement with the result of Proń *et al.*[1]

Fe(II) Species Present in Polyacetylene. The high spin Fe(II) compound of the doublet (A) may be formed by reduction of the doped $FeCl_3$, that is, electron transfer from polyacetylene to $FeCl_3$. Then the Fe(II) species should be either $FeCl_4^{2-}$, anhydrous $FeCl_2$, or hydrated $FeCl_2$. Edwards *et al.*[4] measured the Mössbauer effect of tetrahedrally coordinated $FeCl_4^{2-}$ ions in the temperature range 1.5—363 K. The ΔE_Q value at 78 K for the Fe(II) compound observed in polyacetylene is close to the mean value for the $FeCl_4^{2-}$ ions (ΔE_Q=2.76 mm/s at 77 K), whereas the δ value

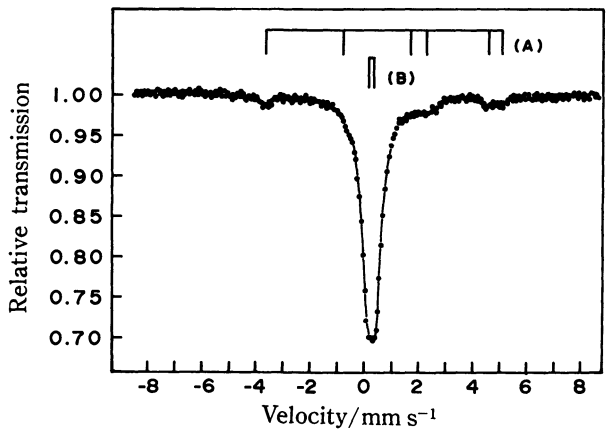

Fig. 2. Mössbauer spectrum of the $[CH(FeCl_3)_{0.074}]_x$ system at 5 K.

for the former is considerably larger than those for the tetrahedral $FeCl_4^{2-}$ ions (δ=0.86 mm/s at 77 K) and is rather close to those in the octahedral Fe(II) compounds. The possibility of anhydrous $FeCl_2$ is immediately ruled out from the Mössbauer spectrum at 5 K, showing six absorption lines due to the internal magnetic field (H_{int}) of 250 kOe (1 Oe=1000/4π A m^{-1}). The Mössbauer spectrum of the anhydrous $FeCl_2$ compound does not show six absorption lines due to the magnetic hyperfine interaction even below the Néel temperature of 24 K.[5,6] Hydrated $FeCl_2$ compounds, $FeCl_2 \cdot H_2O$, $FeCl_2 \cdot 2H_2O$, and $FeCl_3 \cdot 4H_2O$, have been well studied by Mössbauer spectroscopy.[7] $FeCl_2 \cdot 4H_2O$, in which the Fe^{2+} ion is octahedrally surrounded by two chlorine atoms in *trans* configuration with $4H_2O$, is paramagnetic even at 5 K and becomes antiferromagnetic below the Néel temperature of 1.1 K.[8] Therefore, it is clear that the Fe(II) species in polyacetylene is different from $FeCl_2 \cdot 4H_2O$.

The Mössbauer spectra of the dihydrated compound, $FeCl_2 \cdot 2H_2O$, which consists of edge-sharing octahedral chains, are very similar to those of the Fe(II) species present in polyacetylene over the temperature range between 300 and 5 K.[9] $FeCl \cdot 2H_2O_2$ becomes antiferromagnetic below the Néel temperature of 23 K and its Mössbauer spectrum at 4.2 K shows the unsymmetrical six lines due to the internal magnetic field of 255±6 kOe and the quadrupole splitting of +2.48 mm/s with $|\eta|$=0.2.[9] These values of H_{int} and ΔE_Q for $FeCl_2 \cdot 2H_2O$ are in good agreement with those at 5 K for the Fe(II) compound observed in polyacetylene (Table 1).

In the paramagnetic phase, for example at room temperature, the values of ΔE_Q(=2.32 mm/s) and δ(=1.16 mm/s) for $FeCl_2 \cdot 2H_2O$[10] are also very close to those for our Fe(II) species. $FeCl_2 \cdot H_2O$ is also antiferromagnetic below the same temperature of 23 K and the saturation value of the internal magnetic field ($T \rightarrow 0$ K) is about 252 kOe.[11] The value of ΔE_Q at $T=0$ K is evaluated to be +2.50 mm/s. These values of H_{int} and ΔE_Q for $FeCl_2 \cdot H_2O$ in the antiferromagnetic region are in good agreement with those for $FeCl_2 \cdot 2H_2O$. Furthermore, the values of ΔE_Q and δ in the paramagnetic region are also close to those for $FeCl_2 \cdot 2H_2O$. Therefore, the Fe(II) species, formed by reduction of $FeCl_3$ doped in polyacetylene, is determined to be either $FeCl_2 \cdot 2H_2O$ or $FeCl_2 \cdot H_2O$, or their mixture. The Fe(II) compound may exist as clusters in the polyacetylene film because it has the same values of δ, ΔE_Q, and H_{int} at corresponding temperatures as those for the crystalline $FeCl_2 \cdot 2H_2O$ or $FeCl_2 \cdot H_2O$.

Fe(III) Species Present in Polyacetylene. From the doping process of $FeCl_3$, it is expected that one of the $FeCl_4^-$ and $FeCl_6^{3-}$ ions, and anhydrous $FeCl_3$ and $FeCl_3 \cdot 6H_2O$ compounds corresponds to the high spin Fe(III) species of the small quadrupole doublet (B) in the doped polyacetylene. A detailed comparison of our Mössbauer spectra of the doublet (B) with those for the expected compounds is pertinent. The possibility of two neutral compounds, anhydrous $FeCl_3$ and $FeCl_3 \cdot 6H_2O$, is ruled out for the following reasons: (i) the former anhydrous compound becomes antiferromagnetic below the Néel temperature of 15 K and the extrapolated value ($T \rightarrow 0$ K) of the internal magnetic field is about 487 kOe,[12] (ii) the δ value (=0.55 mm/s at 78 K) for the former is also larger than that of the doublet (B), and (iii) the both values of ΔE_Q(=0.91 mm/s at 78 K) and δ(=0.60 mm/s at 78 K) for the latter hydrated compound[13] are considerably larger than those for the Fe(III) species of the doublet (B). Therefore, the Fe(III) species present in polyacetylene is different from the anhydrous $FeCl_3$ and $FeCl_3 \cdot 6H_2O$. It is confirmed that an octahedral $FeCl_6^{3-}$ ion exists in certain solid complexes in association with a smaller, univalent cation. The Mössbauer parameters for the $FeCl_6^{3-}$ ions were reported as δ=0.48—0.52 mm/s and ΔE_Q=0 mm/s at 78 K, respectively.[14] The δ values for the octahedrally coordinated $FeCl_6^{3-}$ ions are slightly larger.

The δ value for the Fe(III) species in polyacetylene suggests that this species is a tetrahedrally coordinated substance. It is well known that the covalency is greater in tetrahedral FeX_4^- ions than in the corresponding octahedral FeX_6^{3-} ions. The tetrahedral $FeCl_4^-$ ion is stable and found in many chemical compounds. The Mössbauer spectra of the typical compounds R_4NFeCl_4 (R=Me, Et, and Ph) were measured in the temperature range 293—1.1 K by Edwards and Johnson.[15] They found that these compounds at 4.2 K showed single absorption peak and still remained paramagnetic. The δ values were found to be about 0.30 mm/s at 77 K. For the compounds containing the small cations, Me_4N^+ and Et_4N^+, the ΔE_Q values are equal to zero, whereas the value is 0.2 mm/s for Ph_4NFeCl_4, indicating that the tetrahedral $FeCl_4^-$ ion is distorted. These values of δ and ΔE_Q for the tetrahedrally coordinated $FeCl_4^-$ ions are in good agreement with those for the Fe(III) species of the doublet (B) over the temperature range 290—5 K. Thus it is concluded that the Fe(III) species present in the doped polyacetylene is a distorted tetrahedral $FeCl_4^-$ ion.

Mechanism of the $FeCl_3$-doping Process. As mentioned above, it was found that two chemical species of $FeCl_2 \cdot nH_2O$ (n=1 and/or 2) and $FeCl_4^-$ existed in the $FeCl_3$-doped polyacetylene. This experimental fact suggests strongly that following reactions occur between the doped $FeCl_3$ molecule and polyacetylene:

$$FeCl_3 + e^- \longrightarrow FeCl_2 + Cl^-,$$

$$FeCl_3 + Cl^- \longrightarrow FeCl_4^-,$$

$$FeCl_2 + nH_2O \longrightarrow FeCl_2 \cdot nH_2O \ (n=1 \text{ and/or } 2).$$

In these reactions there are two kinds of $FeCl_3$ dopants which have individual roles in polyacetylene; one acts as an electron acceptor and the other as a stabilizer for Cl^- produced by reduction of $FeCl_3$. This behavior is similar to that of I_2 dopant in polyacetylene. In the latter system the presence of the triiodide ion (I_3^-), formed by the combination of the I_2 molecule and the resulting I^- ion, has been confirmed by Raman spectroscopy,[16,17] XPS,[16,18,19] and the ^{129}I Mössbauer effect.[20,21]

The finding of no anhydrous $FeCl_2$ in the Mössbauer spectra suggests that the neutral species is removed from the system together with the unreacted $FeCl_3$ dopant by washing with dry nitromethane. In the presence of a small amount of water in the solvent and the doped salt, the hydrated compound, $FeCl_2 \cdot nH_2O$ (n=1 and/or 2), may be formed and no longer removed by washing. Therefore, the content of the hydrated species in the polymer film may be dependent on the water content of the solution. This expectation well interprets the Mössbauer spectra especially at low temperature, indicating that the absorption area of the doublet (B) is much larger than that of the doublet (A) even at 78 K. The Mössbauer absorption area is approximately proportional to the content of each resonant nucleus at a sufficiently low temperature compared with each Debye temperature and in a sufficiently low concentration of each resonant nucleus. Furthermore, the Fe : Cl ratio obtained by the elemental analysis was found to be 1 : 3.9, which also supported strongly the validity of the expectation. If only two chemical species, $FeCl_4^-$ and $FeCl_2 \cdot nH_2O$, exist in the polymer film (no contaminant), the ratio 1 : 3.9 indicates that the content of the $FeCl_4^-$ ion is 19 times greater than that of the hydrated $FeCl_2$ species. This seems reasonable for the absorption area ratio of the Fe(III) to Fe(II) species in the Mössbauer spectrum at 5 K (Fig. 2).

The mechanism of the $FeCl_3$-doping process in polyacetylene differs from that in graphite. In the $FeCl_3$-graphite intercalation compound, the doped $FeCl_3$ is not reduced and its values of δ and ΔE_Q are nearly equal to those for pure anhydrous $FeCl_3$.[22] Many $FeCl_3$ molecules can nevertheless be doped in graphite. In the $FeCl_3$-doped polyacetylene the neutral $FeCl_3$ is completely converted to $FeCl_2$ and $FeCl_4^-$ and the

latter is the dominant dopant species.

This work at University of Tsukuba was supported partly by a Grant-in-Aid for Scientific Research No. 56470083 from the Ministry of Education, Science and Culture.

References

1) A. Proń, I. Kulszewicz, D. Billaud, and J. Przyluski, *J. Chem. Soc., Chem. Commum.* **1981**, 783; A. Proń, D. Billaud, I. Kulszewicz, C. Budrowski, J. Przyluski, and J. Suwalski, *Mat. Res. Bull.*, **16**, 1229 (1981).
2) C. K. Chiang, M. A. Druy, S. C. Gau, A. J. Heeger, E. J. Louis, A. G. MacDiarmid, Y. W. Park, and H. Shirakawa, *J. Am. Chem. Soc.*, **100**, 1013 (1978).
3) H. Shirakawa and S. Ikeda, *Polym. J.*, **2**, 231 (1971); T. Ito, H. Shirakawa, and S. Ikeda, *J. Polym. Sci., Polym. Chem.*, **12**, 11 (1974); **13**, 1943 (1975).
4) P. R. Edwards, C. E. Johnson, and R. J. P. Williams, *J. Chem. Phys.*, **47**, 2074 (1967).
5) K. Ono, A. Ito, and T. Fujita, *J. Phys. Soc. Jpn.*, **19**, 2119 (1964).
6) E. Pfletschinger, *Z. Phys.*, **209**, 119 (1968).
7) N. N. Greenwood and T. C. Gibb, "Mössbauer Spectroscopy," Chapman and Hall, London (1971), Chap. 6.
8) C. E. Johnson and M. S. Ridout, *J. Appl. Phys.*, **38**, 1272 (1967).
9) C. E. Johnson, *Proc. Phys. Soc.*, **88**, 943 (1966).
10) C. D. Burbridge and D. M. L. Goodgame, *J. Chem. Soc., A*, **1968**, 1410.
11) G. Ziebarth, *Z. Phys.*, **212**, 330 (1968).
12) C. W. Kocher, *Phys. Lett. A*, **24**, 93 (1967).
13) N. Thrane and G. Trumpy, *Phys. Rev. B*, **1**, 153 (1970).
14) C. A. Clausen and M. L. Good, *Inorg. Chem.*, **7**, 2662 (1968).
15) P. R. Edwards and C. E. Johnson, *J. Chem. Phys.*, **49**, 211 (1968).
16) S. L. Hsu, A. J. Signorelli, G. P. Pez, and R. H. Baughman, *J. Chem. Phys.*, **69**, 106 (1978).
17) I. Harada, Y. Furukawa, M. Tasumi, H. Shirakawa, and S. Ikeda, *J. Chem. Phys.*, **73**, 4746 (1980).
18) I. Ikemoto, M. Sakairi, T. Tsutsumi, H. Kuroda, I. Harada, M. Tasumi, H. Shirakawa, and S. Ikeda, *Chem. Lett.*, **1979**, 1189.
19) W. R. Salaneck, H. R. Thomas, R. W. Bigelow, C. B. Duke, E. W. Plummer, A. J. Heeger, and A. G. MacDiarmid, *J. Chem. Phys.*, **72**, 3674 (1980).
20) T. Matsuyama, H. Sakai, H. Yamaoka, Y. Maeda, and H. Shirakawa, *Solid State Commun.*, **40**, 563 (1981).
21) G. Kaindl, G. Wortmann, S. Roth, and K. Menke, *Solid State Commun.*, **41**, 75 (1982).
22) R. H. Herber and M. Katada, *J. Inorg. Nucl. Chem.*, **41**, 1097 (1979).

Studies on Aqueous Solutions of Saccharides. I. Activity Coefficients of Monosaccharides in Aqueous Solutions at 25 °C

Koichiro MIYAJIMA,* Masahiro SAWADA, and Masayuki NAKAGAKI
Faculty of Pharmaceutical Sciences, Kyoto University, Yoshida Shimoadachi-cho, Sakyo-ku, Kyoto 606
(Received November 13, 1982)

Activity coefficients of isomeric monosaccharides, D-glucose, D-mannose, and D-galactose were determined by isopiestic comparison method at 25 °C. Excess partial molar entropy of water ($\bar{S}_w^{ex}$) of each monosaccharide solution was negative and the absolute value increased with concentration of solute. From the magnitudes of negative $\bar{S}_w^{ex}$, it was concluded that the structure making ability among three isomers lies in the order D-glucose> D-mannose>D-galactose.

Many papers have been published on the properties of aqueous solutions of monosaccharides, because they are not only biologically important compounds but also the typical hydrophilic nonelectrolytes in the field of solution chemistry.

On the hydration of monosaccharides, Kabayama and Patterson[1] postulated that the spacing of oxygen atoms of equatorial hydroxyl groups of hexopyranose in chair conformations, which are predominant in aqueous solution, are compatible to the spacing of oxygen atoms in tridymite-like structure of water. This model is a so called "specific hydration model."[4] To investigate the validity of the hypothesis, various kinds of experiments, such as partial molar volume,[2,3] compressibility,[2,3] ^{1}H- and ^{17}O-NMR[4-7] and dielectric relaxation[4,8] were carried out. However their conclusions are still in controversy.

From the similar viewpoint, we determined the activity coefficients of three isomeric monosaccharides, *i.e.* D-glucose, D-mannose, and D-galactose in aqueous solution at 25°C and calculated the excess partial molar entropy of water ($\bar{S}_w^{ex}$) from the excess free energy combining the excess enthalpy data[9,10] and investigated the correlation between $\bar{S}_w^{ex}$ and the structure making ability predicted by the special hydration model.

Experimental

Materials. Reagent grade D-glucose, D-mannose, and D-galactose obtained from Wako Chemical Co. Ltd., were dried over P_2O_5 *in vacuo* at room temperature for several days. Reagent grade $CaCl_2 \cdot 2H_2O$ was used without further purification. These compounds were dissolved in purified water by distillation and deionization.

Method. Osmotic coefficients were determined at 25±0.02 °C by isopiestic comparison method described elsewhere.[11] From the osmotic coefficient (ϕ), activity coefficient (γ) was calculated by

$$\ln \gamma = (\phi - 1) + \int_0^m \frac{\phi - 1}{m} dm, \quad (1)$$

where m is the molality of solute. Buoyancy correction was made for monosaccharides assuming that the densities of the solutes in solid states were unity. Experimental determination of isopiestic concentration was precise to ±0.2%. The molalities of isopiestic solution are shown in Table 1. The concentration of $CaCl_2$ used as a reference solute was determined by gravimetric analysis with silver nitrate.

Results and Discussion

Osmotic and activity coefficients of D-monnose and D-galactose are shown in Table 2 together with those of D-glucose. The values of ϕ and γ of D-glucose obtained from this experiment are in a fair agreement with those of Taylor and Rowlinson,[12] but are larger than those of Bonner and Breazeale.[13] The values of γ for three monosaccharides lie in the order D-glucose>D-galactose>D-mannose.

The standard states are taken asymmetrically; taking the infinite dilution and the pure solvent as the standard states of the solute and solvent, respectively, the total excess Gibbs free energy of solution containing a kilogram of solvent is calculated from ϕ and γ by Eq. 2.[14]

$$G^{ex} = mRT(1 - \phi + \ln \gamma). \quad (2)$$

From the heat of dilution of monosaccharides, excess enthalpy of solution (H^{ex}) is expressed in the following form,[9]

$$H^{ex} = h_{xx}m^2 + h_{xxx}m^3, \quad (3)$$

where h_{xx} and h_{xxx} are the interaction parameters. Excess entropy of solution (S^{ex}) is calculated by Eq. 4.

$$S^{ex} = (H^{ex} - G^{ex})/T. \quad (4)$$

Excess quantities *vs.* concentration curves for three monosaccharides are shown in Figs. 1, 2, and 3. The small value of positive excess free energy comes from the difference between largely positive enthalpy and entropy term, that is, the entropy-enthalpy compensation takes place in each system. The predominance of enthalpy term over entropy term characterizes hydrophilic solute in water,[15] in contrast with the hydrophobic solute in aqueous solution, where the entropy term is superior to enthalpy term.[16] The values of TS^{ex} among three isomers decrease in the order D-glucose, D-mannose, and D-galactose.

To investigate the structural change of solvent water, excess partial molar quantities of water were calculated by the following equations.

$$\bar{G}_w^{ex} = mRT(1 - \phi)\frac{M_w}{1000}, \quad (5)$$

$$\bar{H}_w^{ex} = -(h_{xx}m^2 + 2h_{xxx}m^3)\frac{M_w}{1000}, \quad (6)$$

$$\bar{S}_w^{ex} = (\bar{H}_w^{ex} - \bar{G}_w^{ex})/T, \quad (7)$$

where $\bar{G}_w^{ex}$, $\bar{H}_w^{ex}$, and $\bar{S}_w^{ex}$ are the excess partial molar free energy, enthalpy, and entropy of water, respectively.

TABLE 1. MOLALITIES OF ISOPIESTIC SOLUTIONS

D-Glucose					
m(NaCl)[a]	m(Glucose)	m($CaCl_2$)[a]	m(Glucose)	m($CaCl_2$)[a]	m(Glucose)
0.1837	0.3384	0.2838	0.7930	1.1959	3.5996
0.3578	0.6520	0.4733	1.2547	1.2636	3.8538
0.4989	0.9026	0.5993	1.6166	1.3728	4.2811
0.5807	1.0484	0.6645	1.8094	1.4667	4.6536
0.6441	1.1608	0.7206	1.9878	1.5531	5.0090
0.7630	1.3725	0.7966	2.2282	1.6962	5.6249
0.8384	1.5040	0.8545	2.4122	1.7930	6.0510
0.9296	1.6634	0.9466	2.7181	1.8240	6.1977
1.0069	1.8009	1.0435	3.0489		
1.0919	1.9454	1.1447	3.4120		
D-Mannose					
m(NaCl)[a]	m(Mannose)	m($CaCl_2$)[a]	m(Mannose)	m($CaCl_2$)[a]	m(Mannose)
0.2257	0.4160	0.4406	1.1849	1.5956	5.4166
0.4318	0.7927	0.5783	1.5953	1.6110	5.4839
0.4990	0.9162	0.6646	1.8657	1.6670	5.7387
0.5380	0.9884	0.7163	2.0324	1.6843	5.8187
0.5807	1.0662	0.8143	2.3533	1.8352	6.5255
0.7634	1.4026	0.9389	2.7913	1.8781	6.7322
0.8385	1.5416	0.9649	2.8800	1.8798	6.7401
0.8862	1.6242	1.0114	3.0481		
0.9296	1.7065	1.0574	3.2249		
1.0069	1.8496	1.1741	3.6670		
1.0911	2.0045	1.3558	4.3884		
1.3251	2.4375	1.4225	4.6767		
D-Galactose					
m($CaCl_2$)[a]	m(Galactose)[a]	m($CaCl_2$)[a]	m(Galactose)		
0.2532	0.6597	0.7687	2.1946		
0.2973	0.7794	0.8352	2.4117		
0.3855	1.0252	1.0180	3.0534		
0.4839	1.3101	1.0733	3.2622		
0.6381	1.7765	1.1246	3.4489		
0.6843	1.9196				

a) The osmotic coefficients of standard solutions were obtained from the Appendix of "Electrolyte Solutions."[17]

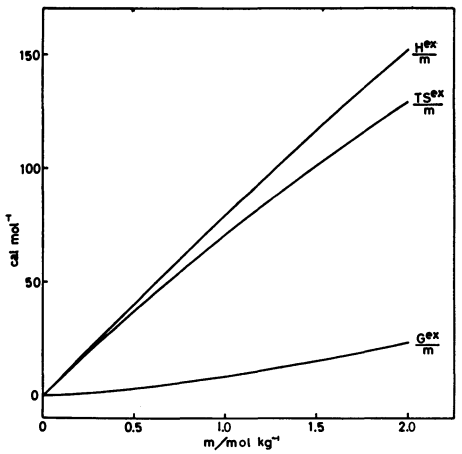

Fig. 1. Excess thermodynamic quantities for aqueous D-glucose solutions at 25 °C.

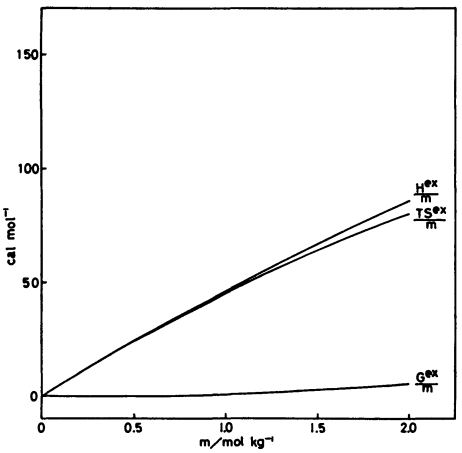

Fig. 2. Excess thermodynamic quantities for aqueous D-mannose solutions at 25 °C.

As shown in Fig. 4, the values of $\bar{S}_w^{ex}$ for D-glucose, D-mannose, and D-galactose are negative and the absolute values increase with concentration of monosaccharide, indicating the ordering of water molecule by the dissolution of these monosaccharides. As shown in Fig. 5, the predominance of enthalpy term over entropy term gives the negative value of $\bar{G}_w^{ex}$. The negative $\bar{S}_w^{ex}$ values which mean the increase of water structure lie in the order D-glucose>D-mannose>D-galactose. Tait[4] calculated the percentage of equatorial

TABLE 2. OSMOTIC AND ACTIVITY COEFFICIENTS OF HEXOSES AT 25 °C

				D-Glucose				
m	ϕ	γ	m	ϕ	γ	m	ϕ	γ
0.1	1.001	1.002	0.9	1.018	1.031	3.0	1.086	1.166
0.2	1.002	1.004	1.0	1.021	1.036	3.5	1.101	1.200
0.3	1.004	1.006	1.2	1.027	1.047	4.0	1.114	1.233
0.4	1.005	1.009	1.4	1.034	1.059	4.5	1.126	1.266
0.5	1.007	1.013	1.6	1.040	1.071	5.0	1.137	1.298
0.6	1.010	1.017	1.8	1.047	1.084	5.5	1.147	1.329
0.7	1.012	1.021	2.0	1.054	1.097	6.0	1.156	1.306
0.8	1.015	1.026	2.5	1.071	1.131			
				D-Mannose				
m	ϕ	γ	m	ϕ	γ	m	ϕ	γ
0.1	1.000	1.000	0.9	1.004	1.005	3.0	1.043	1.068
0.2	1.000	1.000	1.0	1.005	1.006	3.5	1.055	1.088
0.3	1.000	1.000	1.2	1.007	1.010	4.0	1.066	1.109
0.4	1.000	1.000	1.4	1.010	1.014	4.5	1.076	1.130
0.5	1.001	1.001	1.6	1.014	1.019	5.0	1.085	1.150
0.6	1.001	1.001	1.8	1.017	1.025	5.5	1.094	1.169
0.7	1.002	1.002	2.0	1.021	1.031	6.0	1.101	1.189
0.8	1.003	1.003	2.5	1.032	1.048			
				D-Galactose				
m	ϕ	γ	m	ϕ	γ	m	ϕ	γ
0.1	1.000	1.001	0.7	1.003	1.005	1.6	1.016	1.025
0.2	1.001	1.001	0.8	1.004	1.006	1.8	1.021	1.032
0.3	1.001	1.002	0.9	1.005	1.007	2.0	1.026	1.039
0.4	1.001	1.002	1.0	1.006	1.009	2.5	1.039	1.061
0.5	1.002	1.003	1.2	1.008	1.013	3.0	1.051	1.083
0.6	1.002	1.004	1.4	1.012	1.018	3.5	1.061	1.104

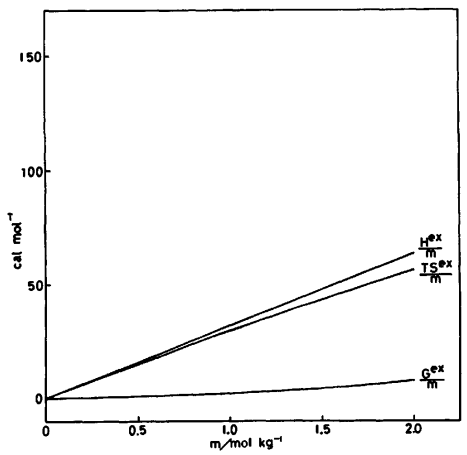

Fig. 3. Excess thermodynamic quantities for aqueous D-galactose solutions at 25 °C.

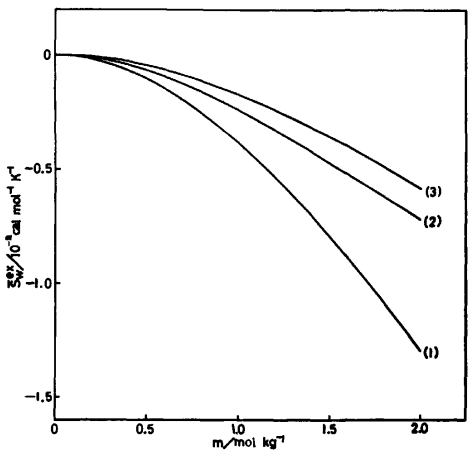

Fig. 4. Excess partial molar entropy of water ($\bar{S}_w^{ex}$) in aqueous D-glucose (1), D-mannose (2), and D-galactose (3) solutions at 25 °C.

OH groups of isomeric monosaccharides assuming that these monosaccharides take chair conformations and are the equilibrium mixtures of α- and β-anomers. Using his results, we calculated the equatorial OH content of D-galactose and D-mannose relative to D-glucose, resulting in 0.78 and 0.71 for D-galactose and D-mannose, respectively. Therefore the structure making ability must be in the order D-glucose>D-galactose>D-mannose. From the ^{17}O-NMR study,[4] Tait could not distinguish the hydration properties of three isomers and concluded that "at least three equatorial hydroxyl groups are required for the monosaccharide to be an effective substitute for the water within structured cluster of water molecules." Judging from the $\bar{S}_w^{ex}$ values of three isomers obtained from this work, the structure making ability lies in the order D-glucose>D-mannose>D-galactose. We cannot explain the discrepancy of structure making ability observed between our result and special hydration model at the present stage. A possible explanation is that the nature of structure promotion of these monosaccharides is affected not only by the number of equatorial hydroxyl groups but also by the relative position of equatorial hydroxyl groups,

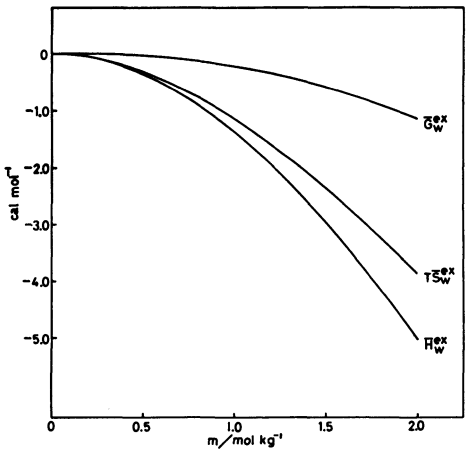

Fig. 5. Excess partial molar free energy, enthalpy, and entropy of water in aqueous D-glucose solutions at 25 °C.

on the assumption that the special hydration model is correct.

References

1) M. A. Kabayama and D. Patterson, *Can. J. Chem.*, **36**, 563 (1958).
2) F. Franks, J. R. Ravenhill, and D. S. Reid, *J. Solution Chem.*, **1**, 3 (1972).
3) H. Høiland and H. Holvik, *J. Solution Chem.*, **7**, 587 (1978).
4) M. J. Tait, A. Suggett, F. Franks, and P. A. Quickenden *J. Solution Chem.*, **1**, 131 (1972).
5) A. Suggett, S. Ablett, and P. J. Lillford, *J. Solution Chem.*, **5**, 17 (1976).
6) A. Suggett, *J. Solution Chem.*, **5**, 33 (1976).
7) J. M. Harvey and M. C. R. Symons, *J. Solution Chem.*, **7**, 571 (1978).
8) A. Suggett and A.H. Clark, *J. Solution Chem.*, **5**, 1 (1976).
9) G. Barone, P. Cacace, G. Castronuovo, and V. Elia, *Carbohydr. Res.*, **91**, 101 (1981).
10) J. J. Savage and R. H. Wood, *J. Solution Chem.*, **5**, 733 (1976).
11) K. Miyajima, K. Inari, N. Hamaguchi, H. Yoshida, and M. Nakagaki, *Nippon Kagaku Kaishi*, **1975**, 1447.
12) J. B. Taylor and J. S. Rowlinson, *Trans. Faraday Soc.*, **51**, 1183 (1955).
13) O. D. Bonner and W. H. Breazeale, *J. Chem. Eng. Data*, **10**, 325 (1965).
14) H. L. Friedman, *J. Chem. Phys.*, **32**, 1351 (1960).
15) F. Franks, "Water, A Comprehensive Treaties," ed by F. Franks, Plenum Press, New York (1975), Vol. 2, p. 366.
16) S. Lindenbaum and G. E. Boyd, *J. Phys. Chem.*, **70**, 814 (1966).
17) R. A. Robinson and R. H. Stokes, "Electrolyte Solutions," 2nd ed, Butterworths, London (1959).

Gravimetric Determination of Copper(II) Using N^1-Hydroxy-N^1-(*m*-tolyl)-N^2-(*o*-chlorophenyl)-*p*-toluamidine Hydrochloride

Hemlata Mohabey, Pramod Kumar Sharma,* and Rajendra Kumar Mishra

Department of Chemistry, Ravishankar University, Raipur, 492 010, India

(Received August 13, 1982)

A simple, rapid, and accurate method has been developed for the gravimetric determination of Copper(II) using a new reagent N^1-hydroxy-N^1-(*m*-tolyl)-N^2-(*o*-chlorophenyl)-*p*-toluamidine hydrochloride (HTCPTH). The proposed reagent reacts quantitatively with copper at 3.3—11.0 pH giving a buff coloured precipitate. The precipitated complex can be easily filtered, dried and directly weighed as $(C_{21}H_{18}N_2OCl)_2Cu$. The complex is thermally stable as is evident from DTA and TGA studies up to 210 °C and insoluble in many organic solvents. Most of the common ions including Ni(II), Co(II), Cr(III), Mn(II), *etc.* do not interfere. The interference due to iron(III) can be eliminated by masking it with tartaric acid. The method has been successfully applied for the determination of copper in some British Chemical Standards alloys.

N^1-Hydroxy-N^1,N^2-diarylbenzamidines have been found to be potential analytical reagents for the determination of various transition elements.[1-3] This communication describes the use of a new *N*-hydroxyamidine, N^1-hydroxy-N^1-(*m*-tolyl)-N^2-(*o*-chlorophenyl)-*p*-toluamidine hydrochloride(I) for the gravimetric determination of copper(II).

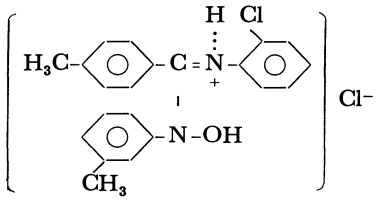

1

The reagent reacts with copper(II) giving a buff coloured precipitate at 2.2—11.5 pH but the reaction is quantitative only at pH 3.3—11.0. The complex is stable towards heat and dilute mineral acids and no weight loss is observed upto 210 °C. The coprecipitated reagent can be completely removed by washing with hot 50% aqueous ethanol as the complex is insoluble in it. The conversion factor (metal/metal complex is very small (0.0833) and therefore small quantities of copper can be accurately determined. The method is free from interference of many foreign ions and is comparable to established methods.[4-9]

Experimental

Reagents and Chemicals. All the chemicals used were of A. R. grade.

Copper stock solution was prepared by dissolving the British Drug House, AnalaR copper metal in dilute nitric acid and the solution boiled to expel nitrogen oxides. The solution was standardized gravimetrically using salicylaldehyde oxime.[10]

The reagent, HTCPTH was prepared by condensing *N*-(*o*-chlorophenyl)-*p*-toluimidoyl chloride and *N*-(*m*-tolyl) hydroxylamine in equimolar amounts in ether as mentioned earlier.[1] A 1% solution of the reagent in ethanol was used for precipitation purposes. The pH of the solution was adjusted to 3.3 to 11.0 with acetic acid and ammonia.

Apparatus. A single pan semimicrobalance SAHM-68 (VEB-Analytic DDR) was used for weighing. The pH of the solution was measured with a Systronic pH meter type −322.

Recommended Procedure. An aliquot of copper solution containing 10—15 mg of copper was diluted to 150 ml. The pH of the solution was adjusted to 3.3 to 11.0 and heated to about 60 °C. To this added 1% reagent solution (20—30 ml per 12.8 mg copper) dropwise with constant stirring. The buff coloured precipitate was digested on water bath for 20 min and filtered through a preweighed G-3 sintered crucible. The complex was washed with hot water followed by 60% ethanol till the washings gave no red-purple colour with iron(III) chloride. It was dried at 120 °C to constant weight and weighed as $Cu(C_{21}H_{18}N_2OCl)_2$ (Found: C, 65.98; H, 4.66; N, 7.28; Cu, 8.30%. Calcd for: C, 66.09; H, 4.72; N, 7.34; Cu, 8.33%).

Properties of the Complex: The copper complex is insoluble in water and sparingly soluble in ethanol, acetone, carbon tetrachloride, chloroform and many other organic solvents. The complex can be dried to constant weight at 110—180 °C with out decomposition. The melting point of the complex is 208 °C and it blackens at this temperature. Though there was change in colour at the melting point of the complex, weight loss was observed only at 220 °C during thermogravimetric studies of the complex.

Precision. The standard deviation of ten independent determinations with 12.8 mg copper is 0.0066 while the relative standard deviation is 0.051%.

Effect of Foreign Ions. Following the procedure described above a known amount of copper (12.8 mg) was accurately determined at pH 3.5—5.5 in presence of many foreign ions. Vanadium(V), iron(II), and iron(III) form coloured complexes with the proposed reagent under the recommended procedure. These ions could be masked with tartaric acid (2 g) and thus the interference due to these ions was eliminated. It is evident from Table 1 that copper can be separated from almost all common ions like Pb(II), Co(II), Ni(II), Bi(III), Sn(IV), V(V), Fe(III), *etc.* and hence the method is suitable for analysis of copper alloys.

Determination of Copper in Alloys. An accurately weighed amount of alloy containing 10—15 mg of copper in 25 ml aliquot of the final solution was dissolved in 40% nitric acid. The solution was evaporated to near dryness to remove the oxides of nitrogen. It was diluted to 100 ml and the precipitated tin and antimony oxides were filtered and washed with hot dilute acetic acid and the solution diluted to 250 ml. Copper was determined by the recommended procedure. It is evident from the results summarised in Table 2, that the amount of copper in its alloys could be determined accurately and precisely.

Thermal Analysis of Copper Complex. Thermogravimetric and differential thermal analysis were carried out to evaluate the thermal stability of the copper complex of HTCPTH. The TGA and DTA curves were obtained using

Table 1. Determination of copper in presence of foreign ions

Copper taken: 12.8 mg, pH: 4.0±0.1.

Ion	Amount of diverse ion added (mg)	Wt of copper complex	Copper found (mg)	Error (%)
Fe(III)	25	153.76	12.81	+0.07
Co(II)	100	153.54	12.79	−0.07
Ni(II)	60	154.06	12.83	+0.23
Mn(II)	50	153.46	12.78	+0.16
Cr(III)	100	153.70	12.80	0.00
W(VI)	25	153.58	12.79	−0.07
Sb(III)	100	153.88	12.82	+0.16
Bi(III)	50	153.77	12.81	+0.07
Ti(IV)	25	153.70	12.80	0.00
Zr(IV)	50	153.60	12.79	−0.07
Al(III)	100	153.66	12.80	0.00
La(III)	100	153.90	12.82	+0.16
Th(IV)	50	153.71	12.80	0.00
U(VI)	50	154.02	12.83	+0.23
Se(VI)	60	153.72	12.80	0.00
Hg(II)	50	153.22	12.76	−0.31
Zn(II)	150	153.72	12.80	0.00
Cd(II)	100	153.65	12.80	0.00
Ca(II)	100	153.70	12.80	0.00
Ba(II)	50	153.58	12.79	−0.07
Na(I)	200	153.78	12.81	+0.07
Vanadate	25	153.70	12.80	0.00
Tartrate	3000	153.46	12.78	−0.16
Citrate	2000	153.60	12.79	−0.07
Chloride	150	153.90	12.82	+0.16
Bromide	150	153.68	12.80	0.00

Table 2. Determination of copper in BCS alloys[a)]

Sample No. and name	Copper found (%)	Certified value (%)	Standard deviation (%)
5 f Brass	70.76, 70.81, 70.78 70.77, 70.79 average value: 70.78	70.80	0.0187
6 f Gun metal	.87.86, 87.88, 87.84 87.85, 87.87 average value: 87.86	87.90	0.0158
8C White metal	4.09, 4.12, 4.09 4.06, 4.09 average value: 4.09	4.10	0.0217

a) BCS: British Chemical Standards.

an automatic unit HOM-BUDAPEST Devitograph (Type-OD-102). The TGA curve (Fig. 1) shows that there is no weight loss upto 220 °C thereby indicating that the chelate is nonhydrated in nature. At 220 °C the complex starts to decompose and 5% weight loss is observed between 220 to 240 °C. Accelerated weight loss takes place in the region 240—760 °C. At about 760 °C nearly 90% weight loss is observed. Here oxide level beings giving a horizontal straight line. It is evident from thermogravimetric analysis that the thermal stability 220 °C of copper-HTCPTH complex is higher than copper-salicylaldehyde oxime[11] *i.e.* 140 °C.

The DTA curve of the complex consists of a pronounced

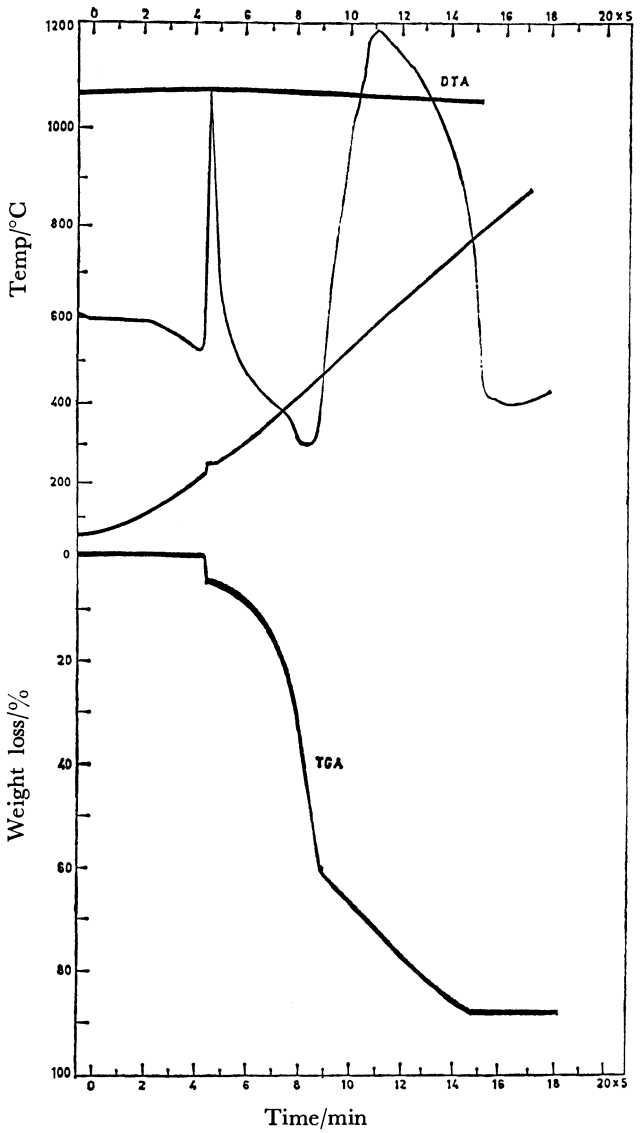

Fig. 1. DTA and TGA curves of copper complex of N^1-hydroxy-N^1-(*m*-tolyl)-N^2-(*o*-chlorophenyl)-*p*-toluamidine hydrochloride.

exothermic peak at about 210 °C which may be due to possible phase transition from solid to liquid (melting). Melting may be accompanied by the loss of organic part of the compound as nearly 5% weight loss takes place at 220 °C (melting with decomposition). The other broad and prominent exothermic peak at about 550 °C may be due to another phase transition in the complex due to loss of ligand molecules as accelerated weight loss is observed in the range 240—760 °C. A small but noticiable endothermic peak is noticed at about 400 °C. There must be some new decomposition products at this temperature as is obvious from weight loss curve. Metal 8-quinolinolates[12] and 2-quinolinecarboxylates[13] also show endothermic decomposition peaks.

Hence the direct weight of copper complex after drying at 110—180 °C for gravimetric determination is justified.

Infrared Spectra. The ligand molecule consists of a broad band at 2550 cm^{-1} confirming the presence of protonated azomethine nitrogen in *N*-hydroxyamidine hydrochloride.[14] The absence of any band in the region 2500—2730 cm^{-1} due to $\overset{+}{N}$–H stretching mode in the spectra of copper

complex suggests that deprotonation of azomethine nitrogen occurs when copper complex is formed. The band due to $C{=}N^+$ stretching (1610 cm^{-1})[15,16] is displaced to lower frequency (1570 cm^{-1}) on complex formation. This indicates the formation of C=N·····Cu coordinate linkage. The N–O stretching mode appears at 930 cm^{-1} in the free ligand.[17,18] Replacement of proton of N–OH group by copper leads to displacement of N–O stretching mode to higher frequency and appears at 950 cm^{-1} in the copper complex.

The authors are thankful to Head, Department of Chemistry, Ravishankar University, Raipur for providing Research facilities and to the Council of Scientific and Industrial Research, New Delhi for the award of a Fellowship to one of them (P.K.S.).

References

1) K. Satyanarayana and R. K. Mishra, *Anal. Chem.*, **46**, 1609 (1976).
2) H. Mohabey and R. K. Mishra, *J. Indian Chem. Soc.*, **57**, 142 (1980).
3) P. K. Sharma and R. K. Mishra, *Croat. Chem. Acta*, **53**, 87 (1980).
4) J. H. Flagg and N. H. Furman, *Ind. Eng. Chem., Anal. Ed.*, **12**, 529 (1940).
5) P. Ray and J. Gupta, *Mikrochemie*, **17**, 14 (1935).
6) S. C. Shome, *Analyst*, **75**, 27 (1950).
7) N. C. Sogani and S. C. Bhattacharya, *Anal. Chem.*, **28**, 1616 (1956).
8) F. Feigl and A. Caldas, *Anal. Chim. Acta*, **8**, 339 (1953).
9) S. P. Gupta, O. P. Malik, and J. Singh, *J. Indian Chem. Soc.*, **52**, 656 (1975).
10) A. I. Vogel, "A Text Book of Quantitative Inorganic Analysis," Longmann, Green, London (1964), p. 498.
11) C. Duval, "Inorganic Thermogravimetric Analysis," Elsevier, London (1953), p. 347.
12) R. G. Charles, *Anal. Chim. Acta*, **27**, 474 (1962).
13) G. Thomas and R. A. Paris, *Anal. Chim. Acta*, **25**, 159 (1961).
14) B. Witkop, *J. Am. Chem. Soc.*, **76**, 5597 (1954).
15) C. N. R. Rao, "Chemical Applications of Infra-red Spectroscopy," Academic Press, New York (1963), p. 267.
16) B. Witkop and T. W. Beiler, *J. Am. Chem. Soc.*, **76**, 5589 (1954).
17) P. A. Gigure and I. D. Liu, *Can. J. Chem.*, **30**, 498 (1952).
18) A. T. Pilipenko, E. A. Shpak, and L. L. Shevchenko, *Zh. Neorg. Khim.*, **121**, 463 (1967).

 © 1983 The Chemical Society of Japan Bull. Chem. Soc. Jpn., 56, 1627—1631 (1983)

Thermal Properties of Solid Bis(2,3-alkanedione dioximato)nickel(II). Crystal Structure Transformation

Mikiya I, Hisanobu WAKITA,* and Isao MASUDA

Department of Chemistry, Faculty of Science, Fukuoka University, Nanakuma, Jonan-ku, Fukuoka 814-02

(Received July 23, 1982)

The thermal behavior in the solid state of the title complexes was investigated. Here 2,3-alkanedione dioximato is CH_3-C(=NOH)-C(=NO)-R; R includes C_2H_5 (**1**), n-C_3H_7 (**2**), n-C_4H_9 (**3**), n-C_5H_{11} (**4**), n-C_6H_{13} (**5**), and n-C_8H_{17} (**6**) groups. The complexes, **1**, **2**, **5**, and **6**, underwent thermal crystal structure transformation; the transformation was irreversible for **1** and **5**, and reversible for **2** and **6**. The ΔH_t values, heats of transformation, were found to fall in the 5.3—32.6 kJ mol^{-1} range. The ΔH_m values, heats of melting, were determined for the complexes, **2**—**6**. On the basis of these data, the thermal characteristics for these complex crystals are discussed in relation to the nature of the R groups.

The nickel(II) complexes of 2,3-alkanedione dioximes have been extensively studied in the fields of analytical and coordination chemistries.[1] The current interest has been concentrated rather on the interpretation of the properties and structures in the solid state of the complexes connected with their solubilities: these solubilities closely relate to the function of these dioximes as a specific precipitant for Ni^{2+} and Pd^{2+} ions and also to the proposed presence of a novel, intermetallic interaction[2] in the crystals of these metal-dioximato complexes.

In the crystal of bis(dimethylglyoximato)nickel(II), $Ni(dmgH)_2$,[3] planar complex molecules are stacked face to face along the c_o axis and are rotated alternately by 90° around the c_o axis;[4] this is referred to as the cross-form. The Ni atoms array along the c_o axis apart by 3.5 Å, posing as if there is an intermetallic Ni–Ni interaction.[2] For the $Ni(emgH)_2$ complex, two different forms of crystal are known. In one form, planar complex molecules array like the slats of a venetian blind inclined with an angle of 44°, when the cord of the blind is likened to the a_o axis of the crystal;[5] this is referred to here as the blind-form. In the other form, molecular packing is considered to be like the above mentioned cross-form of $Ni(dmgH)_2$ according to the analysis of the X-ray powder diffractions.[6] Anex and Krist have reported that the slow evaporation of the complex solution gives rise to the precipitation of the blind-form, whereas the hasty evaporation yields the cross-form.[7]

These facts are thought to imply that a crystal structure transformation occurred in the solid of these complexes. However, there has so far been no report which proved the existence of such a thermal crystal structure transformation.[8] In the present paper, the thermal properties of a series of the bis(2,3-alkanedione dioximato)[3] complexes have been investigated by thermal and X-ray powder diffraction analyses. The crystal structure transformation has been found to occur for the complexes whose dioximato ligand is emgH, prmgH, hxmgH, or omgH,[3] and the thermodynamic data have been determined.

Experimental

Preparation of Ligands. Following the general procedure given in the literature,[9] 2,3-alkanedione dioximes were prepared by the condensation reaction of 3-hydroxyimino-2-alkanone and hydroxylamine; the hydroxyimino derivatives were prepared by the isonitrosation of the corresponding 2-alkanones with ethyl nitrite. The dioximes thus obtained were purified by recrystaliization from methanol–chloroform (3 : 7), and were identified by elemental analysis, melting point, and ^{13}C-NMR spectrum.

Preparation of Complexes. The precipitates of the complexes were obtained in the following general manner: an aqueous solution saturated with nickel acetate was added to a hot methanol solution of the dioximes, and then the precipitate produced was collected on a filter. The recrystallization of the complexes was carried out as follows: the complex was added into the boiling solvent indicated in Table 1 for each complex, and then the saturated solution was filtered while it was hot. If the crystals were separated during the filtration, the crystals were dissolved again by heating the filtrate. Then the filtrate was cooled by allowing it to stand at room temperature. The crystals were separated by filtration, and then dried *in vacuo*.

The X-ray diffractions of crystalline $Ni(emgH)_2$ obtained in the above manner indicated it to be the blind-form.[5] The cross-form of $Ni(emgH)_2$ was prepared by the literature method.[6b]

Measurements. The differential thermal analysis (DTA) and differential scanning calorimetry (DSC) were carried out by use of a Rigaku Denki thermal analyzer, Model 8002; the particle size of samples was under 200 mesh. Heats of transformation and of melting were measured by DTA method for $Ni(prmgH)_2$, and by the DSC method for the other complexes; potassium nitrate (transformation temperature, 127.9 °C; heat of transformation, ΔH_t, 5.4 kJ mol^{-1})[10] was employed as the standard compound.

The X-ray powder diffractograms were recorded on a Rigaku Denki Geigerflex diffractometer using Co *Kα* radiation. The sample was heated in a furnace constructed in our laboratory: a sample placed in a holder equipped with a thermocouple was heated in a porcelain, cylindrical skeleton wrapped with a nichrome wire; the temperature was controlled by a PID action thermal controller constructed in our laboratory.

The reflectance spectra were recorded on a Shimadzu UV-300 spectrophotometer, by means of an opal glass method.[11]

Results

The complexes subjected to the investigation are listed in Table 1 along with their thermal character. The ^{13}C-NMR measurements suggested the trans-coordination of the two 2,3-alkanedione dioximato ligands in these complexes, like that in the $Ni(emgH)_2$ complex.[5] The complexes remained diamagnetic on raising temperature until their decomposition initiated.

TABLE 1. THERMAL CHARACTER OF Ni(2,3-ALKANEDIONE DIOXIMATO)$_2$

Dioximato ligand	Solvent[a)]	Heat of transformation ΔH_t/kJ mol^{-1}	Heat of melting ΔH_m/kJ mol^{-1}	$\Delta H_t + \Delta H_m$	Decomposition t/°C[c)]	Reflectance spectrum peak maximum/nm	
emgH	$C_6H_5NO_2$	9.1 (213)[b)]	——	——	251	490	(cross-form)
prmgH	$(CH_3)_2CO$	5.3 (38)	23.4 (156)[b)]	28.7	210	513 518	(form-I) (form-II)
bmgH	MeOH	——	16.3 (142)	16.3	190	459	
pnmgH	MeOH	——	25.2 (145)	25.2	212	463	
hxmgH	MeOH	24.4 (80)	21.9 (148)	46.3	174	472 471	(form-I) (form-II)
omgH	MeOH	32.6 (78)	14.6 (119)	47.2	219	485 466	(form-I) (form-II)

a) Solvent used for the recrystallization of each complex. b) DTA-peak maximum temperature/°C. c) Initial temperature/°C of decomposition on DTA curve.

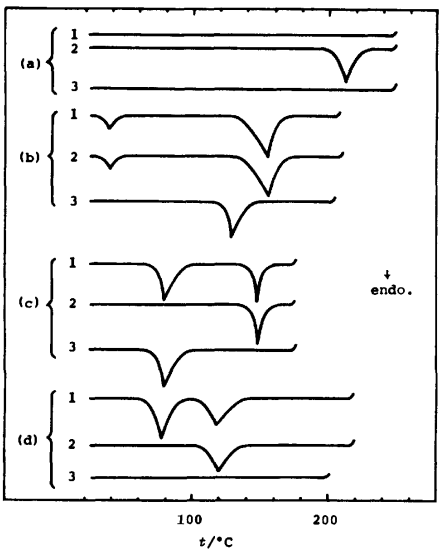

Fig. 1. DTA curves of Ni(2,3-alkanedione dioximato)$_2$. (a) Ni(emgH)$_2$: 1, cross-form; 2, blind-form; 3, cross-form obtained by heating blind-form at *ca.* 200 °C. (b) Ni(prmgH)$_2$: 1, form-II; 2, crystal obtained by heating original form-II at 50—100 °C; 3, sample obtained by heating form-II until melting. (c) Ni(hxmgH)$_2$: 1, form-II; 2, form-I obtained by heating form-II at *ca.* 100 °C; 3, sample obtained by heating form-II until melting. (d) Ni(omgH)$_2$: 1, form-II; 2, form-I obtained by heating form-II at *ca.* 100 °C; 3, sample obtained by heating form-II until melting.

Ni(emgH)$_2$. The DTA curve shown in Fig. 1 indicates that the cross-form crystal of Ni(emgH)$_2$ decomposes exothermally at an initial temperature of 251 °C. The blind-form crystal shows an endothermic DTA peak with a maximum at 213 °C, accompanied by no weight-loss, and then it begins to decompose at 250 °C. The crystal obtained after having heated the blind-form crystal at *ca.* 200 °C no longer shows any DTA peak around 213 °C, and it only shows decomposition initiated at 251 °C, like the authentic cross-form. Moreover, its powder X-ray diffractogram closely corresponded to that of the cross-form.[6b)] These facts indicate that the blind-form is irreversibly transformed into the cross-form in the solid state at *ca.* 200 °C, and the DTA peak at 213 °C is due to this transformation. The thermal analysis showed that the cross-form thus

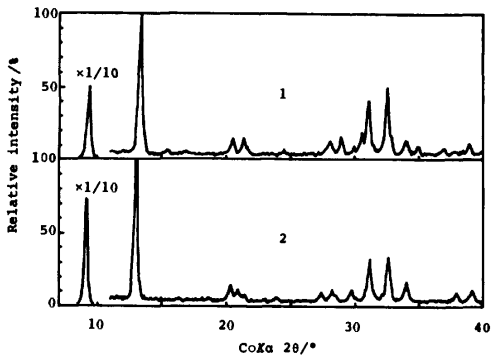

Fig. 2. X-Ray powder diffractograms of Ni(prmgH)$_2$. 1, Form-II; 2, form-I, recorded for form-II at 40 °C.

obtained through the transformation could be reformed as the blind-form by the recrystallization from nitrobenzene solution.

Ni(prmgH)$_2$. As seen in Fig. 1, the crystal of the complex isolated from acetone solution, noted here as form-II, undergoes two endothermic changes, showing DTA peaks with the maxima at 38 and 156 °C; these changes are accompanied by no weight-loss. The peak at 156 °C is due to melting. The crystal initiate decomposition at 210 °C. The crystal obtainable after keeping the form-II crystal at 50—100 °C, still reproduces a DTA curve which corresponds closely to that shown by the original form-II; this is observed to occur repeatedly. Thus, the form-II obviously undergoes reversible transformation to the form-I at 38 °C. As Fig. 2 shows, there is only a little difference in the X-ray diffractograms between form-II and form-I. However, the sample obtained by heating the form-I to melting shows no DTA peak at 38 °C and only shows one due to the melting at 129 °C, lower than that of the original form-I at 156 °C. And its X-ray diffractogram is quite different from those of the form-II and/or -I; this is in line with the above results obtained by DTA.

Ni(hxmgH)$_2$. The DTA curve given in Fig. 1 shows that the crystal obtained from methanol solution, noted as form-II, undergoes two endothermic changes, showing DTA peaks with the maxima at 80 and 148 °C; both changes cause no weight-loss. The peak at 148 °C is due to melting. Its decomposition initiates at 174 °C. The crystal obtained by heating the form-II at 100 °C, denoted as form-I, does not show any DTA

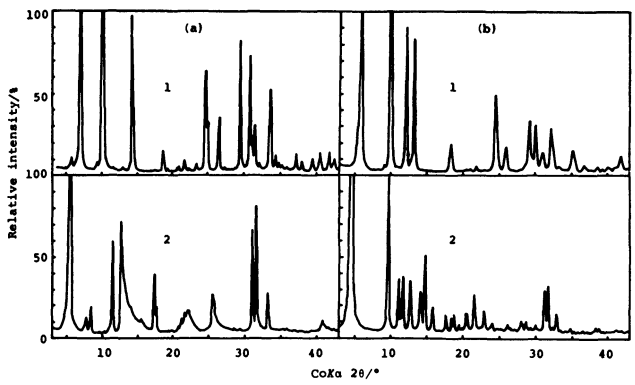

Fig. 3. X-ray powder diffractograms of Ni(hxmgH)$_2$ (a), and Ni(omgH)$_2$ (b).
1, Form-II and 2, form-I.

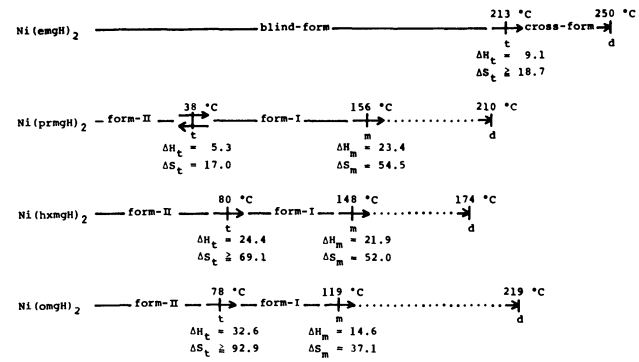

Fig. 4. Illustration for thermal remarks.
t, Transformation; m, melting; d, decomposition. →, Irreversible; and ⇄, reversible changes. ——, Solid; ……, liquid states. Temperature/°C indicates DTA peak maximum temperature for transformation and melting, and initial temperature for decomposition. ΔH values are given in kJ mol^{-1}; and ΔS, in J K^{-1} mol^{-1}.

peak around 80 °C but shows one at 148 °C. Thus, the transformation from form-II to form-I occurs irreversibly at 80 °C. The comparison of the X-ray diffractograms shown in Fig. 3 implies that the above transformation brought about a marked change in the crystal structure. The sample obtained by heating the form-I to melting at 148 °C undergoes melting at 80 °C, lower than the melting point of the form-I at 148 °C.

Ni(omgH)$_2$. As seen in Fig. 1, the thermal character of the crystal obtained from methanol solution, denoted as form-II, resembles those of the form-II crystals of Ni(prmgH)$_2$ and Ni(hxmgH)$_2$; it transforms into its form-I at 78 °C and then melts at 119 °C. For the crystal obtained after having kept the form-II at 100 °C, the DTA peak due to the transformation is not observed at 78 °C. And for the crystal obtained after having heated the form-II until the melting occurred, no DTA peak due either to transformation or to melting is observed. The change in the X-ray diffractogram caused by the transformation at 78 °C is shown in Fig. 3. It is noticed in this case that, on keeping the form-I crystal at room temperature for two or three days, it comes to show the color and X-ray diffractogram characteristic of the form-II, indicating that the transformation of form-I to form-II takes place slowly.

The form-I crystals of Ni(hxmgH)$_2$ and of Ni(omgH)$_2$ yielded by the transformation are rather poorly shaped crystal, as compared with the form-I crystal of Ni(prmgH)$_2$ or with the cross-form crystal of Ni(emgH)$_2$, yielded by the similar transformation. The transformation in the former two cases tends to be accompanied by the formation of an amorphous complex under the conditions employed. The ΔH_t values, heats of transformation, given in Table 1 for the former two cases may partly include the heat needed for a partial crystal-to-amorphous change.

The crystals of Ni(bmgH)$_2$ and Ni(pnmgH)$_2$ were only observed to melt and then to decompose.

The thermal properties for the complexes which undergo the crystal structure transformation are illustrated in Fig. 4.

Discussion

Crystal Structure Transformation. The structure of

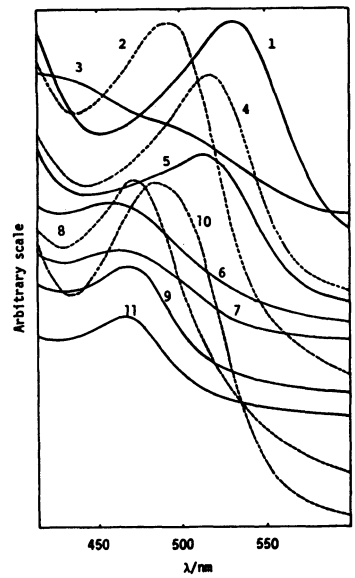

Fig. 5. Reflectance spectra.
1, Ni(dmgH)$_2$; 2, cross-form Ni(emgH)$_2$; 3, blind-form Ni(emgH)$_2$; 4, form-I Ni(prmgH)$_2$; 5, form-II Ni(prmgH)$_2$; 6, Ni(bmgH)$_2$; 7, Ni(pnmgH$_2$); 8, form-I Ni(hxmgH)$_2$; 9, form-II Ni(hxmgH)$_2$; 10, form-I Ni(omgH)$_2$; 11, form-II Ni(omgH)$_2$.

the cross-form crystal of Ni(emgH)$_2$ is similar to that of the cross-form crystal of Ni(dmgH)$_2$; the neighboring Ni atoms in the crystals are 3.44 Å apart for the former and 3.23 Å for the latter.[6b] As seen in Fig. 5, the cross-form Ni(emgH)$_2$ shows the reflectance spectrum with a distinct peak-maximum at 490 nm that may arise from the same origin as the peak at 530 nm observed for Ni(dmgH)$_2$.[12] In the blind-form of Ni(emgH)$_2$, the neighboring Ni atoms in the crystal are separated by a distance of 4.74 Å.[5] This longer Ni–Ni distance, along with the molecular packing in the crystal can hardly indicate the presence of intermetallic Ni–Ni interaction in the blind-form crystal. As Fig. 5 shows, its spectrum

has no clear peak in the visible region.[6b])

It is important that the blind- to cross-form transformation is endothermic with a change of enthalpy $\Delta H_t = 9.1$ kJ mol^{-1}, indicating that thermally the cross-form crystals are less stable than the blind-form crystals. The ΔH_t value is considered to be a measure for the difference in the lattice energy between these two forms; it is found to fall, in fact, in the hydrogen-bond energy range, 4—33 kJ mol^{-1}. Assuming the change in free energy of the transformation to be $\Delta G_t \leqq 0$, change in entropy is calculated to be $\Delta S_t = S_{cross} - S_{blind} \geqq 18.7$ J K^{-1} mol^{-1}. Judging from only the symmetry of the crystal system, the orthorhombic cross-form seems to have less entropy than the monoclinic blind-form. The observed increment in the entropy value caused by the blind- to cross-form transformation could be explained in terms of the change in the density of the crystal, that is, as the transformation progresses, the density 1.58 g cm^{-3} of the blind-form[5] decreases to 1.46 g cm^{-3} of the cross-form crystals.[6]

While the crystal structure of Ni(prmgH)$_2$ has so far not been elucidated,[15] the reflectance spectra of both its form-II and form-I crystals show a peak whose position is close to that of Ni(dmgH)$_2$, as seen in Fig. 5. By comparison of the X-ray data for Ni(prmgH)$_2$ with the ones reported for Ni(dmgH)$_2$,[4] the X-ray diffractions with strong intensity of these form-II and -I crystals could be indexed as those of the orthorhombic system. These suggest that the crystal structure of both forms is similar to that of the cross-form Ni(dmgH)$_2$. This is not inconsistent with the fact that the transformation between the form-II and form-I of Ni(prmgH)$_2$ reversibly took place at the low temperature of 38 °C, with a ΔH_t value as small as 5.3 kJ mol^{-1}. The transformation may include a change not like a molecular displacement but like a small conformational displacement of the propyl groups. Since $\Delta G_t = 0$ in this transformation, the ΔS_t value is calculated to be 17.0 J K^{-1} mol^{-1}, which is smaller than that for Ni(emgH)$_2$.

For Ni(hxmgH)$_2$ and Ni(omgH)$_2$, the ΔH_t values of the form-II to -I transformation are, respectively, 24.4 and 32.6 kJ mol^{-1}, as shown in Table 1 and Fig. 4; these are larger than those for the transformations of Ni(emgH)$_2$ and Ni(prmgH)$_2$. And the ΔH_t value for Ni(hxmgH)$_2$ is as large as its ΔH_m value (heat of melting) and that for Ni(omgH)$_2$ is larger than its ΔH_m value. These ΔH_t values may partly include the heat of the crystal-to-amorphous change. As Fig. 5 shows, the above transformation caused no remarkable change in the position of the visible absorption peaks.

Heat of Fusion. Few investigations have dealt with the characterization of the transition metal complexes by such a value as heat of fusion. The stability of the crystal lattice is considered to be reflected on the heat of fusion, which may be represented by the ΔH_m values obtained here.[14] In the cases of the crystals of Ni(hxmgH)$_2$ and Ni(omgH)$_2$ the form-II to -I transformation occurred with the concomitant crystal-to-amorphous change, which brought about inaccuracy in the ΔH_m values measured with their form-II crystals. In addition, the form-II type crystals in the present series of the complexes were obtainable under the conventional preparative conditions. Therefore, the $\Delta H_t + \Delta H_m$ values of the form-II type crystals will be considered here. As seen in Table 1, the $\Delta H_t + \Delta H_m$ value is the smallest for Ni(bmgH)$_2$. For the complexes with alkyl chains shorter than that of Ni(bmgH)$_2$, the $\Delta H_t + \Delta H_m$ values tend to increase. For Ni(prmgH)$_2$ which has an alkyl chain shorter than that of Ni(bmgH)$_2$, the $\Delta H_t + \Delta H_m$ value is observed to increase again.

Table 1 shows that the crystal having the larger $\Delta H_t + \Delta H_m$ value shows a peak maximum at a higher energy site. From the preliminary result of the X-ray crystallographic investigation on the Ni(prmgH)$_2$ (form-II crystal),[15] the crystal structure may be expected to be similar to that of Ni(dmgH)$_2$ (cross-form),[4] wherein the complex molecules are stacked face to face. This similarity in the molecular array of the crystal is thought to be reflected in the appearance of the peak in the visible reflectance spectrum, as shown in Fig. 2 and Table 1. In fact, the blind-form crystal of Ni(emgH)$_2$ shows no peak.

References

1) Refer to the recent reviews: a) A. Chakravorty, *Coord. Chem. Rev.*, **13**, 1 (1974); b) T. W. Thomas and A. E. Underhill, *Chem. Soc. Rev.*, **1**, 99 (1971); c) R. B. Garg and R. P. Singh, *Talanta*, **26**, 425 (1979).

2) a) S. Yamada and R. Tsuchida, *Bull. Chem. Soc. Jpn.*, **27**, 156 (1954); b) C. V. Banks and D. W. Barnum, *J. Am. Chem. Soc.*, **80**, 3579, 4767 (1958); c) J. C. Zahner and H. G. Drickamer, *J. Chem. Phys.*, **33**, 1625 (1960); d) C. V. Banks and S. Anderson, *Inorg. Chem.*, **2**, 112 (1963).

3) The following abbreviations are used to denote 2,3-alkanedione dioximato, CH_3–C(=NOH)–C(=NO)–R, where R is CH_3 (dmgH), C_2H_5 (emgH), C_3H_7 (prmgH), C_4H_9 (bmgH), C_5H_{11} (pnmgH), C_6H_{13} (hxmgH), and C_8H_{17} (omgH).

4) L. E. Godycki and R. E. Rundle, *Acta Crystallogr.*, **6**, 487 (1953).

5) E. Frasson and C. Panattoni, *Acta Crystallogr.*, **13**, 893 (1960); R. H. Bowers, C. V. Banks, and R. A. Jacobson, *ibid., Sect. B*, **28**, 2318 (1972).

6) a) A. G. Sharpe and D. B. Wakefield, *J. Chem. Soc.*, **1957**, 281; b) B. Egneus, *Anal. Chem. Acta*, **48**, 291 (1969).

7) B. G. Anex and F. K. Krist, *J. Am. Chem. Soc.*, **89**, 6114 (1967).

8) It has been reported that Ni[(*E*, *E*)-benzil dioximato]$_2$, precipitated from solution, alters its crystal color on heating or standing; R. H. Magee, J. C. Rowe, and L. Gordon, *Talanta*, **12**, 303 (1965). However, this change could not be detected by our thermoanalytical inspection.

9) A. H. Blatt, *Org. Synth.*, **2**, 204 (1943).

10) "Kagaku-binran Kiso-hen II," ed by the Chemical Society of Japan, Maruzen, Tokyo (1975), p. 912.

11) K. Shibata, "Methods of Biochemical Analysis," ed by D. Glick, Interscience, New York (1962), Vol. 4, p. 217.

12) Ref. 6b); many reports have appeared which deal with the absorption spectra of the analogous dioximato complexes in suspension. The visible absorption peak is known to occur only in the solid complexes; this has so far been discussed in terms of either a proposed Ni–Ni interaction in the crystals[2] or of the intramolecular nature ($3d_{z^2} \rightarrow 4p_z$ transition) of the complexes.[13] It might be true that this is a characteristic feature of the molecular packing in the crystal.

13) a) J. C. Zahner and H. G. Drickamer, *J. Am. Chem. Soc.*, **80**, 4767 (1958); b) Y. Ohashi, I. Hanazaki, and S. Nagakura, *Inorg. Chem.*, **9**, 2551 (1970).
14) Among the analogous complexes, Ni(glyoximato)$_2$, Ni(methylglyoximato)$_2$, and Ni(dmgH)$_2$ showed similarly to Ni(emgH)$_2$ only decomposition without melting on heating.
15) The crystal structure is under investigation by X-ray diffraction analysis.

Studies of Inorganic Ion Exchangers. VI.[1] The Formation Region and Dehydration Behavior of Various Titanium(IV) Bis(hydrogenorthophosphate) Hydrates

Etsuro KOBAYASHI and Shinsuke YAMAZAKI
National Chemical Laboratory for Industry, Yatabemachi, Tsukuba-gun, Ibaraki 305
(Received August 13, 1982)

The formation region, dehydration behavior, and lattice constants of various types of titanium(IV) bis(hydrogenorthophosphate) hydrates were investigated. α-$Ti(HPO_4)_2 \cdot H_2O$ was formed by refluxing an amorphous titanium phosphate (ATP) with H_3PO_4 at 110—165 °C or by treating it with H_3PO_4 (up to 11.5 mol dm^{-3}) under hydrothermal conditions at temperatures up to 250 °C. (β-γ)-$Ti(HPO_4)_2 \cdot xH_2O$ was obtained by refluxing ATP with H_3PO_4 (15—16 mol dm^{-3}) above 165 °C. γ-$Ti(HPO_4)_2 \cdot 2H_2O$ was formed by a hydrothermal reaction of ATP and H_3PO_4 (10—16 mol dm^{-3}) at 200—300 °C. In the thermal analysis of $Ti(HPO_4)_2$, no difference in weight loss was found at temperatures up to 920 °C of α-form irrespective of the drying conditions of the samples. The (β-γ)-form dried under reduced pressure over P_2O_5 had a composition corresponding to that of a 1/2 hydrate. The γ-form dried at a relative humidity of 75% had a composition identical to that of the dihydrate. In view of the X-ray diffraction, it seemed that the (β-γ)-form (11.6 and 9.2 Å) was changed by drying under reduced pressure over P_2O_5 to the β-form (9.2 Å) as anhydride. The γ-form (11.6 Å) was dehydrated to the β-form by heating. The change in the inter-layer distance upon dehydration was also confirmed by means of a that of the electron diffraction. Thus, it was considered that the (β-γ)-form was a mixture as a quasi stable form.

Various types of titanium(IV) bis(hydrogenorthophosphate) hydrates have been synthesized by refluxing amorophous titanium phosphate with phosphoric acid, and their peculiar ion-exchangeability has been investigated.[1-5] α-$Ti(HPO_4)_2 \cdot H_2O$[6] was formed at phos phoric acid concentrations of 13—62%, while $Ti(HPO_4)_2 \cdot 0$—1/2 H_2O was obtained at 64% or higher.[2,3] Alluli *et al.*[7] synthesized $Ti(HPO_4)_2 \cdot 2H_2O$ by heating amorphous titanium phosphate with 10 mol dm^{-3} of phosphoric acid at temperatures of 200 °C or higher in a sealed tube. They suggested that the crystal structure of this compound was not identical with that of α-$Ti(HPO_4)_2 \cdot H_2O$, but similar to that of γ-$Zr(HPO_4)_2 \cdot 2H_2O$.

In the present study, crystalline titanium phosphates are synthesized by refluxing and by hydrothermal reactions, and the formation regions of the individual modifications are determined.

Experimental

Preparation of Crystalline Titanium(IV) Bis(hydrogenorthophosphate). Refluxing Method: The preparation of $Ti(HPO_4)_2 \cdot xH_2O$ by refluxing phosphoric acid with amorphous titanium phosphate was carried out by the method previously reported.[2,3] The products were dried by storing them in a desiccator charged with a saturated aqueous solution of urea (75—78% in relative humidity at room temperature).

Hydrothermal Reaction Method: One gram of amorphous titanium phosphate was sealed with 10 cm^3 of phosphoric acid (10—16 mol dm^{-3}) in a 20-cm^3 hard glass tube, after the tube was placed in a 200-cm^3 stainless steel autoclave with 80 cm^3 of water to prevent its rupture. The autoclave was then heated at 140—300 °C. The products in the tubes were separated from the mother liquors, washed with water, and then dried at a relative humidity of 75—78%.

Analyses: The chemical analyses of the product were carried out by the method previously reported.[2] The X-ray diffraction was performed with Ni-filtered Cu *Ka* radiation (30 kV P, 20 mA). The thermal analysis was carried out with a microthermal analyzer at a heating rate of 10 °C/min.

Electron Diffraction: The electron diffraction was performed with the aid of a Hitachi HU-12A electron microscope equipped with a standard cooling holder, HC-4. Selected area diffraction patterns were measured at 100 kV.

Results and Discussion

Formation of Various Titanium(IV) Bis(hydrogenorthophosphate). The conditions for the synthesis of $Ti(HPO_4)_2 \cdot xH_2O$ by the reaction of amorphous titanium phosphate with phosphoric acid and the analytical data of the products are shown in Table 1.

Chemical Analysis and X-Ray Diffraction: In No. 1 of Table 1, α-titanium(IV) bis(hydrogenorthophosphate) monohydrate was produced by refluxing amorphous titanium phosphate with phosphoric acid at 140°C. This product was already known to have an interlayer distance of 7.6 Å[7] (Å=10^{-10} m). In Nos. 2—4, the drying conditions for the products obtained by refluxing amorphous titanium phosphate with phosphoric acid of high concentrations were different from that established hitherto, so the products gave analytical data corresponding to those of the 1/2—1 hydrate. In the X-ray diffraction diagram, the products are shown to have interlayer distances of 11.6 and 9.2 Å. When we prepared this product for the first time, we gave it the chemical formulas of $Ti(HPO_4)_2 \cdot 1/2\,H_2O$[2] and also $Ti(HPO_4)_2 \cdot 0$—$1/2H_2O$.[3] In the present study, however, this product gave, as has been described above, values of 1/2—1 hydrate. Accordingly, we will now designate as (β-γ)-$Ti(HPO_4)_2 \cdot xH_2O$ the product shown in the past as $Ti(HPO_4)_2 \cdot 0$—$1/2H_2O$.

In Nos. 5—7, hydrothermal reactions between amorphous titanium phosphate and phosphoric acid having various concentrations were carried out at 175 °C. α-$Ti(HPO_4)_2 \cdot H_2O$ was formed at H_3PO_4 concentrations of 10 and 14.4 mol dm^{-3}. However, a mixture of the α- and γ-forms was formed at a H_3PO_4 concentration of 16 mol dm^{-3}.

In Nos. 8—10, when the hydrothermal reaction was

TABLE 1. SYNTHESIS AND ANALYSIS OF TITANIUM(IV) BIS(HYDROGENORTHOPHOSPHATE)

No.	Reaction conditions: Raw material[a] ATP (g)	Mother liquor H_3PO_4 (mol dm^{-3})	Mother liquor Volume (cm^3)	Method[b]	Temp °C	Time h	Reaction products[c]: TiO_2 (%)	P_2O_5 (%)	H_2O (%)	Estimated formula	X-Ray diagram (form)
1	7.0	12.8	250	REF	140	30	31.8	55.4	14.3	$Ti(HPO_4)_2 \cdot 0.9H_2O$	α
2	5.0	15.9	200	REF	170	100	32.0	56.8	11.2	$Ti(HPO_4)_2 \cdot 0.5H_2O$	$(\beta\text{-}\gamma)$
3	9.0	16.5	275	REF	175	50	31.6	55.9	12.5	$Ti(HPO_4)_2 \cdot 0.8H_2O$	$(\beta\text{-}\gamma)$
4	5.0	15.8	205	REF	170	50	31.0	55.0	14.0	$Ti(HPO_4)_2 \cdot 1.0H_2O$	$(\beta\text{-}\gamma)$
5	1.0	10.0	10	HTR	175	72	31.1	55.2	13.7	$Ti(HPO_4)_2 \cdot 1.0H_2O$	α
6	1.0	14.4	10	HTR	175	72	31.1	55.1	13.8	$Ti(HPO_4)_2 \cdot 1.0H_2O$	α
7	1.0	15.9	10	HTR	175	72	30.0	53.3	16.7	$Ti(HPO_4)_2 \cdot 1.5H_2O$	$\alpha+\gamma$
8	1.0	10.0	10	HTR	200	144	31.0	55.1	13.9	$Ti(HPO_4)_2 \cdot 1.0H_2O$	α
9	1.0	14.4	10	HTR	200	144	29.8	52.0	18.2	$Ti(HPO_4)_2 \cdot 1.8H_2O$	$\alpha+\gamma$
10	1.0	15.9	10	HTR	200	144	29.1	51.5	19.4	$Ti(HPO_4)_2 \cdot 2.0H_2O$	γ
11	1.0	10.0	10	HTR	250	72	31.0	54.9	14.1	$Ti(HPO_4)_2 \cdot 1.0H_2O$	α
12	1.0	14.4	10	HTR	250	72	28.6	50.8	20.6	$Ti(HPO_4)_2 \cdot 2.2H_2O$	γ
13	1.0	15.9	10	HTR	250	72	29.4	52.5	18.1	$Ti(HPO_4)_2 \cdot 1.7H_2O$	γ
14	3.0	10.0	35	HTR	280	18	29.1	51.5	19.4	$Ti(HPO_4)_2 \cdot 2.0H_2O$	γ
15	1.0	10.0	10	HTR	300	30	29.3	51.9	18.8	$Ti(HPO_4)_2 \cdot 1.9H_2O$	γ
16	1.0	12.2	10	HTR	300	30	28.9	51.4	19.7	$Ti(HPO_4)_2 \cdot 2.0H_2O$	γ
17	1.0	15.9	10	HTR	300	30	29.0	51.4	19.6	$Ti(HPO_4)_2 \cdot 2.0H_2O$	γ

a) ATP: Amorphous titanium phosphate. b) REF: Refluxing method, HTR: hydrothermal reaction method.
c) The products are stored for one week in a desiccator with a relative humidity of 75% and then analyzed.

carried out at 200 °C, the product was gradually converted from the α-form to the γ-form *via* a mixture of the α- and γ-forms due to the increasing concentration of H_3PO_4. In Nos. 11—13, the hydrothermal reaction was carried out at 250 °C. The α-form was formed at a H_3PO_4 concentration of 10 mol dm^{-3}, but the γ-form was formed at 14.4 mol dm^{-3}. The hydrothermal reaction was carried out at 280 °C in No. 14 and at 300 °C in Nos. 15—17. At such an elevated temperature, γ-$Ti(HPO_4)_2 \cdot 2H_2O$ was formed at a H_3PO_4 concentration of 10 mol dm^{-3} or higher.

The Formation Regions of Various Titanium(IV) Bis-(hydrogenorthophosphate) Hydrates: The formation regions of various titanium(IV) bis(hydrogenorthophosphate) are shown in Fig. 1.

The curve AB shows the relation between the temperature of phosphoric acid and its concentration. The solid phase formed under the reaction conditions on the curve AB was α-$Ti(HPO_4)_2 \cdot H_2O$. At higher phosphoric acid concentrations, $(\beta\text{-}\gamma)$-$Ti(HPO_4)_2 \cdot xH_2O$ was formed as the solid phase at a refluxing temperature of 165 °C or higher. The conditions for forming this product are shown by a dotted line (BC) as an extension of the solid line (AB). The regions of the formation of the α- and γ-forms by the hydrothermal reaction are separated by a curve MN. A mixture of the α- and γ-forms was formed in the vicinity of the curve.

Water of Crystallization of Various Titanium(IV) Bis-(hydrogenorthophosphate) Hydrates: Table 1 shows the percentages of H_2O calculated from the weight loss at 700 °C of the reaction product stored in a desiccator at a relative humidity of 75—78%. As the water content varies according to the degree of drying, the DTA and TG of α-, $(\beta\text{-}\gamma)$-, and γ-titanium(IV) bis-(hydrogenorthophosphate) differed in drying conditions,

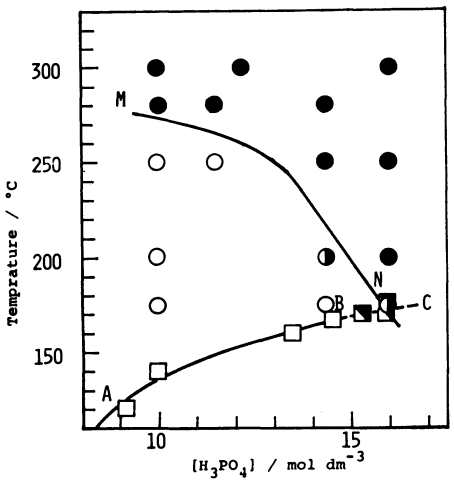

Fig. 1. Formation region of titanium(IV) bis(hydrogenorthorhosphate).
○, ◥: α-$Ti(HPO_4)_2 \cdot H_2O$, □ $(\beta\text{-}\gamma)$ $Ti(HPO_4)_2 \cdot xH_2O$, ◑: $\alpha+\gamma$-$Ti(HPO_4)_2 \cdot 1$—$2\,H_2O$, ●: γ-$Ti(HPO_4)_2 \cdot 2H_2O$. Reflux is indicated with square signs. Hydrothermal reaction is indicated with circular signs.

as Figs. 2, 3, and 4 show.

α-$Ti(HPO_4)_2 \cdot H_2O$: In the DTA curve of Fig. 2, the broad endothermic peak appearing at temperatures below 100 °C is caused by the dehydration of free water attached to the sample. The endothermic peaks at 260 and 510 °C are due to the liberation of the water of crystallization and condensation. The weight losses at 200 °C of the samples dried at relative humidities of 100 and 75% and under reduced pressure over P_2O_5 were as small as 2.0, 0.9, and 0.8% respectively, thus

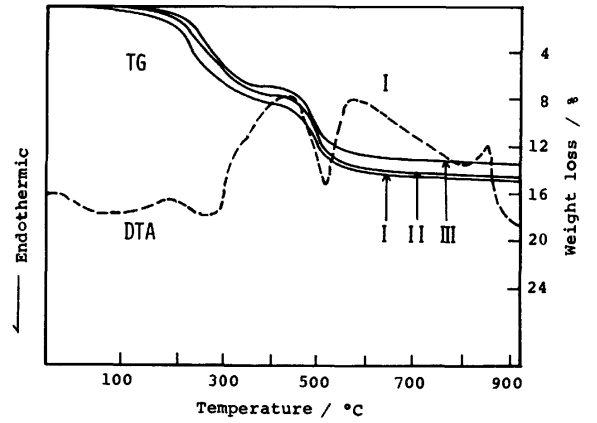

Fig. 2. DTA and TG curves for α-titanium(IV) bis-(hydrogenorthophosphate). I: Product stored in relative humidity 100%. II: Product stored in relative humidity 75%. III: Product vacuum-dried over P_2O_5.

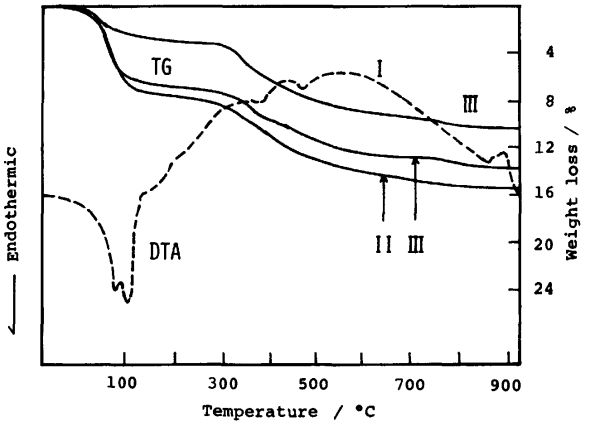

Fig. 3. DTA and TG curves for (β-γ)-titanium(IV) bis-(hydrogenorthophosphate).
I: Product stored in relative humidity 100%. II: Product stored in relative humidity 75%. III: Product vacuum-dried over P_2O_5.

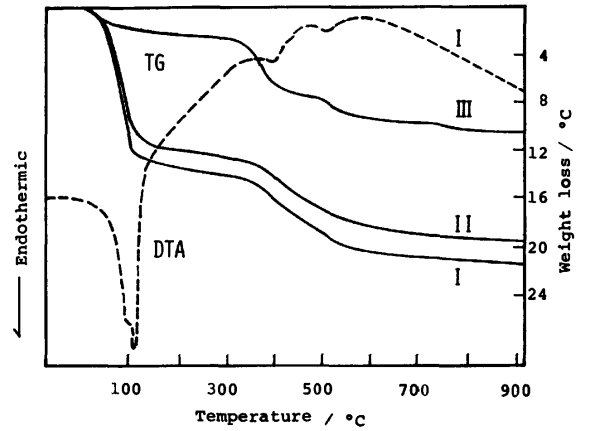

Fig. 4. DTA and TG curves for γ-titanium(IV) bis-(hydrogenorthophosphate).
I: Product stored in relation humidity 100%. II: Product stored in relative humidity 75%. III: Product vacuum-dried over P_2O_5.

permitting the assumption that the water of crystallization of α-$Ti(HPO_4)_2 \cdot H_2O$ is strongly combined with the salt. The weight losses of the individual samples by heating up to 900 °C were 15.0, 14.2, and 13.3% respectively. These values approximately equal a theoretical value of 13.9 (%) ($2H_2O/\alpha$-$Ti(HPO_4)_2 \cdot H_2O \times 100$).

(β-γ)-$Ti(HPO_4)_2 \cdot xH_2O$: In the DTA curve of Fig. 3, a big endothermic peak resulting from dehydration appears at about 100 °C. Two small endothermic peaks resulting from condensation appear at 370 and 464 °C. In the TG curve of Fig. 3, the weight losses at 200 °C of the samples dried at relative humidities of 100 and 75% and under reduced pressure over P_2O_5 were 8.5, 7.0, and 3.0% respectively. These values were extremely large as compared with those of the above described α-$Ti(HPO_4)_2 \cdot H_2O$. In the case of (β-γ)-$Ti(HPO_4)_2 \cdot xH_2O$, the interlayer distance was so great that the water contained therein was easily eliminated by heating at a relatively low temperature. The weight losses at 920 °C of (β-γ)-$Ti(HPO_4)_2 \cdot xH_2O$ dried at relative humidities of 100 and 75% and under reduced pressure over P_2O_5 were 15.5, 12.5, and 10.4% respectively. Only the weight loss of the sample which had been dried under reduced pressure over P_2O_5 agreed with the calculated value of 10.86 (%) ($1.5\ H_2O/Ti(HPO_4)_2 \cdot 1/2\ H_2O \times 100$).

γ-$Ti(HPO_4)_2 \cdot 2H_2O$: Allulli *et al.*[7] measured the TG of titanium(IV) bis(hydrogenorthophosphate), which was regarded identical with the γ-form, and gave this compound the chemical formula of $Ti(HPO_4)_2 \cdot 2H_2O$. In the DTA curve of Fig. 4, a slightly branched endothermic peak by dehydration appears at about 100 °C, while endothermic peaks by condensation appear at 390 and 498 °C, in a tendency similar to that of the DTA curve of the (β-γ)-form. In the TG curve of Fig. 4, the weight losses at 200 °C of the samples dried at relative humidities of 100 and 75% and under reduced pressure over P_2O_5 were 13.6, 12.0, and 2.4% respectively. A substantial part of the water of crystallization in each sample was released up to the above temperature. The weight loss at 920 °C of only the sample dried at a relative humidity of 75% was in agreement with the calculated value of 19.6 (%) ($3H_2O/Ti(HPO_4)_2 \cdot 2H_2O \times 100$).

Change in the Interlayer Distance of (β-γ)- and γ-Titanium-(IV) Bis(hydrogenorthophosphate). Clearfield *et al.*,[8] who first synthesized γ-$Zr(HPO_4)_2 \cdot 2H_2O$ with an interlayer distance of 12.2 Å, obtained β-$Zr(HPO_4)_2$ with an interlayer distance of 9.4 Å by drying the γ-form under reduced pressure over anhydrous calcium sulfate for several weeks at room temperature. In the present studies, we have confirmed whether or not the interlayer distance of titanium(IV) bis(hydrogenorthophosphate) is also changed by drying.

In the case of α-$Ti(HPO_4)_2 \cdot H_2O$, the interlayer distance (7.6 Å) of the samples was not changed by the drying conditions.

(β-γ)-$Ti(HPO_4)_2 \cdot xH_2O$ synthesized by the refluxing method had a composition of approximately 0.7 hydrate at a relative humidity of 75%, and it showed X-ray diffraction peaks at 11.6 and 9.2 Å. The occurrence

TABLE 2. SPACINGS OF VARIOUS TITANIUM (IV) BIS(HYDROGENORTHOPHOSPHATE) HYDRATES DETERMINED BY MEANS OF THE ELECTRON-DIFFRACTION PATTERNS

			α-$Ti(HPO_4)_2 \cdot H_2O$			β-$Ti(HPO_4)_2$				γ-$Ti(HPO_4)_2 \cdot 2H_2O$		
	(1)		(2)	(3)	(4)	(5)	(6)	(7)	(8)	(9)	(10)	(11)
h	k	l	d_{obsd}/Å	d_{calcd}/Å	d_x/Å	d_{obsd}/Å	d_{calcd}/Å	d_x/Å	d_{obsd}/Å	d_{obsd}/Å	d_{calcd}/Å	d_x/Å
0	0	2	7.52	7.618	7.62	9.34	9.211	9.21	9.32	11.26	11.62	11.62
0	1	1	5.03	4.955		6.07	6.037		6.06	6.21	6.026	
0	1	2	4.34	4.317		5.25	5.250	5.21	5.22	5.63	5.633	5.57
1	0	$\bar{1}$		8.634		5.18	5.183			5.29	5.289	
0	1	3	3.59	3.647	3.68		4.428	4.48	4.57	5.00	4.953	
1	0	1		6.647		4.71	4.727				4.778	
1	0	$\bar{3}$	5.12	5.083		4.35	4.332				4.850	
1	0	2	5.03	4.989		4.16	4.176		4.14		4.328	4.28
1	$\bar{1}$	$\bar{1}$	4.53	4.480		4.04	4.025			4.09	4.087	
1	1	0	4.43	4.466		4.01	3.999		4.01	4.00	4.015	
1	$\bar{1}$	$\bar{2}$	4.11	4.147	4.02	3.94	3.869			4.05	4.036	
1	$\bar{1}$	2	3.55	3.613			3.496		3.52		3.592	
1	0	$\bar{5}$	3.09	3.188		3.29	3.281			3.96	3.950	
1	0	3	3.88	3.883			3.631	3.64			3.873	
0	2	0	2.62	2.620	2.61	3.21	3.195		3.18	3.21	3.220	
1	0	4	3.12	3.145	3.15	3.16	3.159			3.45	3.458	3.45
0	2	$\bar{1}$	2.54	2.582	2.53	3.15	3.148			3.19	3.190	
1	0	$\bar{7}$	2.26	2.279	2.24		2.531			3.16	3.155	3.16
0	$\bar{2}$	2	2.34	2.478	2.49	3.03	3.018		3.06		3.103	
1	0	5	2.33	2.328	2.38	2.78	2.768			3.10	3.096	3.02
0	2	4	2.16	2.159	2.24	2.62	2.625		2.63		2.816	
2	0	$\bar{1}$	4.49	4.474			2.603		2.61	2.61	2.622	
1	2	1	2.37	2.437	2.38		2.647			2.67	2.670	
2	0	0	4.27	4.269	4.27	2.56	2.564			2.57	2.567	2.57
2	0	$\bar{2}$	4.34	4.317		2.59	2.591				2.644	
2	$\bar{1}$	$\bar{1}$	3.47	3.403	3.45	2.40	2.411			2.42	2.428	
1	1	6	2.06	2.072			2.287			2.55	2.558	
1	$\bar{2}$	$\bar{5}$	2.05	2.024	2.02		2.289			2.50	2.496	
2	0	2	3.29	3.323		2.36	2.364				2.389	
0	3	2	1.70	1.702		2.08	2.075			2.12	2.111	

Lattice constant		Lattice constant		Lattice constant	
Measured by means of the electron-diffraction patterns	Value calculated by the least-squares method from the face indices and peak values in X-ray diffraction	Measured by means of the electron-diffraction patterns	Value calculated by the least-squares method from the face indices and peak values in X-ray diffraction	Measured by means of the electron-diffraction patterns	Value calculated by the least-squares method from the face indices and peak values in X-ray diffraction
a=8.95 Å	a=9.06 Å	a=5.21 Å	a=5.22 Å	a=5.29 Å	a=5.27 Å
b=5.24 Å	b=5.17 Å	b=6.39 Å	b=6.40 Å	b=6.44 Å	b=6.42 Å
c=15.97 Å	c=16.05 Å	c=18.72 Å	c=18.72 Å	c=23.94 Å	c=24.29 Å
β=107.4°	β=110.93°	β=100.2°	β=100.3°	β=103.9°	β=102.5°

of these two peaks is suggestive of the coexistence of the γ-form with an interlayer distance of 11.6 Å and the β-form with that of 9.2 Å. It is of interest that, when this sample was dried under reduced pressure over P_2O_5, the diffraction peak of the γ-form entirely disappeared, while the diffraction peak of the β-form alone appeaed. This compound can be converted reversible into, the γ-form by the absorption of water and into the β-form by releasing the water.

γ-$Ti(HPO_4)_2 \cdot 2H_2O$ synthesized by the hydrothermal reaction method had a composition corresponding exactly to that of the dihydrate at a relative humidity of 75%, and it showed an intensive diffraction peak at 11.6 Å. When the sample was dried under reduced pressure over P_2O_5, this peak was reduced in intensity, but a diffraction peak at 9.2 Å which characterized the β-form as anhydrous salt did not appear. When the water of crystallization was entirely eliminated from the sample by drying it further under heating (120 °C), the γ-form was converted into the β-form; the latter, however, tended to be converted reversibly into the γ-form by absorption of moisture in the air.

Lattice Constants. *α-$Ti(HPO_4)_2 \cdot H_2O$*: The indices of each lattice of α-$Ti(HPO_4) \cdot {}_2H_2O$ and the calculated values of the corresponding spacing are shown in (1) and (3) of Table 2. The patterns of this crystal may be indexed by assuming an monoclinic unit cell with dimensions of a=8.95 Å, b=5.24 Å, c=15.97

Å, and $\beta=107.45°$. The calculated spacings, "d_{calcd}" were almost entirely consistent with those measured by the selected-area electron diffraction. The results of the calculation are shown in Table 2.

γ-Ti(HPO$_4$)$_2$·2H$_2$O: When the crystals of γ-Ti(HPO$_4$)$_2$·2H$_2$O under cooling below -150 °C with liquid nitrogen, were subjected to selected-area electron diffraction, interlayer water was not released; the crystal structure of the γ-form was also retained.

The values of spacing obtained from the electron-diffraction patterns are shown in Table 2(9). The index of the crystal face and the spacing of γ-Ti(HPO$_4$)$_2$·2H$_2$O were calculated using the lattice constants estimated from the peak values in powder X-ray diffraction and from electron-diffraction net patterns. The values of the spacing are shown in Table 2(10). These values (10) are in agreement with the values (9) obtained from the electron-diffraction patterns, if the axes *a*, *b*, and *c* are 5.29, 6.44, and 23.94 Å, and if the angle β is 103.9°.

β-Ti(HPO$_4$)$_2$: When γ-Ti(HPO$_4$)$_2$·2H$_2$O was irradiated with an electron beam under a high vacuum in the column of an electron microscope, the water of crystallization between the layers was released; the γ-form (dihydrate) was, therefore, converted into the β-form (anhydrate). The values of the lattice constant and of the face index, as determined by the electron-diffraction net patterns are shown in Table 2.

In comparing the lattice constants of β-Ti(HPO$_4$)$_2$ with these of γ-Ti(HPO$_4$)$_2$·2H$_2$O, the a and b axes were found to be almost equal in length in the two forms, while the c axis was 23.9 Å in the γ-form, but as short as 18.7 Å in the β-form. In view of this fact, the β-form was converted from the γ-form when the interlayer water of the γ-form was eliminated from the crystal.

Electron Diffraction of (β-γ)-Ti(HPO$_4$)$_2$·xH$_2$O: To confirm (β-γ)-Ti(HPO$_4$)$_2$·xH$_2$O as a mixture of the β- and γ-form in a quasi-stable form, we observed the electron-diffraction patterns of this compound when the water of crystallization had been eliminated by elevating the temperature by means of irradiation with an electron beam. Table 2(8) shows the measured values of the spacing obtained from the electron-diffraction patterns of the (β-γ)-from. These values were in good agreement with the values of the electron diffraction of the β-form alone, as is shown in Table 2(5). This result apparently shows that a mixture of β-Ti(HPO$_4$)$_2$ and γ-Ti(HPO$_4$)$_2$·2H$_2$O crystals was dehydrated and converted to the β-form.

References

1) a) Presented at the 43rd National Meeting of the Chemical Society of Japan, Tokyo, April 1981; b) Part V: E. Kobayashi and T. Kanayama, *Bull. Chem. Soc. Jpn.*, **53**, 3552 (1980).
2) E. Kobayashi, *Bull. Chem. Soc. Jpn.*, **48**, 3114 (1975).
3) E. Kobayashi, *Bull. Chem. Soc. Jpn.*, **51**, 2305 (1978).
4) E. Kobayashi, *Bull. Chem. Soc. Jpn.*, **52**, 1351 (1979).
5) E. Kobayashi, *Bull. Chem. Soc. Jpn.*, **52**, 1359 (1979).
6) G. Alberti, P. Cardini-Galt, U. Constantio, and E. Torracca, *J. Inorg. Nucl. Chem.*, **29**, 571 (1967).
7) S. Allulli, G. Ferragina, A. La Ginestra, M. A. Massucci, and N. Tomasini, *J. Inorg. Nucl. Chem.*, **39**, 1043 (1977).
8) A. Clearfield, R. H. Blessing, and J. A. Stynes, *J. Inorg. Nucl. Chem.*, **30**, 2249 (1968).

 © 1983 The Chemical Society of Japan Bull. Chem. Soc. Jpn., 56, 1637—1641 (1983)

The Crystal Structure of Bis(2,2′-bipyridine)-*catena*-μ-tetrafluoroborato-copper(II) Tetrafluoroborate

Hisayoshi Nakai

Department of Chemistry, Hyogo College of Medicine, Mukogawa-cho, Nishinomiya, Hyogo 663

(Received September 13, 1982)

The crystal structure of the title compound was determined by means of the X-ray diffraction technique. The crystal is triclinic, space group $P\bar{1}$, $a=11.288(8)$, $b=15.186(17)$, $c=7.368(4)$ Å, $\alpha=74.93(3)$, $\beta=78.23(3)$, $\gamma=65.92(3)°$, and $Z=2$. The structure was solved by the heavy-atom method and refined by the least-squares method to $R=0.068$ for 3678 non-zero reflections. The crystal is composed of BF_4^- ions and polymeric chains of $[Cu(BF_4)(bpy)_2^+]$ in which a tetrafluoroborate ion bridges two adjacent copper atoms through its two fluorine atoms. The coordination polyhedron around the copper atom is a tetragonally distorted octahedron; the four nitrogen atoms of bipyridine molecules in the equatorial plane are arranged in a flattened tetrahedral manner (average Cu–N = 1.99 Å) and the two axial Cu–F distances are 2.566(6) and 2.662(4) Å. In both bipyridine molecules, the two pyridine rings are twisted slightly from each other; the interplanar angle is 3.1° in one bipyridine ligand and 10.2° in the other.

Since the crystal structure of $[CuI(bpy)_2]I$ was reported in 1963,[1] bis(bipyridine)copper(II) complexes have attracted much attention because of the diversity of their stereochemistry. They have been shown to take various stereochemistries such as distorted trigonal bipyramid,[1-3] distorted square pyramid,[4-6] and *cis*- and *trans*-distorted octahedra.[7-10,22] Recently, some attempts to understand such changes in coordination geometry have been made.[4-5]

In this paper, as a part of our structural study on bis(bipyridine)copper(II) complexes, the crystal structure of $[Cu(BF_4)(bpy)_2]BF_4$ will be reported and the structures of some bis(bipyridine)copper(II) complexes will be discussed in terms of the sense of distortion illustrated in Fig. 3.

Experimental

Blue crystals of $[Cu(BF_4)(bpy)_2]BF_4$ were prepared by adding a methanol solution of 2,2′-bipyridine (20 mmol in 30 cm^3 of the solvent) to an aqueous solution of copper(II) tetrafluoroborate (10 mmol in 30 cm^3 of water), and were recrystallized from a water–methanol mixture. Found: C, 43.53; H, 2.99; N, 10.19%. Calcd for $Cu(bpy)_2(BF_4)_2$: C, 43.72; H, 2.93; N, 10.20%.

Preliminary X-ray photographs taken with Cu $K\alpha$ radiation showed $\bar{1}$ Laue symmetry, indicating a triclinic space group. No systematic absences were observed. The space group $P\bar{1}$ was confirmed by a successful refinement of the structure.

A crystal was shaped into a sphere 0.30 mm in diameter and used for data collection. The lattice constants were determined by a least-squares fit using 45 independent θ-values measured accurately on a diffractometer. Crystal data: $[Cu(BF_4)(bpy)_2]BF_4$, $M.W.=549.5$, triclinic, space group $P\bar{1}$, $a=11.288(8)$, $b=15.186(17)$, $c=7.368(4)$ Å, $\alpha=74.93(3)$, $\beta=78.23(3)$, $\gamma=65.92(3)°$, $U=1106.5$ Å^3, $Z=2$, $D_c=1.65$, $D_m=1.65$ g cm^{-3} (by flotation in a benzene–bromoform mixture), Mo $K\alpha$ radiation ($\lambda=0.71069$ Å), μ(Mo $K\alpha$) = 10.7 cm^{-1}.

Intensity data with $2\theta \leqq 55°$ were collected at room temperature by means of the ω-2θ scan techniques on a Philips PW1100 four-circle diffractometer using graphite-monochromated Mo $K\alpha$ radiation. The scan speed and scan width were 0.033° s^{-1} and $(1.00+0.20\tan\theta)°$ respectively. Background counts were measured for scantime/2 at each side of the scan range. A total of 5125 reflections having $I_t - 2\sqrt{I_t} > I_b$ were collected; I_t is the intensity (counts/s) measured at the top of the peak, while I_b is the mean background measurement for 5 s at each side of the peak, but 3678 reflections for which $F_o^2 > 2\sigma(F_o^2)$ were used in the structure analysis. Intensity data were corrected for the Lp factor[11] but not for absorption.

Structure Determination

The structure was solved by the heavy-atom method. The positions of the copper atoms were determined from a three-dimensional Patterson map; all the other non-hydrogen atoms were successively located by means of Fourier syntheses. The positional and thermal parameters were refined by the use of the block-diagonal least-squares method. The minimized function was $\sum w(F_o - |F_c|)^2$. A weighting scheme of the type suggested by Hughes[12] was applied using $w=1.0$ for $F_o \leqq 120.0$ and $w=(120.0/F_o)^2$ for $F_o > 120.0$. The atomic scattering factors were taken from Ref. 13. The positions of hydrogen atoms were obtained from a difference Fourier synthesis. These hydrogen atoms were included in the final refinement with isotropic thermal parameter of 4.0 Å^2. In the final cycle of the refinement, all the parameter shifts were less than one-third of the corresponding standard deviations. The final R value was 0.068 for 3678 non-zero reflections. The final atomic parameters are summarized in Tables 1 and 2 with averaged isotropic temperature factors. The anisotropic thermal parameters for non-hydrogen atoms and complete lists of the F_o and $|F_c|$ values have been preserved by the Chemical Society of Japan (Document No. 8320). All computations were carried out on an ACOS 700S computer at the Crystallographic Research Center, Institute for Protein Research, Osaka University. The computer programs used in the calculation were as follows: HBLS-V[14] (least-squares calculation), RSSFR-5[15] (Fourier synthesis), and DAPH[14] (interatomic distances and coordinates of the H atoms).

Results and Discussion

The crystal structure of $[Cu(BF_4)(bpy)_2]BF_4$ consists of tetrafluoroborate ions and polymeric chains of $[Cu(BF_4)(bpy)_2^+]$ approximately parallel to the c axis, in which $Cu(bpy)_2$-moieties are bridged by tetrafluoro-

TABLE 1. FINAL ATOMIC COORDINATES ($\times 10^4$) AND THERMAL PARAMETERS FOR NON-HYDROGEN ATOMS WITH ESTIMATED STANDARD DEVIATIONS IN PARENTHESES

Atom	x	y	z	B_{eq}/Å^2 a)	Atom	x	y	z	B_{eq}/Å^2 a)
Cu	1398.1(7)	2389.1(5)	4001.3(10)	3.75	C(15)	1905(5)	371(4)	5316(7)	3.83
N(1)	1920(5)	3536(4)	3579(7)	4.42	C(16)	3096(5)	422(4)	4079(7)	3.75
C(1)	3051(7)	3514(5)	3914(10)	6.32	C(17)	4133(6)	−399(5)	3607(9)	4.93
C(2)	3304(9)	4379(7)	3548(11)	8.27	C(18)	5197(6)	−274(5)	2422(9)	5.61
C(3)	2368(10)	5250(6)	2870(10)	8.60	C(19)	5187(6)	654(5)	1734(8)	5.51
C(4)	1192(9)	5282(5)	2599(9)	6.87	C(20)	4111(6)	1452(5)	2229(8)	4.53
C(5)	979(7)	4403(4)	2986(8)	5.00	N(4)	3099(4)	1333(3)	3412(6)	3.23
C(6)	−250(6)	4356(4)	2793(7)	4.45	B(1)	1279(7)	2090(5)	9241(9)	4.19
C(7)	−1314(7)	5163(5)	2104(9)	5.95	F(1)	1738(5)	2318(3)	7383(5)	8.07
C(8)	−2423(7)	5042(6)	1958(10)	6.87	F(2)	1582(4)	2611(3)	10262(5)	6.03
C(9)	−2488(6)	4119(6)	2497(10)	6.34	F(3)	1822(4)	1106(3)	9914(6)	6.84
C(10)	−1390(6)	3338(5)	3170(9)	5.33	F(4)	−60(4)	2378(3)	9409(7)	7.27
N(2)	−308(5)	3453(3)	3348(6)	3.76	B(11)	5881(11)	2798(8)	7457(23)	10.63
N(3)	915(4)	1249(3)	5353(6)	3.36	F(11)	4801(5)	2622(4)	7932(10)	11.90
C(11)	−187(6)	1278(4)	6469(8)	4.59	F(22)	5612(7)	3758(5)	7004(14)	17.16
C(12)	−351(7)	431(5)	7561(9)	5.64	F(33)	6264(10)	2557(6)	5542(14)	19.95
C(13)	651(7)	−464(5)	7529(9)	5.81	F(44)	6799(7)	2223(8)	8354(18)	23.19
C(14)	1802(7)	−496(4)	6390(9)	5.13					

a) Equivalent isotropic temperature factor (W. C. Hamilton, *Acta Crystallogr.*, **12**, 609 (1959)).

TABLE 2. ATOMIC COORDINATES ($\times 10^3$) FOR HYDROGEN ATOMS WITH ESTIMATED STANDARD DEVIATIONS IN PARENTHESES

Atom	x	y	z	Atom	x	y	z
H(C1)	371(6)	283(5)	423(9)	H(C11)	−87(6)	196(5)	664(9)
H(C2)	409(6)	422(5)	386(9)	H(C12)	−117(6)	42(5)	812(9)
H(C3)	251(6)	584(5)	266(9)	H(C13)	52(6)	−110(5)	826(9)
H(C4)	46(6)	593(5)	224(9)	H(C14)	241(6)	−111(5)	624(9)
H(C7)	−112(6)	576(5)	177(9)	H(C17)	406(6)	−101(5)	400(9)
H(C8)	−319(6)	561(5)	139(9)	H(C18)	597(6)	−82(5)	218(9)
H(C9)	−323(6)	390(5)	228(9)	H(C19)	581(6)	80(5)	93(9)
H(C10)	−140(6)	263(5)	335(9)	H(C20)	409(6)	210(5)	182(9)

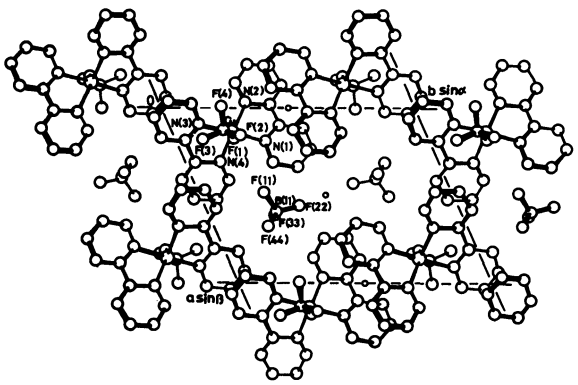

Fig. 1. Crystal structure viewed down the c axis.

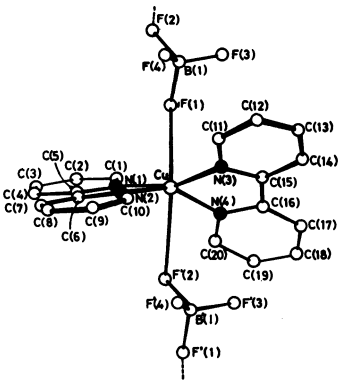

Fig. 2. A schematic drawing of a part of the infinite chain, $[Cu(BF_4)(bpy)_2^+]_\infty$.

borate ligands through the F atoms, as shown in Figs. 1 and 2. The bond lengths and angles with their estimated standard deviations are given in Table 3.

In the complex cation, the coordination polyhedron around the copper atom is a distorted *trans*-octahedron, in which four N atoms of the two bpy chelates form an equatorial plane (mean Cu–N=1.99 Å) and two F atoms of bridging BF_4^- ions occupy the axial positions (Cu–F(1)=2.566(6) Å and Cu–F(2)=2.662(4) Å). Although the four N atoms are arranged around the copper atom in a flattened tetrahedral manner, the copper atom lies almost on the least-squares plane defined by these nitrogen atoms (Table 5). Such a tetrahedral distortion of planar $Cu(bpy)_2$-moiety is now well-known to be due to the steric repulsions between the hydrogen atoms on 6- and 6′-carbon atoms of the bpy chelates. The dihedral angle between the (N(1)–Cu–N(2)) and (N(3)–Cu–N(4)) planes is 36.1°. Analogous stereochemistries have been found in $[Cu(ClO_4)(bpy)_2]ClO_4$[8]

TABLE 3. INTERATOMIC DISTANCES AND BOND ANGLES WITH THEIR ESTIMATED STANDARD DEVIATIONS IN PARENTHESES

Interatomic distance	l/Å		l/Å
Cu-N(1)	1.989(6)	C(16)-C(17)	1.384(9)
Cu-N(2)	1.996(5)	C(17)-C(18)	1.384(10)
Cu-N(3)	1.985(5)	C(18)-C(19)	1.363(11)
Cu-N(4)	1.989(5)	C(19)-C(20)	1.388(11)
Cu-F(1)	2.566(6)	B(1)-F(1)	1.369(9)
Cu-F'(2)	2.662(4)	B(1)-F(2)	1.394(9)
N(1)-C(1)	1.335(10)	B(1)-F(3)	1.359(9)
N(1)-C(5)	1.342(9)	B(1)-F(4)	1.379(9)
C(1)-C(2)	1.404(13)	B(11)-F(11)	1.31(2)
C(2)-C(3)	1.360(15)	B(11)-F(22)	1.33(2)
C(3)-C(4)	1.362(15)	B(11)-F(33)	1.49(2)
C(4)-C(5)	1.398(12)	B(11)-F(44)	1.23(2)
C(5)-C(6)	1.455(10)	C(1)-H(C1)	1.00(7)
N(2)-C(6)	1.350(9)	C(2)-H(C2)	0.88(7)
N(2)-C(10)	1.338(9)	C(3)-H(C3)	0.94(7)
C(6)-C(7)	1.388(11)	C(4)-H(C4)	1.00(7)
C(7)-C(8)	1.366(12)	C(7)-H(C7)	0.98(7)
C(8)-C(9)	1.382(13)	C(8)-H(C8)	1.01(7)
C(9)-C(10)	1.391(12)	C(9)-H(C9)	1.08(7)
N(3)-C(11)	1.335(8)	C(10)-H(C10)	1.06(7)
N(3)-C(15)	1.348(8)	C(11)-H(C11)	1.03(7)
C(11)-C(12)	1.389(10)	C(12)-H(C12)	0.94(7)
C(12)-C(13)	1.371(11)	C(13)-H(C13)	1.03(7)
C(13)-C(14)	1.386(11)	C(14)-H(C14)	0.92(7)
C(14)-C(15)	1.385(10)	C(17)-H(C17)	0.93(7)
C(15)-C(16)	1.481(8)	C(18)-H(C18)	0.96(7)
N(4)-C(16)	1.342(8)	C(19)-H(C19)	0.89(7)
N(4)-C(20)	1.333(8)	C(20)-H(C20)	0.94(7)

Bond angle	ϕ/°		ϕ/°
F(1)-Cu-N(1)	79.6(2)	F(1)-Cu-N(2)	109.8(2)
F(1)-Cu-N(3)	80.3(2)	F(1)-Cu-N(4)	96.7(2)
F'(2)-Cu-N(1)	88.1(2)	F'(2)-Cu-N(2)	76.9(2)
F'(2)-Cu-N(3)	112.1(2)	F'(2)-Cu-N(4)	76.9(2)
N(1)-Cu-N(2)	81.8(2)	N(1)-Cu-N(3)	159.8(2)
N(1)-Cu-N(4)	101.5(2)	N(2)-Cu-N(3)	103.5(2)
N(2)-Cu-N(4)	153.5(2)	N(3)-Cu-N(4)	82.5(2)
C(1)-N(1)-C(5)	119.6(6)	N(1)-C(1)-C(2)	121.0(8)
C(1)-C(2)-C(3)	119.0(9)	C(2)-C(3)-C(4)	120.2(10)
C(3)-C(4)-C(5)	118.9(9)	N(1)-C(5)-C(4)	121.1(7)
N(1)-C(5)-C(6)	115.5(6)	C(4)-C(5)-C(6)	123.4(7)
Cu-N(1)-C(1)	126.5(5)	Cu-N(1)-C(5)	113.8(5)
Cu-N(2)-C(6)	113.2(4)	Cu-N(2)-C(10)	126.9(5)
C(6)-N(2)-C(10)	119.2(6)	C(5)-C(6)-N(2)	115.3(6)
C(5)-C(6)-C(7)	124.2(7)	N(2)-C(6)-C(7)	120.6(6)
C(6)-C(7)-C(8)	119.8(8)	C(7)-C(8)-C(9)	120.1(8)
C(8)-C(9)-C(10)	117.4(8)	N(2)-C(10)-C(9)	122.8(7)
C(11)-N(3)-C(15)	118.7(5)	N(3)-C(11)-C(12)	122.0(6)
C(11)-C(12)-C(13)	119.6(7)	C(12)-C(13)-C(14)	118.6(7)
C(13)-C(14)-C(15)	119.3(7)	N(3)-C(15)-C(14)	121.8(6)
N(3)-C(15)-C(16)	114.5(5)	C(14)-C(15)-C(16)	123.7(6)
Cu-N(3)-C(11)	126.8(4)	Cu-N(3)-C(15)	113.7(4)
Cu-N(4)-C(16)	113.4(4)	Cu-N(4)-C(20)	126.4(4)
C(16)-N(4)-C(20)	119.3(5)	C(15)-C(16)-N(4)	115.1(5)
C(15)-C(16)-C(17)	123.2(6)	N(4)-C(16)-C(17)	121.7(6)
C(16)-C(17)-C(18)	118.8(6)	C(17)-C(18)-C(19)	119.2(7)
C(18)-C(19)-C(20)	119.4(7)	N(4)-C(20)-C(19)	121.5(7)
F(1)-B(1)-F(2)	108.1(6)	F(1)-B(1)-F(3)	110.5(6)
F(1)-B(1)-F(4)	109.6(6)	F(2)-B(1)-F(3)	110.8(6)
F(2)-B(1)-F(4)	108.7(6)	F(3)-B(1)-F(4)	109.2(6)
F(11)-B(11)-F(22)	111(2)	F(11)-B(11)-F(33)	100(2)
F(11)-B(11)-F(44)	115(2)	F(22)-B(11)-F(33)	100(2)
F(22)-B(11)-F(44)	122(2)	F(33)-B(11)-F(44)	104(2)

F'(2) atom is related by the symmetry code $(x, y, -1+z)$ to F(2) atom.

TABLE 4. SOME BOND LENGTHS AND ANGLES OF $[CuN_4X_2]$- AND $[CuN_4X]$-CHROMOPHORES (X=N, O, OR F) IN BIS(BIPYRIDINE)COPPER(II) COMPLEXES[a] (See Fig. 3 for notation)

	Complex	Bond length l/Å			Bond angle ϕ/°				Ref.
		Cu-N(bpy)	Cu-X(1)	Cu-X(2)	θ_1	θ_2	ϕ_1	ϕ_2	
1	$[Cu(S_3O_6)(bpy)_2]$	1.98 —1.99	2.82	2.82					9
2	$[Cu(S_4O_6)(bpy)_2]$	1.985—1.995	2.627	2.627	155.2[b]	155.2[b]			10
3	$[Cu(BF_4)(bpy)_2]BF_4$	1.985—1.996	2.566	2.662	159.8	153.5			This work
4	$[Cu(ClO_4)(bpy)_2]ClO_4$[c]	1.97—2.02	2.45	2.73	161.1	151.0			8
5	$[Cu(NO_3)(bpy)_2]NO_3 \cdot H_2O$	1.982—2.045	2.299		170.9	140.2			4
		1.973—2.051	2.301		170.7	140.7			4
6	$[Cu(S_2O_8)(bpy)_2] \cdot H_2O$	1.959—2.039	2.367		172.2	141.0			5
7	$[Cu(H_2O)(phen)_2](BF_4)_2$[d]	1.985—2.041	2.238		172.8	136.6			16
8	$[Cu(H_2O)(bpy)_2]S_2O_6$[c]	1.98—2.01	2.16		174.6	129.8			2
9	$[Cu(NH_3)(bpy)_2](BF_4)_2$	1.958—2.112	2.045		184.3	108.2	129.5	122.3	3
10	$[Cu(NCS)(bpy)_2]BF_4$	1.980—2.120	1.967		185.3	104.6	137.9	117.5	17
11	$[Cu_2(pydca)_2(bpy)_2] \cdot 4H_2O$[d]	1.985—2.115	2.029		182.5[b]	108.7	138.9	112.4	19
12	$[Cu(H_2O)(bpy)_2]S_5O_6$	1.973—2.123	2.054		180.9	111.4	143.6	104.9	6
13	$[Cu(HCOO)(bpy)_2]BF_4 \cdot 0.5H_2O$	1.978—2.158	2.024		184.2	113.2	146.1	100.5	20
14	$[Cu(CH_3COO)(bpy)_2]ClO_4 \cdot H_2O$	1.971—2.168	2.031		185.5	111.6	147.6	100.7	21
15	$[Cu(CH_3COO)(bpy)_2]BF_4$	1.995—2.209	1.980		181.7	111.0	156.5	92.3	21

a) Distorted *cis*-octahedral $[Cu(NO_2)(bpy)_2]Y$ complexes ($Y=NO_3$[7] and BF_4[22]) are not included. b) Values calculated with the atomic coordinates in the reference. c) Photographic data. d) phen=1,10-Phenanthroline and pydca =pyridine-2,6-dicarboxylate.

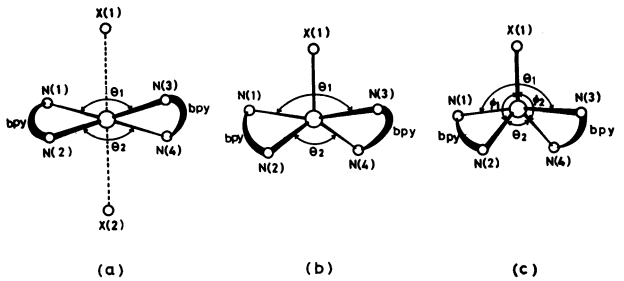

Fig. 3. Structures of bis(bipyridine)copper(II) complexes and their numbering schemes. (a): Distorted *trans*-octahedral structure ((1)—(4) complexes in Table 4), (b): five-coordinate structure with $\theta_1<180°$ ((5)—(8) complexes in Table 4), (c): five-coordinate structure with $\theta_1>180°$ ((9)—(15) complexes in Table 4).

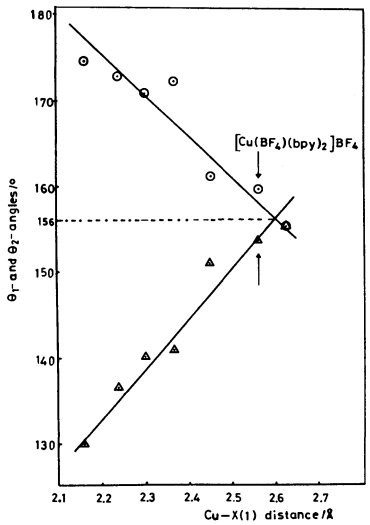

Fig. 4. Correlation between the Cu–X(1) distances (X= O or F) and the angles of θ_1 (⊙) and θ_2 (△) in the (2)—(8) complexes of Table 4. The values denoted by ⊙ and △ line up from right to left in numerical order respectively.

and $[CuX(bpy)_2]$ (X=S_3O_6[9] and S_4O_6[10]).

For comparison, the main bond lengths and angles around the copper atom are given in Table 4; those for $[Cu(S_3O_6)(bpy)_2]$ have not yet been reported in detail. In three *trans*-octahedral complexes (except $[Cu(S_3O_6)(bpy)_2]$), it is very interesting that as the axial Cu–X(1) distances (X=O or F) decrease from 2.627(6) Å in $[Cu(S_4O_6)(bpy)_2]$[10] to 2.566(6) Å in the present complex and to 2.45(2) Å in $[Cu(ClO_4)(bpy)_2]ClO_4$,[8] the θ_1-angles increase from 155.2° to 161.1(8)° and the θ_2-angles decrease from 155.2° to 151.0(7)° systematically. On the other hand, the distances between the X(1) and the N(1) (or N(3)) atoms in those complexes are 2.91, 2.949(8), and 2.79(3) Å respectively; these values are approximately equal to the sum of the van der Waals radii of O(or F) and N atoms. These prove that the enlargement of the θ_1-value with the decrease of the Cu–X(1) distance is due to the steric interference between the X(1) atom and the atoms of N(1) and N(3) in the flattened tetrahedral $Cu(bpy)_2$-moiety. Similar correlations between the Cu–O(1) distances and the

Table 5. Deviations of atoms from least-squares planes and dihedral angles

Deviations (l/Å) of atoms from the planes					
(A) Pyridine ring I					
N(1)	0.023	C(1)	−0.012	C(2)	−0.007
C(3)	0.014	C(4)	−0.005	C(5)	−0.013
(B) Pyridine ring II					
N(2)	−0.011	C(6)	0.006	C(7)	0.001
C(8)	−0.003	C(9)	−0.002	C(10)	0.009
(C) Bipyridine ligand I					
N(1)	0.076	C(1)	0.010	C(2)	−0.033
C(4)	−0.016	C(5)	0.024	C(6)	0.005
C(6)	0.005	C(7)	0.025	C(8)	0.018
C(9)	−0.011	C(10)	−0.025	N(2)	−0.041
(D) Pyridine ring III					
N(3)	0.004	C(11)	−0.006	C(12)	0.004
C(13)	0.001	C(14)	−0.003	C(15)	0.001
(E) Pyridine ring IV					
N(4)	−0.012	C(16)	0.002	C(17)	0.007
C(18)	−0.005	C(19)	−0.005	C(20)	0.014
(F) Bipyridine ring II					
N(3)	0.117	C(11)	0.105	C(12)	0.009
C(13)	−0.099	C(14)	−0.102	C(15)	0.010
C(16)	−0.006	C(17)	0.110	C(18)	0.100
C(19)	−0.006	C(20)	−0.096	N(4)	−0.124
(G) Plane through Cu, N(1), N(2), N(3), and N(4)					
Cu	−0.016	N(1)	−0.511	N(2)	0.445
N(3)	−0.216	N(4)	0.430		
Dihedral angles (ϕ/°) between the planes					
(A)-(B)	3.1	(D)-(E)	10.2	(C)-(F)	44.5

angles of θ_1 and θ_2 have also been found in $[CuN_4O]$-chromophores of bis(bipyridine)copper(II) complexes, having θ_1-values<180° (Table 4). The plots of the θ_1- and θ_2-angles against the Cu–X(1) distances (X=O or F) in the complexes mentioned above are shown in Fig. 4 and have been found to be linear. As a result, the θ_1-angle is expected to become 180° when the Cu–X-(1) distance is about 2.1 Å; on the other hand, in the complexes of (9)—(15) of Table 4 with Cu–X(1) distances(X=N or O)<2.1 Å and θ_1-angles>180°, a great lengthening has been observed in the Cu–N(4) distance from 2.1 Å to 2.2 Å, and, as has been suggested by Hathaway,[2,6] the angle of X(1)–Cu–N(2) (=ϕ_1 in Fig. 3), which is opposite the Cu–N(4) bond, is considered to play an important role in the decision of their stereochemistries.

The bipyridine ligands are not planar, but the pyridine rings are planar within ±0.023 Å. The pyridine rings of the bipyridine molecule are slightly twisted from each other about the 2,2′-carbon bond; the twist angle is 3.1° for the molecule comprising N(1) and N(2) and 10.2° for the other, values of which are in the range of 0.1—13° reported previously.[5,8] Furthermore, the bond angle of α is larger than that of β by 7.9—9.2°. A

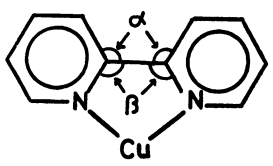

similar difference in these angles (5—10°) has also been observed in the crystal structure of the 2,2′-bipyridine molecule[18] and its copper(II) complexes.[8] Bond lengths and angles in bipyridine ligands are in good agreement with the previously reported ones.[4]

The B–F bond lengths and F–B–F angles of bridging BF_4^- ions are in the range of 1.359(9)—1.394(9) Å and 108.1(6)—110.8(6)° respectively, while those of the uncoordinating BF_4^- anions are less accurate and can not be discussed in detail because of the distorted arrangement in the crystal. The closest approach of the uncoordinating BF_4^- ion to the bipyridine ligand is 3.23(2) Å, between the F(22) and C(3)[$1-x$, $1-y$, $1-z$] positions.

The author is very grateful to Professor Yukinao Noda for his kind advice and encouragement throughout the present work. The author is also grateful to Professor Emeritus Hisao Kuroya and Professor Shun'ichiro Ooi of Osaka City University for their valuable discussions, and to Dr. Keiji Matsumoto, Osaka City University, for the use of a Philips PW1100 diffractometer.

References

1) G. A. Barclay, B. F. Hoskins, and C. H. L. Kennard, *J. Chem. Soc.*, **1963**, 5691.
2) W. D. Harrison and B. J. Hathaway, *Acta Crystallogr., Sect. B*, **35**, 2910 (1979).
3) F. S. Stephens, *J. Chem. Soc., Dalton Trans.*, **1972**, 1350.
4) H. Nakai, *Bull. Chem. Soc. Jpn.*, **53**, 1321 (1980); R. J. Fereday, P. Hodgson, S. Tyagi, and B. J. Hathaway, *J. Chem. Soc., Dalton Trans.*, **1981**, 2070.
5) W. D. Harrison and B. J. Hathaway, *Acta Crystallogr., Sect. B*, **36**, 1069 (1980).
6) W. D. Harrison, B. J. Hathaway, and D. Kennedy, *Acta Crystallogr., Sect. B*, **35**, 2301 (1979).
7) I. M. Procter and F. S. Stephens, *J. Chem. Soc., A*, **1969**, 1248.
8) H. Nakai, *Bull. Chem. Soc. Jpn.*, **44**, 2412 (1971).
9) M. B. Ferrari, G. G. Fava, and C. Pelizzi, *J. Chem. Soc., Chem. Commun.*, **1977**, 8.
10) W. D. Harrison and B. J. Hathaway, *Acta Crystallogr., Sect. B*, **34**, 2843 (1978).
11) J. Hornstra and B. Stubbe, PW1100 Data Processing Program, Philips Research Laboratories, Eindhoven, Holland.
12) E. W. Hughes, *J. Am. Chem. Soc.*, **63**, 1737 (1941).
13) "International Tables for X-Ray Crystallography," Kynoch Press, Birmingham (1974), Vol. IV, p. 71.
14) T. Ashida, "The Universal Crystallographic Computing System–Osaka," The Computation Center, Osaka Univ. (1979), pp. 53 and 61.
15) T. Sakurai, "The Universal Crystallographic Computing System(I)," The Crystallographic Society of Japan (1967), p. 45.
16) H. Nakai and Y. Noda, *Bull. Chem. Soc. Jpn.*, **51**, 1386 (1978).
17) S. Tyagi and B. J. Hathaway, *J. Chem. Soc., Dalton Trans.*, **1981**, 2029.
18) L. L. Merritt, Jr., and E. D. Schroeder, *Acta Crystallogr.*, **9**, 801 (1956).
19) G. Nardin, L. Randaccio, R. P. Bonomo, and E. Rizzarelli, *J. Chem. Soc., Dalton Trans.*, **1980**, 369.
20) W. Fitzgerald and B. J. Hathaway, *J. Chem. Soc., Dalton Trans.*, **1981**, 567.
21) B. J. Hathaway, N. Ray, D. Kennedy, N.O'Brien, and B. Murphy, *Acta Crystallogr., Sect. B*, **36**, 1371 (1980).
22) A. Walsh, B. Walsh, B. Murphy, and B. J. Hathaway, *Acta Crystallogr., Sect. B*, **37**, 1512 (1981).

Noncovalent Interactions in Metal Complexes. VI.[1] Bonding Interaction between Chelate π-System and Menthyl Group in Copper(II), Nickel(II), and Palladium(II) Complexes of 1-*l*-Menthyloxy-3-benzoylacetone

Michio NAKAMURA, Hisashi ŌKAWA,* and Sigeo KIDA
Department of Chemistry, Faculty of Science, Kyushu University 33, Hakozaki, Higashi-ku, Fukuoka 812
(Received December 6, 1982)

Metal complexes, M(*l*-moba)$_2$(H$_2$O)$_n$ (M=Cu(II), n=0; Ni(II), n=2; Pd(II), n=0) and M(bpy)(*l*-moba)ClO$_4$ (M=Cu(II), Pd(II)), where H(*l*-moba) denotes 1-*l*-menthyloxy-3-benzoylacetone, have been synthesized and characterized by means of elemental analyses, NMR spectra, electronic spectra, and circular dichroism spectra. In the NMR spectra of H(*l*-moba), Pd(*l*-moba)$_2$, and Pd(bpy)(*l*-moba)ClO$_4$, the methylene protons adjacent to the *l*-menthyloxy group were observed as AB quartet. The chloroform solutions of Cu(*l*-moba)$_2$ and Cu(bpy)(*l*-moba)ClO$_4$ showed a positive CD band at 15500 and 16200 cm^{-1}, respectively. The chloroform solution of Ni(*l*-moba)$_2$(H$_2$O)$_2$ also showed a weak, positive CD band near 16000 cm^{-1}. When pyridine or *t*-butylamine was added to the chloroform solution of Cu(*l*-moba)$_2$, a negative CD appeared around 17000 cm^{-1} attributable to the five-coordinate species Cu(*l*-moba)$_2$B. On the other hand, with adding an amine to the chloroform solution of Ni(*l*-moba)$_2$(H$_2$O)$_2$, the 16000 cm^{-1} CD band decreased its intensity and finally disappeared. Similar trend was observed when alcohol, DMSO, or DMF was added to the chloroform solution of Ni(*l*-moba)$_2$(H$_2$O)$_2$. NMR and CD spectral results have been rationalized by assuming that the *l*-menthyl group interacts with the chelate ring of *l*-moba$^-$ and this interaction gives rise to a chirality around the metal ion.

Inter-ligand, noncovalent interactions which cause stereoselectivity and stereospecificity in metal complexes are of current interest, because of their importance in biological processes involving metal ion.[2-6] Recently we reported[2] that tris(1-*l*-menthyloxy-3-benzoylacetonato)M(III) complexes, M(*l*-moba)$_3$ (M=Co, Cr, and Mn), prefer the *cis*-Δ-configuration, and this was attributed to an inter-ligand CH/π-interaction between the *l*-menthyl group of the ligand and the phenyl group of the neighbouring ligand in the molecule; on the other hand, no CD induction was observed in the cases of Cu(*l*-moba)$_2$, Ni(*l*-moba)$_2$(H$_2$O)$_2$, Co(*l*-moba)$_2$(H$_2$O)$_2$, and Mn(*l*-moba)$_2$(H$_2$O)$_2$.

In this study, the CD spectra of Cu(*l*-moba)$_2$ and Ni(*l*-moba)$_2$(H$_2$O)$_2$ were reexamined in a highly concentrated chloroform solution, and it was noticed that these complexes show a weak CD band in the d-d band region. It is known that Cu(*l*-moba)$_2$ and Ni(*l*-moba)$_2$(H$_2$O)$_2$ take a square planar and a *trans*-octahedral configuration, respectively.[2] In these configurations, the phenyl group of the ligand is considerably separated from the *l*-menthyl group of the other ligand,and hence it is unlikely that there operates an inter-ligand, CH/π-interaction between these two groups. In this study, new metal complexes, Pd(*l*-moba)$_2$ and M(bpy)(*l*-moba)ClO$_4$ (M=Cu(II), Pd(II)), were prepared and the configurations of the complexes including Cu(*l*-moba)$_2$ and Ni(*l*-moba)$_2$(H$_2$O)$_2$ were examined by means of NMR, electronic absorption, and circular dichroism spectra, in a hope to clarify the mechanism how the *l*-menthyl group of the ligand invokes a chirality around the central metal ion.

Experimental

Preparations. Synthetic methods of H(*l*-moba) and its nickel(II) and copper(II) complexes, Ni(*l*-moba)$_2$(H$_2$O)$_2$ and Cu(*l*-moba)$_2$, are described in the preceding paper.[2] Benzyl *l*-menthyloxyacetate was synthesized by the reaction of *l*-menthyloxyacetyl chloride[7] and benzyl alcohol, in a similar way to that for ethyl *l*-menthyloxyacetate.

1-Ethoxy-3-benzoylacetone (Heoba). This was prepared from ethyl ethoxyacetate and acetophenone by a method similar to that for H(*l*-moba). It was isolated and purified as nickel(II) complex Ni(eoba)$_2$(CH$_3$OH)$_2$.

Found: C, 58.55; H, 6.47%. Calcd for C$_{26}$H$_{34}$O$_8$Ni: C, 58.56; H, 6.43%.

The free ligand was obtained as follows. The nickel complex (2 g) was dissolved in ether (100 cm^3). To this was added 20% sulfuric acid (100 cm^3) and the mixture was vigorously shaken. The ether layer was separated, shaken twice with saturated sodium hydrogencarbonate solution and then twice with water, and dried over sodium sulfate. Evaporation of the solvent left Heoba as a colorless liquid.

Pd(l-moba)$_2$. Palladium chloride (0.2 g, 1.12 mmol) and ammonium chloride (0.12 g, 2.24 mmol) were added to methanol (30 cm^3), and the mixture was vigorously stirred for 2 h to give a brown solution. To this was added dropwise a methanol solution of H(*l*-moba) (0.71 g, 2.24 mmol) and KOH (0.13 g, 2.24 mmol). A cream yellow precipitate thus obtained was collected and recrystallized from methanol.

Found: C, 64.92; H, 7.35%. Calcd for C$_{40}$H$_{54}$O$_6$Pd: C, 65.17; H, 7.38%.

Cu(bpy)(l-moba)ClO$_4$·2H$_2$O. A solution of Cu(bpy)$_2$(ClO$_4$)$_2$ (0.08 g, 0.14 mmol) and Cu(*l*-moba)$_2$ (0.1 g, 0.14 mmol) in methanol (100 cm^3) was heated for an hour. The reaction mixture was concentrated to 20 cm^3 and water was added drop by drop to this mixture to give a green precipitate. It was collected and recrystallized from methanol–water as green crystals. The product appeared to be pure crystals under a microscope observation.

Found: C, 53.17; H, 5.90; N, 4.02%. Calcd for C$_{30}$H$_{39}$N$_2$O$_9$ClCu: C, 53.72; H, 5.86; N, 4.18%.

Pd(bpy)(l-moba)ClO$_4$. To a suspension of Pd(bpy)$_2$Cl$_2$[8] (0.3 g, 1.7 mmol) in methanol (30 cm^3) was added a solution of H(*l*-moba) (0.29 g, 0.9 mmol) and KOH (0.05 g, 0.9 mmol) in methanol (10 cm^3), and the mixture was stirred for 1 h. To this reaction mixture was added a solution of AgClO$_4$ (0.38 g) in methanol to yield a precipitate of AgCl, which was separated by filtration. The filtrate was further

stirred for additional 2 h and was filtered. The filtrate was concentrated to 10 cm^3. When water was added drop by drop to the solution, a yellow precipitate was separated. It was collected and dried *in vacuo* over diphosphorus pentaoxide.

Found: C, 52.36; H, 5.13; N, 4.03%. Calcd for $C_{30}H_{35}N_2O_8ClPd$: C, 52.00; H, 5.09; N, 4.04%.

Measurements. NMR spectra were measured on a Hitachi NMR Spectrometer Model R-20-B in carbon tetrachloride and JEOL Fourier Transform NMR Spectrometer FX90Q in $CDCl_3$, tetramethylsilane being used as an internal standard. Circular dichroism spectra were measured on a JASCO ORD/CD optical dispersion recorder. Electronic absorption spectra were measured on a Shimadzu Multipurpose Spectrophotometer Model MSP-5000. The elemental analyses were carried out at the Service Center of Elemental Analysis, Kyushu University.

Results and Discussion

The proton NMR spectra of H(*l*-moba), Pd(*l*-moba)$_2$, and pd(bpy)(*l*-moba)ClO_4 are given in Fig. 2. The most characteristic feature in these spectra is the AB quartet around 4 ppm attributable to the methylene protons adjacent to the *l*-menthyloxy group. One of the possible origins of the AB quartet of the methylene protons is the effect of the chirality of the neighbouring *l*-menthyl group. In order to examine this, we measured the NMR spectra of benzyl *l*-methyloxyacetate and ethyl *l*-menthyloxyacetate (Fig. 1(b) and (c)) and found that the methylene protons adjacent to the *l*-menthyloxy group of these esters appeared as singlet. Therefore, the AB quartet of the methylene protons of H(*l*-moba), Pd(*l*-moba)$_2$, and Pd(bpy)(*l*-moba)ClO_4 should be attributed to a particular configuration of *l*-moba$^-$. We showed in the previous paper[2] that the ligand assumes the enol form in the metal-free state as well as in the metal complexes. However, benzyl *l*-menthyloxyacetate and ethyl *l*-menthyloxyacetate can not form such an intramolecular hydrogen bonding. Therefore, we assume that an intramolecular interaction is operating between the *l*-menthyl group and the metal chelate ring of the *l*-moba complexes or the hydrogen-bonded ring of H(*l*-moba). This interaction would hinder the free rotation around the methylene group and hence bring about the inequivalence of the methylene protons. In the NMR spectrum of 1-ethoxy-3-benzoylacetone (Fig. 1(d)), the methylene protons appeared as singlet at 4.0 ppm. The Dreiding model consideration has indicated that the ethyl group can not approach so close to the hydrogen-bonded ring as to cause an appreciable interaction with the benzene ring.

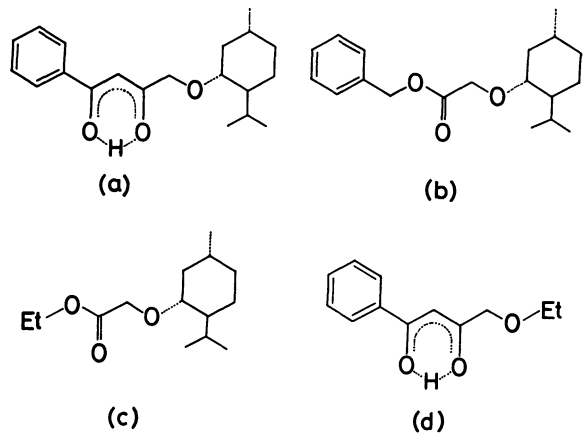

Fig. 1. Chemical structure of (a) 1-*l*-menthyloxy-3-benzoylacetone (H(*l*-moba)), (b) benzyl *l*-menthyloxyacetate, (c) ethyl *l*-menthyloxyacetate, and (d) 1-ethoxy-3-benzoylacetone (Heoba).

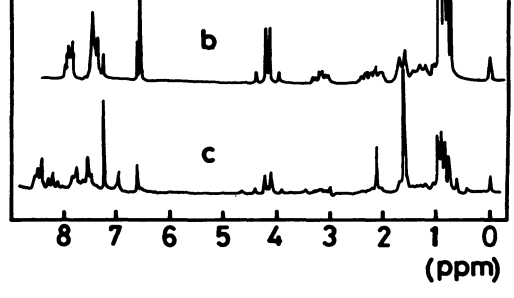

Fig. 2. NMR spectra of (a) H(*l*-moba), (b) Pd(*l*-moba)$_2$, and (c) Pd(bpy)(*l*-moba)ClO_4.

The NMR spectra have revealed that the coupling constants of the methylene protons of Pd(*l*-moba)$_2$ and Pd(bpy)(*l*-moba)ClO_4 are larger than that of H(*l*-moba). This implies that the interaction between the *l*-menthyl group and the ring is enhanced when H(*l*-moba) coordinates to palladium(II) ion. There is little difference between Pd(*l*-moba)$_2$ and Pd(bpy)(*l*-moba)ClO_4 in chemical shift and the coupling constant of the methylene protons. This suggests that in Pd(bpy)(*l*-moba)ClO_4 the *l*-menthyl group does not interact with the π-system of bpy but with the chelate ring of *l*-moba$^-$. This interaction differs from the intramolecular CH/π-interaction observed for the ternary complexes composed of 2,2'-bipyridyl (or 1,10-phenanthroline) and a carboxylic acid,[5] 2,2'-bipyridyl and a sulfonic acid,[5] and 2,2'-bipyridyl and an amino acid.[6] Based on the Dreiding model consideration, no interaction seems to operate between the *l*-menthyl group and the bpy molecule, so long as bpy and *l*-moba$^-$ are planarly coordinated to palladium(II) ion.

Another characteristics in the NMR spectrum of Pd(*l*-moba)$_2$ is two singlets at 6.60 and 6.62 ppm which can be assigned to the methine proton on the chelate ring. This may be reasonably explained by assuming that the sample of Pd(*l*-moba)$_2$ is the mixture of the *cis*- and *trans*-isomers.

In order to investigate further an interaction operating between the *l*-menthyl group and the chelate ring of *l*-moba$^-$, we examined the CD spectra of Cu(*l*-moba)$_2$, Cu(bpy)(*l*-moba)ClO_4, and Ni(*l*-moba)$_2$(H_2O)$_2$. The absorption and CD spectra of Cu(*l*-moba)$_2$ and Cu(bpy)(*l*-moba)ClO_4 in chloroform are shown in Figs. 3 and 4, respectively. The absorption spectrum of Cu(*l*-moba)$_2$ showed three d-d bands at 15200, 17700, and 18900 cm^{-1}; this spectrum resembles that of Cu-

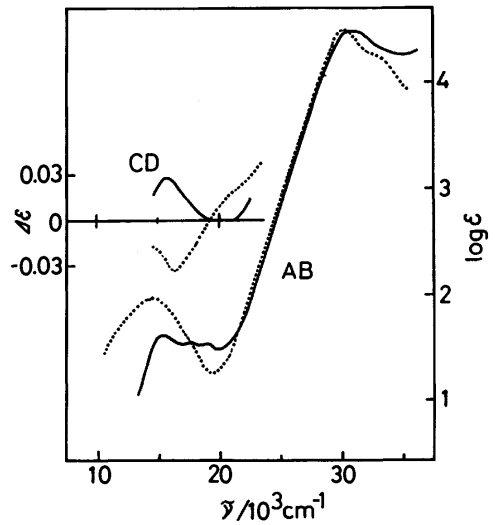

Fig. 3. Absorption and CD spectra of Cu(*l*-moba)$_2$ in $CHCl_3$ (——) and in pyridine (------).

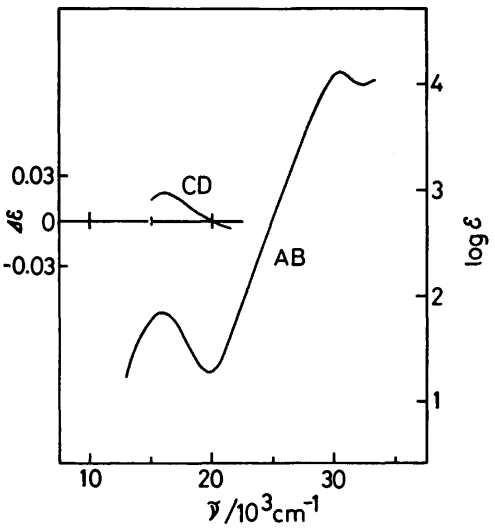

Fig. 4. Absorption and CD spectra of Cu(bpy) (*l*-moba)-ClO_4 in $CHCl_3$.

(acac)$_2$.[9,10] The chloroform solution of Cu(*l*-moba)$_2$ showed a weak, positive CD around 15500 cm^{-1}. On adding excess pyridine or *t*-butylamine to this solution, the CD spectral pattern changed dramatically and a weak, negative CD appeared around 17000 cm^{-1}. In the presence of excess pyridine or *t*-butylamine, Cu(*l*-moba)$_2$ will take a square-pyramidal configuration with the base(B) at the axial site. Because the sixth coordination site is still vacant, one of the *l*-menthyl groups can approach the vacant site of the coordination plane to cause the menthyl/chelate-interaction. The chloroform solution of Cu(bpy)(*l*-moba)ClO_4 showed a d-d band at 16000 cm^{-1} and a weak, positive CD at 16200 cm^{-1}. The marked resemblance in CD spectra between Cu(*l*-moba)$_2$ and Cu(bpy)(*l*-moba)ClO_4 indicates that the *l*-menthyl group of the latter complex does not interact with the π-system of 2,2′-bipyridyl but with the chelate ring of *l*-moba$^-$, similarly to the case of the Pd analogue.

The absorption spectrum of Ni(*l*-moba)$_2$(H_2O)$_2$ in chloroform showed d-d bands at 8800 and 15600 cm^{-1}

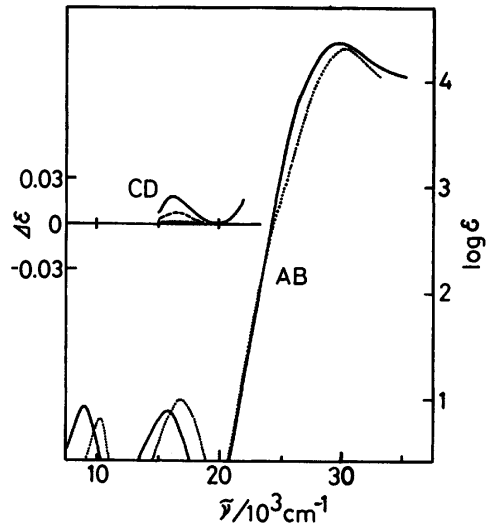

Fig. 5. Absorption and CD spectra of Ni(*l*-moba)$_2$-(H_2O)$_2$ in $CHCl_3$ in the absence and in the presence of propylamine: [propylamine]/[Ni(*l*-moba)$_2$(H_2O)$_2$]=0 (——), 1.5 (------), and 15 (·····).

(Fig. 5), indicating a nearly octahedral symmetry around the metal ion.[11,12] This solution showed a positive CD band near 16000 cm^{-1}. It is likely that the water molecules coordinated at the apical positions do not sterically hinder the interaction between the *l*-menthyl group and the chelate ring. Then, we have examined the CD spectra of Ni(*l*-moba)$_2$(H_2O)$_2$ in the presence of an amine or an alcohol. The CD spectral change for Ni(*l*-moba)$_2$(H_2O)$_2$ on adding propylamine is shown in Fig. 5 as an example. The positive CD at 16000 cm^{-1} gradually decreased its intensity on increasing the amine ratio and finally disappeared. The absorption spectrum of Ni(*l*-moba)$_2$(H_2O)$_2$ in the presence of a large excess of propylamine showed d-d bands at 10000 and 16700 cm^{-1}, implying that the species in the solution is Ni(*l*-moba)$_2$(*n*-prNH_2)$_2$. Thus, the CD spectral change mentioned above can be rationalized by assuming that propylamine coordinated at the apical position sterically hinders the intramolecular interaction between the *l*-menthyl group and the chelate ring of the *l*-moba$^-$ molecule. Similar CD spectral behaviors were also observed when other amines (pyridine, piperidine, *t*-butylamine, and dipropylamine), alcohols (methanol, ethanol, 1-propanol, 1-butanol, 2-methyl-1-propanol, 2-butanol, and 2-methyl-2-propanol), DMF and DMSO were added. In all cases, the interaction between the *l*-menthyl group and the chelate ring must be inhibited due to the steric effect of the molecules coordinated at the apical positions. When triethylamine was added to the chloroform solution of Ni(*l*-moba)$_2$(H_2O)$_2$, no absorption and CD spectral change occured. It is likely that triethylamine can not coordinate to the nickel(II) ion because of the F-strain of the amine.

In the case of addition of excess pyridine, piperidine, *t*-butylamine, 2-methyl-1-propanol, or 2-butanol to the chloroform solution of Ni(*l*-moba)$_2$(H_2O)$_2$, a weak, negative CD peak appeared around 16500 cm^{-1} ($\Delta\varepsilon \approx -0.005$). The origin of this CD is unclear at present, but some intra- or inter-ligand interactions other than

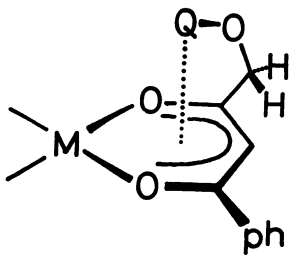

Fig. 6. Schemati· representation of the intramolecular menthyl/chelate-interaction.

the *l*-menthyl/chelate-interaction, such as the interaction between the *l*-menthyl group and the hydrophobic moiety of an amine or an alcohol, might contribute to the weak CD induction.

Based on these facts we conclude that in the *l*-moba metal complexes an intramolecular interaction occurs between the *l*-menthyl group and the chelate ring, and this interaction causes an chirality around the metal ion. It is most likely that the *l*-menthyl group bondingly interacts with the π-system of the chelate ring (Fig. 6). Such a new-type interaction resembles the inter-ligand π/π-interaction suggested for mixed-chelate cobalt(III) complexes containing acetylacetonate ion and (2-aminoethyl)methylphenylphosphine.[13]

References

1) Part V: M. Nakamura, H. Ōkawa, and S. Kida, *Bull. Chem. Soc. Jpn.*, **55**, 2400 (1982).
2) H. Ōkawa, K. Ueda, and S. Kida, *Inorg. Chem.*, **21**, 1594 (1982).
3) H. Ōkawa, Y. Numata, A. Mio, and S. Kida, *Bull. Chem. Soc. Jpn.*, **53**, 2248 (1980).
4) P. R. Mitchell, B. Prijis, and H. Sigel, *Helv. Chim. Acta*, **62**, 1273 (1970).
5) P. R. Mitchell, *J. Chem. Soc., Dalton Trans.*, **1979**, 771.
6) E. Fischer and H. Sigel, *J. Am. Chem. Soc.*, **102**, 2998 (1980).
7) A. W. Ingersoll, "Organic Reactions," Willey, New York (1971), Vol. II, p. 399.
8) B. J. McCormick, E. N. Jaynes, Jr., R. I. Kaplan, *Inorg. Synth.*, **13**, 217 (1792).
9) R. L. Belford, M. Calvin and G. Belford, *J. Chem. Phys.*, **26**, 1165 (1957).
10) H. Kato and J. Gohda, *Bull. Chem. Soc. Jpn.*, **46**, 636 (1973).
11) M. K. Misra and D. V. Ramana Rao, *J. Inorg. Nucl. Chem.*, **34**, 728 (1965).
12) J. T. Hashagen and J. P. Fackler, Jr., *J. Am. Chem. Soc.*, **87**, 2821 (1965).
13) K. Kashiwabara, I. Kinoshita, T. Itoh, and J. Fujita, *Bull. Chem. Soc. Jpn.*, **54**, 725 (1981).

Stereochemical Aspects of the Optical Resolution of *cis*(N)-$[Co(N)_2(O)_4]^-$ Complexes by Reversed-phase Ion-pair Chromatography with Cinchona Alkaloid Cations as the Ion-pairing Reagents[1)]

Shinji Izumoto, Ushio Sakaguchi, and Hayami Yoneda*
Department of Chemistry, Faculty of Science, Hiroshima University, Hiroshima 730
(Received December 24, 1982)

The reversed-phase ion-pair chromatography with cinchona alkaloid cations as the ion-pairing reagents has been used to resolve optically several anionic complexes of the type *cis*(N)-$[Co(N)_2(O)_4]^-$. Complete optical resolution has been achieved for $[Co(edta)]^-$, *cis*-$[Co(ida)_2]^-$, $[Co(cydta)]^-$, $[Co(ox)_2(en)]^-$, and *cis*-*α*-$[Co(ox)(edda)]^-$ by quinine, quinidine, and cinchonidine but not by cinchonine, where edta=ethylenediaminetetraacetate, ida=iminodiacetate, cydta=*trans*-1,2-cyclohexanediaminetetraacetate, ox=oxalate, en=ethylenediamine, and edda=*N*,*N*′-ethylenediaminediacetate. The adjusted retention volumes have been measured for the enantiomers. From comparison of the retention volumes and separation factors obtained for the alkaloids and their derivatives, the mode of chiral discrimination has been proposed.

Cinchona alkaloids, *e.g.*, cinchonine, quinine, quinidine, and cinchonidine, are well-known resolving agents for the optical resolution of anionic metal complexes. The cations of these alkaloids are soluble in water, yet bear a hydrophobic character, which suggests these cations to be likely candidates for good ion-pairing reagents in the reversed-phase ion-pair chromatography.[2)] Recently, Yamazaki[3)] has exploited this technique for the optical resolution of several anionic complexes. Using the cation of quinine as the ion-pairing reagent, complete optical resolution has been achieved for $[Co(edta)]^-$, *cis*-$[Co(ida)_2]^-$, $[Co(ox)_2(en)]^{-1}$, and *cis*-*α*-$[Co(Cl)_2(edda)]^-$, where edta=ethylenediaminetetraacetate, ida=iminodiacetate, ox=oxalate, en=ethylenediamine, and edda=*N*,*N*′-ethylenediaminediacetate. The mechanism of optical resolution has been explained by assuming that both dynamic ion-exchange and ion-pairing are important. The stereochemical aspects has not, however, been considered.

In this work, we have applied the reversed-phase ion-pair chromatography with several cinchona alkaloids as the ion-pairing reagents to the optical resolution of anionic complexes of the type *cis*(N)-$[Co(N)_2(O)_4]^-$. Figure 1 shows the schematic illustration of the structure of the complexes examined in this work. The structure of the cinchona alkaloids used here is depicted in Fig. 2, where the atom numbering scheme is also indicated. The adjusted retention volume has been measured for each enantiomer over a range of pH values. From comparison of these retention volumes obtained for these alkaloids and their derivatives, the stereochemical aspects of the mechanism of optical resolution have been discussed.

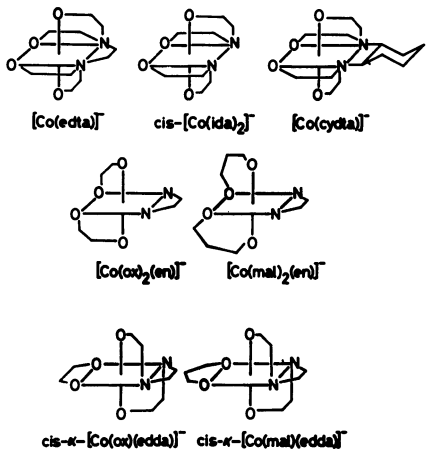

Fig. 1. The structure of the complexes investigated in this work. The figure is drawn for the *Λ* absolute configuration.

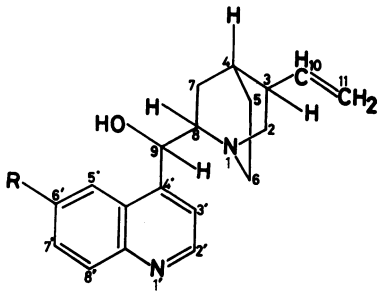

Fig. 2. The structure of the alkaloids used in this work. Cinchonine ((8*R*, 9*S*), R=H); cinchonidine ((8*S*, 9*R*), R=H); quinine ((8*S*, 9*R*), R=OCH_3); quinidine ((8*R*, 9*S*), R=OCH_3). 1-Methylquininium chloride and 9-acetoxyquinine were also employed.

Experimental

Materials. The anionic complexes used in this work were K[Co(edta)],[4)] *cis*-K[Co(ida)$_2$],[5)] K[Co(cydta)](cydta=*trans*-1,2-cyclohexanediaminetetraacetate),[6)] Na[Co(ox)$_2$(en)],[7)] Na[Co(mal)$_2$(en)] (mal=malonate),[8)] *cis*-*α*-K[Co(ox)(edda)],[9)] *cis*-*α*-K[Co(mal)(edda)].[10)] All these complexes were prepared by the literature methods. The absolute configurations of the enantiomers of these complexes were assigned previously.

The following cinchona alkaloids were used as the ion-pairing reagents; (+)-(8*R*, 9*S*)-cinchonine, (−)-(8*S*, 9*R*)-cinchonidine, (−)-(8*S*, 9*R*)-quinine, (+)-(8*R*, 9*S*)-quinidine, 1-methylquininium chloride, and 9-acetoxyquinine. The last two alkaloids were prepared by the literature methods[11,12)] and identified by ^{1}H NMR and chemical analysis. The other alkaloids were obtained from Wako Pure Chemical Industries, Ltd. and used without further purification.

The column packing used in this work was LS-410.ODS.SIL. (Toyo Soda Manufacturing Co., Ltd.), which carries linear

long-chain alkyl groups (octadecyl groups) covalently bonded to the surface of silica gel.

Chromatographic Experiments. A column (4×300 mm) packed with LS-410.ODS.SIL. was equilibrated with an eluent, which was a 0.2 mol dm^{-3} sodium acetate/acetic acid buffered solution containing 0.01 mol dm^{-3} ion-pairing reagent. An aqueous solution of a racemic complex (0.1 mol dm^{-3}) and bis(ethylenediamine)copper(II) chloride (0.1 mol dm^{-3}), which was used as a marker for void volume measurements, was injected by a syringe on top of the column and eluted at an elution rate of 0.50 cm^3/min. The eluate containing an optically resolved anionic complex was fractionally collected and the circular dichroism (CD) spectra were measured to assign the absolute configuration of the resolved complex anion. Interference in the CD spectra due to chiral ion-pairing reagents, an effect called induced CD,[13] was not observed. The pH of the buffered solution was changed from 4.28 to 6.12.

The chromatographic apparatus used here was the same as in previous studies.[3,14] The CD spectra were obtained on a JASCO J-40CS recording spectropolarimeter.

Results and Discussion

Figure 3 shows the elution curves of $[Co(edta)]^-$, $[Co(ox)_2(en)]^-$, and *cis*-α-[Co(ox)(edda)]$^-$, all obtained with quinine at pH 4.28. The $[Co(edta)]^-$ and $[Co(ox)_2(en)]^-$ ions are completely resolved with separation factors of 1.14 and 1.10, respectively. As a rough measure of complete resolution, we may use the separation factor greater than about 1.07 in our experiments. Tables 1 to 4 summarize the results obtained for quinine, quinidine, cinchonidine, and cinchonine, respectively, in terms of the later-eluted enantiomers, their retention volumes, and the separation factors. From these tables, the following points are noted. (i) $[Co(edta)]^-$, *cis*-$[Co(ida)_2]^-$, $[Co(cydta)]^-$, and $[Co(ox)_2(en)]^-$ are completely resolved by any one of quinine, quinidine, and cinchonidine. (ii) $[Co(mal)_2(en)]^-$ and *cis*-α-[Co(mal)(edda)]$^-$ can not be resolved completely by any alkaloids. (iii) *cis*-α-[Co(ox)(edda)]$^-$ can be resolved completely only by quinidine or cinchonidine. (iv) Cinchonine is ineffective in resolving all the complexes and the retention volumes with this alkaloid are much smaller than those with the other alkaloids for all the complexes.

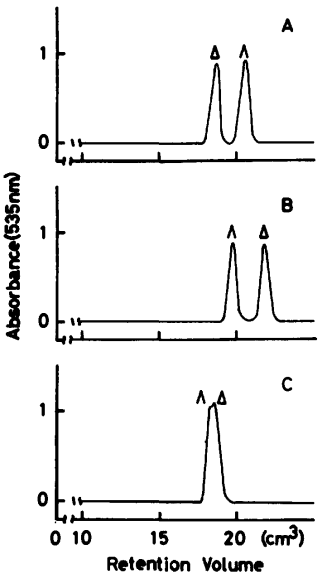

Fig. 3. The elution curves of (A) $[Co(edta)]^-$, (B)$[Co(ox)_2(en)]^-$, and (C) *cis*-α-[Co(ox)(edda)]$^-$, obtained with quinine at pH 4.28.

1. Analysis of Data. In the reversed-phase ion-pair chromatography, the enantiomer that associates more favorably with the ion-pairing reagent is better adsorbed to the hydrophobic stationary phase and eluted later.[2,3] Since protonation of all the alkaloids except 1-methylquininium chloride has been reported[15] to take place at pH 9.70 to 10.03 on the quinuclidine N(1) nitrogen and at pH 5.07 to 5.85 on the quinoline N(1′) nitrogen, the ion-pairing reagents exist as monopositive or dipositive cations in the pH range studied (pH 4.3 to 6.1). Thus, the ion association of the anionic complex ions with the alkaloid cations will take place mainly *via* electrostatic forces. This reasoning has been substantiated clearly by examining the pH dependence of the retention volumes.

(*a*) *Effect of pH*: For all the complex/alkaloid combinations, the retention volume increases substantially as the pH of the eluent solution is lowered beyond the point where the quinoline N(1′) protonation occurs. This is due to an increase in the concentration of alkaloid dications rather than monocations and hence to an increase in the concentration of ion-pairs. The effect of solution pH on the separation factor is, however, rather small, which indicates that the association of metal complex ions to the protonated N(1) nitrogen is effective in chiral discrimination but that to the quinoline N(1′) nitrogen is not. The only mode of association that is effective for chiral discrimination is, therefore, at the protonated N(1) nitrogen. One peculiar result may be noted in Table 4 for the combinations cinchonine/$[Co(edta)]^-$ and cinchonine/$[Co(mal)_2(en)]^-$. For these two combinations, the elution order of enantiomers is inverted by the pH of the eluent. Since these combinations gave only single elution curves and the degree of resolution was very low at any pH, no further investigation on this point was attempted.

(*b*) *Effect of C(8) and C(9) Configurations*: From Tables 1 to 4, it can be seen that the enantiomer eluted faster by the (8*R*,9*S*) alkaloids (cinchonine and quinidine) is eluted later by the (8*S*,9*R*) alkaloids (cinchonidine and quinine). Note here that the latter alkaloids are not the mirror images of the former ones owing to the presence of four asymmetric centers, C(3), C(4), C(8), and C(9).[16] Further, the C(8) and C(9) centers are close to the N(1) nitrogen spatially (see below), this result is considered to be consistent with the inference that the association of complex anions with the protonated N(1) nitrogen is essential in chiral discrimination. Broadly speaking, the (8*S*,9*R*) alkaloids yielded larger separation factors than the (8*R*,9*S*) alkaloids but the reason for this trend is not clear as yet.

(*c*) *Effect of C(6′) Methoxyl Group*: Another point to be noted in Tables 1 to 4 is that the alkaloids with the C(6′) methoxyl group, quinine and quinidine, gave rise to greater retention volumes and separation factors than the alkaloids without the methoxyl group, cinchoni-

Table 1. The absolute configuration of the later-eluted enantiomer, its retention volume (V), and the separation factor (α), obtained with quinine

Complex	pH 4.28			pH 4.93			pH 5.48			pH 6.02		
		V/cm³	α		V/cm³	α		V/cm³	α		V/cm³	α
[Co(edta)]⁻	Λ	21.70	1.14	Λ	13.20	1.10	Λ	9.60	1.10	Λ	8.80	1.09
cis-[Co(ida)$_2$]⁻	Λ	24.80	1.21	Λ	16.10	1.22	Λ	11.60	1.20	Λ	10.20	1.15
[Co(cydta)]⁻	Λ	17.50	1.08	Λ	10.70	1.08	Λ	7.70	1.08	Λ	7.10	1.07
[Co(ox)$_2$(en)]⁻	Δ	22.90	1.10	Δ	13.80	1.14	Δ	10.80	1.09	Δ	9.90	1.09
[Co(mal)$_2$(en)]⁻	Λ	10.10	1.0[a]	b)	6.40	1.0[a]	b)	5.00	1.0[a]	b)	4.80	1.0[a]
cis-α-[Co(ox)(edda)]⁻	Δ	19.60	1.02	Δ	12.40	1.0[a]	Δ	10.10	1.0[a]	Δ	8.80	1.0[a]
cis-α-[Co(mal)(edda)]⁻	Λ	7.40	1.0[a]	b)	4.70	1.0[a]	b)	3.70	1.0[a]	b)	3.50	1.0[a]

a) Single elution curve. b) The absolute configuration of the later-eluted enantiomer could not be determined owing to very low degree of optical resolution.

Table 2. The absolute configuration of the later-eluted enantiomer, its retention volume (V), and the separation factor (α), obtained with quinidine

Complex	pH 4.30			pH 4.97			pH 5.53			pH 6.02		
		V/cm³	α		V/cm³	α		V/cm³	α		V/cm³	α
[Co(edta)]⁻	Δ	22.90	1.07	Δ	14.30	1.07	Δ	10.80	1.07	Δ	9.40	1.06
cis-[Co(ida)$_2$]⁻	Δ	29.30	1.21	Δ	19.30	1.21	Δ	14.50	1.21	Δ	12.30	1.22
[Co(cydta)]⁻	Δ	19.90	1.05	Δ	12.10	1.05	Δ	9.10	1.05	Δ	7.90	1.04
[Co(ox)$_2$(en)]⁻	Λ	23.10	1.13	Λ	15.60	1.15	Λ	11.40	1.11	Λ	9.80	1.10
[Co(mal)$_2$(en)]⁻	Δ	10.60	1.0[a]	Δ	6.70	1.0[a]	Δ	4.90	1.0[a]	Δ	4.60	1.0[a]
cis-α-[Co(ox)(edda)]⁻	Λ	18.60	1.09	Λ	13.40	1.12	Λ	9.65	1.11	Λ	8.70	1.12
cis-α-[Co (mal) (edda)]⁻	Δ	9.80	1.0[a]	b)	6.10	1.0[a]	b)	5.10	1.0[a]	b)	4.40	1.0[a]

a) Single elution curve. b) The absolute configuration of the later-eluted enantiomer could not be determined owing to very low degree of optical resolution.

Table 3. The absolute configuration of the later-eluted enantiomer, its retention volume (V), and the separation factor (α), obtained with cinchonidine

Complex	pH 4.28			pH 4.93			pH 5.30			pH 6.02		
		V/cm³	α		V/cm³	α		V/cm³	α		V/cm³	α
[Co(edta)]⁻	Λ	20.70	1.08	Λ	13.60	1.10	Λ	9.50	1.07	Λ	8.65	1.06
cis-[Co(ida)$_2$]⁻	Λ	25.60	1.15	Λ	18.50	1.15	Λ	11.35	1.12	Λ	10.45	1.12
[Co(cydta)]⁻	Λ	17.55	1.06	Λ	11.10	1.06	Λ	7.90	1.06	Λ	7.15	1.05
[Co(ox)$_2$(en)]⁻	Δ	16.90	1.07	Δ	10.65	1.06	Δ	7.95	1.05	Δ	7.10	1.05
[Co(mal)$_2$(en)]⁻	Λ	9.80	1.0[a]	Λ	6.25	1.0[a]	Λ	4.70	1.0[a]	Λ	4.40	1.0[a]
cis-α-[Co(ox)(edda)]⁻	Δ	16.85	1.07	Δ	10.95	1.06	Δ	8.00	1.06	Δ	7.30	1.06
cis-α-[Co(mal)(edda)]⁻	b)	7.55	1.0[a]	b)	5.10	1.0[a]	b)	3.90	1.0[a]	b)	3.55	1.0[a]

a) Single elution curve. b) The absolute configuration of the later-eluted enantiomer could not be determined owing to very low degree of optical resolution.

Table 4. The absolute configuration of the later-eluted enantiomer, its retention volume (V), and the separation factor (α), obtained with cinchonine

Complex	pH 3.63			pH 4.46			pH 5.76			pH 6.12		
		V/cm³	α		V/cm³	α		V/cm³	α		V/cm³	α
[Co(edta)]⁻	Δ	5.55	1.0[a]	b)	4.40	1.0[a]	Λ	4.10	1.0[a]	Λ	4.10	1.0[a]
cis-[Co(ida)$_2$]⁻	Δ	5.95	1.04	Δ	4.75	1.03	Δ	4.50	1.0[a]	Δ	4.50	1.0[a]
[Co(cydta)]⁻	Δ	4.40	1.0[a]	Δ	3.40	1.0[a]	Δ	3.10	1.0[a]	Δ	3.10	1.0[a]
[Co(ox)$_2$(en)]⁻	Λ	4.75	1.0[a]	Λ	3.80	1.0[a]	Λ	3.60	1.0[a]	Λ	3.60	1.0[a]
[Co(mal)$_2$(en)]⁻	Δ	4.10	1.0[a]	Δ	3.20	1.0[a]	Λ	2.95	1.0[a]	Λ	2.95	1.0[a]
cis-α-[Co(ox)(edda)]⁻	Λ	4.20	1.0[a]	Λ	3.50	1.0[a]	Λ	3.70	1.0[a]	Λ	3.70	1.0[a]
cis-α-[Co(mal)(edda)]⁻	b)	2.40	1.0[a]	b)	2.40	1.0[a]	b)	2.10	1.0[a]	b)	2.10	1.0[a]

a) Single elution curve. b) The absolute configuration of the later-eluted enantiomer could not be determined owing to very low degree of optical resolution.

Table 5. The absolute configuration of the later-eluted enantiomer, its retention volume (V/cm^3), and the separation factor(α), obtained with 1-methylquininium chloride (1-MeQ) and 9-*O*-acetylquinine (9-*O*-acetylQ)

Complex	1-MeQ (pH 4.78)			9-*O*-AcetylQ (pH 4.90)		
		V/cm^3	α		V/cm^3	α
$[Co(edta)]^-$	Λ	13.10	1.03	Λ	10.10	1.10
cis-$[Coi(da)_2]^-$	Λ	12.50	1.05	Λ	11.50	1.28
$[Co(cydta)]^-$	Λ	10.60	1.01	Λ	8.10	1.08
$[Co(ox)_2(en)]^-$	Δ	8.80	1.0[a]	Δ	16.40	1.24
$[Co(mal)_2(en)]^-$	Λ	6.10	1.0[a]	Λ	5.30	1.0[a]
cis-α-$[Co(ox)(edda)]^-$	Δ	10.70	1.10	Δ	11.60	1.15
cis-α-$[Co(mal)(edda)]^-$	Λ	4.50	1.0[a]	Λ	3.90	1.0[a]

a) Single elution curve.

dine and cinchonine (see also Fig. 2). This result indicates that the association with complex anions and also the chiral discrimination are enhanced by the presence of the methoxyl group, which is in turn consistent with the postulated N(1) association, because the C(6′) methoxyl group is spatially in rather close proximity to the N(1) center (see below).

(d) Effect of N(1)-Methylation of Quinine: Now that the association to the protonated N(1) center is seen to play a key role in chiral discrimination, it would be expected that the methylation at this nitrogen reduces the degree of ion association and also the degree of chiral discrimination. Thus, 1-methylquininium cation was employed to measure the retention volumes and separation factors. The results are given in Table 5. The separation factors for all but *cis*-α-$[Co(ox)(edda)]^-$ are in fact reduced greatly compared with those obtained with quinine, as expected. The exceptional behavior of *cis*-α-$[Co(ox)(edda)]^-$ has not been properly explained.

(e) Effect of C(9)-OH Acetylation: The C(9)-OH group is spatially close to the N(1) center (see below), and might be thought to take part in chiral discrimination through, *e.g.*, hydrogen bonding to an oxygen atom of complex anions. This possibility may be tested by measuring retention volumes or separation factors using an acetylated (at C(9)-OH) alkaloid. Thus, 9-*O*-acetylquinine was prepared and measurements were made similarly. The results are given in Table 5. The separation factors with 9-*O*-acetylquinine will be seen to be better somewhat than those with quinine itself. Though this result does not support nor deny that the postulated hydrogen bond with C(9)-OH group takes part in chiral discrimination, this result suggests that the C(9)-OH group is indeed involved in chiral discrimination in some ways.

2. Mode of Chiral Discrimination. Taken all the above experimental results together, we may envisage the mode of association which is effective for chiral discrimination. Before the presentation of the association model, it will be pertinent to see the structure of the alkaloids. The structures of quinidine,[17] quinidinium monocation,[18] cinchonine,[19] and cinchoninium dication[20] have been determined previously by three-

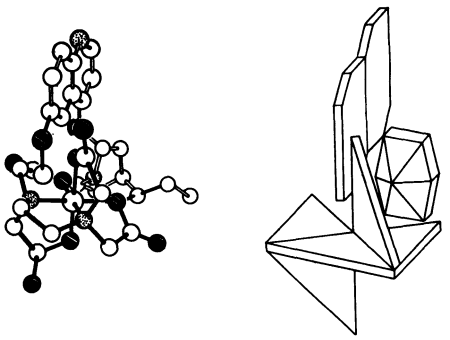

Fig. 4. (a) Proposed mode of chiral discrimination between the quininium cation and Λ-$[Co(edta)]^-$. The dotted and hatched circles represent nitrogen and oxygen atoms, respectively. (b) Simplified version of (a).

dimensional X-ray analysis. Except for the quinidinium salt of (−)-1′,3-dimethyl-1-ferrocenecarboxylic acid, where the conformation about the C(8)–C(9) bond is constrained severely by strong hydrogen bonds between the two carboxyl oxygens and N(1) and C(9)–OH hydrogens,[18] the conformations about C(8)–C(9) and C(9)–C(16) assume surprisingly the same ones (to within $\pm 3.5°$) in all these crystals. This result, as well as considerations using molecular models, suggests strongly that the conformation about these bonds in solution should be rather similar to that in the solid state. Thus, we assume that all the alkaloid cations used in this work have the same conformation in solution (but, of course, not the same absolute configuration); the dihedral angles defined by C(4′)–C(9)–C(8)–N(1) and O–C(9)–C(4′)–C(3′) bonds are about 163° and 22°, respectively.

(a) $[Co(edta)]^-$, cis-$[Co(ida)_2]^-$, and $[Co(cydta)]^-$: The mode of chiral discrimination between the quininium cation and Λ-$[Co(edta)]^-$, as inferred from the results described above, is shown in Fig. 4(a), where hydrogen atoms are omitted for clarity. In Fig. 4(b) is illustrated the mode of fitting of both ions in a very simplified form. It will be seen that the Λ-$[Co(edta)]^-$ ion can fit very nicely with the cation. The Δ-$[Co(edta)]^-$ ion can not fit nicely because the sense of handedness of two R rings is now reversed to that depicted in Fig. 4 and severe steric hindrance with the quinoline ring (including the C(6′) methoxyl group) is anticipated. Thus, in the combination of the quininium cation/$[Co(edta)]^-$, one R ring may be considered as serving as a chiral discriminator. In Fig. 4, the C(6′) methoxyl group may be seen to be useful in chiral discrimination. This mode of association is consistent with the observation that the complexes $[Co(edta)]^-$, *cis*-$[Co(ida)_2]^-$, and $[Co(cydta)]^-$ exhibited the same elution order of enantiomers with similar separation factors, because in this model the substituents ($-CH_2-CH_2-$, H–, and cyclohexane ring) at coordinated nitrogen atoms of complexes are farthest apart from the alkaloid cation.

In the combination with the (8*R*,9*S*) epimers (quinidine and cinchonine) instead of the (8*S*,9*R*) epimers like equinine and cinchonidine, the Δ enantiomers of $[Co(edta)]^-$, *cis*-$[Co(ida)_2]^-$, and $[Co(cydta)]^-$ are

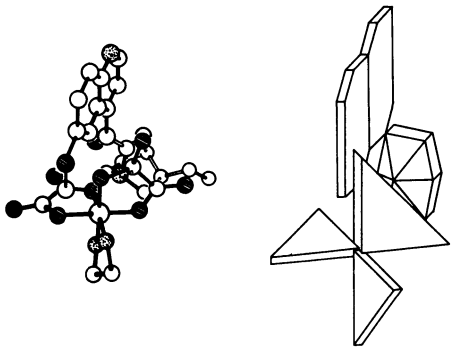

Fig. 5. (a) Proposed mode of chiral discrimination between the quininium cation and Δ-[Co(ox)$_2$(en)]$^-$. The dotted and hatched circles represent nitrogen and oxygen atoms, respectively. (b) Simplified version of (a).

preferred, as opposed to the Λ enantiomer depicted in Fig. 4. If we note that the immediate environment about the N(1) center of these (8*R*,9*S*) epimers is rather similar to the mirror image of the respective (8*S*,9*R*) epimers, this preference is easily understood.

(b) [*Co(ox)$_2$(en)*]$^-$ *and* [*Co(mal)$_2$(en)*]$^-$: Figure 5 illustrates the proposed mode of chiral discrimination between the quininium cation and Λ-[Co(ox)$_2$(en)]$^-$ which is preferred by the cation. The N(1) positive center of the alkaloid cation approaches the complex anion from the side of three anionic oxygen atoms. It will be seen that both ions fit very well from both electrostatic and spatial points of view. If the opposite enantiomer is combined with the cation, a severe steric repulsion is clearly expected. Thus, in the combination of quininium cation/[Co(ox)$_2$(en)]$^-$, the interleaving chelate ring appears to play the role of chiral discriminator.

The [Co(mal)$_2$(en)]$^-$ ion could be resolved very little by any ion-pairing reagents, which makes a sharp contrast to the case of [Co(ox)$_2$(en)]$^-$, where complete optical resolution was attained for all the alkaloids except cinchonine. (Cinchonine was ineffective in the optical resolution of all the complexes investigated, as noted above). Further, the elution order of enantiomers of [Co(mal)$_2$(en)]$^-$ is opposite to that of [Co(ox)$_2$(en)]$^-$ for any alkaloids and at any pH (see, Tables 1 to 5). Two possibilities could be considered as the reason for [Co(mal)$_2$(en)]$^-$ being not resolved. One is that since the malonate chelate ring is more bulky than the oxalate ring and flexible to such an extent that the chelate ring is interconverting rapidly among several conformers,[21] [Co(mal)$_2$(en)]$^-$ can not make a so close contact or can not make a so compact fit to the alkaloids as [Co(ox)$_2$(en)]$^-$ does. The other possibility is that the [Co(mal)$_2$(en)]$^-$ ion is hydrated to a greater degree than [Co(ox)$_2$(en)]$^-$ and its association with hydrophobic alkaloid cations is proportionately weaker. The latter possibility gains some support from the the fact that the retention volume of [Co(mal)$_2$(en)]$^-$ is substantially smaller than that of [Co(ox)$_2$(en)]$^-$ at any pH and for all the alkaloids. A result pointing to greater hydration of [Co(mal)$_2$(en)]$^-$ than [Co(ox)$_2$(en)]$^-$ has been found recently in ion-exchange chromatographic experiments.[14] Further, *cis*-*α*-[Co(ox)(edda)]$^-$ and *cis*-*α*-[Co(mal)(edda)]$^-$ exhibited a similar trend in retention volumes (see Tables 1 to 5), which seems to favor the view that the cobalt(III)-malonate ring is more hydrophilic and hydrated more extensively than the cobalt(III)-oxalate counterpart.

(c) cis-*α*-[*Co(ox)(edda)*]$^-$ *and* cis-*α*-[*Co(mal)(edda)*]$^-$: The *cis*-*α*-[Co(ox)(edda)]$^-$ ion could be resolved completely by quinidine and to a lesser extent by cinchonidine but not by quinine and cinchonine. The separation factors of this ion are generally smaller than those of [Co(edta)]$^-$, *cis*-[Co(ida)$_2$]$^-$, [Co(cydta)]$^-$, and [Co(ox)$_2$(en)]$^-$ for any alkaloids and at any pH. This lower degree of chiral discrimination of *cis*-*α*-[Co(ox)(edda)]$^-$ seems to preclude the proposal of any plausible mode of chiral discrimination for this ion. The distinctive behavior between *cis*-*α*-[Co(ox)(edda)]$^-$ and *cis*-*α*-[Co(mal)(edda)]$^-$ is noted above. As for [Co(ox)$_2$(en)]$^-$ and [Co(mal)$_2$(en)]$^-$, *cis*-*α*-[Co(ox)(edda)]$^-$ and *cis*-*α*-[Co(mal)(edda)]$^-$ appear to show opposite elution orders of enantiomers.

Finally, it will be interesting to compare the present results with the results of the Pfeiffer effect observed[22] for [Cr(ox)$_3$]$^{3-}$, [Cr(ox)$_2$(phen)]$^-$, and [Cr(ox)$_2$(bpy)]$^-$ with the monocations of the cinchona alkaloids as the environment substances, where phen=1,10-phenanthroline and bpy=2,2′-bipyridine. As for the present complexes, the [Cr(ox)$_3$]$^{3-}$ ion was assumed to approach the N(1) positive center of the alkaloids *via* electrostatic forces. For [Cr(ox)$_2$(phen)]$^-$, both electristatic forces (between the oxalate ligands and the N(1) center) and hydrophobic attractive forces (between the phen ligand and the quinolyl ring) were invoked. The mode of chiral discrimination of [Cr(ox)$_2$(phen)]$^-$ was thus utterly different from any of the chiral discrimination modes proposed here.[23]

Acknowledgement is made to Dr. S. Yamazaki, Toyo Soda Manufacturing Co., Ltd. (Tokyo), for the gift of the LS-410. ODS.SIL. resin.

References

1) Part X of "Chromatographic Study of Optical Resolution." Part IX: S. Yamazaki and H. Yoneda, *J. Chromatogr.*, **235**, 289 (1982).

2) For this chromatographic technique, see, *e.g.*; a) B. A. Bidlingmeyer, *J. Chromatogr. Sci.*, **18**, 525 (1980); b) W. R. Melander, K. Kalghatgi, and C. Horvath, *J. Chromatogr.*, **201**, 201 (1980); c) W. R. Melander and C. Horvath, *ibid.*, **201**, 211 (1980); d) C. Peterson and G. Schill, *ibid.*, **204**, 179 (1981), and references cited therein.

3) S. Yamazaki, Ph. D. Thesis, Hiroshima Univ., 1982.

4) a) Synthesis; F. P. Dwyer, E. Gyarfas, and D. Meller, *J. Phys. Chem.*, **59**, 296 (1955); b) CD; C. W. Van Saun and B. E. Douglas, *Inorg. Chem.*, **8**, 1145 (1969).

5) a) Synthesis; J. Hidaka, Y. Shimura, and R. Tsuchida, *Bull. Chem. Soc. Jpn.*, **35**, 567 (1962); b) CD; Ref. 4(b).

6) a) Synthesis; F. P. Dwyer and F. L. Garvan, *J. Am. Chem. Soc.*, **83**, 2610 (1961); b) CD; B. J. Brennan, K. Igi, and B. E. Douglas, *J. Coord. Chem.*, **4**, 19 (1974).

7) a) Synthesis; F. P. Dwyer, I. K. Reid, and F. L. Garvan, *J. Am. Chem. Soc.*, **83**, 1285 (1961); b) CD; B. E. Douglas, R. A. Harnes, and J. B. Brushmiller, *Inorg. Chem.*, **2**, 1194 (1963).

8) a) Synthesis; Ref. 7a; b) CD; Ref. 7b.
9) a) Synthesis; C. W. Van Saun and B. E. Douglas, *Inorg. Chem.*, **8**, 115 (1969); b) CD; C. W. Maricondi and B. E. Douglas, *Inorg. Chem.*, **11**, 688 (1972).
10) a) Synthesis; Ref. 9a; b) CD; W. T. Jordan and J. I. Legg, *Inorg. Chem.*, **13**, 955 (1974).
11) R. T. Major and J. Finkelstein, *J. Am. Chem. Soc.*, **63**, 1368 (1941).
12) G. R. Pettit and S. K. Gupta, *J. Chem. Soc.*, **C**, **1968**, 1208.
13) See, *e.g.*; U, Sakaguchi, H. Nakazawa, K. Sakai, and H. Yoneda, *Bull. Chem. Soc. Jpn.*, **55**, 1862 (1982), and references therein.
14) a) U. Sakaguchi, I. Yamamoto, S. Izumoto, and H. Yoneda, *Bull. Chem. Soc. Jpn.*, **56**, 153 (1983); b) *ibid.*, in press.
15) The protonation occurs at the following pH; 5.85 and 9.92 for cinchonine, 5.80 and 10.03 for cinchonidine, 5.07 and 9.70 for quinine, and 5.40 and 10.00 for quinidine.
16) All the alkaloids used here have the common (3*R*, 4*S*) absolute configuration.
17) R. Doherty, W. R. Benson, M. Maienthal, and J. McD. Stewart, *J. Pharm. Sci.*, **67**, 1698 (1978).
18) O. L. Carter, A. T. McPhail, G. A. Sim, *J. Chem. Soc.*, **A**, **1967**, 365.
19) B. Oleksyn, L. Lebioda, M. Ciechanowicz-Rutkowska, *Acta Crystallogr., Sect. B*, **35**, 440 (1979).
20) B. J. Oleksyn, K. M. Stadnicka, and S. A. Hodorowicz, *Acta Crystallogr., Sect. B*, **34**, 811 (1978).
21) U. Sakaguchi, K. Morito, and H. Yoneda, *Bull. Chem. Soc. Jpn.*, **53**, 2821 (1980), and references cited therein.
22) a) K. Miyoshi, Y. Matsumoto, and H. Yoneda, *Chem. Lett.*, **1980**, 1319; b) H. Ohbo, H. Okazaki, K. Miyoshi, and H. Yoneda, submitted.
23) Additionally, we found that the *cis*-*a*-$[Co(NO_2)_2(edda)]^-$ ion can be resolved completely by cinchonidine and partially by quinine and quinidine but not by cinchonine. Since this ion does not belong to the *cis*(N)-$[Co(N)_2(O)_4]^-$ type, the data for this ion were not included in this paper.

Kinetics of Valinomycin- and Tetranactin-mediated Cation Transport through Liposomal Membrane

Masaharu UENO,* Tomomi YASUI, and Isamu HORIKOSHI
Department of Hospital Pharmacy, Toyama Medical and Pharmaceutical University, 2630 Sugitani, Toyama 930-01
(Received May 28, 1982)

Kinetics of valinomycin- and tetranactin-mediated cation transport were studied. An equation was derived which describes the kinetics of ionophore induced cation leakage from liposomes. The theoretically predicted ion-selectivity of the ionophore-mediated cation transport agreed well with that given by experiments. This supports the assumptions used in the derivation and is consistent with the following characteristics of the ionophores: (1) Ionophore-mediated cation transport is carried out by stoichiometrically forming a ternary complex between ionophore, cation and lipophilic anion. (2) The ion-selectivity of the ionophore is determined primarily by the formation constant of the ionophore cation complex in water. (3) A relative value of the complex formation constant in water can be calculated from both the complex formation constant in methanol, which is estimated more easily than that in water, and the difference between desolvation energy of the cation in water and methanol.

Neutral ionophores, such as valinomycin and tetranactin function as mobile carriers of specific ions through biomembranes or model membranes. Block *et al.* studied the kinetics of valinomycin-induced K^+ leakage from liposomes and determined a partition constant of valinomycin between membrane phase and aqueous phase, and a turnover rate of potassium transport across liposomal membrane.[1] Yamaguchi and Anraku studied the mechanism of SF6847-mediated proton uptake in liposomes and showed that the proton uptake was compensated by valinomycin-induced potassium efflux.[2] Results showed that potassium ion leakage or the exchange transport between proton and potassium ion was induced by ternary complex formation between valinomycin, potassium ion and thiocyanate ion or between valinomycin, potassium ion and SF6847. But in their reports, the ion-selectivity was not discussed.

In the present report, we studied the ion-selective permeation induced by ionophore through liposomal membranes. First, we derived an equation which described the ion selective transport of ionophore through the liposomal membrane. Secondly, we showed experimentally that the equation adequately predicted the ion selectivity of the ionophore. The derivation required two assumptions: (1) It is assumed that ionophore distributes uniformly throughout liposomal membrane. This contrasts with the assumption made by Block *et al.*[1] that ionophore should be localized on the inside and outside membrane surfaces. (2) The association constant for ionophore-cation complexation in water may be expressed in terms of the association constant obtained in methanol and the difference between the desolvation energy of the cation in methanol and water.

Theoretical

In the specific liposomal system under investigation, only the transport of ion through the outer bilayer of the multilamellar liposomes contributes directly to the observed leakage. A model for ionophore-mediated ion transport through membrane is proposed as shown in Fig. 1. In this model it is assumed that only ternary complex (IMX) of ionophore (I), cation (M) and anion (X) can carry ions through membrane, and ionophore is distributed uniformly throughout the membrane phase.

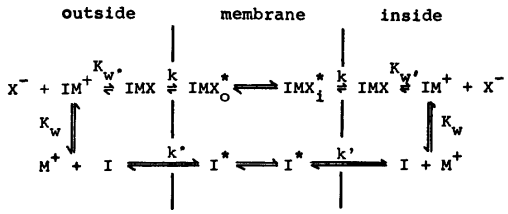

Fig. 1. Model for ionophore-mediated cation leakage from liposomes containing MSCN.

In the water phase inside the bilayer, ionophore (I) and cation (M) form complex (IM) *i.e.* $I+M \overset{K_w}{\rightleftharpoons} IM$. The complex formation constant K_w is expressed by Eq. 1,

$$K_w = \frac{C_{IM}}{C_{IM}C_M}. \quad (1)$$

Complex IM and anion X form ternary complex IMX, $IM+X \overset{K'_w}{\rightleftharpoons} IMX$. K'_w can be expressed by Eq. 2,

$$K'_w = \frac{C_{IM}}{C_{IM}C_X}. \quad (2)$$

Ternary complex IMX is distributed into membrane, $IMX \overset{k}{\rightleftharpoons} IMX^*$, where asterisk (*) indicates the membrane phase. The distribution constant k of the ternary complex is expressed by Eq. 3,

$$k = \frac{C^*_{IMX}}{C_{IMX}}. \quad (3)$$

The distribution constant of ionophore k' is expressed by Eq. 4,

$$k' = \frac{C^*_I}{C_I}. \quad (4)$$

The ternary complex IMX* diffuses through membrane from inside to outside. The flux J of the ternary complex is assumed to be proportional to the concentration gradient of the ternary complex in membrane. We get following equation,

$$J = D\frac{C^*_{IMXi} - C^*_{IMXo}}{d}, \quad (5)$$

where D is the diffusion constant of the ternary complex in methanol and d is the thickness of the membrane.

Subscripts i and o denote inside and outside surfaces of the membrane, respectively. When the distribution equiliblium of IMX between aqueous and membrane phases is achieved quickly, that is, the transmembrane diffusion of the ternary complex is the rate-limiting process of ion transport, $C^*_{MIXo} \ll C_{IMX_i}$ in the initial stage after addition of ionophore, since $C_{IMXo}=0$ in the initial stage. Then the leakage L $(=JS)$ is expressed by Eq. 6,

$$L = JS = D\frac{S}{d}C^*_{IMX_i} = D\frac{S}{d}kC_{IMX}, \tag{6}$$

where S is the surface area of the membrane. From Eqs. 1, 2, 3, and 6, we get

$$L = D\frac{S}{d}kK'_wK_wC_IC_MC_X. \tag{7}$$

If we define b and m as the liposomal volumes of water and membrane phases, and assume the concentration of cation M in extra liposomal water can be regarded as zero in the initial stage after the addition of ionophore, then the total amount of cation a_{MT} and anion a_{XT} are represented by Eqs. 8 and 9.

$$a_{MT} = b(C_M+C_{IM}+C_{IMX}) + m(C^*_M+C^*_{IM}+C^*_{IMX}) \tag{8}$$

$$a_{XT} = b(C_X+C_{IMX}) + m(C^*_X+C^*_{IMX}) \tag{9}$$

In the present case, $C_M \gg C_I$, Eqs. 8 and 9 can be reduced to Eqs. 8′ and 9′,

$$a_{MT} = bC_M, \tag{8'}$$

$$a_{XT} = bC_X. \tag{9'}$$

For uni-valent electrolyte

$$a_T = a_{MT} = a_{XT} = bC_M = bC_X, \tag{10}$$

where a_T is the amount of the salt contained in liposomes before addition of ionophore. When w is the total volume of water (*i.e.* in and out of liposomes), total amount of ionophore a_T is represented as follows;

$$a_T = w(C_I+C_{IM}+C_{IMX})+m(C^*_I+C^*_{IM}+C^*_{IMX}). \tag{11}$$

Since K'_w can be regarded as far less than K_w[1] and ion concentration within the membrane regarded as negligible. Eq. 11 is reduced to Eq. 11′,

$$a_I = w(C_I+C_{IM})+mC^*_I. \tag{11'}$$

From Eqs. 1, 4, and 11′, we get following equation.

$$a_I = w\left(C_I+K_wC_I\cdot\frac{a_T}{b}\right)+mk'C_I \tag{12}$$

From Eqs. 7, 10, and 12, we get following equation.

$$L = D\frac{S}{d}kK'_wK_w\frac{a_I}{w+mk'+\dfrac{wa_T}{b}K_w}\left(\frac{a_T}{b}\right)^2 \tag{13}$$

S, d, m, w, and k' are invariant with cation species. k, D, and K'_w can be regarded as invariant with cation species, because in ionophore-univalent cation complexes cations are enveloped by ionophore and the complexes are similar in shape and size with each other.[3-6] Therefore setting $D\frac{S}{d}kK'_w=A$=constant and $w=mK'=B$=constant, we get

$$L = AK_w\frac{a_I}{B+K_ww\cdot\dfrac{a_T}{b}}\left(\frac{a_T}{b}\right)^2. \tag{14}$$

When the amount of lipid is constant, C_{IT} can be defined as the total amount of ionophore per mg of lipid, and C_T as the concentration of metal thiocyanate in water phase in liposome before addition of ionophore, that is $C_T=\frac{a_T}{b}$, Eq. 14 can be represented as Eq. 15 where A' is A per amount of lipid.

$$L = A'K_w\frac{C_{IT}C_T^2}{B+K_wwC_T} \tag{15}$$

The relation between leakage L and association constant K_w, under the condition where the concentration of ionophore and metal thiocyanate are constant, as defined by Eq. 15, is shown in Fig. 2. When $K_w \ll \frac{B}{wC_T}=\frac{w+mk'}{wC_T}$, Eq. 15 can be reduced to Eq. 16.

$$L = \frac{A'}{B}K_wC_{IT}C_T^2 \tag{16}$$

In this case, leakage L is proportional to K_w, C_{IT}, and C_T^2. According to Eq. 16, the leakage of ion from liposome is proportional to the complex formation constant between ionophore and the cation in water which agrees with the electrical study of Eisenman *et al.*[7-10] When $K \gg \frac{B}{wC_T}=\frac{w+mk'}{wC_T}$, Eq. 15 can be reduced to Eq. 17.

$$L = \frac{A'}{w}C_{IT}C_T \tag{17}$$

In this case, L is proportional to the concentrations of ionophore and metal thiocyanate and has no relation to the association constant.

The ion-selectivity of the ionophore can be evaluated indirectly. It is difficult to estimate the complex formation constant in water (K_w) directly by experimental measurement, because of very low solubility of ionophore in water and small K_w. However, it is only necessary to estimate relative value of K_w in evaluating ion-selectivity and not the absolute value. As discussed in the preceding study,[18] the free energy of complex formation, ΔG^0, is defined as a sum of the conformational energy difference of ionophore between complex form and uncomplex form (ΔU), the desolvation energy of cation with complex formation (ΔG^0_M), and the other factor (I), which includes the solvation effect and the change in entropy of the ionophore upon complex formation and can be regarded as independent of ion

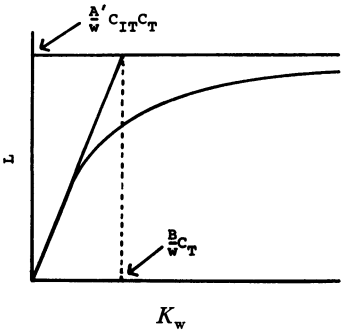

Fig. 2. Scheme of L(leakage) and K_w (complex formation constant) relation under the condition of constant concentration of ionophore and ion.

species.

Then in water,

$$-RT\ln K_w = \Delta G_w^\circ = \Delta U + \Delta G_{Mw}^\circ + I_w \quad (18)$$

and in methanol,

$$-RT\ln K_m = \Delta G_m^\circ = \Delta U + \Delta G_{Mm}^\circ + I_m. \quad (19)$$

By Eqs. 18 and 19, we get

$$K_w = K_m \exp\frac{\Delta G_{Mm}^\circ - \Delta C_{Mw}^\circ}{RT} \exp\frac{I_m - I_w}{RT}. \quad (20)$$

From Eqs. 16 and 20, we get

$$L = \frac{A'}{B} C_{IT} C_T^2 \exp\frac{I_m - I_w}{RT} \cdot K_m \exp\frac{\Delta G_{Mm} - \Delta G_{Mw}}{RT}. \quad (21)$$

Since the $\exp\frac{I_m - I_w}{RT}$ can be regarded as independent of ion species, in the case of C_{IT}=constant and C_T= constant, Eq. 21 is reduced to Eq. 22 with $\frac{A}{B} C_{IT} C_T^2 \exp\frac{I_m - I_w}{RT} = \text{constant} = E$.

$$L = EK_m \exp\frac{\Delta G_{Mm}^\circ - \Delta C_{Mw}^\circ}{RT}. \quad (22)$$

The complex formation constant between ionophore and cation in methanol (K_m) and desolvation energy of cation in methanol (ΔG_{Mm}^0) and in water (ΔG_{Mw}^0) has already been determined.[12-14]

Experimental

Materials. Valinomycin was obtained from Calbiochem Co. Ltd. Tetranactin was gifted from Chugai Pharmaceutical Co. Ltd. Egg lecithin was a purified substance given by Asahi Kasei Co. Ltd. Phosphatidic acid was obtained from Sigma Co. Ltd. The other reagents were special grade of Wako Pure Chemical Industries Ltd.

Methods. Multilayer liposomes were prepared as follows: The inner surface of a 50 ml round-bottomed flask was coated with 10 mg of egg lecithin containing 2% of phosphatidic acid by evaporation of solvent. Then, 5 ml of a 150 mM KSCN/10 mM Tris solution which was adjusted to pH 7.0 by adding H_2SO_4 was poured into the lecithin coated flask and gently shaken until all lipid was removed from the flask. The liposome suspension was centrifuged for 20 min at 40000 g at 4 °C. The liposome preparation was washed with isotonic 150 mM $MgSO_4$/10 mM Tris/H_2SO_4 solution followed by centrifugation at 40000 g for 20 min at 4 °C. The obtained liposome pellet was dispersed in 10 ml of isotonic 150 mM $MgSO_4$/10 mM Tris/H_2SO_4 solution (pH 7.0). Ionophore, dissolved in methanol, was added with a microsyringe (20 μl) to the liposome-dispersed solution. The ion leakage was measured by an ion-meter (Orion Research) with appropriate ion-selective electrodes.

Results and Discussion

When valinomycin was added to the liposomes containing KSCN, the K^+ leakage as well as the SCN^- leakage increased maximally immediately following the addition of the ionophore (Figs. 3-a, b), but when valinomycin was added to the liposomes containing KCL, the increase in K^+ leakage was far smaller than those containing KSCN (Fig. 3-c). These observations suggest that the permeation of K^+ from the liposomes induced by valinomycin is facilitated by lipophilic

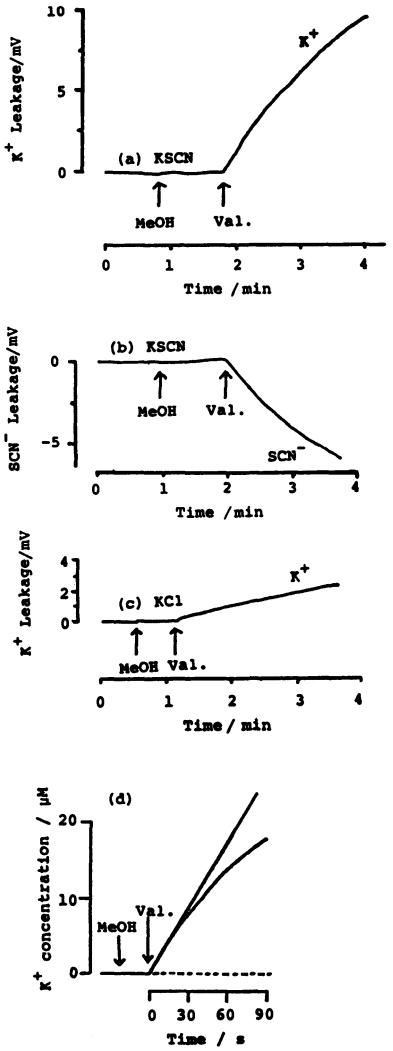

Fig. 3. Recorder trace of the valinomycin-induced ion leakage and the time course of K^+ concentration in medium.
(a) and (b) show K^+ and SCN^- leakages from liposomes containing 150 mM of KSCN. (c) shows K^+ leakage from liposomes containing 150 mM of KCl. (d) shows the time course of K^+ concentration in medium dispersing liposomes containing 150 mM of KSCN.

anions, such as SCN^-. Equation 16 suggests that cation leakage is proportional to the concentration of ionophore, C_{IT}, when C_T and K_w are constant or to the square of the concentration of metal thiocyanate in the liposomes, C_T^2, when C_{IT} and K_w are constant. In Fig. 4, the initial rate of K^+ leakage was plotted against the concentration of valinomycin at constant KSCN concentration. The plot showed a good linear relation. In the Fig. 5, the initial rate of K^+ leakage was plotted against the logarithm of the KSCN concentration at constant valinomycin. The plot showed a linear relation with a slope of near 2. From these observations, Eq. 16 has been found primarily to hold in our experimental condition. Accordingly the assumption, $K_w \ll B/wC_t$, is practically satisfied. In addition, the fact that the slope of the line in Fig. 5 was near 2 supports

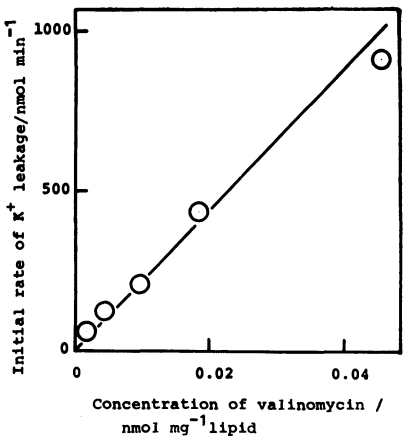

Fig. 4. Initial rate of the K^+ leakage against concentration of valinomycin at constant concentration of KSCN (150 mM) in liposomes.

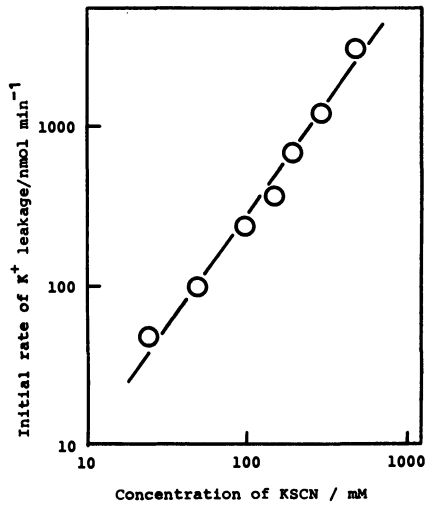

Fig. 5. Initial rate of the K^+ leakage against logarithmic scale of concentration of KSCN in liposomes at constant concentration of valinomycin (0.018 nmol/mg of lipid).

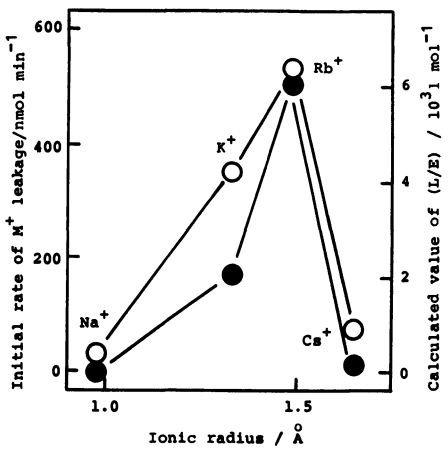

Fig. 6. Initial rate of M^+ leakage and calculated value (L/E) plots against ionic radius for valinomycin.
○: The values obtained from direct experimental measurements. ●: The values summarized in Table 1.

Table 1. Association constant of valinomycin[a] and tetranactin[b] with metal cations in methanol and calculated values, L/E[c]

	$K_m/10^3$ l mol^{-1}	$(L/E)/10^2$ l mol^{-1}
Valinomycin		
Na^+	0.005	0.0003
K^+	80	20
Rb^+	180	61
Cs^+	2.6	2.1
Tetranactin		
Na^+	0.5	0.034
K^+	20	4.9
Rb^+	10	3.4
Cs^+	3	2.4

a) Nishino, Izumiya, *Membrane*, **5**, 338 (1980).
b) M.Ueno *et al.*, *Yakugaku Zasshi*, **97**, 46 (1977).
c) $=K_m\frac{\Delta G^\circ_{Mm}-\Delta G^\circ_{Mw}}{RT}$, see context regarding to Eq. 22.

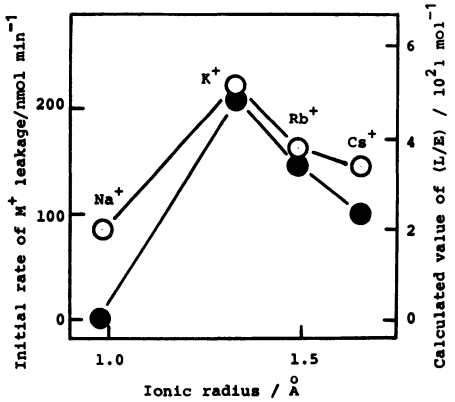

Fig. 7. Initial rate of M^+ leakage and calculated value (L/E) plots against ionic radius for tetranactin.
○: The values obtained from direct experimental measurements. ●: The values summarized in Table 1.

the assumption that valinomycin functions only as a mobile carrier by forming stoichiometrically a ternary complex with K^+ and SCN^-, as described originally by Block *et al.*[1] That the above slope was slightly smaller than 2 may be attributed the <1 activity coefficient of KSCN at 150 mM.

Equation 22 suggests that cation leakage induced by ionophore is proportional to the product of the association constant between the cation and the ionophore in methanol and the exponent of the desolvation energy difference between methanol and water at constant ionophore concentration and constant metal thiocyanate concentration. The association constant in methanol, K_m, and desolvation energy difference, $\Delta G^0_{Mm}-\Delta G^0_{Mw}$, have been reported.[12-14] In Table 1, K_m and $K_m\frac{\Delta G^0_{Mm}-\Delta G^0_{Mw}}{RT}(=L/E)$ were summerized. The experimental values of initial rates of several cations and the calculated values, $K_m\frac{\Delta G^0_{Mm}-\Delta G^0_{Mw}}{RT}$, were plotted against the ionic radii of the cation in Fig. 6 for valinomycin as ionophore and in Fig. 7 for tetranactin. The ion-selectivity of the ionophores given from direct

experimental measurements agreed well with those predicted from Eq. 22. The term, $\Delta G^0_{Mm} - \Delta G^0_{Mw}$, in Eq. 22 ensures the effects of solvation energy of ions on the ion selectivity of the ionophores. The fact that the permeation of Cs^+ or Rb^+ was relatively large as compared with that predicted from the K_m alone shows that the contribution energy of the cation to ion-selectivity of the ionophore is different in methanol and in water. Thus the experimental results justified the validity of application of Eq. 22 to the elucidation of ion selectivity of ionophore-mediated ion transport through liposomal membrane.

References

1) M. C. Block, J. De Gier, and L. L. M. van Deenen, *Biochim. Biophys. Acta*, **367**, 210 (1974).
2) A. Yamaguchi and Y. Anraku, *Biochim. Biophys. Acta*, **501**, 136 (1978).
3) V. T. Ivanov, I. A. Laine, N. D. Abdullaev, L. B. Senyavina, E. M. Popov, Yu. A. Ovchinnikov, and M. M. Shemyakin, *Biochem. Biophys. Res. Commun.*, **34**, 803 (1969).
4) T. Sakamaki, Y. Iitaka, and Y. Nawata, *Acta Cryst., Sect. B*, **23**, 768 (1976).
5) Y. Kyogoku, M. Ueno, H. Akutsu, and Y. Nawata, *Biopolymers*, **14**, 1049 (1975).
6) M. Ueno and Y. Kyogoku, *Biopolymers*, **18**, 2646 (1979).
7) G. Eisenmsn, S. M. Ciani, and G. Szabo, *Fed. Proc.*, **27**, 1289 (1968).
8) S. Ciani, G. Eisenman, and G. Szabo, *J. Membr. Biol.*, **1**, 1 (1969).
9) G. Szabo, G. Eisenman, and S. Ciani, *J. Membr. Biol.*, **1**, 346 (1969).
10) R. Margalit and G. Eisenman, *J. Membr. Biol.*, **61**, 209 (1981).
11) M. Ueno and H. Kishimoto, *Chem. Lett.*, **1979**, 1487 (1979).
12) N. Nishino and N. Izumiya, *Membrane*, **5**, 338 (1980).
13) M. Ueno, M. Miyata, H. Kishimoto, and Y. Kyogoku, *Yakugaku Zasshi*, **97**, 46 (1977).
14) M. Tanaka *et al.*, "Ion and Solvent," ed by the Chemical Society of Japan, Univ. of Tokyo Press, Tokyo (1976), p. 151.

Studies on the β-Turn of Peptides. III[1]. Syntheses and Conformational Properties of *N*-(2,4-Dinitrophenyl)tetrapeptide *p*-Nitroanilides Related to β-Turn Preferring Sequences in Proteins

Kazuki Sato,* Ukon Nagai, and Tsutomu Higashijima†

Mitsubishi-Kasei Institute of Life Sciences, Minamiooya, Machida, Tokyo 194

†*Department of Biophysics and Biochemistry, Faculty of Science, The University of Tokyo, Bunkyo-ku, Tokyo 113*

(Received September 1, 1982)

To confirm the general applicability of CD spectra of *N*-(2,4-dinitrophenyl(Dnp))tetrapeptide *p*-nitroanilides (pNA's) to the analysis of β-turn preference of the tetrapeptide sequences, Dnp-pNA derivatives of some tetrapeptides related to β-turn preferring sequences in proteins were synthesized and subjected to CD and ^{1}H NMR measurements. CD spectra of Dnp–Gly–L-Pro–L-Asn–Gly–pNA (**5a**) were just the mirror image of those of gramicidin S-model peptide, Dnp–Gly–D-Ala–L-Pro–Gly–pNA (**6**). This suggested that **5a** strongly preferred the β-turn and the type of turn was different from that of **6**. The relative intensities of Cotton effects of the tetrapeptide with the general structure Dnp–Gly–L-Pro–Y–Gly–pNA (Y=L-Asn, Gly, L-Ala, or L-Gln) roughly agreed with the bend potentials of the amino acid residues at the third position of β-turns in proteins reported by Chou and Fasman. The effects of changing the amino acid residues at the second position of β-turn were also examined.

In the previous paper, we gave an outline of a new method to study the β-turn conformation of linear tetrapeptides.[2] *N*-(2,4-Dinitrophenyl)tetrapeptide *p*-nitroanilides (Dnp–tetrapeptide–pNA's)[3] exhibited characteristic CD spectra above 300 nm when they took β-turn conformations (Fig. 1). The Cotton effects were considered to be due to the interaction of the two terminal chromophores, namely, the exciton coupling of the transition moments in the two terminal chromophores, and the magnitude of the Cotton effects were shown to reflect the β-turn preference of the peptides. β-Turn preferences of the tetrapeptide derivatives has strong correlation with antibiotic activities of the gramicidin S (GS) analogs containing similar tetrapeptide sequences at their β-turn part.[1] This paper deals with the details of syntheses and conformational properties of Dnp-pNA derivatives of some tetrapeptides related to the β-turn preferring sequences in proteins to confirm the general applicability of the CD spectra of the tetrapeptide derivatives to the analysis of their β-turn conformation.

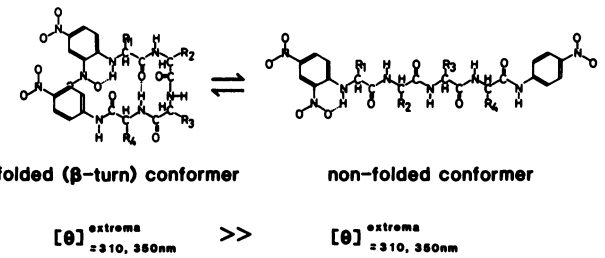

Fig. 1. Models of folded (β-turn) and non-folded conformers of a Dnp–tetrapeptide–pNA.

The first compound synthesized was Dnp–Gly–L-Pro–L-Asn–Gly–pNA (**5a**). The sequence was expected to take the β-turn to a high degree because of the high bend potential of each component amino acid residue at the respective position in the table proposed by Chou and Fasman on the basis of statistical analysis of the X-ray crystallographic data of 29 globular proteins.[4] Kopple and Go,[5] and Fermandjian *et al.*[6] reported that Z–Gly–L-Pro–L-Asn–Gly–NHNH–Boc and H–Gly–L-Pro–L-Asn–Gly–OH, respectively, formed type-I β-turn by NMR analysis. Synthesis of **5a** is outlined in Fig. 2. Boc–L-Asn–Gly–pNA (**1a**) was prepared by coupling of Boc–L-Asn–ONp and H–Gly–pNA, and was deprotected with hydrogen chloride in formic acid to afford H–L-Asn–Gly–pNA·HCl (**2a**·HCl). Coupling of Boc–Gly–L-Pro–OH[7] and **2a** by EDC–HOBt method

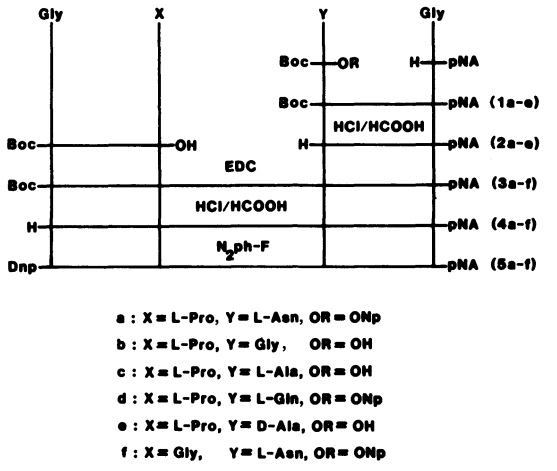

Fig. 2. Syntheses of Dnp–tetrapeptide–pNA's (**5a**—**f**).

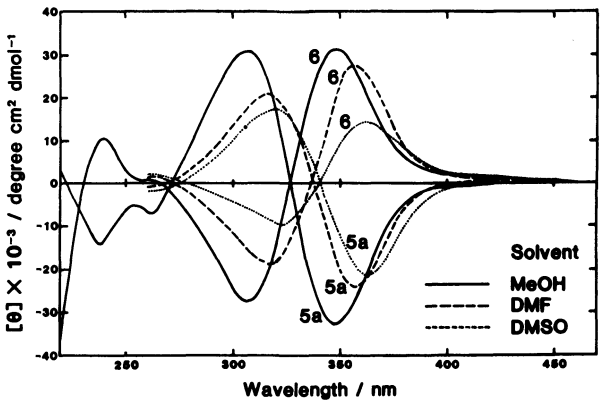

Fig. 3. CD spectra of Dnp–Gly–L-Pro–L-Asn–Gly–pNA (**5a**) and Dnp–Gly–D-Ala–L-Pro–Gly–pNA (**6**).

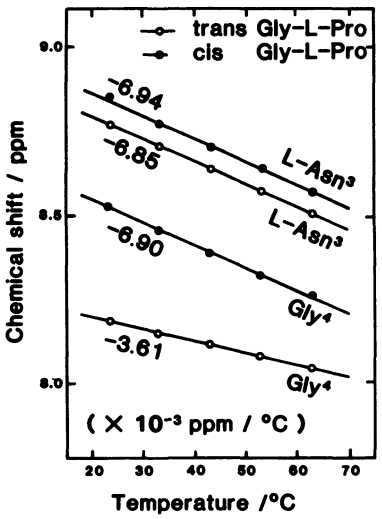

Fig. 4. Temperature dependences of the chemical shifts of the α-amide protons of **5a** in DMSO-d_6 solution.

afforded Boc–Gly–L-Pro–L-Asn–Gly–pNA (**3a**), which was converted into the Dnp derivative, Dnp–Gly–L-Pro–L-Asn–Gly–pNA (**5a**), by deprotection and subsequent treatment with 1-fluoro-2,4-dinitrobenzene. Homogeneities of the synthetic peptides were confirmed by thin-layer chromatography and elemental analysis.

The CD spectra of **5a** were just the mirror image of those of GS-model peptide Dnp–Gly–D-Ala–L-Pro–Gly–pNA (**6**)[1] (Fig. 3). The result indicates that **5a** strongly prefers the β-turn, and the type of the turn would be different from that of the GS model peptide. Certainly, GS is known to take a type II′ β-turn, however **5a** cannot take a type II′ β-turn because of five-membered ring structure of L-Pro residue at the second position. Though it is difficult to discriminate exactly the type of the turn, type II β-turn seems probable for **5a** because of enantiomeric feature of the CD spectra. The ^{1}H NMR spectrum of **5a** in DMSO-d_6 showed two sets of resonances for most of the protons due to *cis-trans* isomerism for the Gly–L-Pro bond. The *cis-trans* ratio was estimated to be 3 : 7 according to the relative peak area of the same proton. Chemical shifts of aromatic protons on the Dnp chromophore of the *trans* isomer (H-3, 8.78 ppm; H-5, 8.25 ppm; H-6, 7.09 ppm) were shifted to higher field compared with those of the *cis* isomer (H-3, 8.78 ppm; H-5, 8.27 ppm; H-6, 7.15 ppm), suggesting the approach of the two terminal chromophores in the *trans* isomer. The Gly^4–NH proton of the *trans* isomer showed smaller temperature dependence than the other NH protons, indicating the presence of 4→1 hydrogen bond essential for β-turn conformation (Fig. 4).[8] Most of the protons other than CO–NH protons show little temperature dependences, suggesting that the conformation of **5a** did not change significantly in the range of this experiment (23—63 °C).

To study the sequence-conformation relationship, a series of compounds having a general structure Dnp–Gly–L-Pro–Y–Gly–pNA (**5b**, Y=Gly; **5c**, Y=L-Ala; **5d**, Y=L-Gln; **5e**, Y=D-Ala) were examined. Syntheses of **5b**—**e** were carried out by a similar manner to that described for the synthesis of **5a** except that EDC coupling was used for the preparation of **1b**, **c**, and **e** (Fig. 2). The CD spectra of **5a**—**e** in DMSO are shown in Fig. 5. They all showed a pair of strong Cotton effects near 310 and 350 nm, and their intensities decreased in the order, L-Asn (**5a**)>Gly (**5b**)>L-Ala (**5c**)>L-Gln (**5d**), which corresponds roughly to that of decreasing bend potentials at the third position in the table of Chou and Fasman.[4] The results suggest that the bend potentials in proteins may be valid also for oligopeptides. When Y was D-Ala (**5e**), the highest ellipticities were observed suggesting that the presence of an D-amino acid at the third position is favorable for the β-turn conformation. Certainly, ^{1}H NMR study of **5e** also indicated that **5e** had higher population of β-turn conformer than **5a**. The ^{1}H NMR spectrum of **5e** in DMSO-d_6 showed two sets of resonances and the *cis-trans* ratio for the Gly–L-Pro bond was about 3 : 7, which is similar to that of **5a**. However, in the *trans* isomer of **5e**, aromatic protons on the Dnp-chromophore showed chemical shifts at higher field (H-3, 8.77 ppm; H-5, 8.20 ppm; H-6, 7.02 ppm) than those of **5a**, and the Gly^4–NH proton showed smaller temperature dependence (-3.27×10^{-3} ppm °C^{-1}) than that of **5a**. This means that CD spectra of Dnp-pNA derivatives are good measures of β-turn preference of tetrapeptide sequences besides GS-model peptides.

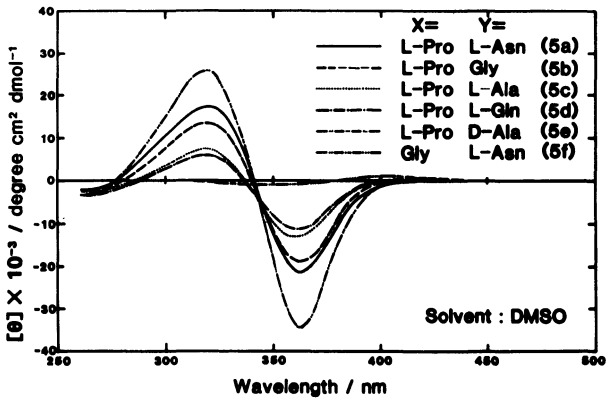

Fig. 5. CD spectra of Dnp–Gly–X–Y–Gly–pNA's (**5a**—**f**) in DMSO.

To examine the contribution of L-Pro at the second position of a tetrapeptide to the β-turn formation, Dnp–Gly–Gly–L-Asn–Gly–pNA (**5f**) was synthesized similarly (Fig. 2). The CD spectrum of **5f** measured in DMSO was compared with those of **5a** and **5b** (Fig. 5). High β-turn preference of the Gly–L-Pro–L-Asn–Gly sequence was not affected so much by replacement of L-Asn^3 with Gly but decreased significantly by replacement of L-Pro^2 with Gly. The results emphasized the importance of L-Pro residue at the second position for the β-turn formation as expected from remarkably high bend potential of the residue at the second position.[4]

It is interesting to note that the β-turn preference of amino acid residues in tetrapeptides well reflects that in proteins. The fact suggests that such a small fragment conformation of a protein is largely governed by short-range interactions of the amino acid residues involved.

Table 1. Yields and analytical data of synthetic peptides

Compound	Yield/%	Mp θ_m/°C	$[\alpha]_D^{22}$ a)/°	Found(%)			Calcd(%)			R_f^1	R_f^2	R_f^3
				C	H	N	C	H	N			
1a	82	202—203	−14.0	49.76	5.48	16.97	49.87	5.66	17.11	0.39	0.09	0.75
1b	77	223—226	—	50.90	5.81	16.18	51.13	5.72	15.90	0.51	0.14	0.88
1c	74	202—203	+11.8	50.88	5.85	14.69	51.19[b]	6.17[b]	14.92[b]	0.71	0.30	0.88
1d	69	183—184	+10.8	51.35	5.90	16.78	51.06	5.95	16.54	0.37	0.09	0.80
1e	65	198—199	−10.8	52.82	5.51	15.23	52.45	6.05	15.29	0.75	0.34	0.88
2a·HCl	93	222—223	+2.0	41.98	4.42	20.49	41.69	4.66	20.26	0.05	0	0.60
2b·HCl	100	115—125	—	40.99	4.31	19.37	41.60	4.54	19.41	0	0	0.49
2c·HCl	100	221—224	+17.4	43.26	4.86	18.18	43.65	4.99	18.51	0.09	0	0.65
2d·HCl	97	204—205	−44.0	43.35	5.02	19.73	43.64	5.07	19.58	0.19	0	0.74
2e·HCl	84	236—237	−31.8	44.10	5.19	18.23	43.65	4.99	18.51	0.10	0	0.67
3a	63	154—156	−44.6	49.72	5.62	16.82	49.56[c]	6.07[c]	16.86[c]	0.43	0.06	0.67
3b	66	139—141	−42.2	51.97	5.95	16.46	52.17	5.97	16.59	0.56	0.12	0.85
3c	80	121—123	−33.4	52.06	6.18	15.82	52.16[b]	6.28[b]	15.87[b]	0.66	0.20	0.74
3d	52	136—138	−33.6	49.76	5.93	16.20	49.66[d]	6.33[d]	16.22[d]	0.47	0.06	0.85
3e	75	125—130	−41.6	53.05	6.26	15.94	53.07	6.20	16.15	0.59	0.18	0.85
3f	53	212—213	−0.4	47.87	5.78	18.90	48.18	5.58	18.73	0.18	0.03	0.71
5a	98	207—209	−84.8	45.68	4.18	19.35	45.73[d]	4.61[d]	19.20[d]	0.26	0.03	0.73
5b	82	157—162	−92.8	46.38	4.20	19.18	46.78[c]	4.44[c]	18.98[c]	0.60	0.10	0.81
5c	78	218—219	−79.2	48.17	4.46	18.50	48.39[b]	4.56[b]	18.81[b]	0.58	0.11	0.83
5d	91	160—161	−77.0	46.92	4.42	19.03	47.19[c]	4.72[c]	19.06[c]	0.31	0.03	0.67
5e	78	256—257	−154.6	47.68	4.34	18.67	47.68	4.67	18.54	0.52	0.13	0.85
5f	93	218—220	+8.0	44.51	3.94	20.57	44.15[b]	4.04[b]	21.06[b]	0.11	0	0.66

a) *c* 1, DMF. b) $1/2H_2O$. c) H_2O. d) $3/2\ H_2O$.

Experimental

Synthesis of Peptides. All the melting points were measured on a Yanagimoto micro melting point apparatus and uncorrected. TLC's were carried out on Merck silica gel 60 F_{254} plates with the following solvent systems: R_f^1, $CHCl_3$–MeOH (5 : 1, v/v); R_f^2, $CHCl_3$–MeOH–AcOH (95 : 5 : 1, v/v); R_f^3, *n*-BuOH–AcOH–pyridine–H_2O (4 : 1 : 1 : 2, v/v). Optical rotations were measured on an Union automatic polarimeter PM-201. Yields, physical constants, and the results of elemental analyses of the synthetic peptides are summarized in Table 1.

*Boc-L-Asn-Gly-pNA (**1a**).* To a solution of H–Gly–pNA (351 mg, 1.8 mmol) in DMF (8 ml) was added Boc–L-Asn–ONp (636 mg, 1.8 mmol). The reaction mixture was stirred overnight at room temperature, evaporated *in vacuo*, and the residue was dissolved in EtOAc. The solution was washed successively with 10% citric acid, 4% $NaHCO_3$, and water, dried (Na_2SO_4), and evaporated to leave crystals, which was recrystallized from EtOH; yield, 601 mg (82%).

Compound **1d** was prepared by a similar manner to that described for the preparation of **1a**.

*Boc-L-Ala-Gly-pNA (**1c**).* To a chilled solution of Boc–L-Ala–OH (378mg, 2 mmol) and H–Gly–pNA (390 mg, 2 mmol) in DMF (8 ml) was added EDC·HCl (383 mg, 2 mmol), and the mixture was stirred at 0 °C for 1 h and at room temperature overnight. The reaction mixture was treated as described for **1a**; yield, 542 mg (74%).

Compounds **1b** and **1e** were prepared by a similar manner to that described for **1c**.

*H-L-Asn-Gly-pNA·HCl (**2a**·HCl).* Compound **1a** (409 mg, 1 mmol) was dissolved in 0.1 M (1 M=1 mol dm^{-3}) hydrogen chloride in formic acid (12 ml). The solution was allowed to stand at room temperature for 30 min and evaporated *in vacuo*. The residue was crystallized by addition of ether; yield, 323 mg (93%).

Compounds **2b—e** were prepared as described for **2a**.

*Boc–Gly–L-Pro–L-Asn–Gly–pNA (**3a**).* To a chilled solution of Boc–Gly–L-Pro–OH[7] (54 mg, 0.2 mmol), **2a**·HCl (69 mg, 0.2 mmol), and TEA (0.028 ml, 0.2 mmol) in DMF (2 ml) were added HOBt (54 mg, 0.4 mmol) and EDC·HCl (38 mg, 0.2 mmol). The reaction mixture was stirred at 0 °C for 1 h and at room temperature overnight and evaporated. After the addition of water, the solid was collected by filtration, washed successively with 10% citric acid, 4% $NaHCO_3$, and water, and dried *in vacuo* over P_2O_5. The crude product dissolved in MeOH (2 ml) was applied to a column (3×170 cm) of Sephadex LH-20 and eluted with MeOH. The fractions with the desired product detected by UV absorption and TLC were collected and evaporated, and the residue was solidified by addition of ether and recrystallized from MeOH–ether; yield, 71 mg (63%).

Compounds **3b—e** were prepared as described for **3a**.

*Boc–Gly–Gly–L-Asn–Gly–pNA (**3f**).* Boc–Gly–Gly–OH[9] (46 mg, 0.2 mmol) and **2a**·HCl (69 mg, 0.2 mmol) were coupled as described for **3a**. The crude product obtained by filtration and subsequent washing, was recrystallized from EtOH; yield, 55 mg (53%).

*H–Gly–L-Pro–L-Asn–Gly–pNA·HCl (**4a**·HCl).* Compound **3a** (56 mg, 0.1 mmol) was dissolved in 0.1 M hydrogen chloride in formic acid (1.2 ml). The solution was allowed to stand at room temperature for 30 min and evaporated to leave an oil. The product was used for the next reaction without further treatment; yield was quantitative.

Compounds **4b—f** were prepared as described for **4a**.

*Dnp–Gly–L-Pro–L-Asn–Gly–pNA (**5a**).* To a solution of **4a**·HCl (50 mg, 0.1 mmol) and TEA (0.042 ml, 0.3 mmol) in DMF (2 ml) was added N_2ph–F (37 mg, 0.2 mmol). The reaction mixture was stirred at room temperature for 3 h and evaporated *in vacuo*. The residue was dissolved in $CHCl_3$ (5 ml) and applied to a column (1.8×20 cm) of silica gel 60

(Merck), and the column was washed with $CHCl_3$. The desired product was eluted with a mixture of $CHCl_3$ and MeOH (5 : 1, v/v). The fractions containing the desired product were collected and evaporated to leave a solid, which was recrystallized from MeOH–ether; yield, 31 mg (98%).

Compounds **5b**—**e** were prepared as described for **5a**.

Dnp–Gly–Gly–L-Asn–Gly–pNA (5f). To a solution of **4f**·HCl (46 mg, 0.1 mmol) and TEA (0.042 ml, 0.3 mmol) in DMF (2 ml) was added N_2ph–F (37 mg, 0.2 mmol). The reaction mixture was stirred at room temperature for 3 h and evaporated *in vacuo*. After the addition of water, the precipitate was collected by filtration, washed successively with 10% citric acid, 4% $NaHCO_3$, and water, and dried *in vacuo* over P_2O_5. The crude product was recrystallized from DMF–ether; yield, 55 mg (93%).

CD Measurements. CD spectra were recorded on a JASCO spectropolarimeter model J-20 or J-40 in a 0.1 mM solution at room temperature (23±2 °C). Concentrations of peptide solutions were corrected by UV absorbances based on the fact that all the peptides showed the same molar absorptivity in the same solvent irrespective of the structures: UV_{max}; 326 nm (MeOH), 337 nm (DMF), 343 nm (DMSO).

^1H NMR Measurements. ^1H NMR spectra were recorded on a Bruker WH-270 spectrometer equipped with a Nicolet-1180 computer and with a Bruker B-ST-100/700 temperature control unit. The spectra were measured at 23±0.5 °C if not mentioned otherwise. Chemical shifts were measured from the internal standard of DSS.[3] The spectra were assigned by spin-decoupling, H–D exchange, and saturation transfer methods.

The authors wish to express their thanks to Professor Tatsuo Miyazawa of The University of Tokyo for helpful discussion. Thanks are also due to the members of Analitical Department of System Engineering Laboratory, Mitsubishi-Kasei Industries Ltd., for elemental analyses.

References

1) Part II of this series: K. Sato, M. Kawai, and U. Nagai, *Bull. Chem. Soc. Jpn.*, **56**, 1527 (1983)

2) K. Sato, M. Kawai, and U. Nagai, *Biopolymers*, **20**, 1921 (1981).

3) The abbreviations used in this paper are those recommended by IUPAC–IUB: *J. Biol. Chem.*, **247**, 977 (1972). Additional abbreviations: Boc, *t*-butoxycarbonyl; Z, benzyloxycarbonyl; Dnp, 2,4-dinitrophenyl; pNA, *p*-nitroanilide; ONp, *p*-nitrophenyl ester; DSS, sodium 2,2-dimethyl-2-silapentane-5-sulfonate; EDC, 1-ethyl-3-(3-dimethylaminopropyl)carbodiimide; N_2ph–F, 1-fluoro-2,4-dinitrobenzene; TEA, triethylamine; DMF, *N,N*-dimethylformamide; DMSO, dimethyl sulfoxide; TLC, thin-layer chromatography; GS, gramicidin S.

4) P. Y. Chou and G. D. Fasman, *J. Mol. Biol.*, **115**, 135 (1977).

5) K. D. Kopple and A. Go, *Biopolymers*, **15**, 1701 (1976).

6) F. Toma, H. Lam-Thanh, F. Piriou, M-C. Heindl, K. Lintner, and S. Fermandjian, *Biopolymers*, **19**, 781 (1980).

7) J. C. Anderson, M. A. Barton, P. M. Hardy, G. W. Kenner, and R. C. Sheppard, *J. Chem. Soc.*, **1967**, 180.

8) M. Ohnishi and D. W. Urry, *Biochem. Biophys. Res. Commun.*, **36**, 194 (1969); K. D. Kopple, M. Ohnishi, and A. Go, *Biochemistry*, **8**, 4087 (1969).

9) H. Kinoshita, K. Inomata, O. Miyano, and H. Kotake, *Bull. Chem. Soc. Jpn.*, **52**, 2619 (1979).

 © 1983 The Chemical Society of Japan Bull. Chem. Soc. Jpn., 56, 1651—1664 (1983)

Studies on Long-range Couplings between ^{77}Se and ^{13}C in Some Aryl Selenides, Dichlorides, and Selenoxides. The Inverse Effect on Couplings in the Selenoxide Formation

Warō Nakanishi* and Yoshitsugu Ikeda

Department of Chemistry, Faculty of Education, Wakayama University, Masagocho, Wakayama 640

(Received September 20, 1983)

Long-range coupling constants between ^{77}Se and ^{13}C in selenoanisole, diphenyl selenide, diphenyl diselenide, and their 2-mono- and 2,2′-disubstituted derivatives, selenoxanthone, selenanthrene, dichlorides, and selenoxides were measured to disclose predominant factors governing the magnitude of the coupling. Extraordinary large values for two- and three-bond couplings are found in selenoxanthone. Three factors are operative: the orientational effect, the coordination number, and the effect of ring formation. The last factor accompanies a stronger inverse effect on the coupling of selenoxides than on that of selenides.

Since selenium has a magnetic isotope ^{77}Se with nuclear spin 1/2 and natural abundance 7.6%, one can study the structure and reactions of organoselenium compounds directly by NMR spectroscopy.[1-4] Chemical shifts have been shown to be correlated with the oxidation state of selenium atom.[1,2] Coupling constants appear to reflect the stereochemistry of organoselenium compounds.[1,2,4] Reich and Trend,[4] for example, have shown a stereochemical dependence of geminal ^{77}Se–^{13}C spin coupling constants in sterically fixed three-coordinated selenium compounds, *i.e.*, a selenonium salt, a selenoxide, and an ylide. In each case, one methyl carbon atom *cis* to the lone pair is substantially more strongly coupled than the other two.

We wish to report here long-range couplings in some aromatic organoselenium compounds which show interesting structural correlations.

Results and Discussion

Orientational Effect of the Lone Pair(s). The two- and three-bond coupling constants between ^{77}Se and ^{13}C (^2J(Se–C) and ^3J(Se–C), respectively) of selenoanisole (**1**), diphenyl selenide (**2**), diphenyl diselenide (**3**), their 2-mono- and 2,2′-disubstituted derivatives, selenoxanthone (**4**), and selenanthrene (**5**) were measured[5] and the results are shown in Tables 1 and 2.

The ^2J(Se–C(2,6)) values of **1**, **2**, and **3** are all about 11 Hz. The ^2J(Se–C(2′,6′)) values of 2-(phenylseleno)-benzoic acid and 2-(hydroxymethyl)phenyl phenyl selenide are 11.1±0.7 Hz, but the ^2J(Se–C(6)) values of these compounds are 6.0±0.5 Hz. Then the ^2J(Se–C) values between selenium and *ortho*-carbon of the benzene ring which has no additional substituent are about 11 Hz, and those associated with substituent attachment

Table 1. Two-bond couplings between ^{77}Se and ^{13}C of some organoselenium compounds[a]

Compound[b]	^2J(Se–C(6))	^2J(Se–C(2′,6′))	Compound[b]	^2J(Se–C(2,2′))	^2J(Se–C(6,6′))
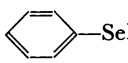 (**1**)	11.0	——	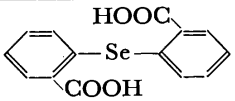	c	<3
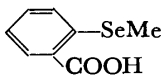	6.6	——	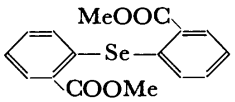	c	<3
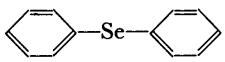 (**2**)	11.0	11.0	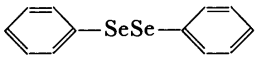 (**3**)	11.0	11.0
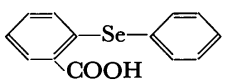	6.4	10.4	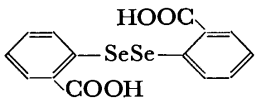	c	4.4
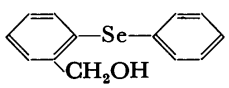	5.5	11.8	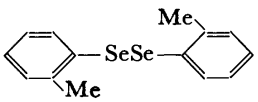	12.8	3.4
			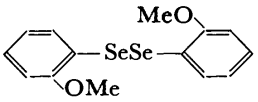	13.7	4.6

a) In Hz. b) Numbers are assigned as follows:

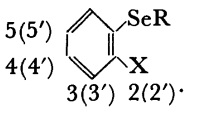

c) Difficult to measure because of low solubility or low sensitivity.

Table 2. ^{13}C NMR chemical shifts and coupling constants of **4**, **5**, **11**, and **12**

Compd	Chemical shift[a]							Coupling constant[b]		
	C(1,1′)	C(2,2′)	C(3,3′)	C(4,4′)	C(5,5′)	C(6,6′)	C=O	^2J(Se–C(6,6′))	^3J(Se–C(5,5′))	^3J(Se–C(3,3′))
4	134.9	130.8	131.2	126.6	132.0	128.1	181.7	34.0	11.9	2.7
11	142.4	130.8	130.3	132.1	134.1	129.5	182.0	22.9	4.7	
5	134.4	134.4	131.1	127.9	127.9	131.1		24.0	6.5	
12	144.7	144.7	128.5	131.2	131.2	128.5		19.0	<3	

a) In ppm from TMS in $CDCl_3$. b) In Hz.

at the other *ortho*-position are about 6 Hz in these five compounds. These results suggest that ^2J(Se–C) values are small when the steric repulsion between the substituent at the *ortho*-position of a benzene ring and the group attached to the selenium increases the population of the group at the selenium in the neighborhood of the carbon of benzene ring carrying the substituent at the other *ortho*-position, *i.e.*, they are small when the lone pair of electrons is on the average far from the carbon under consideration.

This is further confirmed by an examination on ^2J(Se–C) in 2,2′-disubstituted diphenyl selenides and diphenyl diselenides. The ^2J(Se–C(6,6′)) values of 2,2′-diselenodibenzoic acid, di-2-tolyl and bis(2-methoxyphenyl) diselenides are 3.4—4.6 Hz and not affected by electronic properties of the substituents. Those for 2,2′-selenodibenzoic acid and its dimethyl ester are too small to measure. The ^2J(Se–C(2,2′)) values of di-2-tolyl and bis(2-methoxyphenyl) diselenides are 12.8 and 13.7 Hz, respectively, and are larger than that of diphenyl selenide.

When the selenium atom retains at least one lone pair of electrons, the 4s-atomic orbital of selenium to be used for bonding is expected to be low.[6] Namely, most of the s-character of selenium in organoselenium compounds is attributable to its lone pair(s). Since indirect nuclear-nuclear spin couplings are mainly governed by the Fermi contact term[7] and therefore by the s-overlap integral of the bonds under consideration, the orientation of the lone pair of electrons on the selenium atom is important.

Examination of the ^2J(Se–C) values of **4** and **5** is necessary to clarify the effect of the orientation of lone pair of electrons because the ^2J(Se–C(6,6′)) values of **4** and **5**[8] are expected to be larger since the lone pairs of these compounds should spread over carbons C(6) and C(6′). Table 2 shows NMR data for **4** and **5**. Actually, very large ^2J(Se–C) values have been obtained for **4** and **5**, which are 34.0 and 24.0 Hz, respectively. Especially, the ^2J(Se–C) value of **4** is the largest that has ever been obtained for selenides to the best of our knowledge, which is almost the same as that reported for certain ylides.[4] These results provide support for the importance of the orientation of lone pairs for ^2J(Se–C). Three-bond couplings, ^3J(Se–C), were also found in **4** and **5**. The value of ^3J(Se–C(5,5′)) is larger than that of ^3J(Se–C(3,3′)) in **4** and the former is also larger than that of ^3J(Se–C(5,5′ or 4,4′)) of **5**.

The large couplings of selenium with C(6) and C(5) in **4** indicate effective spread of lone pairs over these carbons. The carbonyl group has a smaller covalent radius than selenium, which renders a favorable space

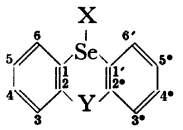

	X	Y
4	None	C=O
5	None	Se
11	O	C=O
12	O	Se=O

to the lone pair of electrons to interact with these carbons, and since the group is likely to arrange the two benzene rings coplanar due to its sp^2 hybridization state, the selenium can interact with the carbons advantageously. That the value of ^3J(Se–C(3,3′)) is smaller than that of ^3J(Se–C(5,5′)) may also indicate the orientational effect of lone pairs.

The large ^2J(Se–C) and ^3J(Se–C) values in **5** may also be explained in terms of the effective spread of lone pairs over these carbons.

After all, these couplings may be well understood on the basis of the orientation of the lone pair of electrons on the selenium.

Effect of the Coordination Number. As ^2J(Se–C) is essentially related to the s-character of selenium and carbon atoms in the bonds,[7] it is expected to vary with change in the coordination number of the selenium atom. Table 3 shows ^{13}C NMR chemical shifts and coupling constants, ^2J(Se–C) and ^3J(Se–C), of **1**, **2**, dichlorides **6** and **7**, selenoxides **8** and **9**, and diphenyl selenone (**10**). The values of ^2J(Se–C) become larger in the order: selenides, dichlorides, and selenoxides. The chemical shift of the C(2) carbons of these organoselenium compounds as well as some aromatic organosulfur compounds[9] moves to higher field if the substituent is electronegative; that is, the ^2J(Se–C) values should be related to the electron-withdrawing ability of the selenium atom and therefore are related to the ^{13}C chemical shift of the C(2) carbons. As shown in Fig. 1, the plots of ^2J(Se–C) value *vs.* ^{13}C chemical shift show a trend in which the slope for the selenoanisoles is more

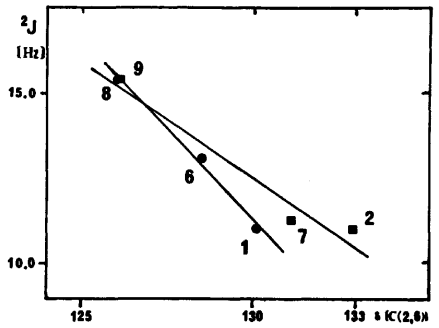

Fig. 1. Plots of ^2J(Se–C(2, 6)) *vs.* δ(C(2, 6)) for selenoanisoles (●) and diphenyl selenides (■).

Table 3. ^{13}C NMR chemical shifts and coupling constants of selenoanisoles and diphenyl selenides

Compound	Chemical shift[a]					Coupling constant[b]	
	C(1)	C(2,6)	C(3,5)	C(4)	C(Me)	^2J(Se–C(2,6))	^3J(Se–C(3,5))
PhSeMe (**1**)	131.7	130.2	128.8	125.9	7.2	11.0	
$PhSeCl_2Me$ (**6**)	141.0	128.5	129.9	131.7	45.7	13.2	
PhSe(O)Me (**8**)	139.6	126.0	129.9	131.6	36.1	15.4	
PhSePh (**2**)	131.0	132.8	129.2	127.2		11.0	
$PhSeCl_2Ph$ (**7**)	142.4	131.2	129.7	131.6		11.2	
PhSe(O)Ph (**9**)	142.7	126.1	129.6	131.2		15.4	
$PhSeO_2Ph$ (**10**)	142.4	126.8	130.2	134.0		13.9	14.6

a) In ppm from TMS in $CDCl_3$. b) In Hz.

negative than that for the diphenyl selenides. Since the sign of ^2J(Se–C) is expected to be positive except **10** with which a negative sign is expected,[6] **10** should be put aside from the plots.

An unexpectedly large ^3J(Se–C) value (14.6 Hz) was found for **10**. This may be due to the increased s-character of the bonds caused by the lack of lone pair of electrons which carry otherwise most of the s-character of the selenium atom.[6]

Effect of the Ring Formation—The Inverse Effect on the Long-range Couplings. The ^{13}C NMR chemical shifts and the long-range coupling constants, ^2J(Se–C) and ^3J(Se–C), of selenoxanthone 10-oxide (**11**) and selenanthrene 9,10-dioxide (**12**) are collected in Table 2. Although the selenoxide formation from **1** and **2** to **8** and **9** increases the ^2J(Se–C) values of these compounds, the values for **11** and **12** are 22.9 and 19.0 Hz, respectively, which are smaller than those for **4** and **5**. The decrease in the long-range couplings between selenium and carbon with the formation of selenoxides relative to that of selenides (the inverse effect) is also found in the three-bond couplings, ^3J(Se–C), of **11** and **12** relative to those of **4** and **5**. The inverse effect may be attributed to the cyclic structure of **11** and **12**. Since ^2J(Se–C) values of **11** and **12** are still larger than those of **8** and **9**, the oxygens in **11** and **12** are supposed to operate in a way to increase the coupling constant but they could not overcome the disadvantageous steric factor. In other words, the s-orbital of the selenium atoms of **11** and **12** could not interact with that of the carbons in the benzene rings so effectively as in **4** and **5**. As mentioned above, the ^2J(Se–C) value of **4** is extraordinary large, which is three times as large as that of **2**, and the value of **5** is twice as large as that of **2**. Then the inverse effect on the long-range coupling in these compounds may be caused by the extraordinary large values resulting from the cyclic structure of these compounds. If the main factor for determining the large coupling constants is the sp^2-character of the selenium atoms in **4** and **5**, the factor should be smaller in **11** and **12** because the formation of selenoxides is expected to increase the sp^3-character of selenium atom. The increased sp^3-character may also decrease the values of ^3J(Se–C) of **11** and **12**. The increase in sp^2-character in **4** and **5** must be due to the cyclic structure with selenium atom(s) in the ring where the steric strain results in change in bond angle.

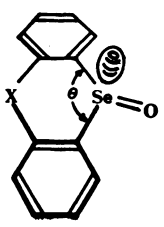

Experimental

^{13}C NMR spectra were obtained on a JEOL FX-60Q spectrometer operating at 15 MHz using chloroform as the solvent and tetramethylsilane as the internal standard. Spectral widths of 600, 1000, 3000, and 3500 Hz with 8 K data points and 30° or smaller pulses were employed. ^{77}Se–^{13}C coupling constants were obtained by observing the ^{77}Se satellites in ^{13}C spectra. A selective decoupling mode was also applied to assignment of ^{13}C chemical shifts if conditions were favorable.

Materials. The following compounds were prepared as described in the literature: 2-(methylseleno)benzoic acid,[10] 2-(phenylseleno)benzoic acid,[11] 2,2′-selenodibenzoic acid[12] and its dimethyl ester,[13] 2,2′-diselenodibenzoic acid,[10] selenoxanthone (**4**)[12] and its 10-oxide (**11**),[12] and selenanthrene 9,10-dioxide (**12**).[14] Physical properties agreed well with those in the literature.

Bis(2-methoxyphenyl) Diselenide. 2-Methoxyselenophenol, which had been prepared from 2-methoxyphenylmagnesium bromide and selenium in ether,[15] was oxidized in hexane with air. Recrystallization from hexane gave the diselenide in good yield, yellow needles, mp 85—87 °C. Found: C, 45.19; H, 3.72%. Calcd for $C_{14}H_{14}O_2Se_2$: C, 45.16; H, 3.76%.

Di-2-tolyl Diselenide. This compound was prepared as above in a red oil. Found: C, 49.82; H, 4.38%. Calcd for $C_{14}H_{14}Se_2$: C, 49.43; H, 4.15%.

Selenanthrene (5). To an ethanol solution (150 ml) of sodium diselenide, which had been prepared from selenium (12 g), sodium borohydride (3.2 g), and sodium hydroxide (3.0 g) according to the methods of Klayman and Griffin[16] and Bogert and Stull,[17] was added a solution of 2-chloronitrobenzene (19.5 g) in 50 ml of ethanol and refluxed for 3 h. After work-up, crystallization from acetic acid gave 2,2′-dinitrodiphenyl diselenide, yellow needles, 10.7 g (43%), mp 209—210 °C (lit,[17] 209 °C).

The diselenide (10.7 g) was dissolved in 30% aqueous dioxane (150 ml) and treated with hydrochloric acid and zinc until the solution became colorless. Then the solution was filtered and the filtrate was diazotized with 3.6 g of sodium nitrite in 50 ml of water at low temperature. The end of the diazotization was monitored with a potassium iodide-starch paper. After 0.5 h at 0 °C, the solution was extracted with ether. The residue obtained after evaporation of the solvent

was dissolved in 10 ml of acetic acid and refluxed for 5 h. After evaporation of the solvent, the product was chromatographed on silica gel to give pale brown needles, 1.7 g (21%), mp 183—184 °C (lit,[18] 181 °C).

2-(Hydroxymethyl)phenyl Phenyl Selenide. This compound was prepared through reduction of 2-(phenylseleno)benzoic acid with lithium aluminium hydride. The details will be described elsewhere.

The authors thank Professor Hiizu Iwamura of IMS for his helpful discussion.

References

1) For a review see H. Iwamura and W. Nakanishi, *Yuki Gosei Kagaku*, **39**, 795 (1981) and references cited therein.

2) W. McFarlane and R. J. Wood, *J. Chem. Soc., Dalton Trans.*, **1972**, 1397; J. E. Trend, Ph. D. Thesis, University of Wisconsin, Wisconsin, USA, 1976.

3) W. Nakanishi, S. Murata, Y. Ikeda, T. Sugawara, Y. Kawada, and H. Iwamura, *Tetrahedron Lett.*, **42**, 4241 (1981); W. Nakanishi, Y. Ikeda, and H. Iwamura, *J. Org. Chem.*, **47**, 2275 (1982); W. Nakanishi, S. Matsumoto, Y. Ikeda, T. Sugawara, Y. Kawada, and H. Iwamura, *Chem. Lett.*, **1981**, 1353; W. Nakanishi, Y. Ikeda, and H. Iwamura, *Org. Magn. Reson.*, **20**, 117 (1982).

4) H. J. Reich and J. E. Trend, *J. Chem. Soc., Chem. Commun.*, **1976**, 310.

5) Kalabin *et al.* also studied the orientational effect of lone pairs in ^2J(Se–C) of some seleno-substituted benzenes; see G. A. Kalabin and D. F. Kushnarev, *Zh. Struct. Khim.*, **20**, 617 (1979); G. A. Kalabin, D. F. Kushnarev, L. M. Kataeva, L. V. Kashurnikova, and R. I. Vinokurova, *Zh. Org. Khim.*, **14**, 2478 (1978).

6) W. McFarlane and D. S. Rycroft, *J. Chem. Soc., Chem. Commun.*, **1973**, 10.

7) E. Breitmaier and W. Voelter, "^{13}C NMR Spectroscopy: Methods and Applications in Organic Chemistry," 2nd ed, Verlag Chemie, Weinheim (1978), pp. 92—110.

8) ^2J(Se–C(3,3′)) is identical with ^2J(Se–C(6,6′)).

9) W. Nakanishi, Y. Ikeda, and H. Iwamura, unpublished results. See also G. L. Nelson and E. A. Williams, *Prog. Phys. Org. Chem.*, **12**, 243 (1976).

10) A. Ruet and M. Renson, *Bull. Soc. Chim. Belges.*, **75**, 157 (1966); *Chem. Abstr.*, **65**, 3785 h (1966).

11) K. Sindelar, E. Svatek, J. Metysova, J. Metys, and M. Protiva, *Collect. Czech. Chem. Commun.*, **34**, 3792 (1969); *Chem. Abstr.*, **72**, 55224 t (1970).

12) R. Lesser and R. Weiss, *Ber.*, **47**, 2510 (1914).

13) R. Lesser and R. Weiss, *Ber.*, **46**, 2640(1913).

14) F. Krafft and A. Kaschau, *Ber.*, **29**, 443 (1896).

15) D. G. Foster, *Org. Synth.*, Coll. Vol. III, 771 (1955).

16) D. L. Klayman and T. S. Griffin, *J. Am. Chem. Soc.*, **95**, 197 (1973).

17) M. T. Bogert and A. Stull, *J. Am. Chem. Soc.*, **49**, 2011 (1927).

18) S. Keimatsu and I. Satoda, *J. Pharm. Soc. Jpn.*, **55**, 1030 (1935).

The Claisen Rearrangement of the Lithium Enolate of 1-(2-Thienyl)alkyl Alkanoate and the Birch Reduction of the Resulting 2-(3-Thienyl)alkanoic Acid

Mitsuo Sado, Hideaki Abe, Nobuki Inuzuka, Kozo Shirai, and Takanobu Kumamoto*
Department of Chemistry, Faculty of Science, Tokai University, Kitakaname, Hiratsuka, Kanagawa 259-12
(Received October 7, 1982)

It was found that the Claisen rearrangement of the lithium enolate of 1-(2-thienyl)alkyl alkanoate in refluxing THF resulted in the formation of 2-(3-thienyl)alkanoic acid (**2**). Similarly, when the lithium enolate of 4-(2-thienyl)-4-butanolide was stirred at room temperature in the presence of hexamethylphosphoric triamide, 5,6-dihydro-4*H*-cyclopenta[*b*]thiophene-4-carboxylic acid was obtained. Further, it was found that the Birch reduction of **2** and subsequent alkylation with benzyl bromide gave a regioselective ring-opening product, 4-benzylthio-3-ethyl-3-alkenoic acid, in a good yield. The Birch reduction of 2-thienylacetic acid, followed by alkylation with benzyl bromide, also gave (*Z*)-3-benzylthio-3-hexenoic acid as the main product.

The Claisen rearrangement is an important and useful synthetic reaction, however, there has been few report,[1] of successfully obtaining 3-substituted thiophene derivatives starting from 1-(2-thienyl)-1-alkanol derivatives by the use of the Claisen rearrangement because of the formation of [1,3] sigmatropic rearrangement products.[2]

During the course of our investigation of the synthetic methodology which utilized thiophene derivatives as the key substances,[3] we needed a convenient method for the preparation of 3-substituted thiophenes. In this investigation, it was found that the Claisen rearrangement of the lithium enolate[4] of 1-(2-thienyl)alkyl alkanoate (**1**) successfully gave 2-(3-thienyl)alkanoic acid (**2**). Further, regioselective ring-opening products, 4-benzylthio-3-ethyl-3-alkenoic acids, were obtained by the Birch reduction of **2** and subsequent alkylation with benzyl bromide.

Results and Discussion

The Claisen Rearrangement of 1. It was found that, when **1a—d** were treated with 2.2 equivalents of lithium *N*-isopropylcyclohexylamide (LICA) at −70 °C in THF under nitrogen and the resulting lithium enolates were subsequently refluxed in THF, **2a—d** were obtained. (See Table 1).

As in shown in Table 1, the reaction of an equimolar amount of LICA with **1a** did not give the rearrangement product because of the formation of lithium salt at the 5-position of the thiophene nuclei (Run 1). Further, when butyryl derivatives, **1b, d**, were used as starting materials, rearrangement products, **2b, d**, were obtained in rather better yields than in the rearrangement of acetyl derivatives, **1a, c**.

Next, we investigated the rearrangement of 4-(2-thienyl)-4-butanolide (**3**) to form the corresponding cyclopentanecarboxylic acid derivative (**4**).

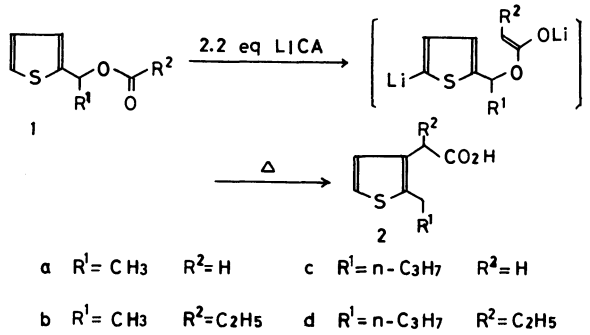

The preparation of **3** was carried out as in the following Scheme, the yields of **5**, **6**, and **3** were 91, 96, and 85% respectively.

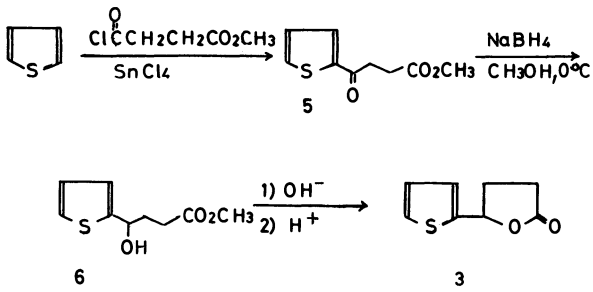

Scheme 1.

As in shown in Table 2, when **3** was treated with LICA under reaction conditions similar to these in the rearrangement of **1**, the expected rearrangement product, **4**, was not obtained, but **3** was recovered

Table 1. Claisen rearrangement of the lithium enolate of 1-(2-thienyl)alkyl alkanoate (**1**)

Run	R^1	R^2	Reaction conditions: LICA(eq)	Reaction conditions: Temp/°C (Time/h)	Yield/% of **2**
1	CH_3	H	1.2	−78(1)→50(5)	—
2	CH_3	H	2.2	−78(1)→66(3)	38
3	CH_3	C_2H_5	2.2	−78(1)→66(5)	82
4	*n*-C_3H_7	H	2.2	−78(1)→66(3)	30
5	*n*-C_3H_7	C_2H_5	2.2	−78(1)→66(3)	81

Table 2. Claisen rearrangement of the lithium enolate of 4-(2-thienyl)-4-butanolide (3)

Run	Reaction conditions				Yield/% of 4
	Solvent	HMPA(eq)	Temp	Time/h	
1	THF	—	Reflux	3	—
2	THF	2.2	Reflux	3	42
3	THF	2.2	rt	18	44
4	THF/HMPA 9 : 1		rt	12	22

completely. However, it was found that the reaction of **3** with 2.2 equivalents of LICA in the presence of 2.2 equivalents of hexamethylphosphoric triamide (HMPA) at −70 °C in THF, and subsequent stirring at room temperature for 18 h, resulted in the formation of **4** in a 44% yield.

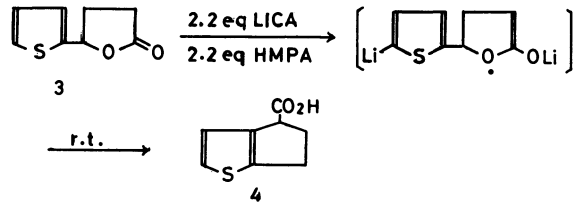

The Birch Reduction of 2. It is well known that the Birch reduction of thiophene derivatives results in the formation of many products. For example, the Birch reduction of thiophene gives 2,5- and 2,3-dihydrothiophenes and a mixture of ring-opening products, butenethiols.[5] However, in recent investigations, it has been reported that the Birch reduction of 2-acyl-[6] or 2-carboxythiophene[7] formed 2,5-dihydrothiophenes selectively. It has been also reported from our laboratory[3] that the selective formation of 2-acyl-2-alkyl-2,5-dihydrothiophene derivatives has been established by the Birch reduction of 2-acylthiophene and subsequent alkylation with alkyl halides. In the present investigation, it was found that a regioselective ring-opening reaction occurred by means of the Birch reduction of **2**.

When **2b** was allowed to react with 5 equivalents of sodium in liquid ammonia in the presence of ethanol, and to the reaction mixture then were subsequently added 3 equivalents of ammonium chloride and benzyl bromide, 4-benzylthio-2,3-diethyl-3-hexenoic acid (**7b**) was obtained in a 72% yield. In a similar manner, the Birch reduction of **2c** and subsequent alkylation with benzyl bromide gave 4-benzylthio-3-ethyl-3-octenoic acid (**7c**) in an 82% yield.

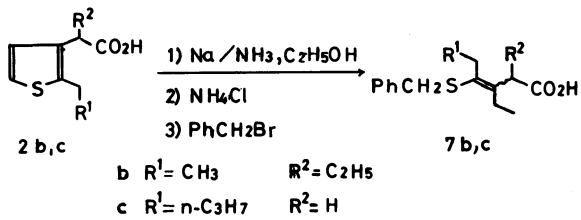

A regioselective ring-opening Birch reduction has been disclosed by Joullié *et al.*[7] It was reported there that the Birch reduction of 2-thiophenecarboxylic acid by 3 equivalents of lithium gave 2,5-dihydro-2-thiophenecarboxylic acid, while that by 5 equivalents of lithium gave (*Z*)-5-mercapto-3-pentenoic acid, which was formed regioselectively by reductive cleavage between the sulfur atom and the carbon atom at the 1-position of the thiophene ring. However, in our reaction, the reductive cleavage of the thiophene ring occurred between the sulfur atom and the carbon atom at the 5-position of thiophene ring regioselectively, while the double bond of the thiophene ring remained at the 1-position. Further, the reaction of **2b** with 3 equivalents of sodium and the subsequent addition of benzyl bromide resulted in the formation of **7b** in a 52% yield while the starting material, **2b**, was recovered in a 32% yield without any formation of dihydrothiophene derivatives. These results show that the regioselective ring-opening reaction occurred predominantly.

Next, the Birch reduction of 2-thienylacetic acid (**8**) was investigated under the assumption that the unusual ring-opening reaction would occurred as the effect of the carboxymethyl group.

When **8** was allowed to react with 5 equivalents of sodium in liquid ammonia, and to this mixture then were subsequently added 3 equivalents of ammonium chloride and benzyl bromide, similar type ring-opening product was obtained in an 84% yield. On the other hand, this product contained (*Z*)-3-benzylthio-3-hexenoic acid (**9**) and the double bond isomerized products, (*Z*)- and (*E*)-3-benzylthio-2-hexenoic acid (**10a, b**), in the ratio of 84 : 12 : 4.

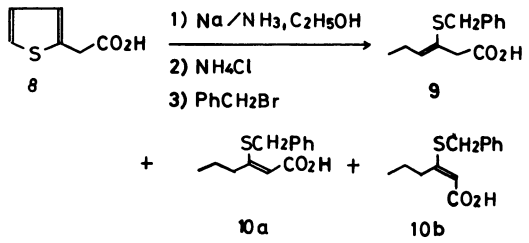

Further, it was found that the Birch reduction of 2-propylthiophene (**11**), which did not contain the carboxyl group, with 4 equivalents of sodium and subsequent alkylation with benzyl bromide also gave a regioselective ring-opening product, (*Z*)-4-benzylthio-3-heptene (**12**), in a 72% yield.

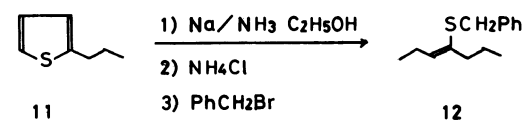

From these results, we could not make clear the reason for the specificity of reductive ring-opening reaction of thiophene derivatives, but we are continuing our investigation of the Birch reduction of many types of thiophene derivatives.

Experimental

Preparation of 1-(2-Thienyl)ethyl Acetate (1a). Into a solution of 1-(2-thienyl)ethanol (3.89 g, 30 mmol) in 20 ml of

dry dichloromethane and 20 ml of dry pyridine, acetyl chloride (2.2 ml, 31 mmol) was added at 0 °C with stirring. The stirring was continued for 2 h at 0 °C and then for additional 22 h at room temperature. The reaction mixture was acidified by 10% hydrochloric acid and extracted with dichloromethane. The dichloromethane layer was dried over sodium sulfate. After the removal of the solvent, the residue was chromatographed on silica gel, **1a** was obtained by the elution of benzene [5.05 g (98%)]. The **1a** was further purified by distillation; bp 93 °C (10 mmHg, 1 mmHg=133.32 Pa). IR (NaCl): 1735 cm^{-1} (C=O), 1230 cm^{-1} (-O-); NMR($CDCl_3$): δ=1.67 (3H, d), 2.08 (3H, s), 6.31 (1H, q), 7.03—7.22 (2H, m), 7.35—7.47 (1H, m); MS: *m/e* 170 (M^+).

Similarly, 1-(2-thienyl)ethyl butyrate (**1b**), 1-(2-thienyl)-butyl acetate (**1c**), and 1-(2-thienyl)butyl butyrate (**1d**) were prepared from the corresponding alcohols and acid chlorides. The spectral and analytical data of **1b**, **1c**, and **1d** are as follows:

1b: Yield 92%, bp 82—85 °C (2.5 mmHg); IR(NaCl): 1730 cm^{-1} (C=O), 1165 cm^{-1} (-O-); NMR($CDCl_3$): δ=0.95 (3H, t), 1.42—2.00 (5H, m), 2.35 (2H, t), 6.35 (1H, q), 7.03—7.25 (2H, m), 7.36—7.47 (1H, m); MS: *m/e* 198 (M^+). Found: C, 60.51; H, 7.18%. Calcd for $C_{10}H_{14}O_2S$: C, 60.56; H, 7.23%.

1c: Yield, 98%, bp 74—75 °C (2 mmHg); IR(NaCl): 1730 cm^{-1} (C=O), 1220 cm^{-1} (-O-); NMR($CDCl_3$): δ=0.95 (3H, t), 1.22—2.03 (4H, m), 2.02 (3H, s), 6.16 (1H, t), 6.95—7.18 (2H, m), 7.27—7.38 (1H, m); MS: *m/e* 198 (M^+). Found: C, 60.56; H, 7.23%. Calcd for $C_{10}H_{14}O_2S$: C, 60.59; H, 7.12%.

1d: Yield, 94%. The **1d** was used for the next reaction without distillation. An oily product; IR(NaCl): 1735 cm^{-1} (C=O), 1170 cm^{-1}, 1095 cm^{-1} (-O-); NMR($CDCl_3$): δ=0.78—1.03 (6H, m), 1.17—2.03 (6H, m), 2.28 (2H, t), 6.05 (1H, t), 6.82—7.30 (3H, m); MS: *m/e* 226 (M^+). Found: C, 63.45; H, 7.95%. Calcd for $C_{12}H_{18}O_2S$: C, 63.70; H, 8.02%.

The Claisen Rearrangement of Lithium Enolate of 1a. To a solution of lithium *N*-isopropylcyclohexylamide, prepared from *N*-isopropylcyclohexylamine (1.56 g, 11 mmol) and butyllithium (11 mmol) in THF (13 ml), a solution of **1a** (0.850 g, 5 mmol) in THF (13 ml) was added at −78 °C under nitrogen. The reaction mixture was stirred at −78 °C for 1 h and then refluxed for 3 h with stirring. After the addition of a 5% potassium hydroxide solution, the mixture was extracted with diethyl ether. The water layer was acidified with concentrated hydrochloric acid and extracted with dichloromethane. The dichloromethane layer was dried over sodium sulfate, and the solvent was removed under reduced pressure. After the residue has been chromatographed on silica gel, (2-ethyl-3-thienyl)acetic acid (**2a**) was obtained as an oily product from the elution of benzene–diethyl ether (4 : 1) [0.329 g (38%)]. IR(NaCl): 3200—2560 cm^{-1} (CO_2H), 1705 cm^{-1} (C=O); NMR($CDCl_3$): δ=1.28 (3H, t), 2.82 (2H, q), 3.62 (2H, s), 6.97—7.30 (2H, m), 12.15 (1H, s); MS: *m/e* 170 (M^+). Found: C, 56.34; H, 5.77%. Calcd for $C_8H_{10}O_2S$: C, 56.46; H, 5.92%.

Further, the structure of the **2a** was established by reductive desulfurization with Raney nickel.[8] The reaction of **2a** (0.319 g, 2 mmol) with Raney nickel, prepared from 20 g of the nickel–aluminum alloy, in refluxing 95% ethanol (100 ml) for 12 h gave a known carboxylic acid,[9] 3-ethylhexanoic acid [0.103 g (38%)]. IR(NaCl): 3400—2300 cm^{-1} (CO_2H), 1705 cm^{-1} (C=O); NMR($CDCl_3$): δ=0.80—1.13 (6H, m), 1.33—1.56 (7H, m), 2.30 (2H, t), 11.06 (1H, s); MS: *m/e* 144 (M^+).

In a similar procedure, the rearrangement of **1b**, **1c**, and **1d** was performed, 2-(2-ethyl-3-thienyl)butyric acid (**2b**), 2-(2-butyl-3-thienyl)acetic acid (**2c**), and 2-(2-butyl-3-thienyl)-butyric acid (**2d**) respectively were thus obtained. The spectral and analytical data are as follows: **2b**: Bp 139—140 °C (4 mmHg); IR(NaCl): 3200—2550 cm^{-1} (CO_2H), 1700 cm^{-1} (C=O); NMR($CDCl_3$): δ=0.90 (3H, t), 1.29 (3H, t), 1.65—2.28 (2H, m), 2.88 (2H, q), 3.67 (1H, t), 7.15 (2H, m), 11.92 (1H, s); MS: *m/e* 198 (M^+). Found: C, 60.78; H, 6.84%. Calcd for $C_{10}H_{14}O_2S$: C, 60.59; H, 7.12%.

2c: An oily product; IR(NaCl): 3200—2550 cm^{-1} (CO_2H), 1700 cm^{-1} (C=O); NMR($CDCl_3$): δ=0.95 (3H, t), 1.25—1.80 (4H, m), 2.63—2.93 (2H, m), 3.63 (2H, s), 6.98—7.25 (2H, m), 12.08 (1H, s); MS: *m/e* 198 (M^+). Found: C, 60.50; H, 7.16%. Calcd for $C_{10}H_{14}O_2S$: C, 60.95; H, 7.12%.

2d: An oily product; IR(NaCl): 3100—2530 cm^{-1} (CO_2H), 1700 cm^{-1} (C=O); NMR($CDCl_3$): δ=0.78—1.03 (6H, m), 1.23—2.27 (6H, m), 2.87 (2H, t), 3.67 (1H, t), 7.07—7.28 (2H, m), 12.11 (1H, s); MS: *m/e* 226 (M^+). Found: C, 63.70; H, 7.83%. Calcd for $C_{12}H_{18}O_2S$: C, 63.70; H, 8.02%.

Preparation of 4-(2-Thienyl)-4-butanolide (3). Methyl 4-oxo-4-(2-thienyl)butyrate (**5**) was prepared from thiophene (8.44 g, 0.1 mol) and methyl 3-(chloroformyl)propionate (15.07 g, 0.1 mol) by the use of the Friedel-Crafts reaction[10] [18.03 g (91%), bp 125—127 °C (2 mmHg)]; IR(NaCl): 1730 cm^{-1}, 1660 cm^{-1} (C=O), 1215 cm^{-1}, 1160 cm^{-1} (-O-); NMR ($CDCl_3$): δ=2.72 (2H, t), 3.24 (2H, t), 3.63 (3H, s), 6.97—7.10 (1H, m), 7.50—7.73 (2H, m); MS: *m/e* 198 (M^+). Found: C, 54.81; H, 5.05%. Calcd for $C_9H_{10}O_3S$: C, 54.54; H. 5.09%.

To a solution of **5** (4.02 g, 20 mmol) in 30 ml of methanol, sodium borohydride (0.391 g, 10 mmol) was added in small portions at 0 °C. After stirring for 1 h at 0 °C, to the reaction mixture we added 1.4 ml of acetic acid and 100 ml of water. The mixture was then extracted with diethyl ether, and the ether layer was washed with a saturated solution of sodium hydrogencarbonate and dried over sodium sulfate. After the removal of the solvent, the residue was chromatographed on silica gel and methyl 4-hydroxy-4-(2-thienyl)butyrate (**6**) was obtained from the elution of benzene and diethyl ether (1 : 1) [3.88 g (96%), an oily product]. IR(NaCl): 3440 cm^{-1} (OH), 1720 cm^{-1} (C=O); NMR($CDCl_3$): δ=1.87—2.60 (4H, m), 3.47 (1H, brs), 3.60 (3H, s), 4.92 (1H, q), 6.77—7.00 (1H, m), 7.12—7.30 (1H, m); MS: *m/e* 200 (M^+). Found: C, 54.00; H, 6.05%. Calcd for $C_9H_{12}O_3S$: C, 53.99; H, 6.04%.

A mixture of **6** (2.02 g, 10 mmol) and sodium hydroxide (0.49 g, 12 mmol) in 10 ml of water and 5 ml of methanol was stirred at room temperature for 0.5 h. The methanol was then removed under reduced pressure and concentrated hydrochloric acid (3 ml) was added to the residue. After the the mixture has been stirred for 2 h at room temperature, 20 ml of water was added and the mixture was extracted with diethyl ether. The ether layer was dried over sodium sulfate. The solvent was removed by distillation, and the residue was chromatographed on silica gel. From the elution of benzene and diethyl ether (3 : 1), 4-(2-thienyl)-4-butanolide (**3**) was obtained as an oily product [1.44 g (85%)]. The **3** was further purified by distillation under reduced pressure [bp 153 °C (5 mmHg)]; IR(NaCl): 1770 cm^{-1} (C=O), 1200 cm^{-1}, 1120 cm^{-1} (-O-); NMR($CDCl_3$): δ=2.30—2.87 (4H, m), 5.68 (1H, t), 6.85—7.03 (2H, m), 7.19—7.32 (1H, m); MS: *m/e* 168 (M^+). Found: C, 57.18; H, 4.78%. Calcd for $C_8H_8O_2S$: C, 57.14; H, 4.80%.

The Claisen Rearrangement of the Lithium Enolate of 3. Into a solution of lithium *N*-isopropylcyclohexylamide, prepared from *N*-isopropylcyclohexylamine (1.555 g, 11 mmol) and butyllithium (11 mmol), and hexamethylphosphoric triamide (1.978 g, 11 mmol) in 25 ml of THF, a solution of **3** (0.843 g, 5 mmol) in 8 ml of THF was added at −78 °C with stirring

under nitrogen. After the temperature has then been elevated to room temperature, the reaction mixture was stirred for 18 h. After the addition of 10% hydrochloric acid, the mixture was extracted with diethyl ether. The ether layer was dried over sodium sulfate and the solvent was removed under reduced pressure. When the residue was chromatographed on silica gel, 5,6-dihydro-4*H*-cyclopenta[*b*]thiophene-4-carboxylic acid (**4**) was obtained as a solid product by the elution of dichloromethane [0.368 g (44%)]; mp 52—53 °C; IR(KBr): 3100—2550 cm^{-1} (CO_2H), 1690 cm^{-1} (C=O); NMR($CDCl_3$): δ= 1.20—2.10 (4H, m), 2.63—2.95 (1H, m), 6.80—7.18 (2H, m), 11.65 (1H, s); MS: *m/e* 168 (M^+). Found: C, 57.05; H, 4.90%. Calcd for $C_8H_8O_2S$: C, 57.14; H, 4.80%.

The Birch Reduction of ***2b****, Followed by Benzylation.* To a mixture of **2b** (0.834 g, 4.2 mmol), 1.5 ml of dry diethyl ether, 1.5 ml of absolute ethanol, and 25 ml of liquid ammonia, small pieces of sodium (0.519 g, 22.6 mmol) were added over the period of 1 h under reflux. After the mixture then been stirred for 1 h in refluxing liquid ammonia, a solid of ammonium chloride (0.721 g, 13.5 mmol) was added and the mixture was stirred for 0.5 h. Next, benzyl bromide (0.6 ml, 5 mmol) was added to the mixture, and the mixture was stirred for 20 min. Further, additional benzyl bromide (0.6 ml, 5 mmol) was added into the mixture, and the mixture was stirred for 1 h with refluxing. The ammonia was then evaporated, and the residue we added 10 ml of 10% hydrochloric acid and 10 ml of chloroform. The mixture was stirred for 1 h, and then the chloroform layer was separated. The chloroform layer was washed with water and dried over sodium sulfate. After the removal of the solvent, the residue was chromatographed on silica gel. From the elution of benzene–diethyl ether (10 : 1), 4-benzylthio-2,3-diethyl-3-hexenoic acid (**7b**) was obtained as an oily product [0.888 g (72%)]. IR(NaCl): 3080—2600 cm^{-1} (CO_2H), 1700 cm^{-1} (C=O); NMR($CDCl_3$): δ=0.68—2.57 (15H, m), 3.43 (1H, t), 3.80 (2H, s), 7.25 (5H, s), 11.32. (1H, s); MS: *m/e* 292 (M^+). Found: C, 69.78; H, 8.29% Calcd for $C_{17}H_{24}O_2S$: C, 69.83; H, 8.27%.

In a similar procedure, the Birch reduction and subsequent benzylation of **2c** and 2-thienylacetic acid (**8**) were performed. The yield and spectral data of products are as follows: 4-Benzylthio-3-ethyl-3-octenoic acid (**7c**): Yield, 82%; an oily product; IR(NaCl): 3050—2550 cm^{-1} (CO_2H), 1700 cm^{-1} (C=O); NMR($CDCl_3$): δ=0.73—1.13 (6H, m), 1.27—1.82 (4H, m), 2.23—2.62 (4H, m), 3.25 (2H, s), 3.92 (2H, s), 7.43 (5H, s), 12.08 (1H, s); MS: *m/e* 292 (M^+). Found: C, 70.08; H, 8.32%. Calcd for $C_{17}H_{24}O_2S$: C, 69.83; H, 8.27%.

(E)-3-Benzylthio-3-hexenoic acid (**9**): Yield, 71%; mp 92.5—94 °C (from petroleum ether); IR(KBr): 3100—2550 cm^{-1} (CO_2H), 1710 cm^{-1} (C=O); NMR($CDCl_3$): δ=0.87 (3H, t), 2.23 (2H, quen), 3.27 (2H, s), 3.89 (2H, s), 5.90 (1H, t), 7.32 (5H, m), 11.45 (1H, s); MS: *m/e* 236 (M^+). Found: C, 66.37; H, 6.78%. Calcd for $C_{13}H_{16}O_2S$: C, 66.08; H, 6.83%.

(Z)-3-Benzylthio-2-hexenoic acid (**10a**): Yield, 9%; mp 117.5—118.5 °C (from petroleum ether); IR(KBr): 3075—2550 cm^{-1} (CO_2H), 1680 cm^{-1} (C=O), 1580 cm^{-1} (C=C); NMR($CDCl_3$): δ=0.98 (3H, t), 1.30—1.87 (2H, m), 2.83 (2H, t), 4.03 (2H, s), 7.36 (5H, s), 11.55 (1H, s); MS: *m/e* 236 (M^+). Found: C, 65.71; H, 6.76%. Calcd for $C_{13}H_{16}O_2S$: C, 66.08; H, 6.83%.

(E)-3-Benzylthio-2-hexenoic acid (**10b**): Yield, 3%; mp 145—146 °C (from petroleum ether); IR(KBr): 3050—2500 cm^{-1} (CO_2H), 1655 cm^{-1} (C=O), 1555 cm^{-1} (C=C); NMR ($CDCl_3$): δ=1.00 (3H, t), 1.30—1.85 (2H, m), 2.53 (2H, t), 4.17 (2H, s), 5.93 (1H, s), 7.50 (5H, s); MS: *m/e* 236 (M^+). Found: C, 66.02; H, 6.83%. Calcd for $C_{13}H_{16}O_2S$: C, 66.08; H, 6.83%.

*The Birch Reduction of 2-Propylthiophene (****11****), Followed by Benzylation.* To a liquid ammonia solution (50 ml) of absolute ethanol (2.5 ml) and **11** (1.269 g, 10 mmol) dissolved in diethyl ether (2.5 ml) we added small pieces of sodium (0.926 g, 40 mmol) over a period of 1.5 h. After refluxing for 1 h, ammonium chloride (1.641 g, 31 mmol) was added to the mixture, and the mixture was stirred for 0.5 h. Next, benzyl bromide (1.5 ml, 12.5 mmol) was added to the mixture, and the mixture was stirred for 20 min. Further, additional benzyl bromide (1.5 ml, 12.5 mmol) was added to the mixture. The reaction mixture was then refluxed for 1 h. The ammonia was subsequently removed, and 10% hydrochloric acid was added to the residue. The mixture was extracted with diethyl ether, and the ether layer was dried over sodium sulfate. After the removal of the solvent, the residue was chromatographed on silica gel and (*Z*)-4-benzylthio-3-heptene (**12**) was obtained as an oily product from the elution of petroleum ether [1.646 g (74%)]. IR(NaCl): 1605 cm^{-1}, 1500 cm^{-1}, 1460 cm^{-1} (Ph); NMR($CDCl_3$): δ=0.73—0.99 (6H, m), 1.28—1.87 (2H, m), 2.28—2.43 (4H, m), 3.82 (2H, s), 5.68 (1H, t), 7.36 (5H, s); MS: *m/e* 220 (M^+). Found: C, 76.72; H, 9.06%. Calcd for $C_{14}H_{20}S$: C, 76.32; H, 9.15%.

References

1) S. Raucher, A. S. Lui, and J. E. MacDonald, *J. Org. Chem.*, **44**, 1885 (1979).

2) In our investigation, when 2-[(1-vinyloxy)ethyl]thiophene was heated at 330 °C for a short time under nitrogen and the resulting aldehyde was reduced by sodium borohydride in methanol, the [1,3] sigmatropic rearrangement product, 3-(2-thienyl)-1-propanol, was obtained in a 44% yield without any formation of the [3,3] sigmatropic rearrangement product.

3) K. Kosugi, A. V. Anisimov, H. Yamamoto, R. Yamashiro, K. Shirai, and T. Kumamoto, *Chem. Lett.*, **1981**, 1341.

4) R. E. Ireland and R. H. Mueller, *J. Am. Chem. Soc.*, **94**, 5897 (1972); R. E. Ireland, R. H. Mueller, and A. K. Willard, *ibid*, **98**, 2868 (1976); *J. Org. Chem.*, **41**, 986 (1972).

5) S. F. Birch and D. T. McAllan, *J. Chem. Soc.*, **1951**, 2565; **1951**, 3411; Ya. L. Goldfarb, A. V. Semenovskii, E. P. Zakharow, G. V. Davydovp, and F. M. Stoyanovich, *Izv. Akad. Nauk. SSSR, Ser. Khim.*, **1979**, 480; *Chem. Abstr.*, **90**, 168011m (1979).

6) K. Nishino, S. Yano, Y. Kohashi, K. Yamamoto, and I. Murata, *J. Am. Chem. Soc.*, **101**, 5059 (1979).

7) W. G. Blenderman, M. M. Joullié, and G. Preti, *Tetrahedron Lett.*, **1979**, 4985.

8) E. J. Modest and J. Szmuszkovicz, *J. Am. Chem. Soc.*, **72**, 577 (1950); H. Wynberg and A. Logothetis, *ibid*, **78**, 1958 (1956).

9) C. P. Casey and C. R. Cyr, *J. Am. Chem. Soc.*, **95**, 2240 (1973).

10) J. R. Johnson and G. E. May, *Org. Synth.*, Coll. Vol. II, 8 (1943).

 © 1983 The Chemical Society of Japan Bull. Chem. Soc. Jpn., 56, 1669—1677 (1983)

Stereoselective Intramolecular Diels-Alder Reactions of α,β-Unsaturated Amides Using Internal Coordination of Metal Salts

Toyonori TAKEBAYASHI,** Nobuharu IWASAWA, Teruaki MUKAIYAMA,* and Tadashi HATA†

Department of Chemistry, Faculty of Science, The University of Tokyo, Hongo, Bunkyo-ku, Tokyo 113

†Analytical and Metabolic Laboratories, Sankyo Co., Ltd., Hiromachi, Shinagawa-ku, Tokyo 140

(Received October 9, 1982)

The intramolecular Diels-Alder reactions between acyclic dienes and α,β-unsaturated amides utilizing the internal coordination of the metal salts have been studied in detail. When the magnesium salts of *N*-(*trans*, *trans*-2,4-alkadienyl)-*N*-(2-hydroxyphenyl)acrylamide derivatives are employed, the intramolecular Diels-Alder reactions are remarkably accelerated and the corresponding cycloadducts are obtained in high yields with isomeric ratios (*exo*-adducts: *endo*-adducts) of about 3 : 2. And the same reactions of *N*-(*trans*, *trans*-2,4-alkadienyl)-*N*-(2-hydroxyphenyl)-1-cyclopentenecarboxamide afford predominantly (60 : 40 to 85 : 15 selectivity) *trans*-fused cycloadducts (*exo*-adducts) in good yields.

The intramolecular Diels-Alder reaction has become one of the most powerful methods for the construction of a variety of interesting ring systems, and has been applied to the syntheses of various natural products.[1]

Though the efficiency of this reaction, derived from the entropical factor, is well established, it sometimes needs high temperature to perform the reaction, and, in some cases, the desired cycloadducts cannot be obtained at all even by the intramolecular Diels-Alder reaction. Moreover, the stereochemical features must be well-defined for this reaction to become widely accepted as a synthetic method.

As for the former problems, we recently reported an efficient method for the acceleration of the intramolecular Diels-Alder reaction between furan derivatives and α,β-unsaturated amide derivatives employing the internal coordination of magnesium salt or internal hydrogen bonding.[2] As for the stereochemical problems, a large amount of work has recently been reported by Roush,[3] Boeckmann,[4] White,[5] and so on. They, in most cases, have dealt with terminally activated trienoate systems, and made it clear that when acyclic diene is employed, two stereoisomers (*endo* and *exo* adducts) are produced, and that non-bonded interaction plays more important role in the stereoselection of this reaction than the secondary orbital control.

In this paper, we would like to describe our recent results about the reaction rate and stereoselection of the intramolecular Diels-Alder reaction between acyclic diene and α,β-unsaturated carbonyl unit connected by the amide bond, with the assumption that the formation of internal chelate complex not only accelerates the reaction but also alters the stereochemical course of this reaction.

Results and Discussion

Only a few examples have been known about the intramolecular Diels-Alder reaction of an acyclic diene and a dienophile linked by the amide bond,[6] and only one report was published on the stereoselection of these compounds by Gschwend *et al.*[7]

Our recent results on the intramolecular Diels-Alder reaction between furan derivatives and α,β-unsaturated amides, utilizing the internal coordination of the magnesium salt and the internal hydrogen bonding, prompted us to examine the reactivity and stereoselection of the reaction between acyclic dienes and α,β-unsaturated carboxyl compounds linked by the amide bond.

Among various conformers of *o*-aminophenol derivative **1**, only conformer **1b** in which diene and dienophile groups are located nearby would contribute to the cycloaddition reaction, and it is assumed that by the employment of the internal interaction (the internal hydrogen bonding or the internal coordination of the metal salt of compound **1**), the conformation of amide **1** would be fixed to **1b** and, combined with the Lewis acid character of the metal salt, the cycloaddition reaction would be accelerated efficiently. Moreover, it is expected that the formation of this rigid internal chelate complex **2** would result in the more efficient stereoregulation by the nonbonding steric repulsion combined with the enhanced secondary orbital control caused by the Lewis acid character of the metal salts (Eq. 1).

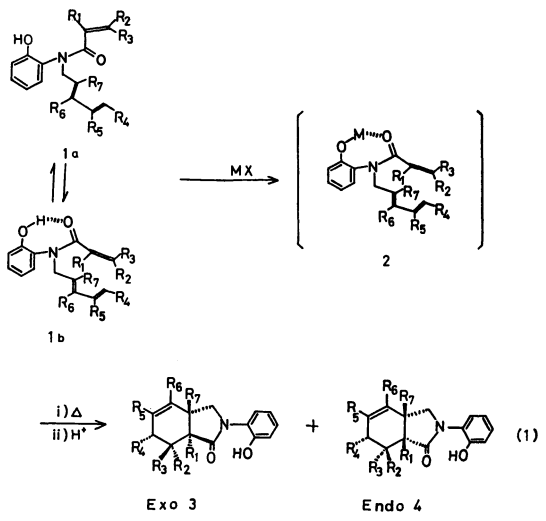

(1)

Based on these assumptions, various *N*-(*trans*,*trans*-2,4-alkadienyl)-*N*-(2-hydroxyphenyl)acrylamide derivatives **9** were prepared as shown in Eq. 2.

In the first place, the intramolecular Diels-Alder reaction of acrylamide derivative **9a** and its magnesium

** Present address: Product Development Laboratories Sankyo Co., Ltd., Hiromachi, Shinagawa-ku, Tokyo 140.

Table 1. The Diels-Alder reaction of the amide **9a**[a)]

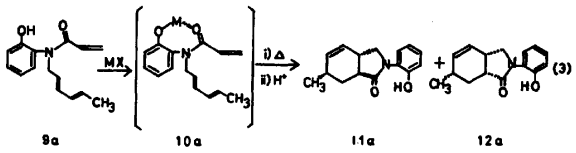

Metal salt	Solvent	Reaction time/h	Yield/% of cycloadduct	Ratio **11a** : **12a**
None	Toluene	20	16	45 : 55
-OMgBr	Toluene	9	72	59 : 41
-OMgBr	Benzene	10	69	55 : 45
-OMgBr	Dichloromethane	36	21	52 : 48
-OMgCl	Toluene	16	77	58 : 42

a) The reaction was performed in refluxing solvent under an argon atmosphere.

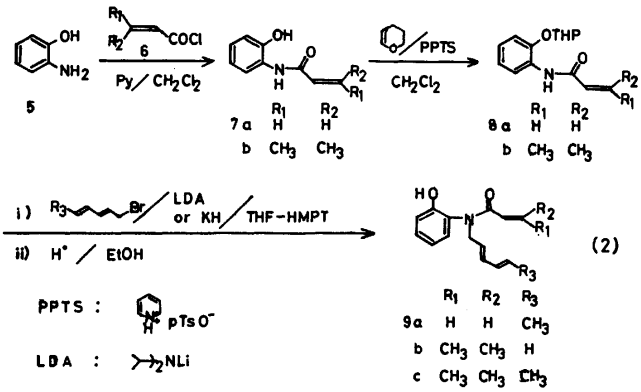

salt was examined and the results were summarized in Table 1.

As shown in this Table, when the toluene solution of amide **9a** was refluxed for 20 h, nearly equal amounts of two cycloadducts (that is, *trans*-fused **11a** and *cis*-fused **12a**) were obtained in only 16% yield along with substantial amount of polymerized product. These two isomers were separated by silica-gel thin-layer chromatography (hexane–ethyl acetate, 3 : 2) and the structures were determined by ^{1}H-NMR (270 MHz).

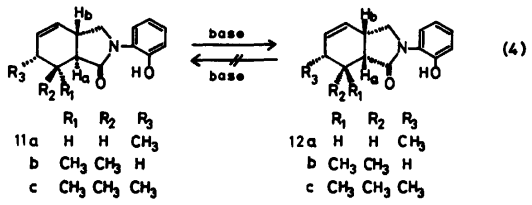

The proton H_a in **11a** appears at δ 2.42 as a doublet-triplet splitting. Coupling constants are $J_{H_a-H_b}=J_{H_a-R_2}=13$ Hz, and $J_{H_a-R_1}=3$ Hz, indicating the trans ring fusion of this compound. On the other hand, the proton H_a in **12a** appears at δ 2.82 as a doublet-doublet-doublet splitting. Coupling constants are $J_{H_a-H_b}=8$ Hz, $J_{H_a-R_1}=5$ Hz, $J_{H_a-R_2}=13$ Hz, indicating the cis ring fusion of this compound. Further, the examination of Dreiding models of **11a** and **12a** suggested the *trans*-fused product is more strained than the *cis*-fused one. In accordance with this, it is observed that trans **11a** was completely isomerized to cis **12a** by the treatment of 0.1 equivalent of sodium methoxide in refluxing methanol. On the other hand, treatment of cis **12a** under the same conditions resulted in the complete recovery of **12a** (Eq. 4).

The IR spectrum of amide **9a** indicates that the internal hydrogen bonding exists in this molecule (carboxyl absorption appears at 1610 cm^{-1}). However, above result indicates that the fixation of the conformation of **9a** by the hydrogen bonding is not enough to promote the cycloaddition reaction effectively.

Next, with the expectation that the formation of internal chelate complex not only accelerate the reaction, but also alter the stereoselection, amide **9a** was converted to its bromomagnesium salt and heated for 9 h in refluxing toluene. As expected, the yield of cycloadducts **11a** and **12a** increased up to 72%, and the ratio of **11a** and **12a** also changed from 45 : 55 to 59 : 41. However, further examination of reaction temperature did not alter the stereoselectivity dramatically.

Next, we examined various metal salts such as Al, Sn, Zn, and B, based on the consideration that stronger Lewis acid than Mg would enhance the secondary orbital control and *endo*-mode of cyclizations would be preferred. And the results are summarized in Table 2.

Table 2. The Diels-Alder reaction of various metal salts of amide **9a**[a)]

Metal salt	Solvent	Reaction time/h	Yield/% of cycloadduct	Ratio **11a** : **12a**
-OAl(Et)Cl	Toluene	11	36	25 : 75
-OAl(Et)$_2$	Toluene	17	37	38 : 62
-OSn(Bu)$_2$Cl	Toluene	17	84	42 : 58
-OZnCl	Toluene	17	43	48 : 52
-OBBr$_2$	Toluene	9	16	38 : 62
-OB [b)]	Toluene	9	43	32 : 68
-OB(OEt)$_2$	Toluene	17	31	41 : 59
-OB(Ph)Cl	Toluene	11	42	14 : 86
-OB(Ph)OH	Toluene	11	28	29 : 71

a) The reaction was performed in refluxing toluene under an argon atmosphere. b) 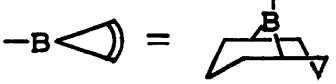

Table 3. The Diels-Alder reaction of amide **9b**[a] (R=H)

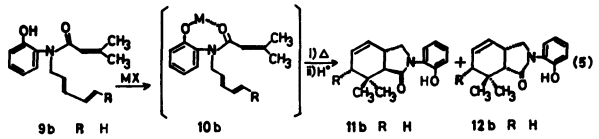

9b R H **9c** R CH_3 **10b** **10c** **11b** R H **11c** R CH_3 **12b** R H **12c** R CH_3

Metal salt	Solvent	Additive[b]	Reaction time/h	Yield/% of cycloadduct	Ratio[c] **11b : 12b**
None	Toluene	—	60	12	55 : 45
–OMgCl	Toluene	—	20	52	52 : 48
–OMgBr	Toluene	—	20	31	62 : 38
–OAl(Et)Cl	Toluene	—	48	24	53 : 47
$-OSn(Bu)_2Cl$	Toluene	—	20	17	52 : 48
None	Xylene	—	20	32	64 : 36
None	Xylene	tBC	20	42	65 : 36
–OMgCl	Xylene	tBC	7	85	59 : 41
–OMgCl	Xylene	tBC	3	75	58 : 42
–OMgBr	Xylene	tBC	7	71	69 : 31
–OAl(Et)Cl	Xylene	tBC	14	27	69 : 31
$-OSn(Bu)_2Cl$	Xylene	tBC	7	41	41 : 59

a) The reaction was performed in refluxing solvent under an argon atmosphere. b) The catalytic amount of 4-*t*-butylcatechol (tBC) was added. c) Two stereoisomers of the cycloadduct were separated by silica-gel chromatography.

Table 4. The Diels-Alder reaction of amide **9c**[a] (R=CH_3)

Metal salt	Solvent	Additive[b]	Reaction time/h	Yield/% of cycloadduct	Ratio **11c : 12c**
None	Toluene	—	30	16	68 : 32
–OMgBr	Toluene	—	24	53	60 : 40
–OAl(Et)Cl	Toluene	—	24	35	40 : 60
$-OSn(Bu)_2Cl$	Toluene	—	24	64	49 : 51
None	Xylene	tBC	20	49	68 : 32
–OMgCl	Xylene	tBC	14	77	57 : 43
–OMgCl	Xylene	tBC	7	78	60 : 40
–OMgBr	Xylene	tBC	14	61	58 : 42
–OAl(Et)Cl	Xylene	tBC	14	54	59 : 41
$-OSn(Bu)_2Cl$	Xylene	tBC	14	55	62 : 38

a) The reaction was performed in refluxing solvent under an argon atmosphere. b) The catalitic amount of 4-*t*-butylcatechol (tBC) was added. c) Two stereoisomers of the cycloadduct were separated by silica-gel thin-layer chromatography.

Though the acceleration of the reaction is rather modest compared to the magnesium salt (one serious problem is the polymerization of starting material caused by the existence of Lewis acid), the preferred formation of *endo*-cycloadduct **12a** should be noted and when phenyldichloroborane is added to the solution of sodium salt of amide **9a**, up to 86 : 14 stereoselection could be achieved.

Next, we examined the reaction of more sterically hindered 3-methyl-2-butenamide derivatives **9b** and **9c** using various metal salts. And the results are summarized in Tables 3 and 4.

As shown in these Tables, the reaction proceeded rather slowly in refluxing toluene even when the magnesium salt was employed. However, the xylene solutions of the magnesium salts of **9b** and **9c** were refluxed with catalytic amount of 4-*t*-butylcatechol as a radical scavenger, high yields of the corresponding cycloadducts were realized. However, remarkable change in the stereoselection of the two cycloadducts was not observed in these cases.

The structures of these stereoisomers were determined by ^{1}H-NMR. The proton H_a in **11b** appears at δ 2.21 as a doublet with a coupling constant of 12 Hz, indicating the trans ring fusion of this compound. On the other hand, the proton H_a in **12b** appears at δ 2.56 as a doublet with a coupling constant of 8 Hz, indicating the cis ring fusion of this compound (Eq. 4). Treatment of **11b** with 0.1 equivalent of sodium methoxide in refluxing methanol completely isomerized **11b** to **12b**. On the other hand, treatment of **12b** under the same conditions resulted in the complete recovery of **12b**. The structures of **11c** and **12c** were assigned similarly. That is, ^{1}H-NMR analysis indicates that coupling constants of proton H_a in **11c** and **12c** are 12 Hz and 8 Hz, respectively, and isomerization of **11c** proceeded smoothly by the treatment of **11c** with NaH in refluxing THF, but when **12c** was treated in the same manner,

TABLE 5. THE DIELS-ALDER REACTION OF AMIDE **14**[a)]

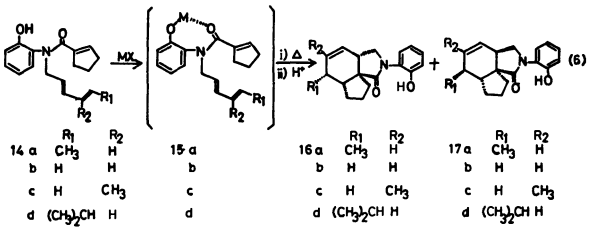

Amide	Metal salt	Reaction time/h	Yield/% of cycloadduct	Ratio **16 : 17**
14a	None	17	46	50 : 50[b)]
	-OMgCl	10	80	85 : 15[b)]
	-OMgBr	10	78	80 : 20[b)]
	-OMgI	10	78	83 : 17[b)]
	-OAl(Et)Cl	24	58	60 : 40[b)]
	$-OSn(Bu)_2Cl$	10	58	54 : 46[b)]
14b	None	6	29	40 : 60[c)]
	-OMgCl	4	91	62 : 38[c)]
	-OMgBr	4	86	62 : 38[c)]
	-OMgI	4	81	60 : 40[c)]
	-OAl(Et)Cl	5	31	38 : 62[c)]
	$-OSn(Bu)_2Cl$	4	43	35 : 65[c)]
14c	None	20	30	42 : 58[c)]
	-OMgCl	10	71	60 : 40[c)]
	-OMgBr	10	75	65 : 35[c)]
	-OMgI	10	75	61 : 39[c)]
	-OAl(Et)Cl	10	38	38 : 63[c)]
	$-OSn(Bu)_2Cl$	10	50	38 : 62[c)]
14d	None	11	25	60 : 40[b)]
	-OMgCl	10	74	76 : 24[b)]
	-OMgBr	10	70	80 : 12[b)]
	-OMgI	10	70	88 : 12[b)]
	-OAl(Et)Cl	10	21	58 : 42[b)]
	$-OSn(Bu)_2Cl$	10	33	62 : 39[b)]

a) The reaction were carried out in refluxing toluene. b) GC analysis were performed on 2 m, 2% OV-17 Chromosorb W column at 200 °C. c) In separable by TLC or GC. Product ratio were determined by ^{1}H-NMR.

complete recovery of **12c** was observed.

Finally, we examined the reaction of cyclic α,β-unsaturated amide compounds to construct polycyclic systems in a single step.

Amides **14** were prepared by the same procedure described in Eq. 1, and the results are shown in Table 5.

As shown in Table 5, when the toluene solution of amide **14a** was refluxed for 17 h, equal amounts of two stereoisomeric adducts **16a** and **17a** were obtained in 46% yield. On the other hand, when toluene solution of the chloromagnesium salt of amide **14a** was refluxed for 10 h, adduct **16a** and **17a** were obtained in 80% yield and the isomeric ratio of the products came up to 85 : 15. The ratio of these two stereoisomers was determined by gas chromatography and the configuration of the predominantly formed adduct was defined from X-ray analysis to be *trans*-fused (*i.e.* **16a**). Similar reactions of the magnesium salts of amides **14b—d** showed that the reaction is surely accelerated by the formation of internal chelate complex and that, in these cases, the *exo*-cycloadducts are predominantly formed.[8)] Recently, Roush[3c)] has reported the Lewis acid catalyzed intramolecular Diels-Alder reaction of terminally activated trienoates, and, in his case, the *endo*-cycloadducts were preferentially obtained, probably because of the enhanced secondary orbital control by the Lewis acid. But in our cases, the *exo*-cycloadducts were predominantly formed by the employment of magnesium salt. This result is interpreted as that, in our magnesium salt mediated intramolecular Diels-Alder reaction, steric control is more important than the secondary orbital control in the stereoselection of the products.

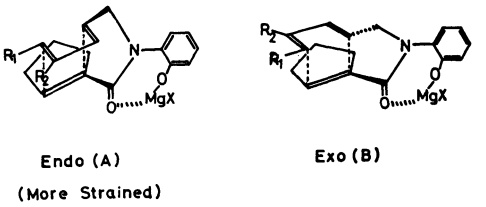

Fig. 1. Transition states of cycloaddition reaction.

When the reaction is carried out without converting to the metal salt, there is little energy difference between

TABLE 6. POSITIONAL PARAMETERS OF THE NON-HYDROGEN ATOMS FOR **18a**, WITH THEIR ESTIMATED STANDARD DEVIATIONS IN PARENTHESES

Positional parameters have been multiplied by 10^4.

Atom	x	y	z	B_{ep}/Å^2	Atom	x	y	z	B_{eq}/Å^2
N(1)	3062(7)	130(4)	5531(7)	4.45(24)	C(17)	−178(9)	1119(5)	3454(10)	5.22(34)
C(2)	3478(8)	69(5)	6773(9)	4.70(31)	C(18)	66(9)	1945(5)	3658(9)	5.20(34)
C(3)	4258(8)	761(5)	7298(8)	4.32(29)	O(19)	1047(6)	2185(4)	4330(7)	6.38(26)
C(4)	5309(9)	738(5)	8577(10)	5.41(35)	C(20)	−935(8)	2467(5)	2924(8)	4.39(30)
C(5)	6544(9)	1025(6)	8438(11)	6.18(38)	C(21)	−626(9)	3175(6)	2662(10)	5.47(35)
C(6)	6271(10)	1693(6)	7591(11)	6.75(42)	C(22)	−1489(9)	3670(6)	1959(10)	5.78(36)
C(7)	5406(10)	1659(6)	6489(10)	6.08(38)	C(23)	−2721(9)	3459(5)	1589(9)	5.32(34)
C(8)	4694(9)	937(5)	6224(10)	5.50(35)	C(24)	−3045(9)	2768(6)	1792(11)	6.31(39)
C(9)	3554(10)	787(6)	5104(10)	5.82(35)	C(25)	−2177(9)	2269(5)	2502(10)	5.82(37)
C(10)	2139(9)	−326(5)	4729(9)	4.81(33)	Br(26)	−3917(1)	4147(1)	624(2)	9.27(7)
C(11)	2277(9)	−1077(5)	4650(11)	6.01(38)	O(27)	3258(6)	−436(4)	7372(6)	5.92(24)
C(12)	1364(10)	−1519(6)	3877(12)	7.13(43)	C(28)	3344(9)	1344(5)	7485(10)	5.37(35)
C(13)	262(10)	−1210(6)	3174(11)	6.60(40)	C(29)	3533(10)	1280(7)	8839(11)	7.24(44)
C(14)	35(9)	−446(6)	3241(10)	5.79(36)	C(30)	4907(10)	1207(6)	9460(10)	6.36(39)
C(15)	972(9)	−4(5)	4026(10)	5.23(35)	C(31)	7522(11)	1162(8)	9696(13)	8.84(52)
O(16)	898(6)	745(3)	4189(6)	5.69(23)					

TABLE 7. THERMAL PARAMETERS OF THE NON-HYDROGEN ATOMS FOR **18a**, WITH THEIR ESTIMATED STANDARD DEVIATIONS

All parameters have been multiplied by 10^4. The thermal parameters are of the form

$$T=\exp[-(B_{11}h_2+B_{22}k^2+B_{33}l^2+2B_{12}hk+2B_{13}hl+2B_{23}kl)].$$

Atom	B_{11}	B_{22}	B_{33}	B_{12}	B_{13}	B_{23}
N(1)	107(8)	30(3)	79(8)	−3(4)	20(7)	5(4)
C(2)	89(10)	25(3)	129(12)	0(5)	39(9)	5(5)
C(3)	94(9)	27(3)	95(11)	8(5)	29(8)	4(5)
C(4)	109(11)	28(4)	140(13)	1(5)	30(10)	9(6)
C(5)	85(10)	44(5)	168(15)	9(6)	28(10)	−2(7)
C(6)	112(12)	44(5)	182(16)	−13(6)	54(11)	−12(7)
C(7)	121(12)	36(4)	157(14)	−5(6)	60(11)	9(6)
C(8)	118(11)	34(4)	125(12)	−1(5)	44(10)	2(6)
C(9)	133(12)	40(4)	113(12)	0(6)	40(10)	12(6)
C(10)	104(11)	30(4)	104(12)	−3(5)	31(9)	−5(5)
C(11)	109(11)	33(4)	166(15)	7(5)	44(11)	0(6)
C(12)	140(13)	29(4)	212(18)	0(6)	52(13)	−16(7)
C(13)	138(13)	39(4)	152(15)	−10(6)	36(11)	−19(7)
C(14)	98(11)	33(4)	151(14)	−5(5)	7(10)	−9(6)
C(15)	117(11)	25(4)	132(13)	3(5)	46(10)	1(5)
O(16)	109(7)	28(2)	148(9)	3(3)	10(6)	−1(4)
C(17)	101(10)	29(4)	135(13)	6(5)	33(10)	−1(5)
C(18)	103(10)	34(4)	124(12)	−4(5)	43(9)	0(6)
O(19)	105(7)	36(3)	171(10)	−2(4)	13(7)	−5(4)
C(20)	99(10)	26(3)	99(11)	2(5)	37(8)	−1(5)
C(21)	97(11)	36(4)	136(13)	−3(5)	36(10)	−8(6)
C(22)	115(11)	35(4)	145(14)	−1(6)	54(10)	13(6)
C(23)	111(11)	32(4)	127(13)	15(5)	42(10)	18(6)
C(24)	90(10)	43(5)	181(16)	2(6)	52(11)	4(7)
C(25)	103(11)	32(4)	167(15)	−4(5)	51(10)	9(6)
Br(26)	133(1)	62(1)	266(2)	31(1)	66(1)	44(1)
O(27)	135(8)	32(3)	132(9)	−11(4)	26(7)	12(4)
C(28)	107(11)	33(4)	131(13)	11(5)	39(10)	0(6)
C(29)	126(13)	59(6)	162(16)	21(7)	63(12)	0(8)
C(30)	145(13)	46(5)	117(13)	−2(6)	44(11)	−3(6)
C(31)	111(13)	81(7)	194(19)	−7(8)	3(13)	−17(9)

endo-mode and *exo*-mode in the transition state. However, when amide **14** is converted to its magnesium salt, the coordination of the Mg to the carbonyl oxygen should make the conformation of the molecule more rigid and the *endo*-mode of cyclization (A) would become more strained compared with the *exo*-mode of cyclization (B), because of the planarity of the amide group (Fig. 1). When the stronger Lewis acid such as

TABLE 8. POSITIONAL AND ISOTROPIC THERMAL PARAMETERS OF THE HYDROGEN ATOMS FOR **18a**, WITH THEIR ESTIMATED STANDARD DEVIATIONS IN PARENTHESES

Positional parameters have been multiplied by 10^3.

Atom	x	y	z	B/Å^2
H(4)	539(6)	21(4)	897(6)	3(2)
H(5)	681(7)	59(5)	795(8)	6(2)
H(6)	677(7)	218(4)	792(7)	5(2)
H(7)	512(7)	203(4)	589(7)	5(2)
H(8)	538(8)	58(5)	622(8)	7(2)
H(9A)	297(8)	118(5)	495(8)	7(2)
H(9B)	376(7)	69(5)	437(7)	6(2)
H(11)	304(8)	−123(5)	517(8)	7(2)
H(12)	143(7)	−201(4)	381(7)	5(2)
H(13)	−36(8)	−149(5)	252(8)	6(2)
H(14)	−70(7)	−17(4)	267(7)	4(2)
H(17A)	−79(6)	99(4)	373(7)	4(2)
H(17B)	−39(7)	103(4)	241(7)	4(2)
H(21)	19(8)	326(5)	291(8)	6(2)
H(22)	−119(9)	407(6)	159(9)	9(3)
H(24)	−382(8)	256(5)	165(8)	7(2)
H(25)	−240(7)	182(4)	258(7)	5(2)
H(28A)	254(8)	122(5)	682(8)	7(2)
H(28B)	366(9)	183(6)	741(9)	9(3)
H(29A)	318(10)	77(6)	916(10)	10(3)
H(29B)	321(9)	169(6)	916(10)	10(3)
H(30A)	515(8)	181(5)	944(8)	7(2)
H(30B)	522(7)	102(4)	1050(7)	4(2)
H(31A)	783(9)	76(5)	1050(9)	8(3)
H(31B)	732(9)	161(6)	1011(10)	9(3)
H(31C)	830(9)	135(6)	969(9)	9(3)

Al or Sn were employed, there would be some delicate balance between steric control and enhanced secondary orbital control, and two cycloadducts were obtained in almost the same ratio with the noncatalyzed reaction.

Thus, magnesium salt is the most effective both for the acceleration of the reaction and for the stereoselective formation of the cycloadducts.

X-Ray analysis revealed the relative configuration of the predominantly afforded cycloadduct to be the *exo*-mode cycloadduct (trans ring junction; **16a**). The analysis was carried out as follows. The preferentially formed cycloadduct was obtained by the recrystallization of the mixture of two stereoisomers from cyclohexane. This isomer was converted to its *p*-bromobenzoylmethyl ether **18a** to get a good single crystal for X-ray analysis (Eq. 7).

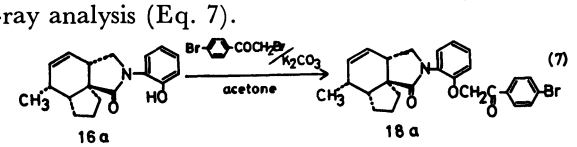

(7)

16a 18a

The crystal data for this compounds are: $a=11.611(4)$ Å, $b=17.874(5)$ Å, $c=11.480(5)$ Å, $\beta=110.50(3)°$, space group $P2_1/c$, $D_c=1.43$ g/cm^3. Intensities of 1896 independent reflection within the limited sphere $2\theta=110°$ were collected on a fully automated diffractometer with graphic-monochromated Cu-$K\alpha$ radiation using ω-2θ scan technique. The structure was solved by the heavy atom method. All non-hydrogen atoms were found in the E-map and subsequent Fourier syntheses. A three dimentional difference Fourier map showed the positions of all H atoms. Block-diagnoal least-squares refinement reduced final R-value and R_w-value to 0.082 and 0.087, respectively. The function minimized was $(\sum w||F_o|-|F_c||^2)$, where the weights w are $1/\sigma(F)$. The atomic parameters with their estimated standard deviations are listed in Tables 6, 7, 8, and 9.[9] The numbering system and a stereoscopic view of the molecule are shown in Figs. 2 and 3, respectively. The bond distances and angles are given in Tables 10 and 11, respectively.

TABLE 10. BOND DISTANCES OF **18a**, WITH THEIR ESTIMATED STANDARD DEVIATIONS IN PARENTHESES

Bond distance	l/Å	Bond distance	l/Å
N(1)–C(2)	1.340(13)	C(23)–Br(26)	1.895(9)
N(1)–C(9)	1.464(14)	C(24)–C(25)	1.379(13)
N(1)–C(10)	1.404(11)	C(28)–(29)	1.496(17)
C(2)–C(3)	1.527(12)	C(29)–C(30)	1.508(15)
C(2)–O(27)	1.216(13)		
C(3)–C(4)	1.547(12)	C(4)–H(4)	1.04(7)
C(3)–C(8)	1.522(16)	C(5)–H(5)	1.06(9)
C(3)–C(28)	1.555(15)	C(6)–H(6)	1.05(8)
C(4)–C(5)	1.583(16)	C(7)–H(7)	0.92(8)
C(4)–C(30)	1.510(17)	C(8)–H(8)	1.02(9)
C(5)–C(6)	1.501(16)	C(9)–H(9A)	0.95(9)
C(5)–C(31)	1.512(15)	C(9)–H(9B)	0.97(9)
C(6)–C(7)	1.313(14)	C(11)–H(11)	0.92(8)
C(7)–C(8)	1.505(14)	C(12)–H(12)	0.91(8)
C(8)–C(9)	1.512(12)	C(13)–H(13)	0.99(8)
C(10)–C(11)	1.359(14)	C(14)–H(14)	1.00(7)
C(10)–C(15)	1.433(12)	C(7)–H(17A)	0.92(8)
C(11)–C(12)	1.370(14)	C(17)–H(17B)	1.15(8)
C(12)–C(13)	1.368(15)	C(21)–H(21)	0.90(8)
C(13)–C(14)	1.397(15)	C(22)–H(22)	0.95(11)
C(14)–C(15)	1.390(13)	C(24)–H(24)	0.95(9)
C(15)–O(16)	1.360(11)	C(25)–H(25)	0.87(8)
O(16)–C(17)	1.409(11)	C(28)–H(28A)	1.00(8)
C(17)–C(18)	1.507(13)	C(28)–H(28B)	0.96(11)
C(18)–O(19)	1.209(11)	C(29)–H(29A)	1.11(12)
C(18)–C(20)	1.499(12)	C(29)–H(29B)	0.96(12)
C(20)–C(21)	1.376(14)	C(30)–H(30A)	1.11(9)
C(20)–C(25)	1.397(13)	C(30)–H(30B)	1.16(7)
C(21)–C(22)	1.368(13)	C(31)–H(31A)	1.12(9)
C(22)–C(23)	1.394(14)	C(31)–H(31B)	0.99(11)
C(23)–C(24)	1.334(15)	C(31)–H(31C)	0.97(11)

As shown in Fig. 3, the ring junction between the ring A and the ring B is *trans*-configuration and the ring B links to the ring C with *cis*-configuration. The ring B is boat conformation, the atom C(5) and C(8) being displaced by 0.57 and 0.65 Å, respectively, form the plane of the other four atoms in this ring. The five-membered ring A and C both take an envelop conformation where the atoms C(8) and C(29) lie 0.63 and 0.59 Å, respectively, out of the plane composed of the other atoms. The atomic configuration of N(1) atom is estimated to be sp^2 hybrid orbital, since this atom is displaced by 0.06 Å from the plane consisted of three attached carbon atoms.

In conclusion, it is noted that an efficient and general method is established for the stereoselective intramolecular Diels-Alder reaction by employing internal coordination of the magnesium salt. By employing this

Table 11. Bond angles of **18a**, with their estimated standard deviations in parentheses

Bond angle	ϕ/°	Bond angle	ϕ/°
C(2)-N(1)-C(9)	112.6(7)	C(11)-C(10)-C(15)	118.0(8)
C(2)-N(1)-C(10)	123.9(8)	C(10)-C(11)-C(12)	122.0(9)
C(9)-N(1)-C(10)	123.0(8)	C(11)-C(12)-C(13)	120.1(10)
N(1)-C(2)-C(3)	107.3(8)	C(12)-C(13)-C(14)	121.2(9)
N(1)-C(2)-O(27)	126.4(8)	C(13)-C(14)-C(15)	118.1(9)
C(3)-C(2)-O(27)	126.3(9)	C(10)-C(15)-C(14)	120.5(8)
C(2)-C(3)-C(4)	121.0(8)	C(10)-C(15)-O(16)	114.3(7)
C(2)-C(3)-C(8)	99.7(8)	C(14)-C(15)-O(16)	125.2(8)
C(2)-C(3)-C(28)	105.0(8)	C(15)-O(16)-C(17)	118.1(7)
C(4)-C(3)-C(8)	113.5(8)	O(16)-C(17)-C(18)	107.0(7)
C(4)-C(3)-C(28)	103.7(8)	C(17)-C(18)-O(19)	122.1(8)
C(8)-C(3)-C(28)	114.2(8)	C(17)-C(18)-C(20)	117.1(7)
C(3)-C(4)-C(5)	109.7(9)	O(19)-C(18)-C(20)	120.7(9)
C(3)-C(4)-C(30)	107.2(8)	C(18)-C(20)-C(21)	118.9(8)
C(5)-C(4)-C(30)	113.1(8)	C(18)-C(20)-C(25)	122.8(8)
C(4)-C(5)-C(6)	109.2(8)	C(21)-C(20)-C(25)	118.3(8)
C(4)-C(5)-C(31)	111.1(11)	C(20)-C(21)-C(22)	122.0(9)
C(6)-C(5)-C(31)	114.0(9)	C(21)-C(22)-C(23)	117.8(10)
C(5)-C(6)-C(7)	120.3(10)	C(22)-C(23)-C(24)	121.3(9)
C(6)-C(7)-C(8)	114.5(10)	C(22)-C(23)-Br(26)	117.8(7)
C(3)-C(8)-C(7)	109.2(9)	C(24)-C(23)-Br(26)	120.6(7)
C(3)-C(8)-C(9)	102.2(9)	C(23)-C(24)-C(25)	120.7(9)
C(7)-C(8)-C(9)	125.5(9)	C(20)-C(25)-C(24)	119.5(9)
N(1)-C(9)-C(8)	100.7(8)	C(3)-C(28)-C(29)	103.4(8)
N(1)-C(10)-C(11)	122.5(8)	C(28)-C(29)-C(30)	104.1(11)
N(1)-C(10)-C(15)	119.3(8)	C(4)-C(30)-C(29)	104.8(9)

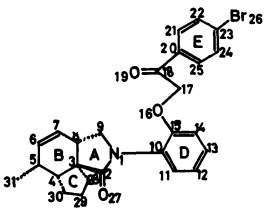

Fig. 2. Atomic numbering system of compound **18a**. Unaccampanied numbers indicate C atoms.

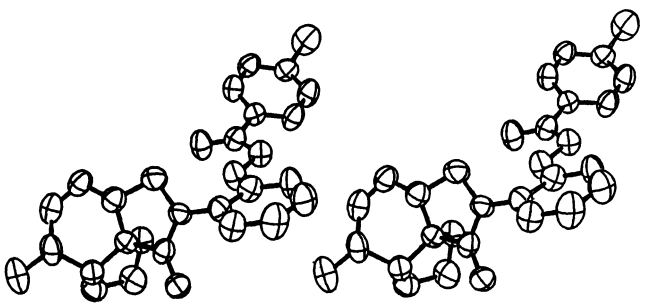

Fig. 3. Stereoscopic view of **18a**. Thermally vibrating Ellipsoids are drawn at the 50% probability level.

method, various cycloadducts, which cannot be prepared in the previous intramolecular Diels-Alder reaction, have become obtainable stereoselectively and in good yield.

Experimental

Measurements. All the melting points were uncorrected. ^{1}H-NMR spectra were recorded on a Bruker WH-270 (270 MHz) or a JEOL FX-90Q (90 MHz)or a Varian Model T-60 (60 MHz). IR spectra were taken on a Hitachi 260-50 spectrometer. Mass spectra were measured with JEOL JMS 01-SG. The intensity of crystal were collected on a Rigaku AFC-5 four-circle diffractomer. GC analyses were done on a Hitachi 163.

Materials. N-*(2-Hydroxyphenyl)acrylamide (7a)*: Under an argon atmosphere acryloyl chloride (9.06 g, 0.1 mol) was added to the suspension of 2-aminophenol **5** (10.91 g, 0.1 mol) and dry pyridine (8.1 ml) in dichloromethane (40 ml) at 0—5 °C and stirred at room temperature for 2 h. To the reaction mixture 2 M hydrochloric acid (5 ml)†† was added and the organic layer was washed with water (15 ml×3). After being dried over Na_2SO_4, the solution was evaporated *in vacuo*. The residue was recrystallized from benzene to afford amide **7a** (13.06 g, 80%). Mp 114.5—115.5 °C (benzene); IR (KBr) 3405, 3092 and 1685 cm^{-1}; NMR ($CDCl_3$) δ=5.50—5.97 (1H, m), 6.17—6.50 (2H, m), 6.70—7.27 (4H, m), 7.50—8.00 (1H, broad), 8.73 (1H, s); Found: C, 66.21; H, 5.49; N, 8.43%. Calcd for $C_9H_9NO_2$: C, 66.24; H, 5.56; N, 8.58%. By similar procedure amide **7b** was prepared. **7b**: Mp 147.0—148.5 °C (benzene); IR (KBr) 3291 and 1627 cm^{-1}; NMR ($CDCl_3$) δ=1.87 (3H, s), 2.17 (3H, s), 5.83 (1H, m), 6.50—6.97 (3H, m), 7.30—7.60 (1H, m), 8.98 (1H, s), 9.33—9.87 (1H, broad); Found: C, 69.03; H, 6.84; N, 7.48%. Calcd for $C_{11}H_{13}NO_2$: C, 69.09; H, 6.85; N, 7.33%.

N-[*2-(Tetrahydropyranyloxy)phenyl*]*acrylamide (8a)*. To the solution of amide **7a** (5.23 g, 32.0 mmol) and pyridinium *p*-toluenesulfonate (0.81 g, 3.2 mmol) in dichloromethane (150 ml), 3,4-dihydro-2*H*-pyran (5.11 g, 60.5 mmol) was added dropwise. After being stirred for 2 h at room temperature, 2 M sodium hydroxide (30 ml) was added to the mixture. The organic layer was washed with water (3×30 ml) and dried over Na_2SO_4. After the solvent was evaporated *in vacuo*,

†† 1 M=1 mol dm^{-3}.

residual oil was crystallized from petroleum ether to afford amide **8a** as white needles (6.42 g, 81%). Mp 81.0—82.0 °C (hexane); IR (KBr) 3408 and 1680 cm^{-1}; NMR ($CDCl_3$) δ= 1.50—2.20 (6H, m), 3.30—4.17 (2H, m), 5.20 (1H, m), 5.47—5.73 (1H, m), 6.03—6.33 (2H, m), 6.70—7.13 (3H, m), 7.73—8.00 (1H, broad), 8.03—8.37 (1H, m); Found: C, 67.92; H, 7.08; N, 5.55%. Calcd for $C_{14}H_{17}NO_3$: C, 67.99; H, 6.93; N, 5.66%. By similar procedure amide **8b** was prepared. **8b**: Mp 88.5—89.5 °C (hexane); IR (KBr) 3354 and 1667 cm^{-1}; NMR ($CDCl_3$) δ=1.40—2.07 (6H, m), 1.90 (3H, s), 2.20 (3H, s), 3.37—4.00 (2H, m), 5.30 (1H, m), 5.33 (1H, m), 6.80—7.23 (3H, m), 7.57—7.97 (1H, broad), 8.07—8.50 (1H, m); Found: C, 69.50; H, 7.83; N, 4.98%. Calcd for $C_{16}H_{21}NO_3$: C, 69.79; H, 7.69; N, 5.09%.

N-(trans, trans-2,4-Hexadienyl)-N-(2-hydroxyphenyl)acrylamide (9a). Under an argon atmosphere, amide **8a** (3.93 g, 15.9 mmol) in dry THF (15 ml) was added slowly at 0 °C to the suspension of potassium hydride (0.64 g, 15.9 mmol) in dry THF (15 ml) and the mixture was further stirred at room temperature for 15 min. To the mixture *trans,trans*-2,4-hexadienyl bromide (2.55 g, 15.9 mmol) was added dropwise at −76 °C over 10 min. After being stirred at room temperature overnight, the reaction mixture was quenched with water (10 ml) and extracted with ethyl acetate (3×20 ml). The extracts were dried over Na_2SO_4 and evaporated *in vacuo*. The residual oil was purified by the silica-gel column chromatography using hexane–ether (2 : 1). Then, the product was dissolved in ethanol (15 ml) and 2 M hydrochloric acid (2 ml). After being heated at 50—55 °C for 2 h, the reaction mixture was neutralized with 5% sodium hydrogencarbonate and extracted with dichloromethane (2×15 ml). The organic layer was washed with water and dried over Na_2SO_4. The solvent was evaporated *in vacuo* and the residual oil was purified by the silica-gel column chromatography using dichloromethane to afford amide **9a** (2.68 g, 70%). Oil; IR (liquid) 3150, 1630, and 1610 cm^{-1}; NMR ($CDCl_3$) δ=1.67 (3H, d, J=6 Hz), 3.87 (1H, dd, J=5 and 14 Hz), 4.70 (1H, dd, J=5 and 14 Hz), 5.13—6.33 (6H, m), 6.70—7.40 (5H, m), 8.60 (1H, s).

N-(trans, trans-2,4-Pentadienyl)-N-(2-hydroxyphenyl)-3-methyl-2-butenamide (9b). Under an argon atmosphere, amide **8b** (5.51 g, 0.02 mol) in dry THF (15 ml) was added dropwise at 0 °C to the solution (THF 50 ml–HMPT 10 ml) of lithium diisopropylamide (0.02 mol) and the mixture was further stirred at room temperature for 30 min. Then *trans,trans*-2,4-pentadienyl bromide (2.96 g, 0.02 mol) was added dropwise to the reaction mixture at −76 °C. After being stirred at room temperature for 2 h, the reaction mixture was quenched with 2 M hydrochloric acid (20 ml) and water (30 ml), and extracted with dichloromethane (3×30 ml). The extracts were washed with water (3×30 ml), dried over Na_2SO_4 and evaporated *in vacuo*. The residual oil was purified by the silica-gel column chromatography using hexane–ether (2 : 1). The product was hydrolyzed with 2 M hydrochloric acid in ethanol in the same way with the preparation of amide **9a** to afford amide **9b** (3.86 g, 75%). Mp 140.5—142.0 °C (hexane); IR (KBr) 3170, 1642, and 1604 cm^{-1}; NMR ($CDCl_3$) δ=1.65 (3H, s), 2.08 (3H, s), 3.58—4.10 (1H, m), 4.28—4.57 (1H, m), 4.83—5.55 (3H, m), 5.62—6.47 (3H, m), 6.67—7.28 (4H, m), 7.42 (1H, s); Found: C, 74.77; H, 7.31; N, 5.72%. Calcd for $C_{16}H_{19}NO_2$: C, 74.68; H, 7.44; N, 5.44%. By similar procedure amides **9c** and **14a—d** were prepared. **9c**: Mp 69.0—70.0 °C (hexane–cyclohexane); IR (KBr) 3220, 1644, and 1608 cm^{-1}; NMR ($CDCl_3$) δ=1.63 (3H, s), 1.70 (3H, d, J=6 Hz), 2.07 (3H, s), 3.50—4.07 (1H, m), 4.20—4.83 (1H, m), 5.10—6.17 (5H, m), 6.53—7.27 (4H, m), 7.67 (1H, s); Found: C, 75.19; H, 7.57; N, 5.25%. Calcd for $C_{17}H_{21}NO_2$: C, 75.24; H, 7.80; N, 5.16%. **14a**: Oil; IR (liquid) 3170, 1610, and 1580 cm^{-1}; NMR ($CDCl_3$) δ=1.33—1.93 (2H, m), 1.67 (3H, d, J=6 Hz), 1.97—2.47 (4H, m), 3.70—4.73 (2H, m), 5.13—6.20 (4H, m), 6.50—7.37 (5H, m), 7.60 (1H, s); Found: *m/e* 283.1603. Calcd for $C_{18}H_{21}NO_2$: M, 283.1572. **14b**: Oil; IR (liquid) 3140, 1604, and 1580 cm^{-1}; NMR ($CDCl_3$) δ=1.27—1.90 (2H, m), 1.93—2.60 (4H, m), 3.60—4.33 (1H, m), 4.40—5.33 (3H, m), 5.37—6.47 (4H, m), 6.53—7.20 (4H, m), 8.73—9.93 (1H, broad); Found: *m/e* 269.1421. Calcd for $C_{17}H_{19}NO_2$: M, 269.1415. **14c**: Oil; IR (liquid) 3140, 1605, and 1580 cm^{-1}; NMR ($CDCl_3$) δ=1.33—1.97 (2H, m), 1.77 (3H, s), 2.03—2.60 (4H, m), 3.70—4.40 (1H, m), 4.47—5.27 (1H, m), 4.83 (2H, s), 5.40—6.37 (3H, m), 6.53—7.20 (4H, m), 8.43—9.43 (1H, broad); Found: *m/e* 283.1607. Calcd for $C_{18}H_{21}NO_2$: M, 283.1572. **14d**: Oil; IR (liquid) 3150, 1610, and 1570 cm^{-1}; NMR ($CDCl_3$) δ=0.93 (6H, d, J=6 Hz), 1.30—1.90 (2H, m), 1.93—2.60 (5H, m), 3.60—4.20 (1H, m), 4.23—4.83 (1H, m), 5.00—6.13 (5H, m), 6.40—7.10 (4H, m), 7.70—8.20 (1H, broad); Found: *m/e* 311.1858. Calcd for $C_{20}H_{25}NO_2$: M, 311.1885.

Intramolecular Diels-Alder Reaction Using Magnesium Salt. 3a,6,7,7a-Tetrahydro-2-(2-hydroxyphenyl)-6-methyl-1-isoindolinone (11a and 12a): To a solution of amide **9a** (314 mg, 1.29 mmol) in dry THF (3 ml) was added dropwise butylmagnesium chloride (1.42 ml, 0.91 mol/l ether solution) at −78 °C under an argon atmosphere. After the solvent was concentrated under the reduced pressure at room temperature, toluene (10 ml) was added and the reaction mixture was refluxed for 16 h under an argon atmosphere. To the solution was added 2 M hydrochloric acid (2 ml) and the products were extracted with ethyl acetate. The extract was washed with water and dried over Na_2SO_4. The solution was evaporated *in vacuo* and the crude product was purified on a silica-gel thin-layer chromatography using hexane–ethyl acetate (3 : 2) to afford the cycloadduct (**11a** and **12a**) (241 mg, 77%). Two stereoisomers **11a** and **12a** were cleanly separable by the silica-gel thin-layer chromatography (**11a** : **12a**=58 : 42). **11a**: Mp 136.0—137.0 °C (cyclohexane); IR (KBr) 3070, 3030, 1658, and 1595 cm^{-1}; NMR (270 MHz) ($CDCl_3$); δ= 1.10 (3H, d, J=7 Hz), 1.84 (1H, dt, J=7 and 13 Hz), 2.00 (1H, dd, J=3 and 13 Hz), 2.42 (1H, dt, J=13 and 3 Hz), 2.56 (1H, m), 2.78 (1H, m), 3.75 (2H, m), 5.77 (1H, dt, J=10 and 3 Hz), 5.81 (1H, dt, J=10 and 1.5 Hz), 6.77—7.40 (4H, m), 8.76 (1H, s); Found: C, 74.00; H, 7.00; N, 5.78%. Calcd for $C_{15}H_{17}NO_2$: C, 74.05; H, 7.04; N, 5.76%. **12a**: Mp 135.0—136.0 °C (hexane); IR (KBr) 3090, 2095, 1658, and 1595 cm^{-1}; NMR (270 MHz) ($CDCl_3$); δ=1.09 (3H, d, J=7 Hz), 1.39 (1H, dt, J=13 and 10 Hz), 2.10 (1H, dt, J=13 and 5 Hz), 2.27 (1H, m), 2.82 (1H, ddd, J=13, 8, and 5 Hz), 3.12 (1H, m), 3.75 (1H, t, J=9 Hz), 3.94 (1H, t, J=9 Hz), 5.65 (1H, ddd, J=10, 3.5, and 2.5 Hz), 5.79 (1H, broad d, J=10 Hz), 6.99—7.37 (4H, m), 8.59 (1H, s); Found: C, 74.04; H, 7.03; N, 5.81%. Calcd for $C_{15}H_{17}NO_2$: C, 74.05; H, 7.04; N, 5.76%. By similar procedure cycloadducts **11b—c** and **12b—c** were afforded. **11b**: Mp 95.0—96.0 °C (cyclohexane); IR (KBr) 3050, 2880, 1652, and 1595 cm^{-1}; NMR (90 MHz) ($CDCl_3$); δ=1.04 (3H, s), 1.36 (3H, s), 1.99 (2H, m), 2.21 (1H, d, J=12 Hz), 2.57—3.17 (1H, broad), 3.70 (2H, d, J=6 Hz), 5.74 (2H, m), 6.81—7.41 (4H, m), 8.80 (1H, s); Found: C, 74.45; H, 7.42; N, 5.47%. Calcd for $C_{16}H_{19}NO_2$: C, 74.68; H, 7.44; N, 5.44%. **12b**: Mp 130.0—131.0 °C (cyclohexane); IR (KBr) 3045, 2950, 1633, and 1595 cm^{-1}; NMR (90 MHz) ($CDCl_3$) δ=1.10 (3H, s), 1.27 (3H, s), 1.60—2.36 (2H, m), 2.56 (1H, d, J=8 Hz), 2.89—3.29 (1H, broad), 3.52 (1H, dd, J=5 and 9 Hz), 4.03 (1H, dd, J=7 and 9 Hz), 5.41—5.99 (2H, m), 6.67—7.36 (4H, m), 8.47 (1H,

s); Found: C, 74.54; H, 7.54; N, 5.46%. Calcd for $C_{16}H_{19}NO_2$: C, 74.68; H, 7.44; N, 5.44%. **11c**: Mp 112.0—113.0 °C (cyclohexane); IR (KBr) 3040, 2960, 1659, and 1595 cm^{-1}; NMR (90 MHz) ($CDCl_3$) $\delta=0.99$ (3H, d, $J=7$ Hz), 1.06 (3H, s), 1.33 (3H, s), 1.68—2.04 (1H, m), 2.24 (1H, d, $J=12$ Hz), 2.64—3.11 (1H, m), 3.68 (2H, m), 5.68 (2H, m), 6.68—7.29 (4H, m), 8.75 (1H, s); Found: C, 75.54; H, 7.73; N, 5.02%. Calcd for $C_{17}H_{21}NO_2$: C, 75.24; H, 7.80; N, 5.16%. **12c**: Mp 142.0—143.0 °C (cyclohexane); IR (KBr) 3040, 2960, 1645, and 1595 cm^{-1}; NMR (90 MHz) ($CDCl_3$) $\delta=0.97$ (3H, s), 1.03 (3H, d, $J=8$ Hz), 1.26 (3H, s), 1.86—2.25 (1H, m), 2.51 (1H, d, $J=8$ Hz), 2.93—3.36 (1H, m), 3.77 (2H, m), 5.60 (2H, s), 6.60—7.29 (4H, m), 8.46 (1H, s); Found: C, 75.38; H, 7.91; N, 5.12%. Calcd for $C_{17}H_{21}NO_2$: C, 75.24; H, 7.80; N, 5.16%. In the case of the cycloaddition reactions of amides **14a—d**, the reactions were carried out in the same way, but two stereoisomers could not be separated eacho ther by silica-gel thin-layer chromatography. The predominantly formed cycloadducts **16a—d** were isolated by the recrystallization from cyclohexane after the purification of cycloadducts (one spot of two stereoisomers) from other miner spots by silica-gel thin-layer chromatography using hexane–ethyl acetate (3 : 2). Physical properties and spectral data of **16a—d** are as follows. **16a**: Mp 100.0—101.0 °C (cyclohexane); IR (KBr) 2960 and 1651 cm^{-1}; NMR ($CDCl_3$) $\delta=1.11$ (3H, d, $J=7$ Hz), 1.23—1.90 (6H, m), 2.07—3.07 (3H, m), 3.50—4.20 (2H, m), 5.50—6.13 (2H, m), 6.67—7.23 (4H, m), 8.77 (1H, s); Found: C, 76.10; H, 7.48; N, 5.00%. Calcd for $C_{18}H_{21}NO_2$: C, 76.29; H, 7.47; N, 4.94%. **16b**: Mp 113.0—114.0 °C (cyclohexane); IR (KBr) 2960 and 1651 cm^{-1}; NMR ($CDCl_3$) $\delta=1.05$—2.38 (8H, m), 2.38—3.28 (2H, m), 3.43—4.10 (2H, m), 5.91 (2H, m), 6.63—7.17 (4H, m), 8.72 (1H, s); Found: C, 75.76; H, 7.13; N, 5.25%. Calcd for $C_{17}H_{19}NO_2$: C, 75.81; H, 7.11; N, 5.20%. **16c**: Mp 129.0—130.0 °C (cyclohexane); IR (KBr) 2970 and 1642 cm^{-1}; NMR ($CDCl_3$) $\delta=1.42$ (3H, s), 1.10—1.90 (6H, m), 1.96—3.08 (4H, m), 3.48—3.98 (2H, m), 5.44—5.60 (1H, m), 6.68—7.28 (4H, m), 8.86 (1H, s); Found: C, 76.27; H, 7.53; N, 4.95%. Calcd for $C_{18}H_{21}NO_2$: C, 76.29; H, 7.47; N, 4.94%. **16d**: Mp 142.0—143.0 °C (cyclohexane): IR (KBr 2960 and 1648 cm^{-1}; NMR ($CDCl_3$) $\delta=1.02$ (6H, d, $J=5$ Hz), 1.08—2.08 (8H, m), 2.58—2.96 (2H, m), 3.58—4.18 (2H, m), 5.98 (2H, s), 6.72—7.24 (4H, m), 8.84 (1H, s); Found: C, 76.92; H, 8.01; N, 4.57%. Calcd for $C_{20}H_{25}NO_2$: C, 77.13; H, 8.09; N, 4.50%.

*Isomerization of Cycloadducts **11a** to **12a**.* A solution of adduct **11a** (99.5 mg, 0.39 mmol) and 28% sodium methoxide (0.15 ml, commercially available in methanol solution) was refluxed for 20 h. The mixture was neutralized with 2 M hydrochloric acid and extracted with dichloromethane. The organic layer was washed with water and dried over Na_2SO_4. The needles obtained by the evaporation of the solvent *in vacuo* was identical in all respects with adduct **12a** (99.0 mg, 99%). By similar procedure adduct **11b** was isomerized to adduct **12b**, but, in the case of adduct **11c**, sodium hydride was used as base instead of sodium methoxide.

*2,3,3a,6,6a,7,8,9-Octahydro-2-[2-(4-bromobenzoylmethoxy)phenyl]-1H-cyclopent[d]isoindol-1-one (**18a**).* To the suspension of adduct **16a** (413.2 mg, 1.46 mmol) and potassium carbonate (111.9 mg, 0.81 mmol) in aceton (20 ml) 4-bromophenacyl bromide (446.6 mg, 1.61 mmol) was added. After the mixture was refluxed for 2 h, water (10 ml) was added. After the extraction with dichloromethane (2×20 ml) the organic layer was dried over $MgSO_4$ and evaporated *in vacuo*. The residue was purified by silica-gel column chromatography using ether–hexane (1 : 1) to afford **18a** (547.1 mg, 80%). Mp: 188.0—189.0 °C (methanol); IR (KBr) 1702, 1681, and 1588 cm^{-1}; NMR ($CDCl_3$) $\delta=1.11$ (3H, d, $J=7$ Hz), 1.21—1.78 (6H, m), 2.20 (1H, m), 2.40—2.80 (2H, m), 3.78 (2H, m), 5.20 (2H, s), 5.76 (1H, m), 5.91 (1H, m), 6.84—7.44 (4H, m), 7.62 (2H, d, $J=8$ Hz), 7.84 (2H, d, $J=8$ Hz).

References

1) W. Oppolzer, *Angew. Chem., Int. Ed. Engl.*, **16**, 10 (1977).

2) a) T. Mukaiyama, T. Tsuji, and N. Iwasawa, *Chem. Lett.*, **1980**, 697; b) T. Mukaiyama and T. Takebayashi, *ibid*, **1980**, 1013.

3) a) W. R. Roush, *J. Org. Chem.*, **44**, 4008 (1979); b) W.R. Roush, A. I. Ko and H. R. Gillis, *ibid*, **45**, 4264 (1980); c) W. R. Roush and H. R. Gillis, *ibid*, **45**, 4267 (1980); d) W. R. Roush and S. M. Peseckis, *J. Am. Chem. Soc.*, **103**, 6696 (1981); e) W. R. Roush and H. R. Gillis, *J. Org. Chem.*, **45**, 4283 (1980); f) W. R. Roush and S. E. Hall, *J. Am. Chem. Soc.*, **103**, 5200 (1981); g) W. R. Roush, H. R. Gillis and I. K. Albert, *ibid.*, **104**, 2269 (1982).

4) a) R. K. Boekman, Jr., and S. S. Ko, *J. Am. Chem. Soc.*, **102**, 7149 (1980); b) R. K. Boeckman, Jr., and S. S. Ko, *ibid*, **104**, 1033 (1982); c) R. K. Boeckmen, Jr., and T. R. Alessi, *ibid*, **104**, 3216 (1982); d) R. K. Boeckman, Jr., and D. M. Demko, *J. Org. Chem.*, **47**, 1792 (1982).

5) a) J. D. White, B. G. Sheldon, B. A. Solheim, and J. Clardy, *Tetrahedron Lett.*, **1978**, 5189; b) J. D. White and B. G. Sheldom, *J. Org. Chem.*, **46**, 2273 (1981).

6) G. Brieger and J. N. Benett, *Chem. Rev.*, **80**, 63 (1980).

7) H. W. Gschwend, A. L. Lee, and H. D. Meier, *J. Org. Chem.*, **38**, 2169 (1973).

8) We did not perform X-ray analysis of predominantly formed cycloadducts **16b—d**, but from the retention time of GC analysis and spectral analogy of ^1H-NMR we assume that cycloadducts (**16b—d**) are the same *exo*-mode cycloadducts as cycloadduct **16a**.

9) Table 9 shows observed and calculated structure factors. The complete F_o-F_c data are deposited as Document No. 8323 at the Office of the Editor of the Bulletin of the Chemical Society of Japan.

Studies of Bitter Peptides from Casein Hydrolyzate. III.[1] Bitter Taste of Synthetic Analogs of BPIa (Arg-Gly-Pro-Pro-Phe-Ile-Val) Containing D-Proline or Glycine in Place of L-Proline[2]

Ichizo MIYAKE, Katsushige KOUGE, Hidenori KANEHISA, and Hideo OKAI*
Department of Fermentation Technology, Faculty of Engineering, Hiroshima University, Shitami, Saijo-cho, Higashihiroshima 724
(Received October 22, 1982)

In order to elucidate the relationship between chemical structure and bitter taste of BPIa, the analogs containing D-proline or glycine in place of the L-proline in the 3- or 4-positions were synthesized. The bitter taste of [D-Pro^{3,4}]-BPIa (**1D-D**), [D-Pro^3]-des-Pro^3-BPIa (**2D**), and [Gly^3]-des-Pro^3-BPIa lacking the L-proline residue was much weaker than that of the peptides containing the L-proline, BPIa (**1L-L**), **1L-D**, **1D-L**, and **2L**. The CD curves of these analogs and BPIa were measured in water. The results suggested that the bitter taste of BPIa is caused by the spatial structure attributed to the L-proline residue.

BPIa is an extremely bitter peptide isolated by Minamiura *et al.* from cow milk casein hydrolyzate by alkaline proteinase of *Bacillus subtilis*. Its amino acid sequence has been determined to be H–Arg–Gly–Pro–Pro–Phe–Ile–Val–OH (**1L-L**).[3] This peptide has been synthesized by the authors and the threshold value of its bitter taste measured.[4] BPIa was found to be one of the most bitter compounds, which include phenylthiourea and quinine; the threshold value of BPIa was 0.05 mM. To study the relationship between chemical structure and bitter taste of BPIa, we prepared a number of fragments and analogs of it, and compared their taste and CD curves with those of BPIa in the previous paper.[1] The report shows that the spatial structure of BPIa might contribute to its bitter taste.

It is of interest to examine the taste variation of BPIa analogs caused by alteration of the spatial structure of BPIa. Among the constituent amino acids of BPIa, the L-proline residue in the 3- or 4-position seems to be very important in the structure. Therefore, we prepared the analogs containing D-proline or glycine residues in place of L-proline residue. The present paper deals with the syntheses and taste of the BPIa diastereomers (**1L-D**, **1D-L**, and **1D-D**), in which L-prolyl-L-proline in the 3- and 4-positions was replaced by L-prolyl-D-proline, D-prolyl-L-proline, and D-prolyl-D-proline respectively. Further, this paper deals with Des-Pro^3-BPIa (**2L**) in which an L-proline residue of BPIa was missing, and with two analogs of BPIa, in which the remaining L-proline residue of **2L** is replaced by D-proline or glycine residues; these are indicated by **2D** and [Gly^3]-des-Pro^3-BPIa(**3**).

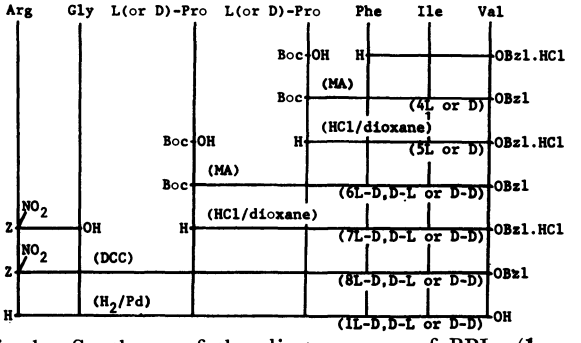

Fig. 1. Syntheses of the diastereomers of BPIa (**1L-D**, **1D-L**, and **1D-D**).

The synthesis of **1L-D** is outlined in Fig. 1. Condensation of Boc–D-Pro–OH with H–Phe–Ile–Val–OBzl·HCl by the mixed anhydride (MA) method gave acyltetrapeptide ester (**4D**). The removal of the Boc group from **4D** with hydrogen chloride in dioxane afforded the corresponding tetrapeptide ester hydrochloride (**5D**). **5D** was coupled with Boc–L-Pro–OH by the MA method to yield acylpentapeptide ester (**6L-D**). It was converted to the corresponding pentapeptide ester hydrochloride (**7L-D**) by the action of hydrogen chloride in dioxane. The protected heptapeptide (**8L-D**) derived from Z–Arg(NO$_2$)–Gly–OH and **7L-D** was hydrogenated in the presence of palladium black to yield the desired product (**1L-D**). A similar procedure was employed for the preparation of **1D-L** and **1D-D**. Des-Pro^3-BPIa (**2L**) and its diastereomer, H–Arg–Gly–D-Pro–Phe–Ile–Val–OH (**2D**), were obtained by hydrogenation of Z–Arg(NO$_2$)–Gly–L(or D)–Pro–Phe–Ile–Val–OBzl (**9L** or **D**) derived from Z–Arg(NO$_2$)–Gly–OH and **5L** or **5D**.

The synthetic procedure of **3** is as follows: Condensation of Boc–Gly–Gly–OH (**10**) with H–Phe–Ile–Val–OBzl·HCl by the MA method gave Boc–Gly–Gly–Phe–Ile–Val–OBzl (**11**). It was converted to the corresponding pentapeptide ester hydrochloride (**12**) by the action of hydrogen chloride in dioxane. Z–Arg(NO$_2$)–OH and **12** were condensed by the MA method to yield the protected hexapeptide, Z–Arg(NO$_2$)–Gly–Gly–Phe–Ile–Val–OBzl (**13**). Hydrogenation of **13** gave H–Arg–Gly–Gly–Phe–Ile–Val–OH (**3**). The homogeneity of the final products was confirmed by paper electrophoresis, amino acid analysis, and elemental

Table 1. The threshold values for bitter taste of BPIa and its analogs

Compounds	Threshold value for bitter taste/mM
Arg–Gly–L-Pro–L-Pro–Phe–Ile–Val(**1L-L**, BPIa)	0.05
Arg–Gly–L-Pro–D-Pro–Phe–Ile–Val (**1L-D**)	0.08
Arg–Gly–D-Pro–L-Pro–Phe–Ile–Val (**1D-L**)	0.11
Arg–Gly–D-Pro–D-Pro–Phe–Ile–Val (**1D-D**)	0.20
Arg–Gly–L-Pro–Phe–Ile–Val (**2L**)	0.05
Arg–Gly–D-Pro–Phe–Ile–Val (**2D**)	0.32
Arg–Gly–Gly–Phe–Ile–Val(**3**)	0.80

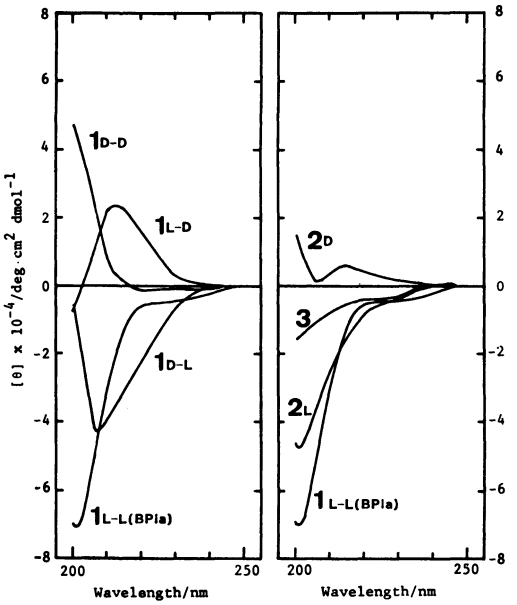

Fig. 2. CD curves of BPIa and its analogs.

analysis.

The taste of the BPIa analogs was organoleptically determined by panel evaluation employing several persons.

The results are listed in the Table. All the synthesized BPIa analogs possessed a bitter taste. The threshold value of BPIa diastereomers shows that the L-proline residue in the 3 position is more necessary for the bitter taste of BPIa than that in the 4-position. The value of **2L** is equal to that of BPIa. However, the bitter taste of **1D-D**, **2D**, and **3** lacking L-proline residue appreciably decreased, compared to that of the peptides containing L-proline residue. This means that L-proline residue is indispensable for the extremely bitter taste of BPIa.

The CD curves of these peptides in water as well as BPIa are shown in Fig. 2. The troughs of **1L-L** and **1D-L** show opposite signs to those of **1D-D** and **1L-D**. **2L** which exhibits the same bitterness as BPIa, has a curve with a negative trough at 202 nm; BPIa possesses a similarly shaped curve. **2D** and **3**, which have much weaker bitterness than BPIa, give different curves. The results of both taste and CD measurements prove that the bitter taste of BPIa is caused by the spatial structure of the molecule attributed to the L-proline residue.

Experimental

All the melting points are uncorrected. The thin layer chromatography was carried out on Merck silica gel G with the solvent systems: R_f^1, 1-butanol–acetic acid–pyridine–water (4 : 1 : 1 : 2, v/v); R_f^2, chloroform–methanol (5 : 1, v/v). Spots of materials possessing a free amino group on a thin layer plate were detected by spraying ninhydrin, and those of amino group blocked materials by spraying 25% hydrogen bromide in acetic acid and then ninhydrin. The optical rotations were measured on a Union PM-101 polarimeter. Amino acid analyses in acid hydrolyzate with 6 M hydrochloric acid (1 M = 1 mol dm^{-3}) at 110 °C for 72 h were performed with a Hitachi amino acid analyzer, KLA-5 type. Molar ratios of amino acids were based on the isoleucine value. Prior to analyses, the compounds were dried over phosphorus pentoxide at 66 °C and 2 mmHg (1 mmHg≈133.322 Pa) for 2 h, except in the case of the peptide ester hydrochlorides.

*Boc-L-Pro-Phe-Ile-Val-OBzl (**4L**).* To a solution of Boc-L-Pro-OH (2.15 g, 10 mmol) and NMM (1.1 ml, 10 mmol) in THF (20 ml), ECF (1.0 ml, 10 mmol) was added at −5 °C with stirring. After 10 min, a solution of H-Phe-Ile-Val-OBzl·HCl[4] (5.04 g, 10 mmol) and NMM (1.1 ml, 10 mmol) in DMF (20 ml) was added to it. The reaction mixture was stored in an ice bath for 1 h and then at room temperature overnight. The mixture was evaporated *in vacuo* and dissolved in ethyl acetate. The solution was washed with 4% sodium hydrogencarbonate, 4% citric acid and water successively, and then dried over anhydrous sodium sulfate. The filtrate was evaporated *in vacuo* and the oily residue was crystallized with ether–petroleum ether: yield 6.06 g (91%); mp 111—112 °C; $[\alpha]_D^{20}$ −83° (*c* 1, methanol); R_f^1 0.98 and R_f^2 0.88.

Found: C, 66.54; H, 8.06; N, 8.37%. Calcd for $C_{37}H_{52}O_7N_4$: C, 66.84; H, 7.88; N, 8.43%.

*Boc-D-Pro-Phe-Ile-Val-OBzl (**4D**).* This was prepared from Boc-D-Pro-OH (2.15 g, 10 mmol) and H-Phe-Ile-Val-OBzl·HCl[4] (5.04 g, 10 mmol) as described above: yield 6.02 g (91%); mp 145—148 °C; $[\alpha]_D^{20}$ −32° (*c* 1, methanol); R_f^1 0.96 and R_f^2 0.78.

Found: C, 66.71; H, 8.11; N, 8.55%. Calcd for $C_{37}H_{52}O_7N_4$: C, 66.84; H, 7.88; N, 8.43%.

*H-L-Pro-Phe-Ile-Val-OBzl·HCl (**5L**).* Compound **4L** (3.32 g, 5 mmol) was dissolved in 4.1 M hydrogen chloride in dioxane (25 ml). The solution was allowed to stand for 1.5 h at room temperature and then evaporated *in vacuo*. The oily residue was solidified by the aid of ether: yield 2.86 g (95%); mp 90 °C (decomp); $[\alpha]_D^{20}$ −66° (*c* 1, methanol); R_f^1 0.88 and R_f^2 0.61.

Found: C, 63.32; H, 7.83; N, 9.11%. Calcd for $C_{32}H_{45}O_5N_4Cl\cdot 1/2\,H_2O$: C, 62.99; H, 7.60; N, 9.18%.

*H-D-Pro-Phe-Ile-Val-OBzl·HCl (**5D**).* This was prepared from **4D** (3.22 g, 5 mmol) as described above: yield 2.67 g (89%); mp 92 °C (decomp); $[\alpha]_D^{20}$ −31° (*c* 1, methanol); R_f^1 0.88 and R_f^2 0.59.

Found: C, 62.72; H, 7.74; N, 8.98%. Calcd for $C_{32}H_{45}O_5N_4Cl\cdot 1/2\,H_2O$: C, 62.99; H, 7.60; N, 9.18%.

*Boc-L-Pro-D-Pro-Phe-Ile-Val-OBzl (**6L-D**).* Boc-L-Pro-OH (0.65 g, 3 mmol) and **5D** (1.80 g, 3 mmol) were coupled by the same method as described for the preparation of **4L**: yield 2.07 g (91%); mp 107 °C; $[\alpha]_D^{20}$ +2° (*c* 1, methanol); R_f^1 0.97 and R_f^2 0.70.

Found: C, 65.92; H, 8.10; N, 9.01%. Calcd for $C_{42}H_{59}O_8N_5$: C, 66.20; H, 7.81; N, 9.19%.

*Boc-D-Pro-L-Pro-Phe-Ile-Val-OBzl (**6D-L**).* Boc-D-Pro-OH (0.65 g, 3 mmol) and **5L** (1.80 g, 3 mmol) were coupled by the same method as described for the preparation of **4L**: yield 1.82 g (80%); mp 68 °C; $[\alpha]_D^{20}$ −50° (*c* 1, methanol); R_f^1 0.94 and R_f^2 0.76.

Found: C, 66.06; H, 8.03; N, 8.98%. Calcd for $C_{45}H_{59}O_8N_5$: C, 66.20; H, 7.81; N, 9.19%.

*Boc-D-Pro-D-Pro-Phe-Ile-Val-OBzl (**6D-D**).* Boc-D-Pro-OH (0.65 g, 3 mmol) and **5D** (1.80 g, 3 mmol) were coupled by the same method as described for the preparation of **4L**: yield 1.60 g (73%); mp 82—84 °C; $[\alpha]_D^{20}$ +10° (*c* 1, methanol); R_f^1 0.97 and R_f^2 0.77.

Found: C, 66.40; H, 7.98; N, 8.83%. Calcd for $C_{42}H_{59}O_8N_5$: C, 66.20; H, 7.81; N, 9.19%.

*H-L-Pro-D-Pro-Phe-Ile-Val-OBzl·HCl (**7L-D**).* Compound **6L-D** (1.52 g, 2 mmol) was treated with hydrogen chloride as described for **5L**: yield 1.33 g (95%); mp 103 °C (decomp); $[\alpha]_D^{20}$ −85° (*c* 1, methanol); R_f^1 0.80 and R_f^2 0.45.

Found: C, 62.74; H, 7.75; N, 9.72%. Calcd for $C_{37}H_{52}O_6N_5Cl \cdot 1/2\ H_2O$: C, 62.82; H, 7.55; N, 9.90%.

*H-D-Pro-L-Pro-Phe-Ile-Val-OBzl·HCl (**7D-L**).* Compound **6D-L** (1.52 g, 2 mmol) was treated with hydrogen chloride as described for **5L**: yield 1.16 g (83%); mp 98 °C (decomp); $[\alpha]_D^{20}$ −73° (*c* 1, methanol); R_f^1 0.81 and R_f^2 0.59.

Found: C, 62.40; H, 7.55; N, 9.51%. Calcd for $C_{37}H_{52}O_6N_5Cl \cdot H_2O$: C, 62.04; H, 7.60; N, 9.78%.

*H-D-Pro-D-Pro-Phe-Ile-Val-OBzl·HCl (**7D-D**).* Compound **6D-D** (1.52 g, 2 mmol) was treated with hydrogen chloride as described for **5L**: yield 1.34 g (96%); mp 115 °C (decomp); $[\alpha]_D^{20}$ −35° (*c* 1, methanol); R_f^1 0.82 and R_f^2 0.62.

Found: C, 62.42; H, 7.60; N, 9.42%. Calcd for $C_{37}H_{52}O_6N_5Cl \cdot H_2O$: C, 62.04; H, 7.60; N, 9.78%.

*Z-Arg(NO2)-Gly-L-Pro-D-Pro-Phe-Ile-Val-OBzl (**8L-D**).* To a solution of Z-Arg(NO_2)-Gly-OH[4] (0.62 g, 1.5 mmol), **7L-D** (1.05 g, 1.5 mmol), and NMM (0.17 ml, 1.5 mmol) in DMF (6 ml), DCC (0.34 g, 1.65 mmol) was added at 0 °C with stirring. The reaction mixture was stirred for 3 h at 0 °C and then at room temperature overnight. DCUrea was filtered off and the filtrate was diluted with ethyl acetate. The solution was washed with 4% sodium hydrogencarbonate, 0.5 M hydrochloric acid, and water successively and then dried over anhydrous sodium sulfate. The filtrate was evaporated *in vacuo* and the residue was collected by the aid of ether. It was recrystallized from methanol–ether: yield 1.22 g (77%); mp 108 °C (decomp); $[\alpha]_D^{20}$ −35° (*c* 1, methanol); R_f^1 0.84 and R_f^2 0.68.

Found: C, 60.17; H, 6.84; N, 14.40%. Calcd for $C_{53}H_{71}O_{12}N_{11}$: C, 60.38; H, 6.79; N, 14.62%.

*Z-Arg(NO2)-Gly-D-Pro-L-Pro-Phe-Ile-Val-OBzl (**8D-L**).* This was prepared from Z-Arg(NO_2)-Gly-OH[4] (0.41 g, 1 mmol) and **7D-L** (0.70 g, 1 mmol) as described above: yield 0.72 g (68%); mp 118 °C (decomp); $[\alpha]_D^{20}$ −62° (*c* 1, methanol), R_f^1 0.87 and R_f^2 0.69.

Found: C, 60.08; H, 6.81; N, 14.48%. Calcd for $C_{53}H_{71}O_{12}N_{11}$: C, 60.38; H, 6.79; N, 14.62%.

*Z-Arg(NO2)-Gly-D-Pro-D-Pro-Phe-Ile-Val-OBzl (**8D-D**).* This was prepared from Z-Arg(NO_2)-Gly-OH[4] (0.62 g, 1.5 mmol) and **7D-D** (1.05 g, 1.5 mmol) as described above: yield 1.10 g (70%); mp 118 °C (decomp); $[\alpha]_D^{20}$ +16° (*c* 1, methanol); R_f^1 0.86 and R_f^2 0.64.

Found: C, 60.09; H, 6.79; N, 14.34%. Calcd for $C_{53}H_{71}O_{12}N_{11}$: C, 60.38; H, 6.79; N, 14.62%.

*H-Arg-Gly-L-Pro-D-Pro-Phe-Ile-Val-OH·AcOH (**1L-D**).* Compound **8L-D** (0.32 g, 0.3 mmol) was dissolved in a mixture of methanol (3 ml) and acetic acid (3 ml) and hydrogenated in the presence of palladium black for 24 h at room temperature. The filtrate from catalyst was evaporated *in vacuo* and the residual oil was solidified by the aid of acetone. The product was recrystallized from methanol–ether: yield 0.20 g (79%); $[\alpha]_D^{20}$ −16° (*c* 1, H_2O); R_f^1 0.68 and R_f^2 0.00. Amino acid ratios in acid hydrolyzate: Arg 0.96, Gly 1.00, Pro 2.06, Phe 1.03, Ile 1.00, Val 0.99.

Found: C, 56.35; H, 7.79; N, 16.13%. Calcd for $C_{38}H_{60}O_8N_{10} \cdot CH_3COOH \cdot 1/2\ H_2O$: C, 56.25; H, 7.75; N, 16.40%.

*H-Arg-Gly-D-Pro-L-Pro-Phe-Ile-Val-OH·AcOH (**1D-L**).* Compound **8D-L** (0.32 g, 0.3 mmol) was hydrogenated as described above: yield 0.19 g (73%); $[\alpha]_D^{20}$ −24° (*c* 1, H_2O); R_f^1 0.69 and R_f^2 0.00. Amino acid ratios in acid hydrolyzate: Arg 1.02, Gly 1.16, Pro 2.31, Phe 1.21 Ile 1.00, Val 0.98.

Found: C, 55.17; H, 7.70; N, 15.96%. Calcd for $C_{38}H_{60}O_8N_{10} \cdot CH_3COOH \cdot 3/2\ H_2O$: C, 55.09; H, 7.74; N, 16.06%.

*H-Arg-Gly-D-Pro-L-Pro-Phe-Ile-Val-OH·AcOH (**1D-D**).* Compound **8D-D** (0.32 g, 0.3 mmol) was hydrogenated as described above: yield 0.16 g (62%); $[\alpha]_D^{20}$ +78° (*c* 1, H_2O); R_f^1 0.62 and R_f^2 0.00. Amino acid ratios in acid hydrolyzate: Arg 0.86, Gly 1.09, Pro 2.18, Phe 1.20, Ile 1.00, Val 0.97.

Found: C, 55.80; H, 7.74; N, 15.90%. Calcd for $C_{38}H_{60}O_8N_{10} \cdot CH_3COOH \cdot H_2O$: C, 55.67; H, 7.71; N, 16.23%.

*Z-Arg(NO2)-Gly-L-Pro-Phe-Ile-Val-OBzl (**9L**).* To a solution of Z-Arg(NO_2)-Gly-OH[4] (0.41 g, 1 mmol) and NMM (0.11 ml, 1 mmol) in THF (2 ml), ECF (0.1 ml, 1 mmol) was added at −5 °C with stirring. After 10 min, a solution of **5L** (0.60 g, 1 mmol) and NMM (0.11 ml, 1 mmol) in THF (2 ml) was added to it. The reaction mixture was stored in an ice bath for 1 h and then at room temperature overnight. The mixture was evaporated *in vacuo* and the residue was solidified with water. It was filtered, washed with 4% sodium hydrogencarbonate, 0.5 M hydrochloric acid, and water successively, and dried. The product was dissolved in methanol and collected by the aid of ethyl acetate: yield 0.72 g (75%); mp 175—180 °C; $[\alpha]_D^{20}$ −24° (*c* 1, DMF); R_f^1 0.88 and R_f^2 0.74.

Found: C, 60.12; H, 6.74; N, 14.52%. Calcd for $C_{48}H_{64}O_{11}N_{10}$: C, 60.23; H, 6.74; N, 14.64%.

*Z-Arg(NO2)-Gly-D-Pro-Phe-Ile-Val-OBzl (**9D**).* This was prepared from Z-Arg(NO_2)-Gly-OH[4] (0.62 g, 1.5 mmol) and **5D** (0.90 g, 1.5 mmol) as described for **8L-D**: yield 1.10 g (77%); mp 175 °C (decomp); $[\alpha]_D^{20}$ +3° (*c* 1, DMF); R_f^1 0.96 and R_f^2 0.78.

Found: C, 59.78; H, 6.84; N, 14.89%. Calcd for $C_{48}H_{64}O_{11}N_{10}$: C, 60.23; H, 6.74; N, 14.64%.

*H-Arg-Gly-L-Pro-Phe-Ile-Val-OH·AcOH (**2L**).* Compound **9L** (0.52 g, 0.5 mmol) was hydrogenated as described for **1L-D**: yield 0.27 g (69%); $[\alpha]_D^{20}$ −114° (*c* 1, H_2O); R_f^1 0.74 and R_f^2 0.00. Amino acid ratios in acid hydrolyzate: Arg 0.91, Gly 1.02, Pro 0.98, Phe 1.00, Ile 1.00, Val 1.13.

Found: C, 55.21; H, 7.95; N, 16.81%. Calcd for $C_{33}H_{53}O_7N_9 \cdot CH_3COOH \cdot 1/2\ H_2O$: C, 55.53; H, 7.72; N, 16.66%.

*H-Arg-Gly-D-Pro-Phe-Ile-Val-OH·AcOH (**2D**).* Compound **9D** (0.29 g, 0.3 mmol) was hydrogenated as described for **1L-D**: yield 0.16 g (69%); $[\alpha]_D^{20}$ +19° (*c* 1, H_2O); R_f^1 0.68 and R_f^2 0.00. Amino acid ratios in acid hydrolyzate: Arg 0.90, Gly 1.19, Pro 1.03, Phe 1.11, Ile 1.00, Val 1.00.

Found: C, 55.94; H, 8.00; N, 16.69%. Calcd for $C_{33}H_{53}O_7N_9 \cdot CH_3COOH$: C, 56.21; H, 7.68; N, 16.86%.

*Boc-Gly-Gly-OH (**10**).* A solution of Boc-Gly-Gly-OBzl[5] (3.22 g, 10 mmol) in methanol (30 ml) was hydrogenated in the presence of palladium black for 10 h. The catalyst was filtered off and the filtrate was evaporated *in vacuo*. The residue was collected by the aid of ether. It was recrystallized from ethanol–ether: yield 2.21 g (95%); mp 136 °C; R_f^1 0.75 and R_f^2 0.40.

Found: C, 46.75; H, 6.95; N, 12.00%. Calcd for $C_9H_{16}O_5N_2$: C, 46.54; H, 6.94; N, 12.06%.

*Boc-Gly-Gly-Phe-Ile-Val-OBzl (**11**).* This was prepared from **10** (0.70 g, 3 mmol) and H-Phe-Ile-Val-OBzl·HCl[4] (1.51 g, 3 mmol) as described for the preparation of **4L**. The product was recrystallized from ethanol–ether: yield 1.79 g (87%); mp 209 °C; $[\alpha]_D^{20}$ −14° (*c* 1, DMF); R_f^1 0.96 and R_f^2 0.65.

Found: C, 63.13; H, 7.56; N, 10.27%. Calcd for $C_{36}H_{51}O_8N_5$: C, 63.41; H, 7.54; N, 10.27%.

*H-Gly-Gly-Phe-Ile-Val-OBzl·HCl (**12**).* Compound **11** (1.36 g, 2 mmol) was treated with hydrogen chloride as described for the preparation of **5L**: yield 1.31 g (98%); mp 227 °C; $[\alpha]_D^{20}$ −23° (*c* 1, DMF); R_f^1 0.76 and R_f^2 0.17.

Found: C, 59.06; H, 7.19; N, 11.03%. Calcd for $C_{31}H_{44}O_6N_5Cl \cdot 1/2\ H_2O$: C, 59.36; H, 7.23; N, 11.17%.

*Z-Arg(NO2)-Gly-Gly-Phe-Ile-Val-OBzl (**13**).* This was prepared from Z-Arg(NO_2)-OH (0.71 g, 2 mmol) and **12** (1.0 g, 1.6 mmol) as described for the preparation of **4L**. The product was recrystallized from ethanol–ether: yield 1.10 g

(75%); mp 139—140 °C; $[\alpha]_D^{20}$ −11° (*c* 1, DMF); R_f^1 0.98 and R_f^2 0.51.

Found: C, 58.65; H, 6.63; N, 15.04%. Calcd for $C_{45}H_{60}O_{11}N_{10}$: C, 58.94; H, 6.60; N, 15.04%.

H–Arg–Gly–Gly–Phe–Ile–Val–OH·AcOH (3). Compound **13** (0.92 g, 1.02 mmol) was hydrogenated as described for **1**L-D: yield 0.64 g (91%); $[\alpha]_D^{20}$ −19° (*c* 1, H_2O); R_f^1 0.74 and R_f^2 0.00. Amino acid ratios in acid hydrolyzate: Arg 0.85, Gly 2.25, Phe 0.92, Ile 1.00, Val 1.03.

Found: C, 53.85; H, 7.85; N, 17.95%. Calcd for $C_{30}H_{49}O_7N_9 \cdot CH_3COOH \cdot 1/2\ H_2O$: C, 53.85; H, 7.59; N, 17.95%.

Paper Electrophoresis. This was carried out under the following conditions: paper, Toyo Roshi No. 51A chromatography paper; solvent, pyridine–acetic acid–water (10 : 0.4 : 90, v/v) (pH 6.4); voltage gradient, 15 V/cm; charge period, 2.5 h. Electrophoretic mobilities were recorded as R_{Arg}, the ratio of the distance the compounds moved to that which a standard arginine spot moved on the same electrophoreogram. The compounds (**1**, **2**, and **3**) migrated toward the cathode and revealed a single spot by spraying Sakaguchi reagent; ninhydrin gave the same result. The R_{Arg} value of each compound was 0.72.

CD Measurements. This was performed with a JASCO J-20 A. A cell of path length 0.2 mm was used. Patterns in water are shown in Fig. 2.

Sensory Test. Taste of the peptides was organoleptically determined by panel evaluation employing four people. A series of solutions of decreasing concentration, each half as strong as the proceeding one, were prepared. Before tasting the sample, the mouth was thoroughly rinsed with deionized water. The sample solution was held in the mouth for *ca.* 10 s and then spit out and the threshold value was determined. The results are listed in the Table.

The authors wish to express their thanks to Associate Professor Michio Kondo of Saga University for the CD measurements. Thanks are also due to Dr. Shinji Okumura of Ajinomoto Co., Inc., for supplying some amino acids.

References

1) Part II. K. Otagiri, I. Miyake, N. Ishibashi, H. Fukui, H. Kanehisa, and H. Okai, *Bull. Chem. Soc. Jpn.*, **56**, 1116 (1983).

2) The abbreviations recommended by IUPAC-IUB commission of Biochemical Nomenclature (*J. Biol. Chem.*, **247**, 977 (1972)) have been used. Amino acid symbols except glycine denoted the L-configuration unless otherwise noted. Additional abbreviations: AcOH, acetic acid; DCC, dicyclohexylcarbodiimide; DCUrea, *N,N'*-dicyclohexylurea; DMF, *N,N*-dimethylformamide; ECF, ethyl chloroformate; NMM, *N*-methylmorpholine; THF, tetrahydrofuran.

3) N. Minamiura, Y. Matsumura, J. Fukumoto, and T. Yamamoto, *Agric. Biol. Chem.*, **36**, 588 (1972).

4) Part I. H. Fukui, H. Kanehisa, N, Ishibashi, I. Miyake, and H. Okai, *Bull. Chem. Soc. Jpn.*, **56**, 766 (1983).

5) V. M. Kozhukhouskaya, S. D. Luova, and R. P. Evstigneeva, *Khim. Prir. Soedin.*, **6**, 599 (1970).

Reaction of Secondary Aromatic Amines with Manganese(III) Acetate

Hiroshi Nishino* and Kazu Kurosawa
Department of Chemistry, Faculty of Science, Kumamoto University, Kurokami 2-39-1, Kumamoto 860
(Received November 18, 1982)

The reaction of 2-(methylamino)benzophenone with manganese(III) acetate afforded 5-[(*o*-benzoylanilino)-methyl]-2-(methylamino)benzophenone, 2-aminobenzophenone, 5-formyl-2-(methylamino)benzophenone, 2-amino-5-[(*o*-benzoylanilino)methyl]benzophenone, 2-formamidobenzophenone, 2-amino-5-formylbenzophenone, and 2-(*N*-methylformamido)benzophenone. It was found that the reaction did not cause oxidative cyclization, but dimerization and conversion of *N*-methyl into *N*-formyl groups. Characterization of the products, the detailed oxidation mechanism, and the effects of the additives are discussed.

It is well known that oxidation of amino compounds with metal salts such as Hg(II), Cu(II), Co(III), Pb(IV), Ce(IV), *etc.* causes metal complex formation, *N*-acylation, *N*-dealkylation, *N,N*-coupling, and cyclization reactions. However, reaction of these compounds with manganese(III) acetate has been scarcely investigated except for the oxidation of *N,N*-dialkylarylamines.[1-3] In connection with our studies on the reaction of manganese(III) acetate with various organic substrates, we decided to investigate in detail the reaction of amino compounds, especially primary and secondary amines, with manganese(III) acetate in acetic acid.

We have previously reported that reaction of some phenolic compounds having an unsaturated side chain or aroyl group with manganese(III) acetate gave cyclic ethers in moderate yields.[4-9] We were interested in the reaction of analogous amines which may give cyclic amines because amino groups have reactivities similar to those of hydroxyl groups. We employed 2-(methylamino)benzophenone (**1**) as an amino compound whose amino group was located in a position suitable for forming a nitrogen containing six membered ring. As the result it was observed that this compound did not undergo the intramolecular oxidative cyclization, but was oxidized to give formamides in higher oxidant/substrate ratio, and dimeric compounds in lower oxidant/substrate ratio which were readily hydrolyzed to yield benzaldehydes and amines. We will describe in the present paper the detailed oxidation mechanism for the secondary amine (**1**), the effect of additives, and the synthetic application of the conversion of *N*-methyl into *N*-formyl group.

Results and Discussion

The 2-(methylamino)benzophenone (**1**) was oxidized with from one-half to eight molar equivalents of manganese(III) acetate in acetic acid at 100 °C or reflux temperature and the products were separated by TLC. The reaction conditions and the yields are summarized in Table 1.

Oxidation of **1** with one-half or one molar equivalent of manganese(III) acetate gave 5-[(*o*-benzoylanilino)-methyl]-2-(methylamino)benzophenone (**2**), 2-aminobenzophenone (**3**), and 5-formyl-2-(methylamino)benzophenone (**4**) (Table 1, Entries 1 and 2). The mass spectrum of **2** showed a parent ion peak at *m/e* 420, indicating that this product was a dimeric compound. Its NMR spectrum revealed two doublets at δ=2.88 (3H, J=4.8 Hz) and 4.26 (2H, J=4.8 Hz) for a methyl and a methylene group both coupled with an amino hydrogen, a multiplet at δ=6.34—7.66 for seventeen aromatic protons, and a broad quartet and

Table 1. Oxidation of 2-(methylamino)benzophenone (**1**) with manganese(III) acetate in acetic acid at 100 °C

Entry	Reaction conditions: Molar ratio of **1** : Oxidant	Reaction conditions: Time/min	Recovery/%	Product (yield/%)[a]: **2**	**3**	**4**	**5**	**6**	**7**	**8**	**9**	**10**
1	1 : 0.5	6	60	5	8	1						
2	1 : 1	7	32	10	10	6						
3	1 : 2	7	6	4	12	8	3	4	2	5		
4[b]	1 : 2	7	4	2	30	10	2	3	2	4		
5[c]	1 : 4	5	Trace		18			42	5	6		
6[b,c]	1 : 4	5	3		31			44	7	5		
7[c]	1 : 6	12	Trace		6			65	6	4		
8[c]	1 : 8	25	Trace		3			59	5	5		
9[d]	1 : 2	6	2	2	8	6	2	4	2	24		
10[e]	1 : 2	7	3	1	5	6				5	52	6
11[f]	1 : 2	7	2	1	24	5	1	5	3	5		

a) The yields were based on the substrate used. b) The reaction was carried out under nitrogen atmosphere. c) The reaction was conducted at reflux temperature. d) Formaldehyde (1 mmol) was added. e) Acetic anhydride (4 mmol) was added. f) Water (3 mmol) was added.

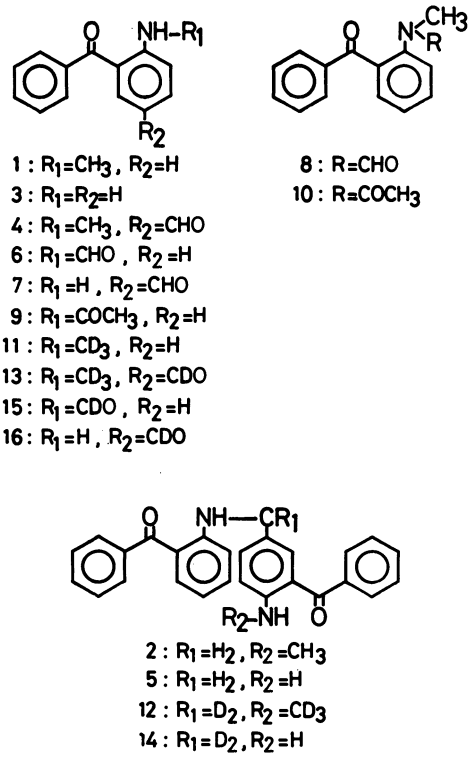

Fig. 1. 2-(Methylamino)benzophenones (**1** and **11**) and the oxidation products (**2**—**10** and **12**—**16**).

triplet at δ=8.43 (1H, J=4.8 Hz) and 8.74 (1H, J=4.8 Hz) for amino groups. The IR spectrum indicated a strong carbonyl absorption band at 1625 cm^{-1} and a broad weak absorption band at 3200—3400 cm^{-1} due to amino groups. Therefore, this spectroscopic evidence supported the structure of 5-[(*o*-benzoylanilino)methyl]-2-(methylamino)benzophenone. The product **3** was identical with an authentic sample. The NMR spectrum of **4** showed the presence of a formyl group at δ=9.61 (1H, s), and an ABX pattern of the aromatic protons at δ=6.82 (1H, d, J=9.0 Hz), 7.88 (1H, dd, J=9.0 and 1.8 Hz), and 7.94 (1H, d, J=1.8 Hz), besides a methylamino group and a phenyl group. The IR spectrum of **4** showed absorption bands at 1615, 1695, and 3300—3500 cm^{-1} due to two carbonyls, and an amino group. Accordingly, the structure of **4** was considered to be 5-formyl-2-(methylamino)benzophenone.

The compound **1** was oxidized with two molar equivalents of manganese(III) acetate to yield **2**, **3**, **4**, 2-amino-5-[(*o*-benzoylanilino)methyl]benzophenone (**5**), 2-formamidobenzophenone (**6**), and 2-amino-5-formylbenzophenone (**7**) (Table 1, Entry 3). The NMR spectrum of **5** was similar to that of **2** except for the absence of a methyl group and the appearance of a primary amino group instead of a secondary amino group. Since the molecular ion peak showed at m/e 406 in its mass spectrum, this product was deduced to be 2-amino-5-[(*o*-benzoylanilino)methyl]benzophenone which was formed by the *N*-demethylation of **2**. In the IR spectrum of **6** two carbonyls and a broad amino absorption appeared at 1640, 1710, and 3100—3600 cm^{-1}. The NMR spectrum of **6** revealed the presence of a formamido group at δ=8.40 (1H, br. s, CHO) and 10.60 (1H, br. s, –NH–). In addition, **6** was hydrolyzed with dil H_2SO_4 at reflux temperature to afford **3** (89%). Therefore, the structure of **6** was confirmed to be 2-formamidobenzophenone. The NMR spectrum of **7** which was an isomer of **6** was analogous to that of **4**, although an amino group was present instead of a methylamino group. Accordingly the structure of **7** was considered to be 2-amino-5-formylbenzophenone which is compatible both with the IR and mass spectra.

Using from four to eight molar equivalents of manganese(III) acetate, four products were obtained; these were determined to be **3**, **6**, **7**, and 2-(*N*-methylformamido)benzophenone (**8**) (Table 1, Entries 5, 7, and 8). The product (**8**) was obtained as pale yellow crystals, mp 96 °C. It showed a parent ion peak at m/e 239 in the mass spectrum, and a strong IR absorption band at 1695 cm^{-1} in chloroform. The NMR spectrum showed the presence of a methyl group (δ=3.00) and a formyl group (δ=8.10). However, the IR and NMR spectra revealed the absence of an amino hydrogen. Accordingly, this evidence suggested that the structure was 2-(*N*-methylformamido)benzophenone.

When **1** was oxidized using six molar equivalents of manganese(III) acetate at reflux temperature, **6** was obtained in the highest yield (65%) for this oxidation reaction. Since in higher oxidant/substrate ratio other products were formed only in small amounts, this reaction may be a useful method for the conversion of *N*-methyl into *N*-formyl compounds.

We then investigated how additions of formaldehyde,[1] acetic anhydride,[10] and/or water[11] influence the product distribution. Addition of formaldehyde to the reaction mixture increased the yield of the *N*-methylformamide (**8**) five times, while the yield of the formamide **6** was not changed (Table 1, Entry 9). When four molar equivalents of acetic anhydride were added, formation of the formamide (**6**) was completely inhibited and acetamides (**9** and **10**) were newly produced; these were identical with compounds obtained by an alternative synthesis (Table 1, Entry 10). The formation of **9** was explained in terms of oxidative *N*-demethylation of tertiary aromatic amines.[2,3,12,13] The product yields

Table 2. Oxidation of 2-(methyl-d_3-amino)benzophenone (**11**) with manganese(III) acetate in acetic acid at 100 °C

Entry	Reaction conditions: Molar ratio of **11**: Oxidant	Reaction conditions: Time / min	Recovery / %	Product (yield/%)[a] **3**	**12**	**13**	**14**	**15**	**16**
1	1 : 2	7	5	14	7	6	4	4	1
2	1 : 4	22	Trace	17	Trace	2		34	7

a) The yields were based on the substrate used.

Table 3. Oxidation of the prodcuts (2—5) with manganese (III)acetate in acetic acid at 100 °C

Entry	Substrate	Reaction conditions: Molar ratio of Substrate : Oxidant	Reaction conditions: Time / min	Recovery / %	Product (yield/%)[a] 2	3	4	5	7	9
1	**2**	1 : 1	4	30		59	52		6	
2	**2**	1 : 2	6	11		67	76		17	
3	**1** and **3**	(1 : 1) : 1	5	47 and 93[b]	7			4		
4	**1** and **3**	(1 : 1) : 2	7	18 and 84[b]	9		1	7	8	
5	**4**	1 : 2	6	28					35	
6	**4**	1 : 4	33	2					37	
7	**3**	1 : 2	15	46						5
8	**3**	1 : 4	15	12						7
9	**5**	1 : 2	5	5		77			84	

a) The yields were based on the substrate used. b) The recoveries correspond to that of **1** and **3**, respectively.

were not appreciably changed by addition of water (3 equiv.) except for **3** (Table 1, Entry 11).

In order to elucidate the reaction mechanism, we prepared and oxidized deuterated 2-(methyl-d_3-amino)-benzophenone (**11**). The reaction conditions and the yields are shown in Table 2.

When **11** was oxidized with two molar equivalents of manganese(III) acetate in acetic acid at 100 °C, **3**, 5-[(*o*-benzoylanilino)methyl-d_2]-2-(methyl-d_3-amino)-benzophenone (**12**), 5-(formyl-*d*)-2-(methyl-d_3-amino)-benzophenone (**13**), 2-amino-5-[(*o*-benzoylanilino)methyl-d_2]benzophenone (**14**), 2-(formyl-*d*-amino)benzophenone (**14**), 2-(formyl-*d*-amino)benzophenone (**15**), and 2-amino-5-(formyl-*d*)benzophenone (**16**) were obtained. This experiment proved that the formyl group of the products, **13** and **16**, must come from the *N*-methyl group. Therefore, it suggests that the precursors of the benzaldehydes **4** or **7** must be the dimeric compound **2** or **5**, respectively. Manganese(III) acetate oxidation was then carried out for **2** and **5**, to confirm the above facts. These oxidations gave the corresponding benzaldehydes (**4** and **7**) and amine (**3**) in good yields as expected (Table 3, Entries 1, 2, and 9). The product (**4**) was also oxidized by manganese(III) acetate to **7** by the oxidative *N*-demethylation (Table 3, Entries 5 and 6).

It was thought that the dimeric compound (**5**) might

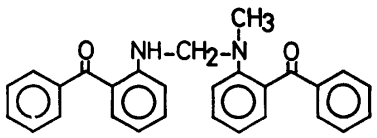

IV

Fig. 2. Dimeric intermediate (**IV**).

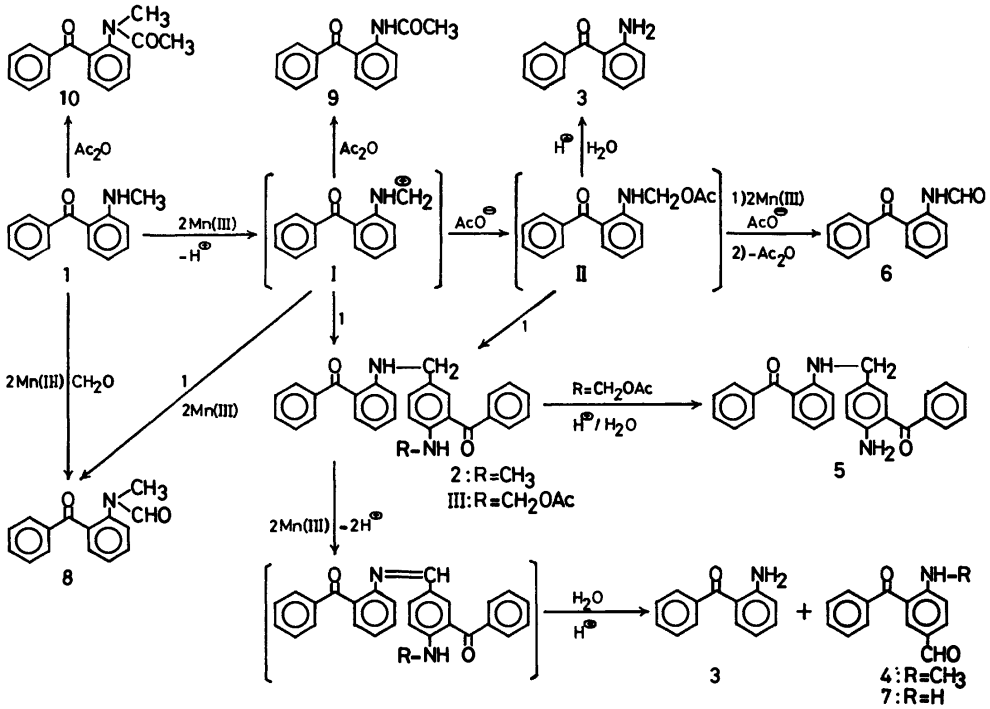

Scheme 1. Oxidation mechanism of 2-(methylamino)benzophenone (**1**) by manganese(III) acetate.

be formed by reaction between the intermediate carbenium cation (**I**) (formed by the oxidation of **1** with manganese(III) acetate) and the amine (**3**), presumably generated by the oxidative *N*-demethylation of **1**. However, oxidation of a 1 : 1 mixture of **1** and **3** under the above conditions gave **5** (Table 3, Entries 3 and 4) in a yield similar to that in the reaction of **1** alone (Table 1, Entry 3). This suggests that primary amines did not exist in the reaction mixture, but were formed during the work-up. We suggest that 2-(acetoxymethylamino)benzophenone (**II**) was produced from the carbenium ion (**I**) by the attack of an acetate ion. It reacted with **I** to give the dimeric compound (**III**), which was hydrolyzed to yield **5** and/or further oxidized to afford **3** and **7** during the work-up.

Reaction of the primary amine (**3**) with manganese(III) acetate gave 2-acetamidobenzophenone (**9**) as the only isolable reaction product (Table 3, Entries 7 and 8).

The mechanism for the formation of the formamide (**6**) can be explained by assuming that the intermediate (**II**) was further oxidized to **6**, since the deuterated isomer (**15**) was obtained from the oxidation of **11** and the yield of **6** was scarcely changed on oxidation of **1** under nitrogen atmosphere (Table 1, Entries 4 and 6). Formation of *N*-methylformamide (**8**), however, might be due to the reaction of **1** with formaldehyde which was produced in the reaction (**II**→**6**), since the yield of **8** was increased by the addition of formaldehyde to the reaction mixture. Alternatively, the intermediate carbenium cation (**I**) might react with the amino group of **1** to give **8** *via* an analogous dimeric intermediate (**IV**). In either event these alternative pathways could not be distinguished. The above reaction mechanism is outlined in Scheme 1.

It is characteristic of this reaction that the use of lower oxidant/substrate ratio induces dimerization, leading to aldehydes and amines. On the other hand, conversion of *N*-methyl into *N*-formyl compounds occurs preferentially at higher oxidant/substrate ratios. By contrast, however, it was found that oxidation of aromatic secondary amines with lead(IV) acetate in chloroform caused *N*-dealkylation and nuclear acetoxylation.[14] The conversion of *N*-methyl into *N*-formyl group by means of manganese(III) acetate can be useful in organic synthesis.

Experimental

Measurements. The IR spectra were measured on a JASCO IRA-1 grating spectrometer. The ^{1}H-NMR spectra were recorded on a Hitachi Perkin-Elmer R-24 spectrometer (60 MHz) with tetramethylsilane as an internal standard; the chemical shifts are reported in δ values. The mass spectra were obtained with a JEOL JMS-DX300 mass spectrometer. The HPLC analyses were performed on an ALTEX model 330/110A/153 isocratic liquid chromatograph equipped with a HY-ODS-5U column, eluting with methanol or 70% aqueous methanol. The melting points were taken on a Yanagimoto micromelting point apparatus and are uncorrected.

Preparation of the Materials. 2-(Methylamino)benzophenone (**1**) was synthesized by the methylation of 2-aminobenzophenone which was obtained from the commercial sample of Wako Pure Chemical Industries, Ltd. The 2-aminobenzophenone (10 mmol) was heated under reflux for 12 h with dimethyl sulfate (15 mmol) in dry acetone (50 ml) containing anhydrous potassium carbonate (2 g). The solvent was removed *in vacuo* and the residue was triturated with water. The aqueous reaction mixture was extracted with chloroform, followed by column chromatography on silica gel (Wakogel C-100) using chloroform as eluent to give **1** (55%); yellow needles (from hexane), mp 68.5 °C (lit,[15] mp 69 °C); IR ($CHCl_3$) 1620 (C=O) and 3250—3400 cm^{-1} (NH); NMR ($CDCl_3$) δ=2.91 (3H, s, CH_3), 6.34—7.69 (9H, m, aromatic), 8.47 (1H, br. s, NH). Found: C, 79.41; H, 6.18; N, 6.41%. Calcd for $C_{14}H_{13}ON$: C, 79.59; H, 6.20; N, 6.63%.

2-(Methyl-d_3-amino)benzophenone (**11**) was also obtained from the same methylation of the 2-aminobenzophenone with dimethyl-d_6 sulfate which was available from E. Merck AG.; 43%; yellow needles (from hexane), mp 69.0—69.5 °C; IR ($CHCl_3$) 1620 (C=O) and 3250—3600 cm^{-1} (NH); NMR ($CDCl_3$) δ=6.32—7.72 (9H, m, aromatic), and 8.48 (1H, br. s, NH). Found: C, 78.46; H+D/2, 6.19; N, 6.51%. Calcd for $C_{14}H_{10}D_3ON$: C, 78.47; H+D/2, 6.11; N, 6.54%.

*Oxidation of **1** and **11**.* The compound **1** (1 mmol) was dissolved in acetic acid (25 ml) and suitable amounts of manganese(III) acetate dihydrate[16] were added. The mixture was heated on a water bath until the brown color of Mn(III) ion disappeared (see Table 1). The solvent was removed *in vacuo* and the residue was triturated with 2 M (1 M = 1 mol dm^{-3}) hydrochloric acid (25 ml), followed by extraction with chloroform. The products were separated on TLC (Wakogel B-10) with chloroform as the developing solvent, and simultaneously tested by HPLC. The deuterated compound **11** (1 mmol) was also oxidized by the procedure described above. It was found that substantial quantities of unidentified tarry materials were formed in both reaction mixture besides the isolated products.

*Oxidation Products of **1**.* *5-[(o-Benzoylanilino)methyl]-2-(methylamino)benzophenone (**2**)*: Yellow liquid; IR ($CHCl_3$) 1625 (C=O) and 3200—3400 cm^{-1} (NH); NMR ($CDCl_3$) δ=2.88 (3H, d, J=4.8 Hz, CH_3), 4.26 (2H, d, J=4.8 Hz, $-CH_2-$), 6.34—7.66 (17H, m, aromatic), 8.43 (1H, q, J=4.8 Hz, –NH–), and 8.74 (1H, t, J=4.8 Hz, –NH–); MS *m/e* (rel intensity), 420 (M^+, 22), 405 (4), 239 (3), 224 (100), 196 (6), 180 (2), 146 (5), 132 (2), 118 (3), 105 (10), 91 (9), and 77 (23). Found: *m/e* 420.19424. Calcd for $C_{28}H_{24}O_2N_2$: M, 420.18378.

*2-Aminobenzophenone (**3**)*: Yellow needles (from hexane), mp 105—106 °C (lit,[17] mp 107 °C).

*5-Formyl-2-(methylamino)benzophenone (**4**)*: Pale yellow needles (from hexane), mp 136 °C; IR ($CHCl_3$) 1615 and 1695 (C=O), and 3300—3500 cm^{-1} (NH); NMR ($CDCl_3$) δ=3.05 (3H, d, J=5.4 Hz, CH_3), 6.82 (1H, d, J=9.0 Hz, $H_{(3)}$), 7.4—7.7 (5H, m, aromatic), 7.88 (1H, dd, J=9.0 and 1.8 Hz, $H_{(4)}$), 7.94 (1H, d, J=1.8 Hz, $H_{(6)}$), 9.20 (1H, br. s, –NH–), and 9.61 (1H, s, CHO); MS *m/e* (rel intensity), 239 (M^+, 100), 238 (70), 210 (5), 134 (6), 105 (16), 91 (5), and 77 (30). Found: C, 75.28: H, 5.50; N, 5.83%. Calcd for $C_{15}H_{13}O_2N$: C, 75.30; H, 5.48; N, 5.85%.

*2-Amino-5-[(o-benzoylanilino)methyl]benzophenone (**5**)*: Yellow liquid; IR ($CHCl_3$) 1625 (C=O) and 3320—3480 cm^{-1} (NH); NMR ($CDCl_3$) δ=4.26 (2H, d, J=4.2 Hz, $-CH_2-$), 6.04 (2H, br. s, NH_2), 6.39—7.67 (17H, m, aromatic), and 8.76 (1H, br. s, –NH–); MS *m/e* (rel intensity), 406 (M^+, 23), 210 (100), 196 (71), 132 (16), 120 (32), 105 (25), 92 (20), and 77 (44). Found: *m/e* 406.16058. Calcd for $C_{27}H_{22}O_2N_2$: M, 406.16813.

*2-Formamidobenzophenone (**6**)*: Pale yellow liquid; IR ($CHCl_3$) 1640 and 1710 (C=O), and 3100—3600 cm^{-1} (NH); NMR ($CDCl_3$) δ=6.90—8.67 (9H, m, aromatic), 8.40 (1H, br. s, CHO), and 10.60 (1H, br. s, –NH–); MS *m/e* (rel intensity), 225 (M^+, 38), 196 (100), 120 (7), 105 (17), and 77

(23). Found: *m/e* 225.08177. Calcd for $C_{14}H_{11}O_2N$: M, 225.07898.

2-Amino-5-formylbenzophenone (7): Pale yellow crystals (from benzene/hexane), mp 131—132 °C; IR ($CHCl_3$) 1615 and 1700 (C=O), and 3320—3490 cm^{-1} (NH); NMR ($CDCl_3$) δ= 6.76 (1H, d, J=8.4 Hz, $H_{(3)}$), 6.95 (2H, br. s, NH_2), 7.25—8.05 (5H, m, aromatic), 7.72 (1H, dd, J=8.4 and 1.8 Hz, $H_{(4)}$), 7.88 (1H, d, J=1.8 Hz, $H_{(6)}$), and 9.56 (1H, s, CHO); MS *m/e* (rel intensity), 225 (M^+, 97), 224 (100), 208 (5), 196 (14), 148 (25), 120 (11), 105 (25), and 77 (32). Found: C, 74.82; H, 4.97; N, 6.02%. Calcd for $C_{14}H_{11}O_2N$: C, 74.65; H, 4.92; N, 6.22%.

2-(N-Methylformamido)benzophenone (8): Pale yellow crystals (from benzene/hexane), mp 96 °C; IR ($CHCl_3$) 1695 cm^{-1} (C=O); NMR ($CDCl_3$) δ=3.00 (3H, s, CH_3), 7.18—7.95 (9H, m, aromatic), and 8.10 (1H, s, CHO); MS *m/e* (rel intensity), 239 (M^+, 27), 210 (100), 194 (92), 134 (92), 105 (47), and 77 (100). Found: *m/e* 239.09281. Calcd for $C_{15}H_{13}O_2N$: M, 239.09463.

Oxidation Products of 11. *5-[(o-Benzoylanilino)methyl-d_2]-2-(Methyl-d_3-amino)benzophenone (12)*: Yellow liquid; IR ($CHCl_3$) 1625 (C=O) and 3200—3600 cm^{-1} (NH); NMR ($CDCl_3$) δ=6.36—7.61 (17H, m, aromatic), 8.41 (1H, br. s, –NH–), and 8.74 (1H, br. s, –NH–); MS *m/e* (rel intensity), 425 (M^+, 20), 229 (100), 151 (20), 105 (22), and 77 (45).

5-(Formyl-d)-2-(methyl-d_3-amino)benzophenone (13): Yellow needles (from hexane), mp 136 °C; IR ($CHCl_3$) 1610 and 1675 (C=O), and 3150—3600 cm^{-1} (NH); NMR ($CDCl_3$) δ=6.83 (1H, d, J=9.0 Hz, $H_{(3)}$), 7.25—7.68 (5H, m, aromatic), 7.88 (1H, dd, J=9.0 and 1.8 Hz, $H_{(4)}$), 7.94 (1H, d, J=1.8 Hz, $H_{(6)}$), and 9.18 (1H, br. s, –NH–); MS *m/e* (rel intensity), 243, (M^+, 100), 197 (20), 166 (26), 105 (27), and 77 (90).

2-Amino-5-[(o-benzoylanilino)methyl-d_2]benzophenone (14): Yellow liquid; IR ($CHCl_3$) 1625 (C=O) and 3340—3500 cm^{-1} (NH); NMR ($CDCl_3$) δ=6.05 (2H, br. s, NH_2), 6.41—7.69 (17H, m, aromatic), and 8.79 (1H, br. s, –NH–); MS *m/e* (rel intensity), 408 (M^+, 12), 212 (36), 167 (10), 105 (43), and 77 (100).

2-(Formyl-d-amino)benzophenone (15): Pale yellow liquid; IR ($CHCl_3$) 1645 and 1680 (C=O), and 3100—3650 cm^{-1} (NH); NMR ($CDCl_3$) δ=6.93—8.71 (9H, m, aromatic), and 10.61 (1H, br. s, –NH–); MS *m/e* (rel intensity), 226 (M^+, 20), 197 (100), 167 (10), 121 (27), and 77 (78).

2-Amino-5-(formyl-d)benzophenone (16): Pale yellow needles (from benzene/hexane), mp 132—133 °C; IR ($CHCl_3$) 1610 and 1690 (C=O), and 3320—3490 cm^{-1} (NH); NMR ($CDCl_3$) δ=6.77 (1H, d, J=9.0 Hz, $H_{(3)}$), 6.95 (2H, br. s, NH_2), 7.22—7.69 (5H, m, aromatic), 7.78 (1H, dd, J=9.0 and 1.8 Hz, $H_{(4)}$), and 7.94 (1H, d, J=1.8 Hz, $H_{(6)}$); MS *m/e* (rel intensity), 226 (M^+, 25), 149 (15), 105 (30), and 77 (100).

Oxidation of a Mixture of 1 and Formaldehyde. The compound **1** (1 mmol) was dissolved in acetic acid (25 ml), and aqueous formaldehyde (37%, 1 mmol) and manganese(III) acetate (2 mmol) were added to it. The mixture was heated at 100 °C for 6 min, followed by treatment in a manner similar to that described above, which gave **2** (2%), **3** (8%), **4** (6%), **5** (2%), **6** (4%), **7** (2%), and **8** (24%).

Oxidation of 1 in Acetic Acid Containing Acetic Anhydride. A mixture of **1** (1 mmol), acetic anhydride (4 mmol), and manganese(III) acetate (2 mmol) were heated at 100 °C for 7 min in acetic acid (25 ml). This oxidation gave **2** (1%), **3** (5%), **4** (6%), **8** (5%), **9** (52%), and **10** (6%).

2-Acetamidobenzophenone (9): Colorless crystals (from hexane), mp 88.0—88.5 °C (lit,[18] mp 88 °C); IR ($CHCl_3$) 1640 and 1710 (C=O), and 3100—3650 cm^{-1} (NH); NMR ($CDCl_3$) δ=2.17 (3H, s, $COCH_3$), 6.88—8.67 (9H, m, aromatic), and 10.74 (1H, br. s, –NH–); MS *m/e* (rel intensity), 239 (M^+, 30), 196 (100), 134 (13), 120 (28), 105 (15), 92 (24), and 77 (55).

2-(N-Methylacetamido)benzophenone (10): Colorless needles (from hexane), mp 80—81 °C; IR ($CHCl_3$) 1650 and 1680 cm^{-1} (C=O); NMR ($CDCl_3$) δ=1.84 (3H, s, $COCH_3$), 3.04 (3H, s, CH_3), and 7.20—7.84 (9H, m, aromatic); MS *m/e* (rel intensity), 253 (M^+, 10), 210 (86), 194 (48), 148 (100), 105 (8), and 77 (20). Found: *m/e* 253.10693. Calcd for $C_{16}H_{15}O_2N$: M, 253.11028.

Acetylation of 1 and 3: The compound **1** (33.3 mg) and acetic anhydride (0.1 ml) were heated at 100 °C for 6 h in pyridine (5 ml) to yield **10** (39.9 mg, 99%). The product **3** (1 mmol) was treated with acetic anhydride (1.5 mmol) in pyridine (5 ml) overnight to give **9** (99%).

Oxidation of a Mixture of 1, Formaldehyde, and Acetic Anhydride. A mixture of **1** (1 mmol), aqueous formaldehyde (37%, 1 mmol), acetic anhydride (3 mmol), and manganese(III) acetate (2 mmol) were heated on a water bath for 6 min in acetic acid (25 ml) to afford **2** (trace), **3** (8%), **4** (6%), **8** (25%), **9** (25%), and **10** (8%).

Oixdation of a Mixture of 1 and Water. The compound **1** (1 mmol), water (3 mmol), and manganese (III) acetate (2 mmol) were heated in acetic acid (25 ml) at 100 °C for 7 min to give **2** (1%), **3** (24%), **4** (5%), **6** (6%), **7** (3%), and **8** (5%).

Oxidation of 2. The product **2** (54.7 mg) was heated at 100 °C for 4 min with manganese(III) acetate (36.5 mg) in acetic acid (5 ml) to yield **3** (15.1 mg, 59%), **4** (16.1 mg, 52%), and **7** (1.7 mg, 6%) which was determined by HPLC.

Oxidation of 3. A mixture of **3** (1 mmol) and manganese(III) acetate (2 mmol) was heated in acetic acid (25 ml) at 100 °C for 15 min. The reaction mixture was treated in a manner similar to that described above to give intractable tarry materials and **9** (5%) as the only isolable reaction product.

Oxidation of 4. A mixture of **4** (31.3 mg) and manganese(III) acetate (76.7 mg) was heated in acetic acid (5 ml) at 100 °C for 6 min to yield **7** (10.2 mg, 35%) and unidentified products (10.2 mg).

Oxidation of 5. A mixture of **5** (32.9 mg) and manganese(III) acetate (45.0 mg) was heated in acetic acid (5 ml) at 100 °C for 5 min to give **3** (12.3 mg, 77%) and **7** (15.3 mg, 84%).

Oxidation of a Mixture of 1 and 3. A mixture of **1** (0.5 mmol) and **3** (0.5 mmol) was dissolved in acetic acid (25 ml) and the mixture was oxidized with manganese(III) acetate (1 mmol) to give **2** (9%), **4** (1%), **5** (7%), and **7** (8%).

Hydrolysis of 6. The product **6** (17.5 mg) was heated under reflux for 1 h in dil H_2SO_4 (5 ml), which was extracted with chloroform, followed by recrystallization from hexane to give **3** (13.7 mg, 89%).

The authors wish to thank Mr. Masanori Tsumura of the Ichikawa Chemical Co. Ltd., Higashi Osaka, for his measurements of the MS spectra, and also wish to thank Dr. John F. W. McOmie of Bristol University, England, for his helpful discussion and for reading the manuscript.

References

1) T. Aratani and M. J. S. Dewar, *J. Am. Chem. Soc.*, **88**, 5479 (1966).

2) B. Rindone and C. Scolastico, *Tetrahedron Lett.*, **1974**, 3379.

3) G. Galliani, B. Rindone, and C. Scolastico, *Tetrahedron Lett.*, **1975**, 1285.

4) K. Kurosawa, *Bull. Chem. Soc. Jpn.*, **42**, 1456 (1969).
5) K. Kurosawa and J. Higuchi, *Bull. Chem. Soc. Jpn.*, **45**, 1132 (1972).
6) K. Kurosawa, Y. Sasaki, and M. Ikeda, *Bull. Chem. Soc. Jpn.*, **46**, 1498 (1973).
7) K. Nogami and K. Kurosawa, *Bull. Chem. Soc. Jpn.*, **47**, 505 (1974).
8) S. Ueda and K. Kurosawa, *Bull. Chem. Soc. Jpn.*, **50**, 193 (1977).
9) K. Kurosawa and F. Araki, *Bull. Chem. Soc. Jpn.*, **52**, 529 (1979).
10) E. I. Heiba, R. M. Dessau, and W. J. Koehl, Jr., *J. Am. Chem. Soc.*, **91**, 138 (1969).
11) E. I. Heiba, R. M. Dessau, and P. C. Rodewald, *J. Am. Chem. Soc.*, **96**, 7977 (1974).
12) G. Galliani and B. Rindone, *J. Chem. Soc., Perkin Trans. 2*, **1976**, 1803.
13) G. Galliani and B. Rindone, *J. Chem. Soc., Perkin Trans. 1*, **1980**, 828.
14) G. Galliani and B. Rindone, *J. Chem. Res. (S)*, **1980**, 178.
15) G. Kempter and E. Schiewald, *J. Prakt. Chem.*, **28**, 169 (1965); *Chem. Abstr.*, **63**, 4236f (1965).
16) P. J. Andrulis, Jr., M. J. S. Dewar, R. Dietz, and R. L. Hunt, *J. Am. Chem. Soc.*, **88**, 5473 (1966).
17) S. Inagaki, *J. Pharm. Soc. Jpn.*, **59**, 1 (1939); *Chem. Abstr.*, **33**, 3790 (1939).
18) W. C. Lothrop and P. A. Goodwin, *J. Am. Chem. Soc.*, **65**, 363 (1943).

Reactions of 2-Methylenebenzothiazolines with Methylenecyclopropenes

Otohiko Tsuge,* Minoru Tanaka, Hiroshi Shimoharada, and Shuji Kanemasa
Research Institute of Industrial Science, Kyushu University 86, Kasuga, Kasuga, Fukuoka 816

(Received December 4, 1982)

Reactions of 2-methylene-3-phenacylbenzothiazoline and 3-benzyl-2-methylenebenzothiazoline, generated *in situ* from the corresponding 2-methylbenzothiazolium bromide and triethylamine, with methylenecyclopropenes gave a variety of products, cross-conjugated systems, spiro-cyclopentafurans and/or cyclopentabenzothiazines, depending on the nature of substituents of the methylenecyclopropenes. The reaction pathways for the formation of products are also described.

It is known that dehydrohalogenation of 3-phenacylthiazolium halide systems generates the corresponding thiazolium *N*-phenacylides whose synthetic utility as 1,3-dipoles has been established in a few recent reports.[1-6] On the treatment with triethylamine (NEt_3), however, 2-methyl-3-phenacylbenzothiazolium bromide does not yield the *N*-phenacylide but generates 2-methylene-3-phenacylbenzothiazoline which was first confirmed by the formation of Michael adducts to electron-deficient olefins and acetylenes.[7] The methylenebenzothiazoline has an electron-rich exocyclic C=C bond and is classified as a cyclic ketene acetal.

Although the reactions between enamines and methylenecyclopropenes have been extensively investigated[8] and known to give different types of products depending on the nature of substituents at the 4-position of methylenecyclopropenes,[9] few examples for the reaction of a ketene acetal, which is expected to show reaction patterns similar to those of enamines, with methylenecyclopropenes have been reported up to date.[10,11]

This paper describes the reactions of 2-methylene-3-phenacyl- (**3**) and 3-benzyl-2-methylenebenzothiazoline (**4**),[12] generated in situ from 2-methyl-3-phenacyl- (**1**) and 3-benzyl-2-methylbenzothiazolium bromide (**2**), and NEt_3 at 0 °C respectively, with methylenecyclopropenes having electron-withdrawing substituents at the 4-position: Different types of products were found to be formed depending on the nature of the substituents of methylenecyclopropenes.

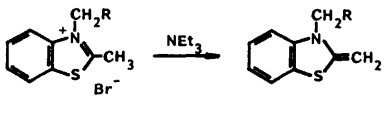

1: R=COPh
2: R=Ph
3: R=COPh
4: R=Ph

Results and Discussion

Reactions with 2-(2,3-Diphenyl-2-cyclopropenylidene)propanedinitrile (5) and Ethyl 2-Cyano-2-(2,3-diphenyl-2-cyclopropenylidene)acetate (6). The reaction of 2-methylenebenzothiazoline **3** with the methylenecyclopropene **5** in dry chloroform at room temperature for 3 h gave a deeply colored 1 : 1 adduct **7** in 95% yield.[13] On the basis of spectral data (Table 1), the 1 : 1 adduct **7** was identified as a cross-conjugated system, 2-(2-dicyanomethylene-1,3-diphenyl-3-butenylidene)-3-phenacylbenzothiazoline. In the ^1H NMR spectrum terminal olefinic protons (2H) are observed, and the ^{13}C NMR spectrum exhibits no sp^3-carbon except for that in the phenacyl group but signals assinable to the olefinic carbons, $=\mathbf{C}(CN)_2$ and $=\mathbf{C}H_2$. The absorption maximum at a long wave region in the electronic spectrum indicates the presence of relatively long conjugation.

Similarly, 2-methylene benzothiazoline **4** reacted with **5** to afford the corresponding cross-conjugated system **8**, whose structure was identified on the basis of spectral data, in an excellent yield. Thus, it can be thought that the behaviour of the methylenebenzothiazolines **3** and **4** toward the methylenecyclopropene **5** is similar to that of enamines.[14]

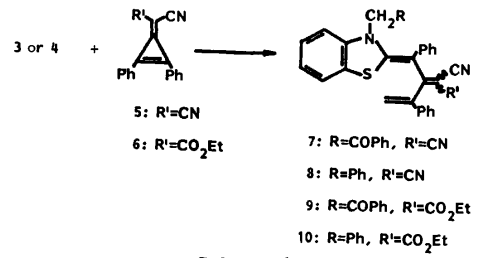

5: R'=CN
6: R'=CO_2Et
7: R=COPh, R'=CN
8: R=Ph, R'=CN
9: R=COPh, R'=CO_2Et
10: R=Ph, R'=CO_2Et

Scheme 1.

Few examples for the reaction of an enamine with the methylenecyclopropene **6** have been reported.[15] 2-Methylenebenzothiazolines **3** and **4** reacted with **6** in dry THF at room temperature for 1 h to give corresponding cross-conjugated systems **9** and **10** in good yields (Scheme 1). Structural elucidation of **9** and **10** was again accomplished on the basis of spectral data.

The yields, physical and spectral data of cross-conjugated system **7**—**10** are listed in Table 1.

Reactions with 2-Benzoyl-2-(2,3-diphenyl-2-cyclopropenylidene)-2,4-pentanedione (12). It has been well established that enamines react with methylenecyclopropenes having an acyl group at the 4-position to produce the corresponding 6,6a-dihydro-5*H*-cyclopenta[*b*]furans.[16] In order to compare with the reaction of enamines, the reactions of 2-methylenebenzothiazolines, **3** and **4**, with methylenecyclopropenes, **11** and **12**, having an acyl group at the 4-position were investigated.

The benzoyl-substituted methylenecyclopropene **11** was found to be less reactive than the above methylenecyclopropenes **5** and **6**, being recovered in the reaction with **3** and **4** at room temperature. When the reaction of **3** and **4** with **11** was performed in dry THF under reflux, however, the corresponding 1 : 1 adducts **13** and **14** were obtained in 36 and 46% yields, respectively.

Table 1. Cross-conjugated systems **7**—**10**

Compd	Yield/%	Mp θ_m/°C	IR (KBr) $\tilde{\nu}$/cm^{-1}	^{1}H NMR ($CDCl_3$) δ	^{13}C NMR ($CDCl_3$) δ	UV λ_{max}[a)]/nm(log ε)
7	95	134—135	2200 (C≡N)	5.47 (2H, s, N**C**H$_2$), 5.67,	55.25 (t, N**C**H$_2$), 64.32(s,	241 (4.35)
			1690 (C=O)	5.73 (each 1H, s, =**C**H$_2$),	=**C**(CN)$_2$), 104.77 (s, N,S>=**C**),	511 (3.87)
			1500—1300	6.80—7.75 (19H, m)	117.93 (t, =**C**H$_2$), 146.62 (s), 165.93(s), 169.01 (s), 189.37 (**C**=O)	
8	99	112—113	2200 (C≡N)	5.09 (2H, s, N**C**H$_2$), 5.73	52.75 (t, N**C**H$_2$), 65.24 (s,	236 (4.32)
			1380	(2H, s, =**C**H$_2$), 6.80—7.44	=**C**(CN)$_2$), 105.07 (s, N,S>=C),	299 (3.96)
			1320	(19H, m)	117.93 (t, =**C**H$_2$), 146.74 (s), 166.22 (s), 168.30 (s)	520 (4.31)
9	80	94	2200 (C≡N)	1.12 (3H, t, J=7.5 Hz),		243 (4.31)
			1690, 1650 (C=O)	4.03 (2H, q, J=7.5 Hz),		522 (4.00)
			1400, 1275	5.40 (4H, s, N**C**H$_2$+=**C**H$_2$),		
				6.75—7.70 (19H, m)		
10	94	97—98	2200 (C≡N)	1.10 (3H, t, J=7.5Hz),	13.95 (q), 52.56 (t, N**C**H$_2$),	243 (4.47)
			1680 (C=O)	4.00 (2H, q, J=7.5 Hz),	60.30 (t), 77.24 (s, =**C**(CN)),	530 (4.09)
			1390	5.10 (2H, s, N**C**H$_2$), 5.46	106.17 (s, N,S>=**C**), 112-.99 (t,	
				(2H, s, =**C**H$_2$), 6.80—7.40 (19H, m)	=**C**H$_2$), 143.31 (s), 148.32 (s), 164.77 (s)	

a) Spectra of **7** and **8** were measured in EtOH, and those of **9** and **10** in $CHCl_3$.

Table 2. Products, **13**—**20**, obtained from the reaction with acyl-substituted methylenecyclopropenes

Compd	Mp θ_m/°C	IR (KBr) $\tilde{\nu}$/cm^{-1}	^{1}H NMR ($CDCl_3$) δ	^{13}C NMR ($CDCl_3$) δ
13	178—179 (decomp)	2200 (C≡N) 1700 (C=O) 1540	3.06, 3.46 (each 1H, d, **C**H$_2$, J=13.0 Hz), 4.33 (2H, s, N**C**H$_2$), 5.70 (1H, m), 6.42—8.05 (23H, m)	49.70 (t, N**C**H$_2$),58.54 (t, **C**H$_2$), 82.60 (s, 3′-**C**), 92.16, 98.92 (each s, spiro-**C**, 6′a-**C**), 115.18 (s, **C**≡N), 174.39 (s, 2′-**C**), 198.88 (s, **C**=O)
14	195 (decomp)	2200 (CN) 1580 1530 1470 1440	3.26, 3.33 (each 1H, d, **C**H$_2$, J=12.0 Hz), 4.03, 4.30 (each 1H, d, N**C**H$_2$, J=18.0 Hz), 5.76 (1H, m), 6.50—8.03 (23 H, m)	47.82 (t, N**C**H$_2$), 58.05 (t, **C**H$_2$), 82.35 (s, 3′-**C**), 93.13, 98.74 (each s, spiro-**C**, 6′a-**C**), 115.00 (s,**C**≡N), 173.97 (s, 2′**C**)
17	180—181	1700 (C=O) 1610 1570 1550	1.76, 1.92 (each 3H, s), 4.41 (1H, s, >**C**H), 4.83, 5.11 (each 1H, d, N**C**H$_2$, J=19.0 Hz), 6.85—7.65 (19H, m), 16.35 (1H, s, **O**H)	23.63 (q, **C**H$_3$), 43.80 (d, 3a-**C**), 55.13 (t, N**C**H$_2$), 108.30, 117.44,120.06 (each s, 1-**C**,3-**C**, **C**=C(OH)Me), 190.11, 191.81, 193.95 (each s, **C**=O)
18	184—185 (decomp)	1660 (C=O) 1550 1470	1.80, 2.22 (each 3H, s), 3.20 (2H, s, **C**H$_2$), 3.90. 4.22 (each 1H, d, N**C**H$_2$, J=18.0 Hz), 5.60—5.73 (1H, m), 6.40—7.53(18H, m)	16.32 (q, **C**H$_3$), 30.70 (q, CO**C**H$_3$), 48.00 (t, N**C**H$_2$), 57.50 (t, **C**H$_2$), 83.20 (s, 3′-**C**), 93.86, 98.90 (each s, spiro-**C**, 6′a-**C**), 175.80(s, 2′-**C**), 193.97 (s, **C**=O)
20	207—208	1610 1540 1470	1.70, 1.90 (each 3H, s), 4.26 (1H, s, >**C**H), 4.60, 4.85 (each 1H, d, N**C**H$_2$, J=18.0 Hz), 6.80—7.65 (19H, m), 16.32 (1H, s, **O**H)	23.51, 23.63 (each q, **C**H$_3$), 43.67 (d, 3a-**C**), 52.08 (t, N**C**H$_2$), 108.43, 117.01, 120.85 (each s, 1-**C**, **C**=C(OH)Me), 190.05, 191.75 (each s, **C**=O)

The compounds, **13**, **14**, **17**, **18**, and **20** are all yellow needles. **13**: UV $\lambda_{max}^{CHCl_3}$/nm (log ε) 270 (4.28), 325 (4.21), 360 (4.27). **14**: UV $\lambda_{max}^{CHCl_3}$/nm (log ε) 265 (4.35), 330 (4.29), 360 (4.34). The ^{1}H NMR spectral data of **15**, **16**, and **19** are given as follows: **15**: δ 1.86, 2.15 (each 3H, s), 3.30, 3.43 (each 1H, d, **C**H$_2$, J=13.0 Hz), 4.20 (2H, s, N**C**H$_2$). **16**: δ 0.73, 2.36 (each 3H, s), 5.06, 5.36 (each 1H, d, N**C**H$_2$, J=18.0 Hz), 5.56 (1H, s, =**C**H), 17.10 (1H, s, **O**H). **19**: δ 0.76, 2.28 (each 3H, s), 5.02, 5.20(each 1H, d, N**C**H$_2$, J=18.0 Hz), 5.78 (1H, s, =**C**H), 16.93 (1H, s, **O**H).

The IR spectra of **13** and **14** showed no carbonyl absorptions came from the benzoyl group in **11**, and two singlets assignable to quaternary carbons appeared in the ^{13}C NMR spectra. Thus, **13** and **14** can be assumed as spiro-cyclopenta[*b*]furans **13a**, **14a** or **13b**, **14b** derived from the participation of the benzoyl group in a cyclization. In the ^{1}H NMR spectra, however, both **13** and **14** showed doublets assignable to allylic methlenes at δ 3.06, 3.46 and 3.26, 3.33, respectively.[17] It is thus reasonable to conclude that 1 : 1 adducts **13** and

14 are spiro[benzothiazole-2(3*H*),6′-cyclopenta[*b*]furan]s **13a**, **14a** rather than isomeric spiro[benzothiazole-2(3*H*),5′-cyclopenta[b]furan]s **13b**, **14b** (Scheme 2).

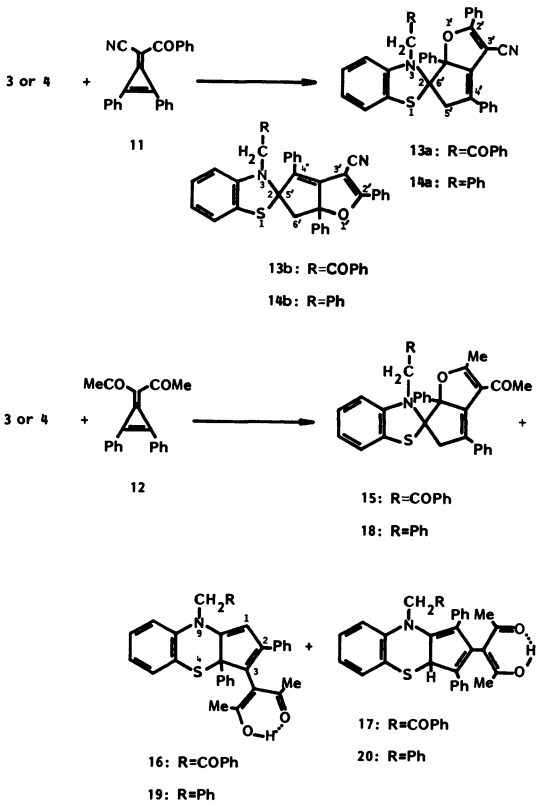

Scheme 2.

In contrast to the above reaction which exhibited a reaction pattern similar to enamines, the methylenebenzothiazolines **3** and **4** reacted with the diacetyl-substituted methylenecyclopropene **12** to give novel rearranged products.

The reaction of **3** with **12** in dry THF at room temperature for 0.5 h afforded a mixture of three isomeric 1 : 1 adducts **15**, **16**, and **17**, from which only the major product **17** was isolated in 87% yield. The yields of **15** and **16** were so poor that their isolation was unsuccessful, but their formation was shown by inspection of the ^{1}H NMR spectrum of reaction mixture. Under the same conditions, **4** reacted with **12** to give three 1 : 1 adducts **18**, **19**, and **20** in 21, 10 and 57% yields, respectively. In the same reaction for a long time (15 h), a yield of the major product **20** increased up to 84% with decreased yields of **18** (10%) and **19** (trace). Although the products **18** and **20** were isolated in pure forms, **19** was too unstable to be isolated. Actually, **19** gradually changed into **20** even at room temperature in solution.

The spectral data of products **15**—**20** are summarized in Table 2. It is quite certain that the minor products **15** and **18** have the same ring structure to the spiro-cyclopenta[*b*]furans, **13a** and **14a**, by comparison of the spectral data.

Structural elucidation of the major products, 2-(1-acetylacetonyl)-9-phenacyl-(**17**) and 2-(1-acetylacetonyl)-9-benzyl-1,3-diphenyl-3a,9-dihydrocyclopenta[*b*]-[1,4]benzothiazine (**20**), was accomplished on the basis of the spectral data. The ^{1}H NMR spectrum showed the signals of a methine and an enolic proton at δ 4.41 and 16.35 for **17** or at δ 4.26 and 16.32 for **20**, respectively, and the ^{13}C NMR spectra indicated the presence of a tertiary carbon in both **17** and **20**. In analogy with cross-conjugated systems, **7**—**10**, methylene protons and carbon in the phenacyl group in **17** or in the benzyl group in **20** are observed at considerably lower fields than those of the spiro-cyclopentafuran **13a** or **14a** respectively, meaning that the phenacyl or benzyl group should be located on an enamino nitrogen atom.[18] The above facts strongly support the assigned benzothiazine structures, **17** and **20**, arisen from a rearrangement of benzothiazoline ring.[19]

As mentioned above, the minor product **19**, whose spectral data are similar to those of **16**, changed into the major product **20**. Thus, **16** and **19** can be regarded as the precursors for **17** and **20**, respectively.

In the ^{1}H NMR spectrum of **16** or **19**, an enolic proton is also observed, but an olefinic proton appears instead of the methine one in **17** or **20**.[19] The phenacyl or benzyl group is under circumstance similar to that in **17** or **20**. Thus, it was deduced that the precursors are 3-(1-acetylacetonyl)-9-phenacyl-(**16**) and 3-(1-acetylacetonyl)-9-benzyl-2,3a-diphenyl-3a,9-dihydrocyclopenta[*b*][1,4]benzothiazine (**19**). In these cases, both the methyl groups are magnetically quite different (δ 0.73, 2.36 for **16** and δ 0.76, 2.28 for **19**) since one of them is forced to face the plane of the phenyl group at the 3a-position. The thermal isomerization of **16** into **17** or **19** into **20** might be driven by release from the steric hindrance around 3a-position.

Reaction Pathways. Although the mechanistic aspects concerning the reactions of enamines with methylenecyclopropenes have not been fully established,[8] the reaction of a cyclic enamine with methylenecyclopropenes leading to pentalene derivatives[20] and cross-conjugated systems[21] has been interpreted as *via* an intermediary [2+2] cycloadduct. The reaction pathways in this paper can be again explained as *via* an intermediary [2+2] cycloadduct (Scheme 3).

The electron-deficient endocyclic C=C bond of methylenecyclopropenes, **5**, **6**, **11**, and **12**, interacts

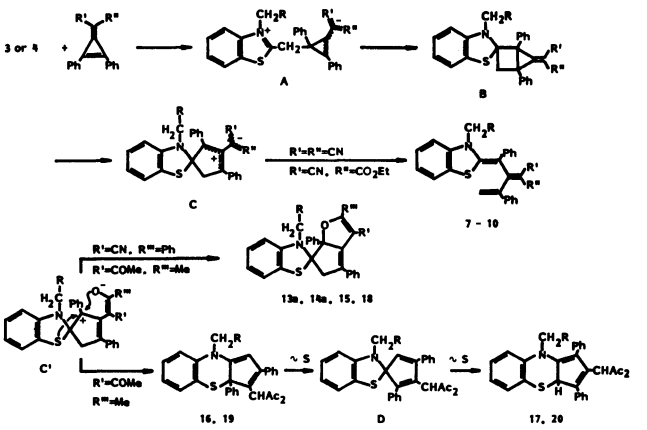

Scheme 3.

with the electron-rich exocyclic one of methylenebenzothiazolines, **3** and **4**, forming an intermediary [2+2] cycloadduct **B**, probably *via* a zwitterion **A**. The intermediate **B** undergoes a ring opening of the fused cyclopropane moiety to yield a new zwitterion **C** that is stabilized by the electron-withdrawing substituents (R′ and R″).

The five-membered ring of cyclopentadienyl cation in **C** opens in a conrotatory manner[21] to give the cross-conjugated systems, **7**—**10**, when the substituents have a relatively weak stabilization effect on the zwitterion **C** (R′ is cyano and R″ is cyano or ethoxycarbonyl).[22] On the other hand, when the substituents strongly stabilize **C** (R′=CN, R″=COPh; R′=R″=COMe)[22] and have at least one acyl moiety, the zwitterion **C** (=**C**′, R″=Ph, Me) takes an opportunity for the cyclization of the acyl group to give the spiro-cyclopentafurans, **13a**, **14a**, **15**, and **18**.

Another novel rearrangement also occurs in the case of **C** having two acetyl groups. The rearrangement of sulfur atom in **C**′ onto the cationic center followed by concurrent proton transfer gives the unstable cyclopenta[*b*][1,4]benzothiazines, **16** and **19**. Their lability might be due to steric hindrance between the phenyl group at the 3a-position and the 1-acetylacetonyl group. Release from the steric hindrance may cause the 1,5-sigmatropic rearrangement of sulfur atom to give a spiro intermediate **D**. A further rearrangement gives rise to the less hindered cyclopenta[*b*][1,4]benzothiazines, **17** and **20**. The reason why only the sulfur atom migrates in the rearrangements would be that the nitrogen migration does not reduce the steric hindrance around the position to which the nitrogen atom migrates.

The reaction pathways depicted in Scheme 3 are supported by the following facts. The cross-conjugated compound **10** canged into the cyclopenta[*b*][1,4]-benzothiazine **21**, whose structure was identified on the basis of the spectral data, when treated with a catalytic amount of hydrochloric acid at room temperature. Contrary to thermal instability of the previous cyclopenta[*b*][1,4]benzothiazines, **16** and **19**, the compound **21** is much more stable on heating. This stability may be due to the less steric hindrance of the cyano(ethoxycarbonyl)methyl substituent. On the treatment with hydrochloric acid, the spiro-cyclopenta[*b*]furan **18** quantitatively isomerized into **19** which further thermally changed into **20** (Scheme 4).

The above isomerizations seem to be explained as follows: Protonation onto the carbon possessing two electron-withdrawing substituents of **10** and a conrotatory cyclization of the resulting pentadienyl cation lead to an intermediate **E** that corresponds to a protonated **C** in Scheme 3. The similar rearrangement of sulfur atom with concurrent deprotonation gives **21**. Similarly, the oxygen atom of furan ring in **18** is protonated and the furan ring opens to form the similar intermediate **F** that gives **19** in the same manner.

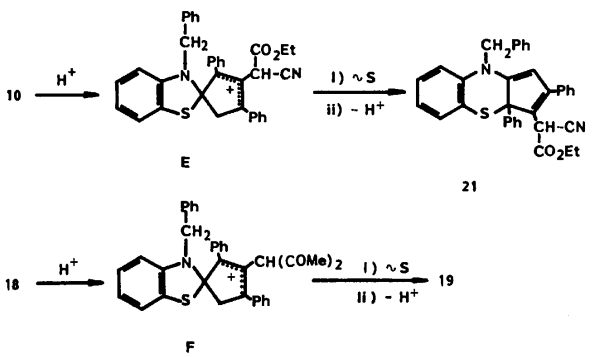

Scheme 4.

As shown in Scheme 3, it is reasonable to say that the degree of stabilization of **C** by the electron-withdrawing substituents (R′ and R″)[22] primarily controls the reaction pathways.

Experimental

All melting points were determined on a Yanagimoto micro melting point apparatus and were uncorrected. The IR spectra were taken with a JASCO IRA-1 or a JASCO A-102 spectrometer. The ^{1}H NMR spectra were recorded on a Hitachi R-40 or a JEOL FX-100 instrument and ^{13}C NMR spectra were obtained on a JEOL FX-100 spectrometer at 25.05 MHz. Chemical shifts are expressed in parts per million downfield from tetramethylsilane. The UV spectra were recorded on a Shimadzu UV-240 spectrometer, and mass spectra were measured with a JEOL JMS-01SG-2 spectrometer at 75 eV of ionization energy. Elemental analyses were performed on a Hitachi 026 CHN analyzer. Thin-layer chromatography was accomplished on 0.2-mm precoated plates of silica gel 60 F-254 (Merck) or on 0.2-mm precoated plates of aluminum oxide 60 F-254 type E (Merck). Visualization was with ultraviolet light (254 and 365 nm) and iodine. Preparatory column chromatography was performed on silica gel Wako C-300 (Wako) or on neutral aluminum oxide Woelm type N (Woelm).

The reactions were performed under nitrogen atmosphere, and solvents were evaporated with a Tokyo Rikakikai rotary vacuum evaporator type V at 50 °C.

Materials. 2-Methyl-3-phenacylbenzothiazolium bromide (**1**)[23] was prepared according to the reported method. 3-Benzyl-2-methylbenzothiazolium bromide (**2**), mp 255—256 °C, was similarly prepared by refluxing equimolar amounts of 2-methylbenzothiazole and benzyl bromide in dry acetone for 7 h: Yield 31%; colorless prisms; IR 1570, 1450, 1430 cm^{-1}. 2-(2,3-Diphenyl-2-cyclopropenylidene)propanedinitrile (**5**),[24] ethyl 2-cyano-2-(2,3-diphenyl-2-cyclopropenylidene)acetate (**6**),[25] 2-benzoyl-2-(2,3-diphenyl-2-cyclopropenylidene)acetonitrile (**11**),[16] and 3-(2,3-diphenyl-2-cyclopropenylidene)-2,4-pentanedione (**12**)[26] were synthesized by the reaction of 1-ethoxy-2,3-diphenylcyclopropenium tetrafluoroborate with the corresponding active methylene compounds, respectively.

Reactions with 2-(2,3-Diphenyl-2-cyclopropenylidene)propanedinitrile (5). A solution of NEt_3 (0.12 g, 1.2 mmol) in dry chloroform (5 mL) was added dropwise, at 0 °C, to a stirred suspension of the benzothiazolium bromide **1** (0.41 g, 1.2 mmol) and **5** (0.3 g, 1.2 mmol) in dry chloroform (40 mL). After 3 h at room temperature, the reaction mixture was poured into water (200 mL) and extracted with chloroform (130 mL). The extract was dried over $MgSO_4$, and evaporated to give a red residue. The residue was chromatographed on silica gel using chloroform as an eluent to give 583 mg (95%) of the cross-conjugated system **7** which was recrystallized from benzene afforded reddish violet prisms. Found: C, 80.01; H, 4.93; N, 6.87%. Calcd for $C_{34}H_{23}N_3OS \cdot C_6H_6$: C, 80.07; H, 4.87; N, 7.00%. MS *m/e* 521 (M^+).

A similar reaction of the benzothiazolium bromide **2** (0.38 g, 1.2 mmol) with **5** (0.3 g, 1.2 mmol) in the presence of NEt_3 (0.12 g, 1.2 mmol) gave 545 mg (99%) of the cross-conjugated system **8** which was purified by recrystallization from benzene to give reddish violet prisms. Found: C, 81.87; H, 5.12; N, 7.50%. Calcd for $C_{33}H_{23}N_3S \cdot C_6H_6$: C, 81.90; H, 5.07; N, 7.35%. MS *m/e* 493 (M^+).

The spectral data of **7** and **8** are shown in Table 1.

Reactions with Ethyl 2-Cyano-2-(2,3-diphenyl-2-cyclopropenylidene)acetate (6). A solution of NEt_3 (0.1 g, 1 mmol) in dry THF (5 mL) was added dropwise, at 0 °C, to a stirred suspension of the benzothiazolium bromide **1** (0.35 g, 1 mmol) and **6** (0.3 g, 1 mmol) in dry THF (40 mL). After 1 h at room temperature, the precipitated triethylammonium bromide was filtered off and the filtrate was evaporated. The residue was chromatographed over neutral alumina using chloroform as an eluent affording 550 mg (80%) of the cross-conjugated system **9** which was purified by recrystallization from benzene to give violet prisms. Found: C, 76.22; H, 5.12; N, 4.95%. Calcd for $C_{36}H_{28}N_2O_3S$: C, 76.06; H, 4.93; N, 4.93%. MS *m/e* 568 (M^+).

A similar reaction of the benzothiazolium bromide **2** (0.32 g. 1 mmol) with **6** (0.3 g, 1 mmol) in the presence of NEt_3 (0.1 g, 1 mmol) yielded 510 mg (94%) of the cross-conjugated system **10** as reddish violet prisms. Found: C, 77.65; H, 5.19; N, 5.20%. Calcd for $C_{35}H_{28}N_2O_2S$: C, 77.76; H, 5.22; N, 5.18%. MS *m/e* 540 (M^+).

The spectral data of **9** and **10** are shown in Table 1.

Reactions with 2-Benzoyl-2-(2,3-diphenyl-2-cyclopropenylidene)-acetonitrile (11). A mixture of the benzothiazolium bromide **1** (0.35 g, 1 mmol), **11** (0.34 g, 1.1 mmol), and NEt_3 (0.1 g, 1 mmol) in dry THF (40 mL) was refluxed for 1 h. The precipitated triethylammonium bromide was filtered off and the filtrate was evaporated to give a colored residue. The residue was chromatographed over silica gel using benzene as an eluent to afford 215 mg (36%) of the spiro-cyclopenta[*b*]-furan **13a** which was purified by recrystallization from benzene–hexane. Found: C, 79.82; H, 4.95; N, 4.36%. Calcd for $C_{40}H_{28}N_2O_2S$: C, 79.98; H, 4.70; N, 4.66%. MS *m/e* 600 (M^+), 105.

Similarly, the benzothiazolium bromide **2** (0.32 g, 1 mmol) reacted with **11** (0.34 g, 1.1 mmol) in the presence of NEt_3 (0.1 g, 1 mmol) to give 264 mg (46%) of the spiro-cyclopenta-[*b*]furan **14a**. Found: C, 81.74; H, 4.90; N, 4.70%. Calcd for $C_{39}H_{28}N_2OS$: C, 81.80; H, 4.93; N, 4.89%. MS *m/e* 572 (M^+), 481, 105.

Reactions with 3-(2,3-Diphenyl-2-cyclopropenylidene)-2,4-pentanedione (12). A solution of NEt_3 (0.3 g, 3 mmol) in dry THF (5 mL) was added dropwise, at 0 °C, to a suspension of the benzothiazolium bromide **1** (1.04 g, 3 mmol) and **12** (0.86 g, 3 mmol) in dry THF (60 mL). After 0.5 h at room temperature, the precipitated triethylammonium bromide was filtered off and the filtrate was evaporated. The residue was dissolved in benzene and the benzene solution was passed through a short column packed with neutral alumina to afford a mixture of **15**, **16**, and **17** (1.48 g, 90%). The formation of the spiro-cyclopentafuran **15** and benzothiazine **16** was indicated by inspection of the ^1H NMR spectrum of the above mixture. Evaporation of the benzene gave yellow pasty material that solidified on trituration with hexane to give 1.45 g (87%) of the benzothiazine **17** which was purified by recrystallization from benzene–hexane.

The same reaction in dry acetonitrile (30 mL) gave **17** in 73% yield. The benzothiazine **17**. Found: C, 78.08; H, 5.49; N, 2.70%. Calcd for $C_{36}H_{29}NO_3S$: C, 77.84; H, 5.23; N, 2.52%. MS *m/e* 555 (M^+), 450, 435, 105.

A similar reaction of the benzothiazolium bromide **2** (0.96 g, 3 mmol) with **12** (0.86 g, 3 mmol) in THF (60 mL) in the presence of NEt_3 (0.3 g, 3 mmol) yielded a mixture of **18**, **19**, and **20** (1.39 g, 88%) whose relative yields were determined on the basis of the ^1H NMR spectrum (**18**: 21%; **19**: 10%; **20**: 57%). The mixture was carefully chromatographed over neutral alumina. The first benzene–hexane eluent afforded almost pure **20** and the next benzene eluent gave **18** which was contaminated with **20**. Both the spiro-cyclopentafuran **18** and benzothiazine **20** were purified by recrystallization from benzene–hexane.

The spirocyclopentafuran **18**. Found: C, 79.96; H, 5.61; N, 2.89%. Calcd for $C_{35}H_{29}NO_2S$: C, 79.67; H, 5.54; N, 2.66%. MS *m/e* 527 (M^+), 436, 91. The benzothiazine **20**. Found: C, 79.97; H, 5.59; N, 2.52%. Calcd for $C_{35}H_{29}NO_2S$: C, 79.67; H, 5.54; N, 2.66%. MS *m/e* 527 (M^+), 436, 394, 350, 91.

The spectral data of **15**—**20** are listed in Table 2.

Acid-catalyzed Isomerization of the Cross-conjugated System 10. An ethanol solution (15 mL) of **10** (0.27 g, 0.5 mmol) containing a catalytic amount of hydrochloric acid was stirred at room temperature for 24 h and evaporated to give a residue. The residue was treated with 10% aqueous potassium carbonate and extracted with chloroform. The chloroform extract was dried over $MgSO_4$ and evaporated. Column chromatography of the residue over neutral alumina using benzene as an eluent afforded the benzothiazine **21** (0.057 g, 31%) which on recrystallization from benzene gave yellow prisms, mp 154—155 °C. IR (KBr) 2230 (C≡N), 1730 (C=O), 1590, 1540, 1440 cm^{-1}; ^1H NMR ($CDCl_3$) δ=1.03 (3H, t), 3.60 (2H, q), 4.56 (1H, s, -CH), 4.90, 5.10 (each 1H, d, NCH_2, J=18.0 Hz), 5.55 (1H, s, =CH), 6.60—7.60 (19H, m); ^{13}C NMR ($CDCl_3$) δ=13.55 (q, CH_3), 35.38 (d, CH), 53.36 (t, NCH_2), 59.01 (s, 3a-C), 62.67 (t, CH_2Me), 103.02 (d, 1-C), 164.17 (s, C–O); MS *m/e* 540 (M^+), 449, 403, 375, 91. Found: C, 77.70; H, 5.33; N, 5.10%. Calcd for $C_{35}H_{28}N_2O_2S$: C, 77.76; H, 5.22; N, 5.18%.

Acid-catalyzed Isomerization of the Spiro-cyclopenta[b]*furan 18.* A drop of hydrochloric acid was added to a solution of **18** in deuteriochloroform and the ^1H NMR spectrum was started to measure at room temperature. The signals for **18** gradually disappeared with the appearance of those for the dihydrocyclopenta[*b*][1,4]benzothiazine **19**. In 0.5 h the change was completed and then **19** was observed to isomerize into **20**. After 15 h, the solvent was evaporated to give **20** in a quantitative yield.

References

1) K. T. Potts, D. R. Choudhury, and T. R. Westby, *J. Org. Chem.*, **41**, 187 (1976).

2) O. Tsuge, H. Shimoharada, and M. Noguchi, *Heterocycles*, **15**, 807(1981).

3) O. Tsuge, H. Shimoharada, and M. Noguchi, *Chem. Lett.*, **1981**, 1199.

4) O. Tsuge, H. Shimoharada, and M. Noguchi, *Chem. Lett.*, **1981**, 1493.

5) O. Tsuge, H. Shimoharada, M. Noguchi, and S. Kanemasa, *Chem. Lett.*, **1982**, 711.

6) O. Tsuge and H. Shimoharada, *Chem. Pharm. Bull.*, **30**, 1903 (1982).

7) O. Tsuge, M. Tanaka, H. Shimoharada, and M. Noguchi, *Heterocycles*, **16**, 1705(1981).

8) Th. Eicher and J. L. Weber, *Topics Current Chem.*, **57**, 1 (1975).

9) The numbering of methylenepropene system is as follows.[8)]

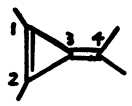

10) Some reactions of a ketene acetal with methylenecyclopropenes have been described as unpublished results in Ref. 8.

11) Part of this work has been reported as a preliminary communication: O. Tsuge, M. Tanaka, H. Shimoharada, and S. Kanemasa, *Chem. Lett.*, **1982**, 1353.

12) It is known that dehydrohalogenation of 3-alkyl-2-methylthiazolium halides generates the corresponding 2-methylenethiazolines (W. König and W. Meier, *J. Prakt. Chem.*, **109**, 324 (1925); G. H. Alt, *J. Org. Chem.*, **33**, 2858 (1968)).

13) The same reaction in THF, in which the methylenecyclopropene **5** is hardly soluble, resulted in quantitative recovery of **5** with the formation of the dimer of **3**. This dimer is the only product in the reaction of the bromide **1** with NEt_3 (see Ref. 7).

14) J. Ciabattoni and E. C. Nathan, III, *J. Am. Chem. Soc.*, **89**, 3081 (1967).

15) It has been described as unpublished results in Ref. 8 that **6** reacts with tautomeric enamine forms derived from Schiff bases to give the 2-pyridones arising from the cross-conjugated systems by loss of alcohol.

16) Th. Eicher and Th. Born, *Justus Liebigs Ann. Chem.*, **762**, 127 (1972).

17) The reported values of chemical shifts of protons in substituted cyclopentenes are as follows (W. Brugel, "Handbook of NMR spectral parameters," Heyden and Son Ltd., London, Philadelphia, Rheine (1979), Vol. 1, p. 235).

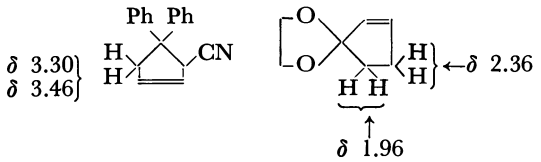

18) It is known that α-hydrogens of alkyl group on an enamino nitrogen occur at considerably lower fields than those on an ordinary nitrogen (E. M. Kosower and T. S. Sorensen, *J. Org. Chem.*, **27**, 3764 (1962); H. Booth and J. H. Little, *Tetrahedron*, **23**, 291 (1967)).

19) The ^1H NMR data of the following tetrahydrophenothiazine are as follows (F. Chioccara and G. Prota, *Synthesis*, **1977**, 876).

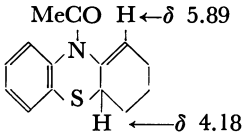

20) O. Tsuge, S. Okita, M. Noguchi, and S. Kanemasa, *Chem. Lett.*, **1982**, 993.

21) O. Tsuge, S. Okita, M. Noguchi, and S. Kanemasa, *Chem. Lett.*, **1982**, 847.

22) The degree of stabilization of the substituents can be estimated with the pK_a values of disubstituted methane derivatives (R. G. Peason and R. L. Dillon, *J. Am. Chem. Soc.*, **75**, 2439 (1953)): $CH_2(COMe)_2$ 9; $CH_2(CN)(COMe)$ 10; $CH_2(CN)_2$ 11; $CH_2(CO_2Et)_2$ 13.

23) F. Krönke and W. Friedrich, *Chem. Ber.*, **96**, 1195 (1963).

24) Th. Eicher, T. Pfister, and N. Kruger, *Org. Prep. Proced. Int.*, **6**, 63 (1974).

25) S. Anfreades, *J. Am. Chem. Soc.*, **87**, 3941 (1965).

26) Th. Eicher and A. Loschner, *Z. Naturforsch.*, **216**, 899 (1966).

Coenzyme Models. 34. Synthesis and Oxidation Ability of a Metal-coordinative Flavin

Seiji SHINKAI,* Yuichi ISHIKAWA, and Osamu MANABE
Department of Industrial Chemistry, Faculty of Engineering, Nagasaki University, Nagasaki 852
(Received December 2, 1982)

A new metal-coordinative flavin(2,4,7-trimethylquino[8,7-*g*]pteridine-9,11(7*H*,10*H*)-dione: (**1**)) which has a phenanthroline-like skeleton within the molecular structure was synthesized. Being different from conventinal flavins, the new flavin showed a significant affinity toward metal ions and the absorption spectra were sensitively affected by added metal ions. The spectral patterns were classified into three types, which were assigned respectively to the different coordination structures. It was demonstrated through oxidation of dihydropyridine derivatives, phenylhydrazine, and L-ascorbic acid that complexed metal ions are able to "activate" **1** as oxidizing agent. The complexes with Zr^{4+} and Fe^{3+} even oxidized alcohols at ambient temperature. Unexpectedly, it was found that tetrahedral coordination metals such as Cd^{2+}, Zn^{2+}, and Co^{2+} frequently give the stable semiquinone radical of **1**. The remarkable stabilization effect of these metals was attributed to a bent, butterflywing structure of the semiquinone radical. These findings suggest that the **1**–metal complexes are useful not only as a model system of metalloflavoproteins but also as an *in vitro* oxidation catalyst.

Flavin coenzymes are versatile redox catalysts in many biological systems and it is now known that more than 100 proteins require flavin coenzymes.[1-3] In contrast to the ability of flavin coenzymes to oxidize a variety of substrates *in vivo*, however, flavin molecules *in vitro* exhibit a rather weak oxidation ability. We have been aiming at "activating" flavin molecules in nonenzymatic systems with the intention of utilizing flavins as an organic turnover oxidation catalyst. There are now recognized two main methods to facilitate flavin-mediated oxidation reactions: That is, (i) to convert substrates into more "specific" ones with the aid of second cofactors or environmental effects and (ii) to shift the redox potential of flavins to more positive values. Method (i) has been achieved by employing cyanide ion,[4-7] thiazolium ions,[8-13] and thiols[14,15] as second cofactors or by conducting flavin-mediated reactions in aqueous micelles and water-soluble polymers.[16-22] Method (ii) is precedented by Cl-, CN-, pyridino-, and nitro-substituted flavins.[19,23-27] To the best of our knowledge, however, no precedent for the metal-activation of flavin catalyses exists, which would be classified as an example of method (ii). The difficulty of the method is solely ascribable to the lack of the metal affinity of flavins, except a few metal ions such as Ag^{+} and Ru^{2+}.[28,29]

It thus occurred to us that it would be of value to synthesize a new flavin which has a metal-coordinative function. With the object in view, we synthesized 2,4,7-trimethylquino[8,7-*g*]pteridine-9,11(7*H*,10*H*)-dione (**1**)† which has a phenanthroline-like skeleton in the molecular structure and examined the influence of complexed metal ions on the oxidation ability of **1**. As control experiments, we used 10-ethylisoalloxazine (**7**). Since flavin coenzymes mediate electron transfers to and from ion-sulfur, molybdenum, and heme in proteins, the investigation would be also of value as a model study of metalloflavoproteins to gain an insight into metal–flavin interactions.

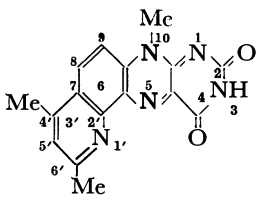

† When the isoalloxazine ring is taken as a basic skeleton, **1** may be named 4′,6′,10-trimethyl-6,7-(2′,3′-pyrido)-isoalloxazine. For the sake of the analogy to conventional isoalloxazines, we will use this naming when we point to the atoms in **1**.

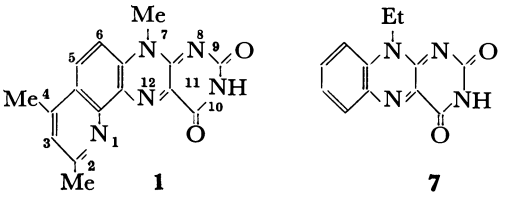

1 **7**

Experimental

Materials. Compound **1** was synthesized according to a following reaction sequence (Ts=tosylate).

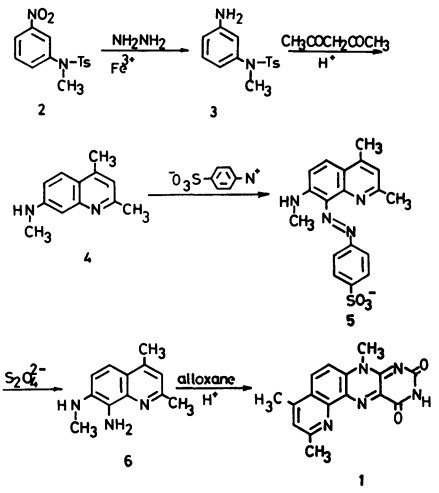

2 **3** **4** **5** **6** **1**

m-*Nitro*-N-*methyl*-N-*tosylaniline* (**2**). *m*-Nitro-*N*-tosylaniline (100 g; 0.34 mol) was dissolved in 800 ml of 1 M NaOH (1 M=1 mol dm^{-3}) aqueous solution and dimethyl

sulfate (45.5 g; 0.34 mol) was added dropwise with stirring at room temperature. After 1 h, 50 ml of 1 M NaOH aqueous solution was added and then dimethyl sulfate (10 g; 0.075 mol) was added dropwise again. The same operation was repeated two more times. The white precipitate was collected by suction, washed with aqueous NaOH, dilute HCl, and water, and then dried *in vacuo*; mp 109.5—110.5 °C, yield 95%. The row product was used for the following synthesis without further purification.

N-Methyl-N-tosyl-m-phenylenediamine (3). The nitro group was reduced by Fe^{3+}–hydrazine.[30] **2** (100 g; 0.33 mol) was dissolved in 100 ml of methanol containing 10 g of active carbon and 1.5 g (5.5×10^{-3} mol) of $FeCl_3\cdot6H_2O$, and the solution was refluxed for 15 min. Hydrazine hydrate (90%) (35 g; 0.495 mol) was added dropwise and then the reaction mixture was heated under reflux for 2.5 h. We here confirmed that the spot of **2** in TLC had disappered. The solution was filtered while it was hot, the solvent being evaporated *in vacuo*. The residue (mp 100—102 °C, yield 94%) was subjected to the following analyses. Found: C, 60.76; H, 5.84; N, 10.17%. Calcd for $C_{14}H_{16}N_2O_2S$: C, 60.85; H, 5.84; N, 10.14%. NMR($CDCl_3$): Ar–CH_3, 2.39 ppm, 3H; *N*-CH_3, 3.09 ppm, 3H; NH_2, 3.69 ppm, 2H; aromatic protons, 6.34 ppm (1H), 6.52 ppm (2H), 7.01 ppm (1H), 7.22 ppm (2H), 7.48 ppm (2H).

2,4-Dimethyl-7-(methylamino)quinoline (4). In 120 ml of acetic acid containing 20 ml of concd sulfuric acid were added **3** (80 g; 0.29 mol) and acetylacetone (34 g; 0.319 mol), and the reaction mixture was refluxed. The progress of the reaction was followed by the TLC method (silica gel–methanol). In order to accelerate the reaction, 3.4 g (0.032 mol) of acetylacetone was added several times so that the total amount of added acetylacetone became 0.49 mol. After 3 d, the solution was concentrated *in vacuo* to one-third and poured into 200 ml of water. The precipitate was collected by suction and washed with hot water. The solid was once dissolved in hot NaOH solution. On cooling, the yellow precipitate was formed, which was recovered by filtration and washed with water: mp 140.0—140.5 °C, yield 28.7%. Found: C, 76.79; H, 7.52; N, 14.91%. Calcd for $C_{12}H_{14}N_2$: C, 77.38; H, 7.58; N, 15.04%. IR(KBr): ν_{NH} 3220 cm^{-1}, ν_{Ar-H} 842, 830, 801 cm^{-1}. NMR ($CDCl_3$): 4-CH_3, 2.56 ppm, 3H; 2-CH_3, 2.64 ppm 3H; *N*-CH_3, 2.94 ppm, 3H; NH, 4.16 ppm 1H; 6-H, 6.82 ppm, 1H(quartet); 3-H, 6.84 ppm, 1H(singlet); 8-H, 7.02 ppm, 1H(doublet); 5-H, 7.88 ppm, 1H(doublet). IR and NMR spectral data support that the product is 2,4-dimethyl-7-(methylamino)quinoline (**4**) but not 2,4-dimethyl-5-(methylamino)quinoline.

4-(2,4-Dimethyl-7-methylamino-8-quinolylazo) benzenesulfonate (5). Compound **4** (11.2 g; 0.06 mol) was dissolved in 60 ml of hot 3.5% HCl solution, and after cooling, the solution was poured into 500 ml of aqueous solution containing the diazonium salt of sulfanilic acid (10.4 g; 0.06 mol). 120 g of urea was added in order to accelerate the coupling reaction. The solution was adjusted to pH 4.5 ± 0.5 with sodium acetate and the reaction was continued for 90 h at 0—10 °C. The precipitate was recovered by filtration. The product solid was once dissolved in aqueous NaOH solution and reprecipitated by adding NaCl. The precipitate was then dissolved in aqueous solution and reprecipitated again by adding concd HCl solution; mp 271—273 °C (red powder), yield 82.4%. IR(KBr): ν_{NH} 3400 cm^{-1}, $\nu_{quinoline\ ring}$ 1620 cm^{-1}, SO_3H, 1219 and 1025 cm^{-1}. Found: C, 55.70; H, 4.80; N, 14.25%. Calcd for $C_{18}H_{18}N_4O_3S$: C, 58.30; H, 4.90; N, 15.13%.

2,4-Dimethyl-7-methylamino-8-quinolinamine (6). Compound **5** (0.5 g; 1.4 mmol) was dissolved in 40 ml of 3% NaOH aqueous solution. 0.7 g (4.0 mmol) of sodium dithionite (practical grade) was added, and the reaction mixture was refluxed for 1 h. The product was extracted with 1-butanol (100 ml×2). Since the product **6** was relatively sensitive to air oxidation, the 1-butanol extract was immediated used for the following reaction. Meanwhile, the aliquot was withdrawn from the solution and cooled in a nitrogen atmosphere. The precipitate was recovered by filtration and subjected to the NMR measurement. NMR($CDCl_3$): 4-CH_3, 2.55 ppm, 3H; 2-CH_3, 2.60 ppm, 3H; *N*-CH_3, 2.96 ppm 3H; 7-NH and 8-NH_2, 3.98 ppm, 3H; 3-H, 6.84 ppm 1H(singlet); 6-H, 7.02 ppm, 1H(doublet); 5-H, 7.37 ppm, 1H(doublet). The NMR spectral data show that diazocoupling occurs at 8-position of **4**.

To the 1-butanol solution containing **6** were added 0.21 g (1.4 mmol) of alloxane and 0.24 g (1.4 mmol) of *p*-toluenesulfonic acid, and the reaction mixture was refluxed for 6 h. The precipitate formed on the addition of several drops of pyridine was collected by suction and washed with water. The product solid **1** was recrystallized from acetic acid with active carbon: mp>293 °C, yield from **5**, 40%. Mass spectrum: M^+ 307. Found: C, 58.39; H, 4.61; N, 20.95%. Calcd for $C_{16}H_{13}N_5O_2\cdot H_2O$: C, 59.07; H, 4.65; N, 21.53%.

Preparations of 10-ethylisoalloxazine (**7**) and 1-benzyl-3-carbamoyl-1,4-dihydroquinoline (BCQH) were described previously.[31,32]

Kinetics. The kinetic measurements of the flavin oxidation of phenylhydrazine, L-ascorbic acid, and alcohols were carried out at 30 °C under anaerobic conditions. The rates were determined by following each absorption maximum of the **1**–metal complexes. The reactions with the dihydro compounds were carried out at 30 °C aerobically under the recycle conditions.[17] The rates were determined by following each absorption maximum of BCQH (340 nm) and 10-methyl-9,10-dihydroacridine (284 nm). The further detailed reaction conditions are recorded in footnotes to each table.

Results and Discussion

Influence of Metal Ions on the Absorption Spectrum of 1. Early spectral studies of model flavin–metal interactions reveal that oxidized flavins exhibit no singificant affinity for most metals, whereas Ag(I), Cu(I), Mo(V), Ru(II), and Fe(II) were found to complex oxidized flavins probably owing to a metal–flavin charge transfer stabilization.[28,29,33-35] The spectral studies suggested that the metal binds to *O*(4) or *N*(5), or both as **8**.[28,29,35] Crystallographic studies of Ag(I) complexes later verified *O*(4)–*N*(5) coordination and in addition revealed second chelate site consisting of *N*(1)–*O*(2).[33,34]

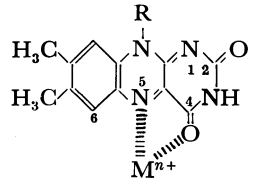

8

We measured absorption spectra of **1** and **7** in methanol at 30 °C. The absorption spectrum of **1**, which features the shift of the S2 band (317 nm) to shorter wavelength and the weakened S1 band (437 nm) relative to the S2 band, is closely akin to that of some 6-substituted flavins[36] rather than to that of conven-

TABLE 1. INFLUENCE OF ADDED METAL IONS ON THE ABSORPTION SPECTRA OF **1** IN METHANOL AT 30 °C

Metal salt ([M^{n+}]/[**1**])	λ_{max}/nm (ε_{max})	
None	317(14300)	437(8910)
$ZrCl_4$(2)	328(27800)	434(13800)
$FeCl_3$(12)	328(22800)	434(10300)
$SbCl_3$(11)	328(23000)	434(11000)
(104)	328(20400)	434(9800)
(218)	328(23500)	434(11200)
$FeCl_2$(5)	327(29800)	434(13800)
(10)	327(31600)	434(15200)
(60)	327(34900)	434(16100)
$HgCl_2$(6)	318(11300)	450(6870)
(12)	320(17500)	452(10500)
(120)	322(21300)	453(12200)
$ZnCl_2$(19)	318(33600)	462(8900)
$CuCl_2$(40)	322(7900)	455(6440)
$AgNO_3$(19)	319(5900)	460(5000)
$Mg(ClO_4)_2$(19)	317(10300)	437(7060)

a) [**1**]$=2.00\times10^{-5}$ M. In the spectral measurements, the sample cell contains **1** and metal salt while the reference cell contains metal salt only.

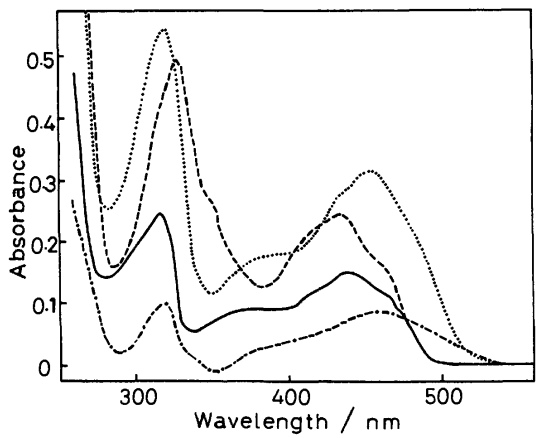

Fig. 1. Influence of added metal ions on the difference absorption spectra of **1** (1.72×10^{-5} M) in methanol at 30 °C. The reference cell contains metal ion equal to that in the sample cell. ——, No metal ion; ------, [Zr^{4+}] $=3.30\times10^{-5}$ M (type A); ·····, [Hg^{2+}]$=3.30\times10^{-4}$ M (type B); ·–·–·, [Ag^+]$=3.30\times10^{-4}$ M (type C).

tional flavins. As reported previously,[28,35] no significant spectral change of **7** occurred on the addition of metals listed in Table 1 (expect Ag(I)). On the other hand, the absorption spectrum of **1** was sensitively affected by various kinds of metal ions (Table 1 and Fig. 1). The influence of metal ions on the absorption spectra would be classified into three types (Table 2). In type A, the absorption bands are enhanced in whole wavelength region of **1**. In type B, a new absorption band spreading to longer wavelength region appears in addition to type A. Type C features the reduction of the flavin bands and the enhancement of the longer wavelength band. On the other hand, the absorption spectrum changed only slightly on the addition of Mg^{2+}, Ca^{2+}, Sr^{2+}, Ba^{2+}, Ni^{2+}, and Mn^{2+}.

Two facts established in the early spectral studies[28,29,35] are very helpful to speculate the coordination structure: That is, (i) conventional flavins do not form complexes with most metals, indicating that the complexation with **1**, when it occurs, must involve the coordination of $N(1')$-position to metal and (ii) the interaction of metal with $O(4)$ is the origin of the longer-wavelength absorption band. Metal ions of type A have not the longer-wavelength absorption band. Thus, the coordination structure possibly involves the interaction at $N(5)$ and $N(1')$ but not at $O(4)$.

TABLE 2. CLASSIFICATION OF METAL IONS FROM SPECTRAL PATTERNS

Type	ε_{max} at 317 nm	ε_{max} at 437 nm	Longer wavelength	Metal
A	Increase	Increase	No	Zr^{4+}, Sb^{3+}, Fe^{3+}, Mo^{5+}
B	Increase	Increase	Increase	Hg^{2+}, Cd^{2+}, Zn^{2+},Co^{2+}
C	Decrease	Decrease	Increase	Cu^{2+}, Ag^+

Type C metals are Cu^{2+} and Ag^+. As described above, Ag^+ is capable of forming the stable complex with conventional flavins through the $O(4)$–$N(5)$ coordination. Also in the present system, Ag^+ would form the complex through the interaction with $O(4)$ and $N(5)$ and would not interact with $N(1')$, because the three-point $O(4)$–$N(5)$–$N(1')$ coordination requires a planar structure while the typical coordination structure of Ag^+ is tetrahedral. In contrast, Cu^{2+} would reasonably interact with **1** at $O(4)$, $N(5)$, and $N(1')$, because it usually adopts a planar coordination structure.

To rationalize the coordination structure of type B metals is very difficult. Since these metal ions do not form the complex with conventional flavins, one must take the interaction with $N(1')$ into account. Since the absorption band at longer wavelength region exists, one must also take the intraction with $O(4)$ into account. Thus, the three-point coordination at $O(4)$–$N(5)$–$N(1')$ becomes a candidate, but this is basically incompatible with the fact that these metal ions favorably adopt a tetrahedral coordination structure. Another reasonable candidate that satisfies the above requirements is the $O(4)$–$N(1')$ coordination. In fact, the basicity of $N(5)$ is very low($pK_a=0$).[37] It is more unlikely, however, that the complex is formed by the $O(4)$–$N(1')$ coordination because the metal complex has an eight-membered ring. It thus seems too complicated to elucidate the coordination structure of type B metals only from the absorption spectroscopy. As a separate attempt, we inquired whether the spectral classification is associated with the ion radius of metal ions but could not find a good correlation between them.

Oxidation of Dihydrophyridine Derivatives. It is interesting to know the co-catalytic effect of complexed metals on the oxidation ability of **1**. The determination of the redox potential of metal–**1** complexes without isolation may be difficult, but one may easily evaluate it through the reaction with NADH model compounds. The reaction is a typical inter-coenzyme reaction and the logarithm of the rate constants is linearly correlated with polarographic half-wave potentials.[38] We first used 1-benzyl-1,4-dihydronicotinamide as a NADH model compound. We found, however, that most of

Table 3. Effect of added metal ions on the oxidation of BCQH, and 10-methyl-9,10-dihydroacridine[a]

Substrate	Metal (concn/mM)	$k' \times 10^4/s^{-1}$ Metal	$k' \times 10^4/s^{-1}$ Metal+**1**	k_2[c] $M^{-1}s^{-1}$
BCQH	None	——	0	0
	NaCl(1.00)	0	0	0
	$HgCl_2$(0.334)	0	0.489	1.76
	$SbCl_3$(0.337)	0	0.057	0.19
	$CuCl_2$(0.660)[b]	1.8	3.2	4.76
	$FeCl_3$(0.330)[b]	24.5	9.7	——
	$ZrCl_4$(0.033)[b]	0.5	0.5	0
N-Methylacridan	None	——	0	0
	$SbCl_3$(0.330)	0.003	0.111	0.44
	$CuCl_2$(0.066)	0.106	0.125	0.06
	$FeCl_3$(0.066)[b]	18.6	8.9	——

a) 30 °C, methanol, O_2, [dihydro compound] = 5.00×10^{-5} M, [**1**] = $(2.5—3.3) \times 10^{-5}$ M. b) 2,6-Lutidine was added: [2,6-lutidine]/[metal] = 5.0. c) $k_2 = (k'_{metal+1} - k'_{metal})/[\mathbf{1}]$.

metal ions are capable of oxidizing (or decomposing) the dihydronicotinamide at ambient conditions in methanol. We thus employed more "deactivated" and "acid-resistant" NADH model compounds, 1-benzyl-3-carbamoyl-1,4-dihydroquinoline (BCQH)[32] (Eq. 1) and 10-methyl-9,10-dihydroacridine. The kinetic results are summarized in Table 3.

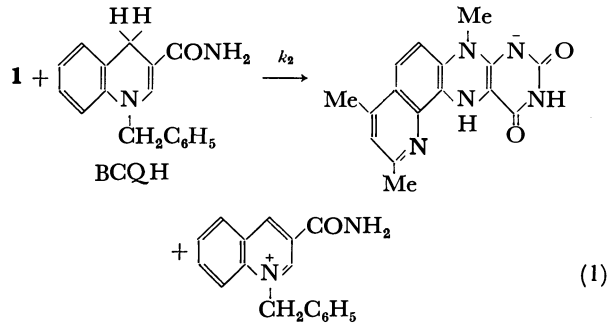

(1)

The reaction rates were monitored spectrophotometrically by following the disappearance of the absorption band of BCQH. The examination of Table 3 reveals that (i) the reaction does not occur in methanol in the absence of metal, (ii) Hg^{2+} ad Sb^{3+}, which do not or scarcely oxidize the dihydro compounds by themselves, serve as efficient co-catalysts for the oxidation by **1**, and (iii) Cu^{2+} is able to oxidize the dihydro compounds by itself but the Cu^{2+}–**1** complex exhibits a markedly higher oxidation ability. As the addition of NaCl provides no catalytic effect on the reaction rate, the co-catalytic behavior of the heavy metals cannot be attributed to a simple salt effect. Strangely, the rate for Fe^{3+} was rather suppressed by the addition of **1**. Compound **1** may weaken the oxidation power of Fe^{3+} through the complex formation. On the other hand, the reaction with **7** which was carried out as a control experiment was not facilitated at all by metal ions listed in Table 3.

Oxidation of Phenylhydrazine. It is known that conventional flavins oxidize phenylhydrazine in the presence of a strong base such as 1,8-diazabicyclo[5.4.0]-undec-7-ene, the product from phenylhydrazine being benzene.[39] The reaction takes place, although slowly, even in the presence of a basic component. The second-order rate constants (k_2) in the absence of metal (Table 4) show that **1** is 18.9 times more reactive than **7**. We found that the oxidation of phenylhydrazine by **1** in ethanol is strongly catalyzed by Cu^{2+} and Fe^{3+}. The examination of Table 4 manifests, however, that the oxidation by **7** is also catalyzed by Co^{2+}, Mg^{2+}, and Fe^{3+}. Hence, the metal catalysis may not be rationalized in terms of the preequilibrium complexation between **1** and metals but rather in terms of the stabilization of the transition state by metal ions.

More interesting is the finding that in the oxidation of

Table 4. Effect of added metal ions on the oxidation of phenylhydrazine[a]

Flavin	Metal	$k_2 \times 10^3/M^{-1}s^{-1}$[b]	Radical species
1	None	17.3	—
	Cu^{2+}	72.6	—
	Co^{2+}	c)	+
	Cd^{2+}	c)	+
	Zn^{2+}	2.84	+
	Mg^{2+}[d]	8.56	—
	Fe^{3+}	66.2	+
	Sb^{3+}	15.9	—
	Zr^{4+}	14.2	—
7	None	0.917	—
	Cu^{2+}	c)	—
	Co^{2+}	2.23	—
	Zn^{2+}	0.23	—
	Mg^{2+}[d]	16.3	—
	Fe^{3+}	9.45	—

a) 30 °C, ethanol, N_2. [**1** or **7**] = 1.50×10^{-5} M, [phenylhydrazine] = 0.510 M, [metal ion (as chloride salt)] = 2.25×10^{-4}M. b) $k_2 = k_1'$ (pseudo-first-order rate constant)/[phenylhydrazine]. c) The increase in the absorption band continued and the absorbance did not satisfy the first-order equation. d) $Mg(ClO_4)_2$.

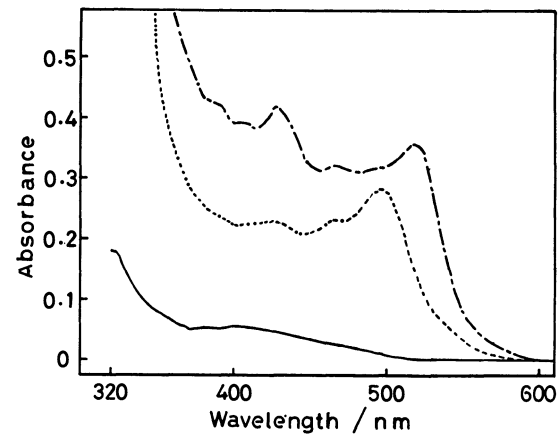

Fig. 2. Absorption spectra of reduced and semiquinone species. ——, Reduced by EDTA and light; ·—·—, semiquinone in phenylhydrazine + Cd^{2+}; ------, semiquinone in phenylhydrazine + Zn^{2+}. 30 °C, [**1**] = 2.80×10^{-5} M, [metal chloride] = 4.20×10^{-4} M, [phenylhydrazine] = 9.67×10^{-1} M, ethanol containing 0.8 vol% *N*,*N*-dimethylformamide.

phenylhydrazine by **1** a new absorption maximum assignable to the semiquinone radical species[28,40] appears at around 510 nm in the presence of Co^{2+}, Cd^{2+}, Zn^{2+}, and Fe^{3+} (Fig. 2). The absorption band immediately disappeared when oxygen was introduced, and the oxidized **1** was regenerated quantitatively. In other cases, the spectrum of oxidized **1** changed to that of reduced **1** without accumulation of any intermediary absorption spectrum. The authentic spectrum of reduced **1** was obtained by photoreduction with disodium salt of ethylenediaminetetraacetic acid([EDTA]/[**1**]=60). It warrants considerable attention that these metal ions (except Fe^{3+}) are classified as type B in Table 1 and usually adopt tetrahedral coordination. It is now unequivocally established that the steric shape of reduced flavins is folded along the $N(5)$–$N(10)$ axis like a butterfly wing.[41,42] It is very conceivable that the semiquinone radical species have a similar bent structure. If so, the tetrahedral coordination metals would be able to specifically stabilize the semiquinone radical species of **1** through a three-point coordination (Scheme 1). Probably, the tetrahedral metals of type B interact with semiquinone **1** at $O(4)$–N(5)–$N(1')$.

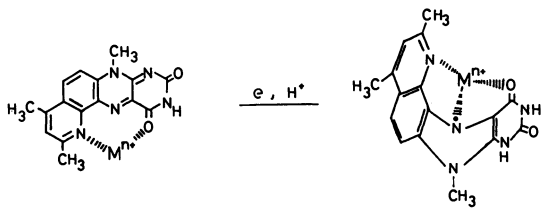

1–M^{n+}(type B) complex(?) Semiquinone–M^{n+} complex

Scheme 1.

TABLE 5. EFFECT OF ADDED METAL IONS ON THE OXIDATION OF L-ASCORBIC ACID[a]

Flavin	Metal	$k_{decomp}\times10^4/s^{-1}$ [b]	$k_1'\times10^4/s^{-1}$ [c]	Radical species
1	None	0.11	89	—
	Mg^{2+}[e]	0.20	164	—
	Ca^{2+}	5.5	308	—
	Zr^{4+}	0.23	184	—
	Zn^{2+}	1.5	59	+
	Cd^{2+}	92	86	+
	Co^{2+}	39	d)	—
7	None	0	19	—
	Mg^{2+}[e]	0	d)	—
	Ca^{2+}	0	d)	—
	Zr^{4+}	0	0.63	—
	Zn^{2+}	0	d)	—
	Cd^{2+}	0	9.3	—
	Co^{2+}	18	52	—

a) 30 °C, 95% ethanol, N_2. [**1** or **7**]$=1.40\times10^{-5}$ M, [DBU] = 0.14 M, [ascorbic acid] $=1.43\times10^{-2}$ M, [metal ion (as chloride salt)]$=2.15\times10^{-4}$M. b) Rate constant for the first-order decrease in the absence of ascorbic acid. c) Rate constant for the first-order decrease in the presence of ascorbic acid. d) The increase in the absorption band continued and the absorbance did not satisfy the first-order equation. e) $Mg(ClO_4)_2$.

Oxidation of L-*Ascorbic Acid.* The oxidation of L-ascorbic acid to dehydroascorbic acid is another diagnostic reaction to estimate the oxidation ability of flavins. In the absence of base the reaction did not occur in 95% ethanol, so that we used excess DBU. The addition of DBU caused not only the oxidation (k_1') but the decomposition (probably hydrolytic) of the isoalloxazines (k_{decomp}) which was observed in the absence of L-ascorbic acid. In particular, Cd^{2+} and Co^{2+} (type B metals) caused a remarkably fast decomposition of **1**. It is known that the base-mediated decomposition of isoalloxazines is usually facilitated by electron-withdrawing substituents.[24] Therefore, the k_{decomp} values in Table 5 suggest that the metal ions complexed with **1** make the isoalloxazine ring more electron-deficient. However, the fact that type B metals efficiently catalyze the (hydrolytic) decomposition may imply that these metals have some specific catalytic mechanism (*e.g.*, nucleophilic attack of metal-coordinated hydroxide). On the other hand, Mg^{2+}, Ca^{2+}, and Zr^{4+} are good catalyst for the oxidation of ascorbic acid by **1**, but other metals play no or little cocatalytic role. We have found that the **1**–Zr^{4+} complex acts as a strong oxidizing agent.[47] On the other hand, Mg^{2+} and Ca^{2+} would stabilize the transition state through the interaction with ascorbate anion. Interestingly, the complex with Zn^{2+} and Cd^{2+}, which are tetrahedral coordination metals, gave a radical peak at around 510 nm. The finding supports again that the type B metals are able to stabilize the semiquinone radical of **1**.

Oxidation of Alcohols. It is known that many electron-deficient organic molecules (*e.g.*, azodicarboxylic diesters, 5-deazaisoalloxazines, 2,3-dichloro-5,6-dicyanobenzene, *etc.*) serve as oxidizing reagents for alcohols.[43–46] However, few of them are able to catalyze the oxidation in a recycle manner because of the insensitivity of the reduced forms to molecular oxygen. If the **1**–metal complexes are able to oxidize alcohols, a new possibility arises that alcohols are oxidized by molecular oxygen with the aid of the ping-pong-type

TABLE 6. EFFECT OF ADDED METAL IONS ON THE OXIDATION OF ALCOHOLS AND HYDROQUINONE[a]

Alcohol (concn/M)	Metal	$k_2\times10^4/M^{-1}s^{-1}$ [b]
Benzyl alcohol (0.29)	None	0
	Cu^{2+}	0
	Co^{2+}	0
	Cd^{2+}	0
	Sb^{3+}	0
	Fe^{3+}	0.1
	Zr^{4+}	1.6
Cyclohexanol(0.57)	None	0
	Zr^{4+}	1.9
Ethanol(1.1)[c]	None	0
	Zr^{4+}	0.5
Hydroquinone(0.067)[c]	None	0
	Zr^{4+}	2.7

a) 30 °C, acetonitrile, N_2. [**1**]$=1.50\times10^{-5}$ M, [metal ion (as chloride salt)]$=2.30\times10^{-4}$ M. b) k_2(apparent second-order rate constant)$=v_{initial}/$[**1**][alcohol]. c) Acetonitrile containing 0.8 vol% *N*,*N*-dimethylformamide.

flavin catalysis. We tested the oxidation of several alcohols by the **1**–metal complexes in various solvents and found out that in acetonitrile the alcohols are in fact oxidized to corresponding aldehydes and ketone (Table 6).[47] The effective metal ions are Zr^{4+} and Fe^{3+}. The result indicates that the complexes with these metal cations are so electron-deficient as to abstract electron(s) from alcohols. The finding suggests that the present **1**–metal complexes are useful not only as a model system of metalloflavoproteins but also as an oxidation catalyst for alcohols and others.

We thank Professor Y. Murakami and Dr. Y. Fuchida for helpful discussions. This work is partly supported by a grant from Toyo Soda Kogyo Co. Ltd.

References

1) P. Hemmerich, G. Nagelschneider, and C. Veeger, *FEBS Lett.*, **8**, 69 (1970).
2) C. Walsh, *Acc. Chem. Res.*, **13**, 148 (1980).
3) T. C. Bruice, *Acc. Chem. Res.*, **13**, 256 (1980).
4) S. Shinkai, T. Ide, and O. Manabe, *Chem. Lett.*, **1978**, 583.
5) S. Shinkai, T. Yamashita, and O. Manabe, *J. Chem. Soc., Chem. Commun.*, **1979**, 301.
6) S. Shinkai, T. Yamashita, Y. Kusano, T. Ide, and O. Manabe, *J. Am. Chem. Soc.*, **102**, 2335 (1980).
7) S. Shinkai, Y. Kusano, and O. Manabe, *Makromol. Chem.*, **181**, 1791 (1980).
8) S. Shinkai, T. Yamashita, and O. Manabe, *Tetrahedron Lett.*, **21**, 2543 (1980).
9) S. Shinkai, T. Yamashita, Y. Kusano, and O. Manabe, *J. Org. Chem.*, **45**, 4947 (1980).
10) S. Shinkai, T. Yamashita, Y. Kusano, and O. Manabe, *J. Am. Chem. Soc.*, **104**, 563 (1982).
11) Y. Yano, Y. Hoshino, and W. Tagaki, *Chem. Lett.*, **1980**, 749.
12) Y. Yano, Y. Tamura, Y. Hoshino, and W. Tagaki, *Bull. Chem. Soc. Jpn.*, **53**, 2340 (1980).
13) H. Inoue and K. Higashiura, *J. Chem. Soc., Chem. Commun.*, **1980**, 549.
14) S. Shinkai, T. Yamashita, Y. Kusano, and O. Manabe, *Chem. Lett.*, **1979**, 1323.
15) S. Shinkai, T. Yamashita, Y. Kusano, and O. Manabe, *J. Am. Chem. Soc.*, **103**, 2070 (1981).
16) S. Shinkai and T. Kunitake, *Bull. Chem. Soc. Jpn.*, **50**, 2400 (1977).
17) S. Shinkai, S. Yamada, and T. Kunitake, *Macromolecules*, **11**, 65 (1978).
18) S. Shinkai, R. Ando, and T. Kunitake, *J. Chem. Soc., Perkin Trans. 2*, **1978**, 1271.
19) S. Shinkai, K. Mori, Y. Kusano, and O. Manabe, *Bull. Chem. Soc., Jpn.*, **52**, 3606 (1979).
20) S. Shinkai, S. Yamada, R. Ando, and T. Kunitake, *Bioorg. Chem.*, **9**, 238 (1980).
21) S. Shinkai, Y. Kusano, O. Manabe, and F. Yoneda, *J. Chem. Soc., Perkin Trans. 2*, **1980**, 1111.
22) W. Spetnagel and I. M. Klotz, *Biopolymers*, **17**, 1657 (1978).
23) I. Yokoe and T. C. Bruice, *J. Am. Chem. Soc.*, **97**, 450 (1975).
24) T. C. Bruice, T. W. Chan, J. P. Taulane, I. Yokoe, D. L. Elliot, R. F. Williams, and M. Novak, *J. Am. Chem. Soc.*, **99**, 6713 (1977).
25) W.-R. Knappe, *Liebigs Ann. Chem.*, **1979**, 1067.
26) T. C. Bruice, L. Main, S. Smith, and P. Y. Bruice, *J. Am. Chem. Soc.*, **93**, 7327 (1971).
27) F. Yoneda, Y. Sakuma, and K. Shinozuka, *J. Chem. Soc., Chem. Commun.*, **1977**, 681.
28) P. Bamberg and P. Hemmerich, *Helv. Chim. Acta*, **44**, 1001 (1961).
29) M. J. Clarke, M. F. Dowling, A. R. Garafalo, and T. F. Brennan, *J. Am. Chem. Soc.*, **101**, 223 (1979) and references cited therein.
30) T. Hirashima and O. Manabe, *Chem. Lett.*, **1975**, 259.
31) F. Yoneda, Y. Sakuma, M. Ichiba, and K. Shinomura, *J. Am. Chem. Soc.*, **98**, 830 (1976).
32) S. Shinkai, H. Hamada, Y. Kusano, and O. Manabe, *J. Chem. Soc., Perkin Trans. 2*, **1979**, 699.
33) C. J. Fritchie, Jr., *J. Biol. Chem.*, **248**, 7516 (1973) and references cited therein.
34) T. D. Wade and C. J. Fritchie, Jr., *J. Biol. Chem.*, **248**, 2337 (1973); C. J. Fritchie, Jr., *ibid.*, **247**, 7459 (1972) and references cited therein.
35) I. F. Baarda and D. E. Metzler, *Biochim. Biophys. Acta*, **50**, 463 (1961).
36) S. Ghisla, W. C. Kenney, W.-R. Knappe, W. McIntire, and T. P. Singer, *Biochemistry*, **19**, 2537 (1980).
37) P. Hemmerich, C. Veeger, and H. C. S. Wood, *Angew. Chem., Int. Ed. Engl.*, **4**, 671 (1965).
38) I. M. Gascoigne and G. K. Radda, *Biochim. Biophys. Acta*, **131**, 498 (1967).
39) Y. Yano, T. Sakaguchi, and S. Asai, private communication.
40) A. Ehrenberg, *Vitamins Hormones*, **28**, 489 (1970).
41) L. Tanscher, S. Ghisla, and P. Hemmerich, *Helv. Chim. Acta*, **56**, 630 (1973).
42) P. Kierkegaard, R. Norrestam, P. Werner, I. Csoregh, M. Glehn, R. Karlsson, M. Leijonmarch, O. Ronnquist, B. Stensland, O. Tillberg, and L. Torbjornsson, "Flavins and Flavoproteins," ed by H. Kamin, University Park Press, Baltimore (1971), p. 1.
43) F. Yoneda, *Yuki Gosei Kagaku Kyokai Shi*, **38**, 679 (1980) and references cited therein.
44) H.-D. Becker, A. Bjork, and E. Alder, *J. Org. Chem.*, **45**, 1596 (1980).
45) F. Yoneda, Y. Sakuma, and P. Hemmerich, *J. Chem. Soc., Chem. Commun.*, **1977**, 825.
46) F. Yoneda, H. Yamato, and M. Ono, *J. Am. Chem. Soc.*, **103**, 5493 (1981).
47) The product analysis for metal-assisted flavin oxidation of alcohols has been reported as a preliminary publication: S. Shinkai, Y. Ishikawa, and O. Manabe, *Chem. Lett.*, **1982**, 809.

Photoresponsive Crown Ethers. 9. Cylindrical and Phane Crown Ethers with Azobenzene Segments as a Light-switch Functional Group[1)]

Seiji SHINKAI,* Yoshihiro HONDA, Takahide MINAMI, Kaori UEDA, Osamu MANABE,* and Masashi TASHIRO†

Department of Industrial Chemistry, Faculty of Engineering, Nagasaki University, Nagasaki 852

†*Department of Molecular Science and Technology, Graduate School of Engineering Sciences, Kyushu University, Kasuga, Fukuoka 816*

(Received December 6, 1982)

Cylindrical and phane crown ethers with azobenzene segments as a light-switch functional group were synthesized. Cylindrical ionophores in which two diazacrown ethers are linked by two photoresponsive azobenzene pillars change their binding ability for polymethylenediammonium salts in response to photoirradiation. Thus, the distance between the two crown rings can be photocontrolled. A phane-type ionophore in which 1,23-bis(*p*-aminophenoxy)-3,6,9,12,15,18,21-heptaoxatricosane is linked by a *trans*-4,4′-azobenzenedicarbonyl segment exhibits no affinity with all alkali metal cations but significantly binds Rb^+ and Cs^+ under UV-light irradiation. This is the example of the "all-or-nothing" control of the ion-binding ability and implies that a crown-like loop emerges only when the azobenzene segment is photoisomerized to the *cis*-configuration. These ionophores are categorized to novel photoresponsive crown ethers.

The importance of macrocyclic ligands has been recognized not only in organic chemistry but also in relation to biological chemistry. One of the recent exploration is associated with the combination of a photoresponsive function with macrocyclic ligands, which leads to photocontrol of chemical and physical functions of a crown ether family by an on-off light switch.[2-7)] For example, we and others have reported that a photoresponsive crown ether that combines within a molecule both a crown ether and a photoresponsible chromophore changes its conformation in response to the photoinduced configurational change in the chromophore,[2-7)] resulting in a change in the complexation ability. The finding has been applied to the novel photocontrol of solvent extraction and ion transport across membranes.[8-10)]

We here wish to address two new classes of photoresponsive crown ethers, cylindrical and phane ionophores. A cylindrical ionophore, in which two macrocyclic ligands are linked by two (or more than two) pillars, is an interesting receptor molecule which is able to bind diammonium ions and plural metal ions.[11-14)] Since the metal affinity of cylindrical ionophores is crucially governed by the pillar length, one may expect that the binding ability and the binding selectivity would be readily controlled by changing the length of the two pillars. Thus, cylindrical ionophores with azobenzene pillars would act as "elastic" ionophores in response to photoinduced *trans-cis* isomerization of the azobenzene pillars. Meanwhile, a phane ionophore, in which a poly(oxyethylene) chain is linked by 4,4′-azobenzene, may exhibit the photoresponsive "all-or-noting" change in the ion-binding ability.[15)] Since the distance between the 4- and 4′-positions of *trans*-azobenzene is 9.0 Å while that of *cis*-azobenzene is 5.5 Å, one may visualize that an ionophoric polyoxyethylene loop would appear in *cis*-isomers and disappear in *trans*-isomers reversibly in response to photoirradiation. With these objects in view we synthesized cylindrical and phane ionophores (**1** and **2**, respectively) and evaluated their photoresponsive behaviors in comparison with their model compounds **3**.

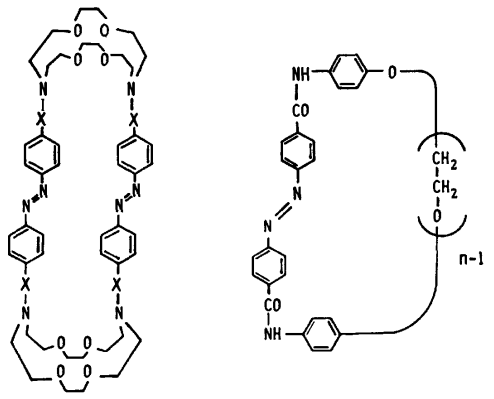

1 (X=CO)

1 (X=OCH_2CO)

2 (n=9)

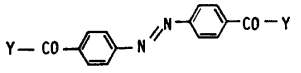

3 (Y=An) : Y=NHC_6H_5

3 (Y=EtAn) : Y=$N(C_2H_5)C_6H_5$

3 (Y=Morph) : Y=N⟨O⟩

Scheme 1.

Experimental

Materials. Compound **1**(X=CO) was synthesized in benzene from equimolar amounts of 1,10-diaza-4,7,13,16-tetraoxa-18-crown-6 and 4,4′-bis(chloroformyl)azobenzene[4)] according to the high-dilution method. In a 1-l three-necked flask with a reflux condenser were placed 200 ml of benzene and 5 ml of triethylamine, and 2.10 g (8.0 mmol) of 1,10-diaza-4,7,13,16-tetraoxa-18-crown-6 in 100 ml of benzene from one dropping funnel and 2.46 g (8.0 mmol) of 4,4′-bis(chloroformyl)azobenzene in 100 ml of benzene from another dropping funnel were added simultaneously. The reaction mixture was stirred vigorously at room temperature. It took about 1 h to complete the addition of two reactants, and the reaction

was continued for 1 h. The precipitate was removed by filtration, the filtrate being washed with water. The benzene was evaporated to dryness *in vacuo*. When the residual red solid was redissolved in 50 ml of benzene, insoluble, viscous material(polymer?) was removed. The benzene solution was concentrated again, and the residue was recrystallized three times from xylene; mp 224—226 °C, yield 21%, hygroscopic. IR(KBr): $\nu_{C=O}$ 1635 cm^{-1}. NMR(Me_2SO-d_6, 80 °C): crown protons, 3.5—3.8 ppm, 48H; 2′-H of azobenzene, 7.56 ppm, 8H; 3′-H of azobenzene, 7.88 ppm, 8H. Mass spectrum: M^+ (*m/e*) 992. Found: C, 62.36; H, 6.64: N, 11.01%. Calcd for $C_{52}H_{64}N_8O_{12}$: C, 62.89; H, 6.50; N, 11.28%. Gel permeation chromatography gave a single peak at 1000±40.

Compound **1**(X=OCH_2CO) was similarly synthesized by the high-dilution method from equimolar amounts of 1,10-diaza-4,7,13,16-tetraoxa-18-crown-6 and 4,4′-bis(chloroformylmethoxy)azobenzene. 4,4′-Bis(carboxymethoxy)azobenzene was prepared from 4,4′-dihydroxyazobenzene and chloroacetic acid in aqueous solution containing NaOH: mp 250 °C, yield 73%. 4,4′-Bis(chloroformylmethoxy)azobenzene was obtained by treating this compound with thionyl chloride: mp 140—145 °C, yield 69%. The condensation to synthesize **1**(X=OCH_2CO) was carried out in benzene in the presence of triethylamine. The raw product was purified by the TLC method(silica gel, chloroform–methanol (8 : 2 v/v)) and finally recrystallized from chlorobenzene: mp 219—221 °C yield 37%. IR(KBr): $\nu_{C=O}$ 1660 cm^{-1}, ν_{C-O-C} 1060—1160 cm^{-1}. NMR($CDCl_3$): crown protons, 3.4—3.8 ppm, 48H; OCH_2, 4.80 ppm, 8H; 3′-H of azobenzene, 6.92 ppm, 8H; 2′-H of azobenzene, 7.72 ppm, 8H. Found: C, 60.47; H, 6.59; N, 9.73%. Calcd for $C_{56}H_{72}O_{16}N_8$: C, 60.42; H, 6.52; N, 10.07%. Gel permeation chromatography gave a single peak at 1000±50.

Compound **2**(*n*=9) was synthesized according to the high-dilution method from equimolar amounts of 1,23-bis(*p*-aminophenoxy)-3,6,9,12,15,18,21-heptaoxatricosane[16] and 4,4′-bis(chloroformyl)azobenzene[4] in benzene in the presence of triethylamine. The precipitate was a mixture of triethylamine hydrochloride and orange solid. The colored solid(polymer?) was insoluble in usual organic solvents. The filtrate was washed with water and concentrated to dryness *in vacuo*. The residue was recrystallized from benzene: mp 179—183 °C, yield 8.4%. IR(KBr): ν_{NH} 3450 cm^{-1}, $\nu_{C=O}$ 1670 cm^{-1}, ν_{C-O-C} 1120—1126 cm^{-1}. NMR(Me_2SO-d_6, 70 °C): central methylene protons at 8, 10, 11, 13, 14, and 16 positions, 3.21 ppm, 12H; 5, 7, 17, and 19 methylene protons, 3.46 ppm, 8H; 4 and 20 methylene protons, 3.57 ppm 4H; 2 and 22 methylene protons, 3.79 ppm, 4H; 1 and 23 methylene protons, 4.22 ppm, 4H; aromatic protons of the aminophenol moiety, 7.02 ppm (4H), 7.40 ppm (4H); aromatic protons of the azobenzene moiety, 7.88 ppm (4H), 8.00 ppm (4H); NH, 10.04 ppm, 2H. Mass spectrum: M^+ (*m/e*) 786. Found: C, 63.57: H, 6.38; N, 7.11%. Calcd for $C_{42}H_{50}O_{11}N_4$: C, 64.11; H, 6.40; N, 7.12%. Gel permeation chromatography gave a single peak at 770±50.

Compound **3**(Y=An) and **3**(Y=EtAn) were prepared by the reaction of 4,4′-bis(chloroformyl)azobenzene[4] with aniline and *N*-ethylaniline, respectively, in benzene in the presence of triethylamine. **3**(Y=An): mp>260 °C. Found: C, 74.37; H, 4.66; N, 13.47%. Calcd for $C_{26}H_{20}N_4O_2$: C, 74.27; H, 4.79; N, 13.32%. **3**(Y=EtAn): mp 135—140 °C. Found: C, 70.23; H, 6.19; N, 10.98%. Calcd for $C_{30}H_{28}N_4O_2 \cdot 2H_2O$: C, 70.29; H, 6.29; N, 10.93%. The preparation of **3**(Y-Morph) was described previously.[4]

Miscellaneous. The method of solvent extraction was described priviously.[4,8] The deteils of the work-up conditions are recorded in footnotes to Table 2. A 500-W high-pressure Hg-lamp with a color glass filter (330 nm<λ<380 nm) was used for the *trans*-to-*cis* photoisomerization unless otherwise stated. The ionophore concentration for the solvent extraction was usually higher than that for the kinetic measurements. In case the concentration was extremely high, the *trans*-to-*cis* photoisomerization was slow and the *cis*-percentage at the photostationary state was not sufficiently high. We thus prepared a thin solution layer between two glass plates and photoirradiated the solution. This method enabled a satisfactory photoconversion to the *cis*-isomers. The *cis*% at the photostationary state was estimated from the decrease in the absorption maximum of the *trans*-isomers, assuming that the absorbance of the *cis*-isomers at the wavelength is neglible in comparison to that of the *trans*-isomers. In all cases, the *cis-trans* isomerism was reversible within the experimental error.

The method of kinetic measurements was also described in the previous papers.[4,8] After a cuvette containing an ionophore solution was photoirradiated, the cuvette was transferred to a thermostated cell-holder (30 °C) in a spectrophotometer. The reaction was monitored by following the appearance of the absorption maximum of the *trans*-isomers.

Results and Discussion

Syntheses, Spectroscopic Properties, and Photoresponsiveness. We previously synthesized an azobenzene-capped azacrown ether **4** (*i.e.*, 1 : 1 adducts) from 1,10-diaza-4,7,13,16-tetraoxa-18-crown-6 and 3,3′-bis(chloroformyl)azobenzene in 23% yield.[4] On the other hand, the reaction between the azacrown ether and 4,4′-bis(chloroformyl)azobenzene mainly gave the polymer.[4] The difference was rationalized in terms of the steric factor that the distance between 1-*N* and 10-*N* of the azacrown ether is almost equal to that between two carbonyl groups of the 3,3′-isomer but significantly shorter than that between two carbonyl groups of the 4,4′-isomer. The present result indicates that when the distances between two reaction centers do not fit each other, the 2 : 2-adduct such as **1** (X=CO) and (**1** X=OCH_2CO) results under high-dilution conditions

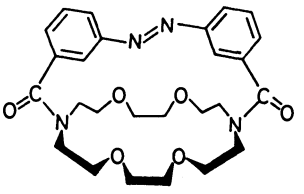

4

An azobenzenophane **2** (*n*=9) was also synthesized according to the high-dilution method. The CPK model of **2** (*n*=9) suggests that the poly(oxyethylene) clain is almost linearly extended when the azobenzene segment adopts the *trans*-configuration. We attempted the synthesis of the homologues with the smaller ring-size (*e.g.*, **2** (*n*=7 and 8)), but we could not isolate any cyclic compound by the TLC method. The result suggests that eight oxyethylene units are the shortest chain to form the cyclic adduct.

In the NMR measurements, the crown protons of **1** (X=CO) and **1** (X=OCH_2CO) appeared at 3.5—3.8 ppm and 3.4—3.8 ppm, respectively, as a broad single

Table 1. Spectroscopic and kinetic properties of cylindrical and phane azobenzene derivatives in o-dichlorobenzene (30 °C)

Properties	**1** (X=CO)[a]	**1** (X=OCH_2CO)	**2** (n=9)[b]	**3** (Y=An)[c]	**3** (Y=EtAn)	**3** (Y=Morph)
λ_{max}/nm	332	356	340	345	343	331
ε_{max}	53200	42900	25240	30200	22300	26200
Time/min to reach photostationary state	60	1.5	30	6	10	10
cis(%) at photostationary state	65	63	10	28	40	26
$k_{cis\rightarrow trans}/s^{-1}$	6.33×10^{-6}	1.55×10^{-3}	*ca.* 1×10^{-5} [d]	1.58×10^{-5}	1.26×10^{-5}	2.22×10^{-5}

a) *o*-Dichlorobenzene: butyl alcohol=86.8 : 13.2 by volume. b) *o*-Dichlorobenzene: butyl alcohol=4 : 1 by volume. c) 9 vol% *N,N*-dimethylformamide in *o*-dichlorobenzene. d) The rate constant could not be determined accurately because the spectral change was slight.

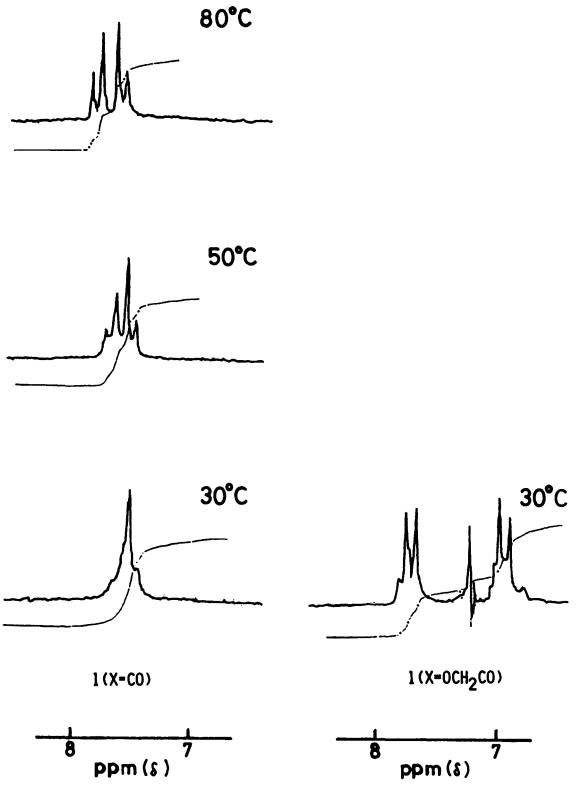

Fig. 1. Temperature dependence of the NMR spectra of **1** (X=CO) (in Me_2SO-d_6) and **1** (X=OCH_2CO) (in $CDCl_3$).

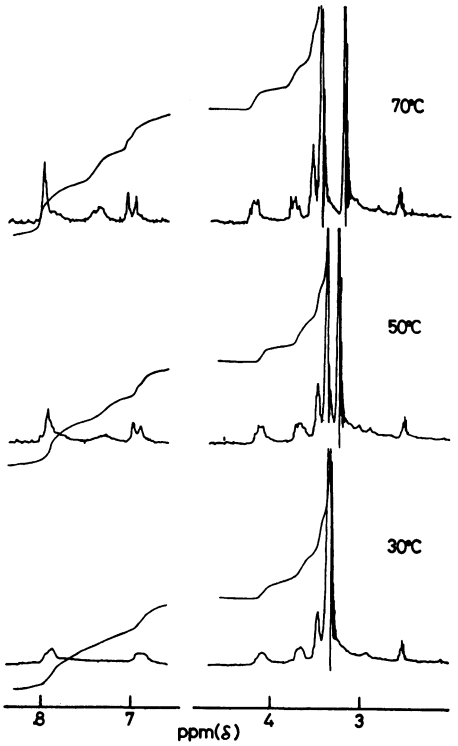

Fig. 2. Temperature dependence of the NMR spectra of **2** (n=9) (in Me_2SO-d_6).

peak. On the other hand, the NMR spectrum of **4** gave two resolved peaks at 3.6—3.9 ppm (8H) and 4.1—4.8 ppm (16H), which were attributed to *N*-CH_2 and *O*-CH_2 of the crown ring, respectively.[4] The comparison of these data suggests that the *O*-methylene protons of **4** are somewhat deshielded by the ring current of the azobenzene moiety. The finding is in line with our previous prediction that the azobenzene moiety of *trans*-**4** stands vertically over the crown ether plane.[4]

Another interesting finding in the NMR measurements is the fact that the NMR peaks of **1** (X=CO) and **2** (n=9) are significantly broad at 30 °C, whereas those of **1** (X=OCH_2CO) are not subject to such a broadening effect (Figs. 1 and 2). The peaks are sharpened with increasing temperature. Conceivably, the broadening effect is induced by the steric rigidity of these molecules and in fact, the CPK models of **1** (X=CO) and **2** (n=9) are more rigid than that of **1** (X=OCH_2CO). It is interesting to know whether the steric rigidity is reflected by photoresponsive behaviors of these molecules. As shown is Table 1, we have found that it takes a long time for **1** (X=CO) and **2** (n=9) to reach the photostationary states as compared with the time required for **1** (X=OCH_2CO) and model compounds such as **3** (Y=An), **3** (Y=EtAn), and **3** (Y=Morph). In contrast, the significant difference was not found for the rate of the thermal *cis*-to-*trans* isomerization: the rate constants ($k_{cis\rightarrow trans}$) for **1** (X=CO) and **2** (n=9) are comparable with those for the model compounds. These results may mean that the transition state of **1** (X=CO) and **2** (n=9) in the photoisomerization process is more destabilized than that of **1** (X=OCH_2CO) and model compounds. Previously, Shiga *et al.*[3] synthesized phane-type crown ether in which a poly(oxyethylene) chain is linked directly by 2,2′-azobenzene. It was found, however, that the photoisomerization of this compound is extremely slow and sometimes accompanied by photodecomposition. This would be also due to the sterically-destabilized transition state. Fortunately, the *trans*-isomers used in the present

study were photochemically converted to the *cis*-isomers and the *cis*-isomers were thermally converted back to the *trans*-isomers: the *cis-trans* isomerism was reversible within the allowable experimental error. Meanwhile, we consider that the enhanced rate constant ($k_{cis \rightarrow trans}$) observed for **1** (X=$OCH_2CO$) is attributable to the electronic effect but not to the steric effect.

Along the isomerization process of the photoresponsive cylindrical ionophores there exist three different isomers: *trans-trans*, *trans-cis*, and *cis-cis*. The thermal isomerization of these cylindrical ionophores satisfied the first-order rate equation for up to four half-lives and the UV-visible spectra of the thermal isomerization showed sharp isosbestic points. The results support that no intermediate is accumulated along the isomerization pathway. One may suppose, therefore, that 65% *cis*-**1** (X=CO) means, for example, 65% *cis-cis*-**1** (X=CO) and 35% *trans-trans*-**1** (X=CO).

Solvent Extraction of Alkali Metal Cations. Solvent extraction of alkali picrates with cylindrical and phane ionophores is summarized in Table 2. Ex% denotes the partition of picrate to organic phase. At the start of this experiment, we expected that *trans-trans*-**1** (X=CO) would form a 1 : 1 crown/metal (*i.e.*, 1 : 2 **1** (X=CO)/metal) complex, whereas *cis-cis*-**1** (X=CO) would form a 2 : 1 crown/metal (*i.e.*, 1 : 1 **1** (X=CO)/metal) sandwich-type complex with large alkali metal cations. The Ex% of picrate salts in Table 2 reveals, however, that the formation of the sandwich-type complex is rather unlikely: *cis-cis*-**1** (X=CO) generally exhibits a metal affinity greater than *trans-trans*-**1** (X=CO), but the enhancement in the Ex% is not limited to large alkali metal cations. We consider at present that the steric rigidity of the crown rings is somewhat relaxed through the photoisomerization of the azobenzene pillars, resulting in the improved affinity toward all alkali metal cations. Similarly, *cis-cis*-**1** (X=OCH_2CO) has the larger Ex% than *trans-trans*-**1** (X=OCH_2CO) and exhibits the selectivity for small alkali metal cations.

It is speculated on the basis of the CPK model building that the poly(oxyethylene) chain of *trans*-**2** (n=9) is almost linearly extended while that of *cis*-**2** (n=9) may form a crown-like loop. The examination of Table 2 reveals that *trans*-**2** (n=9) completely lacks the affinity with metal ions, whereas photoisomerized *cis*-**2** (n=9) is capable of extracting large alkali metal cations such as Rb^+ and Cs^+ in the significant Ex%. Thus, an ionophoric, crown-like loop appears and disappears in response to photoirradiation and the loop size is roughly comparable with that of 21-crown-7.

Solvent Extraction of Polymethylenediammonium Salts. One of the most interesting characteristics of photoresponsive cylindrical ionophores would be the possibility that the distance between two crown rings changes reversibly by an on-off light-switch. The possibility was tested by the solvent extraction of polymethylenediammonium salts as a molecular measure. The inspection of CPK models suggests that, assuming that the polymethylene chain adopts an extended conformation, the distances between the two crown rings of *trans-trans*-**1** (X=CO) and *cis-cis*-**1** (X=CO) are almost equal to those between the two terminal ammonium groups of decamethylenediamine and hexamethylenediamine, respectively.

Table 2. Extraction of picrate salts of alkali metal cations with cylindrical and phane crown ethers (30 °C)

Crown	Ex(%)			
	Na^+	K^+	Rb^+	Cs^+
1 (X=CO)[a], dark	4.4	3.9	5.3	4.7
light (*cis* 54%)	6.5	6.3	6.8	8.5
1 (X=OCH_2CO)[b], dark	4.8	1.7	0	0
light (*cis* 67%)	10.2	2.6	2.6	0
2 (n=9)[c], dark	0	0	0	0
light (*cis* 10%)	0	0	4	1

a) Aqueous phase: [picric acid]=1.00×10^{-4} M, [MOH]=1.00×10^{-2} M, [MCl]=0.49 M. Organic phase: [**1** (X=CO)]=1.00×10^{-3} M, *o*-dichlorobenzene: butyl alcohol=9 : 1 by volume. b) Aqueous phase: [picric acid]=1.00×10^{-4} M, [MOH]=1.00×10^{-2} M, [MCl]=0.49 M. Organic phase: [**1** (X=OCH_2CO)]=3.00×10^{-3} M, chloroform: butyl alcohol=9: 1 by volume. c) Aqueous phase: [picric acid]=3.90×10^{-3} M, [MOH]=6.00×10^{-3} M, [MCl]=0.59 M. Organic phase: [**2** (n=9)]=9.91×10^{-3} M, *o*-dichlorobenzene: butyl alcohol=4: 1 by volume.

Table 3. Extraction of polymethylenediammonium salts with cylindrical crown ethers (30 °C)

Crown	Ex(%) of $H_3N^+(CH_2)_nNH_3^+\cdot(picrate)_2$				
	n=4	6	8	10	12
1 (X=CO)[a], dark	0.5	3.0		20.0	27.2
light(*cis* 22%)	0.8	8.9		12.3	22.0
light(*cis* 38%)	2.4	12.6		9.3	18.9
light(*cis* 54%)	3.0	19.0		6.7	13.1
1 (X=OCH_2CO)[b], dark		0	0	3.0	7.6
light(*cis* 67%)		0	0	0.4	4.2

a) Aqueous phase: [picric acid]=4.00×10^{-4} M, [HCl]=5.96×10^{-2} M, [$H_2N(CH_2)_nNH_2$]=3.00×10^{-2} M. Organic phase: [**1** (X=CO)]=3.00×10^{-3} M, *o*-dichlorobenzene: butyl alcohol=9 : 1 by volume. b) Aqueous phase:[picric acid]=4.00×10^{-4} M, [HCl]=5.96×10^{-2} M, [$H_2N(CH_2)NH_2$]=2.99×10^{-2} M. Organic phase: [**1** (X=OCH_2CO)]=2.98×10^{-3} M in chloroform.

The Ex% was evaluated on the basis of the partition equilibrium of picrate ion added as counter-anion between an organic phase and an aqueous phase (see footnote b) in Table 3). The results in Table 3 substantiates several important points: (i) *trans-trans*-**1** (X=CO) extracts decamethylane and dodecamethylenediammonium salts efficiently but hardly extracts tetramethylene and hexamethylenediammonium salts, (ii) hexamethylenediammonium salt gives the greatest Ex% value under UV-light irradiation, and (iii) with increase in the concentration of *cis-cis*-**1** (X=CO), Ex% of tetramethylene and hexamethylenediammonium salts increases while Ex% of decamethylene and dodecamethylenediammonium salts decreases. The findings are basically compatible with the prediction from CPK model building. Similarly, *trans-trans*-**1** (X=OCH_2CO)

is capable of extracting diammonium salts with long methylene units but scarcely extracts those with short methylene units. As expected, the Ex% of decamethylene and dodecamethylenediammonium salts is suppressed by UV irradiation.

Conclusion

The present paper represents two novel findings. One is the fact that in the photoresponsive cylindrical ionophores, the distance between two crown rings is readily convertible by photoinduced *cis-trans* isomerism of the azobenzene pillars. The other is the all-or-noting change in the metal affinity observed for the azobenzenophane-type ionophore. These novel photoresponsive behaviors would be applicable to the photocontrol of solvent extraction, membrane transport, spatial distance between two metal ions, *etc.*

This research was supported by a Grant-in-Aid from the Ministry of Education, Science and Culture (No. 57470068).

References

1) Preliminary communication: S. Shinkai, Y. Honda, Y. Kusano, and O. Manabe, *J. Chem. Soc., Chem. Commun.*, **1982**, 848.

2) I. Yamashita, M. Fujii, T. Kaneda, S. Misumi, and T. Otsubo, *Tetrahedron Lett.*, **21**, 541 (1980).

3) M. Shiga, M. Takagi, and K. Ueno, *Chem. Lett.*, **1980**, 1021.

4) S. Shinkai, T. Ogawa, T. Nakaji, Y. Kusano, and O. Manabe, *Tetrahedron Lett.*, **1979**, 4569; S. Shinkai, T. Nakaji, Y. Nishida, T. Ogawa, and O. Manabe, *J. Am. Chem. Soc.*, **102**, 5860 (1980).

5) S. Shinkai, T. Ogawa, Y. Kusano, O. Manabe, K. Kikukawa, T. Goto, and T. Matsuda, *J. Am. Chem. Soc.*, **104**, 1960 (1982).

6) S. Shinkai, H. Kinda, and O. Manabe, *J. Am. Chem. Soc.*, **104**, 2933 (1982).

7) H. Bouas-Laurent, A. Castellan, and J.-P. Desvergne, *Pure Appl. Chem.*, **52**, 2633 (1980).

8) S. Shinkai, T. Nakaji, T. Ogawa, K. Shigematsu, and O. Manabe *J. Am. Chem. Soc.*, **103**, 111 (1981).

9) S. Shinkai, T. Minami, Y. Kusano, and O. Manabe, *J. Am. Chem. Soc.*, **104**, 1967 (1982).

10) S. Shinkai, K. Shigematsu, Y. Kusano, and O. Manabe, *J. Chem. Soc., Perkin Trans. 1*, **1981**, 3279.

11) M. R. Johnson, I. O. Sutherland, and R. F. Newton, *J. Chem. Soc., Chem. Commun.*, **1979**, 309.

12) R. Mageswaran, S. Mageswaran, and I. O. Sutherland, *J. Chem. Soc., Perkin Trans. 1*, **1979**, 722.

13) A. H. Alberts, R. Annunziata, and J.-M. Lehn, *J. Am. Chem. Soc.*, **99**, 8502 (1977).

14) J.-P. Kintzinger, F. Kotzyba-Hibert, J.-M. Lehn, A. Pagelot, and K. Saigo, *J. Chem. Soc., Chem. Commun.*, **1981**, 833.

15) S. Shinkai, T. Minami, Y. Kusano, and O. Manabe, *Tetrahedron Lett.*, **23**, 2581 (1982).

16) S. Shinkai, T. Minami, Y. Kusano, and O. Manabe, *J. Am. Chem. Soc.*, **105**, 1851 (1983).

 © 1983 The Chemical Society of Japan Bull. Chem. Soc. Jpn., 56, 1705—1709 (1983)

Photoaddition Reaction of 1,4-Dibromo-2,5-piperazinedione with Cyclohexene

Kuniaki Itoh

Department of Science of Material Reactions, Division of Science of Materials, Graduate School of Science and Technology, Kobe University, Kobe 657

(Received December 27, 1982)

The photo-induced addition reaction of 1,4-dibromo-2,5-piperazinedione (1) with cyclohexene in acetonitrile gave 1 : 1-adducts[1-(2-bromocyclohexyl)-2,5-piperazinediones] and 1 : 2-adducts[1,4-bis(2-bromocyclohexyl)-2,5-piperazinediones] besides 3-bromocyclohexene, 1,2-dibromocyclohexane, and a solvent-incorporated product, *trans*-2-acetylamino-2-bromocyclohexane. Stereochemistry of the adducts was elucidated and mechanism of the addition reaction was discussed.

The characteristic feature of the reactions of *N*-halo imides and amides is their use in well-known allylic halogenation of olefins.[1,2] However, in some instances, the *N*-centered free radicals produced from *N*-halo imides or amides underwent addition to the olefinic double bonds to give addition products.[3-6] The two processes proceed competitively, but the one process can predominate over the other according to the subtle change in the reaction conditions. Thus, Skell and his co-workers[3,7] demonstrated that the photoreaction of *N*-chlorosuccinimide with cyclohexene gave *N*-(2-chlorocyclohexyl)succinimide, 3-chlorocyclohexene, and 4-chlorocyclohexene: the addition and the substitution being closely competitive processes. Chow and his co-workers[4] also showed that the substitution/addition ratio of the photoreaction of *N*-bromosuccinimide (NBS) with cyclohexene was dependent on temperature, solvents, added ethylene oxide (a hydrogen bromide trap), and molar ratio of reactants. The solubility of NBS in organic solvents changed noticeably the reaction pattern (hydrogen abstraction *vs.* addition to double bond) of NBS. Recently, we reported that irradiation of 1,4-dibromo-2,5-piperazinedione (**1**) with cyclohexene in the presence of alcohols efficiently induced alkoxy-bromination of cyclohexene in dichloromethane.[8] A free radical scavenger was employed to avoid possible free radical reactions. However, with less reactive alcohols, especially with *t*-butyl alcohol, the reaction gave an addition product, 1,4-dibromo-2,5-piperazinedione-cyclohexene 1 : 2-adduct, in addition to the expected alkoxybrominated product. Because the *N*-bromo compound (**1**) is almost insoluble in dichloromethane, the photoreaction had been carried out under heterogeneous conditions. The present investigation concerns the photoaddition reaction of **1** with cyclohexene in acetonitrile or halogenated hydrocarbon solvents. Acetonitrile is a poor solvent for **1**, but better than carbon tetrachloride. Structure of the adducts and the stereochemical course of the reaction are discussed.

Results and Discussion

The photoreaction of 1,4-dibromo-2,5-piperazinedione (**1**) was carried out with cyclohexene in a 1 : 10 mole ratio for 3 h at 20 °C in acetonitrile. The reaction mixture was vigorously stirred during the irradiation. After usual work-up, products were separated by silica gel chromatography. The results are given in Table 1.

The photoreaction of NBS with cyclohexene in carbon tetrachloride (heterogeneous conditions) gave no NBS-olefin adduct. In contrast, that in acetonitrile (homogeneous conditions) was reported to yield *N*-(2-bromocyclohexyl)succinimide.[2,4] With 1,4-dibromo-2,5-piperazinedione (**1**), predominant formation of 3-bromo-

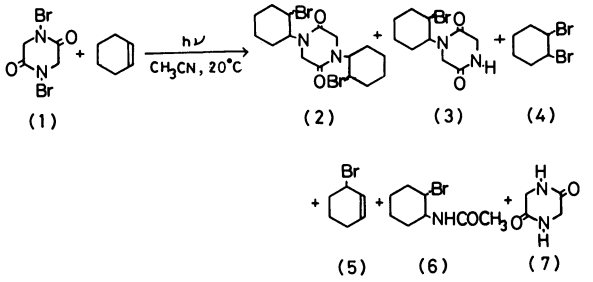

Scheme 1.

Table 1. Products of photoreaction of 1,4-dibromo-2,5-piperazinedione (**1**) with cyclohexene[a]

Solvent	Product yields/%											
	Total **2**	**2a**	**2b**	**2c**	**2d**	Total **3**	**3a**	**3b**	**4**[b]	**5**[b]	**6**	**7**
CH_3CN	34	15	7	10	2	18	13	5	17	24	1	36
CH_2Cl_2	38	17	7	12	2	7	5	2	15	35	0	45
$CHCl_3$	41	17	9	12	3	11	8	3	18	27	0	49
CCl_4	0					0			16	59	0	74[c]
CH_3CN[d]	7	4	1	2	0	0			26	9	0	92
CH_3CN[e]	25	11	5	7	2	12	8	4	17	14	3	39

a) Irradiation of a mixture of **1** (20 mmol) and cyclohexene (200 mmol) in 100 ml of a solvent at 20 °C for 3 h. Isolated yields are given based on **1** employed. b) The yields are determined by GLC. c) Unchangel **1** was recovered in a 25% yield. d) Hydroquinone (0.1 molar equivalent to **1**) was added. e) The molar ratio of **1** to cyclohexene was 1/5.

cyclohexene (**5**) in a carbon tetrachloride solution (heterogeneous conditions) was observed. This implied the intervention of hydrogen abstraction at the allylic position of cyclohexene by means of the Goldfinger mechanism proposed originally for the reaction of NBS with olefins in carbon tetrachloride.[1] However, in better solvents for *N*-bromo imides and amides[9] (*e.g.* acetonitrile and dichloromethane; though the reaction conditions are still not completely homogeneous, they are somewhat more homogeneous than in the carbon tetrachloride solution) the addition of 2,5-dioxo-1-piperazinyl radical to the cyclohexene double bond proceeded rather smoothly to yield the adducts **2** and **3**. The 1,2-adducts, [1,4-bis(2-bromocyclohexyl)-2,5-piperazinedione, **2**], were separated by a silica-gel column to give four stereoisomers (**2a, b, c, d**) in a ratio given in Table 1. In addition, small amounts of the 1 : 1-adducts, [1-(2-bromocyclohexyl)-2,5-piperazinedione(**3**)], were isolated besides *trans*-1,2-dibromocyclohexane (**4**) and 3-bromocyclohexene (**5**). The 1 : 1-adducts were also separated to give a pair of stereoisomers (**3a, b**). Interestingly a small amount of a solvent-incorporated product, *trans*-2-acetylamino-2-bromocyclohexane (**6**), was obtained in case where acetonitrile was employed as the solvent. Other solvents gave no solvent-incorporated products. In all cases, 2,5-piperazinedione (**7**) was obtained in variable amounts.

Stereochemistry of the Adducts. The structures of all the products were determined by means of spectroscopic data and elemental analyses. The 1 : 1-adducts (**3a, b**) and 1 : 2-adducts (**2a—d**) showed characteristic infrared absorptions of the 2,5-piperazinedione moiety. The infrared absorption of these compounds (Table 2) allowed us to assign the adduct structures. Klaeboe, Lothe and Lunde[10] reported that, of the two C–Br stretching frequencies of bromocyclohexanes, the 685 cm^{-1} band should be assigned to the equatorial C–Br bond and the 658 cm^{-1} (lower frequency) band to the axial C–Br bond. In addition, *trans*-*N*-(2-chlorocyclohexyl)piperazine was reported to show its equatorial C–Cl stretching frequency at 730 cm^{-1}. The absorption of the axial C–Cl bond of the corresponding *cis* isomer was observed at 680 cm^{-1} (lower frequency).[5] The structures of the 1 : 1-adducts (**3a, b**) were confirmed to be 1-(2-bromocyclohexyl)-2,5-piperazinedione by means of preliminary spectroscopic analysis. In addition, from Table 2, it was deduced that **3a** has an equatorial bromine atom and **3b** has an axial bromine atom. Thus, **3a** and **3b** are possibly diastereoisomeric to each other. This assignment was reinforced by inspection of their NMR spectra. The axial –CHBr– protons of bromocyclohexane is known to appear at 3.82 ppm whereas the equatorial counterpart does at a lower field, 4.60 ppm. The half-height width of the former signal is wider than that of the latter. For example, Driguez and Lessard[5] reported that in *trans*-*N*-(2-chlorocyclohexyl)piperazine the axial proton on C_2 appeared at 3.72 ppm with a half-height width of 25 Hz, while in the *cis* isomer the equatorial proton on C_2 did at 4.43 ppm with a half-height width of 6.5 Hz. Chemical shifts and half-height widths given in Table 2 clearly

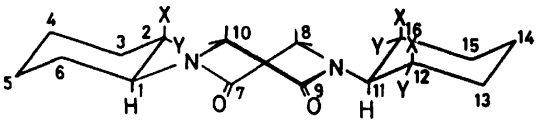

	2		12		16	
	X	Y	X	Y	X	Y
2a	H	Br	H	H	H	Br
2b	H	Br	H	Br	H	H
2c	H	Br	H	H	Br	H
2d	Br	H	H	H	Br	H

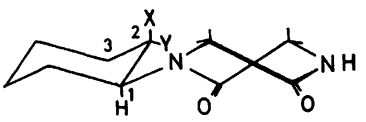

	X	Y
3a	H	Br
3b	Br	H

Scheme 2. The numbering of atoms is the same as in Fig. 1.

Table 2. IR and proton NMR spectral data for adducts

Compound	C–Br Stretching frequency/cm^{-1}		Chemical shifts (δ value) and half-height widths ($\Delta\nu_{1/2}$/Hz, given in parentheses)[a]						
	Equatorial	axial							
1 : 2-Adduct	C–Br	C–Br	H_1	H_2	H_{11}	H_{12}	H_{16}	H_8	H_{10}
2a	690	—	3.7—4.2 (18)	3.9—4.5 (17)	3.7—4.2 (18)	——	3.9—4.5 (17)	3.93[b]	3.93[b]
2b	680	—	3.7—4.2 (18)	4.0—4.6 (18)	3.7—4.2 (18)	4.0—4.6	—— (18)	3.92[b]	3.92[b]
2c	680	650	3.8—4.3 (18)	4.1—4.5 (16)	4.1—4.5 (16)	——	4.75—4.95 (7)	4.17[c] (J=17 Hz)	3.92[b]
2d	—	660	4.1—4.5 (18)	4.75—4.95 (7)	4.1—4.5 (18)	——	4.75—4.95 (7)	4.16[c] (J=16 Hz)	4.16[c] (J=16Hz)
1 : 1-Adduct									
3a	690	—	3.7—4.2 (18)	4.0—4.6 (18)	——	——	——	3.92[b]	4.00[b]
3b	—	655	4.1—4.6 (20)	4.7—4.9 (7)	——	——	——	4.13[c] (J=16 Hz)	3.97[b]

a) The numbering of atoms is the same as in scheme 2 and Fig. 1. b) Singlet. c) An AB-doublet centered at a given chemical shift position with a given J-value.

indicated the structure of **3a** as *trans*-1-(2-bromocyclohexyl)-2,5-piperazinedione, and that of **3b** as the corresponding *cis* isomer having an axial bromine substituent.

Structural elucidation of the 1 : 2-adducts (**2a**—**d**) was achieved taking the following consideration into account. The infrared absorptions of the 1 : 2-adducts showed that **2a** and **2b** have two equatorial bromine atoms, while **2c** has an axial and an equatorial bromine atoms. Interestingly, the presence of two axial bromine atoms in **2d** was indicated by its strong infrared absorption at 660 cm^{-1}. Each 1 : 2-adduct was reduced by tributyltin hydride to give identical 1,4-dicyclohexyl-2,5-piperazinedione. Accordingly these four 1 : 2-adducts were determined to be stereoisomeric to each other at the carbon atoms bound to bromine atoms. The chemical shifts and half-height widths of **2a** and **2b** (Table 2) indicated the presence of the *trans*-diaxial orientation of the vicinal protons (H_1/H_2, H_{11}/H_{12}, or H_{11}/H_{16}), which gave large half-height width absorptions, respectively. The 2,5-piperazinedione ring protons (H_8 and H_{10}) appeared as a singlet, indicating that they experienced an equivalent magnetic environment. A definitive structure assignment for **2a** was made by X-ray crystallography. A suitable single crystal of **2a** was obtained by careful recrystallization from acetone. The unit cell was found to be monoclinic, space group $P2_1/C$, with lattice parameters $a=13.37(1)$ Å, $b=11.59(1)$ Å, $c=11.93(1)$ Å, $\beta=98.55(7)°$, and $Z=4$. Of 4192 independent reflections obtained by using monochromated Mo *Ka* radiation, 1946 reflections with $|F_0|\geq 3\sigma(|F_0|)$ were considered to be observed.[11] The molecular structure of **2a** shown in Fig. 1 reveals that the C–Br bonds and the C=O groups are forced to located at an opposite direction by their dipole-dipole repulsion. The structure of **2b** was similarly determined as a diastereoisomer of **2a** as shown in Scheme 2 by its spectral characteristics.

The other 1 : 2-adducts, **2c** was found to possess an axial and an equatorial bromine substituents. The narrow half-height width observed for one of –CHBr– protons (an axial proton) supported this assignment. A crystal of **2c** obtained from methanol was monoclinic, space group C2/C, with lattice parameters $a=27.043$ (6) Å, $b=12.543(3)$ Å, $c=11.251(3)$ Å, $\beta=109.23(2)°$, and $Z=8$. The molecular structure of **2c** was determined by X-ray analysis, and shown by the ORTEP drawing in Fig. 1.[11] Crystallographic analysis gave the torsional angle of about 90° between the left-hand cyclohexane ring and the central 2,5-piperazinedione ring, and that of about 60° between the right-hand cyclohexane ring and the 2,5-piperazinedione ring. The central 2,5-piperazinedione ring was determined to exist in a flattened boat conformation. This molecular geometry resulted in characteristic NMR signals of **2c**. The structure of **2c** (Fig. 1 [C]) reveals that one of the protons on C_8 is placed close to the axial C_{16}–Br bond of the right-hand cyclohexane ring so that the C_8 methylene protons become magnetic nonequivalent to each other to give an AB quartet centered at 4.17 ppm. The other methylene proton on C_{10} appear at 3.92 ppm (singlet) as the corresponding C_8 and C_{10} protons of **2a** and **2b** do. The other chemical shift data and half hight widths are consistent with those expected from the depicted structure.

The structure of **2d**, which had two axial bromine atoms, was elucidated as shown in Scheme 2 taking the following spectral data into consideration; low field shift and narrow $\Delta\nu_{1/2}$ observed for both H_2 and H_{16}, and AB splitting of H_8 and H_{10} protons.

Course and Stereochemistry of Addition Reaction. The reaction did not occur in the dark. 1,4-Dibromo-2,5-piperazinedione (**1**) was hardly soluble in carbon tetrachloride, and the reaction gave no adducts, but the dominant allylic bromination was observed. The other chlorinated hydrocarbons showed a slightly enhanced solubility for **1**. The photoreaction of **1**

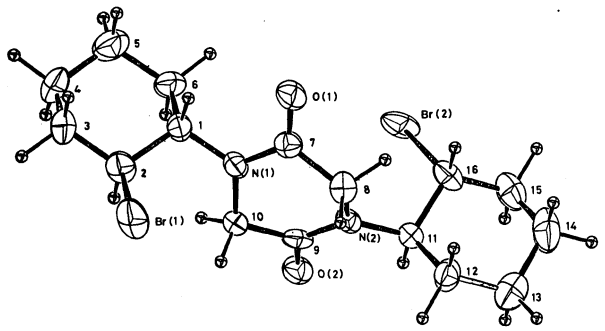

[A]

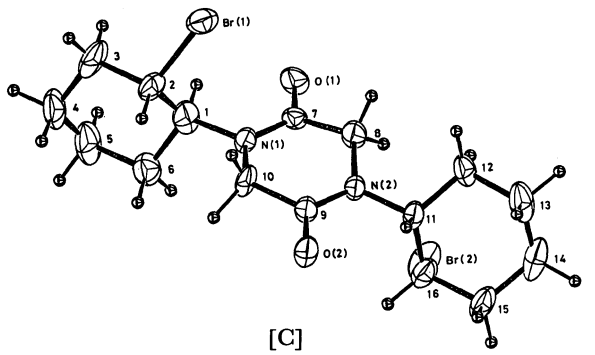

[C]

Fig. 1. ORTEP drawings of the 1 : 2-adducts. The numbering of atoms is the same as in Scheme 2.
[A]: **2a**, [C]: **2c**.

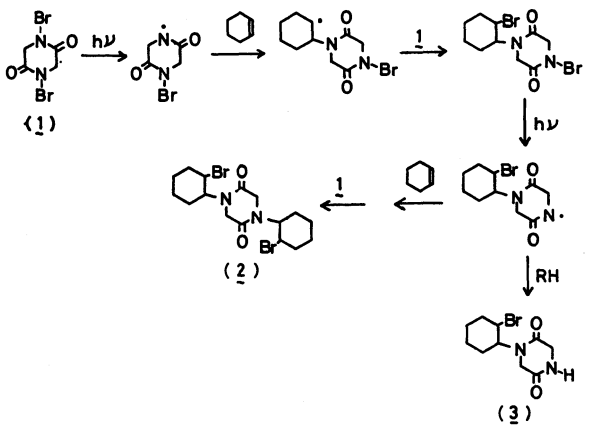

Scheme 3.

with cyclohexene in these solvents gave the adducts **2** and **3**. Acetonitrile was found to be the most convenient solvent for the photoreaction of **1**, although the solubility of **1** was not satisfactory. In acetonitrile the photoreaction of **1** with cyclohexene gave the adducts in considerable amounts. In the presence of hydroquinone, the yield of the adducts (**2** and **3**) decreases down to 7% from 52%. From this observation and the absence of rearranged products in the photoreaction of **1** with 3,3-dimethyl-1-butene,[12] an ionic reaction mechanism was ruled out. Thus the adducts were thought to be produced through a radical process involving the 2,5-dioxo-1-piperazinyl radical as the chain transfer species (Scheme 3).

In acetonitrile, a small amount of *trans*-2-acetylamino-2-bromocyclohexane (**6**) was produced. The yield of **6** was increased with an increased mole ratio of cyclohexene to **1**. The formation mechanism of **6** is to be noted. Photodecompotion of **2** in acetonitrile did not give rise to **6**. This suggests that **2** is not an intermediate to give **6**. Instead, the photoreaction of **1** with cyclohexene in acetonitrile-d_3 gave Me-d_3-**6**, indicating the intervention of a Ritter type reaction.[13] A concomitant reaction which is often encountered in NBS reactions is the ring opening to produce the isomeric 3-bromopropionyl isocyanate.[2] The reaction is reported to be enhanced in the presence of olefins.[14,15] However, in the present investigation, we could not detect any ring opening product.

It is reasonable to expect that the 2,5-dioxo-1-piperazinyl radical attacks the double bond of cyclohexene at the least hindered site, which corresponds to an axial direction in the resulting cyclohexyl radical (Scheme 4, A). The bromine atom is then transferred from **1** to this radical (*trans* addition), and following ring inversion give the adducts with equatorial bromine substituents (**2a, b**, and **3a**). The intermediate radical (A) can invert to give rise to the conformationally more favorable radical (B) having the equatorial 2,5-piperazinedione moiety. Inspection of the stereomodel of B indicates a sterically favored axial bromine attack which gives the adducts **2c, d**, and **3b**. Diastereomers **2a, b** having all substituents at the equatorial position of cyclohexane rings are undoubtedly most stable products, so that the yield of (**2a**+**2b**) is always exceeded that of (**2c**+**2d**). The conformationally unfavored adduct **2d** with two axial bromine substituents was produced in a lowest yield. In addition, it seems that highly symmetrical molecular geometry of **2a** (a center of symmetry, see Fig. 1) is responsible for its predominant formation over **2b**.

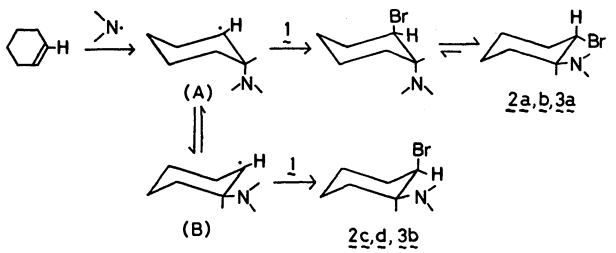

Scheme 4.

The regioselectivity of the addition of **1** to 1-methylcyclohexene and 3,3-dimethyl-1-butene provides a straightforward evidence for the 2,5-dioxo-1-piperazinyl radical as the initial attacking entity to the double bonds (Scheme 2).[12] As pointed out by Skell and Day[15] the radical generated by the processes like **1** + R·→2,5-dioxo-1-piperazinyl radical + R–Br has overwhelmingly σ_N–character (the first exited state). Recent ab initio[16] as well as INDO[17] calculations for the succinimido radical suggested that the ground state (π-radical) is 83 kJ mol^{-1} more stable than the first exited state (σ_N-radical). This energy difference nicely explains the selectivity differences observed for the hydrogen abstraction reactions by **1**, and the enhanced reactivity of the NBS σ_N-radical for aromatics.[2] For other cyclic imido and amido radicals, Apeloig and Schreiber[16] pointed out that the energy differences between the ground state π- and the first exited state σ_N-radical is expected to be greater than 83 kJ mol^{-1}. This difference may be responsible for the enhanced addition reactivity of the radical. However, absence of the radical isomerization and failure of the reaction of **1** with aromatics[12] indicate complex nature of 2,5-dioxo-1-piperazinyl radical.

Experimental

Cyclohexene was dried over Molecular Sieves 4A and distilled over copper(I) chloride prior to use. Acetonitrile was dried over calcium hydride and distilled. 1,4-Dibromo-2,5-piperazinedione (**1**) was prepared according to the procedure reported ealier.[8] IR spectra were recorded as KBr disk with JASCO IR-A-1 and IR-A-3 spectrometers. NMR spectra were measured on JEOL JNM-PMX-60 and JNM-PS-100 spectrometers using tetramethylsilane as the internal standard. Mass spectra were obtained by a Hitachi RMU-6MG spectrometer. GLC anaysis was carried out by a Yanagimoto Model G 1800-F. Irradiation was carried out using a Halos EHB-WU high pressure mercurry arc lamp (100 W).

Reaction of 1,4-dibromo-2,5-piperazinedione (1) with cyclohexene. A typical experimetal procedure is described. Irradiation of a mixture containing 5.44 g (20 mmol) of **1** and 16.43 g (200 mmol) of cyclohexene in acetonitrile (100 ml) was carried out under stirring for 3 h. The mixture was filtered to give 2,5-piperazinedione (**7**) in a 36% yield. A part of the filtrate was directly injected into a GLC column to determine the amounts of low boiling products: *trans*-1,2-dibromocyclohexane (**4**) and 3-bromocyclohexene (**5**) were produced in 17% and 24% yields, respectively. The rest of the filtrate was evaporated up to a syrup, which was separated by a column packed with silica gel using benzene–acetone (4 : 1) as a eluant. Yields are given in Table 1 on the basis of **1** employed. Physical constants of the isolated products are shown below. For characteristic IR absorptions and NMR chemical shifts, see Table 2.

1,4-Bis(2-bromocyclohexyl)-2,5-piperazinediones (2a): Mp 183—184 °C; IR, 1680, 1480, 1185 cm^{-1}; NMR($CDCl_3$), δ=1.1—2.7 (16H, m); MS (*m/e*), 438, 436, 434 (M^+), 357, 355, 275, 195, 115, 81. Found; C, 43.98, H, 5.76%; Calcd for $C_{16}H_{24}Br_2N_2O_2$; C, 44.06, H, 5.55%. **2b**: Mp 213—214 °C; IR, 1680, 1480, 1190 cm^{-1}; NMR($CDCl_3$), δ=1.1—2.6 (16H, m); MS (*m/e*), the same as that of **2a**. Found; C, 44.01, H, 5.93%; Calcd see above. **2c**: Mp 193.5—194.5 °C; IR, 1660, 1460, 1175 cm^{-1}; NMR($CDCl_3$), δ=1.1—2.7 (16H, m); MS (*m/e*), the same as that of **2a**. Found; C, 44.28, H, 5.80%; Calcd;

see above. **2d**: Mp 212—213 °C; IR, 1650, 1470, 1175 cm^{-1}, NMR($CDCl_3$), δ=1.1—2.6 (16H, m); MS (*m/e*), the same as that of **2a**. Found; C, 44.36, H, 5.71%; Calcd see above.

1-(2-Bromocyclohexyl)-2,5-piperazinedione (3a): Mp 165.5—166.5 °C; IR, 3300, 1680, 1470, 1190 cm^{-1}; NMR($CDCl_3$) δ=1.1—2.6 (8H, m), 7.10 (1H, s); MS (*m/e*), 274, 272 (M^+), 194, 115, 81. Found; C, 43.53, H, 5.94%; Calcd for $C_{10}H_{15}BrN_2O_2$; C, 43.65, H, 5.49%. **3b**: Mp 165—166 °C; IR, 3480, 1680, 1630, 1470, 1170 cm^{-1}; NMR($CDCl_3$), δ=1.1—2.5 (8H, m), 6.90 (1H, s); MS (*m/e*), the same as that of **3a**. Found; C, 43.29 H, 5.61%; Calcd see above.

trans-2-acetylamino-2-bromocyclohexane (6): Mp 116.5—117.5 °C (lit,[16] 109—110 °C). IR, 3300, 1620, 690 cm^{-1}; NMR($CDCl_3$), δ=1.1—2.6 (8H, m), 2.00 (3H, s), 3.8—4.1 (2H, m), 5.6—6.0 (1H, m); MS (*m/e*), 221, 219 (M^+), 140, 98, 81. Found; C, 43.62, H, 6.32%; Calcd for $C_8H_{14}BrNO$; C, 43.65, H, 6.41%.

Reduction of 1,4-Bis(2-bromocyclohexyl)-2,5-piperazinedione (2) with Tributyltin Hydride. Compound **2a** (73.5 mg, 0.17 mmol), tributyltin hydride (117 mg, 0.4 mmol), and AIBN (8 mg) were dissolved in 5 ml of benzene, and the mixture was kept in an atmosphere of nitrogen at 80 °C for 3 h. The solvent was evaporated off and the residure was chromatographed through a silica gel column using benzene–acetone (4 : 1) to give 1,4-dicyclohexyl-2,5-piperazinedione in a 85% yield; mp 230.5—232.0 °C; IR, 1650, 1480, 1180 cm^{-1}; NMR ($CDCl_3$), δ=0.9—2.2 (20H, m), 3.93 (4H, s), 3.9—4.6 (2H, m). Found; C, 68.80, H, 9.40%; Calcd for $C_{16}H_{26}N_2O_2$; C, 69.03, H, 9.41%. All the other isomer, **2b—d**, were reduced similarly, and the same 1,4-dicyclohexyl-2,5-piperazinedione was obtained in all cases.

The author is grateful to Professor Akira Sera, Faculty of Science, Kobe University for his comments and suggestions for improvement of the manuscript, and wishes to thank Professor Kazumi Nakatsu and Mr. Kohmei Kafuku, Faculty of Science, Kwansei Gakuin University, for X-ray crystallographic analysis.

References

1) J. S. Pizey, "Synthetic Reagents," Ellis Horword Ltd., Chichester (1974), Vol. II, Chap. 1.
2) P. S. Skell and J. C. Day, *Acc. Chem. Res.*, **11**, 381 (1978).
3) J. C. Day, M. K. Katsaros, W. D. Kocher, A. E. Scott, and P. S. Skell, *J. Am. Chem. Soc.*, **100**, 1950 (1978).
4) F.-L. Lu, Y.M.A. Naguib, M. Kitadani, and Y. L. Chow, *Can. J. Chem.*, **57**, 1967 (1979).
5) H. Driguez and J. Lessard, *Can. J. Chem.*, **55**, 720 (1977).
6) S. Wolfe and D. V. C. Awang, *Can. J. Chem.*, **49**, 1384 (1971).
7) J. C. Day, M. J. Lindstrom, and P. S. Skell, *J. Am. Chem. Soc.*, **96**, 5616 (1974).
8) A. Sera, H. Yamada, and K. Itoh, *Bull. Chem. Soc. Jpn.*, **53**, 219 (1980).
9) The use of carbon tetrachloride (solubility of 0.005 mol/l for NBS) in allylic bromination of olefins with NBS allows the bromine radical to be a chain carrier. In acetonitrile (solubility of 0.8 mol/l for NBS), the increased concentration of NBS changes the dominant chain carrier species from the bromine radical to the succinimido radical, so that double bond addition products can be obtained.[2]
10) P. Kaeboe, J. J. Lothe, and K. Lunde, *Acta Chem. Scand.*, **10**, 1465 (1956).
11) Details of the X-ray analysis will be reported elsewhere.
12) Unpublished results.
13) For a similar results, see Y. Wada and R. Oda, *Bull. Chem. Soc. Jpn.*, **43**, 2167 (1970).
14) R. E. Pearson and J. C. Martin, *J. Am. Chem. Soc.*, **85**, 354, 3142 (1963).
15) P. S. Skell and J. C. Day, *J. Am. Chem. Soc.*, **100**, 1951 (1978).
16) Y. Apeloig and R. Schreiber, *J. Am. Chem. Soc.*, **102**, 6144 (1980).
17) T. Koenig and R. A. Wielsek, *Tetrahedron Lett.*, **1975**, 2007.

Synthesis and Epoxidation of *trans*-5,6-Diacetoxy-1-benzoyloxymethyl-1,3-cyclohexadiene[1]

Seiichiro Ogawa, Tatsushi Toyokuni, Masayasu Ara, Masaru Suetsugu, and Tetsuo Suami*

Department of Applied Chemistry, Faculty of Science and Technology, Keio University, Hiyoshi, Kohoku-ku, Yokohama 223

(Received January 14, 1983)

The title substituted 1,3-cyclohexadiene was prepared in three steps from the readily available DL-1,2-di-*O*-acetyl-(1,3/2)-3-bromomethyl-5-cyclohexene-1,2-diol. Epoxidation of it with *m*-chloroperoxybenzoic acid in 1,2-dichloroethane afforded several stereoisomers of the biologically interesting highly oxygenated cyclohexane derivatives.

Crotepoxide (**1**),[2] senepoxide (**2**),[3] and pipoxide (**3**)[4] belong to a family of highly oxygenated cyclohexane derivatives which exhibit tumor-inhibitory, antileukemic, or antibiotic activity. Very recently, 1,6-desoxypipoxide (**5**), a key intermediary metabolite of **3**, has been isolated from *Uvaria purpurea*.[5] As a part of a synthetic study of mono- and diepoxycyclohexane compounds of biological interest,[6] several stereoisomeric compounds of this class were synthesized by epoxidation of properly functionalized 1,3-cyclohexadiene **6**.

Synthesis of the Substituted 1,3-Cyclohexadiene. Allylic bromination of DL-1,2-di-*O*-acetyl-(1,3/2)-3-bromomethyl-5-cyclohexene-1,2-diol (**7a**)[7] with molar equiv. of *N*-bromosuccinimide (NBS) in carbon tetrachloride in the presence of α,α'-azobisisobutyronitrile (AIBN) was carried out at 80 °C under nitrogen atmosphere for 0.5 h to give, after crystallization followed by fractionation on a silica-gel column, two dibromides **8a** (23%) and **10a** (7%), and one tribromide **12a** (9%), together with a small proportion of an α,β-unsaturated ketone **14** (3.7%).[8] When the same reaction was quenched after heating for 5 min, the new dibromide **11a** could be isolated in 2.6%, together with **8a** (16%). Under these reaction conditions, four dibromides **8a**—**11a** were expected to be obtainable and to be interconvertible by way of an allylic rearrangement. The results indicated that **8a** and **10a** were comparatively stable among them. When excess NBS (3 molar equiv.) was used in the reaction, **12a** was obtained in a quantitative yield. A small proportion of the isomeric tribromide **13** was shown to be present in a crude **12a** by ^{1}H NMR spectroscopy. Formation of **12a** would be rationalized by a readily dehydrobromination of an unstable dibromide **9a** followed by an addition of bromine generated *in situ* by hydrobromic acid and NBS or an addition of bromine to **9a** and/or **11a** followed by dehydrobromination (Scheme 2).

The structures of the dibromides and tribromide were elucidated on the basis of their ^{1}H NMR spectra. Thus, the spectrum of **8a** showed the coupled signals for H-3 and H-4 as a doublet of doublets of triplets (δ 2.59, J= 3, 3, 9, and 12 Hz) and a doublet of quartets (δ 4.90, J=2.5, 2.5, 2.5, and 9 Hz), indicating the axial–pseudoaxial conformations for H-3 and H-4. In the spectrum of **10a**, two protons attached to the carbon atoms bearing the acetoxyl groups appeared as coupled two doublets of doublets (J=8 and 10 Hz) at δ 5.10 and 5.50, being in accord with the assigned structure.

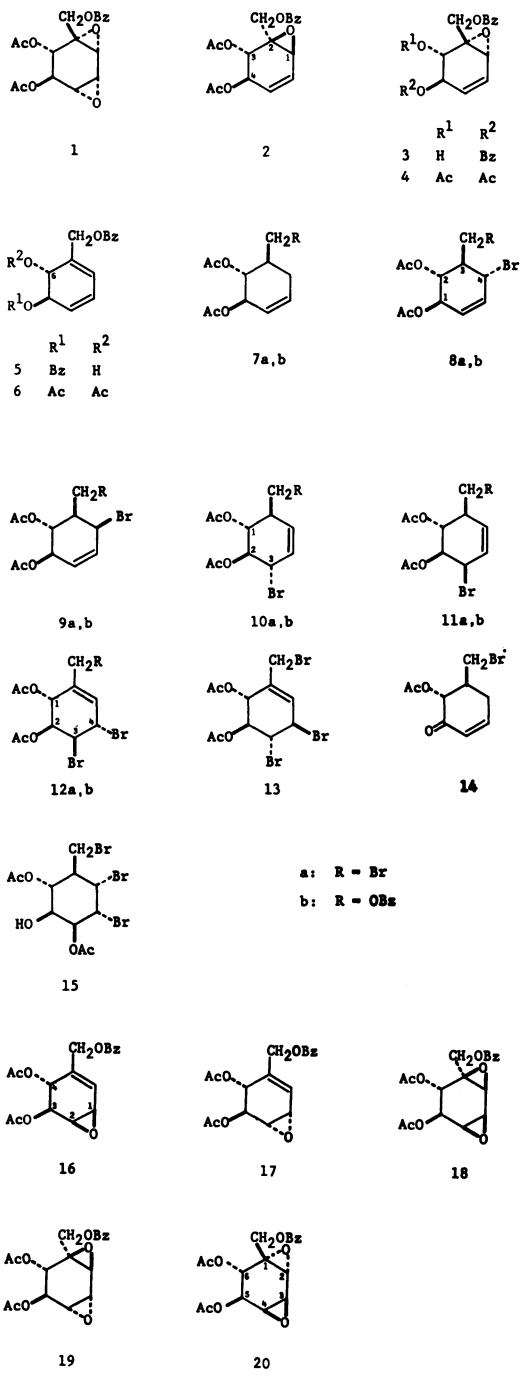

Scheme 1.

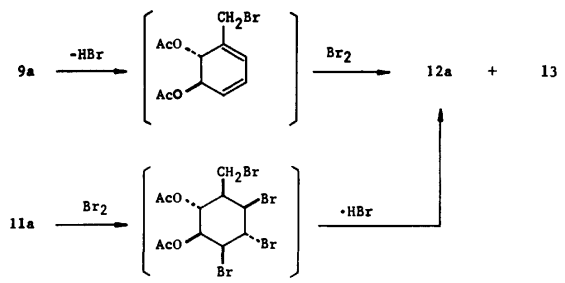

Scheme 2.

In the spectrum of **11a**, one-proton doublet of doublets of doublets (δ 6.10, J=3, 5, and 11 Hz) could be attributed to the C-4 olefinic proton adjacent to the bromo group oriented pseudoaxial conformation. In the spectrum of **12a**, the signals for H-1, H-2, H-3, and H-4 appeared as a doublet (δ 6.04, J=7.5 Hz), a doublet of doublets (δ 5.51, J=3.5 and 7.5 Hz), a triplet (δ 4.63, J=3.5 Hz), and a doublet of doublets (δ 4.96, J=3.5 and 4.5 Hz), respectively, indicating pseudoaxial–axial–equatorial–pseudoequatorial conformations for H-1, H-2, H-3, and H-4. In addition, two doublets of doublets (J=7 and 10 Hz) of small intensity were observed at δ 4.39 and 5.31, which were probably due to C-3 and C-2 protons, respectively, of the isomer **13** contained in crude **12a**.

Compound **8a** was converted into the tribromide **15** by treatment with NBS in aqueous acetic acid. The structure of **15** was fully proved by the ^{1}H NMR spectrum, which further confirmed the assigned structure of **8a**.

A similar bromination of the benzoyloxy derivative **7b**[7] with NBS (1.5 molar equiv.) in carbon tetrachloride yielded a mixture of products, from which two monobromides **8b** (20%) and **11b** (10%), and one dibromide **12b** (18%) were isolated. The structures were correlated with those of the corresponding bromo compounds by ^{1}H NMR spectroscopy. In this case, a use of excess NBS did not increase the yield of **12b**. Compounds **8b** and **11b** seemed to be stable under the reaction conditions, probably due to an inductive effect of the benzoyloxyl function. The desired **12b** was conveniently prepared in 42% overall yield from **7a** by direct treatment of crude **12a** with sodium benzoate in 90% aqueous *N*,*N*-dimethylformamide (DMF) at room temperature for 4 h.

Synthetically useful 1,3-cyclohexadiene **6** was prepared by treatment of **12b** with zinc dust in ethanol at 70 °C for 0.5 h. The product was purified by chromatography on silica gel to give **6** as an oil in 62% yield. The structure of **6** was established by the ^{1}H NMR spectrum, which showed a doublet of doublets (δ 5.25, J=4 and 5 Hz) and a doublet (δ 5.53, J=5 Hz) attributable to two olefinic protons H-3 and H-4, respectively. These data were in good accord with those of the corresponding 1-benzyloxyl derivative reported by White *et al.*[9]

Epoxidation of **6**. Compound **6** was treated with *m*-chloroperoxybenzoic acid (*m*CPBA) in 1,2-dichloroethane at room temperature or at reflux temperature with a radical inhibitor.[10] When an equimolar *m*CPBA was used at room temperature, **6** was consumed within 15 h and three monoepoxides were formed. They were fractionated by use of a silica-gel column to give **4** (14%), **16** (8.4%), and **17** (13%). The structure of **4** was deduced by comparison of the ^{1}H NMR spectrum with those of **2** and **3**. Thus, the signals due to H-3 and H-4 appeared as a two-proton narrow multiplet at δ 5.53 in contrast with those of **2** [H-3 (δ 5.57) and H-4 (δ 5.17)].[3] The C-4 proton of **4** was apparently deshielded by the proximate 1,2-epoxide ring in the half-chair conformation with two acetoxyl groups being diequatorially situated. It was further supported by the spectrum of **3** which revealed the C-4 proton attached to the carbon atom bearing the benzoyloxyl group at δ 5.68.[4b]

The ^{1}H NMR spectra of **16** and **17** showed two epoxide and one olefinic protons, respectively, indicating that they were an epimeric pair of the 3,4-epoxide of **6**. In the spectrum of **16**, the signals due to H-3 and H-4 appeared as a doublet (J=8.2 Hz) at δ 5.28 and 5.79, respectively, being in consistent with the proposed structure in which two acetoxyl groups were oriented diequatorially and the C-4 proton was deshielded by the epoxide group. Whereas, in the spectrum of **17**, two narrow triplets (J=2 Hz) appeared δ 5.30 and 5.46, which could be attributed to H-3 and H-4, respectively, in the preferred conformation with two acetoxyl groups in diaxial disposition.[11] The above data suggested that the conformational preference of these compounds might be due to the configurational relationship between trans-vicinal substituents and epoxide group independent of the steric and polar effect of benzoyloxymethyl group.[12]

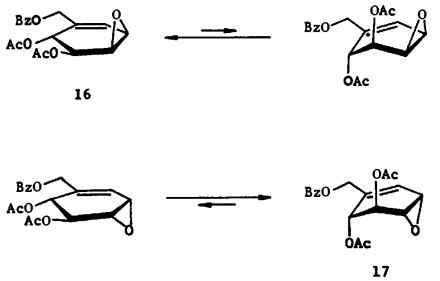

Scheme 3.

When the similar reaction was carried out under forcing conditions[10] (2,6-di-*t*-butyl-*p*-cresol, reflux, 1.5 h), a sole crystalline diepoxide **20** was isolated, after chromatography on silica gel, in 12% yield, along with **4** (3.5%), **16** (1.3%), and **17** (2.6%). The ^{1}H NMR spectrum of **20** showed two coupled sharp doublets (J=8 Hz) at δ 5.28 and 5.65, attributable to H-5 and H-6, respectively. The spectral data were in accord with the proposed structure where the C-5 and C-6 protons adopted the diaxial conformation and the former was deshielded by the proximate 1,2-epoxide group.[13]

The structure was further confirmed by epoxidation of the monoepoxides obtained. Epoxidation of **16** with *m*CPBA occurred smoothly to give **20** selectively. While, **4** did not react with *m*CPBA at room temperature, however, under forcing conditions, formation of **20** was detected by TLC. On the other hand, although **17** was expected to give **1** and/or **19**, it was not oxidized,

but underwent decomposition on prolonged reaction time. The reactivity of **17** may be explained by the steric and electronic effects exerted by diaxial arrangement of two acetoxyl groups.

Accordingly, it was noted that the 1,2-double bond of **6** was deactivated by the inductive effect of the C-1 benzoyloxymethyl group, comparing with that of the corresponding diene with the C-1 benzyloxymethyl group.[9] Stereospecificity of the epoxidation of *trans*-5,6-diacetoxy-1,3-cyclohexadienyl system seems to depend rather on an interaction of the neighboring group than on the spacial steric effect,[14] *e.g.* a conformational requirement of the molecule in the transition state of epoxidation, leading predominantly to the epoxide with two acetoxyl groups in equatorial orientation.

Experimental

Unless otherwise noted, melting points were determined on a Mitamura Riken micro hot stage and are uncorrected. ^{1}H NMR spectra were taken on a Varian EM-360 (60 MHz), EM-390 (90 MHz), or HA-100D (100 MHz) spectrometer in chloroform-*d* ($CDCl_3$) with reference to tetramethylsilane as an internal standard. The peak positions are given in terms of δ-values and values given for coupling constants are of first-order. Mass spectrum was recorded on a Hitachi M-80 mass spectrometer at 70 eV. TLC was performed on silica gel (Wakogel B-10, Wako Pure Chemical Ind., Ltd.). The silica gel used for a column chromatography was Wakogel C-300. Organic solutions were dried over anhydrous sodium sulfate and concentrated below 50 °C under reduced pressure.

Bromination of DL-*1,2-Di*-O-*acetyl-(1,3/2)-3-bromomethyl-5-cyclohexene-1,2-diol (7a) with NBS in Carbon Tetrachloride.* *a)*: To a solution of **7a**[7] (1.46 g) in carbon tetrachloride (15 ml) was added NBS (0.89 g, molar equiv.) and AIBN (10 mg), and the mixture was stirred at 80 °C under nitrogen stream for 0.5 h. After the reaction mixture was cooled to room temperature, succinimide formed was removed by filtration and washed with carbon tetrachloride. The filtrate and washings were combined and concentrated. The oily residue was crystallized from ethanol to give 0.34 g (20%) of DL-1,2-di-*O*-acetyl-(1,3/2,4)-4-bromo-3-bromomethyl-5-cyclohexene-1,2-diol (**8a**) as needles: mp 103—105 °C; ^{1}H NMR ($CDCl_3$, 90 MHz) δ=2.03 (3H, s) and 2.08 (3H, s) (OAc), 2.59 (1H, tdd, $J_{2,3}$=12 Hz, $J_{3,4}$=9 Hz, $J_{3,7}$=$J_{3,7'}$=3 Hz, H-3), 3.73 (1H, dd) and 3.90 (1H, dd) (J_{gem}=12 Hz, H-7 and H-7'), 4.90 (1H, dq, $J_{1,4}$=$J_{4,5}$=$J_{4,6}$=2.5 Hz, H-4), 5.19 (1H, dd, $J_{1,2}$=9 Hz, H-2), 5.42—5.71 (2H, H-1 and H-5) and 6.05 (1H, dt, $J_{5,6}$=10.5 Hz, $J_{1,6}$=2.5 Hz, H-6).

Found: C, 35.43; H, 3.83; Br, 42.96%. Calcd for $C_{11}H_{14}Br_2O_4$: C, 35.70; H, 3.81; Br, 43.19%.

The mother liquor of **8a** was concentrated and the residue was chromatographed on a silica-gel column (65 g) with 2-butanone–toluene (1 : 20) as an eluent. The first fraction [R_f 0.71, 2-butanone–toluene (1 : 8)] gave 0.20 g (9%) of DL-1,2-di-*O*-acetyl-(1,4/2,3)-3,4-dibromo-6-bromomethyl-5-cyclohexene-1,2-diol (**12a**) as an oil: ^{1}H NMR ($CDCl_3$, 100 MHz) δ=2.10 (6H, s, OAc), 3.93 (2H, AB q, J=12 Hz, C$\underline{H}_2$Br), 4.63 (1H, t, $J_{2,3}$=$J_{3,4}$=3.5 Hz, H-3), 4.96 (1H, dd, $J_{4,5}$=4.5 Hz, H-4), 5.51 (1H, dd, $J_{1,2}$=7.5 Hz, H-2), 6.04 (1H, d, H-1) and 6.16 (1H, br d, H-5). Traces of the ^{1}H NMR signals due to the isomer **13** were observed: δ=4.39 (1H, dd, $J_{2,3}$=10 Hz, $J_{3,4}$=7.5 Hz, H-3), 5.31 (1H, dd, $J_{1,2}$=7 Hz, H-2), 5.84 (1H, br d, H-1).

Found: C, 29.82; H, 3.07%. Calcd for $C_{11}H_{13}Br_3O_4$: C, 29.42; H, 2.92%.

The second fraction (R_f 0.58) gave an another crop (90 mg) of **8a** and the combined yield was 23%.

The third fraction (R_f 0.49) gave 0.13 g (7%) of DL-1,2-di-*O*-acetyl-(1,3/2,6)-3-bromo-6-bromomethyl-4-cyclohexene-1,2-diol (**10a**) as prisms: mp 126—128 °C; ^{1}H NMR ($CDCl_3$, 60 MHz) δ=2.06 (3H, s) and 2.09 (3H, s) (OAc), 2.75—3.10 (1H, m, H-6), 4.62 (1H. br d, $J_{2,3}$=8 Hz, H-3), 5.10 (1H, dd, $J_{1,2}$=10 Hz, $J_{1,6}$=8 Hz, H-1), 5.50 (1H, dd, H-2), 5.62 (1H, dt, $J_{3,5}$=$J_{5,6}$=2 Hz, $J_{4,5}$=10 Hz, H-5) and 5.99 (1H, dt, $J_{3,4}$=$J_{4,6}$=2.5 Hz, H-4).

Found: C, 35.87; H, 3.81; Br, 43.05%. Calcd for $C_{11}H_{14}Br_2O_4$: C, 35.70; H, 3.81; Br, 43.19%.

The fourth fraction (R_f 0.42) gave 45 mg (3.7%) of DL-*trans*-6-acetoxy-5-bromomethyl-2-cyclohexen-1-one (**14**) as a glass: ^{1}H NMR ($CDCl_3$, 60 MHz) δ=2.21 (3H, s, OAc), 2.60 (2H, m, H-4 and H-4'), 3.52 (2H, d, $J_{3,5}$=3.5 Hz, C$\underline{H}_2$Br), 5.32 (1H, d, $J_{5,6}$=12 Hz, H-6), 6.03 (1H, dt, $J_{2,3}$=10 Hz, $J_{2,4}$=$J_{2,4'}$=1.5 Hz, H-2) and 6.95 (1H, dt, $J_{3,4}$=$J_{3,4'}$=3.5 Hz, H-3).

Found: C, 43.77; H, 4.44; Br, 32.26%. Calcd for $C_9H_{10}BrO_3$: C, 43.93; H, 4.10; Br, 32.47%.

b): The similar reaction of **7a** (1.46 g) with NBS (0.89 g) was quenched after heating at 80 °C for 5 min, and the reaction mixture was processed similarly as described in a. The product was fractionally crystallized from ethanol to give 0.30 g (16%) of **8a** and 49 mg (2.6%) of DL-1,2-di-*O*-acetyl-(1/2,3,-6)-3-bromo-6-bromomethyl-4-cyclohexene-1,2-diol (**11a**) as cubic crystals: mp 105—108 °C; ^{1}H NMR ($CDCl_3$, 90 MHz) δ=2.08 (3H, s) and 2.10 (3H, s) (OAc), 2.78—3.13 (1H, m, H-6), 3.33 (1H, dd, $J_{6,7}$=6.5 Hz, J_{gem}=10 Hz, H-7), 3.51 (1H, dd, $J_{6,7'}$=4.5 Hz, H-7'), 4.75—4.98 (2H, m, H-2 and H-3), 5.49 (1H, dd, $J_{1,2}$=10.5 Hz, $J_{1,6}$=9 Hz, H-1), 5.56 (1H, dd, $J_{4,5}$=11 Hz, $J_{5,6}$=3 Hz, H-5) and 6.01 (1H, ddd, $J_{3,4}$=5 Hz, $J_{4,6}$=3 Hz, H-4).

Found: C, 35.53; H, 3.88; Br, 43.27%. Calcd for $C_{11}H_{14}Br_2O_4$: C, 35.70; H, 3.81; Br, 43.19%.

c): A mixture of **7a** (2.0 g), NBS (2.45 g, 2 molar equiv.), and AIBN (5 mg) in carbon tetrachloride (20 ml) was heated at reflux under nitrogen atmosphere for 2 h. Succinimide formed was removed by filtration and the filtrate was concentrated to give 3.1 g (100%) of **12a** as an oil.

DL-*1,3-Di*-O-*acetyl-(1,2,4/3,5,6)-5,6-dibromo-4-bromomethyl-1,-2,3-cyclohexanetriol (15).* To a mixture of **8a** (90 mg) in 50% aqueous acetic acid (12 ml) was added NBS (43 mg, molar equiv.) and the reaction mixture was allowed to stand at room temperature for 2 d. Precipitates were collected to give 17 mg (11%) of **15**: mp 198—200 °C; ^{1}H NMR (dimethyl-d_6 sulfoxide, 60 MHz) δ=2.09 (6H, s, OAc), 3.68 (2H, d, J=2 Hz, C$\underline{H}_2$Br), 4.31 (1H, dd, $J_{4,5}$=3.5 Hz, $J_{5,6}$=10 Hz, H-5), 4.71 (1H, t, $J_{3,4}$=3.5 Hz, H-4), 5.07 (1H, t, $J_{1,2}$=$J_{1,6}$=10.5 Hz, H-1) and 5.22 (1H, t, $J_{2,3}$=3.5 Hz, H-3).

Found: C, 28.44; H, 3.24; Br, 51.25%. Calcd for $C_{11}H_{15}Br_3O_5$: C, 28.29; H, 3.24; Br, 51.34%.

Bromination of DL-*1,2-Di*-O-*acetyl-(1,3/2)-3-benzoyloxymethyl-5-cyclohexene-1,2-diol (7b) with NBS in Carbon Tetrachloride.* To a solution of **7b**[7] (0.664 g) in carbon tetrachloride (20 ml) was added NBS (0.356 g, molar equiv.) and AIBN (10 mg), and the mixture was heated at reflux under nitrogen stream for 1 h. An additional amount of NBS (0.18 g) and AIBN (5 mg) was added and heating was continued for 1 h. At this time, **7b** was almost consumed and the formation of four components were detected by TLC [R_f 0.67, 0.60, 0.49, and 0.42 in 2-butanone–toluene (1 : 9)]. An insoluble material was removed by filtration and the filtrate was concentrated to an oil (0.60 g), which was chromatographed on a silica-gel column (30 g) with 2-butanone–toluene (1 : 20) as an eluent. The

first fraction (R_f 0.67) gave, after recrystallization from ethanol, 0.172 g (17.6%) of DL-1,2-di-*O*-acetyl-(1,6/2,5)-3-benzoyloxymethyl-5,6-dibromo-3-cyclohexene-1,2-diol (**12b**) as prisms: mp 132—134 °C; ^{1}H NMR ($CDCl_3$, 90 MHz) δ= 2.03 (3H, s) and 2.07 (3H, s) (OAc), 4.63 (1H, t, $J_{5,6}=J_{1,6}=$ 3 Hz, H-6), 4.78 (2H, br s, C$\underline{H}_2$OBz), 4.93 (1H, br dd, $J_{4,5}=$ 4.5 Hz, H-5), 5.49 (1H, dd, $J_{1,2}=7.3$ Hz, H-1), 6.01 (1H, br d, H-2), 6.11 (1H, br d, H-4), and 7.29—7.68 (3H, m) and 7.91—8.10 (2H, m) (phenyl).

Found: C, 44.29; H, 3.87; Br, 32.85%. Calcd for $C_{18}H_{18}Br_2O_6$: C, 44.12; H, 3.71; Br, 32.60%.

The second fraction (R_f 0.60) gave 0.163 g (20%) of DL-1,2-di-*O*-acetyl-(1,3/2,4)-3-benzoyloxymethyl-4-bromo-5-cyclohexene-1,2-diol (**8b**) as an oil: ^{1}H NMR ($CDCl_3$, 60 MHz) δ= 2.03 (3H, s) and 2.07 (3H, s) (OAc), 2.50—3.20 (1H, m, H-6), 4.30—4.72 (2H, m, C$\underline{H}_2$OBz), 4.91 (1H, ddd, $J_{4,5}=J_{4,6}=2.8$ Hz, $J_{3,4}=9$ Hz, H-4), 5.33 (1H, dd, $J_{1,2}=9.7$ Hz, $J_{2,3}=11.3$ Hz, H-2), 5.59 (1H, ddd, $J_{1,5}=J_{1,6}=2.7$ Hz, H-1), 5.69 (1H, ddd, $J_{5,6}=10.3$ Hz, H-6), 6.09 (1H, ddd, H-5), and 7.30—7.70 (3H, m) and 7.90—8.20 (2H, m) (phenyl).

Compound **8b** was not stable enough to give a satisfactory analytical data.

The third fraction (R_f 0.49) gave 82 mg (10%) of DL-1,2-di-*O*-acetyl-(1,3/2,6)-3-benzoyloxymethyl-6-bromo-4-cyclohexene-1,2-diol (**11b**) as crystals: mp 90—92 °C; ^{1}H NMR ($CDCl_3$, 60 MHz) δ=2.06 (3H, s) and 2.14 (3H, s) (OAc), 2.79—3.22 (1H, m, H-3), 4.22 (1H, dd, $J_{3,7}=5$ Hz, $J_{gem}=11$ Hz, H-7), 4.50 (1H, dd, $J_{3,7'}=4.5$ Hz, H-7'), 4.73—5.03 (2H, m, H-1 and H-6), 5.66 (1H, dd, $J_{3,4}=2$ Hz, $J_{4,5}=10.5$ Hz, H-4), 6.00 (1H, ddd, $J_{3,5}=2.5$ Hz, $J_{5,6}=5$ Hz, H-5), and 7.30—7.60 (3H, m) and 7.90—8.20 (2H, m) (phenyl).

Found: C, 52.72; H, 4.70; Br, 19.43%. Calcd for $C_{18}H_{19}BrO_6$: C, 52.56; H, 4.62; Br, 19.43%.

Practical Synthesis of ***12b***. A mixture of crude **12a** (1.13 g), sodium benzoate (0.40 g), and 90% aqueous DMF (20 ml) was stirred at room temperature for 1 d. TLC indicated the formation of one major (R_f 0.64) and one minor components (R_f 0.35) in 2-butanone–toluene (1 : 8). The reaction mixture was partitioned between ethyl acetate (30 ml) and water (20 ml). The organic layer was washed with water thoroughly, dried, and concentrated. The residue was crystallized from ethanol to give 0.58 g (47% based on **7a** used) of **12b**: mp 129—130 °C.

DL-trans-*5,6-Diacetoxy-1-benzoyloxymethyl-1,3-cyclohexadiene (****6****).* To a stirred solution of **12b** (2.0 g) in ethanol (45 ml) was added zinc dust (1.06 g, 4 atomic equiv.) in portions at 70 °C. The suspension was stirred vigorously at this temperature for 20 min. At this time, **12b** disappeared and one main component (R_f 0.51) and two minor components (R_f 0.16 and 0.12) were formed [TLC: 2-butanone–toluene (1 : 15)]. An insoluble material was removed by filtration and the filtrate was concentrated to give a pale yellow oil (1.2 g), which was chromatographed on a silica-gel column (30 g) with 2-butanone–toluene (1 : 15) as an eluent. The major fraction gave 0.83 g (62%) of **6** as a homogeneous oil: ^{1}H NMR ($CDCl_3$, 60 MHz) δ=1.98 (3H, s) and 2.00 (3H, s) (OAc), 4.74 (2H, s, C$\underline{H}_2$OBz), 5.25 (1H, dd, $J_{4,5}=4$ Hz, $J_{5,6}=5$ Hz, H-5), 5.53 (1H, d, H-6), 5.61—6.20 (3H, br m, H-2, H-3, and H-4) and 6.71—7.92 (5H, m, phenyl).

Found: *m/e* 330.1097. Calcd for $C_{18}H_{18}O_6$: M, 330.1102.[15]

Epoxidation of ***6****. a)*: To a solution of **6** (0.83 g) in 1,2-dichloroethane (20 ml) was added dropwise a solution of *m*CPBA (0.62 g, one molar equiv., purity 70%) in 1,2-dichloroethane (8 ml) at room temperature for 10 min. The reaction mixture was stirred at room temperature for 15 h. At this time, disappearance of **6** and formation of three major components were shown by TLC [R_f 0.51, 0.39, and 0.35 2-butanone–toluene (1 : 8)]. Then the mixture was washed successively with 10% aqueous sodium sulfite, saturated aqueous sodium hydrogencarbonate, and water, and dried. Evaporation of the solvent gave a clear oil which was chromatographed on a silica-gel column (50 g) with 2-butanone–toluene (1 : 15) as an eluent. The first fraction gave an oil which crystallized on standing to give 81 mg (14%) of DL-3,4-di-*O*-acetyl-1,2-anhydro-(1,2,3/4)-2-*C*-benzoyloxymethyl-5-cyclohexene-1,2,3,4-tetrol (**4**) as prisms: mp 112—113 °C; ^{1}H NMR ($CDCl_3$, 90 MHz) δ=2.02 (3H, s) and 2.10 (3H, s) (OAc), 3.51 (1H, dd, $J_{1,5}=1.5$ Hz, $J_{1,6}=3.8$ Hz, H-1), 4.26 (1H, d) and 4.56 (1H, d) ($J_{gem}=12.5$ Hz, C$\underline{H}_2$OBz), 5.53 (2H, m, H-3 and H-4), 5.71 (1H, dt, $J_{4,5}=1.5$ Hz, $J_{5,6}=9.5$ Hz, H-5), 6.00 (1H, ddd, $J_{4,6}=1.5$ Hz, H-6), and 7.47—7.99 (5H, m, phenyl).

The second fraction gave 50 mg (8.4%) of DL-3,4-di-*O*-acetyl-1,2-anhydro-(1,2,3/4)-5-benzoyloxymethyl-5-cyclohexene-1,2,3,4-tetrol (**16**) as a homogeneous oil: ^{1}H NMR ($CDCl_3$, 90 MHz) δ=2.00 (3H, s) and 2.10 (3H, s) (OAc), 3.44 (1H, t, $J_{1,2}=J_{1,6}=4$ Hz, H-1), 3.58 (1H, dd, $J_{2,3}=1.3$ Hz, H-2), 4.73 (2H, s, C$\underline{H}_2$OBz), 5.28 (1H, dd, $J_{3,4}=8.2$ Hz, H-3), 5.79 (1H, br d, H-4), 6.16 (1H, br s, H-6), and 7.43—7.96 (5H, m, phenyl).

The third fraction gave 76 mg (13%) of DL-3,4-di-*O*-acetyl-1,2-anhydro-(1,2,4/3)-5-benzoyloxymethyl-5-cyclohexene-1,2,-3,4-tetrol (**17**) as prisms: mp 116—117.5 °C; ^{1}H NMR ($CDCl_3$, 90 MHz) δ=2.00 (3H, s) and 2.03 (3H, s) (OAc), 3.38 (1H, t, $J_{1,2}=J_{1,6}=4$ Hz, H-1), 3.55 (1H, m, H-2), 4.74 (2H, s, C$\underline{H}_2$OBz), 5.30 (1H, t, $J_{2,3}=J_{3,4}=2$ Hz, H-3), 5.46 (1H, t, $J_{4,6}=2$ Hz, H-4), 6.43 (1H, br d, H-6), and 7.41—7.98 (5H, m, phenyl).

Found for **4**: C, 62.24; H, 5.33%, for **16**: C, 62.17; H, 5.32%, and for **17**: C, 62.50; H, 5.27%. Calcd for $C_{18}H_{18}O_7$: C, 62.42; H, 5.24%.

b): When the similar reaction was carried out in dichloromethane in the presence of phosphate buffer solution (pH 8) under vigorous stirring, **4** (11%); **16** (14%), and **17** (13%) were isolated by chromatography.

c): To a solution of crude **6** prepared from **12b** (0.30 g) were added *m*CPBA (0.20 g, 1.2 molar equiv.) and 2,6-di-*t*-butyl-*p*-cresol (3 mg), and the mixture was refluxed for 90 min. After having been cooled, the reaction mixture was filtered to remove *m*-chlorobenzoic acid and the filtrate was processed similarly as described in a. The mixture of products was chromatographed on silica gel (30 g) with 2-butanone–toluene (1 : 15) as an eluent. The first fraction [R_f 0.51, 2-butanone–toluene (1 : 8)] gave 8 mg (3.5%) of **4** as an oil.

The second fraction (R_f 0.38) gave an oil which crystallized on standing to give 30 mg (12%) of DL-5,6-di-*O*-acetyl-1,2 : 3,4-dianhydro-(1,2,6/3,4,5)-1-*C*-benzoyloxymethyl-1,2,3,4,5,6-cyclohexanehexol (**20**): mp 128—129 °C; ^{1}H NMR ($CDCl_3$, 90 MHz) δ=2.06 (6H, s, OAc), 3.35 (1H, d, $J_{3,4}=4.5$ Hz, $J_{4,5}=1.2$ Hz, H-4), 3.56 (1H, dd, $J_{2,3}=2.5$ Hz, H-3), 3.69 (1H, d, H-2), 4.13 (1H, d) and 4.42 (1H, d) ($J_{gem}=12$ Hz, C$\underline{H}_2$OBz), 5.28 (1H, dd, $J_{5,6}=8$ Hz, H-5), 5.65 (1H, d, H-6), and 7.36—7.98 (5H, m, phenyl).

Found: C, 59.81; H, 5.11%. Calcd for $C_{18}H_{18}O_8$: C, 59.67; H, 5.11%.

The third fraction (R_f 0.37) gave 3 mg (1.3%) of **16**.

The fourth fraction (R_f 0.35) gave 6 mg (2.6%) of **17**.

d): When **6** was treated with excess *m*CPBA (3 molar equiv.) similarly as described in c, **20** was obtained in 20% yield after chromatography, along with a trace of monoepoxides.

Epoxidation of ***4****.* A solution of **4** (0.14 g) and *m*CPBA (0.19 g, 2 molar equiv.) in 1,2-dichloroethane (3.5 ml) was allowed to stand at room temperature for 2 d. At this time,

TLC indicated that **4** remained almost unchanged.

Treatment of **4** (58 mg) with *m*CPBA (42 mg, equimolar) in 1,2-dichloroethane in the presence of 2,6-di-*t*-butyl-*p*-cresol (3 mg) at reflux temperature for 7 h, followed by the conventional acetylation, gave many products, one of which was identified with **20** by TLC. There was no product present, which was identical with **1**.[16]

*Epoxidation of **16**.* Compound **16** (5 mg) was treated with *m*CPBA (7 mg, 2 molar equiv.) in 1,2-dichloroethane (0.6 ml) at room temperature for 3 d. About half of **16** was found to be converted into **20** by TLC.

*Epoxidation of **17**.* Compound **17** (20 mg) was recovered unchanged, after having been treated with *m*CPBA (28 mg, 2 molar equiv.) in 1,2-dichloroethane (2 ml) at room temperature for 2 d. Under the forcing conditions,[10] **17** (62 mg) gave several products, but there was no product identical with **1**. Furthermore, the ^{1}H NMR spectrum of the mixture of products did not show any signals due to epoxide protons.

The authors express their sincere thanks to Mr. Saburo Nakada for the elementary analyses, and to Mr. Isamu Kasahara and Mr. Kenji Kato for assistance in the preparative experiments.

References

1) A preliminary account of portion of this article has previously been presented: S. Ogawa, T. Toyokuni, M. Ara, M. Suetsugu, and T. Suami, *Chem. Lett.*, **1980**, 379. The nomenclature and numbering of cyclitols used in this paper follow IUPAC and IUB Tentative Cyclitol Nomenclature Rule [*J. Biol. Chem.*, **243**, 5809 (1968)]. The formulas depict only one of the respective enantiomers.

2) S. M. Kupchan, R. J. Hemingway, P. Coggon, A. T, McPhail, and G. A. Sim, *J. Am. Chem. Soc.*, **90**, 2982 (1968); S. Takahashi, *Phytochemistry*, **8**, 321 (1969).

3) R. Hollands, D. Becher, A Gaudemer, and J. Polonsky, *Tetrahedron*, **24**, 1633 (1968).

4) a) J. Singh, K. L. Dhar, and K. Atal, *Tetrahedron*, **26**, 4403 (1970); b) B. S. Joshi, D. H. Gawad, and H. Fuher, *Tetrahedron Lett.*, **1979**, 2427.

5) G. R. Schulte, M. Kodpinid, C. Thebtaranonth, and Y. Thebtaranonth, *Tetrahedron Lett.*, **23**, 4303 (1982).

6) S. Ogawa, S. Oki, and T. Suami, *Bull. Chem. Soc. Jpn.*, **52**, 1095 (1979).

7) S. Ogawa, T. Toyokuni, T. Kondoh, Y. Hattori, S. Iwasaki, M. Suetsugu, and T. Suami, *Bull. Chem. Soc. Jpn.*, **54**, 2739 (1981).

8) Under acidic conditions, the C-1 acetoxyl group of **7a** seems to be partly *O*-deacylated and oxidized with NBS.

9) R. Demuth, P. E. Garrett, and J. D. White, *J. Am. Chem. Soc.*, **98**, 634 (1976).

10) Y. Kishi, M. Aratani, H. Tamino, T. Fukuyama, and T. Goto, *J. Chem. Soc., Chem. Commun.*, **1972**, 64.

11) The structures of **16** and **17** were further established by converting them into a single azido compound, respectively: S. Ogawa, M. Suetsugu, T. Toyokuni, and T. Suami, *Nippon Kagaku Kaishi*, **1982**, 1721.

12) S. M. Kupchan, R. J. Hemingway, and R. M. Smith, *J. Org. Chem.*, **34**, 3898 (1969).

13) Diepoxide **20** seems to be identical with epicrotepoxide described by White *et al.*[9]

14) S. G. Davis and G. H. Whitham, *J. Chem. Soc., Perkin Trans. 1*, **1977**, 572.

15) Mass spectrum was measured by Dr. Shigeru Nishiyama to whom our thanks are due.

16) DL-Crotepoxide was kindly supplied by Dr. Masakatsu Matsumoto (Sagami Chemical Research Center, Sagamihara, Kanagawa) to whom our thanks are due.

 © 1983 The Chemical Society of Japan Bull. Chem. Soc. Jpn., 56, 1715—1720 (1983)

The Interaction of a Neutral Polymer with Small Ions in Solution. III. Ionic Association on a Poly(oxyethylene) Chain

Hiroshi Awano, Katsumichi Ono,* and Kenkichi Murakami
Chemical Research Institute of Non-Aqueous Solutions, Tohoku University, Katahira, Sendai 980
(Received August 21, 1982)

Conductivities of NaSCN and KSCN solutions have been measured in ethanol and nitromethane in the presence of poly(oxyethylene). For poly(oxyethylene)-KSCN solutions in ethanol and nitromethane, a distinct minimum appears in conductivity *vs.* polymer concentration curves. In addition, for a poly(oxyethylene)-NaSCN solution in nitromethane, the conductivity curve rises steeply after passing through the minimum. These anomalies cannot be explained by the cation binding to the polymer alone, and the ionic association on the polymer chain should be taken into account at the same time. In order to analyze the results, a theory based on the duplicate ion binding on a one-dimensional lattice has been developed. The theory not only predicts the appearance of the conductivity minima, but also makes it possible to estimate the ionic association constants.

The authors have investigated by conductometry the the binding of alkali metal ions to poly(oxyethylene) (POE) in various solvents.[1-3] It has been found that the equivalent conductivities of the alkali metal salts, Λ, decrease monotonically with an increase in the concentration of POE (monomer base mole), C_p. For solutions of potassium thiocyanate in methanol, acetonitrile, propylene carbonate, and sulfolane, the amount of potassium ion bound to a POE chain has been evaluated from the decrement of Λ. In these cases, it is not necessary to take into account the contribution of the anion to the decrement of Λ, since the specific interaction between the cation and the anion is virtually negligible. A binding constant, K_0, which does not include the contribution of the interaction between the cation bound to a POE chain, has been obtained on the basis of a one-dimensional lattice model.[2] It has been shown that, over a variety of solvents, a linear correlation exists between the logarithmic binding constant, log K_0, and the standard chemical potential of the cation, $\mu^{\ominus}$.[3]

Thus, it can be expected that the binding of potassium ions to POE occurs extensively in ethanol, nitromethane, or the like, in which $\mu^{\ominus}$ is much larger than in methanol, acetonitrile, *etc.* Similarly to the polyelectrolyte systems, in which counter ions are bound to the polyion, it is expected that anions would be bound to the POE–cation complexes and make no contribution to the conductivity, when the charge density of the cation on the chain is enhanced. In addition, ionic association or ion-pair formation also occurs to a large extent even in the polymer free solutions of some alkali metal thiocyanates in ethanol and nitromethane.

In this paper, we assume that the following three equilibria exist in these systems:

1) binding of the cation to a POE chain; 2) ionic association on a POE chain; 3) ionic association in the bulk solvent.

It is necessary to treat the equilibria 1 and 2 on the basis of the one-dimensional lattice model, because both equilibria might be influenced by the interference between the positive charges bound on the chain. In our treatment, an extended one-dimensional lattice model is proposed to interpret the Λ *vs.* C_p curves in such complicated cases. The outline of the treatment has already been published in our preliminary report.[4]

Theory

An Extension of the One-dimensional Lattice Model. When we extend the one-dimensional lattice model to the case of the duplicate ion binding to POE, the following two basic assumptions are made.

In the first place, we must specify the binding state of a site. Three kinds of binding states were assumed for each site according to their energies. The energy of the site was assumed to be 0 if nothing is bound (state $\underline{0}$), E_c if a cation is bound (state $\underline{1}$), and E_c+E_a if not only a cation but also an anion is bound (state $\underline{2}$).

In the second place, we must specify the interaction energy between the sites. When either or both of the i-th and j-th sites are the state $\underline{0}$ or state $\underline{2}$, then the interaction energy J_{ij} between i-th and j-th sites is represented as:

$$J_{ij} = 0. \tag{1}$$

This means that the site specified as state $\underline{2}$ has no effective charges and does not exert electrostatic potential at the other sites. On the other hand, if both of the i-th and j-th sites are in the state $\underline{1}$, J_{ij} is assumed to be represented as:

$$J_{ij} = \begin{cases} J_m, & m \equiv j - i < k \\ 0, & j - i > k, \end{cases} \tag{2}$$

and k is the range of the number of sites, beyond which the interaction is truncated, and J_m is the Debye-Hückel potential. This has the following form:

$$J_m = \frac{e^2 \exp(-\kappa_D r_m)}{4\pi\varepsilon r_m}, \quad \kappa_D^2 = \frac{2N_A e^2 I}{\varepsilon k_B T}, \tag{3}$$

where e is the elementary electronic charge, κ_D the Debye's shielding parameter, r_m the intersite distance, ε the dielectric constant of the solvent, N_A the Avogadro constant, I the ionic strength, k_B the Boltzmann constant, and T the absolute temperature. A statistical weight factor A_m is defined by:

$$A_m \equiv \exp(-J_m/RT). \tag{4}$$

If we denote the chemical potentials of the cation and the anion as μ_c and μ_a, respectively, then the normalized activities of these ions are defined as follows:[2]

$$\xi \equiv \exp[(\mu_c - E_c)/RT] \tag{5}$$

$$\eta \equiv \exp[(\mu_a - E_a)/RT]. \quad (6)$$

The grand partition function of this system may be conveniently described in terms of the following matrix product:

$$\Xi = \boldsymbol{e}\, \boldsymbol{U}_k^N \boldsymbol{e}' \quad (7)$$

where $\boldsymbol{e}$ and $\boldsymbol{e}'$ are row and column vectors such as:

$$\boldsymbol{e} = (1,1,1,\cdots\cdots,1) \qquad \boldsymbol{e}' = \begin{pmatrix} 1 \\ 0 \\ \vdots \\ 0 \end{pmatrix}. \quad (8)$$

In Eq. 7, N is the number of a lattice point on a chain, and $\boldsymbol{U}_k$ is a statistical weight matrix whose order is 3^k. A few examples of the matrix are shown below:

for $k = 1$,

$$\mathrm{U} = \begin{array}{c|ccc} i+1 & \underline{0} & \underline{1} & \underline{2} \\ i & & & \\ \hline \underline{0} & 1 & 1 & 1 \\ \underline{1} & \xi & \xi A_1 & \xi \\ \underline{2} & \xi\eta & \xi\eta & \xi\eta \end{array} \quad (9)$$

for $k = 2$,

$$\boldsymbol{U} = \begin{array}{cc|ccccccccc} i+2 & & \underline{0} & \underline{1} & \underline{2} & \underline{0} & \underline{1} & \underline{2} & \underline{0} & \underline{1} & \underline{2} \\ i & i+1 & \underline{0} & \underline{0} & \underline{0} & \underline{1} & \underline{1} & \underline{1} & \underline{2} & \underline{2} & \underline{2} \\ \hline \underline{0} & \underline{0} & 1 & 1 & 1 & 0 & 0 & 0 & 0 & 0 & 0 \\ \underline{0} & \underline{1} & 0 & 0 & 0 & 1 & 1 & 1 & 0 & 0 & 0 \\ \underline{0} & \underline{2} & 0 & 0 & 0 & 0 & 0 & 0 & 1 & 1 & 1 \\ \underline{1} & \underline{0} & \xi & \xi A_2 & \xi & 0 & 0 & 0 & 0 & 0 & 0 \\ \underline{1} & \underline{1} & 0 & 0 & 0 & \xi A_1 & \xi A_1 \xi A_2 & \xi A_1 & 0 & 0 & 0 \\ \underline{1} & \underline{2} & 0 & 0 & 0 & 0 & 0 & 0 & \xi & \xi A_2 & \xi \\ \underline{2} & \underline{0} & \xi\eta & \xi\eta & \xi\eta & 0 & 0 & 0 & 0 & 0 & 0 \\ \underline{2} & \underline{1} & 0 & 0 & 0 & \xi\eta & \xi\eta & \xi\eta & 0 & 0 & 0 \\ \underline{2} & \underline{2} & 0 & 0 & 0 & 0 & 0 & 0 & \xi\eta & \xi\eta & \xi\eta \end{array} \quad (10)$$

Extrapolation to $k \to \infty$ can be carried out in a similar manner as was shown in our previous paper of this series.[2]

It is convenient to define the degree of binding in terms of the probability that a site is occupied by the cation or the anion, respectively. This probability is *formally* represented for the cation and the anion by;[5]

$$\theta_c = \left(\frac{1}{N}\frac{\partial \ln \Xi}{\partial \ln \xi}\right)_\eta, \quad (11)$$

$$\theta_a = \left(\frac{1}{N}\frac{\partial \ln \Xi}{\partial \ln \eta}\right)_\xi. \quad (12)$$

The binding constants for the cation and the anion are defined as:

$$K_0^c \equiv \exp[(\mu_c^\ominus - E_c)/RT] \quad (13)$$

$$K_0^a \equiv \exp[(\mu_a^\ominus - E_a)/RT], \quad (14)$$

where $\mu_c^\ominus$ and $\mu_a^\ominus$ are the standard chemical potentials of cation and the anion, respectively.

Reproduction of Conductivity Curves. From Eqs. 5, 6, 13, 14, the concentration of the free cation, C_c, and that of the free anion, C_a, are given by:

$$C_c = (\xi/K_0^c y_\pm)C^\ominus, \quad (15)$$

$$C_a = (\eta/K_0^a y_\pm)C^\ominus, \quad (16)$$

where $y_\pm$ is the mean activity coefficient on the molar concentration basis. This is approximately estimated by the Debye-Hückel limiting law, and $C^\ominus$ is the standard value of molar concentration, being equal to 1 mol dm^{-3}. According to the principle of electron-neutrality, C_c and C_a are related to one another, and the following relationship holds:

$$C_c + (\theta_c - \theta_a)C_p/4 = C_a. \quad (17)$$

The second term of the lefthand side of Eq. 17 corresponds to the concentration at the site where only a cation is bound (state $\underline{1}$), and the denominator of this term is introduced on the assumption that a site is compcsed of four oxyethylene units.[1] Substituting Eqs. 15 and 16 into Eq. 17, we obtain:

$$C_p = \frac{4(\eta/K_0^a - \xi/K_0^c)C^\ominus}{y_\pm(\theta_c - \theta_a)}. \quad (18)$$

Next we introduce an ionic association constant K_A.

$$K_\mathrm{A} \equiv \frac{C_{assoc}/C^\ominus}{(C_c y_\pm/C^\ominus)(C_a y_\pm/C^\ominus)}. \quad (19)$$

Where C_{assoc} is the concentration of the ion-pair, the activity coefficient being assumed to be 1. C_{assoc} is obtained by subtracting the concentration of the free anion and that of the bound anion from the total anion concentration, C_s, as follows:

$$C_{assoc} = C_s - C_a - \theta_a C_p/4. \quad (20)$$

Substituting Eq. 20 into Eq. 19, and combining with Eqs. 15 and 16 we finally obtain:

$$\eta = K_0^a y_\pm \frac{(C_s - \theta_a C_p/4)/C^\ominus}{1 + K_\mathrm{A} y_\pm \xi/K_0^c}. \quad (21)$$

For a fixed value of ξ, the set of Eqs. 11, 12, 18, and 21 are simultaneous equations with respect to η, θ_c, θ_a, and C_p. Athough the equations cannot be solved analytically, we can obtain a solution by an iterative method. Then C_c and C_a are calculated from Eqs. 15 and 16.

Molar conductivity is estimated by the following equation,

$$\Lambda = (C_c\lambda_c + C_a\lambda_a)/C_s, \quad (22)$$

where λ_c and λ_a are the molar conductivities of the cation and anion, respectively, in the absence of ionic association. These values are calculated in terms of the Onsager's limiting law.[6]

$$\lambda = \lambda^\infty - (\alpha\lambda^\infty + \beta)\sqrt{I}, \quad (23)$$

where λ^∞, the limiting molar conductivity of the ion, can be found in the literature, α and β are the Onsager parameters, and for a uni-univalent electrolyte;

$$\alpha = \frac{e^2}{3k_\mathrm{B}\varepsilon T}\frac{q}{1+\sqrt{q}}\frac{\kappa_\mathrm{D}}{\sqrt{I}}, \quad q = \frac{1}{2}$$

$$\beta = \frac{Fe}{6\pi\eta_v}\frac{\kappa_\mathrm{D}}{\sqrt{I}}, \quad (24)$$

where η_v is the viscosity of the solvent and F is the Faraday constant. In this way, we can calculate the relationship between Λ *vs.* C_p for a POE–alkali metal salt–solvent system.

Experimental

Poly(oxyethylene) samples, with a nominal molecular weight range from 200 to 5×10^6 (Wako pure chemicals and Union Carbide Co.) were used. Except where indicated, measurements were performed for a sample with molecular weight 2×10^4 (viscosity average MW, 2.47×10^4). Reagent grade potassium and sodium thiocyanates were dried under vacuum before use. Ethanol was stirred with molecular sieve 4A, and distilled. $\kappa=3\times10^{-7}$ S cm^{-1}. Reagent grade nitromethane was used without further purification. $\kappa=2\times10^{-6}$ S cm^{-1}. The measurement of the conductivity was carried out in the manner previously reported.

Results and Discussion

The conductivity curves for the KSCN–EtOH systems are shown in Fig. 1. It may be seen that with increasing C_p conductivity first decreases, passes through a minimum, and then increases gradually at higher C_p. Such a minimum was not observed in the solvent systems studied previously.[3] The minimum becomes more pronounced as C_p becomes greater.

In Fig. 2, the conductivity curve for 5 mmol dm^{-3} NaSCN–EtOH is compared with that of KSCN solution. The minimum is not observed in this case, and the conductivity decreases continually.

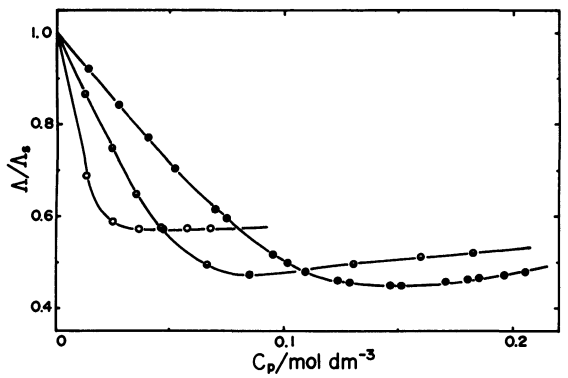

Fig. 1. Plots of relative conductance *vs.* concentration of POE for KSCN–EtOH solutions at 298.15 K. ●, $C_s=10$ mmol dm^{-3}; ◒, $C_s=5$ mmol dm^{-3}; ○, $C_s=1$ mmol dm^{-3}.

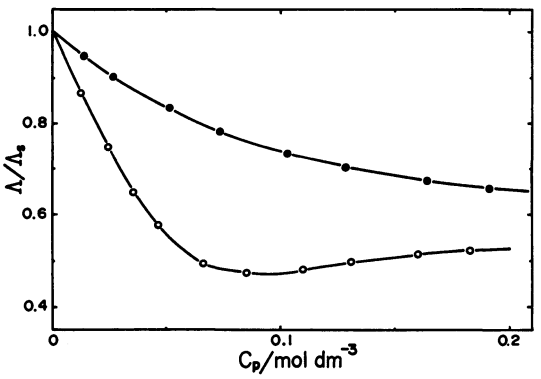

Fig. 2. Plots of relative conductance *vs.* concentration of POE for 5 mmol dm^{-3} KSCN- and NaSCN–EtOH solutions at 298.15 K. ○, KSCN; ●, NaSCN.

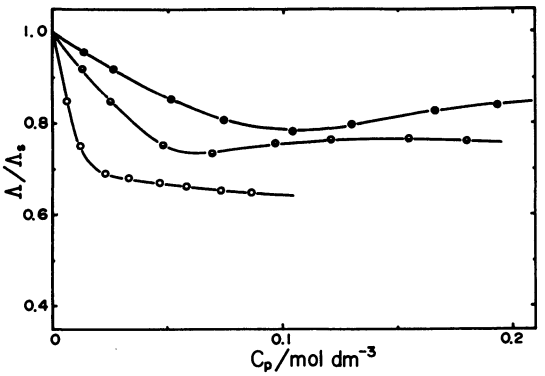

Fig. 3. Plots of relative conductance *vs.* concentration of POE for KSCN–nitromethane solutions at 298.15 K. ●, $C_s=10$ mmol dm^{-3}; ◒, $C_s=5$ mmol dm^{-3}; ○, $C_s=1$ mmol dm^{-3}.

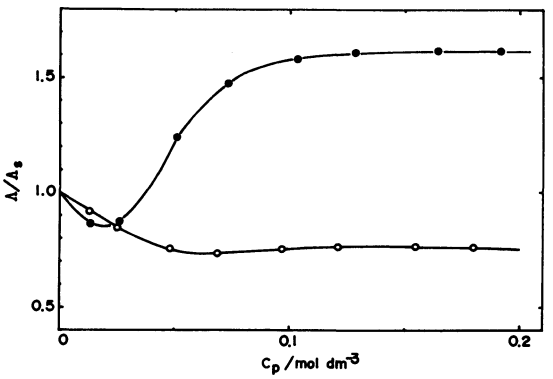

Fig. 4. Plots of relative conductance *vs.* concentration of POE for 5 mmol dm^{-3} KSCN- and NaSCN–nitromethane solutions at 298.15 K. ○, KSCN; ●, NaSCN.

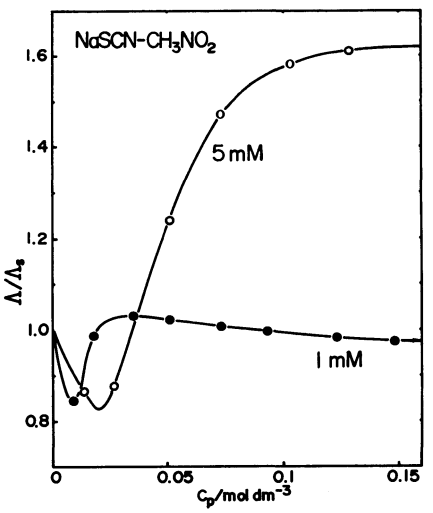

Fig. 5. Plots of relative conductance *vs.* concentration of POE for 5 mmol dm^{-3} and 1 mmol dm^{-3} NaSCN–nitromethane solutions at 298.15 K.

The conductivity curves for KSCN–nitromethane systems are shown in Fig. 3. The minimum in the conductivity is also observed. As is different from that observed in the KSCN–EtOH systems, the intrinsic

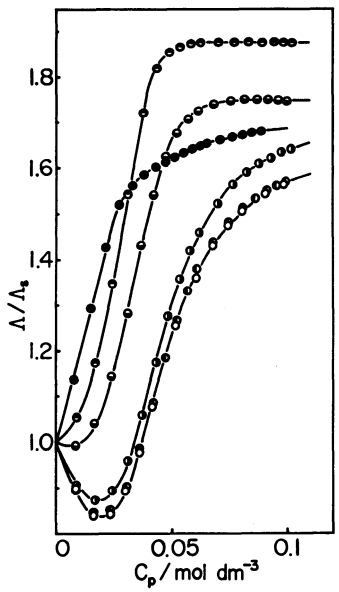

Fig. 6. Molecular weight dependence of the relative conductance *vs.* C_p plots for 5 mmol dm^{-3} NaSCN–nitromethane solutions at 298.15 K. Average molecular weigth; ●, 200; ◓, 400; ◒, 1500; ◑, 7500; ◐, 2×10^4; ○, more than 5×10^6.

value of the conductivity value of the conductivity in the large C_p increases with increasing C_s.

In contrast to the above systems, the behavior in the NaSCN–nitromethane solutions is anomalous. After the conductivity passes through a small minimum, Λ increases tremendously as can be seen in Fig. 4. The degree of the increase in the conductivity is dependent on C_s (Fig. 5). The effect of the molecular weight is shown in Fig. 6. The curves are almost independent of the molecular weight above 2×10^4. This means that the effect of the bulk viscosity of the solution is virtually negligible. In addition, it can be deduced that the electric mobility of the bound ions may be neglected as compared with that of the free ions, if the molecular weight of POE is above 2×10^4. As the molecular weight of POE decreases, the minimum of the curve becomes less prominent and finally diminishes. This is probably due to the increasing contribution of the bound ion to the conductivity.

Similar minima in the conductance plots were also observed by Smid and his coworkers, for the mixture of poly(vinylbenzo crown ether)s and potassium tetraphenylborate in methyl ethyl ketone.[7] The main reason for the appearance of the minima was ascribed to the reduction of viscosity in the higher C_p, where the charge density of the bound cation is relatively low. In view of our results, this is not likely because the conductivity does not depend on molecular weight above 2×10^4, so that the viscosity effect is negligible. We propose alternatively that the ion association on a polymer chain is the main cause of the occurence of the minima.

Before considering the systems quantitatively we should evaluate the ionic association constants in the absence of POE. These constants are calculated by the Fuoss-Kraus method[8] using molar conductivity data

Table 1. Ionic association constants in polymer free solutions calculated by the Fuoss-Kraus method[8]

Solvent	KSCN	NaSCN
EtOH[a]	47.53	32.32
Nitromethane[b]	109.3	1591

a) Ref. 9, b) Ref. 10.

cited in the literatures[9,10] (Table 1). It should be noted that the ionic association constant of NaSCN in nitromethane is extremely large.

To calculate the Λ *vs.* C_p relationships in terms of the extended one-dimensional model, we must know the values for K_A, K_0^c, K_0^a, λ_c^∞, and λ_a^∞. The data in Table 1 can be used for the values for the K_A, and λ_c^∞ and λ_a^∞ values are cited in literatures.

In our previous paper, we have shown that a linear relationship exists between the binding constant and the standard chemical potential of the cation.[3] Using the relative values of the standard chemical potential of potassium ion to that of a reference solvent, reported by Owensby and his coworkers,[11] K_0^c for potassium ion is estimated as 4270 in ethanol and 23400 in nitromethane, respectively. For sodium ion in nitromethane, no reliable estimations of K_0^c are possible, but we tentatively use the same K_0^c value for the potassium ion.

The calculated curves are shown in Figs. 7 through 9, together with the observed values. It is necessary to take into account the ion association on a POE chain in reproducing the conductance minimum. As shown in the figures, the conductance minimum becomes sharper with increasing K_0^a. An optimum fitting is obtained by assuming that $K_0^a \simeq 50$ for KSCN–eth anol, $\simeq 20$ for KSCN–nitromethane, and $\simeq 10$ for NaSCN–nitromethane. Thus, it appears that the ion association occurs to a considerable extent along POE chains.

In Fig. 10, the dependence of the calculated conductivity curves on C_s is shown for KSCN–EtOH solutions. From this figure and Fig. 1, it is noted that the calculated curves well reproduce the qualitative aspect of the C_s dependence of the observed curve as well as that of the conductivity minimum, thereby giving further support on the present model.

The quantitative agreement, however, is rather poor,

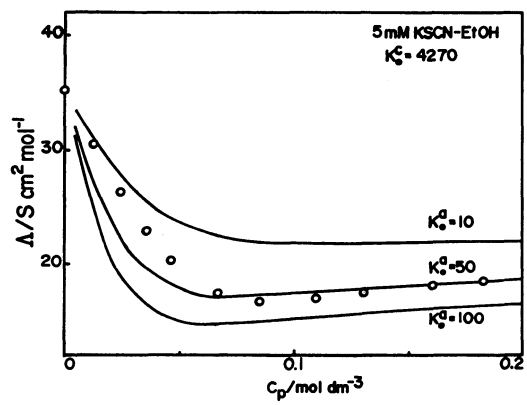

Fig. 7. Calculated Λ *vs.* C_p curves for 5 mmol dm^{-3} KSCN–EtOH solution, together with the observed plots.

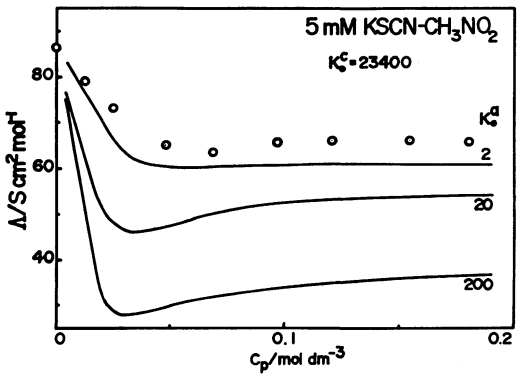

Fig. 8. Calculated Λ *vs.* C_p curves for 5 mmol dm^{-3} KSCN–nitromethane solution, together with the observed plots.

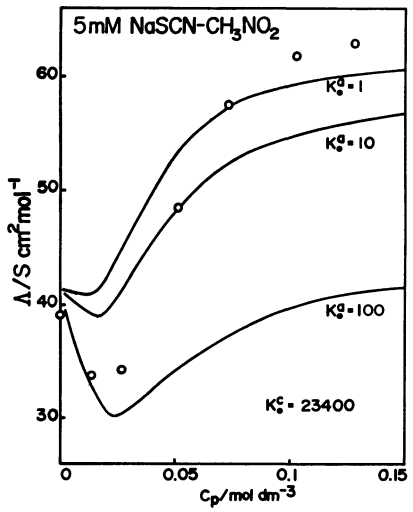

Fig. 9. Calculated Λ *vs.* C_p curves for 5 mmol dm^{-3} NaSCN–nitromethane solution, together with the observed plots.

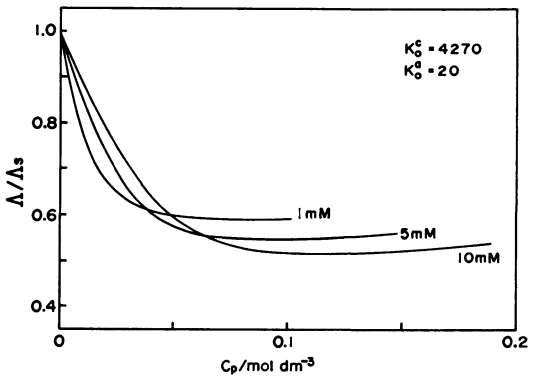

Fig. 10. Dependence of calculated Λ *vs.* C_p curves on total KSCN concentration for KSCN–EtOH solutions.

especially for NaSCN–nitromethane. The theoretical curve can not reproduce the steep rise in conductivity with C_p. One of the causes for the disagreement is the uncertainty in the determination of λ^∞. The precise determination of λ^∞ is difficult in a solvent where the ionic association constant is very large. Another possible cause is the inadequacy of the model where the charge density of the bound cation is high. In the present model, the statistical weight factor of the i-th site being in state $\underline{2}$ is assumed to be $\xi\eta$ irrespective of the binding state of the neighboring sites. In practice, however, this factor may be related to whether $(i+1)$-th site is occupied or not.

It is worth noting that K_0^a values for NaSCN solutions are comparable in ethanol and in nitromethane, despite of the great difference in the ionic association constant, K_A, in the polymer free solution. This result is qualitatively explained by the solvation effects on the sodium ion.[12] In the acidic solvents, such as nitromethane, the solvating power for a cation is very low. On the other hand, basic POE strongly coordinates to sodium ion, which results in the reduction of ionic association if the charge density of the cation on the POE chain is low. This is the reason why the conductance increases in the high C_p for the nitromethane solution.

On the contrary, the hydrogen-bonding solvents, such as ethanol, have well-defined basic sites for the solvation to cation.[12] Consequently, the degree of association is small both in POE free solution and in solutions at high POE concentration. The association is only appreciable in the intermediate regions, where the charge density of the bound cation is high.

We observed a great difference in the behavior of NaSCN and KSCN solutions in nitromethane. As has been stated above, the ionic association constant for sodium ion is much larger than that for potassium ion in the absence of polymer. In the presence of excess POE, almost all the cations are bound to the POE chain. As the effective ion sizes of complexed sodium and potassium ions seem to be identical, the degree of the ionic association of these ions would be similar in magnitude. Consequently, the degree of ionic association for the sodium ion is greatly reduced by the addition of POE, while the reduction is less for the potassium ion.

Finally, we should briefly discuss the correlation with the Manning theory of polyelectrolyte solutions.[13] In his elegant theory, Manning stated that the so-called ion condensation of counter ions is uniquely determined by the charge density parameter ξ_M of the polyion, which is defined by;

$$\xi_M = \frac{e^2}{\varepsilon k_B T b}, \tag{25}$$

where b is the average distance between charges on the polyelectrolyte. According to the theory, for $\xi_M > 1$ the system becomes unstable and the counter ions condense on the polymer chain to achieve the ξ_M value of unity. While the Manning model explains the equilibrium properties of polyelectrolytes in aqueous solutions, the applications to the organic solvent systems are few in the literature.

According to the original theory, the Manning model assumes that the unbound free ions may be treated in the Debye-Hückel approximation. Therefore, the application of the model to the POE–NaSCN–nitromethane system is inadequate, since extensive ionic association occurs even in the POE free solution. We have examined the applicability of the Manning model

to 5 mM KSCN–ethanol and –nitromethane systems, because the ionic association of KSCN is less in these solvents.

It follows from the above that the increase of the conductivity at higher C_p is due to the decrease of ionic association on a POE chain. Thus the POE concentration at the onset of ionic association may be estimated from the point that the increase of the conductivity is no longer detectable in Λ *vs.* C_p curves. From Figs. 1 and 3, for POE–5 mM KSCN–ethanol and –nitromethane systems, this point corresponds to $C_p \simeq 0.2$ and 0.13 M, respectively. Using the intersite distances calculated by a stiff-chain model,[2] ξ_M is estimated to be about 0.4 in both cases. This value is far lower than the limit of the ion condensation predicted from the Manning theory.

It should be noted that the Manning theory is based on the Bjerrum theory[14] of the ionic association between low-molecular weight ions. In the Bjerrum theory, the ionic association is a function only of the dielectric constant of the solvent and the inter-ionic distance. Recent investigations of the solvent effect of ionic association, however, have revealed that this is not true for the ionic association in organic solvents and that it also depends on a specific interaction between the ion and the solvent molecules.[12] This is also the case for the present systems, since the anion binding to the POE chain is related not only to the interaction between the POE–cation complex and the anion but also to that between the cation and the anion in the bulk solvent. As the result, the application of the Manning model to the present systems is inappropriate.

In conclusion, the anomalous conductivity curves for POE-alkali metal ions in ethanol and nitromethane are well explained by a duplicate ion binding model based on the one-dimensional lattice. An improvement of the model would be necessary to achieve a more sufficient agreement between the theoretical and the experimental conductivity curves.

References

1) K. Ono, H. Konami, and K. Murakami, *J. Phys. Chem.*, **83**, 2665 (1 79).
2) Part I of this series: H. Awano, K. Ono, and K. Murakami, *Bull. Chem. Soc. Jpn.*, **55**, 2525 (1982).
3) Part II of this series: H. Awano, K. Ono, and K. Murakami, *Bull. Chem. Soc. Jpn.*, **55**, 2530 (1982).
4) H. Awano, K. Ono, and K. Murakami, *Chem. Lett.*, **1982**, 149.
5) Since from the electro-neutrality principle, ξ and η are dependent with each other, partial differentiations represented in Eqs. 11 and 12 are mathematically impossible. Nevertheless, formal calculations are possible, because Ξ is the functions of ξ and η.
6) L. Onsager, *Phys. Z.*, **28**, 277 (1927).
7) S. C. Shah, S. Kopolow, and J. Smid, *J. Polymer Sci., Polymer Chem. Ed.*, **14**, 2023 (1976).
8) R. M. Fuoss, *Chem. Rev.*, **17**, 27, (1935); D. J. Mead, R. M. Fuoss, and C. A. Kraus, *Trans. Faraday Soc.*, **32**, 594 (1936).
9) M. Barak and H. Hartley, *Z. Phys. Chem.*, **A165**, 272 (1933).
10) C. P. Wright, D. M. Murray-Rust, and H. Hartley, *J. Chem. Soc.*, **1931**, 199.
11) D. A. Owensby, A. J. Parker, and J. W. Diggle, *J. Am. Chem. Soc.*, **96**, 2682 (1974).
12) R. M. Kay, D. F. Evans, and M. A. Matesich, "Solute-Solvent Interactions," ed by J. F. Coetzee and C. D. Richie, Marcel Dekker, New York (1976), Vol. 2, Chap. 10.
13) G. S. Manning, *J. Chem. Phys.*, **51**, 924 (1969).
14) N. Bjerrum, *Dan. Vidensk. Selesk. Mat. Fiz. Medd.*, **7**, 9 (1926).

 © 1983 The Chemical Society of Japan Bull. Chem. Soc. Jpn., 56, 1721—1727 (1983)

Electronic States of Dioxygen Heme Complex Revealed from *ab Initio* LCAO-SCF-MO Calculations

Tsunenori NOZAWA,* Masahiro HATANO, Unpei NAGASHIMA,†,†† Shigeru OBARA,†† and Hiroshi KASHIWAGI*,††

Chemical Research Institute of Non-aqueous Solutions, Tohoku University, Katahira, Sendai 980

†*Department of Chemistry, Faculty of Science, Hokkaido University, Kita-ku, Sapporo 060*

††*Institute for Molecular Science, Myodaiji, Okazaki 444*

Received August 6, 1982)

Ab initio LCAO-SCF-MO calculations of a model oxyheme were carried out on several singlet, triplet and quintet states arising from the three types of configurations, $(d_\epsilon)^6(\pi_g^a)^2$, $(d_\epsilon)^5(d_\gamma)^1(\pi_g^a)^1(\pi_g^b)^1$, and $(d_\epsilon)^5(\pi_g^a)^2(\pi_g^b)^1$. The lowest states in the SCF energy are of the configuration $(d_\epsilon)^5(\pi_g^a)^2(\pi_g^b)^1$ whose electronic structures can be also expressed as Fe(III)–O_2^- from the results of Mulliken's population analysis. Calculated Mössbauer parameters of those states are in good agreement with experiments for oxyhemoglobin, oxymyoglobin and model oxyheme, while those of the closed-shell singlet state $(d_\epsilon)^6(\pi_g^a)^2$ are inconsistent with experiments. The Fe–O_1 overlap populations indicate a bonding nature for the former states and a non-bonding nature for the latter state. These results all predict singlet states of Fe(III)–O_2^- structure as the main configuration of the ground state in the model oxyheme.

The nature of the iron-oxygen bond in oxyhemoglobin and oxymyoglobin is a controversial problem. Although X-ray data from a model oxyheme[1] and oxymyoglobin[2] support the bent Fe–O_1–O_2 geometry proposed by Pauling,[3] questions concerned with the details of the bondings and the charge on the oxygen molecule have not yet been resolved.

Mössbauer resonance of the proteins[4-6] and of the model compound[7] has been used to probe the electron distribution around the iron nucleus. Electronic transitions spectra,[8,9] magnetic circular dichroism spectra,[9,10] infrared stretching frequencies,[11-14] resonance Raman frequencies,[15,16] magnetic susceptibility,[17-22] and the Fe $K\alpha$ fluorescence emission spectrum of oxyhemoglobin[23] have been measured in order to elucidate the bonding of dioxygen to iron porphyrins.

The large quadrupole splitting observed in Mössbauer resonance of the oxyhemoglobin[5,6] and of the model oxyheme compound,[7] would imply the presence of large asymmetric 3d electron distribution caused by covalent bondings if the oxyhemoglobin were to be considered as low-spin iron(II). However the observed negative electric field gradient would be compatible with the loss of electron charge from a $d\pi$ orbital, which may imply an Fe(III)–O_2^- structure.

The oxygen-oxygen stretching frequencies observed in myoglobin (1103 cm^{-1}),[11] in hemoglobin (1107 cm^{-1}),[12] and in the model compounds (1160 cm^{-1})[13] were cited as evidence for the Fe(III)–O_2^- structure, since they fall in the range found for superoxide complexes (KO_2, 1100—1150 cm^{-1}), while the stretching frequencies for the O_2 molecule are 1556 cm^{-1} for the $^3\Sigma_g^-$ state and 1484 cm^{-1} for the $^1\Delta_g$ state. However the force constant of the O–O bond in ozone (6.16 mdyn/Å) displayed a similar value to that for the O_2^- complex (5.7—6.2 mdyn/Å). This suggests that a neutral O_2 unit in heme complexes can have the observed frequencies mentioned above (1 mdyn/Å$=1\times10^{-7}$ N nm^{-1}).

Thus no definite conclusion can be drawn from experimental measurements. Many theoretical calculations[24-35] have been made to try to resolve these uncertainties and to account for the observed properties of oxyhemoglobin.

Recent semi-empirical INDO-SCF-CI calculations on a model oxyheme complex were reported to yield a singlet diamagnetic ground state with a very low-lying paramagnetic triplet state.[31] The diamagnetic ground state has considerable Fe(III)(d^5)–O_2^- character due to extensive charge-transfer but is not described by a single open-shell configuration of the Fe(III)(d^5)–O_2^- type. The calculations gave a quadrupole splitting and an electric field gradient in agreement with experiments, using delicate sets of semi-empirical parameters.

Ab initio LCAO-SCF-MO calculations for the model oxyheme were made by Dedieu *et al.*[33-35] Both minimal and valence-double basis set calculations yielded the lowest energy for a triplet state $^3A'$ with the formal configuration $(d_{x^2-y^2})^2(d_{xz})^2(d_{yz})^1(\pi_g^a)^2(\pi_g^b)^1$. However they assigned the ground state to the closed-shell state ($^1A'$), $(d_{x^2-y^2})^2(d_{xz})^2(d_{yz})^2(\pi_g^a)^2$, which lies at 0.036 a.u. (in the minimal basis) and 0.051 a.u. (in the valence-double basis set calculation) higher than the triplet state, since they estimated the correlation energy to be larger than 0.051 a.u. (1 a.u.$=4.35968\times10^{-18}$ J). This ground state wavefunction could not reproduce experimental Mössbauer parameters.[27,28,34] These calculations of Dedieu *et al.*[33,34] employed a split basis for the iron 3d orbitals consisting of optimized atomic 3d orbitals and additional Gaussian functions with a small exponent of 0.20. In our previous *ab initio* LCAO-SCF-MO calculations on cobalt porphine with a triple zeta 3d set,[36] the Gaussian 3d functions with an exponent of 0.18 were found to be negligible, while those with an exponent of 0.555999 were found to be critical in the description of the electronic structures of high oxidation states (see Discussion). Similarly in the present study we have found that Dediue's description of 3d orbitals is not flexible enough accurately to compare energies between Fe(III)- and Fe(II)-complexes.

In the present investigation we have examined *ab initio* LCAO-SCF-MO calculations using a basis set different from Dedieu's sets with a hope to predict correct energy levels and Mössbauer parameters. In the following sections we give details of the calculation

methods, then present the results, and discuss the total energies, Mössbauer parameters, charge distributions, and bonding natures for the oxyheme model.

Method

The geometry of the iron-porphine core, with the iron atom in the assumed porphine plane, was taken as the experimental geometry of the ($\alpha,\beta,\gamma,\delta$-tetraphenylporphinato)iron(II)(py)(CO)[37] (somewhat idealized) and is shown in Fig. 1a. For the Fe–O_1–O_2 moiety we have used an Fe–O_1 bond length of 1.75 Å, and an O_1–O_2 bond length of 1.24 Å and a Fe–O_1–O_2 angle of 136° corresponding to the experimental values for the dioxygen complex of the picket fence porphyrin.[7] We have used the experimental geometries of the ammonia ligand with an Fe–N bond length of 2.12 Å (Fig. 1b).[38] Our choice of axis is shown in Fig. 1b with the porphine plane being the xy plane. The four nitrogen atoms of the pyrrole rings are along the bisector of the axes x and y. The Fe–O_1 axis is the z axis and the O_1–O_2 axis projects along the axis x. The model system is assumed to have C_s symmetry.

The *ab initio* LCAO-SCF-MO calculations including all electrons have been carried out on the oxyheme model described above with a primitive Gaussian basis set (11s, 7p, 4d/7s, 3p/3s)[39,40] contracted to [4s, 3p, 2d/2s, 1p/1s] which is a minimal set except for the 3d functions with a split basis. The basis sets are shown in Table 1. For H, the (3s) set was contracted to the minimal set. The (7s, 3p) set was contracted to the minimal bases for C, O, and N. The (11s, 7p, 4d) basis set for the Fe atom is constructed from a (12s, 6p, 4d) basis optimized for Fe,[39] where two diffuse s functions were replaced by one s function of exponent 0.26; a set of p functions with an exponent of 0.28 was incremented. A comparison between ours and Dedieu's 3d orbitals is shown in Table 2. To improve the quality of the bases for light atoms, scale factors were used for the valence orbitals. Scale factors are 1.283, 1.098, 1.102, 1.102, 0.966, 1.019, 1.073, 1.073, 0.981, and 0.950 for H(1s), C(2s), C($2p_x$), C($2p_y$), C($2p_z$), N(2s), N($2p_x$) N($2p_y$), N($2p_z$), and O(2s), respectively. The calculations were carried out using the JAMOL 3 program package with a Roothaan's open shell formulation. We adopted a modified scheme of integral approximation[42] based on semi-orthogonalized orbitals.[43–45] The values 3.0×10^{-3} and 1.0×10^{-5} a.u. were taken as the threshold ones, respectively, for the overlap and exchange integrals from the results of the previous studies.[42–45] The calculation of molecular integrals and supermatrices took about 5 h of CPU time on a HITAC M-180 computer at the Computer Center of the Institute for Molecular Science. The HITAC M-180 is faster in speed by a factor of 1.5 as compared with that of an IBM 370-168. Each iteration in the SCF procedure took about 2 min. Iterations were performed to obtain SCF convergence, the criterion of which was less than 1.0×10^{-6} a.u. and 5.0×10^{-4} in the maximum differente between input and output values of the total energy

TABLE 1(A). ORBITAL EXPONENTS (α) AND CONTRACTION COEFFICIENTS OF THE CONTRACTED GAUSSIAN TYPE ORBITALS (CGTO's) FOR Fe

α	Contraction coefficients of CGTO's			
	1s	2s	3s	4s
63509.8	0.00169			
9344.59	0.01320			
2156.66	0.06284			
627.32	0.21100			
208.38	0.44009			
74.8588	0.38283			
19.2876		0.41810		
8.09403		0.67946		
2.14813			0.55185	
0.868997			0.68840	
0.260000				1.00000
α	2p	3p	4p	
424.039	0.02472			
98.9427	0.16155			
30.8593	0.45455			
10.7975	0.48537			
2.91785		0.53686		
0.924889		0.59877		
0.280000			1.00000	
α	$3d_1$	$3d_2$		
23.2006	0.06540			
6.13066	0.28749			
1.84927	0.51785			
0.505755		1.00000		

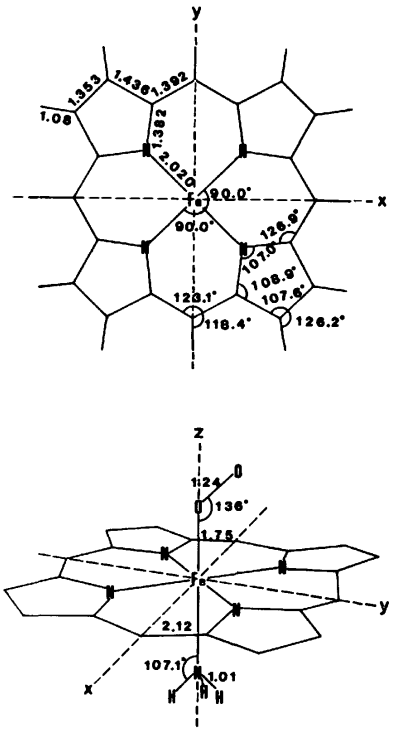

Fig. 1(a). Assumed geometry of the iron-porphine core for the oxyheme model and the choice of axes. Bond lengths are given in angstroms.
(b). The relative orientation and bond lengths (in angstroms) of the dioxygen and ammonia molecules in the oxyheme model.

Table 1(b). Orbital exponents (α) and contraction coefficients of the CGTO's for H, C, N, and O

Atom	α	Contraction coefficients of CGTO's		
		1s	2s	2p
H	4.5018	0.070452		
	0.681444	0.407826		
	0.151398	0.647752		
C	1412.29	0.004813		
	206.885	0.037267		
	45.8498	0.172403		
	12.3887	0.459261		
	3.72337	0.456185		
	0.524194		0.522342	
	0.163484		0.594186	
	4.18286			0.112194
	0.851563			0.466227
	0.199206			0.622569
N	2038.41	0.004479		
	301.689	0.034581		
	66.463	0.164263		
	17.8081	0.453898		
	5.30452	0.468979		
	0.764993		0.513598	
	0.234424		0.605721	
	5.95461			0.119664
	1.23293			0.474629
	0.286752			0.611142
O	2714.89	0.004324		
	415.725	0.032265		
	91.9805	0.15641		
	24.4515	0.447813		
	7.22296	0.481602		
	1.06314		0.504708	
	0.322679		0.616743	
	7.75579			0.129373
	1.62336			0.481269
	0.36503			0.604484

and density matric elements, respectively.

Results

The $3d_{z^2}$, $3d_{xz}$, $3d_{yz}$ orbitals of iron and $1\pi_g$ antibonding orbitals of dioxygen play important roles in the iron-oxygen bond. The π_g orbitals which are degenerate in the oxygen molecule are no longer equivalent in the complex with a bent structure. They are separated into two distinguished orbitals which are labeled as π_g^a and π_g^b in the following. The orbital π_g^a is made of $2p_x$ and $2p_z$ orbitals of the oxygen atoms and is symmetric with respect to the Fe–O_1–O_2 plane which is a plane of symmetry, while π_g^b is made of $2p_y$ orbitals and is antisymmetric with respect to the Fe–O_1–O_2 plane. The π_g^a orbital is stabilized relatively to the π_g^b orbital by the bonding interaction with the iron.

We have studied three groups of configurations $(d_\epsilon)^6(\pi_g^a)^2$, $(d_\epsilon)^5(d_\gamma)^1(\pi_g^a)^1(\pi_g^b)^1$, and$(d_\epsilon)^5(\pi_g^a)^2(\pi_g^b)^1$, where d_ϵ stands for $d_{x^2-y^2}$, d_{yz}, d_{xy} and d_γ represents d_{z^2} or d_{xy}. The closed-shell singlet state $(d_\epsilon)^6(\pi_g^a)^2$ with the $^1A'$ symmetry corresponds to an Fe(II)–O_2 formal configuration. An open-shell singlet state with the configuration $(d_\epsilon)^5(d_\gamma)^1(\pi_g^a)^1(\pi_g^b)^1$ was predicted as the main configuration in the ground state of oxyheme from the *ab initio* GVB-CI calculations on the model oxyheme system composed of O_2–Fe$(NH_2)_4$–NH_3.[29,30] The configuration $(d_\epsilon)^5(\pi_g^a)^2(\pi_g^b)^1$ corresponds to the formal Fe(III)–O_2^- configuration.

The calculated results, summarized in Table 3, indicate that the lowest energies for the oxyheme model were obtained for a group of states having a $(d_\epsilon)^5(\pi_g^a)^2(\pi_g^b)^1$ configuration. The open-shell singlet $^1A''$ (see the footnote (c) in Table 3) with the same formal configuration to that of $^3A''$ is calculated to be only 0.001 a.u. (0.03 eV) above the triplet state. One finds the quintet open-shell states, $^5A''$, and $^5A'$ at 0.032 and 0.047 a.u. (0.87 and 1.3 eV) above the lowest triplet states, respectively. Further above 0.043 a.u. (1.2 eV) from $^5A'$, there exists the closed-shell singlet $^1A'$ which corresponds to the Pauling model. These energy levels are illustrated in Fig. 2c.

The quadrupole splitting ΔE_Q of the present oxyheme model was calculated and is listed in Table 3 with the observed values in Mössbauer spectra. The ΔE_Q was determined as follows. The nine components V_{ij} of the electric field gradient tensor were calculated and the 3×3 tensor was then diagonalized. The principal values were ordered as $|V_{zz}|>|V_{xx}|>|V_{yy}|$. These values were then used in the expression:

$$\Delta E_Q = (1/2)(1/-R)eQq[1+\eta^2/3]^{1/2},$$

where $q=V_{zz}$, $\eta=|(V_{xx}-V_{yy})/V_{zz}|$ $(0<\eta<1)$, R is Sternheimer shielding constant, and Q is nuclear quadrupole moment. The sign of ΔE_Q is the sign of the largest component V_{zz} and $(1-R)eQ$ was taken as an empirical parameter determined to be 2.07 from our previous paper.[48] The calculated values of ΔE_Q, η, and the direction of the largest component of the electric field gradient tensor are listed in Table 3. These

Table 2. Comparison of the orbital exponents (α) and contraction coefficients (not normalized) of the CGTO's for Fe 3d orbitals of ours with those of Dedieu *et al.*

Ours			Dedieu *et al.*'s					
			Basis Set I			Basis Set II		
α	$3d_1$	$3d_2$	α	$3d_1$	$3d_2$	α	$3d_1$	$3d_2$
23.2006	0.0654		12.7344	0.15472		23.2006	0.0654	
6.13066	0.28749		3.15947	0.49782		6.13066	0.28749	
1.84927	0.51785		0.77404	0.61056		1.84927	0.51785	
0.505755		1.00000	0.20000		1.00000	0.505755	0.44311	
						0.200000		1.00000

TABLE 3. SCF TOTAL ENERGIES AND MÖSSBAUER PARAMETERS CALCULATED FOR VARIOUS CONFIGURATIONS OF MODEL OXYHEME

State	Formal occupation number Fe $d_{x^2-y^2}$ a'	Fe d_{xz} a'	Fe d_{yz} a''	Fe d_{z^2} a'	Fe d_{xy} a''	O_2 π_g^a a'	O_2 π_g^b a''	SCF total energy a.u.	Mössbauer parameters ΔE_Q	η	Direction of the principal axis[a]
$^1A''$	2	2	2	0	0	2	0	−2444.6630	0.65	0.50	z
$^5A''$	2	1	2	1	0	1	1	.7216[b]	−1.01	0.98	z
$^5A'$	2	2	1	1	0	1	1	.7064	1.44	0.68	y
$^1A''$[c]	2	1	2	0	0	2	1	.7521	−1.11	0.81	y
$^3A''$	2	1	2	0	0	2	1	.7531	−1.13	0.74	y
$^3A'$	2	2	1	0	0	2	1	.7512	−1.19	0.53	x
		Observed[d]							−2.10	0.23	x or y

a) The symbols x, y, and z denote the molecular axes in Fig. 1. b) The criterion of the SCF convergence is less than 2×10^{-5} (a.u.) and 2×10^{-3} in the maximum differences between input and output values of the total energy and density matrix elements. c) This state is an open-shell singlet state, where the iron spin couples with that in the dioxygen. d) Cited from the reference 5.

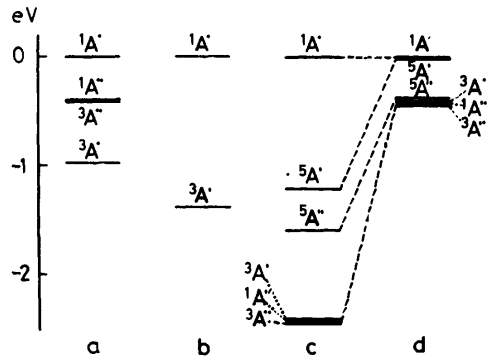

Fig. 2. The SCF energy levels for $^3A''$, $^1A''$, $^3A'$, $^5A''$, $^5A'$ and $^1A'$ from the *ab initio* LCAO-MO calculations (a—c) and the energy levels after correction of correlation energies (d).
(a). The results of Dedieu *et al.*[33-35] with the Basis Set I (minimal basis set except for the 3d orbitals with split functions).
(b). The results of Dedieu *et al.*[35] with the Basis Set II (valence double basis set).
(c). The present results with the minimal basis set except for the 3d orbitals with split functions (refer to Tables 1—3).
(d). The energy levels estimated from the present SCF energies by correction of correlation energies.[49,50]

results indicate that only the open-shell states with the configurations $(d_{x^2-y^2})^2(d_{xz})^2(d_{yz})^1(\pi_g^a)^2(\pi_g^b)^1$ and $(d_{x^2-y^2})^2(d_{xz})^1(d_{yz})^2(\pi_g^a)^2(\pi_g^b)^1$ can give ΔE_Q, and the sign and direction of the principal axis (V_{zz}) in agreement with the experimental low-temperature values ($\Delta E_Q=-2.10$ mm s^{-1}, V_{zz} in plane).[5,6]

Table 4 demonstrates the gross atomic populations and net atomic charges for the iron, oxygen and nitrogen atoms for the $^1A''$ and $^1A'$ states. As seen in Table 4, the net charges on the iron and oxygen atoms for $^1A''$ correspond well to an Fe(III)(d^5)–$O_2^-(\pi_g^3)$ configuration while those for $^1A'$ correspond to an Fe(II)(d^6)–$O_2(\pi_g^2)$ with reduced positive charge on the iron and nearly neutral oxygen atoms.

Table 5 displays the bond overlap populations of the open-shell singlet ($^1A''$) and the closed-shell singlet ($^1A'$) states calculated by Mulliken's population analysis. The

TABLE 4. GROSS AO POPULATIONS OF THE OXYHEME MODEL

AO		$^1A'$ Population	$^1A'$ Net charge	$^1A''$ Population	$^1A''$ Net charge
O_2	2s	1.89		1.88	
	$2p_z$	1.51		1.50	
	$2p_x$	1.56	0.00	1.57	−0.19
	$2p_y$	1.05		1.24	
O_1	2s	1.86		1.80	
	$2p_z$	1.54		1.36	
	$2p_x$	1.60	−0.10	1.56	−0.46
	$2p_y$	1.10		1.75	
Fe	$3d_{x^2-y^2}$	1.99		1.90	
	$3d_{xz}$	1.97		1.08	
	$3d_{yz}$	1.84		1.99	
	$3d_{z^2}$	0.15		0.40	
	$3d_{xy}$	0.24	1.23	0.37	1.50
	4s	0.23		0.27	
	$4p_z$	0.09		0.14	
	$4p_x$	0.20		0.22	
	$4p_y$	0.20		0.22	
N_{pyrr}	2s	1.53		1.15	
	$2p_z$	1.36		1.40	
	$2p_x$	1.25	−0.37	1.24	−0.38
	$2p_y$	1.25		1.24	
N_{axial}	2s	1.47		1.47	
	$2p_z$	1.80		1.78	
	$2p_x$	1.17	−0.60	1.19	−0.62
	$2p_y$	1.17		1.19	

difference (0.15) in the total overlap population of the O_1–O_2 bond between the two states is related mainly to the p orbitals. This indicates that the O_1–O_2 bond of the $^1A''$ state is weakened by the excess electron population in the anti-bonding π_g^b orbital. Another important difference exists in the Fe–O_1 bond, which is non-bonding for the $^1A'$ state but bonding for the $^1A''$ state. Therefore, the Fe–O_1 bond in $^1A''$ state is more stabilized than that in the $^1A'$ state by both covalent and ionic interactions. There exist no significant differences in the overlap populations of the Fe–$N_{pyrrole}$ and the Fe–N_{axial} bonds between the two states.

TABLE 5. OVERLAP POPULATIONS OF THE OXYHEME MODEL

Bond	Type	$^1A'$	$^1A''$
O_1–O_2	s–s	−0.20	−0.18
	s–p	0.05	0.08
	p–s	−0.02	0.00
	p–p	0.61	0.38
	Total	0.44	0.29
Fe–O_1	s–s	−0.02	0.00
	s–p	−0.02	0.02
	p–s	−0.01	0.03
	p–p	−0.02	0.07
	d–s	0.02	0.03
	d–p	0.08	0.12
	Total	0.03	0.27
Fe–N_{pyrr}	s–s	0.01	0.01
	s–p	0.03	0.04
	p–s	0.05	0.05
	p–p	0.08	0.10
	d–s	0.03	0.03
	d–p	0.05	0.06
	Total	0.25	0.29
Fe–N_{axial}	s–s	−0.00	−0.00
	s–p	0.00	0.01
	p–s	0.02	0.02
	p–p	0.05	0.07
	d–s	0.01	0.01
	d–p	0.03	0.03
	Total	0.11	0.14

Discussion

As shown in Fig. 2, the energy gap between $^1A'$ and $^3A'$, $^1A''$ or $^3A''$ in the present SCF calculation is substantially different from those obtained by Dedieu *et al.*[33–35] in the similar *ab initio* SCF-MO calculations with both a minimal set (except for 3d functions) (Basis Set I) and a valence-double basis set (Basis Set II). This difference gives contrary conclusions in the assignment of the ground state of oxyheme model. The total energy of the d^6 closed-shell configuration would be relatively more stabilized than those of the d^5 and d^6 open-shell configurations by the effect of the electron correlation. We have previously estimated that the correlation energy differences of the closed-shell configuration $(d_\epsilon)^6(\pi_g^a)^2$ from the open-shell configurations $(d_\epsilon)^5(\pi_g^a)^2(\pi_g^b)^1$, and $(d_\epsilon)^5(d_\gamma)^1(\pi_g^a)^1(\pi_g^b)^1$ would be ≈2.0 eV[49] and ≈1.2 eV,[50] respectively. Figure 2d illustrates the effect of the electron correlation on the open-shell configurations relative to the closed-shell one. As seen from Fig. 2d, the lowest state is one with the open-shell configuration $Fe(III)(d_\epsilon^5)$–$O_2^-(\pi_g^3)$, even after consideration for the correlation energy. The open-shell state $^3A''$ with the configuration $Fe(II)(d_\epsilon^5 d_\gamma^1)$–$O_2(\pi_g^2)$ stays just above those with the $(d_\epsilon)^5(\pi_g)^3$ configurations, and another open-shell quintet state $^5A'$ lies close to the closed-shell $^1A'$ state in Fig. 2d.

In the calculations with basis set I and II by Dedieu *et al.*[33–35] the energies of the closed-shell state ($^1A'$) are only 0.036 a.u. (0.98 eV) and 0.051 a.u. (1.39 eV), respectively above those of the open-shell state ($^3A'$). They concluded that the closed-shell state ($^1A'$) is the ground state because the SCF energy gap of the two states is smaller than the difference in the correlation energy.

The reason why the SCF energy gap is larger in the present calculation than in their calculations comes from the contents of the basis functions, since the present calculation employed the same oxyheme model as that of Dedieu *et al.*[33–35] Between the present basis set and Dedieu's basis set I, there is no fundamental difference except for the 3d functions. They do differ significantly in the split between ours and those of Dedieu *et al.* as listed in Table 2. Dedieu *et al.* incremented primitive Gaussian functions with an exponent of 0.20 to the atomic 3d orbitals optimized for the iron atom, while we divided the original atomic 3d orbitals into two components (d_1 and d_2) composed of 3 and 1 primitive Gaussian functions, the latter of which has a exponent of 0.505755. Our choice is based on the following argument. In our calculation on cobalt porphine with a triple zeta basis for 3d orbitals[36] the most diffuse d function with an exponent of 0.18 was not effective, while the d function with an exponent of 0.555999 was very important in the proper description of the molecular orbitals. The present form of the split could take account of the effect of the contraction of the 3d orbitals in the change from iron(II) (in $^1A'$) to iron(III) (in $^1A''$). In Table 6, the ratio of coefficients of the two 3d functions (d_1/d_2) is shown for each molecular orbital. The ratios for the iron(II) state are not very different from the ratio of 1.67 for the atomic orbital of the neutral iron. This means that the 3d components in the iron(II) state are as well described as in the iron atom. The large values of the ratio in the iron(III) state indicate the contraction of the 3d components. Therefore the form of the split by Dedieu *et al.*[33–35] is not adequate to describe the iron(III) states, even if it is acceptable for a description of the iron(II) states.

From the observed predominant diamagnetism of oxyhemoglobin and of the dioxygen complex of the picket fence porphyrin, the ground state is assigned to the open-shell singlet $^1A''$ in the present SCF calculation. A strong support for this assignment of the ground state comes from the calculation of the Mössbauer parameters. As shown in Table 3, the open-shell singlet state $^1A''$ yields a large negative electric field gradient whose direction is in the heme plane. These calculated results are in good agreement with low temperature measurements of the single crystal Mössbauer resonance of oxyhemoglobin.[5,6] On the contrary, the closed-shell singlet state $^1A''$, which was assigned as the ground state of the oxyheme by Dedieu *et al.*, can not yield correct Mössbauer parameters, as is seen in Table 3, and as was also shown previously.[27] It should be added that the quintet states do not yield Mössbauer parameters consistent with the low temperature experimental values (Table 3).

The $^1A''$ state can be regarded as a $d\pi$-π_g charge-transfer state of $^1A'$ and has the iron(III) superoxide character as shown in Table 4. This arises from an appreciable amount of charge-transfer from the iron atom to the dioxygen ligand. One electron is transferred from the iron d_{xz} orbital to the oxygen anti-bonding

TABLE 6. COMPARISON OF THE COEFFICIENTS OF THE MOLECULAR ORBITALS WITH PREDOMINANT 3d CHARACTER AND THE RATIOS OFTHOSE FOR $^1A'$ WITH THOSE FOR $^1A''$

MO	$^1A'$ Coefficient (d_1/d_2 Ratio)	Energy a.u.	MO	$^1A''$ Coefficient (d_1/d_2 Ratio)	Energy a.u.
57a' $(d_{xz})_1$	0.4045		42a' $(d_{xz})_1$	0.7318	
$(d_{xz})_2$	0.2472	−0.4520	$(d_{xz})_2$	0.3809	−0.6621
	(1.63)			(1.92)	
58a' $(d_{xz})_1$	0.4147		28a'' $(d_{yz})_1$	0.5786	
$(d_{xz})_2$	0.2537	−0.4394	$(d_{yz})_2$	0.3215	−0.6379
	(1.63)			(1.80)	
59a' $(d_{x^2-y^2})_1$	0.6194		44a' $(d_{x^2-y^2})_1$	0.4804	
$(d_{x^2-y^2})_2$	0.3789	−0.4365	$(d_{x^2-y^2})_2$	0.2661	−0.6213
	(1.63)			(1.81)	
39a'' $(d_{yz})_1$	0.6076				
$(d_{yz})_2$	0.3926	−0.4212			
	(1.55)				

orbital. The ligands donate approximately one electron (0.77) to the formally empty d_{z^2} and d_{xy} orbitals (Table 4). Furthermore the iron 4s and 4p orbitals receive approximately one electron (0.85) from the ligands. This results in atomic charges of 1.50 on the iron atom and −0.65 on the dioxygen ligand in the $^1A''$ state (Table 4).

The following conclusions were obtained from the present *ab initio* LCAO-SCF-MO calculations of the oxyheme model on several singlet, triplet, and quintet states, which arise from the three types of configurations, $(d_\epsilon)^6(\pi_g^a)^2$, $(d_\epsilon)^5(d_\gamma)^1(\pi_g^a)^1(\pi_g^b)^1$, and $(d_\epsilon)^5(\pi_g^a)^2(\pi_g^b)^1$. The lowest states in the SCF energy have the configuration $(d_\epsilon)^5(\pi_g^a)^2(\pi_g^b)^1$ whose electronic structure can be expressed as Fe(III)–O_2^- from the results of Mulliken's population analysis. This configuration remains as the lowest energy states even after consideration of the correlation energy. Calculated Mössbauer parameters of these states are in good agreement with experiments for oxyhemoglobin, oxymyoglobin and oxyheme model, while those of the closed-shell singlet state $(d_\epsilon)^6(\pi_g^a)^2$ are inconsistent with experiment. The Fe–O_1 overlap populations indicate a bonding nature for the $(d_\epsilon)^5(\pi_g^a)^2(\pi_g^b)^1$ states and a non-bonding nature for the $(d_\epsilon)^6(\pi_g^a)^2$ state. From the above discussion, the open-shell singlet state $^1A''$, $(d_\epsilon)^5(\pi_g^a)^2(\pi_g^b)^1$, is the most promising candidate for the ground state of the oxyheme model in the framework of the present Hartree-Fock level calculation. However the ground state and low-lying states would need to be described as a more complex wavefunction than a sigle configuration function if we consider the configuration interaction, the spin-orbit interaction, and the lack of C_s symmetry. Our results indicate singlet configurations $(d_\epsilon)^5(\pi_g)^3$ with the Fe(III)–O_2^- structure as the most important configurations of the ground state in the oxyheme model.

The authors wish to thank Professor Kimio Ohno (Hokkaido University) for his earnest encouragement throughout this study. They also thank Professor Fukashi Sasaki and Dr. Toshikazu Takada (Hokkaido University) for their helpful advices on the program package (JAMOL 3). The author (M. H.) acknowledges the support of a Grant-in-Aid for Scientific Research from the Ministry of Education, Science and Culture.

The calculations reported in this paper were carried out on the HITAC M-180 and M-200H computers at the Computer Center of the institute for Molecular Science. This research was supported by the Joint Studies Program (1979—1980) of the Institute for Molecular Science.

References

1) J. P. Collman, R. R. Gagne, C. A. Reed, W. T. Robinson, and G. A. Rodley, *Proc. Natl. Acad. Sci. U. S. A.*, **71**, 1326 (1974).
2) S. E. V. Phillips, *Nature (London)*, **273**, 247 (1978).
3) L. Pauling, *Nature (London)*, **203**, 182 (1964).
4) G. Lang and W. Marshall, *Proc. Phys. Soc.*, **87**, 3 (1966).
5) K. Spartalian and G. Lang, *J. Chem. Phys.*, **63**, 5375 (1975).
6) Y. Maeda, T. Harami, Y. Morita, A. Trautwein, and U. Gonser, *J. Chem. Phys.*, **75**, 36 (1981).
7) J. P. Collman, R. R. Gagne, C. A. Reed, T. R. Halbert, G. Lang, and W. T. Robinson, *J. Am. Chem. Soc.*, **97**, 1427 (1975).
8) M. W. Makinen and W. A. Eaton, *Ann. N. Y. Acad. Sci.*, **206**, 210 (1973).
9) W. A. Eaton, L. L. Hanson, P. J. Stephens, J. C. Sutherland, and J. B. R. Dunn, *J. Am. Chem. Soc.*, **100**, 4991 (1978).
10) M. Hatano and T. Nozawa, *Adv. Biophys.*, **11**, 95 (1978).
11) J. C. Maxwell, J. A. Vople, C. H. Barlow, and W. S. Caughey, *Biochem. Biophys. Res. Commun.*, **58**, 166 (1974).
12) C. H. Barlow, J. C. Maxwell, W. C. Wallace, and W. S. Caughey, *Biochem. Biophys. Res. Commun.*, **55**, 91 (1973).
13) J. P. Collman, J. I. Brauman, T. R. Halbert, and K. S. Suslick, *Proc. Natl. Acad. Sci. U. S. A.*, **73**, 333 (1976).
14) A. Barbe, C. Secrauer, and P. Jonve, *J. Mol. Spectrosc.*, **49**, 171 (1974).
15) T. Yamamoto, G. Palmer, D. Gill, I. T. Salmen, and L. Rimai, *J. Biol. Chem.*, **248**, 5211 (1973).
16) A. Debois, M. Lutz, and R. Banerjee, *Biochem.*, **18**, 1510 (1979).
17) M. Cerdonio, A. Congiu-Castellano, F. Mogno, B. Pispisa, G. L. Romani, and S. Vitale, *Proc. Natl. Acad. Sci. U. S. A.*, **74**, 398 (1977).
18) L. Pauling and C. D. Coryell, *Proc. Natl. Acad. Sci. U. S. A.*, **22**, 210 (1936).
19) C. D. Coryell, L. Pauling, and R. W. Dodson, *J. Phys. Chem.*, **43**, 825 (1939).

20) D. S. Taylor and C. D. Coryell, *J. Am. Chem. Soc.*, **60**, 1177 (1938).
21) L. Pauling, *Proc. Natl. Acad. Sci. U.S.A.*, **74**, 2612(1977).
22) M. Cerdonio, A. Congiu-Castellano, L. Cal bress, S. Morante, B. Pispisa, and S. Vitale, *Proc. Natl. Acad. Sci. U. S. A.*, **75**, 4916 (1978).
23) A. S. Koster, *J. Chem. Phys.*, **56**, 3161 (1972).
24) M. Zerner, M. Gouterman, and H. Kobayashi, *Theor. Chim. Acta*, **6**, 363 (1966).
25) M. Halton, *Theor. Chim. Acta*, **24**, 89 (1972).
26) R. R. Kirchner and G. H. Loew, *J. Am. Chem. Soc.*, **99** 4639 (1977).
27) B. H. Huynh, D. A. Case, and M. Karplus, *J. Am. Chem. Soc.*, **99**, 6103 (1977).
28) D. A. Case, B. H. Hynh, and M. Karplus, *J. Am. Chem. Soc.*, **101**, 4433 (1979).
29) W. A. Goddard and B. D. Olafson, *Proc. Natl. Acad. Sci. U. S. A.*, **72**, 2335 (1975).
30) B. D. Olafson and W. A. Goddard, *Proc. Natl. Acad. Sci. U. S. A.*, **74**, 1315 (1977).
31) Z. S. Herman and G. H. Loew, *J. Am. Chem. Soc.*, **102**, 1815 (1980).
32) Y. Seno, J. Otsuka, O. Matsuoka, and N. Fuchikami, *J. Phys. Soc. Jpn.*, **33**, 1645 (1972).
33) A. Dedieu, M.-M. Rohmer, and A. Veillard, "Proceeding of the 9th Jerusalem Symposium on Quantum Chemistry and Biochemistry, March 29—April 2, 1976, Metal-Ligand Interactions in Organic Chemistry and Biochemistry," ed by B. Pullman and N. Goldblum, D. Reidel, Holland (1977), p. 101.
34) A. Dedieu, M.-M. Rohmer, and A. Veillard, *J. Am. Chem. Soc.*, **98**, 5789 (1976).
35) A. Dedieu, M.-M. Rohmer, H. Veillard, and A. Veillard, *Nouv. J. Chim.*, **3**, 653 (1978).
36) H. Kashiwagi, T. Takada, S. Obara, E. Miyoshi, and K. Ohno, *Int. J. Quant. Chem.*, **14**, 13 (1978).
37) S. M. Peng and J. A. Ibers, *J. Am. Chem. Soc.*, **98**, 8032 (1976).
38) W. S. Benedict and E. L. Plyler, *Can. J. Phys.*, **35**, 1235 (1975).
39) B. Roos, G. Vinat, and A. Veillard, *Theor. Chim. Acta*, **20**, 1 (1971).
40) B. Roos and P. Siegbahn, *Theor. Chim. Acta*, **17**, 209 (1970).
41) The library program of the Computer Center of Institute for Molecular Science which was coded by H. Kashiwagi, T. Takada, E. Miyoshi, S. Obara, and F. Sasaki, and reported in the paper (H. Kashiwagi and S. Obara, *Int. J. Quant. Chem.*, **20**, 843 (1981)).
42) Y. Osanai and H. Kashiwagi, *Int. J. Quant. Chem.*, **17**, 103 (1980).
43) H. Kashiwagi, *Int. J. Quant. Chem.*, **10**, 135 (1976).
44) H. Kashiwagi and T. Takada, *Int. J. Quant. Chem.*, **12**, 449 (1977).
45) H. Kashiwagi and F. Sasaki, *Int. J. Quant. Chem., Symp.*, **7**, 515 (1973).
46) The present SCF program can not deal with more than two open-shells of the same irreducible representations except for states with parallel spins in all the open-shells.
47) J. J. Weiss, *Nature (London)*, **202**, 83 and 183 (1964).
48) S. Obara and H. Kashiwagi, *J. Chem. Phys.*, **77**, 3155 (1982).
49) The correlation energy was estimated from the differences between calculated and experimental transition energies. The well characterized charge-transfer transition for metmyoglobin cyanide at 6.4×10^3 cm^{-1} (0.79 eV)[51] was utilized for this purpose. Our *ab initio* calculation with a partial-double basis on (porphinato)iron(III)(py)(CN^-) yielded the excited state $^2A_1$ $((d_{x^2-y^2})^2(d_{xz})^2(d_{yz})^2(a_{1u})^2(a_{2u})^1)$ (a d^6 state) at 2.80 eV above the ground state $^2B_2$ $((d_{x^2-y^2})^2(d_{xz})^2(d_{yz})^1(a_{1u})^2(a_{2u})^2$ (a d^5 state) (unpublished results). The difference (2.01 eV) between the calculated transition energy (2.80 eV) and the experimental one (0.79 eV) should be the correlation bias between d^5 states and d^6 states which is the predominant correlation energy difference between $^3A'$, $^3A''$ or $^1A''$, and $^1A'$.
50) The correlation energy between the $^5A'$ or $^5A''$ and $^1A'$ was estimated from the difference between the *ab initio* SCF energies calculated for (porphinato)iron(II)(py) with a partial-double basis[48] and the energy diagram determined by Eicher and Trautwein for deoxyhemoglobin.[52]
51) T. Nozawa, T. Yamamoto, and M. Hatano, *Biochim. Biophys. Acta*, **427**, 28 (1976).
52) H. Eicher and A. Trautwein, *J. Chem. Phys.*, **50**, 2540 (1969).

Zeeman Effect on ^{81}Br NQR in Phosphorus Tribromide-Boron Tribromide

Hiromitsu TERAO,*,† Masanori FUKURA,† Tsutomu OKUDA, and Hisao NEGITA
†Department of Chemistry, Faculty of Education, Tokushima University, Minamijosanjima-cho, Tokushima 770
Department of Chemistry, Faculty of Science, Hiroshima University, Naka-ku, Hiroshima 730

(Received September 18, 1982)

The Zeeman effect on ^{81}Br NQR in a single crystal of $PBr_3 \cdot BBr_3$ was studied at room temperature. The crystal has an orthorhombic symmetry. The bond angles have been f und to be $111.2 \pm 0.1°$ and $111.5 \pm 0.1°$ for Br–B–Br, and $107.0 \pm 0.1°$ and $109.1 \pm 0.3°$ for Br–P–Br. The Br atoms of BBr_3 group have relatively large values of η, 0.151 ± 0.004 and 0.120 ± 0.007, while the Br atoms of PBr_3 group have small values, 0.025 ± 0.005 and 0.020 ± 0.004. The large η values of Br atoms of BBr_3 group are ascribed to the π bonding existing in the B–Br bonds.

It is of interest to investigate the halogen nuclear quadrupole resonance (NQR) of Lewis acid-base complexes $PX_3 \cdot BY_3$ (X, Y=Cl, Br, or I), because both donors PX_3 and acceptors BY_3 contain halogen atoms. Furthermore, the strong interaction between the donors and the acceptors may shift the resonance frequency more than that expected from the crystalline field effects. The previous paper has reported the ^{79}Br and ^{127}I NQR frequencies of $PBr_3 \cdot BBr_3$, $PBr_3 \cdot BI_3$, and $PI_3 \cdot BBr_3$ at 77 K.[1] For these complex-formations, the resonance frequencies (or quadrupole coupling constants) of the donors increased significantly compared to those of the parent molecules, while those of the acceptors also increased by a small extent. The frequency increase in the donors shows that the electric charge on X atoms of PX_3 decreases through p_σ bonds on complexation. In contrast, the charge on Y atoms of BY_3 may increase through both p_σ and p_π bonds. The small increase in frequency in acceptors may be net results of the two opposite effects: frequency lowering and raising due to the increase of the number of p_σ and p_π electrons of the Y atoms, respectively.

The ground state wave function Ψ_N of the complex $PX_3 \cdot BY_3$ may be approximately expressed according to Mulliken[2] by

$$\Psi_N = a\Psi_0(PX_3, BY_3) + b\Psi_1(X_3P^+ - B^-Y_3), \quad (1)$$

where Ψ_0 represents a no-bond structure and Ψ_1 a dative structure. (Chemical experience shows $b^2 > a^2$ in Eq. 1.) This equation shows that a decrease in B–Y π bonding will occur upon progressive increase of the dative structure. On the one hand, the asymmetry parameter η is a measure of the π character of chemical bond when only one of the p_π lone-pair orbitals of halogen atoms can interact to form a π bond.[3] Relatively large values of η, 0.104 and 0.173, were found for $-BI_3$ of $PBr_3 \cdot BI_3$.[1] Another contributions to η arise from the intermolecular bonding in which the relevant atoms participate and the asymmetric distributions of electric charges around the bonds. It is, therefore, desirable to estimate such contributions in order to discuss the bond nature. The η values of X atoms in PX_3 group will offer a clue for this. The η of I atoms in $PI_3 \cdot BBr_3$ have, however, not been obtained owing to the failure to detect these ($m = \pm 3/2 \leftrightarrow \pm 5/2$) transitions. Nor have structural studies of the $PX_3 \cdot BY_3$ been carried out. We examined the Zeeman effect on ^{81}Br NQR for $PBr_3 \cdot BBr_3$ (which is stable on melting, unlike the other complexes stated above) in order to obtain precise NQR parameters as well as information about crystal and molecular structure.

Experimental

The complex was prepared as described previously[1] using Shlenk type glasswares[4] and glove bags; the product was once purified by sublimation at *ca.* 38 °C in a closed Shlenk flask. A single crystal was obtained by the Bridgman method in the sealed glass ampoule of 15 mm diameter.

NQR signals were displayed on an oscilloscope using two superregenerative oscillators: One is a usual LC-oscillator for lower frequency resonances and the other is a Lecher-line oscillator for higher ones. The Zeeman effect was measured by means of a goniometer newly constructed by us. The polar angle Θ is defined by the rotation of the magnetic field which is generated by means of a Helmholtz coil. A field of 7.5×10^{-3} T is generated with a current of 1 A in the Helmholtz coil which has a diameter of 38 cm and a separation of 10 cm between a pair of coils. The azimuthal angle Φ is defined by the rotation of the Φ disk which is attached to a cylinder inserted in the Helmholtz coil. The single crystal is held in the Φ disk. All frames of the goniometer are made of brass. To attain smooth rotation, the heavy Helmholtz coil is supported on 72 pieces of 8 mm diameter brass balls in a circular groove. The scales of Θ and Φ are engraved with marking at 1° intervals. The orthogonality between the rotation axes of Θ and Φ was checked according to the method described by Dean.[5] In the preliminary investigation with a single crystal of $NaClO_3$, the accuracy of the measurement is estimated within ± 0.01 in η and $\pm 0.2°$ in the angle.[6] Zerosplitting cones were obtained using the magnetic field of *ca.* 2×10^{-2} T at room temperature (17—21 °C). The analysis of the data of the Zeeman effect measurement was performed by using a electronic computer HITAC M-180 from Hiroshima University. The resonance signals for $-BBr_3$ of the complex have doublet structures.[1] The measurements were done for the stronger signals of the doublets.

Results and Discussion

Figure 1 shows ^{81}Br NQR spectra of $PBr_3 \cdot BBr_3$ with those of the parent compounds at 77 K. The four resonance lines (labeled ν_1, ν_2, ν_3, and ν_4) are divided into two sets spaced widely in frequency having the signal intensity ratios $I(\nu_1) : I(\nu_2) = I(\nu_4) : I(\nu_3) \approx 1 : 2$. The sets of ν_1 and ν_2, and of ν_3 and ν_4 are ascribed to the bromine atoms of fragments BBr_3 and PBr_3 of the complex, respectively. Thus, the resonance frequencies increase significantly in the donor (*ca.* 30 MHz) but to a small extent for the acceptor (*ca.* 0.5 MHz) on

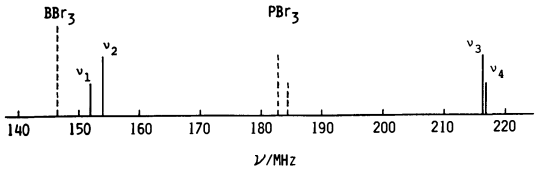

Fig. 1. ^{81}Br NQR spectra of $PBr_3 \cdot BBr_3$ at 77 K.

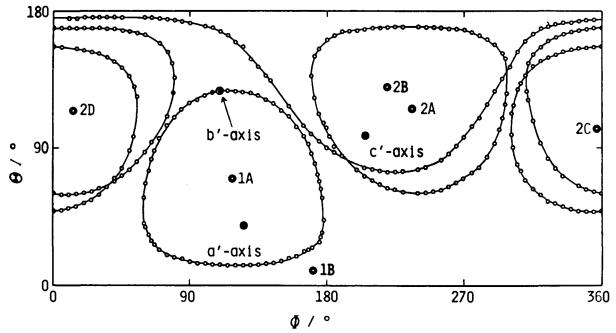

Fig. 2. Zero-splitting patterns of ^{81}Br NQR lines for $-BBr_3$ of $PBr_3 \cdot BBr_3$. 1A, 1B, *etc.*, denote the EFG z-axes of Br_{1A}, Br_{1B}, *etc.*, respectively. The zerosplitting pattern of 1B was not obtained owing to its unfavorable orientation. The direction of 1B was deduced from 1A and the crystal axes.

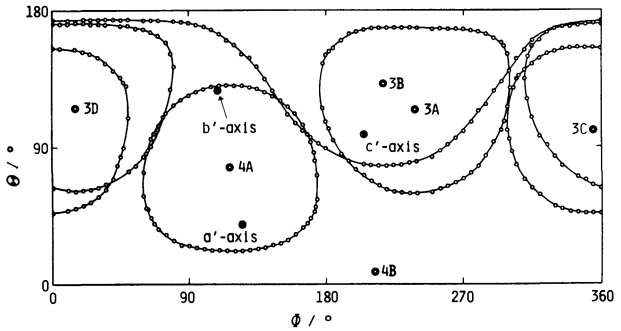

Fig. 3. Zero-splitting patterns of ^{81}Br NQR lines for $-PBr_3$ of $PBr_3 \cdot BBr_3$. 3A, 3B, *etc.*, denote the EFG z-axes of Br_{3A}, Br_{3B}, *etc.*, respectively. The zerosplitting pattern of 4B was not obtained owing to its unfavorable orientation. The direction of 4B was deduced from 4A and the crystal axes.

complexation.

The zero-splitting patterns obtained from the Zeeman effect of the resonance lines for $-BBr_3$ and $-PBr_3$ of the complex are shown in Figs. 2 and 3. The existence of four loci for ν_2 and ν_3, and of two loci for ν_1 and ν_4 was confirmed, but one of the two loci for each of ν_1 and ν_4 could not be determined owing to its unfavorable orientation. The number of the loci shows that the crystal belongs to orthorhombic symmetry. The directions of z-axes of electric field gradients (EFG) obtained from the zero-splitting loci and the crystal axes (tentatively named a', b', and c') which are found from the symmetrical distributions of the z-axes are shown in Figs. 2 and 3. The z-axes of the missing loci 1B and 4B are also shown.

The angles between the z-axes of EFG tensors are listed in Table 1. The bond angle Br–P–Br in gaseous PBr_3 has been found to be 101.0°.[7] In a recent X-ray analysis of solid PBr_3 at 193 K, Enjalbert and Galy[8] have found the bond angles of 101.3° and 99.0°. On the other hand, all the Br–B–Br angles in the few know complexes of the present type $(CH_3)_3N \cdot BX_3$,[9,10] $(CH_3)_3P \cdot BX_3$,[11,12] and $CH_3CN \cdot BX_3$[13] are close to 111° in both gaseous and crystalline states. Taking these angles into consideration and assuming that the z-axes are parallel to the directions of bond axes, the angles Br–M–Br (M=P and B) can be deduced from the angles in Table 1 (and their supplementary angles). These values are listed in Table 2. Further, assuming that the complex molecule has a staggered conformation, (Br_{1A}, Br_{2B}, Br_{2D}, Br_{3B}, Br_{3D}, and Br_{4A}) and (Br_{1B}, Br_{2A}, Br_{2C}, Br_{3A}, Br_{3C}, and Br_{4B}) belong to each molecule which orients in two different directions. The angles Br–B–Br and Br–P–Br in $PBr_3 \cdot BBr_3$ are a little larger than the Br–B–Br and C–M–C (M=P, N) in solid $(CH_3)_3P \cdot BBr_3$[12] and solid $(CH_3)_3N \cdot BBr_3$,[10] respectively. On complexing, the Br–B–Br angles decrease by 7% from the value of a free molecule of BBr_3[14] (Br–B–Br=120°), while the Br–P–Br angles increase by 7% from the value of a free molecule of PBr_3[7] (Br–P–Br=101.0°).

The angles between EFG axes and the crystal axes are listed in Table 3. The B–Br_1 and P–Br_4 bonds exist in the a'b'-plane within experimental errors. For further investigation, the direction of the vector P–Br(G_P) which is directed to the center of mass of three Br atoms in $-PBr_3$, and that of the corresponding vector B–Br(G_B) in $-BBr_3$ were obtained on the assumption that all P–Br or B–Br bonds had equal bond lengths. The angle between the P–Br(G_P) and the B–Br(G_B) in one molecule is $1.4 \pm 0.1°$. The small angle indicates that the molecule

Table 1. Angles between z-axes of EFG (in degrees)

	B–Br_{1A}	B–Br_{1B}	B–Br_{2A}	B–Br_{2B}	B–Br_{2C}	B–Br_{2D}	P–Br_{3A}	P–Br_{3B}	P–Br_{3C}	P–Br_{3D}	P–Br_{4A}
B–Br_{1B}	115.48										
B–Br_{2A}	56.87	111.02									
B–Br_{2B}	68.59	122.86	19.71								
B–Br_{2C}	56.94	111.15	111.43	115.14							
B–Br_{2D}	68.69	122.87	115.24	111.66	19.62						
P–Br_{3A}	54.92	110.10	2.51	22.09	110.01	114.64					
P–Br_{3B}	69.78	124.74	22.28	2.63	114.77	110.39	24.63				
P–Br_{3C}	55.18	109.87	110.26	114.87	2.59	22.17	108.75	114.63			
P–Br_{3D}	69.77	124.43	115.01	110.64	21.84	2.25	114.51	109.28	24.37		
P–Br_{4A}	6.16	109.32	58.08	71.51	58.18	71.62	55.95	72.93	56.19	72.89	
P–Br_{4B}	109.31	6.16	108.07	121.60	108.19	121.59	106.92	123.70	106.70	123.35	103.15

TABLE 2. BOND ANGLES

Compound	Bond angle	θ/°
$PBr_3 \cdot BBr_3$	Br_1–B–Br_2	111.2±0.1
(solid)	Br_2–B–Br_2	111.5±0.1
	Br_3–P–Br_3	107.0±0.1
	Br_3–P–Br_4	109.1±0.3
$(CH_3)_3P \cdot BBr_3$[a]	Br–B–Br	110.4[c]
(solid)	C–P–C	107.2[c]
$(CH_3)_3N \cdot BBr_3$[b]	Br–B–Br	108.4[c]
(solid)	C–N–C	107.5[c]

a) Ref. 12. b) Ref. 10. c) Averaged value.

TABLE 3. ANGLES BETWEEN PRINCIPAL AXES OF EFG AND CRYSTAL AXES (IN DEGREES)

EFG	axis	a′-axis	b′-axis	c′-axis
Br_1	z	32.3±0.4	57.7±0.1	90.0±0.1
	x	58.1±0.1	147.7±0.1	89.2±0.3
	y	89.5±0.3	90.7±0.4	179.2±0.5
Br_2	z	57.6±0.1	80.2±0.2	34.2±0.1
	x	91.0±0.4	167.7±0.3	77.7±0.3
	y	32.4±0.1	97.4±0.6	121.4±0.2
Br_3	z	57.3±0.1	77.8±0.3	35.5±0.1
Br_4	z	38.4±0.4	51.6±0.1	90.0±0.1

TABLE 4. ^{81}Br NQR PARAMETERS AT ROOM TEMPERATURE

Compound		Frequency[a] / MHz	e^2qQ/h / MHz	η	f	Assignment
$PBr_3 \cdot BBr_3$	ν_1	150.31	299.48	0.151±0.004	0.05	BBr_3
	ν_2	151.68	302.63	0.120±0.007	0.04	
	ν_3	212.53	425.01	0.025±0.005		PBr_3
	ν_4	213.22	426.41	0.020±0.004		
BBr_3[b]		146.41	283.80	0.45	0.12	

a) At 293 K. b) Ref. 18; at 77 K.

has effective $3m$ symmetry. The angle between the respective P–Br(G_p) (or B–Br(G_B)) vectors of the two molecules in different orientations is 30.4±1.4°, which is considered as almost coinciding with the angles between the P–B bonds in different orientations.

The asymmetry parameter can be deduced by transforming the zero-splitting locus in the EFG principal axis system,[15] in which the locus is expressed for $I=3/2$ as follows:[16]

$$\sin^2\theta = 2/(3 - \eta\cos 2\phi), \quad (2)$$

where θ and ϕ are polar and azimuthal angles, respectively. Thus, the quadrupole coupling constant $e^2q_{zz}Q/h$ is obtained using the resonance frequency ν and η according to the following equation:

$$\nu = (1/2)(e^2q_{zz}Q/h)[1+(1/3)\eta^2]^{1/2}. \quad (3)$$

The $e^2q_{zz}Q/h$ and η at room temperature are listed in Table 4. It is noted that η values are relatively large for the Br atoms of $-BBr_3$ but very small for the Br atoms of $-PBr_3$ in the complex. This finding may show that the intermolecular contributions to η are very small in the crystal and that the large η of the Br atoms of $-BBr_3$ originate mostly in the π-bonding existing in the B–Br bonds. Neglecting the intermolecular contributions to η, we can estimate the π bonding character of B–Br bonds of $PBr_3 \cdot BBr_3$ according to the following equation:[2]

$$f = (2/3)\eta(e^2q_{zz}Q/h)/(e^2q_{at}Q/h), \quad (4)$$

where f denotes the degree of π character and $e^2q_{at}Q/h$ denotes the atomic quadrupole coupling constant, which is 643.03 MHz for ^{81}Br atom.[17] The values of f are listed in Table 4. On complex-formation, the π character of B–Br bonds reduces from *ca.* 12% to 5%. It is found from Table 3 that the x-axis of the Br_1 atom exists in the mirror plane in which the B–Br_1 bond lies. Furthermore the x-axis of the Br_2 atom makes only a small angle, 5.3±0.3°, with the plane which contains the B–Br_2 bond and the B–Br(G_B) vector in a molecule. This is consistent with the existence of the π bonding in the B–Br bonds of the complex.

The authors express their sincere thanks to Mr. Tokuji Hirakawa of Tokushima University for the construction of the goniometer.

References

1) H. Terao, T. Okuda, and H. Negita, *Bull. Chem. Soc. Jpn.*, **51**, 710 (1978).
2) R. S. Mulliken and W. B. Person, "Molecular Complexes," John Wiley and Sons, New York (1969).
3) R. Bersohn, *J. Chem. Phys.*, **22**, 2078 (1954).
4) D. F. Shriver, "The Manipulation of Air-sensitive Compounds, "McGraw-Hill, New York (1969), Chap. 7.
5) C. Dean, *Rev. Sci. Instrum.*, **31**, 934 (1960).
6) See K. Mano, *J. Magn. Reson.*, **26**, 393 (1977).
7) K. Kuchitsu, T. Shibata, A. Yokozeki, and C. Matsumura, *Inorg. Chem.*, **10**, 2584 (1971).
8) P. R. Enjalbert and J. Galy, *Acta Crystallogr., Sect. B*, **35**, 546 (1979).
9) K. Iijima and S. Shibata, *Bull. Chem. Soc. Jpn.*, **53**, 1908 (1980).
10) P. H. Clippard, J. C. Hanson, and R. C. Taylor, *J. Cryst. Mol. Struct.*, **1**, 363 (1971).
11) K. Iijima and S. Shibata, *Bull. Chem. Soc. Jpn.*, **52**, 3204 (1979); K. Iijima, E. Koshimizu, and S. Shibata, *ibid.*, **54**, 2255 (1981).
12) D. L. Black and R. C. Taylor, *Acta Crystallogr., Sect. B*, **31**, 1116 (1975).
13) B. Swanson, D. F. Shriber, and J. A. Ibers, *Inorg. Chem.*,

8, 2182 (1969).
14) S. Konaka, T. Ito, and Y. Morino, *Bull. Chem. Soc. Jpn.*, **39**, 1146 (1966).
15) K. Yamada, *J. Sci. Hiroshima Univ., Ser. A*, **41**, 77 (1977).
16) C. Dean, *Phys. Rev.*, **96**, 1053 (1954).
17) J. G. King and V. Jaccarino, *Phys. Rev.*, **94**, 1610 (1954).
18) T. Chiba, *J. Phys. Soc. Jpn.*, **13**, 860 (1958).

The Structure of the Cyclodextrin Complex. XVI. Crystal Structure of Heptakis(2,3,6-tri-*O*-methyl)-β-cyclodextrin–*p*-Iodophenol (1 : 1) Complex Tetrahydrate

Kazuaki HARATA,* Kaneto UEKAMA,† Masaki OTAGIRI,† and Fumitoshi HIRAYAMA†

Research Institute for Polymers and Textiles, 1-1-4, Yatabe-Higashi, Tsukuba, Ibaraki 305
†*Faculty of Pharmaceutical Sciences, Kumamoto University, 5-1, Oe-honmachi, Kumamoto 862*
(Received October 7, 1982)

The crystal structure of heptakis(2,3,6-tri-*O*-methyl)-β-cyclodextrin–*p*-iodophenol (1 : 1) tetrahydrate, $C_{63}H_{112}O_{35}\cdot C_6H_5OI\cdot 4H_2O$, was determined by the X-ray method. The crystal is orthorhombic with the space group $P2_12_12_1$, $Z=4$, $a=14.997(2)$, $b=21.368(2)$, and $c=28.205(3)$ Å. The structure was solved by the heavy atom method combined with the rigid-body least-squares technique and refined by the block-diagonal least-squares method to the final *R*-value of 0.094 for 3268 reflections ($\sin\theta/\lambda<0.49$). Heptakis(2,3,6-tri-*O*-methyl)-β-cyclodextrin is in the shape of a truncated elliptical cone. The macrocyclic ring is remarkably distorted from a regular heptagonal structure. The iodophenyl group of the guest is inserted into the host cavity. The phenolic hydroxyl group protrudes from the cavity, forming hydrogen bonds with two water molecules. The iodine atom is located at the center of the macrocyclic ring, while the benzene ring occupies its position at the base side of the cone. The crystal is built up of columns which are formed by the stack of host molecules in a head-to-tail mode along the two-fold screw axis which is parallel to the crystallographic b axis. Four water molecules fill intermolecular spaces in the crystal.

Recently, extensive attention has focused on the chemical modification of cyclodextrins.[1,2] Many substituted cyclodextrins have been studied to improve complexing and catalytic abilities of these macrocyclic oligosaccharides. Methylated cyclodextrins are quite interesting compounds to investigate the effect of substituents on the macrocyclic conformation and host-guest interaction. Previously, we have determined crystal structures of some permethylated α-cyclodextrin complexes.[3-5] In those structures, the macrocyclic ring is distorted by the steric hindrance which is caused by the methyl groups introduced to secondary hydroxyl groups. Permethylated α-cyclodextrin forms inclusion complexes with benzene derivatives, but their host-guest geometry is quite different from the corresponding α-cyclodextrin complexes. On the other hand, Stezowski and his co-workers have reported the structure of heptakis(2,6-di-*O*-methyl)-β-cyclodextrin-adamantanol complex,[6] and shown that the host macrocyclic ring is almost round just like as β-cyclodextrin.[7-11] In this paper, we present the crystal structure of the heptakis-(2,3,6-tri-*O*-methyl)-β-cyclodextrin–*p*-iodophenol (abbreviated to methyl-β-CDx–*p*-IPH) complex. This is the first structural determination of permethylated β-cyclodextrin.

Experimental

Methyl-β-CDx was dissolved in a *p*-IPH saturated aqueous solution. The solution was allowed to stand at 40 °C, then colorless prismatic crystals were obtained. Lattice parameters and reflection intensities were measured on a Nicolet P3/F diffractometer with graphite-monochromated Cu *Kα* radiation. By using θ-2θ scan mode, 3286 independent reflections with $|F_o|\geqq 3\sigma(F)$ were obtained up to 90° in 2θ. No corrections were made for absorption and extinction effects.

Crystal Data: $C_{63}H_{112}O_{35}\cdot C_6H_5OI\cdot 4H_2O$, *F.W.*=1721.6, orthorhombic, space group $P2_12_12_1$, $Z=4$, $a=14.977(2)$, $b=21.368(2)$, $c=28.205(3)$ Å, $V=9026(2)$ Å^3, $D_x=1.267$, $D_m=1.25$ g cm^{-3}.

Determination and Refinement of the Structure

The structure was solved by the heavy atom method. The electron-density map, which was calculated with iodine phases, revealed the outline of methyl-β-CDx. Owing to the low resolution of the map, however, it was quite difficult to estimate coordinates of light atoms. A trial structure of methyl-β-CDx was set up so as to fit the electron-density map, then the orientational and rotational parameters of each 2,3,6-tri-*O*-methylglucose residue were corrected by the rigid-body least-squares technique. After the refinement of the methyl-β-CDx structure by the block-diagonal least-squares method, the light atoms of *p*-IPH and water molecules were found on a difference-Fourier map. Successive refinements of the structure by the block-diagonal least-squares method achieved the *R*-value of 0.094. The quantity minimized was $\sum w(|F_o|-|F_c|)^2$ with $w=1.0$ for all the reflections. The atomic scattering factors were taken from the "International Tables for X-ray Crystallography."[12] The atomic parameters are given in Table 1. Tables of observed and calculated structure factors, anisotropic temperature factors, and bond distances, angles, and conformation angles of methyl-β-CDx are kept at The Chemical Society of Japan (Document No. 8324). The computation was carried out on a FACOM M-200 computer at the RIPS Center, Tsukuba.

Description and Discussion of the Structure

Outline of the Structure. The structure and numbering scheme of the complex are shown in Figs. 1 and 2. Methyl-β-CDx is in the shape of an elliptically-distorted and truncated cone. The guest *p*-IPH molecule is inserted into the methyl-β-CDx ring. The iodine atom is located at the center of the host cavity, while

Table 1. Atomic coordinates ($\times 10^4$) and B_{eq} values (B/Å^2)[a)]

	x	y	z	B_{eq}/Å^2		x	y	z	B_{eq}/Å^2
C(1,G1)	8899(17)	4615(12)	4775(8)	5.84	O(6,G4)	10281(14)	5645(11)	1976(6)	9.04
C(2,G1)	8119(17)	4161(12)	4943(8)	5.55	C(1,G5)	7212(19)	4057(11)	625(8)	5.45
C(3,G1)	7613(16)	3906(12)	4514(8)	5.24	C(2,G5)	7756(17)	3732(11)	268(8)	5.00
C(4,G1)	7212(15)	4522(12)	4272(7)	4.56	C(3,G5)	8762(17)	3697(13)	444(7)	5.83
C(5,G1)	7934(18)	4974(12)	4115(8)	5.90	C(4,G5)	9061(13)	4348(10)	595(6)	3.78
C(6,G1)	7690(18)	5541(12)	3869(8)	5.92	C(5,G5)	8430(15)	4663(12)	942(8)	5.47
C(7,G1)	8855(21)	3761(14)	5646(8)	7.38	C(6,G5)	8659(19)	5332(10)	1078(8)	5.91
C(8,G1)	6912(19)	2920(14)	4443(9)	7.06	C(7,G5)	6690(20)	3090(17)	-87(10)	8.70
C(9,G1)	6519(23)	6344(14)	3931(9)	8.77	C(8,G5)	9573(24)	2843(17)	128(12)	11.08
O(2,G1)	8507(11)	3628(7)	5167(5)	5.35	C(9,G5)	9031(22)	6281(13)	718(9)	7.52
O(3,G1)	6942(11)	3539(8)	4667(5)	6.02	O(2,G5)	7469(12)	3123(8)	188(6)	6.43
O(4,G1)	6733(10)	4270(7)	3880(5)	4.80	O(3,G5)	9297(13)	3482(8)	79(6)	6.76
O(5,G1)	8451(11)	5145(7)	4528(5)	4.87	O(4,G5)	9930(11)	4242(8)	814(5)	5.99
O(6,G1)	6940(14)	5768(8)	4140(6)	7.74	O(5,G5)	7549(10)	4669(7)	734(5)	4.69
C(1,G2)	12086(17)	4121(14)	4125(8)	6.90	O(6,G5)	8838(13)	5635(8)	642(6)	7.13
C(2,G2)	11783(20)	3718(13)	4404(8)	6.71	C(1,G6)	5213(18)	3453(16)	2091(10)	8.71
C(3,G2)	10736(18)	3716(11)	4449(8)	5.53	C(2,G6)	5528(17)	2881(12)	1855(7)	5.45
C(4,G2)	10403(14)	4357(11)	4513(7)	4.54	C(3,G6)	6382(21)	3035(11)	1580(9)	6.82
C(5,G2)	10768(16)	4810(11)	4138(7)	4.88	C(4,G6)	6234(15)	3583(11)	1231(8)	4.88
C(6,G2)	10564(21)	5490(12)	4273(11)	9.01	C(5,G6)	5907(17)	4165(11)	1492(7)	5.40
C(7,G2)	12917(23)	2868(21)	4440(13)	11.85	C(6,G6)	5609(20)	4784(14)	1190(8)	7.55
C(8,G2)	10119(21)	2780(13)	4813(10)	7.52	C(7,G6)	5244(33)	1843(16)	2187(12)	13.21
C(9,G2)	10437(39)	6560(22)	3894(18)	19.03	C(8,G6)	7477(26)	2263(17)	1268(13)	11.36
O(2,G2)	12053(14)	3078(10)	4310(6)	8.45	C(9,G6)	4269(25)	4444(26)	783(12)	15.16
O(3,G2)	10553(12)	3340(8)	4879(5)	5.98	O(2,G6)	5719(17)	2440(10)	2207(6)	9.90
O(4,G2)	9474(9)	4299(7)	4462(4)	4.50	O(3,G6)	6538(16)	2476(9)	1302(6)	8.65
O(5,G2)	11723(11)	4763(8)	4121(5)	5.50	O(4,G6)	7098(11)	3713(8)	1062(5)	5.50
O(6,G2)	10712(23)	5818(12)	3840(10)	14.97	O(5,G6)	5052(11)	4000(8)	1749(5)	6.01
C(1,G3)	12643(19)	3946(13)	2152(9)	6.50	O(6,G6)	5168(14)	4542(12)	747(6)	9.66
C(2,G3)	12596(17)	3274(12)	2430(8)	5.81	C(1,G7)	5919(18)	4591(12)	3750(8)	6.10
C(3,G3)	12004(19)	3344(11)	2876(7)	5.54	C(2,G7)	5187(19)	4146(12)	3672(9)	6.56
C(4,G3)	12350(17)	3894(11)	3190(8)	5.28	C(3,G7)	5389(16)	3681(12)	3247(7)	5.08
C(5,G3)	12235(17)	4492(12)	2877(7)	5.91	C(4,G7)	5541(18)	4143(12)	2810(7)	6.03
C(6,G3)	12505(16)	5130(13)	3096(9)	6.20	C(5,G7)	6353(17)	4568(11)	2924(7)	5.03
C(7,G3)	12770(42)	2276(23)	2157(13)	17.71	C(6,G7)	6639(21)	5040(20)	2540(10)	10.90
C(8,G3)	11354(24)	2444(19)	3275(11)	10.88	C(7,G7)	4749(21)	4064(17)	4505(9)	8.80
C(9,G3)	13676(23)	5610(15)	3552(11)	9.80	C(8,G7)	4600(19)	2683(13)	3322(9)	6.91
O(2,G3)	12260(16)	2820(9)	2124(6)	8.28	C(9,G7)	6312(36)	5880(15)	2037(15)	15.38
O(3,G3)	12159(14)	2788(9)	3121(6)	7.85	O(2,G7)	5051(12)	3732(9)	4084(5)	6.60
O(4,G3)	11704(11)	3924(8)	3581(5)	5.40	O(3,G7)	4591(11)	3328(8)	3150(5)	5.65
O(5,G3)	12850(10)	4437(8)	2480(4)	5.43	O(4,G7)	5898(11)	3705(8)	2443(5)	5.71
O(6,G3)	13361(14)	5046(9)	3310(6)	7.89	O(5,G7)	6013(14)	4961(8)	3321(6)	7.60
C(1,G4)	10625(18)	4634(12)	705(8)	6.24	O(6,G7)	5938(14)	5349(11)	2342(8)	10.51
C(2,G4)	11527(15)	4288(13)	644(7)	5.42	C(1,IP)	8133(24)	2476(16)	3314(11)	9.48
C(3,G4)	11687(17)	3911(13)	1108(8)	5.79	C(2,IP)	8922(22)	2743(15)	3480(10)	8.72
C(4,G4)	11738(15)	4449(12)	1525(7)	4.57	C(3,IP)	9296(27)	3342(17)	3301(12)	11.37
C(5,G4)	10937(18)	4822(11)	1543(7)	5.23	C(4,IP)	8787(23)	3593(15)	2905(10)	8.94
C(6,G4)	11119(20)	5364(13)	1866(8)	6.99	C(5,IP)	8053(24)	3288(15)	2690(12)	10.27
C(7,G4)	11394(37)	4061(21)	-194(9)	15.42	C(6,IP)	7735(23)	2761(15)	2916(11)	9.03
C(8,G4)	12679(23)	3065(17)	900(10)	9.36	O(IP)	7909(19)	1914(11)	3483(8)	11.76
C(9,G4)	10376(29)	6176(13)	2320(12)	11.56	I(IP)	9246(2)	4467(1)	2639(1)	11.29
O(2,G4)	11427(13)	3834(9)	293(6)	7.72	O(W1)	4033(17)	5378(11)	2170(8)	12.20
O(3,G4)	12600(12)	3688(8)	1062(6)	6.74	O(W2)	3689(21)	6343(13)	1613(8)	13.39
O(4,G4)	11730(10)	4057(8)	1948(5)	5.28	O(W3)	3456(20)	6150(14)	654(7)	13.54
O(5,G4)	10765(11)	5113(7)	1079(5)	5.45	O(W4)	1647(21)	6303(15)	749(9)	14.92

a) $B_{eq}=8\pi^2(u_1^2+u_2^2+u_3^2)/3$, where u_i is the root-mean-square deviation in the i-th principal axis of the thermal ellipsoid.

the benzene ring occupies its position at the O(2), O(3) side. The phenolic hydroxyl group protrudes from the O(2), O(3) side and forms hydrogen bonds with two water molecules. Methyl-β-CDx molecules are stacked along the two-fold screw axis parallel to the b axis to form a head-to-tail channel-type structure.

Conformation of Methyl-β-CDx. Average bond distances and angles over seven 2,3,6-tri-*O*-methylglucose residues are shown in Fig. 3. Geometrical data for the methyl-β-CDx ring are given in Tables 2—4. No significant differences in the bond distances and angles are found between methyl-β-CDx and β-cyclodextrin.[8–11] The C(6)–O(6) bonds in the G2 and G4 residues are in a *gauche-trans* conformation, while the other C(6)–O(6) bonds have a *gauche-gauche* conformation. Six of seven C(9)–O(6) bonds are *trans* to the corresponding C(5)–C(6) bonds. The C(9)–O(6) bond in the G6 residue shows a somewhat different orientation; the conformation angle of C(5)–C(6)–O(6)–C(9) is 89°. All the C(7)–O(2) bonds are oriented outside the methyl-β-CDx ring, and give average conformation angles of 96° for C(7)–O(2)–C(2)–C(1) and −147° for C(7)–O(2)–C(2)–C(3). On the other hand, the C(8)–O(3) bonds are extended along the molecular axis of methyl-β-CDx, which is defined as the axis perpendicular to the least-squares plane of seven O(4) atoms. The average conformation angles of C(8)–O(3)–C(3)–C(2) and C(8)–O(3)–C(3)–C(4) are −117° and 127°, respectively. These conformations of the C(7)–O(2) and C(8)–O(3) bonds are quite similar to those of methyl-α-CDx,[3–5] and the orientation of these bonds is scarcely affected by the ring size of macrocycles.

TABLE 2. GEOMETRICAL DATA FOR METHYL-β-CDx

The estimated standard deviations are in the ranges 0.04—0.05 Å for O···O distances and 0.05—0.07 Å for C···O distances.

I. Radius of the O(4) hexagon

Residue	Radius l/Å	Residue	Radius l/Å
G1	4.92	G5	5.27
G2	5.35	G6	5.18
G3	4.99	G7	4.63
G4	4.57	Average	4.99

II. O(4)···O(4) distances between adjacent residues

Distance	l/Å	Distance	l/Å
O(4,G1)···O(4,G2)	4.42	O(4,G4)···O(4,G5)	4.20
O(4,G1)···O(4,G7)	4.41	O(4,G5)···O(4,G6)	4.45
O(4,G2)···O(4,G3)	4.24	O(4,G6)···O(4,G7)	4.29
O(4,G3)···O(4,G4)	4.32	Average	4.33

III. O(2)···O (3) distances between adjacent residues

Distance	l/Å	Distance	l/Å
O(2,G1)···O(3,G2)	3.23	O(2,G5)···O(3,G6)	3.71
O(2,G2)···O(3,G3)	3.41	O(2,G6)···O(3,G7)	3.68
O(2,G3)···O(3,G4)	3.56	O(2,G7)···O(3,G1)	3.30
O(2,G4)···O(3,G5)	3.33	Average	3.46

IV. C(8)···O(2) distances

Distance	l/Å	Distance	l/Å
C(8,G1)···O(2.G1)	3.49	C(8,G1)···O(2,G7)	3.44
C(8,G2)···O(2,G2)	3.29	C(8,G2)···O(2,G1)	3.18
C(8,G3)···O(2,G3)	3.61	C(8,G3)···O(2,G2)	3.39
C(8,G4)···O(2,G4)	3.01	C(8,G4)···O(2,G3)	3.55
C(8,G5)···O(2,G5)	3.21	C(8,G5)···O(2,G4)	3.51
C(8,G6)···O(2,G6)	3.75	C(8,G6)···O(2,G5)	3.56
C(8,G7)···O(2,G7)	3.18	C(8,G7)···O(2,G6)	3.60
Average	3.36	Average	3.46

TABLE 3. TORSION-ANGLE INDICES AND TILT-ANGLES

I. Torsion-angle index[a)]

Residue	Index ϕ/°	Residue	Index ϕ/°
G1	126	G5	122
G2	126	G6	115
G3	100	G7	130
G4	143	Average	123

a) The torsion-angle index is defined as follows: $\phi = |\phi(C(1)-C(2))| + |\phi(C(2)-C(3))| + |\phi(C(5)-O(5))| + |\phi(O(5)-C(1))| - |\phi(C(3)-C(4))| - |\phi(C(4)-C(5))|$, where $\phi(C(1)-C(2))$ is the conformation angle of O(5)-C(1)-C(2)-C(3).

II. Tilt-angle[b)]

Residue	Angle ϕ/°	Residue	Angle ϕ/°
G1	30.4	G5	34.9
G2	16.7	G6	−16.3
G3	−12.7	G7	42.6
G4	43.0	Average	19.8

b) The tilt-angle is defined as the angle made by the plane through seven O(4) atoms and the plane through C(1), C(4), O(4), and O(4′).

Seven glycosidic oxygen atoms (O(4)) form an elliptically distorted heptagon. The radius of the heptagon, which is measured from the center of gravity of seven O(4) atoms to each O(4) atom, is in the range 4.57—5.35 Å (Table 2). The O(4,G2) atom is at the longest distance from the center of gravity, the O(4,G4) atom being nearest to the center. Although the average value of 4.99 Å is in good agreement with the value (5.02 Å) found in the β-cyclodextrin complex with 1,4-diazabicyclo[2.2.2]octane,[11] the distortion of the O(4) heptagon is more remarkable in methyl-β-CDx. In spite of such distortion, the O(4)···O(4) distances between adjacent residues (4.20—4.45 Å) and the torsion-angle indices (100—143°) are similar to those of β-cyclodextrin. This indicates that, unlike methyl-α-CDx, the conformation of the pyranose ring of methyl-β-CDx is less affected by permethylation. The least-

TABLE 4. LEAST-SQUARES PLANES AND DEVIATIONS OF ATOMS FROM THE PLANE

The plane equation is of the $AX+BY+CZ=D$ form, where X, Y, and Z are the coordinates in Å units along the a, b, and c axes, respectively.

I. The plane through seven O(4) atoms

$-0.048X+0.998Y-0.052Z=7.561$

O(4,G1)	0.482	O(4,G5)	0.645
O(4,G2)	0.259	O(4,G6)	−0.316
O(4,G3)	−0.570	O(4,G7)	−0.451
O(4,G4)	−0.048		

II. The benzene plane

$0.575X-0.537Y-0.618Z=-1.578$

C(1,IP)	−0.037	C(5,IP)	0.051
C(2,IP)	0.047	C(6,IP)	−0.013
C(3,IP)	−0.006	O(IP)	0.121
C(4,IP)	−0.042	I(IP)	−0.186

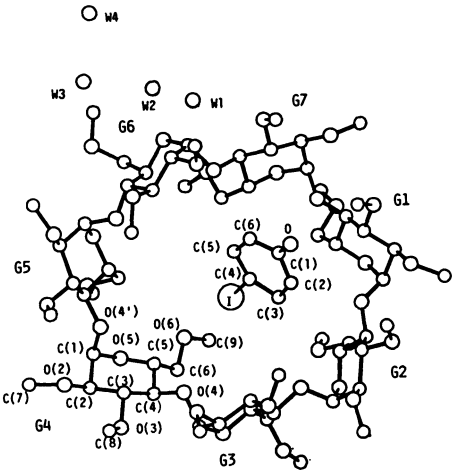

Fig. 1. A numbering scheme of the methyl-β-CDx–p-IPH complex.

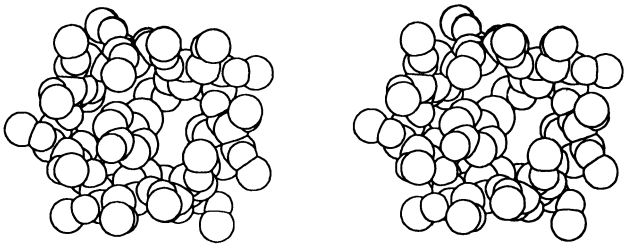

Fig. 2. A stereo-drawing of the structure of the methyl-β-CDx–p-IPH complex. Circles are drawn with three-fourths of van der Waals radii.

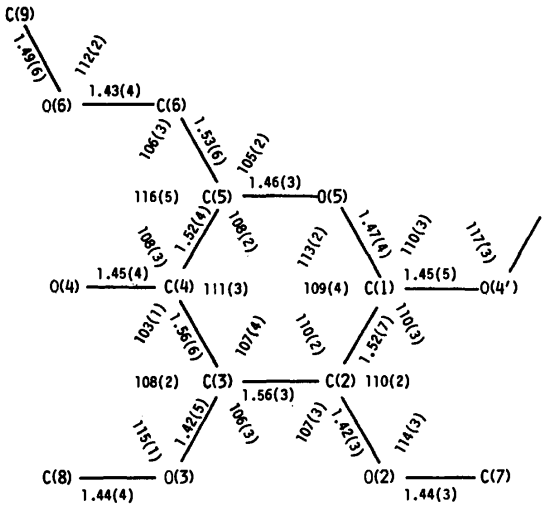

Fig. 3. Average bond distances and angles over seven 2,3,6-tri-*O*-methylglucose residues. Standard deviations in parentheses were estimated according to the equation: $\sigma=[\sum_{i=1}^{7}(x_i-\bar{x})^2/6]^{1/2}$, where x_i refers to the bond distance or angle of the i-th residue and $\bar{x}$ is the average value.

squares plane through seven O(4) atoms and deviation of atoms from the plane are given in Table 4. The maximum deviation of 0.65 Å is remarkably larger than that of β-cyclodextrin.

Compared with β-cyclodextrin, another remarkable difference is found in the tilt-angles of the 2,3,6-tri-*O*-methylglucose residues. The tilt-angles are in the range from −16.3° to 43.0°. The average value of 19.8° is similar to those (16.7—18.8°) found in the methyl-α-CDx complexes,[3-5] but the maximum value of 43.0° is larger than that of 28.1° in methyl-α-CDx.[5] The residues, G1, G2, G4, G5, and G7, incline with their O(6) side nearer to the molecular axis of methyl-β-CDx, while the G3 and G6 residues incline so that their O(2), O(3) sides are nearer to each other. The G6 residue is tilted in a direction opposite to that of the G7 residue. Therefore, the plane through C(1), C(4), O(4), and O(4') of the G6 residue makes a quite large angle, 54.5°, with the corresponding plane of the G7 residue. A similar relationship is found between the G3 and G4 residues, giving an angle of 46.4°. Such a conformational feature of methyl-β-CDx is not observed in β-cyclodextrin. In spite of the inclusion of a variety of guest molecules, the β-cyclodextrin ring is almost round, and the tilt-angle is restricted to a relatively narrow region (from −5° to 23°).[10,11] The C(8)H_3 methyl group is situated between the two O(2) atoms. The average C(8)···O(2) distances are 3.36 and 3.46 Å, which are somewhat larger than the values of 3.20 and 3.35 Å in the methyl-α-CDx–*p*-iodoaniline complex.[3] The O(2)···O(3) distances between adjacent residues are in the range 3.23—3.71 Å, and the average value of 3.46 Å is also larger than the corresponding value (3.28 Å) of the methyl-α-CDx–*p*-iodoaniline complex. These differences in the O(2)···O(3) and C(8)···O(2) distances and the tilt-angles suggest that the 2,3,6-tri-*O*-methylglucose residue of methyl-β-CDx has more flexibility around the glycosidic linkage than that of methyl-α-CDx. The large tilt-angles of the 2,3,6-tri-*O*-methylglucose residues may be ascribed to the inability of methyl-β-CDx for forming intramolecular O(2)···O(3) hydrogen bonds and the steric hindrance between the C(8)H_3 methyl group and O(2) atoms. In unsubstituted cyclodextrins, the adjacent glucose residues are mostly linked by O(2)–H···O(3) or O(3)–H···O(2) hydrogen bonds, and the macrocyclic conformation is held by such intramolecular hydrogen bonds. In the permethylated cyclodextrins, however, the methyl groups require to enlarge the O(2)···O(3) distance to avoid unfavorable interatomic repulsion between the O(2) atoms and C(8)H_3 methyl groups.

Table 5. Intermolecular distances between methyl-β-CDx and *p*-IPH less than 4.0 Å[a]

Distance	*l*/Å	Distance	*l*/Å
O(IP)–C(8,G1)	3.76	C(3,IP)–C(3,G2)	3.97
I(IP)–O(6,G4)	3.50	C(3,IP)–O(4,G3)	3.90
C(1,IP)–C(8,G1)	3.79	C(5,IP)–C(5,G7)	3.80
C(2,IP)–C(8,G3)	3.74	C(6,IP)–O(4,G7)	3.66
C(3,IP)–C(8,G3)	3.63	C(6,IP)–O(2,G6)	3.69
C(3,IP)–O(4,G2)	3.87		

a) Estimated standard deviations are in the range 0.04—0.08 Å.

Host-Guest Interaction. Intermolecular distances between *p*-IPH and methyl-β-CDx are given in Table 5. The iodophenyl group is inserted into the methyl-β-CDx cavity, while the phenolic hydroxyl group protrudes from the O(2), O(3) side of the cavity. The *p*-IPH molecule is included not parallel to the molecular axis of methyl-β-CDx but tilting with the benzene ring nearer to the G1 residue; the benzene plane makes an angle of 57.5° with the O(4) plane. The iodine atom is located at the center of the methyl-β-CDx ring. The O(6) atom of the G4 residue is at the nearest distance (3.50 Å) from the iodine atom, but there are no other contacts less than 4.0 Å between the iodine atom and methyl-β-CDx. The benzene ring is located at the O(2), O(3) side of the cavity. The shortest intermolecular distance between the benzene ring and methyl-β-CDx is 3.63 Å, which is found between C(3,IP) and C(8,G3). Therefore, the *p*-IPH molecule seems to be in weak van der Waals contact with methyl-β-CDx.

The inclusion geometry of the present complex is quite different from that found in the β-cyclodextrin–*p*-IPH complex,[7] in which three *p*-IPH molecules are located in the cylindrical cavity formed by two β-cyclodextrin molecules in a head-to-head dimer-type arrangement. The iodine atom is located at a similar position which is found in the methyl-β-CDx complex, but the benzene ring is located at the O(6) side. On the other hand, in the methyl-β-CDx complex, the large tilt of 2,3,6-tri-*O*-methylglucose residues makes the O(6) side narrower. As a result, the benzene ring is more suitably accommodated to the wider O(2), O(3) side of the cavity. A similar situation has been observed in the methyl-α-CDx–*p*-iodoaniline complex, although the *p*-iodoaniline molecule is included parallel to the molecular axis of methyl-α-CDx. These indicate that the methylation affects not only the macrocyclic

TABLE 6. INTERMOLECULAR DISTANCES LESS THAN 3.5 Å

Distance		l/Å	Distance		l/Å
C(9,G1)–O(3,G5)	(b)	3.48	O(3,G4)–C(9,G6)	(a)	3.08
O(3,G1)–C(9,G5)	(b)	3.33	O(5,G4)–O(W4)	(a)	3.01
O(3,G1)–O(6,G5)	(b)	3.47	O(6,G7)–O(W1)		2.89
O(6,G1)–C(2,G5)	(b)	3.39	O(IP)–O(W4)	(c)	2.62
O(3,G2)–O(W3)	(b)	2.86	O(IP)–O(W2)	(c)	2.70
O(5,G3)–O(W1)	(a)	2.82	O(W1)–O(W2)		2.64
O(6,G3)–C(2,G7)	(a)	3.49	O(W2)–O(W3)		2.76
O(6,G3)–O(W1)	(a)	3.44	O(W3)–O(W4)		2.74

None	x,	y,	z
a	$1+x$,	y,	z
b	$3/2-x$,	$1-y$,	$1/2+z$
c	$1-x$,	$-1/2+y$,	$1/2-z$

conformation of the host molecule but also the geormety of the host-guest interaction.

Molecular Packing. Methyl-β-CDx molecules are stacked to form a channel-type structure in a head-to-tail mode along the two-fold screw axis which is parallel to the b axis. The methyl-β-CDx molecule is nearly parallel to the ac plane; the O(4) plane is tilted by an angle of 4.1° with respect to the ac plane. Two adjacent methyl-β-CDx molecules, which are related by the two-fold screw axis parallel to the b axis, are laterally shifted to each other. As a result, the channel runs not straight but zigzag. This packing feature differs from that of the typical channel-type structure, in which the guest molecule is enclosed within the column formed by the stack of host molecules. The zigzag packing of the methyl-β-CDx molecules enables the *p*-IPH molecule to have contacts with the water molecules, which are located outside the methyl-β-CDx ring as shown in Fig. 4. The phenolic hydroxyl group forms hydrogen bonds with two water molecules, W2 and W4. Intermolecular distances less than 3.5 Å are given in Table 6. There are no significantly short intermolecular contacts. The crystal is built up of columns of methyl-β-CDx. The water molecules are located outside the column. They fill intermolecular spaces between columns, and are linked one another by the W1···W2···W3···W4 hydrogen bonds. These water molecules are also hydrogen-bonded to the oxygen atoms of methyl-β-CDx: O(W1)··· O(5,G3), O(W1)···O(6,G7), and O(W3)···O (3,G2).

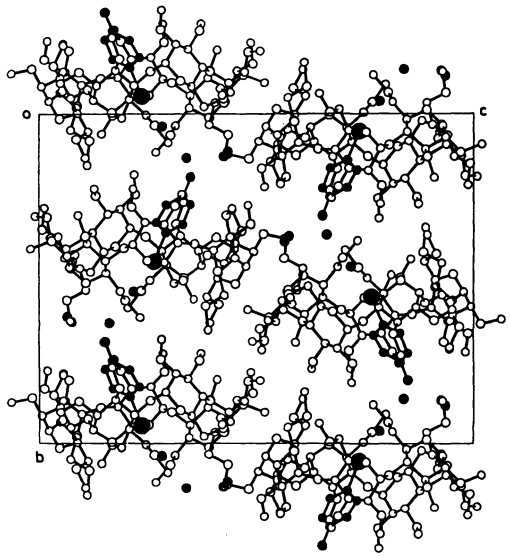

Fig. 4. The crystal structure viewed down along the a axis. Atoms in *p*-IPH and water molecules are denoted by black dots.

References

1) M. L. Bender and M. Komiyama, "Cyclodextrin Chemistry," Springer-Verlag, Berlin (1978).
2) I. Tabushi, *Acc. Chem. Res.*, **15**, 66 (1982).
3) K. Harata, K. Uekama, M. Otagiri, and F. Hirayama, *Bull. Chem. Soc., Jpn.*, **55**, 407 (1982).
4) K. Harata, K. Uekama, M. Otagiri, F. Hirayama, and Y. Sugiyama, *Bull. Chem. Soc. Jpn.*, **55**, 3386 (1982).
5) K. Harata, K. Uekama, M. Otagiri, and F. Hirayama, *Bull. Chem. Soc. Jpn.*, **55**, 3904 (1982).
6) M. Czugler, E. Eckle, and J. J. Stezowsk, *J. Chem. Soc., Chem. Commun.*, **1981**, 1291.
7) J. J. Stezowski, K. H. Jogun, E. Eckle, and K. Bartels, *Nature*, **274**, 617 (1978).
8) J. A. Hamilton, M. N. Sabesan, and L. Steinrauf, *Carbohydr. Res.*, **89**, 33 (1981).
9) R. Tokuoka, T. Fujiwara, and K. Tomita, *Acta Crystallogr., Sect. B*, **37**, 1157 (1981).
10) K. Lindner and W. Saenger, *Carbohydr. Res.*, **99**, 103 (1982).
11) K. Harata, *Bull. Chem. Soc. Jpn.*, **55**, 2315 (1982).
12) "International Tables for X-Ray Crystallography," Kynoch Press, Birmingham (1974), Vol. IV.

 © 1983 The Chemical Society of Japan Bull. Chem. Soc. Jpn., 56, 1737—1739 (1983)

Anomalous Near Infrared Emission Observed in High Energy Electron Excited Xe and Xe-Ar

Masako TANAKA,* Susumu SASAKI, and Meiseki KATAYAMA
Department of Atomic Science and Nuclear Engineering, Faculty of Engineering, Hokkaido University, Sapporo 060
(Received October 30, 1982)

The near infrared emission spectra of Xe and Xe-Ar which were excited by the pulsed irradiation of electrons by using a 45 MeV linear accelerator were investigated. A new broad band, probably due to the transition between the upper molecular states, was observed at 1200 to 1400 nm. The effects of O_2 and SF_6 on this band were studied.

The emission spectra of excited rare gas atoms and excimers have been studied theoretically and experimentally in the vacuum ultraviolet region with respect to the development of bound-free lasers.[1-3] Recent studies are concentrated on the properties of the lowest excited states, 0_u^+ and 1_u, of the Xe excimer, which can be selectively excited by means of synchrotron radiation.[4-8] However, spectroscopic information on the upper molecular states has not been studied well because of the lack of experimental approaches. It is expected from theoretical estimations that the absorption of photons or emission related to the molecular transition should appear in the near infrared region.[9] Arai *et al.* have found the near infrared absorption bands which were assigned to the molecular transition from the first excimer states, $^{1,3}\Sigma_u^+$, for Ne to Xe, which were excited by electron beam pulses.[10] Distefano *et al.* observed the near infrared fluorescence due to the atomic transition from 6p to 6s configuration for vacuum ultraviolet irradiated Xe.[11]

We have investigated the near infrared emission spectra of Xe gas which had been excited by the pulsed irradiation of a high energy electron beam, and have found a new broad band; this is probably due to the transition of the upper to the lower molecular states where the excitation seems to be a nonionic process.

Experimental

The electon beam pulses were generated by a 45 MeV linear accelerator installed at Hokkaido University. The duration of the pulses was 3 μs. The charge provided in one pulse was 5×10^{-6} C. The dose was estimated to be approximately 10 krad per pulse at 700 Torr (1 Torr=133.32 Pa) of N_2O by means of its decomposition.[12]

A block diagram of the experimental system is shown in Fig. 1. A stainless steel cell of 60 mm in diam. by 350 mm long was used. The electron beam entered the cell at one end. The emissions from irradiated sample gases were reflected by a thin mirror which was fixed in the cell just behind the incident window at 45° to the electron beam axis, and directed to the NaCl window, which was attached at a right angle to the beam direction. Thus the emission from the samples was observed in the reverse direction to the electron beam so that interference by the intense Cerenko light in the Xe gas upon irradiation could be avoided in the infrared observation. The detection system for the emission consists of a Bausch and Lomb high-intensity grating monochromator and a PbSe detector (Hamamatsu TV, p 791) with a response time of 2.5 μs. The signals from the detector were amplified 10 fold by an ac amplifier (Keithlel 105) and were followed on a transient

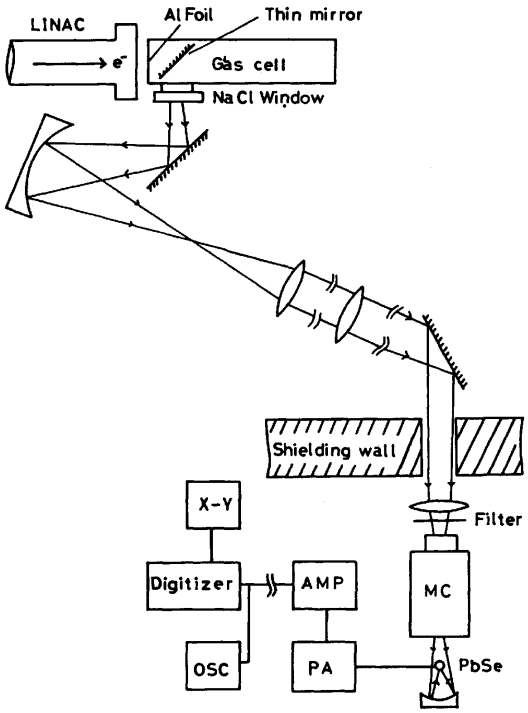

Fig. 1. Block diagram of experimental system.

digitizer (Iwatsu DM901). All the data were recorded on an X-Y recorder. Typical signal traces are shown in the inserts in Fig. 2. Since the response time of the detector was much too long relative to the life time of this kind of emission, the spectra were obtained by plotting the peak intensity of the signal trace against the wavelength. The sensitivity of the detector is known to increase linearly from 1000 to 1600 nm but no correction for this was made. A filter for the cut-off at 650 nm was used to avoid the contribution of higher components.

Research grade Xe (99.995% pure from Nihon Sanso) and ultrahigh pure Ar (99.999% pure from Nihon Sanso) were used. The gases were introduced into the cell through a molecular sieve 5A trap. When necessary, a column of Ba getter at 190 °C was used before the trap to remove any O_2 contained as impurity.

Results

Emission Spectra in Xe. The emission spectrum in the irradiated Xe of 400 Torr is shown in Fig. 2(a). The well known emission lines due to the 6p-6s transitions were observed at 830, 890, and 990 nm, where each band is unresolved but consists of more than one line.

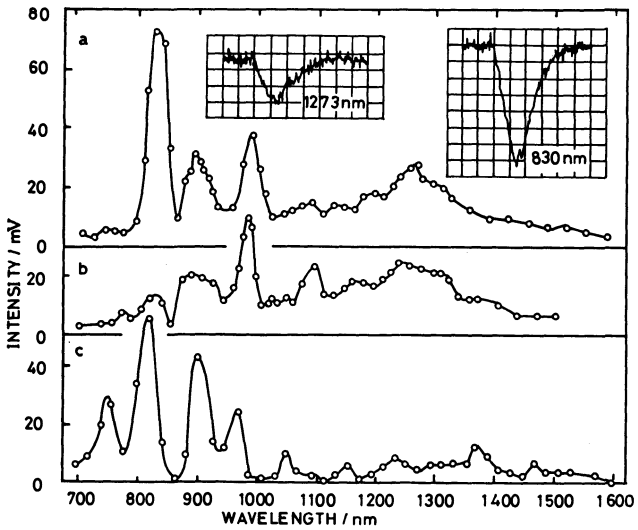

Fig. 2. Emission spectra of irradiated Xe, Xe–Ar and Ar. (a) 400 Torr Xe, inserts: 4 mV/div and 2.5 μs/div, (b) 400 Torr Ar+200 Torr Xe, (c) 500 Torr Ar.

In addition to these lines, a broad band was observed in the region of 1200 to 1400 nm with the maximum at 1270 nm; this has not been reported previously. Since this anomalous emission might originate from the window material having been excited by the Cerenkov light or the second continuum of Xe, the experiment was repeated with a quartz window instead of the NaCl window, and it was confirmed that the intensity of this emission band was not changed. Thus it was concluded that the origin of this band was the irradiated Xe gas.

Emission Spectrum in Xe–Ar. The mixtures of Ar and Xe at various compositions were irradiated. The total pressure of the mixtures was 600 Torr. Figure 2(b) shows the emission spectrum of the irradiated mixture of 200 Torr Xe and 400 Torr Ar. The atomic line at 830 nm, which was the most intense in pure Xe, disappeared, and the intense lines at 990 and 1080 nm were enhanced strongly as the Xe concentration decreased. The emission band similar to that obtained for pure Xe was also observed at around 1270 nm. Assuming that the ionization cross section of Xe is approximately twice that of Ar,[13] the absorption energy for this mixture was calculated to be approximately equal to that of 400 Torr Xe in Fig. 2(a). It is obvious from comparison between Fig. 2(a) and (b) that the equal intensity was obtained for the 1270 nm band under the equal absorption energy. Contrary to the intensity at 990 and 1080 nm lines, the intensity of this band decreased with the decrease of the Xe concentration.

In pure Ar this kind of broad band was not detected between 700 and 1600 nm, as shown in Fig. 2(c).

Effect of O_2. When the 0.01 Torr of O_2 was added to 430 Torr of Xe, the intensity of the broad band at 1270 nm decreased to one-half relative to that in pure Xe, whereas the intensity of the atomic lines was not influenced by the addition of such trace amounts of O_2. The 1270 nm band was quenched completely by 1 Torr of O_2.

Effect of SF_6. Figures 3 and 4 exhibit the effect of a trace amount of SF_6, which was added as a

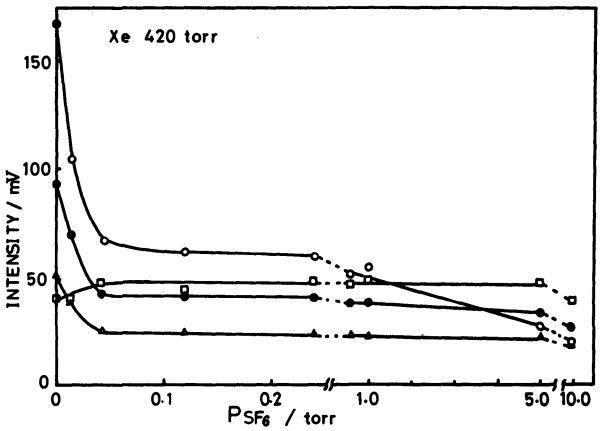

Fig. 3. Effect of SF_6 on the intensities of emission bands in Xe. ○: 830 nm. ●: 990 nm, △: 890 nm, □: 1270 nm.

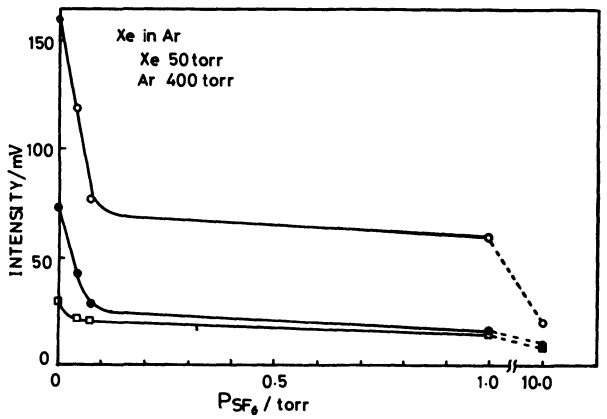

Fig. 4. Effect of SF_6 on the intensity of emission bands in Xe–Ar. ○: 990 nm, ●: 1080 nm, □: 1270 nm.

scanvenger of thermal electrons in Xe and in Xe–Ar respectively. In Xe, as shown in Fig. 3, the intensities of the three atomic lines decreased markedly on the addition of less than 0.05 Torr of SF_6, whereas the intensity of the 1270 nm band was unchanged except for a small increase at the same range of the concentration for which the significant decrease in the intensities of atomic lines occurred. The effect of SF_6 on the emission spectrum in Xe–Ar was essentially the same as in Xe. As shown in Fig. 4, the intensities of the two atomic lines at 990 and 1080 nm decreased to half on adding less than 0.1 Torr of SF_6, while the intensity of the 1270 nm band was almost unchanged except for the small decrease at less than 0.1 Torr of SF_6.

Discussion

A new emission band was observed at around 1270 nm in Xe gas on the bombardment of high energy electrons. Since O_2 is known to be the effective lasing component in the mixture with Xe, the possibility that this new emission band might be caused by contamination with air had to be considered. The result of the experiment on the addition of O_2 indicated that the origin of this emission band was not an impurity but the

excited Xe itself. The large width of this band must be attributed to certain molecular transitions in excited Xe. The recent report by Keto *et al.* about the similar O_2 effect on the intensity of the second continuum in electron excited Ar[14] also supports the above assignment.

As shown in previous publications,[1-3] excited rare gas atoms are produced mainly from the dissociative recombination of Xe_2^+ with the secondary electron; they subsequently form the bound excimer, $^{1,3}\Sigma_u^+$, by three-body collision with atoms in the ground state. Accordingly, these excimer bands should be affected by the addition of SF_6. However, the result shown in Figs. 3 and 4 indicated that the 1270 nm band was not quenched by SF_6. This means that the precursor responsible for the 1270 nm band was not the excited atom. The excimer states observed in this experiment should thus be formed by some direct excitation not *via* the above mentioned ionic process. The small increase in the intensity at 1270 nm on the addition of SF_6 shown in Fig. 3 suggests that the small fraction of the excimer states observed here can be produced directly by the ion recombination of Xe_2^+ and SF_6^-. One of the possible paths of direct excitation under irradiation by high energy electrons is the excitation of the van der Waals (vdW) molecule, Xe_2, to vibrationally excited levels of the upper molecular states by inelastic collision with the secondary electrons, which have kinetic energy higher than thermal electrons. The emission band presented here might be attributed to the transition from the upper molecular states with the shallow minimums of the potential curves, which are located in the vicinity of the vdW distance. Since at least two shoulders were observed at both sides of the 1270 nm peak, several transitions could be associated. The radiative transitions from the 1_u of $7s[3/2]_1$ to the bound states of $6s'[1/2]_1$ or from the 0_u^+ of $6s'[1/2]_1$ to the bound states of $6s[3/2]_1$ were expected to give the emission band at 1200 to 1400 nm. According to Castex, the concentration of vdW bound and quasibound molecules is 0.6% at 760 Torr and at room temperature.[15] In the case of photon excitation, there has been some evidence for the excitation of vdW molecules to upper states both in absorption spectra[16] and in excitation spectra.[4,5,7,8,15,17,18] The vibrational progression was observed in the two-photon excitation spectra of high pressure Xe in the energy range of 6p and 5d configurations by Gornik *et al.*[18] They assigned the molecular bands to the transition from the bound vdW dimers. Recently work on this kind of excitation using monochromatic synchrotron radiation indicated that the red wing in the vicinity of $6s'[1/2]_1$ and $6s[3/2]_1$ excitation band,[4,5,7,8,17] was due to the transition of the vdW dimers to the vibrationally excited molecular states. Analogous with these results for photon excitation, then, the direct excitation of vdW molecules can occur in the high energy and high intensity electron excitation.

In the case of the Xe–Ar system, the disappearance of the emission line at 830 nm due to Xe $6p[1/2]_0$ and the enhancement of the 990 and 1080 nm lines due to Xe $6p[1/2]_1$, which were observed in Fig. 2(b), suggest that the dominant energy transfer occurs from the Ar excimer, $^{1,3}\Sigma_u^+$, to Xe atoms. However, concerning the 1270 nm band in Xe–Ar, the excitation process seems to be completely different, as indicated in Fig. 4, where similar mechanism to that considered in pure Xe can be applicable. The small decrease of the 1270 nm band shown in Fig. 4 can be interpreted to mean that in Xe–Ar the energy transfer from the Ar excimer to the vdW dimers of Xe occurs to a small extent.

The authors would like to thank Professor Yoshihiko Hatano of Tokyo Institute of Technology for his helpful discussions at the early stage of the present investigation. The authors are also indebted to Professor Takeaki Enoto, Messrs. Hiroaki Tanida, and Koichi Sato for the operation of the accelerator.

References

1) C. W. Werner, E. V. George, P. W. Hoff, and C. K. Rhodes, *IEEE. J. Quantum Electron.*, *QE***13**, 769 (1977).
2) M. H. R. Hutchinson, *Appl. Phys.*, **21**, 95 (1980).
3) M. McCusker, "Excimer Lasers," ed by C. K. Rhodes, Springer-Verlag, Berlin Heidelberg (1979), Chap. 3.
4) R. Brodmann, G. Zimmerer, *J. Phys. B: Atom Molec. Phys.*, **10**, 3595 (1977).
5) O. Dutuit, R. A. Gutchek, and J. Le Calve, *Chem. Phys. Lett.*, **58**, 66 (1978).
6) H. D. Wenck, S. S. Hansnain, M. M. Nikitin, K. Sommer, G. Zimmerer, D. Haaks, *Chem. Phys. Lett.*, **66**, 138 (1979).
7) O. Dutuit, M. C. Castex, J. Le Calve, and M. Lavollee, *J. Chem. Phys.*, **73**, 3107 (1980).
8) T. D. Bonfield, F. H. K. Rambow, G. K. Walters, M. V. McCusker, D. C. Lorents, and R. A. Gutcheck, *J. Chem. Phys.*, **72**, 2914 (1980).
9) R. M. Mulliken, *J. Chem. Phys.*, **52**, 5170 (1970).
10) S. Arai, T. Oka, M. Koguma, and M. Imamura, *J. Chem. Phys.*, **68**, 4595 (1978).
11) G. Distefano, M. Lenzi, A. Margani, and C. Nguyenxuan, *Opt. Commun.*, **27**, 85 (1978).
12) S. Takao, Y. Hatano, and S. Shida, *J. Phys. Chem.*, **75**, 3178 (1971).
13) L. G. Christphorou, "Atomic and Molecular Radiation Physics," Wiley-Interscience, London (1971), p. 379.
14) J. W. Keto, C. F. Hart, and Chien-Yu Kuo, *J. Chem. Phys.*, **74**, 4433 (1981).
15) M. C. Castex, *J. Chem. Phys.*, **74**, 759 (1981).
16) M. C. Castex, and N. Damaney, *Chem. Phys. Lett.*, **24**, 437 (1974); M. C. Castex, *Chem. Phys.*, **5**, 448 (1974).
17) Y. Hatano, M. Ohno, N. Kouchi, H. Koizumi, A. Yokoyama, G. Isoyama, H. Kitamura, and T. Sasaki, *Chem. Phys. Lett.*, **84**, 454 (1981).
18) W. Gornik, S. Kindt, E. Matthias, and D. Schmidt, *J Chem. Phys.*, **75**, 68 (1981).

Raman Spectra of Compounds under Inversion Motions. III. *N*-Methylpyrrolidine

Kunio FUKUSHIMA* and Hisayo SASAKI†
Department of Chemistry, Faculty of Science, Shizuoka University 836, Oya, Shizuoka 422
(Received November 8, 1982)

Raman spectra of *N*-methylpyrrolidine were measured in various states and a normal vibration calculation was carried out on its conformers. Results of the measurement and calculation indicate that the Raman band of the inversion vibrational mode is caused to shift remarkably by the formation of hydrogen bond to the nitrogen atom. This phenomenon, along with the enthalpy of hydrogen bond formation obtained from measurements at various temperatures, suggests that the conformer predominant in pure liquid corresponds to one minimum in the potential for the inversion motion, which has a low potential barrier and high anharmonicity.

Some Raman bands of 1,4-dimethylpiperazine and 1-methylpiperazine are caused to shift remarkably by formation of hydrogen bonds to their nitrogen atoms, and this phenomenon has been interpreted as being due to a suppression of the motion of inversion at the nitrogen by the hydrogen bonding.[1,2] The present study is concerned with a five-membered heterocyclic compound, *N*-methylpyrrolidine. Existence of an inversion motion at the nitrogen in this compound was concluded by NMR studies,[3-5] and a value of 33.5 kJ/mol was obtained for the free energy of activation.[5] In addition, dipole moment studies also suggested the existence of the motion.[6,7] An effect of a hydrogen bonding between this compound and chloroform was found in NMR spectral measurements, and a report[8] was made on shifts of its Raman bands of CH stretching vibrations caused by dissolution in water. In the present study, Raman spectra of *N*-methylpyrrolidine in various states were measured, and band shifts found in association with hydrogen bonding are discussed from many points of view.

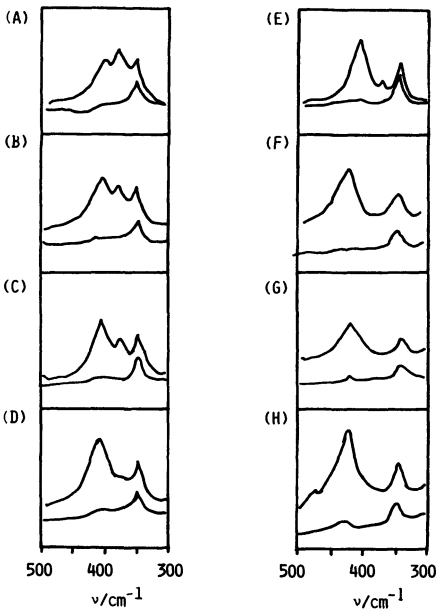

Fig. 1. Raman spectra (350—450 cm^{-1}, $I_{//}$ and $I_{\perp}$) of aqueous solutions of *N*-methylpyrrolidine at room temperature.
(A): x=0.658, (B): x=0.549, (C): x=0.488, (D): x=0.405, (E): x=0.272, (F): x=0.037, (G): x=0.022, (H): x=0.019.
x: Mole fraction of *N*-methylpyrrolidine.

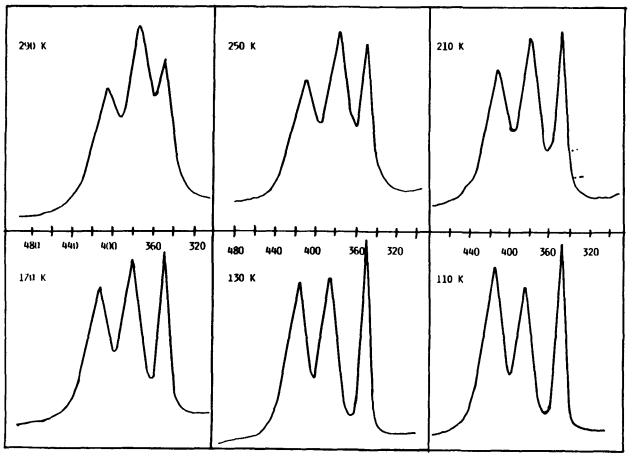

Fig. 2. Raman spectra (350—450 cm^{-1}) of a methanol solution of *N*-methylpyrrolidine (a mixture of *N*-methylpyrrolidine and methanol in mole ratio of 1 to 0.80) at various temperatures.

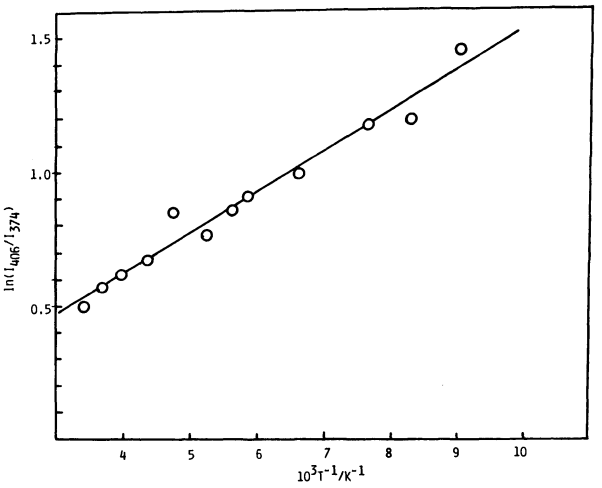

Fig. 3. Relation between $\ln(I_{406}/I_{374})$ and $1/T$. T in K.

Experimental

Sample *N*-methylpyrrolidine was a commercial product from Tokyo Kasei Co. (grade GR). Raman spectra were

† Present address: Department of Chemistry, Faculty of Science, Ochanomizu Women's University.

Table 1. Raman spectra of *N*-methylpyrrolidine[a)]

Pure liquid			Solid		Aq soln (1 : 1.1)			CH_3OH soln (1 : 1.0)			C_6H_6 soln (1 : 1.0)			Dioxane soln (1 : 1.0)			Acetone soln (1 : 1.0)		
ν	I	ρ	ν	I	ν	I	ρ	ν	I	ρ	ν	I	ρ	ν	I	ρ	ν	I	ρ
			120	7															
230	5	0.39	232	6	230	3	0.37	223	3	0.40				223	3	0.31	225	23	0.23
?			292	5															
348	9	0.62	354	15	348	9	0.69	346	9	0.66	342	9	0.55	344	7	0.62	350	9	0.55
											366	14	0.08						
375	15	0.11	388	20	374	8	0.17	372	10	0.13	375	14	0.12	371	12	0.06	376	17	0.09
					406	12	0.13	405	7	0.13									
570	41	0.18	574	56	570	41	0.20	568	43	0.17	565	41	0.12	569	37	0.14	572	43	0.16
?			642	8															
?			734	8							797	4	0.20						
			852	11															
873	23	0.21	876	78	874	33	0.17	870	29	0.18	869	28	0.17	871	28	0.18	874	27	0.21
895	100	0.03	896	100	896	100	0.03	895	100	0.03	890	100	0.03	893	100	0.02	897	100	0.03
941	2	0.75	940	8	940	2	0.75	940	1	0.75							941	1	0.75
961	2	0.75	965	10	960	3	0.64	960	2	0.75							965	2	0.20
1030	9	0.56	1033	27	1032	12	0.71	1030	16	0.48	1027	13	0.46	1027	12	0.24	1032	9	0.52
1040	6	0.75	1044	19				1037	17	0.37									
			1083	6															
1112	4	0.35	1118	7	1117	4	0.55	1110	4	0.55	1108	5	0.32	1105	10	0.58	1112	4	0.24
1148	5	0.75	1148	19	1144	6	0.61	1141	5	0.60	1143	9	0.43	1144	6	0.43	1149	4	0.65
			1177	6															
1201	3	0.40	1201	11	1215	4	0.75	1215	4	0.66	1195	2	0.35				1218	6	0.68
1217	2	0.75	1215	12															
1238	5	0.33	1244	17	1240	6	0.47	1238	5	0.50	1235	5	0.19	1239	6	0.34	1240	6	0.47
1278	3	0.56	1258	12															
1285	3	0.68	1288	22	1285	5	0.67	1280	5	0.50	1280	4	0.41	?		sh	1280	4	0.54
1330	2	0.75	1334	9	1350	4	0.59	1331	2	0.59	1325	2	0.62	1330	6	0.64	1330	2	0.75
1349	3	0.42	1353	13				1347	3	0.56	1345	5	0.32	1344	4	0.29	1350	5	0.41
											1398	3	0.26	1390	3	0.58			
1414	4	0.75	1417	13	1417	4	0.75	1414	5	0.57	1411	4	0.48	1411	6	0.66	1419	4	0.56
1446	10	0.75	1449	29	1449	12	0.75	1447	15	0.75	1443	16	0.74	1440	27	0.71	1447	14	0.72
1467	9	0.75	1465	26	1465	11	0.75	1460	12	0.75	1474	11	0.58						
1480	7	0.75	1483	15													1482	9	0.34

a) ν, frequency in cm^{-1}; I, intensity; ρ, polarization ratio. The ratios in parentheses represent the mole ratio of *N*-methylpyrrolidine to solvent.

recorded on a Model R-800T Raman spe trometer (Japan Spectroscopic Co.) with an excitation effected by use of a Spectra Physics argon ion laser (Model 165) at 514.5 nm (300 mW). Depolarization ratio was measured with a system consisting of a half-wave plate, a lens, and a polarizer. Liquid samples at room temperatures were measured with 0.3 ml Raman cells, while crystals, solutions, and pure liquids at lower temperatures were measured with an Oxford-type cryostat and liquid nitrogen. Experimental results are shown in Table 1 and 2 and Figs. 1, 2, and 3.

Normal Vibration Calculation

Normal vibration calculations on conformers of *N*-methylpyrrolidine (the axial and equatorial conformers and other molecular models) were carried out according to Wilson's GF matrix method[9)] by use of the Computation Center, University of Tokyo and library programs BGLZ and LSMB. The molecular parameters used are: bond lengths, $r(N\text{-}CH_3)=1.49$ Å, $r(NCH_2\text{-}CH_2)=1.53$ Å, $r(CH_2\text{-}CH_2)=1.54$ Å, and $r(C\text{-}H)=1.09$ Å; bond angles, $\alpha(N\text{-}CH_2\text{-}CH_2)=105°$, $\alpha(CH_2\text{-}CH_2\text{-}CH_2)=104°$, and $\alpha(H\text{-}C\text{-}H)(CH_2$ group$)=$bond abgles of CH_3 group$=$bond angles around nitrogen atoms$=$tetrahedral angle. For the molecular models, an envelope structure for the five-membered ring was used on the basis of the existence of depolarized bands in the observed Raman spectra of *N*-methylpyrrolidine in the liquid state. Force constants and results of calculation are shown in Table 3 and Fig. 4, respectively.

Results and Discussion

Spectral Change with State Change from Liquid to Solid. As shown in Table 1, no bands are caused to disappear by the state change from liquid to solid. Therefore, it may reasonably be concluded that one conformer prevails in the pure liquid and that this persists in the solid state. The intensity change of the bands at 1238, 873 and 348 cm^{-1} may be due to a change in their associated polarizabilities.

Spectra of N-*Methylpyrrolidine in Hydrogen-bonding Solvents.* A change in the spectrum of *N*-methylpyrrolidine with

TABLE 2. RAMAN SPECTRA OF *N*-METHYLPYRROLIDINE IN ACIDS[a)]

Pure liquid			HCOOH soln (1 : 2.1)		CH_3COOH soln (1 : 1.0)		HCl soln (1 : 1.5)		DCl soln (1 : 1.0)	
ν	I	ρ	ν	I	ν	I	ν	I	ν	I
230		50.39			216	5				
			335	5			330	6	330	7
348	9	0.62			354	6				
375	15	0.11			375	8				
			450	30	430	9	455	30	443	37
					477	9				
			555	40			552	38	546	42
					571	26				
570	41	0.18								
					662	6				
			697	21						
			790	29			788	26		
873	23	0.21	860	77	880	48	855	69	853	75
895	100	0.03	905	100	900	100	905	100	900	100
			955	9			953	9		
							1006	21	1010	13
1030	9	0.56	1010	21	1036	16	1035	17	1035	17
1040	6	0.75								
							1070	15		
1112	4	0.35			1114	5	1105	18	1100	10
1148	5	0.71								
1201	3	0.40							1190	18
1217	2	0.75								
1238	5	0.33			1240	12	1230	14		
1278	3	0.56								
1285	3	0.68								
1285	3	0.68							1285	19
1330	2	0.75			1333	9				
1349	3	0.42	1348	77			1350	11	1355	14
			1375	45	1380	11				
									1400	8
1414	4	0.75			1413	17				
									1428	
1446	10	0.75	1456	45	1449	30				
1467	9	0.75					1462	39	1458	52
1480	7	0.75								

a) ν, frequency in cm^{-1}; I, intensity; ρ, polarization ratio. The ratios in parentheses represent the mole ratio of *N*-methylpyrrolidine to solvent.

dissolution in water was reported by Hirokawa *et al.*[8] in a spectal region above 2600 cm^{-1}. In a region below 2600 cm^{-1}, a change has been found, as shown in Table 1, that the band at 375 cm^{-1} (pure liquid) remarkably shifts to higher frequencies in aqueous solutions. Relative intensity changes in this band and its shifted band are shown in Fig. 1. With increasing mol fraction of water, the band at 375 cm^{-1} decreases its intensity, while a band appears in the higher frequency side of the band with increasing intensity. In the case of the lowest concentration in the figure, the former disappears and only the latter remains at 424 cm^{-1}. The frequency increase 375 $cm^{-1} \rightarrow 424$ cm^{-1} is a remarkably large one. No other bands in the region below 2600 cm^{-1} show such a remarkable change, although some of them experience smaller frequency change. The valence state of the nitrogen atom of *N*-methylpyrrolidine is expected to resemble an sp^3 state when it is hydrogen-bonded. The observed frequencies for hydrogen-bonded species in Table 1 correspond well to the frequencies calculated for the equatorial conformer by using the first-guess force constants, but not satisfactorily to the axial conformer. The calculated frequencies for the equatorial conformer were made to fit to the observed frequencies so as to give the final force constant set by the method of least squares.[10] The set is shown in Table 3. The calculated frequencies for the skeletal vibrations of the axial conformer for the set of force constants are shown in Fig. 4. They are very different from those of the equatorial conformer included in the figure, which agree well with the observed frequencies. Therefore, it is reasonable to consider that most of hydrogen-bonded species assume equatorial conformations.

Spectral Change with Temperature Change. As discussed in the preceding section, two bands (one at 375 cm^{-1} and the other at the higher frequency side) appear

TABLE 3. FORCE CONSTANTS(mdyn Å^{-1}, 1 dyn$=10^{-5}$ N) OF *N*-METHYLPYRROLIDINE FOR THE MODIFIED UREY-BRADLEY FORCE FIELD

K(N–CH_3)	2.515	F(C–C–C)	0.652	
K(N–C)	3.117	F(H–C–CH_2N)	0.614	
K(NC–C)	1.371	F(H–C–CH_2CH_2N)	0.447	
K(C–C)	1.570	Y(N–CH_3)	0.028	mdyn Å
K(C–H)(CH_3)	4.307	Y(N–CH_2)	0.246	mdyn Å
K(C–H)(CH_2)	3.921	Y(NC–CH_2)	0.157	mdyn Å
H(N–C–H)(CH_3)	0.303	Y(NCH_2CH_2–CH_2)	0.110	mdyn Å
H(H–C–H)(CH_3)	0.363	κ(CH_3)	−0.022	mdyn Å
H(C–N–C)	0.685	κ(N–CH_2–C)	0.090	mdyn Å
H(C–N–CH_3)	0.432	κ(CH_2–CH_2–CH_2)	0.057	mdyn Å
H(N–C–C)	0.106	g	0.067	mdyn Å
H(H–C–N)	0.127	t	−0.040	mdyn Å
H(H–C–$CH_2CH_2CH_2$)	0.261	c	−0.050	mdyn Å
H(H–C–H)(CH_2)	0.376			
H(C–C–C)	0.218			
H(H–C–CH_2N)	0.280			
H(H–C–CH_2CH_2N)	0.222			
F(N–C–H)(CH_3)	0.657			
F(H–C–H)(CH_3)	0.144			
F(C–N–C)	0.466			
F(C–N–CH_3)	0.183			
F(N–C–C)	0.761			
F(H–C–N)	0.633			
F(H–C–$CH_2CH_2CH_2$)	0.623			
F(H–C–H)(CH_2)	0.000			

Y: internal rotation force constant
κ : intramolecular tension force constant
g: gauche-type interaction force constant
t: trans-type interaction force constant
c: cis-type interaction force constant

These force constants are expressed in the unit of mdyn Å.

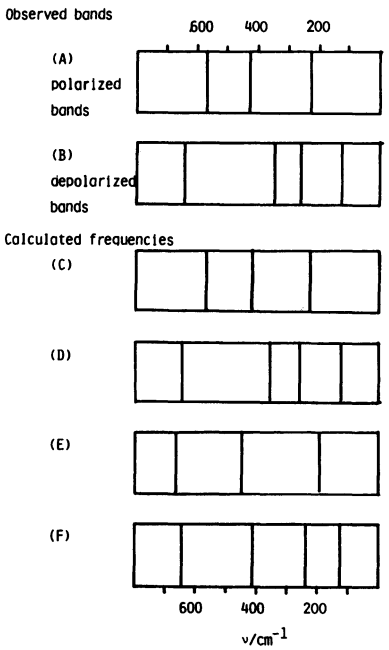

Fig. 4. Observed frequencies of liquid *N*-methylpyrrolidine ((A) and (B)) compared with the calculated frequencies ((C): equatorial form, A′ species, (D): quatorial form, A species, (E): axial form, A′ species, (F): axial form, A″ species).

in the spectra of *N*-methylpyrrolidine solutions in hydrogen-bonding solvents, suggesting two conformers (a hydrogen-bonded equatorial conformer and a conformer having a different conformation) to exist in the solutions. In order to evaluate the energy difference between these two conformers, spectra of a methanol solution were measured at various temperatures between 298 and 110 K. At equilibrium, *N*-methylpyrrolidine ($b-a$ mol)$+CH_3OH$($a-a$ mol)$\rightleftarrows$ hydrogen-bonded complex (a mol), hence the equilibrium constant $K=a/(b-a)(a-a)$, where a and b are the initial quantities in mol of CH_3OH and *N*-methylpyrrolidine, respectively. On the assumption that $b-a$ and a are proportional to the band intensities of the band at 375 cm^{-1} and the one in the higher frequency side, respectively, K was obtained at various temperatures. Plots of ln K *vs.* $1/T$ are shown in Fig. 3. From the figure and the equation $\ln K=-\Delta H/(RT)+$ const, the enthalpy difference for the above reaction is estimated as $\Delta H=-1.3\pm0.2$ kJ/mol.

Spectra of N-*Methylpyrrolidine in Non-hydrogen-bonding Solvents.* Benzene (nonpolar), dioxane (polar), and acetone (polar) were used. They give spectra almost the same as the spectrum of pure liquid. This indicates that the shift of Raman band mentioned above under the second heading is due to hydrogen bonding to the nitrogen atom of the compound.

Spectra of N-*Methylpyrrolidine in Carboxylic Acids and Aqueous Hydrochloric Acid Solutions.* A band corresponding to the band of liquid *N*-methylpyrrolidine at 375 cm^{-1} is observed for each of the solutions shown in Table 2 (HCOOH soln, 450 cm^{-1}; CH_3COOH, 430 cm^{-1}; aqueous hydrochloric acid solution, 455 cm^{-1}). For *N*-methylpyrrolidine in a deuterium chloride–heavy water mixture, the corresponding band appears at 443 cm^{-1}, close to 455 cm^{-1} for the band of aqueous hydrochloric acid solution, indicating that this band is not due to the NH deformation mode but to the skeletal deformation mode. Between these frequency values and 375

cm^{-1} (*N*-methylpyrrolidine, liquid) there lie frequency values for bands of the inversion mode of *N*-methylpyrrolidine in hydrogen-bonding solvents, in agreement with the change in valence state of the nitrogen atom to the sp^3 type with hydrogen bonding.

Concluding Remarks. In liquid *N*-methylpyrrolidine, almost all the molecules are in one conformation different from that for the hydrogen-bonded equatorial conformer.

These two conformers give rise to bands at different frequencies 375 and 424 cm^{-1} for the vibrational mode of inversion at the nitrogen. This may be explained as follows. The hydrogen bonding to the nitrogen atom increases the potential barrier for the inversion motion at the nitrogen and changes the shape of potential for the motion. As a result, for the inversion mode the energy level separation between the ground state ($v=0$) and the first excited state ($v=1$) increases, and the $0\rightarrow1$ transition frequency increases to give the above-mentioned shift of band. On the other hand, the observed enthalpy difference, -1.3 kJ mol, between the hydrogen-bonded equatorial conformer and the abundant conformer in the pure liquid is very small compared with ordinary hydrogen-bond energy values. Therefore, the instability of the non-hydrogen-bonded equatorial form having a nitrogen atom in the sp^3 state may be considered to be compensated by the stabilization energy due to hydrogen bonding. Thus, the potential for the inversion vibrational mode of the conformer in the pure liquid is a low barrier potential with high anharmonicity, one of whose potential minima corresponds to the abundant conformer in the pure liquid. The conformer is stabler than the non-hydrogen-bonded equatorial conformer having a nitrogen atom in the sp^3 state, and the structure around the nitrogen atom is intermediate between the planar and tetrahedral structures.

References

1) K. Fukushima, *Bull. Chem. Soc. Jpn.*, **52**, 2871 (1979).
2) K. Fukushima and H. Takahashi, *Bull. Chem. Soc. Jpn.*, **54**, 2603 (1981).
3) J. B. Lambert and W. L. Oliver, Jr., *J. Am. Chem. Soc.*, **91**, 7774 (1969).
4) K. F. Wong and S. Ng, *J. Chem. Soc., Faraday Trans. 2*, **71**, 622 (1975).
5) J. M. Lehn and J. Wagner, *Tetrahedron*, **26**, 4227 (1970).
6) T. R. Simpson, Jr., J. C. Craig, and W. D. Kumler, *J. Pharm. Sci.*, **56**, 708 (1967).
7) M. R. Favier and M. Gomel, *C. R. Acad. Sci. Paris*, **266**, 1719 (1968).
8) T. Hirokawa, T. Kimura, K. Ohno, and H. Murata, *Spectrochim. Acta, Part A*, **36**, 329 (1980).
9) E. B. Wilson, *J. Chem. Phys.*, **7**, 1047 (1939); **9**, 76 (1941).
10) D. E. Mann, T. Shimanouchi, J. H. Meal, and L. Fano, *J. Chem. Phys.*, **27**, 43 (1957).

 © 1983 The Chemical Society of Japan Bull. Chem. Soc. Jpn., 56, 1745—1748 (1983)

Crystal Structures of Mixed Ligand Copper(II) Complexes Containing L-Amino Acids. III. Aqua(L-histidinato)(L-serinato)copper(II) Trihydrate

Yoshio SASADA,* Akio TAKENAKA, and Toshio FURUYA†

Laboratory of Chemistry for Natural Products, Tokyo Institute of Technology, Nagatsuta, Midori-ku, Yokohama 227

(Received November 19, 1982)

The copper(II) complex containing L-histidine and L-serine crystallizes from an aqueous solution. Crystals of aqua(L-histidinato)(L-serinato)copper(II) trihydrate are monoclinic, space group $P2_1$, $a=11.046(2)$, $b=7.315(1)$, $c=9.737(1)$ Å, $\beta=101.34(2)°$ and $Z=2$. A square-planar coordination around copper consists of α-amino nitrogen and δ-nitrogen atoms in histidine and α-amino nitrogen and α-carboxyl oxygen atoms in serine, the two amino groups being in *cis* position. The fifth coordination site is occupied by a water molecule, and the carboxyl oxygen atom of serine in the adjacent complex makes a weak bond with copper to complete a distorted octahedron. The chelating scheme and overall crystal structure are the same as those of (L-alaninato)aqua(L-histidinato)copper(II) trihydrate (**1**). Crystallization water molecules are situated on the fixed positions in the void space surrounded by the columns of the complexes, but the hydroxyl group of serine takes two sites randomly. The common chelating scheme in the present crystal and **1** is in correspondence with the observation that serine and alanine are of moderate cooperativity with histidine in forming the ternary complexes.

Although most of the copper ions in human serum are bound unexchangeably to ceruloplasmin, the remaining copper ions (10^{-6} mol dm^{-3}) form complexes with albumine, some amino acids and others in complicated equilibria. Binary and ternary complexes, such as L-glutaminatocopper(II) and (L-histidinato)(L-threoninato)copper(II), can be separated by chromatography, and are supposed to be mediators in copper transport between blood and tissues.[1] Neumann and Sass-Kortsak[2] suggested that asparagine, glutamine, and threonine exhibit significant cooperativity with histidine in forming ternary complexes, while alanine, valine, serine, and glutamic acid have weaker effects. Computer simulation also indicated that the content of copper complexes containing histidine is relatively high, although some details are controversial.[3,4] In order to establish the structural basis of these observations, several attempts to synthesize ternary complexes and to determine their geometry have been made, but only a few has been successful.[5]

We have previously reported the structures of (L-asparaginato)(L-histidinato)copper(II) and its hydrate[6] and also (L-alaninato)aqua(L-histidinato)copper(II) trihydrate,[7] (hereafter these complexes are abbreviated as, *e.g.*, Cu(asn his) by using the three-letter code of amino acids). In the former complex, histidine behaves as a terdentate ligand, while in the latter it is a bidentate ligand. It seems that the second amino acid has an effect on the character of the histidine ligand. As found by Freeman *et al.*,[5] Cu(his thr) has the same structure as Cu(asn his). It is interesting to examine whether histidine is a terdentate or bidentate ligand when the second amino acid is serine, which is an amino acid closely related to threonine. We have succeeded in growing suitable crystals of aqua(L-histidinato)(L-serinato)copper(II) trihydrate and have determined its crystal structure by X-ray analysis. The present paper deals with the structure of this complex and discusses the three-dimensional architectures of such ternary complexes.

† On leave from Product Development Laboratories, Yamanouchi Pharmaceutical Co., Ltd., 1-1-8, Azusawa, Itabashi-ku, Tokyo 174

Experimental

Suitable blue single crystals were obtained from aqueous solution placed under an atmosphere of acetone vapour. Preliminary Weissenberg photographs indicated a monoclinic space group $P2_1$ or $P2_1/m$. Since this complex was optically active, the former space group was chosen. Accurate unit cell dimensions were determined by least-squares fits from 2θ values of 20 reflexions measured on a Rigaku four-circle diffractometer. Crystal data are as follows: $C_9H_{16}O_6N_4Cu\cdot 3H_2O$, $P2_1$, $a=11.046(2)$, $b=7.315(1)$, $c=9.737(1)$ Å, $\beta=101.34(2)°$, $Z=2$, $D_m=1.67$, $D_x=1.67$ g cm^{-3}.

Since the crystals gradually deteriorated in air, they were sealed in Lindemann-glass capillaries. Intensity measurements were carried out on a Rigaku four-circle diffractometer, graphite-monochromated Mo $K\alpha$ radiation ($\lambda=0.71073$ Å) being used. Intensities of independent reflexions were collected within the range of $2°<2\theta<55°$. An ω-2θ scan mode was applied with scanning rate of 4° (2θ) min^{-1}. The crystal used had dimensions of $0.6\times0.4\times0.5$ mm^3. Five standard reflexions monitored showed no significant change in intensity. Out of 1917 reflexions measured, 123 reflexions had zero intensity ($I<0$). The observational threshold value, $F_{\rm llm}$, was 1.65. The standard deviations were estimated by the equation, $\sigma^2(F_o)=\sigma_p^2(F_o)+q|F_o|^2$, where $\sigma_p(F_o)$ was evaluated by counting statistics and q (1.22×10^{-5}) was derived from the variations of the monitored reflexions. No correction for absorption was made.

Structure Determination

Although it was expected from the similarity of the unit cell dimensions that the crystal structure of the present complex is close to that of Cu(ala his), the structure determination was made by the straightforward application of the heavy atom method. The first Fourier synthesis based on phases of the copper atom revealed the positions of the three nitrogen and one oxygen atoms that were directly coordinated to copper. Successive Fourier and difference syntheses followed by least-squares refinement led to the location of the other non-hydrogen atoms and to the disordering of the hydroxyl oxygen atom of serine into two sites. Occupancies at

TABLE 1. ATOMIC COORDINATES AND EQUIVALENT ISOTROPIC TEMPERATURE FACTORS

The e.s.d.'s in parentheses refer to last digits. $B_{eq}=8\pi^2(U_1+U_2+U_3)/3$, where U_i's are principal components of the mean square displacement matrix. Values in < > are anisotropicities defined by $\{\sum(B_{eq}-8\pi^2U_i)^2/3\}^{1/2}$.

Atom	x	y	z	B_{eq}/Å^2
Cu	0.19651(6)	0.2500(3)	0.15170(7)	2.71<135>
C(1)	0.4971(7)	0.354(1)	0.5050(7)	3.0<8>
C(2)	0.4369(5)	0.3193(9)	0.3519(6)	2.2<3>
C(3)	0.4791(6)	0.447(1)	0.2511(6)	3.1<15>
C(4)	0.4405(5)	0.396(1)	0.1010(6)	2.4<5>
C(5)	0.3173(5)	0.304(1)	-0.0911(6)	2.6<7>
C(6)	0.4983(7)	0.423(1)	-0.0079(7)	2.7<9>
N(1)	0.2988(4)	0.3228(8)	0.3322(5)	3.1<10>
N(2)	0.3236(4)	0.3242(8)	0.0455(4)	2.4<8>
N(3)	0.4227(4)	0.3631(8)	-0.1266(5)	2.7<10>
O(1)	0.4303(4)	0.3762(8)	0.5925(4)	4.2<19>
O(2)	0.6119(4)	0.3544(9)	0.5341(5)	5.5<33>
C(11)	-0.0303(5)	0.1548(9)	-0.0112(6)	2.6<5>
C(12)	-0.0604(5)	0.150(1)	0.1348(6)	2.8<10>
C(13)	-0.1768(5)	0.259(2)	0.1393(7)	5.3<38>
N(11)	0.0468(4)	0.215(1)	0.2405(5)	3.2<16>
O(11)	0.0802(3)	0.1919(7)	-0.0211(4)	3.2<13>
O(12)	-0.1121(4)	0.1245(8)	-0.1129(4)	3.8<14>
O(13A)	-0.1960(6)	0.299(2)	0.2676(8)	5.5<32>
O(13B)	-0.167(1)	0.405(2)	0.194(2)	5.5<31>
O(1')	0.2720(4)	-0.0625(8)	0.1997(4)	3.9<8>
O(2')	-0.0107(7)	0.212(3)	0.6481(7)	16.5<112>
O(3')	0.1764(6)	0.042(2)	0.5073(7)	13.0<92>
O(4')	0.1760(9)	0.484(2)	0.5787(8)	18.5<136>

these two sites were estimated to be 0.6 and 0.4, respectively, from a difference map constructed at a later stage. Structural parameters were refined by the block-diagonal least-squares method: the quantity minimized was $\sum w(|F_o|-|F_c|)^2$ with $w=1/\sigma^2(F_o)$. Zero reflexions were taken in the least-squares by assuming $F_o=F_{lim}$ and $w=w(F_{lim})$. Hydrogen atoms found on a difference map were included in the calculation. Atomic scattering factors were taken from Ref. 8. The R value dropped to 0.057 for 1767 reflexions with $|F_o|>3\sigma(F_o)$. The final atomic coordinates and equivalent temperature factors are listed in Table 1.[9]

Results and Discussion

Molecular Structure. The geometry of the molecule and the numbering system are presented in Fig. 1, where the bond lengths and angles are also shown.

A square-planar coordination around copper is formed by the chelation of histidine and serine; α-amino nitrogen and imidazole δ-nitrogen atoms in the former and α-amino nitrogen and α-carboxyl oxygen atoms in the latter participate in coordination. Two α-amino nitrogen atoms are in a *cis* position, as found in the mixed ligand copper complexes already reported.[5-7] An apical coordination site is occupied by the water molecule, and the carboxyl oxygen atom in the adjacent complex makes a weak bond to copper from the direction opposite to the water ligand, to complete a distorted octahedron. This coordination scheme is the same as that found in (L-alaninato)aqua(L-histidinato)copper-(II) trihydrate;[7] histidine behaves as a bidentate ligand. Since the value of pK_a of serine is 2.20,[10] slightly smaller than that of alanine, the explanation for modifying the ligating nature of histidine, proposed in the previous paper,[7] could be applied to the present complex.

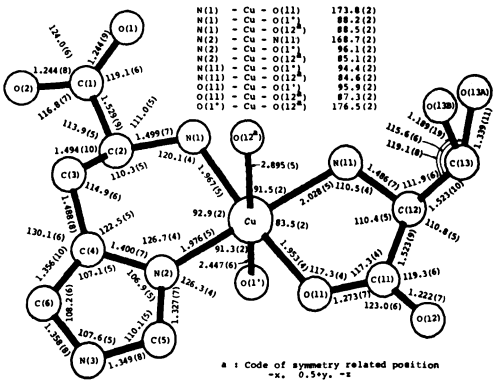

Fig. 1. Bond lengths (l/Å) and angles (ϕ/°) in aqua(L-histidinato)(L-serinato)copper(II). Estimated standard deviations in the last digits are in parentheses.

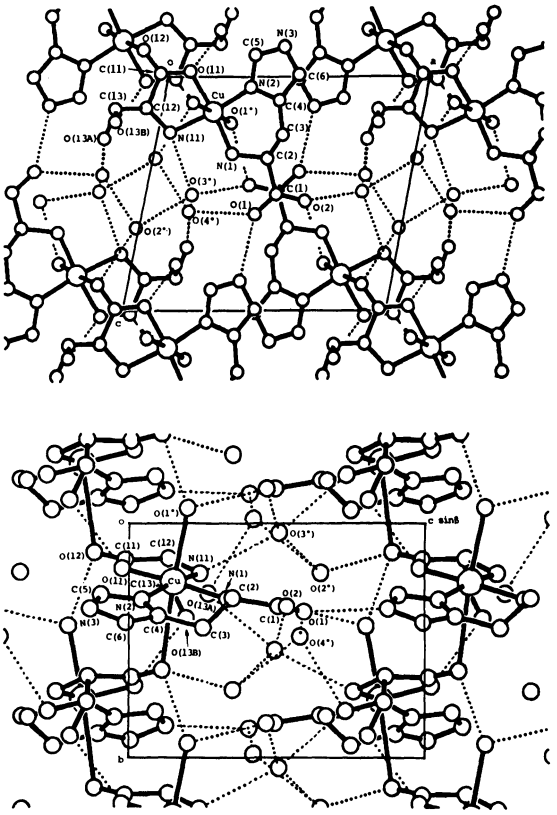

Fig. 2. Crystal structure of aqua(L-histidinato)(L-serinato)copper(II) trihydrate projected along **b** (upper) and **a** (lower).

According to Neumann and Sass-Kortsak,[2] alanine and serine belong to the class of moderate cooperativity with histidine in forming the mixed ligand copper complexes, while asparagine and threonine belong to a class of significant cooperativity. The present serial studies, in addition to the result by Freeman *et al.*,[5] have established that two different chelation modes correspond to the cooperativity classes. These observations reinforce the idea that one of the structural bases for the cooperativity is the chelating mode of histidine.

Coordination distances Cu–N(1), Cu–N(2), Cu–N(11), and Cu–O(11) are 1.967(5), 1.976(5), 2.028(6), and 1.953(4) Å, respectively. The former two Cu–N

Table 2. Hydrogen bond geometry

Donor (D)	Acceptor (A)	Site of A[a)]	l(D···A) Å	ϕ(D–H···A) °
N(3)	O(1)	f	2.755(7)	176(6)
N(11)	O(3′)	o	2.99(1)	128(4)
O(13A)	O(4′)	d	2.74(1)	162(10)
O(13B)	O(11)	a	2.97(1)	113.0(9)[b)]
O(1′)	O(12)	b	2.913(7)	163(6)
O(1′)	O(2)	c	2.726(7)	169(6)
O(2′)	O(12)	e	2.85(1)	166(8)
O(2′)	O(3′)	o	2.97(2)	118(8)[c)]
O(2′)	O(4′)	d	3.07(2)	122(8)[c)]
O(3′)	O(2)	c	2.81(1)	157(10)
O(3′)	O(13A)	d	2.79(1)	147(8)
O(4′)	O(1)	o	2.89(1)	140(9)

a) Site is expressed by symmetry code. o: x, y, z; a: $-x$, $1/2+y$, $-z$; b: $-x$, $-1/2+y$, $-z$; c: $1-x$, $-1/2+y$, $1-z$; d: $-x$, $-1/2+y$, $1-z$; e: $x, y, -1+z$; f: $x, y, -1+z$. Donor atom at o. b) Since the position of hydrogen atom attached to O(13B) is not certain, this is an angle of C(13)-O(13B)···O(11). c) Probably bifurcated hydrogen bond.

distances are slightly shorter than the values (1.98···2.04 Å) reported for rectangular coordination complexes.[11] But these distances, except for Cu–N(1), and two apical coordination distances for Cu–O(12[a]) and Cu–O(1′) seem to be within the fluctuation range found in the related mixed ligand copper complexes.[6,7]

The copper atom is shifted from the mean basal coordination plane toward the apical O(1′) by 0.118(7) Å. The dihedral angle between the planes, N(1)–Cu–N(2) and N(11)–Cu–O(11), is 10.9(2)° (Λ configuration).

The imidazole ring is approximately planar, with maximum deviations of −0.016(6) for C(4) and +0.015(7) Å for C(5). Its mean plane makes a dihedral angle of 2.4(3)° with the plane of N(1)–Cu–N(2).

Crystal Structure. Crystal structures projected along the b and a axes are shown in Fig. 2. As expected from the similarity of the unit cell dimensions, the principal frame of the crystal structure is the same as that of Cu(ala his). The carboxyl oxygen atom, O(12), is weakly coordinated to copper in the complex at $(-x, -1/2+y, -z)$, so that a column extending along the b axis is constructed. ε-Nitrogen atom of the imidazole ring is hydrogen-bonded to the carboxyl oxygen, O(1), in the complex at $(x, y, -1+z)$. These hydrogen bonds connect together the columns above-mentioned, so that a void space extending along the b axis is left, in which three crystallization water molecules and serine side chain are occluded.

While three water molecules are distributed among seven sites randomly in the void space of Cu(ala his), those in the present crystal occupy fixed positions. The serine hydroxyl oxygen atom makes two kinds of hydrogen bonds, by taking two different sites: O(13A) at one site with occupancy of 0.6 links to the water molecule, O(4′), and O(13B) at another site with occupancy of 0.4 is connected to the carboxyl oxygen atom, O(11) in the complex at $(-x, 1/2+y, -z)$.

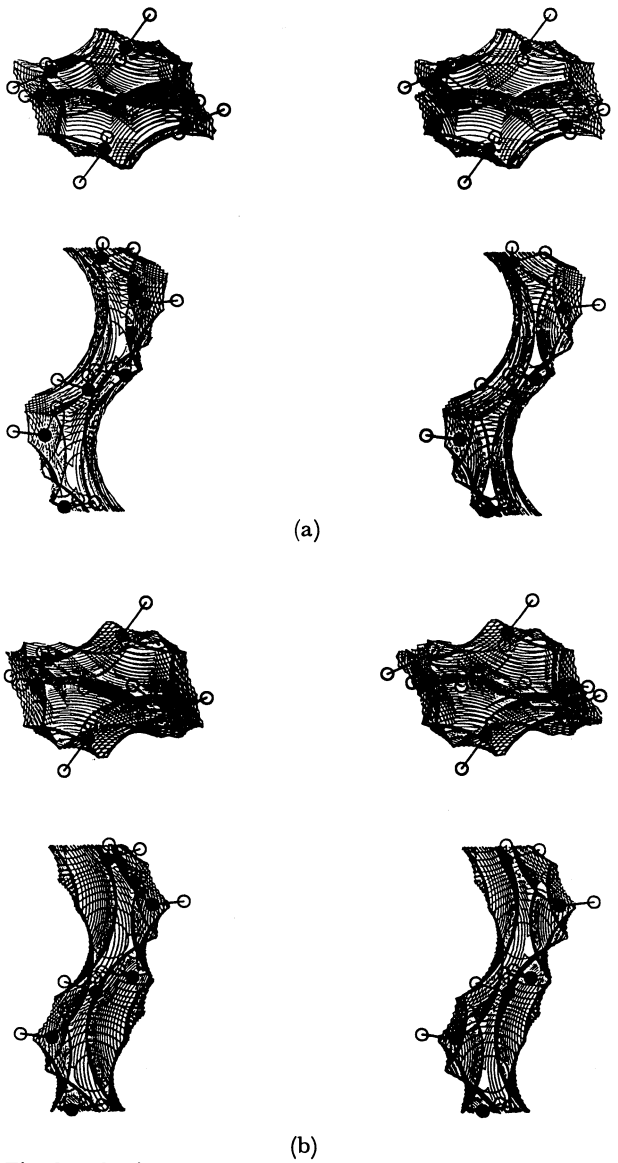

Fig. 3. Cavity for three water molecules viewed along **b** (upper) and **a** (lower), a) when the hydroxyl group of serine takes the site A, b) when the hydroxyl group of serine takes the site B.

Details of these hydrogen bonds are listed in Table 2.

In order to clarify the feature of arrangement of three water molecules, we have drawn the "cavity" for waters, which is defined as a closed space in which the atomic centres of the occluded molecules can be situated (for details of the cavity, see Ref. 12). Taking into account the hydrogen bond formation between water and its surrounding molecules, the radii allotted for hydrogen bond donor and acceptor atoms, O and N, were assumed to be 2.70 and 2.85 Å, respectively (hydrogen atoms attached to these atoms are neglected). Figure 3 shows the cavity viewed along the a and b axes, where the positions of the three water molecules are indicated. As seen from Fig. 3a, the oxygen atoms of water, consisting a triangle, fit very well with the cavity. Hydrogen atoms of water may protrude from the cavity, because the radii of O and N are taken as hydrogen bond distances. Figure 3b indicates the cavity for the case in which the

serine hydroxyl group takes a site with low occupancy. The fit of the water triangle into the cavity is also good. Disordering of serine O(13) gives rise to a slight change for the shape of the cavity, but this does not affect the position and orientation of the triangle. The cavity in the crystal of Cu(ala his) was also drawn, and the shape is nearly the same as that in the present case.

The volumes of the cavities were calculated in the way proposed in the previous paper[12] to be 12.94 Å^3 for the present complex and 17.22 Å^3 for Cu(ala his). The larger cavity of the latter allows the disordering of three water molecules, as discussed in Ref. 7.

Since the side chain of alanine is hydrophobic, while that of seine is hydrophilic, one might expect different crystal structures for Cu(ala his) and Cu(his ser). It is interesting that completely the same building principle applies to those two ternary complexes, perhaps owing to the common chelating mode of the mixed amino acids.

The authors are grateful to Professor Akitsugu Nakahara, Osaka University, for a gift of the sample, to Mr. Taizo Ono in our laboratory for the successful growth of the present crystal, and to Mr. Akira Uchida in our laboratory for drawing the cavities.

References

1) B. Sarkar and T. P. A. Kruck, "The Biochemistry of Copper," ed by J. Peisach, P. Aisen, and W. E. Blumberg, Academic Press, New York (1966), p. 183.

2) P. Z. Neumann and A. Sass-Kortsak, *J. Clin. Invest.*, **46**, 646 (1967).

3) P. M. May, P. W. Linder, and D. R. Williams, *J. Chem. Soc., Dalton Trans.*, **1977**, 588.

4) R. P. Agarwal and D. D. Perrin, *J. Chem. Soc., Dalton Trans.*, **1975**, 268.

5) H. C. Freeman, J. M. Guss, M. J. Healy, R. P. Martin, C. E. Nockolds, and B. Sarkar, *Chem. Commun.*, **1967**, 225.

6) T. Ono, H. Shimanouchi, Y. Sasada, T. Sakurai, O. Yamauchi, and A. Nakahara, *Bull. Chem. Soc. Jpn.*, **52**, 2229 (1979).

7) T. Ono and Y. Sasada, *Bull. Chem. Soc. Jpn.*, **54**, 90 (1981).

8) "International Tables for X-Ray Crystallography," The Kynoch Press, Birmingham (1974), Vol. IV, p. 72.

9) Tables of anisotropic thermal parameters for non-hydrogen atoms, of coordinates and temperature factors for hydrogen atoms, and of the observed and calculated structure factors are kept in the office of the Chemical Society of Japan (Document No. 8318).

10) "Lange's Handbook of Chemistry," Eleventh ed, ed by J. A. Dean, McGraw-Hill, New York (1972), p. 5—37.

11) H. C. Freeman, *Adv. Protein Chem.*, **22**, 257 (1967).

12) Y. Ohashi, A. Uchida, Y. Sasada, and Y. Ohgo, *Acta, Crystallogr., Sect. B*, **39**, 54 (1983).

 © 1983 The Chemical Society of Japan Bull. Chem. Soc. Jpn., 56, 1749—1752 (1983)

The Osmotic and Activity Coefficients of Quaternary Phosphonium Halides in Aqueous Solutions at Freezing Point

Toshiki WAKABAYASHI* and Katsuko TAKAIZUMI
The College of General Education, Tohoku University, Kawauchi, Sendai 980
(Received December 2, 1982)

The osmotic and activity coefficients have been obtained cryoscopically for $(n\text{-Bu})_{4-n}\text{Ph}_n\text{PX}$($n$=0—4, X=Cl, Br) in aqueous solutions at freezing point. The $\gamma_\pm$ decreases with increasing n, for both the chloride and the bromide salts. With the chloride salts, $\gamma_\pm$'s for the salts of n from 0 to 2 show positive deviation from the Debye-Hückel limiting law as concentration increases, whereas $\gamma_\pm$'s for others show negative deviation. Replacement of the anion from Cl^- to Br^- results in lower $\gamma_\pm$'s for the salts of n from 0 to 2, but this elevates the other $\gamma_\pm$'s. These results were interpreted qualit tively in terms of the cosphere overlap model by Desnoyers *et al.*, by assuming a hydrophilic character of the present phenyl group. An attempt was made to evaluate the pairwise interaction coefficients(B^*) and to estimate the contributions to B^* from the interactions, butyl-Cl^- and phenyl-Cl^-.

This paper is part of a continuing study of the thermodynamic properties of aqueous solutions of the quaternary phosphonium halides, $(n\text{-Bu})_{4-n}\text{Ph}_n\text{PX}$($n$=0—4). Since their molal volumes are nearly the same[1,2] we can expect that the size effect of the cations on the solvent water would be commom and the changes with n in their partial molal thermodynamic quantities would reflect directly the effects arising from the systematic variation in the state of cosphere water around the cation.

The activity coefficients of $(C_6H_5)_4MX$ (M=P, As, and Sb) in water at 37 °C were reported by Kalfoglou and Bowen,[3] these values are much lower than those of the usual 1 : 1 electrolytes. The authors attributed the low $\gamma_\pm$'s to the structure-breaking effects of the phenyl groups on the water structures. On the other hand the activity coefficients of tetraalkylammonium chlorides and bromides,[4,5] the higher members of which are known as typical structure-makers, are higher than that given by the Debye-Hückel limiting law. Thus, it is of interest to examine the variation of the osmotic(ϕ) and activity($\gamma_\pm$) coefficients of the present phosphonium halides with successive replacement of the butyl groups of the $n\text{-Bu}_4\text{P}^+$ ion by phenyl groups, this procedure provides an opportunity to test the group contribution to ϕ and $\gamma_\pm$. Also, the concentration dependences of ϕ's and $\gamma_\pm$'s will offer information about the pairwise interactions between each hydrocarbon cosphere and anions as well as those between the hydrocarbon cospheres.

Here, the cryoscopic method is employed to obtain the osmotic and activity coefficients.

Experimental

The phosphonium halides used for the freezing point measurements, $(n\text{-Bu})_{4-n}\text{Ph}_n\text{PX}$($n$=0—4, X=Cl, Br), were synthesized from the phosphines, except for the Ph_4PCl, which was a commercial product (DOTITE). The methods for synthesizing and purifying the salts were almost the same as those reported previously.[1] The sodium chloride delivered from Merck (Suprapur) was used for calibration of a thermistor, after drying. Solutions were prepared with conductivity-grade water by weight and buoyancy corrections were applied.

Cooling curves were obtained on a thermistor-differential amplifier-recorder system, which is essentially the same as that devised by Takahashi *et al.*[6] A sample solution was cooled at a rate of about 0.1 K min^{-1} or less; it was stirred constantly by a magnetic stirrer (1500 min^{-1}) in a Dewar-type cell of about 10 cm^3 inner-capacity, equipped with a rodtype thermistor. The cell was immersed in a cooling bath, the temperature of which was maintained lower by about 10K than the freezing point of the solution. Freezing was initiated by mechanical vibration of the cell assembly if super-cooling of the solution continued even at a temperature lower than the freezing point by 1 K or more. The freezing point was determined, as usual, by extrapolation of the linear part of the cooling curve to the point where the freezing would begin without the supercooling. The electric resistance of the thermistor was about 34 kΩ at 0 °C and the d.c. current which passed was regulated to be about 10 μA. Thus, the Joule's heat evolved is about 0.34 μJ s^{-1} which would hardly affect the temperature measurement under the experimental conditions. The thermistor was standardized against the freezing points of a series of aqueous solutions of sodium chloride, twelve solutions over a concentration range of 0.005 to 1.1 mol kg^{-1}, for which accurate data have been reported by Scatchard and Prentiss.[7]

The thermistor resistance was fitted to this equation as a function of T:

$$\log R = \log R^\circ + b(1/T - 1/T^\circ) + c(1/T - 1/T^\circ)^2,$$

where T° is 273.15 K and R° is the resistance at T°; the parameters b and c were determined by the least-squares method to fit the observed resistances to the freezing points of the aq eous sodium chloride solutions, with a standard deviation, 3×10^{-5}, in log R. The temperature coefficient of the thermistor was about -1.3 kΩ K^{-1}, which enabled us to attain a resolution of 1×10^{-4} K by amplifying. The reproducibility of the freezing point measurements for conductivity-grade water and dilute solutions was within 3×10^{-4} K provided that the stirring was steady and that the reference (R_{ref}) and standard (R_{st}) resistors, decade-types of six figures, were set in a thermostat bath (35±.2 °C), as was the case of the present measurement. Each cooling curve was always preceded and followed by the measurements for the couple, R_{st}-R_{ref}, to compare with the couple, $R_{thermistor}$-R_{ref}. This procedure enables us to eliminate any drift in the recorder or in the amplifier. No aging effect of the thermistor was found, within experimental reproducibility, as confirmed by occasional measurements for the freezing point of pure water.

Results and Discussion

The Lewis-Randall function, j, was obtained from the freezing point depression, θ, by the equation:[8]

TABLE 1. VALUES OF j-FUNCTIONS FOR n-$Bu_{4-n}Ph_nPX$ IN AQUEOUS SOLUTIONS

Molality	j	Molality	j
n-Bu_4PCl		n-Bu_4PBr	
0.00251	0.0164	0.00501	0.0270
0.00657	0.0250	0.01497	0.0527
0.01496	0.0339	0.02455	0.0560
0.04011	0.0458	0.03483	0.0672
0.06716	0.0502	0.05603	0.0816
0.1018	0.0519	0.06497	0.0842
0.1462	0.0517	0.07407	0.0996
0.1991	0.0499	0.08493	0.0979
n-Bu_3PhPCl		n-Bu_3PhPBr	
0.00559	0.0254	0.00633	0.0366
0.01325	0.0356	0.01450	0.0511
0.02344	0.0488	0.03215	0.0696
0.05512	0.0677	0.03401	0.0732
0.09793	0.0820	0.07890	0.1134
0.1478	0.0904	0.1439	0.1597
0.2173	0.1017	0.2338	0.2048
0.2954	0.1076	0.3391	0.2459
0.4006	0.1121	0.4490	0.2822
0.4856	0.1161	0.5533	0.3110
0.6466	0.1127	0.6513	0.3368
0.8068	0.1104	0.7594	0.3646
1.045	0.0993	0.8606	0.3860
1.251	0.0889		
n-Bu_2Ph_2PCl			
0.01363	0.0405	0.4135	0.2198
0.03263	0.0588	0.4791	0.2332
0.04074	0.0704	0.5175	0.2440
0.05587	0.0809		
0.05862	0.0831	n-Bu_2Ph_2PBr	
0.1035	0.1110	0.00516	0.0248
0.1557	0.1336	0.00771	0.0359
0.1606	0.1359	0.01008	0.0370
0.1970	0.1481	0.02419	0.0556
0.2688	0.1723	0.04597	0.0903
0.3620	0.2024	0.07544	0.1120
n-$BuPh_3PCl$		n-$BuPh_3PBr$	
0.01020	0.0432	0.00514	0.0279
0.02037	0.0614	0.00731	0.0313
0.04001	0.0865	0.01499	0.0482
0.06872	0.1162	0.01921	0.0528
0.1158	0.1580	0.02514	0.0649
0.1661	0.2020	0.03088	0.0739
0.2400	0.2614		
Ph_4PCl		Ph_4PBr	
0.00322	0.0272	0.00566	0.0281
0.00645	0.0364	0.00778	0.0367
0.01429	0.0590	0.00964	0.0375
0.02512	0.0780	0.01154	0.0427
0.03514	0.0956	0.01528	0.0536
0.05401	0.1258		
0.06962	0.1525		

TABLE 2. COEFFICIENTS OF j-FUNCTION (Eq. 2)

Salt	a_0	a_1	a_2	σ[a]	B^*[b]
n-Bu_4PCl	2.154	−0.1918	0.05975	0.0004	0.872
n-Bu_3PhPCl	1.350	−0.02855	−0.02804	0.0015	0.467
n-Bu_2Ph_2PCl	1.226	0.1958		0.0022	0.231
n-$BuPh_3PCl$	−0.592			0.0020	−0.194
Ph_4PCl	−1.336			0.0031	−0.437
n-Bu_4PBr	0.326			0.0042	0.107
n-Bu_3PhPBr	−0.124			0.0066	−0.041
n-Bu_2Ph_2PBr	−0.288			0.0036	−0.094
n-$BuPh_3PBr$	−0.444			0.0019	−0.145
Ph_4PBr	−0.724			0.0021	−0.237

a) The standard deviation between the observed and reproduced j-values. b) The coefficient given by Eq. 7 multiplied by 0.4343.

$$j = 1 - \theta/(\lambda\nu m), \tag{1}$$

where λ is the molal lowering of the freezing point of water, 1.860 K mol^{-1} kg, and ν the number of moles of ions formed from 1 mol of electrolyte (*i.e.*, 2 for the present case). The error in j comes mostly from the error in θ and becomes increasingly large as concentration decreases; it amounts to 0.016 due to an error in θ, 3×10^{-4} K, for solution of 5×10^{-3} mol kg^{-1} which was the lowest concentration in the present measurements. The values of j listed in Table 1 are the average values from several measurements for each solution of low concentrations (below 0.1 mol kg^{-1}) and from triple measurements for solutions of higher concentrations.

An empirical form for the j-function was assumed:

$$j = \frac{Am^{1/2}}{1+a_0m^{1/2}} + a_1m + a_2m^2, \tag{2}$$

where A is the Debye-Hückel limiting slope, 0.377 $mol^{-1/2}$ $kg^{1/2}$, and other parameters, a_i, were adjusted to fit the observed j values by the least-squares method. The parameters determined for the n-$Bu_{4-n}Ph_nPX$ salts are summarized in Table 2, where the standard deviations between the observed and reproduced j values are also listed.

The activity coefficients were calculated by the equation:

$$\ln\gamma_\pm = -j - \int_0^m j\,d\ln m + \xi\int_0^\theta \frac{\theta}{\nu m}d\theta, \tag{3}$$

where the last term including $\xi(0.00054)$[8] contributes hardly at all to $\ln\gamma_\pm$, *i.e.*, only a few units in the fourth decimal of $\ln\gamma_\pm$, and was neglected here. Placing Eq. 2 into Eq. 3 and integrating, we obtain the relation:

Table 3. Osmotic coefficients and activity coefficients of n-$Bu_{4-n}Ph_nPX$ in aqueous solutions at freezing point

Molality	ϕ	$\log\gamma_\pm$	Molality	ϕ	$\log\gamma_\pm$
	n-Bu_4PCl			n-Bu_4PBr	
0.01	0.971	−0.041	0.01	0.963	−0.048
0.02	0.963	−0.055	0.02	0.949	−0.067
0.05	0.952	−0.076	0.04	0.929	−0.094
0.1	0.948	−0.093	0.06	0·914	−0.114
0.2	0.950	−0.108	0.08	0.902	−0.131
	n-Bu_3PhPCl			n-Bu_3PhPBr	
0.02	0.956	−0.061	0·01	0.962	−0.049
0.05	0.937	−0.091	0.02	0.946	−0.070
0.1	0.920	−0.120	0.05	0.913	−0.112
0.2	0.902	−0.154	0.1	0.876	−0.159
0.5	0.885	−0.205	0.2	0.821	−0.228
1	0.896	−0.234	0.5	0.708	−0.369
1.2	0.908	−0.236	0.8	0.621	−0.475
	n-Bu_2Ph_2PCl			n-Bu_2Ph_2PBr	
0.01	0.964	−0.047	0.01	0.961	−0.050
0.02	0.951	−0.066	0·02	0.944	−0.071
0.05	0.924	−0.102	0.04	0.920	−0.102
0.1	0.894	−0.142	0.06	0.901	−0.126
0.2	0.852	−0.198	0.08	0.884	−0.147
0.5	0.759	−0.314			
	n-$BuPh_3PCl$			n-$BuPh_3PBr$	
0.01	0.960	−0.051	0.005	0.972	−0.035
0.02	0.942	−0.074	0.01	0.960	−0.051
0.05	0.903	−0.121	0.02	0.943	−0.072
0.1	0.853	−0.178	0.03	0.929	−0.090
0.2	0.771	−0.270			
	Ph_4PCl			Ph_4PBr	
0.01	0.956	−0.054	0.005	0.972	−0.036
0.02	0.934	−0.080	0.01	0.959	−0.052
0.04	0.897	−0.121	0.02	0.941	−0.075
0.06	0.863	−0.157			

$$-\ln\gamma_\pm = \frac{Am^{1/2}}{1+a_0m^{1/2}} + \frac{2A}{a_0}\ln(1+a_0m^{1/2}) + 2a_1m + \frac{3}{2}a_2m^2. \quad (4)$$

In Table 3, the osmotic coefficients ϕ and the activity coefficients $\log\gamma_\pm$ are listed. The present results are, as a whole, accompanied by errors of a few units in the third decimal place of j and are considered to be preliminary ones, especially with the bromide salts, mainly because the measurements for them were confined to low concentration ranges owing to their limited solubilities.

The mean chemical potential for an electrolyte may be described by:[9]

$$\mu_\pm = \mu_\pm^\circ + RT\ln c + Sc^{1/2} + RT[B_2(\kappa)c + B_3(\kappa)c^2 + \cdots], \quad (5)$$

where the coefficient S is given by the Debye-Hückel limiting law. According to Friedman and Krishnan,[9] $B_2(\kappa)$ reflects mainly the effects arising from the pairwise interactions between ions due to the short-range focres, though it depends also on the ionic strength through the Debye κ, and is decomposed into three contributions

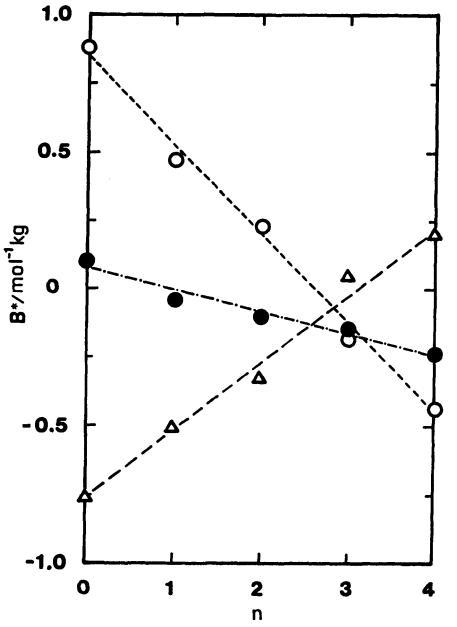

Fig. 1. The B^* coefficient and the difference between the bromide salts and the chloride salts, ΔB^*, as functions of the number of phenyl groups on the cation, n.
---○---, B^*(chloride); -·-●-·-, B^*(bromide); --△--, ΔB^*.

from the pairwise ionic interactions, ++, +−, and −−. For a 1 : 1 electrolyte it can be expressed as

$$B_2(\kappa) = \frac{1}{4}[B_{++}(\kappa) + 2B_{+-}(\kappa) + B_{--}(\kappa)]. \quad (6)$$

Expanding Eq. 4 into polynomial of $m^{1/2}$, we obtain the equation,

$$\ln\gamma_\pm = -Am^{1/2} + Bm + Cm^{3/2} + \cdots,$$

where the first term of the right hand side is the Debye-Hückel limiting term and the coefficient B is given by,

$$B = 2(Aa_0 - a_1). \quad (7)$$

In the last column of Table 2, the values for B^* which is the B coefficient for $\log\gamma_\pm$, *i.e.*, 0.4343 B, are listed. The B^* coefficients may be assumed, as a first approximation, to be proportional to $B_2(\kappa)$, since in dilute solutions the excess part of $\ln\gamma^\pm$ from the Debye-Hückel limiting law would mainly originate from pairwise interactions between ions due to short-range forces and the difference between the two concentration scales is negligible.

The B^*'s for the salts and the differences in B^* between the bromide and chloride salts, ΔB^*, are shown as functions of n in Fig. 1. Some features are to be noted: 1 the B^*, and hence $\log\gamma_\pm$, decreases successively with increasing n for both the chloride and bromide salts, 2) the n dependence of B^* is marked with the chloride salts, while it is not marked with the bromide salts, and 3) the ΔB^* is negative for Bu_4PX, while it is positive for Ph_4PX; those for the intermediate salts appear to distribute between these two ΔB^*'s. Qualitatively, these features are explicable by the structural

hydration interaction model proposed by Desnoyers *et al.*,[10] if the phenyl groups in the present cations are assumed to be hydrophilic rather than hydrophobic, as suggested by Kalfoglou and Bowen[3] and from the volumetric studies.[2,11] In their model, the interactions between ions are classified into four types based on a qualitative consideration about the states of water in the cosphere overlap region: hydrophobic-hydrophobic-(I), hydrophobic-hydrophilic(II), hydrophilic-hydrophilic (ions with opposite charge (III), and hydrophilic-hydrophilic (ions with the same charge) (IV). The contributions to the excess partial molal Gibbs free energy $\bar{G}^{ex}$, and hence also to B_2, are negative for the interactions I and III and positive for those II and IV. This leads to the sign assignment for B_{ij}: for Bu_4PX, $B_{++}<0$ and $B_{+-}>0$, and for Ph_4PX, $B_{++}>0$ and $B_{+-}<0$. Since for each of the two salts the sign of B^* is the same as that of B_{+-}, it comes to be that the cation-anion interactions are dominant for both the cations among the ion-ion interactions $++$, $+-$, and $--$. The chloride ion may be more hydrophilic than the bromide ion in the sense that the former ion is more effective in electrostrictive hydration and B_{+-} for Bu_4PCl would be more positive than that for Bu_4PBr, while the reverse would be true for the Ph_4P^+ ion, *i.e.*, B_{+-} for Ph_4PCl would be more negative than that for Ph_4PBr. The hydrophilic character assumed for the present phenyl groups would be caused by a rather large polarizability due to the π electrons and delocalized charges on them induced by the large electronegativity of $P(V)^+$, as revealed by an NMR study.[12]

With the intermediate cations ($n=1$—3), the opposite effects due to the interactions, butyl-X^- and phenyl-X^-, appear to successively cancel each other, suggesting that the cosphere around each group is affected only weakly by the nearest groups on the same cation. A similar result has been obtained from the volume studies.[2,11]

As examined in the volume studies, the B^* would also be expressed as a quadratic equation of n, if the contribution from the cation-cation interactions are of considerable importance. Although the present results are not accurate enough to discuss the B^*_{++} values the B^* for the chloride salts seems to be a linear function of n. If this is the case, this means that the B^* coefficients are nearly equal to $(1/2)B^*_{+-}$'s (Eq. 6) and hence we can split the contributions, butyl-Cl^- and phenyl-Cl^-. Roughly, they may be given from the B^*'s for Bu_4PCl and Ph_4PCl by dividing $2B^*$ by four, and neglecting B^*_{++} and B^*_{--}, that is, about 0.4 and -0.1 mol^{-1} kg, respectively.

In conclusion, two points are to be noted: First, the present and previous[2,11] results seem to support a simple assumption that the state of cosphere water around any group on the present cations is independent of the nearest groups on the same cation and each of group cospheres(i) interacts with another cosphere(j) around a simple anion or group on another cation with a relative probability proportional to the concentration product, c_ic_j, in dilute solutions. A similar assumption has been used by Wood *et al.*[13,14] for predicting pairwise interaction enthalpies and free energies of nonelectrolytes in dilute aqueous solutions. Applying the Wood method, Visser *et al.*[15] have estimated the enthalpy parameter for the pairwise interaction between the methylene group on tetraalkylammonium ions and the bromide ion. Second, the cosphere overlap model by Desnoyers *et al.*, which is somewhat different from that used by Friedman and his coworkers[16,17] and Streng and Wen,[18] seems to be reasonable and useful to interpret qualitatively ion-ion interactions in aqueous solutions, though the model would be limited to qualitative use until our knowledge on the structures around various ions as well as those of pure water would become more profound.

References

1) K. Takaizumi and T. Wakabayashi, *J. Solution Chem.*, **9**, 809 (1980).
2) T. Wakabayashi and K. Takaizumi, *J. Solution Chem.*, **11**, 565 (1982).
3) G. Kalfoglou and L. H. Bowen, *J. Phys. Chem.*, **73**, 2728 (1969).
4) S. Lindenbaum and G. E. Boyd, *J. Phys. Chem.*, **68**, 911 (1964).
5) S. Lindenbaum, L. Leifer, G. E. Boyd, and J. W. Chase, *J. Phys. Chem.*, **74**, 761 (1970).
6) K. Takahashi, S. Katayama, and R. Tamamushi, *Rep. Inst. Phys. Chem. Res.*, **49**, 13 (1973).
7) G. Scatchard and S. S. Prentiss, *J. Am. Chem. Soc.*, **55**, 4355 (1933).
8) R. A. Robinson and R. H. Stokes, "Electrolyte Solutions," 2nd ed, Butterworths, London (1970), Chap. 8.
9) H. L. Friedman and C. V. Krishnan, "Water," ed by F. Franks, Plenum Press, New York (1973), Vol. 3, Chap. 1.
10) J. E. Desnoyers, M. Arel, G. Perron, and C. Jolicoeur, *J. Phys. Chem.*, **73**, 3346 (1969).
11) K. Takaizumi and T. Wakabayashi, *Bull. Chem. Soc. Jpn.*, in press.
12) S. O. Gim and W. McFarlane, *Can. J. Chem.*, **46**, 2071 (1968).
13) J. J. Savage and R. H. Wood, *J. Solution Chem.*, **5**, 733 (1976).
14) I. R. Tasker and R. H. Wood, *J. Phys. Chem.*, **86**, 4040 (1982) and references cited there.
15) C. de Visser, W. J. M. Heuvelsland, and G. Somsen, *J. Solution Chem.*, **7**, 193 (1977); *J. Chem. Soc., Faraday Trans.*, **76**, 901 (1980).
16) P. S. Ramanathan and H. L. Friedman, *J. Chem. Phys.*, **54**, 1086 (1971).
17) P. S. Ramanathan, C. V. Krishnan, and H. L. Friedman, *J. Solution Chem.*, **1**, 237 (1972).
18) W. H. Streng and W. Y. Wen, *J. Solution Chem.*, **3**, 865 (1974); W. Y. Wen, *ibid.*, **2**, 253 (1973).

 © 1983 The Chemical Society of Japan Bull. Chem. Soc. Jpn., 56, 1753—1760 (1983)

Structure of the Electrical Double Layer at the Interface between Nitrobenzene Solution of Tetrabutylammonium Tetraphenylborate and Aqueous Solution of Lithium Chloride

Takashi KAKIUCHI and Mitsugi SENDA*

Department of Agricultural Chemistry, Faculty of Agriculture, Kyoto University, Sakyo-ku, Kyoto 606

(Received December 22, 1982)

Electrocapillary curves at the polarized interface between a nitrobenzene solution of tetrabutylammonium tetraphenylborate (TBATPB) and an aqueous solution of lithium chloride at various concentrations of TBATPB and LiCl have been measured by the drop time method using a dropping electrolyte solution electrode at 25 °C. The relative surface excesses of tetrabutylammonium and tetraphenylborate ions in the nitrobenzene phase and of lithium and chloride ions in the aqueous phase were well described by the Gouy-Chapman theory of diffuse layers for both sides of the interface. A model of the electrical double layer for the nitrobenzene–water interface is presented, in which an ion-free inner layer consisting of laminated monolayers of water and nitrobenzene is sandwiched by the two diffuse layers on each side of the interface. The potential difference across the inner layer, which was estimated to be *ca.* 20 mV at the potential of zero charge, was found to be dependent on the surface charge density and to be nearly independent of the electrolyte concentration.

In a previous paper[1] we have reported the experimental conditions under which the interface between a nitrobenzene solution of tetrabutylammonium tetraphenylborate (TBATPB) and an aqueous solution of lithium chloride behaves as a polarized interface. Such an interface is amenable to a study of its double structure based on the thermodynamics of an ideal polarized interface between two immiscible electrolyte solutions. Watanabe *et al.*[2] first applied the concept of ideal polarizability to the oil–water interfaces in order to analyze their double layer structure. At such interfaces, however, there always existed a significant amount of ion transfer current through the interface, so that the precise control of the electrical potential difference across the interface was not achieved. Gavach *et al.*[3,4] have studied the double layer structure of the non-polarized nitrobenzene–water interfaces by surface tension measurements. They have shown that the Gouy-Chapman theory of diffuse double layers well describes their experimental results when no specific adsorption of ions at the interface was assumed. In a non-polarized interface, however, the specific adsorption of ions cannot be detected from the electrocapillary measurements, since the surface charge density and surface excesses of ions cannot be independently determined.

In this paper, we describe the results of the experimental study of the double layer structure at the polarized interface between a nitrobenzene solution of TBATPB and an aqueous solution of LiCl on the basis of the electrocapillary measurements and we present an electrical double layer model of the interface. Electrocapillary curves of a polarized interface, in conjunction with the thermodynamics of ideal polarized interface between two immiscible electrolyte solutions[5] and with the Gouy-Chapman theory of electrical double layer, provide us an unequivocal way to examine the adsorption of ions at the interface by determining the surface charge density and surface excesses of individual ionic species.

Experimental

The interfacial tension at the polarized interface between the nitrobenzene solution of TBATPB and the aqueous solution of LiCl was measured with the drop time method using a dropping electrolyte solution electrode.[1] The aqueous lithium chloride solution was dropped upward into the nitrobenzene solution from the tip of a poly(tetrafluoroethylene) capillary of 0.5 mm inner diameter. The flow rate of the aqueous solution and the drop time were typically 0.00036 ml s^{-1} and 50 s. The potential drop across the interface was controlled using a four-electrode potentiostat with a positive feedback device for IR compensation.[6] Details of the measurements and the calculation of the surface tension from the drop time have been reported elsewhere.[1] All the measurements were made at 25.00±0.05 °C in the dark.

TBATPB, tetrabutylammonium chloride (TBACl) and nitrobenzene were purified as described elsewhere.[1] Lithium chloride(spurapur grade, E. Merck) was dissolved into twice distilled water to prepare the stock solution. The concentration of LiCl was determined potentiometrically using a standard silver nitrate solution. Aqueous LiCl solutions of desired concentrations were prepared by serial dilution of the stock solution. Nitrobenzene solutions of TBATPB were prepared in the dark immediately before use.

Results

The electrochemical cell employed in this study is represented by

I	II	III	IV	V
Ag	AgCl	a mol dm^{-3} TBACl	b mol dm^{-3} TBATPB	c mol dm^{-3} LiCl
		(water)	(nitrobenzene)	(water)

VI	VII
AgCl	Ag.

(I)

The interface between phases IV and V is the polarized nitrobenzene–water interface which we are concerned with. The nitrobenzene–water interface between phases III and IV is a non-polarized interface where the potential drop across the interface is determined by the activities of TBA^+ ions in the phases III and IV.[7-9] The electrocapillary equation for the present system at constant temperature and pressure takes the form[5]

$$-d\gamma = q^{W}dE^{W}_{0^+} + \Gamma_{Li/W}d\mu_{LiCl} + \Gamma_{TPB/NB}d\mu_{TBATPB}, \quad (1)$$

where $\Gamma_{Li/W}$ and $\Gamma_{TPB/NB}$ are the relative surface concentrations (the relative surface excesses) of Li^+ and TPB^- ions defined by

$$\Gamma_{Li/W} = \Gamma_{Li} - \frac{x_{NB}^{NB}\Gamma_W - x_W^{NB}\Gamma_{NB}}{x_W^W x_{NB}^{NB} - x_W^{NB} x_{NB}^W} x_{LiCl}^W, \quad (2)$$

and

$$\Gamma_{TPB/NB} = \Gamma_{TPB} - \frac{x_W^W\Gamma_{NB} - x_{NB}^W\Gamma_W}{x_W^W x_{NB}^{NB} - x_W^{NB} x_{NB}^W} x_{TBATPB}^{NB}. \quad (3)$$

Here, γ is the interfacial tension, q^W the surface charge density in aqueous phase defined by $q^W = F(\Gamma_{Li} - \Gamma_{Cl})$, F being the Faraday. x_i^α, μ_i^α, and Γ_i denote the mole fraction, the chemical potential and the surface concentration (the amount of matter in unit area of the interphase),[10] respectively, of i component in α phase (α= NB : nitrobenzene or W : aqueous phase). E_{O+}^{W-} is the potential of the right hand side terminal of the cell (I) with respect to the left, and the subscript O+ and superscript W− on E indicate that the reference electrodes in the nitrobenzene and aqueos phases are reversible to a cation (TBA^+) and an anion (Cl^-), respectively. Since x_W^{NB} and x_{NB}^W are 0.0175 and 0.000295, respectively, for water and nitrobenzene in the absence of an electrolyte at 25 °C,[11] Eqs. 2 and 3 can be approximated by[12]

$$\Gamma_{Li/W} = \Gamma_{Li} - \frac{x_{LiCl}^W}{x_W^W}\Gamma_W, \quad (4)$$

and

$$\Gamma_{TPB/NB} = \Gamma_{TPB} - \frac{x_{TBATPB}^{NB}}{x_{NB}^{NB}}\Gamma_{NB}. \quad (5)$$

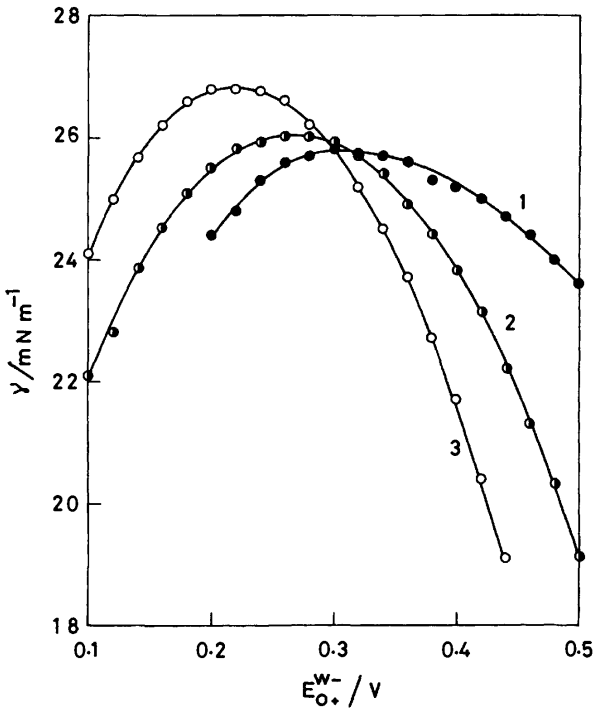

Fig. 1. Electrocapillary curves for the interface between nitrobenzene solution of 0.1 mol dm^{-3} tetrabutylammonium tetraphenylborate and aqueous solution of (1): 0.01, (2): 0.10, and (3): 1.00 mol dm^{-3} lithium chloride at 25 °C.

Table 1. Coordinates of electrocapillary maximum for the interface between nitrobenzene solution of 0.1 mol dm^{-3} tetrabutylammonium tetraphenylborate and aqueous solution of 0.01 to 1.0 mol dm^{-3} lithium chloride at 25 °C

c_{LiCl}^W / mol dm^{-3}	$a_{LiCl}^{\pm,W}$	γ_{pzc} / mN m^{-1}	E_{pzc} / V
0.01	0.009	25.8	0.309
0.02	0.017	25.7	0.289
0.05	0.041	25.8	0.278
0.10	0.079	26.0	0.265
0.20	0.151	26.2	0.245
0.50	0.369	26.5	0.227
1.00	0.776	26.8	0.217

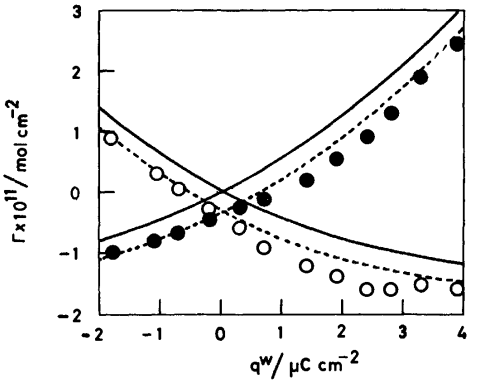

Fig. 2. Relative surface excesses of lithium ion (●) and chloride ion (○) in the aqueous phase as a function of the surface charge density in aqueous phase at 0.1 mol dm^{-3} lithium chloride. The solid lines are the theoretical curves based on Gouy-Chapman theory. Dashed lines are the curves corrected for the exclusion of lithium and chloride ions from the inner layer.

Aqueous Phase. Electrocapillary curves were measured for seven different concentrations of LiCl, c=0.01 to 1.00 mol dm^{-3}, at a=0.1 mol dm^{-3} and b= 0.1 mol dm^{-3} in the cell (I). Some of the results are shown in Fig. 1. The coordinates of the electrocapillary maximum are given in Table 1. The potential of zero charge, E_{pzc}, and the interfacial tension at the potential of zero charge, γ_{pzc}, were determined by a least square fit of an electrocapillary curve around the maximum to a third order polynomial. The mean molar ionic activity of LiCl, $a_{LiCl}^{\pm,W}$, in Table 1 was calculated from Davies' extended equation[13] of the Debye-Hückel theory for the concentrations below 0.1 mol dm^{-3} and was taken from the literature data[14] for the concentrations above 0.1 mol dm^{-3}.

Using Eq. 1, we obtained q^W by numerical differentiation of the electrocapillary curves with respect to E_{O+}^{W-}. $\Gamma_{Li/W}$ was calculated from numerical differentiation of γ *vs.* log $a_{LiCl}^{\pm,W}$ curves with respect to log $a_{LiCl}^{\pm,W}$. The relative surface excess of Cl^- ion, $\Gamma_{Cl/W}$, was evaluated by $q^W = F(\Gamma_{Li} - \Gamma_{Cl}) = F(\Gamma_{Li/W} - \Gamma_{Cl/W})$. Figure 2 shows $\Gamma_{Li/W}$ and $\Gamma_{Cl/W}$ for 0.1 mol dm^{-3} LiCl as a function of q^W.

Nitrobenzene Phase. Electrocapillary curves were measured for seven different concentrations of TBATPB

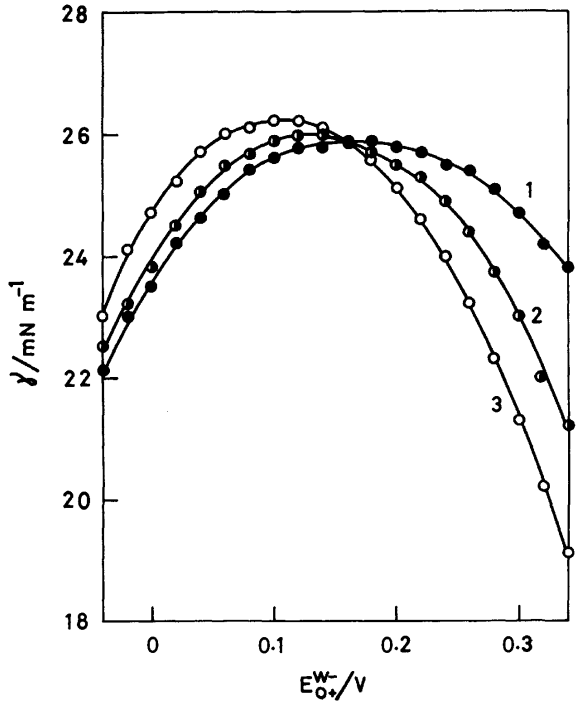

Fig. 3. Electrocapillary curves for the interface between aqueous solution of 0.1 mol dm^{-3} lithium chloride and nitrobenzene solution of (1): 0.02, (2): 0.05, and (3): 0.17 mol dm^{-3} tetrabutylammonium tetraphenylborate at 25 °C.

Table 2. Coordinates of electrocapillary maximum for the interface between aqueous solution of 0.1 mol dm^{-3} lithium chloride and nitrobenzene solution of 0.01 to 0.17 mol dm^{-3} tetrabutylammonium tetraphenylborate at 25 °C

c^{NB}_{TBATPB} / mol dm^{-3}	$a^{\pm,NB}_{TBATPB}$	γ_{pzc} / mN m^{-1}	E_{pzc} / V
0.01	0.008	25.9	0.167
0.02	0.014	25.9	0.153
0.03	0.021	26.0	0.142
0.05	0.033	26.0	0.131
0.07	0.044	26.0	0.129
0.10	0.061	26.1	0.122
0.17	0.099	26.3	0.108

in the nitrobenzene phase, b=0.01 to 0.17 mol dm^{-3}, at a=0.005 mol dm^{-3} and c=0.1 mol dm^{-3} in the cell (I). Some of the results are shown in Fig. 3. The concentration of TBACl in phase III in the cell (I) was kept at such a low value to ensure that the potential across the interface between the phases III and IV would show a Nernstian response for the activity of TBA$^+$ ion in the nitrobenzene phase[9] in the concentration range of TBATPB. Separate measurements showed that the potential of this reference electrode was 0.145 V more negative than that of the reference electrode with 0.1 mol dm^{-3} TBACl used in the measurements of ion adsorption in the aqueous phase.

The coordinates of the electrocapillary maximum are given in Table II. To check the degree of the association

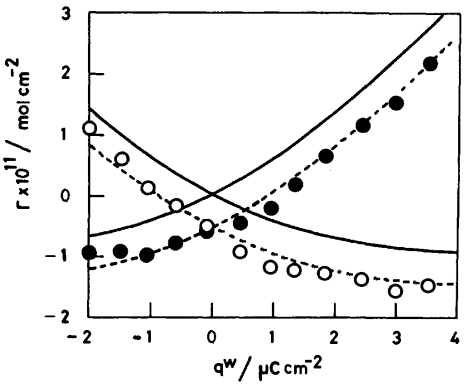

Fig. 4. Relative surface excesses of tetrabutylammonium (○) and tetraphenylborate (●) ions in the nitrobenzene phase as a function of the surface charge density in the aqueous phase at 0.1 mol dm^{-3} tetrabutylammonium tetraphenylborate.

of TBA$^+$ and TPB$^-$ ions in water-saturated nitrobenzene, the conductance of a series of the TBATPB solutions was measured. No indication of the association of the ions was observed in the concentration range used in the electrocapillary measurements. The mean molar ionic activity of TBATPB in the nitrobenzene phase was calculated using the Debye-Hückel theory allowing for a finite size of the ions;[14] here an apparent diameter, 10 Å, was assumed for TBA$^+$ and TPB$^-$ ions.[15] The surface charge density and relative surface excesses of TBA$^+$ and TPB$^-$ ions ($\Gamma_{TBA/NB}$ and $\Gamma_{TPB/NB}$) were calculated similarly. $\Gamma_{TBA/NB}$ and $\Gamma_{TPB/NB}$ at 0.1 mol dm^{-3} TBATPB are plotted against q_W in Fig. 4.

Discussion

We consider that the nitrobenzene–water interface consists of an inner layer which is sandwiched by the two diffuse double layers in the nitrobenzene and the aqueous solution sides.

Ion Adsorption in Aqueous Solution Side. The relative surface excess of Li$^+$ ions defined by Eq. 4 may be divided formally into two parts, that is, the relative surface excess in the inner layer, ${}^{i}\Gamma_{Li/W}$, and that in the diffuse layer, ${}^{d}\Gamma_{Li/W}$;

$$\Gamma_{Li/W} = {}^{i}\Gamma_{Li/W} + {}^{d}\Gamma_{Li/W}, \quad (6)$$

with

$${}^{i}\Gamma_{Li/W} = {}^{i}\Gamma_{Li} - \frac{x^{W}_{LiCl}}{x^{W}_{W}} {}^{i}\Gamma_{W}, \quad (7)$$

and

$${}^{d}\Gamma_{Li/W} = {}^{d}\Gamma_{Li} - \frac{x^{W}_{LiCl}}{x^{W}_{W}} {}^{d}\Gamma_{W}, \quad (8)$$

where ${}^{i}\Gamma_j$ and ${}^{d}\Gamma_j$ (j=Li for lithium ion and W for water) are the surface amounts of j in the inner layer and diffuse layer, respectively, per unit surface area. If we assume that the number of moles of water molecules per unit volume in the diffuse layer, ${}^{d}n^{W}_{W}$, is constant and equal to that in the bulk of the solution, ${}^{b}n^{W}_{W}$, we may write

$${}^{d}\Gamma_{Li/W} = \int_{x=x_2}^{x=\delta} ({}^{d}n^{W}_{Li} - {}^{b}n^{W}_{Li})dx, \quad (9)$$

where ${}^{d}n_{Li}^{W}$ and ${}^{b}n_{Li}^{W}$ are the number of moles of Li^+ ion per unit volume in the diffuse layer and that in the bulk of the solution, respectively, and the integration extends from the outer Helmholtz plane ($x=x_2$) to the boundary plane of the interphase ($x=\delta$) where the composition is identical with that of the bulk of the solution. Similarly, for a Cl^- ion we may write

$$\Gamma_{Cl/W} = {}^{i}\Gamma_{Cl/W} + {}^{d}\Gamma_{Cl/W}, \tag{10}$$

with

$${}^{i}\Gamma_{Ci/W} = {}^{i}\Gamma_{Ci} - \frac{x_{LiCi}^{W}}{x_{W}^{W}} {}^{i}\Gamma_{W}, \tag{11}$$

and

$${}^{d}\Gamma_{Ci/W} = {}^{d}\Gamma_{Ci} - \frac{x_{LiCl}^{W}}{x_{W}^{W}} {}^{d}\Gamma_{W}, \tag{12}$$

and also

$${}^{d}\Gamma_{Cl/W} = \int_{x=x_2}^{x=\delta} ({}^{d}n_{Ci}^{W} - {}^{b}n_{Ci}^{W})dx. \tag{13}$$

The relative surface excesses of Li^+ and Cl^- ions in the diffuse layer defined by Eqs. 8 and 12 can be calculated from the Gouy-Chapman theory and are given, respectively, by ${}^{d}\Gamma_{+}^{W}$ and ${}^{d}\Gamma_{-}^{W}$ as follows:

$${}^{d}\Gamma_{\pm}^{W} = \frac{A^W}{F}\left(\pm\frac{q^W - {}^{i}q^W}{2A^W} + \sqrt{\left(\frac{q^W - {}^{i}q^W}{2A^W}\right)^2 + 1} - 1\right). \tag{14}$$

Here, ${}^{i}q^W$ is the charge density in the inner layer of the aqueous solution side and $A^W=(2RT\varepsilon^W c_{LiCl}^{W})^{1/2}$, where ε^W is the permittivity of water and c_{LiCl}^{W} is the concentration of LiCl. When all the ions are excluded from the inner layer, *i.e.*, in the case of an ion-free inner layer or of no specific adsorption of ions, ${}^{i}\Gamma_{Li}$, ${}^{i}\Gamma_{Cl}$, and ${}^{i}q^W$ reduce to zero. The calculated ${}^{d}\Gamma_{\pm}^{W}$ *vs.* q^W curves when ${}^{i}q^W=0$, $c_{LiCl}^{W}=0.1$ mol dm^{-3} and $\varepsilon^W=6.5\times10^{-10}$ F m^{-1} are shown by solid lines in Fig. 2. We estimated ${}^{i}\Gamma_W$ to be 1.73×10^{-9} mol cm^{-2}, assuming that the density of water in the inner layer is equal to that in the bulk of water and that the inner layer has the thickness of a monomolecular layer of water. Thus, ${}^{i}\Gamma_{Li/W}={}^{i}\Gamma_{Cl/W}=-(x_{LiCl}^{W}/x_{W}^{W}){}^{i}\Gamma_W=-3.1\times10^{-12}$ mol cm^{-2} when $c_{LiCl}^{W}=0.1$ mol dm^{-3}. The dashed lines in Fig. 2 are the calculated curves of the relative surface excess of Li^+ and Cl^- ions obtained by shifting the solid lines by this amount of $-(x_{LiCl}^{W}/x_{W}^{W}){}^{i}\Gamma_W$. The experimental relative surface excesses agree fairly well with the calculated curves for both Li^+ and Cl^- ions. Thus, the results in Fig. 2 can reasonably be explained by assuming the existence of an ion free inner layer, *i.e.*, the absence of specific adsorption of ions, in the aqueous solution side of the interface.

The variation of γ_{pzc} with $\ln(a_{LiCl}^{\pm W})$ can be calculated from the integral form of Eq. 1:

$$\gamma_{pzc} = (\gamma_{pzc})_{c_{LiCl}^{W}=0.1} + 2RT\int_{\ln(0.079)}^{\ln(a_{LiCl}^{\pm W})} -(x_{LiCl}^{W}/x_{W}^{W}){}^{i}\Gamma_W d\ln(a_{LiCl}^{\pm W}), \tag{15}$$

when ${}^{i}\Gamma_{Li}={}^{i}\Gamma_{Ci}=0$ at the pzc. In Eq. 15 R and T have the usual meanings. The lower limit of the integration corresponds to $\ln(a_{LiCl}^{\pm W})$ at $c_{LiCl}^{W}=0.1$ mol dm^{-3}. The observed increase of γ_{pzc} with the increase in $\ln(a_{LiCl}^{\pm W})$ is well reproduced by Eq. 15, as shown in Fig. 5.

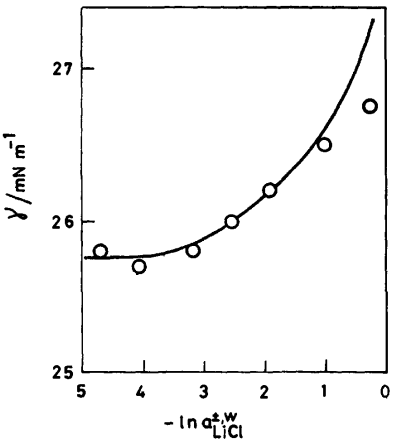

Fig. 5. Variation of interfacial tension at the potential of zero charge with the change of the activity of lithium chloride. Solid line is the calculated curve assuming the exclusion of lithium and chloride ions from the inner layer.

Figure 6 shows E_{0+}^{W-} values plotted against $\ln(a_{LiCl}^{\pm W})$ at several different q^W values. The slope of these plots, analogous to the Esin-Markov coefficient at the mercury-solution interface,[16] is given by

$$\left(\frac{\partial E_{0+}^{W-}}{\partial \ln(a_{LiCl}^{\pm W})}\right)_{q^W,\mu_{J\neq LiCi}} = -2RT \times\left[\left(\frac{\partial {}^{d}\Gamma_{Li/W}}{\partial q^W}\right)_{\mu_J} + \left(\frac{\partial {}^{i}\Gamma_{Li}}{\partial q^W}\right)_{\mu_J} - \frac{x_{LiCl}^{W}}{x_{W}^{W}}\left(\frac{\partial {}^{i}\Gamma_W}{\partial q^W}\right)_{\mu_J}\right]. \tag{16}$$

When both the presence of the ions in the inner layer and the dependence of ${}^{i}\Gamma_W$ on q^W are negligible, the coefficient is given by the first term of the right hand side of Eq. 16, which can be calculated from the Gouy-Chapman theory; from Eq. 14 we have

$$\left(\frac{\partial {}^{d}\Gamma_{Li/W}}{\partial q^W}\right)_{\mu_J} = \frac{1}{F}\left(1+\frac{q^W/2}{[(q^W/2)^2+(A^W)^2]^{1/2}}\right). \tag{17}$$

Therefore, in the case of the absence of specific absorption of ions, the coefficient is expected to become $-2RT/F$, $-RT/F$ and 0 when $q^W\gg0$, $q^W=0$, and $q^W\ll0$, respectively. The experimental plot at the pzc in Fig. 6 is a straight line with the slope of -23 mV which is close to $-RT/F=-25.6$ mV at 25 °C. The small difference might be attributable to a slight dependence of ${}^{i}\Gamma_W$ on q^W and/or a weak specific adsorption of ions in the inner layer. Figure 6 shows that the slope becomes larger with the positive increase of q^W, which is consistent with the prediction of Eq. 15.

We calculated the potential at the outer Helmholtz plane in the aqueous solution side (OHP(W)), ϕ_2^W, referred to the inner potential of the bulk of the aqueous solution, ϕ^W, by using the Gouy-Chapman theory:

$$\phi^W - \phi_2^W = \frac{2RT}{F}\sinh^{-1}[q^W/(2A^W)]. \tag{18}$$

In Fig. 7 $\phi^W-\phi_2^W$ is plotted against the rational potential,[17] $E_{0+}^{W-}-E_{pzc}$, at three different concentrations of LiCl. The variation of $\phi^W-\phi_2^W$ with $E_{0+}^{W-}-E_{pzc}$ is much smaller than those usually observed at the mercury-

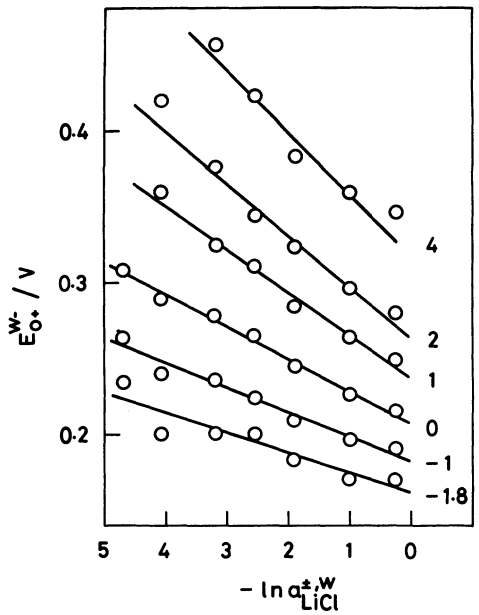

Fig. 6. Esin-Markov plots for aqueous solution phase in contact with nitrobenzene solution of 0.1 mol dm^{-3} tetrabutylammonium tetraphenylborate. The surface charge density in aqueous phase is indicated by each line in μC cm^{-2}.

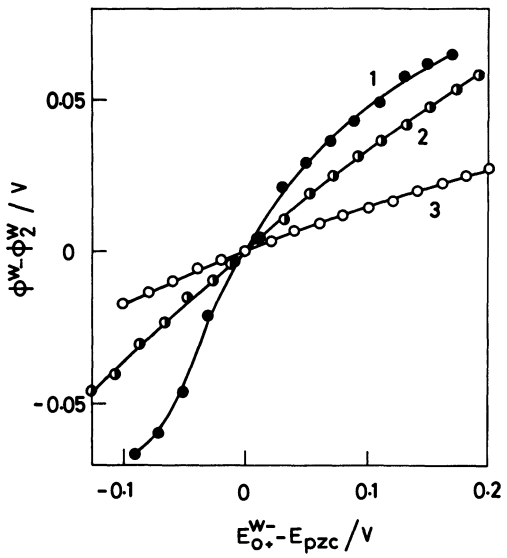

Fig. 7. Potential at the outer Helmholtz plane in aqueous solution side of the interface as a function of rational potential difference at (1): 0.01, (2): 0.1, and (3): 1.0 mol dm^{-3} lithium chloride.

aqueous solution interface in the absence of specific adsorption of ions.[18]

Ion Adsorption in Nitrobenzene Solution Side. The relative surface excesses of TBA^+ and TPB^- ions in the diffuse layer in the nitrobenzene solution side were calculated under the assumption of the ion-free inner layer from the Gouy-Chapman theory:

$$ {}^{d}\Gamma^{o}_{\pm} = \frac{A^{NB}}{F}\left[\mp\frac{q^{W}-{}^{i}q^{W}}{2A^{NB}}\sqrt{\left(\frac{q^{W}-{}^{i}q^{W}}{2A^{NB}}\right)^{2}+1}-1\right]. \quad (19) $$

In Eq. 19 ${}^{d}\Gamma^{o}_{+}$ and ${}^{d}\Gamma^{o}_{-}$ are the surface excesses of TBA^+ and TPB^- ions, respectively, in the diffuse layer,

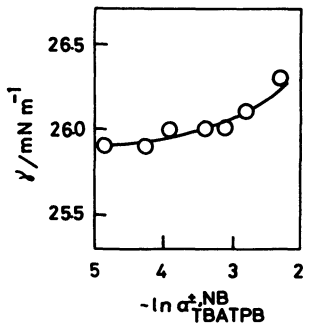

Fig. 8. Variation of interfacial tension at the potential of zero charge with the change of the activity of tetrabutylammonium tetraphenylborate. Solid line is the calculated curve assuming the exclusion of tetrabutylammonium and tetraphenylborate ions from the inner layer.

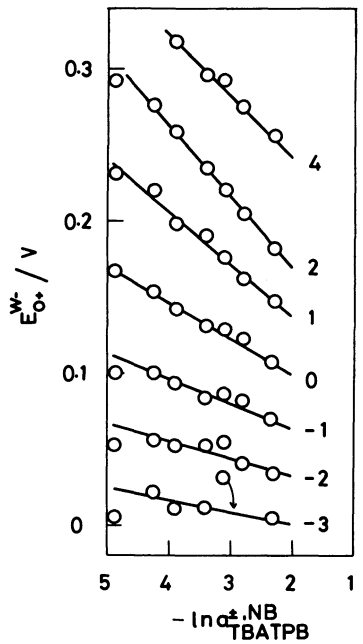

Fig. 9. Esin-Markov plots for nitrobenzene solution phase in contact with aqueous solution of 0.1 mol dm^{-3} lithium chloride. The surface charge density in aqueous phase is indicated by each line in μC cm^{-2}.

and $A^{NB}=(2RT\varepsilon^{NB}c^{NB}_{TBATPB})^{1/2}$ where ε^{NB} and c^{NB}_{TBATPB} are the permittivity of nitrobenzene and the concentration of TBATPB in the nitrobenzene phase. The solid lines in Fig. 4 are the curves calculated according to Eq. 19, when ε^{NB} and c^{NB}_{TBATPB} are 3.08×10^{-9} F m^{-1} and 0.1 mol dm^{-3}, respectively. The number of moles of nitrobenzene molecules in the inner layer per unit surface area was estimated to be 5.40×10^{-10} mol cm^{-2}. The dashed lines in Fig. 4 are the calculated curves corrected for the exclusion of ions from the inner layer. The curves well represent the experimental points, indicating that there exists a certain ion-free inner layer in the nitrobenzene solution side of the interface.

The change of γ_{pzc} with $\ln(a^{\pm,NB}_{TBATPB})$ was calculated from

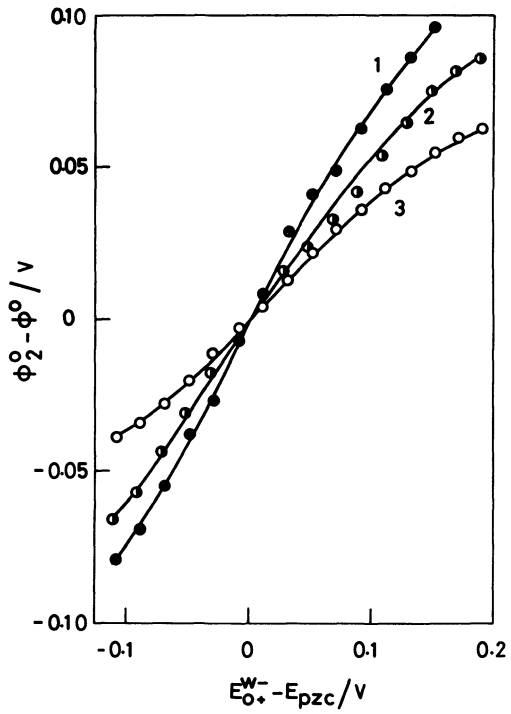

Fig. 10. Potential at outer Helmholtz plane in nitrobenzene solution side of the interface as a function of rational potential difference at (1): 0.02, (2): 0.05, and (3): 0.17 mol dm^{-3} tetrabutylammonium tetraphenylborate.

$$\gamma_{pzc} = (\gamma_{pzc})_{c_{TBATPB}^{NB}=0.1} + 2RT\int_{\ln(0.61)}^{\ln(a_{TBATPB}^{\pm,NB})} -(x_{TBATPB}^{NB}/x_{NB}^{NB})^{i}\Gamma_{NB}\,d\ln(a_{TBATPB}^{\pm,NB}). \quad (20)$$

The lower limit of the integration corresponds to $\ln(a_{TBATPB}^{\pm,NB})$ when $c_{TBATPB}^{NB}=0.1$ mol dm^{-3}. The calculated curve well reproduces the experimental data, as shown in Fig. 8.

The Esin-Markov plots at several constant q^W values for the nitrobenzene phase are shown in Fig. 9. The coefficient of the plot when ${}^{i}\Gamma_{TPB}=0$ (or $\partial^{i}\Gamma_{TPB}/\partial q^W=0$) and $\partial^{i}\Gamma_{NB}/\partial q^W=0$ is given, analogously to the case of the aqueous phase, by

$$\left(\frac{\partial E_{O+}^{W-}}{\partial \ln(a_{TBATPB}^{\pm,NB})}\right)_{q^W,\mu_{j\neq TBATPB}} = -2RT\left(\frac{\partial^{d}\Gamma_{TPB}}{\partial q^W}\right)_{\mu_j} = -\frac{RT}{F}\left(1+\frac{q^W/2}{[(q^W/2)^2+(A^{NB})^2]^{1/2}}\right). \quad (21)$$

Accordingly, the coefficient should reduce to $-2RT/F$, $-RT/F$, and 0 when $q^W \gg 0$, $q^W=0$, and $q^W \ll 0$, respectively. At the pzc, the experimental plot in Fig. 9 has the slope of -24 mV, which is close to $-RT/F=-25.6$ mV. The slope of the plots in Fig. 9 increases with the increase of q^W, which is consistent with the prediction of Eq. 21.

We calculated the potential at the outer Helmholtz plane in the nitrobenzene side (OHP(NB)), ϕ_2^0, referred to the inner potential in the bulk of the nitrobenzene phase, ϕ^0, by using the Gouy-Chapman theory:

$$\phi_2^0 - \phi^0 = \frac{2RT}{F}\sinh^{-1}[q^W/(2A^{NB})]. \quad (22)$$

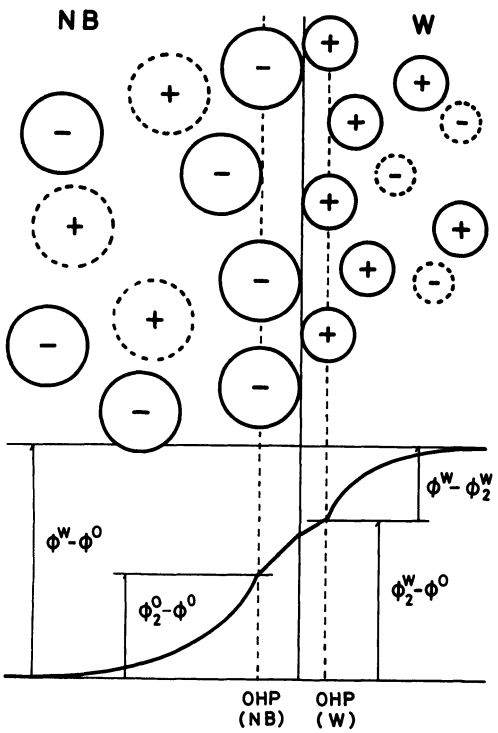

Fig. 11. Schematic representation of the double layer structure and potential profile of the interface between aqueous solution of lithium chloride and nitrobenzene solution of tetrabutylammonium tetraphenylborate.

The calculated values at three concentrations of TBATPB are plotted in Fig. 10.

Electrical Double Layer at Nitrobenzene–Water Interface. The above discussion shows that in the concentration range and the potential range studied, the adsorption of all the ions at the nitrobenzene–water interface primarily occurs in the diffuse parts of the double layer in both sides of the interface and that there exists an ion-free inner layer between the two diffuse layers. The double layer structure of the interface may then be schematically represented by Fig. 11.

The potential drop across the two inner layers, $\Delta\phi_{O2}^{W2}=\phi_2^W-\phi_2^{NB}$, can be expressed by

$$\Delta\phi_{O2}^{W2} = E_{O+}^{W-} - E_{pzc} - (\phi_2^0-\phi^0) - (\phi^W-\phi_2^W) + \Delta\phi_{O,pzc}^{W}, \quad (23)$$

where $\Delta\phi_{O,pzc}^{W}$ is the inner potential difference between the two phases, *i.e.*, $\Delta\phi_O^W=\phi^W-\phi^O$ at the pzc. The value of $\Delta\phi_{O2}^{W2}-\Delta\phi_{O,pzc}^{W}$ at various concentrations of LiCl and TBATPB are plotted in Fig. 12 as a function of q^W. The experimental points in the positive q^W region are scattered on a single curve with only small deviations. This indicates the virtual invariance of the structure of the inner layer with the change of the concentration of the electrolytes at a given value of q^W and is consistent with the previous conclusion of the absence of ions in the inner layers. The slope of the curve at $q^W=2$ μC cm^{-2} gives the inner layer capacity of 90 μF cm^{-2}, which is in agreement with the value of 83 μF cm^{-2} estimated from the differential capacity measurement of the interface.[19] These values are much higher than the inner layer capacity at the interface between mercury and aqueous solution.[17] Figure 12 also shows that

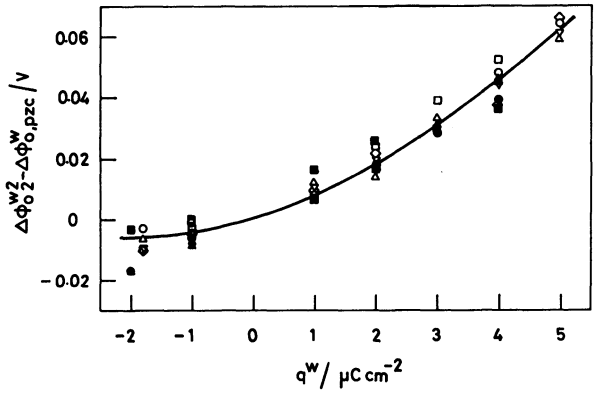

Fig. 12. Change of the inner layer potential difference across the two outer Helmholtz planes $\Delta\phi_{02}^{w2}$ with the change of the surface charge density in aqueous phase at various solution compositions. The concentration of lithium chloride is 0.05 (□), 0.1 (△), 0.2 (◇), 0.5 (▽) and 1.0 (○) mol dm^{-3} when the concentration of tetrabutylammonium tetraphenylborate is 0.1 mol dm^{-3} and the concentration of tetrabutylammonium tetraphenylborate is 0.05 (■), 0.1 (●), and 0.17 (▲) mol dm^{-3} when the concentration of lithium chloride is 0.1 mol dm^{-3}.

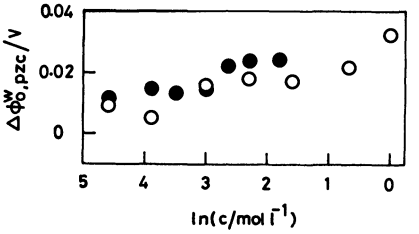

Fig. 13. Potential drop across the two outer Helmholtz planes as a function of the concentrations of tetrabutylammonium tetraphenylborate (●) and of lithium chloride (○).

$\Delta\phi_{02}^{w2}$ increases with the increase of q^w. The slope also becomes larger with increasing q^w, which indicates the decrease of the inner layer capacity with increasing q^w.

The absolute magnitude of $\Delta\phi_{02}^{w2}$ can be evaluated if the value of $\Delta\phi_{0,pzc}^{w}$ is known. In the cell (I) the sum of the potential drops across the phases I and III, and V and VII, $\Delta\phi_{I}^{III}+\Delta\phi_{V}^{VII}$, was calculated from the relation: $\Delta\phi_{I}^{III}+\Delta\phi_{V}^{VII}=(RT/F)\ln(a_{LiCl}^{\pm,w}/a_{TBACl}^{\pm,w})$. The potential drop across the phase III and IV, $\Delta\phi_{III}^{IV}$, was calculated by the theory of the mixed ion transfer potential[9] to be 247.1 mV when $a=b=0.1$ mol dm^{-3} in the cell (I). In the calculation, simultaneous ion transfer of a primary ion (TBA^+) and its co-ion (Cl^-) in the absence of supporting electrolyte was taken into account and the values of the standard ion transfer potentials of ions from water to nitrobenzene were taken as −0.248 and −0.324 V for TBA^+ and Cl^- ions, respectively.[20] Thus, $\Delta\phi_{0,pzc}^{w}$ was estimated by $\Delta\phi_{0,pzc}^{w}=E_{pzc}-(\Delta\phi_{I}^{III}+\Delta\phi_{III}^{IV}+\Delta\phi_{V}^{VII})$. The result is shown in Fig. 13 as a function of the logarithm of the concentrations of TBATPB and LiCl. The $\Delta\phi_{0,pzc}^{w}$ value was always positive and nearly constant at 20 mV when the electrolyte concentration in the two phases was changed. This value is less than one third of the surface potential at the mercury–water interface at the pzc.[21] Such a small surface potential may imply the compensation of the surface potential due to the water dipoles with that of oppositely oriented nitrobenzene dipoles in the inner layer and/or the less oriented structure of the inner layer compared with that at the mercury–water interface.

While this paper was under preparation, Samec *et al.*'s paper[22] on the study of the double structure at the nitrobenzene–water interface appeared. These authors have measured the differential capacity at the interface and analyzed their results with the assumption that the potential at the minimum in the capacity *vs.* potential curve corresponds to the potential of zero charge. However, the capacity minimum occurs at 0.303 V[19] in our system, when $a=b=c=0.1$ mol dm^{-3} in the cell (I), which is 38 mV more positive than the pzc. Also, these authors have estimated $\Delta\phi_{0,pzc}^{w}$ to be 42 mV irrespective of the concentration of LiCl and suggested that the variation of $\Delta\phi_{02}^{w2}$ with q^w is negligible, which is at variance with the present results (see Fig. 12). Gross *et al.*[4] have reported on the basis of the electrocapillary measurements of the non-polarized nitrobenzene–water interface that $\Delta\phi_{0,pzc}^{w}=1$ mV. In their estimation, however, they assumed that the electrocapillary maximum of the non-polarized nitrobenzene–water interface gives the potential of zero charge. This assumption is not generally valid in non-polarized interfaces.[5]

References

1) T. Kakiuchi and M. Senda, *Bull. Chem. Soc. Jpn.*, **56**, 1322 (1983).
2) A. Watanabe, M. Matsumoto, H. Tamai, and R. Gotoh, *Kolloid Z. Z. Polym.*, **220**, 152 (1967).
3) C. Gavach, P. Seta, and B. d'Epenoux, *J. Electroanal. Chem. Interfacial Electrochem.*, **83**, 225 (1977).
4) M. Gros, S. Grom, and C. Gavach, *J. Electroanal. Chem. Interfacial Electrochem.*, **89**, 29 (1978).
5) T. Kakiuchi and M. Senda, to *Bull. Chem. Soc. Jpn.*, in press.
6) T. Kakutani, T. Osakai, and M. Senda, *Bull. Chem. Soc. Jpn.*, **56**, 991(1983).
7) Le Q. Hung, *J. Electroanal. Chem. Interfacial Electrochem.*, **115**, 159 (1980).
8) M. Senda, T. Kakutani, and T. Osakai, *Denki Kagaku*, **49**, 322 (1981).
9) T. Kakiuchi and M. Senda, in preparation.
10) E. A. Guggenheim, "Thermodynamics," 6th ed, North-Holland, Amsterdam (1977), Chap. 5.
11) D. J. Donahue and F. F. Bartell, *J. Phys. Chem.*, **56**, 480 (1952).
12) M. Senda and T. Kakiuchi, paper presented at the 27th Annual Meeting on Polarography, Oct. 1981 (Yokohama) abstract: *Rev. Polarogr. (Kyoto)*, **27**, 49 (1981).
13) C. Davies, "Ion Association," Butterworths, London (1962), p. 39.
14) H. S. Harned and B. B. Owen, "Physical Chemistry of Electrolyte Solutions," 3rd ed, Reinhold, New York (1958), p. 731.
15) J. Kielland, *J. Am. Chem. Soc.*, **59**, 1675 (1937).
16) D. M. Mohilner, "Electroanalytical Chemistry," ed by A. Bard, Marcel Dekker, New York (1966), Vol. 1, p. 321.
17) D. C. Grahame, *Chem. Rev.*, **41**, 441 (1947).

18) R. Parsons, "Advances in Electrochemistry and Electrochemical Engineering," ed by P. Delahay, Interscience, New York (1961), Vol. 1, p. 32.
19) T. Osakai, T. Kakutani, and M. Senda, unpublished result.
20) J. Rais, *Collect. Czech. Chem. Commun.*, **36**, 3253 (1971); J. Rais, P. Selucký, and M. Kyrš, *J. Inorg. Nucl. Chem.*, **38**, 1376 (1976).
21) S. Trasatti, *Croatica Chem. Acta*, **48**, 607 (1976).
22) Z. Samec, V. Mareček, and D. Homolka, *J. Electroanal. Chem. Interfacial Electrochem.*, **126**, 121 (1981).

Electrochemical Oxidation and Reduction of Flavin-Adenine Dinucleotide Adsorbed on a Mercury Electrode Surface

Tadaaki KAKUTANI, Isao KATASHO, and Mitsugi SENDA
Department of Agricultural Chemistry, Faculty of Agriculture, Kyoto University, Sakyo-ku, Kyoto 606
(Received December 23, 1982)

The electrochemical redox reaction of flavin-adenine dinucleotide (FAD) adsorbed on a hanging mercury drop electrode was studied in a pH 6.9 phosphate buffer by means of cyclic d.c. and a.c. voltammetry. Both the oxidized and reduced forms of FAD were strongly adsorbed on the mercury electrode surface. At the surface concentrations of FAD, Γ, lower than 5.0×10^{-11} mol cm^{-2}, the cyclic d.c. and a.c. voltammetric behavior of adsorbed FAD was explained by the theory for a two-step one-electron surface redox reaction. The formal redox potential, semiquinone formation constant, and charge transfer rate constant for the surface redox reaction of FAD and the interaction parameter of adsorbed FAD species were determined. Cyclic d.c. voltammetry and differential capacity measurement showed that, as Γ exceeded 5×10^{-11} mol cm^{-2}, the reorientation of adsorbed FAD molecules occurred. At $\Gamma>5.8\times10^{-11}$ mol cm^{-2}, the semiquinone formation constant was very small and the behavior was interpreted by the theory of a single-step two-electron surface redox reaction. The electrochemical surface redox properties of FAD adsorbed on a mercury electrode surface appear to depend on the orientation mode of adsorbed FAD molecules.

In a previous paper[1] we have shown that a stable adsorption monolayer of flavin mononucleotide (FMN) is formed on a mercury electrode surface and that the electrochemical redox reaction of the adsorbed FMN is well explained by the theory of a two-step one-electron surface redox reaction. The apparent charge transfer rate constants, redox potentials, and semiquinone formation constants of the surface redox reaction have been determined at pH 6.9 and 4.9 using cyclic d.c. and a.c. voltammetry. Recently the electrochemical behavior of flavin-adenine dinucleotide (FAD) irreversibly adsorbed on graphite and glassy carbon electrode has been studied by Gorton and Johansson[2] and Huck[3,4] using cyclic d.c. voltammetry. The (apparent) charge transfer rate constant of *ca.* 1 s^{-1} for FAD adsorbed on graphite electrode at pH 1.05[2] and the semiquinone formation constant of 2.6 for FAD adsorbed on glassy carbon electrode at pH 7[3] are reported. The charge transfer rate constant obtained by the former authors is considerably smaller compared with that for FMN adsorbed on a mercury electrode,[1] though the isoalloxazine moiety is oxidized or reduced in both the redox reactions of the adsorbed FMN and FAD. It seems interesting to determine the charge transfer rate constant of FAD adsorbed on a mercury electrode and to compare the results with those obtained with FAD adsorbed on a carbon electrode and to elucidate whether the difference, if any, should be ascribed to the difference in the electrode material.

In this work the electrochemical redox reaction of FAD adsorbed on a hanging mercury drop electrode has been studied in a pH 6.9 phosphate buffer by means of cyclic d.c. and a.c. voltammetry. We have determined the kinetic and equilibrium parameters of the surface redox reaction of FAD at the various surface concentrations and found that the charge transfer rate constant and the semiquinone formation constant depend on the orientation mode of the adsorbed FAD molecules. The results and discussion are presented here.

Experimental

Flavin-adenine dinucleotide (FAD) and other chemicals were commercially-available reagent grade materials and were used as received.

All voltammetric measurements were performed in a dark box at 25 °C under potentiostatic conditions with a three-electrode system consisting of a hanging mercury drop working electrode, a coiled platinum counter electrode, and a saturated calomel reference electrode (SCE). The hanging mercury drop electrode (HMDE) was a Metrohm drop electrode E410, the surface area being 0.0187 ± 0.0003 cm^2. Buffer solution containing 0.2 mol dm^{-3} sodium dihydrogenphosphate-disodium hydrogenphosphate of pH 6.9 was used as the base solution. The ionic strength was adjusted to 0.5 mol dm^{-3} with potassium nitrate. D.c. and a.c. voltammograms were recorded after a fresh mercury drop from the HMDE had been exposed to a test solution for a given period of time, referred to in the following as the exposure time, t_{exp}, at a constant d.c. potential, E_i. All potentials were measured against a saturated calomel electrode (SCE). The d.c. voltage scan was started from E_i with the scan rates, v, of 98 mV s^{-1} for cyclic d.c. voltammetry and of 18 mV s^{-1} for a.c. voltammetry unless otherwise stated. Other details concerning the apparatus and methods of electrochemical measurements have been described elsewhere[1]

Results

Electrochemical measurements were performed at concentrations of FAD, C_{FAD}, lower than 3.6×10^{-6} mol dm^{-3}, at which the current due to the redox reaction of diffusing, unadsorbed FAD will be negligibly small compared with the current due to the surface redox reaction of FAD confined to the electrode surface by adsorption. The exposure time, t_{exp}, was varied from 0.5 to 5 min. In cyclic d.c. voltammetry FAD gave a pair of peak-shaped cathodic and anodic waves characteristic of the surface redox reaction at -0.40 V, which is attributable to the redox reaction of the isoalloxazine moiety.[1] The waves appeared in various shapes, depending on the exposure time and bulk concentration of FAD (Fig. 1), *i.e.*, on the surface concentration of FAD accumulated on the electrode surface during the exposure time. Figure 1 shows cyclic d.c. voltammograms of 2.7×10^{-6} mol dm^{-3} FAD, recorded after three different exposure times; the voltammograms A, B, and C were recorded at $t_{exp}=70$, 90, and 120 s, respec-

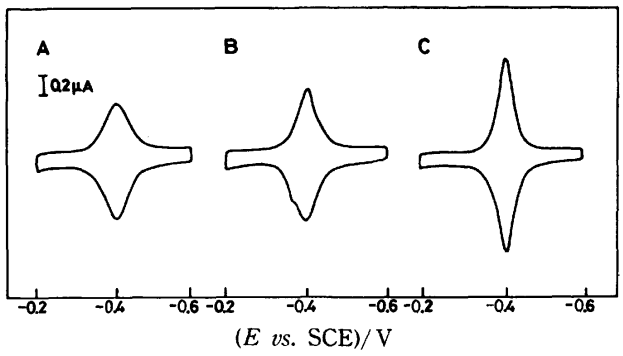

Fig. 1. Cyclic d.c. voltammograms of 2.7×10^{-6} mol dm^{-3} FAD recorded in a pH 6.9 phosphate buffer after three different t_{exp}'s at $E_i=-0.20$ V *vs.* SCE. t_{exp}: (A) 70 s, (B) 90 s, (C) 120 s.

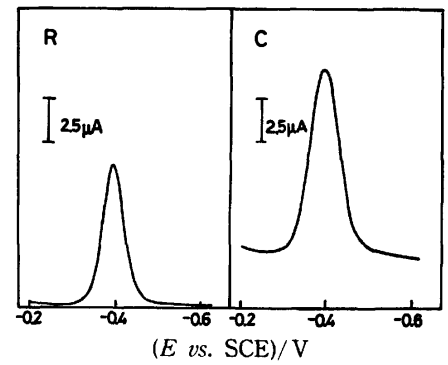

Fig. 2. A.c. voltammograms of 8.1×10^{-7} mol dm^{-3} FAD in a pH 6.9 phosphate buffer at 500 Hz. D.c. voltage scan was started from $E_i=-0.20$ V *vs.* SCE after $t_{exp}=$ 5 min. R Real component, C: imaginary component.

tively, at $E_i=-0.20$ V. In this study the surface concentrations of FAD, Γ, were estimated from the area under the cyclic d.c. wave (corrected for the base current) by assuming that the number of electron transferred for each molecule of FAD is equal to 2 and that $m_1/n_1=m_2/n_2=1$[5] or $m/n=1$.[6] When the surface concentration of FAD was lower than 5.0×10^{-11} mol cm^{-2}, the shapes of the cyclic d.c. waves were broadened and flattened as seen by voltammogram A in Fig. 1, of which Γ was estimated at 4.9×10^{-11} mol cm^{-2}. When Γ exceeded 5.0×10^{-11} mol cm^{-2} and approached 5.8×10^{-11} mol cm^{-2}, the waves became narrower and sharper (see voltammogram C in Fig. 1). In the intermediate surface concentrations of FAD, *i.e.*, 5.0×10^{-11} mol cm^{-2} $<\Gamma<5.8\times10^{-11}$ mol cm^{-2}, the wave shape was asymmetrical and deformed (see voltammogram B in Fig. 1) and changed sensitively with Γ. Quite interestingly the electrochemical behavior of the adsorbed FAD at $\Gamma<5.0\times10^{-11}$ mol cm^{-2} was different from that at $\Gamma>5.8\times10^{-11}$ mol cm^{-2}. In the following the surface concentration of FAD lower than 5.0×10^{-11} mol cm^{-2} will be referred to as the low surface concentration, whereas the surface concentration higher than 5.8×10^{-11} mol cm^{-2} will be referred to as the high surface concentration.

Cyclic d.c. and a.c. Voltammetric Behavior at the Low Surface Concentration. When $\Gamma<5.0\times10^{-11}$ mol cm^{-2}, *i.e.*, at the low surface concentration, the electrochemical behavior of FAD adsorbed on the HMDE was essentially the same[8] as that of FMN adsorbed on the HMDE.[1] In cyclic d.c. voltammetry, the peak heights of the cathodic and anodic waves, I_{pc} and I_{pa}, after correction for the base currents, were proportional to the potential scan rate, v, between 32 and 192 mV s^{-1}, and also to Γ at $\Gamma<5.0\times10^{-11}$ mol cm^{-2} (Fig. 3). The peak height ratio I_{pa}/I_{pc} was unity in the above-stated ranges of v and Γ when corrected for the difference between the amounts of the adsorbed FAD at the cathodic and anodic peak potentials due to the difference in t_{exp}. The peak potentials of the cathodic and anodic waves, E_{Pc}^{DC} and E_{Pa}^{DC}, coincided with each other and were independent of both v and Γ; $E_{Pc}^{DC}=E_{Pa}^{DC}=-0.40$ V. The half-peak widths of the cathodic and anodic waves, $\Delta E_{p/2.c}^{DC}$ and $\Delta E_{p/2.a}^{DC}$, were also independent within experimental errors of both v and Γ; $\Delta E_{p/2.c}^{DC}=\Delta E_{p/2.a}^{DC}=$ 70 ± 3 mV.

Figure 2 shows representative real and imaginary components of a.c. voltammograms of adsorbed FAD at $\Gamma<5.0\times10^{-11}$ mol cm^{-2}; the voltammograms were recorded after the electrode had been exposed to the electrolysis solution containing 8.1×10^{-7} mol dm^{-3} FAD for $t_{exp}=5$ min at $E_i=-0.20$ V, where $\Gamma$was estimated at 3.0×10^{-11} mol cm^{-2} from the cyclic d.c. wave measured under the same conditions. The peak potentials of the real and imaginary components, E_p^{real} and E_p^{imag}, were independent of the ac frequency in the range between 100 and 500 Hz, and also of Γ less than 5.0×10^{-11} mol cm^{-2}. They agreed with each other and with the peak potentials of the cyclic d.c. waves; $E_p^{real}=E_p^{imag}(=E_p^{AC})=-0.40$ V. The ratio of the peak height of the real component ($\delta_1 I_p^{real}$) to that of the imaginary component ($\delta_1 I_p^{imag}$), $(\delta_1 I_p^{real}/\delta_1 I_p^{imag})_{E=E_p^{AC}}$, was proportional to the a.c. frequency between 100 and 500 Hz.

Cyclic d.c. and a.c. Voltammetric Behavior at the High Surface Concentration. When Γ exceeded 5.8×10^{-11} mol cm^{-2}, *i.e.*, at the high surface concentration, the shape of the cyclic d.c. waves became narrower and sharper compared with those observed at the low surface concentration (see Fig. 1). Table 1 shows the scan rate dependence of the peak heights, peak potentials, and half-peak widths of the cyclic d.c. voltammograms. The voltammograms were recorded with various scan rates after the electrode had been exposed to 3.6×10^{-6} mol dm^{-3} FAD solution for $t_{exp}=2$ min at $E_i=-0.20$ V, when the surface concentration of FAD was estimated at 6.7×10^{-11} mol cm^{-2}. E_{Pc}^{DC} and E_{Pa}^{DC} agreed with each other and were independent of both v and Γ; $E_{Pc}^{DC}=E_{Pa}^{DC}(=E_P^{DC})=-0.40$ V. $\Delta E_{p/2.c}^{DC}$ and $\Delta E_{p/2.a}^{DC}$ were practically invariant with both v and Γ; $\Delta E_{p/2.c}^{DC}=\Delta E_{p/2.a}^{DC}=43\pm0.7$ mV. Both I_{pc} and I_{pa} were proportional to v (Table 1) and increased linearly with Γ at $\Gamma>5.8\times10^{-11}$ mol cm^{-2} as shown in Fig. 3. The peak height ratio I_{pa}/I_{pc} was unity independently of v and Γ.

The a.c. voltammetric behavior of adsorbed FAD at the high surface concentration was different from that at the low surface concentration described above. Figure 4 shows a.c. voltammograms of 3.6×10^{-6} mol dm^{-3} FAD at two a.c. frequencies, 100 and 500 Hz;

Table 1. Scan rate dependence of the peak current, peak potential and half-peak width of cyclic d.c. voltammograms of FAD adsorbed at the high surface concentration on mercury electrode at pH 6.9[a)]

Scan rate/mV s^{-1}	$I_{pc}/\mu A$	$I_{pa}/\mu A$	E_{Pc}^{DC}/V[b)]	E_{Pa}^{DC}/V[b)]	$\Delta E_{p/2,c}^{DC}/mV$	$\Delta E_{p/2,a}^{DC}/mV$
32	0.17	0.17	−0.40	−0.40	42	42
48	0.25	0.25	−0.40	−0.40	42	43
98	0.48	0.48	−0.40	−0.40	42	43
193	0.88	0.88	−0.40	−0.40	45	45

a) $C_{FAD}=3.6\times10^{-6}$ mol dm^{-3}, $t_{exp}=2$ min at $E_i=-0.20$ V *vs.* SCE. b) V *vs.* SCE.

Table 2. Peak potential and half-peakwidth of a.c. voltammograms of FAD adsorbed at the high surface concentration on mercury electrode at pH 6.9[a)]

Frequency/Hz	E_p^{real}/V[b)]		E_p^{imag}/V[b)]		$\Delta E_{p/2}^{real}/mV$		$\Delta E_{p/2}^{imag}/mV$	
	Obsd	Calcd[c)]	Obsd	Calcd[c)]	Obsd	Calcd[c)]	Obsd	Calcd[c)]
100	0.40_2	0.4019	0.39_8	0.3984	35	36.4	47	47.0
200	0.40_0	0.4003	0.39_2	0.3946	38	40.4	56	52.4
300	0.39_8	0.3987	0.38_8	0.3905	42	44.2	64	57.4
400	0.39_6	0.3973	0.38_5	0.3870	46	47.4	68	60.9
500	0.39_5	0.3963	0.38_3	0.3842	50	49.8	75	62.9

a) $C_{FAD}=3.6\times10^{-6}$ mol dm^{-3}, $t_{exp}=2$ min at $E_i=-0.20$ V *vs.* SCE($\Gamma=6.7\times10^{-11}$ mol cm^{-2}). b) V *vs.* SCE.
c) Calculated by using $E'_0=-0.400$ V *vs.* SCE, $k_{sap}=5.12\times10^2$ s^{-1}, $J=1.5$, $G=0.13$, and $\theta_t=0.957$.

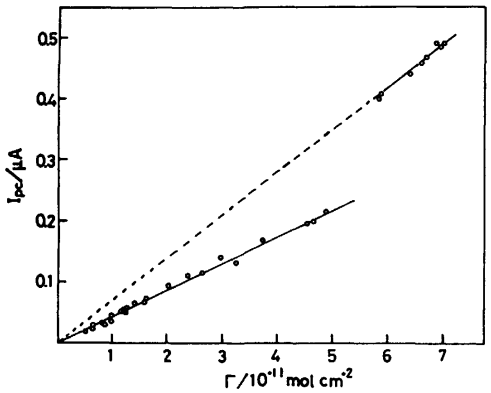

Fig. 3. Plot of I_{pc} against Γ at pH 6.9.

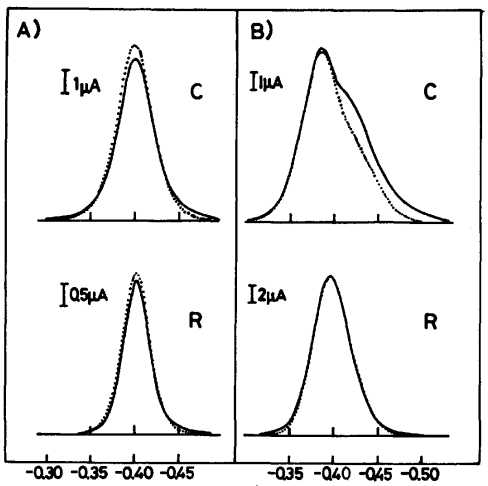

Fig. 4. A.c.voltammograms of 3.6×10^{-6} mol dm^{-3} FAD recorded after $t_{exp}=2$ min at $E_i=-0.20$ V *vs.* SCE at (A) 100 Hz and (B) 500 Hz. R: Real component, C: imaginary component. Dotted lines represent theoretical voltammograms calculated by Eqs. 5 and 6 using $E'_0=-0.400$ V *vs.* SCE, $k_{sap}=5.12\times10^2$ s^{-1}, $J=1.5$, $G=0.13$, $\theta_t=0.957$ and $\Gamma^{max}=7.0\times10^{-11}$ mol cm^{-2}.

the voltammograms were recorded after $t_{exp}=2$ min at $E_i=-0.20$ V, when Γ was estimated at 6.7×10^{-11} mol cm^{-2} from the corresponding cyclic d.c. wave. The peak potentials of the real and imaginary components shifted to a more positive potential with an increase in the a.c. frequency as shown in Table 2. In addition, the wave shapes, in particular, of the imaginary components changed from a nearly symmetrical to an asymmetrical one with a shoulder with increasing a.c. frequency. However, the current ratio of the real component to the imaginary one measured at $E=E_P^{pc}$, $(\delta_1 I_F^{real}/\delta_1 I_F^{imag})_{E=E_P^{pc}}$, was proportional to a.c. frequency as shown in Fig. 5.

Discussion

Adsorption of FAD on Mercury Electrode Surface. The cyclic d.c. voltammetric data given above indicate that both the oxidized and reduced forms of FAD are strongly adsorbed on the HMDE surface. Figure 6 shows the dependence of the cathodic peak height, I_{pc}, on t_{exp} at various concentrations of FAD. In this figure the points below the broken line correspond to the cyclic d.c. voltammograms at the low surface concentration, *i.e.*, at $\Gamma<5.0\times10^{-11}$ mol cm^{-2} (see Fig. 1A), whereas the points above the line correspond to the voltammograms at the high surface concentration, *i.e.*, at $\Gamma>5.8\times10^{-11}$ mol cm^{-2} (see Fig. 1C), and the points in parentheses correspond to the intermediate surface concentration between 5.0×10^{-11} and 5.8×10^{-11} mol cm^{-2}. At $C_{FAD}\leq1.08\times10^{-6}$ mol dm^{-3}, the peak height I_{pc} (and also I_{pa}) increased linearly with the

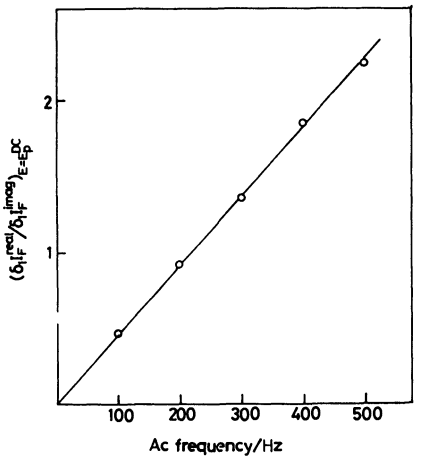

Fig. 5. Frequency dependence of the ac current ratio at $E=E_p^{dc}$, $(\delta_1 I_p^{real}/\delta_1 I_p^{imag})_{E=E_p^{dc}}$. A.c. voltammograms were recorded after the electrode had been exposed to 3.6×10^{-6} mol dm^{-3} FAD solution for $t_{exp}=2$ min at $E_i=-0.20$ V *vs.* SCE.

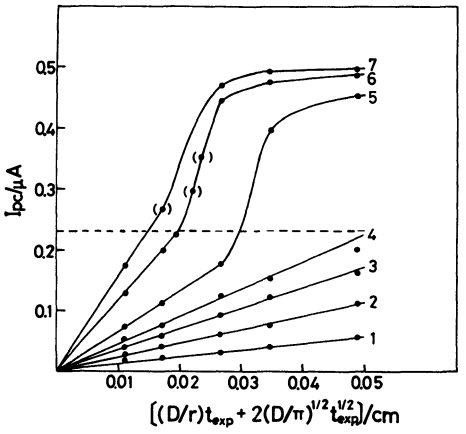

Fig. 6. Plot of I_{pc} against $[(D/r)t_{exp}+2(D/\pi)^{1/2}t_{exp}^{1/2}]$ at pH 6.9. Bulk concentrations of FAD in mol dm^{-3} are: (1) 2.7×10^{-7}; (2) 5.4×10^{-7}; (3) 8.1×10^{-7}; (4) 1.08×10^{-6}; (5) 1.62×10^{-6}; (6) 2.7×10^{-6}; (7) 3.6×10^{-6}.

$[(D/r)t_{exp}+2(D/\pi)^{1/2}t_{exp}^{1/2}]$ function, where D is the diffusion coefficient of FAD, which was estimated to be 2.4×10^{-6} cm^2 s^{-1} from the d.c. polarographic data, using the Ilkovič equation, and r is the radius of the HMDE, which was estimated to be 0.038 cm. In addition, the slopes of the linear plots were proportional to C_{FAD}. These results indicate the diffusion-controlled adsorption of FAD at the mercury electrode surface.[1,9] On the other hand, at $C_{FAD}\geq1.62\times10^{-6}$ mol dm^{-3}, as t_{exp} increased the wave shapes changed from a broad (see Fig. 1A) to a sharp one (see Fig. 1C) and the peak height I_{pc} increased and attained a maximum value, when Γ reached a maximum value, Γ^{max}. The Γ^{max} value was estimated to be 7.0×10^{-11} mol cm^{-2} from the cyclic d.c. voltammogram. If we assume that an FAD molecule is adsorbed on the electrode surface with its isoalloxazine ring plane parallel but its adenine ring plane vertical to the electrode surface, a CPK molecular model gives $\Gamma^{max}=7.5\times10^{-11}$ mol cm^{-2}. On the other hand, when both the ring planes are oriented parallel

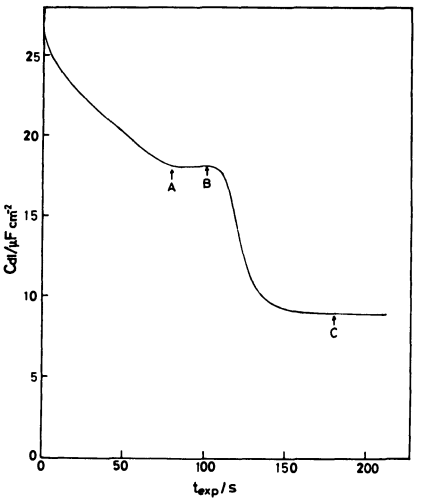

Fig. 7. t_{exp}-dependence of C_{dl} measured in 2.7×10^{-6} mol dm^{-3} FAD solution at -0.20 V *vs.* SCE at pH 6.9.

to the electrode surface, it gives $\Gamma^{max}=5.2\times10^{-11}$ mol cm^{-2}. These results suggest that at the low surface concentrations, *i.e.*, at $\Gamma<5.0\times10^{-11}$ mol cm^{-2} FAD molecule is adsorbed probably with both isoalloxazine and adenine ring planes oriented parallel to the electrode surface, and that, as the surface concentration of FAD exceeds 5.0×10^{-11} mol cm^{-2}, reorientation of the adsorbed FAD molecule occurs, resulting in an adsorbed FAD molecule probably with the isoalloxazine ring plane oriented parallel and the adenine ring plane oriented vertical to the electrode surface. This reorientation of the adsorbed FAD molecule should cause the observed transition in the voltammetric behavior of FAD at the HMDE.

The reorientation of the adsorbed FAD molecules was further indicated by the differential capacity measurement. Figure 7 shows the t_{exp}-dependence of the differential capacity, C_{dl}, at -0.20 V, where no faradaic current takes place, in 2.7×10^{-6} mol dm^{-3} FAD solution. Under these experimental conditions the surface concentrations of FAD at various t_{exp}'s were estimated from the corresponding cyclic d.c. voltammograms as: $\Gamma=5.0$, 5.8, and 6.9×10^{-11} mol cm^{-2} at $t_{exp}=$ 80, 100, and 180 s, respectively (marked by arrows A, B, and C, respectively, in Fig. 7). If the orientation mode of the adsorbed molecules remains unchanged in spite of an increase in Γ and if the relative decrease of the double layer capacitance is proportional to the surface concentration of the adsorbed molecules, then the double layer capacitance can be written as

$$C_{dl} = C_{dl}^{\circ} + (C_{dl}^{max}-C_{dl}^{\circ})(\Gamma/\Gamma^{max}), \quad (1)$$

where C_{dl}° and C_{dl}^{max} are the double layer capacitances in the absence of adsorbed FAD and at the maximum adsorption of FAD, respectively. That is, the double layer capacitance should decrease monotonically with the increase of Γ. Actually, for $t_{exp}<70$ s the decrease in the double layer capacitance, $\Delta C_{dl}=C_{dl}^{\circ}-C_{dl}$, was proportional to the $[(D/r)t_{exp}+2(D/\pi)^{1/2}t_{exp}^{1/2}]$ function as shown in Fig. 8, indicating the diffusion-controlled adsorption of FAD for $t_{exp}<70$ s. Substituting $\Gamma=[(D/r)t_{exp}+2(D/\pi)^{1/2}t_{exp}^{1/2}]C_{FAD}$ into Eq. 1, the slope of

the ΔC_{dl} *vs.* $[(D/r)t_{exp}+2(D/\pi)^{1/2}t_{exp}^{1/2}]$ plot can be given by $[(C_{dl}^{\circ}-C_{dl}^{max})\times C_{FAD}/\Gamma^{max}]$. If we assume that $C_{dl}^{max}=C_{dl}$ at $t_{exq}=80$ s and $\Gamma^{max}=5.0\times10^{-11}$ mol cm^{-2}, the slope can be calculated to be 4.6×10^{2} μF cm^{-3}, which agreed reasonablly well with the experimental value of 4.2×10^{2} μF cm^{-3} obtained from the plot in Fig. 8. These results show that the decrease of C_{dl} with t_{exp} at $t_{exp}<70$ s can be explained by the diffusion-controlled monolayer adsorption of FAD, approaching monotonically to the maximum adsorption near at $t_{exp}=80$ s or $\Gamma=5.0\times10^{-11}$ mol cm^{-2}, which is the maximum adsorption at the low surface concentration. At $t_{exp}>100$ s or $\Gamma>5.8\times10^{-11}$ mol cm^{-2}, C_{dl} decreased abruptly and approached a small value, approximately one half of the value at $\Gamma=5.0\times10^{-11}$ mol cm^{-2}, near at $t_{exp}=180$ s or $\Gamma=7.0\times10^{-11}$ mol cm^{-2}, which is the maximum adsorption at the high surface concentration. The decrease in the capacitance implies an increase in the effective thickness of the adsorbed FAD layer. This interpretation agrees with the above-stated reorientation mechanism of adsorbed FAD molecules when the surface concentration exceeds 5.8×10^{-11} mol cm^{-2}.

Surface Redox Reaction of FAD Adsorbed on the HMDE. A) Surface Redox Reaction at the Low Surface Concentration: As described above the cyclic d.c. and a.c. voltammetric behavior of the adsorbed FAD at the low surface concentration was essentially the same as that of the adsorbed FMN on the mercury electrode surface.[1] The behavior was explained also by the simplified equations[1,5] of the cyclic d.c. and a.c. voltammetry for a two-step surface redox reaction;

$$O_{ad} + e = S_{ad}$$
$$S_{ad} + e = R_{ad}. \quad (I)$$

The semiquinone formation constant, $K=[S_{ad}]^2/[O_{ad}][R_{ad}]$, was determined from the cyclic d.c. voltammograms as $K=1.5$ from $\Delta E_{p/2.c}^{DC}$ or $\Delta E_{p/2.a}^{DC}$ using Eq. 5 in Ref. 1 and $K=1.5$ from the slope of the I_{pc} *vs.* Γ plot (Fig. 3) using Eq. 6 in Ref. 1. The apparent (average) rate constants of the charge transfer, k_{sap}, were determined at several surface concentrations using Eq. 7 in Ref. 1. A linear dependence of ln k_{sap} on the surface coverage θ_t with a slope, a, of 1.0 was obtained, where $\theta_t\equiv\Gamma/\Gamma^{max}$ was estimated by taking $\Gamma^{max}=5.0\times10^{-11}$ mol cm^{-2}. The apparent rate constant at $\theta_t=0$, $k_{sap}(\theta_t\to0)$, was determined by the extrapolation of the ln k_{sap} *vs.* θ_t plot to $\theta_t=0$. Table 3 summarizes the values of the formal redox potential of the adsorbed redox couple O_{ad}/R_{ad}, E_o', as well as K, $k_{sap}(\theta_t\to0)$, Γ^{max}, and a. For reference the values of the electrochemical redox reaction parameters for the surface redox reactions of FMN[1] and riboflavin (RF)[8] at mercury electrode are also given in Table 3.

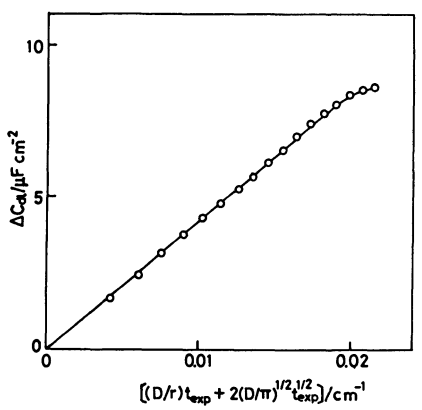

Fig. 8. Plot of ΔC_{dl} against $[(D/r)t_{exp}+2(D/\pi)^{1/2}t_{exp}^{1/2}]$ at pH 6.9. Data were taken from the results presented in Fig. 7.

Table 3. Electroche mical redox properties of flavins adsorbed on mercury electrode at pH 6.9

	RF[8]	FMN[1]	FAD[a]
$(E_o'$ *vs.*SCE)/V	−0.40	−0.41	−0.40
K	1.2	1.1	1.5
$k_{sap}(\theta_t\to0)/10^3$ s^{-1}	9.9	9.5	7.2
$\Gamma^{max}/10^{-11}$ mol cm^{-2}	8.9	8.0	5.0
a	2.0	1.3	1.0

a) Data obtained in this study at the low surface concentration (see text). Previous, less accurate data[8] on FAD were corrected as given here.

B) Surface Redox Reaction at the High Surface Concentration: As described above, at the high surface concentration, *i.e.*, 5.8×10^{-11} mol cm^{-2} $<\Gamma<7.0\times10^{-11}$ mol cm^{-2}, the half-peak widths of the cyclic d.c. waves were 43 mV, which suggest that the semiquinone formation constant K is very small. Therefore, the cyclic d.c. and a.c. voltammetric behavior of adsorbed FAD at the high surface concentration was interpreted in terms of a single-step two-electron surface redox reaction rather than a two-step one-electron surface redox reaction. According to the theory of cyclic d.c.[6,7] and a.c.[6] voltammetry for a single-step n-electron surface redox reaction,

$$O_{ad} + ne = R_{ad}, \quad (II)$$

in which the interactions between the adsorbed reactants are taken into account, the peak heights, I_{pc} and I_{pa}, the peak potentials, E_{Pc}^{DC} and E_{Pa}^{DC}, and the half-peak widths, $\Delta E_{p/2.c}^{DC}$ and $\Delta E_{p/2.a}^{DC}$, of the reversible cyclic d.c. voltammogram, and the real and imaginary components of the a.c. current, $\delta_1 I_F^{real}$ and $\delta_1 I_F^{imag}$, of d.c. reversible surface redox process can be written, for $\alpha=\beta=0.5$ and $n=m=2$ (see Ref. 6 for the details), as:

$$-I_{pc} = I_{pa} = (4F^2/RT)vA\Gamma_t(4-G\theta_t)^{-1} \quad (2)$$

$$E_{pc}^{DC} = E_{pa}^{DC} = E_o' = E_o + (RT/2F) \times[\ln(B_R/B_O) - (H\theta_t/2)] \quad (3)$$

$$\Delta E_{p/2.c}^{DC} = \Delta E_{p/2.a}^{DC} = (RT/F)|\ln(1+\gamma)/(1-\gamma) - (G\theta_t/2)| \quad (4)$$

$$\delta_1 I_F^{real} = 4(F^2/RT)\omega\Gamma_t A\delta_1 E \times \frac{\lambda\exp[-(G-J)\bar{f}\theta_t/2](1-\bar{f})^{3/2}\bar{f}^{3/2}}{\exp[-(G-J)\bar{f}\theta_t][1-G\theta_t(1-\bar{f})\bar{f}]^2+\lambda^2(1-\bar{f})\bar{f}} \quad (5)$$

$$\delta_1 I_F^{imag} = 4(F^2/RT)\omega\Gamma_t A\delta_1 E \times \frac{\exp[-(G-J)\bar{f}\theta_t][1-G\theta_t(1-\bar{f})\bar{f}]\bar{f}(1-\bar{f})}{\exp[-(G-J)\bar{f}\theta_t][1-G\theta_t(1-\bar{f})\bar{f}]^2+\lambda^2(1-\bar{f})\bar{f}}, \quad (6)$$

with

$$G = a_{OO} + a_{RR} - a_{OR} - a_{RO} \quad (7a)$$

$$H = a_{OO} - a_{RR} + a_{OR} - a_{RO} \quad (7b)$$

$$\gamma = [(4-G\theta_t)/(8-G\theta_t)]^{1/2} \quad (7c)$$

$$J = 2(a_{RR}-a_{RO}) \quad (7d)$$

$$\lambda = \omega/k_{sap} \quad (7e)$$

$$k_{sap} = k_s(B_O B_R)^{-1/2}\exp[-(a_{RR}+a_{OR})\theta_t/2], \quad (7f)$$

where B_i is the constant representing the adsorption energy of species i(i=O,R), a_{ij}(i,j=O,R) Frumkin's a-parameter of the interaction between the adsorbed species i and j, E_o^* and E_o are the formal potentials of the adsorbed redox couple O_{ad}/R_{ad} and of the redox couple O/R in the bulk of solution, respectively, ω and $\delta_1 E$ are the angular frequency and amplitude of the applied a.c. voltage, respectively, $\bar{f}$ is the mean ("d.c.") ffraction of the surface coverage defined by $\bar{f}=\bar{\Gamma}_O/\Gamma_t(\Gamma_t=\bar{\Gamma}_O+\bar{\Gamma}_R)$, $\bar{\Gamma}_i$ being the mean ("d.c.") value of the surface concentration of species i, θ_t the total surface coverage defined by $\theta_t=\Gamma_t/\Gamma^{max}$, and A the surface area of the electrode. $\bar{f}$ is related to the d.c. potential, $E_{d.c.}$ by

$$E_{d.c.} = E_o' + (RT/2F)[\ln(\bar{f}/(1-\bar{f})) + (1-2\bar{f})G\theta_t/2]. \quad (8)$$

The interaction parameter G can be determined from the half-peak widths of the cyclic d.c. voltammograms (Eq. 4). Application of Eq. 4 to the experimental results gave the average value of G as 0.13 ± 0.02 in the range of Γ between 5.8×10^{-11} and 7.0×10^{-11} mol cm^{-2}, *i.e.*, $0.83\leq\theta_t\leq1.0$. This G value leads us to the normalized peak heights of the d.c. waves, $\Phi=-I_{pc}/4(F^2/RT)v\Gamma_t A = I_{pa}/4(F^2/RT)v\Gamma_t A$, of 0.257 at $\theta_t=0.83$ and of 0.258 at $\theta_t=1.0$, which means that the peak heights are practically proportional to Γ_t, *i.e.*,

$$-I_{pc} = I_{pa} \cong 0.257(4F^2/RT)v\Gamma_t A. \quad (2')$$

Thus the (theoretical) slope of the I_{pc} *vs.* Γ_t plot can be calculated using Eq. 2′ to be 7.1×10^3 A cm^2 mol^{-1}, which agreed well with the experimental value of 7.0×10^3 A cm^2 mol^{-1}. Equation 3 predicts a linear dependence of E_{Pc}^{pc} or E_{Pa}^{pc} on θ_t for $H\neq0$. However, since θ_t varied between 0.83 and 1.0, the dependence of E_{Pc}^{pc} or E_{Pa}^{pc} on θ_t would not be experimentally detectable when $|H|$ is not so large. For example, the difference in E_{Pc}^{pc}'s between at $\theta_t=0.83$ and 1.0 is calculated to be 2.2 mV for $H=2$, which is well below the magnitude of experimental errors of the present determination. Thus we may conclude that the value of $|H|$ is not so large and should not exceed 2, which is a reasonable conclusion in view of Eq. 7.

Equations 5 and 6 predict that both the real and imaginary components are not symmetrical with respect to the E_o'-axis for $G\neq J$, that their peak potentials, E_p^{real} and E_p^{imag}, should shift positively for $G<J$ or negatively for $G>J$ with increasing a.c. frequency, and that the current ratio $(\delta_1 I_F^{real}/\delta_1 I_F^{imag})_{E_{d.c.}=E_o^*}$ should be proportional to a.c. frequency:

$$(\delta_1 I_F^{real}/\delta_1 I_F^{imag})_{E_{d.c.}=E_o'} = \omega/2k_{sap}\exp[-(G-J)\theta_t/4](1-G\theta_t/4). \quad (9)$$

The linear dependence of current ratio on the a.c. frequency was experimentally found, as shown in Fig. 5. Table 2 gives the experimental and calculated values of E_p^{real}, E_p^{imag}, $\Delta E_{p/2}^{real}$, and $\Delta E_{p/2}^{imag}$ of the surface redox reaction of adsorbed FAD at the high surface concentration, where the calculated values were obtained using the following values of the parameters: $E_o'=-0.400$ V, $k_{sap}=5.12\times10^2$ s^{-1}, $J=1.5$ and $G=0.13$. The a.c. peak currents are plotted against the a.c. frequency in Fig. 9, in which the solid lines are drawn by Eqs. 5 and 6 using the same values of the parameters as above. In Fig. 4 the dotted curves represent the theoretical a.c. voltammograms calculated by using the same values of the parameters as above, which are compared with the experimental voltammograms shown as solid lines. The agreement between the theory and experimental results seems reasonably good, except for curves C in Fig. 4B, in which the experimental asymmetric wave form is reproduced only semi-quantitatively by the present theory. These results indicate that the essential features of the cyclic d.c. and a.c. voltammetric behavior of adsorbed FAD at the high surface concentration can be reproduced by the theory of a single-step surface redox reaction in which the interaction between the adsorbed molecules are taken into account. It is interesting that the orientation mode of the adsorbed FAD molecules has a significant influence on the electrochemical properties of the surface redox reaction of FAD, such as the semiquinone formation constant and the charge transfer rate constant.

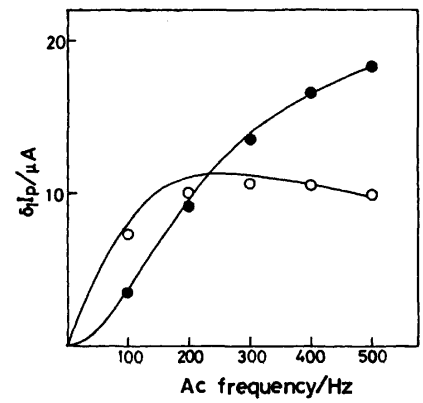

Fig. 9. Dependence of the a.c. peak heights of 3.6×10^{-6} mol dm^{-3} FAD on a.c. frequency at pH 6.9. A.c. voltammograms were recorded after $t_{exp}=2$ min at $E_i=-0.20$ V *vs.* SCE. ●: Real component, ○: imaginary component. Solid lines represent theoretical curves calculated by Eqs. 5 and 6 using the same values of the parameters as used in Fig. 4.

References

1) T. Kakutani, K. Kano, S. Ando, and M. Senda, *Bull. Chem. Soc. Jpn.*, **54**, 884 (1981).
2) L. Gorton and G. Johansson, *J. Electroanal. Chem. Interfacial Electrochem.*, **113**, 151 (1980).
3) H. Huck, *Ber. Bunsenges. Phys. Chem.*, **85**, 221 (1981).
4) H. Huck, *Z. Phys. Chem. NF*, **120**, 39 (1980).
5) T. Kakutani and M. Senda, *Bull. Chem. Soc. Jpn.*, **53**, 1942 (1980).
6) T. Kakutani and M. Senda, *Bull. Chem. Soc. Jpn.*, **52**. 3236 (1979).

7) E. Laviron, *J. Electroanal. Chem. Interfacial Electrochem.*, **52**, 395 (1974).
8) T. Kakutani, I. Katasho, S. Ando, and M. Senda, Paper presented at the annual meeting on polarography and electroanalytical chemistry, Oct. 17—18th, 1981; abstract, *Rev. Polarogr. (Kyoto)* **27**, 92 (1981).
9) J. Koryta, *Collect. Czech. Chem. Commun.*, **18**, 206 (1935).

A Photoelectron Spectroscopic Estimation of the Concentrations of Simple Hydrogen-bonded Dimers Produced in the Temperature-controlled Supersonic Nozzle Beam

Shinji Tomoda and Katsumi Kimura*
Institute for Molecular Science, Myodaiji, Okazaki 444
(Received January 24, 1983)

A photoelectron spectroscopic method is proposed to estimate the ratio of number densities between the monomer and the dimer produced in the supersonic jet. Approximate monomer-dimer ratios have been estimated for water, methanol and formic acid by assuming that the photoionization cross sections of the monomer and dimer are equal to each other. The results show reasonable agreement under similar conditions to those available from mass spectrometric analyses of fragmentation patterns. A simple temperature-controlled supersonic nozzle beam source is described here, which enables us to produce hydrogen-bonded dimers in measurable amounts.

Supersonic nozzle beam technique has recently been drawing a considerable attention not only in the field of molecular beam scattering study but also in various kinds of molecular spectroscopic studies. This seems to be due to the advantageous characters of supersonic nozzle beams which produce molecular clusters (van der Waals molecules, hydrogen-bonded species, *etc.*) with relatively high concentrations and realize low temperature states for internal degrees of molecular freedoms.

Dehmer and Dehmer[1] have first demonstrated the potentiality of this technique in the field of photoelectron spectroscopic studies using inert gas dimers. However, no extensive application of this technique to various chemical species has been published, probably because of the difficulty in controlling the production of their dimers and clusters as well as in analyzing their concentrations quantitatively.

From the chemical points of view, it is important to investigate various kinds of molecular dimers and clusters by photoelectron spectroscopy as well as other molecular spectroscopy. However, in order to apply a supersonic nozzle beam technique to various chemical species which exist in the liquid phase under the normal condition, we have to overcome the following problems. The general criterion to use a supersonic nozzle beam system is to achieve sufficient supersonic expansion under proper stagnation and pumping conditions. For chemical species such as water and many other fundamental chemical compounds, it is essentially important to control the temperature of the whole nozzle beam system both for regulating the vapor pressure stable and for preventing the nozzle from clogging. An electric heating system for the nozzle is not suitable for photoelectron measurements, because of its disturbing electromagnetic field.

In this report we first describe the temperature-controlled supersonic nozzle beam source in detail, which has recently been constructed to measure HeI photoelectron spectra of the water dimer,[2] the methanol dimer,[3] and the formic acid dimer.[4] Secondly, we propose an approximate method to estimate the relative dimer concentration with respect to the monomer concentration from the subtraction procedure between photoelectron spectra of the monomer (reference) and the monomer-dimer mixture. This approach depending on the assumptions is still crude, but it offers a more straightforward interpretation for the dimer concentration than other methods such as mass spectrometry, at least for hydrogen bonded clusters. In the mass analysis of the hydrogen-bonded clusters, it is reported that the fragmentation pattern of these species are rather complicated for the quantitative analysis of neutral concentrations because of a serious protonation in ionization.

Experimental

Design of the temperature-controlled nozzle beam source used in photoelectron measurements is illustrated in Fig. 1. The design and performance of the photoelectron spectrometer combined with this nozzle beam system has been given elsewhere.[4] In the measurements discussed in this paper, a disk with a pinhole of 0.1 mm in diameter and 0.5 mm in thickness has been used in the nozzle.

In the present temperature-controlling system, a copper block ($34\times34\times28$ mm^3) is used as a heat bath for the nozzle, through which a temperature-regulated fluid is circulated. The stainless-steel tubing (8 mm in diameter) is thermally contacted with the heat bath by fastening with screws. The temperature of the top of the nozzle is measured by a copper-constantan thermocouple. A hole of 6 mm in diameter is drilled in the copper block, perpendicular to two parallel holes (6 mm in diameter). The open end of the drilled hole is plugged with a cylindrical block to form a U-shaped tunnel through which the fluid is circulated. The both ends of the U-shaped tunnel are connected with stainless steel bellows (CAJON 1/4″ flexible tubings). The other ends of the bellows are connected to the circulator through the vacuum flange by tubings. All the junctions were carefully brazed to be vacuum tight.

The temperature of the top of the nozzle is controlled by circulating an appropriate fluid from a temperature-regulated bath circulator (NESLAB EX-300). By using water as a circulating fluid, the nozzle temperature is controlled within ±0.3 K between 290 and 370 K. It is possible to raise the nozzle temperature up to about 500 K by using an appropriate circulating fluid and also to lower down to about 250 K by employing a refrigerated circulating bath (NESLAB EN-850). Flowing a cold nitrogen gas, we were able to lower the nozzle temperature down to 175 K in 40 min.

During photoelectron measurements, the vapor pressure of the sample is kept constant by heating a sample container made of stainless steel. Both the container and the pipeline which connects the nozzle to the container can separately be

heated by a mantle-shaped heater and a tape heater, respectively. When a 'seeding method' was employed,[4] a carrier gas such as helium or argon was bubbled through a liquid sample in the container. Three pairs of Helmholtz coils are used to compensate the earth's magnetic field, because of the difficulty in covering the ionization and electron energy analyzing regions by μ-metal plates completely.

Results and Discussion

The approximate dimer concentration with respect to the monomer concentration can be estimated from HeI photoelectron spectra by the following way. In the present analysis we consider some two-component (monomer-dimer) systems for which the resulting monomer-dimer ratio seems to be consistent with those of mass spectrometry under similar conditions.[5,6]

The Method of Analysis. Let us consider a series of photoelectron spectra which consist of (a) a normalized spectrum of a monomer-dimer mixture, (b) a normalized spectrum of the pure monomer (reference), and (c) the stripped spectrum, as illustrated schematically in Fig. 2. The first two spectra (a) and (b) in Fig. 2 are obtained directly from the photoelectron measurements followed by intensity normalization at the maxima. In the mixture spectrum (a), the ratio of the band area (S_d/S_m) between the first bands of the dimer and the monomer, for instance, should reflect the ratio of the concentrations between the dimer and the monomer in the supersonic jet. The stripped spectrum (c) is obtained in such a way that the intense monomer band in the mixture spectrum (a) should be reasonably cancelled by subtraction of the reference spectrum (b) with a proper ractor α. In other words, the following relationship holds for the photoelectron intensity curves which are given as a function of the photoelectron kinetic energy (E).

$$I_s(E) = I_m(E) - \alpha I_r(E), \quad (1)$$

where $I_m(E)$, $I_r(E)$, and $I_s(E)$ are the photoelectron intensities of the mixture spectrum, the reference spectrum and the stripped spectrum, respectively.

The number densities of the monomer (N_m) and the dimer (N_d) in the beam should be proportional to the band areas S_m and S_d, respectively, as can be expressed by the following equations.

$$S_m = \alpha \int_{band} I_r(E)dE = \alpha k_m \sigma_m N_m, \quad (2a)$$

and

$$S_d = \int_{band} I_s(E)dE = k_d \sigma_d N_d, \quad (2b)$$

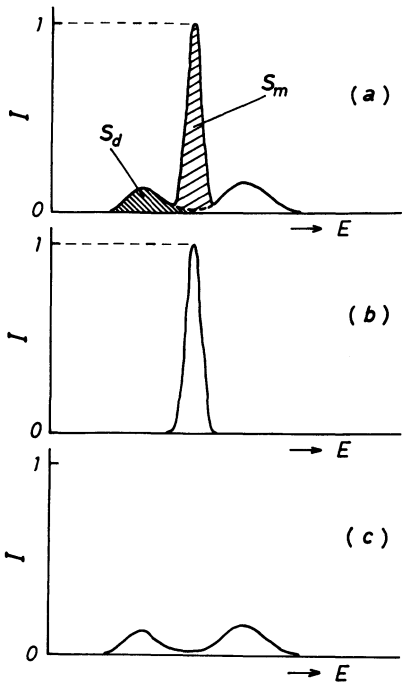

Fig. 2. An illustrative representation of the relation among (a) a normalized photoelectron spectrum of the monomer-dimer mixture ($I_m(E)$), (b) a normalized reference (monomer) spectrum ($I_r(E)$), and (c) the stripped spectrum: $I_s(E)=I_m(E)-\alpha I_r(E)$. Photoelectron intensity in each spectrum is a function of the kinetic energy (E). The monomer and dimer contributions (the shaded areas in spectrum (a)) are indicated by S_m and S_d, respectively.

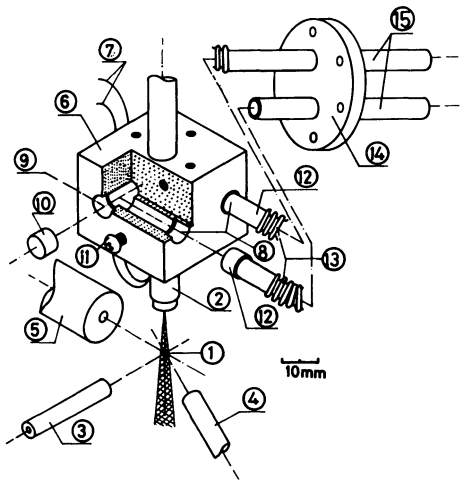

Fig. 1. A schematic drawing of the construction of the temperature-controlled supersonic nozzle beam source: (1) ionization region, (2) nozzle pipe, (3) glass capillary for the light beam, (4) copper tubing for the effusive source, (5) the first piece of an electrostatic lens system, (6) copper block heat bath, (7) copper-constantan thermocouple, (8) two parallel holes, (9) hole connecting the two parallel holes, (10) plug, (11) screw to fasten the nozzle pipe with the heat bath, (12) braze adopters, (13) bellows, (14) vacuum flange, and (15) tubings connected with the fluid circulator.

Table 1. Approximate dimer concentrations estimated from the photoelectron measurements

	Estimated dimer/monomer ratio[a]	Stagnation condition[b] T/K	P/Torr	Ref.
Water	0.06	335	390	2
Methanol	0.2	295—320	100—260	3
Formic acid	3	298	20+130(He)	4

a) Probable errors depend on the validity of the assumptions (see text). b) An aperture of 0.1 mm in diameter is used for the nozzle.

where σ_m and σ_d are the total photoionization cross sections of the monomer and the dimer, respectively. The constants k_m and k_d represent the difference in the angular distribution of photoelectrons, since the photoelectron transmission efficiencies at the same kinetic energy for the monomer and the dimer are equal to each other. It is easily noted from consideration of the differential photoionization cross section[7] that the ratio k_d/k_m would never exceed a factor of two even in the extreme case, when photoelectrons are measured at 90° with respect to the photon beam as in the present case.** Provided that the difference in the angular distribution is negligibly small, the monomer-dimer number density ratio is simply given by

$$N_d/N_m = \alpha(S_d\sigma_m/\sigma_d S_m). \quad (3)$$

Since we have no established knowledge on the ratio of σ_m and σ_d, let us assume $\sigma_d=\sigma_m$ to the crudest approximation. The resulting equation can give the order of the magnitude of the monomer-dimer number density ratio in the sample jet,

$$N_d/N_m \approx \alpha(S_d/S_m). \quad (4)$$

Results of Estimation. The relative dimer concentrations for water, methanol, and formic acid estimated from the previous measurements with a nozzle pinhole of 0.1 mm in diameter are summarized in Table 1, along with the stagnation conditions.

Before making a quantitative comparison between our photoelectron spectroscopic estimation and the available mass spectrometric analysis, we should note the following points.

(1) Production of the dimeric and polymeric species depends on the stagnation conditions and the nozzle characteristics (the shape and the size of the aperture and the depth of the throat), which are different in various studies. Therefore, in order to make proper comparisons of the results, the following experimental conditions should be specified: (a) the diameter and the depth of the aperture of the nozzle (the latter is sometimes not indicated in literatures) and (b) the stagnation pressure and temperature and also the composition of gases if the seeding method is applied.

(2) Fragmentation patterns of the hydrogen-bonded clusters in mass spectrometry seem to be rather complicated, depending on the ionizing projectile (electrons or photons) and its impact energy. No quantitative method to identify the original components from the relative abundance of the ions has been established yet. Under the condition where concentrations of higher polymers are negligible, however, the intensity ratio of the protonated ions (MH^+) or the sum of the protonated ion (MH^+) and the parent ion (M_2^+) with respect to the parent monomer ion (M^+) can be regarded as reflecting the neutral monomer-dimer ratio as a crudest approximation, since hydrogen-bonded dimers yield protonated monomer ions (MH^+) predominantly.[5,6,8-11]

Our monomer-dimer ratio for the water (6%) is in good agreement with the result of the ion intensity ratio ($H_3O^+/H_2O^+\approx 10\%$) reported by Dyke *et al.*[5] under the similar condition. For the methanol dimer, Odutola *et al.*[6] obtained a value of 8% for $(CH_3OH)H^+$ and 4% for $(CH_3OH)_2^+$ with respect to $(CH_3OH)^+$ under the stagnation condition of 317 K and 100 Torr (1 Torr=133.322 Pa). This result also shows a reasonable agreement with our present estimation. Cook *et al.*[8] have recently suggested larger relative concentrations of the dimer to higher polymers for methanol. However, their results cannot be compared directly with our present estimation, because their nozzle (conical, 0.33 mm in diameter) quite differs from ours both in the shape and size of the aperture.[9]

Our estimation of the dimer concentration for the formic acid gives a quite large value which means about three times more dimers than the monomer in the supersonic jet. There seems no available data on the mass analysis of the formic acid dimer for direct comparison. Recently, the temperature dependence of cluster formation for some carboxylic acids in the supersonic jet has been studied by Cook *et al.*[10] and by Mori *et al.*[11] by means of mass spectrometry. These studies have indicated that the dimer formation is extremely dominant for these cyclic dimers and it behaves as a monomer-dimer equilibrium mixture even in the supersonic jet. Therefore, it may be reasonable to understand the high dimer concentration of the present estimation for the formic acid as a "quasi-equilibrium" at a reduced pressure,[4] since about ten times higher dimer concentration (monomer : dimer =10% : 90%) is expected for the saturated formic acid vapor (about 40 Torr at 298 K) from the equilibrium constant by Coolidge.[13]

Conclusion

(1) By using the approximate method described above, the monomer-dimer number density ratio in the supersonic jet has been deduced from careful examinations of the stripping procedure involved in the photoelectron data analysis. The estimated values show reasonable agreements with the available results of mass spectrometric analysis.

(2) The deduction of HeI photoelectron spectra for some hydrogen-bonded dimers has clearly demonstrated the importance and the potentiality of the temperature-controlled nozzle beam source. The present nozzle system is especially suitable for electron spectroscopic measurements, because it is free from electromagnetic fields around the ionization region.

(3) A variety of its applications to molecular beam experiments may be expected not only for electron spectroscopic studies but also for other spectroscopic studies, especially because of its simple structure.

The authors are grateful to Mr. Toshio Horigome of the Institute for Molecular Science for his skilful and thorough work in constructing the present temperature-controlled supersonic nozzle beam source.

** The angular distribution of photoelectrons is given by the following equation,

$$d\sigma(\theta)/d\Omega = (\sigma_{tot}/4)[1-(\beta/4)(3\cos^2\theta-1)],$$

where σ_{tot} is the total photoionization cross section and β is the asymmetry parameter which ranges from -1 to 2.

Reference

1) P. M. Dehmer and J. L. Dehmer, *J. Chem. Phys.*, **67**, 1774 (1977); **68**, 3462 (1978); **69**, 125 (1978).
2) S. Tomoda, Y. Achiba, and K. Kimura, *Chem. Phys. Lett.*, **87**, 197 (1982).
3) S. Tomoda and K. Kimura, *Chem. Phys.*, **74**, 121 (1983).
4) S. Tomoda, Y. Achiba, K. Nomoto, K. Sato, and K. Kimura, *Chem. Phys.*, **74**, 113 (1983).
5) T. R. Dyke, K. M. Mack, and J. S. Muenter, *J. Chem. Phys.*, **66**, 498 (1977).
6) J. A. Odutola, R. Viswanathan, and T. R. Dyke, *J. Am. Chem. Soc.*, **101**, 4787 (1979).
7) J. W. Rabalais, "Priciples of Ultraviolet Photoelectron Spectroscopy," John Wiley and Sons, New York (1977), Chap. 6.
8) K. D. Cook, G. G. Jones, and J. W. Taylor, *Int. J. Mass Spectrom. Ion Phys.*, **35**, 273 (1980).
9) G. R. Parr and J. W. Taylor, *Rev. Sci. Instrum.*, **44**, 1578 (1973).
10) K. D. Cook and J. W. Taylor, *Int. J. Mass Spectrom. Ion Phys.*, **35**, 259 (1980).
11) Y. Mori, T. Kitagawa, T. Yamamoto, K. Yanada, and S. Nagahara, *Bull. Chem. Soc. Jpn.*, **53**, 3492 (1980).
12) A. S. Coolidge, *J. Am. Chem. Soc.*, **50**, 2166 (1928).

Ylide-Metal Complexes. VII.[1] The Preparation and Properties of IIA Group Metal(Be, Mg) and IIIA Group Metal(Al, Ga, In) Complexes of Alkylidenetriphenylphosphoranes

Yoshihisa YAMAMOTO

Faculty of Pharmaceutical Science, Higashi Nippon Gakuen University, Ishikari-Tobetsu, Hokkaido 061-02

(Received November 15, 1982)

The reactions of $(C_6H_5)_3P{=}CH_2$ (**L**) with $BeCl_2$ or $MgCl_2$ in the mole ratio of 2 : 1 or 4 : 1 yield new dimeric compounds of di-μ-chloro-bis[(methylenetriphenylphosphorane)metal] dichloride, $[(C_6H_5)_3PCH_2\text{-}M\langle^{Cl}_{Cl}\rangle M\text{-}CH_2P(C_6H_5)_3]Cl_2$ (M: Be and Mg). The configuration of these metals is trigonal. The reactions of **L** with $AlCl_3$, $GaCl_3$ or $InCl_3$ in the mole ratio of 2 : 1 yield new compounds of di-μ-chloro-bis[bis(methylenetriphenylphosphorane)-metal] tetrachloride, $[\{(C_6H_5)_3PCH_2\}_2M\langle^{Cl}_{Cl}\rangle M\{CH_2P(C_6H_5)_3\}_2]Cl_4$ (M: Al, Ga, and In). The reactions of **L** with $AlCl_3$ or $GaCl_3$ in the mole ratio of 3 : 1 or 5 : 1 yield new compounds of μ-chloro-bis[tris(methylenetriphenylphosphorane)metal] pentachloride, $[\{(C_6H_5)_3PCH_2\}_3M\text{-}Cl\text{-}M\{CH_2P(C_6H_5)_3\}_3]Cl_5$ (M: Al, Ga). These dimers, bridged by chloride anions, are thermally stable.

Many investigations[2] of IIA Group and IIIA Group metal complexes with methylenetri(or di)alkylphosphoranes have been reported, but there have been few investigations of metal complexes with triphenylphosphorane derivatives. A previous paper has been concerned with IVA Group metal (Ge, Sn, Pb) complexes[3] of alkylidenetriphenylphosphoranes. The present paper will deal with the preparation and properties of di-μ-chloro-bis[(methylenetriphenylphosphorane)metal] dichloride, $[(C_6H_5)_3PCH_2M\langle^{Cl}_{Cl}\rangle MCH_2P(C_6H_5)_3]Cl_2$ (M: Be, Mg), di-μ-chloro-bis[bis(methylenetriphenylphosphorane)metal] tetrachloride, $[\{(C_6H_5)_3PCH_2\}_2M\langle^{Cl}_{Cl}\rangle M\{CH_2P(C_6H_5)_3\}_2]Cl_4$ (M: Al, Ga, In), and μ-chloro-bis[tris(methylenetriphenylphosphorane)metal] pentachloride, $[\{(C_6H_5)_3PCH_2\}_3M\text{-}Cl\text{-}M\{CH_2P(C_6H_5)_3\}_3]Cl_5$ (M: Al, Ga).

Results and Discussion

Beryllium, Magnesium, and Calcium Complexes. Di-μ-chloro-bis[(alkylidenetriphenylphosphorane)metal (Be, Mg)] dichlorides have been isolated from a reaction mixture of alkylidenetriphenylphosphorane, $(C_6H_5)_3P{=}CHR$ (**L** (R : H) and **L'** (R: CH_3)), with $BeCl_2$ or $MgCl_2$. Complexes **1** and **2** are soluble only in acidic solvents, such as sulfuric acid, nitric acid, hydrochloric acid, and acetic acid. Complex **3** is soluble in DMF,

$$4(C_6H_5)_3P{=}CH\text{-}R + nMCl_2 \longrightarrow$$

M	Be	Mg
n	2	1

$$[(C_6H_5)_3P\overset{R}{C}H\text{-}M\langle^{Cl}_{Cl}\rangle M\text{-}\overset{R}{C}HP(C_6H_5)_3]Cl_2$$

No.	1	2	3
M	Be	Be	Mg
R	H	Me	H

DMSO, MeOH, and water, but insoluble in chloroform and dichloromethane. They are all highly hygroscopic. No calcium complex could be isolated from the reaction mixture of **L** and $CaCl_2$ in the mole ratio of 2 : 1 or 4 : 1.

The ^1H NMR spectrum of **3** showed a doublet signal for the methylene group at 2.17 ppm and a multiplet signal for phenyl groups at 7.3—8.0 ppm (in the ratio of 2 : 15) in CD_3OD at −80 °C. The chemical shift of the methylene group is at a lower field than that[4] (0.13 ppm) of **L**. The coupling constant ($^2J_{HCP}$) of **3** is 12.3 Hz, larger than that[4] (7.5 Hz) of **L**. These features are similar to those of bis(methylenetriphenylphosphorane)metal chloride, $[(C_6H_5)_3PCHR\text{-}M\text{-}CHRP(C_6H_5)_3]Cl_n$ (**4**) (R: H, M: IB Group and IIB Group metal[5]) and (methylenetriphenylphosphorane)-triphenylmetal chloride, $[(C_6H_5)_3PCH_2\text{-}M(C_6H_5)_3]Cl$ (**5**) (M: IVA Group metal[3]). Thus, the ylide **L** is bonded to the metal atom through the carbanionic donor atom.[3,5] Complexes **1** and **2** are unstable in 3.6 mol dm^{-3} D_2SO_4 at −34 °C, giving a alkyltriphenylphosphonium chloride, $[(C_6H_5)_3PCH_2\text{-}R]Cl$ (R: H (**6a**), CH_3 (**6b**)). The decomposition temperatures did not agree with the melting points of the ylides or salts **6**. Their colors are white. These properties resemble those of **4** (R: CH_3, $CH(CH_3)_2$),[5] and the ylides seem to be bonded to the beryllium atom in the solid state.[3] Two structures for the beryllium compounds have been considered possible: either a tetrahedral (monomeric,[6] dimeric,[7] and polymeric[8]) or a trigonal (monomeric,[9] dimeric,[10] and trimeric[11]) configuration. In the cases of **1**—**3**, they are not soluble in chloroform and dichloromethane. This is different from the **4**[5] (linear configuration), and **5**[3] and IIIA Group metal complexes (tetrahedral configuration). The elemental analyses of **1**—**3** agreed with that of $[LMCl_2]_n$. Complex **3** has free anion from the equivalent conductance. Thus, we suggest that the structure of **1**—**3** can be neither a linear nor tetrahedral configuration, but a dimeric trigonal structure.

Aluminium, Gallium, Indium, and Thallium Complexes. 2 : 1 Complexes: Di-μ-chloro-bis[bis(methylenetriphenylphosphorane)metal (Al, Ga, In)] tetrachlorides have been isolated from a reaction mixture of **L** and $AlCl_3$,

$GaCl_3$ or $InCl_3$ in the mole ratio of 2 : 1. Complexes **7**—**9** are soluble in alcohols, chloroform, dichloromethane, DMF, DMSO, and water, but are unstable in these solvents at room temperature and are changed to the corresponding phosphonium chloride (**6a**). In

$$4(C_6H_5)_3P{=}CH_2 + 2MCl_3 \longrightarrow \left[\begin{matrix}(C_6H_5)_3PCH_2 & Cl & CH_2P(C_6H_5)_3\\ & M \quad M & \\ (C_6H_5)_3PCH_2 & Cl & CH_2P(C_6H_5)_3\end{matrix}\right] Cl_4$$

No.	7	8	9
M	Al	Ga	In

dichloromethane, **7** and **8** are stable at −80 °C. Complex **9** was slowly changed to **6a** in dichloromethane at −80 °C, the ^1H NMR spectrum of **9** showing signals of both **9** and **6a**. No thallium complex could be isolated from the reaction mixture of **L** and TlI in the mole ratio of 2 : 1.

The ^1H NMR spectra of **7** and **8** showed a doublet signal for CH_2P at 3.2 and 2.7 ppm respectively and a multiplet signal for phenyl groups at 7.4—7.9 ppm in a ratio of 2 : 15 at a low temperature in dichloromethane-d_2. In complexes **7**—**9**, the coupling constants ($^2J_{HCP}$) of the methylene group are larger than that of **L** and the chemical shifts are at a lower field than that of **L**, the chemical shift of **7** being the lowest, as is shown in Table 1. The configuration of these metals is assumed to be tetrahedral from the following facts: **7**—**9** are not polymeric, because they are soluble in dichloromethane and alcohols. The elemental analyses of **7**—**9** agreed with that of $[L_2MCl_3]_n$. The structures of $AlCl_3$, $GaCl_3$, $InCl_3$ and related compounds are of a dimeric, tetrahedral configuration.[12] Complexes **7** and **8** have free anion, judging from the equivalent conductance. Thus, it is suggested that **7**—**9** are dimers bridged by chloride anions and with a tetrahedral configuration.

3 : 1 Complexes: μ-Chloro-bis[tris(methylenetriphenylphosphorane)metal (Al, Ga)] pentachlorides have been isolated from a reaction mixture of **L** with $AlCl_3$ or $GaCl_3$ in the mole ratio of 3 : 1 or 5 : 1. The complexes are soluble in alcohols, chloroform, dichloromethane, DMF, DMSO, and water. The gallium complex **11** is stable in dichloromethane at −62 °C, though the aluminium

$$3(C_6H_5)_3P{=}CH_2 + AlCl_3 \longrightarrow 5(C_6H_5)_3P{=}CH_2 + GaCl_3$$

$$\left[\begin{matrix}(C_6H_5)_3PCH_2 & & CH_2P(C_6H_5)_3\\ (C_6H_5)_3PCH_2\text{–}M\text{–}Cl\text{–}M\text{–}CH_2P(C_6H_5)_3\\ (C_6H_5)_3PCH_2 & & CH_2P(C_6H_5)_3\end{matrix}\right] Cl_5$$

No.	10	11
M	Al	Ga

complex **10** is unstable under the same conditions, giving the corresponding phosphonium salt (**6a**). The ^1H NMR spectrum of **11** showed a doublet signal for the methylene group at 2.8 ppm and a multiplet signal for the phenyl groups at 7.4—7.9 ppm, in the ratio of 2 : 15, at −62 °C. The chemical shift and the coupling constant ($^2J_{HCP}$: 16.7 Hz) of the methylene group of **11** are very similar to those of **8** as is shown in Table 1. The

Table 1. ^1H NMR data of complexes

No.	CH_2P δ	CH_2P $^2J_{HCP}$/Hz	C_6H_5 δ	Temp °C	Solvent and standard
3	2.17d(2H)	12.3	7.3—8.0m(15H)	−80	1)
7	3.2d(2H)	14.6	7.4—7.9m(15H)	−80	2)
8	2.7d(2H)	16.7	7.4—7.9m(15H)	−62	2)
9	2.2d	15.2	7.2—7.9m	−80	2)
11	2.8d(2H)	16.7	7.4—7.9m(15H)	−62	2)
L′[a]	0.13d(2H)	7.5	6.2—7.2m(15H)	r.t.	

Solvents: 1) CD_3OD, 2) CD_2Cl_2. Standard: internal TMS (δ=0). a): Ref. 4.

elemental analyses of **10** and **11** agreed with that of $[L_3MCl_3]_n$. Complex **11** has free anion, judging from the equivalent conductance. Thus, **10** and **11** can also be assumed to be dimers bridged by a chloride anion.

The stable alkylidenetriphenylphosphorane complexes in dichloromethane are those with metals of IB Group (Cu, Ag, Au),[5b–d] IIB Group (Zn, Cd)[5a] and IIIA Group (Al, Ga) and with Pb.[3]

Experimental

Measurements. The ^1H NMR spectra were measured with R-40 (Hitachi) and SXP4-100 pulse ST (Bruker) spectrometers. The electric conductivities of solutions were determined by the use of a conductmetric meter, CM-30 (Shimadzu) in methanol for **3** or in dichloromethane for **7**, **8**, and **11** at a low temperature.

Starting Materials. The methylene-[13] and ethylidenetriphenylphosphoranes[5d] were prepared from the corresponding phosphonium bromides by the sodium-amide method.

Preparation of Complexes. Di-μ-chloro-bis[(methylenetriphenylphosphorane)beryllium] Dichloride (1): Beryllium dichloride (0.07 g, 0.876 mmol) was added to a dry THF (6 cm^3) solution of **L** (0.55 g, 1.99 mmol) at room temperature under a nitrogen atmosphere. The mixture was stirred for 12 h, then the white complex thus precipitated was filtered under nitrogen, washed with dry ether, and dried under a vaccum. Yield: 0.27 g (86.5%). Decomp 224 °C. Found: C, 64.81; H, 5.19%. Calcd for $C_{38}H_{34}P_2Be_2Cl_4$ (MW 712.46) C, 64.05; H, 4.81%.

Di-μ-chloro-bis[(ethylidenetriphenylphosphorane)beryllium] Dichloride(2): This complex was prepared from a reaction mixture of beryllium dichloride (0.06 g, 0.751 mmol) and **L′** (0.436 g, 1.50 mmol) in THF (6 cm^3). After 10 h, the white complex thus precipitated was filtered, washed with dry ether, and dried. Yield: 0.10 g (36.0%). Decomp 220 °C. Found: C, 63.41; H, 5.40%. Calcd for $C_{40}H_{38}P_2Be_2Cl_4$ (MW 740.50) C, 64.88; H, 5.17%.

Di-μ-chloro-bis[(methylenetriphenylphosphorane)magnesium] Dichloride (3): Complex **3** was prepared from magnesium dichloride (0.035 g, 0.368 mmol), **L** (0.41 g, 1.48 mmol), and THF (6 cm^3) at room temperature. After 4 d, the white complex thus precipitated was filtered under nitrogen, washed with ether, and dried. Yield: 0.10 g (73.2%). Decomp 60 °C. Found: C, 61.16; H, 4.78%. Calcd for $C_{38}H_{34}P_2Mg_2Cl_4$ (MW 743.06) C, 61.42; H, 4.61%.

Di-μ-chloro-bis[bis(methylenetriphenylphosphorane)aluminium] Tetrachloride (7): Aluminium trichloride (0.12 g, 0.9 mmol) was added to a dry THF (8 cm^3) solution of **L** (0.49 g, 1.77 mmol) under nitrogen. After 22 h, the white complex thus precipitated was filtered under nitrogen, washed with dry pentane, and dried under a vacuum. Yield: 0.4 g (64.8%). Decomp 225 °C. Found: C, 66.67; H, 5.18%. Calcd for $C_{76}H_{68}$-

$P_4Al_2Cl_6$ (MW 1371.92) C, 66.54; H, 5.00%.

Di-μ-chloro-bis[bis(methylenetriphenylphosphorane)gallium] Tetrachloride (8): Gallium trichloride (0.43 g, 2.44 mmol) was added to a THF (20 cm^3) solution of **L** (1.35 g, 4.88 mmol). The color of the **L** changed from yellow to colorless. The white complex thus precipitated was filtered after 2 h, washed with dry ether and dried. Yield: 1.61 g (90.5%). Decomp 187 °C. Found: C, 63.14; H, 5.08%. Calcd for $C_{76}H_{68}P_4Ga_2Cl_6$ (MW 1457.40) C, 62.63; H, 4.70%.

Di-μ-chloro-bis[bis(methylenetriphenylphosphorane)indium] Tetrachloride (9): Indium trichloride (0.08 g, 0.36 mmol) was added to a THF (10 cm^3) solution of **L** (0.20 g, 0.72 mmol). The yellow color of **L** changed to colorless. The white complex thus precipitated was filtered after 10 h, washed with dry ether, and dried. Yield: 0.18 g (64.3%). Decomp 197 °C. Found: C, 59.11; H, 4.21%. Calcd for $C_{76}H_{68}P_4In_2Cl_6$ (MW 1547.62) C, 58.98; H, 4.43%.

μ-Chloro-bis[tris(methylenetriphenylphosphorane)aluminium] Pentachloride (10): This complex was prepared from $AlCl_3$ (0.08 g, 0.6 mmol) and **L** (0.5 g, 1.81 mmol) in THF (10 cm^3). After 22 h, the white complex was filtered. Yield: 0.38 g (65.8%). Decomp 231 °C. Found: C, 70.02; H, 6.08%. Calcd for $C_{114}H_{102}P_6Al_2Cl_6$ (MW 1924.56) C, 71.15; H, 5.34%.

μ-Chloro-bis[tris(methylenetriphenylphosphorane)gallium] Pentachloride (11): This complex was prepared from $GaCl_3$ (0.09 g, 0.511 mmol), **L** (0.77 g, 2.79 mmol), and THF (12 cm^3). After 10 h, the white complex thus precipitated was filtered, washed with ether, and dried. Yield: 0.12 g (23.4%). Decomp 204 °C. Found: C, 67.11; H, 5.47%. Calcd for $C_{114}H_{102}P_6Ga_2Cl_6$ (MW 2010.04) C, 68.12; H, 5.12%.

The present work was partially supported by a Grant-in-Aid for Scientific Research No. 554190 from the Ministry of Education, Science and Culture.

References

1) Part VI: Ref. 3.
2) a) H. Schmidbaur and H. J. Füller, *Chem. Ber.*, **110**, 3528 (1977); b) H. Schmidbaur, O. Gasser, C. Krüger, and J. C. Sekutowski, *ibid.*, **110**, 3517 (1977); c) H. Schmidbaur, H. J. Füller, and F. H. Köhler, *J. Organomet. Chem.*, **99**, 353 (1975); d) H. Schmidbaur and H. J. Füller, *Chem. Ber.*, **107**, 3674 (1974); e) H. Schmidbaur and W. Tronich, *ibid.*, **101**, 595 (1968).
3) Y. Yamamoto, *Bull. Chem. Soc. Jpn.*, **55**, 3025 (1982).
4) H. Schmidbaur, H. Stühler, and W. Vornberger, *Chem. Ber.*, **105**, 1084 (1972).
5) a) Y. Yamamoto and H. Sugimoto, *Bull. Chem. Soc. Jpn.*, **53**, 3176 (1980); b) Y. Yamamoto and Z. Kanda, *ibid.*, **52**, 2560 (1979); b) Y. Yamamoto and H. Schmidbaur, *J. Organomet. Chem.*, **97**, 479 (1975); d) Y. Yamamoto and H. Schmidbaur, *ibid.*, **96**, 133 (1975).
6) V. Amirthalingham, V. M. Padmanabhan, and J. Shanker, *Acta Crystallogr., Sect. B*, **16**, 201 (1960).
7) O. Rahlfs and W. Fischer, *Z. Anorg. Chem.*, **211**, 349 (1933).
8) a) R. E. Rundle and P. H. Lewis *J. Chem. Phys.*, **20**, 132 (1952); b) H. Steinfink and G. D. Brunton, *Acta Crystallogr., Sect. B*, **24**, 807 (1968).
9) L. G. Brisseau, M. G. B. Drew, and J. E. Goulter, *J. Chem. Soc., Chem. Commun.*, **1972**, 916.
10) G. E. Coates and F. Glockling, *J. Chem. Soc.*, **1954**, 22.
11) a) J. L. Atwood and G. D. Stucky, *J. Am. Chem. Soc.*, **91**, 4426 (1969); b) J. L. Atwood and G. D. Stucky, *J. Chem. Soc., Chem. Commun.*, **1967**, 1169.
12) a) K. J. Palmer and N. Elliott, *J. Am. Chem. Soc.*, **60**, 1852 (1938); b) P. H. Lewis and R. E. Rundle, *J. Chem. Phys.*, **21**, 986 (1953); c) N. Müller and D. E. Pritchard, *J. Am. Chem. Soc.*, **82**, 248 (1960); d) M. P. Groenewege, J. Smidt, and H. D. Vries, *ibid.*, **82**, 4425 (1960); e) L. A. Woodward, N. N. Greenwood, J. R. Hall, and I. J. Worrall, *J. Chem. Soc.*, **1958**, 1505; f) S. C. Wallwork and I. J. Worrall, *ibid.*, **1965**, 1816; g) J. D. Forrester, A. Zalkin, and D. H. Templeton, *Inorg. Chem.*, **3**, 63 (1964).
13) R. Köster, D. Simic, and M. A. Grassberger, *Justus Liebigs Ann. Chem.*, **739**, 211 (1970).

The Synthesis and Color of Pyrido[1′,2′ : 1,2]pyrimido[4,5-*b*]-acridine-7,15-diones

Yasukazu YOKOYAMA

Tokyo Laboratory, Toyo Soda Manufacturing Co., Ltd., Hayakawa, Ayase, Kanagawa 252

(Received September 24, 1981)

Some derivatives of pyrido[1′,2′: 1, 2]pyrimido[4,5-*b*]acridine-7,15-diones have been synthesized, their absorption spectra have also been investigated in order to elucidate the relationship between the color and the chemical constitution in contrast to the related compounds, quinacridone and pyrido[2,1-*b*]pyrido[1′,2′ : 1,2]pyrimido-[4,5-*g*]quinazoline-7,15-dione. The absorption spectra in DMSO and in concentrated sulfuric acid show a good correlation with the electronic effect of the substituents. The absorption spectra of the solid are more influenced by the position of the substituents than by the electronic effect.

Linear *trans*-quinacridone (**1**) is a valuable organic pigment because of its excellent properties. Therefore, much attention has heen paid to the synthesis and the electronic spectral studies of quinacridones and some derivatives with similar chemical constitutions.[1] The substituents of quinacridones have little effect on the visible spectra in concentrated sulfuric acid, but a marked effect on the solid color.[2] In a previous paper, we showed that the introduction of methyl groups into the 1,9- and 4,12-positions of pyrido[2,1-*b*]pyrido-[1′,2′ : 1,2]pyrimido[4,5-*g*]quinazoline-7,15-dione (**2**) gives rise to a hypsochromic shift from red to orange in the solid color.[3] Altiparmakin has reported that the effect of the substituents of **2** on the electronic spectra is practically negligible in contrast to the case of **1**, since the substituents are, in fact, isolated from chromophore.[4]

It is interesting to make clear the relationship between the color and the chemical constitution of those compounds. Therefore, in this study, some derivatives of 5*H*-pyrido[1′,2′: 1,2]pyrimido[4, 5-*b*]acridine-7,15-dione (**3a**) were synthesized, and their electronic spectra in solutions and their reflectance spectra in the solid were compared with those of **1** and **2**.

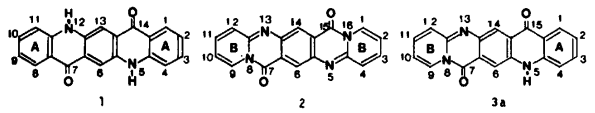

Fig. 1.

Experimental

The IR, VS, and ^{1}H-NMR spectra were recorded on a Shimadzu IR-27G spectrophotometer, a Hitachi 306 spectrophotometer, and a Varian HA-100 spectrometer respectively. The color measurements were obtained using a Hitachi Trichromatic Integrator.

Materials. All the reagents except those listed below were obtained from commercial sources and were used without further purification.

Improved methods for the preparation of **3a** were employed to obtain substituted **3**, whose A or B ring carries substituents (Scheme 1).

The synthetic intermediates, 2-anilino-3-ethoxycarbonyl-1,4-dihydro-9(10*H*)-acridone (**4**) and 7-ethoxycarbonyl-6,9-dihydro-8-hydroxypyrido[2,1-*b*]quinazolin-10-one (**6**) were prepared according to the methods described in the literature.[5]

6, 14-Dihydropyrido[1′, 2′ : 1, 2]pyrimido[4, 5-b]acridine-7, 15-diones (5). *a)*: The reaction of **4** and 2-aminopyridines

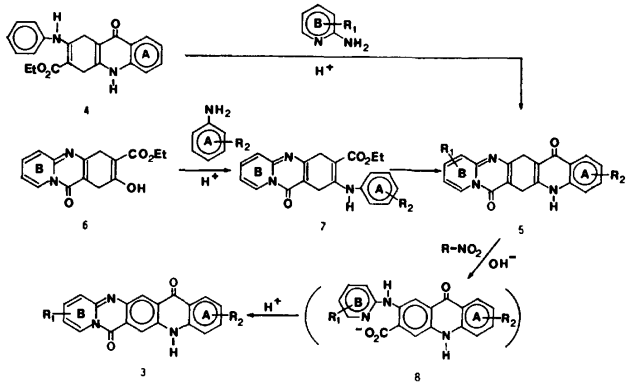

Scheme 1.

were carried out according to the methods described in a previous paper.[4] Pale pink solids of **5a—e** were obtained.

b): A mixture of 5.0 g, of **6** and 19 g of *p*-toluidine was heated to reflux in 50 ml of acetic acid for 2.5 h while being stirred under a nitrogen atmosphere. When the reddish orange solution was then cooled, a pale orange solid precipitated. The solid was collected on a filter, washed with methanol, and dried at 60 °C. The solid (5.0 g) was heated in 70 g of polyphosphoric acid for 1 h. The resulting solution was diluted with large excess of water to give **5f** as a pale pink solid. The other substituted derivatives were prepared analogously.

In this reaction, the methoxyl-group at the 2-position of **5** was hydrolyzed to the 2-hydroxy derivative **5h**. The methoxyl-group at the 4-position of **5** was not hydrolyzed under the same reaction conditions. Some pertinent data on **5** are also shown in Table 1.

Pyrido[1′,2′ : 1,2]pyrimido[4,5-b]acridine-7,15-diones (3).

a): The dehydrogenation of **5** was carried out, using sodium *m*-nitrobenzenesulfonate as a dehydrogenating agent, by the method described in our previous paper.[6]

b): A mixture of 5.0 g of **5b**, 5.0 g of sodium *m*-nitrobenzene-sulfonate, 9 g of a 33% aqueous sodium hydroxide solution, and 100 g of ethylene glycol was heated at 100—130 °C for 2 h. The resulting red solution was cooled and neutralized with an aqueous sulfuric acid solution. The precipitate was filtered, washed with water, and dried at 60 °C.

Three grams of the brown colored powder were heated at 90—100 °C for 2 h in 50 g of polyphosphoric acid. The resulting red solution was cooled to room temperature and then diluted with 200 ml of water. The reddish orange crystals thus precipitated were filtered, washed with water, and dried at 60 °C. The yield was 2.3 g (76.7%).

The compounds **3** were conveniently purified by the following procedure. To a suspension of 3 g of crude **3a—1** in 100

TABLE 1. 6,14-DIHYDROPYRIDO [1′,2′ : 1,2] PYRIMIDO [4,5-*b*] ACRIDINE-7,15-DIONES

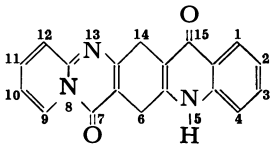

5	Substituent position	Yield %	Found (%) C	Found (%) H	Found (%) N	Calcd (%) C	Calcd (%) H	Calcd (%) N	IR (KBr) ν_{N-H}/cm^{-1}	IR (KBr) $\nu_{C=O}/cm^{-1}$	
5a	None	85	72.41	4.32	13.22	72.37	4.15	13.33	3270	1670	1640
5b	9-CH_3	72.5	73.08	4.65	13.02	72.92	4.60	12.76	3270	1668	1640
5c	10-CH_3	98.0	72.79	4.36	12.93	72.92	4.60	12.76	3270	1720	1665
5d	11-CH_3	92.2	72.50	5.07	12.63	72.92	4.60	12.76	3270	1678	1640
5e	12-CH_3	84.0	73.20	4.76	12.48	72.92	4.60	12.76	3280	1680	1640
5f	2-Cl	94.1	65.05	3.62	12.19	65.24	3.46	12.02	3280	1725	1670
5g	2-CH_3	97.0	72.76	4.33	12.90	72.92	4.60	12.76	3280	1725	1675
5h	2-OH	97.7	69.47	4.03	12.60	68.88	3.93	12.69	3280	1725	1670
5i	2-$COCH_3$	92.8	70.41	4.37	11.86	70.59	4.20	11.76	3280	1725	1670
5j	4-CH_3	86.2	73.16	4.90	12.47	72.92	4.20	12.76	3250	1730	1675
5k	4-OCH_3	86.2	69.04	4.61	12.18	69.55	4.39	12.17	3280	1720	1670
5l	4-Cl	93.0	65.52	3.57	11.89	65.24	3.46	12.02	3280	1690	1670

TABLE 2. PYRIDO [1′,2′ : 1,2] PYRIMIDO [4,5-*b*] ACRIDINE-7,15-DIONES

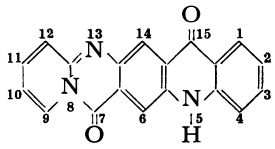

3	Substituent position	Yield %	Found (%) C	Found (%) H	Found (%) N	Calcd (%) C	Calcd (%) H	Calcd (%) N	IR (KBr) ν_{N-H}/cm^{-1}	IR (KBr) $\nu_{C=O}/cm^{-1}$	
3a	None	95.5	72.31	3.74	13.22	72.84	3.54	13.41	3260	1700	1650
3b	9-CH_3	76.7	73.28	4.44	12.86	73.37	4.01	12.84	3250	1710	1660
3c	10-CH_3	90.7	73.86	4.02	12.59	73.37	4.01	12.84	3320	1730	1680
3d	11-CH_3	97.9	73.69	4.27	12.85	73.37	4.01	12.84	3280	1725	1655
3e	12-CH_3	97.2	73.48	4.00	12.58	73.37	4.01	12.84	3250	1690	1650
3f	2-Cl	97.5	65.11	3.69	12.27	65.62	3.49	12.09	3280	1740	1650
3g	2-CH_3	95.9	73.85	4.43	12.96	73.37	4.01	12.84	3250	1740	1650
3h	2-OH	89.4	69.54	4.12	12.70	69.30	3.34	12.77	3250	1740	1650
3i	2-$COCH_3$	93.9	70.61	3.75	11.84	70.99	3.66	11.83	3250	1740	1650
3j	4-CH_3	94.1	73.27	4.18	12.76	73.37	4.01	12.84	3250	1700	1650
3k	4-OCH_3	88.5	69.34	3.92	12.49	69.96	3.82	12.24	3350	1700	1650
3l	4-Cl	96.8	65.31	3.57	12.01	65.62	3.49	12.09	3330	1690	1653

ml of ethylene glycol we added 10 g of a 20% aqueous sodium hydroxide solution. The mixture was heated with continuous stirring at 100—120 °C for 2 h. The resulting red solution was cooled and acidified with 20 g of a 20% aqueous sulfuric acid solution. The slurry thus formed was heated at 70—80 °C for 1 h. The product was collected by filtration and washed with hot ethylene glycol and then water. Recrystallization from DMSO afforded reddish orange crystals (2.7 g, 90% recovery).

The yields and some pertinent data for **3** are listed in Table 2.

Picrate. a): A mixture of 100 ml of ethanol, 2.0 g of **2**, and 5.0 g of picric acid was heated to reflux for 2 h. The resultant yellow solid was collected by filtration, washed with ethanol, and dried at 60 °C. The yield was 4.2 g. The product was determined to be picrate (**2** : picric acid = 1 : 2, M/M, 1 M = 1 mol dm^{-3}) by means of IR spectroscopy and elemental analysis. Found: C; 47.09, H; 2.24, N; 18.29%. Calcd for $C_{30}H_{16}N_{10}O_{16}$: C; 46.64, H; 2.09, 18.13%. IR (KBr) C=O 1705 cm^{-1}. *b)*: From 2.0 g of **3a** and 5.0 g of picric acid, 3.4 g of orange crystals were obtained by means of the procedure described above. The product was determined to be picrate (**3a**: picric acid = 1 : 1, M/M) by IR spectroscopy and elemental analysis. Found: C; 55.51, H; 2.50, N; 15.96%. Calcd for $C_{25}H_{14}N_6O_9$; C; 55.35, H; 2.58, N; 15.50%. IR(KBr) C=O 1723 cm^{-1}. *c)*: The 4,12-dimethyl derivative of **2** and the 4-methyl derivative of **3a**(**3e**) formed no picrate.

Color Measurements. The visible absorption maxima of the solid were obtained from the reflectance spectra on the dispersion of the solid diluted with TiO_2(1/5) in cellulose acetate butyrate.

Spectral Measurements. The visible spectra of **1**, **2**, and **3** were measured on both DMSO and concentrated sulfuric acid solutions, ranging in concentration from 1×10^{-3} to 1×10^{-5} M. The spectra were independent of the concentration in this concentration range.

Table 3. ^{1}H-NMR data for **1**, **2**, and **3** in concd H_2SO_4

Compound	Substituent	Chemical shifts δ										
1		H_1	H_2	H_3	H_4	H_8	H_9	H_{10}		H_{11}		$H_{6,13}$
		9.14	8.42	8.88	8.65	9.14	8.42	8.88		8.65		10.08
		H_1	H_2	H_3	H_4	H_9	H_{10}	H_{11}	H_{12}	H_5	H_6	H_{14}
2		9.83	8.33	9.12	8.52	9.83	8.33	9.12	8.52		9.48	9.48
3a		9.03	8.51	8.94	8.73	9.72	8.25	9.14	8.47	12.96	9.93	9.61
3b	9-CH_3	9.18	8.51	8.8	8.8	$CH_3$3.75	7.92	8.8	8.22	12.88	9.77	9.44
3c	10-CH_3	9.16	8.48	8.91	8.70	9.56	$CH_3$3.10	8.90	8.38	12.92	9.87	9.56
3d	11-CH_3	9.18	8.50	8.92	8.71	9.64	8.06	$CH_3$3.30	8.21	12.93	9.89	9.55
3e	12-CH_3	9.16	8.50	8.9	8.70	9.70	8.17	8.9	$CH_3$3.35	12.94	9.89	9.84
3f	2-Cl	9.10	—	8.83	8.7	9.88	8.24	9.04	8.50	13.11	9.93	9.56
3g	2-CH_3	8.92	$CH_3$3.25	8.88	8.64	9.77	8.24	9.06	8.46	12.93	9.90	9.58
3h	2-OH	8.97	—	8.87	8.74	9.77	8.24	9.06	8.45	13.24	9.95	9.52
3i	2-$COCH_3$	9.1	$COCH_3$4.0	9.0	8.8	9.8	8.3	9.4	8.5	13.30	9.95	9.63
3j	4-CH_3	9.02	8.4	8.75	$CH_3$4.46	9.77	8.23	9.0	8.4	12.34	10.13	9.57
3k	4-OCH_3	9.0	8.40	8.67	$OCH_3$4.80	9.76	8.18	9.04	8.44	13.11	10.05	9.57
3l	4-Cl	8.98	8.46	9.20	—	9.79	8.26	9.08	8.47	12.73	10.18	9.60

Compound	Coupling constants/Hz
1	$J_{1,2}=J_{8,9}=8.0$ $J_{1,3}=J_{8,10}=1.6$ $J_{1,4}=J_{8,11}=0$ $J_{2,3}=J_{9,10}=6.8$ $J_{2,4}=J_{9,11}=1.4$ $J_{3,4}=J_{10,11}=8.2$
2	$J_{1,2}=J_{9,10}=6.8$ $J_{1,3}=J_{9,11}=1.2$ $J_{1,4}=J_{9,12}=0$ $J_{2,3}=J_{10,11}=7.4$ $J_{2,4}=J_{10,12}=0.8$ $J_{3,4}=J_{11,12}=8.0$
3a	$J_{1,2}=8$ $J_{1,3}=1.6$ $J_{1,4}=0$ $J_{2,3}=8$ $J_{2,4}=1.4$ $J_{3,4}=8.4$ $J_{9,10}=7.2$ $J_{9,11}=0.7$ $J_{9,12}=0$ $J_{10,11}=8$ $J_{10,12}=0.8$ $J_{11,12}=8$

Table 4. Visible spectra for **1**, **2**, and **3**

Compound	Substituent	Solid color λ/nm[a]					Solution, in DMSO λ/nm (ε)			in concd H_2SO_4 λ/nm (ε)		
		λ_1	λ_2	λ_3		λ_d[b]	λ_1	λ_2	λ_3	λ_1	λ_2	λ_3
1	H	490	525	560	λ_c	500	462 (3600)	491 (10000)	525 (16000)	517 (4500)	556 (9500)	597 (11500)
2	H	484	516	560		620	458 (4000)	487 (8000)	519 (6000)	420 (3800)	437 (7500)	469 (7500)
3a	H	468	495	523		603	460 (5000)	487 (9200)	519 (9700)	450 (5500)	483 (9000)	516 (8400)
3b	9-CH_3	470s[c]	503	535s		597	460 (3900)	487 (4900)	519 (4400)	458 (3400)	486 (5400)	519 (5100)
3c	10-CH_3	474	502	535		614	460 (5300)	487 (8800)	520 (8800)	455 (3100)	489 (6200)	522 (6200)
3d	11-CH_3	475	505	537		615	462 (4300)	489 (7300)	522 (7400)	455 (4880)	485 (6600)	517 (6200)
3e	12-CH_3	478	507	537		615	459 (4700)	486 (8200)	517 (8500)	455 (3800)	486 (5100)	518 (4800)
3f	2-Cl	485	517	551	λ_c	493	464 (4800)	491 (8000)	524 (8300)	460 (2500)	488 (4300)	521 (4000)
3g	2-CH_3	485	519	552		644	464 (4600)	492 (8000)	525 (8500)	460 (2600)	488 (4600)	520 (4600)
3h	2-OH	480s	512	542s	λ_c	493	464 (3200)	494 (5700)	528 (6100)	452 (4000)	481 (6700)	513 (6400)
3i	2-$COCH_3$	474	505	540		614	452 (5400)	480 (8000)	511 (7500)	464 (4200)	497 (4500)	530 (3900)
3j	4-CH_3	465	490	524		588	458 (4700)	485 (8100)	517 (8100)	460 (4600)	487 (7200)	520 (6700)
3k	4-OCH_3	470	496	530		602	460 (5000)	488 (8200)	520 (8200)	455 (3300)	482 (5500)	513 (5900)
3l	4-Cl	465	493	526		594	456 (5000)	483 (8300)	515 (8300)	463 (4500)	490 (7300)	523 (6900)

a) Obtained from a reflectance spectrum on a dispersion of a solid diluted with TiO_2(1/5) in CAB resin film. b) λ_d shows the dominant wave length, while λ_c represents the complementary wavelength. They were obtained from the C.I.E. Chromaticity Diagram by using Tristimulas Values available from the integration of the reflectance spectra with a trichromatic integrator. c) Shoulder.

Results and Discussion

Dihydro derivatives **5** were synthesized according to the two methods previously reported,[6] as is shown in Scheme 1. The first method gives **5** directly. Amine exchange and intramolecular cyclization spontaneously occurred on the heating of **4** with substituted amino pyridines in acetic acid. The second method involved the preparation of esters **7**, which were obtained by the condensation of **6** with substituted anilines. The cyclization of **7** was carried out in polyphosphoric acid. In this reaction, the *p*-methoxy group (R_2=*p*-OCH_3) of **7** was hydrolyzed to give 2-hydroxy derivative (**5h**), but the *o*-methoxy group was not hydrolyzed under the same reaction conditions. The dehydrogenation of **5** gave the corresponding **3** in high yields.

The compounds **3** are microcrystalline powders and range from orange to red in color. They do not melt or decompose up to 300 °C and are slightly soluble in organic solvents, such as dimethylformamido and dimethylsulfoxide (DMSO). The compounds **3**, as well as compound **2**, are weak bases and are soluble in aqueous solutions of strong acids, such as hydrochloric acid and sulfuric acid. The compounds **2** and **3** formed picrates, the 1 : 2 adduct of **2** and the 1 : 1 adduct of **3** with picric acid. However, the 4,12-dimethyl derivative of **2** and the 4-methyl derivative of **3a**(**3e**) formed no picrate. This is probably due to the steric hindrance between the methyl group adjacent to imino nitrogen and the voluminous nitro group of picric acid.

The absorption spectra of **3** were measured and compared with those of **1** and **2** in order to clarify the influences of substituents and of the measurement medium upon the electronic spectra. The ^{1}H-NMR data for **1**, **2**, and **3** are listed in Table 3. The coupling pattern of **2** is similar to that of **1**, but the proton signals of **2** are distributed over a wider range than those of **1**. The coupling constants for **2** are slightly smaller than those of **1**. The spectra of **3** appear almost as a superimposition of those of **1** and **2**. The chemical shifts of the aromatic protons of **3** are scarcely influenced by the electronic effects of their substituents.

The visible absorption spectra of **1**, **2**, and **3** in various media are listed in Table 4. The compounds **1** and **2** show visible absorptions at considerably shorter wavelengths in DMSO than in a solid. However, in concentrated sulfuric acid the spectrum of **1** shows a strong bathochromic shift, and that of **2**, a remarkable hypsochromic shift. On the other hand, the spectrum of **3a** is little affected by either solvent.

The strong bathochromic shift of **1** in concentrated sulfuric acid can be explained by the increased acceptor capacity of the carbonyl group for the protonation on the carbonyl oxygens. The hypsochromic shift of **2** in concentrated sulfuric acid may be attributed to the protonation at the imino nitrogens.[7] The imino protonation will destroy the polymethine chromophore. In the case of **3**, the bathochromic effect of the protonated acridone skeleton is counteracted by the protonation of the quinazolone skeleton, and the spectral shift is, consequently, small.

These spectral shifts can be interpreted on the basis of the assumption of protonated species, as is shown in Fig. 2. The protonated species **14** and **12** are regarded as the aza-replaced compounds of **1** and its mono protonated structure, **9**, respectively. The aza replacement at the 7a and 14a positions of **1** shows a remarkable hypsochromic shift. The observed shift is in accordance with the color rules.[8]

The compound **3a** absorbs at shorter wavelengths than **1**. This can easily be explained in terms of the replacement of an electron-donor substituent, NH, with an electron-accepter substituent, C=N, at the starred position of an acridone molecule.

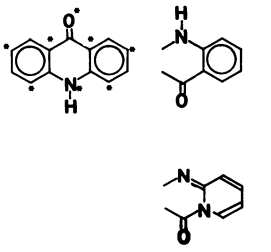

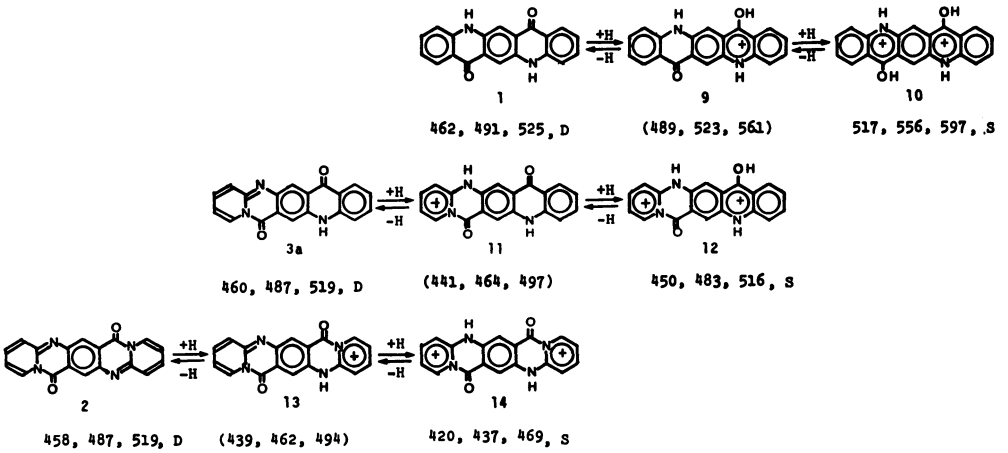

Fig. 2. Structure and spectral wavelength of compounds **1**, **2**, and **3** and their assumed protonated speacies, λ_{max}, (speculated values), nm. D: in DMSO, S: in concentrated sulfuric acid.

In the case of the substituted derivatives of **3a**, it is predictable that an electron-donating substituent at the starred position will show a bathochromic effect. The observed visible spectra of the derivatives of **3a** in the solutions show a good correlation with the electronic effect of the substituents, though the effect is small. Electron-donating substituents cause a bathochromic effect in DMSO and a hypsochromic effect in concentrated sulfuric acid. The substituent effect on protonated **3** is opposed to that on the unprotonated species. The opposite wavelength shifts by the protonation are not observed in the substituents of **1**. The observed wavelength shifts of **3** give straight-line relationship with Hammett σ constants, as is shown in Fig. 3. The relationship to the reactive substituent constant is explained by the fact that the shifts are closely related to the protonation equilibria of **3**. That is, the electron-donating substituents increase the donating ability of the acridone NH group, hence, the bathochromic shift is observed in DMSO. On the other hand, the electron-acceptor groups accelerate the protonation of the acridone skeleton, and the bathochromic shift is observed in concentrated sulfuric acid.

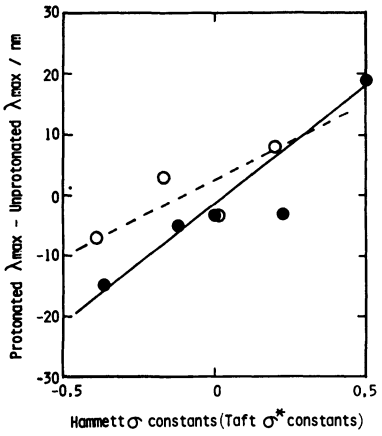

Fig. 3. Spectral longest-wavelength shifts observed with the protonation of **3** plotted against Hammett σ constants (para) ——, and Taft σ^* constants (ortho) ·····.

The substituents of **3** show a pronounced effect on their solid colors. The shades of the solid are also listed in Table 4 in terms of the dominant wavelength values, λ_d or λ_c. The substituents at the 2-position exert a bathochromic effect. The shift is larger than that in DMSO, but shows a poor correlation with the electronic effect of the substituents. The substituents at the 4-position exert almost no effect, and the λ_{max} values are almost the same as those of unsubstituted **3a** either in a solid or in DMSO. The 9, 10, 11, and 12-methyl substituted derivatives absorb light of wavelengths longer than **3a**, but the shift is smaller than that of the 2-methyl substituted derivative, **3g**. On the basis of this spectroscopy, the following conclusions were deduced: the effect of the substituent on the A ring of **3** upon the absorption spectra is larger than that of the substituent on the B ring, and the absorption spectra are more influenced by the position of the substituent than by the electronic effect of the substituent.

The authors wish to thank Professor Mitsuhiko Hida of Tokyo Metropolitan University for his valuable discussion and Mr. Kenichi Sato of the Sagami Chemical Research Center for obtaining the ^{1}H-NMR spectra.

References

1) S. S. Labana and L. L. Labana, *Chem. Rev.*, **67**, 1 (1967).
2) a) K. Hashizume, *Yuki Gosei Kagaku Kyokai Shi*, **20**, 574 (1962); b) K. Takagi, K. Kurosu, and I. Fujii, *Shikizai Kyokai Shi*, **41**, 438 (1968).
3) Y. Yokoyama, *Bull. Chem. Soc. Jpn.*, **51**, 1901 (1978).
4) R. Altiparmakin, *Helv. Chim. Acta*, **61**, 1146 (1978).
5) a) A. Tai, Y. Yokoyama, K. Shindo, and O. Fujii, *Yuki Gosei Kagaku Kyokai Shi*, **31**, 410 (1973); b) Y. Yokoyama, K. Shindo, O. Fujii, and E. Iwamoto, *Bull. CHem. Soc. Jpn.*, **48**, 591 (975).
6) Y. Yokoyama, *Nippon Kagaku Kaishi*, **1979**, 398.
7) Some potential sites of protonation exist in compound **2**. The imino group is inherently much more basic than the amide group, and **14** is considered the most likely structure for protonated **2**.
8) S. Dahne, *Science*, **199**, 1163 (1978).

An Interpretation of the Asymmetric Induction Observed in Rhodium-Bis(dibenzophosphole) Complex Catalyzed Hydroformylation According to an X-Ray Molecular Structure Analysis of an Iridium-(2*R*,3*R*)-2,3-*O*-Isopropylidene-1,4-bis(5*H*-dibenzophosphol-5-yl)-2,3-butanediol Complex

Teruyuki HAYASHI,* Masato TANAKA, Ikuei OGATA, Teruyuki KODAMA,†
Tamotsu TAKAHASHI,† Yasuzo UCHIDA,† and Tokiko UCHIDA††
National Chemical Laboratory for Industry, Higashi, Yatabe, Tsukuba, Ibaraki 305
†*Department of Industrial Chemistry, Faculty of Engineering, The University of Tokyo, Hongo, Bunkyo-ku, Tokyo 113*
††*Department of Industrial Chemistry, Faculty of Science and Technology, Science University of Tokyo Higashikameyama, Yamazaki, Noda, Chiba 278*

(Received April 3, 1982)

An X-ray molecular structure analysis of [(2*R*, 3*R*)-2,3-*O*-isopropylidene-1,4-bis(5*H*-dibenzophosphol-5-yl)-2,3-butanediol((−)-DIPHOL)](1,5-cyclooctadiene)chloroiridium(I) was carried out. The complex takes a distorted trigonal bipyramidal structure, and the chelate ring of (−)-DIPHOL makes a chair form, which decreases the distances of atoms in the chelate ring from the P–Ir–P coordination plane. Thus, the chiral coordination structure of DIPHOL becomes remarkably different from that of DIOP. Through a comparison of the results of X-ray analyses, the results obtained in asymmetric hydroformylation (predominant absolute configuration and optical yield of products) catalyzed by the rhodium-complexes were explained on the basis of some well-grounded assumptions.

X-Ray molecular structure analyses of presumed chiral complex catalysts have been studied in order to elucidate the mechanism of the asymmetric induction, especially in the asymmetric hydrogenation of prochiral olefins catalyzed by rhodium-optically active ligand-complexes.[1] However, no attempt has yet been made in the field of symmetric hydroformylation, probably because the active catalyst species has not yet been made definite, as the reaction is a multistage one and proceeds under more severe conditions than in the case of hydrogenation, namely, at a higher reaction temperature and under a high carbon monoxide pressure.

A rhodium-catalyzed asymmetric hydroformylation reaction had been carried out by the use of chiral monophosphines[2,3] and (2*R*,3*R*)-2,3-*O*-isopropylidene-1,4-bis(diphenylphosphino)-2,3-butanediol[(−)-DIOP][4-6] as ligands. As the present authors reported previously, the enantioselectivity in rhodium-catalyzed asymmetric hydroformylation is considerably enhanced by the use of bis(5*H*-dibenzophosphole)s as chiral ligands in place of the corresponding bis(diphenylphosphine)s (Table 1).[7,8] It was surprising that the prevailing absolute configurations of aldehydes obtained from styrene, 1-butene, and *cis*-2-butene by the use of (−)-DIPHOL or (1*R*,2*R*)-1,2-bis(5*H*-dibenzophosphol-5-ylmethyl)cyclobutane were the opposite of those obtained by the use of (−)-DIOP or (1*R*,2*R*)-1,2-bis(diphenylphosphinomethyl)cyclobutane respectively, though they have the same chiral backbone. An exception was observed in the case of *trans*-2-butene, from which the aldehyde with a very low optical yield was produced.

In the case of the rhodium–triphenylphosphine-complex catalyzed hydroformylation reaction, $HRh(CO)_2PPh_3$ (in the dissociative mechanism) or $HRh(CO)_2(PPh_3)_2$ (in the associative mechanism) is presumed as a key intermediate;[13] only the former follows 18-electron rule upon coordination with a substrate. Similarly, when a bidentate ligand, (−)-DIOP, is used in place of PPh_3, the key intermediate is considered to have only one molecule of DIOP chelating as in HRh(CO)[(−)-DIOP], which may well be supported by the following facts: 1) The optical yield in the hydroformylation of styrene was always higher than those obtained using C-chiral monophosphines,[10] and 2) when the P/Rh atomic ratio in the system was increased, the optical yield levelled out at around the P/Rh value of 3.[14] Therefore, the conformation of (+)-DIOP in an X-ray analysis of a pentacoordinated iridium complex

TABLE 1. OPTICAL PURITY/% AND PREVAILING ABSOLUTE CONFIGURATION OF ALDEHYDES FORMED IN RHODIUM-CATALYZED ASYMMETRIC HYDROFORMYLATION

Substrate (Temp/°C)	Ligand	(2*R*,3*R*)-2,3-*O*-Isopropylidene-1,4-bis(phosphino)-2,3-butanediols		(1*R*,2*R*)-1,2-Bis(phosphinomethyl)-cyclobutanes phosphino=	
		(−)-DIOP	(−)-DIPHOL	Ph_2P	DBP
Styrene (80)[a]		12.3(*R*)	24.9(*S*)	2.8(*R*)	27.1(*S*)
1-Butene (90)		6.8(*R*)	16.2(*S*)	1.5(*R*)	16.2(*S*)
cis-2-Butene (120)		9.5(*S*)	16.6(*R*)	8.0(*S*)	16.8(*R*)
trans-2-Butene (120)		2.4(*S*)	2.3(*S*)	—	—

For the reaction conditions, see Ref. 8. The optical purities in Ref. 8 were recalculated on the basis of the value $[\alpha]_D = -238°$ of optically pure (−)-(*R*)-2-phenylpropanal; see Ref. 8.

—IrCl(COD)[(+)-DIOP] (**A**)[15,16]—is informative with regard to the conformation of (−)-DIOP in the catalytically active species.

The results in Table 1 seem to suggest that (−)-DIPHOL, upon coordination to rhodium, takes a chelate ring conformation essentially different from that of (−)-DIOP, which is a phenomenon caused by 5*H*-dibenzophospholyl (DBP) substitution for Ph_2P.

In order to compare the coordination structures of (−)-DIPHOL and (−)-DIOP, the present authors prepared IrCl(COD)[(−)-DIPHOL] (**B**) complex and determined its X-ray molecular structure. The mechanism of the asymmetric induction in the hydroformylation reaction will be described on the basis of both the structures.

Experimental

[(2*R*,3*R*)-2,3-*O*-Isopropylidene-1,4-bis(5*H*-dibenzophosphol-5-yl)-2,3-butanediol](1,5-cyclooctadiene)chloroiridium(I) (**B**) was prepared according to the procedure used for the corresponding (+)-DIOP complex.[15] Single crystals were obtained from the EtOH–toluene solution as yellow platelets. Found: C, 56.49; H, 4.89%. Calcd for $C_{39}H_{40}ClIrO_2P_2$: C, 56.41; H, 4.86%.

X-Ray Data Collection. A crystal with dimentions of $0.08\times0.32\times0.44$ mm^3 was sealed in a glass capillary under a nitrogen atmosphere. After determining the preliminary data with the Weissenberg photographs, the unit-cell dimensions were refined by the least-squares procedure with the setting angle of 20 reflections ($26.0°<2\theta<34.3°$) on a Rigaku four circle diffractometer with LiF-monochromatized Mo $K\alpha$ radiation ($\lambda=0.71069$ Å). Two sets of intensity data were measured in the θ-2θ scan mode: Data 1 with Mo $K\alpha$ radiation, $2\theta\leq60°$, $\lambda=0.71069$ Å; Data 2 with Co $K\alpha$ radiation, $2\theta\leq82°$, $\lambda=1.5418$ Å. In both cases, the θ scan width was $(1.2°+0.45\tan\theta)$ with the scan rate of 2° min^{-1} (2θ). No significant changes were observed in the intensities of the four standard reflections monitored every 50 measurements throughout the data-collection. Lorentz and polarization corrections were usually applied, but no absorption correction was made. A total of 4075 reflections with $F_o>3\sigma(F)$ in Data 1 were used in the subsequent calculations. The 1181 reflection pairs of $F_o(hkl)$ and $F_o(\bar{h}\bar{k}\bar{l})$ with $F_o>3\sigma(F)$ of Data 2 were used only to confirm the absolute configuration, since the observed number was insufficient for the number of parameters to be refined, and the absorption correction was not taken into account.

Crystal Data: $IrClP_2O_2C_{39}H_{40}$, $M_r=830.4$, orthorhombic, space group $P2_12_12_1$, $a=16.803(3)$, $b=18.969(3)$, $c=10.928(2)$ Å, $V=3483.3(9)$ Å^3, $Z=4$, $D_x=1.56$ gcm^{-3}, μ(Mo $K\alpha$)$=42.1$ cm^{-1}, $F(000)=1608$, μ(Cu $K\alpha$)$=90.2$ cm^{-1}.

Structure Determination and Refinement. The structure was solved by the heavy-atom method and refined by the block-diagonal least-squares method. The quantity minimized was $\sum w(|F_o|-|F_c|)^2$, and the weight parameter was $(14.1/|F_o|)^2$ in the absolute scale. After several cycles with anisotropic non-hydrogen atoms, two enantiomorphic forms, one of which was made by inverting the atomic parameters of the other, were refined separately with anomalous dispersion correction. The R values of the forms were 0.087 and 0.093. Since the R-ratio, the number of observations, and the number of refined parameters were 1.16, 4075, and 407 respectively, the (2*S*,3*S*)-structure could be rejected at the 0.005 significance level.[17] To confirm the configuration, separate refinements with $F_o(hkl)$ and $F_o(\bar{h}\bar{k}\bar{l})$ were carried out with Data 2, which possessed a higher intensity (about four times) than Data 1. The R values and the R ratio were 0.082, 0.087, and 1.061 respectively, so the results agreed with those of Data 1. Table 2 compares the observed and calculated structure amplitudes between several Bijvoet pairs with Data 2.

The final refinement with Data 1 was calculated with anisotropic non-hydrogen atoms, anomalous dispersion corrections for Ir, Cl, and P atoms, and isotropic hydrogen atoms, which were geometrically located and which were given a constant temperature parameter of 4.5 Å^2. The final R and R_w values were 0.076 and 0.079 respectively. The maximun parameter shift to its e.s.d. ratio was less than 0.5. The atomic scattering factors and anomalous dispersion corrections for Ir, Cl, and P atoms were taken from the International Tables for X-ray Crystallography.[18] All the computations were carried out at the Computer Center of the University of Tokyo with the UNICS program system.[19] The final atomic coordinates are shown in Table 3.[20]

Results

Some selected bond distances and angles of **B** are given in Table 4. An ORTEP[21] drawing and the numbering of the atoms are shown in Fig. 1. The Ir–Cl distance (2.549 Å) is fairly large in comparison with those in $IrCl(CO)(P\text{-}o\text{-}Tol_3)_2$[22] (2.43 Å) and in $IrCl(CO)_2$-

Table 2. Observed and calculated structure amplitudes of several Bijvoet pairs

h	k	l	$F_o(hkl)$	$F_o(\bar{h}\bar{k}\bar{l})$	$F_c(hkl)$	$F_c(\bar{h}\bar{k}\bar{l})$	$\frac{F_o(hkl)}{F_o(\bar{h}\bar{k}\bar{l})}$	$\frac{F_c(hkl)}{F_c(\bar{h}\bar{k}\bar{l})}$
4	2	1	43	54	42	54	0.80	0.78
1	1	2	180	160	151	136	1.13	1.11
2	6	2	85	69	83	70	1.23	1.19
5	4	2	49	27	48	25	1.81	1.92
5	6	2	57	45	54	46	1.27	1.17
1	10	3	26	37	32	37	0.70	0.86
7	9	3	61	50	60	50	1.22	1.20
8	4	4	50	40	51	41	1.25	1.24
6	10	5	70	63	70	67	1.11	1.04
3	3	6	49	40	42	32	1.23	1.31
4	5	6	68	58	67	60	1.17	1.12
4	7	6	52	44	53	42	1.18	1.26

TABLE 3. THE POSITIONAL PARAMETERS AND EQUIVALENT ISOTROPIC TEMPERATURE PARAMETERS, WITH THEIR ESTIMATED STANDARD DEVIATIONS IN PARENTHESES

$B_{eq}=4/3\sum_i a_i^2\beta_{ii}$

Atom	x	y	z	B_{eq}/Å
Ir	0.07606(4)	0.16927(4)	0.22104(7)	2.32(1)
Cl	0.2259(3)	0.1579(4)	0.2517(5)	4.4(2)
P(1)	0.1118(3)	0.1990(3)	0.0243(5)	2.6(1)
P(2)	0.0660(3)	0.2831(3)	0.2941(4)	2.4(1)
O(1)	0.248(1)	0.3737(9)	−0.028(2)	4.2(5)
O(2)	0.204(1)	0.436(1)	0.136(2)	5.1(5)
C(01)	0.195(1)	0.2586(9)	−0.005(2)	2.5(5)
C(02)	0.182(1)	0.334(1)	0.016(2)	3.1(5)
C(03)	0.097(1)	0.363(1)	0.208(2)	2.9(5)
C(04)	0.181(1)	0.363(1)	0.149(2)	3.3(5)
C(05)	0.253(2)	0.442(1)	0.033(2)	4.4(7)
C(06)	0.226(2)	0.501(2)	−0.045(3)	7(1)
C(07)	0.342(2)	0.451(2)	0.078(4)	8(1)
C(11)	0.034(1)	0.225(1)	−0.084(2)	3.1(5)
C(12)	−0.022(1)	0.278(2)	−0.066(2)	4.5(7)
C(13)	−0.084(2)	0.282(2)	−0.160(3)	5.2(8)
C(14)	−0.088(2)	0.242(2)	−0.259(3)	6.4(9)
C(15)	−0.035(2)	0.191(2)	−0.262(3)	7(1)
C(16)	0.032(2)	0.178(2)	−0.183(2)	5.7(9)
C(21)	0.140(1)	0.122(1)	−0.073(2)	3.2(5)
C(22)	0.201(2)	0.073(1)	−0.055(3)	5.1(8)
C(23)	0.213(2)	0.021(1)	−0.147(3)	5.1(8)
C(24)	0.166(2)	0.019(1)	−0.247(3)	6(1)
C(25)	0.106(2)	0.067(2)	−0.265(3)	6.1(9)
C(26)	0.093(2)	0.122(1)	−0.178(2)	4.2(7)
C(31)	0.104(1)	0.304(1)	0.446(2)	3.3(5)
C(32)	0.182(1)	0.290(1)	0.488(2)	4.6(7)
C(33)	0.198(2)	0.314(2)	0.610(3)	5.2(8)
C(34)	0.144(2)	0.352(2)	0.677(3)	5.5(9)
C(35)	0.068(2)	0.362(1)	0.635(2)	4.9(7)
C(36)	0.047(1)	0.337(1)	0.518(2)	2.2(5)
C(41)	−0.034(1)	0.315(1)	0.337(2)	3.0(5)
C(42)	−0.101(1)	0.316(1)	0.268(2)	3.9(6)
C(43)	−0.172(1)	0.342(2)	0.320(2)	4.8(7)
C(44)	−0.172(2)	0.370(2)	0.441(3)	5.3(8)
C(45)	−0.102(1)	0.372(2)	0.510(2)	4.7(7)
C(46)	−0.031(1)	0.342(1)	0.458(2)	3.0(5)
C(1)	−0.027(2)	0.117(2)	0.168(3)	5.4(8)
C(2)	0.031(2)	0.071(2)	0.152(3)	6.0(9)
C(3)	0.042(3)	0.010(2)	0.238(6)	4(1)
C(4)	0.054(3)	0.020(2)	0.351(5)	4(1)
C(5)	0.075(2)	0.094(2)	0.382(3)	6.4(9)
C(6)	0.015(2)	0.146(1)	0.405(2)	3.6(7)
C(7)	−0.072(2)	0.129(2)	0.389(3)	6.7(9)
C(8)	−0.097(1)	0.112(2)	0.258(2)	5.3(8)

$(PPh_3)_2$[23] (2.37 Å), while it is similar to that in **A** (2.599 Å).[15] The Ir–P distances (2.303 Å/2.310 Å) are similar not only to those in **A** (2.327 Å/2.339 Å),[15] but also to those in $IrCl(CO)(PMePh_2)_2$[24] (2.342 Å/2.320 Å), $IrCl(CO)_2(PPh_3)_2$[23] (2.341 Å/2.322 Å), and $IrMe(COD)\mathbf{P}_2$ ($\mathbf{P}_2$=2PPhMe$_2$,[25] DPPE,[26] and DPPP[27]) (2.316 Å/2.329 Å, 2.309 Å/2.337 Å, 2.308 Å/2.308 Å). The Ir–(C=C) distances are 2.02 Å for C(1/2) and 2.19 Å for C(5/6), similar to those in $IrMe(COD)\mathbf{P}_2$ (2.078 Å/2.117 Å, 2.033 Å/2.127 Å, 2.011 Å/2.106 Å). C(1/2) and C(5/6) represent the midpoints of the C(1)=C(2) and C(5)=C(6) double bonds. Regarding the DIPHOL ligand, the P–C, C–C, and C–O distances in the chelate ring and in the dioxolane ring are similar to those in DIOP complexes–**A**, HRh[(+)-DIOP]$_2$,[28] and HRuCl-[(+)-DIOP]$_2$.[29] The bond distances and angles in the DBP moieties are reasonable in comparison with those in dibenzophosphole complexes, $Ni(CN)_2(DBP\text{-}R)_3$ (R=Me and Et),[30] $NiBr_2(DBP\text{-}Me)_2$.[31] The distances of the C–C and C=C bonds in the COD ligand are 1.40—1.53 Å for sp^3–sp^3 and sp^2–sp^3 bonds and 1.31—1.38 Å for sp^2–sp^2 bonds, which are comparable with

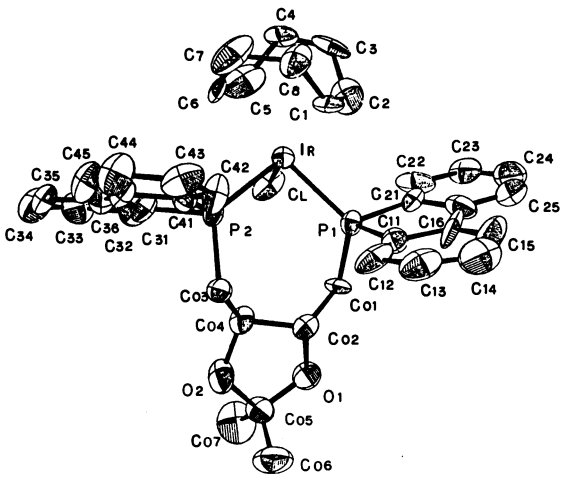

Fig. 1. An ORTEP drawing of IrCl(1,5-COD)[(−)-DIPHOL] (**B**).

the values in IrMe(COD)$\mathbf{P}_2$.[25-27]

The coordination structure around the Ir atom is regarded as a distorted trigonal bipyramid with P(1) and C(5/6) in apical positions, according to the following results: 1) The ∠P(1)IrCl, ∠P(1)IrP(2), and ∠P(1)-IrC(1/2) angles are between 83.4—96.5°, and ∠C(5/6)-IrC(1/2), ∠C(5/6)IrCl, and ∠C(5/6)IrP(2) are between 82.1—94.7°, while ∠P(1)IrC(5/6)=168.5°. 2) The distance of Ir–C(1/2) is smaller than that of Ir–C(5/6). In all trigonal bipyramidal IrMe(COD)$\mathbf{P}_2$ complexes,[25-27] the distances of the equatorial C=C from Ir are shorter than those of the apical one (2.01—2.08 Å/2.11, 2.13 Å). 3) The dihedral angles between the faces of the polyhedron which cross at Cl–C(1/2), C(1/2)–P(2), and P(2)–Cl are 38.9°, 44.1°, and 75.7° respectively. As has been pointed out by Muetterties and Guggenberger,[32] the three smaller angles in the ideal trigonal bipyramid are all 53.1°, while those in the ideal square pyramid are 0.0°, 75.7°, and 75.7°. The comparison of the sum of the squares of each deviation in the angles indicated that the structure of the polyhedron of **B** is nearly trigonal bipyramidal.

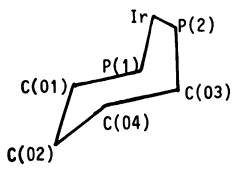

The chelate ring makes a chair form with an almost flat "back" which consists of P(1)–Ir–P(2)–C(03) and a "foot" which consists of C(02). As a result of this chair-form conformation, the dihedral angles between the P(1)–Ir–P(2) plane and the two DBP moieties represented by C(11)–P(1)–C(21) and C(31)–P(2)–C(41) are 60.4° and 82.5° respectively. That is, the DBP moiety containing P(2) is almost perpendicular to the P(1)–Ir–P(2) plane, while that containing P(1) is skewed.

The molecular structures of **A**[15] and **B** are presented in Fig. 2 so that each Cl–P(1)–Ir–P(2) structure takes a similar direction. **A** has (+)-DIOP as the ligand, while the hydroformylation reactions in Table 1 were

Table 4. Bond lenghts and bond angles of IrCl (1,5-COD)[(−)-DIPHOL] (**B**)

Bond length	l/Å		l/Å
Ir–Cl	2.550(7)	Ir–C(1)	2.09(3)
Ir–P(1)	2.302(6)	Ir–C(2)	2.15(3)
Ir–P(2)	2.308(5)	Ir–C(5)	2.27(3)
DIPHOL ligand		Ir–C(6)	2.31(3)
P(1)–C(01)	1.83(2)	COD ligand	
P(1)–C(11)	1.83(2)	C(1)–C(2)	1.31(5)
P(1)–C(21)	1.87(2)	C(2)–C(3)	1.51(7)
P(2)–C(03)	1.86(2)	C(3)–C(4)	1.27(8)
P(2)–C(31)	1.82(2)	C(4)–C(5)	1.48(6)
P(2)–C(41)	1.84(2)	C(5)–C(6)	1.43(4)
C(01)–C(02)	1.46(3)	C(6)–C(7)	1.49(5)
C(02)–O(1)	1.44(3)	C(7)–C(8)	1.53(5)
C(03)–C(04)	1.55(3)	C(8)–C(1)	1.52(4)
C(04)–O(2)	1.45(3)	Ir–C(1/2)	2.02
C(02)–C(04)	1.56(4)	Ir–C(5/6)	2.19
O(1)–C(05)	1.46(3)	Av. of C–C bonds in benzene	
O(2)–C(05)	1.41(3)	rings	
C(05)–C(06)	1.48(5)	Ring 1	1.39
C(05)–C(07)	1.57(5)	Ring 2	1.39
C(16)–C(26)	1.48(5)	Ring 3	1.40
C(36)–C(46)	1.47(3)	Ring 4	1.41

Bond angle	θ/°		θ/°
Cl–Ir–P(1)	83.5(2)	Cl–Ir–C(1/2)	127
Cl–Ir–P(2)	96.1(2)	Cl–Ir–C(5/6)	93
P(1)–Ir–P(2)	96.5(2)	P(1)–Ir–C(1/2)	92
C(1)–Ir–C(5)	84(1)	P(1)–Ir–C(5/6)	169
C(1)–Ir–C(6)	77(1)	P(2)–Ir–C(1/2)	137
C(2)–Ir–C(5)	74(1)	P(2)–Ir–C(5/6)	95
C(2)–Ir–C(6)	89(1)	COD ligand	
DIPHOL ligand		C(1)–C(2)–C(3)	121(4)
Ir–P(1)–C(01)	121.1(8)	C(2)–C(3)–C(4)	120(5)
Ir–P(2)–C(03)	124.8(7)	C(3)–C(4)–C(5)	114(5)
Ir–P(1)–C(11)	118.8(7)	C(4)–C(5)–C(6)	122(3)
Ir–P(1)–C(21)	113.8(8)	C(5)–C(6)–C(7)	121(3)
Ir–P(2)–C(31)	119.4(8)	C(6)–C(7)–C(8)	115(3)
Ir–P(2)–C(41)	117.4(7)	C(7)–C(8)–C(1)	112(3)
C(01)–P(1)–C(11)	105(1)	C(8)–C(1)–C(2)	128(3)
C(01)–P(1)–C(21)	101(1)		
C(11)–P(1)–C(21)	92(1)		
C(03)–P(2)–C(31)	100(1)	C(1/2)–Ir–C(5/6)	82
C(03)–P(2)–C(41)	97(1)		
C(31)–P(2)–C(41)	91(1)		
P(1)–C(01)–C(02)	117(2)	DIPHOL ligand	
C(01)–C(02)–O(1)	110(2)	C(11)–C(16)–C(26)	115(3)
C(01)–C(02)–C(04)	120(2)	C(21)–C(26)–C(16)	115(3)
O(1)–C(02)–C(04)	98(2)	C(31)–C(36)–C(46)	113(2)
C(02)–O(1)–C(05)	111(2)	C(41)–C(46)–C(36)	115(2)
P(2)–C(03)–C(04)	117(2)	Av. of angles in each benzene	
C(03)–C(04)–O(2)	106(2)	ring	
C(03)–C(04)–C(02)	114(2)		120
O(2)–C(04)–C(02)	104(2)		
C(04)–O(2)–C(05)	109(2)		
O(1)–C(05)–O(2)	105(2)		
O(1)–C(05)–C(06)	113(2)		
O(1)–C(05)–C(07)	107(2)		
O(2)–C(05)–C(06)	110(2)		
O(2)–C(05)–C(07)	108(2)		

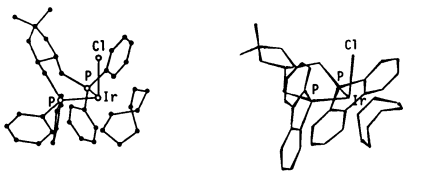

IrCl(COD)[(+)-DIOP] (A) S. Brunie, J. Mazan, N. Langlois, and H. B. Kagan, *J. Organomet. Chem.*, 114, 225 (1976). (Ref. 15)

IrCl(COD)[(-)-DIPHOL] (B) in this work

Fig. 2. X-Ray molecular structures of IrCl(1,5-COD)–chiral diphosphine complexes.

carried out by the use of (−)-DIOP and (−)-DIPHOL, with (2*R*,3*R*)-chirality in the backbones. The chelate-ring conformation in **A**[16] takes a skewed chair form[33,34] with a skewed "back" which consists of CH_2–P–Ir–P and with a "foot" which consists of *t*-CH in DIOP. The displacements of fluxional Ph_2P groups in **A** by rigid DBP groups must increase the steric repulsion between aromatic groups; this may well be removed by a slight distortion of the chelate-ring conformation from the skewed chair form to the chair form described above. Thus, the dihedral angle between the C(03)–P(2)–Ir and P(2)–Ir–P(1) planes, which is 30.0° in **A**,[16] is reduced to 8.4° in **B**. Consequently, C(03)–P(2)–Ir–P(1)–C(21) makes an approximate plane, since a dihedral angle between the P(2)–Ir–P(1) and Ir–P(1)–C(21) planes is also small in **B** (7.2°). These conformational distortions of the chelate ring caused a fairly large difference in the structure of the complex; that is, the distance from the quart-C in the dioxolane ring to the P(1)–Ir–P(2) plane is reduced from 3.98 Å in **A** to 2.22 Å in **B**. Therefore, the mode of the protrusion of aromatic rings of the diphosphines into the coordination site for substrates or reactants, *i.e.*, the steric environment in the site, is profoundly changed, as will be shown below.

Discussion

Although the mechanism of asymmetric induction in hydroformylation has not yet been established, the difference between the stability of the diastereomeric intermediates, the hydridorhodium–(carbonyl)–(π-olefin)–diphosphine complexes, must play a part in the determination of the chirality of products. This is why the three kinds of butenes—1-butene, *cis*-2-butene, and *trans*-2-butene—all of which must go through the same *s*-butyl intermediate to be transformed to optically active 2-methylbutanal, gave aldehydes of different chiralities and different optical yields. (Table 1) The results in Table 1 can be explained on the basis of the molecular structures of **A** and **B** according to the following well-grounded assumptions: 1) The coordination structures of diphosphines in the diastereomeric rhodium–(π-olefin)–intermediate complexes are the same as in the iridium complexes, **A** and **B** respectively. 2) The coordination structures around the rhodium atom in the intermediate complexes are trigonal bipyramidal. 3) H and CO occupy apical positions. 4) The bulkier ligands, a chelating diphosphine and π-olefin, occupy equatorial positions, with angles of about

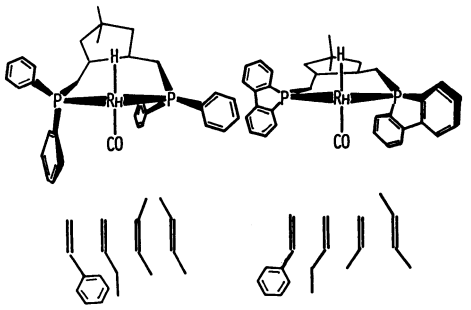

Fig. 3. Schematic coordination structures and conceivable modes of olefin π-coordination.

120° to each other, in order to release the steric congestions. If one of the three bulky ligands happens to occupy an apical position, it must have an angle of 90° with one of the other two in the equatorial position. Assumptions 2—4) can be explained by the X-ray molecular structure of $HRh(CO)(PPh_3)_3$,[35] which has a trigonal bipyramidal structure with H and CO in the apical positions and with three bulkier PPh_3's in the equatorial positions. 5) H in the rhodium intermediate complexes occupies the position of Cl in **A** and **B**; that is, the smallest ligand occupies the same side as the chelating diphosphine with regard to the P–Ir–P plane. This last assumption is acceptable if one considers the steric repulsion between the said apical position and the bridgehead CH or methylene CH_2 in the chelate ring.[36] This repulsion in the DIOP complex may be reduced to some extent in the DIPHOL complex, because the atoms comprising the chelate ring are placed nearer to the P–Ir–P plane, that is, farther from the apical H ligand, in the DIPHOL complex than in the DIOP complex.

In view of the above considerations, the steric environment of the two complexes is considered to be as is schematically drawn in Fig. 3, viewed from the coordination site of π-olefin. Although the difference in the conformations of the chelate rings is small between DIOP and DIPHOL complexes, the steric environment around the π-olefin coordination site is greatly changed, as one can recognize from Fig. 2 and, more directly, from Fig. 3.

As the present X-ray analysis shows, the chelate ring of (−)-DIPHOL is closer to the P–Ir–P coordination plane than is that of (−)-DIOP. Consequently, in the (−)-DIPHOL complex, the plane of the left DBP group becomes perpendicular to the P–Ir–P plane and parallel to the π-olefin coordination site, while the right DBP group protrudes into the middle of the π-olefin coordination site, as if it were a large wing.

In contrast with the case of the asymmetric hydrogenation of enamides or dehydroamino acid derivatives, the substrate olefins in Table 1 have no functional group which can exert an attractive interaction with the rhodium center or other part of the complex. The high reaction temperature and pressure are also disadvantageous to such an interaction. Therefore, the coordination structure of the substrates must be controlled by the steric repulsion only. In addition, olefins need to π-coordinate to the rhodium atom with the

substituents downward (the opposite side to hydrido with regard to the P–Ir–P plane) in order to be transformed into optically active branched aldehydes. Thus, the substrates prefer to π-coordinate to the rhodium center of the (−)-DIPHOL complex as is shown in Fig. 3. (Superimpose the double bonds of the substrates on the rhodium center.)

On the other hand, in the Rh–(−)-DIOP complex, the free rotation of the lower-left phenyl group is restricted by the other phenyl groups, and the steric hindrance by the *ortho*-CH in the coordination site for olefins seems to be significant. Therefore, the substrates prefer to π-coordinate to Rh–(−)-DIOP as is shown in Fig. 3, which leads to the prevailing configuration of products being the opposite of those when Rh–(−)-DIPHOL is used. However, since the upper-right phenyl group is parallel to, but also protrudes into the π-olefin coordination site, the chiral environment around the coordination site for substrates must be less selective. Consequently, the optical yields of products formed by the use of (−)-DIPHOL as a chiral ligand are higher than those formed by the use of (−)-DIOP. Thus, the results in Table 1 can be explained.

The authors wish to express their hearty thanks to Professor H. B. Kagan for sending them his detailed data on the X-ray molecular structure analysis of IrCl(COD)[(+)-DIOP] and for permitting them to reproduce the figure of Ref. 15. They also appreciate very much the permission for the reproduction given by Elsevier Sequoia S. A.

References

1) W. S. Knowles, B. D. Vineyard, M. J. Sabacky, and B. R. Stults, in "Fundamental Research in Homogeneous Catalysis," ed by M. Tsutsui, Plenum, New York (1979), Vol. 3, pp. 537—548.

2) M. Tanaka, Y. Watanabe, T. Mitsudo, K. Yamamoto, and Y. Takegami, *Chem. Lett.*, **1972**, 483.

3) I. Ogata and Y. Ikeda, *Chem. Lett.*, **1972**, 487.

4) C. Salomon, G. Consiglio, C. Botteghi, and P. Pino, *Chimia*, **27**, 215 (1973).

5) G. Consiglio, C. Botteghi, C. Salomon, and P. Pino, *Angew. Chem., Int. Ed. Engl.*, **12**, 669 (1973).

6) R. Stern, A. Hirschauer, and L. Sajus, *Tetrahedron Lett.*, **1973**, 3247.

7) M. Tanaka, Y. Ikeda, and I. Ogata, *Chem. Lett.*, **1975**. 1115.

8) T. Hayashi, M. Tanaka, Y. Ikeda, and I. Ogata, *Bull. Chem. Soc. Jpn.*, **52**, 2605 (1979). When these studies (Refs. 7 and 8) were carried out, the $[\alpha]_D$ value of optically pure 2-phenylpropanal had been claimed in Ref. 9 to be 238°; this value had been indirectly evaluated by extrapolation. The authors of Refs. 7 and 8 adopted the value of 160°,[10] evaluated through the reduction to 2-phenylpropanol. However, in 1982, the value of 238° was directly confirmed as in Refs. 11 and 12, and so the present authors adopt this value in this paper.

9) C. Botteghi, G. Consiglio, and P. Pino, *Justus Liebigs Ann. Chem.*, **1974**, 864.

10) M. Tanaka, Y. Watanabe, T. Mitsudo, and Y. Takegami, *Bull. Chem. Soc. Jpn.*, **47**, 1698 (1974).

11) T. Hayashi, M. Konishi, M. Fukushima, T. Mise, M. Kagotani, M. Tajika, and M. Kumada, *J. Am. Chem. Soc.*, **104**, 180 (1982).

12) C. U. Pittman, Jr., Y. Kawabata, and L. Flowers. *J. Chem. Soc., Chem. Commun.*, **1982**, 473.

13) C. K. Brown and G. Wilkinson, *J. Chem. Soc., A*, **1970**, 2753.

14) M. Tanaka, unpublished results.

15) S. Brunie, J. Mazan, N. Langlois, and H. B. Kagan, *J. Organomet. Chem.*, **114**, 225 (1976).

16) H. B. Kagan, private communication (1980).

17) W. C. Hamilton, *Acta Crystallogr.*, **18**, 502 (1965).

18) "International Tables for X-ray Crystallography," Kynoch, Birmingham (1974), Vol. 4.

19) "UNICS. The Universal Crystallographic Computing System," ed by T. Sakurai, The Crystallographic Society of Japan, Tokyo (1967).

20) Lists of structure factors and anisotropic thermal parameters have been deposited at the office of the Chemical Society of Japan as Document No. 8317.

21) C. K. Johnson, ORTEP. Report ORNL-3794. Oak Ridge National Laboratory, Tennessee (1965).

22) R. Brady, W. H. de Camp, B. R. Flynn, M. L. Schneider J. D. Scott, L. Vaska, and M. F. Werneke, *Inorg. Chem.*, **14**, 2669 (1975).

23) N. C. Payne and J. A. Ibers, *Inorg. Chem.*, **8**, 2714 (1969).

24) J.-Y. Chen, J. Halpern, and J. Molin-Case, *J. Coord. Chem.*, **2**, 239 (1973).

25) M. R. Churchill and S. A. Bezman, *Inorg. Chem.*, **11**, 2243 (1972).

26) M. R. Churchill and S. A. Bezman, *Inorg. Chem.*, **12**, 260 (1973).

27) M. R. Churchill and S. A. Bezman, *Inorg. Chem.*, **12**, 531 (1973).

28) R. G. Ball, B. R. James, D. Mahajan, and J. Trotter, *Inorg. Chem.*, **20**, 254 (1981).

29) R. G. Ball and J. Trotter, *Inorg. Chem.*, **20**, 261 (1981).

30) H. M. Powell, D. J. Watkin, and J. B. Wilford, *J. Chem. Soc., A*, **1971**, 1803.

31) D. J. Watkin, *J. Chem. Soc., Dalton Trans.*, **1976**, 1803.

32) E. L. Muetterties and L. J. Guggenberger, *J. Am. Chem. Soc.*, **96**, 1748 (1974).

33) D. F. Bocian, H. M. Pickett, T. C. Rounds, and H. L. Strauss, *J. Am. Chem. Soc.*, **97**, 687 (1975).

34) W. M. J. Flapper and C. Romers, *Tetrahedron*, **31**, 1705 (1975).

35) S. J. LaPlaca and J. A. Ibers, *J. Am. Chem. Soc.*, **85**, 3501 (1963).

36) R. Graser, *Tetrahedron Lett.*, **1975**, 2127.

Asymmetric Transfer Hydrogenation of Prochiral α,β-Unsaturated Acids and Their Esters by Achiral or Chiral Alcohols with Ruthenium Chiral Diphosphine Complexes

Kohji Yoshinaga,* Taketoshi Kito, and Katsutoshi Ohkubo†

Department of Material Engineering, Kyushu Institute of Technology, Sensui-cho, Tobata-ku, Kitakyushu 804

†*Department of Synthetic Chemistry, Faculty of Engineering, Kumamoto University, Kurokami, Kumamoto 860*

(Received September 30, 1982)

Asymmetric transfer hydrogenations of α,β-unsaturated acids ($MeCH{=}C(Me)CO_2H$, $PhCH{=}C(Me)CO_2H$, $CH_2{=}C(CH_2CO_2H)CO_2H$, and $HO_2CCH{=}C(Me)CO_2H$) and esters ($MeCH{=}C(Me)CO_2R$; R=achiral and chiral group) by alcohols ($PhCH_2OH$, (*RS*)-PhCH(Me)OH, and α-D-glucofuranose derivatives) were carried out with $RuCl_2(PPh_3)_3$ or Ru_2Cl_4((+) or (−)-diop)$_3$ (diop=2,3-*O*-isopropylidene-1,4-bis(diphenylphosphino)-2,3-butanediol) at 160—190 °C. The optical purity (3.4—16.4%) of hydrogenated acids obtained with $PhCH_2OH$ and Ru_2Cl_4((−)-diop)$_3$ is in the order $MeCH{=}C(Me)CO_2H > PhCH{=}C(Me)CO_2H > CH_2{=}C(CH_2CO_2H)CO_2H > HO_2CCH{=}C(Me)CO_2H$, suggesting that the substrates possessing two carboxyl groups would provide an asymmetrically unfavorable coordination to the Ru(II) complex for this asymmetric reaction. In the transfer hydrogenation of $MeCH{=}C(Me)CO_2R$ by $PhCH_2OH$ or (*RS*)-PhCH(Me)OH at 190 °C, the extent of asymmetric induction of Ru_2Cl_4((−)-diop)$_3$ (1.7—11.4% e.e. with $PhCH_2OH$ and 7.4—18.2% e.e. with (*RS*)-PhCH(Me)OH) decreases with increase in bulkiness of groups R (R=H, Me, Et, *n*-Bu, and $PhCH_2$) and is not enhanced by the introduction of any groups R with chiral carbon atoms into esters (maximum 15.4% e.e.). The structural change of hydrogen donors from $PhCH_2OH$ to (*RS*)-PhCH(Me)OH appreciably increases the optical purity of the saturated acids and esters, and the chiral α-D-glucofuranose derivatives afford optically active saturated products, even with achiral $RuCl_2(PPh_3)_3$. Features of the present reaction are discussed in relation to the reaction mechanism.

Catalytic asymmetric synthesis of optically active compounds is recently receiving considerable attention,[1] and rhodium chiral phosphine complexes have successfully been used in homogeneous hydrogenations for formation of α-amino acid derivatives.[2-4] Chiral ruthenium complexes, as compared with rhodium ones, have been subjected to limited investigations on their catalytic activity for the asymmetric synthesis.[5,6]

Since ruthenium chiral phosphine complexes are effective catalysts for enantiomer-differentiating dehydrogenation of racemic secondary alcohols as found in our laboratory,[7] we have investigated the catalytic efficiency of chiral ruthenium complexes for the asymmetric transfer hydrogenation of prochiral olefins by alcohols, to examine the asymmetric hydrogenation without molecular hydrogen at the atmospheric pressure.

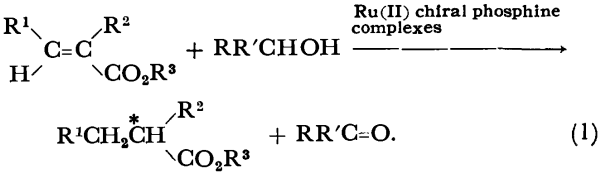

$$R^1R^2C{=}CH(CO_2R^3) + RR'CHOH \xrightarrow{\text{Ru(II) chiral phosphine complexes}} R^1CH_2\overset{*}{C}H(R^2)(CO_2R^3) + RR'C{=}O. \quad (1)$$

In this paper, we describe effects of the chirality and bulkiness of substituent groups in reactants on the extent of asymmetric induction in the transfer hydrogenation of prochiral α,β-unsaturated acids and esters by alcohols with $RuCl_2(PPh_3)_3$ or Ru_2Cl_4((+) or (−)-diop)$_3$ (diop =2,3-*O*-isopropylidene-1,4-bis(diphenylphosphino)-2,3-butanediol), and discuss on the reaction mechanism with particular reference to the enantio-differentiating catalysis by the ruthenium complexes.

Experimental

Materials. (+) and (−)-Diop and Ru_2Cl_4 ((+) or (−)-diop)$_3$ were prepared by Kagan's[8] and James'[5a] methods, respectively. α-D-Glucose derivatives, 1,2-*O*-isopropylidene-1,2 : 5,6-*O*-diisopropylidene-, 1,2-*O*-cyclohexylidene-, and 1,2 : 5,6-*O*-dicyclohexylidene-α-D-glucofuranose were synthesized by the methods reported.[9,10] Several α-methylcrotonates (1-phenylethyl, α-(ethoxycarbonyl)benzyl, (1*R*,2*R*)-1,2-bis(ethoxycarbonyl)-2-hydroxyethyl, and *l*-menthyl esters) were prepared *via* the reaction of α-methycrotonoyl chloride and the corresponding hydroxy compounds (1-phenylethanol, ethyl mandelate, diethyl (2*R*, 3*R*)-tartarate, and *l*-menthol, respectively). Alcohols, prochiral acids, and esters were purified by fractional distillation or recrystallization before use.

Transfer Hydrogenation. A mixture of prochiral olefin and alcohol was allowed to react in the presence of the chiral ruthenium complex in a sealed tube at the desired temperature controlled within ±1 °C in a nitrogen atmosphere. The reaction mixture was refluxed in a 10% NaOH-methanol solution, and the insoluble catalyst was separated from the solution by the filtration. The filtrate was washed with water, acidified with dilute HCl solution in the range of pH 3—4, and extracted with ether. The ethereal phase was washed with water, dried over magnesium sulfate, and evaporated to dryness. The unreacted prochiral olefin and hydrogenated product were identified by GLC analysis (at 170 °C using a 1 m column packed with 15% EGA on Uniport B) or by the proton NMR (100 MHz) method. The optical rotation of the hydrogenated product was measured with a high-sensitivity Union PM-101 polarimeter.

Results and Discussion

Asymmetric Transfer Hydrogenation of α,β-Unsaturated Carboxylic Acids and Esters. The asymmetric reduction of the carbon-carbon double bond in prochiral α,β-unsaturated mono- and dicarboxylic acids by benzyl or *p*-methoxybenzyl alcohol was first carried out with Ru_2Cl_4((−)-diop)$_3$. The results are summarized in Table 1. The optical purity of hydrogenated products for the unsaturated monocarboxylic acids is relatively high as compared with that for the unsaturated dicarboxylic acids. The bulky carboxyl groups might hinder the

Table 1. Asymmetric transfer hydrogenation of prochiral unsaturated carboxylic acids by benzyl alcohol with Ru_2Cl_4((−)-diop)$_3$ at 180 °C[a]

Substrate	Time / h	Yield / %	$[\alpha]_D$ / °	O.P.[b] / %
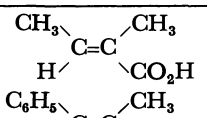	6	10	−1.99	16.4
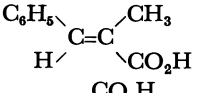	6	36	−3.29	15.9
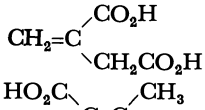	6	31	−0.86	6.1
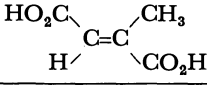	9	9	−0.59	3.4

a) Catalyst, 4 mmol dm^{-3}; substrate, 40 mmol; alcohol, 80 mmol. b) Calculated on the basis of the following values of optically pure acids: $[\alpha]_D^{23}$+12.17° (*c* 5, C_2H_5OH) for (*S*)-(+)-$CH_3CH_2CH(CH_3)CO_2H$;[11] $[\alpha]_D^{25}$+20.68° (neat) for (*S*)-(+)-$CH_3CH_2CH(CH_3)CO_2H$;[12] $[\alpha]_D^{20}$+16.88° (*c* 2.16, C_2H_5OH) for (*R*)-(+)-$CH_3CH(CO_2H)CH_2CO_2H$;[13] $[\alpha]_D^{20}$ −17.27° (*c* 5.0, C_2H_5OH) for (*S*)-(−)-$HO_2CCH_2CH(CH_3)CO_2H$.[14]

asymmetrically favorable coordination of the carbon-carbon double bond in the substrate to the chiral Ru(II) complex in the step of asymmetric induction.

It is also noteworthy that the optical purity of the saturated products derived from α-methylcrotonic or α-methylcinnamic acid (16.4 and 15.4%, respectively) is higher than the reported values (maxima 6.9 and 1.5%, respectively)[6c] for transfer hydrogenations of the same species with $H_4Ru_4(CO)_8$((−)-diop)$_8$ at 120 °C by 2-propanol, indoline, dioxane, *etc.*

Asymmetric transfer hydrogenation of a series of esters of α-methylcrotonic acid by benzyl alcohol or 1-phenylethanol was carried out with the Ru(II)-(−)-diop complex. The results are shown in Table 2. The ester derivatives of α-methylcrotonic acid, as compared with α-methylcrotonic acid itself, are easily hydrogenated to give their hydrogenated products with very low optical purities, which decrease with increasing bulkiness of the ester groups. The bulky ester moiety might decrease the extent of asymmetric induction considerably by suppressing the approach of the ester to the chiral catalyst during the enantio-face differentiating process.

The extent of asymmetric induction is also affected by the structure of hydrogen donor. Such an achiral alcohol as benzyl alcohol results in a low magnitude of asymmetric induction than 1-phenylethanol in the hydrogenation of α-methylcrotonic acid. Although benzyl alcohol gives saturated esters enriched in (*S*)-enantiomer, racemic 1-phenylethanol affords products enriched in the antipode with higher optical purity.

When a hydrogen transfer is effected with the Ru(II)-(−)-diop complex from alcohol to such an unsaturated acid as α-methylcrotonic acid, the reaction is considered to proceed *via* two courses I and II specified in Scheme 1. In course I, a partial esterification of the saturated acid is followed by a reduction of the carbon-carbon double bond of the unsaturated acid, and in course II, an unsaturated ester is formed before the corresponding acid is hydrogenated by alcohol in the presence of Ru(II) catalyst. In order to elucidate which course is predominant in the asymmetric transfer hydrogenation of unsaturated acid, we determined the time dependence of the chemical yield of products in the Ru(II)-(−)-diop complex catalyzed transfer hydrogenation of α-methylcrotonic acid or 1-phenylethyl α-methylcrotonate by 1-phenylethanol.

As can be seen from Fig. 1, α-methylcrotonic acid is

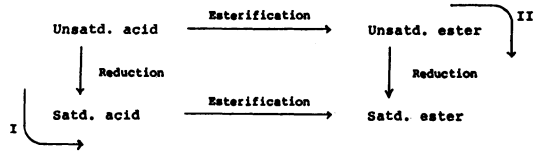

Scheme 1.

Table 2. Asymmetric transfer hydrogenation of α-methylcrotonic acid and its esters by achiral and racemic alcohols with Ru_2Cl_4((−)-diop)$_3$ at 190 °C[a]

Alcohol	$CH_3CH=C(CH_3)CO_2R$ R	Time / h	Yield / %	$[\alpha]_D^{23}$ / °	O.P.[b] / %	Prevailing configuration
$C_6H_5CH_2OH$	H	8	10	−1.39	11.4	*R*
	CH_3	4	35	+0.22	1.8	*S*
	C_2H_5	5	53	+0.28	2.3	*S*
	n-C_4H_9	5	47	+0.28	2.3	*S*
	$C_6H_5CH_2$	5	41	+0.20	1.7	*S*
$C_6H_5CH(CH_3)OH$	H[c]	10	13	−3.21	26.4	*R*
	H	4	10	−2.21	18.2	*R*
	CH_3	3	85	−1.21	10.0	*R*
	C_2H_5	22	59	−1.19	9.8	*R*
	n-C_4H_9	4	94	−0.90	7.4	*R*
	$C_6H_5CH_2$	5	75	−1.02	8.4	*R*
p-$CH_3OC_6H_4CH_2OH$	H	8	9	−1.35	11.1	*R*
	H[d]	8	8	+1.25	10.3	*S*

a) Ru_2Cl_4((−)-diop)$_3$, 4 mmol dm^{-3}; alcohol, 33 mmol; olefin, 67 mmol. b) Optical purities of saturated esters were calculated for the α-methylbutyric acids obtained from the esters by base hydrolysis. c) The reaction was carried out at 170 °C. d) Ru_2Cl_4((+)-diop)$_3$ was used.

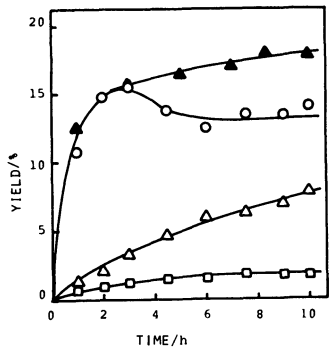

Fig. 1. Changes of product yields with time in the transfer hydrogenation of α-methylcrotonic acid (3.0 mol dm^{-3}) by 1-phenylethanol (5.8 mol dm^{-3}) with Ru_2Cl_4-(−)-diop)$_3$ (4.0 mmol dm^{-3}) at 190 °C.
Product: α-methylbutyric acid (○), 1-phenylethyl α-methylbutyrate (△), 1-phenylethyl α-methylcrotonate (□), 1-phenylethyl α-methylbutyrate (▲) obtained with 1-phenylethyl α-methylcrotonate (2.3 mol dm^{-3}) and 1-phenylethanol (4.7 mol dm^{-3}) at 190 °C.

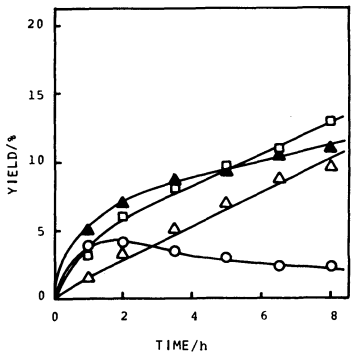

Fig. 2. Changes of product yields with time in the transfer hydrogenation of α-methylcrotonic acid (2.9 mol dm^{-3}) by benzyl alcohol (7.0 mol dm^{-3}) with Ru_2Cl_4-((−)-diop)$_3$ (4.0 mmol dm^{-3}) at 190 °C.
Product: α-methylbutyric acid (○), benzyl α-methylbutyrate (△), benzyl α-methylcrotonate (□); benzyl α-methylbutyrate (▲) obtained with benzyl α-methylcrotonate (1.5 mol dm^{-3}) and benzyl alcohol (6.8 mol dm^{-3}) at 190 °C.

hydrogenated smoothly by 1-phenylethanol with a small extent of esterification of the unsaturated acid, and rates of hydrogen transfers from 1-phenylethanol to α-methylcrotonic acid and to 1-phenylethyl α-methylcrotonate do not differ distinctly from each other. Strictly speaking, the hydrogenation of α-methylcrotonic acid includes a rate drop by the slow esterification of acid. Thus, the chiral Ru(II) complex catalyzed reaction of α-methylcrotonic acid with 1-phenylethanol proceeds mainly *via* course I with formation of α-methylbutyric acid as a main product.

On the other hand, the esterification of α-methylcrotonic acid by benzyl alcohol is relatively rapid, and benzyl α-methylcrotonate is easily reduced to benzyl α-methylbutyrate. From the gradual decrease in the yield of α-methylbutyric acid after the reaction period of 2 h (Fig. 2), it is evident that the saturated ester is produced from α-methylbutyric acid *via* course I, and that benzyl α-methylbutyrate is formed from α-methylcrotonic acid and benzyl alcohol *via* both courses I and II; the later path seems predominant. It should be stressed that in the transfer hydrogenation of α-methylcrotonate with benzyl alcohol or 1-phenylethanol, no hydrolysis of unsaturated or saturated esters was observed. Thus the difference in reactivity between hydrogen donors (alcohols) affects the transfer hydrogenation process, allowing 1-phenylethanol to give a higher optical purity (18.2%) than that (11.4%) obtained with benzyl alcohol in the hydrogenation of α-methylcrotonic acid (Table 2). Since the saturated product from benzyl α-methylcrotonate has a considerably low optical purity (1.7%) and contains the prevailing (*S*)-enantiomer, opposite to the predominant enantiomer found with α-methylcrotonic acid, the easy esterification of α-methylcrotonic acid by benzyl alcohol is taken to be responsible for the decreased optical purity of the saturated product.

For the present reaction the effective asymmetric induction by racemic 1-phenylethanol was actually recognized, and this is attributable to the chiral circumstances enriched in one specific enantiomer of the unreacted alcohol. In fact, in the transfer hydrogenation of α-methylcrotonic acid or its esters by racemic 1-phenylethanol, an enantiomer-differentiation of the alcohol was observed, and the optically active unreacted alcohol (maximum e.e. 4.2%) could be separated; the prevailing enantiomers are the (*S*)-isomer in the case of Ru(II)-(−)-diop complex and the (*R*)-isomer in the case of Ru(II)-(+)-diop complex. One of the enantiomers of 1-phenylethanol might contribute to the asymmetric induction through coordination to the chiral Ru(II) complex.

Asymmetric Transfer Hydrogenation of α-Methylcrotonic Acid by Chiral Alcohol. Since the chirality of hydrogen donors is anticipated to affect the extent of asymmetric induction in the transfer hydrogenation of unsaturated species with the chiral Ru(II) complex, we carried out a reaction of α-methylcrotonic acid with chiral alcohol as follows: (1) an asymmetric transfer hydrogenation using α-D-glucofuranose derivatives as chiral alcohols with an achiral catalyst $RuCl_2(PPh_3)_3$, and (2) a double asymmetric transfer hydrogenation by the chiral hydrogen donors with a chiral catalyst Ru_2Cl_4((+) or (−)-diop)$_3$. Results are listed in Table 3.

$$RR'\overset{*}{C}HOH + CH_3CH{=}C(CH_3)CO_2H \xrightarrow[2.\ Ru_2Cl_4((+)\text{ or }(-)\text{-diop})_3]{1.\ RuCl_2(PPh_3)_3} CH_3CH_2\overset{*}{C}H(CH_3)CO_2H + RR'C{=}O \quad (2)$$

In the case of the transfer hydrogenation of α-methylcrotonic acid with the chiral alcohol and $RuCl_2(PPh_3)_3$, the optically active α-methylbutyric acid (0.3—8.9% e.e.) was produced with the prevailing (*R*)-enantiomer, and the use of 1,2 : 5,6-*O*-diisopropylidene- and 1,2-*O*-isopropylidene-α-D-glucofuranose gave rise to higher optical purities (6.7—8.9%) than those (0.3—3.1%) obtained with 1,2 : 5,6-*O*-dicyclohexylidene- and 1,2-*O*-cyclohexylidene-α-D-glucofuranose.

In the double asymmetric reaction with the chiral

TABLE 3. ASYMMETRIC TRANSFER HYDROGENATION OF α-METHYLCROTONIC ACID BY CHIRAL ALCOHOLS WITH $RuCl_2(PPh_3)_3$ OR Ru_2Cl_4((+) OR (−)-diop)$_3$ AT 160 °C[a]

Alcohol	Catalyst	Yield[b] %	$-[\alpha]_D^{23}$ °	O.P. %
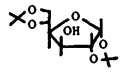	$RuCl_2(PPh_3)_3$	7	0.81	6.7
	Ru_2Cl_4((−)-diop)$_3$	7	1.57	12.9
	Ru_2Cl_4((+)-diop)$_3$	6	0.77	6.4
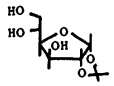	$RuCl_2(PPh_3)_3$	18	1.08	8.9
	Ru_2Cl_4((−)-diop)$_3$	14	2.74	22.5
	Ru_2Cl_4((+)-diop)$_3$	13	−0.47	3.9
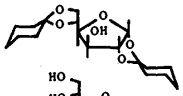	$RuCl_2(PPh_3)_3$	5	0.37	3.1
	Ru_2Cl_4((−)-diop)$_3$	2	0.90	7.4
	Ru_2Cl_4((+)-diop)$_3$	7	0.15	1.2
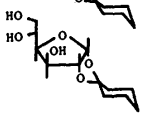	$RuCl_2(PPh_3)_3$	19	0.04	0.3
	Ru_2Cl_4((−)-diop)$_3$	3	0.23	1.9

a) $RuCl_2(PPh_3)_3$, 2.5 mmol dm^{-3}; Ru_2Cl_4((+) or (−)-diop)$_3$, 1.25 mmol dm^{-3}; olefin, 40 mmol; alcohol, 40 mmol in diphenyl ether (300 ml); reaction time, 12 h. b) No products derived from the glucofuranose derivatives were investigated.

TABLE 4. ASYMMETRIC TRANSFER HYDROGENATION OF α-METHYLCROTONATES INCLUDING RACEMIC OR CHIRAL ESTER GROUPS BY 1-PHENYLETHANOL WITH Ru_2Cl_4 ((−)diop)$_3$ AT 190 °C[a]

$CH_3CH=C(CH_3)CO_2R$ R	Time h	Yield %	$[\alpha]_D^{23}$ °	O.P.[b] %
1-Phenylethyl	10	71	+0.10	0.8
α-(Ethoxycarbonyl) benzyl	9	93	−1.88	15.4
(1*R*, 2*R*)-1, 2-Bis(ethoxycarbonyl)-2-hydroxyethyl	4	80	−0.41	1.1
l-Menthyl	9	34	−0.23	1.9
	12[c]	43	+0.06	0.6

a) Catalyst, 4 mmol dm^{-3}; alcohol, 33 mmol; ester, 67 mmol. b) Optical purities were determined in the same way as in Table 2. c) Ru_2Cl_4((+)-diop)$_3$ was used.

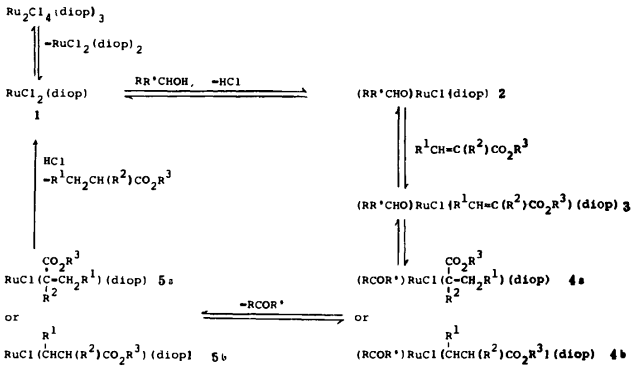

Scheme 2. The sign of the optical rotation of diop is omitted.

alcohol and Ru_2Cl_4((−)-diop)$_3$, the Ru(II) complex substantially increases the optical purity of α-methylbutyric acid enriched in (*R*)-enantiomer with a maximum optical purity of 22.5% in the case of 1,2-*O*-isopropylidene-α-D-glucofuranose. However, the Ru(II)–(+)-diop complex gave a lower optical purity of the saturated product than that obtained with $RuCl_2(PPh_3)_3$, and changed the enriched enantiomer in the product from (*R*)- to (*S*)-isomer in the case of 1,2-*O*-isopropylidene-α-D-glucofuranose.

At any rate, the chiral alcohols (α-D-glucofuranose derivatives) contribute to enhancing the extent of asymmetric induction, even though the maximum optical purity of 22.5% is lower than that (26.4%) attained with 1-phenylethanol.

Asymmetric Transfer Hydrogenation of α-Methylcrotonate Including Racemic or Chiral Ester Groups. In the present transfer hydrogenation, the double asymmetric induction, including the diastereo-face differentiation of unsaturated esters by the chiral catalyst, can also be expected by the use of unsaturated ester substrates containing chiral carbon atoms in the ester moiety, achiral alcohol, and the Ru(II) complex.

When an asymmetric transfer hydrogenation of racemic or optically active α-methylcrotonate by 1-phenylethanol was effected with the Ru(II)–(−)-diop complex, no effective double asymmetric induction was realized (Table 4); optical purities of hydrogenated products were low (maximum 15.4%). Presumably, the steric bulkiness of the ester group in the substrates decreases the enantio-face differentiating ability of the chiral Ru(II) complex through depression of the substrate coordination to the complex.

Reaction Mechanism. It is obvious that the present asymmetric hydrogen transfer from alcohol (RR'CHOH) to unsaturated substrate ($R^1CH=C(R^2)CO_2R^3$) is effected by the coordination of both the reactants to the Ru(II) complex. From the fact that the chirality of the alcohol substantially affects the extent of asymmetric induction by the Ru(II)–(+) or (−)-diop catalyst, the asymmetric induction can be expected in the process of coordination of $R^1CH=C(R^2)CO_2R^3$ to the unsoluble ruthenium–alkoxide complex (*viz.*, the steric approach control over enantio-face differentiation[15]), which has previously been formed from the

active ruthenium species and the alcohol.

As for the catalytically active species in the present catalysis, $RuCl_2$((+) or (−)-diop) (**1**) has already been suggested as the plausible species by our previous ^{31}P NMR analysis of Ru_2Cl_4((−)-diop)$_3$ at −10—70°C;[16] $RuCl_2$((+) or (−)-diop)$_2$ simultaneously formed seems inactive for the present reaction because of the lack of active sites.

Therefore, the present transfer hydrogenation is thought to proceed along the catalytic cycle in Scheme 2, where the participation of HCl in the step of coordination of the alcohol to species **1** and of the elimination of the hydrogenated product has already been proposed by Sasson and Blum[17] in the transfer hydrogenation of unsaturated ketones by alcohols with $RuCl_2(PPh_3)_3$. Ruthenium–alkyl complexes **4a** and **5a** are more plausible than complexes **4b** and **5b** in the light of the contribution of the d-π conjugation between the ruthenium metal and carbonyl group to the stabilization.[18] A more detailed study on the reaction mechanism, especially regarding the asymmetric induction of the Ru(II)-(+) or (−)-diop complex, is now in progress.

References

1) B. Bosnich and M. D. Fryzuk," Topics in Inorganic and Organic Stereochemistry," ed by G. Geofroy, Wiley-Interscience, New York (1981), p. 119; R. E. Merrill, *Chemitech*, **1981**, 118.

2) K. Achiwa, *J. Am. Chem. Soc.*, **98**, 8256 (1976); K. Achiwa, Y. Ohga, Y. Iitake, and H. Saito, *Tetrahedron Lett.*, **1978**, 4683.

3) B. D. Vineyard, W. S. Knowles, M. J. Sabackey, G. L. Bachman, and D. J. Weinkauff, *J. Am. Chem. Soc.*, **99**, 5946 (1977).

4) M. D. Fryzuk and B. Bosnich, *J. Am. Chem. Soc.*, **99** 6262 (1977); **100**, 5491 (1978).

5) a) B. R. James, D. K. Wang, and R. F. Voight, *J. Chem. Soc., Chem. Commun.*, **1975**, 547; b) C. Botteghi, M. Bianchi, and U. Matteoli, *Chemia*, **29**, 257 (1975).

6) a) T. H. Johnson, L. A. Siegle, and V. J. K. Chaffin, *J. Mol. Catal.*, **9**, 307 (1980); b) M. Bianchi, U. Matteoli, G. Menchi, P. Frediani, S. Pratessi, and F. Piacenti, *J. Orgnomet. Chem.*, **198**, 73 (1980); c) M. Bianchi, U. Matteoli, G. Menchi, P. Frediani, and F. Piacenti, *ibid.*, **195**, 337 (1980).

7) K. Ohkubo, I. Terada, and K. Yoshinaga, *Bull. Chem. Soc. Jpn.*, **51**, 2807 (1978); K. Ohkubo, T. Shoji, and K. Yoshinaga, *J. Catal.*, **54**, 166 (1978).

8) H. B. Kagan and T. P. Dang, *J. Am. Chem. Soc.*, **94**, 6429 (1972).

9) W. L. Glen, G. S. Myers, R. J. Barar, and G. A. Grant, U. S. Patent 2715121.

10) J. C. Irvine and J. L. A. Macdonald, *J. Chem. Soc.*, **107**, 1701 (1915).

11) J. Kenyon, H. Phillips, and V. P. Pittman, *J. Chem. Soc.*, **1935**, 1072.

12) D. J. Cram and P. Harberfield, *J. Am. Chem. Soc.*, **83**, 2363 (1961).

13) E. Berner and R. Leonardson, *Ann.*, **539**, 1 (1939).

14) R. Rossi, P. Diversi, and G. Ingrosso, *Gazz. Chim. Ital.*, **98**, 1391 (1968).

15) W. G. Dauben, G. J. Fouken, and D. S. Noyce, *J. Am. Chem. Soc.*, **78**, 2579 (1956).

16) K. Ohkubo, I. Terada, K. Sugahara, and K. Yoshinaga, *J. Mol. Catal.*, **7**, 421 (1980).

17) Y. Sasson and J. Blum, *J. Org. Chem.*, **40**, 1887 (1975).

18) R. W. Goetz and M. Orchin, *J. Am. Chem. Soc.*, **85**, 2782 (1963); R. H. Prince and K. A. Raspin *J. Chem. Soc., A*, **1969**, 612.

 © 1983 The Chemical Society of Japan Bull. Chem. Soc. Jpn., 56, 1791—1794 (1983)

Electrochemical Additions of the Allyl and the Benzyl Groups of Allyl and Benzyl Halides to Acetone

Shohei SATOH,† Hiroshi SUGINOME, and Masao TOKUDA*
Department of Chemical Process Engineering, Faculty of Engineering, Hokkaido University, Sapporo 060
(Received October 12, 1982)

Electrolysis of allyl chloride and five molar excess of acetone in hexamethylphosphoric triamide containing 0.5 M†† tetrabutylammonium perchlorate gave an addition product, 2-methyl-4-penten-2-ol, in a 53% yield. Allyl groups of 1-chloro-2-methyl-2-propene, 1-chloro-2-butene(**3**), 3-chloro-1-butene(**4**), 1-chloro-3-methyl-2-butene(**5**), and 3-chloro-3-methyl-1-butene(**6**), and benzyl groups of benzyl chloride, benzyl bromide, and 1-chloro-1-phenylethane can similarly be added to acetone by electrolysis to give the corresponding alcohols in fair to good yields. Among these electrochemical reactions, those of **3**, **4**, **5**, and **6** with acetone give respectively two isomeric homoallyl alcohols, one of the isomers is not accessible by the usual chemical reaction between allylic organometallics and acetone.

The electrochemical cleavage of the carbon-halogen bond of organic halides generates radical and/or carbanion as the important intermediates.[1] Dimers and hydrocarbons have been the only products isolated in these studies.[1] Although radical or carbanion generated by ordinary chemical reaction is being used in a variety of organic syntheses, carbanion or radical, which was electrochemically generated, has rarely been used for C–C bond formation.[2] For instance, with regard to a nucleophilic addition of a carbanion generated electrochemically to a carbonyl carbon, only the additions of tetrachloromethane[3,4] or ethyl trichloroacetate[3] to carbonyl compounds and the additions of allyl or benzyl chloride to carbon dioxide[2e] have been reported.[5]

In this paper we report successful additions of the carbanions generated electrochemically from substituted allyl and benzyl halides to ketones in hexamethylphosphoric triamide (HMPA) under mild conditions.

Results and Discussions

Electrochemical addition of the allyl group of allyl chloride (**1a**) to acetone was successfully carried out by using HMPA as a solvent. Thus, electrolysis of **1a** in the presence of five molar excess of acetone in HMPA containing 0.5 M tetrabutylammonium perchlorate (TBAP) as a supporting electrolyte using an undivided cell gave 2-methyl-4-penten-2-ol (**9**) in a 53% yield.

$$CH_2{=}CHCH_2X + CH_3COCH_3 \longrightarrow CH_2{=}CHCH_2\overset{\displaystyle CH_3}{\underset{\displaystyle OH}{C}}CH_3$$

1a: X = Cl
b: X = Br
c: X = I

9

Table 1 summarizes the results of this electrochemical addition carried out under several different electrolytic conditions. The Table indicates that HMPA is the best solvent and gives a yield of **9** much higher than that obtained by using other solvents such as DMF or THF (runs 1—3). The ratio of acetone to **1a** is important (runs 3—6) and increasing the ratio of acetone to **1a** generally gives a higher yield of **9**. The use of ten molar excess of acetone, however, resulted in a lower yield of **9**. This lower yield can probably be attributed to a lack of sufficient HMPA (2 ml). (The total volume of the solution was kept nearly constant in all runs and the volume of HMPA in usual runs was 5.5 ml). With regard to the electrode material, platinum cathode gave the best yield of **9** while mercury and carbon as the cathode gave a yield lower than platinum (runs 7 and 8). A change of the current density from 10 to 50 mA/cm^2 did not show any appreciable change in the yield (runs 11—14). The electrolysis at a cathode using a divided cell under the same conditions as that of run 3 in Table 1 gave only 19% yield of **9**. Thus, the use of an undivided cell rather than a divided cell may be preferable although this electrochemical reaction is a cathodic reaction.

Electrochemical reaction of **1a** with cyclohexanone under the same conditions as that of run 3 in Table 1 gave 1-allylcyclohexanol (**10**) in a 42% yield. Controlled potential electrolysis at −2.2 V *vs* Ag/AgI gave **10** in a 55% yield.

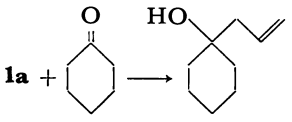

10

Electrochemical additions of the allyl- or the benzyl groups of various allyl halides or benzyl halides to acetone in HMPA containing 0.5 M TBAP gave the corresponding alcohols **9**—**17** and the results are summarized in Table 2. 1,5-Hexadiene from the electrochemical reactions of allyl bromide (**1b**) or allyl iodide (**1c**) with acetone, and bibenzyl from the reaction of benzyl bromide (**7b**) were obtained as by-products. The allyl anion generated by a two electron reduction of **1b** or **1c** underwent a nucleophilic attack on **1b** or **1c** to give 1,5-hexadiene[1e,2e] along with a nucleophilic addition reaction giving **9**. The presence of the side reaction pathway in the reactions of **1b** and **1c** would have led to a lower yield of **9**, whereas the electrochemical reaction of **1a** gave only **9** because of its lower reactivity towards allyl anion.

It should be noted that the addition products such

† Present address: Nippon Engelhard, Ltd., Ichikawa 272.

†† 1 M=1 mol dm^{-3}.

as **13** and **15** obtained in the electrochemical reactions of **3**, **4**, **5**, or **6** with acetone in the present study can not be obtained by the reaction of allylic organometallics derived from these halides with ketone. The organometallic reactions give exclusively the products **12** or **14** having the allyl group attached at the more heavily substituted carbon terminus.[6,7,8] The reactions of a metal with allyl halides **3** and **4** lead to the same organometallic compound which contains mainly the primary type of allylic organometallics, irrespective of the

TABLE 1. RESULTS OF ELECTROHCEMICAL REACTION OF ALLYL CHLORIDE (**1a**) WITH ACETONE[a]

Run	Molar ratio Acetone/**1a**	Solvent	Supporting electrolyte[b]	Curr. dens. mA cm^{-2}	*F*/mol	Yield/% of **9**
1	5	THF	0.5 M TBAP	25	2	9
2	5	DMF	0.5 M TBAP	25	2	10
3	5	HMPA	0.5 M TBAP	25	2	53
4	2	HMPA	0.5 M TBAP	25	2	24
5	1	HMPA	0.5 M TBAP	25	2	13
6	10	HMPA	0.5 M TBAP	25	2	17
7[c]	5	HMPA	0.5 M TBAP	25	2	14
8[d]	5	HMPA	0.5 M TBAP	25	2	36
9	5	HMPA	0.2 M TBAP	25	2	43
10	5	HMPA	0.5 M TEAP	25	2	14
11	5	HMPA	0.5 M TBAP	10	1	24
12	5	HMPA	0.5 M TBAP	25	1	29
13	5	HMPA	0.5 M TBAP	50	1	26
14	5	HMPA	0.5 M TBAP	100	1	17

a) Electrolyzed at 0 °C using an undivided cell with a platinum cathode. Amount of **1a** used was 10 mmol. b) TBAP: Tetrabutylammonium perchlorate; TEAP: tetraethylammonium perchlorate. c) Mercury pool was used as a cathode. d) Carbon was used as a cathode.

TABLE 2. RESULTS OF ELECTROCHEMICAL REACTIONS OF ALLYL OR BENZYL HALIDES WITH ACETONE[a]

Halides	Products (yield/%)[b]		
1a	**9**(53)		
1b	**9**(30)		
1c	**9**(22)		
2	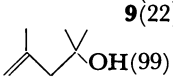 **11**		
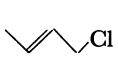 **3**	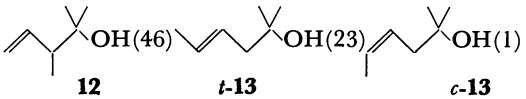 **12**	*t*-**13**	*c*-**13**
4	**12**(44)	*t*-**13**(15)	*c*-**13**(18)
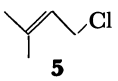 **5**	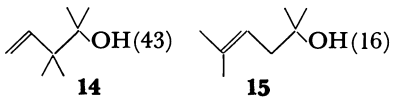 **14**	**15**	
6	**14**(54)	**15**(18)	
$PhCH_2Cl$ **7a**	**16**	$PhCH_3$(21)	
$PhCH_2Br$ **7b**	**16**(46)	$PhCH_3$(15)	$PhCH_2CH_2Ph$(16)
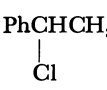 **8**	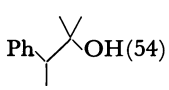 **17**	$PhCH_2CH_3$(9)	

a) A mixture of halide (10 mmol) and acetone (50 mmol) in 5.5 ml of HMPA containing 0.5 M Bu_4NClO_4 was electrolyzed at 0 °C using platinum plate electrodes. Current density was 25 mA/cm^2 and electricity passed was 2.0 *F* per mol of halide. b) Yields are based on halides used. Numbers in parentheses are also a current yield of each product.

structure of the starting halides **3** or **4**.[6] Such organometallics derived from **3** or **4** undergo the addition reaction to acetone to give exclusively **12** with a complete allylic rearrangement.[6] On the other hand, the electrochemical reactions of **3** or **4** with acetone produced different proportions of **12** and **13**. These depended on the properties of the electrode material, the readiness of the reduction of the substrates, or other electrolytic conditions. For instance, the electrochemical addition of **4** to acetone on a platinum cathode gave **12** and **13** in the ratio of 62 : 38 whereas on a carbon cathode the ratio was 29 : 71.[9] An effect of the readiness of the reduction of the substrates on these regiochemistries was observed in the electrochemical conjugate additions of **5** to α,β-unsaturated esters.[20,9] Although the electrochemical conjugate addition of **5** to diethyl fumarate which is more readily reduced than **5** took place at the less heavily substituted carbon terminus of **5**, the addition of **5** to ethyl crotonate which is less readily reduced than **5** occurred at the more heavily substituted carbon of **5**.[20,9] These regiochemistries are of considerable interest from the mechanistic and synthetic points of views, and this will be discussed more fully in later papers.

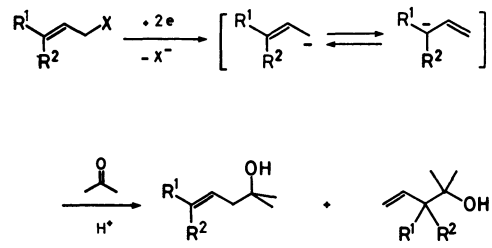

Scheme 1.

A probable path, which involves nucleophilic addition of allyl or benzyl anion to a carbonyl carbon, is shown in Scheme 1. Cyclic voltammetry shows that the reduction peak of acetone does not appear at a potential less negative than −2.5 V *vs.* Ag/AgI whereas the reduction peaks of **1a**, **1b**, **1c**, **2**, **3**, **4**, **7a**, and **7b** were observed at −2.35, −1.90, −1.43, −2.40, −2.40, −2.20, −2.00 and −1.80 V *vs.* Ag/AgI, respectively. Thus, a two electron reduction of allylic or benzylic halides is involved in this electrolysis to give the corresponding carbanions,[1e] which react with a carbonyl carbon.

One of the roles of HMPA as a solvent would be to stabilize carbanion intermediates leading to an increased yield of **9** as compared to those in other solvents. We found that a controlled potential electrolysis of **1a** and acetone in HMPA at −2.0 V or −1.5 V *vs.* Ag/AgI, which is a reduction potential less cathodic than that of **1a**, gave 30—34% yield of **9**. This may be partly due to a specific property of HMPA which has been suggested to be selectively adsorbed on the metal surface.[10] It may be also due to some difference of the reduction potentials between the microelectrolysis and the macroelectrolysis.[11] It should be noted that the electrochemical reduction of naphthalene in HMPA took place at a potential less cathodic than the half-wave potential of naphthalene[11] although this electrolytic system was considerably different from that of the present electrochemical reaction with acetone. The exact roles of HMPA during the course of the present electrochemical reaction are now under investigation.

Experimental

All the products were isolated and purified by distillation and by preparative GLPC with a JEOL JGC-20K or a Varian Autoprep 700 instrument. Spectroscopic measurements were carried out as described previously.[20] Quantitative GLPC analyses were carried out with a Hitachi 063 instrument using an internal standard method.

Materials. Hexamethylphosphoric triamide (HMPA) was dried over calcium hydride and distilled before use over lithium aluminium hydride under nitrogen at a reduced pressure. Acetone was treated with potassium permanganate and distilled. Most of the allyl or benzyl halides were commercially available and were distilled before use. 1-Chloro-3-methyl-2-butene (**5**) and 3-chloro-3-methyl-1-butene (**6**) were prepared from isoprene by the described procedure.[12] **5** (43%): bp 107—109 °C.[20] **6** (70%): bp 10—12 °C/20 mmHg (1 mmHg ≈133.322 Pa); ^{1}H NMR, δ 1.66 (6H, s), 5.15—6.1 (3H, m).

General Procedure for Electrolysis. For most of the preparative electrolyses, a normal undivided cell (2.8 cm dia.) equipped with a magnetic stirrer, a reflux condenser, and a serum cap for introduction of nitrogen gas was used. Electrolysis was carried out under a nitrogen atmosphere at a constant current using two platinum plate electrodes (2×2 cm^2). A typical procedure is as follows: A mixture of halide (10 mmol) and acetone (50 mmol) in 5.5 ml of HMPA containing 0.5 M Bu_4NClO_4 was electrolyzed at 0 °C with a current desity of 25 mA/cm^2 until 2.0 F of electricity per mol of halide was passed. After electrolysis, the reaction mixture was dissolved in diethyl ether and the solution was washed with thiosulfate solution and water, and dried over magnesium sulfate. The usual work-up of the solution gave a product mixture which was subjected to distillation and preparative GLPC to give pure products. Some physical properties of the products are recorded below.

*2-Methyl-4-penten-2-ol (**9**)*: n_D^{21} 1.4240; IR (neat) 3370, 3080, 1150, and 915 cm^{-1}; ^{1}H NMR ,δ 1.13 (6H, s), 1.48 (1H, s), 2.15 (2H, d), 5.1 (2H, m), and 5.85 (1H, m); MS *m/z* (rel intensity) 85 (M^+-CH_3, 4), 59 (100), and 43 (51). Calcd for $C_6H_{11}O$ (M^+-1): *m/z* 99.081. Found: *m/z* 99.081

*1-Allycylohexane (**10**)*: n_D^{25} 1.4729; IR (neat) 3380, 980, and 910 cm^{-1}; ^{1}H NMR, δ 1.19 (1H, s), 1.45 (10H, m), 2.17 (2H, d), 5.1 (2H, m), and 5.85 (1H, m); MS *m/z* (rel intensity) 122 (M^+-H_2O, 19), 99 (86), and 81 (100). Calcd for $C_9H_{16}O$: *m/z* 140.118. Found: *m/z* 140.118.

*2,4-Dimethyl-4-pentent-2-ol (**11**)*: n_D^{25} 1.4318; IR (neat) 3380, 3075, and 890 cm^{-1}; ^{1}H NMR, δ 1.18 (6H, s) 1.30 (1H, s), 1.83 (3H, s), 2.15 (2H, s), 4.73 (1H, m), and 4.90 (1H, m); MS *m/z* (rel intensity) 96 (M^+-H_2O, 10), 81 (73), and 59 (100). Calcd for $C_7H_{14}O$: *m/z* 114.104. Found: *m/z* 114.103.

*2,3-Dimethyl-4-penten-2-ol (**12**)*: n_D^{21} 1.4325; IR (neat) 3400, 3080, and 915 cm^{-1}; ^{1}H NMR, δ 0.95 (3H, d), 0.96 (1H, s), 1.07 (6H, s), 2.07 (1H, qi), 5.00 (2H, m), and 5.75 (1H, m); MS *m/z* (rel intensity) 96 (M^+-H_2O, 16), 81 (71), and 59 (100). Calcd for $C_7H_{14}O$: *m/z* 114.104. Found: *m/z* 114.104.

trans-*2-Methyl-4-hexen-2-ol* (t-*13*): n_D^{20} 1.4321; IR (neat) 3370, 3030, and 970 cm^{-1}; ^{1}H NMR, δ 1.01 (1H, s), 1.08 (6H, s), 1.65 (3H, m), 2.02 (2H, m), and 5.42 (2H, m); MS *m/z* (rel intensity) 96 (M^+-H_2O, 16), 81 (100), and 59 (79). Calcd for $C_7H_{14}O$: *m/z* 114.104. Found: *m/z* 114.104.

cis-*2-Methyl-4-hexen-2-ol* (c-*13*): n_D^{20} 1.4370; IR (neat) 3370,

3020, 1655, and 690 cm^{-1}; ^1H NMR, δ 1.04 (1H, s), 1.13 (6H, s), 1.59 (3H, d), 2.12 (2H, d), and 5.50 (2H, m); MS *m/z* (rel intensity) 96 (M^+-H_2O, 45), 81 (100), and 59 (78). Calcd for $C_7H_{14}O$: *m/z* 114.104. Found: *m/z* 114.105.

*2,3,3-Trimethyl-4-penten-2-ol (**14**)*: n_D^{20} 1.4453; IR (neat) 3450, 3080, 915 cm^{-1}; ^1H NMR, δ 1.03 (6H, s), 1.12 (6H, s), 1.26 (1H, s), 5.05 (2H, m), and 6.05 (1H, m); MS *m/z* (rel intensity) 70 (32), 59 (100), and 43 (57). Calcd for $C_8H_{15}O$: *m/z* 127.112. Found: *m/z* 127.114.

*2,5-Dimethyl-4-hexen-2-ol (**15**)*: n_D^{20} 1.4437; IR (neat) 3370, and 850 cm^{-1}; ^1H NMR, δ 1.15 (6H, s). 1.64 (3H, s), 1.75 (3H, s), 2.10 (2H, d), and 5.24 (1H, m); MS *m/z* (rel intensity) 70 (52), 59 (100), and 43 (57). Calcd for $C_8H_{16}O$: *m/z* 128.120. Found: *m/z* 128.120.

*2-Methyl-1-phenyl-2-propanol (**16**)*: n_D^{24} 1.5110; IR (neat) 3350, 720, and 695 cm^{-1}; ^1H NMR, δ 1.16 (6H, s), 1.64 (1H, s), 2.69 (2H, s), and 7.21 (5H, s); MS *m/z* (rel intensity) 92 (100) and 59 (95). Calcd for $C_{10}H_{14}O$: *m/z* 150.105. Found: *m/z* 150.105.

*2-Methyl-3-phenyl-2-butanol (**17**)*: n_D^{24} 1.5113; IR (neat) 3370, 765, and 695 cm^{-1}; ^1H NMR, δ 1.10 (3H, s), 1.12 (3H, s), 1.32 (3H, d), 1.42 (1H, s), 2.71 (1H, q), and 7.22 (5H, s); MS *m/z* (rel intensity) 106 (100), 91 (97), and 59 (95). Calcd for $C_{11}H_{16}O$: *m/z* 164.120. Found: *m/z* 164.121.

Cyclic Voltammetry. Cyclic voltammetry was carried out with a Yanaco V8 potentiostat at a sweep rate of 0.2 V s^{-1} using a platinum disk electrode (1 mm dia.) in HMPA containing 0.1 M Bu_4ClO_4. A potential was measured in V *vs* Ag/AgI.

References

1) a) A. J. Fry, "Synthetic Organic Electrochemistry," Harper and Row Publishers, New York (1972), p. 170; b) M. R. Rifi, "Organic Electrochemistry," ed by M. M. Baizer, Marcel Dekker, Inc., New York (1973), p. 279; c) M. R. Rifi, F. H. Covitz, "Introduction to Organic Electrochemistry," Marcel Dekker, Inc., New York (1974), p. 194; d) M. R. Rifi, "Technique of Electroorganic Synthesis," ed by N. L. Weinberg, John Wiley and Sons, Inc., New York (1975), Part II, p. 170; e) A. J. Bard and A. Merz., *J. Am. Chem. Soc.*, **101**, 2959 (1979).

2) a) M. R. Rifi, *J. Am. Chem. Soc.*, **89**, 4442 (1967); b) M. R. Rifi, *Collect. Czech. Chem. Commun.*, **36**, 932 (1971); c) R. Gerdil, *Helv. Chim. Acta*, **53**, 2100 (1970); d) A. J. Fry and W. E. Britton, *J. Org. Chem.*, **38**, 4016 (1973); e) M. M. Baizer and J. L. Chruma, *ibid.*, **37**, 1951 (1972); f) W. M. Moore, A. Salajegheh, and D. G. Peters, *J. Am. Chem. Soc.*, **97**, 4954 (1975); g) T. Iwasaki and K. Harada, *J. Chem. Soc., Perkin Trans. 1*, **1977**, 1730; h) T. Shono, I. Nishiguchi, and H. Ohmizu, *Chem. Lett.*, **1977**, 1021; i) F. Barba, M. D. Velasco, and A. Guirado, *Synthesis*, **1981**, 625; j) M. Tokuda, T. Taguchi, O. Nishio, and M. Itoh, *J. Chem. Soc., Chem. Commun.*, **1976**, 606; k) M. Tokuda and O. Nishio, *ibid.*, **1980**, 188; l) S. Satoh, T. Taguchi, M. Itoh, and M. Tokuda, *Bull. Chem. Soc. Jpn.*, **52**, 951 (1979); m) S. Satoh, M. Itoh, and M. Tokuda *J. Chem. Soc., Chem. Commun.* **1978**, 481; n) S. Satoh, M. Itoh, H. Suginome, and M. Tokuda, *Bull. Fac. Eng. Hokkaido Univ.*, **102**, 33 (1981); o) S. Satoh, H. Suginome, and M. Tokuda, *Bull. Chem. Soc. Jpn.*, **54**, 3456 (1981).

3) F. Karrenbrock and H. J. Schäfer, *Tetrahedron Lett*, **1978**, 1521.

4) T. Shono, H. Ohmizu, S. Kawakami, S. Nakano, and N. Kise., *Tetrahedron Lett.*, **22**, 871 (1981); T. Shono, N. Kise, A. Yamazaki, and H. Ohmizu, *ibid.*, **23**, 1609 (1982).

5) Although Wawzonek *et al.* and H. Lund *et al.* have obtained addition products by the electrochemical reduction of benzophenone or 9-fluorenone and alkyl halides, the products probably resulted from a trapping reaction of ketone anion radical by alkyl halide. S. Wawzonek and A. Gudersen., *J. Electrochem. Soc.*, **107**, 537 (1960); H. Lund and J. Simonet, *Bull. Soc. Chim. Fr.*, **1973**, 1843.

6) G. Courtois and L. Miginiac, *J. Organomet. Chem.*, **69**, 1 (1974).

7) V. Rautenstrauch, *Helv. Chim. Acta*, **57**, 496 (1974).

8) J. A. Katzenellenbogen and R. S. Lenox., *J. Org. Chem.*, **38**, 326 (1973).

9) S. Satoh, H. Suginome, and M. Tokuda., *Tetrahedron Lett.*, **22**, 1895 (1981).

10) H. W. Sternberg, R. E. Markby, I. Wender, and D. M. Mohilner, *J. Am. Chem. Soc.*, **89**, 186 (1967); **91**, 4191 (1969).

11) T. Asahara, M. Seno, and H. Kaneko, *Bull. Chem. Soc. Jpn.*, **41**, 2985 (1968).

12) W. J. Jones and H. W. T. Chorley, *J. Chem. Soc*, **1946**, 832.

 © 1983 The Chemical Society of Japan Bull. Chem. Soc. Jpn., 56, 1795—1798 (1983)

A Route from 1,1,1,3-Tetrachloro-3-phenylpropane to Ethynyl Phenyl Ketone Involving Elimination of Hydrogen Chloride and 1,3-Proton Transfer

Takeo Akiyama,* Yasuki Yoshida, Tokiko Hanawa, and Akira Sugimori

Department of Chemistry, Faculty of Science and Technology, Sophia University, Kioi-cho 7-1, Chiyoda-ku, Tokyo 102

(Received October 18, 1982)

The treatment of 1,1,1,3-tetrachloro-3-phenylpropane with alkali in ethanol affords ethynyl phenyl ketone and its acetal in good yields. This reaction proceeds through the elimination of hydrogen chloride and an efficient 1,3-proton transfer catalyzed by base. Ethyl cinnamate is obtained in only 2% yield.

We have already reported the formation of ethynyl metallocenyl ketones in the reaction of 1,1,1-trichloro-3-alkoxy-3-metallocenylpropanes with alkali in ethanol.[1] The expected product, ethyl 3-metallocenylacrylate (Mc–CH=CH–COOEt) has not been obtained.

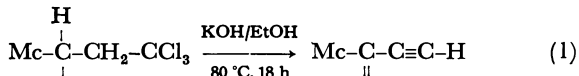

$$\mathrm{Mc{-}\overset{\displaystyle H}{\overset{|}{C}}{-}CH_2{-}CCl_3} \xrightarrow[80\ ^\circ\mathrm{C},\ 18\ \mathrm{h}]{\mathrm{KOH/EtOH}} \mathrm{Mc{-}\overset{\displaystyle OR}{\overset{|}{C}}{-}C{\equiv}C{-}H} \quad (1)$$

Mc: $(\eta^5\text{-}C_5H_5)_2M$, M = Fe, Ru; R = $-CH_3$, $-C_2H_5$

On the other hand, Kharasch *et al.* reported[2] that the treatment of 1,1,1-trichloro-3-bromo-3-phenylpropane, a bromotrichloromethane adduct to styrene, with sodium ethoxide in ethanol followed by hydrolysis gave cinnamic acid.

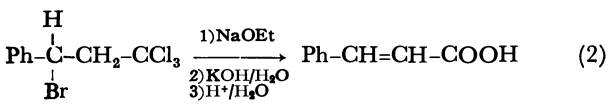

$$\mathrm{Ph{-}\overset{\displaystyle H}{\overset{|}{C}}{-}CH_2{-}CCl_3} \xrightarrow[2)\mathrm{KOH/H_2O}\ 3)\mathrm{H^+/H_2O}]{1)\mathrm{NaOEt}} \mathrm{Ph{-}CH{=}CH{-}COOH} \quad (2)$$
$$\mathrm{Br}$$

In order to clarify whether the unusual reaction shown in Eq. 1 is favored specifically by metallocenyl group attached at 3-position or whether it occurs in the normal carbon tetrachloride adduct of alkenes, we reinvestigated the solvolysis of 1,1,1,3-tetrachloro-3-phenylpropane (**1**) in the alkali–ethanol systems.

Experimental

Materials. Styrene (Wako Pure Chemical Co., G. R.) was distilled under reduced pressure just before use. Chlorotris (triphenylphosphine)ruthenium(II) was prepared according to the method given in the literature.[3] Sodium ethoxide was prepared from sodium metal and absolute ethanol. Ethanol-*d* (CH_3CH_2OD) (Commissariat a l'Energie Atomique, France, deuterium content: 99%) was used as received.

1,1,1,3-Tetrachloro-3-phenylpropane(**1**) was prepared from styrene according to Matsumoto *et al.*[4] Styrene (15.6 g, 0.15 mol) and chlorotris(triphenylphosphine)ruthenium(II) (0.78 g, 0.8 mmol) were dissolved in carbon tetrachloride (76 g, 50 cm³) and the solution was refluxed for 5 h under nitrogen atmosphere. After the reaction, carbon tetrachloride was removed under reduced pressure and the residue was submitted to column chromatography on silica gel (Wakogel C-200, 200 mesh, eluent: C_6H_6). **1** was obtained in 95% yield. The spectral data (IR and ^{1}H NMR spectra) of **1** were identical with those obtained by Matsumoto[5a] and Asahara.[5b] 1,1,1,3-Tetrachloro-4-phenylbutane (**13**) was prepared by the similar method from allylbenzene and carbon tetrachloride in 82% yield. The IR and ^{1}H NMR spectra of **13** were identical with those obtained by Matsumoto.[6]

Measurements. ^{1}H NMR spectra were recorded on a Hitachi R-22 (90 MHz) spectrometer. IR spectra were measured on a Hitachi 260-50 spectrophotometer. Mass spectra and GC-mass spectra were obtained on a JEOL JMA D-300 GC-mass spectrometer (column: OV-1, 5%, 1 m glass column).

Quantitative gas chromatography was performed on a Shimadzu GC-6AFP gas chromatograph (column: OV-1, 5%, 2 m glass column, temperature: 90—120 °C) equipped with an integrator (Shimadzu Chromatopak, E-1a).

Reactions. Reaction of 1,1,1,3-tetrachloro-3-phenylpropane (1) with Potassium Hydroxide in Ethanol Solution: **1** (3.0 g, 11.6 mmol) and potassium hydroxide (10 g, 0.178 mol) were added to ethanol (100 cm³) and the solution was refluxed for 18 h at 80 °C. After the reaction, the reaction mixture was neutralized with aqueous sulfuric acid (0.1 mol dm^{-3}) and the organic substances were extracted with dichloromethane. After the solvent was removed under reduced pressure, the residue was submitted to column chromatography on silica gel (Wakogel C-200, eluent: C_6H_6). Compounds **2**, **3**, **6**, **8**, and **9** were obtained in almost pure form.

Reaction of 1,1,1,3-tetrachloro-4-phenylbutane (13) with Potassium Hydroxide in Ethanol Solution: The procedure is the same as described for the reaction of **1**. **13** (2.0 g, 7.3 mmol) was added to the ethanol solution containing potassium hydroxide (10 g/100 cm³) and the solution was refluxed for 18 h.

Reaction of 1,1,1,3-tetrachloro-3-phenylpropane (1) with Sodium Ethoxide in Ethanol Solution. To the absolute ethanol solution of sodium ethoxide (12.0 g, 0.176 mol in 100 cm³) was added 3 g of **1** (11.6 mmol) and the solution was refluxed for 18 h at 80 °C. The separation method of the reaction products was the same as described above.

Reaction of 1,1-dichloro-3-ethoxy-3-phenylpropane (10) with Sodium Ethoxide in Ethanol Solution: **10** (200 mg, 0.86 mmol) was refluxed in a sodium ethoxide–ethanol solution (3 g in 25 cm³) for 18 h at 80 °C. After the reaction, the solution was neutralized and the organic substances were extracted with dichloromethane. Dichloromethane was removed under reduced pressure and the residue was dissolved in carbon tetrachloride for ^{1}H NMR spectra measurement. The ^{1}H NMR spectra of the product mixture show the presence of only three compounds, **2**, **3**, and **5** (100% conversion). A trace of **4** was detected by GC-mass spectra of the mixture. The yields of the products were calculated from the integrals of the peak areas.

Reaction of 1,1-dichloro-3-ethoxy-3-phenylpropane (10) with Sodium Ethoxide in Ethanol-d (C_2H_5OD) Solution: **10** (300 mg, 1.3 mmol) was refluxed in sodium ethoxide–ethanol-*d* solution (1.0 g in 30 cm³) for 8 h at 80 °C. After the reaction, the products were extracted with dichloromethane and the solvent was removed under reduced pressure. The residue was dissolved in carbon tetrachloride for the measurement of ^{1}H NMR spectra. The ^{1}H NMR spectra showed the presence

of **5**, **5**-*d*, **2**, **2**-*d*, **10**, **10**-*d*, and **3**. The ratio of **5** *versus* **5**-*d* was calculated based on the area of the peak of proton; the ratio of the area $\delta=5.76$ (s, –CH=CDCl) *versus* $\delta=5.76$ (d, $J=13$ Hz, –CH=CHCl) was 2 : 1. Similar calculations were done for **2**, **2**-*d*, **10**, **10**-*d*. The ratios obtained were: 2/2-*d*=2/1, and 10/10-*d*=1/1. No deuterium incorporation was observed for **3**. The similar reaction was carried out at 60 °C for 2 h in order to detect the compound **11**. The ^{1}H NMR spectra showed the peaks of compound **10**, **3**, and **5**. No deuterium incorporation was observed for these compounds. The peak attributable to the presence of **11** could not be observed. The GC-mass spectra of the same sample showed no increase of the intensities of the fragment peaks plus one (P+1) compared with those of the compounds **10**, **3**, and **5** which were obtained in the reaction of **10** in sodium ethoxide–ethanol system.

Identification of the Products. *1-Phenyl-2-propyn-1-one-(Ethynyl Phenyl Ketone) (**2**)*: A colorless liquid substance. IR (neat) 3240 (≡C–H), 3055, 3030 (arom. C–H), 2095 (C≡C), and 1650 cm^{-1} (C=O). ^{1}H NMR (CCl_4) $\delta=3.34$ (1H, s, C≡C–H), 7.30—7.65 (3H, m, meta and para protons of C_6H_5–), and 8.00—8.20 (2H, m, ortho protons of C_6H_5–). GC–MS (OV-1, 110 °C, 23 eV) *m/e* (rel intensity) 130 (M^+, 100), 105 (Ph–CO, 5.27), 102 (M^+-CO, 77.09), 78 (C_6H_6, 5.88), and 77 (C_6H_5, 2.54). Found: *m/e* 130.0440. Calcd for C_9H_6O: M, 130.0418.

*3,3-Diethoxy-3-phenyl-1-propyne (**3**)*: A pale yellow liquid substance. IR (neat) 3270 (≡C–H), 3060, 3030 (arom. C–H), 2980, 2930, 2880 (aliph. C–H), 2110 (C≡C), 1110 and 1045 cm^{-1} (C–O–C). ^{1}H NMR (CCl_4) $\delta=1.19$ (6H, t, $-OCH_2-CH_3$), 2.59 (1H, s, C≡C–H), 3.53 (4H, m, $-OCH_2-CH_3$), and 7.20—7.55 (5H, m, C_6H_5–). GC–MS (OV-1, 126 °C, 70 eV) *m/e* (rel intensity) 204 (M^+, 1.54), ($M^+-C_2H_5$, 29.7), 159 ($M^+-OC_2H_5$, 100), 131 ($M^+-O(C_2H_5)_2+H$, 65.4), and 77 (C_6H_5, 1.9). Found: *m/e* 204.1131. Calcd for $C_{13}H_{16}O_2$: M, 204.1150.

*(Z)3-Chloro-1-phenyl-2-propen-1-one (**4**)*: A colorless liquid substance. IR (neat) 3060, 3030 (arom. C–H), 1670 (C=O), 1650 (C=C), and 670 cm^{-1} (*cis* CH=CHCl). ^{1}H NMR (CCl_4) $\delta=6.63$ (1H, d, $J=8$ Hz, –CH=CHCl), 6.87 (1H, d, $J=8$ Hz, –CH=CHCl), and 7.15—7.6 (5H, m, C_6H_5–). GC–MS (OV-1, 110 °C, 23 eV) *m/e* (rel intensity) 166 (M^+, 41.1, $M^+ +2/M^+=0.322$ (Cl×1)), 138 (M^+-CO, 13.3), 131 (M^+-Cl, 55.5), 105 (Ph–CO, 100), and 77 (C_6H_5, 36.7). Found: *m/e* 166.0168. Calcd for C_9H_7OCl: M, 166.01861.

*(E)1-Chloro-3,3-diethoxy-3-phenylpropene (**5**)*: A colorless liquid substance. IR (neat) 3070, 3030 (arom. C–H), 2980, 2940, 2880 (aliph. C–H), 1660 (C=C), 1070—1060 (C–O–C), and 942 cm^{-1} (*trans* CH=CHCl). ^{1}H NMR (CCl_4) $\delta=1.17$ (6H, t, $-OCH_2-CH_3$), 3.36 (4H, m, $-OCH_2-CH_3$), 5.76 (1H, d, $J=13$ Hz, –CH=CHCl), 6.50 (1H, d, $J=13$ Hz, –CH=CHCl), and 7.10—7.55 (5H, m, C_6H_5–). GC–MS (OV-1, 96 °C, 70 eV) *m/e* (rel intensity) 240 (M^+, 0.12, $M^+ +2/M^+=0.323$ (Cl×1)), 205 (M^+-Cl, 100), 195 ($M^+-OC_2H_5$, 79.23), 167 ($M^+-O(C_2H_5)_2+H$, 60.35), 131 ($M^+-O(C_2H_5)_2-Cl$, 70.84), 105 (Ph–CO, 86.63), and 77 (C_6H_5, 62.92). Found: *m/e* 240.0925. Calcd for $C_{13}H_{17}O_2Cl$: M, 240.09181.

*3,3-Diethoxy-1-phenyl-1-propanone (**6**)*: The dimethyl acetal of **6** which was prepared from **4** with sodium methoxide was reported by T. Matsumoto, *et al.*[7] A colorless liquid substance. IR (neat) 3070, 3030 (arom. C–H), 2980, 2940, 2890 (aliph. C–H), 1690 (C=O), and 1125 cm^{-1} (C–CO–C). ^{1}H NMR (CCl_4) $\delta=1.13$ (6H, t, $-OCH_2-CH_3$), 3.17 (2H, d, $J=5$ Hz, $-CH_2-CH(OC_2H_5)_2$), 3.61 (4H, m, $-CH_2-CH_3$), 5.03 (1H, t, $J=5$ Hz, $-CH_2-CH(OC_2H_5)_2$), 7.11—7.66 (3H, m, meta and para protons of C_6H_5–), and 7.77—8.11 (2H, m, ortho protons of C_6H_5–). GC–MS (OV-1, 110 °C, 23 eV) *m/e* (rel intensity) 222 (M^+, 1.33), 193 ($M^+-C_2H_5$, 29.86), 177 ($M^+-OC_2H_5$, 5.87), 176 ($M^+-HOC_2H_5$, 5.53), 147 ($M^+-O(C_2H_5)_2+H$, 12.27), 133 ($M^+-(OC_2H_5)_2+H$, 13.99), 105 (Ph–CO, 100), and 78 (C_6H_6, 8.59). Found: *m/e* 222.1264. Calcd for $C_{13}H_{18}O_3$: M, 222.12564.

*3,3-Diethoxy-1-phenylpropyne (**7**)*: A colorless liquid substance. IR and ^{1}H NMR spectra of this compound were identical with those reported by Kiely *et al.*[8] Found: *m/e* 204.1164. Calcd for $C_{13}H_{16}O_2$: M, 204.1150.

*Ethyl Cinnamate (**8**)*: The IR and ^{1}H NMR spectra of **8** were identical with those of authentic sample.

*3-Ethoxy-3-phenyl-2-propenal (**9**)*: A colorless liquid substance. IR (neat) 3070, 3030 (arom. C–H), 2980, 2940, 2880 (aliph. C–H), 1660 (–C=C–CHO), and 1378 cm^{-1} (C–H of CHO). ^{1}H NMR (CCl_4) $\delta=1.13$ (3H, t, $-OCH_2-CH_3$), 3.36 (2H, q, $-OCH_2-CH_3$), 5.47 (1H, d, $J=8$ Hz, =CH–CHO), 7.0—7.51 (5H, m, C_6H_5–), and 9.30 (1H, d, $J=8$ Hz, CHO). GC–MS (OV-1, 110 °C, 23 eV) *m/e* (rel intensity) 176 (M^+, 20.92), 175 (M^+-H, 31.98), 147 (M^+-CHO, 25.49), 131 ($M^+-OC_2H_5$, 100), and 78 (C_6H_6, 13.10). Found: *m/e* 176.0841. Calcd for $C_{11}H_{12}O_2$: M, 176.08376.

*1,1-Dichloro-3-ethoxy-3-phenylpropene (**10**)*: A pale yellow liquid substance. IR (neat) 3060, 3030 (arom. C–H), 2960, 2920, 2890 (aliph. C–H), and 1610 cm^{-1} (C=C). ^{1}H NMR (CCl_4) $\delta=1.13$ (3H, t, $-OCH_2-CH_3$), 3.38 (2H, m, $-OCH_2-CH_3$), 5.03 (1H, d, $J=8$ Hz, $-CH(OEt)-CH=CCl_2$), 5.93 (1H, d, $J=8$ Hz, $-CH(OEt)-CH=CCl_2$), and 7.0—7.4 (5H, m, C_6H_5–). GC–MS (OV-1, 110 °C, 23 eV) *m/e* (rel intensity) 230 (M^+, 0.26, $M^+ +2/M^+=0.66$ (Cl×2)), 195 (M^+-Cl, 100), 185 ($M^+-OC_2H_5$, 5.94), 167 ($M^+-Cl-C_2H_5+H$, 36.64), 131 ($M^+-2Cl-C_2H_5$, 15.90), and 105 (Ph–CO, 6.3). Found: *m/e* 230.0198. Calcd for $C_{11}H_{12}OCl_2$: M, 230.0264.

Results and Discussion

When **1** (3.0 g, 11.6 mmol) was refluxed in an ethanolic solution of potassium hydroxide (10 g/100 cm^3) for 18 h followed by neutralization with acid, eight compounds were obtained. The main products were ethynyl phenyl ketone (**2**) (14%) and its acetal (**3**) (33%); these are the phenyl analogs of the compounds obtained in the case of 1,1,1-trichloro-3-ethoxy-3-metallocenylpropane.[1]

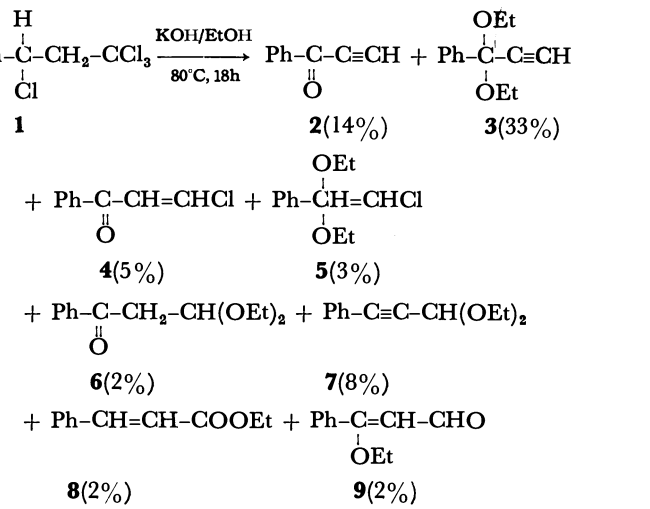

These facts indicate that this type of unusual reaction is favored not only by a metallocenyl group attached to the 3-position but also by a phenyl group at the 3-position.

The products from **1** except for **8** which is the product expected from the report by Kharasch *et al.*[2] have one similar feature, *i.e.* these compounds have a hydrogen atom at the terminal carbon which originally had three chlorine atoms.

When the reaction of **1** was carried out with ethanolic sodium ethoxide (12 g/100 cm^3), compounds **2**, **3**, **4**, **5**, and **10** were obtained in 59, 2, 2, 2, and 22% yields, respectively.

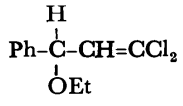

10 (22%)

Compound **10** has a different type of structure from **2**, **3**, **4**, and **5** and is considered to be a precursor to **2** and **3**, since i) **10** is the compound which is formed by the normal substitution of chloride ion by ethoxide ion at benzylic position of **1**; ii) the hydrogen atom at the benzylic position in **1** is still at the original position in **10**; and iii) the terminal carbon has no hydrogen atom yet.

The treatment of **10** (200 mg) with sodium ethoxide in ethanol (3 g/25 cm^3) afforded a mixture of products, the composition of which is similar to that of the product from **1** on treatment with sodium ethoxide except for **10**. **2**, **3**, **4**, and **5** were obtained in 18, 72, <1, and 9% yields, respectively.

The formation of **5** from **10** strongly suggests that the base-catalyzed 1,3-proton transfer[9] takes place effectively and this results in the formation of the rearranged product **11** as shown in Scheme 1.

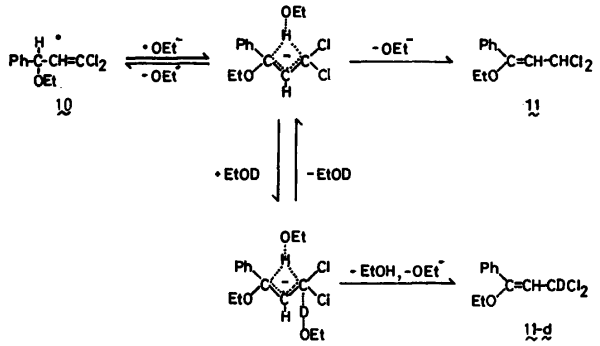

Scheme 1.

If this 1,3-proton transfer occurs intramolecularly, the incorporation of deuterium from the solvent (EtOD) would not be observed in the products. The results that the alkali-solvolysis of **10** (300 mg) with sodium ethoxide in monodeuterated ethanol (EtOD) (1.0 g/30 cm^3) at 80 °C for 8 h shows the 33% incorporation of deuterium in **5** but no incorporation of deuterium in **3** indicate that the 1,3-proton transfer occurs mainly intramolecular fashion. Cram and Uyeda[9] reported the base-catalyzed rearrangement of 3-phenyl-1-butene to *cis*-2-phenyl-2-butene and they showed that both intra- and intermolecular 1,3-hydrogen transfer were involved in the rearrangement. However, the fact that no deuterium incorporation was observed for **3** indicates that the primary reaction of **10** with ethoxide ion to produce **11** is almost intramolecular fashion and the secondary solvolysis of **11** is faster than H–D exchange reaction. When the reaction of **10** with sodium ethoxide in EtOD was carried out at 60 °C for 2 h, formation of **3** and **5** without deuterium were observed, although the formation of **11** was not observed. These results strongly suggest that the intramolecular 1,3-proton transfer occurs effectively in this reaction, when the H–D exchange process is slow enough compared with the solvolysis.

The tentative reaction pathway from **11** to **5** is as follows; i) the rearranged product **11** loses one of the two chlorine atoms as a chloride ion and forms carbenium ion, such as **12**, and ii) **12** is attacked by ethoxide ion at the α-position to phenyl group to produce **5**.

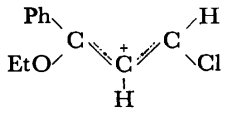

12

No similar reaction involving 1,3-proton transfer was observed in the treatment of 1,1,1,3-tetrachloro-4-phenylbutane (**13**), a carbon tetrachloride adduct to allylbenzene, with potassium hydroxide in ethanol solution.[10]

For this base-catalyzed 1,3-proton transfer reaction, the stabilization of the transition state by conjugation with an aromatic group seems to play an important role: When an ethoxide ion attacks the hydrogen atom at the 3-position of **10** and abstracts it as a proton, the negative charge is delocalized in a conjugate system involving phenyl group. After the proton transfer is completed, the removal of a chloride ion from **11** produces an allyl cation **12** which is also stabilized by the phenyl group. The results that the products **2**, **3**, **4**, **5**, and **6** consist of 82% of the whole products strongly suggest that the carbon atom having phenyl and ethoxyl group in **12** is preferentially attacked by ethoxide ion to produce **5**. These results agree with those obtained in the case of metallocene derivatives of **1**.

The formation of **2**, **3**, **4**, and **5** may be explained by a mechanism in which a transposition of the carbon side chain resulting in the exchange of 1- and 3-positions is involved. However, this mechanism is excluded by the experiment using 1,1,1-trichloro-3-ethoxy-3-(3-ethylferrocenyl)propane. When it was refluxed with potassium hydroxide in ethanol at 80 °C for 18 h, only 3-ethyl ferrocenyl ethynyl ketone was obtained and no product *via* carbon side chain transposition, such as 2-ethylferrocenyl ethynyl ketone or 1′-ethylferrocenyl ethynyl ketone was obtained.

The authors are grateful to Professor Naoki Inamoto for helpful discussions. We also thank Dr. Hideyuki Matsumoto for sending us spectral data of **1** and **13**.

References

1) T. Akiyama, T. Hattori, K. Ito, T. Uryu, M. Kajitani, and Akira Sugimori, *Chem. Lett.*, **1980**, 361.

2) M. S. Kharasch, O. Reinmuth, and W. H. Urry, *J. Am. Chem. Soc.*, **69**, 1105 (1947).

3) P. S. Hallman, T. A. Stephenson, and G. Wilkinson,

Inorg. Synth., **12**, 238 (1972).

4) H. Matsumoto, T. Nakao, and Y. Nagai, *Tetrahedron Lett.*, **1975**, 899; H. Matsumoto and Y. Nagai, *Kagaku No Ryoiki*, **30**, 50 (1976).

5) a) H. Matsumoto, private communication; b) T. Asahara and C. Wu, *Kogyo Kagaku Zasshi*, **72**, 1516 (1969).

6) H. Matsumoto, private communication. IR (neat) 3070, 3040, 2970, 1505, 1460, 1420, 1205, 970, 760, and 699 cm^{-1}. ^1H NMR (CCl_4) $\delta=3.05$—3.29 (4H, m, $-C\underline{H}_2-CHCl-C\underline{H}_2CCl_3$), 4.20—4.58 (1H, m, $-C\underline{H}Cl-$), and 7.21 (5H, s, C_6H_5-). Found: *m/e* 269.9538. Calcd for $C_{10}H_{10}Cl_4$: M, 269.9539.

7) T. Matsumoto and H. Shirahama, *Bull. Chem. Soc. Jpn.*, **38**, 1289 (1965).

8) J. S. Kiely, P. Boudjouk, and L. L. Nelson, *J. Org. Chem.*, **42**, 2626 (1977).

9) D. J. Cram and R. T. Uyeda, *J. Am. Chem. Soc.*, **86**, 5446 (1964).

10) The only product which has molecular weight less than 300 could be identified by GC-MS (OV-1, 110 °C, 23 eV). The parent peak (M^+, *m/e* 208, $M^+ + 2/M^+ = 0.335$) and fragment pattern suggest the presence of 1-chloro-3-ethoxy-4-phenyl-1-butyne.

Reaction of Malonaldehyde with Nucleic Acid. I. Formation of Fluorescent Pyrimido[1,2-*a*]purin-10(3*H*)-one Nucleosides

Hiroshi SETO,* Taisuke OKUDA,† Tomoyuki TAKESUE,† and Tadashi IKEMURA†

Tokyo Metropolitan Research Laboratory of Public Health, Shinjuku-ku, Tokyo 160

†*College of Science and Technology, Nihon University, Chiyoda-ku, Tokyo 101*

(Received November 10, 1982)

The reactions of malonaldehyde with guanosine and 2′-deoxyguanosine proceed slowly under acidic conditions to give new pyrimidopurine nucleosides, **3a** and **3b**, respectively. These compounds emit strong yellow fluorescence and are hydrolyzed by NaOH into malonaldehyde and guanosine from **3a** (2′-deoxyguanosine from **3b**). From chemical and spectroscopic evidence, these compounds were deduced to be 3-β-D-ribofuranosylpyrimido[1,2-*a*]-purin-10(3*H*)-one (**3a**) and 3-(2-deoxy-β-D-*erythro*-pentofuranosyl)pyrimido[1,2-*a*]purin-10(3*H*)-one (**3b**). No products were detected in the reaction mixture of malonaldehyde with 1-methylguanosine, adenosine, cytidine, uridine, thymidine, 2′-deoxyadenosine, or 2′-deoxycytidine.

Malonaldehyde (**1**) has been found to be one of the decomposition products of many oxidized lipid materials.[1,2] The presence of **1** in foods[3–5] and in living organs[6,7] in which the lipid fraction has undergone oxidation may be of physiological significance.

It has been reported that **1** initiates skin carcinogenesis in mice[8] and that it has mutagenic activity.[9,10] DNA is modified by **1** under acidic conditions, and becomes fluorescent.[11] The compound **1** presumably cross-links the amino groups of DNA in solution, probably through the formation of Schiff bases.[11] Brooks *et al.*[12] suggested that **1** is associated preferentially with the guanine and cytosine moieties of the DNA core. However, the mechanism of interaction between DNA and **1** still remains obscure.

When we attempted the reaction of several nucleosides with **1**, guanosine (**2a**) and 2′-deoxyguanosine (**2b**) yielded new orange-yellow fluorescent compounds, **3a** and **3b**, respectively. Lee *et al.*[13] had reported a similar fluorescent compound as a simple guanosine-malonaldehyde adduct. We previously reported a preliminary form[14] and proposed structure for the modified guanosine. In this paper, we describe the formation of the compounds in detail, and present evidence supporting the proposed structures. The physiological significance of these results is discussed.

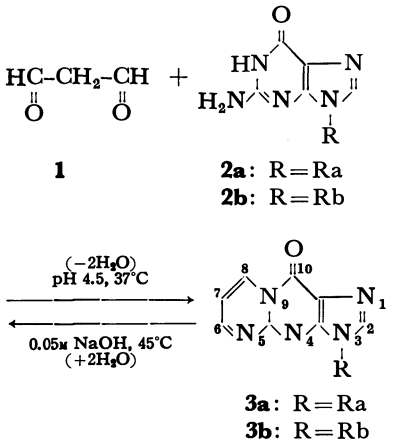

1 **2a**: R=Ra **2b**: R=Rb

3a: R=Ra **3b**: R=Rb

Ra=β-D-ribofuranosyl,
Rb=2-deoxy-β-D-*erythro*-pentofuranosyl

Scheme 1.

Results and Discussion

Product Analysis of Nucleoside-malonaldehyde Reaction Mixture by HPLC. Some HPLC chromatograms are shown in Fig. 1, together with the control. Fluorescent products (p1 and p2) appeared on the reaction of **1** with **2a** and **2b**, respectively. Peaks in the fluorescence (FL) chromatograms appeared later than in the UV traces because of the capacity of the connecting tube, but the FL chromatograms shown in the figure have been corrected for this effect.

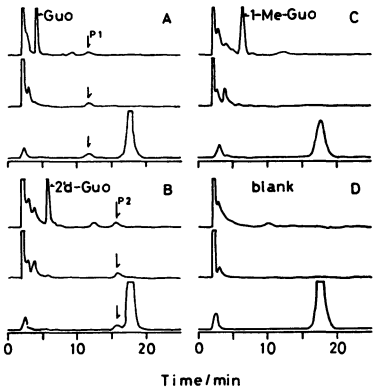

Fig. 1. HPLC chromatograms of nucleoside-malonaldehyde reaction mixtures. (upper): UV 254 nm, range 16, 10 μl inj., (middle): UV 330 nm, range 8, 50 μl inj., (bottom): FL 365—460 nm, 50 μl inj., A time lag of each FL chromatogram is excluded.

DNA was allowed to react with **1** to form fluorescent products with max. emission at 460 nm when excited at 390 nm, and a new absorption peak at 325 nm was also formed.[11] The present products, peaks p1 and p2, showed the same spectral characteristics. However, peaks having these spectral characteristics were not detected in the reaction mixtures of **1** with other nucleosides: 1-methylguanosine, adenosine, cytidine, uridine, thymidine, 2′-deoxyadenosine, and 2′-deoxycytidine. From these findings, it seems that the sugar moiety is not modified by **1**, since **3a** and **3b** have different sugar moieties. Usually, under the chromatographic conditions used, a 2′-deoxyribonucleoside has a longer retention time than the corresponding ribonucleoside.

Our results suggest that one or more sites on the guanine moiety of DNA is reactive to **1**.

Structure of the Modified Nucleoside Formed by Guanosine-malonaldehyde Reaction. Compound **3a** (peak p1) was isolated as a yellow solid (34 mg), mp 195 °C (decomp), by repeated liquid chromatography. The purity of **3a** was 99.7% as determined by HPLC analysis.

Compound **3a** was hygroscopic and highly soluble in water and in dimethyl sulfoxide (DMSO). **3a** was partially hydrolyzed by 0.05 M NaOH (1 M=1 mol dm^{-3}) into **2a** and **1**. The Molish test for sugar was positive. No carbonyl group of ketone and/or aldehyde was detected in the 2,4-dinitrophenylhydrazine test. On the other hand, the TBA (2-thiobarbituric acid) test, which is used for the detection of malonaldehyde and its precursor or adduct, was positive. The pH profile of UV absorption of compound **3a** is shown in Fig. 2. The pK_a value was calculated spectrophotometrically as 1.03.

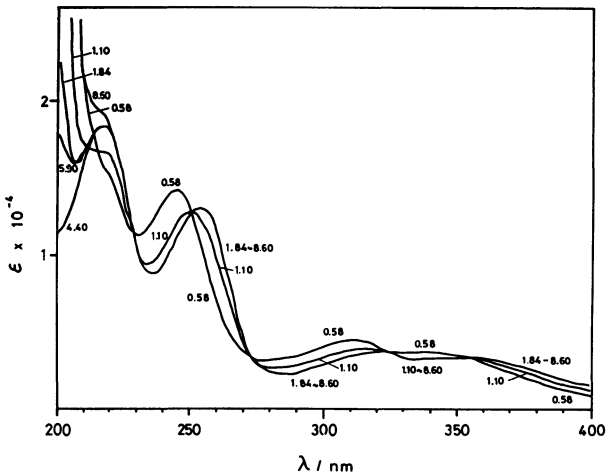

Fig. 2. UV absorption spectra of compound **3a** at various pH.

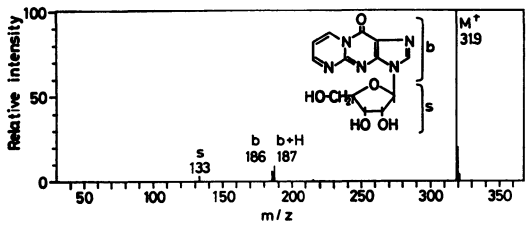

Fig. 3. FD mass spectrum of compound **3a**.

The FD mass spectrum of **3a** indicated m/z values of 319 (M), 187 (base+H) and 133 (ribose) (Fig. 3). The EI and CI mass spectra were obtained after trimethylsilylation of **3a**. The molecular ion peak of the trimethylsilyl (TMS) derivative was observed at an m/z value of 535 (m/z was 536 for CI with methane). Therefore, the number of substitutable active hydrogens by TMS is three. The molecular formula of **3a**, $C_{13}H_{13}N_5O_5$, was established by high resolution mass spectrometry (Found: m/z 535.2099. Calcd for $C_{13}H_{10}N_5O_5(TMS)_3$: M, 535.2102).

The IR(KBr) and UV(H_2O) spectra showed absorption bands at 3350 (O–H), 1723 (C=O) and 1630

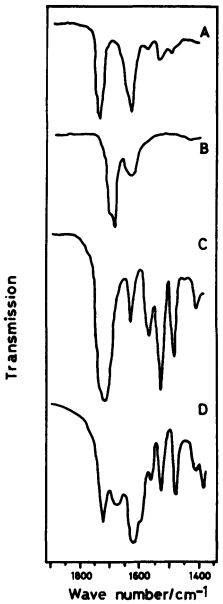

Fig. 4. IR spectra of compound **3a** and **2a**. (A), (B): **3a** and **2a** in acetonitrile, (C), (D): **3a** and **2a** in solid phase.

(C=C, C=N) cm^{-1} and 215 (ε 18600), 251 (ε 13200), 308 (ε 2700), 319 (ε 3140), and 348 (ε 2750) nm, respectively. There were serious differencies between **3a** and **2a** in respect to the absorption in the C=O stretching region. When **3a** was examined in dilute solution (acetonitrile), the relative strength of C=O to C=C and C=N absorption (Fig. 4A) was considerably weaker than that of **2a** (Fig. 4B). On the other hand, in the solid state, the C=O absorption of **2a** was influenced by intermolecular hydrogen bonding, and a complex spectrum was observed (Fig. 4D). In the FL spectrum, the E_x and E_m maxima were 360 and 500 nm, respectively.

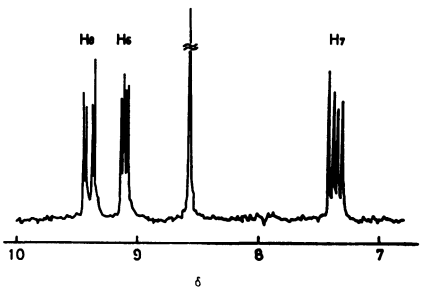

Fig. 5. Proton-NMR spectrum of compound **3a**.

The ^{1}H-NMR spectrum of **3a** (Fig. 5) exhibited typical AMX-type signals due to the –CH=CH–CH= group (δ 7.33 (J=3.9 and 6.8 Hz), 9.08 (J=2.0 and 3.4 Hz) and 9.38 (J=2.0 and 7.3 Hz), each 1H, dd). The signal of the exocyclic amino group of **2a** could no longer be seen. There were no changes in the signals of C_2 methine and ribose protons. The ^{13}C-NMR spectrum showed the existence of three carbons (δ 110.5, 141.0 and 161.8 (each d)) in addition to those of **2a**. The singlet signal of C_{10} was shifted to higher magnetic field in comparison with the original compound **2a**. It

Table 1. Assignment of ^1H chemical shifts of the nucleosides in DMSO-d_6

		3a		3b
C_2–H	8.54	1H(s)	8.47	1H(s)
C_6–H	9.08	1H(dd, J=2.0 and 3.4)	9.05	1H(dd, J=2.2and 3.7)
C_7–H	7.33	1H(dd, J=3.9 and 6.8)	7.30	1H(dd, J=3.9and 7.3)
C_8–H	9.38	1H(dd, J=2.0 and 7.3)	9.35	1H (dd, J=2.2 and 7.1)
$C_{1'}$–H	6.02	1H (d, J=5.9)	6.46	1H (t, J=6.8)
$C_{2'}$–H	4.60	1H (brds., dd)	*	
$C_{3'}$–H	4.20	1H (brds., dd)	4.46	1H (brds., m)
$C_{4'}$–H	4.01	1H (brds., m)	3.94	1H (brds., m)
$C_{5'}$–H	3.65	2H (brds., m)	3.59	2H (brds., m)

s: Singlet, d: doublet, dd: double doublet, t : triplet, m : multiplet, brds: broads, J values are in Hz, *:$C_{2'}$–H gave a overlap with the solvent (δ 2.4—2.6).

seems noteworthy that 1-methylguanosine was unreactive to malonaldehyde (**1**), as shown in Fig. 1C.

These results led us to conclude that the structure of the strongly fluorescent compound is 3-β-D-ribofuranosylpyrimido[1,2-*a*]purin-10(3*H*)-one.

The fluorescent nucleoside (peak p2) from **2b** showed similar properties. Spectroscopic evidence led us to assign the structure 3-(2-deoxy-β-D-*erythro*-pentofuranosyl)pyrimido[1,2-*a*]purin-10(3*H*)-one. The base moieties of these modified nucleosides were the same.

The yields of products were only 1.4% from **2a** and 1.8% from **2b**.

The products formed by reactions of amino compounds[15] or protein[16,17] with **1** were found to be positive in the TBA test. Aldehyde **1** reacted with lysine residues of casein (37 °C for 24 h).[18] The reaction proceeded in two steps: the formation of enamine structure (O=CHCH=CHNHR) and then the formation of aminoiminopropene structure (RN=CHCH=CHNHR) with the characteristic fluorescence spectra.[18] Our results suggest a similar reaction mechanism in the present case. The formation of pyrimidopurine is attributed to an ionic reaction of nucleophilic nitrogen atoms at the 1 and N_2 positions of guanine with carbonium ions of malonaldehyde. The reaction, involving cyclization, is very slow, though some substituted malonaldehydes were reported to react readily with guanine.[19]

The biological significance of our results is not clear at present. Reiss *et al.*[11] reported that the formation of fluorescent products correlates linearly with loss of DNA template activity. It can be assumed that the modified guanine base is unable to form a base-pair with cytosine of DNA. Thus, the decrease of the template activity can probably be attributed to the modification of guanine by **1**. Moreover, such modification is likely to be a major cause of cancer and mutation initiated by **1**. Structural determination of the fluorescent products derived from DNA modified by **1** is in progress.

Experimental

Apparatus. Melting points are uncorrected. IR, UV and FL spectra were recorded on Hitachi EPI-G3, Union Giken SM-401 and Shimadzu RF-500 spectrophotometers, respectively. NMR spectra were obtained on JEOL FX-100 and FX-270 spectrometers with TMS as an internal standard in DMSO-d_6 at room temperature. Mass spectra were recorded on JEOL JMS D-300 (EI, CI and high resolution) and 01SG-2 (FD) mass spectrometers. TLC analyses were carried out with WAKO polyamide FM plates (5 cm × 10 cm). Analytical HPLC was carried out with a Shimadzu LC-2 machine equipped with UV (254 and 330 nm) and FL (E_x 365 nm, E_m 460 nm) detectors, on a Unisil C-18, 5 μm (4 mmϕ × 25 cm) column (the mobile phase was 5% acetonitrile–water). The inlet of the FL detector was connected to the outlet of the UV detector.

Reactions of Malonaldehyde with Nucleosides. All reagents were purchased from commercial sources, and the purity of the nucleosides was checked by HPLC. Aldehyde **1** was prepared by the hydrolysis of 1,1,3,3-tetraethoxypropane. A mixture (pH 4.5) of 0.1 M malonaldehyde (1 ml), 0.01 M nucleosides (1 ml), and 0.1 M dipotassium hydrogenphosphate (8 ml) was heated at 37 °C for 10 d. The mixture was analyzed by HPLC. No growth of microorganisms was apparent during the reaction.

Isolation of the Fluorescent Nucleoside from Guanosine-malonaldehyde Reaction Mixture. Aldehyde **1** was obtained by the hydrolysis of 1,1,3,3-tetraethoxypropane (2.2 g, 0.01 mol) with 0.1 M HCl (100 ml). The mixture was heated at 40 °C for 40 min, then adjusted to pH 4.5. A mixture of **1** (0.01 mol), **2a** (700 mg, 2.5 mmol) and dipotassium hydrogenphosphate (13.6 g, 0.1 mol) in one liter of water was heated at 37 °C for 10 d. The mixture was concentrated to about 100 ml at 40 °C. Acetonitrile (600 ml) was added to the residue. The mixture was stored overnight in a refrigerator (4 °C), then the precipitate was filtered off and washed with 90% acetonitrile. The filtrate was concentrated to 50 ml, then stored overnight at 4 °C. The precipitate was filtered off. The filtrate was cleaned-up by polyamide (Woelm) column chromatography (50 mmϕ × 30 cm) with water as the eluent. The eluate was concentrated to 50 ml. The solution was chromatographed on a Lichroprep RP-18 (Merck, 22 mmϕ × 30 cm) column with 7% acetonitrile as the eluent. The fraction including **3a** was concentrated to 50 ml. The chromatography was repeated twice. Subsequently, the solution was further chromatographed on a Lichroprep RP-18 column (10 mmϕ × 25 cm) with 5% acetonitrile as the eluent. The chromatography was repeated 3 times. All operations of the synthesis and purification procedure described above were repeated 6 times. Guanosine (**2a**) used, therefore, amounted to 4.2 g (14.8 mmol). The final eluate was collected after each synthesis. The pooled eluates were dried and concentrated *in vacuo*.

The fluorescent product **3b** from the 2′-deoxyguanosine-malonaldehyde reaction was synthesized and isolated in a similar manner, but on a smaller scale: 2′-deoxyguanosine (**2b**) used totalled 1.85 g (6.9 mmol).

Trimethylsilylation. To prepare the TMS derivative, acetonitrile (100 μl) and *N,N*-bis(trimethylsilyl)trifluoroacet-

amide containing 1% trimethylchlorosilane (150 μl) were added to the dried nucleoside (100 μg). Then the mixture was heated at 75 °C for 3 h (1.5 h for the 2'-deoxy deriv.) in a reaction vial.

3a: Mp 195 °C (decomp), R_f 0.74 ppc/H_2O, 0.86 polyamide/H_2O, pK_a 1.03, ^{13}C-NMR(DMSO-d_6) 61.3(t), 70.0(d), 74.0(d), 85.7(d), 87.4(d), 110.5(d), 117.9(s), 137.4(d), 141.0(d) 149.0(s), 149.7(s), 152.3(s), 161.8(d).

3b: Mp 145 °C (decomp), R_f 0.80 ppc/H_2O, 0.74 polyamide/H_2O, pK_a 1.05, UV (H_2O) 214 (ε 23700), 253 (ε 16400), 308 (ε 3500), 320 (ε 3800), 350 nm (ε 3200), FL Ex max. 360 nm, Em max. 500 nm, IR(KBr) 3320 (O–H), 1723 (C=O), 1630 cm^{-1} (C=C, C=N), MS FD 303 (M^+), 187 (base+H), 186(base), 117(s), EI(TMS deriv.) 447(M^+), 187(base+H), CI(TMS deriv. isobutane) 448(QM^+), 188(base+2H), ^{13}C-NMR(DMSO-d_6) 61.8(t), 70.9(d), 83.8(d), 88.1(d), 110.7(d), 118.0(s), 137.4(d), 140.9(d), 149.1(s), 149.5(s), 152.5(s), 161.9(d). The $C_{2'}$ signal overlapped with the solvent signal.

We are grateful to Mr. Tsuyoshi Hashimoto for his technical assistance and to Dr. Kazuyuki Akiyama, Tokyo Metropolitan Res. Lab. Pub. Health, for helpful discussions.

References

1) R. O. Sinnhuber, T. G. Yu, and C. T. Yu, *Food Res.* **23**, 624 (1958).
2) B. G. Tarladgis and B. M. Watts, *J. Am. Oil Chemists' Soc.*, **37**, 403 (1960).
3) B. G. Tarladgis, B. M. Watts, and M. T. Younathan, *J. Am. Oil Chemists' Soc.*, **37**, 44 (1960).
4) V. C. Witte, G. F. Kranse, and M. E. Bailey, *J. Food Sci.*, **35**, 582 (1970).
5) K. S. Rhee, *J. Food Sci.*, **43**, 1776 (1978).
6) K. Yagi, *Biochem. Med.*, **15**, 212 (1976).
7) D. H. Boehme, R. Kosecki, S. Carson, F. Stern, and N. Narks, *Brain Res.*, **136**, 11 (1977).
8) R. J. Shamberger, T. L. Andreone, and C. E. Willis, *J. Natl. Cancer Inst.*, **53**, 1771 (1974).
9) F. H. Mukai and B. D. Goldstein, *Science* **191**, 868 (1976).
10) R. J. Shamberger, C. L. Corlett, K. D. Beaman, and B. L. Kasten, *Mutat. Res.* **66**, 349 (1979).
11) U. Reiss, A. L. Tappel, and K. S. Chio, *Biochem. Biophys. Res. Commun.*, **48**, 921 (1972).
12) B. R. Brooks and O. L. Klamerth, *Eur. J. Biochem.*, **5**, 178 (1968).
13) Y. Lee, I. Park, and Y. Y. Lee, *Proc. Coll. Nat. Sci.* Sec. 3 (Seoul Natl. Univ.) **2**, 73 (1977); *Chem. Abstr.*, **89**, 142024x (1978).
14) H. Seto, T. Hashimoto, T. Okuda, T. Takesue, and T. Ikemura, *Chem. Lett.*, **1981**, 707.
15) K. Kikugawa, K. Tsukuda, and T. Kurechi, *Chem. Pharm. Bull.*, **28**, 3323 (1980).
16) T. W. Kwon, D. B. Menzel, and H. S. Olcott, *J. Food Sci.*, **30**, 808 (1965).
17) D. L. Crawford, T. C. Yu, and R. O. Sinnbuber, *J. Food Sci.*, **32**, 332 (1967).
18) H. Chiba, H. Doi, M. Yoshikawa, and E. Sugimoto, *Agric. Biol. Chem.*, **40**, 1001 (1976).
19)R. C. Moschel and N. J. Leonard, *J. Org. Chem.*, **41**, 294 (1976).

Stereospecific and Stereoselective Reactions. IX.[1] Preparation of Ethyl (2*E*,7*R*)-7-Acetoxy-4-oxo-2-octenoate from D-Glucose

Sumio Yokota, Mitsuru Nishida, and Oyo Mitsunobu*

Department of Chemistry, College of Science and Engineering, Aoyama Gakuin University, Chitosedai, Setagaya-ku, Tokyo 157

(Received November 20, 1982)

Reaction of methyl 2,3-anhydro-4,6-dideoxy-α-D-*ribo*-hexopyranoside with MgI_2 exclusively afforded methyl 3,4,6-trideoxy-3-iodo-α-D-*xylo*-hexopyranoside which was dehalogenated by treatment with $LiAlH_4$ to give methyl 3,4,6-trideoxy-α-D-*erythro*-hexopyranoside (**2**). Hydrolysis of **2** and subsequent treatment with ethoxycarbonylmethylenetriphenylphosphorane gave ethyl (2*E*, 4*R*, 7*R*)-4,7-dihydroxy-2-octenoate (**10**). Oxidation of **10** by active MnO_2 resulted in the formation of an equilibrium mixture of ethyl (2*E*, 7*R*)-7-hydroxy-4-oxo-2-octenoate (the carbon skeleton of pyrenophorin) and cyclic hemiacetal. On treatment with acetic anhydride, the mixture afforde dethyl (2*E*, 7*R*)-7-acetoxy-4-oxo-2-octenoate.

Carbohydrates have been utilized as potential starting materials for the construction of natural products having multiple centers of chirality.[2] In spite of many elegant approaches have been reported so far, there is still a need to develop convenient methods for stereospecific and regioselective transformation of a hydroxyl group of carbohydrates. 2,3-Anhydro sugars are attractive chiral intermediates for the transformation of carbohydrates. The opening of the oxirane ring on locked pyranosides system by nucleophiles has been much discussed and a clear pattern has emerged, while the reaction of flexible 2,3-anhydropyranosides with nucleophiles are more complicated and the factors determining the reaction site are not fully elucidated.[3]

We report here a simple synthesis of ethyl (2*E*,7*R*)-7-acetoxy-4-oxo-2-octenoate (**1**), the carbon skeleton of pyrenophorin, from methyl 3,4,6-trideoxy-α-D-*erythro*-hexopyranoside (**2**) which was obtained by a sequence of reactions involving regioselective oxirane ring-opening of readily available methyl 2,3-anhydro-4,6-dideoxy-α-D-*ribo*-hexopyranoside.[4]

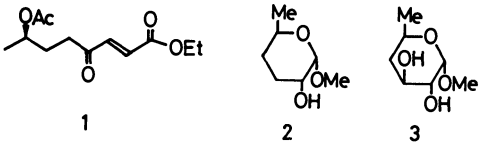

Scheme 1.

Reductive oxirane ring-opening of 2,3-anhydropyranoside has been reported.[5] Thus, methyl 4,6-dideoxy-α-D-*xylo*-hexopyranoside (**3**) was converted into methyl 2,3-anhydro-4,6-dideoxy-α-D-*ribo*-hexopyranoside (**4**) by the reaction with diethyl azodicarboxylate (DEAD) and triphenylphosphine (TPP).[6] It was found, however, that catalytic hydrogenation (Raney-Ni (W-2); 100—120 kg/cm² H_2, 80 °C) or $LiAlH_4$ reduction (−2—0 °C, ether) of **4** afforded the desired **2** in only 18% or 29% yields, respectively.

Next, a two-step procedure was examined. When **4** was allowed to react with MgI_2 in tetrahydrofuran (THF), methyl 3,4,6-trideoxy-3-iodo-α-D-*xylo*-hexopyranoside (**5**) was obtained in 80% yield without any detectable formation of 2-iodo isomer (**6**).[7] The sequence thus allowed net replacement of the 3-hydroxyl group of **3** by iodo substituent with retention of configuration. The reaction of **4** with NaI in the presence of sodium acetate and acetic acid in acetone gave **5** and **6** in 53 and 11% yields, respectively. It is noteworthy that no reaction occurred when **4** was treated with tetrabutylammonium iodide under the similar conditions (THF, refluxed for 6 h). Thus these results suggest that metal cations play an important role in the cleavage of the oxirane-ring of **4**.[8]

Compound **5** reacted smoothly with $LiAlH_4$ to give **2** in 95% yield.

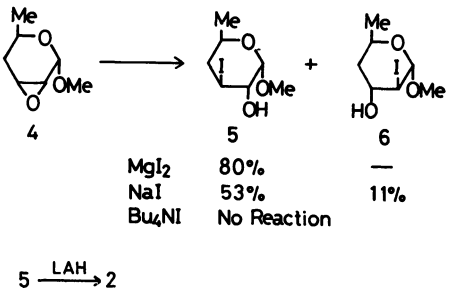

Scheme 2.

An alternative route to **2** was also examined. Methyl 4,6-dideoxy-2-*O*-*p*-tosyl-α-D-*xylo*-hexopyranoside (**7**) was allowed to react with carbon tetrabromide and TPP in THF at room temperature for 24 h giving an oily product which was assumed to be an alkoxyphosphonium bromide (**8**). The solvent was then replaced by toluene and the resulting mixture was refluxed for 2 h affording methyl 3-bromo-3,4,6-trideoxy-2-*O*-*p*-tosyl-α-D-*ribo*-hexopyranoside (**9**) in 54% yield. Although the configuration at the 3-position could not be determined, in view of the nature of the bromination reaction, D-*ribo*-configuration was tentatively assigned.[9] By treatment with $LiAlH_4$, **9** gave **2** in 73% yield.

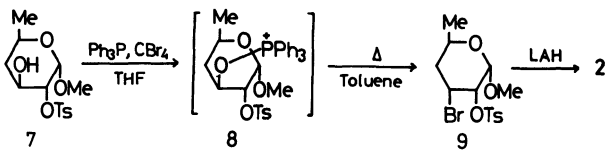

Scheme 3.

Acid hydrolysis of **2** gave free sugar (83% yield) which was converted into ethyl (2*E*,4*R*,7*R*)-4,7-dihy-

droxy-2-octenoate (**10**) by the reaction with ethoxycarbonylmethylenetriphenylphosphorane in 75% yield. Selective oxidation of the 4-hydroxyl group of **10** could be accomplished by the reaction with active MnO_2.[10] As indicated by ^{1}H-NMR spectrum, however, the product is an about 1 : 1 mixture of desired ethyl (2*E*,7*R*)-7-hydroxy-4-oxo-2-octenoate (**11**) and cyclic hemiacetal (**12**; 74% total yield). In order to displace the equilibrium to the open chain compound, the mixture was treated with acetic anhydride in pyridine affording the expected ethyl (2*E*,7*R*)-7-acetoxy-4-oxo-2-octenoate (**1**) in 78% yield. Acetalization of **1** afforded ethyl (2*E*,7*R*)-7-acetoxy-4,4-dimethoxy-2-octenoate (**13**) in 91% yield.

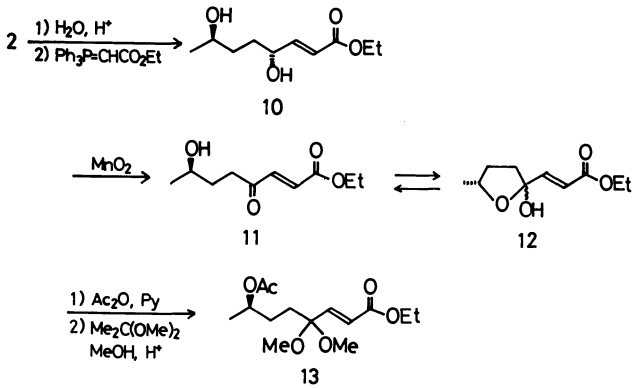

Scheme 4.

Bakuzis *et al.* have reported the synthesis of *dl*-pyrenophorine from ethyl *dl*-7-acetoxy-4,4-ethylenedioxy-2-octenoate by the use of DEAD and TPP in the cyclization step.[11] Since the lactonization using DEAD and TPP has been shown to proceed through inversion of configuration at the reaction site of the alcoholic component,[4,12] the synthesis of **13** indicates a relay approach to (*S*,*S*)-pyrenophorin.

Experimental

Nuclear magnetic resonance (NMR) spectra were measured on Hitachi R-20 spectrometer (60 MHz) using tetramethylsilane as an internal standard. Optical rotations were measured on JASCO DIP-4 digital polarimeter using a 1-dm cell in the solvent indicated. Preparative thin layer chromatography (PLC) and column chromatography were performed on Merck Kieselgel 60 PF_{254} (20 cm × 20 cm or 20 cm × 30 cm plate) and Kieselgel 60 (70—230 mesh), respectively. All evaporations were performed under reduced pressure. For distillation of small amount of product, Kugelrohr (Büchi) apparatus was used and oven temperature is indicated.

*Preparation of Methyl 2,3-Anhydro-4,6-dideoxy-α-*D*-*ribo*-hexopyranoside (**4**) from Methyl 4,6-Dideoxy-α-*D*-*xylo*-hexopyranoside (**3**).* *a) Two-step Procedure*: *p*-Tosyl chloride (35 g, 184 mmol) was added to a suspension of **3** (11.8 g, 73 mmol)[13] in pyridine (150 ml) at 0 °C. After the mixture had been stirred for 80 h at room temperature, chloroform (150 ml) was added. The mixture was washed successively with 10% H_2SO_4 and saturated aqueous $NaHCO_3$, dried ($MgSO_4$), and evaporated. The residue was crystallized from methanol, affording methyl 4,6-dideoxy-2,3-di-*O*-*p*-tosyl-α-D-*xylo*-hexopyranoside (29.7 g, 86%, mp 110—112 °C). NMR ($CDCl_3$ δ=1.15 (d, H-6), 1.45—2.4 (m, H-4), 2.45 (s, $C\underline{H}_3$–C_6H_4–), 3.30 (s, CH_3O–), 3.5—4.15 (m, H-5), 4.2—4.5 (dd, H-2), 4.65—5.2 (m, H-3), 4.83 (d, H-1). Found: C, 53.54; H, 5.58%. Calcd for $C_{21}H_{26}S_2O_8$: C, 53.60; H, 5.57%.

Sodium methoxide in methanol (prepared from 0.87 g of sodium and 20 ml of methanol) was added to a suspension of the ditosylate (6.31 g, 13.4 mmol) in methanol (30 ml) at room temperature. The mixture was refluxed for 6 h with stirring, and then evaporated. Water was added to the residue and extracted with dichloromethane and ether. The organic layer was dried ($MgSO_4$) and evaporated. Methanol was added to the residue and evaporated to a small volume. Unreacted ditosylate was filtered off (1.18 g, 19% recovery). The filtrate was evaporated and the residue was chromatographed (benzene–ethyl acetate=5 : 1) to give **4** (1.11 g, 57%). $[\alpha]_D^{20}$ +61.7° (*c* 0.3, $CHCl_3$). NMR ($CDCl_3$) δ=1.1 (d, H-6), 1.2—2.2 (m, H-4), 3.2—4.2 (m, H-2,3,5), 3.3 (s, CH_3O–), 4.78 (d, H-1, $J_{1,2}$=2.8 Hz). Found: C, 58.65; H, 8.53%. Calcd for $C_7H_{12}O_3$: C, 58.31; H, 8.39%.

b) One-step Procedure: A solution of diethyl azodicarboxylate (1.04 g, 6 mmol) in benzene (2 ml) was added dropwise to a mixture of **3** (0.649 g, 4 mmol) and triphenylphosphine (1.57 g, 6 mmol) in benzene (7 ml) at room temperature. The mixture was refluxed for 2 h, allowed to cool to room temperature, and evaporated. Ether was added to the residue to precipitate triphenylphosphine oxide and diethyl hydrazinedicarboxylate which were filtered off. The filtrate was concentrated and the residue was distilled giving **4** [oven temperature 80—120 °C/22 Torr (1 Torr=133.322 Pa)]. The distillate was contaminated with a small amount of diethyl hydrazinedicarboxylate which was removed by passing through silica-gel column (benzene–ethyl acetate=1 : 5). The yield of **4** was 75% (431 mg). Thin layer chromatography of the crude reaction mixture indicated the presence of a trace of methyl 2,3-anhydro-4,6-dideoxy-α-D-*lyxo*-hexopyranoside. However, the isomer could not be isolated.

*Reaction of Methyl 2,3-Anhydro-4,6-dideoxy-α-*D*-ribo-hexopyranoside (**4**) with Iodide.* *a) Reaction with MgI_2*: MgI_2 was prepared by the reaction of activated magnesium[14] with I_2. After a mixture of potassium (2.54 g, 65 mmol) and $MgCl_2$ (3.22 g, 34 mmol) in THF (20 ml) had been refluxed with stirring under N_2 for 2 h, a solution of I_2 (8.21 g, 32 mmol) in THF (20 ml) was added, followed by a solution of **4** (2.15 g, 15 mmol) in THF (15 ml). The mixture was heated under reflux for 6 h. Saturated aqueous NH_4Cl (10 ml) was added to the cooled reaction mixture and filtered through Hyflosupercel. The filtrate was evaporated, the residue being extracted with chloroform. The organic layer was washed with aqueous sodium thiosulfate, dried ($MgSO_4$), and evaporated affording chromatographically (TLC) pure methyl 3,4,6-trideoxy-3-iodo-α-D-*xylo*-hexopyranoside (**5**; 3.94 g, 97%). Purification by means of PLC (ether–chloroform=1 : 20) afforded pure **5** (80% yield) which was recrystallized from hexane, mp 57—59 °C. $[\alpha]_D^{21}$ +140° (*c* 1.08, $CHCl_3$). NMR ($CDCl_3$) δ=1.16 (d, H-6), 1.9—2.7 (m, H-4, OH), 3.4 (s, CH_3O–), 3.5—4.6 (m, H-2,3,5), 4.66 (d, H-1, $J_{1,2}$=*ca.* 3.5 Hz). Found: C, 31.17; H, 4.95%. Calcd for $C_7H_{13}O_3I$: C, 30.91; H, 4.81%.

b) Reaction with NaI: A mixture of **4** (0.309 g, 2.14 mmol), NaI (1.61 g, 10.7 mmol), sodium acetate (0.0882 g, 1.08 mmol), and acetic acid (2.5 ml) in acetone (10.5 ml) was refluxed with stirring for 2 h. After the solvent had been removed, chloroform was added, washed successively with saturated aqueous $NaHCO_3$ and aqueous sodium thiosulfate, and dried ($MgSO_4$). Solvent was removed and the residue was separated by PLC (ethyl acetate–chloroform=1 : 20) giving **5** (0.309 g, 53%) and **6** (0.0662 g, 11%). NMR for **6** ($CDCl_3$) δ=1.27 (d, H-6), 3.4 (s, CH_3O–), 5.12 (br s, H-1).

c) Reaction with Tetrabutylammonium Iodide: A mixture of **4** (0.144 mg, 1 mmol) and tetrabutylammonium iodide (1.85 g, 5 mmol) in THF (60 ml) was refluxed with stirring for 6 h. The mixture was allowed to cool to room temperature. The precipitated tetrabutylammonium iodide was recovered by filtration (96%). From the filtrate, 76% of **4** was recovered by means of PLC (benzene–ethyl acetate=5 : 1).

*Methyl 3,4,6-Trideoxy-α-*D*-*erythro*-hexopyranoside (**2**).*

*a) From Methyl 3,4,6-Trideoxy-3-iodo-α-*D*-*xylo*-hexopyranoside (**5**)*: A solution of **5** (4.42 g, 16.3 mmol) in THF (30 ml) was added to a suspension of $LiAlH_4$ (0.679 g, 17.9 mmol) in THF (20 ml) with stirring at room temperature, and then refluxed with stirring for 6 h. The mixture was allowed to cool to room temperature, quenched by water (15 ml), filtered through Hyflosupercel, and concentrated. The residue was extracted with dichloromethane. The extracts were washed with water, dried ($MgSO_4$), and evaporated giving **2** (2.27 g, 95%), which was practically pure as indicated by GLC (Carbowax 20M, 1 m, 100 °C). The product could be purified by distillation (oven temperature 60—80 °C/14 Torr) or column chromatography (benzene–ethyl acetate=1 : 5). $[\alpha]_D^{20}+142°$ (*c* 1.08, $CHCl_3$). NMR (CCl_4) δ=1.05 (d, H-6), 1.1—2.0 (m, H-3,4), 3.3—4.0 (m, H-2,5), 3.34 (s, CH_3O–), 4.46 (d, H-1). Found: C, 56.95; H, 9.68%. Calcd for $C_7H_{14}O_3$: C, 57.51; H, 9.65%.

*b) From Methyl 4,6-Dideoxy-2-*O*-p-tosyl-α-*D*-xylo-hexopyranoside (**7**)*: A solution of carbon tetrabromide (1.68 g, 5.06 mmol) in THF (2 ml) was added dropwise to a solution of **7** (949 mg, 3 mmol)[15] and TPP (917 mg, 3.5 mmol) in THF (8 ml) at room temperature with stirring. After the mixture had been stirred for 24 h at room temperature, the solvent was removed. Toluene (10 ml) was added to the residue and refluxed for 2 h. The resulting mixture was concentrated and separated by PLC (ether–petroleum ether=2 : 1) to give methyl 3-bromo-3,4,6-trideoxy-2-*O*-*p*-tosyl-α-D-*ribo*-hexopyranoside as an oil (**9**; 615 mg, 54%) and 8.5% of **7** was recovered. The **9** was used in the next step without further purification. NMR for **9** (CCl_4) δ=1.12 (d, H-6), 1.85—2.25 (m, H-4), 2.4 (s, CH_3–C_6H_4–), 3.2 (s, CH_3O–), 3.85—4.4 (m, H-3,5), 4.12 (d, H-1,2, $J_{1,2}$=*ca.* 2.5 Hz).

A mixture of **9** (570 mg, 1.5 mmol) in THF (5 ml) was added to $LiAlH_4$ (379 mg, 10 mmol) in THF (10 ml) at room temperature and heated under reflux for 20 h. After the addition of water (10 ml) and 2 M (1 M=1 mol dm^{-3}) H_2SO_4 (30 ml), the mixture was extracted with chloroform (120 ml). The organic layer was washed with 2 M Na_2CO_3 and water, dried, and concentrated. The residue was chromatographed (benzene–ethyl acetate=1 : 5) to give **2** (160 mg, 73%) and 20% of **9** was recovered.

*Ethyl (2*E*,4*R*,7*R*)-4,7-Dihydroxy-2-octenoate (**10**).* A mixture of **2**, (1.99 g, 13.6 mmol) and Dowex 50 (H^+) (3.50 g) in water (50 ml) was refluxed with stirring for 4.5 h. After filtration, the filtrate was concentrated to a small volume and extracted with chloroform. The aqueous layer was evaporated to dryness giving 3,4,6-trideoxy-D-*erythro*-hexopyranose (1.30 g, 72%; mp 47—53 °C) which was used in the next step without purification.

A solution of 3,4,6-trideoxy-D-*erythro*-hexopyranose (779 mg, 5.9 mmol), ethoxycarbonylmethylenetriphenylphosphorane (2.222 g, 6.4 mmol), and benzoic acid (30 mg, 0.25 mmol) in benzene (20 ml) was refluxed with stirring for 8 h. After evaporation, ether was added to precipitate triphenylphosphine oxide which was filtered off. The filtrate was evaporated and the residue was separated by chromatography (ethyl acetate) giving about 2 : 1 mixture of desired **10** and triphenylphosphine oxide. The yield of **10** was estimated to be 75% from the integration of the signal of NMR spectrum. The mixture was used in the next step. NMR (CCl_4) δ=1.15 (t, C<u>H</u>$_3$CH$_2$O–), 1.58 (d, H-8), 1.1—2.0 (br one peak, H-5,6), 3.25—5.25 (m, H-4,7 and two OH), 4.08 (q, CH$_3$C<u>H</u>$_2$O–), 5.96 (dd, H-2, $J_{2,3}$=16 Hz, $J_{2,4}$=1.5 Hz), 6.88 (dd, H-3, $J_{3,4}$=4 Hz).

*Ethyl (2*E*,7*R*)-7-Acetoxy-4-oxo-2-octenoate (**1**).* A 2 : 1 mixture of ethyl (2*E*,4*R*,7*R*)-4,7-dihydroxy-2-octenoate (**10**) and triphenylphosphine oxide (containing 4.37 mmol of **10**) was stirred with active MnO_2 (3.00 g)[16] in chloroform (50 ml) for 7 h at room temperature. After filtration, the filtrate was evaporated. The residue was chromatographed (benzene–ethyl acetate=1 : 1), giving about 1 : 1 mixture of ethyl (2*E*,7*R*)-7-hydroxy-4-oxo-2-octanoate (**11**) and cyclic hemiacetal (**12**) in 74% (649 mg) yield. The ratio was determined from the integration of the signal of NMR spectrum.

Acetic anhydride (0.1 ml) was added to a solution of the mixture (105 mg, 0.525 mmol) in pyridine (2 ml) at room temperature. After the solution had been stirred for 22 h at room temperature, water (1 ml) was added. The resulting mixture was evaporated and distilled to give **1** (99 mg, 72%, oven temperature 100—120 °C/0.4 Torr). NMR (CCl_4) δ=1.24 (d, H-8), 1.31 (t, C<u>H</u>$_3$CH$_2$O–), 1.54—2.1 (m, H-6), 1.95 (s, CH_3CO), 2.68 (t, H-5), 4.24 (q, C<u>H</u>$_3$CH$_2$O–), 4.87 (sext, H-7), 6.55 and 7.02 (AB q, olefin, J=16 Hz).

*Ethyl (2*E*, 7*R*)-7-Acetoxy-4,4-dimethoxy-2-octenoate (**13**).* Acetalization was performed by the analogous procedure reported by Hase *et al.*[17] A solution of 2,2-dimethoxypropane (122 mg, 1.17 mmol) in methanol (1 ml) was added to anhydrous *p*-toluenesulfonic acid (6 mg) at −70 °C, followed by ethyl (2*E*,7*R*)-7-acetoxy-4-oxo-2-octenoate (**1**, 49 mg, 0.202 mmol) in methanol (5 ml). The mixture was stirred for 4 h at −50 °C and then for 18 h at room temperature. The mixture was diluted with ether (5 ml), neutralized (3% $NaHCO_3$), and evaporated. The residue was extracted with chloroform. The organic layer was washed with water, dried ($MgSO_4$), and evaporated giving practically pure **13** (53 mg, 91%). Purification by PLC (ether–hexane=2 : 3) gave **13** in 60% yield. $[\alpha]_D^{19}$ +7.9° (*c* 1.53, $CHCl_3$). NMR (CCl_4) δ=1.18 (d, H-8), 1.31 (t, C<u>H</u>$_3$CH$_2$O–), 1.3—2.0 (m, H-5,6), 1.96 (s, CH_3CO), 3.13 (s, two CH_3O–), 4.25 (q, CH$_3$C<u>H</u>$_2$O–), 4.85 (sextet, H-7), 6.03 and 6.56 (AB q, olefin, J=15.6 Hz). An analytical sample was obtained by distillation (oven temperature 125—128 °C/0.4 Torr). Found: C, 58.08; H, 8.27%. Calcd for $C_{14}H_{24}O_6$: C, 58.31; H, 8.39%.

This work was partially supported by a Grant-in-Aid for Scientific Research from Ministry of Education, Science and Culture.

References

1) This work has been presented at 45th National Meeting of Chemical Society of Japan, April 4, 1982, Abstracts No. 4F32. Part VIII, T. Asano, S. Yokota, and O. Mitsunobu, *Chem. Lett.*, **1983**, 343.

2) The use of carbohydrates as starting materials for the construction of chiral products has been reviewed. See for example; S. Hanessian, *Acc. Chem. Res.*, **12**, 159 (1979); A. Vasella, "Modern Synthetic Methods, 1980," ed by R. Scheffold, Otto Salle Verlag-Verlag Sauerlander (1980), pp. 173—267; Y. Nakahara and T. Ogawa, "Kosentakuteki Hanno," ed by H. Nozaki, T. Mukaiyama, and R. Noyori, Kagakudozin, Kyoto (1980), pp. 101—116; H. Ohrui, *Yuki Gosei Kagaku Kyokai Shi (J. Synth. Org. Chem. Jpn.,)* **39**, 275 (1981).

3) R. D. Guthrie, "The Carbohydrates, Chemistry and Biochemistry," 2nd ed, ed by W. Pigman and D. Horton,

Academic Press, New York (1972), Vol. IA, pp. 423—478; J. G. Buchanan and H. Z. Sable, "Selective Organic Transformation," ed by B. S. Thyagarajan, Wiley-Interscience, New York (1972), Vol. 2, pp. 1—95.

4) For the total synthesis of pyrenophorin, see D. Seebach, B. Seuring, H.-O. Kalinowski, W. Lubosch, and B. Renger, *Angew. Chem., Int. Ed. Engl.*, **16**, 364 (1977); B. Seuring and D. Seebach, *Liebigs Ann. Chem.*, **1978**, 2044; R. S. Mali, M. Pohmakotr, B. Weidmann, and D. Seebach, *ibid.*, **1981**, 2272.

5) See for example, D. A. Prins, *J. Am. Chem. Soc.*, **70**, 3955 (1948); Y.-L. Fu and M. Bobek, *J. Org. Chem.*, **41**, 3831 (1976); *ibid.*, **45**, 3836 (1980).

6) O. Mitsunobu, T. Kudo, M. Nishida, and N. Tsuda, *Chem. Lett.*, **1980**, 1613. Guthrie and Jenkins have independently reported the epoxidation of methyl 4,6-*O*-benzylidene-D-aldohexopyranosides by the use of DEAD and TPP; R. D. Guthrie and I. D. Jenkins, *Aust. J. Chem.*, **34**, 1997 (1981). Zbiral and his coworkers have extensively studied the preparation of anhydro sugars by the use of DEAD and TPP. See for example, H. H. Brandstetter and E. Zbiral, *Helv. Chim. Acta*, **63**, 327 (1980); E. Mark, E. Zbiral, and H. H. Brandstetter, *Monatsh. Chem.*, **111**, 289 (1980); E. Mark and E. Zbiral, *ibid.*, **112**, 215 (1981).

7) The reaction of locked and flexible 2,3-anhydropyranosides with metal halides have been reported. See for example, G. N. Richards, L. F. Wiggins, and W. S. Wise, *J. Chem. Soc.*, **1956**, 496; R. U. Lemieux, E. Fraga, and K. A. Watanabe, *Can. J. Chem.*, **46**, 61 (1968); J. Thiem and J. Schwentner, *Chem. Ber.*, **112**, 3126 (1979); J. Thiem, P. Ossowski, and J. Schwentner, *ibid.*, **113**, 955 (1980); J. Thiem, M. Holst, and J. Schwentner, *ibid.*, **113**, 3488 (1980).

8) For the conformation of flexible methyl 2,3-anhydropyranosides, see J. G. Buchanan, R. Fletcher, K. Parry, and W. A. Thomas, *J. Chem. Soc., B*, **1969**, 377. Dwivedi *et al.* have recently reported the importance of magnesium ion-oxygen atom interaction in oxirane ring-opening by $MgBr_2$; S. K. Dwivedi, A. Khare, and M. P. Khare, *Carbohydr. Res.*, **91**, 159 (1981).

9) J. Hooz and S. S. Gilani, *Can. J. Chem.*, **46**, 86 (1968).

10) J. S. Pizey, "Synthetic Reagents," Ellis Horwood Ltd., Chichester, (1974), Vol. II, pp. 143—174; A. J. Fatiadi, *Synthesis*, **1976**, 65, 133.

11) P. Bakuzis, M. L. F. Bakuzis, and T. F. Weingartner, *Tetrahedron Lett.*, **1978**, 2371.

12) O. Mitsunobu, *Synthesis*, **1981**, 1.

13) B. T. Lawton, W. A. Szarek, and J. K. N. Jones, *Carbohydr. Res.*, **14**, 255 (1970); H. Paulsen, B. Sumfleth, and H. Redlich, *Chem. Ber.*, **109**, 1362 (1976).

14) R. D. Rieke and S. E. Bales, *J. Am. Chem. Soc.*, **96**, 1775 (1974).

15) K. Tatsuta, T. Yamauchi, and M. Kinoshita, *Bull. Chem. Soc. Jpn.*, **51**, 3035 (1978).

16) H. B. Henbest, E. R. H. Jones, and T. C. Owen, *J. Chem. Soc.*, **1957**, 4909.

17) T. Hase, A. Ourila, and C. Holmberg, *J. Org. Chem.*, **46**, 3137 (1981).

 © 1983 The Chemical Society of Japan Bull. Chem. Soc. Jpn., 56, 1807—1811 (1983)

Syntheses of 1-Epikanamycin A and Its 1-*N*-[(*S*)-4-Amino-2-hydroxybutyryl] Derivative

Yoshiaki Takahashi, Tsutomu Tsuchiya,* Yukiko Suzuki, Sumio Umezawa, Hamao Umezawa,† and Shunzo Fukatsu††

Institute of Bioorganic Chemistry, 1614 Ida, Nakahara-ku, Kawasaki 211

†*Institute of Microbial Chemistry, Kamiosaki, Shinagawa-ku, Tokyo 141*

††*Central Research Laboratories, Meiji Seika Kaisha, Ltd, Morooka-cho, Kohoku-ku, Yokohama 222*

(Received November 22, 1982)

The titled compounds were prepared from 3,6′-bis(*N*-benzyloxycarbonyl)-3″-*N*-(trifluoroacetyl)kanamycin A (**1**). Oxidation of **1** with hydrogen peroxide in the presence of sodium tungstate gave the 1-hydroxyimino derivative, which, after deblocking, gave 1-deamino-1-dehydro-1-hydroxyiminokanamycin A (**6**). Reduction of **6** with Raney nickel–hydrogen in aqueous ammonia gave a mixture of kanamycin A and 1-epikanamycin A (**9**), which were separated through derivation to the corresponding tetrakis-*N*-(*t*-butoxycarbonyl) derivatives, which showed different solubility in chloroform. 1-*N*-[(*S*)-4-Amino-2-hydroxybutyryl]-1-epikanamycin A was prepared from **9** by the zinc acetate–ethyl trifluoroacetate method [to give 3,6′-bis(*N*-benzyloxycarbonyl)-1-epi-3″-trifluoroacetamidokanamycin A] followed by a regiospecific 1-*N*-acylation with (*S*)-4-benzyloxycarbonylamino-2-hydroxybutyryl group and successive deblocking.

Epimerization of a group at special position of amino glycoside antibiotics is of interest in connection with the role of the group in the antibacterial action. Recently we reported the synthesis of 3″-epidihydrostreptomycin,[1] which was active against resistant bacteria. In this paper we report on the epimerization of the 1-amino group of kanamycin A and the preparation of the 1-*N*-[(*S*)-4-amino-2-hydroxybutyryl] derivative of the epimer of kanamycin A. The (*S*)-4-amino-2-hydroxybutyryl side chain is known to enhance the antibacterial activity of kanamycin A as shown by amikacin.[2] Recently Igarashi *et al.*[3] prepared 1-deamino-1-epihydroxykanamycin A through a 1-oxo intermediate obtained by oxidation of a protected free 1-aminokanamycin A with 3,5-di-*t*-butyl-1,2-benzoquinone.[4]

As the starting material, we utilized 3,6′-bis(*N*-benzyloxycarbonyl)-3″-*N*-(trifluoroacetyl)kanamycin A (**1**),[5] which has a free amino group only at C-1, and prepared readily from kanamycin A by the zinc acetate–ethyl trifluoroacetate method.[5] Since oxidation of the 1-$CHNH_2$ group of **1** to ketoxime (–C=NOH) (not to carbonyl) is desirable for the present synthesis, **1** was treated with hydrogen peroxide in the presence of sodium tungstate according to the procedure by Kahr and Berther.[6] The desired 1-hydroxyimino derivative (**2**) was obtained in 86% yield. To confirm the structure, the compound (**2**) was led to the tris(*N*-benzyloxycarbonyl)-per-*O*-acetyl derivative (**5**). Deacylation of **2** with aqueous ammonia in oxolane gave the 3″-amino derivative (**3**), which, after reprotection of the amino group with *N*-(benzyloxycarbonyloxy)succinimide[2] [to give the 3,6′,3″-tris(*N*-benzyloxycarbonyl) derivative (**4**)], was acetylated with acetic anhydride in pyridine to afford the octaacetyl derivative (**5**). Compound **4** was also prepared directly from **6** in high yield by treating with *N*-(benzyloxycarbonyloxy)succinimide.

The presence of octaacetyl group in **5**, confirmed by the ^{1}H-NMR spectrum, indicated that all hydroxyl groups including the hydroxyimino group were acetylated. The position of the acetoxyimino group (at C-1) evident from the chemical pathway was further confirmed from the ^{1}H-NMR spectrum. The splitting pattern of each of the C-2-methylene protons (δ 3.00 and 3.56) was pure double doublets, one of them being clearly brought from geminal $^2J_{2a,2b}$ (=16.5 Hz) coupling, indicated that the methylene hydrogens had only one vicinal hydrogen (at C-3). This indicates that another adjacent group to the methylene is the C-acetoxyimino group. A doublet (J 6.5 Hz) was recognized at low field (δ 4.99), which is not assigned to H-1′ or -1″ from the J-value, should be assigned to a proton of the methine (C-6) adjacent to the carbon carring the acetoxyimino group, because only the two anomeric and the methine protons can show a doublet, respectively. Furthermore, the proton (H-6) was found to be coupled to a proton, resonating at low field (δ 5.80) as a triplet (J 6.5 Hz, H-5); this indicates that the hydroxyl group at C-5 is acetylated. The above-described result was rather unexpected because, in tetrakis(*N*-benzyloxycarbonyl)-4″,6″-*O*-cyclohexylidenekanamycin A[7] and other related compounds, 5-*O*-acetylation scarcely occurred under reaction conditions similar to that described here. This easy acetylation may be ascribed to the conformation of the aminocyclitol portion of **4**, which is expected not to be chair as in the case of **5** (see ^{1}H-NMR data in Experimental section).

Hydrogenolysis of the *N*-benzyloxycarbonyl groups of **3** in the presence of palladium black gave the 1-(hydroxyimino)kanamycin A (**6**), in 83% yield (based on **2**), with slight kanamycin A. The presence of the hydroxyimino group was supported by appearance of a resonance at low field (δ 154 ppm, C-1) in the ^{13}C-NMR spectrum (see Table 1). Non-chair conformation of the aminocyclitol portion of **6** was also revealed from the ^{1}H-NMR data. This discrepancy from chair conformation, judged from the J values, will be originated from instability of the chair form I caused by interaction between coplaner

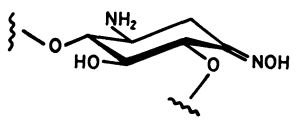

I (unstable)

6-hydroxyl and 1-hydroxyimino groups.[8,9] Possible conformation would be that of slightly flattered skew with 5- and 6-hydroxyl groups pseudoaxial.

Attempts to produce 1-epikanamycin A (**9**) from **6** by catalytic hydrogenation with palladium catalyst under several conditions failed, only giving kanamycin A. However, when **6** was hydrogenated in the presence of Raney nickel in aqueous ammonia, a mixture of kanamycin A and 1-epikanamycin A (**9**) was produced in a ratio approximately 2 : 1. As the direct separation of the products was proved difficult, several *N*-protected derivatives were prepared to seek suitable derivatives for the separation. Among them, a mixture of tetrakis-(*N*-*t*-butoxycarbonyl) derivatives, prepared by treating the mixture of kanamycin A and 1-epikanamycin A with *O*-*t*-butyl *S*-(4,6-dimethyl-2-pyrimidinyl) thiocarbonate[10] (Boc-*S* reagent), was found successful; the tetra-*N*-Boc-kanamycin A (**7**) and tetra-*N*-Boc-1-epikanamycin A (**8**) were separated by the difference of solubility in chloroform.

Deblocking of **7** gave kanamycin A identical with the authentic sample, and deblocking of **8** gave 1-epikanamycin A (**9**). The 1-epi structure of **9** was established by the small *J*-values, in its ^{1}H-NMR spectrum, relating to H-1 (the aminocyclitol portion took chair form). In the ^{13}C-NMR spectrum, large up-field shifts were observed at C-1 and -6, in comparison to the corresponding shifts of kanamycin A (Table 1).

TABLE 1. THE ^{13}C CHEMICAL SHIFTS[a] OF KANAMYCIN A[b] (KMA), 1-DEAMINO-1-DEHYDRO-1-HYDROXYIMINO-KANAMYCIN A (**6**), 1-EPIKANAMYCIN A (**9**), AND 1-*N*-[(*S*)-4-AMINO-2-HYDROXYBUTYRYL]-1-EPIKANAMYCIN A (**14**) MEASURED IN 20% ND_3 IN D_2O

Carbon	KMA	**6**	**9**	**14**
1	51.3	154.4	45.6[d]	44.8
2	36.3	28.3	34.5	32.8
3	49.8	50.0	47.4[d]	48.0
4	88.4	85.0[c]	88.8[c]	87.8[c]
5	74.8	74.9[c]	72.1[f]	72.9[c]
6	88.6	78.6[c]	79.0[c]	76.2
1′	100.5	98.8[c]	100.8[c]	100.7
2′	72.5	72.5[d]	72.8	72.7[c]
3′	73.6[c]	73.6[d•]	73.7[g]	73.6[h]
4′	71.8	72.0[d]	71.8[d•]	71.8
5′	73.9[c]	73.9[d•]	73.9[g]	73.9[h]
6′	42.6	42.7	42.6	42.6
1″	100.8[c]	97.2	95.4	95.3
2″	72.7[c]	72.5[d]	72.1[c]	72.0
3″	55.1	55.3	54.7	54.8
4″	70.0	70.2	70.4[d′]	70.3
5″	73.0	73.4[d•]	72.8[f]	72.9
6″	61.0	61.4	61.3	61.3
1‴				177.3
2‴				70.5[c]
3‴				37.1
4‴				37.8[c]

a) In ppm downfield from TMS calculated as $\delta^{TMS} = \delta^{dioxane} + 67.4$ ppm. b) Shift assignments were based on the shifts of kanamycin A reported[11]. Selective irradiation at (denoted c) or near (denoted d or d′; carried out when c was inadequate) the resonance of the proton attached to the carbon, respectively. e—h) The values cited may be reversed, respectively.

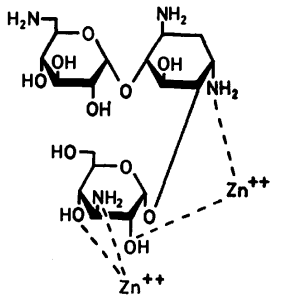

II

The 1-epikanamycin A (**9**) was led to 1-*N*-[(*S*)-4-amino-2-hydroxybutyryl]-1-epikanamycin A (**14**). For that, selective protections of the 3-, 6′-, and 3″-amino groups of **9** are requisite. This was performed by applying the zinc acetate-ethyl trifluoroacetate method.[5] In spite of the 1-epiamino structure of **9**, zinc ions completely protected the 1- and 3″-amino groups as in the case of kanamycin A. If Nagabhushan's proposal[11] for nickel, copper and cobalt is applied to this case, zinc chelation such as II may be considered as a candidate. Treatment of **9** with *N*-(benzyloxycarbonyloxy)succinimide[2] in the presence of zinc acetate in dimethyl sulfoxide gave 3,6′-bis(*N*-benzyloxycarbonyl)-1-epikanamycin A (**10**) in 83% yield after purification. The 3″-amino protection of **10** was also readily carried out by using ethyl trifluoroacetate to give the corresponding 3″-trifluoroacetamide derivative (**11**) in almost quantitative yield.

Coupling (*S*)-4-benzyloxycarbonylamino-2-hydroxybutyric acid to the free amino group at C-1 of **11** was readily performed by utilizing the active ester[2] of the acid to give the product (**12**) in 79% yield. De(trifuoroacetyl)ation of **12** (to give **13**) followed by catalytic de(benzyloxycarbonyl)ation gave the final product (**14**) in 92% yield. The structure of **14** was elucidated by the ^{1}H-NMR spectral data. The resonances of H-1 proton, confirmed by the decoupling method, appeared at δ 4.51 as a narrow quartet, the shift-value being fairly high in comparison to that (δ 3.5) of 1-epikanamycin A (**9**); this difference in shift-value indicates that the 1-amino group of **9** was acylated as expected. The ^{13}C-NMR spectrum of **14** was shown in Table 1.

TABLE 2. MINIMAL INHIBITORY CONCENTRATION (μg/ml) OF **9**, **14**, AND KANAMYCIN A

	Kanamycin A	**9**	**14**
Staphylococcus aureus FDA 209P	0.78	3.12	12.5
Staphylococcus aureus AP01	25	>100	100
Micrococcus luteus PCI 1001	25	>100	>100
Bacillus subtilis NRRL B-558	0.39	3.12	3.12
Escherichia coli K-12	0.78	6.25	12.5
Escherichia coli K-12 ML1629	>100	>100	50
Salmonella typhi T-63	0.39	3.12	25
Pseudomonas aeruginosa A3	25	3.12	25

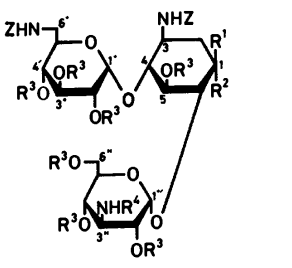

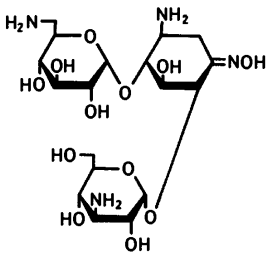

6

	R^1	R^2	R^3	R^4
1	NH_2	H	H	$COCF_3$
2	=NOH		H	$COCF_3$
3	=NOH		H	H
4	=NOH		H	Z
5	=NOAc		Ac	Z

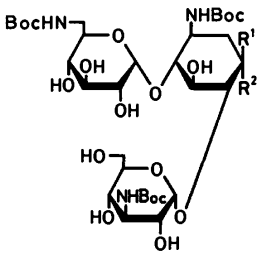

	R^1	R^2
7	NHBoc	H
8	H	NHBoc

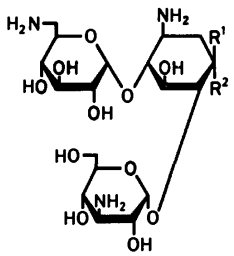

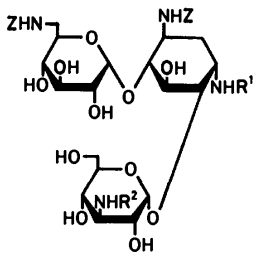

Kanamycin	R^1	R^2
A	NH_2	H
9	H	NH_2

	R^1	R^2
10	H	H
11	H	$COCF_3$
12	(S) $COCHCH_2CH_2NHZ$ OH	$COCF_3$
13	(S) $COCHCH_2CH_2NHZ$ OH	H

14	H	(S) $NHCOCHCH_2CH_2NH_2$ OH

Z: $CO_2CH_2C_6H_5$,
Boc: $CO_2C(CH_3)_3$

Antibacterial spectra of **9** and **14** were shown in Table 2 with the spectrum of kanamycin A. This result shows that epimerization of the 1-amino group of kanamycin A greatly reduced the original activity. 1-(Hydroxyimino)kanamycin A (**6**) was almost devoid of antibacterial activity.

Experimental

Specific rotations were measured with a Perkin-Elmer Model 241 polarimeter. ^{1}H- and ^{13}C-NMR spectra were recorded in the FT mode with a Bruker WM 250 spectrometer operating at 250 and 62.9 MHz, respectively. In the ^{1}H-NMR spectra, tetramethylsilane (δ=0) was used as the internal standard in both organic solvents and deuterium oxide. Thin-layer chromatography (TLC) was carried out on E. Merck precoated silica gel 60 plates with the spray of sulfuric acid or 0.5% ninhydrin in pyridine for detection. For silica-gel column chromatography, Wakogel C-200 was used.

*3,6′-Bis(*N*-benzyloxycarbonyl)-1-deamino-1-dehydro-1-hydroxyimino-3″-*N*-(trifluoroacetyl)kanamycin A (2).* To a solution of **1** (7.73 g, as the base) and sodium tungstate dihydrate (0.6 g) in aqueous oxolane (1 : 2, 160 ml) was added 30% aqueous hydrogen peroxide (8.8 ml), and the solution was kept at room temperature overnight. On checking by TLC with chloroform–methanol–20% aqueous acetic acid (1 : 1.2 : 1, lower layer), the solution showed a single spot at R_f 0.4 (*cf* **1**: R_f 0.25). Concentration of the pale-yellow solution gave a residue, which was washed with water, dried, and washed with ether to give a solid, 6.76 g (86%), $[\alpha]_D^{24}$ +100° (*c* 2, *N*,*N*-dimethylformamide).

^{1}H-NMR (pyridine-d_5–D_2O=30 : 1): δ=4.00 (1H dd, $J_{1'',2''}$ 3.5, $J_{2',3'}$ 9.5 Hz, H-2′), 4.26 (1H dd, $J_{1'',2''}$ 3.5, $J_{2'',3''}$ 10.5 Hz, H-2″), 5.08 (1H t, $J_{3'',4''}$ 10.5 Hz, H-3″), 5.42 (1H d, H-1″), 5.65 (1H d, H-1′).

Found: C, 50.09; H, 5.36; N, 6.48; F, 6.47%. Calcd for $C_{36}H_{45}F_3N_4O_{17}$: C, 50.12; H, 5.26; N, 6.49; F, 6.61%.

*3,6′,3″-Tris(*N*-benzyloxycarbonyl)-1-deamino-1-dehydro-1-hydroxyiminokanamycin A (4).* A solution of **2** (6.38 g) in a mixture of 2 M (1 M=1 mol dm^{-3}) aqueous ammonia–oxolane (1 : 1, 250 ml) was kept at room temperature overnight. The solution showed a single spot at R_f 0.2 (*cf* **2**: R_f 0.3), on TLC with chloroform–methanol–28% aqueous ammonia (1 : 1 : 1, lower layer). Concentration gave a crude solid of **3** (6.58 g). To a solution of the solid (100 mg) in aqueous *N*,*N*-dimethylformamide (1 : 2, 3 ml) was added *N*-(benzyloxycarbonyloxy)-succinimide[2] (32 mg) and the solution was kept for 1 h at room temperature. Concentration gave a syrup, which was washed with water, then with ether to give a chromatographically homogeneous solid, 88 mg (85% based on **2**), $[\alpha]_D^{24}$ +95° (*c* 1, *N*,*N*-dimethylformamide).

Found: C, 55.13; H, 5.78; N, 6.11%. Calcd for $C_{42}H_{52}N_4O_{18}\cdot H_2O$: C, 54.90; H, 5.92; N, 6.10%.

*1-Acetoxyimino-5,2′,3′,4′,2″,4″,6″-hepta-*O*-acetyl-3,5′,3″-tris(*N*-benzyloxycarbonyl)-1-deamino-1-dehydrokanamycin A (5).* To a solution of **4** (140 mg) in pyridine (2.8 ml) was added acetic anhydride (0.3 ml), and the solution was kept overnight at room temperature. Addition of water (0.3 ml) followed by standing for 0.5 h at room temperature and concentration of the solution gave a syrup, which was dissolved in chloroform. The solution was then processed in a usual manner to give a crude product, which was passed through a short column of silica gel with chloroform–ethyl methyl ketone (3 : 1) to give a pure solid of **5**, 147 mg (78%), $[\alpha]_D^{23}$ +90° (*c* 1, chloroform).

^{1}H-NMR (pyridine-d_5): δ=2.00, 2.01, 2.03, 2.05 (6H), 2.16, 2.17, 2.24 (each s, Ac); 3.00 (1H dd, $J_{2a,2e}$ 16.5, $J_{2a,3}$ 11.5 Hz, H-2a), 3.56 (1H dd, $J_{2e,3}$ 5 Hz, H-2e), 4.99 (1H d, $J_{5,6}$ 6.5 Hz, H-6), 5.80 (1H t, $J\approx$6.5 Hz, H-5); Irradiation of H-6 collapsed the triplet of H-5 to a doublet, and irradiation of H-5 caused the signals at $\delta\approx$4.70 (H-4) to simplify.

Found: C, 56.31; H, 5.54; N, 4.53%. Calcd for $C_{58}H_{68}N_4O_{26}$: C, 56.06; H, 5.75; N, 4.42%.

1-Deamino-1-dehydro-1-hydroxyiminokanamycin A (6). A solution of crude **3** (6.20 g; described in the preparation of **4**) in aqueous oxolane (1 : 2, 300 ml) was hydrogenated in the presence of palladium black and acetic acid (5 ml) under atmospheric pressure of hydrogen for 2 h at room temperature. After filtration, the solution was neutralized with 28% aqueous ammonia (5 ml), and concentrated to give a syrup. Separation of the products by column chromatography of the syrup

with CM-Sephadex C-25 with aqueous ammonia (0→0.15 M, the concentration was gradually changed) gave a solid of **6** (from the earlier frations), 3.06 g (83% as the hemicarbonate, based on **2**) and a solid of kanamycin A (from the later fractions), 0.17 g (4.7% as the hemicarbonate, based on **2**). **6**: $[\alpha]_D^{22}$ +180° (*c* 1, water); ^{1}H-NMR (20% ND_3 in D_2O): δ= 2.06 (1H dd, H-2a), 2.74 (1H dd, H-6'a), 3.00 (1H dd, H-6'b), 3.04 (1H t, H-3"), 3.09 (1H dd, H-2e), ≈3.17 (1H m, H-3), 3.25 (1H t, H-4"), 3.27 (1H t, H-4'), 3.41 (1H dd, H-2"), 3.53 (1H dd, H-4), 3.56 (1H dd, H-2'), 3.69 (1H t, H-3'), 3.92 (1H t, H-5), 4.24 (1H d, H-6), 4.92 (1H d, H-1"), 5.35 (1H d, H-1'); $J_{2a,2e}$ 15.0, $J_{2a,3}$ 11.0, $J_{2e,3}$ ≈4.5, $J_{3,4}$ ≈9, $J_{4,5}=J_{5,6}$ 6.0, $J_{1',2'}$ 3.8, $J_{2',3'}=J_{3',4'}=J_{4',5'}$ 9.5, $J_{5',6'a}$ 7.5, $J_{5',6'b}$ 2.5, $J_{6'a,6'b}$ 13.5, $J_{1'',2''}$ 3.8, $J_{2'',3''}=J_{3'',4''}=J_{4'',5''}$ 10.0 Hz.

Found: C, 42.28; H, 6.70; N, 10.43%. Calcd for $C_{18}H_{34}N_4O_{12}\cdot 1/2\,H_2CO_3$: C, 42.04; H, 6.48; N, 10.60%.

*1,3,6',3"-Tetrakis(*N-t-*butoxycarbonyl)kanamycin A* (**7**) *and 1,3,6',3"-Tetrakis(*N-t-*butoxycarbonyl)-1-epikanamycin A* (**8**). A solution of **6** hemicarbonate (2.00 g) in 1 M aqueous ammonia (40 ml) was shaken in the presence of Raney nickel under 3 atmospheric pressure of hydrogen for 5 h at room temperature. On checking by TLC with chloroform–ethanol–1-propanol–17% aqueous ammonia (2 : 7 : 4 : 7), the solution showed a single spot at R_f 0.16 (*cf* **6**: R_f 0.23). Filtration followed by concentration gave a residue, which was passed through a column of CM-Sephadex C-25 with aqueous ammonia (concentration gradually changed from 0 to 0.15 M) and the ninhydrin-positive fractions were concentrated to give a mixture (1.21 g) of kanamycin A and 1-epikanamycin A (**9**).

To an aqueous solution (4 ml) of the mixture (1.00 g) were added triethylamine (3.5 ml) and Boc-*S* reagent (3.0 g, dissolved in 8 ml 1,4-dioxane), and the mixture was stirred for 24 h at 40°C. Concentration gave a residue, which was extracted with chloroform. The nonextractable residue (1.05 g), which gave R_f 0.47 on TLC with chloroform–methanol–20% aqueous acetic acid (1 : 1 : 1, lower layer) was washed successively with acetone to give a solid of **7**, 0.97 g (34%), $[\alpha]_D^{23}$ +79° (*c* 1, pyridine); Found: C, 50.44; H, 7.54; N, 6.46%. Calcd for $C_{38}H_{68}N_4O_{19}\cdot H_2O$: C, 50.54; H, 7.81; N, 6.20%.

The chloroform layer was washed with 0.5 M aqueous sodium hydroxide to remove the concomitant 4,6-dimethyl-2-pyrimidinethiol, and then with 3% aqueous sodium sulfate, dried over sodium sulfate, and concentrated to give a solid of **8**, 0.51 g (18%), which gave R_f 0.55 on TLC with the above-described developing mixture, $[\alpha]_D^{23}$ +81° (*c* 1, pyridine); Found: C, 50.79; H, 7.55; N, 6.16%. Calcd for $C_{38}H_{68}N_4O_{19}\cdot H_2O$: C, 50.54; H, 7.81; N, 6.20%.

1-Epikanamycin A (**9**). A solution of **8** (1.74 g, as the monohydrate) in aqueous trifluoroacetic acid (1 : 19, 17 ml) was kept for 30 min at room temperature. Evaporation *in vacuo* at room temperature with several additions of toluene gave a residue, which was charged on a column of CM-Sephadex C-25 and developed with aqueous ammonia (0→0.15 M) to give **9** as the carbonate, 960 mg (91%), $[\alpha]_D^{25}$ +166° (*c* 2, water); ^{1}H-NMR (20% ND_3 in D_2O): δ=1.45 (1H slightly deformed dt, H-2a), 1.95 (1H dt, H-2e), 2.74 (1H dd, H-6'a), 2.95 (1H dd, H-6'b), 3.10 (1H t, H-3"), ≈3.11 (1H m, H-3), 3.26 (1H t, H-4'), 3.28 (1H t, H-4), 3.28 (1H t, H-4"), 3.45 (1H dd, H-2"), ≈3.48 (1H narrow m, H-1), 3.55 (1H dd, H-2'), 3.63 (1H dd, H-6), 3.67 (1H t, H-3'), ≈3.75 (1H m, H-5'), 3.92 (1H t, H-5), 4.97 (1H d, H-1"), 5.32 (1H d, H-1'); $J_{1,2a}=J_{1,2e}$ ≈3.5, $J_{1,6}$ 4.0, $J_{2a,2e}$ 14.0, $J_{2a,3}$ ≈13, $J_{2e,3}$ ≈3.5, $J_{3,4}=J_{4,5}=J_{5,6}$ 10, $J_{1',2'}$ 3.8, $J_{2',3'}=J_{3',4'}=J_{4',5'}$ 9.5, $J_{5',6'a}$ 7.5, $J_{5',6'b}$ 2.5, $J_{6'a,6'b}$ 13.5, $J_{1'',2''}$ 3.8, $J_{2'',3''}=J_{3'',4''}=J_{4'',5''}$ 10 Hz.

Found: C, 41.91; H, 7.27; N, 9.98%. Calcd for $C_{18}H_{36}N_4O_{11}\cdot H_2CO_3$: C, 41.76: H, 7.01; N, 10.25%.

*3,6'-Bis(*N-*benzyloxycarbonyl)-1-epikanamycin A* (**10**). To a suspended mixture of **9** (100 mg, as the carbonate) in dimethyl sulfoxide (1.5 ml, dried over molecular sieves 4A) was added zinc acetate dihydrate (180 mg), and the mixture was stirred overnight at room temperature. To the resulting clear solution was gradually added *N*-(benzyloxycarbonyloxy)-succinimide (105 mg) and the mixture was kept for 1 h at room temperature. Addition of ether gave a syrup, which was thoroughly washed with ether. The resulting syrup was charged on a column of Amberlite CG 50 (20 ml, an equal-volume mixture of H^+ and NH_4^+ forms was used) and, after washing the column with aqueous oxolane (1 : 1), the product was developed with aqueous oxolane (1 : 1) containing ammonia (the concentration gradually changed from 0.5 to 1 M). The fractions containing **10** [checked by TLC with chloroform–methanol–aqueous 20% acetic acid=5 : 7 : 5 (lower layer) giving R_f 0.32] were concentrated to a volume of ≈5 ml and further concentrated with occasional additions of water and occasional introductions of carbon dioxide (without this procedure, intermolecular *N*-acyl migration or 1,3-ureylene compound[12] may occur to give a contaminated mixture) to give a zinc-ion free (tested by diphenylcarbazide-ammonia[13]) solid of **10** as the carbonate, 124 mg (83%), $[\alpha]_D^{24}$ +95° (*c* 1, aqueous oxolane=1 : 2).

Found: C, 51.56; H, 6.16; N, 6.84%. Calcd for $C_{34}H_{48}N_4O_{15}\cdot H_2CO_3$: C, 51.59; H, 6.19; N, 6.88%.

*3,6'-Bis(*N-*benzyloxycarbonyl)-1-epi-3"-*N-*(trifluoroacetyl)kanamycin A* (**11**). To a solution of **10** (130 mg, as the carbonate) in dry dimethyl sulfoxide (0.8 ml) was added ethyl trifluoroacetate (0.025 ml) and the solution was kept for 20 min at room temperature. On checking by TLC with chloroform–methanol–aqueous 20% acetic acid=5 : 7 : 5 (lower layer), the solution showed a single spot at R_f 0.5. Addition of ether gave a syrup, which was thoroughly washed with ether. The syrup was dissolved in small volume of methanol (0.5 ml) and precipitated by addition of ether. The procedure was repeated twice more to give a dimethyl sulfoxide-free solid of **11**, 137 mg (99%), $[\alpha]_D^{23}$ +93° (*c* 1, methanol).

Found: C, 50.27; H, 5.90; N, 6.19; F, 6.84%. Calcd for $C_{36}H_{47}F_3N_4O_{16}\cdot 1/4\,H_2CO_3$: C, 50.38; H, 5.54; N, 6.48; F, 6.59%.

*3,6'-Bis(*N-*benzyloxycarbonyl)-1-*N-*[(S)-4-benzyloxycarbonylamino-2-hydroxybutyryl]-1-epi-3"-*N-*(trifluoroacetyl)kanamycin A* (**12**). To a solution of **11** (100 mg) in aqueous oxolane (1 : 1, 3 ml) was gradually added *N*-hydroxysuccinimide ester[2] (83 mg) of (*S*)-4-benzyloxycarbonylamino-2-hydroxybutyric acid dissolved in oxolane (1.5 ml), and the mixture was kept at room temperature for 30 min. The resulting acidic solution was neutralized with sodium carbonate (13 mg) and then concentrated. The resulting residue, after being washed with ether, was dissolved in water-saturated 1-butanol (the solid was scarcely soluble in usual organic solvents immiscible with water) and the solution was washed with 1-butanol-saturated aqueous sodium hydrogencarbonate solution (saturated), and 1-butanol-saturated water to remove inorganic impurities. Concentration of the butanol solution gave a residue, which was chromatographed on a silica-gel column with chloroform–methanol=6 : 1 to give a solid of **11**, 98.5 mg (79%), $[\alpha]_D^{25}$ +67° (*c* 1, methanol).

Found: C, 53.11; H, 5.70; N, 6.33; F, 5.16%. Calcd for $C_{48}H_{60}F_3N_5O_{20}$: C, 53.18; H, 5.58; N, 6.46; F, 5.26%.

*1-*N-*[(S)-4-Amino-2-hydroxybutyryl]-1-epikanamycin A* (**14**). A solution of **12** (170 mg) in mixture of 2 M aqueous ammonia–oxolane (1 : 1, 8.5 ml) was kept overnight at room temperature. On checking by TLC with chloroform–methanol–20% aqueous acetic acid (1 : 1 : 1, lower layer), the solution showed a single spot of **13** at R_f 0.15 (*cf* **12**: R_f 0.32). Concentration

gave a residue, which was dissolved in aqueous oxolane (1 : 1, 8 ml) containing acetic acid (1.0 ml), and the solution was hydrogenated in the presence of palladium black under atmospheric pressure of hydrogen for 2 h at room temperature. The resulting product was isolated by column chromatography on CM-Saphadex C-25 with aqueous ammonia (0→0.5 M) to give a solid of **14** as the carbonate, 93 mg (92%), $[\alpha]_D^{23}$ +128° (*c* 1, water); ^{1}H-NMR (20% ND_3 in D_2O): δ=1.52 (1H slightly deformed dt, H-2a), 1.75 (1H apparent sextet, $J\approx$7.5, $\approx$7.5, $\approx$7.5, and 14.5 Hz, H-3″a), 1.90 [1H two dt, J=4, $\approx$7.5, $\approx$7.5, and 14.5 (=$J_{3'''a,3'''b}$) Hz, H-3‴b], 2.09 (1H br dt, H-2e), 2.74 (2H t, J7.5 Hz, H-4″ a,b), $\approx$2.97 (H-3), 2.75 (1H dd, H-6′a), 2.98 (1H dd, H-6′b), 3.04 (1H t, H-3″), 3.27 (1H t, H-4″), 3.28 (1H t, H-4′), 3.36 (1H t, H-4), 3.39 (1H dd, H-2″), 3.57 (1H dd, H-2′), 3.69 (1H t, H-3′), $\approx$3.75 (H-5′), 3.82 (dd, H-6), 3.91 (1H t, H-5), 4.22 (1H dd, $J_{2''',3'''a}$ 8.5, $J_{2''',3'''b}$ 4.0 Hz,H-2‴), 4.51 (1H br q, $J\approx$4 Hz, H-1), 4.91 (1H d, H-1″), 5.35 (1H d, H-1′); $J_{1,2a}$=$J_{1,2e}$ $\approx$3.5, $J_{1,6}\approx$4, $J_{2a,2e}$ 14.0, $J_{2a,3}$ $\approx$12, $J_{2e,3}$ $\approx$3.5, $J_{3,4}$ $\approx$9, $J_{4,5}$=$J_{5,6}$ 9.5, $J_{1',2'}$ 3.8, $J_{2',3'}$=$J_{3',4'}$=$J_{4',5'}$ 9.5, $J_{5',6'a}$ 7.5, $J_{5',6'b}$ 2.5, $J_{6'a,6'b}$ 13.5, $J_{1'',2''}$ 3.5, $J_{2'',3''}$=$J_{3'',4''}$=$J_{4'',5''}$ 10 Hz.

Found: C, 42.62; H, 7.10; N, 10.65%. Calcd for $C_{22}H_{43}N_5O_{13}\cdot H_2CO_3$: C, 42.65; H, 7.00; N, 10.81%.

References

1) T. Tsuchiya and T. Shitara, *Carbohydr. Res.*, **109**, 59 (1982).

2) H. Kawaguchi, T. Naito, S. Nakagawa, and K. Fujisawa, *J. Antibiot.*, **25**, 695 (1972).

3) K. Igarashi, T. Honma, T. Fujiwara, and E. Kondo, *J. Antibiot.*, **33**, 830 (1980).

4) E. J. Corey and K. Achiwa, *J. Am. Chem. Soc.*, **91**, 1429 (1969).

5) T. Tsuchiya, Y. Takagi, and S. Umezawa, *Tetrahedron Lett.*, **1979**, 4951.

6) K. Kahr and C. Berther, *Chem. Ber.*, **93**, 132 (1960).

7) T. Miyake, T. Tsuchiya, S. Umezawa, and H. Umezawa, *Bull. Chem. Soc. Jpn.*, **50**, 2362 (1977).

8) F. Johnson, S. K. Malhotra, *J. Am. Chem. Soc.*, **87**, 5492 (1965).

9) M. T. P. Viet, J. Lessard, and J. K. Saunders, *Tetrahedron Lett.*, **1979**, 317.

10) T. Nagasawa, K. Kuroiwa, K. Narita, and Y. Isowa, *Bull. Chem. Soc. Jpn.*, **46**, 1269 (1973).

11) G. Kotowycz and R. U. Lemieux, *Chem. Rev.*, **73**, 669 (1973).

12) T. Yamaguchi, T. Tsuchiya, and S. Umezawa, *J. Antibiot.*, **30**, 71 (1977).

13) J. C. Touchstone and M. F. Dobbins, "Practice of Thin layer chromatography," John Wiley and Sons, New York (1978), p. 193.

Synthesis of Potential Antineoplastic Anthracenedione Derivatives. II. 1,2-Dihydroxy Derivatives

Katsumi NAKAMURA, Tomoyuki ASAI, Tamio HARA,
Naoki MINORIKAWA, and Tetsuo SUAMI*
Department of Applied Chemistry, Faculty of Science and Technology, Keio University, Hiyoshi, Kohoku-ku, Yokohama, 223

(Received January 17, 1983)

In continuation of the preceding paper in this series,[1] four derivatives of 1,2-dihydroxy-5,8-bis[2-(2-hydroxyethylamino)ethylamino]-9,10-anthracenedione: a positional isomer of mitoxantrone have been prepared to establish a relationship between the position of the hydroxyl groups on the A ring and antineoplastic activity against experimental leukemia L1210 in mice. Two compounds were found to be fairly active.

In continuation of the preceding paper in this series,[1] 1,2-dihydroxy-5,8-bis[2-(2-hydroxyethylamino)ethylamino]-9,10-anthracenedione (**2**): a positional isomer of mitoxantrone has been synthesized, together with the 1-, 2- and 1,2-di-*O*-methyl derivatives in order to establish the role of hydroxyl groups in an appearance of antitumor activity. It has been described by J. R. Brown[2] that 2-substituted anthraquinones were active against leukemia L1210 in mice. Also, 1,2-dihydroxyanthraquinone derivatives were found to be cytotoxic and antileukemic compounds.[3]

While, a DNA-intercalating drug, mitoxantrone is a 1,4-dihydroxy analog of **2** and exhibits high antitumor activity against leukemia L1210 in mice.[4-7] The effective binding to DNA is achieved in the C ring and multiple substitutions with hydroxyl groups in the A ring in an anthraquinone skeleton.[2]

From the facts that mitoxantrone (1,4-dihydroxy analog) and 1-hydroxy analog are active,[5] it has been deduced that an existence of a hydroxyl group on the C-1 position is favorable for antitumor activity. In the present study, a role of another hydroxyl group on the C-2 position will be discussed.

Results and Discussion

A treatment of quinalizarin (**1**) with 2-(2-aminoethylamino)ethanol at elevated temperature gave 1,2-dihydroxy-5,8-bis[2-(2-hydroxyethylamino)ethylamino]-9,10-anthracenedione **2** as a crude product.[7-9] The product was converted into the partially protected compound (**6**) in 19% yield. Removal of the protective groups in **6** with methanolic HCl yielded **2** in 79% yield. Overall yield of **2** from quinalizarin was 15%. Mild hydrolysis of **6** in aq acetic acid afforded the partially deprotected compound (**7**) in 34% yield. Tritylation of **7** gave the ditrityl derivative (**8**) in 73% yield. Also, **8** was obtained by an alternative reaction process as follows. Tritylation of **6** afforded the compound (**9**) in 75% yield, which was converted, by heating with potassium carbonate in acetone, to **8** in 94% yield.

To protect one of the hydroxyl groups on the C-2 position selectively, protection of **8** with *p*-methoxybenzyl chloride yielded 2-*O*-(*p*-methoxybenzyl) derivative (**10**) in 87% yield. Methylation of **10** with dimethyl sulfate and potassium carbonate in acetone gave a 1-*O*-methyl derivative (**11**) in 77%, which was further converted into the dihydrochloride (**3**), by treating with methanolic HCl, in 70% yield.

To prove the structure, **3** was converted into a pentaacetyl derivative (**12**), whose ^{1}H NMR spectrum was identical with the proposed structure.

The positional isomer of **3** (**4**), 2-*O*-methyl derivative was prepared by the following process.

Methylation of **8** with dimethyl sulfate and potassium carbonate gave a 2-*O*-methyl derivative (**13**) exclusively in 93% yield. Deprotection of **13** in methanolic HCl

Table 1. Antitumor activity ofcompounds **2**, **3**, **4** and **5** against mouse leukemia L1210[a]

Compound	Dose (mg/kg)	ILS[b] (%)	60-day survival
2	50	Toxic	0/5
	37.5	>160	2/5
	25	>757	5/5
	12.5	>100	1/5
	6.25	114	0/5
3	200	88	0/5
	100	114	0/5
	50	114	0/5
	25	71	0/5
	12.5	71	0/5
	6.25	71	0/5
4	100	Toxic	0/5
	50	50	0/5
	25	25	0/5
	12.5	25	0/5
	6.25	13	0/5
5	100	14	0/5
	50	14	0/5
	25	0	0/5
	12.5	14	0/5
	6.25	14	0/5
Mitoxantrone	25	Toxic	0/5
	12.5	>157	1/5
	6.25	329	0/5
	3.12	>757	3/5
	1.5	>129	1/5

a) Male BDF_1 hybrid mice were inoculated intraperitoneally with 10^6 cells of lymphoid leukemia L1210. Compounds were dissolved in distilled water and administered intraperitoneally at a volume of 0.1 ml/animal once at 24 h after the tumor implantation. b) Percentage increase in life span of treated animals compared with control tumor bearers [100(T/C-1)].

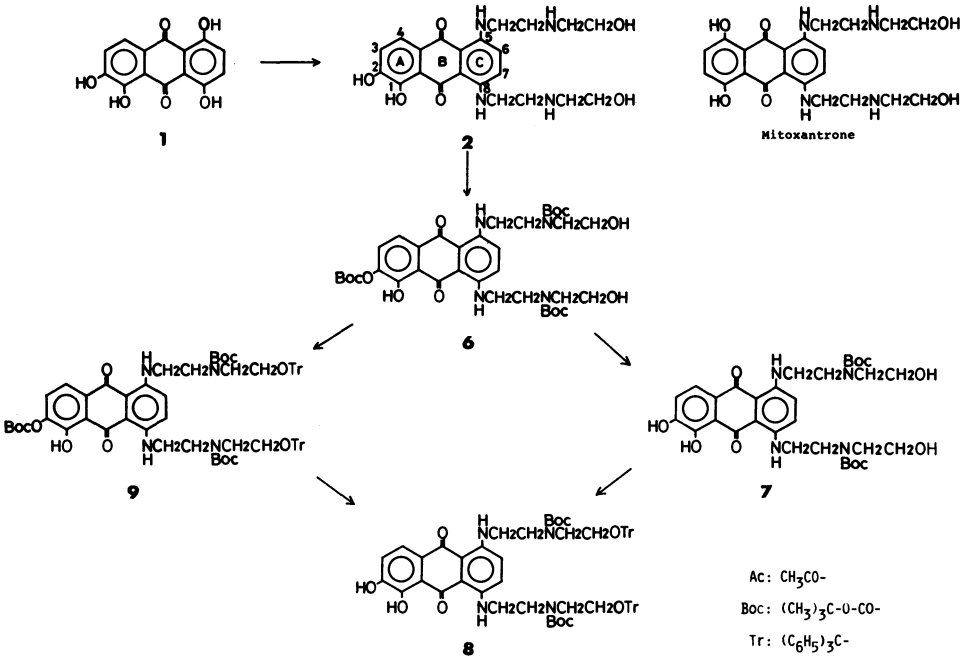

Scheme 1.

gave **4** in 56% yield.

Compound **4** was also obtained by another route as follows. Methylation of **9** with dimethyl sulfate and potassium carbonate afforded a 1-*O*-(*t*-butoxycarbonyl)-2-*O*-methyl derivative (**14**) in 64% yield. The reaction involved a migration of the *t*-butoxycarbonyl (Boc) group from 2-*O* to 1-*O*. Deprotection of **14** in methanolic HCl gave **4** in 87% yield.

Compound **4** was converted to a tetraacetyl derivative (**15**) and a pentaacetyl derivative (**16**), whose ^{1}H NMR spectrum were identical with the proposed structure.

Finally, the 1,2-di-*O*-methyl derivative (**5**) was prepared by the analogous methylation for a prolonged period and successive deprotection in methanolic HCl from **8** *via* compound (**17**).

Acetylation of **5** gave a tetraacetyl derivative (**18**).

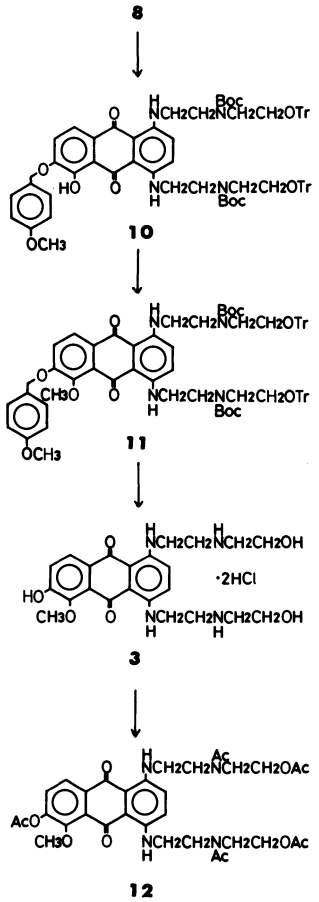

Scheme 2.

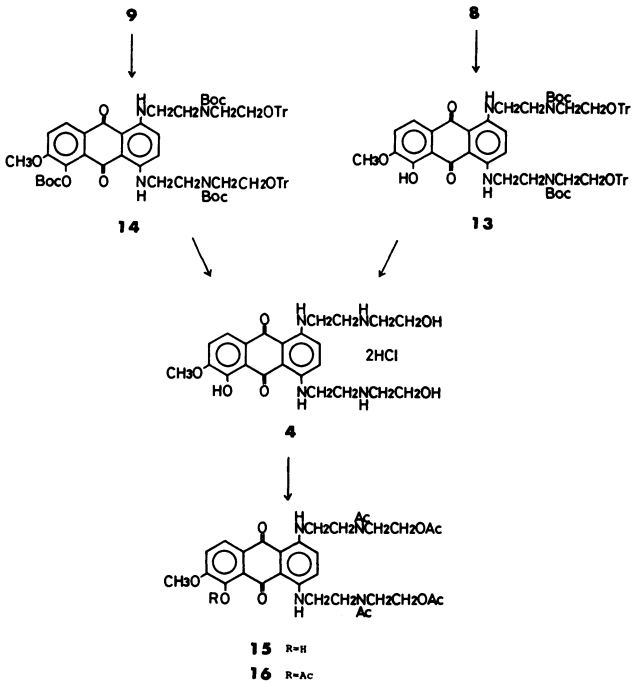

Scheme 3.

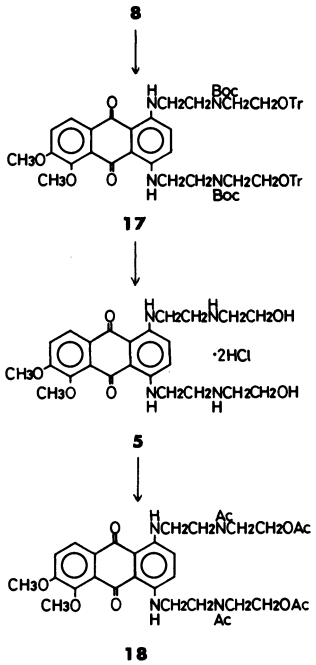

Scheme 4.

When ^{1}H NMR spectra of **12**, **16**, and **18** were compared each other, characteristic chemical shifts of acetoxyl groups on C-1 and 2 provided a good evidence for the structures. The chemical shift of the acetoxyl group on C-2 was attributable to δ 2.37 and that of the acetoxyl group on C-1 was δ 2.46, since the latter was deshielded to the down field by the quinone carbonyl group on C-9.[10]

Antitumor activities of **2**, **3**, **4**, and **5** were determined against experimental leukemia L1210 in mice.[11] Compound **2** was highly active, producing ILS value (>757%) and curing all mice by day 60. While mitoxantrone produced the same ILS value (>757%) but was curing 3 animals in 5 mice by day 60. Therefore, **2** is some what superior to mitoxantrone in number of curing animals by day 60. In the case of **5** where the two hydroxyl groups on C-1 and 2 were methylated, the compound did not show any activity. When the hydroxyl group on C-1 was methylated, **3** retained considerable activity producing 114% ILS value. While, the hydroxyl group on C-2 was methylated, **4** was fairly toxic. Considering from these facts, an existence of the free hydroxyl group on C-2 enhances antitumor activity, together with a presence of the hydroxyl group on C-1.

Experimental

General Methods. The same methods were used as described in the preceding paper.[1]

1,2-Dihydroxy-5,8-bis[2-(2-hydroxyethylamino)ethylamino]-9,10-anhracenedione Dihydrochloride (2). *(a) From quinalizarin (1)*: To a suspension of quinalizarin (**1**, 3.00 g) in 1-butanol (30 ml), a solution of 2-(2-aminoethylamino)ethanol (6.0 g) in 1-butanol (20 ml) was added under N_2 and stirred at 150 °C for 8 h. To the mixture, hexane was added and stirred overnight. The supernatant liquid was removed by decantation and the residue was washed with hot ethanol to give 4.56 g of **2**.

(b) From **6**: Compound **6** (200 mg) was dissolved in methanolic HCl (8 ml) under ice cooling. After 7 h, the precipitates were collected by filtration and recrystallized from 5 : 5 : 2 (v/v) ethanol–methanol–water to give 109 mg (79%) of **2**, mp 214—219 °C; UV (H_2O) 245 (log ε, 4.56), 591 (4.28), 635 nm (4.27); IR (KBr) 1615 cm^{-1} (quinone). ^{1}H NMR (D_2O): δ=3.33—3.93 (12H, m, CH_2 of side chain), 4.00—4.27 (4H, m, CH_2 of side chain), 6.63 (1H, d, J=9.0 Hz, aromatic proton), 6.85—7.33 (3H, m, aromatic protons).

Found: C, 49.72; H, 5.77; N, 10.16; Cl, 12.93%. Calcd for $C_{22}H_{30}N_4Cl_2O_6 \cdot H_2O$: C, 49.35; H, 6.02; N, 10.46; Cl, 13.24%.

2-(t-Butoxycarbonyloxy)-5,8-bis[2-(N-t-butoxycarbonyl-2-hydroxyethylamino)ethylamino]-1-hydroxy-9,10-anthracenedione (6). To a stirred solution of crude **2** (2.00 g) in 1 M NaOH solution (50 ml) and dioxane (25 ml) (1 M=1 mol dm^{-3}), di-*t*-butyl dicarbonate (4.91 g) was added. After 16 h, 1 M HCl solution (50 ml) was added under ice cooling, and the mixture was extracted with ethyl acetate. The Organic layer was washed with water, dried over anhydrous Na_2SO_4 and concentrated. The residue was purified on a column using 1 : 3 (v/v) acetone–toluene. Fractions homogeneous (R_f 0.47) on TLC in 1 : 1 (v/v) acetone–toluene were collected and concentrated. The residue was recrystallized from benzene–hexane to give 651 mg (19%) of **6**, mp 154—155 °C; UV ($CHCl_3$) 260 (log ε, 4.41), 381 (3.68), 606 (4.25), 656 nm (4.36). ^{1}H NMR: δ= 1.46 (18H, s, NBoc×2), 1.61 (9H, s, OBoc), 2.93—3.61 (12H, m, NHC$\underline{H}_2$C$\underline{H}_2$N(Boc)C$\underline{H}_2$CH_2OH), 3.64—3.90 (4H, m, CH_2C$\underline{H}_2$OH), 6.73—6.89 (2H, m, H-6 and 7), 7.29 (1H, d, J=9.0 Hz, H-3), 7.58 (1H, d, J=9.0 Hz, H-4), 10.12 (1H, bs, aromatic NH), 10.77 (1H, bs, aromatic NH), 13.73 (1H, s, 1-OH).

Found: C, 59.43; H, 6.89; N, 7.25%. Calcd for $C_{37}H_{52}N_4O_{12}$: C, 59.66; H, 7.04; N, 7.52%.

5,5-Bis[2-(N-t-butoxycarbonyl-2-hydroxyethylamino)ethylamino]-1,2-dihydroxy-9,10-anthracenedione (7). Compound **6** (400 mg) was dissolved in 80% aqueous acetic acid (10 ml) and stirred at 100 °C for 30 min. The mixture was concentrated and the residue was purified on a column using 1 : 7 (v/v) ethanol–toluene. Fractions homogeneous (R_f 0.43) on TLC in 1 : 5 (v/v) ethanol–toluene were collected and concentrated. The residue was recrystallized from benzene–hexane to give 118 mg (34%) of **7**, mp 164—166 °C; UV ($CHCl_3$) 260 (log ε, 4.36) (shoulder), 274 (4.26) (shoulder), 565 (3.87) (shoulder), 602 (4.19), 650 nm (4.27). ^{1}H NMR: δ=1.47 (18H, s, NBoc×2), 3.44 (12H, bs, NHC$\underline{H}_2$C$\underline{H}_2$N(Boc)C$\underline{H}_2$CH_2OH), 3.76 (4H, bs, CH_2C$\underline{H}_2$OH), 6.54—7.54 (5H, m, aromatic protons and 2-OH), 9.81 (1H, bs, aromatic NH), 10.51 (1H, bs, aromatic NH), 13.48 (1H, s, 1-OH).

Found: C, 59.82; H, 6.89; N, 8.41%. Calcd for $C_{32}H_{44}N_4O_{10}$: C, 59.61; H, 6.88; N, 8.69%.

5,8-Bis[2-[N-(t-butoxycarbonyl)-2-(trityloxy)ethylamino]ethylamino]-1,2-dihydroxy-9,10-anthracenedione (8). *(a) From 7*: To a stirred solution of **7** (80 mg) in pyridine (5 ml), trityl chloride (206 mg) was added. After 17 h at 60 °C, the mixture was poured into ice cold water. Precipitates were collected by filtration and purified on a column using 1 : 10 (v/v) ethyl acetate–toluene. Fractions homogeneous (R_f 0.36) on TLC in 1 : 5 (v/v) ethyl acetate–toluene were collected and concentrated. The residue was recrystallized from ethanol to give 101 mg (73%) of **8**, mp 140—143 °C; UV ($CHCl_3$) 261 (log ε, 4.56) (shoulder), 560 (4.02), (shoulder), 602 (4.36), 652 nm (4.46). ^{1}H NMR: δ=1.40 (18H, bs, NBoc×2), 2.96—4.75 (16H, m, CH_2 of side chain), 6.63 (1H, bs, 2-OH), 6.83—7.54 (33H, m, H-3,6,7 and C($C_6\underline{H}_5$)$_3$), 10.10 (1H, bs, aromatic NH), 10.76 (1H, bs, aromatic NH), 13.65 (1H, bs, 1-OH).

Found: C, 74.24; H, 6.47; N, 4.71%. Calcd for $C_{70}H_{72}$-

N_4O_{10}: C, 74.44; H, 6.43; N, 4.96%.

(b) From ***9***: To a stirred solution of **9** (636 mg) in acetone (15 ml), potassium carbonate (358 mg) was added and heated under reflux. After 7 h, the mixture was filtered and filtrate was concentrated. The residue was dissolved in ethyl acetate, washed with water, dried over anhydrous Na_2SO_4 and concentrated to give 501 mg (94%) of **8**.

*2-(t-Butoxycarbonyloxy)-5,8-bis[2-[N-(t-butoxycarbonyl)-2-(trityloxy) ethylamino] ethylamino]-1-hydroxy-9, 10-anthracenedione (****9****).* Compound **6** (100 mg) was tritylated analogously as described in the preparation of **8**. Fractions homogenous (R_f 0.22) on TLC in 1 : 3 (v/v) ethyl acetate–hexane were collected and concentrated. The residue was recrystallized from ethanol–methanol to give 114 mg (75%) of **9**, mp 190—215 °C; UV (EtOH) 210 (log ε, 4.93), 368 (3.77), 564 (3.96), 603 (4.33), 652 nm (4.45). ^{1}H NMR: δ=1.35 (18H, bs, NBoc×2), 1.53 (9H, s, OBoc), 3.00—3.77 (16H, m, CH_2 of side chain), 6.93—7.60 (33H, m, H-3,6,7 and $C(C_6\underline{H}_5)_3$), 7.80 (1H, d, J=9.0 Hz, H-4), 10.50 (1H, bs, aromatic NH), 11.05 (1H, bs, aromatic NH), 13.85 (1H, bs, 1-OH).

Found: C, 73.38; H, 6.65; N, 4.33%. Calcd for $C_{75}H_{80}N_4O_{12}$: C, 73.27; H, 6.56; N, 4.56%.

*5,8-Bis[2-[N-(t-butoxycarbonyl)-2-(trityloxy)ethylamino]ethylamino]-1-hydroxy-2-(p-methoxybenzyloxy)-9,10-anthracenedione (****10****).* To a stirred solution of **8** (300 mg) in dichloromethane (5 ml) and DMF (5 ml), *p*-methoxybenzyl chloride (0.5 ml) and potassium carbonate (184 mg) were added. After 4 h, the mixture was filtered and filtrate was washed with water, dried over anhydrous Na_2SO_4, and concentrated. The residue was washed with hexane and purified on a column using 1 : 3 (v/v) ethyl acetate–hexane. Fractions homogeneous (R_f 0.40) on TLC in 1 : 2 (v/v) ethyl acetate–hexaen were collected and concentrated. The residue was crystallized from ethanol to give 289 mg (87%) of **10**, mp 103—106 °C; UV ($CHCl_3$) 260 (log ε, 4.51) (shoulder), 280 (4.34) (shoulder), 568 (3.95) (shoulder), 602 (4.28), 654 nm (4.38). ^{1}H NMR: δ=1.17—1.63 (18H, m, NBoc×2), 3.01—3.66 (16H, m, CH_2 of side chain), 3.76 (3H, s, $CH_2C_6H_4OC\underline{H}_3$), 5.17 (2H, s, $C\underline{H}_2C_6H_4OCH_3$), 6.86 (2H, d, J=9.0 Hz, aromatic protons of MBn[13]), 6.99—7.51 (35H, m, aromatic protons), 7.73 (1H, d, J=9.0 Hz, H-4), 10.30 (1H, bs, aromatic NH), 10.83 (1H, bs, aromatic NH), 13.62 (1H, bs, 1-OH).

Found: C, 75.13; H, 6.51; N, 4.41%. Calcd for $C_{78}H_{81}N_4O_{11}$: C, 74.92; H, 6.53; N, 4.48%.

*5,8-Bis[2-[N-(t-butoxycarbonyl)-2-(trityloxy) ethylamino] ethylamino]-1-methoxy-2-(p-methoxybenzyloxy)-9,10-anthracenedione (****11****).* To a stirred solution of **10** (1.43 g) in acetone (20ml), dimethyl sulfate (0.5 ml) and potassium carbonate (794 mg) were added, heated under reflux. After 6 h, the mixture was filtered snd the filtrate was diluted with ethyl acetate. The solution was washed with water, dried over anhydrous Na_2SO_4, and concentrated. The residue was purified on a column using 15 : 1 (v/v) benzene–ethyl acetate. Fractions homogeneous (R_f 0.58) on TLC in 5 : 1 (v/v) benzene–ethyl acetate were collected and concentrated. The residue was recrystallized from ethanol to give 1.11 g (77%) of **10**, mp 101—106 °C; UV ($CHCl_3$) 273 (log ε, 4.56), 597 (4.23), 645 nm (4.26). ^{1}H NMR: δ=1.17—1.59 (18H, m, NBoc×2), 3.02—3.64 (16H, m, CH_2 of side chain), 3.76 (3H, s, $CH_2C_6H_4OC\underline{H}_3$), 3.95 (3H, s, 1-$OCH_3$), 5.15 (2H, s, $C\underline{H}_2C_6H_4OCH_3$), 6.85 (2H, d, J= 9.0 Hz, aromatic protons of MBn), 6.98—7.51 (35H, m, aromatic protons), 8.08 (1H, d, J=9.0 Hz, H-4), 10.23 (2H, bs, aromatic NH).

Found: C, 74.91; H, 6.61; N, 4.44%. Calcd for $C_{79}H_{83}N_4O_{11}$: C, 75.04; H, 6.62; N, 4.43%.

*2-Hydroxy-5,8-bis[2-(2-hydroxyethylamino)ethylamino]-1-methoxy-9,10-anthracenedione dihydrochloride (****3****).* To a stirred solution of **11** (1.11 g) in dichloromethane (5 ml), methanolic HCl (20 ml) was added under ice cooling. The precipitates were collected by filtration and recrystallized from 95% aqueous ethanol to give 342 mg (70%) of **3**, mp 209—211 °C; UV (H_2O) 217 (log ε, 4.50), 239 (4.50), 271 (4.50), 586 (4.20), 629 nm (4.20); IR (KBr) 1640 cm^{-1} (quinone). ^{1}H NMR (D_2O): δ=3.33—3.65 (8H, m, $NHCH_2C\underline{H}_2NHC\underline{H}_2CH_2OH$), 3.68—3.95 (7H, m, $NHC\underline{H}_2CH_2NH$ and 1-OCH_3), 3.95—4.20 (4H, m, $CH_2C\underline{H}_2OH$), 7.00—7.28 (3H, m, H-3,6 and 7), 7.55 (1H, d, J=9.0 Hz, H-4).

Found: C, 49.56; H, 5.83; N, 9.70; Cl, 13.05%. Calcd for $C_{23}H_{30}N_4O_6\cdot 2HCl\cdot 1.5\,H_2O$: C, 49.47; H, 6.31; N, 10.03; Cl, 12.69%.

*2-Acetoxy-5,8-bis[2-(N-acetyl-2-acetoxyethylamino)ethylamino]-1-methoxy-9,10-anthracenedione (****12****).* Compound **3** (15 mg) was acetylated with acetic anhydride (0.5 ml) in pyridine (1 ml) under ice cooling. The mixture was extracted with ethyl acetate and washed with H_2O, dried over Na_2SO_4. The solution was concentrated to give 22 mg (quantative yield) of **12** as an amorphous solid. ^{1}H NMR: δ=2.05, (6H, s, Ac×2), 2.15 (6H, s, Ac×2), 2.37 (3H, s, 2-OAc) 3.09—3.78 (12H, m, $NHC\underline{H}_2C\underline{H}_2N(Ac)C\underline{H}_2CH_2OAc$) 3.92 (3H, s, 1-$OCH_3$), 4.18 (4H, t, J=6.0 Hz, $CH_2C\underline{H}_2OAc$), 7.22—7.48 (3H, m, H-3,6 and 7), 8.15 (1H, d, J=9.0 Hz, H-4), 10.46 (2H, bs, aromatic NH).

*5,8-Bis[2-[N-(t-butoxycarbonyl)-2-(trityloxy) ethylamino] ethylamino]-1-hydroxy-2-methoxy-9,10-anthracedione (****13****).* Compound **8** (70 mg) was methylated analogously as described in the preparation of **11**. The crude product was purified on a column using 1 : 10 (v/v) ethyl acetate–toluene. Fractions homogeneous (R_f 0.43) on TLC in 1 : 5 (v/v) ethyl acetate–toluene were collected and concentrated. The residue was recrystallized from ethanol to give 66 mg (93%) of **13** as amorphous solids, mp 110—114 °C; UV ($CHCl_3$) 262 (log ε, 4.52) (shoulder), 278 (4.38), 564 (3.99) (shoulder), 520 (4.33), 652 nm (4.43). ^{1}H NMR: δ=1.35 (18H, bs, NBoc×2), 2.97—3.63 (16H, m, CH_2 of side chain), 3.82 (3H, s, 2-OCH_3), 6.80—7.67 (33H, m, H-3,6,7 and $C(C_6\underline{H}_5)_3$), 7.78 (1H, d, J=9.0 Hz, H-4), 10.30 (1H, bs, aromatic NH), 10.87 (1H, bs, aromatic NH), 13.79 (1H, bs, 1-OH).

Found: C, 74.75; H, 6.71; N, 4.90%. Calcd for $C_{71}H_{74}N_4O_{10}$: C, 74.58; H, 6.52; N, 4.90%.

*1-(t-Butoxycarbonyloxy)-5,8-bis[2-[N-(t-butoxycarbonyl)-2-(trityloxy)ethylamino]ethylamino]-2-methoxy-9,10-anthracenedione (****14****).* Compound **9** (400 mg) was methylated analogously as described in the preparation of **11**. The crude product was purified on a column using 1 : 4 (v/v) ethyl acetate–hexane. Fractions homogeneous (R_f 0.16) on TLC in 1 : 3 (v/v) ethyl acetate–hexane were collected and concentrated. The residue was recrystallized from ethanol to give 257 mg (64%) of **14**, mp 108—111 °C; UV ($CHCl_3$) 272 (log ε, 4.63), 599 (4.32), 646 nm (4.37). ^{1}H NMR: δ=1.37 (18H, bs, NBoc×2), 1.55 (9H, s, OBoc), 2.90—3.67 (16H, m, CH_2 of side chain), 3.83 (3H, s, 2-OCH_3), 6.90—7.67 (33H, m, H-3,6,7 and $C(C_6\underline{H}_5)_3$), 8.32 (1H, d, J=9.0 Hz, H-4), 10.62 (2H, bs, aromatic NH).

Found: C, 73.13; H, 6.69; N, 4.26%. Calcd for $C_{76}H_{82}N_4O_{12}$: C, 73.41; H, 6.65; N, 4.51%.

*1-Hydroxy-5,8-bis[2-(2-hydroxyethylamino)ethylamino]-2-methoxy-9,10-anthracenedione dihydrochloride (****4****).* *(a) From* ***13***: Compound **13** (150 mg) was treated with methanolic HCl (10 ml) under ice cooling. After 4 h, precipitates were collected and recrystallized from methanol to give 39 mg (56%) of **4**, mp 199—201 °C; UV (H_2O) 227 (log ε, 4.24) (shoulder), 243 (4.45), 260 (4.38), 589 (4.15), 635 nm (4.17); IR (KBr) 1640 cm^{-1} (quinone). ^{1}H NMR (D_2O): δ=6.73—7.00 (4H, m, H-3,4,6 and 7).

Found: C, 48.77; H, 5.85; N, 9.54; Cl, 12.50%. Calcd for $C_{23}H_{30}N_4O_6 \cdot 2HCl \cdot 2H_2O$: C, 48.68; H, 6.39; N, 9.87; Cl, 12.49%.

(b) From ***14***: Compound **14** (150 mg) was treated analogously as described above in (a) to give 56 mg (87%) of **4**,.

*5,8-Bis[2-(*N*-acetyl-2-acetoxyethylamino) ethylamino]-1-hydroxy-2-methoxy-9,10-anthracenedione (**15**).* Compound **4** (30 mg) was acetylated with acetic anhydride (0.5 ml) in pyridine (0.5 ml) under ice cooling. The solution was diluted with ethyl acetate and washed with water, dried over anhydrous Na_2SO_4. The solution was concentrated and the residue was purified on a column using 1 : 6 (v/v) ethanol–toluene were collected and concentrated to give 23 mg (66%) of **15** as syrup. ^{1}H NMR: δ=2.04 (6H, s, Ac×2), 2.14 (6H, s, Ac×2), 3.57 (12H, bs, NHC$\underline{H_2}$C$\underline{H_2}$N(Ac)C$\underline{H_2}$CH$_2$OAc), 3.96 (3H, s, 2-OCH$_3$), 4.17 (4H, t, J=6.0 Hz, CH$_2$C$\underline{H_2}$OAc), 6.87—7.51 (3H, m, H-3,6, and 7), 7.70 (1H, d, J=9.0 Hz, H-4), 10.19 (1H, bs, aromatic NH), 10.72 (1H, bs, aromatic NH), 13.42—13.78 (1H, m, 1-OH).

*1-Acetoxy-5,8-bis[2-(*N*-acetyl-2-acetoxyethylamino) ethylamino]-2-methoxy-9,10-anthracenedione (**16**).* Compound **4** (30 mg) was acetylated analogously as described in the preparation of **15**. Fractions homogeneous (R_f 0.30) on TLC in 1 : 3 (v/v) ethanol–toluene were collected and concentrated to give 13 mg (35%) of **16** as amorphous solids, UV ($CHCl_3$) 274 (log ε, 4.48), 594 (4.14), 640 nm (4.17). ^{1}H NMR: δ=2.02 (6H, s, Ac×2), 2.13 (6H, s, Ac×2), 2.46 (3H, s, 1-OAc), 3.24—3.80 (12H, m, NHC$\underline{H_2}$C$\underline{H_2}$N(Ac)C$\underline{H_2}$CH$_2$OAc), 3.92 (3H, s, 2-OCH$_3$), 4.16 (4H, t, J=6.0 Hz, CH$_2$C$\underline{H_2}$OAc), 6.98—7.67 (3H, m, H-3,6 and 7), 8.25 (1H, d, J=9.0 Hz, H-4), 10.56 (2H, bs, aromatic NH).

Found: C, 59.25; H, 6.01; N, 8.09%. Calcd for $C_{33}H_{40}N_4O_{11}$: C, 59.32; H, 6.03; N, 8.39%.

*5,8-Bis[2-[*N*-(*t*-butoxycarbonyl)-2-(trityloxy) ethylamino]ethylamino]-1,2-dimethoxy-9,10-anthracenedione (**17**).* Compound **8** (110 mg) was methylated analogously as described in the preparation of **11**. The product was purified on a column using 1 : 8 (v/v) ethyl acetate–toluene. Fractions homogeneous (R_f 0.56) on TLC in 1 : 3 (v/v) ethyl acetate–toluene were collected and concentrated. The residue was recrystallized from hexane to give 37 mg (32%) of **17**, mp 85—90 °C; UV (EtOH) 212 (log ε, 4.83), 271 (4.49), 593 (4.18), 640 nm (4.21). ^{1}H NMR: δ=1.22 (18H, bs, NBoc×2), 3.01—3.72 (16H, m, CH$_2$ of side chain), 3.94 (6H, s, OCH$_3$×2), 6.89—7.50 (33H, m, H-3,6,7 and C(C$_6\underline{H_5}$)$_3$), 8.13 (1H, d, J=9.0 Hz, H-4), 10.19 (2H, bs, aromatic NH).

Found: C, 74.18; H, 6.91; N, 4.85%. Calcd for $C_{72}H_{76}N_4O_{10}$: C, 74.72; H, 6.62; N, 4.84%.

*5,8-Bis[2-(2-hydroxyethylamino) ethylamino]-1,2-dimethoxy-9,10-anthracenedione dihydrochloride (**5**).* Compound **17** (100 mg) was dissolved in methanolic HCl (4 ml), after 2 h, precipitates were collected by filtration and recrystallized from ethanol to give 35 mg (81%) of **5**, mp 203—205 °C; UV (H_2O) 221 (log ε, 4.39), 239 (4.41), 272 (6.41), 584 (4.12), 627 nm (4.12); IR (KBr) 1635 cm^{-1}. ^{1}H NMR (D_2O): δ=7.10 (2H, bs, H-6 and 7), 7.32 (1H, d, J=9.0 Hz, H-3), 7.72 (1H, d, J=9.0 Hz, H-4).

Found: C, 51.29; H, 6.03; N, 9.61; Cl, 11.77%. Calcd for $C_{24}H_{32}N_4O_6 \cdot 2HCl \cdot H_2O$: C, 51.16; H, 6.44; N, 9.94; Cl, 12.58%.

*5,8-Bis[2-(*N*-acetyl-2-acetoxyethylamino) ethylamino]-1,2-dimethoxy-9,10-anthracenedione (**18**).* Compound **5** (20 mg) was acetylated analogously as described in the preparation of **15**. Fractions homogeneous (R_f 0.33) on TLC in 1 : 3 (v/v) ethanol–toluene were collected and concentrated to give 14 mg (50%) of **18** as amorphous solids; UV (EtOH) 221 (log ε, 4.08), 239 (4.06), 273 (4.08), 590 (3.78), 635 nm (3.79). ^{1}H NMR: δ=2.04 (6H, s, Ac×2), 2.13 (6H, s, Ac×2), 3.40—3.78 (12H, m, NHC$\underline{H_2}$C$\underline{H_2}$N(Ac)C$\underline{H_2}$CH$_2$OAc), 3.95 (6H, s, OCH$_3$×2), 4.17 (4H, t, J=6.0 Hz, CH$_2$C$\underline{H_2}$OAc), 7.00—7.60 (3H, m, H-3,6 and 7), 8.12 (1H, d, J=9.0 Hz, H-4), 10.12 (2H, bs, aromatic NH).

The authors wish to express their thanks to Dr. Iwao Umezawa for his evaluation of the antineoplastic activity and to Mr. Saburo Nakada for his elementary analysis.

References

1) K. Nakamura, T. Asai, T. Hara, N. Minorikawa, and T. Suami, *Bull. Chem. Soc. Jpn.*, submitted.
2) S. Bennett, D. Sharples, and J. R. Brown, *J. Med. Chem.*, **25**, 369 (1982).
3) P. Chang, K.-H. Lee, T. Shingu, T. Hirayama, and I. H. Hall, *J. Natural Products*, **45**, 206 (1982).
4) D. D. Von Hoff, E. Pollard, J. Kuhn, E. Murray, and C. A. Coltman, Jr., *Cancer Res.*, **40**, 1516 (1980).
5) R. K. Jhonson, R. K. Y. Zee-Cheng, W. W. Lee, F. M. Acton, D. W. Henry, and C. C. Cheng, *Cancer Treat. Res.*, **63**, 425 (1979).
6) R. E. Wallace, K. C. Murdock, R. B. Angier, and F. E. Durr, *Cancer Res.*, **39**, 1570 (1979).
7) R. K. Y. Zee-Cheng and C. C. Cheng, *J. Med. Chem.*, **21**, 291 (1978).
8) R. K. Y. Zee-Cheng, E. G. Podrebarac, C. S. Menon, and C. C. Cheng, *J. Med. Chem.*, **22**, 501 (1979).
9) M. Kikuchi, T. Yamagishi, and M. Hida, *Chem. Lett.*, **1981**, 1391.
10) F. Arcamone, G. Cassinelli, F. DiMatteo, S. Forenza, M. C. Ripamonti, G. Rivola, A. Vigevani, J. Clardy, and T. Ripamonti, G. Rivola, A. Vigevani, J. Clardy, and T. McCabe, *J. Am. Chem. Soc.*, **102**, 1462 (1980).
11) The antitumor activity was determined by Dr. Iwao Umezawa, Kitasato Institute, Shirogane, Minato-ku, Tokyo by the established protocol.[12]
12) J. L. Hartwell, *Cancer Chemother. Rep.*, Part **1**, 25 (1962).
13) MBn: *p*-Methoxybenzyl.

Effects of Additives on Photo-methoxylation of Methyl 2-Pyridinecarboxylate in Acidic Methanolic Solutions. Promotion by 4-Substituted Pyridines

Akira Sugimori,* Teruo Ogishima, Yoshiyuki Miyazawa, Ryo Hasegawa, and Yoko Suzuki

Department of Chemistry, Faculty of Science and Technology, Sophia University, Kioi-cho 7-1, Chiyoda-ku, Tokyo 102

(Received January 20, 1983)

The rate of photo-methoxylation of methyl 2-pyridinecarboxylate(**1**) in acidic methanol is accelerated by 4-substituted pyridines and their analogs, 4,4'-bipyridine and pyrazine. The photo-methoxylation of **1** is not promoted by triplet sensitizers, electron donors, or electron acceptors. Detailed analyses on the **1**–4-pyridinecarbonitrile(**3**) system including wavelength dependence lead to a mechanism for the promotion *via* an excited complex formed from an excited **1** and **3** in the ground state.

The promotion and inhibition of photoreactions are an important theme in the studies of photochemistry from the viewpoints of both mechanistic and synthetic organic photochemistry. The promotion and inhibition *via* energy transfer[1] and electron transfer[2] have been investigated extensively.

The field of photosensitization is, however, wide and studies from new aspects are needed. Increasing interest has been paid to the sensitization *via* excited complexes. For the apparently peculiar "quencher-sensitized" photo-dimerization of anthracene derivatives,[3,4] the participation of an exciplex has been proposed.[3] The selectivity and specificity due to complex formation are important. Photochemical formation of optically active *trans*-cyclooctene and 1,5-cyclooctadiene induced by chiral sensitizers has been explained in terms of the exciplex formation.[5,6]

We describe here the specific promotion of photo-methoxylation of methyl 2-pyridinecarboxylate by 4-substituted pyridines and propose a mechanism for the promotion *via* an exciplex.[7] Concerning the photo-methoxylation of methyl 2-pyridinecarboxylate in the absence of sensitizers, we have observed remarkable concentration dependence and proposed a mechanism *via* an excimer.[8]

Results and Discussion

Indices Describing (Promoting or Inhibiting) Effects of Additives, Y- and A-Value. In the case where the additive and the substrate absorb the incident light competitively, the effects of addititives should be analyzed by taking the distribution of light absorption between the substrate and the additive into consideration.

In a system where the incident light is completely absorbed by the substrate even in the absence of the additive, an index, A, defined below can be used for describing the promoting or inhibiting effect by the additive:

$$A = Y/L$$

$$Y = \frac{\text{Yield in the presence of additive}}{\text{Yield in the absence of additive}}$$

$$L = \frac{\text{Light absorbed by substrate (1)}}{\text{Light absorbed both by substrate (1) and by additive (S)}} = \frac{c_1\varepsilon_1}{c_1\varepsilon_1 + c_S\varepsilon_S},$$

where c_1 and c_S represent the concentrations of **1** and additive, and ε_1 and ε_S are the molar absorption coefficients of **1** and of additive at the wavelength of the photolyzing light, respectively. $A>1$ indicates promotion by the additive and $A<1$ means inhibition.

Effects of Triplet Sensitizer, Triplet Quencher, Electron Donor, and Electron Acceptor. UV-irradiation of methyl 2-pyridinecarboxylate (**1**) in methanol acidified with sulfuric acid gives methyl 6-methoxy-2-pyridinecarboxylate (**2**).

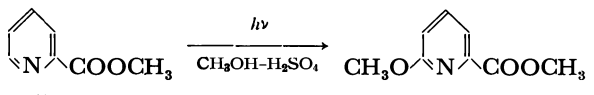

(**1**) (**2**)

Table 1. Effects of triplet sensitizer, electron donor, and electron acceptor on photo-methoxylation of methyl 2-pyridinecarboxylate (**1**) $[H_2SO_4]=5\times10^{-2}$ mol dm^{-3}; Irradiated with 254 nm light.

Additive	10^3 [**1**] / mol dm^{-3}	10^3 [Additive] / mol dm^{-3}	L	Y	A
Benzene	1.0	1.0	0.96	0.83	0.86
	1.0	10	0.68	0.62	0.91
Naphthalene	1.0	6.0	0.16	0.055	0.34
Acetophenone	1.0	1.0	0.45	0.44	1.0
	1.0	3.0	0.21	0.21	1.0
Anisole	1.0	1.0	0.74	0.72	0.97
Ferrocene	1.0	1.0	0.64	0.0	0.0
1, 2, 4, 5-Tetracyanobenzene	0.25	1.0	0.17	0.0	0.0
Nitrobenzene	0.25	1.0	0.27	0.0	0.0

As reported earlier,[8] the photo-methoxylation has a remarkable concentration dependence on **1**: at 32 °C, quantum yields for **2** at $[\mathbf{1}]=5\times10^{-4}$, 1.0×10^{-3}, 2.0×10^{-3}, 5.0×10^{-3}, and 2.0×10^{-2} mol dm^{-3} are 0.009, 0.02, 0.025, 0.051, and 0.17, respectively.

We studied the effects of additives on photo-methoxylation of **1** at $[\mathbf{1}]=1.0\times10^{-3}$ mol dm^{-3}, where the photo-methoxylation is not so efficient. In Table 1 are listed the effects of several typical sensitizers, electron donors, and electron acceptors. The photo-methoxylation of **1** is not promoted by acetophenone, benzene, and naphthalene, and is not inhibited by 1,3-pentadiene (Fig. 1). These results indicate that the photo-methoxylation proceeds *via* a singlet excited state. Anisole, naphthalene, ferrocene, nitrobenzene, and 1,2,4,5-tetracyanobenzene, which can be expected to undergo electron transfer type interactions, have no promoting effect.

Effects of Pyridine Derivatives on Photo-methoxylation of ***1****.* The results of a systematic survey of effects of pyridine derivatives on photo-methoxylation of **1** are shown in Table 2. It should be noted that 4-substituted pyridines

Table 2. Effects of substituted pyridines and related compounds on photo-methoxylation of methyl 2-pyridinecarboxylate (**1**) $[H_2SO_4]=5\times10^{-2}$ mol dm^{-3}; Irradiated with 254 nm light.

Additive	10^3 [**1**] / mol dm^{-3}	10^3 [Additive] / mol dm^{-3}	*L*	*Y*	*A*
2-Methylpyridine	1.0	0.1	0.89	0.92	1.03
	1.0	1.0	0.46	0.59	1.28
2-Pyridinol	1.0	0.2	0.92	0.86	0.93
	1.0	1.0	0.70	0.38	0.55
2-Pyridinamine	1.0	0.2	0.98	1.1	1.1
	1.0	1.0	0.90	0.97	1.1
2-Pyridinecarboxamide	1.0	0.2	0.85	0.77	0.91
	1.0	1.0	0.53	0.44	0.83
2-Pyridinecarbonitrile	1.0	1.0	0.62	0.56	0.90
2-Acetylpyridine	1.0	1.0	0.38	0.19	0.50
3-Methylpyridine	0.25	1.0	0.23	0.0	0.0
3-Pyridinol	1.0	0.2	0.98	0.64	0.65
	1.0	1.0	0.90	0.58	0.64
3-Pyridinamine	1.0	0.2	0.67	0.58	0.87
	1.0	1.0	0.29	0.26	0.89
3-Pyridinecarboxamide	0.25	1.0	0.22	0.0	0.0
3-Pyridinecarbonitrile	1.0	1.0	0.61	0.59	0.97
4-Methylpyridine	0.4	0.2	0.50	0.75	1.5
	0.4	1.0	0.17	0.75	4.4
4-*t*-Butylpyridine	1.0	0.2	0.82	0.67	0.82
	1.0	1.0	0.48	0.37	0.77
4-Phenylpyridine	1.0	1.0	0.44	1.00	2.3
4-Benzylpyridine	1.0	1.0	0.43	0.50	1.2
4-Pyridinol	1.0	1.0	0.87	2.8	3.2
4-Pyridinamine	1.0	0.1	0.76	0.93	1.2
Methyl 4-pyirdinecarboxylate	1.0	0.1	0.93	4.2	4.5
	1.0	0.3	0.81	4.0	4.9
4-Pyridinecarboxamide	1.0	0.2	0.83	1.6	1.9
	1.0	1.0	0.49	1.2	2.4
4-Pyridinecarbonitrile	1.0	0.1	0.96	3.0	3.1
	1.0	1.0	0.71	7.4	10.4
4-Acetylpyridine	0.4	0.2	0.69	0.91	1.3
2, 2′-Bipyridine	1.0	0.1	0.89	0.58	0.65
4, 4′-Bipyridine	1.0	0.2	0.56	1.15	2.1
	1.0	1.0	0.21	2.21	10.5
Dimethyl 2, 4-pyridinedicarboxylate	1.0	0.1	0.97	1.8	1.9
	1.0	1.0	0.74	5.0	6.7
Dimethyl 2, 5-pyridiendicarboxylate	1.0	0.2	0.88	2.9	3.3
	1.0	1.0	0.60	3.1	5.2
Pyridazine	1.0	0.2	0.97	1.5	1.5
	1.0	1.0	0.85	2.1	2.4
Pyrimidine	1.0	0.2	0.94	0.99	1.1
	1.0	1.0	0.77	0.81	1.1
Pyrazine	1.0	0.1	0.91	1.1	1.2
	1.0	1.0	0.49	1.3	2.7

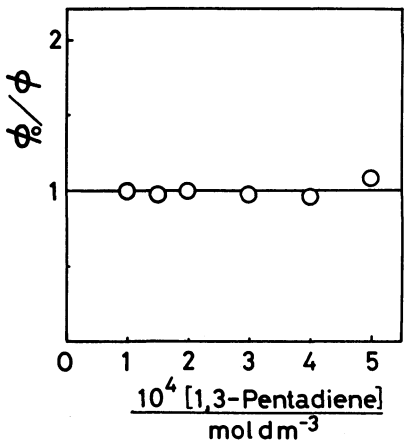

Fig. 1. Stern-Volmer plot for quenching of photo-methoxylation of methyl 2-p ridinecarboxylate (**1**) by 1,3-pentadiene. $[\mathbf{1}]=1.0\times10^{-3}$ mol dm^{-3}; $[H_2SO_4]=5\times10^{-2}$ mol dm^{-3}.

show remarkable promoting effects independently of the electron-accepting or electron-donating character of the substituents. Pyrazine and 4,4'-bipyridine, which can be regarded as analogs of 4-substituted pyridines, show high promoting effects.

Some 2-substituted pyridines accelerate the photo-methoxylation of **1**, but less effectively than 4-substituted pyridines. 3-Substituted pyridines have no promoting effects.

*Characteristics of Promotion by 4-Pyridinecarbonitrile (**3**).* Among 4-substituted pyridines, 4-pyridinecarbonitrile has a large promoting effect. In the methyl 2-pyridine-carboxylate (**1**)-4-pyridinecarbonitrile (**3**) system, the characteristics of the promotion was studied in detail. In Table 3, are shown the data of photosensitization by **3** at $[\mathbf{1}]=1.0\times10^{-3}$ mol dm^{-3} at various concentrations of **3** in the irradiation with 254 nm light. From Table 3 the following points should be noted.

1) The additive, **3**, was recovered almost quantitatively. This means that **3** works as a "true catalyst" (not sacrificially). For example, we analyze the data of line 2 in Table 3. By the irradiation of the solution containing 10^{-3} mol dm^{-3} of **1** and 10^{-4} mol dm^{-3} of **3**, 2.5×10^{-5} mol dm^{-3} of **2** are formed and 5×10^{-7} mol dm^{-3} of **3** are consumed. The formation of **2** is 50 times greater than the consumption of **3**.

2) Both *A*-values, which are indices of promotion normalized on the basis of the light absorbed by **1**, and also *Y*-values, which are indices of promotion without the correction of light absorption are larger than 1.

3) The presence of **3** increases both the consumption of **1** and the selectivity for **3** (selectivity=[**2** formed]/[**1** reacted]). The combination of these two effects results in the large *A*- and *Y*-values.

The promotion by **3** is greater than that *via* self-catalysis by **1**: the addition of 10^{-3} mol dm^{-3} of **3** to 10^{-3} mol dm^{-3} of **1** increased the yield of **2** 7.4 times (in *Y*-value), while the yield of **2** at $[\mathbf{1}]=2\times10^{-3}$ mol dm^{-3} is only 1.23 times of the yield at $[\mathbf{1}]=1\times10^{-3}$ mol dm^{-3} at 32 °C.

Mechanism for Promotion by 4-Pyridinecarbonitrile. For the promotion of photo-methoxylation of **1** by additives, the following mechanisms are conceivable (Scheme 1).

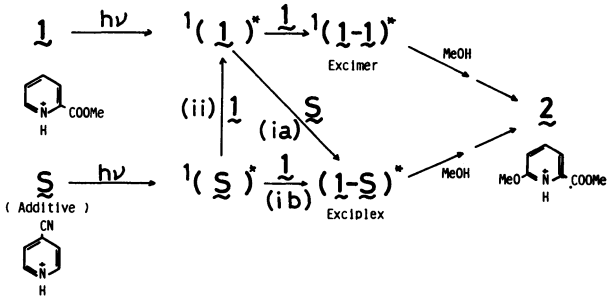

Scheme 1.

(i) Mechanism *via* exciplex formation
It is subdivided into three categories:
(ia) Mechanism *via* an exciplex formed from an excited **1** and a ground state-additive
(ib) Mechanism *via* an exciplex formed from an excited additive and a ground state- **1**.
(ic) Mechanism in which (ia) and (ib) operate simultaneously.
(ii) Singlet energy transfer mechanism

As stated in the previous section, the photo-methoxylation is neither promoted by triplet sensitizer nor inhibited by triplet quencher. A triplet energy transfer mechanism is thus excluded.

The above postulated mechanisms were further examined in the **1**—**3** system.

Table 3. Dependence of promotion of photo-methoxylation of methyl 2-pyridinecarboxylate (**1**) on concentration of added 4-pyridinecarbonitrile (**3**) in irradiation with 254 nm light

Irradiation time, 2 min; $[\mathbf{1}]=1.0\times10^{-3}$ mol dm^{-3}; $[H_2SO_4]=5\times10^{-2}$ mol dm^{-3}.

10^4 [**3**] / mol dm^{-3}	*L*	10^5 [**2**] / mol dm^{-3}	10^5 [**1** reacted] / mol dm^{-3}	*Y*	*A*	[**2** formed] / [**1** reacted]	Recovery of **3** / %
0.0	1.00	0.84	2.3			0.36	
1.0	0.96	2.5	6.2	3.0	3.1	0.40	99.5
3.0	0.89	3.2	7.5	3.9	4.4	0.42	100
5.0	0.83	3.7	7.4	4.7	5.6	0.51	100
6.0	0.80	3.9	6.1	4.8	6.0	0.65	100
7.0	0.78	5.4	7.3	6.7	8.6	0.74	100
8.0	0.75	5.6	6.9	7.0	9.4	0.83	100
10.0	0.71	6.0	7.3	7.4	10.4	0.83	100

A singlet energy transfer mechanism (ii) can be excluded on the basis of the data in Table 3. *Y*-values in the **1**—**3** system are greater than 1. If Mechanism (ii) operates, *Y* can not exceed 1, because in the system, where all the incident light are completely absorbed by **1** and **3**, the sum of singlet excited states of **1** and **3** is constant and the number of the excited **1** in the presence of additive can not exceed the number of the excited **1** in the absence of additive, even if the efficiency of the singlet energy transfer is 100%.

In order to answer the question whether (ia), (ib), or (ic) is more plausible, the wavelength dependence of the promotion is studied. The spectra of **1** differ from those of **3**: 254 nm light is absorbed more efficiently by **1** (ε=4350) than by **3** (ε=1800), while 280 nm light is absorbed more efficiently by **3** (ε=4330) than by **1** (ε=1200).

If the promotion is effected *via* an exciplex from an excited **1** and a ground state- **3** (Mechanism (ia)), *A*-values at the different wavelengths should be the same. In Mechanism (ia), the fate of the excited **1** (to form an excimer (**1**—**1**)* or to form an exciplex (**1**—**3**)*) is determined by the concentrations of **1** and **3**. Therefore, *A*-value, which is the relative yield on the basis of the quantity of the excited **1**, should not change by varying the distribution of light absorption, as long as the concentrations of **1** and **3** remain the same. In Mechanism (ia), the *A*-value, however, should be dependent on the concentrations of **1** and **3**.

In Mechanism (ib) the *A*-value should depend on the wavelength and a higher *A*-value should be expected in the irradiation with light of a wavelength at which **3** absorbs more than **1**.

If the process (ia) and (ib) occur in parallel, the *A*-value for the wavelength at which light is absorbed less by **1** than **3** should be greater than that for the wavelength at which light is absorbed more by **1** than by **3**, because the light absorbed by **3** should be effective for the formation of **2**.

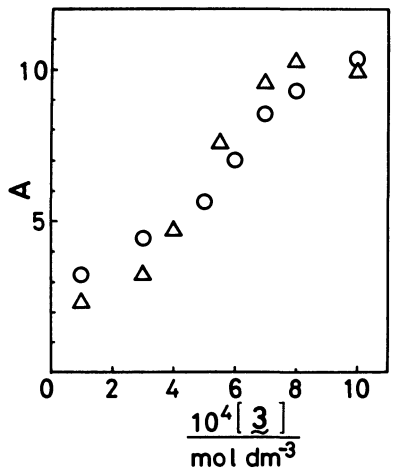

Fig. 2. Wavelength dependence of promotion of photo-methoxylation of methyl 2-pyridinecarboxylate (**1**) by 4-pyridinecarbonitrile (**3**).
Promoting effect is expressed in *A*-value. [**1**]=1.0×10^{-3} mol dm^{-3}. ○, Irradiated with 254 nm light. △, Irradiated with 280 nm light.

Figure 2 shows the wavelength dependence of the promotion of photo-methoxylation of **1** by **3**. The *A*-values in the irradiation at 254 nm light agree with those in the irradiation at 280 nm light in the region of 10^{-4}—10^{-3} mol dm^{-3} of [**3**]. This indicates that Mechanism (ia) should operate in the promotion of photo-methoxylation by **3**.

A question why an exciplex between **1** and **3** has higher reactivity for methoxylation than an excimer of **1** is difficult to answer. However, the higher reactivity of an exciplex could be partially ascribed to the greater polarity of an exciplex than an excimer: The polarity generated in a complex formed between different species should be greater than that in a complex formed from the same species. The greater polarity should result in the increase in the higher reactivity for ionic reaction.

Experimental

Materials. Commercial methyl 2-pyridinecarboxylate (GR grade reagent of Tokyo Kasei Co.) was purified by vacuum distillation (bp, 130—131 °C/27 mmHg, 1 mmHg ≈133.322 Pa). 4-Pyridinecarbonitrile (GR grade of Wako Junyaku Co.) was recrystallized from ether (mp, 82—83 °C). The other reagents used were commercial GR or EP grade reagents.

Preparation of Solution for Irradiation. Solutions (20 cm^3) containing **1** (normally [**1**]=1.0×10^{-3} mol dm^{-3}), sulfuric acid (normally [H_2SO_4]=5×10^{-2} mol dm^{-3}), and additive in methanol were deaerated by bubbling nitrogen through them for at least 45 min.

UV-Irradiation. For the irradiation with 254 nm light, a merry-go-round irradiation apparatus equipped with a 17 W low-pressure mercury lamp was employed. The merry-go-round apparatus was set up in a thermostat and the temperature was maintained at 25.5 °C. For 280 nm light irradiation, a monochrometer (made by Shimadzu-Bausch-Lomb Co.) equipped with a super-high-pressure mercury lamp was used. The resolution in our experimental condition was ±10.5 nm.

Quantitative Analyses. The quantities of **2** formed were determined either by spectrophotometric or by gas-chromatographic method.

i) For the spectrophotometric determination of **2**, its characteristic absorption at 287 nm was used. By means of the spectral method the following systems were analyzed: **1**–benzene, anisole, ferrocene, 1,2,4,5-tetracyanobenzene, nitrobenzene, 2-methylpyridine, 2-pyridinecarboxamide, 3-methylpyridine, 3-pyridinol, 3-pyridinecarboxamide, 3-pyridinecarbonitrile, 4-methylpyridine, 4-*t*-butylpyridine, 4-phenylpyridine, 4-benzylpyridine, 4-pyridinamine, 4-pyridinecarboxamide, 4-acetylpyridine, 2,2′-bipyridine, or pyrimidine.

ii) Gas-chromatographic method was applied for the analyses of the following systems: **1**–naphthalene, acetophenone, 2-pyridinol, 2-pyridinamine, 2-pyridinecarbonitrile, 3-pyridinamine, 4-pyridinol, methyl 4-pyridinecarboxylate, 4-pyridinecarbonitrile, 4,4′-bipyridine, dimethyl 2,4-pyridinedicarboxylate, dimethyl 2,5-pyridinedicarboxylate, or pyrazine.

A typical example applied for the analysis of the **1**—**3** system was done in the following way. After the irradiation, methanol was evaporated under reduced pressure. The solution was neutralized with aqueous $NaHCO_3$ solution and was extracted repeatedly with dichloromethane. The dichloromethane extract was analyzed gas-chromatographically in the following conditions: apparatus, Shimadzu GC-6A; column, 2 m column

of Triton QS-15 (15%) on Uniport B (60/80 mesh); column temperature, 160 °C; internal standard, 3-acetylpyridine.

The present work was partially supported by a Grant-in-Aid from the Asahi Glass Foundation for Industrial Technology.

References

1) M. Koizumi, S. Kato, N. Mataga, T. Matsuura, and Y. Usui, "Photosensitized Reactions," Kagaku Dojin, Kyoto (1978).

2) H. Sakurai and C. Pac, "Kozokan Hanno (Photosensitized Reactions)," in *Kagaku Sosetsu* No. 33, ed by the Chemical Society of Japan, The Scientific Societies Press, Tokyo (1982), p. 75.

3) J. Saltiel and D. E. Townsend, *J. Am. Chem. Soc.*, **95**, 6140 (1973).

4) R. O. Campbell and R. S. H. Liu, *Mol. Photochem.*, **6**, 207 (1974).

5) Y. Inoue, S. Takamuku, Y. Kunitomi, and H. Sakurai, *J. Chem. Soc., Perkin Trans. 2*, **1980**, 1672.

6) S. Goto, S. Takamuku, and H. Sakurai, *J. Chem. Soc., Perkin Trans. 2*, **1980**, 1678.

7) Preliminary report; Y. Miyazawa, R. Hasegawa, E. Tobita, T. Furihata, T. Sugiyama, and A. Sugimori, *Chem. Lett.*, **1977**, 1155.

8) T. Sugiyama, T. Furihata, K. Takagi, M. Sato, S. Akiyama, G. P. Satô, and A. Sugimori, *Bull. Chem. Soc. Jpn.*, **54**, 3785 (1981).

 © 1983 The Chemical Society of Japan Bull. Chem. Soc. Jpn., 56, 1822—1825 (1983)

NAD(P)$^+$-NAD(P)H Model. 43. Formation of 1,4-Dihydronicotinamide in the Reaction of Pyridinium Salt and Glyceraldehyde

Atsuyoshi Ohno,* Satoshi Ushida, and Shinzaburo Oka
Institute for Chemical Research, Kyoto University, Uji, Kyoto 611
(Received January 26, 1983)

It has been found that *N*-substituted 1,4-dihydronicotinamides are produced by the reaction of *N*-substituted 3-carbamoylpyridinium salts with glyceraldehyde and its analogous compounds. A mechanism of the reaction is suggested.

The reduced and oxidized forms of nicotinamide adenine dinucleotide act as redox reagents in biological reactions. The reactions have been accepted with great interest because of a variety of excellent features promised by enzymes and have prompted organic chemists to design model reactions. As one of typical model compounds for NAD$^+$ and NADH, 1-benzyl-3-carbamoylpyridinium salt (BNA$^+$) and 1-benzyl-1,4-dihydronicotinamide (BNAH) have widely been used.

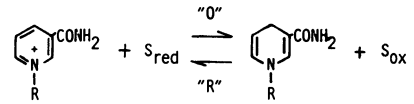

NAD$^+$: R = RPPA NADH : R = RPPA

BNA$^+$: R = CH_2Ph BNAH : R = CH_2Ph

(RPPA represents the dinucleotide residue of NAD$^+$)

As to the reaction of "R" direction many kinds of model reactions have been achieved and valuable insights have been accumulated.[1] However, its reverse reaction, that is, the reduction of pyridinium salt to 1,4-dihydropyridine[2] as a model reaction of "O" direction has not so widely been investigated despite the redox reactions between NAD$^+$ and NADH are reversible in biological systems. This makes it difficult to establish a cyclic reaction system where an NADH model is catalytically used.[3]

For the preparation of BNAH from BNA$^+$ sodium dithionite is an effective and exclusive reductant from the view points of the yield and selectivity toward 1,4-dihydropyridine derivative over its 1,6-isomer. On the other hand, the reducion with sodium borohydride produces large amounts of 1,6-dihydropyridine and tetrahydropyridine derivatives as well as the desired product. The use of other reductants such as sodium cyanoborohydride[4] and formic acid[5] the 1,4-selectivity does not afford good results, neither.

As a model for alcohol dehydrogenases, reduction of pyridinium salt by alkoxides[6] and alcohol[7] has been reported, although the results are not satisfactory. Deazaflavin[8] and 3-hydroxymethylacridinium iodide[9] that have partial structures similar to NAD$^+$ can be reduced by alcohol easily and various excellent reactions including cyclic reaction systems are reported. However, these systems are hardly be regarded as suitable models for NAD$^+$. From this standpoint it is desired to establish more efficient system for "O" directed reaction using, especially, organic compounds as reductants.

It is well known that glyceraldehyde 3-phosphate dehydrogenase (GAPDH) catalyzes the reduction of NAD$^+$ by glyceraldehyde 3-phosphate (**1**) coupled with oxidative phosphorylation of **1**.[10] The model reaction of this enzyme has not been reported yet. Previously it was reported that glyceraldehyde (**2**) reacts with NAD$^+$ to form a product which has a UV-absorption at 340 nm, similarly to NADH. The product, however, had no ability as the reduced coenzyme.[11] This product was thought to be an adduct of NAD$^+$ and **2** containing a 1,4-dihydropyridine moiety. When we tried the reaction of the same type using BNA$^+$ and **2**, reduced product, BNAH, was obtained in addition to such an adduct.[12] We will describe herein the details of the reaction as well as the reaction mechanism.

Results and Discussion

A borate-buffered solution of BNA$^+$ and **2** was refluxed in the presence of chloroform. The color of the aqueous layer turned yellow. At the same time reduced product with a UV-absorption at 355 nm was extracted to the organic layer. The product was ascertained to be BNAH by comparison of its NMR spectrum with that of the authentic sample. It was also confirmed that the extracted product was almost pure *N*-substituted 1,4-dihydronicotinamide contaminated by less than 3% of its 1,6-isomer. No other product was detected. The results are summarized in Table 1.

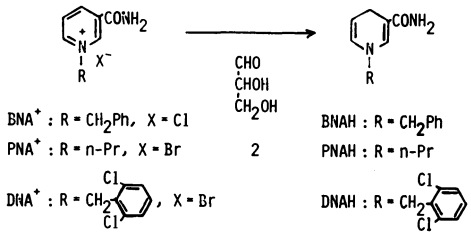

The reduction must be carried out under alkaline conditions. Though the rate of the reaction increased at elevated pH's, the yield of BNAH was not improved appreciably. The yield was also independent of the presence or absence of air and light.

Limitation of structure for the reductant was examined. Sugars such as D-ribose and D-glucose, simple aldehydes such as formaldehyde, acetaldehyde, and glyoxal exerted no ability for the reaction of BNA$^+$. Since α-ketols are known to be good reducing agents for flavins,[13] they might be promising candidates for the

Table 1. Reduction of pyridinium salts[a)]

Pyridinium salt[b)]	α-Ketol[b)]	pH	Reaction time/h	Yield of 1,4-dihydronicotinamide/%[c)]
BNA+[d)]	**3**	9.3— 9.5	18	22
BNA+	**2**	8.5— 8.7	30	22
BNA+	**2**	9.3— 9.5	18	21 (15)
BNA+	**2**	9.9—10.0	18	17 (11)
BNA+	**2**	11.4—11.5	10	8
PNA+	**2**	9.3— 9.5	18	(7)
BNA+	**3**	9.3— 9.5	18	21 (17)
DNA+	**3**	9.3— 9.5	3	(19)
BNA+	**4**	9.3— 9.5	18	22 (17)
DNA+	**5**	9.3— 9.5	18	(14)
BNA+	**6**	9.3— 9.5	14	25
BNA+	**7**[e)]	9.1— 9.2	3 d	(4)

a) In 0.05 M $Na_2B_4O_7$ in the presence of chloroform at its reflux temperature. b) 0.01 M. c) Yields based on pyridinium salt were determined by the intensity of an absorbance at 355 nm (ε=6100 for BNAH). Values in parentheses indicate the yields measured on an NMR spectrometer using *p*-nitrotoluene as an internal standard. d) Reaction under nitrogen in the dark. e) 0.05 M.

present reduction. As shown in Table 1, glycolaldehyde (**3**), dihydroxyacetone (**4**), 2-hydroxypropanal (**5**), acetol (**6**), and L-ascorbic acid (**7**) were effective. On the other hand, acetoin, methyl lactate, lactamide, and lactic acid were not.

In order to confirm the origin of the hydrogen on the 4-position of produced BNAH, several reactions were undertaken using deuterated materials. First of all the reaction of BNA+ with **3** was carried out in D_2O and isotope contents in BNAH were found to be 100% on the 2-position, 35% on the 6-position, and 0% on the 4-position, respectively. Since the hydrogens on the 2- and 6-positions of BNA+ are replaced by protons from the solvent appreciably under the same conditions as that for the reaction described above except for the absence of **3**, there is no doubt that deuteriums in the BNAH produced were introduced before the reduction and the hydrogens on the 4-position came from somewhere else other than water.

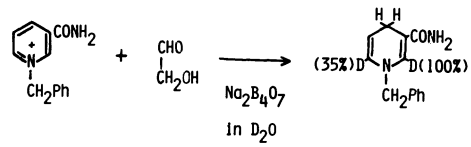

This result excludes the mechanism which, as suggested for the reduction of flavin,[14)] involves an electron-transfer process from the enediol derived from the corresponding α-ketol to the model. The isomerization of initially formed 1,6-isomer to the 1,4-derivative[15)] is also implausible.

Secondly, deuterated glycolaldehydes were employed. Three types of mono- or dideuterated compounds (**8**, **9**, and **10**) were synthesized and subjected to the reaction with BNA+. In any case, however, produced BNAH contained no deuterium so far as in the limitation of NMR spectroscopy.

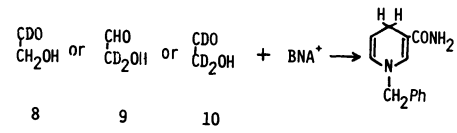

A suggested mechanism for the reduction of NAD+ catalyzed by GAPDH involves a Cannizzaro-type direct hydride transfer from the carbonyl carbon of **1** to the 4-position of NAD+, which is supported by the experiment using tritium labelled on the carbonyl carbon of **1**.[16)] On the other hand, in the present system neither direct hydrogen transfer nor introduction of a proton from water was observed and the oxidized product from **3** could not be detected in spite of our best efforts.

When BNA+ whose 4-position was deuterated (BNA+-*d*) was employed for the reaction with **3**, both hydrogens on the 4-position of BNAH were deuterated.

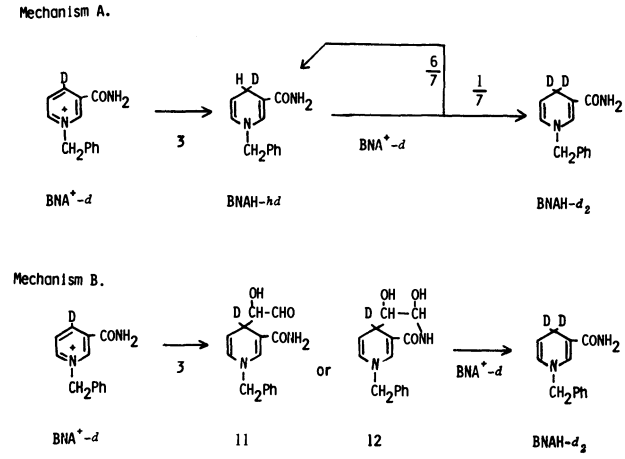

Scheme 1.

In order to account for the result that the origin of the deuterium is not other than that on the 4-position of BNA+-*d*, following two possibilities can be considered. One is a mechanism which involves a fast transhydrogenation between BNAH and BNA+ and the other is the one which involves a formation of an adduct containing a 1,4-dihydropyridine moiety and the adduct is the true reductant (Scheme 1). Mechanism A shown in Scheme 1 indicates that by transhydrogenation, which is a well known reaction,[17)] initially produced BNAH-*hd* reduces BNA+-*d* to afford BNAH-*hd* and BNAH-d_2 with the ratio of 6 to 1 because of the isotope effect of 6.[17)] If the reaction was fast enough to occur 10 times before the BNAH is extracted, BNAH-d_2 might be accumulated in 80% of total BNAH. However, the transhydrogenation is not so fast: when the solution of BNAH-*hd* is added to the aqueous solution of BNA+-*h* dropwise at the reflux temperature of chloroform recovered dihydropyridine in chloroform layer was BNAH-*hd*. If the transhydrogenation occured, BNAH-h_2 should be extracted from the reaction mixture.

This result leads us to the conclusion that the transhydrogenation shown by Mechanism A does not occur before the extraction of BNAH. Moreover, it is also to be referred that the extracted BNAH had no ability for the transhydrogenation: the fact was confirmed by

recovering 90% of BNAH-*hd* after the reflux of aqueous solution of BNA^+-*h* in the presence of a chloroform solution of BNAH-*hd* for 18 h under vigorous stirring.

Alternative mechanism that can explain the result is that the true reductant is an adduct of BNA^+ with **3** (Mechanism B). Burton and Kaplan already reported that, with **2**, **3**, **4**, and so on, NAD^+ forms adducts containing 1,4-dihydropyridine structure[11] and that the adduct has an ability to reduce potassium hexacyanoferrate(III),[18] although they did not isolate NADH from this reaction system.

The same type of adducts were afforded by the reaction of BNA^+ and **2**—**6**. During the reaction colored product with an absorption maximum at around 365 nm was formed in aqueous layer. This product which is not extracted to chloroform is expected to be 1,4-dihydropyridine derivative **11** or **12** as proposed by Burton and Kaplan. It was confirmed that this adduct reduced 1-methylacridinium iodide and BNA^+ in aqueous solution. From the reaction mixture BNAH was isolated by extraction with chloroform and remaining BNA^+ was precipitated as the salt of tetraphenylborate. A number of examples concerning such adducts of pyridinium salts with nucleophiles, especially with carbonyl compounds that have an α-hydrogen, are known.[2,19] It is reported that among them the adduct with pyruvate has an ability to reduce pyridinium salt.[20]

Table 2. Dependency of yields of BNAH on the concentrations of reactants[a]

$[BNA^+]$/M	[**2** or **3**]/M	Yield/%[b]
0.01	0.01(**2**)	21[c]
0.01	0.02(**2**)	20[c]
0.01	0.05(**2**)	17[c]
0.02	0.02(**2**)	24[c]
0.05	0.05(**2**)	26[c]
0.01	0.01(**3**)	22[d]
0.02	0.01(**3**)	29[d]
0.05	0.01(**3**)	37[d]
0.10	0.01(**3**)	45[d]

a) The reaction was carried out in 0.05 M $Na_2B_4O_7$ in the presence of chloroform at its reflux temperature. b) Determined by the intensity of an absorbance at 355 nm. c) Based on BNA^+. d) Based on **3**.

According to the Mechanism B, the yield of the BNAH might increase to 50% when equimolar BNA^+ and **2** are used. However, the yield was not so high as expected as listed in Table 1 because decomposition of the adduct in aqueous media competes with its oxidation. Table 2 shows that the yield of BNAH based on **3** increases as the increase in the concentration of BNA^+. On the other hand, the increase in the concentration of **2** exerts no effect toward the yield. The reaction in relatively concentrated solution affords BNAH in slightly high yield. These results are consistent with the idea that the transhydrogenation from the adduct to BNA^+ is slow enough to compete with its degradation.

In conclusion, by the reaction of BNA^+ with glyceraldehyde or its analogues, BNAH is produced with a high 1,4-selectivity. The mechanism is, however, different from that suggested for the reaction catalyzed by GAPDH.

Experimental

Instruments. UV and NMR spectra were obtained on a Union Giken SM-401 and a JEOL JNMFX-100, respectively.

Materials. BNA^+, PNA^+, and DNA^+ were prepared by quarterization of nicotinamide with benzyl chloride, propyl bromide, and 2,6-dichlorobenzyl bromide, respectively.

BNA^+-*d* was prepared from BNA^+ by twice repetition of reduction with sodium dithionite in D_2O and oxidation by Malachite Green.[21] Deuterium content in BNA^+ was 91± 1%.

2-Hydroxypropanal was synthesized by the condensation of dithiane and acetaldehyde followed by the dethioacetalization with mercury(II) chloride and mercury(II) oxide.[22]

Deuterated glycolaldehydes were prepared by the condensation of 1,3-dithiane and formaldehyde by an appropriate combination of deuterated materials (perdeuterioparaformaldehyde from Merck Inc. and 1,3-dithiane-2,2-d_2 synthesized by three times proton exchange using butyl lithium and D_2O), followed by dethioacetalization with mecury(II) chloride and mercury(II) oxide.

Reaction of BNA^+ and **2**. *A Typical Procedure*: BNA^+ (50 mg) and **2** (16 mg) were dissolved in 20 cm^3 of 0.05 M aqueous solution (1 M = 1 mol dm^{-3}) of sodium tetraborate. The solution was heated in the presence of 20 cm^3 of chloroform at its reflux temperature. After confirming that the intensity of the absorption of extracted BNAH in the organic layer did not increase any more, the chloroform layer was separated, dried over anhydrous sodium sulfate and evaporated to afford the reduced product. The product was identified as BNAH on an NMR spectrometer and the yield of BNAH was measured on a UV-spectrometer by means of absorbance of the chloroform solution at 355 nm(ε=6100)and/or on an NMR spectrometer using *p*-nitrotoluene as an internal standard.

^1H NMR ($CDCl_3$, δ from TMS): 3.16 (m, 2H), 4.25 (s, 2H), 4.75 (dt, 1H), 5.75 (m, 1H), 5.59 (bs, 2H), 7.16 (s, 1H), and 7.28 (s, 5H). The amount of 1,6-isomer measured on the NMR signal from benzyl proton at δ=4.19 was less than 3%.

Reaction of BNA^+-d and **3**. The reaction was carried out in a similar manner as described above. The NMR spectrum of the reduced product was identical with that of BNAH-d_2. No signal for the hydrogen on the 4-position (δ=3.16) was observed and the splitting of the signal for the hydrogen on the 5-position due to the hydrogens on the 4-position disappeared.

Reactivity of the Adduct. The reaction of BNA^+ (50 mg) and **3** (12 mg) was carried out and stopped after an appropriate reaction time. From the aqueous layer BNAH was removed by extraction and remaining BNA^+ was removed as a precipitate of tetraphenylborate. The solution exerted a UV-absorption at around 365 nm which disappeared quantitatively by the addition of 1-methylacridinium iodide. To the aqueous layer, BNA^+ (50 mg) was added again and further reduction was undergone as described above in the typical procedure. BNAH was extracted to the chloroform layer about half amount as compared with the case without interruption.

References

1) R. J. Kill and D. A. Widdowson in "Bioorganic Chemistry," ed by E. E. van Tamelen, Academic Press Inc., New York, N. Y. (1978), Vol. 4, pp. 239—275.

2) D. M. Stout and A. I. Meyers, *Chem. Rev.*, **82**, 223 (1982).

3) Only one example is reported; K. Nakamura, A. Ohno, S. Yasui, and S. Oka, *Tetrahedron Lett.*, **1978**, 4815.
4) Unpublished result from our laboratory (1982).
5) Y. Ohnishi and S. Tanimoto, *Tetrahedron Lett.*, **1977**, 1909.
6) A. Shirra and C. J. Suckling, *Tetrahedron Lett.*, **1975**, 3323; *J. Chem. Soc., Perkin Trans. 2*, **1977**, 759; Y. Ohnishi and M. Kitami, *Tetrahedron Lett.*, **1978**, 4035.
7) K. Wallenfels and W. Hanstein, *Angew. Chem., Int. Ed. Engl.*, **4**, 869 (1965).
8) F. Yoneda, Y. Sakuma, and P. Hemmerich, *J. Chem. Soc., Chem. Commun.*, **1977**, 825.
9) S. Shinkai, H. Hamada, H. Kuroda, and O. Manabe, *Chem. Lett.*, **1980**, 1235.
10) J. I. Harris and M. Waters, in "The Enzymes," 3rd ed, ed by P. D. Boyer, Academic Press Inc., New York, N. Y. (1975), Vol. 13, pp. 1—49.
11) R. M. Burton and N. O. Kaplan, *J. Biol. Chem.*, **206**, 283 (1954).
12) A. Ohno, S. Ushida, and S. Oka, *Tetrahedron Lett.*, **23**, 2487 (1982).
13) J. A. Rynd and M. J. Gibian, *Biochem. Biophys. Res. Commun.*, **41**, 1097 (1970).
14) S. Shinkai, T. Kunitake, and T. C. Bruice, *J. Am. Chem. Soc.*, **96**, 7140 (1974).
15) H. Minato, T. Ito, and M. Kobayashi, *Chem. Lett.*, **1977**, 13.
16) W. S. Allison, H. B. White, III, and M. J. Connors, *Biochemistry*, **10**, 2290 (1971).
17) P. van Eikeren and D. L. Grier, *J. Am. Chem. Soc.*, **99**, 8057 (1977).
18) R. M. Burton, A. san Pietro, and N. O. Kaplan, *Arch. Biochem. Biophys.*, **70**, 87 (1957).
19) U. Eisner and J. Kuthan, *Chem. Rev.*, **72**, 1 (1972).
20) G. Di Sabato, *Biochemistry*, **9**, 4594 (1970).
21) D. Mauzerall and F. H. Westheimer, *J. Am. Chem. Soc.*, **77**, 2261 (1955).
22) E. J. Corey and B. W. Erickson, *J. Org. Chem.*, **36**, 3553 (1971).

Methylation of Deoxynucleotides with Trimethyl Phosphate in Aqueous Phase

Toshizumi TANABE, Kiyoshi YAMAUCHI,* and Masayoshi KINOSHITA
Department of Applied Chemistry, Osaka City University, Sumiyoshi-ku, Osaka 558
(Received February 3, 1983)

Action of trimethyl phosphate on thymidine 5′-phosphate, deoxycytidine 5′-phosphate, deoxyadenosine 5′-phosphate, and deoxyguanosine 5′-phosphate at 37—60 °C, and pH 7—10 gave their methyl esters and base-methylated derivatives. Esterification took place in all deoxyribonucleotides to the almost same extent and its rate was enhanced by the reaction temperature, while being independent of pH in the range 7—10. On the other hand, methylation of the base moieties was affected by both the reaction temperature and pH of the reaction medium. The reactivity order of the four kinds of base moieties w s; at pH 7, cytosine base (N-3)>guanine base (N-7)>adenine base (N-1)≫thymine base (N-3); at pH 10, thymine base (N-3)>guanine base (N-1>N-7)>cytosine base (N-3)>adenine base (N-1).

A wide variety of methylated nucleosides have been found in nucleic acids, especially in the 5′-terminal of mRNA[1] and the loop regions of tTNA.[2] The biological roles of the modified nucleic acid-regions have been discussed with respect to the special structures. On the other hand, factitious alkylation of nucleic acids, especially DNA, by means of alkylating agents has been considered an origin of mutagenic effects since the alkylation may furnish the modified nucleotide units which will no longer be capable of performing the normal biological functions.[3] In this context, alkylations of nucleic acids have been studied using various reagents in order to relate the sites and extents of alkylation with mutagenesis.[4-7] The reactions, however, were conducted in a heterogeneous mixture of water and organic solvents mainly because of water-insoluble and -labile properties of the alkylating agents used. We, therefore, employed recently trimethyl phosphate (TMP) as a water-soluble methylating agent, and estimated the reactivity of nucleic acid-bases and nucleosides.[8-11] This paper deals with the study of an action of TMP toward four principal 5′-deoxyribonucleotides (**1**, **5**, **11**, and **16**). Although these monoalkyl phosphates are not the best models for nucleic acids, it was hoped that the study would furnish information about base-methylation and esterification which would be relevant to the methylation of nucleic acids. The reactivity of four deoxyribonucleotides will be also compared.

Results

The reactions were carried out at 37 and 60 °C by stirring a mixture of deoxynucleotide and TMP in water at an appropriate pH. The yields of the products were determined by a thin-layer chromatography (TLC)-UV method. The products were identified conveniently from the mobilities (R_f) in TLC, and spectral characteristics (UV and NMR), or the comparison of the physical constants with those of authentic samples or literature values. Generally, UV spectra were very useful to determine the sites of methylation in the base-rings. The results are summarized in Tables 1—4.

*Thymidine 5′-Phosphate (**1**).* A treatment of **1** with TMP resulted in the formation of three products

TABLE 1. METHYLATION OF THYMIDINE 5′-PHOSPHATE (**1**, pdT) WITH TRIMETHYL PHOSPHATE (TMP)[a]

Temp °C	pH	Product	R_f[b]	λ_{max}[c]/nm at pH 7	UV-yield/% 12 h	24 h	48 h	72 h
37	7	pdT methyl ester (**2**)	0.22	267.0	8	11	19	25
		3-Methyl-pdT (**3**)	0.39	266.0	0	2	2	4
37	8	**2**			7	12	18	21
		3			4	8	14	17
		3-Methyl-pdT methyl ester (**4**)	0.75	267.0	0	Tr[d]	6	12
37	9	**2**			6	8	10	10
		3			17	23	38	43
		4			3	5	13	21
37	10	**3**			50	73	72	63
		4			7	13	24	33
60	7	**2**			39	53	48	41
		3			6	6	4	2
		4			6	15	38	51
60	10	**3**			42	16	—	—
		4			53	78	—	—

a) Reaction size: pdT (0.05 mmol)–TMP (1.5 mmol)–H_2O (0.5 ml). b) These values were measured on cellulose TLC using 1-propanol–concentrated aqueous ammonia–water (7 : 1 : 2). R_f value of pdT was 0.06. c) UV spectra at pH 1 and pH 13 were identical with literature value. d) Tr refers to a trace yield.

Table 2. Methylation of deoxycytidine 5′-phosphate (**5**, pdC) with trimethyl phosphate (TMP)[a]

Temp °C	pH	Product	R_f[b]	λ_{max}[c] /nm at pH 7	UV-yield/% 24 h	48 h	72 h
37	7	pdC methyl ester (**6**)	0.45	271.0	8	13	17
		3-Methyl-pdC (**7**)	0.16	278.0	11	18	22
		3-Methyl-pdC methyl ester (**8**)	0.66	278.0	0	Tr[d]	6
37	10	**6**			11	19	14
		7			9	13	23
		8			Tr	4	7
60	7	**6**			4	6	5
		7			43	59	62
		8			0	15	22
		3-Methyl-pdU methyl ester[e] (**10**)	0.75	263.0	0	0	3
60	10	**6**			33	17	8
		7			5	Tr	0
		8			19	5	Tr
		3-Methyl-pdU[e] (**9**)	0.22	262.0	5	3	4
		10			24	66	83

a) Reaction size: pdC (0.05 mmol)–TMP (1.5 mmol)–H_2O (0.5 ml). b) These values were measured on cellulose TLC using 1-propanol–concentrated aqueous ammonia–water (7 : 1 : 2). R_f value of pdC was 0.09. c) UV spectra at pH 1 and pH 13 were identical with literature value. d) Tr refers to a trace yield. e) pdU refers to deoxyuridine 5′-phosphate.

Table 3. Methylation of deoxyadenosine 5′-phosphate (**11**, pdA) with trimethyl phosphate (TMP)[a]

Temp °C	pH	Product	R_f[b]	λ_{max}[c] /nm at pH 7	UV-yield/% 24 h	48 h	72 h
37	7	pdA methyl ester (**12**)	0.57	259.0	9	14	—
		N^6-Methyl-pdA (**13**)	0.31	267.0	Tr[d]	5	—
37	10	**12**			11	17	—
		13			0	5	—
		N^6-Methyl-pdA methyl ester (**14**)	0.76	266.0	0	1	—
60	7	**12**			41	43	31
		13			11	8	5
		14			8	22	46
		1-Methyl-pdA methyl ester (**15**)	0.19	258.0	Tr	11	12
60	10	**12**			42	12	10
		13			10	Tr	Tr
		14			31	76	85

a) Reaction size: pdA (0.05 mmol)–TMP (1.5 mmol)–H_2O (0.5 ml). b) These values were measured on cellulose TLC using 1-propanol–concentrated aqueous ammonia–water (7 : 1 : 2). R_f value of pdA was 0.19. c) UV spectra at pH 1 and pH 13 were identical with literature value. d) Tr refers to a trace yield.

(**2**, **3**, and **4**) (Table 1). By comparison of the mobilities in TLC and the UV spectra of the aqueous extracts of the spots with those of authentic samples, they were identified as thymidine 5′-(methyl hydrogenphosphate), 3-methylthymidine 5′-phosphate, and 3-methylthymidine 5′-methyl hydrogenphosphate, respectively. It appeared that TMP did not esterify the dialkyl phosphate (**2** and **4**) to afford the respective 5′-dimethyl phosphates. The N-3 methylation on the thymine ring was accelerated significantly with the increase of the pH value, while the esterification rate was almost independent of the pH (7—10). The increase in the reaction temperature was found to promote both the N-3 methylation and the esterification; *viz.* **1** was converted quantitatively into **4** after 24 h at 60 °C and pH 10.

Deoxycytidine 5′-Phosphate (5). A reaction of **5** with TMP in an aqueous solution afforded five UV-absorbing products (**6**, **7**, **8**, **9**, and **10**), of which **9** and **10** were observed only in the reaction at 60 °C (Table 2). Compound **6** was isolated and identified as deoxycytidine

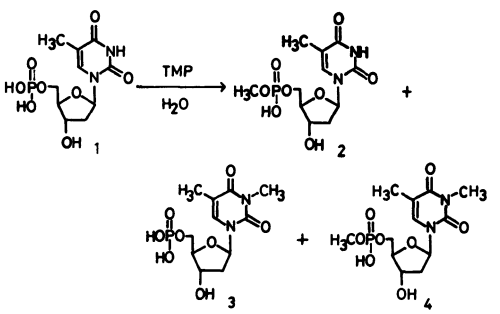

Fig. 1.

TABLE 4. METHYLATION OF DEOXYGUANOSINE 5′-PHOSPHATE (**16**, pdG) WITH TRIMETHYL PHOSPHATE (TMP)[a)]

Temp °C	pH	Product	R_f[b)]	λ_{max}[c)]/nm at pH 7	UV-yield/% 24 h	UV-yield/% 48 h
37	7	pdG methyl ester (**17**)	0.34	252.0 272.0[s)]	6	10
		7-Methyl-pdG (**18**)	0.13	258.0 281.0[s)]	5	6
		7-Methyl- pdG methyl ester (**19**)	0.40	257.0 282.0[s)]	0	2
		7-Methylguanine (**20**)	0.45	284.0	2	6
37	10	1-Methyl-pdG (**21**)	0.14	256.0 269.0[s)]	40	51
		Imidazole ring-opened 7-methyl-pdG (**22**)	0.10	275.0	7	3
		Imidazole ring-opened 1,7-dimethyl-pdG (**23**)	0.18	273.0	Tr[d)]	11
		Unknown A[e)]	0.24	274.0	4	2
		Unknown B[e)]	0.34	258—275	3	11

a) Reaction size: pdG (0.05 mmol)–TMP (1.5 mmol)–H_2O (0.5 ml). b) These values were measured on cellulose TLC using 1-propanol–concentrated aqueous ammonia–water (7 : 1 : 2). R_f value of pdG was 0.06. c) UV spectra of products **17**—**23** at pH 1 and 13 pH were identical with literature value. d) Tr refers to a trace yield. e) The yields of unknown products were determined by postulating their extinction coefficient at λ_{max} as 10000. s) Shoulder.

5′-methyl hydrogenphosphate through its physical properties. Products **7** and **8** were identified tentatively as 3-methyldeoxycytidine 5′-phosphate and its methyl ester, respectively, from their R_f values and UV spectra which were almost similar to those of 3-methyldeoxycytidine. Compounds **9** and **10** were identified as 3-methyldeoxyuridine 5′-phosphate and its methyl ester, respectively, by comparison of their R_f values and UV spectra with those of authentic samples which were prepared from the reaction of deoxyuridine 5′-phosphate with trimethylsulfonium hydroxide.[9)] The compound **9** may be originated from the hydrolysis of the 3-methylcytosine ring of **7**. Similarly, 3-methyldeoxycytidine 5′-(methyl hydrogenphosphate) may be the precursor of **10**, though it may be also produced by the secondary reaction of **9** with TMP.

The esterification of **5** was hardly affected by pH of the solution whereas the N-3 methylation of the cytosine ring was found to decrease slightly with the increase of pH. The increase in the reaction temperature promoted the esterification, the N-3 methylation, and the hydrolysis of **7**, and **8**.

*Deoxyadenosine 5′-Phosphate (**11**).* A treatment of **11** with TMP gave rise to four products (**12**—**15**) as observed in the TLC of the reaction mixture (Table 3). Compounds **12**, **13**, and **14** were identified as deoxyadenosine 5′-(methyl hydrogenphosphate), N^6-methyldeoxyadenosine 5′-phosphate, and N^6-methyldeoxyadenosine 5′-(methyl hydrogenphosphate), respectively, by comparison of R_f values and UV spectra with those of authentic samples. Furthermore, hydrolysis of **12**, and **14** with 1 M hydrochloric acid (1 M=1 mol dm^{-3}) gave adenine and N^6-methyladenine, respectively. Meanwhile, **15** was assigned tentatively 1-methyldeoxyadenosine 5′-(methyl hydrogenphosphate) from the UV spectra (pH 1, 7, and 12) which were very similar to those of 1-methyldeoxyadenosine. As expected, the R_f value was smaller than that of the nucleoside. It would be most likely that the N^6-methylated products (**13**, and **14**) were formed from the Dimroth rearrangement[12)] of the 1-methyl isomers rather than direct methylation at the exocyclic amino groups of the adenine ring, since the external amino group was not as strong in nucleophilicity as the N-1 atom. The esterification, and the N-1 methylation were found to be enhanced by the increase in the reaction temperature, while being almost independent on the pH of the solution.

*Deoxyguanosine 5′-Phosphate (**16**).* Action of TMP on **16** at pH 7 and 37 °C afforded deoxyguanosine 5′-

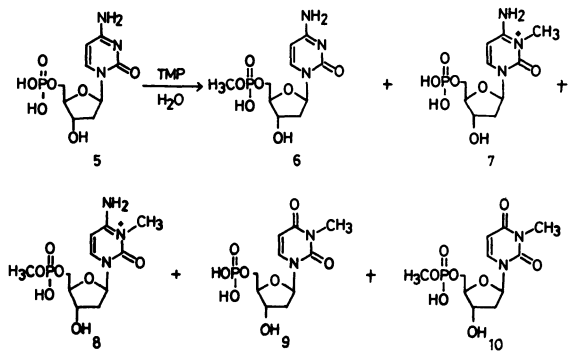

Fig. 2.

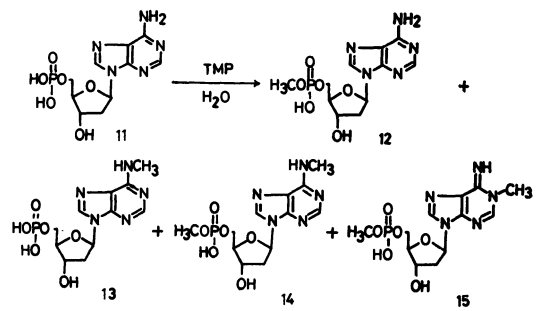

Fig. 3.

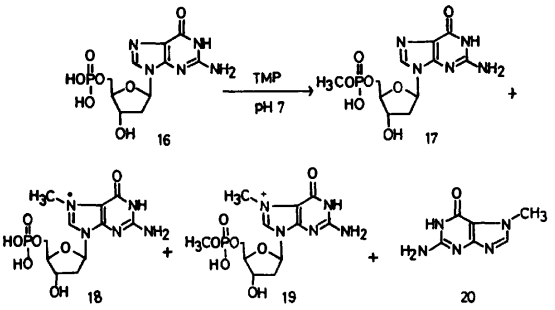

Fig. 4.

(methyl hydrogen phosphate) (**17**), 7-methyldeoxyguanosine 5′-phosphate (**18**), 7-methyldeoxyguanosine 5′-(methyl hydrogenphosphate) (**19**), and 7-methylguanine (**20**).

On the other hand, in the reaction at pH 10 and 37 °C, N-1 methylation took place in preference to both N-7 methylation and esterification, giving chiefly 1-methyldeoxyguanosine 5′-phosphate (**21**). The imidazole ring-opened compounds (**22** and **23**) might be produced by the attack of hydroxide ions at the C-8 position of the 7-methylguanine rings of the corresponding precursors (for instance, **18** for **22**). The reaction mixture also contained two unidentified compounds.

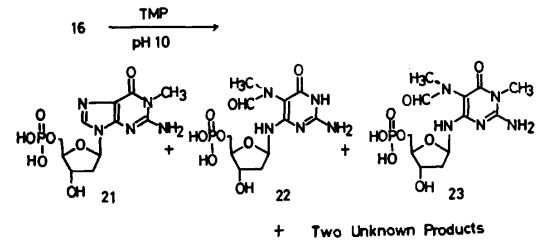

Fig. 5.

All the products other than **22**, and **23** were identified through the comparison of the UV spectra and R_f values with those of authentic samples. Methylation at the N-7 position of the guanine ring was easily acknowledged by the strong fluorescence under the UV light which was characteristic to 7-alkylated guanine ring. The identification of the compounds (**22** and **23**) was tentative, but they had the UV spectra similar to those of the corresponding nucleosides.[11]

Discussion

In a homogeneous aqueous phase TMP was found to methylate the four principal deoxynucleotides at the base moieties (base-methylation) and the phosphate moieties (esterification). As expected, the base methylation proceeded in a manner similar to that of the corresponding nucleosides. Thus, the N-3 of the cytosine ring of **5**, the N-1 of the adenine ring of **11** and the N-7 of the guanine ring of **16** were nucleophilic to be attacked easily by TMP, giving the corresponding products. The pH of the solutions had no effect on methylation at these sites except the N-3 of the cytosine ring which became less susceptive in methylation to the increasing pH. By contrast, the –CO–NH–CO– group of the thymine ring (N^3H) and the –CO–NH– group of the guanine ring (N^1H), which have low pK_a values (9—10), became increasingly active toward methylation with the increasing pH. The reactivity of the base moieties thus can be summarized as follows: pH 7, cytosine (N-3)> guanine (N-7)> adenine (N-1); pH 10, thymine (N-3)> guanine (N-1)> guanine (N-7)> cytosine (N-3).

On the other hand, the esterification was hardly affected by the pH but by temperature. Further, variation of the base moieties had no influence on the degree of esterification. Since the nucleotides are monoalkyl phosphates with pK_a of approximately 1 and 6.[13] TMP should attack the dianionic forms of the nucleotides, furnishing the monomethyl ester such as **2**, **6**, **12**, and **17**. Interestingly, the reagent did not methylate further the monomethyl esters to give the dimethyl esters; the results suggest that nucleic acids which are poly(dialkyl phosphates) may not be methylated by TMP at the internucleotide bonds.

Meanwhile, the 5′-phosphate moieties were found to affect the hydrolysis of the 3-methylcytosine ring to the 3-methyluracil ring, and the rearrangement of 1-methyladenine ring to the N^6-methyladenine ring. For instance,

(a) Under the conditions of pH 10, 37 °C, and 24 h, and TMP/substrate=30 mol/mol, 3-methyldeoxycytidine was hydrolyzed more readily than the nucleotides (**7** and **8**); *e.g.* the extent of total N^3-methylation[14] *vs.* that of the hydrolysis was 18% : 2% in the nucleoside,[8] and 17% : 0% in the 5′-nucleotide (Table 2).

(b) Under the conditions of pH 7, 60 °C, and 24 h, deoxyadenosine 5′-phosphate gave predominantly the N^6-methyl derivatives (**13**, and **14**) in the combined yields of *ca.* 19% (Table 3). By contrast, a treatment of deoxyadenosine with TMP under similar neutral conditions produced 1-methyl-, and N^6-methyldeoxyadenosines in the yields of 38%, and trace, respectively.[9]

Plausibly, the phosphate anionic moieties in **7** and **8** were somewhat effective to shield the C-4 positions of the 3-methylcytosine rings from the attack of OH^- ions, thus decreasing the extent of the hydrolysis. On the other hand, the Dimroth rearrangement, which has been considered to occur by the attack of OH^- ions on the C-2 position of the 1-methyladenine ring, might be

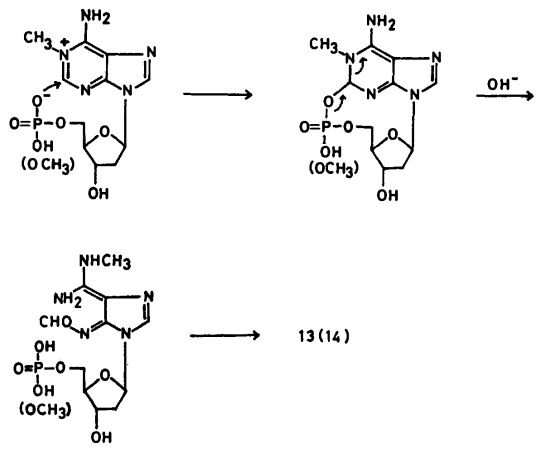

Scheme 1.

assisted by the 5'-phosphate moiety as depicted in the Scheme 1. Indeed, adenosine 2'(3')-phosphate reacted with TMP to give chiefly the 1-methyl derivatives under the conditions (pH 7 and 60 °C) which were the same as those used in the present study.

Dimethyl sulfate, methyl iodide and other S_N2 type reagents have also been reported[4,6,15] to alkylate the deoxynucleotides at the sites similar to those attacked by TMP though the extents of base-alkylation and esterification varied with the reagents used. Highly potent carcinogens, diazomethane and related compounds, have been known to alkylate not only the base nitrogen atoms but also the external oxygen atoms such as thymine ring (O-2 and O-4) and guanine ring (O-6) in addition to the phosphate moieties.[1] The moderate mutagenicity of TMP,[16] thus, may be ascirbed to the predominant methylation at nitrogen atoms, which, except methylation at the N-3 of the cytosine ring, may not disturb significantly the Watson-Crick base pairings.

Experimental

UV spectra were measured with a Hitachi 3T spectrometer. NMR spectra were recorded on a Hitachi Perkin-Elmer R-20 spectrometer, with a dilute solution in deuterioxide and the soldium salt of 3-(trimethylsilyl)propionic-2,2,3,3-d^4 acid as an internal standard. Thin-layer chromatography was performed on cellulose (13254, Eastman) or silica-gel (GF_{254} (type 60), Merck). Column chromatography was carried out using silicagel (Merck, Art. 7734, 70—230 mesh) or aluminium oxide Merck, Art. 1097 .

Commercially available disodium salts of thymidine 5'-phosphate (**1**), deoxyguanosine 5'-phosphate (**16**) and deoxyuridine 5'-phosphate, and the free form of deoxyadenosine 5'-phosphate (**11**) were used without further purification. Deoxycytidine 5'-phosphate (**5**) was prepared according to the procedure of Yoshikawa *et al.*[17] Trimethyl phosphate (TMP) was distilled prior to use.

Reactions of the nucleotides and ethereal diazomethane produced the following known methylated nucleotides,[4,6] which were used to identify the products obtained in the present study: **2**—**4**, **6**, **7**, **9**, **10**, **12**, **15**, **17**—**20**. Some authentic nucleotides were synthesized as follows. They were homogeneous in silica gel- and cellulose-TLC's with the same R_f values as those of known compounds, if any, and had UV spectra and NMR spectra which agreed with the assigned structures.

*Thymidine 5'-(Methyl Hydrogenphosphate) (**2**).* The condensation reaction of thymidine 5'-phosphate (**1**, 93 mg, 0.27 mmol) and methanol (0.25 ml) by dicyclohexylcarbodiimde (300 mg, 1.5 mmol) in pyridine (3.0 ml) at 30 °C for 24 h afforded **2**, which was purified through column chromatography and reprecipitation with diethyl ether (60 mg, 66%); NMR (D_2O) δ=1.94 (3H, d, 5-CH_3, J=1.2 Hz), 3.63 (3H, d, p-OCH_3, J=11 Hz), and 7.77 (1H, d, H^6, J=1.2 Hz); UV, λ_{max} (H_2O) 267.0 nm.

*3-Methylthymidine-5'-(Methyl Hydrogenphosphate) (**4**).* A mixture of **3** (60 mg, 0.2 mmol) and methanolic solution of 0.5 M trimethylsulfonium hydroxide (0.4 ml)[10] was concentrated to give a colorless residue, which was dissolved in DMF (3 ml) and heated at *ca.* 80 °C for 30 min with stirring magnetically. The solvent was evaporated from the reaction mixture, and the resulting residue was applied to a silica-gel column using 1-propanol–concentrated aqueous ammonia–water (7 : 1 : 2 v/v) as a solvent. The title compound was obtained as powder upon mixing the concentrated fraction with diethyl ether, 43 mg (71%), NMR (D_2O) δ=1.96 (3H, d, 5-CH_3, J=1.2 Hz), 3.32 (3H, s, N^3—CH_3), 3.63 (3H, d, p-OCH_3, J=11 Hz), and 7.80 (1H, d, H^6, J=1.2 Hz), UV λ_{max} (H_2O) 266.0 nm.

General Methylation Procedure of Deoxyribonucleotide and TMP. A deoxynucleotide (0.05 mmol) was dissolved in water (0.5 ml) of appropriate pH (7—10), and the solution was treated with TMP (1.5 mmol) at 37 or 60 °C. The pH of the reaction mixture was maintained within $\pm$0.5 unit by the occasional addition of 0.5 M sodium hydroxide throughout the reaction. At an appropriate reaction time, 6 μl of reaction mixture was spotted on a cellulose TLC and developed immediately. The product on each spot was scraped from the plate and extracted with 3 ml of water. The yield of each product was calculated by means of a procedure similar to that mentioned in a previous paper,[10] the result of which is summarized in Tables 1—4. The structure of each product was determined mainly by the comparison of its R_f value and UV spectrum with those of the authentic sample.

Methyl ester of deoxycytidine 5'-phosphate (**6**) was isolated from the reaction mixture as follows. After 50-h stirring of a mixture of disodium salt of deoxycytidine 5'-phosphate (**5**, 350 mg, 1.0 mmol) and TMP (4.25 g, 30.0 mmol) in water (10 ml) at 60 °C, pH 7, TMP was removed by extraction with chloroform. The aqueous layer was concentrated to give a residue, which was subjected to alumina column chromatography (1.5×50 cm). Elution with 1-propanol–concentrated aqueous ammonia–water (7 : 1 : 2) afforded **6** (34 mg, 10%); NMR (D_2O) δ=3.67 (3H, d, p-OCH_3, J=11 Hz), 6.22 (1H, d, H^5, J=8 Hz), and 8.07 (1H, d, H^6, J=8 Hz),

Products from the reaction mixture of deoxyadenosine 5'-phosphate (**11**) with TMP were further analyzed through the isolation and subsequent acid hydrolysis as follows. Each product in the reaction mixture was separated by silica-gel column (1.5×15 cm) which was eluted with 1-propanol–water (3 : 1). Subsequently, each product was hydrolyzed by 1 M hydrochloric acid at 90 °C for 3 h. Adenine was obtained near quantitatively from **12**, and N^6-methyladenine from **13** and **14**, and 1-methyladenine from **15**. The products were identified by UV spectra and comparison of R_f values with those of the authentic sample using several solvent systems.

References

1) H. Busch, *Perspect. Biol. Mid.*, **19**, 549 (1976).
2) J. A. McCloskey and S. Nishimura, *Acc. Chem. Res.*, **10**, 403 (1977).
3) B. Singer, "Molecular and Cellular Mechanisms of Mutagenesis," ed by J. F. Lemontt and R. M. Generoso, Plenum Press, New York, (1981); B. Singer, "Progress in Nucleic Acid Research and Molecular Biology," ed by W. E. Cohn, Academic Press, New York, (1975), Vol. 15, p. 219.
4) J. A. Haines, C. B. Reese, and L. Todd, *J. Chem. Soc.*, **1964**, 1406.
5) B. E. Griffin and C. B. Reese, *Biochim. Biophys. Acta*, **68**, 185 (1963); P. Brookes and P. D. Lawley, *J. Chem. Soc.*, **1960**, 539; J. W. Jones and R. K. Robins, *J. Am. Chem. Soc.*, **85**, 193 (1963).
6) B. Singer, *Biochemistry*, **14**, 4353 (1975).
7) B. Singer, *Biochemistry*, **11**, 3939 (1972); J. T. Kusmierek and B. Singer, *ibid.*, **21**, 5717 (1982).
8) T. Tanabe, K. Yamauchi, and M. Kinoshita, *Bull. Chem. Soc. Jpn.*, **52**, 204 (1979).
9) T. Tanabe, K. Yamauchi, and M. Kinoshita, *Bull. Chem. Soc. Jpn.*, **52**, 3121 (1979).
10) K. Yamauchi, T. Tanabe, and M. Kinoshita, *J. Org. Chem.*, **44**, 638 (1979); **41**, 3691 (1976).

11) K. Yamauchi and M. Kinoshita, *J. Chem. Soc., Perkin Trans. I*, **1978**, 762.
12) D. J. Brown, "Mechanisms of Molecular Migrations," ed by B. S. Thyagarajan, Interscience, New York, N. Y. (1968), p. 209.
13) D. O. Jordan, *Nucl. Acids*, **1**, 459 (1955).
14) Total N^3-methylation=combined yields of the 3-methylcytosine derivatives and 3-methyluracil derivatives.
15) P. Brookes and P. D. Lawley, *J. Chem. Soc.*, **1961**, 3923; H-J. Rhaese and E. Freese, *Biochem. Biophys. Acta*, **190**, 418 (1969); K. K. Ogilvie, S. L. Beaucage, and M. F. Gillen, *Tetrahedron Lett.*, **1978**, 1663. Alkylating characteristics of various reagents are described in Ref. 3.
16) T. H. Conner, *Mutat. Res.*, **65**, 121 (1979); S. S. Epstein, W. Bass, E. Arnold, and Y. Bishop, *Science*, **168**, 584 (1970).
17) M. Yoshikawa, T. Kato, and T. Takanishi, *Tetrahedron Lett.*, **1967**, 5065.

Manufacture of Pure Titanium(IV) Oxide by the Chloride Process. II. Selective Extraction of Titanium(IV) and Iron(III) from Hydrochloric Acid Leach Liquor of Ilmenite Ore by Tributyl Phosphate

Eiichi NARITA,* Hitoshi TAKEUCHI, Hitoshi ICHIKAWA,
Takao ODAGAWA, and Taijiro OKABE
Department of Applied Chemistry, Faculty of Engineering, Tohoku University, Aramaki, Sendai 980

(Received July 29, 1982)

The selective recoveries of titanium(IV) and iron(III) from the synthetic hydrochloric acid leach liquor of ilmenite, *i.e.*, 1.8—11 M (1 M = 1 mol dm^{-3}) hydrochloric acid solutions containing 0.25—0.57 M titanium(IV) and 0.27—0.29 M iron(III), or each single metal ion, were investigated by solvent extraction with benzene solutions of various tributyl phosphate (TBP) concentrations under the volume ratio (Org/Aq) of unity at 25 °C. Iron(III) was extracted into the TBP phase over a wide concentration range of hydrochloric acid studied, and the extraction was considerably accelerated by the salting-out effect of the coexisting titanium(IV). Since no extraction of titanium(IV) was observed at hydrochloric acid concentrations lower than 6 M, iron(III) could be recovered selectively from 3—6 M hydrochloric acid solutions under the conditions of the molar ratio $[TBP]_{org}/[Fe(III)]_{init\ aq} \leqq 3.0$. On the other hand, titanium(IV) in the residual aqueous phase was also extracted as $TiCl_4 \cdot 3TBP$ at a concentration range of chloride ion higher than 7 M. The coextractions of other metal ions and free hydrochloric acid could be prevented by controlling the TBP concentration in the organic phase as $[TBP]_{org}/[Ti(IV)]_{init\ aq} \leqq 3.5$. The problem in applying the solvent extraction technique to actual leach liquor is discussed, as well as the recovery of free hydrochloric acid from the residual leach liquor.

Although titanium(IV) oxide has been produced industrially by the sulfate process and by the vapor phase oxidation of titanium(IV) tetrachloride, both processes have serious disadvantages, such as the treatments of byproducts in the former and the lack of raw rutile minerals in the latter.[1,2] The authors have endeavored to develop a new manufacturing process for titanium(IV) oxide, which would be based on the leaching of ilmenite ore in concentrated hydrochloric acid solution and the selective recovery of titanium(IV) from the resulting leach liquor by solvent extraction with neutral organophosphorus compounds. In this process ilmenite ore, which occurs abundantly in nature, can be used. One other important feature is that the hydrochloric acid used as the leachant allows easier recovery of reusable acid from the waste solution than does sulfuric acid. Therefore, the manufacturing process that we have proposed may solve the serious disadvantages of most methods for the production of titanium(IV) oxide. It is well known that the dissolution of titanium and iron in ilmenite ore can be achieved satisfactorily by using concentrated hydrochloric acid solution over a temperature range of 70—90 °C.[3-5]

A solvent extraction technique has been applied extensively to a hydrometallurgical process not only of highly valuable metals but of nonferrous metals such as Cu, Ni, and Co[6-8] and is becoming more and more common, even for the extraction of iron from the waste solution of steel cleansing,[9] the acid leach liquor of clay,[10] and the waste solution of the sulfate process of titanium(IV) oxide production[11,12] because of the higher selectivity of the solvent extraction operation. For the production of titanium(IV) oxide by leaching ilmenite ore in hydrochloric acid, the preferential removal of iron from the resulting leach liquor has been attempted using trialkyl phosphates,[13] trialkylamines,[13] and organic ketones,[14] However, no attempt has been made to extract titanium(IV) from the leach liquor by solvent extraction with neutral organophosphorus compounds, although several reports concerning solvent extraction of iron(III)[15,16] and titanium(IV)[17-21] with tributyl phosphate (TBP) have been published.

This paper deals with the selective recoveries of titanium(IV) and iron(III) from the synthetic hydrochloric acid leach liquor of ilmenite ore by solvent extraction with TBP in benzene under practical conditions in which the concentrations of metal ions and acid in the leach liquor are sufficiently high.

Experimental

Reagents. All the reagents were of analytical reagent grade. Synthetic hydrochloric acid leach liquor was prepared by dissolving titanium(IV) chloride and/or iron(III) chloride in hydrochloric acid solution. In one part of the experiment, other metal ions incorporated generally to ilmenite ore were also dissolved in the synthetic leach liquor. Since no differences between the extraction results using the commercial and purified TBP were observed, TBP was used without further purification.

Procedure. A 20 cm^3 portion of the hydrochloric acid leach liquor containing known amounts of metal ions was transferred to a 100 cm^3 pear shaped separatory funnel, together with 20 cm^3 portions of benzene solution of various TBP concentration. The extraction was carried out by shaking it vigorously for 10 min at 25 °C, and then leaving it until the phases separated clearly. The metal ions in the aqueous phase were analyzed by colorimetry and atomic absorption spectroscopy. The percentage extractions and distribution coefficients of the metals were calculated from the metal concentrations in the aqueous phase before and after the extraction. In one part of the experiment, the extraction behaviors of acid and chloride ion were also investigated by neutralization and the Volhard method, respectively.

Results and Discussion

Recovery of Iron. The extraction behavior of iron(III) and iron(II) in the presence of titanium(IV) as a function of the initial concentration of hydrochloric

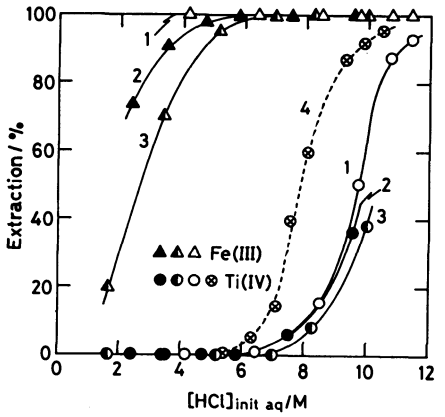

Fig. 1. Extraction of Fe(III) and Ti(IV) *vs.* concentration of HCl in aqueous phase.
1: 0.29 M Fe(III)+0.55 M Ti(IV), 1.8 M TBP, 2: 0.29 M Fe(III) +0.55 M Ti(IV), 0.92 M TBP, 3: 0.29 M Fe(III)+0.29 M Ti(IV), 0.92 M TBP, 4: 0.55 M Ti(IV), 1.8 M TBP.

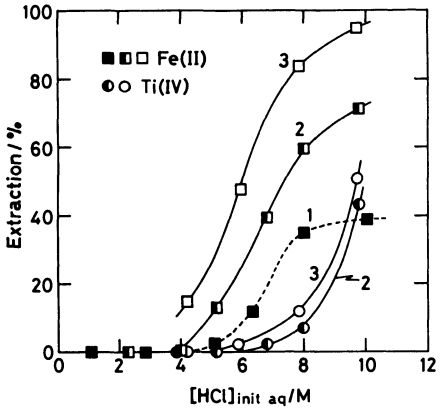

Fig. 2. Extraction of Fe(II) and Ti(IV) *vs.* concentration of HCl in aqueous phase.
1: 0.28 M Fe(II), 2: 0.28 M Fe(II)+0.26 M Ti(IV), 3: 0.28 M Fe(II)+0.57 M Ti(IV), 1, 2, 3: 0.92 M TBP.

acid is shown in Figs. 1 and 2, respectively. The percentage extraction of iron(III) was increased with increasing concentration of hydrochloric acid in the aqueous phase and TBP in the organic phase. Another important feature is that the coexisting titanium(IV) accelerated the extraction of iron(III) by the salting-out effect. Although similar behavior was observed in the extraction of iron(II), the percentage extraction was much lower than that of iron(III). Since the selective recovery of iron(II) was difficult, as can be seen in Fig. 2, iron(II) should be oxidized to iron(III) before applying solvent extraction. Titanium(IV) and minor constituents of ilmenite ore such as manganese(II), aluminum(III), magnesium(II), and chromium(III) were not extracted along with iron(III) from the leach liquor at hydrochloric acid concentrations lower than 6 M. Therefore, it was concluded that the selective recovery of iron from 3—6 M hydrochloric acid leach liquor was possible by solvent extraction with TBP after the oxidation of all iron(II) to iron(III).

The concentration of TBP in organic phase is an important factor in extracting iron(III) without contamination by titanium(IV). Figure 3 shows the plots of log D, distribution coefficient, *versus* log $[TBP]_{org}/[Fe(III)+Ti(IV)]_{init\ aq}$. As expected from Fig. 1, the selectivity, $\beta=D_{(Fe)III}/D_{Ti(IV)}$, was low at high concentrations of hydrochloric acid in aqueous phase because of the coextraction of titanium(IV). At hydrochloric acid concentrations lower than 6 M, β became as high as 1×10^3—1×10^4. The purity of the extracting iron(III) could be increased by controlling TBP concentration in the organic phase as $[TBP]_{org}/[Fe(III)]_{init\ aq} \leqq 3.0$, which was obtained from the result in Fig. 3. Islam *et al.*[22] have reported that the reverse selectivity, $\beta'=D_{Ti(IV)}/D_{Fe(III)}$, by solvent extraction with bis(2-ethylhexyl) hydrogenphosphate (B2EHP) was about 60. For the mutual separation of titanium(IV) and iron(III), TBP was superior to B2EHP.

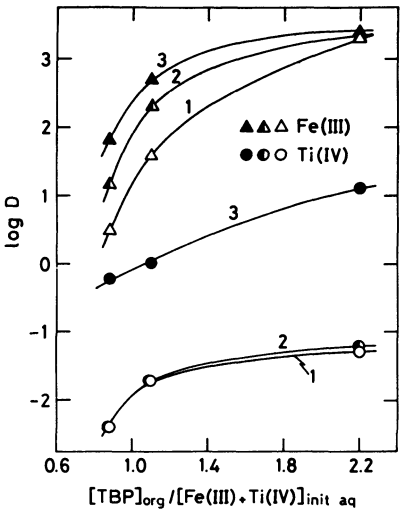

Fig. 3. Dependence of distribution ratios of Fe(III) and Ti(IV) on TBP concentration in organic phase.
1, 2, 3: 0.29 M Fe(III)+0.54 M Ti(IV), HCl(M)—1: 4.2, 2: 6.0, 3: 11.4.

Hydrochloric acid is extracted by an excess of TBP in organic phase.[23,24] The effect of the TBP concentration in the organic phase on the extraction of hydrochloric acid and iron(III) is shown in Fig. 4, which

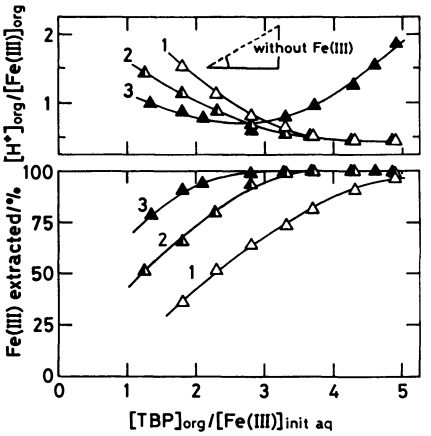

Fig. 4. Dependence of extraction of Fe(III) and acid on TBP concentration in organic phase.
1: 0.27 M Fe(III)+4.9 M HCl, 2: 0.27 M Fe(III)+6.1 M HCl, 3: 0.27 M Fe(III)+10.1 M HCl.

TABLE 1. THE EFFECT OF SALTS ADDED ON THE EXTRACTION OF Ti(IV) WITH 0.92 M TBP IN BENZENE

Concentration in initial solution		Extraction of Ti(IV)/%									
		[H+]/M					[Cl-]/M				
Ti(IV) M	Salt M	6	8	9	10	11	7	9	10	11	12
0.25	—	1	20	65	87	96	1	20	65	87	96
0.25	KCl 0.25	1	25	70	90	93	1	20	64	86	97
0.25	NaCl 0.25	2	27	73	90	92	1	21	66	87	96
0.25	$MgCl_2$ 0.34	4	47	92	93	98	1	18	68	87	97
0.25	$MnCl_2$ 0.27	1	23	74	88	94	1	17	62	83	94
0.25	$AlCl_3$ 0.33	6	63	83	94	99	2	17	63	83	96

gives the percentage extraction of iron(III) and the molar ratio of $[H^+]/[Fe(III)]$ in the organic phase in tests conducted for the leach liquor containing only iron(III). At 4.9—6.1 M acid concentration, the ratio of $[H^+]_{org}/[Fe(III)]_{org}$ decreased with increasing TBP concentration, whereas the percentage extraction of iron(III) increased. This result indicates that the competitive extractions of $FeCl_3$ and HCl would occur at moderate acid concentrations as follows:

$$n[HCl]_{aq} + [TBP]_{org} = [nHCl \cdot TBP]_{org} \quad n=1,2 \qquad (1)$$

$$[FeCl_3]_{aq} + 2[TBP]_{org} = [FeCl_3 \cdot 2TBP]_{org}. \qquad (2)$$

At 10.1 M acid concentration, the ratio of $[H^+]_{org}/[Fe(III)]_{org}$ were approximately constant as 0.75—1.0; which means that iron(III) is extracted mainly as $HFeCl_4$:

$$[H^+]_{aq} + [FeCl_4^-]_{aq} + 2[TBP]_{org} = [HFeCl_4 \cdot 2TBP]_{org}. \qquad (3)$$

Since the slopes of log $D_{Fe(III)}$/log TBP obtained from the results in Fig. 4 were 1.90—1.95, two extractive species of iron(III) such as $FeCl_3 \cdot 2TBP$ and $HFeCl_4 \cdot 2TBP$ have been postulated. On the other hand, the ratio of $[H^+]_{org}/[Fe(III)]_{org}$ became greater than unity under the conditions that the acid concentration was 10.1 M and the ratio of $[TBP]_{org}/[Fe(III)]_{init\ aq}$ was greater than 3.5. The dependence of the acid extraction behavior on the TBP concentration was approximately identical with that obtained without iron(III). Therefore, it is reasonable to assume that the extraction of free hydrochloric acid occurs at high TBP concentration as Eq. 1.

Recovery of Titanium. As shown in Fig. 1, the recovery of titanium(IV) can be performed by increasing the hydrochloric acid concentration in the residual aqueous phase and by extracting with fresh TBP in benzene. The shift of the extraction curve of titanium(IV) toward the low acid side by the removal of iron(III) makes it possible to extract titanium(IV) from the leach liquor at hydrochloric acid concentrations higher than 8 M.

The effect of various chlorides in the leach liquor on the extraction behavior of titanium(IV) is given in Table 1. The extraction of titanium(IV) was apparently accelerated in the presence of these chlorides judged from the same acid concentration, but not accelerated judged from the same chloride ion concentration. This was deduced by following the extraction curves based on the data in the left column in Table 1. This result indicates that these cations did not contribute to the salting-out effect. Under the conditions in which these experiments were conducted, all metal ions listed in Table 1 were not extracted. This result also indicates that the extraction of titanium(IV) will be accelerated by the addition of chlorides of magnesium(II) and aluminum(III) into the leach liquor of acid concentration range of 8—9 M.

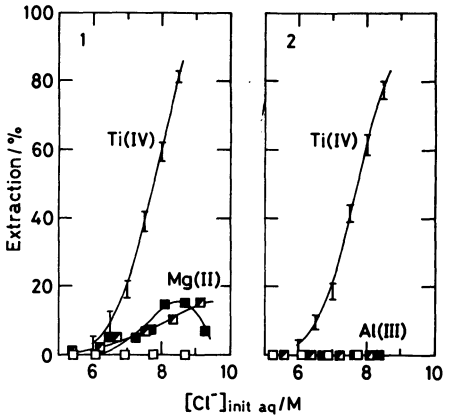

Fig. 5. Extraction of Ti(IV) and other metal ions *vs.* concentration of chloride in aqueous phase.
1: 0.56 M Ti(IV), 1.8 M TBP, 2: 0.27 M Ti(IV), 0.92 M TBP, HCl(M) —□: 4.0, ◩: 5.0, ■: 6.0.

Figure 5 shows the extraction behavior of titanium(IV) from 4—6 M hydrochloric acid solutions as a function of chloride ion concentration when $MgCl_2$ or $AlCl_3$ was added. The extraction of titanium(IV) was accelerated with increasing chloride ion; behavior quite similar to that observed in changing only hydrochloric acid concentration as shown in Fig. 1. The acceleration effect by these compounds was apparently dependent upon the increase of chloride ion. The salting-out effect by chlorides such as $MgCl_2$[25] and $CaCl_2$[20] on the extraction of titanium(IV) into the TBP phase had previously been investigated.

Figure 6 shows the plots of log D *versus* log $[TBP]_{org}$ in tests conducted for 7.0—10.3 M hydrochloric acid solution containing only titanium(IV). The slope of log $D_{Ti(IV)}$/log TBP was about unity at 7 M acid concentration, and increased with increasing acid concentration in aqueous phase; the value of which became 2.7 at 10.3 M acid concentration. It means that the ratio of TBP to titanium(IV) in the extracted

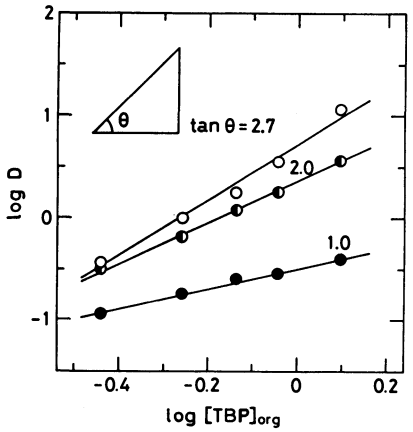

Fig. 6. Dependence of distribution ratio of Ti(IV) on TBP concentration in organic phase.
0.51 M Ti(IV), HCl(M) —●: 7.0, ◐: 8.8, ○: 10.3.

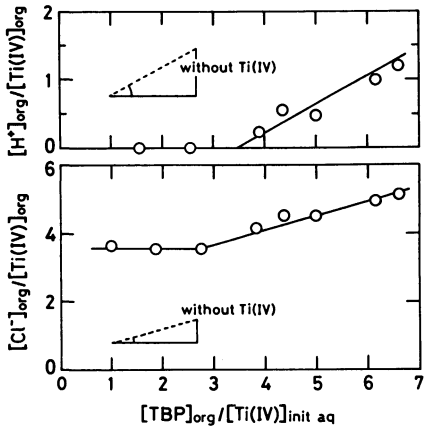

Fig. 7. Dependence of extraction ratio of H^+/Ti(IV) and Cl^-/Ti(IV) on TBP concentration in organic phase.
0.54 M Ti(IV)+10.3 M HCl.

species in organic phase was changed from 1 to 3 according to the acid concentration. Under the conditions conducted here, no free acid was extracted.

The effect of TBP concentration in the organic phase on the extraction of acid and chloride together with titanium(IV) is shown in Fig. 7, which gives the molar ratio of $[H^+]/[Ti(IV)]$ and $[Cl^-]/[Ti(IV)]$ in organic phase in tests conducted for 10.3 M hydrochloric acid solution containing only titanium(IV). At ratios of $[TBP]_{org}/[Ti(IV)]_{init\ aq}$ lower than 3, the ratio of $[Cl^-]_{org}/[Ti(IV)]_{org}$ was constant at 3.6; which suggests that titanium(IV) is extracted as a 1 : 3 complex of $TiCl_4$ and TBP:

$$[TiCl_4]_{aq} + 3[TBP]_{org} = [TiCl_4 \cdot 3TBP]_{org}. \quad (4)$$

As a minor species of titanium(IV) in organic phase, $TiOCl_2$ was inferred. At such high TBP concentration in organic phase as the ratio of $[TBP]_{org}/[Ti(IV)]_{init\ aq} \geqq 3.5$, the equal amounts of Cl^- and H^+ were extracted together with titanium(IV). Because the dependence of acid extraction behavior on TBP concentration in the organic phase was identical with that obtained without titanium(IV), hydrochloric acid would be extracted with an excess of TBP in the organic phase as Eq. 1.

According to Startsev *et al.*,[19,21] titanium(IV) was extracted as $H_2TiCl_6 \cdot 3TBP$, *i.e.*, $[TiCl_4 \cdot 2TBP][2HCl \cdot TBP]$ at high concentrations of hydrochloric acid in aqueous phase and of TBP in organic phase. Our results on the extracted species of titanium(IV) agreed with that reported by Startsev *et al.*

Conclusion

It is generally known that the optimum conditions which realize an effective dissolution of ilmenite ore are as follows: grain size of ore, under 150 mesh; concentration of HCl, higher than 10 M; amount of HCl to ore, 2—4 times in weight; temperature, 70—90 °C.[3,13,14] As can be seen from Eq. 5, the concentration

$$FeTiO_3 + 4HCl = TiOCl_2 + FeCl_2 + 2H_2O \quad (5)$$

of hydrochloric acid decreases with the progress of the leaching reaction, finally becoming 4—6 M. Thus the extraction with TBP can be applied to the leach liquor after the oxidation of iron(II) to iron(III) to recover iron selectively. By the thermal decomposition method,[26,27] iron(III) oxide of higher than pigment grade can be recovered with free hydrochloric acid from the back-extracted solution. This technique is now being applied to the upgrading of ilmenite ore[28] and steel cleansing.[29,30]

Titanium(IV) extracted in organic phase as $TiCl_4 \cdot 3TBP$ should be back-extracted by using 4—6 M hydrochloric acid solutions. The significant acid concentration dependence of the extraction behavior of titanium(IV) was preferable for the back-extraction because titanium(IV) tends to be hydrolyzed easily in weak acid solutions. Since the resulting aqueous solution containing titanium(IV) was not contaminated with any impurities, highly pure titanium(IV) oxide can also be obtained by the thermal decomposition method[28,29] or by the thermal hydrolysis.[31,32] The recovery of free hydrochloric acid from the residual solution after the extractions of iron(III) and titanium(IV) is now a feasible operation.[29,30,33]

References

1) Kirk–Othmer, "Encyclopedia of Chemical Technology," 2nd ed, John Wiley and Sons, Inc., New York (1964), Vol. 14, p. 221.
2) N. Ohta, *Kagaku Keizai*, **28**, 49 (1981).
3) "Gmelins Handbuch der Anorganischen Chemie," 8th ed, No. 41, "Titan," Verlag Chemie, Weinheim (1951), p. 88.
4) M. Imahashi and N. Takamatsu, *Bull. Chem. Soc. Jpn.*, **49**, 1549 (1976).
5) H. Tsuchida, E. Narita, H. Takeuchi, M. Adachi, and T. Okabe, *Bull. Chem. Soc. Jpn.*, **55**, 1934 (1982).
6) K. Murayama, *Shin-Kinzoku Kogyo*, **20**, 315 (1975).
7) K. Murayama, *Bull. Jpn. Petro. Inst.*, **20**, 608 (1977).
8) D. S. Flett, *Chem. Ind.*, **3**, Sept., 706 (1977).
9) S. Kato and M. Ichijo, *Kogai Shigen-Ken Iho*, **10**, 41 (1980).
10) P. Mühl, K. Gloe, C. Fischer, S. Ziegenbalg, and H. Hoffmann, *Hydrometallurgy*, **5**, 161 (1980).
11) R. Sei, *Sangyo Kogai*, **12**, 987 (1975).
12) S. Nishimura, *Kagaku Kogaku*, **41**, 189 (1977).
13) D. A. Ellis, U. S. Patent 3104950 (1963).

14) T. Yamamura, Y. Omote, S. Sato, and T. Hiyama, Japan Patent 49995 (1972).
15) A. K. De, S. M. Khopkar, and R. A. Chalmers, "Solvent Extraction of Metals," Van Nostrand Reinhold Co., London (1970), p. 175.
16) T. Sekine and Y. Hasegawa, "Solvent Extraction Chemistry, Fundamentals and Applications," Marcel Dekker, New York (1977), p. 583.
17) Ref. 15, p. 179.
18) Ref. 16, p. 557.
19) V. N. Startsev, E. I. Krylov, and Y. A. Koz'min, *Russ. J. Inorg. Chem.*, **10**, 1285 (1965).
20) V. N. Startsev and E. I. Krylov, *Russ. J. Inorg. Chem.*, **12**, 399 (1967).
21) V. N. Startsev, Y. I. Sannikov, G. N. Ben'yash, and E. I. Krylov, *Russ. J. Inorg. Chem.*, **13**, 586 (1968).
22) F. Islam, H. Rahman, and M. Ali, *J. Inorg. Nucl. Chem.*, **41**, 217 (1979).
23) Ref. 15, p. 172.
24) Y. Marcus and A. S. Kertes, "Ion Exchange and Solvent Extraction of Metal Complexes," Wiley-Interscience, London (1967), p. 680.
25) A. A. Yadav and S. M. Khopkar, *Anal. Chim. Acta*, **45**, 355 (1969).
26) H. Tsuruta and N. Wakamatsu, *Bunri Gijutsu*, **8**, 346 (1978).
27) H. Tsuruta and K. Murakami, *Kagaku Kojo*, **24**, 29 (1980).
28) N. R. Iammartino, *Chem. Eng.*, **83**, 100 (1976).
29) G. H. Rupy and C. J. Jewell, *CIM Bull.*, **68**, 89 (1975).
30) J. W. Burtch, *CIM Bull.*, **68**, 96 (1975).
31) K. Funaki and Y. Saeki, *Kogyo Kagaku Zasshi*, **59**, 1291 (1956).
32) J. Shiokawa, A. Matsumoto, and H. Kawakami, *Rep. Asahi Glass Found. Ind. Tech.*, **16**, 431 (1970).
33) A. Conners, *CIM Bull.*, **68**, 75 (1975).

 © 1983 The Chemical Society of Japan Bull. Chem. Soc. Jpn., 56, 1837—1840 (1983)

Theoretical Study of Proton and Solvent Effects on Molecular Stacking

Felice ZUCCARELLO,* Antonio RAUDINO, Giuseppe BUEMI, and Carmelo RIGANO†

Istituto Dipartimentale di Chimica e Chimica Industriale, Università di Catania, Viale A. Doria 6, 95125 Catania, Italy

†*Seminario Matematico dell'Università di Catania, Viale A. Doria 6, 95125 Catania, Italy*

(Received November 10, 1981)

Molecular stacking between π-electron systems was analyzed in connection with effects of external charge and solvent. A perturbation approach was used for calculating intermolecular energies and a discrete plus continuum model was used for solvent effects. The solvent favors stacking in unprotonated systems by hydrophobic forces. In the presence of an external charge the solvent induces dissociative effects on the molecular pairs by electrostatic solvation forces.

It is well known that molecular stacking plays an important role in many biological processes. Indeed, intramolecular stacking favors conformational preferences in large flexible molecules (FAD, NAD, *etc.*), while intermolecular stacking is one of the causes for binding of molecules to enzymes, base pairing, *etc.* Generally, these molecular systems are characterized by large π-electron systems which interact with one another essentially through van der Waals-type forces. Since in biological environments these large systems are imbedded in a liquid or quasi-liquid (membrane) medium, and frequently they are in a protonated form ($NAD\text{-}H^+$, $FAD\text{-}H^+$), we think it to be interesting to study associated effects of proton-charge and of solvent on interactions among some π-electron systems.

Following an approach already adopted by us,[1] we select simple systems which partially simulate relevant characteristics of more complex biological systems. Consequently, in the present work we study, both in vacuum and in water, interactions between two π-electron clouds, unperturbed as well as perturbed by a proton localized in a site. In the present approach we study interactions in vacuum between two π-systems, one of which is affected by the presence of a neighboring proton. Successively, we add solvation energy, which allows us to examine effects of both hydrophobic interactions and electrostatic solvation energies on the association of these π-systems.

Intermolecular forces, which are responsible for stacking, can be efficiently described in the framework of the second order perturbation approach of Murrell *et al.*[2] This method is particularly suitable for studying medium- and long-range forces; moreover, it allows an insight into different natures of working intermolecular forces. Practically, to interaction energies we add solvation energies calculated according to the discrete plus continuum model, and draw the trend of total energies at various intermolecular distances.

Description of the Method

The following pair systems were considered in the present work: i) protonated ethylene–ethylene, ii) protonated ethylene–benzene, and iii) protonated benzene–ethylene, each case including the corresponding unprotonated pair. The approaching pathways for the neutral pairs are shown in Fig. 1, where the variable parameters are also defined. The positive charge is located at 1.1 Å[3] from the ethylene plane for systems

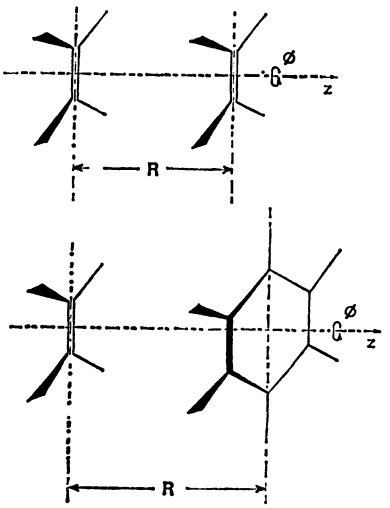

Fig. 1. Approach pathways and variable parameters for ethylene–ethylene and benzene–ethylene pair systems.

i) and ii), and at 0.85 Å from the benzene plane†† for system iii). In all cases it is located along the principal symmetry axis outside the intermolecular space. In evaluating the solvent effect for the unprotonated systems the continuum model was adopted. For the protonated systems the discrete plus continuum model was used; that is, a planar H_3O^+ molecule, perpendicular to the ethylene or benzene plane, was bound to the π-system inside an elliptic cavity of a continuum dielectric medium. Geometrical parameters of H_3O^+ and of the neutral molecules were taken from Refs. 4 and 5. For each value of intermolecular distance, R, and for some relative spatial arrangements, the interaction energy was first calculated, and then the corresponding solvation energy was added.

The intermolecular interaction energy was calculated by the second order perturbation theory of Murrell *et al.*,[2] developed on the LCAO approximation by Fueno *et al.*;[6] this method has been utilized successfully by several authors.[1d,7,8] The method describes quite well the medium and long range forces and allows a useful energy partitioning into five contributions: coulombic (E_Q), exchange repulsion (E_K), induction (E_I), dispersion (E_D), and charge transfer (E_{CT}) energies. The approximations, used in calculating intermolecular integrals, and the structure of the computer

†† This value was optimized by a MINDO/3 calculation.

program used were described in a previous paper.[1d]

Solvation energy was evaluated by means of an approximation††† which divides it into electrostatic, cavitation, dispersion, and short-range contributions. The first contribution was calculated on the reaction field approximation, taking into account the elliptic shape of cavity and the actual position of charges inside. Supermolecule dipole moment was evaluated as the dipole moment induced by a positive charge on polarizable molecules. Polarizability components were evaluated according to a perturbative approach.[9] Cavity contribution was related to the surface tension and to the elliptic surface of solute.[10] Dispersion and short-range energies were calculated by

$$E_{\mathrm{disp}} = \frac{\delta}{2}\int_{\sigma}^{\infty} U(\rho)g^{(2)}(\rho)\langle A(\rho)\rangle d\rho,$$

where δ is the number density of solvent and $U(\rho)$ is a Lennard-Jones potential corrected for the three-body interaction.[11] The coefficient of potential $U(\rho)$ was put equal to

$$\frac{3}{2}\bar{\alpha}_{\mathrm{w}}\bar{\alpha}_{\mathrm{s}}\frac{I_{\mathrm{w}}I_{\mathrm{s}}}{I_{\mathrm{w}}+I_{\mathrm{s}}}(2\sigma)^{-6}.$$

Solute ionization potential (I_{s}) and polarizability (α_{s}) have been theoretically calculated;[9] the ethylene σ value was taken from Ref. 7, while the other values were evaluated from density data.[12,13] $\langle A(\rho)\rangle$ is the spherical average surface of solute, and $g^{(2)}(\rho)$ is the distribution function, here set equal to zero for $\rho<\sigma$ and 1 otherwise.

Results in Gas Phase

Table 1 shows perturbation interaction energy values for the ethylene–ethylene and protonated ethylene–ethylene systems, together with single energy contributions. It can be noted that for the former system, at shorter distances, the exchange repulsion contribution (E_{K}) is the most important, whereas the coulombic (E_{Q}) and dispersion (E_{D}) energies nearly balance each other; at longer distances the total energy arises essentially from the dispersion term, the figures being in agreement with previous calculations.[7] Further calculations showed that the total energy is not affected by rotation of one ethylene molecule around the intermolecular symmetry axis.

When a proton is added (the latter system), we note an increase in E_{K} and a decrease in E_{Q}, while the induction (E_{I}) and charge transfer (E_{CT}) terms are appreciable. Then the total energy shows, with respect to the unprotonated system, a slight deepening of the minimum, which now lies at nearly the same

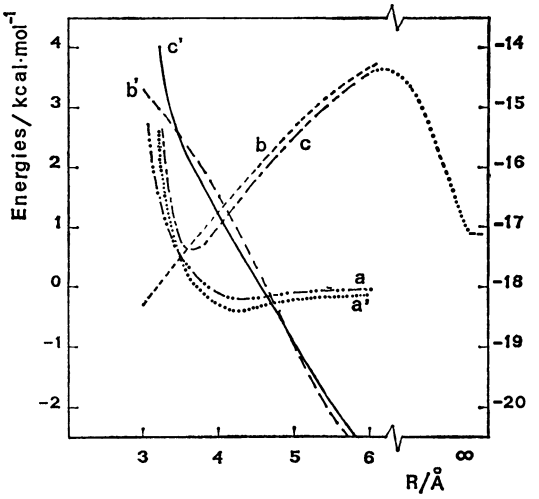

Fig. 2. Ethylene–Ethylene system.
a: Gas-phase energy, unprotonated, a′: gas-phase energy, protonated, b: solvation energy, unprotonated, b′: solvation energy, protonated, c: total energy, unprotonated, c′: total energy, protonated. Scale on the right refers to b′ and c′ curves (1 cal=4.184 J).

Table 1. Perturbation interaction energy terms

R/Å	E_{Q} / kcal mol^{-1}	E_{K} / kcal mol^{-1}	E_{I} / kcal mol^{-1}	E_{D} / kcal mol^{-1}	E_{CT} / kcal mol^{-1}	$E_{\mathrm{tot.}}$ / kcal mol^{-1}
			Ethylene-Ethylene			
2.8	2.32	5.93	0	−1.13	0	7.12
3.0	1.02	3.17	0	−0.80	0	3.39
3.2	0.42	1.63	0	−0.57	0	1.48
3.4	0.18	0.81	0	−0.42	0	0.57
4.0	0.01	0.08	0	−0.18	0	−0.09
5.0	0	0	0	−0.05	0	−0.05
6.0	0	0	0	−0.02	0	−0.02
			H^+-Ethylene-Ethylene			
2.8	1.80	11.64	−0.18	−0.93	−0.48	11.85
3.0	0.36	6.13	−0.14	−0.66	−0.25	5.44
3.2	0.02	3.12	−0.10	−0.47	−0.13	2.44
3.4	−0.17	1.54	−0.08	−0.35	−0.06	0.89
4.0	−0.23	0.16	−0.04	−0.15	−0.01	−0.26
5.0	−0.13	0	−0.01	−0.04	0	−0.19
6.0	−0.08	0	−0.01	−0.02	0	−0.11

††† Details of the method are described in Ref. 1b.

distance as in the neutral system (Fig. 2, a and a' curves).

At first sight it could appear strange that, in Table 1, the coulombic terms vary rapidly with distance as compared with the corresponding exchange terms. However, we must bear in mind that in the ethylene–ethylene system the first nonvanishing term of coulomb interaction is the quadrupole-quadrupole term. A similar situation occurs in the protonated ethylene–ethylene system, where the monopole-quadrupole term is nearly zero on symmetry ground.

Calculations were carried out to test the effect due to the proton–ethylene distance on each energy term: The main effect (at 1—2 Å) is a small increasing of E_K nearly balanced by a small lowering of E_Q when the proton–ethylene distance decreases.

Calculations on the benzene–ethylene system evidenced a higher dispersion energy than the ethylene–ethylene one owing to the increased π-system size, in addition to decreases in E_Q and E_K.** The benzene–ethylene energy curve is shown in Fig. 3 (curve a), together with the corresponding curve for the protonated benzene–ethylene system (curve a').*** We can see that the unprotonated benzene–ethylene system shows a minimum more pronounced and at shorter distances than the ethylene dimer.

Protonation has a stabilizing effect, though small (0.3 kcal mol^{-1}) (1 cal=4.184 J); the energy curves appear deeper and wider with the minima lying at slightly greater distances than in the corresponding unprotonated systems. Indeed, the stabilization should be more extensive; in fact, it is well known that the limited basis set will cause underestimation of dispersive forces,[14,15] so that a more negative dispersion energy is to be expected.

Results in Aqueous Solution

Since the energies involved in these molecular associations are small, we expect that solvation energy plays an important role in determining the stability of molecular pairs. Following the scheme outlined in the calculation section, we added the solvation energy to the energy for the gas phase and constructed curves for the resulting total energy *vs.* intermolecular distance. Figures 2 and 3 show solvation and total energy for the pair systems studied.

The solvation energy for the unprotonated systems (curves b) increases with intermolecular distance, R, the cavitation term prevailing and the dispersion term being nearly constant;§ the slope is greater in the wider benzene–ethylene system (Fig. 3) than in the ethylene dimer (Fig. 2). The solvation causes drastic deepening of the potential well in the short distance range in both the cases (curves c). Moreover, for

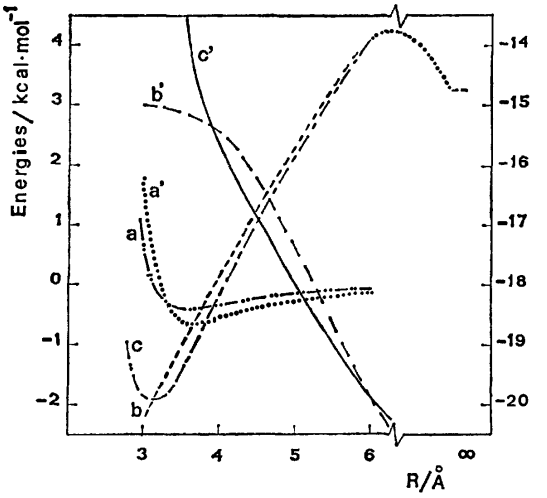

Fig. 3. Benzene–Ethylene system.
a: Gas-phase energy, unprotonated a': gas-phase energy, protonated; b: solvation energy, unprotonated, b': solvation energy, protonated, c: total energy, unprotonated; c': total energy, protonated. Scale on the right refers to b' and c' curves.

each pair in solution the energy minimum is lower than the energy of the two single solvated components at infinite distance. Therefore, to dissociate these unprotonated pairs, we must overcome a potential barrier. This explains how hydrophobic forces induce the stacking of π-electron molecular systems in solution.

The present approach is not capable of allowing us to calculate the exact dissociation barrier, leaving the intermolecular potential variable in a periodic fashion with intermolecular distance as far as this distance is comparable, or greater than, solvent molecular radii.[16,17] However, from an inspection of the curves we expect barriers of 2—3 kcal mol^{-1} for the ethylene–ethylene pair and 5—6 kcal mol^{-1} for the benzene–ethylene one.

When the proton is bound to one of pairing molecules, main consequences from the solvent effect are the disappearence of short range minima and the strong dissociative power in all the cases considered (curves c'). This is accounted for in terms of the appreciable electrostatic contribution to solvation energy. This contribution increases greatly with intermolecular distance because the charge is located in the proximity of cavity wall; this geometric fashion makes remarkable the effect of ellipticity on the electrostatic solvation energy. Such increase in electrostatic solvation energy has been pointed out by several authors[18,19] and evidenced by us in our previous work.[1b] On this ground the cavitation energy here plays a minor role, in contrast to the unprotonated systems.

By comparing the shapes of the solvation energy curves (b') in Figs. 2 and 3, it can be deduced that increasing the size of unsaturated systems will result in lowering the slope of solvation energy curves at short distances. We, therefore, think that the interaction between very extended unsaturated systems could cause inversion in the slope of the above curves for protonated systems so that stacking effects induced by

** No values of the energy components are reported because their trend is quite similar to that of the corresponding ethylene–ethylene system.

*** The curve for the protonated ethylene–benzene system, not reported here, is nearly equal to curve a', apart from a slight destabilization.

§ No significant variations were observed on changing the rotation angle ϕ (see Fig. 1).

the solvent could be reliable. No curves for the protonated ethylene–benzene (both in the gas phase and in solution) are reported in Fig. 3; they are similar to those for the protonated benzene–ethylene system.

We can conclude that in water solution the stacking effect, though weak, can occur between unsaturated molecules, provided that no proton is bound to anyone of the interacting molecules (hydrophobic stacking). On the contrary, when a net charge is held by one of the two molecules, any stacking effects are not possible; at the most, only in very extended unsaturated systems they should be taken into account.

This work was supported partially by the Italian Consiglio Nazionale delle Ricerche (CNR), Rome.

References

1) a) F. Zuccarello, A. Raudino, and G. Buemi, *Chem. Phys. Lett.*, **70**, 565 (1980); b) A. Raudino, F. Zuccarello, and G. Buemi, *J. Chem. Soc., Faraday Trans. 2*, **77**, 1331 (1981); c) F. Zuccarello, A. Raudino, and G. Buemi, *J. Mol. Struct. Theochem*, **87**, 197 (1982); d) A. Raudino, F. Zuccarello, G. Buemi, and C. Rigano, *Bull. Chem. Soc. Jpn.*, **55**, 1628 (1982).

2) J. N. Murrell, M. Randić, and D. R. Williams, *Proc. R. Soc. London, Ser. A*, **284**, 566 (1965).

3) P. C. Hariharom, N. A. Lathan, and J. A. Pople, *Chem. Phys. Lett.*, **14**, 385 (1972).

4) C. H. F. Dierksen, W. P. Kraemer, and B. O. Roos, *Theor. Chim. Acta (Berl.)*, **36**, 249 (1975); M. C. R. Simons, *J. Am. Chem. Soc.*, **102**, 3982 (1980).

5) L. E. Sutton, "Intermolecular Distances," Chem. Soc. Spec. Publ., London (1965).

6) T. Fueno, S. Nagase, K. Tatsumi, and K. Yamaguchi, *Theor. Chim. Acta (Berl.)*, **26**, 43 (1972).

7) K. Suzuki and K. Iguchi, *J. Chim. Phys.*, **75**, 779 (1978).

8) G. R. Pack, G. H. Loew, S. Yamabe, and K. Morokuma, *Int. J. Quantum Chem., Quantum Biol. Symposium*, **5**, 417 (1978).

9) F. T. Marchese and H. H. Jaffe, *Theor. Chim. Acta (Berl.)*, **45**, 241 (1977).

10) O. Sinanoglu, *J. Chem. Phys.*, **75**, 463 (1981).

11) O. Sinanoglu, *Chem. Phys. Lett.*, **1**, 340 (1967).

12) A. Weissberger, E. S. Proskaner, J. A. Riddick, and E. E. Toops, "Organic Solvents," Interscience Publ. Inc., New York (1955).

13) R. B. Hermann, *J. Phys. Chem.*, **79**, 163 (1975).

14) P. E. S. Warmer, F. Mulder, and A. van der Avoird, *Int. J. Quantum Chem.*, **11**, 959 (1977).

15) P. Arrighini, "Lecture Notes in Chemistry, n.25, Intermolecular Forces and their Evaluation by Perturbation Theory," Springer-Verlag, Berlin (1981).

16) R. G. Horn and J. N. Israelachvili, *J. Chem. Phys.*, **75**, 1400 (1981).

17) B. W. Ninham, *J. Phys. Chem.*, **84**, 1423 (1980).

18) Yu. I. Kharkats, *J. Chem. Soc., Faraday Trans. 2*, **1974**, 1345.

19) S. Ehrenson, *J. Am. Chem. Soc.*, **98**, 7510 (1976).

 © 1983 The Chemical Society of Japan Bull. Chem. Soc. Jpn., 56, 1841—1846 (1983)

On the Interaction of CrO_2Cl_2 Vapor with the Surface of γ-Al_2O_3 and the Formation of a Chromium Oxide Covering

Damyan DAMYANOV* and Lubomir VLAEV
Higher Institute of Chemical Technology, 8010 Burgas, Bulgaria
(Received March 31, 1982)

Samples of γ-Al_2O_3 containing different amounts of residual hydroxyl groups were obtained by thermal treatment. The possibility of interaction of the surface hydroxyl groups of γ-Al_2O_3 with chromyl chloride vapor was studied by IR spectroscopy. The hydrogen chloride evolved as a result of the reaction interacts with both strained Al–O–Al bridges and the surface OH groups. Different types of OH groups show different reactivities with respect to the interaction with CrO_2Cl_2. Bands at 3780 and 3700 cm^{-1} are due to OH groups which have a much higher reactivity than the OH groups responsible for bands at 3744 and 3733 cm^{-1}. Not all of the OH groups participate in the surface reaction. Decrease in their surface density results in increase in the reactivity. Modification of the γ-Al_2O_3 surface is achieved by reaction cycles consisting of treatment with CrO_2Cl_2 vapor and hydrolysis of the compounds obtained by water vapor. As a result, an increase in the chromium oxide amount on the surface of γ-Al_2O_3 is observed. This is ascribed to the "secondary" OH groups formed after the hydrolysis.

It is well known that chemical modification of the surface of Al_2O_3 with halogen compounds leads to essential changes in its acidic properties and catalytic activities. In the literature there are a number of studies using hydrogen halides,[1-4] halogenated hydrocarbons,[5,6] $SiCl_4$,[7] various silanes,[8] *etc.* as modifying agents. However, there are no investigations on reactions of the Al_2O_3 surface with vapors of valatile halides or halide oxides of transition metals, which are known to ensure a more uniform deposition of a transition metal and a halogen on the surface than the classical methods of catalysts preparation. In addition, hydrolysis of the surface compound obtained can proceed with formation of "secondary" OH groups, which in turn can interact with the vapor of the same or another halide. Thus, a possibility is found to perform controllable deposition of active components on the surface of supports and to prepare new types of catalysts.

The purpose of the present paper is to investigate the interaction of the surface of γ-Al_2O_3 with CrO_2Cl_2 vapor and the deposition of chromium oxide phases as a result of alternate treatment with chromyl chloride vapor and hydrolysis with water vapor.

Experimental

Samples of γ-Al_2O_3 (Leuna, GDR), with particle sizes of 0.25—0.64 mm, specific surface area of 190 m^2/g, and pore volume of 0.64 cm^3/g, were used for the experiments.

To obtain samples with different amounts of OH groups, the initial γ-Al_2O_3 was calcined for 3 h in air with a view to eliminating organic impurities, after which it was subjected to additional calcination for 3 h *in vacuo* (5×10^{-5} Torr) (1 Torr=133.322 Pa) at suitable temperatures.

The samples thus prepared were brought into contact with CrO_2Cl_2 vapor at an experimentally established temperature of 150 °C. It was found that at lower temperatures, 25 °C, physical adsorption proceeds to a great extent, whereas above 170 °C partial polymerisation of chromyl chloride occurs.[9] The weight gain as a result of chemisorption was determined with a McBain balance. With samples showing no weight change, the residual chromyl chloride vapor and the gaseous products were removed by evacuation for 1 h at 150 °C. The amount of OH groups was determined gravimetrically by assuming complete dehydration of the surface at 1150 °C.

Chromyl chloride was synthesized under laboratory conditions and used after redistillation.[10] Extraction of Cr and Cl^- from the sample was achieved by treatment with 2 M NaOH (1 M=1 mol dm^3). The Cr content was determined iodometrically, and that of Cl^-, by amperometric titration.

The specific surface area was determined by the BET method using low-temperature nitrogen adsorption.

Samples of γ-Al_2O_3 (10×30 mm) weighing 13—15 mg/cm^2 were studied by IR spectroscopy. They were obtained from fine Al_2O_3 powder under a pressure of 200 kg/cm^2. The thermal treatment, the surface modification by CrO_2Cl_2 and the hydrolysis with water vapor as well as the recording of spectra were carried out in a spectral vacuum quartz cell with NaCl windows. The spectra were taken at room temperature with a UR-20 (Carl Zeiss Jena, GDR) apparatus, an optical attenuator being placed in the reference beam.

Results

Table 1 contains data from thermogravimetric measurements of the amount of OH groups. The surface density of OH groups was calculated on the basis of specific surface area. Evidently, all the parameters shown in Table 1 decrease with increasing temperature of precalcination. It should be taken into account that the values of α_{OH} and ω_{OH} are approximate and higher than the real ones. This is indicated by preliminary IR spectroscopy studies. The latter confirmed works of other authors,[11,12] according to which within the above temperature range there is coordination water on the surface of the initial Al_2O_3. It can be assumed that above 400 °C the data on the hydroxyl coverage are real since the weight losses established are due only to dehydration of the surface at the expense of neighboring or favorably oriented OH groups.

Three samples precalcined at 250, 550, and 750 °C, respectively, were treated with CrO_2Cl_2 vapor. It was taken into account that at 250 °C there is still coordination water on the surface of Al_2O_3. At 550 and 750 °C there is no such water but the Al–O–Al bridges formed as a result of dehydration differ in number and stability. In addition, the temperature of 750 °C is limited for the γ-θ-transition of Al_2O_3.

The kinetics of the reaction of CrO_2Cl_2 with the surface of Al_2O_3 are illustrated by the gravimetric

Table 1. Dependence of amount of OH groups (α_{OH}), the specific surface area (S), and surface density of hydroxyl groups (ω_{OH}) on the precalcination temperature of γ-Al_2O_3

	Temp/°C							
	170	250	350	450	550	650	750	850
$\frac{\alpha_{OH} \times 10^{-21}}{\text{numbers g}^{-1}}$	2.37	1.91	1.59	1.20	0.79	0.47	0.27	0.16
$S/m^2\,g^{-1}$	190	188	175	172	179	126	113	90
ω_{OH}/number nm^{-2}	12.49	10.20	9.09	7.00	4.44	3.63	2.35	1.74

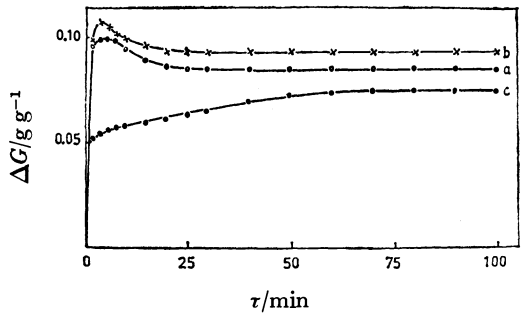

Fig. 1. Kinetic curves of CrO_2Cl_2 chemisorption at 150 °C on γ-Al_2O_3 precalcined at 250 °C (a), 550 °C (b), and 750 °C (c).

Table 2. Dependence of the Cl^- and Cr contents and their ratio on the precalcination temperature of γ-Al_2O_3

No.	Tem/°C	Numbers/10^{-20} g		Cl^-/Cr
		Cl^-	Cr	
1	250	1.93	3.49	0.55
2	550	2.77	3.67	0.75
3	750	2.65	2.35	1.13

curves presented in Fig. 1. The steep course of the curves in their initial portions indicates a rapid interaction. Contrary to the kinetic curves for samples calcined at 250 and 550 °C, the curve for the sample treated at 750 °C shows no maximum, which is probably due to differences in the diffusion of reaction products. After the initial portion of the curves there is a horizontal part indicating equilibrium. The data from chemical analysis (Table 2) show different contents of Cl^- and Cr, their ratios and the weight gain being presented by the kinetic curves. Obviously, the surface density of hydroxyl coverage affects the interaction which, however, is incomplete since the amounts of deposited Cl^- and Cr are much less than the theoretically calculated amounts needed for complete interaction of the available OH groups.

Figure 2 shows changes in IR spectra due to contact of the Al_2O_3 sample calcined at 550 °C with increasing CrO_2Cl_2 amount (the portions of 1.9 μmol).

The spectrum of the initial Al_2O_3 has absorption bands at 3780, 3744, 3733, and 3700 cm^{-1} which, according to the model of Peri,[1] correspond to the srtetching vibrations of isolated OH groups. No bands are discernible in the low-frequency region. The bands at 3780 and 3700 cm^{-1} are not observed in the spec-

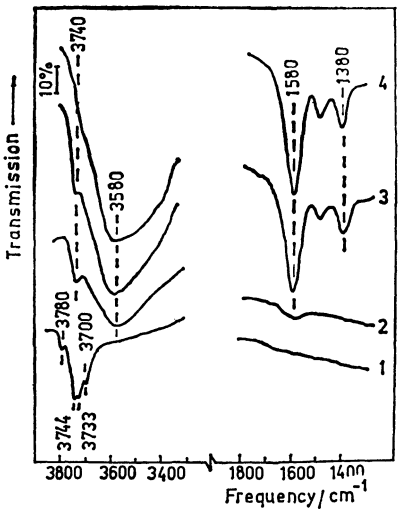

Fig. 2. IR spectra of initial γ-Al_2O_3 calcined for 3 h in air and outgassed in vacuum for 3 h at 550 °C (1), after successive interactions at 150 °C with 1.9 μmol CrO_2Cl_2 vapor (2), with 3.8 μmol CrO_2Cl_2 (3), and upon complete saturation (4).

trum after the first portion of chromyl chloride vapor, whereas the bands at 3744 and 3733 cm^{-1} appear as a single band of lower intensity (spectrum 2). In addition, there is a broad band with a maximum at about 3580 cm^{-1}. According to literature data,[11] this band is due to OH groups interacting by strong hydrogen bonds. Obviously, a chemical reaction with participation of the surface OH groups proceeds. The introduction of new CrO_2Cl_2 portions (spectra 3 and 4) leads to a more pronounced band at 3580 cm^{-1} which is broadened in the low-frequency region where three new bands appear at 1380, 1490, and 1580 cm^{-1}.

To elucidate the nature of the first two bands, spectra of initial γ-Al_2O_3 were taken after its thermal treatment up to 500 °C. A gradual decrease in the intensity of these bands with increasing temperature was observed. At 500 °C they completely disappeared. This means that they are of the same nature and are in some way associated with the presence of coordination water on the γ-Al_2O_3 surface. In Refs. 14 and 15 the band at 1380 cm^{-1} is attributed to the overtone of the Al–OH stretching vibration, where the OH group vibrates as a whole and whose fundamental frequency should be at 660—700 cm^{-1}. In view of what has been mentioned above, the bands at 1380 and 1490 cm^{-1} could, according to our opinion, be the overtone of the coordination bond $>Al{:}OH_2$

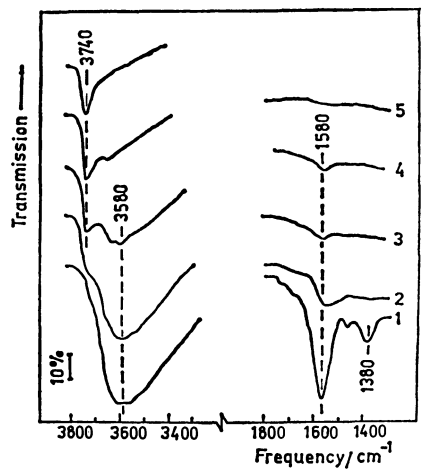

Fig. 3. IR spectra of γ-Al_2O_3 after its modification with CrO_2Cl_2 vapor at 150 °C (1), and after successive outgassing in vacuum and calcination 5 h at 250 °C (2), at 350 °C (3), at 450 °C (4), and at 550 °C (5).

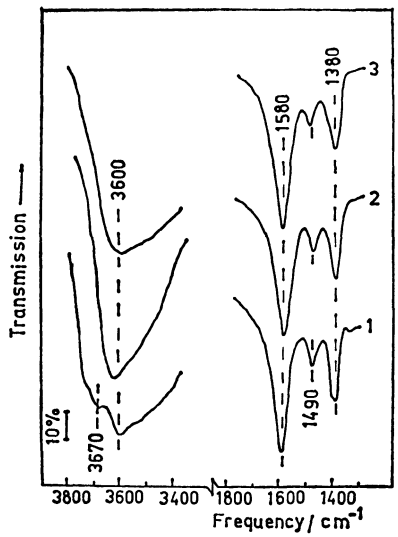

Fig. 4. IR spectra of initial γ-Al_2O_3 calcined for 3 h in air and outgassed in vacuum for 3 h at 250 °C (1), and after successive interactions with 1.9 μmol (2), and 3.8 μmol (3) CrO_2Cl_2.

in tetrahedrally and octahedrally coordinated surface aluminium atoms.

According to Refs. 11, 15, and 16, the band at 1580 cm^{-1} indicates the presence of coordination water. The IR spectra in Fig. 3 demonstrate its thermal stability. Spectrum 1 in Fig. 3 is identical with those given in Figs. 2—4. Evidently, with increasing temperature from 250 to 450 °C, the band at 1580 cm^{-1} gradually reduced its intensity and disappeared at 550 °C. A similar behavior is observed with the broad band at 3580 cm^{-1} which is shifted to higher frequences. Simultaneously, the composite band at 3740 cm^{-1} becomes more pronounced. Its presence may be attributed to (1) the formation of "secondary" OH groups as a result of the interaction of the evolved hydrogen chloride with Al–O–Al bridges; (2) the appearance of unreacted and "masked" OH groups; and

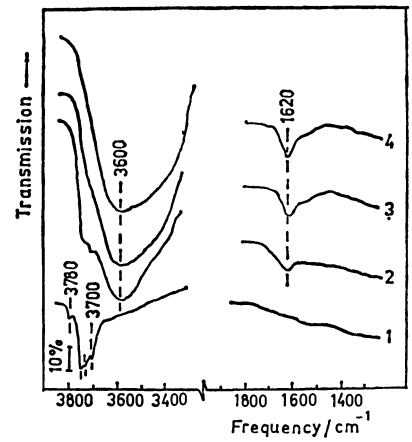

Fig. 5. IR spectra of initial γ-Al_2O_3 calcined for 3 h in air and outgassed in vacuum for 3 h at 750 °C (1), after successive interactions at 150 °C with 1.9 μmol (2), and 3.8 μmol CrO_2Cl_2 (3), and complete saturation (4).

(3) the hydrolysis of the Al–Cl bond by the coordination water during calcination. These assumptions are based on the investigations by Peri[1] on the interaction of Al_2O_3 with hydrogen chloride and on our experimental data indicating an incomplete participation of the free OH groups in the chemical interaction as well as on the absence of chlorine in the samples after their calcination at 550 °C.

The spectrum of the sample preliminarily dehydrated and outgassed at 250 °C (Fig. 4. 1) has no pronounced characteristic bands of free OH groups due to the presence of coordination water (the bands at 1580 and 3600 cm^{-1}). Only a very weak band at 3670 cm^{-1} appears and is no more discernible after the introduction of the CrO_2Cl_2 vapor. The band at 1580 cm^{-1} preserves its intensity, which indicates that the coordination water does not interact with CrO_2Cl_2. The above spectra illustrate very well the behavior of the Al_2O_3 surface in the presence of coordination water and unambiguously confirm that the reaction between this surface and CrO_2Cl_2 leads to the formation of new OH groups and molecular water coordinatively bonded to the surface.

Figure 5 shows changes in the IR spectrum of a sample calcined at 750 °C after interaction with chromyl chloride vapor. The behavior of the bands at 3780 and 3700 cm^{-1} differs from that for the sample calcined at 550 °C. Contrary to the band at 3780 cm^{-1}, the one at 3700 cm^{-1} is also observed after the introduction of the first chromyl chloride portion. In addition, the band at 1620 cm^{-1} appears due to the OH deformation vibration and has a much lower intensity. The above facts confirm the assumption about certain variations in the mechanism of interaction between Al_2O_3 and CrO_2Cl_2 depending on the surface density of the hydroxyl groups.

From the spectra in Fig. 3 it is evident that part of the hydroxyl coverage on the support can be restored. This allows subsequent modification of the surface with CrO_2Cl_2 vapor with a view to increasing the amount of chromium oxide. This possibility is also ensured by the surface compounds with water

vapor. For this reason, the following reaction cycle was carried out: treatment with CrO_2Cl_2 vapor of Al_2O_3 dehydrated at 550 °C; hydrolysis at 100 °C with water vapor of the surface compound obtained; calcination at 550 °C followed by a repetition of the above cycle. Table 3 shows data from chemical analysis of the samples obtained in this way. Here, ΔCr is the increase in Cr amount with each treatment cycle consisting of hydrolysis with water vapor, calcination at 550 °C, and modification with CrO_2Cl_2 vapor. Figure 6 presents changes in the IR spectra. Obviously, the chromium content increases with each treatment cycle. Simultaneously, the Cl^- amount and the $Cl^-/\Delta Cr$ ratio decrease, which is indicative of a hydrolysis process and a participation of the newly formed OH groups in the repeated modification. The spectra in Fig. 6 show a decreasing intensity of the composite band at 3740 cm^{-1} with increasing number of treatment cycles. In addition, the band due to strongly interacting OH groups is shifted from 3560 to 3600 cm^{-1}. It is noteworthy that after the second and subsequent treatments with chromyl chloride the bands at 3780 and 3700 cm^{-1} (coordination water) are not observed. Therefore, the amount of chromium oxides increases as a result of an interaction between chromyl chloride and OH groups giving rise to absorption bands at 3744 and 3733 cm^{-1}.

Table 3. Dependence of the amounts of Cl^- and Cr fixed on the Al_2O_3 surface and $Cl/\Delta Cr$ ratio on the number of modification cycles consisting of treatment with CrO_2Cl_2 and hydrolysis with water vapor

Cycle No.	Numbers/10^{-20} g			$Cl^-/\Delta Cr$
	Cl^-	Cr	ΔCr	
I	2.77	3.67	3.67	0.75
II	1.45	6.75	3.08	0.47
III	0.54	8.19	1.44	0.38

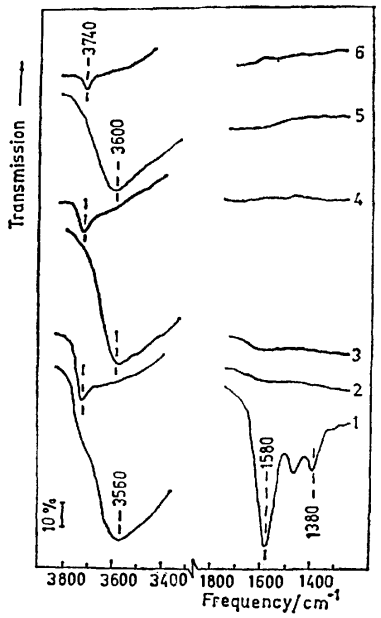

Fig. 6. IR spectra of γ-Al_2O_3 after successive treatments with CrO_2Cl_2 vapor at 150 °C (1, 3, and 5) and hydrolysis with water vapor at 100 °C and calcination at 550 °C (2, 4, and 6).

Discussion

The data from IR spectroscopy indicate defferent chemical activities for the different types OH groups. The OH groups of the highest frequency (absorption band at 3780 cm^{-1}) appear to possess the highest reactivity. Next in reactivity come OH groups of the lowest frequency band (3700 cm^{-1}). After participating in an interaction, these OH groups cannot be restored by hydrolysis. This is evidence for sufficient stability of the Al–O–Cr bond formed. The OH groups responsible for the bands at 3744 and 3733 cm^{-1} are relatively less active. The absence of these bands in the spectrum after the treatment with higher CrO_2Cl_2 amounts should not be interpreted as the indication of complete consumption of these types of OH groups, but should rather be attributed to screening of the latter by the reaction products. As a result, their bands cannot be resolved and appear as one broader band.

The absence of bands at 3780 and 3700 cm^{-1} in the IR spectrum of Al_2O_3 treated with CrO_2Cl_2 and both the decrease in intensity of the bands at 3744 and 3733 cm^{-1} and the presence of Cr^{6+} alone (according to EPR data) indicate electophilic interaction of CrO_2Cl_2 and removal of a proton from the hydroxyl group:

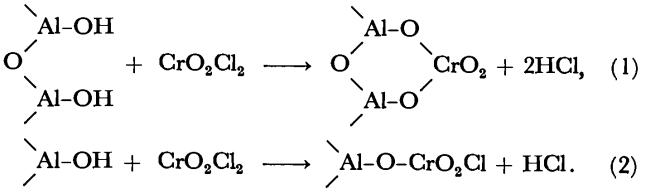

However, the reaction does not stop here. The appearance of a new absorption band at 1580 cm^{-1} indicates formation of water. This can occur only as a result of additional interaction of the hydrogen chloride with the surface OH groups according to the following scheme:

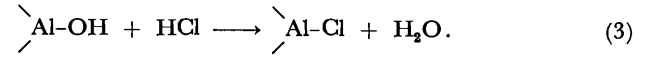

The investigation of Peri[1] on the reaction of hydrogen chloride with Al_2O_3 confirms this scheme.

Since on the surface of Al_2O_3 strained Al–O–Al bridges occurred in addition to the groups, a nucleophilic addition of Cl^- to the surface aluminium atoms can also be expected:

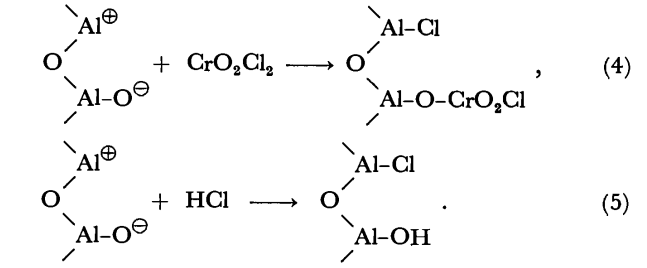

The fact that the first CrO_2Cl_2 portion (Fig. 2) leads to a gecrease in intensity of the bands characterizing the isolated OH groups and that a band of coordination water appears with the subsequent portions, shows that the first stage of the reaction proceeds according to Schemes 1 and 2. The hydrogen chloride evolved interacts first with the strained Al–O–Al bridges according to Scheme 5, which is confirmed by the band at 3680 cm^{-1} due to OH groups connected by hydrogen bonds. Only after this step the hydrogen chloride can interact with hydroxyl groups according to Scheme 3 and form water molecules which are coordinatively bound to the surface (the band at 1580 cm^{-1}). Herewith one answers the question about the constancy in intensity of the band at 1580 cm^{-1} after treatment with CrO_2Cl_2 of γ-Al_2O_3 calcined at 250 °C. The coordination centres of this sample are preliminarily occupied by water molecules and there is no possibility of additional coordination of the water formed as a result of the reaction. This type of reaction is confirmed by the spectra of the samples modified by calcination at 750 °C (Fig. 5). In this case, the band of coordination water is less pronounced due to the decrease in surface density of the hydroxyl groups and the larger amount of Al–O–Al bridges. Since dehydration at 750 °C leads to the formation of "isolated" OH groups alone, the interaction according to scheme 1 should be excluded. In view of the low density of OH groups on the surface (Table 1), the small amount of deposited chromium is quite natural. A comparison of the surface density of the hydroxyl groups with the amount of chromium per unit alumina surface leads to a conclusion that at 750 °C CrO_2Cl_2 interacts mainly according to Scheme 2. At lower temperatures the interaction proceeds partly according to Scheme 1. This is confirmed by the lower Cl^-/Cr ratio at these temperatures of precalcination.

The absence of maximum in the kinetic curve of the sample calcined at 750 °C and the much less pronounced band of deformation vibrations of water which is shifted to a higher frequency in this case, lead us to conclude that during dehydration the nucleophilic addition of Cl^- to the surface of Al_2O_3 is prevailing due to the evolution of hydrogen chloride.

The reaction according to Scheme 4 is not very propable since, in the case of the sample calcined at 750 °C and dehydrated to the highest degree so as to have the largest number of Al–O–Al bridges, the largest amount of chromium should be deposited, and the Cl^-/Cr ratio should be 2, which has not practically been observed. In addition, Scheme 4 shows no evolution of HC which would react according to Eq. 3 and lead to the band observed at 1620 cm^{-1} due to the presence of coordinatively linked water molecules.

The appearance of a band at 3740—3730 cm^{-1} upon hydrolysis or calcination of samples modified by CrO_2Cl_2 is indicative of restoration of part of the hydrate coverage on the carrier. This increase in the chromium amounts Table 3 as a result of successive cycles of halogenation and hydrolysis, which is accompanied by a decrease in intensity of the band at 3740—3730 cm^{-1}, confirms the formation of layers of chromium oxides on the Al_2O_3 surface. The absence of any bands at 3780 and 3700 cm^{-1} after hydrolysis of the samples, on the one hand, and of any band at 1580 cm^{-1} after the second and subsequent halogenations, on the other, confirms that the OH groups responsible for the appearance of the bands of highest and lowest frequencies have the highest reactivity. The OH groups giving rise to bands at 3744 and 3733 cm^{-1} and the eventually formed Cr–OH groups are probably responsible for the subsequent reactions of molecular deposition of chromium oxides. The bands caused by Cr–OH groups were not detected in the range investigated owing to too small an amount of deposited chromium oxide phase and the masking effect of the OH groups on the support.[17,18] The broad absorption band produced by the γ-Al_2O_3 skeleton, which appears in the range 800—1000 cm^{-1}, does not permit any observation of the characteristic band for the Cr–O bond.[17,19] We are of the opinion that the treatment with water vapor leads to hydrolysis of the structure obtained according to Eqs. 2, 3, and 5. Thus, repeated treatment with CrO_2Cl_2 vapor leads to both horizontal densification and vertical growth of the chromium oxide coverage. The continuous increase in the fixed chromium content and the decrease in amount of the chlorides with each cycle of treatment is very significant in this respect.

Conclusion

The surface OH groups of γ-Al_2O_3 react with CrO_2Cl_2 vapor, as a result of which hydrogen chloride is evolved. Part of the latter additionally interacts with the strained Al–O–Al bridges forming new Al–OH and Al–Cl groups. After the consumption of the strained Al–O–Al bridges the hydrogen chloride interacts with the Al–OH groups. As a result, water is formed which is coordinatively bound to the surface. On the sites where the halogen is bound to the surface, new "secondary" OH groups appear due to hydrolysis with water vapor or to calcination. They can interact again with the vapor of CrO_2Cl_2. The hydrogen chloride evolved does not interact with these surface hydroxyl groups. Successive reaction cycles consisting of treatment with CrO_2Cl_2 vapor and hydrolysis with water vapor may increase the amount of chromium oxides of the surface of γ-Al_2O_3.

References

1) J. B. Peri, *J. Phys. Chem.*, **70**, 1482, 3168 (1966).
2) M. Tanaka and S. Ogasawara, *J. Catal.*, **16**, 157 (1970).
3) L. D. Sharma, P. K. Sinhamahaptra, H. P. Sharma, and G. Balamalliah, *J. Catal.*, **48**, 404 (1977).
4) R. R. Bailey and I. P. Wightman, *J. Colloid Interface Sci.*, **70**, 112 (1979).
5) A. G. Goble and P. A. Lawrance, Prepr. Prod. 3rd Int. Congr. Catal., Amsterdam (1964), p. 111.
6) N. P. Bursian, P. N. Borutskii, and N. M. Dvorova, *Zh. Prikl. Khim.*, **48**, 1349 (1975).
7) P. Meallier, I. R. Bernard, C. Camile, and H. Knoche, *C. R. Acad. Sci., Ser. C, Paris*, **281**, 103 (1976).
8) A. A. Chuiko, N. N. Kruglitskii, A. P. Shimanskii,

and V. M. Mashchence, "Adsorption and Adsorbents (in Russian)," Resp. mezhved. Sb. (Coll.), Kiev, Naukova dumka, (1975), Vol. 3, p. 85.

9) S. Z. Makarov and A. A. Vakhrushev, *Izv. AN SSSR, Otd. Khim. Nauk*, (in Russian), **10**, 1931 (1960).

10) G. Brauer, "Rukovodstvo po preparativnoi neorganicheskoi khimii," Moscow (1956).

11) G. D. Chukin, *Zh. Struct. Khim.*, **17**, 122 (1976).

12) H. H. Knozinger and P. Ratnasamy, *Catal. Rev. Sci. Eng.*, **17**, 31 (1978).

13) J. B. Peri, *J. Phys. Chem.*, **69**, 211, 220 (1965).

14) M. R. Basila, *J. Phys. Chem.*, **66**, 2223 (1962).

15) L. A. Ignat'eva and G. D. Chukin, *Zh. Prikl. Khim.*, **10**, 672 (1969).

16) A. I. Trokhimets, P. P. Mardilovich, and G. N. Lysenko, *Zh. Prikl. Spectrosk.*, **30**, 878 (1979).

17) A. A. Davydov, N. A. Rubens, and Yu. M. Shchekochikhin, "Adsorpstiya i adsorbenty," Resp. mezhved. Sb., Kiev, Naukova dumka (1976), Vol. 4, p. 81.

18) A. Zecchina, S. Coluccia, E. Guglielminotti, and G. Chiotti, *J. Phys. Chem.*, **75**, 2774 (1971).

19) D. Shopov, A. Palazov, A. Andreev, L. Prahov, and D. Michajlova, *Izv. Otd, Khim. Nauki, Bulg. Akad. Nauk*, **6**, 787 (1973).

Kinetics of Gas Phase Addition Reactions of Trichlorosilyl Radicals. VI.[1] Orientation of Additions to 2-Pentenes

Takaaki DOHMARU* and Yoshio NAGATA
Radiation Center of Osaka Prefecture, Shinke-cho, Sakai, Osaka 593
(Received October 8, 1982)

Synopsis. Addition reactions of $\cdot SiCl_3$ radicals to *cis*- and *trans*-2-pentene have been studied in the gas phase between 30 and 136 °C. The ratio of the rate of formation of 2- with 3-trichlorosilylpentane, R_2/R_3, was found to vary with temperature or with $HSiCl_3$ concentrations (1.47—17.6 μmol cm^{-3}). This variation was successfully interpreted by the decomposition of an adduct radical, $CH_3CH(SiCl_3)\dot{C}HCH_2CH_3$.

Quantitative studies of silyl radicals are of general interest now. Previously,[2] we reported that the addition of $\cdot SiCl_3$ radicals to *cis*-2-pentene gave 2- and 3-trichlorosilylpentane (2- and 3-TSP) and that the ratio of formation of the two isomers, R_2/R_3, was 0.47 invariant either with temperature (133—182 °C) or with $HSiCl_3$ concentrations (1.34—5.38 μmol cm^{-3}). It was then found, however, that R_2/R_3 was *ca.* 1.2 in a radiation induced reaction of $HSiCl_3$ with *cis*-2-pentene in cyclohexane at room temperature which was performed to prepare authentic samples of 2- and 3-TSP. It is of interest that the value of R_2/R_3 in the liquid phase is quite different from that in the gas phase. Further, orientation of addition in unsymmetrical olefins may be of importance in relation to the nature of the transition state.[3]

In this connection, we studied the variation of R_2/R_3 with $HSiCl_3$ concentrations and with temperature between 30 and 136 °C to cover the temperature range below that of the previous study.

Experimental

Materials and procedures are essentially similar to those described earlier.[2] Mixtures of CH_3COCH_3, 2-pentene, and $HSiCl_3$ were introduced into a cylindrical Pyrex cell of 137 cm^3 which was heated in an electric oven. The light source was a 50 W medium pressure mercury arc. During this series of experiments, the rate of absorption of light was 7×10^{-12} einstein cm^{-3} min^{-1}. After photolysis, the reaction mixture was passed to a gas sampling loop and was immediately analyzed by GLC.

Results and Discussion

Mixtures of CH_3COCH_3 (2.90 μmol cm^{-3}), $HSiCl_3$ (8.70 μmol cm^{-3}) and *cis*- or *trans*-2-pentene (0.58 μmol cm^{-3}) were photolyzed between 30 and 136 °C in the gas phase. Products were almost exclusively $(CH_3)_2CHOSiCl_3$ (A), 2-, and 3-TSP. The ratio of the rate of formation of the two isomers, R_2/R_3, are shown in Fig. 1 as a function of temperature. R_2/R_3 was *ca.* 1.2 at 30 °C but decreased with an increase in temperature. At 136 °C it agreed with the value of 0.47 previously[2] obtained at higher temperatures. In addition, there was no significant difference in reactivity between *cis*- and *trans*-2-pentene.

The Arrhenius plots of the rate of formation of the respective products are given in Fig. 2.

The plot of log R_A against $1/T$ is seen to be linear; the least-mean-squares treatment of the plot gives

$$\log(R_A/\mu mol\ cm^{-3}\ min^{-1}) = 2.52 \pm 0.14 - (2.26\pm0.05)\times10^3/T. \quad (1)$$

In the photolysis of CH_3COCH_3 in the presence of $HSiCl_3$ and 2-pentene, the addition of $\cdot SiCl_3$ radicals to CH_3COCH_3[4] and to 2-pentene[2] is known to constitute chain propagating steps as shown in the following.

$$\cdot SiCl_3 + CH_3COCH_3(Ac) \longrightarrow (CH_3)_2\dot{C}OSiCl_3(\dot{A}) \quad (2)$$

$$\cdot A + HSiCl_3(TCS) \longrightarrow (CH_3)_2CHOSiCl_3(A) + \cdot SiCl_3 \quad (3)$$

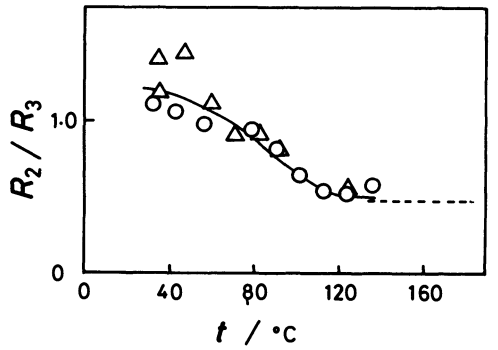

Fig. 1. Variation of R_2/R_3 with temperature.
○: *cis*-Δ^2-C_5H_{10}, △: *trans*-Δ^2-C_5H_{10}, ------: from Ref. 2. $[\Delta^2\text{-}C_5H_{10}]=0.58$, $[CH_3COCH_3]=2.90$, $[HSiCl_3]=8.70$ μmol cm^{-3}.

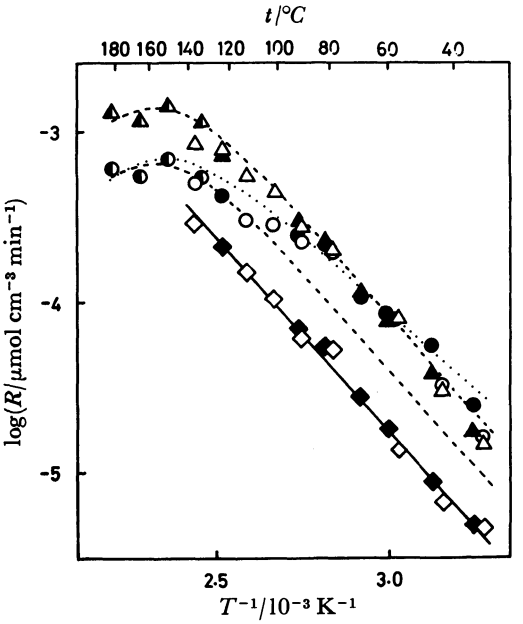

Fig. 2. Arrhenius plots of the rate of formation of the products.
◇: A (Shifted by −0.5), ○: 2-TSP, △: 3-TSP, ◐: 2-TSP from Ref. 2, ▲: 3-TSP from Ref. 2, ------: calculated (see text), ·····: simulation curve based upon Eq. 11. Closed marks are from *trans*-Δ^2-C_5H_{10}.

$$\cdot SiCl_3 + \Delta^2\text{-}C_5H_{10}(P) \rightleftharpoons CH_3\dot{C}HCHCH_2CH_3(\dot{P}_2) \quad (4,-4)$$
$$\qquad\qquad\qquad\qquad\qquad\quad SiCl_3$$
$$\cdot SiCl_3 + \Delta^2\text{-}C_5H_{10}(P) \rightleftharpoons CH_3\dot{C}HCHCH_2CH_3(\dot{P}_3) \quad (4',-4')$$
$$\qquad\qquad\qquad\qquad\qquad\quad SiCl_3$$

$$\cdot P_2 + HSiCl_3 \longrightarrow 2\text{-TSP} + \cdot SiCl_3 \quad (5)$$

$$\cdot P_3 + HSiCl_3 \longrightarrow 3\text{-TSP} + \cdot SiCl_3 \quad (5')$$

Chain terminating radicals are probably[4] $\cdot A$, $\cdot P_2$, and $\cdot P_3$. Irreversibility of reaction (2) up to 253 °C has already been shown[4] in this laboratory.

In the scheme above, three chain cycles resulting in the adducts A, 2-, 3-TSP occur concurrently. Assuming low conversions of the reactants and long reaction chains, one obtain the following rate equations by the conventional steady state treatment.

$$R_2/R_A = ([P]/[Ac])(k_4/k_2)\{1+(k_{-4}/k_5)[TCS]^{-1}\}^{-1}, \quad (6)$$

$$R_3/R_A = ([P]/[Ac])(k_{4'}/k_2)\{1+(k_{-4'}/k_{5'})[TCS]^{-1}\}^{-1}, \quad (6')$$

where R_2, R_3, and R_A denote the rates of formation of 2-, 3-TSP, and A, respectively.

Recently,[2] we obtained the following rate constant ratios for *cis*-2-pentene between 133 and 182 °C using Eqs. 6 and 6'.

$$\log(k_4/k_2) = 0.57,\ \log(k_{4'}/k_2) = 0.89$$
$$\log(k_{-4}/k_5) = 5.39 - 20500/2.3RT(\text{mol cm}^{-3}),$$
$$\text{and}\quad \log(k_{-4'}/k_{5'}) = \log(k_{-4}/k_5). \quad (7)$$

Based upon these values, Eqs. 6, 6', and 1 allow the values of $\log R_2$ and $\log R_3$ to be calculated in the extended temperature range. These calculated values are illustrated in Fig. 2 as dotted lines. It is interesting to note that while $\log R_3$ agrees with the dotted line over the temperature range adopted, $\log R_2$ behaves quite differently with the extended value especially at low temperatures.

The results in Fig. 2 imply that the change in orientation of addition illustrated in Fig. 1 may be caused only by the change in R_2.

Another series of experiments was carried out to ascertain this implication. With other conditions being kept constant, the dependence of the rate of formation of the products on $HSiCl_3$ concentrations was studied at 61 °C. The results are shown in Fig. 3. To check the third body effect, 17.6 μmol cm^{-3} of CO_2 was added at $[HSiCl_3]=1.47$ μmol cm^{-3}, but there was almost no effect.

The results in Fig. 3 show that the variation of $[HSiCl_3]$ has almost no effect on R_3/R_A but has strong effect on R_2/R_A. This fact suggests that some reactions eliminating $\cdot P_2$ radicals compete with reaction (5). The most probable reactions as such are (8), (9), and (−4).

$$\cdot P_2 + \cdot R(\text{any radicals}) \longrightarrow \text{products} \quad (8)$$
$$\cdot P_2 + P \longrightarrow \text{telomer} \quad (9)$$

Reaction (8) is indeed occurring as one of the terminating reactions. But the kinetic chain length of reaction (5) is estimated to be >10 in this experiment, *i.e.*, $R_8/R_2<0.1$, so reaction (8) cannot contribute to the change in R_2 to such an extent as is shown in Fig. 3.

Since $\cdot P_2$ is more reactive than $\cdot P_3$ (stabilized by CH_3–) or $\cdot A$ (tertiary radical), reaction (9) may be reasonably assumed more important than the similar

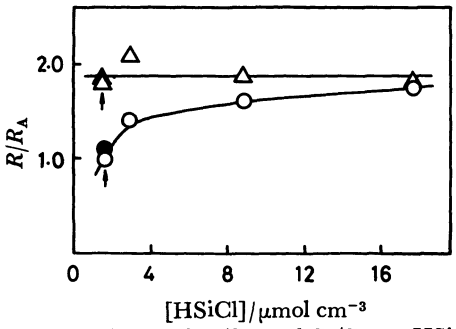

Fig. 3. Dependence of R_2/R_A and R_3/R_A on $HSiCl_3$ concentrations.
△: R_3/R_A, ○: R_2/R_A, ▲, ●: 17.6 μmol cm^{-3} of CO_2 was added. ↑: Formation of *trans*-Δ^2-C_5H_{10} was checked in this run. [*cis*-Δ^2-C_5H_{10}]=0.58, [CH_3COCH_3]=2.90 μmol cm^{-3}.

telomerization reactions involving $\cdot P_3$ or $\cdot A$. When reaction (9) is tentatively included in the mechanism, R_2/R_A is derived as in Eq. 10.

$$R_2/R_A = ([P]/[Ac])(k_4/k_2)\{1+(k_{-4}/k_5)[TCS]^{-1} + (k_9/k_5)([P]/[TCS])\}^{-1} \quad (10)$$

The result in Fig. 3 could be interpreted in terms of Eq. 10 if $k_9/k_5=2.5$ at 61 °C were assumed. But this ratio is clearly too large because alkyl radicals abstract H atoms from $HSiCl_3$[5] faster than they add to alkenes.[6]

Reaction (−4) would accompany *cis-trans* isomerization of 2-pentene. Under the condition indicated in Fig. 3, we checked the formation of *trans*-2-pentene and found that *cis-trans* rearrangement occurred ($R_{trans}=2.3\times10^{-4}$ μmol cm^{-3} h^{-1}) to the extent comparable to the difference between R_3 and R_2 ($R_3-R_2=3.8\times10^{-4}$ μmol cm^{-3} h^{-1}). Without $HSiCl_3$, however, the isomerization occurred ($R_{trans}=1.4\times10^{-4}$ μmol cm^{-3} h^{-1}) as might be expected from the study by Cundall and Davies.[7] Comparison of the rates of isomerization with and without $HSiCl_3$, shows clearly that $\cdot SiCl_3$ radicals enhance isomerization.

Based upon the fact that $\cdot P_2$ radicals decompose at moderate temperatures the values of k_{-4}/k_5 and k_4/k_2 were obtained by iterative calculation to satisfy the result in Fig. 2 (trial and error calculations were made).

$$\log(k_{-4}/k_5) = 4.89 - 19500/2.3RT$$
$$\log(k_4/k_2) = -0.54 + 2190/2.3RT \quad (11)$$

The curve for $\log R_2$ based upon Eq. 11 is shown in Fig. 2.

References

1) Part V: T. Dohmaru and Y. Nagata, *J. Phys. Chem.*, **86**, 4522 (1982).
2) T. Dohmaru and Y. Nagata, *J. Chem. Soc., Faraday Trans. 1*, **78**, 1141 (1982).
3) J. M. Tedder and J. C. Walton, *Acc. Chem. Res.*, **9**, 183 (1976).
4) T. Dohmaru, Y. Nagata, and J. Tsurugi, *Bull. Chem. Soc. Jpn.*, **45**, 2660 (1972).
5) N. L. Arthur and T. N. Bell, *Rev. Chem. Intermediates*, **2**, 37 (1978).
6) J. M. Tedder and J. C. Walton, "Advances in Physical Organic Chemistry," ed by V. Gold and D. Bethell, Academic Press, London (1978), Vol. 16, p. 51.
7) R. B. Cundall and A. S. Davies, *Proc. R. Soc. London, Ser. A*, **290**, 563 (1966).

Induced Circular Dichroism of Two Chromophores Included in γ-Cyclodextrin

Nagao KOBAYASHI,* Yoshihiro HINO, Akihiko UENO,* and Tetsuo OSA
Pharmaceutical Institute, Tohoku University, Aobayama, Sendai 980

(Received October 22, 1982)

Synopsis. Induced circular dichroism (ICD) has suggested that γ-cyclodextrin (γ-CDx) accommodates two molecules of naphthalene and its derivatives with nearly axial inclusion but that it includes two Acridine Orange (AO) molecules with *S*-helicity.

In contrast to α- and β-CDxs which form mainly one host-one guest complexes with small arenes,[1] recent fluorescent studies have suggested that γ-CDx can include two arene molecules.[2-5] However, only a few studies have appeared on the ICD of two arene molecules in γ-CDx,[6-9] although ICD has been substantiated to be a powerful approarch to elucidate types of inclusion and configuration of arene molecules in CDxs.[10,11] Quite recently, we have shown that two pyrene molecules trapped in γ-CDx have *S*-helicity.[7,8] In this report, we describe the results for ICD of AO and naphthalene and its derivatives in the presence of γ-CDx.

Experimental

Materials. Naphthalene and its derivatives were recrystallized several times from appropriate solvents. 3,4-Bis[2-[2-(2-naphthyloxy)ethoxy]ethoxy]benzoic acid (**1**) was prepared in this laboratory.[12] AO (Chroma 1B-307, Germany) was purified according to the literature method.[13] γ-CDx was provided by Dr. N. Nakamura.

Measurements. Fluorescence spectra were recorded on a Shimadzu RF-500 spectrofluorophotometer, absorption spectra on a Shimadzu UV-360 spectrophotometer, and ICD spectra on a JASCO J-400X spectropolarimeter with a DP-500 data-processor at ambient temperature.

Results and Discussion

Figure 1 shows the absorption and ICD spectra of the γ-CDx–AO system. Absorption peaks appeared at 204, 230, 265, and 463 nm. Although the band position and shape of AO are known to be sensitive to temperature, ionic strength, and pH of the solution,[14,15] the present system seems to be composed mainly of dimeric AOs with a little amount of aggregated AOs. This is due to the fact that the bands of monomeric, dimeric, and aggregated AOs occur at *ca.* 490, 470, and 450 nm, respectively.[14,16] In the ICD spectrum, a curve with a change in sign from plus to minus and further to plus viewing from the longer wavelength side was observed in the visible region. As seen, two cross points well correspond to the absorption shoulder and/or peak. These facts indicate that this ICD originates from a dipole coupling between two AO molecules in γ-CDx. The situation is also the same for the UV region. Since the bands at 265 and 463 nm are both assigned to a polarization along the long axis,[17] the results of above ICD indicate that the two AO molecules are included in γ-CDx with *S*-helicity.

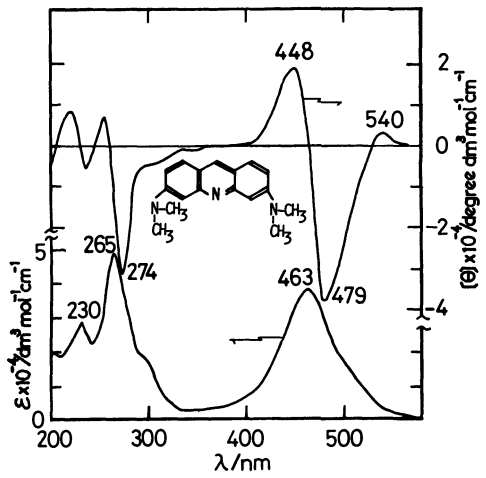

Fig. 1. Absorption (bottom) and ICD (top) spectra of AO in the presence of γ-CDx. [AO]/mol·l^{-1}=1×10^{-4}, [γ-CDx]/mol·l^{-1}=10^{-2}, Solvent: 0.5 mol·l^{-1} phosphate buffer, pH 6.1. Pathlength: 0.2 mm.

Two-guest inclusion of naphthalene and its derivatives into γ-CDx was examined similarly. The results for naphthalene and **1** are demonstrated in Figs. 2 and 3, respectively. As revealed, the intensity ratio of excimer/monomer fluorescence (ratio of emission at 396/334 nm) of naphthalene was larger for a system containing γ-CDx than that containing β-CDx, suggesting inclusion of more than one naphthalene in γ-CDx. Although a monomer fluorescence had still a comparable intensity as that of excimer, ICD spectrum was measured in the presence of γ-CDx. Simple peaks or troughs were

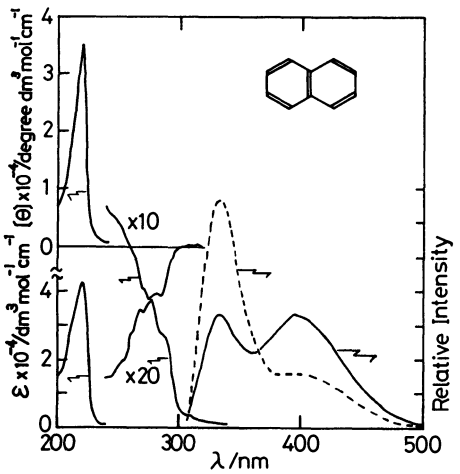

Fig. 2. Absorption (left bottom), ICD (left top), and fluorescence (right) spectra of naphthalene in the presence of γ-CDx (solid line) or β-CDx (dotted line). [naphthalene]/mol·l^{-1}=1.2×10^{-4},[γ-CDx]/mol·l^{-1}=[β-CDx]/mol·l^{-1}=10^{-2}. Solvent: 0.1 mol-l^{-1} phosphate buffer, pH 6.8. Pathlength: 10 mm except for 200—240 nm region (1 mm). In the fluorescence spectra, excitation was at 290 nm.

observed nearly accurately at the wavelengths where ^1L_b, ^1L_a, and ^1B_b transitions appear, but a dipole coupling type spectrum was not recognized.

To clarify the features in Fig. 2, **1** was used (Fig. 3).

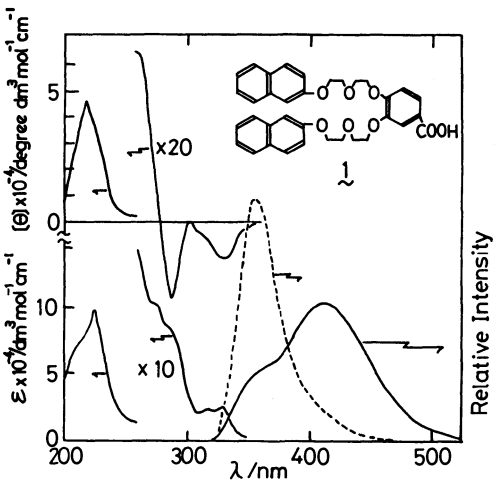

Fig. 3. Absorption (left bottom), ICD (left top), and fluorescence (right) spectra of **1** in the presence (solid line) or absence (dotted line) of γ-CDx. [**1**]/mol·l^{-1}= 1.1×10^{-4}, [γ-CDx]/mol·l^{-1}=10^{-2}. Solvent: 0.1 mol·l^{-1} borate buffer, pH 9.2. Pathlength: 10 mm except for 200—260 nm region (1 mm). In the fluorescence spectra, excitation was at 290 nm.

As shown, **1** showed only monomer fluorescence in the absence of γ-CDx. However, by the addition of γ-CDx, it revealed mainly excimer fluorescence alone, suggesting the inclusion of two naphthalene moieties. The ICD spectrum of this solution showed a single peak associated with the ^1B_b transition. For the interpretation of this phenomenon, two possibilities are deduced. One is that two naphthalene moieties are trapped with their long axes nearly parallel to each other, and another is that even two naphthalene moieties of **1** are not so much bulky for the large cavity of γ-CDx so that it may not have a fixed configuration to produce a clear dipole coupling type spectrum. However, the latter possibility may be small because free movement of the naphthalene moieties of **1** in γ-CDx is restricted by the alkyl chain connecting them.

After convincing the fair development of excimer fluorescence by the addition of γ-CDx, we measured also the ICD spectra of 1- or 2-naphthylacetic acid, 1- or 2-naphthoic acid, and 1- or 2-(naphthyloxy)acetic acid. However, in no case was found a dipole coupling type spectrum.

One plausible reason for the above difference in the ICD spectra between AO and naphthalene derivatives might be ascribed to the difference of the character of guest molecule themselves such as sizes and tendency toward aggregation.

Thus, the ICD spectroscopy coupled with electronic absorption or fluorescence spectroscopy has suggested that γ-CDx accepts two Acridine Orange molecules with *S*-helicity, but that it accommodates two naphthalene molecules with nearly axial inclusion.

We thank Dr. Y. Sato of this institute for his variable comments, and Dr. N. Nakamura (Japan Maize Products Co. Ltd.) for kindly providing γ-CDx. This research was partly supported by a Grant-in-Aid for Scientific Research No. 57771477 from the Ministry of Education, Science and Culture.

References

1) M. L. Bender and M. Komiyama, "Cyclodextrin Chemistry," Springer-Verlag, Berlin (1978).
2) A. Ueno, K. Takahashi, and T. Osa, *J. Chem. Soc., Chem. Commun.*, **1980**, 921; **1981**, 95, 194.
3) J. Emert, D. Kodali, and R. Catena, *J. Chem. Soc., Chem. Commun.*, **1981**, 758.
4) N. J. Turro, T. Okubo, and G. C. Weed, *Photochem. Photobiol.*, **35**, 325 (1982).
5) K. Kano, T. Takenoshita, and T. Ogawa, *J. Phys. Chem.*, **86**, 1833 (1982).
6) N. Kobayashi, A. Ueno, and T. Osa, *J. Chem. Soc., Chem. Commun.*, **1981**, 340.
7) N. Kobayashi, R. Saito, Y. Hino, A. Ueno, and T. Osa, *J. Chem. Soc., Chem. Commun.*, **1982**, 706.
8) N. Kobayashi, R. Saito, H. Hino, Y. Hino, A. Ueno, and T. Osa, *J. Chem. Soc., Perkin Trans. 2*, in press.
9) N. Kobayashi, R. Saito, A. Ueno, and T. Osa, *Makromol. Chem.*, **1983**, 184.
10) H. Shimizu, A. Kaito, and M. Hatano, *Bull. Chem. Soc. Jpn.*, **52**, 2678 (1979); **54**, 513 (1981).
11) K. Harata, *Bull. Chem. Soc. Jpn.*, **51**, 2727 (1978) and references cited therein Nos. 5, 6, 8, and 18.
12) A. Ueno, Y. Hino, and T. Osa, Manuscripts are now in preparation.
13) D. D. Perrin, W. L. F. Armarego, and D. R. Perrin, "Purification of Laboratory Chemicals," Pergamon Press, Oxford (1980), p. 86.
14) V. Zanker, *Z. Phys. Chem.*, **2**, 52 (1954).
15) B. C. Myhr and J. G. Foss, *Biopolymers*, **4**, 949 (1966).
16) D. F. Bradley and M. K. Wolf, *Proc. Natl. Acad. Sci., U. S.*, **45**, 944 (1959).
17) R. E. Ballard, A. J. McCaffery, and S. F. Mason, *Biopolymers*, **4**, 97 (1966).

Solvent Effects on the Nonradiative Relaxation Processes of the Lowest Excited Singlet States of Meso-substituted Bromoanthracenes

Kumao HAMANOUE,* Toshiharu HIDAKA, Toshihiro NAKAYAMA, Hiroshi TERANISHI, Minoru SUMITANI,† and Keitaro YOSHIHARA†

Department of Chemistry, Faculty of Technology, Kyoto Institute of Technology, Matsugasaki, Sakyo-ku, Kyoto 606
†Institute for Molecular Science, Myodaiji, Okazaki 444

(Received November 15, 1982)

Synopsis. From the measurements of the fluorescence lifetimes and the 0-1 emission maxima in solutions, it is concluded that the solvent dependence of the nonradiative transition rates of the lowest excited singlet states of 9-bromoanthracene and 9,10-dibromoanthracene is due to the different extent to which the lowest excited singlet and adjacent higher excited triplet states are stabilized by solvents.

The nonradiative process of the fluorescing state in anthracene derivatives has been studied extensively,[1,2] and it is well known that the fluorescence quantum yields of 9- and 9,10-substituted anthracenes in fluid media decrease as the temperature is increased. This temperature dependence has been attributed to thermally activated intersystem crossing (isc) from the lowest excited singlet state S_1 to an adjacent higher excited triplet state T_n.

Our direct measurements of the temperature dependence of the fluorescence lifetimes of 9-bromoanthracene (BA) and 9,10-dibromoanthracene (DBA)[2] have allowed the determination of the rate constant for isc in the form $k_{isc}=A_{isc}\exp(-\Delta E/kT)$, with activation energies of 600 and 1100 cm^{-1} for BA and DBA in 3-methylpentane, respectively.

From the measurements of the 0-1 emission maxima and of the fluorescence lifetimes by single photon counting method in solutions, Wu and Ware[3] have concluded that the solvent dependence of the nonradiative transition rate of the lowest excited singlet state in DBA is due to the different extent to which S_1 and T_n are stabilized by the solvent.

Since the S_1 lifetimes of BA are very short and the single photon counting method in subnanosecond region sometimes gives some errors, this article reports the results of the solvent effects on the S_1 lifetimes of BA and DBA using a streak camera by picosecond laser photolysis in order to see whether Wu and Ware's relation can generally be applied or not.

Experimental

9-Bromoanthracene (EP grade) was purchased from Tokyo Kasei Kogyo Co., Ltd., and 9,10-dibromoanthracene was synthesized by bromination of anthracene.[4] After repeated crystallization from methanol, both samples were purified by vacuum sublimation. G.R.-grade 3-methylpentane (Wako) and spectral-grade ethanol (Nakarai), diethyl ether (Merck) and all the other solvents (Dojin) were used without further purification. The sample solution were degassed by several freeze-pump-thaw cycles. By the excitation of the sample using the third harmonic (355 nm) with a pulse width of 15 ps from a mode-locked Nd^{3+}: YAG laser, the decay of $S_1\rightarrow S_0$ fluorescence was measured by a Hamamatsu C-979 streak camera with an S-20 cathode. The streak image was detected by a TV camera and treated by a Hamamatsu C-1098 microprocessor. Steady-state fluorescence spectra were taken with a Shimadzu RF-502 fluorescence spectrophotometer. All the experiments were carried out at room temperature (296 K) and the concentration of the sample was about 1×10^{-4} mol dm^{-3}.

Results and Discussion

A typical fluorescence decay of BA is shown in Fig. 1. The smooth curve (dotted line) in Fig. 1 is calculated by

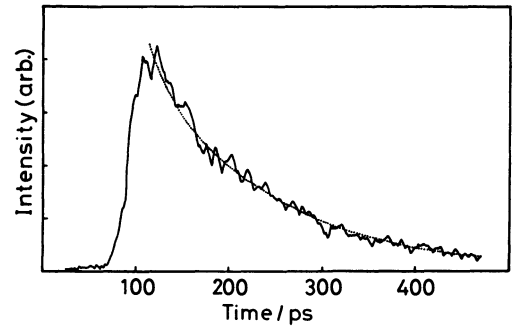

Fig. 1. Fluorescence decay curves of 9-bromoanthracene in acetonitrile at 296 K. ——: Observed curve by a streak camera, ……: simulated curve based on a single exponential decay with $k=6.25\times10^9$ s^{-1}.

a least-squares method assuming a single exponential decay of fluorescence. All the experimental fluorescence decays could be fitted with high precision to a single exponential decay function, that is, the average deviation for fitting to the experimental data was within $\pm0.3\%$ and the standard deviations of the best fit rate constants (k) were between 3 and 8%.

As the relative energy of the S_1 state, the wave number of the 0-1 emission band, $\bar{\nu}(0,1)$, of the fluorescence spectrum was taken instead of that of the 0-0 emission band, $\bar{\nu}(0,0)$, because $\bar{\nu}(0,1)$ could be determined more accurately. Table 1 gives the values of S_1 lifetimes ($\tau=k^{-1}$) and $\bar{\nu}(0,1)$ of BA and DBA.

Although the fluorescence lifetimes of DBA are consistent with those observed by Wu and Ware[3] and Cherkasov *et al.*,[5] the values of BA are an order of magnitude shorter than those observed by Cherkasov *et al.*[5] and Dreeskamp and Pabst.[6] This discrepancy is probably due to uncertainty of their single photon counting method in the subnanosecond region, because the fluorescence lifetimes of BA in acetonitrile are 0.16 ns by the present Nd^{3+} : YAG laser photolysis and 0.5 ns by our single photon counting method, the latter value being the lowest measurable value which the apparatus can give.

As have described in our previous paper,[2] the total rate of the S_1 decay process is expressed as

Table 1. Values of S_1 lifetimes and $\bar{\nu}(0,1)$ of BA and DBA in various solvents

	Solvent	BA		DBA	
		Lifetime τ/ps	$\bar{\nu}(0,1)$ / cm^{-1}	Lifetime τ/ns	$\bar{\nu}(0,1)$ / cm^{-1}
(1)	Hexane	113±6	24100	1.12±0.01	23220
(2)	Diethyl ether	124±8	24040	1.21±0.02	23180
(3)	3-Methylpentane	126	24050	1.11	23250
(4)	Cyclohexane	137	24010	1.46	23150
(5)	Methanol	145±2	24030	0.94±0.02	23220
(6)	Ethanol	148±3	24000	1.39	23170
(7)	Acetonitrile	160	23920	1.27±0.02	23150
(8)	Methylcyclohexane	203±5	24000	3.36	23120
(9)	Acetone	269±2	23920	1.41	23120
(10)	Tetrahydrofuran	291±3	23870	—	—
(11)	Benzene	313	23720	2.54	22890
(12)	Carbon tetrachloride	318	23750	2.62±0.04	22940
(13)	Toluene	322	23720	2.50±0.19	22900
(14)	Chloroform	335	23780	2.73±0.02	22940
(15)	Bromobenzene	483±7	23570	3.67±0.14	22720
(16)	1,2-Dichloroethane	370	—	3.15	22960

$$k = k_r + A_{isc}\exp(-\Delta E/kT), \quad (1)$$

where k_r is the rate constant for the $S_1 \rightarrow S_0$ fluorescence, and the temperature-dependent component for the $S_1 \rightarrow T_n$ intersystem crossing is described by an Arrhenius term of frequency factor A_{isc} and activation energy ΔE.

Assuming the Arrhenius parameter A_{isc} is constant through the series of solvents, Wu and Ware[3] gave the following relation between activation energy and $\bar{\nu}(0,1)$ for DBA,

$$(\alpha-1)[\bar{\nu}(0,1)-\bar{\nu}_0(0,1)] = \Delta E - \Delta E_0, \quad (2)$$

where $\bar{\nu}_0(0,1)$ and ΔE_0 refer to a reference solution and α is the ratio of the solvent stabilization energies of the T_n state to that of the S_1 state, *i.e.*, $\alpha = 0.31 \pm 0.02$.

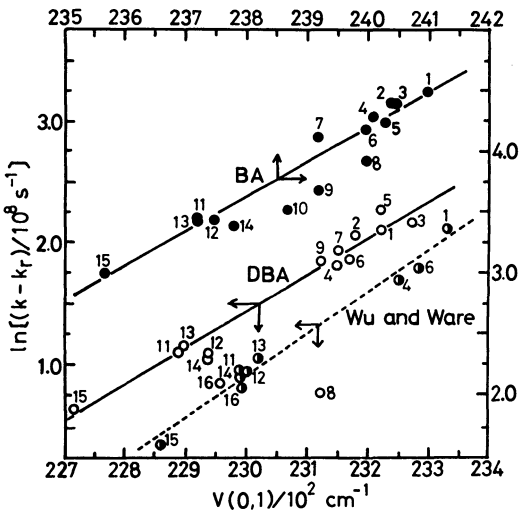

Fig. 2. Plots of $\ln[(k-k_r)/10^8\ s^{-1}]$ *vs.* $\bar{\nu}$ (0, 1). Numbers of the points refer to Table 1. Dotted line show the results of Wu and Ware for DBA.[3]

Plots of $\ln(k-k_r)$ *vs.* $\bar{\nu}(0,1)$ for BA and DBA are shown in Fig. 2 together with the result of Wu and Ware for DBA,[3] where k_r is the average of the radiative rate constants at 77 K in 3-methylpentane and EPA (ether/isopentane/ethanol=5 : 5 : 2 in volume ratio), that is, $k_r = 7.81 \times 10^7$ and $8.20 \times 10^7\ s^{-1}$ for BA and DBA, respectively.[2] It is obvious from Fig. 2 that all the experimental points lie reasonably close to a straight line. The values of α obtained by the least-squares method are 0.43±0.01 for BA and 0.39±0.06 for DBA, that is, the stabilization energy of T_n by solvents is about 40% to that of S_1 stabilization. Our values of α and $(k-k_r)$ for DBA is nearly equal to those obtained by Wu and Ware. As can be seen from Fig. 2, the solid line for DBA comes to the dotted line (Wu and Ware) by the horizontal shift of 1—2 nm. Thus, one can say that our result is identical with that obtained by Wu and Ware for DBA.

In conclusion, the relation obtained by Wu and Ware may be applicable to 9- and 9,10-substituted anthracenes who have activation energies in isc processes.

References

1) K. Hamanoue, S. Hirayama, T. Nakayama, and H. Teranishi, *J. Phys. Chem.*, **84**, 2074 (1980).

2) M. Tanaka, I. Tanaka, S. Tai, K. Hamanoue, M. Sumitani, and K. Yoshihara, *J. Phys. Chem.*, **87**, 813(1983) and references cited therein.

3) Kam-Chu Wu and W. R. Ware, *J. Am. Chem. Soc.*, **101**, 5906 (1979).

4) "Oranic Syntheses," ed by H. Gieman, John Wiley and Sons, New York(1967), p. 207.

5) A. S. Cherkasov, V. A. Molchanov, T. M. Vember, and K. G. Voldaikina, *Sov. Phys. Dokl.*, **1**, 427 (1956).

6) H. Dreeskamp and J. Pabst, *Chem. Phys. Lett.*, **61**, 262 (1979).

Graph-theoretical Formula for Ring Currents Induced in a Polycyclic Conjugated System

Jun-ichi AIHARA* and Tsuyoshi HORIKAWA
Department of Chemistry, Faculty of Science, Shizuoka University, Oya, Shizuoka 422
(Received January 22, 1983)

Synopsis. A graph-theoretical formula was derived for ring currents induced in a polycyclic conjugated system by a uniform magnetic field. Two advantages of this formula are that ring currents can be evaluated by inspecting a geometry of a conjugated system, and that they can be attributed to the individual π-electron rings.

In previous papers[1-6] we developed the theory of London (or ring-currents) diamagnetism[7-9] using graph-theoretical terms. This approach was found to be best suited for analyzing magnetic properties of a polycyclic conjugated system in conjunction with its structural features. We now extend our graph theory to uncover geometrical aspects of ring currents induced in a polycyclic system by a uniform magnetic field. Ring currents themselves were first formulated by Pople and McWeeny in 1958.[9-11]

We clarified before[2] that London (or ring-currents) susceptibility of a polycyclic conjugated system G, χ_G, can be partitioned exactly among the constituent π-electron rings, namely,

$$\chi_G = \sum_i^G \chi_i, \tag{1}$$

where χ_i is a susceptibility contribution from the ith π-electron ring, and i runs over all π-electron rings defined in Sachs' sense.[12] Explicitly, χ_i is expressed as[2]

$$\chi_i = -4\left(\frac{e}{c\hbar}\right)^2 \beta S_i^2 \sum_{j=1}^{n} \frac{P_{G-r_i}(X_j)}{P_G'(X_j)}. \tag{2}$$

Here, $P_G(X)$ is a characteristic polynomial for G; $P_G'(X)$ is a first derivative of $P_G(X)$ with respect to X; X_j is the jth largest root of the equation $P_G(X)=0$, *i.e.*, the jth orbital energy given relative to the carbon Coulomb integral and in units of β; n denotes the highest occupied orbital; r_i is the ith π-electron ring; G-r_i is a subsystem of G, obtained by deleting from G the ith π-electron ring and all π bonds incident to it; S_i is an area of the ith π-electron ring; and e, c, and $\hbar$ are the standard constants with these symbols.

The external magnetic field H provokes an induced moment M_G opposing it and given by the expression:

$$M_G = \chi_G H = \sum_i^G \chi_i H. \tag{3}$$

We define a partial moment of the ith π-electron ring by

$$M_i = \chi_i H. \tag{4}$$

Our hypothesis is that M_i arises from an induced ring current I_i circulating around the ith π-electron ring, *i.e.*,

$$M_i = \frac{I_i S_i}{c}. \tag{5}$$

The assumed ring current I_i is then expressible as

$$I_i = \frac{c\chi_i H}{S_i} = -4\frac{e^2}{c\hbar^2}\beta S_i H \sum_{j=1}^{n} \frac{P_{G-r_i}(X_j)}{P_G'(X_j)}. \tag{6}$$

When there are degenerate orbitals in G, Eq. 2 cannot be applied to them. We instead verified that four π electrons in doubly degenerate orbitals contribute to χ_i by the amount:[2]

$$\Delta\chi_i = -4\left(\frac{e}{c\hbar}\right)^2 \beta S_i^2 \times \frac{U(X_{j*})P_G'_{-r_i}(X_{j*}) - U'(X_{j*})P_{G-r_i}(X_{j*})}{U(X_{j*})^2}, \tag{7}$$

where X_{j*} is a degenerate orbital energy, and

$$U(X) = \frac{P_G(X)}{(X-X_{j*})^2}. \tag{8}$$

Owing to Eq. 7, we can still define a partial moment for each π-electron ring. A ring current induced in benzene, I_0, is calculated as

$$I_0 = -\frac{2}{9}\frac{e^2}{c\hbar^2}\beta S_0 H, \tag{9}$$

where S_0 is an area of the benzene ring.

Finally, a ring current induced in a given π-electron ring of a polycyclic system is estimated in units of I_0 as

$$\frac{I_i}{I_0} = 18\frac{S_i}{S_0}\sum_{j=1}^{n}\frac{P_G'_{-r_i}(X_j)}{P_G'(X_j)}. \tag{10}$$

Ring currents thus calculated for all π-electron rings of four compounds are presented in Fig. 1. We assumed that

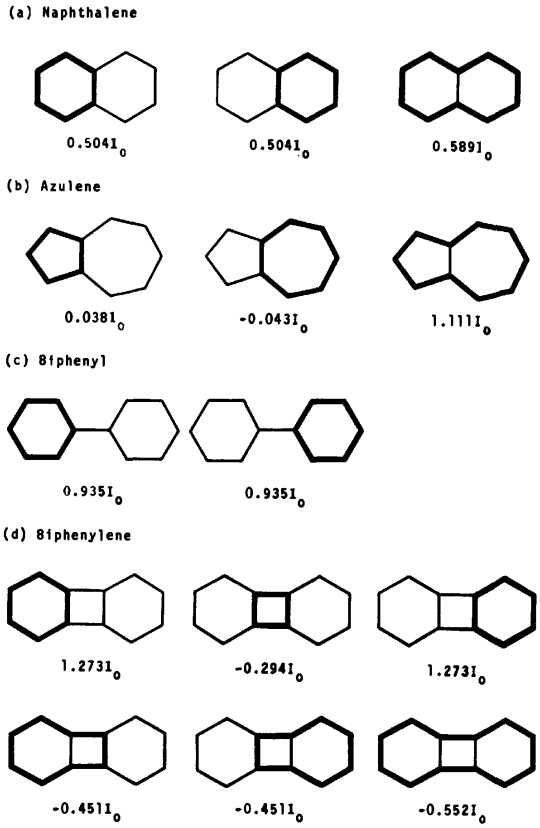

Fig. 1. Constituent π-electron rings and ring currents.

these compounds are structurally combinations of regular polygons with sides equal to a standard carbon-carbon π-bond length. Summing up all ring currents flowing through a given π bond, we obtain an overall current induced there. Overall currents estimated in this manner were found to be exactly the same as those reported by Pople,[10] McWeeny,[13] and Memory.[14] Mathematically, this way of reasoning is identical with that of Pople.[9,10] In this sense, our postulate given as Eq. 5 seems to be quite reasonable. It is to be noted that at the limit of zero field strength ring currents induced in different π-electron rings do not interact with each other, and that the overall current flowing at each π bond is simply an additive sum of individual ring currents defined by Eq. 6.

Salem[9] stated that, for naphthalene and azulene, the central π bond hardly perturbs the annulenic conjugated system formed by the perimeter of ten sp^2-carbon atoms. However, our analysis revealed that the ring current induced in each six-membered ring of naphthalene is comparable in magnitude with that induced in the peripheral ten-membered ring. It is now obvious that the central π bond plays an important role in determining the magnitude of the peripheral current. A weak paramagnetic ring current is predicted along the seven-membered ring of azulene.

In summary, two advantages of our graph theory are that ring currents can be evaluated easily by inspecting the geometry of a cyclic conjugated system, and that they can be assigned uniquely to the individual π-electron rings. We no longer need to expand the field-dependent secular determinant into a polynomial in X and H. The present approach thus presents a novel way of analyzing structural aspects of ring currents and related proton chemical shifts.

References

1) J. Aihara, *J. Am. Chem. Soc.*, **101**, 558 (1979).
2) J. Aihara, *J. Am. Chem. Soc.*, **101**, 5913 (1979).
3) J. Aihara, *Bull. Chem. Soc. Jpn.*, **53**, 1163 (1980).
4) J. Aihara, *Bull. Chem. Soc. Jpn.*, **54**, 1245 (1981).
5) J. Aihara, *J. Am. Chem. Soc.*, **103**, 5704 (1981).
6) J. Aihara, *Pure Appl. Chem.*, **54**, 1115 (1982).
7) F. London, *J. Phys. Radium*, **8**, 397 (1937).
8) B. Pullman and A. Pullman, "Les Théories Electroniques de la Chimie Organique," Masson et Cie, Paris (1952), Chap. 9.
9) L. Salem, "The Molecular Orbital Theory of Conjugated Systems," W. A. Benjamin, New York (1966), Chap. 4.
10) J. A. Pople, *Mol. Phys.*, **1**, 175 (1958).
11) R. McWeeny, *Mol. Phys.*, **1**, 311 (1958).
12) H. Sachs, *Publ. Math. (Debrecen)*, **11**, 119 (1964); A. Graovac, I. Gutman, N. Trinajstić, and T. Živković, *Theor. Chim. Acta*, **26**, 67 (1972).
13) I. J. Maddox and R. McWeeny, *J. Chem. Phys.*, **36**, 2353 (1962).
14) J. D. Memory, *J. Chem. Phys.*, **38**, 1341 (1963).

Kinetics of Oxidative Coupling of Phenols. Oxidation of Guaiacol by Alkaline Hexacyanoferrate(III)

Sukham Nabakishwar SINGH, Mitra BHATTACHARJEE, and Mahendra Kumar MAHANTI*

Department of Chemistry, North-Eastern Hill University, Shillong 793 003, India

(Received May 25, 1982)

Synopsis. The reaction between guaiacol and alkaline hexacyanoferrate(III), at constant ionic strength, gave a coupled product, 3:3′-dimethoxydiphenoquinone. The rate of the reaction was dependent on the first orders of the concentrations of substrate, oxidant, and alkali. The rate determining step involved the formation of a radical intermediate, which was detected by ESR spectroscopy.

Kinetic studies on the oxidation of phenols by hexacyanoferrate(III) in alkaline medium have not received much attention.[1,2] The oxidation of phenols gives rise to radicals, which can yield coupled products. Guaiacol has been chosen for purposes of oxidation by alkaline hexacyanoferrate(III). A survey of the literature revealed that the oxidation of guaiacol had yielded coupled products.[3-5]

Experimental

IR spectra were recorded on an IR-297(Perkin-Elmer) spectrophotometer; NMR spectra on an EM-390(Varian) 90 MHz NMR spectrometer; ESR spectra on an E-4(Varian) EPR spectrometer.

Materials. Guaiacol(SISCO) was distilled before use (bp 204 °C), and its purity confirmed by IR analysis.[6] Methanol (E. Merck) was distilled before use. $K_3Fe(CN)_6$, $K_4Fe(CN)_6$, and NaOH were IDPL samples. $HClO_4$ (E. Merck, 70%) was neutralized with NaOH; the solution was concentrated, and the crystals of $NaClO_4$ obtained were filtered, recrystallized from water, and dried over silica gel under vacuum. The ionic strength of the medium was maintained by the addition of the requisite amount of $NaClO_4$.

Methods. Solutions of guaiacol in aqueous methanol, and $K_3Fe(CN)_6$ in methanol, NaOH, $NaClO_4$, and water were separately thermostated at 30 °C for 3 h under nitrogen, and then mixed in equal volumes. The progress of the reaction was followed by monitoring the disappearance of $[Fe(CN)_6]^{3-}$, spectrophotometrically.[7]

Stoichiometry. Reaction mixtures containing an excess of oxidant were allowed to react to completion, and the $[Fe(CN)_6]^{3-}$ which was left was analyzed, spectrophotometrically. The results gave a ratio of substrate to oxidant according to the equation:

$$2C_7H_8O_2 + 4[Fe(CN)_6]^{3-} + OH^- \longrightarrow C_{14}H_{12}O_4 + 4[Fe(CN)_6]^{4-} + H_2O + 3H^+.$$

Product Analysis. Guaiacol (2.0 g) in 70% methanol (v/v) was mixed with 11.0 g of $K_3Fe(CN)_6$ containing NaOH (0.05 M†) and 70% methanol(v/v), and the mixture refluxed at 60 °C for 3 h under nitrogen. After cooling and filtration, removal of the solvent gave a red residue (0.072 g). The insoluble portion of the mixture was washed with $CHCl_3$, and after removal of $CHCl_3$, a red residue (1.615 g) was obtained. The mp of both these residues was 245 °C. IR analysis of both these residues, in $CHCl_3$, showed them to be identical with 3:3′-dimethoxydiphenoquinone, **4**. A sharp band at 1640 cm^{-1} was obtained, corresponding to the carbonyl stretching of the C=O groups in two rings of an extended quinonoid structure.[8] The $\nu(OCH_3)$ band at 1020 cm^{-1} was also present in the IR spectrum of **4**, indicating that the OCH_3 group was unaffected by the oxidation. The NMR spectrum of **4**, in $CHCl_3$, (internal standard TMS, sweep width 10 ppm), gave a peak at 6.1 τ (OCH_3), and four doublets in the vinylic proton region at 3.20 τ, 3.10 τ, 2.30 τ, and 2.20 τ.

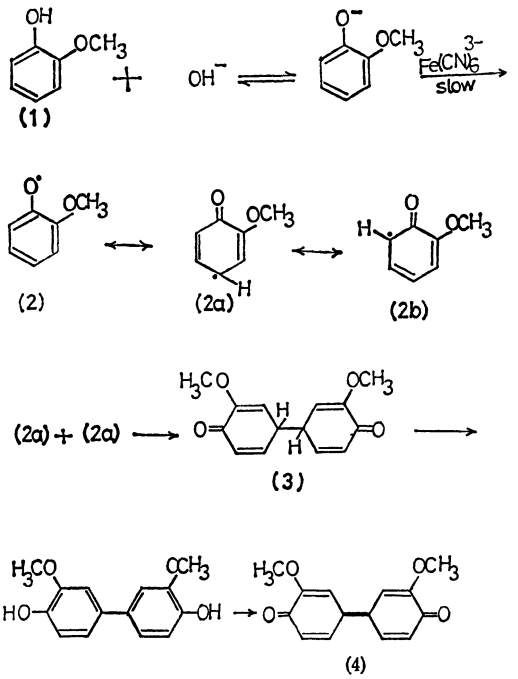

Scheme 1.

Results and Discussion

Kinetic Results. The rate data are shown in Table 1. Under the present experimental conditions, the rate law can be expressed as:

$$\text{Rate} = -\frac{d[Fe(CN)_6]^{3-}}{dt} = k_{obsd}[\text{Guaiacol}][Fe(CN)_6^{3-}][OH^-]. \quad (1)$$

The pseudo first order rate constant, k_{obsd}, was determined by keeping the concentrations of two of the three reactants constant, and was calculated from the equation:[9]

$$k_{obsd} = \frac{2.303}{t}\log\frac{D_0}{D_t}. \quad (2)$$

The effect of temperature was studied (Table 1) and the activation parameters evaluated: $E=23.0\pm0.8$ kJ mol^{-1}; $A=9.5\pm0.5$ s^{-1}; $\Delta H^{\neq}=20.4\pm0.8$ kJ mol^{-1}; $\Delta S^{\neq}=-28.0\pm1.2$ J K^{-1} mol^{-1}.

† 1 M=1 mol dm^{-3}.

Table 1. Rate data for the oxidation of guaiacol

[Guaiacol] 10^3 M	$[K_3Fe(CN)_6]$ 10^4 M	[NaOH] 10^2 M	Temp/°C (±0.1 °C)	$10^3 \times k_{obsd}$ s^{-1}
5.0	10.0	5.0	30.0	1.05
10.0	10.0	5.0	30.0	2.09
20.0	10.0	5.0	30.0	4.20
25.0	10.0	5.0	30.0	5.24
5.0	2.5	5.0	30.0	1.06
5.0	5.0	5.0	30.0	1.10
5.0	7.5	5.0	30.0	1.05
5.0	10.0	2.5	30.0	0.52
5.0	10.0	7.5	30.0	1.57
5.0	10.0	10.0	30.0	2.10
5.0	10.0	5.0	35.0	1.43
5.0	10.0	5.0	40.0	1.86
5.0	10.0	5.0	45.0	2.05
5.0	10.0	5.0	50.0	2.68

Methanol=70%(v/v); μ=0.50 M; all values of rate constants were the average of two or more experiments, with agreements being ±1.5% or better.

The variation of the ionic strength (0.10 M to 0.50 M $NaClO_4$) and the addition of $K_4Fe(CN)_6$ in the concentration range 1.0×10^{-4} M to 1.0×10^{-3} M, did not have any effect on the rate of the reaction.

Increasing proportions of methanol from 60% to 75% (v/v) decreased the rate constant $10^3\times k_{obsd}/s^{-1}$ from 1.41 to 0.90 at [guaiacol]$=5\times10^{-3}$ M, $[K_3Fe(CN)_6]=1\times10^{-3}$ M, [NaOH]$=5\times10^{-2}$ M, μ=0.50 M and temp=30 °C. From the linear plot of $\log k_{obsd}$ *versus* $1/D$, the value of r, the distance of approach between the ions, was calculated from the Scatchard equation[10] to be 3.1 Å, which was of the right order of magnitude.

Radical Intermediate. Phenols are known to give rise to stable radicals, which have been detected and characterized.[11,12] In this investigation, the ESR spectrum of the radical obtained from the oxidation of guaiacol was a spectrum consisting of 9 lines, which were rather broad. This spectrum was interpreted in a manner similar to that in an earlier investigation.[13] For the present, it can be concluded that the rate determining step of the reaction involved the formation of a radical intermediate, which could be stabilized by resonance. It was further observed that this radical intermediate showed a typical absorption band at 1560 cm^{-1} in the IR spectrum. In general, phenoxyl radicals have been characterized by their electronic spectra.[14,15]

Mechanism. Pummerer *et al.*[16,17] had postulated a free phenoxyl radical as the first intermediate in the reactions of phenol coupling. The observed coupling positions, ortho and para, show that a free phenoxyl radical would be reactive only on the oxygen and on the ortho and para carbon atoms of guaiacol. The resonance structures for the radical would symbolize a high density of the unpaired electron at these positions. Guaiacol can be oxidized to the corresponding phenoxyl radical, **2**↔**2a**↔**2b**. Combination of **2a** +**2a** would result in the formation of the dimer, **3**, which would undergo tautomerization rapidly in methanol, and would be oxidized further to yield the extended quinone, **4**. No other intermediate product(s) could be recovered. The mechanism is shown in Scheme 1.

We thank the technical staff of the Regional Sophisticated Instrumentation Centre, IIT, Madras, for recording the ESR spectra. Financial assistance to one of us(MB) from the CSIR, Government of India, is gratefully acknowledged.

References

1) C. G. Haynes, A. H. Turner, and W. A. Waters, *J. Chem. Soc.*, **1956**, 2823.
2) P. S. Radhakrishnamurti and R. K. Panda, *Indian J. Chem.*, **11**, 1003 (1973).
3) F. Fichter and W. Dietrich, *Helv. Chim. Acta*, **7**, 131 (1924).
4) H. Booth and B. C. Saunders, *J. Chem. Soc.*, **1956**, 940.
5) B. O. Lindgren, *Acta Chem. Scand.*, **14**, 2089 (1960).
6) H. A. Szymanski, "Interpreted Infrared Spectra," Vol. 3, Plenum, New York (1967), p. 152.
7) M. Bhattacharjee, A. K. Bhattacharjee, and M. K. Mahanti, *Bull. Chem. Soc. Jpn.*, **54**, 3566 (1981).
8) A. D. Cross and R. A. Jones, "An Introduction to Practical Infrared Spectroscopy," Butterworths (1969).
9) B. Krishna and H. S. Singh, *J. Inorg. Nucl. Chem.*, **31**, 2964 (1969).
10) G. Scatchard, *Chem. Revs.*, **10**, 229 (1932).
11) C. D. Cook, *J. Org. Chem.*, **18**, 261 (1953).
12) E. Müller and K. Ley, Ber., **87**, 922 (1954).
13) T. J. Stone and W. A. Waters, *J. Chem. Soc.*, **1964**, 213.
14) C. D. Cook, C. B. Depatie, and E. S. English, *J. Org. Chem.*, **24**, 1356 (1959).
15) A. Hubele, H. Suhr, and U. Heilmann, *Ber.*, **95**, 639 (1962).
16) R. Pummerer and E. Cherbuliez, *Ber.*, **52**, 1414 (1919).
17) R. Pummerer and A. Rieche, *Ber.*, **59**, 2161 (1926).

The Consecutive Determination of Serum Ammonia and Leucine Amino Peptidase with an Ammonia Gas-sensing Electrode

Masakatsu HATO,* Yukio SHIMURA, Tomiko AKIYAMA, and Hiroko NAKAYAMA
Research Institute for Polymers and Textiles, Yatabehigashi 1-1-4, Tsukuba-gun, Ibaraki-305
(Received October 29, 1982)

Synopsis. A simple method for the consecutive determination of serum ammonia and the activity of leucine amino peptidase (LAP) with an ammonia gas-sensing electrode is described. The values determined by the present method agree with those determined by conventional methods within 6%.

The serum ammonia and LAP level is of clinical significance; *i.e.*, elevated levels have been found in a number of conditions of the liver.[1] Many procedures have been proposed for the determination of serum ammonia.[2-5] However, these methods have various shortcomings;[6] *e.g.*, the ammonia concentration is considerably affected by the diffusion conditions, such as the temperature and the diffusion time. Nitrogenous compounds other than ammonia are destroyed by alkali during the diffusion period, liberating ammonia and giving erroneously high ammonia values. The method proposed by Dienst,[7] which was later improved by Fenton,[8] seems to be complicating.[1] More recently, Okuda *et al.*[9] have developed a usable method. However, their method needs a fairly large amount of serum (0.5—1.0 ml)[10] and requires the deproteinization of the serum and a long incubation time.

In the previous paper, we have reported on the use of an ammonia gas-sensing electrode (abbreviated to an NH_3-electrode) in a kinetic assay of serum LAP,[11,12] where the time course of ammonia production in the reaction, L-leucine amide $\xrightarrow{\text{LAP}}$ L-leucine+NH_3, is directly monitored in buffered serum by means of an NH_3-electrode. The LAP activity thus determined agreed well with that determined by the conventional methods.[12,16] This suggests that, with a minor modification of the procedure, the method can be extended to the determination of serum ammonia as well. In the present communication, the consecutive determination of serum ammonia and LAP with an NH_3-electrode is described.

Experimental

Apparatus and Procedures. The experimental apparatus is illustrated in Fig. 1a. An Orion model 95-10 NH_3-electrode (a) was dipped in a buffer (1.5 ml; 0.2 M TrisHCl pH=8.5, 10 μM NH_4Cl) stirred by a magnetic stirrer (c). The whole apparatus was kept at 25±0.1 °C by circulating thermostated water through a glass jacket (d). The electrode was pre-equilibrated with the buffer. At time $t=0$, male rabbit serum was added through an inlet (e) and the electromotive force (E) was recorded as a function of the time by means of an Orion model 801 mV meter and a Yokogawa 3047 strip-chart recorder. After the equilibrium E value was reached, 0.1 ml of a 110 mM L-leucine amide buffer (a substrate for LAP, 0.2 M TrisHCl pH=8.5) was added to the buffered serum in order to initiate the LAP reaction; the E was recorded as a function of time. The pH was constant throughout the experiment. To examie the accuracy of the present method, the serum ammonia was also determined by means of an Ammonia Test Wako® (Wako Chem. Co.). The LAP activity was also determined by the method of Hjemdahl-Monsen *et al.*[12,16]

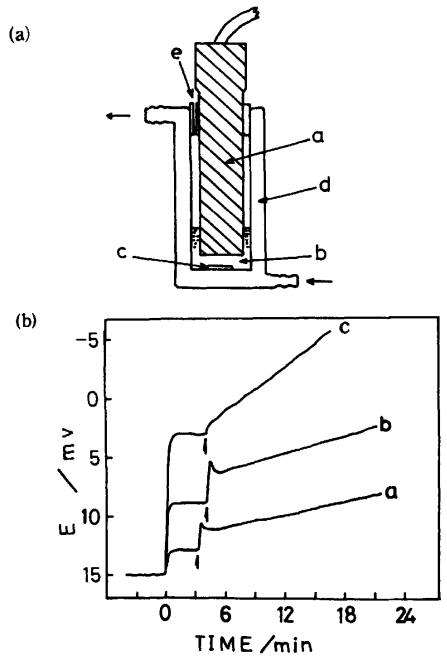

Fig. 1.(a) Schematic illustration of experimental apparatus.
(b) Typical electrode response to serum ammonia and LAP as a function of volume of male rabbit serum (25 °C).

Results and Discussion

Electrode Response to Serum Ammonia and LAP Reaction. Figure 1b shows a typical electrode response to serum ammonia and LAP. With the addition of 10 μl (Curve a), 20 μl (Curve b), and 50 μl (Curve c) of serum at time $t=0$, the E decreased steeply and attained equilibrium values within 1—2 min. The substrate buffer was then added at the times indicated by arrows (+). The initial irregular changes in the E were attributable to the electrode response to the ammonia present in L-leucine amide. The E decreased continuously with time. This reflects the continuous increase in the ammonia concentration due to the LAP reaction in the reaction mixture. The E *vs.* time curves were converted into concentration *vs.* time curves *via* an E *vs.* log (concentration) curve (Fig. 2). The activity of LAP was calculated from the slope of the concentration *vs.* time curve.[12] Measurable activity range is estimated to be from 0.1 μM·min^{-1} to 20 μM·min^{-1}.[11,12] The addition of NH_4Cl in advance to the buffer is important not only to eliminate errors caused by the contamination of ammonia (from the atmosphere or from the

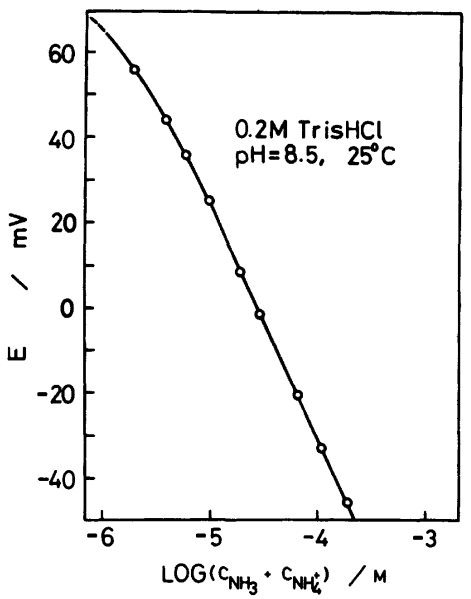

Fig. 2. Electromotive force (E) of the electrode as a function of total ammoniacal concentration (calibration curve).
1 M=1 mol·dm^{-3}. 1 μM=1.4 μg·NH_3-nistrogen/dl.

human body), but also to increase the electrode-response rate.[11] When there is no need to determine the LAP activity, several serum samples can be analyzed consecutively. Five different samples could be analyzed within 7—8 min. The serum ammonia concentration C was calculated from a calibration curve (Fig. 2) and from the equation;

$$C = [(V_i+v)C_f - C_iV_i]/v, \quad (1)$$

where V_i, v, C_i, and C_f are the initial volume of the buffer (or buffered serum), the volume of the added serum, and the initial and final ammonia concentration of the reaction mixture respectively. The measurable ammonia concentration range is estimated to be from 70 to at least 10^4 μgNH_3-nitrogen/dl at $v/V_i=0.01$ and from 20 to at least 10^4 μgNH_3-nitrogen/dl at $v/V_i=0.1$.

Accuracy and Stability of the Electrode Response.

Table 1. Comparison of the serum ammonia and LAP determined by the present method with those determined by conventional methods

Sample	Serum ammonia (μg·NH_3-nitrogen/dl)		LAP activity (μM/min[d])	
	This method[a]	O-F method[b]	This method[a]	H-P-R method[c]
1	134	128	—	—
2	97	92	—	—
3	168	171	0.21	0.20
4	170	175	0.62	0.65

a) Average of 2 measurements. The relative standard deviation for three identical measurements was 6%. b) Average of three measurements[10] c) Average of two measurements[12,16] d) 1 M=1 mol·dm^{-3}.

The serum ammonia and LAP activity determined by the present method are compared with those determined by conventional methods in Table 1. The analytical values agreed with each other within 6%. This indicates that the present method is effective in the determination of serum ammonia and LAP.

Practical difficulties accompanying an NH_3-electrode, *e.g.*, the clogging of the gas-permeable membrane in biological fluid, have often been pointed out.[13,14] However, provided a volume fraction of serum ranging from 0.005—0.25 was used, the electrode response in the buffered serum was stable for at least 3 weeks (10 assays/day). When the fraction exceeded 0.3, errors tended to increase because of the adsorption of serum components on the membrane. Similar effects have also been observed for the case of urea determination in whole blood with an NH_3-electrode based urea electrode.[15] When the fraction was less than 0.005, the electrode response became too small to get accurate results. The NH_3-electrode seems to have no serious practical limitations when employed in moderately diluted serum.

The advantages of the present method are: (1) The consecutive determination of serum ammonia and LAP is possible. (2) Only a small amount of serum is needed; *e.g.*, 10—50 μl is sufficient. (3) A long color-development time for the conventional method is unnecessary. (4) Strong acidic and alkaline reagents are unnecessary, and therefore the procedures for waste disposal are simple.

References

1) M. Sasaki, M. Kitamura, N. Ueda, and T. Nakayama, "Jintaiseibun No Sampling," Kodansha Scientific, Tokyo (1978), p. 103.
2) E. J. Conway, "Microdiffusion Analysis and Volumetric Error," Lockwood, N. Y. (1950).
3) H. Borsook, *J. Biol. Chem.*, **110**, 481 (1935).
4) D. Seligson and K. Hirahara, *J. Lab. Clin. Med.*, **49**, 962 (1957).
5) S. Shibata, *Rinsho Byori*, **6**, 230 (1958).
6) S. Fujii and H. Okuda, *Tokushima J. Exptl. Med.*, **22**, 1 (1975).
7) S. G. Dienst, *J. Lab. Clin. Med.*, **58**, 149 (1961).
8) J. C. B. Fenton, *Clin. Chim. Acta*, **7**, 163 (1962).
9) H. Okuda, S. Fujii, and Y. Kayashima, *Tokushima J. Exptl. Med.*, **12**, 11 (1965).
10) Ammonia Test Wako© Instruction Manual (Wako Chem. Co. Osaka).
11) M. Hato, T. Masuoka, and Y. Shimura, *Anal. Chim. Acta*, **149**, 193 (1983).
12) M. Hato, H. Nakayama, and Y. Shimura, *Anal. Chim. Acta*, **149**, 203 (1983).
13) N. R. Larsen, E. H. Hansen, and G. G. Guilbault, *Anal. Chim. Acta*, **79**, 9 (1975).
14) L. D. Bowers and P. W. Carr, *Anal. Chem.*, **48**, 544A (1976).
15) M. Hato, Y. Suda, and K. Tsuda, *Nippon Kagaku Kaishi*, **1981**, 1172.
16) C. E. Hjemdahl-Monsen, D. S. Papastathopoulos, and G. A. Rechnitz, *Anal. Chim. Acta*, **88**, 253 (1977).

Potassium-selectivities of Bis(benzo-15-crown-5) Derivatives Obtained from Cyclohexanedicarboxylic Acids

Keiichi KIMURA,* Atsuo ISHIKAWA, Hiroshi TAMURA, and Toshiyuki SHONO*
Department of Applied Chemistry, Faculty of Engineering, Osaka University, Yamada-oka 2-1, Suita, Osaka 565
(Received November 25, 1982)

Synopsis. Several bis(benzo-15-crown-5) derivatives containing a cyclohexane or benzene ring in the bridge chain were synthesized as neutral carriers of coated-wire potassium-selective electrodes. The bis(benzocrown ether) derivative obtained from *cis*-1,2-cyclohexanedicarboxylic acid was found to be outstandingly potassium-selective.

Macrobicyclic polyethers containing benzo-15-crown-5 moieties at the end of a short bridge chain, which are commonly referred to as bis(benzo-15-crown-5) derivatives, have received considerable attention because of their attractive cation-binding properties.[1-5] They can form stable sandwich-type 2 : 1 crown ether ring to cation complexes with K^+ intramolecularly, which results in high K^+-selectivity of them on binding alkali and alkaline earth metal ions. Accordingly, some of the bis(benzo-15-crown-5) derivatives have turned out to be good neutral carriers for poly(vinyl chloride) (PVC) membrane K^+-selective electrodes,[6-8] although their K^+-selectivities depend more or less upon the configuration of bis(benzocrown ether) derivatives[7] and the length of the chain connecting two crown ether moieties.[6]

We would like to report here the K^+-selectivities of bis(benzo-15-crown-5) derivatives containing a cyclohexane or benzene ring in the bridge chain in the coated-wire type of K^+-selective electrodes based on them.

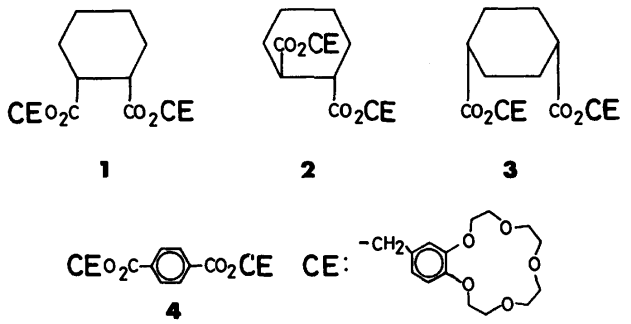

Experimental

Chemicals. Bis(benzo-15-crown-5) derivatives **1** through **4** were synthesized by the reaction of 4'-bromomethylbenzo-15-crown-5 with appropriate dicarboxylic acid potassium salts in acetonitrile, in a similar way to that reported previously.[9] The purification of them was performed by gel permeation chromatography. (**1**—**3**: colorless oil; **4**: colorless crystal, mp 100—102 °C) The plasticizer, *o*-nitrophenyl octyl ether (NPOE), was prepared in a usual manner,[10] and then purified by repeated distillation.

Electrode Construction. The coated-wire ion-selective electrodes were constructed using a silver wire, according to the procedure reported elsewhere.[11] The coating solution consists of 15 mg crown ether, 200 mg NPOE, 100 mg PVC, and 3 ml tetrahydrofuran. The external reference electrode was a standard calomel electrode with a 0.1 M (1 M=1 mol/dm^3) NH_4NO_3 electrolyte bridge. No special conditioning of the ion-selective electrodes was performed before use.

Measurement. All of the emf measurements were made at 25±0.1 °C. Standard K^+ aqueous solutions for calibration plots were obtained by gradual dilution of 1 M KCl solution. Selectivity coefficients (k_{KM}) were determined by a mixed solution method, by taking a constant background of an interfering ion and varying K^+ concentration. The constant concentrations of Na^+, Rb^+, Cs^+, and NH_4^+ are 1×10^{-1}, 1×10^{-3}, 1×10^{-3}, and 1×10^{-2} M, respectively.

Results and Discussion

Three kinds of cyclohexanedicarboxylate-type bis(benzo-15-crown-5) derivatives **1**, **2**, and **3**, which are derived from *cis*-1,2-, *trans*-1,2-, and *cis*-1,4-cyclohexanedicarboxylic acids, respectively, were synthesized for the purpose of obtaining lipophilic and ion-selective neutral carriers for K^+-selective electrodes. Terephthalate-type bis(crown ether) derivative **4** was also prepared for comparison. The K^+-selectivities of the bis(benzo-15-crown-5) derivatives were elucidated by measuring the electrochemical selectivity of coated-wire ion-selective electrodes based on them, which can be easily made up owing to the simple construction.

The electrode properties are summarized in Table 1. The electrodes of bis(crown ether) derivatives **1** and **3** showed a linear response to K^+ activity in the range 10^{-4}—10^{-1} M, the slope of calibration plots being 55 and 58 mV per decade of activity change at 25 °C. The electrodes based on **2** and **4** exhibited a little poorer

Table 1. Electrode properties of coated-wire K^+-selective electrode based on bis(benzo-15-crown-5) derivatives **1** through **4**

Bis(crown ether)	Maximal[a] slope mV/decade	Range[b] pK	k_{KM}			
			Na^+	Rb^+	Cs^+	NH_4^+
1	55	4—1	5×10^{-4}	5×10^{-2}	5×10^{-3}	2×10^{-1}
2	46	4—1	3×10^{-1}	1×10^{-1}	3×10^{-2}	1×10^{-2}
3	58	4—1	3×10^{-3}	2×10^{-1}	5×10^{-2}	3×10^{-1}
4	51	4—2	2×10^{-3}	3×10^{-1}	8×10^{-2}	5×10^{-2}

a) emf change in ten-time change of K^+ activity. b) pK=−log [K^+].

response than that of **1** and **3**.

It should be noted that bis(benzo-15-crown-5) derivatives **1**, **3**, and **4** are better in the K^+-selectivity over Na^+ than **2**. Particularly, the electrode of **1**, *cis*-cyclohexanedicarboxylate type of bis(benzo-15-crown-5) derivative, possesses an excellent k_{KNa} value, 5×10^{-4}. It has been reported previously that a *cis*-bis(benzo-15-crown-5) derivative obtained from maleic acid is easy to form sandwich-type complexes with K^+ intramolecularly, being rather K^+-selective compared to the corresponding *trans* isomer derived from fumaric acid.[3,7] This is also the case in these cyclohexanedicarboxylate type of bis(benzo-15-crown-5) derivatives. That is to say, the bis(benzo-15-crown-5) derivatives containing *cis* configuration, **1** and **3**, are much more K^+-selective than that containing *trans* configuration, **2**. Also, the k_{KNa} value for the electrode based on **1** is about one order of magnitude smaller than that of **3**, implying that the two crown ether moieties in the latter bis(benzo-15-crown-5) derivative are a little too far apart for the formation of the stable intramolecular sandwich-type K^+ complexes. The terephthalate unit of bis(crown ether) derivative **4** may be unfavorable again due to the rigidity of benzene ring.

Thus, the bis(benzo-15-crown-5) derivative obtained from *cis*-1,2-cyclohexanedicarboxylic acid is a highly K^+-selective neutral carrier for the ion-selective electrode. The response time of the electrode was within 10 s on measuring by an incremental method. In the stability and reproducibility of the emf reading, the electrode is similar to that based on the previous bis(benzo-15-crown-5) derivative.[11] Bis(benzo-15-crown-5) derivative **1** is surely superior to the previous ones[6,7] in the lipophilicity which is definitely required as the neutral carrier of the ion-selective electrodes, although they all seem to resemble in the K^+-selectivity.

References

1) M. Bourgoin, K. H. Wong, J. Y. Hui, and J. Smid, *J. Am. Chem. Soc.*, **97**, 3462 (1975).
2) K. Kimura, T. Maeda, and T. Shono, *Talanta*, **26**, 945 (1979).
3) K. Kimura, T. Tsuchida, T. Maeda, and T. Shono, *Talanta*, **27**, 801 (1980).
4) F. Wada, R. Arata, T. Goto, K. Kikukawa, and T. Matsuda, *Bull. Chem. Soc. Jpn.*, **53**, 2061 (1980).
5) S. Shinkai, T. Nakaji, T. Ogawa, K. Shigematsu, and O. Manabe, *J. Am. Chem. Soc.*, **103**, 111 (1981).
6) K. Kimura, T. Maeda, H. Tamura, and T. Shono, *J. Electroanal. Chem. Interfacial. Electrochem.*, **95**, 91 (1979).
7) H. Tamura, K. Kimura, and T. Shono, *Nippon Kagaku Kaishi*, **1980**, 1648.
8) K. W. Fung and K. H. Wong, *J. Electroanal. Chem. Interfacial. Electrochem.*, **111**, 359 (1980).
9) K. Kimura, H. Tamura, T. Tsuchida, and T. Shono, *Chem. Lett.*, **1979**, 611.
10) C. F. H. Allen and J. W. Gates, Jr., *Org. Synth.*, Coll. Vol. III, 140 (1955).
11) H. Tamura, K. Kimura, and T. Shono, *Anal. Chem.*, **54**, 1224 (1982).

Enthalpies of Transfer of Monovalent Ions from Water to Water-Acetonitrile Mixtures

Kiyoshi MIYAJI* and Kenichi MORINAGA
Department of Chemistry, Faculty of Science, Saitama University, Urawa 338
(Received December 3, 1982)

Synopsis. Ionic enthalpies of transfer from water to water–acetonitrile mixtures were estimated for Na^+, K^+, Rb^+, Cs^+, Ag^+, Tl^+, Me_4N^+, Et_4N^+, n-Pr_4N^+, n-Bu_4N^+, Ph_4As^+, Ph_4B^-, Cl^-, Br^-, I^-, NCS^-, NO_3^-, ClO_4^-, and picrate ion on the basis of the assumption $\Delta H_t^\circ(Ph_4As^+)=\Delta H_t^\circ(Ph_4B^-)$.

Several papers are concerned with enthalpies of solution in water–aprotic solvent mixtures.[1] In connection with the conductivity measurement,[2] we measured enthalpies of solution for twenty-three electrolytes in water–acetonitrile (W–AN) mixtures.

Experimental

Tetraphenylarsonium salts were recrystallyzed from acetone.[3] Tetraalkylammonium salts were purified according to the literature.[4] The other salts were of reagent grade and purified by the standard methods. The method for purification of solvents were reported elsewhere.[2] Enthalpies of solution were measured at 25.00±0.02 °C by using a heat-exchange type calorimeter.[5] They were independent of electrolyte concentration (10^{-2}—10^{-3} mol dm^{-3}) within experimental error. Usually three to five measurements were made and the average of values agreeing within ±0.4 kJ mol^{-1} was taken to be the standard enthalpies of solution (ΔH_s°).

Results and Discussion

The ΔH_s° values in Table 1 agree with those in the literature[6] within ±0.7 kJ mol^{-1} in aqueous solutions except for CsI and Et_4NPi (Pi=picrate) and within ±1.1 kJ mol^{-1} in acetonitrile solutions except for Me_4NBr, respectively. The ΔH_t° values for ions estimated on the basis of the assumption $\Delta H_t^\circ(Ph_4As^+)=\Delta H_t^\circ(Ph_4B^-)$ are given in Table 2. The differences between the ΔH_t°(W→AN) values and those in the literature[3,6] are less than ±1.0 kJ mol^{-1} for Na^+, K^+, Me_4N^+, Et_4N^+, n-Pr_4N^+, n-Bu_4N^+, Ph_4As^+, Ph_4B^-, Br^-, and I^- ions, and $-2._7$, $+1._5$, and $+2._0$ kJ mol^{-1} for Rb^+, Cl^-, and ClO_4^- ions, respectively.

As Cox *et al.* have suggested,[1e] there is no doubt that a rapid decrease in ΔH_t° for Ag^+ ion in W-rich region is due to the selective solvation by acetonitrile and an increase in ΔH_t° for Na^+ and Cl^- ions in AN-rich region is due to the selective hydration. Since the specific interaction of Ag^+ ion with acetonitrile at x_{AN} (mole fraction of acetonitrile)=0—1.0 has been established,[8] a slight increase in ΔH_t° at $x_{AN}=0.3$—0.8 and a decrease at $x_{AN}=0.8$—1.0 can be concluded to be characteristic of the type of ion, the cosphere of which is enriched with more acetonitrile than water relative to the bulk composition of solvent mixtures. The ΔH_t° values for alkali metal ions at $x_{AN}=0.2$ follow the order: $Li^+>Na^+>K^+>Rb^+\approx Cs^+$. This is consistent with that of decreasing ΔH_t°-increase in AN-rich region. A marked decrease in ΔH_t° at $x_{AN}=0.2$—0.8 for Li^+ ion can be concluded to be characteristic of a selectively hydrated ion. An endothermic maximum for n-Bu_4N^+, Ph_4As^+, and Ph_4B^- ions at $x_{AN}=0.05$—0.1 is common to a hydrophobic structure-making ion in W–aprotic solvent mixtures.[1a,1g] In contrast to the positive values for n-Bu_4N^+ ion at $x_{AN}=0$—1.0, those for Ph_4As^+ ion are negative at $x_{AN}=0.15$—1.0. The extent of endothermicity for tetraalkylammonium ions decreases with decreasing size, and Me_4N^+ ion behaves like alkali metal ions.[9]

Anions show a variety of ΔH_t° dependences: The ΔH_t° values for all the anions reach a maximum at $x_{AN}=0.15$—0.3, decrease in an intermediate region, and, except for ClO_4^- and Pi^- ions, reach a minimum at $x_{AN}=0.7$—0.95. From the ΔH_t°-increase in AN-rich

Table 1. Enthalpies of solution for electrolytes in water–acetonitrile mixtures. ΔH_s°/kJ mol^{-1}

Electrolyte	x_{AN} 0	0.1	0.2	0.4	0.6	0.8	0.9	1.0
NaCl	$+3.8_9$	$+1.0_9$	-1.0_9	-7.1_1	$-11._7$			
NaBr	-0.6_3	-4.7_3	-7.7_9	$-12._6$	$-17._7$	$-21._3$	$-20._0$	
NaI	-7.4_9	$-12._9$	$-17._8$	$-23._4$	$-28._9$	$-34._6$	$-36._1$	$-28._1$
NaSCN	$+6.7_4$	0	-5.3_3	$-11._8$	$-17._5$	$-22._4$	$-24._2$	$-11._3$
$NaPh_4B$	$-19._8$	$-14._6$	$-43._6$	$-51._8$	$-50._1$	$-51._5$	$-53._4$	$-43._5$[a]
KI	$+20._3$	$+12._1$	$+6.7_4$	$+0.8_9$	-5.4_0	$-11._3$	$-14._2$	$-10._7$
KNO_3	$+34._7$		$+26._0$	$+21._5$	$+15._9$	$+11.0$		
RbI	$+25._6$	$+16._9$	$+11._4$	$+5.1_1$	-0.4_6	-6.9_5	-9.7_1	-7.9_1
CsI	$+32._3$	$+23._4$	$+18._0$	$+11._3$	$+5.9_4$	$+0.8_9$	-1.7	
$AgNO_3$	$+22._7$	$-14._3$	$-18._8$	$-22._4$	$-25._4$	$-28._7$	$-28._5$	$-22._7$
$TlNO_3$	$+40._7$	$+36._0$	$+31._5$	$+26._3$				
Me_4NBr	$+24._5$		$+20._6$	$+17._5$	$+14._1$	$+11._9$	$+12._8$	$+20._3$
Me_4NI	$+43._1$		$+35._5$	$+30._8$	$+28._0$	$+25._3$	$+21._2$	
Et_4NCl	$-12._9$			-8.1_3	$-10._7$	$-11._3$	-8.7_5	$+5.8_6$
Et_4NBr	$+5.6_5$		$+9.2_1$	$+8.5_4$	$+5.9_9$	$+3.4_3$	$+3.6_8$	$+11._5$
Et_4NI	$+27._3$		$+27._6$	$+26._3$	$+23._0$	$+18._7$	$+16._8$	$+18._3$
Et_4NClO_4	$+31._0$	$+33._2$	$+27._0$	$+24._0$	$+20._8$	$+15._3$	$+14._4$	$+12._3$
Et_4NPi	$+33._5$	$+40._6$	$+34._6$	$+30._7$	$+30._2$	$+29._7$	$+29._3$	$+30._3$
n-Pr_4NI	$+11._0$	$+24._4$	$+24._2$	$+22._4$	$+19._5$	$+14._4$	$+12._6$	$+14._0$
n-Bu_4NBr	-9.2_3	$+17._1$	$+16._4$	$+13._5$	$+11._4$	$+9.4_3$	$+8.8_7$	$+16._0$
n-Bu_4NI	$+16._7$[b]	$+41._3$	$+39._7$	$+35._1$	$+32._3$	$+28._3$	$+25._3$	$+27._1$
Ph_4AsBr	$+7.7_0$	$+19._3$	$+11._4$	$+6.2_4$	$+2.6_4$	0	-0.8_4	$+6.2_6$
Ph_4AsI	$+34._7$[c]	$+44._3$	$+33._3$	$+27._3$	$+24._3$	$+18._4$	$+15._1$	$+16._3$

a) Ref. 6. b) Ref. 1a. c) Ref. 7.

Table 2. Ionic enthalpies of transfer from water to water–acetonitrile mixtures. ΔH_t°/kJ mol^{-1}

Ion	x_{AN} 0.1	0.2	0.4	0.6	0.8	0.9	1.0
Li^+[a]	$-6._3$	$-15._8$	$-22._0$	$-26._3$	$-28._9$		$-14._4$
Na^+	$-5._3$	$-16._8$	$-20._8$	$-20._9$	$-21._6$	$-22._3$	$-13._6$
K^+	$-7._9$	$-19._4$	$-23._9$	$-25._1$	$-25._6$	$-26._9$	$-23._3$
Rb^+	$-8._4$	$-20._1$	$-25._0$	$-25._5$	$-26._6$	$-27._8$	$-25._9$
Cs^+	$-8._6$	$-20._3$	$-25._5$	$-25._9$	$-25._5$	$-26._4$	
Ag^+	$-39._5$	$-52._1$	$-55._5$	$-54._4$	$-55._3$	-54	$-55._3$[b]
Tl^+	$-7._3$	$-19._9$	$-24._5$				
Me_4N^+		$-13._6$	$-16._5$	$-14._5$	$-14._3$	$-14._3$	$-13._6$
Et_4N^+		$-6._1$	$-6._0$	$-3._5$	$-3._3$	$-3._5$	$-2._3$
n-Pr_4N^+	$+13._7$	$+7._3$	$+7._0$	$+9._1$	$+9._4$	$+9._3$	$+10._6$
n-Bu_4N^+	$+25._3$	$+16._3$	$+13._7$	$+16._6$	$+17._6$	$+16._1$	$+16._9$
Ph_4As^+,Ph_4B^-	$+10._6$	$-6._9$	$-11._1$	$-9._4$	$-9._9$	$-11._9$	$-10._5$
Cl^-	$+2._5$	$+11._6$	$+10._3$	$+5._7$	$+5._6$	$+8._6$	$+21._6$
Br^-	$+1._3$	$+10._1$	$+9._3$	$+4._1$	$+1._7$	$+3._3$	$+9._4$
I^-	$-0._3$	$+6._6$	$+4._5$	$-0._6$	$-5._9$	$-7._6$	$-7._5$
NCS^-	$-1._4$	$+4._7$	$+2._3$	$-3._3$	$-7._5$	$-8._5$	$-4._9$
NO_3^-	$+2._5$	$+10._7$	$+10._7$	$+6._3$	$+1._9$	$+3$	$+9._9$
ClO_4^-	$+1._3$	$+2._1$	$-1._0$	$-6._5$	$-11._7$	$-12._7$	$-16._6$
Pi^-	$+6._1$	$+7._4$	$+3._3$	$+0._4$	$-0._5$	$+0._3$	$-0._5$

a) The ionic values for Li^+ ion were calculated from ΔH_t° for $LiClO_4$[1b]. b) Ref. 6.

region the order in decreasing hydration can be concluded: $Cl^- > NO_3^- > Br^- > NCS^- > I^- > Pi^- > ClO_4^-$. The x_{AN} value corresponding to ΔH_t° minimum shifts to a higher value from Cl^- through Br^- to I^-. However, the ΔH_t° maximum appears at nearly equal x_{AN}. The extent of endothermicity follows the order: $Cl^- > Br^- > I^-$. As compared with aqueous solution, the solvent structure at x_{AN}=*ca.* 0.3 may be the least favorable for the hydration of halide ions owing to the destruction of water lattice caused by the addition of acetonitrile.[10] In contrast to the positive ΔH_t° values for Cl^- and Br^- ions at x_{AN}=0—1.0, those for I^- ion are negative at x_{AN}=0—0.1 and 0.6—1.0. The behavior of NCS^- ion as a softer ion than I^- ion at x_{AN}=0—0.95 and as a harder ion at x_{AN}=0.95—1.0 may be related to the fact that linear NCS^- ion has two kinds of terminal atoms. The behavior of NO_3^- ion resembles that of Br^- ion. The ΔH_t° values for Pi^- ion suggest that it interacts weakly with either water or acetonitrile.

References

1) a) R. Fuchs and C. P. Hagan, *J. Phys. Chem.*, **77**, 1797 (1973); b) R. P. T. Tomkins, G. M. Gerhardt, L. M. Lichtenstein, and J. P. Turner, *Adv. Chem. Ser.*, **155**, 297 (1976); c) M. F. Estep, D. D. MacDonald, and J. B. Hyne, *J. Solution Chem.*, **6**, 129 (1977); d) C. de Visser, W. J. M. Heuvelsland, and G. Somsen, *Adv. Chem. Ser.*, **177**, 99 (1979); e) B. G. Cox, R. Natarajan, and W. E. Waghorne, *J. Chem. Soc., Faraday Trans. 1*, **75**, 86 (1979); f) B. G. Cox, W. E. Waghorne, and C. K. Piggot, *ibid.*, **75**, 227 (1979); g) M. Castagnolo, G. Petrella, M. D. Monica, and A. Sacco, *J. Solution Chem.*, **8**, 501 (1979).

2) K. Morinaga and K. Miyaji, *Denki Kagaku*, **50**, 736 (1982).

3) B. G. Cox, C. R. Hedwig, A. J. Parker, and D. W. Watts *Aust. J. Chem.*, **27**, 477 (1974).

4) B. E. Conway, R. E. Verrall, and J. E. Desnoyers, *Trans. Faraday Soc.*, **62**, 2738 (1966).

5) M. Nakanishi and S. Fujieda, *Anal. Chem.*, **44**, 574 (1972).

6) C. V. Krishnan and H. L. Friedman, "Enthalpies of Transfer for Solutes in Polar Solvents," in "Solute–Solvent Interactions," ed by J. F. Coetzee and C. D. Ritchie, Marcel Dekker, Inc., New York and Basel (1976), Vol. 2, Chap. 9.

7) E. M. Arnett and D. R. McKelvey, *J. Am. Chem. Soc.*, **88**, 2598 (1966).

8) H. Shneider, "The Selective Solvation of Ions in Mixed Solvents," in "Solute–Solvent Interactions," ed by J. F. Coetzee and C. D. Ritchie, Vol. 2, Chap. 11.

9) C. V. Krishnan and H. L. Friedman, *J. Phys. Chem.*, **73**, 3934 (1967).

10) C. Moreau and C. Douhéret, *J. Chem. Thermodyn.*, **8**, 403 (1976).

Electrocatalytic Reaction of $Fe^{2+/3+}$ Aqua Ions by $[Mo(CN)_8]^{4-/3-}$ Complexes

Keiichi SATO,† Takeo OHSAKA, Hiroaki MATSUDA,† and Noboru OYAMA*

Department of Applied Chemistry for Resources, Tokyo University of Agriculture and Technology, Koganei, Tokyo 184

†*Department of Electronic Chemistry, Tokyo Institute of Technology, Midori-ku, Yokohama 227*

(Received January 24, 1983)

Synopsis. The catalysis of the oxidation of Fe^{2+} aqua ion by $[Mo(CN)_8]^{3-}$ ion, which is formed on an electrode surface, and that of the reduction of Fe^{3+} aqua ion by $[Mo(CN)_8]^{4-}$ ion were examined by means of hydrodynamic voltammetry at a rotating disk pyrolytic graphite electrode. The rate constants of the electron transfer cross-reaction of the $Fe^{2+}/[Mo(CN)_8]^{3-}$ and $Fe^{3+}/[Mo(CN)_8]^{4-}$ systems were estimated to be $(7.0\pm0.5)\times10^6$ and $(6.6\pm0.5)\times10^6$ $cm^3\ mol^{-1}\ s^{-1}$, respectively.

In previous papers[1,2] we have examined the catalysis of the electrode process of $Fe^{2+/3+}$ redox couple by $[Mo(CN)_8]^{4-/3-}$ complexes bound electrostatically to graphite electrodes coated with the protonated poly(4-vinylpyridine) (PVP) film. It has been shown therein that $[Mo(CN)_8]^{4-/3-}$ complexes are strongly incorporated into the protonated PVP film and the resulting metalated film electrode can catalyze both the oxidation of Fe^{2+} aqua ion and the reduction of Fe^{3+} aqua ion present in a bulk solution. The catalytic reaction of the $Fe^{2+}/[Mo(CN)_8]^{3-}$ and $Fe^{3+}/[Mo(CN)_8]^{4-}$ systems can be considered to be simple and outer-sphere electron transfer cross-reaction. However, no kinetic study on the catalytic reaction of both systems in a bulk solution at an uncoated electrode has been reported yet.

In this paper, we will thus examine the catalysis of the oxidation of Fe^{2+} ion by $[Mo(CN)_8]^{3-}$ ion, which is formed on a graphite electrode surface, and that of the reduction of Fe^{3+} ion by $[Mo(CN)_8]^{4-}$ ion by means of hydrodynamic voltammetry at a rotating disk pyrolytic graphite electrode.

Experimental

Electrochemical apparatus and the experimental procedures have been described previously.[1-3,8] The exposed area of each electrode was 0.17 cm^2. Potassium octacyanomolybdate(IV) dihydrate ($K_4[Mo(CN)_8]\cdot2H_2O$) was synthesized according to the standard procedure.[4] Solutions were freed of air with prepurified argon prior to the electrochemical measurements. Experiments were conducted at 25 °C. Potentials are reported with respect to a sodium chloride saturated calomel electrode (SSCE).

Results and Discussion

Current-potential curves A, B, and C shown in Fig. 1 demonstrate typical steady-state current-potential curves obtained at a rotating disk graphite electrode in an each 0.2 M CF_3COONa solution containing 0.2 mM $[Mo(CN)_8]^{4-}$, 2 mM Fe^{2+} and 0.2 mM $[Mo(CN)_8]^{4-}$+2 mM Fe^{2+} ions. When the current-potential curves were measured at a graphite electrode in the solution containing both 0.2 mM $[Mo(CN)_8]^{4-}$ and 2 mM Fe^{2+} ions, two waves were observed and each of their half-wave potentials were about 0.5 and 0.7 V *vs.* SSCE. The first wave observed at about 0.5 V corresponds to the oxidation of $[Mo(CN)_8]^{4-}$ ion. The conventional log-plot of $\log\{i/(i-i_{lim})\}$ against E (where i_{lim} is the limiting current and i is the current at any potential,

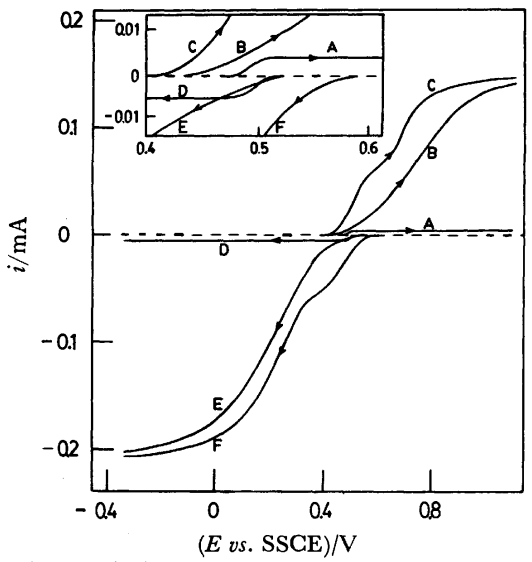

Fig. 1. Typical steady-state current-potential curves demonstrating the catalysis of the oxidation of Fe^{2+} ion by $[Mo(CN)_8]^{3-}$ ion and of the reduction of Fe^{3+} ion by $[Mo(CN)_8]^{4-}$ ion at rotating disk pyrolytic graphite electrodes.
Oxidation of (A): 0.2 mM $[Mo(CN)_8]^{4-}$; (B): 2 mM Fe^{2+}; (C): 0.2 mM $[Mo(CN)_8]^{4-}$+2 mM Fe^{2+}; Reduction of (D): 0.2 mM $[Mo(CN)_8]^{3-}$; (E): 2 mM Fe^{3+}; (F): 0.2 mM $[Mo(CN)_8]^{3-}$ +2 mM Fe^{3+}.
Supporting electrolyte: 0.2 M CF_3COONa-CF_3COOH (pH 1.5). Electrode rotation rate: 800 min^{-1}.

E) of the current-potential curve A yields straight lines with the reciprocal slopes of 59±1 mV, in accordance with the fact that the first wave is the reversible one-electron oxidation wave. From the similar log-plot of the current-potential curve B, the oxidation of Fe^{2+} ion was proved to be close to irreversible. The standard heterogeneous rate constant for the oxidation of Fe^{2+} ion at a graphite electrode is 6×10^{-5} cm s^{-1}.[8] As can readily be seen from the comparison of the limiting currents of the steady-state current-potential curves A and C shown in Fig. 1, the limiting current for the oxidation of $[Mo(CN)_8]^{4-}$ ion in the solution containing Fe^{2+} ion is several times larger than the corresponding limiting current in the absence of Fe^{2+} ion. As the concentration of Fe^{2+} ion increased under the constant concentration of $[Mo(CN)_8]^{4-}$ ion, the height of the first wave increased, but the half-wave potential at about 0.5 V remained constant. At the constant concentrations of Fe^{2+} and $[Mo(CN)_8]^{4-}$ ions, the height of the first wave unchanged with changes in the rotation rate between 400 and 3600 min^{-1}, but the total limiting current was proportional to the square root of the rotation rate. These facts suggest the catalytic oxidation of Fe^{2+} ion by $[Mo(CN)_8]^{3-}$ ion, which is formed on an electrode surface by the electrochemical oxidation of the $[Mo(CN)_8]^{4-}$ ion present in a bulk solution.

Thus, the overall electrode reaction can be expressed by the following scheme:

$$[Mo(CN)_8]^{4-} - e \rightleftharpoons [Mo(CN)_8]^{3-} \quad (1)$$

$$[Mo(CN)_8]^{3-} + Fe^{2+} \underset{k_2}{\overset{k_1}{\rightleftharpoons}} [Mo(CN)_8]^{4+} + Fe^{3+}. \quad (2)$$

Under the conditions that the concentration of Fe^{2+} ion is so high compared with that of $[Mo(CN)_8]^{4-}$ ion, it can be assumed that the concentration Fe^{2+} ion remains constant during the whole electrochemical process. Thus, we obtain Eq. 3 which characterizes the catalytic current, i_{cat}, of the reaction process expressed by Eqs. 1 and 2, together with the conditions expressed by Eq. 5 which must be fulfilled to maintain the validity of Eq. 3:[5,6]

$$\frac{i_{cat}}{i_L} = \frac{\sqrt{\lambda}}{\tanh\sqrt{\lambda}}, \quad (3)$$

with

$$\lambda = (1+K)k_1 C_{Fe^{2+}}\delta^2/D, \quad (4)$$

and

$$\frac{C_{Fe^{2+}}}{C_{[Mo(CN)_8]^{3-}}} \gg \frac{i_{cat}}{i_L}, \quad (5)$$

where i_L is the Levich current[5] for the oxidation of $[Mo(CN)_8]^{4-}$ ion, k_1 and k_2 are the forward and backward rate constants of reaction 2, respectively, the equilibrium constant, K, is k_2/k_1, $C_{[Mo(CN)_8]^{3-}}$ and $C_{Fe^{2+}}$ denote the concentrations of $[Mo(CN)_8]^{3-}$ and Fe^{2+} ions, respectively, D is the common value of the diffusion coefficients of $[Mo(CN)_8]^{4-}$ and $[Mo(CN)_8]^{3-}$ ions and δ is the steady-state thickness of the diffusion layer ($\delta = 1.62\, D^{1/3}\nu^{1/6}\omega^{-1/2}$, ν: the kinematic viscosity, ω: the electrode rotation rate).

Figure 2 shows the plots of the ratio i_{cat}/i_L against the inverse square root of the electrode rotation rate at the various concentrations of Fe^{2+} and $[Mo(CN)_8]^{4-}$ ions, together with the similar plots for the $Fe^{3+}/[Mo(CN)_8]^{4-}$ system. The value of k_1 was evaluated by curve fitting method and estimated to be $(7.0\pm0.5)\times10^6$ cm^3 mol^{-1} s^{-1} by using $\nu = 1\times10^{-2}$ cm^2 s^{-1},[7] $K=4.7$ (calculated using the standard redox potentials,[1] *i.e.*, 0.49 and 0.53 V *vs.* SSCE for $Fe^{2+/3+}$ and $[Mo(CN)_8]^{4-/3-}$ couples, respectively) and $D = 5.0\times10^{-6}$ cm^2 s^{-1}. The value of D was the average value of the diffusion coefficients for $[Mo(CN)_8]^{4-}$ and $[Mo(CN)_8]^{3-}$ ions obtained from the limiting currents of the steady-state current-potential curves by using the Levich equation.[5] The solid lines shown in Fig. 2 represent the best fit curves calculated by using Eq. 3, which are seen to reproduce the experimental results. As can easily be seen from Fig. 2, the plots of i_{cat}/i_L *vs.* $\omega^{-1/2}$ give the straight lines whose slopes are proportional to the square root of the concentration of Fe^{2+} ion, indicating that in this case the r.h.s. of Eq. 3 can be reduced to $\sqrt{\lambda}$, *i.e.*, $\tanh\sqrt{\lambda}\approx1$, as can be expected for a fast catalytic reaction. By introducing the obtained value of k_1 and other known values of D, ν, ω and $C_{Fe^{2+}}$ into the right-hand side of the inequality (Eq. 5), it was confirmed that this inequality is fulfilled under the experimental conditions employed.

From the current-potential curves E and F shown in Fig. 1, it is also apparent that the reduction of Fe^{3+} ion present in a bulk solution is catalyzed by the $[Mo(CN)_8]^{4-}$ ion formed on a graphite electrode surface. By means of the same method as described above, the rate constant (k_2) of the electron transfer cross-reaction between Fe^{3+} and $[Mo(CN)_8]^{4-}$ ions was estimated to be $(6.6\pm0.5)\times10^6$ cm^3 mol^{-1} s^{-1}.

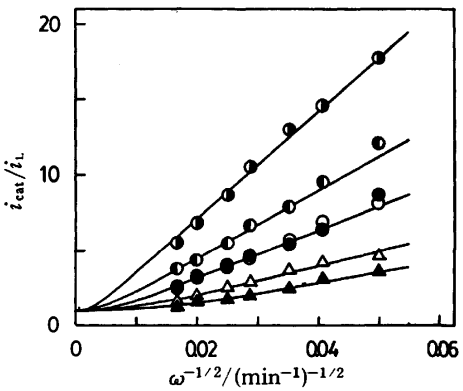

Fig. 2. Plot of the ratio, i_{cat}/i_L, against the inverse square root of the rotation rate, $\omega^{-1/2}$.
○: 0.2 mM $[Mo(CN)_8]^{4-}$+2 mM Fe^{2+}; ◐: 0.2 mM $[Mo(CN)_8]^{4-}$ +4 mM Fe^{2+}; ◑: 0.2 mM $[Mo(CN)_8]^{4-}$ +10 mM Fe^{2+}; ●: 0.05 mM $[Mo(CN)_8]^{4-}$+2 mM Fe^{2+}; ▲: 0.2 mM $[Mo(CN)_8]^{3-}$+2 mM Fe^{3+}; △: 0.2 mM$[Mo(CN)_8]^{3-}$+4 mM Fe^{3+}.
Supporting electrolyte and scan rate of electrode potential are the same as in Fig. 1. Solid lines are the best fit curves calculated by Eq. 3.

The values of k_1 and k_2 are by 1 to 2 orders of magnitude larger than those ($k_1 = 3.8\times10^5$ and $k_2 = 1.0\times10^4$ cm^3 mol^{-1} s^{-1}) reported in a previous paper,[2] where the $[Mo(CN)_8]^{4-}$ or $[Mo(CN)_8]^{3-}$ ion was bound electrostatically to the protonated poly(4-vinylpyridine) (PVP) film on a graphite electrode and Fe^{2+} or Fe^{3+} ion was present in a bulk solution. The similar results have been previously reported in the case of the catalysis of the oxidation of Fe^{2+} ion by the $[IrCl_6]^{2-}$ ion bound to the protonated PVP film on an electrode or present in a bulk solution.[8] This may be mainly attributed to the differences in the reaction media in which the rate constants were measured.

References

1) N. Oyama, K. Sato, and H. Matsuda, *J. Electroanal. Chem.*, **115**, 149 (1980).
2) N. Oyama, N. Ohta, Y. Ohnuki, K. Sato, and H. Matsuda, *Nippon Kagaku Kaishi*, **1983**, 940.
3) N. Oyama, S. Yamaguchi, Y. Nishiki, K. Tokuda, H. Matsuda, and F. C. Anson, *J. Electroanal. Chem.*, **139**, 371 (1982).
4) N. H. Furman and C. O. Miller, *Inorg. Syn.*, **3**, 160 (1950).
5) Z. Galus, "Fundamentals of Electrochemical Analysis," Translation Ed.: G. F. Reynolds, John Wiley and Sons Inc., New York, London, Sydney, Toronto (1976).
6) J. M. Hale, *J. Electroanal. Chem.*, **8**, 332 (1964).
7) A. J. Bard and L. R. Faulkner, "Electrochemical Methods," John Wiley and Sons, New York, Chichester, Brisbane, Toronto (1980), Chap. 8.
8) N. Oyama and F. C. Anson, *Anal. Chem.*, **52**, 1192 (1980).

Solid State Reactions of 2,4-Dinitrotoluene. Detection and Semiquantitative Determination of Indole, Diphenylamine, and *p*-Dimethylaminobenzaldehyde

Syed Ashfaq NABI, Ali MOHAMMAD, and Pushkin Mohammad QURESHI*

Department of Chemistry, Aligarh Muslim University, Aligarh-202001, India

(Received May 24, 1982)

Synopsis. Solid state colour reactions of 2,4-dinitrotoluene have been used for the selective detection of organic compounds and semiquantitative determination of indole, *p*-dimethylaminobenzaldehyde and diphenylamine in a glass capillary. Phloroglucinol and tryptophan do not interfere with the determination of indole. A glass wool plug modification makes the selective test almost specific for indole.

2,4-Dinitrotoluene (DNT) gives interesting colours with a number of compounds.[1-5] A recent study has proposed the use of DNT for the detection of amines.[6] In this note we present methods for the solid state detection and semiquantitative determination of some organic compounds.

Reagents. DNT (Fluka) and *p*-dimethylaminobenzaldehyde (*p*-DAB) (E. Merck) were used. All other reagents were reagent grade and used without further purification. Apparatus: VSU-2(GDR) reflectance spectrophotometer and Perkin Elmer 621 spectrometer were used for obtaining UV-visible reflectance and IR transmission spectra respectively.

Procedure

Solid State Detection. About 5—10 mg of the solid (or 5—10 μl for liquids) was rubbed with several mg of powdered DNT in the depression of a white spot plate. This was to check the colours in neutral medium. To see the effect of acidic or basic medium sodium carbonate or oxalic acid was added to the test substance and DNT; the content was again rubbed and the colour observed was then noted.

Detection by the Capillary Solid State Tests. The well powdered reagent was introduced from one end of a 10 cm capillary (3 mm bore) with the help of an iron rod. The test material was introduced similarly from another end till the two materials came in close contact with one another. Both the ends of the capillary were closed with the help of two cotton plugs. The capillary was kept in an oven at 42±2 °C for one hour. This temperature was chosen as some of the solids used in this study melted at 45 °C. The colour of the product formed at the junction was recorded. No product gave any fluorescence under a UV lamp.

The limits of identification of indole, *p*-DAB, and diphenylamine (DPA) were determined by mixing weighed amounts of well powdered sodium carbonate as a diluent. The mixture was triturated in a small mortar till it became homogeneous. Such a mixture is termed as a synthetic mixture in this paper. The synthetic mixtures contained 1—10% of the test substance. Tests were conducted in the capillary as described above. The synthetic mixture containing the largest percentage of the test substance was tried first and the colour at the junction noted. The procedure was repeated with synthetic mixtures containing lower percentages of the test material till no colour was produced at the junction. In this way the limit of identification was determined for each test substance.

Semiquantitative Determination by Capillary Solid State Tests. Approximately 400 mg of the reagent was introduced from one end of the capillary. Synthetic mixtures containing 10—100% of the test material were then introduced as described above. Three types of synthetic mixtures were tried *i.e.* those diluted with sodium carbonate oxalic acid and starch. The set of capillaries containing different percentages of indole or DPA were heated in an oven at 45± 2 °C for 1 h. This temperature was chosen as indole melts at 52 °C and DPA at 54 °C. As *p*-DAB melts at 75 °C the capillaries containing *p*-DAB were allowed to react at 65 °C for 1 h. The length of the coloured boundary formed at the junction was proportional to the concentration of the test material.

Semiquantitative Determination of Indole in the Presence of Tryptophan and Phloroglucinol. For the semiquantitative determination of indole in phloroglucinol or tryptophan mixtures, various synthetic mixtures of indole were prepared using phloroglucinol or tryptophan as diluents. These two substances were chosen as they generally interfere in the tests of indole.[7] The capillaries containing the reagent and the synthetic mixture were kept at 45±2 °C for 1 h. Capillaries were filled with synthetic mixtures containing 10—100% of indole. The same slope was obtained when a calibration curve for indole was prepared by using potassium chloride or sodium carbonate as a diluent instead of phloroglucinol or tryptophan (Fig. 1). This implies that the latter two compounds do not interfere with the determination of indole. The starch plot does not pass through the origin, hence starch should not be used as a diluent. Similar studies show that DPA can be determined in the presence of *N,N'*-diphenylthiourea and tryptophan.

Glass Wool Plug Modification for Selective Determination of Indole. When a glass wool plug was introduced between DNT and the test samples, a yellow colour was obtained at the DNT-glass wool boundary only in the case of indole. None of the substances in Table 1 and their mix-

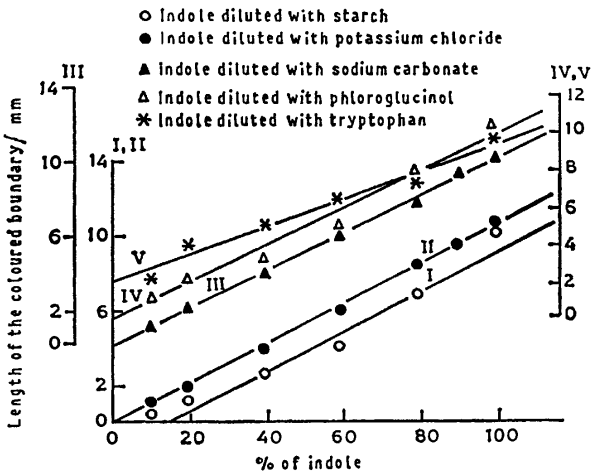

Fig. 1. Semiquantitative determination of indole, in the presence of different diluents.

Table 1. Colour reactions of organic compounds with DNT

No.	Compound	Amount taken/mg	Temperature of the spot test/°C	Colour of the spot test[a)]	Thickness of the coloured boundary/mm at 42±2 °C
1	DPA	100	25	OR	10.0
2	Benzidine	100	35	BR	0.5
3	2-Naphthylamine	100	35	Y	—
4	*p*-Toluidine	100	35	O	16.0
5	*N*-Phenyl-2-naphthylamine	100	35	Y	1.5
6	*o*-Phenylenediamine	100	35	B	1.0
7	*p*-Phenylenediamine	100	35	B	0.0
8	*o*-Nitroaniline	100	35	Y	2.0
9	*m*-Nitroaniline	100	35	Y	TR[b)]
10	*p*-Nitroaniline	100	35	Y	—
11	*p*-DAB	100	35	O	2.5
12	*p*-Dimethylaminocinnamaldehyde (*p*-DAC)	100	35	Y	TR[b)]
13	1-Naphthol	100	35	Y	TR[b)]
14	2-Naphthol	100	35	Y	TR[b)]
15	*o*-Nitrophenol	100	35	Y	12.5
16	*m*-Nitrophenol	100	35	Y	—
17	*p*-Nitrophenol	100	35	Y	2.5
18	2,4-Dinitrophenol	100	35	Y	—
19	Indole	100	35	Y	10.5
20	Brucine(anhydrous)	100	35	Y	TR[b)]
21	8-Quinolinol	100	35	Y	—
22	Phenol	100	35	Y	—
23	Ethylenediamine (liquid)	100	35	Bl	—
24	1,3-Propanediamine (liquid)	100	100	Bl	—

a) Y: Yellow, B: Brown, BR: Brick red, O: Orange, Bl: Blue, OR: Orange red.
b) TR: Thin ring.

tures gave any colour. The test is therefore specific for indole.

Results and Discussion

The colours obtained by direct trituration of test material with DNT are given in Table 1.

The colour reactions with DNT were not altered when performed in the presence of oxalic acid or sodium carbonate. The colour reactions of DNT were studied with representative members of aliphatic amines, phenols, substituted phenols, ketones, aldehydes, ureas, sugars, amino acids, acids, alcohols, hydrocarbons, and their derivatives, and ethers. No substance except those reported in Table 1 gave any colour.

As benzidine gives a characteristic colour with DNT it was detected by triturating with DNT at 35 °C in the presence of phloroglucinol, tryptophan, *p*-DAB, brucine, DPA, *p*-chlorobenzaldehyde, *o*- or *m*-nitroaniline, 2-hydroxy-3-methylbenzaldehyde, maltose, glucose, phenylthiourea, citric acid, nicotinic acid, and *p*-toluidine.

The limits of identification for indole, *p*-DAB and DPA by the capillary solid state test are 7.7, 2.3, and 1.9 μg respectively. The limit of identification for indole when a glass wool gap of 4 mm was introduced between the reagent and indole is 155 μg. Each point in Fig. 1 is an average of five readings with precision and accuracy of 3—4%.

Of the 138 compounds studied, only aromatic amines, phenols, naphthols, indole, *p*-DAC, brucine, and 8-quinolinol gave coloured reactions with DNT.

The UV, visible, and IR spectra of the compounds formed by mixing DNT with DPA, *p*-DAB, or indole

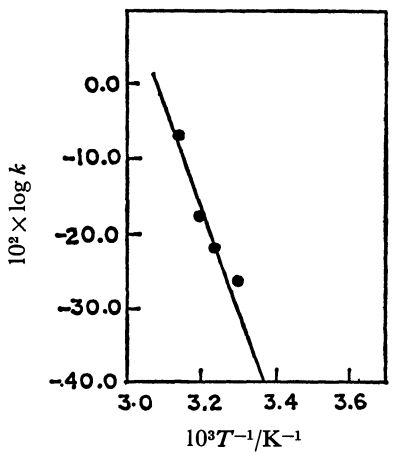

Fig. 2. Dependence of reaction rate on temperature for the DNT–DPA solid-state reaction, whereby:
$$\xi = k \log t,$$
where t is time in h, and ξ is length of coloured boundary.

are in consonance with the formation of weak charge transfer complexes.[8-14)]

The coloured boundary was found to increase with time and temperature. Thus a plot of $\log k$ *vs.* $1/T$ obtained for the DNT–DPA reaction is given in Fig. 2. The plot was used in another connection that is to obtain the energy of activation of the DNT–DPA solid-state reaction.[15)] Similar plots are expected for the DNT–*p*-DAB and DNT–indole reactions.

The authors thank Prof. W. Rahman for research facilities. The C. S. I. R. (India) is thanked for financial assistance.

References

1) T. Sinomiya, *Bull. Chem. Soc. Jpn.*, **15**, 259 (1940).
2) S. J. Stephenes, G. E. Hargis, and J. B. Entrikin, *Proc. Louisiana Acad. Sci.*, **10**, 210 (1948).
3) T. Canback, *Farm. Revy.*, **48**, 217, 234, 849 (1949).
4) H. E. Malone, *Talanta*, **22**, 97 (1975).
5) F. Feigl, "Spot-tests in Organic Analysis," 7th ed, Elsevier, New York (1966).
6) S. A. Nabi, A. Mohammad, and P. M. Qureshi, *Talanta*, **26**, 1179 (1979).
7) V. Anger and S. Ofri, *Microchim. Acta*, **1964**, 772.
8) R. E. Gibson and H. Loeffler, *J. Am. Chem. Soc.*, **62**, 1324 (1940).
9) W. R. Burton and R. E. Richards, *J. Chem. Soc.*, **1950**, 1316.
10) H. Kainer and W. Otting, *Chem. Ber.*, **88**, 1921 (1955).
11) G. Briegleb, "Elektronen-Donator-Acceptor-Komplexe," Springer Verlag, Berlin (1961), pp. 94, 103.
12) L. J. Andrews and R. M. Keefer, "Molecular complexes in organic chemistry," Holden-Day, San Francisco (1964), p. 32.
13) Y. Matsunaga, *J. Chem. Phys.*, **41**, 1609 (1964).
14) Y. Matsunaga, *Nature*, **205**, 72 (1965).
15) M. Qureshi, S. A. Nabi, A. Mohammad, and P. M. Qureshi, *J. Solid. State. Chem.*, (in press).

Polarographic Study of Mixed Ligand (*o*-Mercaptobenzoate–Citrate) Complexes of Cadmium(II), Lead(II), and Thallium(I)

Keval C. GUPTA* and Kalpana K. SHARMA

Post Graduate Department of Chemistry, Govt. College, Kota (Raj), India

(Received July 12, 1982)

Synopsis. The mixed ligand complex formation of *o*-mercaptobenzoic acid and citric acid with Cd(II), Pb (II), and Tl(I) in aqueous KNO_3 ($\mu=1.0$ mol dm^{-3}) solutions containing Triton X-100 (0.001%) has been investigated by polarography. It was shown that only one mixed ligand entity MA_iX_j is formed, where i is two for Cd (II) and one for Tl(I) j is one for all complexes and A and X are the *o*-mercaptobenzoate and citrate ligands respectively. The stability constants have been evaluated.

o-Mercaptobenzoic acid, which figures prominently in the disscussion of sulfur containing ligands has a wide variety of applications in biological, pharmaceutical and analytical fields, such sulfur-containing compounds provide two co-ordination sites *viz.* –COOH and –SH groups. Most of the earlier workers have studied the complexation by using these compounds as simple ligands. Polarography of the *o*-mercaptobenzoic acid in aqueous methanol and dioxone has been studied by K. C. Gupta and Tejinder Kaur.[1] As a part of our investigations on the polarographic study of mixed ligand complexes of sulfur containing organic compounds in combination with several metal ions, the present study of mixed ligand (*o*-mercaptobenzoate and citrate) complexes with Cd(II), Pb(II), and Tl(I), has been initiated, for which no reference could be traced out in the literature. The composition and stability constants of the complexes formed have been studied by polarographic technique.

Experimental

o-Mercaptobenzoic acid (95%, Evan's Chemetics, Inc., New York) and citric acid (B.D.H. AnalaR) as their sodium salts were used as complexing agents. All other reagents used were also of AnalaR (B.D.H.) grade. Stock solutions were prepared in doubly-distilled air-free conductivity-water. Triton X-100 (0.001%) was used as maximum suppressor and KNO_3 ($\mu=1.0$ mol dm^{-3}) as supporting electrolyte. A southern manual polarograph (Surrey, England) with scalmp galvanometer was used for recording current voltage curves. The capillary characterstics in KNO_3 ($\mu=1.0$ mol dm^{-3}) at *Ed.e*$=-0.7$ V in conjuction with respect to SCE were $m^{2/3}t^{1/6}=2.4436$ mg$^{2/3}$ s$^{-1/2}$ ($h=45$ cm). All measurements were done with the cell immersed in thermostatic bath. Dissolved air was removed by bubbling hydrogen through the cell and the necessory corrections for the IR drop and charging current were made as usual.

Results and Discussion

The formation of each mixed ligand complex was studied at 30 °C by recording polarograms of two different sets.

Set I: 1.0 mM Cd $(NO_3)_2$ or Pb $(NO_3)_2$ or Tl NO_3, 0.001% Triton X-100 and KNO_3 ($\mu=1.0$ mol dm^{-3}) with constant citrate concentration ($C_X=40.0\times10^{-3}$ mol dm^{-3}) and varying concentration of *o*-mercaptobenzoate ($C_A=10.0\times10^{-3}$ mol dm^{-3} to 80.0×10^{-3} mol dm^{-3}).

Set II: 1.0 mM Cd $(NO_3)_2$ or Pb $(NO_3)_2$ or Tl NO_3, 0.001% Triton X-100 and KNO_3 ($\mu=1.0$ mol dm^{-3}) with constant *o*-mercaptobenzoate ($C_A=40.0\times10^{-3}$ mol dm^{-3}) and varying concentration of citrate ($C_X=10.0\times10^{-3}$ mol dm^{-3} to 80.0×10^{-3} mol dm^{-3}).

All the plots of $\log(i/(id-i))$ *versus* $-Ed.e.$ yielded straight lines with slopes, which agree with the theoretical value corresponding to $n=2$ for Cd(II) and Pb(II) system and $n=1$ for TI(I) system respectively. The mean values of the slopes for two different series were 0.0302 and 0.0297 for Cd^{2+}, 0.0299 and 0.0301 for Pb^{2+} 0.0589 and 0.0599 for Tl^+ system, showing the reversibility of the reduction. Linear plots of id *versus* $h^{1/2}$ passing through the origin, established the diffusion-controlled nature in each case. The $E_{1/2}$ values from the log plots of the above mentioned c-v curves and corresponding diffusion current values have been recorded (Tables 1a, 1b, and 1c). The $E_{1/2}$ values were found to shift towards more negative values with increasing concentration of complexing agents, showing the complex formation.

Souchay and Faucherre[2] derived an equation where a metal ion complex with two kinds of ligand species simultaneously in solution. If the complexing reaction of the following type is considered.

$$M + iA + jX \rightarrow MA_iX_j \qquad (1)$$

With the restriction that single mixed ligand entity MA_iX_j is formed, then the shift in the $E_{1/2}$ of the polarographic wave of the metal ion as a function of the concentration of added reagents A and X is given by

$$\Delta E_{1/2} = \frac{2.303RT}{nF}\log\left(\frac{D_{free}}{D_{Comp}}\right)^{1/2} - \frac{2.303RT}{nF}\log K_{MA_iX_j} - i\frac{2.303RT}{nF}\log C_A - j\frac{2.303RT}{nF}\log C_X. \qquad (2)$$

The ratio D_{free}/D_{Comp} was obtained from the values of the limiting current. From plots of $\Delta E_{1/2}$ *versus* $\log C_A$ with C_X kept constant and $\Delta E_{1/2}$ *versus* $\log C_X$ with C_A kept constant, values for "i" and "j" can be obtained by intersect method because on differentiation.

$$\left(\frac{\partial(\Delta E_{1/2})}{\partial(\log C_A)}\right)_{C_X} = -\frac{2.303RT}{nF} \qquad (3)$$

$$\left(\frac{\partial(\Delta E_{1/2})}{\partial(\log C_X)}\right)_{C_A} = -\frac{2.303RT}{nF} \qquad (4)$$

Plots of (I) $\Delta E_{1/2}$ *versus* C_A (C_X kept constant), (II) $\Delta E_{1/2}$ *versus* $\log C_X$ (C_A kept constant) yielded straight lines. Figure 1, curves I and II, for Cd^{2+}, curves I′ and II′ for Pb^{2+}, curves I″ and II″ for Tl^+ systems and thus establish the formation of a single mixed ligand entity MA_iX_j. The coordination numbers i

Table 1a. Cd^{2+} Mixed ligand system

Concn C_A/M	0.00	0.01	0.02	0.04	0.06	0.08	0.04	0.04	0.04	0.04
C_X/M	0.00	0.04	0.04	0.04	0.04	0.04	0.01	0.02	0.06	0.08
30 °C id/μA	6.45	5.64	5.28	5.00	4.58	4.24	5.34	5.12	4.73	4.54
$-E_{1/2}$/V	0.596	0.852	0.870	0.892	0.902	0.910	0.870	0.880	0.898	0.902
$K_{MA_iX_j}$	—	13.929	13.922	14.065	14.077	14.099	13.930	13.962	14.107	14.119

Mean $K_{MA_iX_j}$=14.023, standard deviation=0.085.

Table 1b. Pb^{2+} Mixed ligand system

Concn C_A/M	0.00	0.01	0.02	0.04	0.06	0.08	0.04	0.04	0.04	0.04
C_X/M	0.00	0.04	0.04	0.04	0.04	0.04	0.01	0.02	0.06	0.08
30 °C id/μA	7.10	6.20	6.00	5.60	5.20	4.80	5.90	5.70	5.40	5.22
$-E_{1/2}$/V	0.400	0.654	0.674	0.694	0.706	0.714	0.674	0.684	0.700	0.704
$K_{MA_iX_j}$	—	13.864	13.915	13.984	14.069	14.095	13.929	13.958	14.033	14.043

Mean $K_{MA_iX_j}$=13.988, standard deviation=0.077.

Table 1c. Tl^{+} Mixed ligand system

Concn C_A/M	0.00	0.01	0.02	0.04	0.06	0.08	0.04	0.04	0.04	0.04
C_X/M	0.00	0.04	0.04	0.04	0.04	0.04	0.01	0.02	0.06	0.08
30 °C id/μA	5.80	4.42	4.00	3.34	3.00	2.80	3.60	3.50	3.25	3.17
$-E_{1/2}$/V	0.482	4.498	0.516	0.534	0.544	0.552	0.500	0.516	0.542	0.550
$K_{MA_iX_j}$	—	3.715	3.726	3.764	3.785	3.802	3.793	3.755	3.733	3.741

Mean $K_{MA_iX_j}$=3.757, standard deviation=0.031.

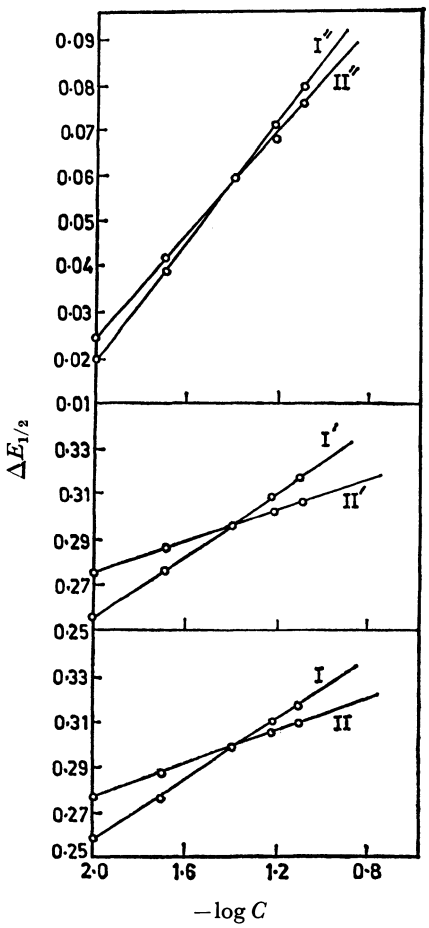

Fig. 1. Plots of $\Delta E_{1/2}$ *versus* $-\log C$.
Curves I and II— for Cd^{2+} system, curves I′ and II′— for Pb^{2+} system, curves I″ and II″— for Tl^{+} system.

and j of ligands A and X were determined from the plot (I) and (II) at 30 °C and found to be i=2.18 for Cd^{2+} 2.05 for Pb^{2+} and 0.94 for Tl^{+} respectively. Integral values of "i" and "j" were used in the calculation of the stability constants $K_{MA_iX_j}$, using Eq. 2 and were found to be 14.023 for Cd^{2+}, 13.988 for Pb^{2+} and 3.757 for Tl^{+} respectively. The present investigation suggests the formation of only one kind of mixed ligand species $[CdA_2X]^{-5}$, $[PbA_2X]^{-5}$, $[TlAX]^{-4}$ with mixed ligand (*o*-mercaptobenzoate–citrate) system.

The authors wish to express their sincere thanks to prof. K. G. Sing, Head of the Chemistry Department and to prof. R. S. Bhargava, Principal, for providing research fascilities.

References

1) K. C. Gupta and Tejinder Kaur, *J. Electrochem. Soc.*, **129**, 90 (1982).
2) P. Souchay and J. Faucherre, *Bull. Soc. Chim. Fr.*, **1947**, 529.

Photochemical Reaction of *S*-Alkyl 3-Oxobutanethioate

Tadashi HASEGAWA,* Toshio SHIMIZU, Kazuhiko IWASAKI, and Shōshichi OGUCHI
Department of Chemistry, Tokyo Gakugei University, Nukuikitamachi, Koganeishi, Tokyo 184
(Received September 6, 1982)

Synopsis. Irradiation of *S*-alkyl 3-oxobutanethioate (**1**) in benzene or ethanol yielded the disulfide **2**. Irradiation of *S*-alkyl α-bromothioacetate also gave the disulfide **2**. The photochemical reaction of the 3-oxobutanethioate **1** involves the Norrish Type I reaction followed by rapid fragmentation of the radical $\cdot CH_2COSR$ to the thiyl radical **5**.

The Norrish Type I reaction of ketones has been thoroughly investigated[1] and work has also been done on the photochemistry of α-substituted β-dicarbonyl compounds.[2] However, β-dicarbonyl compounds which possess no α-substituents are inert toward the Type I reaction.[3,4] We report here that *S*-alkyl 3-oxobutanethioates **1**, which possess no α-substituents, undergo the Type I reaction to give the disulfides **2**, but no thioacetates **6**.

When a benzene solution of *S*-propyl 3-oxobutanethioate (**1a**) was irradiated under nitrogen with a 450 W high-pressure mercury lamp through a Pyrex filter, dipropyl disulfide (**2a**) was obtained in 26% yield. Similarly, irradiation of the 3-oxobutanethioates **1b**—**e** under the same conditions gave the corresponding disulfides **2b**—**e**. In these cases no *S*-alkyl thioacetates, which are expected to be produced through the Type I reaction, and no thiolactones, which are expected to be formed *via* δ-hydrogen abstraction by ketone carbonyl, were detected.

Formation of the disulfide **2** can be explained in terms of the Type I reaction of the 3-oxobutanethioate **1** followed by the fragmentation of the radical $\cdot CH_2COSR$ (**3**) to the thiyl radical **5** (path A).

An alternative path B, which involves the direct cleavage of the sulfur-acyl bond, may be considered. The sulfur-acyl bond of the excited enethiol esters cleaves homolitically to give enethiyl radicals.[5] However, the path B seems to be improbable because the direct or acetone-sensitized irradiation of *S*-propyl thioacetate **6a** in benzene gave no disulfides. More evidence for exclusion of the path B mechanism has been obtained. Loveridge *et al.* reported that irradiation of *S*-phenyl thioacetate in benzene gave diphenyl disulfide; however, no products were obtained when the thioacetate was irradiated in alcohols.[5b] Their results prompted us to investigate the photoreaction of the 3-oxobutanethioate **1** in alcohols. Irradiation of *S*-phenyl 3-oxobutanethioate (**1e**) in ethanol also gave the disulfide **2e** in 22% yield. Similarly, irradiation of the 3-oxobutanethioate **1b** in ethanol gave the disulfide **2b** in 14% yield. These results indicate that the mechanism of the photoreaction of 3-oxobutanethioate **1** is different from that of the photolysis of the enethiol esters. Therefore, path B, which involves the direct sulfur-acyl bond cleavage, seems to be excluded.

TABLE 1. THE YIELDS OF THE DISULFIDE **2** IN THE PHOTOLYSIS OF **1** AND **8**

Compound	Solvent	Yield/% of **2**[a]
1a	PhH	26
1b	PhH	59
	EtOH	14
1c	PhH	5
1d	PhH	2
1e	PhH	49
	EtOH	22
8b	PhH	37
8e	EtOH	19

a) Conversion yield.

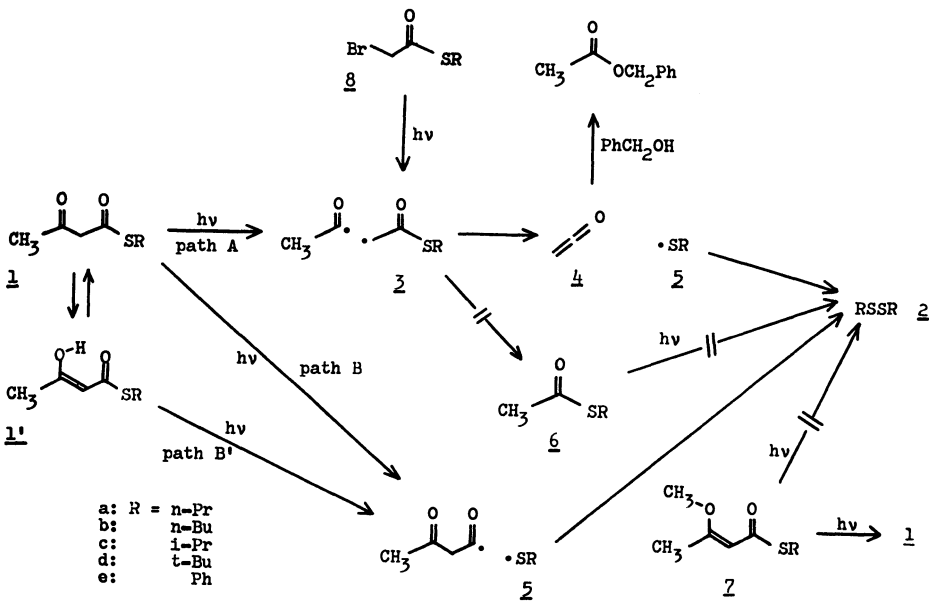

Scheme 1.

The other pathway which involves the direct cleavage of the sulfur-acyl bond from the enol form of the 3-oxobutanethioates may be considered (path B'). The 3-oxobutanethioates **1** exhibited keto-enol tautomerism. The 3-oxobutanethioate **1b** contained 71% of the keto form and 29% of the enol form in deuterated chloroform. However, this pathway seems to be improbable for the following reasons. When a benzene solution of *S*-butyl 3-methoxy-2-butenethioate (**7**), which is a model compound for the enol form of the 3-oxobutanethioate **1b**, was irradiated under the same conditions, *O*-demethylated product **1b** was obtained in 86% yield. A trace of the disulfide **2b** was detected by GLC; however, the disulfide **2b** seems to be a secondary photoproduct from the 3-oxobutanethioate **1b** because of the very low yield.

Although the attempt to trap the radical **3** from **1b** and **1e** with ethanethiol was unsuccessful, evidence in support of the above mechanism (path A) was obtained from the following experiments. When the 3-oxobutanethioate **1b** was irradiated in benzene containing 20% of benzyl alcohol, the ketene **4** was trapped as benzyl acetate which was detected by GLC. Irradiation of an ethanol solution of *S*-phenyl α-bromothioacetate (**8e**), which is expected to form the radical **3**,[6] gave the disulfide **2e** in 19% yield. In this case *S*-phenyl thioacetate could not be detected. Similarly, irradiation of *S*-butyl α-bromothioacetate (**8b**) in benzene gave the disulfide **2b** in 37% yield. These results suggest that the 3-oxobutanethioate **1** undergoes the Type I reaction to yield the radical $\cdot CH_2COSR$ (**3**) and the radical **3** rapidly fragments to the thiyl radical **5**.

The photoreaction of the 3-oxobutanethioate **1b** was efficiently quenched with 1,3-pentadiene, so that the Type I reaction takes place from the n,π^* triplet state of the keto form of the 3-oxobutanethioate **1**.

Experimental

Chemicals. The 3-oxobutanethioates **1a**—**e**, the thioacetate **6a**, and the α-bromothioacetates **8b** and **8e** were prepared according to previously described methods.[7,8] The butenethioate **7** was prepared by treatment of **1b** with diazomethane.[9]

General Procedure for Photolysis of 3-Oxobutanethioate 1 and α-Bromothioacetate 8. A 3-oxobutanethioate **1** or a thioacetate **8** (300 mg) in benzene or ethanol (70 ml) was irradiated for about 100 h under nitrogen with a 450 W high-pressure mercury lamp (Ushio Elec. Co.) through a Pyrex filter. After removal of the solvent, the residue was chromatographed on silica gel. Elution with benzene gave a disulfide **2**. The structure of **2** was determined by direct comparison with authentic samples.[10]

Photoreaction of S-Butyl 3-Methoxy-2-butenethioate (7). A solution of **7** (101 mg) in benzene (50 ml) was irradiated in a Pyrex vessel under nitrogen for 28 h. After removal of the solvent, the residue was chromatographed on silica gel (benzene–ethyl acetate 5 : 1) to give 80 mg of **1b**.

The present work was partially supported by a Grant-in-Aid for Scientific Research No. 56740205 from the Ministry of Education, Science and Culture.

References

1) N. J. Turro, "Modern Molecular Photochemistry," Benjamin/Cummings Co., Menlo Park (1978).

2) C. K. Johnson, B. Dominy, and W. Reush, *J. Am. Chem. Soc.*, **85**, 3894 (1963); M. Tokuda, M. Hataya, J. Imai, M. Itoh, and A. Suzuki, *Tetrahedron Lett.*, **1971** 3133; M. Yoshioka, H. Osawa, and S. Fukuzawa, *Bull. Chem. Soc. Jpn.*, **55**, 877 (1982).

3) R. B. LaCount and C. E. Griffin, *Tetrahedron Lett.*, **1965**, 1549; S. P. Singh and J. Kagan, *J. Chem. Soc., Chem. Commun.*, **1969** 1121; P. Markov, L. Shishkova, and Z. Zdravkova, *Tetrahedron Lett.*, **1972** 4017.

4) We previously reported that β-oxo amides underwent photocyclization *via* δ-hydrogen abstraction by ketone carbonyl; T. Hasegawa, H. Aoyama, and Y. Omote, *J. Chem. Soc., Perkin Trans. I*, **1976** 2054; **1979** 963.

5) a) J. R. Grunwell, *J. Chem. Soc., Chem. Commun.*, **1969** 1437; b) E. L. Loverdge, B. R. Bech, and J. S. Bradshaw, *J. Org. Chem.*, **36**, 221 (1971); c) J. R. Grunwell, N. A. Marron, and S. I. Hanhan, *ibid.*, **38**, 1559 (1973); d) J. R. Grunwell, D. L. Foerst, and M. J. Sanders, *ibid.*, **42**, 1142 (1977).

6) The primary photochemical process of α-haloketones is homolytical fission of the carbon-halogen bond because of weakness of the bond; A. N. Strachan and F. E. Blacet, *J. Am. Chem. Soc.*, **77**, 5254 (1955).

7) S. Motoki and T. Sato, *Bull. Chem. Soc. Jpn.*, **42**, 1322 (1969); K. Konishi, H. Umemoto, and M. Yamamoto, *Nippon Kagaku Kaishi*, **1973**, 118.

8) Y. G. Golobov, L. I. Kruglik, and V. P. Lukyanchuk, *Zh. Org. Khim.*, **13**, 515 (1977).

9) V. Pechmann, *Chem. Ber.*, **28**, 1627 (1895).

10) H. Gilman, L. E. Smith, and H. H. Parker, *J. Am. Chem. Soc.*, **47**, 859 (1925); L. D. Small, J. H. Bailey, and C. J. Cavallito, *ibid.*, **69**, 1712 (1947); F. Mott, E. Motzkus, and H. Rheinboldt, *J. Prakt. Chem.*, **134**, 270 (1932); F. Wessely, and F. Grill, *Monatsh. Chem.*, **77**, 282 (1947).

Stereochemistry of Nucleophilic Substitution of Menthyl Derivatives with Anion of Diphenylphosphine Oxide by an Action of Sodium Dihydridobis(2-methoxyethanolato)aluminate

Mitsuji YAMASHITA,* Yukio SOEDA, Nobuyoshi SUZUKI, Manabu YAMADA, Kenji TSUNEKAWA, Tatsuo OSHIKAWA, and Saburo INOKAWA†

Department of Applied Chemistry, Faculty of Engineering, Shizuoka University, Hamamatsu 432

†*Department of Chemistry, Faculty of Science, Okayama University, Okayama 700*

(Received September 22, 1982)

Synopsis. The reaction of an anion of diphenylphosphine oxide prepared by the action of sodium dihydridobis(2-methoxyethanolato)aluminate on the oxide with various menthyl or neomenthyl halides and sulfonates were studied to clarify the sterochemistry of the substitution. The reaction gave neomenthyl- and methyl-diphenylphosphine oxide in ratios from 100 : 0 to 0 : 100.

In a sequence of reactions to synthesize phosphorus-sugars, that have a phosphorus atom in the hemiacetal ring instead of an oxygen atom, the formation of a phosphorus-carbon bond was the key step. Some addition reactions of phosphorus compounds to C=C, C=N, or C=O double bond have been used to prepare a phosphorus-carbon bond on a sugar skeleton, and the process afforded usually a couple of the stereoisomeric products.[1-3] Therefore stereospecific reactions should be much more desirable for the preparation of phosphorus-carbon bond.

Preparation of phosphide anions by an action of sodium dihydridobis(2-methoxyethanolato)aluminate (SDMA) and the reaction of the anion with alkyl halides have been reported.[4,5] Stereochemistry of nucleophilic substitution reaction of metal phosphide was reported,[6] however, no report has been published concerning that of phosphorus anion prepared by SDMA from a phosphorus compound with alkyl halides or sulfonates. This note deals with the stereochemistry of nucleophilic substitution of an anion prepared by the reaction of diphenylphosphine oxide with SDMA together with the properties of leaving groups of menthyl derivatives.

Results and Discussion

The reaction of diphenylphosphine oxide with SDMA gave the phosphide anion at 0 °C. The reaction of the anion with various types of alkyl halides or *p*-toluenesulfonates gave alkyldiphenylphosphine oxide in good yield.[7] The reaction of several derivatives of menthol with the anion was carried out in order to investigate the stereochemistry of the nucleophilic substitution reaction.

$$Ph_2\overset{O}{\overset{\|}{P}}H \xrightarrow{SDMA} Ph_2\overset{O}{\overset{\|}{P}}^- \qquad (1)$$

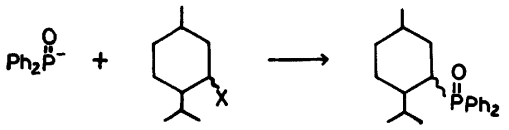

(2)

X = OTs, OMs, OTf, Cl, Br, I

The reaction of the anion of diphenylphosphine oxide with menthyl chloride in tetrahydrofuran for 10 h at 65 °C gave a mixture of neomenthyl- and menthyl-diphenylphosphine oxide in a ratio of 10 : 1. The same reaction with menthyl iodide gave them in a ratio of 1 : 1. The reactions of the anion with menthyl *p*-toluenesulfonate and menthyl methanesulfonate gave

Table 1. Reaction of menthyl or neomenthyl derivatives (RX) with diphenylphosphine oxide in the presence of SDMA

RX		Solvent	Reaction temp/°C	Reaction time/h	Recovered RX/%	Yield of phosphines[a]/%	Ratio of neomenthyl- to menthyl-diphenylphosphine oxide
R	X						
Menthyl	Cl	THF	65	10	40	6	91 : 9
		THF	65	10	37	22	88 : 12[b]
		Toluene	111	16	—[c]	6[d]	86 : 14
	Br	THF	65	10	27	36	82 : 18
	I	THF	65	10	5	37	50 : 50
	OTs[e]	THF	65	5	75	25	100 : 0
		THF	65	10	25	55	99 : 1
	OMs[f]	THF	65	10	33	16	58 : 42
	OTf[g]	THF	65	10	0	26	88 : 12
Neomenthyl	Br	THF	65	10	73	6	0 : 100
		Toluene	111	32	71	10	0 : 100

a) Yields of neomenthyl- and menthyl-diphenylphosphine oxides isolated by preparative TLC. b) One equivalent of sodium iodide was added. c) Not determined. d) Isolated by liquid chromatography. e) *p*-Toluenesulfonate. f) Methanesulfonate. g) Trifluoromethanesulfonate.

the ratios of 99 : 1 and of 82 : 18, respectively. These results are summarized in Table 1.

These findings will suggest that in the reaction the anion of diphenylphosphine oxide attacked on the carbon of menthyl chloride, bromide, and *p*-toluenesulfonate mainly in an S_N2, whereas that the anion attacked on the carbon of menthyl iodide and methanesulfonate mainly in an S_N1 manner.

The lower reactivity and the higher selectivity of inversion for neomenthyl bromide than those for menthyl bromide may attribute to the presence of an assistance by equatorial isopropyl group in breaking the equatorial carbon-bromine bond in menthyl bromide, and to the absence of it in breaking the axial carbon-bromine bond in neomethyl bromide.

Experimental

Apparatus. IR spectra were measured by Hitachi-Perkin-Elmer 337 and Japan Spectroscopic Co., Ltd. JASCO A-3 spectrophotometers, UV spectra were measured by Hitachi 340 Recording Spectrophotometer, ^{1}H-NMR spectra were run on Hitachi R-20 (60 MHz) spectrometer, mass spectra were measured by Hitachi RMU DMG GC-MS spectrometer, optical rotations were determined by Japan Spectroscopic Co., Ltd. DIP-4 digital polarimeter. Liquid chromatography and high performance liquid chromatography were carried out using Toyo Scientific Industry UVICON-540M and Japan Spectroscopic Co., Ltd. UNIFLOW-211, respectively.

Materials. Commercially available SDMA (70% benzene or toluene solution) was used. Menthyl chloride [bp 80.8 °C/8 mmHg,[8] $[\alpha]_D^{15}$ −47.7° (*c* 2.4, EtOH)],[9] menthyl bromide [bp 113 °C/22 mmHg, $[\alpha]_D^{28}$ −29.0° (*c* 1.22, EtOH)],[7] and menthyl *p*-toluenesulfonate [mp 93—95 °C, $[\alpha]_D^{25}$ −70.8° (*c* 1.0, $CHCl_3$)][10] were prepared from *l*-menthol.

Synthesis of Neomenthyl Bromide. Bromination of *l*-menthol (3.1 g) was performed by a treatment of lithium bromide (3.5 g) and chlorotrimethylsilane (5.4 g) in 40 ml of acetonitrile for 20 h under reflux. Extraction of the reaction mixture with ether followed by work-up and evaporation *in vacuo* gave neomenthyl bromide in 72% yield, bp 91 °C/7 mmHg, mp 37—40 °C, $[\alpha]_D^{15}$ −49.8° (*c* 1.04, EtOH). ^{1}H-NMR ($CDCl_3$), δ 0.78 (d, 3H, J=8.0 Hz, CH_3), 0.20—2.55 (m, 15H, C_8H_{15}), and 3.10—3.62 (m, 1H, CHBr).

Iodination of l-*Menthol.* Iodination of *l*-menthol by sodium iodide and chlorotrimethylsilane as described above gave neomenthyl iodide in 40% yield, bp 50 °C/7 mmHg, $[\alpha]_D^{15}$ 0.48° (*c* 1.1, EtOH), ^{1}H-NMR ($CDCl_3$) δ 1.01 [d, 6H, J=4.3 Hz, $CH(C\underline{H}_3)_2$], 0.30—2.77 (m, 12H, C_7H_{12}), and 4.65—5.47 (m, 1H, CHI), and menthyl iodide in 46% yield, bp 93 °C/7 mmHg, $[\alpha]_D^{15}$ −0.58° (*c* 1.0, EtOH), ^{1}H-NMR ($CDCl_3$) δ 0.88 (d, 3H, J=3.8 Hz, CH_3), 0.26—2.85 (m, 9H, C_6H_9), and 3.78—5.39 (m, 1H, CHI).

Synthesis of Menthyl Methanesulfonate. Methanesulfonyl chloride (5.7 g) in pyridine was added to a pyridine solution of *l*-menthol (7.8 g). The work-up of chloroform solution of the product followed by sublimation gave the methanesulfonate in 77% yield, mp 32—36 °C, $[\alpha]_D^{15}$ −63.5° (*c* 1.0, EtOH). ^{1}H-NMR ($CDCl_3$) δ 0.77 (d, 3H, J=3.0 Hz, CH_3), 0.93 (d, 6H, J=7.3 Hz, $CH(C\underline{H}_3)_2$), 2.99 (s, 3H, CH_3SO_2), 0.25—3.64 (m, 9H, C_6H_9), and 4.28—4.88 (m, 1H, CH-O).

Synthesis of Menthyl Trifluoromethanesulfonate. The trifluoromethanesulfonate was prepared by *l*-menthol and trifluoromethanesulfonic anhydride in 32% yield, $[\alpha]_D^{15}$ −6.3° (*c* 1.2, EtOH).

Reaction of Menthyl Derivatives with Diphenylphosphine Oxide in the Presence of SDMA. To a solution of a mixture of diphenylphosphine oxide (1.5 mmol) and SDMA (3.5 mmol) menthyl derivatives (1.5 mmol) were added, and then the solution was allowed to react for several hours. The work-up (addition of water and activated carbon to the reaction mixture followed by filtration, extraction with chloroform, dehydration, and evaporation of the solvent *in vacuo*) of the reaction mixture followed by analysis of the product by HPLC, spectra, and optical rotation revealed that the product consisted of neomenthyldiphenylphosphine oxide and menthyldiphenylphosphine oxide in various ratios. The reaction condition, recovered starting materials, and isolated yields and ratios of the produced phosphine oxides were summarized in Table 1.

Neomenthyldiphenylphosphine oxide showed spectra as follows: ^{1}H-NMR ($CDCl_3$), δ 0.25—3.05 (m, 19H, Me, CH-$(CH_3)_2$, and ring protons) and 7.01—8.02 (m, 10H, 2×Ph); MS, 340 (M^+) and 201 [$P(O)Ph_2$]; IR ν_{max}^{KBr} 1440 (P–Ph), 1193 (P=O), and 720 cm^{-1} (P-C). Menthyldiphenylphosphine oxide showed the similar spectra. HPLC with JASCO SS-05 column eluted by chloroform–hexane (1 : 1) under 100 kg/cm^2 pressure showed peaks of menthyldiphenylphosphine oxide at 15.6 min and of neomenthyldiphenylphosphine oxide at 23.6 min, which were detected by JASCO UVIDEC-100 II UV detector at a wave length of 260.4 nm.

The authors wish to express their thanks to professor M. Suzuki's laboratory of Shizuoka University for giving facility for measurement of optical rotation. This work was partially supported by a Grant-in-Aid for Scientific Research No. 475661 from the Ministry of Education, Science and Culture.

References

1) H. Takayanagi, M. Yamashita, K. Seo, H. Yoshida, T. Ogata, and S. Inokawa, *Carbohydr. Res.*, **38**, C19 (1974).

2) M. Yamashita, Y. Nakatsukasa, M. Yoshikane, H. Yoshida, T. Ogata, and S. Inokawa, *Carbohydr. Res.*, **59**, C12 (1977).

3) P. T. Long, M. Yamashita, and S. Inokawa, *Carbohydr. Res.*, **76**, C4 (1979).

4) R. B. Wetzel and G. L. Kenyon, *J. Am. Chem. Soc.*, **94**, 1774 (1972).

5) R. B. Wetzel and G. L. Kenyon, *J. Org. Chem.*, **39**, 1531 (1974).

6) J. D. Morrison and W. F. Masler, *J. Org. Chem.*, **39**, 270 (1974).

7) M. Yamashita, N. Suzuki, M. Yamada, Y. Soeda, H. Yamashita, K. Nakatani, T. Oshikawa, and S. Inokawa, *Bull. Chem. Soc. Jpn.*, **56**, 219 (1983).

8) 1 mmHg=133.322 Pa.

9) R. B. King, J. Bakos, C. D. Hoff, and L. Markó, *J. Org. Chem.*, **44**, 3095 (1979).

10) H. Phillips, *J. Chem. Soc.*, **127**, 2566 (1925).

Cyclization Reaction of Bis(tributylstannylated) α-Ketols with Heterocumulenes. Preparation of *O,O*-Vinylene Imino- and Thiocarbonates

Shizuyoshi SAKAI,* Masashi MURATA, Nobuto WADA, and Tatsuo FUJINAMI
Department of Applied Chemistry, Faculty of Engineering, Shizuoka University, Johoku 3, Hamamatsu 432
(Received September 27, 1982)

Synopsis. Aromatic α-ketols reacted with diethylaminotributylstannane at 60 °C to afford a mixture of (*Z*)- and (*E*)-1,2-bis(tributylstannyloxy)-1,2-diarylethenes, which were allowed to react with organic isothiocyanates and carbon disulfide to give substituted *O,O*-vinylene imino- and thiocarbonates, respectively. Aliphatic α-ketol, 3-hydroxy-2-butanone, was treated by the aminostannane, followed by the reaction with carbon disulfide to form (*E*)-1,2-bis(tributylstannylthio)-2-butene.

β-Keto derivatives of the group IV organometalloids are well documented.[1,2] These metalloid compounds are generally used as their tautomers, organometallic enol ethers, which are important intermediates in many kinds of carbon-carbon bond formation.[2] Our interest has been focused on both the reactivities of heteroatom-Sn bonds and the cyclization reaction of the saturated compounds having two heteroatom-Sn bonds with sulfur-containing heterocumulenes to form heteroatom-carbon bonds in carbonate syntheses (Eq. 1).

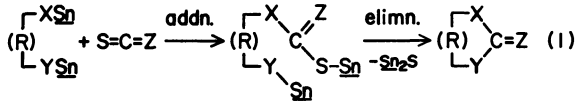

X, Y, Z = O, S, or NR'; (R) = $(CH_2)_{2,3}$; Sn = Bu_3Sn or $Bu_2Sn/2$

This work describes a bis(tributylstannylation) reaction of α-ketol to form bis(tributylstannyloxy)ethenes and their reactions with heterocumulene such as organic isothiocyanates or carbon disulfide to afford imino- or thiocarbonic *O,O*-diester.

Results and Discussion

Formation of Bis(tributylstannyloxy)ethenes. Aromatic α-ketol, 2-hydroxy-1,2-diphenylethane-1-one (**1a**), was allowed to react with an equimolar amount of diethylaminotributylstannane at room temperature to form *O*-tributylstannylated compound (**2a**). A second mole of the aminostannane was added to **2a**, and the mixture was heated at 60 °C to accomplish the stannylation of α-H of carbonyl group in **2a**; this was followed by tautomerization (or *vice versa*) to give **3a** (Eq. 2). The reddish brown liquid (**3a**), prepared *in situ*, showed the strong band of (*E*)-C=C group at 1680 cm^{-1}, the weak band of (*Z*)-C=C group at 1640 cm^{-1}, and the strong band of vinyloxy group at 1330 cm^{-1} in its IR spectrum. These data will suggest that the bis(tributylstannylated) compound (**3a**) exists as a mixture of (*E*)- and (*Z*)-bis(tributylstannyloxy)ethenes. A mixture of (*E*)- and (*Z*)-bis(tributylstannyloxy)-1,2-bis(4-methylphenyl)ethenes (**3b**) was also obtained from the reaction of 2-hydroxy-1,2-bis(4-methylphenyl)ethane-1-one (**1b**) and two equivalents of diethylaminotributylstannane.

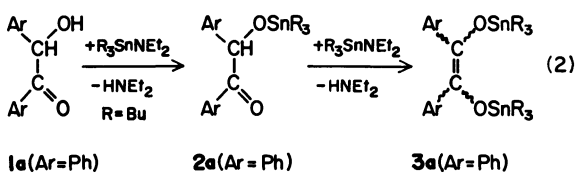

1a(Ar=Ph) 2a(Ar=Ph) 3a(Ar=Ph)
1b(Ar=4-MeC_6H_4) 2b(Ar=4-MeC_6H_4) 3b(Ar=4-MeC_6H_4)

Cyclization Reaction of 3 with Heterocumulenes. An equimolar reaction of **3a**, prepared *in situ* from **1a** and the aminostannane, with phenyl isothiocyanate at room temperature gave a small amount of 2-phenylimino-4,5-diphenyl-1,3-dioxolene (**5**; R'=Ph).

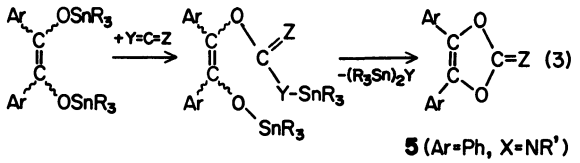

3a or **3b** **4a** or **4b** **5** (Ar=Ph, X=NR') **6a** or **6b** (X=S)
(**a**: Ar=Ph, **b**: Ar=4-MeC_6H_4)

Furthermore, **5** (R'=Ph) was formed in an improved yield (80%), when the reaction mixture was heated for 2 more hours at 100 °C. These results suggest that (*E*)-**3a** will slowly isomerize to (*Z*)-**3a**, which is easily cyclized with an isothiocyanate to give a high yield of **5a**.

4-Methylphenyl isothiocyanate was also allowed to react with **3a** to afford **5** (R'=4-MeC_6H_4). Aliphatic isothiocyanates such as ethyl and cyclohexyl isothiocyanates were less reactive and reacted partially even under severe reaction conditions.

Carbon disulfide is known to be a thiocarbonylating reagent for bis(organostannyloxy)alkanes.[3] Here, unsaturated bis(organostannylated) compound, **3a** or **3b**, was submitted to a reaction with an excess amount of carbon disulfide under reflux for 24 h to afford the substituted *O,O*-vinylene thiocarbonate (**6a** or **6b**) in a moderate yield.[4] On the occasion, *O,O*-vinylene thiocarbonate was prepared from **1** and thiophosgene[5] or from vinylene carbonate and phosphorus pentasulfide.[6] Therefore, the reaction (Eqs. 2 and 3) gives a new route to prepare **6** from the aminostannane, carbon disulfide, and **1**.

Carbonyl sulfide and carbon dioxide inserted across the Sn–O bond in **3a** to afford **4a** (X=O, Y=S or O). However, the starting material **3a** was recovered by distillation. Thus carbonylation of the enediol-type organostannyl compound **3a** was unsuccessful.

Phenyl isocyanate was reported to react with saturated bis(organostannyloxy) compound to form a carbamate-type adduct which was never cyclized even under severe reaction conditions.[3] Bis(organostannyl) enediol-type compound (**3a**) reacted with the isocyanate for 7 h under reflux in toluene to afford 3,4,5-triphenyl-2(3*H*)-oxazolone (**9**). In the light of the scheme for the reaction

of vinylene carbonate with amines to form 2(3*H*)-oxazolones, reaction path (4) was tentatively proposed.

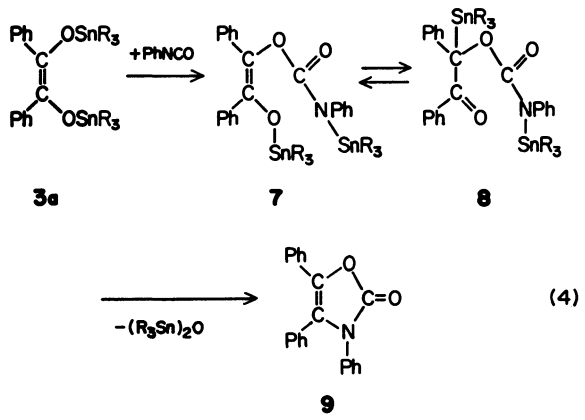

Organostannylation of Aliphatic α-Ketol and Its Reaction with Carbon Disulfide. When 3-hydroxy-2-butanone (**10**) was allowed to react with diethylaminotributylstannane at 60 °C, the methine proton signal in **10** completely disappeared, and methyl and butyl signals only were observed in the NMR spectrum of the reaction mixture; this suggests the formation of bis(tributylstannylated) compound (**11**), which will exist mainly as an (*E*)-enediol-type organostannyl compound, because the band of (*E*)-C=C bond appeared in its IR spectrum. The compound (**11**) reacted with carbon disulfide to form not the corresponding *O,O*-vinylene thiocarbonate but (*E*)-2,3-bis(tributylstannylthio)-2-butene (**12**). Transformation of the bis(organostannyloxy)ethene (**11**) to the bis(organostannylthio)ethene (**12**) is a new type of the reaction of organostannyl-oxygen bond with sulfur-containing heterocumulene.[8]

Experimental

*Reaction of **1a** with Diethylaminotributylstannane.* The compound **1a** (2.12 g, 10.0 mmol) and diethylaminotributylstannane (3.36 g, 10.0 mmol) were stirred under dry nitrogen atmosphere and then *in vacuo* at room temperature to form a transparent liquid (**2a**). IR (neat) 1720 cm^{-1} (C=O); NMR (CCl_4) δ=6.04 (s, 1H, CH). Subsequently, diethylaminotributylstannane (3.36 g, 10.0 mmol) was added to **2a**, and heated at 60 °C for 2 h *in vacuo* to form a reddish brown liquid (**3a**). **3a** could be isolated neither by vacuum distillation nor by recrystallization. **3a**: IR (CCl_4) 1640 ((*Z*)-C=C), 1690 ((*E*)-C=C), and 1330 cm^{-1} (C=C–O).

*Reaction of **3a** with Aryl Isothiocyanate.* Aryl isothiocyanate (10 mmol) was added to **3a** (10 mmol), prepared *in situ*, at room temperature. Soon after the addition, a small amount of white crystals of **5** were precipitated. Then, the reaction mixture was heated at 100 °C for 1 h, filtered, and washed with hexane to afford crude **5**. **5** (R'=Ph): yield 80%; MS *m/e* 313 (M^+); IR ($CHCl_3$) 1730 (C=N) and 1680 cm^{-1} (C=C); NMR ($CDCl_3$) δ=7.3—7.6 (15H, Ph), and **5** (R'=4-MeC_6H_4): yield 60%; mp 148—149 °C; MS *m/e* 327 (M^+); IR ($CHCl_3$) 1735 (C=N) and 1680 cm^{-1} (C=C); NMR ($CDCl_3$) δ=7.1—7.4 (14H, br., Arom.) and 2.30 (3H, s, CH_3). Found: C, 80.50; H, 5.25; N, 4.31%. Calcd for $C_{22}H_{17}NO_2$: C, 80.71; H, 5.23; N, 4.23%.

*Reaction of **3a** or **3b** with Carbon Disulfide.* The compound (**3a** or **3b**; 5.3 mmol) was allowed to react with carbon disulfide (1.5 ml) for 24 h under reflux. Hexane was added to the reaction mixture to precipitate crystals of **6a** or **6b**. **6a**: yield 50%; mp 118—119 °C (Ref. 6 124 °C); IR (CCl_4) 1310 cm^{-1}, and **6b**: mp 183—184 °C; IR ($CHCl_3$) 1320 cm^{-1}; NMR ($CDCl_3$) δ=2.32 (6H, s, CH_3) and 7.3 (8H, d,d-type, Arom.). Found: C, 72.31; H, 5.03; S, 11.12%. Calcd for $C_{17}H_{14}O_2S$: C, 72.31; H, 5.00; S, 11.36%.

*Reaction of **3a** with Phenyl Isocyanate.* Phenyl isocyanate (0.92 g, 7.1 mmol) was added to **3a** (4.9 mmol) in methylbenzene (8 ml) to form **7**; IR 1570 and 1590 cm^{-1}. The reaction mixture was refluxed for 6 h and distilled to remove the solvent. Hexane was added to the residue to separate white crystals of **9**; yield 70%; mp 191—193 °C; IR ($CHCl_3$) 1760 (C=O) and 1685 cm^{-1} (C=C); NMR (CH_2Cl_2) δ=7.0—7.6 (15H, m, Ph). Found: C, 80.52; H, 5.04; N, 4.32%. Calcd for $C_{19}H_{15}NO_2$: C, 80.52; H, 4.82; N, 4.47%.

*Treatment of **10** with Diethylaminotributylstannane Followed by the Reaction with Carbon Disulfide.* Acetoin (**10**; 2.25 g, 25.2 mmol) was treated with two equivalents of diethylaminotributylstannane (21.6 g, 58.6 mmol) *in vacuo* at 60 °C for 5 h to form the bis(tributylstannylated) compound (**11**); IR 1685 cm^{-1} (C=C); NMR ($CDCl_3$) δ=1.8 (6H, br., CH_3) and 0.8—1.9 (m, BuSn). **10** was refluxed with an excess of carbon disulfide. The reaction mixture was then submitted to the sublimation under vacuum (10 Pa) at 130 °C to separate a small amount of **11**; mp 84.5—86.0 °C; MS *m/e* 698 (M^+); IR ($CHCl_3$) 960 cm^{-1} ((*E*)-C=C); NMR (CCl_4) δ=0.7—1.6 (54H, m, Bu) and 1.92 (6H, s, CH_3). Found: C, 48.14; H, 8.85; S, 9.04%. Calcd for $C_{28}H_{60}S_2Sn_2$: C, 48.16; H, 8.66; S, 9.04%.

The present work was partially supported by Grant-in-Aid for Scientific Research No. 165197 from the Ministry of Education, Science and Culture.

References

1) A. G. Brook, "Advances in Organometallic Chemistry," ed by F. A. G. Stone and R. West, Academic Press, New York (1968), Vol. 8, p. 95; R. E. Bruns and P. M. Kuznnesof, *J. Organomet. Chem.*, **56**, 131 (1973).

2) Y. Odic and M. Pereyre, *J. Organoment. Chem.*, **55**, 273 (1973); T. E. Ignacz and N. Serpone, *ibid.*, **127**, 289 (1978); R. H. Fish and B. M. Brolin, *ibid.*, **159**, 255 (1978); J. K. Rasmussen, *Synthesis*, **1977**, 91.

3) S. Sakai, K. Kiyohara, K. Itoh, and Y. Ishii, *J. Org. Chem.*, **25**, 2347 (1970); S. Sakai, T. Fujinami, K. Kosugi, and K. Matsunaga, *Chem. Lett.*, **1976**, 891; S. Sakai, Y. Kobayashi, and Y. Ishii, *J. Organomet. Chem.*, **36**, 1176 (1971).

4) A similar type of reaction was reported for the preparation of acetylenes from bis(trimethylsiloxy)ethenes. D. P. Bauer and R. S. Macomber, *J. Org. Chem.*, **41**, 2640 (1976).

5) W. K. Anderson and R. H. Dewey, *J. Am. Chem. Soc.*, **95**, 7161 (1973).

6) H. M. Fischer and W. Hartman, *Chem. Ber.*, **105**, 2769 (1972).

7) J. C. Sheeham and F. S. Guziec, *J. Org. Chem.*, **38**, 3034 (1973).

8) The Mechanism of the formation of **12** has not been established. A probable scheme is the addition of CS_2 on O–Sn bond in 3-tributylstannyl-3-tributylstannyloxy-2-butanone, an isomer of **11**, to give the xanthate, which will isomerize to dithiocarbonic *S,S*-diester, followed by the elimination of COS to afford 3-tributylstannyl-3-tributylstannylthio-2-butanone, an isomer of 3-tributylstannyl-3-tributylstannyloxybutane-2-thione. These reaction will be repeated again to give **12**.

The Thermal Reactions of Allyl-substituted Germyl Radicals

Kunio MOCHIDA* and Isoo MIYAGAWA
Department of Chemistry, Faculty of Sciences, Gakushuin University, 1-5-1 Mejiro, Tokyo 171
(Received October 20, 1982)

Synopsis. The allyldibutylgermyl and dibutyl(2-methylallyl)germyl radicals in benzene at 80 °C afforded diallyldibutylgermane and dibutylgermane, and dibutylbis(2-methylallyl)germane and dibutylgermane, respectively. The mechanism of these reactions is discussed.

Although numerous publications on addition of organogermyl radicals to olefinic double bonds have appeared,[1] there are few reports on the reactions of olefinic germyl radicals.[1a,2] The reactions of olefinic germyl radicals lead to cyclic products and are of interest both in synthesis and in mechanistic problems. In a previous paper,[2] we have reported on the reactions of ω-alkenyldimethylgermyl radicals, $Me_2\dot{G}e(CH_2)_n$-$CH{=}CH_2$, (n=2—5) (Eq. 1). ω-Alkenyldimethylgermyl

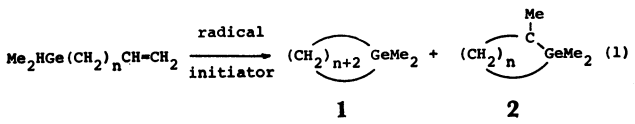

radicals afford cyclization products, with the exo isomer (**1**) predominating. These results are in striking contrast to those of the corresponding ω-alkenyl radicals.[3] This paper deals with the thermal reactions of allyl-substituted germyl radicals which are one group of the ω-alkenylgermyl radicals. It is interesting to compare the present findings with those for carbon analogs.

Results and Discussion

The reactions of allyldibutylgermane (**3**, R=H) and dibutyl(2-methylallyl)germane (**3**, R=Me) were carried out in sealed, degassed tubes in benzene as solvent and dibenzoyl peroxide (BPO) as initiator at 80 °C. Products were isolated by preparative GLC and their structures were verified by comparing the retention times on GLC and IR and NMR spectra with those of authentic samples. The main products obtained in the thermal reactions of allyldibutylgermane (**3**, R=H) and dibutyl(2-methylallyl)germane (**3**, R=Me) under various conditions are summarized in Table 1.

As shown in Table 1, the allyldibutylgermyl radical (**4**, R=H) in benzene afforded diallyldibutylgermane (**6**, R=H) and dibutylgermane. The dibutylbis(2-methylallyl)germyl radicals (**4**, R=Me) in benzene gave dibutylbis(2-methylallyl)germane (**6**, R=Me) and dibutylgermane. Several organic products with much higher boiling points were also detected in both reactions. No cyclization products were detected. The allyldibutylgermyl radical (**4**, R=H) was more reactive than the dibutyl(2-methylallyl)germyl radical (**4**, R=Me). The thermal reactions of allyl-substituted germanes were promoted by BPO, radical generator.

The reversibility of the addition to an olefinic double bond is not a favorable process for carbon radicals at least at low temperature, but is progressively favored for elements lower in group 4B in the periodic table.[4] Therefore, the formation of diallyldibutylgermanes (**6**) and dibutylgermane suggests that the following addition-elimination process may occur in the thermal reactions of allyl-substituted germanes (Scheme **1**):

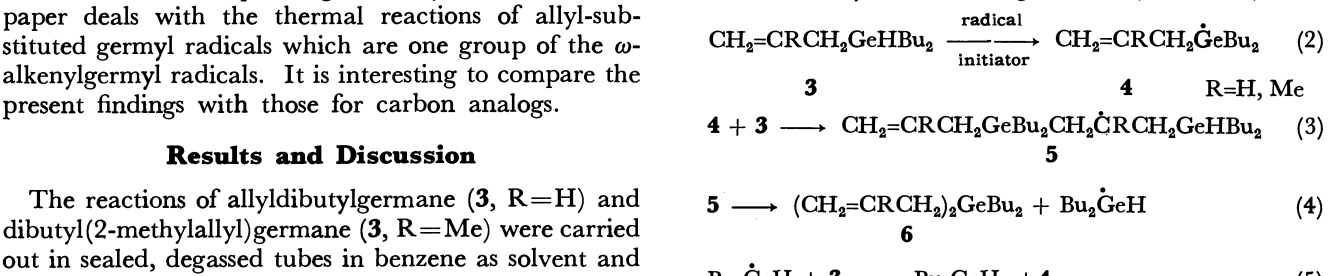

Thus, the addition of the germyl radicals (**4**) generated from the hydrogermanes (**3**) to the carbon-carbon double bond of the hydrogermanes (**3**) intermolecularly gives the intermediate radicals (**5**). The intermediate

Table 1. Thermal reactions of allyl-substituted germanes

Reactants(mmol)			Conditions		Products, Yield/%[a]		
$(CH_2{=}CRCH_2)Bu_2GeH$, **3**	BPO,	C_6H_6	Temp/°C	Time/h	$(CH_2{=}CRCH_2)_2GeBu_2$, **6**	Bu_2GeH_2,	**3**
R=H							
1.01	0.02	31.00	80	15	5.9	7.3	42.2
0.72	0.07	21.52	80	15	3.1	4.8	42.2
0.98	0	30.90	80	15	trace	trace	95.1
0.51	0.02	50.64	80	15	5.5	8.1	48.8
0.59	0.05	53.64	80	15	5.2	7.1	44.4
R=Me							
0.72	0.07	21.20	80	15	4.0	4.0	84.4
0.72	0.05	22.92	80	15	3.3	3.5	88.1
0.51	0	21.20	80	15	trace	trace	98.0
0.77	0.07	77.71	80	15	4.9	6.2	87.6
0.51	0.05	53.28	80	15	3.9	5.2	83.1

a) Based on the consumed hydrogermanes **3**.

radicals (**5**) undergo degradation to form diallyldibutylgermanes (**6**) and dibutylgermyl radical. The dibutylgermyl radical abstracts a hydrogen atom from the hydrogermanes (**3**) to give dibutylgermane and the germyl radicals (**4**). The reactions of allyl-substituted germyl radicals proceed by a free-radical chain mechanism. However, the mass balance in these reactions is bad. Moreover, the theoretical ratio of diallyldibutylgermanes (**6**) and dibutylgermane is not always obtained. These facts suggest that the intermolecular addition of organogermyl radicals to olefinic bonds and/or dimerization of organogermyl radicals, along with the addition-elimination process shown in Scheme 1, may proceed in these reactions resulting in the formation of unidentified materials.

The present results of the thermal reactions of allyl-substituted germyl radicals are clearly different from those of the corresponding 3-butenyl and allylsilyl radicals. 1,2-Vinyl shifts proceeding *via* cyclopropylmethyl radicals are well known in the reactions of 3-butenyl radicals.[3a,4b] It has been reported that vinylsilanes are formed by loss of methylene from the allyl groups[5] or by loss of a methyl group originallyl bound to silicon[6] in the reactions of allylsilyl radicals.

Experimental

Materials. Bu_2GeCl_2: bp 120 °C/10 mmHg,[7] Bu_2GeH_2: bp 86 °C/46 mmHg,[8] Bu_2GeHCl: bp 105 °C/17 mmHg,[8] and $(CH_2{=}CHCH_2)GeBu_2H$: bp 36 °C/0.2 mmHg[9] were prepared as described in the cited references.

Preparation of Dibutyl(2-methylallyl)germane. A (2-methylallyl)magnesium chloride was prepared from 2-methylallyl chloride (3.3 g, 36.0 mmol) and magnesium (0.9 g, 36.0 mmol) in 50 ml of dry THF. To this, (2-methylallyl)magnesium chloride, dibutylchlorogermane (2.0 g, 9.0 mmol) dissolved in 10 ml of dry ether was added. The reaction mixture was stirred with reflux for 3 h. After hydrolysis with water, organic substances were extracted with ether and the extract was dried over sodium sulfate. Fractional distillation gave dibutyl(2-methylallyl)germane (1.6 g, 6.6 mmol, 73.5%), bp 38.5—39.5 °C/0.04 mmHg; n^{20} 1.4689; NMR (δ in $CDCl_3$) 0.88—1.73 (m, 23H), 3.80 (m, 1H), 4.52 (s, 2H); IR (neat, cm^{-1}) 2050 (Ge–H). Found: C, 59.20: H, 10.64%, Calcd. for $C_{12}H_{26}Ge$: C, 59.33; H, 10.79%.

Preparation of Diallyldibutylgermane. An allylmagnesium chloride was prepared from allyl chloride (1.0 g, 14.0 mmol) and magnesium (0.32 g, 14.0 mmol) in 50 ml of dry THF. To this, allylmagnesium chloride, dibutyldichlorogermane (1.5 g, 58 mmol) dissolved in 10 ml of dry ether was added. The reaction mixture was stirred with reflux for 4 h. After hydrolysis with water, organic substances were extracted with ether and the extract was dried over sodium sulfate. Fractional distillation gave diallyldibutylgermane (1.2 g, 4.5 mmol, 76.9%). bp 125 °C/18 mmHg; n^{20} 1.4766; NMR (δ in $CDCl_3$) 0.88—1.32 (m, 18H), 1.69 (d, J=8.0 Hz, 4H), 4.70—4.92 (m, 4H), 5.53—6.02 (m, 2H). Found: C, 62.76: H, 10.24%. Calcd for $C_{14}H_{28}Ge$: C, 62.52: H, 10.49%.

Preparation of Dibutylbis(2-methylallyl)germane. Dibutylbis(2-methylally)germane was prepared from 2-methylallylmagnesium chloride and dibutyldichlorogermane in 76.3% yield, bp 83 °C/0.8 mmHg; n^{20} 1.4818; NMR (δ in CCl_4) 0.80—1.83 (m, 28H), 4.51 (m, 2H). Found: C, 64.64: H, 10.92%. Calcd for $C_{16}H_{32}Ge$: C, 64.70: H, 10.86%.

Thermal Reactions of Hydrogermanes in Benzene. A hydrogermane, BPO, and benzene were placed in a Pyrex glass tubes. The tube was sealed after degassing and immersed in a constant temperature bath kept at 80 °C. The reaction mixture was analyzed by GLC (Shimadzu GC 6A with SE30 20% or Apiezen L 30% 2m). The amounts of products were determined by an internal-standard method. Each product was isolated by preparative GLC and the structure was verified by comparing the retention time on GLC and IR and NMR spectra with those of authentic samples.

References

1) a) M. Lesbre, P. Mazerolles, and J. Satge, "The Organic Compounds of Germanium," John Wiley and Sons, New York (1971), Chap. 4; b) H. Sakurai, "Free Radicals," ed by J. K. Kochi, John Wiley and Sons, New York (1973), Vol. II, Chap. 25; c) H. Sakurai, Proc. IIIrd. Intern. Conf. Organometal. Chem. Germanium, Tin, and Lead, Dortmund, 1980, *J. Organomet. Chem. Library*, **12**, 267 (1981).

2) K. Mochida and K. Asami, *J. Organomet. Chem.*, **232**, 13 (1982).

3) For examples: a) J. W. Wilt, "Free Radicals," ed by J. K. Kochi, John Wiley and Sons, New York (1973), Vol. I, Chap. 8; b) A. L. J. Beckwith and K. U. Ingold, "Rearrangements in Ground and Excited States," ed by P. de Mayo, Academic Press, New York (1980), Vol. I, Chap. 4; c) M. Jullia, *Acc. Chem. Res.*, **4**, 386 (1971).

4) S. W. Bennet, C. Eaborn, R. A. Jackman, and R. Pearce, *J. Organomet. Chem.*, **16**, p 17. (1968).

5) H. Sakurai, A. Hosomi, and M. Kumada, *J. Chem. Soc., Chem. Commun.*, **1970**, 767.

6) S. M. Neider, G. R. Chambers, and M. Jones, Jr., *Tetrahedron Lett.*, **1979**, 3793.

7) H. H. Anderson, *J. Am. Chem. Soc.*, **83**, 3016 (1961).

8) H. H. Anderson, *J. Am. Chem. Soc.*, **82**, 3016 (1960).

9) J. Satgé, *Ann. Chim. (Paris)*, **6**, 519 (1961).

Reactions of 2,4-Azetidinedione with Nucleophilic Reagents

Kazuhiro MARUYAMA* and Yoshihiro ARITA
Department of Chemistry, Faculty of Science, Kyoto University, Sakyo-ku, Kyoto 606
(Received December 21, 1982)

Synopsis. The reaction of 2,4-azetidinedione with a variety of nucleophiles was compared with that of *N*-methylsuccinimide. 2,4-Azetidinedione gave ring-cleaved addition products, while *N*-methylsuccinimide afforded simply addition products to the carbonyl group.

It is known that imide compounds show a variety of reactivity with nucleophilic reagents depending on their structures.[1] For instance, *N*-phenylsuccinimide reacts with ethylmagnesium bromide to give 2-ethyl-2-hydroxy-1-phenylpyrrolidine (**1**), while arylmagnesium bromides react with *N*-substituted maleimides to yield *N*-substituted 5-aryl-5-hydroxy-2-pyrrolidones (**2**) (See Fig. 1).[2] Under certain conditions, the imide ring is

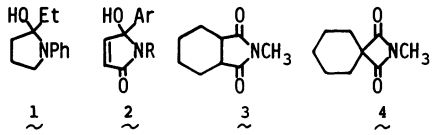

Fig. 1.

cleaved by the Grignard reagent, *i.e.*, *N*-methyl keto amide was the product of the reaction of *N*-methylsuccinimide with ethylmagnesium bromide.[3] Diphenyl and diethyl substituted *N*-phenylmalonimides react with three equivalents of aryl Grignard reagents to give the disubstituted *N*-phenylacetamides and the tertiary alcohols derived from the Grignard reagents.[4]

Recently, the authors[5] reported photochemistry of *N*-methyl-*cis*-1,2-cyclohexanedicarboximide (**3**), which afforded four-membered ring imide, 2,4-azetidinedione **4**.[6] In this report, the reaction of this photoproduct **4** with some nucleophiles has been studied and compared with the reactivity of succinimide **3**.

Results and Discussion

Reactions of **3** and **4** with various Grignard reagents (RMgX) were summarized in Scheme 1 and Table 1. Grignard reagents reacted with **3** to give the hydroxy lactams **5**. The yields of **5** were fairly good. The corresponding reaction of **4** afforded ring-cleaved products **6**, **7**, and **8**. The β-keto amide **6** was the primary product and an excess amount of Grignard reagents reacted with keto carbonyl group of **6** to give the double alkylated products **7** and the reduced products **8**. Because the primary product **6** is sterically hindered by the tertiary carbon, reduction of **6** to **8** occurs mainly when R is bulky. Especially when $R=i$-Pr, t-Bu, octyl, and cyclohexyl, reduction products **8** (**8c**, **8e**, **8f**, and **8g**) were exclusively produced and none of double alkylation products **7** was detected.

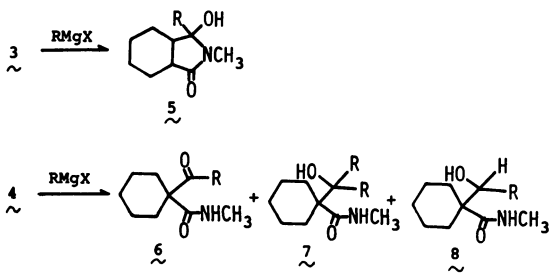

Scheme 1.

Table 1. Yield of the products in the reaction of **3** and **4** with Grignard reagents

R in RMgX		Reaction of **3** Yield of **5**/%	Reaction of **4** Yield of **6**/%	Yield of **7**/%	Yield of **8**/%
a	Me	85	11	63	—
b	Et	99	4	44	52
c	*i*-Pr	96	—	—	85
d	*n*-Bu	95	6	12	79
e	*t*-Bu	47	—	—	50
f	Octyl	95	—	—	96
g	Cyclohexyl	96	—	—	92
h	Ph	97	—	99	—
i	Allyl	95	—	72	—
j	Vinyl	84	—	9 (**7k**,[a] 90)	—

a) **7k**: 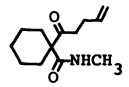

The difference of the reactions between **3** and **4** may be explained as follows. Grignard reagents attack one of the carbonyl carbons of the imide **3** to form the five-membered ring intermediate. The same type of the intermediate is perhaps produced in the reaction of **4**. Since ring strain of four-membered ring is larger than that of five-membered ring, the four-membered ring intermediate could immediately isomerize to the ring-cleaved intermediate,[4] the precursor of **6**, **7**, and **8**.

Reductions of **3** and **4** with sodium borohydride of lithium aluminum hydride proceeded similarly. The imide **3** was reduced to the hydroxy lactam **5**, (R=H), while the imide **4** gave the formyl amide **6**, (R=H). Here, it seems to be general that four-membered imides are ring-cleaved but five-membered imides are not cleaved in the course of the reaction.

When lithium reagents were used as the nucleophile, a new reaction was observed. Thus, phenyllithium reacted with **3** to give the ring-cleaved keto amide **9** as well as **5h**. The imide **4** afforded the amide **10** with addition of an excess amount of phenyllithium in the reacting mixture (See Fig. 2). The lithium reagent is a stronger base than the Grignard reagent and also **3** has a hydrogen at the position adjacent to the carbonyl group. These facts may cause the difference between the reactions of Grignard reagents and lithium reagents. The formation of **10** may be explained by retro-Aldol type reaction. Actually, treatment of **7h** with phenyl-

lithium afforded the same product **10** and triphenylmethanol.

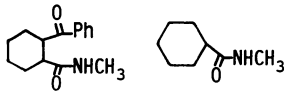

9 10

Fig. 2.

It is general that only one of the carbonyl carbons of imides photochemically behaves like a simple ketone.[7] In the present study, it is realized that ring size of cyclic imides strongly affects its chemical reaction pathway.

References

1) M. K. Hargreaves, J. G. Pritchard, and H. R. Dave, *Chem. Rev.*, **70**, 439, (1970).

2) A. Queen and A. Reipas, *J. Chem. Soc.*, **1967**, 245.

3) R. Lukev and Z. Linhartova, *Collect. Czech. Chem. Commun.*, **25**, 502, (1960).

4) W. Flitsch and R. Heidhues, *Z. Naturforsch.*, *β*, **21**, 1137, (1966).

5) K. Maruyama, T. Ishitoku, and Y. Kubo, *J. Org. Chem.*, **46**, 27, (1981).

6) N. H. Cromwell and B. Phillips, *Chem. Rev.*, **79**, 331, (1979).

7) a) K. Maruyama and Y. Kubo, *J. Org. Chem.*, **42**, 3215, (1977). b) K. Maruyama and Y. Kubo, *J. Org. Chem.*, **46**, 3612, (1981) and references sited therein. c) Y. Kanaoka, *Acc. Chem. Res.*, **11**, 407, (1978).

Substituent Effects on the Dissociation Constants of 1-Aryl-5-hydroxy-2-hydroxymethyl-4-pyridones

Kimiaki IMAFUKU,* Kumio TAKAHASHI,† and Hisashi MATSUMURA††
Department of Chemistry, Faculty of Science, Kumamoto University, Kurokami, Kumamoto 860
(Received December 25, 1982)

Synopsis. Six new 1-aryl-5-hydroxy-2-hydroxymethyl-4-pyridones were synthesized and their dissociation constants were measured. Hammett analysis of pK_a values for proton gain and proton loss gave the following equations: $pK_1 = 2.74 - 0.34\sigma$ and $pK_2 = 8.80 - 0.36\sigma$, respectively.

Hahn *et al.*[1,2] obtained 1-aryl-3-hydroxy-4-pyridones by the reactions of comenic acid and meconic acid with aniline derivatives. However, there is no further investigation in a detailed manner.

In the present work, we wish to report the synthesis of 1-aryl-5-hydroxy-2-hydroxymethyl-4-pyridones from kojic acid and the effects of the substituent in the benzene ring on the dissociation constants.

Results and Discussion

Synthesis. Condensation of kojic acid (**1**) with six anilines (**2a**—**f**) were respectively carried out, according to the Hahn's method,[1,2] to afford 1-aryl-5-hydroxy-2-hydroxymethyl-4-pyridones (**3a**—**f**). However, their yields were not necessarily good. All of the 4-pyridones gave a violet color with iron(III) chloride solution.

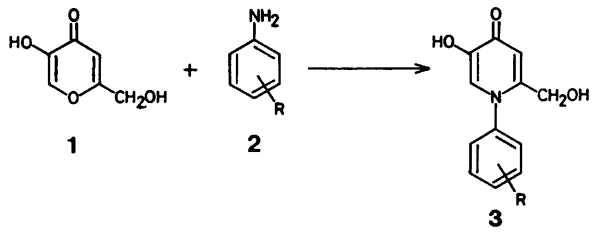

1 2 3

a R=H
b R=*p*-CH_3
c R=*p*-OCH_3
d R=*m*-OCH_3
e R=*p*-Cl
f R=*p*-$COCH_3$

Dissociation Constants. The dissociation constants of six 1-aryl-5-hydroxy-2-hydroxymethyl-4-pyridones were determined spectrophotometrically in water at 25 °C. The results are summarized in Table 1, where pK_1 and pK_2 values represent respectively the dissociation constants for the proton gain and proton loss of the 4-pyridones. Both pK_1 and pK_2 values are respectively smaller than those of 6-substituted 3-hydroxy-1-methyl-4-pyridones,[3] because of inductive effect of the aryl group. When these pK values were plotted against Hammett σ constants,[4] the following equations were obtained by the least-square method.

$$pK_1 = 2.74 - 0.34\sigma \quad (r=0.867,\ s=0.04)$$
$$pK_2 = 8.80 - 0.36\sigma \quad (r=0.980,\ s=0.02)$$

The ratio of the ρ value for **3** against the ρ value for 1-methyl-3-hydroxypyridones[3] is 0.29 for the proton gain and 0.34 for the proton loss. These values are comparable to the transmission factor (π=0.3) for *m*- and *p*-phenylene groups.[5]

Table 1. Dissociation constants

R	pK_1	pK_2
p-OCH_3	2.85	8.89
p-CH_3	2.82	8.86
H	2.64	8.82
m-OCH_3	2.76	8.78
p-Cl	2.39	8.69
p-$COCH_3$	2.57	8.62

Experimental

All the melting points were measured on a Yanagimoto MP-S2 melting point measuring apparatus and are uncorrected. The IR and UV spectra were taken on a JASCO IRA-1 and on a Hitachi EPS-3T spectrophotometer, respectively. The pH values were measured by a Hitachi-Horiba F-5 pH meter. The p*K*a determination was carried out according to the method of Albert and Serjeant.[6]

5-Hydroxy-2-hydroxymethyl-1-phenyl-4-pyridone (3a). A mixture of kojic acid (**1**) (1.0 g) and aniline (**2a**) (1.3 ml) in water (3.3 ml) was heated in the presence of 12 M (1 M=1 mol dm^{-3}) hydrochloric acid (0.5 ml) in a sealed tube on a water bath for 4 h. Water (6.7 ml) was added to the mixture to precipitate **3a** (280 mg, 18.3%). Mp 231 °C (from methanol); IR (KBr) 1653 cm^{-1}; UV (CH_3OH) 224 (sh, log ε 4.33), 287 nm (4.25). Found: C, 66.15; H, 5.18; N, 6.44%. Calcd for $C_{12}H_{11}NO_3$: C, 66.35; H, 5.10; N, 6.45%.

5-Hydroxy-2-hydroxymethyl-1-(p-methylphenyl)-4-pyridone (3b). A mixture of kojic acid (**1**) (1.5 g) and *p*-toluidine (**2b**) (2.4 g) in water (3.5 ml) was treated in the presence of 12 M hydrochloric acid (0.5 ml) and worked up, as mentioned above, to afford **3b** (240 mg, 9.8%). Mp 215—217 °C (from methanol); IR (KBr) 1635 cm^{-1}; UV (CH_3OH) 227 (log ε 4.32), 288 nm (4.28). Found: C, 67.41; H, 5.67; N, 6.08%. Calcd for $C_{13}H_{13}NO_3$: C, 67.52; H, 5.67; N, 6.06%.

5-Hydroxy-2-hydroxymethyl-1-(p-methoxyphenyl)-4-pyridone (3c). A mixture of kojic acid (**1**) (1.5 g) and *p*-anisidine (**3c**) (2.6 g) in water (3.5 ml) was treated in the presence of 12 M hydrochloric acid (0.5 ml) and worked up, as mentioned above, to afford **3c** (130 mg, 5.0%). Mp 231—233 °C (from methanol); IR (KBr) 1635 cm^{-1}; UV (CH_3OH) 244 (log ε 4.43), 288 nm (4.30). Found: C, 63.24; H, 5.23; N, 5.72%. Calcd for $C_{13}H_{13}NO_4$: C, 63.15; H, 5.30; N, 5.67%.

5-Hydroxy-2-hydroxymethyl-1-(m-methoxyphenyl)-4-pyridone (3d) A mixture of kojic acid (**1**) (1.4 g) and *m*-anisidine (**2d**) (1.5 g) in water (1.0 ml) was heated in the presence of 12 M hydrochloric acid (0.5 ml) in a sealed tube at 130—150 °C for 14 h. The reaction mixture was worked up, as mentioned above, to give **3d** (170 mg, 7.0%). Mp 206—208 °C (from methanol); IR (KBr) 1645 cm^{-1}; UV (CH_3OH) 222 (log ε 4.46), 288 nm (4.29). Found: C, 63.10; H, 5.29; N, 5.73%. Calcd for

† Present address: Hiroshima Prefectural Goverment, Hiroshima 730.

†† Present address: Kumamoto Institute of Technology, Ikeda, Kumamoto 860.

$C_{13}H_{13}NO_4$: C, 63.15; H, 5.30; N, 5.67%.

1-(p-Chlorophenyl)-5-hydroxy-2-hydroxymethyl-4-pyridone (3e). A mixture of kojic acid (**1**) (1.5 g) and *p*-chloroaniline (**2e**) (4.0 g) in water (8 ml) was treated in the presence of 12 M hydrochloric acid (0.2 ml), as mentioned above, to give **3e** (30 mg, 1.1%). Mp 230—233 °C (from water); IR (KBr) 1636 cm^{-1}; UV (CH_3OH) 224 (sh, log ε 4.40), 290 nm (4.27). Found: C, 57.14; H, 3.97; N, 5.45%. Calcd for $C_{12}H_{10}ClNO_3$: C, 57.27; H, 4.01; N, 5.57%.

1-(p-Acetylphenyl)-5-hydroxy-2-hydroxymethyl-4-pyridone (3f). A mixture of kojic acid (**1**) (1.0 g) and *p*-aminoacetophenone (**2f**) (2.7 g) in water (8 ml) was treated in the presence of 12 M hydrochloric acid (0.3 ml), as mentioned above, to give **3f** (560 mg, 30.7%). Mp 240—243 °C (from methanol); IR (KBr) 1703, 1737 cm^{-1}; UV (CH_3OH) 228 (log ε 4.31), 292 nm (4.27). Found: C, 65.09; H, 5.07; N, 5.40%. Calcd for $C_{14}H_{13}NO_4$: C, 64.86; H, 5.05; N, 5.40%.

References

1) V. Hahn and S. Kukolja, *Croat. Chim. Acta*, **33**, 137 (1961).

2) K. Blažević and H. Hahn, *Croat. Chim. Acta*, **38**, 113 (1966).

3) K. Imafuku, K. Takahashi, and H. Matsumura, *Bull. Chem. Soc. Jpn.*, **52**, 111 (1979).

4) H. H. Jaffé, *Chem. Rev.*, **53**, 191 (1953).

5) O. Exner, "Advances in Linear Free Energy Relationships," ed by N. B. Chapman and J. Shorter, Plenum Press, London and New York (1972), p. 25.

6) A. Albert and E. P. Serjeant, "Ionization Constants of Acids and Bases," 1st ed, Methuen and Co., London (1962), Chap. 4.

Reduction of Organic Halides with Diethyl Phosphonate and Triethylamine

Toshikazu HIRAO, Shuichiro KOHNO, Yoshiki OHSHIRO,* and Toshio AGAWA
Department of Applied Chemistry, Faculty of Engineering, Osaka University, Yamada-oka, Suita, Osaka 565
(Received December 27, 1982)

Synopsis. Reduction of organic halides [*gem*-bromochlorocyclopropanes, 1,1,1-trichloromethane derivatives, 1,1-dibromo-2-benzyloxyethylene, methyl α-bromocinnamate, α,*p*-dibromoacetophenone, and (1,2-dibromoethyl)benzene] with diethyl phosphonate and triethylamine is surveyed.

We have developed a novel method for reduction of *gem*-dibromocyclopropanes and *gem*-dibromoalkenes with diethyl phosphonate and triethylamine into the corresponding monobromides, respectively.[1] Furthermore, α-bromo-α,β-unsaturated ketones or 1,1-dibromo-2-trimethylsiloxycyclopropanes are shown to be converted to β,γ-unsaturated ketones with diethyl phosphonate and triethylamine.[2] These findings suggest a versatility of diethyl phosphonate–triethylamine as a reducing agent. Now we wish to extend the generality of reduction with diethyl phosphonate–triethylamine.

Treatment of *gem*-bromochlorocyclopropanes **1** with diethyl phosphonate and triethylamine gave the corresponding chlorocyclopropanes **2** exclusively, without formation of bromocyclopropanes (Table 1).

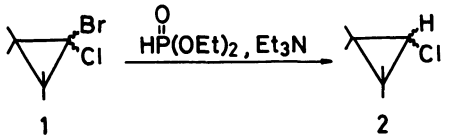

1 2

One of the chlorine atoms of the trichloromethane derivatives **3** was, however, reduced to yield the dichloromethane ones **4**, which were inert under the present reaction conditions, giving no further reduced compounds[3] (Table 1).

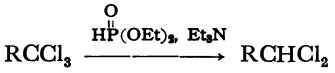

3 **4**

These results are considered to indicate that only activated halogen atom is reactive towards reduction. The following observation also supports this reactivity. Reduction of α-bromostyrene and (*E*)-β-bromostyrene was not achieved even at a high reaction temperature (80 °C), though β,β-dibromostyrene is reduced to (*E*)-β-bromostyrene.[1] The present method is effective for reduction of 1,1-dibromo-2-benzyloxyethylene, producing (*E*)- and (*Z*)-1-bromo-2-benzyloxyethylene in 29 and 51% yields, respectively.

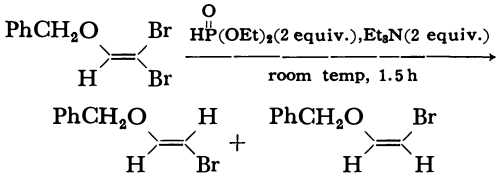

It is of interest to note that methyl α-bromocinnamate was allowed to be reduced into methyl cinnamate in 69% yield, which is in contrast with addition of diethyl phosphonate to methyl cinnamate.[4]

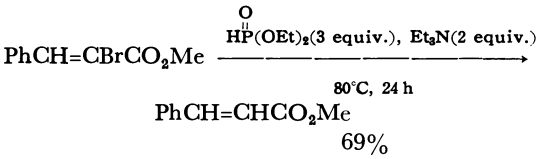

Furthermore, the α-bromine atom of ketones is reduced, as exemplified in the transformation of α,*p*-bromoacetophenone into *p*-bromoacetophenone. In the special cases, the similar kinds of reduction have been reported.[5]

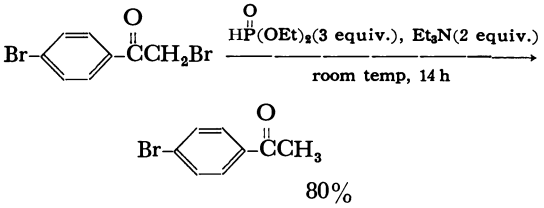

(1,2-Dibromoethyl)benzene was treated with diethyl phosphonate and triethylamine to give styrene as a main product. Since α- and β-bromostyrene were not subjected to reduction as mentioned above, styrene is presumably derived by direct debromination of (1,2-dibromoethyl)benzene, not reduction of the dehydro-

Table 1. Reduction of **1** and **3** with diethyl phosphonate and triethylamine

1 or **3**	$HP(O)(OEt)_2$ (equiv.)	Et_3N (equiv.)	Reaction conditions: Temp/°C	Reaction conditions: Time/h	**2** or **4** (Isolated yield/%)
	4	2	90	20	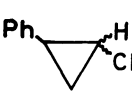 (76)
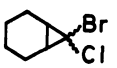	4	2	90	22	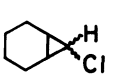 (52)
Cl_3CCMe_2OH	4	3	80	12	Cl_2CHCMe_2OH (73)
$PhCCl_3$	3	2	80	8	$PhCHCl_2$ (86)

brominated compounds (α- or β-bromostyrene).

$$PhCHBrCH_2Br \xrightarrow[\text{room temp, 6 h}]{HP(O)(OEt)_2\text{(3 equiv.)}, Et_3N\text{(2 equiv.)}} PhCH{=}CH_2 + PhCBr{=}CH_2 + PhCH{=}CHBr$$

58% 10% trace

The attack of diethyl phosphonate or its anion on the bromine or chlorine atom is assumed to be the first step in the reduction reaction.[6] The present procedure provides a convenient and selective method for reduction of activated halogenated compounds.

Experimental

Materials. *gem*-Bromochlorocyclopropanes,[7] α-bromostyrene,[8] methyl α-bromocinnamate,[9] and (1,2-dibromoethyl)benzene[10] were prepared by the reported methods. 1,1-Dibromo-2-benzyloxyethylene was obtained by the reaction of dibromocarbene with benzyl formate.[11] The other reagents are commercially available and purified by usual methods before use.

Reduction of 1-Bromo-1-chloro-2-phenylcyclopropane. To a mixture of diethyl phosphonate (1.10 g, 8 mmol) and triethylamine (0.40 g, 4 mmol) was added 1-bromo-1-chloro-2-phenylcyclopropane (0.46 g, 2 mmol) dropwise at room temperature. The resultant mixture was stirred at 90 °C for 20 h. The reaction proceeded with deposition of $Et_3N \cdot HBr$, which was filtered off and washed with ether. Upon evaporation of the filtrate *in vacuo*, the residue was chromatographed on a silica-gel column to give 0.23 g (76%) of 1-chloro-2-phenylcyclopropane. This product was identified by comparison of the IR and NMR spectra with those of the authentic sample.[12]

Reduction of other organic halides was carried out in the similar manner as mentioned above. The molar ratio of diethyl phosphonate or triethylamine, and reaction conditions are shown in Table 1 or equations.

Debromination of (1,2-Dibromoethyl)benzene. A mixture of (1,2-dibromoethyl)benzene (1.32 g, 5 mmol), diethyl phosphonate (2.07 g, 15 mmol) and triethylamine (1.01 g, 10 mmol) was stirred at room temperature for 6 h. The salt was filtered off and washed with ether. Upon concentration of the filtrate *in vacuo*, the residue was chromatographed on a silica-gel column to give 0.30 g (58%) of styrene, 0.09 g (10%) of α-bromostyrene, and a trace amount of β-bromostyrene.

References

1) T. Hirao, T. Masunaga, Y. Ohshiro, and T. Agawa, *J. Org. Chem.*, **46**, 3745 (1981).
2) T. Hirao, T. Masunaga, K.-i. Hayashi, Y. Ohshiro, and T. Agawa, *Tetrahedron Lett.*, **24**, 399 (1983).
3) Reduction of trichloroacetic ester with diethyl phosphonate was reported: V. S. Abramov and N. A. Il'ina, *Zh. Obshch. Khim.*, **39**, 2234 (1969); *Chem. Abstr.*, **72**, 54633 (1970).
4) A. N. Pudovik and I. V. Konovalova, *Synthesis*, **1979**, 81.
5) A. Zwierzak, B. Sledzinski, and L. Cieslak, *Bull. Acad. Pol. Sci., Ser. Sci. Chim.*, **22**, 673 (1974); C.-G. Shin, Y. Yonezawa, K. Suzuki, and J. Yoshimura, *Bull. Chem. Soc. Jpn.*, **51**, 2614 (1978).
6) G. M. Steinberg, *J. Org. Chem.*, **15**, 637 (1950).
7) M. Feboryński, *Synthesis*, **1977**, 783.
8) W. Taylor, *J. Chem. Soc.*, **1937**, 347.
9) G. B. Payne and M. R. Johnson, *J. Org. Chem.*, **33**, 1285 (1968).
10) H. R. Snyder and L. A. Brooks, *Org. Synth.*, Coll. Vol. I, 171 (1943).
11) M. Suda and A. Fukushima, *Tetrahedron Lett.*, **22**, 759 (1981).
12) D. Seyferth, S. P. Hopper, and T. F. Jula, *J. Organomet. Chem.*, **17**, 193 (1969).

Effects of Cation on Transport Efficiency and Selectivity of Amino Acid Derivative Anions through Macrocyclic Carrier-containing Liquid Membrane

Hiroshi TSUKUBE

Department of Chemistry, College of Liberal Arts and Science, Okayama University, Okayama 700

(Received January 7, 1983)

Synopsis. New aspects of amino acid transport mediated by macrocyclic carriers were reported. Its transport "efficiency" and "selectivity" were demonstrated to be controlled by the appropriate choice of co-transported cation and employed carrier-type.

Recently we demonstrated that several macrocyclic crown ethers[1] and their derivatives[2] effectively mediate the passive and active transport of amino acid and oligopeptide derivative anions. In this transport system (see Fig. 1), the macrocyclic carrier, dissolved in the membrane, facilitates the transport of guest anion and co-transported cation from the source phase through the membrane to the receiving phase by solubilizing co-transported cation and guest anion into the membrane.

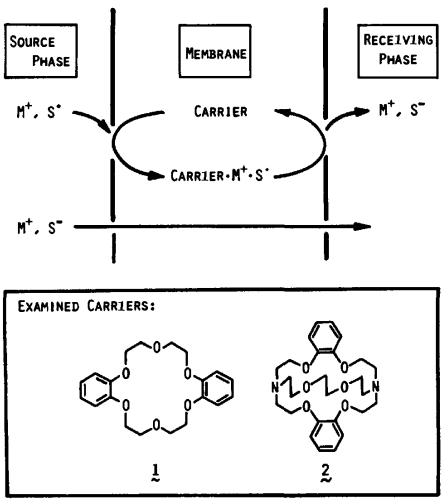

Fig. 1. Liquid membrane and macrocyclic carriers for transport of amino acid derivatives. M^+: Co-transported cation, S^-: guest anion.

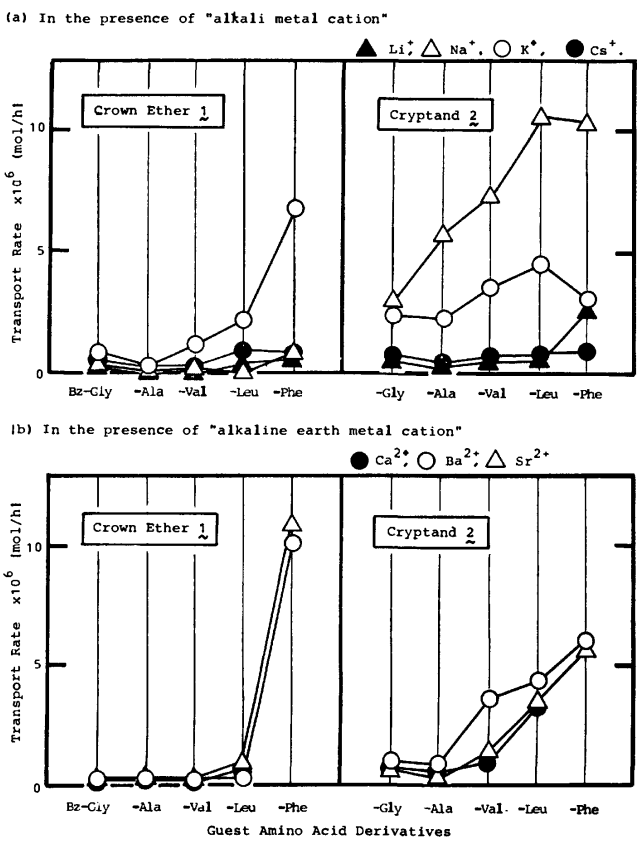

Fig. 2. Transport rates of several *N*-benzoyl amino acid anions by macrocyclic carriers **1** and **2**.
Transport conditions: Source phase; *N*-benzoyl amino acid, 0.250 mmol co-transported cation chloride, 2.50 mmol/0.05 mol dm^{-3} LiOH, 5 ml. Membrane; carrier, 0.0557 mmol/$CHCl_3$, 12 ml. Receiving phase; distilled water, 5 ml. Other conditions were indicated in Experimental.

In the previous publications,[1,2] we showed that the transport rates of some guest anions were largely influenced by the natures and concentrations of co-transported cations. Here we report a further detailed study of co-transported cation effects on the transport phenomena, and provide a new possibility of controlling the transport "selectivity." By using typical two macrocyclic carriers **1** and **2**, we measured the transport rates of amino acid derivatives in the presence of various metal cations (Li^+, Na^+, K^+, Cs^+, Ca^{2+}, Sr^{2+}, and Ba^{2+}), and found that the natures of these cations significantly governed both the transport "selectivity" and "efficiency." Typical results are illustrated in Fig. 2.

Figure 2(a) clearly shows that alkali metal cation has a large effect on the transport "selectivity" and "efficiency" for amino acids. When the crown ether **1** was employed as carrier, Bz–Phe and Bz–Leu anions (Bz= benzoyl) were effectively transported, together with K^+ cation. These transport properties were found to simply depend on the stability constant of crown ether **1**·metal cation complex ($Li^+ < Na^+ < K^+ > Cs^+$)[3] and hydrophobicity of guest anion (Bz–Gly≲Bz–Ala<Bz–Val<Bz–Leu<Bz–Phe). Similar conclusions have been presented in the crown ether-mediated transport of alkali metal–inorganic anion salts by Lamb *et al.*[4] In a marked contrast, the cryptand carrier **2** exhibited unique and interesting transport property. Its transport selectivity was largely affected by the natures of co-transported metal cations: For Li^+; Bz–Gly≈Bz–Ala≈Bz–Val≈Bz–Leu<Bz–Phe. For Na^+; Bz–Gly<Bz–Ala<Bz–Val<Bz–Leu≈Bz–Phe. For K^+; Bz–Gly≈Bz–Ala≲Bz–Val≲Bz–Leu>Bz–Phe. It was of particular interest that Bz–Leu anion was more effectively transported with K^+ cation than Bz–Phe and other guest anions.

Since the cryptand **2** is a much stronger complexing agent for Na^+ and K^+ cations than the crown ether **1**,[5] highly hydrophobic Bz–Phe anion could be accumulated into the membrane as very stable cryptand–cation–guest anion complex rather than being transported. Recently some transition metal complexes were found to successfully mediate the artificial transport of amino acid derivatives anions.[6] In such systems, the amino acid anions with lower hydrophobicities allowed fast transport: Bz–Gly>Bz–Ala>Bz–Val>Bz–Leu>Bz–Phe. Thus, transport selectivity could be dramatically modified and controlled by alterations of the employed metal cation and ligating agent.

The effects of alkaline earth metal cations on this transport process were also examined (Fig. 2(b)). Both two macrocyclic carriers **1** and **2** selectively transported hydrophobic guest anions (Bz–Phe and Bz–Leu), together with Ba^{2+} and Sr^{2+} cations, while they hardly transported hydrophilic anions (Bz–Gly and Bz–Ala). Several investigators have studied the crown ether-mediated transport of alkaline earth metal salts, and found that their transport rates were generally much lower than those of alkali metal salts.[7] Although crown ethers form highly stable complexes with alkaline earth metal cations in the solution systems,[3,5] the heterogeneous complexation reactions at the water/membrane interfaces slowly occurred.[8] Probably, hydrophobic Bz–Phe and Bz–Leu anions could promote the heterogeneous complexation and provide higher transport rates.

These results obtained here clearly show that there is an optimum combination of carrier and metal cation for efficient and selective transport of a given guest anion. This principle[6,9] could be used for effective control of the transport "selectivity" and "efficiency."

Experimental

Materials. The macrocyclic carriers **1** and **2** were purchased from Merck Japan Ltd. The used *N*-benzoyl amino acids were obtained from Nakarai Chem. Ltd. and Tokyo Chem. Ltd. All other chemicals were of analytical grade and employed as received.

Transport Procedure. The transport experiments (Fig. 2) were carried out at room temperature in an U-shaped glass cell (2.0 cm, i.d.) as described before.[6] The carrier in chloroform (12 ml) was placed in the base of the U-tube, and two aqueous phases (5 ml, each) were placed in the arms of the U-tube, floating on the chloroform membrane.The membrane phase was stirred with a magnetic stirrer. The transport rates were calculated from the initial rates of appearance of guest anions into the receiving phase, which were determined spectroscopically. Reproducibility was confirmed as $\pm 15\%$ or better.

The author thanks Professor T. Iwachido of Okayama University for his helpful discussion. This research was supported in part by a Grant-in-Aid for Scientific Research No. 57740267 from the Ministry of Education, Science and Culture.

References

1) H. Tsukube, *Tetrahedron Lett.*, **22**, 3981 (1981); *J. Chem. Soc., Perkin Trans. 1*, **1982**, 2359.

2) H. Tsukube, *J. Polym. Sci., Polym. Chem. Ed.*, **20**, 2989 (1982).

3) M. Hiraoka, "Crown Compounds," Kodansha, Tokyo (1982), p. 98.

4) J. D. Lamb, J. J. Christensen, J. L. Oscarson, B. L. Mielson, B. W. Asay, and R. M. Izatt, *J. Am. Chem. Soc.*, **102**, 6820 (1980); J. D. Lamb, J. J. Christensen, S. R. Izatt, K. Bedke, M. S. Astin, and R. M. Izatt, *ibid.*, **102**, 3399 (1980).

5) B. Dietrich and J. M. Lehn, *J. Chem. Soc., Chem. Commun.*, **1973**, 15.

6) K. Maruyama, H. Tsukube, and T. Araki, *J. Am. Chem. Soc.*, **104**, 5197 (1982).

7) C. F. Reusch and E. L. Cussler, *AIChE J.*, **19**, 736 (1973); J. S. Bradshow, G. E. Maas, J. D. Lamb, R. M. Izatt, and. J. Christensen, *J. Am. Chem. Soc.*, **102**, 467 (1980).

8) S. Kopolow, T. E. Hogen Esch, and J. Smid, *Macromolecules*, **6**, 173 (1973).

9) M. Kirch and J. M. Lehn, *Angew. Chem., Int. Ed. Engl.*, **14**, 555 (1975).

Potassium Fluoride on Alumina. An Efficient Solid Base for Elimination, Addition, and Condensation

Junko YAMAWAKI, Takehiko KAWATE, Takashi ANDO,* and Terukiyo HANAFUSA
The Institute of Scientific and Industrial Research, Osaka University, Mihogaoka, Ibaraki, Osaka 567
(Received January 18, 1983)

Synopsis. Alumina coated with potassium fluoride proved to be a versatile solid base for olefin- and acetylene-forming elimination, the Michael addition, aldol condensation, and the Darzens condensation.

The utility of fluoride salts as potential bases in a variety of synthetic reactions has been recognized in recent years.[1,2] However, low solubilities of fluoride salts in ordinary solvents hamper their wide applications in organic synthesis. On the other hand, there has been increasing use of inorganic solid supports as reagents or reaction media in recent years.[3,4] In our previous papers,[5-7] we reported that alumina coated with potassium fluoride (KF-alumina) is a versatile solid-supported reagent for promoting *C*-, *N*-, *O*-, and *S*-alkylations with alkyl halides. In the present paper, we describe the application of KF-alumina as a solid base for elimination, addition, and condensation.

β-Elimination reaction of alkyl bromides was carried out with KF-alumina (*ca.* 2.5 equiv. KF) in acetonitrile or diglyme with stirring at room temperature or with heating below 100 °C. Typical examples are summarized in Table 1. Elimination of phenethyl, 2-phenoxyethyl, and secondary alkyl bromides proceeded smoothly to give the corresponding olefins. For example, an 86% yield of styrene was obtained from phenethyl bromide at room temperature after 24 h; the elimination did not proceed when KF powder or alumina was used separately. These results show the high reactivity of KF-alumina for β-elimination. When a simple primary alkyl bromide was used as a substrate, hydrolysis became the main reaction in preference to elimination to form substantial amounts of an alcohol and an ether together with an olefin.

KF-Alumina was also applicable to the synthesis of acetylenes. Phenylacetylene and diphenylacetylene were obtained in good yields from the corresponding vicinal bromides under milder reaction conditions than those of

TABLE 1. β-ELIMINATION WITH KF-ALUMINA[a]

Substrate	Solvent	T/°C	Time/h	Product	Yield/%[b]
$PhCH_2CH_2Br$	CH_3CN	25	24	$PhCH{=}CH_2$	86
$PhCH_2CH_2Br$	—[c]	25	20	$PhCH{=}CH_2$	75[d]
$PhOCH_2CH_2Br$	Tetraglyme	45	45	$PhOCH{=}CH_2$	73[d]
$CH_3(CH_2)_6CH_2Br$	Diglyme	100	24	$C_6H_{13}CH{=}CH_2$	14[e]
$CH_3(CH_2)_5CHBrCH_3$	Diglyme	100	15	$C_6H_{13}CH{=}CH_2$	36[f]
				trans-$C_5H_{11}CH{=}CHCH_3$	29
				cis-$C_5H_{11}CH{=}CHCH_3$	13
Cyclohexyl bromide	Diglyme	100	15	Cyclohexene	88
$PhCHBrCH_2Br$	CH_3CN	25	27	$PhC(Br){=}CH_2$	80
$PhCHBrCH_2Br$	Penta ether[g]	100	6	$PhC{\equiv}CH$	70[d]
trans-$PhCH{=}CHBr$	Diglyme	100	24	$PhC{\equiv}CH$	70
meso-$PhCHBrCHBrPh$	Diglyme	100	3	$PhC{\equiv}CPh$	74
meso-$PhCHBrCHBrPh$	DME	85	48	$PhC{\equiv}CPh$	89[d]

a) KF-Alumina containing *ca.* 2.5 equiv. KF was used. b) Unless otherwise mentioned, yields were determined by GLPC using internal standards. c) Without solvent. d) Isolated yields after purification. e) Starting material (8%), 1-octanol (34%), and dioctyl ether (25%) were obtained. f) Starting material (10%) was also detected. g) Tetraethylene glycol dibutyl ether.

TABLE 2. ADDITION AND CONDENSATION WITH KF-ALUMINA[a]

Run	Starting materials A	Starting materials B	Solvent	Time/h	Product	Yield/%[b]
1	$PhCH{=}CHCOPh$	CH_3NO_2	CH_3CN	3.5	$PhCHCH_2COPh$ with CH_2NO_2	74
2	PhCHO	$CH_2(CN)_2$	CH_3CN	3	$PhCH{=}C(CN)_2$	86
3	PhCHO	$PhCH_2CN$	DME	21	$PhCH{=}C(CN)Ph$	82
4		$CH_2(CN)_2$	DME	15	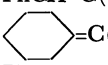	55
5	PhCHO	PhCHClCN	Benzene	4	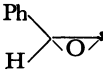	82[c]

a) At room temperature. Molar ratio of A:B:KF-alumina was 1:20:0.2 for run 1, 1:1:0.25 for run 2 and 4, 1:1:0.5 for run 3, and 1 : 1 : 5 for run 5. b) Unless otherwise mentioned, isolated yields after purification are shown. c) Yield determined by ^{1}H-NMR using an internal standard. The ratio of *cis* to *trans* was 56 : 44. When 1,2-dimethoxyethane was used as solvent, the ratio decreased to 28 : 72, while the addition of 0.5 and 1.0 equiv. water to KF in benzene increased the ratio to 61 : 39 and 71 : 29, respectively.

conventional methods using strong bases (Table 1). Interestingly, in the elimination of *meso*-stilbene dibromide there was difference in composition of products by the solvent used. After 44 h at 50 °C in 1,2-dimethoxyethane diphenylacetylene and (*E*)-α-bromostilbene were formed in 24 and 66% yields, respectively. On the other hand, the reaction in acetonitrile gave a 30% yield of *trans*-stilbene, the debromination product, in addition to the above two products in 52 and 12% yields, respectively. This is the first observation of debromination by KF, although the debromination by NaI or LiBr in *N,N*-dimethylformamide has been reported already.[8]

KF-Alumina was found to promote the generation of dichlorocarbene from chloroform, which was trapped with cyclohexene to give a 31% yield of 7,7-dichlorobicyclo[4.1.0]heptane after 48 h at 25 °C. This α-elimination by KF-alumina, however, is not so efficient as the well-known method using phase transfer catalysts.

A catalytic amount of KF-alumina promoted the Michael addition and aldol condensation under mild conditions in satisfactory yields as shown in Table 2. No reaction took place when alumina without KF was added to the mixture of benzaldehyde and benzyl cyanide (run 3). The Darzens condensation of benzaldehyde and α-chlorophenylacetonitrile proceeded smoothly with KF-alumina in benzene to give 2,3-diphenyloxirane-2-carbonitrile (Table 2, run 5). Interestingly, the ratio of *cis*- to *trans*-isomer varied from 3 : 7 to 7 : 3 depending not only on the solvent used but also on the added water to the reaction system (Table 2, footnote c).[9] This phenomenon may give a valuable clue to suggest the characteristics of inorganic solid-organic liquid interfacial reaction, and a further mechanistic study along this line is under way.

In all cases studied, work-up was simple and nonaqueous. Reaction products were isolated by filtration of the solid and evaporation of the solvent; purification by distillation, recrystallization or column chromatography was done when necessary. In conclusion, these results confirmed the utility of KF-alumina as a solid base for a variety of synthetic reactions.

Experimental

General. Unless otherwise mentioned, reagents were obtained commercially and used without further purification. α-Chlorophenylacetonitrile was prepared from α-hydroxyphenylacetonitrile and thionyl chloride.[10] Solvents were dried with molecular sieves 3A or 4A. Neutral alumina was purchased from Merck Japan Ltd. (type 90 for column chromatography, activity I, 70—230 mesh) and used as obtained.

KF-Alumina Reagent. Alumina (30 g) was mixed with KF (20 g) in 200 cm³ of water, and the water was removed at 50—60 °C in a rotary evaporator. This impregnated alumina was then dried in a vacuum drying oven at 75 °C for several hours.

Typical experimental procedures are described in the following three examples.

Styrene: A mixture of phenethyl bromide (3.70 g, 20 mmol) and KF-alumina (15 g, *ca.* 100 mmol KF) without solvent was agitated mechanically by a Mini Vapour S-3 vibrating apparatus (Tokyo Rikakikai Co., Ltd.) at room temperature for 20 h. Purification by distillation gave 1.55 g of the product (74.5%): bp 26—27 °C/2.67 kPa (lit,[11] bp 54 °C/4.00 kPa); purity by GLPC 99.4%.

Phenylacetylene: A mixture of styrene dibromide (12.0 g, 45 mmol) and KF-alumina (74.8 g, *ca.* 450 mmol KF) in 30 cm³ of Penta Ether (tetraethylene glycol dibutyl ether) was mechanically stirred at 100 °C for 6 h. The solid material was filtered off and washed with ether, and the ether was evaporated. Purification by distillation gave 3.13 g of the product (70.4%): bp 62—72 °C/8.00—9.33 kPa (lit,[12] bp 39—40 °C/1.87 kPa); purity by GLPC 97%.

Benzylidenemalononitrile: Condensation of malononitrile (1.32 g, 20 mmol) and benzaldehyde (2.12 g, 20 mmol) in 15 cm³ of acetonitrile in the presence of KF-alumina (0.78 g, *ca.* 5 mmol KF) was carried out at room temperature for 3 h. The alumina was filtered off, and the solvent was evaporated. Purification by column chromatography (silica gel, benzene) gave 2.64 g of the product (85.7%): mp 83.5—84.0 °C (lit,[13] mp 83.5—84.0 °C).

Identification of the Products. All the products are the known compounds, and all the isolated products in Tables 1 and 2 were identified by the spectroscopic (IR, ^{1}H NMR, and UV) and other physical data (mp, bp, and elemental analysis), which were compared with those of the authentic samples or the following literatures: phenoxyethylene,[14] 1,3-diphenyl-4-nitrobutanone,[15] α-phenylcinnamonitrile,[16] cyclohexylidenemalononitrile,[17] and diphenyloxirane-2-carbonitrile.[18]

The present work was supported in part by a Grant-in-Aid for Scientific Research No. 57740264 from the Ministry of Education, Science and Culture.

References

1) J. H. Clark, *Chem. Rev.*, **80**, 429 (1980).
2) T. Ando and J. Yamawaki, *J. Synth. Org. Chem. Jpn.*, **39**, 14 (1981).
3) A. McKillop and D. W. Young, *Synthesis*, **1979**, 401, 481.
4) G. H. Posnor, *Angew. Chem., Int. Ed. Engl.*, **17**, 487 (1978).
5) J. Yamawaki and T. Ando, *Chem. Lett.*, **1979**, 755; **1980**, 533.
6) J. Yamawaki, T. Ando, and T. Hanafusa, *Chem. Lett.*, **1981**, 1143.
7) T. Ando, J. Yamawaki, T. Kawate, S. Sumi, and T. Hanafusa, *Bull. Chem. Soc. Jpn.*, **55**, 2504 (1982).
8) W. K. Kwok and S. I. Miller, *J. Org. Chem.*, **45**, 4034 (1970).
9) Variation of the *cis-trans* ratio was reported for the same reaction with or without a phase transfer catalyst; A. Jończyk, A. Kwast, and M. Makosza, *J. Chem. Soc., Chem. Commun.*, **1977**, 902.
10) F. Barrow and F. J. Thorneycroft, *J. Chem. Soc.*, **1934**, 724.
11) H. B. Dykstra, *J. Am. Chem. Soc.*, **56**, 1625 (1934).
12) J. H. Johnson and W. L. McEwen, *J. Am. Chem. Soc.*, **48**, 474 (1926).
13) B. B. Corson and R. W. Stoughton, *J. Am. Chem. Soc.*, **50**, 2825 (1928).
14) K. Mizuno, Y. Kimura, and Y. Otsuji, *Synthesis*, **1979**, 688.
15) W. Davey and D. J. Tiey, *J. Chem. Soc.*, **1958**, 2276.
16) J. C. Robinson, Jr. and H. R. Snyder, *Org. Synth.*, Coll. Vol. III, 715 (1955).
17) A. C. Cope and K. E. Hoyle, *J. Am. Chem. Soc.*, **63**, 733 (1941).
18) K. Takahashi, T. Nishizuka, and H. Iida, *Tetrahedron Lett.*, **22**, 2389 (1981).

The Structure of Aryldialkyltriazene *N*-Oxides

Angelo G. GIUMANINI,†† Lucia LASSIANI,* Carlo NISI, Andrej PETRIC,† and Branko STANOVNIK†
Istituto di Chimica Farmaceutica, Universita di Trieste, I-34100 Trieste, Italy
†*Department of Chemistry, E. Kardelj University of Ljubljana, 61000 Ljubljana, Yugoslavia*
††*Dipartimento di Chimica, Universita di Udine, I-33100 Udine, Italy*

(Received July 23, 1982)

Synopsis. The structure of 3-aryl-1,3-dimethyltriazene 1-oxides has been demonstrated by comparison with other triazenes and triazene *N*-oxides by mass spectrometry and ^{1}H and ^{13}C NMR.

Aryldimethyltriazene *N*-oxides exhibit interesting pharmacological properties. 1-Aryl-3-hydroxy-3-methyltriazenes, **1a**, which are the proton tautomers of 3-aryl-1-methyltriazene 1-oxides, **1b**, have been described as immunosuppressive[1,2] and antiinflammatory agents.[3]

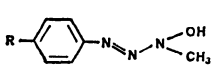

1a

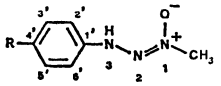

1b

Some 1-aryl-3,3-dimethyltriazene 1-oxides, **2**, were found useful in the treatment of phlogistic processes.[4] The same activity was observed for a third class of triazene *N*-oxides, **3**, obtained from the methylation of 3-aryl-1-methyltriazene 1-oxides, **1b**, with methyl iodide in the presence of the irreversible proton acceptor sodium hydride.[3]

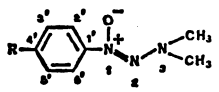

2

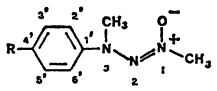

3

In view of preparing new derivatives of **3**, we wished to establish the actual structure of this reaction product; no such evidence could in fact be found in the literature. Bamberger and Renauld[5] reacted the *p*-nitro derivative of **1b** with methyl iodide and potassium hydroxide and postulated structure **4** for the isolated reaction product. Later, Boese *et al.*[6] assumed the same structure for the product resulting from the reaction of *N*,*O*-dimethylhydroxylamine with *p*-nitrobenzenediazonium chloride; evidence for the assignment was obtained by hydrolyzing the product to the starting amine with hydrochloric acid. The melting point of Bamberger's compound differed widely (142 °C *vs.* 66 °C) from that of Boese's. In a recent review this assignment was deemed reasonable on a synthetic basis and structure **4** and **5** were then proposed for Bamberger's compound.[7] We set up to establish the actual structure of the compound on firmer grounds. Incidentally, structure **2** and **5** are of interest, being potential oxidative metabolites of the antitumor agents aryldimethyltriazenes, **6**.[8]

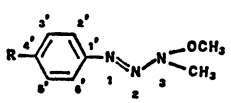

4

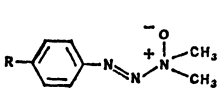

5

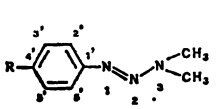

6

Experimental

The following compounds were synthesized for comparative purposes according to reported procedures: 3-aryl-1-methyltriazene 1-oxide (**1b**; R=*p*-nitro,[5] and *p*-chloro,[9] mp 149 °C after recrystallization from methanol, lit,[9] unreported), 1-(*p*-chlorophenyl)-3,3-dimethyltriazene 1-oxide (**2**, R=*p*-chloro[3]), 1-(*p*-chlorophenyl)-3-methoxy-3-methyltriazene (**4**, R=*p*-chloro, mp 18—19 °C after recrystallization from petroleum ether at low temperature), 1-(*p*-nitrophenyl)-3-methoxy-3-methyltriazene (**4**, R=*p*-nitro[6]), Bamberger's triazene[5] and its *p*-chloro analog, synthesized according to the same procedure using four equivalents of potassium hydroxide and methyl iodide in order to drive the reaction to completion, mp 90.5—91.5 °C after recrystallization from hexane.

The ^{1}H and ^{13}C NMR spectra were recorded using TMS as internal standard with JEOL JNM-C60HL and JNM-FX-90Q FT spectrometers respectively. Mass spectra here reported were recorded with an LKB mass Spectrometer, *via* sublimation at room temperature into the ion source kept at 200 °C; ionization energies were at nominal 20 and 70 eV. Reported mp's are uncorrected.

Results and Discussion

^{1}H Spectral characteristics of *p*-chloro- and *p*-nitro-substituted triazenes are summarized in Table 1; the corresponding ^{13}C NMR spectral characteristics are shown in Table 2. The methyl groups in 1-(*p*-chlorophenyl)-3,3-dimethyltriazene, **6** (R=*p*-Cl), appeared as a singlet at δ=3.25 (in $CDCl_3$) and δ=3.26 (in acetone-d_6 at room temperature, whereas in the corresponding 1-(*p*-nitrophenyl)-3,3-dimethyltriazene, **6** (R=*p*-NO_2), the methyl groups appeared as two signals at δ=3.26 and δ=3.60 (in acetone-d_6) or δ=3.28 and 3.50 (in $CDCl_3$) because of the restricted rotation around N_2–N_3 bond, which coalesced at higher temperatures. Similarly, both methyl groups in 1-(*p*-chlorophenyl)-3,3-dimethyltriazene 1-oxide, **2**, appeared as a singlet at room temperature. On the other hand, two methyl groups appeared as two singlets at δ=4.13 and 3.29

TABLE 1. ^{1}H NMR (δ) DATA

Compound	Solvent	N_3-CH_3	N_1-CH_3	O-CH_3	NH	Ar
6 (R=*p*-Cl)	$CDCl_3$	3.25 s				7.25 br s
	CD_3COCD_3	3.26 br s				7.32 s
2 (R=*p*-Cl)	$CDCl_3$	3.22 s				7.88 d, 7.28 d
						$J_{2',3'}=J_{5',6'}$=9.0 Hz
4 (R=*p*-Cl)	$CDCl_3$	3.84 s		3.30 s		7.40 d, 7.25 d
						$J_{2',3'}=J_{5',6'}$=8.0 Hz
1b(R=*p*-Cl)	$CDCl_3$		3.90 s		10.9 br s	7.22 d, 6.95 d
						$J_{2',3'}=J_{5',6'}$=9.0 Hz
3 (R=*p*-Cl)	$CDCl_3$	3.30 s	3.95 s			7.20 d, 6.88 d
						$J_{2',3'}=J_{5',6'}$=9.0 Hz
6 (R=*p*-NO_2)	CD_3COCD_3	3.26 s				8.23 d, 7.54 d
		3.60 s				$J_{2',3'}=J_{5',6'}$=9.0 Hz
	$CDCl_3$	3.28 s				8.10 d, 7.42 d
		3.50 s				$J_{2',3'}=J_{5',6'}$=9.0 Hz
4 (R=*p*-NO_2)	$CDCl_3$	3.88 s		3.65 s		8.15 d, 7.50 d
						$J_{2',3'}=J_{5',6'}$=9.0 Hz
1b(R=*p*-NO_2)	DMSO-d_6		3.98 s		11.85 br s	8.18 d, 7.39 d
						$J_{2',3'}=J_{5',6'}$=9.0 Hz
3 (R=*p*-NO_2)	DMSO-d_6	3.29 s	4.13 s			8.10 d, 7.08 d
						$J_{2',3'}=J_{5',6'}$=9.0 Hz

Table 2. ^{13}C NMR data[a)]

Compound solvent and t/°C	δ	J/Hz
6 (R=Cl) $CDCl_3$	$C_{1'}$ 149.6 t	$J=6.1$
	$C_{4'}$ 130.4 t	$J=7.9$
	$C_{3'}$ 128.8 dd	$J^1=166.4$ $J^2=5.0$
	$C_{2'}$ 121.7 dd	$J^1=163.6$ $J^2=5.0$
	NCH_3 39.3 broad q	$J=142$
2 (R=Cl) $CDCl_3$	$C_{1'}$ 144.0 broad m	
	$C_{4'}$ 136.0 m	
	$C_{3'}$ 128.7 dd	$J^1=170.0$ $J^2=5.9$
	$C_{2'}$ 122.2 dd	$J^1=170.0$ $J^2=5.0$
	NCH_3 43.5 qq	$J^1=138.6$ $J^3=3.6$
4 (R=Cl) $CDCl_3$	$C_{1'}$ 147.9 broad m	
	$C_{4'}$ 133.4 broad m	
	$C_{3'}$ 129.1 dd	$J^1=167.1$ $J^2=5.0$
	$C_{2'}$ 123.0 dd	$J^1=164.3$ $J^2=5.0$
	OCH_3 61.2 q	$J=145.0$
	NCH_3 41.9 q	$J=140.7$
1b(R=Cl) $CDCl_3$	$C_{1'}$ 138.6 broad m	
	$C_{4'}$ 129.4 dd	$J^1=166.4$ $J^2=5.0$
	$C_{3'}$ 127.6 m	
	$C_{2'}$ 115.6 dd	$J^1=164.3$ $J^2=6.0$
	NCH_3 50.1 q	$J=144.3$
3 (R=Cl) $CDCl_3$	$C_{1'}$ 146.1 broad m	
	$C_{4'}$ 128.7 dd	$J^1=166.4$ $J^2=5.4$
	$C_{3'}$ 127.9 broad m	
	$C_{2'}$ 117.9 dd	$J^1=162.9$ $J^2=6.4$
	N_1CH_3 53.1 q	$J=144.3$
	N_3CH_3 37.3 q	$J=140.0$
6 ($R=NO_2$) $CDCl_3$, 24 °C	$C_{1'}$ 155.8 m	
	$C_{4'}$ 144.4 m	
	$C_{3'}$ 124.5 dd	$J^1=170.0$ $J^2=5.0$
	$C_{2'}$ 120.3 dd	$J^1=168.9$ $J^2=6.0$
	NCH_3 43.3 deg qq	$J^1=140.7$ $J^3\simeq3.5$
	NCH_3 36.0 deg qq	$J^1=140.7$ $J^3\simeq3.5$
4 ($R=NO_2$) $CDCl_3$, 24 °C	$C_{1'}$ 153.7 m	
	$C_{4'}$ 145.7 m	
	$C_{3'}$ 124.1 dd	$J^1=170.0$ $J^2=5.0$
	$C_{2'}$ 121.4 dd	$J^1=167.9$ $J^2=6.0$
	OCH_3 61.1 q	$J=146.4$
	NCH_3 41.0 q	$J=142.1$
1b($R=NO_2$) DMSO-d_6, 50 °C	$C_{1'}$ 143.8 m	
	$C_{4'}$ 138.2 m	
	$C_{3'}$ 122.7 dd	$J^1=170.7$ $J^2=5.0$
	$C_{2'}$ 111.0 dd	$J^1=169.3$ $J^2=6.0$
	NCH_3 84.3 q	$J=144.3$
3 ($R=NO_2$) DMSO-d_6, 24 °C	$C_{1'}$ 151.5 m	
	$C_{4'}$ 140.5 m	
	$C_{3'}$ 125.0 deg dd	$J^1=167.1$ $J^2\simeq5.0$
	$C_{2'}$ 113.9 deg dd	$J^1=165.7$ $J^2\simeq5.0$
	N_1CH_3 53.6 q	$J=145.0$
	N_3CH_3 36.7 q	$J=142.9$

a) The ^{13}C chemical shifts of the aryl carbon atoms have been assigned on the basis of literature references: T. Axenrod, P. Mangiaracina, and P. S. Pregosin, *Helv. Chim. Acta*, **59**, 1655 (1976).

in the compound obtained by Bamberger by methylation of the corresponding 3-(*p*-nitrophenyl)-1-methyltriazene 1-oxide, **1b**. The large chemical shift difference observed for these methyl groups ($\Delta\delta=0.84$ ppm) and the absence of coalescence at higher temperatures, indicated that they were attached at different positions, leaving thus the 1-(*p*-nitrophenyl)-1,3-dimethyltriazene 1-oxide (structure **3**) as the most plausible one. Analogous evidence could be found also for the product obtained by methylation of 3-(*p*-chlorophenyl)-3-methyltriazene 1-oxide, **1b**. In ^{13}C NMR spectra, long range coupling constants $J^3_{H-C-N-}{}^{13}C=$

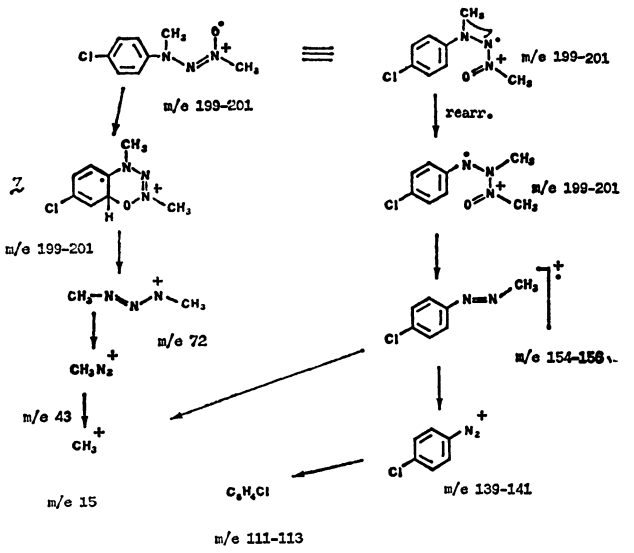

3.6 Hz were observed for all compounds having both methyl groups attached to the same nitrogen atom, *i.e.* in 1-(*p*-nitrophenyl)-3,3-dimethyltriazene, **6** (R=*p*-NO_2), 1-(*p*-chlorophenyl)-3,3-dimethyltriazene, **6** (R=*p*-Cl), and in the corresponding N_1-oxide (**2**, R=*p*-Cl). Since this coupling was not observed for the Bamberger's methylation product and its *p*-chloro analogue, structure **5** had to be excluded, leaving thus the nitrogen close to the phenyl ring as the only possible position at which methylation could occur. Mass spectrometry supported this evidence. Bamberger's *p*-chloro derivative under electron impact at 20 eV showed intense peaks for the parent ions (*m/e* 201 and 199), and doublets separated by two mass units at *m/e* 154—156, 139—141, and 111—113. This fragmentation is clearly incompatible with structure **5**, but could be readily reconciled with structure **3**, by postulating a 3,2-methyl shift in the parent cation radical produced upon ionization. Any thermal rearrangement prior to ionization in the course of sublimation into the ion source could be ruled out by the fact that the process occurred at room temperature. A second pathway could be given by rebonding of the parent ion to the bicyclic system **7**, which eventually collapsed to the dimethyltriazenyl ion (*m/e* 72), then cascading to methane diazonium (*m/e* 43) and methyl (*m/e* 15) cations.

References

1) P. B. Stewart, G. J. Possanza, and F. K. Hess, *J. Immunol.*, **110**, 1180 (1973).

2) F. K. Hess, P. B. Stewart, G. J. Possanza, and K. Freter, German Patent 2301820 (1974); *Chem. Abstr.*, **81**, 104976m (1974).

3) J. L. Miesel, U. S. Patent 3962434 (1976); *Chem. Abstr.*, **85**, 56997c (1976).

4) J. L. Miesel, United States Publ. Pat. Appl. B, 503579 (1976); *Chem. Abstr.*, **85**, 20819g (1976).

5) E. Bamberger and E. Renauld, *Chem. Ber.*, **30**, 2278 (1897).

6) A. B. Boese, Jr., L. W. Jones and R. T. Major, *J. Am. Chem. Soc.*, **53**, 3530 (1931).

7) P. A. Smith, "Open Chain Nitrogen Compounds," ed by W. A. Benjamin, New York (1965), Vol. 2, p. 341.

8) L. Lassiani, C. Nisi, F. Sigon, G. Sava, and T. Giraldi, *J. Pharm. Sci.*, **69**, 1098 (1980).

9) H. K. L. Gupta and N. C. Sogani, *J. Indian Chem. Soc.*, **36**, 87 (1959).

A Practical Synthesis of Olivetol

Ramesh Chander ANAND* and Harish RANJAN

Department of Chemistry, Indian Institute of Technology, Hauz Khas, New Delhi-110 016, India

(Received September 18, 1982)

Synopsis. A simple and practical synthesis of olivetol has been described in 55% overall yield from α-resorcylic acid.

Recently there have been large interests in psychotomimetically active compounds of marijuana (hashish) because of their extensive biological activity.[1] This has stimulated a number of synthetic efforts towards cannabinoids.[2] The syntheses of these compounds depend largely on the availability of the key intermediate olivetol (5-pentyl-1,3-benzenediol) (**1**). This compound was first obtained by degrading lichen acid and olivetonic acid[3] but later a number of synthetic routes have been developed.[4] Most of the syntheses reported involve unsatisfactory overall yields, and/or the intermediates reported are predominantly liquids, the purification of which are relatively cumbersome. Moreover, the syntheses recorded are through the protection of two hydroxyl groups as their methyl ethers, the conversion of which into olivetol requires high temperature and this results in inferior quality product.

In the present communication, we wish to report a simple, efficient and practical synthesis of olivetol starting from commercially available α-resorcylic acid (3,5-dihydroxybenzoic acid) (**2**). The intermediates isolated are solid, crystalline compounds and the deprotection of two benzyloxyl groups at the end is carried out under mild reaction conditions. The synthesis of the title compound is as follows:

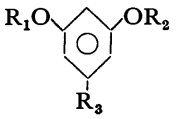

1 $R_1, R_2 = H$; $R_3 = n\text{-}C_5H_{11}$
2 $R_1, R_2 = H$; $R_3 = COOH$
3 $R_1, R_2 = CH_2C_6H_5$; $R_3 = COOCH_2C_6H_5$
4 $R_1, R_2 = CH_2C_6H_5$, $R_3 = CH_2OH$
5 $R_1, R_2 = CH_2C_6H_5$; $R_3 = CHO$
6 $R_1, R_2 = CH_2C_6H_5$; $R_3 = CH(OH)C_4H_9(n\text{-})$

α-Resorcylic acid (**2**) was benzylated with potassium carbonate and benzyl chloride in DMF to give benzyl 3,5-bis(benzyloxy)benzoate (**3**) in 97% yield. Lithium aluminium hydride reduction of the benzyl ester followed by oxidation of the resulting alcohol (**4**) with pyridinium chlorochromate[5] afforded 3,5-bis(benzyloxy)benzaldehyde (**5**). Grignard reaction of butylmagnesium bromide on the aldehyde (**5**) furnished the alcohol (**6**). Refluxing of **6** with *p*-toluenesulfonic acid in benzene under Dean and Stark apparatus followed by hydrogenation of the resulting product with 10% Pd/C at room temperature afforded olivetol in 55% overall yield.

Experimental

Benzyl 3,5-Bis(benzyloxy)benzoate(3). This compound was prepared by refluxing and stirring a mixture of α-resorcylic acid (20 g; 0.129 mol), DMF (150 ml), K_2CO_3(107.64 g, 0.78 mol), and benzyl chloride (98.28 g, 0.78 mol), Reaction was monitored by TLC, after completion of the reaction (12 h), it was diluted with cold water and extracted with ether. Evaporation of solvent and crystallization of the residue with benzene–hexane afforded benzyl-bis(benzyloxy)-benzoate (54.2 g, 97%), mp 63—66 °C, ν_{max} 3090, 3060, 3035, 2925, 1740, 1600, 1490, 1450, 1375, 1350, 1300, 1260, 1225, 1170, 1110, 1060—1030, 985, 945, 920, 875, 855—835, 760 cm^{-1}. NMR: δ 4.88 (s, 4H), 5.24 (s, 2H), 6.64—7.2 (m, 18H).

3,5-Bis(benzyloxy)benzyl Alcohol(4). Benzyl ester (**3**, 54.0 g, 0.12 mol) was reduced with lithium aluminium hydride (9.12 g, 2 mol) in dry ether. It was decomposed with 5% hydrochloric acid. Removal of the solvent followed by crystallization from benzene–hexane gave the alcohol (38.5 g, 95%), mp 81.5—82 °C, ν_{max} 3370, 3040, 2920, 1610, 1470, 1220, 1160, 1050, 840, 770 cm^{-1}. NMR: δ 2.0 (s, 2H), 4.54 (s, 2H), 5.02 (s, 4H), 6.52—6.56 (m, 3H), 7.32 (m, 10H).

3,5-Bis(benzyloxy)benzaldehyde(5). To a stirred mixture of pyridinium chlorochromate (40 g), sodium acetate (3 g) in anhydrous dichloromethane was added the alcohol (**4**) (38 g, 0.118 mol). After stirring for 1 h, it was diluted with dry ether (80 ml) and the dichloromethane–ether layer was decanted. The residue was washed with dry ether and the total organic layer was passed through silica-gel column. Removal of the solvent followed by crystallization with benzene–hexane furnished aldehyde (35.05 g, 93%) mp 76.5—77 °C, ν_{max} 3100—2830, 2740, 1690, 1600, 1460, 1390, 1350, 1260, 1220, 1160, 1085, 1060, 955, 910, 840, 735 cm^{-1}. NMR: δ 4.96 (s, 4H), 6.64—7.28(m, 13H), 9.72(s, 1H).

1-[3,5-Bis(benzyloxy)phenyl]-1-pentanol (6). To a solution of butylmagnesium bromide (prepared from 30.14 g of butyl bromide and 5.76 g of magnesium) in anhydrous ether, was added aldehyde (**5**, 35.0 g, 0.11 mol) in anhydrous ether under N_2 at 0 °C with stirring. It was stirred at room temperature for 2 h and then decomposed with 5% H_2SO_4. Organic layer was separated and the aqueous layer extracted with ether. The combined organic layer after washing with brine was stripped off the solvent and the residue was crystallized from acetone–benzene to give the alcohol (**6**) 38.1 g, 92%), mp 88 °C, ν_{max} 3420, 3085—3035, 2940, 2870, 1610, 1460, 1380, 1300, 1220, 1160, 1060, 910, 840, 735 cm^{-1}. NMR: δ 0.88 (t, 3H), 1.28—2.08 (m, 6H), 4.64 (t, 1H), 4.96 (s, 4H), 6.48 (m, 3H), 7.28 (m, 10H).

5-Pentyl-1,3-benzenediol (Olivetol) (1). A solution of 1-[3,5-bis(benzyloxy)phenyl]-1-pentanol (**6**, 38 g, 0.1 mol), *p*-toluenesulfonic acid (0.6 g) in benzene (350 ml) was refluxed under Dean and Stark apparatus till no more water separated. It was washed with $NaHCO_3$ and brine solutions. Solvent was evaporated and the residue was dissolved in ethanol (300 ml). It was hydrogenated with 10% Pd/C (1 g). After filtration, the solvent was evaporated to have a thick residue which was distilled under vacuum to procure olivetol (12.1 g, 66.7%). IR and NMR are in agreement with those reported for authentic sample.[4d]

References

1) "Marijuana, Chemistry, Pharmacology, Metabolism and Clinical Effects," ed by R. Mechoulam, Academic Press, New York (1973).

2) R. Mechoulam, N. K. McCallum, and S. Burstein, *Chem. Rev.*, **76**, 75 (1976).

3) Y. Asahina and J. Asano, *Ber.*, **65**, 475 (1932).

4) a) T. H. Chan and T. Chaly, *Tetrahedron Lett.*, **1982**, 2935; b) A. J. Birch and J. Slobbe, *ibid.*, **1976**, 2079; c) H. C. Krishnamurthy and S. Prasad, *ibid.*, **1975**, 2511 and references cited therein; d) T. Petrzilka, W. Haefliger, and C. Sikemeier, *Helv. Chim. Acta*, **52**, 1102 (1969); e) A. Focella, S. Teitel, and A. Brossi, *J. Org. Chem.*, **42**, 3456 (1977); f) R. M. Aucker and A. H. Cook, *J. Chem. Soc.*, **1945**, 311; g) C. M. Suter and A. W. Weston, *J. Am. Chem. Soc.*, **61**, 232 (1939).

5) E. J. Corey and J. W. Suggs, *Tetrahedron Lett.*, **1975**, 2647.

 © 1983 The Chemical Society of Japan Bull. Chem. Soc. Jpn., 56, 1891—1895 (1983)

The Molecular Structure of Trimethylamine-Boron Triiodide as Studied by Gas Electron Diffraction

Kinya Iijima and Shuzo Shibata*

Department of Chemistry, Faculty of Science, Shizuoka University, Oya, Shizuoka 422

(Received August 23, 1982)

The molecular structure of trimethylamine–boron triiodide $(CH_3)_3N\cdot BI_3$ has been determined from gas electron-diffraction data. The molecular parameter values and their uncertainties are r_g(B–I) = 2.245±0.004 Å, r_g(N–B) = 1.663±0.013 Å, r_g(C–N) = 1.497±0.005 Å, r_g(C–H) = 1.103±0.010 Å, ∠IBI = 108.6±0.4°, and ∠CNC = 106.0±0.8°. The potential barrier around the N–B bond has also been estimated to be about 3.5 kcal mol^{-1} (1 cal = 4.184 J).

The molecular structures of the trimethylamine complexes of boron trifluoride, boron trichloride, and boron tribromide have been determined in both the gas[1–3] and solid phases,[4–6] while that of the boron triiodide complex has been done only in the solid phase.[6] These studies have given the results that the N–B bond distances of the first three complexes are significantly shorter and the B–X and C–N bond distances are longer in the solid phase than in the gas phase, and thus it is concluded that the dative bonding in trimethylamine–boron trihalides is enhanced in the solid phase.

It has also been reported that in the gas phase the fractional changes of the molecular parameters by the complex formation become larger as the atomic number of the halogen atoms involved in the complex increases,[2] correlating to the reorganization energies of boron trihalides.[7] It has also been found that the height of the rotational barrier about the N–B bond of trimethylamine–boron trihalide varies in the order $(CH_3)_3N\cdot BF_3$[1] < $(CH_3)_3N\cdot BBr_3$[2] < $(CH_3)_3N\cdot BCl_3$.[2] It is therefore interesting to determine the molecular structure of gaseous trimethylamine–boron triiodide, $(CH_3)_3N\cdot BI_3$, and the rotational barrier about the N–B bond by the electron diffraction method.

Experimental

The gas of trimethylamine that was produced by dropwise additions of an aqueous solution of sodium hydroxide to trimethylamine hydrochloride[8] was dried through soda lime and allowed to react with boron triiodide in benzene. The crude complex was dissolved in chloroform and impurities were eliminated by adding activated charcoal. The purity of the complex was checked by IR spectra.[9]

Electron diffraction photographs were taken by the use of an r^3-sector on Kodak Electron-Image plates at camera distances of 294 and 144 mm. The sample was vaporized at 483 K by means of a high temperature nozzle. An accelerating voltage was 40 kV and the wavelength was determined from the diffraction patterns of thallium(I) chloride.[10] The exposure times were about 13 and 30 s for the long and short camera distance photographs, respectively, with an electron-beam current of 0.8 μA. The pressure in the diffraction chamber was 1×10^{-5} Torr (1 Torr = 133.322 Pa) during the experiment. Three plates were selected for each camera distance and their optical densities were measured at 0.4 mm intervals by the use of a digital microphotometer. The electron diffraction unit and the digital microphotometer used in the present study have been described elsewhere.[11]

Analysis and Results

Molecular Intensity and Radial Distribution. The scattering intensities in the range of s = 2.5—14.8 Å^{-1} were obtained from the long camera distance plates and those in the range of s = 7.5—34.6 Å^{-1} from the short camera distance plates. They were leveled by theoretical backgrounds, and then the intensities for each camera distance were averaged. The elastic and inelastic scattering factors were taken from the tables prepared by Schäfer *et al.*[12] and by Cromer and Mann,[13] respectively. The inelastic scattering factor for the hydrogen atom was taken from the table by Tavard *et al.*[14]

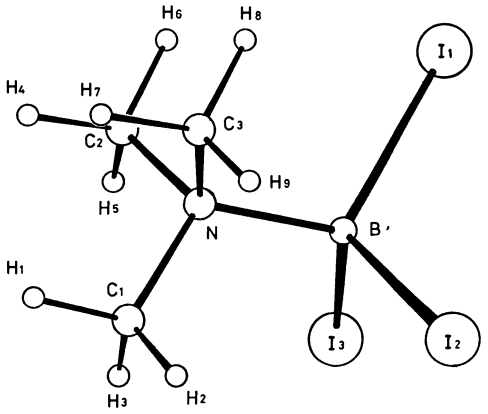

Fig. 1. Numbering of atoms in trimethylamine–boron triiodide (symmetry C_{3v}).

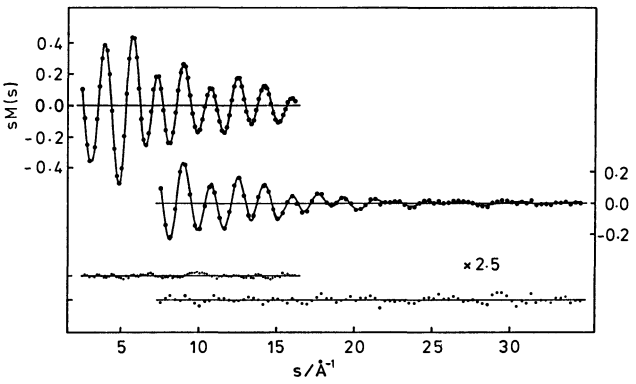

Fig. 2. Molecular intensities for trimethylamine–boron triiodide. The two upper curves are long and short camera-distance data. Dots represent observed ones, solid curves calculated ones, and their residuals are shown below.

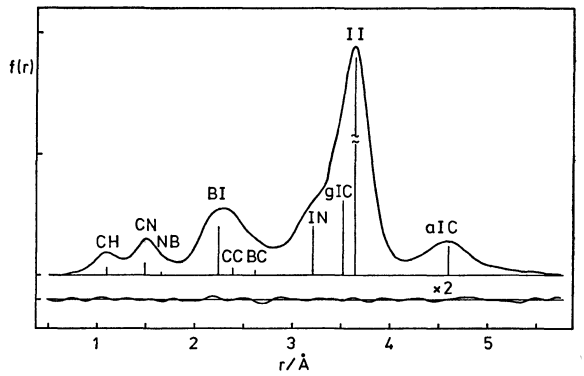

Fig. 3. Experimental radial distribution curve for trimethylamine–boron triiodide. Lower curve represents two times the difference between the experimental and the calculated curves.

The molecular intensities obtained by drawing backgrounds smoothly on the experimental intensities[15] are shown in Fig. 2. The radial distribution function corrected for the large difference[16] in the atomic numbers of the atoms contained in $(CH_3)_3N\cdot BI_3$ is shown in Fig. 3.

Vibrational Amplitudes and Shrinkage Corrections. Root-mean-square amplitudes of the atomic pairs in the staggered form were calculated on the basis of the Urey-Bradley force field obtained from the vibrational spectra of solid $(CH_3)_3N\cdot BI_3$.[9] However, the calculated l(I···I) disagreed with the observed one in the gas phase as will be described later. The force constant F(II) was adjusted to give a better agreement between the calculated and observed l(I···I) amplitudes, since it greatly contributes to the l(I···I). The corrected force constant yielded the decrease of about 50 cm^{-1} in wave numbers for the symmetric and antisymmetric deformations of BI_3. The mean amplitudes and the shrinkage corrections, r_a-r_α,[17] were calculated on the basis of the force constants listed in Table 1, as shown in Table 2.

Molecular Structure and Potential Barrier Height. The molecular parameters of $(CH_3)_3N\cdot BI_3$ have been determined by the least-squares analysis of molecular intensities. Both of the donor and acceptor parts in the complex molecule were assumed to have the C_{3v} symmetry. The methyl groups were also assumed to have the C_{3v} symmetry in a staggered form with respect to the C–N bonds. The geometrical parameters determined by the least-squares analysis are as follows: r(B–I), r(N–B), r(C–N), r(C–H), r(I···I), r(C···C), and ∠NCH. The mean amplitudes of some atom pairs were refined by the least-squares analysis as listed in Table 3. The mean amplitudes of other bonds and atom pairs which are independent of the rotation around the N–B bond were fixed to the values listed in Table 2. The shrinkage corrections for all the atom pairs were also fixed to the values listed in Table 2. The asymmetry parameters, κ, for the B–I, N–B, C–N, and C–H bonds were estimated to be 16, 7.9, 2.6, and 12×10^{-6} Å^3, respectively, by the diatomic approximation[18] and those for the other atom pairs were ignored.

The torsional vibration around the N–B bond contributes greatly to the mean amplitude of the *gauche* I···C atom pair. The analysis assuming a high barrier approximation,[19] however, could not give a reasonable value for that amplitude, so the potential barrier around the N–B bond seemed to be pretty small. Thus the molecule was treated in a low barrier approximation.[19] The mean amplitudes of the rotation-dependent atom pairs were calculated at various torsional angles on the basis of the force field in Table

Table 1. Urey-Bradley force field for $(CH_3)_3N\cdot BI_3$

K(NB)	1.3	H(NCH)	0.3
K(BI)	0.9	F(II)	0.2
K(CN)	2.1	F(IN)	0.7
K(CH)	4.4	F(CC)	0.3
H(IBI)	0.1	F(CB)	0.2
H(IBN)	0.05	F(HH)	0.1
H(CNC)	0.45	F(NH)	0.6
H(CNB)	0.3	Y(CN)	0.17
H(HCH)	0.4	p	−0.05

The torsional force constant, Y, and the internal tension of the methyl carbon, p, are in 10^{-18} N m, while the others are in 10^2 N m^{-1}.

Table 2. Root-mean-square amplitudes and shrinkage corrections for $(CH_3)_3N\cdot BI_3$ (in 10^{-4} Å)

Atomic pair	l	r_a-r_α	Atomic pair	l	r_a-r_α
B–I_1	768	21	N–C_1	551	65
B–N	657	23	N···H_1	1036	238
B···C_1	923	53	C_1···C_2	824	66
B···H_1	1136	192	C_1–H_1	784	333
B···H_2	1763	76	C_1···H_4	1728	102
I_1···I_2	1233	−21	C_1···H_5	1744	88
I_1···N	870	8	C_1···H_6	1067	179
I_1···C_1	920	25	H_1···H_2	1288	473
I_1···C_2	1529	−16	H_1···H_4	2532	39
I_1···H_1	1348	98	H_1···H_5	2732	21
I_1···H_2	1614	54	H_1···H_6	1862	205
I_1···H_4	2015	54	H_2···H_5	1828	193
I_1···H_5	2438	−46	H_2···H_6	1351	243
I_1···H_6	2550	−76	H_2···H_9	2601	26

The numbering of the atoms is shown in Fig. 1. The mean-amplitudes and shrinkage corrections were calculated for the same temperature (483 K) as in the experiment.

Table 3. Root-mean-square amplitudes for $(CH_3)_3N\cdot BI_3$

	l_{obsd}/Å[a]	l_{calcd}/Å[b]
B–I	0.077 (10)	0.077
C–N	0.055 (7)	0.055
C–H	0.081 (11)	0.078
I···I	0.121 (2)	0.123
I···N	0.086 (9)	0.087

a) Results obtained from the least-squares analysis of electron-diffraction data. Limits of error are shown in parentheses. b) Values calculated from the force constants in Table 1.

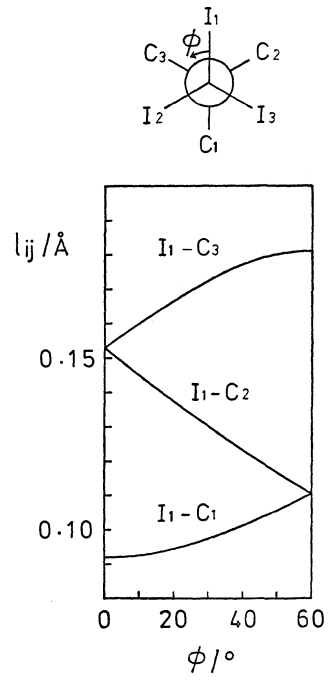

Fig. 4. Calculated mean amplitudes for the atomic pairs which are dependent on the rotation around the N–B bond. The ϕ is the rotational angle from the staggered position.

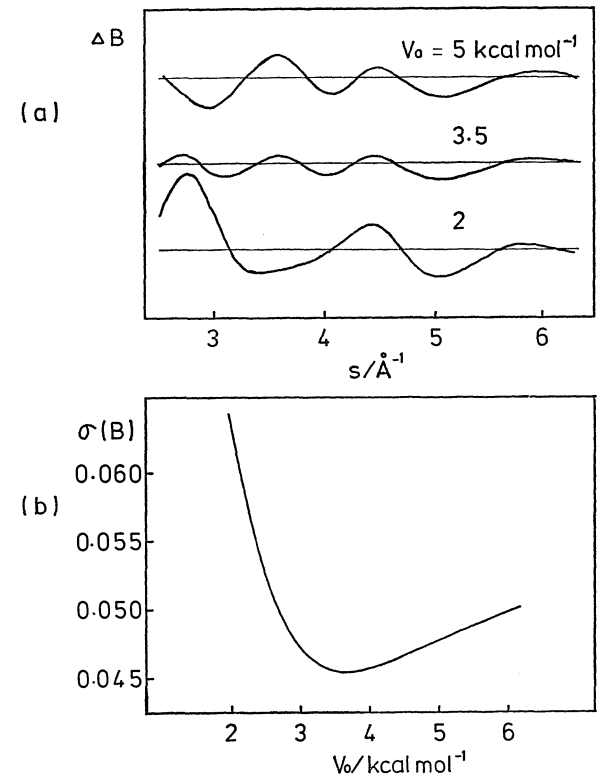

Fig. 5. (a) The difference curves between the smooth and the calculated backgrounds in the small angle range. The V_0 is the assumed potential-barrier height around the N–B bond. (b) The root-mean-square value of ΔB versus the assumed potential-barrier height around the N–B bond.

1. The dependence of these amplitudes on the torsional angle ϕ is shown in Fig. 4. They were fixed throughout the analysis. The molecular intensities were calculated at 6° intervals of the torsional angles and summed with the weights of the Boltzmann distribution. The scattering intensities in a small-angle range depend considerably on the height of the potential barrier. Therefore the potential-barrier height was determined by inspecting the shape of the backgrounds calculated from both the experimental intensities and the theoretical molecular intensities for models with various potential barriers, since the experimental backgrounds should be smooth.[20] The differences between the experimental backgrounds and the calculated backgrounds, ΔB, are shown in Fig. 5(a), and the root-mean-square values of ΔB are shown for each potential-barrier height in Fig. 5(b). These figures indicate that the potential barrier around the N–B bond is about 3.5 kcal mol^{-1}.

The geometrical parameters obtained by the least-squares calculation, in which the potential-barrier height was assumed to be 3.5 kcal mol^{-1}, are listed in Table 4 with the limits of error. The random errors were 2.6 times as large as the errors estimated by the least-squares calculations. The systematic errors were estimated from the errors in both the measurements of camera distance (0.04%) and wavelength (0.09%). The best-fit theoretical molecular intensities are shown in Fig. 2. The experimental intensities, the experimental smooth backgrounds, and the correlation matrix for the molecular parameters are deposited in Document No. 8328 at the Office of the Editor of the Bulletin of the Chemical Society of Japan. The calculations of the mean-amplitudes and the shrinkage corrections and the least-squares analysis were carried out on a HITAC M-200H computer in the Computer Center of the University of Tokyo.

Table 4. Molecular parameters obtained from least-squares analysis for $(CH_3)_3N \cdot BI_3$

	r_a[a]	r_g[a]	ε[b]
B-I	2.240	2.245	0.004
N-B	1.658	1.663	0.013
C-N	1.488	1.497	0.005
C-H	1.064	1.103	0.010
I···I	3.644	3.646	0.004
C···C	2.381	2.390	0.014
∠NCH	110.3		1.7
∠IBI[c]	108.9	108.6	0.4
∠CNC[c]	106.2	106.0	0.8

Bond distance: Å unit; bond angle: degree unit. a) Ref. 17. b) Limits of error. c) Calculated from independent parameters.

Discussion

The molecular parameters for the trimethylamine-boron trihalide complexes in the gas phase are listed in Table 5, together with those in the solid phase[4–6] and those for the component molecules.[21–25] As seen for all of trimethylamine–boron trihalide complexes, the distances of B–X and C–N bonds increase and the angles of XBX and CNC decrease on the complex

TABLE 5. COMPARISON OF MOLECULAR PARAMETERS

		r(N–B)/Å	r(B–X)/Å	r(C–N)/Å	∠XBX/°	∠CNC/°
$(CH_3)_3N\cdot BF_3$	(gas)[a]	1.674 (4)	1.374 (2)	1.485 (2)	112.6 (3)	109.2 (4)
	(solid)[b]	1.585	1.39	1.50	107	114
$(CH_3)_3N\cdot BCl_3$	(gas)[c]	1.652 (9)	1.836 (2)	1.497 (3)	110.9 (2)	108.1 (3)
	(solid)[d]	1.609 (6)	1.864 (4)	1.52 (1)	109.5 (2)	108.6 (14)
$(CH_3)_3N\cdot BBr_3$	(gas)[e]	1.663 (13)	2.001 (3)	1.500 (5)	110.3 (3)	107.8 (5)
	(solid)[d]	1.60 (2)	2.04 (2)	1.52 (1)	108.3 (7)	107.7 (10)
$(CH_3)_3N\cdot BI_3$	(gas)[e]	1.663 (13)	2.245 (4)	1.497 (5)	108.6 (4)	106.0 (8)
	(solid)[d]	1.58 (3)	2.28 (2)	1.52 (1)	108.3 (7)	105.1 (16)
$(CH_3)_3N$[f]				1.461 (2)		110.6 (6)
BF_3[g]			1.313 (1)		120	
BCl_3[h]			1.742 (4)		120	
BBr_3[i]			1.893 (5)		120	
BI_3[j]			2.118 (5)		120	

The values for the gas phase represent r_g parameters. a) Ref. 1. b) Ref. 4. c) Ref. 2. d) Ref. 6. e) Present study. f) Ref. 21. g) Ref. 22. h) Ref. 23. i) Ref. 24. j) Ref. 25.

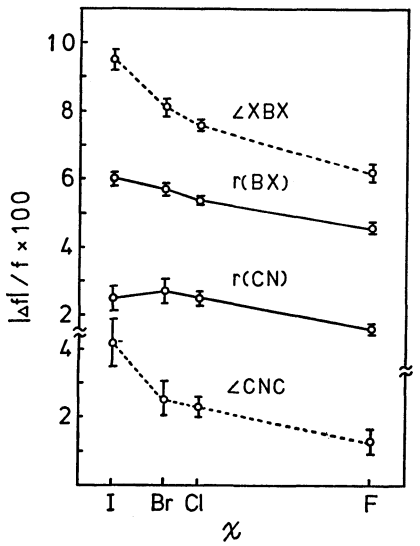

Fig. 6. Parameter changes on complex formation. The abscissa shows the magnitude of the electronegativity χ of the halogen atoms in the acceptor molecules. Solid curves represent positive Δf and dashed curves negative Δf.

formation and the magnitudes of the structural changes of the acceptor molecules are larger than those of the donor molecules. The fractional differences of the parameters, $\Delta f/f$, between the complex and the corresponding free molecules are plotted in Fig. 6 *versus* the electronegativity values of the halogen atoms[26] in the complexes. The differences are in the order $(CH_3)_3N\cdot BF_3 < (CH_3)_3N\cdot BCl_3 < (CH_3)_3N\cdot BBr_3 < (CH_3)_3N\cdot BI_3$, while the N–B bond distances in the trimethylamine complexes are nearly constant in the gas phase as well as in the solid phase with no systematic change by the halogen atoms. This order agrees with the order of heat of reaction of boron trihalides with pyridine from the calorimetric measurements,[27] and also with the order of the relative acceptor power of boron trihalides from the gas-phase displacement reactions,[28,29] though there have been no data for the $(CH_3)_3N\cdot BI_3$ complex. Thus it may be concluded that a complex formed with larger heat of reaction is subject to greater distortion and that a stable complex is not necessarily accompanied by the dative bond with a short distance. However, it is noted that these structural changes found in trimethylamine–boron trihalides are in contrast with those in the complexes of trimethylphosphine–boron trihalides;[30] on the complex formation of trimethylphosphine–boron trihalide the change of the molecular parameters for the complex with larger halogen atom is smaller in spite of the larger heat of reaction.[31,32] This situation cannot be reasonably explained at the present stage.

In the solid phase the B–I and C–N distances are larger and the IBI and CNC angles are smaller than in the gas phase. The structural changes on the complex formation seem to be magnified in the solid phase. The N–B bond distance of $(CH_3)_3N\cdot BI_3$ is smaller than in the gas phase by 0.08 Å. The same trends are seen in other trimethylamine–boron trihalide complexes. Thus it will be concluded that in all trimethylamine–boron trihalides the donor–acceptor bondings are enhanced in the solid phase.

The rotational barrier around the N–B bond in $(CH_3)_3N\cdot BI_3$ is about 3.5 kcal mol^{-1}. In the series of the trimethylamine–boron trihalide complexes, the rotational barriers decrease in the sequence of $(CH_3)_3N\cdot BCl_3$ (>18 kcal mol^{-1}),[2] $(CH_3)_3N\cdot BBr_3$ (10 kcal mol^{-1}),[2] and $(CH_3)_3N\cdot BI_3$. However, the rotational barrier height of $(CH_3)_3N\cdot BF_3$ was found to be 4.3 kcal mol^{-1},[1] which is nearly equal to that of the $(CH_3)_3N\cdot BI_3$ complex. These results are consistent with the results from NMR measurements.[33] The rotation around the N–B bond seems to be mainly hindered by repulsion between the methyl groups and the halogen atoms. The distances of $X_1\cdots H_6$ (see Fig. 1), which are considerably shorter than their van der Waals distances, increase as the atomic numbers of the halogen atoms involved become larger, and therefore their potential barriers are considered to become smaller. However, the barrier height of $(CH_3)_3N\cdot BF_3$ is much smaller than that of $(CH_3)_3N\cdot BCl_3$. This may be due to that the van der Waals radius of a fluorine atom is comparatively small and the $X_1\cdots H_6$ distance is nearly equal to the van der

Waals distance.

References

1) K. Iijima and S. Shibata, *Bull. Chem. Soc. Jpn.*, **52**, 711 (1979).
2) K. Iijima and S. Shibata, *Bull. Chem. Soc. Jpn.*, **53**, 1908 (1980).
3) M. Hargittai and I. Hargittai, *J. Mol. Struct.*, **39**, 79 (1977).
4) S. Geller and J. L. Hoard, *Acta Crystallogr.*, **4**, 399 (1951).
5) H. Hess, *Acta Crystallogr., Sect. B*, **25**, 2338 (1969).
6) P. H. Clippard, J. C. Hanson, and R. C. Taylor, *J. Cryst. Mol. Struct.*, **1**, 363 (1971).
7) F. A. Cotton and J. R. Leto, *J. Chem. Phys.*, **30**, 993 (1959).
8) R. Adams and B. K. Brown, *Org. Synth.*, Coll. Vol. I, 528 (1941).
9) P. H. Laswick and R. C. Taylor, *J. Mol. Struct.*, **34**, 197 (1976).
10) W. Witt, *Z. Naturforsch., Teil A*, **19**, 1363 (1964).
11) S. Shibata, K. Iijima, R. Tani, and I. Nakamura, *Rep. Fac. Sci. Shizuoka Univ.*, **9**, 33 (1974).
12) L. Schäfer, A. C. Yates, and R. A. Bonham, *J. Chem. Phys.*, **55**, 3055 (1971).
13) D. T. Cromer and J. B. Mann, *J. Chem. Phys.*, **47**, 1892 (1967); D. T. Cromer, *ibid.*, **50**, 4857 (1969).
14) C. Tavard, D. Nicolas, and M. Rouault, *J. Chim. Phys.*, **64**, 540 (1967).
15) J. Karle and I. L. Karle, *J. Chem. Phys.*, **18**, 957 (1950).
16) R. M. Gavin and L. S. Bartell, *J. Chem. Phys.*, **48**, 2460 (1968).
17) For the definitions of various distances, see K. Kuchitsu and S. J. Cyvin, "Molecular Structures and Vibrations," ed by S. J. Cyvin, Elsevier, Amsterdam (1972), Chap. 12.
18) K. Kuchitsu, *Bull. Chem. Soc. Jpn.*, **40**, 505 (1967).
19) Y. Morino and E. Hirota, *J. Chem. Phys.*, **28**, 185 (1958).
20) Y. Morino and K. Kuchitsu, *J. Chem. Phys.*, **28**, 175 (1958).
21) B. Beagley and A. R. Medwid, *J. Mol. Struct.*, **38**, 229 (1977).
22) K. Kuchitsu and S. Konaka, *J. Chem. Phys.*, **45**, 4342 (1966).
23) S. Konaka, Y. Murata, K. Kuchitsu, and Y. Morino, *Bull. Chem. Soc. Jpn.*, **39**, 1134 (1966).
24) S. Konaka, T. Ito, and Y. Morino, *Bull. Chem. Soc. Jpn.*, **39**, 1146 (1966).
25) H. Kakubari, S. Konaka, M. Kimura, *Bull. Chem. Soc. Jpn.*, **47**, 2337 (1974).
26) L. Pauling, "The Nature of the Chemical Bond," 3rd ed, Cornell University Press, Ithaca, New York (1960).
27) H. C. Brown and R. R. Holmes, *J. Am. Chem. Soc.*, **78**, 2173 (1956).
28) W. Dutton, W. G. Paterson, and M. Onyszchuk, *Proc. Chem. Soc.*, **1960**, 149.
29) J. M. Miller and M. Onyszchuk, *Can. J. Chem.*, **41**, 2898 (1963).
30) K. Iijima, E. Koshimizu, and S. Shibata, *Bull. Chem. Soc. Jpn.*, **55**, 2551 (1982).
31) D. C. Mente, J. L. Mills, and R. E. Mitchell, *Inorg. Chem.*, **14**, 123 (1975).
32) D. C. Mente and J. L. Mills, *Inorg. Chem.*, **14**, 1862 (1975).
33) C. T. Yim and D. F. R. Gilson, *Can. J. Chem.*, **48**, 515 (1970).

The Cation-Cation Interactions in Aqueous Mixed Electrolyte Solutions of Quaternary Phosphonium Chlorides

Katsuko TAKAIZUMI* and Toshiki WAKABAYASHI
The College of General Education, Tohoku University, Kawauchi, Sendai 980

(Received September 20, 1982)

Density measurements were carried out at six temperatures between 1 and 55 °C for three series of aqueous mixed electrolyte solutions, each of which contained $(n\text{-Bu})_4PCl$ and Ph_4PCl with the mole ratios, 3:1, 1:1, and 1:3, respectively. The mixed solutions are assumed to be the model solutions of the phosphonium chlorides, $(n\text{-Bu})_{4-n}Ph_nPCl$($n=1,2$, and 3), with respect to the pair-wise interactions between the cations, for which a model has been proposed in a previous paper.[1] The volume B-coefficients(B_v) determined for the model salts are in good agreement with those for the corresponding pure salts and those reproduced by the equation derived from the model. The results indicate that the phenyl groups affect weakly the butyl cospheres in both the intermolecular processes and intramolecular processes and that among the ion-ion interactions the cation-cation interactions are the main factor for determining the B_v's. These can be decomposed into three parts, arising from the butyl-butyl, phenyl-phenyl, and butyl-phenyl interactions.

In a previous paper[1], we reported the volume behavior of the quaternary phosphonium salts, $(n\text{-Bu})_{4-n}Ph_nPCl$($n=1$—4) and Bu_4PBr, in aqueous solutions in the temperature range 1—55 °C. The volume B-coefficients(B_v), which would reflect the effects arising from the pair-wise interactions between ions through the ionic cospheres,[2] were determined. It was possible to reproduce the numerical values for B_v of the salts with n from 1 to 3 from those of the salts with n of 0 and 4 by the equation derived from these assumptions: (a) the B_v's are determined mainly by the effects resulting from the cation-cation interactions; (b) when any two cations approach each other, the interaction takes place between a cosphere of one of the hydrocarbon groups on a cation and that on another cation, and we have three types of the interactions, butyl-butyl, phenyl-phenyl, and butyl-phenyl; (c) each interaction takes place on a purely chance basis, that is, in proportion to the 'concentration' of the group. If these assumptions are adequate, we may anticipate that, in the aqueous mixed electrolyte solutions containing $(n\text{-Bu})_4PCl$ and Ph_4PCl with the mole ratio, $(4\text{-}n):n$, the B_v's found for the mixed salts(model salts) should be the same as those found for the pure salts.

In this paper, we report the volumetric properties of three kinds of model salts corresponding to the pure salts with $n=1$, 2, and 3, respectively, and $(n\text{-Bu})_4PCl$ in aqueous solutions at the temperatures 1, 5, 10, 25, 40, and 55 °C.

Experimental

The $(n\text{-Bu})_4PCl$ was obtained from Alfa Division Ventron and was purified as follows. The salt was dissolved in water, washed repeatedly with a small amount of CH_2Cl_2 to remove colored substances, extracted in the presence of NaCl(*ca.* 2 mol kg^{-1}) into $CHCl_3$ phase, which was then washed with a small amount of deionized water, and finally extracted into conductivity-grade water. The aqueous solution was degassed to remove $CHCl_3$ at about 40 °C under reduced pressure and then filtered through a Millipore filter. The clathrate-like hydrate, obtained by cooling the aqueous solution, was collected. The aqueous solution was analyzed gravimetrically for the anion content using $AgNO_3$. The methods for purifying the Ph_4PCl and for preparing the stock solution were the same as previously reported.[1,3]

Three kinds of mixed stock solutions were prepared by mixing both the stock solutions on a weight basis to give the mole ratios of Bu_4PCl to Ph_4PCl, 3:1, 1:1, and 1:3. The solutions for density measurement were obtained by dilution from the mixed stock solutions on a weight basis.

General procedures and reproducibility for the density measurements were essentially the same as those reported previously.[1,3] The measurements were carried out over the concentration range from about 0.04 to 1.5 mol dm^{-3} for each series of the mixed solutions and at the temperatures, 1, 5, 10, 25, 40, and 55 °C. The temperatures of the water bath, in which the pycnometers were immersed, were controlled to 0.01 °C for the measurements at 1, 5, and 55 °C, 0.005 for 25 °C, and 0.007 for 10 and 40 °C.

Results and Discussion

The apparent molar volumes, ϕ_v, for the model salts corresponding to Bu_3PhPCl, Bu_2Ph_2PCl and $BuPh_3PCl$, at six temperatures are listed in Table 1. The ϕ_v's for Bu_4PCl, which had not been determined in the previous work,[1] are also listed.

The ϕ_v's were obtained from the density data by the usual equation:

$$\phi_v = \frac{1}{m}\left(\frac{1000+mM}{d_{soln}} - \frac{1000}{d_o}\right), \quad (1)$$

where m and M are the molality and molecular weight of the model salt which equals that of $(n\text{-Bu})_{4-n}Ph_nPCl$.

The ϕ_v's are assumed to follow the equation;

$$\phi_v = \phi_v^\circ + A_v c^{1/2} + B_v c + C_v c^2 + D_v c^3, \quad (2)$$

where ϕ_v° is the standard partial molar volume of the model salt, A_v the Debye-Hückel limiting slope, and the other coefficients are empirical parameters. The values for A_v at various temperatures were taken from the table compiled by Redlich and Meyer.[4] The other coefficients were determined by the least-squares method to fit the ϕ_v's to the equation.

The numerical values for these coefficients are presented in Table 2, together with the uncertainties (σ_1) of the coefficients and the standard deviations(σ) between the observed and reproduced ϕ_v's. The corresponding coefficients for the pure salts are also listed, for comparison. The differences between ϕ_v's for Bu_4PCl in this work and those in the previous work[1],

which were obtained from ϕ_v's for Bu_4PBr by subtracting the differences in the anionic partial molar volume, $\phi_{v,-}^{\circ}(Br^-) - \phi_{v,-}^{\circ}(Cl^-)$[3], are within 0.08% except for the difference at 1 °C, about 0.15% (Table 2).

Figure 1 shows the ϕ_v's of the mixed salts as a function of the square root of concentration (mol dm^{-3}), together with those of the pure salts. The ϕ_v curves of the three mixed salts are very similar to those for the corresponding pure salts in the low concentration range, while at higher concentrations the similarity in the ϕ_v behavior is not found. This aspect is re-

Table 1. Densities and apparent molar volumes at 1, 5, 10, 25, 40, and 55 °C

	1 °C		5 °C		10 °C		25 °C		40 °C		55 °C	
m	d	ϕ_v	d	ϕ_v	d	ϕ_v	d	ϕ_v	d	ϕ_v	d	ϕ_v
mol kg^{-1}	g cm^{-3}	cm^3 mol^{-1}	g cm^{-3}	cm^3 mol^{-1}	g cm^{-3}	cm^3 mol^{-1}	g cm^{-3}	cm^3 mol^{-1}	g cm^{-3}	cm^3 mol^{-1}	g cm^{-3}	cm^3 mol^{-1}
					Bu_4PCl							
0.07122	0.999516	300.41	0.999490	301.70	0.999109	303.46	0.996270	306.98	0.991254	311.27		
0.08141	0.999499	299.95	0.999459	301.25	0.999056	300.09			0.991121	311.24		
0.10424	0.999408	299.77	0.999364	300.84	0.998940	302.50						
0.11138	0.999407	299.48			0.998914	302.27	0.995856	306.89	0.990770	310.87	0.983977	315.60
0.13630	0.999324	299.31	0.999250	300.35	0.998758	302.18	0.995661	306.42	0.990467	310.81	0.983613	315.56
0.13681	0.999292	299.53	0.999196	300.74	0.998729	302.37	0.995649	306.47	0.990492	310.56	0.983646	315.24
0.18530	0.999201	298.89	0.999050	300.11	0.998517	301.72	0.995253	306.05	0.989940	310.41	0.982972	315.17
0.24685	0.999203	297.94	0.998962	299.26	0.998238	301.34	0.994837	305.45	0.989322	310.03	0.982186	314.92
0.33982	0.999377	296.61	0.998991	298.05	0.998207	299.82	0.994324	304.65	0.988488	309.52	0.981103	314.54
0.44143	0.999663	295.52	0.999131	297.03	0.998180	298.88	0.993879	303.95	0.987633	309.18	0.979988	314.29
0.56538	1.00023	294.23	0.99950	295.86	0.99831	297.85	0.99340	303.36	0.98676	308.69	0.978635	314.16
0.69649	1.00095	293.09	0.99999	294.84	0.99856	296.94	0.99299	302.85	0.98587	308.43	0.97746	313.95
0.87027	1.00020	291.86	1.00074	293.78	0.99897	296.02	0.99250	302.39	0.98469	308.32	0.97584	313.95
1.1033	1.00337	290.76	1.00164	292.88	0.99936	295.38	0.99180	302.13	0.98330	308.18	0.97386	313.97
1.3962	1.00441	290.37	1.00223	292.61	0.99944	295.23	0.99075	302.21	0.98151	308.32	0.97159	314.06
1.7214	1.00463	290.79	1.00206	293.06	0.99887	295.70	0.98935	302.59	0.97959	308.57	0.96933	314.16
1.9738	1.00413	291.54	1.00141	293.74	0.99805	296.29	0.98812	303.02	0.97811	308.85	0.96768	314.36
1.9977	1.00408	291.60	1.00134	293.80	0.99798	296.35	0.98802	303.05	0.97787	308.96	0.96731	314.50
2.7220	1.00133	293.97	0.99850	295.86	0.99495	298.14	0.98449	304.23	0.97391	309.75	0.96301	314.99
3.5674	0.99763	296.22	0.99477	297.90	0.99117	299.92	0.98058	305.44	0.96986	310.57	0.95881	315.53
4.9556	0.99198	298.88	0.98917	300.32	0.98561	302.08	0.97509	306.97	0.96436	311.66	0.95342	316.22
6.8699	0.98587	301.18	0.98311	302.45	0.97968	303.98	0.96930	308.40	0.95879	312.68	0.94798	316.94
					$Bu_4PCl : Ph_4PCl = 3 : 1$							
0.02319									0.992332	312.37		
0.04200	1.000481	300.85	1.000494	302.10								
0.06409	1.000810	300.40	1.000800	301.60	1.000427	303.41	0.997525	308.17	0.992537	312.21		
0.07557	1.000993	300.10	1.000957	301.45	1.000591	302.91	0.997653	307.57	0.992581	312.37	0.985890	316.74
0.09173	1.001227	300.03	1.001172	301.36	1.000743	303.28			0.992664	312.28		
0.11519	1.001634	299.32	1.001541	300.72	1.001079	302.57	0.997983	307.37	0.992793	312.10	0.986001	316.63
0.12982	1.001791	299.76	1.001684	301.12	1.001196	302.99			0.992865	312.08	0.986013	316.83
0.16125	1.002341	299.03	1.002187	300.44	1.001655	302.25	0.998372	307.14	0.993048	311.86	0.986137	316.49
0.17171	1.002484	299.08	1.002304	300.55	1.001774	302.26	0.998460	307.10			0.986139	316.65
0.20487	1.003050	298.58	1.002797	300.21			0.998777	306.78	0.993310	311.59	0.986277	316.34
0.22660	1.003422	298.30	1.003136	299.94	1.002483	301.84	0.998962	306.72	0.993452	311.43	0.986333	316.35
0.29929	1.004552	297.97	1.004201	299.46	1.003451	301.30	0.999657	306.24			0.986588	316.09
0.38903	1.00608	297.17	1.00560	298.71	1.00469	300.63	1.00055	305.69	0.99447	310.77	0.98692	315.81
0.42806	1.00670	297.00	1.00617	298.53	1.00522	300.41	1.00086	305.68	0.99470	310.67	0.98703	315.82
0.64842	1.01041	295.58	1.00955	297.25	1.00821	299.29	1.00296	304.83	0.99609	310.06	0.98786	315.32
0.83176	1.01343	294.65	1.01229	296.41	1.01063	298.55	1.00461	304.35	0.99718	309.73	0.98853	315.03
1.0399	1.01662	293.91	1.01515	295.79	1.01314	298.03	1.00635	303.98	0.99833	309.47	0.98927	314.77
1.3040	1.02021	293.37	1.01840	295.30							0.99011	314.55
1.5986	1.02344	293.27	1.02133	295.22	1.01857	297.54	1.01005	303.66	1.00087	309.15	0.99096	314.38
1.9856	1.02676	293.50	1.02437	295.39	1.02129	297.67	1.01190	303.76	1.00213	309.19	0.99175	314.38
2.3424	1.02902	293.91	1.02663	295.62								
2.6466	1.03028	294.48	1.02766	296.22	1.02420	298.40	1.01413	304.10	1.00373	309.34	0.99294	314.32

TABLE 1. (Continued)

1 °C			5 °C		10 °C		25 °C		40 °C		55 °C	
m	d	ϕ_V	d	ϕ_V	d	ϕ_V	d	ϕ_V	d	ϕ_V	d	ϕ_V
mol kg^{-1}	g cm^{-3}	cm^3 mol^{-1}	g cm^{-3}	cm^3 mol^{-1}	g cm^{-3}	cm^3 mol^{-1}	g cm^{-3}	cm^3 mol^{-1}	g cm^{-3}	cm^3 mol^{-1}	g cm^{-3}	cm^3 mol^{-1}
					$Bu_4PCl : Ph_4PCl = 1 : 1$							
0.02982	1.000923	300.23	1.000940	301.83	1.000632	303.41	0.997847	308.63				
0.04716									0.993331	313.19		
0.07444	1.002433	300.10	1.002380	301.58	1.002002	303.33	0.999030	308.46	0.993966	313.11		
0.11010	1.003627	299.92					0.999965	308.30	0.994790	312.97		
0.15604	1.005179	299.48	1.004994	301.13	1.004441	303.13			0.995839	312.79		
0.19901					1.005735	302.80	1.002257	307.92	0.996801	312.67		
0.26090	1.008590	298.99	1.008286	300.48	1.007553	302.48	1.003837	307.59	0.998190	312.37		
0.31829	1.010436	298.64	1.010037	300.21	1.009219	302.17						
0.39960	1.01296	298.31	1.01247	299.82	1.01152	301.80	1.00725	307.04	1.001210	311.81		
0.48275	1.01553	297.87	1.01491	299.44	1.01382	301.44	1.00922	306.75	1.00294	311.57		
0.57470	1.01828	297.45	1.01754	299.04	1.01630	301.06	1.01137	306.38	1.00481	311.29		
0.68911	1.02157	297.01	1.02059	298.78	1.01922	300.75	1.01386	306.15	1.00701	311.06		
0.81612	1.02503	296.64	1.02395	298.33	1.02237	300.36	1.01654	305.85	1.00934	310.82		
0.96052	1.02869	296.39	1.02743	298.10	1.02566	300.13	1.01944	305.55	1.01194	310.47		
1.1356	1.03294	296.01	1.03148	297.74	1.02951	299.77	1.02268	305.30	1.01474	310.30		
1.2951	1.03659	295.72	1.03493	297.48	1.03281	299.47	1.02552	305.04	1.01727	310.02		
					$Bu_4PCl : Ph_4PCl = 1 : 3$							
0.04255												
0.04262			1.002220	301.06	1.001874	303.28	0.999025	308.62				
0.06785									0.995110	313.45	0.988354	318.82
0.07530					1.003513	303.14	1.000510	308.60				
0.09839	1.005204	299.37							0.996360	313.58	0.989533	318.63
0.13221	1.007008	298.99	1.005110	300.95			1.003020	308.59	0.997801	313.00		
0.13782	1.007289	299.05			1.006564	303.05			0.997937	313.70	0.991004	318.65
0.17833	1.009342	299.10	1.007080	301.05	1.008474	303.08	1.005065	308.20			0.992535	318.33
0.18433	1.009686	298.86	1.009121	300.76	1.008809	302.76	1.005288	308.39	0.999835	313.27	0.992757	318.30
0.23004	1.011970	298.80	1.009462	300.83	1.010931	302.71	1.007241	308.18				
0.23634			1.011664	300.47	1.011238	302.62	1.007523	308.09	1.001903	312.97	0.994712	317.84
0.28033	1.014379	298.90			1.013178	302.78	1.009354	307.95				
0.29739	1.01524	298.71	1.014023	300.48	1.01403	302.42	1.01011	307.71	1.00429	312.60	0.99694	317.47
0.35497	1.01792	298.73			1.01654	302.41						
0.36488	1.01843	298.57	1.01744	300.38	1.01701	302.25	1.01284	307.49	1.00686	312.29	0.99925	317.41
0.44308	1.02206	298.25	1.01793	300.23	1.02040	301.96	1.01591	307.28	1.00970	312.08	1.00197	316.97
0.53283	1.02597	298.18	1.02140	300.05	1.02411	301.77	1.01928	307.09	1.01282	311.89	1.00495	316.63
0.62536	1.02997	297.85	1.02524	299.84	1.02785	301.43	1.02268	306.79	1.01597	311.60	1.00787	316.40
0.73763	1.03450	297.68	1.02913	299.49	1.03208	301.28	1.02656	306.59	1.01959	311.37	1.01130	316.07
0.85839	1.03921	297.40	1.03348	299.39	1.03652	300.96	1.03063	306.24	1.02342	310.94	1.01486	315.71
1.00515	1.04444	297.32	1.03808	299.06					1.02764	310.75		

flected in the agreement of the B_V value for the mixed salts with that for the pure salts(Fig. 2 and Table 2). This may be an important clue for interpreting the physical meaning of the B_V's obtained as empirical parameters. Before discussing the subject, we note that the B_V value is very close to half of B_{2V} which is the coefficient of the linear term of c in the equation for the partial molar volume.[15] Some discussion about B_V will follow.

For dilute solutions, we may reasonably expect that, besides the long-range interactions among ions due to the coulombic force, there may be pairwise interactions between ions at short distances originating from various kinds of potentials. (The potentials other than the coulombic one used by Friedman and coworkers[7,8] are the following; the core repulsion potential, the potential of the ion-cavity interaction between two ions, and the Gurney potential representing the effect of the overlap of the cospheres when the ions come close together. The B_V coefficient would contain the contributions derived from all these potentials.) The agreement in B_V, therefore, suggests strongly that in any given mixed system at low concentrations the ion-ion interactions would take place in a way similar

TABLE 2. STANDARD PARTIAL MOLAR VOLUMES AND COEFFICIENTS FOR Eq. 2

t / °C	ϕ_V° / cm³ mol⁻¹	σ_ϕ	B_V / cm³ mol⁻² dm³	σ_B	C_V / cm³ mol⁻³ dm⁶	σ_C	D_V / cm³ mol⁻⁴ dm⁹	σ_D	σ
				Bu_4PCl[a]					
1	302.10	0.27	−26.89	1.43	16.78	1.62	−2.36	0.48	0.48
	(309.13)	0.18	−25.48	0.79	17.60	0.86	−3.01	0.24	0.31)
	(302.54)[b]								
5	303.13	0.24	−25.25	1.18	16.22	1.33	−2.43	0.40	0.38
	(310.00	0.15	−23.72	0.63	16.90	0.67	−3.00	0.19	0.27)
	(303.34)[b]								
10	304.59	0.18	−23.85	0.93	15.87	1.05	−2.57	0.32	0.30
	(311.14	0.14	−21.21	0.56	15.24	0.58	−2.74	0.16	0.22)
	(304.40)[b]								
25	307.59	0.14	−16.71	0.72	11.64	0.82	−2.02	0.25	0.23
	(314.81	0.06	−15.44	0.24	11.55	0.26	−2.20	0.07	0.10)
	(307.83)[b]								
40	311.48	0.05	−12.85	0.23	9.34	0.27	−1.78	0.08	0.07
	(318.80	0.10	−11.43	0.39	8.64	0.41	−1.71	0.11	0.15)
	(311.59)[b]								
55	315.61	0.08	−9.45	0.37	6.77	0.42	−1.34	0.13	0.10
	(323.12	0.06	−8.19	0.24	5.82	0.26	−1.15	0.07	0.09)
	(315.69)[b]								
				$Bu_4PCl : Ph_4PCl = 3 : 1$[c]					
1	300.92	0.08	−15.89	0.34	6.92	0.23			0.18
	(301.32	0.09	−19.28	0.53	14.20	0.67	−2.80	0.22	0.16)
5	302.13	0.06	−14.68	0.26	6.32	0.18			0.14
	(302.34	0.06	−17.45	0.34	12.79	0.43	−2.53	0.14	0.10)
10	303.72	0.08	−13.62	0.34	5.88	0.23			0.15
	(303.45	0.06	−14.61	0.36	10.54	0.45	−2.08	0.15	0.10)
25	307.84	0.04	−10.44	0.17	4.37	0.12			0.07
	(307.77	0.05	−10.52	0.28	7.08	0.35	−1.38	0.12	0.09)
40	312.29	0.05	−8.90	0.24	3.56	0.15			0.10
	(312.08	0.05	−8.22	0.26	5.19	0.32	−1.06	0.11	0.07)
55	316.60	0.05	−7.00	0.19	2.38	0.14			0.08
	(316.81	0.07	−7.57	0.38	4.51	0.46	−1.01	0.15	0.10)
				$Bu_4PCl : Ph_4PCl = 1 : 1$[d]					
1	300.34	0.04	−9.50	0.22	3.28	0.22			0.06
	(299.84	0.04	−9.82	0.23	6.23	0.30	−1.10	0.10	0.07)
5	301.84	0.07	−9.49	0.28	3.51	0.26			0.05
	(301.30	0.10	−9.23	0.60	5.67	0.77	−1.01	0.26	0.14)
10	303.52	0.06	−8.43	0.31	2.60	0.32			0.08
	(303.04	0.09	−8.08	0.52	4.43	0.35	−0.70	0.23	0.14)
25	308.55	0.07	−8.42	0.28	2.95	0.25			0.04
	(308.26	0.04	−7.87	0.26	4.35	0.35	−0.88	0.10	0.07)
40	313.10	0.03	−8.08	0.16	2.79	0.17			0.04
	(313.14	0.08	−7.66	0.48	3.88	0.63	−0.85	0.22	0.12)
				$Bu_4PCl : Ph_4PCl = 1 : 3$[e]					
1	299.24	0.11	−5.00	0.64	0.97	0.75			0.11
	(299.51	0.07	−5.44	0.31	2.05	0.26			0.11)
5	301.00	0.08	−5.20	0.50	0.91	0.71			0.09
	(301.17	0.08	−5.53	0.36	1.94	0.30			0.13)
10	303.12	0.06	−5.25	0.16					0.11
	(303.04	0.07	−5.17	0.30	1.52	0.25			0.11)
25	308.48	0.06	−5.74	0.16					0.11
	(308.48	0.06	−5.81	0.25	1.45	0.21			0.09)
40	313.48	0.11	−6.43	0.28					0.22
	(313.73	0.05	−7.08	0.23	1.78	0.19			0.08)
55	318.53	0.09	−7.53	0.26					0.17
	(318.86	0.06	−8.58	0.29	2.26	0.25			0.10)

a) The bracketed values are for Bu_4PBr, taken from Ref. 1. b) The values converted into $\phi_V^\circ(Bu_4PCl)$ from $\phi_V^\circ(Bu_4PBr)$ by subtracting $(\overline{V}_-^\circ(Br^-) - \overline{V}_-^\circ(Cl^-))$; *cf.* Ref. 3. c) The bracketed values are for Bu_3PhPCl, taken from Ref. 1. d) The bracketed values are for Bu_2Ph_2PCl, taken from Ref. 1. e) The bracketed values are for $BuPh_3PCl$, taken from Ref. 1.

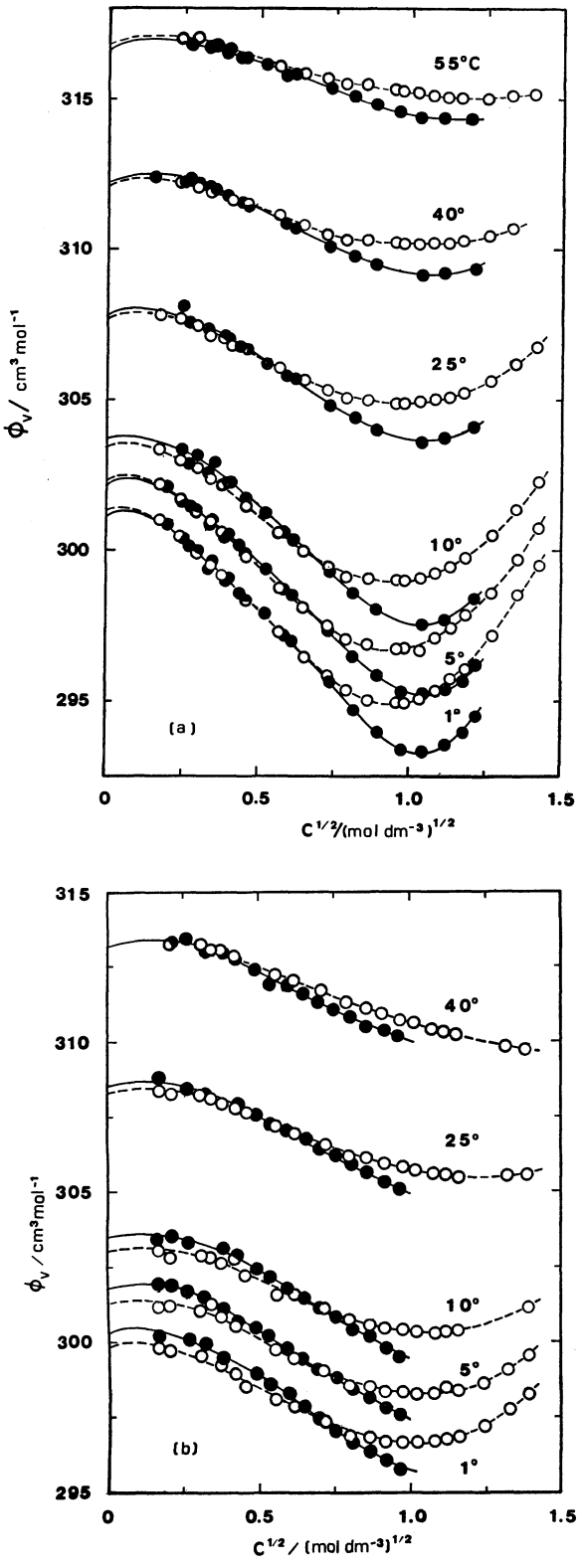

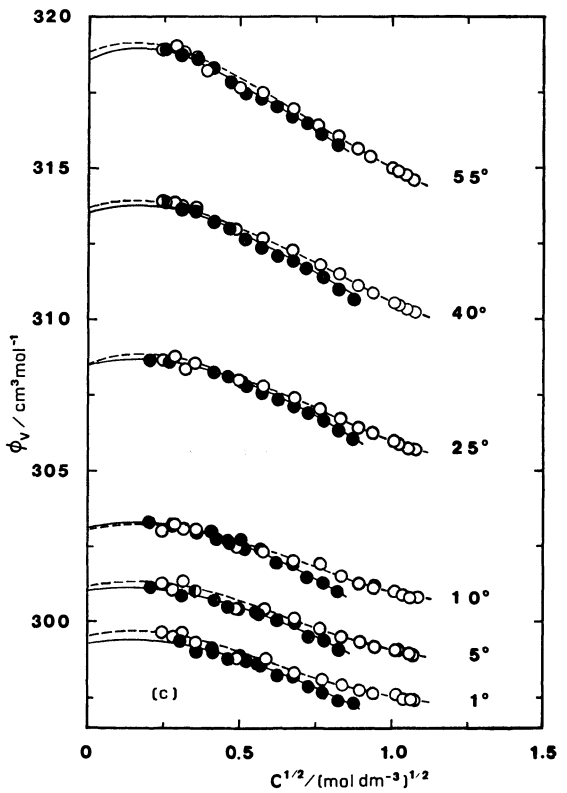

Fig. 1. Comparison of ϕ_V's for the model salts with those for the pure ralts.
Model salt; —●—. Pure salt; --○--. (a) 3:1 model salt and Bu_3PhPCl, (b) 1:1 model salts and Bu_2Ph_2PCl, (c) 1:3 model salt and $BuPh_3PCl$.

to those in the corresponding pure system. Since the actual species in the mixed systems are quite different from those in the pure systems, we should obtain B_V values for the mixed systems different from those for the pure systems, if the B_V's determined from experimental data reflect significantly the effects from short-range interactions among more than two ions, and if the states of cosphere water around a group, say, butyl (or phenyl) group on the cations with n from 1 to 3 differ considerably from those around the butyl(or phenyl) groups on the Bu_4P^+(or Ph_4P^+) ion. Thus we may conclude that the present B_V's reflect mainly pairwise interactions between ions: ++, +−, and −−, and that the cosphere around a group on the cations(n=1—3) is affected weakly by the unlike groups, as concluded in previous papers.[1,18]

There are indications that the cation-cation interactions are the dominant contribution to the excess volumes of some salts containing large-sized organic cations. As may be seen from Table 2, the concentration dependence of ϕ_V of Bu_4PCl at all temperatures examined is very similar to that of Bu_4PBr; the differences between their B_V's are only around 10% and the higher coefficients, C_V and D_V, are in agreement within the experimental uncertainties. If the cation-anion interactions contribute largely to the excess volume, different results would have been obtained because the two anions are known to affect the water structures differently. The situation is similar for the cations containing phenyl groups: the B_V values at 25 °C of Bu_3PhPCl and Bu_3PhPBr are −10.5(±.28) and −11(±.4), and those of Bu_2Ph_2PCl and Bu_2Ph_2PBr, −7.87(±.26) and −7(±.5) cm^3 mol^{-2} dm^3, respectively.[1,3] Volume behavior peculiar to the hydrophobic salts such as n-Bu_4NX[5,6] and (n-Bu)$_3$N(CH$_2$)$_8$N(n-Bu)$_3$Br$_2$[16] in aqueous solutions has been interpreted in terms of the clathrate-like model

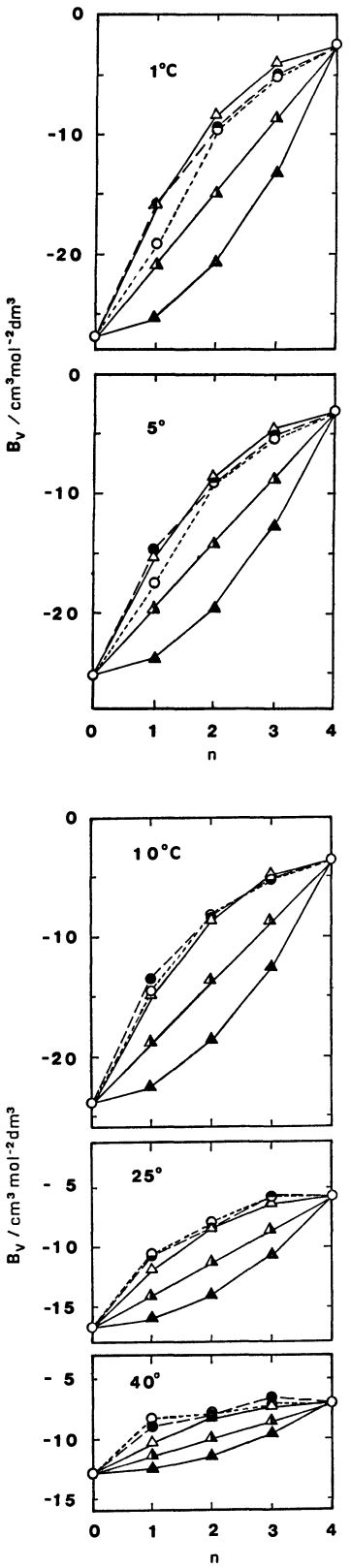

Fig. 2. Comparison of the B_V-coefficients.
Observed B_V; model salt: — —●— —, pure salt: --○--. Calculated B_V; Case 1; —▲—, Case 2; —△—, Case 3; —▲—.

of hydration, in which the cation-cation pairing through water sheath were assumed to be the dominant effect in determining their volume behavior. The results of a model calculation for tetraalkylammonium halides (R_4NX) by Streng and Wen[9,10] shows that, of the three excess volume parameters, V_{++}, V_{+-}, and V_{--}, V_{++} is negative and several times larger in magnitude than V_{+-} for higher three cations(from R=ethyl to *n*-butyl) but is comparable with tetramethylammonium halides, in the calculation V_{--} was assumed to be zero and the anions were the Cl^- and Br^- ions. One reason for these observations is suggested by the cosphere overlap model: the contribution to the excess volume from cosphere overlapping depends on the volume(V_{mu}) of the cosphere-overlap region, from which the cosphere material(water) relaxes to the bulk water. This process results in volume changes of the system caused by the change of the state of water, both in the cosphere region shared by the two ions and in the relaxing part. The V_{mu} is reasonably expected to become increasingly larger as the size of the participant ions increases.

From the above, we assume that the B_V obtained here reflect all the effects resulting from the pairwise interactions between cations. This is of course an oversimplified interpretation for B_V, but is a first step in approaching the volumetric properties of the salts which contain large-sized ions. For a nonelectrolyte solute, the B_V coefficient may have a more distinct meaning,[2] that is, it may be correlated with the pressure derivative of the pair interaction coefficient in the virial-type expression for the chemical potential of the solute.

Based on this assumption, a further analysis for B_V is possible. In a given mixed system, there happen three types of cation-cation interactions: Bu_4P^+–Bu_4P^+, Ph_4P^+–Ph_4P^+, and Bu_4P^+–Ph_4P^+. Since the present cations have nearly the same molar volume and are roughly spherical in shape, we assume approximately that a given cation i would encounter another cation j at a short distance, where the cosphere overlap takes place(cation pairing), with a relative probability proportional only to the number density of species j.[17] Thus, for the mixed system containing Bu_4PCl and Ph_4PCl with the mole ratio, $(4-n):n$, we can express a conditional probability $P_{ij}(n)$, with which we find the cations i and j in a cation pair, by the equation:

$$P_{BB}(n) = \left(\frac{4-n}{4}\right)^2, \quad P_{PP}(n) = \left(\frac{n}{4}\right)^2,$$

$$P_{BP}(n) = 2\left(\frac{4-n}{4}\right)\left(\frac{n}{4}\right), \qquad (3)$$

where the subscripts B and P stand for the cations Bu_4P^+ and Ph_4P^+, respectively. The $B_V(n)$, the B_V coefficient expected for the mixed system, therefore, can be given by

$$B_V(n) = B_V(0)P_{BB}(n) + B_V(4)P_{PP}(n) + bP_{BP}(n), \qquad (4)$$

where $B_V(0)$ and $B_V(4)$ are the observed B_V's for Bu_4PCl and Ph_4PCl in each pure solution, respectively. Here, b is the volume contribution from pairwise interactions between the unlike cations. The b value is unknown and three limiting cases are examined.

1) $b=[B_V(0)+B_V(4)]/2$, 2) $b=B_V(4)$, and 3) $b=B_V(0)$. In Fig. 2, the limiting cases are compared together with the observed B_V's.[14] Clearly, case 2 is most suitable throughout these n values and temperatures. In terms of the cosphere overlap model, case 2 means that when unlike two cations interact at a short distance, a part of the cosphere water around a phenyl group relaxes to the bulk water in a way similar to the case of the Ph_4P^+–Ph_4P^+ interaction, while the butyl cosphere is maintained.

Equation 4 is quite the same as that for the pure systems, if we read the subscripts B and P as the butyl and phenyl group and $P_{ij}(n)$ as the conditional probability with which we find group i and j in a cation pair(two like cations containing n phenyl groups). This is the reason for examining the present systems as the model systems for the aqueous solutions of the $Bu_{4-n}Ph_nPCl$ salts.

In essence, Eq. 4 is derived by neglecting the effects arising from the coulombic interactions, except for the limiting long-range coulombic interaction, which is partially taken into account through the second term in Eq. 2. It is expected, therefore, that the present approach would be more reasonable for nonelectrolyte solutes. Wood and coworkers[11,12] have developed a method to assign pairwise group-group interaction parameters for enthalpies and chemical potentials of nonelectrolytes in aqueous solutions. The basic assumptions in our previous work[1] (the assumptions b and c in this introduction) are essentially the same as theirs. Whether or not the approach presented here is reasonable would depend on the relative magnitudes of two contributions: from short-range pairwise interactions and from the coulombic interactions. It seems that the short-range interactions become relatively more important as ion size increases. In this respect, the result obtained by Visser *et al.*[13] should be noted; they applied Savage and Wood's concept to several tetraalkylammonium bromides in aqueous solutions and found that values of the functional group interaction parameters(enthalpy) for both nonelectrolytes and electrolytes are in reasonable agreement.

We believe that the present results support the simple assumptions made in the previous work for interpreting the B_V coefficients found experimentally for the phosphonium halides in aqueous solutions, and that the present approach can be an empirical way to test the validity of the simple additivity rule assumed for splitting the pairwise interaction parameters for enthalpy and free energy as well as volume into contributions from group-group interactions.

References

1) T. Wakabayashi and K. Takaizumi, *J. Solution Chem.*, **11**, 565 (1982).

2) H. L. Friedman and C. V. Krishnan, "Thermodynamics of Ion Hydration," in "Water: A Comprehensive Treatise," ed by F. Franks, Plenum Press, New York (1973), Vol. 3, Chap. 1, pp. 1—118.

3) K. Takaizumi and T. Wakabayashi, *J. Solution Chem.*, **9**, 809 (1980).

4) O. Redlich and D. M. Meyer, *Chem. Rev.*, **64**, 221 (1964).

5) W. Y. Wen and S. Saito, *J. Phys. Chem.*, **68**, 2639 (1964); **69**, 3569 (1965).

6) W. Y. Wen and K. Nara, *J. Phys. Chem.*, **71**, 3907 (1967).

7) H. L. Friedman and P. S. Ramanathan, *J. Phys. Chem.*, **74**, 3756 (1970); P. S. Ramanathan and H. L. Friedman, *J. Chem. Phys.*, **54**, 1086 (1971).

8) P. S. Ramanathan, C. V. Krishnan, and H. L. Friedman, *J. Solution Chem.*, **1**, 237 (1972).

9) W. Y. Wen, *J. Solution Chem.*, **2**, 253 (1973).

10) W. H. Streng and W. Y. Wen, *J. Solution Chem.*, **3**, 865 (1974).

11) J. J. Savage and R. H. Wood, *J. Solution Chem.*, **5**, 733 (1976).

12) T. R. Tasker and R. H. Wood, *J. Phys. Chem.*, **86**, 4040 (1982); and references cited therein.

13) C. de Visser, W. J. Heuvelsland, and G. Somsen, *J. Solution Chem.*, **7**, 193 (1978).

14) The B_V values for Ph_4PCl were taken from Ref. 1: −2.48, −3.05, −3.54, −5.77, and −6.98 $cm^3\ mol^{-2}\ dm^3$ at 1, 5, 10, 25, and 40 °C, respectively.

15) The partial molar volume of 1:1 salt can be expressed as

$$\overline{V}_2 = \phi_V^\circ + \frac{3}{2}A_V c^{1/2} + B_{2V}c + B_{3V}c^2 + B_{4V}c^3 + \cdots. \quad (A)$$

Converting the ϕ_V to $\overline{V}_2$ by the usual way, we can determine the coefficients B_{2V}, B_{3V}, *etc.* For all the present salts, the B_{2V} values agreed well with the B_V values times 2 within about 0.3%. The agreement is what is expected. Using the coefficients for ϕ_V (Eq. 2), we obtain the expression for $\overline{V}_2$ as a polynomial in $c^{1/2}$:

$$\overline{V}_2 = \phi_V^\circ + \frac{3}{2}A_V c^{1/2} + 2B_V c + [-A_V\phi_V^\circ/2000]c^{3/2} + [\ \ ]c^2 + \cdots.$$

The $c^{3/2}$ term is negligible, *i.e.*, *ca.* 0.3 $cm^3\ mol^{-1}$ even at 1 mol dm^{-3}. Hence B_{2V} in Eq. A is very close to $2B_V$.

16) T. L. Broadwater and D. F. Evans, *J. Phys. Chem.*, **73**, 164 (1969).

17) The pair correlation function g_{ij} is determined by the free energy of pairwise interaction between i and j. The Gurney potential for, say, butyl-butyl overlapping may differ considerably from those for other overlappings, and hence the relative probability to find a cation pair is not proportional to the concentration product(c_ic_j) only, even if other potentials are assumed to be the same. However, the same assumption as used in this work has usually been made in empirical approaches,[11-13] and may be a permissible one in view of the present stage of theory.

18) T. Wakabayashi and K. Takaizumi, *Bull. Chem. Soc. Jpn.*, **56**, 1749 (1983).

Magnetic Susceptibility and ESR Studies of Highly Conductive $CuL(TCNQ)_2$ Incorporating 2,2′-Bipyridine or Ethylenediamine as Ligand

Tomoyoshi SETO,† Motomichi INOUE,*,†† Michiko B. INOUE,†† and Daiyu NAKAMURA†

†*Department of Chemistry, Faculty of Science, Nagoya University, Chikusa-ku, Nagoya 464*

††*Escuela de Ingeniería, CIPM, Universidad de Sonora, Hermosillo, Sonora, Mexico*

(Received October 9, 1982)

Electron spin resonance spectra were recorded on highly conducting $CuL(TCNQ)_2$ (L: 2,2′-bipyridine or ethylenediamine) at different temperatures. The observed g values increased with decreasing temperature. On the basis of the g shift and the static susceptibility observed, a local magnetic susceptibility contributed from Cu and that from TCNQ were evaluated individually. The local Cu susceptibility is of the Curie type. The Curie constant indicates that each Cu atom carries 0.05 umpaired electron on the average in $Cu(bpy)(TCNQ)_2$ and 0.07 in $Cu(en)(TCNQ)_2$: the average oxidation number of copper is equal to 1.05 in the former and 1.07 in the latter. The local susceptibility of TCNQ can be interpreted by a narrow band model in which the susceptibility is given by the sum of the Curie term and a temperature-independent paramagnetic term. This suggests that the TCNQ arrays have inherently metallic nature.

High electrical conductivity has been observed for a series of $CuL(TCNQ)_2$ (L:ethylenediamine, 2,2′-bipyridine, 1,10-phenanthroline, or their derivatives; TCNQ: 7,7,8,8-tetracyanoquinodimethan).[1,2] The powder conductivity amounts to 0.004—1.9 Ω^{-1} cm^{-1} at 300 K depending on the coordinating ligand.[1-3] These values are comparable to the powder conductivities observed for quinolinium$(TCNQ)_2$ and I_2-doped Ni-phthalocyanine whose single crystals exhibit metallic properties.[4-6] The presence of unpaired electrons has been pointed out to be required for the so-called synthetic metals.[7] Therefore, the magnetic study of conducting materials is essential to clarify the mechanism of the electrical conduction. Recently, we have briefly reported the magnetic susceptibilities of some typical $CuL(TCNQ)_2$ complexes.[2] The results suggested that the copper atoms have an intermediate oxidation state due to the so-called equilibrium in solids:

$$\dot{C}u^{2+}L(TCNQ)_2^{2-} \rightleftarrows \ddot{C}u^{+}L(TCNQ)_2^{-}. \quad (1)$$

The resulting incomplete electron transfer yields conduction electrons in TCNQ arrays. The purpose of the present investigation is to obtain further information about the role of unpaired electrons in the electrical conduction. In this point of view, we have recorded the ESR spectra of the Cu complexes at different temperatures, and analyzed the magnetic susceptibilities in detail by taking the ESR results into account.

Experimental

The materials were prepared by the same method as reported previously.[1,2] The ESR spectra were recorded by means of a JEOL SCXA X-band spectrometer in a temperature range of 90—300 K. The temperature of the samples was controlled within ±1 K by a cold-gas flow method, and it was determined by two copper-constantan thermocouples placed near either side of the specimen along the gas flow. Mn^{2+}/MgO was employed as a marker.

Results and Discussion

ESR Spectra. Figure 1 shows ESR spectra observed for $Cu(en)(TCNQ)_2$ and $Cu(bpy)(TCNQ)_2$ at different temperatures. A sharp signal observed at g=2.00 in each spectrum is attributed to free $TCNQ^-$ ions involved as impurities in the samples. The intrinsic spectrum of each compound consists of a simple derivative curve with a g value intermediate between 2.003 of Li(TCNQ) and 2.1 of normal Cu(II) complexes. This indicates that Cu(II) and $TCNQ^-$ ions interact magnetically with a spin-exchange energy

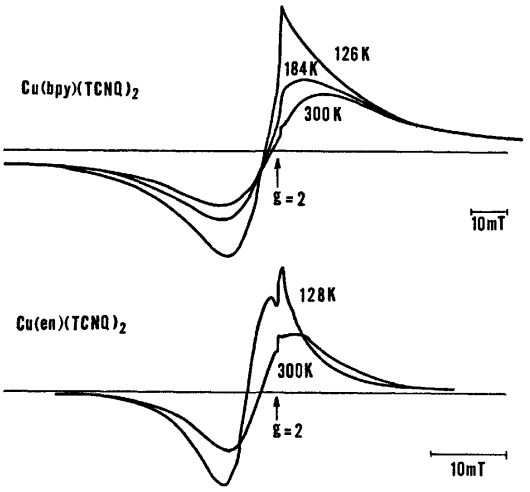

Fig. 1. ESR spectra observed for $Cu(bpy)(TCNQ)_2$ and $Cu(en)(TCNQ)_2$ at different temperatures. They were recorded in the same spectrum condition for each compound.

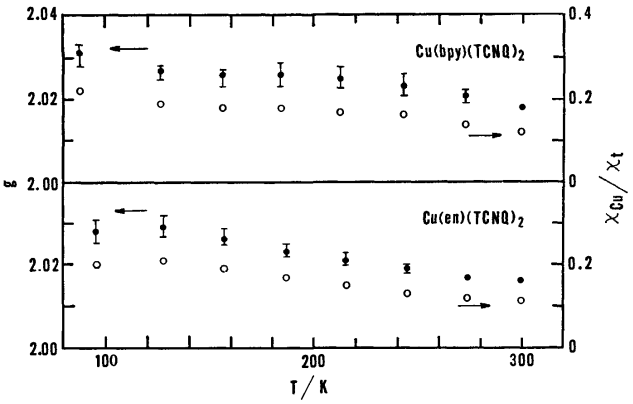

Fig. 2. g factor and the ratio of the local Cu susceptibility to the total susceptibility χ_{Cu}/χ_t.

much larger than that of the g value difference mentioned above. The g value of each compound fluctuated from sample to sample at low temperatures. This is probably due to the fluctuation of the impurity-signal strength. Figure 2, however, shows that the g value obviously increases with decreasing temperature.

Cu(phen)(TCNQ)$_2$ exhibited a spectrum resembling that of Cu(bpy)(TCNQ)$_2$, but an impurity signal at $g=2.00$ was too strong to determine the g value of the intrinsic signal.

Static Magnetic Susceptibility. The magnetic susceptibilities[8] χ of the complexes deviated from the Curie-Weiss law[2] and obeyed the following experimental equation as shown in Figs. 3 and 4:

$$\chi = \gamma/T + \alpha. \quad (2)$$

The parameters[8] were evaluated as $\gamma=0.052$ emu K mol^{-1} and $\alpha=4.6\times10^{-4}$ emu mol^{-1} for Cu(bpy)-(TCNQ)$_2$ and $\gamma=0.093$ emu K mol^{-1} and $\alpha=2.2\times10^{-4}$ emu mol^{-1} for Cu(en)(TCNQ)$_2$. These large α values of the temperature-independent paramagnetic term result in the deviation of the susceptibilities from the Curie-Weiss law. The uncertainty of diamagnetic correction may give an error in determining small spin susceptibility. The α values, however, are comparable to the employed diamagnetic corrections:[2] 3.47×10^{-4} emu mol^{-1} for Cu(bpy)(TCNQ)$_2$ and 2.88×10^{-4} emu mol^{-1} for Cu(en)(TCNQ)$_2$. These values of the corrections were based on diamagnetic susceptibilities observed for the constituent molecules,[9,10] and the uncertainty is estimated to be equal to at most 10%. Therefore, the large α values are not caused by the uncertainty of the diamagnetic corrections, but are ascribed to the intrinsic nature of the complexes. The following ESR results show that the γ/T term also is intrinsic to the complexes. 1) In each spectrum, the integrated intensity of the impurity signal due to isolated TCNQ$^-$ ions was very small compared with that of the intrinsic signal. 2) Every spectrum showed no appreciable impurity signal assignable to isolated Cu(II) ions. 3) The intrinsic signal became strong with decreasing temperature similarly to the temperature dependence of the static susceptibility, although its integrated intensity was difficult to evaluate accurately owing to the impurity signal at $g=2.00$.

g Value and Local Susceptibility. The g value of a spin system in which Cu(II) ions interact with TCNQ$^-$ radical ions is given by an average of the individual g values, g_{Cu} and g_{TQ} (TQ stands for TCNQ), in a strong coupling approximation:[11]

$$g = (\chi_{Cu}g_{Cu}+2\chi_{TQ}g_{TQ})/\chi_t, \quad (3)$$

where χ_{Cu} and χ_{TQ} are local magnetic susceptibilities contributed from Cu and TCNQ, respectively. The total susceptibility χ_t given by

$$\chi_t = \chi_{Cu} + 2\chi_{TQ} \quad (4)$$

can be equated with the observed static susceptibility. The factor 2 comes from the number of TCNQ radicals involved in the chemical unit. If g_{Cu} and g_{TQ} are reasonably assumed, χ_{Cu} and χ_{TQ} can be determined individually from the g factor and the static susceptibility. g_{TQ} can be assumed to be equal to the g value 2.003 of Li(TCNQ). Cu(bpy)$(NO_3)_2\cdot3H_2O$ exhibited an ESR spectrum characteristic of Cu(II) complexes having an axial symmetry: $g_\parallel=2.260$ and $g_\perp=2.067$. The averaged g factor $g_{av}=[(g_\parallel{}^2+2g_\perp{}^2)/3]^{1/2}=2.133$ can be employed as g_{Cu}. Thus, χ_{Cu} and χ_{TQ} of Cu(bpy)(TCNQ)$_2$ were determined as plotted against $1/T$ in Fig. 3. In the same procedure, χ_{Cu} and χ_{TQ} were determined for Cu(en)(TCNQ)$_2$ by use of $g_{av}=2.125$ (calculated with $g_\parallel=2.257$ and $g_\perp=2.056$ observed for Cu(en)$SO_4\cdot3H_2O$) as g_{Cu}. Figure 4 shows the resulting χ_{Cu} and χ_{TQ} as functions of $1/T$.

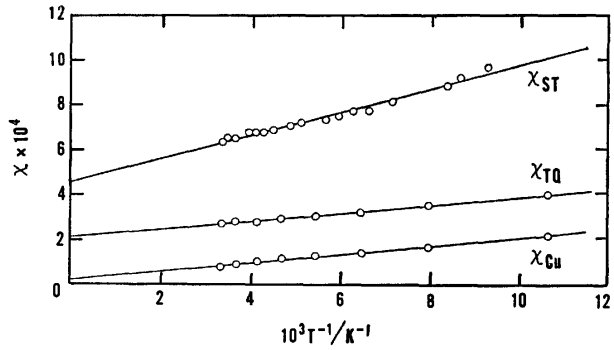

Fig. 3. Static magnetic susceptibility χ_{st}, the local Cu susceptibility χ_{Cu}, and the local TCNQ susceptibility χ_{TQ} (in emu) of Cu(bpy)(TCNQ)$_2$.

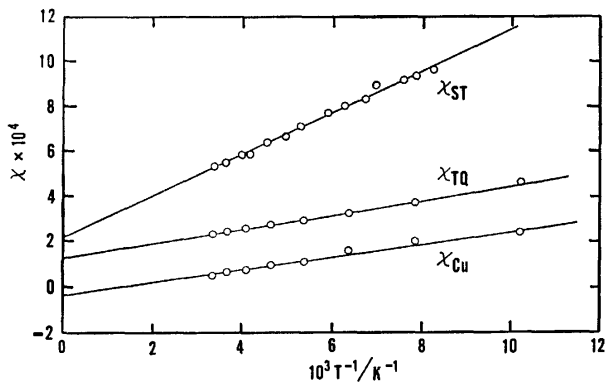

Fig. 4. Static magnetic susceptibility χ_{st}, the local Cu susceptibility χ_{Cu}, and the local TCNQ susceptibility χ_{TQ} (in emu) of Cu(en)(TCNQ)$_2$.

Figure 2 shows that the ratio χ_{Cu}/χ_t signifying the Cu(II) spin contribution to the ESR signal increases with decreasing temperature. If the ratio is temperature independent, it gives the unpaired electron density of Cu atoms.[3] On the contrary, the observed temperature-dependent ratio suggests that more detailed interpretation is required for the local susceptibility.

Local Cu Susceptibility. Figures 3 and 4 show that the local Cu susceptibility changes linearly to $1/T$. The temperature dependence of χ_{Cu} is reproduced by Eq. 2 employed for the interpretation of the static susceptibility. The parameters of Eq. 2 related to χ_{Cu} were determined as $\gamma_{Cu}=0.018$ emu K mol^{-1} and $\alpha_{Cu}=0.3\times10^{-4}$ emu mol^{-1} for Cu(bpy)-(TCNQ)$_2$ and $\gamma_{Cu}=0.028$ emu K mol^{-1} and $\alpha_{Cu}=-0.3\times10^{-4}$ emu mol^{-1} for Cu(en)(TCNQ)$_2$. The Cu(II) contribution to the ESR spectrum increases

with decreasing temperature as mentioned above. This shows that the paramagnetism expressed by γ_{Cu}/T is inherent to the complexes, although the γ_{Cu} values are very small. The absolute values of α_{Cu} fall in the range of the uncertainty (*ca.* 10%) of the diamagnetic corrections made for the static susceptibilities: the α_{Cu} negative in sign may be caused by an underestimation of the correction and the positive α_{Cu} by an overestimation. The α_{Cu} term probably arises from the uncertainty of the corrections and/or the experimental errors. Therefore, the local Cu susceptibilities of the complexes are thought to be of the Curie type intrinsically. Magnetic interaction between a copper atom and its neighboring paramagnetic ions is very weak as compared with the thermal energy in the temperature range investigated.

Local TCNQ Susceptibility. Figures 3 and 4 show that χ_{TQ} can be reproduced with an equation having the same functional form as Eq. 2. The parameters corresponding to χ_{TQ} were evaluated as $\gamma_{TQ}=0.017$ emu K mol^{-1} and $\alpha_{TQ}=2.2\times10^{-4}$ emu mol^{-1} for $Cu(bpy)(TCNQ)_2$, and $\gamma_{TQ}=0.032$ emu K mol^{-1} and $\alpha_{TQ}=1.2\times10^{-4}$ emu mol^{-1} for $Cu(en)(TCNQ)_2$. The α values of the static susceptibilities observed for the complexes agree very well with the respective $2\alpha_{TQ}$ values. Accordingly, the large temperature-independent paramagnetism is ascribed to electrons delocalized extensively in the TCNQ arrays. This supports the previous presumption that TCNQ carries conduction electrons.[2]

The γ_{TQ}/T term shows that the local susceptibility of TCNQ conduction electrons cannot be interpreted simply in terms of the Pauli paramagnetism. As has been pointed out,[7] TCNQ columns hardly form a wide conduction band having a large Fermi energy E_F. If the band has so narrow width that $E_F \gg kT$ does not hold, the paramagnetic susceptibility is temperature-dependent with an effective magnetic moment smaller than that predicted for localized electrons.[12] At high temperatures, χT approaches asymptotically a constant predicted for localized electrons with increasing temperature.[13] No exact expression has been given for the susceptibility. However, a qualitative plot of χT against T suggests that the temperature dependence can be approximated with the following equation in a given narrow temperature range:[13]

$$\chi T = A(T+B). \tag{5}$$

In the expression, the parameters A and B should be temperature-dependent, but they can be presumed to be practically temperature-independent in a very narrow temperature range. The equation is rewritten by the same functional form as Eq. 2 reproducing χ_{TQ}:

$$\chi = AB/T + A. \tag{6}$$

The AB value is equated with γ_{TQ}, which is smaller than the Curie constant of a localized electron system. This shows that Eq. 6 holds for χ_{TQ}, and hence that the narrow band model explains χ_{TQ} satisfactorily.

Other possible explanation may be suggested for the γ_{TQ}/T term: for example, 1) a chain-end effect arising from crystal imperfections, and 2) a thermally activated electron transfer between Cu and TCNQ. If the end effect dominates the paramagnetic increase, the ratio of γ_{TQ} to the Curie constant 0.375 emu K mol^{-1} of a free electron system gives approximately the concentration of the crystal imperfection. It yields an improbable concentration equal to 5% for $Cu(bpy)(TCNQ)_2$ and 9% for $Cu(en)(TCNQ)_2$. If the electron transfer accompanying the equilibrium Eq. 1 is thermally activated, χ_{TQ} exhibits a temperature dependence of thermal activation. The semilogarithmic plot of χ_{TQ} T against $1/T$ (the simplest model of thermal activation) did not yield any straight line. We attempted computer analysis about the observed g shift assuming various models of thermal activation. However, we have obtained no satisfactory result. No conclusive evidence has been obtained for thermally activated electron transfer between Cu and TCNQ.

Electrical Conduction. In $CuL(TCNQ)_2$, two nitrogen atoms from an ethylenediamine or 2,2′-bipyridine molecule are thought to coordinate on a copper atom occupying *cis* positions around the copper atom. Probably, $TCNQ^-$ ions also coordinate to a copper atom to occupy the otherwise vacant positions around the central metal, because the first coordination sphere of copper scarecely has vacant *cis* positions. In spite of the plausible Cu–TCNQ bonding, the magnetic interaction between Cu and TCNQ is very weak. The ratio $\gamma_{Cu}/0.375$ gives an unpaired electron density ρ_{Cu} carried by each copper atom on the average: $\rho_{Cu}=0.05$ for $Cu(bpy)(TCNQ)_2$ and $\rho_{Cu}=0.07$ for $Cu(en)(TCNQ)_2$. The small ρ_{Cu} values are obviously caused by an incomplete electron transfer between Cu and TCNQ accompanying the equilibrium in solids (Eq. 1), in which Cu(II) ions act as electron acceptors against $TCNQ^-$ (on the contrary, Cu(I) ions do as electron donors against $TCNQ^0$). The average oxidation number of copper is equated with $1+\rho_{Cu}$: 1.05 in $Cu(bpy)(TCNQ)_2$ and 1.07 in $Cu(en)(TCNQ)_2$. In our previous paper,[2] the unpaired electron densities were evaluated on the assumption that the paramagnetic term γ/T of the static susceptibility arises only from the copper atoms. The densities reported previously were overestimated. However, the present investigation supports the preceding conclusion that the equilibrium given by Eq. 1 lies so far to the right.[2,3]

The electrical conductivities σ observed for the compressed pellets of the complexes obey

$$\sigma = \sigma_\infty \exp(-E/kT). \tag{7}$$

The activation energy E was determined as 0.036 eV for the bpy complex and 0.12 eV for the en complex.[1] The energy of the former complex is of the order of an energy barrier predicted for contact resistance between powder particles. Possibly, the electrical conduction within the particles is inherently metallic. This is supported by the present magnetic study showing that the local TCNQ susceptibility involving the large temperature-independent paramagnetic term can be interpreted in terms of the narrow band model.

In conclusion, electric current in the $CuL(TCNQ)_2$ complexes flows through a narrow band formed by the TCNQ arrays, and the Cu(II) ions act as electron acceptors against $TCNQ^-$ ions to yield conduction

electrons in the band.

References

1) M. Inoue and M. B. Inoue, *Inorg. Chim. Acta*, **45**, L129 (1980).
2) M. B. Inoue and M. Inoue, *Chem. Phys. Lett.*, **80**, 585 (1981).
3) M. Inoue, M. B. Inoue, T. Seto, and D. Nakamura, *Mol. Cryst. Liq. Cryst.*, **86**, 139 (1982).
4) V. Walatka, Jr., and J. H. Perlstein, *Mol. Cryst. Liq. Cryst.*, **15**, 269 (1971).
5) J. L. Petersen, C. S. Schramm, D. R. Stojakovic, B. M. Hoffman, and T. J. Marks, *J. Am. Chem. Soc.*, **99**, 286 (1977).
6) C. J. Schramm, R. P. Scaringe, D. R. Stojakovic, B. M. Hoffman, J. A. Ibers, and T. J. Marks, *J. Am. Chem. Soc.*, **102**, 6702 (1980).
7) "Low-Dimensional Cooperative Phenomena," ed by H. J. Keller, Prenum Press, New York (1975).
8) χ, γ, and α are given by emu in this paper. Multiplying it by $4\pi \times 10^{-6}$ gives the corresponding value in SI unit.
9) J. C. Scott, A. F. Garito, and A. J. Heeger, *Phys. Rev. B*, **10**, 3131 (1974).
10) "Theory and Applications of Molecular Paramagnetism," ed by E. A. Boudreaux and L. N. Mulay, John-Wiley & Sons, New York (1976).
11) Y. Tomkiewicz, A. R. Taranko, and J. B. Torrance, *Phys. Rev. B*, **15**, 1017 (1977).
12) J. B. Goodenough, "Magnetism and the Chemical Bond," Interscience, New York and London (1963), p. 253.
13) K. Huang, "Statistical Mechanics," John-Wiley & Sons, New York and London (1963), p. 246.

Charge-transfer Interaction of a Series of Trifluoromethylated Benzenes in the Ground and Excited States

Yuji YAMAGUCHI, Takashi NOGAMI,* Hiroshi MIKAWA, Itsumaro KUMADAKI,† and Yoshiro KOBAYASHI†

Department of Applied Chemistry, Faculty of Engineering, Osaka University, Yamada-oka, Suita, Osaka 565
†*Tokyo College of Pharmacy, 1432-1 Horinouchi, Hachioji, Tokyo 192-03*

(Received October 19, 1982)

Charge-transfer interaction of a series of trifluoromethylated benzenes with several donor molecules was investigated by measuring electronic absorption and fluorescence spectra. Half-wave reduction potentials of acceptors were determined by cyclic voltammetry. Charge-transfer absorption bands were observed for several systems. Thermal one-electron transfer reactions were observed for solutions of hexakis(trifluoromethyl)benzene and several aromatic amines even in nonpolar solvents. Charge-transfer fluorescence was observed for solutions of hexakis(trifluoromethyl)benzene or tetrakis(trifluoromethyl)benzene and weak donor molecules such as benzene, toluene, or *p*-xylene.

Spectroscopic studies on the charge-transfer (CT) interaction between donor and acceptor molecules have extensively been made both in the ground and excited states.[1] Acceptors in those studies were mainly aromatic molecules possessing electron withdrawing groups such as halogeno, cyano, nitro, and carbonyl groups. Trifluoromethyl group is known to have a strong electron withdrawing property.[2] However, no study has been made with aromatic acceptor molecule possessing trifluoromethyl group from the viewpoint of CT-interaction. We have measured electronic absorption and fluorescence spectra of the following acceptor molecules (A_2—A_6) with various donor molecules. We have also measured half-wave reduction potentials of these acceptors by cyclic voltammetry.

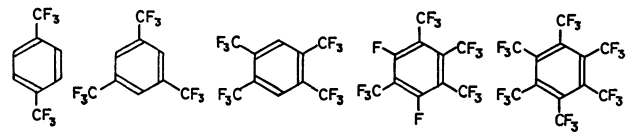

A_2 A_3 A_4 A_{4F} A_6

The names of the acceptor molecules are abbreviated to A_2, A_3, A_4, A_{4F}, and A_6 as specified above. We have found that the above molecules behave as a new family of acceptors both in the ground and excited states.

Experimental

Materials. Hexakis(trifluoromethyl)benzene (A_6) was synthesized *via* a trimerization reaction of bis(trifluoromethyl)acetylene.[3] 1,3-Difluoro-2,4,5,6-tetrakis(trifluoromethyl)-benzene (A_{4F}) was obtained by a pyrolysis of A_6.[4] 1,2,4,5-Tetrakis(trifluoromethyl)benzene (A_4), 1,3,5-tris(trifluoromethyl)benzene (A_3), and 1,4-bis(trifluoromethyl)benzene (A_2) were synthesized *via* reactions of the corresponding carboxylic acids with sulfur tetrafluoride.[5] All of them were purified by vacuum distillation. Aniline, *N,N*-dimethylaniline, *N,N*-diethylaniline, and *N,N*-dibutylaniline were purified by vacuum distillation. *N,N,N′,N′*-Tetramethyl-*p*-phenylenediamine and *N,N*-dimethyl-*p*-phenylenediamine were obtained by neutralizing their dihydrochlorides with aqueous ammonia, followed by extracting them with diethyl ether. The crude materials obtained after evaporating diethyl ether were finally purified by vacuum sublimation. Benzene, toluene, and *p*-xylene were purified by treating them with sulfuric acid, dried over calcium chloride, refluxed over sodium for at least 8 h, and distilled twice. Hexane was purified by treating it with sulfuric acid, and dried over calcium chloride. It was then passed through a column composed successively of acidic, neutral, and basic aluminas, refluxed over sodium for more than 8 h, and finally distilled. Acetonitrile was purified by passing it through a column composed successively of acidic, neutral, and basic aluminas, refluxed over calcium hydride for more than 8 h, and finally distilled.

Cyclic Voltammetry. Cyclic voltammetry was run on an apparatus made by us. Acetonitrile was used as a solvent. Tetrabutylammonium perchlorate (0.1 mol dm^{-3}) was used as the supporting electrolyte; the concentration of the acceptor molecule was 1.0×10^{-3} mol dm^{-3}. An Ag/Ag^+ electrode, comprising an acetonitrile solution of silver nitrate (0.1 mol dm^{-3}) was used as a reference electrode.

Electronic Absorption and Fluorescence Spectra. Electronic absorption spectra were measured on a Shimadzu UV-200 double beam spectrophotometer. Fluorescence spectra were measured on a Hitachi MPF-3 fluorescence spectrometer.

Results and Discussion

Cyclic Voltammetry. An cyclic voltammetry on A_4, A_{4F}, and A_6 in acetonitrile solution was conducted to obtain their reduction potentials. The reduction potentials of 1,2,4,5-tetracyanobenzene (TCNB), 1,3,5-tricyanobenzene (TCB), and *p*-dicyanobenzene (DCB) were also measured for comparison. An Ag/Ag^+ electrode was used as a reference electrode. Table 1 summarizes the half-wave reduction potentials of A_6, A_{4F}, A_4, TCNB, TCB, and DCB. This table shows that the absolute reduction potentials decrease in the order DCB>TCB>A_4>A_{4F}>TCNB≈A_6. The absolute reduction potentials increase with decreasing number of substituent CF_3 groups. From a comparison of the absolute reduction potentials of the CF_3-substituted benzenes with those of the corresponding CN-substituted benzenes, it is clear that the cyano group is a stronger electron withdrawing group than the trifluoromethyl group. The reduction potentials of A_3

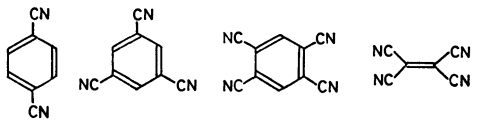

DCB TCB TCNB TCNE

TABLE 1. HALF-WAVE REDUCTION POTENTIALS OF ACCEPTORS

Acceptor	($E_{1/2}$ *vs.* Ag/Ag$^+$)/V
A_6	−1.03
A_{4F}	−1.41
A_4	−1.66
TCNB	−1.06
TCB	−1.32
DCB	−2.00

and A_2 could not be measured due to occurrence of an interference with the cathodic current by the electrolyte.

Charge-transfer Interaction of Trifluoromethylated Benzenes with Weak Aromatic Donor Molecules. CT-interaction of A_4 and A_6 with such a weak aromatic donor molecule as benzene, toluene, or *p*-xylene was investigated by measuring electronic absorption spectra. Figure 1 shows the absorption spectra of cyclohexane solutions of A_6, *p*-xylene, and a mixture of A_6 and *p*-xylene. Subtracting the absorbances of the component molecules from that of the mixture of A_6 and *p*-xylene, a new absorption band shown by the broken lines was obtained as a shoulder. This absorption band is ascribable to a CT-band. CT-absorption bands were also observed as shoulders on the absorption bands of the component molecules in cyclohexane solution for the following systems: A_6–benzene, A_6–toluene, A_4–benzene, A_4–toluene, and A_4–*p*-xylene.

In order to examine the stoichiometry of the CT-complexes in these systems, the absorbance of the CT-band as a function of donor concentration was analysed on the basis of the modified Benesi-Hildebrand equation.[6]

$$\frac{L[A]_0}{I-\varepsilon_A[A]_0L-\varepsilon_D[D]_0L} = \frac{1}{K(\varepsilon_C-\varepsilon_A)}\frac{1}{[D]_0}+\frac{1}{\varepsilon_C-\varepsilon_A}, \quad (1)$$

where, I, ε_D, ε_A, ε_C, $[D]_0$, $[A]_0$, L, and K denote the absorbance, the molar extinction coefficients of the donor, acceptor, and CT-complex, the initial concentrations of the donor and acceptor molecules, the path length, and the equilibrium constant for the CT-complex, respectively. The Benesi-Hildebrand equation[7] could not be used owing to overlap of the absorption band of CT-complex with those of the component molecules. Plots of $L[A]_0/(I-\varepsilon_AL[A]_0-\varepsilon_DL[D]_0)$ against $1/[D]_0$ gave straight lines for all of the above systems. Thus, the compositions of the CT-complexes are one to one in these systems.

Charge-transfer Interaction of A_2, A_3, A_4, and A_6 with Strong Donor Molecules. *N,N,N′,N′*-tetramethyl-*p*-phenylenediamine (TMPD) and *N,N*-dimethyl-*p*-phenylenediamine (DMPD) are known to be strong donor molecules. The CT-interaction of A_2, A_3, A_4, and A_6 with TMPD and DMPD was studied by measuring absorption spectra of mixed solutions of donor and acceptor molecules. In the case of benzene solutions of A_2, A_3, and A_4 with TMPD, new absorptions ascribable to CT-bands were observed as shoulders of the component molecules. The CT-band shifted to the longer wavelength region with increasing electron accepting power of the acceptors. However, when tetrahydrofuran (THF) was used as a solvent, one-electron transfer reaction as well as CT-complex formation was observed in the same donor–acceptor systems. Figure 2 shows the absorption spectra of THF solutions of TMPD mixed with A_2, A_3, or A_4. Besides the CT-absorption bands around at 400—500 nm, characteristic vibrational structures ascribable to the TMPD cation radical (λ_{max}=570, 620 nm)[8] were observed.

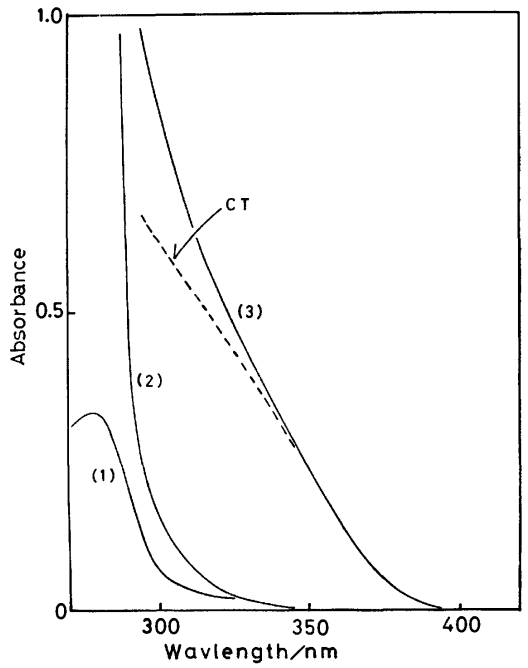

Fig. 1. Electronic absorption spectra of the cyclohexane solutions of (1) A_6, (2) *p*-xylene, and (3) the mixture of *p*-xylene and A_6. The broken line shows the charge-transfer absorption band. $[A_6]=1.23\times10^{-3}$ mol dm^{-3}, [*p*-xylene]=6.53 mol dm^{-3}.

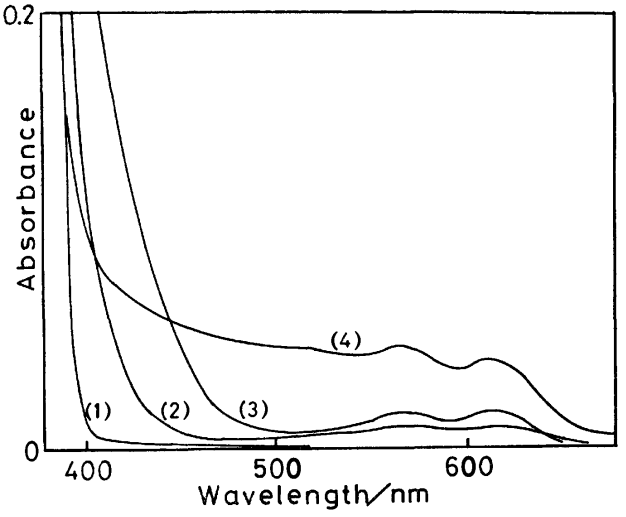

Fig. 2. Electronic absorption spectra of the THF solutions of TMPD and TMPD mixed with acceptors. [TMPD]=0.0743 mol dm^{-3}. (1) TMPD, (2) TMPD–A_2 (0.136 mol dm^{-3}), (3) TMPD–A_3 (0.11 mol dm^{-3}), (4) TMPD–A_4 (0.0139 mol dm^{-3}).

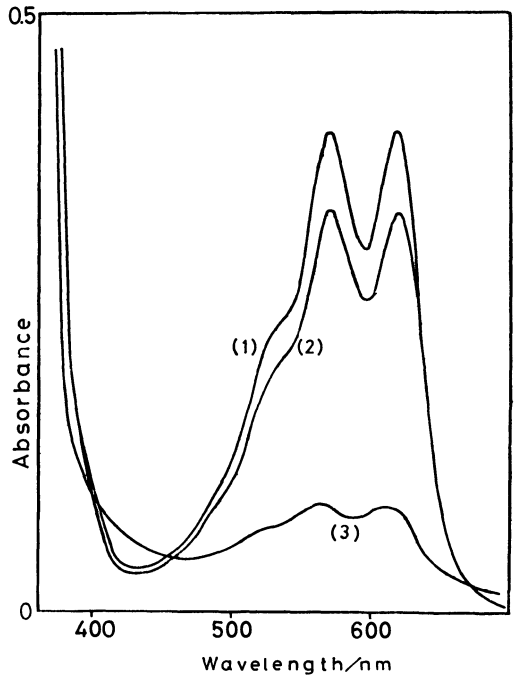

Fig. 3. Electronic absorption spectra of A_6–TMPD system in various solvents. $[A_6]=3.9\times10^{-3}$ mol dm^{-3}, $[TMPD]=3.4\times10^{-3}$ mol dm^{-3}. (1) THF, (2) benzene, (3) cyclohexane.

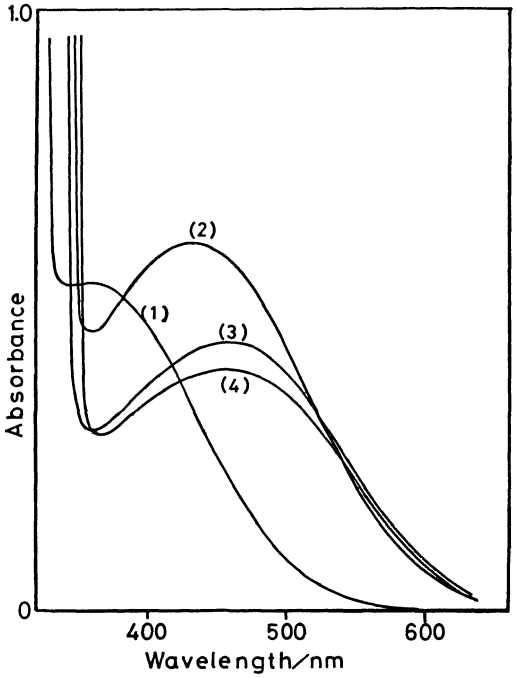

Fig. 4. Charge-transfer absorption spectra of A_6 mixed with liquid donors. $[A_6]=1.8\times10^{-3}$ mol dm^{-3}. (1) A_6–aniline, (2) A_6–*N*,*N*-dimethylaniline, (3) A_6–*N*,*N*-diethylaniline, (4) A_6–*N*,*N*-dibutylaniline.

These findings indicate that A_2, A_3, and A_4 form CT-complexes with strong donors such as TMPD and DMPD in nonpolar solvent. However, in a slightly more polar solvent like THF, these systems allowded not only CT-complex formation but also one-electron transfer from donor to acceptor molecule.

To our surprise, one-electron transfer from TMPD or DMPD to A_6 occurred not only in THF but also in such nonpolar solvents as benzene and cyclohexane. Figure 3 shows the absorption spectra of the TMPD–A_6 system in THF, benzene, or cyclohexane. The absorptions due to the TMPD cation radical were clearly observed in benzene and in cyclohexane. A similar phenomenon was also observed for the DMPD–A_6 system in benzene; the absorption of the DMPD cation radical (λ_{max}=508, 532 nm)[9] as well as that of a dimer cation radical $(CDMPD^+)_2$, (λ_{max}=680 nm)[9] was observed. Tetracyanoethylene (TCNE) is known to be one of the strongest electron acceptor molecules. However, we observed only CT-absorption band even in the TMPD–TCNE system in benzene or cyclohexane. A_6 is, of course, a much weaker electron acceptor than TCNE, judging from its half-wave reduction potential. In spite of this, A_6 behaves as if it were a stronger acceptor than TCNE at least in the nonpolar solvents. We can now give no explanation for these unusual phenomena.

Upon mixing TMPD with A_6, or DMPD with A_6 in such a polar solvent as methanol or acetonitrile, one-electron transfer from donor to acceptor was observed.

Charge-transfer Interaction of A_6 with Aniline and Its Derivatives without Use of Solvents. CT-interaction of liquid donor molecules with A_6 was investigated without use of any solvents. Figure 4 shows the CT-absorption bands observed by mixing A_6 directly with aniline, *N*,*N*-dimethylaniline (DMA), *N*,*N*-diethylaniline (DEA), and *N*,*N*-dibutylaniline (DBA). The absorption bands observed at 380—600 nm are ascribable to CT-bands. The peak positions of the CT-bands shifted to the longer wavelength region with increasing length of alkyl groups attached to the amino-nitrogen: λ_{max}=365 nm (aniline–A_6); λ_{max}=435 nm (DMA–A_6); λ_{max}=465 nm (DEA–A_6); λ_{max}=465 nm (DBA–A_6). These findings can be accounted for in terms of the decrease in the ionization potentials of aniline derivatives due to the hyperconjugation of alkyl groups.

Fluorescence Spectra of Donor–Acceptor Systems. Fluorescence spectra of cyclohexane or hexane solutions of the following systems were measured at room temperature in order to examine the CT-interaction in the excited state: A_4–benzene (in cyclohexane), A_4–toluene (in hexane), A_4–*p*-xylene (in hexane), A_6–benzene (in hexane), A_6–toluene (in hexane), A_6–*p*-xylene (in cyclohexane). Selective excitation of the CT-bands was impossible in these systems except for the A_6–*p*-xylene system due to overlap of the absorption of CT-complex with those of the component molecules. However, the absorbances due to the CT-complexes were much higher than those of the component molecules at the following excitation wavelengths: A_4–benzene, 280 nm; A_4–toluene, 296 nm; A_4–*p*-xylene, 310 nm; A_6–benzene, 325 nm; A_6–toluene, 325 nm; A_6–*p*-xylene, 330 nm. The concentration of the acceptors was kept constant, and that of the donor molecules was varied widely.

Figure 5 shows the fluorescence spectra of the A_4–toluene system as a typical example. The charac-

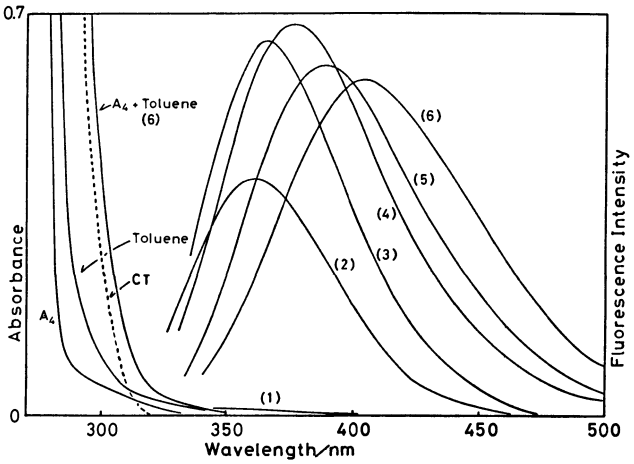

Fig. 5. Absorption and fluorescence spectra of A_4–toluene system in hexane excited at 296 nm. The fluorescence intensities were corrected on the basis of the absorbances at 296 nm. $[A_4]=2.32\times10^{-3}$ mol dm^{-3}. The concentrations of toluene are as follows (mol dm^{-3}); (1) 0, (2) 0.374, (3) 0.751, (4) 1.88, (5) 3.74, (6) 7.51.

teristic points of the system are as follows: (1) new fluorescence bands appeared at the longer wavelength region than the fluorescences of the component molecules; (2) the peak positions of the new fluorescences shifted to the longer wavelength region with increasing donor concentration. These fluorescence bands are ascribed to the CT-fluorescence, since the excitation spectra correspond to the CT-absorption bands. The fluorescence spectra of Fig. 5 were normalized on the basis of the absorbance at the excitation wavelength. The relative intensities of the fluorescences in the A_4–toluene system increased initially and then decreased as the donor concentration increased. The above two characteristic phenomena were also observed in the other systems. However, the dependence of the fluorescence intensity on the donor concentration was somewhat different between the A_4–donor systems and the A_6–donor systems. The fluorescence intensities in the latter systems decreased monotonously with increasing donor concentration.

Discussion on CT-Fluorescence. The fluorescence due to CT-complex was observed in the above systems.[10] It is well known that the Stokes shift of CT-fluorescence is much larger than those of usual organic compounds.[11] The Stokes shifts in the present systems could not be obtained correctly, since the absorption peak positions of the CT-complexes were hidden under the absorptions of the component molecules. However, a rough estimation of Stokes shifts gave values larger than 8×10^3 cm^{-1} in agreement with the above-mentioned tendency.

Let us discuss on the red-shift of the CT-fluorescence with increasing donor concentration. The ground states of the 1:1 CT-complexes are assumed to have mainly no-bond structures, because benzene, toluene, and *p*-xylene are weak donor molecules. The first excited states of the CT-complexes are assumed to have more polar structure than the ground states. The situations of the present systems are quite similar to that of the TCNB–toluene system;[12] the red shift of the CT-fluorescence was also observed as the concentration of toluene increased. Mataga and Murata accounted for the large Stokes shift and red shift of the CT-fluorescence in terms of two factors:[12] (1) the reorientation of the excited CT-complex from the Franck-Condon states to a stabler configuration in the excited CT-states; (2) the reorientation of the Franck-Condon ground states to the stablest configuration of the CT-complex in the ground state.

In the case of the present systems, two possibilities can be considered for the red shift of the CT-fluorescence with increasing donor concentration. One possibility is the same as that mentioned above in connection with the TCNB–toluene system. In this case, as the donor concentration increases, the energy stabilization of CT-complex in the excited states and the energy destabilization in the ground state are induced more and more effectively as a result of the electronic interaction between the CT-complex and donor molecules; this fact accounts for the red shift of CT-fluorescence. The other possibility is that the red shift of CT-fluorescence arises from CT-excited states with different stoichiometries, *e.g.*, different donor to acceptor ratios such as one to one, two to one, three to one,.., *etc.* We cannot conclude which of these two possibilities is applicable to the present systems.

Summary

CT-interaction of a series of trifluoromethylated benzenes with several donor molecules was investigated in the ground and excited states. The trifluoromethylated benzenes acted as electron acceptors to induce CT-complex formation and/or one-electron transfer in the ground state. One-electron transfer reaction was observed for strong donor–A_6 systems even in nonpolar solvents. Fluorescences due to CT-complexes were observed for weak donors–A_4 systems and for weak donor–A_6 systems. The trifluoromethylated benzenes in the present study have been found to be a new family of electron acceptor molecules for study on the electron donor–acceptor interaction.

We are grateful to Dr. Hiroshi Masuhara, Faculty of Engineering Science, Osaka University for his valuable discussion.

References

1) R. S. Mulliken and W. B. Person, "Molecular Complexes," Wiley Interscience, a Division of John Wiley & Sons, New York, London, Sydney, and Toronto (1969).

2) L. M. Stock and M. R. Wasielewski, "Progress in Physical Organic Chemistry," ed by R. W. Taft, Interscience Publication, New York, Chichester, Brisbane, and Toronto (1981), Vol. 13, p. 253.

3) J. H. Harris, R. J. Harder, and G. N. Sansen, *J. Org. Chem.*, **25**, 633 (1960).

4) Y. Kobayashi, I. Kumadaki, and S. Kuboki, *J. Fluorine Chem.*, **19**, 517 (1982).

5) W. R. Hasek, W. C. Smith, and V. A. Engelhaldt, *J. Am. Chem. Soc.*, **82**, 543 (1960).

6) Equation 1 is derived as follows: The following two

relations 1 and 2 are set by definition:

$$I/L = \varepsilon_C[DA] + \varepsilon_D([D]_0-[DA]) + \varepsilon_A([A]_0-[DA]), \quad (1)$$

$$K = [DA]/([D]_0-[DA])([A]_0-[DA]) \quad (2)$$

$$\approx [DA]/[D]_0([A]_0-[DA]), \quad (3)$$

where $[DA]$ denotes the concentration of CT-complex. Since the experiments were performed under the condition $[D]_0 \gg [A]_0$, the equilibrium constant of the CT-complex can be approximated to Relation 3. Cancelation of $[DA]$ from Relations 1 and 3 gives Eq. 1. In the case of $\varepsilon_D=\varepsilon_A=0$, Eq. 1 gives the Benesi-Hildebrand equation.

7) H. A. Benesi and J. H. Hildebrand, *J. Am. Chem. Soc.*, **71**, 2703 (1949).

8) K. Uemura, S. Nakayama, Y. Seo, K. Suzuki, and Y. Ohshika, *Bull. Chem. Soc. Jpn.*, **39**, 1348 (1966).

9) T. Nogami, K. Yoshihara, and S. Nagakura, *Bull. Chem. Soc. Jpn.*, **45**, 122 (1972).

10) We could not measure the life of the CT-fluorescences by use of a nitrogen laser on account of weak absorbances at 337 nm and of low quantum yields of the fluorescences.

11) T. Kobayashi, K. Yoshihara, and S. Nagakura, *Bull. Chem. Soc. Jpn.*, **44**, 2603 (1971).

12) N. Mataga and Y. Murata, *J. Am. Chem. Soc.*, **91**, 3144 (1969).

Direct Measurement of the Interaction Energy between Solids and Gases. IX. Heats of Adsorption of Ammonia and Pyridine on Several Solids at High Temperature

Kazuo Tsutsumi,* Yoshio Mitani,†,†† and Hiroshi Takahashi†

Toyohashi University of Technology, Tempaku-cho, Toyohashi 440

†*Institute of Industrial Science, The University of Tokyo, Roppongi, Minato-ku, Tokyo 106*

(Received October 29, 1982)

Heats of adsorption of ammonia and pyridine on H–Y zeolites and other solids were measured using a microcalorimeter in the temperature range of 313 to 673 K. Infrared spectra of adsorbed ammonia and pyridine were obtained in order to interpret the calorimetric data. There appeared two kinds of the temperature dependence of heats of adsorption. One is that heats of adsorption on H–$Y_{5.0}$ and silica-alumina do change with coverage to a greater extent at high temperature range (above 473 K) than low temperature range. The difference in the shape of the heat curves was found to be attributable to the difference in the selectivity of adsorption at different temperatures, that is, adsorption occurred on stronger acidic sites is preference to weaker or non-acidic sites in the high temperature range, while random adsorption occurred simultaneously on acidic and non-acidic sites in the low temperature range. The other kind of temperature dependence was recognized to appear as a slight decrease in heats of adsorption with a temperature rise, which were observed in cases of ammonia adsorption on H–Y zeolites above 473 K and on Na–Y and silica above 313 K while the shapes of heat curves were similar to one another irrespective of the adsorption temperature. Such decrease may be attributed to the fact that the temperature dependence of the heat of adsorption was thermodynamically defined by the difference in molar heat capacity between adsorbed state and gaseous state.

Heats of adsorption of basic gases on solid acid catalysts have been widely measured using a microcalorimeter near room temperatures in order to estimate their acidic characters.[1–7]

Since solid acid catalysts are generally used for reactions at high temperatures, it will be interesting to measure heats of adsorption at high temperatures. Auroux *et al.*[8] measured heats of adsorption of ammonia at 416 K. However, a temperature dependence of heats of adsorption has not extensively been studied in the range of room temperature to high temperature.

In the present work, heats of adsorption of ammonia and pyridine were respectively measured on H–Y zeolites in the temperature range of 313 to 673 K using a twin-conduction type microcalorimeter. Likewise, heats of adsorption of ammonia on silica-alumina, Na–Y zeolite, and silica were measured.

Experimental

NH_4–Y zeolite was prepared by treating repeatedly Na–Y zeolite, SK-40, with 1 mol dm^{-3} NH_4Cl solution at *ca.* 323 K. The zeolite was then washed with distilled water until no chlorine ion was detected. The chemical composition was $0.72(NH_4)_2O \cdot 0.15Na_2O \cdot Al_2O_3 \cdot 5.0SiO_2$. It was converted to H–$Y_{5.0}$ zeolite by the pretreatment at 673 K before each measurement. Silica-alumina (Al_2O_3 content, 13%) and Aerosil 380 were supplied by Catalysts and Chemicals Ind. Co., Ltd. and Nippon Aerosil Co., Ltd., respectively. All samples were used in granular form of 28—60 mesh.

Ammonia and pyridine were obtained from Matheson Co. and Wako Pure Chemicals Co., respectively. Both were purified by the freeze-thaw method.

Heats of adsorption were measured using a twin-conduction type microcalorimeter. The calorimeter and the procedure of measurements were described in a previous paper.[9] The sample weighing from 0.25 to 1.0 g in the sample cell was outgassed at 673 K under a pressure of 10^{-3} Pa for 5 h and set in the calorimeter. The adsorbed amount was calculated from the pressure change before and after adsorption.

Infrared spectra were obtained by the *in situ* method. The sample was pressed into wafers of thickness of *ca.* 10 mg cm^{-2} under a pressure of 1.6×10^3 kg cm^{-2} and outgassed for 5 h at 673 K before the measurement. The transmission was converted into the absorbance and the spectrum intensity was determined from its band area. The influence of emission was negligible in the temperature range up to 473 K permitting quantitative analysis, but qualitative analysis of the spectra was possible even up to 673 K.

Results and Discussion

Differential Heats of Adsorption of Pyridine and Ammonia on H–$Y_{5.0}$ at 313 and 473 K. Differential heats of adsorption of pyridine on H–$Y_{5.0}$ were measured at 313 and 473 K as shown in Fig. 1. The curve of heats of adsorption obtained at 473 K had a plateau leveling at *ca.* 145 kJ mol^{-1} in the initial stage, thereafter decreasing sharply. On the other hand, the curve obtained at 313 K showed a more monotonic change with coverage, thereafter intersecting the one obtained at 473 K. Differential heats of adsorption of ammonia were measured at 313, 473, 573, and 673 K as shown in Fig. 2. In cases of ammonia adsorption, the difference between heat curves at 313 and 473 K was less explicit than the case of pyridine adsorption. The temperature dependence above 473 K will be discussed later. In case of both adsorbates, measurable pressures of the adsorbate were present even at lower coverage at 473 K or above, while not at 313 K, therefore the equilibrium proved to be obtained in the former system.

The IR measurements were performed to ascertain the temperature dependence of the shape of heat curves. In these experiments, the spectra measured at room temperature were used for contrasting them

†† Present address: Tokuyama Soda Co., Ltd., Mikage-cho, Tokuyama, Yamaguchi 745.

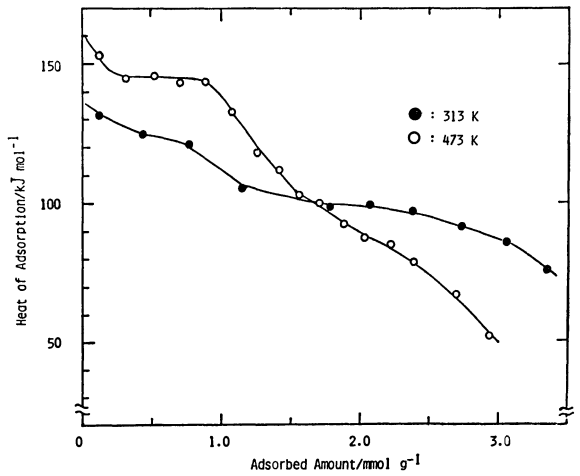

Fig. 1. Differential heats of adsorption of pyridine on H-$Y_{5.0}$. The indicated temperatures represent adsorption temperature.

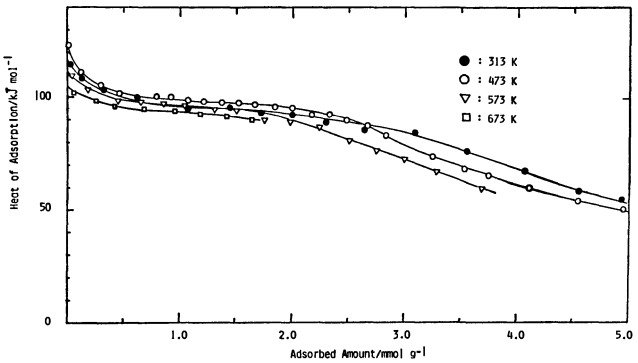

Fig. 2. Differential heats of adsorption of ammonia on H-$Y_{5.0}$.

with the data of heats of adsorption at 313 K because analogous IR data were obtained at these two temperatures. First, the experiment was performed on H-$Y_{5.0}$-pyridine system. Since no Lewis acid site existed judging from the absence of 1450 cm^{-1} band[10] for pyridine, most active sites on H-$Y_{5.0}$ proved to be limited to Brønsted acid sites. Figure 3 shows the spectra of OH bands after pyridine adsorption on H-$Y_{5.0}$ measured at room temperature and 473 K. The spectra measured at 573 and 673 K were analogous to those measured at 473 K. In the temperature range of 473 to 673 K, the 3640 cm^{-1} band was preferentially perturbed, indicating that the selective adsorption occurred on the 3650 cm^{-1}-OH sites in preference to the 3550 cm^{-1}-OH sites. On the other hand, both of the 3640 and 3550 cm^{-1} bands decreased simultaneously in their intensity at room temperature, indicating that random adsorption occurred. The results presented here are in good agreement with the observations of Hughes and White[11] and others[12,13] on the difference in the interaction of two types of hydroxyl groups with pyridine.

In addition to above, temperature dependence of the formation of pyridinium ions was investigated by heating H-$Y_{5.0}$-pyridine system as shown in Table 1. The experimental procedures employed were as follows. After addition of a certain amount of pyridine

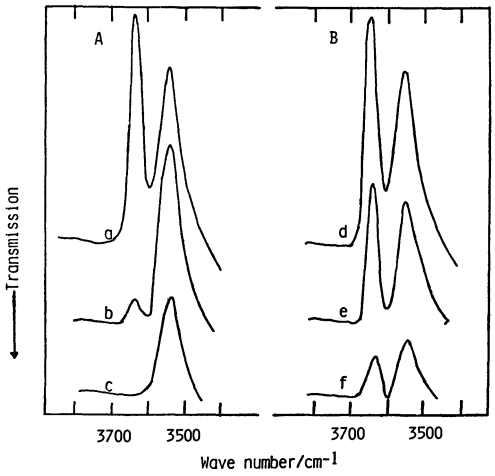

Fig. 3. Changes of bands on H-$Y_{5.0}$ after adsorption of pyridine (A) at 473 K and (B) at room temperature. (a): Evacuated at 673 K then cooled to 473 K; (b): after addition of 1 mmol g^{-1} of pyridine to (a); (c): after addition of 2 mmol g^{-1} of pyridine to (a); (d): evacuated at 673 K then cooled to room temperature; (e): after 1 mmol g^{-1} of pyridine added to (d); (f): after 2 mmol g^{-1} of pyridine added to (d).

Table 1. Enhancement of pyridinium ion formation after heating H-$Y_{5.0}$-pyridine system

	Amount of pyridinium ions/Arb. unit			
	Pyridine adsorbed/mmol g^{-1}			
Temperature/K	0.5	1.0	2.0	3.0
Room temp	0.24	0.47	1.00	1.00
373	—	0.60	—	—
423	—	0.68	—	—
473	0.56	0.85	1.00	1.00
573	—	0.85	—	—
673	—	0.85	—	—

on H-$Y_{5.0}$ at room temperature, the zeolite was heated for 1 h at a desired temperature, then, the relative amount of pyridinium ions formed was determined from the integrated intensities of 1545 cm^{-1} band which is known to be characteristic of pyridinium ions[10] before and after the heat-treatment. The amount at room temperature after pyridine adsorption of 3 mmol g^{-1} was referred to 1.00. At lower coverage, the amount of pyridinium ions increased with a temperature rise below 473 K, then, remained constant up to 673 K. Moreover, spectra in Fig. 4 showed that pyridine molecules adsorbed on the 3550 cm^{-1}-OH sites at room temperature did migrate to the 3640 cm^{-1}-OH sites on heating in agreement with the results in Table 1. It was indicated that the adsorption occurred simultaneously on the 3650 cm^{-1}-OH sites and on other sites at room temperature, but that the adsorbed base on the latter sites migrated to the former sites on heating and was protonated. At higher coverage region, however, the amount remained unchanged on heating, which would tell that the 3650 cm^{-1}-OH sites are wholly saturated at room temperature so that no migration occurred.

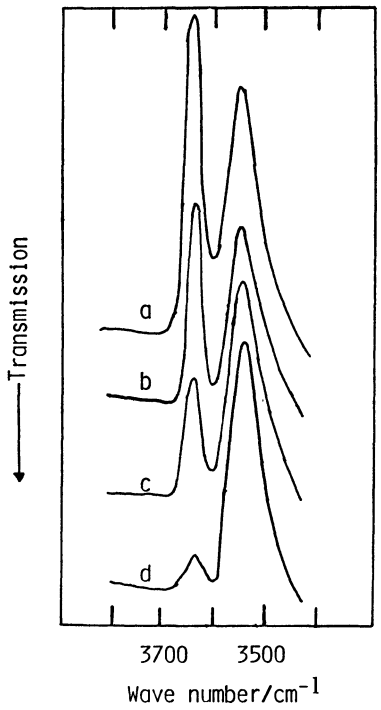

Fig. 4. Redistribution of pyridine on H-$Y_{5.0}$. Spectra were taken at room temperature. (a): Evacuated at 673 K then cooled to room temperature; (b): after adsorption of 1 mmol g^{-1} of pyridine to (a); (c): after heat-treatment of (b) at 423 K for 1 h; (d): after heat-treatment of (c) at 473 K for 1 h.

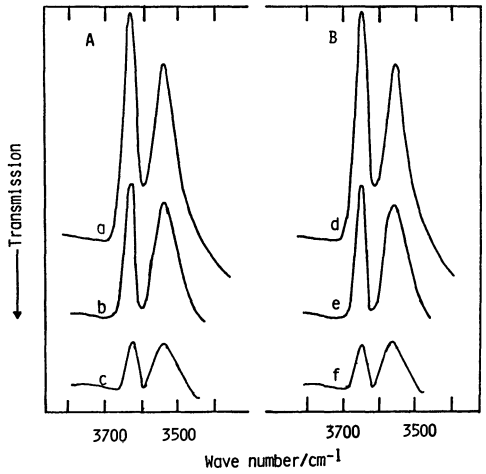

Fig. 5. Changes of bands on H-$Y_{5.0}$ after adsorption of ammonia (A) at 473 K and (B) at room temperature. (a): Evacuated at 673 K then cooled to 473 K; (b): after addition of 1 mmol g^{-1} of ammonia to (a); (c): after addition of 2 mmol g^{-1} of ammonia to (a); (d): evacuated at 673 K then cooled to room temperature; (e): after addition of 1 mmol g^{-1} of ammonia to (d); (f): after addition of 2 mmol g^{-1} of ammonia to (d).

Table 2. Enhancement of ammonium ion formation after heating H-$Y_{5.0}$-ammonia system

	Amount of ammonium ions/Arb. unit				
	Ammonia adsorbed/mmol g^{-1}				
Temperature/K	0.5	1.0	2.0	3.0	4.0
Room temp	0.20	0.38	0.70	0.98	1.00
373	—	0.40	—	—	—
423	—	0.45	—	—	—
473	0.25	0.46	0.74	0.98	1.00
573	—	0.46	—	—	—
673	—	0.46	—	—	—

By direct comparison with IR spectral results, it seems likely that heats of adsorption of pyridine at 473 K reflect the selective adsorption on the 3640 cm^{-1}-OH sites at lower coverages. At 313 K, however, heats were evolved by rather non-selective adsorption either on the 3640 cm^{-1}-OH sites or other sites, then a monotonic heat curve was obtained.

In case of ammonia adsorption on H-$Y_{5.0}$, both of the 3640 and 3550 cm^{-1}-OH bands were effective for the formation of ammonium ions[14] and were almost simultaneously perturbed at 473 K as well as at room temperature as shown in Fig. 5. However, the amount of ammonium ions increased on heating H-$Y_{5.0}$-ammonia system as shown in Table 2, suggesting that migration of adsorbed ammonia occurred at higher temperature. The experimental procedure employed was the same as that employed in case of H-$Y_{5.0}$-pyridine system and the amount of ammonium ions was calculated from integrated intensities of characteristic bands at 1475 and 1435 cm^{-1}.[10] The results obtained by IR measurements imply that some difference should also be observed in the shape of heat curves obtained by ammonia adsorption and that the extent of the difference should be smaller than the case of pyridine adsorption, which was well confirmed by comparing the heat curves in Figs. 1 and 2. In addition, it is also concluded that the strength of acid sites should preferably be determined by the heat curve obtained at 473 K rather than at 313 K because of more selective adsorption.

The temperature dependence of the selective adsorption on the strongest sites observed in our results will not be reasonably explained on the basis of chemical equilibrium, but chemical kinetics should be introduced to explain the behavior of such an irreversible adsorption. The theoretical analysis of selective adsorption on different sites is now in progress and will be published later.

Differential Heats of Adsorption of Ammonia on H-Y Zeolites at 473, 573, and 673 K. The shapes of heat curves of ammonia adsorption on H-$Y_{5.0}$ obtained were almost similar to one another as shown in Fig. 2. However, the heats decreased slightly as a whole with a temperature rise. Provided that the selectivity of adsorption varies in this temperature range as is predicted by chemical equilibrium, the shape of the heat curve should change with temperature. Therefore, analogous shapes of these three heat curves suggest that the effect expected from the aspect of chemical equilibrium may not be so significant as to influence the shape of the heat curves.

A slight decrease of heats should be explained by the following thermodynamic equation representing

Table 3. Temperature dependence of the enthalpy of the reaction; $NH_3(g)+HCl(g) \rightarrow NH_4Cl(s)$

Reaction temperature/K	$-\Delta H$/kJ mol^{-1}
313	177
473	171
573	166
673	160

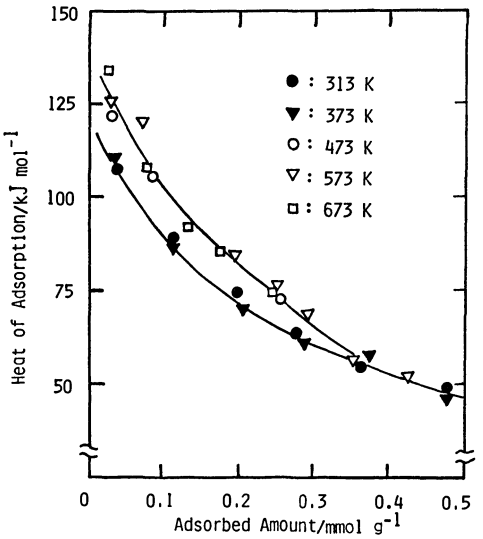

Fig. 6. Differential heats of adsorption of ammonia on silica-alumina.

temperature dependence of a heat evolved from a certain site,

$$(q_{ad})_{T_2} - (q_{ad})_{T_1} = \int_{T_1}^{T_2} \Delta C_v dT, \quad (1)$$

where $(q_{ad})_{T_1}$ and $(q_{ad})_{T_2}$ represent heats of adsorption at temperatures T_1 and T_2, respectively, and ΔC_v, the difference of the molar heat capacity between the gaseous state and the adsorbed state at a constant volume. Since C_v in the adsorption system is difficult to be calculated, the change of the enthalpy in the following reaction in Eq. 2 was calculated as a function of temperature from the tabulated values of molar heat capacities[15] as one of typical instances of the acid-base reactions as shown in Table 3.

$$HCl\ (gas) + NH_3(gas) \longrightarrow NH_4Cl\ (solid) \quad (2)$$

A decrease of the exothermic heats with a temperature rise in Table 4 probably corresponds to that observed in case of ammonia adsorption on the H–Y zeolites.

Differential Heats of Adsorption of Ammonia on Other Solids. Heats of adsorption of ammonia on silica-alumina were measured at 313, 373, 473, 573, and 673 K as shown in Fig. 6. Heats of adsorption at the former two temperatures were smaller than those at the latter three temperatures in the low coverage region. Moreover, the heat-treatment of silica-alumina–ammonia system resulted in the enhancement of the amount of protonated ammonia likewise observed in case of H–$Y_{5.0}$–ammonia system. Accordingly, the relatively low values of heats in the low coverage region measured at 313 and 373 K are considered to be an average of the heats from stronger and weaker or non-acidic sites.

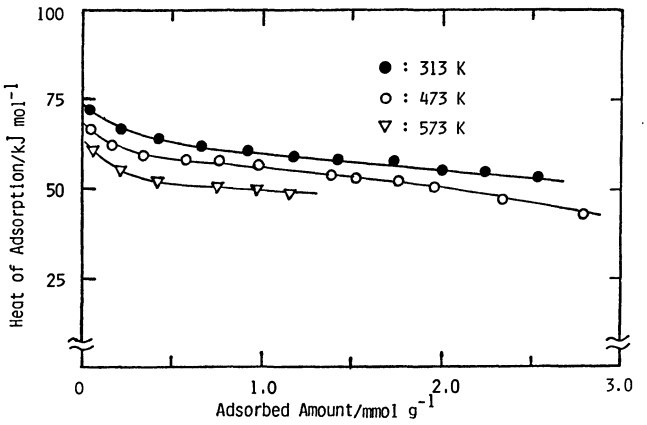

Fig. 7. Differential heats of adsorption of ammonia on Na–$Y_{5.0}$.

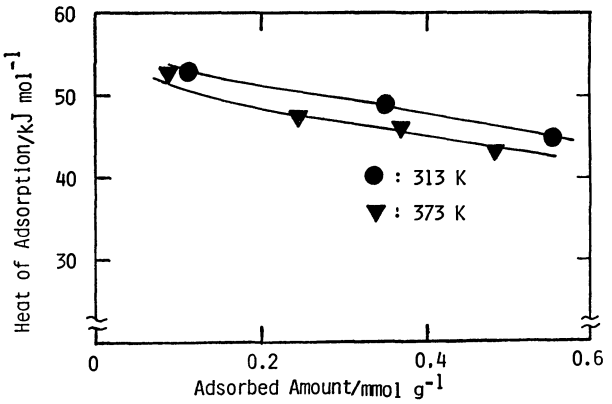

Fig. 8. Differential heats of adsorption of ammonia on silica.

Heats of adsorption of ammonia on Na–Y zeolite resulting from ion-dipole interactions were measured at 313, 473, and 573 K as shown in Fig. 7. Heats on silica resulting from hydrogen bonding were also measured at 313 and 373 K as shown in Fig. 8. In these cases, heats of adsorption showed the same behavior as the case of H–Y zeolites in the temperature range of 473 to 673 K, suggesting similar type of the temperature dependence. In cases of ammonia adsorption on Na–Y and silica, no specific phenomenon was observed on the heat curve because of the weak interaction between ammonia molecule and adsorption site.

References

1) V. Kevorkian and O. Steiner, *J. Phys. Chem.*, **67**, 545 (1963).
2) P. Y. Hsieh, *J. Catal.*, **2**, 211 (1963).
3) F. S. Stone and L. Whalley, *J. Catal.*, **8**, 173 (1967).
4) K. Tsutsumi, H. Q. Koh, S. Hagiwara, and H. Takahashi, *Bull. Chem. Soc. Jpn.*, **48**, 3576 (1975).
5) H. Taniguchi, T. Masuda, K. Tsutsumi, and H. Takahashi, *Bull. Chem. Soc. Jpn.*, **51**, 1970 (1978).
6) T. Masuda, H. Taniguchi, K. Tsutsumi, and H. Takahashi, *Bull. Chem. Soc. Jpn.*, **51**, 1965 (1978).

7) H. Taniguchi, T. Masuda, K. Tsutsumi, and H. Takahashi, *Bull. Chem. Soc. Jpn.*, **53**, 362 (1980).
8) A. Auroux, V. Bolis, P. Wierzchowski, P. C. Gravelle, and J. C. Vedrine, *J. Chem. Soc., Faraday Trans. 1*, **75**, 2544 (1979).
9) K. Tsutsumi, S. Hagiwara, Y. Mitani, and H. Takahashi, *Bull. Chem. Soc. Jpn.*, **55**, 2572 (1982).
10) J. W. Ward, "Zeolite Chemistry and Catalysis," ed by J. A. Rabo, ACS Monograph 171, Washington (1979), p. 225.
11) T. R. Hughes and H. M. White, *J. Phys. Chem.*, **71**, 2192 (1967).
12) J. W. Ward, *J. Catal.*, **9**, 225 (1967).
13) B. V. Liengme and W. K. Hall, *Trans. Faraday Soc.*, **62**, 3229 (1966).
14) J. W. Ward, "Molecular Sieves. Advances in Chemistry Series 101," ACS, Washington (1971), p. 394.
15) "Kagaku Binran (Handbook of Chemistry)," 2nd ed, ed by the Chemical Society of Japan, Maruzen, Tokyo (1975), p. 877.

Direct Measurement of the Interaction Energy between Solids and Gases. X. Acidic Properties of Hydroxyl Sites of H-Y Zeolite Determined by High-temperature Calorimetry

Yoshio MITANI,† Kazuo TSUTSUMI,*,†† and Hiroshi TAKAHASHI

Institute of Industrial Science, The University of Tokyo, Roppongi, Minato-ku, Tokyo 106

††*Toyohashi University of Technology, Tempaku-cho, Toyohashi 440*

(Received October 29, 1982)

Differential heats of adsorption of bases on H-Y zeolite were measured at 473 K and separated into those evolved at 3640 and 3550 cm^{-1}-OH sites respectively by a combined use of calorimetric and IR measurements, and then the acid strength of two OH sites was compared each other. In case of pyridine, heats of adsorption were larger on OH sites at 3640 cm^{-1} than 3550 cm^{-1}, which was in agreement with the results obtained by many authors by IR measurements. However, heats of adsorption on 3640 cm^{-1}-OH sites were only slightly higher than those on 3550 cm^{-1}-OH sites in case of ammonia, and almost the same in case of piperidine. The difference in heats of adsorption between the OH sites was explained by positional difference between the two OH sites, molecular size of the titrated bases and proton mobility induced by a strong base. The order of the strength of bases was determined by replacing a base molecule with another one on H-Y zeolite as follows; piperidine>pyridine>ammonia. This differs from the order expected from their pK_a values in solution.

Infrared measurements have revealed that 3640 cm^{-1}-OH sites were stronger in their acidity than 3550 cm^{-1}-OH sites.[1,2] However, heats of adsorption of bases have not yet been measured on the respective OH sites until now. In the present work, bases were adsorbed on original and poisoned H-Y zeolites at 473 K and heats of adsorption were then measured. Since the selective adsorption on the acid sites occurred at 473 K in each case of pyridine and ammonia as was confirmed previously,[3] heats of adsorption could be separated into those resulted from 3640 and 3550 cm^{-1}-OH sites respectively by a combined use of calorimetric and IR measurements.

Experimental

NH_4-Y zeolite was prepared by treating Y-type zeolite, SK-40, which was supplied by Linde Co. in the sodium form, several times with 1 mol dm^{-3} NH_4Cl solution at *ca.* 323 K. The chemical composition of the sample was analyzed as follows; $0.72(NH_4)_2O \cdot 0.15Na_2O \cdot Al_2O_3 \cdot 5.0SiO_2$. It could be converted to H-Y zeolite by the pretreatment before measurements. The sample was used in granular form of 28—60 mesh for calorimetric measurements. Ammonia was obtained from Matheson Co., and pyridine and piperidine from Wako Pure Chemicals Co. They were purified by the freeze-thaw method.

Differential heats of adsorption were measured at 473 K by a twin-conduction type microcalorimeter as described in a previous paper.[4] IR measurements were carried out by the *in situ* method described elsewhere.[3] Samples were outgassed for 5 h under a pressure of 10^{-3} Pa at 673 K before calorimetric and IR measurements.

Results

Heats of Adsorption and IR Spectra. Heats of adsorption of bases on H-Y were measured at 473 K and shown in Fig. 1. The H-Y was estimated to possess 4.73 mmol g^{-1} of positively charged sites from the view point of chemical composition. Heats of adsorption could be measured over a wide range in case of ammonia, but only below *ca.* 3 mmol g^{-1} in cases of pyridine and piperidine. This can be attributed to pore structure of the zeolite and molecular size of a base. In fact, the amount of adsorption at relative pressure of 0.25 was measured as 3.65 and 3.47 mmol g^{-1} at 293 K for pyridine and piperidine respectively, and as 9.3 mmol g^{-1} at 252 K for ammonia.

Figure 2 shows changes of hydroxyl bands with adsorption or desorption of bases. Since no Lewis acid site on H-Y was detected on the spectra between 1800—1200 cm^{-1} after adsorption of bases, only OH sites (Brønsted acid sites) were taken into account hereafter. In adsorption and desorption processes, only 3640 cm^{-1}-OH band was preferentially perturbed by pyridine (Fig. 2-D,E), while both of the 3640 and 3550 cm^{-1}-OH bands were simultaneously perturbed by ammonia (Fig. 2-B,C) and the behavior of perturbation by piperidine was intermediate between the former two cases (Fig. 2-F,G,H).

Separation of Heats of Adsorption into Heats Evolved at 3640 and 3550 cm^{-1}-OH Sites. Since the 3640 cm^{-1}-OH band was preferentially poisoned by pyridine,

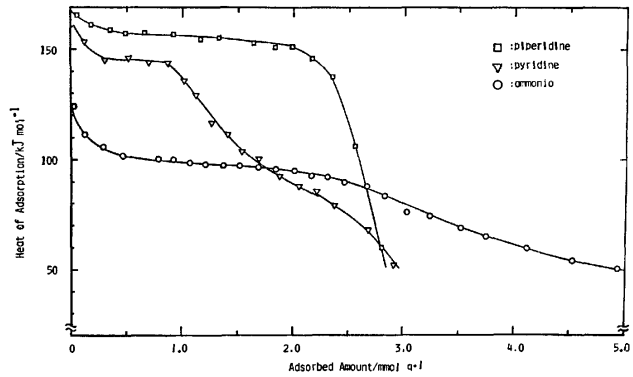

Fig. 1. Differential heats of adsorption of bases measured at 473 K.

† Present address: Tokuyama Soda Co., Ltd., Mikage-cho, Tokuyama, Yamaguchi 745.

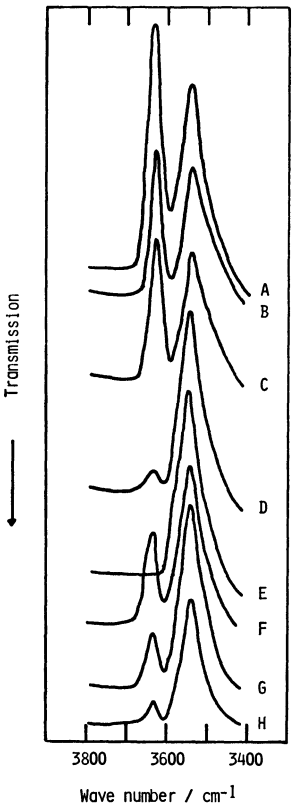

Fig. 2. Hydroxyl bands on H–Y after adsorption or desorption of bases. A: Original H–Y evacuated at 673 K then cooled to 473 K, B: 1 mmol g^{-1} of ammonia added to A, C: evacuated at 473 K after ammonia addition, D: 1 mmol g^{-1} of pyridine added to A, E: evacuated at 473 K after pyridine addition, F: 1 mmol g^{-1} of piperidine added to A, G: evacuated at 673 K after piperidine addition, H: evacuated at 573 K after piperidine addition.

one could easily obtain the H–Y which posessed only 3550 cm^{-1}-OH sites (Fig. 2-E). Heats of adsorption of pyridine were measured on the original and poisoned H–Y as shown in Fig. 3. The heat curve of the poisoned H–Y was almost superimposed on the original H–Y in the coverage above 1.6 mmol g^{-1}. Therefore, heats of adsorption of pyridine on the 3640 cm^{-1}-OH sites proved to correspond to a region above 105 kJ mol^{-1} involving the plateau leveling at *ca.* 145 kJ mol^{-1} and those on the 3550 cm^{-1}-OH sites, to a region below 105 kJ mol^{-1}.

Figure 4 shows heats of adsorption of ammonia on the original and pyridine-poisoned H–Y. On the original H–Y, the heat should result from the simultaneous adsorption on both 3640 and 3550 cm^{-1}-OH sites (Fig. 2-B). In addition, the acid strength of the 3550 cm^{-1}-OH sites must be weakened by poisoning the 3640 cm^{-1}-OH sites with pyridine. In fact, the band near 3550 cm^{-1} shifted by about 8 cm^{-1} to a lower frequency by pyridine adsorption. Moreover, a semi-quantitative IR analysis revealed that the amount of ammonia irreversibly adsorbed on the 3550 cm^{-1}-OH sites of the poisoned H–Y after addition of excess ammonia and subsequent evacuation at 473 K was one-third of that of the original H–Y. For these reasons, the difference between two curves does not necessarily

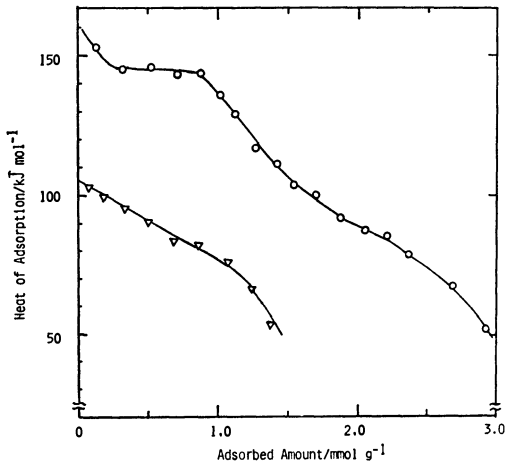

Fig. 3. Differential heats of adsorption of pyridine measured at 473 K. ○: On original H–Y, ▽: on the H–Y after pyridine addition followed by evacuation at 473 K, only 3640 cm^{-1}-OH sites were thus poisoned (see Fig. 2-E)

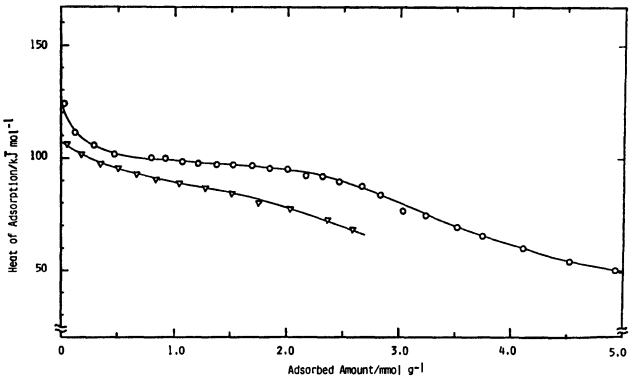

Fig. 4. Differential heats of adsorption of ammonia measured at 473 K. ○: On original H–Y, ▽: on the H–Y after pyridine addition followed by evacuation at 473 K, only 3640 cm^{-1}-OH sites were thus poisoned (see Fig. 2-E).

correspond to actual difference in heats of adsorption between two types of OH sites. However, it seems likely that the difference would not be negligible but remarkably smaller than that obtained in case of pyridine.

In case of piperidine adsorption, the pyridine-poisoned H–Y was not available, because pyridine was easily replaced by piperidine on the surface as discussed later. The H–Y was, therefore, poisoned by piperidine, and heats of adsorption of piperidine were measured on it (Fig. 5). Although the poisoning by piperidine was not necessarily selective as shown in Fig. 2-G,H, the result obtained on the poisoned H–Y by piperidine addition and subsequent evacuation at 673 K could be considered to reflect the heat evolved by adsorption mainly on the 3640 cm^{-1}-OH sites. From the fact that heats of adsorption on this sample and on the original H–Y were almost equivalent, it is suggested that both OH sites were energetically same for piperidine adsorption. A decrease in heats at higher coverage which was more explicit in samples evacuated at lower temperatures after piperidine poi-

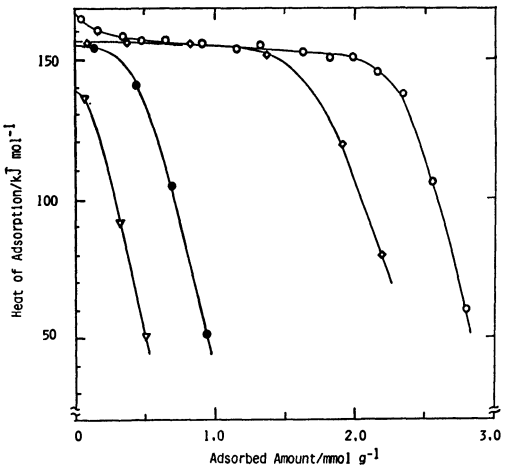

Fig. 5. Differential heats of adsorption of piperidine measured at 473 K. ○: On original H–Y, ◇: on the H–Y after piperidine addition followed by evacuation at 673 K (see Fig. 2-G), ●: On the H–Y after piperidine addition followed by evacuation at 573 K (see Fig. 2-H), ▽: on the H–Y after piperidine addition followed by evacuation at 473 K, both OH bands of this sample were found to be poisoned.

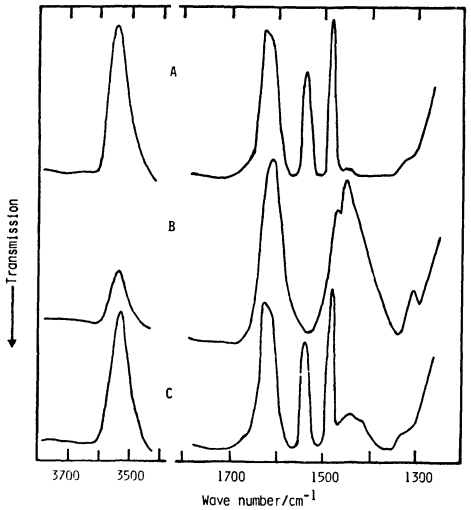

Fig. 6. IR spectra of adsorbed pyridine, piperidine, and ammonia on H–Y at 473 K. (A): Addition of pyridine followed by evacuation at 473 K, (B): addition of piperidine (1 kPa) to (A) followed by evacuation at 473 K, (C): addition of ammonia (1 kPa) to (A) followed by evacuation at 473 K.

soning can best be explained by a decrease in the number of specific adsorption sites.

Determination of the Order of Basic Strength. The order of basic strength has often been taken as piperidine>ammonia>pyridine, considering their pK_a values in aqueous solutions (piperidine, 11.1; ammonia, 9.3; pyridine, 5.2).[1,5] However, in the present work, the order was examined directly by means of replacing basic molecules with another one on H–Y surface. First, in order to compare basic strength of piperidine with that of pyridine, the poisoned H–Y with pyridine (Fig. 2-E or Fig. 6-A) was exposed to excess piperidine under a pressure of *ca.* 1 kPa, and followed by evacuation at 473 K. A band at 1545 cm^{-1} for pyridinium ions almost disappeared, and that at 1610 cm^{-1} for piperidinium ions newly appeared as shown in Fig. 6-B.[6] The spectra obtained after completion of the replacement (Fig. 6-B) were almost the same as those obtained by piperidine adsorption on the original H–Y. On the other hand, no piperidine molecule held on H–Y was replaced upon exposure to pyridine vapour. Moreover, ammonia molecules were also easily replaced by piperidine, while no piperidine molecule was replaced by ammonia. Thus, piperidine proved to be the strongest of the three.

Similar treatments were performed on H–Y zeolite–pyridine–ammonia system. The poisoned H–Y with pyridine (Fig. 6-A) was exposed to excess ammonia under a pressure of *ca.* 1 kPa, and followed by evacuation at 473 K. Bands at 1475 and 1435 cm^{-1} for ammonium ions newly appeared, while that of pyridinium ions at 1545 cm^{-1} was unchanged as shown in Fig. 6-C.[6] Ammonium ions must be formed on 3550 cm^{-1}-OH sites, because 3550 cm^{-1}-OH band was slightly perturbed. They could not be removed by successive addition of pyridine followed by evacuation at 473 K. In addition, these spectra agreed with those obtained on exposure of ammonia-loaded H–Y to pyridine vapor.

In consequence, apparent order of the basic strength seemed to depend on whether acidic sites are 3640 or 3550 cm^{-1}-OH sites. The order at 3640 cm^{-1} was determined as piperidine>pyridine>ammonia, and that at 3550 cm^{-1} as piperidine>ammonia>pyridine. However, since all bases are considered to be accessible to the 3640 cm^{-1}-OH sites as described later, the basic strength should be judged on the 3640 cm^{-1}-OH sites; the order obtained here was in good agreement with the finding of Kebarle *et al.* who determined proton exchange equilibria of bases in vapor phase by mass spectrometer.[7]

Discussion

The positional assignments of hydroxyl sites in H–Y have been widely studied. Eberly[8] assigned the positions on the basis of the interaction of OH groups with olefins. He considered that 3640 cm^{-1}-OH sites existed in supercages having maximum entrance diameter of *ca.* 9 Å and that 3550 cm^{-1}-OH sites existed in hexagonal prisms having maximum entrance diameter of 2.2—2.5 Å (Fig. 7). In contradiction to this, Hughes and White[1] suggested that both OH sites were located on O_1, or O_4 oxygen atoms and accessible to large molecules. Olson and Dempsey[9] assigned 3640 cm^{-1} band to O_1–H groups and 3550 cm^{-1} band to O_3–H groups, using single crystal X-ray techniques. This model was in analogy with Eberly's first observations[8] and agreed with his positional assignments. Additional confirmation was obtained by Ward from exchange of cesium ions into NH_4–Y.[10] Hence, we take Eberly's assignments in order to explain heats of adsorption hereafter.

The 3640 cm^{-1}-OH groups form pyridinium ions in the presence of pyridine while 3550 cm^{-1}-OH groups

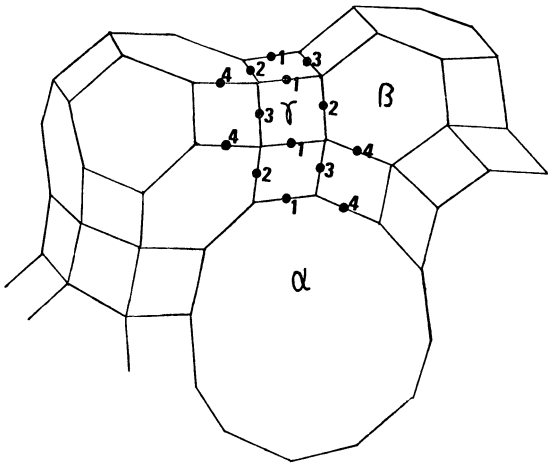

Fig. 7. Framework indication of H–Y zeolite. α: Supercage cavity having maximum entrance diameter of about 9 Å, β: sodalite cavity having maximum entrance diameter of 2.2—2.5 Å, γ: hexagonal prism having maximum entrance diameter 2.2—2.5 Å. The figures 1 through 4 represent oxygen atoms.

form only hydrogen bonds as shown in the formation of 1440 cm^{-1} band. These facts observed by Hughes and White,[1] and other authors[2,11] were confirmed also in the present work. The large molecular size of pyridine prevents it from approaching 3550 cm^{-1}-OH sites and thus it cannot be protonated. Higher heats of adsorption on OH sites at 3640 cm^{-1} must reflect such a situation. Although piperidine is also too large in size to approach the 3550 cm^{-1}-OH sites, it could be actually protonated by these sites as well as the 3640 cm^{-1}-OH sites, which may be rationalized in terms of proton mobility. Strong bases such as piperidine are known to be able to induce proton movement even at lower temperatures.[9,10] The protonation must result in the evolution of similar heats of adsorption on both OH sites at 3550 and 3650 cm^{-1}.

Ammonia was found to be the weakest base of the three, however, it was protonated on the 3550 cm^{-1}-OH sites,[12] then heats of adsorption were not much different on the 3550 and the 3640 cm^{-1}-OH sites. This might originate from the fact that ammonia was small enough to access to the 3550 cm^{-1}-OH sites and to be protonated in spite of its weaker basicity than pyridine. In order to confirm the interaction of ammonia with the 3550 cm^{-1}-OH sites, the following adsorption and/or poisoning measurements of pyridine and ammonia were carried out. The original H–Y (referred to A) was evacuated at 673 K and its weight was taken as reference. Two kinds of poisoned samples were prepared from the evacuated H–Y; one was poisoned with pyridine followed by evacuation at 473 K (B) and the other was further poisoned with ammonia followed by evacuation at 293 K (C). In B, the 3640 cm^{-1}-OH sites were poisoned by pyridine, and in C, the 3550 cm^{-1}-OH sites were also poisoned but by ammonia. All samples were exposed to pyridine vapor at 298 K and their weight change was measured. A weight increase in A coincided with that in B, which reflects the reproducibility in pyridine adsorption. On the other hand, a weight increase in C was higher than that in A by a corresponding value of 1.2 mmol g^{-1} of ammonia. This finding indicates that ammonia interacts with the 3550 cm^{-1}-OH sites, not in supercages but by entering hexagonal prisms or being adsorbed to the 3550 cm^{-1}-OH sites which are inaccessible for pyridine.

References

1) T. R. Hughes and H. M. White, *J. Phys. Chem.*, **71**, 2192 (1967).
2) J. W. Ward, *J. Catal.*, **9**, 225 (1967).
3) K. Tsutsumi, Y. Mitani, and H. Takahashi, *Bull. Chem. Soc. Jpn.*, **56**, 1912 (1983).
4) K. Tsutsumi, S. Hagiwara, Y. Mitani, and H. Takahashi, *Bull. Chem. Soc. Jpn.*, **55**, 2572 (1982).
5) J. W. Ward, "Zeolite Chemistry and Catalysis," ed by J. A. Rabo, ACS Monograph 171, Washington (1979), p. 245.
6) J. W. Ward, "Zeolite Chemistry and Catalysis," ed by J. A. Rabo, ACS Monograph 171, Washington (1979), p. 225.
7) J. P. Briggs, R. Yamdagni, and P. Kebarle, *J. Am. Chem. Soc.*, **94**, 5128 (1972).
8) P. E. Eberly, Jr., *J. Phys. Chem.*, **71**, 1717 (1967).
9) D. H. Olson and E. Dempsey, *J. Catal.*, **13**, 221 (1969).
10) J. W. Ward, *J. Phys. Chem.*, 73, 2086 (1969).
11) B. V. Liengme and W. K. Hall, *Trans. Faraday Soc.*, **62**, 3229 (1966).
12) J. B. Uytterhoeven, L. G. Christner, and W. K. Hall, *J. Phys. Chem.*, **69**, 2117 (1965).

 © 1983 The Chemical Society of Japan Bull. Chem. Soc. Jpn., 56, 1921—1923 (1983)

Direct Measurement of the Interaction Energy between Solids and Gases. XI. Calorimetric Measurements of Acidities of Aluminum Deficient H-Y Zeolites

Yoshio MITANI,†† Kazuo TSUTSUMI,*,† and Hiroshi TAKAHASHI
Institute of Industrial Science, The University of Tokyo, Roppongi, Minato-ku, Tokyo 106
†*Toyohashi University of Technology, Tempaku-cho, Toyohashi 440*
(Received December 2, 1982)

Heats of adsorption of pyridine and ammonia were respectively measured on aluminum deficient H-Y zeolites using a microcalorimeter at 473 K. The calorimetrically determined acidity was discussed in relation to the positional difference between 3640 and 3550 cm^{-1}-OH acidic sites and compared with the catalytic activity. Dealumination generally brings about a decrease in the acid site concentration. However, the extent of the decrease varied with the kind of titrated base and a significant change was observed in the ratio of acid site concentration when titrated with pyridine. This may be explained by the fact that the pore size of the zeolite becomes widely distributed as dealumination proceeds; 3550 cm^{-1}-OH sites in supercages must become accessible to such a large molecule as pyridine. Also observed with dealumination was a slight increase in the heat of adsorption from initial to the middle stage of adsorption, which reflected the enhancement in acid strength of each OH site. The catalytic activity for cumene cracking increased with dealumination, which agreed with the acidity determined by the adsorption of pyridine rather than ammonia.

The acid strength of catalysts has widely been studied in relation to catalytic activity by use of butylamine and coloured indicators.[1-3] However, since it was not certain whether adsorption of butylamine selectively occurred on strong sites in preference to weak sites and whether the molecular size of butylamine was same with that that of reactant, the concentration obtained often deviated from the true value.[4]

In our previous papers,[5,6] the selective adsorption of bases was confirmed to occur onto strong sites in high temperature range above *ca.* 473 K and acid strength was determined as heats of adsorption by calorimetry. In addition, the relative acid strength changed with the kind of titrated base. Thus, the acid strength of solid surfaces should be investiated with respect to basic properties of adsorbate in high temperature range.

In the present work, the acid strength of Al-deficient H-Y zeolites was measured by pyridine and ammonia adsorption. The difference in acid strength between 3640 and 3550 cm^{-1}-OH sites will be discussed in correlation to the positional difference, which is useful for correlating calorimetric acid strength with catalytic activity.

Experimental

NH_4-Y zeolite was obtained by repeated ion exchange of Na-form zeolite (Linde SK 40) in 1 mol/dm^3 NH_4Cl solution at *ca.* 323 K. Al-deficient zeolites were prepared by means of a slow addition of ethylenediaminetetraacetic acid (H_4EDTA) as described by Kerr.[7] Table 1 shows chemical compositions of zeolites determined by chemical analysis. Ammonia and pyridine were purified by the freeze-thaw method before use.

TABLE 1. ZEOLITE COMPOSITIONS

Sample	Composition
$H\text{-}Y_{5.0}$	$0.72(NH_4)_2O\cdot 0.15Na_2O\cdot Al_2O_3\cdot 5.0SiO_2$
$H\text{-}Y_{7.4}$	$0.68(NH_4)_2O\cdot 0.19Na_2O\cdot Al_2O_3\cdot 7.4SiO_2$
$H\text{-}Y_{10.3}$	$0.67(NH_4)_2O\cdot 0.16Na_2O\cdot Al_2O_3\cdot 10.3SiO_2$

After the sample (0.25—0.50 g) was outgassed for 5 h at 673 K under a pressure of 1 mPa, differential heats of adsorption of bases were measured at 473 K using a twin-conduction type microcalorimeter as described previously.[8] IR spectra were obtained at 473 K by the *in situ* method as described elsewhere.[5]

Catalytic activity for cumene cracking reaction was tested in a microreactor made of stainless steel of 0.3 cm in inner diameter, connected to a conventional gas chromatography assembly with a product trap. The catalyst (0.25 g) was pretreated in a stream of helium at 673 K for 3 h. The cracking activity was determined at 543 K by injecting cumene (10^{-2} cm^3 as liquid) into the carrier gas, He, stream (60 cm^3/min). The gas chromatographic separation of the products was carried out with a column of 20 wt% dioctyl sebacate on 100—120 mesh Uniport B at 473 K. Catalytic activity was given in terms of the conversion of cumene to propylene and benzene during the first pulse reaction.

Results and Discussion

Heats of adsorption of ammonia and pyridine were measured on $H\text{-}Y_{5.0}$, $H\text{-}Y_{7.4}$, and $H\text{-}Y_{10.3}$ as shown in Figs. 1 and 2. The change of acid site strength with dealumination could be compared each other in both

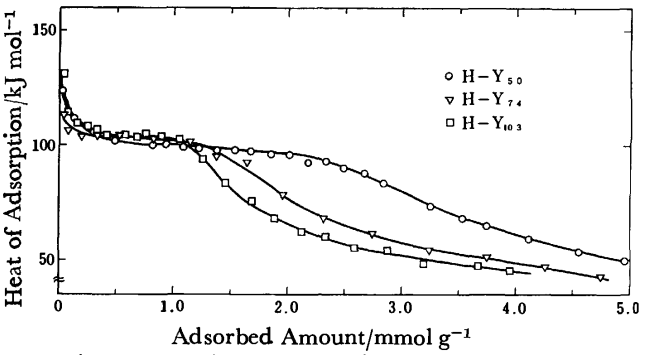

Fig. 1. Differential heats of adsorption of ammonia at 473 K.

†† Present address: Tokuyama Soda Co., Ltd., Mikage-cho, Tokuyama, Yamaguchi 745.

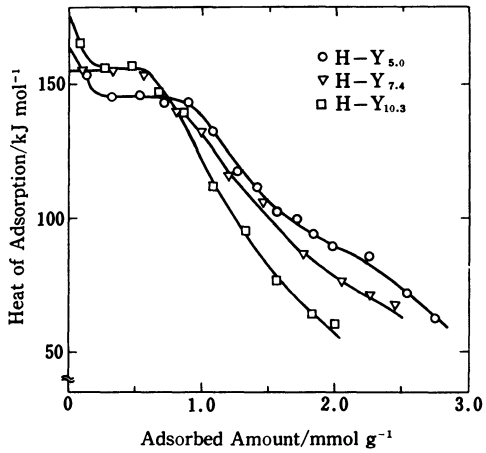

Fig. 2. Differential heats of adsorption of pyridine at 473 K.

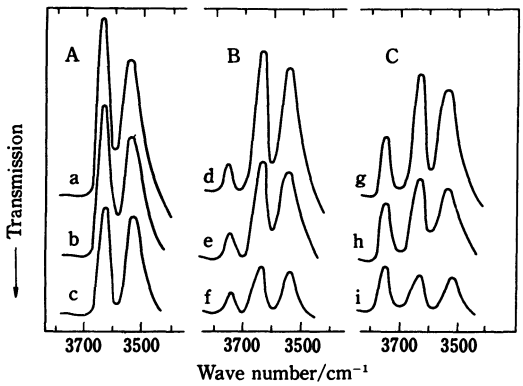

Fig. 3. Infrared spectra of hydroxyl bands measured at 473 K.
(A): On H–$Y_{5.0}$, (B): on H–$Y_{7.4}$, (C): on H–$Y_{10.3}$; (a), (d), and (h): evacuated at 673 K then cooled to 473 K; (b), (e), and (i): 0.5 mmol/g of ammonia added to (a), (d), and (h); (c), (f), and (j): 1 mmol/g of ammonia added to (a), (d), and (h)

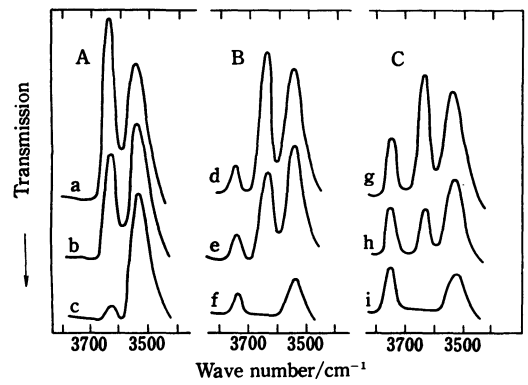

Fig. 4. Infrared spectra of hydroxyl bands measured at 473 K.
(A): On H–$Y_{5.0}$, (B): on H–$Y_{7.4}$, (C): on H–$Y_{10.3}$; (a), (d), and (h): evacuated at 673 K then cooled to 473 K; (b), (e), and (i): 0.5 mmol/g of pyridine added to (a), (d), and (h); (c), (f), and (j): 1 mmol/g of pyridine added to (a), (d), and (h)

cases of ammonia and pyridine adsorption on the basis of heat curves. Dealumination generally brought about a decrease in the number of OH sites, which corresponded to a decrease in the plateau region on heat curves. The ratio of the adsorbed amount in the plateau region to the total number of OH sites which was calculated from zeolite compositions may be assumed to reflect a relative concentration of effective acid sites. Its value depended on the kind of adsorbates, and the proportions of the value obtained by pyridine adsortipn to that by ammonia were 0.4 for H–$Y_{5.0}$, 0.45 for H–$Y_{7.4}$, and 0.55 for H–$Y_{10.3}$. This suggests that some OH sites become accessible to pyridine in progress of dealumination.

Figures 3 and 4 show changes of IR spectra of hydroxyl bands with adsorption of ammonia and pyridine, respectively. Acid sites of H–Y zeolites are known to originate from 3640 and 3550 cm^{-1}-OH sites, and the 3750 cm^{-1}-OH sites are to be silicious sites. On H–$Y_{5.0}$, the strength of both acidic OH sites was found to be approximately similar for the adsorption of ammonia, however, only 3640 cm^{-1}-OH sites acted as strong acid sites for pyridine because of differences in accessibility.[6] A consideration of these facts must account for observations that both OH sites interacted with ammonia on H–$Y_{5.0}$ and their band intensities decreased simultaneously (Fig. 3-A) while that only the 3640 cm^{-1}-OH sites interacted with pyridine and the intensity of the 3550 cm^{-1}-OH band remained unchanged (Fig. 4-A). However, preferential adsorption of pyridine on the 3640 cm^{-1}-sites became less significant as revealed in the change of intensity ratios of the 3640 cm^{-1} band to the 3550 cm^{-1} one with progress of dealumination (Fig. 4-B, C). This suggests that a part of the 3550 cm^{-1}-OH sites became somewhat accessible to pyridine. On the other hand, intensity ratios remained almost constant in case of ammonia adsorption (Fig. 3-B, C), which suggests that accessibility of both OH sites to ammonia seemed not to change with dealumination.

Structural change with dealumination was also examined in relation to accessibility to bases of both OH sites. A half width and integral intensity of X-ray profiles suggested that the framework structure of H–

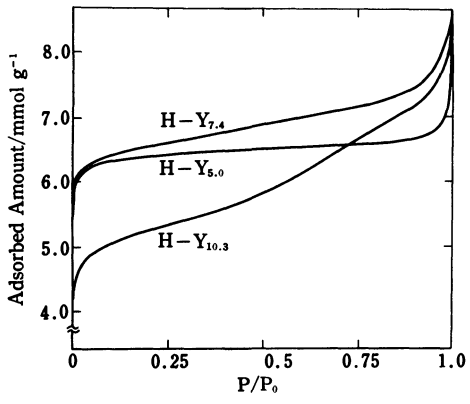

Fig. 5. Nitrogen adsorption isotherms at liquid nitrogen temperature.
(A): On H–$Y_{5.0}$, (B): on H–$Y_{7.4}$, (C): on H–$Y_{10.3}$

Table 2. Catalytic activity for cumene cracking reaction at 543 K

Catalyst	Conversion/%
$H–Y_{5.0}$	56
$H–Y_{7.4}$	76
$H–Y_{10.3}$	76

$Y_{10.3}$ was partially destroyed, while that of $H–Y_{7.4}$ was almost unchanged. Figure 5 shows nitrogen adsorption isotherms on zeolites. The rectangular shape of the isotherm on $H–Y_{5.0}$ suggested that the zeolite was of a regular pore structure. However, the pore size must become widely-distributed with dealmination as revealed in the shapes of isotherms on $H–Y_{7.4}$ and $H–Y_{10.3}$. The positional assignments were demonstrated by Eberly[9] and others[10,11] that H-atoms contained in 3550 cm^{-1}-OH sites existed in hexagonal prisms with maximum entrance diameter of 2.2—2.5 Å and that those in 3640 cm^{-1}-OH sites in supercages with maximum entrance diameter of *ca.* 9 Å. In consideration of both structural change with dealumination and positional assignments of OH sites, 3550 cm^{-1}-OH sites were concluded to become accessible to large molecule of pyridine in respect of size as dealumination proceeded. Since ammonia was considered to be adsorbed close to 3550 cm^{-1}-OH sites even on $H–Y_{5.0}$,[6] the accessibility of OH sites did not change with dealumination. On the other hand, 3640 cm^{-1}-OH sites on these three zeolites were considered to be equally accessible to both pyridine and ammonia in respect of size. These results in Al-deficient zeolites supported the previous discussion[6] that the difference in the acid strength between two OH sites was explained in terms of positional differences. The acid site strength on Al-deficient zeolites proved to be somewhat larger than that on $H–Y_{5.0}$ as judged by heats of adsorption at plateau region in Figs. 1 and 2.

The catalytic activity for cumene cracking was weaker on $H–Y_{5.0}$ than on Al-deficient $H–Y_{7.4}$ and $H–Y_{10.3}$ as shown in Table 2. A comparison of the result with the acidic properties shown in Figs. 1 and 2 suggested that the activity seemed to correlate with the acidity determined by pyridine rather than by ammonia. In case of pyridine adsorption, it was found that the acid site concentration remained nearly constant and its strength was rather enhanced on dealumination. In case of ammonia adsorption, however, the acid site concentration decreased significantly with dealumination. Ward[12] demonstrated on the basis of IR measurements on $H–Y_{5.0}$ that only 3640 cm^{-1}-OH sites were affected by cumene at 523 K. In a previous paper,[6] piperidine was found to affect simultaneously both 3640 and 3550 cm^{-1}-OH sites. This was considered to be attributable to strong basicity of piperidine, while its molecular size is almost the same as that of pyridine. All the data lead to the notion that the activity for acid-catalyzed reaction should be discussed in relation to the surface acidity only in cases in which the basic molecule used has similar size to that of the reactant and selectively interacts with active sites.

References

1) H. A. Benesi, *J. Phys. Chem.*, **61**, 970 (1957).
2) H. A. Benesi, and B. H. C. Winquist, *Adv. Catal.*, **27**, 97 (1978).
3) W. Klading, *J. Phys. Chem.*, **80**, 262 (1976).
4) M. Deeba and W. K. Hall, *J. Catal.*, **60**, 417 (1979).
5) K. Tsutsumi, Y. Mitani, and H. Takahashi, *Bull. Chem. Soc. Jpn.*, **56**, 1912 (1983).
6) Y. Mitani, K. Tsutsumi, and H. Takahashi, *Bull. Chem. Soc. Jpn.*, **56**, 1917 (1983).
7) G. T. Kerr, *J. Phys. Chem.*, **72**, 2594 (1968).
8) K. Tsutsumi, S. Hagiwara, Y. Mitani, and H. Takahashi, *Bull. Chem. Soc. Jpn.*, **55**, 2572 (1982).
9) P. E. Eberly, Jr., *J. Phys. Chem.*, **71**, 1717 (1967).
10) D. H. Olson and E. Dempsey, *J. Catal.*, **13**, 221 (1969).
11) J. W. Ward, *J. Phys. Chem.*, **73**, 2086 (1969).
12) J. W. Ward, *J. Catal.*, **11**, 259 (1968).

A Localized Molecular Orbital Approach to the Bond Moment Theory

Hiroyuki SHINODA*,† and Tomoo MIYAZAKI

Department of Applied Chemistry, Faculty of Science and Engineering, Waseda Uuiversity, Ohkubo, Shinjuku-ku, Tokyo 160

(Received October 29, 1982)

The bond moment theory was reinvestigated by use of localized molecular orbitals derived from INDO canonical orbitals. Bond moments were defined in terms of localized molecular orbital and, together with their derivatives with respect to a C–H stretching motion, were evaluated for some simple molecules; the bond moments of acetylene and hydrogen cyanide in the C–H bending geometry were also calculated. It is concluded that the first-order approximation for the bond moment theory is inadequate to interpret infrared absorption intensity. In the C–H stretching vibration the change in *trans*-sited bond moment is considerably large.

Some properties of a molecule have been analyzed by relating them to several characteristic values of bonds in the molecule. Furthermore, those values for particular kinds of bonds, *e.g.*, the C–H bond, are expected to be capable of being transfered from one molecule to another. A method of analyzing infrared absorption intensities along this line is well known as the bond moment theory.

Experimental approaches to the bond moment theory have been involved in some difficulties. The most serious one is that the number of intensity parameters needed for the application of the theory usually exceeds the number of pieces of experimental information. In practical treatments, therefore, we have been obliged to approximate the theory by neglecting a large part of parameters. Another difficulty is that the sign of dipole moment derivative with respect to the normal coordinate can not be decided uniquely from the experimental intensity.

There are some reports in which infrared absorption intensities were subjected to molecular orbital calculations.[1,2] In most studies molecular orbital calculations played only a supplemental role in the decision of the sign, which constitutes the second difficulty in experimental approach.[1] Recently, with the advance of electronic computer and with the popularization of molecular orbital calculations, infrared absorption intensities as well as vibrational frequencies have been calculated by the molecular orbital method, and successful results have been obtained.[2] Up to now, however, there are not so many reports on the bond moment theory conducted on the basis of molecular orbital calculations.

In this study, localized molecular orbitals (LMOs) which had been transformed from INDO canonical orbitals[3] by the Edmiston and Ruedenberg method[4] were used to define bond moments. The Edmiston and Ruedenberg method is based on maximization of the sum of intraorbital Coulomb repulsion energies and is called the energy localization method. Three other methods for determining LMOs were proposed by Foster and Boys,[5] von Niessen,[6] and Magnasco and Perico.[7] The agreement among results obtained by these four methods was generally good.[8] Figeys *et al.*[9] compared LMOs from *ab initio* canonical orbitals with those from semiempirical canonical orbitals, pointing out that the choice of canonical orbitals is important to gain a quantitative reliability. In this study, however, INDO canonical orbitals were used, because the main aim of the study lies in a qualitative check of the approximations which have been introduced into the bond moment theory and because INDO method gives fairly good electron distributions as compared with the other semiempirical methods. Bond moment derivatives with respect to a C–H stretching were calculated for several small molecules and also bond moments of acetylene and hydrogen cyanide were calculated with a condition of the C–H bond being bent.

The bond moment theory and the approximations introduced into it are described in the following section.

The Bond Moment Theory

The infrared absorption intensity A_a of the fundamental band for a normal vibration a is expressed, with the assumption of the harmonic oscillator approximation, as follows:[10]

$$A_a = \frac{N\pi}{3c}\sum_m\sum_n\left(\frac{\partial\mu}{\partial R_m}\right)_0\cdot\left(\frac{\partial\mu}{\partial R_n}\right)_0 L_{ma}L_{na}, \quad (1)$$

where μ is the molecular total dipole moment, c the velocity of light, N the Avogadro number, L_{ma} the element of the well-known transformation matrix between the internal coordinates $\{R_m\}$ and the normal coordinates $\{Q_a\}$. The starting point of the bond moment theory is that the total dipole moment μ in Eq. 1 is given as the sum of bond moments, μ_k's:

$$\mu = \sum_k \mu_k. \quad (2)$$

Introducing this expression, we rewrite Eq. 1 as follows:

$$A_a = \frac{N\pi}{3c}\sum_m\sum_n\sum_k\sum_l\left(\frac{\partial\mu_k}{\partial R_m}\right)_0\cdot\left(\frac{\partial\mu_l}{\partial R_n}\right)_0 L_{ma}L_{na}. \quad (3)$$

As seen from this equation, the infrared absorption intensity can be interpreted in the terms of $(\partial\mu_k/\partial R_m)_0$'s, bond moment derivatives with respect to the internal coordinates.

In the first stage of investigation, each bond moment was supposed to be parallel to any one bond in the molecule and its magnitude not to be changed without change in the bond length. Therefore, the bending mode which does not change the bond length will

† Present address: Faculty of Pharmaceutical Science, Toyama Medical and Pharmaceutical University, 2630 Sugitani, Toyama 930-01.

cause a variation in the total dipole moment only through a reorientational contribution of the bent bond. Within the restricted supposition, the calculated intensity did not agree with the experimental.[11] Hornig and McKean loosened the supposition,[12] adopting the following three approximations:

(a) When a bond is stretched by an amount dr, a moment $(\partial\mu/\partial r)dr$ is produced in the direction of the bond.

(b) When a bond is bent through an angle $d\alpha$, a moment $\mu^e d\alpha$, where μ^e is the "*effective*" bond moment, is produced in the plane of bending and perpendicular to the direction of the bond.

(c) When any one bond is bent or stretched, no moments are produced in the other bonds.

They investigated experimental infrared intensities of many molecules on the basis of these approximations and concluded that the "*effective*" bond moment of a given bond is not constant, that is, intensities of two different vibrational modes including the bond derive different values of the "*effective*" bond moment. They also concluded that in molecules containing lone pair electrons their effect must be taken into account explicitly. Orville-Thomas and his coworkers studied infrared absorption intensities of several triatomic molecules on the bond moment theory.[13-15] They concluded that the approximations introduced by Hornig and McKean are inadequate to interpret intensities. Therefore, they replaced the approximation (c) given above by a new approximation as follows:

(c′) When a particular bond is bent or stretched, a moment is produced in adjacent bonds.

They called the new set of approximations the "first-order bond moment theory" in contrast with the old one called the "zero-order bond moment theory." The intensity parameters in the new approximations are so many as to make impossible their evaluation from experimental intensities. Then, they had to elaborate some parameters in the form of composite term.[14] They also revealed that in bending modes atomic polarization terms of dipole moment, called rehybridization terms, are significant for interpreting intensities.[15]

Anyway, the investigations described above were founded on the assumption that each bond moment μ_k in Eq. 2 must belong to a certain bond in a molecule. Therefore, the lone pair electrons and the atomic polarization terms had to be treated as if they were new kinds of moments. Some investigations on the bond moment have been carried out by use of some terms of LMOs.[16,17] They will be discussed in comparison with our results.

Methods of Calculation

LMOs $\{\phi_i\}$ were calculated by the Edmiston and Ruedenberg method. The degree of localization was judged in our program as follows: The weight of atom A, w_A, in LMO ϕ_i is calculated by summing the squares of the LCAO coefficients of the atomic orbitals which belong to the atom. When w_A is larger than 0.9, LMO ϕ_i is regarded to be localized on atom A and the degree of localization is given by w_A. When any one w_A does not exceed 0.9 and the sum of w_A and w_B is larger than 0.9, LMO ϕ_i is regarded to be localized at bond A–B and the degree of localization is given by w_A+w_B.

The definition of localized orbital moment for each LMO follows that of Gordan and England[16] as follows:

(1) When LMO ϕ_i is localized at bond A–B, the localized orbital moment is expressed as

$$\mu_i = -2\langle\phi_i|e\boldsymbol{r}|\phi_i\rangle + (\boldsymbol{R}_A+\boldsymbol{R}_B)e. \quad (4)$$

(2) When LMO ϕ_i is localized on atom A as lone pair orbitals or as inner shell orbitals, the localized orbital moment is expressed as

$$\mu_i = -2\langle\phi_i|e\boldsymbol{r}|\phi_i\rangle + 2\boldsymbol{R}_A e. \quad (5)$$

In the above expressions $\boldsymbol{R}_A$ is the position vector of atom A and $\boldsymbol{r}$ is that of an electron. In the INDO calculation the second type of LMO always corresponds to a lone pair orbital. In this study the bond moment is defined as follows:

(1) The bond moment of bond A–B is the sum of the localized bond moments of the LMOs which are localized at the bond.

(2) If LMO ϕ_i is a lone pair orbital, its localized orbital moment itself is regarded as a kind of bond moment. The definitions, particularly (2), are useful in comparing bond moments and their derivatives between various molecules.

Bond moment derivatives with respect to a C–H stretching were calculated from bond moments for the C–H bond displaced +0.1 Å from the equilibrium length.

Results and Discussion

The Cartesian coordinate system used to calculate

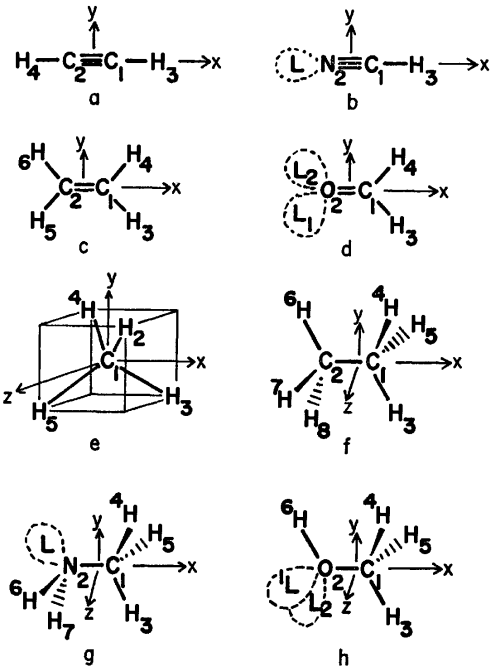

Fig. 1. Numbering of atoms and coordinate system. a: Acetylene. b: Hydrogen cyanide. c: Ethylene. d: Formaldehyde. e: Methane. f: Ethane. g: Methylamine. h: Methanol.

TABLE 1. CALCULATED BOND MOMENTS AND THEIR COMPONENTS AT EQUILIBRIUM MOLECULAR GEOMETRY
(1 D = 3.33564×10^{-30} C m)

Bond[a]	$\frac{\lvert\mu\rvert}{D}$	$\frac{\mu_x}{D}$	$\frac{\mu_y}{D}$	$\frac{\mu_z}{D}$	$\frac{\theta^{b)}}{°}$	s-Character[c] / %
Acetylene						
C_1-H_3	2.000	−2.000	0.0	0.0	0.0	45.7
Hydrogen cyanide						
C_1-H_3	2.049	−2.049	0.0	0.0	0.0	50.5
C_1-N_2	1.182	1.182	0.0	0.0	0.0	
L	3.319	3.319	0.0	0.0		
Ethylene						
C_1-H_3	1.959	−1.044	1.658	0.0	0.854	32.3
Formaldehyde						
C_1-H_3	2.278	−1.225	1.921	0.0	1.514	39.9
C_1-O_2	2.056	2.056	0.0	0.0	0.0	
L_1	2.740	1.146	2.489	0.0		
Methane						
C_1-H_2	2.037	−1.176	−1.176	−1.176	0.0	27.3
Ethane						
C_1-H_3	1.956	−0.646	1.846	0.0	0.303	26.3
Methylamine						
C_1-H_3	2.152	−0.738	2.022	0.0	0.590	28.0
C_1-H_4	2.067	−0.638	−0.978	−1.706	1.470	28.7
C_1-N_2	0.676	0.657	0.158	0.0	13.62	
N_2-H_6	1.221	0.315	0.662	−0.977	7.862	22.8
L	3.338	0.982	−3.190	0.0		
Methanol						
C_1-H_3	2.099	−0.600	2.011	0.0	2.933	30.4
C_1-H_4	2.173	−0.690	−1.032	−1.783	1.087	29.6
C_1-O_2	1.237	1.234	−0.089	0.0	3.995	
L_1	2.875	0.804	1.215	−2.478		
O_2-H_6	0.626	0.058	−0.623	0.0	13.80	18.5

a) The numbering of atoms, designation of lone pair orbitals, and coordinate systems are shown in Fig. 1. b) The angle between the bond and the corresponding bond moment. c) The weight of the 2s-orbital per the overall weight of atom X in the X–H localized orbital.

dipole moment values is shown in Fig. 1. The numbering of atoms and the designation of lone pair orbitals in each molecule are also shown.

Values of bond moments and their components and of angles between bond moments and corresponding bonds were calculated for the equilibrium geometries. The results are listed in Table 1, except those which are clear from the geometrical properties. The values of angles for the C–H bonds are not so large and are in the same order as those reported by Gordon and England.[16] Bruns *et al.*[18] calculated the dipole moment derivatives of ammonia with respect to the symmetry coordinates. In their report the angles between the bond moment and the corresponding N–H bond is 2.15°. On the other hand in our results, the values for the N–H and C–N bonds in methylamine and for the O–H and C–O bonds in methanol are somewhat large. From these results it may be said that the bond moment direction of an X–Y bond, where X and/or Y have lone pair orbitals, largely deviates from the bond and that hydrogen cyanide, formaldehyde, and ammonia fall in special cases where highly symmetrical geometries are possessed.

Since the Edmiston and Ruedenberg method for calculating LMOs has no guarantee for giving full localization, the degree of localization was tested for molecules in equilibrium geometry. It was greater than 0.99 for the bond localized orbital, while for the lone pair orbital it was less than 0.99 with a minimum of 0.969 for hydrogen cyanide. Gordon and England[16] calculated the degree of localization for many hydrocarbons and concluded that the overflow of electrons due to a very small delocalization, which they called tail, was not negligible for some properties of molecules. Therefore, each bond moment of hydrogen cyanide and formaldehyde which reveal the large delocalization was divided into two contribution parts, *i.e.*, the *intra*-LMO part and the *extra*-LMO part. The calculated results are listed in Table 2. It is seen from the table that the contribution of the *extra*-LMO part is at most 5%.

It is found from the first column of Table 1 that the absolute values of the C–H bond moments are varied in the range from 1.96 to 2.28 D (1 D = 3.33564×10^{-30} C m). Their average and standard deviations are 2.077 and 0.096 D, respectively. The deviation is somewhat large as compared with the results of Kapuy and Kozmutza,[17] who investigated prop-

Table 2. Intra-orbital and extra-orbital contribution to bond moments

Bond[a)]	*Intra*		*Extra*	
	μ_x/D	μ_y/D	μ_x/D	μ_y/D
Hydrogen cyanide				
C_1-H_3	−2.078		0.029	
C_1-N_2	1.184		−0.002	
L	3.287		0.033	
Formaldehyde				
C_1-H_3	−1.221	1.940	−0.004	−0.020
C_1-H_4	−1.221	−1.940	−0.004	0.020
C_1-O_2	2.058	0.0	−0.002	0.0
L_1	1.187	2.573	−0.041	−0.084
L_2	1.187	−2.573	−0.041	0.084

a) See footnote a) in Table 1.

erties of LMOs by the *ab initio* molecular orbital calculation. If the LMO of C–H bond is fully localized, the bond moment is a function of the C–H distance vector, the bond polarization of the electron distribution in the LMO, and the s-character of the hybrid orbital in the carbon atom. When the bond polarization does not appear, it is a function of only the s-character and the values of the bond moments are 2.258, 2.128, and 1.955 D for the sp-, sp^2-, and sp^3-hybrid orbitals, respectively; that is, the bond moment changes with the increase in s-character. The s-character of atom X in the X–H bond is shown in the last column of Table 1. It is shown that the order of magnitude for the calculated C–H bond moments does not agree with that of the s-character. Thus it is concluded that the C–H bond moment is determined by not only the s-character but also the bond polarization. The latter factor is dominantly affected by the environment of the C–H bond, so that the

Table 3. Bond moment derivatives with respect to a C–H stretching

Bond[a,b)]	μ'_x / D Å^{-1}	μ'_y / D Å^{-1}	μ'_z / D Å^{-1}	$\lvert\mu'\rvert$ / D Å^{-1}
Acetylene(C_1-H_3)				
C_1-H_3	0.294			0.294
C_1-C_2	−0.096			0.096
C_2-H_4	−0.144			0.144
Total	0.054			0.054
Hydrogen cyanide(C_1-H_3)				
C_1-H_3	0.365			0.365
C_1-N_2	0.118			0.118
L	−0.562			0.562
Total	−0.079			0.079
Ethylene(C_1-H_3)				
C_1-H_3	0.127	0.093		0.157
C_1-H_4	−0.431	0.146		0.455
C_1-C_2	0.149	0.403		0.430
C_2-H_5	−0.057	−0.046		0.073
C_2-H_6	−0.278	0.143		0.313
Total	−0.490	0.739		0.887
Formaldehyde(C_1-H_3)				
C_1-H_3	0.008	0.237		0.237
C_1-H_4	−0.377	0.371		0.529
C_1-O_2	0.342	0.400		0.526
L_1	0.113	−0.062		0.129
L_2	−0.732	0.246		0.772
Total	−0.646	1.192		1.356
Ethane(C_1-H_3)				
C_1-H_3	0.085	0.122	0.0	0.149
C_1-H_4	−0.214	0.177	−0.183	0.278
C_1-H_5	−0.214	0.177	0.183	0.278
C_1-C_2	0.170	0.301	0.0	0.346
C_2-H_6	−0.186	0.109	0.0	0.216
C_2-H_7	−0.013	−0.015	0.026	0.033
C_2-H_8	−0.013	−0.015	−0.026	0.033
Total	−0.385	0.856	0.0	0.939
Methylamine(C_1-H_3)				
C_1-H_3	−0.005	0.307	0.0	0.307
C_1-H_4	−0.196	0.214	−0.180	0.341
C_1-H_5	−0.196	0.214	0.180	0.341
C_1-N_2	0.184	0.291	0.0	0.344
L	−0.479	0.156	0.0	0.560
N_2-H_6	−0.007	−0.035	0.024	0.043
N_2-H_7	−0.007	−0.035	−0.024	0.043
Total	−0.706	1.112	0.0	1.317
Methanol(C_1-H_3)				
C_1-H_3	0.062	0.114	0.0	0.130
C_1-H_4	−0.172	0.209	−0.185	0.328
C_1-H_5	−0.172	0.209	0.185	0.328
C_1-O_2	0.109	0.201	0.0	0.229
O_2-H_6	−0.183	0.107	0.0	0.212
L_1	0.002	−0.003	0.003	0.005
L_2	0.002	−0.003	−0.003	0.005
Total	−0.352	0.834	0.0	0.905
Methylamine(C_1-H_4)				
C_1-H_3	−0.197	0.055	−0.273	0.341
C_1-H_4	0.048	−0.091	−0.149	0.181
C_1-H_5	−0.189	−0.251	−0.075	0.323
C_1-N_2	0.135	−0.128	−0.204	0.276
L	−0.014	0.009	−0.009	0.019
N_2-H_6	−0.016	−0.011	0.024	0.031
N_2-H_7	−0.191	−0.058	−0.094	0.221
Total	−0.424	−0.475	−0.780	1.007
Methanol(C_1-H_4)				
C_1-H_3	−0.175	0.047	−0.280	0.334
C_1-H_4	0.009	−0.116	−0.202	0.233
C_1-H_5	−0.173	−0.267	−0.103	0.334
C_1-O_2	0.156	−0.111	−0.201	0.278
O_2-H_6	−0.006	0.025	0.007	0.027
L_1	0.030	0.008	−0.011	0.033
L_2	−0.359	−0.026	−0.121	0.380
Total	−0.518	−0.440	−0.911	1.137

a) See footnote a) in Table 1. b) The stretching C–H bond is referred to in the parentheses.

transferability of bond moment is permitted only in rather limited congeners.

Bond moment derivatives with respect to the change in C–H bond length were calculated and are listed in Table 3. In most of the molecules the values of many off-diagonal terms are larger than that of the diagonal term. In the cases of acetylene and hydrogen cyanide the derivative of the neighbouring bond moment is small in comparison with that of the non-neighbouring bond moment. Furthermore, the direction of the vector for the non-neighbouring bond moment derivative is opposite to that of the diagonal term so that a large part of derivatives may be cancelled. In ethylene and formaldehyde the derivatives of the neighbouring and the *trans*-sited bond moments are larger than the diagonal term. A similar situation is also found in the results of ethane, methylamine, and methanol. The values of the diagonal terms are in the range of 0.130 to 0.367 D/Å with a standard deviation of 33.5%. Due to their large deviation, the expectation for the transferability between them must be abandoned. In Fig. 2 are illustrated the vectors of the bond moment derivatives for the planar molecules and the projections of the vectors on the plane of symmetry which includes the stretching C–H bond for the nonplanar molecules. The derivatives of the total dipole moments are also shown in the figure. It is found from the figure that the direction of each bond moment derivative is neither along the bond itself nor along the stretching bond, but that the derivative of the total dipole moment has a direction nearly along the stretching bond. It is noteworthy that the overall configuration of bond moment derivatives in a molecule resembles that in another one. It is concluded from the results that if the bond moment theory is developed with LMOs, the first-order approximation is inadequate to explain the change in dipole moment.

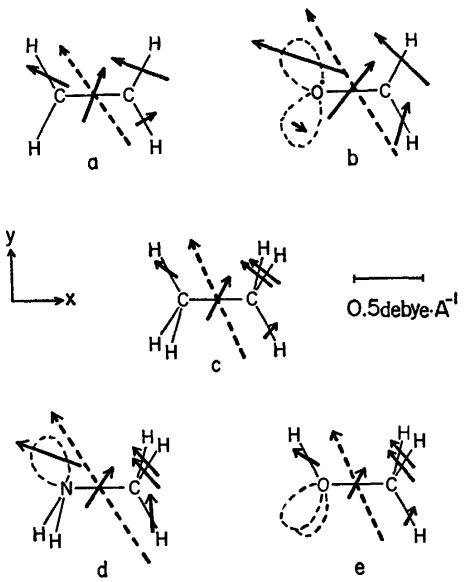

Fig. 2. Projection in xy-plane of bond moment derivatives with respect to a C_1–H_3 stretching.
A C_1–H_3 bond is illustrated in Fig. 1. a: Ethylene. b: Formaldehyde. c: Ethane. d: Methylamine. e: Methanol. ——→: Bond moment derivative; - - - →: total dipole moment derivative.

Some investigators have claimed that the hybridization term of dipole moment is significant to interpret the infrared absorption intensity, especially for bending modes. In our calculations, each bond moment can be divided into the (bond) polarization and hybridization terms. Change in bond moment for a C–H bending motion was studied for acetylene and hydrogen cyanide. The results are listed in Table 4. In the table $\Delta\mu=\mu_{10}-\mu_{eq}$, where μ_{10} is the bond moment when a C–H bond is bent 10° and μ_{eq} is that for the equilibrium geometry. It is concluded from the table that the x-components are caused to change slightly and that a main contribution to the change in the y-component arises from the hybridization terms; in the y-component of the diagonal term, *i.e.*, the bond moment change in the bent bond, the hybridization term is opposite in sign to the polarization term. This conclusion seems similar to the conclusion reported by Galabov and Orville-Thomas.[19] But these two conclusions cannot be regarded as the same since in Ref. 19 the rehybridization term is calculated as the atomic polarization for the central atom of bending, whereas in our results the corresponding atomic polarization is divided into the hybridization terms of two bond moments relating to the central atom. Anyway, it is concluded that the hybridization term is important to interpret the bond moment. It is noticeable that the polarization terms for the y-components of the off-diagonal terms are very small but not to be taken as zero. If the LMOs are fully localized at the bonds, the polarization terms do not change.

TABLE 4. CHANGES IN BOND MOMENTS WITH RESPECT TO A C–H BENDING[a]

Bond[b]	$\Delta\mu_x$[c]/D		$\Delta\mu_y$[c]/D	
	pol.[d]	hyd.[d]	pol.[d]	hyd.[d]
Acetylene				
C_1–H_3	0.002	0.009	0.050	−0.219
C_1–C_2	−0.008	−0.021	−0.000	0.218
C_2–H_4	0.003	−0.001	−0.002	0.045
Total	−0.003	−0.013	0.048	0.044
Hydrogen cyanide				
C_1–H_3	−0.000	0.011	0.051	−0.242
C_1–N_2	−0.010	−0.019	−0.000	0.160
L	0.005	−0.004	−0.007	0.192
Total	−0.004	−0.011	0.044	0.109

a) The molecular geometries for the C–H bending are shown in Fig. 3. b) See footnote a) in Table 1. c) See text. d) Abbreviations pol. and hyd. refer to the bond polarization term and the hybridization term, respectively.

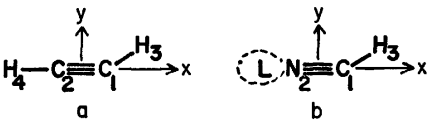

Fig. 3. Molecular geometry at a C–H bending.
a: Acetylene. b: Hydrogen cyanide.

Therefore, their nonzero values are due to the delocalization to the bent bond.

Although localized molecular orbitals are useful to investigate bond moments and their derivatives with respect to an appropriate coordinate, the transferability of intensity parameters in the bond moment theory should carefully and extensively be examined. If the intensity parameters need to be discussed with quantitative accuracy, it is important to use good canonical orbitals.

References

1) R. E. Bruns and R. K. Nair, *J. Chem. Phys.*, **58**, 1849 (1973); R. E. Bruns, *ibid.*, **58**, 1855 (1973); R. E. Bruns and W. B. Person, *ibid.*, **58**, 2585 (1973); R. E. Bruns and P. M. Kuznesof, *ibid.*, **59**, 4362 (1973); see also Refs. 13—15.

2) T. Miyazaki, T. Shigetani, and H. Yamamoto, *Bull. Chem. Soc. Jpn.*, **45**, 678 (1972); T. Miyazaki and H. Yamamoto, *ibid.*, **45**, 1669 (1972); Y. Hamada, M. Tsuboi, and H. Umeyama, *ibid.*, **53**, 48 (1980); Y. Sugawara, Y. Hamada, A. Y. Hirakawa, M. Tsuboi, S. Kato, and K. Morokuma, *Chem. Phys.*, **50**, 105 (1980); Y. Nishimura, M. Tsuboi, S. Kato, and K. Morokuma, *J. Am. Chem. Soc.*, **103**, 1354 (1981); S. Hyodo, K. Tamagake, and T. Fujiyama, *Bull. Chem. Soc. Jpn.*, **55**, 1272 (1982).

3) J. A. Pople and D. L. Beveridge, "Approximate Molecular Orbital Theory," McGraw-Hill, New York (1970).

4) C. Edmiston and K. Ruedenberg, *Rev. Mod. Phys.*, **35**, 457 (1963).

5) J. M. Foster and S. F. Boys, *Rev. Mod. Phys.*, **32**, 300 (1960).

6) W. von Niessen, *J. Chem. Phys.*, **56**, 4290 (1972).

7) V. Magnasco and A. Perico, *J. Chem. Phys.*, **47**, 971 (1967).

8) W. von Niessen, *Theor. Chim. Acta (Berl.)*, **27**, 9 (1972); **29**, 49 (1973).

9) H. P. Figeys, P. Geerlings, and C. van Alsenoy, *J. Chem. Soc., Faraday Trans. 2*, **75**, 528, 542 (1979).

10) E. B. Wilson, Jr., J. C. Decius, and P. C. Cross, "Molecular Vibrations," McGraw-Hill, New York (1955), pp. 162—165.

11) A. M. Thorndike, A. J. Wells, and E. B. Wilson, Jr., *J. Chem. Phys.*, **15**, 157 (1947).

12) D. F. Hornig and D. C. McKean, *J. Phys. Chem.*, **59**, 1133 (1955).

13) P. R. Davies and W. J. Orville-Thomas, *J. Mol. Struct.*, **4**, 163 (1969); G. A. Thomas, J. A. Ladd, and W. J. Orville-Thomas, *ibid.*, **4**, 179 (1969).

14) G. A. Thomas, G. Jalsovszky, J. A. Ladd, and W. J. Orville-Thomas, *J. Mol. Struct.*, **8**, 1 (1971).

15) G. Jalsovszky and W. J. Orville-Thomas, *Trans. Faraday Soc.*, **67**, 1894 (1971); B. Galabov and W. J. Orville-Thomas, *J. Chem. Phys.*, **71**, 4716 (1979).

16) M. S. Gordon and W. England, *J. Am. Chem. Soc.*, **94**, 5168 (1972).

17) E. Kapuy and C. Kozmutza, *Theor. Chim. Acta (Berl.)*, **56**, 259 (1980).

18) R. E. Bruns, A. B. M. S. Bassi, and P. M. Kuznesof, *J. Am. Chem. Soc.*, **98**, 3432 (1976).

19) B. Galabov and W. J. Orville-Thomas, *J. Mol. Struct.*, **18**, 169 (1973).

The Physicochemical Properties of Aqueous Solutions of Sodium Alkanesulfonates. Apparent Molar Volumes, Viscosity *B* Coefficients, Heats of Solution, and Surface Tensions

Kunio Tamaki,* Yōko Ōhara, Masahiro Inabe, Tetsushi Mori, and Fumio Numata

Department of Chemistry, Yokohama City University, Kanazawa-ku, Yokohama 236

(Received November 8, 1982)

The apparent molar volumes, viscosity *B* coefficients, heats of solution, and surface activity of sodium alkanesulfonates (RSO_3Na, methyl to hexyl) in water were measured. The limiting apparent molar volumes at 25 °C increase with the number of carbon atoms in the alkyl chain; the increment per methylene group is about 16 $cm^3\ mol^{-1}$. The viscosity *B* coefficients of $MeSO_3Na$ and $EtSO_3Na$ increase with the temperature, while those of *n*-$BuSO_3Na$ decrease with an increase in the temperature. The changes in heat capacity for dissolution in water, ΔC_p°, as calculated from the heats of solution at 15, 25, and 35 °C, were negative for $MeSO_3Na$ and $EtSO_3Na$, while the ΔC_p° values for *n*-$PrSO_3Na$ and higher homologs were positive. $MeSO_3Na$ raises the surface tension of water, while $EtSO_3Na$ and higher homologs reduce it. The structural changes in the solvent water upon the dissolution of sodium alkanesulfonates are discussed in comparison with those of sodium alkyl sulfates previously reported.

The behavior of amphiphilic organic ions in water may be interpreted approximately in terms of a balance of two types of interaction: hydrophobic hydration due to the nonpolar parts, and electrostrictive hydration due to the ionic parts.[1] Both sodium alkanesulfonates (RSO_3Na) and sodium alkyl sulfates ($ROSO_3Na$) are typical amphiphilic organic electrolytes. The temperature dependence of the heats of solution and the viscosity *B* coefficients for a homologous series of $ROSO_3Na$ were reported in previous papers.[2,3] In this paper, experimental results will be reported on the apparent molar volumes, viscosity *B* coefficients, heats of solution, and surface activity of a series of RSO_3Na in water. The main object of this work is to compare the role of the alkyl group of RSO_3Na in the structural influence in water with that of $ROSO_3Na$ previously reported.

Experimental

Materials. The organic chemicals used were commercial products from the Tokyo Kasei Kogyo Co., Ltd. Sodium methane- and ethanesulfonates were prepared by the neutralization of the corresponding sulfonic acids with a solution of sodium hydroxide, after which the water was evaporated to dryness. The sodium salts were twice recrystallized from ethanol–water solutions. The other sodium alkanesulfanates were synthesized by the Strecker method.[4] Alkyl bromides were refluxed with a saturated water solution of sodium sulfite for several days, after which the mixtures were dried in air. The sodium salts were extracted with ethanol and then further purified by repeated recrystallization from ethanol–water solutions until the salts obtained were free from Br^- ion. All the products of sodium alkanesulfonates were subjected to air-drying under a relative humidity of 50%. Analysis using an electrobalance showed that sodium methanesulfonate was anhydrous, while the other ethane-, 1-propane-, 1-butane-, 1-pentane-, and 1-hexanesulfonates were exactly monohydrates. The monohydrate samples were very stable in air. The conversion from monohydrate salts to anhydrous salts was found to be very troublesome, especially for $EtSO_3Na$; therefore, the monohydrate samples were used for the measurements for density, viscosity, and surface tension. Sodium alkyl sulfates used for the measurements of the surface tension were the same samples as were employed in previous studies.[2,3] Water was triply distilled.

Density Measurement. The densities were measured using a vibrating-tube densimeter, twin-type SS-D-200, manufactured by the Shibayama Scientific Co., Ltd. Two measuring vessels were immersed in a water bath with a capacity of about 40 dm^3 controlled to ±0.002 °C. One of the measuring vessels was used for the density measurement of a solution; the other measuring vessel was used for monitoring the density of water. The apparatus constant of the meter was determined using water and dry air as standard substances; their densities were taken from the literature.[5]

Viscosity Measurement. The viscosities were measured with an automatic viscometer manufactured by the Shibayama Scientific Co., Ltd. The flow times of Ubbelohde-type viscometers were about 250 s at 25 °C for water, measuring to 0.01 s. The viscosity, η, was calculated from the average flow time, t, and the density, ρ, based on the equation:

$$\eta = \rho k_1(t - k_2/t). \quad (1)$$

The k_1 and k_2 constants were determined from the measurements for water at 25 and 40 °C. The viscosity values of water at these temperature were taken from the literature.[6]

Calorimetry. The heats of solution of the anhydrous salts in water were measured at 15, 25, and 35 °C with a twin isoperibol calorimeter TIC-2C, manufactured by the Tokyo Riko Co., Ltd. To obtain anhydrous samples, all the salts were dried *in vacuo* at 100 °C for several days. The glass ampoules filled with samples were further dried *in vacuo* at 100 °C for about 6 h and then sealed. The sample and blank ampoules were, respectively, set in the measuring and reference Dewar vessels, each containing 200 cm^3 of water, resting in depressions in an aluminum block controlled to ±0.01 °C. After thermal equilibrium had been attained, the sample and blank ampoules were broken simultaneously. The difference in temperature, as measured by a pair of thermistors, was recorded on a chart recorder. The calorimeter was checked by measuring the heat of solution of potassium chloride at 25 °C. The value obtained was within 1% of that reported in the literature.[7]

Surface-tension Measurement. The surface tensions were measured at 25±0.01 °C by means of the drop-volume method using a micrometer syringe, similar to that described in a previous paper.[8]

Results and Discussion

Apparent Molar Volumes. The apparent molar volumes, ϕ_v, in $cm^3\ mol^{-1}$ were calculated from the densities using the following equation:

$$\phi_v = \frac{1}{m}\left(\frac{1000+mM}{\rho} - \frac{1000}{\rho_0}\right), \quad (2)$$

where m is the molal concentration in $mol\ kg^{-1}$; M, the molar mass in $g\ mol^{-1}$, and ρ_0 and ρ, the densities in $g\ cm^{-3}$ of water and of a solution respectively. The solutions were made by weight. When the sample of $RSO_3Na \cdot H_2O$ was dissolved in water, the quantity of the water was made equal to the total of the weighed quantity of water in a weighing bottle plus the liberated water from the weighed quantity of solid $RSO_3Na \cdot H_2O$; the quantity of the latter was calculated from the chemical formula. The apparent molar volume of electrolytes is given by the equation:[9]

$$\phi_v = \phi_v^\circ + A_v c^{1/2} + B_v c, \quad (3)$$

where ϕ_v° is the limiting value, which is identical with the partial molar volume at an infinite dilution; A_v and B_v, the constants, and c, the molar concentration in $mol\ dm^{-3}$. The value of constant A_v is 1.868 $cm^3\ dm^{3/2}\ mol^{-3/2}$ for water at 25 °C;[9] the relation ϕ_v—$1.868\,c^{1/2}$ *versus* c for a series of RSO_3Na is shown in Fig. 1. The values of ϕ_v° and B_v are given in Table 1. It is found that the ϕ_v° values increase as the alkyl-chain length increases and that the increments in the ϕ_v° values per methylene group from $EtSO_3Na$ to higher homologs are about 16 $cm^3\ mol^{-1}$; this value corresponds approximately to the value of other homologous compounds, such as alkanoates and alkylammonium salts.[10-13] The B_v values of RSO_3Na are found to decrease with an increase in the number of carbon atoms, as is shown in Table 1; this fact is in accord with the results for other homologous compounds.[10-13]

Table 1. Limiting apparent molar volumes of RSO_3Na at 25 °C

RSO_3Na	ϕ_v°/$cm^3\ mol^{-1}$	B_v/$dm\ cm^3\ mol^{-2}$
Methyl	53.99	0
	53.88[a]	
Ethyl	69.31	−1.15
	71.56[a]	
Propyl	85.08	−1.9
Butyl	101.08	−2.25
Pentyl	117.02	−2.7
Hexyl	132.98	−2.8

a) Ref. 11.

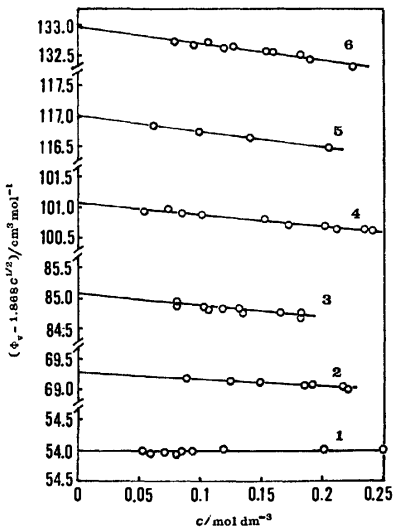

Fig. 1. Apparent molar volumes of RSO_3Na at 25 °C. 1, methyl; 2, ethyl; 3, propyl; 4, butyl; 5, pentyl; 6, hexyl.

Viscosity. The viscosities of RSO_3Na at 25 °C were reported in a previous paper.[1] In this work, the temperature dependence of the viscosity B coefficients for RSO_3Na (methyl to butyl) were reinvestigated by means of a more elaborate apparatus. The viscosity of aqueous electrolyte solution is given by the Jones-Dole equation:[13]

$$\eta/\eta_0 = 1 + A_\eta c^{1/2} + B_\eta c, \quad (4)$$

where η_0 and η are the viscosity of water and the solution respectively; A_η, the constant arising from the interaction between the ions, and B_η, the viscosity B coefficient, which is interpreted in terms of a specific solute-solvent interaction. Equation 4 may be converted to:

$$(\eta/\eta_0 - 1)/c^{1/2} = A_\eta + B_\eta c^{1/2}. \quad (5)$$

For example, Fig. 2 shows the results of the plotting

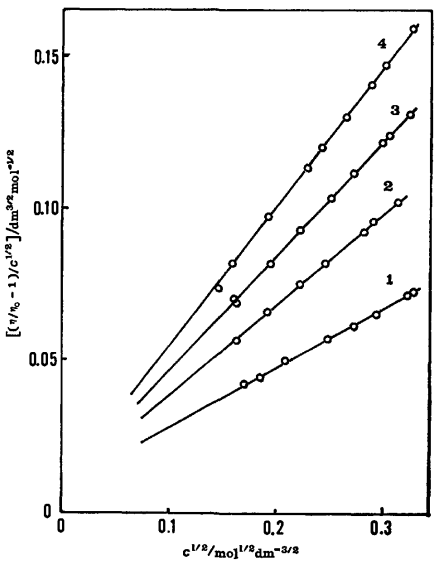

Fig. 2. Plot of $(\eta/\eta_0 - 1)/c^{1/2}$ against $c^{1/2}$ for RSO_3Na at 25 °C. 1, methyl; 2, ethyl; 3, propyl; 4, butyl.

Table 2. Viscosity B/$dm^3\ mol^{-1}$ coefficients of RSO_3Na

RSO_3Na	25 °C	40 °C
Methyl	0.198	0.208
Ethyl	0.304	0.310
Propyl	0.383	0.383
Butyl	0.468	0.436

of Eq. 5 at 25 °C. The B_7 values obtained at 25 and 40 °C are summarized in Table 2. It may be seen in Table 2 that the B_7 values for $MeSO_3Na$ and $EtSO_3Na$ increase with the temperature and that the B_7 values of n-$PrSO_3Na$ are insensitive to the temperature. With n-$BuSO_3Na$, the B_7 values decrease with an increase in the temperature. In a previous work[3] on the viscosity of $ROSO_3Na$ solutions, it was found that $MeOSO_3Na$ showed a slight increase in the B_7 values with the temperature and that the B_7 values of n-$PrOSO_3Na$ decreased slightly with an increase in the temperature. Kay *et al.*,[14] reported an increase in the B_7 values with the temperature for a solvent-structure-breaking salt such as tetramethylammonium salt and a decrease in the B_7 values with an increase in the temperature for a solvent-structure-making salt such as tetrapropyl- and tetrabutylammonium salts. On comparing the viscosity B coefficients of RSO_3Na with those of $ROSO_3Na$, it is found that the hydrophobicity of RSO_3Na is weaker than that of $ROSO_3Na$.

Heat of Solution. Heat-of-solution measurements were carried out in the concentration range of $(1—5)\times10^{-3}$ mol dm^{-3}. In this concentration range, any dependence of the heat of solution on the concentration is within the limit of experimental error, so the average of three or more measurements has been taken as the heat of solution at an infinite dilution, $\Delta H_s°$. The $\Delta H_s°$ values of anhydrous RSO_3Na in water are listed in Table 3. The $\Delta H_s°$ values at 25 °C reported in the literature[15,16] are also included in Table 3. The $\Delta H_s°$ values obtained in this work are slightly more positive than those reported by Krishnan and Friedman.[16] Results from the $\Delta H_s°$ values were used to calculate the change in the heat capacity for dissolution at an infinite dilution, $\Delta C_p°$:

$$\Delta C_p° = d\Delta H_s°/dT, \quad (6)$$

where T is the temperature. The results for $\Delta H_s°$ were represented by the equation:

$$\Delta H_s° = a + bT + cT^2, \quad (7)$$

Table 3. Heats of solution and heat-capacity changes of RSO_3Na

RSO_3Na	$\Delta H_s°$/kJ mol^{-1}			$\Delta C_p°$/J K^{-1} mol^{-1}
	15 °C	25 °C	35 °C	25 °C
Methyl	7.87	6.92	6.17	−85
		6.95[a]		
		6.40[b]		
Ethyl	−2.82	−3.16	−3.48	−33
		−3.60[b]		
Propyl	−6.13	−5.84	−5.63	25
		−6.19[b]		
Butyl	0.08	0.93	1.77	85
		0.84[b]		
Pentyl	−3.59	−2.24	−0.97	131
		−2.68[b]		
Hexyl	−0.96	0.62	2.53	175
		0.25[b]		

a) Ref. 15. b) Ref. 16.

and by:

$$\Delta C_p° = b + 2cT, \quad (8)$$

where a, b, and c are the experimental constants; the $\Delta C_p°$ values obtained at 25 °C are also listed in Table 3. As may be seen in Table 3, $MeSO_3Na$ and $EtSO_3Na$ show negative $\Delta C_p°$ values, while n-$PrSO_3Na$ and higher homologs show the positive $\Delta C_p°$ values, which increase with the number of carbon atoms in the alkyl chain. In an earlier work[2] on a series of $ROSO_3Na$, $MeOSO_3Na$ showed only the negative value of $\Delta C_p°$ and $EtOSO_3Na$ showed insensitive $\Delta H_s°$ values with an increase in the temperature. Further, n-$PrOSO_3Na$ and higher homologs showed positive $\Delta C_p°$ values. Figure 3 shows the $\Delta C_p°$ values as a function of the number of carbon atoms in the alkyl chain of both the RSO_3Na and $ROSO_3Na$ series. The magnitude and sign of $\Delta C_p°$ can be taken as a relative measure of the structural effect upon the solvent water.[17,18] The $\Delta C_p°$ values of simple salts indicate negative values, whereas the $\Delta C_p°$ values of hydrophobic solutes indicate positive values.[18] Therefore, the results (Table 3 and Fig. 3) indicate that the hydrophobic effect of RSO_3Na is weaker than that of $ROSO_3Na$.

Surface Tension. In this paper, the change in the surface tension, $\Delta\sigma$, is defined as:

$$\Delta\sigma = \sigma_0 - \sigma, \quad (9)$$

where σ_0 and σ are the surface tension of water and a solution respectively. Figure 4 shows the change in the surface tension of aqueous solutions of RSO_3Na as a function of the logarithmus of the molar concentration. It may be seen that $MeSO_3Na$ raises the surface tension of pure water, whereas $EtSO_3Na$ and higher homologs reduce the surface tension of water. For comparison, the results[19] for $ROSO_3Na$ presented earlier are shown in Fig. 5. In this case, all the salts represent the surface-active property. The shape of the surface tension-*versus*-concentration curve for an organic salt in aqueous solutions is considered to give a rough criterion of the behavior of the salt in water; simple salt raises the surface tension of water, whereas hydrophobic salts reduce it.[21] In a previous paper[21] on the surface tension of a series of alkylammonium chlorides in aqueous solutions, ethylammonium chloride

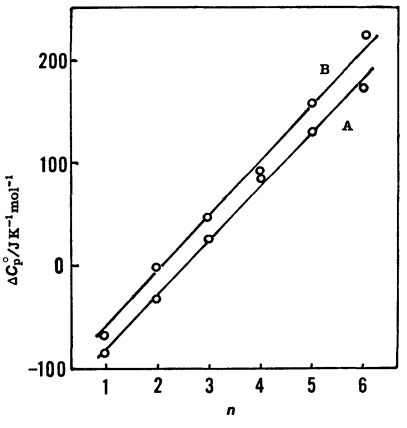

Fig. 3. Plot of $\Delta C_p°$ against number of carbon atoms in the alkyl chain, n. A, RSO_3Na; B, $ROSO_3Na$.

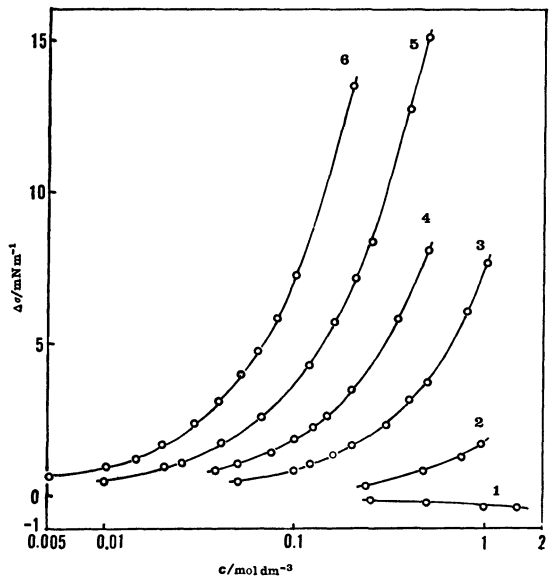

Fig. 4. Change in surface tension as a function of $\log c$ for RSO_3Na. 1, methyl; 2, ethyl; 3, propyl; 4, butyl; 5, pentyl; 6, hexyl.

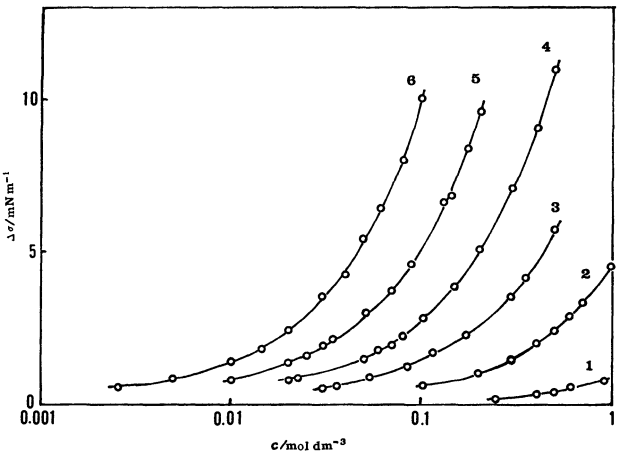

Fig. 5. Change in surface tension as a function of $\log c$ for $ROSO_3Na$. 1, methyl; 2, ethyl; 3, propyl; 4, butyl; 5, pentyl; 6, hexyl.

exhibited a weak surface-active property, while this salt was classified as a weak structure-breaker from the measurement of $\Delta C_p°$.[18] This inclination must be kept in mind when one makes any remark about the behavior of salts in water on the basis of the surface-tension data alone. Nevertheless, as may be seen in Figs. 4 and 5 it is obvious that the surface activity of RSO_3Na in water is rather weaker than that of $ROSO_3Na$.

In order to compare the strength of the surface activity for homologous compounds, the Traube factors are obtained using the $\Delta\sigma$ values *versus* the molar concentration curves shown in Figs. 4 and 5. The Traube factor means the ratio of the molar concentrations of equal $\Delta\sigma$ values when the chain of an aliphatic compound is lengthened by one methylene group. The Traube factors are found to be about 2 for the homologous compounds from *n*-$PrSO_3Na$ to *n*-$C_6H_{13}SO_3Na$ as well as for those from *n*-$PrOSO_3Na$ to *n*-$C_6H_{13}OSO_3Na$ inclusive. This is a characteristic feature of a homologous series of surface-active electrolytes with one alkyl chain.[22]

General Considerations. The classification of the behavior of amphiphilic electrolytes in water is dependent on the experimental method adopted and its interpretation. One should be particularly cautious about the classification when the absolute values of the structural measure are rather small. In general, from the experimental results obtained in this work it may be concluded that the hydrophobic character of RSO_3Na is slightly reduced compared with that of $ROSO_3Na$. In the case of $ROSO_3Na$ studied earlier, $MeOSO_3Na$ is a simple salt, $EtOSO_3Na$ is a borderline solute, and *n*-$PrOSO_3Na$ and higher homologs are hydrophobic structure-makers. On the other hand, in the case of RSO_3Na studied in this work, $MeSO_3Na$ and $EtSO_3Na$ may be classified as simple salts; *n*-$PrSO_3Na$, as a borderline or a weak hydrophobic structure-maker, and *n*-$BuSO_3Na$ and higher homologs, as excellent hydrophobic structure-makers. In this connection, Klevens[23] pointed out that all straight-chain saturated surface-active agents of equal chain length have approximately the same critical micelle concentrations, and that C_{12} sulfonate and C_{11} sulfate belong to the same C_{12} family. In this case, the chain length was measured from the hydrogen of the ultimate carbon to the charged atom at the hydrophilic end of the alkyl chain. From the results of experiments with $\Delta C_p°$, shown in Fig. 3, it is found that the solvent-structure-making effect of the extra –O– group in $ROSO_3Na$ is comparable to about a half of that of a methylene group.

References

1) K. Tamaki, Y. Ōhara, H. Kurachi, M. Akiyama, and H. Odaki, *Bull. Chem. Soc. Jpn.*, **47**, 384 (1974).
2) K. Tamaki, Y. Isomura, and Y. Ōhara, *Bull. Chem. Soc. Jpn.*, **45**, 2939 (1972).
3) K. Tamaki, Y. Ōhara, and Y. Isomura, *Bull. Chem. Soc. Jpn.*, **46**, 1551 (1973).
4) S. Zuffanti, *J. Am. Chem. Soc.*, **62**, 1044 (1940).
5) G. S. Kell, *J. Chem. Eng. Data*, **12**, 66 (1967).
6) L. Korson, W. Drost-Hansen, and F. J. Millero, *J. Phys. Soc.*, **73**, 34 (1969).
7) G. Somsen, J. Coops, and M. W. Tolk, *Recl. Trav. Chim. Pays-Bas*, **82**, 231 (1963).
8) K. Tamaki, *Bull. Chem. Soc. Jpn.*, **40**, 38 (1967).
9) O. Redlich and D. M. Mayer, *Chem. Rev.*, **64**, 221 (1964).
10) J. E. Desnoyers and M. Arel, *Can. J. Chem.*, **45**, 359 (1967).
11) M. Sakurai, *Bull. Chem. Soc. Jpn.*, **46**, 1596 (1973).
12) M. Sakurai, T. Komatsu, and T. Nakagawa, *Bull. Chem. Soc. Jpn.*, **48**, 3491 (1975).
13) G. Jones and M. Dole, *J. Am. Chem. Soc.*, **51**, 1950 (1929).
14) R. L. Kay, T. Vituccio, C. Zawoyski, and D. F. Evans, *J. Phys. Chem.*, **70**, 2336 (1966).
15) D. H. Davies and G. C. Benson, *Can. J. Chem.*, **43**, 3100 (1965).

16) C. V. Krishnan and H. L. Friedman, *J. Solution Chem.*, **2**, 37 (1973).
17) B. Chawla and J. C. Ahluwalia, *J. Solution Chem.*, **4**, 383 (1975).
18) K. Tamaki, S. Yoshikawa, and M. Kushida, *Bull. Chem. Soc. Jpn.*, **48**, 3018 (1975).
19) K. Tamaki and M. Sato, 25th Symposium of Colloid and Surface Chemistry, Fukuoka, Nov. 1972, No. 1A06.
20) K. Tamaki, *Bull. Chem. Soc. Jpn.*, **47**, 2764 (1974).
21) K. Tamaki, *Colloid Polymer Sci.*, **252**, 547 (1974).
22) K. Tamaki, *Bull. Chem. Soc. Jpn.*, **38**, 1987 (1965).
23) H. B. Klevens, *J. Am. Oil Chemists' Assoc.*, **30**, 74 (1953).

 © 1983 The Chemical Society of Japan Bull. Chem. Soc. Jpn., 56, 1935—1943 (1983)

Kinetic Instability of Nonbenzenoid Aromatic Hydrocarbons

Jun-ichi AIHARA

Department of Chemistry, Faculty of Science, Shizuoka University, Oya, Shizuoka 422

(Received November 29, 1982)

Aromatic hydrocarbons have thermodynamically stable cyclic conjugated systems. There is a tacitly accepted view that not only aromatic stabilization but also kinetic stability arise from the same cyclic conjugation of π electrons. In order for this view to be examined criticaly, two reactivity indices, *i.e.*, localization energy and superdelocalizability, were adopted for a variety of cyclic conjugated hydrocarbons, and were compared with those defined for their olefinic reference structures. Interestingly, it was found that chemical reactivity of some constituent carbons might often overcome aromatic stabilization of an entire conjugated system. Not a few nonbenzenoid aromatic hydrocarbons were predicted to have reactive carbons which are olefinic in reactivity. These hydrocarbons constitute unstable aromatic compounds. Thus, it has been clarified that thermodynamic and kinetic stabilities do not always concur in the case of nonbenzenoid hydrocarbons.

An aromatic compound is thermodynamically stable by definition.[1] It is supposed to be more stable than its olefinic reference structure with "localized" π bonds.[1,2] The resonance energy defined in our graph theory of aromaticity is an excellent index of such thermodynamic stability.[3-5] If a given cyclic conjugated system has a large positive resonance energy, it is considered thermodynamically stable and aromatic.[1-5] The predicted aromaticity is due entirely to stabilization by cyclic conjugation.[4]

Our experience tells us that thermodynamic and apparent stabilities of a cyclic conjugated system are closely related to each other. This implies that a thermodynamically stable compound usually has a large kinetic stability. There has been a widely accepted view that aromatic compounds must be stable in a commonplace sense. Thus, thermodynamic stability has long been confused with kinetic stability when one has to decide as to whether a given compound is aromatic or not. Many compounds have been classified as aromatic because of their isolability or low chemical reactivity,[1-5] which are terms of kinetic stability.

Exactly speaking, whether a compound is isolable or not depends not only on the thermodynamic stability, but also on the stability of possible conversion products.[6] A compound predicted to be thermodynamically stable may not be isolable because it can go to still more stable species. Conversely, a high-energy compound may be apparently stable if it has no easy conversion routes available.[6] In principle, all possible reaction paths must be considered to predict kinetic or chemical stability of a cyclic conjugated system.

In fact, all aromatic compounds are neither chemically stable, nor all antiaromatic compounds chemically unstable.[6] Although calicene is predicted to exhibit aromatic stabilization,[2-5,7] it has neither been observed nor isolated. Dimethylenecyclohexadienes are not antiaromatic species,[2-5,8] but they are not isolable. These notable exceptions suggest that chemical stability of a compound might sometimes be determined by factors other than thermodynamic stability. So far there have been few systematic analyses of kinetic stability or instability of cyclic conjugated systems.

The purpose of this paper is to examine kinetic stability of typical aromatic hydrocarbons in conjunction with their aromaticity. I point out that thermodynamic and kinetic stabilities do not always concur in the case of nonbenzenoid aromatic hydrocarbons, and that not a few aromatic hydrocarbons are obviously unstable due to high reactivity toward some kinds of reagents. In order for this feature to be seen explicitly, two reactivity indices, *i.e.*, localization energy[9,10] and superdelocalizability[10,11] are adopted for 42 conjugated hydrocarbons, and are compared with those defined for their olefinic reference structures.

Theoretical Background

The sign and the magnitude of our resonance energy[3-5] are used as an index of aromaticity for cyclic conjugated systems. The degree of aromatic stabilization is given by the resonance energy, divided by the energy of the olefinic reference structure, and then multiplied by 100.[12,13] This quantity is termed a percent resonance energy (%*RE*). Compounds listed in Table 2 are arranged in order of decreasing percent resonance energy. An aromatic compound is said to have as much thermodynamic stability as its resonance energy.

It is impossible to devise a good single index of kinetic stability because there are very many reactions associated with cyclic conjugated systems. In this sense, thermodynamic stability is a much simpler concept than kinetic stability. As will be seen, Wheland's localization energy[9,10] and Fukui's superdelocalizability[10,11] are suitable for surveying one aspect of kinetic stability. These reactivity indices have been defined to elucidate reactivity of conjugated hydrocarbons toward electrophiles and nucleophiles.

Electrophilic substitution, as well as electrophilic addition, involves a reaction with an electrophilic species. Electrophile addition results in a new conjugated system of one less atom and two less π electrons, which is termed a σ complex or Wheland intermediate. Localization energy and superdelocalizability are primary indices when the transition state resembles the σ complex. Abundant evidence has been reported to support the formation of a σ complex as a key intermediate in aromatic substitution.[10]

The reactivity will be different for different hydrocarbons, and also for different positions of attachment of the electrophile in a given hydrocarbon in which there are two or more nonequivalent positions. A conjugated system of a given σ complex is denoted by G-v, where G is a conjugated system of the starting hydrocarbon, and v is a carbon to which the electrophile is attached. Localization energy corresponding to this σ complex with a $+1$ formal charge is denoted by $L_G(v,+1)$. It is defined by[9,10]

$$L_G(v,+1) = E_G(0) - E_{G-v}(+1), \quad (1)$$

where $E_G(0)$ is a total π-electron energy of the starting hydrocarbon with zero formal charge, and $E_{G-v}(+1)$ is that of the σ complex with a $+1$ formal charge. Localization energy is thus a measure of the energy change on going from a given hydrocarbon to the σ complex. Smaller localization energies indicate more susceptible carbons.

Superdelocalizability is another measure of the energy difference between a given hydrocarbon and the σ complex. A possible importance of hyperconjugation through the electrophile-substituted methylene group is stressed in the derivation of superdelocalizability.[11] For a hydrocarbon with N conjugated carbons it is defined by[10,11]

$$S_G(v,+1) = \sum_{i=1}^{N} \frac{g_i P_{G-v}(X_i)}{X_i P_G'(X_i)}. \quad (2)$$

Here, $P_G(X)$ and $P_{G-v}(X)$ are characteristic polynomials for G and G-v, respectively; X_i is the ith energy coefficient, *i.e.*, the ith largest root of the equation $P_G(X)=0$; and g_i is the corresponding occupation number. Superdelocalizability and localization energy are highly correlative with each other.[10]

The fact that stability is always relative leads us to the concept of reference states. We have been using a reference polynomial defined graph-theoretically to describe an olefinic reference structure of a cyclic conjugated system,[3-5,13-17] and interpreted it as a characteristic polynomial for the reference structure. This type of polynomial is denoted by $R_G(X)$. Exactly speaking, $R_G(X)$ is not a characteristic polynomial for the reference structure because it is not a polynomial obtained by expanding the secular determinant; an appropriate secular determinant cannot be defined within the framework of our graph theory.[3-5] Therefore, our olefinic reference structure is hypothetical in nature.

Nevertheless, it is very true that the reference polynomial can be viewed in many respects as a characteristic polynomial for this hypothetical reference structure. Many features of the reference polynomials for cyclic conjugated hydrocarbons are really those of acyclic polyenes:

(a) $R_G(X)$ can be defined in the same manner as a characteristic polynomial for acyclic polyenes,[3] namely,

$$R_G(X) = X^N + \sum_{k=1}^{[N/2]} (-1)^k p(k) X^{N-2k}, \quad (3)$$

where $p(k)$ is the number of ways of choosing k disjoint π bonds from a conjugated system G, and $[N/2]$ is a maximum integer not larger than $N/2$.

(b) The Hess-Schaad reference structure[2] can be considered as an olefinic structure in the singlet ground state since it is constructed using π bonds scissored from acyclic polyenes in the singlet ground state. The energy of this Hess-Schaad reference structure can be reproduced by means of $R_G(X)$, on the assumption that the reference structure defined by this polynomial is in the singlet ground state.[3,16]

(c) The energy levels given as roots of the equation $R_G(X)=0$ satisfy the pairing theorem.[3,4,18] The charge distribution estimated from $R_G(X)$ is uniform over the entire conjugated system.[17] These facts imply that our hypothetical reference structure is a kind of alternant hydrocarbon. Acyclic polyenes are all alternant hydrocarbons.

(d) Neither diamagnetic susceptibility exaltation nor diatropicity are expected in this type of reference structures.[15] The same is true for acyclic polyenes. The above features strongly support our view that $R_G(X)$ is a good characteristic polynomial for the hypothetical reference structure, and that the reference structure defined by $R_G(X)$ is very olefinic in nature. Therefore, we can safely assume that $R_G(X)$ practically represents an olefinic reference structure of a cyclic conjugated system. This interpretation has been consistent with every phase of aromatic chemistry.

On this theoretical basis, we can define reactivity indices for an olefinic reference structure of a cyclic conjugated system. Localization energy for the olefinic reference structure defined by $R_G(X)$ can be defined by

$$L_G^\circ(v,+1) = E_G^\circ(0) - E_{G-v}^\circ(+1), \quad (4)$$

where $E_G^\circ(0)$ and $E_{G-v}^\circ(+1)$ are the total π-electron energies of the reference structures of G and G-v, respectively. In the same manner, superdelocalizability for the reference structure can be defined by

$$S_G^\circ(v,+1) = \sum_{i=1}^{N} \frac{g_i R_{G-v}(X_i^\circ)}{X_i^\circ R_G'(X_i^\circ)}, \quad (5)$$

where X_i° is the ith largest root of the equation $R_G(X)=0$. $L_G^\circ(v,+1)$ and $S_G^\circ(v,+1)$ are reactivity indices which the system G would have if it were free of aromaticity. They are expected to represent the tendency of the reference structure to undergo electrophilic reactions.

Reactivity indices can likewise be defined to describe the tendency to undergo nucleophilic substitution (or addition) reactions. In this case, the intermediate σ complex must have a -1 formal charge. Its total π-electron energy is denoted by $E_{G-v}(-1)$, where v is a carbon to which the nucleophile is attached. Localization energy related to this σ complex is defined by[9,10]

$$L_G(v,-1) = E_G(0) - E_{G-v}(-1). \quad (6)$$

The corresponding superdelocalizability is defined by[10,11]

$$S_G(v,-1) = \sum_{i=1}^{N} \frac{(g_i-2)P_{G-v}(X_i)}{X_i P_G'(X_i)}. \quad (7)$$

For alternant hydrocarbons, such as acyclic polyenes and benzenoid hydrocarbons, $L_G(v,-1)=L_G(v,+1)$ and $S_G(v,-1)=S_G(v,+1)$, so the nucleophilic reactivity

is identical with the electrophilic one. As mentioned before, olefinic reference structures of cyclic conjugated hydrocarbons can also be considered as a kind of alternant hydrocarbons. For these reference structures, indices of nucleophilic reactivity are exactly the same as those of electrophilic reactivity. Therefore,

$$L_G^\circ(v, -1) = L_G^\circ(v, +1) \quad (8)$$

and

$$S_G^\circ(v, -1) = S_G^\circ(v, +1). \quad (9)$$

Localization energy and superdelocalizability can be regarded as indices of kinetic stability (or instability) common to cyclic and acyclic conjugated systems. These indices can be applied equally to aromatic, antiaromatic, and nonaromatic systems to see their electrophilic and nucleophilic reactivities. Whatever the reaction products may be, highly reactive compounds must be very unstable in a kinetic sense. This is a primary reason to choose localization energy and superdelocalizability for the present study of kinetic stability.

Reactivity indices for the olefinic reference structures will give reasonable criteria for estimating the effect of aromaticity on the electrophilic and nucleophilic reactivities. In order to see possible interrelation between aromaticity and reactivity, it is instructive to evaluate the reactivity indices relative to those for the olefinic reference structures, namely,

$$\Delta L_G(v, \pm 1) = L_G(v, \pm 1) - L_G^\circ(v, \pm 1), \quad (10)$$

and

$$\Delta S_G(v, \pm 1) = S_G(v, \pm 1) - S_G^\circ(v, \pm 1). \quad (11)$$

These differences in reactivity index can naturally be ascribed to aromaticity, *i.e.*, cyclic π-electron conjugation of the type $\beta_{ij}\beta_{jk}\cdots\beta_{pq}\beta_{qi}$, where β's are resonance integrals between bonded carbons.[14,15] $\Delta L_G(v, \pm 1)$ and $\Delta S_G(v,\pm 1)$ are hence interpreted as a portion of contribution of aromaticity to kinetic stability. If a given constituent carbon has a small $\Delta L_G(v,\pm 1)$ value or a large $\Delta S_G(v,\pm 1)$ value, it must be olefinic in reactivity.

Results and Discussion

Conjugated carbons in hydrocarbons are classified as shown in Fig. 1. Edge carbons, *i.e.*, exomethylene carbons, are called primary carbons. Carbons shared by two π bonds are called secondary carbons. When a given carbon is shared by three π bonds, it is called a tertiary carbon. Primary, secondary, and tertiary carbons are denoted by Pn, Sn, and Tn, respectively, where the suffixes n indicate nonequivalent carbons.

First, stability considerations are made on the basis of localization energies. Localization energies calculated for all carbons in 42 conjugated hydrocarbons are listed in Tables 1 and 2. Ethylene (**1**), butadiene (**2**), and hexatriene (**3**) in Table 1 are nonaromatic species. In these polyenes, constituent carbons have a variety of localization energies. It is clear that, even in a single conjugated hydrocarbon free of aromaticity, carbons are quite diverse in reactivity. Edge carbons have considerably smaller localization energies than inner carbons. Kinetic stability of a conjugated hydrocarbon is determined by the most reactive carbons. For acyclic polyenes, electrophilic and nucleophilic reactivities are determined primarily by the edge or primary carbons. Each acyclic polyene is identical with its olefinic reference structure.[3-5] Therefore, kinetic stability expressed in terms of localization energy is the same for the two structures.

Table 1. Localization energies for acyclic polyenes

Compound	v	$L_G(v, \pm 1)$
Ethylene (**1**)	P1	2.000
Butadiene (**2**)	P1	1.644
	S1	2.472
Hexatriene (**3**)	P1	1.524
	S1	2.516
	S2	2.159

Let us examine reactivities of cyclic conjugated systems listed in Table 2. Localization energies for the olefinic reference structures, $L_G^\circ(v,\pm 1)$, are now useful for analyzing those for real conjugated systems, $L_G(v, \pm 1)$, in detail. As in the case of acyclic polyenes, $L_G^\circ(v,\pm 1)$ is very small at primary carbons, ranging from 1.22 to 1.48. Secondary carbons have $L_G^\circ(v,\pm 1)$ in the range 1.85—2.40, and tertiary carbons in the range 2.33—3.00. Among tertiary carbons, those next to primary carbons have $L_G^\circ(v,\pm 1)$ larger than 2.81, and those surrounded by three tertiary carbons have $L_G^\circ(v,\pm 1)$ less than 2.41. The values of $L_G^\circ(v,\pm 1)$ at primary carbons never overlap with those at secondary and tertiary carbons. Secondary carbons scarcely overlap with tertiary carbons in this sense. Thus, it is obvious that $L_G^\circ(v,\pm 1)$ is determined by the type of the carbon. If a given conjugated hydrocarbon were deprived of aromaticity, electrophilic and nucleophilic reactivities would be determined primarily by the molecular geometry. Such regularity of the $L_G^\circ(v,\pm 1)$ values further supports the validity of these reference indices.

Benzenoid hydrocarbons **5**—**11** and **14** are highly aromatic since they have large percent resonance energies. These compounds have positive $\Delta L_G(v,\pm 1)$ values at all constituent carbons, so they must be much less reactive than their olefinic reference structures. This means that all the carbons are stabilized by aromaticity, *i.e.*, cyclic π-electron conjugation. All carbons in benzene (**5**) have the same $L_G(v,\pm 1)$ value of 2.536 and the same $\Delta L_G(v,\pm 1)$ value of 0.273. These large values show that benzene is kinetically very stable in accord with its chemical behavior. Naphthalene (**8**) and other condensed benzenoid hydrocarbons are predicted to be a little more reactive than benzene since some of the secondary carbons have smaller $L_G(v,\pm 1)$ values; when $L_G(v,\pm 1)$ is small at carbon v, $\Delta L_G(v,\pm 1)$ usually is small there. Smaller $\Delta L_G(v,\pm 1)$ values naturally indicate enhanced olefinic reactivity. In fact, when appropriate reagents coexist with these compounds, they are not so stable as benzene. In the case of biphenyl (**6**), triphenylene (**7**), naphthelene (**8**), phenanthrene (**9**), and anthracene (**14**), not only substitution but also addition products are formed by reaction with molecular chlorine.[19]

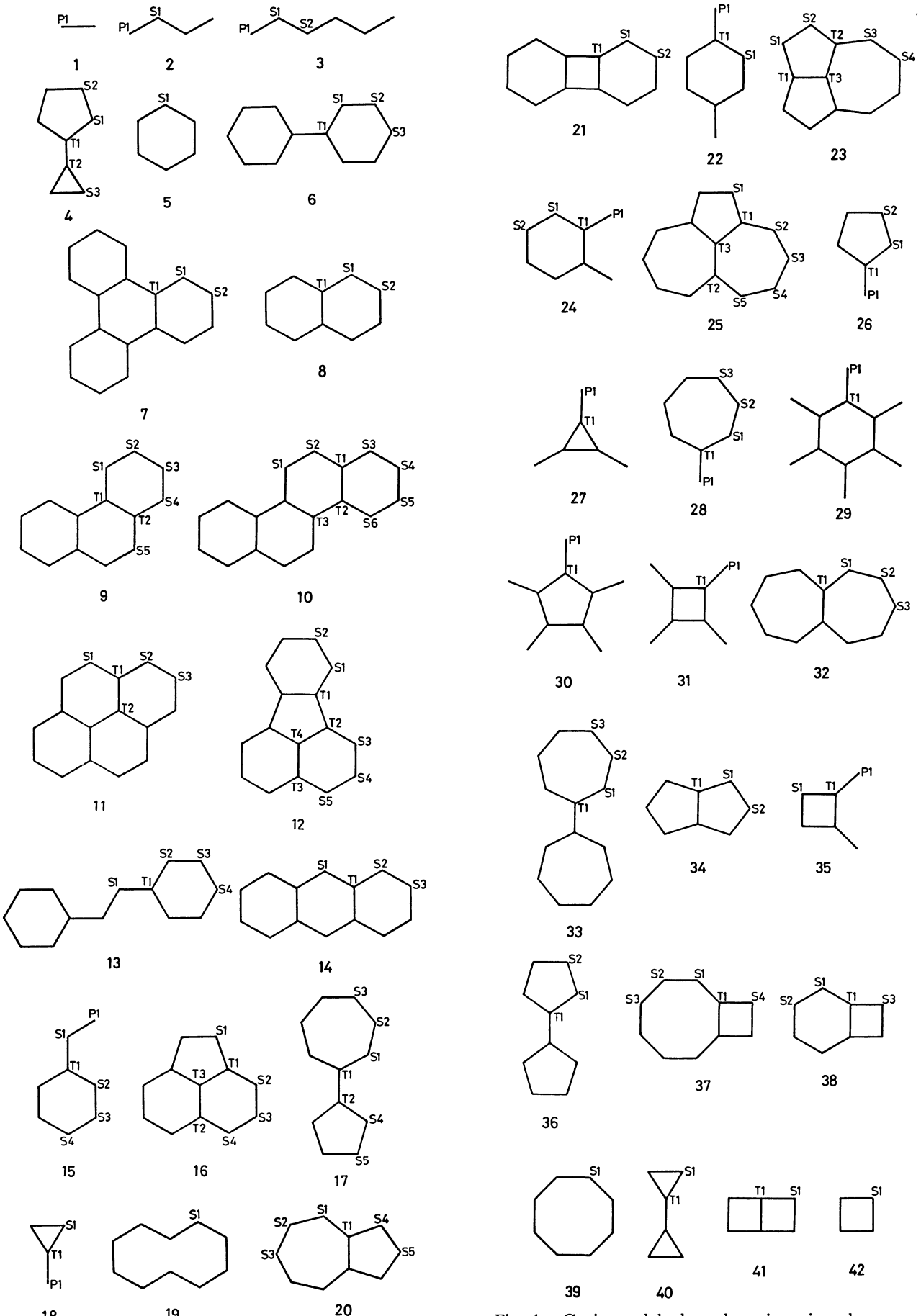

Fig. 1. Conjugated hydrocarbons investigated.

TABLE 2. LOCALIZATION ENERGIES FOR CYCLIC CONJUGATED HYDROCARBONS

Compound	%*RE*	v	$L_G°(v, \pm 1)$	$L_G(v, +1)$	$\Delta L_G(v, +1)$	$L_G(v, -1)$	$\Delta L_G(v, -1)$
Calicene (**4**)	4.13	S1	1.940	1.998	0.058	2.728	0.788
		S2	2.081	2.078	−0.003	3.005	0.924
		S3	1.858	2.863	1.005	2.022	0.164
		T1	2.569	2.467	−0.102	3.703	1.134
		T2	2.350	3.703	1.353	2.467	0.117
Benzene (**5**)	3.53	S1	2.263	2.536	0.273	2.536	0.273
Biphenyl (**6**)	3.16	S1	2.105	2.400	0.295	2.400	0.295
		S2	2.298	2.544	0.246	2.544	0.246
		S3	2.156	2.447	0.291	2.447	0.291
		T1	2.690	2.919	0.229	2.919	0.229
Triphenylene (**7**)	3.01	S1	2.111	2.378	0.267	2.378	0.267
		S2	2.189	2.477	0.288	2.477	0.288
		T1	2.559	2.881	0.322	2.881	0.322
Naphthalene (**8**)	2.92	S1	2.102	2.299	0.197	2.299	0.197
		S2	2.220	2.480	0.260	2.480	0.260
		T1	2.667	3.056	0.389	3.056	0.389
Phenanthrene (**9**)	2.89	S1	2.122	2.365	0.243	2.365	0.243
		S2	2.182	2.453	0.271	2.453	0.271
		S3	2.212	2.497	0.285	2.497	0.285
		S4	2.086	2.317	0.231	2.317	0.231
		S5	2.109	2.298	0.189	2.298	0.189
		T1	2.556	2.889	0.333	2.889	0.333
		T2	2.639	3.007	0.368	3.007	0.368
Chrysene (**10**)	2.81	S1	2.312	2.351	0.219	2.351	0.219
		S2	2.065	2.254	0.189	2.254	0.189
		S3	2.073	2.302	0.229	2.302	0.229
		S4	2.205	2.492	0.287	2.492	0.287
		S5	2.172	2.448	0.276	2.448	0.276
		S6	2.111	2.349	0.238	2.349	0.238
		T1	2.638	3.022	0.384	3.022	0.384
		T2	2.548	2.902	0.354	2.902	0.354
		T3	2.522	2.822	0.300	2.822	0.300
Pyrene (**11**)	2.73	S1	2.099	2.274	0.175	2.274	0.175
		S2	1.995	2.190	0.195	2.190	0.195
		S3	2.263	2.549	0.286	2.549	0.286
		T1	2.648	2.966	0.318	2.966	0.318
		T2	2.467	2.908	0.441	2.908	0.441
Fluoranthene (**12**)	2.64	S1	2.109	2.371	0.262	2.371	0.262
		S2	2.176	2.435	0.259	2.435	0.259
		S3	2.001	2.465	0.464	2.465	0.464
		S4	2.276	2.503	0.227	2.503	0.227
		S5	1.969	2.341	0.372	2.078	0.109
		T1	2.531	2.781	0.250	2.781	0.250
		T2	2.585	2.734	0.149	2.734	0.149
		T3	2.719	3.064	0.345	3.064	0.345
		T4	2.406	2.715	0.309	3.021	0.615
Stilbene (**13**)	2.61	S1	2.104	2.157	0.053	2.157	0.053
		S2	2.051	2.318	0.267	2.318	0.267
		S3	2.309	2.548	0.239	2.548	0.239
		S4	2.113	2.379	0.266	2.379	0.266
		T1	2.758	2.989	0.231	2.989	0.231
Anthracene (**14**)	2.52	S1	1.922	2.013	0.091	2.013	0.091
		S2	2.059	2.231	0.172	2.231	0.172
		S3	2.189	2.423	0.234	2.423	0.234
		T1	2.661	3.025	0.364	3.025	0.364

TABLE 2. (Continued)

Compound	%*RE*	v	$L_G°(v, \pm 1)$	$L_G(v, +1)$	$\Delta L_G(v, +1)$	$L_G(v, -1)$	$\Delta L_G(v, -1)$
Styrene (**15**)	2.45	P1	1.610	1.704	0.094	1.704	0.094
		S1	2.448	2.424	−0.024	2.424	−0.024
		S2	2.120	2.370	0.250	2.370	0.250
		S3	2.297	2.546	0.249	2.546	0.249
		S4	2.175	2.424	0.249	2.424	0.249
		T1	2.711	2.960	0.249	2.960	0.249
Acenaphthylene (**16**)	2.18	S1	2.056	2.124	0.068	2.124	0.068
		S2	1.958	2.525	0.567	1.999	0.041
		S3	2.282	2.513	0.231	2.513	0.231
		S4	1.958	2.417	0.459	1.969	0.011
		T1	2.634	2.812	0.178	2.812	0.178
		T2	2.727	3.066	0.339	3.066	0.339
		T3	2.355	2.566	0.211	3.135	0.780
Sesquifulvalene (**17**)	1.73	S1	1.915	2.454	0.539	1.964	−0.049
		S2	2.075	2.781	0.706	2.073	−0.002
		S3	2.010	2.601	0.591	2.035	0.025
		S4	1.882	1.972	0.090	2.506	0.624
		S5	1.991	2.062	0.071	2.715	0.724
		T1	2.516	3.361	0.845	2.471	−0.045
		T2	2.424	2.471	0.047	3.361	0.937
Triafulvene (**18**)	1.29	P1	1.435	0.962	−0.473	2.962	1.527
		S1	2.071	2.134	0.063	2.134	0.063
		T1	2.899	2.962	0.063	2.962	0.063
[10]Annulene (**19**)	1.25	S1	2.157	2.317	0.160	2.317	0.160
Azulene (**20**)	1.14	S1	2.020	2.551	0.531	1.929	−0.091
		S2	2.197	2.341	0.144	2.341	0.144
		S3	2.070	2.730	0.660	1.988	−0.082
		S4	1.973	1.924	−0.049	2.600	0.627
		S5	2.212	2.362	0.150	2.362	0.150
		T1	2.585	2.736	0.151	2.736	0.151
Biphenylene (**21**)	0.75	S1	2.128	2.408	0.280	2.408	0.280
		S2	2.219	2.352	0.133	2.352	0.133
		T1	2.605	2.522	−0.083	2.522	−0.083
3,6-Dimethylene-1,4-cyclohexadiene (**22**)	0.62	P1	1.298	1.204	−0.094	1.204	−0.094
		S1	2.136	2.197	0.061	2.197	0.061
		T1	2.965	3.026	0.061	3.026	0.061
Cyclopent[*cd*]azulene (**23**)	0.62	S1	2.085	2.352	0.267	1.970	−0.115
		S2	2.056	1.972	−0.084	2.382	0.326
		S3	2.038	2.553	0.515	1.988	−0.050
		S4	2.151	2.638	0.487	2.077	−0.074
		T1	2.557	2.479	−0.078	3.048	0.491
		T2	2.597	3.042	0.445	2.486	−0.111
		T3	2.355	2.313	−0.042	2.882	0.527
5,6-Dimethylene-1,3-cyclohexadiene (**24**)	0.60	P1	1.329	1.233	−0.096	1.233	−0.096
		S1	2.016	2.076	0.060	2.076	0.060
		S2	2.232	2.291	0.059	2.291	0.059
		T1	2.907	2.966	0.059	2.966	0.059
Cyclopenta[*ef*]heptalene (**25**)	0.56	S1	2.052	2.014	−0.038	2.491	0.439
		S2	2.031	2.204	0.173	1.934	−0.097
		S3	2.122	2.061	−0.061	2.463	0.341
		S4	2.144	2.436	0.292	2.060	−0.084
		S5	2.009	1.937	−0.072	2.221	0.212
		T1	2.564	2.505	−0.059	2.981	0.417
		T2	2.600	2.995	0.395	2.513	−0.087
		T3	2.334	2.801	0.467	2.319	−0.015

TABLE 2. (Continued)

Compound	%*RE*	v	$L_G°(v, \pm 1)$	$L_G(v, +1)$	$\Delta L_G(v, +1)$	$L_G(v, -1)$	$\Delta L_G(v, -1)$
Fulvene (**26**)	0.27	P1	1.291	2.230	0.939	0.994	−0.297
		S1	1.982	2.002	0.020	2.002	0.020
		S2	2.220	2.240	0.020	2.240	0.020
		T1	2.974	2.994	0.020	2.994	0.020
[3]Radialene (**27**)	0.12	P1	1.473	1.459	−0.014	1.459	−0.014
		T1	2.819	2.828	0.009	2.828	0.009
Heptafulvene (**28**)	0.09	P1	1.223	1.006	−0.217	1.897	0.674
		S1	1.931	1.940	0.009	1.940	0.009
		S2	2.258	2.267	0.009	2.267	0.009
		S3	2.107	2.116	0.009	2.116	0.009
		T1	2.997	3.006	0.009	3.006	0.009
[6]Radialene (**29**)	0.06	P1	1.468	1.464	−0.004	1.464	−0.004
		T1	2.828	2.837	0.009	2.837	0.009
[5]Radialene (**30**)	0.00	P1	1.468	1.468	0.000	1.468	0.000
		T1	2.828	2.828	0.000	2.828	0.000
[4]Radialene (**31**)	−0.73	P1	1.468	1.504	0.036	1.504	0.036
		T1	2.830	2.758	−0.072	2.758	−0.072
Heptalene (**32**)	−0.89	S1	1.982	1.660	−0.322	2.193	0.211
		S2	2.175	2.032	−0.143	2.032	−0.143
		S3	2.034	1.715	−0.319	2.337	0.303
		T1	2.568	2.427	−0.141	2.427	−0.141
Heptafulvalene (**33**)	−1.20	S1	1.900	1.513	−0.387	1.949	0.049
		S2	2.045	1.626	−0.419	2.248	0.203
		S3	1.988	1.586	−0.402	2.088	0.100
		T1	2.472	2.029	−0.443	2.919	0.447
Pentalene (**34**)	−2.02	S1	2.024	2.380	0.356	1.538	−0.486
		S2	2.247	2.027	−0.220	2.027	−0.220
		T1	2.616	2.401	−0.215	2.401	−0.215
Dimethylenecyclobutene (**35**)	−2.21	P1	1.371	1.612	0.241	1.612	0.241
		S1	2.144	1.982	−0.162	1.982	−0.162
		T1	2.899	2.736	−0.163	2.736	−0.163
Fulvalene (**36**)	−2.28	S1	1.906	1.987	0.081	0.987	−0.919
		S2	2.024	2.236	0.212	1.452	−0.572
		T1	2.471	3.091	0.620	1.855	−0.616
Bicyclo[6.2.0]decapentaene (**37**)	−3.46	S1	2.064	2.191	0.127	2.191	0.127
		S2	2.228	2.046	−0.182	2.046	−0.182
		S3	2.161	2.112	−0.049	2.112	−0.049
		S4	2.176	1.839	−0.337	1.839	−0.337
		T1	2.676	2.215	−0.461	2.215	−0.461
Benzocyclobutene (**38**)	−3.65	S1	2.127	2.261	0.134	2.261	0.134
		S2	2.255	2.173	−0.082	2.173	−0.082
		S3	2.209	1.661	−0.548	1.661	−0.548
		T1	2.719	2.326	−0.393	2.326	−0.393
Cyclooctatetraene (**39**)	−5.80	S1	2.197	1.602	−0.595	1.602	−0.595
Triafulvalene (**40**)	−5.81	S1	1.925	1.035	−0.890	2.114	0.189
		T1	2.461	1.464	−0.997	3.464	1.003
Butalene (**41**)	−7.31	S1	2.261	2.061	−0.200	2.061	−0.200
		T1	2.797	2.193	−0.604	2.193	−0.604
Cyclobutadiene (**42**)	−23.46	S1	2.398	1.172	−1.226	1.172	−1.226

Especially, carbon Sl in anthracene is very reactive and olefinic since $L_G(Sl,\pm1)$ and $\Delta L_G(Sl,\pm1)$ are very small. All other carbons in benzenoid hydrocarbons have $\Delta L_G(v,\pm1)$ in the range 0.172—0.441.

Fluoranthene (**12**) contains a five-membered ring, but this is similar in reactivity to benzenoid hydrocarbons. All constituent carbons are highly stabilized by aromaticity. The same is true for the second member of aromatic annulenes, [10]annulene (**19**). All carbons are moderately stabilized. However, this compound is far from isolable because of heavy steric hindrance.[20]

Stilbene (**13**) and styrene (**15**) are aromatic compounds, but can be regarded as substituted ethylenes. Carbons at ethylenic portions have small $L_G(v,\pm1)$ values and small positive or negative $\Delta L_G(v,\pm1)$ values, and tend to undergo addition reactions. They are located outside of the aromatic rings. Acenaphthylene (**16**) is olefinic in reactivity at carbon Sl. In accord with this, $L_G(Sl,\pm1)$ and $\Delta L_G(Sl,\pm1)$ are very small. Biphenylene (**21**) has small positive resonance energy. However, $\Delta L_G(Tl,\pm1)$ is negative, suggesting that carbon Tl is highly destabilized by the antiaromatic central four-membered ring. Several addition reactions are known to occur around this ring.[21]

Other nonbenzenoid hydrocarbons generally have reactive carbons with smaller localization energies. Azulene (**20**) has long been recognized to be the first example of nonbenzenoid aromatics. This compound undergoes various electrophilic and nucleophilic substitution reactions only under mild conditions.[22] These observations may be rationalized by the negative values of $\Delta L_G(S1,-1)$, $\Delta L_G(S3,-1)$, and $\Delta L_G(S4,+1)$. These negative values, however, indicate that azulene is more reactive than its olefinic reference structure. In fact, oxidative decomposition and hydrogenation easily take place.[23]

Two asymmetric fulvalenes **4** and **17** are predicted to be highly aromatic with large resonance energies. However, there is no experimental evidence for aromatic stabilization.[24] Calicene (**4**) has defied all attempts of isolation. Both compounds are supposed to be very olefinic in reactivity; either $\Delta L_G(v,+1)$ or $\Delta L_G(v,-1)$ is small or negative at each carbon. Therefore, all carbons must be very reactive toward electrophiles or nucleophiles. We might say that the entire π-electron frameworks of these fulvalenes are really aromatic but very unstable.

All radialenes **27** and **29**—**31**, fulvenes **18**, **26**, and **28**, and dimethylenecyclohexadienes **22** and **24** are all predicted to be essentially nonaromatic with small percent resonance energies. They have one or more primary carbons, at which $L_G(v,\pm1)$ is very small as in the case of acyclic polyenes. Secondary and tertiary carbons are also olefinic with $\Delta L_G(v,\pm1)\approx0$. These compounds are very olefinic in their chemical behavior. Triafulvene (**18**) and dimethylenecyclohexadienes are too reactive to be isolated in any form. The same is true for dimethylenecyclobutene (**35**). This compound does readily polymerize in the presence of air.[25] Conjugated hydrocarbons with exomethylene groups are thus extremely reactive. Benzene, fulvene, and dimethylenecyclobutene form an interesting set of isomers, being respectively aromatic, nonaromatic, and antiaromatic, but the first species alone is of great kinetic stability.

Cyclopent[*cd*]azulene (**23**) and cyclopenta[*ef*]heptalene (**25**) are substantially nonaromatic. These nonalternant hydrocarbons are not highly symmetric in shape, so they necessarily have reactive carbons with negative $\Delta L_G(v,+1)$ or $\Delta L_G(v,-1)$ values. These carbons determine the degree of kinetic stability associated with electrophilic and nucleophilic reactivities.

In marked contrast to asymmetric fulvalenes, symmetric fulvalenes **33**, **36**, and **40** are all typically antiaromatic; either $\Delta L_G(v,+1)$ or $\Delta L_G(v,-1)$ at each carbon takes a large negative value. Therefore, they are predicted to be much more reactive than their olefinic reference structures. This is in agreement with their chemistry.[24] Triafulvalene (**40**) has not been isolated yet. Other antiaromatic hydrocarbons belong to the group of such chemically very unstable species. Among them are heptalene (**32**), pentalene (**34**), bicyclo[6.2.0]decapentaene (**37**), benzocyclobutene (**38**), cyclooctatetraene (**39**), butalene (**41**), and cyclobutadiene (**42**). They tend to polymerize readily, or are obtained as a dimer which may arise by way of a self-Diels-Alder reaction. Some carbons in each of these hydrocarbons again have small localization energies together with large negative $\Delta L_G(v,+1)$ or $\Delta L_G(v,-1)$ values. This indicates that antiaromatic instability itself is relaxed by forming appropriate σ complexes. Especially, all carbons in cyclooctatetraene, butalene, and cyclobutadiene have negative $\Delta L_G(v,\pm1)$ values.

We have been examining the values of $L_G(v,\pm1)$ and $\Delta L_G(v,\pm1)$ to discuss the discrepancy between aromaticity and kinetic stability. Essentially the same discussion can be made using Fukui's concept of superdelocalizability, $S_G(v,\pm1)$.[10,11] The magnitude of superdelocalizability for the olefinic reference structure of a cyclic conjugated hydrocarbon, $S_G^\circ(v,\pm1)$, depends primarily on the type of the carbon.[26] Although there are several exceptions, $S_G^\circ(v,\pm1)$ is larger at primary carbons than at secondary carbons, and at secondary carbons than at tertiary carbons. If a given carbon v is stabilized by the cyclic conjugation of π electrons, $S_G(v,\pm1)$ becomes smaller than $S_G^\circ(v,\pm1)$, so the difference $\Delta S_G(v,\pm1)$ becomes negative in sign. When $S_G(v,\pm1)$ is large at carbon v, $\Delta S_G(v,\pm1)$ usually is large there. Reactive carbons specified in terms of $S_G(v,\pm1)$ and $\Delta S_G(v,\pm1)$ are essentially the same as those specified in terms of $L_G(v,\pm1)$ and $\Delta L_G(v,\pm1)$. Such a parallelism can be rationalized partly by noting that $L_G(v,\pm1)$ is theoretically interrelated with $S_G(v,\pm1)$.[27]

In brief, benzenoid hydrocarbons, fluoranthene, and [10]annulene are thermodynamically stable with large $\%_0RE$ values, and are predicted to be rather resistant to electrophiles and nucleophiles. Stilbene, styrene, acenaphthylene, azulene, biphenylene, cyclopent[*cd*]-azulene, cyclopenta[*ef*]heptalene, dimethylenecyclohexadienes, radialenes, and asymmetric fulvalenes must be very reactive toward electrophiles and/or nucleophiles whether these hydrocarbons are aromatic with positive resonance energies or not. All other hydro-

carbons investigated must be much more reactive than nonaromatic polyenes. This aspect of kinetic stability or instability is in good agreement with their chemical behavior.[28]

Concluding Remarks

Thermodynamic stability of a cyclic conjugated system may correlate with its kinetic stability. However, there are such notable exceptions as aromatic compounds for which all synthetic attempts failed. These compounds must have conversion routes to others with still larger kinetic stability. The present approach complements the stability considerations based solely on aromaticity. Using the concepts of localization energy and superdelocalizability, we found that the kinetic stability of a cyclic conjugated system can be conjectured well from its electrophilicity and nucleophilicity. In this sense, localization energy and superdelocalizability are representative indices of kinetic stability. $\Delta L_G(v,\pm 1)$ and $\Delta S_G(v,\pm 1)$ serve as indices of olefinic reactivity. Highly electrophilic and/or nucleophilic carbons were shown to be very olefinic in reactivity. Therefore, hydrocarbons having such carbons are reluctant to retain their original cyclic conjugated systems. When they are attacked by an electrophile or a nucleophile, reaction paths to compounds other than substitution products will be chosen preferentially.

Most nonbenzenoid hydrocarbons have reactive carbons whether they are aromatic or not. In these hydrocarbons not only aromaticity but also reactivity are induced by the same cyclic interactions of π electrons. Many of the anomalies found in the aromaticity-stability relationship can be rationalized in this manner. Examination of reactivities other than electrophilic and nucleophilic ones would further clarify the essence of kinetic stability. In view of excellent correlation between calculated reactivity indices and chemical behavior, we emphasize that aromatic compounds are quite diverse in kinetic stability. Thermodynamic and kinetic stabilities do not always concur in the case of nonbenzenoid hydrocarbons. Some compounds may appear to be chemically stable because their conjugate acids and bases are both stable.[1] According to the present approach, these will be predicted to be reactive and unstable.

If only cyclic unsaturated compounds characterized by low chemical reactivity and high thermodynamic stability are regarded as aromatic compounds, they will be limited to benzenoid hydrocarbons and some semibenzenoids such as fluoranthene. All carbons in these compounds are really stabilized by the cyclic π-electron conjugation. Most nonbenzenoid hydrocarbons will become nonaromatic in this sense. However, we choose to call them unstable aromatic compounds, retaining the original definition of aromaticity based on thermodynamic stability.

It is interesting to see that the most reactive carbons sometimes vary on going from a real conjugated system to its olefinic reference structure. However, the most reactive carbons in benzenoid hydrocarbons usually remain the same in their olefinic reference structures. This indicates that aromaticity, *i.e.*, cyclic π-electron conjugation, scarcely affects relative reactivities of constituent carbons in these compounds.

Finally, one comment must be made concerning the π-electron densities. Localization energy and superdelocalizability are applicable only to the reaction with an electrophile or a nucleophile for which the transition state resembles the σ complex. If the transition state occurs early in the same reaction, that is, if the transition state resembles the initial reactants, the π-electron densities will be a primary index.[10,29] Here, an electrophile or a nucleophile acts as an opposite-charge-seeking species. It follows that if the reaction proceeds via an early transition state, any nonalternant hydrocarbon would be more reactive than its olefinic reference structure, where the charge distribution is uniform as in the case of alternant hydrocarbons.[17] This implies that nonalternant hydrocarbons must be more reactive toward electrophiles and nucleophiles than alternant hydrocarbons including acyclic polyenes. This is possibly another reason why many nonalternant hydrocarbons are much more reactive than are predicted from their resonance energies.

References

1) M. J. S. Dewar and G. J. Gleicher, *J. Am. Chem. Soc.*, **87**, 685, 692 (1965); M. J. S. Dewar and C. de Llano, *ibid.*, **91**, 789 (1969).
2) B. A. Hess, Jr., and L. J. Schaad, *J. Am. Chem. Soc.*, **93**, 305, 2413 (1971); *J. Org. Chem.*, **36**, 3418 (1971).
3) J. Aihara, *J. Am. Chem. Soc.*, **98**, 2750 (1976).
4) J. Aihara, *Pure Appl. Chem.*, **54**, 1115 (1982).
5) I. Gutman, M. Milun, and N. Trinajstić, *J. Am. Chem. Soc.*, **99**, 1692 (1977).
6) B. A. Hess, Jr., and L. J. Schaad, *Aust. J. Chem.*, **25**, 2331 (1972).
7) H. Kollmar, *J. Am. Chem. Soc.*, **101**, 4832 (1979).
8) G. J. Gleicher, D. D. Newkirk, and J. C. Arnold, *J. Am. Chem. Soc.*, **95**, 2526 (1973).
9) G. W. Wheland, *J. Am. Chem. Soc.*, **64**, 900 (1942).
10) A. Streitwieser, Jr., "Molecular Orbital Theory for Organic Chemists," Wiley, New York (1961), Chap. 11.
11) K. Fukui, T. Yonezawa, and C. Nagata, *Bull. Chem. Soc. Jpn.*, **27**, 423 (1954); *J. Chem. Phys.*, **27**, 1247 (1957).
12) J. Aihara, *Bull. Chem. Soc. Jpn.*, **52**, 2202 (1979).
13) J. Aihara, *Bull. Chem. Soc. Jpn.*, **53**, 2689 (1980).
14) J. Aihara, *J. Am. Chem. Soc.*, **98**, 6840 (1976).
15) J. Aihara, *J. Am. Chem. Soc.*, **101**, 558, 5913 (1979); **103**, 5704 (1981).
16) J. Aihara, *Chem. Phys. Lett.*, **73**, 404 (1980).
17) I. M. Gutman, *Bull. Soc. Chim. Beograd*, **43**, 191 (1978). See also Ref. 13.
18) C. A. Coulson and G. S. Rushbrooke, *Proc. Cambridge Phil. Soc.*, **36**, 193 (1940).
19) P. B. D. de la Mare, *Acc. Chem. Res.*, **7**, 361 (1974).
20) S. Masamune and N. Darby, *Acc. Chem. Res.*, **5**, 272 (1972).
21) J. W. Barton, "Nonbenzenoid Aromatics," ed by J. P. Snyder, Academic Press, New York (1969), Vol. I, Chap. 2.
22) A. G. Anderson, Jr., J. A. Nelson, and J. J. Tazuma, *J. Am. Chem. Soc.*, **75**, 4980 (1953).
23) H. Pommer, *Angew. Chem.*, **62**, 281 (1950).
24) H. Prinzbach, *Pure Appl. Chem.*, **28**, 281 (1971).
25) W. D. Huntsman and H. J. Wristers, *J. Am. Chem. Soc.*, **89**, 342 (1967).
26) The list of $S_G(v,\pm 1)$ and $S_G^\circ(v,\pm 1)$ for 42 conjugated hydrocarbons is available on request.
27) K. Fukui, T. Yonezawa, and C. Nagata, *J. Chem. Phys.*, **26**, 831 (1957).
28) D. M. G. Lloyd, "Carbocyclic Non-Benzenoid Aromatic Compounds," Elsevier, Amsterdam (1966).
29) G. A. Olah, *Acc. Chem. Res.*, **4**, 240 (1971).

Excitation Energy Dependence of Intramolecular Exciplex Formation and Electronic Relaxation in the Collision-free Vapor

Michiya ITOH*, Yukio HANASHIMA, Naoko WADA, and Ichiro HANAZAKI†

Faculty of Pharmaceutical Sciences, Kanazawa University, Takara-machi, Kanazawa 920

†*Institute for Molecular Science, Myodaiji, Okazaki 444*

(Received December 14, 1982)

The excitation energy dependence of the intramolecular exciplex formation and the electronic relaxation has been studied in the collision-free vapor of 1-(9,10-dicyano-2-anthryl)-3-(pentamethylphenyl)propane. The fluorescence quantum yields and lifetimes of the 9,10-dicyanoanthryl moiety and the intramolecular exciplex in the collision-free vapor were observed to depend on the excitation energy within the S_1 absorption band. From the quantum yields and the decay rate constants, the excitation energy dependence of the association and dissociation rate constants of the intramolecular exciplex formation were determined. The association rate constant of the exciplex formation increases more remarkably with increasing excitation energy than the nonradiative rate constants of 9,10-dicyanoanthryl moiety and the exciplex. The excitation energy dependence of the association rate constant was discussed in terms of the nonradiative transition from the initial optical state to the final exciplex and the level density of the final state, which were calculated in the simple model system by means of the semi-classical mechanics.

The exciplex formation in the vapor phase was reported in the 9-cyanoanthracene and/or substituted 9-cyanoanthracene and alkylamine systems[1,2] and in the tetracyanobenzene (TCNB) and *p*-xylene system.[3] Okajima and Lim[4] reported that the exciplex formed from the vibrationally hot S_1 state of TCNB and the ground state of *p*-xylene is almost nonfluorescent and decays rapidly via nonradiative process. Recently, Itoh *et al.*[5,6] reported that the intramolecular exciplex of 1-(9,10-dicyano-2-anthryl)-3-(1- or 2-naphthyl)propane ($\beta\alpha$- or $\beta\beta$-DCAN) in the collision-free vapor phase exhibits the excitation energy dependence of the fluorescence spectra and lifetimes of the exciplex. They suggested that exciplex formation from the vibrationally hot S_1 state of the electron acceptor and the ground state donor moieties followed by the fluorescent relaxation from the upper vibrational state of the exciplex takes place. In the intermolecular electron donor acceptor system, the concentration of the electron donor (or acceptor) amounts to 10^{-2}—10^{-3} mol dm^{-3} in the vapor phase, which corresponds to the gas pressure of approximately 50 Torr (1 Torr=133.322 Pa). The donor molecules in this pressure may act as a collisional relaxer of the vibrationally hot S_1 state of the acceptor.[7] Therefore, the vibrational effect on the exciplex formation and the electronic relaxation can not be measured in the intermolecular system. The electronic interaction between the electron donor–acceptor system can be investigated only in the isolated molecular condition of the intramolecular electron donor acceptor system. Further, Itoh and Hanashima[8] reported the excitation energy dependence of the rate constants of intramolecular exciplex formation in the collision-free vapor. The rate constant of the exciplex formation increases remarkably on the excitation of the upper vibrational S_1 state. Very recently, Felker *et al.*[9] also reported the excess energy dependence of the exciplex fluorescence in the jet-cooled molecules of the intramolecular electron donor acceptor system.

On the other hand, the excitation energy dependence of the fluorescence lifetimes, quantum yields, and the radiative and nonradiative rate constants has been reported in the single vibronic level (SVL) fluorescence of some aromatic compounds. Further, numerous investigations of the vibrational level dependence of the photochemical reaction such as dissociation and isomerization of small molecules have been published.[10] However, no excitation energy dependence of the molecular complex formation and bimolecular reaction in the excited state has been reported except two papers mentioned above, though the important role of the S_1 excess energy on the photochemical reaction was pointed out.[11] This paper is further concerned with the excitation energy dependence of the association and dissociation rate constants of the exciplex formation in the collision-free vapor of 1-(9,10-dicyano-2-anthryl)-3-(pentamethylphenyl)propane (DCAB).[12] The rate constants of the exciplex formation and dissociation increase with increasing vibrational energy of the S_1 state of the 9,10-dicyanoanthryl (DCA) moiety. In order to investigate the excitation energy dependence, the transition probability from the initial locally excited state of DCA to the final exciplex was estimated in the model system by means of the semi-classical mechanics. The results suggest that the excess energy dependence may be mostly attributable to the density of the vibrational levels of the exciplex state.

Experimental

Preparation and purification of the sample were described in the previous papers.[12] 2-Methyl-9,10-dicyanoanthracene was prepared by bromination and cyanogenation of 2-methylanthracene (Nakarai Chem. GR), and purified by repeated column chromatography (silica gel. benzene–hexane) followed by recrystallization. 1-(9,10-Dicyano-2-anthryl)-3-(pentamethylphenyl)propane was synthesized from the starting materials of 2-anthraldehyde and pentamethylacetylbenzene, and purified by repeated column chromatography and recrystallization.[12] The rectangular quartz cell (10 mm) with graded seals containing samples was degassed and sealed off from the vacuum line. Fluorescence and absorption spectra were measured in a quartz dewar at controlled temperature by heated air flow. The fluorescence and absorption spectra were measured by Hitachi MPF-4 and 220 spectrophotometers, respectively. The fluorescence lifetimes

and decay curves were measured in the excitations by a nitrogen laser and its pumped dye laser (Molectron UV-12 and DL-14), and by an HTVR666 photomultiplier and a Tektronix 7904 (7A19 and 7B85) oscilloscope. Observed decay curves were analyzed by a computer-simulated deconvolution. The fluorescence quantum yields were determined by using a quinine sulfate solution as a standard (1×10^{-5} mol dm^{-3} in 0.25 mol dm^{-3} sulfuric acid; $\phi=0.54$ at room temperature)[13] where the fluorescence spectra of the standard solution were measured in the almost completely same experimental set-up as those of the vapor phase.

Results and Discussion

The absorption spectrum of DCAB in the vapor phase at 500—550 K shows a very weak absorption intensity as shown in Fig. 1, because of a very low vapor pressure. Assuming that the absorption intensity of DCAB in the vapor phase may be almost identical to that in the nonpolar solution, the concentration and pressure of DCAB in the vapor phase at this temperature were estimated to be 10^{-6}—10^{-7} mol dm^{-3} and 10^{-2}—10^{-3} Torr, respectively. Since the intermolecular collisional rate of the S_1 state of the molecule in the gas pressure of p is estimated to be 10^7p Torr^{-1} s^{-1} by a hard sphere collision model,[14] the molecules of DCAB in the experimental condition may be regarded to be an intermolecularly collision-free condition, that is the isolated molecular condition.

The fluorescence and excitation spectra of this collision free vapor of DCAB are shown in Fig. 1. The excitation spectra monitored at 450 and 500 nm are in good consistency with that of the absorption spectrum. Further, the fluorescence spectrum of 2-methylanthracene (2-Me-DCA) in the collision-free condition is also shown in Fig. 1. From comparison of the fluorescence spectrum of DCAB with that of 2-Me-DCA, the shorter wavelength fluorescence (400—460 nm) and the longer wavelength one (450—520 nm) are ascribed to the 9,10-dicyanoanthryl (DCA) moiety and the intramolecular exciplex in the vapor phase, respectively. The fluorescence intensity of the collision-free vapor of DCAB was observed to exhibit a remarkable excitation energy dependence. Figure 2 shows the relative fluorescence quantum spectra in the excitations at several wavelengths, the relative intensity decreases with increasing excitation energy. Further, the fluorescence spectral distribution shifts to the shorter wavelength region with increasing excitation energy, as shown in Fig. 3.

The photochemical reaction scheme and kinetics in the intramolecular exciplex formation are expressed by the following wellknown equations;[15]

$$\mathrm{D} + \mathrm{A}^* \underset{k_4}{\overset{k_3}{\rightleftharpoons}} (\mathrm{DA})^*$$

$$(\mathrm{DA})^* \xrightarrow{k_1} \mathrm{D} + \mathrm{A} + h\nu, \quad (\mathrm{DA})^* \xrightarrow{k_2} \mathrm{D} + \mathrm{A}$$

$$(\mathrm{DA})^* \xrightarrow{k_5} \mathrm{D} + \mathrm{A} + h\nu', \quad (\mathrm{DA})^* \xrightarrow{k_6} \mathrm{D} + \mathrm{A}$$

$$[\mathrm{A}^*] = c_1\exp(-\lambda_1 t) + c_2\exp(-\lambda_2 t), \tag{1}$$

$$[(\mathrm{DA})^*] = c_3\exp(-\lambda_1 t) - c_3\exp(-\lambda_2 t), \tag{2}$$

$$2\lambda_1,\ 2\lambda_2 = (X+Y) \pm \{(Y-X)^2 + 4k_3k_4\}^{1/2},$$

$$X = k_1 + k_2 + k_3, \qquad Y = k_4 + k_5 + k_6,$$

where A and D are DCA and phenyl moieties, respec-

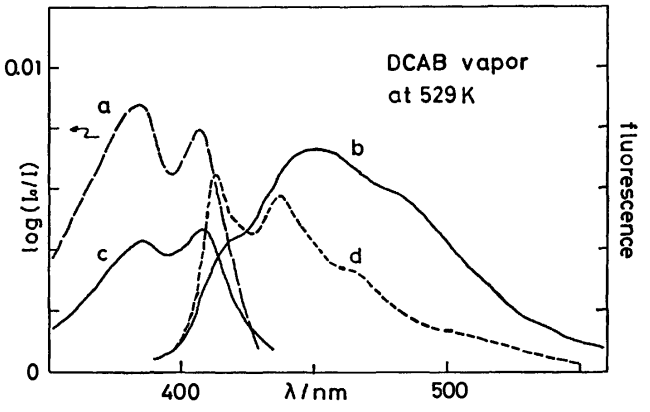

Fig. 1. (a) Electronic absorption spectrum of DCAB in the vapor phase. (b) Fluorescence (excited at 385 nm) and (c) excitation (monitored at 500 nm) spectra of the collision-free vapor of DCAB at 529 K. (d) Fluorescence spectrum of the collision-free vapor of 2-Me-DCA (excited at 385 nm) at 458 K. The fluorescence spectra are uncorrected.

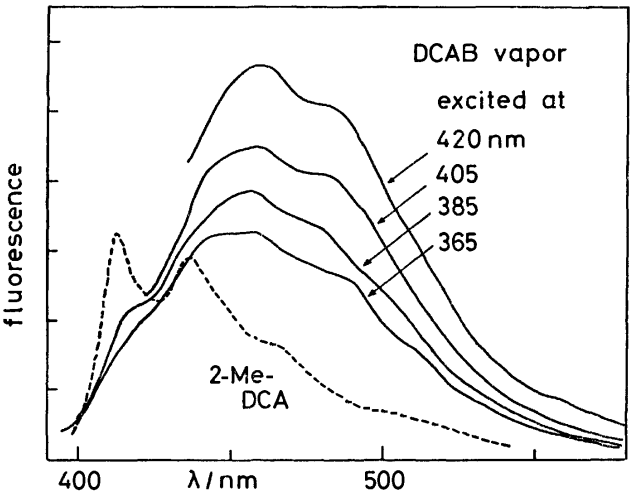

Fig. 2. The relative fluorescence quantum spectra of the collision free vapor of DCAB in the excitations at several wavelengths at 529 K. The spectra are corrected.

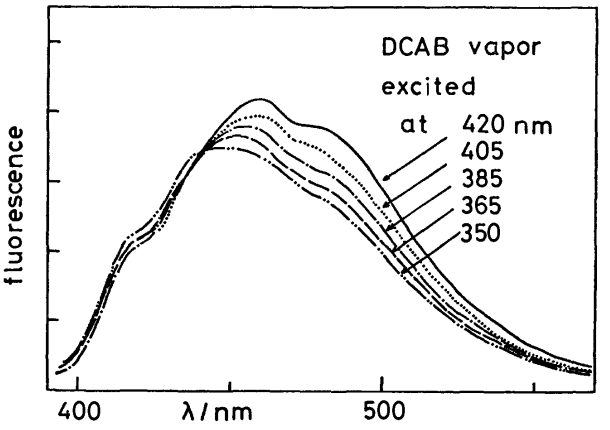

Fig. 3. The excitation wavelength dependence of the fluorescence spectral distribution of the collision-free vapor of DCAB at 529 K. The spectra are normalized in intensity at 440 nm and uncorrected.

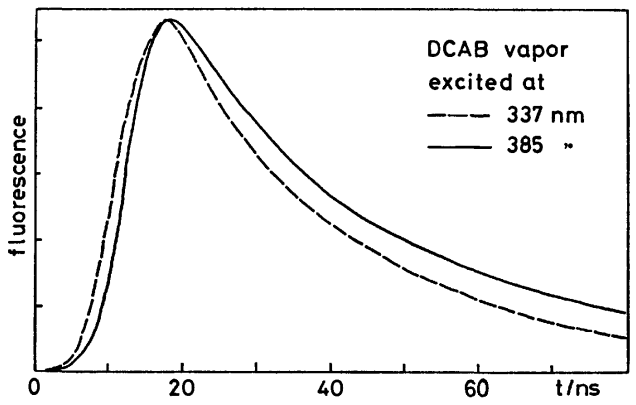

Fig. 4. Typical fluorescence decay curves (monitored at 430 nm) of the DCAB vapor at 525 K. The curve (— — —) was excited at 337 nm (pulse FWHM $\approx$10 ns) and analyzed for $A\exp(-\lambda_2 t)+(1-A)\exp(-\lambda_1 t)$, $\lambda_1^{-1}=28.94$, $\lambda_2^{-1}=1.47$ ns, and $A=0.7675$; the curve (——) excited at 385 nm (pulse FWHM $\approx$7 ns), $\lambda_1^{-1}=41.42$, $\lambda_2^{-1}=7.09$ ns, and $A=0.4984$.

tively. In the collision-free vapor, A* and (DA)* imply the upper vibrational states of their S_1 states depending on the excitation energy. Spears and Rice reported that the quantum yields and the lifetimes of the SVL fluorescence of benzene vapor exhibit different excitation energy dependences from each other according to the vibrational sequence.[16] However, the intramolecular vibrational energy redistribution (randomization) might take place at a rather high temperature.[17] If the considerable fast redistribution of the vibrational energy may take place, A* and (DA)* may be expressed by each sum of several vibrational states, and the decay of these states may be expressed by multi-exponential or an average from these vibrational states. The decay curves of A* and (DA)* were observed to be approximately double (at 430 nm) and single (at 580 nm) exponentials, respectively. Therefore, A* and (DA)* are considered as a quasi-single vibronic state in equilibrium. The typical decay curves of the collision-free vapor of DCAB excited at 337 and 385 nm are shown in Fig. 4. Therefore, the decay rate constants λ_1 and λ_2 were obtained from the A* fluorescence decay (Eq. 1) for respective excitation energies. However, no significant rise time (λ_2^{-1}) of the (DA)* fluorescence (Eq. 2) was observed because of the spectral overlap of A* and (DA)* fluorescences, as will be mentioned later, though the same decay rate constant λ_1 was obtained from the (DA)* fluorescence as that of A*. These decay rate constants are summarized in Table 1 for several excitation wavelengths.

The fluorescence quantum yield and lifetime of the collision free vapor of 2-Me-DCA were observed to depend on the excitation energy. From these excitation energy dependences, radiative and nonradiative rate constants were determined at 523 K, as summarized in Table 1. On the other hand, the fluorescence quantum yields of A* (ϕ_a) and (DA)* (ϕ_e) in DCAB are expressed as follows;

$$\phi_a = k_1 Y/(XY-k_3k_4) \quad (4)$$

$$\phi_e = k_3k_5/(XY-k_3k_4). \quad (5)$$

Table 1. Excitation wavelength dependence of fluorescence quantum yields (ϕ_a and ϕ_e), and decay (10^7 s^{-1}) and reaction rate constants (10^7 s^{-1}) of the intramolecular exciplex formation in DCAB vapor at 523—526 K

Excitation	337 nm	365 nm	385 nm	405 nm
ϕ_a[a]	0.07	0.15	0.19	0.28
ϕ_e	0.23	0.33	0.33	0.27
k_1[a]	1.8	2.5	2.7	2.8
k_2[a]	11	6.8	5.8	4.3
λ_1	3.4	3.0	2.4	2.2
λ_2	66	18	14	10
k_3[b]	50.6	8.5	5.6	3.3
k_4[b]	5.8	0.9	0.2	—
k_5[b]	2.3	2.4	2.1	1.7
k_6[b]	0.4	0.3	0.2	2.3

a) Determined from the collision-free vapor of 2-Me-DCA; errors are approximately $\pm$10%. b) Errors are approximately $\pm$20%.

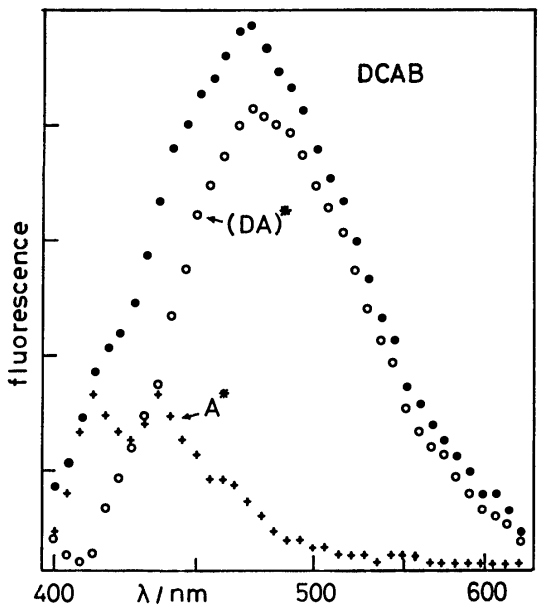

Fig. 5. An example of the separation of the fluorescence spectra (corrected) of the collision-free vapor of DCAB into those of DCA moiety and exciplex.

The fluorescence spectra of A* and (DA)* overlap very close each other. Therefore, assuming that the fluorescence spectrum of DCA moiety (A*) in DCAB is identical to that of 2-Me-DCA in the several excitation energies, the fluorescence spectrum (corrected) obtained was divided into the A* and (DA)* fluorescence spectra by the computer simulation as shown in Fig. 5. Then, the quantum yields ϕ_a and ϕ_e were obtained in the respective excitation energies. Furthermore, assuming k_1 and k_2 to be identical to the radiative and nonradiative rate constants of 2-Me-DCA, respectively, the rate constants k_3, k_4, k_5, and k_6 were determined from decay rate constants λ_1 and λ_2, and quantum yields (ϕ_a and ϕ_e). These data

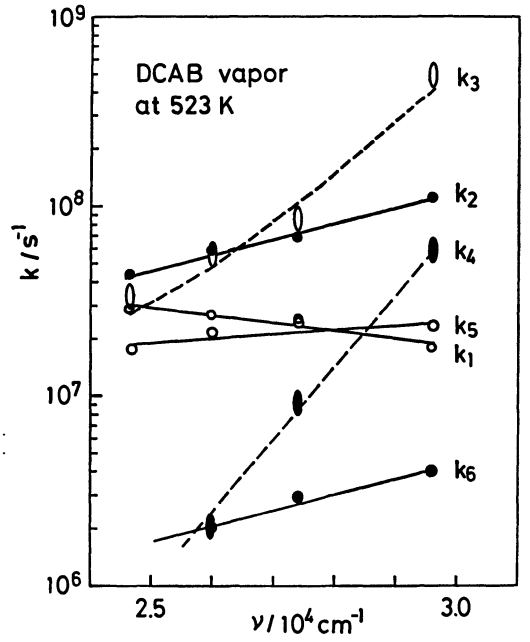

Fig. 6. The plots of rate constants *vs.* excitation energy (wavenumber unit) shown in Table 1.

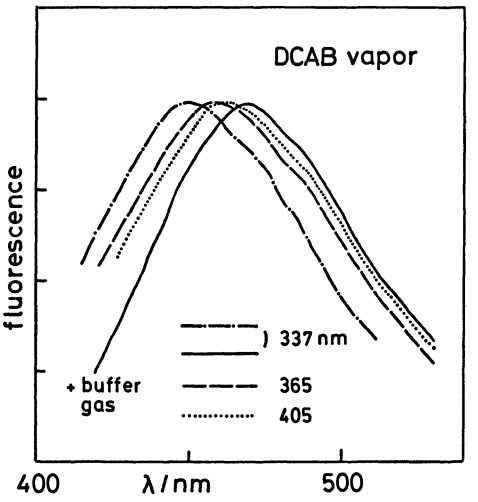

Fig. 7. Time-resolved fluorescence spectra of the DCAB vapor (523 K) in the excitations at several wavelengths. The spectra were depicted at 50 ns after a laser pulse; (—●—●—) 337 nm, (— — —) 365 nm, (·····) 405 nm for the collision-free vapor. The spectrum (——) of the collisionally relaxed vapor by 50 Torr hexane gas excited at 337 nm. The spectra are normalized in intensity.

are summarized in Table 1.

The quantum yield of the DCA moiety, ϕ_a, decreases remarkably and λ_2 increases with increasing excitation energy. As the results, the association (k_3) and dissociation (k_4) rate constants of the exciplex formation increase with increasing excitation energy in the DCAB vapor. Similar excitation energy dependence of the exciplex formation in the collision-free vapor of $\beta\beta$-DCAN and also the intramolecular excimer formation in *N,N,N',N'*-tetramethylpropanediamine vapor were reported in the previous papers.[8,18] Figure 6 shows log plots of these rate constants *vs.* excitation energy (wave number). The nonradiative rate constants of the DCA moiety (k_2) and the exciplex (k_6) increase markedly with increasing excitation energy. The nonradiative rate constants of polyatomic molecules are known to depend linearly on the exponential of the excitation energy.[19,20] The observed excitation energy dependence of k_2 and k_6 exhibits a reasonable trend from this point of view. However, it is noteworthy that $\log k_3$ and $\log k_4$ increase extraordinarily with increasing vibrational energy level, and shows a significant deviation from a linear relationship with respect to the energy; the reason will be discussed later.

The collision-free vapor of DCAB shows the excitation energy dependence of the spectral distribution of the exciplex, as mentioned above. Figure 3 exhibits that the exciplex fluorescence seems to shift to the longer wavelength region with decreasing excitation energy, while the fluorescence of 2-Me-DCA was observed to exhibit conversely a little blue shift. In order to demonstrate the shift of the exciplex fluorescence, the time-resolved fluorescence (Fig. 7) was depicted at ≈50 ns after a laser pulse. The spectral distribution shows red shift with decreasing excitation energy. However, the spectra of the collisionally relaxed vapor of DCAB by the buffer gas (≈500 Torr hexane gas) shows the longest wavelength fluorescence irrespective of the excitation energy. Halpern and Gartmen reported the similar excitation energy dependence of the fluorescence spectrum of *N,N'*-dimethylpiperidine vapor and suggested it to be the fluorescence from the unrelaxed state.[21] The fluorescence spectral distribution depending excitation energy is attributable to the fluorescent deactivation from the upper vibronic S_1 states. The excitation energy dependence of the spectra provides an important information of potential energy surfaces of both ground and excited states of the exciplex. The fluorescence spectra of usual aromatic compounds such as 2-Me-DCA in the collision-free vapor exhibit a faint red shift with increasing excitation energy. The fact is usually interpreted by a consideration that the potential curve of the fluorescent state may be shallower than that of the ground state. In the exciplexes, however, the ground state corresponding to the exciplex is considered to be repulsive and very shallow. Therefore, the fluorescence from the upper vibrational level may shift to the shorter wavelength region than that from the lower level.

An extraordinary vibrational energy dependence of the rate constant was reported in an atom molecular reaction such as $KCl+H=K+HCl$.[22] The rate constant from the vibrational state $v=1$ of HCl is approximately 100 times as large as that from $v=0$. Numerous experimental and theoretical investigations have been reported in the vibrational and rotational energy dependence on the reaction rate constants.[23,24] However, it is not properly interpreted how these observed effects of vibrational energy to the reaction rate constants are to be attributable to the activation energy and/or the pre-exponential factor in the reaction rate equation. Further, in the excited-state electron donor–acceptor interaction, the rate constant of the

exciplex formation between the vibrationally hot S_1 state (*via* S_2) of TCNB and the ground state of *p*-xylene (7×10^{12} mol^{-1} dm^3 s^{-1}) was suggested to be an order of magnitude greater than that from the vibrationally relaxed S_1 state (7×10^{11} mol^{-1} dm^3 s^{-1}).[4] It is noteworthy that these rate constants of the excited-state interaction show an unusual dependence on the vibrational energy of the S_1 state reported here and also in the previous papers.[8,18] Very recently, Felker *et al.* reported the excitation energy dependence of the exciplex fluorescence spectra and decay rate in the jet-cooled molecular EDA system, as mentioned in the introductory section. The extent of the excitation energy dependence of the exciplex fluorescence lifetimes seems to be more remarkable in the jet-cooled molecule than those in the collision-free vapor at rather high temperature,[6-8,18] though Felker *et al.* did not determine any excitation energy dependence of the association and dissociation rate constants of the exciplex in the jet-cooled molecule. These facts are quite reasonable in the jet-cooled molecule, because the randomization of the vibrational energy may be limited at low temperature. However, the kinetic determination of the association rate constant of the exciplex formation seems to be almost impossible, since the estimation of the fluorescence quantum yield is very difficult in the supersonic expansion.

The nonradiative rate constant of the electronic excited state is usually discussed in terms of the transition probability of the Fermi Golden rule for the nonradiative process.[25-28] Further, the excited-state proton transfer is also considered as the nonradiative process between the double minimum potential of the hydrogen bonding system.[29] However, this theory of the nonradiative transition can not be strictly applicable to (DA)* formation because of the repulsive potential in the initial optical state of A* and D, as shown in Fig. 8. In the excitation into the upper vibrational states of the 9,10-dicyanoanthryl moiety in DCAN and DCAB, which is connected to the electron donor moiety by trimethylene chain, the vibrational energy in the aromatic ring system seems to dissipate to the methylene chain by the vibrational-vibrational ($V-V$) energy transfer. Then, stretching and/or bending vibrations in trimethylene chain of DCAN and DCAB are induced by the $V-V$ energy transfer. This means that the vibrational to translational ($V-T$) energy transfer occurs through the trimethylene chain, and that the DCA moiety obtains translational energy.

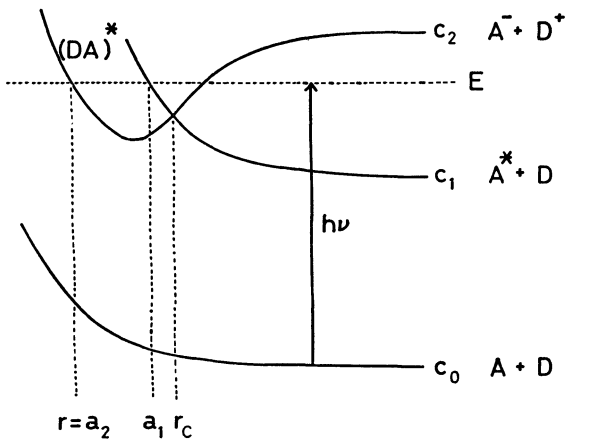

Fig. 8. Schematic potential energy curves of the exciplex formation.

In order to simplify the theoretical consideration, the electronic interaction between the electron donor acceptor is assumed to be a kind of Coulomb interaction between D and A* which are assumed simply to be two atoms. Figure 8 shows the potential energy curves of D+A (C_0), D+A* (C_1), and $(D^+ + A^-)$* (C_2) along the reaction coordinate. Here, the following assumptions are made in order to solve the problem by means of the semi-classical mechanics; the C_2 potential is considerably lower than C_1 at the stable interatomic distance of (DA)* and the CT interaction between C_1 and C_2 is small so that the potential curve for (DA)* can be approximately by C_2. The transition from the initial state (D+A*) to the complex state (DA)* occurs at the crossing point of $r=r_c$, where the energy and also momentum are conserved. According to the Landau's theory,[30] the transition probability (w) from the initial state (D+A*) to the (DA)* state is expressed as following equation;

$$w=\frac{2\pi}{h\nu}\left\{\left|\int X_2^* V(r) X_1 \mathrm{d}r\right|\right\}^2, \tag{6}$$

where $V(r)$ is a perturbation energy of interaction between two states, and X_1 and X_2 are semi-classical wave functions in the (D+A*) and (DA)* states, respectively. From the simple model calculation, the estimated transition probability (w) was ploted *vs.* the excess energy from the potential barrier, as shown in Fig. 9. The transition probability exhibits a considerable decrease with increasing excess energy, but does not depend greatly on the excess energy.

Okajima and Lim[4,31] suggested an importance of the Franck Condon factor associated with the transition

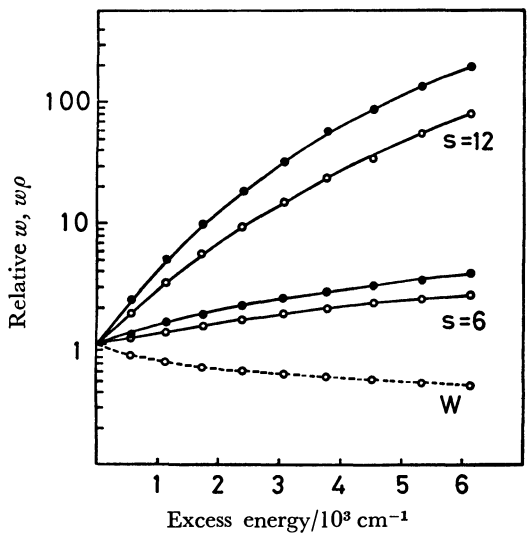

Fig. 9. Relative transition porbability (w, --O--O--) and the product of w and the level density (ρ) calculated by the semiclassical mechanics for the simple model system; (—●—●—) $\Delta E=1800$ cm^{-1}, (—O—O—) $\Delta E=2500$ cm^{-1}. Data are normalized at zero excess energy (see text).

from the uncomplexed to complexed component molecules in the vibrational energy dependence of the association rate constant (k_3). The Franck-Condon factor is expected to be large for a vibration. Further, they suggested that the vibrational excitation in a good accepting mode render the vibration a better accepting mode, then the rate constant may be increased by vibrational excitation.[31] On the other hand, since the actual molecules such as DCAB and DCAN have a large number of vibrational and rotational energy levels, the reaction rate constant of the exciplex formation may be proportional to the product of the transition probability (w) and the vibrational level density (ρ) of the final exciplex state. The semiclassical approximation for the density of vibrational energy levels of polyatomic molecules was proposed by Haarhoff,[32] where the density is expressed as follows;

$$\rho = (E+E_0)^{s-1}/[(s-1)!h\nu_1]. \quad (9)$$

Here ν_1 is the wave number of normal mode i; s is the number of the vibrational freedom. In this paper, the level density of the final state (ρ) was estimated at several excess energies (E_x) for a simple model system of two atoms as mentioned above. Figure 9 shows the product of transition probability and the estimated level density *vs.* the excess energy from the potential barrier (ΔE), of which level is higher than the zero point energy; $E=E_x+\Delta E$. The excess energy dependence of $w\rho$ in the case of $s=10$—12 and $\Delta E=1800\ \mathrm{cm}^{-1}$ seems qualitatively to interpret that of the rate constant k_3 (Fig. 6), though the model calculation of $w\rho$ is not accurate and the profiles of the curves of the excess energy dependence are considerably different from each other. Therefore, Fig. 9 may tentatively suggest that the excess energy dependence of k_3 seems to be attributable to the level density of the final exciplex state.

References

1) S. Hirayama, G. C. Abbott, and D. Phillips, *Chem. Phys. Lett.*, **56**, 497 (1978).
2) S. Hirayama, *Chem. Phys. Lett.*, **63**, 596 (1979).
3) J. Prochorow, S. Okajima, and E. C. Lim, *Chem. Phys. Lett.*, **66**, 590 (1979).
4) S. Okajima and E. C. Lim, *Chem. Phys. Lett.*, **70**, 283 (1980).
5) M. Itoh, T. Kotani, and Y. Hanashima, *Chem. Phys. Lett.*, **75**, 307 (1980).
6) M. Itoh, T. Kotani, and Y. Hanashima, *J. Am. Chem. Soc.*, **103**, 3271 (1980).
7) M. Itoh and Y. Hanashima, *Bull. Chem. Soc. Jpn.*, **54**, 3271 (1981).
8) M. Itoh and Y. Hanashima, *Chem. Phys. Lett.*, **83**, 405 (1981).
9) P. M. Felker, J. S. Syage, Wm. R. Lambert, and A. H. Zewail, *Chem. Phys. Lett.*, **92**, 1, (1982).
10) (a) R. S. Lewis, K. Y. Tang, and E. K. C. Lee, *J. Chem. Phys.*, **65**, 2910 (1976); (b) K. Y. Tang and E. K. C. Lee, *ibid.*, **65**, 1833 (1976).
11) N. J. Turro, W. Ramaurthy, W. Cherry, and W. Farmethy, *Chem. Rev.*, **78**, 125 (1978), and references therein.
12) M. Itoh, Y. Kumano, and T. Okamoto, *Bull. Chem. Soc. Jpn.*, **49**, 42 (1976).
13) J. N. Demas and G. A. Grosby, *J. Phys. Chem.*, **75**, 991 (1971).
14) H. Baba, "Laser and Chemical Reaction," ed by S. Tsuchiya, Japan Scientific Societies Press, Tokyo (1980), p. 62.
15) W. R. Ware, D. Watt, and D. Holmes, *J. Am. Chem. Soc.*, **96**, 7853 (1974).
16) K. G. Spears and S. A. Rice, *J. Chem. Phys.*, **55**, 6561 (1971).
17) Y. Hirata and E. C. Lim, *Chem. Phys. Lett.*, **71**, 167 (1980).
18) M. Itoh, Y. Hanashima, and I. Hanazaki, *J. Phys. Chem.*, **87**, 569 (1983).
19) S. A. Rice "Excited States," ed by E. C. Lim, Academic Press, New York (1975), Vol. 2, p. 111.
20) K. F. Freed, "Topics in Applied Physics," ed by F. K. Fong, Springer, Berlin (1976), Vol. 15, p. 23, and references therein.
21) A. M. Halpern and T. Gartman, *J. Am. Chem. Soc.*, **96**, 1393 (1974).
22) F. E. Bartoszek, D. M. Manos, and J. C. Polanyi, *J. Chem. Phys.*, **69**, 933 (1978).
23) I. P. Herman and J. B. Marling, *J. Chem. Phys.*, **71**, 643 (1979).
24) H. Schor, S. Chapman, S. Green, and R. N. Zare, *J. Chem. Phys.*, **68**, 3790 (1978).
25) D. F. Heller, K. F. Freed, and W. M. Gelbert, *J. Chem. Phys.*, **56**, 2309 (1972).
26) K. F. Freed and J. Jortner, *J. Chem. Phys.*, **52**, 6272 (1970).
27) R. Euglman and J. Jortner, *Mol. Phys.*, **18**, 145 (1970).
28) G. S. Beddard, G. P. Fleming, O. L. J. Gijzemann, and G. Porter, *Chem. Phys. Lett.*, **18**, 48 (1973).
29) H. Shizuka, K. Matsui, Y. Hirata, and I. Tanaka, *J. Phys. Chem.*, **80**, 2070 (1976), and references therein.
30) L. Landau and E. Lifshitz, "Quantum Mechanics," Addison-Wesley, Mass. (1968).
31) S. Okajima and E. C. Lim, *J. Phys. Chem.*, **86**, 4120 (1982).
32) P. C. Haarhoff, *Mol. Phys.*, **7**, 101 (1963).

 © 1983 The Chemical Society of Japan Bull. Chem. Soc. Jpn., 56, 1950—1953 (1983) [Vol. 56, No. 7

Thermodynamic Study on Penetration of Pentadecanoic Acid Monolayer by Dodecylammonium Chloride

Yoshiteru HAYAMI,† Makoto ARATONO, Shozo URYU, Kinsi MOTOMURA, and Ryohei MATUURA*

Department of Chemistry, Faculty of Science, Kyushu University 33, Fukuoka 812

(Received January 5, 1983)

In order to show that our thermodynamic treatment [*J. Colloid Interface Sci.*, **87**, 333 (1982)] is useful in the study on the monolayer penetration, the surface tension has been measured with the system consisting of pentadecanoic acid monolayer and dodecylammonium chloride solution. Applying the thermodynamic equations to the experimental data, the surface density of dodecylammonium chloride, and entropy and energy of penetration have been estimated numerically. It has been found that the surface density, entropy, and energy all decrease with increasing the concentration of film-forming substance. Therefore, it has been concluded that the penetration of monolayer of this system is caused by the decrease of the energy of penetration which compensates the decrease of the entropy of penetration.

The investigation of monolayer penetration has been made by many workers from the practical and biological points of view.[1-9] Since the penetrated monolayer is a mixed monolayer consisting of film-forming and penetrating molecules, it is also important from the physico-chemical viewpoint to clarify the monolayer penetration. In the previous paper,[10] rigorous thermodynamic equations have been derived for the penetrated monolayer. Application of these equations to experimental data is expected to provide useful information regarding the behavior of film-forming and penetrating molecules in the monolayer state. It seems useful to employ the system consisting of spread monolayer of pentadecanoic acid and adsorbed monolayer of dodecylammonium chloride because they show the phase transitions from an expanded to a condensed state and from a gaseous to an expanded state.

The object of this paper is to measure the surface tension of the pentadecanoic acid monolayer penetrated by dodecylammonium chloride and to evaluate the thermodynamic quantity of penetration with the aid of the thermodynamic equations.

Experimental

Pentadecanoic acid was recrystallized from hexane after fractionation by vacuum distillation, and its purity was checked by gas-liquid chromatography. Dodecylammonium chloride was prepared by the method described previously.[11] Water was distilled from aqueous alkaline permanganate solution after reflux for one day. Hexane used as the spreading solvent was distilled after passing through an activated alumina column.

Surface tension was measured by a Wilhelmy plate technique combined with a Shimadzu recording microbalance. The aqueous solution of dodecylammonium chloride was placed in a glass culture dish of 12 cm diameter, and it was covered doubly so as for the solution not to evaporate and contaminate. On spreading, a micro pipette of 10 μl was used to facilitate the evaporation of hexane. After about half an hour, as the surface tension reached a constant value, the spreading was repeated. This equilibration time varied from 15 min to 2 h as the surface pressure was raised in this experimental range.

† Present address: Chikushi Jogakuen Junior College, Dazaifu, Fukuoka, 818-01.

Results and Discussion

The surface tension γ of pentadecanoic acid monolayer on the aqueous solution of dodecylammonium chloride was measured as a function of area A per pentadecanoic acid molecule, concentration m_2^w of dodecylammonium chloride, and temperatrue T under atmospheric pressure. The variation of the γ *vs.* A curve with m_2^w at 293.15 K is shown in Fig. 1. In the absence of dodecylammonium chloride (curve 1), the pentadecanoic acid monolayer is heterogeneous in the range between areas indicated by A and B; gaseous and expanded films coexist in equilibrium.[12] The monolayer becomes the expanded film at the area B and remains homogeneous up to the area C where the monolayer is transformed into the condensed film. Increasing the concentration of dodecylammonium chloride, the homogeneous expanded monolayer region is found to shift to a larger area and broaden significantly. It is also seen that the surface tension decreases greatly with increasing m_2^w. Such a behavior can clearly be ascribed to the penetration of penta-

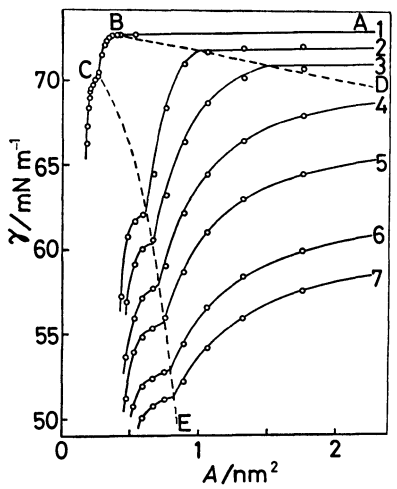

Fig. 1. Surface tension *vs.* area curves of pentadecanoic acid monolayer on dodecylammonium chloride solution at constant concentration at 293.15 K: (1) m_2^w = 0 mmol kg^{-1}; (2) 0.315; (3) 0.714; (4) 1.31; (5) 1.83; (6) 2.62; (7) 3.07.

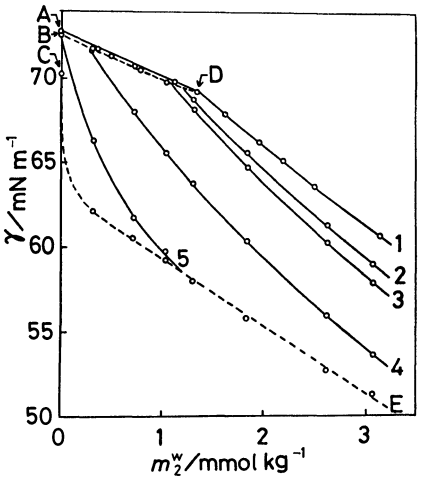

Fig. 2. Surface tension *vs.* molality curves at constant area at 293.15 K: (1) $A=\infty$ nm^2; (2) 3.00; (3) 2.00; (4) 1.00; (5) 0.70.

decanoic acid monolayer by dodecylammonium chloride molecules.

It has been shown previously[13] that the adsorbed film of dodecylammonium chloride at air/water interface transfers from a gaseous to an expanded phase at 1.38 mmol kg^{-1}. To specify the state of the penetrated monolayer, it may be necessary to recognize how the transition point between two phases on the γ *vs.* m_2^w curve varies with A. The variation of γ *vs.* m_2^w curve with A is shown in Fig. 2, where the curve of the condensed film is excluded because of its uncertainty. The break point, denoted by D, on the curve 1 represents the phase transition of dodecylammonium chloride film from the gaseous to the expanded state. On the other hand, the point B on the ordinate represents the corresponding phase transition of pentadecanoic acid monolayer. Therefore, the broken line BD is the equilibrium γ *vs.* m_2^w curve between gaseous and expanded phases. Moreover, the broken line CE is proved to be the equilibrium γ *vs.* m_2^w curve between expanded and condensed phases. Comparing Fig. 1 with Fig. 2, we notice that the penetrated monolayer behaves as the expanded film in the area DBCE on Fig. 1 and the gaseous film is never realized at concentrations larger than 1.38 mmol kg^{-1}.

Let the penetrated monolayer be an expanded film at the area A. When the concentration m_2^w is larger than 1.38 mmol kg^{-1}, the monolayer is homogeneous in the area range from A to infinity. In this instance we can use Eq. [10] of Ref. 10, referred to as Eq. (Ref. 10, 10), to calculate the surface density Γ_2^H of dodecylammonium chloride:

$$\Gamma_2^H = \Gamma_2^H(0) - [1/A(\partial\mu_2/\partial m_2^w)]\int_A^\infty (\partial\Pi/\partial m_2^w)_{T,p,A}\mathrm{d}A, \quad (1)$$

where $\Gamma_2^H(0)$ is the value of Γ_2^H at $A=\infty$, μ_2 the chemical potential of dodecylammonium chloride, and Π the surface pressure defined as the difference between the surface tension of a subsolution and that of a monolayer on the subsolution by Eq. (Ref. 10, 8). On the solution of the concentration $m_2^w<1.38$ mmol kg^{-1}, on the other hand, the monolayer is attended by the phase transition from gaseous to expanded film, the value of Γ_2^H being not calculated by Eq. 1. Evidently Eq. (Ref. 10, 40) is applicable to the calculation of Γ_2^H at the area A^e of the expanded film which is in equilibrium with the gaseous film. Integrating Eq. (Ref. 10, 9) from A to A^e and combining the resulting equation with Eq. (Ref. 10, 40), we can obtain the expression

$$\Gamma_2^H = \Gamma_2^H(0) - [1/A(\partial\mu_2/\partial m_2^w)]\left[\int_A^{A^e}(\partial\Pi/\partial m_2^w)_{T,p,A}\mathrm{d}A + \int_{A^e}^{A^g}(\partial\Pi^{eq}/\partial m_2^w)_{T,p}\mathrm{d}A + \int_{A^g}^{\infty}(\partial\Pi/\partial m_2^w)_{T,p,A}\mathrm{d}A\right], \quad (2)$$

where A^g is the area of the gaseous film in equilibrium with the expanded film and Π^{eq} the equilibrium surface pressure.

Now we can calculate the value of Γ_2^H from the experimental data. Inspecting Fig. 3 which is made from Fig. 2, it is seen that the slope of Π *vs.* m_2^w curve decreases markedly with increasing A. This is clearly shown in Fig. 4 where $\partial\Pi/\partial m_2^w$ is plotted against A. Furthermore, the slope of Π^{eq} *vs.* m_2^w curve (broken line BD in Fig. 3) is found to be negligibly small. In the case of the system under consideration, it might be possible to assume that the values of $\partial\Pi/\partial m_2^w$ at large areas give negligible contributions to the integrals of Eqs. 1 and 2, and these equations are replaced by the approximation

$$\Gamma_2^H = \Gamma_2^H(0) - (m_2^w/2ART)\int_A^{A'}(\partial\Pi/\partial m_2^w)_{T,p,A}\mathrm{d}A, \quad (3)$$

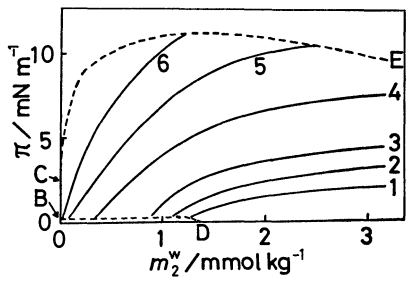

Fig. 3. Surface pressure *vs.* molality curves at constant area at 293.15 K: (1) $A=3.00$ nm^2; (2) 2.00; (3) 1.50; (4) 1.00; (5) 0.80; (6) 0.70.

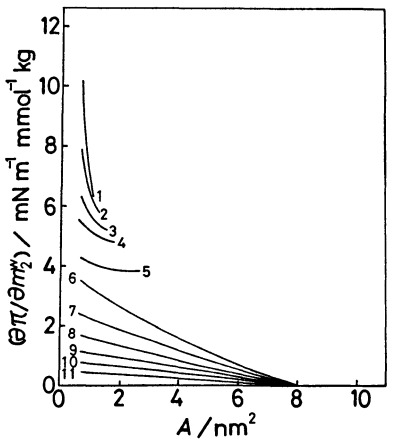

Fig. 4. $(\partial\Pi/\partial m_2^w)$ *vs.* A curves at constant m_2^w at 293.15 K: (1) $m_2^w=0.4$ mmol kg^{-1}; (2) 0.6; (3) 0.8; (4) 1.0; (5) 1.2; (6) 1.4; (7) 1.6; (8) 1.8; (9) 2.0; (10) 2.4; (11) 3.0.

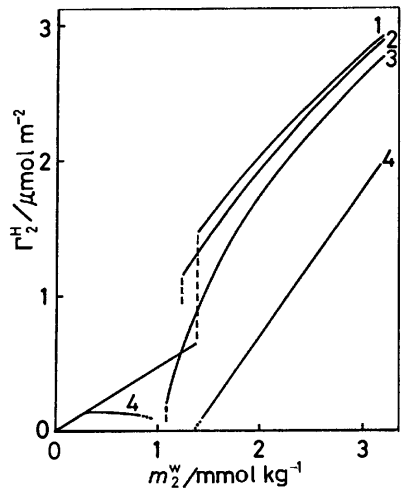

Fig. 5. Surface density of dodecylammonium chloride *vs.* molality curves at constant area at 293.15 K: (1) $A=\infty$ nm^2; (2) 3.00; (3) 2.00; (4) 1.00.

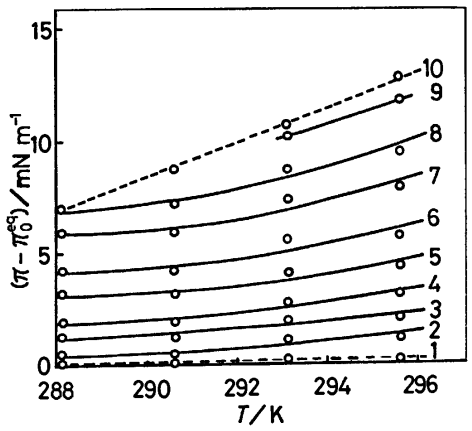

Fig. 6. Surface pressure difference *vs.* temperature curves at constant area at $m_2^w=1.00$ mmol kg^{-1}: (1) $A^e<A<A_0^g$; (2) $A=1.50$ nm^2; (3) 1.30; (4) 1.15; (5) 1.00; (6) 0.90; (7) 0.80; (8) 0.75; (9) 0.70; (10) $A^c<A<A^e$.

where A' is taken as the area extrapolated to $\partial\Pi/\partial m_2^w=0$ when $m_2^w>1.38$ mmol kg^{-1} and as A^e when $m_2^w<1.38$ mmol kg^{-1}. We have also assumed that the dodecylammonium chloride solution behaves ideally. The calculation of Γ_2^H was performed on a FACOM OS IV computer. The values calculated at several areas at 293.15 K are plotted against m_2^w in Fig. 5. The curve at $A=\infty$ is the $\Gamma_2^H(0)$ *vs.* m_2^w curve and accordingly its discontinuous change displays the phase transition between gaseous and expanded phases.[13] It is observed from Fig. 5 that the value of Γ_2^H decreases with decrease in A. At first glance this looks like a strange result. Adding the surface density of pentadecanoic acid Γ_1^I to Γ_2^H, however, the sum is undoubtedly larger than the value of $\Gamma_2^H(0)$. Therefore, we may conclude that the present result is reasonable and the adsorption of dodecylammonium chloride is enhanced by the presence of pentadecanoic acid monolayer. Here, attention should be called to the fact that Γ_2^H has a negative value at a concentration around 1 mmol kg^{-1}. It might be said that Eq. 3 is a poor approximation of Eq. 2 at this concentration because of a considerable contribution of the term involving $\partial\Pi^{eq}/\partial m_2^w$ which is positive. In order to shed light on this point, it will be required to measure the surface pressure accurately at large areas.

Let us now proceed to evaluate the entropy of penetration Δs. Since the pure pentadecanoic acid monolayer carries out the phase transition, Eq. (Ref. 10, 45) can be used when the concentration of dodecylammonium chloride is higher than 1.38 mmol kg^{-1}:

$$\Delta s=\Delta s(0)-(1/A)\left[\int_A^{A_0^g}(\partial(\Pi-\Pi_0^{eq})/\partial T)_{p,A,m_2^w}dA+\int_{A_0^g}^{\infty}(\partial(\Pi-\Pi_0)/\partial T)_{p,A,m_2^w}dA\right], \quad (4)$$

where A^g is the area of the aqueous phase of the pure pentadecanoic acid monolayer in equilibrium with the expanded phase and Π_0 the surface pressure of the pure monolayer. At concentration lower than 1.38 mmol kg^{-1}, we must use the extended equation of Eq. 4:

$$\Delta s=\Delta s(0)-(1/A)\left[\int_A^{A^e}(\partial(\Pi-\Pi_0^{eq})/\partial T)_{p,A,m_2^w}dA+\int_{A^e}^{A_0^g}(\partial(\Pi^{eq}-\Pi_0^{eq})/\partial T)_{p,m_2^w}dA+\int_{A_0^g}^{A^g}(\partial(\Pi^{eq}-\Pi_0)/\partial T)_{p,A,m_2^w}dA+\int_{A^g}^{\infty}(\partial(\Pi-\Pi_0)/\partial T)_{p,A,m_2^w}dA\right], \quad (5)$$

where we have assumed $A^e<A_0^g<A^g$.

Further measurements of the surface tension were made at 288.15, 290.65, and 295.65 K. In Fig. 6, the results at $m_2^w=1.00$ mmol kg^{-1} are depicted in the form of $\Pi-\Pi_0^{eq}$ *vs.* T plot. It appears that the values of $\Pi-\Pi_0^{eq}$ show some scatter. This might be attributable partly to a small change of the surface tension with temperature and partly to the difficulty of measuring the equilibrium surface tension. It is found by drawing a smooth curve that the slope of the curve decreases with increase in A. At the areas between A^e and A_0^g, the value of $\Pi^{eq}-\Pi_0^{eq}$ seems to be nearly independent of T. Therefore, Eqs. 4 and 5 may be approximated by the expression

$$\Delta s=\Delta s(0)-(1/A)\int_A^{A'}(\partial(\Pi-\Pi_0^{eq})/\partial T)_{p,A,m_2^w}dA, \quad (6)$$

which corresponds to Eq. 3 for Γ_2^H. By applying Eq. 6 to the experimental data, the value of Δs was computed. The variation of the Δs *vs.* m_2^w curve with A at 293.15 K is shown in Fig. 7. The curve at $A=\infty$ represents the $\Delta s(0)$ *vs.* m_2^w curve which has the small, although definite, discontinuous change corresponding to the change of the $\Gamma_2^H(0)$ *vs.* m_2^w curve. As the area is reduced, the curve is found to shift significantly to a negative value of Δs. It is also seen that the value of Δs decreases remarkably with increasing m_2^w. These facts indicate that the entropy of penetrated monolayer is smaller than that of spread

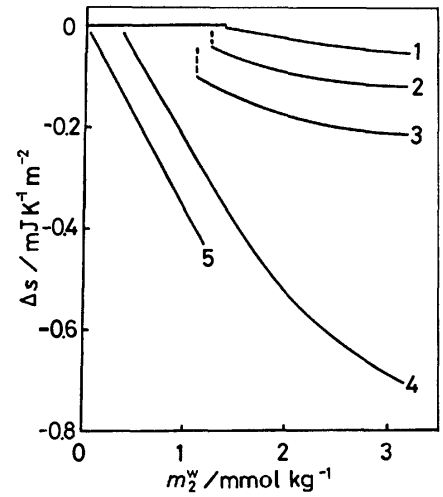

Fig. 7. Entropy of penetration *vs.* molality curves at constant area at 293.15 K: (1) $A=\infty$ nm^2; (2) 3.00; (3) 2.00; (4) 1.00; (5) 0.70.

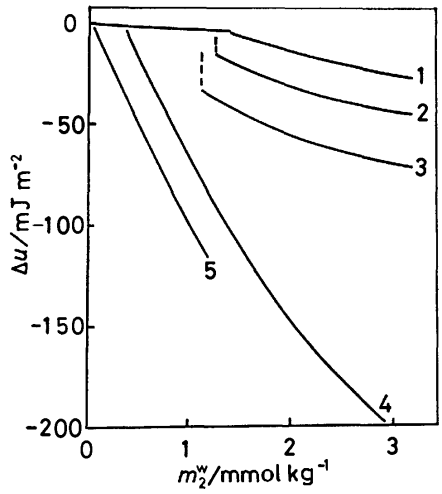

Fig. 8. Energy of penetration *vs.* molality curves at constant area at 293.15 K: (1) $A=\infty$ nm^2; (2) 3.00; (3) 2.00; (4) 1.00; (5) 0.70.

film of pentadecanoic acid and decreases with increase in the total surface density. Therefore it is proved that the penetration is an unfavorable process from the viewpoint of entropy. We may also say that the film-forming and penetrating molecules are forced to take highly restricted conformation in the penetrated monolayer.

Further, we can evaluate the energy of penetration Δu. Evidently an equation similar to Eqs. 3 and 6 is expected to hold. Taking account of Eqs. (Ref. 10, 27) and (Ref. 10, 46), it may be written in the form

$$\Delta u = \Delta u(0) + (1/A)\int_A^{A'} (\partial[(\Pi-\Pi_0^{eq})/T]/\partial(1/T))_{p,A,m_2^w} dA. \quad (7)$$

Now we can use Eq. 7 to calculate the value of Δu from the experimental data. The value obtained at 293.15 K is plotted against m_2^w at constant A in Fig. 8. Comparing Fig. 8 with Fig. 7, the variation of Δu with m_2^w and A is observed to be quite similar to that of Δs. It is clear that the penetration by dodecylammonium chloride diminishes the energy of pentadecanoic acid monolayer. Therefore, we may conclude that the penetration is brought about by the energy decrease which results predominantly from the mutual interaction between pentadecanoic acid and dodecylammonium chloride. This is in harmony with the observation that the mixed monolayer of tetradecanoic acid and octadecylammonium chloride shows a negative azeotropic transformation between expanded and condensed films.[14]

The above thermodynamic analysis of experimental results demonstrates that the equations derived by us[10] are useful to make clear the penetration of monolayers.

References

1) R. Matalon and J. H. Schulman, *Trans. Faraday Soc.*, **43**, 479 (1947); E. D. Goddard and J. H. Schulman, *J. Colloid Interface Sci.*, **8**, 309, 329 (1953).
2) B. A. Pethica, *Trans. Faraday Soc.*, **51**, 1402 (1955); P. J. Anderson and B. A. Pethica, *ibid.*, **51**, 1080 (1955).
3) R. Shimozawa and R. Matuura, *Bull. Chem. Soc. Jpn.*, **34**, 457 (1961); A. Matsubara, *ibid.*, **38**, 1254 (1965).
4) F. M. Fowkes, *J. Phys. Chem.*, **65**, 355 (1961); **66**, 385, 1863 (1962); **68**, 3515 (1964).
5) J. Ahmad, J. A. Mann, and M. J. Povich, *J. Colloid Interface Sci.*, **49**, 1 (1974).
6) K. S. Birdi, *J. Colloid Interface Sci.*, **57**, 228 (1976).
7) S. S. Chen and H. L. Rosano, *J. Colloid Interface Sci.*, **61**, 207 (1977).
8) M. Nakagaki and T. Handa, *Bull. Chem. Soc. Jpn.*, **49**, 2934 (1976); M. Nakagaki and E. Okamura, *ibid.*, **55**, 1352, 3381 (1982).
9) M. A. McGregor and G. T. Barnes, *J. Colloid Interface Sci.*, **49**, 362 (1974); **54**, 439 (1976); **62**, 213 (1977); *J. Pharm. Sci.*, **67**, 364 (1978); *J. Colloid Interface Sci.*, **65**, 291 (1978); D. M. Alexander and G. T. Barnes, *J. Chem. Soc., Faraday Trans. 1*, **76**, 118 (1980).
10) K. Motomura, Y. Hayami, M. Aratono and R. Matuura, *J. Colloid Interface Sci.*, **87**, 333 (1982).
11) M. Aratono, M. Yamanaka, N. Matubayashi, K. Motomura, and R. Matuura, *J. Colloid Interface Sci.*, **74**, 489 (1980).
12) K. Sekita, M. Nakamura, K. Motomura, and R. Matuura, *Mem. Fac. Sci. Kyushu Univ.*, **C10**, 51 (1976).
13) K. Motomura, S. Iwanaga, Y. Hayami, S. Uryu, and R. Matuura, *J. Colloid Interface Sci.*, **80**, 32 (1981).
14) K. Motomura, M. Ikematsu, Y. Hayami, H. Matuo, and R. Matuura, *Bull. Chem. Soc. Jpn.*, **53**, 2217 (1980).

Studies on Aqueous Solutions of Saccharides. II. Viscosity *B*-Coefficients, Apparent Molar Volumes, and Activity Coefficients of D-Glucose, Maltose, and Maltotriose in Aqueous Solutions

Koichiro MIYAJIMA,* Masahiro SAWADA, and Masayuki NAKAGAKI

Faculty of Pharmaceutical Sciences, Kyoto University, Yoshida Shimoadachi-cho, Sakyo-ku, Kyoto 606

(Received January 14, 1983)

Viscosities, apparent molar volumes, and activity coefficients of aqueous solutions for D-glucose, maltose, and maltotriose were measured at various concentrations. The signs of B_{st}, the increment of viscosity *B*-coefficient arising from structural change of water, were positive for these three saccharides, and the signs of dB/dT, the temperature dependence of B, were negative. The magnetudes of B_{st} and $|dB/dT|$ increased with the number of glucose residue. Activity coefficients were larger than unity and increased with concentration, and their magnitudes also increased with the number of glucose residue. These results indicate that D-glucose, maltose, and maltotriose are structure forming solutes, and that their abilities lie in the order of D-glucose < maltose < maltotriose.

Many studies[1,2] concerning the properties of aqueous solutions of saccharides have been published, because they are not only biochemically important compounds but also the typical nonelectrolytes with hydrophilic hydoxyl groups, which are capable of hydrogen bonding. Stokes and Robinson[3] interpreted the concentration dependences of activity coefficients of D-glucose and sucrose in terms of the semi-ideal solution theory.† This idea that the solute-solvent interactions govern the concentration dependences of thermodynamic quantities seems to be fundamentally correct, since Raman[4] and NMR relaxation[5] studies of aqueous solutions of mono- and disaccharides suggested an absence of solute-solute interactions even at relatively high concentrations.

Kabayama and Patterson[6] postulated that not only the number of hydroxyl groups but also the stereochemical orientation of hydroxyl groups, *i.e.* axial and equatorial, play an important role on the hydration of saccharides. In other words, the spacing of oxygen atoms of equatorial OH groups of monosaccharides in chair conformation nearly fit the spacing of oxygen atoms of ice-like structure of water. This hydration model for saccharides is so called "specific hydration model." The people who favour this model, Franks school of England, regard monosaccharide, which takes mainly the chair conformation, as a structure maker. Harvey *et al.*[7] are suspicious of the validity of this model because of the similarity of NMR spectra of monosaccharides between aqueous and alcoholic solutions. Rowlinson *et al.*[8] and Kawaizumi *et al.*[9] classified mono- and disaccharides as structure makers in terms of excess partial molar entropy and heat capacity. While Goring *et al.*[10] classified the hydrophilic solutes including D-glucose and sucrose as structure breakers, on the basis of positive temperature dependences of apparent molar volumes.

To solve the puzzling situation of the effect of saccharide on water structure, we measured viscosity *B*-coefficients, apparent molar volumes and activity coefficients of D-glucose homologues; D-glucose, maltose and maltotriose, and discussed the effects of these compounds on water structure.

† Water molecules and hydrated saccharide molecules mix ideally.

Experimental

Materials. Reagent grade D-glucose, maltose, and maltotriose purchased from Nakarai Chemical Co. Ltd., were dried *in vacuo* over P_2O_5 at room temperature for several days before use. Under these conditions, the water of hydration of maltose monohydrate was reported to be stable.[11] Reagent grade sodium chloride obtained from Matsunaga Chemical Co. Ltd., was dried *in vacuo* at 110 °C for a day. These compounds are dissolved in purified water by distillations and deionization.

Method. The viscosity measurements were carried out at 15, 25, and 35±0.03 °C using an Ostwald type viscometer with an efflux time of *ca.* 540 s for water at 25 °C. The detail procedure and kinetic correction of viscometer were described elsewhere.[12] The experimental determination of an efflux time was precise to ±0.05 s.

Density of a solution was measured by Seiko SDM 420 and 421 vibration densimeter at 15, 25, and 35±0.01 °C. Pure water and 6 mol dm^{-3} aqueous sodium chloride solution were used as the standards for the calibration of the apparatus. Measurements were done at least twice for every solution and were accurate within $\pm 10^{-5}$ g cm^{-3}. Apparent molar volume, ϕ_v of solute was calculated by Eq. 1.

$$\phi_v = 1000(d_o - d)/cd_o + M_2/d, \quad (1)$$

where d_o and d are the densities of solvent and solution, respectively. M_2 is molecular weight of solute.

Osmotic coefficients of maltose and maltotriose were measured at 25±0.02 °C by isopiestic comparison method described elsewhere.[13] Sodium chloride was used as a reference solute. Experimental determination of isopiestic concentration was precise to ±0.2%.

Results and Discussion

Relative viscosity, η_{rel}, of nonelectrolyte solution in relatively high concentration range (0.1—1.0 mol dm^{-3}) is expressed by

$$\eta_{rel} = \eta/\eta_o = 1 + Bc + Dc^2, \quad (2)$$

where η_o and η are the viscosities of solvent and solution, respectively, and c is the molarity of solute. At constant pressure and temperature, B and D are the characteristic constants depending on the combination of solute and solvent. The constant B is so called "viscosity *B*-coefficient", which is related to the solute-solvent interaction. The constant D is the coefficient

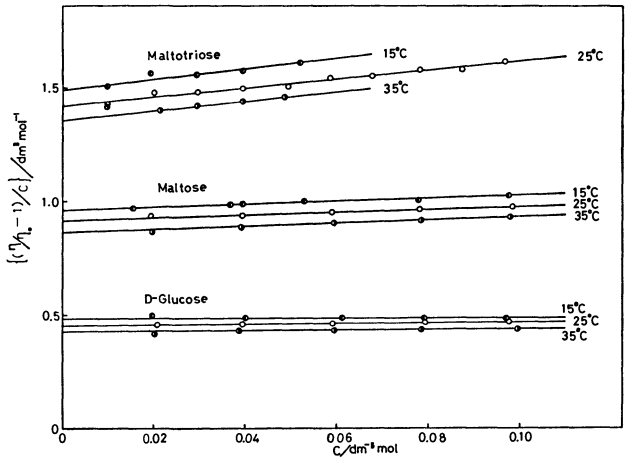

Fig. 1. Relations between $(\eta/\eta_0-1)/c$ and c for saccharides at 15, 25, and 35 °C.

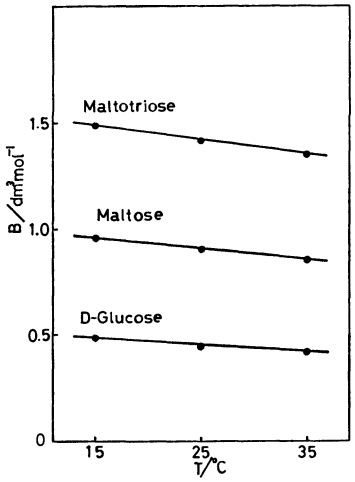

Fig. 2. Temperature dependences of B-coefficients for saccharides.

representing the interactions of solute-solvent and solute-solute, but the physical meaning of D-coefficient is not yet clarified.

As shown in Fig. 1, B and D coefficients are obtained from the intercepts and the slopes of $(\eta_{rel}-1)/c$ *vs.* c curves. B-coefficient is usually expressed by the sum of two terms, *i.e.* B_{size} and B_{st}. The former is the contribution of hydrodynamic obstruction effect arising from the size and the shape of solute molecule, and the latter the contribution of the structural change of solvent by solute-solvent interactions. For the estimation of B_{size}, the Einstein-Simha viscosity equation for colloidal suspension is usually applied to the solution of low molecular weight solute.

$$\eta_{rel} = 1 + \nu\phi, \tag{3}$$

where ϕ is the volume fraction of colloidal particle and ν is a function of the axial ratio of ellipsoid. The ν value is equal to 2.5 for spherical colloidal suspension, which corresponds to the Einstein equation. Assuming that the effective rigid volume of solute equals to the partial molar volume of solute at infinite dilution ($\overline{V}^\circ$), ϕ is equal to $c\overline{V}^\circ/1000$. Hence B_{st} can be expressed by

$$B_{st} = B - \nu\overline{V}^\circ/1000. \tag{4}$$

Scheraga's table[14] was combined with the axial ratio of oblate given by Edward[15] to obtain the ν value for D-glucose. We adopted the ν values of cellobiose and cellotriose as those of maltose and maltotriose. The values of $\overline{V}^\circ$ were obtained from the densities of the solutions described later.

The temperature dependences of B-coefficients for three saccharides are shown in Fig. 2. Each slope of the curves (dB/dT) is negative, and the absolute values increase with the number of glucose residue. The values of B at 15, 25, and 35 °C, and the values of B_{st} and dB/dT at 25 °C are listed in Table 1. The values of B and dB/dT for D-glucose are in fair agreement with those calculated from Goring's data[16]. As seen in Table 1, the positive signs of B and the negative signs of dB/dT indicate that these solutes are structure makers. As shown in Fig. 3(a), the negative values of dB/dT increase with the number of glucose

Table 1. The values of B, B_{st}, dB/dT, $\overline{V}^\circ$, and α^* for saccharides

	Temp/°C	D-Glucose	Maltose	Maltotriose
B/dm³ mol⁻¹	15	0.49	0.96	1.49
	25	0.45	0.91	1.42
	35	0.43	0.86	1.36
B_{st}/dm³ mol⁻¹	25	0.14	0.31	0.41
$(dB/dT)\times10^3$ / dm³ mol⁻¹ K⁻¹	25	−3.0	−5.0	−6.5
$\overline{V}^\circ$/cm³ mol⁻¹	15	110.3	205.5	304.0
	25	111.3	209.0	309.0
	35	112.5	211.0	312.5
$\alpha^*\times10^3$ / cm³ mol⁻¹ K⁻¹	25	1.0	1.3	1.4

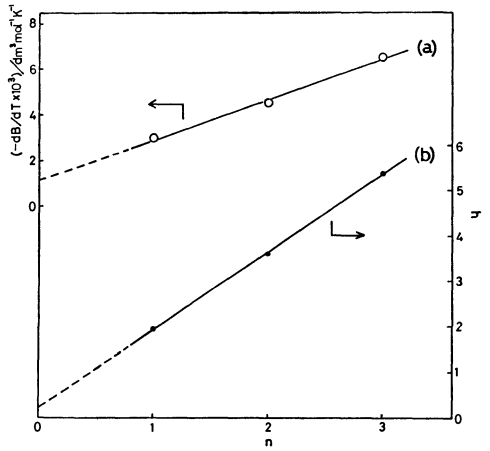

Fig. 3. Plots of dB/dT (a) and h (b) against n.

residue (n). It is noteworthy that the intercept of the straight line drawn through the three points gives positive value in dB/dT *vs.* n plots. This fact means the structure making effects of maltose and maltotriose are not twice and three times as large as that of D-glucose, indicating that the formation of α-1,4 linkage reduces the structure making effects of saccharides.

Apparent molar volume of nonelectrolyte is expressed by

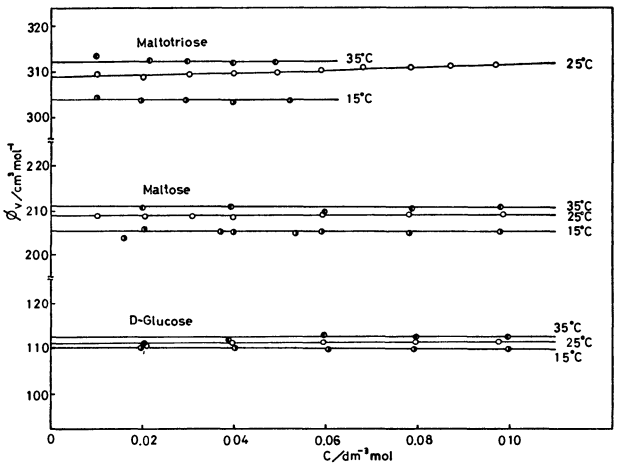

Fig. 4. Relations between ϕ_V and c for saccharides at 15, 25, and 35 °C.

$$\phi_V = \overline{V}^\circ + b_V c, \tag{5}$$

where $\overline{V}^\circ$ is the partial molar volume at infinite dilution and b_V is an empirical constant reflecting the solute-solute interactions. As shown in Fig. 4, ϕ_V values for three saccharides at 15, 25, and 35 °C are linearly related to the concentration. The slopes of ϕ_V *vs.* c curves correspond to b_V, which are nearly zero at 15 °C and slightly positive at 25 and 35 °C. The small values of b_V indicate that the solute-solute interactions are weak in the systems. Table 1 shows the partial molar volumes at infinite dilution at 15, 25, and 35 °C and the coefficients of thermal expansion (α^*) at 25 °C. The values of $\overline{V}^\circ$ for these three saccharides at 25 °C are in fair agreement with the literature.[11] The volume increment for glucose residue is about 100 cm³ mol⁻¹. α^* values were calculated by Eq. 6.

$$\alpha^* = (\mathrm{d}\overline{V}^\circ/\mathrm{d}T)/\overline{V}^\circ. \tag{6}$$

The values of α^* increase with the number of glucose residue, indicating that the amount of unstructured water per glucose residue increases with the number of glucose residue, because the expansibility of disordered water must be larger than that of structured water.

Osmotic (ϕ) and activity (γ) coefficients for maltose and maltotriose are shown in Table 2. The values of ϕ for maltose are in fair agreement with those reported by Uedaira.[17] As seen in Fig. 5, activity coefficients for three saccharides increase with concentration and their magnitudes lie in the order of D-glucose<maltose<maltotriose. The fact that activity coefficients for these saccharides are larger than unity implies that strong solute-solvent interactions exist in these solutions, since solute-solute interactions are weak or absent.[4,5] Using the following equation derived from the semi-ideal theory,

$$\phi = -\frac{1}{0.018m}\ln\left[\frac{1-0.018mh}{1-0.018m(h-1)}\right], \tag{7}$$

the hydration numbers (h) for these saccharides were calculated from osmotic coefficients at 2 mol kg⁻¹, and relation between h and n is shown in Fig. 3(b). The hydration number increases linearly with the number of glucose residue (n), indicating that the hydration number per glucose residue is nearly constant among these low molecular weight homologues. The point given by extrapolating the straight line to $n=0$ shows the positive value. As seen in Fig. 3(a), this behavior is similar to the relation between $\mathrm{d}B/\mathrm{d}T$ and n, and indicates that the formation of α-1,4 ether linkage from the two monosaccharides results in the decrease of hydration numbers of saccharides. The possible explanation for these results may be due to the decrease of the sites of hydrogen bond and/or the increase of structural incompatibility by the formation of α-1,4 ether linkage, because the disagreement of geometric factors of oligosaccharide with ice-like structure of water is considered to occur due to the fact that C–O–C linkage has two degrees of rotational freedom.

TABLE 2. OSMOTIC AND ACTIVITY COEFFICIENTS FOR SACCHARIDES AT 25 °C

	Maltose		Maltotriose	
m	ϕ	γ	ϕ	γ
0.1	1.002	1.003	1.002	1.003
0.2	1.004	1.007	1.006	1.010
0.3	1.006	1.010	1.010	1.016
0.4	1.010	1.014	1.016	1.023
0.5	1.015	1.020	1.022	1.030
0.6	1.021	1.027	1.030	1.040
0.7	1.028	1.036	1.038	1.049
0.8	1.035	1.044	1.048	1.061
0.9	1.042	1.052	1.059	1.074
1.0	1.050	1.061	1.071	1.088
1.1	1.058	1.070	1.084	1.103
1.2	1.067	1.081	1.098	1.120
1.3	1.076	1.091	1.113	1.138
1.4	1.086	1.103	1.129	1.158
1.5	1.096	1.114	1.146	1.179
1.6	1.106	1.126	1.162	1.199
1.7	1.116	1.138	1.179	1.220
1.8	1.126	1.150	1.196	1.242
1.9	1.137	1.163	1.213	1.265
2.0	1.148	1.176	1.231	1.288

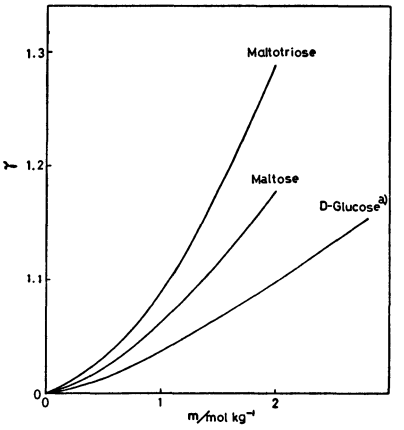

Fig. 5. Activity coefficients of saccharides at 25 °C.
a) see Ref. 2.

Judging from the specific hydration model, it seems to be reasonable that the value of dB/dT or hydration number per glucose residue decrease with increase of the number of glucose residue, because the incompatibility of orientation of hydrogen bond between a saccharide molecule and water molecules of ice-like structure would increase with the number of α-1,4 ether linkage as stated above.

As seen in Fig. 3, however, the value of dB/dT or hydration number is nearly proportional to the number of glucose residue. This result implies that the hydration behavior of di- and trisaccharides are more consistent with the prediction of simple hydration model[††] rather than that of the specific hydration model. As stated previously, the validity of the specific hydration model for monosaccharide solutions is still in controversy. Our results seem to indicate the inadequacy of the specific hydration model for the application of oligosaccharide solutions.

Based on the results of viscosity B-coefficients, apparent molar volumes, and activity coefficients, these saccharides are structure forming solutes, and their abilities lie in the order of D-glucose<maltose<maltotriose.

†† The hydration number of saccharide depends on the number of hydroxyl group in the molecule at the constant water activity.[1)]

References

1) A. Suggett, "Water, A Comprehensive Treatise," ed by F. Franks, Plenum Press, New York (1975), Vol. 4, p. 533.
2) K. Miyajima, M. Sawada, and M. Nakagaki, this Bulletin submitted.
3) R. H. Stokes and R. A. Robinson, *J. Phys. Chem.*, **70**, 2126 (1966).
4) G. A. Walrafen, *J. Chem. Phys.*, **44**, 3726 (1966).
5) A. Sugget, S. Albett, and P. J. Lillford, *J. Solution Chem.*, **5**, 17 (1976).
6) M. A. Kabayama and D. Patterson, *Can. J. Chem.*, **36**, 563 (1958).
7) J. M. Harvey and M. C. R. Symons, *J. Solution Chem.*, **7**, 571 (1978).
8) J. B. Taylor and J. S. Rowlinson, *Trans. Faraday Soc.*, **51**, 1183 (1955).
9) F. Kawaizumi, N. Nishio, H. Nomura, and Y. Miyahara, *J. Chem. Thermodyn.*, **13**, 89 (1981).
10) J. L. Neal and D. A. I. Goring, *J. Phys. Chem.*, **74**, 658 (1970).
11) F. Shahidi, P. G. Farrell, and J. T. Edward, *J. Solution Chem.*, **5**, 807 (1976).
12) K. Miyajima, M. Sawada, and N. Nakagaki, *Bull. Chem. Soc. Jpn.*, **55**, 3101 (1982).
13) K. Miyajima, K. Inari, N. Hamaguchi, H. Yoshida, and M. Nakagaki, *Nippon Kagaku Kaishi*, **1975**, 1447.
14) H. A. Scheraga, *J. Chem. Phys.*, **23**, 1526 (1955).
15) J. T. Edward, *Can. J. Chem.*, **35**, 571 (1957).
16) M. Ihnat, A. Szabo, and D. A. I. Goring, *J. Chem. Soc., A*, **1968**, 1500.
17) H. Uedaira and H. Uedaira, *Bull. Chem. Soc. Jpn.*, **42**, 2137 (1969).

 © 1983 The Chemical Society of Japan Bull. Chem. Soc. Jpn., 56, 1958—1962 (1983) [Vol. 56, No. 7

Competitive Effects in Polymer Adsorption and Exchangeability of Adsorption Layer

Kunio FURUSAWA* and Kazuaki YAMAMOTO†

The University of Tsukuba, Department of Chemistry, Sakura-mura, Ibaraki 305

(Received January 28, 1983)

Critical experimental data on competitive adsorption and exchangeabllity of adsorbed polymer are produced under the various conditions using the gel permeation chromatography technique. It is apparent that the competitive effects and the exchangeability were found to depend not only on the molecular weight of the polymer, but also on the concentration of each component at which the corresponding adsorption is carried out. This can be explained as follows; the conformation of the adsorbed polymer would be influenced extensively by the polymer concentration in bulk. The polymer molecules adsorbed from a dilute solution would take on a flat conformation being rich in train segments, but the polymer layer formed under a concentrated solution would occupy a small of sites and adopt an extended loop configuration which would be desorbed more easily than the flat one. Also, in the mixed sample the effects of adsorption Kinetics play an important role on the structure of the adsorption layer, because at first the surface is convered by an adsorption layer of small components due to its rapid adsorption rate.

Among the various branches of surface and polymer chemistry, the problem on polymer adsorption at solid-liquid interface is still new and much attention has been paid to it, both theoretically and experimentally. Especially, the problems on (ir)reversibility of polymer adsorption are fundamental and essential ones, because these are concerned with the thermodynamic background in these approaches.

On the question of whether or not polymer molecules adsorb reversibly on a solid surface, experimental data sometimes give conflicting answers. For example, often no detectable desorption can be observed upon dilution,[1,2] whereas the adsorbed polymer is easily desorbed by altering the quality of the solvent.[3] Similar confusing facts can be observed in the theoretical field.[4] Some theories predict irreversible properties, and others reversible ones.

Recently, Cohen Stuart *et al.*[5] showed that many experimental observations ascribed to irreversibility can be explained in therms of polydispersity of the sample, *i.e.*, in a polydisperse sample, preferential adsorption of a large molecule over a smaller one occurs.[6,7] Especially, with increasing molecular weight(M) the polymers adsorb progressively more strongly and exchanges for molecules of smaller M. If the polymer concentration is increased, larger molecules are available to replace smaller ones. Therefore, the molecular weight distribution on the adsorption layer changes with the amount of adsorption and may differ considerably from that in the bulk phase. This fractionation process continues as long as there are larger molecules in the bulk phase than on the adsorption layer and the adsorption isotherm is strongly influenced by the molecular weight distribution of the sample. Hence, in such an adsorption, it is impossible practically to follow the isotherm back by dilution alone and the process appears to be irreversible.

Under the concept proposed by Cohen Stuart *et al.*, it is important to obtain an exact knowledge of competitive effects of polymer molecules and exchangeability of the adsorbed polymer. In this work, competitive and displacement effects in a polymer adsorption process, were examined in some detail using polystyrene samples with narrow-molecular-weight distribution at the Θ-conditions. Furthermore, much attention has been paid to the effects from adsorption kinetics which were neglected in the Cohen Stuart theory, because at the beginning the adsorption layer of a mixed sample is occupied entirely by the small components due to their rapid adsorption rate. These analyses were performed quantitatively by the gel permeation chromatography technique. We believe that these data will shed some light on the problem of (ir)reversibility of polymer adsorption.

Experimental

Materials. Linear polystyrene samples having a narrow molecular weight distribution were supplied by Toyo Soda Co. Ltd., (Shinnanyo, Yamaguchi, Japan). The characteristics of the samples used are given in Table 1.

Cyclohexane, employed as the theta solvent, was purified by the procedure described in a previous paper.[8] Commercial porous glass beads with a particle size of 120—200 mesh were mainly used as substrate which were supplied by Electron-Nucleonics Inc.(Fairfield, N.J.) and designated as CPG-10. The surface area and the average pore-radius of these beads were reported by the supplier to be 15.0 m^2/g and 1000 A, respectively. The pore radius is about 3—30 time larger than the radius of gyration of the dissolved polymers in cyclohexane at 35 °C. Under these conditions, the effect of the porosity of the adsorbent can be ignored

TABLE 1. CHARACTERISTIC OF POLYSTYRENE SAMPLES

Sample	M_w	M_w/M_n
S-1.7[a]	16 700	1.02
S-5[b]	50 000	1.06
S-10.7[a]	107 000	1.01
S-18.6[a]	186 000	1.07
S-41.1[b]	411 000	1.06
S-77.5[a]	775 000	1.01
S-128[a]	1280 000	1.05
S-200[b]	2000 000	1.06

a) Supplied by Toyo Soda Co. Ltd., (Yamaguchi, Japan).
b) Supplied by Pressure Chemicals (Pittsburg, Pa. U.S.A.).

† Present address: Toyo Soda Co. Ltd., Tonda, Shinnanyo, Yamaguchi 746.

in the adsorption process of these polymers.[9] The glass beads were cleaned carefully by the method described previously.[9]

Adsorption Experiments. The determination of the amount of polymer adsorbed was carried out by measuring the change in concentration of the supernatant liquid using a digital precision density meter(Anton paar. K.G. PHA02C). The temperature of the adsorption tube was controlled within 0.05 °C. The details concerning the adsorption process and the analysis of these data were reported previously.[9]

GPC Measurements. The measurements were carried out with a Toyo Soda Model 803-A GPC at 25 °C, with chloroform as a solvent. The GPC chromatograph was equipped with two 7.5 mm×600 mm stainless-steel columns, types TKS-DMH and G200H. 0.4-ml portions of the polymer solution with 1.0 to 2.0 g m^{-3} was injected and eluted at 25 °C under a flow rate of 1-ml/min.

Measurements of Competitive Adsorbability. In order to determine the competitive(or preferential) adsorbability between different molecular weight species, adsorption isotherms of mixtures were constructed. The total adsorption amounts of the mixtures were determined by the usual procedure using the density meter. For evaluation of each component in the adsorption layers, the GPC technique was employed. After the adsorption period(usual adsorption time is 24 h), the supernatant solution of the mixture and the original solution were evaporated, and the polystyrene films obtained were subsequently dissolved in benzene for freeze drying. The polymer was allowed to remain to a vacuum line for 12 h in 10^{-3} Torr (1 Torr≈133.322 Pa). Both samples were finally dissolved in chloroform within the concentration range 1.0 to 2.0 g m^{-3} so as to present no appreciable concentration effect on the elution curve. In Fig. 1, an example of GPC chromatograms obtained for both samples is illustrated. The amounts of adsorption for individual components in the binary mixture were calculated by the following relations deduced from a simple mass balance analysis:

$$A_a = A_t(\alpha+\alpha\beta'-\alpha'\beta),$$
$$A_b = A_t(\beta+\alpha'\beta-\alpha\beta'). \quad (1)$$

Here, A_a, A_b, and A_t indicate the amounts of adsorption for the components a, b, and their total, and α, β, α', and β' show the areas of normalized chromatograms for components a and b before and after the adsorption process. For a tertiary mixture, the chromatogram was also analyzed under the same consideration.

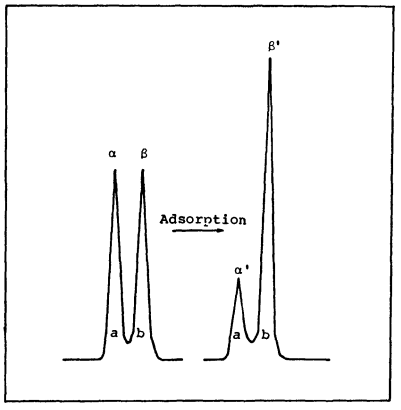

Fig. 1. Gel permeation chromatograms showing relative change of two components before (a,b) and after (a',b') the adsorption process. (α,β), (α',β'): Areas of normalized chromatogram for the components before and after adsorption.

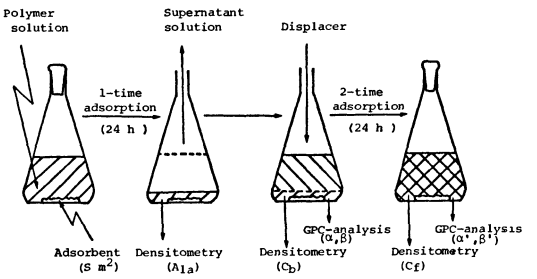

Fig. 2. A schematic picture for showing the procedure to determine the exchangeability of absorption layer.

Measurements of Exchangeability of Adsorption Layer. The exchangeability of the adsorbed polymer was also measured by the GPC technique. A schematic picture of the procedure is shown in Fig. 2. The surface of the adsorbent was first occupied with one polymer species according to the usual adsorption process and then the amounts of adsorption was determined by measuring the residual concentration of the polymer. Thereafter, the supernatant was substituted with another polymer solution used as displacer(usually the concentration of displacer is 35 g m^{-3}). The half-volume of the new supernatant was immediately taken from the tube and after determining the concentration(C_b), the solution was prepared as the GPC sample to analyse the components at the beginning time. Then, the "second-time adsorption" was performed in the other half-volume of the displacer. After the adsorption period of 24 h, the determination of polymer concentration(C_f) and the GPC analysis for the supernatant were conducted in the same way as described above. From these measurements, the adsorption amounts of the total(A_{2t}) and each component(A_{2a}, A_{2b}) in the adsorption layer after completion of the second adsorption process, can be calculated by the following relations which were deduced by a simple analysis and the mass balances,

$$A_{2t} = A_{1a} + \frac{(C_b-C_f)}{S}, \quad (2)$$

$$A_{2a} = A_{1a} + \frac{(C_b-C_f)}{S}(\alpha+\alpha\beta'-\alpha'\beta), \quad (3)$$

$$A_{2b} = \frac{(C_b-C_f)}{S}(\beta+\alpha'\beta-\alpha\beta'). \quad (4)$$

Where A_{1a} is the amount of adsorption for the component "a" after the first-time adsorption, S the total surface area of adsorbent employed, C_b and C_f the total polymer concentrations before and after the second-time adsorption.

Results and Discussion

Adsorption Rate of Mixed Sample. To measure the apparent rate of adsorption, the adsorbed amounts of mixed polymers were determined at various time intervals from 0.1 to 24 h at an initial polymer concentration of 60 g m^{-3} which gives enough saturated amount of adsorption. Figure 3 shows a plot of adsorption rate for a mixture containing two components of different molecular weight samples(S-18.6 and S-77.5) in 1:1 ration. In the same figure, the calculated adsorptions of individual component in the mixture which were determined by the GPC analysis, are also shown. It is seen that the apparent adsorption of

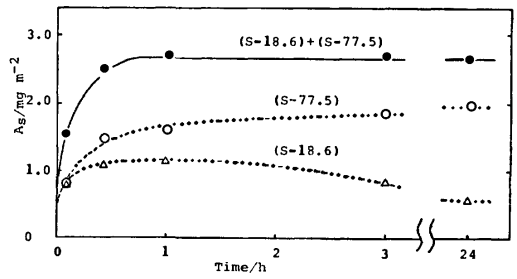

Fig. 3. Adsorption rate of a mixture containing two components (C_p=60 g m^{-3}, in cyclohexane, 35 °C).
(●): Mixture (S-18.7+S-77.5), (△): S-18.6 in mixture, (○): 8-77.5 in mixture.

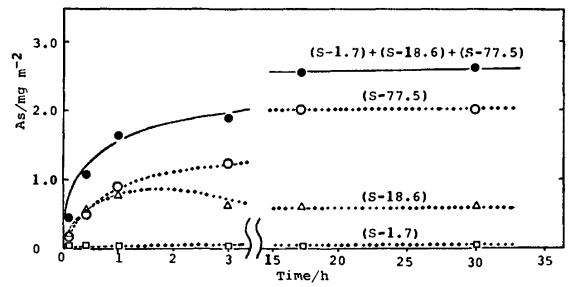

Fig. 4. Adsorption rate of a mixture containing three components (C_p=60 g m^{-3}, in cyclohexane, 35 °C).
(●): Mixture(S-1.7+S-18.6+S-77.5), (□): S-1.7 in mixture (△): S-18.6 in mixture, (○): S-77.5 in mixture.

the mixture reach an equilibrium within 1 h, but the relative change of each component in the adsorption layer continued for a long time. This tendency can be explained by the differences of the adsorption rates of each polymer species. The surface of the adsorbent will be occupied at first by the law molecular weight species because of their rapid adsorption rate and then exchanged by the later arrivals with higher molecular masses, displaying, as a rule preferential adsorbability. In Fig. 4, we have plotted adsorption rates for a mixture containing three components of different molecular weights(S-1.7, S-18.6, and S-77.5) in 1:1:1 ratio. As may be seen in the figure, the time required for attaining real equilibrium is very long and is barely established after 20 h. From these data, we can imagine that an enormous period will be necessary for a polydisperse sample to attain real equilibrium of adsorption.

Competitive Effects of Polymers Having Different Molecular Weights. In Fig. 5, a molecular weight dependence of saturated adsorption, A_s, for a series of different molecular weight species, is shown in the form of a $\log A_s$ *vs.* $\log M_w$ plot. As may be seen in the figure, $\log A_s$ and $\log M_w$ are related by a straight line and the molecular weight dependence parameter for the adsorption($\nu=\mathrm{dlog}\, A_s/\mathrm{dlog}\, M_w$) was calculated to be $\nu=0.29_5$ from the slope of the line. Thus there will be a competitive effect between the different molecular weight species when a mixed sample is used as the adsorbate.

Figure 6 shows an example of an adsorption isotherm for a mixture containing three components of different molecular weights in 1:1:1 ratio. The mixture isotherm shows a round shape as may be expected from the Cohen Stuart's theory and finally tends to an adsorption of the highest-molecular-weight component. In the same figure, the calculated adsorptions of individual components in the mixture are also shown. It appears that the preference for large molecules over smaller ones can be seen over the whole concentration region and the composition of the adsorption layer is much dependent on the solution concentration at which the corresponding adsorption is carried out. However, it is noteworthly that some adsorption of the lowest-molecular-weight species are found over the the whole concentration region. This result suggests that preferential adsorption of large molecules over smaller ones is not complete and the composition of both the bulk and the adsorption layer varies smoothly with the molecular weight of the polymer.

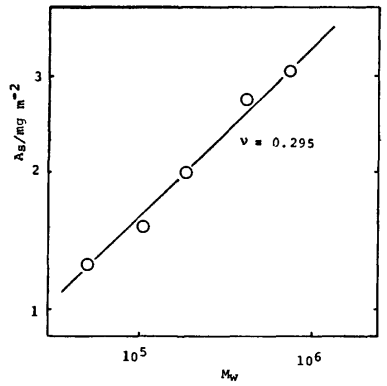

Fig. 5. Molecular weight dependence of saturated adsorption of polystyrene on porous glass from cyclohexane solution at 35 °C.

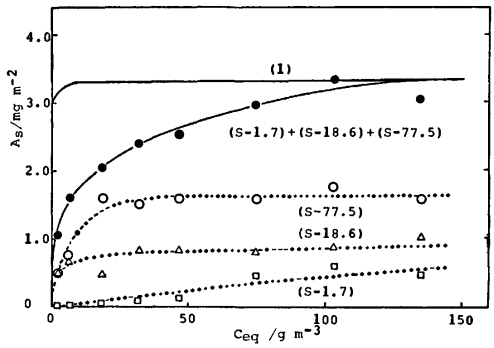

Fig. 6. Adsorption isotherms for a mixture containing three components of different molecular weights (in cyclohexane, 35 °C).
(○): Mixture (S-1.7+S-18.6+S-77.5), (□): S-1.7 in mixture, (△): S-18.6 in mixture, (○): S-77.5 in mixture.

Exchangeability of the Adsorption Layer. From analysis of the exchange process of one adsorbed polymer by another, we can get much knowledge on the peculiarity of polymer adsorption. Figures 7, 8, and 9 show the results for three combinations of different molecular weight species. In these figures, demonstrating the degree of displacement of adsorption layers formed under the various residual concentrations (C_{eq-1}) by a definite displacer solution(usually we

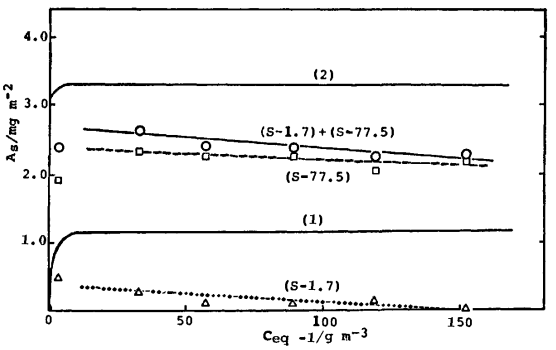

Fig. 7. Exchangeability of adsorption layers formed under the various equilibrium concentrations of primal adsorbate (C_{eq-1}) by a definite displacer solution ($C_{dis.}$: 35 g m^{-3}).
(○): Total adsorption amounts after 2-time adsorption, (△): residual amounts of adsorbate after 2-time adsorption, (□): exchanged amounts of displacer after 2-time adsorption, (1): adsorption isotherm of primal adsorbate (S-1.7), (2): adsorption isotherm of displacer (S-77.5).

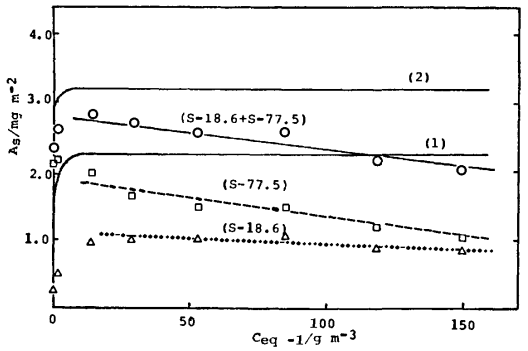

Fig. 8. Exchangeability of adsorption layers formed under the various equilibrium concentrations of primal adsorbate (C_{eq-1}) by a definite displacer solution ($C_{dis.}$: 35 g m^{-3}).
(○): Total adsorption amounts after 2-time adsoption, (△): residual amounts of adsorbate after 2-time adsorption, (□): exchanged amounts of displacer after 2-time adsorption, (1): adsorption isotherm of primal adsorbate (S-18.6), (2): adsorption isotherm of displacer (S-77.5).

fixed the concentration at 35 g m^{-2}). For the sake of comparison, Figs. 7 and 8 include isotherms of the adsorbate and the displacer themselves. As may be seen from these figures, the small component adsorbing on the surface is displaced extensively by the large-size molecules used as a displacer. The degree of displacement is greatly dependent on the difference of molecular weights of both polymers: *i.e.*, in a much different combination(Fig. 7), the degree of displacement is extensive and in the small differences(Figs. 8 and 9), the degree is not so extensive. A striking feature seen from these figures is that the exchangeability is found to depend not only on the molecular weight of the adsorbed polymer but also on the solution concentration at which the corresponding initial adsorption was carried out. It appears that the polymer molecules adsorbed at high concentrations are ex-

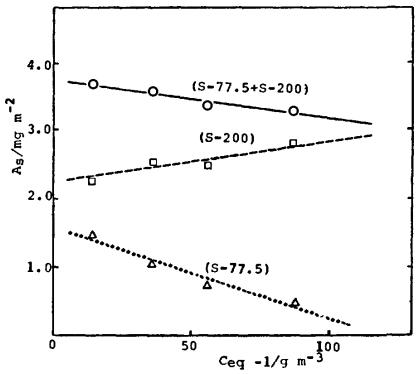

Fig. 9. Exchangeability of adsorption layers formed under the various equilibrium concentrations of primal adsorbate (C_{eq-1}) by a definite displacer solution ($C_{dis.}$: 35 g m^{-3}).
(○): Total adsorption amounts after 2-time adsorption, (△): residual amounts of adsorbate after 2-time adsorption, (□): exchanged amounts of displacer after 2-time adsorption.

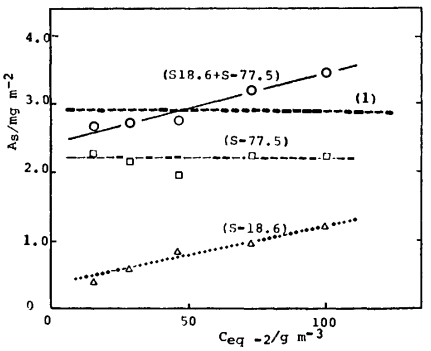

Fig. 10. Exchangeability of adsorption layer of big molecules (S-77.5) formed under a definite concentration (C_{eq-1}=27 g m^{-3}) by different concentrated solutions (C_{eq-2}) of small molecules (S-18.6).
(○): Total adsorption amounts after 2-time adsorption, (△): residual amounts of adsorbate after 2-time adsorption, (□): exchanged amounts of displacer after 2-time adsorption, (1): line showing adsorption amount of primale adsorbate, (S-77.5).

changed more easily than the polymer layer formed at low concentrations. If the exchangeability is related to the number of adsorbed segments, this suggests that the polymer layer formed at high concentrations has smaller adsorbed segments than the layer formed at low concentrations. This can be explained by the polymer molecules in a dilute solution arriving at the sparsely populated surface and adopting a relatively flat conformation; however the polymer molecules in a more concentrated solution, especially when some later arrivals come to the surface, would occupy a smaller number of sites and therefore must adopt a considerably extended loop conformation which would be desorbed more easily than the flat ones. Also, it is interesting to notice that the total adsorbances after the second-time adsorption show an increasing tendency with decreasing the equivalent concentrations of the displacer. This will be due to different couples of residual molecules with a flat conformation and dis-

placed molecules with an extended conformation.

Another peculiarity in the polymer adsorption is shown in Fig. 10, where the large molecules adsorbed previously are exchanged by a displacer having a small molecular weight, though such a trend is not as pronounced as those found in the opposite combination. However, this result shows crucially that the preference in polymer adsorption depends not only on the molecular weight of the adsorbate, but also on the solution concentration of each species. Furthermore, Fig. 10 shows another indication that the big molecules remaining in the adsorption layer are maintained constant over the whole concentration region of the displacer. This shows that there are "weakly adsorbed matters" in the adsorption layer(*ca.* 25%) and they are classified essentially with the other firmly adsorbed components. Existence of the "weakly adsorbed matters" were also found by Terashima *et al.*[10] in their direct adsorption measurements using microbalance.

In this article, we have attempted to produce critical experimental data on the competitive effects in the polymer adsorption and exchangeability of the adsorption layer. All these data support the Cohen Stuart's theory and are well explained by the concept of reversible adsorption of the polymer.

References

1) W. H. Grant, L. E. Smith, and R. R. Stromberg, *Faraday Discuss. Chem. Soc.*, **59**, 209 (1975).

2) G. J. Howard and P. Mc Connel, *J. Phys. Chem.*, **71**, 2981 (1967).

3) M. Kawaguchi and A. Takahashi, *J. Polym. Sci., Polym. Phys. Ed.*, **18**, 2069 (1980).

4) J. M. G. Lankveld and J. Lyklema, Vth Intern. Congr. Surface Activity (Barcelona), Proceeding Vol. 2, 633 (1968); L. K. Koopal and J. Lyklema, *Faraday Discuss. Chem. Soc.*, **59**, 230 (1975).

5) M. A. Cohen Stuart, J. M. H. M. Scheutjens, and G. J. Fleer, *J. Polym. Sci., Polym. Phys. Ed.*, **18**, 559 (1980); M. A. Cohen Stuart, Thesis, Agricultural University, Wageningen, The Netherlands, 1980.

6) C. Vander Linden and R. Van Leemput, *J. Colloid Interface Sci.*, **67**, 63 (1978).

7) G. J. Howard and S. J. Woods, *J. Polym. Sci., Part A-2*, **10**, 1023 (1970).

8) K. Furusawa, H. Nakanishi, and K. Kotera, Intern. Conf. Colloid and Surface Science(Budapest), Proceeding Vol. 1, 221 (1975).

9) Kunio Furusawa, K. Yamashita, and K. Konno, *J. Colloid Interface. Sci.*, **86**, 35 (1982).

10) H. Terashima, J. Klein, and P. F. Luckham, "Adsorption from Solution," ed by R. H. Ottewill, C. H. Rochester, and A. L. Smith, Academic Press, London (1983), p. 299.

 © 1983 The Chemical Society of Japan Bull. Chem. Soc. Jpn., 56, 1963—1967 (1983)

Polarographic Studies of the Ion-pair Formation and Conjugation Reactions of Acetate and Benzoate Ions in Acetonitrile

Masashi Hojo* and Yoshihiko Imai

Department of Chemistry, Faculty of Science, Kochi University, Kochi 780

(Received May 25, 1982)

An acetate ion (A^-) formed a homoconjugated species, $A^-(HA)_2$, with 2 molecules of acetic acid (HA) in the presence of a large excess of HA in an acetonitrile solution. In the presence of both acetic acid and $LiClO_4$, one molecule of HA was derived from $A^-(HA)_2$ by means of a lithium ion to from an ion-paired species, HA_2^-Li, as follows: $A^-(HA)_2+Li^+ \overset{K_{ex}}{\rightleftharpoons} HA_2^-Li^+ + HA$. The equilibrium constant, K_{ex}, was evaluated as 1.1×10^4 from the shift in the anodic half-wave potential of the acetate ion. As for the benzoate ion (A'^-) and HA', similar reactions occured, and the constant of the exchange reaction was evaluated as 6×10^3. The effect of the sodium ion and HA (or HA') on the A^- (or A'^-) ion was complicated. On the other hand, the presence of $[M(A')_2]^-$ (M=Li, Na, K) was proved by the shift of the cathodic wave of the alkali metal. The addition of water caused the apparent stability constant of $[Li(A')_2]^-$ to decrease extremely.

Polarography has been a powerful means to determine the stability constants of metal complexes. The difference in half-wave potential between a complex and the free metal ion is used in a usual calculation. In some cases,[1] however, the anodic wave-height was measured in order to evaluate the concentration of the uncomplexed ligand in the solution.

Reilley *et al.*[2] have reported an interesting method to obtain a stability constant; their method is based on the shift of the anodic wave of the complex-forming agent in the presence of an excess of the metal ions. At the same time, however, they pointed out a limiting feature of that method: the wave-height decreased in the cases of interactions between EDTA and Pb^{2+}, *etc.* in aqueous solutions. Therefore, we have modified the relationship proposed by Reilley *et al.* and successfully applied it to an ion-pair formation reaction in a nonaqueous solvent. Using this method, we have evaluated the equilibrium constants from the shift in the half-wave potential of the anodic wave of acetate or benzoate ions in the presence of an excess of alkali metal ions. This method was also extended to a reaction for not only an ion-pair formation, but also a homo- or heteroconjugation.

Kolthoff *et al.*[3,4] have reported, based on potentiometric or conductometric measurements, that acetate or benzoate ions associate (homoconjugate) with one molecule of acetic or benzoic acid in acetonitrile. In the same solvent, on the other hand, Pawlak *et al.*[5] showed the association of acetate and other carboxylate ions with 2 molecules of the corresponding acid. We were much interested in the above inconsistency and the fact that the solubilities of alkali carboxylates are much increased by the addition of a large amount of acetic acid in a protophobic solvent.

In the present paper, we studied, by means of polarography, the conjugation and ion-pair formation reactions for acetate and benzoate ions in the presence of large amounts of acetic and benzoic acids, and alkali metal ions in acetonitrile. In acetonitrile, the acetate ion or its homoconjugated ion gives a well-defined anodic wave,[6] although the polarographic anodic wave of the acetate ion is difficult to observe in an aqueous solution. On the other hand, the formation of alkali metal dibenzoate complexes were proved by the shift of the cathodic wave of the alkali metal in the presence of a large excess of the benzoate ion. Moreover, the effect of water on the apparent stability constant for the lithium dibenzoate complex was examined in the solvent.

Experimental

The tetraethylammonium acetate and benzoate were prepared according to the procedure of Kolthoff *et al.*[3,7] The methods of purifying acetonitrile (MeCN) and of preparing Et_4NClO_4, $LiClO_4$, $NaClO_4$, and $KClO_4$ have been described elsewhere.[8] Benzoic acid of a GR grade was dried in a vacuum at room temperature. The other GR-grade chemicals were used without further purification. Polarograms were recorded with a Yanagimoto Polarograph, Model p-1000, and a Watanabe X-Y recorder, Model WX-4401-L0. The rate of the potential sweep was 2 mV/s. The dropping mercury electrode had the following open-circuit characteristics: $m=1.26$ mg/s and $\tau=3.2$ s in a 0.1 M** Et_4NClO_4-MeCN solution at $h=50$ cm. All the polarographic measurements were carried out in an H-type cell at 25.0+0.2 °C. The reference electrode was a silver-silver perchlorate electrode, Ag/0.1 M $AgClO_4$-MeCN.

Results and Discussion

Effects of Acetic Acid and Lithium Ion on Anodic Wave of Acetate Ion. The acetate ion gave an anodic wave at −0.45 V (0.35 mM) in acetonitrile containing 0.1 M Et_4NClO_4 as a supporting electrolyte. The wave height was linear to the concentration of the acetate ion over the range of 0.1—1 mM. The half-wave potential shifted slightly to the negative side with an increase in the concentration of the depolarizer. The anodic wave is certainly based on the dissolution of the mercury(I) ion in an acetonitrile solution, judging from the linearity of the relation of E *vs.* $\log(i_d-i)$ and the extremely small solubility of $Hg_2(CH_3COO)_2$ in the solvent. The variation in the limiting current with the height of the mercury head (h) indicated diffusion control.

When acetic acid (HA) was added to the solution of the acetate ion, the half-wave potential of the anodic wave shifted greatly to the positive potential. Figure 1 shows the shift of the half-wave potential in the presence of acetic acid. The ten-fold increase in the

** Throughout this paper, 1 M=1 mol dm^{-3}.

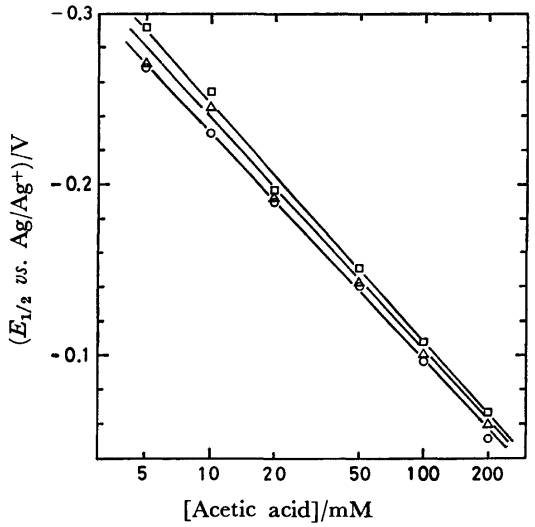

Fig. 1. Effect of acetic acid on the anodic half-wave potential of acetate ion in acetonitrile solutions containing 0.1 M Et_4NClO_4. (○) 0.18, (△) 0.35, (□) 0.70 mM of acetate ion.

concentration of acetic acid caused the half-wave potential for the acetate ion to shift 120 mV positively. The anodic waves were diffusion-controlled and reversible when 10 mM or more of acetic acid was added to 0.35 mM of the acetate ion. We applied the following equation to the homoconjugation reaction:

$$(E_{1/2})_c = (E_{1/2})_s + \frac{0.059}{n}\log K_{homo} + \frac{0.059}{n}p\log[HA], \quad (1)$$

assuming the activity and diffusion coefficients of A^- and the homoconjugated species to be equal to each other; here, $(E_{1/2})_s$ is the half-wave potential of the acetate ion, $(E_{1/2})_c$ is the $E_{1/2}$ of the homoconjugated species for the acetate ion, and K_{homo} is the formation constant of the homoconjugation reaction. We obtained $p=2.0$ and $K_{homo}=ca.\ 5.7\times10^7\ M^{-2}$ from the slope of the graph and the $(E_{1/2})_c-(E_{1/2})_s$ value, since $n=1$ in the case of the formation of the mercury(I) salt.[9] The above results show that the acetate ion forms a very stable homoconjugated species, $A^-(HA)_2$ with 2 molecules of acetic acid (see also Scheme 1):

$$A^- + 2HA \overset{K_{homo}}{\rightleftarrows} A^-(HA)_2. \quad (2)$$

The addition of another acid, such as propionic and benzoic acid or phenol, to a solution of the acetate ion also gave a slope of *ca.* 120 mV, which indicated that heteroconjugated species, $A^-(HX)_2$ were formed.

Acetate ion gave an anodic wave in a 0.1 M $LiClO_4$–MeCN solution at an extremely positive potential (+0.06 V) compared with that in an Et_4NClO_4 solution. The shift of $E_{1/2}$ to the positive potential was

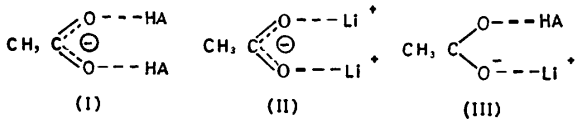

Scheme 1.

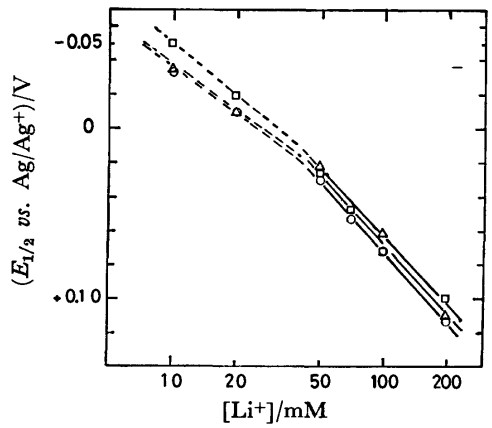

Fig. 2. Effect of Li^+ on the $E_{1/2}$ of acetate ion. (○) 0.18, (△) 0.35, (□) 0.70 mM of acetate ion. Total ionic strength was kept formally 0.1 M with Et_4NClO_4, except 0.2 $LiClO_4$ solution.

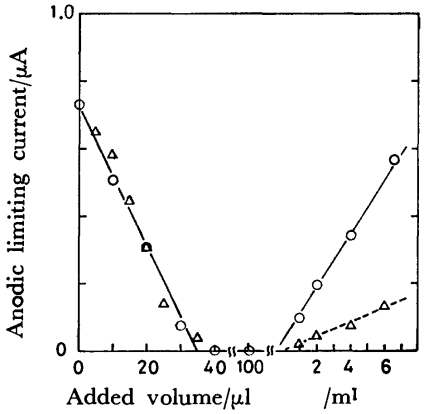

Fig. 3. Amperometric titration curves for 0.35 mM acetate ion of 20 ml by 0.2 M $LiClO_4$ and $NaClO_4$. (○) $LiClO_4$, (△) $NaClO_4$. The changes of total volume were corrected.

considered to be caused by ion-pair (or complex) formation between Li^+ and the acetate ion. The effect of the Li^+ concentration on the half-wave potential for the acetate ion was also examined, as shown in Fig. 2. However, when the concentration of $LiClO_4$ was low (1—20 mM) for the 0.35 mM acetate ion, the wave-height of the acetate ion was extremely depressed. The decrease in the anodic wave-height would be caused by the precipitation of CH_3COOLi. This strange phenomenon was clearly exhibited when 20 ml of a 0.35 mM acetate-ion solution was titrated by a 0.2 M $LiClO_4$–MeCN solution, as shown in Fig. 3. The anodic wave (−0.45 V) of the acetate ion disappeared at the 1:1 equivalent point. Again, an anodic wave from the acetate ion appeared at −0.05—+0.06 V for the addition of a large excess of Li^+. From an analysis similar to that above, with 50—200 mM of $LiClO_4$, we concluded that, in the presence of a large excess of Li^+, the acetate ion exists in the form of $CH_3COO^-(Li^+)_2$, which is electrochemically active. We had the formation constant of $K_f=1\times10^{11}\ M^{-2}$ for the following reaction:

$$CH_3COO^- + 2Li^+ \overset{K_f}{\rightleftarrows} CH_3COO^-(Li^+)_2. \quad (3)$$

When 0.1 M $NaClO_4$ was used as the supporting electrolyte, the solution of the acetate ion formed a white precipitate (CH_3COONa, $pK_{sp}=9.1$ by Kolthoff and Chantooni[10]) and showed only a very small anodic wave at −0.1 V. A titration curve for the 0.35 mM acetate ion obtained by the use of 0.2 M $NaClO_4$ is also shown in Fig. 3.

Next, we shall consider the interaction between $A^-(HA)_2$ and Li^+. We added both acetic acid and the Li^+ ion in various concentrations to solutions of the acetate ion, and then recorded the half-wave potentials. The waves were diffusion-controlled and were reversible when sufficient amounts of acetic acid and Li^+ were added. If the $E_{1/2}$ of $A^-(HA)_2$ is taken as the standard,[11] we obtain the following equation by assuming conditions similar to Eq. 1:

$$(E_{1/2})_c = (E_{1/2})_s + 0.059 \log K_{ex} + 0.059\, p \log[HA] + 0.059\, q \log[Li^+], \quad (4)$$

where $(E_{1/2})_s$[12] is the half-wave potential of $A^-(HA)_2$ and $(E_{1/2})_c$ is the $E_{1/2}$ of the resultant species. From the data in Fig. 4, we obtained $p=-1$ and $q=1$. If the value of p were zero ($p=0$), the following equation would be realized. $A^-(HA)_2+Li^+ \rightleftharpoons A^-(HA)_2Li^+$. However, in practice, $p=-1$, which shows that one HA is present on the right-hand side of the reaction equation. Also, the fact that $q=1$ shows that one

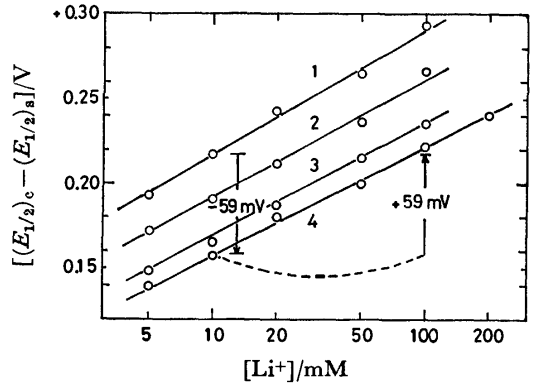

Fig. 4. Shift in $E_{1/2}$ of acetate ion by the presence of both acetic acid and Li^+ ion. (1) 20, (2) 50, (3) 100, (4) 200 mM of the acid. $[CH_3COO^-]=0.35$ mM. See the text for $(E_{1/2})_c-(E_{1/2})_s$.

Table 1. The difference in half-wave potential for acetate ion in solutions containing the same concentration of acetic acid and Li^+

Concn of HA and Li^+/mM	$[(E_{1/2})_c-(E_{1/2})_s$[a)]]/V		
	0.18	0.35	0.70 mM of acetate ion
20	0.247	0.243	0.232
50	0.246	0.238	0.240
100	0.241	0.235	0.240
200	0.237	0.238	0.236
Av.	0.243	0.238	0.237
$\log K_{ex}$	4.10	4.02	4.01
	$K_{ex}=1.1\times10^4$		

a) See the text.

Li^+ ion reacts with $A^-(HA)_2$ as follows:

$$A^-(HA)_2 + Li^+ \overset{K_{ex}}{\rightleftharpoons} HA_2^-Li^+ + HA. \quad (5)$$

The above equation shows the formation of the species HA_2^- Li^+, which consists of an acetate ion, an acetic acid, and a lithium ion. In Eq. 4, if we take [HA]=[Li^+], the value of K_{ex} can be easily obtained from the value of $(E_{1/2})_c-(E_{1/2})_s$, since $-p=q=1$. The experimental results are shown in Table 1. The obtained values coincide well with one another for 0.18—0.7 mM) of the acetate ion containing 20—200 mM of the acid and the Li^+ ion (*e.g.*, [HA]=[Li^+]=50 mM). As an average, we obtain the equilibrium constant of the exchange reaction (the formation constant of the species) $K_{ex}=1.1\times10^4$. Therefore, when the acetate ion is present with both acetic acid and the Li^+ ion in acetonitrile, $HA_2^-Li^+$ is the predominant species and the concentration of $A^-(HA)_2$ becomes negligibly small.

Kolthoff *et al.*[3] reported $K_{homo}=5\times10^3$ M^{-1} as the homoconjugation reaction of the acetate ion ($A^-+HA \overset{K_{homo}}{\rightleftharpoons} HA_2^-$) in acetonitrile. With the help of the value given by them, we obtained the ion-pair formation constant $K_{ion}=ca.$ 1×10^8 M^{-1} for the following reaction: $HA_2^-+Li^+ \overset{K_{ion}}{\rightleftharpoons} HA_2^-$ Li^+.

Effects of Benzoic Acid and Lithium Ion on Anodic Wave of Benzoate Ion. The benzoate ion gave an anodic wave at a slightly more positive potential (−0.36 V at 0.3 mM) than the acetate ion in an acetonitrile solution containing 0.1 M Et_4NClO_4 as the supporting electrolyte. The wave-height was linear to the concentration of the benzoate ion over the range of 0.2—1 mM. The other behavior of the anodic wave of the benzoate ion was similar to that of the acetate ion.

The addition of benzoic acid (HA′) to the benzoate solution caused the half-wave potential of the anodic wave to shift positively. From the analysis of Eq. 1, we obtained $p=2.0$ and $K_{homo}=ca.$ 1×10^7 M^{-2} with 0.2—0.4 mM of the benzoate ion and 20—200 mM of benzoic acid. Here, the formation of homoconjugated species, $A'^-(HA')_2$, with 2 molecules of benzoic acid (HA′) was proved to be present, as in the case of the acetate ion.

In a 0.1 M $LiClO_4$–MeCN solution, the anodic wave from the benzoate ion appeared at *ca.* +0.085 V. However, the calibration curve did not show a linearity, for the solution formed a white precipitate (C_6H_5COOLi) at higher concentrations of benzoate (more than 0.4 mM). Despite this, the formation constant of $C_6H_5COO^-(Li^+)_2$ was evaluated to be *ca.* 1×10^9 M^{-2} with 0.2 mM benzoate and 100—200 mM $LiClO_4$.

When both benzoic acid and Li^+ were present with the benzoate ion, the half-wave potential of the benzoate ion shifted in a manner similar to that in the case of the acetate ion, shown in Fig. 4. From the same analysis as Eq. 4, we obtained the equilibrium constant of 6×10^3 for the following exchange reaction:

$$A'^-(HA')_2 + Li^+ \overset{K_{ex}}{\rightleftharpoons} HA'^-_2Li^+ + HA'. \quad (6)$$

The addition of benzoic acid and Na^+ instead of Li^+

to a benzoate solution caused the half-wave potential of the benzoate ion to shift in a strange manner: the value of $q=1$, but $p=ca.$ −0.5, so the results could not be explained well. Incidentally, the behavior of the acetate ion in the presence of acetic acid and Na^+ was much more complicated.

Other Interactions between Benzoate Ion and Alkali-metal Cations. When a benzoate-ion solution was amperometrically titrated by $LiClO_4$, the height of the anodic wave of the benzoate ion decreased and the wave disappeared at 1:1 equivalent point. Then, again, with a large excess of $LiClO_4$ an anodic wave from the benzoate ion appeared at a much more positive potential (+0.05—0.08 V) than the initial potential (−0.36 V), in a manner similar to that in the case of the acetate ion, shown in Fig. 3. However, the decrease in the benzoate wave-height was completely different from that in the case of the acetate ion: the wave of the acetate ion decreased linearly with the addition of $LiClO_4$. On the other hand, the total wave of the benzoate ion did not decreased so much with the addition of $LiClO_4$, at first, but then it suddenly disappeared at the equivalent point (see Fig. 5). By a detailed examination of the wave, the anodic wave of benzoate could be divided into two parts, that is, the first wave of *ca.* −0.36 V and the second wave of around −0.16 V. The first wave disappeared at a half of the 1:1 equivalent point. The second wave gradually became large and reached its maximum at the half-equivalent point. The composition ratio of Li^+ to the benzoate ion is 1:2 at the maximum point. Therefore, the formation of the lithium dibenzoate complex, $[Li(C_6H_5COO)_2]^-$, was suggested in the presence of an excess of benzoate ions. Therefore, the following experiments were performed in order to prove the formation of the complex. The cathodic wave of the lithium ion (0.5 mM) being used as the indicator, the shift of the wave was measured in the presence of a large amount of benzoate ions (5—20 mM). The half-wave potential of lithium shifted greatly to a negative potential, *e.g.*, 0.75 V at 10 mM of benzoate, and the presence of more than 50 mM of benzoate caused a wave shift behind the cut-off. The analysis of the results proved the presence of a 1:2 complex and gave the formation constant, K_f, of $10^{16.7}\ M^{-2}$;

$$Li^+ + 2C_6H_5COO^- \overset{K_f}{\rightleftarrows} [Li(C_6H_5COO)_2]^-. \quad (7)$$

When 0.48 mM of the benzoate ion was titrated by the use of 0.2 M $NaClO_4$, the anodic wave of the benzoate ion did not decrease linearly; therefore, the formation of the sodium dibenzoate complex was suggested. Similar experiments for 0.5 mM of sodium ions with 50—100 mM of benzoate ions gave the formation constant, K_f, of $10^{8.4}\ M^{-2}$ for $[Na(C_6H_5COO)_2]^-$. Even the potassium ion was complexed by the benzoate ion in an acetonitrile solution. The formation constant for $[K(C_6H_5COO)_2]^-$ was given as $10^{4.2}\ M^{-2}$ by experiments with 0.5 mM K^+ and 30—100 mM benzoate ions. When the 0.48 mM benzoate ion was titrated by $KClO_4$, however, the anodic wave of the benzoate ion did not completely disappear, even in the presence of a large excess of $KClO_4$. This phenomenon is probably the result of the large solubility of C_6H_5COOK in acetonitrile. The value of the solubility products for potassium benzoate could not easily be found in the literature, although the values for lithium and sodium benzoates in acetonitrile have been reported to be $pK_{sp}=10.5$[4] and 8.7[10] respectively.

The effect of water on the stability constant of the lithium dibenzoate complex was also examined. As is shown in Fig. 6, the apparent stability constant of the lithium dibenzoate complex decreased extremely with an increase in the concentration of water. In the calculation of the constant, the shift of the half-wave potential of the free lithium ion was corrected because the half-wave potential of the lithium ion was negatively shifted by the addition of water to an acetonitrile solution without a benzoate ion. The shift in the half-wave potential might be caused by the difference in the liquid-junction potential or solvation. By extrapolation, the formation constant of the lithium dibenzoate complex was estimated to be $\log K_f \approx 0$ for 100% water. This fact suggests that the lithium dibenzoate complex does not actually form in an aqueous

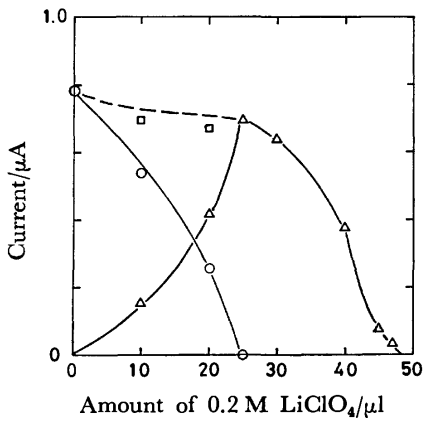

Fig. 5. Amperometric titration curves for 0.48 mM benzoate ion of 20 ml by 0.2 M $LiClO_4$. (○) the first wave of ca. −0.36 V, (△) the second wave of around −0.16 V, (□) total of the two waves.

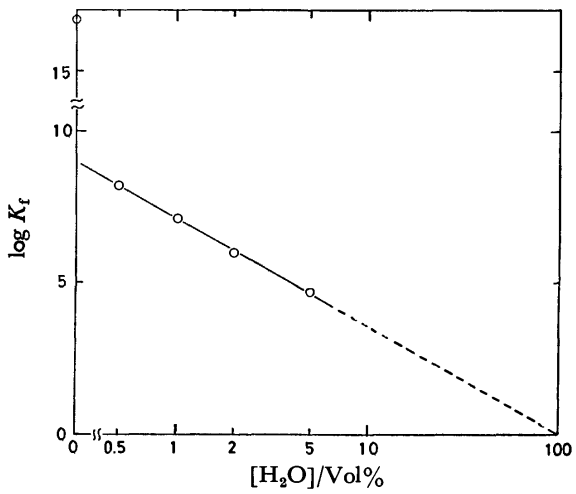

Fig. 6. Effect of water on the apparent stability constant, K_f.

solution. Another experiment showed that a benzoate ion is conjugated by 2 molecules of H_2O in an acetonitrile solution.

The interaction between the acetate ion and alkali metal cations was not fully examined because the behavior of complex reactions for them was complicated, and also because the solubility of tetraethylammonium acetate was much smaller (less than 30 mM) than that of the benzoate (≈200 mM) in acetonitrile.

Conclusion

The results reported in this paper indicate that the formation of homoconjugation for acetate or benzoate is affected by the alkali metal ions in acetonitrile; this is the cause of the difficulty in measuring the precise formation constant of a conjugation reaction by the solubility method.

The authors wish to express their thanks to Emeritus Professor Taitiro Fujinaga and Dr. Satoshi Okazaki, Kyoto University, for their helpful discussions. This work was partly supported by a Grant-in-Aid for Scientific Research from the Ministry of Education, Science and Culture.

References

1) H. Ogino, *Bull. Chem. Soc. Jpn.*, **38**, 771 (1965).
2) C. N. Reilley, W. G. Scribner, and C. Temple, *Anal. Chem.*, **28**, 450 (1956).
3) I. M. Kolthoff, M. K. Chantooni, Jr., and S. Bhowmik, *J. Am. Chem. Soc.*, **90**, 23 (1968).
4) M. K. Chantooni, Jr., and I. M. Kolthoff, *J. Am. Chem. Soc.*, **92**, 7025 (1970).
5) Z. Pawlak, Z. Szponar, and C. Dobrogowska, *Ann. Soc. Chim. Pol.*, **48**, 501 (1974).
6) M. Hojo, *Bull. Chem. Soc. Jpn.*, **53**, 2856 (1980).
7) I. M. Kolthoff and M. K. Chantooni, Jr., *J. Phys. Chem.*, **70**, 856 (1966).
8) T. Fujinaga, S. Okazaki, and M. Hojo, *Bull. Inst. Chem. Res., Kyoto Univ.*, **56**, 139 (1978).
9) Because of the formation of the insoluble salt with mercury, $E=E^0_{Hg_2^{2+}}+\frac{0.059}{2}\log S-0.059\log[A^-]_0 = E^{0\prime}-0.059\log[A^-]_0$, where $S=[Hg_2^{2+}]_0[A^-]_0^2$. The diffusion of acetate ions towards the electrode surface is governed by the Ilkovic equation: $-i=\kappa([A^-]-[A^-]_0)=-I_d-\kappa[A^-]_0$. Substituting for $[A^-]_0$ in the former equation leads to: $E=E^{0\prime}-0.059\log\frac{i-I_d}{\kappa}$, $E_{1/2}=E^{0\prime}-0.059\log\frac{(-I_d)}{2\kappa}=E^{0\prime}-0.059\log\frac{[A^-]}{2}$. As for the homoconjugated species; $-i=\kappa'([A^-(HA)_p]-[A^-(HA)_p]_0)=-I_d'-\kappa'[A^-(HA)_p]_0=-I_d'-\kappa'[A^-]_0K[HA]_0^p$, $E=E^{0\prime}-0.059\log\frac{i-I_d'}{\kappa'}+0.059\log K[HA]_0^p$. As sufficient [HA] is present, $E_{1/2}=E^{0\prime}-0.059\log\frac{(-I_d')}{2\kappa'}+0.059\log K[HA]^p=E^{0\prime}-0.059\log\frac{[A^-(HA)_p]}{2}+0.059\log K[HA]^p$. When $[A^-]\approx[A^-(HA)_p]$, $(E_{1/2})_c-(E_{1/2})_s=0.059\log K+0.059\,p\log[HA]$. Therefore, $n=1$ in Eq. 1.
10) I. M. Kolthoff and M. K. Chantooni, Jr., *J. Phys. Chem.*, **76**, 2024 (1972).
11) We can take $A^-(Li^+)_2$ as the standard, and the conclusion is as follows: $A^-(Li^+)_2+HA \overset{K}{\rightleftharpoons} HA_2^-Li^+ + Li^+$, $K=ca.\ 1.4\times10$.
12) For example, when [HA]=50 mM and $[Li^+]=100$ mM, $(E_{1/2})_s$ is the $E_{1/2}$ of $A^-(HA)_2$ at [HA]=50 mM and Li^+-free.

Spectrophotometric Determination of Palladium and Bismuth(III) with Semimethylxylenol Blue

Joichi UEDA* and Kyoko KADOWAKI

Department of Chemistry, Faculty of Education, Kanazawa University, Marunouchi, Kanazawa 920

(Received October 26, 1982)

Procedures are described for the spectrophotometric determination of palladium and bismuth(III) with Semimethylxylenol Blue (SMXB). SMXB reacts with palladium and bismuth(III) to form reddish-violet 1:1 complexes. The optimum pH ranges for the color development are pH 1.0—1.7 for palladium and pH 1.0—1.4 for bismuth(III). The absorption maxima of the colored solutions lie at 565—568 nm and at 568—570 nm, respectively. Beer's law is obeyed over the range of 0.4—3.2 μg cm^{-3} of palladium and 0.4—4.0 μg cm^{-3} of bismuth(III), and the sensitivities of the determinations are 4.0×10^{-3} μg Pd cm^{-2} and 6.1×10^{-3} μg Bi cm^{-2} for 0.001 of absorbance. For the palladium determination, gallium, tin(IV), bismuth(III), scandium, zirconium, and iron(III) interfere, but tin(IV), scandium, zirconium, and iron(III) can be masked by the addition of fluoride. For the bismuth(III) determination, gallium, tin(IV), scandium, zirconium, and iron(III) interfere, but the effect of iron(III) is eliminated by the addition of L-ascorbic acid, and tin(IV) and scandium can be masked by fluoride. A consecutive determination of palladium and bismuth(III) by the difference of the rates of color developments for their complexes was also studied.

Semimethylxylenol Blue (SMXB) is obtained as one of the products in the synthesis of Methylxylenol Blue. In the previous papers, we described photometric methods for the determination of thorium,[1] iron(III),[2] aluminium,[2] zirconium,[3] and gallium[4] using SMXB. In this work, we examined the usefulness of this reagent as the spectrophotometric reagent for palladium and bismuth(III), and observed that SMXB was a suitable reagent for these elements in respect to sensitivity and selectivity. Comparing the present methods for palladium and bismuth(III) with other methods which use reagents with structures similar to that of SMXB, for bismuth(III), SMXB is less sensitive than Semixylenol Orange,[5] but more sensitive than Xylenol Orange,[5,6] Methylxylenol Blue,[7,8] and Methylthymol Blue.[9] For palladium, this reagent has nearly the same sensitivity as Xylenol Orange.[10] As for the selectivity, the present methods are nearly as specific as the methods using the above reagents.[5-10] In the proposed methods, the color development for the bismuth(III) complex is rapid at room temperature, but that for the palladium complex is very slow, especially in the presence of chloride. Thus, utilizing the difference of the rates of color developments, 20—80 μg of palladium and 20—120 μg of bismuth(III) could be determined consecutively from the solution containing both elements. This paper describes the fundamental conditions for the spectrophotometric determination of palladium and bismuth(III), and for the consecutive determination of the two elements.

Experimental

Reagents. *Standard Palladium Solution*: A solution containing about 1 mg cm^{-3} of palladium was prepared by dissolving guaranteed reagent grade palladium chloride in 1.5 mol dm^{-3} nitric acid. The solution was standardized by the complexometric back titration with a standard solution of thorium using Xylenol Orange as an indicator. This solution was diluted as required.

Standard Bismuth(III) Solution: A solution containing about 1 mg cm^{-3} of bismuth(III) was prepared by dissolving guaranteed reagent grade bismuth(III) nitrate in 2 mol dm^{-3} nitric acid. The solution was standardized by the complexometric titration using Xylenol Orange as an indicator. This solution was diluted as required.

SMXB Solution: A 0.05% SMXB solution was prepared by dissolving in distilled water a weighed amount of the SMXB which had been synthesized by the Mannich condensation and purified by means of cellulose column chromatography.[1,2]

1 mol dm^{-3} nitric acid and 1 mol dm^{-3} aqueous ammonia was used for pH adjustments.

All the other reagents used were of guaranteed reagent grade.

Apparatus. A Hitachi-Perkin-Elmer model 139 spectrophotometer with 1 cm glass cells was used for the absorbance measurements, and a Hitachi-Horiba model M-5 glass electrode pH meter for the pH measurements.

Recommended Procedures. *Determination of Palladium*: A sample solution containing 10—80 μg of palladium is taken into a 50 cm^3 Erlenmeyer's flask, and adequate amounts of 1 mol dm^{-3} nitric acid and 3 cm^3 of 0.05% SMXB solution are added. Then, the total volume is made about 20 cm^3 with water. After being kept for 5 min in a boiling water bath, the solution is cooled with running water, transferred to a 25 cm^3 volumetric flask, and diluted to the mark with water (the final pH:1.1). The absorbance is measured at 568 nm against the reagent blank.

Determination of Bismuth(III): A sample solution containing 10—100 μg of bismuth(III) is transferred to a 25 cm^3 volumetric flask. Then, adequate amounts of 1 mol dm^{-3} nitric acid and 3 cm^3 of 0.05% SMXB solution are added. After increasing the volume to 25 cm^3 (the final pH:1.1), the absorbance is measured at 568 nm against the reagent blank.

Consecutive Determination of Palladium and Bismuth(III): The sample solution containing 20—80 μg of palladium and 20—120 μg of bismuth(III) is divided equally. In one solution, the absorbance of bismuth(III) complex is measured by the recommended procedure for bismuth(III), by adding 3 mg of chloride before the addition of the SMXB solution. In this case, the measurements must be done within 4 min after color development. From this absorbance, bismuth(III) is determined by using calibration curve III in Fig. 3. In the other, the total absorbance of the palladium and bismuth(III) complexes is measured by the recommended procedure for palladium, by adding 3 mg of chloride before the addition of the SMXB solution. Then, palladium is determined by subtracting the absorbance due to bismuth(III) from the total absorbance and using calibration curve

II in Fig. 3.

Result and Discussion

Absorption Curves. Figure 1 shows the absorption curves of palladium and bismuth(III) complexes obtained by the recommended procedures. The absorption maxima of the colored solutions of the complexes are at 565—568 nm and at 568—570 nm, respectively.

The Effect of pH. The effect of pH on the color development of the complexes was examined. As shown in Fig. 2, the ranges in which the maximum and nearly constant absorbance was obtained were pH 1.0—1.7 for palladium and pH 1.0—1.4 for bismuth(III). When sulfuric acid, perchloric acid and hydrochloric acid were used instead of nitric acid for the pH adjustment on the palladium determination, sulfuric acid and perchloric acid gave nearly the same results as nitric acid, while hydrochloric acid reduced the absorbance. In the bismuth(III) determination, all of these acids gave almost the same results.

The Effect of the Reagent Concentration. Various amounts of 0.05% SMXB solution were added to a solution containing 40 μg of palladium or 50 μg of bismuth(III). The maximum and reasonably constant absorbances were obtained by adding from 1.5 to 7 cm^3 of SMXB solution for each element.

The Stability of the Color. The color development for the palladium complex is very slow at room temperature. However, heating in a boiling water bath hastened the color development and the maximum absorbance was obtained within a few minutes. Heating for 5 min in a boiling water bath, therefore, was adopted in further experiments. On the other hand, the full color development for bismuth(III) complex occurred immediately after the reagent was added, and the color intensity was independent of heating for at least 20 min in a boiling water bath. The color of the both complexes, once developed, was very stable, and the absorbances remained constant for at least 3 h.

Calibration Curves. The calibration curves for palladium and bismuth(III) which were prepared by the recommended procedures are shown in Fig. 3. Linear relationships between absorbance and concentration held over the range of 0.4—3.2 μg cm^{-3} of palladium and 0.4—4.0 μg cm^{-3} of bismuth(III); the molar absorptivities calculated from the curves were 2.64×10^4 and 3.43×10^4, respectively. The relative standard deviations for five replicate determinations were 1.4% for 40 μg of palladium and 1.2% for 50 μg of bismuth(III). In Fig. 3, the calibration curve for palladium in the presence of 3 mg of chloride is also shown. In this case, the absorbance decreased about 10% compared with that in the absence of chloride, but Beer's law was obeyed over the range of 0.4—3.2 μg cm^{-3} of palladium.

The Effect of Diverse Ions. Table 1 shows the effect of diverse ions on the determination of 40 μg of palladium and 50 μg of bismuth(III). Palladium could be determined within 5% errors in the presence of 1 mg each of 20 cations such as alkali metals, alkaline earth metals, lead, zinc, lanthanoids, manganese(II), cobalt, and nickel, and in the presence of 10 mg each of 6 anions such as fluoride, oxalate, citrate, *etc.*

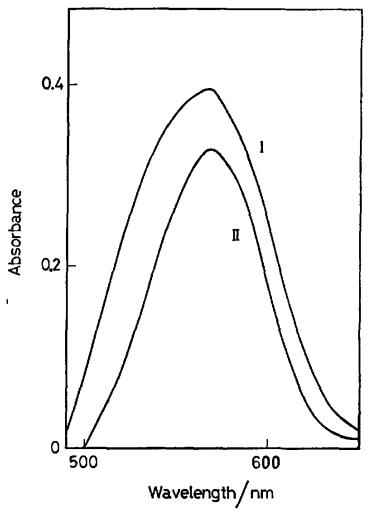

Fig. 1. Absorption curves.
0.05% SMXB: 3 cm^3, pH: 1.1, reference: reagent blank, I: Pd 40 μg/25 cm^3, II: Bi(III) 50 μg/25 cm^3.

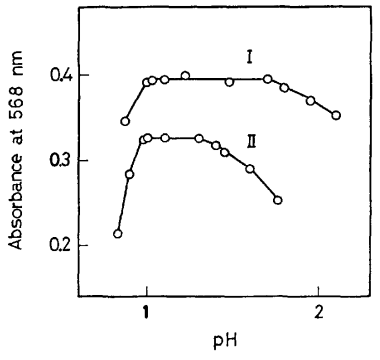

Fig. 2. Effect of pH.
0.05% SMXB: 3 cm^3, reference: reagent blank, I: Pd 40 μg/25 cm^3, II: Bi(III) 50 μg/25 cm^3.

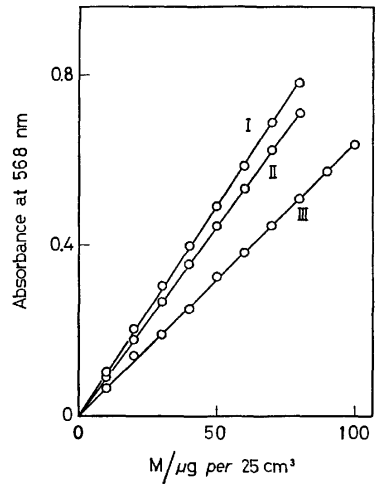

Fig. 3. Calibration curves.
0.05% SMXB: 3 cm^3, pH: 1.1, reference: reagent blank, M—I, II: Pd, III: Bi(III), II: 3 mg of chloride was added.

TABLE 1. EFFECTS OF DIVERSE IONS

Ion	A		B	
	Amount added (mg)	Pd found (μg)	Amount added (mg)	Bi(III) found (μg)
Li^+	1	39.8	1	51.5
K^+	1	40.6	1	49.6
Be^{2+}	1	41.0	1	51.2
Mg^{2+}	1	40.0	1	50.9
Ca^{2+}	1	40.0	1	49.0
Sr^{2+}	1	40.9	1	48.9
Ba^{2+}	1	40.3	1	50.0
Al^{3+}	0.04	40.2	1	49.6
Al^{3+}	1[a]	40.8	—	—
Ga^{3+}	0.04	74.2	0.05	51.4
In^{3+}	0.5	38.4	0.1	51.2
Sn^{4+}	0.04	45.6	0.05	83.0
Sn^{4+}	1[a]	39.8	0.05[b]	51.8
Pb^{2+}	1	40.9	1	50.0
As(V)	0.5	41.1	1	51.6
Bi^{3+}	0.04	65.1	—	—
Cu^{2+}	0.04	40.2	0.05	50.5
Zn^{2+}	1	40.9	1	50.0
Cd^{2+}	1	40.8	1	49.6
Hg^{2+}	1	40.0	1	49.6
Sc^{3+}	0.04	47.1	0.05	97.7
Sc^{3+}	0.5[a]	40.0	0.5[b]	52.0
Y^{3+}	1	39.8	1	50.0
La^{3+}	1	39.2	1	48.5
Ce^{3+}	1	40.3	1	49.1
Zr^{4+}	0.04	129.7	0.01	101.0
Zr^{4+}	1[a]	40.3	—	—
Th^{4+}	0.04	41.1	0.05	89.7
Th^{4+}	1[a]	41.4	0.5[b]	51.6
V(V)	0.1	38.8	0.1	50.0
Cr^{3+}	1	41.5	1	50.3
Mo(VI)	0.04	40.0	0.05	51.0
W(VI)	1	40.8	0.1	50.4
UO_2^{2+}	1	40.0	1	48.9
Mn^{2+}	1	38.9	1	49.1
Fe^{3+}	0.04	97.8	0.01	83.3
Fe^{3+}	0.04[a]	40.0	1[c]	50.5
Co^{2+}	1	40.0	1	50.0
Ni^{2+}	1	40.6	1	48.5
Rh^{3+}	1	39.4	1	48.9
Pd^{2+}	—	—	0.05[d]	51.5
Pt(IV)	1	41.1	1	49.6
F^-	10	38.9	1	49.0
Cl^-	1	39.0	10	48.9
PO_4^{3-}	10	40.2	10	51.3
SO_4^{2-}	10	40.0	10	48.3
Oxalate	10	39.8	0.05	49.0
Tartrate	10	40.8	10	51.5
Citrate	10	40.0	10	51.0

A: Effect on palladium determination (40 μg of palladium was taken). B: Effect on bismuth(III) determination (50 μg of bismuth(III) was taken). a) 10 mg of fluoride was added. b) 1 mg of fluoride was added. c) 3 cm^3 of 4% L-ascorbic acid solution was added. d) Absorbance was measured immediately after color development.

Gallium, tin(IV), bismuth(III), scandium, zirconium, and iron(III) interfered with the determination, but tin(IV), scandium, zirconium, and iron(III) could be masked by the addition of fluoride. For the bismuth(III) determination, interfering ions such as tin(IV) and scandium, could be masked by fluoride and the effect of iron(III) is eliminated by ascorbic acid. Gallium and zirconium, however, interfered seriously.

Consecutive Determination of Palladium and Bismuth(III). The color development for the palladium complex is slow at room temperature. The speed of this reaction becomes slower by the addition of chloride, and as a result, no color development occurs for about 3 min immediately after preparation of the color system. After that, the color development occurs gradually, but the increase of the absorbance in the next 5 min is only about 4% of the absorbance which is obtained when the color develops fully. So, if the absorbance is measured within 4 min after preparation of the color system, the absorbance from palladium complex is negligible. The order of the addition of chloride is important, and if chloride is added after the addition of the SMXB solution, it has no effect on the rate of color development. On the other hand, the color formation of the bismuth(III)

TABLE 2. CONSECUTIVE DETERMINATION OF PALLADIUM AND BISMUTH(III)

Taken (μg)		Found (μg)	
Pd	Bi(III)	Pd	Bi(III)
10	10	9.3	10.2
10	60	9.2	59.5
30	30	30.3	30.8
40	10	41.0	10.9
40	50	40.9	49.9
40	60	40.9	61.2

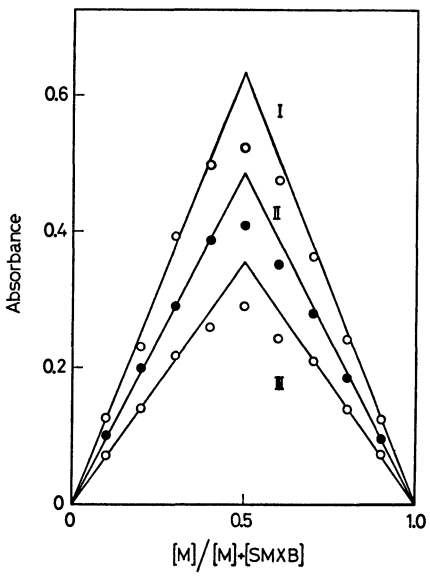

Fig. 4. Continuous variation method.
pH: 1.1, [M]+[SMXB] (mol dm^{-3})—I, III: 5.64×10^{-5}, II: 3.23×10^{-5}, M—I, III: Pd, II: Bi(III), wavelength(nm)—I, II: 568, III: 520.

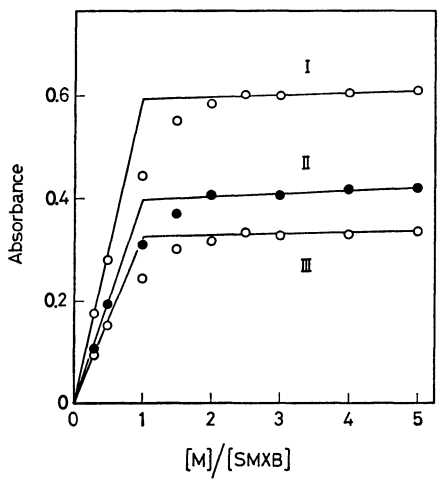

Fig. 5. Mole ratio method.
pH: 1.1, [M] (mol dm^{-3})—I, III: 2.26×10^{-5}, II: 1.34×10^{-5}, M—I, III: Pd, II: Bi(III), wavelength (nm)—I, II: 568, III: 520.

complex is rapid, and the maximum absorbance is obtained instantaneously. Utilizing these facts, the fundamental conditions for the consecutive determination of the two elements have been examined. As shown in Table 2, satisfactory results of the determinations were obtained with the solution containing 20—80 μg of palladium and 20—120 μg of bismuth(III).

The Composition of the Complexes. As shown in Figs. 4 and 5, the continuous variation and the mole ratio methods indicated that both palladium and bismuth(III) formed the 1:1 complexes with SMXB.

References

1) J. Ueda, *Nippon Kagaku Kaishi*, **1977**, 350.
2) J. Ueda, *Bull. Chem. Soc. Jpn.*, **51**, 773 (1978).
3) J. Ueda, *Nippon Kagaku Kaishi*, **1979**, 1115.
4) J. Ueda and T. Kitadani, *Nippon Kagaku Kaishi*, **1982**, 1914.
5) K. Sonoda, M. Otomo, and K. Kodama, *Bunseki Kagaku*, **27**, 429 (1978).
6) H. Onishi and N. Ishiwatari, *Bull. Chem. Soc. Jpn.*, **33**, 1581 (1960).
7) T. Enoki, I. Mori, M. Yamazaki, and M. Inoue, *Bunseki Kagaku*, **21**, 31 (1972).
8) M. Deguchi, I. Okumura, and K. Sakai, *Bunseki Kagaku*, **19**, 836 (1970).
9) T. Enoki, I. Mori, and Y. Izumi, *Bunseki Kagaku*, **18**, 963 (1969).
10) M. Otomo, *Bull. Chem. Soc. Jpn.*, **36**, 889 (1963).

Kinetic Studies of Fast Equilibrium by Means of High-performance Liquid Chromatography. IV. Separation of Rotamers of Palladium(II) Dithiocarbamates

Masataka Moriyasu,* Yohei Hashimoto, and Masaru Endo†

Kobe Women's College of Pharmacy, Motoyamakita-machi, Higashinada-ku, Kobe 658

†*Kinki District Narcotic Control Office, Uchikyuhoji-machi, Higashi-ku, Osaka 540*

(Received October 28, 1982)

The restricted rotation about carbon-nitrogen bonds of unsymmetrical palladium(II) dithiocarbamate chelates has been investigated by high-performance liquid chromatography. At higher temperatures, the rotation is so rapid that two rotamers have not been distinguished, and a single sharp peak has appeared on chromatograms, whereas at lower temperatures, they have been separated. The activation energy of the rotation of palladium(II) dithiocarbamate ($\Delta H^{*}=83\pm5$ kJ mol^{-1} for $Pd(C_6H_5CH_2CH_2NHCSS)_2$) is smaller than usual values of the energy barrier to rotate double bonds, but larger than those to rotate single bonds.

In our previous reports[1-3] it was shown that fast equilibrium including ternary complex formation between two different dithiocarbamate chelates of nickel(II) or copper(II) ($MA_2+MB_2\rightleftharpoons 2MAB$) could be traced by high-performance liquid chromatography (HPLC), while the labile ternary complex MAB was eluted without disproportionation. When kinetically unstable species are chromatographed, they are transformed gradually into other species in the column. The chromatogram patterns vary whether or not the separation is faster than the transformation. When the separation is much faster, the transformation during chromatography will be negligible, and kinetically unstable species will be eluted without any change in the column. On the other hand, when the separation is much slower, unstable species is not detected. Between these two extremes, the separation and the transformation will compete and complicated chromatograms will be obtained. Therefore, in order to trace fast reactions in solution by HPLC, kinetically unstable species should be stabilized in the column by some ways, and the following methods are suggested. (1) Temperature control: Since the rate of reaction decreases with decreasing temperature, kinetically unstable species will be stabilized when HPLC is performed at low temperatures. (2) Flow rate control: Since the residence time of each species in the column decreases with increasing flow rate of the eluent, this brings a similar result to temperature decrease. (3) Sample amount: The effect of sample amount on chromatograms should differ whether the reaction proceeds according to the first-order or the second-order rate law. The progress of second-order reactions is slow, when low initial concentrations of reactants are chosen. Thus, different chromatogram patterns will be obtained, when samples of different initial concentrations with the same sample volume are supplied to HPLC. Contrary to this, when a reaction proceeds according to the first-order rate law, the progress of the reaction should be indifferent to sample amounts, giving unchanged chromatogram patterns. Thus the change of sample concentrations might give a useful information on the reaction mechanism.

In this report equilibria between various kinetically unstable species present in the solution of palladium(II) dithiocarbamate chelates have been scrutinized by means of HPLC.

Experimental

Reagents. Sodium or ammonium salts of various *N,N*-disubstituted and *N*-monosubstituted dithiocarbonic acids were prepared by mixing corresponding aliphatic amine, carbon disulfide, and sodium hydroxide (or aqueous ammonia).[4] The following amines were used: symmetrical secondary amines (dimethylamine, diethylamine, dipropylamine, dibutylamine, pyrrolidine, piperidine, perhydroazepine, morpholine, and dibenzylamine), unsymmetrical secondary amines (*N*-methylbenzylamine, *dl*-2-methylpiperidine, and *l*-ephedrine), and primary amines (methylamine, ethylamine, propylamine, butylamine, benzylamine, and phenethylamine). Standard solutions of palladium(II) and nickel(II) (0.1 mol dm^{-3}) were prepared by dissolving $PdCl_2$ and $NiCl\cdot 6H_2O$ in dilute hydrochloric acid.

Apparatus. The HPLC apparatus is of our own construction. A two-plunger reciprocal pump (Model KHD-W-294, Kyowa Seimitsu Co. Ltd.), a variable sample injector (Model KHP-U1-130, Kyowa Seimitsu Co. Ltd.), a silica-gel column, and a variable wavelength UV-visible detector (Model SPD-1, Shimadzu) were combined. Silica-gel packings (LiChrosorb SI 100, 5 μm, E. Merck Darmstadt; Polygosil 50-5, 5 μm, M. Nagel, Duren; Wako-gel LC 10 H, 10 μm, Wako Pure Chemicals Co. Ltd.) were slurry-packed into stainless steel columns (diameter 4 mm, length 25 cm). Absorbance of palladium(II) dithiocarbamate chelates was measured by a double-beam spectrometer (Model 124, Hitachi).

Procedure. In order to carry out HPLC at low temperatures, column and solvent reservoir were immersed into refrigerant composed of water-methanol in a bath (Model Cryocool CC-80f, Neslab Instruement Inc.). When sillica-gel packings and mixed solvent sysrems of hexane-isopropyl acetate were combined, HPLC was made possible even at −70 °C, though column efficiency was reduced below −40 °C. For the determiantion of rate constants, the HPLC apparentus was modified as depicted in Fig. 1. The procedure was as follows. An equilibrated solution composed of two isomers ($X\rightleftharpoons Y$) was supplied to HPLC through injector I and the portion corresponding to X (or Y) was collected into a reservoir thermostated in the bath. The collected solution was stirred and then stood for a few minutes. After the flow path was changed by the six-way valve, the solution in the reservoir was sucked in from injector II. The injection was repeated for a definite interval. Since the reaction $X\rightarrow Y$ (or $Y\rightarrow X$) proceeded gradually in the thermostated solution, peak of Y (or X) grew while that of X (or Y) fell with each injection. Thus the progress of the

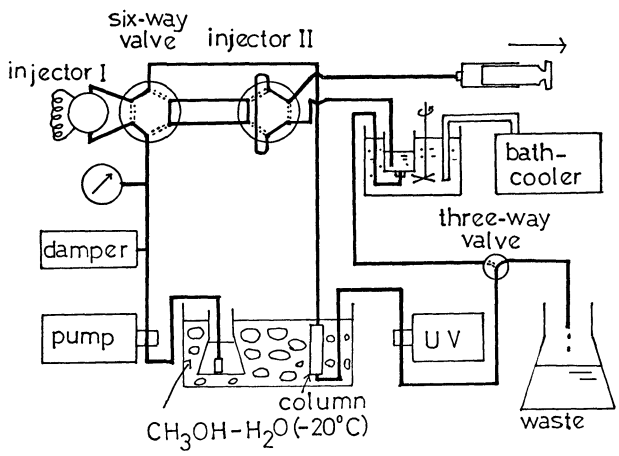

Fig. 1. Block diagram of HPLC apparatus.

reaction was traced by HPLC. All the measurements were repeated three times.

Theoretical

HPLC of Two Isomers in the Equilibrium State. Two different species (X and Y) exist in the equilibrated state in solution, fast interconversion of two isomers being an example.

$$X \underset{k_{-1}}{\overset{k_1}{\rightleftharpoons}} Y , \quad (1)$$

$$K_1 = y_e/x_e = k_1/k_{-1}. \quad (2)$$

Here, x_e and y_e are concentrations of X and Y in the equilibrium state, respectively. Possible chromatogram patterns will be considered first. It is assumed that intrinsic retention time of X is smaller than that of Y, and K_1 is close to 1.0. (1) When k_1 and k_{-1} are very small and separation is achieved promptly, two species X and Y will be eluted separately without interconversion. In this case the obtained chromatograms will be similar to those of the separation of two stable species (Fig. 2(a)). (2) With the increase of k_1, partial interconversion will commence to occur during the course of chromatography. When a part of species X with smaller retention time is converted into Y, its linear velocity passing through the column is reduced, and the peak of X tends to cause tailing (Fig. 2(b)). Similarly the peak of Y will cause leading. (3) When the rate of interconversion is moderately fast, and separation and interconversion occur competitively in the column, complicated chromatograms will be obtained (Figs. 2(c) and 2(d)). (4) When the interconversion is much faster than the separation and consequently the equilibrium in Eq. 1 is maintained throughout the HPLC process, a single peak will appear on chromatograms, and the retention time is the mean of the intrinsic retention times of X and Y (Fig. 2(e)). A fall of column temperature and an increase of flow rate will bring the change of chromatogram patterns, Fig. 2(e)→Fig. 2(d)→Fig. 2(c)→Fig. 2(b)→Fig. 2(a), because interconversion will be retarded by these procedures. The decrease of initial concentration of the sample will bring a similar result provided that the interconversion proceeds according to the second-order rate law.

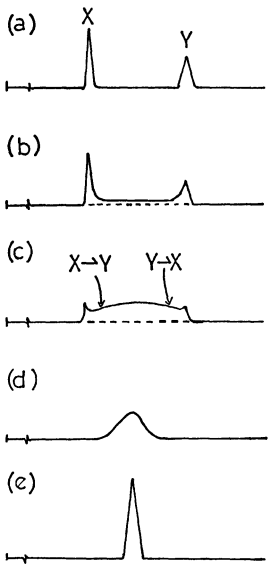

Fig. 2. Possible chromatogram patterns of the system of two kinetically unstable species in equilibrium state.

Determination of Equilibrium and Rate Constants. There exists some difficulty in the determination of the equilibrium and the rate constants, since species X and Y are hardly obtained in a pure state. The measurement of two peak areas in Fig. 2(a) does not give K_1 values directly due to the difference of absorption coefficients of X and Y. The determination of K_1 should thus be carried out by the following procedure, if a chromatogram pattern shown in Fig. 2(a) is obtained. The equilibrated solution is supplied to HPLC, and two fractions corresponding to X and Y are collected. These two solutions are diluted to a definite volume with an HPLC solvent. After standing enough time to attain the equilibrium ($X \rightleftharpoons Y$), K_1 can be determined by one of the following alternative methods. (1) The measurement of absorbance of these two solutions gives K_1 values. (2) When a portion of these two solutions is rechromatographed, chromatogram patterns shown in Fig. 2(a) will be obtained again. The measurements of peak heights (or peak areas) of these two solutions give K_1 values. The calibration curves of X and Y are obtained when K_1 values are determined.

The determination of k_1 and k_{-1} will be carried out as follows. If X (or Y) can be obtained in a pure state, k_1 and k_{-1} are determined easily. This assumption, though being hardly attained in case of a fast equilibrium, will be useful to extend the discussion. Therefore, we consider first using this assumption. In this case, rate constants are determined by dissolving pure X (or Y) and after standing for a definite time a portion of the solution is supplied to HPLC. When the injection is repeated at a definite interval, the peak of Y (or X) will grow while that of X (or Y) will fall. The rate constants are expressed by the following alternative equations whether the reaction proceeds according to the first-order (3) or the second-order (4) rate law.[5]

$$k_1 = (y_e/x_0t)\ln\{y_e/(y_e-y)\}, \quad (3)$$

$$k_1 = [y_e/\{2x_0t(x_0-y_e)\}] \times \ln[\{y(x_0-2y_e)+x_0y_e\}/\{x_0(y_e-y)\}]. \quad (4)$$

Here, x_0, y, and y_e denote initial concentration of X, concentration of Y at t and at equilibrium state, respectively.

Since the aforementioned premise is not satisfied actually, some modification of the formulation is required. The fraction of X (or Y) is collected by HPLC and then the solution is kept in the thermostated bath. After standing for some minutes, a portion of the thermostated solution is rechromatographed. At this time t', the reaction X→Y (or Y→X) already proceeds partially, and we denote the concentrations of X and Y at t' as x' and y', respectively. After a definite interval Δt, a portion of the solution is injected repeatedly. Eqs. 3 and 4 are modified as follows.

$$k_1 = \{y_e/x_0(t'+\Delta t)\}\ln\{y_e/(y_e-y'-\Delta y)\}, \quad (3')$$

$$k_1 = [y_e/\{2x_0(t'+\Delta t)(x_0-y_e)\}] \times \ln[\{(y'+\Delta y)(x_0-2y_e)+x_0y_e\}/\{x_0(y_e-y'-\Delta y)\}]. \quad (4')$$

Here, $y'+\Delta y$ is the concentration of Y at $t'+\Delta t$.

Results and Discussion

Comparison of HPLC of Palladium(II) and Nickel(II) Dithiocabamate Chelates. Chromatographic behavior of various palladium(II) dithiocarbamate chelates was compared with that of nickel(II) dithiocarbamate chelates. As mentioned in our previous report,[6] retention times of each palladium(II) dithiocarbamate were very close to those of corresponding nickel(II) dithiocarbamate when silica gel packings and mixed solvent systems of hexane–isopropyl acetate were used. The characteristic feature of the chromatograms of palladium(II) chelates is an appearance of very broad peaks in some cases, as exemplified in Fig. 3. When

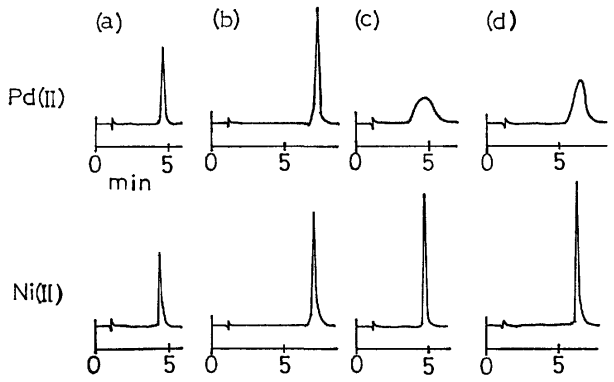

Fig. 3. Comparison of HPLC of dithiocarbamate chelates of Pd(II) and Ni(II).
Column: Polygosil 50-5 (4 mm×25 cm). Eluent: hexane:isopropyl acetate=100:15 (water saturated). Flow rate: 1.5 cm³/min. Detector: 305 nm (Pd), 325 nm (Ni). Sample size: 0.01 cm³. Sample: MA_2 A= (a) $(CH_3)_2NCSS^-$, (b) O(CH₂CH₂)₂NCSS⁻, (c) $(C_6H_5CH_2CH_2)HNCSS^-$, (d) $(CH_3CH_2)HNCSS^-$.

palladium(II) chelates were derived from symmetrical secondary amines such as diethylamine and piperidine, peaks were always sharp. However, *N*-monosubstituted dithiocarbamate chelates derived from primary amines gave broad peaks. This seems to be attributable to the decomposition of the chelates since *N*-monosubstituted dithiocarbamate chelates of some metal ions are less stable chemically than *N*,*N*-disubstituted dithiocarbamate chelates.[7] This explanation, however, is not valid because solutions of *N*-monosubstituted dithiocarbamate chelates of palladium(II) did not give any change in absorption spectra after 10 d. Furthermore, dithiocarbamate chelates derived from unsymmetrical secondary amines such as *N*-methylbenzylamine also gave broad peaks. The characteristic feature of the chromatograms is summarized that peaks are broadened when unsymmetrical palladium(II) dithiocarbamates are chromatographed.

Separation of Two Rotamers of Palladium(II) Dithiocarbamates. The X-ray conformational study of nickel(II) diethyldithiocarbamate has shown[8] that this chelate has a structure as shown below. All the atoms except terminal methyl groups lie in the same plane.

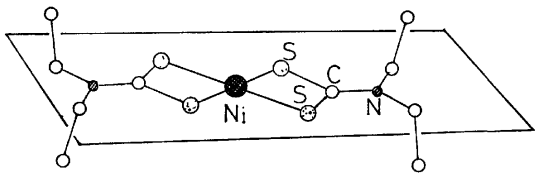

The carbon-nitrogen bond length is 1.33 Å (1 Å= 10^{-10} m), which is much shorter than that of the usual carbon–nitrogen single bond (1.47 Å), but slightly longer than that of the carbon-nitrogen double bond (1.30 Å). The bond lengths of two carbon-sulfur bonds are identical (1.71 Å) within the experimental error. These results suggest that the contribution of the following three canonical forms is possible and that of the last form is largest.

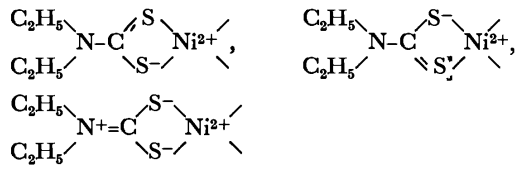

It is well known that the carbon-nitrogen double bonds are rigidly fixed, similarly to the carbon-carbon double bonds. On the other hand, the carbon-nitrogen single bonds rotate freely at room temperature. When two different substituents (R_1 and R_2) are linked to each nitrogen atom, two geometric isomers shown below might be separated, provided that the carbon-nitrogen bond has a double bond character.

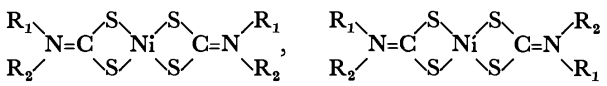

A similar explanation is valid for palladium(II) chelates because palladium(II) has been well known to form square-planer complexes. We chromatographed several unsymmetrical palladium(II) dithiocarbamates at various temperatures. An example of chromatograms of palladium(II) dithiocarbamate derived from

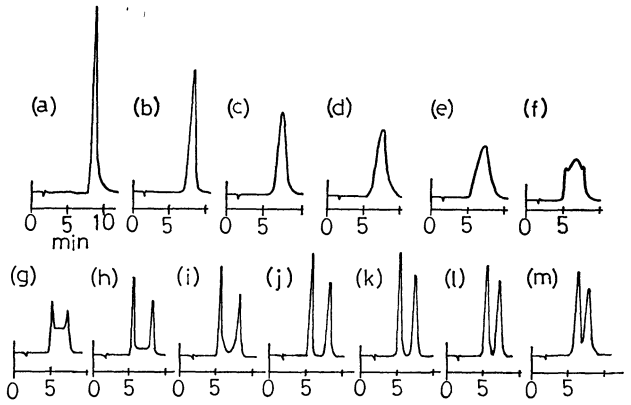

Fig. 4. Chromatograms of Pd(II) dithiocarbamate derived from phenethylamine at various temperatures. Column: Wakogel LC-10H (4 mm×25 cm). Eluent: hexane:isopropyl acetate=100:15 (water saturated). Flow rate: 1.5 cm³/min. Detector: 305 nm. Sample size: 0.01 cm³. Sample: 1.0×10^{-3} mol dm^{-3} Pd-$[(C_6H_5CH_2CH_2)HNCSS]_2$ (a) 50 °C, (b) 40 °C, (c) 30 °C, (d) 25 °C, (e) 20 °C, (f) 15 °C, (g) 10 °C, (h) 0 °C, (i) −10 °C, (j) −20 °C, (k) −30 °C, (l) −40 °C, (m) −50 °C.

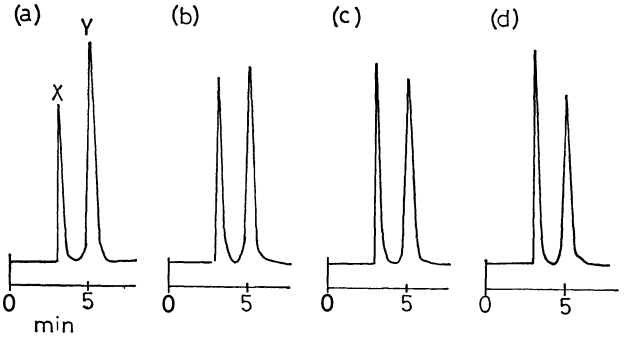

Fig. 5. Change of chromatogram patterns during the course of interconversion of two rotamers of Pd(II) dithiocarbamate derived from phenethylamine. Column: LiChrosorb SI 100 (5 μm, 4 mm×25 cm). Eluent : hexane : isopropyl acetate=100:15 (water saturated). Flow rate: 2.5 cm³/min. Detector: 305 nm. Sample size: 0.2 cm³. Sample: A 0.025 cm³ solution of 2×10^{-3} mol dm^{-3} Pd$[(C_6H_5CH_2CH_2)$-$NHCSS]_2$ was supplied to HPLC and the fraction corresponding to the latter peak was collected. After thermostated at 0 °C for a few minutes, a 0.2 cm³ portion of the solution was supplied to HPLC. The initial concentration of Y ($=y_0$) was determined to be 2.0×10^{-5} mol dm^{-3}. (a) at t_0, (b) at $t_0+5.0$ min, (c) at $t_0+10.0$ min, (d) at t_0+30 min(equilibrium). The value k_1 ($=k_{-1}$) was determined to be 1.1×10^{-3} s^{-1} in this case.

phenethylamine is shown in Fig. 4, which gave the broadest peak at room temperature. These chromatograms suggest that partial rotation around the carbon-nitrogen bond does occur during chromatography at intermediate temperatures. At lower temperatures (<−20 °C), the rotation is negligible because neither tailing nor leading was observed. When the temperature was lowered down to −40 °C, two peaks gradually overlapped due to the decrease of column efficiency. At higher temperatures (>50 °C), the rotation is so rapid that two isomers cannot be distinguished by HPLC. Other palladium(II) chelates derived from unsymmetrical amines such as ethylamine and *N*-methylbenzylamine gave similar results. Contrary to palladium(II) chelates, unsymmetrical nickel(II) chelates always gave single peaks at any temperatures. From these results, it can be concluded that palladium(II) chelates undergo relatively slow intramolecular carbon-nitrogen bond rotation, while for nickel(II) chelates the rotation is rapid even at lower temperature. This suggests that a lone-pair electron on the nitrogen atom is withdrawn by palladium(II) ion more strongly than by nickel(II) ion.

Reaction Mechanism of the Rotation. In order to elucidate whether the rotation proceeds according to the first- or second-order rate law, HPLC conditions such as flow rate and initial concentration of the sample were varied. When the flow rate was doubled at 15 °C, the chromatogram was found to be similar to that shown in Fig. 4(g) (at 10 °C), suggesting that the reaction is approximately doubled with 5 °C rise in temperature. Then the sample solution was diluted various times, and 0.01 cm³ each of the solution was supplied to HPLC at 15 °C. The chromatogram pattern was independent of initial concentration, suggesting the first-order reaction mechanism.

Determination of K_1 and k_1. The equilibrium constants K_1 and the rate constants k_1 of palladium(II) chelate derived from phenethylamine were determined at various temperatures according to the procedure described in the previous theoretical section. The K_1 values were always equal to 1.0 within the experimental error. Two peak areas in Figs. 4(i)—4(l) were also the same, suggesting that two rotamers have almost the same absorption coefficients. These results seem to be in good agreement with the fact that no steric hindrance exists for these two rotamers. Since $K_1=1.0$, Eq. 3′ will be simplified to

$$k_1 = k_{-1} = \{0.5/(t'+\Delta t)\} \ln \{x_0/(x_0-2y'-2\Delta y)\}. \quad (5)$$

An example of the change of chromatogram patterns at 0 °C is shown in Fig. 5. Here X and Y denote the former and the latter peaks, respectively, because it is not always possible to conclude which rotamer is eluted faster. The k_1 value at 0 °C was thus determined to be $(1.1\pm0.1)\times10^{-3}$ s^{-1}. The energy barrier of rotation ΔH^* was obtained by measuring k_1 at different temperatures, and the results are plotted in Fig. 6. Since the rotation is so rapid at higher temperatures that the determination of k_1 was impossible above 10 °C. The energy barrier ΔH^* was determined to be 83±7 kJ mol^{-1}. This value is much larger than that to rotate usual single bonds, but smaller than that to rotate double bonds. For example, the activation energy to rotate carbon–carbon single and double bonds are well known to be about 12 and 260 kJ mol^{-1}, respectively.[9] Since the upper limit of the thermal energy of molecules in solution is 63—85 kJ mol^{-1},[9] a value of 83 kJ mol^{-1} seems to be near the limit that the reaction proceeds promptly at room temperature. The k_1 value at room temperature is extraporated to be 3.6×10^{-2} s^{-1} (at 25

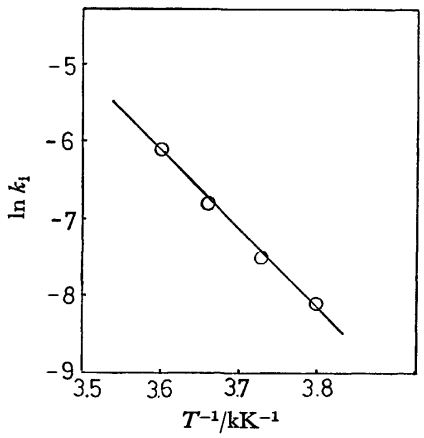

Fig. 6. Activation energy of the carbon-nitrogen bond rotation. Chromatographic conditions were similar to those shown in Fig. 5. The values of k_1 were determined at various temperatures with the similar procedure shown in Fig. 5. The value ΔH^* was determined from the following equation: $k_1 = A_0 \exp(-\Delta H^*/RT)$.

°C) from Fig. 6. From this result it is calculated that the interconversion reaction X→Y proceeds to 50% within 10 s at 25 °C.

Ternary Complex Formation. When chloroform solutions of two different dithiocarbamate chelates of palladium(II) (MA_2 and MB_2) were mixed, ternary complex formation was found to occur similarly to the cases of nickel(II) and copper(II).[1]

$$MA_2 + MB_2 \underset{k_-}{\overset{k}{\rightleftharpoons}} 2MAB, \quad (6)$$

$$K = [MAB]^2/[MA_2][MB_2]. \quad (7)$$

An example of chromatograms of ternary complex formation is shown in Fig. 7. The equilibrium constant K is 4.0, which suggests that similarly to copper(II) and nickel(II) ternary complex formation is controlled by a statistical factor. Rate constants k were measureed for several systems, and the results were tabulated in Table 1 together with the data on nickel(II) and copper(II) complexes described in our previous reports.[1,3] The values of palladium(II) complexes are much smaller than those of nickel(II), which is in agreement with the fact that palladium(II) forms more inert complexes than nickel(II).

Ternary complex formation, which was found to proceed according to the second-order rate law, should

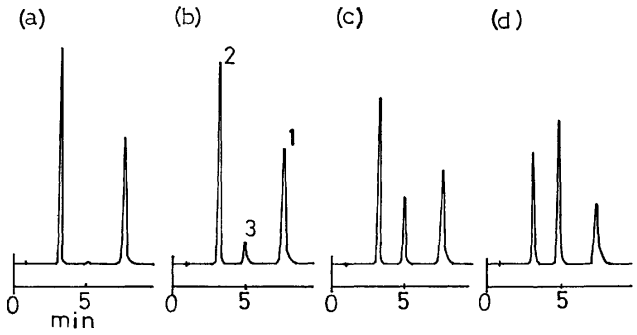

Fig. 7. Ternary complex formation of two Pd(II) dithiocarbamates.
Column: Polygosil 50-5 (4 mm×25 cm). Eluent: hexane:isopropyl acetate=100:3 (water saturated). Flow rate: 2.0 cm^3/min. Detector: 305 nm. Sample size: 0.01 cm^3. Sample: 5×10^{-4} mol dm^{-3} PdA_2+ 5×10^{-4} mol dm^{-3} PdB_2 in $CHCl_3$, A=Pd[$(CH_3CH_2)_2$-NCSS]$_2$, B=Pd[$(CH_3CH_2CH_2)_2$NCSS]$_2$. 1) PdA_2, 2) PdB_2, 3) PdAB. (a) After mixing 1.0 min, (b) 10 min, (c) 290 min, (d) 3 d (equilibrium). The mixed solution was thermostated at 25 °C.

be accompanied by cleavage of metal–sulfur bond and the exchange of ligand, dithiocarbamates. A similar reaction occurs when B=A in Eq. 6.

$$MA_2 + MA_2^* \rightleftharpoons 2MAA^*. \quad (8)$$

Here * is added to distinguish two MA_2. When A is a symmetrical dithiocarbamate, no net reaction will occur and the reaction cannot be traced by HPLC. On the other hand, when A is an unsymmetrical dithiocarbamate, the reaction shown in Eq. 9 should occur.

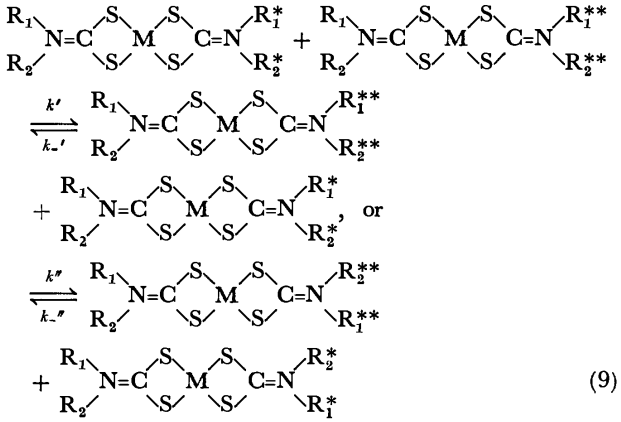

(9)

Table 1. Summary of rate constants of ternary complex formation

$$MA_2 + MB_2 \underset{k_-}{\overset{k}{\rightleftharpoons}} 2MAB, \quad K=[MAB]^2/[MA_2][MB_2]=4.0$$

B	k/mol^{-1} dm^3 s^{-1}		
	M=Cu(II)	M=Ni(II)	M=Pd(II)
$(CH_3CH_2CH_2)_2NCSS^-$	$(6.4\pm0.3)\times10^3$ a)	$(2.4\pm0.2)\times10^2$ a)	$(4.0\pm0.3)\times10^{-2}$ c)
$(C_6H_5CH_2)_2NCSS^-$	$(3.4\pm0.8)\times10^3$ a)	$(1.9\pm0.2)\times10^2$ a)	$(7.2\pm0.5)\times10^{-3}$ c)
$(CH_3CH_2)HNCSS^-$	——	$(1.6\pm0.3)\times10^2$ b)	$(1.2\pm0.2)\times10^{-2}$ c)
$(C_6H_5CH_2CH_2)HNCSS^-$	——	——	$(1.9\pm0.2)\times10^{-2}$ c)

A: $(CH_3CH_2)_2NCSS^-$ a) Ref. 1, b) Ref. 3, c) this work. For experimental conditions of a) and b), see Refs. 1 and 3. Experimental conditions of c) are described in Fig. 7.

The latter pathway in Eq. 9 should be accompanied by the isomerization reaction, while the former does not bring any reaction. Thus, the presence of another path of the isomerization reaction is suggested. Since the reactions shown in Eqs. 6 and 8 are essentially similar, it will reasonably be concluded that $k'+k''$ is close to k shown in Table 1. Both k_1 and k'' of palladium(II) dithiocarbamates will be of the order 10^{-2} on the assumption that $k' \approx k''$. There exists, however, an essential difference between k_1 and k'' that k_1 is a first-order rate constant, while k'' second-order. Therefore, at higher concentrations such as 1 mol dm^{-3}, the isomerization will occur according to two competitive pathways (Eqs. 1 and 9). On the other hand, at lower concentrations such as 10^{-3} mol dm^{-3} at which the major parts of the present experiments were carried out, bond rotation will be a predominant process.

References

1) M. Moriyasu and Y. Hashimoto, *Bull. Chem. Soc. Jpn.*, **53**, 3590 (1980).
2) M. Moriyasu and Y. Hashimoto, *Bull. Chem. Soc. Jpn.*, **54**, 2470 (1981).
3) M. Moriyasu and Y. Hashimoto, *Bull. Chem. Soc. Jpn.*, **54**, 3374 (1981).
4) A. W. Hofman, *Chem. Ber.*, **1**, 25 (1868).
5) For exampie, K. J. Laidler, "Chemical Kinetics," 2nd ed, McGraw-Hill, London (1965), p. 21.
6) M. Moriyasu, Y. Hashimoto, and M. Endo, *Bull. Chem. Soc. Jpn.*, **54**, 3369 (1981).
7) A. Hulanicki, *Talanta*, **14**, 1371 (1967).
8) M. Bonamico, G. Dessy, C. Mariani, A. Vaciago, and L. Zambonelli, *Acta Crystallogr.*, **19**, 619 (1965).
9) For example, J. B. Hendrickson, D. J. Cram, and G. S. Hammond, "Organic Chemistry," 3rd ed, McGraw-Hill, London (1970), p. 185.

Partial Molal Volumes and Volume Changes for Complex Formation of $[M(phen)_3]Cl_2$ in Aqueous Solutions

Kouzou Yoshitani,* Manabu Yamamoto,† and Yuroku Yamamoto†

Faculty of General Education, Gifu University, Nagara, Gifu 502

†*Department of Chemistry, Faculty of Science, Hiroshima Uuiversity, Higashisenda, Naka-ku, Hiroshima 730*

(Received November 1, 1982)

The partial molal volumes, $\overline{V}°$, of $[M(phen)_3]Cl_2$ (M=Fe(II), Co(II), Ni(II), Cu(II), and Zn(II)) and 1,10-phenanthroline were determined from density measurements at 25 °C. From the values for $\overline{V}°$ of $[M(phen)_3]^{2+}$, M^{2+} and phen the volume changes for complex formation of $[M(phen)_3]^{2+}$, $\Delta\overline{V}°$, were caluculated. Values for $\overline{V}°$ of $[M(phen)_3]Cl_2$ varied from 445.1 $cm^3\ mol^{-1}$ for $[Fe(phen)_3]Cl_2$ to 458.1 $cm^3\ mol^{-1}$ for $[Zn(phen)_3]Cl_2$ and were in the order, $[Fe(phen)_3]^{2+}<[Co(phen)_3]^{2+}>[Ni(phen)_3]^{2+}<[Cu(phen)_3]^{2+}<[Zn(phen)_3]^{2+}$. The $\Delta\overline{V}°$ of $[Fe(phen)_3]^{2+}$ was significantly small, 4.7 $cm^3\ mol^{-1}$. While those of other metal chelate ions were similar values, *ca.* 20 $cm^3\ mol^{-1}$. The smaller $\Delta\overline{V}°$ of $[Fe(phen)_3]^{2+}$ is considered to be due to the spin change from the high-spin aqua ion, $[Fe(OH_2)_6]^{2+}$, to the low-spin complex ion, $[Fe(phen)_3]^{2+}$.

Metal chelate cations such as $[Fe(phen)_3]^{2+}$ are widely used for the determination of a large number of anions by solvent extraction of ion pairs.[1] Extensive studies have been reported to understand the mechanisms of solvent extraction of ion pairs and solute-solvent interactions of metal chelate electrolytes through viscosities,[2] conductivities,[3] solubilities,[4] and salting effects on the solubilities on nonelectrolytes in water.[5] The partial molal volumes and volume changes of complexation are effective in elucidating the solute-solvent interactions, yet few studies have been reported, especially for volume changes of the complex formation reactions of these metal chelates.

In this study, the partial molal volumes of tris(1,10-phenanthroline) complexes of the first transition metal ions (Fe(II), Co(II), Ni(II), Cu(II), and Zn(II)) are determined and volume changes on complex formation are estimated. The specific aspect of $[Fe(phen)_3]^{2+}$ has been discussed by the spin change on complexation.

Experimental

The metal chelate electrolytes, $[Fe(phen)_3]Cl_2\cdot 7.5H_2O$, $[Ni(phen)_3]Cl_2\cdot 7.5H_2O$ and $[Co(phen)_3]Cl_2\cdot 7.5H_2O$ were prepared by the literature methods.[2,6,7] $[Cu(phen)_3]Cl_2\cdot 7.5H_2O$ and $[Zn(phen)_3]Cl_2\cdot 7.5H_2O$ were prepared by a method similar to that for the Ni-complex. 1,10-Phenanthroline monohydrate (Hanawa Pure Chemical Industries, Ltd.) was used without further purification. Purity of the products was checked by analysis.

The metal chelate electrolytes were dehydrated by drying to constant weigh under reduced pressure over P_2O_5. All solutions were prepared by weight with deionized and distilled water.

The densities of the sample solutions were measured using a digital densimeter (Shibayama Scientific Co., Ltd. Model SS-D-200) with an external measuring cell which was completely immersed in a water bath controlled to 25.00± 0.002 °C. The system was calibrated with dry air and pure water. The accuracy of the system was checked by measuring the densities of NaCl solutions.[8] The errors in the density measurements were estimated within 3×10^{-6} g cm^{-3}.

Results

The apparent molal volumes, ϕ_v, of the solutes have been calculated from the densities of the solutions using the equation:

$$\phi_v = \frac{1000(d°-d)}{md°d} + \frac{M}{d}, \quad (1)$$

where M is the molecular weight of the solute, m is the molality, $d°$ and d are the densities of the solvent and the solution, respectively. The density of pure water at 25 °C was taken from the literature.[9]

The apparent molal volumes of the metal chelate electrolytes were fitted to the Redlich-Mayer equation in order to extrapolate them to infinite dilution:[10]

$$\phi_v = \phi_v° + S_vC^{1/2} + b_vC, \quad (2)$$

where $\phi_v°$ is the apparent molal volume at infinite dilution (equal to the partial molal volume, $\overline{V}°$), S_v is given by the limiting Debye-Hückel law as 9.706 $cm^3\ dm^{3/2}\ mol^{-3/2}$ for 2:1 electrolytes in water at 25 °C, b_v is a constant and c is the concentration.[10] Equation 2 was rearranged to

$$(\phi_v - S_vC^{1/2}) = \overline{V}° + b_vC, \quad (3)$$

and plots of the left side of Eq. 3 against C are shown in Fig. 1. The parameters, $\overline{V}°$ and b_v, for the molal volumes of $[Fe(phen)_3]Cl_2$ and $[Ni(phen)_3]Cl_2$ are obtained by the least squares method and are given in Table 1. The plots of Eq. 3 for the molal volumes of $[Co(phen)_3]Cl_2$, $[Cu(phen)_3]Cl_2$ and $[Zn(phen)_3]Cl_2$ deviated from linearity at low concentrations due to partial ligand dissociations. However, when measurements were done in 0.01 mol dm^{-3} solutions of 1,10-phenanthroline, the molal volumes showed normal concentration dependences as shown in Fig. 1. Then, by fitting the apparent molal volumes of these chelates in 0.01 mol dm^{-3} solutions of 1,10-phenanthroline to the equation:

$$\phi_v = \overline{V}° + A_vC^{1/2} + B_vC, \quad (4)$$

$\overline{V}°$ and fitting parameters, A_v and B_v, are obtained. These $\overline{V}°$ values are assumed to be those in pure water and are given in Table 1.

The apparent molal volumes of free 1,10-phenanthroline in water were determined at five different concentrations, (1.0×10^{-2}—1.5×10^{-2} mol dm^{-3}), which did not show any concentration dependence over the range of experimental errors. Therefore, the mean value of ϕ_v, (142.2±0.1 $cm^3\ mol^{-1}$), is regarded as the value at infinite dilution.

The volume changes of the complex formation of

Table 1. Standard partial molal volumes at 25 °C

Solute	$\overline{V}^\circ$ / cm³ mol⁻¹	b_v [a] / cm³ dm³ mol⁻²	A_v [b] / cm³ dm³/² mol⁻³/²	B_v [b] / cm³ dm³ mol⁻²
$[Fe(phen)_3]Cl_2$	445.1 (443) [c]	−21.8		
$[Co(phen)_3]Cl_2$	456.3 [d]		11.39	−25.2
$[Ni(phen)_3]Cl_2$	454.2	−26.1		
$[Cu(phen)_3]Cl_2$	456.5 [d]		9.86	−26.8
$[Zn(phen)_3]Cl_2$	458.1 [d]		7.75	−19.8
phen	142.2			

a) An adjustable parameter of Eq. 2. b) Parameters of Eq. 4. c) Ref. 2. d) $\overline{V}^\circ$ in 0.01 mol dm⁻³ 1,10-phenanthroline solutions.

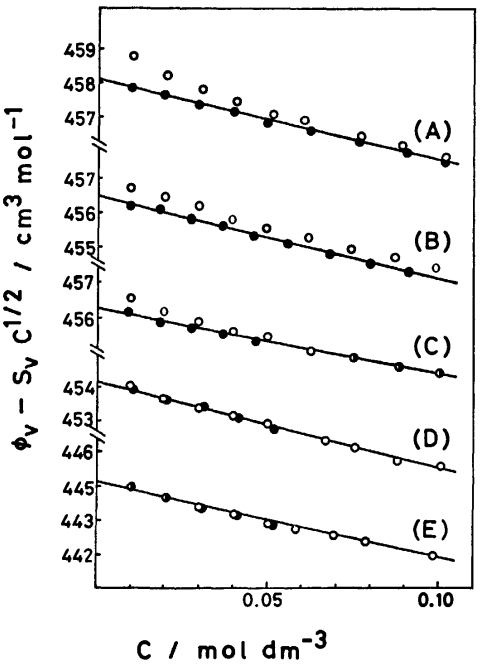

Fig. 1. Apparent molal volumes of $[M(phen)_3]Cl_2$ at 25 °C.
(A): $[Zn(phen)_3]Cl_2$, (B): $[Cu(phen)_3]Cl_2$, (C): $[Co(phen)_3]Cl_2$, (D): $[Ni(phen)_3]Cl_2$, (E): $[Fe(phen)_3]Cl_2$. ○: In water, ●: in 0.01 mol dm⁻³ solutions of 1,10-phenanthroline.

tris(1,10-phenanthroline) complexes, $\Delta\overline{V}^\circ$, can be estimated with the partial molal volumes of the reactants and products according to the relationship:

$$\Delta\overline{V}^\circ = \overline{V}^\circ([M(phen)_3]^{2+}) + 6\overline{V}^\circ(H_2O) - \overline{V}^\circ([M(OH_2)_6]^{2+}) - 3\overline{V}^\circ(phen), \quad (5)$$

where $\overline{V}^\circ([M(phen)_3]^{2+})$, $\overline{V}^\circ(H_2O)$, $\overline{V}^\circ([M(OH_2)_6]^{2+})$, and $\overline{V}^\circ(phen)$ are the partial molal volumes of metal chelate ions, water, aqua ions and 1,10-phenanthroline, respectively. The partial molal volumes of the hexaaqua complex ions can be estimated in good approximation by the equation:

$$\overline{V}^\circ([M(OH_2)_6]^{2+}) = \overline{V}^\circ(M^{2+}) + 6\overline{V}^\circ(H_2O), \quad (6)$$

where $\overline{V}^\circ(M^{2+})$ is the partial molal volume of the transition metal cation, which is generally obtained in the literature. By substituting Eq. 6 into Eq. 5, we obtain a simpler relation:

$$\Delta\overline{V}^\circ = \overline{V}^\circ([M(phen)_3]^{2+}) - \overline{V}^\circ(M^{2+}) - 3\overline{V}^\circ(phen), \quad (7)$$

Table 2. Ionic partial molal volumes and volume changes for the formation of $[M(phen)_3]^{2+}$ [a]

M(II)	$\overline{V}^\circ(M^{2+})$ / cm³ mol⁻¹	$\overline{V}^\circ([M(phen)_3]^{2+})$ / cm³ mol⁻¹	$\Delta\overline{V}^\circ$ / cm³ mol⁻¹
Fe(II)	−32.6 [b]	398.7	4.7
Co(II)	−36.2 [c]	409.9	19.5
Ni(II)	−39.2 [c]	407.8	20.4
Cu(II)	−35.9 [d]	410.1	19.4
Zn(II)	−35.5 [c]	411.7	20.6

a) Estimated values using $\overline{V}^\circ(Cl^-) = 23.2$ cm³ mol⁻¹ and $\overline{V}^\circ(ClO_4^-) = 49.5$ cm³ mol⁻¹. b) Ref. 11. c) Ref. 13. d) Ref. 12.

which means that $\Delta\overline{V}^\circ$ can be estimated from the partial molal volumes of metal chelate ions, transition metal cations and 1,10-phenanthroline. The partial molal volumes of the transition metal cations were estimated from the literature values for $FeCl_2$, $Co(ClO_4)_2$, $Ni(ClO_4)_2$, $Cu(ClO_4)_2$, and $Zn(ClO_4)_2$ using the additivity principle with $\overline{V}^\circ(Cl^-) = 23.2$ and $\overline{V}^\circ(ClO_4^-) = 49.5$ cm³ mol⁻¹.[11-13] The ionic partial molal volumes are given in Table 2.

Discussion

Partial Molal Volumes and the Solvation of the $[M(phen)_3]^{2+}$ Ions. The $\overline{V}^\circ$ of the aqua ions are in a sequence, $[Fe(OH_2)_6]^{2+} > [Co(OH_2)_6]^{2+} > [Ni(OH_2)_6]^{2+} < [Cu(OH_2)_6]^{2+} < [Zn(OH_2)_6]^{2+}$. The molal volumes of the chelate cations are in the same sequence except for the molal volume of $[Fe(phen)_3]^{2+}$, that is, $[Fe(phen)_3]^{2+} < [Co(phen)_3]^{2+} > [Ni(phen)_3]^{2+} < [Cu(phen)_3]^{2+} < [Zn(phen)_3]^{2+}$. From the results of X-ray analysis, the bond lengths of M–N are 1.97 Å and 2.09 Å in $[Fe(phen)_3]^{2+}$ and $[Ni(phen)_3]^{2+}$, respectively.[14,15] The Cu–N distances in $[Cu(phen)_3]^{2+}$ are 2.04 Å and 2.33 Å in the equatrial position and in the axial position, respectively.[16] From the M–N bond lengths, the molal volumes of these chelate cations are expected in the order, $[Fe(phen)_3]^{2+} < [Ni(phen)_3]^{2+} < [Cu(phen)_3]^{2+}$, which is in agreement with the observed sequence of the molal volumes of these chelate cations. However the M–N bond lengths could not be a direct measure of the molal volumes of these chelate ions. That is, if one assumes a rigid sphere for these chelates, then the radius of $[M(phen)_3]^{2+}$ is estimated about 5.5 Å from

its molal volume. For such a sphere, a difference of 0.1 Å in radius due to the M–N bond length yields a difference about 20 to 25 $cm^3 mol^{-1}$ in the molal volume, which is about one order larger than the observed differences of these complexes except for $[Fe(phen)_3]^{2+}$.

The radius of the circumscribed sphere of $[Fe(phen)_3]^{2+}$ was estimated as 7 Å,[17] with the volume of 865 $cm^3 mol^{-1}$.[5] However, the molal volumes are in the range from 398.7 $cm^3 mol^{-1}$ for $[Fe(phen)_3]^{2+}$ to 411.7 $cm^3 mol^{-1}$ for $[Zn(phen)_3]^{2+}$, which are about 4 to 6% smaller than the three times of the molal volume of the free 1,10-phenanthroline, (426.6 $cm^3 mol^{-1}$). These facts indicate that water creates a solvation cage closely surrounding the three-bladed propeller of 1,10-phenanthroline, each moiety around each 1,10-phenanthroline is almost the same as the solvation cage of the free 1,10-phenanthroline molecule except around the nitrogen atoms. Such a closely surrounding solvation cage is consistent with a fact that, in aqueous solutions of the complex $[Cr(phen)_3]^{2+}$, water molecules can enter into the pockets between the ligands, penetrating the radius about 7 Å of the complex by about 2 Å.[18]

Volume Changes on Complexation. The partial molal volumes in the present work allow one to estimate the volume changes, $\Delta\overline{V}^\circ$, on the complex formation of,

$$[M(OH_2)_6]^{2+} + 3phen \rightarrow [M(phen)_3]^{2+} + 6H_2O.$$

As shown in Table 2, the $\Delta\overline{V}^\circ$ values are almost equal except for the very small $\Delta\overline{V}^\circ$ of $[Fe(phen)_3]^{2+}$.

The exceptionally small $\overline{V}^\circ$ and the resultant small $\Delta\overline{V}^\circ$ of $[Fe(phen)_3]^{2+}$ can be related to the contraction of the volume due to the spin change from high to low on the complex formation. Such an effect of spin change on complex formation was also observed for the entropy change.[19] That is, the formation of $[Fe(phen)_3]^{2+}$ at 20 °C is accompanied by a negative change in the entropy but for the other chelate cations the changes are positive.

On complexation of alkali or alkaline earth ions with crown ethers or criptands, the $\Delta\overline{V}^\circ$ values vary in a wide range from 0 to 28 $cm^3 mol^{-1}$ depending on the sizes of the ions and ligands.[20,21] In these complexes, metal ions have more than one water molecule and the charges are not completely screened from the water.[20]

For the complexation of Ni^{2+} with EDTA and MIDA, $\Delta\overline{V}^\circ$ are 25.5 and 26.8 $cm^3 mol^{-1}$, respectively.[22] These rather larger values are attributed to the partial neutralization of charges on complexation and to the delocalization of the residual charges on the chelate complexes.[22]

A volume change due to the electrostriction for a 2:2 electrolyte can be estimated from $\Delta\overline{V}^\circ$ on an ion pair formation. The $\Delta\overline{V}^\circ$ for $CaSO_4$ is 25.2 $cm^3 mol^{-1}$,[23] but $\Delta\overline{V}^\circ$ of $MgSO_4$ is less than 10 $cm^3 mol^{-1}$,[24] where the former is known to form a contact ion pair, but the latter, predominantly an outer sphere one.

In the present system, though charges are not neutralized, they are delocalized in the large aromatic ligands, which is responsible for the hydrophobic character on these complexes.[2,5] The volume changes of the present reaction, which are comparable to those of the contact ion pair formation and the complexation of Ni–EDTA or Ni–MIDA, may be due to the volume changes of water molecules released from the electronic fields of the central metal ions.

The Change of the Hydration Number on Complexation. On complexation, it may be assumed that the ligand hydration is almost the same for the free and coordinated ligand and only the hydration water of the aqua ions are released to the bulk. By using a simple model for the electrostriction of the ions the change of the hydration number, Δn_H, accompanied on the complexation can be estimated through an equation:[23–26]

$$\Delta n_H = \Delta\overline{V}^\circ/(\overline{V}^\circ_B - \overline{V}^\circ_E), \quad (8)$$

where $\overline{V}^\circ_B$ and $\overline{V}^\circ_E$ are partial molal volumes of the bulk and electrostricted water, respectively. Using Padova's estimation,[25] $\overline{V}^\circ_E - \overline{V}^\circ_B = -2.1$ $cm^3 mol^{-1}$, Δn_H of about 10 is obtained for these chelates except for $[Fe(phen)_3]^{2+}$. Of course this calculation depends on the estimation of the molal volume of the electrostricted water, and the number of released water molecules is not absolute. However the present estimation of Δn_H of 10 seems reasonable in comparison with the hydration number of the transition metal cations. That is, most of these were found in the range of 8 to 12,[27–29] except for the value of 6 estimated for coordinated water from NMR[30] and adiabatic compressibility[31] measurements.

References

1) Y. Yamamoto and S. Kinuwaki, *Bull. Chem, Soc. Jpn.*, **37**, 434 (1964); Y. Yamamoto and K. Kotsuji, *ibid.*, **37**, 594, 785 (1964); Y. Yamamoto, S. Uchikawa, and K. Akabori, *ibid.*, **37**, 1718 (1964); Y. Yamamoto, T. Kumamaru, Y. Hayashi, and M. Yamamoto, *Anal. Chim. Acta*, **69**, 321 (1974).

2) Y. Yamamoto, T. Tominaga, and T. Tagashira, *Inorg. Nucl. Chem. Lett.*, **11**, 825 (1975).

3) Y. Yamamoto, E. Sumimura, K. Miyoshi, and T. Tominaga, *Anal. Chim. Acta*, **64**, 225 (1973).

4) Y. Yamamoto, T. Tarui, E. Iwamoto, and T. Tarumoto, *Anal. Chim. Acta*, **84**, 217 (1976).

5) E. Iwamoto, Y. Hiyama, and Y. Yamamoto, *J. Solution Chem.*, **6**, 371 (1977); E. Iwamoto, Y. Tanaka, H. Kimura, and Y. Yamamoto, *ibid.*, **9**, 841 (1980).

6) F. P. Dwyer and E. G. Gyarfas, *J. Proc. R. Soc., N. S. Wales*, **83**, 232 (1949).

7) F. Blau, *Monatsh. Chim.*, **10**, 372 (1970).

8) F. J. Millero, *J. Phys. Chem.*, **74**, 356 (1970).

9) G. S. Kell, *J. Chem. Eng. Data*, **20**, 97 (1975).

10) O. Redlich and D. M. Mayer, *Chem. Rev.*, **64**, 221, (1964).

11) F. J. Millero, "Water and Aqueous Solutions, Structure, Thermodynamics and Transport Processes," ed by R. A. Horne, Wiley-Interscience, a Division of John Wiley and Sons, Inc., New York (1972), Chap. 13.

12) J. J. Spitzer, P. P. Singh, K. G. McCurdy, and L. G. Hepler, *J. Solution Chem.*, **7**, 81 (1978).

13) J. J. Spitzer, P. P. Singh, I. V. Olofsson, and L. G. Hepler, *J. Solution Chem.*, **7**, 623 (1978).
14) A. Zalkin, D. H. Templeton, and T. Ueki, *Inorg. Chem.*, **12**, 1641 (1973).
15) B. A. Fenz and J. A. Ibers, *Inorg. Chem.*, **11**, 1109 (1972).
16) O. P. Anderson, *J. Chem. Soc., Dalton Trans.*, **1972**, 2597.
17) F. M. Van Meter and H. M. Neuman, *J. Am. Chem. Soc.*, **98**, 1382 (1976).
18) G. M. LaMar and G. R. van Hecke, *Inorg. Chem.*, **12**, 1767 (1973).
19) G. Anderegg, *Helv. Chim. Acta*, **46**, 2813 (1963).
20) H. Høiland, J. A. Ringseth, and T. S. Brun, *J. Solution Chem.*, **8**, 779 (1979).
21) N. Morel-Desrosiers and J. P. Morel, *J. Am. Chem. Soc.*, **103**, 4743 (1981).
22) Y. K. Sze and W. A. E. McBryde, *Can. J. Chem.*, **58**, 1795 (1980).
23) F. J. Millero, F. Gomber, and J. Oster, *J. Solution Chem.*, **6**, 269 (1977).
24) F. J. Millero and W. L. Masterton, *J. Phys. Chem.*, **78**, 1287 (1974); F. J. Millero, G. S. Ward, F. K. Lepple, and E. V. Hoff, *ibid.*, **78**, 1636 (1974).
25) J. Padova, *J. Chem. Phys.*, **39**, 1552 (1963); **40**, 691 (1964).
26) F. J. Millero, *Chem. Rev.*, **71**, 147 (1971).
27) B. E. Conway and J. O'M. Bockris "Modern Aspects of Electrochemistry," ed by J. O'M. Bockris, Butterworths, London (1954), Vol. 1, Chap. 2.
28) J. F. Hinton and E. S. Amis, *Chem. Rev.*, **71**, 627 (1971).
29) B. E. Conway, "Ionic Hydration in Chemistry and Biophysics," Elsevier, Amsterdam (1981), Chap. 29.
30) A. M. Chmelnick and D. N. Fiat, *J. Am. Chem. Soc.*, **93**, 2875 (1971).
31) J. Padva, *Bull. Res. Coun. Israel*, **10A**, 63 (1961).

Crystal and Molecular Structure of (+)-(3*R*,4*S*,8*R*,9*S*)-Quinidinium *Δ*-(−)$_{546}$-Bis(oxalato)(1,10-phenanthroline)chromate(III) Monohydrate and Its Implication in the Pfeiffer Effect of the Corresponding System

Hiroyuki Ohbo, Hiroshi Okazaki, Katsuhiko Miyoshi, and Hayami Yoneda*

Department of Chemistry, Faculty of Science, Hiroshima University, Higashi-senda-machi, Naka-ku, Hiroshima 730

(Received December 3, 1982)

The crystal structure of the title compound *d*-quinidinium (−)$_{546}$-[Cr(ox)$_2$(phen)]·H$_2$O has been determined by a single-crystal X-ray analysis and refined to $R=0.078$ for 2172 reflections. The crystals are orthorhombic, space group $P2_12_12_1$ with unit cell dimensions of $a=9.943(2)$, $b=11.265(2)$, $c=30.716(6)$ Å, and $Z=4$. The known configurations of *d*-quinidinium ion revealed that (−)$_{546}$-[Cr(ox)$_2$(phen)]$^-$ has a *Δ* configuration in accord with the earlier assignment based on its CD spectrum. Following characteristics were noted with regard to intermolecular interactions in the crystal; i) complex anions are linked with one another through the hydrogen bonds to intervening water molecules, to form chains along two-fold screw axes parallel to the a-axis, ii) intermolecular hydrogen bonds connect the complex anion closely with *d*-quinidinium cation which is further hydrogen-bonded to each other forming infinite chains along two-fold axes parallel to the b-axis, and iii) partial stacking is observed between aromatic phen and quinoline rings. These interaction modes were discussed in relation to the Pfeiffer Effect of the corresponding system in water.

The Pfeiffer Effect[1] is a shift in chiral equilibrium between two antipodes of an initially racemic complex upon the addition of a certain chiral compound called an environment substance in solution. It is, thus, a prototype of so-called first-order asymmetric transformations of coordination compounds. In our previous paper,[2] it was reported that an appreciable equilibrium shift is attained for a mixed-chelate complex, [Cr(ox)$_2$(phen)]$^-$ (ox=oxalate dianion and phen=1,10-phenanthroline), when monohydrochloride salts of cinchona alkaloids are mixed with in water. In particular, *d*-quinidinium chloride (=6′-methoxy-*d*-cinchoninium

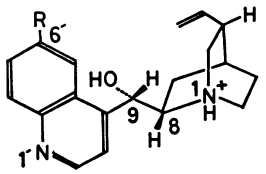

R = H; cinchoninium ion
R = MeO; quinidinium ion

chloride) and *l*-quininium chloride (=6′-methoxy-*l*-cinchonidinium chloride) are found much more effective in inducing an equilibrium shift of [Cr(ox)$_2$(phen)]$^-$ than their parent alkaloids *d*-cinchoninium and *l*-cinchonidinium chlorides, suggesting some important roles played by the MeO group on the quinoline ring in the stereoselective interaction with the complex anion in water. These observations led us to presume that more extensive association takes place between the cinchona alkaloid cations and the complex anion than is expected for usual 1:1 electrolytes. In fact, molecular model consideration indicates that hydrophobic stacking interaction is possible between aromatic phen and quinolyl groups in addition to electrostatic and/or hydrogen-bonding interactions of ox ligand(s) with the protons on the N(1) atom and of the OH group on the C(9) atom of the alkaloid cation.

In the present study, an X-ray analysis was performed on a diastereomeric salt of *d*-quinidinium ion with (−)$_{546}$-[Cr(ox)$_2$(phen)]$^-$ to get some information on their intermolecular interactions in the solid state, which, we expect, might help us to elucidate their stereoselective interactions involved in the Pfeiffer Effect of the corresponding system in water.

Experimental

Preparation of Compounds. Potassium salt of [Cr(ox)$_2$(phen)]$^-$ was prepared as described in the literature,[3] and was identified by its absorption spectrum.[4] Aqueous *rac*-K[Cr(ox)$_2$(phen)]·4H$_2$O (8 mM, 50 ml) was mixed with aqueous *d*-quinidinium chloride dihydrate (8 mM, 50 ml), and a small amount of ethanol (1—2 ml) was added to facilitate the crystal formation. After the solution was allowed to stand at room temperature in the dark for 2 d, purple-red plate-like crystals were separated out. Found: C, 57.67; H, 4.57; N, 7.59%. Calcd for $C_{36}H_{35}CrN_4O_{11}$: C, 57.52; H. 4.69; N, 7.45%.

Data Collection. A crystal with the size of 0.49×0.42×0.09 mm^3 was used for reflection data collection. Determination of the unit cell dimensions and data collection were carried out on a Syntex R3 automated four-circle diffractometer with Mo *Kα* radiation monochromated by a graphite plate ($\lambda=0.71069$ Å). In Table 1 are given cell constants and their estimated standard deviations which were derived from a least-squares refinement for 22 strong, general reflections ($20°<2\theta<35°$). Other crystal data are also collected in Table 1. From systematic absences for *h*00 with *h* odd, 0*k*0 with *k* odd, and 00*l* with *l* odd, the space group was uniquely identified as $P2_12_12_1$. Reflection intensities were measured up to $2\theta=50°$ using the *ω*-scan technique with a scan speed of 3—30°/min (50 kV, 20 mA). Three reference reflections monitored after every cycle of 200 measurements, showed no significant variation in intensity during the data collection. Out of 3470 reflections measured, 2172 reflections with $|F_o|>3\sigma(F_o)$ were selected and were used for the structure determination. They were corrected for the Lorentz-polarization factor, but no absorption correction was

Table 1. Crystal data

Orthorhombic Space Group $P2_12_12_1$	
a = 9.943(2) Å	$D_o=1.41$ g cm^{-3}
b = 11.265(2) Å	$D_c=1.43$ g cm^{-3}
c = 30.716(9) Å	$Z=4$
$U=3440(1)$ Å^3	μ(Mo *Kα*) = 4.2 cm^{-1}

applied since the linear absorption coefficient was low.

Solution and Refinement of Crystal Structure

The structure was solved by a conventional heavy-atom method. Atomic scattering factors for all atoms were taken from Ref. 5 and were corrected for real and imaginary parts of anomalous scattering.[6]

The position of the Cr atom was deduced from the three-dimensional Patterson synthesis. The remaining atoms were located from successive difference Fourier syntheses. After all nonhydrogen atoms were located, the block-diagonal least-squares refinement using anisotropic thermal parameters for these atoms reduced an R value, $\Sigma||F_o|-|F_c||/\Sigma|F_o|$, to 0.091. At this stage, initial positions of hydrogen atoms were deduced from the geometrical calculations, and the least-squares refinement was continued with all the parameters fixed for hydrogen atoms. Two cycles of the refinement finally performed with all parameters variable, converged an R value to 0.078 and an R_w value,

Table 2. Atomic coordinates and thermal parameters

Atom	x	y	z	B_{eq}/Å^2 a)	Atom	x	y	z	B_{eq}/Å^2 a)
Cr	−0.00086(19)	0.23326(12)	0.39232(5)	3.61	C(E5)	0.1913(9)	0.2764(8)	0.2090(3)	3.12
N(A1)	0.1510(8)	0.1734(6)	0.3526(2)	3.56	C(E6)	0.0853(10)	0.3359(10)	0.2276(3)	4.33
C(A2)	0.1429(10)	0.1163(9)	0.3158(3)	4.63	C(E7)	0.0992(10)	0.4088(10)	0.2640(3)	4.71
C(A3)	0.2540(12)	0.0726(9)	0.2940(3)	5.25	C(E8)	0.2223(10)	0.4303(9)	0.2807(3)	4.41
C(A4)	0.3805(12)	0.0879(9)	0.3118(4)	6.33	C(E9)	−0.0683(10)	0.2589(11)	0.1761(3)	5.81
C(A5)	0.5169(11)	0.1762(10)	0.3725(4)	7.40	C(E10)	0.3362(10)	0.3724(8)	0.2632(3)	4.09
C(A6)	0.5203(11)	0.2338(10)	0.4100(4)	7.52	C(E11)	0.3207(9)	0.2952(7)	0.2271(3)	2.90
C(A7)	0.3979(12)	0.3356(11)	0.4714(4)	7.19	O(E12)	−0.0445(6)	0.3248(7)	0.2139(2)	5.52
C(A8)	0.2799(14)	0.3713(10)	0.4883(3)	7.50	O(W)	−0.2583(11)	0.4742(10)	0.5251(3)	13.70
C(A9)	0.1622(11)	0.3503(9)	0.4663(3)	5.07	H(CA2)	0.048(8)	0.095(8)	0.302(3)	4.6
N(A10)	0.1614(8)	0.2947(6)	0.4272(2)	4.07	H(CA3)	0.240(9)	0.028(7)	0.264(2)	3.2
C(A11)	0.2820(9)	0.2567(8)	0.4099(3)	4.11	H(CA4)	0.466(9)	0.059(8)	0.295(3)	4.6
C(A12)	0.2769(9)	0.1948(8)	0.3695(3)	4.11	H(CA5)	0.596(8)	0.149(7)	0.356(3)	4.2
C(A13)	0.3952(9)	0.1525(9)	0.3502(4)	5.82	H(CA6)	0.608(8)	0.246(8)	0.425(3)	3.6
C(A14)	0.4032(10)	0.2791(9)	0.4307(3)	5.13	H(CA7)	0.484(9)	0.352(8)	0.487(2)	3.1
O(B1)	−0.0262(6)	0.3817(5)	0.3607(2)	4.20	H(CA8)	0.271(9)	0.417(8)	0.516(3)	5.4
O(B2)	−0.1294(6)	0.3041(5)	0.4321(2)	4.84	H(CA9)	0.072(8)	0.373(7)	0.481(2)	2.7
C(B3)	−0.1184(10)	0.4464(9)	0.3762(3)	4.49	H(ND1)	0.341(9)	0.099(8)	0.095(3)	4.3
C(B4)	−0.1780(10)	0.4039(9)	0.4184(3)	4.60	H(CD2a)	0.499(8)	0.059(7)	0.045(2)	2.2
O(B5)	−0.1563(8)	0.5411(6)	0.3611(3)	7.12	H(CD2b)	0.564(8)	0.076(8)	0.095(2)	3.4
O(B6)	−0.2646(8)	0.4599(6)	0.4376(2)	6.76	H(CD3)	0.601(7)	0.215(7)	0.020(2)	1.8
O(C1)	−0.1362(6)	0.1480(6)	0.3606(2)	4.76	H(CD4)	0.615(8)	0.404(8)	0.065(3)	4.1
O(C2)	0.0120(7)	0.0876(5)	0.4257(2)	4.84	H(CD5a)	0.365(9)	0.430(8)	0.066(3)	6.6
C(C3)	−0.1585(11)	0.0423(9)	0.3735(4)	5.74	H(CD5b)	0.423(8)	0.377(8)	0.018(3)	4.1
C(C4)	−0.0681(11)	0.0056(9)	0.4119(4)	5.68	H(CD6a)	0.232(8)	0.273(7)	0.066(2)	2.5
O(C5)	−0.2405(8)	−0.0250(6)	0.3599(3)	7.76	H(CD6b)	0.330(8)	0.203(7)	0.027(2)	4.9
O(C6)	−0.0717(8)	−0.0930(7)	0.4288(3)	8.99	H(CD7a)	0.622(7)	0.284(7)	0.137(2)	1.3
N(D1)	0.3951(7)	0.1665(7)	0.0887(2)	2.78	H(CD7b)	0.520(8)	0.402(7)	0.136(2)	3.5
C(D2)	0.5237(10)	0.1180(9)	0.0705(3)	4.46	H(CD8)	0.330(8)	0.294(7)	0.134(2)	1.3
C(D3)	0.6109(9)	0.2227(9)	0.0540(3)	4.78	H(CD9)	0.352(8)	0.108(7)	0.173(2)	3.2
C(D4)	0.5525(10)	0.3364(9)	0.0722(3)	4.50	H(CD10)	0.832(9)	0.279(8)	0.050(3)	6.1
C(D5)	0.4170(11)	0.3569(10)	0.0507(4)	5.56	H(CD11a)	0.766(9)	0.056(7)	0.094(2)	4.6
C(D6)	0.3298(10)	0.2472(9)	0.0558(3)	4.41	H(CD11b)	0.932(9)	0.139(8)	0.086(3)	4.7
C(D7)	0.5355(9)	0.3230(8)	0.1218(3)	3.31	H(OD12)	0.546(8)	0.021(8)	0.184(2)	4.3
C(D8)	0.4168(9)	0.2410(8)	0.1293(3)	2.98	H(CE2)	0.656(9)	0.349(8)	0.280(2)	3.3
C(D9)	0.4309(9)	0.1583(8)	0.1702(3)	3.09	H(CE3)	0.641(8)	0.217(7)	0.218(2)	2.4
C(D10)	0.7609(12)	0.2125(10)	0.0644(3)	6.47	H(CE5)	0.180(8)	0.220(7)	0.183(2)	1.4
C(D11)	0.8205(13)	0.1327(12)	0.0823(4)	8.55	H(CE7)	0.015(8)	0.445(7)	0.279(2)	2.3
O(D12)	0.5503(6)	0.0907(6)	0.1658(2)	4.26	H(CE8)	0.231(9)	0.486(8)	0.306(3)	2.7
N(E1)	0.4592(8)	0.3936(7)	0.2823(2)	4.12	H(CE9a)	0.020(8)	0.280(7)	0.153(2)	3.9
C(E2)	0.5625(10)	0.3350(9)	0.2662(3)	4.43	H(CE9b)	−0.156(9)	0.278(8)	0.162(3)	5.8
C(E3)	0.5580(9)	0.2583(9)	0.2309(3)	3.94	H(CE9c)	−0.065(8)	0.171(8)	0.181(3)	4.2
C(E4)	0.4384(9)	0.2412(9)	0.2105(3)	3.13					

a) For the nonhydrogen atoms, anisotropic thermal parameters are listed in Table 6 (supplementary material). $B=8\pi^2(U_{11}+U_{22}+U_{33})/3$.

$[\Sigma w(|F_o|-|F_c|)^2/\Sigma w|F_c|^2]^{1/2}$, to 0.055. The quantity minimized was $\Sigma w(|F_o|-|F_c|)^2$ and the weighting scheme employed was $w=[\sigma^2+g^2|F_o|^2]^{-1}$ for the final refinement, where σ is a standard deviation obtained from the counting statistics for each reflection and the value of g used is 0.01. The final electron density difference map showed no unusual features, and there was no residual peak higher than 0.3 e/Å^3.

Fourier syntheses, least-squares refinement, and geometrical calculations were performed using programs $P2_12_12_1$,[7] HBLS,[8] and DAPH[9] with slight modification, respectively on a HITAC M-200H computer at the Hiroshima University Information Processing Center.

The final atomic parameters and their estimated standard deviations are listed in Table 2 with averaged isotropic thermal parameters. Anisotropic thermal parameters and complete lists of the $|F_o|$ and $|F_c|$ values have been preserved by the Chemical Society of Japan (Document No. 8327).

Results and Discussion

The asymmetric unit within the unit cell is illustrated in Fig. 1 with the numbering scheme adopted for respective atoms.

Molecular Structure of Complex Anion. The bond distance and selected bond angles in $[Cr(ox)_2(phen)]^-$ are given in Table 3. The mean C–O bond distance is 1.939(7) Å somewhat shorter than the corresponding distances of 1.969(2) Å found in *rac*-$K_3[Cr(ox)_3]\cdot 3H_2O$[10] and of 1.965(2), 1.952(7), and 1.962(5) Å in *fac*-$[Cr(gly)_3]\cdot H_2O$,[11] *rac*-$[Cr(acac)_3]$,[12] and Δ-$[Cr(acac)_3]$,[13] respectively. Somewhat greater anisotropy in the thermal parameters might be in part responsible for the shorter Cr–O distances found in the present crystal. The mean Cr–N bond distance found is 2.065 (8) Å, which coincides well with the corresponding distances of 2.066(10) Å in $[Cr(phen)_2(OH)]_2I_4\cdot 4H_2O$[14] and of 2.068(5) Å in *fac*-$[Cr(gly)_3]\cdot H_2O$.[11]

The averaged O–Cr–O and N–Cr–N bond angles are 83.5(3)° and 81.5(3)°, respectively. They compare well within e.s.d.'s with the values of 82.3(1)° and 79.7(3)° reported for *rac*-$K_3[Cr(ox)_3]\cdot 3H_2O$[10] and $[Cr(phen)_2(OH)]_2I_4\cdot 4H_2O$,[14] respectively.

Intramolecular bond distances within phen and ox chelate ligands are all in good agreement with the comparable values reported in the literature.[10,14] Ox chelates have two kinds of C–O bonds; one forms a "free" carbonyl group and the other is directly associated with the complex formation with Cr(III) ion. A general trend[10] that the latter bond is longer, is also noted in this case. In a phen chelate, the N(A1)–C(A2) and N(A10)–C(A9) distances, for example, are a little shorter than the N(A1)–C(A12) and N(A10)–C(A11) distances, respectively, as is usually the case.[14] Similarly, some deviations are also seen in the C–C bond distances. If e.s.d.'s are taken into account, the C–N and C–C bond distances in a phen chelate seem to correlate with their π-bond orders estimated.[14,15]

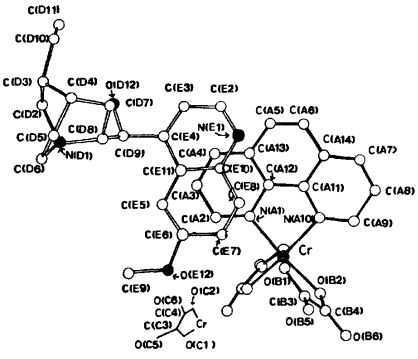

Fig. 1. Asymmetric unit within the unit cell of *d*-quinidinium Δ-$[Cr(ox)_2(phen)]\cdot H_2O$ with the numbering scheme.

In Table 4 are presented the equations of the least-squares plane through the chelate ligands and the distances from the plane to the respective atoms. The Cr(III) atom lies approximately on the plane of one ox chelate (C), but off the plane of another ox chelate (B) which is hydrogen-bonded to both the H–N$^+$(D1) and H–O(W) protons. Similarly, the Cr(III) atom is not coplanar with the phen chelate plane (A), which is probably due to the repulsive interaction with the neighboring quinolyl group of *d*-quinidinium ion.

The absolute configuration of $(-)_{546}$-$[Cr(ox)_2(phen)]^-$ forming a less-soluble diastereomer with *d*-quinidinium cation is assigned as Δ on the basis of the known configurations (3*R*,4*S*,8*R*,9*S*) of *d*-quinidinium cation.[16] This assignment is in accord with that made earlier by the CD spectrum.[4]

Molecular Structure of d-*Quinidinium Cation.* The bond distances and angles within *d*-quinidinium cation (Table 3) are very close to those reported earlier by an X-ray analysis on several cinchona alkaloids,[16–18] with somewhat a shorter C(D10)–C(D11) bond distance. The quinuclidine part has a skew conformation. When it is viewed along the N(D1)–C(D4) direction, the bonds N(D1)–C(D2), N(D1)–C(D6), and N(D1)–C(D8) are rotated about 10° from the eclipsed position over the bonds C(D4)–C(D3), C(D4)–C(D5), and C(D4)–C(D7), in keeping with the results obtained by earlier studies.[16,17] The quinoline ring is regarded as planar within experimental error.

Crystal Packing. The molecular packing in the crystal seen down the a-axis is depicted in Fig. 2. The crystal structure is characterized simply by four types of intermolecular hydrogen bonds by which the composite molecules, complex ion, *d*-quinidinium ion, and water are held together; other intermolecular

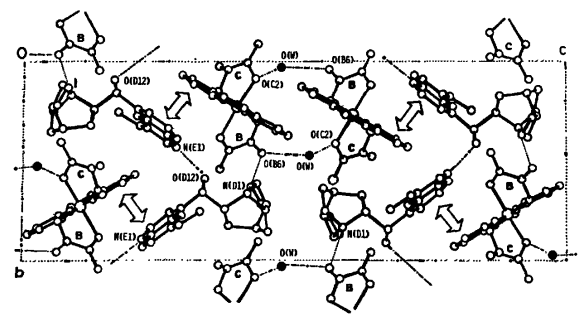

Fig. 2. Crystal packing in *d*-quinidinium Δ-$[Cr(ox)_2(phen)]\cdot H_2O$ viewed down the a-axis.

contacts being due to normal van der Waals interactions. The intermolecular distances shorter than 3.4 Å are given in Table 5. In the following, the crystal packing is discussed with particular reference to intermolecular interactions involved.

First of all, infinite chains of *d*-quinidinium cations hydrogen-bonded to one another (O(D12)–H···N(E1)) are aligned along the two-fold screw axes parallel to the b-axis (O(D12)···N(E1) 2.74 Å). Each *d*-quinidinium cation in the chain is further connected to the ox chelate (B) through the N^+(D1)–H···O(B6) hydrogen bond (N(D1)···O(B6) 2.78 Å). In short, a particular *d*-quinidinium ion participates in the two types of intermolecular hydrogen-bonding, *i.e.*, the N(E1) and H–O(D12) atoms are employed for the interaction with another *d*-quinidinium ion and the H–N^+(D1) proton for the interaction with the complex anion.

The crystal structure of *d*-quinidinium salt with 1,1′-dimethylferrocene-3-carboxylate has been reported.[16] In this crystal, both of the H–N^+(D1) and H–O(D12) protons are associated with the hydrogen

Table 3. Selected intramolecular distances and angles

Intramolecular distances	*l*/Å		*l*/Å
Cr-N(A1)	2.058(8)	Cr-O(B1)	1.948(6)
Cr-N(A10)	2.071(8)	Cr-O(B2)	1.943(7)
N(A1)-C(A2)	1.291(13)	Cr-O(C1)	1.920(7)
N(A10)-C(A9)	1.322(14)	Cr-O(C2)	1.943(7)
N(A1)-C(A12)	1.385(12)	O(B1)-C(B3)	1.265(12)
N(A10)-C(A11)	1.371(12)	O(B2)-C(B4)	1.291(12)
C(A2)-C(A3)	1.391(15)	O(C1)-C(C3)	1.281(13)
C(A9)-C(A8)	1.399(18)	O(C2)-C(C4)	1.298(13)
C(A3)-C(A4)	1.381(16)	C(B3)-O(B5)	1.212(13)
C(A8)-C(A7)	1.334(18)	C(B4)-O(B6)	1.223(13)
C(A4)-C(A13)	1.377(16)	C(C3)-O(C5)	1.189(14)
C(A7)-C(A14)	1.357(16)	C(C4)-O(C6)	1.235(15)
C(A13)-C(A5)	1.416(17)	C(B3)-C(B4)	1.514(14)
C(A14)-C(A6)	1.423(16)	C(C3)-C(C4)	1·533(16)
C(A12)-C(A13)	1.405(15)		
C(A11)-C(A14)	1.412(14)		
C(A5)-C(A6)	1.346(17)		
C(A11)-C(A12)	1.439(14)		
N(D1)-C(D2)	1.510(12)	N(E1)-C(E2)	1.300(13)
C(D2)-C(D3)	1.544(15)	C(E2)-C(E3)	1.398(14)
C(D3)-C(D4)	1.518(15)	C(E3)-C(E4)	1.351(14)
C(D4)-C(D5)	1.528(15)	C(E4)-C(E11)	1.399(13)
C(D4)-C(D7)	1.551(14)	C(E5)-C(E11)	1.422(13)
C(D5)-C(D6)	1.534(15)	C(E5)-C(E6)	1.355(14)
C(D6)-N(D1)	1.501(13)	C(E6)-C(E7)	1.414(15)
C(D7)-C(D8)	1.524(12)	C(E7)-C(E8)	1.325(15)
C(D8)-N(D1)	1.518(11)	C(E8)-C(E10)	1.403(15)
C(D8)-C(D9)	1.556(12)	C(E10)-N(E1)	1.372(13)
C(D9)-O(D12)	1.426(11)	C(E10)-C(E11)	1.440(14)
C(D9)-C(E4)	1.567(13)	C(E6)-O(E12)	1.371(13)
C(D3)-C(D10)	1.548(16)	C(E9)-O(E12)	1.396(14)
C(D10)-C(D11)	1.192(17)		
Intramolecular angles	**ϕ/°**		**ϕ/°**
N(A1)-Cr-N(A11)	81.5(3)	C(D10)-C(D3)-C(D2)	115(1)
O(B1)-Cr-O(B2)	82.8(3)	C(D10)-C(D3)-C(D4)	111(1)
O(C1)-Cr-O(C2)	84.2(3)	C(D3)-C(D10)-C(D11)	128(1)
Cr-N(A1)-C(A2)	129.2(7)	C(D9)-C(D8)-N(D1)	111(1)
Cr-N(A10)-C(A9)	128.3(7)	C(D9)-C(D8)-C(D7)	114(1)
Cr-N(A1)-C(A12)	112.5(6)	C(D8)-C(D9)-O(D12)	109(1)
Cr-N(A10)-C(A11)	111.4(6)	C(D8)-C(D9)-C(E4)	107(1)
Cr-O(B1)-O(B3)	114.0(6)	C(D12)-C(D9)-C(E4)	111(1)
Cr-O(B2)-O(B4)	113.6(6)	C(E5)-C(E6)-O(E12)	124(1)
Cr-O(C1)-O(C3)	115.1(7)	C(E7)-C(E6)-O(E12)	113(1)
Cr-O(C2)-C(C4)	112.3(7)	C(E5)-C(E6)-C(E7)	123(1)
		C(E6)-O(E12)-C(E9)	117(1)

Table 4. Least-squares planes

Deviations of atoms from the planes in Å

plane(A)		plane(B)		plane(E)	
N(A1)	−0.010	O(B1)	−0.014	N(E1)	0.030
C(A2)	−0.013	O(B2)	0.003	C(E2)	−0.021
C(A3)	−0.016	C(B3)	0.020	C(E3)	−0.028
C(A4)	−0.036	C(B4)	0.003	C(E4)	0.026
C(A5)	0.009	O(B5)	−0.003	C(E5)	−0.014
C(A6)	−0.000	O(B6)	−0.010	C(E6)	−0.007
C(A7)	−0.042	Cr*	0.134	C(E7)	−0.039
C(A8)	−0.047			C(E8)	0.019
C(A9)	−0.010	plane(C)		C(E9)	0.061
N(A10)	0.043	O(C1)	0.020	C(E10)	0.018
C(A11)	0.033	O(C2)	−0.028	C(E11)	0.005
C(A12)	0.042	C(C3)	0.011	O(E12)	−0.042
C(A13)	0.019	C(C4)	0.006		
C(A14)	0.032	O(C5)	−0.027		
Cr*	−0.155	O(C6)	0.018		
		Cr*	−0.003		

Dihedral angles between the planes

plane(A)-plane(B)	103.2°	plane(B)-plane(C)	89.1°
plane(A)-plane(C)	85.0°	plane(A)-plane(E)	9.5° (stacking)

Plane equations[a)]

plane	l	m	n	p
A	0.0809	0.8646	−0.4959	3.5504
B	−0.6998	−0.4940	−0.5161	7.6448
C	0.6878	−0.3340	−0.6445	8.6477
E	0.1528	0.7735	−0.6151	1.2365

* The Cr atom is not included for plane calculations. a) The equation of a plane is expressed as $lx'+my'+nz'+p=0$, where x', y', and z' are coordinates in Å. All atoms are given equal weight.

bonds to the carboxylate group on the ferrocene, and the N(E1) atom on the quinolyl group is completely indifferent to the intermolecular interaction. Similarly, the N(E1) atom does not participate at all in any intermolecular interactions in the crystal of free *d*-cinchonine where both of the H–O(D12) and N(D1) atoms are used for the hydrogen-bonding interactions with another *d*-cinchonine molecule.[18] In this way, our present crystal structure seems peculiar in that the N(E1) atom plays as a proton acceptor an essential role in the crystal packing.

Remaining two types of hydrogen bonding found in the present crystal structure are associated with water molecules of crystallization; the complex anions are linked with one another through the hydrogen bonds to the intervening water molecules (O(W)–H···O(B6) and O(W)–**H**···O(C2)) to form another screw chain parallel to the a-axis. The intermolecular distances are as follows; O(W)···O(B6) 2.69 Å and O(W)···O(C2) 2.83 Å.

One more interaction mode to be noted is partial intermolecular stacking between aromatic phen and quinoline rings (Fig. 1). The spacing between the two rings is 3.3—3.5 Å and the tilt angle between the normals of the ring planes is 9.5°. Similar stacking is often observed in the crystal structures of mixed-ligand metal complexes having phen or bpy ligand(s) as a chelate.[19]

Implication to the Interactions Involved in the Pfeiffer Effect. As noted in the introduction, the chiral equilibrium of $[Cr(ox)_2(phen)]^-$ is substantially shifted in favor of its *Δ*- and *Λ*-enantiomers in the presence of *d*-quinidinium and *l*-quininium cations, respectively. Under certain experimental conditions, the enantiomer excess actually attained amounts to almost 20%, which is by far greater than those usually observed (2—3%).[2] In order to account for the much greater Pfeiffer Effect observed, a following association model is proposed for the stereoselective interaction between *Δ*-$[Cr(ox)_2(phen)]^-$ and *d*-quinidinium ions in aqueous solution (Fig. 3-a).

In this model, it is one ox chelate(B) of the complex anion that interacts with quinidinium cation through the two hydrogen bonds; one between the free carbonyl oxygen atom and the H–N$^+$(1) proton, and the other between another carbonyl oxygen atom coordinated to the Cr(III) ion and the OH group on the C(9) atom. Similar hydrogen-bonding interactions have been actually found between the carboxylate group and *d*-quinidinium ion in the solid state.[16] The other ox chelate(C) is not concerned at all with the interaction with *d*-quinidinium ion. In addition to these hydrogen bonds, hydrophobic stacking[20] interaction between the aromatic phen and quinoline rings contributes to the stereoselective association. The presence of stacking interaction is suggested by the findings

TABLE 5. INTERMOLECULAR DISTANCES

1) Hydrogen bonds of the type A-H···B

No.	A-H···B		tr.[a]	A-H···B *l*/Å
1	O(W)	O(B6)	1	2.69
2	O(W)	O(C2)	2	2.83
3	O(D12)	N(E1)	3	2.74
4	N(D1)	O(B6)	4	2.78

2) Contacts related to hydrogen bonds

No.[b]	A′	B′	tr.[a]	A′···B′ *l*/Å
1	C(A7)	O(B2)	5	3.37
1	C(A8)	O(B2)	5	3.27
2	O(W)	C(A11)	2	3.30
3	O(D12)	C(E8)	3	3.33
4	N(D1)	O(B5)	4	3.16
4	C(D9)	O(B5)	4	3.18
4	C(D2)	O(B6)	4	3.14
4	C(D6)	O(B6)	4	3.31

3) Other close contacts (<3.4 Å)

A′	B′	tr.[a]	A′···B′ *l*/Å
C(A3)	C(E11)	1	3.31[c]
O(B1)	C(E7)	1	3.24
C(D6)	O(C6)	6	3.17
C(D8)	O(C5)	6	3.18
C(E5)	O(C5)	6	3.12
C(D4)	O(W)	7	3.29
C(A5)	O(C5)	8	3.33
C(E9)	C(D11)	8	3.40

a) tr. refers to the following translations of "B" atom from the coordinates listed in Table 2.: 1) *x*, *y*, *z*; 2) $-0.5+x$, $0.5-y$, $1-z$; 3) $1-x$, $-0.5+y$, $0.5-z$; 4) $-x$, $-0.5+y$, $0.5-z$; 5) $0.5+x$, $0.5-y$, $1-z$; 6) $-x$, $0.5+y$, $0.5-z$; 7) $0.5-x$, $1-y$, $-0.5+z$; 8) $-1+x$, *y*, *z*. b) Number given to the hydrogen bond listed in 1). c) Related to stacking interaction. The e.s.d. is at most 0.02 Å for each distance.

that organic additives like dioxane[21] diminish the Pfeiffer Effect of the present system greatly and the association constant estimated is 57 which is too great to be accounted for by the electrostatic attraction alone.[22] Furthermore, if the MeO group on the quinoline ring also participates in the hydrophobic interaction[23,24] with the phen chelate, stronger association with the complex anion is expected, and thus a much greater equilibrium shift induced by *d*-quinidinium (6′-methoxy-*d*-cinchoninium) ion than by *d*-cinchoninium ion may be rationalized.

In short, the association model shown in Fig. 3-a is constructed on the assumption that *d*-quinidinium cation recognizes the chirality of $[Cr(ox)_2(phen)]^-$ by interacting with the two chelate ligands, ox and phen, simultaneously through the hydrogen-bonding and hydrophobic stacking interactions, respectively. The simultaneous interactions with *d*-quinidinium cation come into play effectively when the complex anion has a *Δ* configuration, as seen in Fig. 3-a. The *Δ*-enantiomer cannot associate with *d*-quinidinium ion in such a way that the two interactions contribute simultaneously. In this way, the *Δ*-enantiomer is favored over the *Λ*-enantiomer, the former being thereby enriched at equilibrium in the presence of *d*-quinidinium

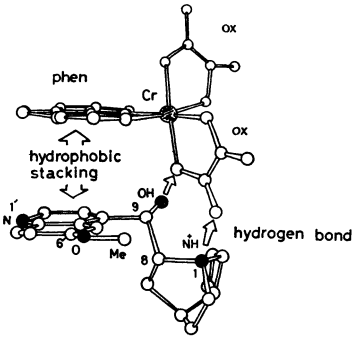

Fig. 3-a. Proposed model for stereoselective association between *Δ*-$[Cr(ox)_2(phen)]^-$ and *d*-quinidinium ions. The conformations of the latter are the same as those assumed in the solid state.

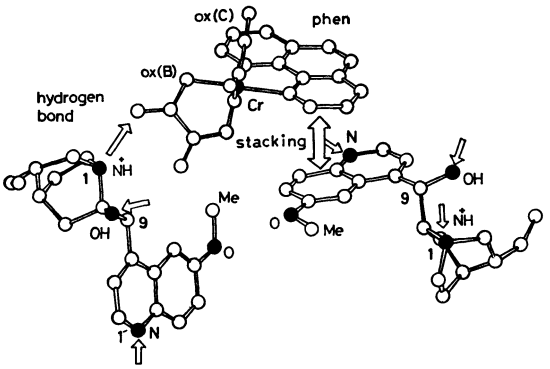

Fig. 3-b. Intermolecular interactions found in *d*-quinidinium *Δ*-$[Cr(ox)_2(phen)]\cdot H_2O$.

ion.

Now, turning to the intermolecular interactions found in the crystal structure of *d*-quinidinium *Δ*-$[Cr(ox)_2(phen)]\cdot H_2O$, one ox chelate(B) of the complex anion actually interacts with *d*-quinidinium cation through the hydrogen bond between the free carbonyl group and the H–N^+(1) proton, but the OH group on the C(9) atom is hydrogen-bonded not to the ox chelate but to the N(1′) atom of another *d*-quinidinium ion, thereby forming infinite chains of *d*-quinidinium cations. Furthermore, the phen ring of the complex anion is stacked with *d*-quinidinium cation, but the stacking is partial (Fig. 1) and is with the quinoline ring of another *d*-quinidinium ion hydrogen-bonded to another complex anion. The above-mentioned situations are easily visualized in Fig. 3-b, where a particular complex anion and two *d*-quinidinium cations interacting with it are projected along an appropriate axis.

It cannot be stated whether the intermolecular interactions found in the solid state persist also in solution. In fact, the metal complex anion interacts directly with two *d*-quinidinium cations simultaneously in the present crystal structure, while 1:1 association is dominant in solution.[2] Thus, the association modes in solution are not directly deduced from the crystal structure. However, the intermolecular interactions found in the solid state are often informative in discussing how the composite ions interact with each other in solution.[19]

As seen in Fig. 3-b, both the OH and N^+–H groups

of *d*-quinidinium ion are associated with the intermolecular hydrogen bonds, and the quinolyl group is stacked, though partially, with the phen chelate in the present crystal structure. These observations imply that the complex and *d*-quinidinium ions are held together in solution also by both the hydrogen-bonding and hydrophobic stacking interactions. As a result, we suppose that the association modes shown in Fig. 3-a are fairly plausible and are probably responsible for the substantial equilibrium shift attained by the Pfeiffer Effect in water.

Finally, the MeO group on the quinoline ring is found not to participate at all in the interaction with the phen chelate in the solid state (Fig. 1). However, an appreciable up-field shift[23,24] has been observed in the pmr spectrum of the MeO group of *l*-quininium ion upon the addition of $[Co(ox)_2(phen)]^-$ in D_2O,[22] suggesting attractive interaction of the MeO group with the phen chelate of the complex anion in water. This observation supports the idea that the MeO group is also involved in the hydrophobic interaction with the phen part of the complex anion. Our proposed model allows the above interaction to work at least for the Δ-enantiomer and thus provides a possible interpretation to the fact that *d*-quinidinium and *l*-quininium cations induce a much greater equilibrium shift in $[Cr(ox)_2(phen)]^-$ than *d*-cinchoninium and *l*-cinchonidinium cations.

References

1) For reviews, S. Kirschner, N. Ahmad, C. Munir, and R. J. Pollock, *Pure Appl. Chem.*, **51**, 913 (1979); S. Kirschner and I. Bakker, *Coord. Chem. Rev.*, **43**, 325 (1982).

2) K. Miyoshi, Y. Matsumoto, and H. Yoneda, *Chem. Lett.*, **1980**, 1319.

3) J. A. Broomhead, *Aust. J. Chem.*, **15**, 228 (1962).

4) S. Kaizaki, J. Hidaka, and Y. Shimura, *Bull. Chem. Soc. Jpn.*, **42**, 988 (1969).

5) "International Tables for X-ray Crystallography," Kynoch Press, Birmingham (1968), Vol. III, pp. 202—205.

6) "International Tables for X-ray Crystallography," Kynoch Press, Birmingham (1974), Vol. IV, p. 149.

7) Y. Kushi, unpublished work.

8) T. Ashida, "The Universal Crystallographic Computation Program System," ed by T. Sakurai, The Crystallographic Society of Japan (1967).

9) T. Ashida, "The Universal Crystallographic Computing System Osaka," The Computation Center, Osaka University (1973).

10) D. Taylor, *Aust. J. Chem.*, **31**, 1455 (1978).

11) R. F. Bryan, P. T. Greene, P. F. Stokely, and E. W. Wilson, Jr., *Inorg. Chem.*, **10**, 1468 (1971).

12) B. Moroshin, *Acta Crystallogr.*, **19**, 131 (1965).

13) R. Kuroda and S. F. Mason, *J. Chem. Soc., Dalton Trans.*, **1979**, 273.

14) R. P. Scaringe, P. Singh, R. P. Eckberg, W. E. Hatfield, and D. J. Hodgson, *Inorg. Chem.*, **14**, 1127 (1975).

15) B. A. Frenz and J. A. Ibers, *Inorg. Chem.*, **11**, 1109 (1972); J. T. Veal, W. E. Hatfield, and D. J. Hodgson, *Acta Crystallogr., Sect. B*, **29**, 12 (1973).

16) O. L. Carter, A. T. McPhail, and G. A. Sim, *J. Chem. Soc., A*, **1967**, 365.

17) B. J. Oleksyn, K. M. Stadnicka, and S. A. Hodorowicz, *Acta Crystallogr., Sect. B*, **34**, 811 (1968).

18) B. J. Oleksyn, L. Lebioda, and M. Ciechanowicz-Rutkowska, *Acta Crystallogr., Sect. B*, **35**, 440 (1975).

19) For example, K. Aoki, *J. Chem. Soc., Chem. Commun.*, **1977**, 600; **1979**, 589; *J. Am. Chem. Soc.*, **100**, 7106 (1978); K. Aoki and H. Yamazaki, *ibid.*, **102**, 6878 (1980); B. E. Fischer and R. Bau, *Inorg. Chem.*, **17**, 27 (1978); C.-Y. Wei, B. E. Fischer, and R. Bau, *J. Chem. Soc., Chem. Commun.*, **1978**, 1053; P. Orioli, R. Cini, D. Donati, and S. Mangani, *J. Am. Chem. Soc.*, **103**, 4446 (1981).

20 P. R. Mitchell and H. Sigel, *J. Am. Chem. Soc.*, **100**, 1564 (1978) and references therein.

21) Organic additives are known to reduce the hydrophobic interaction, see Refs. 39 and 40 in B. E. Fischer and H. Sigel, *J. Am. Chem. Soc.*, **102**, 2998 (1980).

22) H. Yoneda, *et al.*, unpublished results.

23) B. E. Fischer and H. Sigel, *J. Am. Chem. Soc.*, **102**, 2998 (1980); H. Okawa, K. Ueda, and S. Kida, *Inorg. Chem.*, **21**, 1594 (1982) and references therein.

24) P. R. Mitchell, *J. Chem. Soc., Dalton Trans.*, **1979**, 771.

Kinetics and Mechanisms of Anation and Exchange Reactions in Pentakis(*N,N*-dimethylformamide)dioxouranium(VI) Ion in Nonaqueous Media

Hideo Doine, Yasuhisa Ikeda, Hiroshi Tomiyasu, and Hiroshi Fukutomi*

Research Laboratory for Nuclear Reactors, Tokyo Institute of Technology, O-okayama, Meguro-ku, Tokyo 152

(Received December 8, 1982)

The exchange reaction of *N,N*-dimethylformamide (dmf) in $[UO_2(dmf)_5]^{2+}$ ion and the anation reactions by SCN^- and N_3^- have been studied by the NMR method in CD_2Cl_2 and the stopped-flow method in DMF, respectively. For the dmf exchange reaction, rate $=(k_d+k_IK_{os}[DMF])[UO_2(dmf)_5^{2+}]/(1+K_{os}[DMF])$, where k_d, k_I, and K_{os} are $(1.30\pm0.21)\times10^2$ s^{-1}, $(2.94\pm0.07)\times10^3$ s^{-1}, and 1.59 ± 0.11 mol^{-1} kg at -50 °C, respectively. For the anation reactions by SCN^- and N_3^-, the pseudo-first-order rate constant (k_{obsd}) is expressed by $k_{obsd}=\{k_{-1}+(k_1+k_{-1})K_{os}[X]\}/(1+K_{os}[X])$ (X=SCN^- and $[UO_2(dmf)_5]^{2+}$ for the anation reactions by SCN^- and N_3^-, respectively). The values of k_1, k_{-1}, and K_{os} at 25 °C are 1.95×10^2 s^{-1}, 4.27×10^2 s^{-1}, 1.48×10^2 M^{-1} (1 M=1 mol dm^{-3}), and 1.64×10^3 s^{-1}, 3.72×10^2 s^{-1}, 1.80×10^2 M^{-1} for SCN^- and N_3^- anation reactions, respectively. These results suggest that the substitution reaction in $[UO_2(dmf)_5]^{2+}$ ion proceeds through the associative interchange mechanism. The difference of reactivities for SCN^- and N_3^- toward $[UO_2(dmf)_5]^{2+}$ ion seems to be related to the pK_a values for acids, HSCN and HN_3.

Ligand exchange reactions in the equatorial plane of uranyl complexes have been extensively studied by using NMR,[1–7] and it is proposed that the ligand exchange reactions in most of the uranyl complexes proceed through the dissociative(D) or dissociative interchange(I_d) mechanism.[8] There have been a few studies on the anation reactions of uranyl aqua complex with some anions in aqueous solution,[9–11] and very few studies have been concerned with the ligand substitution of uranyl complexes in nonaqueous solvent.

Hence a detailed kinetic analysis of ligand substitution reactions for $[UO_2(dmf)_5]^{2+}$ ion was performed for the following reactions,

$$[UO_2(dmf)_5]^{2+} + DMF^* \rightleftharpoons [UO_2(dmf)_4dmf^*]^{2+} + DMF, \quad (1)$$

$$[UO_2(dmf)_5]^{2+} + SCN^- \rightleftharpoons [UO_2(dmf)_4NCS]^+ + DMF, \quad (2)$$

$$[UO_2(dmf)_5]^{2+} + N_3^- \rightleftharpoons [UO_2(dmf)_4N_3]^+ + DMF, \quad (3)$$

where an asterisk is used to denote the exchanging species. The dmf exchange reaction has been already reported by Lincoln *et al.*[5] They studied the dmf exchange by measuring the NMR line-broadening of the methyl protons of free and coordinated DMF and proposed that the dmf exchange proceeded through the D mechanism.

In the present study, the NMR line broadening of the formyl proton in DMF was measured by changing the free DMF concentration over a 50 fold concentration range and compared with the Lincoln's results. The reaction mechanism is discussed by comparing the results of kinetic studies of reactions (1), (2), and (3).

Experimental

Synthesis of Complexes. The $[UO_2(dmf)_5](ClO_4)_2$ complex was prepared in the atomosphere of nitrogen by refluxing hydrated uranyl perchlorate with triethyl orthoformate at 50—60 °C for one hour, followed by the addition of *N,N*-dimethylformamide at room temperature. The resulting light yellow crystals were filtered, washed with ethyl ether and dried *in vacuo* for 2 d. Anal. Calcd for $[UO_2(dmf)_5](ClO_4)_2$: C, 21.59; H, 4.22; N, 8.39. Found: C, 21.65; H, 4.20; N, 8.50. Elemental analysis of the complexes was carried out in the Institute of Physical and Chemical Research.

Other Materials. Dichloromethane-d_2 (CD_2Cl_2, Merck 99%), which was used as a solvent in the exchange reaction of dmf in $[UO_2(dmf)_5]^{2+}$ complex, was died over 4A molecular sieves (Wako Pure Chemical Ind., Ltd.). *N,N*-Dimethylformamide (Wako) was distilled twice under reduced pressure and stored over 4A molecular sieves. Triethyl orthoformate (Wako) was of guaranteed grade and used without further purification. Sodium thiocyanate (Wako) was used without further purification. The concentration of azide ion in DMF solution was determined by measuring sodium ion concentration with a Varian-Techtron 1100 flamespectrophotometer. The amount of water contained in DMF solvent was measured by a Mitsubishi CA-02 moisturemeter and the maximum concentration was found to be less than 0.01 M. Anhydrous sodium prechlorare (Wako) was used to adjust the ionic strength of solutions.

Preparations of NMR Samples. Sample solutions for NMR measurements were prepared by weighing sample substances in a 1 cm^3 volumetric flask and some of each solution was placed in an NMR sample tubes and sealed. All samples were prepared in a glove box filled with dry nitrogen. Sample solutions were placed in a dark room to avoid the photochemical redox reactions.[12]

Measurement of NMR and IR Spectra. ^{1}H NMR spectra were measured at 100 MHz on a JEOL JNM-FX 100 FT-NMR spectrometer equipped with a JNM-VT-3B temperature controller. Infrared spectra of $[UO_2(dmf)_5]^{2+}$ complex in CD_2Cl_2 were recorded in 200—4000 cm^{-1} range by using a JASCO DS-701G IR spectrophotometer.

Measurement of Equilibrium Constants. The equilibrium constants between $[UO_2(dmf)_5]^{2+}$ and SCN^- or N_3^- ions were measured spectrophotometrically by using a Shimadzu UV-210A double-beam spectrophotometer with a cell compartment thermostated at 25 °C. The ionic strength of sample solutions was adjusted to 0.2 M by using sodium perchlorate.

Kinetic Measurements. The dmf exchange reaction in $[UO_2(dmf)_5]^{2+}$ complex was measured by the NMR line-broadening method as described in the previous paper.[13]

As is mentioned later, the methyl proton signal of the coordinated dmf, which should have two peaks, gave a single peak. This implies that the use of the methyl proton signal for the kinetic measurements is liable to produce an uncertain error. From this reason, the formyl proton signal was employed in the present study.

The anation rates were measured by using a Durrum 110 stopped-flow spectrophotometer with a thermostated cell compartment. The pseudo-first-order rate constants were obtained from the plot of $\ln\{(A_t-A_\infty)/(A_0-A_\infty)\}$ *vs.* time. The symbols, A_0, A_∞, and A_t represent the absorbance at time zero, infinity, and t, respectively.

Results and Discussion

Structure of $[UO_2(dmf)_5](ClO_4)_2$ *in* CD_2Cl_2. Figure 1 shows the ^1H NMR spectrum of a solution containing $[UO_2(dmf)_5](ClO_4)_2$, DMF, and CD_2Cl_2 at -80 °C. From the comparison with the ^1H NMR spectrum of pure DMF, the signals (a) and (b) were assigned to the methyl protons of free and coordinated DMF, respectively. The signals (c) and (d) were attributed to the formyl protons of free and coordinated DMF, respectively. It is noted that the methyl proton signal of the coordinated dmf is a single peak, while that of the free DMF has two equivalent peaks. This result is consistent with that of Lincoln *et al.*[5] The signal of methyl protons of the coordinated dmf should originally have two peaks. In fact, this kind of single peak has not been observed in other dmf complexes, *e.g.* $[Al(dmf)_6]^{3+}$, $[Ga(dmf)_6]^{3+}$, and $[Be(dmf)_4]^{2+}$.[14-16] This phenomenon may be due to the rotation round the C–N bond in coordinated dmf molecules, which is assumed to be too fast on the NMR time scale at this temperature, or to the equalization of chemical shifts of both methyl groups of the coordinated dmf molecules caused by the magnetic anisotropy of the uranyl ions as proposed by Lincoln *et al.*[5] The former is not likely because the IR spectrum of $[UO_2(dmf)_5]^{2+}$ complex in CD_2Cl_2 gives the value of 1642 cm^{-1} for the C–O stretching of dmf, which is 33 cm^{-1} lower than that observed for pure DMF (1675 cm^{-1}). This fact suggests that the dmf molecules coordinate to the uranyl ion through oxygen, since the C–O stretching, so called Amide I, is shifted to a lower side when the dmf molecule coordinates to metal ion through oxygen.[17-19] This coordination tends to increase the double bond character of the C–N group and hence make more difficult the rotation round the C–N bond.

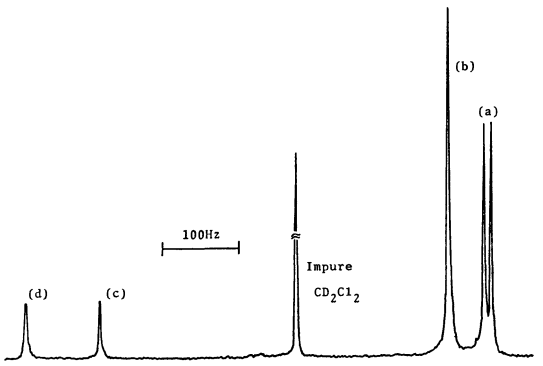

Fig. 1. The ^1H NMR spectrum of a solution consisting of $[UO_2(dmf)_5]^{2+}$ (0.00433 mol kg^{-1}), DMF (0.0216 mol kg^{-1}), and CD_2Cl_2 (11.4 mol kg^{-1}) at -80 °C.

On the other hand, it is more likely that the magnetic anisotropy of the uranyl ion may introduce the degeneration of two signal peaks arising from the methyl groups of the coordinated dmf. Pople *et al.*[20] give the equation for the chemical shift ($\Delta\delta$) caused by the anisotropic field

$$\Delta\delta = \Delta\chi_{atomic}(1-3\cos^2\gamma)/3R^3, \quad (4)$$

where $\Delta\chi_{atomic} = \chi_{atomic}$(parallel to axis) $- \chi_{atomic}$ (perpendicular to axis), in which the axis is taken to be the O=U=O axis, R is the distance between the proton and the uranium atom, and γ is the angle between a straight line connecting the proton and uranium atom and the O=U=O axis. From this equation, it is expected that the chemical shifts of both methyl groups of the coordinated dmf become identical at the particular values of γ and R. Lincoln *et al.*[5] estimated the value of $\Delta\delta$ for both methyl groups of the coordinated dmf by using Eq. 4 and found that the calculated values were consistent with the experimental ones. Furthermore, the dmf methyl proton signal of $UO_2(acac)_2dmf$ (acac=acetylacetonate) in CD_3COCD_3 and CD_2Cl_2 has two equivalent peaks[12] in spite of the coordination of dmf in the same equatorial plane of uranyl ion and the differences of chemical shifts between two peaks are 0.03 and 0.14 ppm in CD_3COCD_3 and CD_2Cl_2, respectively. These phenomena can be explained by the differences of the values for γ and R in $UO_2(acac)_2dmf$ and $[UO_2(dmf)_5]^{2+}$ complexes.

The number of the coordinated dmf molecules were determined by area integrations of the methyl and formyl proton signals of free and coordinated DMF, respectively and the results are listed in Table 1. The absence of any significant variation of the number

Table 1. Solution compositions and coordination numbers (CN) for the exchange of dmf in $[UO_2(dmf)_5]^{2+}$

No.	$[UO_2(dmf)_5^{2+}]$ / 10^{-3} mol kg^{-1}	DMF / 10^{-2} mol kg^{-1}	$[CD_2Cl_2]$ / mol kg^{-1}	CN[a]
i	2.54	0.871	11.5	5.2±0.1
ii	4.33	2.16	11.4	5.1±0.3
iii	4.59	5.24	11.4	5.1±0.1
iv	4.30	9.73	11.4	4.8±0.2
v	21.7	44.0	10.9	5.0±0.1

a) The quoted errors represent the standard deviations.

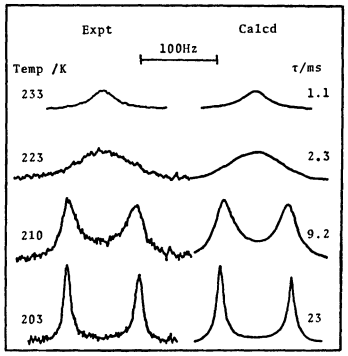

Fig. 2. Experimental (left-hand side) and best-fit calculated ^1H NMR lineshapes of a solution consisting of $[UO_2(dmf)_5]^{2+}$ (0.00433 mol kg^{-1}), DMF (0.0216 mol kg^{-1}), and CD_2Cl_2 (11.4 mol kg^{-1}). Temperatures and best-fit τ-values are shown at left- and right-hand side of the figure, respectively.

of coordinated dmf molecules over a wide concentration range (Table 1) indicates that neither CD_2Cl_2 nor perchlorate ion enters into the first coordination sphere of uranyl ion. The absence of any splitting of the coordinated dmf formyl proton signal indicates also that the five molecules of the coordinated dmf occupy the equivalent equatorial positions of the uranyl ion. These results confirm that the structure of $[UO_2(dmf)_5]^{2+}$ ion in CD_2Cl_2 is pentagonal bipyramidal.

Exchange Reaction of DMF in $[UO_2(dmf)_5]^{2+}$ Ion in CD_2Cl_2. A typical temperature dependence of lineshape for the formyl proton signals of the coordinated and free DMF is shown at the left side in Fig. 2. This figure shows that the dmf exchange reaction occurs between the coordinated and free sites. The best-fit life times (τ-values) were determined by using the computer program for two site exchange[21] and are shown at the right side in Fig. 2 together with the corresponding lineshapes. From these τ-values, the first-order rate constants, k_{ex}, were calculated by the following equations,

$$\tau = P_F\tau_c = P_c\tau_F, \tag{5}$$

$$k_{ex} = 1/\tau_c = \text{rate}/5[UO_2(dmf)_5^{2+}] = (kT/h)\exp(-\Delta H^*/RT)\exp(\Delta S^*/R), \tag{6}$$

where τ and P with the subscripts of F and c are the life times and mole fractions of the free and coordinated sites, respectively.

The same measurements were carried out for the solutions with different compositions listed in Table 1. Figure 3 shows the plots of k_{ex} against the DMF concentration, which do not yield a simple linear relationship but the intercepts and the limiting values at high concentration region. This result suggests that the dmf exchange reaction proceeds through two paths, that is, one is the independent path of the DMF concentration and another is the path which depends on the DMF concentration in its low region and becomes independent of the DMF concentration in its high region.

These paths are assumed to proceed through the D and I mechanism[8] as follows.

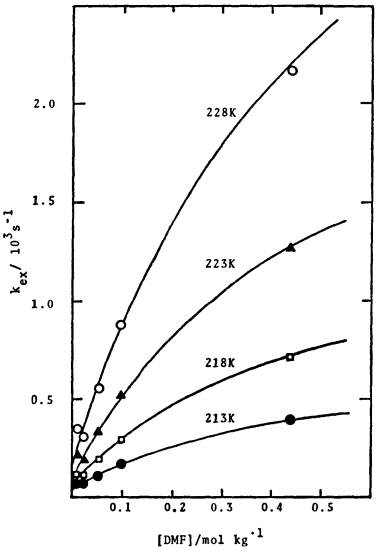

Fig. 3. Plots of k_{ex} *vs.* [DMF] for the exchange of dmf in $[UO_2(dmf)_5]^{2+}$. The solid lines denote the least-squares best-fit lines.

$$[UO_2(dmf)_5]^{2+} + DMF^* \xrightarrow[\text{slow}]{k_d} [UO_2(dmf)_4]^{2+} + DMF + DMF^* \xrightarrow[\text{fast}]{} [UO_2(dmf)_4dmf^*]^{2+} + DMF,$$

$$[UO_2(dmf)_5]^{2+} + DMF^* \overset{K_{os}}{\rightleftharpoons} [UO_2(dmf)_5]^{2+}\cdots DMF^* \xrightarrow[\text{slow}]{k_I} [UO_2(dmf)_4dmf^*]^{2+}\cdots DMF \xrightarrow[\text{fast}]{} [UO_2(dmf)_4dmf^*]^{2+} + DMF,$$

where K_{os} is the outer-sphere complex formation constant. These mechanisms lead to the following equation for k_{ex}[22]

$$k_{ex} = \frac{k_d + k_I K_{os}[DMF]}{1 + K_{os}[DMF]}. \tag{7}$$

This equation can be simplified to $k_{ex} = k_d + k_I K_{os} \times [DMF]$ when $K_{os}[DMF] \ll 1$. This corresponds to the dependence of k_{ex} on the DMF concentration in the low concentration region. If the value of $K_{os}[DMF]$ is much larger than unity, Eq. 7 becomes $k_{ex} \simeq k_I$, which agrees with the fact that the dmf exchange rate becomes independent of the DMF concentration in its high region.

The values of k_d, k_I, and K_{os} were calculated by

Table 2. Kinetic parameters of ligand exchange reaction[a]

Temp / K	k_d / 10^2 s^{-1}	k_I / 10^3 s^{-1}	K_{os} / mol^{-1} kg
228	2.10±0.39	5.08±0.12	1.59±0.19
223	1.30±0.21	2.94±0.07	1.59±0.11
218	0.72±0.10	1.51±0.03	1.88±0.06
213	0.43±0.05	0.83±0.01	1.88±0.03

a) The quoted errors represent the standard deviations.

Table 3. Kinetic data for the ligand substitution reactions in $[UO_2(dmf)_5]^{2+}$ at 298 K

Ligand	Solvent	Method	Rate constant / s^{-1}	Mechanism	ΔH^{*} b) / kJ mol^{-1}	ΔS^{*} b) / J K^{-1} mol^{-1}
DMF	CD_2Cl	NMR	$k_d=4.70\times10^4$	D	42.0±2.1	−15.1±3.3
			$k_I=2.34\times10^6$	I	48.3±0.9	38.6±2.6
SCN^-	DMF	Stopped-flow	$k_1=1.95\times10^{2}$ a)	I	67.6±3.5	24.4±4.0
			$k_{-1}=4.27\times10^{2}$ a)	—	38.6±3.1	−68.0±5.7
N_3^-	DMF	Stopped-flow	$k_1=1.64\times10^{3}$ a)	I	50.6±2.0	−14.5±4.8
			$k_{-1}=3.72\times10^{2}$ a)	—	47.2±2.3	−38.0±7.2

a) Ionic strength=0.2 M($NaClO_4$). b) The quoted errors represent the standard deviations.

using the nonlinear least-squares method. The results are shown in Table 2. The solid lines in Fig. 3 are the best-fit lines obtained from the calculated values of k_d, k_I, and K_{os} and indicate that the calculated values are in fair agreement with the experimental data. The activation parameters for k_d and k_I were obtained from the Eyring plot and are listed in Table 3.

The present results are different from those of Lincoln *et al.*[5] They reported that the rate of dmf exchange was independent of the free DMF concentration and that this exchange reaction proceeded through the D mechanism. In their experiments, the first-order rate constants are obtained from the lineshape analysis of the methyl proton signals of the free and coordinated DMF and the concentration range of free DMF (0.00213—0.04323 M) is lower than that of the present experiment (0.0123—0.588 M). Hence the different results in two works might be due to the differences in the experimental conditions.

Equilibrium between $[UO_2(dmf)_5]^{2+}$ and SCN^-. Figure 4 shows spectral changes of $[UO_2(dmf)_5]^{2+}$ with varying the concentration of thiocyanate ion from 0.01 M to 0.04 M in DMF. Although an isosbestic point is not observed, the most probable reaction corresponding to the spectral change is

$$[UO_2(dmf)_5]^{2+} + SCN^- \overset{K}{\rightleftharpoons} [UO_2(dmf)_4NCS]^+ + DMF. \quad (8)$$

The equilibrium constant K for this process was obtained from the following equation.

$$\frac{[UO_2(dmf)_5^{2+}]}{Abs-\varepsilon_1[UO_2(dmf)_5^{2+}]} = \frac{1}{\varepsilon_2-\varepsilon_1} + \frac{1}{(\varepsilon_2-\varepsilon_1)K[SCN^-]}, \quad (9)$$

where Abs is the observed absorbance, and ε_1 and ε_2 are the molar extinction coefficients of $[UO_2(dmf)_5]^{2+}$ and $[UO_2(dmf)_4NCS]^+$, respectively. If $[UO_2(dmf)_5^{2+}]/(Abs-\varepsilon_1[UO_2(dmf)_5^{2+}])$ is plotted against $1/[SCN^-]$, the plot should be linear. Indeed, Fig. 5 shows this linear relationship, which supports the validity of the reaction given by Eq. 8. From the slope and the intercept, the value of K was calculated and is listed in Table 4.

Equilibrium between $[UO_2(dmf)_5]^{2+}$ and N_3^-. When azide ions were added to a DMF solution of $[UO_2(dmf)_5]^{2+}$, a change in the absorption spectrum of $[UO_2(dmf)_5]^{2+}$ was much larger than that by the addition of thiocyanate ion. Therefore, the measurement of the equilibrium constant K for $[UO_2(dmf)_4N_3]^+$, was carried out under the conditions of $[UO_2(dmf)_5^{2+}] \gg [N_3^-]$ in order to avoid other complex formation. In this case, the value of K was calculated from the slope and the intercept in the plot of $[N_3^-]/(Abs-\varepsilon_1[UO_2(dmf)_5^{2+}])$ *vs.* $1/[UO_2(dmf)_5^{2+}]$ at 437 nm. The result is shown in Table 4.

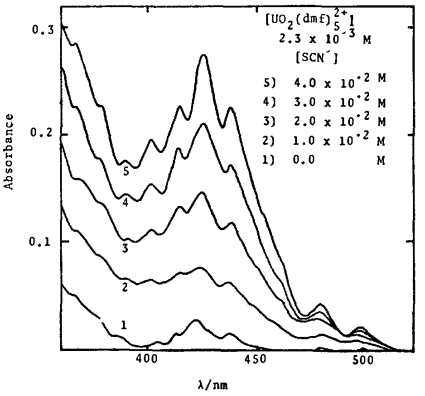

Fig. 4. The spectral change of $[UO_2(dmf)_5]^{2+}$ with varying the concentration of thiocyanate ion in DMF at 25 °C and μ=0.2 M ($NaClO_4$).

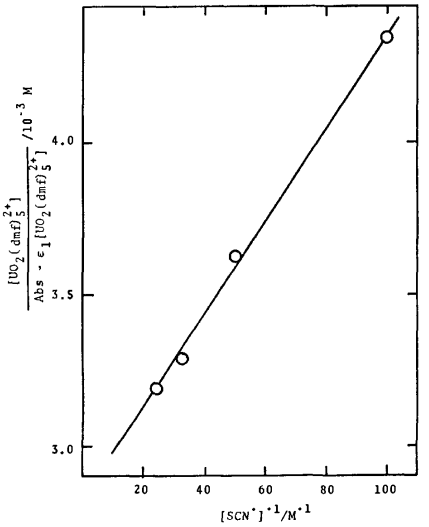

Fig. 5. The plot of $[UO_2(dmf)_5^{2+}]/(Abs-\varepsilon_1[UO_2(dmf)_5^{2+}])$ *vs.* $[SCN^-]^{-1}$ for the substitution reaction of $[UO_2(dmf)_5]^{2+}$ by thiocyanate ion at 25 °C, 437 nm, and μ=0.2 M ($NaClO_4$).

Anation Reaction. On the basis of the results of equilibrium constants measured spectrophotometrically, the pseudo-first-order rate constants, k_{obsd}, for the anation reactions by SCN^- and N_3^- were measured under the conditions of $[SCN^-]>[UO_2(dmf)_5^{2+}]$ and $[UO_2(dmf)_5^{2+}]>[N_3^-]$, respectively.

Figures 6 and 7 show the plots of k_{obsd} against $[SCN^-]$ and $[UO_2(dmf)_5^{2+}]$, respectively, which do not display a simple linear relationship, and the values of k_{obsd} approach each limiting value at high concentration region of $[SCN^-]$ and $[UO_2(dmf)_5^{2+}]$. Attempts were also made to examine the effect of the water on the anation reaction, in which the concentration of water was changed from 0.01 M to 0.1 M. It was found that water made no effect on the present anation reaction in this concentration range.

Table 4. Equilibrium constants at 298 K[a)]

Ligand	K / M^{-1}	K_{calcd} / M^{-1}
SCN^-	186±26	215±42
N_3^-	974±73	974±43

Ionic strength=0.2 M($NaClO_4$). a) The quoted errors represent the standard deviations.

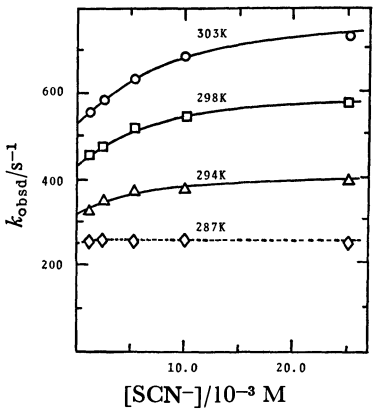

Fig. 6. Plots of k_{obsd} *vs.* $[SCN^-]$ for the anation reaction by SCN^-.
The solid lines denote the least-squares best-fit lines.

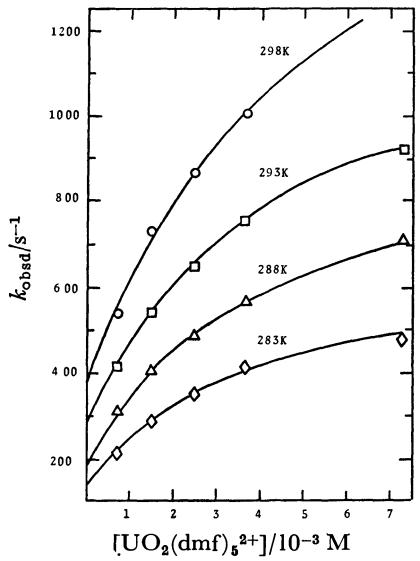

Fig. 7. Plots of k_{obsd} *vs.* $[UO_2(dmf)_5^{2+}]$ for the anation reaction by N_3^-.
The solid lines denote the least-squares best-fit lines.

Taking into account the result that the dmf exchange reaction in $[UO_2(dmf)_5]^{2+}$ seems to proceed predominantly through the I mechanism as described above, the following I mechanism appears to be the most plausible mechanism for the present anation reactions.

$$[UO_2(dmf)_5]^{2+} + L^- \overset{K_{os}}{\rightleftharpoons} [UO_2(dmf)_5]^{2+}\cdots L^-$$

$$[UO_2(dmf)_5]^{2+}\cdots L^- \underset{k_{-1}}{\overset{k_1}{\rightleftharpoons}} [UO_2(dmf)_4L]^+ + DMF,$$

where L^- is the SCN^- or N_3^- ion, and K_{os} is the outer-sphere complex formation constant. According to this mechanism, the observed rate constant, k_{obsd}, is given by Eq. 10

$$k_{obsd} = \frac{k_{-1}+(k_1+k_{-1})K_{os}[X]}{1+K_{os}[X]} \quad (10)$$

where X is SCN^- and $[UO_2(dmf)_5]^{2+}$ for the anation reactions by SCN^- and N_3^-, respectively, since these anation reactions were carried out under the conditions of $[UO_2(dmf)_5^{2+}]<[SCN^-]$ and $[UO_2(dmf)_5^{2+}]>[N_3^-]$, respectively. When $K_{os}[X]\ll 1$, Eq. 10 can be simplified to $k_{obsd}=k_{-1}+(k_1+k_{-1})K_{os}[X]$. This is in good agreement with the dependence of k_{obsd} on [X] in the low concentration region. If the value of $K_{os}[X]$ is much larger than unity, Eq. 10 becomes $k_{obsd}=k_1+k_{-1}$, which is consistent with the fact that the limiting values of k_{obsd} are obtained at high [X].

The values of k_1, k_{-1}, and K_{os} were calculated by the nonlinear least-squares method and are listed in Table 5. The solid lines obtained from the calculated values agree with the experimental results. The activation parameters for k_1 and k_{-1} obtained from the Eyring plots are shown in Table 3.

The outer-sphere complex formation constants for both reactions are nearly the same as shown in Table 5, while the interchange rate constants are fairly different. This seems to be reasonable since SCN^- and N_3^- ions have the same charge, nearly the same size and structure. Thus the interatomic distance between $[UO_2(dmf)_5]^{2+}$ and SCN^- or N_3^- in the outer-sphere

Table 5. Kinetic parameters of ligand substitution reaction[a)]

Temp / K	k_1 / s^{-1}	k_{-1} / s^{-1}	K_{os} / M^{-1}
$[UO_2(dmf)_5]^{2+}+SCN^-$			
293	116±8	320±25	154
298	195±12	427±30	148
303	273±19	528±35	126
$[UO_2(dmf)_5]^{2+}+N_3^-$			
283	520±35	132±12	300
288	784±37	181±15	270
293	1077±41	274±21	220
298	1640±49	372±30	180

Ionic strength=0.2 M($NaClO_4$). a) The quoted errors represent the standard deviations.

complexes is assumed to be the same. In this case, the Fuoss equation[23] gives the same value for the outer-sphere complex formation constant. When the anation reaction proceeds through the interchange mechanism, the relationship between the equilibrium constant (K) and the outer-sphere complex formation constant (K_{os}) is generally given by the following equation.[24]

$$K = K_{ob}(1+k_1/k_{-1}) \quad (11)$$

The calculated values of K were obtained from Eq. 11 by using the values of k_1, k_{-1}, and K_{os} derived from kinetic measurements. It is found that the calculated K values (Table 4) are in remarkable agreement with those obtained spectrophotometrically. This fact also supports that the anation reactions by SCN^- and N_3^- proceed through the interchange mechanism. Table 3 indicates that the interchange rate constants (k_1) for the anation by SCN^- and N_3^- are smaller than that of dmf exchange reaction by a factor of about 10^3, and the values of ΔH^* for the anation reactions are larger than that for the dmf exchange reaction. These facts suggest that the anation reactions by SCN^- and N_3^- proceed through the associative interchange (I_a) mechanism. If the anation reaction proceeds through the dissociative interchange (I_d) mechanism, the interchange rate constants and ΔH^* values for the anation reactions should be consistent with those for the dmf exchange reaction. Additional evidence for the I_a mechanism is given by the interchange rate constants k_1 (Table 5), which depend strongly on the nature of the entering ligands SCN^- and N_3^-. The difference of the reactivities, *i.e.* $k_1^{N_3^-}/k_1^{SCN^-} \approx 10$, cannot be attributed to the outer-sphere complex formation, because the value of this ratio is much larger than the corresponding value for K_{os}, $K_{os}^{N_3^-}/K_{os}^{SCN^-}=1.2$ at 25 °C. Thus the different reactivity may be due to a difference in the nucleophilicity of SCN^- and N_3^- toward $[UO_2(dmf)_5]^{2+}$. The value of pK_a for HN_3 is much larger than that for HSCN.

It is concluded that the anation reactions by SCN^- and N_3^- proceed through the I_a mechanism since the interchange rate constants depend strongly on the nature of entering ligands, SCN^- and N_3^-. If it is reasonable to regard the anation reaction as a special case of the solvent exchange reaction where an anion in the second coordination sphere becomes the entering ligand rather than a solvent molecule in the same region,[22] it may be supposed that the k_I path in the dmf exchange reaction also proceeds through the I_a mechanism.

The authors wish to express their thanks to Dr. Roderick D. Cannon of the University of East Anglia, Messrs. Takashi Kojima and Masayuki Harada for their helpful discussions. This work was partly supported by the Grant-in-Aid for Scientific Research from the Ministry of Education, Science and Culture.

References

1) Y. Ikeda, S. Soya, H. Tomiyasu, and H. Fukutomi, *J. Inorg. Nucl. Chem.*, **41**, 1333 (1979).
2) Y. Ikeda, H. Tomiyasu, and H. Fukutomi, *Bull. Res. Lab. Nucl. Reac.*, **4**, 47 (1979).
3) R. P. Bowen, S. F. Lincoln, and E. H. Williams, *Inorg. Chem.*, **15**, 2126 (1976).
4) J. Crea, R. Digiusto, S. F. Lincoln, and H. E. Williams, *Inorg. Chem.*, **16**, 2825 (1977).
5) R. P. Bowen, G. J. Honan, S. F. Lincoln, T. M. Spotswood, and E. H. Williams, *Inorg. Chim. Acta*, **33**, 235 (1979).
6) G. J. Honan, S. F. Lincoln, and E. H. Williams, *J. Chem. Soc., Dalton Trans.*, **1979**, 1220.
7) A. M. Hounslow, S. F. Lincoln, P. A. Marshall, and E. H. Williams, *Aust. J. Chem.*, **34**, 2543 (1981).
8) C. H. Langford and H. B. Gray, "Ligand Substitution Processes," Benjamin, London (1974).
9) M. P. Whiiaker, E. M. Eyring, and E. Dibble, *J. Phys. Chem.*, **69**, 2319 (1965).
10) P. Hurwitz and K. Kustin, *J. Phys. Chem.*, **71**, 324 (1967).
11) A. Ekstrom and D. A. Johnson, *J. Inorg. Nucl. Chem.*, **36**, 2549 (1974).
12) E. Rabinowitch and R. L. Belford, "Spectroscopy and Photochemistry of Uranyl Compounds", Pergamon Press, New York (1964).
13) Y. Ikeda, H. Tomiyasu, and H. Fukutomi, *Bull. Chem. Soc. Jpn.*, **56**, 1060 (1983).
14) W. G. Movius and N. A. Matwiyoff, *Inorg. Chem.*, **6**, 847 (1967).
15) W. G. Movius and N. A. Matwiyoff, *Inorg. Chem.*, **8**, 925 (1969).
16) N. A. Matwiyoff and W. G. Movius, *J. Am. Chem. Soc.*, **89**, 6077 (1967).
17) W. Gerrard, M. F. Lappert, H. Pyszora, and J. W. Wallis, *J. Chem. Soc.*, **1960**, 2144.
18) C. D. Schmulbach and R. S. Drago, *J. Am. Chem. Soc.*, **82**, 4484 (1960).
19) S. J. Kuhn and J. S. McIntyre, *Can. J. Chem.*, **43**, 375 (1965).
20) J. A. Pople, W. G. Schneider, and H. G. Bernstein, "High Resolution Nuclear Magnetic Resonance," McGraw-Hill, New York, N. Y. (1959).
21) G. Binsch, "Topics in Stereochemistry," ed by E. L. Eliel and N, L. Allinger, Wiley Interscience, New York (1968), Vol. 3, p. 97.
22) S, T. D. Lo and T. W. Swaddle, *Inorg. Chem.*, **15**, 1881 (1976).
23) R. M. Fuoss, *J. Am. Chem. Soc.*, **89** 5059 (1958).
24) S. Yamada and M. Tanaka, *J. Inorg. Nucl. Chem.*, **37**, 587 (1975).

 © 1983 The Chemical Society of Japan Bull. Chem. Soc. Jpn., 56, 1995—1999 (1983)

Preparation and Spectroscopic Studies of (Diethylenetriamine)cobalt(III) Complexes with L-Penicillaminate or Its Derivative

Katsuhiko WAKAYAMA,† Ken-ichi OKAMOTO,* Hisahiko EINAGA,†† and Jinsai HIDAKA

Department of Chemistry, University of Tsukuba, Sakura, Ibaraki 305

(Received December 11, 1982)

The (diethylenetriamine)(L-penicillaminato)cobalt(III) complex, $[Co(L\text{-pen})(dien)]^+$, was chromatographically separated into three isomers, *trans*(N_1N), *trans*(N_1O) and *trans*(N_1S). Each of these gave a corresponding isomer of the (diethylenetriamine)(*S*-methyl-L-penicillaminato)cobalt(III) complex, $[Co(L\text{-smp})(dien)]^{2+}$, by the reaction with dimethyl sulfate. The (triammine)(*S*-methyl-L-penicillaminato)cobalt(III) complex was also derived from the corresponding L-pen complex, $[Co(L\text{-pen})(NH_3)_3]^+$. The absorption and CD spectra of the L-pen complexes were compared with those of the L-smp ones to specify the geometrical configurations. The L-pen complexes exhibited characteristic absorption behavior and CD spectra in the region of $(14—30)\times10^3$ cm^{-1}.

Cobalt(III) complexes with the thioether type terdentate-*N*,*S*,*O* ligands such as *S*-methyl-L-cysteinate and L-methioninate have been characterized on the basis of their absorption and CD spectra.[1-6] However, the absorption and CD spectral behaviors of the complexes with the thiolato type ligands have not been clarified yet.[6,7] The thiolato type complexes generate the thioether ones by the reaction with dimethyl sulfate.[6] This reaction is useful for the investigations of the spectrochemical and stereochemical properties for the thiolato type complexes.

In this work, the (diethylenetriamine)(L-penicillaminato)cobalt(III) complex, $[Co(L\text{-pen})(dien)]^+$, was prepared and chromatographically separated into three geometrical isomers, *trans*(N_1N), *trans*(N_1O), and *trans*(N_1S) (Fig. 1). Each of the L-pen isomers gave the corresponding isomer of the (diethylenetriamine)(*S*-methyl-L-penicillaminato)cobalt(III) complex, $[Co(L\text{-smp})(dien)]^{2+}$, on reaction with dimethyl sulfate. The (triammine)(*S*-methyl-L-penicillaminato)cobalt(III) complex, $[Co(L\text{-smp})(NH_3)_3]^{2+}$, was derived from the corresponding L-pen complex, $[Co(L\text{-pen})(NH_3)_3]^+$, by the same reaction as that for the dien complex. The structural assignments of the isomers for $[Co(L\text{-smp})(dien)]^{2+}$ are fairly difficult, because the three L-smp isomers which belong to a *cis*(*SO*)-$[Co(S)(O)(N)_4]$ type show quite similar absorption spectra. Therefore, one of $[Co(L\text{-pen})(dien)]^+$ isomers was preliminarily determined to have a *trans*(N_1N) configuration by the X-ray crystal structure analysis.[8] On the basis of the absorption and CD spectra of *trans*(N_1N)-$[Co(L\text{-pen})(dien)]^+$ and the result derived from the reaction of the *trans*(N_1N) L-pen isomer with dimethyl sulfate, the absorption and CD spectra of the L-pen and L-smp complexes will be discussed to specify their geometrical configurations.

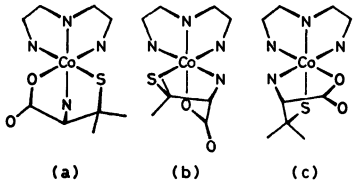

Fig. 1. Three geometrical isomers of $[Co(L\text{-pen or L-smp})(dien)]^{+ \text{ or } 2+}$; (a) *trans*($N_1N$), (b) *trans*($N_1O$), and (c) *trans*($N_1S$).

Experimental

1) (Diethylenetriamine)(L-penicillaminato)cobalt(III) Chloride. *[Co(L-pen)(dien)]Cl*: This complex was prepared and separated into three isomers by the method described in the previous paper.[8] Dark-brown needle crystals were obtained from the first eluate (A-1) of the three brown bands eluted, A-1, A-2, and A-3. The A-1 isomer was determined to have a *trans*(N_1N) isomer by the X-ray crystal structure analysis.[8] Found for A-1: C, 30.51; H, 6.73; N, 15.12%. Found for A-2: C, 30.04; H, 6.67; N, 15.56%. Calcd for $[Co(L\text{-pen})(dien)]Cl\cdot H_2O = CoC_9H_{22}N_4O_2SCl\cdot H_2O$: C, 29.80; H, 6.69; N, 15.44%. Found for A-3: C, 30.37; H, 6.28; N, 16.00%. Calcd for $[Co(L\text{-pen})(dien)]Cl\cdot 0.25H_2O$: C, 30.95; H, 6.49; N, 16.04%.

2) (Diethylenetriamine)(S-methyl-L-penicillaminato)cobalt(III) Chloride. *[Co(L-smp)(dien)]Cl_2*: This complex was prepared by the reaction of $[Co(L\text{-pen})(dien)]^+$ obtained in 1) with dimethyl sulfate. About 10 cm^3 of dimethyl sulfate was added drop by drop to a solution containing 0.5 g of the A-1 isomer of $[Co(L\text{-pen})(dien)]^+$ in 10 cm^3 of water and the mixture was mechanically stirred for a few minutes. When the mixture had been allowed to stand at room temperature for a while, it separated into two layers: a brown (upper) layer and a cloudy colorless (lower) layer. The former changed gradually from brown to reddish orange. After being allowed to stand at room temperature for about 5 h, the reddish orange solution was separated and poured onto a column of SP-Sephadex C-25 (Na^+ form, 3×40 cm). After the column was swept with water, the adsorbed reddish orange band was eluted with a 0.15 mol dm^{-3} aqueous solution of sodium chloride. Only one reddish orange band was eluted and fractionated. It was found, from the absorption and CD spectra of the fractionated eluates, that the eluate contained only one isomer (B-1). Then the fractions were combined and concentrated to a small volume with a rotary evaporator at about 20 °C. The deposited sodium chloride was filtered off. After a large amount of ethanol was added to the filtrate, the solution was kept in a refrigerator overnight. The B-1 isomer obtained was recrystallized from a small amount of water by the addition of acetone. Similarly, the B-2 and B-3 isomers were derived from the A-2 and A-3 isomers by a reaction with dimethyl

† Present address: TDK Electronics Co., Ltd., 1-13-1, Nihonbashi, Chuo-ku, Tokyo 103.

†† Present address: Institute of Materials Science, University of Tsukuba, Sakura, Ibaraki 305.

sulfate. Found for B-1: C, 29.82; H, 6.46; N, 13.68%. Calcd for $[Co(L\text{-}smp)(dien)]Cl_2 \cdot 0.5H_2O = CoC_{10}H_{25}N_4O_2SCl_2 \cdot 0.5H_2O$: C, 29.71; H, 6.48; N, 13.86%. Found for B-2: C, 28.00; H, 6.62; N, 13.31%. Calcd for $[Co(L\text{-}smp)(dien)]Cl_2 \cdot 1.5H_2O$: C, 28.44; H, 6.68; N, 13.27%. Found for B-3: C, 26.92; H, 6.82; N, 12.95%. Calcd for $[Co(L\text{-}smp)(dien)]Cl_2 \cdot 2.5H_2O$: C, 27.28; H, 6.87; N, 12.73%.

3) (Triammine)(L-penicillaminato)cobalt(III) Ion. *[Co(L-pen)(NH$_3$)$_3$]$^+$*: A hot solution (*ca.* 40 °C) containing 4.5 g of $[Co(NH_3)_6]Cl_3$[9] in 50 cm^3 was adjusted to pH *ca.* 2.5 by the addition of 15% hydrochloric acid. To this solution were added 2 g of L-penicillamine and a small amount of activated charcoal. The mixture was mechanically stirred at 40 °C for 15 min. The resultant mixture was filtered in order to remove the activated charcoal, after cooling to room temperature. The filtrate was poured onto a column of SP-Sephadex C-25 (Na^+ form, 5×40 cm). After the column was swept with water, the adsorbed brown band was eluted with a 0.075 mol dm^{-3} aqueous solution of sodium perchlorate. Two colored bands, a large amount of the brown band and a small amount of the yellow one, were eluted in this order. Of the two eluates, the yellow eluate was found to contain a by-product without the coordinated sulfur atom, because the absorption spectrum of this eluate did not show the charge transfer band in the region of (30—35)×10^3 cm^{-1}. The absorption spectrum of the brown eluate was similar to that of *trans(N$_1$N)*-[Co(L-pen)(dien)]$^+$[8] in the whole region and showed the charge transfer band at 34.7×10^3 cm^{-1}. As described in 4), furthermore, the brown eluate gave $[Co(L\text{-}smp)(NH_3)_3]^{2+}$ after treatment with dimethyl sulfate. These facts suggest that the brown eluate contained only $[Co(L\text{-}pen)(NH_3)_3]^+$. However, the complex was so unstable that it could not be isolated in solid state. The absorption and CD spectra of $[Co(L\text{-}pen)(NH_3)_3]^+$ were measured with a solution passed through a cation exchange column; they are illustrated with an arbitrary scale in Fig. 5.

4) (Triammine)(S-methyl-L-penicillaminato)cobalt(III) Perchlorate. *[Co(L-smp)(NH$_3$)$_3$](ClO$_4$)$_2$*: This complex was prepared by the same procedure as in 2), using the brown eluate obtained in 3) instead of $[Co(L\text{-}pen)(dien)]^+$. The complex treated with dimethyl sulfate was chromatographed on the column (SP-Sephadex C-25, Na^+ form) as in 2). Only one reddish orange band was eluted. It was found, from the comparison of the absorption spectrum of the brown eluate to those of $[Co(L\text{-}smp)(dien)]^{2+}$ isomers in 2), that the eluate contained only $[Co(L\text{-}smp)(NH_3)_3]^{2+}$. The eluate was concentrated to a small volume with a rotary evaporator at about 20 °C. The deposited sodium perchlorate was filtered off and to the filtrate was added a small amount of ethanol. The complex which precipitated was collected and recrystallized from as little water as possible by the addition of acetone. The pure complex was washed with ethanol and ether, and then dried in a vacuum desiccator over $CaCl_2$. Found: C, 15.08; H, 4.50; N, 11.66%. Calcd for $[Co(L\text{-}smp)(NH_3)_3](ClO_4)_2 \cdot 0.25H_2O = CoC_6H_{21}N_4O_{10}SCl_2 \cdot 0.25H_2O$: C, 15.15; H, 4.56; N, 11.78%.

Measurements. The electronic absorption spectra were recorded with a JASCO UVIDEC-1 spectrophotometer, and the CD spectra with JASCO J-20 and J-500 spectropolarimeters. All measurements were carried out in aqueous solution at room temperature.

The ^{1}H NMR spectra were recorded in deuterium oxide on a JEOL JNM-FX-100 NMR spectrometer at the probe temperature. Sodium 2,2-dimethyl-2-silapentane-5-sulfonate (DSS) was used as an internal reference.

Results and Discussion

Structural Assignment. For $[Co(L\text{-}pen)(dien)]^+$ and for $[Co(L\text{-}smp)(dien)]^{2+}$, three geometrical isomers are possible. These isomers are designated as *trans(N$_1$N)*, *trans(N$_1$O)*, and *trans(N$_1$S)* with respect to the coordinated atoms as shown in Fig. 1, where N_1 denotes the imino nitrogen atom of the coordinated dien. The three isomers, B-1, B-2, and B-3, of $[Co(L\text{-}smp)(dien)]^{2+}$ were derived from the A-1, A-2, and A-3 isomers of $[Co(L\text{-}pen)(dien)]^+$ by the reaction with dimethyl sulfate. Of the three L-pen isomers, the A-1 isomer was preliminarily determined to have a *trans(N$_1$N)* configuration by the X-ray crystal structure analysis[8] which is a basis of the present work. As shown in Figs. 2—4 and Table 1, the absorption spectra of the three L-smp isomers resemble one another

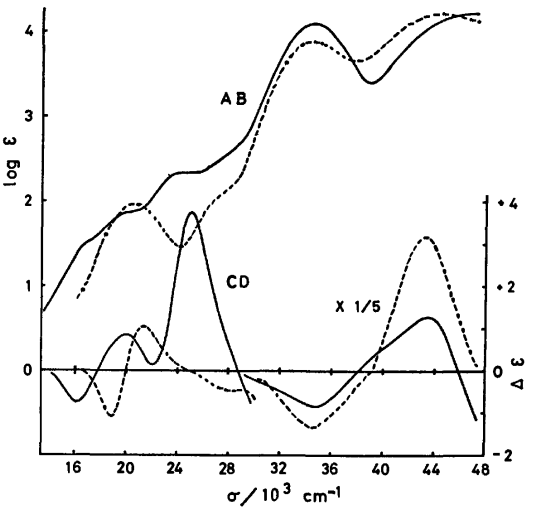

Fig. 2. Absorption and CD spectra of *trans(N$_1$N)*-$[Co(L\text{-}pen)(dien)]^+$ (——) and *trans(N$_1$N)*-$[Co(L\text{-}smp)(dien)]^{2+}$ (----).

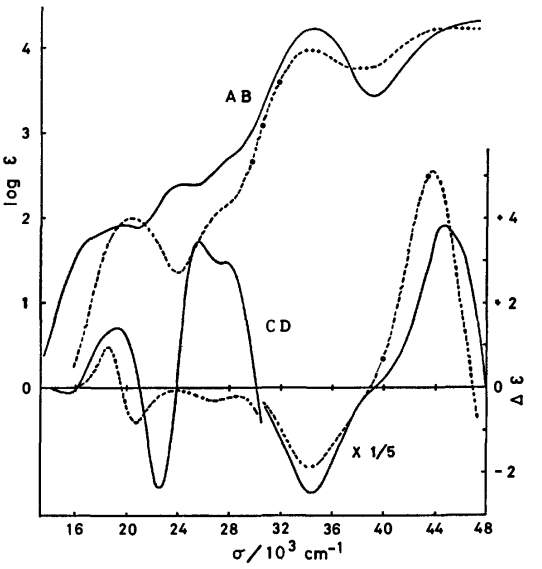

Fig. 3. Absorption and CD spectra of *trans(N$_1$O)*-$[Co(L\text{-}pen)(dien)]^+$ (——) and *trans(N$_1$O)*-$[Co(L\text{-}smp)(dien)]^{2+}$ (----).

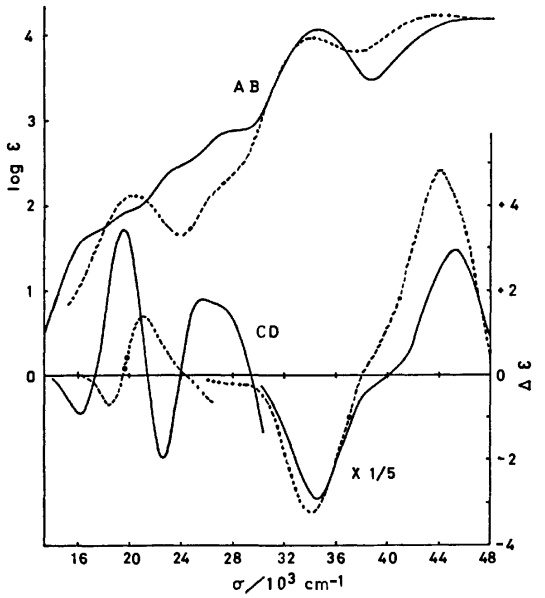

Fig. 4. Absorption and CD spectra of *trans*(N_1S)-[Co(L-pen)(dien)]$^{+}$ (——) and *trans*(N_1S)-[Co(L-smp)-(dien)]$^{2+}$ (----).

in the whole region, because these isomers belong to a *cis(SO)*-[Co(S)(O)$(N)_4$] type having a thioether group. The absorption spectra of the three L-pen isomers, which have a thiolato instead of a thioether group, differ remarkably from those of the L-smp isomers in the region of $(14—30)\times10^3$ cm^{-1}. A difference in absorption spectral behavior is also observed between the triammine complexes, [Co(L-pen)$(NH_3)_3$]$^{+}$ and [Co(L-smp)$(NH_3)_3$]$^{2+}$, as shown in Fig. 5 and Table 1.

Trans(N_1N*)*-[Co(L-pen)(dien)]$^{+}$ (A-1 isomer) did not isomerize in aqueous solution and gave only one isomer (B-1) of [Co(L-smp)(dien)]$^{2+}$ by the reaction with dimethyl sulfate. In a previous paper,[6] the reaction of the coordinated thiolato donor atoms of *trans(N)*- or *trans(O)*-[Co(D-pen)$_2$]$^{-}$ with dimethyl sulfate was accompanied by the geometrical isomerization and the three isomers of [Co(D-smp)$_2$]$^{+}$, *trans(N)*, *trans(O)*, and *trans(S)*, were obtained. Similar isomerization in aqueous solution was also observed for the cobalt(III) complexes with the tripod-like terdentate ligands such as *S*-methyl-L-cysteinate, L-histidinate, and L- or D-aspartate.[6,10-12] When these facts are taken into account, the present result suggests that the reaction of the A-1 isomer with dimethyl sulfate proceeded with retention of the *trans(*N_1N*)* configuration, namely, the B-1 isomer of [Co(L-smp)-(dien)]$^{2+}$ held the *trans(*N_1N*)* configuration because of the rigidity of the coordinated dien.[13] Each of the remaining two L-pen isomers (B-2 and B-3) also gave only one isomer of the L-smp complex by the reaction with dimethyl sulfate, respectively. Namely, the B-2 isomer of [Co(L-smp)(dien)]$^{2+}$ was derived from the A-2 isomer of [Co(L-pen)(dien)]$^{+}$ and the B-3 L-smp isomer from the A-3 L-pen one. The consideration used for the *trans(*N_1N*)* isomers suggests that the B-2 and B-3 isomers retain the geometrical configurations of the A-2 and A-3 ones.

Table 1. Absorption and CD spectral data of [Co(L-pen or L-smp)(dien)]$^{+ \text{ or } 2+}$ and [Co(L-pen or L-smp)$(NH_3)_3$]$^{+ \text{ or } 2+}$

Complex	Absorption $\sigma/10^3$ cm^{-1} (ε/mol^{-1} dm^3 cm^{-1})	CD $\sigma/10^3$ cm^{-1} ($\Delta\varepsilon$/mol^{-1} dm^3 cm^{-1})
trans(N_1N)-[Co(L-pen)(dien)]$^{+}$	16.69(1.5 sh[a])	16.23(−0.75)
	20.20(1.9 sh)	20.00(+0.85)
	24.27(2.35)	25.00(+3.75)
	28.01(2.6 sh)	34.84(−4.14)
	34.48(4.10)	43.29(+6.40)
trans(N_1O)-[Co(L-pen)(dien)]$^{+}$	17.30(1.8 sh)	15.48(−0.14)
	19.80(1.93)	19.31(+1.43)
	24.39(2.41)	22.60(−2.35)
	28.01(2.7 sh)	25.55(+3.47)
	34.48(4.23)	27.78(+2.98)
		34.48(−12.3)
		44.64(+19.2)
trans(N_1S)-[Co(L-pen)(dien)]$^{+}$	16.89(1.7 sh)	16.13(−0.87)
	19.42(1.9 sh)	19.53(+3.45)
	23.47(2.45 sh)	22.52(−1.90)
	28.01(2.7 sh)	25.64(+1.82)
	34.72(4.07)	34.60(−14.5)
		45.25(+14.8)
trans(N_1N)-[Co(L-smp)(dien)]$^{2+}$	20.62(1.97)	18·87(−1.08)
	27.10(2.06 sh)	21.37(+1.06)
	34.30(3.88)	28.17(−0.45)
	44.44(4.20)	34.42(−6.65)
		43.48(+15.9)
trans(N_1O)-[Co(L-smp)(dien)]$^{2+}$	20.37(2.01)	18.52(+0.98)
	27.78(2.1 sh)	20.76(−0.79)
	34.25(3.96)	26.88(−0.27)
	44.84(4.20)	34.25(−9.28)
		43.68(+25.6)
trans(N_1S)-[Co(L-smp)(dien)]$^{2+}$	20.37(2.12)	18.52(−0.71)
	26.25(2.1 sh)	21.05(+1.42)
	34.25(3.96)	33.78(−16.0)
	44.25(4.23)	44.05(+24.1)
[Co(L-pen)$(NH_3)_3$]$^{+}$	16.9 (sh)	15.64(−)
	20.0 (sh)	18.01(+)
	24.6 (sh)	21.82(−)
	27.8 (sh)	24.78(+)
	34.68	34.85(−)
		45.24(+)
[Co(L-smp)$(NH_3)_3$]$^{2+}$	20.06(2.02)	18.35(−0.28)
	27.78(2.2 sh)	20.79(+0.96)
	34.48(3.82)	27.78(−0.53 sh)
	45.87(4.14)	34.25(−10.8)
		45.25(+12.4)

a) sh denotes a shoulder.

In the first absorption band region, the B-1, B-2, and B-3 isomers of the L-smp complex commonly show a sharp band at around 20×10^3 cm^{-1} (Figs. 2—4 and Table 1), as in the isomers of [Co(ida)(dien)]$^{+}$ (ida; iminodiacetate),[14] [Co(L-alama)(dien)]$^{+}$ (L-alama; *N*-

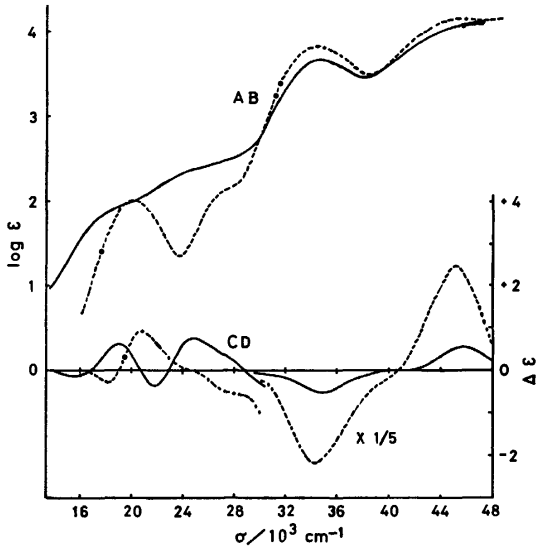

Fig. 5. Absorption and CD spectra of [Co(L-pen)-$(NH_3)_3]^+$ (——) and $[Co(L\text{-smp})(NH_3)_3]^{2+}$ (----). The L-pen complex is illustrated with arbitrary scale.

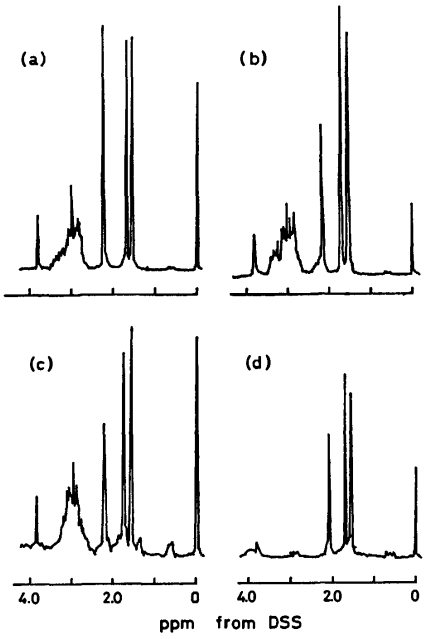

Fig. 6. ^1H NMR spectra of the L-smp complexes; (a) *trans*(N_1N), (b) *trans*(N_1O), and (c) *trans*(N_1S) for $[Co(L\text{-smp})(dien)]^{2+}$, and (d) $[Co(L\text{-smp})(NH_3)_3]^{2+}$.

(carboxylatomethyl)-L-alaninato),[14] and [Co(L- or D-asp)(dien)]$^+$ (asp; aspartate),[15] indicating the proximity of the thioether and COO^- groups in the spectrochemical series.[3-6] The CD spectra of the L-smp isomers in the corresponding region give useful information for the assignments of their geometrical configurations. As shown in Fig. 1, (b) and (c) are quasi-antipodal in overall form, while (a) is symmetrical in comparison with (b) and (c), as in the case of the three isomers of [Co(D-asp)(dien)]$^+$.[15] Indeed, the CD spectrum of the B-1 isomer assigned to *trans*-(N_1N) configuration shows a quite similar CD pattern to that of $[Co(L\text{-smp})(NH_3)_3]^{2+}$, which has no chirality arising from the skew pair of the chelate rings (Figs. 2 and 5, and Table 1). On the other hand, the B-2 and B-3 isomers exhibit an almost enantiomeric CD spectral pattern in the first absorption band region, reflecting a quasi-antipodal relationship between the two isomers. The relationship of the B-2 and B-3 isomers is comparable with that of the u^1-*cis* and u^2-*cis* isomers of [Co(L-asp)(dien)]$^+$,[16] namely, the CD spectra of the B-2 and B-3 isomers correspond to those of the u^2-*cis* and u^1-*cis* isomers of [Co(L-asp)(dien)]$^+$,[15] respectively, in the first absorption band region. From this viewpoint, the B-2 and B-3 isomers are tentatively assigned to *trans*(N_1O) and *trans*(N_1S), respectively. The same conclusion is also obtained by comparing the CD spectra of the B-2 and B-3 isomers with those of the *Δ*- and *Δ-unsym-cis*(*O*) isomers of [Co(ida)-(dien)]$^+$ and [Co(L-alama)(dien)]$^+$.[14] Namely, in the first absorption band region, the B-2 isomer shows the CD pattern corresponding to the *Δ-unsym-cis*(*O*) isomer and prefers *trans*(N_1O), while the B-3 isomer shows the pattern appropriate to the *Δ-unsym-cis*(*O*) isomer and prefers *trans*(N_1S). The CD spectral behavior of the L-smp isomers in the first absorption band region and the results that the reaction of the L-pen isomers with dimethyl sulfate proceeded with retention of their geometrical configurations allow us to assign the A-2 and B-2 isomers as *trans*(N_1O), and the A-3 and B-3 isomers as *trans*(N_1S).

The thioether type sulfur atom takes the *R*(*S*) or *S*(*S*) configuration when coordinated with a cobalt(III) ion. As shown in Fig. 6, each isomer of [Co(L-smp)-(dien)]$^{2+}$, and $[Co(L\text{-smp})(NH_3)_3]^{2+}$ exhibit a single peak in the *S*-methyl protons region (2.23 ppm for *trans*(N_1N), 2.22 ppm for *trans*(N_1O) and 2.18 ppm for *trans*(N_1S) of the dien complex, and 2.07 ppm for the triammine complex). In general, for the cobalt-(III) complexes with the thioether type ligands having *S*-methyl group, the *S*-methyl protons signals of the *R*(*S*) and *S*(*S*) configurations can be distinguished.[5,6,17,18] The present results suggest that the sulfur atoms of the four complexes take either *R*(*S*) or *S*(*S*). If the sulfur center in the *trans*(N_1N) and *trans*(N_1O) isomers takes *R* configuration, a repulsion exists between an *S*-methyl group and an ethylenediamine moiety of the dien. There is no such repulsion in the *S*-form coordination. Accordingly, it is probable that the sulfur atoms of the *trans*(N_1N) and *trans*-(N_1O) isomers take *S* configuration. Similarly, model inspection of the interligand interaction between the *S*-methyl group and amino group for the *trans*(N_1S) isomer or ammine group for the triammine complex suggests that the coordinated sulfur atoms have *S* configuration.

Absorption and CD Spectra. In the energy region higher than the charge transfer band at about 34×10^3 cm^{-1}, the absorption and CD spectra of the isomers of [Co(L-pen)(dien)]$^+$ are quite similar to those of the L-smp isomers (Figs. 2—4 and Table 1). The triammine complexes, $[Co(L\text{-pen})(NH_3)_3]^+$ and $[Co(L\text{-smp})(NH_3)_3]^{2+}$, also exhibit similar absorption and CD spectral behavior to the dien complexes (Fig. 5 and Table 1). The CD pattern of the triammine complexes are due to the coordination of L-pen and

L-smp, respectively. In this region, the CD pattern of the present complexes seems to depend mainly on the absolute configuration of L-thiolato and L-thioether type ligands. In the higher energy region, the similarity of CD pattern in the present L-pen and L-smp isomers should be noted and compared with the difference in CD pattern between the corresponding isomers of $[Co(D\text{-pen})_2]^-$ and $[Co(D\text{-smp})_2]^+$.[6] In the lower energy region [$(14—30)\times10^3$ cm^{-1}], in contrast to the higher energy region, the absorption and CD spectra of the L-pen isomers deviate from those of the L-smp ones. First, the first absorption bands of the L-pen isomers shift to lower energy than those of the L-smp ones and are broader because of a thiol coordination.[6,7,19] The CD spectra of the [Co(L-pen)(dien)]$^+$ isomers consist of three components in the first absorption band region, as seen in Figs. 2—4. This CD pattern corresponds well with that of $[Co(L\text{-pen})(NH_3)_3]^+$ and it seems that the coordinated dien contributes little to the CD pattern in the first absorption band region. Secondly, the absorption and CD spectral differences between the L-pen and L-smp isomers are remarkable in the region of $(24—30)\times10^3$ cm^{-1}. The L-smp isomers exhibit the second absorption band as a shoulder, while the L-pen isomers exhibit two more intense absorption bands in the corresponding region (Figs. 2—4 and Table 1). The CD spectra of the *trans(N$_1$O)* and *trans(N$_1$S)* isomers of [Co(L-pen)(dien)]$^+$ consist of two positive bands, which correspond well with the two absorption components in this region. *Trans(N$_1$N)* isomer of [Co(L-pen)(dien)]$^+$ and $[Co(L\text{-pen})(NH_3)_3]^+$ which are more symmetrical in configuration than the *trans(N$_1$O)* and *trans(N$_1$S)* isomers show a positive CD band with a vague shoulder in the higher energy side (Figs. 2 and 5). Similar absorption and CD spectral behavior can also be observed for the other penicillaminato mixed complexes of [Co(L-pen)(terdentate)] type, where terdentate denotes L-histidinate, L-2,4-diaminobutylate and L-ornithinate.[20] The sign of the two CD bands depends on the absolute configuration of the optically active penicillaminate coordinated, namely, a positive sign for the L-pen and negative one for the D-pen,[20] as in the case of *trans(N)*- and *trans(O)*-$[Co(D\text{-pen})_2]^-$.[6] The L-pen mixed complexes commonly show two positive CD bands, while the $[Co(D\text{-pen})_2]^-$ isomers seem to show a negative CD band in the corresponding region.[6] This difference in CD pattern may be due to the lowering of symmetry of the thiolato type complexes.

References

1) J. Hidaka, S. Yamada, and Y. Shimura, *Chem. Lett.*, **1974**, 1487.
2) P. de Meester and D. J. Hodgson, *J. Chem. Soc., Dalton Trans.*, **1976**, 618.
3) K. Yamanari, J. Hidaka, and Y. Shimura, *Bull. Chem. Soc. Jpn.*, **50**, 2299 (1977).
4) K. Yamanari, J. Hidaka, and Y. Shimura, *Bull. Chem. Soc. Jpn.*, **50**, 2451, 2643 (1977).
5) T. Isago, K. Igi, and J. Hidaka, *Bull. Chem. Soc. Jpn.*, **52**, 407 (1979).
6) K. Okamoto, K. Wakayama, H. Einaga, S. Yamada, and J. Hidaka, *Bull. Chem. Soc. Jpn.*, **56**, 165 (1983).
7) K. Yamanari, N. Takeshita, T. Komorita, and Y. Shimura, *Chem. Lett.*, **1981**, 861.
8) K. Okamoto, K. Wakayama, H. Einaga, M. Ohmasa, and J. Hidaka, *Bull. Chem. Soc. Jpn.*, **55**, 3473 (1982).
9) J. Bjerrum and J. P. McReynolds, *Inorg. Synth.*, **2**, 216 (1946).
10) M. Watabe, S. Kawaai, and S. Yoshikawa, *Bull. Chem. Soc. Jpn.*, **49**, 1845 (1976).
11) M. Watabe, M. Zamma, and S. Yoshikawa, *Bull. Chem. Soc. Jpn.*, **51**, 1354 (1978).
12) M. Watabe, H. Yano, and S. Yoshikawa, *Bull. Chem. Soc. Jpn.*, **52**, 61 (1979).
13) F. R. Keene and G. M. Searle, *Inorg. Chem.*, **11**, 148 (1972).
14) K. Okamoto, J. Hidaka, and Y. Shimura, *Bull. Chem. Soc. Jpn.*, **48**, 2456 (1975).
15) J. I. Legg and D. W. Cooke, *J. Am. Chem. Soc.*, **89**, 6854 (1967).
16) The *u^1-cis* (IV-A) and *u^2-cis* (III-B) isomers in Ref. 15 correspond to (c) and (b) in Fig. 1, respectively, of the present paper.
17) W. G. Jackson and A. M. Sargeson, *Inorg. Chem.*, **17**, 2165 (1978).
18) K. Okamoto, T. Isago, M. Ohmasa, and J. Hidaka, *Bull. Chem. Soc. Jpn.*, **55**, 1077 (1982).
19) V. H. Houlding, H. Mäcke, and A. W. Adamson, *Inorg. Chem.*, **20**, 4279 (1981).
20) K. Wakayama, K. Okamoto, and J. Hidaka, unpublished data.

Spectrophotometric Determination of Iron(II) after Separation by Collection of Its Ternary Complex of 1,10-Phenanthroline and Tetraphenylborate on Microcrystalline Naphthalene

Lih-Fen CHANG, Masatada SATAKE,* B. K. PURI,† and Saswati P. BAG††

Faculty of Engineering, Fukui University, Fukui 910

†*Department of Chemistry, Indian Institute of Technology, Hauz Khas, New Delhi-110016, India*

††*Chemistry Department, Jadavpur University, Calcutta-700 032, India*

(Received January 20, 1983)

A new procedure for the spectrophotometric determination of iron(II) after collection of its ternary complex with 1,10-phenanthroline and tetraphenylborate on microcrystalline naphthalene is described. In the presence of tetraphenylborate, the tris(1,10-phenanthroline)iron(II) ion is quantitatively collected on microcrystalline naphthalene as the ion-association complex. The system conforms to Beer's law over the range 3—50 μg of iron in 10 ml of the solvent. The molar absorptivity was 1.2×10^4 l mol^{-1} cm^{-1} at 514 nm. The effect of various factors, such as wavelength, pH, amounts of reagent and naphthalene, shaking time, and diverse ions, were also studied. The procedure method was satisfactorily applied to the determination of iron in standard aluminium alloy, aluminium, and magnesium metals.

1,10-Phenanthroline is a sensitive and selective reagent for iron(II) and it has been widely employed for the spectrophotometric determination of iron and the method has been applied to the determination of iron[1] in alloys, metals and water samples.

The water-soluble complex ferroin, $[Fe(phen)_3]^{2+}$ produced with this is insoluble in organic solvents, but some of its ion-association complexes with colorless inorganic anions, such as ClO_4^-, I^-, SCN^-, CN^-, BF_4^-, $PtCl_6^-$, $AuCl_4^-$, $AuBr_4^-$, and with some organic anions such as pentachlorophenolate, trichloroacetate, and 1,2-bis(octyloxycarbonyl)ethanesulfonate, are extractable by suitable organic solvents and may be used for the extractive colorimetric determination of metals[2-4] or of the associated anions.[5-7]

Since 1969, we have developed a new method[8-12] for the spectrophotometric determination of trace metals using naphthalene as an extractant or collector, as well as by solvent extraction in chloroform or benzene. In the present communication, the technique described above was used for the collection of iron ion which forms ion-association complex with complexing reagent at room temperature.

We have observed that the cationic complex $[Fe(phen)_3]^{2+}$ reacts with sodium tetraphenylborate to form a very stable water-insoluble colored ternary complex. This ternary complex is difficult to be dissolved in organic solvents except with nitrobenzene because of low solubility of the complex in solvent. However, this complex can be easily collected on microcrystalline naphthalene even by vigorous shaking for a few seconds and is freely soluble in acetonitrile and *N,N*-dimethylformamide, which are miscible with water. This simple and inexpensive procedure can be successfully applied for analysis of iron in metal alloys.

Experimental

Reagents. Standard iron(III) solution, 1000 ppm. Prepared by dissolving 0.8635 g of ammonium iron(III) sulfate dodecahydrate in 100 ml of 0.5 M (1 M = 1 mol dm^{-3}) H_2SO_4 and by diluting to 500 ml with water.

1,10-Phenanthroline(phen) solution, 0.2%. Prepared by dissolving 0.2 g of the reagent in a small volume of concentrated hydrochloric acid and diluting to 100 ml with water.

Hydroxylammonium chloride solution, 2% in water.

Sodium tetraphenylborate solution, 1% water.

Naphthalene solution, 20% in acetone.

Buffer solutions were prepared by mixing 1 M acetic acid and 1 M ammonium acetate solution for pH 3—6, and 1 M aqueous ammonia and 1 M ammonium acetate solution for pH 8—11.

Naphthalene, acetone, *N,N*-dimethylformamide, and all other reagents were of analytical-reagent grade, and were used without further purification.

Apparatus. The absorbance measurements were made with a Bausch and Lomb spectronic-70 spectrophotometer, using 1 cm cells.

All the pH measurements were done with a Beckman Model H-2 pH meter.

Procedure. Transfer a sample solution containing 3—50 μg of iron(III) to a tightly stoppered Erlenmeyer flask (100 ml), add 1.0 ml of 2% hydroxylammonium chloride solution and 5.0 ml of 0.2% 1,10-phenanthroline solution and adjust pH to 4.5 with 2.0 ml of acetate buffer. Mix the solution, add 1.0 ml of 1% sodium tetraphenylborate solution and let stand for 10 min. Add 2.0 ml of 20% naphthalene solution in acetone to this sample solution using a small nozzled pipe attached to a rubber bulb, and shake the mixture vigolously for 30 s. Collect the colored naphthalene mixture on a filter paper placed flat on a Teflon filter plate in a funnel or a sintered glass filter (No. 2) by filtration. Wash it with water and dry at 50—60 °C. Then dissolve the mixture in *N,N*-dimethylformamide and dilute to exactly 10 ml. Measure the absorbance of the solution in a 1-cm glass cell against the reagent blank.

Results and Discussion

Absorption Spectra. Sample solution containing 30 μg of iron(II), 5.0 ml of 0.2% 1,10-phenanthroline solution and 1.0 ml of 1% sodium tetraphenylborate solution was prepared by the procedure. The absorption spectrum of the iron(II)–phen–TPB complex in naphthalene–*N,N*-dimethylformamide solution is shown in Fig. 1, together with that of the reagent blank. The ternary complex has its absorbance maximum at 514 nm. The reagent blank does not absorb at wavelengths longer than 430 nm. Therefore, 514 nm was

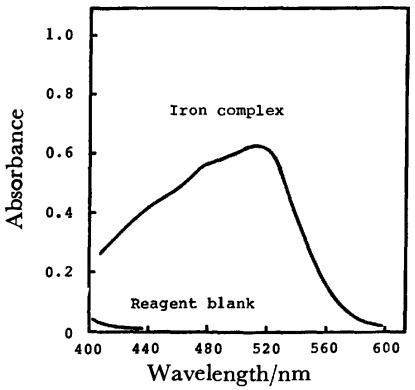

Fig. 1. Absorption spectra of 1,10-phenanthroline and ternary complex with sodium tetraphenylborate in naphthalene-*N*,*N*-dimethylformamide solution.
Iron(II): 30 μg; pH: 4.5; 0.2% 1,10-phenanthroline: 5.0 ml; 1% sodium tetraphenylborate: 1.0 ml; reference: water.

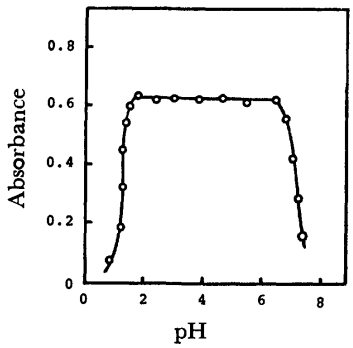

Fig. 2. Effect of pH.
Iron(II): 30 μg; wavelength: 514 nm; 0.2% 1,10-phenanthroline: 5.0 ml; 1% sodium tetraphenylborate: 1.0 ml; naphthalene: 1.5 g; shaking time: 30 s; standing time: 30 min, reference: reagent blank.

chosen as an optimum wavelength.

Effect of pH. The effect of pH on the absorbance of the ternary complex was investigated with a sample containing 30 μg of iron. The pH of the solution after collection was measured at room temperature. The pH for the collection of the ternary complex on microcrystalline naphthalene was varied between 0.5 and 7.7. The optimum pH for quantitative collection was 1.7—6.4, as shown in Fig. 2. Hence pH 4.5 was chosen for convenience.

Effect of Hydroxylammonium Chloride Concentration. Varying amounts of hydroxylammonium chloride as a reducing agent were added to the sample containing 30 μg of iron(III). Iron(III) was completely reduced to iron(II) with 0.2 ml of 2% solution to 5.0 ml of 10% hydroxylammonium chloride solution. In this study, 1.0 ml of 2% solution was used.

Effect of 1,10-Phenanthroline and Sodium Tetraphenylborate Concentration. The effect of 1,10-phenanthroline concentration on the absorbance was examined with a solution containing 30 μg of iron. With other variables held constant, 0.3 ml of 0.2% 1,10-phenanthroline solution was found to be sufficient for full color development for 30 μg of iron. The absorbance remained constant even with 8.0 ml of the reagent (Fig. 3).

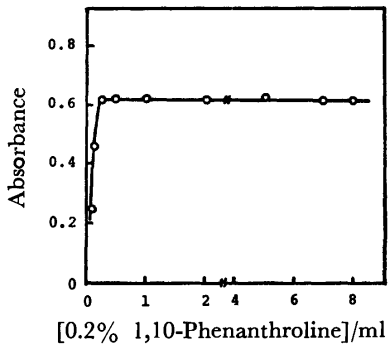

Fig. 3. Effect of 1,10-phenanthroline concentration.
Iron(II): 30 μg; wavelength: 514 nm; pH: 4.5; rest of the conditions were the same as above. Reference: reagent blank.

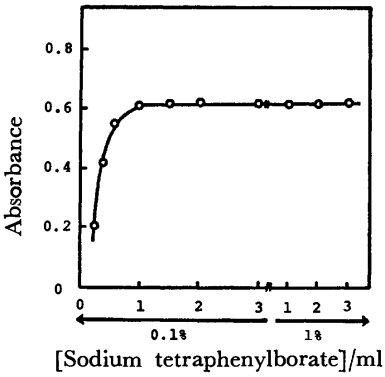

Fig. 4. Effect of sodium tetraphenylborate concentration.
Iron(II): 30 μg; wavelength: 514 nm; rest of the conditions were the same as above. reference: reagent blank.

Similar studies with a sodium tetraphenylborate showed that the absorbance remained unchanged over the range of 1.0 ml of 0.1% TPB solution to 3.0 ml of 1% TPB solution (Fig. 4). In this work, 5.0 ml of 0.2% 1,10-phenanthroline solution and 1.0 ml of 1% sodium tetraphenylborate solution were used.

Effect of Addition of Buffer Solution and Digestion Time. Addition of 0.5—5.0 ml of the acetate buffer did not cause practically variation in the absorbance. Thus 1.5 ml of the buffer was added for collection. A solution containing the iron(II)-phen-TPB complex was digested at room temperature (20—25 °C). The rate of formation of this ion-association complex is very fast at room temperature. The complex was found to be stable even at a temperature of 81 °C. It was scarcely dissociated in aqueous solution.

Effect of Naphthalene Concentration and Shaking Time. The collection of the ternary complex in the solution was carried out with addition of 0.5—4.0 ml of 20% naphthalene solution in acetone by vigorous shaking for 30 s. The collection did not cause any change with increasing amount of naphthalene. Thus, 2.0 ml of 20% naphthalene solution was taken as the suitable amount. Two ml of 20% naphthalene solution was added to the solution containing the ternary complex, and the mixed solution was shaken vigorously for 90 s. The complex was completely collected on naphthalene by vigorous shaking for a few seconds. Shaking

for 30 s was found to be satisfactory for complete collection.

Effect of Volume of Aqueous Phase. The volume of aqueous phase was varied between 40 and 2400 ml, and the effect of volume of aqueous phase on the absorbance was examined. The absorbance was almost constant over the range of up to 2200 ml, but decreased gradually with increase in the volume of aqueous phase. For larger volumes of aqueous phase, the collection of the complex on naphthalene was carried out by using a larger volumes of the reagent solutions and shaking and digestion for longer time. In this series of tests, 10 ml of 0.2% 1,10-phenanthroline solution and 2.5 ml of 1% sodium tetraphenylborate solution were taken; the mixed solution was shaken for 2 min and digested for 20 min, 3.0 ml of 20% naphthalene solution being used.

Effect of Standing Time. The collected naphthalene mixture was dissolved in *N,N*-dimethylformamide. The color of the complex thus obtained is very stable, and the absorbance remained constant for a long time.

Calibration Curve. Based on the optimum conditions described above, a calibration curve was constructed according to the procedure. Beer's law was obeyed for 3—50 μg of iron(II) in 10 ml of *N,N*-dimethylformamide, at 514 nm. The molar absorptivity at 514 nm was found to be 1.2×10^4 l mol^{-1} cm^{-1}. The sensitivity was 0.0047 μg/cm^2 in *N,N*-dimethylformamide and 0.0050 μg/cm^2 in aqueous medium for 0.001 absorbance. Ten parallel determinations of 30 μg of iron gave a standard deviation of 0.00421 μg with relative standard deviation of 0.66%.

Choice of Solvent. Tests were made with various organic solvents to dissolve the collected naphthalene mixture. This mixture is easily soluble in *N,N*-dimethylformamide and acetonitrile, but insoluble in dioxane, chloroform, benzene, toluene, xylene, *o*-dichlorobenzene, isopentyl acetate, isobutyl methyl ketone (MIBK), carbon tetrachloride, methanol, ethanol, chlorobenzene, *etc*, at room temperature.

Effect of Diverse Ions. The effect of diverse ions on the iron determination was studied by adding various amounts of diverse ions in question to a solution containing 30 μg of iron and applying the procedure. The tolerance limits (error<5%) for the diverse ions are listed in Table 1. Most of the alkali salts did not interfere, but only 2 and 7 mg of KCN and sodium oxalate respectively could be tolerated. Larger amounts of inorganic anions such as thiocyanate and perchlorate, which form the ion-association complex, did not interfere in the determination. Bi^{3+} (100 μg) and Sn^{2+}(300 μg) also would be tolerated. If the iron content in practical samples is lower and diverse metal ions interfere with iron determination, extraction by organic solvents(MIBK or diethyl ether) is very efficient for the iron determination.

Analysis of Iron in Reference Material and Metal Samples. The proposed method was applied to the determination of iron in the reference material(aluminium alloy), metallic aluminium and magnesium samples, and the results (Table 2) are in reasonably good agreement with those obtained by the standard spectrophotometric procedure employing 2,4,6-tripyridyl-*s*-triazine (TPTZ) method[13-14]. The analytical procedures were as follows: 1.0 g of standard aluminium alloy (NBS, SRM-85b) was accurately taken in a 100-ml beaker to which were added 40—50 ml of hydrochloric acid (1+1) and 3 ml of 30% hydrogen peroxide. This was heated over the boiling water for about 10 min, the mixture dissolved completely and the excess of hydrogen peroxide decomposed. After cooling the volume of sam-

TABLE 1. TOLERANCE LIMITS FOR DIVERSE METAL SALTS AND METAL IONS

Diverse metal salt	Tolerance limit[a)]	Diverse ion	Tolerance limit[a)]
KSCN	9 g	Al^{3+}	20 mg
NaI	10 g	Bi^{3+}	100 μg
$CH_3COONa\cdot3H_2O$	2 g	Cr^{6+}	11 mg
KNO_3	7 g	Ca^{2+}	500 mg
Na_2SO_4	6 g	Cd^{2+}	1500 μg
KH_2PO_4	0.5 g	Co^{2+}	400 μg
$KClO_4$	0.5 g	Cu^{2+}	500 μg
NaCl	0.1 g	Hg^{2+}	2000 μg
Na_2tartrate	1.5 g	Mn^{2+}	70 mg
Na_3citrate	20 mg	Mg^{2+}	200 mg
Na_2oxalate	7 mg	Ni^{2+}	700 μg
KCN	2 mg	Pb^{2+}	3000 μg
		Sn^{2+}	300 μg
		Zn^{2+}	4000 μg

Iron(II): 30 μg; pH: 4.5; 0.2% 1,10-phenanthroline: 5.0 ml. a) Error <5%.

TABLE 2. ANALYSIS OF SAMPLES FOR ION

Sample	Composition of alloy/%	Iron, certified value/%	Iron content[a)]/%	
			Present method	TPTZ method
N. B. S. SRM-85b Al alloy	Cu:3.99, Cr:0.21 Mn:0.61, Ni:0.089 Si:0.18, Ti:0.022 Zn:0.03, Ga:0.019 V:0.006, Pb:0.021	0.24	0.239±0.002	0.238±0.001
Aluminium metal (powder)	—	—	0.136±0.001	0.138±0.001
Magnesium metal (powder)	—	—	0.0024±0.0002	0.0025±0.0001

a) Average of 5 individual samples.

ple was completed to 200 ml with water. An aliquot of this sample was taken in a separatory funnel, followed by 40 ml of hydrochloric acid (1+1). Iron(III) in this sample was extracted by vigorous shaking for 5 min with 20 ml of MIBK.[15] It was then back-extracted from the organic phase with 25 ml of water and the proposed method and TPTZ procedure were applied.

Metallic aluminium powder was analyzed in the same way as for the case of the standard aluminium alloy.

Metallic magnesium powder was analyzed in the same way as described above.

In the present work, the collection of the ternary complex on naphthalene is easily achieved merely by contact with microcrystalline naphthalene or by vigorous shaking for a few seconds. A very small amount (0.5 g) of the organic phase (naphthalene) is required for the complete collection which enhances the sensitivity as the whole of the organic phase may be taken for the analysis. Generally diverse metal ions and alkali metal salts (Table 1) even at higher concentrations level have very little influence on the analytical determination compared with the 1,10-phenanthroline procedure in aqueous medium[1] or organic solvent extraction.[16] Furthermore no remarkable difference was observed in the molar absorptivity, sensitivity and precision of the ternary complex for the above described procedures.

In conclusion, this inexpensive and relatively simple procedure can be successfully employed for the determination of iron in standard aluminium alloy and metal samples.

References

1) W. B. Fortune and M. G. Mellon, *Ind. Eng. Chem., Anal. Ed.*, **10**, 60 (1938).
2) F. G. Nasouri, S. A. F. Shahine, and R. J. Magee, *Anal. Chim. Acta*, **36**, 346, (1966).
3) Y. Yamamoto, M. Tsubouchi, and K. Okimura, *Bunseki Kagaku*, **16**, 1176 (1967).
4) Y. Yamamoto, M. Tsubouchi, K. Okimura, and T. Takagi, *Nippon Kagaku Zasshi*, **88**, 745 (1967).
5) Y. Yamamoto, T. Kumamaru, Y. Hayashi, T. Kobayashi, and R. Tanaka, *Chem. Pharm. Bull. (Tokyo)*, **15**, 1437 (1967).
6) Y. Yamamoto, T. Kumamaru, and Y. Hayashi, *Talanta*, **14**, 661 (1967).
7) Y. Yamamoto, T. Kumamaru, and Y. Uemura, *Anal. Chim. Acta*, **39**, 51 (1967).
8) T. Fujinaga, M. Satake, and T. Yonekubo, *Bull. Chem. Soc. Jpn.*, **48**, 899 (1975).
9) M. Satake, *Anal. Chim. Acta*, **92**, 423 (1977).
10) M. Satake, Y. Matsumura, and M. C. Mehra, *Mikrochim. Acta*, 1980 **I**, 455.
11) M. Satake, Y. Matsumura, and M. C. Mehra. *Analusis (France)*, **9**, 389 (1981).
12) M. Satake and M. C. Mehra, *Microchem. J.*, **27**, 182 (1982).
13) P. F. Collins and H. Diehl, *Anal. Chem.*, **31**, 1862 (1959).
14) P. F. Collins and H. Diehl, *Anal. Chim. Acta*, **22**, 125 (1960).
15) JIS H 1353 (1972).
16) V. P. R. Rao, K. V. Rao, and P. V. R. B. Sarma, *Talanta*, **16**, 277 (1969).

Use of Normal Pulse Voltammetry in Diagnosing Electrode Kinetics of Octacyanomolybdate(IV/V) Complexes Bound Electrostatically to Graphite Electrodes Coated with Polyelectrolytes

Keiichi SATO, Shuichiro YAMAGUCHI, Hiroaki MATSUDA,
Takeo OHSAKA,† and Noboru OYAMA*,†

Department of Electronic Chemistry, Graduate School at Nagatsuta, Tokyo Institute of Technology Nagatsuta, Midori-ku, Yokohama 227

†*Department of Applied Chemistry for Resources, Tokyo University of Agriculture and Technology, Koganei, Tokyo 184*

(Received January 24, 1983)

An electron transfer process of $[Mo(CN)_8]^{4-/3-}$ redox couple at the graphite electrode/protonated poly(4-vinylpyridine) (PVP) interfaces was examined by the normal pulse voltammetry. It became apparent that electrode reaction of the electroactive species confined in the polymer film on electrode surface obeys the conventional Butler-Volmer equation which characterizes the ordinary electrode reaction at electrode/solution interface. From the analysis of the dependences of the current-potential curves upon the sampling time the relevant kinetic parameters (*i.e.*, the standard rate constant, k° and the transfer coefficient, α) of the electrode reaction were evaluated. The value of k° decreased from 9.7×10^{-4} to 1.7×10^{-4} cm s^{-1} and the value of α was almost constant (0.50), when the molar ratio of the incorporated $[Mo(CN)_8]^{4-}$ to pyridine group of the PVP film, Γ_M/Γ_{PVP}, was increased from 0.0025 to 0.22. The apparent diffusion coefficient, D_{app}, for the process of charge transport within the film was also determined from the dependence of the limiting current upon the sampling time. The value of D_{app} decreased from 4.4×10^{-8} to 2.5×10^{-9} cm^2 s^{-1}, when the ratio Γ_M/Γ_{PVP} was increased from 0.0025 to 0.22.

Electrochemical reaction of solution species mediated by "redox polymer" films bound to the electrode surfaces, where the polymer itself is electroactive or the electroactive species are confined in the electroinactive polymer film, has recently received considerable attention.[1-4] It is now well recognized that the kinetics of electrochemical reactions mediated by "redox polymer" films is controlled by the interplay of the three rate-limiting factors, *i.e.*, (1) the diffusion-like propagation of the electrons through the film from the electrode surface toward the film/solution interface, (2) the diffusion of the substrate from the film/solution interface toward the electrode surface and (3) the electron cross-exchange reaction between the substrate and the active form of the redox mediator.[1,2,5-13] The theoretical approaches that take into account the interplay of these three factors, together with the diffusion of substrate in the solution, have been developed with regard to rotating disk electrode voltammetry.[4,9,14] Experimental studies also have actively been carried out in line with much success of such theoretical approaches.[1,2,6-8,11-15] However, no attempt to study in detail the kinetics on the electron transfer process at the electrode/film interface has yet been reported to our knowledge.

In order to conduct such a kinetic study, it seems to be at first indispensable to examine whether the Butler-Volmer theory[16] being proposed for the conventional electrode reaction at the electrode/solution interface is applicable to the electrode reaction of electroactive species confined in the polymer domains on electrode surface or not. For this purpose, it seems to be convenient to examine the behavior of the electrode coated with polymer film, in which electroactive species are confined by some interaction (*e.g.*, electrostatic interaction,[1,2,6,15,17-22] hydrophobic interaction,[23,24] and coordination bond[20-22,25] between the electroactive species and the polymer domain), in a solution containing only the supporting electrolyte. In this case, the overall electrode reaction consists of the electron transfer process at the electrode/film interface and the process of charge transport within the film. The latter process has been considered as the diffusion process of electroactive species to the electrode surface within the film and/or the hopping process of a series of electrons between adjacent pairs of oxidized and reduced reactants that serves to shuttle electrons from the electrode to reactants which are located away from the electrode surface.[1,2,15,17-19,23,24,26-35] So far, it has become apparent that in either case (or with combinations of the two) the process of charge transport within the film can be described in terms of apparent diffusional motion.[36,37]

This paper represents a first example on the kinetic study of the electron transfer process at the electrode/film interface. The main purpose of this work is to examine if the current-potential relationship[16] of the Butler-Volmer type usually employed for the electrode reactions at electrode/solution interface is applicable to the electron transfer process of electroactive species confined in the polymer films on electrode surface. The $[Mo(CN)_8]^{4-/3-}$ redox couple which is electrostatically bound to the protonated poly(4-vinylpyridine) (PVP) film on a pyrolytic graphite electrode is chosen as a suitable system for this purpose, because the process of charge transport of this system within the film has been previously studied in detail by means of chrono-amperometry, -coulometry and -potentiometry and has been recognized to be treated as a diffusion process which obeys Fick's second law.[19] The normal pulse voltammetric technique (NPV) is employed as a means of the measurement. Among the numerous pulse techniques, NPV has proved to be most suitable for the examination of electrode kinetics in polarographically quasi-reversible electrode processes and the current-potential curves of NPV are similar to that of d.c. polarography, so that the analysis

of the current-potential curves in NPV can be easily carried out by using a similar procedure to that of d.c. polarography.[38-42] The apparent diffusion coefficients for the process of charge transport within the film are also determined by using NPV.

Experimental

Materials. The pyrolytic graphite (Union Carbide Corp.) disk electrodes were prepared and mounted in a glass holder as previously described.[21] The exposed area of each electrode was 0.17 cm^2. The average molecular weight of PVP reprecipitated from methanol-diethyl ether was 7.4×10^5. $K_4[Mo(CN)_8]\cdot2H_2O$ was synthesized according to the standard procedure.[43]

Apparatus and Procedures. Adherent coatings of PVP were produced by transferring aliquots of a 0.5 weight percent methanolic solution of the polymer to the surface of a freshly cleaved graphite electrode and then evaporating the solvent at room temperature. The resulting coatings were swelled in an aqueous solution but remained insoluble.

The $[Mo(CN)_8]^{4-}$ complex was firmly held within the domain of the protonated PVP film.[2] The quantities of $[Mo(CN)_8]^{4-}$ incorporated into the protonated PVP coatings were determined by the following procedure: After incorporation of the $[Mo(CN)_8]^{4-}$ complex, the electrodes were washed and transferred to solutions containing only supporting electrolyte (0.2 M $CF_3COONa+CF_3COOH$, pH 1.5) (1 M=1 mol dm^{-3}). Then, the electrode potential was scanned from a value before the oxidation of the incorporated $[Mo(CN)_8]^{4-}$ ion to a value well beyond the voltammetric peak potential for oxidation and thereafter maintained until the current falls to background levels. The quantity of incorporated reactant was calculated from the integration of the current with correction for background contributions.

Normal pulse voltammograms and cyclic voltammograms were obtained with instruments which were constructed in our laboratory and were recorded with a X-Y recorder (Watanabe Corp.). Positive feed-back circuitry was employed to compensate the resistances associated with the PVP coatings as much as possible. In normal pulse voltammetric experiments, the pulse width of 50 ms and the interval of 20 to 50 s between successive pulses were employed. Thus it can be safely considered that the depletion layer of reactants produced during the precedent pulse completely disappears before the following pulse starts. Solutions were deaerated with pre-purified argon and experiments were conducted at 25 °C. Potentials were measured and are quoted with respect to a sodium chloride saturated calomel electrode (SSCE).

Results and Discussion

It has been well known that multiply-charged transition metal complexes can be incorporated into and confined in various polyelectrolytes coated on electrode surfaces by electrostatic interaction between the polyelectrolyte layer and metal complexes carrying the opposite charge.[1,2,6,15,17-22] The $[Mo(CN)_8]^{4-}$ complex can also be electrostatically attached to the protonated PVP coating on electrode.[2] When the PVP film is sufficiently thin, the cyclic voltammogram for the oxidation and reduction of the $[Mo(CN)_8]^{4-/3-}$ couple bound to the protonated PVP coatings yields symmetrical, identically shaped, anodic and cathodic

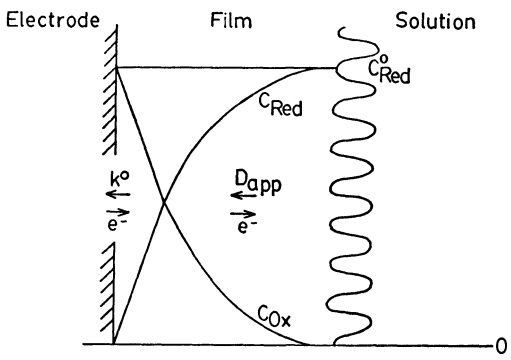

Fig. 1. Concentration profile of redox couple within polymer film at limiting current.

waves and peak currents vary linearly with scan rates. These results are characteristic of the surface redox-reaction.[37,44] With thickening the polymer film, the shape of the cyclic voltammograms becomes less symmetric and the peak currents exhibit the proportionality to the square root of scan rate.[22] The separation between anodic and cathodic peak potentials becomes large even at the ordinary scan rate such as 50 mV s^{-1} and at fast scan rate (*e.g.*, 0.5 V s^{-1} with IR compensation) the separation is larger than $\approx$59 mV, typical of a Nernstian solution process. This suggests that the overall rate of the electrode reaction is limited by the charge transport within the film and the electron transfer at the electrode/film interface.[22,34,37]

From the results obtained previously[19] by means of potential-step chronoamperometry, potential-step chronocoulometry and chronopotentiometry, the process of charge transport within the film can be treated as a semi-infinite diffusion process (Fig. 1), when the electrolysis time is below *ca.* 30 ms. In the present work, normal pulse voltammograms were taken at the sampling times between 2 and 16 ms. Therefore, the present experimental condition satisfies the condition of such a semi-infinite diffusion.

According to the usual kinetic theory[16] of a simple electrode reaction, Red$\rightleftharpoons$Ox+ne, the faradaic current, i, can be expressed by

$$i = nFA\{\vec{k}(E)C^s_{Red} - \overleftarrow{k}(E)C^s_{Ox}\}, \quad (1)$$

where $\vec{k}(E)$ and $\overleftarrow{k}(E)$ are the forward and backward rate constants, respectively, C^s_{Ox} and C^s_{Red} are concentrations of Ox and Red at the electrode surface, respectively, A is the electrode area, n is the number of electrons involved in the electron-transfer process and F is the Faraday constant.

By assuming that the Nernst equation can be applicable to an equilibrium situation of Ox and Red, Eq. 1 can be transformed into

$$i = nF\vec{A}k(E)\left\{C^s_{Red} - C^s_{Ox}\exp\left[-\frac{nF}{RT}(E-E^\circ)\right]\right\}, \quad (2)$$

where E is the electrode potential, E° is the formal standard potential of the reaction: Red$\rightleftharpoons$Ox+ne, and R and T have their usual significance. In the case of normal pulse voltammetry, the forward rate constant, $\vec{k}(E)$, can be given by[41]

$$\ln\{\vec{k}(E)\} = -\ln\left(\frac{4}{\sqrt{3}}\frac{\sqrt{\tau}}{\sqrt{D_{\mathrm{Red}}}}\right) + \ln\left\{x\left[\frac{1.75+x^2(1+\exp(-\zeta))^2}{1-x(1+\exp(-\zeta))}\right]^{1/2}\right\}, \quad (3)$$

with

$$\zeta = (nF/RT)(E-E^{\tau}_{1/2}), \quad (4)$$

$$x = i/(i_{\mathrm{d}})_{\mathrm{Cott}}, \quad (5)$$

$$E^{\tau}_{1/2} = E^{\circ} - (RT/nF)\ln\sqrt{D_{\mathrm{Ox}}/D_{\mathrm{Red}}}, \quad (6)$$

where $E^{\tau}_{1/2}$ is the reversible half-wave potential, τ is the sampling time, D_{Red} and D_{Ox} are the diffusion coefficients of Red and Ox, respectively, $(i_{\mathrm{d}})_{\mathrm{Cott}}$ denotes the diffusion current expressed by the Cottrell equation in the following manner:[45]

$$(i_{\mathrm{d}})_{\mathrm{Cott}} = nFAC^{\circ}\sqrt{D_{\mathrm{app}}/\pi\tau}, \quad (7)$$

with

$$D_{\mathrm{app}} = (D_{\mathrm{Ox}})^{\alpha}(D_{\mathrm{Red}})^{1-\alpha}, \quad (8)$$

where C° is the bulk concentration of Ox or Red in the film, and α is the anodic transfer coefficient.

Figure 2 shows the typical normal pulse voltammograms for the oxidation of $[Mo(CN)_8]^{4-}$ incorporated into the PVP film at various sampling times. The S-shaped waves shown in Fig. 2 are similar to those observed for redox species present in a solution at an uncoated electrode. The half-wave potential of the normal pulse voltammograms shifted to anodic direction with decreasing sampling times.

As shown in Fig. 3, plots of the anodic limiting currents of these normal pulse voltammograms against the inverse square root of the sampling times were found to be linear. This means that the limiting current is diffusion-controlled and the values of diffusion coefficients, D_{app}, for the process of charge transport within the film can be obtained from the anodic limiting currents by using Eq. 7.

Figure 4 shows the logarithmic plot of D_{app} *vs.* the molar ratio of the incorporated $[Mo(CN)_8]^{4-}$ ion to pyridine group of the protonated PVP, $\Gamma_{\mathrm{M}}/\Gamma_{\mathrm{PVP}}$, together with D_{app} for the reduction of $[Mo(CN)_8]^{3-}$.[38] This plot shows clearly the dependence of D_{app} on the concentration of the incorporated $[Mo(CN)_8]^{4-}$. As the ratio $\Gamma_{\mathrm{M}}/\Gamma_{\mathrm{PVP}}$ decreases, the apparent diffusion coefficient increases. Similar results have also been obtained in a previous work[19] where anionic reactants, $[Mo(CN)_8]^{4-/3-}$, $[Fe(CN)_6]^{4-/3-}$, and $[W(CN)_8]^{4-/3-}$, were incorporated into the PVP coating and the diffusion coefficients of the incorporated anions were evaluated by chronoamperometric, chronocoulometric and chronopotentiometric measurements.[46] The results shown in Fig. 4 and the previous data[19] suggest that the physical motion of $[Mo(CN)_8]^{4-}$ through the polymer film dominates its diffusional rate at the lower concentrations. One factor that contributes to the larger values of D_{app} may be the smaller extent of electrostatic cross-linking[6,15,17-19,30] of the $[Mo(CN)_8]^{4-}$ ion with the surrounding cation sites, as the concentration of the $[Mo(CN)_8]^{4-}$ ion decreases. At higher concentrations of $[Mo(CN)_8]^{4-}$, *i.e.* $\Gamma_{\mathrm{M}}/\Gamma_{\mathrm{PVP}} > 15\%$, the value of D_{app} becomes smaller but constant. In this

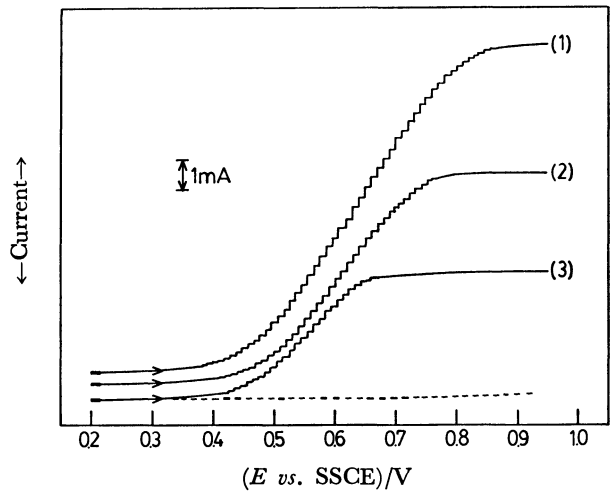

Fig. 2. Typical normal pulse voltammograms for the oxidation of $[Mo(CN)_8]^{4-}$ incorporated into the protonated PVP film on BPG electrode in 0.2 M CF_3COONa–CF_3COOH (pH 1.5) solution. Sampling time; (1) τ=2 ms, (2) 4 ms, and (3) 8 ms. Concentration of $[Mo(CN)_8]^{4-}$ incorporated into PVP, Γ_{M}: 7.0×10^{-8} mol cm^{-2}; Concentration of PVP coated on electrode, Γ_{PVP}: 4.6×10^{-7} mol cm^{-2} of pyridine as PVP. Dotted line shows a residual current.

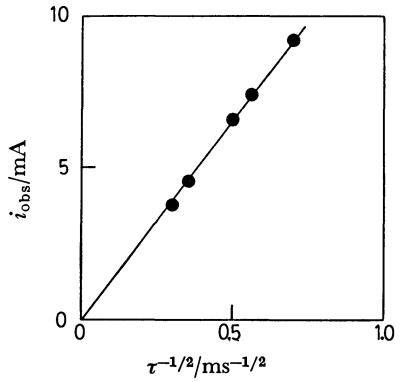

Fig. 3. Plots of observed limiting current (i_{obs}) *vs.* (sampling time)$^{-1/2}$ for the oxidation of $[Mo(CN)_8]^{4-}$ incorporated into the protonated PVP film on BPG electrode. Other conditions are the same as in Fig. 2.

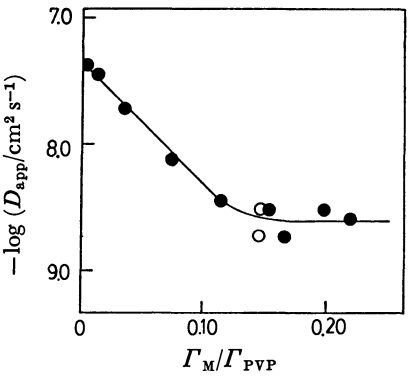

Fig. 4. Logarithmic plot of D_{app} *vs.* the molar ratio of incorporated $[Mo(CN)_8]^{4-}$ ions to protonated pyridine groups of PVP, $\Gamma_{\mathrm{M}}/\Gamma_{\mathrm{PVP}}$. Anion incorporated: (●) $[Mo(CN)_8]^{4-}$; (○) $[Mo(CN)_8]^{3-}$. Supporting electrolyte: 0.2 M CF_3COONa–CF_3COOH (pH 1.5).

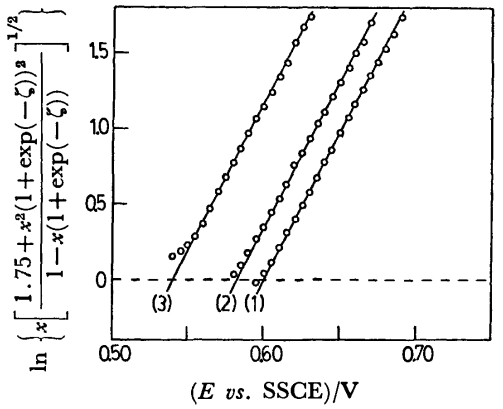

Fig. 5. Modified log-plots of normal pulse voltammograms for the oxidation of $[Mo(CN)_8]^{4-}$ incorporated into the protonated PVP film. Sampling time; (1) $\tau=2$ ms, (2) 4 ms, and (3) 8 ms. Other experimental conditions are the same as in Fig. 2.

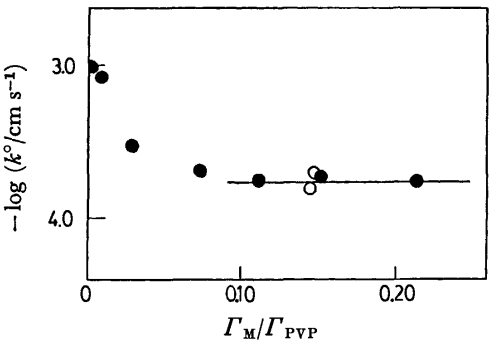

Fig. 6. Logarithmic plot of the standard rate constant, k°, against the molar ratio of incorporated $[Mo(CN)_8]^{4-}$ ions to protonated pyridine groups of PVP. Anion incorporated: (●) $[Mo(CN)_8]^{4-}$; (○) $[Mo(CN)_8]^{3-}$. Other experimental conditions are the same as in Fig. 5.

case, physical motion of the $[Mo(CN)_8]^{4-}$ ions through the film may be more difficult because of the higher extent of electrostatic cross-linking.[6,15,17-19,30] The fact that the D_{app} values are independent of the concentration of the incorporated $[Mo(CN)_8]^{4-}$ ion probably suggests that the structural changes caused by cross-linking may have reached their limit so that this factor no longer affects the measured values of D_{app}.[19]

Equation 3 indicates that the plot of $\ln(x[\{1.75+x^2(1+\exp(-\zeta))^2\}/\{1-x(1+\exp(-\zeta))\}]^{1/2})$ *vs.* E manifests the potential dependence of the forward rate constant. Figure 5 shows the typical examples of such log-plots of the normal pulse voltammograms, in which the logarithm of the second term on r.h.s. of Eq. 3 is plotted against E for the oxidation of $[Mo(CN)_8]^{4-}$ incorporated into the protonated PVP coatings. These plots gave the straight lines the slopes of which were constant at the different sampling times within experimental errors. This fact concludes that the electrode reaction of the electroactive species confined in the polymer film on electrode surfaces obeys the conventional Butler-Volmer equation[16] which characterizes the electrode reaction at electrode/solution interface. Thus, the forward rate constant, $\vec{k}(E)$, can be expressed as follows:

$$\vec{k}(E) = k^\circ \exp[(\alpha nF/RT)(E-E^\circ)], \quad (9)$$

where k° is the standard rate constant.

As can readily be seen from the comparison of Eqs. 3 and 9, the slope of the straight lines shown in Fig. 5 is equal to $(\alpha nF/RT)$ and the value, E^*, of the intersect of these lines with the zero-line can be expressed by

$$E^* = E^r_{1/2} - \frac{RT}{\alpha nF}\ln\left(\frac{4}{\sqrt{3}}\frac{k^\circ\sqrt{\tau}}{\sqrt{D_{app}}}\right), \quad (10)$$

under the assumption that $D_{Red}=D_{Ox}$, so that $E^\circ=E^r_{1/2}$. Thus, the anodic transfer coefficient was evaluated from the slopes of the straight lines shown in Fig. 5 and its value was 0.50 ± 0.05. The values of α were independent of Γ_M/Γ_{PVP}. The standard rate constants of electron transfer process at electrode/film interface were evaluated by introducing the experimental values of D_{app}, α and $E^r_{1/2}$ into Eq. 10, where the value of $E^r_{1/2}$ was estimated as the average of the anodic and cathodic peak potentials of the cyclic voltammogram for the oxidation-reduction of $[Mo(CN)_8]^{4-/3-}$ couple.

Figure 6 shows the dependence of k° upon the ratio of Γ_M to Γ_{PVP}. The value of k° decreased gradually with increasing the ratio Γ_M/Γ_{PVP} and in the region of $\Gamma_M/\Gamma_{PVP}=10$—20% the values of k° were constant and 2×10^{-4} cm s^{-1}. This value of the standard rate constant was in agreement with that obtained from the reduction of $[Mo(CN)_8]^{3-}$ confined in the protonated PVP on a graphite electrode (see open circles in Fig. 6) and the value of cathodic transfer coefficient was 0.50 ± 0.02. The standard rate constant of the electrode reaction of $[Mo(CN)_8]^{4-/3-}$ redox couple at an uncoated platinum electrode has been reported as 5×10^{-1} cm s^{-1}, which has been obtained with $[Mo(CN)_8]^{4-/3-}$ redox couple dissolved in an aqueous solution.[49] It is very interesting that the largely different values of k° were obtained, depending upon the experimental conditions where the electroactive species exist in the polymer film or the solution. In the former case, the electroactive species are firmly bound to the polymer films by electrostatic force. There is no such a special interaction in the latter case.

From the fact that there is a linear relation between $\ln(x[\{1.75+x^2(1+\exp(-\zeta))^2\}/\{1-x(1+\exp(-\zeta))\}]^{1/2})$ and electrode potential (E) (see Fig. 5), in the case of the electrode reaction at the polymer-coated electrode the formation of electrical double layer and the electron transfer process at the electrode/film interface can be considered to be essentially the same as those in an ordinary electrode reaction at electrode/solution interface. As can readily be seen from the essential ground (*i.e.*, electrostatic interaction) of the incorporation of $[Mo(CN)_8]^{4-/3-}$ redox couple into the protonated PVP film, $[Mo(CN)_8]^{4-/3-}$ couple is strongly interacting with its surroundings, *i.e.*, polymeric domains.[2,19] Under these circumstances, thus, the formation of "activated complex"[47,48] prior to the electron transfer seems to be more difficult than in the case of electron transfer reactions in a bulk solution.

The free energy required to reorganize the surrounding medium (outer shells) prior to the electron transfer becomes to be larger,[50-53] under the assumption that the free energy required to reorganize the inner coordination shells of the reactants can be almost the same for the electrode reactions of both the electroactive species present in a bulk solution and the electroactive species confined in the polymer film. Thus it seems to be likely that a large difference between the values of k° obtained in this study and the value obtained with $[Mo(CN)_8]^{4-/3-}$ redox couple dissolved in a bulk solution originates from the difference of the energy needed for the solvent reorganization occuring outside the inner coordination shells of $[Mo(CN)_8]^{4-/3-}$ couple prior to (and necessary for) electron transfer in the reaction media in which the rate constants were measured. Similarly, the dependence of k° on Γ_M/Γ_{PVP} shown in Fig. 5 appears to arise from the change of the solvent reorganization energy by Γ_M/Γ_{PVP}.

A kinetic study on the electrode reactions at polymer-coated electrodes has just been started[38,42] and the present experimental data concerning the electrode reactions of this type are scarce. Many experimental data should thus be accumulated in order to give a successful explanation for some interesting problems mentioned above. It is of great interest to examine the dependence of k° on temperature and to obtain the activation parameters of these electrode reactions. Study on the effect of ion strength and the kind of supporting electrolyte upon the kinetic parameters of electrode reactions would also give further information.

References

1) N. Oyama and F. C. Anson, *Anal. Chem.*, **52**, 1192 (1980).
2) N. Oyama, K. Sato, and H. Matsuda, *J. Electroanal. Chem.*, **115**, 149 (1980).
3) R. W. Murray, *Philos. Trans. R. Soc. London*, **302**, 237 (1981) and references therein.
4) C. P. Andrieux, J. M. Dumas-Bouchiat, and J. M. Saveant, *J. Electroanal. Chem.*, **131**, 1 (1982).
5) C. P. Andrieux and J. M. Saveant, *J. Electroanal. Chem.*, **93**, 163 (1978).
6) K. Shigehara, N. Oyama, and F. C. Anson, *Inorg. Chem.*, **20**, 518 (1981).
7) W. J. Albery, A. W. Foulds, K. J. Hall, and A. R. Hillman, *J. Electrochem. Soc.*, **127**, 654 (1980).
8) P. Daum, J. R. Lenhard, D. Robinson, and R. W. Murray, *J. Am. Chem. Soc.*, **102**, 4649 (1980).
9) C. P. Andrieux, J. M. Dumas-Bouchiat, and J. M. Saveant, *J. Electroanal. Chem.*, **114**, 159 (1980).
10) F. C. Anson, *J. Phys. Chem.*, **84**, 3336 (1980).
11) P. Daum and R. W. Murray, *J. Phys. Chem.*, **85**, 389 (1981).
12) R. D. Rocklin and R. W. Murray, *J. Phys. Chem.*, **85**, 2104 (1981).
13) T. Ikeda, C. R. Leidner, and R. W. Murray, *J. Am. Chem. Soc.*, **103**, 7422 (1981).
14) N. Oyama, N. Ohta, Y. Ohnuki, K. Sato, and H. Matsuda, *Nippon Kagaku Kaishi*, **1983**, 940.
15) F. C. Anson, T. Ohsaka, and J. M. Saveant, *J. Phys. Chem.*, **87**, 640 (1983).
16) For example, K. J. Vetter, "Electrochemical Kinetics," Academic Press, New York and London (1967), p. 107; J. O'M. Bockris and A. K. N. Reddy, "Modern Electrochemistry," Plenum Press, New York (1973), Vol. 2, Chap. 8.
17) N. Oyama and F. C. Anson, *J. Electrochem. Soc.*, **127**, 247 (1980).
18) N. Oyama, T. Shimomura, K. Shigehara, and F. C. Anson, *J. Electroanal. Chem.*, **112**, 271 (1980).
19) N. Oyama, S. Yamaguchi, Y. Nishiki, K. Tokuda, H. Matsuda, and F. C. Anson, *J. Electroanal. Chem.*, **139**, 371 (1982).
20) N. Oyama and F. C. Anson, *J. Am. Chem. Soc.*, **101**, 739 (1979).
21) N. Oyama and F. C. Anson, *J. Am. Chem. Soc.*, **101**, 3450 (1979).
22) N. Oyama and F. C. Anson, *J. Electrochem. Soc.*, **127**, 640 (1980).
23) I. Rubinstein and A. J. Bard, *J. Am. Chem. Soc.*, **102**, 6641 (1980).
24) I. Rubinstein and A. J. Bard, *J. Am. Chem. Soc.*, **103**, 5007 (1981).
25) M. C. Pham, G. Tourillon, P. C. Lacaze, and J. E. Dubois, *J. Electroanal. Chem.*, **111**, 385, (1980).
26) K. Shigehara, N. Oyama, and F. C. Anson, *J. Am. Chem. Soc.*, **103**, 2552 (1981).
27) K. Kuo and R. W. Murray, *J. Electroanal. Chem.*, **131**, 37 (1982).
28) J. A. Bruce and M. S. Wrighton, *J. Am. Chem. Soc.*, **104**, 74 (1982).
29) J. Facci and R. W. Murray, *J. Electroanal. Chem.*, **124**, 339 (1981).
30) J. Facci and R. W. Murray, *J. Phys. Chem.*, **85**, 2870 (1981).
31) D. A. Buttry and F. C. Anson, *J. Electroanal. Chem.*, **130**, 333 (1981).
32) R. J. Mortimer and F. C. Anson, *J. Electroanal Chem.*, **138**, 325 (1982).
33) H. S. White, J. Leddy, and A. J. Bard, *J. Am. Chem. Soc.*, **104**, 4811 (1982).
34) C. R. Martin, I. Rubinstein, and A. J. Bard, *J. Am. Chem. Soc.*, **104**, 4817 (1982).
35) D. A. Buttry and F. C. Anson, *J. Am. Chem. Soc.*, **104**, 4824 (1982).
36) C. P. Andrieux and J. M. Saveant, *J. Electroanal. Chem.*, **112**, 377 (1980).
37) E. Laviron, *J. Electroanal. Chem.*, **112**, 1 (1981).
38) N. Oyama, K. Sato, S. Yamaguchi, and H. Matsuda, *Denki Kagaku*, **51**, 91 (1983).
39) S. Yamaguchi, H. Matsuda, T. Ohsaka, and N. Oyama, *Bull. Chem. Soc. Jpn.*, in press (1983).
40) T. Ohsaka, N. Oyama, S. Yamaguchi, and H. Matsuda, *Bull. Chem. Soc. Jpn.*, **54**, 2475 (1981).
41) H. Matsuda, *Bull. Chem. Soc. Jpn.*, **53**, 3439 (1980).
42) N. Oyama, T. Ohsaka, M. Kaneko, K. Sato, and H. Matsuda, *J. Am. Chem. Soc.*, in press (1983).
43) N. H. Furman and C. O. Miller, *Inorg. Synth.*, **3**, 160 (1950).
44) E. Laviron, *J. Electroanal. Chem.*, **39**, 1 (1972).
45) F. G. Cottrell, *Z. Phys. Chem.*, **42**, 385 (1903).
46) A. J. Bard and L. Faulkner, "Electrochemical Methods," John Wiley and Sons, New York, N.Y. (1980), Chap. 7.
47) R. Parsons, *Trans. Faraday Soc.*, **47**, 1332 (1951).
48) S. Glasstone, K. J. Laidler, and H. Eyring, "The Theory of Rate Processes," McGraw-Hill, New York (1941).
49) T. Saji, Y. Maruyama, and S. Aoyagui, *J. Electroanal. Chem.*, **86**, 219 (1978).
50) R. A. Marcus, *Can. J. Chem.*, **37**, 155 (1959).
51) R. A. Marcus, *J. Phys. Chem.*, **67**, 853 (1963).
52) R. A. Marcus, *Electrochim. Acta*, **13**, 995 (1968).
53) N. S. Hush, *Trans. Faraday Soc.*, **57**, 557 (1961).

The Preparation and Photoreation of Spiro[oxirane-2,6′-tricyclo[3.2.1.0^{2,7}]-oct[3]en]-8′-ones. An Intramolecular Cycloaddition of Photochemically Generated Ketene with the Epoxide Ring[1]

Makoto NITTA,* Akihiko OMATA, and Hazime NAKATANI

Department of Chemistry, School of Science and Engineering, Waseda University, Shinjuku-ku, Tokyo 160

(Received August 13, 1982)

The oxidations of 1,5-dimethyl- and 1,3,5-trimethyl-6-methylenetricyclo[3.2.1.0^{2,7}]oct-3-en-8-ones with 3-chloroperbenzoic acid or thallium(III) acetate resulted in the formation of 1′,5′-dimethyl and 1′,3′,5′-trimethylspiro[oxirane-2,6′-tricyclo[3.2.1.0^{2,7}]oct[3]en]-8′-ones (**2a** and **2b**). The oxidation occured stereoselectively on the exocyclic double bond from the *exo*-side. The photochemical reactions of **2a** and **2b** resulted in the formation of 4,8-dimethyl- and 4,6,8-trimethyl-3,4-dihydro-1H-2-benzopyran-3-ones, both of which would be derived from an ene-type reaction of the ketene intermediate with the exoxide ring involved in the [$4\pi+2\sigma$] electronic system. The intermediacy of the ketene was assessed by low-temperature infrared spectroscopy as well as by a trapping experiment, the mechanistic pathways were confirmed by conducting the photoreaction in deuterated methanol.

Recently, the stereoselectivities of the electrophilic reaction of molecules containing a proximal π-bond have been explored.[2] In connection with these studies and our own previous work,[1,3] the peroxy-acid oxidation and the thallium(III) acetate-induced oxidation of 1,5-dimethyl- and 1,3,5-trimethyl-6-methylenetricyclo[3.2.1.0^{2,7}]oct-3-en-8-ones (**1a** and **1b**) were investigated. The products, 1′,5′-dimethyl and 1′,3′,5′-trimethylspiro[oxirane-2,6′-tricyclo[3.2.1.0^{2,7}]oct[3]en]-8′-ones (**2a** and **2b**), have a skeleton of photolabile 3-methyl-4-caren-2-one, which has been shown to photoisomerize to a ketene derivative.[4] Therefore, **2a** and **2b** were expected to be promising precursors of a ketene possessing another functional group of an epoxide involved in the [$4\pi+2\sigma$] electronic system.

Although the intramolecular cycloaddition of photochemically generated ketenes has been widely known,[5] little is known about the reaction of such ketenes with an electronic system which involves both π-bonds and a polar or bent σ-bond such as an epoxide ring. Some information on the reaction of an epoxide

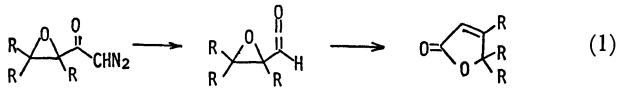

(1)

with a ketene has, however been shown. The epoxide attacks the C=O or C=C bond to afford the acetal or lactone.[6] The epoxyketene, on the other hand, undergoes a vinylcyclopropane–cyclopentene-type rearrangement, leading to butenolide (Eq. 1)[7] On understanding some unknown behavior of the epoxide toward a reactive ketene, the photochemical reactions of **2a** and **2b** were investigated.

Results and Discussion

*The Epoxidation of 1,5-Dimethyl- and 1,3,5-Trimethyl-6-methylenetricyclo[3.2.1.0^{2,7}]oct-3-en-8-ones (**1a** and **1b**).* The treatment of **1a** with 3-chloroperbenzoic acid afforded 1′,5′-dimethylspiro[oxirane-2,6′-tricyclo-[3.2.1.0^{2,7}]oct[3]en]-8′-one (**2a**) in a 55% yield, along with the starting meterial, **1a**, in a 29% yield. The structure of **2a** was deduced from its spectral properties. The stereochemistry of the epoxide ring was determined by means of the pseudo-contact NMR spectra obtained by using Eu(fod)$_3$. The relative downfield shifts of δ's are given in parentheses in the structural formula **2a**. The relatively small shifts for the hydrogens of the allylic moiety suggest that the coordination of Eu(fod)$_3$ occurs on the epoxide-oxygen. The large shifts of the two methyl groups and the proton at the 7′-position suggest that the epoxide-oxygen is located *syn* to the carbonyl group. Thus, the stereochemistry of the epoxide was assessed.

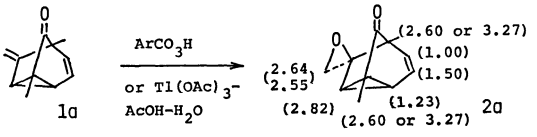

1a 2a

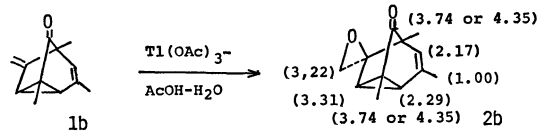

1b 2b

The epoxidation of alkenes with thallium(III) acetate has also been shown.[8] Thus, the reaction of **1a** with thallium(III) acetate in H_2O–AcOH afforded the epoxide **2a** in a 61% yield. The reaction of the trimethyl analogue **1b** in a similar way also afforded the epoxide **2b** in a 59% yield, along with *ca.* 5% of an unidentified compound, **6**. The orientation of the epoxide-oxygen for **2b** was deduced to be *syn* to the carbonyl group from the pseudo-contact NMR spectra, which were obtained by using Eu(fod)$_3$. The relative downfield shifts of δ's, which are presented in parentheses in the structural formula **2b**, exhibited a trend similar to that of **2a**.

In our previous papers, the solvomercuration-demercuration reaction on the exocyclic double bond of **1a** and its related compounds with the general structure of [**A**] was described as exhibiting a remarkable stereoselectivity to give [**B**].[3] The stereoselectivity was ex-

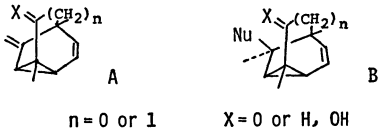

plained by the steric and/or electronic factor of the mercurinium-ion formation and the subsequent incorporation of the nucleophile.[3] In the present reactions, epoxide-oxygen was also stereoselectively incorporated on the exocyclic double bond from the *exo*-side.

Photochemical Reactions of the Epoxide ***2a*** *and* ***2b***. The photoirradiation of **2a** in acetonitrile under a nitrogen atmosphere resulted in the formation of 4,8-dimethyl-3,4-dihydro-1*H*-2-benzopyran-3-one (**7a**) in a 61% yield. Similarly, **2b** afforded 4,6,8-trimethyl-3,4-dihydro-1*H*-2-benzopyran-3-one (**7b**) in a 77% yield. The structures of **7a** and **7b** were deduced from the spectral properties, as well as by comparison with the spectral data of 1,5-dimethyl-3,4-dihydro-1*H*-2-benzopyran-3-one, which had been derived from the oxidation of 1,4-dimethyl-2-indanone.[9] The irradiation of **2a** was also carried out in acetonitrile containing a ten-fold excess of diethylamine, **7a** and the amide **8** were then obtained in 44% and 15% yields respectively.

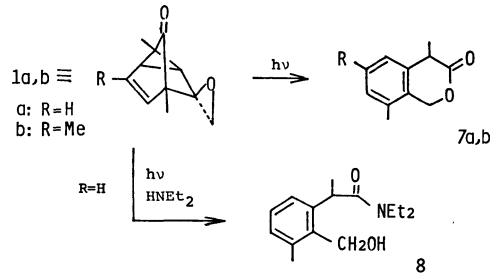

From the formation of **1a**, **7b**, and **8**, the ketene **9** was proposed as the common intermediate. Support for the intermediacy of this ketene was obtained by conducting the irradiation of the film of **2a** at 77 K. During the irradiation, the intensity of the band due to the carbonyl group in the low-temperature IR spectrum slowly decreased. A distinct new band, attributable to the ketene function, appeared at 2120 cm^{-1} after 3 h. On warming to room temperature, the 2120 cm^{-1} band disappeared completely, while there appeared a new band at 1730 cm^{-1} corresponding to **7a**, hence, the intermediacy of the ketene was clarified.

The photoreaction of **2a** in methanol also gave **7a**, while the methanol adduct to the ketene moiety was not obtained. Thus, the pathway for the formation of **7a,b** seems to be the concerted ene-type cyclization represented in the structural formula **9-A** (Scheme 1, Path a). Another possible routes can be envisaged to explain the formation of **7a,b** in acetonitrile or methanol: i) the intramolecular cycloaddition of the ketene moiety with the $[4\pi+2\sigma]$ electronic system to give the norcaradiene intermediate **10** *via* **9-B** or **9-C**, followed by aromatization (Path b),[10] ii) the nucleophilic reaction of the epoxide ring assisted by methanol *via* **11** (Path C), iii) the rearrangement of the ketene **9** to **12** followed by methanol-assisted lactonization to give **7a,b** *via* **13** (Path d).[11] Judging from the forbidden 1,3-hydrogen migration required for the isomerization of **9** to **12**, however, the intermediacy of 12 seems unlikely under neutral conditions.[12] In order to clarify the possibilities of Path b, Path C, or

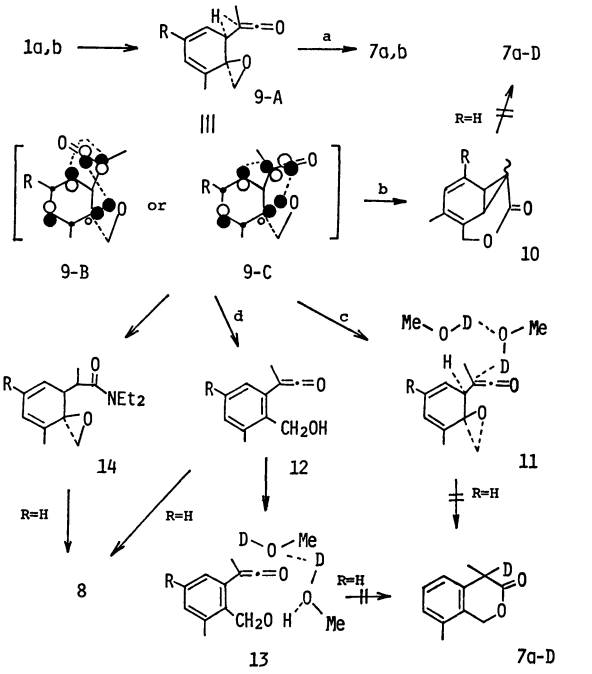

Scheme 1.

TABLE 1.

Time/h	4	7	14
7a/**7a**—**D**	10	2.3	1.0
2a (%)	60	30	16

Path d, the photoreaction of **2a** was carried out in 98%-deuterated MeOD. However, the deuterium-incorporated product **7a**—**D**, which could be expected from Path b, Path c, or Path d, could not be obtained at the early stage of the reaction. The prolonged irradiation, which continued to about 50% of the **2a** has been consumed, caused a deuterium-incorporation at the C-4 position of **7a** (Table 1). Furthermore, the independent irradiation of **7a** in MeOD underwent deuterium exchange at the C-4 position of **7a**. Therefore, the deuterium-incorporation to **7a** seems to result from the subsequent photoreaction of **7a**. This fact suggests that Path b, Path c, or Path d could not be involved in the present photoreaction in methanol or acetonitrile.

On the other hand, the formation of the amide **8** in the presence of diethylamine is suggestive of the isomerization of the ketene **9** to the ketene **12**, which undergoes the addition of diethylamine to give **8**, and/or the amine addition to **9** to give **14**, which undergoes aromatization to give **8**, under the basic conditions in the presence of diethylamine.

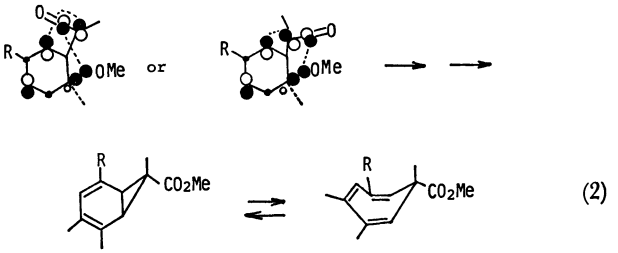

(2)

In the present photoreaction, the intramolecular cycloaddition of the ketene with the suitably located [4π+2σ] electronic system represented by **9-B** or **9-C** (Path b) is prohibited. The photochemical or thermal reaction of *exo*-6-methoxy-1,5,6-trimethyltricyclo-[3.2.1.0^{2,7}]oct-3-en-8-one has been shown to undergo this type of cycloaddition (Eq. 2).[10] Since compound **10** seems to be very constrained, therefore, this reaction pathway (Path b) is less energetically favored than the ene-type reaction (Path a).

Experimental

The IR spectra were recorded on a Shimadzu IR-400 spectrometer The mass spectral studies were conducted using an Hitachi, RMU-60 spectrometer, All the NMR spectra were recorded on a JEOL PS-100 high-resolution spectrometer, using tetramethylsilane as the internal standard. The shift data were obtained by adding small increments of Eu(fod)$_3$ to the sample and by then nothing the extent to which each peak was shifted. The relative-shift slopes were obtained by dividing each slope by the slope of the least-shifted signal. The VPC analyses and separation were performed on a Shimadzu GC-6A or a Varian Model-920 chromatograph, using a column packed with 5% SE-30 on Chromosorb W. The analyses were performed by the Science and Engineering Research Ladoratory of Waseda University.

Irradiation was carried out using a Rayonet RPR-100 Photoreactor fitted with RPR-300 nm lamps. The solution to be irradiated was placed in a Pyrex tube and was, after deoxygenation with a stream of nitrogen, sealed with a serum cap.

*Oxidation of 1,5-Dimethyl-6-methylenetricyclo[3.2.1.0^{2,7}]oct-3-en-8-one (**1a**) and 3-Chloroperbenzoic Acid.* A solution of **1a** (800 mg, 5 mmol) and 3-chloroperbenzoic acid (860 mg, 5 mmol) in dichloromethane (10 cm^3) was stirred at room temperature for 2 h. The 3-chlorobenzaic acid thus precipitated was removed by filtration, and the filtrate was washed with aqueous sodium hydrogencarbonate and dried over sodium sulfate. The subsequent removal of the solvent gave 671 mg of an oil, which was then chromatographed on silica gel, using benzene as the eluent, to give 228 mg (29%) of the starting material **1a** and 443 mg (55%) of the epoxide **2a**: IR (film), 3040, 2974, 2939, 2865, 1742, 993 cm^{-1}; NMR (CCl), δ=0.72 (3H, s), 1.25 (3H, s), 1.64 (1H, d, J=8.0 Hz), 2.02—2.34 (1H, m), 2.64 (1H, d, J=4.0 Hz), 2.68 (1H, d, J=4.0 Hz), 5.42 (1H, dxd, J=8.0, 3.0 Hz), 6,02 (1H, dxd, J=8.0, 5.5 Hz); MS, *m/e* (rel intensity), 176 (M$^+$, 13) 118 (11). Found: C, 74.91; H, 6.68%. Calcd for $C_{11}H_{12}O_2$: C, 74.97; H, 6.86%.

*Oxidation of **1a** with Thallium(III) Acetate.* A solution of **1a** (1.6 g, 10 mmol) and thallium(III) acetate (7.62 g, 20 mmnl) in 60 cm^3 of an acetic acid-water (1/1) mixture was stirred at room temperature overnight and then neutralized with aqueous sodium hydrogencarbonate. To this reaction mixture, was added saturated aqueous sodium chloride, after which the percipitate was removed by filtration. The filtrate was extracted with ether and dried over sodium sulfate. After the removal of the solvent, the residue was distilled to give 1.07 g (61%) of **2a**.

*Oxidation of 1,3,5-Trimethyl-6-methylenetricyclo[3.2.1.0.^{2,7}]-oct-3-en-8-one (**1b**) with Thallium(III) Acetate.* The oxidation was carried out as has been described above, using 1.0 g (0.57 mmol) of **1b** and 4.57 g (12 mmol) of thallium-(III) acetate. A subsequent workup similar to that described above gave an oil. This oil was separated by TLC on silica gel using chloroform-benzene (1/1) as the eluent. The first band from the TLC plates afforded 640 mg (59%) of **2b**: bp 108—111 °C/798.6 Pa (bath temperature); IR (CCl_4), 3040, 2949, 2859, 1737, 992 cm^{-1}; NMR (CCl_4), δ=0.80 (3H, s), 1.33 (3H, s), 1.64 (1H, d, J=8.0 Hz), 1.80—2.08 (1H, m), 1.94 (3H, d, J=3.0 Hz), 2.78 (1H, d, J=4.5 Hz), 2.89 (1H, d, J=4.5 Hz), 5.22—5.37 (1H, m). Found: C, 75.82; H, 7.47%. Calcd for $C_{12}H_{14}O_2$: C, 75.76; H, 7.42%.

The second band for the TCL plates contained 50 mg (5%) of **6**: IR (CCl_4), 3049, 2976, 2941, 2874, 1742, 1689 (shoulder), 1449, 1379 cm^{-1}; NMR (CCl_4), δ=1.08 (3H, s), 1.25 (3H, s), 1.09 (3H, s), 2.17—2.43 (3H, m), 2.44 (2H, s), 5.30 (1H, m).

*Irradiation of **2a**.* A solution of **2a** (50 mg, 0.28 mmol) in 10 cm^3 of anhydrous acetonitrile was irradiated at room temperature. The photoreaction, followed by VPC, was completed in 32 h. The photolysate was separated by TLC on silica gel, using benzene as the eluent, to give 41 mg (80%) of **7a**: mp 75—76 °C; IR (KBr), 1730 cm^{-1}; NMR (CCl_4), δ=1.60 (3H, d, J=7.0 Hz), 2.36 (3H, s), 3.50 (1H, q, J=7.0 Hz), 5.18 (1H, d, J=14.0 Hz), 5.38 (1H, d, J=14.0 Hz), 7.00—7.36 (3H, m); MS, *m/e* (rel intensity), 176 (M$^+$, 17), 132 (100). Found: C, 74.77; H, 7.11%. Calcd for $C_{11}H_{12}O_2$: C, 74.97; H, 6.88%.

Oxidation of 1,4-Dimethyl-2-indanone with 3-Chloroperbenzoic Acid. A solution of 1,4-dimethyl-2-indanone (480 mg, 3 mmol) and 3-chloroperbenzoic acid (692 mg, 4 mmol) was stirred overnight. To this reaction mixture, we then added 5 cm^3 of saturated aqueous $Na_2S_2O_3$ and water, after with the reaction mixture was extracted with dichloromethane. The evaporation of the dried organic portion and subsequent recrystallization gave 288 mg (55%) of 1,5-dimethyl-3,4-dihydro-1*H*-2-benzopyran-3-one: mp 114—115 °C; IR (CCl_4), 1754 cm^{-1}; NMR (CCl_4), δ=1.73 (1H, d, J=6.6 Hz), 2.34 (3H, s), 3.62 (1H, d, J=18.6 Hz), 3.87 (1H, d, J=18.6 Hz), 5.55 (1H, q, J=6.6 Hz), 7.20—7.50 (3H, m); MS, *m/e* (rel intensity), 176 (M$^+$, 27), 132 (100). Found: C, 75.36; H, 6.81%. Calcd for $C_{11}H_{12}O_2$: C, 74.94; H, 6.86%.

*Irradiation of **2b**.* A solution of **2b** (64 mg, 0.36 mmol) in 10 cm^3 of anhydrous acetonitrile was irradiated for 19 h. The photolysate was purified by column chromatography on Florisil, using benzene as the eluent, to give 49 mg (77%) of lactone **7b**: mp 117—118 °C; IR (CCl_4), 1736 cm^{-1}; NMR ($CDCl_3$), δ=1.77 (3H, d, J=7.5 Hz), 2.53 (3H, s), 2.60 (3H, s), 3.94 (1H, q, J=7.5 Hz), 5.80 (1H, d, J=13.5 Hz, 5.94 (1H, d, J=13.5 Hz), 7.66—7.83 (2H, broad s); MS, *m/e* (rel intensity), 190 (M$^+$, 100), 146 (84). Found: C, 75.44; H, 7.25%. Calcd for $C_{12}H_{14}O_2$: C, 75.76; H, 7.42%.

*Irradiation of **2a** in the Presence of Diethylamine.* A solution of **2a** (88 mg, 0.5 mmol) and diethylamine (365 mg, 5 mmol) in 10 cm^3 of anhydrous acetonitrile was irradiated for 3 h in a quartz tube with RPR-300 nm lamps at room temperature. After the evaporation of the solvent, the photolysate was separated by TLC on silica gel, using benzene as the eluent. The first band from the TLC plates gave 39 mg (44%) of **7a**. The second band contained 19 mg (15%) of the amide **8**: mp 121—122 °C; IR ($CHCl_3$), 3300, 1610 cm^{-1}; NMR ($CDCl_3$), δ=0.80—1.30 (6H, broad m), 1.40 (3H, d, J=6.5 Hz), 2.16 (1H, s), 2.41 (3H, s), 2.82—3.80 (4H, broad m), 4.21 (1H, q, J=6.5 Hz), 4.78 (2H, s), 7.00—7.30 (3H, m); MS, *m/e* (rel intensity), 249 (M$^+$, 16), 100 (100). Found: C, 72.53; H, 9.41; N, 5.66%. Calcd for $C_{15}H_{23}O_2N$: C, 72.25; H, 9.30; N, 5.62%.

Trap of the Ketene Intermediate by Low-temperature IR Spectroscopy. A glassy film of **2a** was placed on an infrared cell and irradiated externally with a 450-W medium-pressure mercury lamp through a CaF_2 cell window for infrared spectroscopy at *ca.* 77 K. A distinct new band, attributable to the ketene intermediate, appeared at 2120 cm^{-1} after 3 h. This ketene band gradually disappeared with the rise in the temperature to the ambient temperature, a new band appeared at 1730 cm^{-1} due to the carbonyl group of **7a**.

*Irradiation of **2a** in Methanol-*d_1. Three Pyrex tubes containing 27 mg (0.15 mmol) of **2a** in 0.4 cm^3 of MeOD were irradiated for several hours. The irradiation time and the ratio of the photoproducts of **7a**—**D** to **7a** (as determined by NMR spectroscopy using the signals of the methine proton at δ 3.50 and the methyl protons at δ 1.60), and the recovery yields of **2a** after separation through TLC, are listed in Table 1.

*Irradiation of **7a** in Methanol-*d_1. A solution of **7a** (22 mg, 0.13 mmol) in 1 cm^3 of MeOD was irradiated for 8 h. The photolysate was purified by TLC on silica gel, using benzene as the eluent, to give 18 mg (85%) of a mixture of **7a** and **7a**—**D** in a ratio of 1/1, as determined by means of the NMR spectrum.

The authors wish to thank to Professor Masaru Tada of Waseda University for low-temperature infrared spectroscopy and Mr. Shuji Okada for a part of the experimental work.

References

1) Preliminary account of the photoreaction has appeared: M. Nitta and H. Nakatani, *Chem. Lett.*, **1978**, 957.

2) K. Okada and T. Mukai, *J. Am. Chem. Soc.*, **100**, 6509 (1978); L. A. Paquette, L. W. Hertel, R. Gleiter, and M. C. Bohm, *ibid.*, **100**, 6510 (1978); L. W. Hertel and L. A. Paquette, *ibid.*, **101**, 7620 (1979); L. A. Paquette, L. W. Hertel, R. Gleiter, M. C. Bohm, M. A. Beno, and G. G. Christph, *ibid.*, **103**, 7106 (1981); L. A. Paquette, F. Klinger, and L. W. Hertel, *J. Org. Chem.*, **46**, 4403 (1981).

3) M. Nitta, A. Omata, and H. Sugiyama, *Chem. Lett.*, **1980**, 1615; *Bull. Chem. Soc. Jpn.*, **55**, 569 (1982).

4) J. E. Baldwin and S. N. Kruger, *J. Am. Chem. Soc.*, **91**, 2396 (1969).

5) K. N. Houk, *Chem. Rev.*, **76**, 1 (1976), and the references cited therein.

6) K. Gulbins and K. Hamann, *Chem. Ber.*, **94**, 3287 (1961).

7) P. M. M. van Hard, L. Thijis, and B. Zwannenberg, *Tetrahedron Lett.*, **1975**, 803.

8) W. Kruse and T. M. Bednarski, *J. Org. Chem.*, **36**, 1154 (1971).

9) J. P-Katalinic, J. Zsindely, and H. Schmid, *Helv. Chim. Acta*, **57**, 223 (1974).

10) M. Nitta, A. Omata, and M. Namiki, *Chem. Lett.*, **1982**, 227.

11) P. J. Lillford and D. P. N. Satchell, *J. Chem. Soc., B.* **1968**, 889.

12) W. J. Bailey and R. A. Baylounty, *J. Org. Chem.*, **27**, 3476 (1962); R. B. Woodward and R. Hoffman, *Angew. Chem., Int. Ed. Engl.*, **8**, 781 (1969).

Revision of Structures of Nellionol and Dehydronellionol

Takashi MATSUMOTO,* Sachihiko IMAI, Shoji TAKEDA, and Masanori MITSUKI

Department of Chemistry, Faculty of Science, Hiroshima University, Higashisenda-machi, Naka-ku, Hiroshima 730

(Received November 29, 1982)

The structures of nellionol and dehydronellionol were revised respectively to 6α,11,12,16-tetrahydroxyabieta-8,11,13-trien-7-one (**12**) and 6,11,12,16-tetrahydroxyabieta-5,8,11,13-tetraen-7-one (**13**) by the following syntheses. A mixture of (15*R*)- and (15*S*)-12-methoxyabieta-8,11,13-trien-16-ol, prepared from 13-acetyl-12-methoxypodocarpa-8,11,13-triene, was converted into 11,12,16-triacetoxyabieta-8,11,13-trien-7-one (**22**) *via* 16-acetoxy-12-benzoyloxyabieta-8,11,13-trien-11-ol. Treatment of **22** with isopropenyl acetate, followed by oxidation with *m*-chloroperbenzoic acid and subsequent acetylation, afforded 6α,11,12,16-tetraacetoxyabieta-8,11,13-trien-7-one, which was hydrolyzed with dilute hydrochloric acid to **12**. The ketone **22** was also converted into **13** *via* 11,12,16-triacetoxyabieta-8,11,13-trien-6-one. The spectral data of **12** and **13** were in good agreement with those of natural nellionol and dehydronellionol.

The novel tricyclic aromatic diterpenes, nellionol and dehydronellionol, have recently been isolated from the root bark of *Premna latifolia* Roxb. by Rao *et al.*[1] On the basis of chemical and spectroscopic studies, they deduced the structures of nellionol and dehydronellionol to be 6α,11,14,16-tetrahydroxyabieta-8,11,13-trien-7-one (**1**) and 6,11,14,16-tetrahydroxyabieta-5,8,11,13-tetraen-7-one (**2**), respectively. Among many naturally-occurring tricyclic diterpenes possessing abietane skeleton, several compounds have two oxygen functions in the C-ring. In these compounds, the oxygen functions are usually present at the C-11 and C-12 positions; this is true for cryptojaponol (**3**),[2] galdosol (**4**),[3] carnosolone (**5**),[4] and carnosic acid (**6**).[5,6] However, Rao *et al.* proposed very unique structures (**1** and **2**) possessing two oxygen functions at the C-11 and C-14 positions and no oxygen function at the C-12 position. It is of interest to confirm the validity of their proposed structures. We therefore examined the published spectral data of these natural products. The ^{1}H NMR spectra of nellionol tetraacetate and dehydronellionol tetraacetate showed, respectively, an aromatic proton signal at δ 8.04 and 8.12. These chemical shifts assigned to the C-12 protons in the proposed structures are in an unusually low field; similar compounds, methyl 11,14-diacetoxy-7-oxoabieta-8,11,13-trien-18-oate (**7**) and 11,14-diacetoxy-13-(acetoxymethyl)podocarpa-8,11,13-trien-7-one (**8**),[7] showed the C-12 proton signals at δ 7.04 and 7.09, respectively. On the other hand, the ^{1}H NMR spectra of carnosolone diacetate (**9**),[4] methyl 11,12-diacetoxy-7-oxoabieta-8,11,13-trien-20-oate (**10**),[3] and methyl 11,12-diacetoxy-7-oxoabieta-5,8,11,13-tetraen-20-oate (**11**)[5] showed singlet signals due to the C-14 aromatic proton at δ 8.23, 8.04, and 8.15, respectively. These spectral data strongly suggested that the aromatic protons in the new natural products are placed at the C-14 position ortho to a carbonyl group. From these ^{1}H NMR spectral analyses together with consideration of the other spectral data, we deduced 6α,11,12,16-tetrahydroxyabieta-8,11,13-trien-7-one (**12**) and 6,11,12,16-tetrahydroxyabieta-5,8,11,13-tetraen-7-one (**13**) to be more preferable structures of nellionol

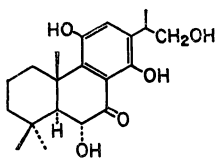

1

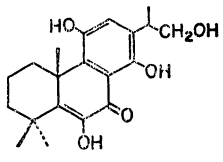

2

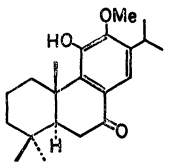

3

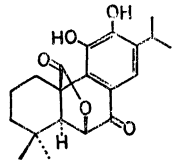

4

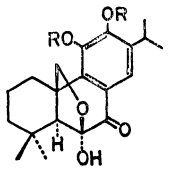

5 R=H
9 R=Ac

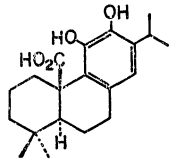

6

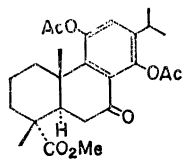

7

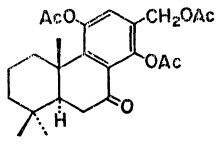

8

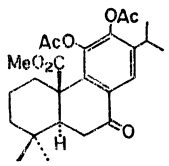

10

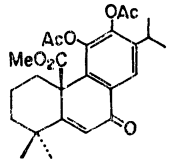

11

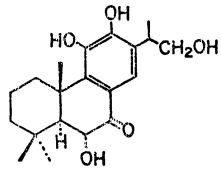

12

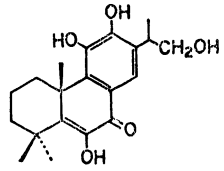

13

and dehydronellionol, respectively. To confirm the validity of our proposal, independent syntheses of **12** and **13**, starting from 13-acetyl-12-methoxypodocarpa-8,11,13-triene (**14**),[8,9] have been attempted.

Grignard reaction of **14** with methylmagnesium iodide in refluxing ether, followed by dehydration of the resulting alcohol (**15**: 86%) in refluxing acetic acid, afforded 12-methoxyabieta-8,11,13,15-tetraene (**16**: 95%), whose ^{1}H NMR spectrum showed singlet signals at δ 2.06 (3H) and 4.96 (2H) due to an isopropenyl group. The tetraene **16** was converted into an epimeric mixture at C-15 of 12-methoxyabieta-8,11,13-trien-16-ol (**17**: 70%) by hydroboration and subsequent oxidation with alkaline hydrogen peroxide. Separation of these epimeric alcohols was unsuccessful. Therefore, the mixture was used in the following reactions. Acetylation of **17** with acetic anhydride in pyridine yielded the corresponding acetate (**18**: 94%), which was treated at room temperature with anhydrous aluminium chloride and ethanethiol in dichloromethane to give 16-acetoxyabieta-8,11,13-trien-12-ol (**19**: 91%). To introduce an oxygen function at the C-11 position, the phenol **19** was oxidized at room temperature with benzoyl peroxide[10] in chloroform to afford 16-acetoxy-12-benzoyloxyabieta-8,11,13-trien-11-ol (**20**: 40%). This was then converted into 11,12,16-triacetoxyabieta-8,11,13-triene (**21**: 90%) by treatment with lithium aluminium hydride in refluxing ether, followed by acetylation with acetic anhydride in pyridine. The ^{1}H NMR spectrum of **21** showed signals due to three acetoxyl groups at δ 1.95 (3H) and 2.22 (6H), and an aromatic proton signal at δ 6.77. Oxidation of **21** with chromium trioxide in acetic acid afforded the corresponding 7-oxo compound (**22**: 73%), whose ^{1}H NMR spectrum showed a singlet signal at δ 8.03 due to an aromatic proton. The downfield shift of the aromatic proton signal from δ 6.77 in **21** to δ 8.03 in **22** must be caused by a deshielding effect of the carbonyl group at the C-7 position. This supported the location of the aromatic proton at C-14. The 7-oxo compound **22** was refluxed with isopropenyl acetate in the presence of *p*-toluenesulfonic acid monohydrate to give 7,11,12,16-tetraacetoxyabieta-6,8,11,13-tetraene (**23**). The ^{1}H NMR spectrum of **23** showed a doublet signal due to an olefinic proton at δ 5.61 and a singlet signal due to an aromatic proton at δ 6.95. Oxidation of **23** with *m*-chloroperbenzoic acid in dichloromethane, followed by acetylation[11] with acetic anhydride in pyridine, afforded 6α,11,12,16-tetraacetoxyabieta-8,11,13-trien-7-one (**24**: 86% from **22**). The α-configuration of the acetoxyl group at the C-6 position in **24** was supported by its ^{1}H NMR spectrum, which showed a doublet signal due to the C-6 proton at δ 5.83 with a coupling constant of 14 Hz, suggesting the β orientation. Hydrolysis of **24** with dilute hydrochloric acid in refluxing ethanol yielded the desired **12** (55%). The ^{1}H NMR spectra of the synthetic **12** and **24** were in good agreement with those of natural nellionol and its tetraacetate.

Subsequently the 7-oxo compound **22** was reduced at room temperature with sodium borohydride in methanol to give a mixture of epimeric alcohols at C-7, which was immediately converted into 11,12,16-triacetoxyabieta-6,8,11,13-tetraene (**25**) by treatment with dilute hydrochloric acid in refluxing methanol and subsequent acetylation[12] with acetic anhydride in pyridine. The ^{1}H NMR spectrum of **25** showed two double doublet signals due to two olefinic protons at δ 5.93 (J=9 and 3 Hz, C_6–H) and 6.45 (J=9 and 3 Hz, C_7–H). The tetraene **25** was further converted into 11,12,16-triacetoxyabieta-8,11,13-trien-6-one (**26**: 40% from **22**) by a series of reactions: oxidation with *m*-chloroperbenzoic acid in dichloromethane at room temperature, treatment with dilute hydrochloric acid in refluxing methanol, and acetylation[12] with acetic anhydride in pyridine. Oxidation of **26** with Jones reagent, followed by treatment with sodium acetate in refluxing acetic anhydride, afforded 6,11,12,16-tetraacetoxyabieta-5,8,11,13-tetraen-7-one (**27**: 52%). Hydrolysis of **27** with dilute hydrochloric acid in refluxing methanol produced the desired **13** (38%). The ^{1}H NMR spectra of the synthetic **13** and **27** were also in good agreement with those of natural dehydronellionol and its tetraacetate.

From the present studies, it is clear that the proposed structures (**1** and **2**) of nellionol and dehydronellionol must be revised to **12** and **13**. However, the stereochemistry of the C-15 position in these natural com-

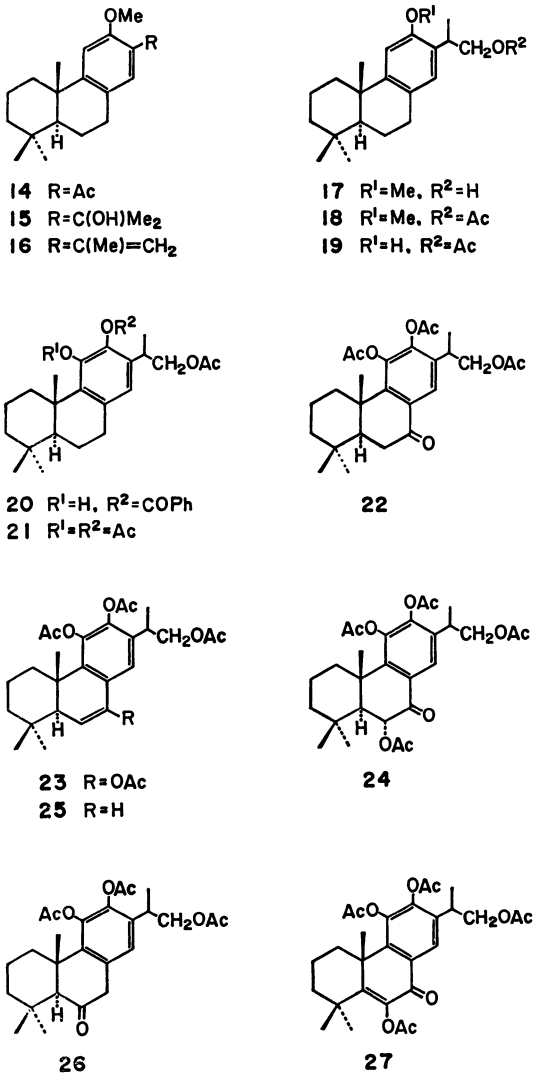

pounds remained unsettled.

Experimental

The IR spectra were measured in chloroform and the ^{1}H MNR spectra in carbon tetrachloride at 60 MHz, with tetramethylsilane as an internal standard, unless otherwise stated. The chemical shifts are presented in terms of δ values; s: singlet, bs: broad singlet, d: doublet, bd: broad doublet, dd: double doublet, m: multiplet. The column chromatography was performed using Merck silica gel (0.063 mm).

*Methyl 11,14-Diacetoxy-7-oxoabieta-8,11,13-trien-18-oate (**7**).* A mixture of methyl 11,14-dihydroxy-7-oxoabieta-8,11,13-trien-18-oate[13] (19 mg), acetic anhydride (0.4 ml), and pyridine (0.4 ml) was refluxed for 1 h. After the usual work-up, the crude product was chromatographed on silica gel (5.0 g), using ether-benzene (3:97) as the eluent, to give methyl 11-acetoxy-14-hydroxy-7-oxoabieta-8,11,13-trien-18-oate (2 mg: 9%), whose IR spectrum was identical with that of the authentic sample.[13] Further elution with ether-benzene (5:95) gave **7** (15 mg: 64%) as an oil; IR: 1760, 1723, 1684 cm^{-1}; ^{1}H NMR ($CDCl_3$), 90 MHz): 1.05 (3H, d, J=7 Hz) and 1.09 (3H, d, J=7 Hz) (-CH($C\underline{H}_3$)$_2$), 1.29 (3H, s) and 1.33 (3H, s) (C_4-CH_3 and C_{10}-CH_3), 2.32 (3H, s) and 2.34 (3H, s) (2-OCOCH_3), 3.65 (3H, s, -CO_2CH_3), 7.04 (1H, s, C_{12}-H). Found: C, 67.84; H, 7.51%. Calcd for $C_{25}H_{32}O_7$: C, 67.55; H, 7.26%.

*12-Methoxyabieta-8,11,13-trien-15-ol (**15**).* 13-Acetyl-12-methoxypodocarpa-8,11,13-triene (**14**)[8,9] was prepared from (+)-dehydroabietic acid. A solution of **14** (13.1 g) in dry ether (40 ml) was added dropwise to an ethereal solution of methylmagnesium iodide prepared from magnesium turnings (1.3 g) and methyl iodide (3.3 ml) in dry ether (40 ml). The mixture was refluxed for 1.5 h, cooled, poured into ice-dilute hydrochloric acid, and then extracted with ether. The ether extract was washed successively with aqueous sodium thiosulfate and brine, dried over sodium sulfate, and evaporated *in vacuo*. The residue was chromatographed on silica gel (150 g), using benzene and then ether-benzene (9:91) as the eluent, to give **15** (11.8 g: 86%); IR: 3530 cm^{-1}; ^{1}H NMR: 0.96 (6H, s, -$\dot{C}(CH_3)_2$), 1.18 (3H, s, C_{10}-CH_3), 1.52 (6H, s, -C($C\underline{H}_3$)$_2$OH), 3.57 (1H, s, -OH), 3.83 (3H, s, -OCH_3), 6.67 (1H, s) and 6.88 (1H, s) (C_{11}-H and C_{14}-H).

*12-Methoxyabieta-8,11,13,15-tetraene (**16**).* A solution of **15** (11.5 g) in acetic acid (30 ml) was refluxed for 5 min, cooled, neutralized with aqueous sodium hydroxide, and extracted with ether. The ether extract was weshed with brine, dried over sodium sulfate, and evaporated *in vacuo*. The residue was chromatographed on silica gel (100 g), using hexane-benzene (1:1) as the eluent, to give **16** (10.3 g: 95%); ^{1}H NMR: 0.96 (6H, s, -$\dot{C}(CH_3)_2$), 1.19 (3H, s, C_{10}-CH_3), 2.06 (3H, s, C_{15}-CH_3), 3.73 (3H, s, -OCH_3), 4.96 (2H, bs, -$\dot{C}$=CH_2), 6.61 (1H, s) and 6.72 (1H, s) (C_{11}-H and C_{14}-H).

*12-Methoxyabieta-8,11,13-trien-16-ol (**17**).* A solution of boron trifluoride etherate (2.4 ml) in dry tetrahydrofuran (4.0 ml) was added dropwise at −5—0 °C to a stirred mixture of **16** (4.0 g) and sodium borohydride (530 mg) in dry tetrahydrofuran (35 ml) in a stream of nitrogen. After the mixture had been stirred at 0—5 °C for 2 h, there were added successively aqueous tetrahydrofuran (50%: 6.0 ml), aqueous sodium hydroxide (12%: 6.3 ml), and hydrogen peroxide (30%: 6.3 ml) at −5—0°C. The mixture was stirred at −5—0 °C for 30 min and then at room temperature for 1 h, diluted with water, and extracted with ether. The ether extract was washed with brine, dried over sodium sulfate, and evaporated *in vacuo*. The residue was chromatographed on silica gel (200 g), using benzene as the eluent, to give a mixture of C-15 epimers (**17**) (2.9 g: 70%); IR: 3592, 3456 cm^{-1}; ^{1}H NMR: 0.96 (6H, s, -$\dot{C}(CH_3)_2$), 1.16 (3H, bd, J=7 Hz, C_{15}-CH_3), 1.17 (3H, s, C_{10}-CH_3), 1.52 (1H, s, -OH), 3.22 (1H, m, C_{15}-H), 3.46 (2H, bs, -$C\underline{H}_2$OH), 3.74 (3H, s, -OCH_3), 6.59 (1H, s) and 6.67 (1H, s) (C_{11}-H and C_{14}-H).

*16-Acetoxy-12-methoxyabieta-8,11,13-triene (**18**).* A mixture of **17** (1.2 g), acetic anhydride (2.0 ml), and pyridine (5.0 ml) was stirred at 80—85 °C for 1.5 h. After the usual work-up, the crude product was purified by column chromatography on silica gel (50 g), using benzene as the eluent, to give **18** (1.3 g: 94%); IR: 1725 cm^{-1}; ^{1}H NMR: 0.97 (6H, s, -$\dot{C}(CH_3)_2$), 1.19 (3H, s, C_{10}-CH_3), 1.20 (3H, d, J=7 Hz, C_{15}-CH_3), 1.97 (3H, s, -$OCOCH_3$), 3.78 (3H, s, -OCH_3), 4.05 (2H, bd, J=7 Hz, -CH_2O-), 6.63 (1H, s) and 6.70 (1H, s) (C_{11}-H and C_{14}-H).

*16-Acetoxyabieta-8,11,13-trien-12-ol (**19**).* A mixture of **18** (1.3 g), anhydrous aluminium chloride (2.9 g), and ethanethiol (2.7 ml) in dichloromethane (20 ml) was stirred at 0—5 °C for 5 min and then at room temperature for 1 h. The mixture was poured into dilute hydrochloric acid and extracted with ether. The ether extract was washed with brine, dried over sodium sulfate, and evaporated *in vacuo*. The residue was chromatographed on silica gel (50 g), using ether-benzene (1:99) as the eluent, to give **19** (1.1 g: 91%); IR: 3605, 3405, 1720 cm^{-1}; ^{1}H NMR: 0.95 (6H, s, -$\dot{C}(CH_3)_2$), 1.13 (3H, s, C_{10}-CH_3), 1.26 (3H, d, J=7 Hz, C_{15}-CH_3), 2.05 (3H, s, -$OCOCH_3$), 3.8—4.4 (2H, m, -CH_2O-), 6.38 (1H, s, C_{12}-OH), 6.55 (1H, s) and 6.64 (1H, s) (C_{11}-H and C_{14}-H).

*16-Acetoxy-12-benzoyloxyabieta-8,11,13-trien-11-ol (**20**).* A solution of **19** (862 mg) and benzoyl perpxide (3.0 g) in chloroform (10 ml) was allowed to stand at room temperature for 50 h. The chloroform solution was diluted with ether. This ether solution, after addition of acetic acid (9.0 ml) and aqueous potassium iodide (30%: 30 ml), was stirred at room temperature for 4 h. The mixture was washed successively with water, aqueous sodium thiosulfate, aqueous sodium hydrogencarbonate, and brine. After being dried over sodium sulfate, the solvent was evaporated *in vacuo* and the residue was purified by column chromatography on silica gel (70 g), using benzene as the eluent, to give **20** (446 mg: 40%). IR: 3575, 3375, 1730 cm^{-1}; ^{1}H NMR: 0.97 (6H, s, -$\dot{C}(CH_3)_2$), 1.15 (d, J=7 Hz) and 1.18 (d, J=7 Hz) (3H, C_{15}-CH_3), 1.34 (3H, s, C_{10}-CH_3), 1.86 (3H, s, -$OCOCH_3$), 3.93 (2H, m, -CH_2O-), 5.65 (1H, s, C_{11}-OH), 6.45 (1H, s, C_{14}-H), 7.30—7.65(m) and 8.00—8.30(m) (5H, -C_6H_5).

*11,12,16-Triacetoxyabieta-8,11,13-triene (**21**).* A stirred mixture of **20** (327 mg) and lithium aluminium hydride (60 mg) in dry ether (7.0 ml) was refluxed for 2 h. The mixture was poured into ice-dilute hydrochloric acid and extracted with ether. The ether extract was washed with brine, dried over sodium sulfate, and evaporated *in vacuo* to give the crude triol (289 mg).

The crude triol (289 mg) was acetylated with acetic anhydride (1.0 ml) in pyridine (1.0 ml) at room temperature for 17 h. After the usual work-up, the crude product was purified by column chromatography on silica gel (15 g), using ether-benzene (3:97) as the eluent, to give **21** (290 mg: 90%). IR: 1761, 1731 cm^{-1}; ^{1}H NMR: 0.95 (6H, s,

$-\dot{C}(CH_3)_2$), 1.20 (3H, bd, $J=7$ Hz, C_{15}-CH_3), 1.22 (3H, s, C_{10}-CH_3), 1.95 (3H, s, C_{16}-$OCOCH_3$), 2.22 (6H, s, C_{11}-$OCOCH_3$ and C_{12}-$OCOCH_3$), 3.97 (2H, bd, $J=7$ Hz, $-CH_2O-$), 6.77 (1H, s, C_{14}-H).

*11,12,16-Triacetoxyabieta-8,11,13-trien-7-one (**22**).* A mixture of **21** (340 mg) and chromium trioxide (120 mg) in acetic acid (5.0 ml) was stirred at 0—5 °C for 15 min and then at room temperature for 22 h. The mixture was diluted with water and extracted with ether. The ether extract was washed successively with aqueous sodium hydrogencarbonate and brine, dried over sodium sulfate, and evaported *in vacuo*. The residue was chromatographed on silica gel (15 g), using ether-benzene (4:96) as the eluent, to give **22** (255 mg: 73%). IR: 1773, 1727, 1683, 1607 cm^{-1}; ^1H NMR ($CDCl_3$): 0.96 (3H, s) and 0.98 (3H, s) ($-\dot{C}(CH_3)_2$), 1.24 (d, $J=7$ Hz) and 1.28 (d, $J=7$ Hz) (3H, C_{15}-CH_3), 1.35 (3H, s, C_{10}-CH_3), 2.03 (3H, s, C_{16}-$OCOCH_3$), 2.35 (6H, s, C_{11}-$OCOCH_3$ and C_{12}-$OCOCH_3$), 4.06 (d, $J=7$ Hz) and 4.09 (d, $J=7$ Hz) (2H, $-CH_2O-$), 8.03 (1H, s, C_{14}-H).

*7,11,12,16-Tetraacetoxyabieta-6,8,11,13-tetraene (**23**).* A mixture of **22** (112 mg) and *p*-toluenesulfonic acid monohydrate (10 mg) in isopropenyl acetate (2.0 ml) was refluxed for 14 h. The mixture was cooled and diluted with ether. The ether solution was washed with brine, dried over sodium sulfate, and evaporated *in vacuo* to give the crude **23** (139 mg) which, without purification, was used in the next reaction. ^1H NMR: 0.97 (3H, s) and 1.05 (3H, s) ($-\dot{C}(CH_3)_2$), 1.25 (3H, s, C_{10}-CH_3), 5.61 (1H, d, $J=2.5$ Hz, C_6-H), 6.95 (1H, s, C_{14}-H).

*6α,11,12,16-Tetraacetoxyabieta-8,11,13-trien-7-one (**24**).* A mixture of the crude **23** (139 mg) and *m*-chloroperbenzoic acid (85%: 58 mg) in dichloromethane (3.0 ml) was stirred at 0—5 °C for 10 min and then at room temperature for 24 h. The mixture was diluted with ether and washed successively with aqueous potassium iodide, aqueous sodium thiosulfate, aqueous sodium hydrogencarbonate, and brine. After being dried over sodium sulfate, the ether solution was evaporated *in vacuo* to give a mixture of 6α-acetoxy and 6α-hydroxy derivatives (147 mg), which was immediately acetylated with acetic anhydride (1.0 ml) in pyridine (1.0 ml) at room temperature for 20 h. After the usual work-up, the crude product was chromatographed on silica gel (5.0 g). Elution with ether-benzene (5:95) gave **24** (101 mg: 86% from **22**); IR: 1774, 1734, 1700, 1607 cm^{-1}; ^1H NMR ($CDCl_3$: 90 MHz): 1.07 (3H, s) and 1.14 (3H, s) ($-\dot{C}(CH_3)_2$), 1.25 (3H, d, $J=7$ Hz, C_{15}-CH_3), 1.52 (3H, s, C_{10}-CH_3), 2.00 (3H, s, C_{16}-$OCOCH_3$), 2.23 (1H, d, $J=14$ Hz, $C_{5\alpha}$-H), 2.24 (3H, s) and 2.31 (6H, s) (C_6-$OCOCH_3$, C_{11}-$OCOCH_3$, and C_{12}-$OCOCH_3$), 3.1—3.5 (1H, m, C_{15}-H), 4.05 (d, $J=7$ Hz) and 4.08 (d, $J=7$ Hz) (2H, $-CH_2O-$), 5.83 (1H, d, $J=14$ Hz, $C_{6\beta}$-H), 7.99 (1H, s, C_{14}-H). The ^1H NMR spectrum of **24** was in good agreement with that of natural nellionol tetraacetate,[1] except for the signals due to the corresponding C-15 epimer. Found: C, 65.14; H, 7.11%. Calcd for $C_{28}H_{36}O_9$: C, 65.10; H, 7.02%.

*6α,11,12,16-Tetrahydroxyabieta-8,11,13-trien-7-one (**12**).* A mixture of **24** (83 mg) and dilute hydrochloric acid (10%: 0.5 ml) in ethanol (2.0 ml) was refluxed for 3 h. The mixture was cooled, diluted with water, and extracted with ether. The ether extract was washed with brine, dried over sodium sulfate, and evaporated *in vacuo*. The residue was chromatographed on silicic acid (Mallinckrodt CC-4: 4.0 g), using hexane-chloroform (1:4) as the eluent, to give **12** (32 mg: 55%). IR: 3492, 3400—3050, 1663, 1608 cm^{-1}; ^1H NMR (DMSO-d_6: 90 MHz): 1.16 (3H, s) and 1.18 (3H, s) ($-\dot{C}(CH_3)_2$), 1.18 (3H, d, $J=6$ Hz, C_{15}-CH_3), 1.48 (3H, s, C_{10}-CH_3), 1.68 (1H, bd, $J=12$ Hz, $C_{5\alpha}$-H), 3.55 (2H, bd, $J=6$ Hz, $-CH_2O-$), 4.47 (1H, bd, $J=12$ Hz, $C_{6\beta}$-H), 7.33 (1H, s, C_{14}-H). The ^1H NMR spectrum of **12** was in good agreement with that of natural nellionol,[1] except for the signals due to the corresponding C-15 epimer.

*11,12,16-Triacetoxyabieta-6,8,11,13-tetraene (**25**).* A mixture of **22** (167 mg) and sodium borohydride (30 mg) in methanol (3.0 ml) was stirred at 0—5 °C for 30 min and then at room temperature for 1 h. The mixture was acidified with dilute hydrochloric acid (10%: 0.5 ml) refluxed for 1 h, and evaporated *in vacuo*. The residue was extracted with ether. The ether extract was washed with brine, dried over sodium sulfate, and evaporated *in vacuo*. The residual oil was acetylated[12] with acetic anhydride (1.0 ml) in pyridine (1.0 ml) at 60—70 °C for 3 h to give the crude **25** (160 mg) which, without purification, was used in the next reaction. IR: 1765, 1730 cm^{-1}; ^1H NMR: 0.96 (3H, s) and 1.03 (3H, s) ($-\dot{C}(CH_3)_2$), 1.11 (3H, s, C_{10}-CH_3), 1.18 (d, $J=7$ Hz) and 1.23 (d, $J=7$ Hz) (3H, C_{15}-CH_3), 1.95 (3H, s, C_{16}-$OCOCH_3$), 2.20(3H, s) and 2.23 (3H, s) (C_{11}-$OCOCH_3$ and C_{12}-$OCOCH_3$), 3.93 (d, $J=7$ Hz) and 4.00 (d, $J=7$ Hz) (2H, $-CH_2O-$), 5.93 (1H, dd, $J=9$ and 3 Hz, C_6-H), 6.45 (1H, dd, $J=9$ and 3 Hz, C_7-H), 6.77 (1H, s, C_{14}-H).

*11,12,16-Triacetoxyabieta-8,11,13-trien-6-one (**26**).* A mixture of the crude **25** (160 mg) and *m*-chloroperbenzoic acid (85%: 180 mg) in dichloromethane (4.0 ml) was stirred at 0—5 °C for 1 h and then at room temperature for 14 h. The mixture was diluted with ether and washed successively with aqueous potassium iodide, aqueous sodium thiosulfate aqueous sodium hydrogencarbonate, and brine. The ether solution was dried over sodium sulfate and evaporated *in vacuo*. The residual oil was refluxed with dilute hydrochloric acid (10%: 0.5 ml) in methanol (4.0 ml) for 1 h. The mixture was evaporated *in vacuo*, diluted with water, and extracted with ether. The ether extract was washed with water, dried over sodium sulfate, and evaporated *in vacuo* to give an oil (155 mg). This oil was acetylated[12] with acetic anhydride (0.5 ml) in pyridine (0.5 ml) at 75—85 °C for 3 h. After the usual work-up, the crude product was purified by column chromatography on silica gel (7.0 g), using ether-benzene (3:97) as the eluent, to give **26** (64 mg: 40% from **22**). IR: 1767, 1733, 1720 cm^{-1}; ^1H NMR ($CDCl_3$): 1.05 (3H, s) and 1.23 (3H, s) ($-\dot{C}(CH_3)_2$), 1.22 (d, $J=7$ Hz) and 1.24 (d, $J=7$ Hz) (3H, C_{15}-CH_3), 1.34 (3H, s, C_{10}-CH_3), 2.05 (3H, s, C_{16}-$OCOCH_3$), 2.34 (6H, s, C_{11}-$OCOCH_3$ and C_{12}-$OCOCH_3$), 2.60 (1H, bs, C_5-H), 3.64 (2H, br, $-COCH_2-$), 4.06 (d, $J=7$ Hz) and 4.09 (d, $J=7$ Hz) (2H, $-CH_2O-$), 6.90 (1H, s, C_{14}-H).

*6,11,12,16-Tetraacetoxyabieta-5,8,11,13-tetraen-7-one (**27**).* A solution of **26** (84 mg) in acetone (2.0 ml) was oxidized with Jones reagent [2.5 M (1 M=1 mol dm^{-3}): 0.1 ml] at 0—5 °C for 10 min and then at room temperature for 2 h. The mixture was diluted with water and extracted with ether. The ether extract was washed with brine, dried over sodium sulfate, and evaporated *in vacuo*. The residual oil (78 mg) was refluxed with acetic anhydride (4.0 ml) in the presence of anhydrous sodium acetate (200 mg) for 2.5 h with stirring. The mixture was diluted with water and benzene, evaporated *in vacuo*, and extracted with ether. The ether extract was washed successively with aqueous sodium hydrogencarbonate and brine, dried over sodium sulfate, and evaporated *in vacuo*. The residue was chromatographed on silica gel (4.0 g), using ether-benzene (5:95) at the eluent, to give **27** (49 mg: 52%). IR: 1776, 1728, 1658, 1612 cm^{-1}; ^1H NMR ($CDCl_3$: 90 MHz): 1.29 (d, $J=$

7 Hz) and 1.31 (d, $J=7$ Hz) (3H, C_{15}-CH_3), 1.40 (6H, s, -$\dot{C}(CH_3)_2$), 1.65 (3H, s, C_{10}-CH_3), 2.00(s) and 2.01(s) (3H, C_{16}-$OCOCH_3$), 2.32 (3H, s) and 2.36 (6H, s) (C_6-$OCOCH_3$, C_{11}-$OCOCH_3$, and C_{12}-$OCOCH_3$), 3.24 (1H, m, C_{15}-H), 4.07 (d, $J=7$ Hz) and 4.10 (d, $J=7$ Hz) (2H, -CH_2O-), 8.11 (1H, s, C_{14}-H). The ^{1}H NMR spectrum of **27** was in good agreement with that of natural dehydronellionol tetraacetate,[1] except for the signals due to the corresponding C-15 epimer. Found: C, 65.06; H, 6.74%. Calcd for $C_{28}H_{34}O_9$: C, 65.36; H, 6.66%.

*6,11,12,16-Tetrahydroxyabieta-5,8,11,13-tetraen-7-one (**13**).* A mixture of **27** (35 mg) and dilute hydrochloric acid (10%: 0.3 ml) in methanol (2.0 ml) was refluxed for 1 h. The mixture was diluted with water and extracted with ether. The ether extract was washed with brine, dried over sodium sulfate, and evaporated *in vacuo*. The residue was chromatographed on silicic acid (Mallinckrodt CC-4: 3.0 g), using hexane-chloroform (1:4) as the eluent, to give **13** (8.9 mg: 38%). IR: 3515, 3450—3050, 1630, 1600 cm^{-1}; ^{1}H NMR ($CDCl_3$: 90 MHz): 1.38 (3H, d, $J=7$ Hz, C_{15}-CH_3), 1.46 (6H, s, -$\dot{C}(CH_3)_2$), 1.67 (3H, s, C_{10}-CH_3), 3.70—4.14 (2H, m, -CH_2O-), 7.09 (1H, s, -OH), 7.59 (1H, s, C_{14}-H). The ^{1}H NMR spectrum of **13** was in good agreement with that of natural dehydronellionol,[1] except for the signal due to the corresponding C-15 epimer.

The authors are grateful to Arakawa Chemical Co. Ltd. for a generous gift of rosin. Thanks are also due to Professor Ch. B. Rao for kindly supplying the spectral data of the natural products.

References

1) Ch. B. Rao, T. N. Rao, and E. K. S. Vijayakumar, *Curr. Sci.*, **47**, 455 (1978); *Indian J. Chem.*, **18B**, 513 (1979).
2) T. Kondo, M. Suda, and M. Teshima, *J. Pharm. Soc. Jpn.*, **82**, 1252 (1962).
3) A. G. Gonzalez, B. M. Fraga, J. G. Luis, and A. G. Ravelo, *Experientia*, **29**, 1471 (1973).
4) F. Yoshizaki, P. Rüedi, and C. H. Eugster, *Helv. Chim. Acta*, **62**, 2754 (1979).
5) H. Linde, *Helv. Chim. Acta*, **47**, 1234 (1964).
6) E. Wenkert, A. Fuchs, and J. D. McChesney, *J. Org. Chem.*, **30**, 2931 (1965).
7) T. Matsumoto, S. Imai, and S. Yuki, *Bull. Chem. Soc. Jpn.*, **55**, 3836 (1932).
8) H. Burnell and M. Ringuet, *Can. J. Chem.*, **56**, 517 (1978).
9) H. Akita and T. Oishi, *Chem. Pharm. Bull.*, **29**, 1567 (1981).
10) T. Matsumoto, Y. Ohsuga, S. Harada, and K. Fukui, *Bull. Chem. Soc. Jpn.*, **50**, 266 (1977); T. Matsumoto, S. Usui, and T. Morimoto, *ibid.*, **50**, 1575 (1977); T. Matsumoto, H. Kawashima, and K. Iyo, *ibid.*, **55**, 1168 (1982).
11) The oxidation gave a mixture of 6α-hydroxy and 6α-acetoxy derivatives which was acetylated to facilitate the purification.
12) Under these conditions, the acetoxyl groups were partially hydrolyzed.
13) T. Matsumoto, S. Imai, S. Yuki, A. Katayama, and M. Furutani, *Bull Chem. Soc. Jpn.*, **55**, 527 (1982).

The Synthesis of (+)-Pisiferol and (+)-Pisiferal

Takashi Matsumoto,* Yoshinori Endo, and Masaru Okimoto

Department of Chemistry, Faculty of Science, Hiroshima University, Higashisenda-machi, Naka-ku, Hiroshima 730

(Received January 12, 1983)

Reduction of abieta-8,11,13,-trien-6-one with lithium aluminium hydride, followed by treatment with lead tetraacetate and iodine, afforded 6*β*,20-epoxyabieta-8,11,13-triene. This was converted into a separable mixture of abieta-8,11,13-trien-20-ol (**13**) and 5*βH*-abieta-8,11,13-trien-20-ol (**14**) by a series of reactions; ether cleavage with acetic *p*-toluenesulfonic anhydride, catalytic hydrogenation, and reduction with lithium aluminium hydride. Acetylation of **13** and **14** gave the corresponding acetates, 20-acetoxyabieta-8,11,13-triene (**11**) and 20-acetoxy-5*βH*-abieta-8,11,13-triene (**12**). Friedel-Crafts acylation of **11** with acetyl chloride in the presence of anhydrous aluminium chloride afforded 20-acetoxy-12-acetylabieta-8,11,13-triene, which was converted into pisiferol by oxidation with *m*-chloroperbenzoic acid and subsequent treatment with lithium aluminium hydride. The synthetic pisiferol was oxidized with Jones reagent to give pisiferal. Similarly, 5*βH*-abieta-8,11,13-triene-12,20-diol was synthesized from **12**. Conversion of the cis A/B ring junctions in **12** into the trans ones is also described.

Pisiferol (**1**) and pisiferal (**2**), rare naturally-occurring tricyclic diterpenes possessing an oxidized angular methyl group, have recently been isolated from the leaves of *Chamaecyparis pisifera* (Cupressaceae) by Yatagai *et al.*[1,2] As a part of our synthetic studies on the naturally-occurring diterpenes, we have attempted the syntheses of these rare natural compounds. This paper will describe the syntheses of (+)-pisiferol (**1**) and (+)-pisiferal (**2**), starting from (+)-abieta-8,11,13-trien-6-one (**3**)[3-5] which was prepared from an epimeric mixture of 7*α*- and 7*β*-acetoxyabieta-8,11,13-triene (**4**)[3] in an improved yield.

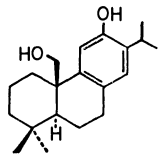

1

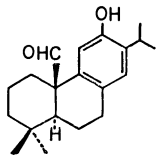

2

Treatment of the mixture **4** with 10% hydrochloric acid in refluxing ethanol afforded abieta-6,8,11,13-tetraene (**5**)[3-5] (84.4%). The tetraene **5** was oxidized at 0—5 °C with *m*-chloroperbenzoic acid in dichloromethane to give an epoxide (**6**) which, without purification, was converted into **3** (82.3% from **5**) by refluxing with *p*-toluenesulfonic acid in benzene. Reduction of **3** with lithium aluminium hydride in refluxing ether yielded abieta-8,11,13-trien-6*β*-ol (**7**: 87.3%). The stereochemistry of the hydroxyl group at C-6 in **7** was assigned to be *β*-configuration from its ^{1}H NMR spectrum, which showed a signal due to the angular methyl group at C-10 in a lower field (δ 1.51) than that of the corresponding signal (δ 1.29) in **3**. These down-field shift suggested a 1,3-diaxial *cis*-relationship between the angular methyl group and the hydroxyl group at C-6. In order to oxidize the angular methyl group by transannular oxidation, the alcohol **7** in benzene was treated with lead tetraacetate in the presence of iodine at room temperature under a stream of nitrogen. Purification of the crude product by column chromatography on silica gel afforded 6*β*,20-epoxyabieta-8,11,13-triene (**8**: 86.3%). The structure of **8** was supported by the appearance of signals due to methylene protons [ABq at δ 3.51 (d, J=8 Hz) and 3.82 (d, J=8 Hz)] in its ^{1}H NMR spectrum and by the disappearance of the signal due to the angular methyl group. Treatment of **8** with acetic *p*-toluenesulfonic anhydride[6] in dichloromethane at room temperature produced a mixture of 20-acetoxyabieta-5,8,11,13-tetraene (**9**) and 20-acetoxyabieta-6,8,11,13-tetraene (**10**) in 87.1% yield. The ^{1}H NMR spectrum of the mixture showed the presence of **9** [δ 3.33 (2H, d, J=4 Hz, C_7–H_2) and 6.17 (1H, t, J=4 Hz, C_6–H)] and **10** [δ 2.31 (1H, t, J=3 Hz, C_5–H), 5.97 (1H, dd, J=3 and 10 Hz, C_6–H), and 6.55 (1H, dd, J=3 and 10 Hz, C_7–H)] in a ratio of *ca.* 5:8. The mixture of **9** and **10** in acetic acid was submitted to catalytic hydrogenation over PtO_2 at room temperature to afford a mixture of 20-acetoxyabieta-8,11,13-triene (**11**) and its cis isomer (**12**). Because of the difficulty of the separation of **11** and **12**, the mixture was immediately treated with lithium aluminium hydride in refluxing ether. The repeated column chromatography of the crude product using silica gel afforded abieta-8,11,13-trien-20-ol (**13**) and its cis isomer (**14**) in 66.1% and 20.0% yields from the mixture of **9** and **10**. The *cis*-configuration of the A/B ring junction in **14** was supported by the appearance of a signal due to one of the *gem*-dimethyl groups at C-4 in very high field (δ 0.41) owing to the shielding effect of the aromatic C ring. Acetylation of **13** and **14** with acetic anhydride in pyridine gave the corresponding acetates, **11** (98.4%) and **12** (93.5%). The Friedel-Crafts acylation of **11** with acetyl chloride in dichloromethane in the presence of anhydrous aluminium chloride yielded 20-acetoxy-12-acetylabieta-8,11,13-triene (**15**: 85.4%), whose IR spectrum showed carbonyl bands at 1732 and 1680 cm^{-1}. The ^{1}H NMR spectrum of **15** showed two singlets at δ 6.94 and 7.30 due to the two aromatic protons. These spectral data of **15** supported the presence of an acetyl group at C-12. The Baeyer-Villiger oxidation of **15** with *m*-chloroperbenzoic acid in the presence of *p*-toluenesulfonic acid in refluxing 1,2-dichloroethane afforded 12,20-diacetoxyabieta-8,11,13-triene (**16**: 69.3%). Treatment of **16** with lithium aluminium hydride in refluxing ether yielded abieta-8,11,13-triene-12,20-diol (pisiferol) (**1**: 96.4%) which, on methylation with methyl iodide and anhydrous potassium carbonate in refluxing ethyl methyl ketone, afforded 12-methoxyabieta-8,11,13-trien-20-ol (**17**: 98.4%). The IR and

^{1}H NMR spectra of the synthetic **1** were identical with those of natural pisiferol. Oxidation[1] of **1** with Jones reagent at 0—5 °C afforded 12-hydroxyabieta-8,11,13-trien-20-al (pisiferal)[1,2] (**2**: 47.6%). Similarly, the cis acetate **12** was also converted into 5βH-abieta-8,11,13-tricne-12,20-diol (**20**: 98.5%) *via* 20-acetoxy-12-acetyl-5βH-abieta-8,11,13-triene (**18**: 57.2 %) and 12,20-diacetoxy-5βH-abieta-8,11,13-triene (**19**: 61.8%).

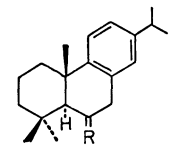

3 R=O
7 R=α-H, β-OH

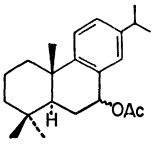

4

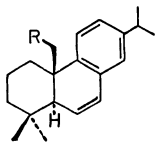

5 R=H
10 R=OAc

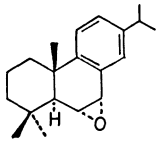

6

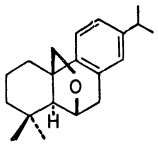

8

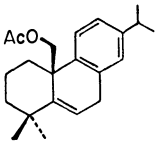

9

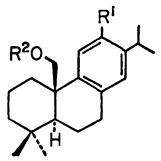

11 R^1=H, R^2=Ac
13 R^1=R^2=H
15 R^1=R^2=Ac
16 R^1=OAc, R^2=Ac
17 R^1=OMe, R^2=H

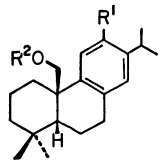

12 R^1=H, R^2=Ac
14 R^1=R^2=H
18 R^1=R^2=Ac
19 R^1=OAc, R^2=Ac
20 R^1=OH, R^2=H

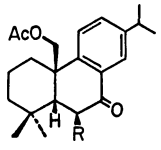

21 R=H
23 R=Br

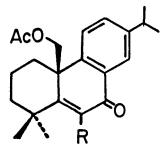

24 R=H
25 R=OAc

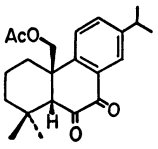

22

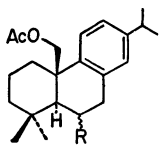

26 R=α-OAc
27 R=β-OAc

Subsequently, conversion of the cis A/B ring junctions into the trans ones was carried out as follows. The cis acetate **12** was oxidized with Jones reagent at room temperature to give 20-acetoxy-5βH-abieta-8,11,13-trien-7-one (**21**: 52.3%[7]) and 20-acetoxy-5βH-abieta-8,11,13-triene-6,7-dione (**22**: 28.8[7]). Bromination of **21** with pyridinium tribromide in dichloromethane at room temperature afforded 20-acetoxy-6β-bromo-5βH-abieta-8,11,13-trien-7-one (**23**: 97.3%) which was converted into 20-acetoxyabieta-5,8,11,13-tetraen-7-one (**24**: 87.8%) by treatment with lithium carbonate and lithium bromide in *N,N*-dimethylformamide at 110—130 °C under a stream of nitrogen. The tetraene **24** in ethyl acetate was catalytically hydrogenated with 10% Pd–C in the presence of perchloric acid to give the trans acetate (**11**: 98.9%). The 6,7-dioxo acetate **22** was refluxed with anhydrous sodium acetate in acetic anhydride to give the corresponding enol acetate (**25**: 77.9%). The enol acetate **25** in ethyl acetate was then submitted to catalytic hydrogenation over 10% Pd–C in the presence of perchloric acid. Purification of the crude product by column chromatography on silica gel afforded **11** (28.8%) and a mixture (53.2%) of 6α,20- (**26**) and 6β,20-diacetoxyabieta-8,11,13-triene (**27**) (*ca.* 1:1 ratio).

Experimental

All melting points are uncorrected. The IR spectra and optical rotations were measured in chloroform and the ^{1}H NMR spectra in carbon tetrachloride at 60 MHz, with tetramethylsilane as an internal standard, unless otherwise stated. The chemical shifts are presented in terms of δ values; s: singlet, bs: broad singlet, d: doublet, bd: broad doublet, dd: double doublet, t: triplet, m: multiplet. The column chromatography was performed using Merck silica gel.

*Abieta-6,8,11,13-tetraene (**5**).* The epimeric mixture of 7α- and 7β-acetoxyabieta-8,11,13-triene (**4**)[3] was prepared from (+)-dehydroabietic acid.

A mixture of **4** (5.830 g) and dilute hydrochloric acid 10%: 8.5 ml) in ethanol (50 ml) was refluxed for 2.5 h and evaporated *in vacuo*. The residue was diluted with water and extracted with ether. The ether extract was washed with brine, dried over sodium sulfate, and evaporated *in vacuo*. The crude product was purified by column chromatography on silica gel (50 g), using hexane as the eluent, to give **5**[3-5] (4.023 g: 84.4%), $[\alpha]_D$ −124° (*c* 4.67).

*Abieta-8,11,13-trien-6-one (**3**).* A mixture of **5** (16.77 g) and *m*-chloroperbenzoic acid (80%: 17.50 g) in dichloromethane (170 ml) was stirred at 0—5 °C for 1.5 h. The mixture was diluted with ether and then washed successively with aqueous potassium iodide, aqueous sodium thiosulfate apueous sodium hydrogencarbonate, and brine. The solution was dried over sodium sulfate and evaporated *in vacuo* to give a crude epoxide (**6**) (17.38 g); ^{1}H NMR: 1.09, 1.14, and 1.20 (each 3H and s, $-\underline{C}(CH_3)_2$ and C_{10}-CH_3), 1.26 (6H, d, J=7 Hz, $-CH(C\underline{H}_3)_2$), 2.83 (1H, m, $-C\underline{H}(CH_3)_2$), 3.29 (1H, t, J=4 Hz, $C_{6\beta}$-H), 3.61 (1H, d, J=4 Hz, $C_{7\beta}$-H), 6.98 (2H, bs, C_{11}-H and C_{12}-H), 7.24 (1H, bs, C_{14}-H).

A mixture of the crude epoxide **6** (17.38 g) and *p*-toluenesulfonic acid monohydrate (1.50 g) in dry benzene (250 ml) was refluxed for 1 h. The benzene solution was washed successively with water, aqueous sodium hydrogencarbonate, and brine. The solution was dried over sodium sulfate and evaporated *in vacuo*. The crude product was chromatographed on silica gel (300 g), using hexane-benzene (1:1) as the eluent, to give **3**[3-5] (14.63 g: 82.3% from **5**), $[\alpha]_D$ +125° (*c* 2.64), IR: 1710 cm^{-1}.

Abieta-8,11,13-trien-6β-ol (7). A mixture of **3** (3.196 g) and lithium aluminium hydride (420 mg) in dry ether (50 ml) was stirred at 0—5 °C for 5 min and then refluxed for 1.5 h. The mixture was poured into ice-dilute hydrochloric acid, and exteacted with ether. The ether extract was washed with brine, dried over sodium sulfate, and evaporated *in vacuo*. The residue was chromatographed on silica gel (150 g), using benzene as the eluent, to give **3** (89 mg: 2.8%). Further elution with the same solvent afforded **7** (2.808 g: 87.3%) as a solid, mp 100—101 °C, $[\alpha]_D$ +40.8° (*c* 5.15); IR: 3615, 3480 cm^{-1}; ^1H NMR: 0.99 and 1.23 (each 3H and s, $-\dot{C}(CH_3)_2$), 1.22 (6H, d, J=7 Hz, $-CH(C\underline{H}_3)_2$), 1.51 (3H, s, C_{10}-CH_3), 4.50 (1H, bs, $W_{1/2}$=9.5 Hz, $C_{6\alpha}$-H), 6.73 (1H, bs, C_{14}-H), 6.85 (1H, bd, J=8 Hz, C_{12}-H), 7.10 (1H, d, J=8 Hz, C_{11}-H). Found: C, 83.85; H, 10.75%. Calcd for $C_{20}H_{30}O$: C, 83.86; H, 10.56%.

6β,20-Epoxyabieta-8,11,13-triene (8). A mixture of **7** (13.18 g), lead tetraacetate (87.5%: 32.2 g), and iodine (16.6 g) in dry benzene (250 ml) was stirred for 2 h under a stream of nitrogen with cooling in a water bath. The mixture was diluted with benzene and the organic solution was washed successively with aqueous sodium thiosulfate, aqueous sodium hydrogencarbonate, and brine. The dried solution was evaporated *in vacuo*. The crude product was purified by column chromatography on silica gel (500 g), using benzene as the eluent, to give **8** (11.30 g: 86.3%), $[\alpha]_D$ −64.4° (*c* 2.10); ^1H NMR: 0.93 and 1.02 (each 3H and s, $-\dot{C}(CH_3)_2$), 1.20 (6H, d, J=7 Hz, $-CH(C\underline{H}_3)_2$), 2.76 (1H, m, $-C\underline{H}(CH_3)_2$), 2.92 (2H, bd, J=2.5 Hz, C_7-H_2), 3.51 and 3.82 (ABq, each 1H and d, J=8 Hz, $-CH_2O-$), 4.35 (1H, t, J=2.5 Hz, $-\dot{C}HO-$). Found: C, 84.53; H, 10.21%. Calcd for $C_{20}H_{28}O$: C, 84.45; H, 9.92%.

Ether Cleavage of 8. A mixture of **8** (8.131 g) and acetic *p*-toluenesulfonic anhydride (18.40 g) in dichloromethane (150 ml) was stirred at room temperature for 2.5 h and then diluted with ether. The ether solution was washed successively with aqueous sodium hydrogencarbonate and brine, dried over sodium sulfate, and evaporated *in vacuo*. The crude product was chromatographed on silica gel (500 g), using benzene as the eluent, to give a mixture (8.13 g: 87.1%) of 20-acetoxyabieta-5,8,11,13-tetraene (**9**) and 20-acetoxyabieta-6,8,11,13-tetraene (**10**) in a ratio of *ca.* 5:8 by ^1H NMR spectrum analysis. ^1H NMR of **9** ($CDCl_3$, 90 MHz): 1.85 (3H, s, $-OCOCH_3$), 3.33 (2H, d, J=4 Hz, $=CHC\underline{H}_2-$), 4.13 (2H, s, $-C\underline{H}_2OCOCH_3$), 6.17 (1H, t, J=4 Hz, C_6-H). ^1H NMR of **10** ($CDCl_3$, 90 MHz): 1.74 (3H, s, $-OCOCH_3$), 2.31 (1H, t, J=3 Hz, $C_{5\alpha}$-H), 4.23 and 4.38 (ABq, each 1H and d, J=11 Hz, $-C\underline{H}_2OCOCH_3$), 5.97 (1H, dd, J=3 and 10 Hz, C_6-H), 6.55 (1H, dd, J=3 and 10 Hz, C_7-H).

Abieta-8,11,13-trien-20-ol (13) and 5βH-Abieta-8,11-13-trien-20-ol (14). A mixture (9.180 g) of **9** and **10** in acetic acid (25 ml) was submitted to catalytic hydrogenation using PtO_2 (1.0 g) at room temperature.

The crude product (8.848 g) was immediately treated for 2 h with lithium aluminium hydride (2.04 g) in refluxing ether (100 ml). The excess lithium aluminium hydride was decomposed with ethyl acetate. The mixture was poured into ice-dilute hydrochloric acid and extracted with ether. The ether extract was washed with brine, dried over sodium sulfate, and evaporated *in vacuo*. The residue was purified by repeated column chromatography on silica gel, using ether-benzene (1:99) as the eluent, to give **13** (5.323 g: 66.1%) and **14** (1.614 g: 20.0%). Alcohol **13**: $[\alpha]_D$ +41.6° (*c* 4.93); IR: 3580, 3440 cm^{-1}; ^1H NMR: 0.97 (6H, s, $-\dot{C}(CH_3)_2$), 1.20 (6H, d, J=7 Hz, $-CH(C\underline{H}_3)_2$), 3.45 and 3.73 (ABq, each 1H and bd, J=11 Hz, $-C\underline{H}_2OH$). Found: C, 84.02; H, 10.61%. Calcd for $C_{20}H_{30}O$: C, 83.86; H, 10.56%. Alcohol **14**: $[\alpha]_D$ +17.4° (*c* 2.24); IR: 3610, 3580, 3430 cm^{-1}; ^1H NMR: 0.41 (3H, s, $C_{4\alpha}$-CH_3), 0.95 (3H, s, $C_{4\beta}$-CH_3), 1.21 (6H, d, J=7 Hz, $-CH(C\underline{H}_3)_2$), 3.27 (2H, bs, $-C\underline{H}_2OH$), 6.77 (1H, bs, C_{14}-H), 6.83 (1H, dd, J=1.5 and 8 Hz, C_{12}-H), 7.10 (1H, d, J=8 Hz, C_{11}-H). Found: C, 83.98; H, 10.70%. Calcd for $C_{20}H_{30}O$: C, 83.86; H, 10.56%.

20-Acetoxyabieta-8,11,13-triene (11). A mixture of **13** (885 mg) and acetic anhydride (1.0 ml) in pyridine (2.0 ml) was heated at 70—80 °C for 2 h. After the usual work-up, the crude product was chromatographed on silica gel (40 g), using benzene as the eluent, to give **11** (999 mg: 98.4%), $[\alpha]_D$ +56.0° (*c* 3.89), IR: 1733 cm^{-1}; ^1H NMR: 0.99 (6H, bs, $-\dot{C}(CH_3)_2$), 1.21 (6H, d, J=7 Hz, $-CH(C\underline{H}_3)_2$), 1.79 (3H, s, $-OCOCH_3$), 4.03 and 4.43 (ABq, each 1H and d, J=11 Hz, $-C\underline{H}_2OCOCH_3$). Found: C, 80.17; H, 10.01%. Calcd for $C_{22}H_{32}O_2$: C, 80.44; H, 9.83.

20-Acetoxy-5βH-abieta-8,11,13-triene (12). A mixture of **14** (403.1 mg) and acetic anhydride (0.5 ml) in pyridine (1.0 ml) was heated at 70—80 °C for 2 h. After the usual work-up, the crude product was chromatographed on silica gel (30 g), using ether-benzene (1:99) as the eluent, to give **12** (432.0 mg: 93.5%), $[\alpha]_D$ +29.0° (*c* 8.14), IR: 1726 cm^{-1}; ^1H NMR: 0.39 (3H, s, $C_{4\alpha}$-CH_3), 0.94 (3H, s, $C_{4\beta}$-CH_3), 1.21 (6H, d, J=7 Hz, $-CH(C\underline{H}_3)_2$), 1.93 (3H, s, $-OCOCH_3$), 3.63 and 3.97 (ABq, each 1H and d, J=11 Hz, $-C\underline{H}_2OCOCH_3$), 6.78 (1H, bs, C_{14}-H), 6.86 (1H, bd, J=8 Hz, C_{12}-H), 7.13 (1H, d, J=8 Hz, C_{11}-H). Found: C, 80.56; H, 10.13%. Calcd for $C_{22}H_{32}O_2$: C, 80.44; H, 9.83%.

20-Acetoxy-12-acetylabieta-8,11,13-triene (15). Anhydrous aluminium chloride (1.20 g) was added at 0—5 °C to a stirred solution of **11** (962.3 mg) and acetyl chloride (0.65 ml) in dichloromethane (16 ml). The mixture was stirred at this temperature for 5 min and then at room temperature for 3 h, poured into ice-dilute hydrochloric acid, and extracted with ether. The ether extract was washed successively with aqueous sodium hydrogencarbonate and brine, dried over sodium sulfate, and evaporated *in vacuo*. The residue was chromatographed on silica gel (60 g), using ether-benzene (3.97) as the eluent, to give **15** (927.8 mg: 85.4%), $[\alpha]_D$ +30.6° (*c* 13.02); IR: 1732, 1680 cm^{-1}; ^1H NMR: 0.99 (6H, s, $-\dot{C}(CH_3)_2$), 1.18 (6H, d, J=7 Hz, $-CH(C\underline{H}_3)_2$), 1.80 (3H, s, $-OCOCH_3$), 2.44 (3H, s, C_{12}-$COCH_3$), 3.45 (1H, m, $-C\underline{H}(CH_3)_2$), 4.01 and 4.47 (ABq, each 1H and d, J=11 Hz, $-C\underline{H}_2OCOCH_3$), 6.94 (1H, bs, C_{14}-H), 7.30 (1H, s, C_{11}-H). Found: C, 78.07; H, 9.39%. Calcd for $C_{24}H_{34}O_3$: C, 77.80;H, 9.25%.

12,20-Diacetoxyabieta-8,11,13-triene (16). A mixture of **15** (906.0 mg), *m*-chloroperbenzoic acid (80%: 1.05 g), and *p*-toluenesulfonic acid monohydrate (30 mg) in 1,2-dichloroethane (23 ml) was refluxed for 2 h. The mixture was cooled, diluted with ether, and washed successively with aqueous potassium iodide, aqueous sodium thiosulfate,

aqueous sodium hydrogencarbonate, and brine. The dried ether solution was evaporated *in vacuo*. The residue was chromatographed on silica gel (60 g), using ether–benzene (0.5:99.5) as the eluent, to give **16** (655.4 mg: 69.3%), $[\alpha]_D$ +51.9° (*c* 2.37·; IR: 1750 sh, 1732 cm^{-1}; ^1H NMR: 0.97 6H, s, $-C(CH_3)_2$), 1.15 (6H, d, J=7 Hz, $-CH(CH_3)_2$), 1.82 (3H, s, C_{20}-$OCOCH_3$), 2.21 (3H, s, C_{12}-$OCOCH_3$), 4.00 and 4.37 (ABq, each 1H and d, J=11 Hz, $-CH_2OCOCH_3$), 6.69 and 6.13 (each 1H and s, C_{11}-H and C_{14}-H). Found: C, 74.58; H, 8.95%. Calcd for $C_{24}H_{34}O_4$: C, 74.57; H, 8.87%.

*Abieta-8,11,13-triene-12,20-diol (Pisiferol) (**1**).* A mixture of **16** (495.7 mg) and lithium aluminium hydride (195 mg) in dry ether (5.0 ml) was refluxed for 2 h. The mixture was poured into ice-dilute hydrochloric acid and extracted with ether. The ether extract was washed with brine, dried over sodium sulfate, and evaporated *in vacuo*. The crude product was purified by column chromatography on silica gel (25 g), using ether–benzene (7:93) as the eluent, to give **1** (373.9 mg: 96.4%), which was recrystallized from hexane, mp 147—148.5 °C, $[\alpha]_D$ +79.6° (*c* 2.21); IR: 3580, 3330 cm^{-1}; H^1 NMR ($CDCl_3$, 90 MHz): 0.90 and 0.94 (each 3H and s, $-C(CH_3)_2$), 1.22 (6H, d, J=7 Hz, $-CH(CH_3)_2$), 3.18 (1H, m, $-CH(CH_3)_2$), 3.57 and 3.98 (ABq, each 1H and d, J=11 Hz, $-CH_2OH$), 6.03 (1H, bs, -OH), 6.71 (1H, s) and 6.91 (1H, bs) (C_{11}-H and C_{14}-H). Found: C, 79.71; H, 10.19%. Calcd for $C_{20}H_{30}O_2$: C, 79.42; H, 10.00%. The IR and ^1H MNR spectra of the synthetic **1** were identical with those of natural pisiferol. However, the melting point of the synthetic **1** was higher than that reported (mp 108—110 °C) for natural pisiferol.[8]

*12-Hydroxyabieta-8,11,13-trien-20-al (Pisiferal) (**2**).* A solution of **1** (127.3 mg) in acetone (4.0 ml) was oxidized with Jones reagent [2.5 M (1 M=1 mol dm^{-3}): 0.2 ml] at 0—5°C for 1 min. The mixture was diluted with water and extracted with ether. The ether extract was washed with brine, dried over sodium sulfate, and evaporated *in vacuo*. The residue was chromatographed on silica gel (10 g), using ether–benzene (1:99) as the eluent, to give **2** (60.2 mg: 47.6%), which was recrystallized from hexane, mp 125.5—127 °C, $[\alpha]_D$ +386° (*c* 0.29); IR: 3595, 3360, 2745, 1700 cm^{-1}; ^1H NMR ($CDCl_3$, 90 MHz): 0.82 and 1.00 (each 3H and s, $-C(CH_3)_2$), 1.20 (6H, d, J=7 Hz, $-CH(CH_3)_2$), 2.92 (2H, *t*, J=6 Hz, C_7-H_2), 3.15 (1H, m, $-CH(CH_3)_2$), 5.63 (1H, bs, C_{12}-OH), 6.64 (1H, s) and 6.92 (1H, bs) (C_{11}-H and C_{14}-H), 9.90 (1H, d, J=1.5 Hz, -CHO); MS (*m/e*): 300 (M^+). The IR and ^1H NMR spectra of the synthetic **2** were identical with those of natural pisiferal. However, the melting point of the synthetic **2** was also higher than that reported (mp 80—82 °C[9]) for natural pisiferal.

*12-Methoxyabieta-8,11,13-trien-20-ol (**17**).* A stirred mixture of **1** (48.3 mg), methyl iodide (0.1 ml), and anhydrous potassium carbonate (220 mg) in ethyl methyl ketone (2.0 ml) was refluxed for 8 h. The mixture was diluted with water and extracted with ether. The ether extract was washed successively with aqueous sodium thiosulfate and brine, dried over sodium sulfate, and evaporated *in vacuo*. The residue was chromatographed on silica gel (5.0 g), using ether–benzene (2:98) as the eluent, to give **17** (49.6 mg: 98.4%), $[\alpha]_D$ +61.9° (*c* 0.70); IR: 3580, 3450 sh cm^{-1}; ^1H MNR: 0.97 (6H, s, $-C(CH_3)_2$), 1.16 (6H, d, J=7 Hz, $-CH(CH_3)_2$), 3.78 (3H, s, $-OCH_3$), 6.61 (1H, s) and 6.73 (1H, bs) (C_{11}-H and C_{14}-H). Found: C, 79.70; H, 10.47%. Calcd for $C_{21}H_{32}O_2$: C, 79.70; H, 10·19%.

*20-Acetoxy-12-acetyl-5βH-abieta-8,11,13-triene (**18**)* Anhydrous aluminium chloride (540 mg) was added at 0—5 °C to a stirred solution of **12** (428.3 mg) and acetyl chloride (0.29 ml) in dichloromethane (7.0 ml). The mixture was stirred at this temperature for 5 min and then at room temperature for 3 h. After the same work-up as described for the preparation of **15**, the crude product was purified by column chromatography on silica gel (20 g), using benzene and then ether–benzene (1:99) as the eluent, to give **18** (276.4 mg: 57.2%), $[\alpha]_D$ +18.8° (*c* 5.32); IR; 1733, 1680 cm^{-1}; ^1H NMR: 0.41 (3H, s, $C_{4\alpha}$-CH_3) 0.97 (3H, s, $C_{4\beta}$-CH_3), 1.20 (6H, d, J=7 Hz, $-CH(CH_3)_2$), 1.96 (3H, s, $-OCOCH_3$), 2.50 (3H, s, C_{12}-$COCH_3$), 3.70 and 3.97 (ABq, each 1H and d, J=11 Hz, $-CH_2OCOCH_3$), 6.98 (1H, bs, C_{14}-H), 7.40 (1H, s, C_{11}-H). Found: C, 77.65; H, 9.42%. Calcd for $C_{24}H_{31}O_3$: C, 77.80; H, 9.25%.

*16,20-Diacetoxy-5βH-abieta-8,11,13-triene (**19**)* A mixture of **18** (283.9 mg), *m*-chloroperbenzoic acid (80%: 330 mg), and *p*-toluenesulfonic acid monohydrate (5.0 mg) in 1,2-dichloroethane (6.0 ml) was refluxed for 2 h. After the same work-up as described for the preparation of **16**, the crude product was chromatographed on silica gel (50 g), using ether–benzene (1:99) as the eluent, to give **19** (185.8 mg: 61.8%), $[\alpha]_D$ +25.9° (*c* 3.13); IR: 1750 sh, 1732 cm^{-1}; ^1H NMR: 0.39 (3H, s, $C_{4\alpha}$-CH_3), 0.94 (3H, s, $C_{4\beta}$-CH_3), 1.17 (6H, d, J=7 Hz, $-CH(CH_3)_2$), 1.94 (3H, s, C_{20}-$OCOCH_3$), 2.24 (3H, s, C_{12}-$OCOCH_3$), 3.86 (2H, s, $-CH_2OCOCH_3$), 6.80 (1H, s) and 6.85 (1H, bs) (C_{11}-H and C_{14}-H). Found: C, 74.74; H, 9.11%. Calcd for $C_{24}H_{34}O_4$: C, 74.57; H, 8.87%.

*5βH-Abieta-8,11,13-triene-12,20-diol (**20**).* A mixture of **19** (153.3 mg) and lithium aluminium hydride (60 mg) in dry ether (5.0 ml) was refluxed for 2 h. After the same work-up as described for the preparation of **1**, the crude product was chromatographed on silica gel (10 g), using ether–benzene (8:92) as the eluent, to give **20** (125.7 mg: 98.5%). This was recrystallized from hexane, mp 113.5—115 °C, $[\alpha]_D$ +27.4° (*c* 2.60); IR: 3600, 3350 cm^{-1}; ^1H NMR ($CDCl_3$): 0.44 (3H, s, $C_{4\alpha}$-CH_3), 0.93 (3H, s, $C_{4\beta}$-CH_3), 1.22 (6H, d, J=7 Hz, $-CH(CH_3)_2$), 3.15 (1H, m, $-CH(CH_3)_2$), 3.38 (2H, bs, $-CH_2OH$), 6.65 (1H, s) and 6.79 (1H, bs) (C_{11}-H and C_{14}-H). Found: C, 79.37; H, 10.27%. Calcd for $C_{20}H_{30}O_2$: C, 79.42; H, 10.00%.

*Oxidation of **12**.* A solution of **12** (175.0 mg) in acetone (3.0 ml) was oxidized with Jones reagent (2.5 M: 0.3 ml) at room temperature for 2.5 h and then diluted with ether. The ether solution was washed with brine, dried over sodium sulfate, and evaporated *in vacuo*. The residue was chromatographed on silica gel (10 g), using benzene as the eluent, to give the starting **12** (79.7 mg: 45.5%). Subsequent elution with ether–benzene (3:97) afforded 20-acetoxy-5β*H*-abieta-8,11,13-trien-7-one (**21**) (52.0 mg: 28.5%; 52.3%[7]), $[\alpha]_D$ +40.0° (*c* 5.88); IR: 1735, 1672, 1608 cm^{-1}; ^1H NMR: 0.69 (3H, s, $C_{4\alpha}$-CH_3), 0.99 (6H, d, J=7 Hz, $-CH(CH_3)_2$), 1.05 (3H, s, $C_{4\beta}$-CH_3), 1.66 (3H, s, $-OCOCH_3$), 2.49 (2H, bd, J=5.5 Hz, $-CH_2CO-$), 2.64 (1H, m, $-CH(CH_3)_2$), 3.43 and 3.74 (ABq, each 1H and d, J=12 Hz, $-CH_2OCOCH_3$), 6.98 (2H, bs, C_{11}-H and C_{12}-H), 7.52 (1H, bs, C_{14}-H). Found: C, 77.31; H, 9.05%. Calcd for $C_{22}H_{30}O_3$: C, 77.15; H, 8.83%.

Further elution with the same solvent afforded 20-acetoxy-5β*H*-abieta-8,11,13-triene-6,7-dione (**22**) (29.8 mg: 15.7%; 28.8%[7]), $[\alpha]_D$ +50.2° (*c* 6.15); IR: 1748, 1727, 1688, 1608 cm^{-1}; ^1H NMR: 0.66 (3H, s, $C_{1\alpha}$-CH_3), 1.00 (6H, d, J=7 Hz, $-CH(CH_3)_2$), 1.06 (3H, s, $C_{4\beta}$-CH_3), 1.48 (3H, s, $-OCOCH_3$), 2.21 (1H, s, $C_{5\beta}$-H), 3.25 and 3.65 (ABq, each 1H and d, J=11 Hz, $-CH_2OCOCH_3$), 6.99 (1H, d, J=9 Hz C_{11}-H), 7.18 (1H, dd, J=1.5 and 9 Hz, C_{12}-H),

7.58 (1H, d, $J=1.5$ Hz, C_{14}-H); MS (*m/e*): 356 (M^+).

20-Acetoxy-6β-bromo-5βH-abieta-8,11,13-trien-7-one (23) A mixture of **21** (68.5 mg) and 80% pyridinium tribromide (80 mg) in dichloromethane (1.5 ml) was stirred at room temperature for 1 h. The mixture was diluted with water and extracted with ether. The ether extract was washed successively with aqueous sodium thiosulfate and water, dried over sodium sulfate, and evaporated *in vacuo*. The residue was chromatographed on silica gel (10 g), using ether-benzene (3:97) as the eluent, to give **23** (82.0 mg: 97.3%); IR: 1735, 1680, 1608 cm^{-1}; ^1H NMR: 0.26 (3H, s, $C_{4\alpha}$-CH_3), 1.13 (3H, s, $C_{4\beta}$-CH_3), 1.29 (6H, d, $J=7$ Hz, -CH($C\underline{H}_3$)$_2$), 1.99 (3H, s, -OCOCH_3), 2.61 (1H, s, $C_{5\beta}$-H), 2.94 (1H, m, -C$\underline{H}$(CH_3)$_2$), 3.81 and 4.12 (ABq, each 1H and d, $J=11.5$ Hz, -C$\underline{H}_2$OCOCH_3), 4.72 (1H, s, $C_{6\alpha}$-H), 7.15—7.5 (2H, m, C_{11}-H and C_{12}-H), 7.77 (1H, bs, C_{14}-H); MS (*m/e*): 422 (M^++2), 420 (M^+),

20-Acetoxyabieta-5,8,11,13-tetraen-7-one (24). A mixture of **23** (364.0 mg), lithium carbonate (192 mg), and lithium bromide (150 mg) in *N*,*N*-dimethylformamide (4.5 ml) was stirred at 110—130 °C for 4 h under a stream of nitrogen. The mixture was cooled, poured into ice-dilute hydrochloric acid, and extraced with ether. The ether extract was washed successively with aqueous sodium thiosulfate and brine, dried over sodium sulfate, and evaporated *in vacuo*. The crude product was purified by column chromatography on silica gel (20 g), using ether-benzene (3:97) as the eluent, to give **24** (258.3 mg: 87.8%). This was recrystallized from hexane, mp 75—76 °C, $[\alpha]_D$ −17.5° (*c* 5.15); IR: 1735, 1650, 1608 cm^{-1}; ^1H NMR: 1.28 (6H, d, $J=7$ Hz, -CH($C\underline{H}_3$)$_2$), 1.30 (6H, s, -$\dot{C}$(CH_3)$_2$), 1.72 (3H, s, -OCOCH_3), 2.95 (1H, m, -C$\underline{H}$(CH_3)$_2$), 4.05 and 4.43 (ABq, each 1H and d, $J=11$ Hz, -C$\underline{H}_2$OCOCH_3), 6.45 (1H, s, C_6-H), 7.28 (2H, bs, C_{11}-H and C_{12}-H), 7.79 (1H, bs, C_{14}-H). Found: C, 77.46; H, 8.34%. Calcd for $C_{22}H_{28}O_3$: C, 77.61; H, 8.29%.

Catalytic Hydrogenation of 24. A mixture of **24** (280 mg), 10% Pd-C (200 mg), and 60% perchloric acid (0.2 ml) in ethyl acetate (7.0 ml) was stirred at room temperature for 7.5 h in an atmosphere of hydrogen. The mixture was filtered and the filtrate was washed with brine. The dried solution was evaporated *in vacuo* to give an oil (267 mg: 98.9%), whose IR and ^1H NMR spectra were identical with those of the authentic **11**.

6,20-Diacetoxyabieta-5,8,11,13-tetraen-7-one (25). A mixture of **22** (220.0 mg) and anhydrous sodium acetate (900 mg) in acetic anhydride (9.0 ml) was refluxed for 28.5 h. The reaction mixture was cooled and diluted with ether. The ether solution was washed with water and evaporated *in vacuo*. The residue was extracted with ether. The ether extract was washed successively with aqueous sodium hydrogencarbonate and brine, dried over sodium sulfate, and evaporated *in vacuo*. The crude product was purified by column chromatography on silica gel (20 g), using ether-benzene (3:97) as the eluent, to give **25** (191.6 mg: 77.9%), $[\alpha]_D$ +13.1° (*c* 2.68); IR: 1760, 1740, 1664, 1614 cm^{-1}; ^1H NMR: 1.28 (6H, d, $J=7$ Hz, -CH($C\underline{H}_3$)$_2$), 1.29 and 1.34 (each 3H and s, -$\dot{C}$(CH_3)$_2$), 1.77 (3H, s, C_{20}-OCOCH_3), 2.30 (3H, s, C_6-OCOCH_3), 2.94 (1H, m, -C$\underline{H}$(CH_3)$_2$), 3.88 and 4.56 (ABq, each 1H and d, $J=11$ Hz, -C$\underline{H}_2$OCOCH_3), 7.33 (2H, bs, C_{11}-H and C_{12}-H), 7.80 (1H, bs, C_{14}-H); MS (*m/e*): 398 (M^+).

Catalytic Hydrogenation of 25. A mixture of **25** (175.0 mg), 10% Pd-C (175 mg), and 60% perchloric acid (0.2 ml) was submitted to catalytic hydrogenation at room temperature for 9 h. After the same work-up as described for the preparation of **11**, the crude product was chromatographed on silica gel (15 g), using benzene as the eluent, to give **11** (41.6 mg: 28.8%). Further elution with ether-benzene (1:99) afforded, without further separation, a mixture (90.3 mg: 53.2%) of 6α,20-diacetoxyabieta-8,11,13-triene (**26**) and 6β,20-diacetoxyabieta-8,11,13-triene (**27**) in a ratio of *ca.* 1:1. ^1H NMR of **26** ($CDCl_3$): 0.87 and 1.04 (each 3H and s, -$\dot{C}$(CH_3)$_2$), 1.69 and 1.98 (each 3H and s, C_6-OCOCH_3 and C_{20}-OCOCH_3), 4.32 (2H, s, -C$\underline{H}_2$OCOCH_3), 5.44 (1H, m, $W_{1/2}=14$ Hz, $C_{6\beta}$-H). ^1H NMR of **27** ($CDCl_3$): 1.04 and 1.07 (each 3H and s, -$\dot{C}$(CH_3)$_2$), 1.99 and 2.02 (each 3H and s, C_6-OCOCH_3 and C_{20}-OCOCH_3), 4.45 and 4.80 (ABq, each 1H and d, $J=12$ Hz, -C$\underline{H}_2$OCOCH_3), 5.65 (1H, m, $W_{1/2}=10$ Hz, $C_{6\alpha}$-H).

The authors are grateful to Dr. M. Yatagai, Forestry and Forest Products Research Institute, for kindly supplying the spectral data of natural products.

References

1) M. Yatagai, T. Shirato, Y. Hayashi, N. Fukuhara, and T. Takahashi, *Mokuzai Gakkaishi*, **24**, 267 (1978).
2) M. Yatagai and T. Takahashi, *Phytochemistry*, **18**, 176 (1979); **19**, 1149 (1980).
3) J. W. Huffman and J. J. Gibbs, *J. Org. Chem.*, **39**, 2501 (1974).
4) G. Defaye-Duchateau, *Bull. Soc. Chim. Fr.*, **1964**, 1469.
5) G. Defaye-Duchateau, *Chem. Abstr.*, **72**, 79254d (1970).
6) M. H. Karger and Y. Mazur, *J. Org. Chem.*, **36**, 528 (1971).
7) Yields are based on the starting material consumed.
8) A personal communication from Dr. Yatagai informed us that the melting point of natural piciferol was raisen to 146.6—148.2 °C by recrystallization and no depression resulted when it was mixed with the synthetic pisiferol (**1**).

 © 1983 The Chemical Society of Japan Bull. Chem. Soc. Jpn., 56, 2023—2028 (1983)

Synthesis of [0]Orthocyclo[2]orthocyclo[0](1,1′)ferrocenophane and [0]Paracyclo[2]paracyclo[0](1,1′)ferrocenophane

Iwao Shimizu, Hiroshi Umezawa, Toshihiro Kanno, Taeko Izumi, and Akira Kasahara*

Department of Applied Chemistry, Faculty of Engineering, Yamagata University, Yonezawa 992

(Received December 10, 1982)

syn- and *anti*-[0]Orthocyclo[2]orthocyclo[0](1,1′)ferrocenophan-7-enes were synthesized *via* an intramolecular reductive coupling of 1,1′-bis(*o*-formylphenyl)ferrocene with low valent titanium reagents. *syn*- and *anti*-[0]Orthocyclo[2]orthocyclo[0](1,1′)ferrocenophanes and [0]paracyclo[2]paracyclo[0](1,1′)ferrocenophane were prepared by the reaction of 1,1′-bis[*o*-(bromomethyl)phenyl]ferrocene and 1,1′-bis[*p*-(bromomethyl)phenyl]-ferrocene with butyllithium. The transannular π-electronic interactions between two aromatic rings in these compounds were examined on the basis of the NMR and electronic spectra.

Recently a wide variety of cyclophane compounds containing benzene or heteroaromatic rings has been synthesized in order to study the effect of transannular π-electronic interactions on their physical and chemical properties.[1] Many ferrocenophanes of [*m*] (1,2)-, [*m*]-(1,1′)- or [*m.n*] (1,1′)-type are known in which one or more intramolecular bridges link homo- or heteroannular positions within one or two ferrocene moieties,[2] but there have been only a few investigations of ferrocenophanes having transannular π-electronic interactions: [2.2]ferrocenophane-1,13-diyne,[3] [2.2]ferrocenophane-1,13-diene,[4] [3.3]- and [5.5] (1,1′)ferrocenophane derivatives,[5] and [2]paracyclo[2]paracyclo-[2] (1,1′)ferrocenophane derivatives.[6] Moreover, as a part of our studies on metallocenophane chemistry, we have reported the synthesis of [0]metacyclo-[2]metacyclo[0](1,1′)ferrocenophan-7-ene, in which substantial repulsive interactions exist between the two aryl rings.[7] These results have encouraged us to study the synthesis of [0]orthocyclo[2]orthocyclo[0]-(1,1′)ferrocenophanes (**1**) and [0]paracyclo[2]paracyclo[0] (1,1′)ferrocenophane (**2**).

Results and Discussion

Synthesis. Although a number of synthetic methods have recently been developed for [2.2]paracyclophanes,[8] a reductive coupling of carbonyl compounds with low valent titanium reagents[9] is still very convenient and advantageous for the synthesis of cyclophane compounds because of the availability of the intermediary compounds.[5–7,10] In the present work, we attempted to synthesize by the same method the unsaturated ferrocenophanes: [0]orthocyclo[2]orthocyclo[0] (1,1′)ferrocenophan-7-enes (**3s** and **3a**) and [0]-paracyclo[2]paracyclo[0] (1,1′)ferrocenophan-7-ene (**4**). In connection with the synthesis of **3s**, **3a**, and **4**, it became desirable to synthesize 1,1′-bis(*o*-formylphenyl)ferrocene (**5a**) and 1,1′-bis(*p*-formylphenyl)ferrocene (**5b**) in quantity.

The syntheses of the intermediates, **5a** and **5b**, were carried out by the Gomberg's arylation of ferrocene with diazonium salts (**6a** and **6b**) derived from methyl anthranilate and ethyl *p*-aminobenzoate, subsequent reduction with $LiAlH_4$, and oxidation with MnO_2 in chloroform.

The reductive coupling of **5a** to the ferrocenophanes (**3s** and **3a**) with low valent titanium reagents was carried out according to Mukaiyama's procedure ($TiCl_4$–Zn).[9a] Separation of the reaction products by silica-gel column chromatography gave 1,1′-di-*o*-tolylferrocene (**8a**), **3s**, and **3a**, and 1,1′-bis[*o*-(hydroxymethyl)phenyl]ferrocene (**7a**). On the other hand, the intramolecular reductive coupling of **5b** with $TiCl_4$–Zn for preparing the unsaturated ferrocenophane **4**, was unfortunately unsuccessful and led to the formation of reduction products: 1,1′-bis[*p*-(hydroxymethyl)phenyl]ferrocene (**7b**) and 1,1′-*p*-tolylferrocene (**8b**).

The ferrocenophanes, **3s** and **3a**, are exceedingly insoluble in common solvents and olefinic bond of the compounds is sterically hindered. Therefore, attempts to reduce catalytically to saturated ferrocenophanes, **1s** and **1a**, were made without results. Thus, the **1s** and **1a**, were prepared by the ring closure of 1,1′-bis[*o*-(bromomethyl)phenyl]ferrocene (**9a**) with butyllithium according to Trampe's procedure.[11] The separation of the reaction products by silica-gel column chromatography led to the isolation of **1s**, **1a**, and the dimer: [0]orthocyclo[2]orthocyclo[0] (1,1′)-ferroceno[0]orthocyclo[2]orthocyclo[0] (1,1′)ferrocenophane (**10**). The reaction of 1,1′-bis[*p*-(bromomethyl)-phenyl]ferrocene (**9b**) with butyllithium afforded the saturated ferrocenophane **2**.

The synthesis of the intermediates, **9a** and **9b**, were carried out by the reaction of the alcohols, **7a** and **7b**, with chlorotrimethylsilane and lithium bromide.[12]

Structures. The structures of the ferrocenophanes, **1s**, **1a**, **2**, **3s**, and **3a**, were determined on the basis of the IR, NMR, and mass spectra, and the elementary analyses. The NMR and IR spectra data of all ferrocenophanes and the reference compounds are summarized in Tables 1 and 2, respectively.

In the unsaturated ferrocenophanes (**3s** and **3a**), the mass spectra show the pattern containing a molecular ion peak at *m/e* 362, indicating that the two are isomeric. The configuration of olefinic bond in **3s** was confirmed to be *cis*, because the IR spectrum of **3s** exhibited a band of 730 cm^{-1} which was characteristic of *cis* vinylene linkage and the characteristic C–H out of deformation modes of *trans* vinylene linkage at near 960 cm^{-1} were absent. On the other hand, the configuration of olefinic bond in **3a** was confirmed to be *trans*, because the IR spectrum of **3a** exhibited a band of 960 cm^{-1} which was characteristic of *trans* vinylene linkage.

In ferrocene, the distance between the two cyclo-

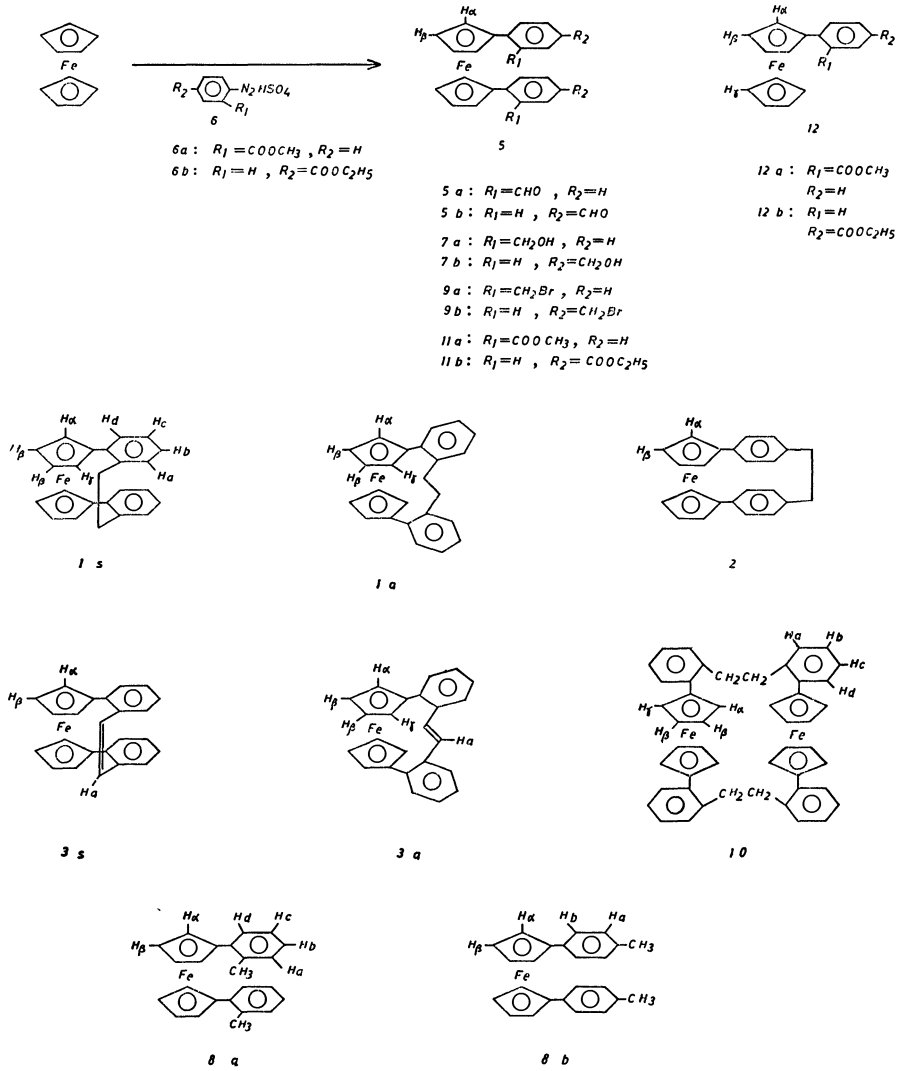

Scheme 1.

pentadienyl rings is 3.32 Å,[13] while the van der Waals separation between parallel π-system is 3.4 Å.[14] Thus, in **3s**, substantial repulsive interactions exist probably between the two aromatic rings which are bound together by vinylene bridges at both *ortho*-positions. In the NMR spectrum of **3s**, the aromatic protons (δ, 6.87) appear at higher fields than the corresponding protons of **3a** (δ, 7.18—7.33) and the reference compound **8a** (δ 7.13 and 7.60). This phenomenon indicates that the two benzene rings in **3s** are held face to face in close proximity by a vinylene bridge and the *syn*-conformation for **3s** can be accommodated. The aromatic proton signals of **3a** were observed at nearly the same positions as those of the reference compound **8a**. This suggests that the two benzene rins in **3a** are not held in a face to face conformation and the *anti*-conformation for **3a** can be accommodated.

In the saturated cyclophanes (**1s** and **1a**), the mass spectra also show the same pattern containing a molecular ion peak at *m/e* 364. This fact confirms that the two are isomeric, similar to the case of **3s** and **3a**. The structural difference between **1s** and **1a** is unequivocally realized in the NMR spectra. The aromatic protons of **1s** (δ, 6.58 and 7.06) exhibit an upfield shift, due to the diamagnetic shielding effect of the opposed aromatic ring, whereas the aromatic proton signals of **1a** were observed at nearly the same positions as those of the reference compound **8a**. These data are best accommodated by the *syn*-structure for **1s** and the *anti*-structure for **1a**.

In ferrocenophane **2**, the IR spectra revealed the presence of 1,1′-disubstituted ferrocene and *p*-disubstituted benzene rings. The molecule probably exists in the conformation with the phenyl rings approximately parallel to one another and approximately coplanar to the plane of the cyclopentadienyl ring. Thus, in **2**, substantial repulsive interactions must exist between the two benzene rings which are bound together by a methylene bridge at both *para*-positions. In the NMR spectra of **2**, as expected, the aromatic protons (δ, 6.62) appeared at higher fields than the corresponding protons of the reference compound, **8b** (δ, 6.98 and 7.18). This phenomenon is probably due to diamagnetic shielding effect due to opposed aromatic ring.

The electronic spectra of the ferrocenophanes (**1s**, **1a**, **2**, **3s**, **3a**, and **10**) and the reference compounds (**8a** and **8b**) are shown in Figs. 1 and 2. It is well known that the transannular electronic interactions in cyclophanes result in the bathochromic and hyperchromic shifts of absorption bands in electronic spectra.[1,8] Toluene shows no absorption in the long wavelength region above 270 nm.[15] The electronic spectra of **1s**, **3s**, and **2** showed somewhat bathochromic and hyperchromic shifts and unambiguous broadening in a range 220—300 nm, compared with those of the reference compounds, **8a** and **8b**. This may be due to transannular π-electronic interactions between the two benzene chromophores in **1s**, **3s**, and **2**; these phenomena are also explained by *syn*-structure, but not by *anti*-structure. On the other hand, in 240—300 nm region, the electronic spectra of **1a** and **3a**, are very similar to the spectra of the reference compound, **8a**. This phenomenon and the small shielding effects on aromatic protons in the NMR spectra of **1a** and **3a** indicate that the interactions between the two benzene rings in **1a** and **3a** are relatively weak and the *anti*-conformations are accommodated.

The IR, NMR, and mass spectra of the dimer **10** were all consistent with the proposed structure. The fragmentation pattern observed in the mass spectra of **10** consisted of only three predominant peaks: *m/e* 56, 364, and 728, corresponding to Fe^+, a doubly charged parent species, and a parent ion respectively. This fragmentation pattern is normally observed in [0.0]-,[16] [1.1]-,[17] [2.2]-,[3,4] and [3.3] (1,1′)ferrocenophanes.[5] The IR spectra revealed the presence of 1,1′-disubstituted ferrocene and *o*-disubstituted benzene rings. In the NMR spectrum of **10**, the aromatic proton signals were observed at nearly the same positions as those of the reference compound, **8a**. Moreover, in the 240—300 nm region of the electronic spectrum of **10**, the intensity was somewhat increased, but the shape of the spectrum was very similar to that of **8a**. These phenomena indicate that the interactions between the benzene rings in **10** are relatively weak.

The electronic spectrum of ferrocene have two main absorptions, *viz.*, 325 and 440 nm. Both the position and the intensity of the 440 nm are particularly sensitive to ferrocene ring-tilt distortion.[18] In the 330—450 nm region, the intensity of the spectra of **1s**, **1a**, **3s**, **3a**, and **10** was somewhat increased, but the shape of the spectra was practically identical with that of the reference compound **8a** bearing an untilted ferrocene ring. These phenomena suggest that, due to the short length of the side chain which is bridging at the *ortho* position of the benzene ring, the planes of the cyclopentadienyl and benzene rings in these compounds have a nonplanar orientation, and accordingly the ferrocene ring tilt distortions are relatively weak. The electronic spectrum of **2** in the 330—450 nm region shows an increased intensity and a bathochromic shift to higher wavelength (475 nm), compared with that of **8b** bearing an untilted ferrocene ring. This suggests that, in **2**, a ferrocene ring-tilt distortion occurs due to the short length of the side chain which is bridging at the *para* position in benzene rings.

The IR spectra of [2.2]paracyclophane system have several obvious features.[19] One is the increase of the intensity of the band in 1530—1600 cm^{-1}, which is related to the increased double bond character due to the distortion of the benzene rings. The other is the appearance of a strong new maximum near the 710 cm^{-1} region. Longgone and Warren[19b] reported that the strong maximum at 725 cm^{-1} in [2.2]paracyclophane and at 710 cm^{-1} in 4,7,12,15-tetramethyl[2.2]-paracyclophane might be a characteristic band associated with the distortion benzene ring in [2.2]paracyclophane system. Otsubo *et al.*[19c] also reported the same phenomena in the multilayered [2.2]paracyclophane system. In practice, besides the strong peak around 1600 cm^{-1}, the ferrocenophane **2** exhibits a strong new band around 710 cm^{-1}, whereas the reference compound **8b** bearing strain-free benzene rings exhibits no band in this region. This indicates that the compound **2** bears strained benzene rings due to the interactions between the two aromatic rings. On

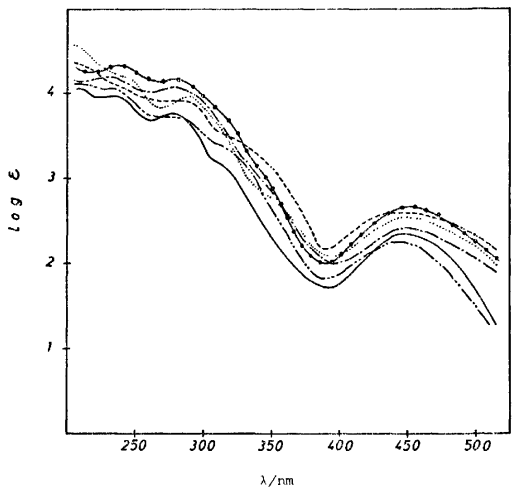

Fig. 1. Electronic spectra of **1s**, **1a**, **3s**, **3a**, **8a**, and **10** in dioxane.
·····: **1s**, ——: **1a**, ----: **3s**, ——-: **3a**, ——: **8a**, —•—•: **10**.

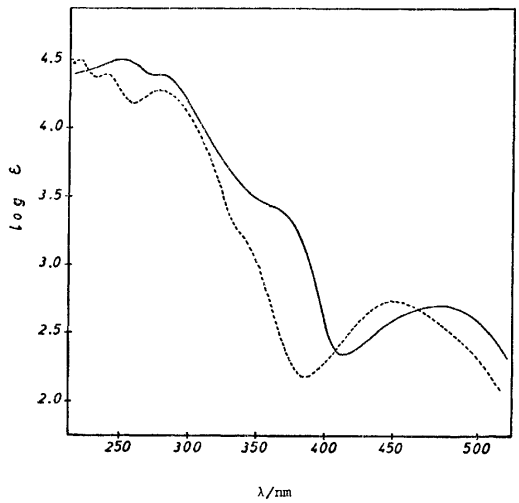

Fig. 2. Electronic spectra of **2** and **8b** in dioxane.
——: **2**, ·····: **8b**.

Table 1. The ^{1}H NMR spectra of the ferrocenophanes (**1s**, **1a**, **2**, **3s**, **3a**, and **10**) and the reference compounds (**8a** and **8b**) (δ from TMS, in $CDCl_3$)

Compound	Aromatic ring protons	Ferrocene ring protons	Other protons
1s	6.58 (m, 2H, $\underline{H}_a$) 7.06 (m, 6H, $\underline{H}_{b,c,d}$)	4.27 (m, 4H, $\underline{H}_\beta$) 4.49 (m, 4H, $\underline{H}_\alpha+\underline{H}_\gamma$)	4.15 (m, 2H, $\underline{H}_e$) 4.34 (m, 2H, $\underline{H}_f$)
1a	7.20 (m, 8H)	4.40 (m, 4H, $\underline{H}_\beta$) 4.51 (m, 4H, $\underline{H}_\alpha+\underline{H}_\gamma$)	4.06—4.18 (m, 4H, $-C\underline{H}_2-$)
3s	6.87 (m, 8H)	4.41 (m, 8H, $\underline{H}_\alpha+\underline{H}_\beta$)	6.98 (s, 2H, $\underline{H}_a$)
3a	7.18—7.33 (m, 8H)	4.31 (m, 4H, $\underline{H}_\beta$) 4.41 (m, 4H, $\underline{H}_\alpha+\underline{H}_\gamma$)	7.46 (s, 2H, $\underline{H}_a$)
10	7.08 (m, 6H, $\underline{H}_{a,b,c}$) 7.62 (m, 2H, $\underline{H}_d$)	4.28 (m, 4H, $\underline{H}_\beta$) 4.51 (m, 4H, $\underline{H}_\alpha+\underline{H}_\gamma$)	4.04—4.15 (m, 8H, $-C\underline{H}_2-$)
8a	7.13 (m, 6H, $\underline{H}_{a,b,c}$) 7.60 (m, 2H, $\underline{H}_d$)	4.22 (t, 4H, $\underline{H}_\beta$) 4.41 (t, 4H, $\underline{H}_\alpha$)	2.31 (s, 6H, $-C\underline{H}_3$)
2	6.62 (b-s, 8H)	4.25 (t, 4H, $\underline{H}_\beta$) 4.62 (t, 4H, $\underline{H}_\alpha$)	3.20 (s, 4H, $-C\underline{H}_2-$)
8b[23]	6.98 (d, 4H, $\underline{H}_a$) 7.18 (d, 4H, $\underline{H}_b$)	4.17 (t, 4H, $\underline{H}_\beta$) 4.44 (t, 4H, $\underline{H}_\alpha$)	2.28 (s, 6H, $-C\underline{H}_3$)

Table 2. The IR spectra of the ferrocenophanes (**1s**, **1a**, **2**, **3s**, **3a**, and **10**) and the reference compounds (**8a** and **8b**) (KBr cm^{-1})

Compound	
1s	3100, 815 (1,1′-disubstituted ferrocene ring), 1600, 1500, 760 (*o*-disubstituted benzene ring)
1a	3100, 815 (1,1′-disubstituted ferrocene ring), 1600, 1500, 760 (*o*-disubstituted benzene ring)
3s	3100, 805 (1,1′-disubstituted ferrocene ring), 1600, 1500, 740 (*o*-disubstituted benzene ring), 1635 720 (*cis* -CH=CH-)
3a	3100, 810 (1,1′-disubstituted ferrocene ring), 1600, 1500, 750 (*o*-disubstituted benzene ring), 1640, 960 (*trans* -CH=CH-)
10	3100, 810 (1,1′-disubstituted ferrocene ring), 1600, 1500, 760 (*o*-disubstituted benzene ring)
8a	3100, 810 (1,1′-disubstituted ferrocene ring), 1600, 1500, 745 (*o*-disubstituted benzene ring)
2	3100, 810 (1,1′-disubstituted ferrocene ring), 1600, 1500, 820 (*p*-disubstituted benzene ring), 710, 685 (distorted benzene ring)
8b	3100, 805 (1,1′-disubstituted ferrocene ring), 1600, 1500, 825 (*p*-disubstituted benzene ring)

the other hand, near the 700 cm^{-1} region, the IR spectra of **1s**, **1a**, **3s**, **3a**, and **10** are quite similar to those of the open-chain model **8a**. This may be due to the non-distortion of benzene rings in these compounds.

Experimental

Measurements. All the melting points are uncorrected. The IR, NMR, mass, and electronic spectra were recorded with Hitachi 260-10, Hitachi R-22, Hitachi RMU-6M, and Hitachi 200-10 spectrometers, respectively.

1,1′-Bis[o-(*methoxycarbonyl*)*phenyl*]*ferrocene* (**11a**). Methyl anthranilate (15.1 g, 0.10 mol) was diazotized in 10% sulfuric acid (300 cm^3) at 0—5 °C with sodium nitrite (7.1 g, 0.102 mol). After diazotization had been completed, the diazotized salt solution was added rapidly to a solution of ferrocene (7.44 g, 0.04 mol) in acetic acid (500 cm^3) under an atmosphere of nitrogen. The resulting dark brown solution was stirred overnight at room temperature, and was then poured into water. The reaction mixture was extracted with chloroform and the chloroform extract was washed with 5% aqueous sodium hydrogencarbonate solution, and brine, dried over anhyd $MgSO_4$, filtered, and concentrated. The residue was purified by column chromatography (silica gel-benzene). First elution with benzene gave the starting material: ferrocene (1.23 g, 16.5%), mp 173 °C.

Second elution with benzene afforded 1.34 g (10.4% yield based on ferrocene) of [*o*-(methoxycarbonyl)phenyl]ferrocene (**12a**), raddish crystals, mp 74—76 °C (lit,[20] mp 74—75 °C). IR (KBr): 3100, 1100, 1000. 805 (monosubstituted ferrocene ring), 1720 (-COOMe), 1600, 1500, 760, 735 cm^{-1} (*o*-disubstituted benzene ring). ^{1}H NMR ($CDCl_3$): δ=3.68 (s, 3H, $-C\underline{H}_3$), 4.02 (s, 5H, $\underline{H}_\gamma$), 4.26 (t, 2H, $\underline{H}_\beta$), 4.42 (t, 2H, $\underline{H}_\alpha$), 7.11—7.82 (m, 4H, Ar-$\underline{H}$). Found: C, 67.47; H, 4.87%; M^+, 320. Calcd for $C_{18}H_{16}FeO_2$: C, 67.52; H, 5.03%; M, 320.

Third elution with benzene gave 4.42 g of **11a** (23.3% yield based on ferrocene), reddish crystals, mp 92—94 °C. IR (KBr): 3100, 805 (1,1′-disubstituted ferrocene ring), 1720 (-COOMe), 1600, 1500, 760, 735 cm^{-1} (*o*-disubstituted benzene ring). ^{1}H NMR ($CDCl_3$): δ=3.69 (s, 6H, $-C\underline{H}_3$), 4.19 (t, 4H, $\underline{H}_\beta$), 4.33 (t, 4H, $\underline{H}_\alpha$), 7.18—7.60 (m, 8H, Ar-$\underline{H}$). Found: C, 68.86; H, 4.95%; M^+, 454. Calcd for $C_{25}H_{22}FeO_4$: C, 68.73; H, 4.88%; M, 454.

1,1′-Bis[p-(*ethoxycarbonyl*)*phenyl*]*ferrocene* (**11b**). Gomberg's arylation of ferrocene with diazonium salts (**6b**) derived from ethyl *p*-aminobenzoate, was carried out in the same way as descrived for **11a**, and [*p*-(ethoxycarbonyl)-phenyl]ferrocene (**12b**, mp 87—88 °C, reddish crystals, (lit,[21] mp 88—90 °C) and **11b** (reddish yellow crystals, mp 130—131 °C) were obtained in 14 and 26% yields, respectively.

12b: IR (KRr): 3100, 1100, 800 (monosubstituted ferrocene ring), 1715 (-COOEt), 1600, 820 cm^{-1} (*p*-disubsti-

tuted benzene ring). ^{1}H NMR ($CDCl_3$): δ=1.33 (t, 3H, -CH$_3$), 3.97 (s, 5H, H$_\gamma$), 4.33 (t, 2H, H$_\beta$), 4.37 (q, 2H, -CH$_2$-), 4.65 (t, 2H, H$_\alpha$), 7.44 (d, 2H, Ar-H), 7.92 (d, 2H, Ar-H). Found: C, 68.16; H, 5.26%; M$^+$, 334. Calcd for $C_{19}H_{18}FeO$: C, 68.28; H, 5.42%; M, 334.

11b: IR (KBr): 3100, 805 (1,1′-disubstituted ferrocene ring), 1720 (-COOEt), 1600, 820 cm^{-1} (*p*-disubstituted benzene ring). ^{1}H NMR ($CDCl_3$): δ=1.36 (t, 6H, -CH$_3$), 4.24 (t, 4H, H$_\beta$), 4.37 (q, 4H, -CH$_2$-), 4,49 (t, 4H, H$_\alpha$), 7.22 (d, 4H, Ar-H), 7.80 (d, 4H, Ar-H). Found: C, 69.25; H, 5.37%; M$^+$, 482. Calcd for $C_{28}H_{26}FeO_4$: C, 69.37; H, 5.43%; M, 482.

1,1′-Bis[o-*(hydroxymehyl)phenyl*]*ferrocene* (**7a**). To a suspension of $LiAlH_4$ (1.41 g, 0.037 mol) in anhydrous diethyl ether (160 cm^3) was added dropwise a solution of **11a** (8.17 g, 0.018 mol) in dry benzene (100 cm^3) at room temperature during 1 h, and the reaction mixture was then heated under reflux for an additional 5 h. After the mixture had been decomposed with a small amount of cold water, the organic layer was washed successively with 5% hydrochloric acid, 5% sodium hydrogencarbonate solution, and brine, and dried over anhyd $MgSO_4$. After removal of the solvents, the residue was purified by column chromatography on silica gel (chloroform) to afford **7a** as reddish yellow crystals, which were recrystallized from ethanol, mp 103—104 °C (6.73 g, 94% yield). IR (KBr): 3300, 1020 (-OH), 3100, 810 (1,1′-disubstituted ferrocene ring), 1600, 1500, 750 cm^{-1} (*o*-disubstituted benzene ring). ^{1}H NMR ($CDCl_3$): δ=2.20 (br-s, 2H, -OH), 4.24 (m, 4H, H$_\beta$), 4.36 (m, 4H, H$_\alpha$), 4.56 (s, 4H, -CH$_2$-), 7.13—7.35 (m, 8H, Ar-H). Found: C, 72.49; H, 5.67%; M$^+$, 398. Calcd for $C_{24}H_{22}FeO_2$: C, 72.37; H, 5.56%, M, 398.

1,1′-Bis[p-*(hydroxymethlyl)phenyl*]*ferrocene* (**7b**). A reduction of **11b** with $LiAlH_4$ was carried out in the same way as described above, and **7b** (reddish crystals mp 210—212 °C) was obtained in 89% yield. IR (KBr): 3200 (-OH), 3100, 805 (1,1′-disubstituted ferrocene ring), 1600, 1500, 820 cm^{-1} (*p*-disubstituted benzene ring). ^{1}H NMR ($CDCl_3$): δ=4.12 (t, 4H, H$_\beta$), 4.47 (m, 8H, H$_\alpha$+-CH$_2$-), 5.07 (br-s, 2H, -OH), 7.11 (d, 4H, Ar-H), 7.26 (d, 4H, Ar-H). Found: C, 72.31; H, 5.48%; M$^+$, 398. Calcd for $C_{21}H_{22}FeO_2$: C, 72.37; H, 5.56%; M, 398.

1,1′-Bis(o-*formylphenyl*)*ferrocene* (**5a**). At room temperature, active manganese(IV) oxide (100 g) was added to a solution of **7a** (6.76 g, 0.017 mol) in chloroform (200 ml) and the mixture was stirred in the dark for 12 h. After filtration to remove MnO_2, the reddish chloroform solution was evaporated to dryness and the residue was chromatographed by elution of benzene on silica gel to afford reddish crystals **5a** (5.88 g, 87% yield), mp 124—125 °C. IR (KBr): 2820, 1680 (-CHO), 3100, 810 (1,1′-disubstituted ferrocene ring), 1600, 1500, 740 cm^{-1} (*o*-disustituted benzene ring). ^{1}H NMR ($CDCl_3$): δ=4.38 (m, 4H, H$_\beta$), 4.47 (m, 4H, H$_\alpha$), 7.33—7.85 (m, 8H, Ar-H), 10.31 (s, 2H, -CHO). Found: C, 73.27; H, 4.73%; M$^+$, 384. Calcd for $C_{24}H_{18}FeO_2$: C, 73.11; H, 4.60%; M, 384.

1,1′-Bis(p-*formylphenyl*)*ferrocene* (**5b**). An oxidation of **7b** with active manganese(IV) oxide was carried out in the same way as described above, and reddish crystal **5b** (mp 220—221 °C) were obtained in 54% yield. IR (KBr): 2820, 1695, (-CHO), 3100, 805 (1,1′-disubstituted ferrocene ring), 1600, 1500, 820 cm^{-1} (*p*-disubstituted benzene ring). ^{1}H NMR ($CDCl_3$): δ=4.33 (m, 4H, H$_\beta$), 4.58 (m, 4H, H$_\alpha$), 7.28 (d, 4H, Ar-H), 7.61 (d, 4H, Ar-H), 9.92 (s, 2H, -CHO). Found: C, 73.02; H, 4.45%; M$^+$, 384. Calcd for $C_{24}H_{18}FeO_2$: C, 73.11; H, 4.60%; M, 384.

1,1-Bis[o-*(bromomethyl)phenyl*]*ferrocene* (**9a**). Under an atmosphere of nitrogen, chlorotrimethylsilane (5.43 g, 0.05 mol) was added to a solution of anhyd lithium bromide (3.48 g, 0.04 mol) in dry acetonitrile (50 cm^3) with stirring at room temperature. The alcohol **7a** (3.62 g, 0.01 mol) was then added and the reaction mixture was heated under reflux for 12 h. After cooling, the mixture was extracted with diethyl ether (300 cm^3), and the extract was washed successively with water, 5% sodium hydrogencarbonate solution, and brine, and dried over anhyd $MgSO_4$ Removal of the solvents and subsequent recrystallization from benzene-hexane afforded orange crystals **9a** (2.10 g, 40% yield), mp 150—152 °C. IR (KBr): 3100, 810 (1,1′-disubstituted ferrocene ring), 1600, 1500, 760 cm^{-1} (*o*-disubstituted benzene ring). ^{1}H NMR ($CDCl_3$): δ=4.27 (m, 4H, H$_\beta$), 4.34 (s, 4H, -CH$_2$-), 4.51 (m, 4H, H$_\alpha$), 7.11—7.64 (m, 8H, Ar-H). Found: C, 54.87; H, 3.73%. MS: 364 (M$^+$ −2Br), 444 (M$^+$ −Br), 524 (M$^+$). Calcd for $C_{24}H_{20}Br_2Fe$: C, 55.00; H, 3.48%; M, 524.

1,1′-Bis[p-*(bromomethyl)phenyl*]*ferrocene* (**9b**). The reaction of the alcohol **7b** with Me_3SiCl-LiBr in acetonitrile was carried out in the same way as described above, and the reaction product **7b** was purified by column chromatography on silica gel using benzene as eluent in 43% yield, reddish crystals, mp 136—138 °C (decomp). IR (KBr): 3100, 805 (1,1′-disubstiuted ferrocene ring), 1600, 1500, 825 cm^{-1} (*p*-disubstituted benzene ring). ^{1}H NMR ($CDCl_3$): δ=4.23 (t, 4H, H$_\beta$), 4.48 (m, 8H, H$_\alpha$+-CH$_2$-), 7.17 (br-s, 8H, Ar-H). Found: C, 54.87; H, 3.33%. MS: 364 (M$^+$ −2Br), 444 (M$^+$−Br), 524 (M$^+$). Calcd for $C_{24}H_{20}Br_2Fe$: C, 55.00; H, 3.48%; M, 524.

The Intramorecular Reductive Coupling of **5a** *with* $TiCl_4$-*Zn*. Under an atomosphere of nitrogen, zinc dust (7.8 g, 0.12 mol) was added in small portions to a stirred solution of $TiCl_4$ (11,3 g, 0.06 mol) in dry THF (180 cm^3) at 0—5 °C. After the mixture was refluxed for 2 h, a solution of **5a** (4.72 g, 0.012 mol) and dry pyridine (0.90 g) in dry THF (600 cm^3) was added over 21 h under refluxing, followed by an additional 10 h period of reflux and quenched by addition of 200 cm^3 of saturated K_2CO_3 solution. The mixture was stirred for 0.5 h, diluted with chloroform, and filtered through Celite. The chloroform layers were washed with brine and dried over anhyd $MgSO_4$. After removal of the solvents, the residue was dissolved in hexane and chromatographed on silica gel.

The first fraction, eluted with hexane and followed by evaporation and recrystallization from ethanol, gave yellow orange crystals (0.10 g, 2.3% yield). These were identified as 1,1′-*o*-tolylferrocene (**8a**, mp 67—68 °C), by a comparison of the IR, NMR, and mass spectra and by a mixed-melting-point determination with the authentic sample, which was prepared by Gomberg's reaction of ferrocene with diazonium salts derived from *o*-toluidine.[22] Found: C, 78.55; H, 5.04%; M$^+$, 366. Calcd for $C_{24}H_{22}Fe$: C, 78.69; H, 6.05%; M, 366.

The second fraction, eluted with hexane-benzene (1:1) and followed by evaporation and recrystallization from ethanol, gave reddish crystals (0.62 g, 14.3% yield), mp 181—182 °C, which were determined to be *syn*-[0]orthocyclo[2]-orthocyclo[0](1,1′)ferrocenophan-7-ene (**3s**). Found: C, 79.65; H, 5,11%; M$^+$, 362. Calcd for $C_{24}H_{18}Fe$: C, 79.57; H, 5.03%; M, 362.

The third fraction, eluted with benzene and followed by evaporation and recrystallization from benzene-hexane gave yellowish red crystals (5.23 g, 5.3% yield), mp 230—231 °C, which were determined to be *anti*-[0]orthocyclo[2]orthocyclo-[0](1,1′)ferrocenophan-7-ene (**3a**). Found: C, 79.51; H, 5.08%; M$^+$, 362. Calcd for $C_{24}H_{18}Fe$: C, 79.57; H, 5.03%;

M, 362.

The fourth fraction, eluted with chloroform and followed by evaporation and recrystallization from ethanol gave reddish yellow crystals (0.79 g, 16.5% yield), mp 103—104 °C, which were identified as 1,1′-bis[*o*-(hydroxymethyl)phenyl]-ferrocene (**7a**) by a comparison of the IR and NMR spectra and by a mixed-melting-point determination with **7a**.

The Reaction of ***5b*** *with* $TiCl_4$*–Zn.* The reaction of **5b** with $TiCl_4$–Zn was carried out in the same way as described above, and 1,1′-di-*p*-tolylferrocene [**8b**, reddish crystals, mp 167—169 °C (lit,[23] mp 168—169 °C)] and 1,1′-bis[*p*-(hydroxymethyl)phenyl]ferrocene (**7b**), mp 103—104 °C, were obtained in 47 and 24% yields, respectively.

The Intramolecular Coupling of ***9a*** *with Butyllithium.* Under an atmosphere of nitrogen, a 15% solution of butyllithium in hexane (8 cm^3) was added dropwise to a solution of **9a** (2.41 g, 0.0046 mol) in dry THF (320 cm^3) at −50 °C, followed by stirring at the same temperature for 2 h and then at 0 °C for 2 h. After a successive addition of water (20 cm^3) and 1 M hydrochloric acid (40 cm^3), the mixture was extracted with chloroform. The chloroform extracts were washed successively with 1 M hydrochloric acid, brine, 5% sodium hydrogencarbonate solution, and brine, and dried over anhyd $MgSO_4$. After removal of the solvents, the residue was dissolved in benzene–hexane (1:1) and chromatographed on silica gel.

The first fraction, eluted with benzene–hexane (1:1) and followed by evaporation and recrystallization from benzene–hexane, gave reddish crystalls (0.10 g, 6% yield), mp 164—165°C, which were determined to be *syn*-[0]orthocyclo[2]-orthocyclo[0](1,1′)ferrocenophane (**1s**). Found: C, 79.01; H, 5.39%; M^+, 364. Calcd for $C_{24}H_{20}Fe$: C, 79.13; H, 5.53%, M, 364.

The second fraction, eluted with benzene–hexane (1:1) and followed by evaporation and recrystallization from ethanol affored reddish crystals (0.10 g, 6% yield), mp 182—183 °C, which were determined to be *anti*-[0]orthocyclo[2]-[2]orthocyclo[0](1,1′)ferrocenophane (**1a**). Found: C, 78.96; H, 5.41%; M^+, 364. Calcd for $C_{24}H_{20}Fe$: C, 79.13; H, 5.53%; M, 364.

The third fraction, eluted with benzene–hexane (1:1) and followed by evaporation and recrystallization from ethanol gave yellow orange crystals (0.70 g, 42% yield), mp 245—247 °C (decomp), which were determined to be [0]orthocyclo [2] orthocyclo [0] (1, 1′) ferroceno [0] orthocyclo [2] orthocyclo[0](1,1′)ferrocenophane (**10**). Found: C, 78.91; H, 5.44%. MS: 56 (Fe^+), 364 ($M^+/2$), 728 (M^+). Calcd for $C_{48}H_{40}Fe_2$: C, 79.13; H, 5.53%; M, 728.

*[0]Paracyclo[2]paracyclo[0](1,1′)ferrocenophane (****2****).* The intramolecular coupling of **9b** with butyllithium was carried out in the same way as described above, and the ferrocenophane **2** was separated by column chromatography on silica gel using benzene as eluent, followed by recrystallization from benzene (yield 20%), mp 230 °C (decomp), reddish crystals. Found: C, 78.98; H, 5.44%; M^+, 364. Calcd for $C_{24}H_{20}Fe$: C, 79.13; H, 5.53%; M, 364.

This work was supported by Grant-in-Aid for Science Research No. 554137 from the Ministry of Education, Science and Culture.

References

1) S. Misumi and T. Otsubo, *Acc. Chem. Res.*, **11**, 251 (1978).
2) G. B. Shul'pin and M. I. Rybinskaya, *Usp. Khim.*, **43**, 1524 (1974).
3) M. Rosenblum, N. M. Brawn, D. Clappenelli, and J. Tancrede, *J. Organomet. Chem.*, **24**, 469 (1970).
4) A. Kasahara and T. Izumi, *Chem. Lett.*, **1978**, 21.
5) A. Kasahara, T. Izumi, and I. Shimizu, *Chem. Lett.*, **1979**, 1317.
6) A. Kasahara, T. Izumi, and I. Shimizu, *Chem. Lett.*, **1979**, 1119.
7) A. Kasahara, T. Izumi, and H. Umezawa, *Chem. Lett.*, **1980**, 1039.
8) S. Misumi, *Kagaku No Ryoiki*, **28**, 927 (1974); **32**, 651 (1978); Y. Sakata, *Yuki Gosei Kagaku Kyokai Shi*, **38**, 164 (1980).
9) a) T. Mukaiyama, T. Sato, and J. Hanna, *Chem. Lett.*, **1973**, 1041; b) J. E. McMurry and M. P. Fleming, *J. Am. Chem. Soc.*, **96**, 4708 (1974); c) J. E. McMurry and L. R. Krepski, *J. Org. Chem.*, **41**, 3929 (1976); d) A. Ishida and T. Mukaiyama, *Chem. Lett.*, **1976**, 1127; e) J. E. McMurry, M. P. Fleming, K. L. Kees, and L. R. Krepski, *J. Org. Chem.*, **43**, 3255 (1978).
10) D. Tanner and O. Wennerstrom, *Tetrahedron Lett.*, **22**, 2313 (1981).
11) S. Trampe, K. Menke, and H. Hopf, *Chem. Ber.*, **110**, 371 (1977).
12) G. A. Olah, B. G. Gupta, R. Malhotra, and S. C. Narang, *J. Org. Chem.*, **45**, 1638 (1980).
13) M. Rosenblum, "Chemistry of the Iron Group Metallocenes," Interscience Publishers, New York (1965), Part 1, p. 31.
14) L. Pauling, "The Nature of the Chemical Bond," 3rd ed, Cornell University Press, Ithaca, New York (1960), p. 262.
15) L. Doub and J. M. Vandenbelt, *J. Am. Chem. Soc.*, **69**, 2714 (1947).
16) F. L. Hedberg and H. Rosenberg, *J. Am. Chem. Soc.*, **91**, 1258 (1969).
17) W. E. Watts, *J. Am. Chem. Soc.*, **88**, 855 (1966); T. H. Barr, H. L. Lentzner, and W. E. Watts, *Tetrahedron*, **25**, 6001 (1969).
18) T. H. Barr and W. E. Watts, *J. Organomet. Chem.*, **15**, 177 (1968); A. G. Osborne and R. H. Whitely, *ibid.*, **193**, 345 (1980).
19) a) D. J. Cram and H. Steinberg, *J. Am. Chem. Soc.*, **73**, 5691 (1951); b) D. J. Longone and C. L. Warren, *ibid.*, **84**, 1507 (1962); c) T. Otsubo, S. Mizogami, I. Otsubo, Z. Tozuka, A. Sakagami, Y. Sakata, and S. Misumi, *Bull. Chem. Soc. Jpn.*, **46** 3419 (1973).
20) W. F. Little, C. N. Reilley, J. D. Johnson, K. N. Kynn, and A. P. Sanders. *J. Am. Chem. Soc.*, **86**, 1376 (1964).
21) A. N. Nesmeyanov, *Proc. R. Soc. London, Ser. A*, **246**, 495 (1958).
22) G. D. Broadhead and P. L. Pauson, *J. Chem. Soc.*, **1955**, 367 (not isolated in a pure state).
23) E. G. Perevalova, N. A. Simkova, T. V. Nikitia, P. D. Reshetov, and A. N. Nesmeyanov, *Izv. Akad. Nauk SSSR, Otd. Khim, Nauk*, **1961**, 77.

Baeyer-Villiger Oxidation with $Me_3SiOOSiMe_3$ under Assistance of $SnCl_4$ or $BF_3 \cdot OEt_2$

Seijiro MATSUBARA, Kazuhiko TAKAI,* and Hitosi NOZAKI

Department of Industrial Chemistry, Faculty of Engineering, Kyoto University, Yoshida, Sakyo-ku, Kyoto 606

(Received January 25, 1983)

Treatment of ketones with bis(trimethylsilyl) peroxide and Lewis acid such as $SnCl_4$ or $BF_3 \cdot OEt_2$ in dichloromethane at room temperature affords esters in fair to excellent yields. Jasmine lactone is synthesized from 2-[(*Z*)-2-pentenyl]cyclopentanone by means of $Me_3SiOOSiMe_3$–$BF_3 \cdot OEt_2$ system without any protection of the carbon-carbon double bond. The oxidation of enol acetates of ketones to α-hydroxy (or α-acetoxy) ketones with $Me_3SiOOSiMe_3$–$FeCl_3$ system is also disclosed.

The Baeyer-Villiger oxidation is one of the most important processes in organic synthesis.[1] Recent publication[2] by Noyori and his coworkers on this oxidation using $Me_3SiOOSiMe_3$–Me_3SiOTf prompted us to disclose our independent work.

Usual Baeyer-Villiger oxidants[3] such as H_2O_2 or peroxy acids react with the coexisting carbon–carbon double bond of the substrate under epoxidation.[4] To overcome this difficulty, we examined the oxidation with $Me_3SiOOSiMe_3$[5] in the presence of Lewis acids[6] being added in order to activate the carbonyl function (Table 1). Among those examined, $SnCl_4$ was found to effectively assist the oxidation in general. No reaction occurred in the absence of Lewis acid.

The reaction rate with $BF_3 \cdot OEt_2$ is comparable with that by means of $SnCl_4$ in the case of cyclopentanones. Other cycloalkanones reacted in the presence of $BF_3 \cdot OEt_2$ to produce generally cyclic peroxides,[7] which decomposed slowly to afford a mixture of the desired lactones and the starting ketones. The results of the Baeyer-Villiger oxidation with $Me_3SiOOSiMe_3$–$SnCl_4$ or –$BF_3 \cdot OEt_2$ system are summarized in Table 2.

Although aliphatic ketones were oxidized in good to excellent yields (runs 1,2), aromatic ketones such as acetophenone gave complex mixtures.[8] The observed Baeyer-Villiger reaction in preference to C=C bond attack (runs 3—6) features the present oxidation procedure over the peroxy acid one.

TABLE 1. EFFECTS OF VARIOUS LEWIS ACIDS ON THE TRANSFORMATION OF 4-*t*-BUTYLCYCLOHEXANONE TO 4-*t*-BUTYL-6-HEXANOLIDE[a]

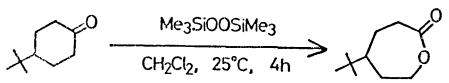

1 **2**

Lewis acid	Yield/%	Lewis acid	Yield/%
$SnCl_4$	84	$ZrCl_4$	34
$BF_3 \cdot OEt_2$	88[b]	$TiCl_4$	27
$FeCl_3$	72	$ZnCl_2$	<5
$AlCl_3$	38		

a) Two mol of $Me_3SiOOSiMe_3$ and one mol of Lewis acid were employed per mol of 4-*t*-butylcyclohexanone. b) The reaction rate was inconveniently low. The reaction required 2 d for completion.

TABLE 2. BAEYER-VILLIGER OXIDATION WITH $Me_3SiOOSiMe_3$–$SnCl_4$ AND –$BF_3 \cdot OEt_2$ SYSTEMS[a]

Run	Ketone	Lewis acid (mol equiv)	Time / h	Ester	Yield[b] / %
1	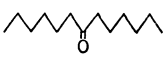	$SnCl_4$ (1.0)	5	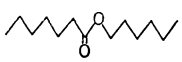	93
2	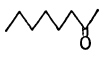	$SnCl_4$ (1.0)	11	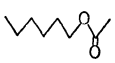	69
3		$SnCl_4$ (1.0) $BF_3 \cdot OEt_2$ (2.0)	9 7		25, 38[c] 17, 28[c]
4		$SnCl_4$ (1.0)	4	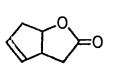	80[d]
5		$SnCl_4$ (1.0) $BF_3 \cdot OEt_2$ (2.0)	3 4	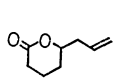	64 58
6	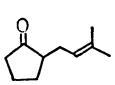	$BF_3 \cdot OEt_2$[e] (2.0)	4	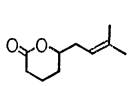	44[e,f]

a) Reactions were performed on 1.0 mmol scale at 25 °C. b) Isolated yield. c) Based on the consumed starting material. d) Ref. 1a. e) Ref. 4. f) Reaction with $SnCl_4$ gave a complex mixture in which the desired lactone was absent.

TABLE 3. OXIDATION OF SIMPLE CYCLIC KETONES TO GIVE THE CORRESPONDING LACTONES AND/OR α-HYDROXY KETONES[a]

n		5	6	7	8	10	11	12
Time/h		3	3	3.5	4	3	4	2.5
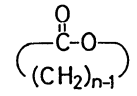	Yield[b] %	85	83	50	11	24	30	62
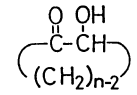	Yield %	0[c]	0[c]	4[c]	42	35	33	20

a) Reactions were done at 25 °C in CH_2Cl_2. Two mol of $Me_3SiOOSiMe_3$ and 1 mol of $SnCl_4$ were employed per mol of carbonyl compounds. b) Isolated yield. c) GLPC yield.

Table 3 summarizes the reaction of simple cyclic ketones[9] in the presence of $SnCl_4$. The product distributions depend on the sizes of the ring. In the case of 5, 6, 7, and 12 membered ring the corresponding lactones were obtained in good yields. Meanwhile, medium ring (8, 10, and 11 membered) cycloalkanone gave α-hydroxy ketones.[10] This is tentatively ascribed to the oxidation of enol forms of the substrates.[11]

Treatment of silyl enol ethers with $Me_3SiOOSiMe_3$ in the presence of $SnCl_4$, $BF_3 \cdot OEt_2$, or $FeCl_3$ gave the starting ketones. In contrast, enol acetates are oxidized to the corresponding α-acetoxy and/or α-hydroxy ketones by means of $Me_3SiOOSiMe_3$–Lewis acid system. Yields of α-acetoxy and α-hydroxy acetophenone in the oxidation of 1-phenylethenyl acetate and $Me_3SiOOSiMe_3$ in dichloromethane at 25 °C for 12 h were as follows: $SnCl_4$, 28%, 41%; $BF_3 \cdot OEt_2$, 28%, 0%. Iron(III) chloride proved to be the best promoter for the oxidation (Fig. 1).[12]

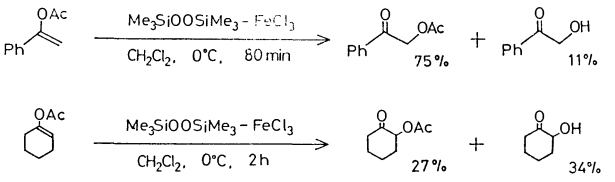

Fig. 1.

Relative migratory aptitude in the cleavage of unsymmetrical ketones with $Me_3SiOOSiMe_3$–$SnCl_4$ and –$BF_3 \cdot OEt_2$ systems were examined (Fig. 2). The present reactions have the same tendency as those with peroxy acids.[13] The selectivity was poor in the case of 2-methylcyclohexanone.

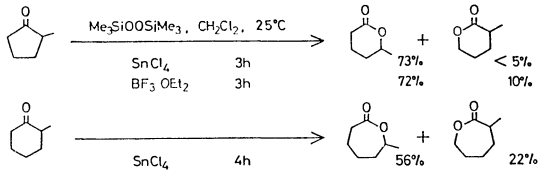

Fig. 2.

Jasmine lactone (**4**) is synthesized from 2-[(*Z*)-2-pentenyl]cyclopentanone (**3**) in several steps.[14] Protection of the olefinic bond is prerequisite in the previous procedures with perbenzoic acid, as treatment of the ketone **3** with *m*-chloroperbenzoic acid (1.5 equiv) in dichloromethane gave epoxide in 89% yield in our hand. The Baeyer-Villiger oxidation in preference to the epoxidation has now been achieved with $Me_3SiOOSiMe_3$–$BF_3 \cdot OEt_2$ system (Fig. 3). Addition of portions of $Me_3SiOOSiMe_3$ (2.2 equiv) and $BF_3 \cdot OEt_2$ (2.0 equiv) to the ketone **3** in dichloromethane gave the lactone **4** in 50% yield along with the hydroxy carboxylic acid (**5**) in 8% yield.[15]

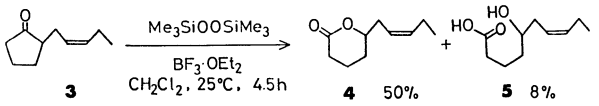

Fig. 3.

Although the yields of the oxidation with $Me_3SiOOSiMe_3$–$SnCl_4$ (or $BF_3 \cdot OEt_2$) system are better than, or at least comparable to, those with Me_3SiOTf, easy accessibility of the Lewis acids characterizes this system as a useful method for the Baeyer-Villiger oxidation.

Experimental

The IR Spectra were determined on a Shimadzu IR-27-G spectrometer, the mass spectra on a Hitachi M-80 machine, and the NMR spectra on a Varian EM-390 spectrometer. The chemical shifts are given in δ, with TMS as an internal standard. The analyses were carried out by the staff at the Elemental Analyses Center of Kyoto University. Dichloromethane was dried on P_2O_5 and distilled. Bis(trimethylsilyl) peroxide was prepared according to the reported procedure and purified by distillation (bp 40—41 °C/30 Torr, 1 Torr = 133.322 Pa).[5] All the experiments were carried out under an argon atmosphere. Purification of products were performed by preparative thin layer chromatography (TLC) or column chromatography on silica gel (Wakogel C-100). Analytical GLPC was performed with a Yanagimoto GCG-550-F and a Shimadzu GC-4CPT.

4-t-Butyl-6-hexanolide (**2**): To a stirred solution of 4-*t*-butylcyclohexanone (**1**, 0.15 g, 1.0 mmnl) and bis(trimethylsilyl) peroxide (0.18 g, 1.0 mmol) in CH_2Cl_2 (10 ml) at 0 °C tin(IV) chloride (0.26 g, 1.0 mmol) was added slowly at this temperature. After being stirred at 0 °C for 15 min and 25 °C for 1 h, bis(trimethylsilyl) peroxide (0.18 g, 1.0 mmol) was added and the whole was stirred at 25°C for 3 h. The resulting mixture was poured into aq $Na_2S_2O_3$ (10 ml) and extracted with ether. The combined organic layers were washed with aq $NaHCO_3$ (10 ml) and brine, dried and con-

centrated. Purification by preparative TLC on silica gel (hexane-ethyl acetate, 2:1) gave **2** as a white solid (0.14 g, 84%). Mp 55 °C (hexane); IR (CCl_4): 1743, 1200, 1190, 1140, 1080 cm^{-1}; NMR (CCl_4): δ=0.90 (s, 9H), 1.10—2.30 (m, 5H), 2.40—2.66 (m, 2H), 3.80—4.40 (m, 2H); MS *m/e* (%): 170 (M^+, 2), 155 (2), 114 (80), 86 (60), 68 (13), 57 (100). The compound was identical with an authentic sample.[16]

Hexyl Heptanoate:[17] Bp 120 °C (bath temp, 3 Torr); IR (neat): 1742, 1380, 1170, 1102 cm^{-1}; NMR (CCl_4): δ= 0.72—1.83 (m, 22H), 2.17 (t, J=7 Hz, 2H), 3.94 (t, J= 7 Hz, 2H), MS *m/e* (%): 131 (7), 84 (25), 69 (18), 61 (19), 60 (12), 56 (44), 43 (100), 42 (27).

9-Decenyl Acetate:[18] Bp 100 °C (bath temp, 3 Torr); IR (neat): 1750, 1645, 1245, 910 cm^{-1}; NMR (CCl_4): δ=1.10—2.20 (m, 14H), 1.96 (s, 3H), 3.94 (t, J=7 Hz, 2H), 4.70—5.10 (m, 2H), 5.68 (ddt, J=16.5, 10, 7 Hz, 1H); MS *m/e* (%): 198 (M^+, 0.3), 155 (6), 138 (24), 110 (40), 96 (80), 82 (90), 68 (100), 54 (50).

2-Oxabicyclo[3.3.0]oct-6-en-3-one:[1] Bp 80 °C (bath temp, 1 Torr); IR (neat): 3090, 1780, 1180, 1020, 923, 720 cm^{-1}; NMR (CCl_4): δ=2.10—2.90 (m, 4H), 3.30—3.66 (m, 1H), 5.00—5.20 (m, 1H), 5.50—6.10 (m, 2H); MS *m/e* (%): 124 (M^+, 16), 96 (54), 95 (49), 79 (60), 68 (38), 67 (100), 66 (54).

7-Octen-5-olide:[14] Bp 75 °C (bath temp, 3 Torr); IR (neat): 3090, 1740, 1645, 1245, 1050, 996, 924 cm^{-1}; NMR (CCl_4): δ=1.15—2.95 (m, 8H), 3.96—4.10 (m, 1H), 4.78—5.30 (m, 2H), 5.30—6.10 (m, 1H); MS *m/e* (%): 140 (M^+, 5), 100 (57), 99 (92), 71 (96), 67 (21), 55 (100), 43 (87).

8-Methyl-7-nonen-5-olide: Bp 95 °C (bath temp, 0.15 Torr); IR (neat): 1740, 1242, 1175, 1048, 920 cm^{-1}; NMR (CCl_4): δ=1.13—2.50 (m, 8H), 1.63 (s, 3H), 1.72 (s, 3H), 3.80—4.40 (m, 1H), 4.90—5.30 (bt, 1H); MS *m/e* (%): 168 (M^+, 6), 99 (85), 71 (100), 69 (12), 55 (34), 43 (54): Found: C, 71.41; H, 9.47%, Calcd for $C_{10}H_{16}O_2$: C, 71.39, H, 9.59%.

7-Heptanolide: The above procedure using cycloheptanone (0.11 g, 1.0 mmol) afforded after usual workup and purification by preparative TLC (hexane-ethyl acetate, 2:1) a mixture of 7-heptanolide and 2-hydroxycycloheptanone in 54% yield (69 mg) in a ratio of 93:7 as determined by GLPC (5% PEG 20 M, 1.5 m, 128 °C). 7-Heptanolide (T_r=4.5 min) and 2-hydroxycycloheptanone (T_r=6.5 min) were identical with authentic sample.[19,10] 7-Heptanolide had bp 90 °C (bath temp, 20 Torr); IR (neat): 1715, 1240, 1150, 1098 cm^{-1}; NMR (CCl_4): δ=1.36—2.13 (m, 8H), 2.35 (t, J=6 Hz, 2H), 4.25 (t, J=6 Hz, 2H): MS *m/e* (%): 128 (M^+, 12), 110 (44), 100 (78), 98 (100), 96 (60), 82 (74), 81 (85), 71 (55), 68 (92), 67 (52), 57 (75).

2-Hydroxycycloheptanone: Bp 83 °C (bath temp, 3 Torr); IR (neat): 3490. 1705, 1078, 930 cm^{-1}; NMR (CCl_4): δ=1.10—3.00 (m, 10H), 3.45 (d, J=4 Hz, 1H), 3.90—4.30 (m, 1H); MS *m/e* (%): 128 (M^+, 0.3), 126 (0.4), 110 (5), 82 (7), 67 (100), 44 (32).

8-Octanolide: The above procedure with cyclooctanone (0.13 g, 1.0 mmol) gave a mixture of 8-octanolide (16 mg, 11%) and 2-hydroxycyclooctanone (60 mg, 42%). These compounds were identical with authentic samples.[19,10] 8-Octanolide had bp 130 °C (bath temp, 20 Torr); IR (neat): 1740, 1142, 1032 cm^{-1}; NMR (CCl_4): δ=1.10—2.00 (m, 10H), 2.10—2.36 (m, 2H), 4.28 (t, J=6 Hz, 2H); MS *m/e* (%): 142 (M^+, 5), 124 (6), 112 (25), 99 (77), 96 (48), 84 (50), 82 (69), 70 (43), 68 (100), 43 (46).

2-Hydroxycyclooctanone: Bp 100 °C (bath temp, 3 Torr); IR (neat): 3500, 1705, 1450, 1100, 950 cm^{-1}; NMR (CCl_4): δ=0.80—2.80 (m, 12H), 3.30—3.75 (m, 1H), 4.00 (dd, J =3, 6 Hz, 1H); MS *m/e* (%): 142 (M^+, 2), 124 (52), 98 (100), 81 (57), 80 (39), 68 (38), 57 (93), 55 (60), 44 (43).

10-Decanolide:[19] Bp 130 °C (bath temp, 20 Torr), IR (neat): 1720, 1480, 1450, 1080 cm^{-1}; NMR (CCl_4): δ= 1.10—1.93 (m, 14H), 2.05—2.40 (m, 2H), 4.00—4.30 (m, 2H); MS *m/e* (%): 170 (M^+, 2), 144 (6), 111 (14), 98 (100), 84 (34), 69 (16), 55 (20).

2-Hydroxycyclodecanone:[10] Bp 110 °C (bath temp, 0.15 Torr): IR (neat): 3500, 1700, 1475, 1100, 1085, 995 cm^{-1}; NMR (CCl_4): δ=0.83—3.40 (m, 16H), 3.50 (bs, 1H), 3.97—4.27 (m, 1H); MS *m/e* (%): 170 (M^+, 2), 134 (4), 96 (19), 82 (31), 68 (47), 57 (100), 55 (44).

11-Undecanolide:[19] Bp 105 °C (bath temp, 3 Torr): IR (neat): 1705, 1480, 1192. 1090 cm^{-1}; NMR (CCl_4): δ= 1.10—3.00 (m, 18H), 4.20 (dd, J=6, 8Hz, 2H); MS *m/e* (%): 184 (M^+, 25), 166 (14), 125 (23), 112 (25), 98 (100), 84 (33), 82 (39), 69 (66).

2-Hydroxycycloundecanone:[10] Bp 140°C (bath temp, 3 Torr); IR (neat): 3500, 1705, 1470, 1100, 1045 cm^{-1}; NMR (CCl_4): δ=1.10—3.00 (m, 18H), 3.20—3.50 (bs, 1H), 4.15 (t, J= 4.5 Hz, 1H); MS *m/e* (%): 184 (M^+, 10), 119 (41), 111 (53), 98 (58). 82 (100), 81 (58), 68 (78), 55 (54).

12-Dodecanolide:[19] Bp 120 °C (bath temp, 1 Torr); IR (neat): 1740, 1465, 1280, 1140, 1050 cm^{-1}; NMR (CCl_4): δ=1.20—1.95 (m, 18H), 2.20—2.50 (m, 2H), 4.25 (t, J= 4.5 Hz, 2H); MS *m/e* (%): 198 (M^+, 6), 180 (16), 138 (33), 110 (34), 98 (100), 96 (67), 84 (72), 82 (63).

2-Hydroxycyclododecanone:[10] Mp 79 °C (hexane/ether); IR (CCl_4): 3500, 1710, 1470, 1075, 1010 cm^{-1}; NMR (CCl_4): δ=0.80—3.30 (m, 21H), 4.25 (t, J=4 Hz, 1H); MS *m/e* (%): 198 (M^+, 6), 180 (10), 136 (20), 124 (22), 111 (23), 98 (53), 96 (49), 95 (47), 82 (100), 81 (44), 68 (56), 67 (37), 57 (36).

5-Hexanolide:[20] The same procedure with 2-methylcyclopentanone (98 mg, 1.0 mmol) and $BF_3 \cdot OEt_2$ gave a mixture of 5-hexanolide and 2-methyl-5-pentanolide in 81% yield (92 mg). GLPC (5% PEG 20 M, 1.5 m, 130 °C) indicated two peaks, T_r=24 min (5-hexanolide, 88%), T_r=22 min (2-methyl-5-pentanolide, 12%). 5-Hexanolide had bp 70 °C (bath temp, 3 Torr); IR (neat): 1745, 1380, 1250, 1070 cm^{-1}; NMR (CCl_4): δ=1.33 (d, J=6 Hz, 3H), 1.44—2.10 (m, 4H), 2.20—2.50 (m, 2H), 4.33 (qt, J=6, 3 Hz, 1H); MS *m/e* (%): 114 (M^+, 0.5), 71 (11), 70 (17), 55 (36), 42 (100).

2-Methyl-5-pentanolide:[21] Bp 70 °C (bath temp, 3 Torr); IR (neat): 1745, 1380, 1150, 1075 cm^{-1}; NMR (CCl_4): δ= 1.28 (d, J=6 Hz, 3H), 1.30—2.73 (m, 5H), 4.28 (t, J= 6 Hz, 2H); MS *m/e* (%): 114 (M^+, 28). 70 (22), 56 (48), 55 (100), 42 (82).

6-Heptanolide:[20] The same procedure with 2-methylcyclohexanone (0.11 g, 1.0 mmol) and $SnCl_4$ (0.26 g, 1.0 mmol) afforded a mixture of 6-heptanolide and 2-methyl-6-hexanolide in 93% yield (0.12 g) in a ratio of 72:28 as determined by ^1H-NMR (the absorption of the methyl proton). 6-Heptanolide had bp 93 °C (bath temp, 3.5 Torr); IR (neat): 1735, 1180. 1078. 1018 cm^{-1}; NMR (CCl_4): δ=1.31 (d, J=6 Hz, 3H), 1.20—2.10 (m, 6H), 2.35—2.73 (m, 2H), 4.10—4.50 (m, 1H); MS *m/e* (%): 128 (M^+, 2), 84 (40), 56 (69), 55 (73), 41 (100).

2-Methyl-6-hexanolide: Bp 88 °C (bath temp, 3 Torr); IR (neat): 1735, 1175, 1080, 1050 cm^{-1}; NMR (CCl_4): δ=1.13 (d, J=5 Hz, 3H), 1.20—2.13 (m, 6H), 2.30—2.80 (m, 1H), 4.00—4.30 (m, 2H); MS *m/e* (%): 128 (M^+, 4), 70 (5), 69 (14), 56 (32), 55 (38), 43 (20), 42 (100), 41 (63), 40 (14); Found: C, 65.56; H, 9.52%, Calcd for $C_7H_{12}O_2$: C, 65.59, H, 9.44%.

(Z)-7-Decen-5-olide (4):[14] To a stirred solution of 2-[(*Z*)-2-pentenyl]cyclopentanone (**3**, 0.15 g, 1.0 mmol) and

$Me_3SiOOSiMe_3$ (0.21 g, 1.2 mmol) in CH_2Cl_2 (10 ml) under an argon atmosphere $BF_3 \cdot OEt_2$ (0.14 g, 1.0 mmol) was added slowly at 0 °C. The resulting mixture was stirred at 0 °C for 15 min and 25 °C for 1.5 h. Additional $BF_3 \cdot OEt_2$ (0.14 g, 1.0 mmol) and $Me_3SiOOSiMe_3$ (0.18 g, 1.0 mmol) were added and the whole was stirred at 25 °C for 3 h. The mixture was poured into aq $NaHCO_3$ (10 ml) and extracted with ether. The combined organic layer was washed with brine, dried and concentrated. Purification by preparative TLC (hexane-ethyl acetate, 2:1) gave (*Z*)-7-decen-5-olide (jasmine lactone, **4**, 84 mg, 50%) along with the hydroxy carboxylic acid **5**. The hydroxy carboxylic acid **5** was heated at 100 °C under reduced pressure (10 Torr) for 1 h. Purification by preparative TLC afforded the desired lactone **4** in 8% yield (13 mg): Bp 125 °C (bath temp, 0.2 Torr); IR (neat): 3020, 1740, 1240, 1049, 928 cm^{-1}; NMR (CCl_4): δ=0.99 (t, J=7 Hz, 3H), 1.20—2.93 (m, 10 Hz), 4.00—4.50 (m, 1H), 5.06—5.75 (m, 2H); MS *m/e* (%): 168 (M^+, 14), 150 (10), 127 (6), 108 (6), 99 (100), 81 (10), 71 (40), 55 (18).

2-Acetoxyacetophenone:[22] Iron(III) chloride (0.16 g, 1.0 mmol) was added in portions to a stirred solution of 1-phenylethenyl acetate (0.16 mg, 1.0 mmol) and $Me_3SiOOSiMe_3$ (0.21 g, 1.2 mmol) at 0°C under an argon atmosphere. After stirring at 0 °C for 80 min, the resulting mixture was poured into brine (5 ml) and extracted with ether. The combined organic layers were dried and concentrated. Purification by preparative TLC (hexane-ethyl acetate, 2:1) gave 2-acetoxyacetophenone in 75% yield (0.13 g) and 2-hydroxyacetophenone in 11% yield (14 mg). 2-Acetoxyacetophenone had bp 107 °C (bath temp, 3 Torr); IR (neat): 1755, 1708, 1600. 1215. 1080, 955. 750, 685 cm^{-1}; NMR (CCl_4): δ=2.13 (s, 3H), 5.13 (s, 2H), 7.15—7.63 (m, 3H), 7.70—7.93 (m, 2H); MS *m/e* (%): 178 (M^+, 1), 118 (12), 106 (23), 105 (100), 91 (12), 77 (71).

2-Acetoxycyclohexanone:[23] Bp 90 °C (bath temp, 3 Torr); IR (neat): 1755, 1728, 1375, 1240, 1082, 1065 cm^{-1}; NMR (CCl_4): δ=1.00—2.55 (m, 8H), 2.10 (s, 3H), 4.96 (dd, J=7, 11 Hz, 1H); MS *m/e* (%): 156 (M^+, 14), 114 (27), 113 (76), 85 (26), 76 (38), 57 (10), 43 (100).

2-Hydoxycyclohexanone:[10] Bp 78 °C (bath temp, 3 Torr); IR (neat): 3500, 1715, 1262, 1100, 1025, 885 cm^{-1}; NMR (CCl_4): δ=1.10—2.70 (m, 8H), 3.36 (m, 1H), 3.94 (dd, J=8, 11 Hz, 1H); MS *m/e* (%): 114 (M^+, 11), 96 (7), 68 (9), 67 (15), 58 (16), 43 (100).

Financial support by the Ministry of Education, Science and Culture, Japanese Government, (Grant-in-Aid Nos. 57750744, 57307007) is acknowledged.

References

1) For example see: a) E. J. Corey and R. Noyori, *Tetrahedron Lett*, **1970**, 311; b) P. A. Grieco, *J. Org. Chem.*, **37**, 2363 (1972).

2) M. Suzuki, H. Takada, and R. Noyori, *J. Org. Chem.*, **47**, 902 (1982).

3) For general reviews, see: C. H. Hassall, *Org. React.*, **9**, 73 (1957); H. O. House, "Modern Synthetic Reactions," W. A. Benjamin, Inc., Menlo Park (1972), pp. 321—329, J. B. Lee and B. C. Uff, *Q. Rev. Chem. Soc.*, **21**, 449 (1967). Recent examples of the Baeyer-Villager oxidation cited in Ref. 2.

4) Treatment of 2-(3-methyl-2-butenyl)cyclopentanone with *m*-chloroperbenzoic acid (*m*CPBA) in CH_2Cl_2 gave the corresponding epoxide in 89% yield as a sole product. The same substrate was treated with H_2O_2–$BF_3 \cdot OEt_2$ system[6a] to afford the desired lactone in 28% yield along with the complex by-products arising from the epoxide.

5) $Me_3SiOOSiMe_3$ was prepared according to the literature: P. G. Cookson, A. G. Davies, and N. Fazal, *J. Organomet. Chem.*, **99**, C31 (1975); A. A. Oswald and D. L. Guertin, *J. Org. Chem.*, **28**, 651 (1963).

6) a) H_2O_2–$BF_3 \cdot OEt_2$: J. D. McClure and P. H. Williams, *J. Org. Chem.*, **27**, 24 (1962); b) CH_3CO_3H–$BF_3 \cdot OEt_2$: B. D. Mookherjee, R. W. Trenkel, and R. R. Patel, *ibid.*, **37**, 3846 (1972).

7) For the dimeric and trimeric cyclic peroxide thus formed see: P. R. Story, B. Lee, C. E. Bishop, D. D. Denson, and P. Bush, *J. Org. Chem.*, **35**, 3059 (1970) and references cited therein.

8) $Me_3SiOOSiMe_3$–Me_3SiOTf system has also been reported to give the undesired mixture in aromatic ketone cases (Ref. 2). For hydroxylation of benzene ring by means of $Me_3SiOOSiMe_3$–$AlCl_3$ system, see: J. O. Apatu, D. C. Chapman, and H. Heaney, *J. Chem. Soc., Chem. Commun.*, **1981**, 1079.

9) The reaction rate for oxidation of simple cyclic ketones with $PhCO_3H$ has been reported. S. L. Friess, *J. Am. Chem. Soc.*, **71**, 2571 (1949); S. L. Friess and P. E. Frakenburg, *ibid.*, **74**, 2679 (1952).

10) E. Friedrich and W. Lutz, *Chem. Ber.*, **113**, 1245 (1980).

11) Enol forms of simple medium ring ketones play an important role in the iodonium ion attack case, see: A. Gero, *J. Org. Chem.*, **26**, 3156 (1961) and N. L. Allinger, L. W. Chow, and R. A. Ford, *ibid.*, **32**, 1994 (1967).

12) P. D. Gardner, *J. Am. Chem. Soc.*, **78**, 3421 (1956).

13) M. F. Hawthorne, W. D. Emmons, and M. S. McCallum, *J. Am. Chem. Soc.*, **80**, 6393 (1958) and M. F. Hawthorne and W. D. Emmons, *ibid.*, **80**, 6398 (1958).

14) E. Demole and M. Winter, *Helv. Chim. Acta*, **45**, 1256 (1962); A. Ijima, H. Mizuno, and K. Takahashi, *Chem. Pharm. Bull.*, **20**, 197 (1972).

15) Jasmine lactone was obtained only in 19% yield by using $Me_3SiOOSiMe_3$–$SnCl_4$ system.

16) P. A. Grieco, Y. Yokoyama, S. Gilman, and Y. Ofune, *J. Chem. Soc., Chem. Commun.*, **1977**, 870.

17) M. P. J. Brennan and R. Brettle, *J. Chem. Soc., Perkin Trans. 1*, **1973**, 257.

18) J. Levisalles and D. Villemin, *Tetrahedron*, **36**, 3181 (1980).

19) R. Huisgen and H. Ott, *Tetrahedron*, **6**, 253 (1959).

20) W. H. Pirkle and P. E. Adams, *J. Org. Chem.*, **44**, 2169 (1979).

21) J. Falbe, N. Huppes, and F. Korte, *Chem. Ber.*, **97**, 863 (1964).

22) G. M. Rubbotom, J. M. Gruber, and K. Kincaid, *Synth. Commun.*, **6**, 59 (1976) and A. L. Stockburn and C. W. Thomas, *Org. Mass. Spectrom.*, **9**, 1027 (1974).

23) G. M. Rubbotom, R. C. Mott and H. D. Juve, Jr., *J. Org. Chem.*, **46**, 2717 (1981).

Further Polarographic Studies on the Condensation Products of Dehydro-L-ascorbic Acid with *o*-Phenylenediamine in Acetate Buffer, pH 3.6

Mitsuaki OHMORI,† Yuji TSUJIMOTO,† and Masanosuke TAKAGI*

Laboratory of Food Chemistry, College of Agriculture, University of Osaka Prefecture, Sakai 591

†*Osaka City Institute of Public Health and Environmental Sciences, Tennoji-ku, Osaka 543*

(Received January 28, 1983)

Three polarographic reduction waves, which appear when dehydro-L-ascorbic acid (DAA) is treated with *o*-phenylenediamine (OPD) in acetate buffer, pH 3.6, were reinvestigated by comparing with those of the synthesized products from DAA and OPD. A reaction scheme of DAA with OPD is presented and the characteristics of the reactions are discussed.

As previously known, dehydro-L-ascorbic acid (DAA), the oxidized form of L-ascorbic acid (AA), reacts with *o*-phenylenediamine (OPD) in acidic buffers to give three cathodic DC-waves ($E_{1/2}$: −0.240, −0.412, and −0.634 V *vs.* SCE, at pH 3.6), and this polarographic behavior differs appreciably from that of the other dehydro-reductones with OPD.[1] The third wave ($E_{1/2}$: −0.634 V), observed at an early stage of the measurement, is characteristic of DAA and can be used to detect both AA and DAA.[1,2] When the amount of OPD exceeds that of DAA, the ratio of the three wave heights changes with time, the sum of the three decreasing slightly.

With regard to the condensation products of DAA with OPD, many works have been reported.[3-12] Repeated discussions on the formulae of the products from 1 mole of DAA with 1 or 2 mol of OPD have not successfully assigned them to the three cathodic DC-waves.[1,13]

In the present work, each compound, synthesized according to the literature,[4,5,8,12] is studied polarographically at pH 3.6 and its polarographic behavior is compared with that of the three waves obtained when DAA is treated with OPD in the same buffer. In addition, the reaction mechanism of DAA with OPD is discussed, considering the bicyclic DAA structure recently suggested.[14-16]

Experimental

Chemicals. *o*-Phenylenediamine (reagent grade, Katayama Chemical Co., Osaka) was recrystallized before use. L-Ascorbic acid, acetone, methanol, and the chemicals used were of reagent grade. A pH 3.6 acetate buffer [0.2 M (mol dm^{-3})] was chosen. Norit "Extra" activated charcoal and O_2 gas of high purity were also employed.

Preparation of DAA. DAA-methanol solution was first prepared as before.[17] The evaporation of methanol under reduced pressure gave a viscous DAA-methanol adduct, which was directly diluted to a desired concentration of DAA with buffer solution of pH 3.6, for electrolyte solution. For solid preparation, DAA was prepared as previously described.[18]

Synthesis of the Condensation Products of DAA with OPD and Related Compounds. The condensation product of 1 mol DAA with 1 mol OPD (**A**)[5,12] was prepared according to Ogawa[5] or El Ashry *et al.*[12] and that of 1 mol DAA with 2 mol OPD (**B**)[4,5,8] according to Hasselquist.[4] The product **B** was refluxed in absolute methanol to give yellow crystals (**B′**).[4,8] A hydrolysis product from **B** in dilute HCl (**C**) was prepared according to Hasselquist.[4] The product **C** was also obtained from **B′**.

Apparatus. Polarographic measurements were carried out with a Yanagimoto Polarograph Type P-8, the characteristics of the capillary being $m=1.86$ mg/s, $t=4.50$ s^{-1} when the Hg level was 72.5 cm, and −0.6 V was applied. All the polarographic experiments were carried out at 25± 0.2 °C. ^{13}C-NMR Spectra were recorded on a JEOL FX-100 spectrometer.

*Preparation of Electrolyte Solutions of **B** and **B′**.* Neither **B** nor **B′** dissolved sufficiently in pH 3.6 acetate buffer, but both were freely soluble in *N,N*-dimethylformamide (DMF). For a stock solution, 0.1 M **B** or **B′** DMF solution was prepared. The solution was diluted 100 times with the acetate buffer before use, and the diluted solution was directly applied to the polarographic measurements.

Results and Discussion

Polarograms of the Condensation Products of DAA with OPD. The DAA concentration was kept constant at approximately 1×10^{-3} M, and the OPD concentration was changed. The polarograms shown in Fig. 1 were taken 1 h after mixing OPD with DAA in the buffer solution. As shown in Fig. 1(a), when the OPD concentration was below the DAA concentration, two reduction waves were observed, the half-wave potentials being −0.240 and −0.634 V (*vs.* SCE). The wave with more negative $E_{1/2}$ was much higher in

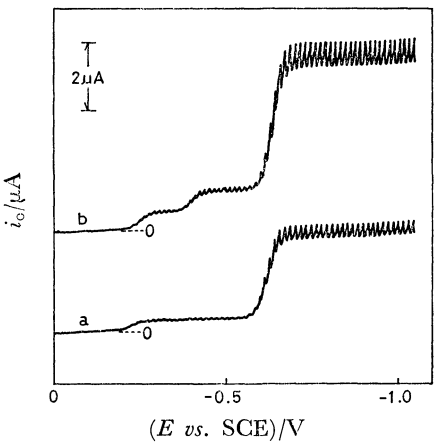

Fig. 1. Polarograms of the condensation products of DAA with OPD in acetate buffer pH 3.6.
Concn of DAA: *ca.* 1×10^{-3} M, concn of OPD: (a) 5×10^{-4} M, (b) 5×10^{-3} M, temp: 25 °C. Polarograms were taken 1 h after mixing OPD with DAA in the buffer solution.

wave height than the other. The relationships between the condensation time and the wave heights of the two reduction waves are shown in Fig. 2(a). The wave heights did not change after they reached equilibrium. When the OPD concentration was higher than the DAA concentration, another reduction wave appeared between the two waves (Fig. 1(b)). The half-wave potential was −0.412 V (*vs.* SCE). The three wave heights changed in a complex way with time as shown in Fig. 2(b). The third wave height decreased, while the first and second wave heights increased gradually. The total wave height of the three waves gradually decreased, though not large, as seen in Fig. 2(b).

Cyclic Voltammograms of the Condensation Products of DAA with OPD. Cyclic voltammograms (CV)

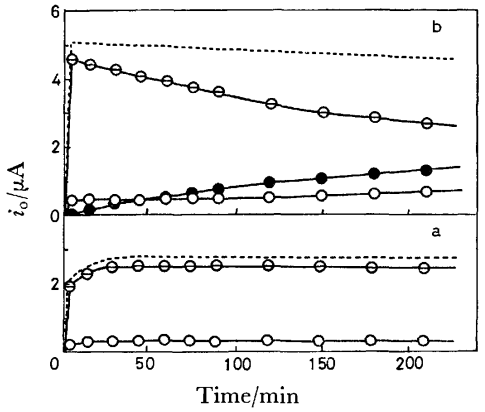

Fig. 2. Relationships between the condensation time and the wave height.
Concn of DAA: *ca.* 1×10^{-3} M, concn of OPD: (a) 5×10^{-4} M, (b) 5×10^{-3} M, temp: 25 °C, pH 3.6. ○: 1st wave, ●: 2nd wave, ⊖: 3rd wave, ---: total wave height.

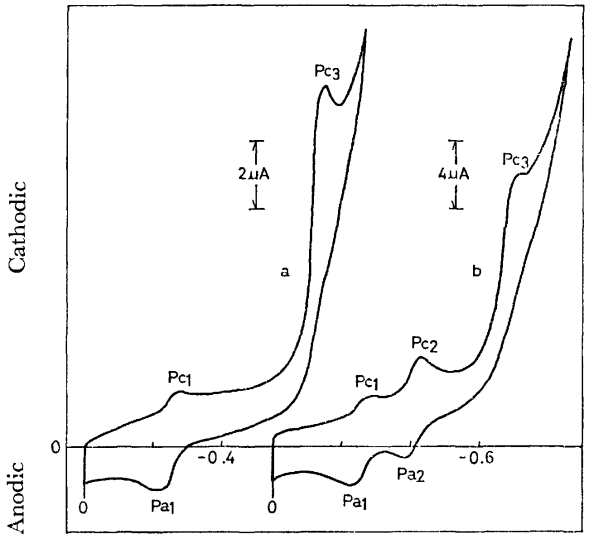

Fig. 3. CV curves of the condensation products of DAA with OPD in acetate buffer pH 3.6.
Concn of DAA: *ca.* 1×10^{-3} M, concn of OPD: (a) 5×10^{-4} M, (b) 5×10^{-3} M, temp: 25 °C, sweep rate: 50 mV/s, electrode: hanging mercury electrode (HME).

were recorded under the same experimental conditions as for the DC-polarograms. When the OPD concentration was below that of DAA, two cathodic peaks (P_{c1} and P_{c3}) corresponding to the first and the third DC-waves, respectively, and one anodic peak (P_{a1}) corresponding to the P_{c1} product, were observed, as shown in Fig. 3(a). When the OPD concentration was higher than that of DAA, three cathodic peaks (P_{c1}, P_{c2}, and P_{c3}) corresponding to the first, the second and the third DC-waves, and two anodic peaks (P_{a1} and P_{a2}) corresponding to the P_{c1} and P_{c2} products, were observed as shown in Fig. 3(b). These results indicate that the first and the second waves are reversible but the third wave is irreversible.

Polarograms of the Synthesized Products from DAA with OPD and Related Compounds. The polarogram of **A** (Fig. 4) was identical with that in Fig. 1(a), since the two reduction waves corresponded to the first and third waves. We attributed the polarogram shown in Fig. 1(a) to the equimolar condensation product of DAA with OPD.

For the polarograms of **B**, as shown in Fig. 5, two reduction waves were observed, whose wave heights changed with time. The two waves corresponded to the first and the second waves. The polarograms of

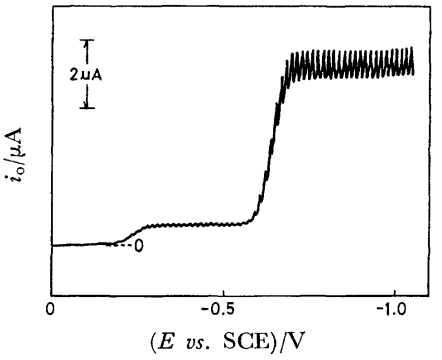

Fig. 4. Polarogram of **A**.
Concn of **A**: 2.64 mg/10 ml of buffer solution, temp: 25 °C, pH 3.6.

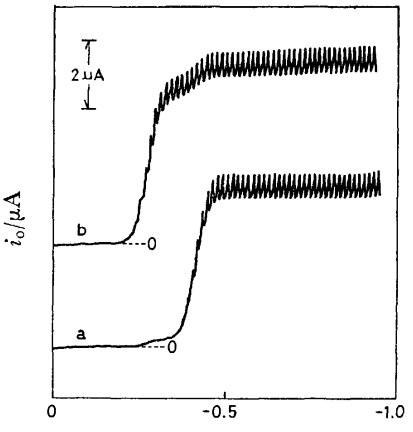

Fig. 5. Polarograms of **B**.
Concn of **B**: 3.54 mg/10 ml of buffer solution, temp: 25 °C, a: immediately after dissolving **B**, b: one day after.

B′ were similar to those of **B** shown in Fig. 5. It was also found by a separate experiment that **B′** changed to **B** quantitatively when refluxed with a mixture of methanol and water (4:1). The electronic spectra showed that **B** is favored whenever water is added.

The polarogram of **C** is shown in Fig. 6. Only one reduction wave, corresponding to the first wave, was observed.

The polarograms of the further reaction products of **A** with OPD were recorded after the direct dissolution of excess OPD into the buffer solution containing **A**. Three reduction waves appeared, and the polarogram which was recorded 1 h after the addition of OPD agreed with that shown in Fig. 1(b). The time courses of the reaction of **A** with OPD observed by the change of heights of three waves are shown in Fig. 7. The polarographic behavior of the reaction products of **A** with OPD in the buffer was similar to that previously observed in Fig. 2(b). It is probable that, when DAA is treated with excess OPD, the condensation product, corresponding to **A**, is first produced and then it reacts further with another 1 mol of OPD.

By comparing this behavior with that of **B** or **B′**, and considering that the total wave height of the three waves began to decrease gradually as soon as the second wave appeared, we came to the conclusion that the appearance of the second wave and the increase in the first wave were caused by the formation of the condensation product of 1 mol DAA with 2 mol OPD as either **B** or **B′**.

The decrease of the total wave height with time may be explained by a decrease of the diffusion constant of the depolarizer caused by the addition of one more OPD to **A**. However, the total wave height reaches its maximum value at the final equilibrated state, when the chemical species corresponding to **B** or **B′** is scarce. That is, when DAA reacts with OPD, the formation of **B** or **B′** is transitory, if the concentration of OPD is not much larger than that of the DAA; say maximum 3 times of DAA. When OPD is more than 10 times of DAA, the final state shows the presence of **C** and **B** or **B′** only. The equilibrium between **C** and **B** (**B′**) is approximately 3:1, coinciding with the observation by Erlbach and Ohle for iso-DAA with OPD.[3]

Reaction Mechanism of DAA with OPD. Recently, it has been confirmed that the structure of DAA is predominantly a bicyclic form, shown as **1** at the top of Scheme 1, in solution, and the bicyclic form of DAA changes to the compound **2** with time.[14,16] We measured ^{13}C-NMR spectra of DAA in the mixture of D_2O and hydrochloric acid (about pH 3.0) to identify the structure of DAA in acidic solution. Six signals at 174.2, 92.0, 106.3, 73.6, 88.3, and 76.8 ppm were found. They were in accord with the chemical shifts in D_2O solution (C-1: 174.2, C-2: 92.0, C-3: 106.3, C-4: 73.5, C-5: 88.2, and C-6: 76.8 ppm), which were assigned to **1** by Hvoslef and Pedersen.[14] We thus conclude that DAA is predominantly in the form of structure **1** in acidic solution.

The structure of **A** has recently been correctly described as **3** by El Ashry *et al.*[11] The anomeric structure of **C** was first reported to be that of **4** by Erlbach and Ohle[3] in a reaction system of iso-DAA with OPD, and then **4** was reported by Ogawa,[5] Hasselquist,[4] and Dahn and Moll[8] in a reaction system of DAA with OPD.

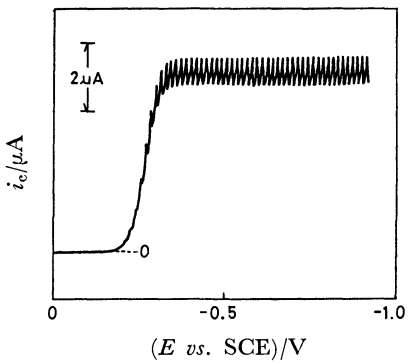

Fig. 6. Polarogram of **C**.
Concn of **C**: 2.46 mg/10 ml of buffer solution, temp: 25 °C, pH 3.6.

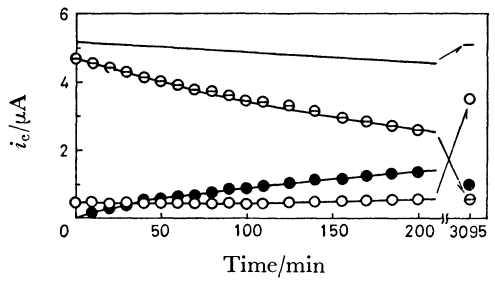

Fig. 7. Time courses of the reaction of **A** with OPD by the change of heights of the three waves.
Concn of **A**: 2.64 mg/10 ml of buffer solution, concn of OPD: 4×10^{-3} M, temp: 25 °C, pH 3.6. ○: 1st wave, ●: 2nd wave, ⊖: 3rd wave, ——: total wave height.

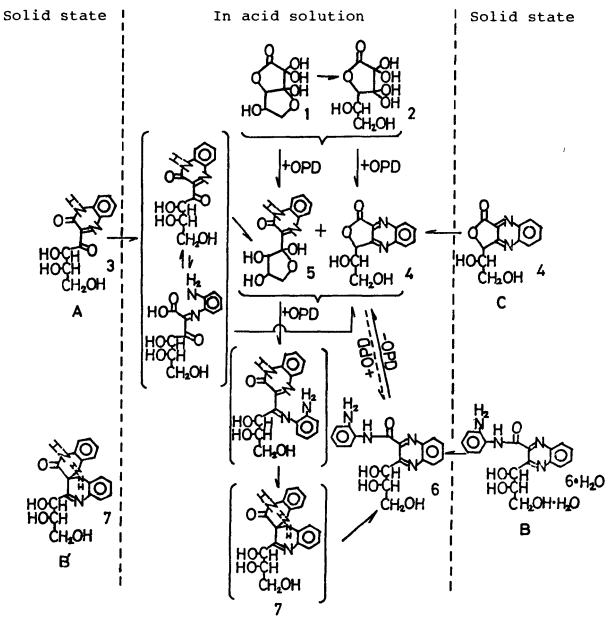

Scheme 1. Reaction mechanism of DAA with OPD in acetate buffer pH 3.6.

As previously mentioned, DAA reacts equimolarly with OPD to exhibit two reduction waves. The first wave seems to be caused by **C**, which is formed by the reaction of **2** with OPD, whereas the characteristic wave, corresponding to the third, seems to be due to the reaction product of bicyclic DAA with OPD.

With regard to the structure of **B**, Dahn and Moll[8] corrected the structure suggested by earlier workers[3,4] and reported **6** for **B**, while **B'** has not been confirmed. Recently, we have studied the structures of **B** and **B'** on the basis of elemental analysis and spectroscopic data, and have concluded that **B** seemed to be a monohydrate of **6** and that **B'** might be 7.[19]

When OPD is in excess in the reaction with DAA the condensation product of 1 mol DAA with 2 mol OPD seems to be produced *via* **5**. Because **B'** could easily change to **B** in aqueous solution, **B'** is probably first produced *via* product **5** and seems to change immediately to **B**. This possibility is supported by the fact that the polarographic behavior of **B'** was identical with that of **B**. The product **B** was then hydrolyzed to **C**. When the polarogram of **C** was recorded with a large excess of OPD, the second wave was observed as well as the first. The reverse reaction from **C** to **B** seems to proceed when there is a large excess of OPD. This explains why the increment of the first wave was low in Fig. 2(b) and in Fig. 7.

Consequently, the reaction mechanism may be as shown in Scheme 1. Refering to the two-electron transfer found for each electrode reaction,[1] and the cyclic voltammetric results of the three waves, it is reasonable to assume that the electrode reaction of the first and the second waves occurs reversibly with a two-electron transfer for the quinoxalines of **4** and **6**. In contrast, the electrode reaction of the third wave occurs irreversibly in a two-electron transfer which results in the quinoxalinone, **5**.

The authors are grateful to the staff of the Application Center, Scientific Instrument Project, JEOL, Ltd., for the measurement of ^{13}C-NMR spectra of DAA in aqueous solution.

References

1) T. Wasa, M. Takagi and S. Ono, *Bull. Chem. Soc. Jpn.*, **34**, 518 (1961).
2) M. Ohmori, H. Akehashi, S. Shigeoka, S. Kitaoka, and M. Takagi, *Bunseki Kagaku*, **26**, 56 (1977).
3) H. Erlbach und H. Ohle, *Ber.*, **67**, 555 (1934).
4) H. Hasselquist, *Ark. Kemi.*, **4**, 369 (1952).
5) S. Ogawa, *J. Pharm. Soc. Jpn.*, **73**, 309 (1953).
6) G. Henseke und K. Dittrich, *Chem. Ber.*, **92**, 1550 (1959).
7) G. Henseke, D. Lehmann, und K. Dittrich, *Chem. Ber.*, **94**, 1743 (1961).
8) H. Dahn und H. Moll, *Helv. Chim. Acta*, **47**, 1860 (1964).
9) G. Henseke, *Z. Chem.*, **6**, 329 (1966).
10) E. S. H. El Ashry, I. E. El Khnly, and Y. El Kilany, *Carbohydr. Res.*, **60**, 303 (1978).
11) E. S. H. El Ashry, M. M. A. Abdel Rahman, M. Nassr, and A. Amer, *Carbohydr. Res.*, **67**, 403 (1978).
12) E. S. H. El Ashry, M, M, A, Abdel Rahman, N. Rashed, and A. Amer, *Carbohydr. Res.*, **67**, 423 (1978).
13) M. Takagi, R. Hosogaki, and S. Ono, *Rev. Polarog.*, **14**, 367 (1967).
14) J. Hvoslef and B. Pedersen, *Acta. Chem. Scand., Ser. B*, **33**, 503 (1979).
15) K. Pfeilsticker, F. Marx, und M. Bockisch, *Carbohydr. Res.*, **45**, 269 (1975).
16) R. Matusch. *Z. Naturforsch., B*, **32**, 562 (1977).
17) M. Ohmori and M. Takagi, *Agric. Biol. Chem.*, **42**, 173 (1978).
18) M. Ohmori, H. Higashioka, and M. Takagi, *Agric, Biol. Chem.*, **47**, 607 (1983).
19) Y. Tsujimoto, M. Ohmori, and M. Takagi, unpublished result.

 © 1983 The Chemical Society of Japan Bull. Chem. Soc. Jpn., 56, 2037—2043 (1983)

Synthesis of 6- and 8-Phenyl-substituted Flavonoids

Hisashi Matsumura,† Toshio Tsuchiya,†† Tsuneko Takeda,†††
and Kimiaki Imafuku*

Department of Chemistry, Faculty of Science, Kumamoto University, Kurokami, Kumamoto 860

(Received Junuary 29, 1983)

3-Acetylbiphenyl-4-ol and -2-ol were condensed with substituted benzaldehydes to give respectively 5′- and 3′-phenyl-substituted chalcones (**1a—k**), which were cyclized to afford 6- and 8-phenylflavanones. The chalcones (**1a—k**) also gave the corresponding 6- and 8-phenylflavones *via* dibromides. The effects of the phenyl group on the spectral data are also discussed.

Flavonoids are well-known as the main constituent of yellow pigments of plant and possess many pharmacological actions. These flavonoids occur as hydroxy or methoxy-substituted compounds or glucosides. On the other hand, compounds having alkyl, halogen, amino, or nitro group have been obtained in synthetic materials. However, phenyl-substituted flavonoids have not been found in nature and in synthetic materials, except for a few reports.[1-3] One of them described synthesis of 5′-phenylchalcones[1] and the others described synthesis of 4-phenylchalcones[2] and 4′-phenyl-substituted flavanones and flavones.[3]

In this paper, we wish to report the synthesis of 5′- and 3′-phenylchalcones and the corresponding 6- and 8-phenyl-substituted flavanones and flavones.

Results and Discussion

The starting materials, 3-acetylbiphenyl-4-ol and -2-ol, were already prepared from biphenyl-4-ol and -2-ol by their *O*-acetylation and Fries rearrangement.[4] When Nencki-type reaction with boron trifluoride–acetic acid complex was applied to biphenyl-4-ol, 3-acetylbiphenyl-4-ol was easily obtained in one step and in good yield. However, the preparation of 3-acetylbiphenyl-2-ol by this method was failed.

These 3-acetylbiphenyl-4-ol and -2-ol were condensed with substituted benzaldehydes to give 2′-hydroxy-5′-phenylchalcones (**1a—h**) and 2′-hydroxy-3′-phenylchalcones (**1i—k**) in good yields, except for **1e** (16%) and **1h** (20%). The spectral data are summarized in Table 1. The IR spectra show the carbonyl absorption at 1635—1645 cm^{-1}. The UV spectra of **1a** and **1i** are shown in Fig. 1, together with the spectrum of the parent 2′-hydroxychalcone [λ (CH_3OH):[5] 221 (log ε 4.11) and 316 nm (4.36)]. The phenyl group at the 3′- and 5′-positions of **1a** and **1i** shows no appreciable effect because the phenyl group exists at the *meta* position against the cinnamoyl group. Substituents in the B ring caused bathochromic shift of the maximum of absorption band at *ca.* 320 nm of **1a** and **1i** to 330—390 nm. Particularly, the spectrum of a red colored compound **1d** showed maximum of absorption bands at 260 and 437 nm. In the NMR spectra of all the chalcones (**1a—k**), the signal for the hydrogen-bonded 2′-OH group was found at δ *ca.* 13.

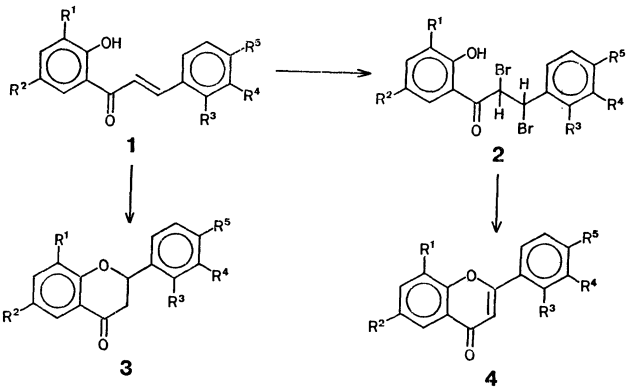

	R^1	R^2	R^3	R^4	R^5
a	H	Ph	H	H	H
b	H	Ph	H	H	CH_3
c	H	Ph	H	H	OCH_3
d	H	Ph	H	H	$N(CH_3)_2$
e	H	Ph	OH	H	H
f	H	Ph	H	Cl	H
g	H	Ph	H	H	Cl
h	H	Ph	H	OCH_3	OH
i	Ph	H	H	H	H
j	Ph	H	H	H	CH_3
k	Ph	H	H	H	OCH_3

Scheme 1.

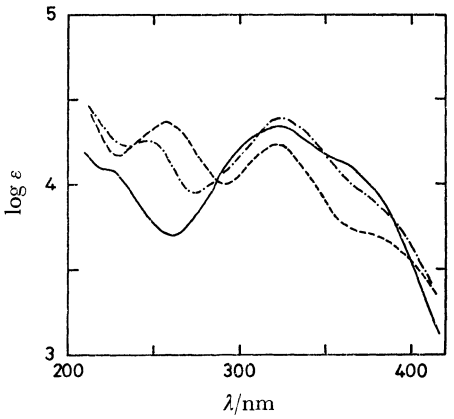

Fig. 1. UV Spectra of chalcones.
——: 2′-Hydroxychalcone, ----: **1a**, —·—·—: **1i**.

The bromination of the chalcones (**1a—k**) gave the corresponding their dibromides, 2′-hydroxy-5′- and 3′-phenylchalcone dibromides (**2a—k**), whose results are

† Present address: Kumamoto Institute of Technology Ikeda, Kumamoto 860.

†† Present address: Nagasaki-Prefectural Kenhoku Kogyo Gijutsu Center, Hirota-cho, Sasebo, Nagasaki 859-32.

††† Née: Aso,

Table 1. Characteristics for the chalcones (1)

Compd	Reaction time h	Appearance	Yield %	Mp θ_m/°C	IR (KBr) $\nu_{C=O}$/cm^{-1}	UV (CH_3OH) λ/nm(log ε)	NMR ($CDCl_3$) δ	Formula	Found(Calcd) (%) C	H	N
1a	3	Yellow needles	73	116.5—117.5 (116—117)[a]	1645	255(4.21) 318(4.35)	7.0—8.1(m, 15H), 12.90(s, 1H, OH)	$C_{21}H_{16}O_2$	84.01 (83.98	5.33 5.37)	
1b	20	Yellow needles	95	128.5—129 (122—123)[a]	1640	255(4.44) 330(4.36)	2.49(s, 3H, CH_3), 7.0—7.8 (m, 12H) 8.00(d, 1H, J=2.0 Hz, 6′-H) 8.22(d, 1H, J=15.5 Hz, β-H) 12.73(s, 1H, OH)	$C_{22}H_{18}O_2$	83.99 (84.05	5.63 5.77)	
1c	1/6	Yellowish orange needles	82	148.5—149 (127—128)[a]	1640	254(4.54) 361(4.40)	3.80(s, 3H, OCH_3), 6.86(dm, 2H, J= 9.0 Hz, 3,5-H), 7.0—8.0(m, 10H) 7.88(d, 1H, J=14.0 Hz, β-H) 7.97(d, 1H, J=2.0 Hz, 6′-H) 12.86(s, 1H, OH)	$C_{22}H_{18}O_3$	79.78 (79.98	5.34 5.49)	
1d	1	Red prisms	90	161.5—162 (160—161)[a]	1635	260(4.52) 437(4.40)	2.93(s, 6H, N-CH_3×2), 6.63 (d, 2H, J=9.5 Hz, 3,5-H), 7.02(d, 1H, J= 8.0 Hz, 3′-H), 7.2—7.9(m, 9H) 7.92(d, 1H, J=14.5 Hz, β-H) 8.02(d, 1H, J=2.5 Hz, 6′-H) 13.12(s, 1H, OH)	$C_{23}H_{21}O_2N$	80.50 (80.44	6.03 6.16	4.02 4.08)
1e	5	Yellowish orange needles	16	189.5—191	1640	258(4.41) 314(4.00) 378(4.07)	3.18(br.s, 1H, OH)[b], 1.7—8.1(m, 13H), 8.09(d, 1H, J=2.5 Hz, 6′-H) 12.86(s, 1H, OH)	$C_{21}H_{16}O_3$	80.01 (79.73	5.07 5.10)	
1f	1/12	Orange needles	48	100.5—101.5	1640	258(4.44) 313(4.37)	6.84(d, 1H, J=8.0 Hz, 3′-H) 7.0—8.0(m, 12H), 7.89(d, 1H, J= 2.5 Hz, 6′-H), 13.17(s, 1H, OH)	$C_{21}H_{15}O_2Cl$	75.61 (75.33	4.39 4.52)	
1g	1/12	Yellow needles	95	135.5—136 (135—136)[a]	1640	258(4.44) 326(4.42)	7.01(d, 1H, J=9.5 Hz, 3′-H) 7.2—7.95(m, 11H), 7.84(d, 1H, J= 14.5 Hz, β-H), 7.93(d, 1H, J=2.5 Hz, 6′-H), 12.64(s, 1H, OH)	$C_{21}H_{15}O_2Cl$	75.35 (75.33	4.53 4.52)	
1h	24	Yellowish orange needles	20	157—158	1645	258(4.52) 384(4.40)	3.91(s, 3H, OCH_3), 6.02(s, 1H, 4-OH) 6.88(d, 1H, J=8.5 Hz, 3′-H) 7.0—7.7(m, 10H), 7.89(d, 1H, J= 14.0 Hz, β-H), 7.99(d, 1H, J=2.5 Hz, 6′-H), 12.88(s, 1H, OH)	$C_{22}H_{18}O_4$	76.16 (76.28	5.16 5.24)	
1i	3	Yellow scales	90	103—104	1640	240(4.26) 322(4.45)	6.8—8.2(m, 15H), 13.30(s, 1H, OH)	$C_{21}H_{16}O_2$	83.93 (83.98	5.20 5.37)	
1j	1	Yellow scales	86	120—121	1645	244(4.29) 335(4.45)	2.35(s, 3H, CH_3), 6.8—8.1(m, 14H) 13.28(s, 1H, OH)	$C_{22}H_{18}O_2$	83.88 (84.05	5.66 5.77)	
1k	1/6	Yellow needles	88	134.5—136	1635	248(4.36) 366(4.48)	3.83(s, 3H, OCH_3), 6.87(d, 2H, J= 8.0 Hz, 3,5-H), 6.7—8.1(m, 12H) 13.41(s, 1H, OH)	$C_{22}H_{18}O_3$	79.95 (79.98	5.57 5.49)	

a) Ref. 1. b) In DMSO-d_6.

Table 2. Characteristics for the chalcone dibromides (**2**)

Compd	Appearance	Yield %	Mp θ_m/°C	IR (KBr) $\nu_{C=O}$/cm^{-1}	Formula	Found(Calcd) (%) C	H
2a	Yellow crystals	65	178—179	1635	$C_{21}H_{16}O_2Br_2$	55.03 (54.81	4.48 3.51)
2b	Yellow crystals	65	184—185	1635	$C_{22}H_{18}O_2Br_2$	55.68 (55.72	3.81 3.83)
2c	Yellow prisms	100	150—152	1635	$C_{22}H_{18}O_3Br_2$	54.12 (53.90	3.61 3.70)
2e	Brown microcrystals	82	140.5(decomp)	1635	$C_{21}H_{16}O_3Br_2$	53.21 (52.97	3.43 3.39)
2f	Yellow crystals	97	160—162	1640	$C_{21}H_{15}O_2Br_2Cl$	50.80 (50.99	3.15 3.06)
2g	Yellow crystals	84	192—193	1630	$C_{21}H_{15}O_2Br_2Cl$	51.21 (50.99	3.22 3.06)
2h	Pale yellow crystals	51	136(decomp)	1630	$C_{22}H_{18}O_4Br_2$	51.98 (52.20	3.66 3.58)
2i	Pale yellow microcrystals	69	207—210	1640	$C_{21}H_{16}O_2Br_2$	55.08 (54.81	3.45 3.51)
2j	Yellow microcrystals	79	205—206	1640	$C_{22}H_{18}O_2Br_2$	55.51 (55.72	3.83 3.83)
2k	Pale yellow needles	86	173—174	1645	$C_{22}H_{18}O_3Br_2$	53.74 (53.90	3.72 3.70)

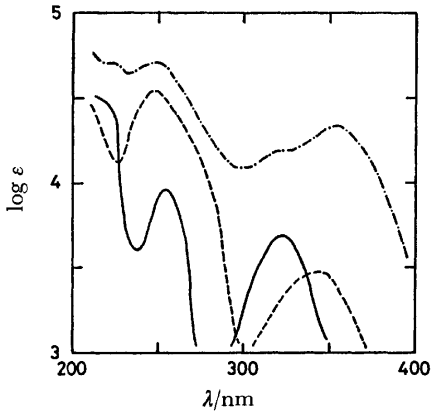

Fig. 2. UV Spectra of flavanones.
——: Flavanone, ----: **3a**, —·—·—: **3i**.

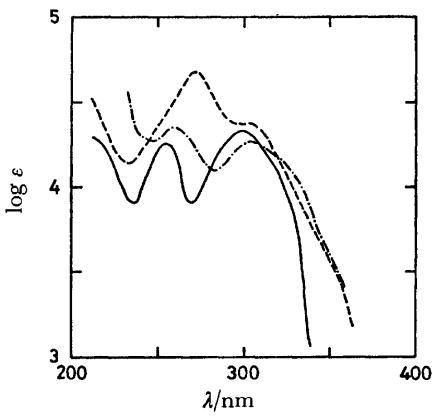

Fig. 3. UV Spectra of flavones.
——: Flavone, ----: **4a**, —·—·—: **4i**.

listed in Table 2. The compound **2d** was not isolated as crystal form and used for the flavone synthesis in this semisolid state.

The chalcones (**1a**—**k**) in acetone–ethanol were refluxed for 2 h in the presence of alkali to cyclize to 6- and 8-phenylflavanones (**3a**—**k**). The characteristic data are summarized in Table 3. In the IR spectra, the carbonyl absorptions were observed at 1705—1710 cm^{-1}, except for **3e** (1670 cm^{-1}). The UV spectra of 6- and 8-phenylflavanones (**3a** and **3i**) are shown in Fig. 2, together with the spectrum of flavanone itself [λ (CH_3OH):[5] 250 (log ε 3.86) and 320 nm (3.37)]. Introduction of the phenyl group at the 6- or 8-position produced bathochromic shifts of the absorption band at 320 nm by 15—25 nm. The NMR spectra showed the typical ABX pattern of 2-, 3e-, and 3a-protons.

The chalcone dibromides (**2a**—**k**) were treated with alkali to afford 6- and 8-phenylflavones (**4a**—**k**) in good yields. These results are summarized in Table 4. The IR spectra showed the carbonyl absorption at 1640—1650 cm^{-1}. The UV spectra of 6- and 8-phenylflavones (**4a** and **4i**) are shown in Fig. 3, together with flavone itself [λ (CH_3OH):[5] 250 (log ε 4.06) and 297 nm (4.20)]. The spectra of the flavones (**4a**—**k**) also showed bathochromic shifts of the absorption maximum at 300—330 nm by introduction of substituent in the B ring. Particularly, the maximum of absorption bands of the dimethylamino-substituted compound **4d** was observed at 257, 333, and 400 nm. In the NMR spectra, the 3-H protons were recorded at δ 6.6—6.8 as a sharp singlet peak.

Experimental

The melting points were determined with a Yanagimoto MP-S2 melting point-measuring apparatus and are uncorrected. The IR spectra were taken on a JASCO IRA-1

Table 3. Characteristics for the the flavanones (**3**)

Compd	Reaction time / h	Appearance	Yield / %	Mp θ_m/°C	IR (KBr) $\nu_{C=O}$/cm^{-1}	UV (CH_3OH) λ/nm(log ε)	NMR ($CDCl_3$) δ	Formula	Found(Calcd) (%) C	H	N
3a	24	Pale yellow prisms	30	99—100	1705	247(4.55) 345(3.34)	2.85(dd, 1H, J=18.0, 5.5 Hz, 3e-H) 3.00(dd, 1H, J=18.0, 11.0 Hz, 3a-H) 5.45(dd, 1H, J=11.0, 5.5 Hz, 2-H) 6.8—7.9(m, 12H) 8.09(d, 1H, J=2.5 Hz, 5-H)	$C_{21}H_{16}O_2$	83.69 (83.98	5.57 5.37)	
3b	7	Colorless scales	33	144—145	1710	247(4.57) 346(3.44)	2.36(s, 3H, CH_3) 2.90(dd, 1H, J=15.5, 3.5 Hz, 3e-H) 3.11(dd, 1H, J=15.5, 12.0 Hz, 3a-H) 5.45(dd, 1H, J=12.0, 3.5 Hz, 2-H) 7.10(d, 1H, J=8.5 Hz, 8-H) 7.1—7.7(m, 9H) 7.73(dd, 1H, J=8.5, 2.0 Hz, 7-H) 8.10 (d, 1H, J=2.0 Hz, 5-H)	$C_{22}H_{18}O_2$	83.98 (84.05	5.83 5.77)	
3c	2	Pale yellow needles	80	151—152	1710	246(4.58) 340(3.28)	2.88(dd, 1H, J=16.0, 5.0 Hz, 3e-H) 3.10(dd, 1H, J=16.0, 11.0 Hz, 3a-H) 3.78(s, 3H, OCH_3) 5.42(dd, 1H, J=11.0, 5.0 Hz, 2-H) 6.92(dm, 2H, J=9.0 Hz, 3′,5′-H) 7.1—7.6(m, 8H) 7.68(dd, 1H, J=8.5, 2.0 Hz, 7-H) 8.09(d, 1H, J=2.0 Hz, 5-H)	$C_{22}H_{18}O_3$	79.88 (79.98	5.57 5.49)	
3d	3	Yellow plates	48	192—192.5	1705	265(4.64) 346 sh	2.5—3.0(m, 2H, 3e, 3a-H) 2.92(s, 6H, N-CH_3×2) 5.35(dd, 1H, J=11.5, 5.0 Hz, 2-H) 6.64(dm, 2H, J=9.5 Hz, 3′,5′-H) 7.00(d, 1H, J=8.0 Hz, 8-H) 7.1—7.6(m, 9H) 7.65(dd, 1H, J=8.0, 2.0 Hz, 7-H) 8.07(d, 1H, J=2.0 Hz, 5-H)	$C_{23}H_{21}O_2N$	80.21 (80.44	6.24 6.16	4.18 4.08)
3e	5	Yellow crystals	46	207—208.5	1670	249(4.39) 347(3.32)	2.7—3.5(m, 2H, 3e,3a-H)[a] 5.83(dd, 1H, J=10.0, 5.0 Hz, 2-H) 6.7—7.9(m, 11H) 8.01(d, 1H, J=2.0 Hz, 5-H) 9.67(br.s, 1H, OH)	$C_{21}H_{16}O_3$	79.62 (79.73	5.09 5.10)	
3f	2	Pale yellow crystals	19	98—100	1710	249(4.46) 340(3.28)	2.87(dd, 1H, J=17.5, 6.0 Hz, 3e-H) 3.03(dd, 1H, J=17.5, 11.0 Hz, 3a-H) 5.45(dd, 1H, J=11.0, 6.0 Hz, 2-H) 7.07(d, 1H, J=8.5 Hz, 8-H) 7.2—7.7(m, 9H) 7.72(dd, 1H, J=8.5, 2.0 Hz, 7-H) 8.10(d, 1H, J=2.0 Hz, 5-H)	$C_{21}H_{15}O_2Cl$	75.33 (75.33	4.49 4.52)	

Table 3. (Continued)

Compd	Reaction time / %	Appearance	Yield / %	Mp θ_m/°C	IR (KBr) $\nu_{C=O}$/cm^{-1}	UV (CH_3OH) λ/nm(log ε)	NMR ($CDCl_3$) δ	Formula	Found(Calcd) (%) C	H	N
3g	24	Yellow scales	30	150.5—151	1710	247(4.57) 346(3.23)	2.88(dd, 1H, J=15.0, 5.5 Hz, 3e-H) 3.03(dd, 1H, J=15.0, 10.0 Hz, 3a-H) 5.43(dd, 1H, J=10.0, 5.5 Hz, 2-H) 7.06(d, 1H, J=8.0 Hz, 8-H) 7.1—7.7(m, 9H) 7.68(dd, 1H, J=8.0, 2.0 Hz, 7-H) 8.08(d, 1H, J=2.0 Hz, 5-H)	$C_{21}H_{15}O_2Cl$	75.61 (75.33	4.52 4.52)	
3h	25	Pale yellow needles	42	103—104	1705	246(4.60) 345(3.46)	2.88(dd, 1H, J=16.0, 4.0 Hz, 3e-H) 2.99(dd, 1H, J=16.0, 11.0 Hz, 3a-H) 3.88(s, 3H, OCH_3) 5.37(dd, 1H, J=11.0, 4.0 Hz, 2-H) 5.74(s, 1H, OH) 6.9—7.7(m, 9H) 7.68(dd, 1H, J=8.5, 2.0 Hz, 7-H) 8.10(d, 1H, J=2.0 Hz, 5-H)	$C_{22}H_{18}O_4$	76.26 (76.28	5.31 5.24)	
3i	24	Colorless prisms	71	117.5—118.5	1705	240(4.42) 334(4.66)	2.88(dd, 1H, J=17.5, 6.5 Hz, 3e-H) 3.00(dd, 1H, J=17.5, 9.5 Hz, 3a-H) 5.44(dd, 1H, J=9.5, 6.5 Hz, 2-H) 6.9—7.7(m, 12H) 7.90(dd, 1H, J=7.5, 2.0 Hz, 5-H)	$C_{21}H_{16}O_2$	83.89 (83.98	5.44 5.37)	
3j	1	Colorless prisms	38	113—114	1705	240(4.42) 338(3.57)	2.28(s, 3H, CH_3) 2.88(dd, 1H, J=17.5, 7.0 Hz, 3e-H) 2.97(dd, 1H, J=17.5, 9.0 Hz, 3a-H) 5.41(dd, 1H, J=9.0, 7.0 Hz, 2-H) 6.93(d, 1H, J=7.0 Hz, 7-H) 6.9—7.7(m, 10H) 7.89(dd, 1H, J=7.0, 2.0 Hz, 5-H)	$C_{22}H_{18}O_2$	83.98 (84.05	5.80 5.77)	
3k	2	Pale yellow needles	23	139—140	1710	232(4.49) 336(3.57)	2.88(dd, 1H, J=18.0, 6.5 Hz, 3e-H) 3.02(dd, 1H, J=18.0, 10.0 Hz, 3a-H) 3.75(s, 3H, OCH_3) 5.43(dd, 1H, J=10.0, 6.5 Hz, 2-H) 6.80(dm, 2H, J=9.5 Hz, 3′,5′-H) 7.10(d, 1H, J=9.0 Hz, 7-H) 7.2—7.7(m, 8H) 7.91(dd, 1H, J=8.5, 2.0 Hz, 5-H)	$C_{22}H_{18}O_3$	79.74 (79.98	5.41 5.49)	

a) In DMSO-d_6.

Table 4. Characteristics for the flavones (**4**)

Compd	Appearance	Yield %	Mp θ_m/°C	IR (KBr) $\nu_{C=O}$/cm^{-1}	UV (CH_3OH) λ/nm(log ε)	NMR ($CDCl_3$) δ	Formula	Found(Calcd) (%) C	H	N
4a	Yellow prisms	86	156—157	1645	273(4.64) 304(4.32)	6.72(s, 1H, 3-H), 7.2—8.0(m, 12H) 8.32(d, 1H, J=2.0 Hz, 5-H)	$C_{21}H_{14}O_2$	84.32 (84.54	4.80 4.73)	
4b	Pale yellow needles	90	201—202	1640	275(4.58) 314(4.42)	2.40(s, 3H, CH_3), 6.76(s, 1H, 3,H) 7.1—8.0(m, 11H) 8.36(d, 1H, J=2.5 Hz, 5-H)	$C_{22}H_{16}O_2$	84.54 (84.59	5.21 5.16)	
4c	Pale yellow scales	87	181—182	1640	249(4.36) 278(4.42) 331(4.51)	3.85(s, 3H, OCH_3), 6.68(s, 1H, 3-H) 6.95(d, 2H, J=8.5 Hz, 3′,5-H) 7.2—8.1(m, 9H) 8.38(d, 1H, J=2.0 Hz, 5-H)	$C_{22}H_{16}O_3$	80.23 (80.47	4.93 4.91)	
4d	Yellow needles	81[a)]	226—227	1640	257(4.58) 333(4.05) 400(4.60)	2.97(s, 6H, N-CH_3×2) 6.61(s, 1H, 3-H) 6.63(dm, 2H, J=8.5 Hz, 3′,5′-H) 7.2—8.0(m, 9H) 8.38(d, 1H, J=2.0 Hz, 5-H)	$C_{23}H_{19}O_2N$	79.96 (80.91	5.41 5.61	3.91 4.10)
4e	Yellowish orange needles	60	115—117	1635	258(4.31) 318(4.12)	7.09(d, 1H, J=10.0 Hz, 8-H) 7.2—7.9(m, 11H) 8.49(d, 1H, J=2.0 Hz, 5-H) 11.80(s, 1H, OH)	$C_{21}H_{14}O_3$	80.03 (80.24	4.28 4.49)	
4f	Yellow plates	53	162—163.5	1640	273(4.67) 306 sh(4.29)	6.69(s, 1H, 3-H), 7.2—8.0(m, 11H) 8.32(d, 1H, J=2.0 Hz, 5-H)	$C_{21}H_{13}O_2Cl$	75.62 (75.79	3.95 3.94)	
4g	Plae yellow needles	25	231—232	1640	276(4.62) 310(4.39)	6.71(s, 1H, 3-H), 7.2—8.1(m, 11H) 8.33(d, 1H, J=2.0 Hz, 5-H)	$C_{21}H_{13}O_2Cl$	75.53 (75.79	3.84 3.94)	
4h	Yellow crystals	22	203—204	1645	257(4.52) 276 sh(4.36) 347(4.46)	3.94(s, 3H, OCH_3), 6.42(br.s, 1H, OH) 6.64(s, 1H, 3-H), 7.2—7.8(m, 8H) 7.83(dd, 1H, J=9.0, 2.5 Hz, 7-H) 8.40(d, 1H, J=2.5 Hz, 5-H)	$C_{22}H_{16}O_4$	77.01 (76.73	4.67 4.68)	
4i	Pale yellow needles	94	131—131.5	1640	253(4.36) 302(4.29)	6.74(s, 1H, 3-H), 7.1—8.0(m, 12H) 8.22(dm, 1H, J=8.0 Hz, 5-H)	$C_{21}H_{14}O_2$	84.65 (84.54	4.51 4.73)	
4j	Pale yellow needles	70	149—150	1650	253(4.30) 312(4.39)	2.36(s, 3H, CH_3), 6.76(s, 1H, 3-H) 7.11(dm, 2H, J=9.0 Hz, 3′,5′-H) 7.3—7.9(m, 9H) 8.15(dd, 1H, J=8.0, 2.5 Hz, 5-H)	$C_{22}H_{16}O_2$	84.70 (84.59	5.33 5.16)	
4k	Yellow needles	93	189—191	1650	225(4.50) 263 sh(4.14) 329(4.46)	3.76(s, 3H, OCH_3), 6.64(s, 1H, 3-H) 6.77(dm, 2H, J=8.5 Hz, 3′,5′-H) 7.2—7.9(m, 9H) 8.11(dd, 1H, J=7.0, 2.5 Hz, 5-H)	$C_{22}H_{16}O_3$	80.35 (80.47	4.94 4.91)	

a) Based on **1d**.

and JASCO 403G spectrophotometers, and the UV spectra on a Hitachi EPS-3T spectrophotometer. The NMR spectra were recorded with a Hitachi R-24 spectrometer (60 MHz).

3-Acetylbiphenyl-2-ol. This compound was prepared by the method of Cheetham and Hey.[4]

3-Acetylbiphenyl-4-ol. A mixture of biphynyl-4-ol (21.3 g) and boron trifluoride-acetic acid complex (50 ml) was heated on a water bath for 2 h. The mixture was treated with water and extracted with ether. The ethereal solution was washed with water and dried over anhydrous sodium sulfate. After removal of the solvent, the residue was recrystallized from ethanol to afford 3-acetylbiphenyl-4-ol. Yield, 16.5 g (62%). Mp 61—62.5 °C (lit,[4] 61.5—62 °C).

*2'-Hydroxy-5'- or 3'-phenylchalcones (**1a—k**).* A solution of 3-acetylbiphenyl-4-ol or -2-ol (2.1 g, 10 mmol) and substituted benzaldehyde (10 mmol) in ethanol (10 ml) was stirred at 50—60 °C in the presence of 60% potasium hydroxide solution (7.5 ml). The mixture was neutralized with 3 M hydrochloric acid (1 M=1 mol dm^{-3}) to give a precipitate of 2'-hydroxy-5'- or 3'-phenylchalcone (**1a—k**), which was collected and recrystallized from methanol or acetone.

*2'-Hydroxy-5'- or 3'-phenylchalcone Dibromides (**2a—k**).* A bromine (320 mg, 2 mmol) solution in carbon tetrachloride (2 ml) was added dropwise to a solution of 2'-hydroxy-5'- or 3'-phenylchalcone (**1a—k**) (500 mg, 1.5—1.6 mmol) in carbon tetrachloride (5 ml) at room temperature. The mixture was allowed to stand for 30 min. After evaporation of an excess of bromine and the solvent under reduced pressure, the residue was treated with benzene to afford 2'-hydroxy-5'- or 3'-phenylchalcone dibromide (**2a—k**).

*6- and 8-Phenylflavanones (**3a—k**).* To a solution of 2'-hydroxy-5'- or 3'-phynylchalcone (**1a—k**) (500 mg, 1.5—1.6 mmol) in acetone (5 ml)-ethanol (10 ml) was added 1% potassium hydroxide solution (1 ml). After refluxing for 2 h on a water bath, the reaction mixture was slightly acidified with 3 M hydrochloric acid and allowed to stand overnight at room temperature to precipitate 6- or 8-phenylflavanone (**3a—k**), which was collected and recrystallized from methanol or acetone.

*6- and 8-Phenylflavones (**4a—k**).* To a suspended solution of 2'-hydroxy-5'- or 3'-phenylchalcone dibromide (**2a—k**) (500 mg) in acetone (1 ml) was added 20% potassium hydroxide solution (1 ml) at room temperature. The mixture was diluted with water and slightly acidified with 3 M hydrochloric acid to give 6- or 8-phenylflavone (**4a—k**) as a precipitate, which was collected and recrystallized from methanol or acetone.

We are grateful to Sanko Chemical Co., Ltd. for a supply of biphenyl-2-ol and -4-ol.

References

1) K.-K. Hsu and T.-S. Wu, *Tai-Wan Ko Huseh*, **27**, 19 (1973).

2) K.-K. Hsu and J.-Y. Shi, *J. Chinese Chem. Soc.*, **19**, 45 (1972).

3) K.-K. Hus and J.-Y. Shi, *J. Chinese Chem. Sci.*, **20**, 51 (1973).

4) K. H. Cheetham and D. H. Hey, *J. Chem. Soc.*, **1937**, 770.

5) L. Jurd, "The Chemistry of Flavonoid Compounds," ed by T. A. Geissman, Pergamon Press, Oxford (1962), p. 107.

Synthetic Study on Peptide Antibiotic Nisin. I. The Synthesis of Ring A[1]

Tateaki WAKAMIYA, Kuniaki SHIMBO, Akihiko SANO, Koichi FUKASE, and Tetsuo SHIBA*

Department of Chemistry, Faculty of Science, Osaka University, Toyonaka, Osaka 560

(Received February 8, 1983)

Synthesis of the ring A, a cyclic sulfide peptide part containing dehydroalanine residue, in peptide antibiotic nisin was successfully achieved by applications of two novel procedures. First, a sulfide ring was derived from a cyclic disulfide peptide by desulfurization with $P(Et_2N)_3$. Secondly, for the preparation of dehydroalanyl residue, a simple and convenient method through Hofmann degradation of 2,3-diaminopropionyl residue was newly exploited in the presence of sulfide linkage.

Nisin, a peptide antibiotic, was isolated from culture broth of *Streptococcus lactis* by Mattick *et al.* in 1947,[2] and Berridge *et al.* in 1952.[3] However, in spite of the early isolation, the structure of nisin was first proposed by Gross *et al.* in 1970.[4] As shown in Fig. 1, nisin has a quite unique structure composed of thirty four amino acids including three dehydroamino acid residues and five sulfide rings named A, B, C, D, and E from the *N*-terminal in the molecule.

An antimalarial activity as well as an inhibition of growth of *Staphylococcus aureus* were known as typical biological activities of this peptide.[5] However, few works are reported about the structure-biological activity relationships except a role of dehydroalanine residue for an exhibition of the antibacterial activity.[5] Thus, we started the synthetic study of nisin from the standpoint of not only a synthetic interest in such a complicated structure but also a confirmation of its unique structure and detailed elucidation on structure-activity relationships of this antibiotic.

For accomplishment of the synthesis of nisin, we are required to resolve two problems in the synthetic procedures, *i.e.*, i) introduction of the dehydroamino acid residue; ii) formation of the sulfide ring. Especially, both points are very important to carry out the synthesis of the ring A (Fig. 2) as the first target of the total synthesis of nisin. We attempted to solve the first problem by application of our novel method for the dehydroalanine synthesis through Hofmann degradation of 2,3-diaminopropionic acid (A_2pr).[6]

The second problem concerns to how to prepare lanthionine moiety in a cyclic peptide. For synthetic strategies of cyclic lanthionine peptide, possibly the following three procedures may be considered (Fig. 3). First of all, a cyclization can be performed by amide bond formation between carboxyl and amino groups at suitable positions in a lanthionyl peptide. Indeed, Photaki and her coworkers applied this concept to prepare ring A of nisin based on their extensive knowledge of lanthionine chemistry.[7] Although, a route a) seems to be quite reasonable, much efforts are required for preparation of the *meso*-lanthionyl residue. For instance, four functional groups in lanthionine moiety must be differentially protected and also made free step by step. This is not so easy task, and furthermore, a yield of cyclization by amide bond formation is sometimes not so high.

Therefore, we attempted to find more convenient method for sulfide ring formation. One of the promising ways may be an addition of mercapto group to the dehydroalanyl residue as described in route b). Although highly expensive D-cysteine is not required in this case, crucial disadvantage of this route is no assurance of stereoselective addition to obtain a desired steric form of lanthionine. Therefore, a final route c) seems to be most attractive procedure, if desulfurization of a cyclic disulfide peptide will successfully proceed, because a formation of –S–S– bond is rather easier than a cyclization by amide bond formation.

Based on the above considerations, the linear peptide **8** containing two cysteine residues of D- and L-configurations and 2,3-diaminopropionic acid residue as precursors of *meso*-lanthionine and dehydroalanine, respectively, was prepared as shown in Fig. 4. Protection of the mercapto groups in Cys residues and S–S bond formation were made by reference to Kamber's elucidation, which suggested an oxidative disulfide formation effected with I_2 from ~~Cys(Acm)~~Cys(Acm)~~ in DMF or ~~Cys(Trt)~~Cys(Acm)~~ in MeOH.[8] For reasons of easiness of *S*-tritylation compared to *S*-acetamidomethylation, convenience of experimental procedure in MeOH than DMF, and possible prevention of the intermolecular S–S linkage formation, the latter combination of protecting groups seemed to be preferable. On the other hand, N^{β}-amino group of A_2pr residue was protected with benzyl-

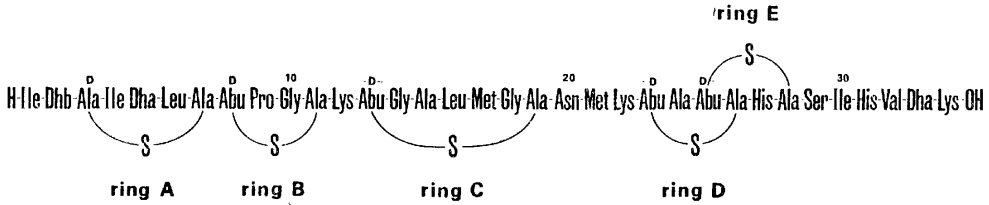

Fig. 1. The proposed structure of nisin. Abu: 2-aminobutyric acid; Dha: dehydroalanine; Dhb: dehydrobutyrine (=3-methyldehydroalanine); Ala Ala: lanthionine; Abu Ala: β-methyllanthionine.

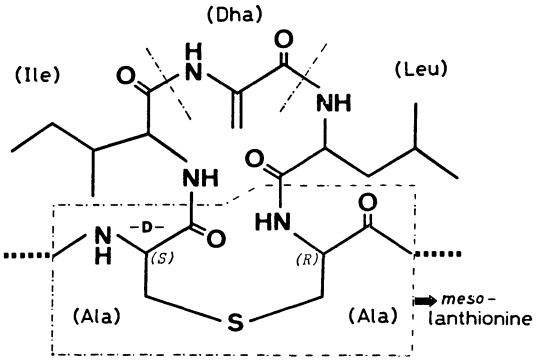

Fig. 2. The chemical structure of the ring A part in nisin.

oxycarbonyl (Z) group which is removable by the catalytic hydrogenation even though in the presence of sulfide moiety.[9] The peptide elongation was performed starting from the *C*-terminal by use of an active ester method.

The fully protected linear pentapeptide **8** thus obtained was then subjected to the preparation of the cyclic disulfide **9**. The oxidation was carried out smoothly to give the monomeric disulfide, whose molecular weight was confirmed by both mass spectrometry (FD, *m/z* 782; calcd 782) and osmometry (750± 37; calcd 783), in a good yield as expected.

The desulfurization reaction for the cystine peptide **9**, one of the important targets in this study, was achieved using tris(diethylamino)phosphine ($P(Et_2N)_3$) reported by Harpp for the preparation of lanthionine itself.[10] When the reaction was carried out in $CHCl_3$, the yield of the sulfide compound **10** was not reproducible and always poor. In order to check the reaction conditions, we then examined an effect of solvent on the desulfurization using a model compound, $(Z\text{-}Cys\text{-}OCH_3)_2$. The desirable lanthionine derivative was obtained only in DMF presumably *via* path (a) based on the concerted mechanism as shown in Fig. 5, while in solvents such as $CHCl_3$, THF, dioxane, or benzene, the dehydroalanine derivative was found to be a major product as a result of intramolecular β-elimination as shown in path (b). Thus, the cyclic disulfide compound **9** was successfully desulfurized in DMF to produce cyclic *meso*-lanthionyl peptide **10** without a formation of dehydroalanyl peptide. In this case, care must be taken to dry DMF absolutely, otherwise another side reaction as shown in Fig. 6 occurs.[11] The formation of *meso*-lanthionyl residue in this reaction was clearly ascertained by amino acid analysis of the hydrolyzate of **10**. (Fig. 8b)

A conversion of the A_2pr residue into the dehydroalanine residue was originally performed by a permethylation with CH_3I in the presence of $KHCO_3$.[6] However, according to this procedure, a methylation onto sulfur atom also occurred resulting in the undesirable formation of another dehydroalanyl residue. For example, *S*-methylcysteinyl peptide **14** as a model peptide gave a mixture of monodehydroalanyl peptide **15** and didehydroalanyl peptide **16**. (Fig. 7) Even under the most preferable conditions, the yield of **15** was less than 70% and the by-product **16** was still obtained in a yield of 10%.[6a] In order to prevent this undesirable *S*-methylation, we attempted to increase a reactivity of β-amino group of A_2pr compared to that of sulfide part. For this purpose, the β-amino group was once methylated to increase its basicity by an application of reductive *N*-alkylation with $NaBH_3CN$ and HCHO.[12] From model experiments using two simple peptides **14** and **18**, it was revealed that the former compound **14** gave dimethyl derivative **17**, while the latter **18** gave monomethyl one **19**. (Fig. 7) Probably, N^{α}-Boc group might sterically hinder the introduction of the second methyl group in the case of the methylation of **18**. These compounds were then subjected to Hofmann degradation. Interestingly, both **17** and **19** produced solely monodehydroalanyl peptides in good yields by use of a limited amount of CH_3I in the presence of an excess $KHCO_3$, respectively. The fact clearly indicated that the first *N*-methylation would be a rate-determining step during permethylation procedure in Hofmann reaction. By this modification, it has become feasible that our method for dehydroalanine synthesis is applicable to the A_2pr peptide involving the sulfide amino acid.

Along the above consideration, a final step of our synthesis of ring A was performed. Cyclic pentapeptide **10** was first debenzyloxycarbonylated by hydrogenation in the presence of Pd black catalyst which was required in more amount than that in usual case. When the hydrogenation did not proceed smoothly, the first catalyst was removed and then fresh catalyst

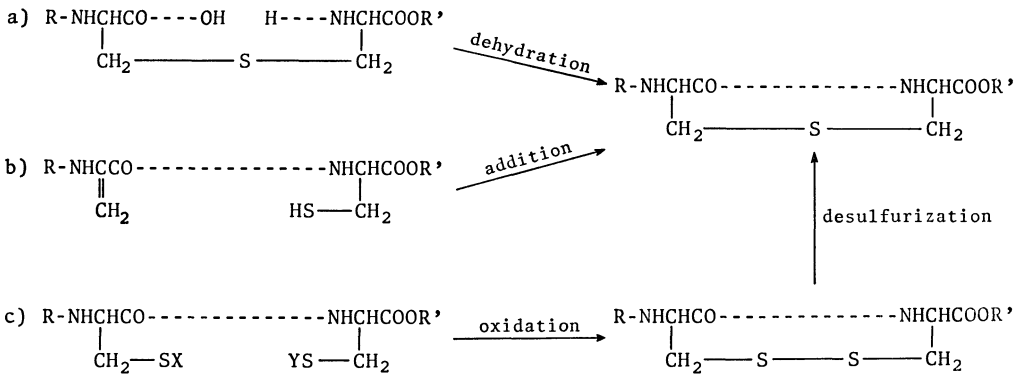

Fig. 3. Synthetic strategies of the cyclic lanthionyl peptide.

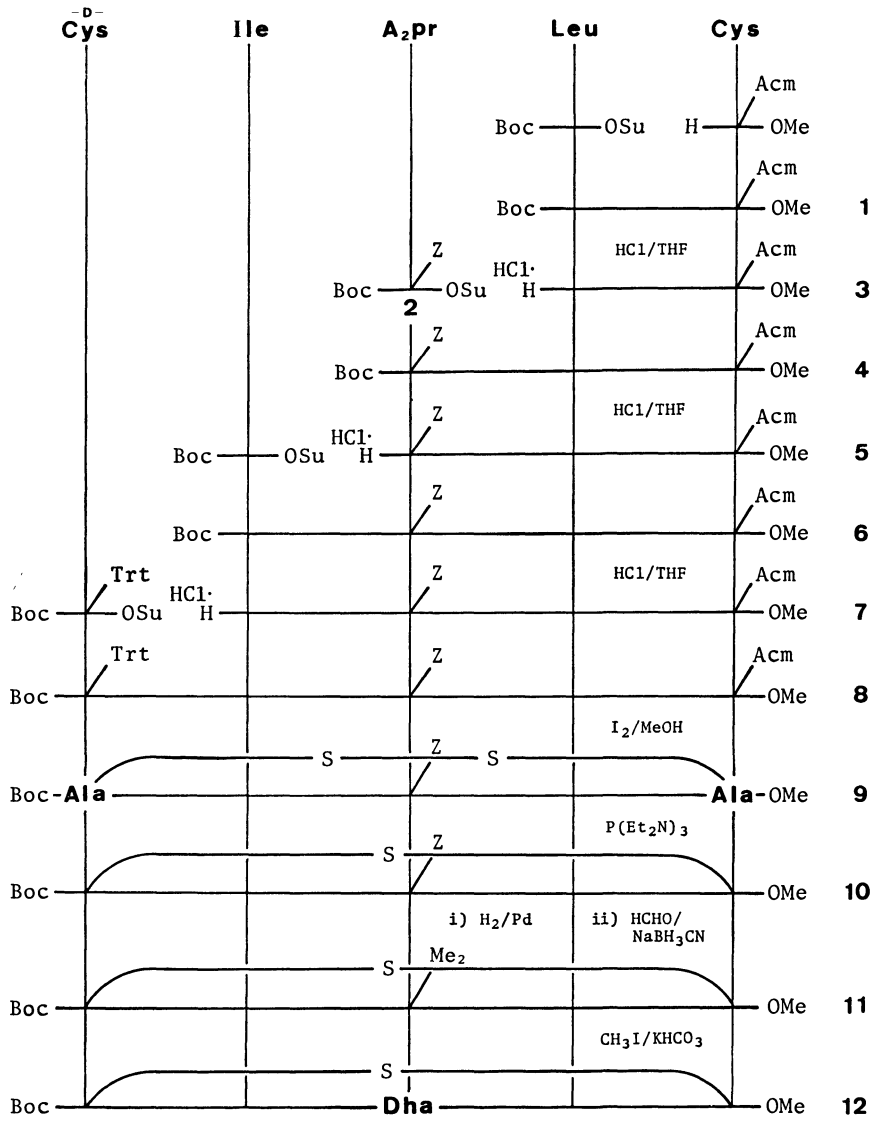

Fig. 4. The synthetic scheme of the protected ring A.

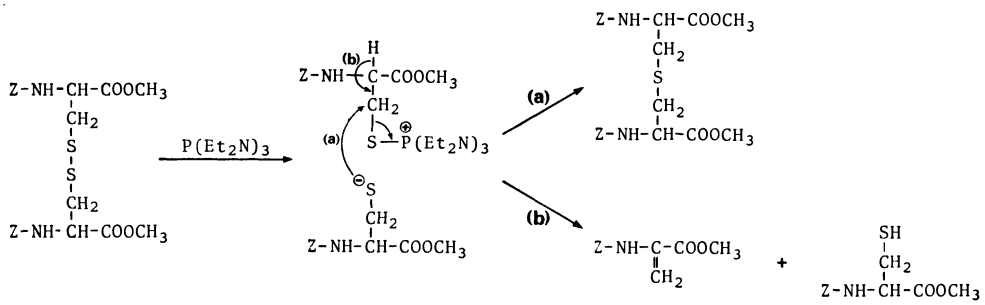

Fig. 5. The plausible reaction mechanism of the desulfurization.

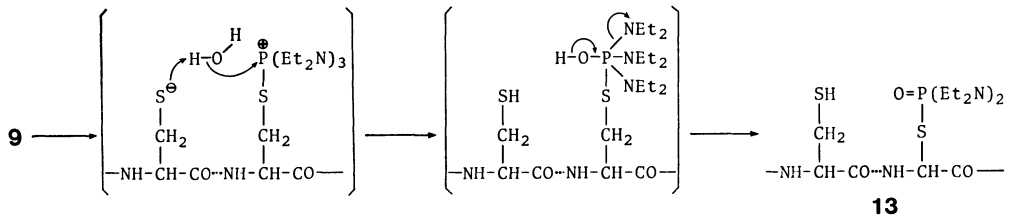

Fig. 6. The plausible by-product formation in the presence of water molecule during the desulfurization reaction.

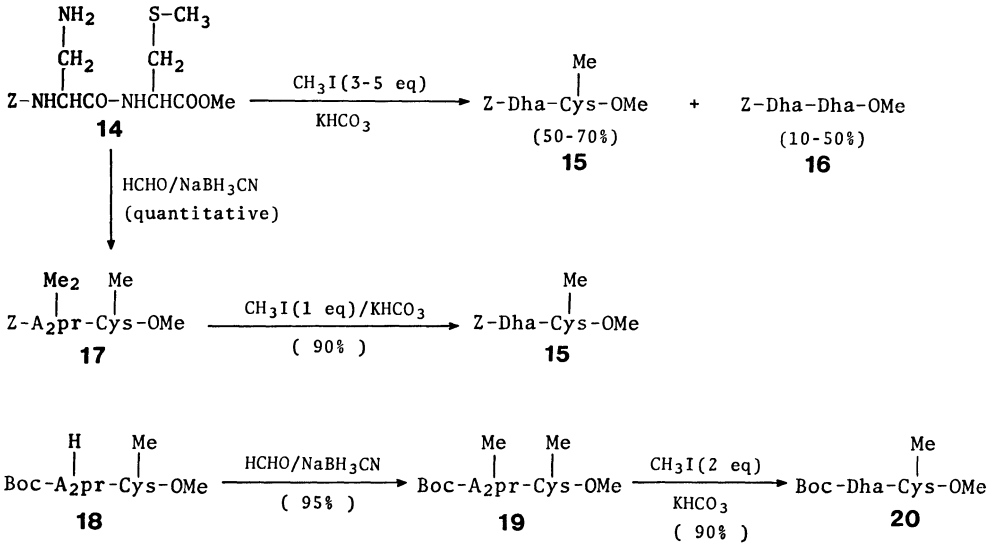

Fig. 7. An improved method of the dehydroalanine synthesis through Hofmann degradation *via* the N^{β}-methyl derivative of A_2pr residue.

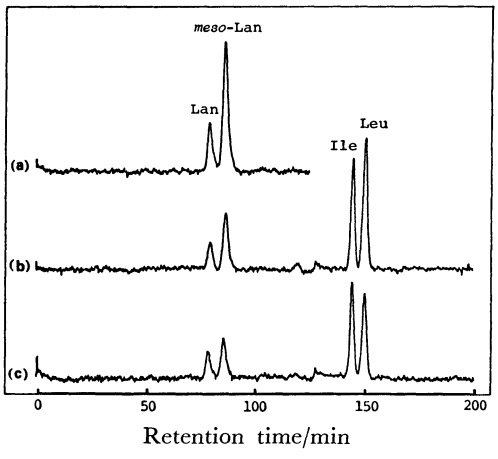

Fig. 8. Amino acid analyses of compounds **11** and **12**.
(a) When *meso*-lanthionine (*meso*-Lan) was treated under the hydrolytic conditions (6 M HCl, 110 °C, 20 h), a part of the sample was racemized to produce DL-lanthionine (Lan). (b) The hydrolyzate of desulfurization product **11** with 6 M HCl at 110 °C for 20 h. A chart of neutral component was shown. (c) The hydrolyzate of protected ring A **12**. A longer hydrolysis (6 M HCl, 110 °C, 40 h) caused more racemization of the *meso*-lanthionine residue.

must have been added. The hydrogenation product was immediately subjected to *N*-methylation with $NaBH_3CN$ and HCHO. Actually in the case of the cyclic peptide **10**, we could obtain dimethyl derivative **11** whose structure was confirmed by the molecular weight determination with FD-MS. Finally, the pentapeptide **11** could be converted through addition of 1.0—1.5 equivalent of CH_3I into desired dehydroalanyl peptide **12**, *i.e.*, protected ring A. The structure of the final product was definitely ascertained both chemically and physically. For example, the molecular weight was confirmed by FD-MS and the existence of the dehydroalanyl residue was confirmed from NMR spectrum. Furthermore, amino acid analysis of a hydrolyzate of the final product proved the presence of 11 amino acids constituting ring A. (Fig. 8c)

As mentioned above, we could satisfactorily exploit a novel method for preparation of the dehydroalanine through Hofmann degradation in the synthesis of ring A in peptide antibiotic nisin. Thereby, it proved that this method is very useful and applicable even for syntheses of other complex natural products containing dehydroalanine residue such as AM-toxins. Furthermore, the successful application of desulfurization reaction from cystinyl peptide made the preparation of lanthionyl peptide possible and opened a promising way for the convenient syntheses of other rings in nisin. Indeed, we recently performed the synthesis of ring B in this extention and the result will be reported elsewhere.

Experimental

All melting points are uncorrected. NMR spectra were obtained with a Varian XL-100-15 and JEOL FX-90Q spectrometers using TMS as an internal standard. FD-MS spectra were obtained with a JEOL 01SG spectrometer. Molecular weights were measured with a Knauer vapor pressure osmometer. The specific rotations were obtained with a Perkin-Elmer 141 polarimeter. UV spectra were recorded on a Hitachi 124 spectrophotometer. Amino acid analyses were carried out with a Hitachi KLA-5 analyzer using the following conditions: neutral and acidic amino acids were run on 0.9×55 cm column warmed at 55 °C with citrate buffer of pH 3.25 to 4.25 and basic components were analyzed on 0.9×7 cm column with citrate buffer of pH 5.28. Samples for the analysis were hydrolyzed with constant boiling 6 M (1 M=1 mol dm^{-3}) HCl in a sealed tube at 110 °C for 20 h.

*Boc-Leu-Cys(Acm)-OMe (**1**).* To a solution of Boc-Leu-OSu[13] (20 g, 60.9 mmol) and HCl·H-Cys(Acm)-OMe[14] (17.7 g, 72.8 mmol) in 200 ml of DMF was added triethylamine (14.8 g, 0.146 mol) under ice cooling. The reaction mixture was stirred at room temperature overnight. Triethylamine hydrochloride was filtered off and the filtrate

was concentrated *in vacuo*. Ethyl acetate solution of the residue was washed with aqueous 10% citric acid, saturated $NaHCO_3$, and saturated NaCl solutions. The organic layer was dried over $MgSO_4$ and then concentrated *in vacuo*. The oily residue was crystallized from hexane to obtain colorless needles in a yield of 24.5 g (96.1%). Analytical sample was prepared by recrystallization from ethyl acetate and hexane: mp 79—81 °C; $[\alpha]_D^{17}$ −16.4° (*c* 1.42, AcOEt).

Found: C, 51.32; H, 7.85; N, 9.82; S, 7.71%. Calcd for $C_{18}H_{33}N_3O_6S$: C, 51.53; H, 7.93; N, 10.02; S, 7.64%.

*HCl·H-Leu-Cys(Acm)-OMe (**3**).* Compound **1** (1.00 g, 2.38 mmol) was dissolved in 5.4 ml of 4.4 M HCl/THF. To a reaction mixture allowed to stand at room temperature for 1 h was added 300 ml of ether under cooling in an ice bath. The precipitate filtered was reprecipitated from isopropyl alcohol and ether: yield 0.69 g (82%); mp 156—158 °C; $[\alpha]_D^{15}$ −14.5° (*c* 1.45, MeOH).

Found: C, 43.33; H, 7.33; N, 11.24; S, 8.83; Cl, 9.71%. Calcd for $C_{13}H_{26}N_3O_4SCl\cdot 0.4H_2O$: C, 43.00; H, 7.44; N, 11.57; S, 8.83; Cl, 9.76%.

*Boc-A_2pr(Z)-Leu-Cys(Acm)-OMe (**4**).* To a solution of **3** (4.05 g, 11.4 mmol) in 80 ml of DMF were added Boc-A_2pr(Z)-OSu[15] (4.50 g, 10.3 mmol) and triethylamine (2.08 g, 20.6 mmol) under cooling in an ice bath. After stirring at room temperature overnight, triethylamine hydrochloride precipitated was filtered off. The residue obtained by concentration of the filtrate was dissolved in ethyl acetate. The solution was washed with aqueous 10% citric acid, saturated $NaHCO_3$, and saturated NaCl solutions. The organic layer was dried over $MgSO_4$ and concentrated *in vacuo*. Crystalline residue obtained was recrystallized from AcOEt: yield 5.60 g (84.7%); mp 119—122 °C; $[\alpha]_D^{13}$ −53.6° (*c* 1.45, MeOH).

Found: C, 54.29; H, 7.03; N, 10.71; S, 4.79%. Calcd for $C_{29}H_{45}N_5O_9S$: C, 54.44; H, 7.09; N, 10.95; S, 5.01%.

*HCl·H-A_2pr(Z)-Leu-Cys(Acm)-OMe (**5**).* Protected tripeptide **4** (1.00 g, 1.56 mmol) was dissolved in 5.7 ml of 4.1 M HCl/THF. After the solution was allowed to stand at room temperature for 40 min, ether was added to precipitate **5** under cooling in an ice bath. White powder obtained was filtered and reprecipitated from isopropyl alcohol and hexane: yield 0.91 g (quantitative); mp 103—105 °C; $[\alpha]_D^{13}$ −46.4° (*c* 1.01, MeOH).

Found; C, 48.56; H, 6.60; N, 11.73; S, 5.75; Cl, 6.23%. Calcd for $C_{24}H_{38}N_5O_7SCl$: C, 48.81; H, 6.76; N, 11.86; S, 5.43; Cl, 6.00%.

*Boc-Ile-A_2pr(Z)-Leu-Cys(Acm)-OMe (**6**).* To a solution of tripeptide hydrochloride **5** (7.46 g, 13.0 mmol) in 50 ml of DMF were added Boc-Ile-OSu [3] (4.26 g, 13.0 mmol) and triethylamine (2.63 g, 26.0 mmol) under ice cooling. The reaction mixture was stirred at room temperature overnight. Triethylamine hydrochloride was filtered off and the filtrate was concentrated *in vacuo*. The residue was once dissolved in a small amount of hot AcOEt and the solution was cooled in an ice bath. The gelatinous precipitate filtered was reprecipitated from methanol and water: yield 8.65 g (88.6%); mp 169—170 °C (decomp); $[\alpha]_D^{15}$ −56.5° (*c* 1.00, MeOH).

Found: C, 55.46; H, 7.42; N, 11.15; S, 4.30%. Calcd for $C_{35}H_{56}N_6O_{10}S\cdot 1/4\,H_2O$: C, 55.50; H, 7.52; N, 11.10; S, 4.23%.

*HCl·H-Ile-A_2pr(Z)-Leu-Cys(Acm)-OMe (**7**).* To a solution of protected tetrapeptide **6** (5.60 g, 7.44 mmol) in 22 ml of MeOH was added 16 ml of 4.7 M HCl/THF. The mixture was allowed to stand at room temperature for 1 h and then ether was added to precipitate hydrochloride under cooling in an ice bath. Crude product was reprecipitated from methanol and ether: yield 4.80 g (93.6%); mp 197—198 °C; $[\alpha]_D^{17}$ −36.0° (*c* 1.00, MeOH).

Found: C, 51.59; H, 7.15; N, 12.03; S, 4.87; Cl, 5.11%. Calcd for $C_{30}H_{49}N_6O_8SCl$: C, 51.60; H, 7.22; N, 12.04; S, 4.59; Cl, 5.08%.

*Boc-D-Cys(Trt)-Ile-A_2pr(Z)-Leu-Cys(Acm)-OMe (**8**).* Boc-D-Cys(Trt)-OH·DCHA[16] (1.40 g, 2.18 mmol) was treated with ethyl acetate and 10% aqueous citric acid. Ethyl acetate layer taken was washed with water three times and dried over $MgSO_4$. Oily residue obtained by vacuum concentration was dissolved in 10 ml of absolute THF. To the solution was added *N*-hydroxysuccinimide (250 mg, 2.18 mmol) and then DCC (448 mg, 2.18 mmol) under ice cooling. The mixture was stirred at 0 °C for 1 h and at room temperature for 2 h. *N,N'*-Dicyclohexylurea precipitated was filtered off and the filtrate was concentrated *in vacuo*. Oily residue thus obtained and **7** (1.50 g, 2.18 mmol) were dissolved in 20 ml of DMF. To the solution was added triethylamine (0.44 g, 4.4 mmol) under cooling in an ice bath. The reaction mixture was stirred at 0 °C for 30 min and at room temperature overnight. Triethylamine hydrochloride was filtered off and the filtrate was concentrated *in vacuo*. Oily residue was triturated with cold ether to make powder which was reprecipitated from methanol and 2% aqueous acetic acid. The precipitate filtered was washed with water and ether: yield 1.85 g (77.4%); mp 169—172 °C; $[\alpha]_D^{26}$ −45.4° (*c* 1.00, MeOH).

Found: C, 61.09; H, 6.84; N, 8.93; S, 5.62%. Calcd for $C_{57}H_{75}N_7O_{11}S_2\cdot H_2O$: C, 61.30; H, 6.95; N, 8.82; S, 5.74%.

*Boc-D-Cys-Ile-A_2pr(Z)-Leu-Cys-OMe (**9**).* To a solution of linear peptide **8** (4.60 g, 4.19 mmol) in 840 ml of MeOH was added I_2 (3.19 g, 12.6 mmol) in 125 ml of MeOH under vigorous stirring in a minute. The oxidation was accomplished for 1 h at room temperature and stopped by an addition of 0.1 M $Na_2S_2O_3$ solution until the color of I_2 disappeared. The reaction mixture was concentrated *in vacuo* and the residue was dissolved in water. Extraction with $CHCl_3$ was performed three times and the extract was concentrated *in vacuo* after drying over $MgSO_4$. The oily residue thus obtained was crystallized by an addition of ether to obtain pure material as a powder: yield 2.63 g (80.2%); mp 178—180 °C; $[\alpha]_D^{26}$ +2.3° (*c* 1.0, DMF); MW 750±37 (Calcd 783); FD-MS, *m/z* 782 (M^+).

Found: C, 53.12; H, 6.93; N, 10.42; S, 8.33%. Calcd for $C_{35}H_{54}N_6O_{10}S_2\cdot 1/2\,H_2O$: C, 53.08; H, 7.00; N, 10.61; S, 8.10%.

*Boc-D-Ala-Ile-A_2pr(Z)-Leu-Ala-OMe (**10**).* To a solution of the cyclic disulfide **9** (200 mg, 0.255 mmol) in 80 ml of anhydrous DMF was added tris(diethylamino)-phosphine (1.26 g, 5.11 mmol) in 20 ml of anhydrous DMF. The reaction mixture was stirred at 50 °C for 2 d and then concentrated *in vacuo*. The residue was once dissolved in AcOEt and washed with 10% citric acid and saturated NaCl solution. Organic layer was dried over $MgSO_4$ and concentrated *in vacuo*. The oily residue was easily crystallyzed by trituration with hexane in a yield of 164 mg (85.4%). Although the product was pure enough to be supplied for the next reaction, a part of the sample was recrystallized from methanol to obtain an analytical sample: mp 226.5—227 °C; $[\alpha]_D^{26}$ −47.6°C (*c* 1.00, DMF); FD-MS, *m/z* 750 (M^+). Amino acid analysis: Lan[17] (0.33), *meso*-Lan (0.72), Ile (0.76), Leu (1.00), A_2pr (1.15).

Found: C, 55.56; H, 7.18; N, 11.04; S, 4.31%. Calcd for $C_{35}H_{54}N_6O_{10}S$: C, 55.98; H, 7.25; N, 11.19; S, 4.27%.

Boc-D-Ala-Ile-$A_2pr(Me_2)$-Leu-Ala-OMe (**11**). The sulfide compound **10** (279 mg, 0.356 mmol) in 60 ml of methanol was hydrogenated in the presence of acetic acid (2.0 ml) by use of Pd black catalyst (*ca.* 2 g) under a gentle bubbling of hydrogen. A progress of the reaction was followed on TLC. After the hydrogenolysis was finished, the catalyst was filtered off. The filtrate was concentrated *in vacuo* and the residue was immediately dissolved in 25 ml of methanol for the following permethylation. To the solution were added 35% formaldehyde (153 mg, 1.78 mmol) and $NaBH_3CN$ (45 mg, 0.72 mmol). The reaction mixture was stirred at room temperature for 2 h and then concentrated *in vacuo*. The residue was treated with ethyl acetate and a saturated aqueous $NaHCO_3$. The organic layer was washed once with a saturated $NaHCO_3$ solution and three times with a saturated NaCl solution. The ethyl acetate extract was dried over $MgSO_4$ and concentrated *in vacuo*. The residue was reprecipitated from ethyl acetate and hexane: yield 179 mg (78.3%); mp 192—193 °C; $[\alpha]_D^{24}$ −44.0° (*c* 1.00, MeOH); FD-MS, *m/z* 644 (M^+).

Found: C, 54.24; H, 8.09; N, 13.02; S, 4.61%. Calcd for $C_{29}H_{52}N_6O_8S$: C, 54.02; H, 8.13; N, 13.03; S, 4.97%.

Boc-D-Ala-Ile-Dha-Leu-Ala-OMe (Boc-Ring A-OMe) (**12**). To a solution of dimethyl derivative **11** (140 mg, 0.217 mmol) in 5 ml of methanol were added $KHCO_3$ (326 mg, 3.26 mmol) and CH_3I (30.8 mg, 0.217 mmol). Since a part of CH_3I vaporized during the reaction at room temperature, a small amount of CH_3I (3.1 mg) was added four times every 10—12 h. The reaction mixture was finally cooled in an ice bath to precipitate a desired product. The precipitates filtered were washed with a 10% critic acid solution and water to remove inorganic salts: yield 40.6 mg (31.2%); mp 228—229 °C; $[\alpha]_D^{17}$ −68.2° (*c* 1.00, DMF); FD-MS, *m/z* 599 (M^+); UV(MeOH)λ_{max}, 250 nm (ε, 1500). Amino acid analysis: Lan[17] (0.40), *meso*-Lan (0.70), Ile (0.94), Leu (1.00).

Found: C, 53.91; H, 7.56; N, 11.55; S, 5.27%. Calcd for $C_{27}H_{45}N_5O_8S$: C, 54.07; H, 7.56; N, 11.68; S, 5.35%.

The authors are deeply indebted to Professor Kenji Okawa and Dr. Kiichiro Nakajima, Kwansei Gakuin University, for their kindness given for the use of an osmometer. The present work was partially supported by a Grant-in-Aid for Scientific Research No. 57540305 from the Ministry of Education, Science and Culture.

References

1) A part of this work was presented at 1st Symposium on Synthetic Organic Chemistry, Kyoto (Japan), September 1980, Abstr. No. I-4; 43rd National Meeting of the Chemical Society of Japan, Tokyo, April 1981, Abstr. No. 3F34; 4th International Conference on Organic Synthesis, Tokyo (Japan), August 1982, Abstr. No. B-I-2103.

2) A. T. R. Mattick and A. Hirsh, *Lancet*, **ii**, 5 (1947).

3) N. J. Berridge, G. G. F. Newton, and E. P. Abraham, *Biochem. J.*, **52**, 529 (1952).

4) E. Gross and J. L. Morell, *J. Am. Chem. Soc.*, **92**, 2919 (1970); **93**, 4634 (1971).

5) E. Gross and J. L. Morell, *J. Am. Chem. Soc.*, **89**, 2791 (1967).

6) a) S. Nomoto, A. Sano, and T. Shiba, "Peptide Chemistry 1978," ed by N. Izumiya, Protein Research Foundation, Osaka (1979), p. 35; b) S. Nomoto, A. Sano, and T. Shiba, *Tetrahedron Lett.*, **1979**, 521.

7) I. Photaki, S. Caranikas, I. Samouilidis, and L. Zervas, *J. Chem. Soc.*, Perkin *Trans 1*, **1980**, 1965.

8) B. Kamber, A. Hartmann, K. Eiser, B. Riniker, H. Rink, P. Sieber, and W. Rittel, *Helv. Chim. Acta*, **63**, 899 (1980). Abbreviations: Trt=trityl, Acm=acetoamidomethyl.

9) C. A. Dekker, S. P. Taylor Jr., and J. S. Fruton, *J. Biol. Chem.*, **180**, 155 (1949); K. Hoffmann, A. Johl, A. E. Furlenmeier, and H. Kappler, *J. Am. Chem. Soc.*, **79**, 1636 (1957); C. H. Li, J. Meienhofer, E. Schnabel, D. Chung, T. B. Lo, and J. Ramachandran, *ibid.*, **83**, 4449 (1961); K. Medzihradszky, V. Bruckner, M. Matjar, M. Löw, S. Bajusz, and L. Kisfaludy, *Acta Chim. Acad. Sci. Hung.*, **30**, 105 (1962); K. Medziharadszki and H. M. Schweiger, *ibid.*, **44**, 15 (1965); H. Yajima, K. Kawasaki, Y. Kinomura, T. Oshima, S. Kimoto, and M. Okamoto, *Chem. Pharm. Bull.*, **16**, 1342 (1968).

10) D. N. Harpp and J. G. Gleason, *J. Org. Chem.*, **35**, 3259 (1970); **36**, 73 (1971).

11) The structure of the by-product **13** was ascertained by FD mass spectrum in which the molecular peak (*m/z* 975 $(M+H)^+$) was observed.

12) R. F. Borch, M. D. Bernstein, and H. D. Durst, *J. Am. Chem. Soc.*, **93**, 2897 (1971); R. F. Borch and A. I. Hossid, *J. Org. Chem.*, **37**, 1673 (1972); C. F. Lane, *Synthesis*, **1975**, 135.

13) G. W. Anderson, J. E. Zimmerman, and F. M. Callahan, *J. Am. Chem. Soc.*, **86**, 1839 (1964).

14) B. Kamber, *Helv. Chim. Acta*, **54**, 927 (1971); P. Sieber, B. Kamber, K. Eisler, A. Hartmann, B. Riniker, and W. Rittel, *Helv. Chim. Acta*, **59**, 1489 (1976).

15) T. Teshima, S. Nomoto, T. Wakamiya, and T. Shiba, *Bull. Chem. Soc. Jpn.*, **50**, 3372 (1977).

16) R. G. Hiskey, L. M. Beacham, III, and V. G. Matl, *J. Org. Chem.*, **37**, 2472 (1972). The derivative of D-cysteine prepared showed reasonable optical rotation, *i.e.*, $[\alpha]_D^{20}$ −23.0° (*c* 1.00, MeOH) which was opposite in sign compared to that of L-form, while mp was identical with that of L-form in this reference.

17) See the note in the caption of Fig. 8, (a).

 © 1983 The Chemical Society of Japan Bull. Chem. Soc. Jpn., 56, 2050—2054 (1983)

Synthesis of Some New Aza Tricyclic Compounds with a Cyclopropane Ring *via* Photolysis of Dihydromayurone Oximes and the Related Compounds

Hajime Takahashi and Masaaki Ito*

Chemistry Laboratory, Department of General Education, Higashi Nippon Gakuen University, Ombetsu, Hokkaido 088-01

(Received October 12, 1982)

Oximation of dihydromayurone and 6,10,10-trimethyltricyclo[4.4.0.0^{1,3}]decan-4-one gives new isomeric oximes, respectively. The Beckman rearrangement of (*Z*)- or (*E*)-dihydromayurone oxime and (*Z*)- or (*E*)-6,10,10-trimethyltricyclo[4.4.0.0^{1,3}]decan-4-one oxime with polyphosphoric acid takes place prior to the *Z*-*E* equilibration of these isomers, respectively. Photolysis of the oximes gives two pairs of the isomeric lactams, 4-aza-8,12,12-trimethyltricyclo[6.4.0.0^{1,3}]dodecan-5-one, 5-aza-8,12,12-trimethyltricyclo[6.4.0.0^{1,3}]dodecan-4-one, 4-aza-7,11,11-trimethyltricyclo[5.4.0.0^{1,3}]undecan-5-one, and 5-aza-7,11,11-trimethyltricyclo[5.4.0.0^{1,3}]undecan-4-one. The reaction of either dihydromayurone or 6,10,10-trimethyltricyclo[4.4.0.0^{1,3}]decan-4-one with hydroxylamine-*O*-sulfonic acid in acetic acid affords only the lactam arising from the migration of the less substituted carbon.

Since the first study on the photo-Beckmann rearrangement of aromatic aldoximes by de Mayo,[1] a number of the related investigations have been reported. The mechanistic aspects of this intriguing and potentially useful photo chemical rearrangement have also been discussed for aromatic aldoximes,[2] and naphthalenone oxime,[3] styryl ketone oximes,[4] and alicyclic ketone oximes.[5–13] The formation of amides by photolysis of oximes is considered to take place *via* oxaziridine intermediates formed rapidly from the excited state oximes, which have been proved to be of a singlet state for the aromatic aldoximes[2] and the styryl ketone oxime rearrangement.[4]

In the photo-Beckmann rearrangement of the steroidal ketone oximes, we have recently reported[8,9] that the original configuration of C-α in the produced lactam with respect to the hydroxyimino group of the starting oxime was retained, irrespective of the configuration of the hydroxyimino group of the starting oxime.

We wish to report the photolysis and the Beckmann rearrangement of dihydromayurone oximes and 6,10,10-trimethyltricyclo[4.4.0.0^{1,3}]decan-4-one oximes, derived[14,15] both from a sesquiterpene thujopsene. We also report the reaction of the starting ketones (**1**) and (**4**) with hydroxylamine-*O*-sulfonic acid.[16,17] Considering that photolysis and the Beckmann rearrangement of an α,β-unsaturated ketone oxime are generally inferior to those of an alicyclic ketone oxime, we believe that the reactions of cyclopropyl ketone system which has a partial property of α,β-unsaturated ketone are important both from the synthetic and mechanistic points of view.

Results and Discussion

Preparation of Dihydromayurone Oximes (2), (3), and 6,10,10-Trimethyltricyclo[4.4.0.0^{1,3}]decan-4-one Oximes (5), (6). It was found that oximation of dihydromayurone[14] (**1**) gave a 2 : 1 mixture of new two isomeric oximes, which could be separated by preparative TLC into a less polar crystlline **2**, mp 136—137 °C and a more polar crystalline **3**, mp 160—161 °C. On the other hand, oximation of 6,10,10-trimethyltricyclo[4.4.0.0^{1,3}]decan-4-one[15] (**4**) also afforded the two isomeric crystalline oximes **5**, mp 103—105 °C and **6**, mp 106—107 °C in the ratio of 1.3:1, which could be separated by TLC.

The configurations of **2**, **3**, **5**, and **6** were established both by the following ^{1}H NMR spectra and the Beckmann rearrangement.

Generally, hydrogens on an α-carbon atom to the oximino group are known to appear downfield[18] and especially, a *Z*-hydrogen disposed coplanar with a hydroximino hydroxyl group considerably downfield in the ^{1}H NMR spectrum.

In the ^{1}H NMR spectra of **2**, **3**, **5**, and **6**, the signals of C-5-H$_2$ of **2** and **5** appeared more downfield, and the signals of C-3-H of **2** and **5** appeared more upfield

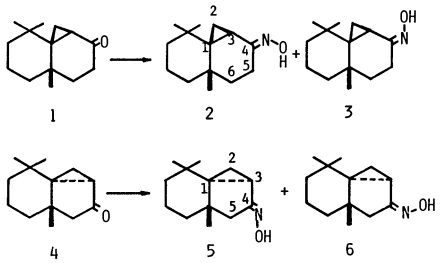

Scheme 1.

Table 1. ^{1}H NMR spectra [δ, $CDCl_3$, TMS] of C-3-H and C-5-H$_2$ of the oximes (**2**), (**3**), (**5**), and (**6**)

Oxime	C-3-H(J/Hz)[a]	C-5-H$_2$(J/Hz)
2	1.90 (dd, J=5 and 10 Hz)	2.20—2.40 (m)
3	2.41 (dd, J=5 and 10 Hz)	2.10 (m)
5	2.03 (dd, J=4 and 8 Hz)	1.71 and 2.50 (AB-q, J=17 Hz)
6	2.56 (dd, J=4 and 8 Hz)	1.81 and 2.00 (AB-q, J=16 Hz)

a) This assignment was confirmed by the decoupling study with C-2-H$_2$.

than those of **3** and **6**, as shown in Table 1. These results indicated that **2**, **5** and **3**, **6** were assigned to *E*- and *Z*-configuration, respectively. These assignments were supported by the following Beckmann rearrangement.

Beckmann Rearrangement of the Oximes (2) and (3). Treatment of **2** with polyphosphoric acid[19] (PPA) at 90 °C for 10 min afforded the two new lactams (**7**), mp 156—161 °C, and (**8**), mp 118—120 °C, in 40 and 7% yields (by GLC analysis), respectively. On the other hand, the Beckmann rearrangement of **3** under the same conditions afforded **7** and **8** in 10 and 41% yields. The new lactams **7** and **8** were identified as 4-aza-8,12,12-trimethyltricyclo[6.4.0.0^{1,3}]dodecan-5-one and 5-aza-8,12,12-trimethyltricyclo[6.4.0.0^{1,3}]dodecan-4-one, respectively, on the ^{1}H NMR spectral ground.

In the spectrum of **7**, signals due to protons at C-3, C-6, and N atoms appeared as a double doublet at δ 2.57 (J=4 and 9 Hz), as a multiplet at δ 2.10, as a broad singlet at δ 6.62 (W_H=12 Hz), respectively. It is noteworthy that one proton signal was observed abnormally at down field as a double doublet at δ 2.91 (J=8, 12, and 12 Hz). Irradiation at δ 2.10 (C-6-H$_2$) collapsed the double double doublet at δ 2.91 into a double doublet (J=8 and 12 Hz), indicating the signal in question to be assigned to one proton at C-7. With an aim to clarify the structure of **7**, dihydromayurone (**1**) was treated with *m*-chloroperbenzoic acid (MCPBA) in dichloromethane giving a lactone, 8,12,12-trimethyl-4-oxatricyclo-[6.4.0.0^{1,3}]dodecan-5-one (**9**). The ^{1}H NMR spectrum of **9** was similar to that of **7**; the signals of C-3-H, C-7-H, and C-6-H$_2$ appeared as a double doublet (δ 3.77, J=4 and 8 Hz), a double double doublet (δ 3.01, J=8, 12, and 12 Hz), and a multiplet (δ 2.30), respectively. While the C-7 proton of **9** appeared downfield by 0.1 ppm from the corresponding proton of **7**, and displayed the same splitting pattern, supporting the structure of **7** and **9**.

In the ^{1}H NMR spectrum of **8**, the signal due to N-proton was observed as a broad singlet at δ 7.18 (W_H=20 Hz). Moreover, the signal due to two C-6-protons appeared as two multiplets at δ 3.13 (1H) and 3.82 (1H). By addition of D_2O, the signal due to N-proton disappeared and the two multiplets were converted into a double double doublet and a double doublet centered at δ 3.82 (J=5, 12, and 14 Hz) and 3.13 (J=6 and 14 Hz), respectively. This also supports the structure of **8** as depicted in Scheme 2.

In the Beckmann rearrangement of oximes in general, it is well known[20] that the C–C bond oriented at the antiposition with respect to the hydroximino hydroxyl group migrates. Our results indicated that the equilibration between **2** and **3** took place to some extent prior to rearrangement under our experimental conditions. However, judging from the results, its rearrangement proceeded faster than the isomerization. These facts strongly suggested that the *E*- and *Z*-configurations were reasonably assigned to **2** and **3**, respectively.

Beckmann Rearrangement of the Oximes (5) and (6). Treatment of **5** with PPA at 90 °C for 5 min gave the two new lactams (**10**), mp 206—207 °C, and (**11**), mp 149—151 °C in 46 and 10% yields, respectively. On the other hand, the same treatment of **6** afforded **10** and **11** in 12 and 40% yields. On the basis of the ^{1}H NMR spectra, these lactams were assigned to the respective formulas, 4-aza-7,11,11-trimethyltricyclo[5.4.0.0^{1,3}]undecan-5-one and 5-aza-7,11,11-trimethyltricyclo[5.4.0.0^{1,3}]undecan-4-one, shown in Scheme 2. In the spectrum of **10**, signals due to protons at C-3, C-6, and N atoms appeared as a double doublet at δ 2.81 (J=5 and 10 Hz), as an AB-quartet at δ 1.80 and 2.12 (J=16 Hz) and as a broad singlet at δ 8.27 (W_H=16 Hz), respectively. Moreover, a new lactone, 7,11,11-trimethyl-4-oxatricyclo[5.4.0.0^{1,3}]-undecan-5-one (**12**) was prepared by treatment of **4** with MCPBA, and the structure of **10** was confirmed by the comparison with the spectra of **12**.

In the ^{1}H NMR spectrum of **11**, the signals of two C-6-protons appeared as a doublet at δ 2.91 (1H, J=13 Hz) and a double doublet at δ 2.48 (1H, J= 6 and 13 Hz). Addition of D_2O collapsed the double doublet at δ 2.48 into a doublet (J=13 Hz). The signal due to C-3-proton was not observed at downfield in the spectrum, again supporting the structure of **11** as indicated in Scheme 2.

These results confirmed the orientation of each hydroximino hydroxyl group of **5** and **6**.

Reaction of the Ketones (1) and (4) with a Hydroxylamine-O-sulfonic Acid. It has been reported that treatment of ketone with hydroxylamine-*O*-sulfonic acid[16] produced lactam, and camphor was converted into only α-camphidone[17] which is produced from less substituted α-carbon. Since the migration in the Beckmann rearrangement usually occurs from the more substituted α-carbon, the above result suggests "unusual" Beckmann rearrangement. Then, we attempted the reaction of the cyclopropyl ketone systems **1** and **4**.

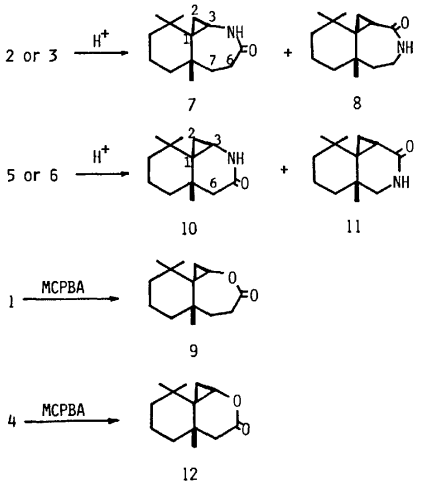

Scheme 2.

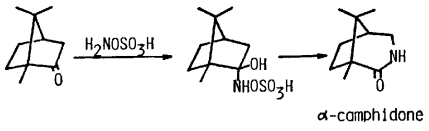

Scheme 3.

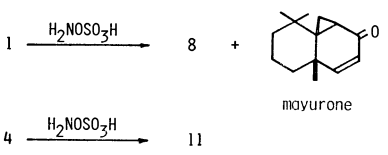

Scheme 4.

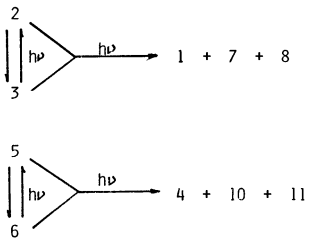

Scheme 5.

Treatment of **1** with hydroxylamine-*O*-sulfonic acid in acetic acid under reflux for 20 h gave **8** and mayurone in 33 and 24% yields, respectively. On the other hand, treatment of **4** under the same conditions afforded only **11** in 86% yield. These results indicated that the migration of less substituted α-carbon (C-5) took place predominantly (unusual Beckmann type).

Photolysis of Dihydromayurone Oximes (2) and (3). The photo-Beckmann rearrangement of **2** and **3** was carried out in methanol under nitrogen atmosphere at room temperature with a 15 W low pressure mercury lamp placed in the solution. Examination of the reaction by TLC indicated that a rapid photostationary equilibration between the *E*- and *Z*-forms took place, and, after 3 h, nearly equal amounts of *E*- and *Z*-forms were present in the solution. However, the photolysis for 20 h led to formation of several products, which were separated roughly into three fractions by column chromatography over silica gel. The least polar fraction consisted mainly of **1** in 40% yield, while the middle and the most polar fractions were found to contain **4** and **5** in the 10 and 13% yields, respectively. These products were identified by direct comparison with the spectra of the authentic samples.

The Photo-Beckmann Rearrangement of 5 and 6. The photo-Beckmann rearrangements of **5** and **6** were carried out under the same conditions as in the case of **2** and **3**. Examination of the reaction mixture after 5 h by TLC also revealed the presence of nearly equal amounts of *E*- and *Z*-forms in the solution. Further photolysis for 20 h resulted only in partial transformation of the oximes giving several products. Since further irradiation appeared to cause secondary photochemical decomposition of the initial products, the irradiation was stopped at this stage. The products were separated into four fractions by column chromatography over silica gel. The least polar fraction was found to be **4** in 24% yield by its spectra. The second least polar fraction (41%) consisted of a 1:1 mixture of the unreacted oximes. The third least and most polar fractions (3 and 5%) contained lactams **10** and **11**, respectively.

The results of the photolysis were summarized as follows. (i) The photo-Beckmann rearrangement of the conjugated cyclopropyl ketone oximes afforded the corresponding lactams. (ii) However, the yields of lactams were poor probably owing to the steric effect in the starting oximes and a property of a partial unsaturation of the cyclopropane ring. The major portion of products was the parent ketone arising from elimination of the nitrogen moiety of the intermidiary oxaziridines.

Experimental

All melting points were determined with a Shimadzu micro-apparatus. IR and ^1H NMR were determined with a Shimadzu IR-400 spectrometer and with a JEOL JNM-PMX-60 and/or a JEOL PS 100 high resolution spectrometer (solvent, chlorofrom-*d*; internal reference, tetramethylsilane), respectively. TLC and column chromatography were carried out on Wakogel B and on Cica Silica gel. GLC was carried out on a Shimadzu 4BM (column; 1.5% SE-30, 1.5 m). Elemental analysis were determined with a Hitachi CHN Analyzer. Mass spectra were taken by the staff of the Faculty of Pharmaceutical Science, Hokkaido University, with a RMU-6E spectrometer.

Dihydromayurone Oximes (2) and (3). Dihydromayurone (**1**) (2.06 g) in 90% aq ethanol (150 ml) was refluxed for 2 h with hydroxylamine hydrochloride (1.00 g) and sodium acetate (1.50 g). After removal of solvent, the reaction mixture was mixed with ether. The ether layer was washed with water, dried (Na_2SO_4), and evaporated to leave crystals, which were found to consist of two isomeric compounds by the ^1H NMR and TLC. These compounds were separated by repeated preparative TLC with a 4:1 mixture of benzene and acetone into **2** (1.04 g) and **3** (0.50 g).

Oxime **2**, mp 136—137 °C (from ethanol); MS, *m/e* 221 (M^+, 18%), 204 ($M^+ - OH$); IR ν_{max} (KBr) 3250 (-OH), 3020 (cyclopropane), and 1650 cm^{-1} (-C=N-); ^1H NMR, δ 1.90 (dd, 1H, $J=5$ and 10 Hz, C-3-H), 2.20—2.40 (m, 2H, C-5-H_2), 0.64, 1.14 and 1.19 each (s, 3H, -CH_3); Found: C, 75.76; H, 10.61; N, 6.20%. Calcd for $C_{14}H_{23}NO$: C, 75.97; H, 10.47; N, 6.33%.

Oxime **3**, mp 160—161 °C (from ethanol); MS, *m/e* 221 (M^+, 22%), 204 ($M^+ - OH$, 7); IR, ν_{max} (KBr) 3250 (-OH), 3020 (cyclopropane), and 1650 cm^{-1} (-C=N-); ^1H NMR, δ 2.41 (dd, 1H, $J=5$ and 10 Hz, C-3-H), 2.10 (m, 2H, C-5-H_2), 0.66, 1.10, and 1.16 each (s, 3H, -CH_3), Found: C, 75.88; H, 10.58; N, 6.32%. Calcd for $C_{14}H_{23}NO$: C, 75.97; H, 10.47; N, 6.33%.

6,10,10-Trimethyltricyclo[4.4.0.0^{1,3}]decan-4-one Oximes (5) and (6). The starting ketone (**4**) (0.96 g) in 90% aq ethanol (50 ml) was refluxed for 1 h with hydroxylamine hydrochloride (0.50 g) and sodium acetate (0.54 g). After removal of solvent, the reaction mixture was mixed with ether. The ether solution was washed with water, dried (Na_2SO_4), and evaporated to leave crystals, which were separated by repeated preparative TLC with a 5:1 mixture of benzene and acetone to afford **5** (460 mg) and **6** (350 mg).

Oxime **5**, when recrystallized from ethanol, had mp 103—105 °C; MS, *m/e* 207 (M^+, 17%), 190 ($M^+ - OH$, 25); IR, ν_{max} (KBr) 3280 (-OH), 1650 cm^{-1} (-C=N-); ^1H NMR, δ 2.03 (dd, 1H, $J=4$ and 8 Hz, C-3-H), 2.50 and 1.71 (AB-q, $J=17$ Hz, C-5-H_2), 0.60, 1.06, and 1.16 each (s, 3H, -CH_3); Found: C, 75.25; H, 10.05; N, 7.01%. Calcd for $C_{13}H_{21}NO$: C, 75.31; H, 10.21; N, 6.76%.

Oxime **6**, when recrystallized from ethanol, had mp 206—207 °C; MS, *m/e* 207 (M^+, 14%), 190 ($M^+ - OH$, 28); IR; ν_{max} (KBr), 3300 (OH), and 1650 cm^{-1} (-C=N-); ^1H NMR, δ 2.56 (dd, 1H, $J=4$ and 8 Hz, C-3-H), 1.81 and 2.00 (AB-

q, 2H, J=16 Hz, C-5-H_2), 0.63, 1.06, and 1.14 each (s, 1H, -CH_3); Found: C, 75.31; H, 10.24; N, 7.22%. Calcd for $C_{13}H_{21}NO$: 75.31; H, 10.21; N, 6.76%.

Rearrangement of ***2*** *with PPA.* **2** (400 mg) was added into polyphosphoric acid (20 g) at 90 °C, stirred with glass stick for 10 min, and cooled. To the reaction mixture was added 10% aq sodium carbonate and ether. The ether solution left oily residue, which was separated by column chromatography over silica gel to afford lactam **7** (123 mg) and **8** (25 mg).

Lactam **7**, mp 156—160 °C (from hexane); MS, *m/e* 221 (M^+, 19%); IR, ν_{max} (KBr) 3010 (cyclopropane), 3200 (-NH), and 1670 cm^{-1} (carbonyl); ^1H NMR, δ 2.57 (dd, 1H, J=4 and 9 Hz, C-3-H), 2.10 (m, 2H, C-6-H_2), 2.91 (ddd, 1H, J=8, 12, and 12 Hz, C-7-H), 6.62 (broad s, 1H, W_H=12 Hz, NH), 0.56, 0.85, and 1.18 each (s, 3H, -CH_3); Found: C, 75.68; H, 10.58; N, 6.18%. Calcd for $C_{14}H_{23}NO$: C, 75.97; H, 10.47; N, 6.33%.

Lactam **8**, mp 118—120 °C (from hexane); MS, *m/e* 221 (M^+, 24%); IR, ν_{max} (KBr) 3200 (-NH) and 1670 cm^{-1} (carbonyl); ^1H NMR, δ 3.13 and 3.82 each (m, 1H, C-6-H), 7.18 (broad s, 1H, W_H=20 Hz), 0.63, 0.83, and 1.13 each (s, 3H, -CH_3); Found C, 75.69; H, 10.55; N, 6.06%. Calcd for $C_{14}H_{23}NO$: C, 75.97; H, 10.47; N, 6.33%.

Rearrangement of ***3*** *with PPA.* **3** (400 mg) was added into polyphosphoric acid (20 g) at 90 °C and stirred with glass stick for 10 min. Usual work-up afforded **7** (400 mg) and **8** (164 mg).

*8,12,12-Trimethyl-4-oxatricyclo[6.4.0.0^{1,3}]dodecan-5-one (**9**).* **1** (300 mg) and *m*-chloroperbenzoic acid (700 mg) in dichloromethane (20 ml) were refluxed for 20 h, and then cooled. After addition of 10% aq sodium carbonate, the mixture was extracted with dichloromethane. The dichloromethane solution was washed with water and dried (Na_2SO_4). The residue, obtained by removal of solvent by column chromatography over silica gel to afford crystals (154 mg), which on recrystallization from hexane gave lactone **9**, mp 120—122 °C; MS, *m/e* 222 (M^+, 0.3%); IR, ν_{max} (KBr) 1750 and 1270 cm^{-1} (lactone); ^1H NMR δ 3.77 (dd, 1H, J=4 and 8 Hz, C-3-H), 2.30 (m, 2H, C-6-H_2), 3.01, (ddd, 1H, J=8, 12, and 12 Hz, C-7-H), 0.59, 0.88, and 1.19 each (s, 3H, -CH_3); Found: C, 75.68; H, 9.81%. Calcd for $C_{14}H_{22}O_2$: C, 75.63; H, 9.97%.

Rearrangement of ***5*** *with PPA.* **5** (200 mg) was added into warm polyphosphoric acid (10 g) at 100 °C and stirred with grass stick for 10 min, and cooled. To the reaction mixture was added 10% aq sodium carbonate, and ether. The ether sulution was washed with water, and dried (Na_2SO_4); the residue obtained by removal of solvent was separated by column chromatography over silica gel to give two lactams **10** (92 mg) and **11** (20 mg).

Lactam **10**, when recrystallized from hexane, had mp 206—207 °C; MS, *m/e* 207 (M^+, 25%); IR, ν_{max} (KBr) 3180 (NH) and 1680 cm^{-1} (carbonyl); ^1H NMR, δ 2.81 (dd, 1H, J=5 and 10 Hz, C-3-H), 1.80 and 2.12 (AB-q, J=16 Hz, C-6-H_2), 8.27 (broad s, 1H, W_H=16 Hz, NH), 0.59, 1.07, and 1.22 each (s, 3H, -CH_3); Found: C, 74.96; H, 9.91; N, 6.69%. Calcd for $C_{13}H_{21}NO$: C, 75.30; H, 10.21; N. 6.76%.

Lactam **11**, when recrystallized from hexane, had mp 149—151 °C; MS, *m/e* 207 (M^+, 25%); IR, ν_{max} (KBr) 3330 (NH), and 1670 cm^{-1} (carbonyl); ^1H NMR, δ 2.91 (d, 1H, J=13 Hz, C-6-H) and 2.48 (dd, 1H, J=6 and 13 Hz, C-6-H), 7.35 (broad s, 1H, W_H=8 Hz, NH), 0.62, 1.55, and 1.55 each (s, 3H, -CH_3); Found: C, 75.10; H, 10.20; N, 6.54%. Calcd for $C_{13}H_{21}NO$: C, 75.31; H, 10.21; N, 6.76%.

Rearrangement of ***6*** *with PPA.* **6** (200 mg) was converted into lactams **10** (23 mg) and **11** (80 mg) under the same conditions with rearrangement of **5**.

*7,11,11-Trimethyl-4-oxatricyclo[5.4.0.0^{1,3}]undecan-5-one (**12**)* **4** (220 mg) and *m*-chloroperbenzoic acid (700 mg) in dichloromethane (20 ml) were refluxed for 20 h. After being cooled, the reaction mixture was washed with 10% aq sodium carbonate and water, dried (Na_2SO_4), and evaporated to leave oily residue, which was purified by column chromatography over silica gel to yield lactone **12** (150 mg) in pure state.

Lactone **12**, recrystallization from hexane, mp 129—131 °C; MS, *m/e* 208 (M^+, 0.3%); IR, ν_{max} (KBr) 1740 and 1240 cm^{-1} (lactone); ^1H NMR, δ 4.13 (dd, 1H, J=4 and 8 Hz, C-3-H), 1.98 and 2.22 (AB-q, 2H, J=17 Hz, C-6-H_2), 0.61, 1.05, and 1.21 each (s, 3H, -CH_3); Found: C, 74.75; H. 9.63%. Calcd for $C_{13}H_{20}O_2$; C, 74.96; H, 9.68%.

Reaction of ***1*** *with Hydroxylamine-O-sulfonic Acid.* **1** (412 mg) and hydroxylamine-*O*-sulfonic acid (452 mg) in acetic acid (5 ml) were refluxed for 20 h under nitrogen atmosphere. After being cooled, to the reaction mixture was added 10% aq sodium hydroxide (20 ml) and ether. The ether layer was washed with water, and dried (Na_2SO_4). The products were separated by column chromatography over silica gel, using benzene, ether and acetone as solvent. Elution with 2:1 mixture of benzene and ether gave a single crystal (100 mg), which was identified with authentic mayurone. On the other hand, elution with 1:1 mixture of ether and acetone afforded a single crystal **8** (140 mg).

Reaction of ***4*** *with Hydroxylamine-O-sulfonic Acid.* **4** (190 mg) and hydroxylamine-*O*-sulfonic acid (170 mg) in acetic acid (3 ml) were refluxed for 20 h. After being cooled, to the reaction mixture was added 10% aq sodium hydroxide and ether. The ether layer was washed with water and dried (Na_2SO_4). Removal of solvent gave a crystal (176 mg), which was identified with **11**.

Photolysis of ***2*** *and* ***3***. A 2:1 mixture of **2** and **3** (1.50 g) in methanol (400 ml) was irradiated for 20 h with 15 W low pressure arc Hg lamp, while nitrogen was slowly bubbled through the solution. Removal of methanol left oily residue, which was separated by column chromatography over silica gel to give **1** (600 mg, from 2:1 mixture of benzene and ether), **7** (150 mg, from ether), and **8** (200 mg, from 1:1 mixture of ether and acetone). They were identical with authentic compounds, respectively.

Photolysis of ***5*** *and* ***6***. A 1.3:1 mixture of **5** and **6** (2.0 g) in methanol (400 ml) was irradiated for 20 h with 15 W low pressure arc Hg lamp, while nitrogen was slowly bubbled through the solution. The oily residue, obtained removal of methanol, was separated by column chromatography over silica gel to afford **4** (447 mg, from 2:1 mixture of benzene and ether), **5** and **6** (825 mg, from 1:1 mixture of benzene and ether), **10** (67 mg, from ether) and **11** (100 mg, from 1:1 mixture of ether and acetone), which were identical with the respective authentic compounds.

The authors wish to express their thanks to Professor Tadashi Masamune and Professor Hiroshi Suginome of Hokkaido University for many helpful suggestions.

References

1) J. H. Amin and P. de Mayo, *Tetrahedron Lett.*, **1963**, 1585.

2) H. Izawa, P. de Mayo, and T. Tabata, *Can. J.*

Chem., **47**, 51 (1969).
3) T. Oine and T. Mukai, *Tetrahedron Lett.*, **1969**, 157.
4) T. Oine, T. Mukai, and K. Kikuchi, *Sci. Rep. Tohoku Univ. Ser.*, **54**, 1 (1971).
5) T. Sasaki, S. Eguchi, and T. Toru, *J. Chem. Soc., Chem. Commun.*, **1970**, 1239.
6) B. L. Fox and H. M. Losenberg. *J. Chem. Soc., Chem. Commun.*, **1966**, 1115.
7) G. Just and L. S. NG. *Can. J. Chem.*, **46**, 3381 (1968).
8) H. Suginome, H. Takahashi, *Tetrahedron Lett.*, **1970**, 5119.
9) H. Suginome, H. Takahashi, and T. Masamune, *Bull. Chem. Soc. Jpn.*, **45**, 1836 (1975).
10) H. Suginome and H. Takahashi, *Bull. Chem. Soc. Jpn.*, **48**, 576 (1975).
11) H. Suginome and T. Uchida, *Tetrahedron Lett.*, **1973**, 2293.
12) H. Suginome and T. Uchida, *Bull. Chem. Soc. Jpn.*, **46**, 678 (1974).
13) H. Suginome and F. Yagihashi, *J. Chem. Soc., Perkin Trans. 1*, **1977**, 2488.
14) M. Ito, K. Abe, H. Abe, K. Yamada, and T. Masamune, *Bull. Chem. Soc. Jpn.*, **47**, 3173 (1974).
15) H. Sekizaki, M. Ito, and S. Inoue, *Bull. Chem. Soc. Jpn.*, **51**, 2439 (1978).
16) G. A. Olah and A. P. Fung, *Synthesis*, **1972**, 187.
17) G. R. Krow and S. Szcaepanski, *Tetrahedron Lett.*, **21**, 4593 (1980).
18) W. D. Phillips, *Ann. N. Y. Acad. Sci.*, **70**, 871 (1958); H. Saito, K. Nukada, and M. Ohno, *Tetrahedron Lett.*, **1964**, 2124; W. F. Trager and A. C. Huitric, *ibid.*, **1966**, 825.
19) E. C. Hornig, V. L. Stromberg, and H. A. Lloyd, *J. Am. Chem. Soc.*, **74**, 5153 (1952).
20) R. H. Mazur, *J. Org. Chem.*, **28**, 248 (1963); C. G. Malarty, in "The Chemistry of the Carbon-Nitrogen Double Bond," ed by S. Patai, Interscience Publ., N.Y. (1970).

Photochemical Activation of Zinc-Carbon and Zinc-Sulfur Bonds in Zinc Porphyrins

Masahiro NUKUI, Shohei INOUE,* and Yasukazu OHKATSU

Department of Synthetic Chemistry, Faculty of Engineering, The University of Tokyo, Hongo, Bunkyo-ku, Tokyo 113

(Received December 3, 1982)

Ethyl(*N*-methyltetraphenylporphinato)zinc (NMTPPZnEt **2**) reacts with thiol (RSH: R=Pr^n, Bu^t, Ph) and hydrogen sulfide (H_2S) to form *N*-methyltetraphenylporphinatozinc sulfide (NMTPPZnSR: R=Pr^n, Bu^t, Ph, H). Irradiation with visible light enhances the reactivity of **2** in the reaction with Bu^{t}SH and brings about the homolytic cleavage of the zinc-sulfur bond of NMTPPZnSPr^n in dichloromethane.

The photochemistry of metalloporphyrins is of current interest in connection with the conversion of solar energy into chemical energy.[1-3] We have been studying the photochemical behavior of metalloporphyrins of aluminium and zinc which have an axial ligand bound to the metal *via* a σ-bond, and have found some very interesting effects of visible light on the reactivity of the axial ligand of the metalloporphyrins.

Ethyl(tetraphenylporphinato)aluminium (TPPAlEt **1**), which is unreactive to carbon dioxide in the dark, is activated by visible light and carbon dioxide is inserted into the aluminium-carbon bond in the presence of *N*-methylimidazole (Im).[4]

$$\underset{\mathbf{1}}{\text{TPPAlEt}} + CO_2 \xrightarrow[\text{Im}]{h\nu\ (>420\text{ nm})} \text{TPPAl-OC-Et} \quad (1)$$

The zinc-carbon bond of ethyl(*N*-methyltetraphenylporphinato)zinc (NMTPPZnEt **2**) was found to be subject to homolytic cleavage under irradiation with visible light in dichloromethane solution.[5]

$$\underset{\mathbf{2}}{\text{NMTPPZnEt}} \xrightarrow[\text{in } CH_2Cl_2]{h\nu\ (>420\text{ nm})} [\text{NMTPPZn}\cdot] + \text{Et}\cdot \quad (2)$$

In these reactions, the metal-carbon bond which may not absorb visible light is indirectly activated by photoexcitation of the porphyrin macrocycle.

In this paper we report the photochemical activation of the zinc-carbon bond of NMTPPZnEt (**2**) in the reaction with thiol having a bulky group, and of the zinc-sulfur bond in porphinatozinc alkyl sulfide (NMTPPZnSR), resulting in the homolytic cleavage of zinc-sulfur bond.

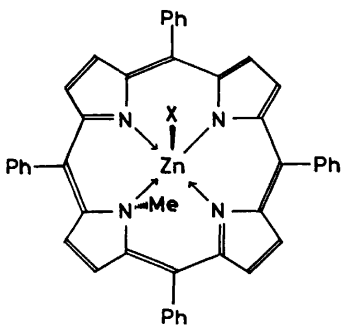

Scheme X=Et (**2**)
SPr^n (**3**)
SBu^t (**4**)
SPh (**5**)
SH (**6**)

Experimental

Materials. Benzene and hexane were distilled under nitrogen over sodium wire. Dichloromethane was refluxed and distilled over calcium hydride under nitrogen. Diethylzinc was distilled under reduced pressure and stored in nitrogen. *N*-Methyltetraphenylporphyrin (NMTPPH) was prepared from α, β, γ, δ-tetraphenylporphyrin and methyl fluorosulfate.[6] NMTPPZnEt (**2**) was prepared by the reaction of NMTPPH and diethylzinc according to the method previously reported.[5] 1-Propanethiol and 2-methyl-2-propanethiol were dried over calcium sulfate (Drierite), distilled and stored under nitrogen. Benzenethiol was dried over calcium sulfate, distilled under reduced pressure, and stored under nitrogen. Hydrogen sulfide was generated by heating "H_2S Powder" (Kanto Chemical Co., Inc.) and used after passing through a column packed with calcium chloride.

Measurements. ^{1}H NMR spectra were recorded using a JEOL-CW-PS-100. Visible spectra were obtained on a JASCO UVIDEC-1 spectrometer. ESR spectra were recorded on a JEOL JES-PE spectrometer under irradiation with visible light (Xe lamp, >420 nm) using nitrosodurene as the radical trapping reagent.

Synthesis of Ethylzinc Propyl Sulfide (EtZnSPr^n). EtZnSPr^n was synthesized according to the method for the preparation of MeZnSPr^n.[7] Diethylzinc (1.10 cm^3, 10.7 mmol) was added to dry, oxygen-free hexane (15 cm^3) in a Pyrex flask (20 cm^3 capacity, fitted with a three-way cock) using a syringe under nitrogen, and the solution was cooled to 0 °C in an ice bath. 1-Propanethiol (0.90 cm^3, 10.0 mmol) was then added dropwise with a syringe to the stirred solution, and the mixture was allowed to warm slowly to room temperature. When gas evolution had ceased, the mixture was heated to reflux to dissolved the solid. The product crystallised on cooling the mixture to room temperature. Ethylzinc propyl sulfide was obtained as colorless short broad needles (1.03 g, 61%), soluble in benzene and dichloromethane. ^{1}H NMR (CH_2Cl_2) δ= 0.36 (2H, q, CH_2-Zn), 0.94 (3H, t, CH_3-CH_2-Zn), 1.15 (3H, t, CH_3-CH_2-CH_2-S), 1.66 (2H, m, -CH_2-CH_2-S), 2.68 (2H, t, -CH_2-S). Found: Zn, 38.3%. Calcd for $C_5H_{12}SZn$: Zn, 38.6%.

Reaction of NMTPPH with EtZnSPr^n. In an attempt to prepare *N*-methyltetraphenylporphinatozinc propyl sulfide (NMTPPZnSPr^n **3**), NMTPPH was allowed to react with an equimolar amount of EtZnSPr^n. NMTPPH (15.7 mg, 0.025 mmol) was dissolved in dichloromethane (1 cm^3) under nitrogen in a Pyrex tube (10 cm^3 capacity) wrapped in aluminium foil and equipped with a three-way cock, and a dichloromethane solution (0.1 cm^3) of EtZnSPr^n (0.025 mmol) was added using a syringe at room temperature in the dark. The reaction mixture was transferred to an NMR tube with a syringe under nitrogen in the

dark and subjected to NMR analysis. The NMR investigation indicated that $EtZnSPr^n$ can react with NMTPPH by both zinc-ethyl bond and zinc-propylthio bond to give NMTPPZnSPr^n (**3**) and NMTPPZnEt (**2**), respectively (Eqs. 3 and 4), and the propylthio group is substituted for the ethyl group of NMTPPZnEt (**2**) thus formed (Eq. 5).

$$\text{NMTPPH} + \text{EtZnSPr}^n \rightarrow \text{NMTPPZnSPr}^n + \text{EtH} \quad (3)$$

$$\text{NMTPPH} + \text{EtZnSPr}^n \rightarrow \text{NMTPPZnEt} + \text{Pr}^n\text{SH} \quad (4)$$

$$\text{NMTPPZnEt} + \text{Pr}^n\text{SH} \rightarrow \text{NMTPPZnSPr}^n + \text{EtH} \quad (5)$$

The last reaction suggests a good procedure for the formation of NMTPPZnSR, as described below.

Reaction of NMTPPZnEt (2) with Thiol (RSH). To a benzene solution (1 cm^3) of NMTPPZnEt (**2**) (0.025 mmol) was added 1-propanethiol (0.09 cm^3, 1 mmol), 2-methyl-2-propanethiol (0.11 cm^3, 1 mmol), or benzenethiol (0.10 cm^3, 1 mmol) using a syringe in nitrogen at room temperature. The resulting mixture was stirred for an hour in the dark. Removal of the solvent and unreacted thiol under reduced pressure at room temperature left a green solid, which was dissolved in benzene or dichloromethane and subjected to NMR analysis.

Reaction of NMTPPZnEt (2) with H_2S. Hydrogen sulfide was bubbled through a benzene solution (1 cm^3) of NMTPPZnEt (**2**) (0.025 mmol) for 5 min. After being stirred for an hour at room temperature in the dark, the solution was evaporated under reduced pressure to give green powder as the residue; this was dissolved in benzene and subjected to NMR analysis.

Reaction of NMTPPZnEt (2) and Bu^{t}SH under Irradiation. To a benzene solution (0.4 cm^3) of NMTPPZnEt (**2**) (0.01 mmol) in an NMR tube, a benzene solution (0.04 cm^3) of 2-methyl-2-propanethiol (0.01 mmol) was added using a syringe under nitrogen in the dark. The reaction was carried out under irradiation using 500 W Xe lamp (Ushio UXL-500 D-O). The distance between the NMR tube and the lamp was about 30 cm, and a glass filter was used to cut the light of wave length shorter than 420 nm. After the prescribed time of irradiation, the ^{1}H NMR spectrum of the reaction mixture was measured in the dark. The conversion of NMTPPZnEt (**2**) was determined on the basis of the signal intensities due to ethyl protons of **2** and *N*-methyl protons.

Results and Discussion

Photochemical Activation of Zinc-Carbon Bond of NMTPPZnEt (2) in the Reaction with Thiol. The reaction of NMTPPZnEt (**2**) with a large excess of thiol RSH (R=Pr^n, Bu^t, Ph) in the dark in benzene was examined by inspecting the ^{1}H NMR spectrum of the reaction mixture (Fig. 1). The reaction generally proceeded rapidly at room temperature. The signals due to ethyl protons of NMTPPZnEt (**2**) (δ= −2.10 (t), −5.00 (q)) disappeared, and new signals due to strongly shielded protons ascribed to alkylthio (or arylthio) group appeared at much higher magnetic field than those of thiol (Table 1), indicating that alkylthio (or arylthio) group is attached to the zinc atom in the porphyrin ring and is affected by its ring current. The equimolar ratio of the alkylthio (or arylthio) group and the *N*-methyl group of the porphyrin was confirmed on the basis of the signal intensities of their protons. The visible spectrum of the reaction mixture changed from that of NMTPPZnEt (**2**) (Table 2). These results suggest that NMTPPZnEt (**2**) reacts with thiol to form a porphinatozinc alkyl (aryl) sulfide. Similarly, the reaction of NMTPPZnEt (**2**) with hydrogen sulfide was found to give a porphinatozinc hydrogensulfide.

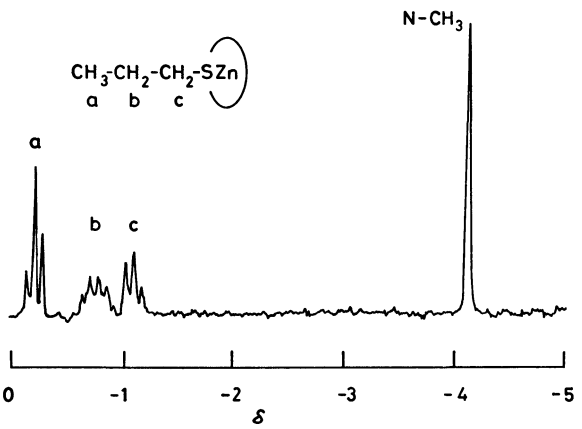

Fig. 1. ^{1}H NMR spectrum of the reaction mixture of NMTPPZnEt (**2**) and Pr^{n}SH in benzene.

$$\text{NMTPPZnEt} + \text{RSH} \rightarrow \text{NMTPPZnSR} + \text{EtH} \quad (6)$$

(R=Pr^n, Bu^t, Ph, H)

The reaction of NMTPPZnEt (**2**) was rather slow in the case of a thiol with bulky group such as 2-methyl-2-propanethiol (Bu^{t}SH). For example, when NMTPPZnEt (**2**) was allowed to react with Bu^{t}SH in an equimolar ratio at room temperature in the dark, it was found by ^{1}H NMR spectroscopy that the conversion of NMTPPZnEt (**2**) was 21% after 25 min. On the other hand, the substitution reaction was accelerated by irradiation with visible light (Fig. 2); NMTPPZnEt (**2**) reacted with Bu^{t}SH completely under irradiation after 20 min, and NMTPPZnSBu^t (**4**) was

Table 1. ^{1}H NMR data of NMTPPZnSR[a)]

NMTPPZnSR	Chemical shift δ (Intensity, Multiplicity)	
R	Protons of R	Protons of *N*-CH$_3$
$CH_3CH_2CH_2$- (**3**)	−0.20(3H, t), −0.74(2H, m), −1.06(2H, t)	−4.12(3H, s)
$(CH_3)_3C$- (**4**)	−0.92(9H, s)	−4.20(3H, s)
C_6H_5- (**5**)[b)]	+6.34(1H, t), +6.10(2H, t), +3.90(2H, d)	−4.07(3H, s)
H- (**6**)	−6.96(1H, s)	−3.97(3H, s)

a) Measured at room temperature in benzene (except for **5**), 2.5×10^{-2} mol dm^{-3}. b) Measured in dichloromethane.

Table 2. Visible spectroscopic data of NMTPPZnSR[a)]

R	λ_{max}/nm ($\varepsilon \times 10^{-3}$)				
	Soret				
Pr^n (**3**)	438(230) 450(sh)	530(sh)	567(6.8)	619(12)	661(7.2)
Bu^t (**4**)	438(190) 450(sh)	528(sh)	566(6.3)	615(9.2)	661(5.5)
Ph (**5**)	438(180) 450(sh)	530(sh)	566(4.8)	619(8.4)	661(5.1)
H (**6**)	438(230) 450(sh)	527(sh)	565(7.7)	616(12)	661(6.9)

a) Measured in dichloromethane (5×10^{-4}—5×10^{-5} mol dm^{-3}) at room temperature under nitrogen. The optical pathlength was 0.1 cm. b) sh: shoulder inflection.

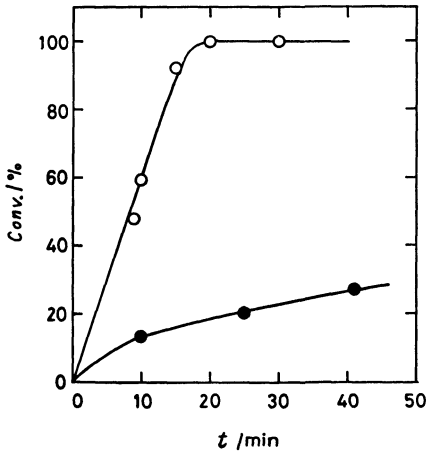

Fig. 2. Formation of NMTPPZnSBu^t by the reaction of NMTPPZnEt (**2**) and Bu^{t}SH at room temperature in benzene. ○: Under irradiation, ●: in the dark. [NMTPPZnEt]=[Bu^{t}SH]=0.01 mmol. Conversion of NMTPPZnEt was determined by ^{1}H NMR spectrum on the basis of ethyl protons of NMTPP-ZnEt and N-CH_3 protons.

found to be the sole product on the basis of the ^{1}H NMR spectrum of the reaction mixture.

Thus, irradiation with visible light has an interesting effect in enhancing the nucleophilicity of the ethyl group of NMTPPZnEt (**2**) in the reaction with thiols.

Photochemical Cleavage of Zinc-Sulfur Bond in Porphinatozinc Alkyl Sulfide (NMTPPZnSR). N-Methyltetraphenylporphinatozinc propyl sulfide (NMTPP-ZnSPr^n **3**) was found to be decomposed in dichloromethane by the irradiation with visible light, although it was stable under nitrogen in the dark. The ^{1}H NMR spectrum of NMTPPZnSPr^n (**3**) showed that the intensity of signals due to propylthio group decreased upon irradiation, while the signals due to dipropyl disulfide appeared [^{1}H NMR (CH_2Cl_2) δ= +0.80 (6H, t), +1.54 (4H, m), +2.45 (4H, t)]. When the signals of the propylthio group of NMTPPZnSPr^n (**3**) disappeared completely (2 h), the formation of dipropyl disulfide was quantitative. The main product derived from porphyrin macrocycle is considered to be N-methyltetraphenylporphinatozinc chloride (NMTPPZnCl) on the basis of the chemical shift of N-methyl protons (δ (CH_2Cl_2)=−3.90[5]) observed in the irradiated solution.

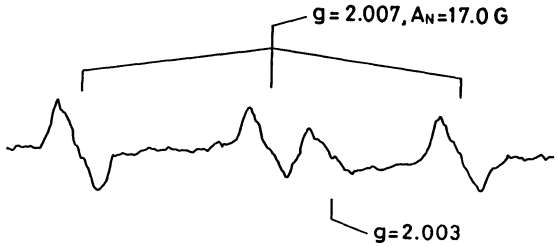

Fig. 3. ESR spectrum of photo-irradiated NMTPP-ZnSPr^n (**3**) in dichloromethane at r. t. using nitrosodurene as trapping reagent.

$$\underset{\mathbf{3}}{\text{NMTPPZnSPr}^n} \xrightarrow[\text{in } CH_2Cl_2]{h\nu\ (>420\text{nm})} \text{NMTPPZnCl} + \text{Pr}^n\text{SSPr}^n \quad (7)$$

In contrast with NMTPPZnSPr^n (**3**), EtZnSPr^n was unchanged in dichloromethane under irradiation with visible light. These results indicate that zinc-sulfur bond of NMTPPZnSPr^n (**3**), which does not absorb visible light, is activated by the photoexcitation of the porphyrin ring. In the solution in benzene or in the solid state, NMTPPZnSPr^n (**3**) was found to be almost unaltered by the irradiation with visible light. In the cases of NMTPPZnSBu^t (**4**), NMTPPZnSPh (**5**), and NMTPPZnSH (**6**), the ^{1}H NMR spectra in dichloromethane did not show any change after irradiation with visible light.

Figure 3 shows the ESR spectrum of the dichloromethane solution of NMTPPZnSPr^n (**3**) in the presence of nitrosodurene under visible light. NMTPPZnSPr^n (**3**) did not show any ESR signal in the dark. When the solution of NMTPPZnSPr^n (**3**) in the ESR cavity was irradiated with visible light, two different signals appeared immediately, at g=2.007 (A_N=17.0 G) and g=2.003. The former signal was assigned to propylthio radical trapped by nitrosodurene.[8] The g value of the latter radical was in agreement with that observed in the irradiation of NMTPPZnEt (**2**) with visible light.[5]

$$\underset{\mathbf{3}}{\text{NMTPPZnSPr}^n} \xrightarrow[\text{in } CH_2Cl_2]{h\nu\ (>420\text{ nm})} [\text{NMTPPZn}\cdot] + \text{Pr}^n\text{S}\cdot \quad (8)$$

This study was supported by Grant-in-Aid for Scientific Research No. 56045029 from the Ministry of Education, Science and Culture. The authors are grateful to Mr. Masaru Hirai and Miss Mitsue Inada for their assistance in some of the experiments.

References

1) F. R. Hopf and D. G. Whitten, "Photochemistry of Porphyrins and Metalloporphyrins," in "Porphyrins and Metalloporphyrins," ed by K. M. Smith, Elsevier, Amsterdam-Oxford-New York (1975), pp. 667—700.

2) I. Okura and N. Kim-Thuan, *J. Mol. Catal.*, **6**, 227 (1979).

3) G. McLendon and D. Miller, *J. Chem. Soc., Chem. Commun.*, **1980**, 533.

4) S. Inoue and N. Takeda, *Bull. Chem. Soc. Jpn.*, **50**, 984 (1977).

5) S. Inoue, H. Murayama, N. Takeda, and Y. Ohkatsu, *Chem. Lett.*, **1982**, 317.

6) D. K. Lavelle and A. E. Gebala, *Inorg. Chem.* **13**, 2004 (1974).

7) G. E. Coates and D. Ridley, *J. Chem. Soc.*, **1965**, 1870.

8) S. Terabe, K. Kuruma, and R. Konaka, *J. Chem. Soc., Perkin Trans. 2,* **1973**, 1252.

Synthesis of 2-(1-Azulenyl)ethanamine Derivatives by Aminoethylation of Azulenes with Aziridines

Shinji KUROKAWA* and Arthur G. ANDERSON, Jr.†

Department of Chemistry, Faculty of Education, Saga University, Honjo-machi, Saga 840

†*Department of Chemistry, University of Washington, Seattle, Washington 98195, U.S.A.*

(Received October 6, 1982)

Azulene analogs of biological active amines were synthesized. Reaction of azulene or guaiazulene with 1-butanoylaziridine or with 1-butanoyl-2-methylaziridine in the presence of Lewis acid catalyst formed the corresponding *N*-butanoyl-1-(1-azulenyl)-, *N*-butanoyl-2-(1-azulenyl)-, and *N*-butanoyl-2-(1-guaiazulenyl) derivatives of ethanamine, or 1-propanamine, or of 2-propanamine, respectively (**5**—**9**). Reaction of guaiazulene with 2-methyl-, or 1,1-dimethylaziridinium, or with 1,1,2,2-tetramethylaziridinium ions gave the corresponding 1-(1-guaiazulenyl)- and 2-(1-guaiazulenyl) derivatives of ethanamine, or 1-propanamine, or of 2-propanamine. 2-(1-Azulenyl)- and 2-(4,6,8-trimethyl-1-azulenyl) derivatives of ethanamine were also obtained by the action of 1,1-diethylaziridinium ion on azulene or on 4,6,8-trimethylazulene. Compounds **5**, **6**, and **9** were active *in vitro* in the inhibition of prostaglandin 15-hydroxydehydrogenase and of cyclic AMP-phosphodiesterase.

2-Arylethanamine derivatives constitute an important class of physiologically active compounds.[1] Natural compounds exhibit a variety of structural modifications and hundreds of additional derivatives have been synthesized in the search for therapeutic agents. A literature search did not reveal any examples having a nonbenzenoid aryl moiety. The low toxity of guaiazulene as an anti-inflammatory agent[2] led us to investigate the preparation of some 2-(1-azulenyl)ethanamine derivatives.

An earlier study had revealed that azulene reacted readily with tetracyanoethylene oxide to give concomitant epoxide ring opening and aromatic substitution.[3] An analogous behavior toward the aziridine ring would lead to the desired structure.

Results and Discussion

1-Butanoylaziridine (**1**) and 1-butanoyl-2-methylaziridine (**2**) were selected as reactants and were readily formed by the method of Brown and Tsukamoto,[4] with variation of the solvent as needed. From the treatment of **1** with azulene (**3**) in dichloromethane in the presence of aluminium chloride a 21% yield of *N*-butanoyl-2-(1-azulenyl)ethanamine (**5**) was obtained.

Similarly, from **2** and azulene (**3**) 20% of *N*-butanoyl-2-(1-azulenyl)-1-propanamine (**6**) was isolated. When the solvent was changed to benzene, the reaction of **3** with **2** formed **6** (21%) and a product (15%) having spectral and analytical data consistent with the isomeric structure **7**. Analogous reactions with guaiazulene (**4**) with **1** (in ether) and **2** (in dichloromethane) gave **8** (8%) and **9** (57%), respectively.

The structural assignments for **5**—**9** were based on spectral analyses. These were consistent with substitution at the azulene 1-position and the presence of the amide function for all the products. ^{1}H NMR spin-decoupling was used for the characterization of the propyl side-chain moieties in **6** and **9**. In **6**, for example, irradiation at δ 3.68 (–CH) caused the doublet at δ 1.40 ($-CH_3$) to become a singlet, and irradiation at δ 3.42 and δ 3.92 ($-CH_2-$) did not affect the doublet at δ 1.40 ($-CH_3$). The $-CH_2-$ pattern exhibited coupling with the amide hydrogen (J=5 Hz) and with the methine hydrogen (J=5 and 7 Hz).

The isolation only of **6** in one experiment, and of **6** and **7** in another, suggests two reaction paths, one (*a*) dominant in dichloromethane and both (*a* and *b*) appreciably operative in benzene, as proposed by Milstein[5] and shown in Scheme 1. In *a* the more stable of the two possible carbocations is formed and leads to **6**. In *b* direct nucleophilic attack on the aziridinium ion occurs at the less hindered methylene and leads to **7**.

A second approach to this type of compound was by the reaction of guaiazulene with a simple (protonated) or quaternary aziridinium ion. 2-Methylaziri-

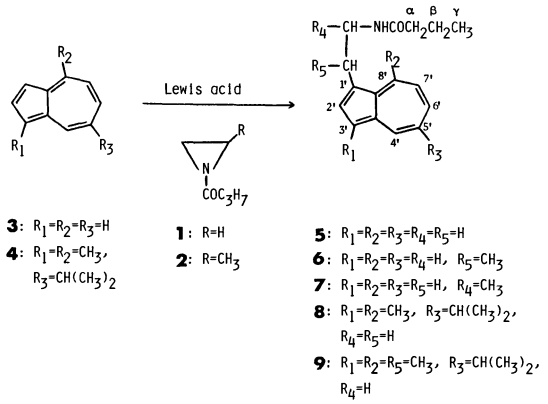

Chart 1.

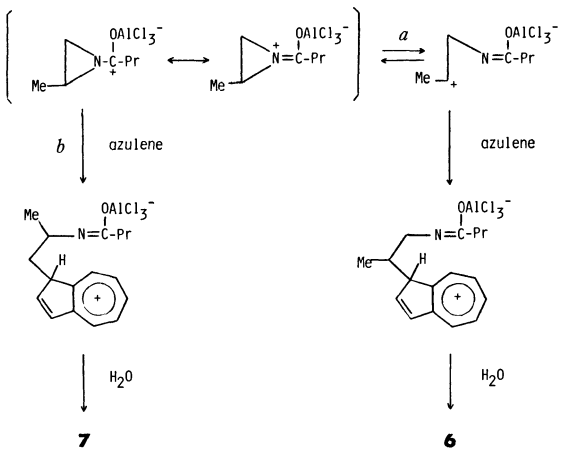

Scheme 1.

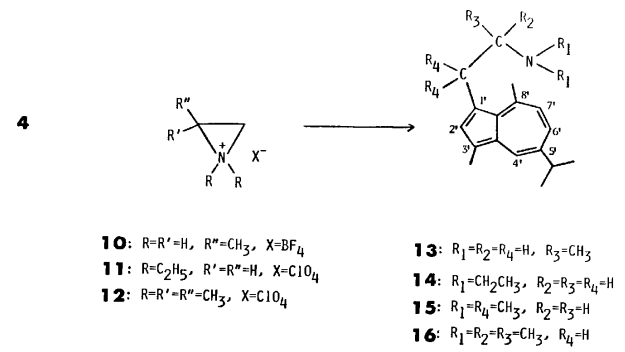

Chart 2.

dinium tetrafluoroborate (**10**)[6] was used for the former. A number of solvents, temperatures, and reaction times were tried (neat, 160—180 °C, 20 min; dichloromethane, *ca.* 20 °C, 1 h; 1,2-dimethoxyethane, 93 °C, 48 h; 1,2-diethoxyethane, 124 °C, 16 h; bis(2-methoxyethyl) ether, 160 °C, 4 h; bis(2-ethoxyethyl) ether, 190 °C, 1 h) but the yields of **13** were uniformly low (0.08—8%) and appreciably unchanged guaiazulene was recovered. The aziridinium salt was only slightly soluble in the solvents.

Treatment of guaiazulene with 1,1-diethylaziridinium perchlorate (**11**) in 1,2-dichloroethane gave a 35% yield of **14**. Under the same conditions but with a thirteen times longer reaction time, however, reaction with 1,1,2,2-tetramethylaziridinium perchlorate (**12**) afforded only 0.07% of **15** and 0.1% of **16** with 79% recovery of unchanged guaiazulene.

Similarly, reaction of azulene (**3**) with **11**, followed by treatment with hydrochloric acid, gave a 12% yield of the hydrochloride (**20**), from which **18** (78%) was regenerated by alkali treatment. Moreover, 4,6,8-trimethylazulene (**17**) reacted with **11** to afford 53% of **19**. The identities of **13**—**16**, **18**, and **19** were shown by ultraviolet-visible, infrared, ^{1}H nuclear magnetic resonance, and mass spectral characteristics, all of which were in agreement with the assigned structures.

However, some ambiguity was observed in ^{1}H NMR of **14**, **18**, and **19**. For instance, 1- and 2-methylene protons showed two multiplets, the pattern of which was exactly the same in three compounds. Thus, ^{13}C NMR was used for the characterization of **18** (in the form of **20**) and **19**. In this case, the methylene carbon signals appeared as clear triplets in good accordance with the structure. In the mass spectra of all 2-(1-azulenyl)ethanamine derivatives, allyl fission of aminoethyl side chain gave rise the most abundant ion, which was also used for structural assignments.

Compounds **5**, **6**, and **9** have been found to be

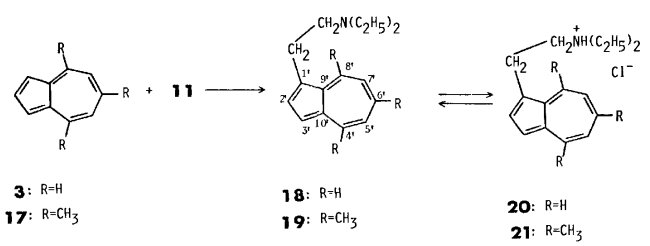

Chart 3.

active *in vitro* (20 μg in 1 cm^3) in the inhibition of prostaglandin 15-hydroxydehydrogenase (71, 69, and 50%, respectively), and of cyclic AMP–phosphodiesterase (24, 47, and 70%, respectively).[7] Details of the biological activities will be described elsewhere.

Experimental

Spectral data were recorded on the following instruments: UV, Hitachi 624 digital spectrometer with a Hitachi 056 recorder; IR, Hitachi 260-10 spectrometer; ^{1}H NMR, JEOL MH-100 except for JNM-FX 100 for **13**; ^{13}C NMR, JNM-FX 100; MS, JEOL-D300 at 70 eV. GLC were done on a Shimadzu GC-3AH instrument and TLC were done on Merck precoated alumina sheet, silica gel 70 (Art. 5553), or neutral alumina 60F$_{254}$ type E (Art. 5550). A Schlenk apparatus[8] was used to exclude moisture for the preparation of **5**—**9**.

N-Butanoyl-2-(1-azulenyl)ethanamine (5). To an ice-cooled, stirred solution of 643 mg (5.02 mmol) of azulene in 50 cm^3 of dry dichloromethane was added 1.33 g (9.98 mmol) of aluminium chloride (washed in with 5 cm^3 of dichloromethane) (blue color changed to light yellow) and then, dropwise, a solution in 17 cm^3 of dry ether of *ca.* 10 mmol of 1-butanoylaziridine [prepared from 1.1 g (10.3 mmol) of butanoyl chloride, 430 mg (9.98 mmol) of aziridine, and 1.01 g (9.98 mmol) of triethylamine].[4] The light yellow color changed to blue. Stirring was continued at 0 °C for 1 h and the mixture was then added to 500 cm^3 of cold (0 °C) 10% sodium chloride–10% hydrochloric acid. The blue solution obtained by extraction (twice each) with 150, 100, and 50 cm^3 portions of chloroform was washed with 150 cm^3 of saturated sodium chloride, twice with 150 cm^3 of 10% sodium hydroxide and then dried (sodium sulfate). Removal of the solvent (reduced pressure) gave blue crystals (two major components by TLC on silica gel). Chromatography on a silica-gel column (elution with 3:1 hexane–THF) gave 549 mg of violet crystals, which on rechromatography (elution with hexane) afforded 429 mg (3.35 mmol) of unchanged azulene. Successive blue eluates (3:1 hexane–THF) yielded 545 mg of blue oil, which was rechromatographed to give 254 mg (1.05 mmol, 21%) of **5**. Further colored fractions removed by hexane–THF, acetone, and methanol were not characterized. In order to get analytical specimen, **5** was further purified by extraction of a benzene (30 cm^3) solution with 10 cm^3 of 85% phosphoric acid, washing the acid extract with 3×20 cm^3 of benzene, dilution with 300 cm^3 of 17% sodium chloride, and extraction with 3×100 cm^3 of benzene. Chromatography of the concentrate from the dried (potassium carbonate) benzene solution over silica gel (3:1 hexane–THF) gave 61.6 mg (11%) of **5** as a blue oil which formed tiny prisms, mp 48—50 °C, on refrigeration: UV (C_2H_5OH) 237 (log ε 4.12), 259 (sh, 4.13), 264 (sh, 4.30), 268 (sh, 4.44), 274 (sh, 4.57), 278 (4.64), 282 (sh, 4.39), 287 (sh, 4.44), 297 (sh, 3.64), 320 (sh, 3.22), 328 (sh, 3.39), 334 (sh, 3.42), 343 (3.58), 358 (3.27), 516 (ε sh, 104), 534 (sh, 144), 558 (sh, 199), 580 (sh, 232), 597 (226), 618 (sh, 234), 652 (223), 683 (sh, 111), and 722 nm (80); IR (CCl_4) 3460 (nonassoc N-H), 3350 (assoc N-H), and 1685 cm^{-1} (amide C=O); ^{1}H NMR ($CDCl_3$) δ=0.88 (3H, t, J=7.5 Hz, γ-CH_3), 1.60 (2H, sext, J=7.5 Hz, β-CH_2), 2.06 (2H, t, J=7.5 Hz, α-CH_2), 3.30 (2H, t, J=7.0 Hz, 2-CH_2), 3.66 (2H, sext, J=7.0 and 5.0 Hz, 1-CH_2), 5.52 (1H, br m, NH), 7.16 (2H, t, J=10.0 Hz, 5'- and 7'-H), 7.40 (1H, d, J=4.0 Hz, 3'-H), 7.62 (1H, t, J=10.0 Hz, 6'-H), 7.82 (1H, d, J=4.0 Hz, 2'-H), 8.32 (1H, d,

J=10.0 Hz, 4′-H), and 8.36 (1H, d, J=10.0 Hz, 8′-H); MS *m/e* (rel intensity) 241 (M^+, 18), 154 ($M^+-C_4H_9NO$, 90), and 141 ($M^+-C_3H_7CONHCH_2$, 100).

Found: C, 79.60; H, 7.92; N, 5.72%. Calcd for $C_{16}H_{19}NO$: C, 79.63; H, 7.94; N, 5.80%.

N-*Butanoyl-2-(1-azulenyl)-1-propanamine (**6**).* *A*: The reaction of 640 mg (4.99 mmol) of azulene in 50 cm³ of dichloromethane, 1.33 g (9.98 mmol) of aluminum chloride and *ca.* 9.9 mmol of 1-butanoyl-2-methylaziridine [from 1.10 g (10.3 mmol) of butanoyl chloride, 570 mg (9.98 mmol) of 2-methylaziridine, and 1.01 g (9.98 mmol) of triethylamine in 17 cm³ of ether][4] was carried out as described for **5** except that the crude reaction mixture was added to 500 cm³ of cold (0 °C) 10% hydrochloric acid prior to extraction successively with 150, 50 (thrice), and 60 cm³ of dichloromethane. The organic extracts were washed with 100 cm³ (thrice) of water before drying (sodium sulfate) and removal of the solvent. Chromatography of the residue over alumina (9:1 benzene-chloroform) gave 586 mg of violet crystals and 667 mg of blue oil. Rechromatography of the violet crystals (silica gel; hexane) gave 440 mg (69%) of unchanged azulene. From the blue oil after chromatography over silica gel twice (elution with chloroform and then 5:1 hexane-THF) was obtained 254 mg (20%) of **6** as a blue oil. This compound was further purified by washing a benzene (150 cm³) solution with 150 cm³ (thrice) of 10% sodium hydroxide and 100 cm³ (thrice) of water, drying (sodium sulfate), removal of the solvent, resolution into 120 cm³ of 5:1 hexane-benzene, and extraction into 85% phosphoric acid (50 cm³, then 30 cm³ twice). Dilution of the acid extract with 500 cm³ of water and basification with solid potassium carbonate was followed by extraction into benzene (200 cm³ then 100 cm³ twice). Chromatography on silica gel (3:1 hexane-THF) of the residue from the washed (3×105 cm³ of water), dried (sodium sulfate) benzene solution gave 68.2 mg (6%) of analytical specimen of **6** as a blue oil: UV (C_2H_5OH) 238 (log ε 4.03), 258 (sh, 4.00), 263 (sh, 4.18), 268 (sh, 4.35), 274 (sh, 4.49), 278 (4.55), 282 (sh, 4.51), 288 (sh, 4.34), 296 (sh, 3.55), 320 (sh, 3.12), 333 (sh, 3.33), 343 (3.51), 359 (3.23), 517 (ε sh, 82), 534 (sh, 116), 557 (sh, 162), 579 (sh, 192), 597 (221), 621 (sh, 190), 686 (sh, 81), and 722 nm (60); IR (CCl_4) 3450 (nonassoc N-H), 3350 (assoc N-H), and 1680 cm⁻¹ (amide C=O); ¹H NMR ($CDCl_3$) δ=0.81 (3H, t, J=7.0 Hz, γ-CH_3), 1.40 (3H, d, J=7.0 Hz, 3-CH_3), 1.50 (2H, sext, J=7.0 Hz, β-CH_2), 1.94 2H, t, J=7.0 Hz, α-CH_2), 3.42 (1H, sext, J=13.0, 5.0, and 5.0 Hz, one H of 1-CH_2), 3.68 (1H, decet, J=7.0, 7.0, and 5.0 Hz, 2-CH), 3.92 (1H, octet, J=13.0, 7.0, and 5.0 Hz, one H of 1-CH_2), 5.60 (1H, br t, J=5.0 Hz, NH), 7.09 (2H, t, J=10.0 Hz, 5′- and 7′-H), 7.36 (1H, d, J=4.0 Hz, 3′-H), 7.54 (1H, t, J=10.0 Hz, 6′-H), 7.82 (1H, d, J=4.0 Hz, 2′-H), 8.25 (1H, d, J=10.0 Hz, 4′-H), and 8.35 (1H, d, J=10.0 Hz, 8′-H); MS *m/e* (rel intensity) 255 (M^+, 9), 168 ($M^+-C_3H_7CONH_2$, 24), and 155 ($M^+-C_3H_7CONHCH_2$, 100).

Found: C, 79.68; H, 8.37; N, 5.43%. Calcd for $C_{17}H_{21}NO$: C, 79.96; H, 8.29; N, 5.49%.

B: The reaction of 128 mg (1.00 mmol) of azulene in 30 cm³ of dry benzene, 400 mg (3.00 mmol) of aluminum chloride and *ca.* 3.00 mmol of 1-butanoyl-2-methylaziridine [from 321 mg (3.0 mmol) of butanoyl chloride, 171 mg (3.00 mmol) of 2-methylaziridine, 303 mg (3.00 mmol) of triethylamine in 7 cm³ of benzene at 5 °C][4] was carried out as described for **5** except for the change in solvent and a reaction temperature of 5 °C. The hydrolyzed (10% hydrochloric acid) mixture was extracted with 100 cm³ of ether (4 times) and the extracts washed successively with 150 cm³ of water (twice), 150 cm³ of sodium hydroxide (twice), and 175 cm³ of water (thrice). Chromatography of the crude product (isolated as described for **5**) over silica gel (3:1 hexane-THF) gave 101 mg of violet crystals, 37 mg of blue oil, and 171 mg of blue oil. Rechromatography of the violet crystals (silica gel; hexane) gave 70.6 mg (55%) of unchanged azulene. The first blue fraction was characterized as *N*-butanoyl-1-(1-azulenyl)-2-propanamine (**7**) (15%): IR (CCl_4) 3460 (nonassoc N-H), 3350 (assoc N-H), and 1680 cm⁻¹ (amide C=O); ¹H NMR ($CDCl_3$) δ=0.93 (3H, t, J=7.0 Hz, γ-CH_3), 1.47 (3H, d, J=7.0 Hz, 3-CH_3), 1.58 (2H, sext, J=7.0 Hz, β-CH_2), 2.17 (2H, t, J=7.0 Hz, α-CH_2), 3.59 (2H, m, 1-CH_2), 4.10 (1H, 12 lines, J=7.0 and 3.0 Hz, 2-CH), 6.74 (1H, br d, J=3.0 Hz, NH), 7.03 (1H, t, J=10.0 Hz, 5′-H), 7.07 (1H, t, J=10 Hz, 7′-H), 7.36 (1H, d, J=4.0 Hz, 3′-H), 7.57 (1H, t, J=10.0 Hz, 6′-H), 7.82 (1H, d, J=4.0 Hz, 2′-H), 8.25 (1H, d, J=10.0 Hz, 4′-H), and 8.37 (1H, d, J=10.0 Hz, 8′-H);[9] MS *m/e* (rel intensity) 255 (M^+, 33), 226 ($M^+-C_2H_5$, 83) 156 ($M^+-C_5H_9NO$, 100), and 141 ($M^+-C_3H_7CONHCHCH_3$, 10).

Found: N, 5.39%. Calcd for $C_{17}H_{21}NO$: N, 5.49%.

Rechromatography of the last blue fraction afforded 53.6 mg (21%) of blue oil identical (TLC, IR, MS) with **6** obtained from *A*.

N-*Butanoyl-2-(1-guaiazulenyl)ethanamine (**8**).* To an ice-cooled, stirred solution of *ca.* 9.9 mmol of 1-butanoylaziridine [from 430 mg (9.98 mmol) of aziridine, 1.10 g (10.3 mmol) of butanoyl chloride, 1.01 g (9.98 mmol) of triethylamine][4] in 6 cm³ of ether was added slowly (syringe) a solution of 990 mg (5.00 mmol) of guaiazulene in 3 cm³ of ether and then 2.60 g (10.0 mmol) of tin(IV) chloride. The color changed from blue to green and the mixture solidified. After 1 h at room temperature, 50 cm³ of water was added and the solution was made alkaline with aqueous ammonium hydroxide. The mixture was extracted with ether and the ether solution filtered. The green-blue filtrate, including ether washings of the precipitate, was extracted with 50 cm³ of saturated sodium carbonate (twice), 50 cm³ of water (four times) and dried (sodium sulfate). Removal of the solvent and chromatography of the residue (silica gel; 9:1 benzene-chloroform) gave 660 mg of blue oil and 129 mg (8%) of **8** as blue crystals. Rechromatography of the blue oil over silica gel (hexane) separated unchanged guaiazulene (494 mg, 50%) and a green oil which, after rechromatography (silica gel; 9:1 hexane-benzene) amounted to 12.5 mg of green crystalline product identical (mp, TLC, UV, IR, MS) with authentic specimen of 3,3′-biguaiazulene.[10]

Rechromatography (silica gel; chloroform) and recrystallization (from 80% ethanol) of the blue crystals gave the analytical sample of **8** as tiny blue prisms, mp 108—109 °C: UV (C_2H_5OH) 202 (log ε 4.13), 218 (4.06), 247 (4.26), 287 (4.54), 290 (sh, 4.54), 306 (4.08), 338 (sh, 3.47), 352 (3.66), 369 (3.63), 577 (ε sh, 275), 621 (344), 673 (sh, 278), and 744 nm (sh, 95); IR ($CHCl_3$) 3470 (nonassoc N-H), 3350 (assoc N-H), and 1685 cm⁻¹ (amide C=O); ¹H NMR ($CDCl_3$) δ=0.90 (3H, t, J=7.0 Hz, γ-CH_3), 1.32 (6H, d, J=7.0 Hz, 5′-CH(C$\underline{H}_3$)$_2$), 1.62 (2H, sext, J=7.0 Hz, β-CH_2), 2.08 (2H, t, J=7.0 Hz, α-CH_2), 2.59 (3H, s, 3′-CH_3), 2.94 (3H, s, 8′-CH_3), 3.08 (1H, sept, J=7.0 Hz, 5′-C$\underline{H}$(CH$_3$)$_2$), 3.51 (4H, quint, J=6.8 Hz, 1- and 2-CH_2), 5.82 (1H, br s, NH), 6.81 (1H, d, J=10.6 Hz, 7′-H), 7.24 (1H, q, J=10.6 and 2.0 Hz, 6′-H), 7.44 (1H, s, 2′-H), and 8.06 (1H, d, J=2.0 Hz, 4′-H); MS *m/e* (rel intensity), 311 (M^+, 23), 224 ($M^+-C_3H_7CONH_2$, 48), and 211 (M^+

$-C_3H_7CONHCH_2$, 100).

Found: C, 81.16; H, 9.38; N, 4.50%. Calcd for $C_{21}H_{29}NO$: C, 80.98; H, 9.38; N, 4.50%.

Reaction of Guaiazulene with 1-Butanoyl-2-methylaziridine. To an ice-cooled, stirred solution of 990 mg (5.00 mmol) of guaiazulene and *ca.* 15 mmol of 1-butanoyl-2-methylaziridine [from 860 mg (15.1 mmol) of 2-methylaziridine, 1.60 g (15.0 mmol) of butanoyl chloride, and 1.52 g (15.0 mmol) of triethylamine in 10 cm³ of dichloromethane at *ca.* −5 °C][4] in 50 cm³ of dichloromethane was added gaseous boron trifluoride below the surface until the solution was saturated. The mixture was then stirred for 1 h, added to 500 cm³ of ice water, and extracted with one 200 cm³ and three 150 cm³ portions of chloroform. The green-blue organic extracts were washed with 150 cm³ of 10% sodium hydroxide (twice), 150 cm³ of water (thrice) and dried (sodium sulfate). The solvent was removed and chromatography of the residue (silica gel; 3:1 hexane–THF) gave three fractions. From fraction 1 (blue oil) was recovered 46.9 mg (0.237 mmol) of unchanged guaiazulene. Fraction 2 (blue oil) was rechromatographed (silica gel; 3:1 hexane–THF) and the main blue fraction combined with fraction **3** (blue oil) to give 932 mg (57%) of blue oil. The spectral properties of this product were in good agreement with those expected for *N*-butanoyl-2-(1-guaiazulenyl)-1-propanamine (**9**): UV (C_2H_5OH) 202 (log ε 4.31), 218 (4.14), 247 (4.22), 287 (4.40), 305 (4.04), 353 (3.55), 369 (3.47), 574 (ε sh, 250), 617 (283), 670 (sh, 226), and 752 nm (sh, 76); IR (CCl_4) 3470 (nonassoc N–H), 3360 (assoc N–H), and 1690 cm⁻¹ (amide C=O); ¹H NMR ($CDCl_3$) δ=0.82 (3H, t, *J*=7.0 Hz, γ-CH_3), 1.36 (9H, t, *J*=7.0 Hz, 5′-CH($C\underline{H}_3$)$_2$ and 3-CH_3), 1.46 (2H, sext, *J*=7.0 Hz, β-CH_2), 2.00 (2H, t, *J*=7.0 Hz, α-CH_2), 2.64 (3H, s, 3′-CH_3), 2.98 (3H, s, 8′-CH_3), 3.05 (1H, sept, *J*=7.0 Hz, 5′-C$\underline{H}$(CH_3)$_2$), 3.42 (1H, sext, *J*=13.0, 5.0, and 5.0 Hz, one H of 1-CH_2), 3.74 (1H, decet, *J*=7.0, 7.0, and 5.0 Hz, 2-CH), 4.10 (1H, octet, *J*=13.0, 7.0, and 5.0 Hz, one H of 1-CH_2), 5.64 (1H, br m, NH), 6.92 (1H d, *J*=10.0 Hz, 7′-H), 7.34 (1H, q, *J*=10.0 and 2.0 Hz, 6′-H), 7.68 (1H, s, 2′-H), and 8.18 (1H, d, *J*=2.0 Hz, 4′-H); MS *m/e* (rel intensity) 325 (M^+, 18), 238 ($M^+-C_3H_7CONH_2$, 20), and 225 ($M^+-C_3H_7CONHCH_2$, 100).

Found: N, 4.54%. Calcd for $C_{22}H_{31}NO$: N, 4.30%.

*1-(1-Guaiazulenyl)-2-propanamine (**13**).* A suspension of *ca.* 15 mmol of colorless 2-methylaziridinium tetrafluoroborate in dichloromethane was prepared from 860 mg (15.1 mmol) of 2-methylaziridine in 10 cm³ of dry dichloromethane and 2.46 g (15.1 mmol) of tetrafluoroboric acid in ether (54%, Merck) according to the method of Harder *et al.*[11] and was used without further purification.

To the salt suspension was added, under nitrogen with stirring, dropwise (10 min) a solution of 990 mg (5.00 mmol) of guaiazulene in 20 cm³ of 1,2-dimethoxyethane (monoglyme). After distillative removal of the ether and dichloromethane, the mixture was refluxed for 48 h and then cooled and poured onto 300 g of crushed ice. A 50% solution of potassium carbonate (200 g) was added and the mixture then extracted with 3×100 cm³ of chloroform. The combined extracts were washed twice with a 29% sodium chloride (100 g) solution and dried (sodium sulfate). Removal of the solvent (ambient temperature at 2700 Pa and then 30 °C at 133—266 Pa) left a blue oil which gave two major TLC spots (alumina, chloroform: R_f 0.12 for **13** and 0.86 for guaiazulene). Chromatography over alumina with chloroform separated 1072 mg of material which yielded 510 mg (52%) of pure, unchanged guaiazulene after rechromatography over silica gel (hexane). The blue oil fractions obtained by further elution with chloroform and, finally, with acetone amounted to 420 mg. Rechromatography (alumina, 95:5 benzene–methanol) gave 101 mg (8%) of **13** as a blue oil: UV (C_2H_5OH) 217 (log ε 4.07), 247 (4.22), 287 (4.47), 306 (4.05), 341 (sh, 3.48), 353 (3.62), 369 (3.55), 581 (ε sh, 290), 622 (334), 673 (sh, 288), and 751 nm (sh, 111); IR (CCl_4) 3380 and 3310 (nonassoc N–H), 3190 (assoc N–H), and, 1380 and 1370 cm⁻¹ (δ_s CH_3); ¹H NMR ($CDCl_3$) δ=1.16 (3H, d, *J*=6.0 Hz, propane-CH_3), 1.34 (6H, d, *J*=7.0 Hz, 5′-CH($C\underline{H}_3$)$_2$, 1.36 (2H, s, NH_2), 2.63 (3H, s, 3′-CH_3), 2.98 (3H, s, 8′-CH_3), 3.02—3.72 (4H, m, CH-CH_2 and 5′-C$\underline{H}$(CH_3)$_2$, 6.90 (1H, d, *J*=11.0 Hz, 7′-H), 7.33 (1H, q, *J*=11.0 and 2.0 Hz, 6′-H), 7.54 (1H, s, 2′-H), and 8.14 (1H, d, *J*=2.0 Hz, 4′-H); MS *m/e* (rel intensity) 255 (M^+, 6%), 211 ($M^+-CH_3CHNH_2$, 100), and 44 (CH_3CHNH_2, 75%).

Found: C, 84.24; H, 9.88; N, 5.33%. Calcd for $C_{18}H_{25}N$: C, 84.65; H, 9.87; N, 5.48%.

N,N-*Diethyl-2-(1-guaiazulenyl)ethanamine (**14**).* From 17.1 g (0.100 mol) of *N*,*N*-diethyl-2-chloroethanamine hydrochloride was prepared a 44% solution of the corresponding amine in benzene as determined by GLC analysis (Silicone SE 30 on Chromosorb W, 1 m column, 50 °C, 20 cm³ min⁻¹ He, t_R=1.8 min), and a solution of 5.02 g (37.0 mmol) of this amine (obtained from an aliquot portion of the benzene solution) was converted to 1,1-diethylaziridinium perchlorate [7.00 g, 95%, IR (CCl_4) 3125 cm⁻¹, mp 188—192 °C decomp] (Ref. 12; 192 °C decomp) as described by Leonard and Paukstelis[12] except that the crude salt was purified twice by dissolving it in 10 cm³ of dichloromethane and then precipitation by the addition of 200 cm³ of ether.[13]

A mixture of 200 mg (1.01 mmol) of guaiazulene, 300 mg (1.50 mmol) of 1,1-diethylaziridinium perchlorate and 5 cm³ of 1,2-dichloroethane was refluxed for 6 h, then taken up in 100 cm³ of chloroform, washed with 2×50 cm³ of saturated aqueous potassium carbonate, 3×50 cm³ of water and dried (sodium sulfate). Solvent removal (reduced pressure) left a green oil which gave two TLC spots (alumina, chloroform; R_f 0.65 for **14** and 0.82 for guaiazulene). Chromatography (alumina, 9:1 benzene–chloroform then chloroform) gave 85.1 mg of blue oil, which yielded 67.8 mg (34%) of guaiazulene on rechromatography (silica gel, hexane), and 161 mg of green-blue oil. Rechromatography (alumina, chloroform) of the green-blue oil afforded 104 mg (35%) of **14** (green-blue oil, R_f=0.65 on alumina with chloroform): UV (C_2H_5OH) 218 (log ε 4.06), 246 (4.22), 287 (4.46), 304 (sh, 4.04), 339 (sh, 3.49), 352 (3.68), 369 (3.56), 582 (ε sh, 256), 622 (298), 675 (sh, 235), and 751 nm (sh, 78); IR (CCl_4) 2960 (ν_{as} CH), 2925 (ν_{as} CH_2), 2870 (ν_s CH), 1460 (δ_{as} CH_3), and, 1380 and 1370 cm⁻¹ (δ_s CH_3); ¹H NMR ($CDCl_3$) δ=1.08 (6H, t, *J*=7.0 Hz, $CH_2C\underline{H}_3$), 1.32 (6H, d, *J*=7.0 Hz, 5′-CH($C\underline{H}_3$)$_2$), 2.61 (3H, s, 3′-CH_3), 2.66 (4H, q, *J*=7.0 Hz, $C\underline{H}_2CH_3$), 2.78 (2H, m, 1-CH_2), 3.37 (2H, m, 2-CH_2), 6.84 (1H, d, *J*=10.5 Hz, 7′-H), 7.28 (1H, q, *J*=10.5 and 2.0 Hz, 6′-H), 7.52 (1H, s, 2′-H), and 8.10 (1H, d, *J*=2.0 Hz, 4′-H); MS *m/e* (rel intensity) 297 (M^+, 2), 211 ($M^+-CH_2NEt_2$, 7), and 86 ($Et_2NCH_2^+$, 100).

Found: C, 84.13; H, 10.45; N, 4.88%. Calcd for $C_{21}H_{31}N$: C, 84.79; H, 10.50; N, 4.71%.

N,N-*Dimethyl-2-(1-guaiazulenyl)-2-methyl-1-propanamine (**15**) and* N,N-*Dimethyl-1-(1-guaiazulenyl)-2-methyl-2-propanamine (**16**).* From 13.0 g (70.0 mmol) of *N*-isopropylidenedimethylammonium perchlorate, mp 298—300 °C,[6] was prepared 5.57 g (40%) of 1,1,2,2-tetramethylaziridinium

perchlorate [^{1}H NMR (CH_2Cl_2) δ=1.74 (6H, s, C(CH_3)$_2$), 3.08 (2H, s, CH_2), and 3.18 (6H, s, $(CH_3)_2N^+$] [Ref. 14; δ=1.72 (6H, 3.02 (2H), and 3.16 (6H)] as described.[14]

A mixture of 990 mg (5.00 mmol) of guaiazulene and 2.00 g (10.0 mmol) of the above aziridinium salt in 25 cm^3 of 1,2-dichloroethane under nitrogen was stirred at reflux temperature for 80 h, then treated as described for the preparation of **14** (500 cm^3 of chloroform; 2×100 cm^3 of 25% potassium carbonate; 2×100 cm^3 of water). From the chromatography of the crude blue oil (alumina; 9:1 benzene–chloroform) were obtained 942 mg of blue oil and 24.4 mg of green-blue oil. Rechromatography of the blue oil (silica gel, hexane) gave 786 mg (79%) of unchanged guaiazulene. Preparative TLC on alumina (9:1 benzene–chloroform) of the green-blue oil afforded 1.04 mg (0.07%) of **15** as a green oil (R_f=0.25) and 1.69 mg (0.1%) of **16** as a blue oil (R_f=0.15).

15: UV (C_2H_5OH) 247 (log ε 4.03), 289 (4.00), 305 (sh, 3.93), 590 (ε 146), and 665 nm (sh, 109); IR ($CHCl_3$) 2970 (ν_{as} CH_2), 2870 (ν_s CH), 1460 (δ_{as} CH_3), and 1380 and 1370 cm^{-1} (δ_s CH_3); MS *m/e* (rel intensity) 297 (M^+, 10), 222 ($M^+-CH_2N(CH_3)_2-2H$, 40), 58 ($CH_2\overset{+}{N}(CH_3)_2$, 96), and 43 ($CH_2\overset{+}{N}CH_3$, 100).

16: UV (C_2H_5OH) 218 (log ε 4.16), 247 (4.29), 289 (4.48), 306 (sh, 4.13), 342 (sh, 3.61), 353 (3.69), 371 (3.65), 575 (ε 258), 618 (300), 672 (sh, 237), and 755 nm (sh, 70); IR (CCl_4) 2970 (ν_{as} CH), 2930 (ν_{as} CH_2), 1460 (δ_{as} CH_3), and, 1380 and 1360 cm^{-1} (δ_s CH_3); ^{1}H NMR ($(CD_3)_2C=O$) δ=1.36 (6H, s, 1-C(CH_3)$_2$), 1.64 (6H, d, J=6.0 Hz, 5′-CH(CH_3)$_2$), 2.39 (6H, s, $N(CH_3)_2$), 2.57 (3H, s, 3′-CH_3), 2.86 (3H, s, 8′-CH_3), 2.92 (1H, sept, J=6.0 Hz, 5′-CH(CH_3)$_2$), 3.19 (2H, s, 2-CH_2), 5.74 (1H, d, J=9.0 Hz, 7′-H), 6.08 (1H, q, J=9.0 and 1.5 Hz, 6′-H), 6.37 (1H, s, 2′-H), and 6.66 (1H, d, J=1.5 Hz, 4′-H); MS *m/e* (rel intensity) 297 (M^+, 8), 211 ($M^+-(CH_3)_2NC(CH_3)_2$, 13), and 86 ($(CH_3)_2\overset{+}{N}C(CH_3)_2$, 100).

N,N-*Diethyl-2-(1-azulenyl)ethanamine* (**18**). From 128 mg (1.00 mmol) of azulene and 300 mg (1.50 mmol) of 1,1-diethylaziridinium perchlorate was obtained, as described for **14**, a green-blue oil as the crude product. Chromatography (alumina, 98:2 benzene–methanol) separated 11.9 mg (9%) of unchanged azulene from 309 mg of blue oil. A benzene (70 cm^3) solution of the latter was extracted with 1 mol dm^{-3} hydrochloric acid (3×70 cm^3) and the combined acid solutions were extracted with chloroform (4×70 cm^3). Removal of the solvent from the dried (sodium sulfate) chloroform solution and chromatography of the residue (silica gel, 7:3 chloroform–methanol) gave 30.7 mg (12%) of hydrochloride (**20**) as tiny blue prisms, mp 150—151 °C: UV (C_2H_5OH) 238 (log ε 4.36), 267 (sh, 4.57), 273 (sh, 4.69), 277 (4.74), 282 (sh, 4.71), 288 (sh, 4.55), 298 (sh, 4.03), 328 (sh, 3.90), 331 (3.90), 344 (3.97), 359 (3.84), 547 (s sh, 252), 563 (sh, 290), 589 (340), 610 (sh, 312), 636 (289), and 705 nm (111); IR ($CHCl_3$) 2520, 2390, and 2330 (NH^+), and 1186 cm^{-1} (C–N); ^{1}H NMR ($CDCl_3$) δ=1.42 (6H, t, J=7.5 Hz, CH_2CH_3), 3.18 (4H, q, J=7.5 Hz, CH_2CH_3), 3.22 (2H, m, 1-CH_2), 3.68 (2H, m, 2-CH_2), 7.14 (2H, br t, J=*ca.* 10 Hz, 5′- and 7′-H), 7.31 (1H, d, J=4.0 Hz, 3′-H), 7.58 (1H, t, J=10.0 Hz, 6′-H), 7.74 (1H, d, J=4.0 Hz, 2′-H), 8.28 (1H, d, J=9.5 Hz, 4′-H), and 8.46 (1H, d, J=9.5 Hz, 8′-H); ^{13}C NMR ($CDCl_3$) δ=8.8 (q, CH_2CH_3), 22.5 (t, 2-C), 46.3 (t, CH_2CH_3), 52.9 (t, 1-C), 116.9 (d, 3′-C), 122.7 (d, 7′-C), 123.0 (d, 5′-C), 123.7 (s, 1′-C), 133.7 (d, 8′-C), 136.1 (s, 4′-C), 136.5 (s, 9′-C), 136.9 (d, 6′-C), 138.1 (d, 2′-C), and 140.7 (s, 10′-C).[15]

To a mixture of 28.7 mg (0.109 mmol) of **20** and 52 cm^3 of 50:2 benzene–methanol was added slowly 100 cm^3 of ice-cooled 50% aqueous potassium carbonate. The separated aqueous layer was extracted with benzene (3×40 cm^3). Removal of the solvent from the combined, dried (sodium sulfate) original benzene layer and extracts gave 19.4 mg (78%, 10% overall) of **18** (blue oil, R_f=0.37 on alumina with 7:3 benzene–ethyl acetate): UV (C_2H_5OH) 238 (log ε 4.27), 263 (sh, 4.44), 268 (sh, 4.46), 273 (sh, 4.71), 277 (4.76), 281 (sh, 4.73), 287 (sh, 4.58), 297 (sh, 3.96), 315 (sh, 3.34), 322 (sh, 3.43), 334 (3.59), 344 (3.74), 359 (3.48), 537 (ε sh, 222), 560 (sh, 294), 581 (sh, 343), 601 (387), 622 (sh, 343), 655 (322), 687 (sh, 169), and 724 nm (123); IR (CCl_4) 2980 and 2940 (ν_{as} CH), 2880 (ν_s CH), 1465, 1457, and 1439 (δ_{as} CH_3), and, 1397, 1388 and 1378 cm^{-1} (δ_s CH_3); ^{1}H NMR ($CDCl_3$) δ=1.09 (6H, t, J=7.5 Hz, CH_2CH_3), 2.69 (4H, q, J=7.5 Hz, CH_2CH_3), 2.84 (2H, m, 1-CH_2), 3.26 (2H, m, 2-CH_2), 7.08 (1H, t, J=10.0 Hz, 5′-H), 7.12 (1H, t, J=10.0 Hz, 7′-H), 7.37 (1H, d, J=4.0 Hz, 3′-H), 7.57 (1H, t, J=10.0 Hz, 6′-H), 7.85 (1H, d, J=4.0 Hz, 2′-H), 8.29 (1H, d, J=10.0 Hz, 4′-H), and 8.34 (1H, d, J=10.0 Hz, 8′-H); MS *m/e* (rel intensity) 227 (M^+, 3), 141 ($M^+-CH_2N(C_2H_5)_2$, 8), and 86 ($CH_2N(C_2H_5)_2^+$, 100).

Found: C, 84.50; H, 9.29; N, 6.08%. Calcd for $C_{16}H_{21}N$: C, 84.53; H, 9.31; N, 6.16%.

N,N-*Diethyl-2-(4,6,8-trimethyl-1-azulenyl)ethanamine* (**19**). From 172 mg (1.01 mmol) of 4,6,8-trimethylazulene and 300 mg (1.50 mmol) of 1,1-diethylaziridinium perchlorate was obtained, as described for **14** except that the mixture was refluxed for 23 h; a violet oil was obtained as the crude product. Chromatography (alumina, 9:1 hexane–ethyl acetate) of a solution of the oil in a small volume of acetone separated 25.1 mg (15%) of unchanged trimethylazulene from 143 mg (53%) of **19** (blue oil, R_f=0.30 on alumina with 9:1 hexane–ethyl acetate): UV (C_2H_5OH) 246 (log ε 4.42), 278 (sh, 4.40), 284 (sh, 4.57), 288 (4.66), 293 (4.65), 298 (sh, 4.61), 327 (sh, 3.46), 338 (3.58), 352 (3.68), 367 (sh, 3.18), 555 (ε sh, 368), 564 (428), 607 (sh, 340), and 667 nm (sh, 129); IR (CCl_4) 2975 (ν_{as} CH), 2930 (ν_{as} CH_2), 2880 (ν_s CH), 1470, 1462, 1445 and 1426 (δ_{as} CH_3), and, 1382 and 1372 cm^{-1} (δ_s CH_3); ^{1}H NMR ($CDCl_3$) δ=1.06 (6H, t, J=7.0 Hz, CH_2CH_3), 2.48 (3H, s, 6′-CH_3), 2.63 (4H, q, J=7.0 Hz, CH_2CH_3), 2.75 (3H, s, 4′-CH_3), 2.76 (2H, m, 1-CH_2), 2.96 (3H, s, 8′-CH_3), 3.34 (2H, m, 2-CH_2), 6.81 (2H, s, 5′- and 7′-H), 7.22 (1H, d, J=4.0 Hz, 3′-H), and 7.44 (1H, d, J=4.0 Hz, 2′-H); ^{13}C NMR ($CDCl_3$) δ=11.5 (q, CH_2CH_3), 25.4 (q, 4′-CH_3), 27.4 (q, 8′-CH_3), 28.3 (q, 6′-CH_3), 29.6 (t, 2-C), 46.8 (t, CH_2CH_3), 56.0 (t, 1-C), 115.2 (d, 3′-C), 126.0 (d, 5′-C), 128.2 (d, 7′-C), 129.0 (s, 1′-C), 132.2 (s, 9′-C), 135.8 (d, 2′-C), 137.0 (s, 10′-C), 144.7 (s, 4′-C), 145.5 (s, 6′-C), and 146.1 (s, 8′-C); MS *m/e* (rel intensity) 269 (M^+, 4), 183 ($M^+-CH_2N(C_2H_5)_2$, 4), and 86 ($(C_2H_5)_2NCH_2^+$, 100).

A solution of 111 mg (0.412 mmol) of **19** in 60 cm^3 of benzene was extracted with 1 mol dm^{-3} hydrochloric acid (3×35 cm^3), and the hydrochloric acid layer was extracted with chloroform (6×35 cm^3). The chloroform solution was dried (sodium sulfate), concentrated (reduced pressure), and chromatographed on a silica gel column (elution with 8:2 chloroform–methanol) to give 84.4 mg (67%) of **21** as a purple oil: UV (C_2H_5OH) 247 (log ε 4.44), 277 (sh, 4.38), 283 (sh, 4.55), 288 (4.63), 293 (4.63), 297 (sh, 4.60), 336 (3.56), 345 (sh, 3.57), 351 (3.61), 552 (ε 334), 592 (sh, 276), and 647 nm (sh, 108); IR ($CHCl_3$) 2470, 2440, 2400, 2355, and 2330 (NH^+), and 1195 cm^{-1} (C–N);

^{1}H NMR ($CDCl_3$) δ=1.43 (6H, t, J=7.0 Hz, $CH_2C\underline{H}_3$), 2.16 (1H, s, NH^+), 2.60 (3H, s, 6′-CH_3), 2.84 (3H, s, 4′-CH_3), 3.07 (3H, s, 8′-CH_3), 3.25 (q, 4H, J=7.0 Hz, $C\underline{H}_2CH_3$), 3.27 (2H, m, 1-CH_2), 3.85 (2H, m, 2-CH_2). 7.08 (2H, s, 5′- and 7′-H), 7.39 (1H, d, J=4.0 Hz, 3′-H), and 7.60 (1H, d, J=4.0 Hz, 2′-H).

Found: C, 74.99; H, 9.88; N, 4.71; Cl, 11.23%. Calcd for $C_{19}H_{28}NCl$: C, 74.60; H, 9.23; N, 4.58; Cl, 11.59%.

References

1) See, for example, W. E. Coyne, "Medicinal Chemistry,"3rd ed, ed by A. Burger, Wiley Interscience, New York (1970), Part II, pp. 953—968; W. T. Comer and A. W. Gomoll, *ibid.*, pp. 1019—1056; D. J. Triggle, *ibid.*, pp. 1235—1282.

2) H. Janistyn, *Deut. Apoth.-Ztg.*, **91**, 319 (1951); C. Wolfgramm, *Pharmazie*, **7**, 604 (1952); F. Jung, *ibid.*, **6**, 192 (1951).

3) A. G. Anderson, Jr., and S. Kurokawa, *J. Org. Chem.* **40**, 3224 (1975).

4) H. C. Brown and A. Tsukamoto, *J. Am. Chem. Soc.*, **83**, 2016 (1961).

5) N. Milstein, *J. Heterocycl. Chem.*, **5**, 339 (1968).

6) N. J. Leonard and J. V. Paukstelis, *J. Org. Chem.*, **28**, 3021 (1963).

7) These tests were performed by Masao Kidokoro at the Central Research Laboratory of Sankyo Co. Ltd., using established procedures.

8) D. F. Shriver, "The Manipulation of Air-Sensitive Compounds," McGraw-Hill, New York (1969); translated into Japanese by Y. Takeuchi, H. Mikuni, and S. Tomoda, "Fuantei-kagobutsu Sosa Ho," Hirokawa, Tokyo (1972), pp. 139—149.

9) Due to insufficient amount of **7**, a mixture of **6** and **7** was used for the ^{1}H NMR measurement. Subtraction of signals of **6** from the spectrum enabled the assignment for **7**.

10) S. Kurokawa, K. Kohara, K. Watanabe, and T. Baba, *J. Fac. Educ. Saga Univ.*, **21**, 151 (1973); *cf.* R. Hagen, E. Heilbronner, and P. A. Straub, *Helv. Chim. Acta*, **51**, 45 (1968).

11) U. Harder, E. Pfeil, and K.-F. Zenner, *Chem. Ber.*, **97**, 510 (1964).

12) N. J. Leonard and J. V. Paukstelis, *J. Org. Chem.*, **30**, 821 (1965); except 100 cm^3 of 1.0 mol dm^{-3} NaOH was used. The reported 0.1 mol dm^{-3} NaOH appeared to be a misprint.

13) Recrystallization from 2-propanol, as specified, gave material of mp 230—232 °C thought to be the perchlorate salt of *N*,*N*-dimethyl-2-isopropoxyethanamine.

14) N. J. Leonard, J. V. Paukstelis, and L. E. Brady, *J. Org. Chem.*, **29**, 3383 (1964).

15) S. Braun and J. Kinkeldei, *Tetrahedron*, **33**, 1827 (1977).

 © 1983 The Chemical Society of Japan Bull. Chem. Soc. Jpn., 56, 2065—2068 (1983)

The Copper-catalyzed Autoxidation of Cysteine. The Amount of Hydrogen Peroxide Produced under Various Conditions and the Stoichiometry of the Reaction

Akira HANAKI* and Hiroko KAMIDE

National Institute of Radiological Sciences, Anagawa-4-chome, Chiba 260

(Received January 31, 1983)

Hydrogen peroxide is shown to be produced as an intermediate from oxygen in the copper-catalyzed autoxidation of cysteine. The amounts of cysteine oxidized and of hydrogen peroxide formed varied depending on the reaction conditions employed. The perpxide upon forming was spontaneously utilized for the oxidation of cysteine. As a result, the ratio of the concentration of hydrogen peroxide formed to cysteine oxidized is variable depending on the conditions. But, in dilute solutions, where the oxidation by the peroxide was slow, a stiochiometric relation of 2:1 was obtained between cysteine consumed and hydrogen peroxide produced. The rate of autoxidation is dependent on the concentration of oxygen dissolved. The double reciprocal plot of the rate against the concentration of oxygen gives a straight line, which indicates a possibility of the Michaelis-Menten type mechanism concerning the reoxidation or oxygenation of Cu(I) species.

Copper ion catalyzes effectively the autoxidation of cysteine (CySH) to cystine(CyS–SCy). Typical features of this autoxidation are that the substrate forms very strong complexes with both Cu(I) and Cu(II) ions and the redox process is assumed to take place within a copper thiolate complex.[1] At high pH and in the presence of excess cysteine, a 2:1(CySH/Cu) complex is formed,[2,3] but this complex is not considered as an intermediate; because it is relatively stable under the conditions.[4] Therefore, a 1:1(CySH/Cu) complex, which has not hitherto been detected by spectroscopic methods, is postulated as a reaction intermediate. During the autoxidation, various amounts of H_2O_2 are formed and subsequently decomposed depending on pH.[2,5] Thus, the primary process of the reaction can be written by Eq. 1, but the stoichiometric relation between cysteine consumed and H_2O_2 formed has not been reported so far.

$$2CySH + O_2 \longrightarrow CyS\text{-}SCy + H_2O_2 \quad (1)$$

Aims of the present work are to verify the stiochiometric relation shown in Eq. 1 and to elucidate the role of oxygen in the reaction. In this paper, we wish to report the following results. 1) The rate of autoxidation depends on the concentration of oxygen. The double reciprocal plot of the rate against the concentration of oxygen gives a straight line, which indicates a possibility that the reoxidation or oxygenation process of Cu(I) species obeys the Michaelis-Menten type mechanism. 2) The stiochiometric relation between cysteine and H_2O_2 was proved to be 2:1. The Cu(I) species may be reoxidized *via* a two-equivalent process.

Experimental

A stock solution of Cu(II) ion was prepared from copper foil of 99.999% purity (Kishida Chemical & Co., Ltd.), which was weighed out and dissolved in a small amount of concd HNO_3. The Cu(II) nitrate solution thus prepared was diluted with deionized, doubly distilled water to a desired concentration. The concentration of the Cu(II) solution was determined by titration with standard 0.01 M EDTA (1M=1 mol dm^{-3}) in ammonium-ammonia buffer at pH 10 with murexide as an indicater[6]. Cysteine, 5,5′-dithiobis(2-nitrobenzoic acid), abbreviated as DTNB, $TiCl_4$ and other reagents were of analytical grade and were used without further purification.

The oxidation was conducted in a 200 ml water-jacketted beacker under pure oxygen or oxygen-nitrogen mixtures (4:1—1:4) at 20 °C. The solution was saturated with oxygen or oxygen-nitrogen mixtures by bubbling for 20 min prior to the kinetic run. The reaction was started by adding the cysteine solution last. Gas bubbling at a rate of 100 ml/min and vigorous agitation by a magnetic stirrer were continued during the reaction. Aliquots were withdrawn at periodic intervals from the reaction mixtures, and applied to the determination of cysteine and H_2O_2. The determination of cysteine and H_2O_2 was carried out spectrophotometrically by using a Hitachi 101 spectrophotometer. Cysteine was determined at 415 nm with DTNB[7], and H_2O_2 at 410 nm with a $TiCl_4$ reagent[8]. The determination of the dissolved oxygen was done before a kinetic run with a Beckman Fieldlab oxygen analyzer, which had been calibrated against air saturated water.

Plots of the decrease of cysteine against time gave a straight line for over 60% reaction. In the kinetic study, the initial rate was calibrated with a graphical method.

Results and Discussion

The oxidation was conducted over the pH range of 6.5 and 7.8. The rate of cysteine autoxidation depended on the concentration of the dissolved oxygen in the medium. Martell *et al.* reported that the rate of the ascorbate oxidation catalyzed by iron chelates was linearly proportional to the concentration of oxygen, and on the basis of this observation they postulated the formation of the ascorbate–Fe(III)–O_2 ternary complex as an intermediate.[9] But, in the autoxidation of cysteine, the rate *vs.* the concentration of oxygen plot did not give a straight line.

Of much importance is that the double reciprocal plot; *i.e.*, the Lineweaver-Burk plot, of the rate against the oxygen concentration gives a straight line as shown in Fig. 1. A series of reciprocal plots for various cysteine concentrations appear to intercept at one point on the abscissa. Only the slope is affected by the variation in the cysteine concentration. The intercept at the abscissa is $-1/K_{0.5}$, where $K_{0.5}$ represents the half saturation concentration of oxygen for the autoxidation. The intercept at the ordinate is $1/V_{max}$,

where V_{max} represents the maximal velocity. The existence of the linear Lineweaver-Burk plot suggests the kinetic association of the metal catalyst and oxygen during the course of the reaction. Probably, the oxygen dissolved in the medium may associate with Cu(I) to form an adduct, Cu(I)–O_2, through which the electron transfer from Cu(I) to oxygen proceeds.

When a small amount of EDTA, less than 10^{-4} M, was added to the medium, the reaction was considerably enhanced.[10] In this case, a Lineweaver-Burk plot also gives a straight line, but a series of the plots appear to be parallel. The $K_{0.5}$ value becomes significantly small in the presence of a small amount of EDTA. Those kinetic parameters are summarized in Table 1.

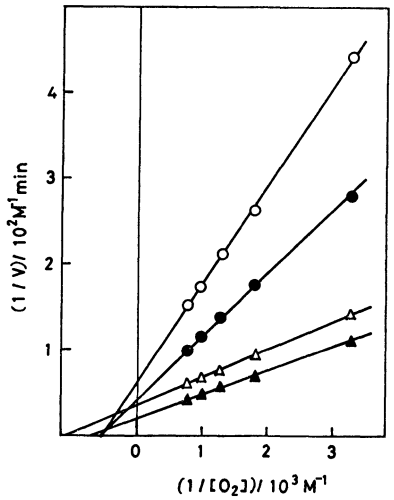

Fig. 1. Double reciprocal plot of the rate against the concentration of the oxygen dissolved in the medium. $[Cu(II)]_0 = 1.38 \times 10^{-6}$ M, $[CySH]_0 = 2.00 \times 10^{-3}$ M(○) and 4.00×10^{-3} M(●) in the absence of EDTA; $[CySH]_0 = 2.00 \times 10^{-3}$ M(△) and 4.00×10^{-3} M(▲) in the presence of EDTA, Buffer: 0.016 M glycylglycine.

The rate of autoxidation was affected by buffers with chelating abilities. Glycylglycine used as a buffer appeared to retard the oxidation, while phosphate did not affect or rather increased the rate of reaction. When the reaction was carried out in buffers containing both glycylglycine and phosphate and the concentration of phosphate was varied, the rate increased significantly with an increase of phosphate ion. This trend is obvious in the pH range of 7—7.5. The examples are shown in Table 2. When the oxidation was conducted in the buffer containing phosphate only, the rate increased approximately 20% as compared with the rate observed in both glycylglycine and phosphate containing buffer. Thus, phosphate is considered to enhance the oxidation.

Since glycylglycine is present excessively; *i.e.*, approximately at 10^4-fold concentration over copper ion, the main species for Cu(II) complex in the medium is $[Cu^{II}(H_{-1}glygly)(glygly)]^-$ (λ_{max}=620 nm, ε=85 $M^{-1}\,cm^{-1}$).[11-13] This 2:1 complex competes with cysteine for coordination site on the Cu(II) catalyst. In addition, glycylglycine is present at tenfold concentration over the substrate. Then, the competition

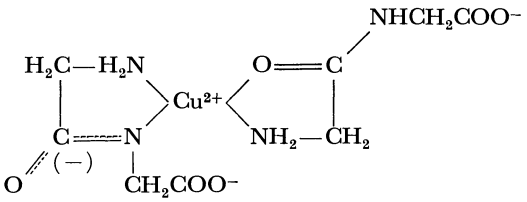

Structure of $[Cu^{II}(H_{-1}glygly)(glygly)]^-$.

Table 1. Kinetic parameters for the autoxidation of cysteine

[Cysteine] / 10^{-3} M	With EDTA		Without EDTA	
	$K_{0.5}$ / 10^{-3} M	V_m / 10^{-4} M min^{-1}	$K_{0.5}$ / 10^{-3} M	V_m / 10^{-4} M min^{-1}
2.00	1.05	3.12	2.13	1.79
4.00	1.43	5.00	2.13	2.70

$[Cu(II)]_0 = 1.38 \times 10^{-6}$ M, T=20 °C, pH 7.5.

Table 2. Effect of phosphate ion on the enhancement of the rate of cysteine autoxidation

Buffer [Glygly.] / 10^{-2} M	Buffer [Phosphate] / 10^{-2} M	Rate/10^{-5} M min^{-1} pH 7.10 Partial pressure of O_2 100%	pH 7.10 40%	pH 7.35 100%	pH 7.35 40%
1.6	0	6.58	3.80	6.78	3.74
1.6	0.1	6.68	3.92	6.74	3.58
1.6	0.25	7.70	3.95	8.98	4.90
1.6	0.5	7.88	4.06	12.4	6.52
0	0.5			14.7	7.60
1.6	1.0	8.48	4.10	14.7	7.70
0	1.0			16.9	8.78

$[Cu(II)]_0 = 1.48 \times 10^{-6}$ M, $[CySH]_0 = 2.00 \times 10^{-3}$ M.

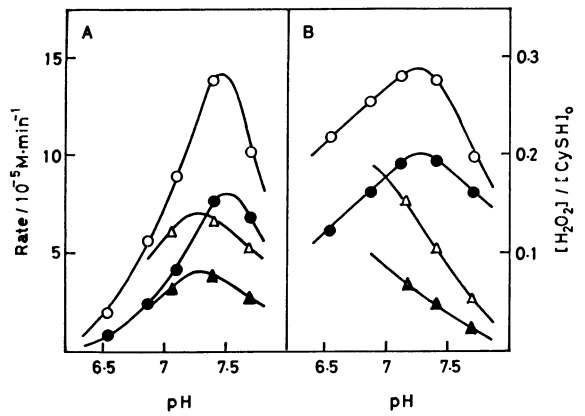

Fig. 2. Effects ot buffers on the pH-rate and pH-$[H_2O_2]/[CySH]_0$ Plots.
$[Cu(II)]_0 = 1.38 \times 10^{-6}$ M, $[CySH]_0 = 2.00 \times 10^{-3}$ M, buffer: 0.016 M glycylglycine(△; 100% O_2, ▲; 40% O_2), 0.016 M glycylglycine-0.01 M phosphate(○; 100% O_2, ●; 40% O_2).

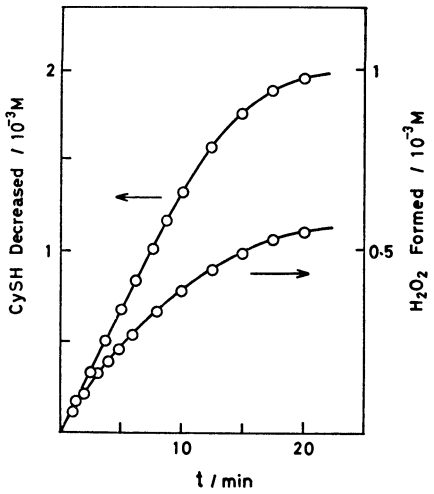

Fig. 3. Time course of the cysteine consumption and the formation of H_2O_2 at pH 7.4.
$[Cu(II)]_0 = 1.38 \times 10^{-6}$ M, $[CySH]_0 = 2.00 \times 10^{-3}$ M, buffer: 0.016 M glycylglycine-0.01 M phosphate, partial pressure of O_2: 100% at 760 mmHg.

of cysteine with glycylglycine; *i.e.*, the ligand substitution from glycylglycine to cysteine in the Cu(II) ion, may be much more retarted. When an equivalent amount of phosphate to glycylglycine is added to the medium, the absorption spectrum of $[Cu^{II}(H_{-1}glygly)(glygly)]^-$ undergoes red shift ($\lambda_{max} = 640$ nm, $\varepsilon = 83$ M^{-1} cm^{-1} at pH 7.1), which suggests that the chelation between Cu(II) and glycylglycine is loosed and is likely dissociated. Under these conditions, the association of cysteine with Cu(II) becomes facilitated and the oxidation is stimulated.

The rate of autoxidation and the amounts of H_2O_2 formed depended on pH. The pH-rate profile gave bell-shaped curves in both buffer systems as shown in Fig. 2A. But, the profile is different in detail. The maximal rates appeared at pH 7.25 in glycylglycine and at pH 7.45—7.5 in glycylglycine–phosphate buffers. The most considerable differences appeared in the relation between the amounts of H_2O_2 formed and pH. Typical examples are shown in Fig. 2B. The amounts of H_2O_2 formed in glycylglycine buffer, which was determined after cysteine had been completely consumed, decreased monotonously with pH, while in phosphate containing buffer the pH profile also gave a bell-shaped curve. In the latter case, a maximal value for the ratio of the concentration of H_2O_2 formed to the initial concentration of cysteine; *i.e.*, $[H_2O_2]/[CySH]_0$, is approximately 0.3 under pure oxygen. As mentioned above, Cu(II) in glycylglycine buffer possesses a relatively low catalytic ability. In the presence of excess cysteine and at high pH, the 2:1(CySH/Cu) complex is formed increasingly and stabilized with an increase of pH.[14] As a result, the oxidation of cysteine by copper in glycylglycine buffer is reduced at high pH, while the rate of oxidation of cysteine by H_2O_2, which is also catalyzed by copper, is shown to increase with pH.[15] Then, the formation and subsequent decomposition of H_2O_2 may be concerted and thereby the amounts of detectable H_2O_2 is apparently reduced.

Various amounts of H_2O_2 were formed concomitantly with the decrease of cysteine. Under the condition at $[Cu(II)]_0 = 1.38 \times 10^{-6}$ M, $[CySH]_0 = 2.00 \times 10^{-3}$ M and the partial pressure of oxygen in the gas phase=20—100% at 760 mmHg (1 mmHg≈133.322 Pa), a certain stoichiometric relation between the concentrations of cysteine consumed and H_2O_2 formed did not exist. A reason why the stoichiometry does not observed may be due to the consumption of H_2O_2 during the reaction. When cysteine has been almost consumed, the concentration of H_2O_2 remained is kept at constant, which indicates that H_2O_2 is utilized; *i.e.*, decomposed, in the presence of the substrate but not decomposed in the absence of the substrate. The time course for the cysteine consumption and H_2O_2 formation at pH 7.4 is shown in Fig. 3.

H_2O_2 is assumed to be a primary product from oxygen in the autoxidation process. If H_2O_2 formed were inert to the substrate, it would be accumulated quantitatively relative to the amounts of cysteine consumed. But, H_2O_2 upon forming does react inevitably and rapidly with cysteine. If the reaction proceeds at a very slow rate, the stoichiometric relation might be estimated; because the extent of H_2O_2 decomposition may be negligible. In an attempt to estimate the stoichiometry of the cysteine autoxidation, the reaction was carried out at various concentrations of cysteine from 5×10^{-4} M to 4×10^{-3} M, where the concentration of the copper catalyst and oxygen were kept at constant. The plot of the initial concentration of cysteine against $[H_2O_2]/[CySH]_0$ is shown in Fig. 4. Expectedly, as the initial concentration of cysteine reduced, the rate decreased and the ratio increased. The value of $[H_2O_2]/[CySH]_0$ was extraporated to 0.5 at the infinitively dilute concentration of cysteine. This fact indicates that the first-step in the autoxidation process involves naturally a two-equivalent oxidoreduction, in which oxygen is reduced to H_2O_2 directly, or two one-equivalent reduction, in which oxygen is reduced *via* superoxide as an intermediate. But. the

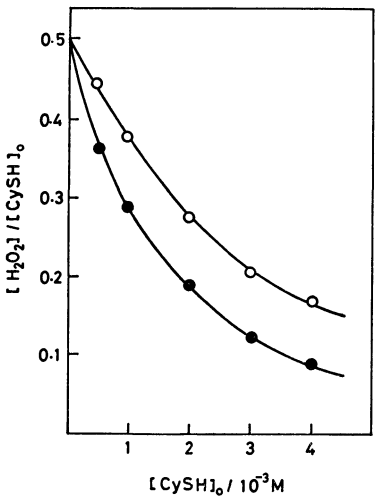

Fig. 4. Relation between the initial concentration of cysteine and $[H_2O_2]/[CySH]_0$; estimation of the stoichiometric relation of the cysteine autoxidation. $[Cu(II)]_0 = 1.38 \times 10^{-6}$ M, partial pressure of O_2: 100%(○) and 40%(●).

superoxide, O_2^-, could not be detected. Accordingly, it is proposed that the autoxidation of cysteine catalyzed by copper involves a two-equivalent process as shown by Eq. 1.

References

1) H. Gampp and A. D. Zuberbuhler, "Metal Ions in Biological Systems," ed by H. Sigel, M. Dekker, Inc., New York (1981), Vol. 12, Chap. 4.
2) C. de Marco, S. Duprè, C. Crifo, G. Rotilio, and D. Cavallini, *Arch. Biochem. Biophys.*, **144**, 496 (1971).
3) D. Cavallini, C. de Marco, D. Duprè, and G. Rotilio, *Arch. Biochem. Biophys.*, **130**, 354 (1969).
4) A. Hanaki, *Chem. Lett.*, **1981**, 139.
5) A. Hanaki and H. Kamide, *Chem. Pharm. Bull.*, **23**, 1671 (1975).
6) G. Schwarzenbach, "Die Komplexometrische Titration," F. Enke Verlag, Stuttgart (1955), pp. 68—69.
7) G. L. Ellman, *Arch. Biochem. Biophys.*, **82**, 70 (1959).
8) E. W. Weissler, *Ind. Eng. Chem., Anal. Ed.*, **17**, 695 (1945).
9) M. M. Taqui Khan and A. E. Martell, *J. Am. Chem. Soc.*, **89**, 4176 (1967).
10) A. Hanaki and H. Kamide, *Chem. Pharm. Bull.*, **26**, 325 (1978). The oxidation is retarded in the presence of EDTA over 2×10^{-4} M.
11) H. Dobbie and W. O. Kermack, *Biochem. J.* **59**, 246 (1955).
12) A. Kaneda and A. E. Martell, *J. Coord. Chem.*, **4**, 137 (1975).
13) M. Sheinblatt and E. D. Becker, *J. Biol. Chem.*, **242**, 3159 (1967).
14) A. Hanaki, unpublished result.
15) A. Hanaki and H. Kamide, *Chem. Pharm. Bull.*, **21**, 1421 (1973).

Lead Tetraacetate Oxidation of Humulene and Conformational Analysis of the Produced Humulatrienediols

Haruhisa SHIRAHAMA,* Kiyoharu HAYANO, Gurdial Singh ARORA, Eiji ŌSAWA and Takeshi MATSUMOTO

Department of Chemistry, Faculty of Science, Hokkaido University, Sapporo 060

(Received February 12, 1983)

Humulene was oxidized by lead tetraacetate in benzene to give 2,5,9-humulatrien-7-ol acetate and 1,5,9-humulatriene-3,7-diol diacetates. Conformational analysis of 1,5,9-humulatriene-3,7-diols was performed by NMR spectroscopy and molecular mechanics calculations.

Oxidation of the double allylic methylene group (C-8) of humulene (**1**) was previously attempted by Sukh Dev[1] in order to make a conversion of humulene to zerumbone (8-ketohumulene) (**2**). The oxidation seemed to be facile. However, even by using various reagents it was practically so difficult that the conversion was not fruitful. We also tried the oxidation of humulene and all of attempts at oxidizing C-8 methylene group of humulene were unsuccessful. The conversion to zerumbone was recently achieved through a roundabout way after all.[2] During these studies, a rather clean oxidation reaction of humulene by lead tetraacetate was realized.[3] The reaction could be applicable to syntheses and modifications of humulanoids.

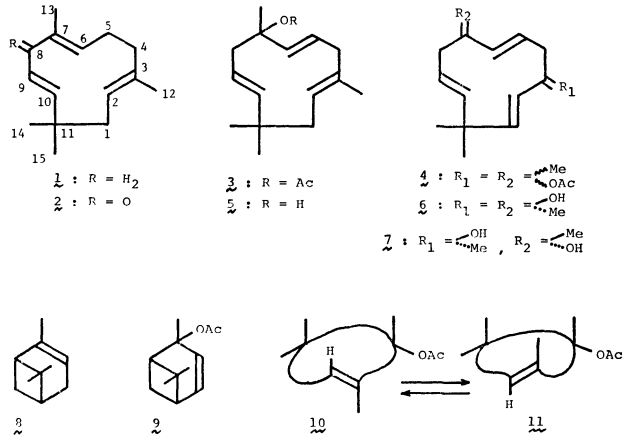

Fig. 1.

Humulene (1 mol) was treated with 1 mol of lead tetraacetate in benzene at 70 °C to give an acetate **3** (45%) and a diastereoisomeric mixture of diacetates **4** (23%). Oxidation with 3 mol of the reagent afforded the mixture of diacetates **4** exclusively. The ^{1}H NMR spectrum of the acetate **3** in the presence of a shift reagent (LIS-^{1}H NMR) (Table 1) showed that following partial structures were there in the molecule:

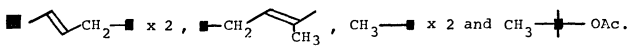

They led us readily to figuring formula **3**. The ^{13}C NMR and MS spectra also supported the formula. On treatment with $LiAlH_4$ the acetate **3** gave an alcohol **5** whose ^{1}H NMR spectrum was identical to that of the compound obtained also through oxidation of humulene by Matsubara *et al.*[3b,4]

The mixture of diacetates **4** first seemed to be a single compound whose structure was presumed to be **4** by its ^{1}H NMR and molecular weight referring to the structure of monoacetate **3**. It was, however, found to be a mixture of two diacetates (1:1) after converting it to corresponding alcohols which could be separated by chromatography. Both diols **6** and

Table 1. ^{1}H NMR spectra of the compounds **3**, **6**, and **7** in the presence of Eu(fod)$_3$

Compound [Eu]/[S]	**3** 0.22	**6** 0.30		**7** 0.44	
proton	δ	δ	$S^{b)}$	δ	$S^{b)}$
14, 15	1.2(3H, s) 1.24(3H, s)	1.74(3H, s) 1.98(3H, s)	1.5 2.6	2.18(6H, s)	2.4
12[a)]	1.8(3H, s)	3.85(3H, s)	8.8	4.70(3H, s)	8.1
13[a)]	3.43(3H, s)	4.08(3H, s)	8.9	4.74(3H, s)	8.3
8	2.72(2H, d, J=7 Hz)	4.41(1H, dd, J=13, 9 Hz) 5.14(1H, dd, J=13, 5 Hz)	8.6 10.1	5.84(1H, dd, J=12, 7 Hz) 6.59(1H, dd, J=12, 7 Hz)	9.1 10.8
4	3.4(1H, dd, J=7, 14 Hz) 4.05(1H, dd, J=7, 14 Hz)	4.92(1H, dd, J=15, 10 Hz) 5.78(1H, dd, J=15, 5 Hz)	9.4 11.4	6.05(1H, dd, J=12, 6 Hz) 6.84(1H, dd, J=12, 6 Hz)	9.1 11.2
10	5.40(1H, dd, J=15 Hz)	6.74(1H, d, J=16 Hz)	5.3	7.18(1H, d, J=16 Hz)	5.1
9	5.82(1H, dt, J=15, 7 Hz)	7.13(1H, ddd, J=16, 9, 5 Hz)	5.1	7.70(1H, dt, J=16, 7 Hz)	6.8
1	2.1(2H, d, J=8 Hz)	8.33(1H, d, J=16 Hz)	8.9	8.63(1H, d, J=16 Hz)	8.3
6	7.29(1H, d, J=16 Hz)	7.88(1H, d, J=15 Hz)	9.6	9.26(2H, d, J=16 Hz)	8.3
2	5.40(1H, t, J=8 Hz)	7.9(1H, d, J=16 Hz)	10.0		
5	6.74(1H, dt, J=16, 7 Hz)	8.02(1H, ddd, J=15, 10, 5 Hz)	11.3	9.63(1H, dt, J=16, 6 Hz)	11.5
Ac	4.20(3H, s)				

a) Assignment to 12 and 13 alternates for **6** and **7**. b) LIS values = $\Delta\delta$/[Eu]/[substrate].

7 exhibited the same M^+ by high resolution MS and their ^1H NMR spectra were so similar that these were implied to be stereoisomers. LIS-^1H NMR revealed that the both diols **6** and **7** and the following structural fragments:

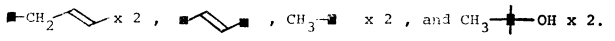

Assembling these parts on a humulene skeleton gave readily formula **6** or **7** except stereochemistry. Relative configuration of the two hydroxyl groups was deduced from LIS value ($\Delta\delta$/[Eu]/[Substrate]). The compound whose *gem*-dimethyl group shifted separately by addition of the shift reagent, namely, **6** was assigned to a *cis*-diol and the other one showing equivalent shift for each of the *gem*-dimethyl groups was allotted to a *trans*-diol.

The mode of lead tetraacetate oxidation of olefinic compounds is not uniform but the above reaction followed the one that exhibited by the oxidation of α-pinene (**8**→**9**).[5] Reaction of 6,7-double bond first took place and then the oxidation of 2,3-double bond followed. The ratio (1:1) of formation of the diastereoisomeric diacetates **6** and **7** could be regarded as a support[6] for equal existence of two stable conformers (**10** and **11**) of the acetate **3** because three *trans* double bonds must have been placed perpendicular to the 11-membered ring and attack of reagent must have been made from outside of the ring.

Conformational Analysis of 1,5,9-Humulatriene-3,7-diol. The coupling constants of methylene protons of **6** were not averaged and suggested that the compound existed either in a predominant conformation or in an equilibrium among several conformations. Strain energy and population for each of eight possible conformations[7] of **6** were thus estimated by means of molecular mechanics calculations.[8] Analysis of possible conformers for **6** followed our previous work[9] in which the conformations of humulene were fully analysed. Arrangement of three double bonds of **6** in cycloundecane ring was the same as those of humulene itself (1,4,8-undecatriene) and thus basic four conformations of humulene (CT, CC, TC, and TT)[9] were modified by proper substitutions (Fig. 2). Energy minimization of the eight conformers were successfully achieved to give their precise geometries and strain energies (Table 2). The conformation *RRR*-CC[10] was found to be most stable and the compound **6** was suggested to be equilibrated mostly among three conformers (*RRR*-CC, *SSS*-CC, and *RRS*-TC). The coupling constants (J_{AC}, J_{BC}, J_{DF}, and J_{EF}) (see Fig. 2) allotted to partial structures, $C(4)H_2C(5)H=$ and $C(8)H_2$–$C(9)H$–, were

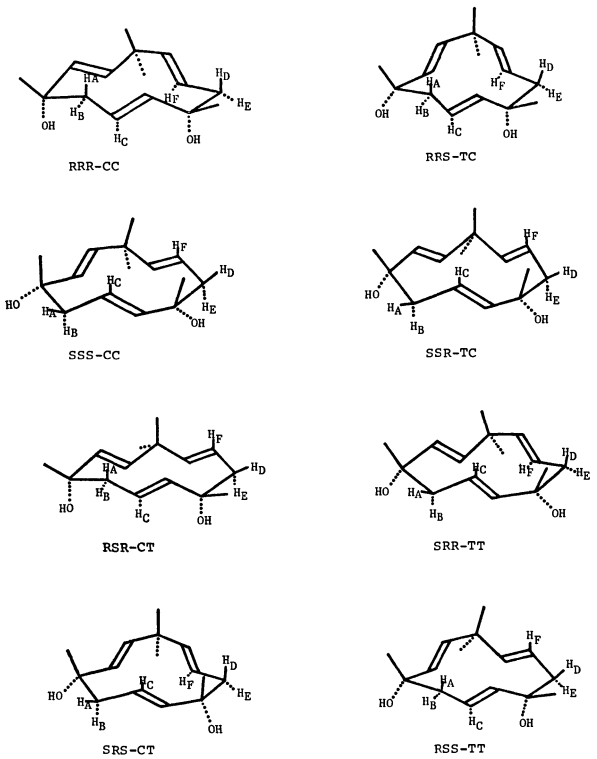

Fig. 2. Eight possible conformations of (3*S*,7*S*)-(*E*,*E*,*E*)-1,5,9-humulatriene-3,7-diol.

TABLE 2. DIHEDRAL ANGLES, RELATIVE STRAIN ENERGY, AND POPULATION FOR EIGHT POSSIBLE CONFORMATIONS OF (3*S*,7*S*)-(*E*,*E*,*E*)-1,5,9-HUMULATRIENE-3,7-DIOL

Dihedral angles	*RRR*-CC	*SSS*-CC	*RRS*-TC	*SSR*-TC	*RSR*-CT	*SRS*-CT	*RSS*-TT	*SRR*-TT
1-2=3-4	−175.3	176.7	−176.9	174.6	−174.2	174.4	−173.8	168.3
2=3-4-5	106.5	−97.2	114.0	−120.2	111.1	−100.8	114.8	−112.3
3-4-5-6	−45.9	40.2	−40.0	45.1	−36.6	33.4	−26.6	27.6
4-5-6-7	125.8	−124.4	110.7	−100.5	−91.4	99.1	−85.0	101.0
5-6=7-8	−174.6	175.8	−116.6	169.9	167.4	−168.6	168.7	−175.4
6=7-8-9	51.1	−49.7	75.8	−95.7	−70.3	64.0	−62.4	47.9
7-8-9=10	51.0	−51.0	−98.0	69.0	93.0	−100.0	−76.4	50.8
8-9=10-11	−174.7	175.3	170.6	−167.9	−169.9	170.7	169.7	−174.9
9=10-11-1	126.1	−124.1	−61.6	95.4	100.7	−89.1	−64.7	104.8
10-11-1-2	−47.1	−42.9	−41.7	37.4	−47.7	42.4	−35.7	27.8
11-1-2=3	106.2	−110.7	119.4	−109.0	120.9	−124.6	129.2	−113.3
2=3-4-OH	−12.2	146.5	−5.1	123.7	−8.1	142.7	−2.9	131.1
9=10-11-OH	8.1	119.7	−179.8	−22.8	−17.1	154.8	179.5	−14.5
Relative strain / kcal mol^{-1}	0.00	1.01	0.73	2.72	1.87	3.42	3.32	3.84
Population/%	65.2	11.8	19.0	0.7	2.8	0.2	0.2	0.1

Table 3. Dihedral angles calculated for $-CH_2-CH=$ moieties and estimated and observed J values

		H_A-4 -5-H_C	H_B-4 -5-H_C	H_D-8 -9-H_F	H_E-8 -9-H_F
RRR-CC	*a*	167.9	52.6	−172.6	68.7
	J	12	4	12	1
	J'	7.8	2.6	7.8	0.7
SSS-CC	*a*	−58.0	−172.9	−70.7	172.3
	J	3	12	1	12
	J'	0.4	1.4	0.1	1.4
RRS-TC	*a*	176.7	60.8	176.1	58.2
	J	13	3	13	3
	J'	2.5	0.6	2.5	0.6
SSR-TC	*a*	−57.7	−173.7	−52.0	−166.2
	J	3	12	4	12
	J'	0.0	0.1	0.0	0.1
RSR-CT	*a*	−178.4	63.2	−43.6	−158.5
	J	13	2	6	11
	J'	0.4	0.1	0.2	0.3
SRS-CT	*a*	−70.8	172.8	161.1	46.9
	J	1	12	11	6
	J'	0.0	0.0	0.0	0.0
RSS-CT	*a*	−169.9	71.7	−39.3	−152.8
	J	12	1	7	10
	J'	0.0	0.0	0.0	0.0
SRR-TT	*a*	−64.0	179.1	158.6	46.2
	J	2	13	10	6
	J'	0.0	0.0	0.0	0.0
	J_{calcd}	11.0	4.8	10.6	2.8
	J_{obsd}	10	5	9	5

a: Dihedral angles for the moieties indicated in the first line. *J*: *J* values estimated for the dihedral angles shown in the upper line. *J'*: Contributing fraction = *J* × population.

obtained from the estimated conformations referring Karplus relationship.[11] Weighted averages (sum of each conformer's *J* × population) of the calculated *J* values well coincided with observed values (Table 3).

The coupling constants of methylene protons of **7** were averaged and indicated that this compound was freely mobile and did not exist in a particular stable conformation. The different situation between the two diastereoisomers, **6** and **7**, may be readily understood since in **6** two methyl groups at C(3) and C(7) will take equatorial-like orientation while in **7** the both will take always opposite (equatorial- and axial-like) orientations each other.

Experimental

Melting point was uncorrected. IR spectra were measured with JASCO IR-S spectrometer. ^{1}H NMR and ^{13}C NMR spectra were recorded on a HITACHI R20B (60 MHz) and a JEOL JNM FX-100 (25 MHz) instrument using TMS as an internal standard respectively. High resolution mass spectra were measured on a JEOL JMS D-300 mass spectrometer.

Lead Tetraacetate Oxidation of Humulene (1). To a stirred mixture of $Pb(OAc)_4$ (1.2 g, 2.71 mmol) and dry benzene (20 ml) was added a solution of humulene (500 mg, 2.45 mmol) in benzene (10 ml) under argon. The mixture was stirred at 65—70 °C for 8 h and washed with water, aqueous $NaHCO_3$ solution and brine. The benzene solution was dried over Na_2SO_4 and evaporated under reduced pressure to leave paste. The crude product was chromatographed on a silica-gel column using hexane, 5% Et_2O-hexane and 13% Et_2O-hexane in turn as eluents to give an acetate **3** (289 mg, 45%) and a diasteroisomeric mixture of diacetates **4** (180 mg, 23%) which was not separable on TLC and VPC.

(E,E,E)-2,5,9-Humulatrien-7-ol Acetate (3): IR (neat) 1745, 1245, and 965 cm^{-1}; ^{1}H NMR δ=1.0, 1.02, and 1.99 (each 3H, s), 1.59 (6H, s), 2.4—2.8 (3H, m), and 4.8—5.9 (5H, complex); ^{13}C NMR δ=17.6(q), 22.0 (q), 22.3 (q), 26.4 (q), 27.4 (q), 38.9 (s), 40.5 (t×2), 47.3 (t), 82.8 (s), 120.2 (d), 123.6 (d), 129.1 (d), 134.3 (d), 137.9 (s), 143.5 (d), and 169.6 (s). Found: *m/z* 262.1924. Calcd for $C_{17}H_{26}O_2$: M, 262.1926.

(E,E,E)-1,5,9-Humulatriene-3,7-diol Diacetates (4): IR (neat) 1745, 1240, and 965 cm^{-1}; ^{1}H NMR δ=1.19 (6H, s), 1.51 (3H, bs), 1.58 (3H, s), 1.95, 1.96 (each 3H, s), and 4.9—5.7 (6H, complex). Found: *m/z* 320.2026. Calcd for $C_{19}H_{28}O_4$: 320.1980.

(E,E,E)-2,5,9-Humulatrien-7-ol (5). A solution of the acetate **3** (29 mg) in dry THF (1 ml) was stirred with $LiAlH_4$ (8 mg) at 0 °C under argon. The reaction was followed by TLC. After completion of the reaction, aqueous NH_4Cl solution was added and the mixture was extracted with ether three times. The combined extracts were dried (Na_2SO_4) and evaporated to leave an oil **5** (23 mg, 95%) which was purified by chromatography (silica gel, 5% AcOEt-hexane): IR (neat) 3420, 1660, 1110, and 965 cm^{-1}; ^{1}H NMR δ=1.03 and 1.37 (each 3H, s), 1.65 (3H, d, *J*=1 Hz), 1.94 (2H, d, *J*=8 Hz), 2.55 (2H, d, *J*=7 Hz), 5.05 (3H, m), 5.33 (1H, d, *J*=16 Hz), and 5.73 (1H, dt, *J*=16 and 7 Hz). Found: *m/z* 220.1815. Calcd for $C_{15}H_{24}O$: 220.1821.

*(E,E,E)-1,5,9-Humulatriene-*cis*-3,7-diol (6) and (E,E,E)-1,5,9-Humulatriene-*trans*-3,7-diol (7).* A solution of the diacetates **4** (40 mg) in dry THF (0.5 ml) was added to a well stirred slurry of $LiAlH_4$ (15 mg) and dry THF (0.5 ml) at 0 °C under argon. After completion of the reaction (checked by TLC), an excess of the $LiAlH_4$ was decomposed by addition of ice-water and extracted with EtOAc three times. The combined extracts were dried and evaporated to give 30 mg (quantitative) of paste which was shown to be a mixture (1:1) of two diols by its NMR spectrum. The mixture was separated by chromatography on a silica-gel column using a mixed solvent of hexane and ether (4:1) to afford a pair of diastereomeric diols **6** and **7**.

Diol 6: Mp 124—125 °C, IR ($CHCl_3$) 3640, 3480, 1090, and 970 cm^{-1}; ^{1}H NMR δ=1.18, 1.22, 1.28, and 1.35 (each 3H, s), 1.66—2.6 (6H, m), 5.08 and 5.46 (2H, ABq, *J*=16 Hz), and 5.1—5.5 (4H, m). Found: *m/z* 236.1772, Calcd for $C_{15}H_{24}O_2$: 236.1777.

Diol 7: Colorless oil, IR ($CHCl_3$) 3640, 3480, 1090, and 970 cm^{-1}; ^{1}H NMR δ=1.18 (6H, s), 1.27 and 1.33 (each 3H, s), 1.9—2.5 (6H, m), and 4.8—5.6 (6H, m). Found: *m/z* 236.1763. Calcd for $C_{15}H_{24}O_2$: 236.1777.

We thank Prof. Y. Matsubara (Kinki University) for sending ^{1}H NMR spectrum of compound **5**.

References

1) N. P. Damodaran and Sukh Dev, *Tetrahedron Lett.*, **1965**, 1977.

2) H. Shirahama, B. R. Chhabra, and T. Matsumoto,

Chem. Lett., **1981**, 717.

3) a) "Many of the reactions of lead tetraacetate with olefin systems are characterized by complex mixture of products which often render these reactions of little synthetic value." R. N. Butler, "Lead Tetraacetate" in "Synthetic Reagents," ed by J. S. Pizey, Ellis Horwood Ltd., Chichester, England (1977), Vol. 3, Chap. 4, p. 288; b) In fact, humulene gave many oxidation products by use of lead tetraacetate in acetic acid: H. Iwamuro, M. Hashimoto, and Y. Matsubara, *Nippon Nogei Kagaku Kaishi*, **55**, 793 (1981).

4) They have given the same structure as ours to their compound without showing any supporting data and without discussing the geometry of rearranged double bond (Δ^5).

5) G. H. Witham, *J. Chem. Soc.*, **1961**, 2232.

6) This is not real evidence, of course. However, a medium size cyclopolyolefin reserves often its stable conformation during the reactions. K. Takeda, *Tetrahedron*, **30**, 1525 (1974); J. K. Sutherland, *ibid*, **30**, 1651 (1974); P. D. Cradwick and G. A. Sim, *J. Chem. Soc., D*, **1971**, 31; F. H. Allen, E. D. Brown, D. Rogers, and J. K. Sutherland, *ibid*, **1967**, 1116; R. M. Gipson, H. W. Guin, S. H. Simonsen, C. G. Skinner, and W. Shive, *J. Am. Chem. Soc.*, **88**, 5366 (1966).

7) Their enantiomers were not considered.

8) Allinger's program "MMI" was used. QCPE 318. N. L. Allinger; J. T. Sprague, and J. Liljefors, *J. Am. Chem. Soc.* **96**, 5100 (1974); D. H. Wertz and N. L. Allinger, *Tetrahedron* **30**, 1579 (1974).

9) H. Shirahama, E. Ōsawa, and T. Matsumoto, *J. Am. Chem. Soc.*, **102**, 3208 (1980).

10) A prefix RRR represents the chiralities of the three double bonds, $\Delta^{1,2}$, $\Delta^{5,6}$, and $\Delta^{9,10}$, in this order. Conformations only for 3*S*,7*S*-diol were considered here.

11) L. M. Jackman and S. Sternhell, "Applications of Nuclear Magnetic Resonance Spectroscopy in Organic Chemistry," 2nd ed, Pergamon Press, Oxford (1969), Chap. 4-2.

Double Cycloaddition Reaction of Imidazolium Methylides. Intermolecular 1,3-Dipolar and Intramolecular Diels-Alder Cycloaddition Reactions

Otohiko Tsuge,* Shuji Kanemasa, and Shigeori Takenaka

Research Institute of Industrial Science, and Department of Molecular Science and Technology, Interdisciplinary Graduate School of Engineering Sciences, Kyushu University, Kasuga, Kasuga, Fukuoka 816

(Received February 21, 1983)

Such imidazolium methylides as imidazolium dicyanomethylide and bis(ethoxycarbonyl)methlide react with the methylenecyclopropenes with unsaturated substituents at the 4-position in the fashion of double cycloaddition reaction, leading to the novel cage compounds, which involves an intermorecular 1,3-dipolar cycloaddition reaction and an intramolecular Diels-Alder reaction.

Since the reaction of thiazolium methylides with the methylenecyclopropenes having unsaturated substituents at the 4-position presented the first example of double cycloaddition reaction that included at least a 1,3-dipolar cycloaddition reaction,[1,2] it has been reported that pyridinium methylides can be also employed in the similar reaction with methylenecyclopropenes leading to the cage compounds.[3]

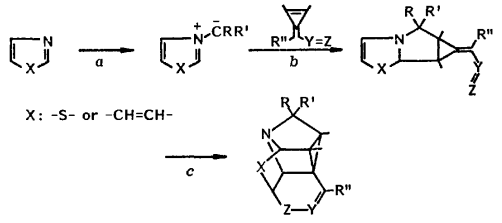

Scheme 1.

As shown in Scheme 1, these reactions have provided a new methodology for the double functionalization of nitrogen-containing aromatic heterocycles such as thiazole and pyridine: The heterocycles are converted into the corresponding azomethine ylide 1,3-dipoles (the step *a* as the first functionalization), the 1,3-dipolar cycloaddition reaction of the ylides across the endocyclic double bond of methylenecyclopropenes forms the [3+2] cycloadducts leading to the collapse of aromatic character of the starting heterocycles (the step *b* as the second functionalization), and the intramolecular Diels-Alder reaction takes place across the newly formed olefinic double bond giving the cage compounds (the step *c*).

According to the general reaction pattern mentioned above, imidazole would be also doubly functionalized by the ylide formation and the reaction with methylenecyclopropenes having unsaturated substituents at the 4-position, while no examples for the 1,3-dipolar cycloaddition reaction of imidazolium ylides to olefinic dipolarophiles have been reported so far.[4]

This paper describes the first example for the double cycloaddition reaction of imidazolium methylides that react with methylenecyclopropenes having unsaturated substituents at the 4-position leading to the novel cage compounds.

Results and Discussion

The Reaction with 2-Benzoyl-2-(2,3-diphenyl-2-cyclopropenylidene)acetonitrile. The reaction of 1-methyl-1*H*-imidazol-3-ium dicyanomethylide (**1**) with 2-benzoyl-2-(2,3-diphenyl-2-cyclopropenylidene)acetonitrile (**3**) in ethanol under reflux gave the 1:1 adduct **4** as a colorless solid in a good yield (Table 1). The IR spectrum exhibits no carbonyl stretching indicating that the benzoyl group of **3** has participated in a cyclization. The structure of **4** was easily assigned to the pentacyclic cage structure shown in Scheme 2 by comparison of the NMR spectral data with those of the similar cage compounds obtained in the reaction of thiazolium methylides.[1] The ^{1}H-NMR spectrum shows three methine hydrogens, two of which couple each other (J_{5-12}=4.0 Hz), and the ^{13}C-NMR indicates the existence of a cyclopropane ring (28.17, 41.85, and 50.28 ppm as each singlet), three methine carbons (66.18, 88.59, and 97.56 ppm as each doublet), and another quaternary carbon (65.69 ppm as a singlet).

Although the zwitterionic dicyanomethylides of nitrogen-containing heterocycles are stable enough to be isolated and have been conveniently used in the study of cycloaddition reactions, the major problem is their hard solubility in organic solvents. So a new imidazolium methylide, 1-methyl-1*H*-imidazol-3-ium bis(ethoxycarbonyl)methylide (**2**), was synthesized. The reaction of 1-methylimidazole with diethyl 2-bromomalonate in acetone afforded 1-methyl-3-[bis(ethoxycarbonyl)methyl]-1*H*-imidazol-3-ium bromide (**6**) in a quantitative yield. Treatment of the salt **6** with aqueous sodium carbonate gave the expected ylide **2** as a colorless solid also in a quantitative yield. The ylide **2** is less stable than the dicyanomethylide **1**,[5] but readily soluble in aprotic organic solvents such

Table 1. Reaction of imidazolium methylides with methylenecyclopropenes

Reactant		Reaction conditions: Temperature	Time / h	Solvent	Product	Yield / %
1	**3**	Reflux	29	Ethanol	**4**	76
2	**3**	Reflux	2	THF	**5**	99
7	**8**	Room temperature	4	THF	**9**	28
1	**8**	Reflux	24	Ethanol	**10**	36
					11	30
2	**8**	Reflux	48	THF	**12**	90

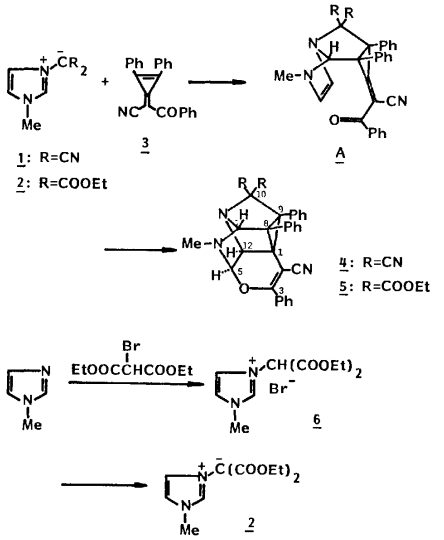

Scheme 2.

as chloroform and tetrahydrofuran.

The imidazolium bis(ethoxycarbonyl)methylide **2** thus synthesized reacted with **3** under reflux in tetrahydrofuran for 2 h to give the similar cage compound **5** in an almost quantitative yield (Table 1). The structure of **5** was confirmed on the basis of the spectral data.

The reaction pathway for the formation of the pentacyclic cage compounds **4** and **5** is illustrated in Scheme 2. It should be emphasized that the imidazolium methylides **1** and **2** have cycloadded stereo- and regioselectively to the endocyclic double bond of the methylenecyclopropene **3** to form the intermediary *endo* [3+2] cycloadducts **A** whose structures are favored for the subsequent intramolecular Diels-Alder cycloaddition reaction.

The Reaction with 2-Phenyl-2-(2,3-diphenyl-2-cyclopropenylidene)acetonitrile. The reaction of 1-methyl-1*H*-imidazol-3-ium phenacylide (**7**), which was generated *in situ* from 1-methyl-3-phenacyl-1*H*-imidazol-3-ium bromide and triethylamine, with 2-phenyl-2-(2,3-diphenyl-2-cyclopropenylidene)acetonitrile (**8**) in tetrahydrofuran at room temperature gave a red-colored product **9** in 28% yield. The product **9** has a molecular formula derived from the 1:1 adduct between **7** and **8** with the loss of 1-methylimidazole, and was determined as 2-(α-cyanobenzylidene)-3,4,6-triphenyl-2*H*-pyran on the basis of the IR (no carbonyl stretching), ^{1}H-NMR (an olefinic singlet at 6.47 ppm), and ^{13}C-NMR spectra (no sp^3 carbon). The elimination of heterocyclic moiety from the N-ylides of nitrogen-containing heterocycles has been observed quite often.[6] In the reaction of pyridinium phenacylide with 4,4-diacylmethylenecyclopropenes, Eicher has reported the formation of red-colored pyran derivatives as the pyridine-eliminated products.[7] The formation of **9** is explained by the reaction pathway shown in Scheme 3: The nucleophilic addition of the ylide carbon of **7** to the endocyclic double bond of **8** forms the intermediary zwitterion **B**, 1-methylimidazole is kicked out to give the allene intermediate **C**, and finally the 6π-cyclization occurs leading to the isolated product **9**.

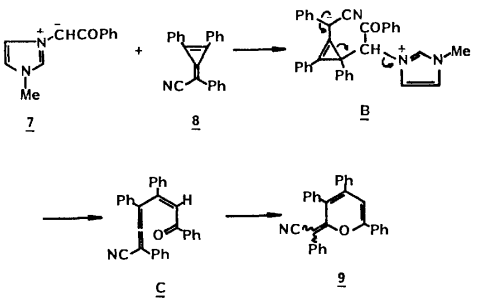

Scheme 3.

On the other hand, the reaction of the dicyanomethylide **1** with the methylenecyclopropene **8** under reflux in ethanol gave two kinds of the 1:1 adducts **10** and **11** in 36 and 30% yields, respectively. The analysis of the spectral data confirmed the pentacyclic cage structure of **10** and the imidazoindenopyridine structure of **11**.

The ^{1}H-NMR and ^{13}C-NMR spectra of **10** show four methine hydrogens and carbons (4.11^s, 4.15^d (J= 4.0 Hz), 4.50^d, and 4.92^s ppm in the ^{1}H-NMR, and 27.53, 66.99, 68.10, and 93.17 ppm as each doublet in the ^{13}C-NMR spectra) and three singlet carbons assigned to the carbons of cyclopropane moiety (33.17, 36.93, and 48.14 ppm). The stereochemistry at the 2-position was determined as shown in Scheme 4 on the ground of the high chemical shift of the 2-methine hydrogen.[8]

The ^{1}H-NMR spectrum of **11** shows only two methine hydrogens which couple each other with a coupling constant of 7.0 Hz (5.58 and 6.10 ppm). The ^{13}C-NMR spectrum exhibits two quaternary carbons (67.36 and 68.05 ppm) as well as two methine carbons (40.28 and 94.81 ppm). The absence of a cyclopropane moiety in **11** indicates that the cyclopropane ring and one of the phenyl groups of **8** have interacted to give the product **11**. Although there are two skeletons possible for **11** (the 5,7,11b,11c-tetrahydro-1*H*-imidazo-[1,2-*a*]indeno[1,2-*c*]pyridine(**11-1**) and 5,10,11,11a-tetrahydro-1*H*-imidazo[1,2-*a*]indeno[2,1-*d*]pyridine (**11-2**)) on the basis of the reaction modes mentioned later, it was impossible to assign the correct structure.

On the other hand, the bis(ethoxycarbonyl)methylide **2** gave the pentacyclic cage compound **12** as the single product in an excellent yield (Table 1). The spectral data are consistent with the proposed structure.

The reaction of the imidazolium methylides **1** and **2** with the methylenecyclopropene **8** proceeds also stereo- and regioselectively forming the *endo* [3+2] cycloadducts **D** which then cyclize through the intramolecular Diels-Alder reaction to give the other intermediates **E**. A 1,3-hydrogen shift of the 4-methine hydrogen to the 2-position affords the cage compounds **10** and **12**. In the case of the intermediate **D** derived from the dicyanomethylide **1**, another type of cyclization takes place. The Cope rearrangement concerned with the phenyl group at the 6a- or 5a-position leads to the intermediate **F-1** or **F-2**, respectively, while it is not clear which phenyl group has participated in the rearrangement. A 1,3-hydrogen shift of the 7a-hydrogen of **F-1** or a 1,5-hydrogen shift of the 9a-

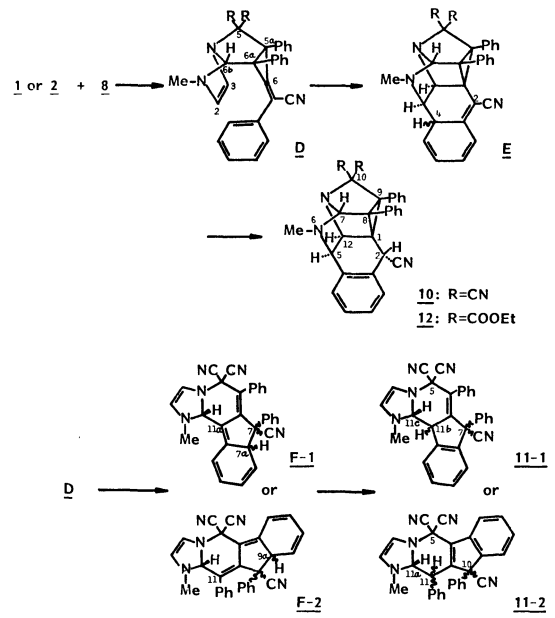

Scheme 4.

hydrogen of **F-2** gives the product **11-1** or **11-2**, respectively. The similar Cope rearrangement has been observed in the [2+2] cycloadduct of an enamine to **8**.[9]

Experimental

General. Melting points were determined on a Yanagimoto micro melting point apparatus and are uncorrected. IR spectra were taken with a JASCO IRA-1 or a JASCO A-102 spectrometer. ^{1}H-NMR spectra were recorded on a Hitachi R-40 at 90 MHz or a JEOL FX-100 spectrometer at 100 MHz and ^{13}C-NMR spectra were obtained on a JEOL FX-100 instrument at 25.05 MHz. Chemical shifts are expressed in parts per million downfield from tetramethylsilane. Mass spectra were measured with a JEOL JMS-01SG-2 spectrometer at 75 eV of ionization energy. Elementary analyses were performed on a Hitachi 026 CHN analyzer. Thin-layer chromatography (TLC) was accomplished on 0.2-mm precoated plates of silica gel 60 F-254 (Merck) or on 0.2-mm precoated plates of aluminum oxide 60 F-254 type E (Merck). Visualization was with ultraviolet light (254 and 365 nm) and iodine. Preparatory column chromatography was performed on silica gel Wako C-300 (Wako). Solvents were evaporated with a Tokyo Rikakikai rotary vacuum evaporator type V at about 50 °C unless otherwise stated.

Tetrahydrofuran was distilled from sodium immediately before use. Triethylamine was distilled and stored on potassium hydroxide. Acetone was dried over anhydrous potassium carbonate.

Materials. 2-Benzoyl-2-(2,3-diphenyl-2-cyclopropenylidene)acetonitrile(**3**) (pale yellow needles from 2-propanol, mp 168—170 °C (lit,[10] mp 162—163 °C)) and 2-phenyl-2-(2,3-diphenyl-2-cyclopropenylidene)acetonitrile (**8**) (orange needles from benzene-hexane, mp 178—180 °C (lit,[11] mp 182—183 °C)) were prepared according to the reported methods. 1-Methyl-1*H*-imidazol-3-ium dicyanomethylide (**1**) (beige leaflets from ethanol, mp 142—143 °C (lit,[12] mp 143—144 °C)) was synthesized by the reaction of 1-methylimidazole with tetracyanoethylene oxide. 1-Methyl-3-phenacyl-1*H*-imidazol-3-ium bromide (colorless needles from acetonitrile, mp 154 °C (lit,[13] mp 153—155 °C) was obtained in 96% yield in the reaction of 1-methylimidazole with phenacyl bromide. 1-Methylimidazole and diethyl 2-bromomalonate are commercially avaliable.

*Reaction of 1-Methyl-1*H*-imidazol-3-ium Dicyanomethylide (**1**) with 2-Benzoyl-2-(2,3-diphenyl-2-cyclopropenylidene)acetonitrile (**3**).* A mixture of **1** (73 mg, 0.5 mmol) and **3** (169 mg, 0.5 mmol) in ethanol (20 ml) was refluxed for 29 h during which time all the starting materials were consumed (on TLC). After complete evaporation of the solvent *in vacuo*, the residue was chromatographed over silica gel using benzene as an eluent to give **4** (182 mg, 76%): Colorless needles from ether-hexane, mp 185—188 °C (decomp)). IR (KBr) 2180 cm^{-1} (C≡N); ^{1}H-NMR ($CDCl_3$) δ=2.94 (3H, s, 6-Me), 4.13 (1H, d, J_{12-5}=7.0 Hz, 12-H), 5.13 (1H, s, 7-H), 5.58 (1H, d, J_{5-12}=7.0 Hz, 5-H), and 6.70—7.82 ppm (15H, m, ArH); ^{13}C-NMR ($CDCl_3$) δ=28.17 (s, 1-C), 41.18 (q, 6-Me), 41.85, 50.28 (each s, 8- and 9-C), 65.69 (s, 10-C), 66.18 (d, 12-C), 88.59 (d, 7-C), 97.56 (d, 5-C), 110.71, 116.22 (each s, 10-CN), 121.97 (s, 2-CN), and 168.94 ppm (s, 3-C); MS *m/e* 479 (M^+, 4%). Found: C, 77.39; H, 4.41; N, 14.59%. Calcd for $C_{31}H_{21}ON_5$: C, 77.66; H, 4.38; N, 14.67%.

*1-Methyl-1*H*-imidazol-3-ium Bis(ethoxycarbonyl)methylide (**2**).* A mixiture of 1-methylimidazole (2.5 g, 0.03 mol) and diethyl 2-bromomalonate (7.2 g, 0.03 mol) in dry acetone (50 ml) was stirred at room temperature for 24 h. The acetone was evaporated *in vacuo* giving a colorless viscous oil of **6** (9.7 g, 100%). The salt **6** (9.7 g, 0.03 mol) was dissolved in water (5 ml) and treated with saturated aqueous sodium carbonate under vigorous stirring precipitating colorless solid of **2** (7.2 g, 100%): Colorless prisms from chloroform-acetone, mp 164—165 °C. IR (KBr) 1690, 1640 (C=O), and 1580 cm^{-1}; ^{1}H-NMR ($CDCl_3$) δ=1.24 (6H, t, $CH_2C\underline{H}_3$), 3.92 (3H, s, *N*-Me), 4.09 (4H, q, $C\underline{H}_2CH_3$), 7.09 (2H, m, 4- and 5-H), and 8.25 ppm (1H, br, s, 2-H).

*Reaction of **2** with **3**.* A mixture of **2** (120 mg, 0.5 mmol) and **3** (167 mg, 0.5 mmol) in dry tetrahydrofuran (20 ml) was refluxed until **3** no longer showed its spot on a TLC plate (2 h). The tetrahydrofuran was evaporated *in vacuo* and then the residue was chromatographed over silica gel using benzene as an eluent to give **5** (284 mg, 99%): Colorless prisms from ether-light petroleum, mp 175 °C. IR (KBr) 2204 (C≡N) and 1738 cm^{-1} (C=O); ^{1}H-NMR ($CDCl_3$) δ=1.02, 1.19 (each 3H, t, 10-$COOCH_2C\underline{H}_3$), 2.94 (3H, s, 6-Me), 3.97 (1H, d, J_{12-5}=4.0 Hz, 12-H), 4.12, 4.22 (each 2H, q, 10-$COOC\underline{H}_2CH_3$), 5.40 (1H, s, 7-H), 5.54 (1H, d, J_{5-12}=4.0 Hz, 5-H), and 6.60—7.58 ppm (15H, m, ArH); ^{13}C-NMR ($CDCl_3$) δ=13.56, 13.74 (each q, 10-$COOCH_2\underline{C}H_3$), 29.53 (s, 1-C), 41.10 (q, 6-Me), 44.09, 47.61 (each s, 8- and 9-C), 61.82 (t, 10-$COOCH_2CH_3$), 65.52 (d, 12-C), 85.30 (s, 10-C), 87.77 (d, 7-C), 97.93 (d, 5-C), 117.18 (s, 2-CN), 166.15 (s, 10-$\underline{C}OOEt$), and 168.26 ppm (s, 3-C); MS *m/e* 573 (M^+, 63%) and 500 ($M^+-COOEt$, 33%). Found: C, 73.00; H, 5.45; N, 7.33%. Calcd for $C_{35}H_{31}O_5N_3$: C, 73.28; H, 5.45; N, 7.33%.

*Reaction of 1-Methyl-1*H*-imidazol-3-ium Phenacylide (**7**) with 2-Phenyl-2-(2,3-diphenyl-2-cyclopropenylidene)acetonitrile (**8**).* To a stirred suspension of 1-methyl-3-phenacyl-1*H*-imidazol-3-ium bromide (141 mg, 0.5 mmol) and **8** (153 mg, 0.5 mmol) in 25 ml of dry tetrahydrofuran was added dropwise triethylamine (0.07 ml, 0.5 mmol). After the mixture was stirred at room temperature for 4 h, a colorless solid precipitated (triethylammonium bromide) was filtered off

and washed with 5 ml of tetrahydrofuran. The combined filtrate and washing were evaporated *in vacuo*. The residue was chromatographed over silica gel using benzene as an eluent to afford **3** (60 mg, 28%): Red needles from 2-propanol, mp 187 °C. IR (KBr) 2250 cm^{-1} (C≡N); ^{1}H-NMR ($CDCl_3$) δ=6.47 (1H, s, 5-H) and 6.80—7.85 ppm (20H, m, ArH); ^{13}C-NMR ($CDCl_3$) δ=104.95 (s, CN), 124.90 (d, 5-C), 127.36 (s, =C(CN)Ph), 143.33 (s, 4-C), 154.68 (s, 6-C), and 161.40 ppm (s, 2-C); MS *m/e* 423 (M^+, base peak), 105 ($PhCO^+$, 57%), and 77 (Ph^+, 37%). Found: C, 88.12; H, 5.09; N, 3.56%. Calcd for $C_{31}H_{21}ON$: C, 87.94; H, 4.96; N, 3.31%.

Reaction of **1** *with* **8**. A solution of **1** (73 mg, 0.5 mmol) and **8** (153 mg, 0.5 mmol) in ethanol (20 ml) was refluxed for 24 h. No trace of **8** was detected on a TLC plate after 24 h. The solvent was completely removed off by evaporation *in vacuo*. The residue was chromatographed over silica gel using benzene as an eluent. The first colorless fraction gave **10** (82 mg, 36%) and the second yellow fraction afforded **11** (68 mg, 30%).

10: Colorless needles from ether-light petroleum, mp 251—252 °C (decomp). IR (KBr) 2250 cm^{-1} (C≡N); ^{1}H-NMR ($CDCl_3$) δ=2.81 (3H, s, 6-Me), 4.11 (1H, s, 2-H), 4.15 (1H, d, J_{12-5}=4.0 Hz, 12-H), 4.50 (1H, d, J_{5-12}=4.0 Hz, 5-H), 4.92 (1H, s, 7-H), and 6.40—7.64 ppm (14H, m, ArH); ^{13}C-NMR ($CDCl_3$) δ=27.53 (d, 2-C), 33.17 (s, 1-C), 36.93, 48.14 (each s, 8- and 9-C), 44.56 (q, 6-Me), 63.30 (s, 10-C), 66.99 (d, 12-C), 68.10 (d, 5-C), 93.17 (d, 7-C), 111.08, 111.95 (each s, 10-CN), and 119.00 ppm (s, 2-CN); MS *m/e* 451 (M^+, base peak). Found: C, 79.91; H, 4.70; N, 15.55%. Calcd for $C_{30}H_{21}N_5$: C, 79.80; H, 4.69; N, 15.51%.

11: Yellow prisms from ether-light petroleum, mp 132—133 °C. IR (KBr) 2250 cm^{-1} (C≡N); ^{1}H-NMR ($CDCl_3$) δ=2.84 (3H, s, 1-Me), 5.58 (1H, d, J=7.0 Hz, CH), 6.10 (1H, d, J=7.0 Hz, CH), and 6.75—7.64 ppm (16H, m, ArH, 2- and 3-H); ^{13}C-NMR ($CDCl_3$) δ=40.28 (d, CH), 44.44 (q, 1-Me), 67.36, 68.05 (each s, quart-C), 94.81 (d, CH), 111.72, 114.42, and 118.34 ppm (each s, CN); MS *m/e* 451 (M^+, base peak). Found: C, 79.63; H, 4.60; N, 15.53%. Calcd for $C_{30}H_{21}N_5$: C, 79.80; H, 4.69; N, 15.51%.

Reaction of **2** *with* **8**. A mixture of **2** (120 mg, 0.5 mmol) and **8** (153 mg, 0.5 mmol) in dry tetrahydrofuran (20 ml) was refluxed for 48 h. The tetrahydrofuran was eveporated *in vacuo* and the residue was chromatographed over silica gel using benzene as an eluent to give **12** (245 mg, 90%): Colorless prisms from ether-light petroleum, mp 192 °C. IR (KBr) 2220 (C≡N) and 1740 cm^{-1} (C=O); ^{1}H-NMR δ=1.13, 1.19 (each 3H, t, 10-$COOCH_2C\underline{H}_3$), 2.77 (3H, s, 6-Me), 4.02 (1H, d, J_{12-5}=4.3 Hz, 12-H), 4.14, 4.23 (each 2H, q, 10-$COOC\underline{H}_2CH_3$), 4.16 (1H, s, 2-H), 4.40 (1H, d, J_{5-12}=4.3 Hz, 5-H), 5.11 (1H, s, 7-H), and 6.50—7.50 ppm (14H, m, ArH); ^{13}C-NMR ($CDCl_3$) δ=13.77 (q, 10-$COOCH_2\underline{C}H_3$), 28.86 (d, 2-C), 33.98 (s, 1-C), 39.16, 45.31 (each s, 8- and 9-C), 44.82 (q, 6-Me), 62.01, 62.16 (each t, 10-$COO\underline{C}H_2CH_3$), 66.36 (d, 12-C), 67.53 (d, 5-C), 83.25 (s, 10-C), 92.62 (d, 7-C), 120.16 (s, 2-CN), 167.09 and 167.72 ppm (each s, 10-$\underline{C}OOEt$); *m/e* 545 (M^+, 15%) and 472 (M^+−COOEt, base peak). Found: C, 74.82; H, 6.12; 7.51%. Calcd for $C_{34}H_{31}O_4N_3$: C, 74.84; H, 5.73; N, 7.70%.

References

1) O. Tsuge and H. Shimoharada, *Chem. Pharm. Bull.*, **30**, 1903 (1982).

2) O. Tsuge, H. Shimoharada, M. Noguchi, and S. Kanemasa, *Chem. Lett.*, **1982**, 711.

3) O. Tsuge, S. Kanemasa, and S. Takenaka, *Chem. Lett.*, **1983**, 519.

4) The cycloaddition reaction of imidazolium methylides to acetylenic dipolarophiles has been reported (see Ref. 13). The only example for the reaction of benzimidazolium ylide with acrylonitrile (I. Zugravescu, J. Herden, and I. Druta, *Rev. Roumaine de Chim.*, **19**, 659 (1974)) and some reports of the reaction with acetylenic dipolarophiles (H. Ogura and K. Kikuchi, *J. Org. Chem.*, **37**, 2679 (1972); I. Zugravescu, J. Herdan, and I. Druta, *Rev. Roumaine de Chim.*, **19**, 649 (1974); O. Meth-Cohn, *Tetrahedron Lett.*, **1975**, 413) are known.

5) The purification of the bis(ethoxycarbonyl)methylide **2** by recrystallization failed. Once the ylide **2** is dissolved in organic solvents, it hardly crystallizes again. Evaporation of the solvents gives a pasty material whose ^{1}H-NMR spectrum, however, is identical to that of **2**.

6) As a review: I. Zugravescu and M. Petrovanu, "N-Ylide Chemistry", McGraw-Hill, New York (1976), p. 155.

7) Th. Eicher, E. V. Angerer, and A. -M. Hansen, *Justus Liebigs Ann. Chem*, **746**, 102 (1971).

8) The reaction of thiazolium dicyanomethylide with **8** afforded two stereoisomeric cage compounds in which the 2-methine hydrogens were observed at 4.29 and 5.03 ppm (see Ref. 2).

9) O. Tsuge, S. Okita, M. Noguchi, and S. Kanemasa, *Chem. Lett.*, **1982**, 993.

10) Th. Eicher and T. Born, *Justus Liebigs Ann. Chem.*, **762**, 127 (1972).

11) H. -U. Wagner, R. Seidl, and H. Faß, *Tetrahedron Lett.*, **1972**, 3883.

12) W. J. Linn, O. W. Webster, and R. E. Benson, *J. Am. Chem. Soc.*, **87**, 3651 (1965).

13) V. Boekelheide and N. A. Fedoruk, *J. Am. Chem. Soc.*, **90**, 3830 (1965).

Pseudo-sugars. X. Synthesis of Several Branched-chain Unsaturated Cyclitols and Their Derivatives[1]

Seiichiro Ogawa, Takao Hattori, Tatsushi Toyokuni, and Tetsuo Suami*

Department of Applied Chemistry, Faculty of Science and Technology, Keio University, Hiyoshi, Kohoku-ku, Yokohama 223

(Received February 23, 1983)

Some racemic (hydroxymethyl)cyclohexenepolyols and their derivatives of biological interest have been synthesized from DL-1,2,3-tri-*O*-acetyl-(1/2,3)-4-methylene-5-cyclohexene-1,2,3-triol derived from the corresponding dibromide by treatment with sodium acetate in hexamethylphosphoric triamide.

In connection with the previous paper,[2] several (hydroxymethyl)cyclohexenepolyols and its derivatives have been synthesized as peracetates from readily available DL-1-*O*-acetyl-2,3-anhydro-(1/2,3,4,6)-4-bromo-6-bromomethyl-1,2,3-cyclohexanetriol (**1**).[3]

Compound **1** was treated with aqueous acetone containing 1% concd sulfuric acid at reflux, followed by acetylation with acetic anhydride in pyridine, to produce DL-1,2,3-tri-*O*-acetyl-(1,2/3,4,6)-4-bromo-6-bromomethyl-1,2,3-cyclohexanetriol (**2**) in 87% yield. Opening of the epoxide ring proceeds selectively *via* an anchimeric assistance of the C-1 acetoxyl group at C-2. As the corresponding (1,3/2,4,6)-isomer,[3] **2** was expected to be a versatile synthetic intermediate for various kinds of branched-chain cyclitol derivatives.[4,5]

Treatment of **2** with 4 molar equiv. of sodium acetate in *N*,*N*-dimethylformamide (DMF) at 80 °C for 8 h resulted in a preferential replacement of the primary bromo group with an acetate ion to give the tetraacetate **3** in 75% yield, along with the elimination product, DL-1,2,3-tri-*O*-acetyl-(1/2,3)-4-methylene-5-cyclohexene-1,2,3-triol (**4**, 14%). When the similar reaction was carried out at an elevated temperature (110 °C) for 32 h, the elimination of hydrobromic acid between C-4 and C-5 further occurred to give DL-1,2,3-tri-*O*-acetyl-(1,4/2,3)-4-acetoxymethyl-5-cyclohexene-1,2,3-triol (**5**) in 48% yield, along with **4** (22%). On the other hand, hexamethylphosphoric triamide (HMPA) was used as the solvent instead of DMF, **4** was obtained predominantly in 69% yield, after having been heated at 120 °C for 2 h. Whereas, a reaction of **3** with zinc dust in acetic acid at 65 °C for 35 h gave DL-1,2-di-*O*-acetyl-(1,2/3)-3-acetoxymethyl-5-cyclohexene-1,2-diol (**6**) in 51% yield. The structures of **5** and **6** were deduced on the basis of analytical data and ^{1}H NMR spectra, and finally established by converting them into branched-chain cyclitols. Thus, the conventional osmium tetraoxide-oxidation of **5** and **6**, followed by acetylation, afforded mainly the peracetyl (hydroxymethyl)cyclohexanepentol **7** and tetrol **8**[6] in 33 and 70% yields, respectively. The ^{1}H NMR spectrum of **7** showed the signals due to six acetoxyl methyl groups as four singlets with 2:1:2:1 relative intensity, indicative of the presence of the plane of the symmetry in the molecule, being consistent with the assigned structure. The postulated structure of **8** was supported by the ^{1}H NMR spectral

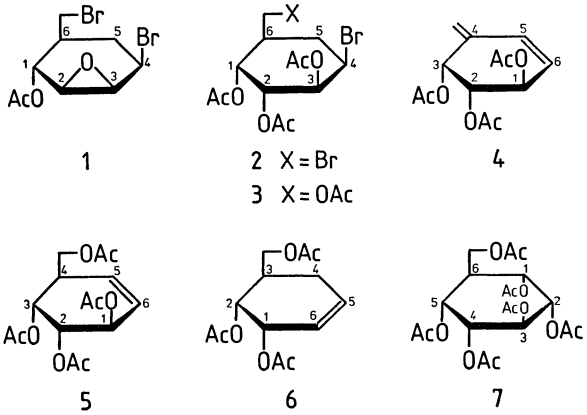

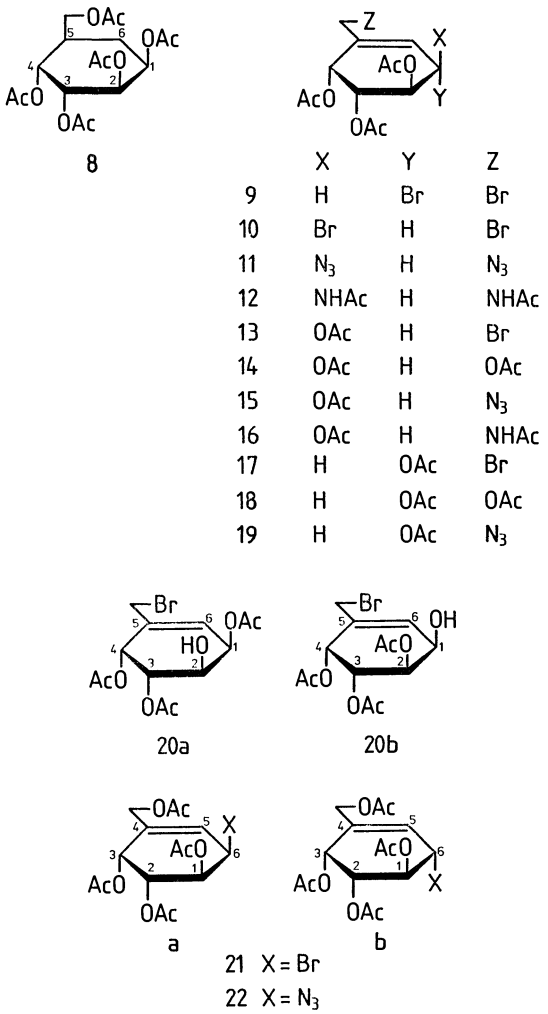

Scheme 1.

signal-pattern similar to that of **3** in the region of the ring protons attached to the carbon atoms bearing the acetoxyl groups, and finally confirmed by identification with the compound derived by the alternative synthetic route.[7]

The structure of **4** was confirmed by the appearance of the signal for the exocyclic methylene protons at δ=5.22 as a two-proton doublet (J=6 Hz) and that for the olefinic proton at δ=6.19 as a doublet (J=10 Hz) in the ^{1}H NMR spectrum. In contrast to the corresponding (1,3/2)-isomer,[8] **4** is unstable and readily polymerizes during purification. But it can be preserved as an ethyl acetate solution for several days.

Bromination of **4** with bromine in acetic acid–acetic anhydride (1:3) at room temperature gave a mixture of the 1,4-addition products, which were fractionated by a silica-gel column to give the dibromides **9** (30%) and **10** (3%), along with the monobromide **13** (5%). The ^{1}H NMR spectrum of **9** revealed the olefinic proton as a narrow doublet (J=3 Hz) at δ=6.12, in support of a pseudoequatorial orientation of the C-6 bromo group.[9] Compounds **9** and **10** are interconvertible each other in the presence of a bromide ion, and the more thermodynamically stable isomer **9** predominates in the reaction mixture. Compound **13** seems to be formed from **9** by an attack of an acetate ion at C-6 from the pseudoaxial direction.

The structure of **9** was further confirmed by the reaction with silver acetate (4 molar equiv.) in acetic acid, which proceeded through a neighboring group participation reaction of the C-1 acetoxyl group at C-6 giving rise to an intermediate 1,6-cyclic acetoxonium ion.[4] When the reaction was carried out in aqueous acetic acid, the acetoxonium ion was attacked by water to give a mixture of DL-1,3,4- (**20a**) and 2,3,4-tri-*O*-acetyl-(1,2/3,4)-5-bromomethyl-5-cyclohexene-1,2,3,4-tetrol (**20b**) in 72% yield. While, under anhydrous conditions (in acetic acid–acetic anhydride), the acetoxonium ion was likely to undergo a back side attack by an acetate ion at the allylic position giving the pentaacetate **18** with the inversion of the configuration at C-6. On the other hand, a molar equiv. of silver acetate was used in the above reaction, the secondary bromo group was only displaced to give the bromo tetraacetate **17** in 48% yield. The mixture of **20a** and **20b** was converted into the pentaacetate **14** by further treatment with sodium acetate in aqueous DMF, followed by acetylation.

Nucleophilic substitution reactions of the bromides thus obtained were then studied. Treatment of **9** with an azide ion in DMF at room temperature gave smoothly a single diazido compound **11** in 67% yield

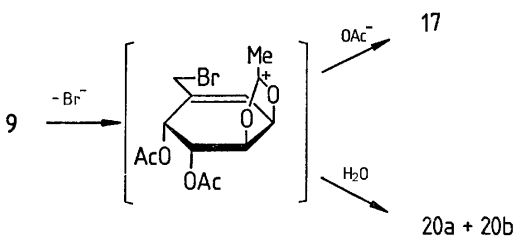

Scheme 2.

via an S_N2 reaction with inversion of the configuration at C-6. In the ^{1}H NMR spectrum of **11**, the signal for the olefinic proton appeared as a doublet (J=4.5 Hz) at δ=5.86, in support of the assigned structure. Reduction of **11** with hydrogen sulfide, followed by acetylation, gave bis(acetamide) **12** in 78% yield. Similar azidolysis of **17** and **20a,b** gave the corresponding azides **19** and **15** (after acetylation) in 59 and 69% yields, respectively. Compound **15** could easily be converted into the acetamide **16** in 52% yield.

Finally, in order to introduce a desired nucleophile into the C-6 position, attempts to displace first the primary bromo group of **9** by an acetate ion were made. Treatment of **9** with a molar equiv. of sodium acetate in DMF at room temperature gave a mixture of the unstable 6-bromo compounds **21a** and **21b** in 67% yield. Compounds **21a** and **21b** are interconvertible each other in the presence of a bromide ion, and are isolated as an equilibrium mixture. Without further purification, the mixture was directly treated with sodium azide in DMF at room temperature yielded a mixture of the azides **22a** and **22b** in 74% yield. The ^{1}H NMR spectrum of the mixture showed the methylene signal as a singlet at δ=4.44, in support of the presence of the acetoxyl group at the branched-chain carbon atom. Therefore, **21a,b** would be useful as a synthon for preparation of some isomeric validoxylamine A[10] and α-glucosidase inhibitors.[11]

Experimental

General. Melting points were determined on a Büchi 510 capillary melting point apparatus and are uncorrected. Unless otherwise noted, ^{1}H NMR spectra were taken on Varian EM-390 (90 MHz) in chloroform-*d* with reference to tetramethylsilane as an internal standard. The peak positions were given in terms of δ-values and values given for coupling constants were of first-order. TLC was performed on a precoated silica gel 60 F-254 plates (Merck, Darmstadt; 0.25 mm thickness). The silica gel used for a column chromatography was Wakogel C-300 (Wako Pure Chemical Industries, Ltd.).

DL-*1,2,3-Tri*-O-*acetyl-(1,2/3,4,6)-4-bromo-6-bromomethyl-1,2,3-cyclohexanetriol (2).* A solution of DL-1-*O*-acetyl-2,3-anhydro-(1/2,3,4,6)-4-bromo-6-bromomethyl-1,2,3-cyclohexanetriol (**1**)[3] (3.0 g) in acetone (27 ml) containing 10% sulfuric acid (3 ml) was refluxed for 3 h. The reaction mixture was neutralized with sodium hydrogencarbonate and then evaporated to dryness. The residue was treated with acetic anhydride (6 ml) and pyridine (6 ml) at room temperature overnight. The reaction mixture was poured into ice water and the precipitates were collected by filtration. Recrystallization of the crude product from ethanol gave 3.4 g (87%) of **2** as plates: mp 126.5—127.5 °C; ^{1}H NMR ($CDCl_3$) δ=2.00 (3H, s), 2.11 (3H, s), and 2.19 (3H, s) (OAc), 3.18—3.54 (2H, m, CH_2Br), 4.40 (1H, ddd, J=3, 5.5, and 12 Hz, H-4), 4.98 (1H, dd, J=3 and 10.5 Hz, H-1), 5.25 (1H, dd, J=3 and 4 Hz, H-3), and 5.34 (1H, dd, J=3 and 4 Hz, H-4).

Found: C, 36.08; H, 4.01; Br, 36.84%. Calcd for $C_{13}H_{18}Br_2O_6$: C, 36.30: H, 4.22; Br, 37.16%.

DL-*1,2,3-Tri*-O-*acetyl-(1,2/3,4,6)-6-acetoxymethyl-4-bromo-1,2,3-cyclohexanetriol (3).* A mixture of **2** (0.30 g), sodium acetate (0.25 g), and *N,N*-dimethylformamide (DMF)

(5 ml) was stirred at 80 °C for 8 h. The reaction mixture was concentrated and coevaporated with 1-butanol and toluene. The residue was extracted with chloroform and the extracts were filtered through a short column of alumina. The filtrate was concentrated and the residue was fractionated on a silica-gel column (12 g) with ethyl acetate–hexane (1 : 2) as an eluent. The first fraction (R_f 0.14) gave an oil, which was recrystallized from ethanol to give 0.21 g (75%) of **3** as prisms: mp 104.5—105 °C; ^{1}H NMR ($CDCl_3$) δ=1.97 (3H, s), 2.06 (3H, s), 2.11 (3H, s), and 2.18 (3H, s), (OAc), 3.97 (2H, d, J=4 Hz, C$\underline{H}_2$OAc), 4.37 (1H, ddd, J=3, 6, and 11 Hz, H-6), 4.95 (1H, dd, J=3 and 11 Hz, H-3), 5.20 (1H, dd, J=3 and 4 Hz, H-1), and 5.25 (1H, dd, J=3 and 4 Hz, H-2).

Found: C, 44.00; H, 5.01; Br, 19.06%. Calcd for $C_{15}H_{21}BrO_8$: C, 44.03; H, 5.17; Br, 19.53%.

The second fraction (R_f 0.29) gave 24 mg (14%) of DL-1,2,3-tri-*O*-acetyl-(1/2,3)-4-methylene-5-cyclohexene-1,2,3-triol (**4**) as an oil: ^{1}H NMR ($CDCl_3$) δ=2.04 (3H, s) and 2.08 (6H, s) (OAc), 5.09 (1H, dd, J=3 and 7.5 Hz, H-2), 5.22 (2H, d, J=6 Hz, C=C$\underline{H}_2$), 5.58—5.80 (3H, m, H-1, H-3, and H-6), and 6.19 (1H, d, J=10 Hz, H-5).

This compound was very unstable and a satisfactory analytical data were not obtained. Therefore, practically pure sample was directly used in the succeeding reactions.

Reaction of **2** *with Sodium Acetate.* *a) In DMF*: A mixture of **2** (4.0 g), sodium acetate (3.3 g, 4 molar equiv.), and DMF (35 ml) was stirred at 110 °C for 32 h. TLC indicated the formation of two products [R_f 0.47 and 0.25, ethyl acetate–hexane (1 : 5)]. The reaction mixture was concentrated and the residue was chromatographed on a silica-gel column (120 g) with ethyl acetate–hexane (1 : 2) as an eluent. The first fraction gave 0.48 g (22%) of **4** as an oil, which was identical with the compound obtained before. The second fraction gave 1.45 g (47.5%) of DL-1,2,3-tri-*O*-acetyl-(1,4/2,3)-4-acetoxymethyl-5-cyclohexene-1,2,3-triol (**5**) as an oil: ^{1}H NMR ($CDCl_3$) δ=2.05 (6H, s) and 2.06 (6H, s) (OAc), 2.75 (1H, br q, J=*ca.* 5 Hz, H-4), 4.09 (2H, d, J=5 Hz, C$\underline{H}_2$OAc), 5.05—5.36 (3H, m, H-1, H-2, and H-3), and 5.71 (2H, s, H-5 and H-6).

Found: C, 54.68; H, 6.02%. Calcd for $C_{15}H_{20}O_8$: C, 54.88; H, 6.14%.

b) In Hexamethylphosphoric Triamide (HMPA): A mixture of **2** (0.30 g), sodium acetate (0.23 g, 4 molar equiv), and HMPA (5 ml) was stirred at 120 °C for 2 h. TLC indicated the formation of one main component [R_f 0.55, ethyl acetate–hexane (1 : 4)], along with four minor components. The reaction mixture was diluted with ethyl acetate (20 ml) and washed thoroughly with water, and dried over anhydrous sodium sulfate. Evaporation of the solvent gave an oil, which was rapidly chromatographed on a silica-gel column (6 g) with ethyl acetate–hexane (1 : 4) as an eluent. The main fraction gave 0.12 g (69%) of **4** as an oil, which could be preserved as an ethyl acetate solution in a refrigerator.

DL-*1,2-Di*-O-*acetyl-(1,2/3)-3-acetoxymethyl-5-cyclohexene-1,2-diol (***6***).* A mixture of **3** (0.40 g) and zinc dust (1.95 g) in acetic acid (10 ml) was stirred at 65 °C for 35 h. The reaction mixture was filtered and the insoluble material was washed thoroughly with acetic acid. The filtrate and washings were combined and concentrated to give crystals, which were recrystallized from ethanol to give 0.14 g (51%) of **6** as prisms: mp 57.5—59 °C; ^{1}H NMR ($CDCl_3$) δ=1.99 (3H, s), 2.01 (3H, s), and 2.05 (3H, s) (OAc), 3.85—4.25 (2H, m, C$\underline{H}_2$OAc), 4.93 (1H, dd, J=3.5 and 11 Hz, H-2), 5.42 (1H, br t, J=3.5 Hz, H-1), 5.61 (1H, br dd, J=3.5 and 10 Hz, H-6), and 5.92 (1H, ddd, J=2.5, 4, and 10 Hz, H-5).

Found: C, 57.51; H, 6.64%. Calcd for $C_{13}H_{18}O_6$: C, 57.77; H, 6.71%.

Osmium Tetraoxide-oxidation of **5**. To a solution of **5** (0.34 g) in *t*-butyl alcohol (8 ml) containing 30% hydrogen peroxide (2 ml) was added *t*-butyl alcohol (2.5 ml) containing osmium tetraoxide (0.01 g), and the mixture was stirred at room temperature for 1 d. The reaction mixture was diluted with water and the excess hydrogen peroxide was destroyed by addition of sodium sulfite. The mixture was concentrated to dryness and the residue was treated with acetic anhydride and pyridine in the usual way. The product was purified by passage through a short column of alumina with chloroform. The filtrate was concentrated to give crystals, which were recrystallized from ethanol to give 0.15 g (33%) of 1,2,3,4,5-penta-*O*-acetyl-(1,2,4,5/3,6)-6-acetoxymethyl-1,2,3,4,5-cyclohexanepentol (**7**) as prisms: mp 170.5—171.5 °C; ^{1}H NMR ($CDCl_3$) δ=2.01 (6H, s), 2.02 (3H, s), 2.06 (6H, s), and 2.11 (3H, s) (OAc), 2.65 (1H, m, H-6), 4.11 (2H, d, J=3 Hz, C$\underline{H}_2$OAc), and 5.10—5.30 (5H, m, H-1, H-2, H-3, H-4, and H-5).

Found: C, 50.81; H, 5.88%. Calcd for $C_{19}H_{26}O_{12}$: C, 51.12; H, 5.87%.

Osmium Tetraoxide-oxidation of **6**. Compound **6** (0.62 g) was treated with osmium tetraoxide in *t*-butyl alcohol similarly as described in the preparation of **7**. The product was acetylated and then purified by a short column of alumina with chloroform. Recrystallization of the crude product from ethanol gave 0.62 g (70%) of DL-1,2,3,4-tetra-*O*-acetyl-(1,2,5/3,4)-5-acetoxymethyl-1,2,3,4-cyclohexanetetrol (**8**) as prisms: mp 105—106.5 °C; ^{1}H NMR ($CDCl_3$) δ=1.97 (6H, s), 2.01 (3H, s), 2.07 (3H, s), and 2.09 (3H, s) (OAc), 4.03 (2H, d, J=5 Hz, C$\underline{H}_2$OAc), 5.03 (1H, dd, J=3.5 and 10 Hz, H-4), and 5.03—5.36 (3H, m, H-1, H-2, and H-3); (Found: C, 52.87; H, 6.24%). It was identical with the compound (mp 106—107 °C) derived by the alternative route.[7]

The mother liquor of **8** was concentrated and the residue was chromatographed on a silica-gel column (15 g) with ethyl acetate–hexane (1 : 2) as an eluent. The first fraction (R_f 0.55) gave 12 mg (1.8%) of 2,6-diacetoxy-4-methylene-2,5-cyclohexadiene-1-one as an oil: ^{1}H NMR ($CDCl_3$) δ=2.04 (3H, s) and 2.23 (3H, s) (OAc), 4.94 (2H, s, C=C$\underline{H}_2$), and 7.08 (2H, s, H-3 and H-5). The second fraction (R_f 0.43) gave 19 mg (2.1%) of DL-(hydroxymethyl)-cyclohexanetetrol pentaacetate as an oil: ^{1}H NMR ($CDCl_3$) δ=1.93 (3H, s), 1.97 (3H, s), 2.00 (3H, s), 2.04 (3H, s), and 2.08 (3H, s) (OAc), 3.90 (1H, dd, J=3.5 and 11 Hz) and 4.09 (1H, dd, J=5 and 11 Hz) (C$\underline{H}_2$OAc). These compounds were not further characterized because of minute quantities.

Reaction of **4** *with Bromine in Acetic Acid and Acetic Anhydride.* An 1 : 3 mixture of acetic acid and acetic anhydride was heated at reflux for 2 h before use as a solvent. To a stirred solution of crude **4** (0.35 g) in the mixture of solvent (7 ml) was added dropwise 5% bromine-acetic acid (1.35 ml) at room temperature, and then the stirring was continued for 1.5 h. TLC indicated the formation of one major component (R_f 0.53), along with two mionr components (R_f 0.51 and 0.36) [irrigated two times in ethyl acetate–hexane (1 : 4)]. The reaction mixture was diluted with ethyl acetate, washed thoroughly with saturated sodium hydrogencarbonate, and dried. Evaporation of the solvent gave an oil, which was fractionated on a silica-gel column (30 g) with ethyl acetate–hexane (1 : 4) as an eluent.

The first fraction gave crystals, which were recrystallized

from ethanol to give 0.17 g (30%) of DL-1,2,3-tri-*O*-acetyl-(1/2,3,6)-6-bromo-4-bromomethyl-4-cyclohexene-1,2,3-triol (**9**) as prisms: mp 108.5—109 °C; ^{1}H NMR ($CDCl_3$) δ= 1.99 (3H, s), 2.08 (3H, s), and 2.13 (3H, s) (OAc), 3.87 (2H, s, C$\underline{H}_2$Br), 4.54 (1H, br dd, J=3 and 7.5 Hz, H-6), 5.02 (1H, dd, J=4 and 10.5 Hz, H-2), 5.63 (1H, dd, J= 7.5 and 10.5 Hz, H-1), 5.80 (1H, d, J=4 Hz, H-3), and 6.12 (1H, d, J=3 Hz, H-5).

Found: C, 36.18; H, 3.77; Br, 37.15%. Calcd for $C_{13}H_{16}Br_2O_6$: C, 36.48; H, 3.77; Br, 37.33%.

The second fraction gave 16 mg (3%) of DL-1,2,3-tri-*O*-acetyl-(1,6/2,3)-6-bromo-4-bromomethyl-4-cyclohexene-1,2,3-triol (**10**) as an oil: ^{1}H NMR ($CDCl_3$) δ=2.00 (3H, s), 2.08 (3H, s), and 2.12 (3H, s) (OAc), 3.84 (2H, s, C$\underline{H}_2$Br), 4.90—5.16 (2H, m, H-2 and H-6), 5.27—5.62 (1H, m, H-1), 5.86 (1H, d, J=4 Hz, H-3), and 6.15 (1H, d, J=4 Hz, H-5). Compound **10** was not stable enough to give satisfactory analytical data. The third fraction gave crystals, which were recrystallized from ethanol to give 26 mg (5%) of DL-1,2,3,4-tetra-*O*-acetyl-(1,2/3,4)-5-bromomethyl-5-cyclohexene-1,2,3-triol (**13**) as prisms: 120.5—121 °C; ^{1}H NMR ($CDCl_3$) δ=2.00 (3H, s), 2.02 (3H, s), 2.06 (3H, s), and 2.08 (3H, s) (OAc), 3.84 (2H, s, C$\underline{H}_2$Br), 5.20—5.50 (2H, m, H-2 and H-3), 5.63 (1H, br dd, J=2.5 and 5 Hz, H-1), 5.87 (1H, d, J=3 Hz, H-4), and 5.94 (1H, d, J=5 Hz, H-6).

Found: C, 43.98; H, 4.62; Br, 19.29%. Calcd for $C_{15}H_{19}BrO_8$: C, 44.25; H, 4.70; Br, 19.62%.

DL-*1,2,3,4-Tetra*-O-*acetyl-(1,2/3,4)-5-acetoxymethyl-5-cyclohexene-1,2,3,4-tetrol* (**14**). A mixture of **9** (0.30 g), silver acetate (0.13 g, 4 molar equiv.), and 90% aqueous acetic acid (10 ml) was stirred at room temperature for 20 h in the dark. The reaction mixture was filtered and the filtrate was concentrated to an oil, which was chromatographed on a silica-gel column (15 g) with 2-butanone-toluene (1 : 3) as an eluent. The main fraction gave 0.18 g (72%) of a mixture of 1,3,4- (**20a**) and 2,3,4-tri-*O*-acetyl-(1,2/3,4)-5-bromomethyl-5-cyclohexene-1,2,3,4-tetrol (**20b**) as an oil: ^{1}H NMR ($CDCl_3$) for **20a** δ=2.05 (3H, s), 2.06 (3H, s), 2.10 (3H, s), and 2.12 (3H, s) (OAc), 2.27—2.53 (1H, m, O$\underline{H}$), 3.81 (2H, s, C$\underline{H}_2$Br), 4.12 (1H, dd, J=4 and 9 Hz, H-2), 5.16—5.50 (2H, m, H-1 and H-3), 5.82 (1H, d, J=4 Hz, H-4), and 5.97 (1H, d, J=4 Hz, H-6). The signal due to the C-1 proton of **20b** appeared as a narrow multiplet at δ=4.43—4.54, of which intensity was estimated at *ca.* one third of that of **20a**.

Found: C, 42.39; H, 4.66; Br, 22.20%. Calcd for $C_{13}H_{17}BrO_7$: C, 42.76; H, 4.69; Br, 21.88%.

A 0.12 g portion of the mixture was treated with sodium acetate (30 mg) in 90% aqueous DMF (3 ml) for 8 h. The reaction mixture was diluted with ethyl acetate, washed with water, and dried. The residue was acetylated in the usual way and the product was purified by a short column of alumina with chloroform. The product was recrystallized from ethanol to give 63 mg (49%) of **14** as prisms: mp 118.5—119 °C; ^{1}H NMR ($CDCl_3$) δ=1.98 (3H, s), 2.00 (3H, s), and 2.06 (9H, s) (OAc), 4.45 (2H, br s, C$\underline{H}_2$-OAc), 5.36 (2H, m, H-2 and H-3), 5.55—5.80 (2H, m, H-1 and H-4), and 5.87 (1H, br d, J=5.5 Hz, H-6).

Found: C, 53.08; H, 5.80%. Calcd for $C_{17}H_{22}O_{10}$: C, 52.85; H, 5.74%.

DL-*1,2,3,4-Tetra*-O-*acetyl-(1,3,4/2)-5-acetoxymethyl-5-cyclohexene-1,2,3,4-tetrol* (**18**). A mixture of silver acetate (0.31 g, 4 molar equiv.) in acetic acid (6 ml) and acetic anhydride (6 ml) was refluxed for 2 h, and then **9** (0.20 g) was added to it, and the mixture was refluxed for 8 h. The reaction mixture was filtered and the filtrate was concentrated. The residue was chromatographed on a silica-gel column with ethyl acetate-hexane (1 : 1) as an eluent. The product was recrystallized from ethanol to give 79 mg (26%) of **18** as prisms: mp 93—94 °C; ^{1}H NMR ($CDCl_3$) δ=1.95 (3H, s), 2.00 (3H, s), 2.04 (6H, s), and 2.07 (3H, s) (OAc), 4.43 (2H, s, C$\underline{H}_2$OAc), 5.07 (1H, ddd, J=3.5, 8.5, and 12 Hz, H-2), 5.45 (1H, br d, J=8.5 Hz, H-1), 5.62 (1H, d, J=3.5 Hz, H-4), and 5.74 (1H, br s, H-6).

Found: C, 52.91; H, 5.72%. Calcd for $C_{17}H_{22}O_{10}$: C, 52.85; H, 5.74%.

DL-*1,2,3,4-Tetra*-O-*acetyl-(1,3,4/2)-5-bromomethyl-5-cyclohexene-1,2,3,4-tetrol* (**17**). A mixture of silver acetate (0.12 g, a molar equiv.), acetic acid (8 ml), and acetic anhydride (8 ml) was refluxed for 2 h, and then **9** (0.30 g) was added to it, and the mixture was refluxed for 2 h. The reaction mixture was processed as described in the preparation of **18**. The product was chromatographed on a silica-gel column with ethyl acetate-hexane (1 : 2) to give 0.14 g (48%) of **17** as an oil: ^{1}H NMR ($CDCl_3$) δ=1.97 (3H, s), 2.00 (3H, s), 2.04 (3H, s), and 2.10 (3H, s) (OAc), 3.83 (2H, s, C$\underline{H}_2$Br), 5.03 (1H, m, H-3), 5.42 (1H, d, J=7.5 Hz, H-2), 5.33—5.53 (1H, m, H-1), 5.79 (1H, d, J=3.5 Hz, H-4), and 5.83 (1H, br d, J=1.5 Hz, H-6).

Found: C, 44.42; H, 4.68; Br, 19.35%. Calcd for $C_{15}H_{19}BrO_8$: C, 44.25; H, 4.70; Br, 19.62%.

DL-*1,2,3-Tri*-O-*acetyl-(1,6/2,3)-6-azido-4-azidomethyl-4-cyclohexene-1,2,3-triol* (**11**). A mixture of **9** (0.30 g), sodium azide (0.18 g, 3 molar equiv.), and DMF (10 ml) was stirred at room temperature for 1 h. The reaction mixture was diluted with ethyl acetate, washed with water, and dried. Evaporation of the solvent gave an oil, which was purified by a silica-gel column (7 g) with ethyl acetate-hexane (1 : 2) to give crystals. Recrystallization from ethanol gave 0.17 g (67%) of **11** as needles: mp 80—81 °C; ^{1}H NMR ($CDCl_3$) δ=2.00 (3H, s), 2.07 (3H, s), and 2.12 (3H, s) (OAc), 2.75 (2H, s, C$\underline{H}_2N_3$), 4.30—4.55 (1H, br s, H-6), 5.33 (2H, br s, H-1 and H-2), 5.61 (1H, br s, H-3), and 5.86 (1H, br d, J=4.5 Hz, H-5).

Found: C, 44.15; H, 4.60; N, 23.55%. Calcd for $C_{13}H_{16}N_6O_6$: C, 44.32; H, 4.58; N, 23.85%.

DL-*1,2,3-Tri*-O-*acetyl-(1,6/2,3)-6-acetamido-4-acetamidomethyl-4-cyclohexene-1,2,3-triol* (**12**). Compound **11** (0.11 g) was dissolved in a mixture of pyridine (4 ml) and water (4 ml), and hydrogen sulfide was bubbled into it at room temperature for 1 h. Excess hydrogen sulfide was removed by a nitrogen stream and then the reaction mixture was concentrated. The residual product was acetylated in the usual way and the product was chromatographed on a silica-gel column (5 g). The column was eluted in turn with toluene and with ethanol-toluene (1 : 3). The product was recrystallized from acetone to give 95 mg (78%) of **12** as prisms: mp 224—225 °C; ^{1}H NMR (DMSO-d_6) δ=1.77 (6H, s), 1.88 (3H, s), 1.90 (3H, s), and 2.00 (3H, s) (NAc and OAc), 3.59 (2H, br d, J=5.5 Hz, C$\underline{H}_2$-NHAc), 4.68 (1H, br dt, J=4.5, 4.5, and 9 Hz, H-6), 4.95 (1H, dd, J=4.5 and 10.5 Hz, H-1), 5.22 (1H, dd, J=4 and 10.5 Hz, H-2), 5.36 (1H, d, J=4 Hz, H-3), 5.51 (1H, br d, J=4.5 Hz, H-5), and 7.80—8.00 (2H, m, N$\underline{H}$Ac).

Found: C, 52.51; H, 6.21; N, 7.19%. Calcd for $C_{17}H_{24}N_2O_8$: C, 53.12; H, 6.29; N, 7.29%.

DL-*1,2,3,4-Tetra*-O-*acetyl-(1,2/3,4)-5-azidomethyl-5-cyclohexene-1,2,3,4-tetrol* (**15**). A mixture of **20a** and **20b** (0.18 g) was treated with sodium azide (65 mg, 2 molar equiv.) in DMF (5 ml) at room temperature for 2.5 h. The reaction mixture was processed as described in the preparation of **11**. The product, after the conventional acetylation, was purified by

crystallization from ethanol to give 0.13 g (69%) of **15** as prisms: mp 109.5—110 °C; ^{1}H NMR ($CDCl_3$) δ=1.98 (3H, s), 2.00 (3H, s), 2.04 (3H, s), and 2.06 (3H, s) (OAc), 3.74 (2H, s, C$\underline{H}_2N_3$), 5.33 (2H, m, H-2 and H-3), 5.50—5.73 (2H, m, H-1 and H-4), and 5.86 (1H, br d, J=4.5 Hz, H-6).

Found: C, 48.99; H, 5.17; N, 11.56%. Calcd for $C_{15}H_{19}N_3O_8$: C, 48.78; H, 5.19; N, 11.38%.

DL-*1,2,3,4-Tetra*-O-*acetyl-(1,3,4/2)-5-azidomethyl-5-cyclohexene-1,2,3,4-tetrol* (**19**). Compound **17** (0.14 g) was treated with sodium azide (44 mg, 2 molar equiv.) in DMF (5 ml) at room temperature for 18 h. The reaction mixture was processed as described in the preparation of **11** to give 73 mg (59%) of **19** as an oil: ^{1}H NMR ($CDCl_3$) δ=1.98 (3H, s), 2.03 (3H, s), 2.09 (3H, s), and 2.14 (3H, s) (OAc), 3.79 (2H, s, C$\underline{H}_2N_3$), 5.11 (1H, m, H-3), 5.50 (1H, d, J=7 Hz, H-2), 5.35—5.60 (1H, m, H-1), 5.64 (1H, d, J=3.5 Hz, H-4), and 5.88 (1H, br s, H-6).

Found: C, 48.60; H, 5.26; N, 11.12%. Calcd for $C_{15}H_{19}N_3O_8$: C, 48.78; H, 5.19; N, 11.38%.

DL-*1,2,3,4-Tetra*-O-*acetyl-(1,2/3,4)-5-acetamidomethyl-5-cyclohexene-1,2,3,4-tetrol* (**16**). Compound **15** (61 mg) was reduced with hydrogen sulfide as described in the preparation of **12**. The product was acetylated in the usual way. Recrystallization of the crude crystals from ethanol gave 33 mg (52%) of **16** as prisms: mp 181—182 °C; ^{1}H NMR ($CDCl_3$) δ=1.99 (3H, s), 2.01 (6H, s), 2.06 (3H, s), and 2.09 (3H, s) (NAc and OAc), 3.85 (2H, d, J=6 Hz, C$\underline{H}_2$NHAc, changing to a singlet on deuteration), 5.37 (2H, m, H-2 and H-3), 5.51—5.81 (4H, m, H-1, H-4, H-6, and N$\underline{H}$).

Found: C, 53.12; H, 6.06; N, 3.46%. Calcd for $C_{17}H_{23}NO_9$: C, 52.98; H, 6.02; N, 3.64%.

DL-*1,2,3-Tri*-O-*acetyl-(1,6/2,3)-* (**22a**) *and -(1/2,3,6)-4-acetoxymethyl-6-azido-4-cyclohexene-1,2,3-triol* (**22b**). A mixture of **9** (0.20 g), sodium acetate (38 mg, a molar equiv.), and DMF (5 ml) was stirred at room temperature for 38 h. TLC indicated the disappearance of **9** (R_f 0.48) and the formation of one major component [R_f 0.33, ethyl acetate-hexane (1 : 2)]. The reaction mixture was diluted with ethyl acetate and washed with water and dried. Evaporation of the solvent gave an oil, which was chromatographed on a silica-gel column with ethyl acetate-hexane (1 : 2) to give 0.13 g (67%) of a mixture of the 6-bromo compounds (**21a** and **21b**) as an unstable oil. Without further purification, these compounds were used in the next step.

A 0.13 g portion of the mixture was treated with sodium azide (41 mg, 2 molar equiv.) in DMF (5 ml) at room temperature for 19 h. The reaction mixture was processed as described above and the product was purified by use of a silica-gel column with ethyl acetate-hexane (1 : 2) to give 85 mg (74%) of a mixture of the azides (**22a** and **22b**) as a pale yellow oil: ^{1}H NMR ($CDCl_3$) δ=1.98, 1.99, 2.01, 2.02, 2.03, and 2.07 (12H, six s, OAc), 3.90—4.50 (1H, m, H-6), 4.44 (2H, s, C$\underline{H}_2$OAc), 4.98 (0.5H, dd, J=3.5 and 11 Hz, H-2 of **22a**), 5.27—5.48 (1.5 H, m, H-1 and H-2), 5.56—5.71 (1H, m, H-3), and 5.73—5.90 (1H, m, H-5).

Found: C, 48.75; H, 5.27; N, 11.36%. Calcd for $C_{15}H_{19}N_3O_8$: C, 48.78; H, 5.19; N, 11.38%.

The authors wish to express their thanks to Mr. Saburo Nakada for elemental analyses.

References

1) The preceding paper of this series: S. Ogawa, T. Nakamura, N. Chida, and T. Suami, *Bull. Chem. Soc. Jpn.*, **56**, 1563 (1983). The nomenclature is based on the IUPAC-IUB Tentative Cyclitol Nomenclature Rule [*J. Biol. Chem.*, **243**, 5809 (1968)]. For convenience, the formulas of racemic compounds depict only one of the respective enantiomers.

2) S. Ogawa, T. Toyokuni, and T. Suami, *Chem. Lett.*, **1980**, 713.

3) S. Ogawa, K. Nakamoto, M. Takahara, Y. Tanno, N. Chida, and T. Suami, *Bull. Chem. Soc. Jpn.*, **52**, 1174 (1979).

4) T. Toyokuni, Y. Abe, S. Ogawa, and T. Suami, *Bull. Chem. Soc. Jpn.*, **56**, 505 (1983).

5) T. Toyokuni, S. Ogawa, and T. Suami, *Bull. Chem. Soc. Jpn.*, **56**, 1161 (1983).

6) In addition, small amount of an isomeric (hydroxymethyl)cyclohexanetetrol pentaacetate and a β-elimanation product were isolated. Their structures were tentatively deduced on the basis of the ^{1}H NMR spectra, but further characterization were not carried out.

7) S. Ogawa, M. Ara, T. Kondoh, M. Saitoh, R. Masuda, T. Toyokuni, and T. Suami, *Bull. Chem. Soc. Jpn.*, **53**, 1121 (1980).

8) S. Ogawa, T. Toyokuni, M. Omata, N. Chida, and T. Suami, *Bull. Chem. Soc. Jpn.*, **53**, 455 (1980).

9) The configuration of **9** is considered to correspond with that of conduritol F, the C-6 proton being located in pseudoaxial orientation ($J_{5,6}$=1.9 Hz). While, in **10**, out of two possible half-chair conformation, the one in which two acetoxyl groups at C-1 and C-2 oriented in diequatorial positions seems to be favorable, the observed $J_{5,6}$ (4 Hz) being in accord with the calculated value (5.3 Hz): R. J. Abraham, H. Gottschalck, H. Paulsen, and W. A. Thomas, *J. Chem. Soc.*, **1965**, 6268.

10) S. Ogawa, T. Toyokuni, and T. Suami, *Chem. Lett.*, **1981**, 947.

11) S. Ogawa, Y. Iwasawa, T. Toyokuni, and T. Suami, *Chem. Lett.*, **1982**, 1729; **1983**, 337; N. Sakairi and H. Kuzuhara, *Tetrahedron Lett.*, **23**, 5327 (1982).

 © 1983 The Chemical Society of Japan Bull. Chem. Soc. Jpn., 56, 2082—2085 (1983)

Restricted Rotation Involving the Tetrahedral Carbon. IL. Singly *peri*-Substituted 9-Isopropyltriptycenes Revisited[1)]

Gaku YAMAMOTO and Michinori ŌKI*

Department of Chemitsry, Faculty of Science, The University of Tokyo, Hongo, Bunkyo-ku, Tokyo 113

(Received March 16, 1983)

9-Isopropyltriptycene derivatives carrying a fluoro, chloro, bromo, or *t*-butyl substituent in a *peri*-position were synthesized and their dynamic NMR behavior was studied to see the dependence of the barrier to rotation of the bridgehead substituent upon the bulkiness of the *peri*-substituent. The data obtained in this work together with those reported earlier disclose that, among the derivatives in which the *peri*-substituent is not buttressed by the 2-substituent, the *peri*-methoxy compound has the highest barrier and the barrier decreases as the bulkiness of the *peri*-substituent increases. 1,2,3,4-Tetrachloro and tetrabromo derivatives show the slightly positive buttressing effect.

In 1974, we reported the rotational barriers in a *peri*-unsubstituted 9-isopropyltriptycene (**1**) and several singly *peri*-substituted derivatives (**2**—**5**).[2)] The data are included in Table 2 and Fig. 1. One of the interesting features is that the barrier heights have no apparent correlation with the bulkiness of the *peri*-substituent as judged from the van der Waals radii of the groups. The low barrier of **3** was ascribed to the gearing of the *peri*-methyl group[2)] but the explanation was criticized that the results could be interpreted on the basis of the buttressing effect.[4)]

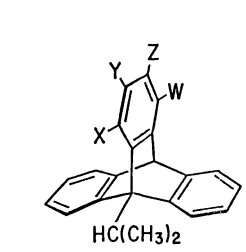

	X	Y	Z	W
1	H	CH_3	H	CH_3
2	OCH_3	H	H	OCH_3
3	CH_3	H	H	CH_3
4	Cl	Cl	Cl	Cl
5	Br	Br	Br	Br
6	F	H	H	H
7	Cl	H	H	H
8	Br	H	H	H
9	t-Bu	H	t-Bu	H
10	H	t-Bu	H	t-Bu

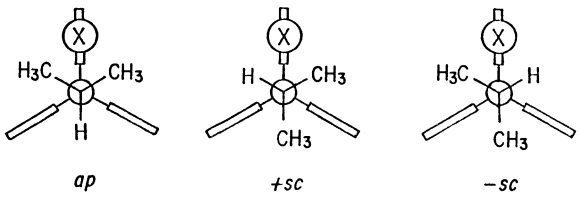

In view of the intriguing dependence of the rotational barriers in singly *peri*-substituted 9-(1,1-dimethyl-2-phenylethyl)triptycenes upon the *peri*-substituents, in which the *peri*-fluoro derivative has the highest barrier in the series,[5,6)] a reexamination of the rotational barriers in 9-*s*-alkyltriptycenes will be of value. 9-Isopropyltriptycenes exhibited a plateau in the diagram of the rotational barrier *vs.* the bulkiness of the *peri*-substituent.[2)] Other 9-*s*-alkyltriptycenes hitherto studied appear to give the maximal barriers in the 1,2,3,4-tetrachloro or tetrabromo derivatives.[7)] However it is desirable to erase the buttressing effect if we wish to discuss the relationship between the rotational barrier and the bulkiness of the *peri*-substituent in any detail. Such a work will also constitute a partial answer to the criticism for neglecting the buttressing effect.[4)] We therefore prepared 1-halo-9-isopropyltriptycenes (**6**—**8**) and determined the barriers to rotation in these compounds to compare with those in the tetrahalo counterparts **4** and **5**. In order to see the effect of an extremely bulky *peri*-substituent, the 1-*t*-butyl derivative (**9**) was also prepared.

Results and Discussion

1-Halo-9-isopropyltriptycenes (**6**—**8**) were synthesized by reactions of benzyne with 1-halo-9-isopropylanthracenes (**12**: X=F, Cl, and Br), which were prepared by Grignard reactions of isopropylmagnesium bromide with 1-haloanthrones (**11**) followed by dehydration. The reaction of 3,5-di-*t*-butylbenzyne[8)] with **12** (X=H) afforded two isomeric 9,10-adducts, **9** and **10**, in a ratio of *ca.* 1:2, which were separated by liquid chromatography.

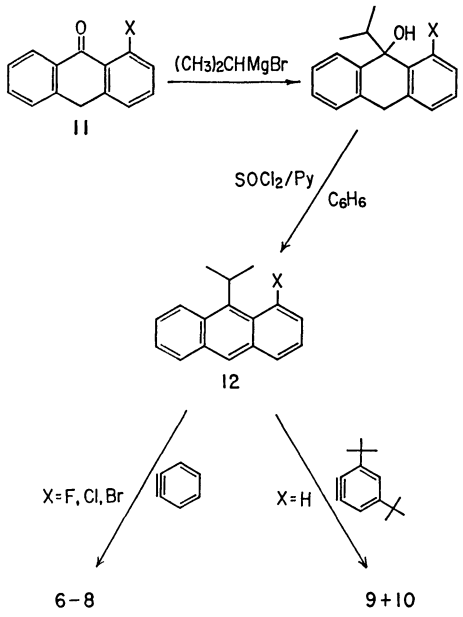

NMR Spectra and Rotamer Distributions. ^1H NMR spectral data of compounds **6**—**10** taken in chloroform-*d* at *ca.* 35 °C are given in Table 1. Rotation about the bridgehead-to-substituent bond in these compounds is sufficiently slow on the NMR time scale under these conditions to observe the signals due to the diastereotopic methyl groups separately.

Compound **6** carrying a fluoro substituent in a *peri*-position is shown by NMR spectroscopy to exist in

Table 1. ^{1}H NMR data in $CDCl_3$ at *ca.* 35 °C[a)]

Compound	Rotamer	$(C\underline{H}_3)_2CH$	$(CH_3)_2C\underline{H}$	10-H	$(C\underline{H}_3)_3C$
6	$\pm sc$	1.80 dd (6.8, *0.9*) 1.85 dd (6.7, *5.8*)	3.82 d sep (6.8, *2.0*)	5.26 d (*1.6*)	
	ap	1.81 dd (6.7, *5.8*)	3.58 d sep (6.7, *2.0*)	5.28[b)]	
7	$\pm sc$	1.76 d (6.7) 1.92 d (6.8)	4.29 sep (6.8)	5.20	
8	$\pm sc$	1.76 d (6.8) 1.93 d (7.0)	4.43 sep (6.9)	5.19	
9	$\pm sc$	1.73 d (7.1) 1.78 d (6.8)	4.26 sep (7.0)	5.10	1.22, 1.35
10	$\pm sc$	1.88 d (6.8) 1.90 d (6.8)	3.60 sep (6.8)	6.08	1.24, 1.53
	ap	1.90 d (6.8)	3.62 sep (6.8)	6.06	1.27, 1.61

a) Chemical shifts are given in δ. Signals are singlets unless otherwise noted; d: doublet, dd: double doublet, sep: septet, d sep: double septet. In parentheses are coupling constants in Hz. Those in italics are couplings with ^{19}F. b) Presumably a doublet. Obscured by overlap with the signal due to $\pm sc$.

two rotameric states, *ap* and $\pm sc$. ^{19}F NMR spectrum of **6** exhibits a small peak at 58.9 ppm downfield from internal hexafluorobenzene together with a large peak at 49.7 ppm with an intensity ratio of 1:9. The ^{1}H NMR spectrum of **6** is complex not only because of the existence of two rotamers but also due to the presence of long-range ^{1}H-^{19}F spin-spin couplings. The methyl protons of the isopropyl group of the major rotamer appear as two sets of double doublets suggesting the diastereotopicity of the two methyl groups, while those of the minor rotamer as a double doublet reflecting the enantiotopicity of the methyl groups. These features clearly show that the major isomer is the $\pm sc$ rotamer and the minor *ap*. The existence of the *ap* rotamer in **6** should be a reflection of the small bulkiness of the *peri*-fluoro group, because the *ap* rotamer is not detected if the *peri*-substituent is bulkier than fluorine: Methyl protons of the isopropyl group in compounds **7**—**9** appear as a pair of equally intense doublets, indicating that these compounds reside solely in the $\pm sc$ rotamer.

Compound **10** lacking a *peri*-substituent shows two singlets with an intensity ratio of 2.1:1 for each of the *t*-butyl groups indicating the existence of the $\pm sc$ and *ap* rotamers in almost a statistical ratio. The slight preference for the $\pm sc$ rotamer may be due to the larger effective bulkiness of the 1-hydrogen than the other *peri*-hydrogens because of the buttressing effect of the 2-*t*-butyl group.

Dynamic NMR Studies. The double doublet signal for the isopropyl methyl groups of compounds **7**—**9** broadened and coalesced into a doublet upon raising the temperature. Rate constants (k_c) for the $+sc \rightleftharpoons -sc$ interconversion at the coalescence temperatures (T_c) were obtained graphically according to Jaeschke *et al.*,[9)] regarding the signal as two overlapping sets of mutually coalescing singlets. The coalescence phenomenon of the *t*-butyl signals in compound **10** gave the rate constants for the $ap \rightleftharpoons \pm sc$ interconversion at two temperatures. The kinetic data obtained are compiled in Table 2 together with those obtained before, some of which are recalculated to express in terms of the free energies of activation at the coalescence temperatures.

As for the methyl signals in **6**, three overlapping sets of double doublets coalesce into a double doublet on elevation of the temperature by two processes of $+sc \rightleftharpoons -sc$ and $ap \rightleftharpoons \pm sc$. The change should therefore be analyzed as a three-site exchange problem of an eight-spin system ($A_3B_3MX \rightleftharpoons B_3A_3MX \rightleftharpoons C_6KY$). Such an analysis was beyond the capacity of the computer simulation program available[10)] and was abandoned. Neglecting the presence of a small amount of the *ap* rotamer and simulating the spectra as a mutually exchanging four spin system (ABMX$\rightleftharpoons$BAMX) gave a rough estimate of the barrier to the $+sc \rightleftharpoons -sc$ interconversion as 22—23 kcal mol^{-1} (1 cal=4.184 J) at the temperature range of 110—150 °C.

The dependence of the barrier in **1**—**10** on the bulkiness of the *peri*-substituent as represented by the van der Waals radii is shown in Fig. 1. Although the data for **1** were obtained by observing the $ap \rightleftharpoons \pm sc$ process, the barrier height should not differ significantly from that for the $+sc \rightleftharpoons -sc$ process, because the two processes should have the identical barrier height in the absence of the buttressing effect by the 2-substituent; the buttressing effect of the 2-methyl group is negligible. Points for the unbuttressed compounds form a flat curve with a maximum at the *peri*-methoxy compound (**2**) and those for the tetrahalo compounds (**4** and **5**) deviate upward from the curve manifesting the positive buttressing effect.

Appearance of a maximum at a rather small *peri*-substituent is a similar trend as was found in 9-(1,1-dimethyl-2-phenylethyl)triptycene derivatives,[5)] although the variation of the barrier heights is far smaller. It can therefore be inferred that the lowering of the barrier height with a bulky *peri*-substituent is not a special phenomenon exhibited only by 9-*t*-alkyl derivatives but is also observable in 9-*s*-alkyltriptycenes.

As discussed in some detail in the previous paper,[5)]

TABLE 2. DYNAMIC NMR DATA[a)]

Compound	van der Waals radius of X[b)]/Å	T_c / °C	$\Delta\nu_c$ / Hz	k_c / s^{-1}	ΔG_c^{*} [c)] / kcal mol^{-1}	Solvent[d)]
1	1.20	100			20.6[e)]	TCE
10[f)]		99	2.3	2.1	21.4	TCE
		106	4.4	4.4	21.3	
2	1.52	140			23.2[e)]	HCB
7	1.75	158	10.6	23	22.9	HCB
3		164			23.3[e)]	HCB
8	1.85	153	11.0	23	22.6	HCB
4[g)]		175	9.4	19	24.0	HCB
5	1.97[h)]	128			22.0[e)]	HCB
9	2.79[h)]	89	1.6	2.2	20.8	TCE

a) Data for **1** and **10** refer to the $ap \rightarrow \pm sc$ process, and those for the others to the $+sc \rightleftarrows -sc$ process. b) According to Charton: M. Charton, *J. Am. Chem. Soc.*, **91**, 615 (1969). c) Reliable to ± 0.1 kcal mol^{-1}, which comes from the uncertainty of ± 2 °C for determination of T_c. d) TCE: Tetrachloroethylene. HCB: Hexachloro-1,3-butadiene. e) Calculated using ΔH^{*} and ΔS^{*} values reported in Ref. 2. f) Values in the upper row are obtained from the higher field pair of the *t*-butyl signals due presumably to the one at 2-position. g) Re-evaluated. *cf.* Ref. 7a. h) $(r_{v,min}+r_{v,max})/2$.

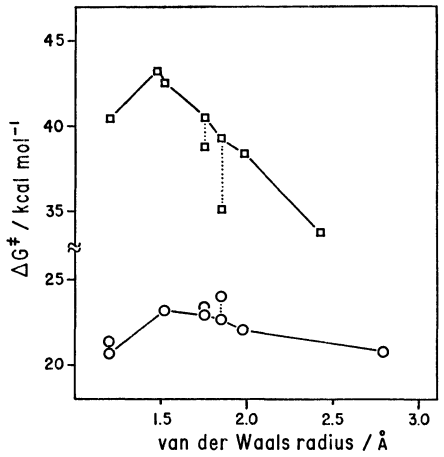

Fig. 1. Dependence of the rotational barriers on the bulkiness of the *peri*-substituent. ○: ΔG_c^{*} for 1-substituted 9-isopropyltriptycenes. □: ΔG_{500}^{*} for 1-substituted 9-(1,1-dimethyl-2-phenylethyl)triptycenes. Points for the unbuttressed compounds are connected by a solid line. Points deviated from the lines are those for the buttressed derivatives.

the phenomenon seems to be partly explained in terms of the molecular deformation in highly congested systems which causes the lesser stabilization of the transition state for rotation than the ground state upon introduction of a bulky *peri*-substituent. Because the congestion in the 9-*s*-alkyl series is considerably smaller than that in the 9-*t*-alkyl one, even such a bulky *peri*-substituent as a *t*-butyl group destabilizes the ground and the transition states rather similarly, resulting in only a small decrease in the barrier.

The small positive buttressing effect found in **4** and **5** is in sharp contrast with the large negative effect found in 1,2,3,4-tetrachloro- and tetrabromo-9-(1,1-dimethyl-2-phenylethyl)triptycenes.[6)] In the less congested system, the transition state may be destabilized to a greater extent than the ground state upon introduction of the buttressing substituent reflecting the increased rigidity of the 1-halogen substituent.

The barrier to the $ap \rightleftarrows \pm sc$ process in the 2,4-di-*t*-butyl derivative (**10**) is somewhat higher than that in the 2,4-dimethyl one (**1**). This may be ascribed to the positive buttressing effect on the 1-hydrogen exerted by the 2-*t*-butyl group. The $+sc \rightleftarrows -sc$ barrier in **10** may be slightly lower than the $ap \rightleftarrows \pm sc$ barrier because the 1-hydrogen eclipses the methyl group in the latter process while it eclipses the methine hydrogen in the former.

We have made it clear through our investigation on the dependence of the rotational barrier of the 9-substituent of triptycene systems upon the *peri*-substitution that the barrier height does not always increase with the bulkiness of the *peri*-substituent and shows a rather complex behavior. This comes from the fact that *peri*-substituents affect not only the transition state for rotation but also the ground state in congested sp^3–sp^3 systems. This is quite different from the cases in sp^2–sp^2 systems in which substituents close to the rotating bond does not significantly affect the ground state energy of the system and even a quantitative correlation between the barrier heights and the bulkiness of the substituents can be made.[11)]

From the data presented above, the low barrier to rotation in the 1,4-dimethyl compound (**3**) can be attributed to the raise of the ground state energy, although the possibility of gearing is not completely erased.

Experimental

Melting points are not corrected. The routine ^1H and ^{19}F NMR spectra were recorded on a Varian EM-390 spectrometer at 90.0 and 84.67 MHz, respectively, at *ca.* 35 °C. ^{19}F chemical shifts are shown in ppm downfield from internal hexafluorobenzene. Variable temperature ^1H NMR spectra were obtained on a Hitachi R-20B spectrometer operating at 60.0 MHz. Temperatures were calibrated by using an ethylene glycol sample.[12)] High performance liquid chromatography was carried out on a Waters M6000A system using a Microporasil semipreparative column with

hexane as an eluent.

*1-Bromoanthrone (**11**: X=Br).* To a magnetically stirred solution of 2.87 g (10.0 mmol) of 1-bromoanthraquinone in 50 mL of concentrated sulfuric acid was added portionwise 1.0 g of aluminium powder. The mixture was stirred at room temperature for 20 h and poured onto ice. The solid formed was collected by filtration, washed with water and dried in air. Recrystallization from benzene-hexane gave 1.71 g (63%) of **11** (X=Br) as yellow crystals, mp 129—130 °C. Found: C, 61.35; H, 3.18; Br, 29.72%. Calcd for $C_{14}H_9BrO$: C, 61.56; H, 3.32; Br, 29.26%. ^{1}H NMR ($CDCl_3$, δ): 4.31 (2H, s), 7.2—7.7 (6H, m), 8.24 (1H, s).

*General Procedure for Preparation of 1-Halo-9-isopropylanthracenes (**12**).* To an ethereal solution of the Grignard reagent prepared from 1.0 g (8.1 mmol) of isopropyl bromide was added portionwise 3.0 mmol of 1-haloanthrone. The mixture was stirred under reflux for 1 h and decomposed with aqueous ammonium chloride to afford 1-halo-9,10-dihydro-9-isopropyl-9-anthrol. The alcohol was, without further purification, heated with 1.5 mL of thionyl chloride and 3 mL of pyridine in 50 mL of benzene for 15 min. The reaction mixture was washed with water and dried over magnesium sulfate. Column chromatography on alumina with hexane as an eluent gave the desired anthracene as a yellow oil, which was used in the subsequent reaction.

*1-Fluoro-9-isopropylanthracene (**12**: X=F)* was obtained from 1-fluoroanthrone[5] in 38% yield by way of 1-fluoro-9,10-dihydro-9-isopropyl-9-anthrol [^{1}H NMR ($CDCl_3$, δ): 0.65 (3H, dd, J=6.8 and 0.6 Hz), 0.92 (3H, dd, J=6.8 and 1.2 Hz), 2.14 (1H, m), 3.21 (1H, br s), 3.90 (2H, s), 6.7—8.1 7H, m)]. ^{1}H NMR ($CDCl_3$, δ): 1.67 (6H, dd, J=7.3 and 2.4 Hz), 4.71 (1H, d sept, J=7.3 and 5.0 Hz), 6.8—8.7 (8H, m).

*1-Chloro-9-isopropylanthracene (**12**: X=Cl)* was obtained from 1-chloroanthrone[13] in 33% yield by way of 1-chloro-9,10-dihydro-9-isopropyl-9-anthrol [^{1}H NMR ($CDCl_3$, δ): 0.54 (2H, d, J=6.7 Hz), 1.03 (3H, d, J=6.9 Hz), 2.50 (1H, sept, J=6.8 Hz), 3.73 (1H, br s), 3.95 (2H, s), 6.8—8.0 (7H, m)]. ^{1}H NMR ($CDCl_3$, δ): 1.70 (6H, d, J=7.0 Hz), 5.07 (1H, sept, J=7.0 Hz), 7.0—8.0 (6H, m), 8.17 (1H, s), 8.4—8.6 (1H, m).

*1-Bromo-9-isopropylanthracene (**12**: X=Br)* was obtained from 1-bromoanthrone in 35% yield by way of 1-bromo-9,10-dihydro-9-isopropyl-9-anthrol [^{1}H NMR ($CDCl_3$, δ): 0.49 (3H, d, J=7.0 Hz), 1.01 (3H, d, J=7.0 Hz), 2.54 (1H, sept, J=7.0 Hz), 3.10 (1H, br s), 3.83 and 4.00 (2H, AB-q, J=19.5 Hz), 6.8—8.3 (7H, m)]. ^{1}H NMR ($CDCl_3$, δ): 1.70 (6H, d, J=7.2 Hz), 5.13 (1H, sept, J=7.2 Hz), 6.9—8.0 (6H, m), 8.15 (1H, s), 8.4—8.6 (1H, m).

*General Procedure for Preparation of 1-Halo-9-isopropyltriptycenes (**6**—**8**).* To a boiling solution of 3.0 mmol of 1-halo-9-isopropylanthracene (**12**) and 1.5 mL of isopentyl nitrite in 30 mL of 1,2-dimethoxyethane (DME) was added a solution of 1.0 g (7.3 mmol) of anthranilic acid in 15 mL of DME during the course of 1 h and the mixture was heated under reflux for 1 h. Column chromatography on alumina with hexane as an eluent followed by recrystallization from tetrahydrofuran-hexane gave the desired triptycene as colorless crystals.

*1-Fluoro-9-isopropyltriptycene (**6**)* was obtained from **12** (X=F) in 74% yield, mp 202—203 °C. Found: C, 87.89; H, 5.80%. Calcd for $C_{23}H_{19}F$: C, 87.87; H, 6.09%. ^{19}F NMR ($CDCl_3$): 49.65 (m, $\pm sc$), 58.86 (m, *ap*).

*1-Chloro-9-isopropyltriptycene (**7**)* was obtained from **12** (X=Cl) in 32% yield, mp 178—180 °C. Found: C, 83.33; H, 5.49; Cl, 10.83%. Calcd for $C_{23}H_{19}Cl$:C, 83.50; H, 5.79; Cl, 10.71%.

*1-Bromo-9-isopropyltriptycene (**8**)* was obtained from **12** (X=Br) in 60% yield, mp 211—213 °C. Found: C, 73.87; H, 5.25; Br, 21.17%. Calcd for $C_{23}H_{19}Br$: C, 73.60; H, 5.10; Br, 21.30%.

*1,3-Di-t-butyl-9-isopropyltriptycene (**9**) and 2,4-Di-t-butyl-9-isopropyltriptycene (**10**).* To a boiling solution of 683 mg (3.1 mmol) of 9-isopropylanthracene (**12**: X=H)[14] and 1 mL of isopentyl nitrite in 20 mL of DME was added dropwise a solution of 1.10 g (4.4 mmol) of 3,5-di-*t*-butylanthranilic acid[8] in 20 mL of DME during the course of 1.5 h and the mixture was heated under reflux for 1 h. ^{1}H NMR spectrum of the crude reaction mixture indicated the presence of **9** and **10** in a ratio of *ca.* 1:2. Separation of the isomers was affected by liquid chromatography. The 2,4-di-*t*-butyl derivative (**10**) eluted faster than the other isomer and was recrystallized from tetrahydrofuran-ethanol, mp 170—172 °C. Found: C, 90.95, H, 8.94%. Calcd for $C_{31}H_{36}$: C, 91.12; H, 8.88%. The 1,3-di-*t*-butyl derivative (**9**) was recrystallized from dichloromethane-hexane, mp 202—204 °C. Found: 91.34; H, 9.04%. Calcd for $C_{31}H_{36}$: C, 91.12; H, 8.88%.

References

1) Part XLVIII: F. Kakizaki, N. Nakamura, and M. Ōki, *Chem. Lett.*, **1983**, 81.

2) F. Suzuki, M. Ōki, and H. Nakanishi, *Bull. Chem. Soc. Jpn.*, **47**, 3114 (1974).

3) The free energy of activation at the coalescence temperature is used in the present discussion as the parameter for the energy barrier.

4) W. D. Hounshell, L. D. Iroff, D. J. Iverson, R. J. Wroczynski, and K. Mislow, *Isr. J. Chem.*, **20**, 65 (1980).

5) G. Yamamoto, M. Suzuki, and M. Ōki, *Bull. Chem. Soc. Jpn.*, **56**, 306 (1983).

6) G. Yamamoto, M. Suzuki, and M. Ōki, *Bull. Chem. Soc. Jpn.*, **56**, 809 (1983).

7) a) M. Suzuki, G. Yamamoto, H. Kikuchi, and M. Ōki, *Bull. Chem. Soc. Jpn.*, **54**, 2383 (1981); b) H. Kikuchi, S. Hatakeyama, G. Yamamoto, and M. Ōki, *ibid.*, **54**, 3832 (1981).

8) R. W. Franck and E. G. Leser, *J. Org. Chem.*, **35**, 3932 (1970).

9) A. Jaeschke, G. Munsch, H. G. Schmid, H. Friebolin, and A. Mannschreck, *J. Mol. Spectrosc.*, **31**, 14 (1969).

10) A modified version of the DNMR-3 program by Binsch: G. Binsch, *Top. Stereochem.*, **3**, 97 (1968).

11) G. Bott, L. D. Field, and S. Sternhell, *J. Am. Chem. Soc.*, **102**, 5618 (1980). See also H. Förster and F. Vögtle, *Angew. Chem., Int. Ed. Engl.*, **16**, 429 (1977).

12) A. L. Van Geet, *Anal. Chem.*, **40**, 2227 (1968).

13) E. de B. Barnett and M. A. Matthews, *J. Chem. Soc.*, **123**, 2549 (1923).

14) E. de B. Barnett and M. A. Matthews, *Ber.*, **59**, 1429 (1926).

The Adsorption of Chloromethanes on KCl. The Role of the Surface Ions as Adsorption Sites

Masatoshi Chikazawa, Masatoshi Amada, and Takafumi Kanazawa*

Department of Industrial Chemistry, Faculty of Technology, Tokyo Metropolitan University, Fukasawa, Setagaya-ku, Tokyo 158

(Received September 6, 1982)

The adsorbed amounts of chloro-substituted methanes, such as CH_2Cl_2, $CHCl_3$, and CCl_4, for KCl particles were measured by a volumetric method at various temperatures, and the isosteric heats of adsorption and differential entropies of the adsorbed molecules were estimated from the adsorption isotherms. The order of magnitude of the heats of adsorption at a coverage of $\theta=0.5$ was found to be $CH_2Cl_2>CHCl_3>CCl_4$. Moreover, a plot of the dipole moments of the three adsorbates *vs.* the adsorption heat values gave a straight line. Therefore, the differences among the adsorption heats of the three adsorbates is mainly caused by an orientation of their dissimilar dipoles to the surface. It may be concluded that the chloro-substituted methanes are adsorbed on surface anions of KCl powder.

Alkali halide crystals are used as adsorbents to investigate various adsorption phenomena, because of their simple surface structure and a regular configuration of the surface ions. Many theoretical calculations have been carried out about the heats of adsorption of nonpolar gasses on alkali halides.[1-3] On the other hand, in cases of polar substances, such heat calculations have been made for only a few systems,[4] and the subjects concerning adsorption sites, *i.e.* the role of surface ions in their adsorptions has not yet been resolved.

In the present study, the adsorbed amounts of chloro-substituted methanes, such as $CHCl_3$, CH_2Cl_2, and CCl_4, on KCl particles were measured at various temperatures, and the isosteric heats of adsorption and the differential entropies of the adsorbed molecules were calculated from the adsorption isotherms obtained. The adsorption characteristics of chloro-substituted methanes are discussed in relation to the dipole moments and the cross-sectional areas of the polar adsorbates.

Experimental

Materials. Potassium chloride was purified by twice recrystallization of special-grade reagents using distilled water. An aqueous solution of KCl was added to about a five-fold volume of ethanol cooled to −80—−90 °C with stirring. The sample thus obtained was filtered and washed four times with absolute ethanol and then dried at a reduced pressure of 1.33×10^{-1} Pa. This precipitate was found to be very small cubic crystals (≈5 μm) by electron microscopy. The sample was evacuated with an oil diffusion pump under a reduced pressure of 1.33×10^{-4} Pa for 20—30 h at room temperature prior to the adsorption measurements. The three adsorbates were purified by twice distillation of the respective special-grade reagents, and their purities were confirmed to be apporoxymatly 100% by gas chromatography.

Adsorption Measurement. The apparatus for measuring adsorbed amounts was reported previously by the present authors.[5] The equilibrium pressures of the adsorbates were determined using a mercury manometer and a reading magnifier with a resolution of 10 μm.

Surface Area Measurement. The specific surface areas of the samples were determined prior to the adsorption measurements of the chloro-substituted methanes by applying the BET equation to the nitrogen-adsorption data obtained at 77 K, assuming the cross-sectional area of a nitrogen molecule to be 16.2 Å^2. The obtained values were about 0.21 m^2/g.

Results and Discussion

Adsorption Isotherms. The adsorption isotherms of CH_2Cl_2 on KCl are given in Fig. 1. In this case, a linear BET plot was not obtained in the BET region. On the other hand, the adsorption isotherms at adsorbed amounts above 0.13 cm^3 STP/m^2 gave a straight line with increasing pressure, and the point "B" showing a monolayer completion was determined easily. The capacity of the monolayer adsorption was estimated to be 0.13 cm^3 STP/m^2. This value is slightly smaller than the monolayer capacity (0.15 cm^3 STP/m^2) which is calculated from the cross-sectional area (24.3 Å^2) of CH_2Cl_2 and the surface area obtained by N_2 adsorption, assuming that the sample surface is covered with the close-packed monolayer. The cross-sectional area is estimated from the liquid density of CH_2Cl_2 at the measurement temperature. The relative vapor pressure at the point B was higher, compared with the values determined from the adsorptions of polar substances such as CH_3OH,[6] $(CH_3)_2CO$,[7] and H_2O.[8]

The isosteric heats of CH_2Cl_2 adsorption and the differential entropies of the adsorbed molecules are shown in Fig. 2. The latter values are calculated by Eq. 1, where $\overline{S_s}$, S, and S_g are the differential entropy of the adsorbed molecule on KCl, molar entropies

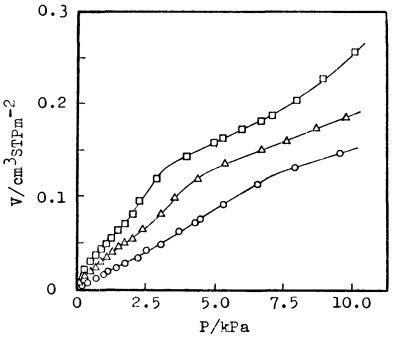

Fig. 1. Adsorption isotherms of CH_2Cl_2 on KCl. Temperature/°C: □: −6, △: 0, ○: 10,

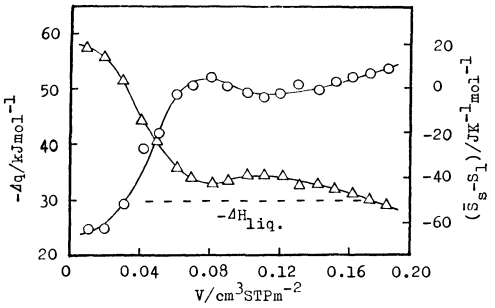

Fig. 2. Isosteric heat of CH_2Cl_2 adsorption and differential entropy of CH_2Cl_2 adsorbed on KCl.
△: Isosteric heat of adsorption, ○: differential entropy.

of liquid adsorbate and vapor molecule, respectively, A is the heat of vaporization and x a relative vapor pressure.

$$(\bar{S}_s - S_l) = (\bar{S}_s - S_g) + A/T - R \ln x \quad (1)$$

The adsorption heat at low coverage was found to be large, but it decreased rapidly with adsorbed amounts. A peak was observed at $V=0.12$ cm³ STP/m². This value is nearly equal to the monolayer capacity described above. Therefore, the appearance of such a peak can be explained in terms of a lateral interaction among the adsorbed molecules. A slightly stepwise rise recognized in the isotherm before the monolayer completion may be also due to this lateral interaction.

On the other hand, the differential entropies obtained in the region of the adsorbed amount 0—0.06$_5$ cm³ STP/m² were smaller than the molar entropy of liquid CH_2Cl_2 at the measurement temperature, and at the adsorbed amounts above 0.06$_5$ cm³ STP/m² the entropy values were approximately equal to the molar entropy of liquid CH_2Cl_2. The former result shows that CH_2Cl_2 molecules are adsorbed strongly on the KCl surface and the mobility of the adsorbed molecules are restrained. Whereas, the latter fact indicates that the adsorbed molecules can move easily in the adsorbed layer as in liquid CH_2Cl_2. Figure 2 indicates a minimum at the monolayer completion in the entropy curve. Such change in the differential entropy corresponds to the existence of the lateral interaction described above.

Figure 3 shows the adsorption isotherms of $CHCl_3$ on KCl. The isosteric heat of $CHCl_3$ adsorption and the differential entropies of the adsorbed molecules are given in Fig. 4. The isotherms resembled in shape those obtained for the CH_2Cl_2 adsorption. A maximum was also recognized in the heat curve at about the monolayer completion ($V=0.11$ cm³ STP/m²). Therefore, it is considered that a lateral interaction will occur similarly as is shown in the case of CH_2Cl_2 adsorption. The differential entropies of adsorbed $CHCl_3$ at low coverage are larger than the molar entropy of liquid $CHCl_3$. This result is different from the case of CH_2Cl_2 adsorption.

The adsorption isotherms of CCl_4 on KCl are given

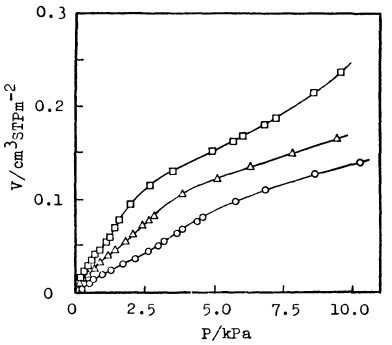

Fig. 3. Adsorption isotherms of $CHCl_3$ on KCl.
Temperature/°C: □: 10, △: 20, ○: 30.

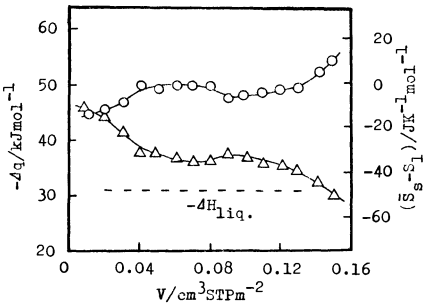

Fig. 4. Isosteric heat of $CHCl_3$ adsorption and differential entropy of $CHCl_3$ adsorbed on KCl.
△: Isosteric heat of adsorption, ○: differential entropy.

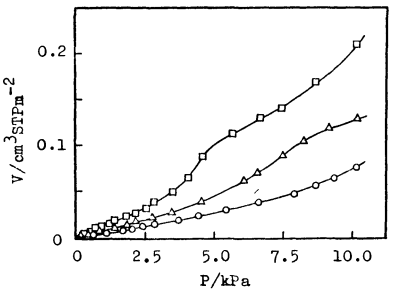

Fig. 5. Adsorption isotherms of CCl_4 on KCl.
Temperature/°C: □: 20, △: 30, ○: 40.

in Fig. 5. The isotherms were classified into the BDDT III type, judging only from their profile in the early stage $V<0.1$ cm³ STP/m². However, the point B was determined at a high vapor pressure and the monolayer capacity was obtained. According to the BDDT classification, an interaction between the surface of a KCl particle and CCl_4 molecules will be weaker than those in cases of CH_2Cl_2 and $CHCl_3$ adsorptions. In Fig. 6 the isosteric heats of CCl_4 adsorption and the differential entropies of the adsorbed molecules are shown. The adsorption heats at low coverages were determined precisely in this case on account of the large equilibrium pressures. As is shown in Fig. 6, the adsorption heat value at adsorbed amounts below 0.01 cm³ STP/m² is higher than the liquefaction heat of CCl_4 vapor, but it becomes less

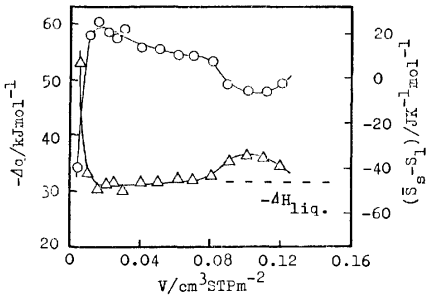

Fig. 6. Isosteric heat of CCl_4 adsorption and differential entropy of CCl_4 adsorbed on KCl.
△: Isosteric heat of adsorption, ○: differential entropy.

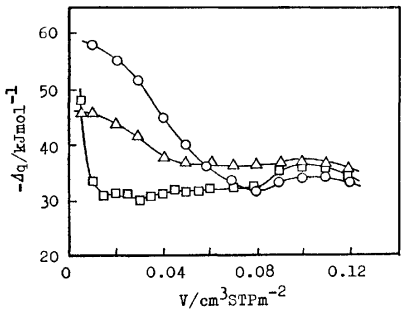

Fig. 7. Change in isosteric heat of adsorption with adsorbed amount.
○: CH_2Cl_2, △: $CHCl_3$, □: CCl_4.

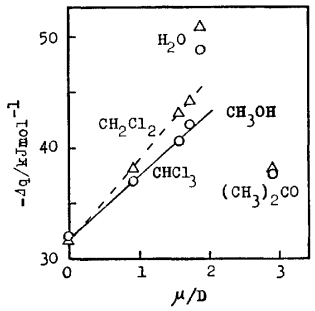

Fig. 8. Effect of dipole moment on isosteric heat of adsorption.
Coverage (θ): △: 0.4, ○: 0.5.

than the liquefaction heat at amounts above 0.01 cm^3 STP/m^2. The latter result indicates that the interaction between the KCl surface and CCl_4 molecules is weak as described above. Such estimation of the surface property is supported by the fact that the differential entropy of adsorbed CCl_4 is larger than the molar entropy of liquid CCl_4. Then the adsorption heat increased gradually with the increment of the adsorbed amount and a peak produced by the lateral interaction was observed in the heat curve at V=0.11 cm^3 STP/m^2. This value is equal to the monolayer capacity obtained from the isotherm. Moreover, the height of the peak was the largest among the three adsorbates. However, the differential entropy at the monolayer completion is less than the molar entropy of liquid CCl_4 and shows a minimum. From these results, the lateral interaction in CCl_4 adsorption is considered to be stronger than those of CH_2Cl_2 and $CHCl_3$ adsorptions. For the two polar adsorbates, if the molecules are adsorbed on the KCl surface orienting their dipole moments to the surface at the monolayer completion, the lateral interaction will decrease owing to the repulsive forces generated by the dipole moments which are parallel oriented. On account of this effect, the height of the peak observed in the heat curve is expected to diminish in CH_2Cl_2 and $CHCl_3$ adsorptions.

The large heat of adsorption observed in the early stage indicates the existence of active sites on the salt surface. The fraction of the active sites on the KCl surface for CCl_4 adsorption is estimated to be about 9% of the total sites. In the case of NaF prepared by the same method in the present study, Yao[9] concluded that 4% of the total surface is active from the comparison of adsorption characteristics of four polar substances he used. This fact shows that such an assessment concerning the active sites on KCl surface is reasonable.

Adsorption Mechanism. The heats of adsorption of the three adsorbates for KCl surface are, for convenience, repeatedly shown in Fig. 7. At low coverage, the adsorption heats of the chloromethanes differ considerably from each other and the value is influenced by the dipole moment of the adsorbate molecule. To clarify this point, the heats of adsorption of chloromethanes at coverages of 0.4 and 0.5 are plotted in Fig. 8 as a function of the dipole moments of the adsorbates. The other polar substances, $(CH_3)_2CO$, CH_3OH and H_2O, are also given in this figure. A linear relationship was found between the heats of adsorption and the dipole moments, expect for $(CH_3)_2CO$ and H_2O. The present authors have clarified already that one CH_3OH molecule is adsorbed on a surface anion of KCl particles,[6] whereas one $(CH_3)_2CO$ molecule is adsorbed on a surface cation conversely.[7] The adsorption heat value of CH_3OH was plotted in the straight line. However, in case of $(CH_3)_2CO$ adsorption where the mechanism is different from that of CH_3OH adsorption, the plot deviates greatly from linearity. Therefore, we conclude that the adsorption of chloromethanes on a KCl surface will occur by a similar mechanism to that proposed for CH_3OH adsorption. In other words, chloromethanes having dipole moments are adsorbed on the surface anions orienting their dipoles to the KCl surface. For H_2O adsorption one water molecule is adsorbed on two adjacent surface anions.[8] The plot of heat of H_2O adsorption also deviates from a straight line on account of the difference of the adsorptive mechanism. Considering these results, it will be concluded that the surface anions or cations play an important role in the adsorptions of polar substances on a KCl surface and that the adsorptive mechanisms largely depend on the molecular structures of the adsorbates used.

References

1) W. J. C. Orr, *Trans. Faraday Soc.*, **35**, 1247 (1939).
2) T. Hayakawa, *Bull. Chem. Soc. Jpn.*, **30**, 332 (1957).
3) D. M. Young, *Trans. Faraday Soc.*, **48**, 548 (1952).
4) P. B. Barraclough and P. G. Hall, *Surf. Sci.*, **46**, 393 (1947).
5) M. Chikazawa, F. Yamamoto, E. Saita, M. Kaiho, and T. Kanazawa, *Bull. Chem. Soc. Jpn.*, **50**, 337 (1977).
6) M. Chikazawa and T. Kanazawa, *Bull. Chem. Soc. Jpn.*, **50**, 2837 (1977).
7) M. Chikazawa and T. Kanazawa, *Nippon Kagaku Kaishi*, **1977**, 445.
8) M. Chikazawa and T. Kanazawa, to be published.
9) Y. Y. Yao, *J. Colloid Interface Sci.*, **28**, 376 (1968).

 © 1983 The Chemical Society of Japan Bull. Chem. Soc. Jpn., 56, 2090—2092 (1983) [Vol. 56, No. 7

IR Spectra of Solid State Reaction Products of TTF and Iodine

Susumu MATSUZAKI, Naoto KOGA, Ichiro MORIYAMA,
and Koichi TOYODA*

Department of Chemistry, Faculty of Science, Kumamoto University, Kumamoto 860

(Received October 12, 1982)

IR spectra of the mixture of tetrathiafulvalene (TTF) and iodine showed that the two components react with each other in the solid state. Spectral changes with an increase in iodine content were analyzed on the basis of the spectra of TTF and the cations, and it was found that TTF is oxidized by iodine up to the dication in the solid state in contrast to the reaction in solution.

Tetrathiafulvalene (TTF) is known to form good electric conductors with various organic acceptors, *e.g.*, tetracyano-*p*-quinodimethan (TCNQ). The high electrical conductivity of the organic charge transfer salts such as TTF–TCNQ arises from the segregated stack crystal structure and the mixed-valence ground electronic state.[1] Such charge transfer salts have two stacks of donors and acceptors, both of which can potentially conduct, so that considerable complexities are encountered in the analysis of the solid state properties. On the other hand, TTF forms good conductors also with some inorganic anions, *e.g.*, halogens, which have only donor stacks. The single stack compounds should in principle provide simpler model systems for study on the electrical conductivity.

Recently Scott *et al.*[2] studied the crystal chemistry and phase compositions of TTF–halide systems to determine the compositional phase diagrams and to relate them to the important questions of structure and stability of these compounds. They obtained the salts by the reaction in solution. However, all the possible phases of the system are not always obtained as solid precipitates by the method because of the solubilities and the equilibria between the species. Other preparation methods should, therefore, be tried to obtain the whole phase diagram. We found the solid state reaction of TTF–iodine system. In this report, the IR spectra of the reaction products are measured and some information on the compositional phase diagram is obtained from the analysis of the spectra.

Experimental

TTF was synthesized by the method of Wudl *et al.*,[3] and recrystallized twice from hexane–cyclohexane and sublimed *in vacuo*. Iodine was obtained commercially and sublimed *in vacuo* from potassium iodide. Solid state reaction products were obtained by mixing of TTF and iodine in an agate mortar for several minutes at room temperature. A ratio of iodine atoms to TTF molecules is represented by the symbol "*n*". Composition of the mixtures ranged from $n=0.2$ to 40. A mixed-valence salt, $TTF \cdot I_{0.7}$, was prepared by the mixing of the stoichiometric amounts of the components in acetonitrile, and recrystallized from the solvent. A cation salt, $TTF \cdot I_3$, was prepared by the dropwise addition of the acetonitrile solution of TTF into the solution of excess iodine, and recrystallized from the solvent. A dication salt, $TTF \cdot Br_x$, was also obtained by the similar dropwise method in acetonitrile, but the recrystallization was not feasible because of the poor solubility. Elemental analyses showed that $x=ca.$ 6; therefore, this salt is probably formulated as TTF^{2+} $(Br_3^-)_2$. All the sample prepared were dispersed in KBr, and the IR spectra were recorded on a JASCO DS-403G spectrometer.

Results and Discussion

IR spectra of TTF, $TTF \cdot I_{0.7}$, and $TTF \cdot I_3$ are shown in Fig. 1. The spectra of TTF and $TTF \cdot I_{0.7}$ agreed with those in the literature.[4,5] The spectrum of $TTF \cdot I_3$ also agreed with that of $TTF \cdot Br_{1.0}$ reported by Bozio *et al.*[4] except the small frequency shifts which are probably due to the difference in the counter ions. IR spectrum of $TTF(Br_3)_2$ is shown in Fig. 3a, which is similar to that of $TTF(BF_4)_2$ reported by Siedle *et al.*[6] except additional bands of BF_4^- in the latter. These results support the identification of the salts.

Of the features in these spectra, two absorption bands near 1500 and 1350 cm^{-1} are most suitable indications of the valence of TTF. The former, assigned to b_{1u} ν_{18} of TTF,[4] shows a large frequency shift with the change of the valence. The frequencies are: TTF, 1528 cm^{-1}; $TTF \cdot I_{0.7}$, 1500 cm^{-1}; $TTF \cdot I_3$, 1474 cm^{-1}; $TTF(Br_3)_2$, 1422 cm^{-1}. The other characteristic band near 1350 cm^{-1} is assigned to the out-of-phase combination mode of TTF a_g ν_3.[4] The vibronic interaction between the unpaired electron and the molecular vibration of TTF is responsible for the IR activity of this band;[4] therefore, the band appears only in the spectra of $TTF \cdot I_{0.7}$ and $TTF \cdot I_3$. The band of the former is much broader than that of the latter, and the two species, $TTF \cdot I_{0.7}$ and $TTF \cdot I_3$, are easily distinguished from the difference in the width. We analyze the IR spectrum of the solid state

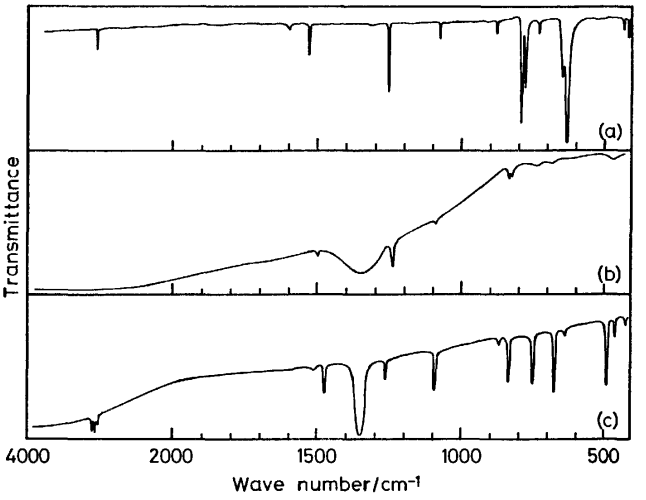

Fig. 1. IR spectra of (a) TTF, (b) $TTF \cdot I_{0.7}$, and (c) $TTF \cdot I_3$.

reaction products on the basis of the results for these TTF salts.

Spectral changes of TTF–iodine system with an increase in n are shown in Fig. 2. The changes may be interpreted as the stepwise oxidation of TTF, *i.e.*, $TTF \rightarrow TTF^{0.7+} \rightarrow TTF^{+} \rightarrow TTF^{2+}$, although a controversial feature is observed in the range, $n<0.7$: this will be discussed later. Absorption bands of TTF are decreasing with an increase in n. At $n=1$, features of $TTF^{0.7+}$ dominate the spectra and those of $TTF \cdot I_3$ also appear. The features of $TTF \cdot I_3$ grow up with n, and absorption bands of a new species appear at $n=4$. When n increases further, the new species comes to dominate the spectra, and only absorption bands of this species are observed at $n=20$. No further spectral changes occurred when n was increased up to 40; therefore, this species is probably the end product of this solid state reaction. The spectrum at $n=20$ is practically the same as that of $TTF(Br_3)_2$ as shown in Fig. 3. The result shows that iodine oxidizes TTF up to the dication in the solid state reaction. The sample of $n=20$ gave practically the same IR spectrum in Nujol mull as in the KBr disk. The former is black because of excess iodine whereas the latter is brown which may be attributed to the presence of I_2Br^- ion.

In the solution reaction, no dication salts have been obtained for TTF–iodine system. We also attempted to react TTF with a large excess of iodine to prepare the dication salt, but $TTF \cdot I_3$ was only obtained. Chlorine and bromine, on the other hand, easily oxidize TTF to the dication in solution.[2] The difference among the halogens is probably attributable to the weaker oxidizing ability of iodine than the others. Formation constant of the dication is expected to be rather small in the equilibrium, $TTF^{+}+nI_2 \rightleftharpoons TTF^{2+}\text{-}(I_x^-)_2$. In the solid state, the environment of TTF remains iodine-rich during the whole oxidation processes and the dication species is formed. In solution, on the other hand, no dication salts will be obtained because TTF probably escapes from the iodine-rich environment, *i.e.*, the solution, as a precipitate of $TTF \cdot I_3$ before the further oxidation occurs.

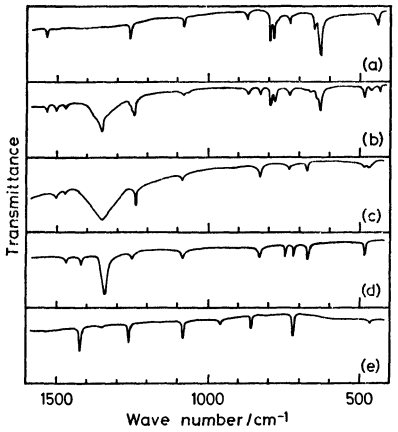

Fig. 2. IR spectra of solid state reaction products of TTF and iodine. (a) $n=0$; (b) 0.4; (c) 1; (d) 4; (e) 20.

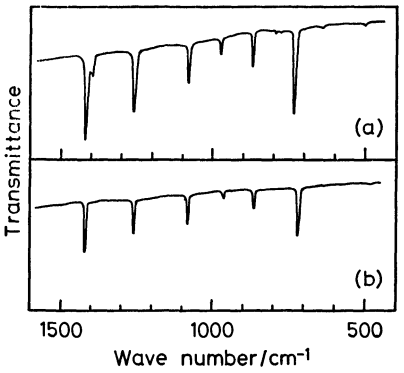

Fig. 3. IR spectra of (a) $TTF(Br_3)_2$ and (b) sample of $n=20$.

No IR features of species other than TTF^{+} and TTF^{2+} are observed in the spectrum of $n>4$. The result shows that no homogeneous mixed-valence salt exists between the cation and the dication in contrast to the case between the neutral molecule and the cation, where $TTF^{0.7+}$ exists. Siedle *et al.*[6] reported a mixed-valence salt formulated as $(TTF^{+})(TTF^{2+})_2\text{-}(CuCl_2^-)_5$, but the vibrational spectra are reasonably explained as a superposition of those of TTF^{+} and TTF^{2+}. Therefore, no valence fluctuation[7] occurs in this salt, in the time scale of molecular vibrations. The result shows striking difference in comparison with the case of homogeneous mixed-valence compounds such as $TTF \cdot I_{0.7}$, where two valence states, TTF and TTF^{+}, are indistinguishable from the vibrational spectra because the features of the two species are averaged out by the valence fluctuation.[8] The salt of Siedle *et al.* should, therefore, be considered inhomogeneous from the viewpoint of the vibrational characteristic time. The result in the present work does not rule out the possibility that such an inhomogeneous mixed-valence salt exists in TTF–iodine system.

In the range, $0<n<0.7$, an anomaly is observed

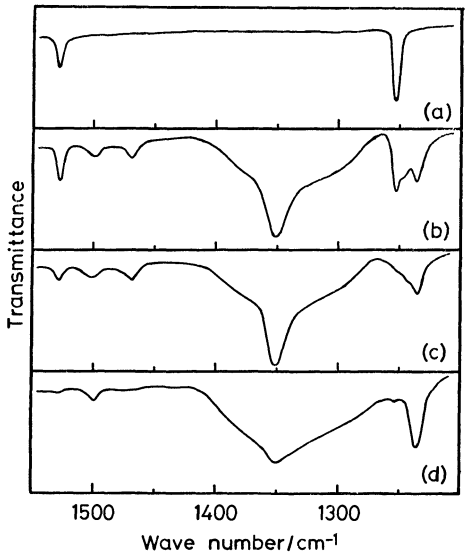

Fig. 4. IR spectra of solid state reaction products of TTF and iodine. (a) $n=0$; (b) 0.3; (c) 0.4; (d) 0.7.

in the spectra, as mentioned above. In order to show the detailed feature of the spectra, the region of 1200—1600 cm^{-1} is given in an expanded scale (Fig. 4). IR spectra of the samples were obtained also in Nujol and hexachlorobutadiene mull, and the spectra agreed well with those in the KBr disk. The samples of $n=$ 0.3 and 0.4 clearly exhibit three absorption bands at 1528, 1500, and 1470 cm^{-1}, which are attributable to the b_{1u} ν_{18} modes of TTF, $TTF^{0.7+}$, and TTF^{+}, respectively. Another triplet structure is observed also in the region of b_{2u} ν_{23}, 1230—1250 cm^{-1}.[4] Furthermore, the characterictic broad band near 1350 cm^{-1} has an anomalous profile, which is probably due to the superposition of sharp and broad features of TTF^{+} and $TTF^{0.7+}$. These results clearly show that the reaction product contains not only $TTF^{0.7+}$ but also TTF^{+} even under the condition of a fairly small iodine content. The equilibrium is expected to shift to TTF^{+}, if n is increased. However, the result was obtained contrary to this expectation as shown in Fig. 4; *i.e.*, $TTF^{0.7+}$ came to dominate the spectrum with an increase in n. The TTF^{+} species above is not probably the triiodide salt because the iodine content is fairly small and the frequency of the vibronically allowed band, 1355 cm^{-1}, is distinct from that of $TTF \cdot I_3$, 1345 cm^{-1}. Only the candidate will be $TTF \cdot I_{1.0}$, which has not been obtained by the reaction in solution.

The cause of this anomaly may be attributable to a cluster structure of the cation in TTF–iodine mixture. The ionization potential of TTF is small and the electron affinities of halogens are large, so that TTF is present only as the fully ionic form, TTF^{+} and $(TTF^{+})_2$,[9] in the solution of TTF–halides. In the crystals of nonstoichiometric TTF–halides, on the other hand, the mixed-valent state is stabilized by the balance of the energy cost with the ionization of the donor–acceptor pairs and the energy gain by the electrostatic interaction (crystal Madelung energy);[10] in other words, mixed-valent states are stable only in the crystal. These facts suggest that TTF molecules have the fully ionic and the mixed-valent states in the small and large clusters respectively, *i.e.*, the state changes at a boundary size of the cluster. The fraction of the large clusters increases with an increase in n, and this will result in the spectral change observed. Such a fully ionic-to-mixed-valent transition of TTF state is interesting from the viewpoint of the stability of mixed-valent TTF salts. Some information will be obtained from, *e.g.*, vibrational spectra of the aggregates of TTF^{+} in an inert gas matrix at low temperature.

References

1) J. B. Torrance, "Synthesis and Properties of Low-Diemensional Materials," ed by J. S. Miller and A. J. Epstein, Ann. N. Y. Acad. Sci. (1978), p. 210, and references therein.

2) B. A. Scott, S. J. La placa, J. B. Torrance, B. D. Silverman, and B. Welber, *J. Am. Chem. Soc.*, **99**, 6631 (1977).

3) F. Wudl, M. L. Kaplan, E, J. Hufnagel, and E. W. Southwick Jr., *J. Org. Chem.*, **39**, 3608 (1974).

4) R. Bozio, I. Zanon, A. Girlando, and C. Pecile, *J. Chem. Phys.*, **71**, 2282 (1979).

5) R. Bozio, A. Girlando, I. Zanon, and C. Pecile, "Quasi One-Dimensional Conductors. I," ed by S. Barišić, J. R. Cooper, and B. Leontic, Spiringer-Verlag, Berlin (1979), p, 217.

6) A. R. Siedle, G. A. Candela, T. F. Finnegan, R. P. Van Duyne, T. Cape, G. F. Kokoszka, P. M. Woyciejes, and J. A. Hashmall, *Inorg. Chem.*, **20**, 2635 (1981).

7) J. M. Lawrence, P. S. Riseborough, and R. D. Parks, *Rep. Prog. Phys.*, **44**, 1 (1981).

8) S. Matsuzaki, T. Moriyama, and K. Toyoda, *Solid State Commun.*, **34**, 857 (1960).

9) J. B. Torrance, B. A. Scott, B. Welber, F. B. Kaufman, and P. E. Seiden, *Phys. Rev. B*, **19**, 730 (1979).

10) J. B. Torrance and B. D. Silverman, *Phys. Rev. B*, **15**, 788 (1977).

 © 1983 The Chemical Society of Japan Bull. Chem. Soc. Jpn., 56, 2093—2100 (1983)

The Heat Capacities of Lithium, Sodium, Potassium, Rubidium, and Caesium Nitrates in the Solid and Liquid States

Kazuhiko Ichikawa* and Toshiyuki Matsumoto

Department of Chemistry, Faculty of Science, Hokkaido University, Sapporo 060

(Received December 24, 1982)

The heat capacities, C_p, of the alkali metal nitrates, MNO_3 (M=Li, Na, K, Rb, and Cs), in the solid and liquid states have been measured between 50 and 450 °C by means of adiabatic calorimetry. We have measured with a fair degree of accuracy the C_p values for the MNO_3 systems, because the existing data on $NaNO_3$ and KNO_3 above 250 °C are quite scanty. Some empirical rules, some of which may extend to other salts, have been obtained from the results on C_p for the five alkali nitrates in the solid and liquid states. For the molten MNO_3, the heat capacities at a constant volume, C_V, were obtained from the thermodynamical relationship between C_V and C_p, using the experimental values of C_p; the C_V values have been interpreted in terms of the interionic and intraionic portions.

It has become a common theme of research to develop technology for the storage of thermal energy and for heat transfer, employing molten salts; the study of their thermal properties has thus acquired a practical meaning. The salt of most interest is molten alkali-metal nitrate, for it has better physical and chemical properties than other salts. Some of these properties are its low melting point, t_{mp}, its nonvolatile, nondecomposite, and noncorrosive characteristics, and its high heat capacity. The existing data on the heat capacity at constant pressure C_p, for $NaNO_3$ and KNO_3, which were obtained from the slopes of the curves of the heat content *versus* temperature,[1] are quite scanty, in particular just below and above t_{mp}. The thermal property[2] of most interest in this paper is the heat capacity as an important parameter. This work describes briefly an adiabatic calorimeter used to measure high-temperature heat capacities with a fair degree of accuracy (2.0%). The C_p results are shown for the five alkali-metal nitrates MNO_3 (M= Li, Na, K, Rb, and Cs) in the solid and liquid states between 50 and 450 °C. Their heat-capacity data have given rise to some empirical rules, which may extend to other salts. The high heat-capacities observed will also be discussed in terms of their interionic and intraionic contributions.

Experimental

Materials. The salts used were pure-grade recrystallized reagents. The KNO_3 was supplied by Prof. G. J. Janz, Rensselaer Polytechnic Institute, and the $NaNO_3$ and $LiNO_3$ of a special grade, by Wako. The purity of the $RbNO_3$ and $CsNO_3$ purchased from Alfa was 99.9%. Metallic impurities indicated: for KNO_3, Si 0.1—0.5, Mg 0.1—0.5, Fe 0.1—0.5, and Ca 0.5—2.0 ppm; for $NaNO_3$, Pb 0.007, K 0.008, Cu 0.002, Fe 0.003 mass percentage; for $LiNO_3$, Pb 0.001, Na 0.05, K 0.05, Cu 0.0005, Mg 0.005, Ca 0.01, Ba 0.001, Fe 0.005 mass percentage.

Apparatus and Procedure. Measurements of the high-temperature heat capacity, C_p, were made with an adiabatic calorimeter. The adiabatic shield control consists of a PID-SCR circuit, a constant wattage supply, a heater of platinum-wire, and multi-junction thermocouples. The temperature difference between the sample in a calorimetric ampoule (*i.e.*, a platinum cylindrical vessel of *ca.* 7.5 cm^3) and the adiabatic shield was controlled within 0.1 °C between 50 and 450 °C. Since the heat emissivity of the gold metal is very small, the inner adiabatic jacket and the outer vessel of the sample container are gold-plated. The adiabatic calorimeter may be sufficiently protected from the heat leakage due to thermal radiation. In order to get avoid any oxidation and corrosion of the interior of the calorimeter over the entire temperature range of this work, heat-capacity measurements were made under Ar gas of *ca.* 2.5×10^4 Pa at room temperature introduced into the vacuum cell of the calorimeter. The values of C_p in J K^{-1} g^{-1} were computed from the following equation:

$$C_p = (W\cdot\Delta t)/(M\cdot\Delta\theta) - (M'/M)C_p', \quad (1)$$

where W (in watts) is the electric power supplied by the internal heater, Δt (in seconds) is the time required for increasing the temperature by $\Delta\theta$ degrees and is determined by the clock timer unit, and M is the weight (*i.e.*, 10—15 g) of the sample. The heat capacity of the empty calorimeter, $M'C_p'$, was obtained in a preliminary measurement. The temperature measurement was carried out with a Pt-Rh thermocouple calibrated by a cryoscopic method for pure-grade recrystallized reagents, KNO_3, K_2SO_4, Ag_2SO_4, and $KClO_4$.

The experimental errors may originate from two major sources. Firstly, sample characteristics associated with endothermic reactions, such as decomposition and evaporation, should be considered.[3] In this work, however, the weight-loss of the sample between 50 and 450 °C ranged from 0.01% to 0.06%. Thus, the endothermic heat resulting from the decomposition or evaporation of MNO_3 may not affect any magnitudes of C_p within the present experimental uncertainty. Secondly, the calorimeter operation was tested by measuring the C_p of standard synthetic sapphire (99.99 wt% purity). The magnitude of the experimental error

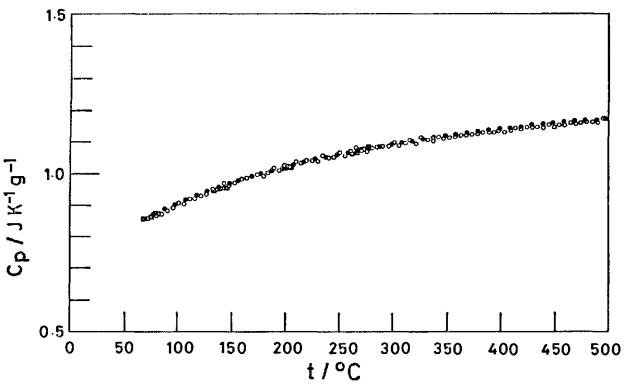

Fig. 1. Temperature dependence of the heat capacity of synthetic sapphire: ○, this work; ●, Ref. 4; □ Ref. 5.

attributable to the heat leakage was less than two per cent of C_p of the sample for the temperatures of interest; Fig. 1 shows that our results of synthetic sapphire agree with the selected values cited in the text published by TPRC[4] and with the existing data, which were measured by a reliable adiabatic calorimeter and which prove the precision to be ±0.3% and give an accuracy of ±0.6%.[5] This agreement is sufficient for our present purposes. The amount of argon gas in the interior of the stainless-steel vacuum vessel did not affect the data of C_p within the limits of experimental uncertainty of ±1.0% between 50 and 500 °C.

Results and Discussion

The experimental results on C_p in J K^{-1} g^{-1} of $LiNO_3$ and $NaNO_3$ between 50 and 400 °C, and of KNO_3, $RbNO_3$, and $CsNO_3$ between 50 and 450 °C are presented in Figs. 2—6 respectively. Their molar heat capacities in J K^{-1} mol^{-1} are listed in Table 1. It is worthy while focussing on the accuracy of the results, because the literature data are quite scattered above the level of precision of each of the data (*e.g.*, Fig. 3 for $NaNO_3$).[1,6–16]

$NaNO_3$: Figure 3 demonstrates that the many existing data on the C_p of $NaNO_3$ in the solid and liquid states are quite scanty and not in good agreement. Our data are in close agreement with the data of Sokolov and Schmidt,[11] and of Carling[16] except for the neighborhood of the solid-state transition temperature, t_{tr}, which depends on the literature (*i.e.*,

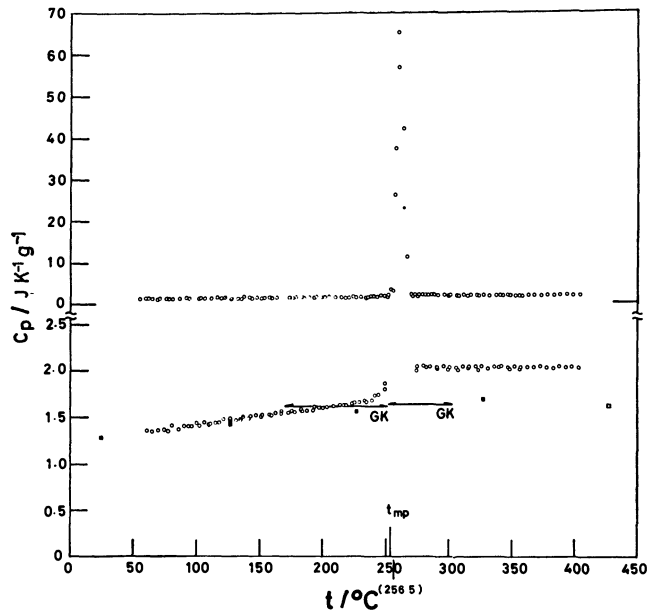

Fig. 2. Temperature dependence of the heat capacity of $LiNO_3$: ○, this work; GK, Ref. 1; ■(solid) and □(liquid), Ref. 21. In this and in Figs. 3—6 the temperatures of t_{tr} and t_{mp} shown by the vertical lines were referred from the literature data and the temperature in parentheses, the location of which is pointed out by an arrow, was determined in this work.

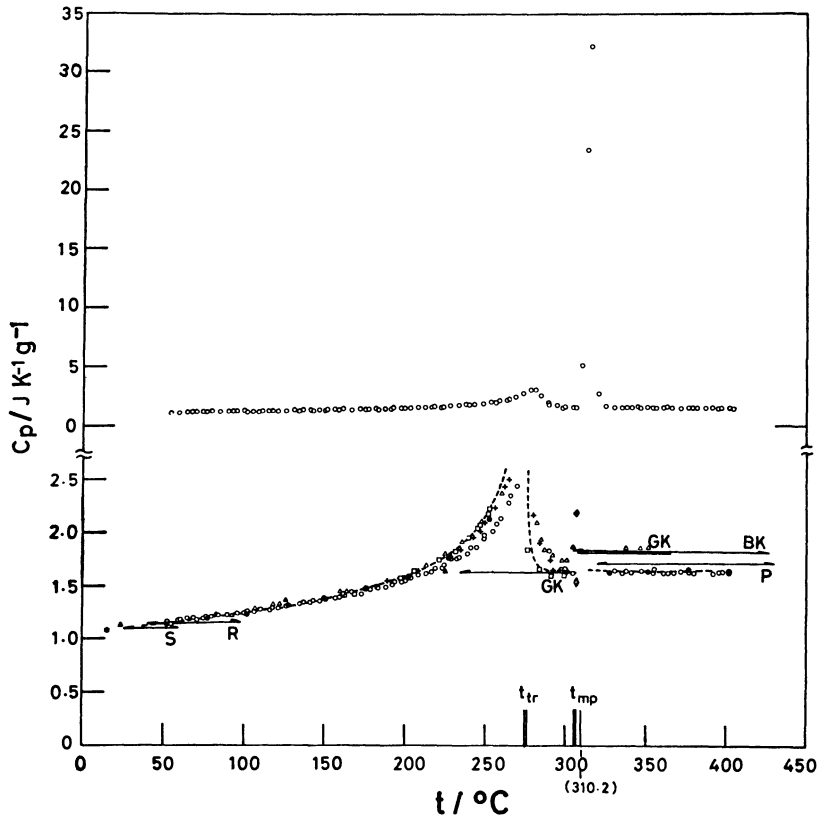

Fig. 3. Temperature dependence of the heat capacity of $NaNO_3$: ○, this work; R, Ref. 6; P, Ref. 7; S, Ref. 8; GK, Ref. 1; ★ Ref. 9; +, Ref. 10; ----, Ref. 11; △, Ref. 12; ◆(solid) and ◇(liquid), Ref. 13; □, Ref. 14; ▲ and BK, Ref. 15; ●, Ref. 16.

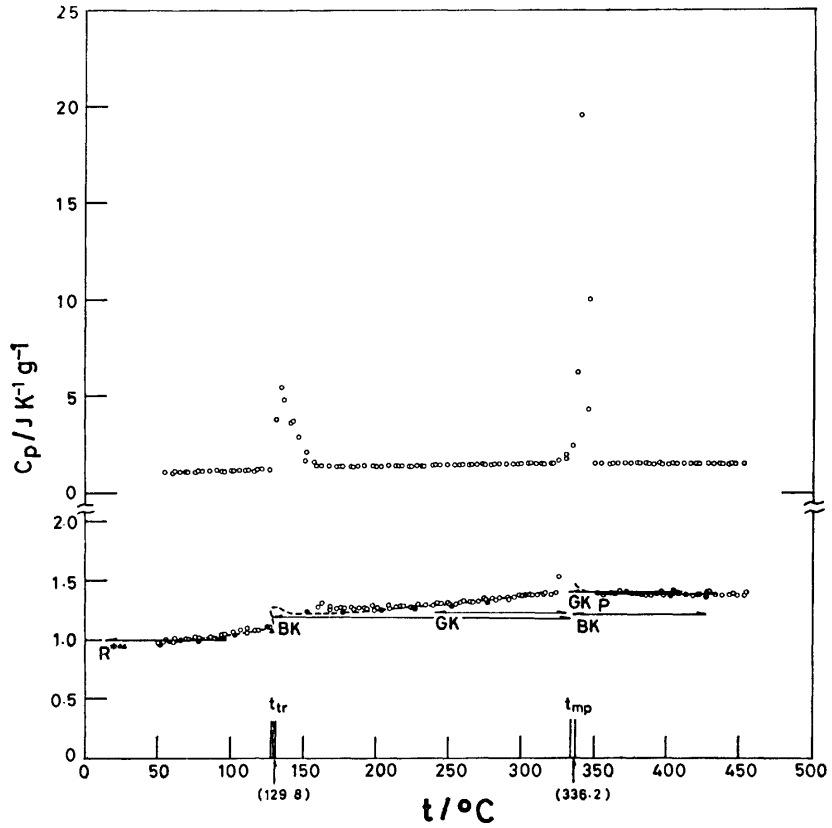

Fig. 4. Temperature dependence of the heat capacity of KNO_3: ○, this work; ----, Ref. 17; the other symbols should be referred in Fig. 3.

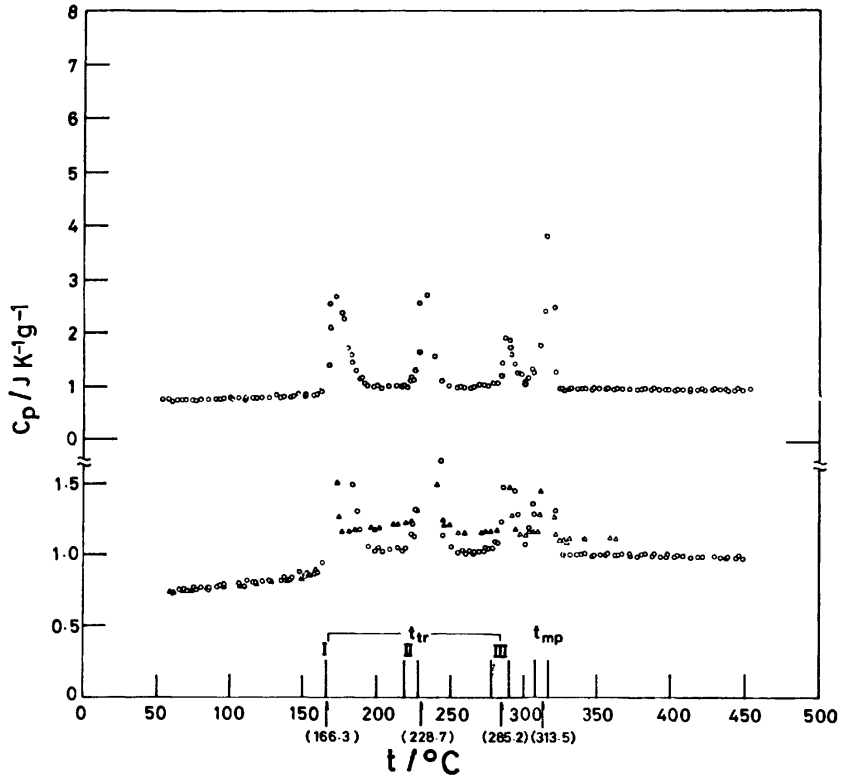

Fig. 5. Temperature dependence of the heat capacity of $RbNO_3$: ○, this work; △, Ref. 19. The three reversible solid-transitions I, II, and III,[33] have been observed and their temperatures and t_{mp} are some what scattered in the literature data.

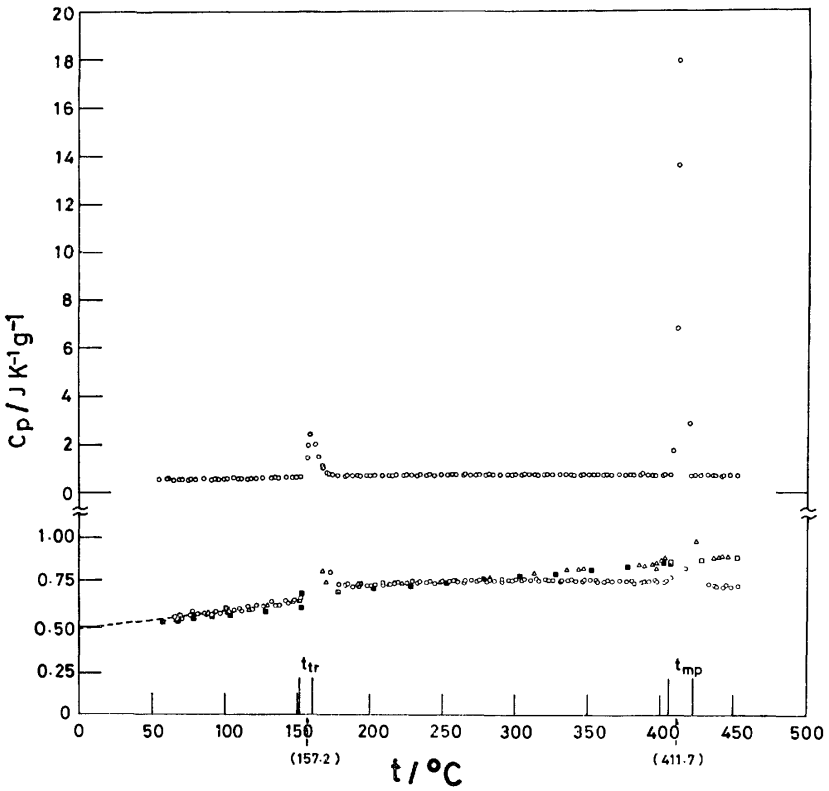

Fig. 6. Temperature dependence of the heat capacity of $CsNO_3$: ○, this work; ----, Ref. 22; △, Ref. 20; ■(solid) and □(liquid), Ref. 23.

275 and 276 °C). Our data also agree with the data of Miekk-oja[10] between t_{tr} and t_{mp}; the data of Reinsborough and Wetmore[14] immediately below t_{mp} are slightly less than ours. On the other hand, Mustajoki's data[12] (for heating) above t_{mp}, which are located above the C_p values (see the horizontal arrows in Fig. 3) obtained from the temperature dependence of enthalpy by Goodwin and Kalmus[1] and by Barir and Knacke,[15] are larger than the data of this work, Sokolov and Schmidt,[11] and Carling[16] by *ca.* 14% above the level of precision of each of the data. It may also be noted that Goodwin and Kalmus'[1] data just below t_{mp} agree satisfactorily with those of this work, Sokolov and Schmidt,[11] and Carling,[16] but the former does not show any broad cusp-shaped peak in the heat capacity curve. The change in the heat capacity on fusion at t_{mp}, $\Delta C_p^\circ(t_{mp})$, is given as the difference between the heat capacities just below t_{mp} and immediately above t_{mp}, wherein the experimental values which show the peak of C_p around the temperature, t_p, located slightly higher than t_{mp} should be omitted. Thus, $\Delta C_p^\circ(t_{mp})$ may be defined by:

$$\Delta C_p^\circ(t_{mp}) \equiv \lim_{\delta\to 0}[C_p^l(t_{mp}+\delta)] - \lim_{\delta'\to 0}[C_p^s(t_{mp}-\delta')], \qquad (2)$$

where the suffixes l and s stand for the liquid and solid states respectively. The mark of $\lim_{\delta \text{ or } \delta'\to 0}$ indicates the extrapolation of C_p until t_{mp}; δ and δ' are positive. Under an ideal condition that both δ and δ' are equal to zero, t_p should be equal to t_{mp}. Figure 3 shows that $\Delta C_p^\circ(t_{mp})$ for $NaNO_3$ is almost zero, as well as KNO_3. On the other hand, $\Delta C_p^\circ(t_{mp})$ in the literature data is either negative or positive (*i.e.*, Goodwin and Kalmus[1]: 15.0 J K^{-1} mol^{-1}, Mustajoki[12]: 3.3, Janz *et al.*[13]: −56.0, Barin and Knacke[15]: −2.6, and Sokolov and Schmidt[11]: 2.9). The magnitude of *ca.* 3 J K^{-1} mol^{-1} is almost comparable with the experimental uncertainty in the C_p values.

KNO_3: There exist data in the literatures which are scattered similar to $NaNO_3$. Our data are in close agreement with the data of Sokolov and Schmidt[17] and of Carling[16] as in the case of $NaNO_3$. Further, our data have reproduced also the data of Person[7] and of Goodwin and Kalmus.[1] To our knowledge there exist no data for KNO_3 above t_{tr} (*i.e.*, the 129.8 °C observed in this work), though Mustajoki[18] reported the data for MNO_3 (M=Na,[12] Rb,[19] and Cs[20]) in the solid and liquid states. In this work, $\Delta C_p^\circ(t_{mp})=0$, and in Carling's data it also seems to be zero, but in the literature data 17.4 J K^{-1} mol^{-1} has been reported by Goodwin and Kalmus[1] and 2.9 by Barin and Knacke.[15] For both $NaNO_3$ and KNO_3, the values extrapolated to room temperature agree well with their heat capacities at the low temperatures measured by Southard and Nelson,[9] as is shown in Figs. 3 and 4.

The magnitudes and the temperature dependence of the C_p values were not determined from the slopes of the curves of the heat content and the corresponding temperatures with sufficient accuracy, for the differences in the C_p values between our data and the data of Goodwin and Kalmus or the data tabulated by Barin and Knacke are dependent on the systems above

TABLE 1. EXPERIMENTAL HEAT CAPACITIES OF ALKALI METAL NITRATES MNO_3 (M=Li, Na, K, Rb, AND Cs) IN THE SOLID AND LIQUID STATES

t / °C	C_p / J K^{-1} mol^{-1}	t / °C	C_p / J K^{-1} mol^{-1}	t / °C	C_p / J K^{-1} mol^{-1}
			$LiNO_3$		
59.7	91.6	131.7	101.4	192.2	108.7
60.7	93.6	134.7	101.2	193.2	111.1
64.8	93.4	136.8	104.0	198.3	110.6
70.0	94.1	141.9	103.6	200.3	110.6
75.1	94.5	142.9	104.0	203.4	110.9
77.2	93.8	147.0	104.9	208.5	111.7
85.4	95.4	151.1	104.0	208.5	111.9
85.4	95.1	152.2	105.7	213.7	112.7
90.6	97.2	157.3	105.8	216.7	112.6
93.6	96.7	159.4	104.5	218.8	112.8
95.7	97.0	162.4	106.5	223.9	114.0
100.8	99.1	167.6	106.5	224.9	114.2
106.0	99.7	167.6	107.4	229.0	114.9
110.1	98.7	172.7	107.6	233.1	116.0
111.1	99.2	175.8	108.3	234.1	115.2
116.2	99.8	177.8	107.9	239.2	116.2
118.3	99.3	182.9	110.0	241.3	118.9
121.4	102.7	184.0	108.2	244.3	120.0
126.5	102.5	188.1	108.8		
			Solid-Liquid transition		
275.0	141.4	315.8	141.3	356.6	140.8
280.1	141.8	320.9	141.6	361.7	140.5
282.2	140.3	326.0	141.3	366.8	140.9
285.2	140.8	331.1	139.3	371.9	141.4
290.3	139.3	331.1	139.7	377.0	140.5
290.3	140.5	336.2	141.0	382.0	140.0
295.4	141.4	339.3	140.7	387.1	141.6
298.5	138.9	341.3	141.3	392.2	140.7
300.5	140.7	346.4	140.5	397.3	141.1
305.6	140.5	347.4	138.9	402.4	140.3
310.7	140.9	351.5	141.6		
314.8	140.1	355.6	139.1		
			$NaNO_3$		
59.7	98.9	90.6	104.1	126.5	111.0
60.7	100.6	95.7	105.9	131.7	112.6
64.8	100.9	100.8	106.3	134.7	114.4
69.0	100.8	101.9	107.8	136.8	114.3
70.0	100.1	106.0	106.5	141.9	115.1
75.1	101.4	110.1	108.9	142.9	116.2
77.2	102.7	111.1	108.8	147.0	116.1
80.3	102.9	116.2	108.6	151.1	117.8
85.4	101.9	118.3	110.6	152.2	117.6
85.4	103.7	121.4	110.5	157.3	117.7
159.4	118.5	184.0	126.2	208.5	135.5
162.4	121.0	188.1	126.5	208.5	136.7
167.6	122.1	192.2	128.8	213.7	137.1
162.6	122.7	193.2	130.2	216.7	139.2
175.8	125.2	198.3	130.9	218.8	141.3
177.8	125.3	200.3	132.2	223.9	142.3
182.9	126.4	203.4	133.4		
			Phase transition		
298.5	139.1	300.5	141.1	305.6	138.8
			Solid-Liquid transition		
331.1	140.0	347.4	139.8	371.9	139.7
331.1	139.9	351.5	139.3	377.0	138.6
336.2	138.5	355.6	138.5	380.0	138.5
339.3	139.9	361.7	138.6	396.3	138.6
341.3	138.7	363.7	139.1	397.3	138.7
346.4	139.2	366.8	138.5	402.4	139.0
			KNO_3		
54.6	101.2	77.2	102.1	106.0	109.3
59.7	99.7	85.4	103.2	110.1	107.0
60.7	101.9	85.4	103.9	111.1	110.4
64.8	100.6	93.6	105.2	116.2	109.1
69.0	101.9	95.7	106.9	118.3	109.2
70.0	101.5	100.8	107.0	126.5	110.9
75.1	103.0	101.9	106.6		
			Phase transition		
159.4	128.4	218.8	129.3	269.9	133.4
162.4	131.5	223.9	129.9	274.0	136.3
167.6	128.7	224.9	128.8	275.0	134.7
167.6	126.0	229.0	130.9	280.1	135.5
172.7	127.0	233.1	131.3	285.2	136.0
175.8	127.7	234.1	129.9	290.3	136.1
177.8	126.8	239.2	130.2	295.4	137.1
182.9	127.6	241.3	132.4	298.5	138.7
184.0	127.0	244.3	131.6	300.5	137.8
188.1	127.5	249.5	131.4	305.6	139.0
192.2	127.4	249.5	132.5	306.6	138.4
198.3	128.2	254.6	130.9	310.7	138.5
200.3	127.6	257.6	132.9	314.8	140.1
208.5	128.7	259.7	134.0	315.8	140.7
213.7	128.2	264.8	133.1	320.9	139.1
216.7	129.6	265.8	132.7	323.0	140.4
351.5	140.8	388.1	139.4	422.7	139.8
355.6	139.6	392.2	139.7	427.8	140.4
361.7	140.4	396.3	141.6	428.8	142.0
363.7	141.1	397.3	139.5	432.9	139.2
371.9	141.4	402.4	139.4	436.9	140.0
371.9	141.6	404.4	140.0	438.0	139.1
377.0	139.8	407.5	140.4	443.0	138.9
380.0	140.8	412.6	139.5	445.1	141.0
382.0	139.5	412.6	139.6	453.2	140.2
387.1	140.0	420.7	140.0		
			Solid-Liquid transition		
			$RbNO_3$		
60.7	108.1	93.6	115.5	126.5	120.5
64.8	110.9	95.7	116.4	134.7	120.2
69.0	111.6	106.0	117.7	136.8	122.3
70.0	110.3	110.1	118.2	141.9	122.0
75.1	112.4	111.1	119.9	147.0	128.8
77.2	110.6	116.2	118.4	151.1	124.2
80.3	113.7	118.3	118.3	152.2	127.7
85.4	112.5	121.4	119.5	157.3	127.6
90.6	114.0	126.5	120.1	159.4	127.7
			Phase transition I		
198.3	149.8	208.5	151.9	216.7	151.5
200.3	153.7	208.5	152.1	218.8	153.5
203.4	149.1	213.7	154.3		
			Phase transition II		
254.6	149.0	264.8	148.8	275.0	153.2
257.6	150.4	265.8	148.5	280.1	160.8
259.7	147.2	274.0	153.8	282.2	160.0
			Phase transition III		
300.5	156.6				
			Solid-Liquid transition		
326.0	145.9	366.8	147.0	412.6	145.6
331.1	146.3	371.9	145.1	417.6	145.3
336.2	146.9	371.9	146.8	420.7	145.9
339.3	146.9	377.0	144.7	427.8	145.7
341.3	147.9	380.0	146.9	428.8	146.2
346.4	145.1	382.0	147.6	436.9	144.8
347.4	146.2	387.1	145.4	438.0	145.1
351.5	146.8	392.2	144.5	445.1	146.0
355.6	146.3	397.3	146.9	453.2	145.1
356.7	147.9	404.4	146.2	453.2	144.7
361.7	146.0	407.5	146.0		
363.7	146.8	412.6	144.4		
			$CsNO_3$		
64.8	108.2	95.7	111.5	131.7	124.0
69.0	109.9	101.9	111.9	134.7	119.5
70.0	106.0	106.0	114.6	136.8	120.1
75.1	110.1	110.1	114.2	141.9	124.7
77.2	113.1	111.1	114.2	142.9	121.4
80.3	111.5	116.2	117.9	147.0	125.5
85.4	111.1	118.3	115.6	151.1	125.5
85.4	110.9	121.4	119.5	152.2	128.5
90.6	109.9	126.5	116.6		
93.6	111.5	126.5	117.9		
			Phase transition		
177.8	142.9	257.6	147.0	331.2	148.1
182.9	143.1	259.7	147.7	336.2	149.1
184.0	143.3	264.8	146.4	339.3	147.9
188.1	140.9	265.8	147.7	341.3	147.7
192.2	141.2	269.9	148.7	346.4	147.4
193.2	143.1	274.0	147.4	347.4	148.1
198.3	142.3	275.0	148.9	351.5	149.1
200.3	141.5	280.1	147.7	355.6	147.4
203.4	143.3	282.2	147.9	356.6	146.8
208.5	145.4	285.2	147.9	361.7	147.9
208.5	144.0	290.3	147.7	363.7	147.7
213.7	143.5	290.3	149.3	366.8	147.7
216.7	143.5	295.4	149.1	371.9	148.3
218.8	145.8	298.5	147.7	371.9	147.4
224.9	144.6	300.5	149.3	377.0	147.9
229.0	147.2	305.6	148.9	380.0	148.1
233.1	145.6	306.6	148.5	382.0	145.8
234.1	146.6	310.7	148.3	387.1	147.6
139.2	145.8	314.8	149.3	388.1	146.6
241.3	147.0	315.8	147.9	392.2	147.9
244.3	145.0	320.9	149.3	396.3	147.7
249.5	147.4	323.0	147.2	397.3	146.8
249.5	147.2	326.0	148.1	402.4	146.2
254.6	147.6	331.1	147.6	404.4	147.4
			Solid-Liquid transition		
432.9	143.9	443.0	141.7	448.1	141.1
436.9	142.5	445.1	142.7	453.2	142.7
438.0	141.7				

t_{mp}. In comparison with the former our data are larger by *ca.* 23% for $LiNO_3$, smaller by *ca.* 10% for $NaNO_3$ and equivalent in magnitude for KNO_3; in comparison with the latter, our data are smaller by *ca.* 12% for $NaNO_3$ and larger *ca.* 12% for KNO_3. The temperature coefficients of C_p below t_{mp} are quite different between the previously reported data (*i.e.*, Barin and Knacke,[15] Goodwin and Kalmus,[1] Schüller,[8] and Regnault,[6]) and our data for $NaNO_3$ and KNO_3. It may thus be concluded that the reli-

ability of the literature data above t_{mp} is satisfactory only in the cases of Sokolov and Schmidt, and Carling. We had better say that the thermodynamic values of Gibbs free energy tabulated by Barin and Knacke are sufficiently accurate.

$LiNO_3$: Above 150 °C no satisfactory results were previously obtained.[1,21] No broad peaks associated with the reversible solid-state transition have been observed in the C_p measurements with an increase in the temperature. The substance of $LiNO_3$ is unique among the other alkali-nitrates because the difference $\Delta C_p^\circ(t_{mp})$ is not zero: $\Delta C_p^\circ(t_{mp})=23.2$ J K^{-1} mol^{-1}, and no reversible solid-state transition takes place.

$RbNO_3$: To our knowledge, the only existing data on C_p are the data measured by Mustajoki.[19] The three reversible thermal transitions below t_{mp} and the solid-liquid transition are shown in Fig. 5. The data of Mustajoki above the first solid-phase transition temperature, which varies with the authors (*e.g.*, 160 °C was reported by Mustajoki while it is 166.3 °C in this work), are larger than ours by *ca.* 11%, as in the system of $NaNO_3$. The value of $\Delta C_p^\circ(t_{mp})$ may be slightly negative or almost zero, though it can not be estimated with accuracy because of the phase transition immediately below t_{mp}; the value reported by Mustajoki[19] is -14.2 J K^{-1} mol^{-1}.

$CsNO_3$: The data of this work agree satisfactorily with the data by Sato[22] (see the dashed line in Fig. 6 between 0 and 100 °C but these temperatures are located below t_{tr}). The data of Mustajoki[20] and Flotow *et al.*[23] above 300 °C are larger than ours by less than *ca.* 19%. The values of t_{tr} and t_{mp} (*i.e.*, 151.5 °C and 405.5 °C, and 152 °C and 406 °C as reported by Mustajoki and by Flotow *et al.*, respectively) are rather low compared with ours (*i.e.*, 157.2 °C and 411.7 °C, which lie below each of the data in the other literature), as is shown in Fig. 6. The experimental values of C_p reported by Flotow *et al.* increase linearly with an increase in the temperatures over the entire temperature range above t_{tr}, except for the neighborhood of t_{mp}. Our data show that the heat capacities in the liquid state are almost independent of temperature for all the alkali metal nitrates. The C_p values below t_{tr} in the Flotow *et al.* data are smaller than ours and Mustajoki's. The value of $\Delta C_p^\circ(t_{mp})$ measured by Mustajoki depends on the systems, *i.e.*, 15.0 J K^{-1} mol^{-1} for $NaNO_3$, -14.2 for $RbNO_3$ and *ca.* 0 for $CsNO_3$; in this work $\Delta C_p^\circ(t_{mp})=0$ J K^{-1} mol^{-1} for all the alkali metal nitrates which show a reversible solid-state transition. The values of t_{tr} and t_{mp} determined in this work are given by the figures in parentheses. The literature values are shown by the vertical lines in Figs. 2—6.

Some empirical rules which are possibly suitable for other typical salts have been obtained from the experimental results of C_p for the five alkali metal nitrates:

(1) The $\Delta C_p^\circ(t_{mp})$ defined in Eq. 2 is almost zero for MNO_3 accompanying the reversible solid-state transitions, *i.e.*, $NaNO_3$, KNO_3, $RbNO_3$, or $CsNO_3$.

(2) The heat capacities are independent of the temperatures above t_{mp} for all the nitrates. They increase linearly with an increase in the temperature until the first phase-transition temperatures (*i.e.*, 1.8×10^{-3} J K^{-2} g^{-1} between 50 and 230 °C for $LiNO_3$, 2.3×10^{-3} between 50 and 150 °C for $NaNO_3$, 1.5×10^{-3} between 50 and 125 °C for KNO_3, 1.2×10^{-3} between 50 and 150 °C for $RbNO_3$, and 1.0×10^{-3} between 50 and 150 °C for $CsNO_3$); according to Southard and Nelson,[9] whose data near room temperature are shown by ★ in Figs. 3 and 4, the temperature coefficients of C_p for $NaNO_3$ and KNO_3 over the 100 °C range below room temperature are 2.1×10^{-3} J K^{-2} g^{-1} and 1.5×10^{-3}, respectively. Therefore, between -100 °C and 150 °C the C_p values of $NaNO_3$ and KNO_3 increases linearly with an increase in the temperatures.

(3) Roughly speaking, the magnitude of the discontinuity, ΔC_p^{app}, at the temperature, t_p, corresponding to the maximum value of C_p is in inverse proportion to the thermal expansion α_T for the molten MNO_3 systems except for $RbNO_3$, which has three phase transition points below t_{mp}.

(4) Each of the $NaNO_3$, KNO_3, and $RbNO_3$ systems has nearly the same magnitude of enthalpy required for all the reversible solid-transitions, though the profile of C_p at t_{tr} and the number of the transitions below t_{mp} are dependent on the specific substances.

We shall confine our attention here to the heat capacities of MNO_3 in the liquid state. Starting from a formula for the difference between C_p and C_V, one obtains

$$\frac{C_p}{C_V}-1=\frac{u^2\alpha_T^2MT}{C_p} \tag{3}$$

or:

$$C_p-C_V=\frac{\alpha_T^2v_mT}{\beta_T}, \tag{4}$$

where u, α_T, M, v_m, and β_T are the sound velocity, the thermal expansivity, the molar weight, the molar volume and the isothermal compressibility, respectively.[24] Equation 3 or 4 is useful because we can determine C_V directly from the measured values of C_p and u or β_T. The values of C_V at $1.1\times T_{mp}$ are listed in Table 2, together with the data of β_T, u, α_T, and v_m. The magnitudes of C_V obtained from the compressibility data[25,26] are slightly larger than the C_V values obtained from the velocity data,[27-29] for the molten $CsNO_3$ or $RbNO_3$ with a large molar volume, as is shown in Table 2. No substantial difference between the values of C_V determined using the ultrasonic velocity data[27] and using the hypersonic velocity data[28,29] was found for fused $LiNO_3$ and $NaNO_3$. It is very interesting that the γ ratio, which is defined as C_p/C_V or β_T/β_s (β_s: adiabatic compressibility), increases roughly with an increase in the molar volume, v_m, among the five alkali-metal nitrates in the liquid state. The heat capacity C_V at a constant volume for the MNO_3 melts, consisting of monatomic univalent cations, M^+, and complex univalent anions, NO_3^-, can be divided into the interionic and intraionic portions:

$$C_V=C_V^{inter}+C_V^{intra}, \tag{5}$$

where C_V^{inter} is the sum of the contributions from the translation and configuration for both M^+ and NO_3^- ions and where C_V^{inter} is constructed of vibrational,

TABLE 2. HEAT CAPACITY AT A CONSTANT PRESSURE OR VOLUME OF MOLTEN ALKALI-METAL NITRATES

Sample	$T(=1.1\times T_m)$ / K	$10^{11}\beta_T$ [a] / N m^{-2}	u [b] / ms^{-1}	$10^4\alpha_T$ [2] / K^{-1}	$10^6 v_m$ / m^3	C_p [c] / J K^{-1} mol^{-1}	C_V [d] / $N_A k_B$	γ	10^3 M / kg	t_{mp} [c] / °C
$LiNO_3$	582.7	18.1[25]	—	2.88	36.6		15.7	1.08	68.95	256.5
		20.0[26]	—			140.6 $^{+1.2}_{-1.7}$	15.9	1.07		
		—	1783[27]				15.7	1.08		
		—	1751[28]				15.8	1.07		
$NaNO_3$	641.7	19.8[25]	—	3.46	41.3		14.8	1.13	85.01	310.2
		19.6[26]	—				14.8	1.13		
		—	1740[27]			139.1 $^{+0.9}_{-0.6}$	14.6	1.15		
		—	1761[28]				14.6	1.15		
		—	1762[29]				14.6	1.15		
KNO_3	670.5	22.4[25]	—	3.60	49.9		15.2	1.11	101.1	336.3
		22.7[26]	—				15.2	1.11		
		—	1683[27]			140.3 $^{+1.3}_{-1.4}$	15.3	1.10		
		—	1766[28]				14.8	1.14		
		—	1751[29]				14.8	1.14		
$RbNO_3$	645.4	23.5[25]	—	3.62	54.9		15.2	1.16	147.49	313.5
		20.9[26]	—			146.0 $^{+1.9}_{-1.6}$	14.9	1.18		
		—	1506[28]				14.7	1.19		
$CsNO_3$	753.4	33.6[25]	—	3.81	63.7		14.6	1.17	194.92	411.7
		30.6[26]	—			142.3 $^{+1.6}_{-1.2}$	14.4	1.19		
		—	1198[28]				14.1	1.21		

a) Obtained from the measurement of $(\partial T/\partial P)_s$ in 26) and from the p-V-T studies in 25). b) Hypersonic velocities in 28) and 29), and ultrasonic velocities in 27). c) This work. d) Obtained using Eq. 3 or 4.

rotational and electronic parts in the NO_3^- ion.[30] The values of C_V^{vib}/N_Ak_B and C_V^{rot}/N_Ak_B are 6 and 1.5 respectively, in accord with the classical theory of the heat capacity of an assembly of independent, rigid, non-linear molecules for NO_3^- ions.[30]

Under the assumption of a point charge model for the univalent melts, the C_V^{trans}, C_V^{config}, and C_V^{elec} values of the molten MNO_3 are equal to 3, 3, and 0 respectively in units of N_Ak_B. The estimated value of C_V/N_Ak_B, 13.5, should be compared with the results of the C_V/N_Ak_B values of the five molten MNO_3 at $1.1\times T_{mp}$ cited in Table 2, in which the disagreement may originate mainly from the short estimation of C_V^{config} for molten MNO_3. The molten alkali nitrates have a higher heat capacity (*i.e.*, *ca.* $15\times N_Ak_B$) at a constant volume than that (*ca.* $6.0\times N_Ak_B$) of molten alkali chlorides because of the vibrational and rotational contributions associated with NO_3^-. The hard-sphere models[31,32] applied to the thermodynamic properties of simple molten salts are not adequate for the molten nitrates which consist of complex anions, NO_3^-, and monatomic cations M^+.

Once again let us focus on the difference, ΔC_p^{app}, between the maximum value of C_p near t_{mp} and the value of C_p corresponding to the horizontal line linking the open circles shown in the upper part of Figs. 2—6. The ΔC_p^{app} quantity should not be confused with the $\Delta C_p^{\circ}(t_{mp})$ defined in Eq. 2 and should be infinite, though it is apparently finite in the experimental results. Such values of ΔC_p^{app} may originate from the sudden appearance of the communal entropy at the melting point because each ion can move anywhere in the liquid, whereas in the crystal the ions are localized systems.

Some of the techniques used have serious drawbacks, since some previously reported data on heat capacities in the liquid state are much too high, and their temperature coefficients are not certainly less than the positive values in the solid state.[34] The conclusion in this work is that the heat capacity of each molten alkali-metal nitrate is in the range from 138 to 148 J K^{-1} mol^{-1} and is probably independent of the temperature. At this point, it should be possible to regard some sets of results above t_{mp} as better than others.

We wish to thank Professor Hideaki Kita for his encouragement during the course of this work. We also greatly appreciate the help of Professor G. J. Janz in supplying the sample of KNO_3 used in this work and for showing us a number of references on the heat capacities of ionic melts which were retrieved by the Molten Salt Data Center, Rensselaer Polytechnic Inst., USA. We also wish to thank Dr. D. K. Tödheide for his comments on the compressibility and velocity data of the molten nitrates. This work was supported by a Grant-in-Aid for Scientific Research No. 56470001 from the Ministry of Education, Science and Culture.

References

1) *E.g.* H. M. Goodwin and H. T. Kalmus, *Phys. Rev.*, **28**, 1 (1909).
2) G. J. Janz, "Molten Salts Handbook," Academic Press, New York (1967), p. 184.
3) W. W. Wendlandt, "Thermal Methods of Analysis," Interscience Pub., New York (1964), p. 132.

4) Y. S. Touloukian and C. Y. Ho, "Thermophysical Properties of Matter, Specific Heat (Vol. 4)," Heyden Pub., London.
5) N. Onodera, A. Kimoto, M. Sakiyama, and S. Seki, *Bull. Chem. Soc. Jpn.*, **44**, 1463 (1971).
6) H. V. Regnault, *Ann. Chim. Phys.*, **1**, 129 (1841).
7) C. C. Person, *Ann. Chim. Phys.*, **21**, 295 (1847).
8) J. H. Schüller, *Pogg. Ann.*, **136**, 70 and 235 (1869).
9) J. C. Southard and R. A. Nelson, *J. Am. Chem. Soc.*, **55**, 4865 (1933).
10) H. Miekk-Oja, *Ann. Acad. Sci. Fenn., Ser. A*, **1**, 7 (1941).
11) V. A. Sokolov and N. E. Schmidt, *Izv. Sekt. Fiz-Khim. Anal. Inst. Obsh. Neorg. Khim. Acad. Nauk. SSSR*, **26**, 123 (1955).
12) A. Mustajoki, *Ann. Acad. Sci. Fenn., Ser. A*, **6**, 5 (1957).
13) G. J. Janz, F. J. Kelly, and J. L. Perano, *J. Chem. Eng. Data*, **9**, 133 (1964).
14) V. C. Reinsborough and F. E. W. Wetmore, *Aust. J. Chem.*, **20**, 1 (1967).
15) I. Barin and O. Knacke, "Thermochemical Properties of Inorganic Substances," Springer-Verlag, Berlin (1973).
16) R. W. Carling, "Proc. of the Third Inter. Symp. on Molten Salts," ed by G. Mamantov, M. Blander, and G. P. Smith, Elect. Soc., Pennington (1981), p. 485.
17) V. A. Sokolov and N. E. Schmidt, *Izv. Fiz-Khim. Anal. Inst. Obsh. Neorg. Khim. Acad. Nauk. SSSR*, **27**, 217 (1956).
18) A Mustajoki, *Ann. Acad. Sci. Fenn., Ser. A*, **6**, 99 (1962).
19) A. Mustajoki, *Ann. Acad. Sci. Fenn., Ser. A*, **6**, 9 (1958).
20) A. Mustajoki, *Ann. Acad. Sci. Fenn., Ser. A*, **6**, 7 (1957).
21) "Landolt-Börnstein, Zahlenwerte und Funktionen, II. Band 4. Teil: Kalorische Zustandsgroßen," Springer-Verlag, Berlin (1961), p. 502.
22) S. J. Sato, *Sci. Res. Inst. Tokyo*, **48**, 59 (1954).
23) H. E. Flotow, P. A. G. O'Hare, and J. J. Boerio-Goates, *Chem. Thermodyn.*, **13**, 477 (1981).
24) E.g., K. S. Pitzer and L. Brewer, "Thermodynamics," McGraw-Hill, New York (1961), p. 102.
25) J. E. Bannard and A. F. M. Barton, *J. Chem. Soc., Faraday Trans. 1*, **74**, 153 (1978).
26) B. Cleaver and P. Zain, *High Temp.-High Pressures*, **10**, 437 (1978).
27) J. O'M. Bockris and N. E. Richards, *Proc. R. Soc. London, Ser. A*, **241**, 44 (1957).
28) H. E. G. Knape and L. M. J. Torell, *Chem. Phys.*, **62**, 4111 (1975).
29) T. Ejima, K. Shimakage, T. Yamamura, Y. Sato, T. Yoko, H. Nakatao, and Y. J. Kobayashi, *Jpn. Inst. Metals.*, **46**, 43 (1982).
30) E.g., G. S. Rushbrook, "Introduction to Statistical Mechanics," Clarendon Press, Oxford (1951), pp. 84 and 127.
31) H. Reiss, *Adv. Chem. Phys.*, **9**, 1 (1965).
32) T. Itami and M. Shimoji, *J. Chem. Soc., Faraday Trans. 2*, **76**, 1347 (1980).
33) C. N. R. Rao and K. J. Rao, "Phase Transitions in Solids," McGraw-Hill, New York (1978), p. 17.
34) E.g., P. Nguyen-Duy and E. A. Dancy, *Thermochim. Acta*, **39**, 95 (1980).

Self-diffusion and Melting in the Plastic Phases of Neopentane as Studied by NMR Relaxation at High Pressures

Sadamu TAKEDA, (the late) Gen SODA, and Hideaki CHIHARA*

Department of Chemistry, Faculty of Science, Osaka University, Toyonaka, Osaka 560

(Received December 2, 1982)

Proton spin-lattice relaxation time T_1 in the plastic phase of 2,2-dimethylpropane (neopentane) was measured at 10 MHz up to 170 MPa between 192.7 and 308.2 K. T_1 near the melting point is determined by self-diffusion. The enthalpy and volume of activation of this motion suggest that self-diffusion occurs through a single vacancy mechanism. The correlation time of self-diffusion at the melting point (T_f) is $(3.2 \pm 0.5) \times 10^{-7}$ s irrespective of external pressure. The diffusion rate is a function only of T_f/T, *i.e.* the law of corresponding states holds. The feature of activation properties of self-diffusion is strongly correlated with the melting phenomenon. The melting curve of the phase diagram was also determined and a possibility of existence of another plastic phase was found above 40 MPa.

Molecular motions in plastic crystals (ODIC, the orientationally disordered crystals) have been studied by a variety of experimental methods.[1] These crystals are characterized by a small entropy of fusion (less than 21 J K^{-1} mol^{-1}) and existence of a phase transition below which the crystal becomes brittle. In general, overall rotation of a molecule is highly excited in the plastic phase and even self-diffusion is seen by the NMR and other methods below the melting point in many plastic crystals.[2] There is an empirical law that the correlation time of self-diffusion becomes about 10^{-7} s at the melting temperature in different plastic crystals.[2] It leads us to believe that on-set of self-diffusion acts as a dynamical trigger of the melting phenomenon in these crystals. A large amount of experimental data have already been accumulated about the self-diffusion in plastic crystals but most of them are the results under ordinary pressure. It is the purpose of the present study to make a "corresponding state" type of analysis of the melting from the self-diffusion data on 2,2-dimethylpropane (neopentane) obtained under different pressures.

Neopentane is a typical compound having a plastic crystalline phase and a relatively large amount of experimental information is now available. The plastic phase of neopentane has the f.c.c. structure (a= 8.82 Å)[3,4] containing four molecules a unit cell. The melting and transition temperatures are 256.5 and 140.5 K, respectively, and their associated entropy changes are 12.0 and 18.7 J K^{-1} mol^{-1}.[5] The state of molecular motion in the plastic and brittle crystalline phases are fairly well understood by the NMR[6-10] and other methods.[11-13] Thus, it is generally substantiated that overall molecular tumbling is highly excited in the plastic phase with an activation enthalpy of 4.2 kJ mol^{-1}, while the activation enthalpy for self-diffusion was reported to be between 25 and 34 kJ mol^{-1}.[6,8,9]

The pressure dependence of molecular motion in the plastic neopentane has also been reported by Allen *et al.*[7] However, they dealt only with a limited temperature range. Therefore, we now extended the measurements of proton spin-lattice relaxation time of the plastic phase of neopentane under pressure up to the melting point and also determined its melting curve. The results were then analyzed to derive motional parameters related to self-diffusion and melting.

Experimental

High Pressure Vessel and Pressure Measurement. The high pressure vessel used in this experiment was a clamped type which is essentially the same as the one that has been reported elsewhere.[14] The seal materials were fluoride rubber, Teflon, and lead metal, which constitute a conventional Bridgeman-type pressure seal. The design of the electrical leads from the interior of the pressure vessel to the outside is similar to that used by Terry and Ruoff,[15] with a heat shrinkable Teflon tube (NSTube-910-2, Nitto Denko, Japan) and epoxy putty XD580 (Japan CIBA GEIGY) used for the seal materials.[14]

The pressure-transmitting medium is the sample itself and its pressure was measured by means of a "manganin gage" whose resistance was determined by the four-terminal method. The gage was calibrated for temperature- and pressure-coefficients. First, the pressure coefficient was determined at 293 K with reference to the standard Heise gage up to 200 MPa. Secondly, the temperature coefficient was determined at the ambient pressure between 175 and 330 K. The pressure coefficient also depends on temperature but it is reported that the effect is small; if we put $\Delta = \{R(P) - R(0)\}/R(0)$, the value of $(d\Delta/dT)/\Delta$ is less than 3×10^{-4} K^{-1}.[16-18] Therefore, we used $\Delta/P = 2.442 \times 10^{-5}$ $(MPa)^{-1}$ (at 293 K) throughout the temperature range studied in the present work (192 K to 308 K). The temperature coefficient of the resistance of manganin is not very small at low temperatures, *e.g.* 2×10^{-4} K^{-1} at 200 K, and this required a good precision of temperature measurement and control. The temperature of the specimen could be controled to within $\pm 1/30$ K and it was measured by several Chromel-P-Constantan thermocouples attached on the outside periphery of the vessel. The overall uncertainty in the pressure determination was about ± 2.5 MPa.

Preparation of the Sample and T_1 Measurement. A sample of neopentane of commercial origin (Takachiho Kagakukogyo, Co.) was dried over Molecular Sieves 3A, 4A, and 5A in vacuum, purified by repeated vacuum distillation, and degassed by several freeze-pump-thaw cycles. The specimen was then distilled into the high pressure vessel through an adapter which connected the pressure vessel to the purification line.[14] The final purity of the specimen was better than 99.8 mol% by gas chromatography. The specimen was compressed at room temperature by use of a hydraulic press and the T_1 measurements were made under conditions of effectively constant volume.

Proton spin-lattice relaxation time (T_1) was measured using 90° train$-\tau-$90° pulse sequences at an operating frequency of 10.0 MHz. A series of T_1 values under pres-

sure were measured by varying the temperature after the specimen had been compressed at room temperature. The temperatures at which the T_1 measurement was performed were fixed within ± 0.1 K throughout the different series. Because the pressure inside the vessel changed when the specimen temperature changed, the primary experimental results of the different series were reorganized to show the pressure dependence of T_1 at a constant temperature.

It should be noted that the materials used to pressure-seal of the vessel did not contaminate the specimen as far as the T_1 values were concerned; we obtained completely reversible and reproducible results within the experimental uncertainty for the 10-d old sample held in the vessel as well as for a virgin specimen.

Results and Discussion

Self-diffusion and Its Activation Properties. The representative pressure dependence of the proton spin-lattice relaxation time in the plastic phase of neopentane at various temperatures are shown in Fig. 1. The plots for the measurements at seven additional intermediate temperatures (308.2, 293.2, 272.4, 252.5, 233.8, 214.0, and 192.7 K) fall between the curves but for the sake of clarity they were not included in this figure. The two motional processes, molecular rotation and self-diffusion, have been discussed from the continuous wave and pulsed NMR experiments in the plastic phase.[6-10]

There is a maximum in T_1 when it is plotted as a function of pressure for a constant temperature. This has been clearly demonstrated by Allen *et al.*[9] and its high-pressure side corresponds to the region where molecular tumbling is the dominant mechanism of the spin-lattice relaxation. The present study is essentially restricted to the low-pressure side of the T_1 maximum where self-diffusion mainly governs the relaxation rate. Where comparison is possible, our results are in reasonable agreement with the results of Allen *et al.* (who used 24.4 MHz for measurements).[9] Therefore, we will deal only with self-diffusion in this paper.

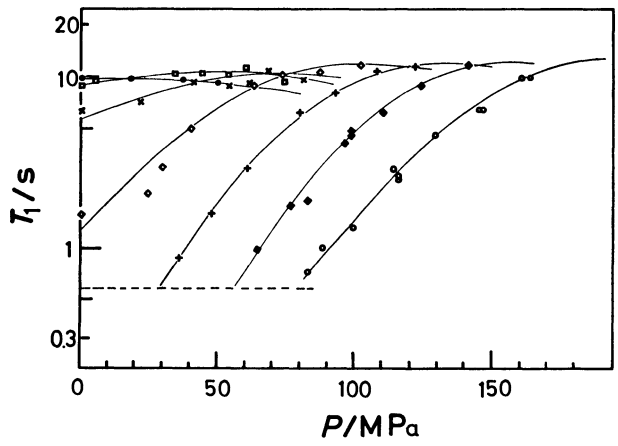

Fig. 1. Pressure dependence of the proton spin-lattice relaxation time at different temperatures; ○ 297.4 K, ◆ 281.0 K, + 263.6 K, ◇ 242.9 K, × 223.9 K, □ 214.0 K, ● 202.5 K. The dashed line shows the alignment of the melting points.

We assume the Arrhenius type of activation process for self-diffusion,

$$\tau_{SD} = A \exp(\Delta G^*/RT) = \tau^0_{SD} \exp(\Delta H^*/RT), \quad (1)$$

where τ_{SD} is the correlation time of self-diffusion and ΔG^*, the Gibbs energy of activation, is defined by

$$\Delta G^* = \Delta H^* - T\Delta S^*$$

or

$$\Delta G^* = \Delta E^* + P\Delta V^* - T\Delta S^*. \quad (2)$$

Then, the activation volume ΔV^* and the activation enthalpy ΔH^* can be derived from the equations,[19]

$$\Delta V^* = RT\{\partial(\ln\tau_{SD})/\partial P\}_T, \quad (3)$$

$$\Delta H^* = R\{\partial(\ln\tau_{SD})/\partial(1/T)\}_P, \quad (4)$$

where the activation entropy ΔS^* has been assumed to be constant over the present temperature and pressure region.[19] Because what we observed is the low temperature branch ($\omega_0\tau_{SD} \gg 1$) of the T_1 curve due to self-diffusion, τ_{SD} is proportional to $T_{1\,SD}$, where $T_{1\,SD}$ is the relaxation time due to self-diffusion. Thus, τ_{SD} in Eqs. 3 and 4 can be replaced by $T_{1\,SD}$ because the change of intermolecular dipole-dipole interaction can be safely ignored in the present pressure range.[9] One can obtain $T_{1\,SD}$ from the equation,

$$T_1^{-1}{}_{obsd} = T_1^{-1}{}_{SD} + T_1^{-1}{}_{RO}, \quad (5)$$

where $T_1^{-1}{}_{obsd}$ is the observed spin-lattice relaxation rate (Fig. 1) and $T_1^{-1}{}_{RO}$ is the spin-lattice relaxation rate due to molecular reorientation. Now, we try to separate the two contributions in Eq. 5. The second term of Eq. 5 was evaluated in the following way. Since the slope of $T_{1\,obsd}$ on the high pressure side of the maximum (Fig. 1) agrees with the slope as determined by Allen *et al.* where comparison is possible, we used their slope so that smooth extrapolation of our T_1 curve to high pressure may be made. This extrapolation enables us to estimate $T_1^{-1}{}_{RO}$ from the high-pressure branch of the $T_1^{-1}{}_{obsd}$ curve.

The activation volume ΔV^* was then derived from linear plots of $\ln(T_{1\,SD})$ against P at different temperatures. The activation volume ΔV^* (Fig. 2) thus derived was 133 ± 18 cm^3 mol^{-1} between 252.5 and

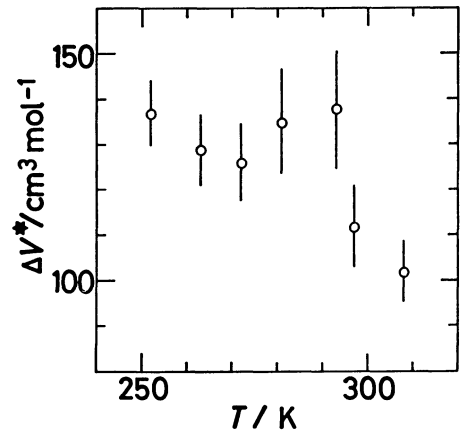

Fig. 2. Temperature dependence of the activation volume of self-diffusion.

293.2 K. The result is nearly equal to that obtained by Allen *et al.*[9] The two points above 297.4 K in Fig. 2 lie much lower than the other points; this may indicate possible existence of another phase transition as will be discussed below. The ratio of ΔV^* to the molecular volume V_m, which was determined to be 102 $cm^3\ mol^{-1}$ at 220 K from X-ray experiments,[3,4] is about 1.3. Because each of the formation and migration volume of a vacancy is not considered to be equal to V_m, the comparison of ΔV^* with V_m does not have a definite meaning. But the fact, $\Delta V^*/V_m = 1.3$, probably suggests that the self-diffusion in plastic neopentane is mainly controled by a single vacancy.

The feature of single-vacancy diffusion in plastic neopentane is assisted by the value of activation enthalpy ΔH^*. The plot in Fig. 1 can be rearranged to show the temperature dependence of T_1 at constant pressure. Through a similar procedure to the derivation of ΔV^*, the activation enthalpy ΔH^* of self-diffusion was calculated by use of Eq. 4 from the $\ln(T_{1\,SD})$ *vs.* $1/T$ plot. Unfortunately, large errors involved in the determination of ΔH^* did not permit to determine its temperature coefficient but the average value of ΔH^* was 43.5 ± 8.4 kJ mol^{-1} between 0.1 and 80 MPa which is somewhat larger than the value reported by Stejeskal *et al.*,[6] Roeder and Douglass,[8] and Allen *et al.*[9] The activation enthalpy ΔH^* is the sum of enthalpy of vacancy formation and enthalpy of migration,[20] each of which is usually considered to be nearly equal to the heat of sublimation L_s if self-diffusion proceeds *via* single vacancy mechanism.[2,21,22] In the case of neopentane, the ratio of ΔH^* to L_s[23] is

$$\Delta H^*/L_s = 43.5\ \text{kJ mol}^{-1}/23.4\ \text{kJ mol}^{-1} = 1.9 \quad (6)$$

at an ordinary pressure, which fact therefore suggests that self-diffusion in plastic neopentane is also controled by a single vacancy.

Phase Diagram. The melting point of neopentane under pressure was determined from the point where dP/dT changed its slope. It was also seen by a discontinuous change in T_1. The results are shown in Fig. 3. The equilibrium curve must follow the Clapeyron-Clausius equation,

$$dT_f/dP = \Delta V_f T_f/\Delta H_f, \quad (7)$$

where ΔH_f is the enthalpy of fusion and ΔV_f is the change in molecular volume at T_f, the melting temperature. By substituting the appropriate values to ΔH_f (3.09 kJ mol^{-1}),[5] ΔV_f (7×10^{-6} $m^3\ mol^{-1}$),[24] and T_f (256.5 K),[5] one obtains $dP/dT_f = 1.7$ MPa K^{-1}. The value found from Fig. 3 is 1.8 MPa K^{-1}, being consistent with Eq. 7.

There is possibility for existence of another solid phase which we designate Phase I′ between the plastic f.c.c. solid and the liquid phases above 40 MPa. It was inferred from a break in the curve of pressure *vs.* temperature at a prefixed volume. This curve is also shown in Fig. 3 as a dotted curve. According to Art-Ming Chen and Kai-Chow Chan who measured the density at 50 MPa at different temperatures, the density linearly decreases up to 273.5 K but it is smaller

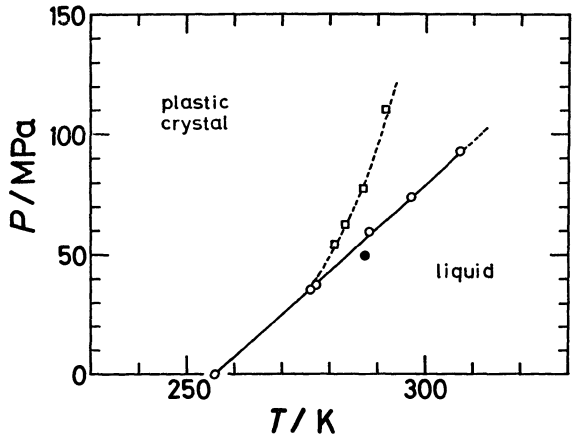

Fig. 3. Phase diagram of neopentane. Solid line shows the melting curve (○), while dashed line indicates a new transition line (see text). Full circle (●) is the melting point at 50 MPa determined by Art-Ming Chen and Kai-Chow Chain.[24]

by about 3.2% at 286.3 K than may be predicted from a linear extrapolation. This also supports existence of a new Phase I′. It is difficult to speculate about the nature of Phase I′ or the new transition at this point, but there is no discernible change in the T_1 values on going from the f.c.c. phase to Phase I′. Also the fact that the melting curve of Fig. 3 is almost linear suggests that changes in physical properties at the new transition point will be small.

The two points in Fig. 2 above 297.4 K correspond to the region where Phase I′ is stable. It is interesting to note that ΔV^* is smaller in Phase I′ than in Phase I (f.c.c.).

Corresponding State. If $\log(T_{1\,SD})$ is plotted against T_f/T, one obtains a good straight line irrespective of the pressure. This is illustrated for some selected pressures in Fig. 4. The fact that they all fall on a single straight line indicates that the law of corresponding states holds for the spin-lattice relaxation time at least to within the bounds of scatter of points in Fig. 4. In other words, the diffusion rate is also a function of T_f/T only, since the correlation time τ_{SD} is related to $T_{1\,SD}$ in the present case through

$$T_1^{-1}{}_{SD} = 2.29\gamma^2 M_2(\omega_0{}^2\tau_{SD})^{-1}, \quad (8)$$

which is derived using Torrey's correlation functions[25-27] for random walk in a f.c.c. lattice, where M_2 is the part of intermolecular second moment that is modulated by self-diffusion.

The threshold value of τ_{SD} at the melting point may be calculated from Eq. 8 using $M_2 = 1.1$ G^2 obtained at the ambient pressure.[7,10] It is $(3.2 \pm 0.5) \times 10^{-7}$ s at T_f although T_f varies from 256.5 K (at 0.1 MPa) to 306 K (at 90 MPa). It seems that the threshold value of τ_{SD} is not only independent of pressure but it is a kind of constant of plastic crystal because most of the plastic crystals ever examined melt when the threshold value of τ_{SD} reaches a value of about 10^{-7} s.[2,28]

The linear relation of Fig. 4 shows that τ_{SD} is em-

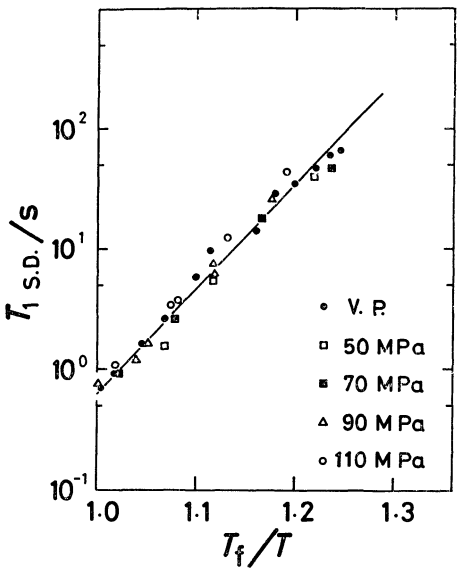

Fig. 4. Spin-lattice relaxation time due to self-diffusion ($T_{1\,SD}$) is plotted against the reduced temperature T_f/T, where T_f is the melting temperature at each pressure. V.P. means the vapor pressure of the sample itself.

pirically given by

$$\tau_{SD} = \tau^0_{SD}\exp\{b(T_f/T)\}, \tag{9}$$

where b is 20.2±2.6 for neopentane. If one substitutes Eq. 9 to Eqs. 3 and 4, b is shown to be related to the enthalpy and volume of activation for self-diffusion through the formulas

$$\Delta H^* = bRT_f \tag{10}$$

and

$$\Delta V^* = bR(dT_f/dP). \tag{11}$$

By substituting Eqs. 10 and 11 into the Clapeyron-Clausius equation (Eq. 7), we obtain

$$\Delta V^*/\Delta H^* = \Delta V_f/\Delta H_f. \tag{12}$$

If we use the values observed in the present experiment, *i.e.* $\Delta V^* = 133\pm17$ cm^3 mol^{-1} and $\Delta H^* = 43.5\pm8.4$ kJ mol^{-1}, we obtain $\Delta V^*/\Delta H^* = 3.3\pm1.1$ cm^3 (kJ)$^{-1}$ which is in reasonable agreement with the value $\Delta V_f/\Delta H_f = 2.3$ cm^3 (kJ)$^{-1}$ where $\Delta V_f = 7$ cm^3 mol^{-1} [24] and $\Delta H_f = 3.093\pm0.001$ kJ mol^{-1}.[5] Equation 12 which is an almost exact consequence of the relation (9) shows that the activation process for diffusion is in a way related to the melting process.

The activation energy ΔE^* of diffusion is the sum of the energy of formation (E_f) of a vacancy and its migration (E_m). Cauchman and Reynolds[29] derived a relation between the energy of migration of a vacancy (E_m) and the melting temperature (T_f),

$$E_m = \frac{K_1}{D}\left(\frac{k}{\hbar}\right)^2 T_f, \tag{13}$$

where K_1 and D are constants determined primarily by geometry of the lattice. By combining Eq. 13 with the formula for E_f due to Glyde,[30] we obtain a relation between ΔE^* and T_f similar to Eq. 13,

$$\begin{aligned}\Delta E^* &= E_m + E_f \\ &= \left(\frac{k}{\hbar}\right)^2\left(\frac{K_1+K_2}{D}\right)T_f \\ &= CT_f,\end{aligned} \tag{14}$$

where K_2 is also a constant. Because the contribution of the $P\Delta V^*$ term to the activation enthalpy, $\Delta H^* = \Delta E^* + P\Delta V^*$, is small (less than 1%), the comparison between Eq. 10 and Eq. 14 is possible. The constant b in Eq. 9 must therefore depend on the properties of the lattice in which diffusion takes place. In many plastic crystals, the value of b ($=C/R$) in Eq. 9 is also about 20[31] and similar values of C/R were also found for many metals. This fact is very suggestive but the theory is only of qualitative nature and does not warrant any quantitative calculation.

Finally, it is perhaps significant to note that the straight line of Fig. 4 covers both situations of melting of Phase I and Phase I'. This is related to the fact that we failed to detect any change in T_1 on going from Phase I to Phase I'. Probably, Phase I' is also a plastic crystal which has a similar property to that of Phase I (f.c.c.).

The authors would like to express their gratitude to Dr. Akifumi Onodera for help provided in the calibration of the pressure gage (manganin gage).

References

1) "The plastically crystalline state, orientationally disordered crystals," ed by J. N. Sherwood, John Wiley & Sons, New York (1979).
2) J. M. Chezeau and J. H. Strange, *Phys. Repts.*, **53**, 1 (1979), and references cited therein.
3) A. H. Mones and B. Post, *J. Chem. Phys.*, **20**, 755 (1952).
4) R. Rudman and B. Post, *Mol. Cryst.*, **5**, 95 (1968).
5) H. Enokido, T. Shinoda, and Y. Mashiko, *Bull. Chem. Soc. Jpn.*, **42**, 84 (1969).
6) E. O. Stejeskal, D. E. Woessnor, T. C. Farrar, and H. S. Gutowsky, *J. Chem. Phys.*, **31**, 55 (1959).
7) J. G. Powles and H. S. Gutowsky, *J. Chem. Phys.*, **21**, 1965 (1953).
8) S. B. W. Roeder and D. C. Douglass, *J. Chem. Phys.*, **52**, 5525 (1970).
9) W. C. Allen, N. Liu, and J. Jonas, *J. Chem. Phys.*, **63**, 3312 (1975).
10) S. Takeda, G. Soda, and H. Chihara, *Mol. Phys.*, **47**, 501 (1982).
11) R. E. Lechner, *Solid State Commun.*, **10**, 1247 (1972).
12) R. C. Livingston, W. G. Rothschild, and J. J. Rush, *J. Chem. Phys.*, **59**, 2498 (1973).
13) C. Steenbergen and L. A. de Graaf, *Physica*, **96B**, 1 (1979).
14) T. Hasebe, G. Soda, and H. Chihara, *Bull. Chem. Soc. Jpn.*, **54**, 2583 (1981).
15) R. E. Terry and A. L. Ruoff, *Rev. Sci. Instr.*, **43**, 1379 (1972).
16) S. Yamamoto, *Bull. Natl. Res. Lab. Metrol.*, **24**, 23 (1972).
17) S. Yamamoto, *Bull. Natl. Res. Lab. Metrol.*, **25**, 1 (1972).
18) G. Fujii, N. Mori, H. Nagano, and S. Minomura, *Cryog. Eng.*, **4**, 226 (1969).

19) S. M. Ross and J. H. Strange, *J. Chem. Phys.*, **68**, 3078 (1978).
20) A. V. Chadwick and H. R. Glyde, "Rare gas solids," ed by M. L. Klein and T. A. Venable, Academic Press, New York and London (1977), Vol. II, Chap. 19, p. 1151.
21) J. N. Sherwood, "Surface and defect properties of solids, Specialist periodical reports," The Chemical Society, London (1973), Vol. 2, p. 250.
22) R. Folland, R. C. Jackson, J. H. Strange, and A. V. Chadwick, *J. Phys. Chem. Solids*, **34**, 1713 (1973).
23) S. M. Breitling, A. D. Jones, and H. Boyd, *J. Chem. Phys.*, **54**, 3959 (1971).
24) H. Art-Ming Chen and R. Kai-Chow Chan, *Can. J. Chem.*, **51**, 2141 (1973).
25) H. C. Torrey, *Phys. Rev.*, **92**, 962 (1953).
26) H. C. Torrey, *Phys. Rev.*, **96**, 690 (1954).
27) H. A. Resing and H. C. Torrey, *Phys. Rev.*, **131**, 110 (1973).
28) H. Chihara and N. Nakamura, *Mol. Cryst. Liq. Cryst.*, **41**, 21 (1977).
29) P. R. Couchman and C. L. Reynolds, Jr., *Philos. Mag.*, **34**, 327 (1976).
30) H. R. Glyde, *J. Phys. Chem. Solids.*, **28**, 2061 (1967).
31) N. Boden, *Chem. Phys. Lett.*, **46**, 141 (1977).

Oxygen Evolution Reaction on Composite Cobalt Borides

Tetsuya Osaka,* Yoshio Iwase, Hiroshi Kitayama, and Toshihiro Ichino

Department of Applied Chemistry, School of Science and Engineering, Waseda University, Okubo, Shinjuku-ku, Tokyo 160

(Received December 4, 1982)

The Oxygen evolution reaction on cobalt borides and composite cobalt borides was investigated in a 6 M KOH solution (1 M = 1 mol dm^{-3}) using the factor of the magnetic properties. In the system of cobalt borides (Co:B = 3:1) prepared at various sintering temperatures, the boride having a higher saturation magnetization revealed a higher activity of the oxygen evolution reaction. In the system of composite cobalt borides which have various magnetic moments, μ_B, a clear correlation between the activity of the oxygen evolution reaction and the saturation magnetization (or magnetic moment, μ_B) was observed for several composite cobalt boride species (*i.e.*, Co-Fe-B, Co-Ni-B, Co-Mn-B, and Co-B). Among the composite cobalt boride species, the cobalt iron boride (Co:Fe:B = 1:2:1) sintered at 450 °C showed the highest activity of oxygen evolution reaction in a 6 M KOH solution. The conditions of oxide formation on Co-Fe-B(1:2:1) and on Co-B(3:1) in a 6 M KOH solution were compared with those on cobalt by means of voltammetry and chronopotentiometry. It was concluded that the ease and stability of oxide films in higher oxidation states are strongly correlated to the activity of the oxygen evolution reaction which occurs on more highly oxidized oxide films.

Oxygen evolution reaction on non-noble metals or alloys is attractive in the field of oxygen electrode catalysts because of the demand for low-cost electrocatalyst materials for water electrolyzers. The transition metal borides have been reported to have a high activity for an oxygen evolution reaction in an alkaline solution.[1] In the present paper, we will focus on the cobalt boride and investigate the activity of the oxygen evolution reaction on composite cobalt borides in terms of the factor of magnetic properties.

Experimental

The composite cobalt borides were prepared by mixing the powders of cobalt, the other transition metal (Fe, Ni, or Mn), and amorphous boron in a proper atomic ratio. The mixed powders, whose particle sizes were adjusted by means of 200 mesh sieve, were pressed with 10 t cm^{-2} into a cylinder shape (0.7 cm in diameter). The cylindrical samples were sintered for 4 h in an Ar gas atmosphere at several temperatures. The identification and characterization of the composite cobalt borides were performed by means of an X-ray diffractometer, a differential thermal analyzer, an X-ray photoelectron spectroscopy, and a magnetic-property analyzer (sensitive vibrating sample magnetometer). The surface conditions and roughness of the electrodes were examined by means of a scanning electron microscope and a stylus technique (Talystep). The mean surface roughness† of the boride electrodes became lower with the increase in the sintering temperature, reaching a constant value of 0.6 μm at a sintering temperature of more than 400 °C. The SEM observation showed that the surface of borides sintered at more than 300 °C for 4 h is non-porous.†† The current *vs.* potential curves with IR correction for oxygen evolution reaction on the composite cobalt borides were measured potentiostatically in a 6 M KOH solution at 25 °C under an N_2 atmosphere. After having been covered by epoxy resin, the working electrode was carefully polished with emery paper, and then it was washed with ethanol and water. The boride electrode was used after pretreatment consisting of anodic oxidation for 1 h at 0.80 V (Hg-HgO) in the case of the oxygen evolution reaction in order to obtain stable oxidized surface condition. The activation energy of the oxygen evolution reaction was evaluated by means of the apparent activation energy at 0.60 V (Hg-HgO) (or at proper potential) and it was determined in the temperature range between 0 °C and 50 °C with the temperature correction. The electrochemical investigation of electrode surface oxides was done in a 6 M KOH solution by means of linear potential sweep voltammetry and chronopotentiometry. A mercury-mercury(II) oxide electrode in the same solution was used as the reference electrode, and all the potential was referred to the Hg-HgO electrode. The stability of the borides was evaluated by means of the amount of boron dissolved after 24 h electrolysis at 0.70 V in the 6 M KOH solution. The amount of boron dissolved in the solution was examined by means of photospectroscopy using the Methylene Blue method. A small amount of boron dissolved was detected as having values between 2 and 4 mg after 24 h electrolysis for the three cases of Co-B(3 : 1), Fe-B(3 : 1), and Co-Fe-B(1 : 2 : 1), which were sintered at 400 or 450 °C.

† The mean surface roughness is evaluated by averaging 10 point data of ΔR_{max} (difference between top and bottom positions as measured by Talystep).

Results and Discussion

Oxygen Evolution Reaction on Cobalt Borides. It was found that the cobalt boride at proper conditions has a higher activity for oxygen evolution reaction than does nickel or cobalt in an alkaline solution.[1] The activity of the oxygen evolution reaction depends

†† The double layer capacities of Co, Co-B(3 : 1) sintered at 400 °C, and Co-Fe-B(1 : 2 : 1) sintered at 450 °C, measured at −1.0 V and at 1 kHz in 6 M KOH, were observed as the reasonable values of 110, 60, and 110 μF cm^{-2} respectively. The current-potential curve on the Co electrode, which was prepared by the same method as the borides, was observed to show the same behavior as on an usual Co electrode. These two facts also strongly support the theory that these borides can be used as non-porous states.

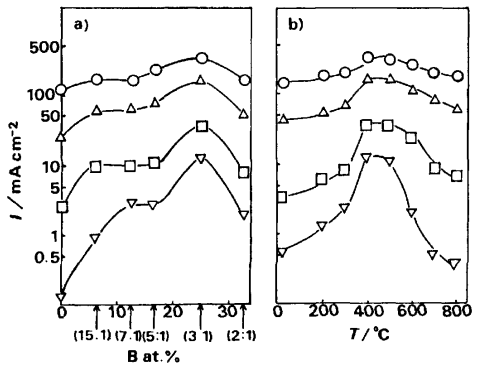

Fig. 1. Effects of sintering temperature and boron content of cobalt borides on oxygen evolution current in 6 M KOH at 25 °C.
a) Oxygen evolution current *vs.* boron content curves on Co-B sintered at 400 °C for 4 h. b) Oxygen evolution current *vs.* sintering temperature curves on Co-B(3 : 1), ○: at 0.80 V, △: at 0.70 V, □: at 0.60 V, ▽: at 0.50 V.

largely on the composition ratio of Co:B and the sintering temperature. The effects of the boron content and the sintering temperature on the activity of the oxygen evolution reaction (*i.e.*, current values at several constant potentials) are demonstrated in Fig. 1. The best conditions for a high activity of oxygen evolution were obviously observed to be at the composition ratio of Co:B=3:1 and at the sintering temperature=400—500 °C, as may be seen in Fig. 1. The apparent activation energy, ΔH, at 0.60 V, of the oxygen evolution reaction on cobalt boride sintered at 400—500 °C, gave the lowest value of 8.6 kcal mol^{-1}.††† As has already been pointed out in Ref. 1, the cobalt boride sintered at 400 °C is considered to be amorphous or in a transition state, judging from the combined results of X-ray diffraction analysis, differential thermal analysis, and magnetic property measurement. The magnetic properties which are sensitive to the structure change in materials were measured and discussed in Ref. 1 in connection with the function of the sintering temperature. A rapid decrease in coercivity, Hc, was observed in the range of sintering temperature between 350 and 400 °C. The saturation magnetization, σ_s, also started to change from the sintering temperature of 300 °C and showed its maximum in the sintering temperature region between 350 and 500 °C. In the region of sintering temperatures, higher than 500 °C, the value of σ_s abruptly decreased. The change in magnetic properties from the lower sintering temperature, at which the peaks of X-ray diffraction analysis and DTA caused by the formation of compounds are not recognized (*cf.* Ref. 1), may indicate that the amorphous or transition state compounds are formed in the range between 400 and 500 °C.**

††† 1 kcal mol^{-1}=4.184 J mol^{-1}.

** The X-ray diffraction peak of CoB was partially observed at 400 °C, while the peaks of Co_3B were detected from 600 °C.

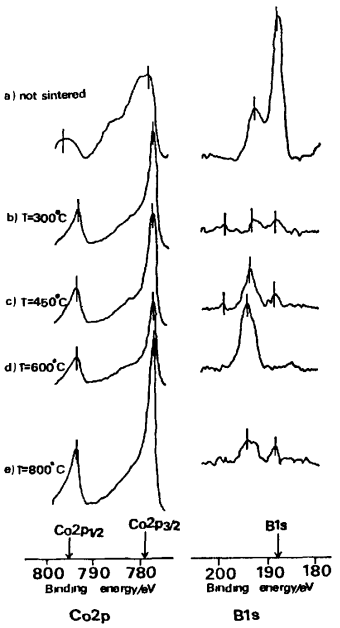

Fig. 2. Photoelectron spectra of Co 2p levels and B 1s level for Co-B(3 : 1) at various sintering temperatures.

Since X-ray photoelectron spectroscopy (XPS) is a powerful technique for the investigation of bonding in transition metal compounds, the XPS measurements were performed in order to confirm the formation of compounds. The XPS spectra of the Co 2p and B 1s levels are shown in Fig. 2 as a function of the sintering temperature. The spectra were measured after pretreatment of 5 min Ar^+ sputtering. The peak values of the metal states, which are given by arrows in the figure, have been reported to be 794.0 and 779.0 eV for Co $2p_{1/2}$ and $2p_{3/2}$ respectively and 188.1 eV for the B 1s state.[2,3] The chemical shifts for the Co $2p_{3/2}$ and $2p_{1/2}$ were observed to become the lower energy level at a sintering temperature of more than 300 °C. The chemical shifts for the Co $2p_{3/2}$ level reach a constant value of 1.0 eV from the sintering temperature of 300 °C. In the case of the Co $2p_{1/2}$ level, the shifts give 0.7 eV at 300 °C and close to the final value of 1.0 eV at 800 °C with the increase in the sintering temperature. In the spectra of the B 1s level, there appear two peaks, at 188.9 eV and in the range between 193 and 194 eV. In the range of sintering temperatures between 300 and 450 °C, where the oxygen evolution reaction on cobalt borides shows the highest activity, the spectra show unclearly three small peaks (the peak at 199.5 eV was newly observed), which might be satellite peaks caused by the exchange splitting of the B 1s level with the unpaired valence electrons under amorphous conditions. It can be also confirmed from the above results, shown in Fig. 2, that the compounds of cobalt borides showing amorphous or transition state conditions are formed in the range of sintering temperatures between 300 °C and 500 °C.

The magnetic properties of 3d transition-metal alloys are strongly connected to the electron numbers of 3d

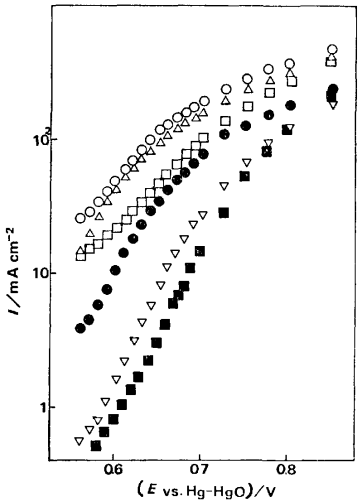

Fig. 3. Oxygen evolution current *vs.* potential curves on various composite cobalt borides in 6 M KOH at 25 °C.
○: Co-Fe-B(1 : 2 : 1) sintered at 450 °C, ●: Co-Ni-B(3 : 3 : 2) sintered at 400 °C. □: Co-B(3 : 1) sintered at 400 °C, △: Co-Fe-B(3:3:2) sintered at 450 °C, ▽: Co-Mn-B(3 : 3 : 2) sintered at 400 °C, ■: Co.

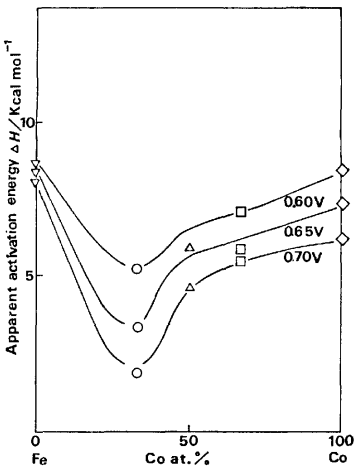

Fig. 4. Effect of cobalt or iron content of Co-Fe-B (Metal : B=3 : 1) on apparent activation energy at various potentials (0.60, 0.65, and 0.70 V) in 6 M KOH.
○: Co-Fe-B(1 : 2 : 1) sintered at 450 °C, △: Co-Fe-B(3 : 3 : 2) sintered at 450 °C, □: Co-Fe-B(2 : 1 : 1) sintered at 450 °C, ◇: Co-B(3 : 1) sintered at 450 °C, ▽: Fe-B(3 : 1) sintered at 400 °C.

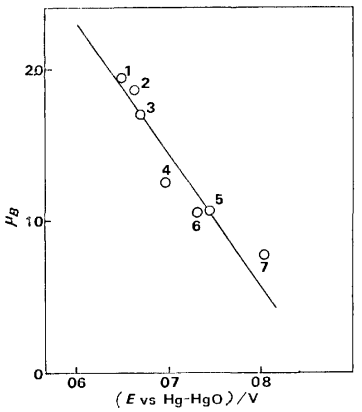

Fig. 5. Relationship between magnetic moment and activity of oxygen evolution reaction (expressed as potential at 0.1 A cm^{-2}) on composite cobalt borides in 6 M KOH at 25 °C.
1: Co-Fe-B(1 : 2 : 1) sintered at 450 °C, 2: Co-Fe-B(3 : 3 : 2) sintered at 450 °C, 3: Co-B(3 : 1) sintered at 400 °C, 4: Co-B(3 : 1) sintered at 600 °C, 5: Co-B (3 : 1) sintered at 800 °C, 6: Co-Ni-B(3 : 3 : 2) sintered at 400 °C, 7: Co-Mn-B(3 : 3 : 2) sintered at 400 °C.

plus 4s, and they are usually discussed with the magnetic moment, μ_B, expressed by Bohr magnetons. The magnetic moment, μ_B, can be calculated from σ_s by using the following equation:

$$\mu_B = M/\beta = A \cdot \sigma_s/(N \cdot \beta), \quad (1)$$

where M, A, N, and β are magnetic moment per atom, the atomic mass, the Avogadro constant, and the unit of the Bohr magneton respectively. Since the saturation magnetization of cobalt borides reaches a maximum in the range where the activity of oxygen evolution reaction becomes the highest, the saturation magnetization, σ_s, or the magnetic moment, μ_B, may be one of the most important factors which are correlated to the activity. Therefore, we tried to form the composite cobalt borides by referring to the Slater-Pauling curves,[5] which demonstrate the relationship between μ_B and the electron number of the outer-most orbitals (3d+4s) in the case of 3d transition-metal alloys. In the Slater-Pauling curves, the 30% Co-Fe alloy has the maximum value of μ_B=2.5.

Oxygen Evolution Reaction on Composite Cobalt Borides. The current *vs.* potential curves for oxygen evolution reactions with IR correction on several composite cobalt borides and cobalt in a 6 M KOH solution are demonstrated in Fig. 3. Among the composite cobalt borides, the cobalt boride containing iron (Co-Fe-B), which has a higher saturation magnetization value than that of the cobalt boride species, gives the highest activity of oxygen evolution reaction, as may be seen in Fig. 3. The activity order of composite cobalt borides is as follows:

Co-Fe-B(1:2:1) > Co-Fe-B(3:3:2) > Co-B(3:1) > Co-Ni-B(3:3:2) > Co-Mn-B(3:3:2) > Co,

where the almost composite cobalt borides were sintered at 400 or 450 °C for 4 h. The effect of the iron composition ratio of composite cobalt borides (Co-Fe-B) was evaluated by means of the apparent activation energy at 0.60, 0.65, and 0.70 V as is shown in Fig. 4, where the sintering temperature was fixed at 450 °C, at which temperature the Co-Fe-B species usually gives the highest activity of the oxygen evolution reaction. In Fig. 4, the cobalt iron boride with Co:Fe:B=1:2:1 shows the lowest apparent activation energy, namely, the highest activity of the oxygen evolution reaction (*e.g.*, ΔH at 0.60 V=5.2 kcal

mol^{-1}). The results correspond well to the information from the Slater-Pauling curves, where the 30% Co–Fe alloy has the maximum μ_B value of 2.5.

The relationship between the activity of the oxygen evolution reaction and the magnetic moment, μ_B, is demonstrated in Fig. 5, where the activity is expressed as the potential at a constant oxygen evolution current, 0.10 A cm^{-2}. As has previously been supposed, the above relation has a clear linear correlation, the composite cobalt boride with the higher μ_B gives the higher activity of the oxygen evoulution reaction. Since the magnetic moment, μ_B, is correlated to the numbers of unpaired electrons in the 3d transition metal alloys, the number of unpaired electrons is considered to be the most important factor in determining the activity of the oxygen evolution reaction in the composite cobalt boride species. The oxygen evolution reaction, however, occurs not on bare boride, but on oxidized boride. Therefore, the magnetic moment or the number of unpaired electrons may be connected with the ease of surface oxide film formation, which frequently affects the oxygen evolution reaction because the oxygen evolution reaction occurs in many cases on oxide films. Since the formation and conditions of oxide films can be strongly correlated to the activity of the oxygen evolution reaction on composite cobalt borides, the conditions of oxide films on Co–Fe–B and on Co–B with the higher activity will, in the next section, be investigated by means of linear potential sweep voltammetry and chronopotentiometry by comparing the oxide conditions of cobalt in a 6 M KOH solution.

Electrochemical Investigation of Surface Oxide on Cobalt, Cobalt Boride, and Cobalt Iron Boride in a 6 M KOH Solution. A Typical linear potential sweep voltammogram and a chronopotentiogram on cobalt in a 6 M KOH solution are shown in Fig. 6. The behavior of the linear potential sweep voltammogram is almost the same as that in 0.2—8 M KOH solutions reported by Behl and Toni.[6] They discussed the five peaks and concluded that the following reaction scheme holds for the electrooxidation of cobalt in a KOH solution:

$$Co + 2OH^- \rightarrow Co(OH)_2 + 2e \quad \text{Peak 1 and 2} \quad (2)$$

$$Co + 2OH^- \rightarrow CoO + H_2O + 2e \quad \text{Peak 2} \quad (3)$$

$$3Co(OH)_2 + 2OH^- \rightarrow Co_3O_4 + 4H_2O + 2e \quad \text{Peak 3} \quad (4)$$

$$Co(OH)_2 + OH^- \rightarrow CoOOH + H_2O + e \quad \text{Peak 4} \quad (5)$$

$$CoOOH + OH^- \rightarrow CoO_2 + H_2O + e \quad \text{Peak 5} \quad (6)$$

In Fig. 6, the Peak 3 is not clear in the voltammogram, but it is detectable at an enlarged scale. It is likely that the first film formed on cobalt is cobalt(II) hydroxide and that the cobalt(II) oxide films are formed after hydroxide formation. Finally, the more highly oxidized oxide films, such as Co_3O_4, CoOOH, and CoO_2, begin to form at the more anodic oxidation. The same conclusion can be drawn from our results for linear potential sweep voltammogram judging from the similar behavior in Fig. 6(a). The behavior of the chronopotentiogram shown in Fig. 6(b) is similar to that of the linear potential sweep voltammogram, but only three waves are observed. The first large wave corresponds to the hydroxide film formation, while the small second and third waves are connected with the more highly oxidized oxide film formation.

The linear potential sweep voltammograms and

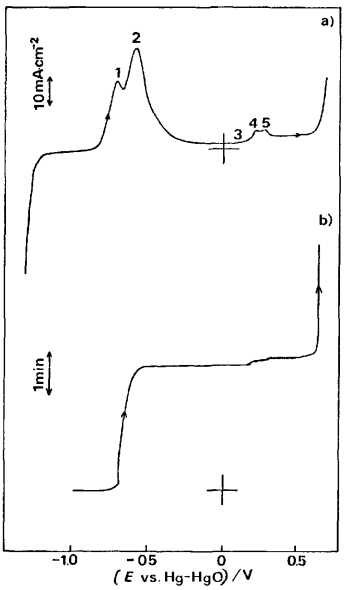

Fig. 6. Typical linear potential sweep voltammogram and chronopotentiogram on Co electrode in 6 M KOH at N_2 atmosphere at 25 °C. a) Linear potential sweep voltammogram, 50 mV s^{-1}, b) chronopotentiogram, 4.1 mA cm^{-2}.

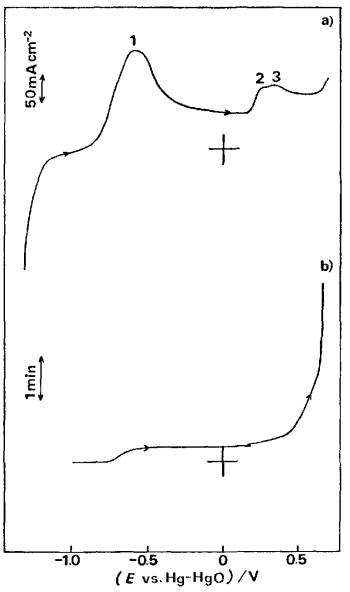

Fig. 7. Typical linear potential sweep voltammogram and chronopotentiogram on Co-B(3 : 1) sintered at the 400 °C electrode in 6 M KOH at N_2 atmosphere at 25 °C. a) Linear potential sweep voltammogram, 50 mV s^{-1}, b) chronopotentiogram, 37.7 mA cm^{-2}.

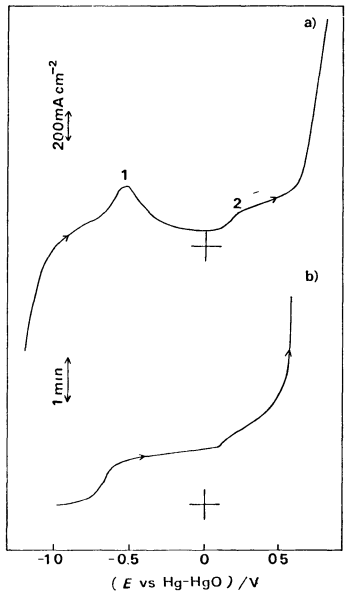

Fig. 8. Typical linear potential sweep voltammogram and chronopotentiogram on Co-Fe-B(1 : 2 : 1) sintered at the 450 °C electrode in 6 M KOH atmosphere at 25 °C. a) Linear potential sweep voltammogram, 50 mV s^{-1}, b) chronopotentiogram, 37.7 mA cm^{-2}.

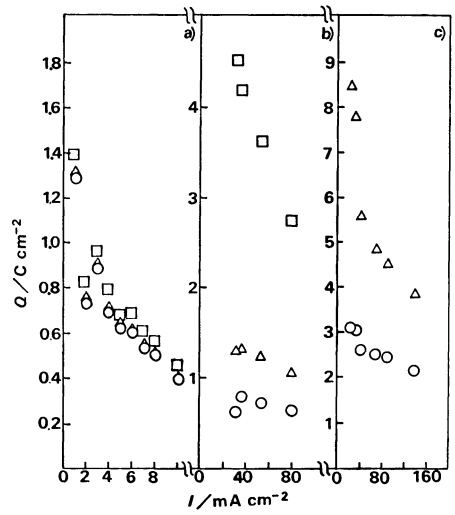

Fig. 9. Relation between amount of charge and current density at chronopotentiometry. a) Co, b) Co-B(3 : 1) sintered at 400 °C, c) Co-Fe-B(1 : 2 : 1) sintered at 450 °C. ○: 1st wave, △: 2nd wave, □: 3rd wave, where the charges for the 2nd and the 3rd waves are, for convenience, calculated from the initial potential of the 1st wave.

chronopotentiograms on the most active cobalt boride and cobalt iron boride are shown in Figs. 7 and 8. The behavior of the voltammogram and chronopotentiogram on cobalt boride (3:1) shown in Fig. 7 is similar to that on cobalt; however, the current peaks in the voltammogram due to the formation of hydroxide, shown as 1, or oxides, shown as 2 and 3, in Fig. 7, become larger (*i.e.*, the unit of the current axis in the voltammogram for Co–B is five times that for Co), and the initial potential at which the hydroxide film starts to form shifts to the more cathodic side. In the case of Co–Fe–B(1:2:1) the linear potential sweep voltammogram and chronopotentiogram are also very similar to those for Co–B(3:1), and the anodic peaks due to hydroxide (shown as 1) and oxide (shown as 2 in Fig. 8) formations become very large (*i.e.*, the unit of the current axis in the voltammogram for Co–Fe–B is twenty times that for Co). The order of the potential at which the hydroxide film starts to form is as follows:

$$\text{Co-Fe-B}(1:2:1) = -1.00\,\text{V},\ \text{Co-B}(3:1) = -0.93\,\text{V},$$
$$\text{Co} = -0.83\,\text{V}.$$

The order of the amount of charge due to hydroxide and oxide films can easily be determined by means of chronopotentiometry. Figure 9 represents the amount of charge due to the waves in the chronopotentiograms. The total charges due to hydroxide and oxide film formations on the borides are much larger than on cobalt. Moreover, the charge due to oxide formation in the case of cobalt is much smaller than that due to hydroxide formation (*cf.* Fig. 9(a)), while in the case of borides, the charge due to the oxide formation is much larger than that of hydroxide film formation. Therefore on the borides, the hydroxide film may change completely to oxide films on the anodic side and the thicker oxide films in higher oxidation states are easily formed on the surface. It may be concluded from the above results that the composite cobalt boride and the cobalt boride with the higher activity of the oxygen evolution reaction form the thicker and more stable oxide films in higher oxidation states in which the oxygen evolution reaction occurs. The very thick oxide layer in higher oxidation states might act as an intermediate in accelerating the oxygen evolution reaction on the borides. The above conclusion corresponds fairly well with the information, deduced from the relation between the magnetic moment, μ_B, and its activity, seen in Fig. 5, considering that the formation of oxide films becomes easier with the increase in the number of unpaired valence electrons.

Therefore, the oxide films on composite cobalt borides are considered to play an important role in the oxygen evolution reaction, and it may be concluded that the ease and stability of more highly oxidized oxide film formation are strongly connected with the activity of the oxygen evolution reaction.

The authors would like to thank Mr. Haruo Sekiguchi, Analytical Centre, Shimadzu Corporation, for his experimental support of the XPS measurements.

References

1) T. Osaka, O. Ishibashi, T. Endo, and T. Yoshida, *Electrochim. Acta*, **26**, 339 (1981).

2) "Surface Analysis," ed by M. Someno and I. Yasumori, Kodansha, Tokyo (1976).
3) D. C. Frost, C. A. McDowell, and I. S. Woolsey, *Mol. Phys.*, **27**, 1473 (1974).
4) "Handbook of Metals," 3rd ed, ed by Japan Institute of Metals, Maruzen, Tokyo (1971), p. 1028.
5) S. Chikazumi, "Physics of Ferromagnetism No. 1," Shokabo, Tokyo (1978), p. 183; R. M. Bozorth, "Magnetic Properties of Metals and Alloys," American Soc. Metals (1959), p. 349.
6) W. D. Behl and J. E. Toni, *J. Electroanal. Chem.*, **31**, 63 (1971).

Crystal and Molecular Structure of Methyl D-Tetronitroside

Noriaki HIRAYAMA,* Masaji KASAI, Kunikatsu SHIRAHATA,
Yuji OHASHI,† and Yoshio SASADA†

Tokyo Research Laboratries, Kyowa Hakko Kogyo Co., Ltd., 3-6-6 Asahimachi, Machida, Tokyo 194

†*Laboratory of Chemistry for Natural Products, Tokyo Institute of Technology, Nagatsuta, Midori-ku, Yokohama 227*

(Received January 21, 1983)

The structure of the novel sugar, methyl D-tetronitroside [methyl 2,3,4,6-tetradeoxy-4-(methoxycarbonylamino)-3-*C*-methyl-3-nitro-D-*xylo*-hexopyranoside], was determined by X-ray analysis. This compound is a structural component of the antitumor antibiotics, tetrocarcins. The space group is $P2_1$ with $a=11.782(3)$, $b=10.271(2)$, $c=11.636(3)$ Å, $\beta=105.12(4)°$, and $Z=4$. The structure was solved by direct methods, and least-squares refinement using 2503 reflexions gave the final R value of 0.079. Both the two independent molecules take a $^4C_1$ chair conformation and they are connected together through two hydrogen bonds. Although the average C-C distance in the rings is 1.527 Å, the C(2)-C(3) distance is significantly long (average 1.546 Å) due to the steric hindrance by the nitro groups.

D-Teronitrose is a structually important component of antitumor antibiotics, tetrocarcins,[1] and is the third naturally occuring nitro sugar discovered in antibiotics. The nitro sugar is so rare in nature that its detailed molecular structure has not yet been reported. Only the structure of the tetronitrose was spectroscopically and chemically elucidated but the molecular configuration was not confirmed because of having the asymmetric carbon atom with the nitro group as a side chain. In this paper we will report the X-ray analysis of methyl D-teronitroside in order to describe the stereochemical features of the nitro sugar. Recently a nitro sugar with the same composition as D-tetronitrose has been isolated from kijanimicins.[2]

Experimental and Structure Determination

The crystals of methyl D-teronitroside prepared by methanolysis of tetrocarcin A[1] were obtained by evaporation from a hexane-dichloromethane solution. A crystal, $0.4\times0.3\times0.3$ mm^3 in size, was used for data collection on a Rigaku four-circle automated diffractometer with graphite monochromated Mo $K\alpha$ radiation ($\lambda=0.71069$ Å). Preliminary unit cell dimensions and space group were obtained from photographs. Accurate cell dimensions were determined by least-squares calculations with the 2θ values of 15 high-angle reflexions measured on the diffractometer. Crystal data are as follows: $C_{10}H_{18}N_2O_6$; $M.W.=262.26$; $P2_1$; $Z=4$; $a=11.782(3)$, $b=10.271(2)$, $c=11.636(3)$ Å, $\beta=105.12(4)°$; $D_x=1.282$ g cm^{-3}; μ(Mo $K\alpha$) $=1.141$ cm^{-1}. All independent reflexions within the range $2\theta\leqq55°$ were collected by use of the ω-2θ scan mode with a scanning rate of $4°(2\theta)$ min^{-1}. Stationary background counts were accumulated for 10 s before and after each scan. Periodic check of the intensities of three standard reflexions showed no significant X-ray damage or decay. Correction for absorption or extinction was not applied. A total of 3308 independent reflexions were obtained, of which 2503 ($|F_o|>3.0\sigma(|F_o|)$) were considered as observed.

The structure was solved by direct methods using MULTAN.[3] The structural parameters were refined by block-diagonal least-squares methods with a modified HBLS program.[4] All the hydrogen atoms were found on a difference Fourier map and included in further refinement with isotropic thermal parameters. The final R value was 0.079 for 2503 observed reflexions. The weighting scheme used in the final stage was $w=(\sigma(F_o)^2+(0.015F_o)^2)^{-1}$. Atomic scattering factors were taken from Ref. 5. The final positional and thermal parameters are given in Table 1.**

Results and Discussion

The stereoscopic drawing of the two independent molecules are shown in Fig. 1, together with the atom numbering system. The absolute configuration of the tetronitrose, D-configuration, has been determined by applying Hudson's rules of isorotation to its α- and

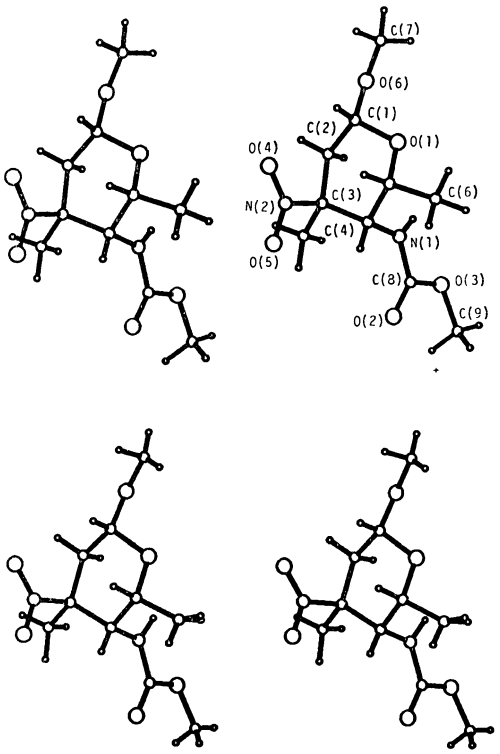

Fig. 1. Stereoscopic drawings of the two independent molecules and the numbering system. a) Molecule A. b) Molecule B.

** The tables of observed and calculated structure factors, and anisotropic thermal parameters are kept as Document No. 8332 at the Chemical Society of Japan.

Table 1-a. Final atomic coordinates with their estimated standard deviations, multiplied by 10^4

Atom	Molecule A				Molecule B			
	x	y	z	B_{eq}/Å^2	x	y	z	B_{eq}/Å^2
O(1)	5793(3)	4154(3)	1761(3)	3.46	8213(3)	6401(3)	3384(3)	3.49
O(2)	5682(3)	4919(4)	5917(3)	4.97	9816(3)	2750(4)	1744(5)	6.38
O(3)	7335(3)	5859(5)	5719(3)	5.18	7898(3)	2275(4)	1412(4)	4.46
O(4)	2490(3)	4451(5)	1329(4)	5.95	10001(4)	8504(5)	1575(5)	7.18
O(5)	2493(4)	4358(6)	3147(4)	7.14	11062(4)	6865(5)	1634(6)	8.98
O(6)	5408(3)	5442(4)	109(3)	4.30	6943(3)	8073(4)	2722(3)	3.75
N(1)	6035(3)	5184(5)	4103(4)	4.12	8474(3)	4299(4)	1812(4)	3.73
N(2)	2931(3)	4721(5)	2352(4)	4.31	10127(4)	7367(5)	1539(4)	4.26
C(1)	4892(4)	4870(5)	937(5)	3.59	8024(4)	7572(5)	2679(4)	3.13
C(2)	4428(4)	5931(5)	1592(4)	3.54	7971(4)	7232(5)	1396(4)	3.14
C(3)	4092(4)	5498(5)	2700(4)	3.50	9035(4)	6461(5)	1269(4)	3.11
C(4)	5003(4)	4537(6)	3438(4)	3.67	9320(4)	5341(5)	2190(5)	3.56
C(5)	5316(4)	3507(6)	2623(5)	3.91	9333(4)	5836(6)	3428(5)	4.16
C(6)	6171(6)	2489(7)	3250(6)	6.12	9549(6)	4801(9)	4361(6)	7.05
C(7)	5579(5)	4555(8)	-766(5)	5.83	6960(5)	8711(7)	3802(5)	5.01
C(8)	6303(4)	5296(6)	5311(5)	3.92	8827(5)	3081(5)	1671(5)	3.96
C(9)	7760(5)	5974(8)	7011(5)	6.00	8170(6)	910(6)	1383(7)	5.90
C(10)	3851(5)	6662(7)	3419(6)	5.44	8888(5)	6000(6)	-2(5)	4.99

Table 1-b. Final atomic coordinates of hydrogen atoms with their estimated standard deviations, multiplied by 10^3

Atom	Molecule A				Molecule B			
	x	y	z	B/Å^2	x	y	z	B/Å^2
HC(1)	425(3)	422(5)	49(4)	3(1)	865(3)	820(4)	300(3)	2(1)
HAC(2)	502(3)	652(4)	185(3)	2(1)	729(3)	672(4)	110(4)	2(1)
HBC(2)	381(3)	628(4)	104(4)	3(1)	790(3)	803(4)	95(3)	2(1)
HC(4)	466(4)	414(5)	395(4)	4(1)	1005(3)	505(4)	224(4)	3(1)
HC(5)	458(4)	317(5)	219(4)	4(1)	991(4)	662(5)	364(4)	6(1)
HAC(6)	581(4)	201(5)	375(4)	4(1)	954(5)	463(7)	497(5)	8(2)
HBC(6)	705(5)	279(6)	379(5)	6(1)	1027(4)	456(5)	442(4)	4(1)
HCC(6)	635(5)	190(7)	266(5)	8(2)	878(7)	421(9)	416((7)	11(2)
HAC(7)	484(4)	421(6)	-118(4)	5(1)	740(4)	836(5)	444(4)	4(1)
HBC(7)	626(4)	415(6)	-53(4)	5(1)	629(4)	913(6)	373(4)	6(1)
HCC(7)	582(6)	494(9)	-149(6)	11(2)	766(5)	942(7)	395(5)	7(2)
HAC(9)	777(4)	508(6)	736(5)	5(1)	893(5)	80(7)	202(5)	8(2)
HBC(9)	855(4)	647(6)	714(5)	6(1)	749(6)	37(8)	122(6)	9(2)
HCC(9)	720(6)	654(8)	733(7)	10(2)	850(4)	87(6)	89(4)	5(1)
HAC(10)	444(4)	705(5)	372(4)	4(1)	810(5)	551(7)	-36(5)	8(2)
HBC(10)	321(4)	707(6)	298(5)	6(1)	887(4)	669(5)	-51(4)	4(1)
HCC(10)	359(6)	630(8)	412(6)	10(2)	955(4)	535(6)	-1(5)	5(1)
HN(1)	653(4)	551(5)	384(4)	4(1)	775(4)	448(5)	189(4)	3(1)

Table 2. Bond lengths and angles

Bond length	l/Å A	l/Å B	Bond angle	θ/° A	θ/° B
C(5)-C(4)	1.527(8)	1.525(8)	C(5)-C(4)-N(1)	110.5(5)	111.7(5)
C(4)-C(3)	1.544(8)	1.548(7)	C(3)-C(4)-N(1)	112.0(5)	109.3(4)
C(3)-C(2)	1.511(8)	1.522(7)	C(4)-N(1)-C(8)	122.4(5)	121.0(5)
C(2)-C(1)	1.512(8)	1.519(7)	N(1)-C(8)-O(3)	110.6(5)	110.0(5)
C(1)-O(1)	1.433(6)	1.440(6)	N(1)-C(8)-O(2)	124.3(6)	125.7(6)
O(1)-C(5)	1.435(7)	1.430(7)	O(3)-C(8)-O(2)	125.1(6)	124.3(6)
C(5)-C(6)	1.503(9)	1.493(11)	C(8)-O(3)-C(9)	116.3(5)	115.6(5)
C(4)-N(1)	1.424(8)	1.450(7)	C(4)-C(3)-N(2)	104.8(4)	106.7(4)
N(1)-C(8)	1.363(8)	1.341(7)	N(2)-C(3)-C(10)	105.7(5)	105.2(4)
C(8)-O(2)	1.205(7)	1.196(8)	C(2)-C(3)-C(10)	111.4(5)	111.6(4)
C(8)-O(3)	1.318(8)	1.343(7)	C(4)-C(3)-C(10)	113.4(5)	113.0(4)
O(3)-C(9)	1.460(9)	1.441(9)	C(2)-C(3)-N(2)	109.9(4)	109.2(4)
C(3)-C(10)	1.527(9)	1.519(8)	C(3)-N(2)-O(4)	120.3(5)	119.7(5)
C(3)-N(2)	1.544(7)	1.552(7)	C(3)-N(2)-O(5)	118.5(5)	117.1(5)
N(2)-O(4)	1.200(7)	1.180(8)	O(4)-N(2)-O(5)	121.2(6)	123.1(6)
N(2)-O(5)	1.229(8)	1.194(9)	C(2)-C(1)-O(6)	108.9(4)	108.6(4)
C(1)-O(6)	1.395(7)	1.387(6)	O(1)-C(1)-O(6)	107.4(4)	107.2(4)
O(6)-C(7)	1.420(9)	1.413(8)	C(1)-O(6)-C(7)	113.2(5)	113.8(4)
O(1)-C(5)-C(4)	108.4(4)	108.6(5)	O(1)-C(5)-C(6)	109.1(5)	107.2(5)
C(5)-C(4)-C(3)	110.0(5)	110.7(5)	C(4)-C(5)-C(6)	114.8(5)	114.1(6)
C(4)-C(3)-C(2)	111.3(5)	110.8(4)	C(5)-C(4)-N(1)	110.6(5)	111.7(5)
C(3)-C(2)-C(1)	115.3(5)	113.1(4)	C(3)-C(4)-N(1)	112.0(5)	109.3(4)
C(2)-C(1)-O(1)	109.5(4)	109.2(4)	C(4)-N(1)-C(8)	122.4(5)	121.0(5)
C(1)-O(1)-C(5)	110.4(4)	111.3(4)	C(5)-O(1)-C(7)	110.4(4)	111.3(4)
O(1)-C(5)-C(6)	109.1(5)	107.2(5)	O(1)-C(5)-C(4)	108.4(4)	108.6(5)
C(4)-C(5)-C(6)	114.8(5)	114.1(6)	C(5)-C(4)-C(3)	110.0(5)	110.7(5)
C(3)-C(2)-C(1)	115.3(5)	113.1(4)	C(4)-C(3)-C(2)	111.3(5)	110.8(4)
C(2)-C(1)-O(1)	109.5(4)	109.2(4)			

β-glycosides; $[M]_{D\alpha}-[M]_{D\beta}=363.5°-66.4°=297.1°$. Very recently α-D-tetronitroside has been synthesized from D-mannose by Yoshii, and its D-absolute configuration was confirmed.[6]

Bond Lengths and Angles. The bond lengths and angles are shown in Table 2. Although most of the corresponding bond lengths in molecules A and B agree within the experimental error, the differences between them by greater than 3σ are observed in the amide bond. The average C–C distance of 1.527 Å in the rings agree with those observed in usual monosaccharides,[7] but the C(2)–C(3) distance (average 1.546 Å) is significantly longer than the other C–C distance in the rings and its reason will be discussed later. The two C–C bonds in the ring are almost equal to the average of 1.435 Å. The average distance of N(2)–C(3) bond (1.548 Å) is in good agreement with the corresponding N–C bond (1.541(3) Å) in *c*-5-methyl-*t*-5-nitro-1,3,2-dioxathian *r*-2-oxide.[8] The C(1)–O(6) bond (average 1.391 Å) is significantly shorter than the O(6)–C(7) bond (average 1.417 Å), which indicates large anomeric effect.

The differences between the corresponding bond angles in the two molecules are rather large compared to those of bond lengths. The average bond angles in the pyranose ring are 110.8 and 110.6° for molecules A and B, respectively, which are in agreement with

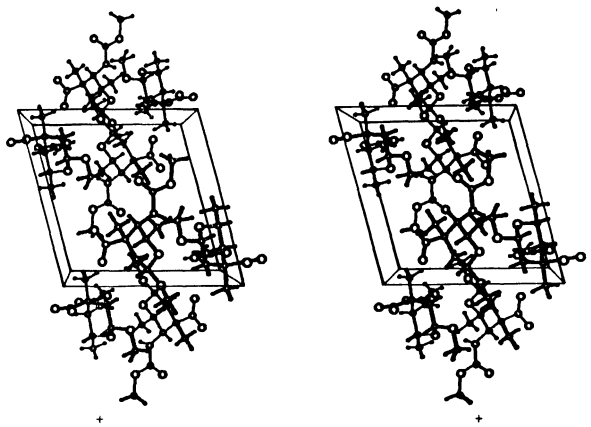

Fig. 2. Stereoscopic drawing of the crystal structure viewed along the b axis. The vertical and the holizontal axes are a and c, respectively. This figure and Fig. 1 were drawn by TSD : XTAL, a program for NOVA 3 computer.[9]

those found in pyranoses.[7]

Conformation. Both of the two independent molecules take a $^4C_1$ chair conformation. Selected torsion angles are tabulated in Table 3. The average torsion angles in the ring, 54.9 and 56.4° in A and B, respectively, are within the range observed for monosaccharides.[7] The *d* values (the deviation of the two atoms from the least-squares plane of the other four atoms forming the seat of a chair)[9] of the ring atoms in two molecules are averaged as follows; O(1) 0.706, C(1) 0.657, C(2) 0.569, C(3) 0.574, C(4) 0.651, C(5) 0.717 Å. The O(1) and C(5) atoms are most puckered, while the C(3) and C(2) atoms are less puckered. The O(4) atom is nearly eclipsed to the C(2) atom (O(4)–N(2)–C(3)–C(2) torsion angle is 6.2° for A and −13.9° for B). Therefore, the O(4) has short contact with C(2); the O(4)···C(2) nonbonded distance is 2.693(8) in A and 2.685(8) Å in B. The less puckering of C(3) and C(2) and the lengthening of C(2)–C(3) bond may cause the relief of steric hindrance, and it eventually causes the large puckering of the O(1) and C(5) atoms.

Table 3. Torsional angles

Torsional angle	ϕ/° A	ϕ/° B
C(1)-O(1)-C(5)-C(4)	68.9	67.9
O(1)-C(5)-C(4)-N(1)	64.7	64.1
O(1)-C(5)-C(4)-C(3)	-59.6	-58.0
C(6)-C(5)-C(4)-N(1)	-57.5	-55.3
HC(1)-C(5)-C(4)-HC(2)	-64.0	-63.8
C(5)-C(4)-C(3)-C(2)	45.9	48.0
C(5)-C(4)-C(3)-N(2)	-72.9	-70.7
N(1)-C(4)-C(3)-C(2)	-77.5	-75.4
HC(4)-C(4)-C(3)-C(10)	-69.8	-69.7
N(1)-C(4)-C(3)-C(10)	49.0	50.8
HC(4)-C(4)-C(3)-N(2)	44.9	45.4
C(4)-C(3)-C(2)-C(1)	-41.9	-46.3
N(2)-C(3)-C(2)-C(1)	73.7	70.9
N(2)-C(3)-C(2)-HBC(2)	-46.3	-50.5
C(10)-C(3)-C(2)-HAC(2)	-51.1	-54.5
C(3)-C(2)-C(1)-O(1)	49.6	53.5
HAC(2)-C(2)-C(1)-O(6)	49.7	50.6
HBC(2)-C(2)-C(1)-O(6)	-69.1	-67.4
HBC(2)-C(2)-C(1)-HC(1)	51.9	54.4
C(3)-C(2)-C(1)-HC(1)	-72.3	-68.1
C(2)-C(1)-O(1)-C(5)	-63.5	-64.6
HC(1)-C(1)-O(1)-C(5)	61.3	57.4
O(4)-N(2)-C(3)-C(2)	-6.2	13.9
O(5)-N(2)-C(3)-C(10)	55.7	70.0
O(5)-N(2)-C(3)-C(4)	-64.4	-50.3
C(7)-O(6)-C(1)-O(1)	-77.8	-76.6
C(7)-O(6)-C(1)-HC(1)	39.6	43.6
C(8)-N(1)-C(4)-C(3)	-109.6	-124.3
C(8)-N(1)-C(4)-HC(4)	8.2	-4.8
HN(1)-N(1)-C(4)-C(3)	72.0	72.7
HN(1)-N(1)-C(4)-C(5)	-51.1	-50.2
C(4)-N(1)-C(8)-O(2)	-3.4	6.0
C(4)-N(1)-C(8)-C(3)	-176.0	175.1
HN(1)-N(1)-C(8)-O(3)	2.8	-13.5
C(9)-O(3)-C(8)-O(2)	-2.7	-8.5
C(9)-O(3)-C(8)-N(1)	176.7	-172.6

Crystal Structure. Crystal structure viewed along the b axis is shown in Fig. 2. The two independent molecules make pairs through the two NH···O hydrogen bonds with following geometry: N(1A)···O(1B) =3.157(6), N(1B)···O(1A)=3.147(6) Å, ∠N(1A)–H···O(1B)=170.1(5), ∠N(1B)–H···O(1A)=157.8(5)°. The paired molecules are packed together with usual van der Waals contacts.

References

1) M. Kasai and K. Shirahata, *J. Antibiot.*, in press.
2) A. K. Mallams, M. S. Puar, and R. R. Rossman, *J. Am. Chem. Soc.*, **103**, 3938 (1981).
3) P. Main, S. E. Hull, L. Lessinger, G. Germain, J. P. Declerq, and M. M. Woolfson, "MULTAN78. A System of Computer Program for the Automatic Solution of Crystal Structures from X-Ray Diffraction Data," Univs. of York, England, and Louvain, Bergium (1978).
4) Y. Ohashi, unpublished version of an original Program by T. Ashida (1975).
5) "International Tables for X-Ray Crystallography," The Kynoch Press, Birmingham (1974), Vol. IV, pp. 72—102.
6) E. Yoshii, private communications.
7) S. H. Kim and G. A. Jeffrey, *Acta Crystallogr.*, **22**, 537 (1967).
8) G. H. Petit, A. T. H. Lensen, H. J. Geise, and P. Swepston, *Cryst. Struct. Commun.*, **9**, 187 (1980).
9) N. Hirayama, K. Shirahata, Y. Ohashi, and Y. Sasada, *Bull. Chem. Soc. Jpn.*, **53**, 3104 (1980).
10) A. Takenaka and Y. Sasada, *J. Cryst. Soc. Jpn.*, **22**, 214 (1980).

The Structure of Liquid Formamide Studied by Means of X-Ray Diffraction and *ab Initio* LCGO-MO-SCF Calculations

Hitoshi Ohtaki,* Atsushi Funaki, Bernd M. Rode,†
and Gilbert J. Reibnegger†

Department of Electronic Chemistry, Tokyo Institute of Technology at Nagatsuta, Nagatsuta-cho, Midori-ku, Yokohama 227

†*Institute of Inorganic and Analytical Chemistry, The University of Innsbruck, Innrain 52a, Innsbruck A-6020, Austria*

(Received February 7, 1983)

The molecular and liquid structures of formamide have been studied by means of X-ray diffraction. Relative stabilities of aggregates of formamide molecules have been calculated by using the *ab initio* LCGO-MO-SCF procedure and minimal basis sets. The atomic distances within a formamide molecule and the intermolecular N···O distance between the hydrogen-bonded molecules are determined by the X-ray diffraction experiment as follows: C=O: 1.24(1) Å, C–N: 1.33(1) Å, N···O (intramolecular): 2.25(2) Å, and N···O (intermolecular): 3.05(5) Å. The intermolecular -HNH···O=C< bond angle (θ) is about 120°. It is concluded from the X-ray diffraction experiment that liquid formamide mainly consists of the chain-like hydrogen-bonded structure of formamide molecules by combining through $-NH_2\cdots O=CH-$ interactions. The conclusion is supported by the *ab initio* calculations. Formation of ring-dimers in the liquid formamide has not been confirmed by the X-ray diffraction study, although a possibility of the formation of the ring-dimer structure as another constituent of liquid formamide is suggested from the *ab initio* calculations.

Formamide ($HCONH_2$) has a relatively large dielectric constant ($\varepsilon/\varepsilon_0=107$ at 25 °C, where ε and ε_0 represent the dielectric constants of formamide and vacuum, respectively), and thus can dissolve many electrolytes. Since the oxygen and nitrogen atoms within a formamide molecule are negatively charged and the carbon and hydrogen atoms have partially positive charges, a formamide molecule has a dipole moment of about 12.4×10^{-30} C m *in vacuo*. The donor number of formamide ($DN=24$) is larger than that of water ($DN=18.0$), although the acceptor number of the former ($AN=39.8$) is smaller than that of the latter ($AN=54.8$). Therefore, rather strong interactions between formamide molecules can be expected in the condensed phase.

Molecular and crystal structures of formamide have been determined by X-ray and electron diffraction methods,[1,2] and it has been found that all atoms within one molecule lay on a plane. A similar structure is kept even in the gas phase.[3] Therefore, we can expect that molecules of formamide in the liquid state have the planar structure similar to that observed in the gas and solid phases.[1–3] In crystal, formamide molecules form ring dimers which construct a large ring structure through hydrogen bonds (see Fig. 1).[1,2] However, the stable ring structure exisiting in the solid state may be rather unfavorable to give the high dielectric constant of formamide and high solubilities of electrolytes in it in the liquid phase.

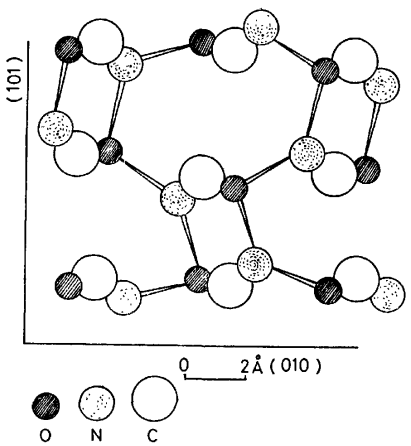

Fig. 1. Structure of formamide in the solid state,[1]

The aim of the present study is to determine the molecular arrangement, as well as the molecular structure of formamide in the liquid phase, in order to compare the structures with those in the gas and solid phases. The liquid structure of formamide estimated by the X-ray diffraction method will be compared with structural models of various aggregates examined by the *ab initio* LCGO-MO-SCF calculations.

Experimental

Preparation of Sample Solution. Formamide of reagent grade, purchased from Wako Pure Chemicals Co., Tokyo, was distilled twice under a reduced pressure. The water content of the formamide was determined by means of the Karl-Fischer titration. Since the amount of water (about 0.02% w/w) was very small, it was neglected in the course of the data analysis of X-ray diffraction.

Method of Measurement and Treatment of X-Ray Scattering Data. The X-ray diffractometer, JEOL DX-GO-Y (θ-θ type), was employed in combination with Philips 2255/20 Mo $K\alpha$ X-ray tube ($\lambda=0.7107$ Å) and an NaI-Tl scintillation counter. Scattered X-rays were monochromatized by a Johansson-type LiF monochromator and a pulse-height analyzer. The scattering angle (2θ) measured was in the range of 2° to 140°, and the data were recorded twice over the whole angle range. Corrections and analysis of the scattering data were performed by the same ways as those described elsewhere.[4] The scattering and correction factors of atoms in the system were taken from the literature.[5]

The reduced intensities $i(s)$ were obtained by the following equation:

$$i(s) = KI_{\mathrm{corr}}(s) - \sum_i n_i[\{f_i(s)+\Delta f_i'\}^2+(\Delta f_i'')^2], \qquad (1)$$

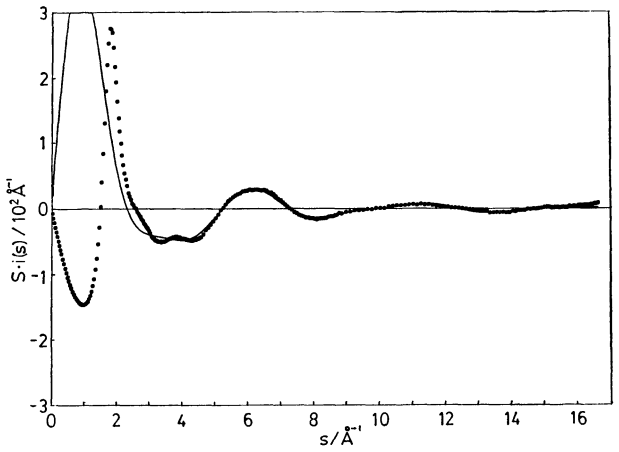

Fig. 2. Reduced intensities, $s \cdot i(s)$, experimentally obtained (circles) and calculated values ($s \cdot i_{\text{calcd}}^{\text{intra}}(s)$, solid line) by taking into account only intramolecular interactions.

where K denotes a factor for transforming measured intensities $I_{\text{corr}}(s)$, which had been corrected for absorption, polarization and multiple scatterings of X-rays by the usual methods,[4] to the absolute ones. The factor had been obtained by the high-angle method[6] and the method by Krogh-Moe[7] and Norman.[8] The K values obtained by the two methods agreed with each other within 1%. $\Delta f_i'$ and $\Delta f_i''$ in Eq. 1 represent the real and imaginary parts of the anomalous dispersion of atom i, respectively.

The reduced intensities multiplied by s ($=4\pi\lambda^{-1}\sin\theta$) of the test solution are shown in Fig. 2.

The radial distribution function $D(r)$ was calculated by the Fourier transform of the reduced intensities according to Eq. 2.

$$D(r) = 4\pi r^2\rho_0 + \frac{2r}{\pi}\int_0^{s_{\max}} s \cdot i(s) \cdot M(s) \cdot \sin(sr)\mathrm{d}s, \qquad (2)$$

where ρ_0 is the average scattering density in the stoichiometric volume V of the test solution, and $s_{\max}$ denotes the maximum s-value attained in the measurement ($s_{\max}=16.6$ Å^{-1}). $M(s)$ represents the modification function

$$M(s) = \frac{[\sum_i n_i f_i(0)^2]}{[\sum_i n_i f_i(s)^2]} \cdot \exp(-ks^2), \qquad (3)$$

where n_i denotes the number of atom i in the stoichiometric volume. $f_i(0)$ and $f_i(s)$ stand for the scattering factors of atom i at $s=0$ and s, respectively. The damping factor k was chosen as 0.01 Å^2 in the present experiment.

Calculations for data treatments were carried out by using the KURVLR program developed by Johansson and Sandström.[9]

Raman spectra of the test solution were measured before and after X-ray radiation, and it was confirmed that formamide was not decomposed by the X-ray radiation.

Computations for treating the X-ray data were performed at the Tokyo Intitute of Technology at Nagatsuta by using HITAC M-170.

Theoretical Treatment

In order to investigate the relative stabilities of various possible aggregates of formamide molecules in the condensed phase, varying structural models were examined by means of *ab initio* LCGO-MO-SCF calculations with a minimal basis set (2s/1p),[10] which has been successfully employed in other cases.[11–13] The molecular geometry of formamide was kept constant at the experimental values obtained by the present work, except for the C–H and N–H bond lengths which were taken from the literature,[2] throughout the calculations. The dimer models which were investigated by the *ab initio* calculations were selected on the basis of knowledges obtained by the present X-ray diffraction experiment. Some possible structural models were also examined in order to compare their relative stabilities with those of the selected geometries. The computations were carried out by using computers at the University of Innsbruck and partly at the Interuniversity Computer Center of the Technical University of Vienna.

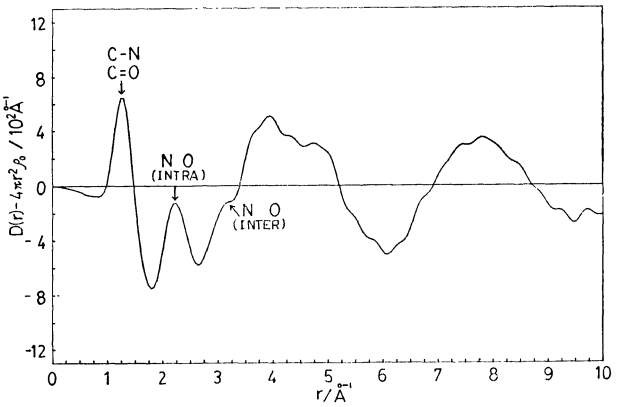

Fig. 3. Differential radial distribution curve of liquid formamide.

Results and Discussion

X-Ray Diffraction. The differential radial distribution curve, $D(r)-4\pi r^2\rho_0$, of formamide is shown in Fig. 3. The first peak appearing at about 1.2 Å is ascribed to the C–N and C=O bonds within a formamide molecule, and the second peak at 2.3 Å is attributed to the intramolecular N···O distance. A shoulder is observed at about 3 Å, which may be due to the intermolecular N···O distance according to the data by X-ray crystallography of formamide.[1,2] The reduced intensity curve calculated by using the intramolecular bond distances found from the differential radial distribution curve well reproduced the experimental curve in the range $s>5$ Å^{-1} (see Fig. 2). At the lower s range the two curves are remarkably discrepant, the discrepancy being due to intermolecular interactions between formamide molecules which have not been taken into account at the present stage of the X-ray data analysis.

The intramolecular distances thus roughly estimated from the differential radial distribution curve were further refined by applying the least-squares method to the reduced intensities $s \cdot i(s)$ over various s ranges, where $s_{\max}$ was fixed at 16.6 Å^{-1} and $s_{\min}$ was varied from 4 Å^{-1} to 6 Å^{-1}. The least-squares refinement was carried out by using the following equation:

$$U = \sum_{s_{min}}^{s_{max}} s^2\{i(s) - i_{calcd}^{intra}(s)\}^2, \quad (4)$$

where $i_{calcd}^{intra}(s)$ denotes the calculated $i(s)$ values by taking into account the intramolecular interactions only.

The results obtained for the intramolecular distances within a formamide molecules, as well as the temperature factors of each atom pair, in the liquid state are summarized and compared with those found in the gas and solid states in Table 1. No significant difference was noticed in the bond distances within a formamide molecule in the different phases.

At the second stage of the analysis of the X-ray scattering data, intermolecular interactions between formamide molecules in the liquid state were estimated from intensities due to the intermolecular interactions only which were obtained by subtracting the intensities due to the intramolecular interactions thus evaluated from the experimental values:

$$i^{inter}(s) = i(s) - i_{calcd}^{intra}(s). \quad (5)$$

Intensities $s \cdot i^{inter}(s)$ due to the intermolecular interactions thus estimated are shown in Fig. 4.

In order to interprete the $s \cdot i^{inter}(s)$ data, various dimer models were examined. In Fig. 5 the models examined are summarized. In each model the C–N and N–H bonds were rotated in order to compare the theoretical scattering intensities calculated from the models having various configurations with the experimentally obtained $s \cdot i(s)$ values. However, those except two models did not give theoretical intensities which satisfactorily fitted the experimental curves. The two models were the extremes of model (3) in Fig. 5. One was a linear dimer bonded through the N–H···O hydrogen bond with $\Theta=0°$ (two molecules were in the same plane) and $\Theta'=0°$ (Fig. 6A) and the other was a ring dimer ($\Theta=0°$ and $\Theta'=180°$) (Fig. 6B). A model at an intermediate configuration ($\Theta=0°$ and $0°<\Theta'<180°$) gave a theoretical intensity curve between those of the two extremes. In the course of the calculations of the theoretical intensity curve $s \cdot i_{calcd}^{inter}(s)$, the N···O distance was fixed at 3.05 Å in each model, which was experimentally determined by the present X-ray diffraction work. Theoretical intensities calculated on the basis of the two models were compared with the experimental ones in Fig. 4. The theoretical $s \cdot i_{calcd}^{inter}(s)$ curve drawn by using

TABLE 1. INTRA- AND INTERMOLECULAR DISTANCES OF FORMAMIDE. r AND b DENOTE THE BOND DISTANCE AND TEMPERATURE FACTOR, RESPECTIVELY[a)]

Bond	Liquid	Solid	Gas
C=O	$r=1.24(1)$ Å, $b=0.0017(3)$ Å^2	$r=1.24$ Å[2)]	$r=1.21$ Å[3)]
C–N	$r=1.33(1)$ Å, $b=0.0018(3)$ Å^2	$r=1.32$ Å[2)]	$r=1.37$ Å[3)]
N···O (intra)	$r=2.25(2)$ Å, $b=0.0028(5)$ Å^2	$r=2.27$ Å[2)]	$r=2.29$ Å[3)]
N···O (inter)	$r=3.05(5)$ Å	$r=2.88$ Å[1)], 2.94 Å[1)]	

a) Numbers in parentheses indicate standard uncertainties.

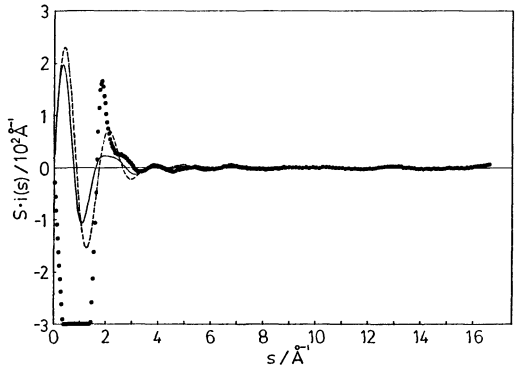

Fig. 4. Reduced intensities, $s \cdot i^{inter}(s)$, defined by Eq. 5 (circles). The solid and broken lines represent calculated $s \cdot i(s)$ values for intermolecular atom-pair interactions in models (A) and (B) given in Fig. 6, respectively.

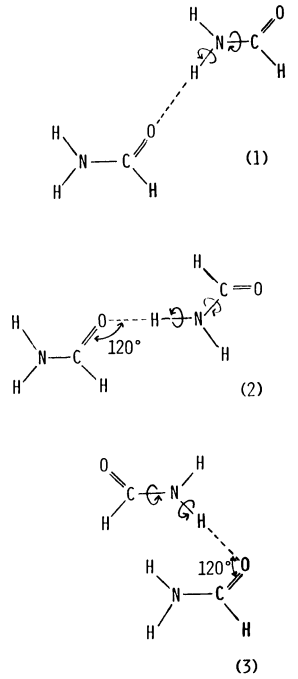

Fig. 5. Structural models of various dimers. The second molecule is allowed to rotate along the C–N and O···H–N bonds.

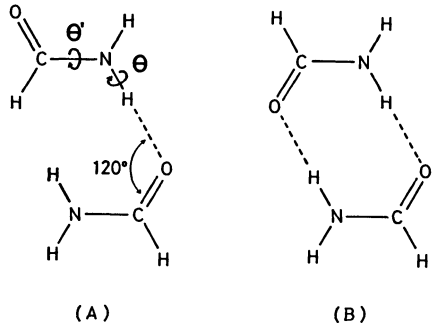

Fig. 6. Structural models of linear (A) and cyclic (B) dimers of formamide.

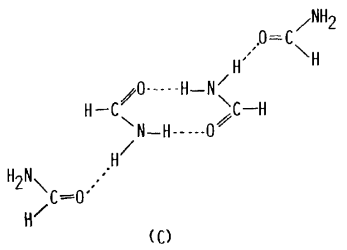

Fig. 7. A structural model consisting of linear and cyclic constituents.

the linear dimer model shown in Fig. 6A gave a better agreement with the experimental values than that calculated from the ring dimer model (Fig. 6B) in the range 3.5 Å^{-1}<s<5.5 Å^{-1}, and moreover, the hump appearing around $s\simeq2.8$ Å^{-1} was better reproduced by the former model than the latter.

A possibility of formation of a mixture of the two models were also examined at various mole ratios. However, an increase in the content of the ring dimers in the mixture enhanced the discrepancy between the theoretical and experimental intensity curves in the range 2.5 Å^{-1}<s<3.5 Å^{-1}, and therefore, the mixture model could not give a satisfactory interpretation for the $s\cdot i^{\text{inter}}(s)$ curve.

A chain-like structure consisting of the linear and the ring dimer units was taken into consideration in order to interprete the experimental $s\cdot i^{\text{inter}}(s)$ curve. The model employed is shown in Fig. 7 (model C). However, no noticeable improvement could be achieved in the interpretation of the experimentally obtained $s\cdot i^{\text{inter}}(s)$ curve by the introduction of the mixture model.

The intra- and intermolecular distances thus determined on the basis of the linear dimer model are summarized in Table 1. Disagreement between the experimental and theoretical $s\cdot i(s)$ curves observed at s<3.5 Å^{-1} is due to a disregard of longer range intermolecular and inter-chain interactions.

Although the linear model gave a better interpretation than the ring model for the experimental X-ray scattering data, the difference between the $s\cdot i(s)$ curve calculated by using the two models was so small that the existence of the ring dimers in the liquid formamide could not be completely excluded by the X-ray diffraction method examined in the present study. Therefore, we examined *ab initio* calculations for estimating energies of intermolecular interactions between formamide molecules in order to compare relative stabilities of the linear and ring dimer structures.

Ab Initio *LCGO-MO-SCF Calculations.* Relative stabilities of intermolecular interactions of dimeric, trimeric and even tetrameric polymers of formamide were calculated by the *ab initio* LCGO-MO-SCF procedure with a minimal basis set, which had been employed for calculations in other systems.[10-13] The geometry of the formamide molecules was kept constant at the experimental values given in Table 1 which were obtained by the present work, except for the C–H and N–H distances which were taken from the literature,[1] throughout the calculations, and the intermolecular –NH_2···O=CH– distances were allowed to change in order to search the energy minimum of the interaction at a given aggregate model.

Table 2. Energies at optimized C-H···O and N-H···O hydrogen bond distances (R) and energies per hydrogen bond (E_h) within formamide dimers[a]

Model	R/Å	E_h/kJ mol^{-1}
(a) 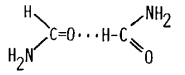	3.27	−8.4
(b) 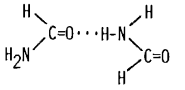	2.75	−43.9
(c) 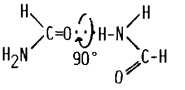	2.80	−45.2
(d) 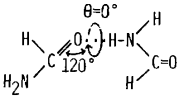	2.80	−67.8
(e) 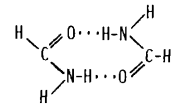	2.80	−63.2

a) The total energy of monomer is −143.34210 hartrees. 1 hartree=2625.34 kJ mol^{-1}.

For dimers, five different models as shown in the first column of Table 2 were examined as selected ones on the basis of considerations described in the previous section for the X-ray diffraction experiment. In models (a), (b), (d), and (e) we assumed that the two molecules were situated in the same plane. In model (c), on the other hand, the planes containing each molecule differed by 90°.

The optimized distance (R) of the intermolecular hydrogen bonds and energies for each hydrogen bonding (E_h) are listed in Table 2. In agreement with previous results,[14,15] model (d) gave the largest stabilization energy for the hydrogen bonding among the chain-like structures examined here. The stabilization energy for the formation of the dimers becomes largest in model (e), because the dimer has two hydrogen bonds within the unit structure (*i.e.*, −63.2 kJ per hydrogen bond×2=−126.4 kJ per dimer). Thus we can say that the cyclic structure is most stable in the formation of dimeric formamide. Nevertheless, as we will discuss in later sections, the structure shown in the linear model (d) can be more favorable than the cyclic dimer model (e) at a high degree of polymerization of the molecules in the condensed phase in which a large number of formamide molecules interact each other.

In model (d) the change in the relative stability of the linear dimer with changing angle of rotation (Θ in Fig. 6A) of the second molecule around the axis of the hydrogen bond was examined. The changes in the total energy (ΔE_{tot}) by the rotation are tabulated in Table 3. A shallow minimum appeared at

Table 3. The energy change (ΔE_{tot}) of the linear dimer model (d) at various rotation angles (Θ)

Θ/°	ΔE_{tot}/kJ mol^{-1}
0	—
30	6.7
60	9.7
90	7.5
120	9.5
150	11.6
180	11.6

$\Theta=90°$, which suggested that the rotated structure of model (d) could have some contribution to the liquid structure of formamide, although the minimum was very shallow and the basis set employed in the present calculations was not highly sophisticated.

The hydrogen-bond distance between two formamide molecules through either C–H···O or N–H···O interaction was calculated by optimizing the distance at the lowest energy of interactions of a given configuration of the formamide dimers by the *ab initio* method (Table 2). Except for model (a) which had a longer hydrogen bond than the experimental value (3.05 Å), the distance found in models (b) to (e) was in the range 2.75—2.80 Å independent of the configurations. The result suggested that the intermolecular hydrogen-bonded distance of formamide molecules is rather insensitive to the molecular arrangement.

The distances of the hydrogen bond in models (b) to (e) were all slightly shorter than the observed value. The shortening of the calculated distance of the hydrogen bond may mainly be due to a more or less simplified basis set used in the present calculations, although the minimal basis set employed in the present calculations can give rather reasonable distances for hydrogen bonds between molecules compared with other minimal basis sets used so far.[16]

Stabilization energies of formation of trimers were estimated by the same procedure for five kinds of trimeric aggregates, four of them being shown in Fig. 8. The other one is the trimeric moiety of the chain-like structure of the mixed linear-and-ring structure shown in Fig. 7 (structure C). The energy of the hydrogen bonds within the last trimer model was a simple sum of the energies of the linear dimer (d in Table 2) and the ring dimer (e), *i.e.* $(-67.8+(2\times -63.2))$ kJ per trimer. The stabilization energies of the other trimers shown in Fig. 8 are summarized in Table 4. Structure (II), which is an extension of the linear dimer (d) (or model A in Fig. 5), has the largest energy per hydrogen bond among the five models. However, the total energy of stabilization of the trimers is largest in the mixed linear-and-ring model. Therefore, this type of the chain-like structure may contribute to some extent to the construction of liquid formamide, although the existence of the ring-dimer structure was not well accepted as the model explainable for the X-ray diffraction data.

It should be noted that the energy of hydrogen bonding in the formation of trimer (II) was the same as that in dimer (d). This result suggests that the

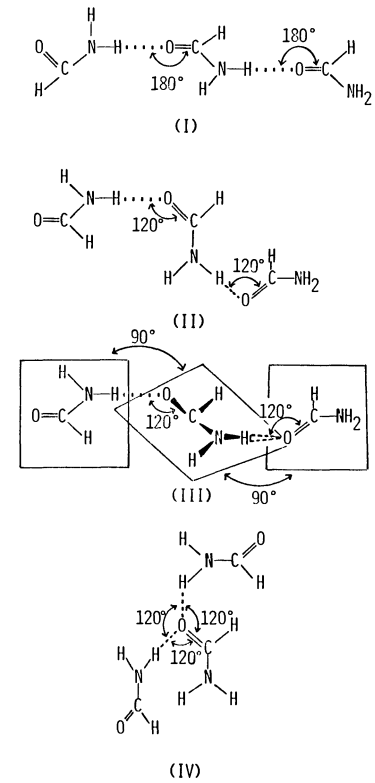

Fig. 8. Structural models of trimers.

Table 4. Stabilization energies for trimeric structures due to hydrogen bonding (E_h)

Model	E_h/kJ mol^{-1}
(I)	−48.5
(II)	−67.8
(III)	−60.2
(IV)	−44.4

energy of hydrogen-bonding of this type seems to be additive. On the other hand, trimer model (I), which is an extension of dimer (b), had an increased energy of the hydrogen bond by polymerization, although the stabilization energy of the formation of trimer (I) was still smaller than that of trimer (II). A relatively large stabilization energy of the hydrogen bond in trimer (III) suggested that rotation of molecules in trimer (II) might be easy. Trimer (IV) seems to be rather unstable compared with trimers (II) and (III) and has almost the same stability as trimer (I).

Stabilization energies for the formation of some tetramers were also calculated. For a tetramer similar to trimer (I) (*i.e.*, a linear polymer with the N–H···O angle of 180°), a slight increase by 1.3 kJ mol^{-1} (the total energy of the hydrogen bond was −49.8 kJ mol^{-1}) was observed in the stabilization energy of the aggregate, which was much less than the increment in the formation of trimer (I) from dimer (b) (4.6 kJ mol^{-1}). This suggests that the stabilization energy due to hydrogen bonding of this type may reach a constant value of about −50 kJ mol^{-1} at a pentamer or a hexamer of formamide. Since the stabilization energy of the formation of hydrogen bonds of this type is much

less compared with that of the type of dimer (d) or trimer (II) (67.8 kJ mol^{-1}), the chain-like structure of the trimer (I)-type may be less important in liquid formamide. The stabilization energy per hydrogen bond of the trimer (II)-type (or the dimer (d)-type) within a linear tetramer was essentially the same as that of the corresponding trimer and dimer, which indicated that the additivity of the stabilization of the aggregates was held in this configuration, and the chain structure of this type thus becomes the most stable one in liquid formamide.

Although the ring dimer has a larger stabilization energy due to the formation of two hydrogen bonds within it than any of the open-chain structures examined, the open structure consisting of dimer (d)-units becomes more stable than the ring structure, if the chains is formed with more than 16 molecules. Entropy effects due to easier bond rupture between molecules in the chain structure than in the ring structure and due to rotation of molecules in the chain will probably make the chain structure more favorable than the ring structure, so that the number of molecules for polymerization necessary to form stable chains might be much less than 16. Thus it can be concluded from the results of the MO-calculations that the open structures consisting of the trimer (II)-units and, to some extent the trimer (III)-units, should be dominant in liquid formamide. The ring-dimer structure may contribute to some extent to the chain structure as a link between the linear chain structures, as indicated in structure C, although the contribution was not detectable by the X-ray diffraction experiments.

A long chain structure and a mixed linear-and-ring structure did not give improved interpretations to the X-ray diffraction data, because interactions between the chain structures could hardly be estimated in the interpretation of the intensities of scattered X-rays.

The work has been partially supported by the Grant-in-Aid for Special Project Research (No. 510806) from the Ministry of Education, Science and Culture of Japan, and by the International Research Cooperation Project (Erl. zl. 18 889/25-10/79) from the Austrian Federal Ministry.

References

1) J. Ladell and B. Post, *Acta Crystallogr.*, **7**, 559 (1954).
2) E. D. Stevens, *Acta Crystallogr., Sect. B*, **34**, 544 (1978).
3) M. Kitano and K. Kuchitsu, *Bull. Chem. Soc. Jpn.*, **47**, 67 (1974).
4) H. Ohtaki, M. Maeda, and S. Ito, *Bull. Chem. Soc. Jpn.*, **47**, 2217 (1974); H. Ohtaki, T. Yamaguchi, and M. Maeda, *ibid.*, **49**, 701 (1976); T. Yamaguchi and H. Ohtaki, *ibid.*, **51**, 3227 (1978).
5) A. H. Compton and S. K. Allison, "X-Ray in Theory and Experiment," Van Nostrand, New York (1935); R. F. Stewart, E. R. Davidson, and W. T. Simpson, *J. Chem. Phys.*, **42**, 3175 (1964); D. T. Cromer and J. T. Waber, *Acta Crystallogr.*, **18**, 104 (1965); D. T. Cromer, *J. Chem. Phys.*, **50**, 4857 (1969); D. T. Cromer and D. Liberman, *ibid.*, **53**, 1891 (1970).
6) K. Furukawa, *Rep. Prog. Phys.*, **25**, 395 (1962).
7) J. Krogh-Moe, *Acta Crystallogr.*, **9**, 951 (1956).
8) N. Norman, *Acta Crystallogr.*, **10**, 370 (1957).
9) G. Johansson and M. Sandström, *Chem. Scr.*, **4**, 195 (1973).
10) B. M. Rode and K. Sagarik, *Chem. Phys. Lett.*, **88**, 337 (1982).
11) R. Fusseneger and B. M. Rode, *Chem. Phys. Lett.*, **44**, 95 (1976).
12) B. M. Rode and R. Fussenegger, *J. Chem. Soc., Faraday Trans. 2*, **71**, 1958 (1975).
13) J. F. Hinton and R. D. Harpool, *J. Am. Chem. Soc.*, **99**, 346 (1977).
14) A. Pullman, H. Berthod, C. Giessner-Prettre, J. F. Hinton, and D. Harpool, *J. Am. Chem. Soc.*, **100**, 3991 (1978).
15) N. R. Carlsen, L. Random, N. V. Riggs, and W. R. Rodwell, *J. Am. Chem. Soc.*, **101**, 2233 (1979).
16) Minimal basis sets such as the STO-3G basis set sometimes give a very short distance for a hydrogen-bond compared with hydrogen-bond distances calculated by extended basis sets. The basis set employed here has a much small effect for the shortening of the calculated distances of hydrogen-bonds. An example may be given for an O···N distance in an NH_3-H_2O system, in which the O···N distance has been estimated to be 3.000 Å by using the present (2s/1p) basis set (B. M. Rode and K. Sagarik, *Chem. Phys. Lett.* **88**, 337 (1982)) and 3.075 Å by a more extended basis set (8s/4p/1d).

Electrochemical Kinetic Parameters of Geometric Isomers of Singly Charged Cobalt(III) Complexes

Akifumi YAMADA* and Tadatsugu YOSHIKUNI†

Department of Materials Science and Technology, Technological University of Nagaoka, Kamitomioka, Nagaoka 949-54

†*Research Laboratory of Otsuka Chemical Co., Ltd., Kagasuno 463, Kawauchi, Tokushima 771-01*

(Received Decembar 3, 1982)

The kinetic parameters of electrode reactions of several geometric isomers of singly charged cobalt(III) complexes have been determined by means of Tast polarography. The complexes studied are *trans*-$[Co(NCS)(NO_2)(en)_2]Cl\cdot H_2O$, *cis*-$[Co(NCS)(NO_2)(en)_2]Cl\cdot 2H_2O$, *trans*-$[Co(NO_2)_2(en)_2]NO_3$, *cis*-$[Co(NO_2)_2(en)_2]NO_3$, *trans*-$[Co(NO_2)_2(NH_3)_4]NO_3\cdot 0.5H_2O$, *cis*-$[Co(NO_2)_2(NH_3)_4]NO_3$, *trans*-$[CoCl(NO_2)(en)_2]NO_3$, and *cis*-$[CoCl(NO_2)(en)_2]NO_3$. These complexes showed two irreversible reduction waves; the first corresponds to $Co^{III}\rightarrow Co^{II}$, and the second, to $Co^{II}\rightarrow Co^0$. The electrochemical kinetic parameters for the one-electron reduction wave were obtained in 0.1 and 1.0 M acetate buffer solutions. The half-wave potentials for the first wave of the complexes were more positive for the *cis* isomers than for the corresponding *trans* isomers. The cathodic rate constants at $E=0$ for the *cis* isomers were also larger than those for the corresponding *trans* isomers. A slight increase in the rate constant with the decrease in ionic strength was observed.

A number of electrochemical studies of cobalt(III) complexes[1] have been carried out. Among these studies, the polarography of geometric isomers of cobalt(III) complexes has been discussed by Holtzclaw and Sheetz,[2] Holtzclaw,[3] Inoue and Imai,[4] and Vlček.[5] However, no systematic work on geometric isomers under the same conditions has yet been done. In this paper, the electrochemical kinetic parameters of geometric isomers of singly charged cobalt(III) complex ions are determined, and the differences in kinetic parameters between isomeric pairs are discussed.

Experimental

Materials. The complexes, *trans*-$[Co(NCS)(NO_2)(en)_2]Cl\cdot H_2O$,[6] *cis*-$[Co(NCS)(NO_2)(en)_2]Cl\cdot 2H_2O$,[7] *trans*-$[Co(NO_2)_2(en)_2]NO_3$,[8] *cis*-$[Co(NO_2)_2(en)_2]NO_3$,[9] *trans*-$[Co(NO_2)_2(NH_3)_4]NO_3\cdot 0.5H_2O$,[10] *cis*-$[Co(NO_2)_2(NH_3)_4]NO_3$,[11] *trans*-$[CoCl(NO_2)(en)_2]NO_3$,[12] and *cis*-$[CoCl(NO_2)(en)_2]NO_3$,[7] were prepared by the literature methods. The ionic strength of the solution was adjusted with a sodium acetate buffer(pH=5.0). A portion of 0.005% gelatin was used as the maximum suppressor. All the other chemicals used were of a guaranteed reagent grade.

Electrochemical Measurements. A three-electrode cell[13] equipped with a saturated calomel electrode (Yanagimoto MR-P2-05-1) and a platinum-wire electrode was employed. A dropping mercury electrode (flow rate, 1.17 mg s^{-1} and drop time, 3.97 s in 0.1 M (1 M=1 mol dm^{-3}) acetate buffer solutions) served as a working electrode. The kinetic parameters of the electrode reactions were determined by means of Tast polarography. The Tast polarograms were recorded by means of a Fuso Model 312 polarograph with a Watanabe Model WX441 X-Y recorder. A Takeda Riken digital multimeter, Model TR-6355, was used, the current and the potential were thus measured precisely. Dissolved oxygen was removed by bubbling purified nitrogen gas through the solution. All the measurements were made at 25 °C.

Results and Discussion

In every complex studied, two polarographic waves were obtained. The height of the second step was about twice that of the first, which suggests that a one-electron reduction is followed by a two-electron reduction. Both steps were found to be proportional to the bulk concentration of the complex and to be diffusion-controlled. The present investigation is concerned only with the reduction of Co^{III} to Co^{II}. Slopes of the log-plots for the Tast polarogram indicate an irreversible reduction throughout. Figure 1 shows a Tast polarogram of the first waves of the *cis* and *trans* isomers obtained in 0.1 M acetate buffer solutions.

The Tast polarograms were analyzed by applying the following relations for a totally irreversible electrode process:[14]

$$(\boldsymbol{RT}/\alpha n\boldsymbol{F})\ln[2x(3-x)/5(1-x)] = E_{1/2}-E, \quad (1)$$

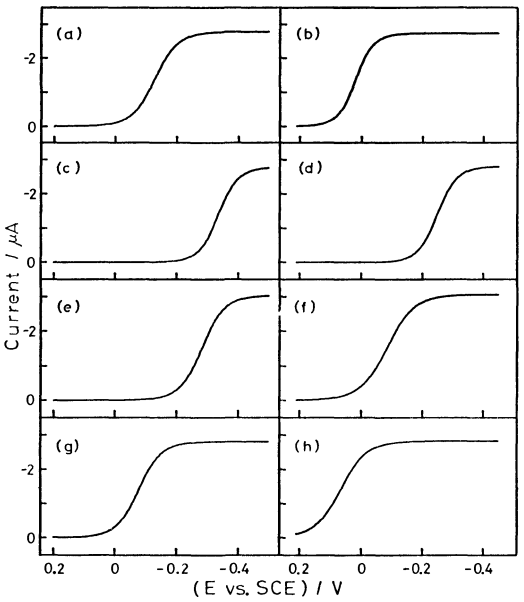

Fig. 1. Tast polarograms for the first wave of several isomeric cobalt(III) complex ions obtained in 0.1 M acetate buffer and 0.005% gelatin at 25 °C.
(a) *trans*-$[Co(NCS)(NO_2)(en)_2]^+$, (b) *cis*-$[Co(NCS)(NO_2)(en)_2]^+$, (c) *trans*-$[Co(NO_2)_2(en)_2]^+$, (d) *cis*-$[Co(NO_2)_2(en)_2]^+$, (e) *trans*-$[Co(NO_2)_2(NH_3)_4]^+$, (f) *cis*-$[Co(NO_2)_2(NH_3)_4]^+$, (g) *trans*-$[CoCl(NO_2)(en)_2]^+$, (h) *cis*-$[CoCl(NO_2)(en)_2]^+$.

with

$$x = I/I_d, \quad (2)$$

and

$$E_{1/2} = (\boldsymbol{R}T/\alpha n\boldsymbol{F})\ln[1.35k_c^\circ(t_d/D)^{1/2}], \quad (3)$$

where I is the current at the potential, E; I_d, the diffusion-controlled current; D, the diffusion coefficient; t_d, the drop time; α, the transfer coefficient; k_c°, the cathodic rate constant at $E=0$; n, the number of electrons; $\boldsymbol{R}$, the gas constant; $\boldsymbol{F}$, the Faraday constant, and T, the absolute temperature. According to Eq. 1, a plot of $\ln[2x(3-x)/5(1-x)]$ *vs.* E should be a straight line. The transfer coefficient, α, can be obtained from the slope, and the half-wave potential, $E_{1/2}$, from the intersection. The rate constant, k_c°, can be obtained from $E_{1/2}$ by applying Eq. 3.

The kinetic parameters of the electrode reactions thus obtained in 0.1 M acetate buffer solutions are given in Table 1. The kinetic parameters thus obtained were checked by calculating the current according to this relation:

$$2x(3-x)/5(1-x) = 1.35k_c^\circ(t_d/D)^{1/2}\exp(-\alpha n\boldsymbol{F}E/\boldsymbol{R}T). \quad (4)$$

The calculated currents were in good agreement with the observed ones.

The diffusion coefficient of the cobalt complexes was measured by means of a method previously reported[15] by using $[Co(NH_3)_6]^{3+}$ as the reference substance; the results are also given in Table 1. The magnitude of the diffusion coefficients of these isomers decreased in this order; *cis*- and *trans*-$[Co(NO_2)_2(NH_3)_4]^+$ > *cis*- and *trans*-$[CoCl(NO_2)(en)_2]^+$ > *cis*- and *trans*-$[Co(NO_2)_2(en)_2]^+$ > *cis*- and *trans*-$[Co(NCS)(NO_2)(en)_2]^+$. According to the Stokes-Einstein equation, a diffusion coefficient increases with a decrease in the ion size. Since the size of the complex depends on that of the ligand, the magnitude of the diffusion coefficient reflects the bulkiness of the ligand.

An examination of Table 1 shows that the half-wave potentials for the first wave of the complex containing negative groups in two of the coordination positions and neutral groups in the other four are more positive for the *cis* isomer than for the corresponding *trans* isomer. This tendency is in good agreement with the earlier polarographic observation which dealt with *cis* and *trans* isomers of cobalt(III).[2] The order of the half-wave potential in the series of isomers is: *cis*- and *trans*-$[CoCl(NO_2)(en)_2]^+$ > *cis*- and *trans*-$[Co(NCS)(NO_2)(en)_2]^+$ > *cis*- and *trans*-$[Co(NO_2)_2(NH_3)_4]^+$ > *cis*- and *trans*-$[Co(NO_2)_2(en)_2]^+$. This may be attributed to the electronegativity of the ligand.

The specific rate constant, k_c°, of the *cis* complex which contains two negative groups and four neutral groups was found to be larger than that of the symmetrical *trans* isomer. In this type of complex, a dipole exists within the coordination sphere of the *cis* form, but not in that of the symmetrical *trans* isomer. Because of the mutual electrostatic repulsion of these adjacent centers of electronegativity, the *cis* complex may be less stable than the symmetrical *trans* isomers. This may be expected to lead to faster specific rate constants for the *cis* isomer, indicating an easier reduction. The transfer coefficients of the *cis* complex in Table 1 tend to be slightly smaller than those of the corresponding *trans* isomers except for the *cis*- and *trans*-isothiocyanatonitrobis(ethylenediamine)cobalt-

Table 1. Kinetic parameters of one-electron reduction of several isomeric cobalt(III) complex ions obtained in 0.1 M acetate buffer (pH=5.0) at 25 °C

Complex ion	α	$E_{1/2}$ *vs.* SCE / V	k_c° / cm s^{-1}	D / 10^{-6} cm^2 s^{-1}
trans-$[Co(NCS)(NO_2)(en)_2]^+$	0.61	−0.129	4.86×10^{-5}	7.96
cis-$[Co(NCS)(NO_2)(en)_2]^+$	0.74	−0.003	9.41×10^{-4}	7.68
trans-$[Co(NO_2)_2(en)_2]^+$	0.73	−0.335	8.16×10^{-8}	8.00
cis-$[Co(NO_2)_2(en)_2]^+$	0.68	−0.287	5.10×10^{-7}	8.10
trans-$[Co(NO_2)_2(NH_3)_4]^+$	0.64	−0.283	1.04×10^{-6}	9.51
cis-$[Co(NO_2)_2(NH_3)_4]^+$	0.50	−0.114	1.28×10^{-4}	9.68
trans-$[CoCl(NO_2)(en)_2]^+$	0.63	−0.079	1.51×10^{-4}	8.10
cis-$[CoCl(NO_2)(en)_2]^+$	0.52	+0.046	2.72×10^{-3}	8.21

Table 2. Kinetic parameters of one-electron reduction of several isomeric cobalt(III) complex ions obtained in 1.0 M acetate buffer (pH=5.0) at 25 °C

Complex ion	α	$E_{1/2}$ *vs.* SCE / V	k_c° / cm s^{-1}
trans-$[Co(NCS)(NO_2)(en)_2]^+$	0.65	−0.143	2.82×10^{-5}
cis-$[Co(NCS)(NO_2)(en)_2]^+$	0.72	−0.014	7.03×10^{-4}
trans-$[Co(NO_2)_2(en)_2]^+$	0.72	−0.346	6.46×10^{-8}
cis-$[Co(NO_2)_2(en)_2]^+$	0.69	−0.317	2.12×10^{-7}
trans-$[Co(NO_2)_2(NH_3)_4]^+$	0.62	−0.293	9.73×10^{-7}
cis-$[Co(NO_2)_2(NH_3)_4]^+$	0.49	−0.123	1.10×10^{-4}
trans-$[CoCl(NO_2)(en)_2]^+$	0.61	−0.085	1.40×10^{-4}
cis-$[CoCl(NO_2)(en)_2]^+$	0.53	+0.038	2.32×10^{-3}

(III) complexes. Since the thiocyanate ion is strongly adsorbed on mercury, the transfer coefficient of *cis*-$[Co(NCS)(NO_2)(en)_2]^+$ is probably larger than that of the corresponding *trans* isomer.

The effect of the ionic strength on the kinetic parameters of the electrode reaction was tested in solutions of a 1 M acetate buffer. The results are shown in Table 2. With the increase in the ionic strength, the half-wave potential shifted toward negative potentials. This would be expected for the reduction of the positive-charge complex ions in this potential region. The specific rate constant decreased slightly with the increase in the ionic strength. The effect of the ionic strength on the rate constant may be estimated by means of Frumkin's equation as a first approximation:[16]

$$k_c^\circ = (k_c^\circ)_t \exp[(\alpha n - z)\boldsymbol{F}\phi/\boldsymbol{R}T], \quad (5)$$

where $(k_c^\circ)_t$ is a true cathodic rate constant at $E=0$; z, the ionic charge of the reactant, and ϕ, the double-layer potential. In this work, the value of $(\alpha n - z)$ is negative, as may be seen from Table 1. The double-layer potential of acetate salt has a small negative value in this potential region and decreases with the decrease in the ionic strength;[17] this may cause the slight increase in the rate constant with the decrease in the ionic strength.

It is difficult to compare the electrochemical kinetic parameters obtained in this work with those reported in the literature since the experimental conditions are quite different and only few data have been reported. Inoue and Imai[4] have determined the kinetic parameters for the reduction of *trans*- and *cis*-$[Co(NO_2)_2(NH_3)_4]^+$ at the DME in 1 M $NaNO_2$: the values are $k_c^\circ = 2.9\times10^{-3}$ cm s^{-1}; $\alpha=0.65$ for *trans*-$[Co(NO_2)_2(NH_3)_4]^+$ and $k_c^\circ = 7.1\times10^{-2}$ cm s^{-1}; $\alpha=0.58$ for *cis*-$[Co(NO_2)_2(NH_3)_4]^+$ at 25 °C. Vlček[5] has also reported the kinetic parameters of the same complex in 0.14 M $HClO_4$+1.26 M $NaClO_4$: $k_c^\circ/\sqrt{D} = 1.9\times10^{-4}$ s$^{-1/2}$; $\alpha=0.6$ for *trans*-$[Co(NO_2)_2(NH_3)_4]^+$ and $k_c^\circ/\sqrt{D} = 2.3\times10^{-2}$ s$^{-1/2}$; $\alpha=0.54$ for *cis*-$[Co(NO_2)_2(NH_3)_4]^+$.

The authors wish to express their deep thanks to Prof. Yu Yokoyama of the Technological University of Nagaoka and also to Prof. Nobuyuki Tanaka and to Dr. Yoshikiyo Kato of Tohoku University for their encouragement. This work was supported by Grant-in-Aid for Scientific Research No. 364205 from the Ministry of Education, Science and Culture.

References

1) N. Maki and N. Tanaka, "Encyclopedia of Electrochemistry of the Elements," ed by A. J. Bard, Marcel Dekker, New York (1975), Vol. 3, pp. 43—210.
2) H. F. Holtzchow, Jr., and D. P. Sheetz, *J. Am. Chem. Soc.*, **75**, 3053 (1953).
3) H. F. Holtzchow, Jr., *J. Phys. Chem.*, **59**, 300 (1955).
4) S. Inoue and H. Imai, *Rev. Polarog.* (Kyoto), **12**, 163 (1964).
5) A. A. Vlček, "Advances in Chemistry of Coordination Compounds," ed by S. Kirschner, Macmillan, New York (1961), pp. 590—603.
6) A. Werner, *Ann. Chem.*, **386**, 240 (1912).
7) A. Werner, *Ann. Chem.*, **386**, 230 (1912).
8) A. Werner, *Ber.*, **44**, 2450 (1911).
9) J. Sprinborg and C. E. Schaffer, "Inorganic Syntheses," ed by A. Wold and J. K. Ruff, McGraw-Hill, New York (1973), Vol. 14, p. 72.
10) S. M. Jørgensen, *Z. Anorg. Chem.*, **17**, 469 (1898).
11) S. M. Jørgensen, *Z. Anorg. Chem.*, **17**, 473 (1898).
12) A. Werner, *Ann. Chem.*, **386**, 251 (1912).
13) A. Yamada, T. Yoshikuni, Y. Kato, and N. Tanaka, *Anal. Chim. Acta*, **133**, 421 (1981).
14) K. B. Oldham and E. P. Parry, *Anal. Chem.*, **40**, 65 (1968).
15) A. Yamada, Y. Kato, T. Yoshikuni, Y. Tanaka, and N. Tanaka, *Anal. Chim. Acta*, **112**, 55 (1979).
16) N. Tanaka and A. Yamada, *Electrochim. Acta*, **14**, 491 (1969).
17) D. C. Grahame and B. A. Soderberg, *J. Chem. Phys.*, **22**, 449 (1954).

 © 1983 The Chemical Society of Japan Bull. Chem. Soc. Jpn., 56, 2125—2128 (1983)

Structure and Properties of Dichloro(L-proline)cadmium(II) Hydrate

Yasuhiko YUKAWA,* Yoshie INOMATA, and Toshio TAKEUCHI

Department of Chemistry, Faculty of Science and Technology, Sophia University, Kioi-cho, Chiyoda-ku, Tokyo 102

(Received December 8, 1982)

An X-ray diffraction study of the title complex has been carried out. The crystal is orthorhombic, with the space group $P2_12_12_1$; $Z=4$, $a=10.021(3)$, $b=13.562(4)$, $c=7.298(3)$ Å. Block-diagonal least-squares refinements have led to the final R value of 0.035. The structure is very similar to that of dichloro(4-hydroxy-L-proline)cadmium(II), which has a one-dimensional polymer bridged by chlorine atoms and a carboxyl group like an infinite folding screen. The thermal behavior is, however, different from that of dichloro(4-hydroxy-L-proline)cadmium(II). The difference is likely to be due to a difference of the crystal structure, whether it contains intermolecular hydrogen bonds or not.

Amino acids such as 4-hydroxy-L-proline (Hhpro) and proline (Hpro), which have a pyrrolidine ring, are important to biochemists who investigate the constitution and configuration of proteins. There are few studies, however, about metal complexes with Hhpro and Hpro. The crystal and molecular structure of $CdCl_2$(Hhpro) was previously determined in order to investigate how Hhpro coordinates to the metal.[1]

In this work, the complex with Hpro was prepared and characterized, including the determination of its structure. These results were compared with those from $CdCl_2$(Hhpro).

Experimental

Preparation of Dichloro(L-proline)cadmium(II) Hydrate; *$CdCl_2$-(Hpro)·H_2O.* The complex was prepared in almost the same way as used for $CdCl_2$(Hhpro);[1] equimolar amounts of $CdCl_2\cdot 2.5H_2O$ and Hpro were mixed in aqueous solution, and the solution was adjusted to pH 4 with *ca.* 2 mol dm^{-3} HCl. All chemicals used were reagent grade. The obtained colorless prisms were air-dried.

Found: C, 18.91; H, 3.01; N, 4.58; Cl, 22.45; Cd, 35.4%. Calcd for $CdCl_2(C_5H_9NO_2)\cdot H_2O$: C, 18.98; H, 3.50; N, 4.43; Cl, 22.41; Cd, 35.52%.

X-Ray Measurements. The crystal data are given in Table 1.

The crystal for data collection was shaped into a sphere ($\phi=0.34$ mm) and covered by cyanoacrylate resin to prevent the loss of H_2O from the crystal. The reflections were collected by the ω-2θ scan technique ($2\theta<65°$) on a Philips PW 1100 automated four-circle diffractometer, using Mo $K\alpha$ radiation (0.7107 Å). The 1464 independent reflections with $|F_o|>3\sigma(|F_o|)$ were used for the structure refinement. The intensities were corrected for Lorentz and polarization factors, but no correction was made for the absorption because of the low magnitude of μr ($=0.45$). All the calculations were carried out on a HITAC M-200H computer at the Computer Center of the University of Tokyo, using the local version of UNICS.[2] The atomic scattering factors were taken from tables.[3]

Table 1. Crystal data

$CdCl_2(C_5H_9NO_2)\cdot H_2O$	F.W. = 316.45
Orthorhombic	Space group $P2_12_12_1$
$a=10.021(3)$ Å	
$b=13.562(4)$ Å	
$c=7.298(3)$ Å	
$Z=4$	$U=991.8(6)$ Å^3
$D_m=2.13$ g cm^{-3}	$D_x=2.12$ g cm^{-3}
μ(Mo $K\alpha$) = 26.7 cm^{-1}	

Structure Determination. The structure was solved by a heavy-atom method. The positions of the cadmium atom and chlorine atoms were obtained from a three-dimensional Patterson function, while the positions of all the other non-hydrogen atoms were successively located by Fourier syntheses. Since the positions of only a few hydrogen atoms were obtained by a difference-Fourier syntheses, all of the positions were calculated and fixed. Their isotropic temperature factors were all assumed to be 5.0 Å^2. Since the absolute configuration of Hpro was known, the structure analysis was based on this configuration.

All other positions and thermal parameters were refined by a repeated block-diagonal least-squares method. The weighting scheme was $W=1/[\{\sigma(|F_o|)\}^2+(0.04\times|F_o|)^2]$. In the last cycle of the refinement with anisotropic temperature factors for all non-hydrogen atoms, all the parameter shifts were less than one-third of the corresponding standard deviations. The final R value ($R=\Sigma||F_o|-|F_c||/\Sigma|F_o|$) was 0.035.

The Other Measurements. The simultaneous thermogravimetric (TG) and differential thermal (DTA) analyses were carried out with a Rigaku Denki "Thermoflex" M-8075 using a sample weighing about 10 mg in each operation; the heating rate was 5 °C min^{-1} in air and α-alumina was used as the reference.

The infrared spectra of the samples were obtained by means of a Hitachi EPI-G2 infrared spectrophotometer, using Nujol and hexachloro-1,3-butadiene mull, and KBr disks.

Results and Discussion

The final atomic parameters are listed in Table 2,[4] the interatomic distances in Table 3, and the bond angles in Table 4. The perspective drawing of the complex and the numbering scheme of the atoms are shown in Fig. 1.

The complex has a very similar structure to that of $CdCl_2$(Hhpro); it consists of a one-dimensional polymer bridged by chlorine atoms and carboxyl oxygen atoms. The four chlorine atoms which coordinate to a cadmium atom are almost on a plane; the deviations of these atoms from the calculated best plane are shown in Table 5. The planes extended zigzag in the direction of the c axis like an infinite folding screen, sharing opposite edges. The dihedral angle between adjacent planes is 146°. From the trough positions in the zigzag folding structure, the two carboxyl oxygen atoms of Hpro coordinate to the two cadmium atoms. All the angles around the cadmium

TABLE 2. FINAL POSITIONAL PARAMETERS ($\times 10^4$ FOR NON-HYDROGEN ATOMS; $\times 10^3$ FOR HYDROGEN ATOMS) AND EQUIVALENT ISOTROPIC TEMPERATURE FACTORS (B_{eq}/Å^2),[a] WITH THE ESTIMATED STANDARD DEVIATIONS

Atom	x	y	z	B_{eq}/Å^2
Cd	2463.0(4)	21.2(2)	3333.7(5)	1.81
Cl(1)	4324(1)	344(1)	872(2)	2.12
Cl(2)	3726(2)	1026(1)	5844(2)	2.60
O(1)	1299(5)	1414(4)	2398(6)	2.99
O(2)	1386(5)	1359(4)	−652(5)	2.64
N	−919(6)	2225(4)	−1214(7)	3.05
C(1)	831(6)	1536(4)	799(8)	2.14
C(2)	−540(7)	2027(6)	706(9)	3.00
C(3)	−1607(7)	1309(10)	1353(14)	5.71
C(4)	−1929(10)	719(9)	−291(21)	6.94
C(5)	−1835(9)	1422(7)	−1815(15)	5.23
O(W)	896(8)	2516(6)	5890(8)	5.43
H(21)[b]	−48	269	152	
H(31)	−248	170	184	
H(32)	−123	84	243	
H(41)	−292	41	−20	
H(42)	−122	12	−46	
H(51)	−144	106	−302	
H(52)	−281	172	−213	
H(N1)	−50	254	−231	
H(N2)	−144	274	−53	

a) The equivalent isotropic temperature factors for non-hydrogen atoms were computed using the following expression: $B_{eq}=4/3(B_{11}a^2+B_{22}b^2+B_{33}c^2+B_{12}ab\cos\gamma+B_{13}ac\cos\beta+B_{23}bc\cos\alpha)$. The B_{ij}'s are defined by: $\exp[-(h^2B_{11}+k^2B_{22}+l^2B_{33}+2klB_{23}+2hlB_{13}+2hkB_{12})]$. b) The numbering scheme of hydrogen atoms is based on the number of the atom attached to the hydrogen atom.

TABLE 3. INTERATOMIC DISTANCES WITH THE ESTIMATED STANDARD DEVIATIONS IN PARENTHESES

Interatomic distance	l/Å	Interatomic distance	l/Å
Cd-Cd^{I}	3.650(3)	C(1)-C(2)	1.528(10)
		C(2)-N	1.477(11)
Cd-Cl(1)	2.627(3)	C(2)-C(3)	1.520(13)
Cd-Cl(2)	2.611(3)	C(3)-C(4)	1.479(20)
Cd-Cl(1)^{I}	2.624(3)	C(4)-C(5)	1.468(19)
Cd-Cl(2)^{II}	2.596(3)	C(5)-N	1.490(11)
Cd-O(1)	2.323(5)	N···O(2)	2.624(9)
Cd-O(2)^{I}	2.319(5)		
O(1)-C(1)	1.268(8)	N···O(W)^{III}	2.816(11)
O(2)-C(1)	1.220(8)		

Key to symmetry operations in this table and subsequent tables: I. $0.5-x$, $-y$, $0.5+z$; II. $0.5-x$, $-y$, $-0.5+z$; III. x, y, $-1.0+z$.

atom with four chlorine atoms and two carboxyl oxygen atoms are approximately 90°. The average bond distance of Cd–Cl is 2.61 Å, and that of Cd–O is 2.32 Å. Thus the cadmium atom has octahedral coordination. The bond distance of Cd–Cl and the angle of Cd–Cl–Cd (=88°) are comparable with those of $CdCl_2(biuret)_2$, which consists of an infinite linear ribbon of $CdCl_2$: Cd–Cl, 2.55(1), 2.62(1) Å; Cd–Cl–Cd, 91.5(3)°.[5] The ligand is a zwitter ion in the complex.

TABLE 4. BOND ANGLES WITH THE ESTIMATED STANDARD DEVIATIONS IN PARENTHESES

Bond angle	ϕ/°	Bond angle	ϕ/°
Cl(1)-Cd-Cl(2)	92.80(5)	O(2)-C(1)-C(2)	117.2(6)
Cl(1)-Cd-O(1)	91.17(13)	C(1)-C(2)-C(3)	109.9(7)
Cl(1)-Cd-O(2)^{I}	89.97(12)	C(1)-C(2)-N	110.7(6)
Cl(2)-Cd-O(1)	91.45(13)	C(3)-C(2)-N	103.3(7)
Cl(2)-Cd-O(2)^{I}	87.49(13)	C(2)-C(3)-C(4)	104.4(1.0)
Cd-Cl(1)-Cd^{II}	88.09(4)	C(3)-C(4)-C(5)	104.4(1.0)
Cd-Cl(2)^{II}-Cd^{II}	89.02(5)	C(4)-C(5)-N	107.0(1.0)
O(1)-C(1)-O(2)	127.2(6)	C(5)-N-C(2)	107.7(6)
O(1)-C(1)-C(2)	115.5(6)		

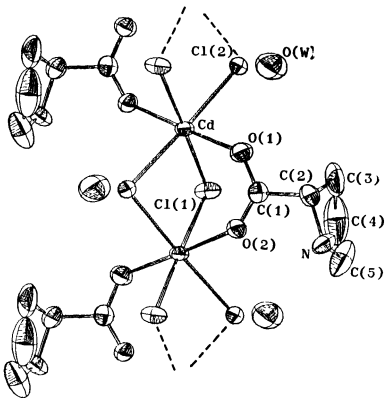

Fig. 1. The perspective drawing of $CdCl_2(Hpro)\cdot H_2O$ and the numbering scheme of non-hydrogen atoms.

In $CdCl_2(Hhpro)$, there are intermolecular hydrogen bonds between the nitrogen atom in the pyrrolidine ring and the hydroxyl oxygen atom. In contrast, $CdCl_2(Hpro)\cdot H_2O$ does not contain any intermolecular hydrogen bonds. Thus the pyrrolidine ring is not fixed and the positions far from the coordination atoms in Hpro have rather large temperature factors. Therefore, the calculated bond lengths of C(3)–C(4) (1.479(20) Å) and C(4)–C(5) (1.468(19) Å) are slightly shorter than the normal C–C bond length. A water molecule is connected to the nitrogen atom in the pyrrolidine ring by hydrogen bonding, instead of by intermolecular hydrogen bonds.

On coordination, the pyrrolidine ring in Hpro is bent on the line from N to C(3), and C(4) and C(5) atoms deviate from the best-plane of the pyrrolidine ring. The intramolecular hydrogen bond exists between N and O(2).

The projections of $CdCl_2(Hpro)\cdot H_2O$ along the c axis and of $CdCl_2(Hhpro)$ along the b axis are given in Fig. 2. In both cases, the zigzag folding screen is parallel to 2_1 axis. In $CdCl_2(Hhpro)$ it is connected with the neighboring one by hydrogen bonds between the nitrogen atom in the pyrrolidine ring and the hydroxyl oxygen atom; a sheet forms parallel to the (101) plane. In $CdCl_2(Hpro)\cdot H_2O$, there are no such hydrogen bonds and individual zigzag folding

Table 5. Least-squares planes and the deviations of atom (l/Å)

Plane(1) [Cl(1), Cl(2), Cl(1)^{I}, Cl(2)^{II}]
$-0.4971X+0.8181Y-0.2892Z+1.954=0$
Cl(1), −0.0029; Cl(2), 0.0029; Cl(1)^{I}, −0.0029; Cl(2)^{II}, 0.0029
(Cd, 0.0471)

Plane(2) [O(1), O(2), C(1), C(2)]
$-0.4199X-0.9075Y+0.01406Z+2.254=0$
O(1), −0.0079; O(2), −0.0082; C(1), 0.0223; C(2), −0.0059

Plane(3) [Cd, O(1), O(2), Cd^{III}]
$-0.8510X-0.5250Y-0.01089Z+2.139=0$
Cd, −0.0033; O(1), 0.0055; O(2), −0.0056; Cd^{III}, 0.0035
(C(1), 0.3301)

X, Y, and Z are coordinates expressed by the following equation:

$$\begin{pmatrix} X \\ Y \\ Z \end{pmatrix} = \begin{pmatrix} a & b\cos\gamma & c\cos\beta \\ 0 & b\sin\gamma & -c\cos\alpha^* \sin\beta \\ 0 & 0 & c\sin\alpha^* \sin\beta \end{pmatrix} \begin{pmatrix} x \\ y \\ z \end{pmatrix}.$$

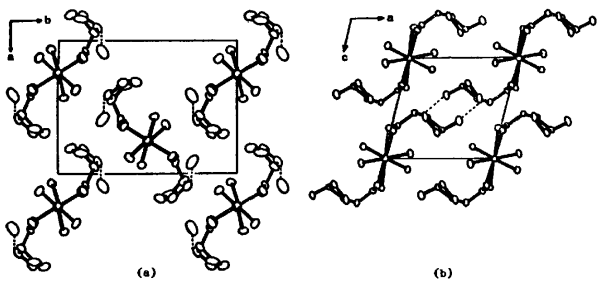

Fig. 2. The projection of (a) $CdCl_2(Hpro)\cdot H_2O$ along the c axis and (b) $CdCl_2(Hhpro)$ along the b axis. (----: Hydrogen bonding)

screens are bundled only by van der Waals' contacts.

The infrared spectra of the free ligand, the deuterated ligand, $CdCl_2(Hpro)\cdot H_2O$, and the deuterated complex are shown in Fig. 3. The deuterated compounds were obtained by recrystallization from 99.75% D_2O. It was already confirmed that the free ligand is a zwitter ion.[6] According to Herlinger and Long,[7] the peaks at 3050 and 1555 cm^{-1} are assigned to NH stretching vibration and NH_2^+ scissors vibration, respectively. The antisymmetric and symmetric stretching vibrations of COO^- are observed at 1619 and 1402 cm^{-1}, respectively. In $CdCl_2(Hpro)\cdot H_2O$, the peak at 3550 cm^{-1} is assigned to the OH stretching vibration of H_2O. Although there is a peak at 3180 cm^{-1} corresponding to the NH stretching vibration, the peak of NH_2^+ scissors vibration can not be assigned because it overlaps with the peaks of H_2O bending and COO^- antisymmetric stretching vibrations. To discuss the carboxyl stretching vibrations, the deuteration of NH_2^+ and H_2O is required since the peak near 1600 cm^{-1} (COO^- antisymmetric stretching) is probably coupled to NH_2^+ modes in Hpro;[7] there are also overlapping NH_2^+ bending and H_2O scissors vibrations[8,9] in $CdCl_2(Hpro)\cdot H_2O$, as mentioned above.

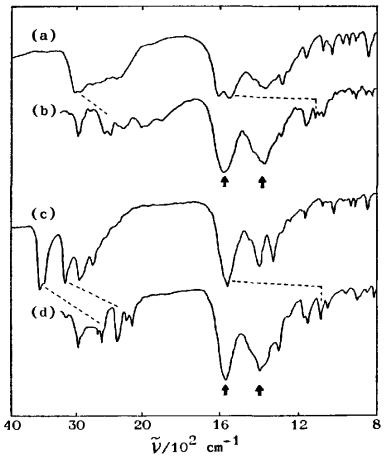

Fig. 3. Infrared spectra of (a) Hpro, (b) the deuterated ligand, (c) $CdCl_2(Hpro)\cdot H_2O$, and (d) the deuterated complex. The shifts of the peaks by deuteration are indicated by the dotted lines. The arrows indicate the peaks of COO^- antisymmetric (left) and symmetric (right) stretching vibrations.

The carboxylate ion may coordinate to a metal in one of the following modes:

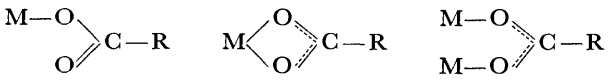

(I) (II) (III)

In the unidentate complex (structure (I)), the separation between COO^- anti- and symmetric stretching vibrations is much larger than that of the free ion, while it is smaller than that of the free ion in structure (II). In the bridging complex (structure (III)), however, two COO^- stretching vibrations are close to the free ion values.[10] In the present case, this separation evaluated from the deuteration spectrum is 180 cm^{-1}, and the separation for the free ligand is 185 cm^{-1}. This accords with the trend in the structure (III). The trend is also observed in $CdCl_2(Hhpro)$. Thus the trends in the carboxylate ion are likely to be observed in the amino acids which have a pyrrolidine ring.

The results of the simultaneous TG and DTA of $CdCl_2(Hpro)\cdot H_2O$ and of $CdCl_2(Hhpro)$ are shown in Fig. 4. In the former, an endothermic peak on the DTA with a mass loss corresponding to one water molecule is observed at about 80 °C. At about 180 and 210 °C, endothermic peaks on the DTA without mass loss are observed. The complex seems to become an amorphous state; this was confirmed from the X-ray powder pattern. It then melts at 210 °C. At about 230 °C the ligand is thought to decompose and the complex changes into cadmium chloride. About 35% mass loss occurs in the region 230—300 °C. Moreover, from 410 °C about 60% mass loss begins and becomes constant at about 800 °C, where no residue is obtained. Therefore in the region cadmium chloride changes into cadmium oxide and then it is sublimed.[11] The observation of an endothermic peak at 560 °C may indicate that cadmium chloride melts.[12]

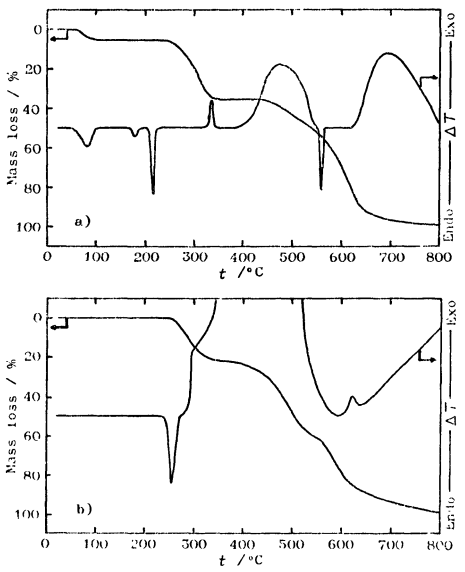

Fig. 4. Thermogravimetric and differential thermal analysis curves of a) $CdCl_2(Hpro)\cdot H_2O$ and b) $CdCl_2$-(Hhpro).

This thermal behavior is not observed in $CdCl_2$-(Hhpro); the DTA curve shows only an endothermic peak at about 210 °C and the complex burns with a gradual mass loss. This difference of the behavior between $CdCl_2(Hhpro)$ and $CdCl_2(Hpro)\cdot H_2O$ is thought to be due to the difference of the crystal structure, whether it contains intermolecular hydrogen bonds which connect with the neighboring zigzag folding screen or not.

The authors wish to express their thanks to Professor Yoichi Iitaka for the X-ray diffractometer measurements, and to Dr. Shoichi Sato and Dr. Shin-ichi Nishikiori, The University of Tokyo, for helpful discussions. They would also like to thank Dr. F. S. Howell of Sophia University for correcting this manuscript. The present work was partially supported by a Grant-in-Aid for Scientific Research No. 57430011 from the Ministry of Education, Science and Culture.

References

1) Y. Yukawa, Y. Inomata, T. Takeuchi, M. Shimoi, and A. Ouchi, *Bull. Chem. Soc. Jpn.*, **55**, 3135 (1982).
2) The Universal Crystallographic Computation Program System (UNICS), ed by T. Sakurai, Crystallographic Society of Japan, Tokyo (1967).
3) "International Tables for X-ray Crystallography," Kynoch Press, Birmingham, U. K. (1974), Vol. IV.
4) The final thermal parameters and the final F_o-F_c table are deposited as Document No. 8331 at the Office of the Editor of the Bulletin of the Chemical Society of Japan.
5) L. Cavalca, M. Nardelli, and G. Fava, *Acta Crystallogr.*, **13**, 594 (1960).
6) R. L. Kayushina and B. K. Vainshtein, *Kristallografiya*, **10**, 833 (1965).
7) A. W. Herlinger and T. V. Long, II, *J. Am. Chem. Soc.*, **92**, 6481 (1970).
8) T. Shimanouchi, "Sekigaisen-kyushu Supekutoru Kaiseki-ho (Analysis of Infrared Spectra)," enlarged ed, Nankodo, Tokyo (1976), p. 122.
9) S. Mizushima and T. Shimanouchi, "Sekigaisen-kyushu To Raman-Koka," in "Kyoritsu Zensho," Kyoritsu Shuppan, Tokyo (1958), pp. 155—156.
10) K. Nakamoto, "Infrared and Raman Spectra of Inorganic and Coordination Compounds," 3rd ed, John Wiley and Sons, New York (1978), pp. 230—233.
11) "Kagaku Binran Kisohen I," ed by the Chemical Society of Japan, Maruzen, Tokyo (1975), p. 82.
12) "Kagaku Binran Kisohen I," ed by the Chemical Society of Japan, Maruzen, Tokyo (1975), p. 70.

Complex Formation between Molybdate and Alizarin Red S

Takanori KATO and Teisuke MURAYAMA*

Department of Industrial Chemistry, Faculty of Engineering, Shizuoka University, Johoku, Hamamatsu 432

(Received December 24, 1982)

The complex formation between molybdate and Alizarin Red S (ARS) has been studied by spectrophotometry and pH titration. Results by the former method confirm that the composition of the complexes formed corresponds to a ratio of 1:1 for molybdate to ARS and that the complexes are stable between pH 2 to 6. Those by the latter are summarized by the following stability constants at 25 °C and an ionic strength of 0.1: $MoO_4^{2-} + ars^{3-} + 2H^+ = MoO_3ars^{3-} + H_2O$, $\log(\beta_1/mol^{-3}\,L^3) = 20.18 \pm 0.01$; $MoO_4^{2-} + ars^{3-} + 3H^+ = MoO_3(Hars)^{2-} + H_2O$, $\log(\beta_2/mol^{-4}\,L^4) = 24.93 \pm 0.04$ (the completely deprotonated species of ARS is denoted by ars^{3-}, and the concentration of H_2O is not included in the definition of stability constants). Protonation constants of MoO_4^{2-} and ars^{3-} were also determined under the same conditions.

Nearly three decades ago, Nazarchuk[1] observed the formation of a complex between molybdate and Alizarin Red S (9,10-dihydro-3,4-dihydroxy-9,10-dioxo-2-anthracenesulfonic acid monosodium salt, abbreviated to ARS) at pH 2—5, and used for colorimetric determinations of molybdenum. He considered that the composition of the complex was 1:1. However, Dey *et al.*,[2] Ishibashi *et al.*,[3] and Csanyi[4] reported it as 1:2. Krizan and Nozaki[5] wrote it as 1:1. Although these authors all have used spectrophotometry and conditions employed for the measurements are not so different each other (except Krizan and Nozaki who used 1:1 ethanol–water mixture as solvent), their conclusions are not in harmony. The present investigation aimed at determining the composition of the complex and its stability constant. We have used pH titration in conjunction with a spectrophotometric method, and found the formation of, instead of one, two complexes, one protonated and another unprotonated both with the composition corresponding to a ratio of 1:1 for molybdate to ARS.

Experimental

All chemicals used were of guaranteed reagent grade. Solutions were prepared with usual precautions, and the ionic strength was controlled to 0.1 with sodium nitrate. Sodium molybdate was used as a source of the molybdate ion.

Absorption spectra were recorded with a HITACHI UV-VIS spectrophotometer Model 200-10 and 10-mm quartz cells. A glass electrode (TOA HGS-2005) and a reference electrode (TOA HS-205S) were used with a TOA pH-meter Model HM-20E for pH titrations, and nitrogen was bubbled through the solution to exclude carbon dioxide. All measurements were made at 25.0 °C.

The refinement of equilibrium constants was carried out by a SHARP personal computer PC-3200.

Results and Discussion

Determination of the Composition of the Complex by Spectrophotometry. Figure 1 shows absorption spectra of ARS and its mixture with sodium molybdate at pH 4.00. An absorption maximum of ARS at 420 nm shifts to longer wavelengths on the complex formation with molybdate which is transparent in the visible region. A continuous variation curve at this pH and 475 nm indicates that the composition of the complex or complexes formed was 1:1, though it has

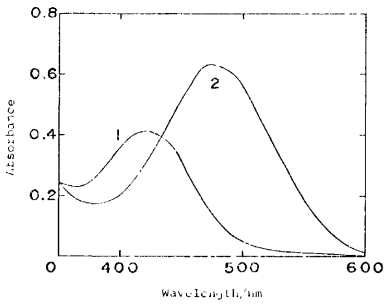

Fig. 1. Absorption spectra of ARS in the absence and presence of sodium molybdate. Concentration of ARS, 8.0×10^{-5} mol/L; pH 4.00. Concentration of sodium molybdate: curve 1, 0 mol/L; curve 2, 17.6×10^{-5} mol/L.

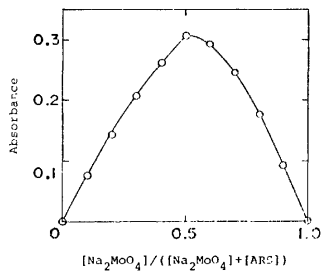

Fig. 2. Continuous variation curve for sodium molybdate and ARS mixture at 475 nm. Total concentration, 1.00×10^{-4} mol/L; pH 4.00.

a slight distortion (Fig. 2). The same conclusion was drawn from measurements at other pH's. The pH dependence of the ordinate of the continuous variation curve at the 1:1 composition is given by curve 1 in Fig. 3. The curve illustrates that the complex or complexes formed in a range of pH 2—6, and that they became unstable at outside of these limits. These facts are in accord with results reported by previous authors.[1-5]

Determination of Protonation Constants of MoO_4^{2-} by pH Titration. Measurements were carried out by titrating dilute mixtures of sodium molybdate and nitric acid with a sodium hydroxide solution. The protonation of MoO_4^{2-} proceeds through following two steps:

$$H^+ + MoO_4^{2-} = HMoO_4^- \quad K_1^M = \frac{[HMoO_4^-]}{[H^+][MoO_4^{2-}]}, \quad (1)$$

TABLE 1. PROTONATION CONSTANTS OF MoO_4^{2-} AND ars^{3-}, AND STABILITY CONSTANTS OF THEIR COMPLEXES IN 0.1 mol L^{-1} $NaNO_3$ SOLUTION AT 25 °C

Protonation constant

$\log \frac{K_1^M}{mol^{-1}\,L}$ 3.77±0.02	$\log \frac{K_2^M}{mol^{-1}\,L}$ 2.35±0.16	$\log \frac{K_{78}^M}{mol^{-14}\,L^{14}}$ 53.00±0.05
$\log \frac{K_1^L}{mol^{-1}\,L}$ 10.34±0.02	$\log \frac{K_2^L}{mol^{-1}\,L}$ 5.66±0.01	$\log \frac{K_3^L}{mol^{-1}\,L}$ 2.12±0.07

Stability constant

$\log \frac{\beta_1}{mol^{-3}\,L^3}$ 20.18±0.01	$\log \frac{\beta_2}{mol^{-4}\,L^4}$ 24.93±0.04

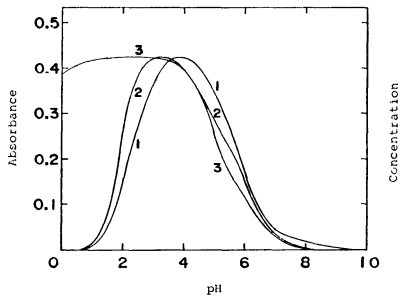

Fig. 3. pH dependence of the absorbance of the continuous variation curve for sodium molybdate and ARS mixture at the 1 : 1 composition. Wavelength, 475 nm; concentration of sodium molybdate, 8.0×10^{-5} mol/L; concentration of ARS, 8.0×10^{-5} mol/L. Curve 1, observed pH dependence of the absorbance; curve 2, $[MoO_3ars^{3-}]+[MoO_3(Hars)^{2-}]$; curve 3, $[MoO_3ars^{3-}]+[MoO_2ars^-]$. The concentration curves were drawn on arbitrary scales to make their highest points on equal level with the highest point of the absorbance curve.

and

$$H^+ + HMoO_4^- = H_2MoO_4 \qquad K_2^M = \frac{[H_2MoO_4]}{[H^+][HMoO_4^-]}, \tag{2}$$

where [X] is the concentration of species X in mol/L. Besides, molybdate ion in acidified solutions is known to produce many kinds of isopolyanions.[6] Under the experimental conditions adopted in this study, an assumption of the formation of heptamolybdate ion, $Mo_7O_{24}^{6-}$, is sufficient to explain titration curves.

$$8H^+ + 7MoO_4^{2-} = Mo_7O_{24}^{6-} + 4H_2O$$

$$K_{78}^M = \frac{[Mo_7O_{24}^{6-}]}{[H^+]^8[MoO_4^{2-}]^7}. \tag{3}$$

Protonation constants were calculated by the method for two-pK systems by Briggs and Stuehr[7] with some modifications for the formation of heptamolybdate ion. Instead of Eq. 9 in their paper, the computation was carried out by using the equation

$$\frac{(1+K_1^M[H^+]+7K_{78}^M[H^+]^8[MoO_4^{2-}]^6)(V+R-\Delta V)}{2+K_1^M[H^+]+6K_{78}^M[H^+]^8[MoO_4^{2-}]^6} = -\frac{K_1^M[H^+]^2(V+R-\Delta V)}{2+K_1^M[H^+]+6K_{78}^M[H^+]^8[MoO_4^{2-}]^6}K_2^M + V_e, \tag{4}$$

where

$$R = ([H^+]-[OH^-])V_t/C_B, \tag{5}$$

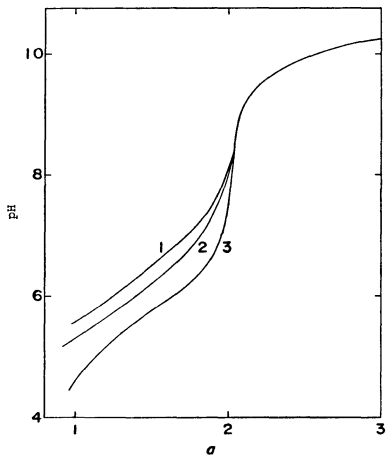

Fig. 4. Titration curves of ARS in the absence and presence of sodium molybdate. Concentration of ARS, 4.90×10^{-4} mol/L. Concentration of sodium molybdate: curve 1, 5.33×10^{-4} mol/L; curve 2, 2.67×10^{-4} mol/L; curve 3, 0 mol/L. The abscissa *a* is the ratio of the volume of sodium hydroxide solution added to the theoretical volume of the base per proton required to neutralize the acid H_3ars.

and C_B is the concentration of sodium hydroxide in the titrating solution, V is the volume of the base added, V_t is the total volume of the solution titrated, V_e is the theoretical volume of the base per proton required to neutralize the acid H_2MoO_4, and ΔV is the volume of the base neutralized by any strong acid present in the solution at the beginning of the titration. Protonation constants obtained are given in Table 1.

Determination of Protonation Constants of ARS by pH Titration. Curve 3 in Fig. 4 is a titration curve of ARS in the absence of the molybdate. The protonation of ARS consists of following three steps:

$$H^+ + ars^{3-} = Hars^{2-} \qquad K_1^L = \frac{[Hars^{2-}]}{[H^+][ars^{3-}]}, \tag{6}$$

$$H^+ + Hars^{2-} = H_2ars^- \qquad K_2^L = \frac{[H_2ars^-]}{[H^+][Hars^{2-}]}, \tag{7}$$

and

$$H^+ + H_2ars^- = H_3ars \qquad K_3^L = \frac{[H_3ars]}{[H^+][H_2ars^-]}. \tag{8}$$

In the above, ars^{3-} represents the completely deprotonated species of ARS with three negative charges.

Protonation constants were calculated by the method for three-pK systems.[7] The constants obtained are

shown in Table 1.

Identification of the Complex Species Formed and Determination of Their Stability Constants by pH Titration. Figure 4 shows titration curves of ARS in the presence and absence of the molybdate. Titration curves in the presence of the molybdate lie above the curve in the absence of the molybdate in the lower pH range and coincide with it in the upper range. Titration curves of this kind represent the formation of the ester between participating species, *i.e.* molybdate and ARS. The corresponding formation reaction of the complex consumes protons and thereby increases pH of the solution.

Conditions of the 1:1 composition and of the instability in acid solutions limit possible complex species to ones whose formation reactions are given by

$$MoO_4^{2-} + ars^{3-} + mH^+ = MoO_{4-n}(H_{m-2n}ars)^{(5-m)-} + nH_2O, \quad (9)$$

where $5>m\geqslant 2n>0$. This restriction leaves only three candidate complexes to be considered: MoO_3ars^{3-}, $MoO_3(Hars)^{2-}$, and MoO_2ars^-. Formation reactions of these complexes are

$$MoO_4^{2-} + ars^{3-} + 2H^+ = MoO_3ars^{3-} + H_2O, \quad (10)$$

$$MoO_4^{2-} + ars^{3-} + 3H^+ = MoO_3(Hars)^{2-} + H_2O, \quad (11)$$

and

$$MoO_4^{2-} + ars^{3-} + 4H^+ = MoO_2ars^- + 2H_2O. \quad (12)$$

Stability constants are defined as follows:

$$\beta_1 = \frac{[MoO_3ars^{3-}]}{[MoO_4^{2-}][ars^{3-}][H^+]^2}, \quad (13)$$

$$\beta_2 = \frac{[MoO_3(Hars)^{2-}]}{[MoO_4^{2-}][ars^{3-}][H^+]^3}, \quad (14)$$

and

$$\beta_3 = \frac{[MoO_2ars^-]}{[MoO_4^{2-}][ars^{3-}][H^+]^4}. \quad (15)$$

As shown in Fig. 4, the titration of ARS in the presence of the molybdate was carried out at above pH 5, where the atomic ratio of molybdenum of the heptamolybdate to the total molybdenum was below 10^{-5}. Hence the concentration of heptamolybdate ions is ignored in the following derivation of equations.

Total concentrations of the molybdate, ARS, and dissociable hydrogen ions are respectively given as follows:

$$M_t = [MoO_4^{2-}] + [HMoO_4^-] + [H_2MoO_4] + [MoO_3ars^{3-}] + [MoO_3(Hars)^{2-}] + [MoO_2ars^-], \quad (16)$$

$$L_t = [ars^{3-}] + [Hars^{2-}] + [H_2ars^-] + [H_3ars] + [MoO_3ars^{3-}] + [MoO_3(Hars)^{2-}] + [MoO_2ars^-], \quad (17)$$

and

$$H_t = [H^+] - [OH^-] + [HMoO_4^-] + 2[H_2MoO_4] + [Hars^{2-}] + 2[H_2ars^-] + 3[H_3ars] + 2[MoO_3ars^{3-}] + 3[MoO_3(Hars)^{2-}] + 4[MoO_2ars^-]. \quad (18)$$

Combination of these equations and equilibrium constants results Eqs. 19 and 20:

$$f_1f_5[MoO_4^{2-}]^2 + (f_2f_3-f_1f_4-f_5f_6)[MoO_4^{2-}] + (f_4f_6-f_3f_7) = 0, \quad (19)$$

and

$$(L_t-F[MoO_4^{2-}])\beta_3[H^+]^4 + \{(L_t-F[MoO_4^{2-}])\beta_2-K_1^LK_2^LK_3^LF\}[H^+]^3 + \{(L_t-F[MoO_4^{2-}])\beta_1-K_1^LK_2^LF\}[H^+]^2 - K_1^LF[H^+] - F = 0, \quad (20)$$

where

$$f_1 = 1 + K_1^M[H^+] + K_1^MK_2^M[H^+]^2, \quad (21)$$

$$f_2 = 4 + 3K_1^M[H^+] + 2K_1^MK_2^M[H^+]^2, \quad (22)$$

$$f_3 = 1 + K_1^L[H^+] + K_1^LK_2^L[H^+]^2 + K_1^LK_2^LK_3^L[H^+]^3, \quad (23)$$

$$f_4 = K_1^L[H^+] + 2K_1^LK_2^L[H^+]^2 + 3K_1^LK_2^LK_3^L[H^+]^3, \quad (24)$$

$$f_5 = 2\beta_1[H^+]^2 + \beta_2[H^+]^3, \quad (25)$$

$$f_6 = M_t - L_t, \quad (26)$$

$$f_7 = 4M_t - H_t + [H^+] - [OH^-], \quad (27)$$

and

$$F = M_t/[MoO_4^{2-}] - f_1. \quad (28)$$

The procedure for obtaining a set of the best values of stability constants involves the following steps:

(1) Estimate β_1, β_2, and β_3.
(2) Calculate f_i's for data points in the appropriate pH region using the estimates of stability constants and the values of other equilibrium constants.
(3) Solve Eq. 19 for $[MoO_4^{2-}]$, and calculate F.
(4) Solve Eq. 20 for $[H^+]$.
(5) Convert $[H^+]$ to pH, and find the standard error of estimate from the experimental and calculated pH values.
(6) Vary β_3 by small amounts, and repeat steps 4—5 until a minimum in the standard error of estimate is obtained.
(7) Repeat steps 2—6 using new estimates of β_2 until the smallest standard error of estimate is found.
(8) Repeat steps 2—7 using new estimates of β_1 until the lowest standard error of estimate of pH is gotten. A set of values of β_1, β_2, and β_3 which yields the lowest standard error of estimate is chosen as the most probable set of values.

Although it is possible to compute the three stability constants with the above method by adopting the three-complex-species (*i.e.* MoO_3ars^{3-}–$MoO_3(Hars)^{2-}$–MoO_2ars^-) model, this is not the best way to explain titration curves. This unnecessarily increases the number of new species, which must be a minimum indispensable.

Three one-complex-species models were tried at first. However they failed to reproduce titration curves. Two of two-complex-species models were equally successful to reproduce the curves. These are the MoO_3ars^{3-}–$MoO_3(Hars)^{2-}$ and MoO_3ars^{3-}–MoO_2ars^- models. The concentrations of respective complex species were calculated as functions of pH by using resulted values of stability constants, and examined whether they were in accord with observed results illustrated by curve 1 in Fig. 3 or not. Curves 2 and 3 in this figure are, respectively, the sum of concentrations of MoO_3ars^{3-} and $MoO_3(Hars)^{2-}$, and the sum of con-

centrations of MoO_3ars^{3-} and MoO_2ars^-. If the difference of molar absorption coefficient between different species is taken into account, the discrepancy between curve 1 (absorbance) and curve 2 (sum of the concentrations) is explicable, but the one between curve 1 and curve 3 (sum of the concentrations) is not. Hence, the MoO_3ars^{3-}–$MoO_3(Hars)^{2-}$ model is acceptable, but the MoO_3ars^{3-}–MoO_2ars^- model is not.

Values of stability constants of MoO_3ars^{3-} and $MoO_3(Hars)^{2-}$ in Table 1 are ones based on the MoO_3ars^{3-}–$MoO_3(Hars)^{2-}$ model. Dey *et al.* reported two values of 9.5[2b] and 9.2[2c] for logarithm of the stability constant of the 1:2 complex at pH 3.5. Csanyi gave a value of 7.7 for the same constant at pH 3.8.[4] Krizan and Nozaki reported a value of 5.4 for the logarithmic constant of the 1:1 complex at pH 5.[5] These are all apparent constants, however. Hence it is not profitable to compare these with the values in Table 1.

It seems natural that the ester formation takes place at a site where the protonation occurs most easily in free ars^{3-}. Yampol'skii *et al.*[8] stated that the protonation in ars^{3-} occurs at the anionic 1-O at first. Therefore the MoO_3 group is concented to ARS through the 1-O in MoO_3ars^{3-}. The protonation of this complex is given by

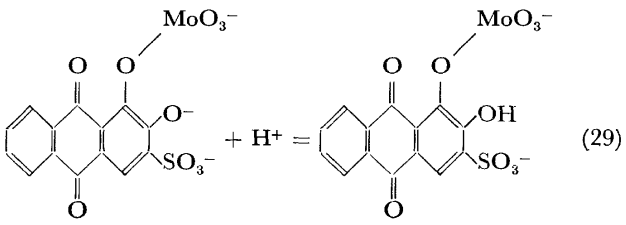

(29)

and the protonation constant was calculated to be $10^{4.75}$ mol^{-1} L from values shown in Table 1. This value is about an eighth of K_2^L, the corresponding protonation constant of uncomplexes $Hars^{2-}$. The decrease of the protonation constant is a reflection of the difficulty of proton's arriving at the anionic 2-O due to the overcrowding around the O-atom by complexation with the MoO_3 group at the 1-O.

References

1) T. N. Nazarchuk, *Ukr. Khim. Zh. (Russ. Ed.)*, **20**, 417 (1954).

2) a) A. K. Dey and S. K. Banerji, "Proc. Symposium Chem. Co-ordination Compounds," Agra, India (1959), Part 2, p. 198; b) S. K. Banerji and A. K. Dey, *Z. Phys. Chem. (Leipzig)*, **218**, 173 (1961); c) R. L. Seth and A. K. Dey, *Z. Anorg. Allg. Chem.*, **321**, 278 (1963).

3) N. Ishibashi, H. Kohara, and K. Abe, *Bunseki Kagaku*, **17**, 154 (1968).

4) L. J. Csanyi, *Mikrochim. Acta*, **1980**, I, 277.

5) M. Krizan and J. Nozaki, *Mikrochim. Acta*, **1975**, II, 435.

6) K.-H. Tytko and O. Glemser, "Isopolymolybdates and Isopolytungstates," in "Advances in Inorganic Chemistry and Radiochemistry," ed by H. J. Emelcus and A. G. Sharpe, Academic Press, New York, N. Y. (1976), Vol. 19, pp. 239—315.

7) T. N. Briggs and J. E. Stuehr, *Anal. Chem.*, **47**, 1916 (1975).

8) M. A. Yampol'skii, L. I. Gen, and P. D. Tyutyunnikova, *Nauchn. Tr., Kursk. Gos. Pedagog. Inst.*, **23**, 185 (1974); *Chem. Abstr.*, **82**, 65087w (1975).

Determination of Diffusion Coefficients of Metals Dissolved in Mercury by Double Potential Step Chronoamperometry at Hanging Mercury Drop Electrodes

Sang Yun PARK,† Koichi AOKI, Koichi TOKUDA, and Hiroaki MATSUDA*

Department of Electronic Chemistry, Graduate School at Nagatsuta, Tokyo Institute of Technology, Nagatsuta, Midori-ku, Yokahama 227

(Received January 31, 1983)

Double potential step chronoamperometry at the hanging mercury drop electrode is proposed for determination of diffusion coefficients of metals dissolved in mercury. The expression for chronoamperometric curves is obtained, from which the algorithm is derived for evaluating diffusion coefficients of metals. The diffusion coefficients of lead, zinc, and cadmium in mercury at 25 °C were determined by the present technique.

Symbols

- c_O^s Concentration of substance O at the electrode surface.
- c_R^s Concentration of substance R at the electrode surface.
- c_O^* Bulk concentration of substance O.
- D_O Diffusion coefficient of substance O.
- D_R Diffusion coefficient of substance R.
- E_i Initial potential.
- F Faraday constant.
- j_a Anodic current density.
- j_c Cathodic current density.
- n Charge number of the electrode reaction.
- p Intercept of the extrapolated line in the plots of $\phi(\xi)\sqrt{\xi}$ *vs.* $\sqrt{\xi}$.
- q Slope of the extrapolated line in the plots of $\phi(\xi)\sqrt{\xi}$ *vs.* $\sqrt{\xi}$.
- t Electrolysis time.
- r Radius of the hanging mercury drop electrode.
- τ Duration of the first potential step.
- γ Ratio of square root of D_R to that of D_O, defined by Eq. 9.
- ϕ Dimensionless anodic current, defined by Eq. 10.
- θ Dimensionless duration of the first potential step, defined by Eq. 8.
- ξ Dimensionless electrolysis time during the second potential step, defined by Eq. 7.

Electrochemical methods have often been applied to a study on determination of the solubility of metals and the diffusion coefficients of metal atoms in mercury.[1] A classical electrochemical method for determination of the diffusion coefficients of metals in mercury is amalgam polarography developed extensively by Furman and Cooper,[2] Stromberg,[3] and Stackelberg and Toome.[4] This method has difficulties in determining accurately the concentration of dissolved metal, especially when the amalgam is unstable. The other method is linear sweep voltammetry at a hanging mercury drop electrode (HMDE) which was proposed by Stromberg and Zakharova[5] and Baransky[6] and later investigated quantitatively by Tokuda *et al.*[7] This can be undertaken with a simple electrochemical instrument in relatively short time but this method is often subjected to complexity when the charge transfer is slow. A new technique leading to more accurate determination was introduced by Stevens and Shain,[8] which is chronoamperometry following the amalgam formation by a pre-electrolysis at the HMDE. In this method, amalgam is prepared by the long-term electroreduction of the metal ion in solution such that the concentration of metal may be uniform over the whole mercury drop. Stevens and Shain took advantages of characteristics of the spherical diffusion at the HMDE and proposed the method of plotting $It^{1/2}$ against $t^{1/2}$ so that the plots fall into a straight line, where I is the anodic current at electrolysis time, t. Fitak determined the diffusion coefficients of many metals in mercury by this method.[9] However, this method is not necessarily an extensively applicable technique because, during the pre-electrolysis, unstable amalgam may be altered in properties and further the HMDE may be influenced by unexpected fluctuations of temperature and undesirable mechanical vibrations. Therefore it is required to develop a method with a short time window.

We present here a technique of double potential step chronoamperometry at the HMDE, of which conditions are as follows: (a) The HMDE does not contain initially any foreign metal while metal ions are in the solution phase. (b) The potential of the HMDE is initially set at E_i, which is positive enough for no faradaic process to occur. (c) The potential is stepped to a sufficiently negative region corresponding to the limiting diffusion-controlled current for the reduction of the metal ions in the solution, and then switched back to E_i. (d) The duration of the cathodic electrolysis is ranged from a few seconds to some ten seconds and the subsequent anodic current is measured within one second. The equations for the double potential step chronoamperometric curves are derived and the procedures of evaluating the diffusion coefficients of metals in mercury are presented. Furthermore this method is applied to the determination of the diffusion coefficients of lead, zinc and cadmium in mercury.

Theoretical

We consider a simple electrode reaction, $O+ne \rightleftarrows R$, without any chemical complication. We assume that the limiting currents are governed by the spherical diffusion of substance O in the solution and of sub-

† Present address: The Korea Meritime University, 1, Dongsam-Dong, Yongdo-ku, Busan, Korea.

stance R in the mercury drop. This means that the shielding effect of capillary tip and the deviation of the shape of the drop from a perfect sphere are neglected. Further it is assumed that the solution initially contains only the spicies O and supporting electrolytes.

The diffusion equation within the finite spherical region has been solved and the concentrations of O and R at the electrode surface have been expressed as functions of the current density and the electrolysis time.[7]

[*A*] *First Potential Step.* Concentrations of the ion and the metal at the surface of the HMDE are given by[7]

$$c_O^s = c_O^* - (\pi D_O)^{-1/2}\int_0^t (j/nF)(t-x)^{-1/2}dx + (1/r)\int_0^t G(D_O(t-x)/r^2)(j/nF)dx, \quad (1)$$

$$c_R^s = (1/r)\int_0^t H(D_R(t-x)/r^2)(j/nF)dx, \quad (2)$$

with

$$G(x) = \exp(x)\,\mathrm{erfc}\sqrt{x} \quad (3)$$

$$H(x) = 1/\sqrt{\pi x} + \exp(x)(1+\mathrm{erf}\sqrt{x}) \quad \text{for } 0<x<0.06, \quad (4)$$

where the function $H(x)$ is the inverse Laplace transform of the asymptotic expansion for $1/(\sqrt{s}\coth\sqrt{s}-1)$. Taking c_O^s to be zero yields the well-known expression for the limiting current density controlled by spherical diffusion,[10]

$$j_c = nFc_O^*\sqrt{D_O}(1/\sqrt{\pi t}+\sqrt{D_O}/r). \quad (5)$$

This equation has been applied to determination of diffusion coefficients of several metal ions with high accuracy in the elaborate operation of the HMDE.[12,13]

[*B*] *Second Potential Step.* After the first potential step, of which duration is described as τ, the electrode potential is stepped back to E_i to make the concentration of species R effectively zero at the electrode surface, *i.e.*,

$$c_R^s = 0 \quad \text{for } t>\tau. \quad (6)$$

Substituting condition (6) into Eq. 2 and introducing the dimensionless variable, parameters and function as follows:

$$\xi = D_O(t-\tau)/r^2, \quad (7)$$

$$\theta = D_O\tau/r^2, \quad (8)$$

$$\gamma = (D_R/D_O)^{1/2}, \quad (9)$$

$$\phi(\xi) = -(j_a/nF)[\sqrt{\pi}\,r/c_O^*D_O], \quad (10)$$

then we have

$$\int_0^\xi H[\gamma^2(\xi-x)]\phi(x)dx = \int_0^\theta H[\gamma^2(\xi+\theta-x)](1/\sqrt{x}+\sqrt{\pi})dx, \quad (11)$$

where j_a is the anodic current density and $\phi(\xi)$ the dimensionless anodic current. Since it is somewhat complicated to solve the above integral equation, details of the derivation are given in Appendix. Then $\phi(\xi)$ is expressed as

$$\phi(\xi) = (1+\gamma)[2\exp(\gamma^2\theta)-G(\gamma^2\theta)][1/\gamma\sqrt{\xi}-\sqrt{\pi}\,G(\gamma^2\xi)] + (2/\sqrt{\pi})[\gamma^2(\xi+\theta)+1]\arctan\sqrt{\xi/\theta} + 2\gamma(\gamma+1)\sqrt{\theta}\,G(\gamma^2\xi) - 2\gamma(\gamma+1)\sqrt{\xi+\theta} + (2/\sqrt{\pi})\gamma^2(\gamma+1)\sqrt{\xi\theta} - 1/\sqrt{\xi+\theta} - 1/\gamma\sqrt{\xi} - 2(1+\gamma)\gamma^3\int_0^\xi(\xi+\theta-x)^{1/2}G(\gamma^2x)dx. \quad (12)$$

Equation 12 represents the current-time curve for the second potential step, with the parameters of ξ and θ given by Eqs. 7 and 8, respectively.

In Fig. 1, numerically calculated values of $\phi(\xi)\sqrt{\xi}$, which corresponds to $j_a(t-\tau)^{1/2}$, are plotted against $\sqrt{\xi}$ for $\theta=0.06$ and various values of γ. The integral involved in Eq. 12 was evaluated by Simpson's 1/3 rule. The figure shows that a difference between any two curves increases with a decrease in ξ and that every curve becomes almost a straight line as $\sqrt{\xi}$ tends to zero. Therefore extrapolation of $\phi(\xi)\sqrt{\xi}$ to $\sqrt{\xi}\to 0$ is a useful procedure for determinating D_R. The function, $\phi(\xi)\sqrt{\xi}$, can be expanded about $\sqrt{\xi}=0$, as follows:

$$\phi(\xi)\sqrt{\xi} = p + q\sqrt{\xi} + \cdots, \quad (13)$$

with

$$p = [(1+\gamma)\exp(\gamma^2\theta)(1+\mathrm{erf}(\gamma\sqrt{\theta}))-1]/\gamma, \quad (14)$$

$$q = (4/\sqrt{\pi}-2)\sqrt{\theta}\,\gamma(1+\gamma)-1/\sqrt{\theta}-2(1+\gamma) \times\exp(\gamma^2\theta)[1+\mathrm{erf}(\gamma\sqrt{\theta})]. \quad (15)$$

The parameter p is a main factor for evaluating D_R. If the value of D_O is determined from the cathodic current-time curves during the first potential step by plotting j_c against $t^{-1/2}$ and applying Eq. 5, p and q become experimentally accessible quantities. Since the radius of the HMDE, r, can readily be evaluated, θ becomes a known value. Hence it is possible to obtain γ, that is, D_R, from Eq. 14 in principle. In Fig. 2 theoretical values of p calculated from Eq. 14 are plotted against γ for several values of θ, demonstrating that the slopes of the curves increase with an increase in θ. This indicates that making longer the duration of the first potential step and/or using the HMDE with a smaller radius leads to more accurate determination of the diffusion coefficients.

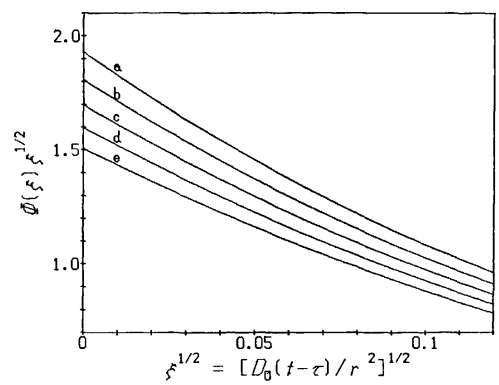

Fig. 1. Variations of $\phi(\xi)\sqrt{\xi}$ with $\sqrt{\xi}$ for $\theta=0.06$ and γ=(a) : 1.4, (b): 1.2, (c): 1.0, (d): 0.8, (e): 0.6,

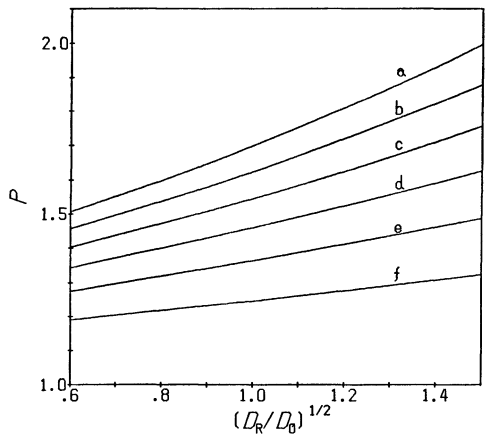

Fig. 2. Dependence of extrapolated values of $\phi(\xi)\sqrt{\xi}$ upon γ for $\theta=$(a): 0.06, (b): 0.05, (c): 0.04, (d): 0.03, (e): 0.02, (f): 0.01.

Since the curves in Fig. 1 have concave forms, extrapolating the curves from the region corresponding to large values of $\sqrt{\xi}$ may yield smaller values of γ than the true ones. We examined the extrapolation procedure of a number of theoretical curves and found that the values of γ can be obtained within 2.5% errors if values of $\sqrt{\xi}$ less than 0.03 are used for extrapolation.

It is not so convenient or elegant to use the working curves in Fig. 2 for evaluating γ from chronoamperometric data. It might be more desirable to utilize the explicit form of γ than to use Fig. 2. Unfortunately, we could not find the inverse function for p. Instead we propose the algorithm for evaluating γ with reasonably high accuracy by Newton-Raphson's method as follows:

$$\gamma_{k+1} = \gamma_k - \frac{[(1+\gamma_k)h_k - 1 - \gamma_k p]\gamma_k}{\left[\begin{array}{l}\{2\gamma_k{}^2\theta(1+\gamma_k)-1\}h_k \\ \quad +2\sqrt{\theta/\pi}(1+\gamma_k)\gamma_k \exp(-\gamma_k{}^2\theta)+1\end{array}\right]}, \quad (16)$$

$$h_k = \exp(\gamma_k{}^2\theta)[1+\mathrm{erf}(\gamma_k\sqrt{\theta})],$$

$$(k=0,\ 1,\ 2,\ \cdots).$$

The initial value of γ,γ_0, is usually taken to be unity. Substituting γ_0 and measured value of p into Eq. 16 gives a new value of γ_1, which is again inserted into Eq. 16 to yield γ_2. We confirmed that accuracy with four digits is ensured after two or three iterations.

The values of γ thus evaluated should be consistent with those calculated from slopes of the straight lines by the use of Eq. 15. Since the slope, q, is a secondary term, it is desirable to make use of the slopes for a criterion of the value obtained from p by means of extrapolation. In other words, inserting a value of γ calculated from p into Eq. 15 yields q, which should be the same as that obtained experimentally. If one fails to reach the consistency, the data may be invalid or one can try again to determine γ by varying the slope slightly.

Experimental

Apparatus and Chemicals. A micrometer-type HMDE assembly MCI AS01 (Mitsubishi Chemical Industries, Ltd.) was employed. In order to avoid the shielding of the diffusion space by the capillary wall and to ensure the spherical diffusion as completely as possible, the capillary end was drawn to give a tip of *ca.* 0.2 mm in outer diameter as has been done by Ikeuchi *et al.*[13] Five capillaries were prepared but two of them had good performance in the relation of the size of a mercury sphere to the reading of the micrometer. We paid special attention to the temperature of the cell and mechanical vibrations, to both of which the characteristics of the HMDE are quite sensitive. The H-typed cell with the capillary was dipped into a thermostat at (25± 0.1) °C, which was supported by four semiinflated balls.

All the solutions were made up using Analar grade chemicals and twice-distilled water. Solutions of 3 mmol dm^{-3} of Pb(II) and Cd(II) were prepared by dissolving known amounts of lead oxide and cadmium oxide into solutions of nitric acid, respectively. A supporting electrolyte was sodium sulfate (1.0 mol dm^{-3}).

The electrode potential was controlled with the aid of a home-made potentiostat equipped with a current limiter and a signal generator for clock-controlled potential-time sequences. Transition of the currents was measured with a 12-bit digital oscilloscope (Nicolet 1090A explorer digital oscilloscope).

Procedures. Five glass cups in one centimeter height were placed on the bottom of the cell before passing nitrogen gas through a solution. They function as a vessel for collecting a mercury drop after each experimental run. The initial and the first-step potentials were selected to be about 200 mV more positive and more negative than the half-wave potential, respectively. Durations of the first step used were 3, 7, and 12 s and the current responses were sampled after a 30 ms lapse. Currents during the second potential step were measured in the range from 50 ms to 1 s. Five different radii of the HMDE's were examined. After an experimental run, the HMDE was dropped into one of the glass cups, which was taken out from the cell when five cups were occupied with mercury drops. The mercury drop was rinsed with water, ethanol and acetone in turn and dried. It was weighed immediately after most of acetone was evapolated, because evapolation of mercury causes serious error in determining the radius of a drop. The radius and the area of the HMDE were evaluated from the weight of the drop. Radii of the HMDE were varied from 0.36 mm to 0.55 mm.

Results and Discussion

Plots of the cathodic currents for lead against the reciprocal of the square root of time are shown in Fig. 3. As expected from Eq. 3, the plots fall into a straight line, of which slope gives $nFc_0{}^*D_0{}^{1/2}$. The values of D_0 for Pb(II),Cd(II), and Zn(II) ions thus calculated from slopes and Eq. 3 are summarized in Table 1. They were constant regardless of the variations in radii of the HMDE and are quite reasonable values. Unfortunately, we could not find the literature values of D_0 under the same conditions as in this experiment. If we take into account the fact that accuracy of the balance was 0.1 mg, *i.e.*, 4% of relative errors, it turns out that the errors involved in D_0 values can be attributed mainly to errors of weighing mercury drops.

The plots in Fig. 3 deviate upward from the straight line when t ($t<\tau$) is less than 60 ms. Since we confirmed that the residual cathodic current decays almost

Table 1. Diffusion coefficients of ions in 1 mol dm^{-3} Na_2SO_4 solution and metals in mercury at 25 °C

		$10^{10}D$ / m^2 s^{-1}	Number of runs	Literature values[1] of $10^{10}D$/m^2 s^{-1}
Pb	ion	7.74±0.08(0.50)[a]	33	
	metal	10.5 ±0.26(1.50)	33	11.7
Cd	ion	7.84±0.08(0.29)	12	
	metal	11.4 ±0.2 (0.66)	12	15.2
Zn	ion	7.41±0.08(0.24)	9	
	metal	17.6 ±1.2 (3.00)	6	19.0

a) Digits in the parenthese indicate the standard deviation.

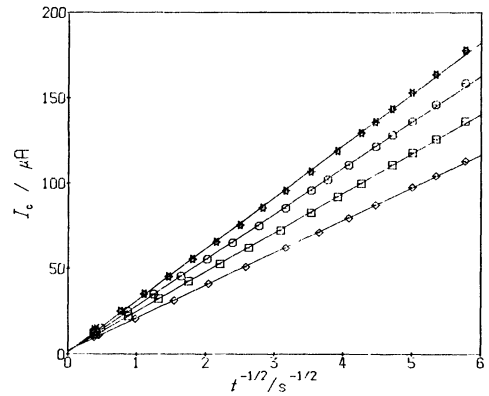

Fig. 3. Plots of cathodic currents *vs.* inverse square roots of time at the HMDE with radii of (★): 0.545, (○): 0.475, (□): 0.445, and (◇): 0.410 mm. The solution was 3 mmol dm^{-3} of Pb^{2+} in 1.0 mol dm^{-3} Na_2SO_4 at 25 °C.

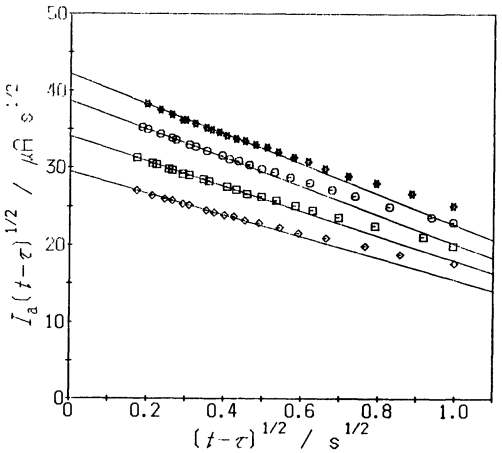

Fig. 4. Plots of products of anodic currents by square roots of time against square roots of time at the HMDE with radii of (★): 0.545, (○): 0.475, (□): 0.445, and (◇): 0.410 mm. The solution was 3 mmol dm^{-3} of Pb^{2+} in 1.0 mol dm^{-3} Na_2SO_4 at 25 °C.

to zero at 4 ms, the deviation cannot be attributed to the charging current. One of the causes of the enhancement of the currents may be the saturation of the potentiostat due to extremely high currents at short times although a current limiter was employed.[13]

The plots of $I_a(t-\tau)^{1/2}$ *vs.* $(t-\tau)^{1/2}$ corresponding to the curves given in Fig. 3 are presented in Fig. 4. The curves in Fig. 4 are quite similar in shape to those of Fig. 1. Since an extrapolated value is required for determination of D_R, it is desirable to measure currents at short electrolysis times. As described above, however, currents obtained at the times less than 60 ms may involve some extraneous components. Plots at the times $(t-\tau)$ more than 0.35 s, which correnspond to $\sqrt{\xi}>0.03$, are ineffective for the extrapolation because of the nature of the concave curves, as predicted from the theoretical curves in Fig. 1. Hence a straight line was drawn for the extrapolation so as to fit the plots in the restricted region (60—350 ms). The procedure for evaluation of D_R is illustrated below by taking the third plot in Fig. 4 as an example. The extrapolated value is 34.0 μA s$^{1/2}$. Substituting this value and the corresponding D_O value ($=7.71\times10^{-10}$ m^2 s^{-1}) into the following equation:

$$p = \lim_{t\to\tau} j_a[\pi(t-\tau)]^{1/2}/nFc_O^*D_O^{1/2}, \quad (17)$$

we obtain $p=1.48$. Since $\tau=7.0$ s, θ is equal to 0.027. Inserting the values of p and θ into Eq. 16, we obtained the recurrent values of γ such as 1.348, 1.326, 1.327, and 1.326, indicating that the convergent value is 1.326. Hence it follows that $D_R=1.02\times10^{-10}$ m^2 s^{-1}. The value of q calculated from Eq. 15 with the values of θ and γ was −12.0, which is in good agreement with the dimensionless slope, −11.6, of the third straight line.

The diffusion coefficients of lead, zinc and cadmium in mercury were determined in this way for some different values of the cathodic pre-electrolysis time, τ, (3—12 s) and the radius of the HMDE, r, (0.36—0.55 mm). The values of D_R obtained are given in Table 1, together with the values suggested by Galus in the light of his present knowledge.[1] These values were constant regardless of variations not only in τ but also in r. We did not observe any dependence of diffusion coefficient of zinc on r although Dowgird and Galus did.[14]

The precision of the values of D_R is twice as poor as that of D_O. The errors may partly result from the extrapolation shown in Fig. 4 and partly be attributed to the double potential perturbation.

Conclusion

The expression for the double potential step chronoamperometric curve has been derived and the procedure for determining the diffusion coefficient of metal in mercury has been developed on the basis of examination of the theoretical curves. The procedure is as follows: (1) D_O is evaluated from the slope of the plots of cathodic currents against $t^{-1/2}$ $(t<\tau)$. (2) Anodic currents multiplied by $(t-\tau)^{1/2}$ are plotted against $(t-\tau)^{1/2}$. (3) A part of the straight line of the plots is extrapolated up to $(t-\tau)^{1/2}\to 0$. (4) This extrapolated value and the values of D_O determined in process (1) are inserted into Eq. 16, and the ratio of D_R to D_O is obtained by iterative computation. (5) The slope of the straight line is used for checking whether the extrapolation is reasonable or not.

The measurements for lead, zinc, and cadmium in mercury gave the diffusion coefficients in agreement with literature values. This method is suitable for short time measurement of diffusion coefficients of unstable metals in mercury regardless of the degree of reversibility.

Appendix

The appendix describes details of the derivation of $\phi(\xi)$ from integral equation 11. Applying Laplace transformation with respect to ξ to Eq. 11 yields

$$\begin{aligned}\mathrm{L}[\phi(\xi)]/\gamma(\sqrt{s}-\gamma) &= (s-\gamma^2)^{-1}\\ &\times\int_0^\theta[(\sqrt{s}/\gamma)\exp[s(\theta-x)]\mathrm{erfc}\sqrt{s(\theta-x)}\\ &+\exp[\gamma^2(\theta-x)](1+\mathrm{erf}\sqrt{\gamma^2(\theta-x)})]\\ &\times(1/\sqrt{x}+\sqrt{\pi})\mathrm{d}x, \qquad \text{(A-1)}\end{aligned}$$

where L denotes the operator of the Laplace transformation. The left-hand side has been obtained with the aid of the convolution theorem, whereas the right-hand side has been derived by the direct Laplace integration. Since the integral in Eq. A-1 is of the form of convolution with respect to θ, it is convenient to evaluate the integrals using the convolution theorem for the Laplace transformation. One of the examples is given below.

$$\begin{aligned}&\int_0^\theta\exp[s(\theta-x)]\mathrm{erfc}\sqrt{s(\theta-x)}x^{-1/2}\mathrm{d}x\\ &=\mathrm{L}_\theta^{-1}[\mathrm{L}(1/\sqrt{\theta})\mathrm{L}_\theta(\exp(s\theta)\mathrm{erfc}\sqrt{s\theta})]\\ &=\mathrm{L}_\theta^{-1}[\sqrt{\pi}/u(\sqrt{u}+\sqrt{s})]\\ &=\sqrt{\pi/s}[1-\exp(s\theta)\mathrm{erfc}\sqrt{s\theta}],\end{aligned}$$

where L_θ denotes the Laplace transformation operator with respect to θ and u the Laplace transformed variable of θ. Then the Laplace transformed function of $\phi(\xi)$ becomes

$$\begin{aligned}\mathrm{L}[\phi(\xi)] &= \sqrt{\pi}(1+\gamma)[2\exp(\gamma^2\theta)-G(\gamma^2\theta)]/\gamma(\sqrt{s}+\gamma)\\ &-\sqrt{\pi/s}/\gamma+\sqrt{\pi}G(\theta s)/\gamma\sqrt{s}\\ &-\sqrt{\pi}(1+\gamma)G(\theta s)/\gamma(\sqrt{s}+\gamma). \qquad \text{(A-2)}\end{aligned}$$

Carrying out the inverse Laplace transformation of Eq. A-2 with the help of a table of the transformation[11] yields Eq. 12.

References

1) Z. Galus, *CRC Crit. Rev. Anal. Chem.*, **6**, 359 (1975).
2) N. H. Furman and W. C. Cooper, *J. Am. Chem. Soc.*, **72**, 5647 (1950); W. C. Cooper and N. H. Furman, *J. Am. Chem. Soc.*, **74**, 6183 (1952).
3) A. G. Stromberg, *Dokl. Akad. Nauk SSSR*, **85**, 831 (1952).
4) M. v. Stackelberg and V. Toome, *Z. Elektrochem.*, **58**, 226 (1954).
5) A. G. Stromberg and E. A. Zakharova, *Sov. Electrochem.*, **1**, 922 (1965).
6) A. Baranski, Ph. D. thesis, University of Warsaw, 1974.
7) K. Tokuda, N. Enomoto, H. Matsuda, and N. Koizumi, *J. Electroanal. Chem.*, in press.
8) W. G. Stevens and I. Shain, *J. Phys. Chem.*, **70**, 2276 (1966).
9) S. Fitak, M. Sc. thesis, University of Warsaw, 1973.
10) A. J. Bard and L. R. Faulkner, "Electrochemical Methods: Fundamentals and Applications," John Wiley & Sons, New York (1980), p. 145.
11) G. E. Roberts and H. Kaufman, "Table of Laplace Transforms," W. B. Saunders Company, Philadelphia (1966).
12) H. Ikeuchi, Y. Fujita, K. Iwai, and G. P. Satô, *Bull. Chem. Soc. Jpn.*, **49**, 1883 (1976).
13) H. Ikeuchi, K. Iwai, M. Kaneko, M. Maya, and G. P. Satô, *Bull. Chem. Soc. Jpn.*, **52**, 1863 (1979).
14) A. Dowgird and Z. Galus, *Bull. Acad. Pol. Sci., Ser. Sci. Chim.*, **18**, 225 (1970).

Thermal Properties and Raman Spectra of Crystalline and Vitreous $BaZrF_6$, $PbZrF_6$, and $SrZrF_6$

Yoji KAWAMOTO* and Fumiko SAKAGUCHI

Department of Chemistry, Faculty of Science, Kobe University, Rokkodai, Nada-ku, Kobe 657

(Received February 3, 1983)

Differential thermal analysis and Raman spectroscopic studies have been performed of crystalline and vitreous $BaZrF_6$, $PbZrF_6$, and $SrZrF_6$ compounds in order to examine the thermal properties and the F coordination of Zr. The differential thermal analyses clarified the definite phase transformation characteristics of crystalline $BaZrF_6$, and $SrZrF_6$ and also suggested that the low- and high-temperature modifications are present in $PbZrF_6$ as well as in $BaZrF_6$ and $SrZrF_6$. The Raman spectra of crystalline $BaZrF_6$, $PbZrF_6$, and $SrZrF_6$ were discussed in relation to the F coordination of Zr in fluorozirconate compounds. The crystallization behaviors and Raman spectra of vitreous $BaZrF_6$, $PbZrF_6$, and $SrZrF_6$ revealed that Zr in the vitreous compounds is eight-coordinated by F although small amounts of seven-coordinated Zr may exist in vitreous $BaZrF_6$.

Zirconiumtetrafluoride-based glasses recently developed[1] are a new family of glasses and are noted in properties of high F ion conductivity and mid infrared transparency.[2] Currently various properties of the glasses are being examined to evaluate the possibility of the potential applications.[2] However, the structural studies are a few[3–5] so that the glass structures are not thoroughly understood yet.

The binary systems BaF_2–, PbF_2–, and SrF_2–ZrF_4 yield vitreous materials in given composition ranges[6] and besides the combination of the binaries and other fluorides gives a number of polynary fluorozirconate glasses.[2] Accordingly the binary systems can be regarded as mother systems for fluorozirconate glasses. Thus, elucidating the structures of the binary glasses is indispensable for the structural understanding of ZrF_4-based fluoride glasses. As the first step of the structural studies of the BaF_2–, PbF_2–, and SrF_2–ZrF_4 glasses, the present authors dealt with Ba, Pb, and Sr metafluorozirconate glasses, that is, vitreous $BaZrF_6$, $PbZrF_6$, and $SrZrF_6$.

The objective of this work is to elucidate the short-range structure, mainly the F coordination environment of Zr, of the vitreous $BaZrF_6$, $PbZrF_6$, and $SrZrF_6$. Differential thermal analysis and Raman spectroscopy were employed for the investigation. A method frequently employed for inferring the structure of a glass is to compare the various spectra of the glass with those of the related crystalline compounds. In the present study the thermal properties and Raman spectra of crystalline $BaZrF_6$, $PbZrF_6$, and $SrZrF_6$ that were not reported were first studied. Then the thermal behaviors and Raman spectra of vitreous $BaZrF_6$, $PbZrF_6$, and $SrZrF_6$ were examined and compared with those of the crystalline compounds.

Experimental

Materials. Raw materials employed for the preparation of crystalline and vitreous $BaZrF_6$, $PbZrF_6$, and $SrZrF_6$ were ZrF_4 (Morita Chemicals, 99.9% purity), BaF_2(Merck, suprapur), PbF_2 (Merck, suprapur), and SrF_2(Merck, suprapur). About 5 g stoichiometric mixtures of the raw materials with addition of small amounts of NH_4HF_2 were melted in platinum crucibles in an N_2 gas atmosphere using a simple SiC resistance furnace and the melts were kept at about 850 °C for 10 min. The low-temperature modifications(α) of $BaZrF_6$, $PbZrF_6$, and $SrZrF_6$ were obtained by cooling the melts slowly to room temperature in the furnace. On the other hand, the high-temperature forms(β) of $BaZrF_6$ and $SrZrF_6$ were prepared by crystallizing the melts at temperatures a few degrees below their melting points and then quenching them by liquid nitrogen. Vitreous $BaZrF_6$, $PbZrF_6$, and $SrZrF_6$ were prepared by quenching the melts rapidly using a twin roller. The synthesized crystalline compounds were polycrystalline and were identified by X-ray powder diffraction to be the respective single phases. In the identification the reference X-ray powder patterns were computed from the available crystal structure data. The prepared vitreous compounds were thin films of about 20 μm thickness and amorphous in X-ray diffraction.

Differential Thermal Analyses. Differential thermal analyses were undertaken to examine the phase transformation (T_t) and melting (T_m) temperatures of crystalline $BaZrF_6$, $PbZrF_6$, and $SrZrF_6$ compounds and the glass transition(T_g) and crystallization (T_c) temperatures of the vitreous compounds. The measurements were made in an Ar gas stream with a heating or cooling rate of 5 °C min^{-1}.

Raman Spectra. Raman scattering of crystalline and vitreous $BaZrF_6$, $PbZrF_6$, and $SrZrF_6$ were measured with a Spex 14018 double monochromator in the 90° scattering configuration using the Ar^+ 488.0 nm laser line at ambient temperature. In the measurements the slits were opened to 400 μm and the pressed-disc samples were used. No sample deterioration was observed under irradiation with an about 150 mW beam.

Results and Discussion

Differential Thermal Analyses. So far the followings have been reported on the modifications and crystal structures of $BaZrF_6$, $PbZrF_6$, and $SrZrF_6$: Both $BaZrF_6$ and $SrZrF_6$ have the low- and high-temperature modifications but $PbZrF_6$ is present only in a single modification.[7] The structures of β-$BaZrF_6$, $PbZrF_6$, and α-$SrZrF_6$ are crystallographically isomorphous and are composed of $(ZrF_8)^{4-}$ dodecahedra connected by two edges to form chain linked by Ba^{2+}, Pb^{2+}, and Sr^{2+} ions.[7] The structure of α-$BaZrF_6$ is built up of $(Zr_2F_{12})^{4-}$ complex anions linked by Ba^{2+} cations, where a Zr atom is coordinated by seven F atoms.[8]

Although the presence of α- and β-modifications in $BaZrF_6$ and $SrZrF_6$ is confirmed in crystal structure studies the α-β phase transformation temperatures are

not well-defined. Furthermore, even the melting temperatures of $BaZrF_6$, $PbZrF_6$, and $SrZrF_6$ are not reported. In the present work, therefore, thermal studies were first made of crystalline $BaZrF_6$, $PbZrF_6$, and $SrZrF_6$ compounds with differential thermal analysis. In the analyses the products at endotherm or exotherm peaks were identified by X-ray diffraction measurements of the quenched samples. The results of α- and β-$BaZrF_6$, $PbZrF_6$, and α- and β-$SrZrF_6$ are shown in Figs. 1(a, b), 2(a), and 3(a, b), respectively, where

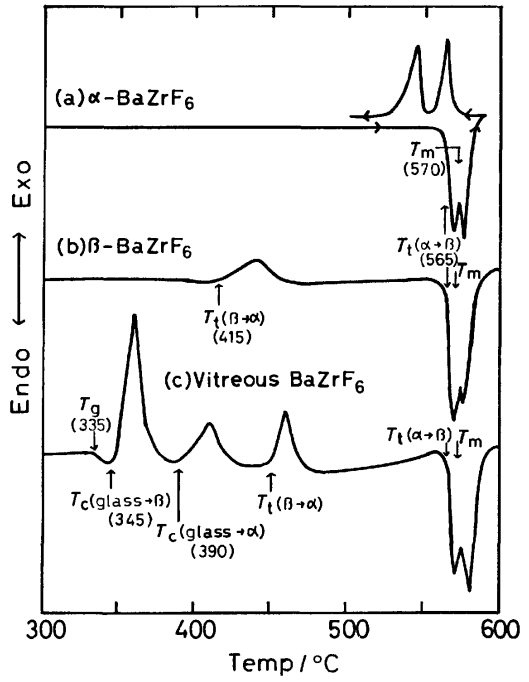

Fig. 1. Differential thermal analysis curves of α- and β-$BaZrF_6$ and vitreous $BaZrF_6$. Numerals in parentheses are temperatures in °C.

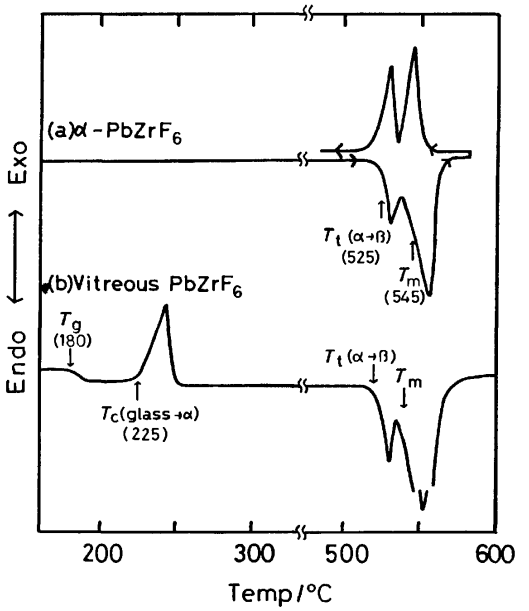

Fig. 2. Differential thermal analysis curves of crystalline and vitreous $PbZrF_6$. Numerals in parentheses are temperatures in °C.

the subscripts (α→β) and (β→α) of T_t refer to transformation from α-form to β-form and from β-form to α-form, respectively. As shown in Figs. 1(a, b) and 3(a, b), the phase transformation characteristics of $BaZrF_6$ and $SrZrF_6$ were clearly defined. As can be seen from Fig. 2(a), on the other hand, $PbZrF_6$ showed a differential thermal analysis curve very similar to those of α-$BaZrF_6$ and α-$SrZrF_6$. This indicates that $PbZrF_6$ also may exhibit the α-β phase transformation and that crystalline $PbZrF_6$ already known may be the α-modification. The attempt of preparing β-$PbZrF_6$ according to the method described in Experimental was unfortunately unsuccessful. So the presence of α- and β-modifications in $PbZrF_6$ could not be firmly established in this work.

The differential thermal analysis curves of vitreous $BaZrF_6$, $PbZrF_6$, and $SrZrF_6$ compounds are shown in Figs. 1(c), 2(b), and 3(c), respectively, where the subscripts (glass→α) and (glass→β) of T_c indicate that α- and β-form compounds crystallized from glasses, respectively. The crystallization behaviors show that the crystallized products of vitreous $BaZrF_6$, $PbZrF_6$, and $SrZrF_6$ were β-$BaZrF_6$ and small amounts of α-$BaZrF_6$, α-$PbZrF_6$, and α-$SrZrF_6$, respectively.

Raman Spectra. The Raman spectra observed for crystalline $BaZrF_6$, $PbZrF_6$, and $SrZrF_6$ compounds are shown in Figs. 4—6. In the figures the Raman peaks with asterisks may be bands assigned to symmetric stretching vibration (ν_s).

Here the Raman spectra of crystalline fluorozirconates are discussed in relation to the F coordination of Zr. It is known that, in crystalline fluorozirconates, Zr atoms exhibit three kinds of F coordination numbers (six, seven, and eight) to form fluorozirconate complex anions. Toth *et al.* measured the Raman spectra of

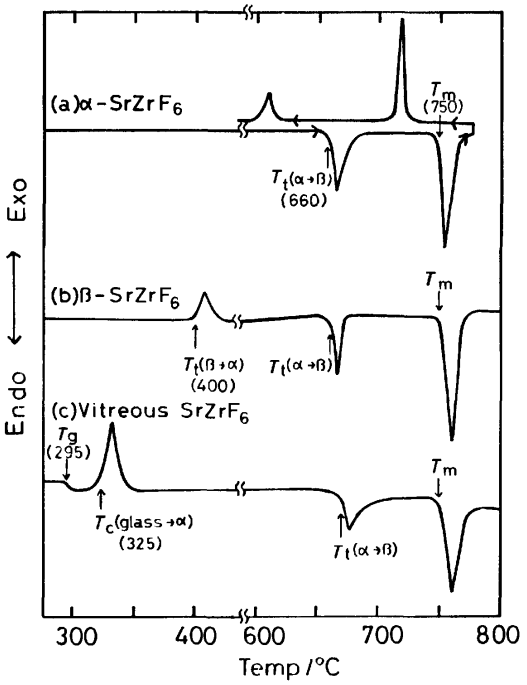

Fig. 3. Differential thermal analysis curves of α- and β-$SrZrF_6$ and vitreous $SrZrF_6$. Numerals in parentheses are temperatures in °C.

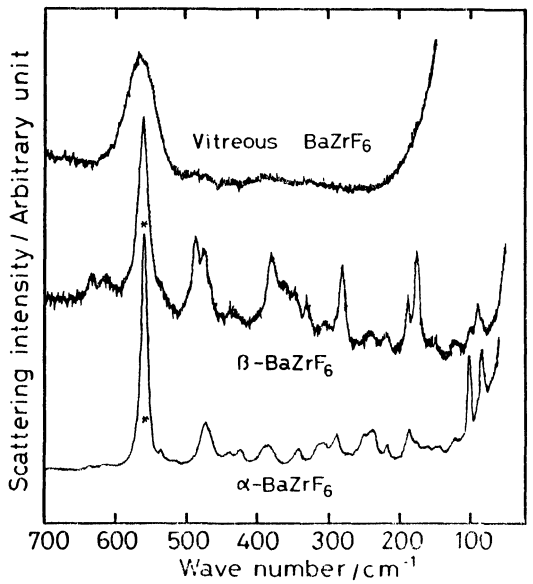

Fig. 4. Raman spectra of α- and β-$BaZrF_6$ and vitreous $BaZrF_6$.

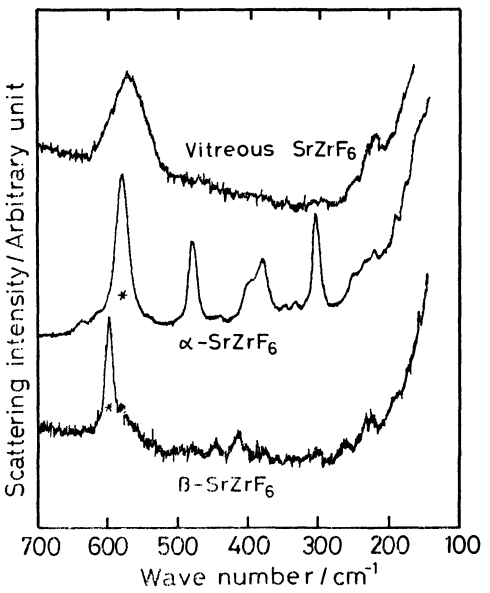

Fig. 6. Raman spectra of α- and β-$SrZrF_6$ and vitreous $SrZrF_6$.

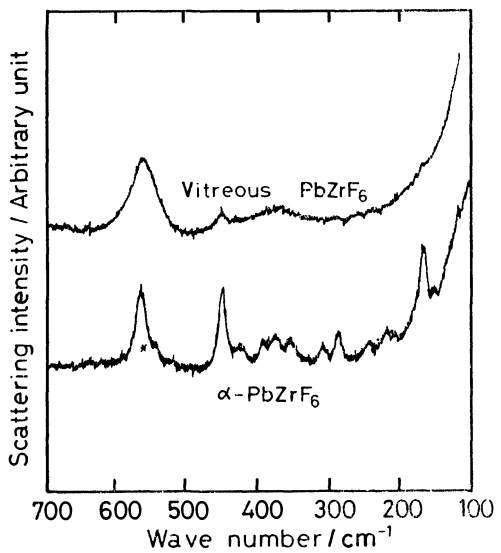

Fig. 5. Raman spectra of crystalline and vitreous $PbZrF_6$.

several alkali fluorozirconate compounds with known crystal structures and discussed the correlation between the ν_s and the F coordination number of Zr.[9] They mentioned that, only in the absence of bridging between F complex ions of Zr, an inverse correlation between the ν_s and the coordination number holds.

The ν_s frequencies observed for the present compounds and alkali fluorozirconate compounds are classified according to the F coordination number of Zr and tabulated in Table 1. In the table the average Zr–F bond lengths and structural characteristics in the respective compounds are also given. In the series of alkali fluorozirconates an inverse correlation is found between the ν_s and the F coordination number, but throughout alkali and alkaline earth fluorozirconates such a correlation does not hold at all. In particular the Zr atoms in β-$BaZrF_6$, α-$PbZrF_6$, and α-$SrZrF_6$ have the same F coordination number(eight) and the same dodecahedral coordination.[7] Nevertheless the ν_s frequencies in the three compounds are significantly different from each other, though the ν_s frequency differences might be probably attributed to the Badger rule, *i.e.*, an inverse correlation between ν_s and Zr–F bond length.[15] The same situation can be seen in a set of Li_2ZrF_6 and Cs_2ZrF_6. Thus no consistent correlation can be deduced between the ν_s and the F coordination number of Zr in fluorozirconate compounds. The following reasons for this may be supposed: Even if the F coordination number is identical the coordination environment may be highly different, especially in large coordination numbers. Moreover, when bridging takes place between the F complex ions it should give many complicated effects on the ν_s vibrations. The bridging manner also may be different in the respective compounds. The above concludes that the Raman ν_s frequency can not be utilized as a reliable guide for identifying the F coordination number of Zr in a fluorozirconate complex with unknown structure.

F Coordination Numbers of Zr in Vitreous $BaZrF_6$, $PbZrF_6$, and $SrZrF_6$. The Raman spectra of vitreous $BaZrF_6$, $PbZrF_6$, and $SrZrF_6$ are shown in Figs. 4, 5, and 6, respectively, together with those of the corresponding crystalline compounds to facilitate the comparison between both the spectra. In the vitreous Raman spectra only the polarized bands were strong and prominent, and all other bands were very weak and broad. In a comparison of vitreous spectra and crystalline spectra, very close resemblance in spectral features can be seen between vitreous $BaZrF_6$ and β-$BaZrF_6$, between vitreous $PbZrF_6$ and α-$PbZrF_6$, and between vitreous $SrZrF_6$ and α-$SrZrF_6$. As already described, on the other hand, the crystallization products of vitreous $BaZrF_6$, $PbZrF_6$, and $SrZrF_6$ compounds were predominantly β-$BaZrF_6$, only α-$PbZrF_6$, and only α-$SrZrF_6$, respectively. In general it is antic-

TABLE 1. F COORDINATION NUMBERS OF Zr AND RAMAN ν_S FREQUENCIES IN VARIOUS FLUOROZIRCONATE COMPOUNDS

Coordination number	Compound	ν_S/cm^{-1}	Average Zr-F bond length/nm	Structural characteristics	Ref.
8	β-$BaZrF_6$	562	0.2138	Edge-shared $(ZrF_8)^{4-}$ chain[a]	7
	α-$PbZrF_6$	567	0.2095	Edge-shared $(ZrF_8)^{4-}$ chain[a]	7
	α-$SrZrF_6$	578	0.2080	Edge-shared $(ZrF_8)^{4-}$ chain[a]	7
	K_2ZrF_6	525[c]	0.2112	Edge-shared $(ZrF_8)^{4-}$ chain	10
	$Na_7Zr_6F_{31}$	548[c]	0.2113	Bridged $(ZrF_8)^{4-}$ complex	11
7	α-$BaZrF_6$	560	0.2082	Edge-shared $(ZrF_7)^{3-}$ dimer	8
	Na_3ZrF_7	556[c]	0.2280	Free $(ZrF_7)^{3-}$ ion	12
6	Cs_2ZrF_6	577[c]	0.2035	Free $(ZrF_6)^{2-}$ ion[b]	13
	Li_2ZrF_6	585[c]	0.2016	Free $(ZrF_6)^{2-}$ ion[b]	14
?	β-$SrZrF_6$	598	?	?	

a) Isostructural ZrF_8 dodecahedron. b) Isostructural ZrF_6 octahedron. c) Ref. 9.

ipated that compounds which crystallize from a glass are crystals with the structures closer to the glass structures. Therefore the crystallization behaviors and Raman spectra of vitreous $BaZrF_6$, $PbZrF_6$, and $SrZrF_6$ conclude that the Zr atoms in the vitreous compounds are eight-coordinated by the F atoms like the Zr atoms in crystalline β-$BaZrF_6$, α-$PbZrF_6$, and α-$SrZrF_6$. Furthermore it may be proposed that the basic structures of the vitreous compounds consist of chains of ZrF_8 dodecahedra. Radial distribution analyses of the vitreous $BaZrF_6$ and $PbZrF_6$ compounds are now in progress to verify the present proposal.[16] Here it is a wonder that vitreous $BaZrF_6$ has a β-$BaZrF_6$-like structure and, on the contrary, vitreous $PbZrF_6$ and $SrZrF_6$ possess the α-form crystal-like structures. Elucidating the crystal structures of β-$PbZrF_6$ and β-$SrZrF_6$ should answer to this question.

Almeida and Mackenzie have inferred that the Ba metafluorozirconate glass is composed of six- and seven-coordinated Zr atoms.[3] In their study, however, they have compared the Raman spectra of fluorozirconate glasses with those of alkali fluorozirconate compounds. This comparison is not proper, as described in the preceding section. In addition it is questioned that the crystallized product of the glass has been reported to be α-$BaZrF_6$. Probably the product identified by Almeida and Mackenzie would be the phase-transformed product of β-$BaZrF_6$ that crystallized initially from the glass.

This work was supported in part by Grant-in-Aid for Special Research, Project "New Investigation of Functional Ceramics" from Ministry of Education, Science and Culture and also in part by Hyogo Prefecture Foundation for Promotion of Science and Technology.

References

1) M. Poulain, M. Poulain, and J. Lucas, *Mater. Res. Bull.*, **10**, 243 (1975).
2) C. M. Baldwin, R. M. Almeida, and J. D. Mackenzie, *J. Non-Cryst. Solids*, **43**, 309 (1981).
3) R. M. Almeida and J. D. Mackenzie, *J. Chem. Phys.*, **74**, 5954 (1981).
4) C. A. Angell, Proceedings of 1st International Symposium on Halide and Other Nonoxide Glasses, Abstr. 7A, ed by Society of Glass Technology, held at Cambridge in England in 1982.
5) D. Louër, R. Coupe, J. Lucas, and A. J. Leonard, Proceedings of 1st International Symposium on Halide and Other Nonoxide Glasses, Abstr. 8B.
6) T. Manabe, *Ceram. Jpn., (Bull. Ceram. Soc. Jpn.)*, **17**, 271 (1982).
7) J. P. Laval, D. Mercurio-Lavaud, and B. Gaudreau, *Rev. Chim. Miner.*, **11**, 742 (1974).
8) J. P. Laval, R. Papiernik, and B. Frit, *Acta Crystallogr., Sect. B*, **34**, 1070 (1978).
9) L. M. Toth, A. S. Quist, and G. E. Boyd, *J. Phys. Chem.*, **77**, 1384 (1973).
10) R. Hoppe and B. Mehlhorn, *Z. Anorg. Allg. Chem.*, **425**, 200 (1976).
11) J. H. Burns, R. D. Ellison, and H. A. Levy, *Acta Crystallogr., Sect. B*, **24**, 230 (1968).
12) L. A. Harris, *Acta Crystallogr., Sect. B*, **12**, 172 (1959).
13) V. H. Bode and G. Teufer, *Z. Anorg. Chem.*, **283**, 18 (1956).
14) G. Brunton, *Acta Crystallogr., Sect. B*, **29**, 2294 (1973).
15) R. M. Badger, *J. Chem. Phys.*, **2**, 128 (1934); **3**, 710 (1935).
16) Y. Kawamoto and T. Horisaka, to be presented in International and VIIth University Conference on Glass Science which will be held in West Germany in 1983.

Synthesis and Characterization of Imidazolate-bridged Copper(II) Complexes of Triangular Skeleton

Hisashi Ōkawa,* Masahiro Mikuriya, and Sigeo Kida

Department of Chemistry, Faculty of Science, Kyushu University 33, Higashi-ku, Fukuoka 812

(Received February 16, 1983)

New polynuclear copper(II) complexes of the composition [CuL(im)]X (L=*N,N,N',N'*-tetramethylethylenediamine (tmen), bip, phen; X=ClO_4, PF_6, BF_4; im=imidazolate ion) have been prepared. Cryomagnetic measurements have indicated that the complexes involve a trianglar-trinuclear skeleton and an antiferromagnetic spin-exchange interaction operates between copper(II) ions; exchange integrals being evaluated at -37—-45 cm^{-1}. Based on the Dreiding model consideration of the complexes and the crystal structure of $[Cu(tmen)(imH)_2](ClO_4)_2$, a trinuclear structure of the triangular skeleton with imidazolate bridges, Cu-Im-Cu-Im-Cu-Im-┐, was supposed for the complexes.

Bovine erythrocyte superoxide dismutase (BESOD) is known to involve an imidazolate-bridged copper(II)–zinc(II) unit at the active site.[1] Cryomagnetic investigation of the copper-substituted enzyme Cu_4-BESOD revealed that an antiferromagnetic spin-exchange interaction operates within each Cu^{2+}–Im–Cu^{2+} unit, the exchange integral being evaluated at -26 cm^{-1}.[2] Therefore, imidazolate-bridged polynuclear copper(II) complexes are of current interest.

So far binuclear and tetranuclear copper(II) complexes with imidazolate bridge have been prepared and characterized. Syntheses of the complexes were achieved (1) by the use of polynucleating ligands containing imidazolate group,[3-6] (2) by the use of biimidazolate or bibenzimidazolate as bridging group,[7] (3) by the reaction of a tridentate or tetradentate ligand, copper(II) ion and imidazole (or 2-methylimidazole) in the 2:2:1 mole ratio,[4,6,8-11] and (4) by the reaction of a binucleating macrocycle, copper(II) ion and imidazole in the 1:2:1 mole ratio.[12,13] Haddad and Hendrickson also prepared and characterized the imidazolate-bridged complexes $[Cu_2(bip)_4(im)](PF_6)_3$ and $[Cu_2(phen)_4(im)](ClO_4)_3$.[7]

In this study we have synthesized new imidazolate-bridged trinuclear copper(II) complexes of the composition CuL(im)X (L=*N,N,N',N'*-tetramethylethylenediamine (tmen), bip, phen; X=ClO_4, PF_6, BF_4; im=imidazolate ion). The triangular structure has been characterized on the basis of cryomagnetic properties, Dreiding model consideration, and the crystal structure of $[Cu(tmen)(imH)_2](ClO_4)_2$.

Experimental

Syntheses. *[CuL(im)]X (L=tmen, bip, phen; X=ClO_4, PF_6, BF_4)*: The synthetic methods for the complexes are nearly the same and exemplified by $[Cu(tmen)(im)]ClO_4$. Copper(II) acetate monohydrate (2.0 g) and tmen (1.2 g) were dissolved in a methanol–water mixture (1:1, 100 cm^3) and warmed at 60 °C. To this was added an aqueous solution of NaOH (0.4 g) and $NaClO_4$ (1.4 g) with stirring to give a di-μ-hydroxo complex $[Cu_2(tmen)_2(OH)_2](ClO_4)_2$. Imidazole was added to this mixture with stirring and warming. When the most part of the di-μ-hydroxo complex was dissolved, the reaction mixture was quickly filtered to separate insoluble materials and the filtrate was allowed to stand overnight. The crystals thus obtained were filtered, washed with methanol and dried *in vacuo*.

$[Cu(phen)(im)]ClO_4$ was practically insoluble in water and in methanol. In order to avoid the contamination of $[Cu_2(phen)_2(OH)_2](ClO_4)_2$, it was prepared by adding a small excess of imidazole to the di-μ-hydroxo complex and the product was throughly washed with hot water.

$[Cu(tmen)(imH)_2](ClO_4)_2$. Copper(II) perchlorate hexahydrate (3.7 g), tmen (1.2 g), and imidazole (1.5 g) were dissolved in hot water (30 cm^3), and the resulting purple solution was filtered and left stand overnight to give bluish purple crystals.

Elemental analyses of the complexes are given in Table 1.

Measurements. Electronic spectra were recorded on a Shimadzu Multipurpose Spectrophotometer model MSP-1000 by reflection on powder samples. Magnetic susceptibilities were measured by the Faraday method, the apparatus being calibrated by the use of $[Ni(en)_3]S_2O_3$.

X-Ray Crystal Structure Analysis of $[Cu(tmen)(imH)_2](ClO_4)_2$. A crystal with dimensions of 0.02 mm×0.17 mm×0.45 mm

Table 1. Elemental analyses of complexes

Complex	Found(%)			Calcd(%)		
	C	H	N	C	H	N
$[Cu(tmen)(im)]PF_6$	27.22	4.93	14.23	27.59	4.89	14.30
$[Cu(tmen)(im)]ClO_4$	30.70	5.43	16.07	31.22	5.53	16.18
$[Cu(tmen)(im)]BF_4$	32.13	5.70	16.68	32.40	5.74	16.79
$[Cu(bip)(im)]PF_6$	35.78	2.90	12.90	36.16	2.59	12.98
$[Cu(bip)(im)]ClO_4$	40.04	3.03	14.08	40.43	2.87	14.51
$[Cu(bip)(im)]BF_4$	40.73	3.16	14.38	40.80	3.16	14.64
$[Cu(phen)(im)]PF_6$	39.53	2.77	11.80	39.53	2.43	12.29
$[Cu(phen)(im)]ClO_4$	43.07	2.74	13.65	42.97	2.88	13.36
$[Cu(phen)(im)]BF_4 \cdot H_2O$	43.21	3.13	13.54	43.35	3.15	13.48

was used for the X-ray analysis. The unit-cell parameters and intensities were measured on a Rigaku AFC-5 automated four-circle diffractometer with graphite-monochromated Mo $K\alpha$ radiation (λ=0.71069 Å) at 20±1 °C. The unit-cell parameters were determined by the least-squares refinement based on the 25 reflections in the range of $17<2\theta<29°$.

Crystal Data: $C_{12}H_{24}Cl_2CuN_6O_8$, F.W.=514.81; monoclinic; $P2_1/n$; a=12.920(5), b=16.171(9), and c=10.084(4) Å; β=97.15(3)°; D_m=1.62; D_c=1.64 g cm^{-3}; Z=4.

The intensity data were collected by the 2θ-ω scan technique with a scan rate of 4° min^{-1}. Three standard reflections were monitored every 100 reflections, and their intensities showed a good stability. A total of 4030 reflections with $2\theta<50°$ were collected. The intensity data were corrected for the Lorentz and the polarization effects, but not for absorption. Independent 1838 reflections with $|F_o|>3\sigma(|F_o|)$ were considered as "observed" and were used for the structure analysis.

The structure was solved by the heavy-atom method and refined by the block-diagonal least-squares method. To identify the nitrogen atoms of the imidazole rings which are not coordinated to the copper atom, the two possible atoms of each ring were both labelled nitrogen. Then the atoms with the lower temperature factors were distinctly labelled nitrogen. Hydrogen atoms were located from the difference Fourier map and included in the refinement. In the least-squares refinement the weighting scheme,[14] $w=(15.56+|F_o|+0.0078|F_o|^2)^{-1}$, was employed. The final R values were R=0.097 and R_w=0.126.

Table 2. Fractional positional parameters ($\times10^4$) and thermal parameters of non-hydrogen atoms with their estimated standard deviations in parentheses

Atom	x	y	z	B_{eq}/Å^2
Cu	1187(1)	2387(1)	3773(2)	2.8
Cl(1)	1059(3)	3695(2)	6960(4)	3.9
Cl(2)	1851(3)	920(3)	303(4)	4.1
O(1)	1060(13)	3107(7)	5926(12)	7.0
O(2)	1619(12)	4404(8)	6605(13)	6.9
O(3)	1555(15)	3312(13)	8135(14)	9.8
O(4)	88(12)	3904(11)	7143(25)	11.6
O(5)	1487(13)	1515(9)	1158(15)	7.8
O(6)	2539(14)	414(11)	1168(14)	9.5
O(7)	1039(12)	427(11)	−323(19)	9.3
O(8)	2336(20)	1332(16)	−619(17)	15.1
N(1)	579(10)	3277(7)	2473(11)	3.5
N(2)	−332(9)	1915(9)	3597(11)	4.0
N(3)	2634(9)	2837(8)	3801(11)	3.7
N(4)	4003(10)	3634(9)	4117(13)	4.6
N(5)	1761(11)	1413(8)	4870(10)	4.2
N(6)	2317(10)	635(8)	6559(12)	3.9
C(1)	376(15)	4061(11)	3146(18)	5.3
C(2)	1229(16)	3486(13)	1383(17)	5.9
C(3)	−401(14)	2898(11)	1777(17)	4.8
C(4)	−1004(12)	2525(10)	2766(17)	4.7
C(5)	−390(16)	1115(11)	2962(18)	5.2
C(6)	−744(14)	1833(17)	4914(16)	6.8
C(7)	3448(12)	2449(12)	3253(14)	4.7
C(8)	4272(14)	2948(11)	3422(14)	4.5
C(9)	2990(12)	3545(9)	4328(13)	3.3
C(10)	2210(16)	718(12)	4429(15)	5.5
C(11)	2549(16)	247(9)	5457(16)	4.8
C(12)	1867(12)	1353(10)	6196(13)	3.7

The atomic scattering factors and the anomalous dispersion corrections were taken from the International Tables for X-ray Crystallography.[15] All the calculations were carried out on the FACOM M-200 computer in the Computer Center of Kyushu University by the use of a local version[16] of the UNICS-III[17] and the ORTEP[18] programs. The final positional and thermal parameters with their estimated standard deviations are given in Table 2. The anisotropic thermal parameters of the nonhydrogen atoms, the coordinates and isotropic temperature factors of hydrogen atoms, and the F_o-F_c tables have been deposited as a Document No. 8330 at the Office of the Editor.

Results and Discussion

All the complexes except for [Cu(phen)(im)]BF_4 were isolated as anhydrous purple crystals, while [Cu(phen)(im)]BF_4 crystallized as blue-colored monohydrate. Deprotonation of imidazole nitrogen in these complexes was evidenced by no N–H stretching mode in the region 3200—3500 cm^{-1}.

Reflectance spectra of the complexes show a d-d band at about 17,000 cm^{-1}. Judging from the fact that the d-d frequency of [Cu(tmen)(im)]ClO_4 (17,300 cm^{-1}) is nearly the same as that (17,500 cm^{-1}) of [Cu(tmen)(imH)$_2$]$(ClO_4)_2$ which possesses a nearly coplanar [CuN_4] chromophore as will be shown later, all the complexes (except for [Cu(phen)(im)]$BF_4\cdot H_2O$ are assumed to have a planar configuration with four nitrogen donor atoms. This suggests that the complexes contain imidazolate group acting as a bridge.

Magnetic moments of the complexes fall in the range 1.59—1.65 BM lower than the spin-only value 1.73 BM. This again implies that the complexes are of polynuclear structure bridged by imidazolate group. In order to obtain further informations on the structure of the complexes, magnetic susceptibilities were measured in the temperature range from liquid nitrogen temperature to room temperature. Magnetic susceptibility of each complex (except for [Cu(phen)(im)]-$BF_4\cdot H_2O$) increases with lowering of temperature, while magnetic moment decreases with lowering of temperature and reaches to 1.2—1.3 BM near liquid nitrogen temperature. This behavior suggests that the complexes involve odd, probably three, copper(II) ions within each molecule.

Since a cyclic-polynuclear structure is more likely than a linear-chain structure for the present complexes, it was attempted to explain the magnetism in terms of the susceptibility equation for triangular-trinuclear copper(II) system. Based on the Heisenberg model, magnetic susceptibility expression for the triangular copper(II) system (Fig. 1) is given by

$$\chi_A=\frac{Ng^2\beta^2}{12kT}\frac{5+\exp(-3J/kT)}{1+\exp(-3J/kT)}+N\alpha,$$

on the assumption of equal exchange integrals ($J_{12}=J_{23}=J_{31}=J$). Each symbol in the equation has its conventional meaning. Magnetic susceptibilities of the complexes except for [Cu(phen)(im)]$BF_4\cdot H_2O$ were satisfactorily explained by the use of the equation as is exemplified by [Cu(tmen)(im)]PF_6 in Fig. 2. Mag-

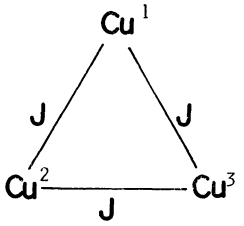

Fig. 1.

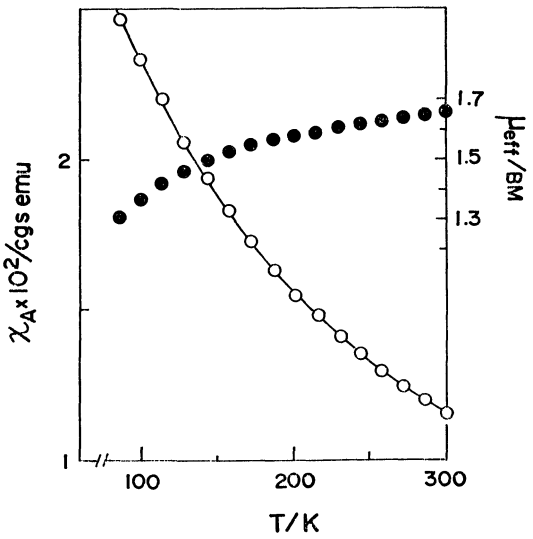

Fig. 2. Temperature variations of magnetic susceptibility and magnetic moment of $[Cu(tmen)(im)]PF_6$.

Table 3. Magnetic parameters, $-J$, g and $N\alpha$, of complexes

Complex	$-J$/cm^{-1}	g	$N\alpha\times10^6$ / cgs mol^{-1}
$[Cu(tmen)(im)]PF_6$	37	2.08	40
$[Cu(tmen)(im)]ClO_4$	45	2.08	60
$[Cu(tmen)(im)]BF_4$	43	2.08	50
$[Cu(bip)(im)]PF_6$	40	2.07	45
$[Cu(bip)(im)]ClO_4$	44	2.08	60
$[Cu(bip)(im)]BF_4$	45	2.08	50
$[Cu(phen)(im)]PF_6$	38	2.07	45
$[Cu(phen)(im)]ClO_4$	37	2.08	60

netic parameters, J, g, and $N\alpha$, obtained by the best fit technique are given in Table 3. The exchange integrals are in the range -37——-45 cm^{-1}, which are moderate or a little larger in absolute value compared with the exchange integrals of the imidazolate-bridged binuclear and tetranuclear copper(II) complexes so far studied.

Magnetic susceptibility of $[Cu(phen)(im)]BF_4\cdot H_2O$ is also subnormal but does not obey the above equation. Judging from its magnetic behavior, this complex is presumed to be composed of even copper(II) ions. However, its structure was not further investigated in this study.

The structure of the present complexes was considered by means of the Dreiding model. The projec-

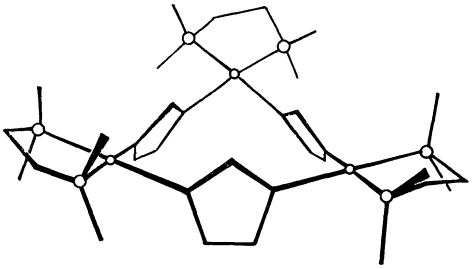

Fig. 3. The projection of Dreiding model for $[Cu(tmen)(im)]^+$.

Table 4. Bond lengths (l/Å) and bond angles (ϕ/°) with their estimated standard deviations in parentheses

(a) Copper coordination spheres			
Cu–N(1)	2.037(11)	Cu–N(5)	2.013(13)
Cu–N(2)	2.093(13)	Cu–O(1)	2.487(12)
Cu–N(3)	2.003(12)	Cu–O(5)	3.058(15)
N(1)–Cu–N(2)	85.5(5)	N(2)–Cu–O(5)	88.7(5)
N(1)–Cu–N(3)	92.1(5)	N(3)–Cu–N(5)	89.8(5)
N(1)–Cu–N(5)	173.1(5)	N(3)–Cu–O(1)	88.9(5)
N(1)–Cu–O(1)	99.8(4)	N(3)–Cu–O(5)	87.8(5)
N(1)–Cu–O(5)	81.4(4)	N(5)–Cu–O(1)	86.9(4)
N(2)–Cu–N(3)	176.0(4)	N(5)–Cu–O(5)	92.0(4)
N(2)–Cu–N(5)	92.2(5)	O(1)–Cu–O(5)	176.5(5)
N(2)–Cu–O(1)	94.7(5)		
(b) Tmen moiety			
N(1)–C(1)	1.477(22)	N(2)–C(4)	1.499(20)
N(1)–C(2)	1.502(23)	N(2)–C(5)	1.442(22)
N(1)–C(3)	1.500(21)	N(2)–C(6)	1.496(21)
C(3)–C(4)	1.470(25)		
Cu–N(1)–C(1)	112.8(9)	C(3)–C(4)–N(2)	109.3(13)
Cu–N(1)–C(2)	115.1(10)	Cu–N(2)–C(4)	106.2(9)
Cu–N(1)–C(3)	104.4(9)	Cu–N(2)–C(5)	111.2(11)
C(1)–N(1)–C(2)	106.9(13)	Cu–N(2)–C(6)	113.0(9)
C(1)–N(1)–C(3)	112.2(13)	C(4)–N(2)–C(5)	110.3(12)
C(2)–N(1)–C(3)	105.4(12)	C(4)–N(2)–C(6)	108.0(13)
N(1)–C(3)–C(4)	109.8(13)	C(5)–N(2)–C(6)	108.0(15)
(c) Im moiety			
N(3)–C(7)	1.396(21)	N(4)–C(9)	1.360(20)
C(7)–C(8)	1.330(25)	C(9)–N(3)	1.321(19)
C(8)–N(4)	1.379(23)		
Cu–N(3)–C(7)	125.4(11)	C(7)–C(8)–N(4)	107.8(15)
Cu–N(3)–C(9)	126.7(11)	C(8)–N(4)–C(9)	107.6(13)
C(7)–N(3)–C(9)	107.9(13)	N(4)–C(9)–N(3)	108.8(13)
N(3)–C(7)–C(8)	107.9(15)		
N(5)–C(10)	1.364(23)	N(6)–C(12)	1.329(20)
C(10)–C(11)	1.318(23)	C(12)–N(5)	1.330(16)
C(11)–N(6)	1.343(21)		
Cu–N(5)–C(10)	127.4(9)	C(10)–C(11)–N(6)	107.1(15)
Cu–N(5)–C(12)	126.5(11)	C(11)–N(6)–C(12)	108.4(12)
C(10)–N(5)–C(12)	105.8(13)	N(6)–C(12)–N(5)	109.1(13)
N(5)–C(10)–C(11)	109.5(14)		
(d) ClO_4			
Cl(1)–O(1)	1.411(12)	Cl(1)–O(3)	1.417(16)
Cl(1)–O(2)	1.425(15)	Cl(1)–O(4)	1.334(18)
O(1)–Cl(1)–O(2)	108.0(8)	O(2)–Cl(1)–O(3)	111.8(10)
O(1)–Cl(1)–O(3)	106.3(10)	O(2)–Cl(1)–O(4)	110.3(10)
O(1)–Cl(1)–O(4)	111.1(12)	O(3)–Cl(1)–O(4)	109.3(13)
Cl(2)–O(5)	1.410(16)	Cl(2)–O(7)	1.404(17)
Cl(2)–O(6)	1.425(17)	Cl(2)–O(8)	1.359(23)
O(5)–Cl(2)–O(6)	104.4(9)	O(6)–Cl(2)–O(7)	108.9(11)
O(5)–Cl(2)–O(7)	112.0(10)	O(6)–Cl(2)–O(8)	113.3(13)
O(5)–Cl(2)–O(8)	107.5(13)	O(7)–Cl(2)–O(8)	110.7(12)

tion of the model for $[Cu(tmen)(im)]^+$ is shown as an example in Fig. 3. Two coordination sites around planar copper(II) ion are occupied by tmen and remaining sites by imidazolate nitrogens. Triangular-trinuclear skeleton is built up of three copper atoms at the apices and three imidazolate groups combining these copper atoms. The plane of each imidazolate group is nearly perpendicular (*ca.* 70—80°) to the plane described by the donor atoms and are arranged "*cis*" to each other with respect to nitrogen atoms (see Fig. 3). The alternative configuration in which one of the imidazolate groups is placed "*trans*" to the remaining two is also possible, but this configuration seems unfavorable to that in Fig. 3. This trinuclear skeleton is quite rigid, but this is reasonably constructed without changing bond distances and distorting bond angles from the usual ones. ESR spectra of the complexes in *N,N*-dimethylformamide showed a very broad signal both at room temperature and near liquid nitrogen temperature. This implies that the polynuclear structure of the complexes is considerably stable and is maintained even in *N,N*-dimethylformamide solution. Since such a rigid skeleton can not be formed in the cases of cyclic polynuclear structure larger than triangular structure, the stability of the complexes in *N,N*-dimethylformamide seems to be associated with the triangular-trinuclear skeleton shown in Fig. 3.

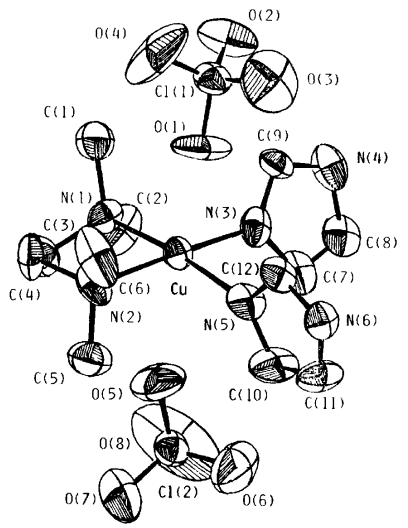

Fig. 4. Crystal structure of $[Cu(tmen)(imH)_2](ClO_4)_2$.

So far all efforts to obtain a single crystal suitable for X-ray analysis have been in vain. In order to obtain an additional support for the triangular-trinuclear structure with the imidazolate bridges for [CuL(im)]X, we have examined the crystal structure of $[Cu(tmen)(imH)_2](ClO_4)_2$ which contains the $[CuN_4]$-chromophore relevant to [Cu(tmen)(im)]X. A perspective drawing of the complex and the numbering system are illustrated in Fig. 4. Bond lengths and angles are listed in Table 4.

The copper atom is coordinated by two amino nitrogen atoms of tmen, N(1) and N(2), and two imidazole nitrogen atoms, N(3) and N(5), at distances 2.037(11), 2.093(13), 2.003(12), and 2.013(13) Å, respectively. These in-plane atoms form an approximate square plane (Table 5). The copper atom is further coordinated by the oxygen atoms of the perchlorate ions, O(1) and O(5), at the distances of 2.487(12) and 3.058(15) Å, respectively. Thus, the coordination geometry may be described as an elongated octahedron. The copper atom lies above the equatorial plane toward the oxygen atom O(1) by 0.09 Å. The tmen moiety forms a five-membered chelate ring with the copper atom. The Cu–N(1)–C(3)–C(4)–N(2) chelate rings has a gauche conformation, C(3) and C(4) being located 0.538 Å below and 0.144 Å above the plane defined by Cu, N(1), and N(2), respectively.

The most striking characteristic in the structure of $[Cu(tmen)(imH)_2](ClO_4)_2$ is that two imidazole rings are nearly perpendicular to the equatorial plane (the rings being inclined by 66.0 and 85.3° to the plane, respectively) and are arranged "*cis*" to each other with respect to the non-coordinating nitrogen atom. It should be noted that the local coordination environment of [CuL(im)]X considered on the basis of the Dreiding model (Fig. 3) is substantially the same as that of $[Cu(tmen)(imH)_2](ClO_4)_2$. Although this is

Table 5. Deviations of the atoms from least-squares planes (l/Å) and dihedral angles between them (ϕ/°)

(I) Plane through N(1), N(2), N(3), N(5)
$-0.2533X+0.5371Y+0.8299Z=4.7546$[a]
[N(1) −0.029, N(2) 0.028, N(3) 0.028, N(5) −0.028, Cu 0.088][b]
(II) Plane through Cu, N(1), N(2)
$-0.2932X+0.5684Y+0.7992Z=4.7857$
[Cu 0.000, N(1) 0.000, N(2) 0.000, C(3) −0.538, C(4) 0.144]
(III) Plane through N(3), C(7), C(8), N(4), C(9)
$0.1893X-0.4558Y+0.8394Z=1.7794$
[N(3) −0.009, C(7) 0.012, C(8) −0.011, N(4) 0.005, C(9) 0.002]
(IV) Plane through N(5), C(10), C(11), N(6), C(12)
$0.8860X+0.4577Y-0.0366Z=2.8939$
[N(5) −0.012, C(10) 0.004, C(11) 0.006, N(6) −0.014, C(12) 0.016]
Dihedral angles between the planes (ϕ/°)
(I) and (III) 66.0 (I) and (IV) 85.3 (III) and (IV) 88.6

a) The equation of the plane is expressed as $LX+MY+NZ=D$, where X, Y, and Z are in Å units referred to the crystallographic axes. b) Deviations (l/Å) of atoms from the planes are listed in square brackets.

not a direct evidence, it may afford a support for the structure of [CuL(im)]X with "*cis*"-arranged imidazolate bridges.

Based on these facts we may conclude that the [CuL(im)]X complexes are imidazolate-bridged trinuclear complexes with a triangular skeleton.

References

1) J. S. Richardson, K. A. Thomas, B. H. Rubin, and D. C. Richardson, *Proc. Natl. Acad. Sci. U.S.A.*, **72**, 1349 (1975).
2) J. A. Fee and R. G. Briggs, *Biochim. Biophys. Acta*, **400**, 439 (1975).
3) G. Kolks, C. R. Freihart, H. N. Rabinowitz, and S. J. Lippard, *J. Am. Chem. Soc.*, **98**, 5720 (1976).
4) G. Kolks and S. J. Lippard, *J. Am. Chem. Soc.*, **99**, 5804 (1977).
5) Y. Nakao, W. Mori, N. Okuda, and A. Nakahara, *Inorg. Chim. Acta*, **35**, 1 (1979).
6) G. Kolks, S. J. Lippard, J. V. Waszczak, and H. R. Lilienthal, *J. Am. Chem. Soc.*, **104**, 717 (1982).
7) M. S. Haddad and D. N. Hendrickson, *Inorg. Chem.*, **17**, 2622 (1978).
8) Y. Nakao, W. Mori, T. Sakurai, and A. Nakahara, *Inorg. Chim. Acta*, **37**, L507 (1979); **55**, 103 (1981).
9) K. Matsumoto, S. Ooi, Y. Nakao, W. Mori, and A. Nakahara, *J. Chem. Soc., Dalton Trans.*, **1981**, 2045.
10) C. O'Yang, J. C. Dewan, H. R. Lilienthal, and S. J. Lippard, *J. Am. Chem. Soc.*, **100**, 7291 (1978).
11) T. Suzuki, H. Kanatomi, H. Koyama, and I. Murase, *Inorg. Chim. Acta*, **44**, L41 (1980).
12) P. K. Coughlin, J. C. Dewan, S. J. Lippard, E. Watanabe, and J. M. Lehn, *J. Am. Chem. Soc.*, **101**, 265 (1979).
13) P. K. Coughlin, S. J. Lippard, A. E. Martin, and J. E. Bulkowski, *J. Am. Chem. Soc.*, **102**, 7616 (1980).
14) D. W. J. Cruickshank, "Computing Methods in Crystallography," ed by J. S. Rollet, Pergamon Press, Oxford (1965).
15) "International Tables for X-Ray Crystallography," Kynoch Press, Birmingham (1974), Vol. IV.
16) S. Kawano, *Rep. Comp. Cent. Kyushu Univ.*, **13**, 39 (1980).
17) T. Sakurai and K. Kobayashi, *Rep. Inst. Phys. Chem. Res.*, **55**, 69 (1979).
18) C. K. Johnson, Report No. 3794, Oak Ridge National Laboratory, Oak Ridge, Tennessee (1965).

Reactions of Dialkylnickel(II) Complexes NiR_2L_2 with Alkyl (or Aryl) Halides, R'COY (Y=Cl, Br, OPh, OCOPh), and CS_2

Takakazu YAMAMOTO,* Teiji KOHARA, Kohtaro OSAKADA, and Akio YAMAMOTO

Research Laboratory of Resources Utilization, Tokyo Institute of Technology, 4259 Nagatsuta, Midori-ku, Yokohama 227

(Received February 24, 1983)

Reactions of $Ni(CH_3)_2(bpy)$ (**1**), $Ni(C_2H_5)_2(bpy)$ (**2**) (bpy=2,2'-bipyridine), *trans*-$Ni(CH_3)_2(triethylphosphine)_2$ (**3**), $Ni(CH_3)_2$(1,2-bis(diphenylphosphino)ethane) (**4**), and $Ni(CH_3)_2$(1,3-bis(diphenylphosphino)propane) (**5**) with alkyl or aryl halides, R'COY (Y=Cl, Br, OC_6H_5, $OCOC_6H_5$), and CS_2 have been investigated. The reactions of NiR_2L_2 with alkyl or aryl halides are classified into three types of reactions by their reactirn products: Type A: $NiR_2L_2+R'X\rightarrow NiX(R')L_2+R\text{-}R$, Type B: $NiR_2L_2+R'X\rightarrow$alkane (RH)+olefin (R'(-H)), and Type C: $NiR_2L_2+R'X\rightarrow NiR(X)L_2+R\text{-}R'$. Complexes **1** and **2** undergo mainly Type A reaction. Complex **3** gives Type A reaction product on treatment with C_6H_5Br, but it gives Type B reaction product on treatment with C_2H_5Br. On the other hand, **4** undergoes Type C reaction on interaction with C_6H_5Cl. The reactions with R'COY (Y=Cl, Br, OPh, OCOPh) are classiffed into two types of reactions by their reaction products: Type D: $NiR_2L_2+R'COY\rightarrow NiY(R)L_2+RCOR'$ and Type E: $NiR_2L_2+R'COY\rightarrow NiY(R')L_2+RCOR$. Complexes **1**—**3** undergo mainly Type D reaction, whereas complexes **4** and **5** mainly Type E reaction. The difference in the reaction route is discussed on the basis of presence or absence of vacant coordination site for attack by R'COY. The reaction of **4** with CS_2 affords $Ni(CS_2)$(1,2-bis(diphenylphosphino)ethane) with evolution of a reductive elimination product, ethane, whereas the reaction of **3** with CS_2 gives a 1:1 adduct of **3** and CS_2.

Although chemistry of organonickel complexes has been developed in the past two decades,[1] examples of isolated dialkylnickel(II) complexes[2-7] are still limited and chemical reactivities of the dialkylnickel complexes have been poorly understood in comparison with the chemical reactivities of much more stable dialkylplatinum(II) complexes. Our research group has been dealing with the dialkylnickel(II) complexes and has reported isolation and chemical reactivities of the dialkylnickel(II) complexes.[2,7-9] As an extension of the study on the dialkylnickel(II) complexes, we have examined chemical reactivities of the following dialkylnickel(II) complexes, NiR_2L_2, with organic halides and their analogues (R'X and R'COY) and CS_2. We now report the results of the reactions.

$NiMe_2(bpy)$ (**1**), $NiEt_2(bpy)$ (**2**), *trans*-$NiMe_2(PEt_3)_2$ (**3**), $NiMe_2(dpe)$ (**4**), $NiMe_2(dpp)$ (**5**). Me=CH_3, Et=C_2H_5. bpy=2,2'-Bipyridine. PEt_3=triethylphosphine. dpe=1,2-Bis(diphenylphosphino)ethane. dpp=1,3-Bis(diphenylphosphino)propane.

To clarify the process of the reaction of NiR_2L_2 with R'X is particularly important, since it often induces C–C coupling between R and R or R and R' which is considered to be a crucial elemental step of Ni-catalyzed C–C coupling reactions between metal alkyls (*e.g.*, RMgX) and organic halides.[10]

Results and Discussion

Reactions with R'X. Table 1 shows results of the reactions of complexes **1**—**4** with R'X. It includes results of a previously reported reaction of **2** with C_6H_5Cl.[11] The reactions listed in Table 1 can be classified into the following three types of reactions according to their products,

Type A: Formation of the reductive elimination product, R–R, and $NiX(R')L_2$.
$NiR_2L_2+R'X\rightarrow NiX(R')L_2+R\text{-}R$.

Type B: Hydrogen migration from R' to R to release alkane, RH, and olefin, R'(–H).
$NiR_2L_2+R'X\rightarrow RH+R'(-H)$.

Type C: Cross coupling of R and R' to form R–R' and $NiR(X)L_2$.
$NiR_2L_2+R'X\rightarrow NiR(X)L_2+R\text{-}R'$.

Each type of reaction is discussed below.

Type A: The reaction of **1**, a homologue of **2**, with 2-chlorotoluene leads to the evolution of the reductive elimination product, ethane, which is accompanied by formation of NiCl(2-tolyl)(bpy), similarly to the reaction of **2** with chlorobenzene.[11] The results indicate that the Ni–R bonds in $NiR_2(bpy)$ is activated by interaction with haloarene to induce the reductive elimination of R–R,

$$NiR_2(bpy) + \text{chloroarene} \longrightarrow NiCl(aryl)(bpy) + R\text{-}R. \quad (1)$$

Since it is known that electron transfer from Ni in $NiR_2(bpy)$ to an electron accepting ligand causes activation or weakening of the Ni–R bonds,[2d,12] we assume that the elimination of R–R is promoted by the electron transfer from nickel to the coordinating chloroarene in reaction intermediates such as

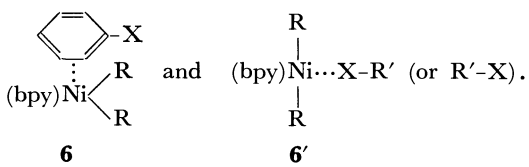

6 **6'**

In the intermediate **6**, the haloarene coordinates with nickel through the aromatic ring and an electron migration from Ni to π^* orbital(s) of chloroarene is assumed. On the other hand, in the intermediate **6'**, chloroarene (R'X) approaches to Ni through the electron-withdrawing halogen atom or positively charged R' carbon bonded to X. When the reductive elimination takes place, the reaction is considered to be followed by a rapid oxidative addition of chloroarene

Table 1. Reactions of NiR_2L_2 with R'X

No.	NiR_2L_2	R'X[a]	Temp °C	Time h	Product(%-yield/NiR_2L_2) Complex	Gaseous product[b] RH	R(-H)	R-R	R-R'	R'H	R'(-H)
1	**1**	2-Chlorotoluene	50	3	NiCl(2-tolyl)(bpy) (73)	sm	—	84	—	—	—
2	**2**	PhCl	r.t.	2	NiCl(Ph)(bpy)(0.5 PhCl) (60)[e]			Major[e]			
3	**2**	$(CH_3)_3CCl$	r.t.	72	$NiCl_2$(bpy) (70)	2	1	64	0	4	50
4	**2**	$\{CH_2\text{-}CH(Cl)\}_n$	r.t.	1	$\{CH_2\text{-}CH(NiCl(bpy))\}_n$	sm	sm	70	—	—	—
5	**3**	PhBr	r.t.	24	$NiBr(Ph)(PEt_3)_2$ (36)	9	0	35	17	0	—
6	**3**	PrBr	r.t.	12	$NiBr_2(PEt_3)_2$ (71)	115	0	46	sm	35	127
7[c]	**3**	EtBr	r.t.	24	$NiBr_2(PEt_3)_2$ (66)	(53)	(98)	(117)		(53)	(98)
8	**4**	PhCl	r.t.	120	NiCl(Me)(dpe) (*ca.* 55)[f]	11	sm	14	50	0	—
9[d]	**4**	EtBr	35	48	$NiBr_2$(dpe) (48)	78	0	(70)	10	(70)	33

a) R'X=Excess. Ph=Phenyl. Pr=Propyl. b) sm=Small. c) In this reaction, R equals R'. Therefore total yields of RH and R'H, R(-H) and R'(-H), and R-R R-R' are given in parentheses. d) In this case, both R-R and R'H represents ethane, whose amount is given in the parentheses. e) Data from Ref. 11. f) Based on weight of a solid recovered after the reaction and $^{31}P\{^1H\}$-NMR data of the solid (see Experimental).

Table 2. Reactions of NiR_2L_2 with acyl halides and its analogues

No.	NiR_2L_2	R'COX (R'COX/Ni)	Temp °C	Time h	Product(%-yield/NiR_2L_2) Ni-complex	Ketone RCOR'	RCOR	RCOR'/RCOR	Others[a]
1	**1**	C_6H_5COCl (3)	r.t.	24	b)	74	11	6.7	C_1(13), C_2(13)
2[c]	**2**	CH_3COCl (1)	r.t.	0.2	$NiCl(Et)L_2$ (47)	96	0	Large	
3[c]	**2**	CH_3COBr (1)	r.t.	0.2	$NiBr(Et)L_2$ (35)	76	0	Large	C_1(2), C_2(13), C_2'(9)
4	**2**	C_6H_5COCl (3)	r.t.	24	b)	70	0	Large	C_2'(4), C_4(23), C_6(15)
5	**2**	$(C_6H_5CO)_2O$ (3)	r.t.	24	$NiEt(OCOPh)L_2$, d)	36	0	Large	R'COR'(6), C_2(30), C_4(10)
6	**3**	C_2H_5COCl (2)	r.t.	24	$NiCl_2L_2$ (40)	66	sm	Large	R'COR'(6), C_1, d)
7	**3**	C_6H_5COCl (3)	0—15	24	b)	54	sm	Large	R'COR'(2), C_1(28), C_2(53), Toluene(2), C_6(8)
8[c]	**3**	$(C_6H_5CO)_2O$ (1)	r.t.	24	$NiMe(OCOPh)L_2$ (66)	70	0	Large	C_1(41)
9[e]	**3**	$C_6H_5COOC_6H_5$ (2)	r.t.	120	b)	21	12	1.75	C_1(14), C_2(39), Toluene(2), Ph-Ph(16)
10[e]	**4**	C_6H_5COCl (1)	r.t.	24	$NiCl(Ph)L_2$ (83)	sm	51	*ca.* 0	C_1(28), C_2(2)
11	**4**	C_2H_5COCl (2.6)	r.t.	24	$NiCl_2L_2$ (88)	0	21	0	C_1(51), C_2(8), C_2'(15)
12	**4**	$(C_6H_5CO)_2O$ (3)	r.t.	24	b)	1	34	0.03	PhCOPh(1), C_1(43), Ph-Ph(4)
13	**5**	C_6H_5COCl (3)	r.t.	24	b)	0	26	0	C_1(9), C_2(41)
14	**5**	$(C_6H_5CO)_2O$ (3)	r.t.	24	b)	0	46	0	C_1(40), C_2(5)

a) $C_1=CH_4$. $C_2=C_2H_6$. $C_2'=C_2H_4$. $C_4=C_4H_{10}$. $C_6=C_6H_6$. $Ph=C_6H_5$. b) Isolation of complexes was not feasible. c) Reported previously.[8b] d) Formation of the complex was confirmed by IR or GLC, but its yield was not measured. e) Reactions were carried out twice, and average of the yields is given.

to Ni^0 species.

An alternative reaction mechanism involving oxidative addition of chloroarene to $NiR_2(bpy)$ to form a quadrivalent $Ni(R)_2(aryl)(Cl)(bpy)$ species and elimination of R–R from the intermediate is also conceivable. However, this mechanism is less plausible as judged from selective formation of R–R and no liberation of the cross coupling product, R–aryl, although formation of such a four valent nickel species as a reaction intermediate is assumed as for the Types B and C reactions (*vide infra*).

The reaction of **1** with 2-chlorotoluene requires a somewhat higher temperature than for a similar reaction of **2**,[11] reflecting stronger Ni–R bonds in **1** than in **2**.[2d]

When an alkyl halide, *t*-butyl chloride, was employed in the reaction with **2**, the reaction also led to liberation of R–R, butane, with formation of a reddish brown complex, which may be assignable to NiCl(*t*-butyl)(bpy). Attempts to isolate this complex failed due to its instabilities, and prolonged reaction caused formation of light green $NiCl_2(bpy)$ (proved by IR) and evolution of isobutene and a small amount of isobutane which are considered to be formed through the thermal decomposition of the *t*-butyl–Ni complex. When poly(vinyl chloride) is employed in the reaction with **2**, the chloro(alkyl)nickel complex produced, $\{CH_2\text{-}CH(NiCl(bpy))\}_n$ (see experimental), has some stabilities and can be used for further reaction with CO to afford an acylnickel group pending in poly(vinyl chloride),

$$\mathbf{2} + \{CH_2\text{-}CHCl\}_n \longrightarrow \{CH_2\text{-}CH(NiCl(bpy))\}_n + R\text{-}R \quad (2)$$

$$\{CH_2\text{-}CH(NiCl(bpy))\}_n + CO \longrightarrow \{CH_2\text{-}CH(CONiCl(bpy))\}_n. \quad (3)$$

In the case of the activation of the Ni–Et bonds in **2** by the alkyl halides, formation of the intermediate complex of type **6** is not possible and the reaction is considered to proceed through formation of the intermediate of type **6'**.

Similar reductive elimination of R–R in the PEt_3-coordinated dimethylnickel complex **3** is also induced by the interaction with an haloarene, bromobenzene. The reductive elimination is again accompanied by the formation of an oxidative addition product, *trans*-

$$\mathbf{3} + PhBr \xrightarrow[\text{2) oxidative addition}]{\text{1) reductive elimination}} Me\text{-}Me + NiBr(Ph)(PEt_3)_2 \quad (4)$$

$NiBr(Ph)(PEt_3)_2$, which was prepared by Morrell and Kochi[13] through a different reaction pathway. The formation of a small amount of toluene in the reaction of **3** with PhBr suggests that the following cross coupling reaction (Type C reaction) partially occurs,

$$\mathbf{3} + PhBr \longrightarrow \left[\begin{array}{c} Ph \\ \vdots \\ Br \cdots Me \\ \vdots \\ L_2Ni \\ Me \end{array} \right] \text{or} \left[\begin{array}{c} Me \\ | \\ L_2Ni\text{—}Ph \\ | \\ Me \end{array} \begin{array}{l} \\ \\ \\ \\ Br \end{array} \right]$$

7a **8a**

$$\longrightarrow (NiBr(Me)(PEt_3)_2) + CH_3C_6H_5. \quad (5)$$

9a

In the above reaction, formation of a bromo(methyl)-nickel complex **9a** is assumed. However, detection of **9a** was not feasible.

Type B: When propyl bromide is employed in the reaction with **3**, a similar inductive effect of the alkyl bromide on the reductive elimination of R–R, ethane, was observed. However, in this case, methane and propylene became the major gaseous products, suggesting that occurrence of hydrogen migration from the propyl group to the methyl group on a Ni^{IV} species formed by oxidative addition of propyl bromide to **3**.

$$\mathbf{3} + C_3H_7Br \longrightarrow \left[\begin{array}{c} Me \\ | \\ (PEt_3)_2Ni\text{—}C_3H_7 \\ | \\ Me \end{array} \begin{array}{l} \\ \\ \\ \\ Br \end{array} \right] \longrightarrow$$

8b

$$\left[(PEt_3)_2Ni \begin{array}{l} Br \\ Me \end{array} \right] + CH_4 + C_3H_6$$

9b

$\downarrow C_3H_7Br$

$$\left[\begin{array}{c} Br \\ | \\ (PEt_3)_2Ni\text{—}Br \\ | \\ Me \end{array} \begin{array}{l} \\ \\ \\ \\ C_3H_7 \end{array} \right]$$

10b

$$CH_4 + C_3H_6 + NiBr_2(PEt_3)_2$$

Scheme 1.

The formation of C_3H_8 in this reaction indicates that certain hydrogen abstraction reaction by the C_3H_7 group in the intermediate species takes place. Although the number of isolated Ni^{IV} complexes is not large,[14] various Pt^{IV} complexes including alkylplatinum(IV) complexes are known[15] and the results of the reaction of **3** with propyl bromide is most straightforwardly explained by assuming the Ni^{IV} intermediate as shown in Scheme 1. The agreement of the amount of CH_4 evolved with that of C_3H_6 supports the mechanism shown above.

Type C: In the case of the reaction of **4** with PhCl, a cross coupling reaction such as expressed by Eq. 5 constitutes the main reaction route, and a complex of type **9**, NiCl(Me)(dpe) (**9c**), is formed as the main nickel product.

$$\mathbf{4} + PhCl \longrightarrow \left[\begin{array}{c} Ph \\ \vdots \\ Cl \cdots Me \\ \vdots \\ (dpe)Ni \\ Me \end{array} \text{or} \begin{array}{c} Me \\ | \\ (dpe)Ni\text{—}Ph \\ | \\ Cl \end{array} \right]$$

7c **8c**

$$\longrightarrow NiCl(Me)(dpe) + CH_3C_6H_5 \quad (6)$$

The partial formation of ethane and NiPh(Cl)(dpe) (proved by acidolysis) indicates that the reductive

elimination of Me–Me in **8c** or the reductive elimination induced by PhCl as discussed for the reactions of **1** and **2** with aryl halides also takes place (see Experimental),

$$\mathbf{4} + \mathrm{PhCl} \xrightarrow{\text{minor route}} [\mathbf{6}, \mathbf{6}', \text{or } \mathbf{8c}] \longrightarrow \mathrm{Me\text{-}Me} + \mathrm{NiCl(Ph)(dpe)}. \quad (7)$$

In contrast to the reaction of **4** with PhCl, that with an alkyl halide, ethyl bromide (No. 9), affords the cross coupling product, propane, in only a small yield, and the reaction causes evolution of other gaseous products which are produced through the Type A (ethane) and Type B (methane and ethylene) reaction routes.

The results shown above indicate that subtle differences in the structures of the dialkylnickel complex and R'X cause a considerable change in the reaction route. It may be noted that the intermediate formed in the reaction of a diphosphine-coordinated dialkylnickel complex with alkyl halide having β-hydrogen has a trend to undergo the hydrogen shift reaction (or β-elimination reaction) from R' to R, and this may be related to the fact that the C–C coupling catalyzed by nickel–phosphine complexes does not give good results when alkyl halides are used as the reactants.[10]

Reactions with R'COY. Table 2 shows results of the reactions of the dialkylnickel(II) complexes with acyl halides and their analogues, R'COY. It includes some previously reported results[8b] of the reactions of NiR_2L_2 with R'COY. The reaction listed in Table 2 can be classified into the following two types of reactions according to the product distribution:

Type D: Formation of asymmetric ketone, RCOR', and $NiX(R)L_2$.
$NiR_2L_2 + R'COY \rightarrow NiY(R)L_2 + RCOR'$

Type E: Formation of symmetric ketone RCOR, accompanied by formation of $NiX(R')L_2$.
$NiR_2L_2 + R'COY \rightarrow NiY(R')L_2 + RCOR$.

Each type of the reaction is discussed below.

Type D: Complexes **1**—**3** undergo Type D reaction on treatment with R'COY or its analog (Nos. 1—9 in Table 2). The formation of these products is explained by assuming the following four-center mechanism.

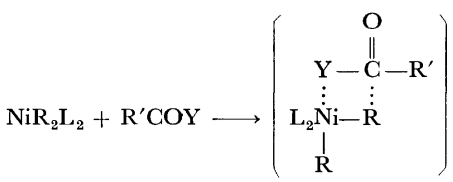

$$\longrightarrow NiY(R)L_2 + RCOR' \quad (8)$$

Scheme 2.

The isolation of NiY(Et)(bpy) in Nos. 2 and 3 indicates that NiY(Et)(bpy) is less reactive toward R'COY than **2**. The isolation of $NiMe(OCOPh)(PEt_3)_2$ in No. 8 also indicates the isolated complex is not reactive toward $(C_6H_5CO)_2O$. When an excess of C_2H_5COCl is added, complex **3** is transformed to *trans*-$NiCl_2(PEt_3)_2$, suggesting that $NiCl(Me)(PEt_3)_2$ initially formed reacts further with C_2H_5COCl.

In most cases, the formation of RCOR' and $NiY(R)L_2$ is accompanied by evolution of alkanes (RH and R–R) and alkene (ethylene from **2**), indicating that activation of the Ni–R bond on interaction with R'COY takes place. The formation of RCOR in Nos. 1 and 9 suggests that Type E reaction occurs partly. R'COR' obtained in Nos. 5—7 seems to be formed through oxidative addition of R'COY to Ni^0 complex(es) which is formed in the reaction system, *e.g.*,

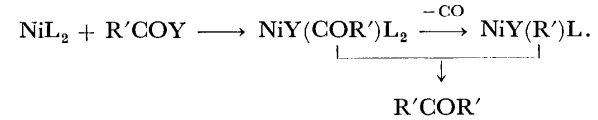

Type E: The diphosphine-coordinated dialkylnickel(II) complexes, **4** and **5**, undergo Type E reaction to afford RCOR. In the case of the reaction of **4** with PhCOCl (No. 10), the complex of the type $NiY(R')L_2$ is isolable. $NiCl_2(dpe)$ obtained in No. 11 is considered to be formed by a reaction of initially formed NiCl(Et)(dpe) with C_2H_5COCl.

The formation of RCOR clearly indicates migration of CO from R'COCl to NiR_2L_2. As for the process to produce RCOR, we consider the following two mechanisms.

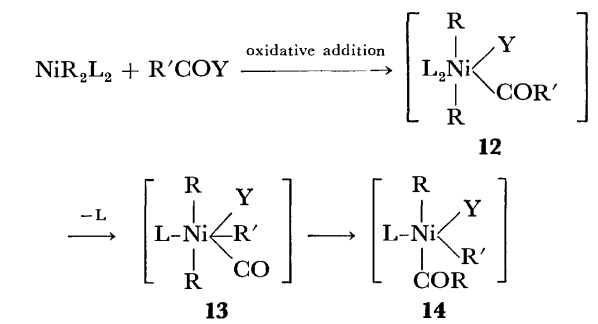

Scheme 3.

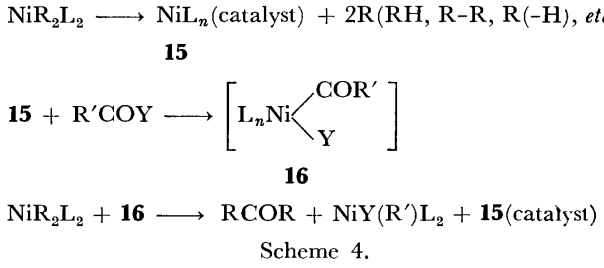

Scheme 4.

Scheme 3 involves oxidative addition of R'COX to NiR_2L_2 to form a Ni^{IV} species **12**, decarbonylation from the R'CO– ligand in **12**, insertion of the CO ligand into the Ni–R bond, and reductive elimination of RCOR from the four-valent nickel intermediate. Ruddick and Shaw showed that pyrolysis of $PtCl(Me)_2(COMe)(PMe_2Ph)_2$ gave acetone and *trans*-$PtCl(Me)(PMe_2Ph)_2$ as the sole products.[16a]

In Scheme 4, we assume initial formation of Ni^0 complex, NiL_n, by thermal decomposition of NiR_2L_2. The Ni^0 species thus formed is assumed to react with

R'COY to give the oxidative addition product **16**, which further reacts with NiR_2L_2 to yield RCOR with resumption of NiL_n, which thus serves as a catalyst to carry the decarbonylative CO transfer agent. Oxidative addition of RCOX to Ni^0 complexes is well known,[17] and we previously reported[18] formation of RCOR and the $NiY(R')L_2$ type complex by reactions of an acylnickel(II) complex, *trans*-Ni(COMe)(phthalimido)$(PEt_3)_2$ (Y=phthalimido), with NiR_2(bpy) (R=Me, Et).

$$Ni(COMe)Y(PEt_3)_2 + NiR_2(bpy) \longrightarrow RCOR + NiMeY(PEt_3)_2$$

Y=phthalimido

At the moment, we have no strong evidence to prove or disprove the mechanisms. However, the decarbonylation reaction from the coordinatively saturated **12** to **13** seems to require partial or full dissociation of the bidentate diphosphine ligand. Therefore, if we take into account the previously observed fact[9] that the diphosphine ligands have much higher coordinating abilities toward nickel complexes than PEt_3 and bpy, the present observation that Type E reaction does not proceed with the dialkylnickel(II) complexes having the weakly coordinating PEt_3 or bpy ligand but with the complexes having the strongly coordinating dpe or dpp ligand seems not compatible with the mechanism shown in Scheme 3. Moreover, if the reaction proceeds by Scheme 3, the reaction would give RCOR' besides RCOR.

If we assume Schemes 2 and 4, the variation of the products depending on the nature of the dialkylnickel(II) may be explained by the presence or absence of an open coordination site in the dialkylnickel complexes for interaction with R'COY to form the active intermediate **11**. Complexes **1** and **2** having the flat bpy ligand possess an open vacant site for R'COX at their apical positions as can be seen on the CPK molecular model, and **3** has a trend to liberate the PEt_3 ligand as shown by variable temperature NMR spectroscopy[7] which shows a rapid exchange between the coordinating PEt_3 ligand and free PEt_3 in solutions even at low temperatures (*e.g.*, −60 °C). Under these circumstances, R'COY has an access to coordinate to Ni in **1**—**3**, and thus can undergo Type D reaction. On the other hand, the bulky and strongly coordinating diphosphine ligands in **4** and **5** block the coordination site in the nickel dialkyls. Therefore, the production of the unsymmetrical ketone RCOR' in the reactions of **4** and **5** with R'COY is hindered, and complexes **4** and **5** take a different reaction course as shown in Scheme 4.

Reaction with CS_2. The reductive elimination of R–R from **4** is induced by interaction with CS_2, and the Ni(0) complex thus formed takes up one molecular of CS_2 per the nickel complex,

$$\underset{}{\mathbf{4}} + CS_2 \longrightarrow \underset{69\%}{Me\text{-}Me} + \underset{\mathbf{17}(84\%)}{Ni(CS_2)(dpe)}. \quad (9)$$

Baird and Wilkinson reported formation of a similar CS_2 adduct of $Ni(PPh_3)_2$ by a reaction of $Ni(PPh_3)_4$ with CS_2.[19] An absorption band at 1190 cm^{-1} in an IR spectrum (KBr) of **17** is comparable with reported ν(C=S) vibrations of $Ni(CS_2)(PPh_3)_2$ (1196, 1117 cm^{-1} in CS_2),[19] $Pd(CS_2)(PPh_3)_2$ (1193 cm^{-1} in CS_2),[19] and $Pd(CS_2)$(dpe) (1178, 1167, 1152 cm^{-1}).[20] The CS_2 in **17** is strongly coordinated with Ni, and it is not replaced even by CO at 1 atm. The reaction of **3** with CS_2, on the contrary, does not lead to the reductive elimination of R–R, but it gives a 1:1 adduct of **3** and CS_2 as shown by elemental analysis of the adduct. IR spectrum of the adduct shows new bands at 1430, 1270, and 605 cm^{-1}, suggesting a different mode of the coordination of CS_2 to Ni from that in **17**.

Experimental

Manipulation, Material, and Analysis. Manipulation of complexes and reactions were carried out under atmosphere of N_2 or Ar or under vacuum. Complexes **1**—**5** were prepared according to literature.[2,7] Solvents were dried over Na, distilled under N_2, and stored under N_2. Microanalysis of C, H, N, and S was performed by Mr. T. Saito of our research laboratory. The amount of gas produced was measured with a Toepler pump and the gas collected was analyzed by GLC using a Shimadzu GC-3BT gas chromatograph. IR and NMR spectra were recorded on a Hitachi Model 295 infrared spectrometer and a JEOL JNM-PS-100 spectrometer, respectively.

*Reaction with R'X (*cf. *Table 1).* *No. 1*: 2-Chlorotoluene (3 cm^3) was added to a tube containing 360 mg (1.5 mmol) of deep green **1** at −78 °C. After the tube was evacuated, the mixture was warmed to 50 °C and stirred for 3 h at the temperature. Evolution of 1.23 mmol of C_2H_6 (84% per **1**) and a small amount of CH_4 was observed. The reddish brown precipitate formed was filtered off and crystallized from acetone (yield=250 mg, 73%). The reddish brown complex was characterized as NiCl(2-tolyl)(bpy) by comparing its IR spectrum with that of an authentic sample prepared according to literature.[11b]

No. 3: $(CH_3)_3CCl$ (3 cm^3) was added by trap-to-trap distillation to a tube containing 176 mg (0.64 mmol) of deep green **2** by using a vacuum line. When the green solution was stirred at room temperature, a smooth reaction proceeded to give a brown solution and a precipitate. At this point, evolution of butane was checked by GLC. Further stirring of the reaction mixture at room temperature for 3 d gave a greenish gray precipitate. Analysis of the gas phase showed evolution of gases shown in Table 1. The gaseous and liquid materials in the reaction system was removed by evaporation under vacuum and the gray precipitate was identified as $NiCl_2$ (bpy) from its IR spectrum.[2d]

No. 4:[21] When **2** (230 mg, 0.86 mmol) was added into a THF solution (20 cm^3) of poly(vinyl chloride) (M.W.=103000, 1.0 g, 16 mmol), the deep green homogeneous solution initially obtained rapidly changed to a deep red color with evolution of butane (0.60 mmol). The nickelated poly(vinyl chloride) was recovered by adding hexane, washed with hexane repeatedly, and dried under vacuum. The visible spectrum of the nickelated poly(vinyl chloride) showed a strong band assignable to a CT band at 535 nm ($\varepsilon=2\times10^3$), the λ_{max} and ε values being the same as that of a low molecular weight analogue of the polymer–nickel adduct, NiEt(Cl)(bpy)[8b] ($\lambda_{max}=533$ nm, $\varepsilon=2\times10^3$). The reaction of the nickelated poly(vinyl chloride) with carbon monoxide was carried out as follows. Carbon monoxide (atmospheric pressure) was introduced into a vessel containing a THF solution of the nickelated poly(vinyl chloride). After stirring

the solution for 20 min, the polymer was recovered by adding hexane to the THF solution and dried under vacuum. The infrared spectrum of the product of the reaction with carbon monoxide showed a ν(C=O) band at 1640 cm^{-1}. The infrared spectrum of a low molecular weight analogue of $\{CH_2-CH(CONiCl(bpy))\}_n$, Ni(COEt)Cl(bpy),[18] shows the ν(C=O) band at 1660 cm^{-1}. The carbonylated complex, $\{CH_2-CH(CONiCl(bpy))\}_n$ reacts with methanol to give a $\{CH_2-CHCOOCH_3\}_n$ monomer unit introduced into poly (vinyl chloride) as proved by IR (ν(C=O)=1730 cm^{-1}). This also supports the formation of $\{CH_2-CH(CONiCl(bpy))\}_n$.

No. 5: Bromobenzene (82×10^{-3} cm^3, 0.78 mmol) was added into a diethyl ether (2 cm^3) solution of **3** (120 mg, 0.36 mmol) at −50 °C. After evacuation of the reaction vessel, the reaction mixture was stirred at room temperature for 1 d. GLC analysis showed formation of gaseous and liquid products shown in Table 1. A yellow precipitate obtained by adding hexane to the reaction mixture was collected by filtration and dried under vacuum to yield 57 mg (36%) of a yellow solid, which was characterized as *trans*-$NiBr(Ph)(PEt_3)_2$ by comparing its IR and NMR spectra with those of an authentic sample prepared according to literature.[13]

No. 6: Propyl bromide (0.10 cm^3, 1.1 mmol) was added into a toluene (1 cm^3) solution of **3** (120 mg, 0.37 mmol). The reaction mixture was stirred at room temperature for 12 h. GLC analysis showed the formation of the gaseous and liquid products shown in Table 1. After removing toluene under vacuum, the complex formed was crystallized from a mixture of diethyl ether and hexane to yield reddish purple crystals (120 mg, 0.26 mmol, 71%), which were characterized as *trans*-$NiBr_2(PEt_3)_2$ from its IR spectrum and elemental analysis. The reactions of **3** and **4** with EtBr (Nos. 7 and 9) were carried out analogously.

No. 8: A mixture of **4** (380 mg, 0.79 mmol) and chlorobenzene (6 cm^3) was stirred at room temperature for 5 d. Analysis of the gaseous and liquid products by GLC showed evolution of 0.90 mmol of CH_4, 0.11 mmol of C_2H_6, and 0.39 mmol of toluene. Addition of hexane to the reaction mixture gave a brownish yellow precipitate. The precipitate was dissolved in THF and a yellow solid (260 mg) was recovered by addition of hexane to the THF solution. ^1H and $^{31}P\{^1H\}$-NMR spectra showed that it contained NiMe(Cl)dpe as a chief component and $NiCl_2$(dpe) and NiPh(Cl)dpe (*cf.* No. 10 in Table 2, *vide infra*) as minor. The ratios between these three complexes were determined as 79:7:14 from the area ratios of their peaks in $^{31}P\{^1H\}$-NMR spectrum. Attempts to separate these compounds have not been successful. Acidolysis of 46 mg of this yellow solid gave 0.08 mmol of CH_4 and 0.01 mmol of C_6H_6 in accord with its $^{31}P\{^1H\}$-NMR data. An authentic sample of NiMe(Cl)dpe was prepared separately from a 1:1 reaction of **4** with HCl according to the procedure shown below.

To a THF (25 cm^3) solution of **4** (500 mg, 1.0 mmol), a THF (5 cm^3) solution of dry HCl (0.95 mmol) was added dropwise at −50 °C. After stirring for 30 min at this temperature, the solvent was reduced to 10 cm^3 by evaporation. The yellow solid thus obtained was filtered, washed with hexane, and dried under vacuum. Recrystallization from THF–diethyl ether (1:1) gave orange yellow crystals of NiMe(Cl)dpe (160 mg). Found: C, 64.2; H, 5.3; Cl, 7.5%. Calcd for $C_{27}H_{27}ClNiP_2$: C, 63.9; H, 5.4; Cl, 7.0%. ^1H-NMR(*N*,*N*-dimethylformamide-d_7): δ=0.1 (3H, multiplet, CH_3–Ni), 1.9—2.8 (4H, multiplet, CH_2–P), and 7.3—8.1 (20H, multiplet, C_6H_5–P). $^{31}P\{^1H\}$-NMR(CH_2Cl_2): 67.7 (d, J_{P-P}=8 Hz) and 43.7 (d, J=8 Hz) ppm from external PPh_3.

*Reaction with R'COY (*cf. *Table 2). No. 1*: When a mixture of **1** (110 mg, 0.42 mmol) and PhCOCl (0.16 cm^3, 1.4 mmol) in THF (1.5 cm^3) was stirred at room temperature, the color of the solution changed instantly from deep green to purple. The color of the solution, then, turned to brown gradually with formation of a brown precipitate. The GLC analysis after 1 d showed formation of ketones and other products shown in Table 2. Reactions Nos. 2 and 3 were carried out analogously as reported in our previous paper.[8b] Reactions Nos. 4—9 were also carried out analogously. The nickel complexes obtained in Nos. 5 and 8 were characterized by comparing their IR spectra with authentic samples.[8b]

No. 10: Toluene (5 cm^3) and PhCOCl (0.15 cm^3) were added into a reaction vessel containing 0.30 g of **4** at −196 °C. After evacuation of the vessel, the reaction mixture was stirred at room temperature for 1 d. GLC analysis of the gas and liquid phase indicated the formation of the gaseous and liquid products shown in Table 2. The yellow precipitate formed during the reaction was collected by filtration and crystallized from a mixture of THF and diethyl ether. The nickel complex thus isolated was identified as NiCl(Ph)dpe from its elemental analysis and IR and NMR spectra. The same complex was prepared by a ligand exchange reaction of known $NiCl(Ph)(PPh_3)_2$[22] with dpe. Found: C, 67.2; H, 5.1; Cl, 6.2. Calcd for $C_{32}H_{29}ClNiP_2$: C, 67.5; H, 5.1; Cl, 6.2. IR(KBr, cm^{-1}): 1560s, 1460vs, 320 m. ^1H NMR: δ=1.6—2.8 (4H, multiplet, CH_2–P), 6.6 (3H, *o*, *m*- or *m*, *p*-H of Ni–C_6H_5), 6.9—8.2 (22H, multiplet, C_6H_5–P and *o*- or *m*-H of Ni–C_6H_5). $^{31}P\{^1H\}$-NMR-(CH_2Cl_2): 60.3 (d, J_{P-P}=20 Hz) and 43.4 (d, J=20 Hz) ppm from external PPh_3. Reactions Nos. 11—14 were carried out analogously. $NiCl_2$(dpe) obtained in No. 11 was characterized by comparing its IR spectrum with that of an authentic sample.[23]

Reaction with CS_2. Toluene (6 cm^3) and CS_2 (0.10 cm^3, 1.7 mmol) were added into a vessel containing **4** (0.28 g, 0.58 mmol) at −196 °C. After evacuation of the vessel, the reaction mixture was stirred at room temperature. After 1 h, formation of a green precipitate was observed. Analysis of the gas phase by gas chromatography indicated formation of 0.40 mmol (69%) of ethane and a small amount of CH_4. The green precipitate was collected by filtration, washed repeatedly with diethyl ether, and dried under vacuum to yield 260 mg of Ni(CS_2)(dpe). Found: C, 61.6; H, 4.7; S, 12.2. Calcd: C, 60.8; H, 4.5; S, 12.0. The complex was soluble in CH_2Cl_2, but it decomposes in the solvent as judged from IR spectra of a solid recovered from the CH_2Cl_2 solution. Ni(CS_2)(dpe) was sparingly soluble in other solvents, and recrystallization has not been succesful.

The reaction of **3** with CS_2 was carried out analogously by using 0.19 g (0.60 mmol) of **3** and 0.078 cm^3 (1.30 mmol) of CS_2 at −25 °C for 2 d (solvent=2 cm^3 of diethyl ether). The pale brown precipitate was collected by filtration at −30 °C, washed with diethyl ether at −30 °C, and dried under vacuum to yield 220 mg (85%) of a nickel complex having an approximate composition of $NiMe_2(PEt_3)_2(CS_2)$. Found: C, 43.9; H, 9.4; S, 16.2%. Calcd: C, 44.9; H, 9.0; S, 16.0%. Acidolysis of $NiMe_2(PEt_3)_2(CS_2)$ gave methane quantitatively.

References

1) P. W. Jolly and G. Wilke, "The Organic Chemistry of Nickel," Academic Press, New York (1974), Vol. 1 and (1975), Vol. 2.

2) a) A. Yamamoto, K. Morifuji, S. Ikeda, T. Saito, Y. Uchida, and A. Misono, *J. Am. Chem. Soc.*, **87**, 4652 (1965);

b) T. Saito, Y. Uchida, A. Misono, A. Yamamoto, K. Morifuji, and S. Ikeda, *ibid.*, **88**, 5198 (1966); c) A. Yamamoto and S. Ikeda, *ibid.*, **89**, 5989 (1967); d) T. Yamamoto, A. Yamamoto, and S. Ikeda, *ibid.*, **93**, 3350, 3360 (1971).

3) G. Wilke and J. Herrmann, *Angew. Chem.*, **78**, 591 (1966).

4) H.-F. Klein and H. H. Karsch, *Chem. Ber.*, **106**, 2438 (1973).

5) M. L. H. Green and M. J. Smith, *J. Chem. Soc., A*, **1971**, 639.

6) E. A. Jeffery, *Aust. J. Chem.*, **26**, 219 (1973).

7) T. Yamamoto, M. Takamatsu, and A. Yamamoto, *Bull. Chem. Soc. Jpn.*, **55**, 325 (1982).

8) a) T. Yamamoto, T. Kohara, and A. Yamamoto, *Bull. Chem. Soc. Jpn.*, **54**, 1720 (1981); b) **54**, 2010 (1981).

9) T. Kohara, T. Yamamoto, and A. Yamamoto, *J. Organomet. Chem.*, **192**, 265 (1980).

10) K. Tamao, K. Sumitani, Y. Kiso, M. Zembayashi, A. Fujioka, S. Kodama, I. Nakajima, A. Minato, and M. Kumada, *Bull. Chem. Soc. Jpn.*, **49**, 1958 (1976).

11) a) M. Uchino, A. Yamamoto, and S. Ikeda, *J. Organomet. Chem.*, **24**, C63 (1970); b) **84**, 93 (1975).

12) T. Yamamoto and A. Yamamoto, *J. Organomet. Chem.*, **57**, 127 (1973).

13) D. G. Morrell and J. K. Kochi, *J. Am. Chem. Soc.*, **97**, 7262 (1975).

14) D. Nicholls, "The Chemistry of Iron, Cobalt, and Nickel," Pergamon Text in Inorg. Chem., Vol. 24, Pergamon, Oxford (1973); R. S. Nyholm, *J. Chem. Soc.*, **1951**, 2602.

15) a) F. R. Hartley, "The Chemistry of Platinum and Palladium," Applied Science Publishers, London (1973); b) S. E. Livingstone, "Comprehenxive Inorganic Chemistry," Pergamon, Oxford (1973), Vol. 3, p. 1330.

16) a) J. D. Ruddick and B. L. Shaw, *J. Chem. Soc., A*, **1969**, 2969; b) M. P. Brown, P. J. Puddephatt, and C. E. E. Upton, *J. Chem. Soc., Dalton Trans.*, **1974**, 1613.

17) *E.g.*, a) H.-F. Klein, *Angew. Chem.*, **85**, 403 (1973); b) B. Corain and G. Favero, *J. Chem. Soc., Dalton Trans.*, **1975**, 283.

18) T. Yamamoto, T. Kohara, and A. Yamamoto, *Bull. Chem. Soc. Jpn.*, **54**, 2161 (1981).

19) M. C. Baird and G. Wilkinson, *J. Chem. Soc., A*, **1967**, 865.

20) T. Kashiwagi, N. Yasuoka, T. Ueki, N. Kasai, S. Takahashi, and N. Hagihara, *Bull. Chem. Soc. Jpn.*, **41**, 296 (1968).

21) T. Yamamoto, *Chem. Ind. (London)*, **1981**, 28.

22) M. Hidai, T. Kashiwagi, T. Ikeuchi, and Y. Uchida, *J. Organomet. Chem.*, **30**, 279 (1971).

23) G. Booth and J. Chatt, *J. Chem. Soc.*, **1965**, 3238.

Metal Complexes in Organic Synthesis. VIII.[1,2] Allylic Alcohols as Starting Materials in Palladium-catalyzed Wittig-type Olefinizations

Marcial MORENO-MAÑAS* and Antonio TRIUS

Departamento de Química Orgánica, Universidad Autónoma de Barcelona, Bellaterra, Barcelona, Spain

(Received July 28, 1982)

Allylic alcohols, aldehydes, and triphenylphosphine participate in a one-pot process catalyzed by palladium, which is formally equivalent to the Wittig olefinization. It can be applied to both aliphatic and aromatic aldehydes. The resulting olefins which appear as mixtures of stereoisomers were fully hydrogenated. Two different mechanisms can account for the observed results.

Palladium catalyzed and promoted reactions have attracted the interest of the chemical community since this transition metal provides us with the possibility of performing several interesting transformations.[3]

In the course of our study on the alkylation of 2,4-pentanedione with allylic and related alcohols under palladium catalysis,[4] we observed the formation of *ca.* 0.7% of (*Z*)- and (*E*)-stilbene in the reaction of sodium 2,4-pentanedionate with benzyl alcohol in the presence of catalytic amounts of bis(2,4-pentanedionato)palladium ($Pd(acac)_2$), and triphenylphosphine. Since benzaldehyde is formed together with toluene by disproportionation of benzyl alcohol, we first reasoned that the phosphine present in the reaction media could somehow react with the alcohol to yield benzyltriphenylphosphonium hydroxide, which should be the precursor of the Wittig reagent. The ylide could finally react with benzaldehyde in a conventional way.

We then started a study on the reaction of several different aldehydes with allylic alcohols and triphenylphosphine under palladium catalysis, the metal being always added in the form of $Pd(acac)_2$. The general reaction can be formulated as indicated in Eq. 1, and the results of the most significant experiments are collected in Table 1.

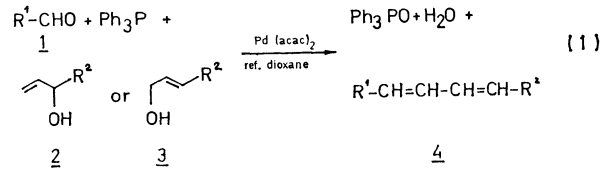

1 2 3 4 (1)

Some experimentation was performed before appropriate experimental conditions could be found. Dioxane was shown to be superior as solvent to THF, DME, diglyme, and toluene. The refluxing dioxane was passed through a molecular sieve pad before returning to the reaction flask. This shortened the required reaction times although the yields were not affected. Triphenylphosphine was the most suitable phosphorus compound for this reaction since tributylphosphine, tri-*o*-tolylphosphine, tris(*o*-methoxyphenyl)-phosphine, triethyl phosphite and bis(1,2-diphenylphosphino)ethane gave clearly lower yields of condensation products.

The olefinization method has been extended to aliphatic aldehydes, both saturated and α,β-unsaturated, as well as to aromatic aldehydes with different

Table 1. The reactions of aldehydes, allylic alcohols, and triphenylphosphine in the presence of $Pd(acac)_2$[a] · structures of products **5**

Op.	Ald.	Alc.[b]	Molar ratio Ald./Alc.	Time/h	Products **4** (Yield/%)	Products **4** R_1	Products **4** R_2	Products **5**	Products **5** R_2	Products **5** R_3
1	**1a**	**2**	1.0/1.1	40	**4a**(49)	4-ClC_6H_4	*n*-C_5H_{11}	**5a**	*n*-C_5H_{11}	4-ClC_6H_4
2	**1a**	**2**	1.0/2.2	70	**4a**(68)[c]					
3[d]	**1a**	**2**	1.0/1.1	72	**4a**(49)					
4	**1a**	**3a**	1.0/5.0	75	**4b**(41)	4-ClC_6H_4	CH_3	**5b**	CH_3	4-ClC_6H_4
5	**1b**	**2**	1.0/1.1	5	**4c**(48)[e]	4-$NO_2C_6H_4$	*n*-C_5H_{11}	**5c**	*n*-C_5H_{11}	4-$NH_2C_6H_4$
6	**1b**	**3b**	1.0/1.1	5	**4d**(45)	4-$NO_2C_6H_4$	*n*-C_3H_7	**5d**	*n*-C_3H_7	4-$NH_2C_6H_4$
7	**1c**	**2**	1.0/1.1	65	**4e**(20)	4-$MeOC_6H_4$	*n*-C_5H_{11}	**5e**	*n*-C_5H_{11}	4-$MeOC_6H_4$
8	**1d**	**2**	1.0/1.1	72	**4f**(51), **4g**(4)	4-$HOCC_6H_4$[f]	*n*-C_5H_{11}	**5f**[g]	*n*-C_5H_{11}[g]	4-MeC_6H_4[g]
9	**1d**	**2**	1.0/4.0[h]	72	**4f**(65), **4g**(28)					
10	**1f**	**2**	1.0/1.1	7 d	**4h**(32)	*n*-C_5H_{11}	*n*-C_5H_{11}	**5h**	*n*-C_5H_{11}	*n*-C_5H_{11}
11[i]	**1f**	**2**-OAc	1.0/1.1	65	**4h**(30)					
12	**1g**	**2**	2.0/1.1	24	**4i** (12)[j]	MeCH=CH	*n*-C_5H_{11}	**5i**	*n*-C_5H_{11}	*n*-C_3H_7
13	**1h**	**2**	1.0/1.1	88	**4j** (27)[k]	*n*-PrCH=CH	*n*-C_5H_{11}	**5h**	*n*-C_5H_{11}	*n*-C_5H_{11}

a) One equivalent of PPh_3 and a 5% molar of Pd were used unless otherwise stated. b) 1-Octen-3-ol (**2**), (*E*)-2-buten-1-ol (**3a**), (*E*)-2-hexen-1-ol (**3b**). c) 1,3-Octadienes were also detected. d) 10% molar of Pd was used. e) 3-((*E*)-2-Octenyl)-2,4-pentanedione and 3,3-bis((*E*)-2-octenyl)-2,4-pentanedione could also be isolated.[4] f) For **4f**. See text for **4g**. g) See text for **5g**. h) Two equivalents of PPh_3 were used. i) Two drops of hydrazine were added to reduce the Pd(II). j) 2-Pentyltoluene was also detected. k) 1-Pentyl-2-propylbenzene was also detected.

substituents at the ring. 4-Chlorobenzaldehyde (**1a**), 4-nitrobenzaldehyde (**1b**), 4-methoxybenzaldehyde (**1c**), terephthalaldehyde (**1d**), phthalaldehyde (**1e**), hexanal (**1f**), (*E*)-2-butenal (**1g**), and (*E*)-2-hexenal (**1h**), were shown to react with triphenylphosphine and one or more of the following allylic alcohols: 1-octen-3-ol (**2**), its acetate (**2**-OAc), (*E*)-2-buten-1-ol (**3a**) and (*E*)-2-hexen-1-ol (**3b**). However, a simple ketone, 6-methyl-2-heptanone was recovered after refluxing in dioxane for seven days with **2**, triphenylphosphine and 5% molar $Pd(acac)_2$.

Irrespective of primary or secondary nature of the allylic alcohols, products **4** were always formed by reaction at the terminal end of the allylic system (see ops. 4 and 6 in Table 1). The regioselectivity of the reaction is always higher than 99% as shown by GLC analysis of the hydrogenated products **5** (see below).

The olefins **4** were formed as mixtures of stereoisomers. We did not study the stereochemical outcome of our reactions. However, ratios of isomers as determined by GLC are indicated in the experimental part.

When the unsaturated aldehydes **1g** and **1h** were used as starting materials, only reaction at the carbonyl group was observed, products arising from attack at the electrophilic β position not being detected.

Terephthalaldehyde (**1d**) reacted with one equivalent of **2** to yield mainly the product of monocondensation, 1-(4-formylphenyl)-1,3-nonadiene (**4f**) (51%), and only minor amounts of the corresponding product of dicondensation, 1,4-bis(1,3-nonadienyl)benzene (**4g**) (4%) (see op. 8). Even working with a large excess of alcohol, **4f** was formed as the major product (op. 9). A similar selectivity in the reactions of the aldehyde **1d** in Wittig olefinizations has been described.[5]

In our first experiments aimed at preparing 1-(4-chlorophenyl)-1,3-nonadiene (**4a**), we realized that the reaction stopped when both the aldehyde **1a** and triphenylphosphine, but not the alcohol **2**, were still present in the reaction media. Elimination of water or acetic acid from allylic alcohols and acetates through the intermediacy of π-allylpalladium complexes is well documented[4,6] and we could demonstrate that dehydration of **2** was indeed a side reaction. In op. 2 a ratio **1a**/**2** of 1.0/2.2 was adopted, the yield of **4a** being raised to 68%. Also, the solvent, which was carefully recovered after the reaction and analyzed by GLC, showed two additional peaks. Hydrogenation under 10% Pd–C catalysis led to a dioxane containing octane as the only accompanying product, thus allowing us to assign the (*Z*)- and (*E*)-1,3-octadiene structures to the products present in the dioxane before hydrogenation.

The reactions were quite clean except when the nitroaldehyde **1b** was used. In such cases (ops. 5 and 6) no triphenylphosphine was recovered, a complicated array of products without nitro group being also formed. The reduction of nitro groups by trivalent phosphorus compounds is a well known fact[7] which can account for the observations made.

Since the olefins **4** were formed as mixtures of stereoisomers, we hydrogenated them under 10% Pd–C

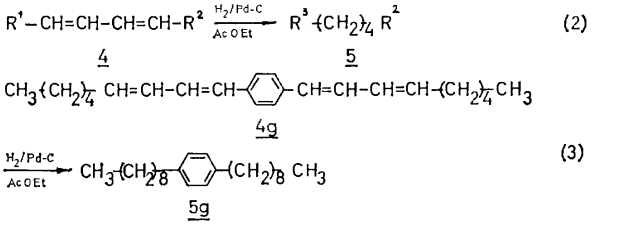

(2)

(3)

catalysis to the corresponding saturated compounds **5** as indicated in Eqs. 2 and 3. The results are collected in Table 1. Products **5** were homogeneous in GLC to an extent higher than 99%. They were fully characterized by elemental analysis and the usual spectroscopic techniques, or by comparison (GLC) with authentic specimens.

When trienes **4i** and **4j** were hydrogenated, the corresponding paraffins, dodecane (**5i**) and tetradecane (**5h**), were contaminated with *ca.* 6% of another components which presented a molecular ion in mass spectrometry at *m/e* eight units lower than the corresponding **5**, and aromatic absorptions in the ^{1}H-NMR spectrum. On these grounds the structures of 2-pentyltoluene and 1-pentyl-2-propylbenzene can be attributed to the contaminant products. They can arise from electrocyclic ring closures on the pertinent isomers of constitutions **4i** and **4j** followed by oxidative aromatization (Eq. 4).

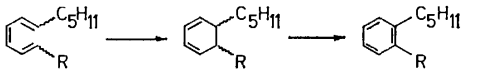

(4)

We turned next to **1e** as starting aldehyde. Its reactions were much more complicated than those previously described. When **1e** was treated with a tenfold excess of **3a** and two equivalents of triphenylphosphine under palladium catalysis, a 17% of a complex mixture of products without carbonyl group was isolated. Also triphenylphosphine was recovered, but no **1e** could be detected in the mixture. This was hydrogenated to only two products formed in a ratio of *ca.* 2/1. Mass spectrometric analysis coupled with GLC allowed us to assign the structure of 1,2-dipentylbenzene (**6**), and the constitution of 1,2-dimethyl-1,2,3,4,4a,9,10,10a-octahydrophenanthrene (**7**) to the products (Eq. 5).

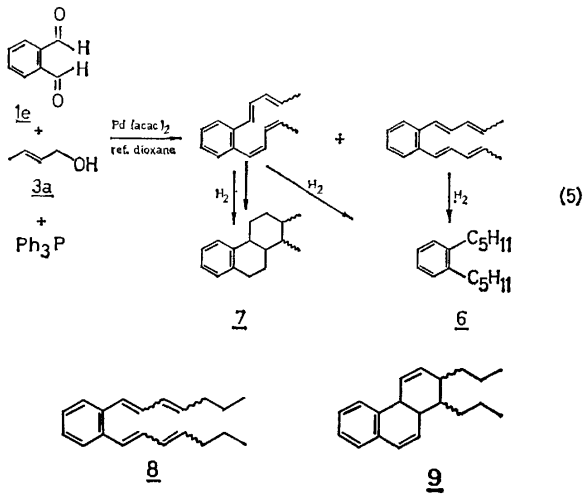

(5)

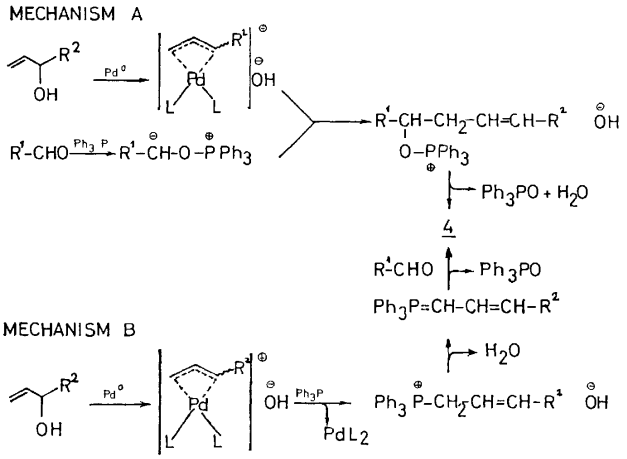

Fig. 1. Possible mechanisms accounting for the observed olefinizations.

Similar experiments were performed with **3b** as starting alcohol. In this case a 48% of diolefinization products could be isolated as a mixture of no less than eight components with the constitutions of 1,2-bis(1,3-heptadienyl)benzene (**8**), and probably 1,2-dipropyl-1,2,4a,10a-tetrahydrophenanthrene (**9**). A sample of **8** was isolated by column chromatography and inequivocally characterized by ^{1}H-NMR spectroscopy and mass spectrometry.

Two different mechanisms can account for the observed olefinizations. They are indicated in Fig. 1. Both mechanisms involve the intermediacy of π-allyl complexes formed by reaction of allylic alcohols with palladium(0) species. It should be recalled that allylic alcohols can indeed act as precursors for such complexes,[4] palladium(0) being formed by *in situ* reduction of the bivalent palladium compound really added to the reaction mixture. The inversion of reactivity at the carbonyl group needed for mechanism A to be operative has been previously postulated.[8] However, the reaction between phosphines and π-allylnickel[9] and palladium[10] complexes as exemplified by mechanism B has been described. At this point we can not decide through which mechanism the reactions proceed.

Experimental

Infrared and ^{1}H-NMR spectra were respectively recorded with a Perkin-Elmer Infracord 720 and a Perkin-Elmer R-12 models. Mass spectra were run with a Hewlett-Packard 5930 spectrometer. Only peaks with a *m/e* value above 20 are indicated unless they correspond to the molecular ion. GLC determinations were carried out in the Hewlett-Packard 5831A and Perkin-Elmer Sigma 1 models, both provided with flame ionization detection and UCW columns (0.5 m) unless otherwise stated.

Reaction between ***1a***, ***2***, *and Triphenylphosphine (op. 2); Preparation of 1-(4-Chlorophenyl)-1,3-nonadiene (****4a****).* The aldehyde **1a** (1.405 g, 10.0 mmol), alcohol **2** (2.816 g, 22.0 mmol), triphenylphosphine (2.751 g, 10.5 mmol) and Pd(acac)$_2$ (0.153 g, 0.5 mmol) were refluxed in dioxane (8 ml) for 70 h under magnetic stirring and dry nitrogen. The refluxing solvent was passed through a molecular sieve (4 Å) pad. The solvent was distilled off and the residue was chromatographed through a silica-gel column to afford **4a** (eluted with hexane), triphenylphosphine, **1a**, and triphenylphosphine oxide (eluted respectively with hexane(85)–dichloromethane(15), dichloromethane and chloroform).

4a: 1.591 g (68%). Ratio of isomer peaks in GLC: 38/15/13/34. IR (film): 1640, 1600, 980, 840, 790 cm^{-1}. ^{1}H-NMR (CCl_4): δ 0.75—1.10 (broad t, 3H), 1.10—1.75 (m, 6H), 1.9—2.4 (m, 2H), 5.50—6.95 (m, 4H), 7.25 (s, 4H). MS: *m/e* 236(7), mol wt 234(M$^+$, 30), 177(46), 163(49), 142(80), 129(100), 115(38), 96(34), 67(28), 41(44).

The distilled dioxane was analyzed by GLC showing two additional peaks in a 44/56 ratio. The mixture was treated with hydrogen at atmospheric pressure under 10% Pd–C (0.035 g) catalysis. When the uptake of hydrogen was over the catalyst was filtered off and the filtrate was analyzed by GLC. Only one additional peak was observed which was shown to correspond to octane by comparison with an authentic specimen.

The following products were prepared in a similar manner (see Table 1):

*1-(4-Chlorophenyl)-1,3-pentadiene (****4b****)*: Ratio of isomer peaks in GLC: 25/35/40. IR (film): 1640, 1590, 980, 940, 920, 840, 810, 790, 720 cm^{-1}. ^{1}H-NMR (CCl_4): δ 1.80 (d, J=6 Hz, 3H), 5.50—6.77 (m, 4H), 7.28 (broad s, 4H). MS: *m/e* 180(4), mol wt 178(M$^+$, 17), 143(67), 128(100), 115(46), 89(21), 75(25), 53(26).

*1-(4-Nitrophenyl)-1,3-nonadiene (****4c****)*: Ratio of isomer peaks in GLC: 9 (including a shoulder)/11/80. IR (film): 1630, 1590, 1510, 1330, 980 cm^{-1}. ^{1}H-NMR (CCl_4): δ 0.7—1.1 (m, 3H), 1.15—1.80 (m, 6H), 1.85—2.50 (m, 2H), 5.7—7.3 (m, 4H), 7.45, 7.60, 8.15, 8.30 (4H). MS: *m/e* mol wt 245(M$^+$, 6), 158(26), 142(50), 141(54), 137(26), 128(100), 119(48), 117(44), 115(58), 102(32), 96(40), 91(64), 83(38), 77(34), 67(36), 65(32), 63(26), 57(26), 44(76).

*1-(4-Nitrophenyl)-1,3-heptadiene (****4d****)*: Ratio of isomer peaks in GLC: 28.5/4.5/11.5/55.5. IR (film): 1640, 1580, 1510, 1340, 990, 950, 860, 740 cm^{-1}. ^{1}H-NMR (CCl_4): δ 0.92 (t, J=7 Hz, 3H), 1.15—1.80 (m, 2H), 2.15 (q, J=7 Hz, 2H), 5.5—7.2 (m, 4H), 7.30, 7.45, 8.00, 8.15 (4H). MS: *m/e* mol wt 217(M$^+$, 43), 188(36), 174(21), 143(83), 142(69), 129(50), 128(100), 115(58), 83(40), 77(23), 55(73), 41(77), 39(69).

*1-(4-Methoxyphenyl)-1,3-nonadiene (****4e****)*: Ratio of isomer peaks in GLC: 40.5/11.5/10.5/37.5. IR(film): 1610, 990, 820 cm^{-1}. ^{1}H-NMR (CCl_4): δ 0.75—1.10 (broad t, 3H), 1.1—1.8 (m, 6H), 1.85—2.65 (m, 2H), 3.78 (s, 3H), 5.45—6.83 (m, 4H), AA'BB' system centered at 7.17 (4H). MS: *m/e* mol wt 230(M$^+$, 25), 204(21), 202(32), 187(21), 173(28), 168(21), 159(32), 134(100), 121(57), 119(46), 91(34), 89(25).

*1-(4-Formylphenyl)-1,3-nonadiene (****4f****) and 1,4-Bis(1,3-nonadienyl)benzene (****4g****).* ***4f***: Ratio of isomer peaks in GLC: 42/10/13/35. IR (film): 2890, 2750, 1690, 1600, 990, 950, 860, 840, 820, 800 cm^{-1}. ^{1}H-NMR (CCl_4): δ 0.7—1.1 (broad t, 3H), 1.1—1.7 (m, 6H), 1.90—2.05 (m, 2H), 5.25—7.20 (m, 4H), 7.30, 7.45, 7.65, 7.80 (4H), 9.90 (broad s, 1H). MS: *m/e* mol wt 228(M$^+$, 12), 157(21), 143(20), 129 (100), 115(28), 91(28), 67(23), 41(20).

4g: Ratio of isomer peaks in GLC: 13/10/12/29/11/11/14. IR (film): 1640, 980, 940, 860 cm^{-1}. ^{1}H-NMR (CCl_4): δ 0.70—1.80 (m, 18H), 1.90—2.60 (m, 4H), 5.40—7.15 (m, 8H), 7.22 (s, 4H). MS: *m/e* mol wt 322(M$^+$, 7), 181(35), 167(82), 155(80), 141(100), 129(51), 128(48), 115(36), 91(20), 67(27), 55(23), 41(28).

*6,8-Tetradecadiene (****4h****)*: Ratio of isomer peaks in GLC (Carbowax 20 M column, 2 m): 71/29. IR (film): 990, 950 cm^{-1}. ^{1}H-NMR (CCl_4): δ 0.75—1.15 (m, 6H), 1.15—1.85 (m, 12H), 1.85—2.45 (m, 4H), 5.15—6.65 (m, 4H).

MS: *m/e* mol wt 194(M^+, 46), 124(25), 110(50), 109(36), 96(92), 95(78), 82(72), 81(96), 67(100), 55(21), 54(20), 41 (32).

*2,4,6-Dodecatriene (**4i**)*: Ratio of peaks in GLC: 3/6.5 (this belongs to *2-pentyltoluene*)/90.5. IR (film): 1640, 990, 940, 920 cm^{-1}. ^{1}H-NMR (CCl_4): δ 0.90 (t, J=6 Hz, 3H), 1.10—1.70 (m, 6H), 1.78 (d, J=6 Hz, 3H), 1.95—2.45 (m, 2H), 5.30—6.85 (m, 6H). MS: *m/e* mol wt 164(M^+, 19), 107(22), 105(26), 93(52), 91(61), 79(100), 77(39), 65(21), 41(26).

*4,6,8-Tetradecatriene (**4j**)*: Ratio of peaks in GLC: 23/11/7.5 (this belongs to *1-pentyl-2-propylbenzene*)/58. IR (film): 990, 960 cm^{-1}. ^{1}H-NMR (CCl_4): δ 0.7—1.2 (m, 6H), 1.20—1.75 (m, 8H), 1.8—2.6 (m, 4H), 5.2—6.6 (m, 6H). MS: *m/e* mol wt 192(M^+, 17), 121(25), 105(27), 93(42), 92(35), 91(87) 79(100), 77(50), 71(46), 67(33), 65(25), 55(21), 53 (20), 43(79).

*Hydrogenation of **4a**; Preparation of 1-Chloro-4-nonylbenzene (**5a**).* The diene **4a** (0.850 g, 3.6 mmol) in ethyl acetate (25 ml) was hydrogenated at atmospheric pressure for 20 min in the presence of 10% Pd–C (0.050 g). The catalyst was filtered off and the solvent was evaporated to yield 0.848 g (98%) of **5a**, bp 127 °C (oven temp)/0.5 mmHg (1 mmHg= 133.322 Pa), which was homogeneous in GLC. ^{1}H-NMR (CCl_4): δ 0.7—1.1 (m, 3H), 1.1—2.0 (broad s, 14H), 2.6 (t, J=7 Hz, 2H), 7.2 (m, 4H). MS: *m/e* 240(7), 239(7), mol wt 238(M^+, 20), 125(100), 91(40), 57(30), 44(47). Found: C, 75.40; H, 9.84; Cl, 15.20%. Calcd for $C_{15}H_{23}Cl$: C, 75.44; H, 9.71; Cl, 14.85%.

The following products were prepared in a similar manner (see Table 1):

*1-Chloro-4-pentylbenzene (**5b**)*: Bp 112 °C (oven temp)/0.9 mmHg, 98% yield, homogeneous to an extent of more than 99% in GLC. ^{1}H-NMR (CCl_4): δ 0.65—1.95 (m, 9H), 2.50 (t, J=8 Hz, 2H), 7.0, 7.15, 7.20, 7.35 (4H). MS: *m/e* 184(3), mol wt 182(M^+, 7), 127(29), 125(100), 91(64), 89(36), 77(22), 63(34), 51(32), 41(91). Found: C, 71.98; H, 8.29; Cl, 19.74%. Calcd for $C_{11}H_{15}Cl$: C, 72.32; H, 8.27; Cl, 19.41%.

*1-Amino-4-nonylbenzene (**5c**)*: Bp 158 °C (oven temp)/1 mmHg, homogeneous in GLC. IR (film): 3500, 3400 cm^{-1}. ^{1}H-NMR (CCl_4): δ 0.9 (t, J=5 Hz, 3H), 1.25 (broad s, 14H), 2.45 (t, J=7 Hz, 2H), 3.35 (s, 2H), 6.35, 6.50, 6.80, 6.95 (4H). MS: *m/e* mol wt 219(M^+, 13), 106(100). Found: C, 81.94; H, 11.70; N, 6.45%. Calcd for $C_{15}H_{25}N$: C, 82.13; H, 11.49; N, 6.38%.

*1-Amino-4-heptylbenzene (**5d**)*: Bp 135 °C (oven temp)/1 mmHg, homogeneous to an extent of more than 99% in GLC. IR (film): 3450, 3380 cm^{-1}. ^{1}H-NMR (CCl_4): δ 0.60—1.05 (m, 3H), 1.10—1.75 (broad s, 10H), 2.45 (t, J= 8 Hz, 2H), 3.75 (s, 2H), 6.30, 6.45, 6.70, 6.85 (4H). MS: *m/e* mol wt 191(M^+, 12), 106(100). Found: C, 81.31; H, 11.17; N, 7.41%. Calcd for $C_{13}H_{21}N$: C, 81.62; H, 11.06; N, 7.32%.

*1-Methoxy-4-nonylbenzene (**5e**)*: Bp 140 °C (oven temp)/0.5 mmHg, homogeneous to an extent of more than 99% in GLC. ^{1}H-NMR (CCl_4): δ 0.55—1.05 (m, 3H), 1.05—1.95 (broad s, 14H), 2.53 (t, J=7 Hz, 2H), 3.70 (s, 3H), AA′BB′ system centered at 6.85 (4H). MS: *m/e* mol wt 234(M^+, 5), 121(100). Found: C, 81.95; H, 11.37%. Calcd for $C_{16}H_{26}O$: C, 81.99; H, 11.18%.

*4-Nonyltoluene (**5f**)*: Bp 120 °C (oven temp)/0.6 mmHg, homogeneous to an extent of more than 99% in GLC. ^{1}H-NMR (CCl_4): δ 0.90 (t, J=5 Hz, 3H), 1.25 (broad s, 14H), 2.25 (s, 3H), 2.50 (t, J=7 Hz, 2H), 6.87 (s, 4H). MS: *m/e* mol wt 218(M^+, 0.5), 105(100), 41(51). Found: C, 87.92; H, 12.14%. Calcd for $C_{16}H_{26}$: C, 88.00; H, 12.00%.

*1,4-Dinonylbenzene (**5g**)*: Bp 205 °C (oven temp)/0.5 mmHg, homogeneous to an extent of more than 99% in GLC. ^{1}H-NMR (CCl_4): δ 0.90 (t, J=7 Hz, 6H), 1.27 (broad s, 28H), 2.52 (t, J=7 Hz, 4H), 6.95 (s, 4H). MS: *m/e* mol wt 330(M^+, 0.3), 105(100), 92(60), 91(63), 77(21). Found: C, 87.29; H, 12.90%. Calcd for $C_{24}H_{42}$: C, 87.19; H, 12.81%.

*Tetradecane (**5h**)*: It was compared with an authentic specimen and homogeneous to an extent of more than 99% in GLC when it was produced from **4h**. However, **5h** originated from **4j** was contaminated with an 8% of *1-pentyl-2-propylbenzene* which gave peaks in MS at *m/e* 190, 91, and 77.

*Dodecane (**5i**)*: It was compared with an authentic specimen. An analysis by GLC coupled with mass spectrometry revealed that it was contaminated with a 7% of *2-pentyltoluene* which gave peaks in MS at *m/e* 162(M^+, 2), 105(77), 92(24), 91(45), 79(30), 77(35), 65(28), 55(20), 53(24), 51(30), 43(54), 41(100).

*Reaction of **1e**, **3a**, and Triphenylphosphine.* The aldehyde **1e** (1.340 g, 10.0 mmol), the alcohol **3a** (7.200 g, 0.1 mol), triphenylphosphine (5.502 g, 21.0 mmol) and $Pd(acac)_2$ (0.152 g, 0.5 mmol) were refluxed in dioxane (10 ml) for 72 h under magnetic stirring and dry nitrogen. The refluxing solvent was passed through a molecular sieve (4 Å) pad. The solvent was distilled off and the residue was extracted with hexane leaving insoluble triphenylphosphine oxide. The hexane was evaporated and the new residue was chromatographed through a silica-gel column giving 0.460 g (17%) of a hydrocarbon mixture eluted with hexane and 2.089 g of the starting phosphine eluted with hexane(4)–dichloromethane(1). All the other eluted fractions were complex mixtures of unidentified products. The hydrocarbon mixture (0.402 g, 1.9 mmol) was hydrogenated at atmospheric pressure in ethyl acetate (10 ml) in the presence of 10% Pd–C (0.040 g). The catalyst was filtered off and the solvent evaporated to afford a colourless liquid (0.409 g) which analyzed by GLC gave two peaks in a ratio 66.5/33.5. An analysis by GLC coupled to mass spectrometry was consistent with, respectively, the structure of *1,2-dipentylbenzene* (**6**) and the constitution of *1,2-dimethyl-1,2,3,4,4a,9,10,10a-octahydrophenanthrene* (**7**).

6: MS: *m/e* mol wt 218(M^+, 12), 105(100), 91(26).

7: MS: *m/e* mol wt 214(M^+, 2), 129(100), 115(21).

*Reaction of **1e**, **3b**, and Triphenylphosphine.* The aldehyde **1e** (1.340 g, 10 mmol), the alcohol **3b** (4.000 g, 40 mmol) triphenylphosphine (5.502 g, 21 mmol), and $Pd(acac)_2$ (0.152 g, 0.5 mmol) were refluxed in dioxane (10 ml) for 64 h under magnetic stirring and dry nitrogen and the refluxing solvent being passed through a molecular sieve (4 Å) pad. The solvent was evaporated and the residue was chromatographed through a silica-gel column. A mixture (1.845 g) of hydrocarbons and triphenylphosphine was eluted with hexane. Further elutions gave triphenylphosphine (0.761 g), a mixture (0.267 g) of triphenylphosphine, **3b** and unidentified products (all eluted with hexane(4)–dichloromethane(1)), **3b** (0.247 g) (eluted with hexane(7)–dichloromethane(3)), and triphenylphosphine oxide (eluted with chloroform). The mixture of hydrocarbons and triphenylphosphine was treated in benzene (25 ml) with methyl iodide (1.5 g) at room temperature for 2 h. The precipitate of methyltriphenylphosphonium iodide formed was filtered off and the remaining solution evaporated to afford 1.284 g (48%) of a mixture of *1,2-bis(1,3-heptadienyl)benzene* (**8**) and probably *1,2-dipropyl-1,2,4a,10a-tetrahydrophenanthrene* (**9**), which presented eight peaks in GLC with relative areas 10/33/13.5/5/12/9.3/6.8/10.4. A further chromatography through

a silica-gel column gave 0.052 g of pure **8**.

8: ^{1}H-NMR (CCl_4): δ 0.95 (t, J=7 Hz, 6H), 1.10—1.80 (m, 4H), 2.15 (dt, J *ca.* 6 and 6 Hz, 4H), 5.40—6.90 (m, 8H), 6.95—7.60 (m, 4H). MS: *m/e* mol wt 266(M^+, 12), 183(34), 181(37), 167(100), 166(27), 165(47), 155(28), 153 (34), 152(32), 141(97), 128(53), 115(37), 91(26), 79(25), 77(20), 67(25), 55(31).

The authors express their gratitude to the "Comisión Asesora de Investigación Científica y Tecnica" and to "INAPE" (Ministerio de Educación y Ciencia of Spain) for financial support and for a grant (to A. T.). The authors are also indebted to Dr. P. de March and A. Virgili for kindly registering the mass spectra.

References

1) Part VII: P. de March, J. Marquet, M. Moreno-Mañas, R. Pleixats, I. Ripoll, and A. Trius, *An. Quim., Ser. C*, **79**, 15 (1983).

2) A. short communication has been previously published: M. Moreno-Mañas and A. Trius, *Tetrahedron Lett.*, **22**, 3109 (1981).

3) J. Tsuji, "Organic Synthesis with Palladium Compounds," Springer-Verlag, Berlin (1980).

4) M. Moreno-Mañas and A. Trius, *Tetrahedron*, **37**, 3009 (1981).

5) J. Castells, J. Font, and A. Virgili, *J. Chem. Soc., Perkin Trans. 1*, **1979**, 1.

6) K. Dunne, and F. J. McQuillin, *J. Chem. Soc., C*, **1970**, 2200 and 2203; J. Tsuji, T. Yamakawa, M. Kaito, and T. Mandai, *Tetrahedron Lett.*, **1978**, 2075; T. Mandai, H. Yasuda, M. Kaito, J. Tsuji, R. Yamaoka, and H. Fukami, *Tetrahedron*, **35**, 309 (1979); B. M. Trost, T. R. Verhoeven, and J. M. Fortunak, *Tetrahedron Lett.*, **1979**, 2301; R. O. Hutchins, K. Learn, and R. P. Fulton, *ibid.*, **21**, 27 (1980); K. Yamamoto, S. Suzuki, and J. Tsuji, *Bull. Chem. Soc. Jpn.*, **54**, 2541 (1981).

7) "Comprehensive Organic Chemistry," ed by D. Barton and W. D. Ollis, Pergamon Press, Oxford (1979), Vol. 2, p. 344.

8) a) I. J. Borowitz, M. Anschel, and P. D. Readio, *J. Org. Chem.*, **36**, 553 (1971); b) F. Ramírez, N. Ramanathan, and N. B. Desai, *J. Am. Chem. Soc.*, **85**, 3465 (1963).

9) F. Guerrieri and G. P. Chiusoli, *J. Organomet. Chem.*, **15**, 209 (1968).

10) T. Yamamoto, O. Saito, and A. Yamamoto, *J. Am. Chem. Soc.*, **103**, 5600 (1981).

© 1983 The Chemical Society of Japan

NOTES

Bull. Chem. Soc. Jpn., 56, 2159—2160 (1983)

Nb_2O_5 Supported on TiO_2. Catalytic Activity for Reduction of NO with NH_3

Susumu Okazaki* and Tetsuhiro Okuyama

Department of Industrial Chemistry, Faculty of Engineering, Ibaraki University, Nakanarusawa-cho Hitachi 316

(Received May 26, 1982)

Synopsis. Niobium(V) oxide supported on TiO_2 showed a high catalytic activity for the reduction of NO with NH_3 at temperatures higher than 450 °C. The presence of SO_4^{2-} in Nb_2O_5 or in Nb_2O_5 supported on TiO_2 brought about an increase in the catalytic activity.

Vanadium(V) oxide[1] supported on TiO_2 is commonly used for the reduction of NO with NH_3. Other metal oxides such as MoO_x[2] and FeO_x[3] supported on TiO_2 also show considerable catalytic activity for this reaction. Although Nb is a neighbor of Mo or V in the periodic table, the catalytic activity of Nb_2O_5 for denitration has not been well-studied; this topic is presented here. In particular, the effect of SO_4^{2-} on the catalytic activity was carefully studied, since in industrial denitration processes small amounts of SO_2 included in the reacting gas combine with O_2 to form SO_4^{2-}, which may be adsorbed and further combined with the catalysts.

Most catalyst samples were prepared by a coprecipitation method in which a mixture of niobium(V) oxide hydrate and titanium tetraisopropoxide was neutralized with 28% aqueous ammonia, followed by washing and drying. The niobium(V) oxide hydrate, supplied by the CBMM Company, contained about 55 wt% of Nb and no detectable amounts of alkali components such as Na and K, which would decrease the catalytic activity for denitration. For comparison of the activities as catalyst carriers, Al_2O_3, ZrO_2, and SiO_2 were prepared from $Al(NO_3)_3$, $Zr(OH)_4$, and colloidal silica respectively.

To elucidate the effect of the preparation method on the catalytic activity, some catalyst samples were prepared by impregnating TiO_2 with niobium(V) oxide hydrate dissolved in a 20 wt% aqueous solution of oxalic acid. Other niobium(V) oxide catalysts supported on Al_2O_3, ZrO_2, and SiO_2 were prepared by impregnation similarly to the TiO_2 supported niobium(V) oxide.

The samples containing definite amounts of SO_4^{2-} were prepared by adding ammonium sulfate to a solution containing the catalyst components.

All the catalyst samples were heat-treated at 500 °C for 3 h immediately before use as catalysts in the same reactor used for the denitration.

The specific surface area was determined by applying the BET equation to the adsorption of N_2 at −196 °C. The solid acidity was measured by NH_3 adsorptions at 250 and 450 °C. The acidity was further examined by the catalytic activity for isomerization of cyclopropane to propene which is promoted only by Brönsted acid sites.[4]

The reaction of NO with NH_3 was carried out at 200—500 °C by using a conventional flow reactor. The mixture of NO and NH_3, which was diluted with air so that the concentrations of both gases were 500 ppm, was passed through 2 g of catalyst, the flow rate and space velocity being 35 ml min^{-1} and 50000 h^{-1}, respectively. After the reaction, the amount of unreacted NO was measured by a NO_x meter(Kyoto Denki Kogyo, NX 22 or Takeda Kikai, KN 400 type).

The catalytic activity of Nb_2O_5 supported on TiO_2 for the reduction of NO with NH_3 in the presence of air was much higher than those of Nb_2O_5 supported on other oxides(Fig. 1). As is shown in Fig. 2, the activities of Nb_2O_5–TiO_2 were also higher than those of the component oxides. The catalytic activity for the mixed oxides prepared by coprecipitation had a maximum at the atomic ratio(Nb/Ti) of 1/1.

Figure 3 shows that the specific surface area of the mixed oxide is maximum at the atomic ratio of, not 1/1, but 1/9. Further, the specific activity(conversion/surface area) is especially high at the ratio(1/1). So, the higher activity is not merely due to the high dispersibility of the Nb component on TiO_2. It has been observed that the solid acidity is closely related to

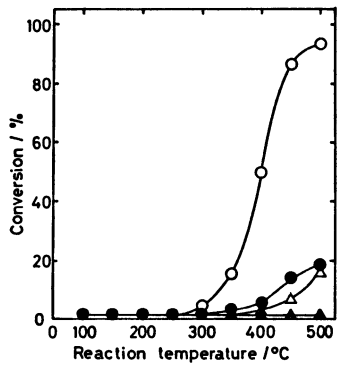

Fig. 1. Catalytic activities of Nb_2O_5 supported on various oxides at different temperatures.
○: Nb_2O_5-TiO_2(Nb/Ti=1/9), △: Nb_2O_5-Al_2O_3(Nb/Al=1/9), ●: Nb_2O_5-ZrO_2(Nb/Zr=1/9), ▲: Nb_2O_5-SiO_2(Nb/Si=1/9).

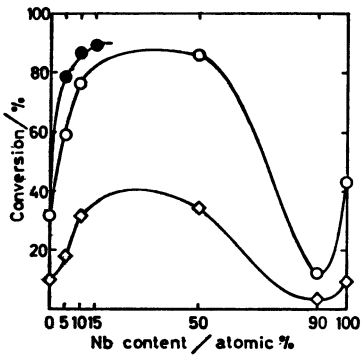

Fig. 2. Effect on catalytic activity of Nb_2O_5 content in Nb_2O_5–TiO_2 prepared by coprecipitation and impregnation.
○: Coprecipitation(reaction temperature: 450 °C), ◇: coprecipitation(350 °C), ●: impregnation(450 °C).

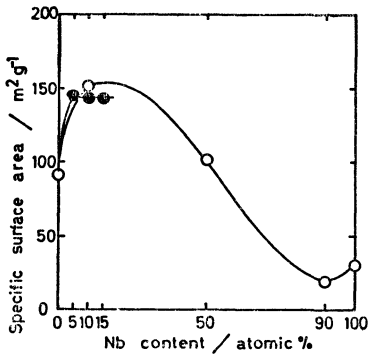

Fig. 3. Effect on specific surface area of Nb_2O_5 content on Nd_2O_5-TiO_2 prepared by coprecipitation and impregnation. ○: Coprecipitation, ●: impregnation. All the samples were heat-treated at 500 °C for 3 h immediately before determinations.

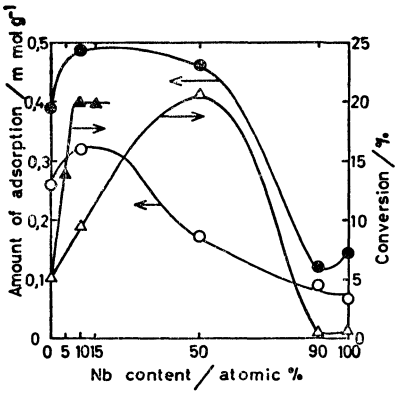

Fig. 4. Effects on adsorptive activity for NH_3 and catalytic activity for cyclopropane isomerization of Nb_2O_5 content.
○: NH_3 adsorption at 450 °C, ●: NH_3 adsorption at 250 °C, △: cyclopropane isomerization over mixed oxides prepared by coprecipitation, ▲: cyclopropane isomerization over mixed oxides prepared by impregnation. The condition of cyclopropane isomerization are as following; pulse method; pulse size: 1.09 ml, catalyst weight: 50 mg, reaction temperature: 250 °C, carrier gas: He, 40 ml/min.

the catalytic activity for the denitration of MoO_x-TiO_2.[5] However, as Fig. 4 shows, the total acidity measured by NH_3 adsorptions at 250 and 450 °C, was maximum at the atomic ratio of 1/9; thus this observation is unable to explain the catalytic activity of Nb_2O_5-TiO_2 prepared by coprecipitation. The catalytic activity is more adequately explicable by the Brönsted acidity determined by the catalytic activity for the isomerization of cyclopropane. Also, the fact that the activity of the mixed oxide of low Nb/Ti atomic ratio prepared by impregnation is higher than that prepared by coprecipitation may be due to the high Brönsted acidity of the sample prepared by impregnation. In the reduction of NO with NH_3, the NH_3 molecules are considered to be adsorbed on Brönsted acid sites as NH_4^+.[6] Thus, the Brönsted acid sites formed on the mixed oxides may contribute to activation of NH_3.

The catalytic activities of the oxides containing SO_4^{2-} shown in Figure 5 are considerably higher than those

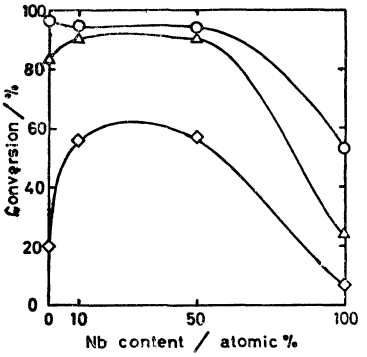

Fig. 5. Effect on catalytic activity of Nb_2O_5 content in Nb_2O_5-TiO_2 containing SO_4^{2-}.
Reaction temperature; ○: 450 °C, △: 400 °C, ◇: 350 °C. Mixed oxides were prepared by coprecipitation. The atomic ratio of S to the sum of Nb and Ti, S/(Nb+Ti) was kept constant at 5/95.

of oxides free from SO_4^{2-} (shown in Fig. 2). The effect of SO_4^{2-} addition is especially remarkable for the activities of TiO_2 and mixed oxides of high Ti content. Since it is already known that an addition of small amount of SO_4^{2-} greatly increases the solid acidity of TiO_2,[7] the enhancement in catalytic activity may also be due to the increase in Brönsted acidity. The addition of SO_4^{2-} to an extent that an atomic ratio of S to the sum of Nb and Ti, (S/(Nb+Ti)) equaled 5/95 appeared to be enough for the enhancement of the catalytic activity of Nb_2O_5-TiO_2 prepared by coprecipitation.

Compared to the catalytic activities of V_2O_5-TiO_2 and MoO_3-TiO_2,[5] that of Nb_2O_5-TiO_2 was still lower, especially at temperatures lower than 300 °C. Unlike V_2O_5 and MoO_3, Nb_2O_5 is not readily reduced, as is shown by the fact that NbO_2 is formed with difficulty by treating Nb_2O_5 with H_2 at temperatures as high as 1000—1200 °C.[8] Hence, the redox activity of Nb component may be not so large as V and Mo components. This seems to be the reason why Nb_2O_5-TiO_2 shows only relatively low catalytic activity, even though it has a considerable amount of Brönsted acid sites.

The authors wish to express their thanks to the CBMM Company for their financial support of this study.

References

1) Kokai Tokkyo Koho 50 65466(Mitsubishi Kasei); 57 3417 (Sumitomo Kinzoku Kogyo).
2) H. Hattori, K. Tanabe, K. Tanaka, and S. Okazaki, Proc. 3rd Intern. Conf. on Chem. Uses of Mo (1979), p. 188.
3) Kokai Tokkyo Koho 50 89290 (Hitachi Seisakusho).
4) L. Jacono and W. K. Hall, *J. Colloid Interface Sci.*, **58**, 76 (1977).
5) S. Okazaki, M. Kumasaka, J. Yoshida, K. Kosaka, and K. Tanabe, *IEC Product Res. Develop.*, **20**, 301 (1981).
6) M. Takagi, K. Kawai, M. Soma, T. Ohnishi, and K. Tamaru, *J. Catal.*, **50**, 441 (1979).
7) A. Kurosaki and S. Okazaki, *Nippon Kagaku Kaishi*, **1976**, 1816.
8) M. Taniguchi and H. Endo, "Shin Jikken Kagaku Koza," ed by the Chemical Society of Japan, Maruzen (1976), Vol. 8, p. 276.

Rapid Diffusion of Oxygen Ions in Indium Oxide during Reduction-oxidation

Kiyoshi Otsuka,* Takao Yasui, and Akira Morikawa

Department of Chemical Engineering, Tokyo Institute of Technology, Ookayama, Meguro-ku, Tokyo 152

(Received January 12, 1983)

Synopsis. Rapid diffusion of oxygen ions in indium oxide particles has been suggested by measuring the distribution of ^{18}O ions after oxidation of reduced-indium oxide by $^{18}O_2$ (gas). This result explains the observation that the reduced-indium oxide is one of the most efficient compounds among the reduced metal oxides for reduction of H_2O, CO_2, or NO.

In the previous works we have demonstrated that In_2O_3 is one of the most effective metal oxides to the two step hydrogen production from water which applies reduction (Step 1) and oxidation (Step 2) cycles of the oxide.[1,2] If the Step 1 is operated by using hydrogen for simplicity, the Steps 1 and 2 can be expressed by the following forward and reverse reactions, respectively:[1,3]

$$In_2O_3 + 3H_2 \rightleftharpoons 2In + 3H_2O. \quad (1)$$

When CO_2, NO, or O_2 instead of H_2O was used in Step 2, the following reactions proceeded smoothly at 673 K:[3]

$$2In + 3CO_2 \longrightarrow In_2O_3 + 3CO \quad (2)$$

$$2In + 3NO \longrightarrow In_2O_3 + 3/2\,N_2 \quad (3)$$

$$2In + 3/2O_2 \longrightarrow In_2O_3. \quad (4)$$

In the previous studies we have proposed a mechanism of reduction of In_2O_3 and that of reoxidation of the reduced oxide which assume a rapid diffusion of oxygen ions from the reaction interface at the surface of indium oxide particles into the bulk or vice versa, respectively (homogeneous model).[4] This model inevitably requires an apparent homogeneous distribution of the oxygen ions and indium metals throughout a oxide particle. With regard to this requirement, we intend to describe in this note an experimental proof that the oxygen ions in indium oxide particles distribute homogeneously during their redox cycles.

Experimental

The In_2O_3 used was a reagent-grade powder (purity>99.9 %) obtained from Wako Pure Chemical Co. The BET surface area of the oxide was 13.9 $m^2\,g^{-1}$. The apparatus employed was a conventional mercury-free, greese-free, static gas-circulation system of *ca.* 320 cm^3 volume. The water vapor evolved during the reduction of In_2O_3 by hydrogen was always condensed in a trap which had been placed in the gas-circulation line and cooled at 77 K. Contents of oxygen isotopes in oxygen or water were determined by mass-spectroscopic analysis.

Results and Discussion

After the reduction of In_2O_3 by hydrogen to the degree of reduction of 19.7%, which was estimated from the quantity of oxygen removed from the oxide, the reoxidation by $^{18}O_2$ (98.5% ^{18}O content) was carried out at 673 K. The oxygen ions of the sample thus oxidized by $^{18}O_2$ were stripped by reduction with hydrogen at 623—673 K. The contents of $H_2{}^{18}O$ in the produced water at certain range of reduction levels were measured by mass spectrometer. The change in contents of ^{18}O ions thus determined is demonstrated in Fig. 1 as a function of the degree of reduction of In_2O_3 (solid lines). The hight of bars in the figure indicates the average percentage of ^{18}O ions observed between the each two levels of reduction of the sample oxide.

Let us consider first the distribution of ^{18}O ions in a indium oxide particle. If the reduction of In_2O_3 proceeds from the surface of In_2O_3 particle into the bulk, leaving indium metal layer covering the particle (Fig. 2, model A), we expect the distribution of ^{18}O ions after reoxidation by $^{18}O_2$ as indicated by the chain line (— — —) in Fig. 1. On the other hand, if the oxide ions diffuse rapidly into or from the bulk, resulting in seemingly homogeneous distribution of ^{18}O ions (Fig. 2, model B), the distribution of ^{18}O ions in a particle should be the one indicated by the broken line (– – – –). The experimental results (bars) suggest that the distribution of ^{18}O ions is roughly homogeneous, supporting the propriety of the latter model.

The formation of In_2O by the reduction of In_2O_3 was assumed by several workers.[5-7] However, there are no evidence suggesting the existence of crystalline In_2O.[8-10] Our X-ray spectroscopic studies of the partially reduced In_2O_3 could establish only the existence of In_2O_3 and indium metal. Brewer[8] concluded in

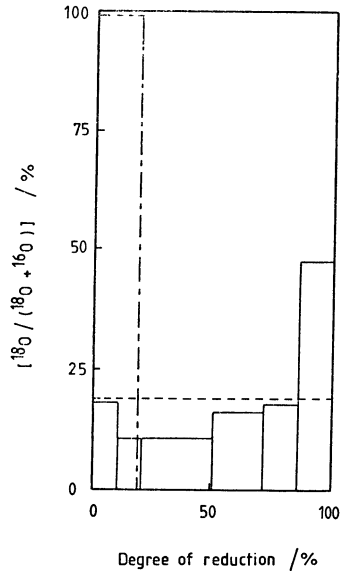

Fig. 1. ^{18}O ions distribution in a particle of the reoxidized indium oxide by $^{18}O_2$(gas). (——); Experimental observation, (— — —); idealized distribution according to the model A, (- - - -); idealized distribution according to the model B or C.

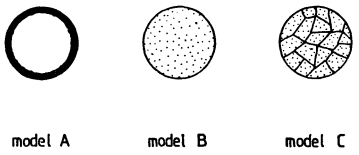

Fig. 2. Schematic model of the distribution of indium metal in the bulk of a particle (sectional views of a particle). Black part or spots are indium metal layer or nuclei. The lines in model C are grain boundaries.

his review that the supporsedly crystalline In_2O is a stoichiometric mixture of indium and In_2O_3 or is a metastable homogeneous phase. Wit *et al.*[10] commented that an indium(I) oxide like In_2O exists only as a parasitic phase, in combination with the contacting indium metal and In_2O_3, and is highly nonstoichiometric. We consider that the model B in Fig. 2 corresponds to the homogeneous mixture of indium metal and In_2O_3 as described above.

The mean dimension of the In_2O_3 crystallites estimated from the half width of X-ray diffraction peaks using the Scherrer's equation[11] was 23 nm. The SEM picture of the sample indicated that the sizes of the particles are in the range of 100—1000 nm. Therefore, the netwarks of the grain boundaries can be assumed to spread over in a particle. The rapid transport of oxygen ions in a particle may be enabled by the short circuit diffusion through these grain boundaries (model C in Fig. 2).

The exchange of $^{18}O_2$ in gas phase with ^{16}O ions of fresh In_2O_3 occurred at temperatures higher than 673 K. The sample of In_2O_3, whose oxygen ions had been exchanged by $^{18}O_2$ at 773 K to the extent of 7.3 atomic percentage of the total oxygen ions of the oxide, was reduced by hydrogen at 623 K stepwise to the degree of reduction of 62% and at 673 K to 90%. The analysis of the produced water indicated the distribution of ^{18}O in the oxide as demonstrated in Fig. 3. The broken line indicates the ideal homogeneous distribution of ^{18}O ions in a In_2O_3 particle or grain. The observed distribution demonstrated by the bar graph in Fig. 3 suggests that the ^{18}O ions have penetrated deep into a In_2O_3 particle or crystal grain, supporting the easy diffusion of oxygen ions from the surface or grain boundaries into the bulk. The high content of ^{18}O at the lowest range of reduction level (0—10%) may be ascribed either to adsorbed

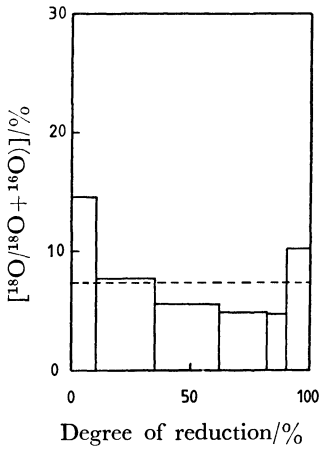

Fig. 3. ^{18}O ions distribution in a particle of In_2O_3 which had been exchanged by $^{18}O_2$(gas). (——); Experimental observation, (----); idealized distribution according to the model B or C.

oxygen atoms on the surface or to the oxygen atoms at grain boundaries which were equilibrated with $^{18}O_2$ in gas phase during the exchange pretreatment. The rather high concentration of ^{18}O ions at the highest reduction levels indicated both in Figs. 1 and 3 cannot be explained at the moment. They might be the one trapped in dislocations or defects of crystals, resulting in their total stabilization.

References

1) K. Otsuka, T. Yasui, and A. Morikawa, *Bull. Chem. Soc. Jpn.*, **55**, 1768 (1982).
2) K. Otsuka, Y. Takizawa, and A. Morikawa, *Fuel Process. Tech.*, **6**, 215 (1982).
3) K. Otsuka, T. Yasui, and A. Morikawa, *J. Chem. Soc., Faraday Trans. 1*, **78**, 3281 (1982).
4) K. Otsuka, S. Shibuya, and A. Morikawa, submitted.
5) W. Klemm and H. U. V. Vogel, *Z. Anorg. Alleg. Chem.*, **219**, 45 (1934).
6) K. A. Klinedinst and D. A. Stevenson, *J. Chem. Thermodyn.*, **5**, 21 (1973).
7) T. J. Anderson and L. F. Donaghey, *J. Chem. Thermodyn.*, **9**, 617 (1977).
8) L. Brewer, *Chem. Rev.*, **52**, 38 (1953).
9) N. C. Broch and A. N. Christensen, *Acta Chem. Scand.*, **20**, 1996 (1966).
10) A. J. Van Dillen, J. W. Geus, and J. H. W. de Wit, *J. Chem. Thermodyn.*, **10**, 895 (1978).
11) P. Scherrer, *Gött. Nachr.*, **2**, 98 (1918).

Mechanochemical Decomposition of Dipotassium Peroxodisulfate by Dry Grinding

Itaru MOTOOKA,* Hiroyuki NARIAI, and Mitsutomo TSUHAKO†
Department of Chemistry, Faculty of General Education, Kobe University, Nada-ku, Kobe 657
†*Kobe Women's College of Pharmacy, Motoyamakitamachi, Higashinada-ku, Kobe 658*
(Received August 2, 1982)

Synopsis. The mechanochemical decomposition of dipotassium peroxodisulfate by dry grinding was investigated by X-ray diffractometry, infrared spectrophotometry, electron spin resonance (ESR) spectrometry, and thermal and volumetric analyses. When dipotassium peroxodisulfate ($K_2S_2O_8$) was ground, type I of $K_2S_2O_8$ was transformed into type II and then into type III. With prolonged grinding, the O–O linkage in $K_2S_2O_8$ was severed to produce $KSO_4\cdot$ radicals, which reacted with a little moisture to give $KHSO_4$.

Mechanochemical phenomena have recently been noted in the wide field of scientific and technical investigations because mechanical treatment influences structures, physical and chemical properties, and reactivity of solids. Although effects of pressure and heat on the mechanochemical phenomena were observed,[1] mechanical force, particularly shear stress, has an important influence on the scission of chemical bonds.[2]

The chemical bonds in solid substances are reported to be severed by mechanical treatment[3] as in the case of grinding sodium pyrophosphate which gives orthophosphates by severing the P–O–P linkage.[4]

Peroxide is liable to decompose and produce radicals since the O–O bond energy is relatively small. Dipotassium peroxodisulfate gives $SO_4^{-}\cdot$ radicals by heating or exposing to ultraviolet light.[5,6] Therefore, it is used as an initiator for radical polymerization. If treated mechanically, the O–O bonds in peroxodisulfate are expected to be severed easily to produce radicals such as $SO_4^{-}\cdot$.

In the present paper, the mechanochemical decomposition of dipotassium peroxodisulfate by dry grinding is investigated.

Experimental

Reagent grade dipotassium peroxodisulfate was used without further purification. All other reagents used were of analytical grade.

The X-ray diffraction patterns were obtained with a Rigaku Geigerflex diffractometer using nickel-filtered Cu $K\alpha$ radiation. Infrared spectra were recorded on a JASCO IR-E spectrophotometer equipped with gratings. Thermal analyses (DTA and TG) were carried out by a Rigaku 8002 SD thermal analyzer. The ESR spectra were recorded on a JEOL JES-3BX electron spin resonance spectrometer equipped with an X-band microwave units and 100 kHz field modulation.

The grinding apparatus was an Ishikawa's grinder equipped with an agate mortar and installed in a steel box. Five grams of crystalline dipotassium peroxodisulfate was ground for the specified lengths of time with the relative humidity of 30—40% at room temperature because the mechanochemical effects are affected by the atomosphere, particularly moisture.

The amount of peroxodisulfate ($S_2O_8^{2-}$) was determined volumetrically by adding excess Mohr's salt to a solution of the ground sample and titrating excess iron(II) ion with a standard solution of potassium permanganate. The amount of sulfate (SO_4^{2-}) was determined as follows. Potassium ions in the solution of the ground sample were exchanged for hydrogen ions using a cation-exchange resin. The resulting peroxodisulfuric acid was thoroughly hydrolyzed to sulfuric acid (total sulfate) by heating for 20 min in boiling water, which was titrated with a standard solution of sodium hydroxide. The amount of sulfate in the ground sample was calculated by subtracting the amount of peroxodisulfate from total sulfate.

Results and Discussion

Figure 1 shows X-ray diffraction patterns of $K_2S_2O_8$ at various stages of grinding. The intensity of each diffraction line decreased, the line-width broadened for all the diffraction lines, and the different diffraction lines appeared. That is, with the distortion in crystal lattice, type I of $K_2S_2O_8$ was transformed into type II after a grinding period of 6 h and into type III after 168 h. With further grinding (250 h), the diffraction lines of $KHSO_4$ appeared and became stronger after 430 h. Type I of $K_2S_2O_8$ is apparently converted to $KHSO_4$ through types II and III. The infrared spectra of the samples ground for more than 250 h also indicated the presence of $KHSO_4$.[7]

Figure 2 shows the DTA and TG diagrams of the ground samples. The DTA and TG curves for 6 and 168 h were essentially the same as those of the original sample. In Fig. 2 an exothermic peak in the 200 °C region with a weight loss is due to the decomposition of $K_2S_2O_8$ with the evolution of oxygen, and the two endothermic peaks at about 330 and 370 °C are due to the order-disorder transformation and melting of $K_2S_2O_7$, respectively.[8] The melting point lowered with an increase in the grinding time because the particle size became smaller by grinding, and then it coincided in position with the transformation point. The samples ground for 250 h and 430 h also had an endothermic peak at about 200 °C. This peak may be attributed to the pyrolysis of $KHSO_4$ produced by

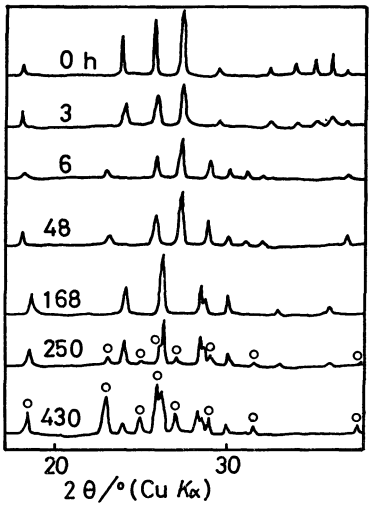

Fig. 1. X-Ray diffraction diagrams of ground samples.
○: $KHSO_4$.

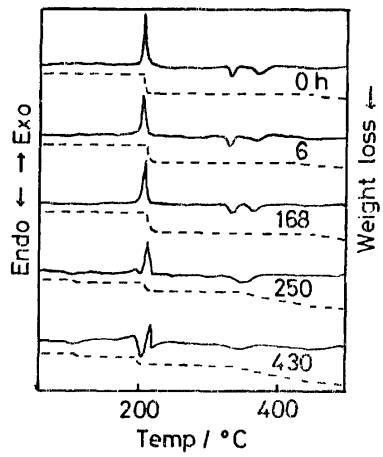

Fig. 2. DTA-TG curves of ground samples.
Solid line: DTA, dotted line: TG.

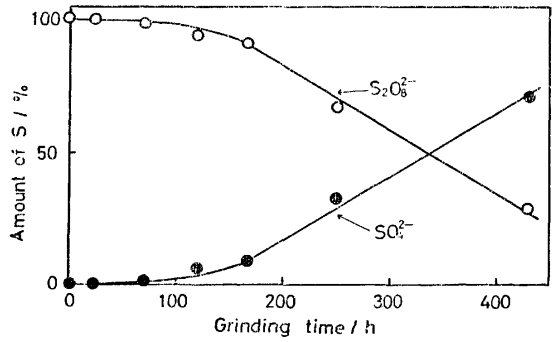

Fig. 3. Changes of distribution of sulfur in ground samples upon grinding.

the grinding of $K_2S_2O_8$. The intensity of this peak increased with an increase in the grinding time, while the weight loss in the 200 °C region decreased. This finding indicates that $K_2S_2O_8$ changes to $KHSO_4$ by grinding. This fact is compatible with the results of X-ray diffractometry and infrared spectrophotometry.

Figure 3 shows the distribution of sulfur in the ground samples. In the first stage of grinding (less than 72 h), sulfate was produced to a small extent and increased with decreasing amount of peroxodisulfate after grinding for more than 120 h.

The absence of peroxomonosulfate (SO_5^{2-}) in the ground samples was confirmed by paper chromatography.[9]

Above findings indicate that $K_2S_2O_8$ decomposes to $KHSO_4$ by prolonged grinding.

Figure 4 shows ESR spectra of the ground $K_2S_2O_8$. A singlet signal with two g values, $g_1=2.011$ and $g_2=2.007$, indicates the presence of radicals, probably $KSO_4\cdot$.[6] In the first stage of grinding, this signal was very weak, reached a maximum in 168 h, and decreased gradually with grinding time. This fact indicates the presence of radicals which are larger in the beginning of the severing of O–O linkages than after grinding for more than 250 h. Thus, it is considered that the radicals produced in the beginning are relatively stable, but that those produced by prolonged grinding react immediately with the moisture adsorbed on the powder surface which is very active due to prolonged grinding.

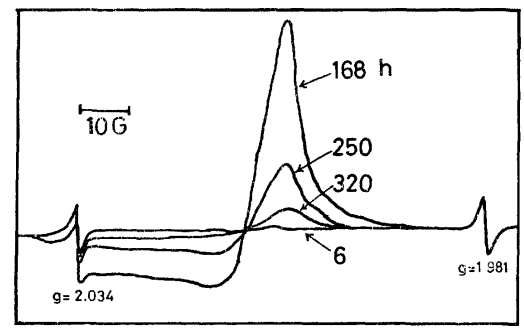

Fig. 4. ESR spectra of ground samples.

It is concluded that the following changes take place when $K_2S_2O_8$ is ground.

$$K_2S_2O_8(\text{type I}) \xrightarrow{\text{Grinding}} K_2S_2O_8(\text{type II}) \xrightarrow{\text{Grinding}} K_2S_2O_8(\text{type III}) \xrightarrow{\text{Grinding}} 2KSO_4\cdot \xrightarrow{+H_2O} 2KHSO_4 + 1/2\,O_2$$

After conversion I→II→III, the O–O linkages in $K_2S_2O_8$ are severed to produce the $KSO_4\cdot$ radicals which react with a little moisture adsorbed on the powder surface and are stabilized as $KHSO_4$ accompanied by oxygen evolution. The reaction of the $KSO_4\cdot$ radical with H_2O seems to take place by the following mechanism proposed by Kolthoff and Miller.[10]

$$2KSO_4\cdot + H_2O \longrightarrow 2KHSO_4 + 2\cdot OH$$
$$2\cdot OH \longrightarrow H_2O + 1/2\,O_2$$

The authors wish to thank Professor Yukio Kanaji, Faculty of Engineering, Kobe University, for his advice in making the ESR measurements.

References

1) P. S. De Carli and J. C. Jamieson, *J. Chem. Phys.*, **31**, 1674 (1959); F. Dachille and R. Roy, *Nature*, **186**, 34 (1960); Y. Horiguchi, Y. Nomura, and T. Funayama, *Kogyo Kagaku Zasshi*, **68**, 170 (1965); A. C. Greenham and B. P. Richards, *J. Br. Ceram. Soc.*, **69**, 115 (1970).

2) K. Bishof, *Int. Chem. Engr.*, **3**, 80 (1963); H. Takahashi, *Bull. Chem. Soc. Jpn.*, **32**, 235, 381 (1959); H. Takahashi and K. Tsutsumi, "Funtai No Bussei, Kagaku Zokan 31st," ed by K. Iinoya *et al.*, Kagaku Dojin, Kyoto (1967), p. 55; G. Natta and I. Giachetti, *Chim. Ind. (Milan)*, **39**, 1002 (1957); T. Kubo, "Mechanochemistry Gairon," 2nd ed, Tokyo Kagaku Dojin, Tokyo (1978), p. 44; Y. Ogo, N. Nishiguchi, and Y. Okuri, *Bull. Chem. Soc. Jpn.*, **54**, 520 (1981).

3) I. Motooka, G. Hashizume, and M. Kobayashi, *Nippon Kagaku Zasshi*, **87**, 255 (1966); G. Walters *et al.*, *J. Appl. Phys.*, **32**, 1854 (1961); H. Devel *et al.*, *Helv. Chim. Acta*, **39**, 1585 (1956).

4) I. Motooka and M. Kobayashi, "Topics in Phosphorus Chemistry," ed by M. Grayson and E. J. Griffith, John Wiley & Sons, New York (1980), Vol. 10, p. 177.

5) "Kagaku Binran, Oyo-hen," ed by the Chemical Society of Japan, Maruzen, Tokyo (1973), p. 808.

6) P. D. Bartllet and J. D. Cotwan, Jr., *J. Am. Chem. Soc.*, **71**, 1419 (1949); S. B. Barnes and M. C. R. Symons, *J. Chem. Soc.*, *A*, **1966**, 66.

7) F. A. Miller and C. H. Wilkins, *Anal. Chem.*, **24**, 1253 (1952).

8) K. D. Cleaver and J. E. D. Davies, *J. Raman Spectrosc.*, **9**, 376, (1980).

9) Peroxophosphate (PO_5^{3-}) was found to be present when tetrapotassium peroxodiphosphate was ground (unpublished data).

10) I. M. Kolthoff and I. K. Miller, *J. Am. Chem. Soc.*, **73**, 3055 (1951).

Polarography of Pb(II) Complexes with *N,N'*-Bis(2-hydroxyethyl)-ethylenediamine-*N,N'*-diacetic Acid

Tsutomu MATSUO,* Yoshitaka MASUDA,† and Eiichi SEKIDO†

Kobe Technical College, Tarumi-ku, Kobe 655

†*Department of Chemistry, Faculty of Science, Kobe University, Nada-ku, Kobe 657*

(Received August, 1982)

Synopsis. The electrochemical behaviour of the Pb(II)–*N,N'*-Bis(2-hydroxyethyl)ethylenediamine-*N,N'*-diacetic acid(H_2bhedda=H_2L) system has been examined by means of d.c. polarography. Two well-defined polarographic reduction waves were observed. The mechanisms of the electrode reaction for the two waves were elucidated. The kinetic parameters of the irreversible reduction of the complexes have been evaluated; $k_{f1}=3.80\times10^{-5}$ cm/s and $k_{f2}=5.25\times10^{-16}$ cm/s. The stability constant of the $PbHL^+$ species is calculated to be $10^{1.45}$.

Many workers[1,2] have reported on the electrochemical behaviour of H_4edta derivative complexes with several kinds of metals. We ourselves have previously studied the mechanisms of the electrode reactions of Pb(II)–H_6ttha(triethylenetetramine-*N,N,N',N'',N''',N'''*-hexaacetic acid) and Cd(II)–H_2bhedda(*N,N'*-bis(2-hydroxyethyl)ethylenediamine-*N,N'*-diacetic acid) complexes.[3-5] Little is known, however, concerning the properties of the H_2bhedda ligand and its metal complexes, except for the acid-dissociation constants.[6] In this report, the mechanisms and parameters of the electrode reactions for Pb(II)–H_2bhedda complexes are investigated. The influence of the hydroxymethyl groups on the stability constant and the rate constant of the reduction is also discussed.

Experimental

A Pb(II) solution(Pb(II) aquo ion) was prepared by dissolving reagent-grade lead nitrate. The ligand, H_2bhedda (Clewat OH-300, Tcikoku Chemical Co.) was twice recrystallized from hot water, and 0.01 mol dm^{-3} solution was prepared. The acetate buffer solutions were used to adjust the pH values of the test solutions. A sodium perchlorate solution (1.0 mol dm^{-3}) was added to keep the ionic strength constant (μ=0.4).

Results and Discussion

Polarograms of Pb(II)–H_2bhedda System. The polarogram of the Pb(II)–H_2bhedda system exhibited a maximum(−0.84 V *vs.* SCE). Triton X-100 (up to 1.7×10^{-4}%) was added to suppress the maximum. In an excess of the metal ion to the ligand, the polarograms gave two well-defined reduction waves(Fig. 1). The two waves are referred to as Wave A (first wave) and Wave B(second wave). In an excess of the ligand, the limiting current for Wave A was independent of the mercury-head height below pH 4.0. The temperature coefficient of the limiting current for Wave A was 3.5% (pH=3.28, M:L=1:5). From the analysis of *i-t*(*i*:current, *t*:time) curves for Wave A, the value of γ in the equation, $i=kt^{\gamma}$, was calculated to be 0.67(pH=3.28, 1:5, −0.7 V *vs.* SCE). The limiting current for Wave A involves a kinetic characteristic below pH 4.0 in an excess of the ligand.

As the limiting current for Wave B was proportional to the square root of the mercury-head height at any pH, and the temperature coefficient of the limiting current for Wave B was 1.5%(1:5, pH=4.9), the limiting current for Wave B can safely be said to be diffusion-controlled. The average value of the reciprocal slope of the conventional log-plot for Wave B was 47.1 mV, and so Wave B is considered to be an irreversible two-electron reduction wave.

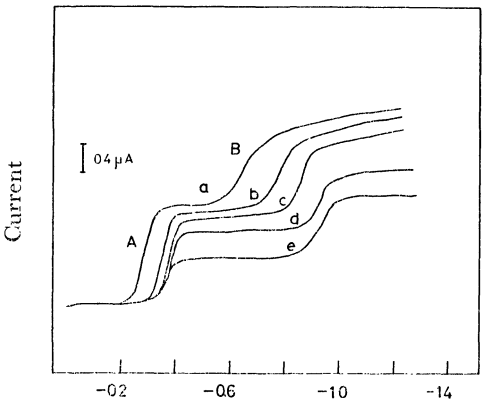

Fig. 1. Polarograms of Pb(II)–H_2bhedda system varying with pH.
$[Pb]_t=5.0\times10^{-4}$ mol dm^{-3}, $[H_2bhedda]_t=2.5\times10^{-4}$ mol dm^{-3}, μ=0.4($NaClO_4$), acetate buffer, pH —— (a) 3.05, (b) 3.53, (c) 4.08, (d) 5.19, (e) 7.72. A: Wave A, B: Wave B.

Test of Kinetic Current Theory for Wave A. The rate-determining step of the kinetic process for Wave A in an acetate buffer is expressed as follows;

$$PbHL^+ + qH^+ \xrightarrow{k_d} Pb^{2+} + H_{q+1}L, \quad (1)$$

$$Pb^{2+} + jOAc^- \rightleftharpoons Pb(OAc)_j^{2-j}. \quad (2)$$

The following relationship, derived by Koryta,[7] is applicable to such a kinetic current;

$$\left(\frac{(i_k)_a}{(i_d)_a-(i_k)_a}\right)\left(1+\frac{(i_k)_a}{(i_d)_a}\cdot\frac{C_M}{C_L}\cdot\frac{K_{PbHL}\cdot\delta_{HL}/\sum_{p=0}^{1}K_{PbHL_p}\cdot\delta_{H_pL}}{\delta_{H_{(q+1)}L}}\right)^{1/2}$$

$$=0.886[H^+]^q\sqrt{\frac{k_d\cdot t_d\sum_{j=0}^{p}(K_0'\cdots K_j'[OAc]^j)}{K_{eq}\cdot C_L\cdot\delta_{H_{(q+1)}L}}}, \quad (3)$$

where C_M is the total concentration of Pb(II); δ_{H_pL}, the molar distribution ratio of H_pL species; q, the number of the proton participating in reaction (1); k_d, the dissociation rate constant of the complex; t_d, the dropping time; [OAc], the concentration of the acetate ion, and $K_{eq}=[PbHL][H^+]^q/[Pb^{2+}][H_{(q+1)}L]$. The effect of the acetate buffer solution on the kinetic current $(i_k)_a$ was also considered. The value of $\Sigma(K_0'\cdots K_j'[OAc]^j)$ was obtained from the shift of the half-wave potential. The plot of

$$F_1=\log\frac{(i_k)_a}{(i_d)_a-(i_k)_a}+\frac{1}{2}\log\left(1+\frac{(i_k)_a}{(i_d)_a}\cdot\frac{C_M}{C_L}\cdot\frac{K_{PbHL}\cdot\delta_{HL}/\sum_{p=0}^{1}K_{PbH_pL}\cdot\delta_{H_pL}}{\delta_{H_{(q+1)}L}}\right)vs.$$

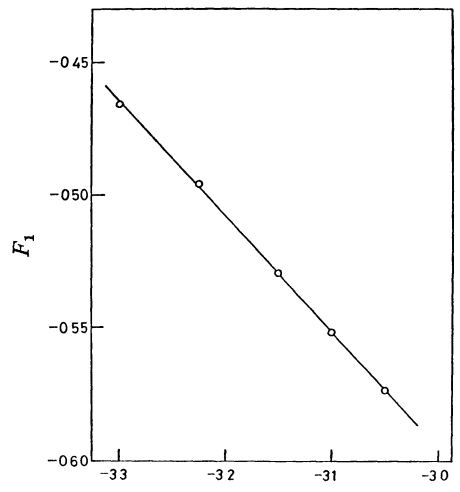

Fig. 2. Test of kinetic current theory for Wave A (Plot of F_1 *vs.* $\log C_L \cdot \delta_{H_2L}$)

$$\left(F_1 = \log\frac{(i_k)_a}{(i_d)_a-(i_k)_a} + \frac{1}{2} \times \log\left(1 + \frac{(i_k)_a}{(i_d)_a} \cdot \frac{C_M}{C_L} \cdot \frac{K_{PbHL} \cdot \delta_{HL} / \sum_{p=0}^{1} K_{PbH_pL} \cdot \delta_{H_pL}}{\delta_{H_{(q+1)}L}}\right)\right)$$

$[Pb]_t = 5.0 \times 10^{-4}$ mol dm^{-3}, $[H_2bhedda]_t = 5.0 \times 10^{-4}$, -9.0×10^{-4} mol dm^{-3}, $\mu = 0.4(NaClO_4)$, acetate buffer

$\log C_L \cdot \delta_{H_2L}$ is shown in Fig. 2. The slope of the straight line (−0.43) is consistent with the theoretical value of Eq. 3 (−0.5). Thus, the number of the proton participating in the above reaction mechanism could be obtained by plotting F_1 *vs.* pH ($q=1$). The average dissociation rate constant(k_d) of the complex was also calculated($k_d = 1.49 \pm 0.43$ s^{-1}, pH=2.95—3.53).

Electrode Reaction for Wave B. The dependence of the half-wave potential $(E^{irr}_{1/2})_b$ on the pH was remarkably changed from −92 mV/pH to −4.0 mV/pH at pH 5.4. In order to analyze the irreversible reduction mechanisms for Wave B, a theoretical equation proposed by Vlček,[3] could be used. By assuming that the complex species, PbL, participates in the reaction in the pH range from 4.0 to 5.4, the number of the proton is found to be 2. The electrode reaction mechanism is expressed as follows:

$$PbL + 2H^+ + 2e + Hg \xrightarrow[k_{j_1}]{} Pb(Hg) + H_2L. \quad (4)$$

The electrode reaction rate constant, k_{j_1}, was calculated ($k_{j_1} = 3.80 \times 10^{-5}$ cm/s at $E^{irr}_{1/2} = -0.888$ V *vs.* SCE). Above pH 5.4, the mechanism of the electrode reaction can also be expressed as follows:

$$PbL + 2e + Hg \xrightarrow[k_{j_2}]{} Pb(Hg) + L^{2-}, \quad (5)$$

where k_{j_2} was calculated to be 5.25×10^{-16} cm/s($E^{irr}_{1/2} = -0.947$ V *vs.* SCE).

The stability constants[7,8] of the Pb(II)–H_2bhedda and Pb(II) complexes with the analogous H_2bhedda ligands are shown in Table 1. Both of the stability constants, K_{PbL} and K_{PbHL}, become smaller in the order of the ligands: H_4edta > H_3hedta > H_2bhedda. This results from the drop in the coordinating ability of the ligand due to the substitution of the hydroxymethyl group for the carboxyl group in the ligand. The small value of k_{j_2} (pH>5.4) for H_2bhedda results from the increase on the transfer coefficient, the negative shift of the half-wave potential, and the steric hindrance caused by uncoordinated hydoxymethyl groups in H_2bhedda.

Table 1. Logarithmic stability constants and kinetic parameters

	(1) Stability constants		
	PbL	PbHL	Ref.
H_4edta	18.04	10.61	7
H_3hedta	14.85	7.68	8
H_2bhedda	11.1	4.45	Authors

	(2) Kinetic parameters						
	α		$(-E^0_p$ *vs.* SCE)/V		k_j/cm s^{-1}		
	(PbHL)	(PbL)	(PbHL)	(PbL)	(PbHL)	(PbL)	Ref.
H_4edta	0.26	0.26	0.718	—	8.7×10^{-6}	1.2×10^{-6}	2
H_3hedta	0.36	0.36	0.618	—	2.4×10^{-4}	7.9×10^{-5}	2
H_2bhedda	—	0.63	—	0.715[a]	a kinetic nature	3.8×10^{-5}(k_{j_1}) (4.0<pH≦5.4) 5.25×10^{-16}(k_{j_2}) (pH>5.4)	Authors

α: Transfer coefficient, k_j: formal electrode-reaction rate constant.
a) $E^0_p = -0.388 - 0.0295 \log(\beta_{101}/\beta_{001})$ ($\beta_{101} = K_{PbL}$, $\beta_{001} = 1$).

Table 2. Dissociation rate constants (pH=3.2)

	k_d/s^{-1}	Ref.
$Pbhedta^- + H^+ \rightarrow Pb^{2+} + Hhedta^{2-}$	47.6	9
$Pbedta^{2-} + H^+ \rightarrow Pb^{2+} + Hedta^{3-}$	0.442	9
$Pbcydta^{2-} + H^+ \rightarrow Pb^{2+} + Hcydta^{3-}$	2.52×10^{-4}	9
$Pbdtpa^{3-} + H^+ \rightarrow Pb^{2+} + Hdtpa^{4-}$	0.183	9
$PbHbhedda^+ + H^+ \rightarrow Pb^{2+} + H_2bhedda$	1.5	Authors

H_3hedta: *N*-(2-Hydroxyethyl)ethylenediamine-*N*,*N*′,*N*′-triacetic acid. H_4edta: Ethylenediamine-*N*,*N*,*N*′,*N*′-tetraacetic acid. H_4cydta: *trans*-1,2-Cyclohexylenedinitrilotetraacetic acid. H_5dtpa: Diethylenetriamine-*N*,*N*,*N*′,*N*″,*N*″-pentaacetic acid.

Some dissociation-rate constants[9] for Pb(II) complexes with H_3hedta, H_4edta, H_4cydta, H_5dtpa, and H_2bhedda are shown in Table 2. All these dissociation-rate constants except for that of H_2bhedda correspond to the dissociation of the unprotonated Pb(II) complex participating with each proton. The result for the Pb(II)–H_2bhedda complex indicates that the reaction scheme differs from the other complexes given in Table 2.

References

1) J. Koryta, *Collect. Czech. Chem. Commun.*, **24**, 2903, 3057 (1959).
2) N. Oyama, T. Shirato, and H. Matsuda, *J. Electroanal. Chem.*, **81**, 67 (1977).
3) Y. Masuda, T. Nakamori, and E. Sekido, *Nippon Kagaku Kaishi*, **1978**, 190.
4) T. Matsuo, Y. Masuda, and E. Sekido, *Electrochim. Acta*, **27**, 461 (1982).
5) T. Matsuo, Y. Masuda, and E. Sekido, *Nippon Kagaku Kaishi*, **1979**, 1708.
6) Y. Masuda, Y. Ago, and E. Sekido, 29th National Meeting of the Chemical Society of Japan, Hiroshima, Sep. 1973, Abstr. I, p. 5.
7) A. E. Martell and L. G. Sillen, "Stability Constants of Metal-Ion Complexes," Organic Part, Part II, Supplement No. 1 to Special Publication No. 17, The Chem. Soc., London (1971), p. 627.
8) N. Oyama, T. Shirato, H. Matsuda, and Ohtaki, *Bull. Chem. Soc. Jpn.*, **49**, 3047 (1976).
9) T. Fujisawa and N. Tanaka, *Nippon Kagaku Zasshi*, **92**, 962 (1971).

The Determination of 5-Iodouracil Using the *o*-Hydroxyhydroquinonephthalein–Palladium(II) Complex†

Yoshikazu FUJITA, Itsuo MORI,* and Shoko KITANO
Osaka College of Pharmacy, 2-10-65, Kawai, Matsubara, Osaka 580
(Received November 11, 1982)

Synopsis. A simple and sensitive spectrophotometric procedure was studied for the determination of 5-iodouracil (IU) using the *o*-hydroxyhydroquinonephthalein(Qn.Ph.)–palladium(II) complex and avoiding any effect of iodide ions. This method could be used in the concentration range of 0—15 μg/10 ml of IU, where the Sandell sensitivity was 0.0020 μg/cm² for at 630 nm; the coexistence of the iodide ion did not interfere with the determination of IU, even when it was present in a 500-fold excess.

The determination of organic iodine compounds involves, in general, a preliminary ashing step to release iodide ions.[1,2] Moreover, organic iodine compounds tend to decompose upon exposure to ambient light and so liberate iodide ions. Therefore, it is important that organic iodine compounds be determined without any interference by iodide ions.

We have already reported simple and sensitive spectrophotometries[3–5] for the determination of cephalexin, ampicillin, *etc.* based on the decrease in the absorbance of the *o*-hydroxyhydroquinonephthalein(Qn.Ph.)–palladium(II) complex solution.

This paper will describe a procedure for the determination of 5-iodouracil(IU) using the Qn.Ph.–palladium(II) complex without any effect of the coexistence of iodide ions.

Experimental

Apparatus. The absorption spectra and absorbance were measured with a Shimadzu Model 240 recording spectrophotometer using matched 1.0-cm quartz cells. A Hitachi-Horiba Model F-7 AD glass electrode pH meter was used for the pH measurements.

Reagents. A stock solution(1.0×10^{-3} M, 1 M=1 mol dm^{-3}) of IU(Tokyo Kasei Kogyo Co., Ltd., Tokyo) was prepared by dissolving IU in a 20% methanol solution, while the working solution was made by the suitable dilution of this stock solution as required. A 5.0×10^{-4} M aqueous solution of palladium(II) and a 5.0×10^{-4} M methanol solution of Qn.Ph. were prepared according to the method of a previous report.[3] A 1.0×10^{-2} M solution of hexadecyltrimethylammonium chloride(HTAC) was prepared by dissolving the respective compound in water. A 0.1 M sodium carbonate–0.1 M sodium hydrogencarbonate buffer solution[6] was used for the pH adjustment. All the other reagents were of an analytical grade.

Standard Procedure. 0.5 ml of the 5.0×10^{-4} M palladium(II) solution, 2.0 ml of the 1.0×10^{-2} M HTAC solution, 2.0 ml of the buffer solution(pH 9.8), 0.75 ml of the 5.0×10^{-4} M Qn.Ph. solution, and a solution containing up to 15 μg of IU were placed in a 10-ml calibrated flask. The mixture was diluted to 10 ml with water, kept at 60 °C for 15 min, and then cooled 5 min in water. The difference in absorbance [ΔA] between the Qn.Ph.–palladium(II)–IU and the Qn.Ph.–palladium(II) solutions was measured at 630 nm against water.

Results and Discussion

Absorption Spectra. The absorption spectra of Qn.Ph.–palladium(II) in the presence of IU at pH 9.8 are shown in Fig. 1. On the addition of IU to the Qn.Ph.–palladium(II) solution, the decrease in the absorbance of the Qn.Ph.–palladium(II) complex at 630 nm was proportional to the concentration of IU.

Effect of pH and Surfactants. The effects of the pH and the surfactants were examined. The maximum and constant ΔA value was obtained in the pH range from 9.3 to 10.5 with a 0.1 M sodium carbonate–0.1 M sodium hydrogencarbonate buffer solution. Subsequent measurements were carried out by the addition of 2.0 ml of the pH buffer solution(pH 9.8). Compared with nonionic surfactants, such as poly(vinyl alcohol) and poly(*N*-vinylpyrrolidone), or an anionic surfactant such as sodium dodecyl sulfate, the ΔA value in the presence of a cationic surfactant was more than 30 times as large. HTAC was superior to the other cationic surfactants examined in terms of sensitivity; the maximum and constant ΔA value could be obtained over the range of 1.5—2.5 ml of the 1.0×10^{-2} M HTAC solution in the final 10 ml.

Effects of Palladium(II) and Qn.Ph. Concentration. The effect of the amount of Qn.Ph. on ΔA was examined by varying the molar ratio of Qn.Ph. to palladium(II), the amounts of palladium(II) and IU

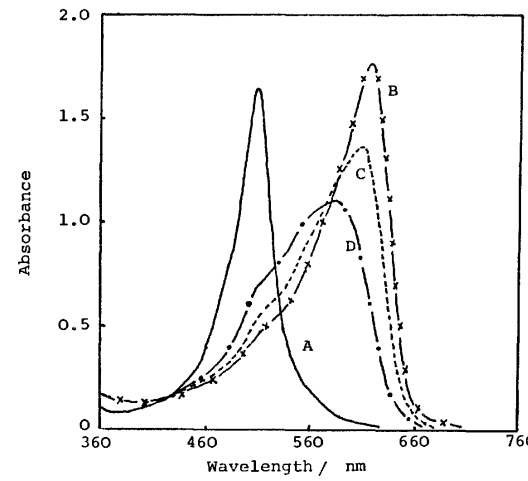

Fig. 1. Absorption spectra of Qn.Ph. and Qn.Ph.–palladium(II) solutions in the presence of IU at pH 9.8.
Pd(II): 1.5×10^{-5} M; Qn.Ph.: 2.25×10^{-5} M; HTAC: 2.0×10^{-3} M; Reference: water; curve A: Qn.Ph. solution; curves B, C, and D: Qn.Ph.–Pd(II) solutions(IU concentration: curve B, 0; curve C, 6.0×10^{-6} M; curve D, 1.8×10^{-5} M).

† Application of Xanthene Derivatives for Analytical Chemistry. Part XXIX. Part XXVIII: Y. Fujita, I. Mori, and S. Kitano, *Chem. Pharm. Bull.*, **31**, 1289 (1983).

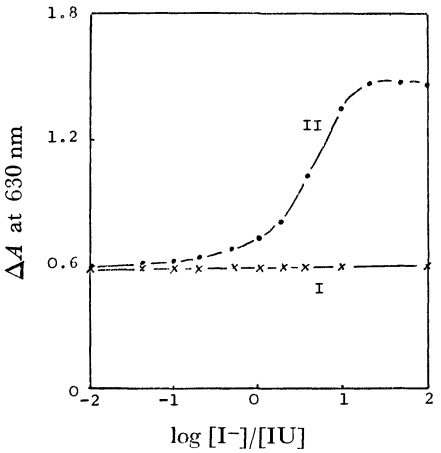

Fig. 2. Effect on ΔA with sequence of addition of iodide ion.
IU: 5.0×10^{-6} M; Pd(II): 2.5×10^{-5} M; Qn.Ph.: 3.75×10^{-5} M; HTAC: 2.0×10^{-3} M; pH: 9.8; Reference: water; sequence of addition of reagents, curve I, Pd(II)→HTAC→Buffer→Qn.Ph.→IU, iodide ion; curve II, IU, iodide ion→Pd(II)→HTAC→Buffer →Qn.Ph.

being kept constant. The molar ratio of palladium(II) 2:Qn.Ph. 3 was most effective. Further, the molar ratio of palladium(II) to Qn.Ph. was found to be 2:3 by using the molar ratio method. Accordingly, all further work was carried out with 2.5×10^{-5} M palladium(II) and 3.75×10^{-5} M Qn.Ph. solutions in the final 10 ml.

Sequence of Addition. The identical ΔA value was obtained in the determination of IU even when the order of the addition of the reagents was varied. However, the influence of iodide ions could be completely eliminated when a solution containing iodide ions was added to the solution obtained after the color reaction between palladium(II) and Qn.Ph. The effect on ΔA of the sequence of addition is shown in Fig. 2.

Stability and Calibration Curve. The maximum ΔA value at 630 nm was given by heating at 60 °C for 15 min. The ΔA value was constant for at least 90 min. The calibration curve for the determination of IU was prepared according to the standard procedure. It obeyed Beer's law over the range of 0—15 μg of IU in the final 10 ml. The Sandell sensitivity was estimated to be 0.0020 μg/cm² IU at 630 nm, and the effective "desorptivity" was 1.15×10^5 l mol^{-1} cm^{-1}. When 5 solutions containing 11.3 μg/10 ml were determined by the standard procedure, the coefficient of variation was 0.95%.

Effects of Foreign Substances. The interfering effects of various substances were examined under the standard conditions. The results are summarized in Table 1. Various metal ions, such as iron(III), copper(II), zinc(II), and cobalt(II) reacted with Qn.Ph. to form a colored complex, thus interfering with the determination of IU. Large amounts of chloride, nitrate, sulfate, organic acids ions, *etc.* did not interfere, while small amounts of cyanide, thiosulfate and thiocyanate ions did so. Uracil, thiourea, purine, orotic acid, amino acids, *etc.* in small amounts affected the determination of IU. Large amounts of salicylic acid, glucose, phenol, urea, *etc.* did not, however, interfere. Uracil present up to 4 times the amount of IU could be permitted by determining the IU according to the standard addition method. As has been described above, iodide ions did not interfere, even in a 500-fold excess. Therefore, the present method could be used to determine IU in the presence of large amounts of iodide ions without a preliminary ashing step to release the iodide ions.

Table 1. Effects of foreign substances

Foreign substances	Added as	Added (μg/10 ml)	ΔA at 630 nm
—	—	—	0.576
Cu(II)	Nitrate	1.6	0.432
Zn(II)	Chloride	3.2	0.408
Fe(III)	Sulfate	2.8	0.498
S^{2-}	Sodium	1.6	0.660
SCN^-	Potassium	5.8	0.618
2-Thiouracil	—	0.6	0.618
Thiourea	—	0.4	0.640
Uracil	—	8.4	0.652
Barbital	—	18.4	0.630
Glycine	—	7.5	0.655

IU taken: 11.3 μg/10 ml; Pd(II): 2.5×10^{-5} M; Qn.Ph.: 3.75×10^{-5} M; HTAC: 2.0×10^{-3} M; pH: 9.8; Reference: water.

References

1) "Muki Oyo Hishoku Bunseki(Inorganic Applied Colorimetric Analysis)," Kyoritsu Shuppan, Tokyo (1973), Vol. 3, p. 50.
2) "Commentary of the Japanese Pharmacopoeia," Tenth ed, Hirokawa Publishing Co., Tokyo (1981).
3) I. Mori, Y. Fujita, and K. Sakaguchi, *Chem. Pharm. Bull.*, **30**, 2599 (1982).
4) I. Mori, Y. Fujita, S. Kitano, and K. Sakaguchi, *Bunseki Kagaku*, **31**, E 305 (1982).
5) I. Mori, Y. Fujita, and S. Kitano, *Chem. Pharm. Bull.*, **31**, 1289 (1983).
6) D. D. Perin and B. Dempsey, "Buffer for pH and Metal Ion Control," trans. by K. Tsuji Kodansha, Tokyo (1981).

Macroscopic and Microscopic Behavior of the Eluent in Liquid Chromatography

Ken-ichi FUKUHARA,* Asao NAKAMURA, and Masamichi TSUBOI†

Central Research Laboratories, Ajinomoto Co., Inc. Suzuki-cho, Kawasaki-ku, Kawasaki 210

†*Faculty of Pharmaceutical Sciences, The University of Tokyo, Hongo, Bunkyo-ku, Tokyo 113*

(Received December 18, 1982)

Synopsis. By injecting an isotope pulse into the eluent of liquid chromatography, it has been shown that the eluent flow does not go into the stationary phase, while each of the molecules in the eluent is replaced by an equivalent molecule originally contained in the stationary phase. Meanwhile, an appropriate method for determining the t_0 value is given.

Liquid chromatography is useful, not only for the preparation and/or analysis of chemical substances, but also for deriving some thermodynamic functions of intermolecular interactions. For this purpose, it is convenient to regard a chromatogram as free-energy spectrum and to assign to each molecule in question a proper, standard free energy on the basis of the observed chromatogram.[1,2] It is essential in this procedure to determine the t_0 value, which is the time required for the eluent to go through the column, in other words, t_0 is the retention time of a hypothetical molecule which is kept always in the mobile phase and which never goes into the stationary phase.[2] In the present note, our examination of how to determine t_0 will be briefly discussed.

An example of our present experimental results is shown in Fig. 1. Here is a series of chromatograms in which the eluent is always CH_3CN (50%)+H_2O (50%). In every case, a small amount of a sample solvent was injected at zero time. Whenever its composition was different from that of the eluent (chromatograms b,c,d,e,f, and j), a peak (or a negative peak) appeared 6.7 min after the injection. The peak height depends upon the composition of the sample solvent, but its position (6.7 min) is independent of it. This position is considered to correspond to the total volume of the mobile phase of the particular column now in question. In other words, 6.7 min must be the time required for the sample solvent (having a different index of refraction from that of the eluent) to go through the mobile phase of the column. This is taken as the above-defined t_0 for this particular column system.

Next, in order to confirm the above determination of the t_0 value, the microscopic behavior of the eluent in this system is examined. Whenever an isotopic acetonitrile CD_3CN is involved in a sample solvent, another negative peak appears at a definite position: t_c=7.9 min after the injection, *i.e.*, at a somewhat retarded time (see chromatograms c,g,i, and j). This means that CD_3CN in the present column system, with the CH_3CN (50%)+H_2O (50%) eluent, has a relative retention time (t_c-t_0) of 7.9—6.7=1.2 min. Figure 1 indicates also that, after the injection of isotopic water D_2O, a negative peak appears at t_w=10.5 min (chromatograms e,h,i,j) and that the relative retention time (t_w-t_0) is 10.5—6.7=3.8 min.

In order to determine whether the relative retention times (1.2 min or 3.8 min) come from the microscopic behavior of the individual solvent molecule (acetonitrile or water) in the eluent or from simple isotope effects (CH_3CN–CD_3CN or H_2O–D_2O), radioisotopic water T_2O was examined in this system. When a small amount of T_2O is added to the D_2O injected, a radioactivity peak of T_2O is found to be superimposed on the refractive index peak of D_2O (Fig. 1,f). We could not find any difference among T_2O, D_2O, THO, TDO, and HDO in their retention time t_w, nor could we detect any isotopic effect.

Therefore, it is evident that H_2O has the same retention time t_w as those mentioned above. It is also evident that CH_3CN has the same retention time t_c as that of CD_3CN.

It can now be stated that the molecules constituting the solvent are retained to a proper extent in the stationary phase, while the solvent sample as a mac-

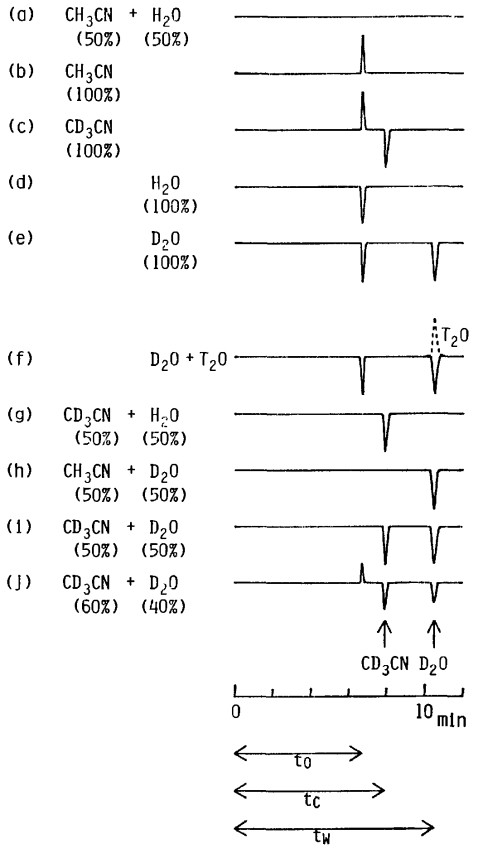

Fig. 1. A series of chromatograms for the determination of t_0, t_c, and t_w values.
Column, Hitachi #3013-N (8ϕ×500 mm); eluent, CH_3CN: H_2O: 1 M phosphate buffer (pH 7)=50 : 49 : 1 (v/v); flow rate, 2 ml/min; temperature, 50 °C; detection, refractive index.

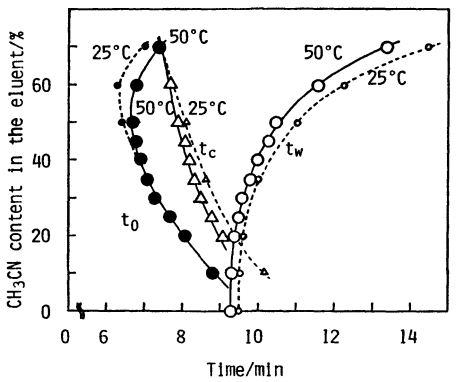

Fig. 2. The values of t_0, t_c, and t_w in a chromatograph system (Hitachi #3013-N with CH_3CN+H_2O as eluent), as functions of the CH_3CN content in the eluent.
Here t_0 is the time required for the solvent to go through the mobile phase (—●—, at 50 °C; --●--, at 25 °C); t_c is the time required for the CD_3CN molecule to come out from the column after its injection (—△—, at 50 °C; --△--, at 25 °C); and t_w is the time required for the D_2O (or HOD or T_2O) molecule to come out from the column after its injection (—○—, at 50 °C; --○--, at 25 °C).

roscopic mass goes through the mobile phase without any retention. In other words, the sample solvent does go down through the mobile phase without changing its composition, but a certain amount of microscopic exchange of the solvent molecules is considered to take place between the mobile phase and the stationary phase. Without an isotopic injection, we cannot detect such a retention of the solvent or eluent molecule (Fig. 1,a), but it is evident that a similar microscopic molecular exchange takes place in every eluent used.

As for how to determine t_0, we have now found an answer: we should inject a solvent pulse with a slightly different composition from that of the eluent. Quite often one does this without intention, for the solvent of a sample solution is actually often slightly different in its composition from that of the eluent, and this causes a small peak in chromatogram which corresponds to t_0. One might think that an isotopic solvent should directly indicate t_0, but actually this does not work, as has been shown here.

We have made similar series of experiments, with different eluents, to see how the t_0, t_c, and t_w values depend upon the eluent composition. These results are given in Fig. 2. As may be seen in the figure, the effective volume of the mobile phase gives a minimum at about 50% of CH_3CN. The retention time (t_w) of D_2O increases, while that (t_c) of CD_3CN decreases, with the increase in the CH_3CN content in the eluent. There is a small temperature effect for each of the t_0, t_c, and t_w values.

References

1) K. Fukuhara, A. Nakamura, and M. Tsuboi, *Chem. Pharm. Bull.*, **30**, 1121 (1982).
2) M. Tsuboi, *Gendai Kagaku (Chemistry Today)*, April **1981**, 46—53.

Nitration of Aromatic Heterocycles with Palladium(II) Acetate and Sodium Nitrite

Toshio ITAHARA,* Reiko EBIHARA, and Kazukuni KAWASAKI
Institute of Chemistry, College of Liberal Arts, Kagoshima University, Kagoshima 890
(Received August 9, 1982)

Synopsis. Treatments of 1,3-dimethyluracil, 1-methyl-2-pyridone, and thiophene with palladium(II) acetate and sodium nitrite gave the corresponding nitro-substituted products.

The treatment of benzene with palladium(II) salts and sodium nitrite in acetic acid was reported to give nitrobenzene.[1] We have studied the oxidation of aromatic heterocycles with palladium(II) acetate.[2] In the course of the studies, we have found that the treatments of 1,3-dimethyluracil (**1a**), 1-methyl-2-pyridone (**2a**), and thiophene (**4a**) with palladium acetate and sodium nitrite gave the corresponding nitro-substituted products in good yields.

The treatment of **1a** with palladium acetate and sodium nitrite in acetic acid at the reflux temperature gave 1,3-dimethyl-5-nitrouracil (**1b**) in a good yield. In the absence of palladium acetate, the treatment of **1a** with sodium nitrite gave only a small amount of **1b**, although it was reported that the reaction of **1a** with nitronium tetrafluoroborate gave **1b**.[3] These results are summarized in Table 1. Previously it was reported that the oxidation of **1a** with palladium acetate in acetonitrile gave a mixture of dimeric compounds.[4] However, under the present conditions no dimeric compounds were obtained. The attempted nitration of **1a** with other metal acetates and sodium nitrite were unsuccessful, as listed in Table 1.

The treatments of 1-methyl-2-pyridone (**2a**) and of thiophene (**4a**) with palladium acetate and sodium nitrite also resulted in the nitration, although it is known that the treatment of **2a** with nitric acid gives 1-methyl-3-nitro-2-pyridone, 1-methyl-5-nitro-2-pyridone (**2b**), and 3,5-dinitro-1-methyl-2-pyridone (**3b**),[5] and a similar treatment of **4a** gives 2-nitrothiophene, 2,5-dinitrothiophene, and 2,4-dinitrothiophene (**4b**).[6] When **2a** was treated with palladium acetate and sodium nitrite, **3b** was obtained in the yield of 49% together with a small amount of **2b**. The treatment of **4a** under similar conditions also gave **4b**, but no mononitrothiophenes were obtained. It was previously reported that the nitration of 3-nitrothiophene gave

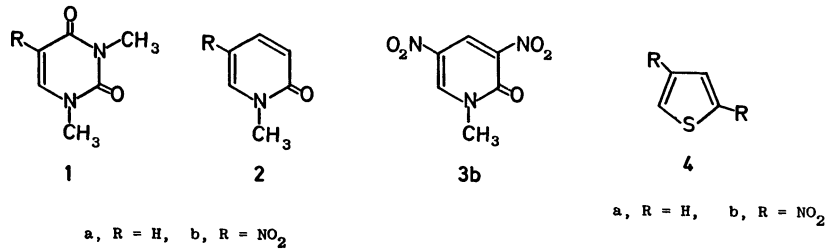

Fig. 1.

TABLE 1. NITRATION OF **1a**, **2a**, AND **4a** WITH METAL ACETATES AND SODIUM NITRITE[a]

Substrate	Metal acetate (mmol)	$NaNO_2$ (mmol)	Reaction time/h	Conversion %	Products Isolated (yield/%)
1a (1 mmol)	$Pd(OAc)_2$ (1)	2	7	63	**1b** (81)[b]
1a (1 mmol)	$Pd(OAc)_2$ (1)	2	18	82	**1b** (74)[b]
1a (1 mmol)		2	7	15	**1b** (77)[b]
1a (1 mmol)	$Cu(OAc)_2$ (1)	2	7	24	**1b** (50)[b]
1a (1 mmol)	AgOAc (1)	2	7	20	**1b** (55)[b]
1a (1 mmol)	$Ni(OAc)_2 4H_2O$ (1)	2	7	17	**1b** (70)[b]
1a (1 mmol)	$Co(OAc)_2 4H_2O$ (1)	2	7	7	**1b** (trace)
1a (1 mmol)	$Mn(OAc)_2 4H_2O$ (1)	2	7	8	**1b** (trace)
2a (1 mmol)	$Pd(OAc)_2$ (1)	3	7	55	**2b** (7)[b]; **3b**(49)[b]
2a (1 mmol)		3	7	14	**2b** (10)[b]; **3b**(50)[b]
4a (2 mmol)	$Pd(OAc)_2$ (1)	3	7		**4b** (22)[c-e]
4a (20 ml)	$Pd(OAc)_2$ (1)	10	10		**4b** (66)[c,d,f]
4a (20 ml)		20	10		**4b** (trace)[d,f]

a) The reactions were carried out in acetic acid (30 ml) at the reflux temperature under nitrogen unless otherwise noted. b) Yields based on the substrate **1a** or **2a** consumed. c) Yields (mol/mol%) based on $Pd(OAc)_2$ used. d) The amount of **4a** recovered was not determined. e) The reaction was carried out at 80 °C. f) The reactions were carried out in AcOH (40 ml) at 80 °C in air.

only **4b**, while 2-nitrothiophene gave a mixture of 2,5-dinitrothiophene and **4b**,[6] suggesting that the formation of **4b** from **4a** proceeded *via* 3-nitrothiophene. The attempted nitration reactions of pyrroles such as 1-methyl-, 1-acetyl-, and 1-benzoylpyrroles, 1-acetylindole, and furan with palladium acetate and sodium nitrite in acetic acid were unsuccessful.

Experimental

*1,3-Dimethyl-5-nitrouracil (**1b**).* A solution of 1,3-dimethyluracil **1a** (1 mmol), $Pd(OAc)_2$ (1 mmol), and $NaNO_2$ (2 mmol) in acetic acid (30 ml) was heated at the reflux temperature under nitrogen for 18 h. The reaction mixture was evaporated to give a brown residue which was then chromatographed on a silica-gel plate with ethyl acetate as the developer to give **1a** (0.18 mmol), and **1b** (0.61 mmol), the latter being identical with the sample prepared by the method of Huang and Torrence.[3]

*1-Methyl-5-nitro-2-pyridone (**2b**) and 1-Methyl-3,5-dinitro-2-pyridone (**3b**).* A solution of 1-methyl-2-pyridone (**2a**) (1 mmol), $Pd(OAc)_2$ (1 mmol), and $NaNO_2$ (3 mmol) in acetic acid (30 ml) was heated at the reflux temperature under nitrogen for 7 h. The reaction mixture was evaporated and chromatographed on a silica-gel plate with ethyl acetate as the developer to give **2a** (0.45 mmol), **2b** (0.04 mmol; mp 173—174 °C, lit,[7] 173—174 °C), and **3b** (0.27 mmol) which was identical with the sample prepared by the method of Matsumura *et al.*[5] The structure of **2b** was further confirmed by comparing its ^{1}H-NMR spectrum with that of the compound reported by Mohrle and Weber.[7]

*2,4-Dinitrothiophene (**4b**).* A solution of $Pd(OAc)_2$ (1 mmol) and $NaNO_2$ (10 mmol) in a mixture of thiophene **4a** (20 ml) and acetic acid (40 ml) was heated at 80 °C in air for 10 h. The reaction mixture was evaporated and chromatographed on a silica-gel plate with benzene as the developer to give **4b** (0.66 mmol); mp 54—56 °C (lit,[6] 56 °C); IR (Nujol) 1540, 1510, 1340 cm^{-1}; NMR ($CDCl_3$) δ=8.43—8.66(m); Mass: *m/e* (relative intensity) 174 (M^+, 100), 144(12), 82(49), 81(36), 70(22), 69(44).

The authors wish to thank Professor Tsunao Hase and Professor Tsutomu Sakakibara of Kagoshima University for their encouragement throughout the study.

References

1) T. Tisue and W. J. Downs, *J. Chem. Soc., Chem. Commun.*, **1969**, 410; P. M. Henry, *J. Org. Chem.*, **36**, 1886 (1971); R. O. C. Norman, W. J. E. Parr, and C. B. Thomas, *J. Chem. Soc., Perkin Trans. 1*, **1974**, 369.

2) T. Itahara, *Chem. Lett.*, **1982**, 1151.

3) G. Huang and P. F. Torrence, *J. Org. Chem.*, **42**, 3821 (1977).

4) I. Arai, R. Hanna, and G. D. Daves, Jr., *J. Am. Chem. Soc.*, **103**, 7684 (1981).

5) N. P. Shusherina and T. I. Likhomanova, *Khim. Geterotsikl. Soedin*, **1973**, 1671; *cf. Chem. Abstr.*, **80**, 82588m (1973); E. Matsumura, M. Ariga, and Y. Tohda, *Bull. Chem. Soc. Jpn.*, **52**, 2413 (1979).

6) A. H. Blatt, S. B. Rosenberg, and L. W. Kresch, *J. Org. Chem.*, **22**, 1693 (1957).

7) H. Mohrle and H. Weber, *Chem. Ber.*, **104**, 1478 (1971).

Aromatic Nucleophilic Substitution. XVII.[1] Formation and Decomposition of Anionic σ Complexes in Reactions of 2-Acetylaminoethyl 2,6-Dinitrophenyl Ether and *N*-Acetyl-*N*-(2-hydroxyethyl)-2,6-dinitroaniline with Potassium *t*-Butoxide

Shizen SEKIGUCHI,* Ohtomo HOSHINO, Motohiko HIRAI, Keiji OKADA, and Noboru TOMOTO
Department of Synthetic Chemistry, Gunma Uuiversity, Kiryu, Gunma 376

(Received September 1, 1982)

Synopsis. Reactions of 2-acetylaminoethyl 2,6-dinitrophenyl ether and *N*-acetyl-*N*-(2-hydroxyethyl)-2,6-dinitroaniline with *t*-butyl alcoholic $KOC(CH_3)_3$ in DMSO were followed by UV-VIS and NMR spectroscopies. In both reactions the same spiro anionic σ complex was formed.

Previously we reported the kinetics of the base-catalyzed Smiles rearrangement of 2-acetylaminoethyl 2-X-4-nitrophenyl ether (X: NO_2, Br, and CN) giving *N*-(2-acetoxyethyl)-2-X-4-nitroaniline in aqueous DMSO.[2] We have been successful in preparing 2-acetylaminoethyl 2,6-dinitrophenyl ether (**1**) and *N*-acetyl-*N*-(2-hydroxyethyl)-2,6-dinitroaniline (**8**).

This paper reports the formation and decomposition of the same anionic σ complexes in the reactions of **1** and **8** with $KOC(CH_3)_3$ in DMSO–*t*-BuOH mixtures by UV-VIS and NMR spectroscopies.

Results and Discussion

*Absorption Spectra. Reaction of 2-Acetylaminoethyl 2,6-Dinitrophenyl Ether (**1**) with $KOC(CH_3)_3$*: Upon addition of *t*-butyl alcoholic $KOC(CH_3)_3$ [1.10×10^{-2} M (1 M=1 mol dm^{-3})] to **1** (2.68×10^{-5} M) in DMSO, the solution was colored purple instantly [λ_{max} 340 (m) and 585 nm (s)], which could be attributed to the formation of **2** (Scheme 1),[3] and then the color slowly faded away. The absorption spectrum after 4 h [λ_{max} 368 nm (m)] could be attributed to the anionic species **5** (Scheme 2).[4] These results show that the respective O→N and N→O migrations of 2,6-dinitrophenyl and acetyl groups take place concurrently, and would be compatible with Scheme 1.

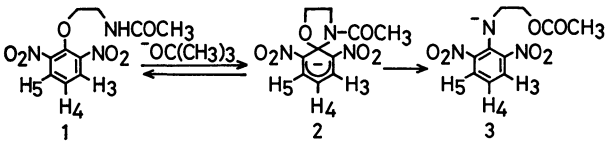

Scheme 1.

Reaction of N-*(2-Acetoxyethyl)-2,6-dinitroaniline (**4**) with $KOC(CH_3)_3$*: In order to elucidate further the final species in the reaction of **1** with $KOC(CH_3)_3$, the reaction of **4** with $KOC(CH_3)_3$ was carried out. Upon addition of *t*-butyl alcoholic $KOC(CH_3)_3$ (1.10×10^{-2} M) to **4** (4.71×10^{-5} M) in DMSO, the solution was colored purple instantly [λ_{max} 320 (m), 368 (m), and 585 nm (w)], and then the color slowly faded away. From a consideration of the results of Crampton *et al.*[3,4] Pollitt and Saunders,[3] and ours[2] together with the NMR spectral evidence, these bands could be attributed to a mixture of **3** (585 nm), **5** (368 nm), and **6** (320 nm). After 2 h the absorption peak at 368 nm (**5**) increased at the expense of that at 320 nm (**6**). Therefore Scheme 2 would be compatible with the results.

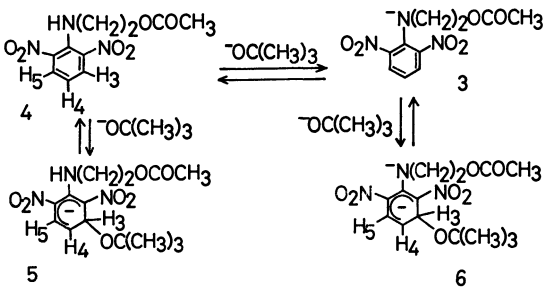

Scheme 2.

Reaction of N-*Acetyl*-N-*(2-hydroxyethyl)-2,6-dinitroaniline (**8**) with $KOC(CH_3)_3$*: In order to elucidate the processes described above in detail the reaction of **8** with $KOC(CH_3)_3$ was carried out.

Upon addition of *t*-butyl alcoholic $KOC(CH_3)_3$, almost similar absorption spectra to that obtained at the initial stage in the reaction of **1** with $KOC(CH_3)_3$ appeared [λ_{max} 340 (m) and 585 nm (s)] indicating the presence of the complex **2**. In course of time the absorption peak at 368 nm increased at the expense of the peak at 585 nm, indicating that after the complex **2** had been formed, the anionic species **5** was produced *via* **3** (Scheme 2).

*NMR Spectra. Reaction of 2-Acetylaminoethyl 2,6-Dinitrophenyl Ether (**1**) with $KOC(CH_3)_3$*: Upon addition of 1 equiv. of *t*-butyl alcoholic $KOC(CH_3)_3$ amide proton signal (δ=8.00) of **1** disappeared instantly, and $H_{3,5}$ and H_4 signals shifted upfield respectively (δ=8.33→7.77; 7.57→5.15) (Fig. 1). Such shifts are quite the same as the results observed in the reaction of 2-acetylaminoethyl 2,4-dinitrophenyl ether with $NaOCH_3$ in DMSO,[5] indicating the proton abstraction by $^-OC(CH_3)_3$ followed by the intramolecular nucleophilic attack of amide ion on C-1 position (Scheme 3).

Reaction of N-*(2-Acetoxyethyl)-2,6-dinitroaniline (**4**) with $KOC(CH_3)_3$*: Upon addition of 1 equiv. of *t*-butyl alcoholic $KOC(CH_3)_3$ amide proton signal (δ=8.10) of **4** disappeared instantly, and $H_{3,5}$ and H_4 signals shifted upfield instantly (δ=8.27→8.00; 6.93→6.43), which are due to the formation of **3** (Fig. 2b). After 2 h, collapsed doublets appeared at δ=*ca.* 7.87 and 5.30, attributed to H_5 and H_3 protons of **6**, respectively (Fig. 2c). Further, $H_{3,5}$ doublet (δ=8.27) of **4** reappeared, indicating the reversion of **6**⇄**3**⇄**4** (Scheme 2). This is also strongly evidenced by the presence of amino proton signal at δ=*ca.* 8.10, although it partly overlapped $H_{3,5}$ doublet (δ=8.27) of **4** (Fig. 2c). Collapsed triplet at δ=6.93 could be attributed to H_4 proton of **4**. The weak signals at δ=*ca.* 5.45 would be a part of the doublet due to H_3 proton of **5**. H_3 doublet (δ=*ca.* 5.20) of **5** partly overlapped collapsed H_3 doublet (δ=*ca.* 5.40) of **6**.

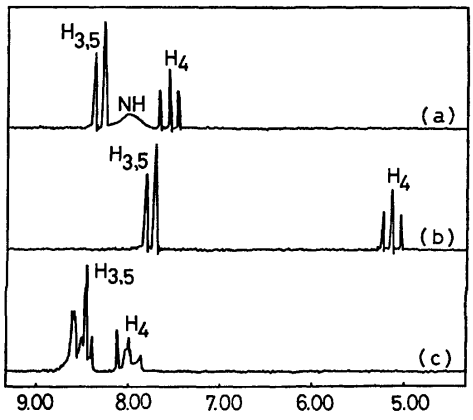

Fig. 1. NMR spectral change relevant to the reactions of 2-acetylaminoethyl 2,6-dinitrophenyl ether (**1**) and *N*-acetyl-*N*-(2-hydroxyethyl)-2,6-dinitroaniline (**8**) with $KOC(CH_3)_3$ in DMSO. a: **1**, b: just after addition of 1 equiv. of *t*-butyl alcoholic $KOC(CH_3)_3$, c: **8**.

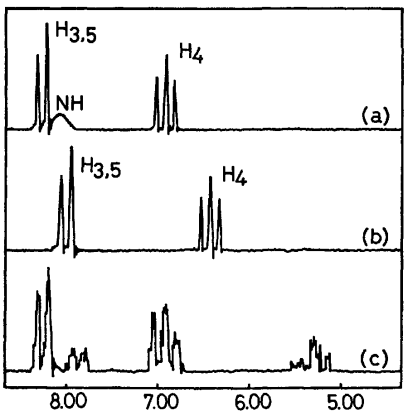

Fig. 2. NMR spectral change relevant to the reaction of *N*-(2-acetoxyethyl)-2,6-dinitroaniline (**4**) with $KOC(CH_3)_3$ in DMSO. a: **4**, b: just after addition of 1 equiv. of *t*-butyl alcoholic $KOC(CH_3)_3$, c: 6 h after addition.

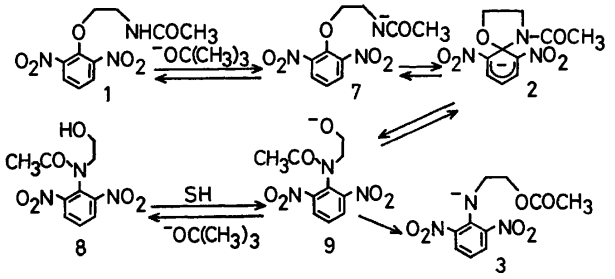

Scheme 3.

These results show that just after addition of $KOC(CH_3)_3$ **4** is transformed to **3**, which partly reverts to **4**, producing **5**, and partly changes into **6** (Scheme 2).

Reaction of N-*Acetyl*-N-*2-(hydroxyethyl)-2,6-dinitroaniline (8) with* $KOC(CH_3)_3$: Upon addition of 1 equiv. of *t*-butyl alcoholic $KOC(CH_3)_3$ to **8** in DMSO (Fig. 1c), the same signal pattern as Fig. 1b appeared, indicating the formation of the complex **2**. Complicated $H_{3,5}$ and H_4 signals (Fig. 1c) are considered to be due to the coexistence of (*E*) and (*Z*) isomers of **8**.

In conclusion, it is confirmed that **1** undergoes the base-catalyzed Smiles rearrangement, producing **4** *via* the spiro anionic σ complex **2**, producing **4** *via* **9** and **3**, and that **8** is base-catalyzed to at first produce **2**, which reverts to **9**, producing **4** *via* **3**.[2]

Experimental

Mps were uncorrected. Compounds **1**, **4**, and **8** were identified by NMR, IR, and MS. Their results of the elementary analysis were in good agreement with those calculated ones within the experimental errors.

2-Acetylaminoethyl 2,6-Dinitrophenyl Ether (1). According to the method described in the literature[6] was prepared 2,6-dinitroaniline (DNA) from chlorobenzene (yield 20%), and 2,6-dinitrochlorobenzene (DNC) prepared from DNA (yield 69%).

After a nitrobenzene (10 g) solution of KF (6 g, 0.103 mol) and DNC (14 g, 0.0069 mol) was stirred at 190 °C for 5 h and, then, the nitrobenzene distilled off under reduced pressure, the residue was further distilled at 145—150 °C/6 mmHg to produce 8.4 g of 2,6-dinitrofluorobenzene (DNF) (yield 61%), mp 60—62 °C (lit, 60—63 °C).[10]

From DNF and 2-acetylaminoethanol was prepared **1** according to the method described previously.[5] Recrystallization from ligroin gave pure **1** crystals (yield 13%); mp 92—93 °C; UV_{max} (DMSO) 305 nm (ε=1970).

N-(2-Acetoxyethyl)-2,6-dinitroaniline (4). A 30 ml DMSO solution of 2.4 g (0.0039 mol) of 2-aminoethanol was added dropwise to a 60 ml DMSO stirred solution of 4 g (0.020 mol) of DNC for 3 h at room temperature, and then the mixture poured into an ice-water. The precipitate formed was filtered and recrystallization from ethanol gave 2 g of pure *N*-(2-hydroxyethyl)-2,6-dinitroaniline (HDNA) (yield 44.5%). After a 100 ml dioxane solution of 2 g (0.0088 mol) of HDNA and 1.4 g (0.018 mol) of acetyl chloride was stirred at 80 °C for 1 h, the mixture was poured into an ice-water and extracted with benzene. The benzene layer was dried over anhydrous Na_2SO_4 overnight, filtered and evaporated. The residue was chromatographed over silica gel (benzene) and recrystallized from methanol to give 1.7 g of **4** (yield 75.5%); mp 55—56 °C; UV_{max} (DMSO): 428 nm ($\varepsilon=6.05\times10^3$).

N-Acetyl-N-(2-hydroxyethyl)-2,6-dinitroaniline (8). A 50 ml dioxane solution of 5.5 g (0.053 mol) of 2-acetylaminoethanol, and 1.0 g (0.027 g-atom) of potassium was refluxed until potassium was dissolved. To this solution was rapidly added a 50 ml dioxane solution of 5.0 g (0.027 mol) of DNF, and the mixture swirled for *ca.* 3 min (short reaction time should be necessary). Then, the mixture was poured into an ice-water, neutralized with dilute HCl (10%), and extracted with chloroform. The chloroform layer was dried over anhydrous Na_2SO_4 overnight, filtered, evaporated, and chromatographed over silica gel (benzene:acetone 5:1 v/v), and recrystallized from ligroin to give 0.09 g (yield 1.3%) of **1** and 0.32 g (yield 4.4%) of **8**; mp 118—119 °C; UV_{max} (DMSO) 320 nm ($\varepsilon=4.13\times10^3$).

References

1) Part XVI: S. Sekiguchi, N. Tone, T. Takei, and N. Tomoto, *Bull. Chem. Soc. Jpn.*, **56**, 753 (1983).
2) K. Okada and S. Sekiguchi, *J. Org. Chem.*, **43**, 441 (1978).
3) M. Strauss, *Chem. Rev.*, **70**, 667 (1970).
4) M. R. Crampton and M. J. Willison, *J. Chem. Soc., Perkin Trans. 2*, **1974**, 1681.
5) K. Okada, K. Matsui, and S. Sekiguchi, *Bull. Chem. Soc. Jpn.*, **51**, 2601 (1978).
6) *Org. Synth.*, Coll. Vol. IV, 160, 364 (1963).
7) R. E. Parker and T. O. Read, *J. Chem. Soc.*, **1962**, 3149.

Reinvestigation of the Synthetic Reaction of Dimethylamino-1,3-indandione

Masaaki Ito*, Kazuo Abe, Teruji Sasaki, and Kenzo Misono†

Chemistry Laboratory, Department of General Education, Higashi-Nippon-Gakuen University, Onbetsu, Hokkaido 088-01

†*Hokkaido-Togyo Co., Ltd., 1, 2-Kandajinbocho, Chiyoda-ku, Tokyo 101*

(Received October 9, 1982)

Synopsis. One step preparation of dimethylamino-1,3-indandione (**1**) from salicylaldehyde with glycine betaine was reinvestigated. Reaction conditions to give the best yield of **1**, characterization of a minor product (2-acetoxybenzylidene diacetate), and reaction pathway were described.

The reaction of salicylaldehyde with (carboxymethyl)trimethylammonium hydroxide inner salt (glycine betaine) in acetic anhydride provides a convenient procedure for the preparation of dimethylamino-1,3-indandione (**1**).[1,2]

The pathway of the reaction is proposed as depicted in Scheme 1. The reaction is based on an acetylation of the hydroxyl group of salicylaldehyde, a nucleophilic attack of α-carboxy(dimethylamino)methanide ion which is formed from the glycine betaine, and an acetylation of the benzene ring accompanied by elimination of the acetoxyl group.

The reaction mixture containing salicylaldehyde and the glycine betaine in acetic anhydride was refluxed at 150 °C for 7 h. After removal of the volatile matters, the resulting residue was recrystallized from benzene to give pale yellow crystals of **1**. The optimum reaction conditions for this reaction were investigated on several ratios of acetic anhydride and the glycine betaine *versus* the salicylaldehyde, and on the reaction time as shown in Tables 1 and 2. To obtain optimum

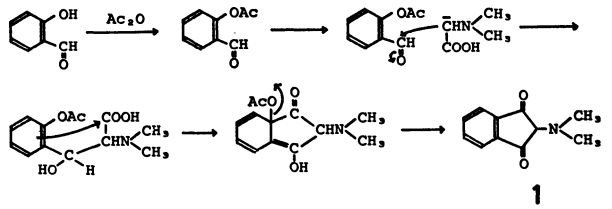

Scheme 1.

Table 1. Yields of the 1,3-indandione **1** and by-product **2**[a]

Run	Molar ratio of glycine betaine : salicylaldehyde : Ac_2O	Yield[b]/% **1**	Yield[b]/% **2**
1	1 : 1 : 1	42.6	none
2	1 : 1 : 2	53.5	10.2
3	1 : 1 : 5	52.5	21.0
4	1.5 : 1 : 2	69.3	5.4
5	2 : 1 : 2	78.7	2.4
6	2.5 : 1 : 2	80.1	1.6
7	3 : 1 : 2	77.8	trace
8	1 : 2 : 2	61.1	trace

a) The reaction was carried out at 150 °C for 7 h. b) Yields are based on salicylaldehyde used. Determined by GLC.

Table 2. Effect on reaction time for yields

Run	Reaction time/min	Yield/% **1**	Yield/% **2**
9	15	55.1	4.9
10	30	61.5	3.6
11	60	68.4	4.5
12	180	72.6	3.6

Reaction conditions: Molar ratio of the glycine betaine : salicylaldehyde : acetic anhydride = 2 : 1 : 2, temp: 150 °C. Yields are based on salicylaldehyde used. Determined by GLC.

yield of **1**, the reaction must be conducted at 150 °C for 7 h using 2—2.5 mol of the glycine betaine and 2 mol of acetic anhydride *versus* one mol of salicylaldehyde.

It is found that this reaction is accompanied by formation of 2-acetoxybenzylidene diacetate (**2**) as a minor product. By-product **2** will be formed by acetalyzing and acetylation of salicylaldehyde with acetic anhydride. The formation of **2** increases in yield when acetic anhydride is used in large quantities. The structure of **2** was confirmed by the analytical and spectral data, and by the fact that compound **2** is hydrolyzed to salicylaldehyde.

The similar reaction using hydroxybenzoic acids, methyl salicylate in place of salicylaldehyde did not give the product **1**, and in the case of methyl salicylate it gave only methyl 2-acetoxybenzoate.

Experimental

All melting points were uncorrected. The IR, ^{1}H NMR, UV, and Mass spectra were recorded on a Shimadzu IR-400, a JEOL JNM-PMX-60 using TMS as internal standard, a Shimadzu MPS-5000, and a Shimadzu LKB-9000 spectrometer, respectively. The analytical GLC were performed on a Shimadzu GC-4B apparatus equipped with a data processor, Chromatopac C-R1B, and with a 1.5 m glass column packed 10% Silicone OV-17 at 210 °C. Acetic anhydride was purified by refluxing with CaC_2 and by distillation before use.

*Preparation of Dimethylamino-1,3-indandione (**1**).* A mixture of the glycine betaine (29.3 g, 0.25 mol) and salicylaldehyde (12.2 g, 0.1 mol) in acetic anhydride (20.4 g, 0.2 mol) was refluxed at 150 °C for 7 h. After sufficient water was added to decompose the excess acetic anhydride, the mixture was extracted with benzene, washed with water, dried over sodium sulfate, and evaporated to leave a crude product 15.2 g of the 1,3-indandione **1** in 80.1% yield (based on salicylaldehyde, obtained on GLC datum). An analytical sample was recrystallized from benzene, a pale yellow crystal: mp 85—86 °C; UV_{max} (EtOH) 245 (ε 8100) and 340 nm (ε 14400); ^{1}H NMR ($CDCl_3$): δ=2.98 (6H, s), 6.69 (1H,

s), 7.27 (4H, s); IR (KBr): 1705 (C=O) cm^{-1}; MS (*m/e*) 189 (M^+); Found: C, 69.56; H, 5.77; N, 7.40%. Calcd for $C_{11}H_{11}NO_2$: C, 69.82; H, 5.86; N, 7.40%.

The reactions shown in Tables 1 and 2 were carried out under the full range of the reaction conditions noted above.

*2-Acetoxybenzylidene Diacetate (**2**). Isolation of **2***: A mixture of the glycine betaine (5.9 g, 0.05 mol), salicylaldehyde (6.1 g, 0.05 mol) in acetic anhydride (25.5 g, 0.25 mol) was refluxed at 150 °C for 7 h. After the usual work-up, the residue was chromatographed on silica-gel column. From a benzene elute, 2.4 g, (18.0%) of **2** was obtained. Colorless crystals; mp 102.7—103.4 °C; ^1H NMR ($CDCl_3$): δ=2.12 (6H, s), 2.34 (3H, s), 7.06—7.73 (4H, m), 7.91 (1H, s); IR (KBr): 1755—1745 (C=O) cm^{-1}; Found: C, 58.57; H, 5.33%. Calcd for $C_{13}H_{14}O_6$: C, 58.64; H, 5.30%. Mol wt (Rast, benzene) 267. Calcd 266.24. E.V. 48.24. Calcd 48.51. The saponification value was determined by hydrolysis with a 0.5 M ethanolic KOH solution for 1 h.

*Preparation of **2***: A mixture of salicylaldehyde (12.2 g, 0.1 mol) in acetic anhydride (25.5 g, 0.25 mol) was refluxed at 150 °C for 2 h. After cooling, a crystalline product was filtered and recrystallized from benzene to give **2** (19.3 g, 72.5%). The product was identified by means of gas chromatography in comparison with the isolated product described above.

*Reaction of 2-Acetoxybenzylidene Diacetate (**2**) with the Glycine betaine and Acetic Anhydride.* A mixture of 2.7 g (0.01 mol) of **2** and 2.3 g (0.02 mol) of the glycine betaine in 3 g (0.03 mol) of acetic anhydride was refluxed at 150 °C for 4.5 h. After the usual work-up, 0.19 g (47.6% based on **2** used) of the 1,3-indandione (**1**) was obtained on GLC. Its IR and ^1H NMR spectra data agreed with those of **1** obtained as noted above.

The authors wish to express their thanks to Hokkaido-Togyo Co., Ltd. for its finacial support, to Dr. Hajime Takahashi of Department of General Education, Higashi-Nippon-Gakuen University for his helpfull discussion, and to Mr. Akiyo Sakushima of Faculty of Pharmaceutical Sciences, Higashi-Nippon-Gakuen University for Mass spectra measurement.

References

1) M. ITO, U. S. Patent 4302602 (Nov. 24, 1981).
2) On using anhydrous sodium acetate instead of anhydrous glycine betaine a Perkin's reaction occurs.

Preparation and Properties of Polymers Anchoring Biphenyl-2-ol

Tomomichi ISHIKAWA* and Satoshi ASAI

Department of Industrial Chemistry, Faculty of Technology, Tokyo Metropolitan University, Fukasawa, Setagaya-ku, Tokyo 158

(Received December 18, 1982)

Synopsis. The monomer, 2-biphenylyl acrylate (BPA), was prepared and was polymerized and copolymerized with vinyl acetate (VAc), styrene and *N*-vinylpyrrolidone. The reactivity ratios of BPA(M_1) with VAc were evaluated as $r_1=4.6+0.4$ and $r_2=0.37+0.08$. The polymers were hydrolyzed in methanol–phosphate buffer solution(pH 6 and 8), and the release rate of biphenyl-2-ol from the polymer was investigated.

Recently, there has been a great deal of interest in drugs,[1–3] agricultural medicines[4,5] and coatings[6,7] with long-lasting biological activity. Polymers of which fungicidal biphenyl-2-ol(*o*-phenylphenol, abbreviated to OPP) is anchored *via* hydrolyzable ester link to the main chain may be available to control the release of the fungicide over an extended period. Preparation of the polymers is accomplished by polymerization and copolymerization of 2-biphenylyl acrylate (BPA). In this work we describe the synthesis of both the monomer and polymer, and a study of the hydrolytic release of OPP from the polymer.

Experimental

Materials. Vinyl acetate(VAc), *N*-vinylpyrrolidone (NVP), styrene(St), and acryloyl chloride were distilled under reduced pressure prior to use. OPP and α,α′-azobisisobutyronitrile (AIBN) were purified by recrystallization. Benzene used as reaction media was dried and purified by distillation.

Synthesis of BPA. Previously dried benzene(100 cm³), OPP(34.0 g, 0.2 mol) and triethylamine(22 g, 0.22 mol) were placed in a 200 cm³ four necked round-bottom flask equipped with a stirrer, condenser and dropping funnel with a nitrogen inlet tube. The mixture was then maintained at 20—25 °C while acryloyl chloride(20.0 g, 0.22 mol) was added through the dropping funnel. Stirring was continued for additional 4 h. After the precipitate was filtered, the benzene solution was washed with 5% aqueous $NaHCO_3$ solution and twice with water. The benzene layer was dried over Na_2SO_4, and then the benzene was removed by vacuum evaporation. The pale yellow solution which remained was distilled under reduced pressure in the presence of 4-*t*-butylcatechol to yield 31.0 g (64.0%) BPA: bp 120—122 °C(200 Pa); IR (liquid) 1740(C=O), 1630(C=C), 1190, 1145(C–O–C) cm^{-1}; ^{1}H-NMR ($CDCl_3$) $\delta=5.60$, 6.25 (3H, m, CH_2=CH) and 7.30 (9H, m, aromatic proton). Found: C, 83.43; H, 6.29%. Calcd for $C_{15}H_{12}O_2$: C, 83.36; H, 6.18%.

General Procedure for Polymerization. All the polymerization experiments were carried out using a bulk technique at 60 °C in the presence of 0.5 wt% AIBN. The polymers obtained were purified by repeated precipitation from a solvent system into a non-solvent system. The purified polymers were dried at 60 °C under vacuum to constant weight and submitted to elemental analysis.

General Procedure for Hydrolysis. The polymer (converted into 0.5—0.6 mmol OPP) and the phosphate buffered methanol–water solution (pH 6 or 8; 200 cm³) were placed in 300 cm³ Erlenmeyer flask, and then maintained at 30 °C with a regulated water bath. The mixture was shaken often, and a part of this mixture (1 cm³) was taken out periodically. The polymers was removed by filtration. The filtrate was diluted with the buffer solution (4 cm³). The solution was put into a cubic quartz cell (1 cm) and detection of OPP was performed by UV at 244.0 nm.

Synthesis of 2-Biphenylyl Propionate (BPP). BPP was prepared from OPP with propionyl chloride by a similar procedure to that of BPA-synthesis: yield 54.0%; bp 156—158 °C (1333 Pa); IR (liquid) 1760(C=O), 1180 and 1140 (C–O–C) cm^{-1}; ^{1}H-NMR ($CDCl_3$) $\delta=1.00$ (3H, t, CH_3), 2.30 (2H, m, CH_2) and 7.30 (9H, m, aromatic proton). Found: C, 79.46; H, 6.44%. Calcd for $C_{15}H_{14}O_2$: C, 79.62; H, 6.24%.

Results and Discussion

Polymerization and Copolymerization of BPA. The BPA obtained was a colorless viscous liquid. The

TABLE 1. POLYMERIZATION AND COPOLYMERIZATION OF BPA

Run	Monomer		Polymer			
	BPA (mol%)	Comonomer	Conversion %	Analysis (%)	BPA (mol%)	$[\eta]^{a)}$ $dm^3\ g^{-1}$
1	20.0	VAc	23.4	C 74.34	54.3	—
2	50.0	VAc	22.4	C 77.87	77.5	—
3	80.0	VAc	24.2	C 79.74	93.9	—
4	20.0	VAc	82.0	C 66.50	22.9	0.12
5	50.0	VAc	91.6	C 73.72	51.0	0.35
6	79.7	VAc	79.8	C 77.70	76.1	0.35
7	20.0	St	76.8	C 90.32	8.26	0.37
8	50.0	St	75.7	C 84.26	48.6	0.32
9	80.0	St	72.0	C 81.04	88.1	0.34
10	50.0	NVP	78.3	N 3.46	56.7	0.26
11	80.0	NVP	79.3	N 1.81	74.7	0.37
12	100	—	81.0	—	100.0	0.03

a) Measured in benzene at 30 °C.

Table 2. Hydrolysis of BPA polymer

Run	Polymer BPA (mol%)	Comonomer	Conversion/% pH 8 1 week	pH 8 2 weeks	pH 6 1 week	pH 6 2 weeks
5	51.0	VAc	4.3	12.0	0.1	0.2
6	76.1	VAc	9.5	18.7	1.2	1.8
7	8.26	St	4.0	6.5	0.3	0.6
8	48.6	St	8.0	13.5	0.5	0.8
9	88.1	St	13.1	18.4	1.3	2.1
10	56.7	NVP	6.4	7.5	2.8	3.3
11	74.7	NVP	16.4	19.5	4.9	6.0
12	100	—	23.0	30.0	1.8	3.0

homopolymer was purified by reprecipitation from dichloromethane and methanol. Purification of the copolymers with NVP were by repeated precipitation from benzene and hexane. The copolymers with VAc or St were redissolved in dichloromethane and reprecipitated in methanol. Results are shown in Table 1. These polymers are colorless powders, soluble in organic solvents such as acetone, benzene, tetrahydrofuran and dichloromethane.

For BPA(M_1) with VAc, the reactivity ratios were determined by the integral form of the general copolymerization equation from the results for Runs 1—3 in Table 1. The r_1 and r_2 values obtained were $r_1=4.6\pm0.4$ and $r_2=0.37\pm0.08$. The conversion was calculated using Spinner and co-worker's equation[8] from these r_1 and r_2 values were fairly consistent with the results for Runs 4—6.

Release of OPP from Polymer. The polymers were hydrolyzed at pH 6 and 8. OPP released during the hydrolysis was dissolved in methanol–phosphate buffer solution(1/1 volume ratio) because of their lower solubility in water. The amount of OPP released was determined by measuring its absorbance at 244.0 nm. Table 2 shows the results after one and two weeks. It appears that the release rate of OPP are faster at pH 8 than at pH 6. After one week at pH 8, BPA–NVP copolymer was hydrolyzed faster than the other two copolymers, but much slower than the BPA homopolymer. In the period between one and two weeks, however, BPA–VAc copolymer was more susceptible to hydrolysis than the others. In this copolymer also, it was observed that the time-conversion plots are nearly linear and release the incorporated OPP by zero-order kinetics for at least two weeks.

As Table 2 shows, when the OPP content becomes higher, the conversion increases. But the BPA homopolymer was hydrolyzed very slowly and even after two weeks, about 70% of OPP unit remained on the polymer chain. In order to compare with the hydrolysis rate of the BPA homopolymer, a model compound, BPP, was hydrolyzed. The results were shown in Fig. 1. From these results, it seems that the polymers were resistant to hydrolysis and released OPP gradually. When the polymers are used as coating films, the above results suggest that the polymers will lose few OPP under a natural environment such as in the rain.

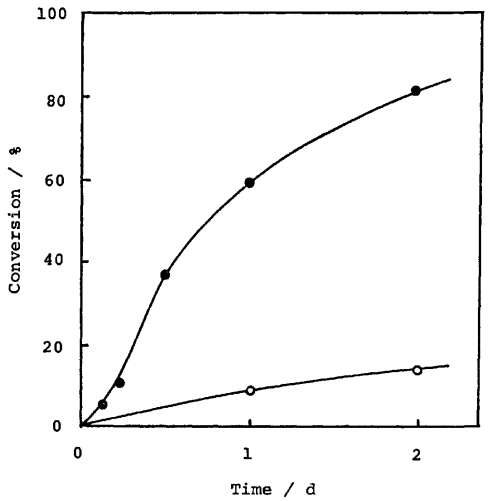

Fig. 1. Hydrolysis of BPP and BPA-homopolymer at pH 8.
●: BPP, ○: BPA-homopolymer

References

1) P. P. Umrigar, S. Ohashi, and G. B. Butler, *J. Polym. Sci., Polym. Chem. Ed.*, **17**, 351 (1979).
2) H. Ritter, *Makromol. Chem., Rapid Commun.*, **3**, 431 (1982).
3) J. Pitha, S. Zawadzki, and B. A. Hughes, *Makromol. Chem.*, **183**, 781 (1982).
4) M. B. Shambhu, G. A. Digenis, D. K. Gulati, K. Bowman, and P. S. Sabhrwal, *J. Agric. Food Chem.*, **24**, 666 (1976).
5) J. Bartulin and B. L. Rivas, *Makromol. Chem., Rapid Commun.*, **2**, 375 (1981).
6) C. U. Pittman, Jr., G. A. Stahl, and H. Winters, *J. Coatings Tech.*, **50**, 49 (1978).
7) C. U. Pittman, Jr., and G. A. Stahl, *J. Appl. Polym. Sci.*, **26**, 2403 (1981).
8) I. H. Spinner, B. C. Y. Lu, and W. F. Graydon, *J. Am. Chem. Soc.*, **77**, 2198 (1955).

Synthesis of 4*H*-Cyclopenta[*def*]phenanthrene from Fluorene Skeleton

Masaaki Yoshida*, Masahiro Minabe, and Kazuo Suzuki†

Department of Industrial Chemistry, Faculty of Engineering, Utsunomiya University, Ishiicho, Utsunomiya 321

†*Akita Technical College, Iijima-bunkyocho, Akita 011*

(Received January 10, 1983)

Synopsis. 4-Fluoreneacetic acid was prepared and its chloride was cyclized with $AlCl_3$ to give 4*H*-cyclopenta-[*def*]phenanthren-8-ol accompanied by the 8,9-dione. These were both reduced to 4*H*-cyclopenta[*def*]phenanthrene: the overall yield was 40—50% from diphenic acid. The phenol was converted to acetoxy and amino substrates.

Hydrocarbon 4*H*-cyclopenta[*def*]phenanthrene (**1**) involves an active methylene, a located C_8–C_9 double bond, and strained aromatic rings, and is of interest for carcinogenic screening tests. The characterized aromatic **1** possesses features of naphthalene, fluorene, and phenanthrene, thus **1** is one of the key compounds for studying arenes[1] and annulenes.[2] Reported synthetic pathways of **1** could be classified in three types, according to the ring which is built up at the last step from the component skeleton: (a) formation of the five-membered ring from phenanthrene derivatives;[3] (b) formation of the side six-membered ring from acenaphthene derivatives;[4] (c) formation of the center six-membered ring from fluorene derivatives. The first two methods require many steps, resulting in very low yields, and the third type has not yet succeeded.[5,6]

We wish to report here a convenient preparation of **1** from diphenic acid (**2**) *via* fluorene derivative (Scheme 1). The preparation of 4-fluorenecarboxylic acid (**3a**) in a good yield was reported by one of us.[7] Extension of the carbon chain of **3a** to **4d** has been carried out by means of the Arndt-Eistert reaction;[5] however, no diazomethane is available for mass production. The synthesis of **4d** from **3a** proceeded by the following stepwise sequence: esterification to **3b**, reduction to **4a**, bromination to **4b**, substitution to **4c**, and hydrolysis to **4d**. All these reactions gave very high yields and required only easy treatment.

Ring closures of 4-fluoreneacetic acid (**4d**) and 9-oxo-4-fluoreneacetic acid to the **1** derivatives were attempted unsuccessfully under the conditions which has sufficed to convert biphenyl-2-acetic acid to phenanthrene derivative.[5,8] This may be due to an increase of the distance between C_4 and C_5 of **4d**. This experiment shows that only 4-fluoreneacetyl chloride (**5**) was cyclized under the Friedel-Crafts conditions to 4*H*-cyclopenta[*def*]phenanthren-8-ol (**7a**) accompanied by 4*H*-cyclopenta[*def*]phenanthrene-8,9-dione (**8**). Both **7a** and **8** were reduced to the hydrocarbon **1** with hydriodic acid and red phosphorus[9] in good yields. Also, from the crude products of the ring closure reaction, the hydrocarbon was obtained in a 66% overall yield from **5**.

The phenol **7a** is a tautomer with 4*H*-cyclopenta-[*def*]phenanthren-8(9*H*)-one (**6**), which failed to separate for **6**, probably forming a complex with aluminium, but was confirmed as an intermediate by the NMR spectrum of the reaction mixture in $CDCl_3$ (Fig. 1). The singlets of 4.73 and 4.18 ppm were assigned to the methylene protons of 9- and 4-position of **6**, respectively, by comparison with the spectrum of 9,9-dimethyl-4*H*-cyclopenta[*def*]phenanthren-8(9*H*)-one.[10] Owing to the tautomer with **6**, **7a** may be readily oxidized to dione **8** on exposure to air. So, for storage during a long period, the hydroxyl group of **7a** was protected as the acetate (**7b**: X=OAc) which was hydrolyzed quantitatively to **7a**.

Consequently, this procedure appears more simple and easier than the methods hitherto available. One of the merits of this facile method is a moderate yield of **1** (40—50% based on **2**). The second is a ready transformation to the 8-derivatives which are difficult to obtain by electrophilic substitution of **1**.[11] **7a** was

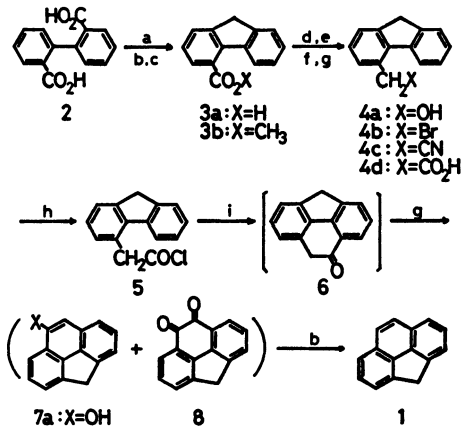

a: H_2SO_4. b: HI, P. c: MeOH, H_2SO_4 d: $LiAlH_4$. e: HBr. f: KCN. g: $H_3{}^+O$. h: $SOCl_2$. i: $AlCl_3$

Scheme 1.

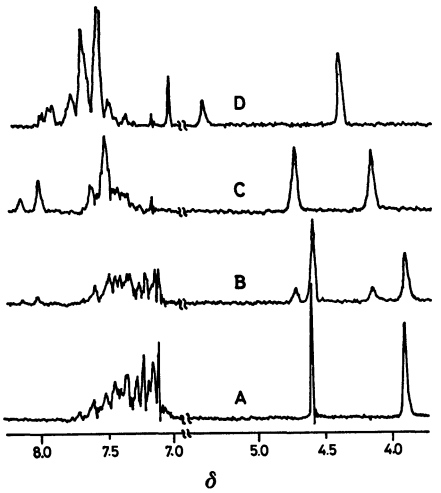

Fig. 1. ^1H NMR spectra on the ring closure reaction of **5** in $CDCl_3$. A: Starting material **5**. B: In the course of the reaction. C: End of the reaction. D: Upon hydrolysis (**7a**).

derived to 4*H*-cyclopenta[*def*]phenanthren-8-amine (**7c**: X=NH_2)[12] which was converted easily into many 8-substituted 4*H*-cyclopenta[*def*]phenanthrenes.

Experimental

All the melting points are uncorrected. The following spectrometers were used: ^1H NMR, JEOL C-60-HL (downfield from internal Me_4Si); IR, JASCO IR-G (KBr pellets); mass spectra, Hitachi RMU-6E or M-80 (direct inlet system). Elemental analyses were determined on a Yanagimoto CHN-corder.

4-(Bromomethyl)fluorene (4b). Dicarboxylic acid **2** was treated with concentrated sulfuric acid at 130—140 °C for 15 min to afford 9-oxo-4-fluorenecarboxylic acid (yield 97%). The keto acid was reduced with hydriodic acid and red phosphorus in acetic acid under refluxing for 20 h to give **3a** (yield 95%).[7] 4-Fluorenemethanol (**4a**) was obtained from methyl 4-fluorenecarboxylate (**3b**) with lithium aluminium hydride in a 99% yield.[13] A solution of **4a** (11.8 g, 60 mmol) in acetic acid (150 ml) was saturated with hydrogen bromide, followed by standing overnight at room temperature. The resulting mixture was extracted with benzene (60 ml) and the extract was washed with water to neutrality. The organic layer was dried and recrystallized from cyclohexane to give **4b** (14.4 g, 93%): mp 126—127 °C (lit,[13] mp 115—118 °C); NMR (CCl_4) δ=3.80 (s, 2H), 4.77 (s, 2H), and 7.02—8.01 (m, 7H). Found: C, 65.19; H, 4.07%.

4-Fluoreneacetonitrile (4c). To a solution of **4b** (4.50 g, 17.3 mmol) in *N,N*-dimethylformamide (100 ml) was added aqueous potassium cyanide (3 normal, 10 ml) and the mixture was refluxed for 4 h. The resulting mixture was poured into water (300 ml) and the precipitate was recrystallized from cyclohexane to give **4c** (3.05 g, 86%): mp 101—102 °C; IR 2270 cm^{-1}; NMR ($CDCl_3$) δ=3.87 (s, 2H), 4.10 (s, 2H), and 7.12—7.76 (m, 7H); MS *m/e* 205 (M^+), 178, and 165. Found: C, 87.94; H, 5.39; N, 6.62%. Calcd for $C_{15}H_{11}N$: C, 87.77; H, 5.40; N, 6.82%.

4-Fluoreneacetyl Chloride (5). Nitrile **4c** was hydrolyzed with dilute sulfuric acid in acetic acid to give carboxylic acid **4d** in a 96% yield; mp 178—179 °C (lit,[5] mp 178.5—179.0 °C). A mixture of **4d** (2.1 g, 9.4 mmol) in thionyl chloride (10 ml) was gently refluxed for 0.5 h and was dried *in vacuo*. The residue was recrystallized from hexane to afford **5** (2.13 g, 94%): mp 98.0—98.5 °C; IR 1786 cm^{-1}; NMR ($CDCl_3$) δ=3.92 (s, 2H), 4.60 (s, 2H), and 7.11—7.81 (m, 7H); MS *m/e* 244 and 242 (M^+), 206, and 165. Found: C, 74.31; H, 4.51%. Calcd for $C_{15}H_{11}OCl$: C, 74.20; H, 4.57%.

Ring Closure of 5. To a suspension of anhydrous aluminium chloride (0.53 g, 4 mmol) in 1,2-dichloroethane (30 ml), a solution of **5** (485 mg, 2 mmol) in 1,2-dichloroethane (5 ml) was added slowly at 20 °C and stirring was continued for 2 h. The mixture was hydrolyzed with dilute hydrochloric acid and extracted with benzene. The extract was submitted to silica-gel column chromatography to afford **7a** from the first eluate (269 mg, 65%): mp 167—168 °C decomp; IR 3330 and 1126 cm^{-1}; NMR ($CDCl_3$) δ=4.32 (s, 2H), 5.55 (s, 1H, OH), 7.04 (s, 1H), and 7.32—8.00 (m, 6H); MS *m/e* 206 (M^+) and 178. Found: C, 87.21; H, 5.05%. Calcd for $C_{15}H_{10}O$: C, 87.35; H, 4.89%.

The second eluate of the column gave **8** (44 mg, 10%): mp 254—256 °C decomp (lit,[10] mp 256 °C decomp).

4H-Cyclopenta[def]*phenanthrene (1).* Upon the intramolecular Friedel-Crafts reaction of **5** (242 mg, 1 mmol), the mixture containing **7a** and **8** was treated with hydriodic acid (57%, 10 ml) and red phosphorus (1.0 g) in acetic acid (50 ml) to reflux under nitrogen for 90 h. The resulting mixture was poured into aqueous sodium hydrogensulfite (1%, 100 ml) and was extracted with benzene. The organic layer was chromatographed on a silica gel to give **1** from the colorless eluate (126 mg, 66% from **5**): mp 113—114 °C (lit,[14] mp 116 °C).

The reductions of **7a** and **8** were carried out: **1** was obtained in yields of 27, 53, 88, and 78% from **7a** during the reaction times of 16, 24, 48, and 90 h, respectively, by a method similar to that described above. Also, **1** was afforded from **8** in yields of 26, 37, 58, and 80%, respectively.

8-Acetoxy-4H-cyclopenta[def]*phenanthrene (7b).* The mixture of **7a** (721 mg, 3.5 mmol) and acetic anhydride (100 ml) was refluxed for 1 h and was then quenched with cold water. The precipitate was recrystallized from ethanol, affording **7b** (780 mg, 90%): mp 97—98 °C; IR 1758 and 1199 cm^{-1}; NMR ($CDCl_3$) δ=2.48 (s, 3H), 4.31 (s, 2H), 7.50 (s, 1H), and 7.28—7.87 (m, 6H); MS *m/e* 248 (M^+) and 206. Found: C, 82.50; H, 4.96%. Calcd for $C_{17}H_{12}O_2$: C, 82.24; H, 4.87%.

Hydrolysis of **7b** (248 mg, 1 mmol) was carried out in aqueous ethanol (30%, 15 ml) with potassium hydroxide (1.0 g) at 60 °C for 10 min to give 200 mg (97%) of **7a**.

4H-Cyclopenta[def]*phenanthren-8-amine (7c).* A mixture of **7a** (103 mg, 0.5 mmol), sulfur dioxide (3 g), and aqueous ammonia (28%, 40 ml) was heated in an autoclave (50 ml volume) at 150—160 °C at 8.5 kg/cm^2 for 10 h. The resulting product was purified by silica-gel column chromatography to yield **7c** (52 mg, 56%): mp 139.5—140.0 °C decomp (lit,[12] mp 136—138 °C).

References

1) W. J. Archer and R. Taylor, *J. Chem. Soc., Perkin Trans. 2*, **1981**, 1153.

2) W. E. Barth and R. G. Lawton, *J. Am. Chem. Soc.*, **93**, 1730 (1971); B. M. Trost and P. L. Kinson, *ibid*, **97**, 2438 (1975).

3) M. Bergmann and A. Weizmann, *J. Org. Chem.*, **11**, 592 (1946); H. Medenwald, *Chem. Ber.*, **86**, 287 (1953); K. G. Rutherford and M. S. Newman, *J. Am. Chem. Soc.*, **79**, 213 (1957); D. H. R. Barton, P. G. Sammes, and G. G. Weingarten, *J. Chem. Soc., C*, **1971**, 729; D. S. C. Chang and N. Filipescu, *J. Am. Chem. Soc.*, **94**, 4170 (1972).

4) W. E. Bachmann and J. C. Sheehan, *J. Am. Chem. Soc.*, **63**, 204 (1941).

5) W. E. Bachmann and J. C. Sheehan, *J. Am. Chem. Soc.*, **62**, 2687 (1940).

6) A photocyclization of 1-(4-fluorenyl)-1-phenylethylene to 8-phenyl-4*H*-cyclopenta[*def*]phenanthrene was reported but it is difficult to obtain **1** by removing the phenyl group: see R. Koussini, R. Lapouyade, and P. F. de Violet, *J. Am. Chem. Soc.*, **100**, 6679 (1978).

7) K. Suzuki, *Technol. Rept. Tohoku Univ.*, **19**, 63 (1954).

8) A. Schönberg and F. L. Warren, *J. Chem. Soc.*, **1939**, 1837.

9) The reactions were carried out under more vigorous conditions than those of 9-phenanthrol and phenanthrenequinone to phenanthrene: see M. Konieczny and R. G. Harvey, *J. Org. Chem.*, **44**, 4813 (1979).

10) M. Yoshida, A. Kadokura, M. Minabe, and K. Suzuki, *Bull. Chem. Soc. Jpn.*, **53**, 1179 (1980).

11) M. Yoshida, K. Hishida, M. Minabe, and K. Suzuki, *J. Org. Chem.*, **45**, 1783 (1980).

12) M. Yoshida, S. Nagayama, M. Minabe, and K. Suzuki, *J. Org. Chem.*, **44**, 1915 (1979).

13) K. D. Warren and J. R. Yandle, *J. Chem. Soc.*, **1965**, 4221.

14) O. Kruber, *Chem. Ber.*, **67**, 1000 (1934).

The Stereochemistry of Cross-coupling Adducts of Norbornenes with Butadiene Catalyzed by Ni Complex

Yasutaka Ishii,* Masakazu Kawahara, Toshimitsu Noda, Hiroyuki Ishigaki, and Masaya Ogawa*

Department of Applied Chemistry, Faculty of Engineering, Kansai University, Senriyama, Suita Osaka 564

(Received January 31, 1983)

Synopsis. The stereochemistry of cross-coupling adducts of norbornenes with butadiene catalyzed by Ni complex generated in situ by $NiBr_2(Ph_3P)_2$ and $NaBH_4$ in ethanol was investigated. The configuration of four-member cross-coupling products could be confirmed by means of independent synthesis.

The Ni catalyzed cross-coupling reaction of butadiene (**1**) with strained olefins, such as *endo*-tricyclo[5.2.1.$0^{2,6}$]-deca-3,8-diene (**2**), gives the four-member cross-coupling product (**3**) together with a small amount of 1-methylene-2-vinylcyclopentane (**4**) (Eq. 1).[1,2]

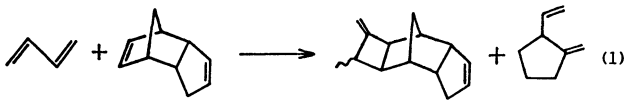

(1)

1 **2** **3** **4**

Unfortunately, the stereochemistry on coupling reactions has not been established because of the difficulty in determining the configuration of the coupling products. However, this unusual coupling reaction is of interest from the synthetic and mechanistic aspects. Thus, the coupling reactions of **1** with some strained olefins having a bicyclo[2.2.1]heptene skeleton catalyzed by $NiBr_2(Ph_3P)_2$ and $NaBH_4$ were studied to confirm the stereochemistry of cross-coupling products; the stereochemical course of coupling reactions is briefly discussed here.

In order to obtain the most simple cross-coupling product, **1** was allowed to react with bicyclo[2.2.1]-heptene (**5**), in the presence of $NiBr_2(Ph_3P)_2$ and $NaBH_4$ in ethanol (Eq. 2).

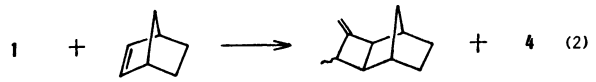

(2)

5 **6**

The four-member coupling product (**6**) was obtained in 60% yields together with **4** (12%). The exo-configuration of adduct **6** was readily assigned from the characteristic ^{13}C NMR chemical shift of the bridge carbon (C-9).[3] The hydrogenation of **6** on Pd/C suggested the formation of **7** or **8**, but not **9**, because the ^{13}C NMR spectrum of the hydrogenation product consisted of six carbon signals. The determination of configuration, either **7** or **8**, could be achieved by the independent synthesis of **8**.

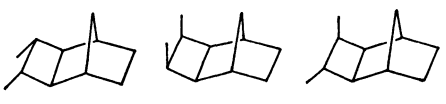

7 **8** **9**

Under the influence of $RuH_2(Ph_3P)_4$ catalyst, **5** reacts with dimethyl acetylenedicarboxylate (**10**) to give [2+2] cross-adduct (**11**) which on subsequent hydrogenation on Pd/C is converted into a saturated compound (**12**), whereupon both methoxycarbonyl groups are oriented in the syn-direction.[4]

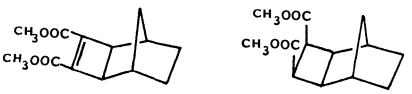

11 **12**

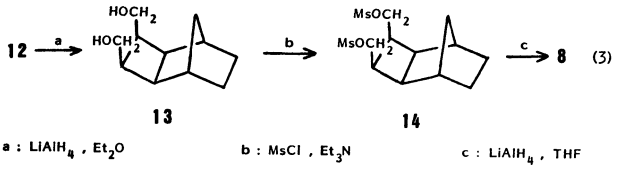

(3)

13 **14**

a : $LiAlH_4$, Et_2O b : MsCl, Et_3N c : $LiAlH_4$, THF

Since the subsequent interconversion of **12** to **8** proceeds with complete retention of the stereochemistry, **12** was converted into *syn,syn*-3,4-dimethyl-*exo*-tricyclo[4.2.1.$0^{2,5}$]nonane (**8**) (Eq. 3). From the comparison of spectral data of **8** with those of the compound obtained by the hydrogenation of **6** derived from Ni catalyzed reaction, it was identified as *anti,anti*-3,4-dimethyl-*exo*-tricyclo[4.2.1.$0^{2,5}$]nonane (**7**). Thus the configuration of **6** could be assigned to *anti*-3-methyl-4-methylene-*exo*-tricyclo[4.2.1.$0^{2,5}$]nonane.

On the other hand, the reaction of **1** with **2** catalyzed by Ni-complex gave cross-coupling products which consisted of two components[5] with approximately 1:1 ratio, whose NMR spectral patterns were very similar. The hydrogenation of coupling products led to the same saturated compound, which was identified to *anti,anti*-9,10-dimethyl-2-*endo*-8-*exo*-tetracyclo[5.4.2.1.$0^{2,6}$.$0^{8,11}$]dodecane (**17**), since the Ru-catalyzed reaction of **2** with **10** followed by the interconversion of functional groups afforded the corresponding *syn,syn*-dimethyl compound (**18**).

Thus the configuration of cross-coupling products of **1** with **2** was established as *anti*-9-methyl-10-meth-

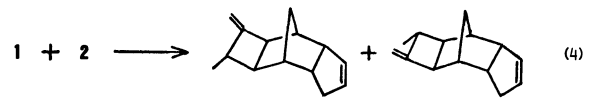

(4)

15 **16**

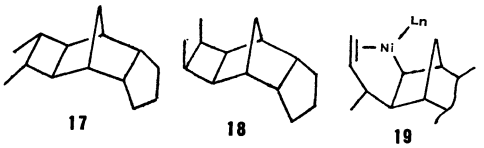

17 **18** **19**

ylene-2-*endo*-8-*exo*-tetracyclo[5.4.1.$0^{2,6}$.$0^{8,11}$]dodec-3-ene (**15**) and its regioisomer (**16**).

Kiji[2] suggested that the active species of coupling reaction of **1** with **2** catalyzed by $NiCl_2(n\text{-}Bu_3P)_2$ and $NaBH_4$ is a nickel hydride such as $HNiBr(n\text{-}Bu_3P)_2$,[6] and that the reaction proceeds through a π-crotyl nickel intermediate. Consequently, π-crotyl nickel thus generated couples with a strained olefin coordinated to nickel to form an intermediate such as **19** which subsequently undergoes β-elimination after coupling to give the four-member cross-coupling adduct. This reaction path explains satisfactorily the formation of regioisomers of **15** and **16** for the coupling reaction of **1** with **2**.

Experimental

The ^{1}H NMR and ^{13}C NMR spectra were recorded with a JEOL PMX-60 and a JNM-PS-100 FT-NMR spectrometer, respectively. The IR spectra were taken with a JASCO-A202 spectrometer. The GLC analyses were carried out on a Yanagimoto G1800 apparatus. The melting and boiling points are uncorrected.

Materials. Unless otherwise noted, the materials were obtained from commercial suppliers and used without further purification, except for solvents. *endo*-Tricyclo[5.2.1.$0^{2,6}$]-deca-3,8-diene (**2**) was prepared from the dimerization of cyclopentadiene obtained by the destructive distillation of commercially available **2**. Solvents were purified by the conventional methods.

*Coupling Reactions of **1** with **2** and **5** Catalyzed by $NiBr_2(Ph_3P)_2$–$NaBH_4$.* A solution of $NiBr_2(Ph_3P)_2$[7] (4 mmol) and $NaBH_4$ (4 mmol) in ethanol (30 cm^3) was placed in an autoclave and then **1** (72 mmol) and **5** (60 mmol) was added to this solution at −78 °C under nitrogen stream. The mixture was allowed to react under stirring at 80 °C for 24 h, and the reaction mixture was extracted with hexane (50 cm^3×4). After evaporation of solvents, the residue was distilled under reduced pressure to give (**6**) (60%), bp 118—120 °C/3300 Pa; IR(neat) 3050, 2940, 1680, 1450, 880 cm^{-1}; ^{13}C NMR($CDCl_3$) δ=158.2(s), 105.2(t), 49.1(d), 46.6(d), 40.8(d), 39.4(d), 39.3(d), 32.9(t), 28.4(t), 27.4(t), 20.1(q). Found: C, 89.10; H, 10.85%. Calcd for $C_{11}H_{16}$: C, 89.12; H, 10.88%.

The hydrogenation of **6** (1 mmol) in hexane (10 cm^3) on 5% Pd/C (30 mg) under 50 kg/cm^2 H_2 gave a saturated compound **7** (95%), bp 119—123 °C/3300 Pa; IR(neat) 2930, 2850, 1450, 1210, 750 cm^{-1}; ^{13}C NMR($CDCl_3$) δ= 48.1(d), 38.5(d), 33.2(t), 33.0(d), 27.8(t), 15.6(q).

The coupling reaction of **1** with **2** was carried out in a similar manner to that above to give a regioisomeric mixture of **15** and **16** in 70% yields; this was hydrogenated to give **17** (95%), bp 124—126 °C/2660 Pa; IR(neat) 2940, 1470, 1450, 1060, 890 cm^{-1}; ^{13}C NMR($CDCl_3$) δ=44.7(d), 43.7 (d), 41.7(d), 37.7(t), 32.9(d), 29.2(t), 15.8(q). Found: C, 88.38; H, 11.60%. Calcd for $C_{14}H_{22}$: C, 88.35; H, 11.65%.

*Preparation of **8** and **18**.* To a solution of $LiAlH_4$ (18 mmol) in ether (70 cm^3) was added dropwise an etheral solution of **12** (15 mmol) prepared according to the literature procedure,[4] and then the mixture was refluxed for 5 h. After decomposition of unreacted $LiAlH_4$ with ethyl acetate, followed by H_2O, the reaction mixture was extracted with ether. Removal of solvents yielded **13** (85%); the immediate mesylation of **13** according to the method of Jung[8] gave dimesylate (**14**) (42%). The treatment of **14** (4.5 mmol) with $LiAlH_4$ (10.8 mmol) in THF (20 cm^3) by the method of Mitsudo[9] afforded hydrocarbon **8** (44%), which was separated by MPLC on silica gel (elution with 10% ether in hexane); IR(neat) 2920, 2850, 1450, 1090, 660 cm^{-1}; ^{13}C NMR($CDCl_3$) δ=44.7(d), 36.7(t), 35.5(d), 31.9(d), 29.3 (t), 9.2(q). Found: C, 87.85; H, 12.10%. Calcd for $C_{11}H_{18}$: C, 87.93; H, 12.07%.

Compound **18** was prepared by the same method as above; IR (neat) 2940, 1470, 1440, 1050, 760 cm^{-1}; ^{13}C NMR ($CDCl_3$) δ=46.2(d), 41.1(t), 40.4(d), 37.8(d), 31.5(d), 29.1 (t), 26.9(t), 9.1(q). Found: C, 88.30; H, 11.70%. Calcd for $C_{14}H_{22}$: C, 88.35, H, 11.65%.

References

1) S. Yoshikawa, S. Nishimura, J. Kiji, and J. Furukawa, *Tetrahedron Lett.*, **1973**, 3071.

2) J. Kiji, S. Yoshikawa, E. Sasakawa, S. Nishimura, and J. Furukawa, *J. Organomet. Chem.*, **80**, 267 (1974).

3) A series of ^{13}C NMR spectra of bicyclo[2.2.1]heptane derivatives were measured in our previous paper: K. Nakagawa, S. Iwase, Y. Ishii, S. Hamanaka, and M. Ogawa, *Bull. Chem. Soc. Jpn.*, **49**, 2017 (1976).

4) T. Mitsudo, K. Kokuryo, T. Shinsagi, Y. Nakagawa, Y. Watanabe, and Y. Takegami, *J. Org. Chem.*, **44**, 4492 (1979).

5) The formation of isomers in the coupling of **1** with **2** is not described in Ref. 2.

6) J. Kiji, K. Yamamoto, S. Mitani, S. Yoshikawa, and J. Furukawa, *Bull. Chem. Soc. Jpn.*, **46**, 1791 (1973).

7) L. M. Venanzi, *J. Chem. Soc.*, **1958**, 719.

8) M. E. Jung and T. J. Shaw, *J. Am. Chem. Soc.*, **102**, 6304 (1980).

9) Y. Fujimoto and T. Tatsuno, *Tetrahedron Lett.*, **1976**, 3325.

Synthesis of Lepiochlorin, a Chlorinated Antibiotic, by Use of Electrochemical Haloalkoxylation

Sigeru Torii,* Tsutomu Inokuchi, and Kazumi Kondo
Department of Industrial Chemistry, School of Engineering, Okayama University, Okayama 700
(Received February 4, 1983)

Synopsis. The fungal metabolite lepiochlorin was synthesized from 2-methyl-4-oxopentanoic acid by the electrochemical chloromethoxylation of 2-methyl-2,4-pentadien-4-olide in MeOH–NH_4Cl–(Pt–Pt) system followed by hydrolysis in a mixed solution of dioxane–H_2O–concd HCl (25/10/1 V/V/V) in 38% overall yield.

γ-Oxygenated butenolides appeared in naturally occurring products exhibit interesting biological activities.[1] Synthetic methodology for the butenolide has been well documented in a recent review.[2] As a new antibiotic butenolide, lepiochlorin (**4b**), a chlorinated metabolite of a fungus (a *Lepiota* species) cultivated by a leaf-cutting ants, has been isolated.[3] In the previous study,[4] we reported a convenient haloalkoxylation of enol ethers by the electrolysis in ROH–NH_4X (X=Cl, Br, I)–(Pt–Pt) system. This procedure is expected to be potentially useful for the preparation of chlorohydrin moiety of **4b**. We describe here a short-step synthesis of the butenolide **4b** by introducing the electrochemical chloromethoxylation of γ-methylenebutenolide **3a**.

The target molecule **4b** has been synthesized recently by McMorris *et al.* in 18—20% overall yields in a laborious seven-step synthesis from α-phenylthiopropionic acid and allyl methoxyethoxymethyl ether.[5] In our route to **4b** we started with 2-methyl-3-penten-4-olide **2** which can be obtained from commercially available 2-methyl-4-oxopentanoic acid (**1**)[6] by the procedure of Helberger *et al.*[7] (Scheme 1).

Bromination of **2**, obtained by dehydration of **1** with phosphoric acid, with one equivalent of bromine and subsequent treatment with 1,8-diazabicyclo[5.4.0]-undec-7-ene (DBU) at −20 to 10 °C in benzene provided the key intermediate, γ-methylenebutenolide **3a**,

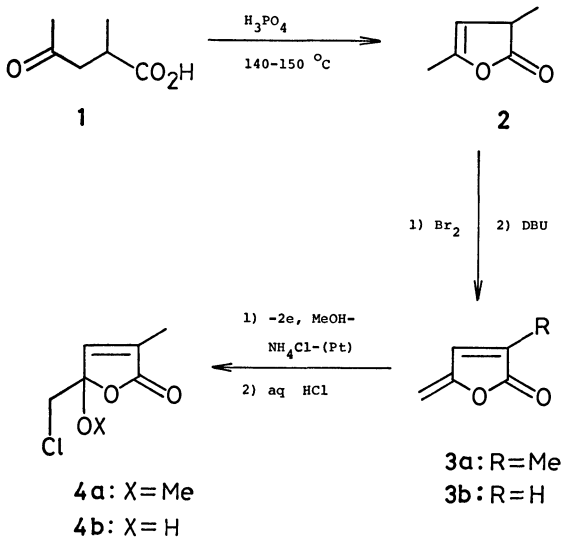

Scheme 1.

in 51% yield (from **1**).[8]

It is interesting to note that the butenolide **3a** is stable to heat in contrast to unstable protoanemonine (**3b**) which lacks methyl group at C-2 position of **3a** and dimerizes spontaneously at room temperature.[7b,9] For example, Diels-Alder reaction of **3a** with 1,3-dienes, *i.e.*, isoprene and 2-trimethylsiloxy-1,3-butadiene, took place on heating at 110—120 °C for 10 h in toluene to give the corresponding diene adducts **5** in 80—83% yields (Scheme 2). In addition, the reaction of **3a** with appropriate nucleophiles has been explored to give the corresponding 1,6-adducts.[10]

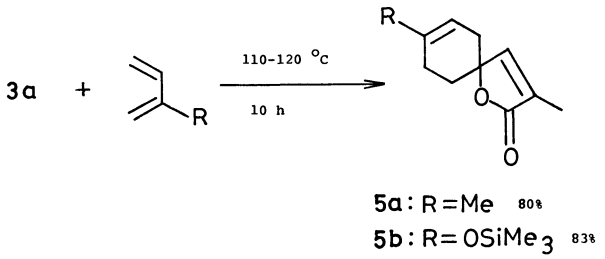

Scheme 2.

Electrochemical halogenation of **3a** in a MeOH–NH_4Cl (1.5 equiv.)–(Pt–Pt) system was carried out under a current of 3.5—6.7 mA/cm² (applied voltage: 2.0 V, cell voltage: 0.8—1.0 V *vs.* Ag wire) in a beaker type undivided cell. The passage of 3.0 F/mol of electricity (10 h) at room temperature afforded the chlorinated acetal **4a** in 88% yield. On the other hand, attempts at the direct electrochemical chlorohydroxylation of **3a** employing a MeCN–H_2O (3/1 V/V)–NH_4Cl–(Pt–Pt) system resulted in the low yield of **4b** (10—20% yields). Hydrolysis of acetal group of **4a** by heating to reflux in a mixed solvent of dioxane–H_2O–concd HCl (25/10/1 V/V/V) afforded the desired **4b** in 86% yield.[11]

Experimental

Melting point is uncorrected and boiling points are indicated by an air-bath temperature without correction. IR spectra were determined with a JASCO IRA-1 grating spectrometer. NMR spectra were obtained with a Hitachi R-24 (60 MHz for proton) and/or a JEOL FX-100 (100 MHz for proton and 25.05 MHz for carbon-13) spectrometers. Samples were dissolved in $CDCl_3$ and the chemical shift values (δ) are expressed in parts per million downfield from an internal Me_4Si. Elemental analyses were performed in our laboratory.

2-Methyl-3-penten-4-olide (2). According to the procedure reported in the literature,[7b] **1** (5.0 g, 38.4 mmol) was heated with H_3PO_4 (0.25 g) at 140—150 °C for 4 h. The mixture was distilled at 140—150 °C/20 Torr and the distillate was chromatographed (SiO_2, hexane–AcOEt 8:1) to give 2.6 g of **2** (89% yield based on 1.06 g of unchanged

1). **2**: bp 77—78 °C/41 Torr (lit,[12] 53 °C/6 Torr).

*2-Methyl-2,4-pentadien-4-olide (**3a**).* To a solution of **2** (107.3 mg, 0.97 mmol) in CS_2 (2 ml) was added dropwise Br_2 (155 mg, 0.97 mmol) at −20 °C. After the solution had become colorless, the CS_2 was removed *in vacuo* with cooling in a water bath. The residue was dissolved in benzene (5 ml) containing a catalytic amount of 2,5-di-*t*-butylhydroquinone, and to this solution was added DBU (433 mg, 2.91 mmol) with immediate cooling to about −20 °C. The mixture was stirred for 30 min and warmed gradually to room temperature over about 5 h. Concentration and chromatography (SiO_2,[13] hexane–Et_2O 3:1) gave 62 mg (58%) of **3a**: bp 52—53 °C/2 Torr (lit,[14] 25 °C/0.05 Torr); MS, *m/e* (rel int.) 111 (M^++1, 8.2), 110 (M^+, 100), 82 (29.0), 68 (27.1), 54 (25.4). Spectroscopic properties were identical with those reported previously.[14]

*5-Chloro-4-methoxy-2-methyl-2-penten-4-olide (**4a**).* The electrochemical halogenation was carried out in an undivided cell fitted with two platinum foil (2.0×1.5 cm^2) electrodes.[4] A solution of **2a** (15 mg, 0.14 mmol) and NH_4Cl (11.3 mg, 0.21 mmol) in MeOH (4 ml) was electrolyzed under a constant applied voltage of 2.0 V (3.5—6.7 mA/cm^2). After 3.0 F/mol of electricity has been passed, the mixture was concentrated and the residue was taken up in ether. The extract was washed with brine and dried (Na_2SO_4). Evaporation of the solvent followed by chromatography (SiO_2, hexane–AcOEt 3:1) gave 21.2 mg (88%) of **4a**: bp 88—89 °C/1.0 Torr; IR (neat) 3040, 1775 (lactone C=O), 1665 cm^{-1} (C=C); ^1H NMR (100 MHz) δ 1.99 (d, J=1.5 Hz, 3H, CH_3), 3.26 (s, 3H, OCH_3), 3.61 (d, J=12 Hz, 1H, CHCl), 3.85 (d, J=12 Hz, 1H, CHCl), 6.82 (q, J=1.5 Hz, 1H, HC=C); ^{13}C NMR δ 10.7 (q, C-2 Me), 48.5 (t, C-5), 51.7 (q, OMe), 106.7 (s, C-4), 135.8 (s, C-2), 143.5 (d, C-3), 170.4 (s, C-1); MS, *m/e* (rel int.) 179 (M^++2, 0.34), 177 (M^+, 0.94), 159 (0.51), 147 (6.9), 145 (21.6), 127 (100), 99 (35.3), 97 (18.3), 79 (17.0), 77 (48.4). Found: C, 47.56; H, 5.20. Calcd for $C_7H_9ClO_3$: C, 47.61; H, 5.13.

*5-Chloro-4-hydroxy-2-methyl-2-penten-4-olide (Lepiochlorin, **4b**).* A solution of **4a** (29 mg, 0.16 mmol) in a mixed solution of dioxane–H_2O–concd HCl (25/10/1 V/V/V, 2 ml) was heated to reflux for 6 h. The mixture was extracted with benzene–ether (1:1). The usual workup and chromatography (SiO_2,[13] hexane–AcOEt 3:1) gave 20 mg (86%) of **4b**: mp 69—70 °C (from petroleum ether) (lit,[3] 68—70 °C,[5] 74—74.5 °C); ^{13}C NMR δ 10.4 (q, C-2 Me), 46.7 (t, C-5), 103.8 (s, C-4), 134.1 (s, C-2), 145.0 (d, C-3), 172.0 (s, C-1). IR and ^1H NMR spectra were identical with those reported.[3]

The present work was partially supported by a Grant-in-Aid for the Special Project Research No. 57118002 (Innovative Studies on Highly Selective Synthesis) from the Ministry of Education, Science and Culture.

References

1) G. Pattenden, *Fortschr. Chem. Org. Naturst.*, **35**, 133 (1978).
2) Y. S. Rao, *Chem. Rev.*, **76**, 625 (1976).
3) M. S. R. Nair and A. Hervey, *Phytochemistry*, **18**, 326 (1979).
4) S. Torii, T. Inokuchi, S. Misima, and T. Kobayashi, *J. Org. Chem.*, **45**, 2731 (1980).
5) J. R. Donaubauer and T. C. McMorris, *Tetrahedron Lett.*, **21**, 2771 (1980).
6) Available from Aldrich Chemical Co., Milwaukee, WI.
7) a) J. H. Helberger, S. Ulubay, and H. Civelekoglu, *Ann.*, **561**, 215 (1949); b) C. Grundmann and E. Kober, *J. Am. Chem. Soc.*, **77**, 2332 (1955).
8) For the alternative methods of the preparation of γ-ylidenebutenolides: G. A. Kraus and H. Sugimoto, *J. Chem. Soc., Chem. Commun.*, **1978**, 30; T. Nakano and Y. Nagai, *ibid.*, **1981**, 815; M. Asaoka, N. Yanagida, K. Ishibashi, and H. Takei, *Tetrahedron Lett.*, **22**, 4269 (1981).
9) C. B. Chapleo, K. L. Svanholt, R. Martin, and A. S. Dreiding, *Helv. Chim. Acta*, **59**, 100 (1976); J. Cardellach, C. Estopa, J. Font, M. Moreno-Mañas, R. M. Ortuño, F. Sanchez-Ferrando, S. Valle, and L. Vilamajo, *Tetrahedron*, **38**, 2377 (1982).
10) H. Wyss, L. Révész, and R. Scheffold, *Helv. Chim. Acta*, **64**, 2272 (1981).
11) D. P. Marriott and J. R. Bantick, *Tetrahedron Lett.*, **22**, 3657 (1982).
12) J. A. Hirsch and A. J. Szur, *J. Heterocycl. Chem.*, **9**, 523 (1972).
13) SILICAR CC-7 SPECIAL silica gel purchased from Mallinckrodt, Inc. (Paris, Kentucky 40361) was used.
14) L.-C. Yu and P. Helquist, *J. Org. Chem.*, **46**, 4536 (1981).

A Convenient Synthesis of C(2)-Substituted Cephalosporins

Sigeru Torii,* Hideo Tanaka, Norio Saitoh, Takashi Siroi,
Michio Sasaoka, Nobuhito Tada, and Junzo Nokami
Department of Industrial Chemistry, School of Engineering, Okayama University, Okayama 700
(Received March 3, 1983)

Synopsis. Replacement of the C(2)-substituents of 2-acetoxy- or 2-methoxycephalosporin with nucleophiles was performed efficiently in dichloromethane in the presence of acid-catalysts, affording cephalosporins bearing heteroaromatic moieties, sulfenyl, and alkoxyl groups at the C(2)-position.

Chemical modification of natural penicillins and cephalosporins has been intensively investigated in order to obtain new clinically significant drugs with greater antibacterial activity.[1] In this connection, much attention has been paid to introduction of a desired functional group to the C(2)-position of cephalosporins.[2] However, the C(2)-substituents so far introduced are only known of alkyl,[3] alkylidene,[4] and/or a few simple functional groups, *e.g.*, acetoxyl,[5] methoxyl,[6] and methylthio groups.[7]

The development of synthesis procedures of C(2)-acetoxy- and methoxycephalosporins[5,6] prompted us to investigate the replacement of the acetoxyl and methoxyl groups of **2** with more complex substituents. We now found that the replacement of the C(2)-substituents of **2** can be successfully performed by treatment with various nucleophiles in dichloromethane in the presence of an acid catalyst.

Table 1. C(2)-Substitution of 2-acetoxy- or 2-methoxycephalosporin with nucleophiles[a]

Entry	Compound 2 R	Nu-H	Acid	Temp °C	Time h	Product 4	Yield[b] %
1	CH_3CO		$TiCl_4$	-25	4	4a	87
2	CH_3CO		$AlCl_3$	3	1.5	4a	84
3	CH_3CO		p-TsOH	5	8	4a	78
4	CH_3		$AlCl_3$	25	0.6	4a	67
5	CH_3		p-TsOH	25	3	4a	67
6	CH_3		p-TsOH	25	3	4b	55
7	CH_3CO		$TiCl_4$	-30	0.2	4c	96
8	CH_3CO		$AlCl_3$	-30	1.6	4d	91
9	CH_3CO	C_4H_9S–H [c]	$TiCl_4$	-30	0.6	4e	64
10	CH_3CO	$HOCOC_2H_4S$–H [c]	$TiCl_4$	-40	3	4f	59
11	CH_3CO	[c]	$AlCl_3$	-30	1.1	4g	90
12	CH_3CO	[c]	$AlCl_3$	-30	2	4h	81
13	CH_3CO	[c]	$AlCl_3$	-20	2	4i	74
14	CH_3CO	CH_2=$CHCH_2O$–H [c]	$TiCl_4$	3	3	4j	83

a) Unless otherwise noted, reaction was carried out according to the general procedure described in the experimental. b) Isolated yield after column chromatography (SiO_2, benzene–AcOEt). c) 1.2—1.5 molar equiv of nucleophiles were used.

The reaction conditions along with the yield of the desired products **4** are summarized in Table 1. Treatment of **2a** (R=CH_3CO) with 2-methylfuran in dichloromethane in the presence of titanium(IV) chloride at −25 °C for 25 min afforded 2-(5-methyl-2-furyl)cephalosporin **4a** in 87% yield (entry 1). Aluminum (III) chloride and *p*-toluenesulfonic acid were also effective catalysts for this transformation (entries 2 and 3). Reaction of **2b** (R=CH_3) with 2-methylfuran in the same media afforded same product **4a** (entries 4 and 5). In a similar manner, the reaction of **2a** with furan, 2-methylthiophene, and *N*-methylpyrrole afforded the corresponding C(2)-substituted cephalosporins **4b—d**. Replacement of the acetoxyl group of **2a** with sulfenyl and allyloxyl groups was performed by treatment with various thiols and allyl alcohol in dichloromethane in the presence of titanium (IV) chloride and/or aluminum (III) chloride (entries 9—14).

In the present acid-catalyzed substitution reaction, no detectable amounts of by-products resulting from the C(2)-carbon-sulfur bond fission were isolated. This suggests that in the initial stage of the reaction, selective attack of Lewis acids or proton on the acetoxyl and methoxyl groups of **2** generates cation **3**, which, in turn, reacts with the nucleophiles to give **4** (Scheme 1).

Experimental

All melting points are uncorrected. IR spectra were determined with a JASCO IRA-I infrared spectrometer. ^1H NMR spectra were obtained at 60 MHz with a Hitachi R-24 spectrometer and/or at 100 MHz with a JEOL FX-100 spectrometer. Elemental analyses were performed in our

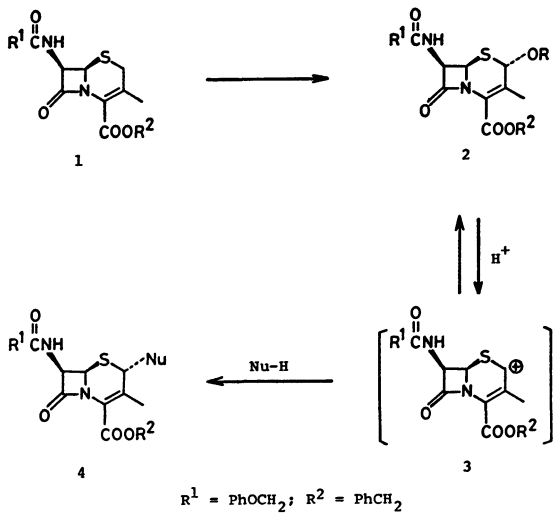

R^1 = $PhOCH_2$; R^2 = $PhCH_2$

Scheme 1.

laboratory.

Benzyl 2-acetoxy-3-methyl-7-phenoxyacetoamido-Δ^3-cephem-4-carboxylate (**2a**) was prepared from benzyl 3-methyl-7-phenoxyacetoamido-Δ^3-cephem-4-carboxylate (**1**) as previously described:[2] mp 63—65 °C (from ether); IR ($CHCl_3$) 3450, 1790, 1745, 1730, and 1690 cm^{-1}; ^1H NMR ($CDCl_3$) δ=1.98 (3H, s), 2.00 (3H, s), 4.40 (2H, s), 5.00 (1H, d, J=5 Hz), 5.16 (2H, s), 5.76 (1H, dd, J=5 and 9 Hz), 6.17 (1H, s), and 6.6—7.4 (11H, m).

Found: C, 60.43; H, 5.15%. Calcd for $C_{25}H_{24}N_2O_7S$: C, 60.47; H, 4.87%.

Benzyl 2-methoxy-3-methyl-7-phenoxyacetoamido-Δ^3-cephem-4-carboxylate (**2b**) was prepared from **1** in accordance with the reported procedure:[3] mp 121—122 °C (from ether); IR ($CHCl_3$) 3250, 1775, 1730, and 1675 cm^{-1}; ^1H NMR ($CDCl_3$) δ=2.14 (3H, s), 3.38 (3H, s), 4.49 (2H, s), 4.70 (1H, s), 4.96 (1H, d, J=5 Hz), 5.20 (2H, s), 5.80 (1H, dd, J=5 and 9 Hz), 6.7—7.4 (10H, m), and 7.45 (1H, d, J=9 Hz).

Found: C, 61.66; H, 5.23%. Calcd for $C_{24}H_{24}N_2O_6S$: C, 61.53; H, 5.16%.

Replacement of the C(2)-Substituents of 2-Acetoxy- or 2-Methoxycephalosporin with Nucleophiles. The reaction conditions and results are summarized in Table 1. The general procedure is exemplified by the preparation of **4a** (Nu=5-methyl-2-furyl) (entry 1 in Table 1). To a stirred solution of **2a** (34.2 mg, 0.069 mmol) and 2-methylfuran (0.5 mL, 5 mmol) in CH_2Cl_2 (0.5 mL) was added $TiCl_4$ (0.8 μL, 0.007 mmol) at −25 °C. After being stirred at −25 °C for 4 h, the reaction was quenched with two drops of an aqueous $NaHCO_3$. The mixture was diluted with CH_2Cl_2, dried over Na_2SO_4, and filtered. The filtrates were concentrated and chromatographed (SiO_2, benzene–AcOEt=20:1) to give **4a** (31.3 mg, 87%) as a colorless foam: IR ($CHCl_3$) 1782, 1724, and 1698 cm^{-1}; ^1H NMR ($CDCl_3$) δ=2.12 (3H, s), 2.28 (3H, s), 4.57 (2H, s), 4.61 (1H, s), 5.10 (1H, d, J=5 Hz), 5.35 (2H, s), 5.96 (1H, dd, J=5 and 8.4 Hz), 5.98 (2H, s), and 6.9—7.7 (11H, m).

Found: C, 64.99; H, 5.32%. Calcd for $C_{28}H_{26}N_2O_6S$: C, 64.85; H, 5.05%.

Compound **4b** (Nu=2-furyl): IR ($CHCl_3$) 1787, 1730, and 1697 cm^{-1}; ^1H NMR ($CDCl_3$) δ=2.08 (3H, s), 4.49 (2H, s), 4.58 (1H, s), 5.01 (1H, d, J=5 Hz), 5.28 (2H, s), 5.88 (1H, dd, J=5 and 9 Hz), 5.95—6.40 (2H, m), and 6.7—7.6 (12H, m).

Found: C, 64.13; H, 4.85%. Calcd for $C_{27}H_{24}N_2O_6S$: C, 64.27; H, 4.79%.

Compound **4c** (Nu=5-methyl-2-thienyl): IR ($CHCl_3$) 1783, 1725, and 1693 cm^{-1}; ^1H NMR ($CDCl_3$) δ=2.14 (3H, s), 2.44 (3H, s), 4.54 (2H, s), 4.26 (1H, s), 4.95 (1H, d, J=5.2 Hz), 5.32 (2H, s), 5.94 (1H, dd, J=5.2 and 8 Hz), 6.55 (2H, s), and 6.78—7.26 (11H, m).

Found: C, 63.14; H, 4.98%. Calcd for $C_{28}H_{26}N_2O_5S_2$: C, 62.90; H, 4.90%.

Compound **4d** (Nu=1-methyl-2-pyrrolyl): IR ($CHCl_3$) 1784, 1725, and 1698 cm^{-1}; ^1H NMR ($CDCl_3$) δ=2.07 (3H, s), 3.60 (3H, s), 4.50 (2H, s), 4.54 (1H, s), 4.80 (1H, d, J=5 Hz), 5.29 (2H, s), 5.6—6.05 (3H, m), and 6.5—7.6 (13H, m).

Found: C, 65.02; H, 5.25%. Calcd for $C_{28}H_{27}N_3O_5S$: C, 64.97; H, 5.26%.

Compound **4e** (Nu=butylthio): IR ($CHCl_3$) 1780, 1720, and 1695 cm^{-1}; ^1H NMR ($CDCl_3$) δ=0.90 (3H, m), 1.55 (4H, m), 2.22 (3H, s), 2.74 (2H, m), 4.45 (1H, s), 4.49 (2H, s), 5.30 (2H, s), 5.39 (1H, d, J=5 Hz), 6.00 (1H, dd, J=5 and 10 Hz), and 6.8—7.6 (11H, m).

Found: C, 61.65; H, 5.46%. Calcd for $C_{27}H_{30}N_2O_5S_2$: C, 61.57; H, 5.74%.

Compound **4f** (Nu=2-carboxylethylthio): IR ($CHCl_3$) 1780, 1710, and 1690 cm^{-1}; ^1H NMR ($CDCl_3$) δ=2.18 (3H, s), 2.5—3.1 (4H, m), 4.54 (3H, s), 5.25 (2H, s), 5.32 (1H, d, J=5 Hz), 5.95 (1H, dd, J=5 and 9 Hz), and 6.7—8.6 (12H, m).

Found: C, 57.62; H, 5.13%. Calcd for $C_{26}H_{26}N_2O_7S_2$: C, 57.55; H, 4.83%.

Compound **4g** (Nu=1-phenyl-1,2,3,4-tetrazol-5-ylthio): IR ($CHCl_3$) 1795, 1735, and 1700 cm^{-1}; ^1H NMR ($CDCl_3$) δ=2.22 (3H, s), 4.51 (2H, s), 5.06 (1H, d, J=4.2 Hz), 5.24 (2H, s), 5.87 (1H, s), 5.87 (1H, dd, J=4.2 and 8.8 Hz), and 6.7—7.7 (16H, m).

Found: C, 58.66; H, 4.40%. Calcd for $C_{30}H_{26}N_6O_5S_2$: C, 58.62; H, 4.26%.

Compound **4h** (Nu=1-methyl-1,2,3,4-tetrazol-5-ylthio): IR ($CHCl_3$) 1785, 1723, and 1692 cm^{-1}; ^1H NMR ($CDCl_3$) δ=2.26 (3H, s), 3.90 (3H, s), 4.48 (2H, s), 5.23 (1H, d, J=5 Hz), 5.27 (2H, s), 5.71 (1H, s), 5.93 (1H, dd, J=5 and 8 Hz), and 6.7—7.5 (11H, m).

Found: C, 54.57; H, 4.56%. Calcd for $C_{25}H_{24}N_6O_5S_2$: C, 54.33; H, 4.38%.

Compound **4i** (Nu=5-methyl-1,3,4-thiadiazol-2-ylthio): IR ($CHCl_3$) 1790, 1730, and 1698 cm^{-1}; ^1H NMR ($CDCl_3$) δ=2.30 (3H, s), 2.78 (3H, s), 4.58 (2H, s), 5.34 (1H, d, J=4.4 Hz), 5.35 (2H, s), 5.81 (1H, s), 6.05 (1H, dd, J=4.4 and 9.6 Hz), and 6.7—7.6 (11H, m).

Found: C, 55.11; H, 4.38%. Calcd for $C_{26}H_{24}N_4O_5S_3$: C, 54.91; H, 4.25%.

Compound **4j** (Nu=allyloxy): IR ($CHCl_3$) 1782, 1722, and 1690 cm^{-1}; ^1H NMR ($CDCl_3$) δ=2.15 (3H, s), 4.15 (2H, m), 4.54 (2H, s), 4.92 (1H, s), 5.10 (1H, d, J=4.4 Hz), 5.28 (2H, s), 5.0—5.5 (3H, m), 5.94 (1H, dd, J=4.4 and 8.8 Hz), and 6.8—7.5 (11H, m).

Found: C, 63.23; H, 5.28%. Calcd for $C_{26}H_{26}N_2O_6S$: C, 63.14; H, 5.30%.

References

1) a) S. Torii, H. Tanaka, M. Sasaoka, N. Saitoh, T. Siroi, and J. Nokami, *J. Bull. Soc. Berg.*, **91**, 951 (1982); b) "Topics in Antibiotic Chemistry," ed by E. D. Sammes, Ellis Horwood Limited, Chichester (1980), Vol. 4; c) "Recent Advances in the Chemistry of β-Lactam Antibiotics," ed by G. I. Gregory, The Royal Society of Chemistry, Burlington House, London (1980).

2) For the review see, Ref. 1b, p. 173.

3) a) T. Kamiya, T. Teraji, M. Hashimoto, O. Nakaguchi, and T. Oku, *J. Am. Chem. Soc.*, **98**, 2342 (1976); b) D. O. Spry, *Tetrahedron Lett.*, **1977**, 3611; c) D. H. Bremner and M. M. Campbell, *J. Chem. Soc., Perkin Trans. 1*, **1977**, 2298.

4) D. O. Spry, *Tetrahedron Lett.*, **21**, 1289 (1980).

5) a) W. H. Koster, J. E. Dolfini, and B. Toeplity, *J. Org. Chem.*, **43**, 79 (1978); b) G. Franceschi, M. Foglio, P. Masi, A. Surato, G. Palamidessi, L. Bernardi, F. Arcamone, and G. Cainelli, *J. Am. Chem. Soc.*, **99**, 248 (1977); c) D. O. Spry, *Tetrahedron Lett.*, **1972**, 3717.

6) C. U. Kim and D. N. McGregor, *Tetrahedron Lett.*, **1978**, 409; see also Refs. 2 and 5.

7) a) H. E. Applegate, C. M. Cimarusti, J. E. Dolfini, P. T. Funke, W. H. Koster, M. S. Puar, W. A. Slusarchyk, and M. G. Young, *J. Org. Chem.*, **44**, 811 (1979); b) W. A. Slusarchyk, H. E. Appligate, C. M. Cimarusti, J. E. Dolfini, P. Funke, and M. Puar, *J. Am. Chem. Soc.*, **100**, 1886 (1978); see also Ref. 5a.

Conversion of Lupeol into Dammarane Derivatives

Shinya OHTA, Motoo TORI, Takahiko TSUYUKI, and Takeyoshi TAKAHASHI*

Department of Chemistry, Faculty of Science, The University of Tokyo, Hongo, Bunkyo-ku, Tokyo 113

(Received February 5, 1983)

Synopsis. On treatment with potassium carbonate in aqueous dioxane, 3β-tetrahydropyranyloxybaccharan-18β-yl mesylate, prepared from lupeol, underwent D-ring contraction. The solvolytic products were hydrolyzed and acetylated to give Δ^{20}-, $\Delta^{20(22)}$-, $\Delta^{17(20)}$-, and $\Delta^{13(17)}$-dammaren-3β-yl acetates and (20*S*)-20-hydroxydammaran-3β-yl acetate together with bacchar-13(18)- and -12-en-3β-yl acetates.

It has been proposed that dammarane derivatives undergo D-ring enlargement to afford baccharane derivatives, which yield lupane derivatives by E-ring formation in succession in the biogenesis of triterpenes. In connection with a study on the behavior of C-20 cation on dammarane derivatives, such as **1**,[1] we examined reactivities of C-18[2] cation on baccharane derivatives (**2**). In this paper, a conversion of baccharane derivatives into dammarane derivatives is described. Baccharane derivatives being prepared from lupeol (**3**), this conversion constitutes a reverse transformation[3] from the biogenetic pathway described above.

3β-Hydroxybaccharan-18-one (**4**) was prepared from **3** by a known procedure.[4] Reduction of **4** with lithium aluminium hydride gave a 3β,18α-dihydroxy derivative (**5**) exclusively, which on partial acetylation afforded a 3β-monoacetate (**6**). On the other hand, Birch reduction of **4** afforded a 3β,18β-dihydroxy derivative (**7**). Although selective acetylation of the 3β-hydroxyl group of **7** was attempted under various conditions, a satisfactory selectivity was not attained; a diacetate (**8**) appeared at the early reaction stage. Protection of the 3β-hydroxyl group of **4** by tetrahydropyranylation gave a tetrahydropyranyloxy ketone (**9**), which was subjected to Birch reduction to afford a 3β-tetrahydropyranyloxy-18β-hydroxy derivative (**10**).

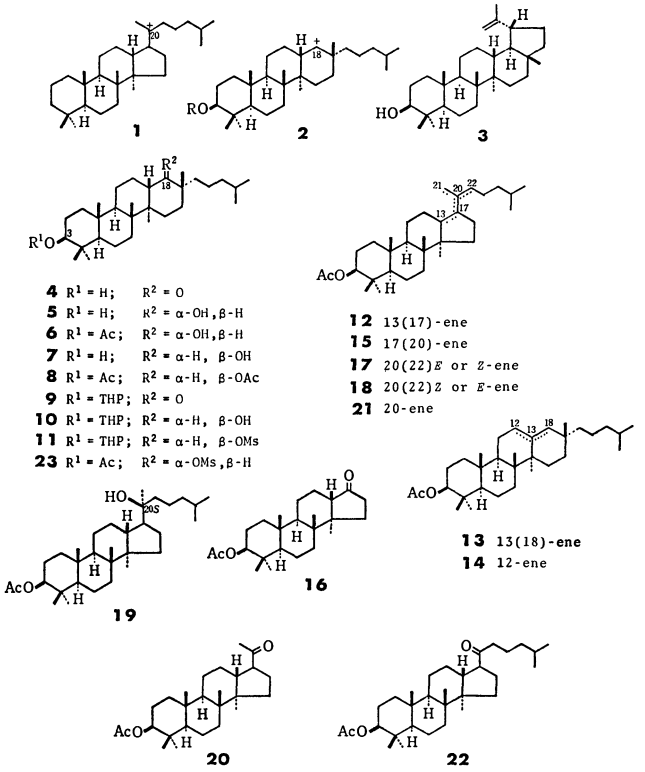

The mesylate (**11**; *ca.* 50 mg), prepared from **10**, was treated with potassium carbonate in boiling aqueous dioxane for 4 h and the products were treated with 10% hydrochloric acid to give a mixture of alcohols, which was acetylated. The acetylation product was separated by column chromatography into three fractions, A, B, and C. The fraction A, a mixture of unsaturated acetates, was further separated by column chromatography of silica gel impregnated with silver nitrate into five components. The first (the least polar) component was found to be a mixture of dammar-13(17)-en-3β-yl acetate (**12**) and bacchar-13(18)- and bacchar-12-en-3β-yl acetates (**13** and **14**) by comparison of their retention times with those of authentic samples[5,6] in GLC examination. The second component was shown to be a tetrasubstituted olefinic acetate by ^{1}H NMR and high resolution mass spectrum. This compound, on oxidation with ruthenium tetraoxide, afforded an octanor keto acetate (**16**),[7] showing a molecular ion at *m/e* 374. Therefore, the original acetate (**15**) is inferred to be dammar-17(20)-en-3β-yl acetate.

The third component showed an olefinic proton at δ 5.14 (1H, m), IR 1730 cm^{-1}, and a molecular ion at *m/e* 470.4221. The fourth component gave almost the same fragmentation pattern as that of the third one in the mass spectrum and showed an olefinic proton at δ 5.08 (1H, m) and a molecular ion at *m/e* 470.4106. These two compounds were found to be identical with an *E,Z*-isomeric pair of dammar-20(22)-en-3β-yl acetates (**17** and **18**), prepared from dammaranediol II monoacetate (**19**).[6] On oxidation with ruthenium tetraoxide, **17** and **18** gave the same product, hexanordammaran-20-one (**20**).[6,7]

The most polar component showed the presence of an *exo*-methylene moiety by ^{1}H NMR, IR, and a molecular ion. Spectral comparison showed that the compound was identical with dammar-20-en-3β-yl acetate (**21**),[6] prepared from **19**. Oxidation of the acetate (**21**) with ruthenium tetraoxide gave 22-nor-20-oxodammaran-3β-yl acetate (**22**).[6,7]

The fraction B was identical with baccharane-3β,18β-diyl diacetate (**8**). The fraction C was shown to be dammaranediol II monoacetate (=(20*S*)-20-hydroxydammaran-3β-yl acetate) (**19**).[6] A 20*R*-epimer was not detected in the solvolytic product.

3β-Acetoxy-18α-hydroxy derivative (**6**) was treated with mesyl chloride in a mixture of triethylamine and dichloromethane to give a mesylate (**23**), which was subjected to solvolysis under the same conditions as before. The product was found to be a mixture of bacchar-13(18)- and bacchar-12-en-3β-yl acetates (**13** and **14**)[5] by ^{1}H NMR and GLC examination.

Experimental[8]

Baccharane-3β,18α-diol (5) and 18α-Hydroxybaccharan-3β-yl Acetate (6). 3β-Hydroxybaccharan-18-one (**4**; 27 mg)[4]

was treated with $LiAlH_4$ (*ca.* 5 mg) in THF and the reaction product was worked up as usual to afford **5** as white crystals, NMR δ 3.20 (1H, m) and 3.25 (1H, br s); MS *m/e* 446 (M^+), 428, and 410. The diol (**5**) was acetylated with Ac_2O (0.1 ml) in pyridine (0.1 ml) at room temperature overnight. Usual work-up and crystallization from $CHCl_3$–MeOH gave **6** (26 mg) as white needles, mp 199—202 °C; IR (Nujol) 3560, 1720, and 1260 cm^{-1}; NMR δ 0.80—1.10 (24H), 2.03 (3H, s), 3.23 (1H, br s), and 4.47 (1H, dd-like); MS *m/e* 488 (M^+), 470, 455, 428, 413, 410, 385, 344, 189, 135 (base peak); Found: *m/e* 488.4220. Calcd for $C_{32}H_{56}O_3$: M 488.4229.

Baccharane-3β,18β-diol (7) and Baccharane-3β,18β-diyl Diacetate (8). A solution of **4** (40 mg) in THF (1 ml) and MeOH (0.1 ml) was added to Li (*ca.* 30 mg) in liquid NH_3 (3 ml) at −78 °C with stirring and the reaction mixture was kept at −33 °C for 15 min. An aqueous NH_4Cl solution was added and the solution was warmed to remove NH_3 and extracted with Et_2O. The ethereal layer was worked up to give **7** in a quantitative yield, NMR δ 0.77—1.02 (24H), 3.16 (1H, d, J=10 Hz), and 3.18 (1H, dd-like); MS *m/e* 446 (M^+), 428, 220, 207, 189, and 95 (base peak).

A solution of diol (**7**; *ca.* 40 mg) in Ac_2O (0.1 ml) and pyridine (0.1 ml) was allowed to stand overnight at room temperature. The reaction was stopped by addition of MeOH and the usual work-up was followed to give **8** (*ca.* 45 mg); mp 183—184 °C ($CHCl_3$–MeOH); IR (film) 1740 and 1245 cm^{-1}; NMR δ 0.82—1.03 (24H), 2.06 (6H, s), 4.48 (1H, dd-like), and 4.76 (1H, d, J=11 Hz); MS *m/e* 530 (M^+), 470 (base peak), 455, 410, 249, 220, 207, 202, and 189; Found: C, 76.75; H, 10.84%. Calcd for $C_{34}H_{58}O_4$: C, 76.93; H, 11.01%.

3β-Tetrahydropyranyloxybaccharan-18β-ol (10). A solution of **4** (46 mg) and 3,4-dihydro-2*H*-pyran (0.1 ml) in $CHCl_3$ (2 ml) was kept with a catalytic amount of TsOH for 1 h. After addition of an aqueous $NaHCO_3$ solution, organic layer was worked up to give a residue, which was purified by silica gel column chromatography. Elution with 5—10% EtOAc in hexane afforded **9** (50 mg), mp 183—185 °C ($CHCl_3$–MeOH); IR (KBr) 1695 cm^{-1}; MS *m/e* 528 (M^+), 444, 427, 426, 411, 388, 383, 360 (base peak), 342, 237, 223, 207, 196, and 189; Found: *m/e* 528.4530. Calcd for $C_{35}H_{60}O_3$: M 528.4540.

The ketone (**9**; 50 mg), dissolved in a mixture of THF (2 ml) and MeOH (0.1 ml), was added to Li (40 mg) in liquid NH_3 (3 ml) kept at −78 °C, and the reaction mixture was subjected to the same treatment as in the case of **7** to afford **10** (49 mg), NMR δ 0.80—1.01 (24H) and 3.07 (1H, d, J=11 Hz); MS *m/e* 530 (M^+), 446, 429, 428, 410, 395, 344, 220, 207, 189, and 85 (base peak).

Solvolysis of 3β-Tetrahydropyranyloxybaccharan-18β-yl Mesylate (11). Mesyl chloride (0.1 ml) was added to a solution of **10** (50 mg) in Et_3N (0.2 ml) and CH_2Cl_2 (1 ml) and the mixture was allowed to stand for 1 h. The usual work-up afforded a mesylate (**11**), which, without further purification, was subjected to solvolysis. The mesylate (**11**) was dissolved in a solution of K_2CO_3 in H_2O (2 ml) and dioxane (2 ml), and refluxed for 4 h. The reaction mixture was slightly acidified with 10% HCl and warmed for 10 min to complete the deprotection at C-3. The usual work-up afforded a residue, which was acetylated with Ac_2O (0.1 ml) and pyridine (0.1 ml). The reaction product was separated by silica gel (2.5 g) column chromatography into three fractions A, B, and C.

Fraction A (32 mg), eluted with 5—10% EtOAc in hexane, was further subjected to separation by column chromatography of silica gel (3 g) impregnated with $AgNO_3$ (0.5 g). Elution with 10% $CHCl_3$ in hexane gave two components. One component (*ca.* 1.2 mg) gave three peaks at t_R 18.3, 20.3, and 21.4 min in GLC analysis. These retention times were identical with those of **12**, **13**, and **14**, respectively. The other component (**15**; 1.2 mg) showed ^1H NMR δ 2.05 (3H, s) and 4.48 (1H, m); MS *m/e* 470 (M^+), 410, 357, 249, 205, 190, and 69 (base peak); Found: *m/e* 470.4077. Calcd for $C_{32}H_{54}O_2$: M 470.4121. On oxidation with RuO_4 in CCl_4, **15** affoded 17-oxooctanordammaran-3β-yl acetate (**16**); IR (KBr) 1738 cm^{-1}; MS *m/e* 374 (M^+), 314, 299, 271, 191, 190, and 189.

Elution with 33% $CHCl_3$ in hexane afforded a geometrical pair of dammar-20(22)-en-3β-yl acetates (**17** and **18**); the isomer (**17**; 3.7 mg) with a large R_f value: mp 143—144 °C, IR (KBr) 1730 and 1250 cm^{-1}; NMR δ 0.82—0.97 (24H), 2.03 (3H, s), 4.46 (1H, m), and 5.14 (1H, m); MS *m/e* 470 (M^+), 410, 344, 289, 249, 229, 220, 189, and 69 (base peak); Found: *m/e* 470.4221. Calcd for $C_{32}H_{54}O_2$: M 470.4121. The other isomer (**18**) with a small R_f value: mp 159.5—161 °C; IR (KBr) 1730 and 1250 cm^{-1}; NMR δ 0.80—0.96 (24H), 2.03 (3H, s), 4.46 (1H, m), and 5.08 (1H, m); MS *m/e* 470 (M^+), 410, 395, 344, 289, 249, 229, 220, 189, and 95 (base peak); Found: *m/e* 470.4106. Calcd for $C_{32}H_{54}O_2$: M 470.4121. Oxidation of **17** and **18** with RuO_4 in CCl_4 afforded hexanordammaran-20-one (**20**), mp 202.5—204 °C; IR (KBr) 1730, 1710, and 1250 cm^{-1}; NMR δ 0.83—0.90 (12H), 0.97 (3H, s), 2.03 and 2.11 (each 3H, s), and 4.47 (1H, dd-like); MS *m/e* 402 (M^+), 359, 342, 327, 299 (base peak), 229, 204, 191, and 189; Found: *m/e* 402.3108. Calcd for $C_{26}H_{42}O_3$: M 402.3133.

The most polar component (**21**; 9 mg) was eluted with 50% $CHCl_3$ in hexane, mp 142.5—144 °C (MeOH); IR (KBr) 1730, 1260, and 885 cm^{-1}; NMR δ 0.83—0.97 (21H), 2.03 (3H, s), 4.46 (1H, m), and 4.68 (2H, br s); MS *m/e* 470 (M^+), 410, 395, 344, 289, 249, 229, 220, 189, and 95 (base peak); Found: *m/e* 470.4055. Calcd for $C_{32}H_{54}O_2$: M 470.4121. Oxidation of **21** with RuO_4 gave 22-nor-20-oxodammaran-3β-yl acetate (**22**), IR 1740 (sh) and 1730 cm^{-1}; NMR δ 0.82—0.91 (18H), 0.98 (3H, s), 2.03 (3H, s), 2.25—2.55 (2H, m), and 4.48 (1H, m).

Solvolysis of 3β-Acetoxybaccharan-18α-yl Mesylate (23). 3β-Acetoxybaccharan-18α-ol (**6**; *ca.* 10 mg) was dissolved in Et_3N (0.1 ml) and CH_2Cl_2 (0.3 ml). The solution was treated with mesyl chloride (1 drop) and worked up to give **23**, which was subjected to solvolysis as before. The solvolytic product was a mixture of **13** (t_R=20.3 min) and **14** (t_R=21.4 min) by GLC examination.

References

1) M. Tori, T. Tsuyuki, and T. Takahashi, *Bull. Chem. Soc. Jpn.*, **50**, 3349 (1977).

2) Numbering of baccharane refers to the nomenclature described in the Chemical Abstracts.

3) Synthesis of the skeleton of dammarane-type triterpene from hydroxyhopanone was reported by H. Fujimoto and O. Tanaka (*Chem. Pharm. Bull.*, **18**, 1440 (1970)).

4) E. Suokas and T. Hase, *Acta Chem. Scand.*, **25**, 2359 (1971).

5) K. Suemura, T. Irokawa, M. Tori, S. Ohta, Y. Moriyama, T. Tsuyuki, T. Takahashi, A. Itai, and Y. Iitaka, *Chem. Lett.*, **1982**, 1617.

6) J. S. Mills, *J. Chem. Soc.*, **1956**, 2196.

7) P. Crabbé, G. Ourisson, and T. Takahashi, *Tetrahedron*, **3**, 279 (1958); J.-F. Biellmann, P. Crabbé, and G. Ourisson, *ibid.*, **3**, 303 (1958).

8) General procedures are the same as those described in *Bull. Chem. Soc. Jpn.*, **54**, 234 (1981).

Branched-chain Sugars. XXXIV. Synthesis of Methyl Dihydroeurekanate[1]

Juji YOSHIMURA,* Kazutoshi HARA, and Masafumi MATSUZAWA†

Laboratory of Chemistry for Natural Products, Faculty of Science, Tokyo Institute of Technology, Nagatsuta, Midori-ku, Yokohama 227

(Received February 9, 1983)

Synopsis. Methyl dihydroeurekanate; methyl 6-deoxy-4-*C*-[(*S*)-1-hydroxyethyl]-2,3-*O*-methylene-D-galactonate was synthesized from benzyl 6-deoxy-4-*C*-[(*S*)-1-hydroxyethyl]-2,3-*O*-methylene-D-galactopyranoside.

Up to the present, three branched-chain aldonolactones have been found in oligosaccharide antibiotics of orthothomycin family,[2] and they were characterized as their methyl aldonate. The structure of the first one in everninomicins[3] was determined to be 4-*C*-[(*S*)-1-methoxyethyl]-2,3-*O*-methylene-L-arabinono-1,5-lactone by X-ray analysis,[4] and the corresponding aldonate, methyl 6-deoxy-4-*C*-hydroxymethyl-5-*O*-methyl-2,3-*O*-methylene-L-idonate[5] was synthesized from L-arabinose *via* the introduction of equatorial 4-*C*-vinyl group by us.[6] The structure of methyl eurekanate obtained from flambamycin[2] and avilamycin A[7] was determined to be methyl 4-*C*-acetyl-6-deoxy-2,3-*O*-methylene-D-galactonate by a similar synthesis[8] and X-ray analysis.[7] D-*galacto* configuration of the remaining methyl dihydroeurekanate (**1**) from avialamycin C was proved by the fact that one of the epimers obtained by reduction of the 4-*C*-acetyl group of methyl eurekanate was identical with **1**,[9] but, the chirality of its 1-hydroxyethyl group was unknown. As was commonly observed in naturally occuring branched-chain sugars such as L-*γ*-octose[10] and D-aldgalose,[11] the chirality of 1-hydroxyethyl group of **1** was deduced to be (*S*), and in fact, it was recently proved by X-ray analysis.[12] This paper describes a simple preparation of **1** from benzyl 6-deoxy-4-*C*-[(*S*)-1-hydroxyethyl]-2,3-*O*-methylene-α-D-galactopyranoside [(1′*S*)-**2**].[13]

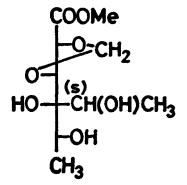

1

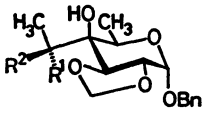

(1′R)-**2** R^1=OH, R^2=H
(1′S)-**2** R^1=H, R^2=OH
(1′R)-**3** R^1=OAc, R^2=H
(1′S)-**3** R^1=H, R^2=OAc

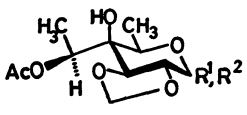

4 R^1,R^2=H, OH
5 R^1,R^2=O

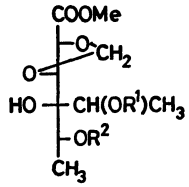

6 R^1=Ac, R^2=H
7 R^1=H, R^2=Ac
8 R^1=R^2=Ac

Results and Discussion

In our previous report,[13] (1′*R*)-**2** and (1′*S*)-**2** obtained by reduction of (1′*R*)- and (1′*S*)-mixture of the corresponding 4-*C*-(oxiranyl) derivative were directly separated by silica-gel column chromatography, but, the separation proceeded more smoothly after the usual acetylation into (1′*R*)-**3** and (1′*S*)-**3**. The both epimers were thoroughly characterized by ^{1}H- and ^{13}C-NMR. However, the hydrogenolysis of (1′*S*)-**3** into **4** gave an unstable complex mixture which showed two acetyl signals in the ratio of 3:1 and aldehydic proton at *δ* 9.73 in ^{1}H-NMR spectrum. This fact indicates the presence of acyclic species and/or the occurrence of acetyl migration. Oxidation of crude **4** into **5** with bromine–water gave again a mixture which showed two acetyl signals. Therefore, crude **5** was converted into the corresponding methyl aldonate by treatment with diazomethane in methanol. ^{1}H-NMR spectrum of the product indicated the presence of two monoacetate (**6** and **7**) in the ratio of 1.5:1, indicating the acetyl migration during these conversions. Usual acetylation of the mixture gave diacetate (**8**) in fairly good yield. The ^{1}H NMR spectrum and the specific rotation of **8** shown in Table 1 revealed its structure. Deacetylation of **8** in methanol with catalytic amount of sodium methoxide gave **1** in 76% yield. ^{1}H-NMR and ^{13}C-NMR spectra shown in Table 2 together with that of **8** proved that **1** was identical with that obtained from avilamycin C.

Experimental

Specific rotations were measured with JASCO DIP-4 polarimeter in chloroform. ^{1}H- and ^{13}C-NMR were recorded in chloroform-*d* with JEOL PS-100 and JEOL FX-100 spectrometers, respectively. Chemical shifts and Coupling constants were recorded in *δ* (ppm) and Hz units, respectively.

*Isolation of (1′*R*)-3 and (1′*S*)-3.* The mixture of (1′*R*)-**1** and (1′*S*)-**1** (3.2 g, 10.3 mmol) in pyridine (25 ml) was acetylated in the usual procedure to give a syrupy product which was separated on a silica-gel (WAKO C-200) column (1:2 ethyl acetate–hexane). (1′*R*)-**3** (R_f 0.28) and (1′*S*)-**3** (R_f 0.41) were obtained in 49% (1.79 g) and 34% (1.23 g) yields, respectively.

(1′*R*)-**3**: $[\alpha]_D$ +167° (*c* 1.0), ^{1}H-NMR (*δ*): 7.41 (s, 5H, Ph), 5.36 (d, $J_{1,2}$ 3.0, H-1), 5.14 and 5.24 (ABq, 2H, *J* 1.4, OCH_2O), 5.00 (q, $J_{1',2'}$ 6.8, H-1′), 4.79 (s, 2H, CH_2Ph), 4.03 (d, $J_{2,3}$ 9.8, H-3), 3.92 (dd, H-2), 3.70 (q, $J_{5,6}$ 6.8, H-5), 2.85 (bs, OH), 2.14 (s, 3H, OAc), 1.28 (d, 3H, H-2′), 1.19 (d, 3H, H-6); ^{13}C-NMR (ppm): 13.4 and 15.7 (each q, C-6,2′), 21.3 (q, CH_3CO), 68.1, 73.2, 73.3 and 73.6 (each d, C-2,3,5,1′), 70.1 (t, CH_2Ph), 76.6 (s, C-4), 96.4 (t, OCH_2O), 96.7 (d, C-1), 127.9 and 128.5 (each d, Ph), 137.3 (s, Ph), 171.2 (s, C=O).

† Present address: K. I. Chemicals Research Institute, Fukude-cho, Iwata, Shizuoka 437-12.

Table 1. Comparison of physical properties for **1** and **8** with those reported for samples obtained from avilamycin C

	$[\alpha]_D$ (in $CHCl_3$)	Chemical shift (δ) and coupling constant (Hz)									
		H-2 ($J_{2,3}$)	H-3	H-5 ($J_{5,6}$)	H-6	H-1′ ($J_{1',2'}$)	H-2′	OCH_2O	CO_2Me	OH	OAc
1	—	4.26 d (5.5)	4.88 d	3.7—4.3 m (6.6)	1.28 d	3.7—4.3 m (6.6)	1.32 d	4.90 s 5.23 s	3.79 s	2.02 s 2.23 s	—
(Reported)	−36.9°	4.38 d (5.5)	4.88 d	3.8—4.3 m (6.5)	1.30 d	3.8—4.3 m (6.5)	1.32 d	4.90 s 5.22 s	3.78 s	2.52 d 2.70 d 3.18 s	—
8	−48°	4.36 d (4.8)	4.92 d	5.30 q (7.0)	1.30 d	5.16 q (7.0)	1.32 d	4.91 s 5.20 s	3.80 s	2.80 s	2.03 s 2.07 s
(Reported)	−50°	4.35 d (5.2)	4.92 d	5.30 q (7.1)	1.30 d	5.16 q (7.1)	1.31 d	4.90 s 5.18 s	3.75 s	2.73 s	2.00 s 2.04 s

Table 2. ^{13}C-NMR data of **1** and **8**

Position[a]	**1**	Reported **1**	**8**[b]
1	52.6 (q)	52.6 (q)	52.5 (q)
2	172.3 (s)	172.1 (s)	171.5 (s)
3	82.4 (d)	82.1 (d)	80.9 (d)
4	74.6 (d)	74.5 (d)	74.8 (d)
5	76.2 (s)	76.1 (s)	76.2 (s)
6	69.6 (d)**[c]	69.6 (d)**	71.9 (d)**
7	17.6 (q)*	18.0 (q)*	15.4 (q)*
8	95.6 (t)	95.6 (t)	95.6 (t)
9	69.9 (d)**	69.9 (d)**	71.9 (d)**
10	18.1 (q)*	18.2 (q)*	15.5 (q)*

a) The numbering of carbon atoms is shown below.
b) **8** showed additional signals of acetyl carbons: 21.2 (q, 2×C), 170.0 and 174.8 (each s, 2×C=O) ppm.
c) Each pairs of marked assignments may be reversed although those given here are preferred.

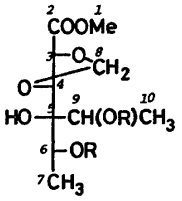

(1′*S*)-**3**: $[\alpha]_D$ +116° (*c* 0.64); ^{1}H-NMR (δ): 7.42 (s, 5H, Ph), 5.36 (d, $J_{1,2}$ 3.6, H-1), 5.15 and 5.24 (ABq, 2H, *J* 1.0, OCH_2O), 5.07 (q, $J_{1',2'}$ 6.6, H-1′), 4.78 (s, 2H, CH_2Ph), 4.17 (d, $J_{2,3}$ 10.0, H-3), 3.85 (dd, H-2), 3.78 (q, $J_{5,6}$ 6.6, H-5), 2.36 (bs, OH), 2.04 (s, 3H, OAc), 1.38 (d, 3H, H-2′), 1.16 (d, 3H, H-6); ^{13}C-NMR (ppm): 13.4 and 15.7 (each q, C-6,2′), 21.3 (q, CH_3CO), 68.1, 73.2, 73.3 and 73.6 (each d, C-2,3,5,1′), 70.1 (t, CH_2Ph), 76.6 (s, C-4), 96.4 (t, OCH_2O), 96.7 (d, C-1), 127.9 and 128.5 (each d, Ph), 137.3 (s, Ph), 171.2 (s, CO). Found for (1′*R*)-**3**: C, 60.97; H, 6.79 and for (1′*S*)-**3**: C, 60.96; H, 6.88%. Calcd for $C_{18}H_{24}O_7$: C, 61.35; H, 6.86%.

Conversion of (1′S)-3 into 6 and 7. A suspension of (1′*S*)-**3** (540 mg, 1.46 mmol) and palladium–carbon (10%, 500 mg) in ethanol (100 ml) containing 1 M HCl (2 ml) was hydrogenolyzed in an autoclave under hydrogen atmosphere (60 kg/cm^2) for 7 h at room temperature. The usual work-up of the reaction mixture gave crude **4** in 76% (292 mg) yield. To a suspension of the above **4** (241 mg, 0.92 mmol) and trilead (II) dicarbonate dihydroxide (2.84 g) in water (5 ml) was added bromine (94.9 μl) and the mixture was shaken in dark for 12 h at room temperature. After aeration the mixture was filtered, and the filtrate was passed through IR 120 (H^+) column and then evaporated to give a syrupy **5** in 95% (194 mg) yield. This syrup was esterified with diazomethane in the usual manner gave a mixture of **6** and **7**. The predominant product showed the following ^{1}H-NMR data: 5.40 (q, $J_{1',2'}$ 7.0, H-1′), 5.20 (q, $J_{5,6}$ 6.4, H-5), 5.19 and 5.00 (each s, 2H, OCH_2O), 4.88 (d, $J_{2,3}$ 4.4, H-3), 4.72 (d, H-2), 3.83 (s, 3H, MeO), 2.14 (s, 3H, OAc), 1.51 (d, 3H, H-2′), 1.32 (d, 3H, H-6).

Methyl Dihydroeurekanate Diacetate (8). The mixture of **6** and **7** (58 mg, 0.199 mmol) in pyridine (0.5 ml) was acetylated by the usual manner to give syrupy **8** in 66% (42 mg) yield, which was purified by a preparative TLC (2:3 acetone–hexane). Found: C, 50.01; H, 6.72%. Calcd for $C_{14}H_{22}O_9$: C, 50.29; H, 6.63%.

Methyl Dihydroeurekanate (1). A solution of **8** (23 mg, 0.1 mmol) in methanol (1 ml) containing catalytic amount of sodium methoxide was kept at room temperature for 6 h, passed through a IR 120 (H^+) column, evaporated, to give a sirup which was purified on a preparative TLC (1:1 acetone–hexane). Yield, 76% (15 mg).

References

1) Part XXXIII: J. Yoshimura and K. Sato, *Carbohydr. Res.*, in contribution.
2) W. D. Ollis, C. Smith, and D. E. Wright, *Tetrahedron*, **35**, 105 (1979).
3) A. K. Ganguly, "Oligosaccharide Antibiotics," in "Topics in Antibiotic Chemistry," ed by P. G. Sammes, Wiley, New York (1978), Vol. 2, p. 59.
4) A. K. Ganguly, O. Z. Sarre, A. T. McPhall, and R. W. Miller, *J. Chem. Soc., Chem. Commun.*, **1979**, 22.
5) A. K. Ganguly, O. Z. Sarre, D. Greeves, and J. Morton, *J. Am. Chem. Soc.*, **97**, 1982 (1975).
6) M. Matsuzawa and J. Yoshimura, *Carbohydr. Res.*, **81**, C5 (1980).
7) E. Kupfer, K. Neupert-Laves, M. Dobler, and W. Keller-Schierlein, *Helv. Chim. Acta*, **63**, 1141 (1980).
8) J. Yoshimura and M. Matsuzawa, *Carbohydr. Res.*, **85**, C1 (1980); **100**, 283 (1982).
9) W. Keller-Schierlein, W. Heilman, W. D. Ollis, and C. Smith, *Helv. Chim. Acta*, **62**, 7 (1979).
10) H. Paulsen and V. Sinnwell, *Chem. Ber.*, **111**, 869 (1978).
11) H. Paulsen, B. Sumfleth, and H. Redlich, *Chem. Ber.*, **109**, 1362 (1976).
12) E. Kupfer, K. Neupert-Laves, M. Dobler, and W. Keller-Schierlein, *Helv. Chim. Acta*, **65**, 3 (1982).
13) J. Yoshimura and M. Matsuzawa, *Carbohydr. Res.*, **96**, 7 (1981).

Hydrolysis of *p*-Nitrophenyl Esters by Hydrophobic Linear Molecule Containing Two Histidine Residues

Masato KODAKA

National Chemical Laboratory for Industry, Tsukuba 305

(Received March 1, 1983)

Synopsis. A new type of linear nucleophile, CH_3O–His–CO–$(CH_2)_8$–CO–His–OCH_3(HisC$_8$His), was designed, and its catalytic behavior for the hydrolysis of *p*-nitrophenyl acetate, hexanoate and laurate was investigated. It was shown that HisC$_8$His enhanced the hydrolysis of *p*-nitrophenyl laurate and hexanoate as compared with imidazole both in the absence and presence of methyltrioctylammonium chloride.

Hydrophobic interaction has proved to be very significant for the enzyme activity by the use of simple model compounds, such as functional polymers,[1,2] peptides,[3–5] cyclodextrins,[6,7] micelles[8–13] or other hydrophobic aggregates.[14,15] In the present paper, the author wishes to describe the catalytic behavior of a new type of simple-structure nucleophile which is composed of a long alkyl chain and two histidine residues placed on both sides of the long alkyl chain. The linear molecule with such a structure will have enough hydrophobicity but simultaneously have enough solubility in water. Furthermore, in the present study the effect of the hydrophobic quaternary ammonium salt, methyltrioctylammonium chloride (MTAC), was investigated, since there is a possibility that the hydrolysis might be considerably activated due to the formation of hydrophobic ion pairs between imidazolate anion and ammonium cation.[14,15] In relation to this, the author tried to combine MTAC with histidine residue covalently.

Experimental

CH_3O–His–CO–$(CH_2)_8$–CO–His–OCH_3(HisC$_8$His) or $CH_3(CH_2)_4$CO–His–OCH_3(C$_5$His) was synthesized from L-histidine methyl ester and sebacoyl chloride or hexanoyl chloride. $Br(CH_2)_5$CO–His–OCH_3 was prepared from L-histidine methyl ester and 6-bromohexanoyl chloride, and then it was converted to $Br^-[CH_3(CH_2)_7]_3N^+(CH_2)_5$CO–His–$OCH_3$(N$^+C_5$His) by the reaction with trioctylamine. Imidazole, *N*-*t*-butoxycarbonyl-L-histidine methyl ester (Boc–His–OCH_3), methyltrioctylammonium chloride (MTAC), and *p*-nitrophenyl esters were commercially available.

The hydrolysis was carried out in 10 v/v% ethanol–water at 25 °C, μ=0.5(KCl), buffered with 1/10 mol dm^{-3} potassium dihydrogenphosphate–1/20 mol dm^{-3} sodium borate for pH 7—9, 1/20 mol dm^{-3} sodium borate–1/20 mol dm^{-3} sodium carbonate for above pH 9. The reaction rate was determined by using the absorbance of *p*-nitrophenolate at 400 nm with a Hitachi Model 100-10 spectrophotometer. Pseudo-first-order rate constant (k_1) was estimated by correcting the total rate constant (k_{total}) for the spontaneous hydrolysis as follows:

$$k_1 = k_{total} - k_{spont}.$$

In the presence of MTAC, k_{spont} means the rate constant for the hydrolysis only by MTAC. Second-order rate constant (k_2) was obtained by dividing k_1 by the total catalyst concentration per histidine residue.

Results and Discussion

Second-order rate constants (k_2) for the hydrolysis of *p*-nitrophenyl esters are summarized in Table 1. It should be noted that HisC$_8$His showed much higher activity than imidazole, Boc–His–OCH_3 and C$_5$His for the hydrolysis of *p*-nitrophenyl laurate (PNPL). For *p*-nitrophenyl hexanoate (PNPH), HisC$_8$His showed a little higher activity than imidazole and 2—4 times higher activity than Boc–His–OCH_3 and C$_5$His. HisC$_8$His gave a little greater activity for *p*-nitrophenyl acetate (PNPA) than Boc–His–OCH_3 and C$_5$His but smaller activity than imidazole. These results suggest that the rate enhancement for PNPL and PNPH was primarily ascribed to the hydrophobic interaction between the long alkyl chain of HisC$_8$His and those of the substrates. The significance of the hydrophobic interaction is also indicated by the following results. When 3 mol dm^{-3} urea was added the hydrolytic rate of PNPL by HisC$_8$His was decreased by *ca.* 80%, while that of PNPA only by *ca.* 20%. It is generally known that urea denaturates enzymes partly owing to the inhibition of hydrophobic interaction.[16] The analogous linear molecules which have a long alkyl chain but only one histidine residue, $CH_3(CH_2)_6$CO–His–OCH_3(C$_7$His) and $CH_3(CH_2)_{14}$CO–His–OCH_3(C$_{15}$His), also seem to be hydrophobic but they are poorly soluble in water, and therefore these catalysts could not be investigated in the present study. In this respect, the bi-histidine catalyst like HisC$_8$His designed in the present study is superior to the mono-histidine catalysts like C$_7$His and C$_{15}$His.

As reported by Kunitake *et al.*, hydrophobic nucleophiles having imidazoles gave enormously large rate enhancement in the hydrolysis of *p*-nitrophenyl ester in the presence of MTAC, due to the increase in the fraction of imidazolate anion facilitated by the formation of hydrophobic ion pairs between imidazolate anion and quaternary ammonium cation.[14,15] In the present study, therefore, the author has attempted the hydrolysis in the presence of both HisC$_8$His and MTAC in order to increase the catalytic ability of HisC$_8$His. The kinetic data are summarized in Table 2. Also in this case, HisC$_8$His gave considerably high catalytic activity for PNPL and PNPH as compared with the other nucleophiles, while it gave virtually no enhancement for PNPA. The hydrolysis of PNPL by HisC$_8$His was enhanced by *ca.* 20 times in the presence of MTAC. Figure 1 shows the relation between the pseudo-first-order rate constant (k_1) and the concentration of HisC$_8$His in the presence of MTAC. The k_1 values increase almost linearly with the HisC$_8$His concentration for both PNPH and PNPL. In Fig. 2 are shown the pH profiles of k_2 for PNPH and PNPL in the presence of HisC$_8$His and MTAC, where k_2 begins to increase exceedingly above pH 8.5—9.0. This suggests that the imidazolate anion is the catalytic nucleophile mainly contributing to the hydrolysis.[11,14,15] Since HisC$_8$His showed considerably higher catalytic activity on addition of MTAC, the author attempted then to design the catalyst, N$^+$C$_5$His, which has both MTAC

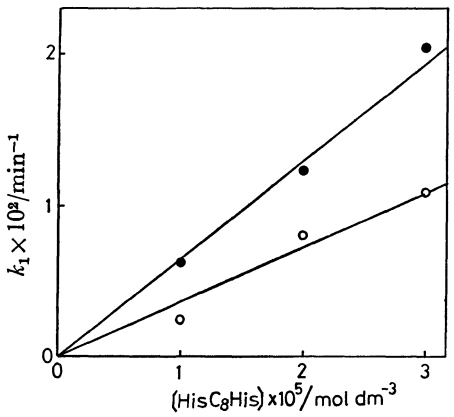

Fig. 1. Dependence of the pseudo-first-order rate constant (k_1) on the HisC$_8$His concentration in the presence of MTAC: (●) PNPL, (○) PNPH; 25 °C, pH 8.0, μ=0.5(KCl), 1/10 mol dm^{-3} KH_2PO_4-1/20 mol dm^{-3} $Na_2B_4O_7$ buffer, [PNPL]=[PNPH]=2.0×10^{-5} mol dm^{-3}, [MTAC] = 2.0 × 10^{-5} mol dm^{-3}. 10 v/v% EtOH was contained.

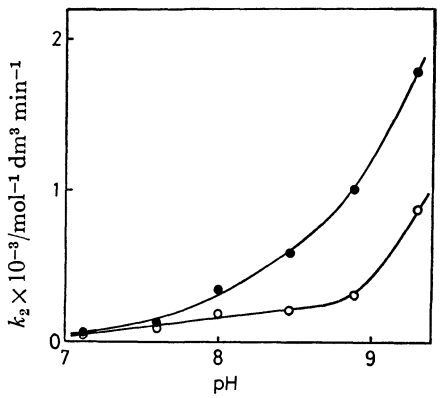

Fig. 2. pH-rate profiles for the hydrolysis of *p*-nitrophenyl esters in the presence of HisC$_8$His and MTAC: (●) PNPL, (○) PNPH; 25 °C, μ=0.5(KCl), 1/10 mol dm^{-3} KH_2PO_4-1/20 mol dm^{-3} $Na_2B_4O_7$ buffer(pH 7—9), 1/20 mol dm^{-3} $Na_2B_4O_7$-1/20 mol dm^{-3} Na_2CO_3 buffer(pH>9), [PNPL] = [PNPH] = 2.0 × 10^{-5} mol dm^{-3}, [HisC$_8$His] = 3.0 × 10^{-5} mol dm^{-3}, [MTAC] = 2.0 × 10^{-5} mol dm^{-3}. 10 v/v% EtOH was contained.

Table 1. Second-order rate constants (k_2) for the hydrolysis of *p*-nitrophenyl esters[a]

Catalyst	k_2 / mol^{-1} dm^3 min^{-1}		
	PNPA	PNPH	PNPL
Imidazole	20	15	0.3
Boc-His-OCH$_3$	6.7	5.7	0.5
C$_5$His	7.0	7.9	1.7
HisC$_8$His[b]	9.0	20	15
N$^+$C$_5$His	9.7	8.1	2.2

a) 25 °C, pH 8.0, μ=0.5(KCl), 1/10 mol dm^{-3} KH_2PO_4-1/20 mol dm^{-3} $Na_2B_4O_7$ buffer, [PNPA]=[PNPH]=[PNPL]=2.0×10^{-5} mol dm^{-3}, [catalyst]=1.0×10^{-3} mol dm^{-3} except for HisC$_8$His, [HisC$_8$His]=5.0×10^{-4} mol dm^{-3}. 10 v/v% EtOH was contained. b) The values of k_2 were estimated per histidine residue.

Table 2. Second-order rate constants (k_2) for the hydrolysis of *p*-nitrophenyl esters in the presence of methyltrioctylammonium chloride(MTAC)[a]

Catalyst	$k_2 \times 10^{-1}$ / mol^{-1} dm^3 min^{-1}		
	PNPA	PNPH	PNPL
Imidazole	<0.05	2.1	0.4
Boc-His-OCH$_3$	<0.05	0.8	2.0
C$_5$His	<0.05	0.3	1.9
HisC$_8$His[b]	<0.05	18	34
N$^+$C$_5$His	<0.05	0.8	1.8

a) 25 °C, pH 8.0, μ=0.5(KCl), 1/10 mol dm^{-3} KH_2PO_4-1/20 mol dm^{-3} $Na_2B_4O_7$ buffer, [PNPA]=[PNPH]=[PNPL]=2.0×10^{-5} mol dm^{-3}, [catalyst]=3.0×10^{-5} mol dm^{-3}, [MTAC] = 2.0 × 10^{-5} mol dm^{-3}. 10 v/v% EtOH was contained. b) The values of k_2 were estimated per histidine residue.

and histidine parts intramolecularly. The kinetic data for N$^+$C$_5$His are also shown in Table 1. As a whole, N$^+$C$_5$His does not have so large activity, although it gives a little enhancement for PNPA. As shown in Table 2, N$^+$C$_5$His does not give so large enhancement even in the presence of MTAC, too. N$^+$C$_5$His studied in the present report might not be able to form hydrophobic aggregates like MTAC in itself and not be able to be incorporated into MTAC aggregates, although there is still great room for improvement in this catalyst.

References

1) C. G. Overberger, T. St. Pierre, C. Yaroslavsky, and S. Yaroslavsky, *J. Am. Chem. Soc.*, **88**, 1184 (1966).
2) C. G. Overberger and H. Maki, *Macromolecules*, **3**, 214 (1970).
3) M. J. Heller, J. A. Walder, and I. M. Klotz, *J. Am. Chem. Soc.*, **99**, 2780 (1977).
4) Y. Murakami, A. Nakano, K. Matsumoto, and K. Iwamoto, *Bull. Chem. Soc. Jpn.*, **51**, 2690 (1978).
5) Y. Imanishi, T. Sugihara, M. Tanihara, and T. Higashimura, *Chem. Lett.*, **1975**, 261.
6) P. L. VanEtten, J. F. Sebastian, G. A. Clowes, and M. L. Bender, *J. Am. Chem. Soc.*, **89**, 3242 (1967).
7) K. Fujita, A. Shinoda, and T. Imoto, *J. Am. Chem. Soc.*, **102**, 1161 (1980).
8) C. Gitler and A. Ochoa-Solano, *J. Am. Chem. Soc.*, **90**, 5004 (1968).
9) W. Tagaki, D. Fukushima, T. Eiki, and Y. Yano, *J. Org. Chem.*, **44**, 555 (1979).
10) T. Kunitake, Y. Okahata, and T. Sakamoto, *Chem. Lett.*, **1975**, 459.
11) Y. Murakami, A. Nakano, A. Yoshimatsu, and K. Matsumoto, *J. Am. Chem. Soc.*, **103**, 2750 (1981).
12) K. Ogino, I. Tomita, K. Machiya, and W. Tagaki, *Chem. Lett.*, **1982**, 1875.
13) R. A. Moss, R. C. Nahas, and S. Ramaswami, *J. Am. Chem. Soc.*, **99**, 627 (1977).
14) Y. Okahata, R. Ando, and T. Kunitake, *J. Am. Chem. Soc.*, **99**, 3067 (1977).
15) Y. Okahata, R. Ando, and T. Kunitake, *Bull. Chem. Soc. Jpn.*, **52**, 3647 (1979).
16) Y. Nozaki and C. Tanford, *J. Biol. Chem.*, **238**, 4074 (1963).

 © 1983 The Chemical Society of Japan Bull. Chem. Soc. Jpn., 56, 2193—2197 (1983)

Lattice Dynamical Analysis of MgO

Akiko KIDA,*,† Mitiko MIURA, and Hiromu MURATA
Department of Chemistry, Faculty of Science, Hiroshima University, Higashisenda-machi, Hiroshima 730
†*Hiroshima Prefectural Research Center for Environmental Science, Minami-machi, Hiroshima 734*
(Received December 4, 1981)

The lattice dynamical properties of MgO are studied using a model based on the Birman method, which is different from the conventional point-like atom model. The model includes three kinds of forces: the short-range, the long-range Coulomb, and the long-range polarization interactions. The long-range interactions are dependent on the magnitude of the expansion of the electron distribution. The degrees of the expansion for Mg and O (w_{Mg} and w_O) are estimated from the X-ray data. The calculated phonon dispersion curves agree with the observed curves in the case of $w_{Mg}=0.35$ Å and $w_O=0.73$ Å, which are nearly equal to the estimated values, 0.35 and 0.65 Å.

Many theoretical treatments have been accumulated in order to interpret and describe the dielectric and dynamical behavior of lattices observed by means of inelastic neutron scattering in ionic crystals. In these attempts, two processes of the theoretical treatments have been developed: (1) from the rigid-ion model (RIM) through the rigid-shell model to the three-body-force shell model;[1-7] (2) from the RIM through the polarizable-ion model (PIM) to the modified PIM.[8,9]

In the previous paper,[10] the lattice dynamics of wurzite has been studied on the basis of the PIM, which is a point-like atom model like the RIM. Later this model was modified by taking the expansion of the electron distribution (electron expansion or expansion of electrons) on the basis of the Birman method;[11,12] this new model was called the modified PIM,[9] where attention was paid only to the influence of the electron expansion on the macroscopic quantities.

Then this method was applied to CaO[13] in order to see the relation between the expansion estimated by the modified PIM method and that obtained by the X-ray analysis; discrepancy was found between them because only the electron expansion of one side of an ion pair in CaO was taken into account.

This paper, therefore, will be concerned with the lattice dynamics of MgO using further modified treatment regarding the electron expansion of both the Mg and O ions. On this occasion, since the Birman method includes many hard problems when it is applied explicitly to lattice dynamics, some assumptions are introduced into the practical treatment in order to simplify the procedure. The last section shows the relation between the further modified PIM treatment and the shell-model treatment, which has been the most frequently used one and which has achieved a close reproduction of the observed data.

Theoretical Treatment

The Modified PIM. In the conventional method of calculating the electrostatic lattice potential, called the Ewald method,[14] the contribution of any ion to the potential at a point in a crystal consists of the sum of two terms including a Gaussian function with a width parameter w for a rapid convergence on the evaluation of the crystal potential. These two terms we previously symbolized as Φ_r and Φ_t.[12] The potential $\Phi(=\Phi_r+\Phi_t)$ based on the Ewald method is independent of w after summation. Birman[11] noticed the physical meaning of the two terms and the Gaussian function: Φ_t represents the potential due to a neutral configuration (core plus compensating Gaussian), and Φ_r, the potential due to the unbalanced Gaussian charge, while a half-width parameter w of a Gaussian indicates the degree of electron expansion of an atom. Under the Birman method, two potentials are differently weighted with the ion and the core (nucleus and inner electrons) charge, z and q^c, and total:

$$\begin{aligned}\phi(w) &= z\Phi_r(w) + q^c\Phi_t(w), \text{ or}\\ &= q^v\Phi_r(w) + q^c\Phi,\end{aligned} \tag{1}$$

where q^v represents the valence-electron charge ($q^v=z-q^c$). The electron-charge distribution is assumed to be described by a single normalized Gaussian:

$$\rho(\mathbf{x}) = \exp[-\mathbf{x}^2/w^2]/w^3\pi^{3/2}. \tag{2}$$

The interaction energy between the kth and k'th ions is represented as the sum of the products of the charge and the potential, and expressed by:

$$\begin{aligned}\phi(kk') &= q_k^c\{z_{k'}\Phi_r(w_{k'},\mathbf{x}_{k'}) + q_{k'}^c\Phi_t(w_{k'},\mathbf{x}_{k'})\}\\ &+ q_k^v\int\{z_{k'}\Phi_r(w_{k'},\mathbf{x}_{k'}-\mathbf{x}') + q_{k'}^c\Phi_t(w_{k'},\mathbf{x}_{k'}-\mathbf{x})\}\\ &\times \rho_k^v(\mathbf{x}_k-\mathbf{x}')d\mathbf{x}',\end{aligned} \tag{3}$$

where $\rho_k^v(\mathbf{x}_k-\mathbf{x}')$ denotes the valence-electron charge-density distribution of the kth ion, the center of which resides at the position $\mathbf{x}_k(=0)$.[11,13]

The dynamical matrix for the PIM is written by its constituents as:[8]

$$\boldsymbol{D}(\boldsymbol{y},kk') = \boldsymbol{D}^N(\boldsymbol{y},kk') + \boldsymbol{D}^C(\boldsymbol{y},kk') + \boldsymbol{D}^P(\boldsymbol{y},kk'), \tag{4}$$

where $\boldsymbol{y}$ is the wave vector. Three interaction terms, $\boldsymbol{D}^N$, $\boldsymbol{D}^C$, and $\boldsymbol{D}^P$, are concerned with the short-range force, the long-range Coulomb force, and the long-range polarization force respectively. In the MPIM, long-range interactions are dependent upon the degree of the width parameter w in a Gaussian related to the electron expansion. The model parameters are the effective ionic charge z, the polarizabilities α_+ and α_-, four short-range force coefficients, A, A', B, and B', and the width parameter w. The formulas for the calculation of macroscopic quantities, such as the wavenumbers and elastic constants in the MPIM, have been shown in previous papers.[9,10,13]

Electron Expansion of Both Side Ions. In a previous paper,[13] we assumed $\rho(\mathbf{x}_k-\mathbf{x}')=\delta(\mathbf{x}_k-\mathbf{x}')$ in Eq. 3, that is, in the interaction between k and k', one side of

an ion pair is always assumed to be a point charge. This approximation is called the first approximation. Though the expansion of both ions is taken into account in the treatment, the overlap between two expanded ions is not considered. The present treatment is a PIM further modified by taking into consideration the overlap effect due to both sides of the Mg and O ions. This approximation is called the second approximation.

When $\phi^{(1)}$ denotes the first term of Eq. 3 with respect to the charge, it can be represented as:

$$\phi^{(1)} = q_k^c q_{k'}^v \times \text{Gaussian}(w_{k'}) + q_k^c q_{k'}^c \times \text{Dot(Point)}, \quad (5)$$

where the first Gaussian term represents the interaction between the dotty (point-like) core of k and the Gaussian valence electron of the k' ion, and the second, the Dot term between the dotty core of k and that of k'. The remaining interactions of $q_k^v q_k^c \times$ Gaussian and $q_k^v q_{k'}^v \times$ Gaussian are included in the second term of Eq. 3, $\phi^{(2)}$. This term is rewritten by means of the constitutive charge-density distributions as:

$$\phi^{(2)} = q_k^v \iint \sum_l \{[q_k^v q_{k'}^v(\mathbf{x}''-\mathbf{x}_{lk'}) + q_k^c q_{k'}^c(\mathbf{x}''-\mathbf{x}_{lk'})] / |\mathbf{x}''-\mathbf{x}'|\} d\mathbf{x}'' \rho_k(\mathbf{x}_{lk}-\mathbf{x}')d\mathbf{x}', \quad (6)$$

and hence:

$$\phi^{(2)} = q_k^v \sum_l \iint \{q_k^v q_{k'}^v(\mathbf{x}''-\mathbf{x}_{lk'})/|\mathbf{x}''-\mathbf{x}'|\} d\mathbf{x}'' \rho_k(\mathbf{x}')d\mathbf{x}' + q_k^v q_{k'}^c \sum_l \int \rho_k\{(\mathbf{x}_k-\mathbf{x}')/(\mathbf{x}_{lk}-\mathbf{x}')\} d\mathbf{x}', \quad (7)$$

where l indicates the cell index. The second term in this equation represents the contribution to the potential field at $\mathbf{x}_{lk}$ due to the Gaussian charge distribution, the center of which resides at $\mathbf{x}_k$ and the sum of which as regards l is represented by means of Φ_r.

The double integrals appearing in the first term in Eq. 7 are troublesome or scarcely calculable. A practical treatment is, therefore, carried out as follows. The overlap integral of the charge distributions $\rho(\mathbf{x})$ between the ions is given as:

$$\int \{\exp[-(\mathbf{x}_k-\mathbf{x}')^2/w_k^2]/w_k^2\pi^{3/2} \times \{\exp[-(\mathbf{x}_{k'}-\mathbf{x}')^2/w_{k'}^2]/w_{k'}^3\pi^{3/2}\} d\mathbf{x}' = \exp[-(\mathbf{x}_k-\mathbf{x}_{k'})^2/(w_k^2+w_{k'}^2)]/[(w_k^2+w_{k'}^2)\pi]^{3/2}. \quad (8)$$

This result can be considered to represent the charge density at the point $\mathbf{x}_k$ due to the Gaussian residing at $\mathbf{x}_{k'}$ and with the width parameter of $(w_k^2+w_{k'}^2)^{1/2}$. Accordingly, the double integral term is approximately represented by means of Φ_r with the with the width parameter of $(w_k^2+w_{k'}^2)^{1/2}$. Though this approximation is mathematically not valid, this simplifies Eq. 3 to:

$$\begin{aligned}\phi(kk') &= q_k^c[z_{k'}\Phi_r(w_{k'},\mathbf{X}) + q_{k'}^c\Phi_t(w_{k'},\mathbf{X})] \\ &+ q_k^v q_{k'}^c\Phi_r(w_k,\mathbf{X}) + q_k^v q_{k'}^v\Phi_t(\sqrt{w_k^2+w_{k'}^2},\mathbf{X}) \\ &= (z_k z_{k'} - q_k^v q_{k'}^c - q_k^c q_{k'}^v)\Phi_r(w_{k'},\mathbf{X}) \\ &+ q_k^c q_{k'}^c\Phi_t(w_{k'},\mathbf{X}) + q_k^v q_{k'}^c\Phi_r(w_k,\mathbf{X}) \\ &+ q_k^v q_{k'}^v\Phi_t(\sqrt{w_k^2+w_{k'}^2},\mathbf{X}), \end{aligned} \quad (9)$$

where $\mathbf{X}=\mathbf{x}_k-\mathbf{x}_{k'}$. The signs of the terms with regard to the interaction between the valence charges of different kinds of ions have to be inverted. Though a physical reason for this inversion can not yet be given explicitly, it seems that the interaction between the valence charges of different kinds of ions makes a different contribution in comparison with that of the same kind.

The phonon dispersion is calculated by means of Eq. 9, where the calculation is performed by assuming $\phi(kk')=\phi(k'k)$.

Calculation and Results

Determination of w and q^c. In the Birman method, the electrons of an ion are divided into two parts, the "inner" (tightly bound) and the "valence" (loosely bound) parts.[11] The inner-core part is built of the nucleus and the inner electrons, while the electron expansion is formed of the outer, valence electrons. The division of electrons into the valence and the core may be unequivocal. In this paper the electrons are divided in accordance with the experimental charge-density distribution, though in the case of CaO[13] the division was based on the atomic arrangement of the neighbors.

Vidal-Valat *et al.*[16] have determined the atomic charge-density distribution for MgO by means of X-ray analysis, as is shown in Fig. 1. The dense inner distributions are assigned to the core electrons, shown by the shadow in the figure. The partitions of the electrons are illustrated in Fig. 2, together with their charges. The integration of these distributions leads to the findings that the total charge of the inner electrons of Mg is nearly equal to $4e$ and that of O to $2e$. Accordingly, the core charges, q^c, become $8|e|$ and $6|e|$ for Mg and O respectively. The dense outer distributions are assigned to the valence electrons. The width parameter w of the normalized Gaussian function for each ion is determined so as to reproduce the corresponding dense outer distributions. The results are that the w for Mg

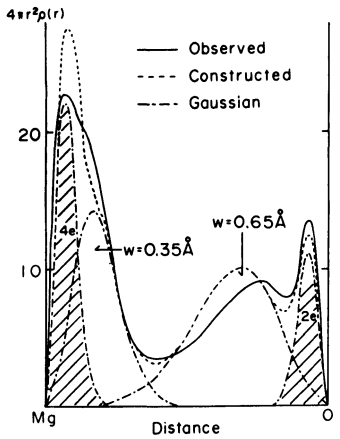

Fig. 1. The radial charge-density distribution for MgO. Shaded part indicate the inner electrons.

	Z	Core part 1s	Core part 2s	Valence part 2p	Valence part 3s	q^c/e	q^v/e	w^v/Å
Mg	12	↑↓	↑↓	↑↓ ↑↓ ↑↓	↑↓	8	-6	0.35
O	8	↑↓	↑↓	↑↓ ↑ ↑		6	-8	0.65

Fig. 2. Partitions of the electrons of Mg^{2+} and O^{2-}.

Table 1. Macroscopic quantities of MgO.

Lattice parameter	a/Å	4.21	Ref. 3a
High-frequency dielectric constant	ε_∞	2.96	Ref. 3a
Wave numbers	ν_{LO}/cm^{-1}	730	Ref. 3b
	ν_{TO}/cm^{-1}	400	Ref. 3b
Elastic constants	c_{11}/GPa	294	Ref. 17
	c_{12}/GPa	93	Ref. 17
	c_{44}/GPa	155	Ref. 17

Table 2. The model parameters determined for MgO on the first approximation

w_O/Å	z/e	α_-/Å^3	A/mdyn Å^{-1}	B/mdyn Å^{-1}	A'/mdyn Å^{-1}	B'/mdyn Å^{-1}
0.65	1.22	1.64	0.935	0.076	0.105	−0.029
0.90	1.40	1.67	0.910	0.018	0.080	−0.019
1.00	1.57	1.71	0.840	−0.020	0.050	−0.011
1.10	1.81	1.76	0.740	−0.065	0.007	0.

α_+ is fixed as 0.12 Å^3.

(w_{Mg}) is equal to 0.35 Å, while the w for O (w_O) is 0.65 Å. The effective ionic charge determined roughly by the use of this experimental charge distribution is nearly equal to the formal charge. The manner in which the experimental charge distribution is reconstructed with the Gaussian having these w values is shown in Fig. 1 by broken curves. Though the charge distribution constructed of the Gaussian in this way does not closely reproduce the observations up to the inner part, this is not important, for the interaction due to the electronic overlap occurs mostly in the outer part.

The accuracy of these evaluated w values is governed by the experimental error allowed for the X-ray measurements. By taking into account the experimental error and assuming that the charge distribution is represented by the Gaussian with only one parameter, the error of these w values was estimated at about ± 0.1 Å.

Reproduction of Macroscopic Quantities. The macroscopic quantities are tabulated in Table 1. The effective ionic charge, $z(=q^c+q^v)$, and the electronic polarizability, a, are determined respectively from the observed *TO-LO* splitting and high-frequency dielectric constants.[10] The Coulomb and the polarization force terms in the dynamical matrix in Eq. 4 are estimated from z and a. The short-range force coefficients are adjusted towards agreement between the calculated and observed Γ-point optical mode wavenumbers and the elastic constants by successive approximations.

To make it clear that the second approximation is reasonable, the result calculated by means of the first approximation is given. Table 2 summarizes reasonable parameter sets producing observed macroscopic quantities against several different values of w_O, fixing $w_{Mg}=$ 0.35 Å. In order to examine the reasonableness of the parameters determined, the phonon dispersions are calculated by the use of these parameters, where $w_{Mg}=$ 0.35 Å and $w_O=0.65$ Å, both determined by the X-ray analysis, are adopted. However, certain marked discrepancies in the acoustic-branch mode towards higher wave vectors along the [y00] and [yy0] directions are seen (dotted curves in Fig. 3) and are improved by taking into account the further electron expansion, that is, when the w_O is expanded so far as to 1.1 Å (full curves in Fig. 3).

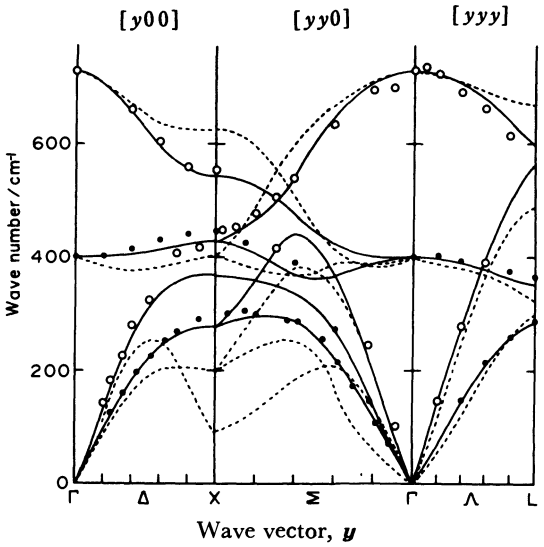

Fig. 3. The dispersion curves of MgO along three symmetry directions using the modified PIM on the assumption $\rho(\mathbf{x}_k-\mathbf{x}')=\delta(\mathbf{x}_o-\mathbf{x}')$. ------ Calculated results for $w_{Mg}=0.35$ Å and $w_O=0.65$ Å; —— those for $w_{Mg}=0.35$ Å and $w_O=1.1$ Å. Observation; ○ transverse branches; ● longitudinal branches.

Under the second approximation, where the overlap effect is due to both side ions, Mg and O, a closer reproduction of the phonon dispersion is given, as can be seen in Fig. 4, when the w_{Mg} and w_O are equal to 0.35 Å and 0.73 Å respectively, which are nearly equal to the values determined by the X-ray analysis. Even if the w_O changes from 0.65 Å to 0.73 Å, the total density is not far different from the observation. The model parameters for the further modified PIM are as follows: z/e, 1.97; a_-/Å^3, 1.82; A, A', B, and B'/mdyn Å^{-1}, 0.76, −0.14, −0.012, and 0.0025. Table 3 gives the calculated macroscopic quantities and the contributions of each kind of force to them. The value of the effective ionic charge, z, increases toward the formal charge with an increase in the value of w_O (see Table 2). The increase in the z value may be interpreted as indicating that all the electrons, spreading in accordance with the width parameter, can be explicitly assigned to each domain of

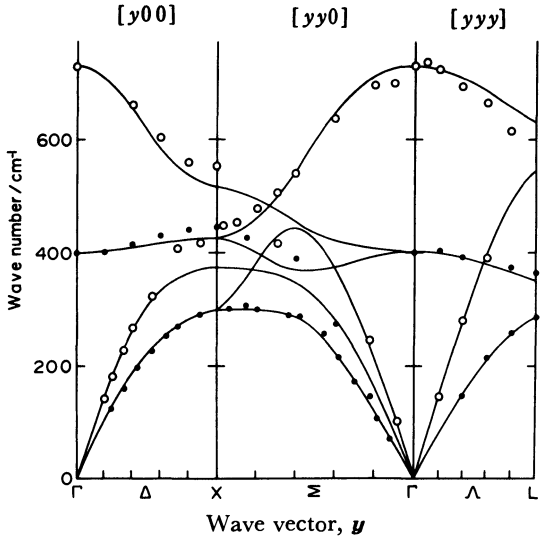

Fig. 4. The dispersion curves of MgO for $w_{Mg}=0.35$ and $w_o=0.73$ Å using the further modified PIM taking account of valence electron expansion of both the side ions.

TABLE 3. CALCULATED MACROSCOPIC QUANTITIES AND CONTRIBUTION OF EACH KIND OF FORCE TO THEM UNDER THE SECOND APPROXIMATION

	Calcd	Contribution (%)		
		D^N	D^C	D^P
ν	400.4	105	−5	−0
c_{11}	282	125	−25	
c_{12}	98	56	44	
c_{44}	163	−42	142	

an expanded ion. Usually the z value is smaller than the formal charge because of the neglect of the overlap or because of the interaction between the valence electrons. In the present treatment, as can be seen, by taking the electron expansion explicitly into account the z is estimated as the formal charge.

Thus, we have improved the previous finding that the electron expansion determined on the basis of the assumption that one side of an ion pair is a point charge is larger than that expected from the experimental data, and the w values determined from the phonon dispersion agree with those determined by means of the X-ray data.

Discussion

The origin of the polarization has been assumed to be the effective field at the lattice sites, which is composed of the externally applied field and the field due to the point dipoles of the crystal.[8] Woods *et al.*[12] have given an extended treatment so as to consider the short-range interaction causing the polarization—a treatment which has been termed the shell-model method. In this model, the polarizability is made finite by an arbitrary short-range harmonic restoring force with a spring constant k that acts between the core and the shell of an ion, while the relative displacement between the shell and the core produces a dipole moment at the ion site. The calculated phonon dispersions given by Sangster *et al.* on the basis of the shell model have reproduced the observed values very closely.[3b]

The value of k represents the strength of the bond between the core and the shell. If $k\to\infty$, the shell shrinks down to the core and the ion, therefore, becomes rigid. This rigid-shell model corresponds to the PIM. This feature of k is just the same as that of the width parameter w in the modified PIM, which can be determined by the X-ray data. As has been mentioned previously in the study on CaO[13] the shell charge, the core-shell coupling parameters, *etc.*, are the adjustable parameters in the shell model, whereas in the modified PIM treatment the only adjustable parameters are four short-range force coefficients. The other parameters, w, z, and α, can be determined independently from the results of the electron-charge distribution by means of the X-ray analysis, the *TO-LO* splitting phenomenon, and the dielectric property respectively. In conclusion, the further modified PIM treatment deserves well of the examination of lattice dynamics as well as the shell model because the parameter w reproducing the observed phonon dispersion curve agrees with the one estimated from the electron-density distribution. This treatment has, moreover, two advantages; the ease of handling because of the less adjustable parameters and the electronic overlap effect obtained by describing the valence-electron expansion by the Gaussian function.

The author wish to express their thanks to Professor Yosio Sakamoto and Mr. Hitoshi Arimori, Hiroshima University, for their indespensable help in the preparation of this paper.

References

1) E. W. Kellerman, *Philos. Trans. R. Soc. London*, **238**, 513 (1940).
2) A. D. B. Woods, W. Cochran, and B. N. Brockhous, *Phys. Rev.*, **119**, 980 (1960).
3) a) G. Peckham, *Proc. Phys. Soc. London*, **90**, 657 (1967); b) M. J. L. Sangster, G. Peckham, and D. H. Saunderson, *J. Phys. C*, **3**, 1026 (1970).
4) K. S. Upadhyaya and R. K. Singh, *J. Phys. Chem. Solids*, **36**, 293 (1975).
5) S. S. Jaswal and V. D. Dilly, *Solid State Commun.*, **24**, 577 (1977).
6) S. K. Agarwal, *Solid State Commun.*, **39**, 513 (1981).
7) R. K. Singh and S. P. Sanyal, Proc. Nucl. Phys. Solid State Phys. Symp., 1981, 24C, 203; *Chem. Abstr.*, **97**, 47519u (1982).
8) M. Born and K. Huang, "Dynamical Theory of Crysta. Lattices," Clarendon Press, Oxford (1954).
9) M. Miura, T. Satô, H. Murata, and Y. Shiro, *J. Phys. Chem. Solids*, **41**, 189 (1980).
10) M. Miura, H. Murata, and Y. Shiro, *J. Phys. Chem. Solids*, **38**, 1071 (1977); **39**, 669 (1978).
11) J. Birman, *Phys. Rev.*, **97**, 897 (1955).
12) M. Miura, Y. Sakamoto, A. Kida, and H. Murata, *J. Sci. Hiroshima Univ., Ser. A*, **45** (3) 419 (1982).
13) M. Miura, H. Arimori, H. Murata, A. Kida, and K. Iishi, *J. Phys. Chem. Solids*, in press.
14) P. P. Ewald, *Ann. Phys. (Leipzig)*, **64**, 253 (1921).

15) M. P. Tosi, *Solid State Phys.*, **16**, 1 (1964).
16) G. Vidal-Valat, J. P. Vidal and K. Kurki-Suonio, *Acta Crystollogr., Sect. A*, **34**, 594 (1978).
17) M. M. Choy, W. R. Cood, R. F. S. Hearmon, H. Jaffe. J. Jerphagnon, S. K. Kurz, S. T. Liu, and D. F. Nelson, "Elastic, Piezolectric, Piezooptic Electrooptic Constants, and Nonlinear Dielectric Susceptibilities of Crystals," in "LANDORT-BÖRNSTEIN Numerical Data and Functional Relationships in Science and Technology," ed by K.-H, Hellwege, Springer Verlag, Berlin (1979), III/7, p. 28.

An NMR Study on Molecular Interactions in 3-Methylsydnone and Its Aqueous Mixtures

Shoji TANAKA† and Masatoki YOKOI*
Department of Chemistry, Faculty of Science, Shinshu University, Asahi, Matsumoto 390
(Received August 16, 1982)

Molecular motion in neat 3-methylsydnone and molecular interaction in 3-methylsydnone–water mixtures were studied by the multinuclear FT-NMR method. The estimated rotational correlation times of the methine carbon and the carbonyl oxygen atom in neat sydnone are 8.6 and 8.1 ps at 40 °C, respectively. According to shift variations of the ^{13}C, ^{14}N, and ^{17}O nuclei of the sydnone molecule in sydnone–water mixtures, the sydnone forms a hydrogen bond with water at the carbonyl oxygen and not at the ring oxygen site. The effect of dissolved paramagnetic ions was investigated on the ^{13}C spin-lattice relaxation time of the carbon atoms of sydnone, and a discussion was made on the possible relative configuration of cation and anion to the solvent sydnone molecule.

The group of sydnones is a prototype for the general class of mesoionic compounds which cannot satisfactory be represented by Lewis forms involving no charge separation. The structure and reactions of sydnones were studied extensively.[1-3] Recently Lemire and Sears[4] measured bulk physical properties of 3-methylsydnone (Fig. 1), pointing out that it would be a

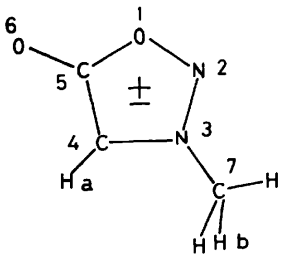

Fig. 1. Structure and numbering of the atoms of 3-methylsydnone.[5]

promising nonaqueous solvent; its dipole moment is 7.3 D (1 D$=3.3356\times10^{-30}$ cm) and its relative permittivity for the liquid phase is 144.0 (40 °C). In their subsequent work,[5] interaction of 3-methylsydnone with water and solvation of ions dissolved in the sydnone were studied by determining bulk properties of sydnone–water mixtures and conductivities of ions in the sydnone, respectively. In the present study, we examined four aspects of solvent properties of 3-methylsydnone by the multinuclear FT-NMR method: First, to investigate the self-association of the sydnone, we measured the ^{13}C spin-lattice relaxation time of the methine carbon C(4) and the ^{17}O spin-spin relaxation time of the carbonyl oxygen O(6), and discussed on the molecular motion in neat 3-methylsydnone. Second, to investigate the electron accepting ability of the sydnone, pyridine was used as a probe; we measured the ^{13}C spin-lattice relaxation time of the pyridine carbon atoms in an equimolecular mixture with the sydnone to detect any association of pyridine with the sydnone at the pyridine nitrogen atom. Third, to identify proton-accepting sites in 3-methylsydnone, measurements were made of chemical shift variations of the ^{1}H, ^{13}C, ^{14}N, and ^{17}O nuclei of the sydnone with dilution of the sydnone with D_2O. On the basis of these data we attempted to determine the site at which the sydnone is hydrogen-bonded to water. Fourth, to investigate solvation of ions in 3-methylsydnone paramagnetic ions were used; we measured the ^{13}C spin-lattice relaxation time of the sydnone carbon atoms before and after addition of a paramagnetic cation or anion, and then attempted to determine the relative configuration of the ion to the sydnone molecule.

† Prestnt address: Department of Chemistry, Faculty of Science, Tohoku University, Aoba, Aramaki, Sendai 980.

Experimental

3-Methylsydnone was synthesized from *N*-methylglycine by the method of Vasil'eva and Yashunskii,[6] and purified by the zone melting method. The final freezing point of the purified sydnone was 36 °C. Pyridine, paramagnetic reagents, and deuterium oxide were commercially available and used without further purification. 3-Methylsydnone–D_2O and –pyridine mixtures were prepared on the weight basis. NMR sample tubes for relaxation time measurement were degassed on a vacuum line by at least three freeze-pump-thaw cycles and sealed before use. All NMR experiments were performed on naturally abundant materials.

NMR measurements were carried out on a JEOL FX-90Q spectrometer operating in the Fourier transform mode. A JEOL Temperature-controller (NM-VTS) with a thermocouple external to the sample was used to monitor the probe temperature within 1 K. The ^{13}C spin-lattice relaxation time was obtained from satandard inversion-recovery FT-NMR experiments. The ^{14}N spectrometer frequency was 6.42 MHz and 8192 data points were used for a 4 kHz spectral width. Pulses with 8 μs width and 1.0 s interval were used for each scan. Averaging 1000 scans were sufficient to get a reasonable S/N ratio for the signal of the N(3) atom of sydnone. The experimental error for the reported ^{14}N chemical shifts is within ±0.1 ppm. The ^{17}O spectral parameters were as follows: spectrometer frequency, 12.10 MHz; spectral width, 10 kHz; pulse interval, 40 ms; pulse width, 10 μs: 512 data points were used. Normally, 10^6 scans were adequate for obtaining a well resolved ^{17}O NMR signal. The ^{17}O spin-spin relaxation time was calculated from $T_2=(\pi\Delta\nu_{1/2})^{-1}$, where $\Delta\nu_{1/2}$ is the full width at the half height of absorption signal in Hz. The accuracies for the reported T_2 and chemical shifts were estimated as ±10% and ±10 ppm, respectively. The temperature was 40±1 °C except for the shift measurement for the O(1) atom in 3-methylsydnone. Since the absorption signal of O(1) was too broad at 40 °C, we could obtain no precise shift values. The shift variation was measured at 100 °C.

Table 1. Chemical shifts of atoms in neat 3-methylsydnone

Atom	Chemical shift/ppm	Reference[a)]
O(1)	389	External D_2O
N(2)	Very broad	—
N(3)	252.1	External NH_4^+ (NH_4NO_3)
C(4)	97.66	External TMS
C(5)	170.66	External TMS
O(6)	234	External D_2O
C(7)	40.43	External TMS
H(a)	6.895	Internal DSS
H(b)	4.307	Internal DSS

a) The relative shift based on the external referencing was corrected for the difference in bulk susceptibility between the sample and the reference compound.

Results and Discussion

Assignment of NMR Signals. Table 1 presents the chemical shifts of the ^1H, ^{13}C, ^{14}N, and ^{17}O atoms of neat 3-methylsydnone. The assignment of the NMR signals, except for the ^{17}O atoms, is based on shift data reported in the literature.[7-11] The assignment of the two ^{17}O NMR signals is based on the assumption that the NMR signal of the ^{17}O atom with higher local electron density appears at higher field.[12] Eckert-Maksić and Maksić[13] estimated the local electron density of the atoms in 3-methylsydnone by means of MO calculation (MNDO). We utilized their results on the assignment of the ^{17}O signals.

Molecular Motion and Self-association in Neat 3-Methylsydnone. Table 2 presents the ^{13}C spin-lattice relaxation time of the methine carbon C(4) and the ^{17}O spin-spin relaxation time of the carbonyl oxygen O(6) together with the estimated values for the rotational correlation time τ_c. The estimation of τ_c's is based on the assumption that the ^{13}C atom relaxes primarily through dipolar interaction with the directly bonded proton, whereas the ^{17}O atom does through quadrupole interaction with the filed gradient tensor of the molecule. The dipolar relaxation expression is given by

$$\frac{1}{T_1^{DD}} = \frac{n_H \gamma_C \gamma_H \hbar^2}{r_{C-H}^6} \tau_c, \quad (1)$$

where n_H is the number of protons directly attached to the carbon of interest. The quadrupole relaxation expression is given by the following equation within the limits of extreme narrowing condition:[14]

$$\frac{1}{T_1^Q} = \frac{1}{T_2^Q} = \frac{3(2I+3)}{40I^2(2I-1)}\left(1+\frac{\eta^2}{3}\right)\left(\frac{e^2qQ}{\hbar}\right)^2 \tau_c, \quad (2)$$

where I is the spin quantum number, η is the asymmetric parameter, and e^2qQ/h is the quadrupole coupling constant (NQCC). The calculation of τ_c for the ^{13}C atom requires the value of carbon-hydrogen bond distance. We employed a C–H distance of 1.09 Å which is reasonable for the sp^2 carbon. The calculation of τ_c for the ^{17}O atom requires the value of NQCC and asymmetry parameter. There have been reported only a few ^{17}O NQR studies, and therefore we employed a NQCC of 10.2 MHz, which is the value for urea, and an asymmetric parameter $\eta=0.45$, which is the nominal value for the carbonyl oxygen.[15] Since the NQCC is included squared in the relaxation equation, the molecular correlation time as calculated from nuclear quadrupolar relaxation data is dependent highly on the NQCC value. The coupling constant for urea is in good agreement with the 10.6—10.9 MHz range of constants obtained for substituted benzaldehydes.[16]

Table 2. ^{13}C spin-lattice and ^{17}O spin-spin relaxation times and rotational correlation times of C(4) and O(6) atoms of 3-methylsydnone at 40 °C

Atom	T_1, T_2	τ_c /ps
$^{13}C(4)$	5.4 s	8.6
$^{17}O(6)$	1.1_8 ms	8.1

The estimated rotational correlation times for the methine carbon C(4) and carbonyl oxygen O(6) are nearly equal to each other. Since 3-methylsydnone is not a spherical top, it is possible that there will be a preferred axis of molecular rotation. Both Eqs. 1 and 2 essentially correspond to the isotropic molecular reorientation. The carbon $\tau_c(^{13}C)$, however, reflects the motions effective for reorienting each C–H vector, and the oxygen τ_c (^{17}O) reflects the motion most effective for reorienting the electric field gradients at the ^{17}O atom. Therefore, it can be inferred that the estimated correlation time for the methine carbon $\tau_c(^{13}C)$ corresponds to that for the reorientation of the C(4)–H vector and that the correlation time for the carbonyl oxygen $\tau_c(^{17}O)$ corresponds to that for the reorientation of the C(5)–O(6) vector. These two vectors are not parallel to each other. Thus the agreement between $\tau_c(^{13}C)$ and $\tau_c(^{17}O)$ leads us to a conclusion that the molecular reorientation of 3-methylsydnone is fairly isotropic.

If chain-like association as found in some amide systems[17] takes place in neat sydnone, the reorientation of aggregates is expected to be highly anisotropic. Thus, from the above discussion it may be concluded that such "anisotropic" association does not take place in neat 3-methylsydnone. We have estimated the radius of the molecule from the average correlation time for C(4) and O(6) by the Debye relation

$$\tau_c = \frac{4\pi r^3 \eta}{3kT}, \quad (3)$$

where r is the molecular radius, η is the macroscopic shear viscosity, k is the Boltzmann constant, and T is the absolute temperature. The estimated molecular

radius is 1.2 Å. This result suggests that 3-methylsydnone does not form large aggregates. The intermolecular interactions in neat 3-methylsydnone seem weak and nonspecific. It is important, however, that the above discussion do not disprove the formation of aggregates which are small and rotating isotropically.

The Electron-accepting Ability of 3-Methylsydnone. Campbell *et al.*[18] proposed that pyridine is a useful probe for studying association of molecules when the interaction is weak and the life time of the complex is short. Pyridine has a basic lone electron pair at its nitrogen. The reorientation of pyridine, when the lone pair is free, is effectively isotropic and thus pyridine has nearly equal ^{13}C spin-lattice relaxation times for C(2), C(3), and C(4). When pyridine associates with a molecule on the lone pair site, the reorientation of the molecule becomes anisotropic. The formation of such complexes slows down the tumbling about the axis perpendicular to the C(4)–N(1) axis, and a change in rotational diffusion tensor can be detected by measuring the spin-lattice relaxation times for C(2), C(3), and C(4). They introduced a parameter R, defined as the ratio of the mean of the relaxation times of C(2) and C(3) to that of C(4), *i.e.*

$$R = \frac{T_1(C2) + T_1(C3)}{2T_1(C4)}. \quad (4)$$

Table 3 presents the relaxation times of C(2), C(3), and C(4) of pyridine in the neat liquid and in an equimolar mixture with 3-methylsydnone, together with the estimated values of R. The addition of 3-methylsydnone does not change the R value. This result indicates that any charge-transfer complexes between pyridine and the sydnone do not form, and that 3-methylsydnone has no site on which the sydnone interacts with a basic lone pair.

Identification of the Proton-aceepting Site in 3-Methylsydnone. Chemical shifts of all the atoms except N(2) in 3-methylsydnone were measured in sydnone–D_2O mixtures at 40 °C. Figures 2 and 3 present chemical shift differences relative to the neat sydnone as a function of mole fraction of D_2O. 3-Methylsydnone has four lone-pair sites where the sydnone can be expected to form hydrogen bonds to water. As shown in Fig. 2,

TABLE 3. ^{13}C SPIN-LATTICE RELAXATION TIMES OF PYRIDINE

	T_1/s			R
	C(2)	C(3)	C(4)	
Neat pyridine	14.8	14.3	15.3	0.95
Pyridine–Sydnone mixture	12.0	12.6	13.0	0.94

TABLE 4. ^{13}C SPIN-LATTICE RELAXATION TIMES IN Mn^{2+}–SYDNONE AND $Cr(C_2O_4)_3^{3-}$–SYDNONE SYSTEMS

Ion	Atom	T_{1dia}/s	T_{1ob}/s	T_1^e/s
Mn^{2+}	C(7)	5.3	2.3	4.1
	C(4)	5.4	0.98	1.2
	C(5)	50.5	0.25	0.25
$Cr(C_2O_4)_3^{3-}$	C(7)	5.3	0.37	0.40
	C(4)	5.4	0.43	0.47
	C(5)	50.5	0.83	0.84

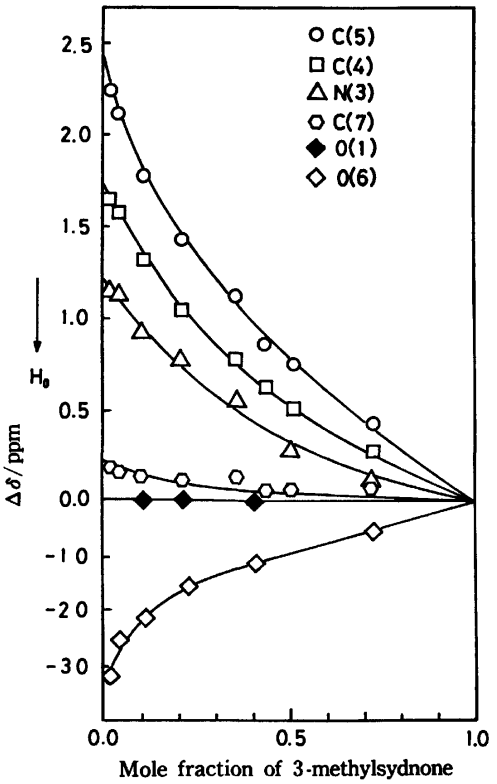

Fig. 2. The shift variations of ^{13}C, ^{14}N, and ^{17}O atoms in 3-methylsydnone–D_2O system.

when 3-methylsydnone is diluted with D_2O, the carbonyl oxygen O(6) show a very large up-field shift, up to about 34 ppm at infinite dilution. It has been reported that the hydrated carbonyl oxygens of acetone, *N*-substituted formamides, and *N*-substituted acetamides show a large up-fieled shift (20—50 ppm).[12,19] As a significant aspect the experimental results show that the shift variation of the other atoms C(5), C(4), N(3), and C(7) decreases in this order; this indicates that an electron transfer from the ring to carbonyl oxygen takes place. These results lead us to the conclusion that 3-methylsydnone forms a hydrogen bond with water at the carbonyl oxygen site. The chemical shift of the ring oxygen O(1) is almost unchanged. Though the shifts were measured at 100 °C, we may conclude that no hydrogen bond is formed on this site of the sydnone. The NMR signal of the N(2) atom is too broad to be observed. We can, however, rule out the possibility that hydrogen bond will be formed only on this site: First, on the basis of MO calculation results,[13] protonation at the N(2) atom decreases the local electron density at the O(6) atom and thus if a hydrogen bond is to be formed at the N(2) atom, the carbonyl oxygen O(6) should show a down-field shift. This is against the experimental results. Second, formation of hydrogen bond at the N(2) atom will change electronic states of the atom adjacent to N(2) most effectively. Nevertheless, the shift variations of the O(1) and N(3) atoms are smaller than those of the other atoms of the ring. The above discussions are based on the assumption that the chemical shifts of ^{13}C, ^{14}N, and ^{17}O atoms are dependent predominantly on the paramagnetic nuclear screening

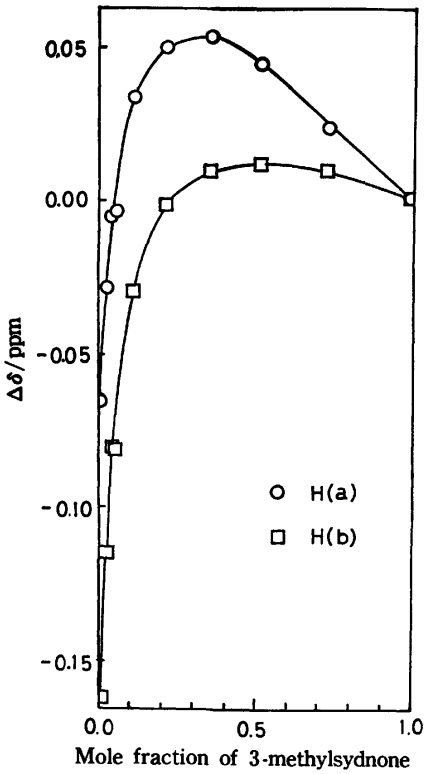

Fig. 3. The shift variations of the ^1H atoms of 3-methylsydnone in the sydnone–D_2O system.

constant σ_P so that the changes in chemical shift are due primarily to alternation in the local electron density at the atom.[12]

As shown in Fig. 3, as 3-methylsydnone is diluted with D_2O, the protons of the sydnone show a down-field shift at low dilution and an up-field shift at high dilution. The down-field shift variation can be explained in terms of the hydrogen bonding effect. The hydrogen bonds between the sydnone and water decrease the electron density of the sydnone ring so as to give rise to down-field shift of the proton. To interpret the up-field shift change, we assume that part of the sydnone molecules associate to form aggregates, whose protons are capable of resonance at lower fields than those of the monomer, possibly by the ring current effect. Thus, in sufficiently diluted solution, aggregates break out until the up-field shift effect has outweighed the hydrogen bonding effect.

The Solvation of Ions in 3-Methylsydnone. Table 4 presents the spin-lattice relaxation rates $1/T_1$ of the ^{13}C atoms in 3-methyl sydnone before and after addition of paramagnetic ions. From these results the relative configuration of ions to the sydnone molecule is to be considered. Paramagnetic relaxation reagents can interact with organic compounds to form collision type or electron-transfer type complexes and to change T_1's of the atoms in the molecule according to the electron-nuclear dipole-dipole relaxation mechanism. This relaxation mechanism has a reciprocal sixth-power distance dependence and no angle dependence. Atoms close to the site of complexation will have shortest T_1 values. We have estimated the electron-nuclear d-d relaxation time of the atoms in the molecule. The effect of a paramagnetic reagent on T_1 is given by

$$\frac{1}{T_{1\,ob}} = \frac{1}{T_{1\,dia}} + \frac{1}{T_1^e}, \tag{5}$$

where $1/T_{1\,op}$ is the observed relaxation rate, $1/T_{1\,dia}$ is the sum of all diamagnetic relaxation rates, and $1/T_1^e$ is the relaxation rate according to the electron-spin d-d relaxation mechanism. Levy and Komoroski[20] pointed out that the atoms in a given molecule may be under a considerable effect from relaxation reagent ions that are not complexed, being led to formulate

$$\frac{1}{T_1^e} = \frac{X_f}{T_{1f}^e} + \frac{X_c}{T_{1c}^e}, \tag{6}$$

where $1/T_1^e$ is the total relaxation rate for the electron-nuclear dipolar interaction, $1/T_{1f}^e$ and $1/T_{1c}^e$ are the rates when the molecule is free and complexed, respectively, and X_f and X_c are the respective molar fractions. Since X_f, X_c, and T_{1f}^e are common for given atoms in a molecule, T_{1c} may be taken to be proportional to the reciprocal sixth power of distance R from the atom of interest to the relaxation reagent. Thus we have

$$\frac{1}{T_1^e} = \alpha\frac{1}{R^6} + \beta, \tag{7}$$

where α and β are positive constants. By positioning systematically the paramagnetic ion relative to the 3-methylsydnone molecule, we have calculated the distances from the carbon atoms to the ion. The bond lengths and angles for the sydnone used in the calculation are based on the X-ray analysis on 4,4'-dichloro-3,3'-ethylenebissydnone by Thiessen and Hope.[21] From these distances and the experimental relaxation rates, parameters α and β were calculated by the least-square procedure, and then the variances was estimated by

$$\text{Variance} = \log\left(\sum\left\{\frac{1}{T_{1\,ob}^e} - \frac{1}{T_{1\,cal}^e}\right\}\right), \tag{8}$$

where $1/T_{1\,ob}^e$ and $1/T_{1\,cal}^e$ are the observed and calculated relaxation rates, respectively. If the variance is less than -4 and both α and β are positive for a given position, the ion can be taken to exist at the position.

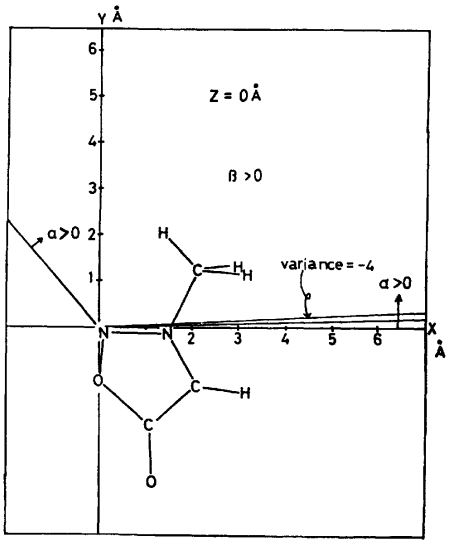

Fig. 4. Parameter diagram of $Cr(C_2O_4)_3^{3-}$–sydnone system.

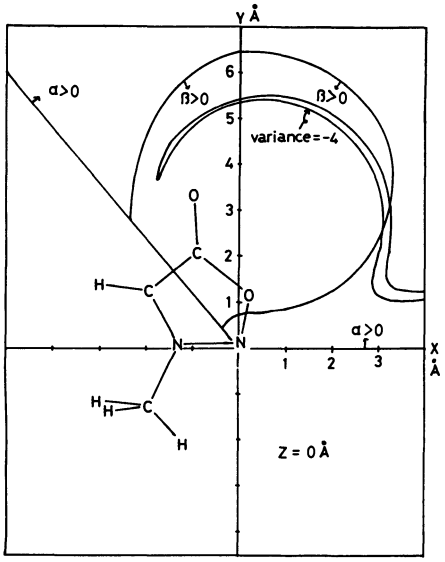

Fig. 5. Parameters diagram of Mn^{2+}–sydnone system.

This threshold value of −4 has been determined from the experimental error for the T_1 measurement of ±5%. Figures 4 and 5 illustrate contour diagrams of the variance for anion and cation, respectively. Since we have not a fitting point but a fitting surface as shown in these figures, we cannot quantitatively specify the relative positions of the ions. We can, however, obtain information on the site of ion solvation in 3-methylsydnone from these results. The methine proton and methyl group with large positive formal charge[13] are closest to the anion. For the cation, on the other hand, the carbonyl oxygen and ring oxygen with large negative formal charge and lone pairs of electron are closest to the ion. The NMR signal of the carbonyl carbon is broadened by addition of Mn^{2+} ion. The broadening can be explained in terms of contact interaction of the unpaired electron of the ion with the carbon.

The authors are particularly indebted to Professor Hiroshi Kato of the Shinshu University for many useful suggestions on the preparation and purification of 3-methylsydnone.

References

1) W. Baker and W. D. Ollis, *Q. Rev. Chem. Soc.*, **11**, 15. (1957).
2) F. H. C. Stewart, *Chem. Rev.*, **64**, 129 (1964).
3) M. Ohta and H. Kato, "Nonbenzenoid Aromatics," ed by J. P. Snyer, Academic Press, New York, N. Y. (1969), Vol. 1, Chap. 4, p. 117.
4) R. J. Lemire and P. G. Sears, *J. Chem. Eng. Data*, **22**, 376 (1977).
5) R. J. Lemire and P. G. Sears, *J. Solution Chem.*, **9**, 553 (1980).
6) V. F. Vasil'eva and V. G. Yashuskii, *J. Gen. Chem. USSR* (Engl. Transl.), **32**, 2845 (1962).
7) K. D. Lawson, W. S. Brey, Jr., and L. B. Kier, *J. Am. Chem. Soc.*, **86**, 463 (1964).
8) G. A. Olah, D. P. Kelly, and N. Suciu, *J. Am. Chem. Soc.*, **92**, 3133 (1970).
9) M. T. W. Hearn and K. T. Potts, *J. Chem. Soc., Perkin Trans. 2*, **1974**, 875.
10) A. J. Buglass, *J. Chem. Soc., Chem. Commun.*, **1974**, 313
11) L. Stefaniak, *Tetrahedron*, **33**, 2571 (1977).
12) T. Sugawara Y. Kawada, M. Katoh, and H. Iwamura, *Bull. Chem. Soc. Jpn.*, **52**, 3391 (1979).
13) M. Eckert-Maksić and Z. B. Maksić, *J. Chem. Soc., Perkin Trans. 2*, **1981**, 1462.
14) A. Abragam, "The Principles of Nuclear Magnetism," Oxford University Press, Oxford (1961), p. 314.
15) M. I. Burger, T. E. Amour, and D. Fiat, *J. Phys. Chem.*, **85**, 502 (1981).
16) C. P. Cheng and T. L. Brown, *J. Am. Chem. Soc.*, **101**, 2327 (1979).
17) L. A. LaPlanche, H. B. Thompson, and M. T. Rogers, *J. Phys. Chem.*, **69**, 1482 (1965).
18) I. D. Cambell, R. Freeman, and D. L. Turner, *J. Magn. Reson.*, **20**, 172 (1975).
19) J. Reuben, *J. Am. Chem. Soc.*, **91**, 5725 (1969).
20) G. C. Levy and R. A. Komoroski, *J. Am. Chem. Soc.*, **96**, 678 (1974).
21) W. E. Thiessen and H. Hope, *J. Am. Chem. Soc.*, **89**, 5977 (1967).

 © 1983 The Chemical Society of Japan Bull. Chem. Soc. Jpn., 56, 2203—2207 (1983)

Catalysis by "Copper Chromite". I. The Effect of Hydrogen Reduction on the Composition, Structure, and Catalytic Activity for Methanol Decomposition

Akira IIMURA,* Yasunobu INOUE,† and Iwao YASUMORI

Department of Chemistry, Tokyo Institute of Technology, Meguro-ku, Tokyo 152

†*Analytical Center, Nagaoka Technological University, Kamitomioka, Nagamine, Nagaoka, Niigata 949-54*

(Received November 27, 1982)

The effect of hydrogen reduction on the composition, structure, and catalytic activity of dichromium(III) copper(II) tetraoxide (copper chromite), $CuCr_2O_4$, was investigated. In this oxide, the surface and the bulk Cu^{II} was reduced into Cu^{I} and further to Cu^{0} by heating in hydrogen. The methanol decomposition on fresh copper chromite proceeded in a manner similar to that on metallic copper formed as the result of strong reduction and dispersed on chromium(III) oxide. The contribution of Cu^{II}, Cu^{I}, and Cu^{0} species to catalytic activity was examined and the similarity in the character of reaction on these two samples with different surface states was discussed. The role of Cr_2O_3 interacting with zerovalent copper was postulated.

Dichromium(III) copper(II) tetraoxide (copper chromite), $CuCr_2O_4$, having the spinel structure has been used as a catalyst for the hydrogenation[1-3] of carbonyl compounds or olefins and for the decomposition of alcohols.[4] The durability of $CuCr_2O_4$ to heat and inhibitor seems to be superior to that of metallic copper. The catalytic activities of this oxide, however, often vary with the method of preparation and the conditions of pretreatment.[5] Especially, under reductive conditions, surface or bulk reduction may occur, and the catalytic activity would be influenced by these processes. Accordingly, the study on the structural and activity changes, occurring in reduction treatment is considered to be important. Furthermore the study provides useful information on the structure of the active sites available for catalytic reactions.

Stroupe[6] found that Adkins' catalyst,[1,2] which is composed mainly of $CuO \cdot CuCr_2O_4$ and is active for the hydrogenolysis of esters, was reduced to Cu and $Cu_2Cr_2O_4$ during the course of reaction. Although there are several reports[6,7] on the reduction of the CuO/Cr_2O_3 system, few investigations about the changes of the surface structure of copper chromite by reducing treatments have been made.

Recently, Capece *et al.* reported that the structure of "copper chromite" was elucidated by means of X-ray photoelectron spectroscopy.[8] However, the changes in the surface structure of spinels by reduction have not been clearly discussed because the samples measured by them are commercial "copper chromite" catalysts which contain CuO as well as $CuCr_2O_4$. Thus, in the present study, the copper chromite catalyst was treated in various reducing conditions and the changes of the composition and the structure of the bulk and the surface of the catalyst were investigated. The difference of the catalytic activities between fresh and reduced catalysts was also examined by using the decomposition of methanol as a test reaction. The effect of reducing treatments on the composition and the structure of the simple oxides, CuO and Cr_2O_3 was also studied in comparison with that on $CuCr_2O_4$.

Experimental

Catalysts. $CuCr_2O_4$ was prepared by co-precipitation with aqueous ammonia from an aqueous solution of chromium(III) nitrate and an excess of copper(II) nitrate in relation to the stoichiometric amount of copper, followed by calcination in air at 600—650 °C for 6 h. The crude product was washed with 3 M HNO_3 (1 M = 1 mol dm^{-3}) until there was no detectable Cu^{II} species in the filtrate, and then heated in air at 400 °C for 4 h. This sample will be designated F catalyst in this paper.

The F catalyst was heated under an initial pressure of hydrogen of 50 Torr (1 Torr = 133.322 Pa) in a circulating system for 2 h at various temperatures. Then, the system was evacuated for a few minutes. After evacuation, the catalyst was heated to 500 °C in a closed system, and the water produced was collected in a trap cooled with liquid nitrogen. Finally, the sample catalyst was evacuated at 500 °C for 1 h. The temperatures chosen for the heating in hydrogen were 100, 200, 300, and 400 °C, and the catalysts obtained by these treatments were designated R100, R200, R300, and R400, respectively.

In order to obtain a strongly reduced copper chromite, the F catalyst was placed in a circulating reactor with a liquid nitrogen trap and heated in hydrogen at 500 °C until the rate of water formation became lower than 10 μmol/h g catalyst. Then the catalyst was evacuated for 1 h at the same temperature and was designated SR catalyst.

Commercial CuO(elemental analysis grade) was used for the experiment after pulverization. Chromium(III) oxide was prepared by decomposition of ammonium dichromate, followed by heating in air at 600—650 °C for 6 h.

Characterization of the Catalysts. The X-ray powder diffraction of the prepared catalysts was measured using the Cu $K\alpha_1$ line as an X-ray source.

XP spectra of these catalysts were recorded with a Hewlett-Packard 5950A ESCA Spectrometer. The monochromatized Al $K\alpha$ line (1486.6 eV) was used as an X-ray source. The F catalyst sample was used for the measurement both without treatment and after evacuation at 500 °C in the XPS apparatus for 45 min. R200 and R400 catalyst sample were prepared by heating F catalyst at 200 and 400 °C, respectively in the preparation chamber of the spectrometer under 4 Torr of hydrogen followed by evacuation at 500 °C for 45 min. The SR catalyst was also used for the measurement after evacuation at 500 °C for 45 min in the XPS apparatus. The binding energy values of emitted electrons were corrected by using the carbon Cls value, 285 eV, as an internal standard.

BET surface areas of the catalysts were measured by the use of krypton at liquid nitrogen temperature.

Catalytic Activities. Catalytic activities were examined

for the decomposition of methanol and the initial reaction rates were measured in a circulating system of 470 ml in volume. The reaction was followed by analyzing the products with a gas chromatograph. A good reproducibility of catalytic activity was obtained by evacuation at the reaction temperature for one hour.

For purposes of comparison, the rates of propene hydrogenation on these catalysts were measured using the circulating system described above. To obtain reproducibility of rate measurement, the catalysts were evacuated at 500 °C for one hour before each experimental run of the hydrogenation.

Results

Reduction Behavior. In Fig. 1, the X-ray powder diffraction patterns of F, R100-R400, and SR catalysts are shown and the percentage fractions of reduction are summerized in the column 2 of Table 1. The latter values were estimated from the partial pressure of water formed, by assuming that the reduction was completed when all $CuCr_2O_4$ was turned into Cu and Cr_2O_3.

As shown in the figure, the diffraction lines assigned to $Cu_2Cr_2O_4$, which would be produced by the partial reduction of $CuCr_2O_4$, appeared in the pattern of R200, and the lines became more distinct on the patterns of R300 and R400. In the pattern of SR catalyst, however, the lines corresponding to $Cu_2Cr_2O_4$ completely disappeared and, on the contrary, only the lines assigned to copper metal and Cr_2O_3 appeared. As the (311) diffraction was most intense in all the diffractions of $CuCr_2O_4$, the values of full width at half maximum (FWHM) of this line and the crystallite sizes[9] calculated from these FWHM values are listed in column 3 and 4 of Table 1, respectively. The table shows that the decrease in the crystallite size takes place by reduction at temperatures between 200 and 300 °C. The degree of reduction of R300 is also largely different from that of R200.

It was found that simple oxides of copper, CuO and Cu_2O, were easily reduced into metallic copper by heating at 50 Torr of hydrogen at 300 °C, while the X-ray diffraction patterns of Cr_2O_3 were almost the same before and after heating in hydrogen at 500 °C.

In Fig. 2, $Cu2p_{3/2}$ X-ray photoelectron spectra for F, R200, R400, and SR catalysts are shown. In the spectrum of F catalyst, there are two peaks at about 936 and 940—945 eV which are characteristic of the Cu^{II} species and are assigned to a main peak and its shake-up satellite peak, respectively.[10] A peak which was assigned to photoelectrons from Cu^{I} or Cu^{0} species was also

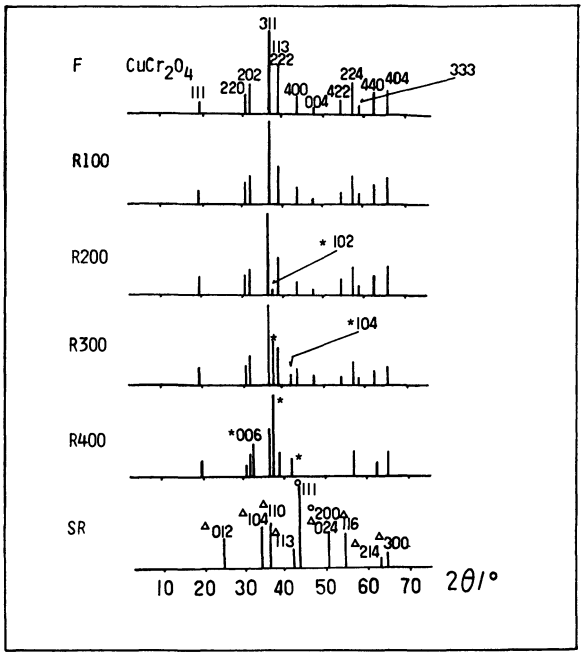

Fig. 1. Changes in X-ray diffraction patterns.
*: $Cu_2Cr_2O_4$, △: Cr_2O_3, ○: Cu.

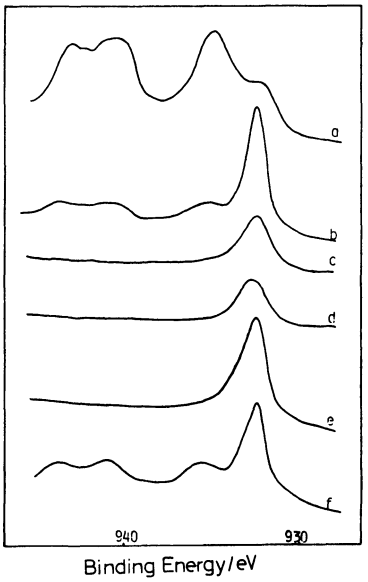

Fig. 2. $Cu2p_{3/2}$ XP spectra. (a) F catalyst, (b) F catalyst after heating at 500 °C, (c) R200, (d) R400, (e) SR catalyst, (f) reoxidized R400 (heated under 4 Torr of oxygen at 400 °C).

TABLE 1. REDUCTION PERCENTAGE, FWHM OF 311 LINE, CRYSTALLITE SIZE, AND SURFACE AREA OF F, R100—R400, SR, AND REOXIDIZED R400 CATALYSTS

Sample	Reduction/%	FWHM/°	D_{311}/Å	Specific surface area/$m^2\ g^{-1}$
F	0	0.24	347	5.7
R100	2	0.24	347	5.6
R200	4	0.24	347	5.9
R300	11	0.30	278	8.4
R400	20	0.42	199	9.9
SR	73	—	—	16.3
Reox.	—	0.42	199	6.4

observed at about 932 eV in all the spectra in the figure. For F, R400, and SR catalysts, peaks were observed at about 917.6, 916.8, and 919.1 eV of kinetic energies, respectively, and assigned to the $L_3M_{4,5}M_{4,5}$ Auger electrons from Cu^{II}, Cu^{I}, and Cu^{0}, respectively.[11] The intensity ratio was estimated at 2 : 1 : 5.

From the spectrum **a** in Fig. 2, the $Cu^{I}/(Cu^{I}+Cu^{II})$ intensity ratio was determined as about 0.15. By assuming that the cross sections of photoionization for Cu^{I} and Cu^{II} species were equal, it was estimated that 15% of the Cu species existed as Cu^{I} in the surface layer of the F catalyst.

Since photoelectrons from Cu^{II} species are scarcely observed in the spectrum of R200, the amount of Cu^{II} species existing in the surface layer of R200 is negligible.

In order to see the changes in the ratio of copper to chromium atoms existing in the surface layer, the intensity ratio of $Cu2p_{3/2}$ to $Cr2p_{3/2}$ in the XP spectra were determined. The results are shown in Table 2; the Cu/Cr ratios of R200 and R400 were significantly lower than that of F catalyst. This indicated that the Cr^{III} species was exposed preferentially to the surface of the catalyst when F was reduced into R200 or R400. The Cu/Cr ratio of SR was the highest all over the catalysts, so that it is concluded that the metallic copper produced by strong reduction is enriched in the surface layer. Therefore, it seems that the SR catalyst has the structure of dispersed metallic copper on Cr_2O_3.

In the bottom of the figure, the spectrum of an R400 sample heated at 400 °C in 4 Torr of oxygen for a further 45 min is shown. The observed main peak at about 936 eV and the satellites at 940—945 eV indicate clearly that the sample surface was partly reoxidized.

Table 2. XPS Intensity ratio of $Cu(2p_{3/2})$ to $Cr(2p_{3/2})$

Sample	$Cu(2p_{3/2})/Cr(2p_{3/2})$
F	1.6
R200	0.2
R400	0.2
SR	1.7
Reoxidized R400	0.6

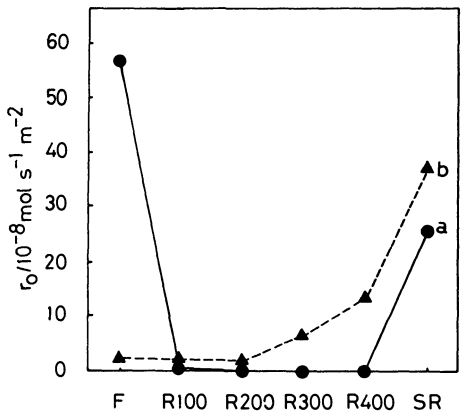

Fig. 3. Relationship between reduction conditions and initial rates of the reactions.
a: Decomposition of methanol at 200 °C, $p_0(CH_3OH) \simeq$ 20 Torr. b: Hydrogenation of propene at 0 °C, $p_0(C_3H_6) \simeq p_0(H_2) \simeq 17$ Torr.

In the spectrum of copper(II) oxide, CuO, no characteristic peaks of the Cu^{I} species were observed.

Catalytic Activities. In Fig. 3, the initial rates of methanol decomposition and propene hydrogenation on F, R100—R400, and SR catalysts are shown. In the case of methanol decomposition, the initial pressure of methanol and reaction temperature were fixed at 20 Torr and 200 °C, respectively. The rates were evaluated from the initial decreases in the partial pressure of methanol. As shown in the plot **a** of the figure, the catalytic activity decreased abruptly on increasing the degree of reduction to 2% (F→R100), and the decomposition did not occur on R200, R300, and R400 catalysts. However, on SR catalyst which was the highest in the extent of reduction, the catalytic activity was observed. The hydrogenation of propene was examined at 0 °C using a equimolar mixture of H_2 and C_3H_6, 35 Torr in total pressure. The product of the hydrogenation was found to be propane only. The reaction rate was evaluated by the initial decrease in the total pressure of the reactant. The plot **b** of the figure shows that the rates of propene hydrogenation were relatively low on F, R100, and R200, whereas the rate became higher on R300 and attained the highest point on the SR catalyst.

Typical runs of methanol decomposition on F and SR catalysts are shown in Fig. 4. The reaction products consisted of methyl formate, hydrogen, and carbon monoxide and there was no obvious difference between the courses of reaction on these catalysts. The changes in the composition of the gaseous product during the course of reaction on F and SR catalysts are appreciably different from that for the reaction on copper wire reported by Miyazaki and Yasumori;[12] the decay of methyl formate as the intermediate was faster than that in the reaction on copper wire.

The initial rates, r_0, of the decomposition on these catalysts were both expressed in the form as

$$r_0 = kKp/(1+Kp),$$

where p is the partial pressure of methanol, k and K are the rate constant and the adsorption constant, respectively: the linear relationships between $1/r_0$ and $1/p$ hold as shown in Fig. 5. From the dependence of ln k against $1/T$, the true activation energies of the reactions on F and SR were evaluated as 62 ± 5 and 60 ± 4 kJ mol^{-1},

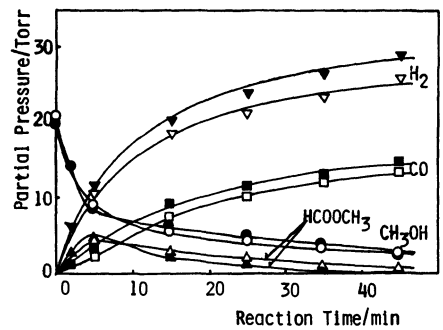

Fig. 4. Courses of methanol decomposition on F and SR catalyst.
Catalyst amount: 1.5×10^{-3} mol. ○△□▽: F catalyst at 200 °C. ●▲■▼: SR catalyst at 180 °C.

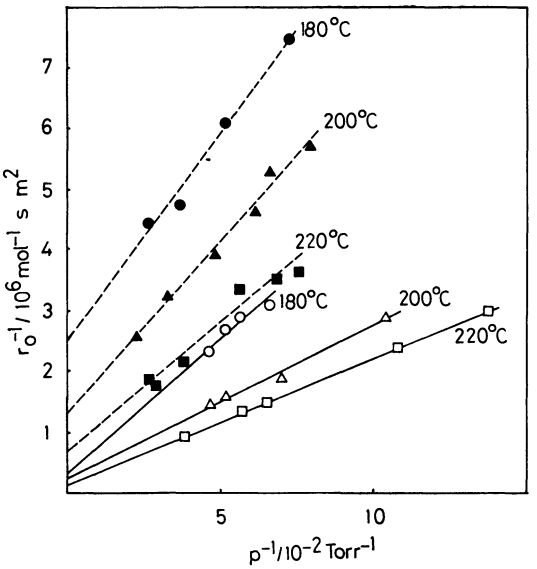

Fig. 5. Relationship between $1/p$ and $1/r_0$.
○△□: F catalyst, ●▲■: SR catalyst.

respectively.

The reactions of methanol on CuO and Cu_2O were examined at 200 °C. In these cases, the formation of CO_2, H_2O, and H_2 was observed in the initial stage of the reaction and methyl formate was produced later. This result shows that the reduction of the oxides proceeded simultaneously with the methanol decomposition, and, the reaction became similar to that on copper wire after the completion of reduction.

The decomposition of methanol on Cr_2O_3 was not observed up to 250 °C.

Discussion

Reduction-Reoxidation Behavior. The present work revealed the details of the effect of reduction conditions upon the composition and structure of copper chromite, $CuCr_2O_4$. Namely;

i) When the catalyst was heated in hydrogen below 200 °C, the bulk composition remained unchanged (Fig. 1 and Table 1), while Cu^{II} ions in surface layer were reduced to the state of Cu^{I} as revealed by the XPS data.

ii) The data shown in Table 1 indicated that the effects of hydrogen reduction began to penetrate deeper at about 300 °C. Under such conditions, the reaction,

$$2CuCr_2O_4 \xrightarrow{H_2} Cu_2Cr_2O_4 + Cr_2O_3 + H_2O, \quad (1)$$

was considered to occur even in the bulk, and the crystallites of starting material, $CuCr_2O_4$, would became smaller. Absence of the Cr_2O_3 lines on the X-ray diffraction chart indicated that the Cr_2O_3 produced by Reaction 1 did not crystallize.

iii) On heating at 500 °C, the catalyst was further reduced to Cu and Cr_2O_3. This suggested that $Cu_2Cr_2O_4$ produced in the Reaction 1 was converted to metallic copper and Cr_2O_3,

$$Cu_2Cr_2O_4 \xrightarrow{H_2} 2Cu + Cr_2O_3 + H_2O. \quad (2)$$

The X-ray data showed that Cr_2O_3 began to crystallize under this condition. On SR catalyst, therefore, the fine crystals of metallic copper were considered to be dispersed over Cr_2O_3.

The reoxidation of the reduced sample provides us with additional information about the structure of the catalyst. When R400 was heated in 25 Torr of oxygen at 400 °C for 1 h, the bluish green sample changed to black in color. The X-ray diffraction pattern of this reoxidized sample was similar to the pattern of R400; the positions, the widths, and the intensity ratios of the diffraction lines of the former sample were almost identical with the corresponding values of the latter sample. This result suggests that reoxidation scarcely occurred in the bulk of R400 under the conditions described above. However, as shown in Fig. 2, reoxidation occurred in the sample surface even under milder conditions. In addition, Table 1 shows that the surface area of the R400 sample decreased appreciably on heating at 400 °C in oxygen. On the basis of these findings, the reduction-reoxidation processes of the present copper chromite catalyst are indicated as follows;

i) The starting material F: The catalyst is the aggregates of polycrystalline particles of $CuCr_2O_4$. Since a small amount of Cu^{I} species is contained in the surface layer of the particles, $Cu_2Cr_2O_4$ and amorphous Cr_2O_3 coexists with $CuCr_2O_4$.

ii) Reduction to R100-R200: Oxygen atoms are removed from the catalyst surface by reduction with hydrogen and Cu^{II} ions are converted into Cu^{I} ions on the surface. The Cr_2O_3 produced covers most of the catalyst surface.

iii) Reduction to R300-R400: Oxygen atoms at the grain boundaries in the polycrystalline particles are also removed; the surface area of the catalyst increases since the original polycrystalline particles are divided into smaller ones.

iv) Reoxidation: When the reduced catalyst to the stage (iii) is heated in oxygen, Cu^{I} ions are oxidized to Cu^{II} ions in the surface layer, and the polycrystalline particles are sintered, so that the surface area of the catalyst decreases again. The crystallite size of $CuCr_2O_4$ in the catalyst particle which is covered with $Cu_2Cr_2O_4$ does not change because the reoxidation occurs only in a few layers of $Cu_2Cr_2O_4$ near the surface. These processes are illustrated by Fig. 6.

As described in the preceding section, the simple oxides of copper, CuO and Cu_2O, were more sensitive to hydrogen treatments than F catalyst, and metallic copper readily formed by heating in hydrogen at 200 °C. Thus it is possible to consider than Cu^{II} ions are somewhat stabilized in the bulk of the spinel structure of $CuCr_2O_4$. The Cu^{I} ions in $Cu_2Cr_2O_4$ are also stable up to 400 °C in 50 Torr of hydrogen, whereas Cu_2O

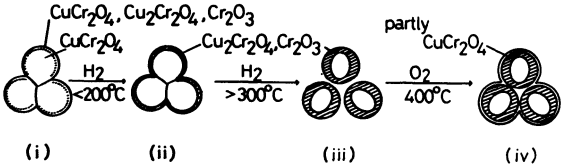

Fig. 6. Reduction-reoxidation process of $CuCr_2O_4$.

is reduced into metallic copper at 200 °C in the same pressure of hydrogen.

Cr_2O_3 formed on the catalyst surface was stable against reduction in the hydrogen treatment under conditions of the present study.

Catalytic Activities. For the decomposition of methanol, high activities were observed only on F and SR catalysts. Cu^{II} species exists only on the F catalyst. On R200—R400, the surface concentration of Cu^{I} species became quite small and methanol decomposition did not occur. These results indicate that Cu^{I} and/or Cu^{II} species are responsible for the methanol decomposition on F catalyst.

From the data of XPS intensity in Table 2, it is considered that the surfaces of R200—R400 catalysts are almost covered with amorphous Cr_2O_3. Therefore, their poor activities may be attributed to the low degree of exposure of Cu^{I} species or the absence of Cu^{II} species.

In SR catalyst, the main surface component is metallic copper; the Auger spectrum of SR catalyst indicates that the Cu^{I} species were rarely exposed on the surface. It is well known[12] that metallic copper has an activity for methanol decomposition, so it is possible to consider that metallic copper is the active component in the SR catalyst.

It has been reported by several authors that olefin hydrogenation proceeds on dehydrated chromium oxide gel,[13] and metallic copper:[14] The high activity of SR catalyst for propene hydrogenation reflects the formation of the dehydrated Cr_2O_3 and Cu^0 species on the surface.

The rate equation applied to the decomposition on these catalysts indicates that the rate determining step of the reaction is a unimolecular process on the catalyst surface. Wachs and Madix[15] reported that, in the reaction of methanol over oxygen preadsorbed Cu(110), a stable surface intermediate, CH_3O, existed on the catalyst below room temperature. By taking their results into consideration, it can be suggested that the O–H bond in methanol adsorbed on F and SR catalysts is weakened to some extent. Accordingly, the sequence of reaction on these catalysts can be represented as follows:

$$CH_3OH(g) \rightleftarrows CH_3O\cdots H(a),$$
$$CH_3O\cdots H(a) \nrightarrow H_2CO(a) + 2H(a),$$
$$2H_2CO(a) \rightleftarrows HCOOCH_3(g),$$
$$2H(a) \rightleftarrows H_2(g).$$

The results obtained for methanol decomposition show that the characteristics of the reaction on F and SR catalysts are very similar to each other, although the surface compositions and the valence states of copper are greatly different between these catalysts. The view that chromium ions act as the main active sites is excluded since the reaction was not observed on Cr_2O_3. Thus these similarities in the catalytic activities have to be attributed to the similarity in the nature of Cu^0 on Cr_2O_3 and that of Cu^{I} or Cu^{II} in F catalyst. Although the characteristics of methanol decomposition of F and SR catalysts (the rate equation and the value of real activation energy) are similar to those for the reactions on copper wire reported by Miyazaki and Yasumori,[12] the changes in the composition of the gas phase product during the course of the reaction are appreciably different. Wachs and Madix[15] reported that the ability of the copper surface to chemisorb methanol was greatly enhanced by surface oxygen. It is expected that Cu^0 on SR catalyst shows characteristics similar to that of Cu^{I} or Cu^{II} species if the oxygen atoms of Cr_2O_3 interact strongly with metallic copper under the present reaction conditions.

In order to reveal clearly the reason for the poor activities of R100-R400 as well as the mechanisms of catalyses by F and SR, it is necessary to analyze precisely the adsorbed state of reactant molecule and its behavior on the catalyst surfaces.

This study was supported by Grant-in-Aid for Special Project Research No. 56119004 from the Ministry of Education, Science and Culture.

References

1) H. Adkins, *J. Am. Chem. Soc.*, **72**, 2626 (1950).
2) H. Adkins and R. Connor, *J. Am. Chem. Soc.*, **53**, 1091 (1931).
3) Z. Kyrideo, *J. Am. Chem. Soc.*, **68**, 1385 (1946).
4) "Organic Syntheses," John Wiley and Sons, Inc., New York, N. Y. (1939), Vol. XIX., pp. 31—35.
5) W. A. Lazier and J. V. Vangen, *J. Am. Chem. Soc.*, **54**, 3080 (1932).
6) J. D. Stroupe, *J. Am. Chem. Soc.*, **71**, 589 (1949).
7) É. É. Rachkovskii and G. K. Boreskov, *Kinet. Catal.*, **11**, 1036 (1970).
8) F. M. Capece, V. Dicastron, C. Furlani, G. Mattogno, C. Fragale, M. Gargano, and M. Rossi, *J. Electron Spectrosc. Relat. Phenom.*, **27**, 119 (1982).
9) B. E. Warren, *Z. Krist.*, **99**, 488 (1938) and references therein.
10) N. S. McIntire and M. G. Cook, *Anal. Chem.*, **47**, 2208 (1975).
11) P. E. Larson, *J. Electron Spectrosc. Relat. Phenom.*, **4**, 213 (1974).
12) E. Miyazaki and I. Yasumori, *Bull. Chem. Soc. Jpn.*, **40**, 2012 (1967).
13) R. L. Burwell, Jr., A. B. Littlewood, M. Cardew. G. Pass, and C. T. H. Stoddart, *J. Am. Chem. Soc.*, **82**, 6272 (1960).
14) E. Nishimura, Y. Inoue, and I. Yasumori, *Bull. Chem. Soc. Jpn.*, **48**, 803 (1975).
15) I. E. Wachs and R. D. Madix, *J. Catal.*, **53**, 208 (1978).

NMR Study of Protonated Halothiophenes. I. ^{1}H NMR Study of Chlorothiophenium Ions[1)]

Yukihiro YOKOYAMA, Yukihide YAMASHITA, Kensuke TAKAHASHI,* and Tyo SONE†
Department of Industrial Chemistry, Nagoya Institute of Technology, Gokiso-cho, Showa-ku, Nagoya 466
†*Department of Applied Chemistry, Faculty of Engineering, Yamagata University, Jonan, Yonezawa 992*
(Received November 30, 1982)

Well-resolved ^{1}H NMR signals of the cations formed from chlorothiophenes were observed in the HSO_3F or $AlCl_3$–HCl–CH_2Cl_2 system. Chlorothiophenes are protonated exclusively at the position adjacent to sulfur, either with or without substituents. The protonation of 2-chloro-5-methylthiophene occurs at the 5-position, and, in the HSO_3F system, the cation 5*H*-2-chloro-5-methylthiophenium ion thus formed undergoes an irreversible 2,5-hydrogen shift.

It was recently reported that 2-chlorothiophene reacted with active benzene derivatives such as aromatic ethers in the presence of aluminum chloride to give 2-arylthiophenes.[2)] In this reaction, the existence of a

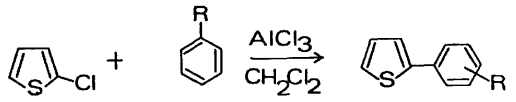

Scheme 1.

protonated intermediate (**1**) was assumed because a proton was presumably derived from the contact of aluminum chloride with water in the moist air.

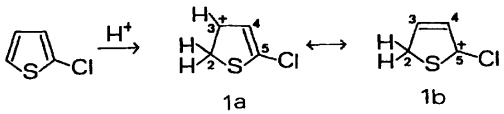

1a 1b

Scheme 2.

Studies of various kinds of arenium ions in the super acids have been energetically performed by many researchers.[3)] These studies are important and interesting in connection with the direct observation of the protonation of aromatic rings and the kinetics of arenium-ion rearrangement. However, the cations in the super acids are not necessarily the same as the species produced in ordinary cationic reaction processes, *e.g.*, in the $AlCl_3$–HCl–solvent system. In general, it is difficult to observe such species directly during the reaction process.

This study was undertaken to get proof of the formation of chlorothiophenium ions involving **1** in the $AlCl_3$–HCl–CH_2Cl_2 system as well as in the HSO_3F system, and, in addition, to obtain information about the structures of the chlorothiophenium ions. A few works have been carried out so far by Okami *et al.*[4)] and Belen'kii *et al.*[5)] aimed at the direct NMR spectroscopic observation of some protonated benzenes and thiophenes in the $AlCl_3$–HCl–solvent system, but they were concerned with compounds having active substituents such as alkyl groups. There has not yet been reported any work concerning thiophenes having inactive substituents such as halogens. Our preliminary results have previously been reported.[6)]

Experimental

All the compounds studied were synthesized by one of the present authors (T.S.). The reagents used were commercial ones and were used without further purification.

The ^{1}H NMR measurements were carried out by means of a Hitachi R-20B spectrometer at 60 MHz with a variable-temperature controller (R-202-VTC). The ^{1}H chemical shifts are referred to the signal of tetramethylsilane in a sealed Pyrex capillary inserted into each sample tube.

The cations studied were prepared by the following general procedures.

Preparation of the Cations in HCl–$AlCl_3$–Solvent Systems. In the reaction of 2-chlorothiophene with active benzene derivatives, once a small amount of the products has been formed, it can provide HCl, which in turn can prompt a further reaction. However, for the ^{1}H NMR measurements of the cation, the second material (benzene derivative) is not brought into the system; therefore, the addition of HCl gas is necessary.

A hand-made Pyrex container (*ca.* 10 ml) is filled with *ca.* 1 g of $AlCl_3$ powder. The container has an inlet for HCl gas, and the gas is blown into the container from a HCl-generator for about 5 min. The container is then immersed in a low-temperature bath (methanol–Dry Ice), which is kept at about −40 °C, and *ca.* 5 ml of solvent is introduced. Further HCl gas is then blown into the container for about 90 min or more. The solvent in the container is thus thoroughly saturated with HCl and $AlCl_3$. A small reactor, connected to an NMR sample tube, is first filled with $AlCl_3$ in an amount corresponding to the 1 : 1 mole ratio of the sample (chlorothiophene) used, and then kept at −40 °C. About 1 ml of the previously prepared solvent is then added into the reactor, and the mixture is stirred by means of a magnetic stirrer. The starting material, chlorothiophene, is then added into the reactor. A suitable reaction time is about 2—6 min depending upon the reactivity of the material. When enough time has passed, the material seems to be polymerized. When the amount of the material is in excess of that of HCl or $AlCl_3$ in the solvent, a polymerization of the material occurs. The NMR spectra of the polymerized products give broad signals. When the protonation is considered to have progressed to a desired extent, the mixture is transferred into the connected NMR tube and kept at −40 °C in the bath. Then the NMR tube is moved into another Dry Ice–methanol bath at *ca.* −80 °C, cut off from the reactor, and sealed by means of a Teflon cap. The sample is then used for the NMR measurements. When it is kept at −80 °C, the reaction seems to be frozed, showing no progress for several hours.

Preparation of the Cations in Fluorosulfonic Acid or in the Magic Acid. The magic acid used in this study contains 7.7 mol/l of SbF_5 in HSO_3F, which has been prepared by mixing the two reagents in a stream of nitrogen in a dry box. The acid is kept in several sealed Pyrex glass tubes until it is used. The

NMR samples of the cations are prepared by the following procedure. An ordinary NMR sample tube is filled with about 0.5 g of the magic acid or HSO_3F, and then kept in a Dry Ice–methanol bath at −80 °C. The starting material (*ca.* 0.05—0.10 g) is then added to the tube. The material ordinarily keeps in the solid state on the wall of the tube and does not react with the acid under these conditions. The tube is then pulled out from the bath, shaken in the air for a few seconds, and again put into the bath. The shaking is repeated several times until the solution in the tube shows a homogeneous coloration. In this instance, when the shaking in the air has continued long enough, the reaction products are too complex to be analyzed by means of the ^1H NMR. However, when the shaking time is too short, the reaction will not start at all. The coloration of the solution is a most suitable indication of the reaction progress. When the sample exhibits a suitable and characteristic coloration, it is kept in the bath at −80 °C until it is used for the NMR measurements.

Results and Discussion

The ^1H NMR data of the eight cations produced are given in Table 1. The site of the protonation is taken to be the 2-position to make clear the comparison of the species.[7]

A typical ^1H NMR spectrum of protonated 2-chlorothiophene (**1**) in HSO_3F and an $AlCl_3$–HCl–solvent system is given in Figs. 1a and 1b respectively. It is shown that the two cations produced under the two different circumstances are of the same kind, although the chemical shifts of the signals of the cation (**1**) are

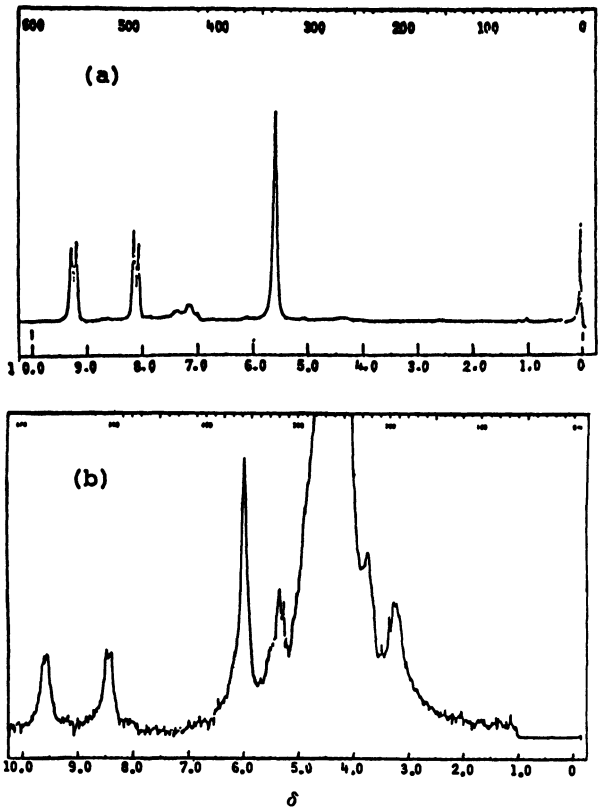

Fig. 1. ^1H NMR spectra of protonated 2-chlorothiophene (**1**) at 60 MHz. (a) In HSO_3F at −50 °C, (b) in $AlCl_3$–HCl–dichloroethane at −30 °C.

Table 1. ^1H NMR data of protonated chlorothiophenes[a]

No.	Substituent	Solvent	Temp °C	Chemical shift/ppm[b] 2-H	3-H	4-H	5-H
1	5-Cl	A[c]	−50	5.50 (1.3)[d]	9.15(5.5,1.3)	8.03(5.5)	—
		C	−70	[e]	9.69	8.51	—
		D	−40	6.19	9.78	8.65	—
2	2-CH_3, 5-Cl	A	−70	2.13(CH_3,7.5) 5.75(7.5)	9.07(5.5)	7.92(5.5)	—
		B	−50	2.22(CH_3) 5.83	9.14	8.00	—
		C	−70	2.61(CH_3) [e]	9.60	8.42	—
3	2-Cl, 5-CH_3	A	−70	6.92	8.64(5.5)	7.84(5.5)	3.51(CH_3)
		B	−50	7.00	8.70	7.92	3.59(CH_3)
4	3-Cl	A	−50	5.39(2.0)	—	8.09(4.5)	11.00(4.5, 2.0)
5	4,5-Cl_2	A	−50	5.45(2.0)	9.07(2.0)	—	—
6	2,5-Cl_2	A	−70	7.10(1.5)	8.83(5.6,1.5)	7.89(5.6)	—
		B	−70	7.18	8.90	7.96	—
		C	−70	7.78	9.41	8.43	—
		D	−40	7.80	9.47	8.51	—
7	2,5-Cl_2, 3-CH_3	A	−50	6.82	2.99(CH_3)	7.79	—
		B	−50	6.90	3.03(CH_3)	7.84	—
		C	−50	7.38	3.44(CH_3)	8.27	—
		D	−40	7.39	[e]	8.29	—
8	2, 3, 5-Cl_3	B	−50	6.89	—	7.99	—

a) As stated in the text, the site of the protonation is taken to be the 2-position. b) ^1H chemical shifts are referred to an external neat TMS contained in a capillary. c) Abbreviations: A, HSO_3F; B, HSO_3F–SbF_5; C, $AlCl_3$–HCl–dichloromethane; D, $AlCl_3$–HCl–1,2-dichloroethane. d) The values in parentheses are the coupling constants between protons in Hz; they are given only for the first example of each starting material. e) Not available because of the large solvent peaks.

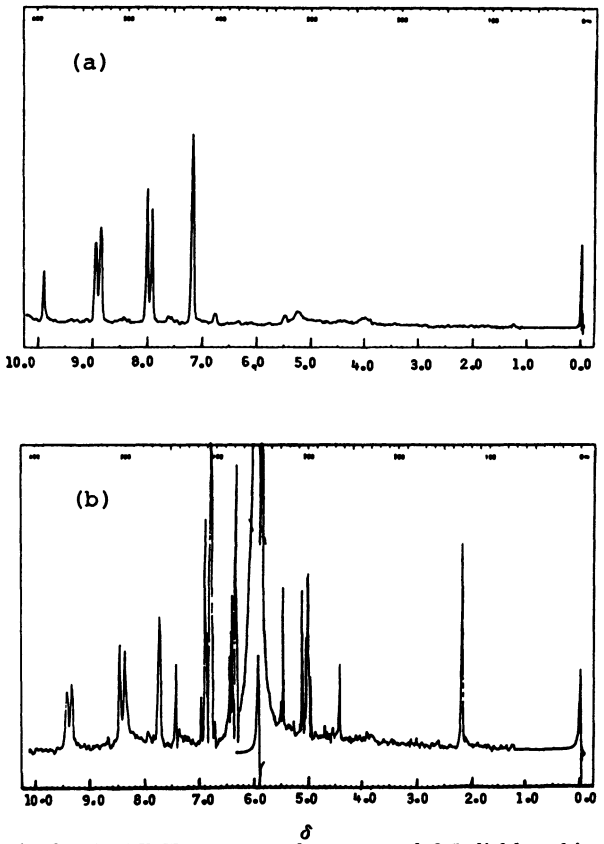

Fig. 2. ^{1}H NMR spectra of protonated 2,5-dichlorothiophene (**6**) at 60 MHz. (a) In the magic acid (see text) at −50 °C and the signal at near 10.0 ppm is due to the sideband of the acid proton, (b) in $AlCl_3$–HCl–dichloromethane at −50 °C and a signal at 2.17 ppm is unknown.

larger by about 0.5 ppm in the latter than those in the former system. The chemical shifts are quite apart from each other, so the signals can easily be assigned. The intensity ratio of the three peaks is 1 : 1 : 2 from low to high field in Fig. 1a, as would be expected for the cation (**1**). The protonation of 2-chlorothiophene at the 5-position is consistent with the ordinary concept of thiophene chemistry. The protonation of 2,3-dichlorothiophene also occurs at the 5-positioned carbon atom not carrying the substituent.

In the cases where the two α-positions have already been substituted, the protonations still occur at the α-position. Thus, the protonation of 2,5-dichlorothiophene has occurred at the chlorine-bearing α-position and produced the cation (**6**), as is shown in Fig. 2, in sharp contrast to those of chlorobenzenes, which occur at the unsubstituted ring position,[8] although Olah *et al.* have reported that the protonation of the halogen-bearing carbon can be assumed in explaining a Friedel-Crafts-type isomerization.[9]

The protonation of 2-chloro-5-methylthiophene has

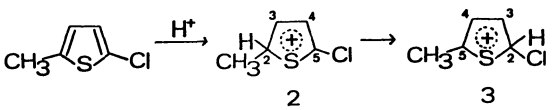

Scheme 3.

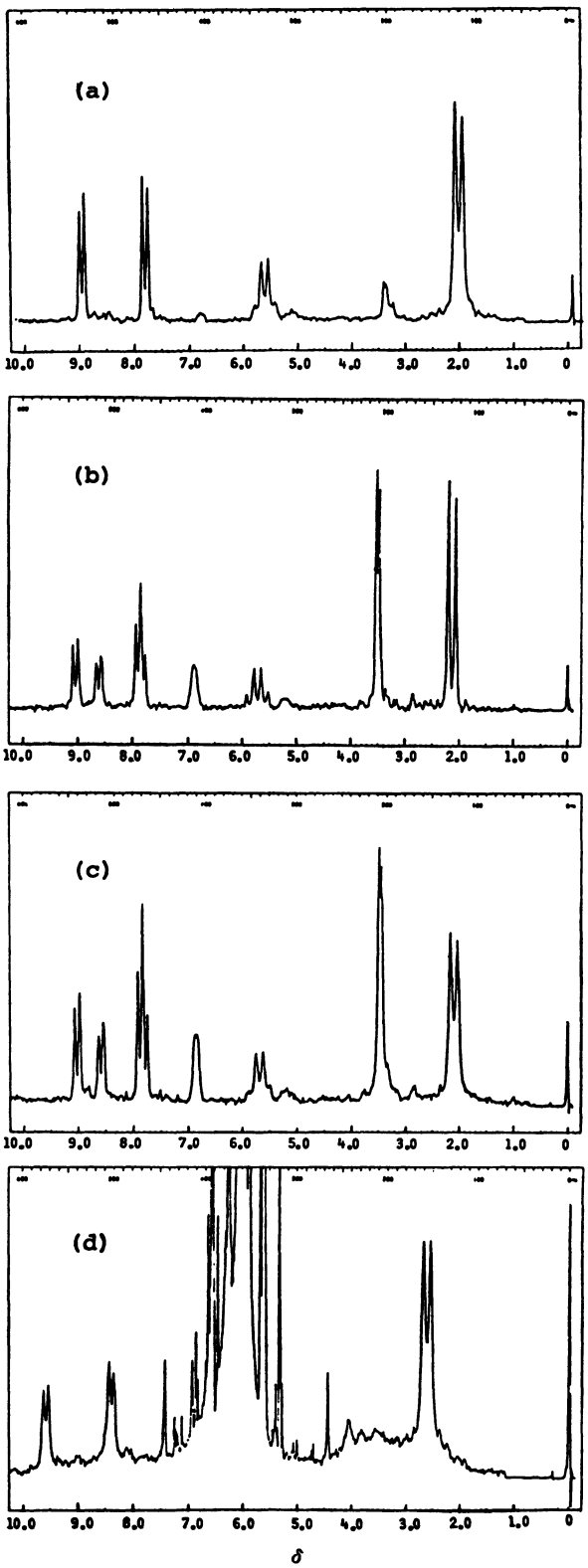

Fig. 3. ^{1}H NMR spectra of protonated 2-chloro-5-methylthiophene (**2** and **3**) at 60 MHz. (a) In HSO_3F at −70 °C, (b) at −30 °C, (c) again at −70 °C after observing the spectrum b, (d) in $AlCl_3$–HCl–dichloromethane at −70 °C.

produced two cations, (**2**) and (**3**), in HSO_3F in ratios from 3 : 1 to 10 : 1, depending on the shaking time described in the Experimental part. The signals of **2**

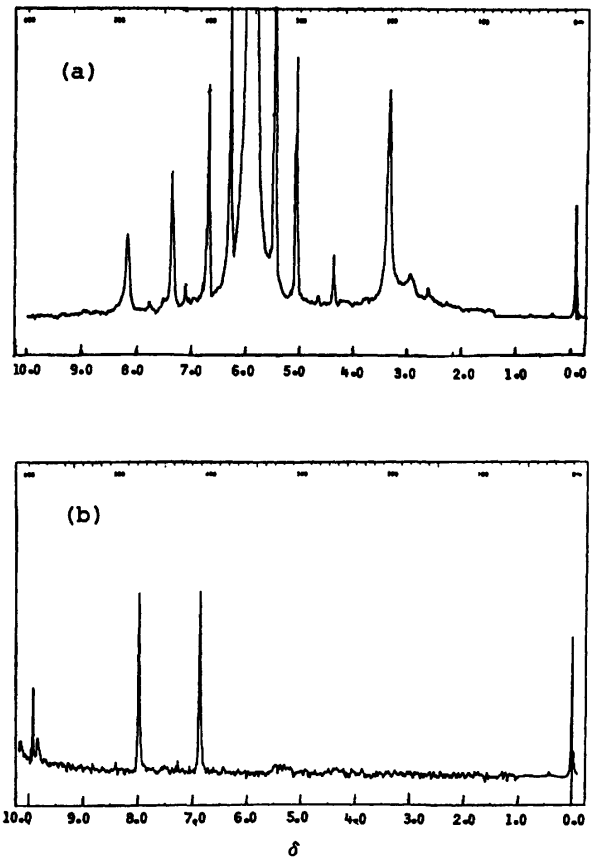

Fig. 4. ^1H NMR spectra of (a) protonated 2,5-dichloro-3-methylthiophene (**7**) in $AlCl_3$–HCl–dichloromethane at −70 °C, (b) protonated 2,3,5-trichlorothiophene (**8**) in the magic acid at −30 °C.

are considerably stronger than those of **3** at low temperatures, as is shown in Fig. 3a. When the temperature is carefully raised from −70 °C to −30 °C, the signals of **3** increase in intensity to the same extent as those of **2** (Fig. 3b). When the temperature is again lowered, the signals of **3** do not show any decrease (Fig. 3c). The conversion from **2** to **3** is not reversible. These results clearly indicate that the protonation occurs at the 5-position to give the cation (**2**), which later rearranges to the thermodynamically stable cation (**3**).[10] In the $AlCl_3$–HCl–CH_2Cl_2 system, the cation (**2**) is produced exclusively, as is shown in Fig. 3d.

The protonation of the compounds having one β- and two α-substituents occurred at the α-position neighbouring the β-substituent. This was the case with the cations (**7** and **8**), whose spectra are given in Fig. 4. In such cases, the electron-donating ability of the β-substituent seems to play a role.

The cations produced in this study are stable until the temperature reaches about −30 °C. Above −30 °C, the spectra gradually become complex, probably because of the rearrangement and/or polymerization of the molecule.

The data given in Table 1 are those obtained at the lower temperature rather than at the higher, because the proton-exchange effects are then suppressed and so are small. However, the resolution of the absorption lines is ordinarily better at a higher temperature than at a lower one.

A characteristic point of the couplings in thiophenium ions appears in the values of J_{23} and J_{34}. The J_{34} values of the thiophenium ions are larger than those of thiophenes. The J_{23} and the J_{34} of **1** are 1.3 and 5.5 Hz, while the corresponding values of 2-chlorothiophene are 6.1 and 4.0 Hz respectively. The change in these coupling constants shows the change in the system caused by protonation. It means that the distance between C_2 and C_3 increases, while that between C_3 and C_4 decreases, upon the protonation at the 2-position. The structural change in the system is clearly expressed by the change in the interproton couplings. The J_{24} of **1** is about 0.5 Hz, as estimated from the line broadening of the H_4 signal. The same is true for that of **6**. This may be compared with the J_{35} of 2-chlorothiophene (1.1 Hz).

The chemical shifts of the H_3 are always larger than those of the H_4 in thiophenium ions. Two limiting resonance structures of the ions are shown in Scheme 2. The positive charge is localized at C_3, but not at C_4, in the Scheme. This fact is consistent with the chemical-shift difference between H_3 and H_4 in Table 1.

This study provides a proof of the formation of the 2-chlorothiophenium ion (**1**) as a key intermediate in the reaction shown in Scheme 1. The cations observed here become reaction intermediates in similar acid-catalyzed reactions, one example of which is given in the case of 2,5-dichlorothiophene.[11] The study is now being extended to other halothiophenes; the synthetic use of halothiophenium ions is also under investigation.

References

1) Y. Yokoyama, Y. Yamashita, K. Takahashi, and T. Sone, Presented at the 20th Symposium on NMR spectroscopy of the Chemical Society of Japan, Tokyo, Nov. 1981, Preprint, p. 207.

2) T. Sone, R. Yokoyama, and Y. Okuyama, The 41st National Meeting of the Chemical Society of Japan, Suita, April 1980, Abstr. 2N10.

3) G. A. Olah and P. von R. Schleyer, "Carbonium Ions," John Wiley and Sons, New York (1973), Vols. 1—4.

4) Y. Okami, N. Otani, D. Katoh, S. Hamanaka, and M. Ogawa, *Bull. Chem. Soc. Jpn.*, **46**, 1860 (1973).

5) L. I. Belen'kii, A. P. Yakubov, and Ya. L. Gol'dfarb, *Zh. Org. Khim.*, **11**, 424 (1975).

6) Y. Yokoyama, Y. Yamashita, K. Takahashi, and T. Sone, *Chem. Lett.*, **1981**, 813.

7) In the previous paper (Ref. 6), the site of protonation was taken to be the 5-position.

8) D. M. Brouwer, *Recl. Trav. Chim. Pays-Bas*, **87**, 335 and 342 (1968).

9) G. A. Olah, W. S. Tolgyesi, and R. E. A. Dear, *J. Org. Chem.*, **27**, 3449 (1962).

10) The statement in our previous communication (Ref. 6) that the two cations, **2** and **3**, were produced in the ratio of 3 : 1 at the same time must be corrected.

11) T. Sone and M. Inoue, Presented at the 8th International Congress of Heterocyclic Chemistry, August 1981, Graz, Abstr., p. 352.

The Ultraviolet Photoelectron Spectroscopy of Aliphatic Hydrocarbons and Tetramethylsilane in the Solid State

Kazuhiko Seki* and Hiroo Inokuchi
Institute for Molecular Science, Myodaiji, Okazaki 444
(Received January 5, 1983)

He I, Ne I, and Ar I ultraviolet photoelectron spectra were measured for solid hexane, 3-methylpentane, 2,2-dimethylbutane, neopentane, tetramethylsilane, cyclohexane, and 1-hexene deposited on a substrate at the temperature of liquid nitrogen. The spectra of all the compounds except hexane showed valence-band features. The threshold ionization potential was 7.6—8.9 eV, with a lowering of the threshold from the gas to the solid phase (polarization energy P_S) of 1.2—1.8 eV. These P_S values are in reasonable agreement with theoretical model calculations. To clarify the effect of intra- and intermolecular factors on P_S, the observed P_S values were compared with those of liquid-phase and solid-aromatic hydrocarbons. For compounds in which the bottom of the conduction band lies above the vacuum level, the polarization energy data showed that electrons with energies between these states are also emitted, possibly without any excitation of electrons to the conduction band in the bulk of the solid.

Ultraviolet photoelectron spectroscopy (UPS) is a powerful tool for studying the electronic structure and electron-transport properties of solids, including organic compounds.[1] Although extensive studies have been carried out on aromatics,[2-4] however, few results have been reported for aliphatics. We have already reported UPS studies of long-chain alkanes (n-$C_{28}H_{58}$, n-$C_{36}H_{74}$, and polyethylene),[5-9] whilst others[10] have concentrated more on small compounds containing one or two carbon atoms. We wish here to report a UPS study of aliphatic hydrocarbons containing five to seven carbon atoms, and of tetramethylsilane.

This work has two aims. One is to study the energetics of the ionized states of these solids. An important quantity obtained by UPS is the threshold ionization potential of a solid, which gives the location of the top of the occupied valence band. Together with the reported energy of the bottom of the conduction band, V_0 (relative to the vacuum level),[11,12] it gives a basic picture of the electronic structure of these solids. Further, a comparison of the threshold with that in the gas phase gives the interaction energy between the ionized molecule and the surroundings. This is mainly to be ascribed to the electric polarization of the surroundings and is called the polarization energy.[13,14] It is a fundamental quantity in discussing the ionized state of molecular solides.[14] However, the values of the polarization energies of aliphatic solids have not been experimentally determined except in a few small-molecule compounds. The experimental values observed here are discussed in comparison with theoretical-model calculations, the polarization energies in liquid phase,[15,16] or aromatic hydrocarbon solids.[3]

The second aim of this study is to obtain information as to the photoemission mechanism from aliphatic solids. In most of the solids studied here, the bottom of conduction band has been reported to lie above the vacuum level ($V_0>0$), with no bulk electronic state in-between.[11,12] Some compounds have V_0's as high as $\approx$1 eV (1 eV=0.1602 aJ). It is of interest to determine whether or not electrons which do have energies between these two levels are emitted. This problem could be elucidated by the measured photoemission threshold and the polarization energies.

There is also a question about the origin of features in the photoelectron spectra. In our previous studies of long-chain alkane solids,[6,7] the UPS spectra for 11 eV $\leq h\nu \leq$ 21 eV were dominated by conduction-band features, unlike those of most other organic solids, dominated by valence-band features.[1-4] The present study will elucidate if similar behavior is also exhibited by smaller aliphatic compounds.

Since the electronic properties of aliphatic compounds in the condensed phase are known to depend significantly on the molecular structure,[11,12,17,18] we chose to study the following species: hexane, 3-methylpentane, 2,2-dimethylbutane, neopentane, tetramethylsilane, cyclohexane, methylcyclohexane, and 1-hexene.

Experimental

The samples were commercially obtained, of the purity indicated: Hexane (99.8%, gas chromatographic standard), cyclohexane (99.7%), and tetramethylsilane (99.7%, NMR standard) from Merck; 3-methylpentane (99%), 2,2-dimethylbutane (99.8%), and methylcyclohexane (99.9%) from Tokyo Kagaku Seiki; neopentane (96.3%) and 1-hexene (99%) from Tokyo Kasei. All were further purified by vacuum distillation and the freeze-and-thaw technique in a system with a base pressure of 5×10^{-6} Pa.

The photoelectron spectra were recorded on a retarding-potential-type photoelectron spectrometer. The base pressure of the vacuum chamber was 2×10^{-8} Pa. A copper substrate 12 mm in diameter was located at the center of a nearly spherical collector coated inside with gold. The sample vapor was deposited through a variable-leak valve onto a substrate cooled to about 80 K by means of liquid nitrogen. The light source was a dc discharge lamp capable of He I (21.22 eV), Ne I (16.67 and 16.85 eV), and Ar I (11.62 and 11.83 eV) emission. For Ne I and Ar I, the mean values, 16.8 and 11.7 eV, were taken to be the incident energies respectively. As an exception, the higher energy components were used to calculate the photoemission thresholds. The energy analysis was performed by means of the ac-modulated retarding-potential technique reported previously,[2a] with a 0.2 V peak-to-peak modulation of 4 Hz. The energy resolution was 0.2—0.3 eV, determined by the Fermi edge of gold.

Although the film thickness was not measured, it was increased step-by-step until no essential change in the spectra could be observed on further deposition. Figure 1 shows such

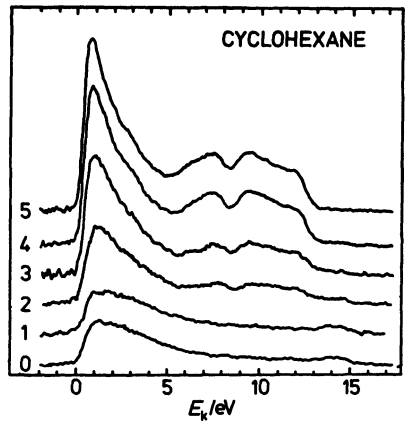

Fig. 1. He I photoelectron spectra of condensed cyclohexane against kinetic energy of electron E_k with a different degree of sample deposition. 0, copper substrate; 1 to 5, spectra showing the larger amount of condensation of cyclohexane.

a series for the He I photoelectron spectra of cyclohexane, plotted against the kinetic energy of photoelectrons E_k. The spectral profile appears to become settled at Curve 5, apart from the increasing secondary electron peak at $E_k \approx 0$ eV. A further increase in thickness resulted in the charging of the deposited sample, which could be detected as the tailing at the left-hand cutoff of the spectrum. Since 3-methylpentane, methylcyclohexane, and 1-hexene are known to form glass on rapid cooling, with their glass-transition temperatures above the temperature of liquid nitrogen,[19] they should form such glasses under the present experimental conditions. For the other compounds, it is not clear whether they form crystalline films or become amorphous.

Results and Discussion

General Aspects of the Photoelectron Spectra. Figures 2—9 (a) show the solid UPS spectra of the aliphatic

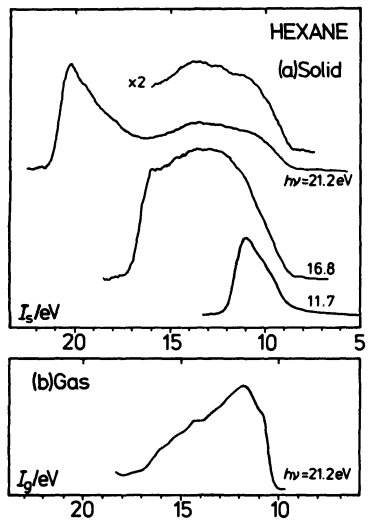

Fig. 2. Photoelectron spectra of hexane in solid (a) and gas (b) phases. Energy scales are shifted by 0.6 eV. The correspondence between the spectra of the two phases is dubious for this compound. The units of the ordinate are arbitrary and not common to the different curves (the same also in Figs. 5(a)—9(a)).

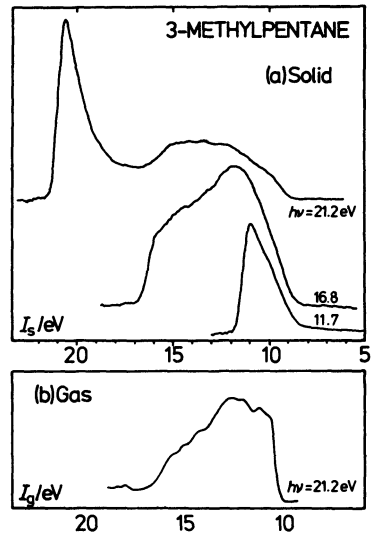

Fig. 3. Photoelectron spectra of 3-methylpentane in solid (a) and gas (b) phases. Energy scales are shifted by 0.8 eV for a good peak correspondence between the two phases.

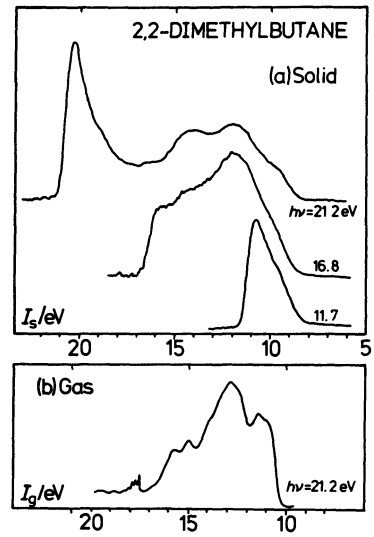

Fig. 4. Photoelectron spectra of 2,2-dimethylbutane in solid (a) and gas (b) phases. Energy scales are shifted by 0.9 eV for a good peak correspondence between the two phases.

compounds studied here. The abscissa is the solid ionization potential, I_s, relative to the vacuum level of the sample, converted from E_k as:

$$I_s = h\nu - E_k. \quad (1)$$

For all the compounds some features in the low I_s region correspond to constant values of I_s, independent of $h\nu$. which indicates that they originate from valence bands. In particular, the right-hand edge of the spectrum corresponds to the top of the valence bands, and its I_s gives the threshold ionization potential of the solid. For the sake of comparison, the gas-phase photoelectron spectra reported by other workers[20] are shown in Figs. 2—9 (b). The valence-band features of a solid corre-

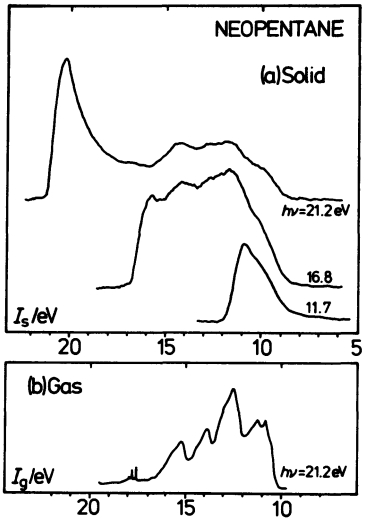

Fig. 5. Photoelectron spectra of neopentane in solid (a) and gas (b) phases. Energy scales are shifted by 1.1 eV for a good peak correspondence between the two phases.

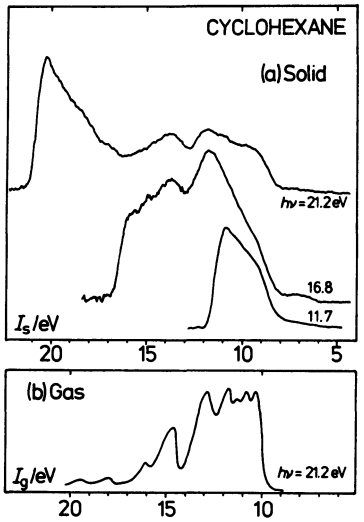

Fig. 7. Photoelectron spectra of cyclohexane in solid (a) and gas (b) phases. Energy scales are shifted by 1.0 eV for a good correspondence between the two phases.

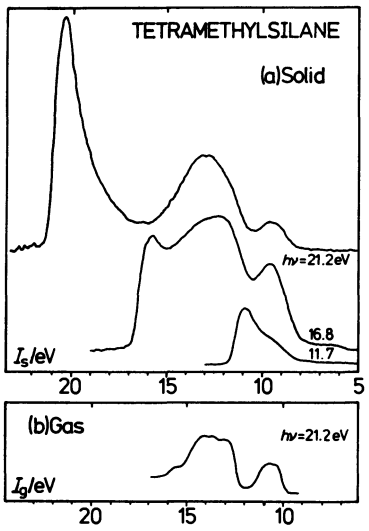

Fig. 6. Photoelectron spectra of tetramethylsilane in solid (a) and gas (b) phases. Energy scales are shifted by 1.1 eV for a good peak correspondence between the two phases.

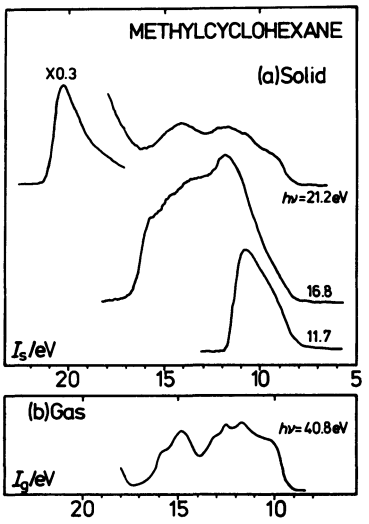

Fig. 8. Photoelectron spectra of methylcyclohexane in solid (a) and gas (b) phases. Energy scales are shifted by 0.7 eV for a good peak correspondence between the two phases.

spond well with the gas-spectrum features, when we make a shift between I_s and the gas-phase ionization potential I_g, as is indicated in each figure caption. Such a good correspondence shows that the photoemission from an organic solid may be regarded as the ionization of a molecule in the solid.[2,3]

If the conduction band gives rise to a band in the photoelectron spectrum its value of E_k should be independent of $h\nu$.[6,21] No such features are seen except for the secondary-electron peak at $E_k \approx 0$ eV. The features in the spectra of 1-hexene and hexane at $I_s \approx 9$ eV cannot be ascibed unambiguously to either the valence- or the conduction-band. These results show that the dominance of conduction-band features observed in the spectra of long-chain alkanes for $h\nu \leq 21.2$ eV[6,7] is not common to aliphatic compounds. Rather, they suggest that linear-chain aliphatics, maybe including hexane and 1-hexene, form a special group in terms of the photoemission from organics. Naturally, the cause of such variation in valence- or conduction-band dominance is of great interest, but here we will not discuss this point in detail, leaving it to a later publication.

The relative intensity of the secondary-electron peak at $E_k \approx 0$ eV is much larger in the He I spectrum than in the Ne I spectrum. This intensity difference can be ascribed to inelastic electron-electron (e-e) scattering, which can occur only when the photon energy exceeds the threshold energy E_1 given by:[21,22]

$$E_1 = E_g + E_x, \tag{2}$$

where E_g and E_x are the band gap and the energy of the lowest electronic excitation in the solid respectively. The values of E_1 in condensed aliphatic compounds are

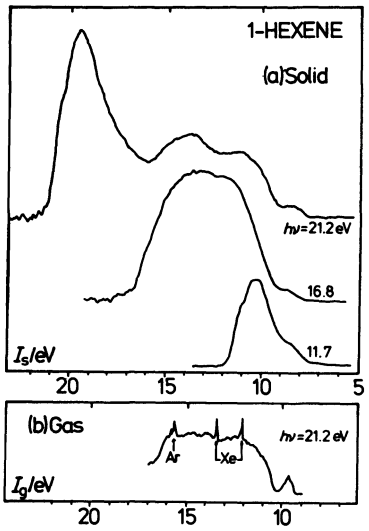

Fig. 9. Photoelectron spectra of 1-hexene in solid (a) and gas (b) phases. Energy scales are shifted by 1.0 eV for a good correspondence of the lowest ionization potential peaks between the two phases. The correspondence is dubious for the region of $I_s > 9$ eV.

estimated to be ≈16 eV (*e.g.*, for liquid hexane, E_g= 8.7 eV[16] and E_x=7.4 eV).[23] In the Ne I ($h\nu$=16.8 eV) spectra, $h\nu$ is comparable with E_1, and most of the photoexcited electrons cannot undergo e-e scattering. In the He I spectra, $h\nu$ is sufficiently large to cause appreciable e-e scattering, and hence secondary-electrons. In contrast to the present results, the smaller E_1 values of 4—8 eV in aromatics result in strong secondary-electron bands, even in the Ne I spectra.[2b]

Photoemission Threshold and Polarization Energy. Table 1 lists the values of the threshold ionization energy I_s^{th} determined as the intercept of the low I_s linear extrapolation of the spectrum with the energy axis. The values obtained from the spectra for three photon energies agreed within ±0.1 eV, including a reproducibility for several samples.

There is a problem in the determination of the I_s^{th} of amorphous solids, for the ionization potential of a molecule in the solid may depend on the arrangement of the surrounding molecules. However, the onsets in the lowest I_s region of the observed spectra are fairly distinct, which suggests that the fluctuation of this kind is minimal.

Using these values and the reported values of V_0,[11,12] which are also listed in Table 1, we can construct basic energy diagrams for these compounds. The band gap between the valence and conduction bands is 8—9 eV, which is consistent with the onset energies of the electronic absorption[23] and the photoconduction[16,24] of these compounds in the condensed phase.

The ionization potential of a molecule in the bulk of a solid is determined as the gas-phase ionization potential lowered by the polarization energy, P_s of the surroundings.[13,14] We can determine P_s from a comparison of the gas and solid-state photoelectron spectra. According to an analysis of the contribution of molecules in the bulk and at the surface, we have already noted[3] that we should compare the thresholds of these spectra, rather than the peak energies, to obtain the bulk polarization energy. That is, P_s should be determined as:

$$P_s = I_g^a - I_s^{th}, \quad (3)$$

where I_g^a is the threshold (adiabatic) ionization potential

Table 1. Observed photoemission thresholds and related energy-structure parameters

Compound	$I_s^{tha)}$ / eV	$V_0^{b)}$ / eV	$I_g^{ac)}$ / eV	$P_s^{d)}$ / eV	$P_s^{*e)}$ / eV
Hexane	8.5_5	0.62[f]	10.2_5	1.7(2.1)	2.3
		0.98[g]			2.7
		0.9[i]			2.6
3-Methylpentane	8.8_5	1.29[g]	10.2	1.3(1.7)	2.6
		1.20[h]			2.5
		0.6[i]			1.9
2,2-Dimethylbutane	8.8	−0.013[f]	10.2	1.4	—
		0.59[g]			2.0
Neopentane	8.7	0.33[g]	10.2	1.5	1.8
		<0[i]			—
Tetramethylsilane	8.2	0.440[f]	9.79	1.6	2.0
		<0[i]			—
Cyclohexane	8.2	0.47[f]	9.88	1.7(1.7)	2.2
		0.9[i]			2.6
Methylcyclohexane	8.3	1.00[g]	9.5	1.2(1.6)	2.2
		1.43[f]			2.6
		1.24[h]			2.4
1-Hexene	7.6	0.6[i]	9.37	1.8(2.4)	2.4

a) Photomission threshold observed in the present study. b) Energy of the bottom of the conduction band relative to the vacuum level. c)Gas-phase adiabatic (thereshold) ionization potential taken from Ref. 20. The values of hexane, 3-methylpentane, and 2,2-dimethylbutane were read from the spectra. d) Polarization energies calculatcd from Eq. 3 (correct values). The values in parentheses are from Ref. 12. e) Polarization energies calculated from Eq. 6 (wrong values, see text). f—i) Values from Refs. 11a,b,c, and 12 respectively.

Table 2. Polarization energies calculated by means of Eq. 5 and parameters used

Compound	ε[a] Crystal	ε[a] Glass	ρ[b] / pm	P_s[c] / eV
Hexane	2.33 (A)	2.23 (B)	214	1.92 (A)
				1.86 (B)
3-Methylpentane	—	2.31 (A)	214	1.91 (A)
		2.24 (B)		1.86 (B)
2,2-Dimethylbutane	2.18 (A)	2.23 (B)	219	1.78 (A)
				1.81 (B)
Neopentane	1.98 (A)	2.14 (B)	216	1.65 (A)
				1.78 (B)
Tetramethylsilane	2.19 (A)	2.20 (B)	225	1.74 (A)
				1.75 (B)
Cyclohexane	2.48 (A)	2.39 (B)	213	2.02 (A)
				1.97 (B)
Methylcyclohexane	—	2.53 (A)	213	2.04 (A)
		2.38 (B)		1.96 (B)
1-Hexene	—	2.36 (A)	210	1.98 (A)
		2.28 (B)		1.92 (B)

a) Optical permittivity estimated as described in the Appendix. Symbols in the parentheses indicate the methods given there. b) Effective radius of the cation evaluated from the density. c) Polarization energy estimated using Eq. 5.

in the gas phase. The values of I_g^a reported by other workers and the P_s values calculated by means of Eq. 3 are listed in Table 1. The maximum error in P_s is estimated to be ± 0.2 eV from those (± 0.1 eV) for both I_g^a and I_s^{th}. As has already been noted, the shift between I_s and I_s to give the best peak correspondence (relaxation shift) is shown in each caption of Figs. 2—9, which may be convenient in comparing our results with those of other workers.

Recently Hiraoka[12] estimated the P's for several of the compounds studied here. He estimated I_s^{th}, from the values of E_g and V_0 measured by an electron-transmission experiment, as:

$$I_s^{th} = E_g - V_o, \tag{4}$$

and used Eq. 3. His values are also listed in Table 1. They are, on the average, 0.4 eV larger than the present directly measured ones, but the latter are within the estimated error of his values, ± 0.4 eV for E_g and $^{+0.2}_{-0.3}$ eV for V_0.

We will discuss the observed values of the polarization energy P_s in some detail, for it is an important quantity in the energestics of the ionized state of a molecular solid.

Comparison with Theoretical Models. Two models have been reported for the theoretical estimation of the polarization energy. In the first model, by Lyons and his-coworkers,[13,25,26] the polarization energy is calculated as the sum of the interaction energy between the cation and the multipoles induced on surrounding molecules. Lyons and Mackie[25] reported $P_s = 1.7$ eV for hexane, which is in good agreement with the present experimental result. Unfortunately, no calculations are reported for the other compounds studied here.

In the second model, by Born,[27] the ion is treated as a point charge at the center of a spherical cavity, while the surrounding molecules are regarded as a continuous medium. The polarization energy is given by:

$$P_s = (e^2/2\rho)(1 - 1/\varepsilon), \tag{5}$$

where e is the electronic charge: ρ, the effective radius of the ionic cavity, and ε the optical permittivity of the medium. This model can be applied not only to crystals but also to liquids[15-17] and amorphous solids.[11,12]

In order to calculate P_s by means of this model, the values of ρ and ε are needed. We estimated ε (solid) at the temperature of liquid nitrogen in two ways (A and B), as will be described in the Appendix. For compounds whose state of aggregation is not clear, ε was evaluated for both crystalline and glassy states. The effective radius was calculated as $v^{1/3}/2$, where, $v = 1/N$ and where N is the number density of molecules, as evaluated from the density; this gave a reasonable agreement with the experimental values in the case of aromatic hydrocarbons.[3] The values of these parameters and of P_s as calculated by means of Eq. 5 are listed in Table 2.

The agreement between the experimental and calculated values is reasonable, considering the estimated error of ± 0.2 eV in the observed values. The state of aggregation or the method of estimation of ε do not affect the calculated P_s so much. Calculations using two other kinds of effective radius: (1) the van der Waals radius used in the hard-core model of the critical volume[28] and (2) the electron-molecule hard-core radius,[16,27] gave larger P_s values, with poorer agreement with the experimental values. We note that the above trends are common in molecules from spherical to linear, which have varying degrees of matching to the assumption of spherical cavity. This suggests that the anisotropy in the molecular shape of these compounds is not yet so large as to break the validity of this model.

The reasonable success of the present way of evaluating ρ tempts us to calculat the ρ of TMPD (N,N,N',N'-tetramethyl-p-phenylenediamine), which has been frequently used as a photoionizing dopant in these compounds. The crystal structure[30] gives 316 pm, which is comparable with one of the previous estimates, 324 pm,[31a] but which shows a discrepancy from the 249 and 193 pm in Refs. 31b and 11c.

In conclusion, theoretical calculations, both the Lyons model and Born's, predict reasonably accurate values for P_s. However, a very detailed discussion of the correlation between the calculated and observed values does not appear feasible at this time.

Comparison with Aromatic Hydrocarbons. Aromatic hydrocarbons form another representative group of organic compounds. The P_s values of aliphatics range from 1.2 to 1.8 eV, which is, on the average, a little smaller than the almost constant value of ≈1.7 eV for condensed aromatic hydrocarbons with planar structures.[3]

We can analyze these values in terms of molecular polarizability and molecular packing.[3] In aliphatics, ε is much smaller than those in aromatics (ε=4.8—5.9 from naphthalene to coronene). As may be seen in Eq. 5, this will make the P_s values of aliphatics smaller. However, ρ is also smaller in aliphatics than in aromatics (ρ=280—360 pm for the aromatics described above). This tends to increase the P_s. The observed P_s values should be the result of the balance between these two factors.

Such a difference in P_s preserves or even enlarges the difference between the I_g^a's of aliphatics and aromatics in going to the solid phase. Thus, the I_s^{th} values of saturated compounds exceed 8 eV and are higher than those of aromatics (*e.g.*, 7.1 eV for benzene[32]). A similar preservation also exists between saturated and unsaturated (*e.g.*, 7.1 eV for 1-hexene) aliphatic hydrocarbons.

Comparison with Polarization Energies of Liquid Phase. Recently, data have accumulated on the polarization energies of pure liquid P_l. Schmid *et al.*[15] and Casanovas *et al.*[16] measured the band gap of tetramethylsilane and some alkanes as the photoconduction thresholds. The polarization energies were calculated by means of Eqs. 4 and 3 using reported values of I_g^a and V_0. Their results are listed in Table 3, together with the $\Delta P_{sl}=P_s-P_l$ calculated with P_s in Table 1. For most compounds, P_s and P_l are rather similar, indicating that the polarization energy and the ionization threshold do not change very much in these condensed states. The small positive values of ΔP_{sl} (except for 2,2-dimethylbutane) may be understood as being due to the decrease in density, and thus in ε, at the transition from the solid to the liquid phase. The calculation of ΔP_{sl} by means of Eq. 5, using the ρ and ε of these two states, gives an almost common value of 0.2—0.3 eV. Considering the possible errors in P_l and P_s, however, it is difficult to discuss these values further.

Interpretation of the Observed Photoemission Threshold Energies. Most of the compounds studied here have been reported to have fairly large positive V_0 values (Table 1). This means that the lower boundary of the conduction band (CB) lies above the vacuum level (VL) (Fig. 10), with no bulk electronic states in between. This raises a question as to whether photoelectrons with energies between CB and VL may be emitted by direct photoemission from the valence band into the vacuum (Case I), or whether the electron must first be excited to the conduction band in the bulk of the solid, and hence may not possess an energy between the two levels

Table 3. Polarizatuion energies of liquid phase and their differences from solid phase

Compound	P_l[a] / eV	ΔP_{sl}[b] / eV
Hexane	1.61[c]	0.1
2,2-Demethylbutane	1.46[c]	−0.1
Neopentane	1.2$_6$[e]	0.2
Tetramethylsilane	1.17[c]	0.4
	1.12[d]	0.5
Cyclohexane	1.46[c]	0.2

a) Polarization energy of the liquid phase. b) $\Delta P_{sl}\equiv P_s-P_l$. c) Ref. 16. The values are slightly different from theoriginal values due to the use of the I_g's in Table 1 instead of tho se used in Ref. 16. d) Ref. 15.

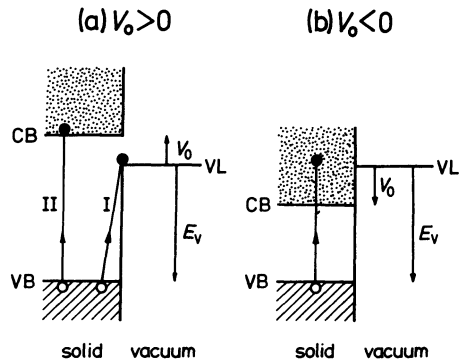

Fig. 10. Schematic energy diagram of photoemission process. VB, top, of the valence band; CB, bottom of the conduction band; VL, vacuum level; V_0, the energy of CB relative to VL; E_v, the energy differnce between VL and VB. (a) The case of $V_0>0$. I denotes the direct photoemission into vacuum and II denotes the photoexcitation process in the rigorous three-step model. (b) The case of $V_0<0$.

(Case II). The latter case was favored by Delahay[33] and by Less and Wilson[24] on the basis of a three-step photoemission model (photoexcitation in the bulk/electron transport/escape into the vacuum).[21]

An examination of the photoemission thresholds and polarization energies enables us to determine which model is most probably correct. In Case I, the experimentally observed threshold I_s^{th} corresponds to the excitation energy from the top of the valence band to the vacuum E_v (VB→VL in Fig. 10(a)), as in the case of $V_0<0$ (Fig. 10(b)). This was our assumption in the preceding part of this paper. In Case II, I_s^{th} gives the band gap $E_g=E_v+V_0$ (VB→CB in Fig. 10(a)). Since the polarization energy is defined as $I_g^a-E_v$, the "true" polarization energy in Case II, P_s^*, is:

$$P_s^* = I_g^a - (I_s^{th}-V_0), \quad (6)$$

instead of $I_g^a-I_s^{th}$ (Eq. 3). The values of P_s^* calculated using the reported V_0's are listed in Table 1.

The theoretical results of Lyons and Mackie[25] give the polarization energies for hexane and anthracene as 1.7 and 2.1 eV respectively. This indicates that the polarization energy of hexane is unlikely to exceed that of anthracene. For anthracene, the negative value of V_0[14] assures that Eq. 3 gives the polarization energy. The observed P_s=1.7 eV for anthracene[3] shows that

the idea that $P_s^* = 2.3_2$ to 2.6_8 eV for hexane is very improbable, while $P_s = 1.7$ eV in Table 1 is reasonable. Therefore, Case I applies, and I_s^{th} corresponds to the VB→VL excitation. Thus, the discussion in the preceding part of this paper is substantiated. To support this, Koch *et al.*[34] showed that $E_g > I_s^{th}$ for solid Ne and Ar, from independent measurements of E_g and I_s^{th} by means of optical spectra and photoemission respectively. This gives another example where Case I applies.

It was shown that the photoemission experiment can provide the energy of electrons relative to the vacuum level, even for organic solids with positive V_0 values. Considering that an advantage of UPS is that one can get the absolute energy of electrons relative to the vacuum level, this is an important conclusion. Furthermore, the above discussion suggests that the photoemission in aliphatic solids most probably cannot be rigorously divided into three steps (only because at present we cannot exclude the possibility of the existence of defect states between CB and VL, which may allow optical excitation and the transport of electrons in this energy range[12]).

Concluding Remarks

The ultraviolet photoelectron spectra of seven aliphatic hydrocarbons and tetramethylsilane were measured in an attempt to elucidate the energetics of the ionized state and the photoemission mechanism. Most of the spectra revealed valence-band features, but linear compounds (hexane and 1-hexene) showed some spectral features which may be due to conduction-band structures. Together with the dominance of the conduction band observed in longer-chain normal alkanes, this suggests that long linear aliphatics may form a special group in terms of photoemission from organics.

Although it has been reported that the conduction bands lie above the vacuum level, with no bulk electronic states in between, electrons with energies between the two levels are emitted. That is, we can determine the location of the valence-band features relative to the vacuum level. This ensures the usefulness of UPS as a tool for probing the electronic structures of organic solids with positive V_0 values. By virtue of this fact, the experimental values of the photoemission thresholds and the polarization energies could be obtained directly from the observed spectra.

The reasonable agreement of the observed polarization energies with the model calculations confirmed the validity of these models, and also indicated that both aliphatics and aromatics can be treated in a common theoretical frame. Further studies of other aliphatics are desired in order to confirm this point.

Although the present study gave these important pieces of general information on the electronic structure and photoemission mechanism of aliphatic solids, more studies are required in order to clarify such problems as the peculiarity of long-chain molecules and the difference between solid and liquid states. The accumulation of data on other compounds is required for the former, while the continuous examination of the solid and liquid states, using the same photoelectron spectrometer, will be useful for the latter. We have already started these kinds of studies.

The authors are grateful to Professors Edgar Heilbronner and R. A. Burgess for providing some of the gas-phase photoelectron spectra, to Professor Yoshihiko Hatano and his collaborators for the data on the density of solid tetramethylsilane, to Dr. J. Casanovas for sending preprints, to Dr. Nobuo Ueno and Professor Kenzo Hiraoka for useful information and comments, and to Dr. Naoki Sato and Professor Kosuke Shobatake for their critical reading of the manuscript.

This work was partly supported by a Grant-in-Aid for Scientific Research (No. 474210) from the Ministry of Education, Science and Culture.

Appendix

Here we will describe the two methods[11] of evaluating the optical permittivity ε of aliphatic solids at the temperature of liquid nitrogen, methods which were used for the calculation of P_s by means of Eq. 5.

One of them (Method A) applies the Clausius–Mosotti relation $(\varepsilon-1)/(\varepsilon+2)(M/d) = N_A\alpha/3$, where M is the molecular weight; d, the density; N_A, the Avogadro constant, and α, the molecular polarizability. Assuming that α is independent of the temperature, we first calculated its value using ε and d[35] for the liquid at room temperature. The value of ε was taken as the square of the refractive index n for the Na D emission lines.[35] The procedure was then reversed to obtain ε at low temperatures from the solid density.

In the other method (Method B), the value of n at a low temperture was estimated by the extrapolation of n using dn/dT (liquid), and ε was taken as equal to n^2.

Method A is applicable for both crystalline and glassy states, while B may be used only for the glassy state because of the discrete change in n at the liquid-crystal transition. For compounds whose state of aggregation was not clear, ε was evaluated for both states. The low-temperature values of d for crystalline states were calculated for the nearest temperature phase whose crystal structure data are available.[36] For tetramethylsilane, a directly measured value for d is available.[37] For glasses, d and dn/dT are available for several compounds.[19,36] For compounds with no observed data, dn/dT of similar compounds were used. The various values of ε thus obtained are listed in Table 2.

References

1) For example, "Photoemission in Solid," ed by M. Cardona and L. Ley, Springer-Verlag, Berlin (1978), Vols. I and II, and the references cited therein.

2) For example, a) T. Hirooka, K. Tanaka, K. Kuchitsu, M. Fujihira, H. Inokuchi, and Y. Harada, *Chem. Phys. Lett.*, **18**, 390 (1973); b) K. Seki, T. Hirooka, Y. Kamura, and H. Inokuchi, *Bull. Chem. Soc. Jpn.*, **49**, 904 (1976). See also the references cited therein.

3) N. Sato, K. Seki, and H. Inokuchi, *J. Chem. Soc., Faraday Trans. 2*, **77**, 1621 (1981). See also the references cited therein.

4) For reviews, see a) W. D. Grobman and E. E. Koch, Ref. 1, Vol. II, Chap. 5; b) E. A. Silinsh, "Organic Molecular Crystals," Springer-Verlag, Berlin (1980).

5) M. Fujihira and H. Inokuchi, *Chem. Phys. Lett.*, **17**, 554 (1972).

6) K. Seki, S. Hashimoto, N. Sato, Y. Harada, K. Ishii H. Inokuchi, and J. Kanbe, *J. Chem. Phys.*, **66**, 3644 (1977).

7) N. Ueno, T. Fukushima, K. Sugita, S. Kiyono, K. Seki, and H. Inokuchi, *J. Phys. Soc. Jpn.*, **48**, 1254 (1980).
8) S. Hashimoto, S. Hino, K. Seki, and H. Inokuchi, *Chem. Phys. Lett.*, **40**, 279 (1976); S. Hashimoto, K. Seki, N. Sato, and H. Inokuchi, *J. Chem. Phys.*, **76**, 163 (1982).
9) K. Seki and H. Inokuchi, *Chem. Phys. Lett.*, **89**, 268 (1982).
10) a) J. E. Demuth and D. E. Eastman, *Phys. Rev. Lett.*, **32**, 1123 (1974); b) F.-J. Himpsel, N. Schwentner, and E. E. Koch, *Phys. Status Solidi B*, **71**, 615 (1975); c) K. Y. Yu, J. C. McMenamin, and W. E. Spicer, *Surf. Sci.*, **50**, 149 (1975); d) G. W. Rubloff, W. D. Grobman, and H. Luth, *Phys. Rev. B*, **14**, 1450 (1976); e) T. Takahashi and Y. Harada, *Bull. Chem. Soc. Jpn.*, **54**, 81 (1981).
11) a) J. Bullot and M. Gauthier, *Can. J. Chem.*, **55**, 1821 (1977); b) D. Grand and A. Bernas, *J. Phys. Chem.*, **81**, 1209 (1977); c) S. Noda, L. Kevan, and K. Fueki, *ibid.*, **79**, 2886 (1975). See also the references cited therein.
12) K. Hiraoka, *J. Phys. Chem.*, **85**, 4008 (1981).
13) L. E. Lyons, *J. Chem. Soc.*, **1957**, 5001.
14) F. Gutmann and L. E. Lyons, "Organic Semiconductors," John-Wiley & Sons, New York (1967).
15) W. F. Schmidt, W. Döldissen, U. Hahn, and E. E. Koch, *Z. Naturforsch., A*, **33**, 1393 (1978).
16) J. Casanovas, R. Grob, D. Delacroix, J. P. Guelfucci, and D. Blanc, private communication.
17) R. A. Holroyd, *J. Chem. Phys.*, **57**, 3007 (1972).
18) W. F. Schmidt, "Electron-Solvent and Anion-Solvent Interactions," ed by L. Kevan and B. C. Webster, Elsevier, Amsterdam (1976), Chap. 7.
19) L. Kevan, *Adv. Rad. Chem.*, **4**, 181 (1974).
20) a) Hexane, 3-methylpentane, and 2,2-dimethylbutane: E. Heilbronner, private communication; b) neopentane and tetramethylsilane: A. E. Jones, G. K. Schweitzer, F. A. Grimm, and T. A. Carlson, *J. Electron Spectrosc.*, **1**, 29 (1972/73); c) cyclohexane: P. Bischof, J. A. Harshmall, E. Heilbronner, and J. P. Maier, *Helv. Chim. Acta*, **60**, 2213 (1977), and K. Kimura, S. Katsumata, Y. Achiba, T. Yamazaki, and S. Iwata, "Handbook of He I Photoelectron Spectra of Fundamental Organic Molecules," Japan Scientific Societies Press, Tokyo, and Halsted Press, New York (1981); d) methylcyclohexane: G. Biere, F. Burger, E. Heilbronner, and J. P. Maier, *Helv. Chim Acta*, **60**, 2213 (1977); e) 1-hexene: F. S. Ashmore and A. R. Burgess, *J. Chem. Soc., Faraday Trans. 2*, **74**, 734 (1978); F. A. Ashmore, Ph. D Thesis, University of London, London, United Kingdom, 1975.
21) W. E. Spicer, "Optical Properties of Solids," ed by F. Abelés, North-Holland, Amsterdam (1972).
22) N. Schwentner, M. Skibowski, and W. Steinmann, *Phys. Rev. B*, **8**, 2965 (1973).
23) B. L. Sowers, M. W. Williams, R. N. Hamm, and E. T. Arakawa, *J. Chem. Phys.*, **57**, 167 (1972).
24) K. J. Less and E. G. Wilson, *J. Phys. C*, **6**, 3110 (1973).
25) L. E. Lyons and J. C. Mackie, *Proc. Chem. Soc.*, **1962**, 71.
26) For recent developments, see, *e.g.*, P. J. Bounds and R. W. Munn, *Chem. Phys.*, **44**, 103 (1979).
27) M. Born, *Z. Phys.*, **1**, 45 (1920).
28) B. Chu, "Molecular Forces: Based on the Baker Lectures of Peter J. Debye," John-Wiley & Sons, New York (1967).
29) K. Fueki, D.-F. Feng, and L. Kevan, *Chem. Phys. Lett.*, **13**, 616 (1972); H. T. Davis and L. D. Schmidt, *Can. J. Chem.*, **51**, 3443 (1973).
30) I. Ikemoto, G. Katagiri, S. Nishimura, K. Yakushi, and H. Kuroda, *Acta Crystallogr., Sect. B*, **35**, 2264 (1979).
31) a) Y. Nakato, T. Chiyoda, and H. Tsubomura, *Bull. Chem. Soc. Jpn.*, **47**, 3001 (1974); b) R. A. Holroyd and R. L. Russel, *J. Phys. Chem.*, **78**, 2128 (1974).
32) Ref. 4a (read from the spectrum) and K. Seki, unpublished result.
33) P. Delahay, Ref. 12, Chap. 4.
34) E. E. Koch, R. Nurnberger, and N. Schwentner, *Ber. Bunsenges. Phys. Chem.*, **82**, 110 (1978), and the references cited therein.
35) "Handbook of Physics and Chemistry," ed by R. C. Weast and M. J. Astle, CRC Press, West, Palm Beach (1978).
36) a) Hexane: N. Norman and H. Mathieson, *Acta Chem. Scand.*, **15**, 1747, 1755 (1961); b) 2,2-dimethylbutane: B. Post, R. Schwartz, and I. Fankuchen, *J. Am. Chem. Soc.*, **73**, 5113 (1951); c) neopentane: H. Mark and W. Noethling, *Z. Kryst.*, **65**, 435 (1927); d) cyclohexane: R. Kahn, R. Fourme, D. Andre, and K. Renaud, *Acta Crystallogr., Sect. B*, **29**, 131 (1973).
37) Y. Nakamura, H. Namba, K. Shinsaka, and Y. Hatano, *Chem. Phys. Lett.*, **76**, 311 (1980), and private communication.

One-electron Oxidation Potentials of an NADH Model Compound and a Dimeric Rhodium(I) Complex in Irreversible Systems. A Convenient Determination from the Fluorescence Quenching by Electron Acceptors

Shunichi Fukuzumi, Katsuhiko Hironaka, Nobuaki Nishizawa, and Toshio Tanaka*
Department of Applied Chemistry, Faculty of Engineering, Osaka University, Suita, Osaka 565
(Received February 19, 1983)

A new methodology for experimental determinations of redox potentials of oxidants or reductants in both reversible and irreversible systems is presented. The Rehm-Weller free energy relationship between the activation free energy $\Delta G^{\ddagger}$ and the free energy change ΔG for the electron transfer quenching of the excited states of oxidants or reductants by a series of reductants or oxidants is converted to a linear correlation between $\Delta G^{\ddagger}-\Delta G$ and $(\Delta G^{\ddagger})^{-1}$, which can be utilized in convenient determinations of redox potentials of oxidants or reductants. This methodology is established in various reversible systems where the redox potentials of oxidants or reductants determined based on the Rehm-Weller free energy relationship agree well with those determined independently by electrochemical methods. By using this method, one-electron oxidation potentials of two quite different compounds, one is an NADH model compound, 1-benzyl-1,4-dihydronicotinamide (BNAH), and the other $[Rh_2(dicp)_4]^{2+}$ (dicp=1,3-diisocyanopropane), in MeCN have been determined as 0.60 ± 0.10 and 0.38 ± 0.10 V *vs.* SCE, respectively. The relation between the oxidation potential and the oxidation peak potential of BNAH measured by the cyclic voltammetry is discussed in the context of free energy relationships.

Electron transfer processes are receiving increased attention in oxidation-reduction reactions especially in those related to biological redox systems which play a dominant role in energy conversion and substrate metabolism in living systems.[1] Electrons are transferred in the direction of increasing redox potentials. Therefore, redox potentials of oxidants and reductants are of great importance for an understanding of electron transfer processes from reductants to oxidants. Redox potentials of a number of oxidants or reductants, however, have not been determined precisely by electrochemical methods because of the irreversible nature of these one-electron oxidation or reduction on the time scale of electrochemical measurements. In such irreversible systems, there have been no established methodology for experimental determinations of redox potentials of oxidants or reductants. In principle, however, redox potentials of oxidants or reductants in irreversible systems as well as reversible systems can be determined from the activation free energy $\Delta G^{\ddagger}$ for one-electron transfer reactions between oxidants and reductants, since $\Delta G^{\ddagger}$ is known to be expressed as a monotonous function of the redox potentials of the oxidants and reductants.[2-5] Thus, if the other parameters in the relation between $\Delta G^{\ddagger}$ and the redox potential of an oxidant (or a reductant) are somehow obtained, the redox potential can be determined from $\Delta G^{\ddagger}$. When the excited states of oxidants (or reductants) show the emissions, the $\Delta G^{\ddagger}$ values for electron transfer reactions of the excited states of the oxidants (or reductants) are readily determined experimentally from the electron transfer quenching of the excited states by a series of appropriate reductants (or oxidants).[3,6-9]

In the present study, we wish to show how free energy relationships between $\Delta G^{\ddagger}$ and ΔG obtained from the emission quenching by electron transfer reactions can be utilized in convenient determinations of redox potentials of oxidants or reductants in both reversible and irreversible systems. First, the methodology of experimental determinations of redox potentials will be established in various reversible systems reported in the literatures,[3,6-9] where the redox potentials of oxidants or reductants determined by the method based on the free energy relationships for electron transfer quenching of the excited states are compared with those obtained independently by conventional electrochemical methods. Next, the methodology thus established is applied to irreversible systems of current interest to determine one-electron oxidation potentials of 1-benzyl-1,4-dihydronicotinamide (BNAH), a model compound of NADH, which is one of the principal coenzymes for biochemical oxidation-reduction reactions[10] and also of a dimeric rhodium(I) complex $[Rh_2(dicp)_4]^{2+}$ (dicp=1,3-diisocyanopropane) which has recently merited a special attention as offering a possibility for photochemical energy storage.[11,12] The one-electron oxidation potential of BNAH in the irreversible system will be compared with the oxidation peak potential measured by the cyclic voltammetry in the context of free energy relationships for electron transfer reactions.

Experimental

Materials. 1-Benzyl-1,4-dihydronicotinamide (BNAH) and the 4-deuterio compound (BNAH-4-d_1) were prepared according to the literature,[13] and purified by recrystallization from ethanol. Preparation of $[Rh_2(dicp)_4]^{2+}$ was described previously.[14] Electron acceptors used in this study are commercially available and were purified by the standard methods.[15] Acetonitrile was purified and dehydrated with calcium hydride by the standard procedure.[15]

Fluorescence Quenching Experiments. Fluorescence measurements were performed using a Hitachi 650-10S fluorescence spectrophotometer. The excitation wavelengths of BNAH, BNAH-4-d_1, and $[Rh_2(dicp)_4]^{2+}$ were chosen so that the absorption by quenchers may be neglected (normally 360 nm for BNAH and BNAH-4-d_1 but 400 nm when acetophenone derivatives are used as quenchers, and 553 nm for $[Rh_2(dicp)_4]^{2+}$). The monitoring wavelengths were those corresponding to the maxima of the respective emission bands (BNAH and BNAH-4-d_1, 443 nm; $[Rh_2(dicp)_4]^{2+}$, 656 nm). Relative fluorescence

intensities were measured for an MeCN solution of BNAH, BNAH-4-d_1, or $[Rh_2(dicp)_4]^{2+}$ with a quencher at various concentrations. There has been no change in the shape but intensity of the fluorescence spectrum by the addition of a quencher. The Stern-Volmer relationship (Eq. 1) was obtained

$$I_f^0/I_f = 1 + K_{sv}[Q] \quad (1)$$

between the ratio of the fluorescence intensities in the absence and presence of a quencher I_f^0/I_f and the quencher concentration [Q]. The quenching rate constant k_q was determined from the Stern-Volmer constant K_{sv} and the fluorescence lifetime τ (BNAH, 0.76 ns;[16] $[Rh_2(dicp)_4]^{2+}$, 1.3 ns[17]) by using

$$k_q = K_{sv}\tau^{-1} \quad (2)$$

Eq. 2. Degassing of an MeCN solution of BNAH, BNAH-4-d_1, or $[Rh_2(dicp)_4]^{2+}$ with a quencher has been found to cause no effect on the fluorescence intensity in accordance with the quenching of the singlet excited state.

Cyclic Voltammetry. Reduction potentials of some electron acceptors were determined by the cyclic voltammetry (CV) measurements which were performed on a Hokuto Denko Model HA-301 potentiostat/galvanostat at 298 K in MeCN containing 0.1 mol dm^{-3} n-Bu_4NClO_4 as a supporting electrolyte, using a standard NaCl calomel reference electrode (SCE) or a Ag/Ag^+ reference electrode ($Ag/AgNO_3$ 0.1 mol dm^{-3}); the reduction potential *vs.* Ag/Ag^+ is 0.34 V lower than that *vs.* SCE.[18] The oxidation peak potentials of BNAH and BNAH-4-d_1 were measured by changing the sweep rate in the range 10—1000 mV s^{-1}.

Results and Discussion

Determination of Redox Potentials of Oxidants or Reductants from the Electron Transfer Quenching of the Excited States. The increase of the donor or acceptor abilities of electron donors or acceptors by the electronic excitation often results in electron transfer quenching of the excited states by the ground states of acceptors or donors.[3,6-9] Rehm and Weller[3] have formulated the following reaction scheme for the fluorescence quenching by electron transfer reactions in polar solvents such as MeCN,

$$D^* + A \underset{k_{21}}{\overset{k_{12}}{\rightleftharpoons}} (D^*\,A) \underset{k_{32}}{\overset{k_{23}}{\rightleftharpoons}} (D^+\,A^-) \xrightarrow{k_{30}} D + A, \quad (3)$$

where asterisk stands for the excited state which can be either the donor (D*) or the acceptor (A*) molecule, k_{12} and k_{21} are the diffusion and the dissociation rate constants, k_{23} and k_{32} are the rate constants of forward electron transfer for the actual electron transfer process and the back electron transfer to the excited state, respectively, and k_{30} is the rate constant of back electron transfer to the ground state. The over-all rate constant k_q of fluorescence quenching is given by Eq. 4,

$$k_q = \frac{k_{12}k_{23}}{k_{23}+k_{21}(1+k_{32}/k_{30})}, \quad (4)$$

which is reduced to Eq. 5 under the condition that the

$$k_q = \frac{k_{12}k_{23}}{k_{23}+k_{21}} \quad (5)$$

back electron transfer to the ground state is much faster than that to the excited state, *i.e.*, $k_{30} \gg k_{32}$. Then, the activation free energy ΔG^* for the actual electron transfer process k_{23}, encounter complex (D* A)→ion pair ($D^+\,A^-$), is obtained from the quenching rate constant k_q by using Eq. 6 derived from Eq. 5,

$$\Delta G^* = \frac{RT}{F}\ln\left[Z\left(\frac{1}{k_q}-\frac{1}{k_{12}}\right)\right], \quad (6)$$

where ΔG^* is given in the unit of V, Z is the collision frequency which is generally taken as 1×10^{11} mol^{-1} dm^3 s^{-1},[1,2,16] F is the Faraday constant, the k_{12} value has been reported as 2×10^{10} mol^{-1} dm^3 s^{-1} for neutral organic molecules,[3,8,9,16] and the other notations are conventional. The Rehm-Weller free energy relationship for the quenching of excited states of oxidants or reductants by electron transfer reactions (Eq. 3) has well been established as represented by Eq. 7,[3,6-9]

$$\Delta G^* = \frac{\Delta G}{2} + \left[\left(\frac{\Delta G}{2}\right)^2 + (\Delta G_0^*)^2\right]^{1/2}, \quad (7)$$

where ΔG_0^* is the intrinsic barrier representing the activation free energy for electron transfer when the driving force is zero, *i.e.*, $\Delta G^* = \Delta G_0^*$ at $\Delta G = 0$. According to the thermochemical cycle in Scheme 1, the free energy change ΔG of the actual electron transfer process, (D* A)→(D^+ A^-), is expressed in terms of the redox potentials of electron donors (E_{ox}^0) and acceptors (E_{red}^0) as shown in Eq. 8,

$$\begin{array}{ccc} & D^* + A \xrightarrow{w_r} (D^*\,A) & \\ E_{ox}^0 - E_{red}^0 - \Delta E_{0,0} \downarrow & & \downarrow \Delta G \\ & D^+ + A^- \xrightarrow{w_p} (D^+\,A^-) & \end{array}$$

Scheme 1.

$$\Delta G = E_{ox}^0 - E_{red}^0 + w_p - \Delta E_{0,0}, \quad (8)$$

where w_p is the work term required to bring the products D^+ and A^- together, w_r which is the corresponding term for the reactants has been neglected in Eq. 8,[19] and $\Delta E_{0,0}$ is the zero-zero transition energy which is obtained from the frequencies of the absorption (ν) and fluorescence (ν_f) maxima by using Eq. 9.[3,20]

$$\Delta E_{0,0} = (h\nu + h\nu_f)/2 \quad (9)$$

A simple mathematical consideration of Eq. 7 yields a linear formulation between $\Delta G^* - \Delta G$ and $(\Delta G^*)^{-1}$ (Eq. 10),

$$\Delta G^* - \Delta G = (\Delta G_0^*)^2/\Delta G^*, \quad (10)$$

which is rewritten by Eq. 11, using Eq. 8. Thus, the $E_{red}^0 - w_p$ value of the acceptor can be evaluated from

$$\Delta G^* - E_{ox}^0 + \Delta E_{0,0} = \frac{(\Delta G_0^*)^2}{\Delta G^*} - (E_{red}^0 - w_p) \quad (11)$$

the intercept of the linear correlation between $\Delta G^* - E_{ox}^0 + \Delta E_{0,0}$ and $(\Delta G^*)^{-1}$ based on Eq. 11. This methodology for determining reduction potentials of electron acceptors (oxidants) is tested for reductive quenching of fluorescent aromatic hydrocarbons Ar* (acceptors) by a series of electron donors (amines and methoxybenzenes) having various known oxidation potentials (Eq. 12).[3]

$$Ar^* + D \xrightarrow{k_q} Ar^- + D^+ \quad (12)$$

The plots of $\Delta G^* - E_{ox}^0 + \Delta E_{0,0}$ *vs.* $(\Delta G^*)^{-1}$ for the

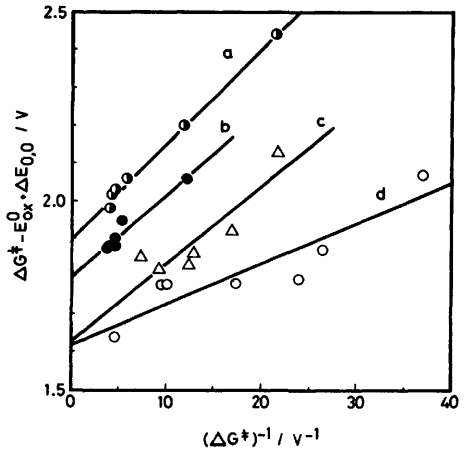

Fig. 1. Plots of Eq. 11 ($\Delta G^* - E^0_{ox} + \Delta E_{0,0}$ *vs.* $(\Delta G^*)^{-1}$) for the reductive quenching of the excited states of electron acceptors ((a) benz[*a*]anthracene, (b) 4-pyrencarboxylic acid, (c) benz[*c*]acridine, and (d) 3-pyrenecarboxylic acid) by a series of electron donors (amines and methoxybenzenes) in MeCN (Eq. 12); the data of the quenching rate constants k_q from which the ΔG^* values are obtained by using Eq. 6, E^0_{ox} of the donors, and $\Delta E_{0,0}$ were taken from Ref. 3. Note that the intercepts correspond to the $-(E^0_{red} - w_p)$ values of the acceptors, see Eq. 11 in text.

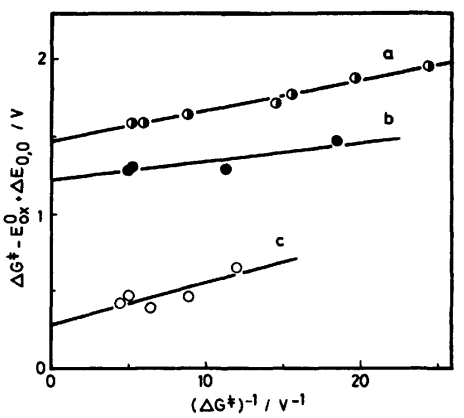

Fig. 2. Plots of Eq. 11 ($\Delta G^* - E^0_{ox} + E_{0,0}$ *vs.* $(\Delta G^*)^{-1}$) for the reductive quenching of the excited states of electron acceptors ((a) $[Ru(bpy)_3]^{2+}$, (b) $[Ir(Me_2phen)_2Cl_2]^+$, and (c) $[Cr(bpy)_3]^{3+}$) by a series of electron donors (aromatic amines and methoxybenzenes) in MeCN (Eq. 13); the data of the quenching rate constants k_q from which the ΔG^* values are obtained by using Eq. 6, E^0_{ox} of the donors, and $\Delta E_{0,0}$ were taken from Ref. 7. The intercepts correspond to the $-(E^0_{red} - w_p)$ values of the acceptors, see Eq. 11 in text.

Table 1. Comparison of the $E^0_{red} - w_p$ or $E^0_{ox} + w_p$ values of oxidants or reductants determined by the plots of Eq. 11 or 14, respectively, with the corresponding electrochemical values of E^0_{red} or E^0_{ox}

Oxidant	$E^0_{red} - w_p$ / V	E^0_{red} / V	w_p / V
Organic[a]			
3-Pyrenecarboxylic acid	−1.62	−1.67	−0.05
Benz[*c*]acridine	−1.63	−1.75	−0.12
4-Pyrenecarboxylic acid	−1.80	−1.92	−0.12
Benz[*a*]anthracene	−1.90	−2.02	−0.12
Inorganic[b]			
$[Ru(bpy)_3]^{2+}$	−1.47	−1.35	0.12
$[Cr(bpy)_3]^{3+}$	−0.28	−0.26	0.02
$[Ir(Me_2phen)_2Cl_2]^+$	−1.22	−1.16	0.06
Inorganic reductants[c]	$E^0_{ox} + w_p$	E^0_{ox}	w_p
$[Ru(bpy)_3]^{2+}$	1.45[d]	1.32[e]	0.13[f]
$[Ru(phen)_2(CN)]$	0.79	0.84	−0.05
$[Ru(bpy)_2(CN)]$	0.80	0.83	−0.03
$[Ru(bpy)_3]^{2+}$	1.31	1.32	−0.01

a) Used in reactions (Eq. 12) taken from Ref. 3. b) Used in reactions (Eq. 13) taken from Ref. 7. c) Used in reactions (Eqs. 15—17) taken from Refs. 8,9,6. d) This value corresponds to $E^0_{ox} + w_p - w_r$ (Ref. 25). e) N. E. Tokel-Takvoryan, R. E. Hemingway, and A. J. Bard, *J. Am. Chem. Soc.*, **95**, 6582 (1973). f) This value corresponds to $w_p - w_r$.

fluorescence quenching of some aromatic acceptors (benz[*a*]anthracene, 4-pyrenecarboxylic acid, benz[*c*]-acridine, and 3-pyrenecarboxylic acid) by a series of electron donors in MeCN are shown in Fig. 1.[21] The $E^0_{red} - w_p$ values for the acceptors obtained from the intercepts in Fig. 1 by the least squares analysis are listed in Table 1 together with the E^0_{red} values determined independently by electrochemical methods.[3] Although the linear correlations in Fig. 1 are not very impressive,[22] the $E^0_{red} - w_p$ values obtained from the intercepts in Fig. 1 agree well with the electrochemical values of E^0_{red} (Table 1) by taking into account the work terms w_p which are considered as being small negative values for the product ions of opposite charge in outer-sphere electron transfer reactions.[23]

Transition metal complexes containing bpy (2,2'-bipyridine) or phen (1,10-phenanthroline) as ligands have recently been shown to act excellent donors or acceptors in the excited state electron transfer reactions and thus the rate data for both reductive[7] and oxidative[6,8,9] quenching of excited states by electron transfer reactions are now available. The linear plots of Eq. 11 for the reductive quenching of excited states of transition metal complexes M^{n+} ($[Ru(bpy)_3]^{2+}$, $[Ir(Me_2phen)_2Cl_2]^+$, and $[Cr(bpy)_3]^{3+}$) by a series of electron donors D (aromatic amines and methoxybenzenes) in MeCN (Eq. 13)[7] are shown in Fig. 2. The $E^0_{red} - w_p$ values of

$$M^{n+*} + D \longrightarrow M^{(n-1)+} + D^+ \qquad (13)$$

M^{n+} determined from the intercepts in Fig. 2 are slightly more negative than the corresponding electrochemical values of E^0_{red} (Table 1). Therefore, the work terms w_p obtained by subtracting $E^0_{red} - w_p$ from E^0_{red} are small positive values, which agree with those expected for the product ions of the same charge type (Eq. 13)[24] in contrast with those of opposite charge (Eq. 12).

The oxidation potentials of electron donors (reductants) can also be determined from oxidative quenching of excited donors by appropriate electron acceptors (oxidants) having various reduction potentials, based on the plots of Eq. 14 ($\Delta G^* + E^0_{red} + \Delta E_{0,0}$ *vs.* $(\Delta G^*)^{-1}$) which is obtained by rearranging Eq. 11. Figure 3 depicts the plots of $\Delta G^* + E^0_{red} + \Delta E_{0,0}$ *vs.*

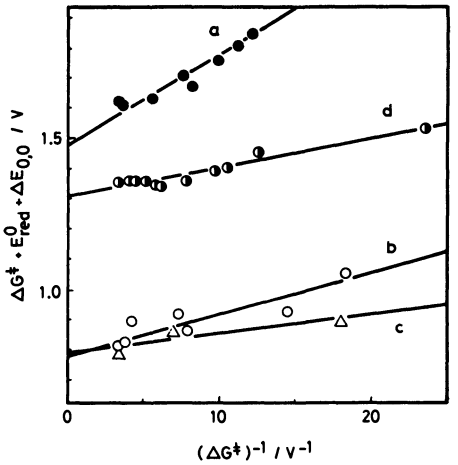

Fig. 3. Plots of Eq. 14 ($\Delta G^* + E^0_{red} + \Delta E_{0,0}$ *vs.* $(\Delta G^*)^{-1}$) for the oxidative quenching of the excited stated of electron donors ((a) $[Ru(bpy)_3]^{2+}$, (b) $[Ru(phen)_2(CN)]$, and (c) $[Ru(bpy)_2(CN)]$) by pyridinium ions (Eqs. 15 and 16; the data were taken from Refs. 8 and 9 and of (d) $[Ru(bpy)_3]^{2+}$ by nitrobenzene derivatives (Eq. 17); the data were taken from Ref. 6. Note that the intercepts correspond to the $E^0_{ox}+w_p$ values of the donors, see Eq. 14 in text.

$$\Delta G^* + E^0_{red} + \Delta E_{0,0} = \frac{(\Delta G^*_0)^2}{\Delta G^*} + E^0_{ox} + w_p, \quad (14)$$

$(\Delta G^*)^{-1}$ for the oxidative quenching of $[Ru(bpy)_3]^{2+*}$ by bipyridinium ions BP^{2+} as electron acceptors (Eq. 15),[8] that of $[RuL_2(CN)]^*$ (L=bpy and phen) by pyridinium ions P^+ (Eq. 16)[9] and also that of $[Ru(bpy)_3]^{2+*}$ by nitrobenzene derivatives (Eq. 17).[6]

$$[Ru(bpy)_3]^{2+*} + BP^{2+} \longrightarrow [Ru(bpy)_3]^{3+} + BP^+ \quad (15)$$

$$[RuL_2(CN)]^* + P^+ \longrightarrow [RuL_2(CN)]^+ + P^0 \quad (16)$$

$$[Ru(bpy)_3]^{2+*} + Ar\text{–}NO_2 \longrightarrow [Ru(bpy)_3]^{3+} + Ar\text{–}NO_2^{\cdot -} \quad (17)$$

The $E^0_{ox}+w_p-w_r$ value of $[Ru(bpy)_3]^{2+}$, the E^0_{ox} values of $[RuL_2(CN)]$, and the $E^0_{ox}+w_p$ value of $[Ru(bpy)_3]^{2+}$ determined from the respective intercepts in Fig. 3 by using Eq. 14[25] show reasonable agreement with the corresponding E^0_{ox} values determined electrochemically by taking into account the small work terms.[23]

Thus, the methodology of experimental determinations of both reduction and oxidation potentials based on the Rehm-Weller free energy relationship (Eqs. 11 and 14) for electron transfer quenching of excited states of oxidants and reductants, respectively, has well been established. The experimental errors in the determinations of redox potentials by this method are considered to be comparable with those by electrochemical methods.[26] Of course, as far as the determinations of the redox potentials in reversible systems are concerned, electrochemical methods are more suitable and convenient than the present method. It should be emphasized, however, that the method based on Eq. 11 or 14 does not depend on the systems whether oxidation of reductants (or reduction of oxidants) is reversible or irreversible, since with regard to reductants or oxidants of interest, only the kinetic data (k_q or ΔG^*) are required in Eq. 11 or 14.

A Comparison between the Rehm-Weller and the Marcus Free Energy Relationships. The Marcus free energy relationship (Eq. 18) also has frequently been used for electron transfer reactions.[2,5,8] From Eqs. 8 and 18 is obtained Eq. 19. According to Eq. 19, the intercept

$$\Delta G^* = \Delta G^*_0 \left(1+\frac{\Delta G}{4\Delta G^*_0}\right)^2 \quad (18)$$

$$(\Delta G^*)^{1/2} = (\Delta G^*_0)^{1/2} + (16\Delta G^*_0)^{-1/2}(E^0_{ox} - E^0_{red} + w_p - \Delta E_{0,0}) \quad (19)$$

to the abscissa of the linear plot between $(\Delta G^*)^{1/2}$ and E^0_{ox} or $-E^0_{red}$ gives the relation of Eq. 20. Then, the

$$E^0_{ox} - E^0_{red} + w_p - \Delta E_{0,0} + 4\Delta G^*_0 = 0 \quad (20)$$

$E^0_{red}-w_p$ or $E^0_{ox}+w_p$ value can be evaluated from Eq. 20 by using the ΔG^* value obtained from the slope $(16\Delta G^*)^{-1/2}$ of the plot between $(\Delta G^*)^{1/2}$ and E^0_{ox} or $-E^0_{red}$ (Eq. 19).

As pointed out by Indelli and Scandola,[27] however, the Marcus equation (Eq. 18) cannot be applied to electron transfer quenching of excited states because of the serious disagreement with experimental results especially in the largely exothermic region (Eq. 18 predicts the increase of ΔG^* as ΔG decreases in the region $\Delta G < -4\Delta G^*_0$, although most experimental results have shown that $\Delta G^* \to 0$ in the largely exothermic region).[6-9] Thus, the application of the Marcus equation is restricted to the region $\Delta G > -4\Delta G^*_0$.[28] In order to compare the Marcus free energy relationship (Eq. 18 or 19) with the Rehm-Weller's (Eq. 7 or 11), the data for the fluorescence quenching of 1,2-benzanthracene by electron donors (Fig. 1a) are replotted according to Eq. 19, *i.e.*, $(\Delta G^*)^{1/2}$ *vs.* E^0_{ox}, as shown by open circles in Fig. 4, where the solid line represents the plot corresponding to the Rehm-Weller equation (Eq. 7). A significant deviation from the linear relation between $(\Delta G^*)^{1/2}$ and E^0_{ox} is observed in the region $E^0_{ox} < 1.3$ V. However, the extrapolation of the linear

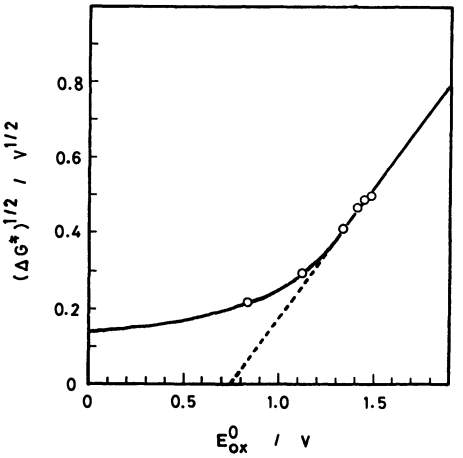

Fig. 4. A plot of $(\Delta G^*)^{1/2}$ *vs.* E^0_{ox} (Eq. 19) for the reductive quenching of 1,2-benzanthracene by electron donors; the solid line represents the plot corresponding to the Rehm-Weller equation (Eq. 7 or 11) for the data shown in Fig. 1a. For the deviation of the solid line from the linear correlation between $(\Delta G^*)^{1/2}$ and E^0_{ox} in the region $E^0_{ox} < 1.3$ V, see the discussion in text.

Table 2. Quenching rate constants k_q^h and k_q^d of the BNAH and BNAH-4-d_1 fluorescence, respectively, by electron acceptors having various reduction potentials E^0_{red}, and the kinetic isotope effect k_H/k_D.

Acceptor	E^0_{red} [a] / V	k_q^h / mol^{-1} dm^3 s^{-1}	k_q^d / mol^{-1} dm^3 s^{-1}	k_H/k_D [b]
Diethyl fumarate	−1.50	1.4×10^{10} [c]	1.4×10^{10}	1.0
Acetophenone	−2.10	9.1×10^{9} [c]	8.5×10^{9}	1.1
Propiophenone	−2.15	9.1×10^{9}	8.6×10^{9}	1.1
trans-Stilbene	−2.20	5.8×10^{9} [c]		
4-Methoxyacetophenone	−2.29	5.9×10^{9}	5.8×10^{9}	1.0
Cyanobenzene	−2.35	4.9×10^{9} [c]	4.6×10^{9}	1.1
Methyl benzoate	−2.37	4.4×10^{9} [c]	4.6×10^{9}	0.9
Ethyl benzoate	−2.40	3.6×10^{9}	3.6×10^{9}	1.0

a) Relative to a standard NaCl calomel reference electrode (SCE), measured by cyclic voltammetry. b) Determined from k_q^h and k_q^d by using Eq. 21. c) Similar values are reported in Ref. 16.

part in the region $E^0_{ox}>1.3$ V to the abscissa gives the intercept value $E^0_{ox}=0.74$ V with the slope of 0.69, which yields essentially the same $E^0_{red}-w_p$ value (−1.92 V) of benz[*a*]anthracene using Eq. 20 as the value (−1.90 V in Table 1) obtained from the intercept to the ordinate in the plot of Eq. 11 (Fig. 1a).

In conclusion, from a purely empirical point of view, the use of the Rehm-Weller free energy relationship (Eq. 11 or 14) is preferable to that of the Marcus free energy relationship (Eq. 19), since the method based on the plot of Eq. 11 or 14 directly gives the $E^0_{red}-w_p$ or $E^0_{ox}+w_p$ value from the intercept, respectively, while that of Eq. 19 is restricted to the region $\Delta G>-4\Delta G_0^*$ (Fig. 4) and also requires both the slope and intercept in determining the $E^0_{red}-w_p$ or $E^0_{ox}+w_p$ value.

One-electron Oxidation Potentials of an NADH Model Compound and $[Rh_2(dicp)_4]^{2+}$ in Irreversible Systems. The excitation of the absorption band (350 nm) of an MeCN solution of BNAH or the 4-deuterio compound BNAH-4-d_1 results in fluorescence ($\lambda_{max}=443$ nm, $h\nu_f=2.80$ eV, and $\tau=0.76$ ns).[16] The BNAH or BNAH-4-d_1 fluorescence was quenched by electron acceptors which have various reduction potentials. The quenching rate constants k_q determined by the Stern-Volmer plots (see Experimental, Eq. 1) are listed in Table 2 together with the reduction potentials of the acceptors. The kinetic isotope effect k_H/k_D has also been determined from the ratio of the quenching rate constants of BNAH (k_q^h) and BNAH-4-d_1 (k_q^d) by using Eq. 21.[29] No isotope

$$k_H/k_D = (2k_q^d/k_q^h-1)^{-1} \quad (21)$$

effect for the fluorescence quenching of BNAH by the electron acceptors is observed (Table 2), indicating that the quenching process is one-electron transfer from BNAH* to an acceptor (Eq. 22). One-electron transfer from BNAH is known to be irreversible since $BNAH^+$

$$BNAH^* + A \xrightarrow{k_q} BNAH^+ + A^- \quad (22)$$

formed by the electron transfer reaction (Eq. 22) is unstable to undergo the disproportionation reaction (Eq. 23).[30] The ΔG^* values for the actual electron

$$2BNAH^+ \longrightarrow BNA^+ + (BNAH)H^+ \quad (23)$$

transfer process k_{23} (Eq. 3) are obtained from the k_q values in Table 2 by using Eq. 6. The zero-zero transition energy $\Delta E_{0,0}$ of BNAH and BNAH-4-d_1 is obtained as 3.17 eV from the $h\nu$ and $h\nu_f$ values (3.54 and 2.80 eV, respectively) by using Eq. 9. In order to determine the one-electron oxidation potential E^0_{ox} of BNAH and BNAH-4-d_1, the values of $\Delta G^*+E^0_{red}+\Delta E_{0,0}$ are plotted against the $(\Delta G^*)^{-1}$ values in Fig. 5a which shows the same linear correlation for BNAH and BNAH-4-d_1. Thus, the intercept in Fig. 5a gives the $E^0_{ox}+w_p$ value of BNAH and BNAH-4-d_1 as 0.50 V.

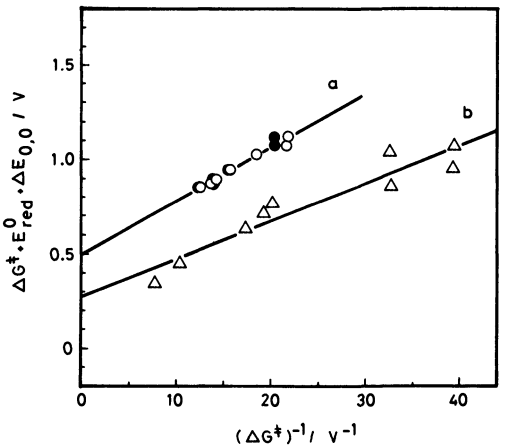

Fig. 5. Plots of $\Delta G^*+E^0_{red}+\Delta E_{0,0}$ *vs.* $(\Delta G^*)^{-1}$ (Eq. 14) for the fluorescence quenching of (a) ○ BNAH and ● BNAH-4-d_1 by the electron acceptors in Table 2 (Eq. 22) and that of (b) ◑ $[Rh_2(dicp)_4]^{2+}$ by the acceptors in Table 3 (Eq. 24). The intercepts 0.50 and 0.28 V give the $E^0_{ox}+w_p$ values of BNAH (or BNAH-4-d_1) and $[Rh_2(dicp)_4]^{2+}$, respectively, according to Eq. 14.

Similarly, the one-electron oxidation potential of $[Rh_2(dicp)_4]^{2+}$ whose one-electron oxidation also is irreversible[14] has been determined from the fluorescence quenching of $[Rh_2(dicp)_4]^{2+}$ by a series of electron acceptors A (Eq. 24). The k_q values of $[Rh_2(dicp)_4]^{2+*}$

$$[Rh_2(dicp)_4]^{2+*} + A \xrightarrow{k_q} [Rh_2(dicp)_4]^{3+} + A^- \quad (24)$$

as well as the reduction potentials of the acceptors are listed in Table 3. The $E^0_{ox}+w_p$ value of $[Rh_2(dicp)_4]^{2+}$ is obtained as 0.28 V from the intercept of the linear plot between $\Delta G^*+E^0_{red}+\Delta E_{0,0}$[31] and $(\Delta G^*)^{-1}$, as shown in Fig. 5b. Thus, the one-electron oxidation

Table 3. Quenching rate constants k_q of the $[Rh_2(dicp)_4]^{2+}$ fluorescence by electron acceptors having various reduction potentials E^0_{red}

Acceptor[a)]	E^0_{red} / V	k_q / mol^{-1} dm^3 s^{-1}
1,4-Dinitrobenzene	−0.69	1.8×10^{10}
1,3-Dinitrobenzene	−0.90	1.5×10^{10}
Methyl 4-nitrobenzoate	−0.95	1.4×10^{10}
3-Nitrobenzaldehyde	−1.02	1.3×10^{10}
1-Chloro-4-nitrobenzene	−1.06	1.2×10^{10}
Nitrobenzene	−1.15	1.3×10^{10}
2-Nitroaniline	−1.27	1.2×10^{10}
4-Nitroaniline	−1.36	8.3×10^{9}
1-Methoxy-2-nitrobenzene	−1.40	7.7×10^{9}
Diethyl fumarate	−1.50	6.8×10^{9}
1,4-Dicyanobenzene	−1.72	1.9×10^{9}
Benzophenone	−1.86	5.9×10^{8}

a) Taken from Ref. 31 unless otherwise noted. b) This study.

potentials E^0_{ox} of BNAH (or BNAH-4-d_1) and $[Rh_2(dicp)_4]^{2+}$ are determined as 0.60 ± 0.1 and 0.38 ± 0.1 V, respectively, by taking into account the value −0.1 V as the work term w_p.[32)]

Thus, the oxidation potentials in irreversible systems can be determined based on the Rehm-Weller free energy relationship (Eq. 14) for the electron transfer quenching of the excited states of reductants by a series of oxidants. Although this method requires the knowledge of the emission lifetime τ of the excited states to determine the electron transfer rate constants k_q from the quenching constants K_{sv} (Eq. 2), the k_q values can be estimated from the K_{sv} values without the direct measurement of τ by assuming that the K_{sv} value which reaches a constant value with increasing E^0_{red} of oxidants is equivalent to the diffusion rate constant k_{12}.

A Comparison between the Oxidation Potential E^0_{ox} and the Oxidation Peak Potential E^p_{ox} in an Irreversible System.

In the foregoing sections, we have shown that how free energy relationships between ΔG^* and ΔG obtained from the electron transfer quenching of the excited states of oxidants or reductants can be successfully used in determining the redox potentials of the oxidants or reductants in irreversible systems as well as reversible systems. In this section, such free energy relationships are shown to be utilized also for the irreversible electrochemical oxidation of BNAH to determine the oxidation potential E^0_{ox} of BNAH from the cyclic voltammetry (CV) measurements, which is compared with the E^0_{ox} value determined from the electron transfer quenching study of the BNAH fluorescence.

The cyclic voltammogram of BNAH is illustrated in Fig. 6, which shows an anodic wave with a current maximum but no cathodic wave on the reverse scan as confirmed by changing the sweep rates in the range 10 to 1000 mV s^{-1}. The anodic oxidation of BNAH is thus irreversible, indicating that the follow-up chemical reaction (Eq. 23)[30)] is fast on the time scale of the CV measurements. The width of the anodic wave $E^p_{ox}-E^{p/2}_{ox}$ in such an irreversible system has been shown

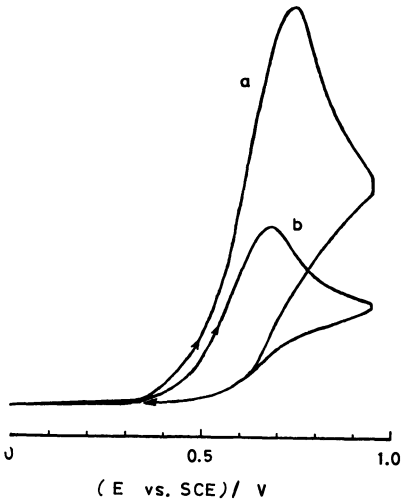

Fig. 6. Cyclic voltammograms of BNAH in MeCN containing 0.1 mol dm^{-3} n-Bu_4NClO_4 at the sweep rates of (a) 0.5 V s^{-1} and (b) 0.1 V s^{-1}.

to depend only on the transfer coefficient β according to Eq. 25.[33,34)] Then, the transfer coefficient β defined by

$$E^p_{ox} - E^{p/2}_{ox} = 1.857\,(RT/\beta F) \tag{25}$$

the tangent of the free energy relationship $\partial\Delta G^*/\partial\Delta G$ at the oxidation peak potential E^p_{ox} is obtained from the width of the anodic wave $E^p_{ox}-E^{p/2}_{ox}$ by using Eq. 26,

$$\beta = \frac{1.857\,RT}{F(E^p_{ox}-E^{p/2}_{ox})}, \tag{26}$$

which is derived from Eq. 25. The β value can be determined also from the dependence of the oxidation peak potential E^p_{ox} on the sweep rate v (V s^{-1}) by using Eq. 27,[33,34)]

$$E^p_{ox} = \frac{2.3\,RT}{2\beta F}\log v + \text{Const}, \tag{27}$$

in which the constant is given by Eq. 28,

$$\text{Const} = E^0_{ox} + \frac{2.3\,RT}{\beta F}\log\frac{2.18\,D\beta F}{k(E^0_{ox})RT}, \tag{28}$$

where $k(E^0_{ox})$ (cm s^{-1}) is the electron transfer rate constant at the oxidation potential E^0_{ox}. On the other hand, the transfer coefficient β is expressed as a function of $\Delta G(=E^0_{ox}-E)$ (Eq. 29) by differentiating the Rehm-

$$\beta = \frac{1}{2} + \frac{\Delta G}{4[(\Delta G/2)^2+(\Delta G^*_0)^2]^{1/2}} \tag{29}$$

Weller free energy relationship (Eq. 7) with respect to ΔG. From Eq. 29 is derived a relation between the oxidation potential E^0_{ox} and the oxidation peak potential E^p_{ox} (Eq. 30) when $\Delta G=E^0_{ox}-E^p_{ox}$. According to Eq. 30,

$$E^p_{ox}=E^0_{ox} + \frac{(1-2\beta)}{[\beta(1-\beta)]^{1/2}}\Delta G^*_0 \tag{30}$$

the oxidation potential E^0_{ox} can be evaluated from the intercept of the linear plot between E^p_{ox} and $(1-2\beta)/[\beta(1-\beta)]^{1/2}$. The E^p_{ox} values of BNAH obtained from the cyclic voltammograms of BNAH measured at various sweep rates are plotted against the corresponding values of $(1-2\beta)/[\beta(1-\beta)]^{1/2}$ in which β is determined by Eq. 26, as shown in Fig. 7a. The intercept of the linear correlation in Fig. 7a gives the E^0_{ox} value of BNAH as 0.57 V which agrees well with the E^0_{ox} value $0.60\pm$

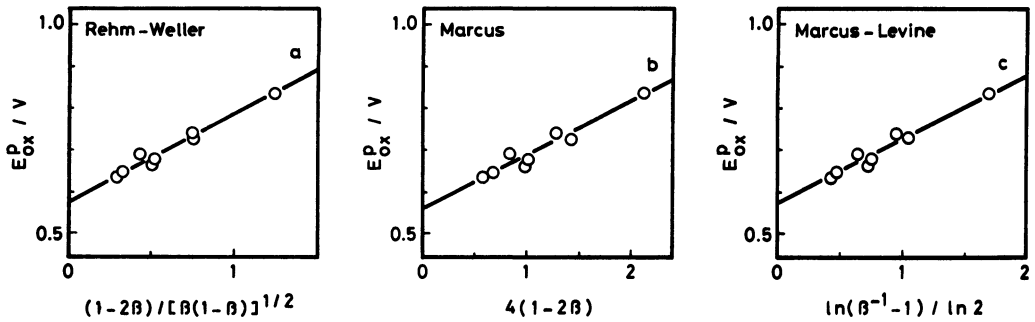

Fig. 7. The oxidation peak potential E^p_{ox} of BNAH plotted as a function of the transfer coefficient β based on (a) the Rehm-Weller (Eq. 7), (b) the Marcus (Eq. 18), and (c) the Marcus-Levine (Eq. 30) free energy relationships. See Eqs. 28, 29, and 31 in text, respectively. Note that the intercept corresponds to the E^0_{ox} value of BNAH.

0.10 V determined by the fluorescence quenching study described above. The same E^0_{ox} value of BNAH-4-d_1 was obtained from the cyclic voltammograms of BNAH-4-d_1 at various sweep rates by the plot of Eq. 30.

The other free energy relationships which are currently used also are applied to the determination of the E^0_{ox} value of BNAH from the CV measurements. One is the Marcus free energy relationship being already given by Eq. 18, from which Eq. 31 is derived. The other is

$$E^p_{ox} = E^0_{ox} + 4(1-2\beta)\Delta G_0^{\ddagger} \quad (31)$$

the Levine free energy relationship (Eq. 32)[4] which has the equivalent formulation to that derived by

$$\Delta G^{\ddagger} = \Delta G + \frac{\Delta G_0^{\ddagger}}{\ln 2} \ln\left[1+\exp\left(-\frac{\Delta G \ln 2}{\Delta G_0^{\ddagger}}\right)\right] \quad (32)$$

Marcus.[35] From Eq. 32 is derived a relation between E^p_{ox} and E^0_{ox} as well (Eq. 33). The plots according to Eqs. 31 and 33 are shown in Figs. 7b and 7c, respectively. The intercept values in Figs. 7a—c are essentially the

$$E^p_{ox} = E^0_{ox} + \frac{\Delta G_0^{\ddagger}}{\ln 2} \ln(\beta^{-1}-1) \quad (33)$$

same, and thereby the same E^0_{ox} value of BNAH is obtained irrespective of the use of different free energy relationships for electron transfer reactions (Eqs. 7, 18, and 32).

In conclusion, reliable values of redox potentials of oxidants or reductants in irreversible systems can be determined based on the free energy relationships for the electron transfer quenching of the excited states of oxidants or reductants (Eq. 11 or 14) as well as for the electrochemical electron transfer measured by cyclic voltammetry (Eqs. 30, 31, and 33).

References

1) R. A. Marcus, "Tunneling in Biological Systems," ed by B. Chance *et al.*, Academic Press, New York (1979), p. 109; N. Sutin, "Inorganic Biochemistry," ed by G. L. Eichhorn, Elsevier, Amsterdam (1973), Vol. 2, p. 611; G. Dryhurst, K. M. Kadish, F. Scheller, and R. Renneberg, "Biological Electrochemistry," Academic Press, New York (1982), Vol. 1; R. D. Cannon, "Electron Transfer Reactions," Butterworths, Boston (1982); L. Eberson, *Adv. Phys. Org. Chem.*, **18**, 79 (1982).

2) R. A. Marcus, *J. Phys. Chem.*, **67**, 853 (1963); *Ann. Rev. Phys. Chem.*, **15**, 155 (1964).

3) D. Rehm and A. Weller, *Ber. Bunsenges. Phys. Chem.*, **73**, 834 (1969); *Isr. J. Chem.*, **8**, 259 (1970).

4) R. D. Levine, *J. Phys. Chem.* **83**, 159 (1979); N. Agmon and R. D. Levine, *Chem. Phys. Lett.*, **52**, 197 (1977).

5) F. Scandola, V. Balzani, and G. B. Schuster, *J. Am. Chem. Soc.*, **103**, 2519 (1981).

6) C. R. Bock, T. J. Meyer, and D. G. Whitten, *J. Am. Chem. Soc.*, **97**, 2909 (1975).

7) R. Ballardini, G. Varani, M. T. Indelli, F. Scandola, and V. Balzani, *J. Am. Chem. Soc.*, **100**, 7219 (1978).

8) C. R. Bock, J. A. Connor, A. R. Gutierrez, T. J. Meyer, D. G. Whitten, B. P. Sullivan, and J. K. Nagle, *J. Am. Chem. Soc.*, **101**, 4815 (1979).

9) J. K. Nagle, W. J. Dressick, and T. J. Meyer, *J. Am. Chem. Soc.*, **101**, 3993 (1979).

10) H. Sund, "Biological Oxidations," ed by T. P. Singer, Wiley-Interscience, New York (1968), p. 603, 641; U. Eisner and J. Kuthan, *Chem. Rev.*, **72**, 1 (1972); D. M. Stout and A. I. Meyers, *ibid.*, **82**, 223 (1982); R. J. Kill and D. A. Widdowson, "Bioorganic Chemistry," ed by E. E. van Tamelen, Academic Press, New York (1978), Vol. 4, Chap. 8.

11) A. W. Maverick and H. B. Gray, *Pure Appl. Chem.*, **52**, 2339 (1980); H. B. Gray, K. R. Mann, N. S. Lewis, J. A. Thich, and R. M. Richman, *Adv. Chem. Ser.*, **168**, 44 (1978).

12) I. S. Sigal, K. R. Mann, and H. B. Gray, *J. Am. Chem. Soc.*, **102**, 7252 (1980).

13) A. G. Anderson, Jr., and G. Berkelhammer, *J. Am. Chem. Soc.*, **80**, 992 (1958); D. Mauzerall and F. H. Westheimer, *ibid.*, **77**, 2261 (1955).

14) S. Fukuzumi, N. Nishizawa, and T. Tanaka, *Bull. Chem. Soc. Jpn.*, **55**, 2892 (1982).

15) D. D. Perrin, W. L. F. Armarego, and D. R. Perrin, "Purification of Laboratory Chemicals," Pergamon Press, New York (1966).

16) F. M. Martens, J. W. Verhoeven, R. A. Gase, U. K. Pandit, and Th. J. de Bore, *Tetrahedron*, **34**, 443 (1978); the fluorescence lifetime τ of the deuterio compound BNAH-4-d_1 is assumed to be the same as that of BNAH since the fluorescence quantum yield of BNAH-4-d_1 was the same as that of BNAH.

17) S. J. Milder, R. A. Goldbeck, D. S. Kliger, and H. B. Gray, *J. Am. Chem. Soc.*, **102**, 6761 (1980); V. M. Miskowski, G. L. Nobinger, D. S. Kliger, G. S. Hammond, N. S. Lewis, K. R. Mann, and H. B. Gray, *ibid.*, **100**, 485 (1978).

18) C. K. Mann, *Electroanal. Chem.*, **4**, 57 (1969).

19) The work term w_r for the neutral reactants is known to be negligible (see Ref. 3).

20) The energy difference $\Delta E_{0,0}$ between the thermally equilibrated excited and ground states of the donor D or the

acceptor A is larger than the energy corresponding to the emission maximum $h\nu_f$ and smaller than the energy corresponding to the absorption maximum $h\nu$ since the absorption and emission are vertical processes.

21) The ΔG^{*} values are evaluated for the quenching rate constant k_q smaller than 1.3×10^{10} mol^{-1} dm^3 s^{-1} since the experimental errors in determining ΔG^{*} by using Eq. 6 become large when the k_q values are close to the diffusion rate constant $k_{12}=2\times10^{10}$ mol^{-1} dm^3 s^{-1}.

22) The correlation coefficients ρ of the plots in Fig. 1 are 0.995 for benz[*a*]anthracene, 0.97 for 4-pyrenecarboxylic acid, 0.87 for benz[*c*]acridine, and 0.90 for 3-pyrenecarboxylic acid.

23) The work term w_r or w_p can be estimated from Debye-Hückell theory by using the equation w (in V)$=(0.395z_Az_B/d)/(1+0.48d\mu^{1/2})$, in which z_A and z_B are the ion charges, μ is the ionic strength, and d is the distance (in Å) between the ion centers (Ref. 8). The w_p values of the product ions of opposite charge have been evaluated as -0.01——-0.08 V depending on the systems (Refs. 3, 6—8), which are the same order of magnitude as those in Table 1.

24) In the case of $[Ir(Me_2phen)_2Cl_2]^+$, however, the work term w_p is expected to be negligiblly small since the product $[Ir(Me_2phen)_2Cl_2]$ is an uncharged species.

25) In the case of the oxidative quenching of $[Ru(bpy)_3]^{2+*}$ by BP^{2+} (Eq. 15), the intercept corresponds to $E^0_{ox}+w_p-w_r$, since the work term w_r of the reactants which are charged species cannot be neglected. The work terms w_r and w_p for the reactions of $[RuL_2(CN)]^*$ (Eq. 16) may be negligibly small since both reactants and products contain uncharged species.

26) The experimental errors in the $E^0_{red}-w_p$ or $E^0_{ox}+w_p$ values determined by the present method (Table 1) are considered to be less than ±0.1 V by taking into account the small w_p values (Ref. 23).

27) M. T. Indelli and F. Scandola, *J. Am. Chem. Soc.*, **100**, 7733 (1978).

28) In the endothermic region, the application of the Marcus equation is resticted also to the region $\Delta G<4\Delta G^{*}_0$, since $\Delta G^{*}\rightarrow\Delta G$ for $\Delta G\gg4\Delta G^{*}_0$.

29) J. J. Steffens and D. M. Chipman, *J. Am. Chem. Soc.*, **93**, 6694 (1971).

30) W. J. Blaedel and R. G. Haas, *Anal. Chem.*, **42**, 918 (1970); S. Fukuzumi, Y. Kondo, and T. Tanaka, *Chem. Lett.*, **1982**, 1591.

31) The $\Delta E_{0,0}$ value of $[Rh_2(dicp)_4]^{2+}$ is taken as 2.07 eV; S. Fukuzumi, N. Nishizawa, and T. Tanaka, *Bull. Chem. Soc. Jpn.*, **56**, 709 (1983).

32) The averaged value of w_p for organic oxidants (Table 1) is used as the w_p value for the reactions in Eqs. 22 and 24.

33) R. S. Nicholson and I. Shain, *Anal. Chem.*, **36**, 706 (1964).

34) R. J. Klingler and J. K. Kochi, *J. Am. Chem. Soc.*, **102**, 4790 (1980); *J. Phys. Chem.*, **85**, 1731 (1981); W. H. Tamblyn, R. J. Klingler, W. S. Hwang, and J. K. Kochi, *J. Am. Chem. Soc.*, **103**, 3161 (1981).

35) R. A. Marcus, *J. Phys. Chem.*, **72**, 891 (1968).

Electronic Relaxation Processes from Single Vibronic Levels in the $S_1(n, \pi^*)$ State of Pyridine Vapor

Kazuyoshi SUSHIDA, Masahisa FUJITA, Iwao YAMAZAKI,† and Hiroaki BABA*
Division of Chemistry, Research Institute of Applied Electricity, Hokkaido University, Sapporo 060
†*Institute for Molecular Science, Myodaiji, Okazaki 444*
(Received February 24, 1983)

The rate constants of radiative decay (k_F), internal conversion (k_{IC}), and intersystem crossing (k_{ISC}) for single vibronic levels in the $S_1(n, \pi^*)$ state of pyridine-d_0 and -d_5 vapors have been determined from measured fluorescence quantum yields (Φ_F), intersystem crossing quantum yields (Φ_{ISC}), and picosecond fluorescence lifetimes. The Φ_{ISC} values are fairly constant in the region of lower excess vibrational energy (<1000 cm^{-1}), while the Φ_F values are particularly large for vibronic levels involving non-totally symmetric vibrations, ν_{16b} and ν_{10a}. The latter observation is attributed to both an increase of k_F and a decrease of k_{IC} and k_{ISC} (relative to the zero-point level) for the ν_{16b} levels ($16b^2$ and $16b^26a^1$), and to an increase of k_F for the ν_{10a} levels. The relative values of k_F are discussed using the Herzberg-Teller theory of vibronic coupling. The values of k_F for $16b^1$ and $16b^2$ are significantly larger than that for the zero-point level, though no absorption band corresponding to $16b_0^1$ can be observed. In both pyridine-d_0 and -d_5, the value of k_{IC} is as large as 1.7×10^{10} s^{-1} even for the zero-point level, which is more than twice the k_{ISC} value for the same level.

In previous papers,[1] we reported the results of experimental studies on the excitation-energy dependence of nonradiative electronic relaxation in pyridine vapor. It was shown that the fluorescence quantum yield of pyridine is almost constant in the neighborhood of the zero-point vibrational level of the $S_1(n, \pi^*)$ state and decreases rapidly as the vibrational energy in excess of the zero-point energy, ΔE, becomes higher than 800 cm^{-1}. This observation was interpreted as due to an increase in rate of the internal conversion $S_1 \rightsquigarrow S_0$. In these studies, however, on account of the extreme weakness of the fluorescence of pyridine, the bandwidth of the exciting light employed was so great (>100 cm^{-1}) that the individual vibronic bands could hardly be resolved.

In the present study, we have re-examined the fluorescence and intersystem-crossing quantum yields of pyridine-d_0 and -d_5 with a small excitation bandwidth of ≈1 cm^{-1}, using a high-resolution laser spectrophotometric system. The resulting data, along with the picosecond fluorescence lifetimes obtained using a mode-locked dye laser, have made it possible to determine precisely the rate constants for the radiative and nonradiative processes that start from single vibronic levels in the S_1 state of pyridine-d_0 and -d_5. In the absorption spectrum of pyridine, the long-wavelength tail of the $S_2 \leftarrow S_0$ absorption has a significant intensity in the $S_1 \leftarrow S_0$ absorption region. The present paper is concerned with a region of ΔE lower than 1600 cm^{-1} where the contribution of $S_2 \leftarrow S_0$ absorption is relatively small.

The vibrational analyses of the $S_1 \leftarrow S_0$ absorption spectra of pyridine-d_0 and -d_5 were made, respectively, by Sponer and Stücklen[2] and Shukla *et al.*[3] More recently, Mochizuki *et al.*[4] analyzed vibronic bands of the pyridines, and showed that the $\nu_{10a}(a_2)$ vibration induces a vibronic interaction between $S_1(^1B_1)$ and $S_2(^1B_2)$ states. The band at $\nu_{0-0}+139$ cm^{-1} of pyridine-d_0 was assigned by Jesson *et al.*[5] to an overtone of the $16b(b_1)$ mode with two quanta, *i.e.* $16b_0^2$. (Jesson *et al.* adopted a wavenumber of 138 cm^{-1} instead of 139 cm^{-1}). Mochizuki *et al.*[6] had a doubt about this assignment, because they could not observe any progression involving the ν_{16b} vibration in their single vibronic level (SVL) fluorescence spectrum from the $16b^2$ level. In the present study, attention was directed to the role of these non-totally symmetric vibrations in the electronic relaxation processes in pyridine.

Experimental

Pyridine-d_0 (Merck, Uvasol) was allowed to stand over potassium hydroxide for a few days, and was fractionally distilled under a stream of nitrogen. Pyridine-d_5 (Aldrich, Spectrograde) and biacetyl (Nakarai Chemicals, G. R.) were purified by repeated distillation under reduced pressure. Sulfur hexafluoride (SF_6, Seitetsu Chemicals, 99.65%) was used as an inert foreign gas without further purification.

Absorption spectra and excitation spectra of fluorescence or sensitized phosphorescence were measured simultaneously at room temperature with a high-resolution laser spectrophotometric system, the details of which were described in previous papers.[7] In this system, a pulsed dye laser (Molectron DL14) pumped by a nitrogen laser (Molectron UV22) is used as a light source. The dye laser is operated by the use of a mixture of Coumarin 495 and Rhodamine 6G, and the frequency is doubled by a KDP crystal to generate UV laser pulses with a repetition rate of 20 pulses/s, a spectral bandwidth of about 0.5 cm^{-1}, and a pulse duration of 3 ns. A somewhat wide spacing was taken between the successive wavelengths of the laser light, so that the overall resolution was about 1 cm^{-1} for both absorption and excitation spectra. All the emission measurements were made by the use of 35 mm square quartz cells.

For obtaining the fluorescence quantum yield (Φ_F), the fluorescence spectrum was measured and corrected for the spectral sensitivity of the emission monochromator-photomultiplier system. The absolute Φ_F value of pyridine-d_0 or -d_5 was determined for excitation at the 0–0 band of the $S_1 \leftarrow S_0$ absorption by comparing the corrected fluorescence spectrum of the pyridine with that of quinine sulfate in (1/2) M sulfuric acid (1 M = 1 mol dm^{-3}), which has a Φ_F value of 0.51.[8]

The intersystem-crossing quantum yields (Φ_{ISC}) of the pyridines were determined by means of the sensitized-biacetyl-phosphorescence method based on T–T energy transfer.[9] To a mixture of 0.5 Torr (1 Torr = 133 Pa) of pyridine-d_0 or -d_5 (donor) with 0.5 Torr of biacetyl (acceptor) was added 160

Torr of SF_6. Under such high pressure conditions, the energy transfer takes place from the thermally equilibrated T_1 levels of the donor to the isoenergetic triplet levels of the acceptor, irrespective of the initially excited singlet level of the donor. The energy transfer is followed by rapid vibrational relaxation into the thermally equilibrated triplet of biacetyl, from which the biacetyl phosphorescence is emitted. The intensity of the sensitized biacetyl phosphorescence (I_p) was measured following excitation of the donor at 0–0 band of its $S_1 \leftarrow S_0$ absorption. On the other hand, for a mixture composed of 0.5 Torr of biacetyl and 160 Torr of SF_6, the intensity of biacetyl phosphorescence (I_p^0) was measured by exciting biacetyl at 453 nm, *i.e.*, at the 0–0 band of its $S_1 \leftarrow S_0$ absorption. The Φ_{ISC} value of biacetyl is known to be unity when excitation is made at long wavelengths including 453 nm.[10] The Φ_{ISC} value of the donor can then be obtained by comparing I_p with I_p^0 after the usual corrections are made.

The pressure of the pyridines was determined from the absorption intensity, while that of biacetyl was determined by measuring the intensity of its phosphorescence excited at 453 nm; biacetyl vapor is known to give a definite phosphorescence quantum yield when it is excited at this wavelength and at a pressure higher than 1 Torr.[10]

For measuring the excitation spectra, the fluorescence was monitored through filters, UV-D35 (Toshiba) and 2,6-lutidine (25% by volume) in hexane, and the sensitized phosphorescence was monitored through a cut filter, VY-45 (Toshiba). The excitation spectra were corrected for the spectral intensity distribution of the exciting laser light and for the inner filter effect. Relative values of Φ_F and Φ_{ISC} at various excitation positions were obtained by taking the ratios of the intensities of the corrected excitation spectra to the intensities of the corresponding absorption spectra. By combining the resulting relative yields with the absolute quantum yield which had been determined, as mentioned earlier, at a particular excitation position for the fluorescence or sensitized phosphorescence, the absolute values of Φ_F and Φ_{ISC} were obtained as a function of excitation energy for pyridine-d_0 and -d_5.

The fluorescence lifetimes (τ_F) of pyridine-d_0 and -d_5 were obtained by using a synchronously-pumped, mode-locked dye laser[11] as an exciting light source. The details of the experiments have been reported elsewhere.[12]

Results

Figures 1(a) and 2(a) show, respectively, the $S_1 \leftarrow S_0$ absorption spectra of pyridine-d_0 and -d_5 in the vapor phase. Band assignments are given in the figures and also in Table 1, where FR means Fermi resonance. These assignments are the ones made by Mochizuki *et al.*[4] except for the bands involving the ν_{16b} vibration, the assignments of which are taken from a paper by Jesson *et al.*[5]

The spectrum of pyridine-d_0 consists mainly of bands that correspond to fundamentals, overtones, or combinations of two totally symmetric vibrations $\nu_{6a}(a_1)$ and $\nu_{12}(a_1)$, which in the excited state S_1 have frequencies of 542 cm^{-1} (ν_{6a}') and 995 cm^{-1} (ν_{12}'). The progression $6a_0^n$, starting with the 0–0 band ($n=0$), is seen to be most prominent. Note that the 0–0 band is located at 34769 cm^{-1}. Some other bands are observed which

Table 1. Quantum yields, lifetimes, and radiative and nonradiative rate constants for pyridine-d_0 and -d_5 vapors

Compound	Vibronic level[a]	ΔE[b] / cm^{-1}	Φ_F / 10^{-5}	Φ_{ISC}	τ_F / ps	k_F / $10^6\ s^{-1}$	k_{IC} / $10^{10}\ s^{-1}$	k_{ISC} / $10^{10}\ s^{-1}$
Pyridine-d_0	0	0	5.9	0.30	42	1.40	1.67	0.71
	$16b^1$	59[c]	9.4	0.22	41	2.29	1.91	0.53
	$16b^2$	139	11.9	0.28	60	1.98	1.20	0.47
	$16b^3$	237[c]	10.6	0.24				
	$10a^1$	331	8.3	0.24	34	2.44	2.23	0.71
	$16b^4$	347[c]	10.9	0.26				
	$16b^5$	464[c]	8.4	0.30				
	$6a^1$	542	7.0	0.30	42	1.67	1.67	0.71
	$16b^2 6a^1$	681	12.8	0.27	54	2.37	1.36	0.49
	$10a^1 6a^1$	864	6.3	0.15	35	1.80	2.43	0.43
	12^1	995	7.0	0.23	35	2.00	2.21	0.65
	$6a^2$	1084	6.3	0.20	38	1.66	2.10	0.53
	$10a^1 6a^2$	1406	3.0	0.08	30	1.00	3.07	0.27
	$12^1 6a^1$	1537	2.7	0.06	28	0.96	3.36	0.21
	$6a^3$	1626	0.9	0.03				
Pyridine-d_5	0	0	6.0	0.30	42	1.43	1.66	0.72
	$16b^2$	118	12.0	0.31	50	2.40	1.38	0.62
	$10a^1$	253	8.2	0.28	40	2.05	1.80	0.70
	FR($6a^1$, $10a^2$)	510	10.0	0.30	34	2.94	2.06	0.88
		560	9.7	0.29	45	2.16	1.57	0.65
	12^1	954	7.7	0.23	30	2.57	2.56	0.77
	FR($6a^2$, $16b^2 12^1$)	1075	6.2	0.15				
		1082	2.5	0.07				
	FR($10a^2 12^1$, $6a^1 12^1$)	1465	11.0	0.13	34	3.24	2.56	0.38
		1516	6.1	0.10				

a) See Figs. 1 and 2 for the absorption transitions which lead to the vibronic levels in this column. The 0–0 band for pyridine-d_0 is located at 34769 cm^{-1} and that for pyridine-d_5 at 34950 cm^{-1}. b) From Ref. 4 except for c). c) From Ref. 5.

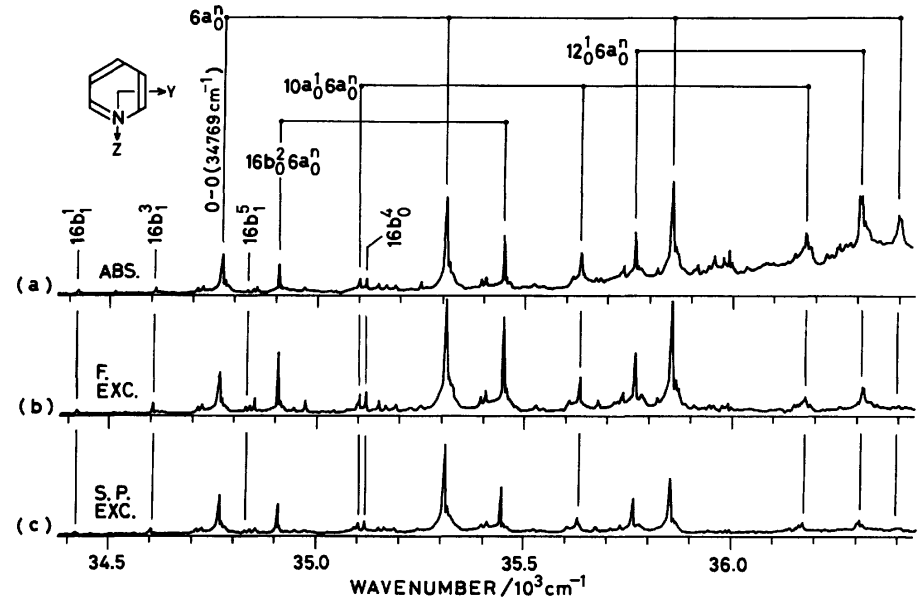

Fig. 1. (a) Absorption spectrum, (b) fluorescence excitation spectrum, and (c) sensitized biacetyl phosphorescence excitation spectrum for pyridine-d_0 vapor. The pressures of pyridine-d_0: (a) 5.4, (b) 0.5, and (c) 1.0 Torr. In the case of (c), 0.8 Torr of biacetyl and 160 Torr of SF_6 are added to the pyridine-d_0 vapor. In the notation of vibronic transitions, the superscript and subscript denote the vibrational quantum numbers in the S_1 and S_0 states, respectively.

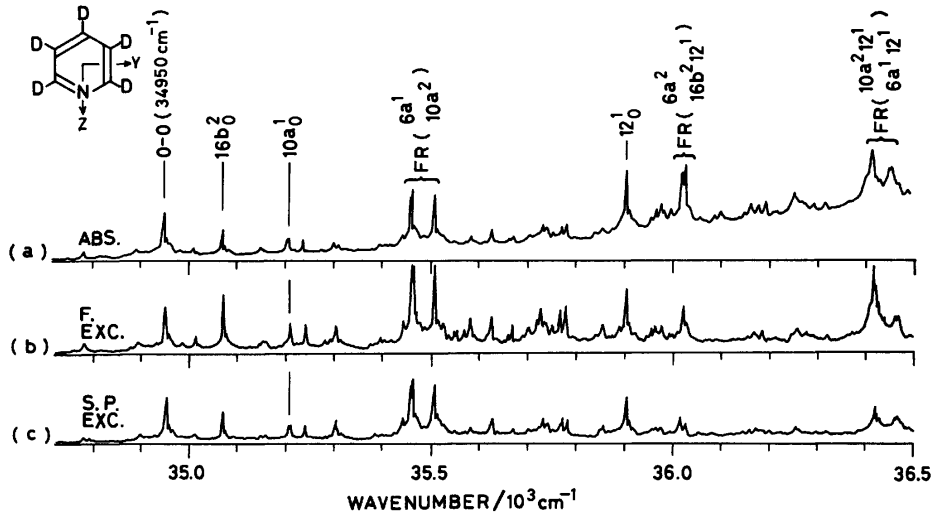

Fig. 2. (a) Absorption spectrum, (b) fluorescence excitation spectrum, and (c) sensitized biacetyl phosphorescence excitation spectrum for pyridine-d_5 vapor. The pressures of pyridine-d_5: (a) 7.6, (b) 1.8, and (c) 0.8 Torr. In the case of (c), 1.1 Torr of biacetyl and 160 Torr of SF_6 are added to the pyridine-d_5 vapor. In the notation of vibronic transitions, the superscript and subscript denote the vibrational quantum numbers in the S_1 and S_0 states, respectively.

involve non-totally symmetric vibrations, $\nu_{16b}(b_1)$ and $\nu_{10a}(a_2)$. Thus the bands at $\nu_{0-0}+139$ cm^{-1} and $\nu_{0-0}+331$ cm^{-1} can be assigned to $16b_0^2$ and $10a_0^1$, respectively. The combination band $16b_0^2 6a_0^1$ and weak hot bands $16b_1^n$ ($n=1, 3, 5$) also appear in the spectrum. A progression in ν_{6a}', denoted by $10a_0^1 6a_0^n$ in the figure, starts with the $10a_0^1$ band. On the other hand, the absorption spectrum of pyridine-d_5 does not show any regular progressions of bands. This is due mainly to the occurrence of Fermi resonance, as is seen in Fig. 2(a). The 0-0 band is located at 34950 cm^{-1} in this case.

Figures 1(b) and 1(c) show the excitation spectra of the fluorescence and sensitized biacetyl phosphorescence for pyridine-d_0, and Figs. 2(b) and 2(c) the same spectra for pyridine-d_5. Band positions in these excitation spectra agree very well with those in the corresponding absorption spectra, indicating that the observed fluorescence and sensitized phosphorescence originate from pyridine-d_0 or -d_5 itself. It was confirmed that no change in shape of the fluorescence excitation spectra occurs

upon adding the foreign gas, SF_6, up to 160 Torr. In Figs. 1 and 2, it can be seen at a glance that, so far as the lower excitation energy region is concerned, the sensitized phosphorescence excitation spectrum is similar to the absorption spectrum, but that the fluorescence excitation spectrum is substantially different from the absorption spectrum in intensity distribution. In fact, in the fluorescence excitation spectra of pyridine-d_0 and -d_5, some bands which involve the ν_{16b} mode have particularly high intensities.

The values of fluorescence quantum yields (Φ_F) and of the intersystem-crossing quantum yields (Φ_{ISC}) from various vibronic levels are shown in Table 1, and the excess vibrational energy (ΔE) dependence of Φ_F and Φ_{ISC} is illustrated in Figs. 3 and 4. These yield values were determined according to the method described in the preceding section. As is seen in Figs. 1 and 2, each of the bands is characterized by a peak. However, the peak is accompanied by a background which is due to superposition of the rotational contours of neighboring bands and, at higher frequencies, also to overlap of the tail of the $S_2 \leftarrow S_0$ absorption. In the evaluation of Φ_F and Φ_{ISC}, therefore, care was taken to eliminate the contribution of the background to the spectral intensity.[13] It is seen from Figs. 1—4 that the values of Φ_F are significantly large for levels involving the ν_{16b} mode, *i.e.*, $16b^2$ and $16b^26a^1$ of pyridine-d_0 and $16b^2$ of pyridine-d_5. The value of Φ_F for the $10a^1$ level is about 1.4 times that for the zero-point level in both molecules. In pyridine-d_0, Φ_F rapidly decreases as ΔE exceeds about 1100 cm^{-1}. In pyridine-d_5, the values of Φ_F for the Fermi resonance levels are larger than that for the zero-point level except for the level at 1082 cm^{-1}. On the other hand, the values of Φ_{ISC} for both pyridine-d_0 and -d_5 are fairly constant regardless of the nature of the vibronic level in the lower ΔE region ($<$1000 cm^{-1}). In the case of pyridine-d_0, Φ_{ISC} is found to decrease rapidly in the higher ΔE region.

The observed fluorescence lifetimes (τ_F) of pyridine-d_0 and -d_5 are summarized in Table 1. When ΔE increases, τ_F does not decrease monotonously, but varies in a characteristic way. The lifetimes for $16b^2$ and $16b^26a^1$ levels are seen to be notably long.

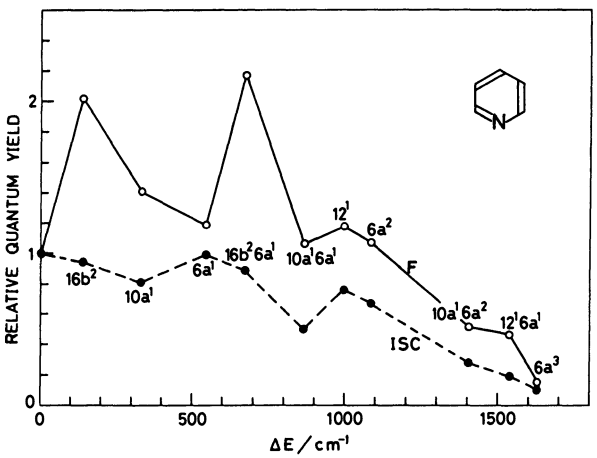

Fig. 3. Relative quantum yields plotted aginst ΔE for pyridine-d_0: ——, fluorescence (Φ_F^v/Φ_F^0); ------, intersystem crossing ($\Phi_{ISC}^v/\Phi_{ISC}^0$).

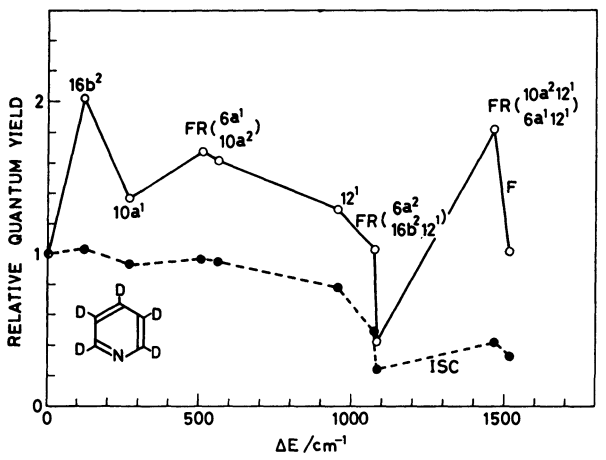

Fig. 4. Relative quantum yields plotted against ΔE for pyridine-d_5: ——, fluorescence (Φ_F^v/Φ_F^0); ------, intersystem crossing ($\Phi_{ISC}^v/\Phi_{ISC}^0$).

Discussion

Since pyridine is considered to belong to the statistical limit rather than to the intermediate case,[1,12] the experimental results described in the preceding section can be analyzed on the basis of a simple kinetic scheme. Suppose that the pyridine molecule is excited into a vibronic level v in the S_1 state. The molecule will then relax through radiative and nonradiative decay processes. The rate constant for the radiative fluorescence decay is denoted by k_F^v, and those for the $S_1 \rightsquigarrow S_0$ internal conversion and the $S_1 \rightsquigarrow T$ intersystem crossing are denoted by k_{IC}^v and k_{ISC}^v, respectively. So far as lower excitation energies are concerned, nonradiative processes other than the latter two processes may safely be neglected in the case of pyridine, because the quantum yield of the photochemical reaction in pyridine vapor is known to be negligibly low, as was described in a previous paper.[1] The quantum yield of the fluorescence (Φ_F^v) and that of the intersystem crossing (Φ_{ISC}^v) from a vibronic level v can thus be expressed as $\Phi_F^v = k_F^v/(k_F^v+k_{IC}^v+k_{ISC}^v)$ and $\Phi_{ISC}^v = k_{ISC}^v/(k_F^v+k_{IC}^v+k_{ISC}^v)$. The radiative rate constant k_F^v is given by

$$k_F^v = \Phi_F^v/\tau_F^v, \tag{1}$$

where τ_F^v represents the lifetime of the fluorescence from v. The nonradiative rate constants can be written as

$$k_{IC}^v = k_F^v(1-\Phi_F^v-\Phi_{ISC}^v)/\Phi_F^v, \tag{2}$$

$$k_{ISC}^v = k_F^v\Phi_{ISC}^v/\Phi_F^v. \tag{3}$$

On the basis of Eqs. 1—3, the rate constants k_F^v, k_{IC}^v, and k_{ISC}^v were determined from the experimental values of τ_F^v, Φ_F^v, and Φ_{ISC}^v, with the results summarized in Table 1. The relative values of the rate constants, k_F^v/k_F^0, k_{IC}^v/k_{IC}^0, and k_{ISC}^v/k_{ISC}^0, are shown in Figs. 5 and 6, the values for the zero-point level (v=0) being normalized to unity.

An increase of the quantum yield of fluorescence from an excited vibronic level will result, in general, from an increase of the radiative rate and/or a decrease of the nonradiative rate. We first consider pyridine-d_0. For

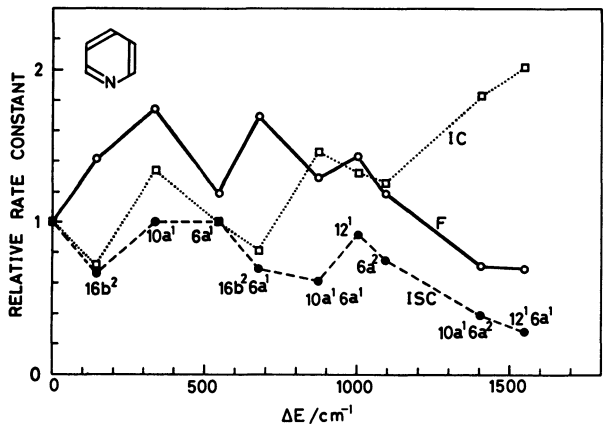

Fig. 5. Relative rate constants plotted against ΔE for pyridine-d_0: ——, k_F^v/k_F^0; ·····, k_{IC}^v/k_{IC}^0; ------, k_{ISC}^v/k_{ISC}^0.

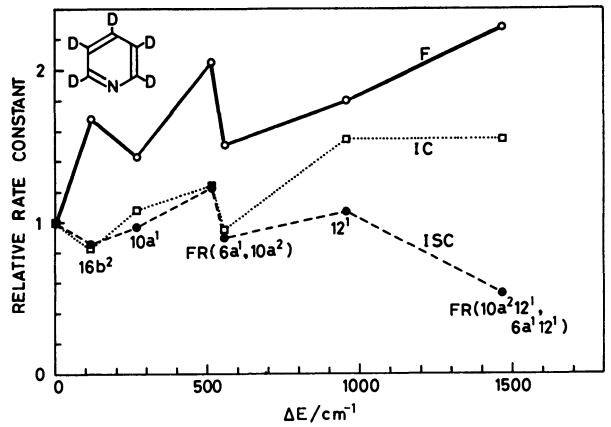

Fig. 6. Relative rate constants plotted against ΔE for pyridine-d_5: ——, k_F^v/k_F^0; ·····, k_{IC}^v/k_{IC}^0; ------, k_{ISC}^v/k_{ISC}^0.

its $16b^2$ level, k_F^v is 1.41 times as large as k_F^0, while the values of k_{IC}^v and k_{ISC}^v are about 70% of the values of k_{IC}^0 and k_{ISC}^0. These relations existing among the rate constants account for the finding that Φ_F^v is particularly large for the $16b^2$ level ($\Phi_F^v/\Phi_F^0=2.02$). The $16b^26a^1$ level is in a similar situation, as is seen from Table 1 and Fig. 5. For the $10a^1$ level, Φ_F^v is significantly larger than Φ_F^0, *i.e.*, $\Phi_F^v/\Phi_F^0=1.41$. This observation is interpreted as due solely to the fact k_F^v/k_F^0 is as large as 1.74. Note that in this case k_{IC}^v/k_{IC}^0 and k_{ISC}^v/k_{ISC}^0 are greater than or equal to unity. Inspection of the kinetic data given in Table 1 will reveal that the relatively high values of Φ_F for the $16b^2$ and $10a^1$ levels of pyridine-d_5 be explained in essentially the same manner as the corresponding values of pyridine-d_0.

Since the $S_1(^1B_1)$ state of the pyridine molecule is of an (n, π^*) type, the rate of the radiative decay from S_1 may be noticeably enhanced by the vibronic interaction. Let us first discuss vibronic levels involving the ν_{10a} vibration after the method adopted by Yamazaki, Fujita, and Baba[14] in their discussion about the radiative rate constant of the fluorescence of pyrazine. According to these authors, the ratio of the radiative rate constant for the $10a^j$ level to that for the zero-point level, *i.e.*, $k_F(10a^j)/k_F^0$ is given by

$$\frac{k_F(10a^j)}{k_F^0}=\frac{1+(\zeta/u)(2j+1)}{1+\zeta/u}, \tag{4}$$

where ζ is the ratio of the intensity of the $10a_0^1$ absorption band to that of the 0–0 absorption, and u is a numerical factor introduced to allow for the difference between $\nu_{10a'}$ and $\nu_{10a''}$, which denote the frequencies of ν_{10a} in S_1 and S_0, respectively. Equation 4 is based on the Herzberg-Teller theory of vibronic coupling. From the integrated intensities for the rotational contours of the $10a_0^1$ and 0–0 absorption bands, ζ is determined to be 0.28 for pyridine-d_0 and 0.24 for pyridine-d_5. There is a great difference between $\nu_{10a'}$ and $\nu_{10a''}$. In fact, $\nu_{10a'}=331\ cm^{-1}$ and $\nu_{10a''}=886\ cm^{-1}$ for pyridine-d_0, while $\nu_{10a'}=253\ cm^{-1}$ and $\nu_{10a''}=690\ cm^{-1}$ for pyridine-d_5. By the use of these frequency values, the numerical factor u is calculated to be 0.30 for pyridine-d_0 and 0.29 for pyridine-d_5. These data lead to the results that $k_F(10a^1)/k_F^0=1.97$ and 1.91 for pyridine-d_0 and -d_5, respectively. The corresponding experimental values are 1.74 and 1.43, so that in either case the calculated value is higher than the experimental. However, in view of the fact that no allowance has been made for the mixing of vibrational modes due to the Duschinskii effect, which is likely to occur between ν_{10a} and ν_{16a} in pyridine,[6] as well as for the anharmonicity of the ν_{10a} vibration,[4] it may be said that the theoretical results obtained from Eq. 4 account, to a good extent, for the experimental data on the radiative rate constants.

As is seen in Table 1, the ν_{16b} vibration, the out-of-plane "boat" vibration, seems to have an effect on k_F which is similar to the one observed for the ν_{10a} vibration. In the case of ν_{16b}, however, if an equation analogous to Eq. 4 is used, $k_F(16b^j)/k_F^0$ is estimated to be unity regardless of j. The reason for this is that the ratio ζ between the intensities of $16b_0^1$ and 0–0 absorption bands is zero, because no absorption band can be observed which is to be assigned to $16b_0^1$. In contrast to the above theoretical estimation, the experimental values of k_F for both $16b^1$ and $16b^2$ levels are significantly larger than k_F^0, as is seen from Table 1.

Mochizuki *et al.*[6] recently reported that the SVL fluorescence spectrum from "the $16b^2$ level" of pyridine-d_0 or -d_5 is essentially the same as the corresponding fluorescence spectrum from the zero-point level except for a relative shift by $139\ cm^{-1}$ in pyridine-d_0 and by $118\ cm^{-1}$ in pyridine-d_5, and that no fluorescence band is observed which is to be related to the ν_{16b} vibration. Accordingly, they pointed out that one cannot decide whether the absorption band at $\nu_{0-0}+139\ cm^{-1}$ (or $\nu_{0-0}+118\ cm^{-1}$) should be assigned as a cold band like $16b_0^2$ or as a hot band of an unknown vibration. In a later report, on the basis of the absorption spectrum measured in a supersonic cold beam, these authors showed that the band in question must be regarded as a cold one.[15] To sum up it may be said that the assignments involving the ν_{16b} vibration, given by Jesson *et al.*[5] for some absorption bands at lower frequencies of pyridine-d_0 and -d_5, are considered to be reasonable, but that the spectral or kinetic properties associated with these bands appear to be unusual.

Another point to be noted is that the values of k_F for some vibronic levels involving totally symmetric vibra-

tions 6a and 12 are observed to be larger than k_F^0. At present, we are not in a position to give an adequate explanation for the above observation. It is possible, however, that a higher energy singlet state having the same symmetry as S_1 may be vibronically coupled to S_1 through mode 6a or 12 to enhance the rate of the radiative decay from the vibronic levels in question.

The Φ_{ISC} value of pyridine vapor is obviously smaller than unity even for the zero-point level and decreases with increasing ΔE, in marked contrast to pyrazine and pyrimidine vapors whose Φ_{ISC} values are known to be close to unity over a wide range of ΔE.[14] This is due to the fact that in pyridine k_{IC} is more than twice as large as k_{ISC} even at the zero-point level, whereas in pyrazine and pyrimidine k_{IC} is much smaller than k_{ISC}. The anomalously large k_{IC} value in pyridine, which is responsible for the extreme weakness of its fluorescence, suggests that there should be a strong vibronic coupling between $S_1(n, \pi^*)$ and S_0. The detailed mechanism of such a coupling, however, remains to be elucidated.

References

1) I. Yamazaki, K. Sushida, and H. Baba, *J. Chem. Phys.*, **71**, 381 (1979); K. Sushida, I. Yamazaki, and H. Baba, *Bull. Res. Inst. Appl. Elec., Hokkaido Univ.*, **32**, 36 (1980).

2) H. Sponer and H. Stücklen, *J. Chem. Phys.*, **14**, 101 (1946).

3) J. V. Shukla, K. N. Upadhya, and S. N. Thakur, *Appl. Spectrosc.*, **26**, 283 (1972).

4) Y. Mochizuki, K. Kaya, and M. Ito, *J. Chem. Phys.*, **65**, 4163 (1976).

5) J. P. Jesson, H. W. Kroto, and D. A. Ramsay, *J. Chem. Phys.*, **56**, 6257 (1972).

6) Y. Mochizuki, K. Kaya, and M. Ito, *Chem. Phys.*, **54**, 375 (1981).

7) H. Baba, M. Fujita, N. Ohta, and Y. Shindo, *J. Spectrosc. Soc. Jpn.*, **29**, 387 (1980); H. Baba, M. Fujita, and K. Uchida, *Chem. Phys. Lett.*, **73**, 425 (1980).

8) W. H. Melhuish, *J. Phys. Chem.*, **65**, 229 (1961).

9) T. L. Brewer and S. H. Jones, *J. Phys. Chem.*, **75**, 3769 (1971); S. H. Jones and T. L. Brewer, *J. Am. Chem. Soc.*, **94**, 6310 (1972).

10) A. Z. Moss and J. T. Yardley, *J. Chem. Phys.*, **61**, 2883 (1974).

11) I. Yamazaki, T. Murao, and K. Yoshihara, *Chem. Phys. Lett.*, **87**, 384 (1982); T. Murao, I. Yamazaki, Y. Shindo, and K. Yoshihara, *J. Spectrosc. Soc. Jpn.*, **31**, 96 (1982).

12) I. Yamazaki, T. Murao, K. Yoshihara, M. Fujita, K. Sushida, and H. Baba, *Chem. Phys. Lett.*, **92**, 421 (1982).

13) N. Ohta and H. Baba, *J. Chem. Phys.*, **76**, 1654 (1982).

14) I. Yamazaki, M. Fujita, and H. Baba, *Chem. Phys.*, **57**, 431 (1981).

15) K. Kaya, Y. Mochizuki, J. Murakami, and M. Ito, Symposium on Molecular Structure, Fukuoka (1980).

Crystal Structure of Adenine-1-(2-Carboxyethyl)uracil (1 : 1) Complex. A Model for Interactions of Amino Acid Side Chains with Nucleic Acid Base Pair

Shigeo FUJITA, Akio TAKENAKA, and Yoshio SASADA*

Laboratory of Chemistry for Natural Products, Tokyo Institute of Technology, Nagatsuta, Midori-ku, Yokohama 227

(Received March 15, 1983)

As a model for protein-nucleic acid interactions, crystals of the title complex were prepared from a water-ethanol (1 : 1) solution containing equimolar amounts of adenine and 1-(2-carboxyethyl)uracil. The space group is $P2_1/c$ with the unit cell dimensions of $a=12.567(1)$, $b=13.358(1)$, $c=8.032(1)$ Å and $\beta=93.28(1)°$. The crystal structure was determined by X-ray analysis. The final R value was 0.053. The adenine and uracil moieties form a reversed Hoogsteen base pair in which N(7) and N(6) of adenine are hydrogen-bonded with N(3) and O(2) of uracil, respectively. The carboxyl group is dissociated and hydrogen-bonded to the protonated N(1) of adenine in the adjacent base pair at a distance of 2.542(3) Å. It is suggested that the protonation of adenine–uracil reversed Hoogsteen base pair could occur to make the base pair more stable, and the dissociated carboxyl group may be hydrogen-bonded to it in the protein–nucleic acid interactions.

Protein–nucleic acid interactions are essential for gene expression and its regulation.[1] Recently, the three-dimensional structures of cro repressor,[2] λ repressor[3] and catabolite gene activator protein[4] were determined by the X-ray method, and a binding model of cro repressor to its operator site on DNA was constructed by adjusting the structure so as to make hydrogen bonds, assuming the two-fold symmetry.[5] This model suggests that the hydrogen bonds between the nucleotide bases and the amino acid side chains must be the leading part of the specific protein–nucleic acid interactions. For understanding of the molecular basis of recognition between the two kinds of macromolecules, it is important to know the hydrogen bonds between their components. There should be some elementary patterns of hydrogen bonding with different degree of preference or stability, and their suitable combination would give a specificity of the interactions.

Protein crystallography has shown that the atoms located at the protein–protein or protein–substrate interface are packed as close as those in crystals of small molecules.[6] It may be expected that the recognition between different biomolecules are performed in a circumstance similar to crystalline field and the suitable model crystals give us information at atomic level for interpreting the specificity. By X-ray analyses of model crystals in which both the components coexist, we have been studying the elementary binding patterns between nucleotide bases and amino acid side chains.[7–14] We have found the three different binding patterns between adenine and carboxyl group: a carboxyl group is (i) hydrogen-bonded to N(3),[10] (ii) doubly hydrogen-bonded to N(6) and N(7),[15] and (iii) dissociated and doubly hydrogen-bonded to N(6) and protonated N(1).[11] In combination with uracil, a carboxyl group is hydrogen-bonded to O(2)[12] or doubly hydrogen-bonded to N(3) and O(4).[16] Thus, a carboxyl group interacts with both adenine and uracil in the binary model systems. What preference is displayed by a carboxyl group if both adenine and uracil bases are present? We have prepared model crystals that contain these components and revealed the binding geometry by the X-ray method.

Experimental and Structure Determination

1-(2-Carboxyethyl)uracil was prepared from uracil and β-propiolactone, according to Kondo *et al.*[17] The titration curve of 1-(2-carboxyethyl)uracil (0.01 mol dm^{-3}) with NaOH (0.008 mol dm^{-3}) was recorded using Toshiba-Beckman pH meter, and the value of pK_a was evaluated to be 4.1 from the curve. Colorless plate crystals were obtained by slow evaporation of a water–ethanol (1 : 1) solution containing equimolar amounts of adenine and 1-(2-carboxyethyl)uracil. The syste-

TABLE 1. FRACTIONAL COORDINATES AND ISOTROPIC TEMPERATURE FACTORS

The B values accompanied with < > are the equivalent isotropic temperature factors calculated from anisotropic thermal parameters using the equation $B=8\pi^2(U_1+U_2+U_3)/3$, where U_1, U_2, and U_3 are principal components of mean square displacement matrix U. Values in < > are anisotropicity defined by $(\sum(B-8\pi^2U_i)^2/3)^{1/2}$ and those in ( ) are e.s.d.'s; they refer to last decimal places.

Atom	x	y	z	B/Å^2
N(1)	0.3663(2)	-0.0302(2)	0.0976(3)	2.9<13>
C(2)	0.3117(2)	0.0517(2)	0.0369(4)	2.9<9>
O(2)	0.2340(2)	0.0444(1)	-0.0633(3)	4.0<25>
N(3)	0.3488(2)	0.1420(2)	0.0918(3)	3.1<16>
C(4)	0.4331(2)	0.1604(2)	0.2060(4)	3.2<10>
O(4)	0.4569(2)	0.2466(1)	0.2434(3)	4.6<27>
C(5)	0.4839(2)	0.0710(2)	0.2681(4)	3.6<17>
C(6)	0.4505(2)	-0.0186(2)	0.2143(4)	3.4<14>
C(9)	0.3341(2)	-0.1313(2)	0.0370(4)	3.1<10>
C(10)	0.2438(3)	-0.1711(2)	0.1329(5)	3.8<11>
C(11)	0.2111(2)	-0.2748(2)	0.0707(4)	3.0<8>
O(12)	0.1264(2)	-0.2855(1)	-0.0178(3)	3.8<16>
O(13)	0.2702(2)	-0.3462(1)	0.1102(3)	4.8<34>
N(1')	-0.0061(2)	0.3312(2)	-0.3065(3)	2.9<9>
C(2')	-0.0152(2)	0.4314(2)	-0.2944(4)	3.5<12>
N(3')	0.0464(2)	0.4920(2)	-0.2056(3)	3.4<17>
C(4')	0.1267(2)	0.4408(2)	-0.1218(4)	4.9<10>
C(5')	0.1440(2)	0.3380(2)	-0.1260(3)	2.5<8>
C(6')	0.0716(2)	0.2790(2)	-0.2186(4)	2.6<3>
N(6')	0.0737(2)	0.1803(2)	-0.2231(4)	3.2<13>
N(7')	0.2326(2)	0.3129(2)	-0.0255(3)	2.9<12>
C(8')	0.2659(2)	0.3990(2)	0.0358(4)	3.2<13>
N(9')	0.2065(2)	0.4794(2)	-0.0161(3)	3.17<151>
H(3)	0.318(2)	0.193(2)	0.054(4)	0.9(7)
H(5)	0.531(2)	0.079(2)	0.342(4)	1.8(8)
H(6)	0.479(2)	-0.087(2)	0.257(3)	1.2(6)
H(9A)	0.309(2)	-0.127(2)	-0.087(4)	1.4(7)
H(9B)	0.393(3)	-0.184(3)	0.054(4)	3.2(8)
H(10A)	0.274(3)	-0.178(3)	0.252(5)	3.6(9)
H(10B)	0.182(3)	-0.128(3)	0.129(5)	4.0(10)
H(1')	-0.065(2)	0.289(2)	-0.388(4)	2.9(8)
H(2')	-0.073(2)	0.461(2)	-0.355(3)	1.1(6)
H(6A')	0.029(3)	0.145(3)	-0.277(4)	2.9(9)
H(6B')	0.128(3)	0.148(2)	-0.157(4)	2.6(8)
H(8')	0.325(2)	0.406(2)	0.120(3)	1.1(6)
H(9')	0.221(3)	0.558(3)	0.023(4)	3.9(9)

matic absence of reflections showed the space group to be $P2_1/c$. The density was measured by the flotation method in hexane and carbon tetrachloride mixture.

A crystal, $0.5\times0.4\times0.1$ mm^3 in size, was used for data collection on a Rigaku four-circle diffractometer with Ni-filtered Cu $K\alpha$ radiation ($\lambda=1.5418$ Å). Accurate unit cell dimensions were derived from 2θ values of 80 high-angle reflections. The crystal data are as follows: $C_5H_5N_5\cdot C_7H_8N_2O_4$ F.W. 319.3, monoclinic, space group $P2_1/c$, $a=12.567(1)$, $b=13.358(1)$, $c=8.032(1)$ Å, $\beta=93.28(1)°$, $Z=4$, $D_m=1.57$ g cm^{-3}, and $D_c=1.575$ g cm^{-3}.

Intensities were measured in the $\omega/2\theta$ scan mode with a scan width of $2.6°(2\theta)$ plus α_1—α_2 divergence and a scan speed of $4°(2\theta)$ min^{-1}. Five reference reflections monitored showed no significant intensity deterioration. Correction was not made for absorption effect. Of 2087 independent reflections within the range $2°<2\theta<125°$, 154 weak reflections below background were considered zero-reflections. The structure was solved by the direct method and its parameters were refined by the full-matrix least-squares method. The weighting scheme and the treatment of the zero-reflections were the same as those in Ref. 11. The value of q and $F_{\rm lim}$ were taken as 2.99×10^{-5} and 1.108, respectively. All the hydrogen atoms were found on a difference map and included in the refinement. The R value was 0.053 for 1914 reflections with $F_o>3\sigma$; the maximum shift in atomic parameters was 0.3σ in the last cycle. The final atomic parameters are listed in Table 1.[18] The atomic scattering factors were taken from Ref. 19.

Results and Discussion

Molecular Structure. The carboxyl group in 1-(2-carboxyethyl)uracil is dissociated and a proton acceptor is N(1′) of adenine, as confirmed by the difference synthesis.

Bond lengths and angles are shown in Fig. 1. The dimensions of the carboxyl group are typical of carboxylate ion. The pyrimidine ring is planar within 0.015 Å. The bond lengths and angles are similar to those found in 1-(2-carboxyethyl)uracil.[12] Closer examination shows, however, that the C(2)–N(3) bond is slightly shortened and the C(2)–O(2) bond is lengthened. These changes indicate the increase of the contribution from the quinonoidal form, accompanied by the polarization at H(3)–N(3)–C(2)–O(2). The polarization must be induced by the hydrogen bonds with the adenine monocation. The methylene chain is extended, contrary to the folded form found in 1-(2-carboxyethyl)uracil.[12]

As compared with the neutral adenine, the N(1′)–C(6′) bond is lengthened, the C(6′)–N(1′)–C(2′) bond angle is expanded and the C(5′)–C(6′)–N(1′) and N(1′)–C(2′)–N(3′) bond angles are contracted. Such changes are typical of adenine monocation protonated at N(1′).[20–24] The six-membered ring is ruffled, as usually observed in the purine ring.[25]

Hydrogen Bond in Crystal. As shown in Figs. 2 and 3, the uracil moiety and the adeninium cation form a reversed Hoogsteen base pair[26] through the two hydrogen bonds N(3)–H···N(7′) (2.842(3) Å for N···N) and N(6′)–H···O(2) (2.951(3) Å for N···O). The geometries of both the hydrogen bonds are similar to those of the reversed Hoogsteen base pair without protonation, found in the complexes of 9-ethyladenine: 1-methyl-5-bromouracil[27] and adenosine: 5-bromouridine.[28] The

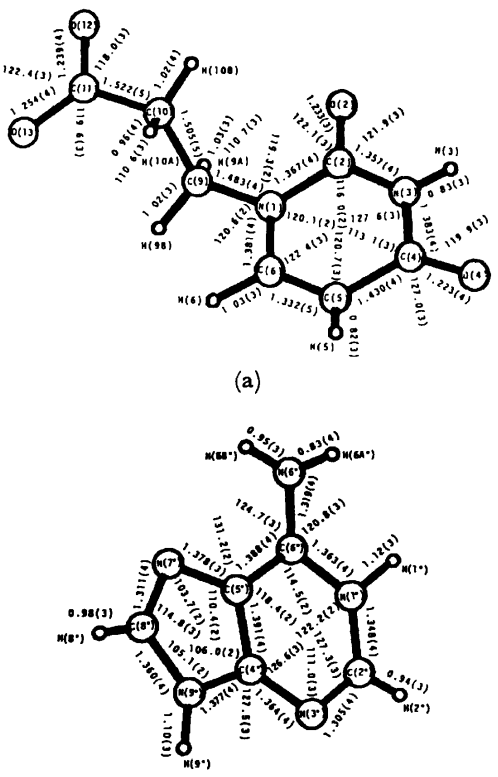

Fig. 1. Bond lengths (l/Å) and angles (ϕ/°) with e.s.d.'s in the parentheses. (a) 1-(2-Carboxyethyl)uracil and (b) adenine. Bond angles involving hydrogen atoms are deposited.

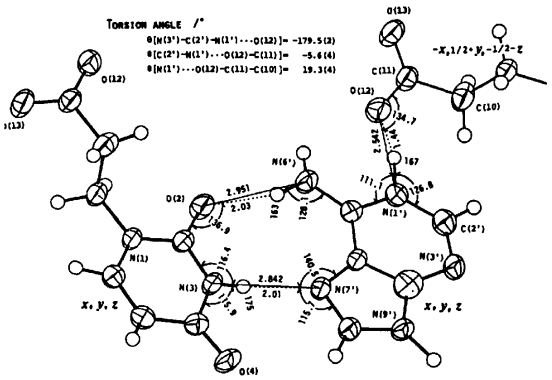

Fig. 2. A projective view of binding mode of the carboxyl group to the adenine–uracil base pair with hydrogen bond distances (l/Å) and angles (ϕ/°). E.s.d.'s are 0.003 Å and 0.2°, respectively, for distances and angles involving nonhydrogen atoms. The corresponding values involving hydrogen atoms are 0.03 Å and 2°, respectively.

two ring systems are nearly coplanar with a dihedral angle of 5.0(1)° between their respective least-squares planes; similar values are reported for the other reversed Hoogsteen base pairs.[27–28]

The carboxyl group interacts with the protonated N(1′) of adenine through the strong N(1′)–H···O(12) hydrogen bond; the N···O distance is 2.542(3) Å and the torsion angles, θ[N(3′)–C(2′)–N(1′)···O(12)], θ[C(2′)–N(1′)···O(12)–C(11)], and θ[N(1′)···O(12)–C(11)

TABLE 2. HYDROGEN BOND DISTANCES AND ANGLES[a)]
Standard deviations are given in parentheses.

Hydrogen bond distance	l/Å		l/Å
N(3′)···N(6′) (i)[b)]	2.972(4)	N(9′)···O(13) (ii)	2.646(3)
N(3′)···H(6A′) (i)	2.26(4)	H(9′)···O(13) (ii)	1.57(3)
Hydrogen bond angle	ϕ/°		ϕ/°
N(3′)···H(6A′)–N(6′) (i)	145(3)	N(9′)–H(9′)···O(13) (ii)	163(3)
C(2′)–N(3′)···N(6′) (i)	98.1(2)	C(4′)–N(9′)···O(13) (ii)	115.4(2)
C(4′)–N(3′)···N(6′) (i)	150.8(2)	C(8′)–(9′)···O(13) (ii)	139.5(2)
N(3′)···N(6′)–C(6′) (i)	147.1(2)	N(9′)···O(13)–C(11) (ii)	114.5(2)
N(3′)···N(6′) (i)···O(2) (i)	83.7(1)		

a) The other hydrogen bonds found in the present crystal are shown in Fig.2. b) Symmetry codes: (i) $-x$, $1/2+y$, $-1/2-z$; (ii) x, $1+y$, z.

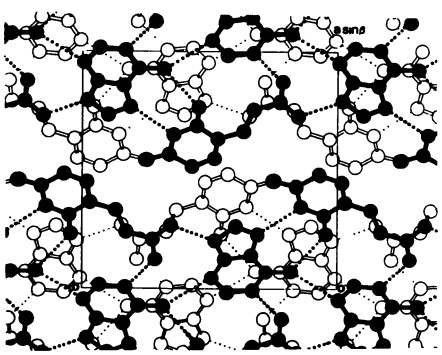

Fig. 3. Crystal structure of adenine: 1-(2-carboxyethyl)-uracil (1 : 1) complex, projected along the c axis. The broken lines indicate the hydrogen bonds.

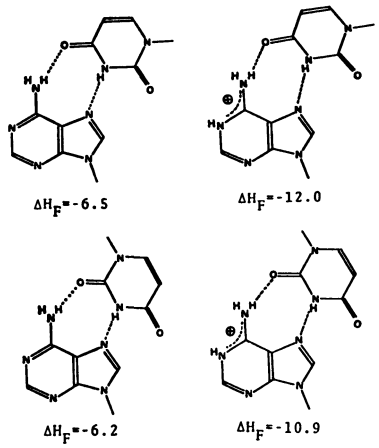

Fig. 4. Formation energies (ΔH_F/kcal mol^{-1}) of four types of adenine–uracil base pairs calculated with the CNDO/2 method.

C(10)] are −179.5(2), −5.6(4), and 19.3(4)°, respectively. The other oxygen atom O(13) is hydrogen-bonded to N(9′) at a distance of 2.646(3) Å. These two hydrogen bonds are very short compared with normal N–H···O hydrogen bonds. Between adeninium cations related by 2_1 screw, the N(6′)–H···N(3′) hydrogen bond is formed; the distance of 2.972(4) Å is normal, but this hydrogen bond deviates to some extent from linearity, the N(6′)–H···N(3′) being 145(3)°. The O(4) atom of uracil moiety does not participate in hydrogen bonding and surrounded by the hydrophobic groups. The O(4) atom points to the hydrogen atom of C(6) at $1-x$, $1/2+y$, $1/2-z$ at a distance of 3.357(3) Å for O···C. The base pairs related by 2_1 screw around $x=0$ and $z=1/4$ form a ribbon along the b axis. The detailed hydrogen bond distances and angles are given in Fig. 2 or Table 2.

Hydrogen Bonding between Carboxyl Group and Adenine–Uracil Base Pair. The present crystal structure suggests that the proton transfer from the carboxyl group to N(1) of adenine, accompanied by hydrogen bonding between them, makes the reversed Hoogsteen base pair more stable. This is confirmed by a CNDO/2 calculation[29)] of the formation energies; it is obvious from Fig. 4 that the protonation at N(1) stabilizes by about 5 kcal mol^{-1} both the reversed and normal Hoogsteen base pair.** It is plausible that the base pair to which a suitable proton donor is close may be protonated in a hydrophobic conditions. But such stabilization may be unlikely for the Watson-Crick base pair because of the small pK_a value for N(7) or N(3) of adenine (pK_a<1). If the protonation is compelled, it would occur at N(1) of adenine (pK_a=4.25) to lead a break-down of Watson-Crick base pair.[30)]

The dissociation constant, as an indication, of 1-(2-carboxyethyl)uracil (pK_a=4.1) is comparable to those of the acidic side chains of amino-acid derivatives and peptides,[31)] which shows that the chemical behavior of the carboxyl group of model compound is similar to that of the acidic side chains of protein. Therefore, one could expect that the interaction between the carboxylate ion and the charged reversed Hoogsteen base pair found in the present model crystal is also realized in a living system and takes some part in recognition of the special type of base pair by protein side chains.

As mentioned in the previous section, the specificity in protein–nucleic acid interactions would arise from the suitable combinations of preferred hydrogen bonds between their components which are supported by the three-dimensional structure of macromolecule. It is important to examine if the hydrogen bonding found in the present model crystal could be applied to the binding of the amino acid side chain with bases in a particular secondary or tertiary structure of nucleic acid.

The Hoogsteen base pair commonly exists between U8 and A14 residues in t-RNA for which, it is known,

** 1 cal=4.186 J.

aminoacylsynthetase,[32] elongation factor Tu,[33] ethidium bromide[34] and Mg^{2+} ion[35] can be accessible. Based on the geometry of the present hydrogen bond, model fitting of the dissociated carboxyl group into the t-RNA^{phe} molecule[36] was tried by interactive computer graphics. The carboxyl group is close to the G20 residue which does not form a pair with other bases. X-Ray studies have shown that this residue, located at the surface of the molecule, is mobile even in crystalline state.[37] If the guanine moiety of G20 is rotated by 60° around its glycosidic bond (the resulting χ^{CN} of 51.2° is within the range reported for purine nucleosides and nucleotides[38]), there is no abnormal contacts between atoms. Therefore, the present binding could be justified as one of possibilities of the extention from the model crystal structure to the protein-nucleic acid interactions.

Recently, it has been reported that the carbamoyl group is also hydrogen-bonded to N(1) of adenine in the normal Hoogsteen base pair between adenine and thymine in the crystalline complex of 9-(2-carbamoylethyl)adenine:1-methylthymine.[14] So, N(1) of adenine may be a preferential binding site in the normal and reversed Hoogsteen pairs.

The present work was supported in part by a Grant-in-Aid for Scientific Research No. 57380026 from the Ministry of Education, Science and Culture, and Kawakami Foundation, to which the authors' thanks are due. A part of calculation was carried out on a HITAC M200 at the Computer Center of the Institute for Molecular Science.

References

1) "The Mechanism of Protein Synthesis and Its Regulation," ed by L. Bosch, North-Holland Publishing Company, Amsterdam, London (1972).
2) W. F. Anderson, D. H. Ohlendorf, Y. Takeda, and B. W. Matthews, *Nature (London)*, **290**, 754 (1981).
3) C. O. Pabo and M. Lewis, *Nature (London)*, **298**, 443 (1982).
4) D. B. Mckay and T. A. Steitz, *Nature (London)*, **290**, 744 (1981).
5) D. H. Ohlendorf, W. F. Anderson, R. G. Fisher, Y. Takeda, and B. W. Matthews, *Nature (London)*, **298**, 718 (1982).
6) D. M. Segal, E. A. Padlan, G. H. Cohen, S. Rudikoff, M. Potter, and D. R. Davies, *Proc. Natl. Acad. Sci. U.S.A.*, **71**, 4298 (1974); H. Frauenfelder, G. A. Petsko, and D. Tsernoglou, *Nature (London)*, **280**, 558 (1979); J. Baldwin and C. Chothia, *J. Mol. Biol.*, **129**, 175 (1979).
7) M. Ohki, A. Takenaka, H. Shimanouchi, and Y. Sasada, *Bull. Chem. Soc. Jpn.*, **48**, 848 (1975).
8) M. Ohki, A. Takenaka, H. Shimanouchi, and Y. Sasada, *Bull. Chem. Soc. Jpn.*, **50**, 2573 (1977).
9) A. Takenaka, M. Ohki, and Y. Sasada, *Bull. Chem. Soc. Jpn.*, **53**, 2724 (1980).
10) A. Takenaka and Y. Sasada, 38th National Meeting of the Chemical Socirty of Japan, Nagoya, October 1978, Abstr. 1004.
11) A. Takenaka and Y. Sasada, *Bull. Chem. Soc. Jpn.*, **55**, 680 (1982).
12) S. Fujita, A. Takenaka, and Y. Sasada, *Acta Crystallogr., Sect. B*, **38**, 2936 (1982).
13) M. Takimoto, A. Takenaka, and Y. Sasada, *Bull. Chem. Soc. Jpn.*, **54**, 1635 (1981).
14) M. Takimoto, A. Takenaka, and Y. Sasada, *Bull. Chem. Soc. Jpn.*, **55**, 2734 (1982).
15) T. Ishida, M. Inoue, A. Ota, and T. Kurihara, *J. Chem. Soc., Chem. Commun.*, **1980**, 1074.
16) R. Destro and R. E. Marsh, *Acta Crystallogr., Sect. B*, **28**, 2971 (1972).
17) K. Kondo, T. Sato, and K. Takemoto, *Chem. Lett.*, **1973**, 967.
18) Lists of structure factors, anisotropic thermal parameters and least-squares plane equations and deviations of atoms from these planes have been deposited as Document No. 833, at the office of the Chemical Society of Japan.
19) "International Tables for X-ray Crystallography," Kynoch Press, Birmingham (1974), Vol. IV, p. 71.
20) K. Shikata, T. Ueki, and T. Mitsui, *Acta Crystallogr., Sect. B*, **29**, 31 (1973).
21) T. J. Kistenmacher and T. Shigematsu, *Acta Crystallogr., Sect. B*, **30**, 166 (1974).
22) H.-S. Shieh and D. Voet, *Acta Crystallogr., Sect. B*, **31**, 2192 (1975).
23) V. Langer, K. Huml, and L. Lessinger, *Acta Crystallogr., Sect. B*, 34, 2229 (1978).
24) B. E. Hingerty, J. R. Einstein, and C. H. Wei, *Acta Crystallogr., Sect. B*, **37**, 140 (1981).
25) J. Sletten and L. H. Jensen, *Acta Crystallogr., Sect. B*, **25**, 1608 (1969).
26) T. D. Sakore, S. S. Tavale, and H. M. Sobell, *J. Mol. Biol.*, **43**, 361 (1969).
27) L. Katz, K. Tomita, and A. Rich, *Acta Crystallogr.*, **21**, 754 (1966).
28) A. E. Haschemeyer and H. M. Sobell, *Acta Crystallogr.*, **18**, 525 (1965).
29) J. A. Pople and G. A. Segal, *J. Chem. Phys.*, **44**, 3289 (1966).
30) Ph. Hermann and E. Fredericq, *Nucleic Acids Res.*, **4**, 2939 (1977).
31) T. Miyazawa, private communication.
32) S. Yamashiro-Matsumura and M. Kawata, *J. Biol. Chem.*, **256**, 9308 (1981).
33) S. Bertram and R. Wagner, *Biochem. Int.*, **4**, 117 (1982).
34) M. Liebman, J. Rubin, and M. Sundaralingam, *Proc. Natl. Acad. Sci. U. S. A.*, **74**, 4821 (1977).
35) S. R. Holbrook, J. L. Sussman, R. W. Warrant, G. M. Church, and S.-H. Kim, *Nucleic Acids Res.*, **4**, 2811 (1977).
36) F. C. Bernstein, T. F. Koetzle, G. J. B. Williams, E. F. Meyer, J. M. D. Brice, J. R. Rodgers, O. Kennard, T. Shimanouchi, and M. Tasumi, *J. Mol. Biol.*, **112**, 535 (1977).
37) C. D. Stout, H. Mizuno, S. T. Rao, P. Swaminathan, J. Rubin, T. Brennan, and M. Sundaralingam, *Acta. Crystallogr., Sect. B*, **34**, 1529 (1978).
38) C. Altona and M. Sundaralingam, *J. Am. Chem. Soc.*, **94**, 8205 (1972).

Pressure-Volume-Temperature Relations and Isotropic-nematic Phase Transitions for 4-(*trans*-4-Pentylcyclohexyl)benzonitrile

Hajime Ichimura, Toshiaki Shirakawa,* Taneki Tokuda, and Tsutomu Seimiya
Department of Chemistry, Faculty of Science, Tokyo Metropolitan University, Setagaya-ku, Tokyo 158
(Received April 7, 1983)

Pressure-volume isotherms of 4-(*trans*-4-pentylcyclohexyl)benzonitrile were directly measured by means of piston-cylinder method at various temperatures. From the relation of the molar volume and the transition temperature which was determined by its clearing point, the parameter $\partial \ln T_c/\partial \ln V_c$, was found to assume a value of -5.24, which should be closely related with the intermolecular potential energy. The value of this parameter increased correlatively with the alkyl chain length in the homologous series of 4-(*trans*-4-alkylcyclohexyl)benzonitriles.

The liquid crystal molecules generally have a long and thin rod-like structure. The straight-chain hydrocarbon molecule also has a similar linear structure, however, it never shows liquid crystalline behavior. The characteristic difference between them lies in the flexibility of the linear structure. The flexibility of the straight-chain hydrocarbon molecule is dustributed uniformly over an entire molecule, while an ordinary liquid crystal molecule is roughly regarded to consist of two characteristic parts. One is a flexible part such as chain structure and the other is a rigid core part such as aromatic ring group. Such morphological classification of liquid crystal molecule is well known in the practical application field, whereas it has still been unsuccessful in phase transition theory to take the characteristic chemical structure into account.

Several phase transition theories have hitherto been proposed to explicate the nematic-isotropic phase transition. The intermolecular potential function assumed in those theories is roughly divided into the contributions of two parts, one is the orientation dependent part and the other is the volume dependent part. The volume dependent part determines the type of interaction which is dominant in the nematic-isotropic phase transition. From the intermolecular potential function thus derived, the clearing temperature is expressed as a function of the volume at clearing point:

$$T_c \propto V_c^{-\gamma}. \quad (1)$$

The exponent γ in Eq. 1 differs by the type of interaction assumed in the theory. Equation 1 may be transformed into the following expression:

$$\gamma = -\frac{\partial \ln T_c}{\partial \ln V_c}. \quad (2)$$

In Maier-Saupe theory,[1] dispersion force is assumed as the intermolecular force, in which the value γ is calculated to be 2, while in Pople-Karasz theory,[2] γ become 4 where they assumed repulsive force. It is clear in Eq. 2 that the value γ can be determined from a series of *P-V-T* measurements for liquid crystalline substances from which the actual interaction operating among the liquid crystal molecules may be analyzed.

In this study, *P-V-T* relations were measured for 4-(*trans*-4-pentylcyclohexyl)benzonitrile, hereafter refered as 5PCH. The volume dependent part of the intermolecular potential energy was also discussed.

Experimental

5PCH of 99% purity (Merck and Co., Inc.) was used as obtained without further purification. Density of this sample was measured by Lipkin-Devison type pycnometer. *P-V-T* relations were measured by using a piston-cylinder apparatus shown in Fig. 1. Variation of the pressure was detected by a manganin pressure gauge mounted in the cylinder. The degree of compression of the sample was estimated by a differential transformer attached to one end of a piston. Both the analog output of the differential transformer and that of the manganin pressure gage were acquisited to a microcomputer after the proper amplification and digital conversion. The microcomputer also served to control an oil pressurizing pump to compress the sample at a predetermined sequence by monitoring these signals. The volume of the cylinder was about 10 cm^3. The details of the present computer-controlled apparatus for *P-V-T* measurement will appear elsewhere.[3] The error of measurements of pressures and volumes were with ± 0.03 MPa and $\pm 0.002\%$, respectively. The piston-cylinder apparatus was kept in air bath which was thermocontrolled within ± 0.01 K.

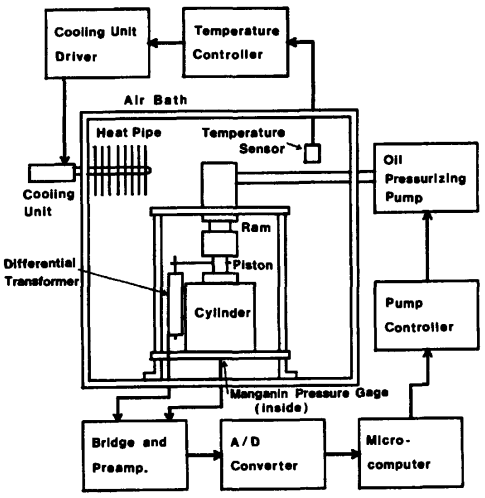

Fig. 1. The schematic diagram for the *P-V-T* measurement apparatus.

Results and Discussion

In Fig. 2, the density of 5PCH at atmospheric pressure is plotted as a function of temperature. The clearing temperature is read to be 327.59 ± 0.08 K from the

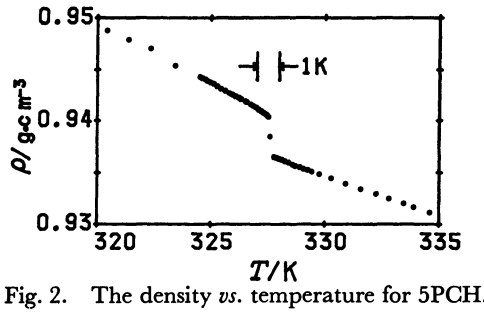

Fig. 2. The density *vs.* temperature for 5PCH.

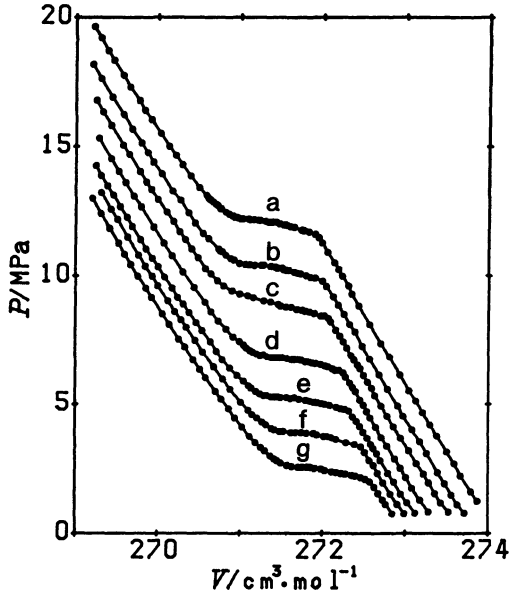

Fig. 3. The pressure-volume isotherms for 5PCH near the clearing transition. a: 333.19, b: 332.24, c: 331.40, d: 330.49, e: 329.79, f: 329.20, g: 328.60 K.

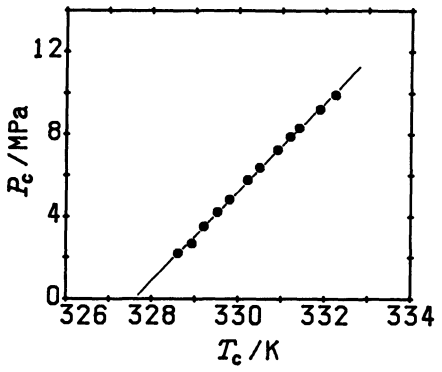

Fig. 4. The transition pressure *vs.* temperature for 5PCH.

figure. Transition occurs sharply within the temperature range of about 0.2 K. Figure 3 shows the series of pressure-volume isotherms for 5PCH in the vicinity of a clearing point at various temperatures. The plots are approximately linear in the isotropic side, and slightly curved in the nematic side. Drastic volume change at the transition is clearly observed. The molar volume at a clearing point decreased as temperature increased. From these isotherms, the pressure at a clearing point is obtained and plotted in Fig. 4 as a function of temperature. The plots show almost linear relation with a slope of 2.09 ± 0.02 MPa/K. The clearing temperature at atmospheric pressure is estimated by extrapolation to be 327.55 ± 0.03 K. This value agrees well with that obtained by the density measurement shown in Fig. 2. Figure 5 shows a full logarithmic plot of the temperature and the molar volume relation at a clearing point. The slope of this curve, $\partial \ln T_c/\partial \ln V_c$, is estimated to be -5.24 ± 0.09.

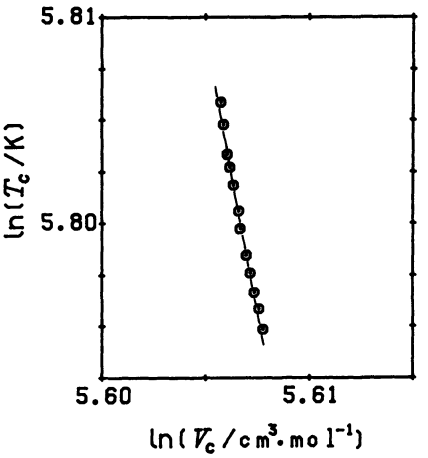

Fig. 5. The transition temperature *vs.* molar volume for 5PCH.

According to Maier-Saupe theory,[1] the intermolecular potential energy is expressed as follows:

$$U = -\frac{A}{2V^2}\cdot S\cdot(3\cos^2\theta - 1), \tag{3}$$

where V is the molar volume, A is the constant which is independent of pressure, volume and temperature, θ is the angle the long axis of molecule forms with the uniaxial direction of medium, and S is an order parameter. At the transition point, following well-known equation is obtained:

$$T_c = \frac{A}{4.541\, kV_c^2}. \tag{4}$$

Equation 4 indicates that the transition temperature is inversely proportional to the square of molar volume at the transition point. The value of γ as calculated from Eqs. 2 and 4 is found to be 2. This value does not agree with our experimentally observed value.

Pople and Karasz have also proposed a theory[2] which is an extension of Lennard-Jones and Devonshire model of melting. They assumed the anisotropic intermolecular potential energy to be expressed by

$$W = W_0\left(\frac{V_0}{V}\right)^4, \tag{5}$$

where W_0 and V_0 are constants. The transition temperature is expressed in their theory as follows:

$$T_c = \frac{zW(2S-1)}{2k\ln\dfrac{S}{1-S}}, \tag{6}$$

where z is the coordination number of a given molecule and S is the order parameter at the transition. The substitution of Eq. 5 in Eq. 6 leads to the relation in

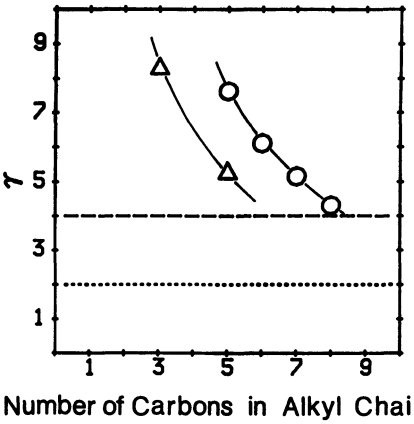

Fig. 6. The value γ *vs.* carbon number in alkyl chain. —○—: Data for CB series, —△—: data for PCH series, ·····: Maier-Saupe model, ------: Pople-Karasz model.

which the transition temperature is inversely proportional to the fourth power of the molar volume at the transition point, which means that γ assumes the value 4. This value is much closer to ours than that calculated after Maier-Saupe theory. Hence, our observation seems to indicate that the repulsive interaction should have a dominant contribution to the nematic-isotropic transition. Some liquid crystals, however, show rather big γ value,[5,6] which do not agree with Pople-Karasz theory.

It was also found in the recent study[5] that the value γ decreases with increasing alkyl chain length for homologous series of 4′-alkyl-4-cyanobiphenyls (abbreviated as CB series). The value γ is plotted against the carbon number of alkyl chain for CB series and PCH series in Fig. 6,[4-6] and compared to above-mentioned values theoretically predicted. The dotted and the dashed horizontal lines each represents the expected relation by the Maier-Saupe and the Pople-Karasz theories, respectively. These lines show constant γ values which are independent of carbon number. The value γ for PCH series varies in a similar manner as that for CB series.

There have been several attempts in the theories to take into account the molecular shape factor to interpret the properties of the nematic-isotropic phase transition. The typical one may be represented by scaled particle theory.[7] Savithramma and Madhusudana have extended the Andrews method of deriving thermodynamic properties of an assembled particles, and compared their results with those obtained on the basis of scaled particle theory.[8] The common feature of both theories is the assumption that molecules are good regarded as rigid spherocylinders. Their calculations showed that the value γ assumes the value close to 4 for a spherocylinders having particular length to breadth ratio. This value seems to be in reasonably good agreement with the experimental data for 4,4′-azoxydianisole.[9] Their results, however, contrary to ours show that the value γ becomes exceedingly greater as the length to breadth ratio of molecule increases. Our experimental data indicates that the value γ becomes smaller as the molecule lengthens. They assumed the shape of molecule to be the spherocylinder. This is the obvious reason why their theoretical calculation showed inverse tendency against the experimental data, because it will not be favorable to assume rigid rod for the actual liquid crystal molecule.

As mentioned earlier, a liquid crystal molecule generally considered to be made up of a core part and a chain part. In homologous series of a compound PCH we have chosen, the core part of molecule is the same: For example, each molecule has a cyclohexylbenzonitrile core shown below. For the core parts are the same, the

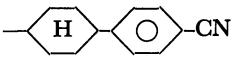

variation of γ in a homologous series may be attributed to the difference in the alkyl chain parts. An alkyl chain has a conformational freedom, because it is made of linear framework of C–C single bonds. As the length of a chain increases, the conformational freedom increases. Therefore, decrease of γ in Fig. 6 may be caused by the increased flexibility of alkyl chain part. It should be noted next that the difference in the values γ between 5CB and 5PCH may be rendered to the structural difference of their core parts. The core part of CB series is made of a biphenyl structure. The core part of PCH series includes cyclohexane ring. The conformational freedom for the core of CB series should be lower than that of PCH. The value γ for 5CB is 7.62,[5] while that for 5PCH is 5.24, the difference is comparable to that between 5CB and 6CB, and is attributed to the change of flexibility between benzene ring and cyclohexane ring. Perrin and Bergès reported lately that the flexibility of the core is comparable to that of the alkyl chain.[10]

Though the evaluation of the effect of flexibility on liquid crystal formation still needs further analysis, it is clear that the value γ is closely related to the conformational character of liquid crystal molecule: Especially, the flexibility of alkyl chain part and that of core part where it plays an important role in the nematic-isotropic phase transition.

References

1) W. Maier and A. Saupe, *Z. Naturforsch.*, *A*, **14**, 882 (1959).
2) J. A. Pople and F. E. Karasz, *J. Phys. Chem. Solids*, **18**, 28 (1961).
3) T. Shirakawa and H. Ichimura, manuscript in preparation.
4) T. Shirakawa, T. Inoue, and T. Tokuda, *J. Phys. Chem.*, **86**, 1700 (1982).
5) T. Shirakawa, T. Hayakawa, and T. Tokuda, *J. Phys. Chem.*, **87**, 1406 (1983).
6) T. Shirakawa, M. Arai, and T. Tokuda, *Mol. Cryst. Liq. Cryst.*, submitted.
7) M. A. Cotter, *J. Chem. Phys.*, **66**, 1098 (1977).
8) K. L. Savithramma and N. V. Madhusudana, *Mol. Cryst. Liq. Cryst.*, **62**, 63 (1980).
9) J. R. McColl and C. S. Shih, *Phys. Rev. Lett.*, **29**, 85 (1972).
10) H. Perrin and J. Bergès, *J. Phys. (Paris), Lett.*, **43**, 531 (1982).

 © 1983 The Chemical Society of Japan Bull. Chem. Soc. Jpn., 56, 2241—2249 (1983)

Syntheses, Structure, and Properties of Several Bis{(alkylthio)acetato}copper(II)-Amine Adducts[1)]

Akira Ouchi,* Yoshiyuki Sato, Yasuhiko Yukawa,† and Toshio Takeuchi†

Department of Chemistry, College of Arts and Sciences, The University of Tokyo, Komaba 3-8-1, Meguro-ku, Tokyo 153

†*Department of General Sciences, Faculty of Science and Technology, Sophia University, Kioi-cho 7, Chiyoda-ku, Tokyo 102*

(Received October 30, 1982)

The crystal and molecular structure of tetrakis{(isopropylthio)acetato}bis(quinoline)dicopper(II) (**1**), bis(dibenzylamine)bis{(ethylthio)acetato}copper(II) (**2**), and bis{(isopropylthio)acetato}tris(isoquinoline)copper(II) (**3**) were determined by the X-ray diffraction method. The final R values obtained are 0.041, 0.055, and 0.078 for **1**, **2**, and **3** respectively. **1** is green in color and is orthorhombic with the space group Pcab. It has a dimer structure similar to that of the copper(II) acetate hydrate, where four (alkylthio)acetate liagnds bridge both copper(II) atoms. **2** is violet in color and is monoclinic with the space group A2/a. It has a square-palnar geometry, and no atoms are coordinated to the copper(II) atom from the axial direction, probably because of the steric effect of the large dibenzylamine molecules. **3** is blue in color and is triclinic with the space group P$\bar{1}$. It has potentially a hepta-coordinate geometry, where one nitrogen atom and two oxygen atoms ligate from the axial direction of the CuN_2O_2 plane.

(Alkylthio)acetic acids are interesting ligands, as they have a carboxyl group as well as a sulfide sulfur atom which can be coordinated to a metal atom. In the cases of cobalt(II) or copper(II) (alkylthio)acetate dihydrates, the ligand is bidentate, forming a five-membered chelate ring by the coordination of its oxygen and sulfur atoms.[2-4)] On the other hand, in the anhydrous cobalt(II) (propylthio)acetate hexamer, it was found that the ligands bridge the metal atoms; half of them bridge two cobalt atoms by both of the carboxyl oxygen atoms, while the other half bridge three cobalt atoms with both of carboxyl oxygen and the sulfide sulfur atoms.[5)]

This time, the authors planned the synthesis of the anhydrous copper(II) (alkylthio)acetate. However, the dehydration of the hydrated copper(II) (alkylthio)acetates by the azeotropic method, *i.e.*, evaporating the benzene–alcohol solution to dryness as in the cases of cobalt(II) or nickel(II) salts, was not successful; the copper(II) salts were destroyed during the process. On the other hand, when quinoline or some such kind of amine was added to the solution before the evaporation process, the water in the complex was completely replaced by the amine, and their mono-, bis-, and tris-(amine) adducts were obtained without decomposing the (alkylthio)acetate ligand. They are easily soluble in nonpolar solvents such as benzene, and they are stable in air. Each of them has a characteristic color; *i.e.*, the mono(amine) adducts are green; the bis(amine) adducts, violet, and the tris(amine) adducts, blue. The absorption coefficients of their benzene solution (containing excess of amine) are rather high (about 150—200 $cm^{-1}\,mol^{-1}\,dm^3$) compared with those of the common copper(II) salts. Therefore, it seems that it would be interesting to clarify their geometries around the copper(II) atom, and so we began to study their structures by means of the X-ray diffraction technique.

Experimental

Synthesis of Tetrakis{(isopropylthio)acetato}bis(quinoline)dicopper(II) (1) and the Related Mono(amine) Adduct Dimers. The ligand, (isopropylthio)acetic acid, was obtained by a condensation reaction between 2-bromopropane and mercaptoacetic acid (Larsson's method).[6)] The copper(II) (isopropylthio)acetate dihydrate was obtained according to the method described in early papers.[7)] (The other ligands and the starting copper(II) salts were obtained similarly.) The hydrated copper(II) salt (violet isomer) (0.55 g, 1.5 mmol) and quinoline (0.40 g, 3.1 mmol) were boiled with about 10 cm^3 of benzene for several minutes, and then cooled. Then the supernatant fluid was separated into another open vessel; the water in the hydrate remained on the wall of the original vessel. About 10 cm^3 of petroleum benzine was then added, and the mixture was left standing for several hours. The deposited crystals were filtered off, washed with a small portion of benzene–petroleum ether mixture (1 : 1=v/v), and dried in a vacuum desiccator (yield, 0.47 g, 68%). They were purified by reprecipitation: the product was dissolved into benzene containing an excess of quinoline, and the solution in an open vessel was left standing in petroleum benzine vapor (in a desiccator) for several days to obtain the crystals.

The other mono(amine) adduct dimers with the formula of $[Cu_2(RSCH_2CO_2)_4(amine)_2]$ (where R=CH_3, C_2H_5, or $(CH_3)_2CH$, and amine=quinoline, isoquinoline, or pyridine) were obtained similarly; their yields were comparable to that of **1**.

Synthesis of Bis(dibenzylamine)bis{(ethylthio)acetato}copper(II) (2). Diaquabis{(ethylthio)acetato}copper(II) (0.50 g, 1.5 mmol) and dibenzylamine (1.2 g, 6.0 mmol) were boiled in 5 cm^3 of benzene, and they dissolved. The supernatant fluid was mixed with 5 cm^3 of petroleum benzine in a beaker, after which the mixture was left standing overnight in petroleum benzine vapor (in a desiccator). A deep violet product was thus precipitated (yield, 0.73 g, 70%). It was purified by the reprecipitation process (see the process for **1**). The same type of adducts were similarly obtained using (methylthio)- or (isopropylthio)acetate of copper(II) in place of the (ethylthio)-acetate mentioned above.

Synthesis of Bis{(isopropylthio)acetato}bis(isoquinoline)copper(II). Bis{(isopropylthio)acetato}copper(II) dihydrate (violet isomer) (0.55 g, 1.5 mmol) and isoquinoline (0.40 g, 3.1 mmol), were dissolved into about 5 cm^3 of a benzene–ligroine mixture (1 : 1=v/v) by heating them. To the supernatant fluid, about 15 cm^3 of ligroine was then added. After the mixture had been left standing for several hours, a violet precipitate was deposited; the precipitate was filtered off and washed with

Table 1. Analyses and magnetic moments of the complexes, $[Cu(RSCH_2CO_2)_2(amine)_n]$**

n	R	Amine		Cu (%)	C (%)	H (%)	N (%)	μ_{eff} a) / BM
1	CH_3	Isoquinoline	Found	15.55	45.61	4.29	3.40	1.3_6
			Calcd	15.77	44.71	4.25	3.48	
1	CH_3	Quinoline	Found	15.59	45.03	4.28	3.56	1.3_2
			Calcd	15.77	44.71	4.25	3.48	
1	CH_3	Pyridine	Found	17.78	37.05	4.20	3.89	1.4_2
			Calcd	18.01	37.44	4.28	3.97	
1	C_2H_5	Isoquinoline	Found	14.89	47.52	4.98	3.14	1.3_5
			Calcd	14.74	47.37	4.91	3.25	
1	C_2H_5	Quinoline	Found	14.90	47.36	4.91	3.21	1.3_8
			Calcd	14.74	47.37	4.91	3.25	
1	C_2H_5	Pyridine	Found	16.63	41.20	5.08	3.64	1.4_1
			Calcd	16.68	40.99	5.03	3.68	
1	$(CH_3)_2CH$	Isoquinoline	Found	13.66	49.88	5.54	3.05	1.3_8
			Calcd	13.84	49.71	5.49	3.05	
1	$(CH_3)_2CH$	Quinoline	Found	13.61	50.00	5.56	3.08	1.3_3
			Calcd	13.84	49.71	5.49	3.05	
2	CH_3	Dibenzylamine	Found	9.30	61.36	6.07	4.18	1.7_3
			Calcd	9.51	61.10	6.03	4.19	
2	C_2H_5	Dibenzylamine	Found	9.19	61.70	6.35	4.02	1.7_6
			Calcd	9.12	62.09	6.37	4.02	
2	$(CH_3)_2CH$	Isoquinoline	Found	10.70	57.23	5.63	4.58	1.7_9
			Calcd	10.80	57.17	5.48	4.76	
2	$(CH_3)_2CH$	Dibenzylamine	Found	8.51	62.82	6.68	3.60	1.6_9
			Calcd	8.77	63.00	6.68	3.87	
3	CH_3	Isoquinoline	Found	10.00	57.63	4.60	6.08	1.8_2
			Calcd	9.61	57.94	4.73	6.35	
3	C_2H_5	Isoquinoline	Found	9.16	60.68	5.07	5.83	1.8_2
			Calcd	9.22	60.98	5.12	6.10	
3	$(CH_3)_2CH$	Isoquinoline	Found	9.09	62.07	5.46	5.84	1.8_5
			Calcd	8.86	61.95	5.48	5.86	

a) 1 BM$=9.274078(36)\times10^{-24}$ J T^{-1}.
** Mono (amine) adducts are shown by the experimental formula.

ligroine (yield 0.50 g, 57%). When isoquinoline is present in a large excess, and when the volume ratio of benzene to ligroine of the mixed solvent is high, only the blue tris(isoquinoline) adduct was obtained. On the other hand, when the amount of added isoquinoline was less than twice that of the starting copper(II) salt in mol/mol, only the green mono(isoquinoline) adduct was obtained. No bis(amine) adduct was obtained by using quinoline in place of isoquinoline.

Synthesis of Bis{(isopropylthio)acetato}tris(isoquinoline)copper(II) (3). Bis{(isopropylthio)acetato}copper(II) (violet isomer) (0.55 g, 1.5 mmol) and isoquinoline (1.0 g, 7.8 mmol) were boiled with 5 cm^3 of benzene, and they dissolved. The supernatant fluid was mixed with 8 cm^3 of ligroine, after which the mixture was left standing for several hours until blue crystals were precipitated (yield, 0.7 g, 65%). The crude product was recrystallized from toluene–ligroine (1 : 1.5=v/v) containing about 2 mol dm^{-3} of isoquinoline.

The same type of complexes were also obtained using (methylthio)- or (ethylthio)acetato of copper(II) and/or pyridine in place of the starting materials mentioned above, but the pyridine adducts were unstable and they lost pyridine even when they were washed with petroleum benzine, changing into green mono(amine) adduct dimers. Even when the blue pyridine adduct crystals obtained without washing were kept in a bottle at room temperature, they decomposed within several days. The same type of adducts were not obtained using quinoline.

Their analyses and the magnetic moments as measured by means of Gouy balance at room temperature (15—20 °C), are shown in Table 1. The yields of the complexes were between 55 and 68%.

Single-crystal X-Ray Analyses. The crystals used were in the shape of parallelepipeds (**1**, $0.3\times0.3\times0.2$ mm^3; **2**, $0.3\times0.3\times0.3$ mm^3; and **3**, $0.3\times0.3\times0.4$ mm^3). All their edges were ground off, though they were not shaped into perfect spheres. The reflections within the range of $2\theta<55°$ were collected on a Philips PW 1100 automated four-circle diffractometer with graphite monochromated Mo $K\alpha$ radiation (0.7107 Å), the θ-2θ scan technique being employed (scan speed 4° min^{-1}; scan width, $1.0+0.3\tan\theta$°). The intensities were corrected for Lorentz and polarization factors, but no correction was made for absorption and extinction. As a representative bis(amine) adduct, bis(dibenzylamine)bis{(isopropylthio)acetato}copper(II) had been studied first, because **1** and **3** are the adducts of (isopropylthio)acetates and it was thought to be convenient to compare its data with those of the other types of adducts. However, the attempt was not successful, because the complex was decomposed under the X-ray radiation within several hours. On the other hand, the crystals of **2** did not decompose even under X-ray radiation for several weeks.

The crystallographic and X-ray measurement data of **1**, **2**, and **3** are as follows:

1. $Cu_2C_{38}H_{50}S_4O_8N_2$, F.W.=918.17; orthorhombic; space group Pcab (The systematic absences of the reflections were

those of $kk0(k=\text{odd})$, $0kl(l=\text{odd})$, and $h0l(h=\text{odd})$; $a=17.525(6)$, $b=28.068(18)$, $c=8.870(4)$ Å, $Z=4$,[8] $D_m=1.40(3)$, $D_x=1.38$ g cm^{-3}, μ(Mo $K\alpha$)$=1.24$ mm^{-1}. In total, 2323 independent reflections with $|F_o|>3\sigma(|F_o|)$ among the 2485 measured ones were used for the structure refinement.

2. $CuC_{36}H_{44}S_2O_4N_2$, F.W.$=696.43$; monoclinic; space group A2/a (the systematic absences of the reflections were $hkl(k+l=\text{odd})$ and $h0l(h=\text{odd})$; $a=19.235(8)$, $b=11.944(2)$, $c=17.137(5)$ Å, $\beta=111.13(3)°$, $Z=4$, $D_m=1.26(2)$, $D_x=1.25$ g cm^{-3}, μ(Mo $K\alpha$)$=0.592$ mm^{-1}. In total, 2090 independent reflections with $|F_o|>3\sigma(|F_o|)$ among the 2188 measured ones were used for the structure determination.

3. $CuC_{37}H_{39}S_2O_4N_2$, F.W.$=717.41$; triclinic; space group P$\bar{1}$; $a=11.550(10)$, $b=16.912(6)$, $c=9.792$ Å, $\alpha=100.32(5)$, $\beta=109.96(13)$, $\gamma=79.50(5)°$, $Z=2$, $D_m=1.36(2)$, $D_x=1.34$ g cm^{-3}, μ(Mo $K\alpha$)$=0.553$ mm^{-1}. In total, 3404 independent reflections with $|F_o|>3\sigma(|F_o|)$ among the 3832 measured ones were used for the structure refinement.

The Structure Determination. The calculations were carried out on a HITAC M200H computer at the Computer Center of The University of Tokyo, using the local version of the UNICS program.[9]

The atomic scattering factors were taken from the tables.[10] The structure was solved by the heavy-atom method. The positional and thermal parameters were refined by the block-diagonal least-squares method. The positions of several hydrogen atoms were obtained from a difference Fourier synthesis, and some others, by calculation on the assumption of C–H$=1.0$ Å; they were also refined assuming $B_{iso}=8.0$. In the last cycle of the refinement, all the parameter shifts were less than $\sigma/3$'s. The final R values[11] were 0.041, 0.055, and 0.078 for **1**,**2**, and **3** respectively.

The Spectroscopic Measurements. The infrared absorption spectra of the samples were obtained by means of a JASCO 403G infrared spectrophotometer, using nujol and hexachloro-1,3-butadiene mull.

The visible absorption spectra in a benzene solution, and the reflectance spectra of their solids, were measured by means of a Hitachi 124 spectrophotometer.

Results and Discussion

The final atomic parameters of non-hydrogen atoms are listed in Table 2, while their interactomic distances and bond angles are tabulated in Table 3.[12] A perspective drawing of each complex and the numbering scheme are shown in Figs. 1, 2, and 3.

No abnormal intermolecular contact is found in the crystal structures of **1**—**3**.

As is shown in Fig. 1, the **1** complex has a dimer structure, in which four (isopropylthio)acetate ions bridge two copper atoms. The complex has a center of symmetry at the middle point of the Cu–Cu bond (2.676(4) Å).

All of the Cu–O bond lengths are normal (1.964(5)—1.981(5) Å).[13] The average plane of the CuO_4 is shown by this equation:

$$-0.651x - 0.729y - 0.211z + 1.164 = 0$$

(where x, y, z, are taken in the a-, b-, and c-axis directions respectively and are shown in Å units), and the distances from the average plane are: Cu, −0.174; O(12), 0.051; O(22), 0.052; O(11^I), 0.050; and O(21^I), 0.052 Å. Thus, the Cu atom deviates a little to the N(31) side from the plane. The ∠Cu^I–Cu–N(31) is about 8° less than 180°, and ∠O–Cu–N(31) are in the 90.84(12)—102.18(13)° range. The Cu–N(31) (2.222(6) Å) is a little longer than the common Cu–N bond (2.00 Å).[13] The dihedral angle between the CuO_4 plane and the quinoline one is 81.5°. Both of the carboxyl groups of the carboxylate ligands are almost symmetric. Neither of the sulfur atoms, S(1) and S(2), is coordinated. Thus, the structure is similar to that of tetrakis(acetato)-diaquadicopper(II) or some such bis(amine)tetrakis-(carboxylato)copper(II) dimers;[14] and the bond lengths and bond angles of **1** are comparable to those of the dimers.

The complexes with the same chemical formula, $[Cu(RSCH_2CO_2)_4(amine)_2]$, where amine=isoquinoline or pyridine, are expected to have similar structures, though those of some aromatic amines are expected to have different structures, as has been shown for bis-(propionato)-*p*-toluidinecopper(II).[15]

Table 2. Final atomic coordinates ($\times 10^4$) and equivalent isotropic temperature factors (B/Å^2) of non-hydrogen atoms, with estimated standard deviations in parentheses

(1) Tetrakis{(isopropylthio)acetato}bis(quinoline)dicopper(II)

Atom	x	y	z	B_{eq}/Å^2 [a]	Atom	x	y	z	B_{eq}/Å^2 [a]
Cu	493.5(3)	352.9(2)	279.9(6)	2.8	C(23)	−1417(3)	1554(2)	521(6)	4.6
S(1)	545(1)	−1322(1)	3920(2)	4.9	C(24)	−1740(4)	1877(2)	−686(6)	6.0
S(2)	−2114(1)	1088(1)	898(2)	4.4	C(25)	−1206(4)	1830(2)	1899(7)	5.7
O(11)	−65(2)	−648(1)	1540(4)	4.2	N(31)	1418(2)	859(1)	897(4)	3.0
O(12)	755(2)	−60(1)	2014(3)	3.6	C(32)	2011(3)	659(2)	1564(5)	3.6
O(21)	−1187(2)	29(1)	988(4)	4.2	C(33)	2604(3)	910(2)	2269(6)	4.4
O(22)	−369(2)	620(1)	1415(4)	3.8	C(34)	2580(3)	1387(2)	2249(6)	4.6
C(11)	465(2)	−458(2)	2276(5)	3.4	C(35)	1931(3)	2126(2)	1409(7)	5.4
C(12)	801(3)	−713(2)	3630(6)	4.9	C(36)	1363(4)	2337(2)	673(7)	5.6
C(13)	−469(3)	−1309(2)	4293(5)	4.4	C(37)	787(3)	2062(2)	−22(6)	5.0
C(14)	−688(4)	−1806(3)	4840(9)	8.4	C(38)	811(3)	1575(2)	78(5)	3.6
C(15)	−703(4)	−931(3)	5393(8)	8.1	C(39)	1405(2)	1346(2)	836(5)	3.0
C(21)	−1013(3)	428(2)	1515(5)	3.3	C(30)	1986(3)	1628(2)	1511(5)	3.8
C(22)	−1634(3)	714(2)	2265(6)	4.1					

a) The equivalent isotropic temperature factors for non-hydrogen atoms were computed using the following expression: $B_{eq}=4/3(B_{11}a^2+B_{22}b^2+B_{33}c^2)$. The B_{ij}'s are defined by: $\exp[-(h^2B_{11}+k^2B_{22}+l^2B_{33}+2klB_{23}+2hlB_{13}+2hkB_{12})]$.

(2) Bis(dibenzylamine)bis{(ethylthio)acetato}copper(II)

Atom	x	y	z	B_{eq}/Å^2 b)	Atom	x	y	z	B_{eq}/Å^2 b)
Cu	0.0	0.0	0.0	3.9	C(13)	−3174(3)	1419(5)	−2999(4)	6.7
S	1485(1)	−2958(2)	−678(1)	8.9	C(14)	−3219(3)	630(6)	−3591(4)	6.9
O(1)	479(2)	−1029(3)	−502(2)	6.0	C(15)	−2743(3)	−240(5)	−3400(4)	7.5
O(2)	−372(2)	−1528(3)	−1706(2)	6.4	C(16)	−2217(3)	−340(5)	−2621(4)	6.4
N	−796(2)	455(3)	−1098(2)	4.0	C(20)	−655(3)	1596(4)	−1341(3)	4.9
C(1)	266(3)	−1509(4)	−1200(3)	4.5	C(21)	133(3)	1694(4)	−1310(3)	4.9
C(2)	889(3)	−2020(5)	−1427(3)	6.3	C(22)	669(3)	2203(5)	−640(4)	7.3
C(3)	1005(5)	−4298(7)	−1024(6)	12.7	C(23)	1408(3)	2279(7)	−615(5)	9.8
C(4)	342(5)	−4355(8)	−827(7)	14.9	C(24)	1592(3)	1827(6)	−1227(5)	9.4
C(10)	−1574(3)	305(4)	−1137(3)	4.9	C(25)	1083(4)	1324(6)	−1879(4)	8.1
C(11)	−2148(2)	433(4)	−1997(3)	4.4	C(26)	351(3)	1256(5)	−1923(3)	6.5
C(12)	−2636(3)	1324(5)	−2204(3)	5.4					

b) The equivalent isotropic temperature factors for non-hydrogen atoms were computed using the following expression: $B_{eq}=4/3(B_{11}a^2+B_{22}b^2+B_{33}c^2+B_{13}ac\cos\beta)$. The B_{ij}'s are defined by: $\exp[-(h^2B_{11}+k^2B_{22}+l^2B_{33}+2klB_{23}+2hlB_{13}+2hkB_{12})]$.

(3) Bis{(isopropylthio)acetato}tris(isoquinoline)copper(II)

Atom	x	y	z	B_{eq}/Å^2 c)	Atom	x	y	z	B_{eq}/Å^2 c)
Cu	5852(1)	2552(1)	3396(1)	2.8	C(36)	2860(9)	116(6)	5840(11)	4.6
S(1)	1776(2)	4455(2)	4081(3)	4.4	C(37)	2589(9)	−36(6)	4327(11)	4.4
S(2)	8243(3)	388(2)	1091(3)	4.6	C(38)	3087(8)	365(5)	3613(10)	3.7
O(11)	5298(5)	3551(3)	4575(6)	3.3	C(39)	3905(7)	936(5)	4425(9)	2.7
O(12)	3565(6)	3324(4)	2749(6)	4.0	C(30)	4186(7)	1093(5)	5965(9)	2.7
O(21)	6428(5)	1572(3)	2272(6)	3.0	C(41)	6737(8)	3775(5)	2325(9)	3.5
O(22)	4704(6)	1291(4)	468(7)	4.5	C(43)	5248(8)	3094(6)	519(10)	3.9
N(32)	5223(6)	1889(4)	4494(7)	2.7	C(44)	5293(9)	3517(6)	−542(10)	4.4
N(42)	5964(6)	3234(4)	1932(7)	3.1	C(45)	6246(10)	4551(6)	−1212(11)	4.6
N(52)	7872(7)	2502(4)	5104(7)	3.5	C(46)	7047(11)	5128(6)	−686(13)	6.1
C(11)	4129(8)	3698(5)	3934(9)	3.2	C(47)	7730(11)	5267(6)	739(12)	5.5
C(12)	3442(9)	4377(6)	4711(11)	4.3	C(48)	7644(11)	4839(6)	1777(11)	5.0
C(13)	1508(9)	3450(7)	4211(12)	5.2	C(49)	6834(9)	4251(5)	1303(10)	3.7
C(14)	120(11)	3457(8)	3803(16)	7.7	C(40)	6128(9)	4093(5)	−170(10)	3.8
C(15)	2167(14)	3185(8)	5723(16)	8.2	C(51)	8205(8)	3011(5)	6308(10)	3.6
C(21)	5850(8)	1180(5)	1076(9)	3.2	C(53)	8698(8)	1824(5)	4962(10)	3.7
C(22)	6583(9)	524(5)	321(10)	4.2	C(54)	9787(9)	1647(6)	6024(11)	4.4
C(23)	8715(9)	1337(6)	976(11)	4.7	C(55)	11290(9)	2030(7)	8522(11)	5.1
C(24)	10080(11)	1276(8)	1697(13)	6.5	C(56)	11554(11)	2557(7)	9760(11)	5.8
C(25)	8358(13)	1503(10)	−593(16)	9.6	C(57)	10745(11)	3265(7)	9891(12)	6.2
C(31)	4465(8)	1364(5)	3757(8)	3.0	C(58)	9636(10)	3435(6)	8805(11)	4.5
C(33)	5498(8)	2037(5)	5964(9)	3.2	C(59)	9339(8)	2878(6)	7477(9)	3.8
C(34)	5010(8)	1659(5)	6725(9)	3.2	C(50)	10147(8)	2177(6)	7337(9)	3.7
C(35)	3642(9)	659(5)	6671(10)	4.1					

c) The equivalent isotropic temperature factors for non-hydrogen atoms were computed using the following expression: $B_{eq}=4/3\,(B_{11}a^2+B_{22}b^2+B_{33}c^2+B_{12}ab\cos\gamma+B_{13}ac\cos\beta+B_{23}bc\cos\alpha)$. The B_{ij}'s are defined by: $\exp[-(h^2B_{11}+k^2B_{22}+l^2B_{33}+2klB_{23}+2hlB_{13}+2hkB_{12})]$.

As is shown in Fig. 2, the copper atom of **2** lies at the center of symmetry, forming a N_2O_2 tetra-coordinate square-planar complex. Both the Cu–O and Cu–N bond lengths are normal,[13] but the ∠O–Cu–N angle is 4.6° more than the right angle. Although the axially elongated octahedral geometry is the most common coordination site around a copper(II) ion, there are not many complexes with the pure square-planar configuration. In the case of bis(oxalato)copper(II), two oxygen atoms of other chelates are coordinated weakly from both the axial directions,[16] while in the cases of β-diketonates,[17–21] which are typical square-planar complexes, weak Cu–C bondings between the copper(II) and the γ-carbon atoms of other chelates were found. Recently, a long-distance interaction of the type was also reported in copper(II) metalaacetylacetonate.[22]

Especially in crystaline state, copper(II) complexes coordinated to four unidentate ligands arer are, although $Na_4[Cu^{II}(NH_3)_4][Cu^{I}(S_2O_3)_2]_2$,[23] $Cu(C_5H_5NO)_4X_2$ (where $X=BF_4$ or ClO_4),[24] and $Cu(diazepam)_2Cl_2\cdot 2H_2O\cdot 1/3\,CHCl_3$ (where diazepam=7-chloro-1,3-dihydro-1-methyl-5-phenyl-3*H*-1,4-benzodiazepin-2-one)[25] have been reported.

In the case of **2**, the phenyl rings of the ligand effectively block the axial coordination site, as in the case of the diazepam complex.[25] In **2**, all distances between any carbon atoms of a phenyl ring and any one of the other phenyl rings of the same dibenzylamine ligand are over 4.0 Å. From the molecular-structure-model study of the **2** complex, using the HGS model and assuming that

TABLE 3. INTERATOMIC DISTANCES AND BOND ANGLES, WITH ESTIMATED STANDARD DEVIATIONS IN PARENTHESES

(1) Tetrakis{(isopropylthio)acetato}bis(quinoline)dicopper(II)

Bond length	l/Å	Bond length	l/Å
Cu–Cu^{I}	2.676(4)	Cu–O(12)	1.981(5)
Cu–O(22)	1.964(5)	Cu–O(11^{I})	1.965(6)
Cu–O(21^{I})	1.971(6)	Cu–N(31)	2.222(6)
O(11)–C(11)	1.255(6)	O(12)–C(11)	1.248(6)
C(11)–C(12)	1.518(8)	C(12)–S(1)	1.786(6)
S(1)–C(13)	1.808(6)	C(13)–(14)	1.525(10)
C(13)–C(15)	1.498(10)	O(21)–C(21)	1.252(7)
O(22)–C(21)	1.254(6)	C(21)–C(22)	1.505(8)
C(22)–S(2)	1.812(7)	S(2)–C(23)	1.821(6)
C(23)C–(24)	1.515(9)	C(23)–C(25)	1.493(9)
N(31)–C(32)	1.323(7)	C(32)–C(33)	1.403(8)
C(33)–C(34)	1.338(8)	C(34)–C(30)	1.403(8)
C(30)–C(35)	1.403(8)	C(35)–C(36)	1.331(9)
C(36)–C(37)	1.411(9)	C(37)–C(38)	1.371(8)
C(38)–C(39)	1.397(7)	C(39)–C(30)	1.423(7)
C(39)–N(31)	1.368(6)		
Bond angle	ϕ/°	**Bond angle**	ϕ/°
Cu^{I}–Cu–O(22)	83.09(9)	Cu^{I}–Cu–O(12)	81.93(12)
Cu$_{I}$–Cu–O(11^{I})	85.02(9)	Cu^{I}–Cu–O(21^{I})	83.74(9)
Cu^{I}–Cu–N(31)	171.74(9)	O(12)–Cu–O(22)	90.18(12)
O(12)–Cu–N(31)	90.84(12)	O(22)–Cu–O(11^{I})	88.06(13)
O(11^{I})–Cu–O(21^{I})	89.77(13)	Cu–O(12)–C(11)	125.1(3)
Cu^{I}–O(11)–C(11)	122.1(3)	O(11)–C(11)–O(12)	125.8(4)
O(11)–C(11)–C(12)	119.9(4)	C(11)–C(12)–S(1)	118.0(4)
C(12)–S(1)–C(13)	104.7(2)	S(1)–C(13)–C(14)	106.8(4)
S(1)–C(13)–C(15)	113.7(4)	Cu–O(22)–C(21)	124.4(3)
Cu^{I}–O(21)–C(21)	123.3(3)	O(21)–C(21)–O(22)	125.3(4)
O(21)–C(21)–C(22)	117.7(4)	C(21)–C(22)–S(2)	110.4(3)
C(22)–S(2)–C(23)	103.2(2)	S(2)–C(23)–C(24)	108.0(4)
S(2)–C(23)–C(25)	112.8(4)	Cu–N(31)–C(32)	114.3(3)
N(31)–C(32)–C(33)	124.6(4)	C(32)–C(33)–C(34)	118.3(5)
C(33)–C(34)–C(30)	120.9(5)	C(34)–C(30)–C(39)	117.2(4)
C(39)–C(30)–C(35)	118.5(4)	C(30)–C(35)–C(36)	121.9(5)
C(35)–C(36)–C(37)	120.3(5)	C(36)–C(37)–C(38)	119.7(5)
C(37)–C(38)–C(39)	120.87(4)	C(38)–C(39)–C(30)	118.7(4)
C(39)–N(31)–C(32)	117.1(4)	N(31)–C(39)–C(30)	121.9(4)

Key to symmetry operations: I. $-x$, $-y$, $-z$.

(2) Bis(dibenzylamine)bis{(ethylthio)acetato}copper(II)

Bond length	l/Å	Bond length	l/Å
Cu–O(1)	1.916(5)	Cu–N	2.026(6)
O(1)–C(1)	1.255(9)	O(2)–C(1)	1.221(7)
C(1)–C(2)	1.513(10)	C(2)–S	1.776(8)
S–C(3)	1.836(9)	C(3)–C(4)	1.434(20)
N–C(10)	1.483(10)	N–C(20)	1.479(7)
C(10)–C(11)	1.498(10)	C(11)–C(12)	1.377(7)
C(11)–C(16)	1.382(11)	C(12)–C(13)	1.386(12)
C(13)–C(14)	1.364(13)	C(14)–C(15)	1.345(9)
C(15)–C(16)	1.360(12)	C(20)–C(21)	1.502(9)
C(21)–C(22)	1.378(11)	C(21)–C(26)	1.367(13)
C(22)–C(23)	1.410(12)	C(23)–C(24)	1.334(18)
C(24)–C(25)	1.335(12)	C(25)–C(26)	1.384(11)
Cu···C(21)	3.100(9)	Cu···C(22)	3.286(9)
Cu···C(26)	3.985(11)	Cu···O(2)	3.300(7)
Bond angle	ϕ/°	**Bond angle**	ϕ/°
O(1)–Cu–N	94.6(2)	Cu–O(1)–C(1)	132.7(4)
O(1)–C(1)–O(2)	125.8(6)	O(1)–C(1)–C(2)	114.5(5)
C(2)–S–C(3)	101.4(4)	C(1)–C(2)–S	115.7(7)
Cu–N–C(10)	115.0(4)	S–C(3)–C(4)	110.6(9)

(Continued)

Bond angle	ϕ/°	Bond angle	ϕ/°
C(10)–C(11)–C(12)	121.7(6)	N–C(10)–C(11)	114.0(6)
C(12)–C(11)–C(16)	116.8(6)	C(11)–C(12)–C(13)	121.0(7)
C(12)–C(13)–C(14)	119.9(6)	C(13)–C(14)–C(15)	119.9(8)
C(14)–C(15)–C(16)	120.4(8)	C(15)–C(16)C(11)	122.1(6)
Cu–N–C(20)	110.8(3)	N–C(20)–C(21)	110.3(4)
(C20)–C(21)–C(22)	120.4(7)	C(21)–C(22)–C(23)	119.9(9)
C(22)–C(21)–C(26)	117.7(7)	C(23)–C(24)–C(25)	121.2(9)
C(22)–C(23)–C(24)	120.0(9)	C(21)–C(26)–C(25)	121.5(7)
C(24)–C(25)–C(26)	119.8(10)	O(1)–Cu···C(21)	85.1(2)
O(1)–Cu···O(2)	39.9(2)	O(1)–Cu···C(26)	67.0(2)
O(1)–Cu···C(22)	93.1(2)	N–Cu···O(2)	58.4(2)

(3) Bis{(isopropylthio)acetato}tris(isoquinoline)copper(II)

Bond length	l/Å	Bond length	l/Å
Cu–O(11)	2.002(7)	Cu–O(12)	2.642(10)
Cu–O(21)	1.960(6)	Cu···O(22)	3.282(10)
Cu–N(32)	2.050(9)	Cu–N(42)	2.044(9)
Cu–N(52)	2.359(11)	O(11)–C(11)	1.278(12)
O(12)–C(11)	1.241(11)	C(11)–C(12)	1.515(14)
C(12)–S(1)	1.797(12)	S(1)–C(13)	1.815(13)
C(13)–C(14)	1.513(18)	C(13)–C(15)	1.522(20)
O(21)–C(21)	1.268(11)	O(22)–C(21)	1.246(12)
C(21)–C(22)	1.512(14)	C(22)–S(2)	1.792(12)
S(2)–C(23)	1.821(13)	C(23)–C(24)	1.483(16)
C(23)–C(25)	1.513(21)	C(31)–N(32)	1.303(11)
N(32)–C(33)	1.351(12)	C(33)–C(34)	1.368(16)
C(34)–C(30)	1.403(13)	C(30)–C(35)	1.435(17)
C(35)–C(36)	1.362(14)	C(36)–C(37)	1.391(16)
C(37)–C(38)	1.365(18)	C(38)–C(39)	1.415(13)
C(39)–C(30)	1.415(14)	C(39)–C(31)	1.415(15)
C(41)–N(42)	1.313(13)	N(42)–C(43)	1.352(12)
C(43)–C(44)	1.383(17)	C(44)–C(40)	1.408(16)
C(40)–C(45)	1.442(17)	C(45)–C(46)	1.377(17)
C(46)–C(47)	1.351(17)	C(47)–C(48)	1.387(19)
C(48)–C(49)	1.398(16)	C(49)–C(40)	1.398(14)
C(49)–C(41)	1.434(16)	C(51)–N(52)	1.315(11)
N(52)–C(53)	1.370(12)	C(53)–C(54)	1.354(14)
C(54)–C(50)	1.410(13)	C(50)–C(55)	1.446(14)
C(55)–C(56)	1.348(15)	C(56)–C(57)	1.393(17)
C(57)–C(58)	1.379(16)	C(58)–C(59)	1.439(13)
C(59)–C(50)	1.386(13)	C(59)–C(51)	1.427(13)
Bond angle	ϕ/°	Bond angle	ϕ/°
O(11)–Cu–O(12)	55.1(2)	O(11)–Cu–N(32)	88.0(3)
O(11)–Cu–N(42)	90.7(3)	O(11)–Cu–N(52)	90.2(2)
O(12)–Cu–N(52)	145.3(2)	O(21)–Cu–O(22)	41.4(2)
O(21)–Cu–N(32)	92.1(3)	O(21)–Cu–N(42)	89.6(3)
O(22)–Cu–N(52)	129.8(2)	Cu–O(11)–C(11)	104.7(5)
Cu–O(12)–C(11)	76.0(4)	O(11)–C(11)–O(12)	123.9(8)
O(11)–C(11)–C(12)	115.6(7)	C(11)–C(12)–S(1)	116.9(6)
C(12)–S(1)–C(13)	102.6(5)	S(1)–C(13)–C(14)	107.5(7)
S(1)–C(13)–C(14)	107.5(7)	S(1)–C(13)–C(15)	113.2(8)
Cu–O(21)–C(21)	130.1(5)	Cu···O(21)–C(21)	63.3(4)
O(21)–C(21)–O(22)	124.6(8)	O(21)–C(21)–C(22)	118.6(7)
C(21)–C(22)–S(2)	118.3(6)	C(22)–S(2)–C(23)	104.9(5)
S(2)–C(23)–C(24)	107.0(7)	S(2)–C(23)–C(25)	111.8(8)
Cu–N(32)–C(31)	119.6(6)	Cu–N(32)–C(33)	120.9(6)
C(31)–N(32)–C(33)	119.3(8)	N(32)–C(31)–C(39)	123.0(8)
N(32)–C(33)–C(34)	122.7(8)	C(33)–C(34)–C(30)	119.5(8)

(Continued)

Bond angle	ϕ/°	Bond angle	ϕ/°
C(30)–C(35)–C(36)	119.1(9)	C(35)–C(36)–C(37)	121.6(11)
C(36)–C(37)–C(38)	121.1(10)	C(37)–C(38)–C(39)	119.6(9)
C(30)–C(39)–C(31)	117.9(8)	C(38)–C(39)–C(30)	119.7(9)
C(34)–C(30)–C(39)	117.7(9)	C(35)–C(30)–C(39)	118.9(8)
Cu–N(42)–C(41)	121.7(6)	Cu–N(42)–C(43)	118.2(6)
C(41)–N(42)–C(43)	120.1(8)	N(42)–C(41)–C(49)	122.1(8)
N(42)–C(43)–C(44)	121.6(9)	C(43)–C(44)–C(40)	120.0(9)
C(40)–C(45)–C(46)	117.5(9)	C(45)–C(46)–C(47)	123.0(12)
C(46)–C(47)–C(48)	121.3(11)	C(47)–C(48)–C(49)	118.0(9)
C(40)–C(49)–C(41)	118.2(9)	C(48–(C(49)–C(40)	121.6(10)
C(44)–C(40)–C(49)	117.9(10)	C(45)–C(40)–C(49)	118.6(9)
Cu–N(52)–C(51)	124.5(5)	Cu–N(52)–C(53)	117.6(5)
C(51)–N(52)–C(53)	117.0(7)	N(52)–C(51)–C(59)	123.8(7)
N(52)–C(53)–(54)	123.1(8)	C(53)–C(54)–C(50)	120.7(8)
C(50)–C(55)–C(56)	120.5(9)	C(55)–C(56)–C(57)	120.3(10)
C(56)–C(57)–C(58)	121.9(10)	C(57)–C(58)–C(59)	118.6(9)
C(50)–C(59)–C(51)	118.6(7)	C(58)–C(59)–C(50)	119.7(7)
C(54)–C(50)–C(59)	116.9(7)	C(55)–C(50)–C(54)	119.1(8)

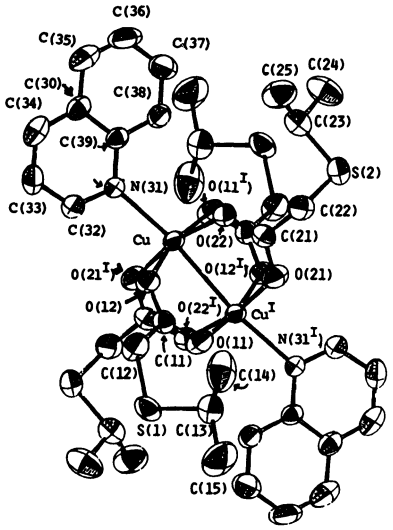

Fig. 1. A perspective drawing of tetrakis{(isopropylthio)-acetato}bis(quinoline)dicopper(II) (**1**), and the numbering scheme of atoms.

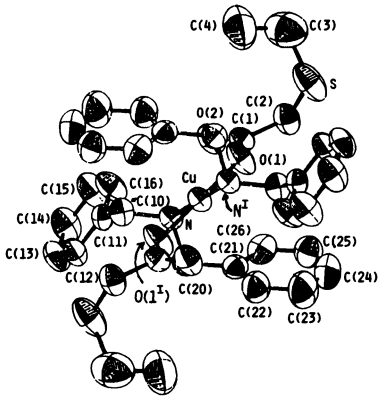

Fig. 2. A perspective drawing of bis(dibenzylamine)bis-{(ethylthio)acetato}copper(II) (**2**), and the numbering scheme of atoms.

each bond length is kept to the value shown by the X-ray analysis and that all sigle-bonded atoms can rotate freely around the axis, it was found that the phenyl

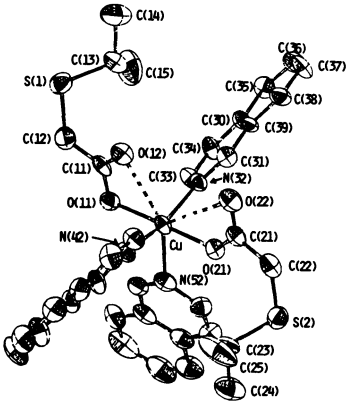

Fig. 3. A perspective drawing of bis{(isopropylthio)-acetato}tris(isoquinoline)copper(II) (**3**), and the numbering scheme of atoms.

groups of the amine ligand must approach each other when one more oxygen or sulfur atom of an (alkylthio)-acetate ligand bonds to the copper(II) atom. In the real structure, the intra-molecular interaction between phenyl groups of the amine is likely to be dominant, because the phenyl groups spread to prevent the bonding of the additional ligand atoms like a "*picket fence*."[12]

As is shown in Fig. 3, the copper atom of **3** is coordinated to two oxygen and two nitrogen atoms in a O_2N_2 square planar geometry. These Cu–O as well as Cu–N bond lengths are normal compared with those of common copper(II) complexes.[13] The average plane of the CuO_2N_2 is shown by this equation:

$$-0.773x + 0.057y - 0.631z + 6.591 = 0$$

and the shifts from the plane are: Cu, −0.105; N(32), 0.201; N(42), 0.170; O(11), −0.135; and O(21), −0.117 Å. The ∠(Nor O)–Cu–N(or O) angles between side-by-side atoms in the plane are 88.0(3)—92.1(3)°.

The copper(II) atom is surrounded by seven atoms. Among them, the O(11), O(21), N(32), N(42), and N(52) atoms are situated in the axially elongated octahedral geometry, where one axially ligating atom is absent. While ∠O(11)–Cu–O(12) is 55.1°, and Cu–

O(12) is 2.642(10) Å, the deviation of the O(12) position from the octahedral environment is rather extreme compared with the positions of other five atoms mentioned above. Moreover, as ∠O(21)–Cu–O(22) is 41.4(2)° and Cu–O(22) is 3.282(10) Å, Cu–O(22) should not be considered as the common coordination bond. However, the three axial atoms, N(52), O(12), and O(22), together with the Cu, O(11), and O(21) atoms, are almost all on one plane, shown by the following plane equation:

$$0.552\,x + 0.631\,y - 0.545\,z + 3.301 = 0.$$

The shifts of the atoms are: Cu, 0.026; O(11), 0.001; O(12) −0.002; O(21), 0.047; O(22), −0.032; and N(52), −0.037 Å. An abnormally long-distance Cu–O bonding has already been reported in copper(II) oxalate[16] or in the nitrate.[26] In some carboxylate complexes of large metal ions, two oxygen atoms of a carboxylate ion are coordinated to the same metal ion.[27] Consequently, although both Cu–O(12) and Cu–O(22) are too long, and the bonds can be expected to be weak, it seems that both O(12) and O(22) atoms are coordinated to the copper atom, cooperating with each other. Therefore, the configuration of **3** is, tentatively, named the "*potentially hepta-coordinated configuration.*"

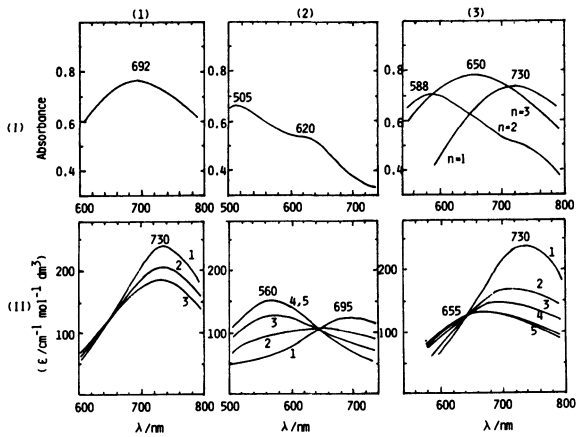

Fig. 4. Reflectance and absorption spectra of the complexes. (The wavelengths of absorption maxima are shown in figures.) (I): Diffuse reflectance spectra (upper figures). (II): Absorption spectra in benzene solution (lower figures). The concentration of Cu(II) in the solution: (1) 4.54×10^{-3}; (2) 4.72×10^{-3}, (3) 4.42×10^{-3} mol dm^{-3}.
(1) (Left figs.) : tetrakis{(isopropylthio)acetato}bis(quinoline)dicopper(II). Amine: Cu(II) in the solution: 1, 6; 2, 175; 3, 406 (mol/mol). (2) (Middle figs.): bis (dibenzylamine)bis{(ethylthio)acetato}copper(II). Amine: Cu(II) in the solution: 1, 5; 2, 7; 3, 12; 4, 53; 5, 214 (mol/mol). (3) (Right figs.): $n=1$, tetrakis-{(isopropylthio) acetato}bis (isoquinoline) dicopper (II) ; $n=2$, bis{(isopropylthio)acetato}bis(isoquinoline)copper-(II); $n=3$, bis{(isopropylthio)acetato}tris(isoquinoline)-copper(II). Amine: Cu(II) in the solution: 1, 6; 2, 45; 3, 80; 4, 150; 5, 400 (mol/mol). (For the absorption spectra in benzene solution, the same result was obtained when the mol ratio of Cu(II): amine in the solution is the same, when the $n=1$, $n=2$, or $n=3$ complex was used.)

A similar type of structure was found in tris(pyridine)-copper(II) nitrate,[28] where two oxygen atoms of each nitrate ion are coordinated to the copper(II) atom, and where the geometry of the CuO_4N_3 configuration closely resembles that of **3**.

The diffuse reflectance spectra of the solid, and the absorption spectra in a benzene solution of **1**, **2**, and **3**, as well as those of mono- and bis(isoquinoline) adducts of copper (isopropylthio)acetate, are shown in Fig. 4. The reflectance spectra of **1** are characteristic of a copper(II) carboxylate dimer,[14,29,30] as the d-d band maximum appears at about 690—730 nm. Its benzene solution shows an absorption maximum of almost the same wavelength as that of the reflectance spectra of its solid. Consequently, their dimer structure is likely kept, even in the benzene solution.

When an excess of quinoline is added to the benzene solution of **1**, the absorption maximum does not move. On the other hand, when as excess of isoquinoline or pyridine is added to a solution of their adduct of the respective Type-**1** complex, the formation of Type-**3** complex is found by the change in color and in spectra. For example, as is shown in Fig. 4, in the case of the solution of Type-**1** isoquinoline adduct, the wavelength of the absorption maximum decreased from 730 to 655 nm depending on the increase in the isoquinoline concentration in the solution. The final wavelength, 655 nm, is almost the same as that of the maximum of the reflectance spectra of the solid **3**. During the process, as the minimum wavelength of the absorption maximum observed was 655 nm, its bis(amine) adduct is probably not the dominant species under these conditions, because the reflectance spectra of the solid bis(amine) adduct of the Type-**2**, bis{(isopropylthio)acetato}bis-(isoquinoline)copper(II), has an absorption maximum at 588 nm. As has been shown in the experimental part, the solid Type-**2** adducts were obtained from a benzene–ligroine mixture solution containing both the starting copper(II) complex and the amine in higher concentrations.

The reflectance spectra of **2** shows an absorption maximum at about 505 nm, which is shorter than that of common copper complexes.[31] Such a short wavelength maximum is found only in D_{4h}-type complexes, where the axial atoms are bonded very weakly or where no axially ligating atoms exist.[32] (An additional shoulder appears at about 620 nm).

For example, bis{(isopropylthio)acetato}copper(II) dihydrate (violet isomer) shows a similar absorption maximum at 566 nm in its reflectance spectra of the solid, which has an axially elongated D_{4h} geometry.[2]

When a benzene solution of **2** is diluted, the change in the spectra and in the color of the solution shows the formation of the Type-**1** dimer complex. Therefore, in the solution, the amine ligand of **2** is in dissociation equilibrium, and a part of it is dissociated. Even when a large excess of dibenzylamine (about amine : Cu= 200, in mol/mol) is added to the solution, the absorption maximum shifts at most to 560 nm, not to 505 nm.

The reflectance spectra of **3** has an absorption maximum at about 650 nm, which is intermediate

Table 4. Infrared absorption spectral data of the complexes, $[Cu(RSCH_2CO_2)_2(amine)_n]$ (cm^{-1})[a]

n	Amine	R= CH_3		C_2H_5		$(CH_3)_2CH$	
		ν_{as}	ν_s	ν_{as}	ν_s	ν_{as}	ν_s
1	Isoquinoline	1623	1393	1620	1390	1627	1393
1	Quinoline	1630	1393	1629	1393	1628	1391
1	Pyridine	1620 (1600)	1395	1620 (1597)	1395	1620 (1598)	1390
2	Dibenzylamine	1590	1353	1588	1352	1594	1352
2	Isoquinoline					1610	1365 1349
3	Isoquinoline	1623 1600	1388 1352	1618 1598	1390 1355	1619 1598	1388 1353

a) The $n=1$ complexes are shown by the experimental formula.

between those of **1** and **2**, probably because its axial atom bondings are of medium strength.

The wave numbers of the $\nu_{as}(COO)$ and $\nu_s(COO)$ of the adducts are shown in Table 4. As each of these complexes has Type-**1**, **-2**, or **-3** structure, the maximum wave numbers should also be classified into three groups.

In **1**, the carboxyl group of the ligand bridges the copper atoms with both of its oxygen atoms, and the group is almost completely symmetric. The $\nu_{as}(COO)$ of Type-**1** adducts is about 1600—1630 cm^{-1}, which is typical of the bridging carboxylate group of the copper-(II) carboxylate dimer.[33,34]

In **2**, the carboxyl group bonds with the metal ion by only one oxygen atom, and the group is rather asymmetric. However, the $\nu_{as}(COO)$ of **2** appears in a relatively low wave number region, *i.e.*, at about 1590 cm^{-1}.

In **3**, as Cu–O(12) and Cu–O(22) are different in their bond lengths, the grades of asymmetry of the two carboxyl groups can be expected to be different, too. Therefore, two types of $\nu_{as}(COO)$ as well as $\nu_s(COO)$ bands overlap in its spectra.

The authors wish to thank Professor Yoichi Iitaka, The Faculty of Pharmaceutical Sciences, The University of Tokyo, for the collection of the intensity data. The present work was partially supported by a Grant-in-Aid for Scientific Research (No. 57430011) from the Ministry of Education, Science and Culture.

References

1) Part of this paper has been presented previously: a) Y. Sato, A. Ouchi, Y. Yukawa, and T. Takeuchi, *Chem. Lett.*, **1982**, 1495; b) Y. Sato and A. Ouchi, *ibid.*, **1982**, 1995.

2) T. Ogawa, M. Shimoi, and A. Ouchi, *Acta Crystallogr., Sect. B*, **36**, 3114 (1980).

3) T. Ogawa, M. Shimoi, and A. Ouchi, *Bull. Chem. Soc. Jpn.*, **55**, 126 (1982).

4) A. Ouchi, M. Shimoi, T. Takeuchi, and H. Saito, *Bull. Chem. Soc. Jpn.*, **54**, 2290 (1981).

5) M. Shimoi, F. Ebina, A. Ouchi, Y. Yoshino, and T. Takeuchi, *J. Chem. Soc., Chem. Commun.*, **1979**, 1132.

6) E. Larsson, *Ber.*, **63**, 1347 (1930).

7) A. Ouchi, Y. Ohashi, T. Takeuchi, and Y. Yoshino *Bull. Chem. Soc. Jpn.*, **43**, 1088 (1970); Y. Ohashi, T. Takeuchi, A. Ouchi, and Y. Yoshino, *ibid.*, **43**, 2845 (1970); A. Ouchi, T. Takeuchi, and Y. Ohashi, *ibid.*, **44**, 731, 3461 (1971).

8) This number of Z is for the dimer molecules. As the dimer has the center of symmetry, the structural data in Tables 2 and 3 are shown for a half of it; in this case, the other half of the dimer is shown by the symmetry operation of $-x$, $-y$, and $-z$, and the Z number is 8.

9) "The Universal Crystallographic Computation Program System (UNICS)," ed by T. Sakurai, Crystallographic Society of Japan, Tokyo (1967).

10) "International Tables for X-Ray Crystallography," Kynoch Press, Birmingham, U. K. (1974), Vol. IV.

11) $R=\sum||F_o|-|F_c||/\sum|F_o|$

12) The atomic coordinates of hydrogen atoms, the final thermal parameters, the F_o-F_c table, and the crystal packing diagrams of **1**, **2**, and **3**, as well as their stereoscopic views, are kept at the office of the editor of the Bull. Chem. Soc. Jpn., as Document No. 8325.

13) A. F. Wells, "Structural Inorganic Chemistry," 4th ed, Clarendon Press, Oxford, U. K. (1975), p. 897.

14) J. Catterick and P. Thornton, "Advances in Inorganic Chemistry and Radiochemistry," Academic Press, New York, N. Y. (1977), p. 291, and the references cited there in.

15) D. B. W. Yawney, J. A. Moreland, and R. J. Doedens, *J. Am. Chem. Soc.*, **95**, 1164 (1973).

16) A. Gleizes, J. Maury, and J. Galy, *Inorg. Chem.*, **19**, 2074 (1980).

17) H. Koyama, Y. Saito, and H. Kuroya, *J. Inst. Polytech. Osaka City Univ.*, **C4**, 43 (1953); *Chem. Abstr.*, **48**, 3097a (1954).

18) G. A. Barclay and A. Cooper, *J. Chem. Soc.*, **1965**, 3746.

19) D. Hall, A. J. McKinnon, and T. N. Waters, *J. Chem. Soc., A*, **1966**, 615.

20) P. K. Hon, C. E. H. Pfluger, and R. L. Belford, *Inorg. Chem.*, **5**, 516 (1966).

21) I. Robertson and M. R. Truter, *J. Chem. Soc., A*, **1967**, 309.

22) P. G. Lenhert, C. M. Luckehart, and L. T. Warfield, *Inorg. Chem.*, **19**, 311 (1980).

23) A. Ferrari, A. Braibanti, and A. Tiripicchio, *Acta Crystallogr.*, **21**, 605 (1966).

24) D. S. Brown, J. D. Lee, and B. G. A. Melsom, *Chem. Commun.*, **1968**, 852.

25) A. Mosset, J. P. Tuchagues, J. J. Bonnet, R. Haran, and P. Sharrock, *Inorg. Chem.*, **19**, 290 (1980).

26) C. C. Addison, N. Logan, S. C. Wallowrk, and C. D. Garner, *Quart. Rev.*, **25**, 289 (1971), and the references cited there in.

27) S. Kondo, M. Shimoi, A. Ouchi, and T. Takeuchi, *Bull. Chem. Soc. Jpn.*, **55**, 2840 (1982).

28) A. F. Cameron, D. W. Taylor, and R. H. Nuttall, *J. Chem. Soc., Dalton Trans.*, **1972**, 1603.

29) E. Kokot and R. L. Martin, *Inorg. Chem.*, **3**, 1306 (1964).

30) S. Yamada, H. Nakamura, and R. Tsuchida, *Bull. Chem. Soc. Jpn.*, **31**, 303 (1958).

31) B. N. Figgis, "Introduction to Ligand Fields," Interscience, New York, N. Y. (1966). pp. 218, 316.

32) S. Yamada and S. Miki, *Bull. Chem. Soc. Jpn.*, **36**, 680 (1963).

33) K. Nakamoto, "Infrared and Raman Spectra of Inorganic Coordination Compounds," 3rd ed, Wiley, New York, N. Y. (1978), p. 232.

34) Y. Mathey, D. R. Greig, and D. F. Shreiver, *Inorg. Chem.*, **21**, 3409 (1982).

A Calorimetric Study on the Relative Thermal Stability of Some Bis(diamine)cobalt(III) Complexes in a Solid Phase

Ryokichi Tsuchiya,* Akira Uehara, Toshio Wazumi, and Yoshinori Muramatsu
Department of Chemistry, Faculty of Science, Kanazawa University, Kanazawa 920

(Received November 18, 1982)

The enthalpy changes (ΔH) in the reaction of *trans*-$[CoX_2(AA)_2]X\cdot mHX\cdot nH_2O$-type complexes with an alkaline sodium sulfide solution were calorimetrically measured at 25 °C, where AA is diamine and X is Cl^-, Br^-, or ClO_4^-; $m=0$ or 1, and $n=0$, 0.5, 1, or 2. The thermal stabilities were found to decrease in the following orders for both dichloro and dibromo complexes: 1,2-ethanediamine>*l*- or *d*-1,2-propanediamine>racemic 1,2-propanediamine, *d,l*-2,3-butanediamine>meso-2,3-butanediamine>2-methyl-1,2-propanediamine, 1,2-ethanediamine>1,3-propanediamine, and *meso*-2,4-pentanediamine>*d,l*-2,4-pentanediamine. The complexes containing six-membered diamine chelate rings were less stable than those containing five-membered diamine chelate rings. The dibromo complex bromides were less stable than the corresponding dichloro complex chlorides.

Neither trans-to-cis nor cis-to-trans isomerization has so far been found in the solid $[CoX_2en_2]X$-type complexes (X: Cl^- or Br^-). Our previous paper, however, calorimetrically predicted that the above complexes undergo cis-to-trans isomerization in a solid phase, and the prediction was actually verified.[1] The enthalpy change was predominant relative to the entropy change in the free energy change of the above isomerization. The relative thermal stability among the trans-complexes in a solid phase is, therefore, considered to depend principally upon the difference in enthalpy changes of complex formation from each component in a gaseous state. On the basis of such idea, the strain energy calculation by conformational analysis has been carried out by many workers[2] for mono-, bis- and tris-diamine Co(III), Mo(0), Cr(III), Cr(0), Pt(II), and Pd(II) complexes. On the other hand, the relative strain enthalpies have been obtained calorimetrically by Woldbye *et al.*[3] for some tris(diamine)cobalt(III) complexes in an aqueous solution. The strain enthalpies by conformational analysis and by calorimetry have never been obtained for these diamine complexes in a solid phase. In the present study, the thermal stability of $[CoX_2(AA)_2]X\cdot mHX\cdot nH_2O$-type complexes in a solid phase was discussed on the basis of lattice energies evaluated from the enthalpy changes for the reaction with an alkaline sodium sulfide solution, where AA is a diamine, m is 0 or 2, and n is 0, 0.5, 1, or 2.

Experimental

Preparation of Diamines. 1,2-Ethanediamine (en), 1,2-propanediamine (pn), and 1,3-propanediamine (tn) were commercially available. 2,3-Butanediamines (*dl*-bn and *m*-bn)[4] and 2,4-pentanediamines (*dl*-ptn and *m*-ptn)[5] were prepared by the literature methods and characterized by NMR spectra.[6,7] 2-Methyl-1,2-propanediamine (*i*-bn) was supplied by Aldrich Chemical Co. Inc.

Preparation of Complexes. The following complexs were prepared by the literature methods slightly modified: *trans*-$[CoCl_2en_2]Cl\cdot HCl\cdot 2H_2O$, *trans*-$[CoCl_2en_2]Cl$,[8] *trans*-$[CoCl_2pn_2]Cl\cdot HCl\cdot 2H_2O$, *trans*-$[CoCl_2pn_2]Cl\cdot H_2O$, *trans*-$[CoCl_2(l\text{-pn})_2]Cl\cdot H_2O$,[9] *trans*-$[CoCl_2(dl\text{-bn})_2]ClO_4$, *trans*-$[CoCl_2(m\text{-bn})_2]ClO_4$, *trans*-$[CoCl_2(i\text{-bn}_2)]ClO_4$,[5] *trans*-$[CoCl_2tn_2]Cl$,[10] *trans*-$[CoCl_2(dl\text{-ptn})_2]Cl\cdot 0.5H_2O$, *trans*-$[CoCl_2(m\text{-ptn})_2]Cl\cdot 0.5H_2O$,[11] *trans*-$[CoBr_2en_2]Br\cdot HBr\cdot 2H_2O$, *trans*-$[CoBr_2en_2]Br$,[12] *trans*-$[CoBr_2pn_2]Br\cdot HBr\cdot 2H_2O$, *trans*-$[CoBr_2pn_2]Br\cdot H_2O$, *trans*-$[CoBr_2(d\text{-pn})_2]Br\cdot H_2O$,[9] *trans*-$[CoBr_2(dl\text{-bn})_2]ClO_4$, *trans*-$[CoBr_2(m\text{-bn})_2]ClO_4$, *trans*-$[CoBr_2(i\text{-bn})_2]ClO_4$,[5] *trans*-$[CoBr_2tn_2]Br$,[10] *trans*-$[CoBr_2(dl\text{-ptn})_2]Br\cdot 0.5H_2O$, and *trans*-$[CoBr_2(m\text{-ptn})_2]Br\cdot 0.5H_2O$.[11]

Calorimetric Measurements. The enthalpy changes in the reaction of the complexes in the powder state with an alkaline sodium sulfide solution were measured with a Tokyo-Riko twin isoperibol calorimeter TIC-2S at 25 °C. In each run, the diamine complexes were accurately weighed and the reacting solution was 100 cm^3 of a mixture containing 2×10^{-2} mol dm^{-3} Na_2S and 1 mol dm^{-3} NaOH.

Results and Discussion

Thermal Stability of $[CoX_2(AA)_2]X\cdot mHX\cdot nH_2O$-type Complexes with Various Diamines. The enthalpy changes measured for the reaction of these complexes with an alkaline sodium sulfide solution are summarized in Table 1. The enthalpy changes for *trans*-$[CoCl_2en_2]Cl\cdot HCl\cdot 2H_2O$l and *trans*-$[CoCl_2pn_2]Cl\cdot HCl\cdot 2H_2O$, are given as below,

$$\text{trans-}[CoCl_2en_2]Cl\cdot HCl\cdot 2H_2O(s)+3/2\ S^{2-}(aq)+OH^-(aq) = 1/2\ Co_2S_3(s)+4Cl^-(aq)+2en(aq)+3H_2O(l)\qquad \Delta H=-117.4\ \text{kJ mol}^{-1},\quad (1)$$

$$\text{trans-}[CoCl_2pn_2]Cl\cdot HCl\cdot 2H_2O(s)+3/2\ S^{2-}(aq)+OH^-(aq) = 1/2\ Co_2S_3(s)+4Cl^-(aq)+2pn(aq)+3H_2O(l)\qquad \Delta H=-136.7\ \text{kJ mol}^{-1}.\quad (2)$$

On the other hand, the heats of dissolution of diamines into an alkaline sodium sulfide solution in the same concentration as above were also measured with the calorimeter, and their heats of vaporization were calculated from the boiling points and Trouton's constants. The values for en and pn are as follows:

$$\left.\begin{array}{ll} en(l) = en(aq) & \Delta H=-30.4\ \text{kJ mol}^{-1} \\ en(l) = en(g) & \Delta H=34.3\ \text{kJ mol}^{-1} \end{array}\right\},\quad (3)$$

$$\left.\begin{array}{ll} pn(l) = pn(aq) & \Delta H=-33.4\ \text{kJ mol}^{-1} \\ pn(l) = pn(g) & \Delta H=34.5\ \text{kJ mol}^{-1} \end{array}\right\}.\quad (4)$$

Combining these values with those of Eqs. 1 and 2, the enthalpy change for the reaction,

$$\text{trans-}[CoCl_2en_2]Cl\cdot HCl\cdot 2H_2O(s)+2pn(g) = \text{trans-}[CoCl_2pn_2]Cl\cdot HCl\cdot 2H_2O(s)+2en(g),$$

Table 1. Enthalpy changes, ΔH, for the reaction of cobalt(III) complexes with sodium sulfide solution

Complex	X=Cl⁻ ΔH/kJ mol⁻¹	X=Br⁻ ΔH/kJ mol⁻¹
trans-$[CoX_2en_2]X\cdot HX\cdot 2H_2O$	−117.4	−89.8
trans-$[CoX_2en_2]X$	−60.5	−40.5
trans-$[CoX_2pn_2]X\cdot HX\cdot 2H_2O$	−136.7	−107.7
trans-$[CoX_2pn_2]X\cdot H_2O$	−70.1	−64.3
trans-$[CoX_2(l\text{-pn})_2]X\cdot H_2O$	−65.1	—
trans-$[CoX_2(d\text{-pn})_2]X\cdot H_2O$	—	−59.1
trans-$[CoX_2(dl\text{-bn})_2]ClO_4$	−69.8	−73.0
trans-$[CoX_2(m\text{-bn})_2]ClO_4$	−81.2	−80.5
trans-$[CoX_2(i\text{-bn})_2]ClO_4$	−84.0	−85.4
trans-$[CoX_2tn_2]X$	−89.6	−57.5
trans-$[CoX_2(dl\text{-ptn})_2]X\cdot 0.5H_2O$	−121.0	−87.9
trans-$[CoX_2(m\text{-ptn})_2]X\cdot 0.5H_2O$	−101.9	−80.5

Table 2. Enthalpy changes, ΔH, for the substitution reaction of diamine

Substitution reaction	X=Cl⁻ ΔH/kJ mol⁻¹	X=Br⁻ ΔH/kJ mol⁻¹
trans-$[CoX_2en_2]X\cdot HX\cdot 2H_2O\rightarrow pn_2$ [a]	12.9	11.5
trans-$[CoX_2en_2]X\rightarrow tn_2$	17.9	5.8
trans-$[CoX_2(l\text{-pn or }d\text{-pn})_2]X\cdot H_2O\rightarrow pn_2$	5.0	5.2
trans-$[CoX_2(dl\text{-bn})_2]ClO_4\rightarrow(m\text{-bn})_2$	9.6	5.7
trans-$[CoX_2(dl\text{-bn})_2]ClO_4\rightarrow(i\text{-bn})_2$	14.2	12.4
trans-$[CoX_2(m\text{-ptn})_2X\cdot 0.5H_2O\rightarrow(dl\text{-ptn})_2$	20.5	8.8

a) Represents the substitution reaction, *trans*-$[CoX_2en_2]X\cdot HX\cdot 2H_2O(s)+2pn(g) =$ *trans*-$[CoX_2pn_2]X\cdot HX\cdot 2H_2O(s)+2en(g)$. Such expressions are similarly used for the respective reactions.

was calculated as $\Delta H=12.9$ kJ mol^{-1}. The enthalpy change in substituting pn for en in the corresponding bromide was obtained as $\Delta H=11.5$ kJ mol^{-1} in the same way. These values should correspond to the difference in lattice energies between the bis(en) and bis(pn) complexes in chlorides and bromides. Thus, the bis(pn) complexes are thermally less stable than the corresponding bis(en) complexes (Table 2).

In order to compare the thermal stability between the complexes containing racemic pn and optically active *l*-pn or *d*-pn, the enthalpy changes for the following reactions were calculated by using the data in Table 1 and those in Eq. 4:

trans-$[CoCl_2pn_2]Cl\cdot H_2O(s) + 2(l\text{-pn})(g)$
$= $ *trans*-$[CoCl_2(l\text{-pn})_2]Cl\cdot H_2O(s) + 2pn(g)$
$\Delta H = -5.0$ kJ mol^{-1},

trans-$[CoBr_2pn_2]Br\cdot H_2O(s) + 2(d\text{-pn})(g)$
$= $ *trans*-$[CoBr_2(d\text{-pn})_2]Br\cdot H_2O(s) + 2pn(g)$
$\Delta H = -5.2$ kJ mol^{-1}.

These data suggest that the complexes containing optically active pn are thermally more stable than those containing racemic pn in both the chloride and the bromide.

By similar calculations, the enthalpy changes for the following reactions substituting tn for en were obtained:

trans-$[CoCl_2en_2]Cl(s) + 2tn(g)$
$= $ *trans*-$[CoCl_2tn_2]Cl(s) + 2en(g)$
$\Delta H = 17.9$ kJ mol^{-1},

trans-$[CoBr_2en_2]Br(s) + 2tn(g)$
$= $ *trans*-$[CoBr_2tn_2]Br(s) + 2en(g)$
$\Delta H = 5.8$ kJ mol^{-1}.

Here, the following data,

tn(l) = tn(aq) $\Delta H = -34.4$ kJ mol^{-1},
tn(l) = tn(g) $\Delta H = 35.9$ kJ mol^{-1},

were used. These data show that the bis(tn)cobalt(III) complexes with six-membered chelate rings are thermally less stable than the corresponding bis(en)cobalt(III) complexes with five-membered chelate rings in a solid phase.

By using the following data,

dl-bn(l) = *dl*-bn(aq) $\Delta H = -35.9$ kJ mol^{-1},
dl-bn(l) = *dl*-bn(g) $\Delta H = 35.9$ kJ mol^{-1},
m-bn(l) = *m*-bn(aq) $\Delta H = -37.1$ kJ mol^{-1},
m-bn(l) = *m*-bn(g) $\Delta H = 35.6$ kJ mol^{-1},
i-bn(l) = *i*-bn(aq) $\Delta H = -36.2$ kJ mol^{-1},
i-bn(l) = *i*-bn(g) $\Delta H = 35.6$ kJ mol^{-1},

the enthalpy changes for the following reactions were calculated:

trans-$[CoX_2(dl\text{-bn})_2]ClO_4(s) + 2m\text{-bn}(g)$
$= $ *trans*-$[CoX_2(m\text{-bn})_2]ClO_4(s) + 2dl\text{-bn}(g)$,
for X = Cl⁻ $\Delta H = 9.6$ kJ mol^{-1},
for X = Br⁻ $\Delta H = 5.7$ kJ mol^{-1},

trans-$[CoX_2(dl\text{-bn})_2]ClO_4(s) + 2i\text{-bn}(g)$
$= $ *trans*-$[CoX_2(i\text{-bn})_2]ClO_4(s) + 2dl\text{-bn}(g)$,
for X=Cl⁻ $\Delta H = 14.2$ kJ mol^{-1},
for X=Br⁻ $\Delta H = 12.4$ kJ mol^{-1}.

In these three dichloro and three dibromo complexes, the thermal stabilities decrease in the following orders,

trans-$[CoCl_2(dl\text{-bn})_2]ClO_4 >$ *trans*-$[CoCl_2(m\text{-bn})_2]ClO_4$
$>$ *trans*-$[CoCl_2(i\text{-bn})_2]ClO_4$,
trans-$[CoBr_2(dl\text{-bn})_2]ClO_4 >$ *trans*-$[CoBr_2(m\text{-bn})_2]ClO_4$
$>$ *trans*-$[CoBr_2(i\text{-bn})_2]ClO_4$.

These orders coincide with those of the stability of tris(*l*-bn), tris(*m*-bn), and tris(*i*-bn) complexes in solution calculated from strain enthalpy.[3] The difference in the stabilities between bis(*dl*-bn) and bis(*m*-bn) or bis(*i*-bn) complexes can be understood from the fact that two methyl groups in the coordinated *dl*-bn (*S*, *S*-δ or *R*, *R*-λ) are equatorial,[2c] whereas one of two methyl groups in the *m*-bn (*R*, *S*-δ or *R*, *S*-λ) and *i*-bn (δ or λ) are in the axial position.

By using the following data,

dl-ptn(l) = *dl*-ptn(aq) $\Delta H = -39.0$ kJ mol^{-1},
dl-ptn(l) = *dl*-ptn(g) $\Delta H = 37.0$ kJ mol^{-1},
m-ptn(l) = *m*-ptn(aq) $\Delta H = -39.6$ kJ mol^{-1},
m-ptn(l) = *m*-ptn(g) $\Delta H = 37.1$ kJ mol^{-1},

the enthalpy changes for the following reactions are calculated:

$$trans\text{-}[CoX_2(dl\text{-ptn})_2]X\cdot 0.5H_2O(s) + 2m\text{-ptn}(g) = trans\text{-}[CoX_2(m\text{-ptn})_2]X\cdot 0.5H_2O(s) + 2dl\text{-ptn}(g),$$

for $X = Cl^-$ $\Delta H = -20.5$ kJ mol^{-1},

for $X = Br^-$ $\Delta H = -8.8$ kJ mol^{-1}.

In these cases, the complexes containing the meso-form of ptn are thermally more stable than those containing the racemic form in contrast to the bis(bn) complexes. Such a difference will be ascribed to the difference in the conformation of the chelates, although the orientation of methyl groups is all equatorial in both complexes.[13]

The enthalpy changes for the substitution reaction of diamines are listed in Table 2.

Thermal Stability Differences between Dichloro Complex Chlorides and the Corresponding Dibromo Complex Bromides. Considering the following data,

$Cl^-(aq) = Cl^-(g)$ $\Delta H = -76.5$ kJ mol^{-1},[14]

$Br^-(aq) = Br^-(g)$ $\Delta H = -110.5$ kJ mol^{-1},[14]

the enthalpy changes for the following reactions,

$$trans\text{-}[CoCl_2(AA)_2]Cl\cdot m HCl\cdot nH_2O(s) + (3+m)Br^-(g) = trans\text{-}[CoBr_2(AA)_2]Br\cdot m HBr\cdot nH_2O(s) + (3+m)Cl^-(g),$$

were calculated, which are summarized in Table 3.

These values correspond to the decrement of lattice energies of the solid complexes when chloride ions coordinated and/or those present as counter ions are replaced by bromide ions. It is shown that the dibromobis(diamine)cobalt(III) bromides are thermally less stable than the corresponding dichloro chlorides by about 35—70 kJ mol.$^{-1}$ Especially, a tendency seems to exist that, in the complexes containing 1,2-ethanediamine or the diamines with two methyl groups attached to the distant carbon atoms like ptn, the enthalpy increments in the replacement of Cl^- by Br^- are about 40 kJ mol.$^{-1}$ On the other hand, for the other complexes containing the diamines with two methyl groups at the adjacent carbon atoms like bn, the enthalpy increments are about 60 kJ mol.$^{-1}$

Thermal Stability Diagram of the Bis(en), Bis(pn) and Bis(tn) Complexes. The enthalpy change for the reaction of *trans*-$[CoCl_2en_2]Cl$ with an alkaline sodium sulfide solution is, as Table 1 shows, given as,

$$trans\text{-}[CoCl_2en_2]Cl(s) + 3/2\ S^{2-}(aq) = 1/2\ Co_2S_3(s) + 3Cl^-(aq) + 2en(aq)$$

$$\Delta H = -60.5 \text{ kJ mol}^{-1}. \quad (5)$$

Combining the value of Eq. 5 with that of Eq. 1 and the values[14] shown below,

$HCl(g) = H^+(aq) + Cl^-(aq)$ $\Delta H = -75.2$ kJ mol^{-1},

$H_2O(l) = H^+(aq) + OH^-(aq)$ $\Delta H = 55.9$ kJ mol^{-1},

$H_2O(l) = H_2O(g)$ $\Delta H = 44.0$ kJ mol^{-1},

the enthalpy change for the reaction,

$$trans\text{-}[CoCl_2en_2]Cl\cdot HCl\cdot 2H_2O(s) = trans\text{-}[CoCl_2en_2]Cl(s) + HCl(g) + 2H_2O(g),$$

was calculated as $\Delta H = 162.2$ kJ mol^{-1}. Using this value, and taking account of the other data concerned, the enthalpy levels of some bis(en) and bis(pn) complexes are obtained, which are diagramatically shown in Fig. 1.

Table 3. Enthalpy changes, ΔH, for the reaction substituting Br^- for Cl^- in cobalt (III) complexes

Complex	ΔH/kJ mol^{-1}
trans-$[CoX_2en_2]X\cdot HX\cdot 2H_2O$	40.4
trans-$[CoX_2en_2]X$	48.0
trans-$[CoX_2pn_2]X\cdot HX\cdot 2H_2O$	39.0
trans-$[CoX_2\ pn_2]X\cdot H_2O$	62.2
trans-$[CoX_2(l\text{-pn or } d\text{-pn})_2]X\cdot H_2O$	62.0
trans-$[CoX_2(dl\text{-bn})_2]ClO_4$	71.2
trans-$[CoX_2(m\text{-bn})_2]ClO_4$	67.3
trans-$[CoX_2(i\text{-bn})_2]ClO_4$	69.4
trans-$[CoX_2tn_2]X$	35.9
trans-$[CoX_2(dl\text{-ptn})_2]X\cdot 0.5H_2O$	34.9
trans-$[CoX_2(m\text{-ptn})_2]X\cdot 0.5H_2O$	46.6

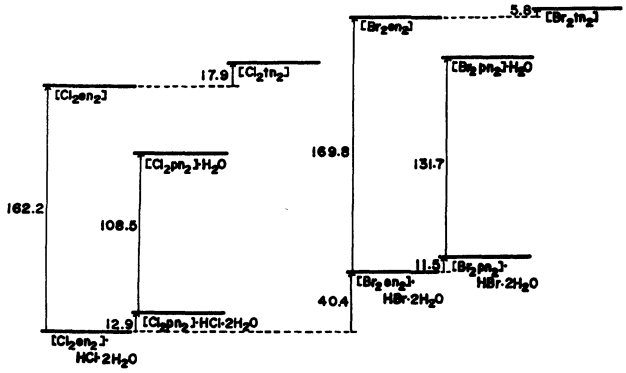

Fig. 1. Enthalpy level diagram for bis(en), bis(pn), and bis(tn) complexes. $[Cl_2en_2]\cdot HCl\cdot 2H_2O$ and $[Cl_2en_2]$ are abbreviations of *trans*-$[CoCl_2en_2]Cl\cdot HCl\cdot 2H_2O$ and *trans*-$[CoCl_2en_2]Cl$, respectively. Other abbreviations are similarly used. The numerals are expressed by the unit of kJ mol^{-1}.

Comparing the data in Table 2 with those in Table 3, the enthalpy changes for the substitution reaction of halide ions are considerably larger than those for the diamines. Such a tendency is obviously illustrated in Fig. 1 for each of the bis(en), bis(pn), and bis(tn) complexes. In summary, the thermal stability based on the lattice energy difference was found to be largely affected by the kind of halide ions rather than that of diamines.

References

1) R. Tsuchiya, A. Uehara, and Y. Muramatsu, *Bull. Chem. Soc. Jpn.*, **55**, 3770 (1982).

2) a) S. R. Niketić, and F. Woldbye, *Acta Chem. Scand.*, **27**, 621 (1973); b) C. J. Hawkins and R. M. Peachey, *Aust. J. Chem.* **29**, 33 (1976); c) S. R. Niketić, and K. Rasmussen, *Acta Chem. Scand., Ser. A*, **32**, 391 (1978); d) T. W. Hambley, C. J. Hawkins J. A. Palmer, and M. R. Snow, *Aust. J. Chem.*, **34**, 2525 (1981); e) C. J. Hawkins and J. A. Palmer, *Coord. Chem. Rev.*, **44**, 1 (1982).

3) S. Bagger, O. Bang, and F. Woldbye, *Acta Chem. Scand., Ser. A*, **30**, 98 (1976).

4) F. H. Dickey, W. Fickett, and H. J. Lucas, *J. Am. Chem. Soc.*, **74**, 944 (1952).

5) B. Bosnich and J. M. Harrowfield, *J. Am. Chem. Soc.*, **94**, 3425 (1972).
6) J. L. Sucmeier and C. N. Reilley, *Anal. Chem.*, **36**, 1707 (1964).
7) a) F. Mizukami, H. Ito, J. Fujita, and K. Saito, *Bull. Chem. Soc. Jpn.*, **44**, 3051 (1971); b) T. G. Appleton and J. R. Hall, *Inorg. Chem.*, **9**, 1800 (1970).
8) W. C. Fernelius, *Inorg. Synth.*, Vol. II, 222 (1946).
9) A. Werner and A. Fröhlich, *Ber.*, **40**, 2225 (1907).
10) Y. Kojima, *Bull. Chem. Soc. Jpn.*, **48**, 2033 (1975).
11) H. Boucher and B. Bosnich, *Inorg. Chem.*, **15**, 2322 (1975).
12) A. Werner, L. Gerb, S. Lorie, and J. Rapiport, *Ann.*, **386**, 111 (1912).
13) S. R. Niketić, K. Rasmussen, F. Woldbye, and S. Lifson, *Acta Chem. Scand., Ser. A*, **30**, 485 (1976).
14) F. D. Rossini, D. D. Wagman, W. H. Evans, S. Levine, and I. Jaffe, "Selected Values of Chemical Thermodynamic Properties," U. S. Government Printing Office, Washington, D. C. (1952).

Simultaneous Determination of Trace Amounts of Carbazole and Anthracene in Dibenzofuran by Synchronous Fluorescence Spectrometry after Zone-melting Separation

Masaki TACHIBANA* and Motohisa FURUSAWA
Faculty of Engineering, Yamanashi University, Takeda, Kofu 400
(Received December 4, 1982)

Trace amounts of carbazole and anthracene in dibenzofuran can be simultaneously determined by measuring the synchronous fluorescence intensities at 336 and 381 nm respectively. The determination limit is 2 ppm. For the application of this method to the practical samples containing interfering impurities, a zone-melting technique was applied successfully to remove the impurities prior to the determination. The recoveries of carbazole and anthracene were 99 and 92% respectively.

Synchronous fluorescence spectrometry was introduced by Lloyd[1] and has been further developed as a technique for the multicomponent analysis of polynuclear aromatic compounds.[2-5] In this spectrometry, a fluorescence signal is recorded while both excitation and emission wavelengths are scanned simultaneously with a fixed wavelength interval between them. Consequently, this method offers several advantages compared with conventional fluorimetry, an enhancement in selectivity by a narrowing of the spectral band, and a decrease of spectral interference from other luminescent species.

The determination of small amounts of carbazole and anthracene by ultraviolet spectrophotometry[6] has been developed. The determination limit is approximately 0.01% and it is difficult to apply to samples containing colored substances. Other spectrophotometric methods[7-8] have been also developed for the determination of carbazole. The determination limits are more than 0.004%.

In the present paper, simultaneous determination of trace amounts of carbazole and anthracene by synchronous fluorescence spectrometry is described. The determination limit is 2 ppm. Carbazole and anthracene in dibenzofuran can be selectively separated from the impurities by the zone-melting technique because each distribution coefficient is greater than unity. The proposed method, therefore, has a wide applicability to the determination of trace amounts of carbazole and anthracene in the practical samples containing interfering impurities. Due to the zone-melting separation, however, this method requires a relatively large amount of the sample and is time-consuming.

Experimental

Reagents. Commercially available dibenzofuran was dissolved in warm acetic acid and the solution was stirred for a while after the addition of a small amount of chromium trioxide. The crystals precipitated by the addition of water were collected, washed with water, dried, and dissolved in benzene. The benzene solution was shaken 4 times with 85% sulfuric acid, washed with water, dried over anhydrous calcium chloride, and passed through an alumina column, and then the benzene was evaporated off. The dibenzofuran thus obtained was further purified by zone refining. The content of carbazole and anthracene was less than 0.1 ppm. Cyclohexane and xylene were of guaranteed reagent grade and used without further purification.

Apparatus. All the measurements of synchronous fluorescence spectra were made on a Hitachi 650-40 fluorescence spectrophotometer equipped with a Hitachi 056 recorder. The spectral bandpass was set at 2 nm. A 150-W xenon lamp was used as the exciting source. A $10\times10\times45$ mm^3 quartz cell was used.

For zone melting a Shibayama SS-950 high-speed zone refiner was used. In this apparatus six zones are produced by six ring heaters placed at equal spacings on the charge, and each zone is set to travel by moving the heater along the charge.

Procedure. In a glass tube with an i.d. of 4 mm, 4.0 g of the sample was charged to a length of about 26 cm, and then the zone-pass was repeated 20 times. The molten zones about 30 mm long were set to travel at the speed of 100 mm/h. During the travels, the zones were stirred by spinning the tube at 1200 min^{-1} with reversal of the rotation direction at intervals of 1.0 s. Exactly 2.0 g of the zone-molten sample was cut out from the beginning part of the ingot and dissolved in 50 ml of xylene. Then 2 ml of the solution was transferred into a 20-ml volumetric flask and diluted to the mark with cyclohexane. The synchronous fluorescence intensity of the solution was measured at 336 nm for carbazole and at 381 nm for anthracene with the wavelength interval of 5 nm. As the standard, the synchronous fluorescence intensity of a dibenzofuran solution (0.1 μg/ml) in cyclohexane was used, which was measured at 303 nm with a wavelength interval of 6 nm. The calibration curves for carbazole and anthracene were prepared by using their solutions (0—0.2 μg/ml) containing dibenzofuran (4 mg/ml). Carbazole was almost recovered quantitatively, but the recovery of anthracene was 92%. The incomplete recovery of anthracene was corrected for by using the reciprocal of 0.92 as the correction factor.

Results and Discussion

Synchronous Fluorescence Spectra. A wavelength interval is one of the important factors in the measurement of synchronous fluorescence spectrum. For the determination of carbazole and anthracene, the wavelength interval of 3 nm is suitable under ordinary conditions.[5] For the determination of more minute amounts of these compounds, however, a larger wavelength interval is necessary for enhancement of the signal-to-noise ratio, and a wavelength interval of 5 nm was effective. The synchronous fluorescence spectrum of a mixed solution containing carbazole (0.2 μg/ml), anthracene (0.2 μg/ml) and dibenzofuran (4 mg/ml) is shown in Fig. 1(1). For comparison, the spectrum of

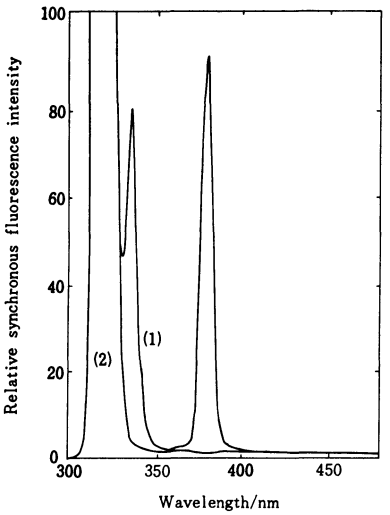

Fig. 1. Synchronous fluorescence spectra of carbazole, anthracene, and dibenzofuran.
Wavelength interval ($\Delta\lambda$): 5 nm; solvent: cyclohexane–xylene mixture (9 : 1); standard: synchronous fluorescence intensity of a dibenzofuran solution (0.100 μg/ml) in cyclohexane measured at 303 nm ($\Delta\lambda$=6 nm) was taken as 70 div.; (1): dibenzofuran (4.0 mg/ml) containing both carbazole (0.20 μg/ml) and anthracene (0.20 μg/ml); (2): dibenzofuran (4.0 mg/ml).

dibenzofuran solution (4 mg/ml) measured under identical experimental conditions is shown in Fig. 1(2). In Fig. 1 the spectral bands of these compounds are well-resolved, and the peaks at 336 and 381 nm are due to carbazole and anthracene, respectively.

Calibration Curves. For the determination of minute amounts of carbazole and anthracene in dibenzofuran, it is desirable to use a concentrated solution of the sample for the measurement of synchronous fluorescence spectrum. On the other hand, the concentrated solution shows the interferences due to both absorption and fluorescence of dibenzofuran at the characteristic wavelength of carbazole. From the result of experiments the concentration of 4 mg/ml was found suitable. In this concentration, the interference seems to be correctable by using a calibration curve, which is prepared under the presence of dibenzofuran. The calibration curves of carbazole and anthracene were prepared by using their solutions (0—0.2 μg/ml) containing dibenzofuran (4 mg/ml). The synchronous fluorescence intensities of carbazole and anthracene were measured at 336 and 381 nm respectively. As the standard, the synchronous fluorescence intensity of a dibenzofuran solution (0.1 μg/ml) in cyclohexane was used, which was measured at 303 nm with a wavelength interval of 6 nm. The calibration curves thus obtained were linear. However, the curve for carbazole did not pass the origin, and the gradient showed a slight decrease compared with the corresponding curve of carbazole alone.

Separation by Zone-melting Technique. To remove the impurities contained in the practical samples, a zone-melting method was applied. The dibenzofuran sample containing both carbazole (66 ppm) and anthracene (65 ppm) was charged in the tube for the zone melting. The zone-molten ingot obtained was divided into 15 portions. The concentrations of the carbazole and the anthracene were simultaneously measured by the synchronous fluorescence method, and then each relative concentration, C/C_0, was calculated, where C_0 and C were initial and final concentrations, respectively. Their concentration profiles in dibenzofuran are shown in Figs. 2(1) and (2), which indicate that both compounds are concentrated toward the beginning of the zone-molten ingot. The profile for acenaphthene which interferes the determination of carbazole is shown in Fig. 2(3). The initial content of acenaphthene was 0.24%. Acenaphthene was evaluated by ultraviolet spectrophotometry. Figure 2(3) shows that acenaphthene is removed from the beginning of the ingot. Some practical samples of dibenzofuran contain colored substances which show the interference due to absorption, and they were found to be accumulated in the end of the ingot. By these experiments carbazole and anthracene in dibenzofuran were found to be effectively separated from the interfering impurities.

Recoveries of Carbazole and Anthracene. After the zone melting had been performed on the dibenzofuran sample containing carbazole (66 ppm) and anthracene (65 ppm), the zone-molten ingot was divided into 13 portions. The quantities of both compounds in each portion were determined, and the relations between the amounts of the dibenzofuran cut out from the beginning of the ingot and the recoveries of both compounds were calculated. The results illustrated in Fig. 3 indicate that the use of 2.0 g of the zone-molten ingot was preferable for the determination judging from the recoveries of both compounds and the removal of the interfering impurities. Approximately 100% of carbazole and 92% of anthracene are recovered. To measure the recoveries more precisely, the zone melting was

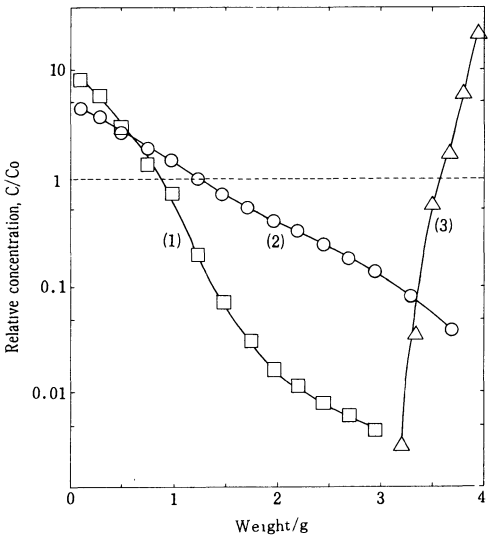

Fig. 2. Concentration profiles for carbazole, anthracene, and acenaphthene in dibenzofuran.
C_0 and C are initial and final contents of the solute; (1): carbazole, C_0=66 ppm; (2): anthracene, C_0=65 ppm; (3): acenaphthene, C_0=0.24%.

TABLE 1. RECOVERIES OF CARBAZOLE AND ANTHRACENE

Added (μg)		Found (μg)		Recovery %					
Carbazole	Anthracene	Carbazole	Anthracene	Carbazole			Anthracene		
265	282	265	261	$100._0$			$92._6$		
265	282	263	260	$99._2$			$92._2$		
265	282	268	264	$101._1$	$\bar{x}=99._1$		$93._6$	$\bar{x}=92._1$	
169	191	167	177	$98._8$	$\sigma=1.2$		$92._7$	$\sigma=0.92$	
93.4	101	92.0	91.6	$98._5$	C.V.=1.2%		$90._7$	C.V.=1.0%	
59.9	70.7	59.6	65.6	$99._5$			$92._8$		
59.9	70.7	59.1	64.5	$98._7$			$91._2$		
29.9	29.9	28.9	27.3	$96._7$			$91._3$		

TABLE 2. ANALYTICAL RESULTS FOR CARBAZOLE AND ANTHRACENE IN SYNTHETIC MIXTURES

Content ppm		Relative synchronous fluorescence intensity[a]		Found ppm	
Carbazole	Anthracene	Carbazole	Anthracene	Carbazole	Anthracene
1.9	1.9	6.2	5.7	$2._1$	$1._7$
3.8	3.8	11.2	12.2	$3._7$	$3._6$
7.5	8.8	22.9	29.2	$7._6$	$8._6$
11.7	12.6	36.2	43.1	$11._9$	$12._5$
21.5	24.2	66.2	84.0	$22._0$	$24._8$
3.1	22.8	9.4	78.6	$3._1$	$23._2$
18.2	3.5	54.4	11.4	$18._1$	$3._4$
32.8	36.3	51.8[b]	61.4[b]	$33._8$	$36._3$
48.4	52.7	74.0[b]	87.2[b]	$48._3$	$51._5$

a) Synchronous fluorescence intensity of the dibenzofuran solution (0.100 μg/ml) in cyclohexane measured at 303 nm (wavelength interval=6 nm) was taken as 70 div. b) 2 mg/ml solution of the mixture was used for the measurement.

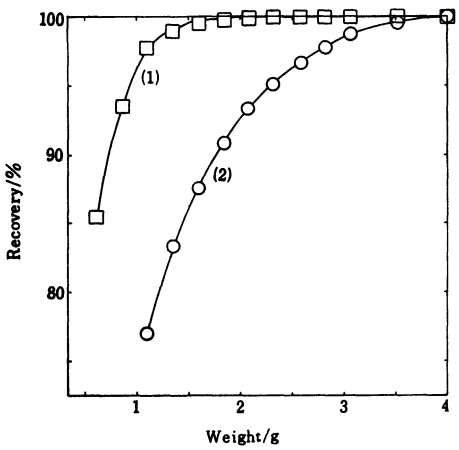

Fig. 3. Recovery profiles for carbazole and anthracene. (1): Carbazole, C_0=66 ppm; (2): anthracene, C_0=65 ppm.

carried out by the use of the dibenzofuran samples containing various amounts of both compounds. The quantities of both compounds in a 2.0 g portion of the zone-molten ingot are shown in Table 1. The recoveries of carbazole and anthracene are 99% with a coefficient of variation of 1.2%, and 92% with that of 1.0%, respectively. Carbazole can be almost quantitatively recovered, but anthracene cannot. The incomplete recovery of anthracene, however, can be corrected for by use of the reciprocal of 0.92 as the correction factor because a reproducible value is obtained.

Determination of Carbazole and Anthracene in Synthetic Mixtures. The analytical results for carbazole and anthracene in synthetic mixtures of dibenzofuran are shown in Table 2. Each mixture contains 0.3% of biphenyl, naphthalene, acenaphthene, fluorene, and phenanthrene, and 0.02% of pyrene, fluoranthene, 9-fluorenone, 1,4-naphthoquinone, and 9,10-phenanthrenequinone. Table 2 indicates that the analytical results agree closely with the individual contents of carbazole and anthracene in the synthetic mixtures. Therefore, trace amounts of carbazole and anthracene in dibenzofuran containing impurities can be simultaneously determined by the present method.

Determination of Carbazole and Anthracene in Practical Samples. Carbazole and anthracene in three different commercial dibenzofuran samples were determined by the present method. The analytical results for carbazole were 61, 41, and 12 ppm, and those for anthracene, 65, 41, and 24 ppm, respectively. The shapes of the synchronous fluorescence spectra, one of which is shown in Fig. 4(1), agree closely with that of the spectrum shown in Fig. 1(1). The solutions used for the determination did not show the absorption based on interfering impurities. The synchronous fluorescence spectra of the remaining parts of the zone-molten ingot of the practical samples were also measured by the same procedure. From these spectra, one of which is shown in Fig. 4(2), the interfering impurities in dibenzofuran are found to be accumulated toward the end of the zone-molten ingot. As the results of the above experi-

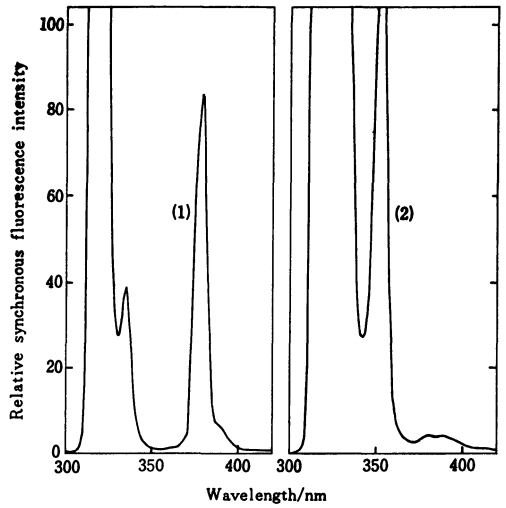

Fig. 4. Synchronous fluorescence spectra of zone-molten commercial dibenzofuran.
$\Delta\lambda$: 5 nm; solvent: cyclohexane–xylene mixture (9 : 1); standard: synchronous fluorescence intensity of a dibenzofuran solution (0.100 μg/ml) in cyclohexane measured at 303 nm ($\Delta\lambda$=6 nm) was taken as 70 div.; (1): solution used for the determination, 4.0 mg/ml; (2): solution prepared by dissolving the opposite end of the same ingot, 4.0 mg/ml.

ments, the method proposed in the present paper can be applied to the practical samples of dibenzofuran.

The authors are indebted to Miss Sumiko Yamada and Mr. Tadayuki Yano for their technical assistance. The present work was partially supported by a Grant-in-Aid for Scientific Research from the Ministry of Education, Science and Culture.

References

1) J. B. F. Lloyd, *Nature (London), Phys. Sci.*, **231**, 64 (1971).
2) Tuan Vo-Dinh, *Anal. Chem.*, **50**, 396 (1978).
3) Tuan Vo-Dinh, R. B. Gammage, and P. R. Martinez, *Anal. Chem.*, **53**, 253 (1981).
4) T. Katoh, S. Yokoyama, and Y. Sanada, *Fuel*, **59**, 845 (1980).
5) M. Furusawa, M. Tachibana, and Y. Hayashi, *Bunseki Kagaku*, **31**, 229 (1982).
6) K. Kihara, *Bunseki Kiki*, **11**, 436 (1973).
7) M. Furusawa, S. Yamada, M. Tachibana, and T. Natori, *Yamanashi Daigaku Kohgakubu Kenkyu Hohkoku*, **28**, 142 (1977).
8) M. Furusawa, M. Tachibana, S. Yamada, and Y. Ishida, *Bunseki Kagaku*, **28**, 130 (1979).

The Affinity for Carbon Monoxide, Electrochemical and Spectral Properties of Binuclear Copper(I) Complexes

Susumu KITAGAWA, Megumu MUNAKATA,* and Noboru MIYAJI
Department of Chemistry, Faculty of Science and Technology, Kinki University, Kowakae, Higashi-Osaka, Osaka 577
(Received December 15, 1982)

Binuclear copper(I) complexes $[CuXL]_2$(X=Cl^- and I^-; L=2,2′-bipyridine, 1,10-phenanthroline, and their derivatives) have been synthesized in acetone, which react with CO reversibly to give crystalline carbonyl adducts $[Cu_2X_2L_2(CO)]$. The cyclic voltammograms of $[CuXL]_2$ and $[Cu_2X_2L_2(CO)]$ show two couples of copper-centered oxidation-reduction waves, indicative of binuclear structure. One couple of waves in $[Cu_2X_2L_2(CO)]$ alone shifts to the anodic region, exhibiting the formation of monocarbonylated complexes. All the half-wave potentials are primarily governed by the basicity of a ligand L, and the contribution of a coordinated CO to the stabilization of Cu^I state by π back-bonding is found. The equilibrium constants of the reaction, $[CuXL]_2+CO\overset{K_{CO}}{\rightleftharpoons}[Cu_2X_2L_2(CO)]$, are lowered with the decrease in the transition energy of the ligand←metal charge transfer of $[CuXL]_2$. On this basis, it is concluded that CO competes with L concerning π back-bonding with copper(I). The ν_{CO} values of the coordinated CO exhibit apparent L-dependence, which is accounted for by the competition between Cu–L and Cu–CO π-bonding, and hence, ν_{CO} values are useful probe to inquire into the nature of Cu–CO bonding among these copper(I) complexes.

A greater knowledge of coordination chemistry of copper(I) particularly of binuclear structure, is important in view of current interest in understanding the structure-function relationship of the "type 3" copper proteins. We have recently reported novel binuclear copper(I) complexes,[1] which have two bridging halogen atoms. It has been demonstrated that the binuclear complexes reversibly react with carbon monoxide (CO) to form a monocarbonylated complex which have the stoichiometry of 1CO/2Cu, corresponding to that of hemocyanin,[2,3] and their affinity for CO is remarkably influenced by the bridging halogens and solvent.

To gain further insight into the nature of copper(I)-ligand binding, we present here a systematic electrochemical properties of binuclear copper(I) complexes containing several 2,2′-bipyridine (bpy) and 1,10-phenanthroline (phen) derivatives (Figs. 1; **1a—f**, **2a**, and **2b**), and their carbonyl adducts. Furthermore, the relationship between the affinity for CO and the bonding nature of Cu^I–L or Cu^I–CO is examined on the basis of visible absorption and infrared spectra.

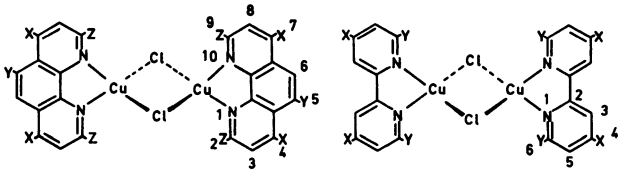

1a X=Z=H; Y=Cl 1d X=Z=H, Y=CH_3 2a X=Y=H
1b X=Z=H; Y=Br 1e X=CH_3; Y=Z=H 2b X=CH_3; Y=H
1c X=Y=Z=H 1f X=ph; Y=Z=H

Fig. 1. $[CuClL]_2$.

Experimental

Materials. The reagent grade copper(I) chloride was purified according to literature.[4] Reagent grade copper(I) iodide was used without further purification. They were all dried *in vacuo* (75—100 °C). 2,2′-Bipyridine (bpy), 4,4′-dimethyl-2,2′-bipyridine (4,4′-dmbp), 1,10-phenanthroline (phen), 5-chloro-1,10-phenanthroline (5-Cl-phen), 5-bromo-1,10-phenanthroline (5-Br-phen), 5-methyl-1,10-phenanthroline (5-mp), 4,7-dimethyl-1,10-phenanthroline (4,7-dmp), 4,7-diphenyl-1,10-phenanthroline (4,7-dpp), and 2,9-dimethyl-1,10-phenthroline (2,9-dmp) were commercially available (Wako Pure Chemical Ltd). 6,6′-Dimethyl-2,2′-bipyridine (6,6′-dmbp) was prepared according to literature.[5] They were recrystallized several times from acetone, and dried *in vacuo* before use.

Acetone was dried over anhydrous potassium carbonate, and distilled from 4 Å molecular sieves before use. Tetrabutylammonium perchlorate (TBAP) was prepared by the usual method.

Cyclic Voltammograms. Cyclic voltammetric (CV) measurement were made with a Hokuto model HA104 potentiostat/galvanostat driven by a Hokuto model HB107A function generator. Scans were recorded with a Rika Denki X-Y recorder. A conventional three-electrode system was utilized. A Pt wire served as the working electrode, and a Pt coil was used as the counter electrode. A commercial saturated calomel electrode (SCE) was utilized as the reference electrode. Current-voltage curves were measured at 0.05—0.5 V/s. The SCE was separated from the bulk of the solution with a fritted-glass bridge filled with solvent and supporting electrolyte. All potentials are reported in volts *vs.* SCE.

A solution of phen (1.0×10^{-4} mol) and anhydrous CuCl (1.0×10^{-4} mol) in 50 cm^3 of acetone was stirred under argon at 25 °C for 4 h. Complete complex formation was checked by monitoring the band at 440 nm (peak maxima). This solution was transferred anerobically into the electrolytic cell containing TBAP (5.0×10^{-3} mol), and maintained at constant temperature. Temperature was set at 5 and 25 °C. During measurments, argon atmosphere was kept over the solution in the electrolytic cell. The carbonyl adduct was prepared by directly passing CO gas into the stock solution prepared in a similar way. It was then transferred into the electrolytic cell in which CO atmosphere (1 atm) was maintained during measurements. The partial pressure of CO in the gas bubbled through the stock solution and the electrolytic cell was adjusted by mixing pure argon with pure CO, using two Kusano KG-1 rotameters and two precission needle valves. Partial pressure effect was examined only for $[CuCl(bpy)]_2$. The cyclic voltammograms of the copper(I) complexes containing the other phen or bpy derivatives were measured in similar ways.

Solution Equilibria. Visible spectra were recorded on Hitachi 200-10 spectrophotometer. The cell used for the

determination of CO equilibria consisted of 1.0-cm quartz cuvette with gas inlet and outlet tubes, by means of which N_2 gas containing varying partial pressure of CO can be bubbled through the copper(I) complex solution. The change in absorbance maxima was measured as a function of the partial pressure of CO. The equilibrium constants given by Eqs. 1 and 2 were obtained.

$$[CuClL]_2 + CO \overset{K_{co}}{\rightleftharpoons} [Cu_2Cl_2L_2(CO)] \quad (1)$$

$$K_{co} = [Cu_2Cl_2L_2(CO)]/[[CuClL]_2](P_{co}) \quad (2)$$

The detailed procedure to obtain the equilibrium constants has been described elsewhere.[1]

Measurements of Infrared Spectra. Infrared spectra were recorded on Hitachi 260-10 spectrophotometer. The spectra of saturated solutions of $[Cu_2Cl_2L_2(CO)]$ were measured in 0.05-cm cavity KCl cells, with polystyrene film as calibration standard. KBr disk pellet was prepared as follows. A solution of $L(1.0\times10^{-3}$ mol) and $CuCl(1.0\times10^{3}$ mol) in 50 cm^3 acetone was stirred under argon for 4 h. A suspended brown solution was obtained. Carbon monoxide was then added to this solution; the initially brown color turned pale yellow and the precipitate dissolved into acetone. When the solution was cooled at −70 °C, a pale yellow crystals were obtained. This was stable at low temperature. The quick preparation of KBr disk pellets provided IR spectra of $[Cu_2Cl_2L_2(CO)]$. The carbonyl adduct in KBr disk was stable for many hours.

Results and Discussion

Electrode Reactions. Figure 2 illustrates a typical cyclic voltammogram of $[CuCl(phen)]_2$ (**1c**) in acetone/0.1 M TBAP (1 M=1 mol dm^{-3}). The oxidation-reduction reactions noted here correspond to the metal-centered reactions, Cu^I/Cu^{II} at 0.3—0.7 V *vs.* SCE, because the ligand phen encounters no reaction in this region. The cyclic voltammogram of **1c** (Fig. 2) shows two oxidation processes. The ^1H NMR spectrum of **1c** in acetone showed the signals attributed to only a single species indicative of no dissociation of **1c**. The first two peaks(1) in cyclic voltammogram at 0.22 and 0.44 V in Fig. 2 are coupled to the initial oxidation-reduction process of the other copper of **1c**. These are chemically reversible and non-Nernstian at a platinum electrode ($E_{p,a}-E_{p,c}$=0.1—0.2 V). These electrode reactions are represented by Eqs. 3 and 4.

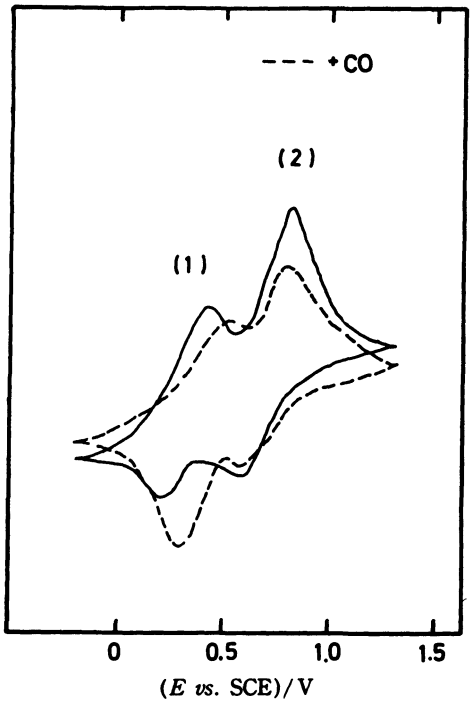

Fig. 2. Cyclic voltammograms of $[CuCl(phen)]_2$(solid line) and $[Cu_2Cl_2(phen)_2(CO)]$(dotted line) in acetone.

$$(phen)Cu^ICl_2Cu^I(phen) \overset{-e}{\rightleftharpoons} (phen)Cu^{II}Cl_2Cu^I(phen) \quad (3)$$

$$(phen)Cu^{II}Cl_2Cu^I(phen) \overset{-e}{\rightleftharpoons} (phen)Cu^{II}Cl_2Cu^{II}(phen) \quad (4)$$

On the other hand, copper(I) complex containing 2,9-dmp or 6,6′-dmbp showed a single oxidation process; this indicates that the dominant species is a mononuclear form. Appearance of the two oxidation peaks[6] at this region is a good measure of the binuclear structure of the copper(I) complex in question. The other binuclear copper(I) complexes, **1a**, **1b**—**f**, **2a**, and **2b**, also have similar anodic properties. If differences in diffusion coefficients between the oxidation and reduction halves of redox couples are ignored, value of $E_{1/2}$ obtained in the above electrochemical experiments can be used. These formal half-wave potentials ($E_{1/2}$s) are listed in Table 1. Knowledge of these formal potentials enables one to quantify some interesting properties of the system.

Electrode Reactions under CO Atmosphere. In this electrode reaction, both two sets of coupled peaks should shift anodically if a dicarbonyl adduct is formed. The ^1H NMR and visible spectra have demonstrated that $[CuCl(phen)]_2$ binds to CO at room temperature to give a monocarbonyl adduct $[(phen)CuCl_2Cu(CO)(phen)]$.[1] It is worth noting in Fig. 2 that the couple(1) alone moves anodically and the other couple(2) remains. This also support the formation of monocarbonyl adduct. In order to firmly assign this cyclic voltammogram, the partial pressure of CO is varied. When the partial pressure increases, the peak current of the couple(1) of $[CuCl(phen)]_2$ decreases and a new couple(1) (a dashed curve in Fig. 2) appears.[7] The high pressure of CO causes the increase in the peak current of the new couple(1) but it does not influence the redox potential. This fact exhibits that the monocarbonylated complex

Table 1. Oxidation-reduction potentials of $[CuClL]_2$ and $[Cu_2Cl_2L_2(CO)]$

L	($E_{1/2}$ *vs.* SCE)/V[a]			
	$[CuClL]_2$		$[Cu_2Cl_2L_2(CO)]$	
	(1)	(2)	(1)	(2)
5-Cl-phen	0.37	0.72	0.43	0.70
phen	0.33	0.69	0.40	0.68
5-mp	0.31	0.67	0.40	0.69
4,7-dmp	0.26	0.66	0.38	0.67
4,7-dpp	0.32	0.67	0.41	0.68
bpy	0.31	0.74	0.41	0.68
4,4′-dmbp	0.26	0.70	0.39	0.70
2,9-dmp	0.66		0.69	
6,6′-dmbp	0.69		0.65	

a) [Complex]=2.0×10^{-3} M and [TBAP]=0.1 M in acetone at 25°C.

forms with the increase of the CO pressure. Hence, the new couple(1) is attributable to the copper coordinated with CO. The selective anodic shift of the copper coordinated by CO has also been found in $Cu^{I}Cu^{I}L'(CO)$,[6] in which the stabilization of the copper(I)(Cu–CO) is attributable to the π back-bonding interaction between CO and Cu. It is interesting to compare the relative stability of two copper(I) ions in the binuclear monocarbonyl complex. In the case of $[Cu_2Cl_2L_2(CO)]$ studied here, the first oxidation occurs at $Cu^{I}(CO)$, while it occurs at the Cu^{I} without coordinated CO in the case of $[Cu^{I}Cu^{I}(CO)L']$. It should be remembered that copper(I) prefers the tetrahedral geometry while copper(I) favors the square-planar one. $[Cu_2Cl_2L_2(CO)]$ has a flexible structure[1] and the geometry around each copper atom is different and may not be simply square-planar; one is distorted square-pyramidal (CO-coordinated) and the other is tetrahedral.[8] On this basis, the five-coordinate copper(I) is less stable than the tetrahedral one in spite of the coordination of CO. On the other hand, [CuCu(CO)L'][6] has square-planar and square-pyramidal geometry around each copper atom. The square-planar copper is less stable than the square-pyramidal copper because the latter is stabilized by π back-bonding interaction with CO. Consequently, the contribution of geometry around the copper atom may predominate over the effect of stabilization of CO as the fifth ligand in the carbonyl copper(I) complexes studied here.

Relationship between $E_{1/2}$ and pK_a of Ligands. Figure 3 shows that the $E_{1/2}$ values for copper(I) complexes containing phen derivatives are plotted against the pK_a values of phens. The straight lines exhibit a good relationship between $E_{1/2}$ and pK_a: the negative slope reveals that the ligand having the higher pK_a destabilizes the copper(I) complexes. Similar results have been found in copper(I) complex in aqueous solution.[9] This is accounted for by the following two reasons. Firstly, when the coordinated ligand gives a more negative charges to the copper(I) ion, this ion will be more unstable. In fact, the aliphatic amines having the greater basicity (pK_a=10—11) form very unstable complexes with copper(I) ion, which are readily oxidized to copper(II) complexes. On the other hand, copper(II) ion favors the ligand having the greater basicity and forms the stable complex.[10] Hence, the ligand having the greater basicity contributes to the stabilization of its copper(II) complexes more effectively than that of copper(I) complex. Secondly, the π conjugated structure of the ligand can accept electronic

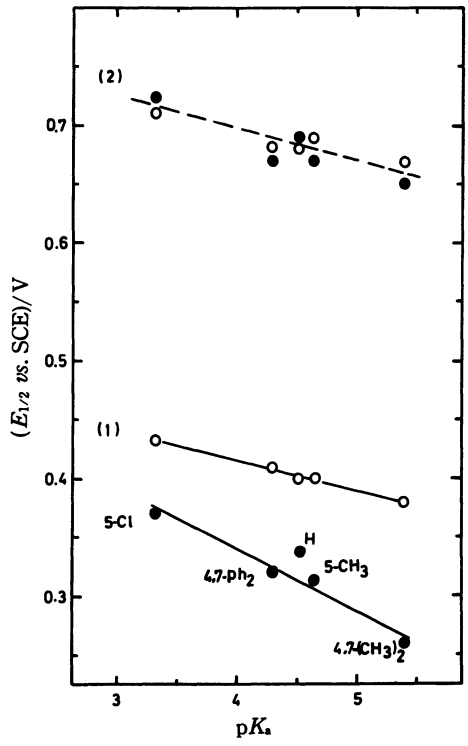

Fig. 3. Plots of half-wave potentials ($E_1/_2$) of $[CuClL]_2$ (●) and $[Cu_2Cl_2L_2(CO)]$ (○) *vs.* pK_a of the ligand (L; phen derivatives).

Table 2. Metal-to-ligand charge transfer bands of $[CuClL]_2$ and formation constants of their carbonyl adducts

Complex	pK_a[a]	λ_{MLCT}/nm[b]	K_{CO}/atm^{-1}[c]
1a	3.43	445	0.9
1c	4.53	440	1.2
1d	4.65	443	1.1
1e	5.40	437	1.6
1f	4.30	463	—
2a	3.62	440	1.3[d]
2b	4.40	433	—
$[Cu(2,9\text{-dmp})_2]$	—	455	—[e]
$[Cu(6,6'\text{-dmbp})_2]$	4.23	455	—[e]

a) The pK_a values of the coordinated ligands; 50% v/v dioxane–water. Ref. 9. b) Error limit, ±1 nm. c) Error limit, ±0.1 atm^{-1}. d) Ref. 1. e) No reaction with CO.

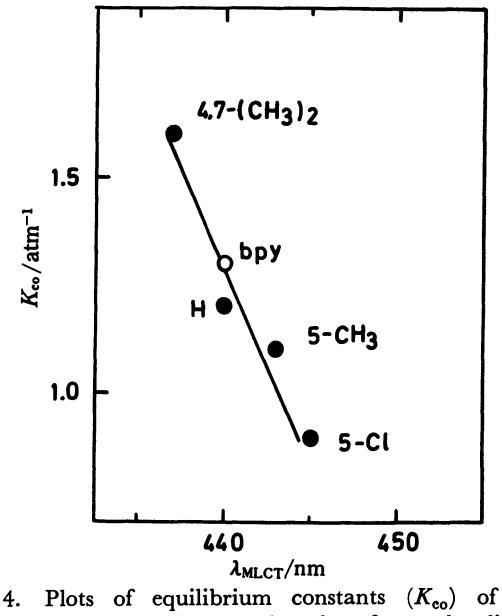

Fig. 4. Plots of equilibrium constants (K_{co}) of the reaction (1) *vs.* the wavelengths of metal-to-ligand charge transfer (MLCT) band of $[CuClL]_2$ (L; phen derivatives (●) and bpy (○)).

charge from copper(I) ion through π back-bonding. The substituent which enhances the donor ability of the nitrogen of the ligand tends to destabilize the lowest vacant (LV) π^* orbital[11,12] of the ligand which is significantly associated with the π back-bonding. This effect has been demonstrated in the case of 4-substituted pyridines.[13] On this basis, the ligand with the greater basicity is disadvantageous for π back-bonding interaction with copper(I) ion, and it lowers the redox potential of the resultant copper(I) complex. Consequently, in a series of bidentate ligands possessing donor atoms which have both σ and π bonding natures, their copper(I) complexes are destabilized with an increase in their pK_a values.

It is worth noting in Fig. 3 that the gradient of the straight line(1) of the CO adducts is smaller than that of the precursor complex, indicative of the contribution of a coordinated CO to the stabilization of copper(I) ion: even if phen derivatives with the higher basicity destabilizes Cu^I state in a moiety ($LCu(CO)<^{x}_{x}$) of a CO adduct, coordinated CO stabilizes Cu^I state through π back-bonding. On the other hand, the copper(I) ion in the residual moiety ($^{x}_{x}>CuL$) shows a pK_a-dependence of $E_{1/2}$ similar to that of the precursor one. In this sense, CO is a good π acceptor. This nature of CO leads to the expectation that CO competes with L for π back-bonding. In fact, the intense MLCT band between L and copper(I) ion in the visible region disappears[1] when CO binds [$LCuCl_2CuL$]. This indicates that CO is significantly associated with π back-bonding and subsequently, it enhances the stabilization of copper(I) state, competing with a bidentate ligand L.

Relationship between K_{CO} and λ_{MLCT}. The stability of the CO adduct is examined with the aid of the equilibrium constants. The K_{CO} values obtained for the binuclear complexes (Eqs. 1 and 2) are listed in Table 2, together with the peak maxima of the metal-to-ligand charge transfer (MLCT) band of $[CuClL]_2$, λ_{MLCT}. This K_{CO} exhibits the affinity for CO of copper(I) ion. K_{CO} reflects the competition of L with CO concerning the metal-ligand binding. A good measure to depict the Cu–L π back-bonding is λ_{MLCT}, whose greater value indicates the significant association of π back-bonding in Cu–L bond. In order to examine the relationship between stability of CO adducts and their π back-bonding nature of Cu–CO bonding, K_{CO} is plotted against λ_{MLCT} (Fig. 4). Figure 4 shows the good correlation between K_{CO} and λ_{MLCT}, indicative of considerable contribution of π back-bonding to the stabilization of CO adducts. The stronger Cu–L π back-bonding (the greater λ_{max}) results in the weaker CO-affinity (the smaller K_{CO}). It is concluded that L controls the affinity for CO of copper(I) through π-bonding although overall stability of the CO adduct, of course, results from the delicate balance between bondings of Cu–CO and Cu–L and the resultant geometry.

Coordinated Carbonyl Stretching Frequencies. To gain further insight into the nature of the Cu–CO bonding, CO-stretching frequencies of the copper(I) complexes have been measured. These ν_{CO} values are presented in Table 3. Inspection of Table 3 reveals that they fall within the range 2063—2088 cm^{-1}. It is well known that π back-bonding plays an important role in the metal–CO bond. This π back-bonding brings about a shift of ν_{CO} toward the lower frequency region.[14] On this basis, the smaller value of ν_{CO} indicates the stronger π back-bonding in the Cu–CO bond. Floriani *et al.*[15-18] have synthesized several four-coordinate carbonyl copper(I) complexes containing aliphatic amines such as ethylenediamine and their derivatives. These ν_{CO} values fall within 2055—2080 cm^{-1}, and the bond distances of Cu–CO(r_{Cu-CO}) and C–O(r_{C-O}) are 1.73—1.80 Å, and 1.11—1.17 Å, respectively. They, however, could not find the evident relationship between the ν_{CO} and r_{Cu-CO} or r_{C-O} in their four-coordinate copper(I) complexes containing the terminal CO. A five-coordinate carbonyl, copper(I) complex has been synthesized by Gagne *et al.*[19,20] This gave ν_{CO}=2068 cm^{-1}. Five coordinate [$Cu_2X_2L_2(CO)$] studied here also encounters ν_{CO} values of 2063—2088 cm^{-1}. These terminal CO provides no ν_{CO} values characteristic of the five-coordinate form. The stretching frequencies of CO coordinated to Cu^I seem to have no evident correlation with a coordination number and geometry around copper, such as tetrahedral or square-pyramidal. Then, a question arises. What does the ν_{CO} inform us about carbonyl copper(I) complexes? It is worth noting that most of carbonyl copper(I) complexes are ternary ones containing Cu, CO, and L. On the basis of the discussion in the previous section, we are now in a position to focus on the ν_{CO} in relation to the Cu–CO bonding influenced by L through the Cu–L bonding. This effect of the coordinated ligand should be examined by use of a series of structural analogs of carbonyl copper(I) complexes in order to exclude the contribution of other structural factors. We have explored the Cu–CO bonding of [$Cu_2X_2L_2(CO)$] with the aid of the formation constants of carbonyl copper(I) complexes,[1] which depend on the coordinated ligands and halide ions. We now refer to monocarbonyl copper(I) complexes studied here. These are relevant to inquire into the nature of Cu–CO bonding as a function of L and X^-. Table 3 shows that the ligand L influences the ν_{CO} values appreciably: the CO adduct of **1a** (or **1b**) has a greater ν_{CO} value than that of **1c** while the affinity for CO of these complexes is cataloged with the increasing order **1a**<**1c** (Table 2). This is accounted for by the π-acceptor capability of phen derivatives. As is discussed in the previous section, 5-Cl-phen π encounters stronger π back-bonding from copper(I) ion than non-substituted phen,

Table 3. CO-stretching frequencies of carbonyl adducts

Precursor complex	ν_{CO}/cm^{-1}	
	In the solid state[a]	In solution[b]
1a	2088	2085
1b	2082	—
1c	2063	2076
1d	2068	—
2a	2066	2075
$[CuI(bpy)]_2$	2064	—

a) KBr disk. Error limit, ± 1 cm^{-1}. b) In acetone. Error limit, ± 2 cm^{-1}.

and it should weaken the π back-bonding between copper(I) and CO, leading to the decrease in CO-affinity of the precursor complex. The similar trend in ν_{CO} is also obtained from $[Cu_2X_2L_2(CO)]$ in solution, as shown in Table 3. As is expected from the affinity for CO in Table 2, ν_{CO} obtained for **1d** is similar to that for **1c**. Hence, the effect of the methyl group at 5-position of phen is smaller than that of the halogeno groups.

The ν_{CO} of **2a** containing bpy is close to that of **1c**, both in solution and in solid states. Substitution of I^- for Cl^- in **2a** causes ν_{CO} signal to shift slightly to the lower frequency region. Similar phenomena are also found in $[Cu_2(tmen)_2(CO)_2X]$ ($X=Cl^-$, Br^-, and I^-).[17] This trend in ν_{CO} is reasonable in the light of the fact that $[CuI(bpy)]_2$ has stronger affinity for CO than $[CuCl(bpy)]_2$ (Table 3 in the Ref. 1). This slight change in ν_{CO} upon substitution of halide ion indicates that L is more effective for carbonyl stretching frequencies than halide ions, and this is in good contrast to the fact that a halide ion exerts its drastic effect upon the affinity for CO of the precursor complex. In conclusion, ν_{CO} values are available to investigate the bonding nature of Cu–CO among the structural analogs of carbonyl copper(I) complexes. The ν_{CO} values as well as K_{CO} reflect the competition of CO with L concerning the π-bonding.

We appreciate the assistance of Mr. Yonezawa. This work was supported in part by a Grant-in-Aid Scientific Research No. 57740326 from the Ministry of Education, Science and Culture.

References

1) S. Kitagawa and M. Munakata, *Inorg. Chem.*, **20**, 2261 (1981).
2) J. O. Alben, L. Yen, and N. J. Farrier, *J. Am. Chem. Soc.*, **92**, 8234 (1970).
3) W. Vannester and H. S. Mason, "The Biochemistry of Copper," ed by J. Peisach, P. Aisen, and W. E. Blumberg, Academic Press, New York (1966).
4) L. F. Andrieth, J. C. Bailar, W. C. Fernelius, W. C. Johnson, and R. E. Kirk, *Inorg. Synth.*, **2**, 1 (1946).
5) W. H. F. Sasse and C. P. Whittle, *J. Chem. Soc.*, **1961**, 1347.
6) R. R. Gagné, C. A. Koval, T. J. Smith, and M. C. Cimolino, *J. Am. Chem. Soc.*, **101**, 4571 (1979). L′ is a condensed-ring compounds which is obtained from 1,3-diaminopropane and 5-methyl-2-hydroxyisophthalaldehyde.
7) In addition to this, a single anodic peak at 0.20 V appears, when the sweep range was set between −1.5 and +1.0 V. This may be ascribed to the two electron redox reaction($Cu^0 \rightleftharpoons Cu^{II}$) of another species which forms under CO atmosphere. This is excluded from the present consideration.
8) In $[Cu_2Cl_2L_2(CO)]$, one is four-coordinate copper(I) and another is five-coordinate copper(I). This type of complex is more flexible than a complex containing a macrocyclic ligand because there are no restraints between two moieties of bpy and bridging halogen atoms. Hence, the most possible structure is tetrahedral and square-pyramidal geometry around copper(I) atoms.
9) B. R. James and R. J. P. Williams, *J. Chem. Soc.*, **1961**, 2007.
10) W. R. McWinnie and J. D. Miller, *Adv. Inorg. Chem. Radiochem.*, **12**, 135 (1969).
11) I. Nenner and G. J. Schultz, *J. Chem. Phys.*, **62**, 1747 (1975).
12) G. N. LaMar, *J. Am. Chem. Soc.*, **94**, 9055 (1972).
13) S. Kitagawa, M. Munakata, and A. Higashie, *Inorg. Chim. Acta*, **59**, 219 (1982).
14) F. A. Cotton and G. Wilkinson, "Advanced Inorganic Chemistry," 2nd ed, Wiley, New York (1972), Chap. 27.
15) M. Pasquali, F. Marchetti, and C. Floriani, *Inorg, Chem.*, **17**, 684 (1978).
16) M. Pasquali, C. Floriani, and A.G-Manfredotti, *Inorg. Chem.*, **19**, 1191 (1980).
17) M. Pasquali, G. Marini, and C. Floriani, *J. Chem. Soc., Chem. Comm.*, **1979**, 937.
18) M. Pasquali, G. Marini, C. Floriani, A. G-Manfredotti. and C. Guastini, *Inorg. Chem.*, **19**, 2525 (1980).
19) R. R. Gagné, J. L. Allison, R. S. Gall, and C. A. Koval, *J. Am. Chem. Soc.*, **98**, 6709 (1976).
20) R. R. Gagné, *J. Am. Chem. Soc.*, **99**, 7170 (1977).

 © 1983 The Chemical Society of Japan Bull. Chem. Soc. Jpn., 56, 2263—2266 (1983)

A Kinetic Study of a Zn^{2+}-catalyzed Transamination Reaction between Pyridoxamine Analogs with a Pyridinophane Structure and α-Keto Acids

Yoji TACHIBANA,† Makoto ANDO, and Hiroyoshi KUZUHARA*
The Institute of Physical and Chemical Research, Wako, Saitama 351
(Received January 6, 1983)

The kinetics of the nonenzymatic transamination reaction from pyridoxamine analogs with a pyridinophane structure to α-keto acids catalyzed by Zn^{2+} were investigated by monitoring the changes in the absorption spectra in methanol. It was found that these reactions obeyed first-order kinetics for the formation of the Zn^{2+} chelate of an aldimine. No appreciable change in the reaction rate was observed when the concentration of the α-keto acid was increased, indicating that the isomerization of the ketimine chelate to the aldimine chelate is the rate-determining step. There was a considerable enhancement of the reaction rate when the molar ratio of the zinc ion to the pyridoxamine analogs was reduced from 1/1 to 0.5/1. The reaction rates corresponding to the various α-keto acids employed in the presence of an amount of Zn^{2+} equimolar to the pyridoxamine analog decreased in this order; phenylpyruvic acid>pyruvic acid≈4-methyl-2-oxopentanoic acid>3-methyl-2-oxobutanoic acid, whereas those in the presence of half-molar equivalents of Zn^{2+} to the pyridoxamine analog decreased in this order; pyruvic acid>phenylpyruvic acid ≈4-methyl-2-oxopentanoic acid>3-methyl-2-oxobutanoic acid. Furthermore, the use of the pyridoxamine analog with a linear "ansa" bridge resulted in a larger reaction rate than the use of the one with a branched "ansa" bridge. The solvent isotope effect is also described.

In a series of studies of the vitamin B_6-dependent enzyme mimics, we have succeeded in the asymmetric synthesis of various α-amino acids by employing the chiral pyridoxamine analogs with an "ansa" bridge between the 2- and the 5-positions of the pyridine ring as the donor of an amino group to the corresponding α-keto acids.[1,2] This stereoselective nonenzymatic transamination reaction was catalyzed by Zn^{2+}, like the usual transamination model reactions.[3] The mechanism of the transamination reaction involves the formation of the zinc chelate complex of the ketimine Schiff base (**4**) and the subsequent isomerization to the aldimine Sciff base (**6**) within the complex.[4] In order to obtain further information about the mechanism of this system, we investigated the kinetics of this nonenzymatic transamination reaction.

All the reactions examined here with the racemates of the pyridoxamine analogs proceeded quite smoothly at room temperature, and all could be followed by means of the spectral change in a methanol solution. This paper will describe the influence of the molar ratio of Zn^{2+} to the pyridoxamine analogs, and also that of the bulkiness of the "ansa" bridge in the pyridoxamine analog molecules, on the reaction rates of the nonenzymatic transamination reaction; our results indicate some different aspects from those reported for the reactions using pyridoxamine itself.[3,5]

Experimental

The pyridoxamine analogs, 15-aminomethyl-14-hydroxy-5,5-dimethyl-2,8-dithia[9](2,5)pyridinophane (**1**)[6] and 15-aminomethyl-14-hydroxy-2,8-dithia[9](2,5)pyridinophane (**2**),[1] and pyridoxal analogs, 15-formyl-14-hydroxy-5,5-dimethyl-2,8-dithia[9](2,5)pyridinophane (**7**)[6] and 15-formyl-14-hydroxy-2,8-dithia[9](2,5)pyridinophane (**8**),[7] were prepared as has been reported previously. The other materials were obtained from commercial sources. The UV spectra were recorded with a Hitachi 124 spectrometer.

† Present address: Central Research Laboratory, Nisshin Flour Milling Co., Ltd., Ooimachi, Iruma-gun, Saitama 354.

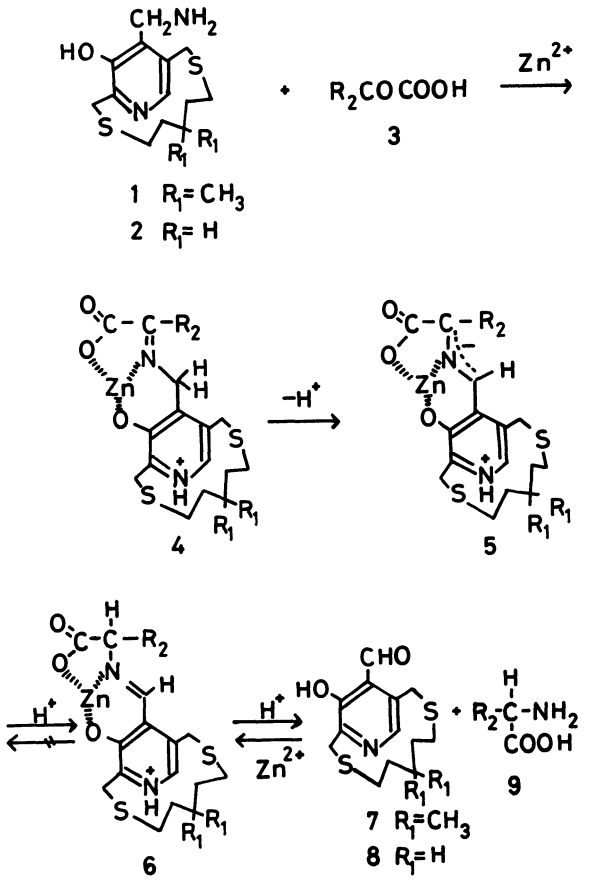

Fig. 1. Nonenzymatic transamination reaction between pyridoxamine analogs and α-keto acid.

Theree methanolic solutions (100 ml each) of a pyridoxamine analog (0.1 mmol), of α-keto acid (0.2—1.6 mmol), and of $Zn(ClO_4)_2 \cdot 6H_2O$ (0.025—0.3 mmol) were prepared. To the pyridoxamine analog solution (10 ml) we added an α-keto acid solution (10 ml) and a zinc perchlorate solution (10 ml) successively; we then immediately diluted them with methanol until the total volume of the solution was 100 ml. The solution was stirred at 23 °C, and aliquots of the solution were taken at

regular time intervals for recording the electronic-absorption spectrum.

Results and Discussion

Spectral Changes. The rates of the changes in the absorption spectra that occur when the pyridoxamine analog (**1**), sodium pyruvate, and zinc perchlorate solutions are mixed simultaneously in the molar ratios of 1 : 4 : 0.5 and 1 : 4 : 1 are shown in Figs. 2 and 3 respectively. When the molar ratio of Zn^{2+} to the pyridoxamine analog (**1**) was 0.5/1, only one peak at 305 nm was formed initially. As the intensity of the 305 nm peak decreased with time, a newly formed peak at 395 nm increased, accompanied by the formation of a couple of isosbestic points at 290 and 340 nm (Fig. 2).

When the molar ratio of Zn^{2+} to the pyridoxamine analog (**1**) was 1/1, the initial spectrum in the reaction had an absorption maximum at 305 nm and a shoulder at 320 nm. As the peak at 305 nm disappeared, the absorption at 320 nm became a single absorption maximum within 3 h. With the gradual decrease in the peak at 320 nm with time, the band at 395 nm is strengthened, with its isosbestic points at 290 and 350 nm (Fig. 3). Although the final spectra were quite similar in both cases, the rate of the absorption spectral change was much smaller in the latter case (Zn^{2+}/**1**=1/1) than in the former case (Zn^{2+}/**1**=0.5/1). The final absorption spectra in both cases were the same as those of the Zn^{2+}–aldimine chelates (**6**) prepared from the pyridoxal analog (**7**), sodium salt of alanine, and zinc perchlorate in the molar ratios of 1 : 4 : 0.5 and 1 : 4 : 1 respectively. These facts suggest that the transformation of the ketimine (**4**) to the aldimine (**6**) was completed within the chelated complex, in each cases including a different amount of Zn^{2+}; the mode of the chelation also seemed to be different.

Matsushima and Martell have reported kinetic studies of the reaction between pyridoxamine, potassium 3-methyl-2-oxobutanoic acid, and zinc acetate to produce Zn^{2+} chelate of pyridoxylidenevaline.[3] They used the absorption band of the Zn^{2+} chelate of pyridoxylidenevaline at 385 nm for these kinetic studies because of its large molecular extinction coefficient, and also because the pyridoxylidenevaline chelate is the only substance that might be present which absorbs at that wavelength. In the same manner, we employed for the present kinetic studies the 395 nm band, which should be assigned to the Zn^{2+}–aldimine chelate (**6**). The plot of $\ln A_\infty/(A_\infty - A_t)$ against the time t (where A_∞ and A_t indicate the optical densities at 395 nm at the completion of the reaction and the time t respectively) gave straight lines. This indicates that these reactions obeyed first-order kinetics for the formation of the Zn^{2+}–aldimine chelate. The first-order rate constant, k_{opsd}, was obtained for the slopes of the straight lines.

Influence of the Concentration of Keto Acid. The results of kinetic runs in which the concentration of the pyridoxamine analog (**1**) was kept at 1.0×10^{-4} M (1 M=1 mol dm^{-3}), while those of the α-keto acids and zinc perchlorate were varied, are shown in Table 1. When the molar ratio of Zn^{2+} to the pyridoxamine

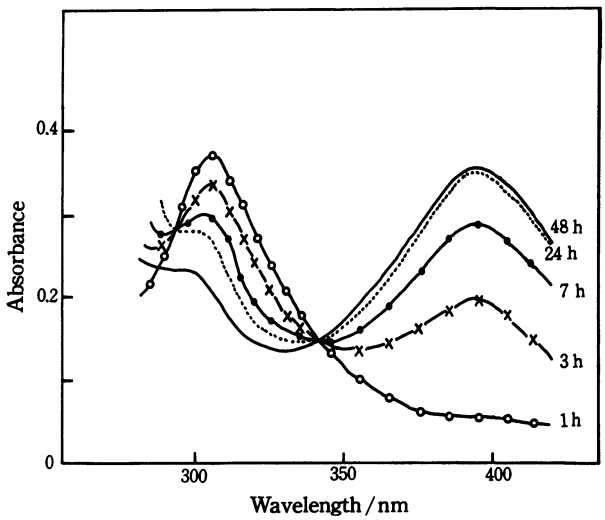

Fig. 2. Changes of electronic absorption spectra with time for a methanolic solution of pyridoxamine analog (**1**) (1.0×10^{-4} M), zinc perchlorate (0.5×10^{-4} M), and sodium pyruvate (4.0×10^{-4} M).

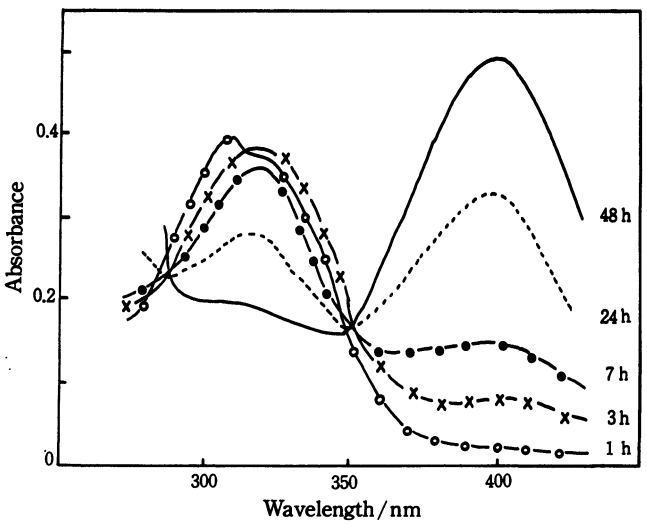

Fig. 3. Changes of electronic absorption spectra with time for a methanolic solution of pyridoxamine analog (**1**) (1.0×10^{-4} M), zinc perchlorate (1.0×10^{-4} M), and sodium pyruvate (4.0×10^{-4} M).

analog (**1**) was 0.5/1, the rate constants increased very slightly with the increase in the α-keto acid concentration from 2.0×10^{-4} M up to 6.0×10^{-4} M, while they were almost constant at higher α-keto acid concentrations ($\approx8.0\times10^{-4}$ M). When the molar ratio of Zn^{2+}/**1** was 1/1, the rate constants were little influenced by the concentration of the α-keto acids. Such an essential independence of the rate constants from the concentration of the α-keto acids indicates that the rate-determining step in the nonenzymatic transamination reaction is not the formation of the Zn^{2+}–ketimine chelates (**4**), but its isomerization to the Zn^{2+}–aldimine chelates (**6**), which is comprised of two reaction stages: the deprotonation of **4** and the protonation of the resulting **5**. The electronic absorption ascribable to **5** has not been observed,[8] suggesting that the protonation of **5** takes

Table 1. Observed rate constants for Zn^{2+}-catalyzed transamination reaction between **1**[a] and RCOCOONa

R	$[Zn^{2+}]$ 10^{-4} M	[RCOCOONa] 10^{-4} M	k_{obsd} 10^{-5} s^{-1}
CH_3	0.5	2.0	8.0
	0.5	4.0	9.0
	0.5	6.0	10.4(9.6)[b]
	0.5	8.0	9.5
	0.5	16.0	6.7
	1.0	2.0	1.3
	1.0	4.0	1.3
	1.0	6.0	1.4
	1.0	8.0	1.4
$C_6H_5CH_2$	0.5	2.0	6.2
	0.5	4.0	7.5
	0.5	6.0	7.8(7.1)[b]
	0.5	8.0	7.4
	0.5	16.0	4.9
	1.0	2.0	3.1
	1.0	4.0	3.1
	1.0	6.0	3.1
	1.0	8.0	3.7
$(CH_3)_2CHCH_2$	0.5	2.0	4.8
	0.5	4.0	6.4
	0.5	6.0	7.8(7.1)[c]
	0.5	8.0	7.4
	0.5	16.0	5.8
	1.0	2.0	0.9
	1.0	4.0	1.1
	1.0	6.0	1.4(1.1)[c]
	1.0	8.0	1.3
$(CH_3)_2CH$	0.5	2.0	1.2
	0.5	4.0	1.1
	0.5	6.0	1.2
	0.5	8.0	1.2
	1.0	2.0	0.6
	1.0	4.0	0.6
	1.0	6.0	0.7
	1.0	8.0	0.7

a) **1**: 1.0×10^{-4} M. b) (*S*)-**1**: 1.0×10^{-4} M. c) (*R*)-**1**: 1.0×10^{-4} M.

place rapidly to give **6**. The observation that the employment of a large excess of α-keto acid reduced the rate constant might be explained by the chelation with the α-keto acid that lowers the concentration of the utilizable Zn^{2+}.

Influence of the Kind of Keto Acid. The rate constants decreased in this order; phenylpyruvic acid> pyruvic acid ≈4-methyl-2-oxopentanoic acid>3-methyl-2-oxobutanoic acid when Zn^{2+} and the pyridoxamine analog (**1**) were used in a molar ratio of 1/1. The largest rate constant of phenylpyruvic acid might be explained by assuming that the electron-withdrawing ability of the phenyl group stabilizes the carbanion intermediates (**5**).[9,10] On the other hand, the employment of half-molar equivalents of Zn^{2+} to **1** resulted in this order; puruvic acid>phenylpyruvic acid≈4-methyl-2-oxopentanoic acid>3-methyl-2-oxobutanoic acid. Since the amount of Zn^{2+} is restricted under these

Table 2. Observed rate constants for Zn^{+2}-catalyzed transamination reaction between **2**[a] and RCOCOONa

R	$[Zn^{2+}]$ 10^{-4} M	[RCOCOONa] 10^{-4} M	k_{obsd} 10^{-5} s^{-1}
CH_3	0.5	2.0	10.0
	0.5	6.0	16.0
	1.0	2.0	2.7
	1.0	6.0	3.1
$C_6H_5CH_2$	0.5	2.0	8.2
	1.0	2.0	4.6
	1.0	6.0	5.2
$(CH_3)_2CHCH_2$	0.5	2.0	5.6
	0.5	6.0	8.2
	1.0	2.0	1.0
	1.0	6.0	1.5
$(CH_3)_2CH$	0.5	2.0	1.3
	0.5	6.0	1.4
	1.0	2.0	0.6
	1.0	6.0	0.9

a) **2**: 1.0×10^{-4} M.

conditions, a rigid octahedral Zn^{2+} intermediate coordinated with 2 mol of the ketimine ligands is formed.[11,12] The reaction rate is influenced more by the steric factor than by the electronic factor in this situation.[13,14] This is the reason why the order of the rate constants between pyruvic acid and phenylpyruvic acid was reversed when Zn^{2+}/**1** ratio was changed from 1/1 to 0.5/1.

Influence of the Bulkiness of the "Ansa" Bridge in the Pyridoxamine Analogs. A comparison of Table 2 with Table 1 shows that the rate constants of the transamination reaction using **2** was larger than those using **1**. The branched-bridge chain in **1** seems to affect the reaction rate more negatively than the linear one in **2**.

Influence of the Molar Ratio of Zn^{2+} to Pyridoxamine Analogs. According to Matsushima and Martell,[3] the rate constants for the formation of the Zn^{2+} chelate of pyridoxylidenevaline decreased with the decrease in the Zn^{2+} concentration in the range from 2.0×10^{-4} M to 0.5×10^{-4} M (pyridoxamine: 1.0×10^{-4} M and potassium 3-methyl-2-oxobutanoate: 1.0×10^{-3} M). In contrast to their results, the rate constants of our nonenzymatic transamination reaction using the pyridoxamine analogs with a pyridinophane structure such as **1** increased almost linearly as the Zn^{2+} concentration was decreased from 1.0×10^{-4} M to 0.5×10^{-4} M; they then decreased at lower concentrations of Zn^{2+} ($\approx0.25\times10^{-4}$ M). When the concentration of Zn^{2+} was above 1.0×10^{-4} M, the rate constants were constant. The results are illustrated in Fig. 4. The mechanism of such interesting changes in the reaction rates is obscure at this stage. However, they remind us of a similar correlation between the ratio of Zn^{2+}/**1** and the enantiomeric excesses of the α-amino acids that was obtained through the same transamination reaction using chiral **1**[2]; *i.e.*, an enhancement of the enantiomeric excesses was observed with a lowering of the ratio of Zn^{2+}/chiral **1** from 1/1 to 0.5/1, like the enhancement of the reaction rates with the racemate in this paper. The figures in

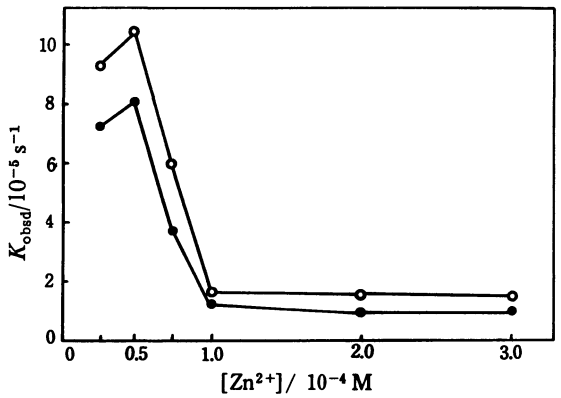

Fig. 4. Variation of k_{obsd} as a function of zinc perchlorate concentration; solutions contained 1.0×10^{-4} M pyridoxamine analog (**1**) with 6.0×10^{-4} M sodium pyruvate (○) and with 6.0×10^{-4} M sodium 4-methyl-2-oxopentanoate (●).

parentheses in Table 1 indicate that there was little difference in the reaction rates between the racemic pyridoxamine analog and the chiral one. This means all discussions of the reaction rates concerning the racemate in this paper are also applicable to the reactions with the chiral one. Consequently, it may be concluded in the chiral system that the enhancement of both the reaction rate and stereoselectivity at the same time can be attained by lowering the ratio of Zn^{2+}/**1**. These interesting phenomena are suggestive of some role of the "ansa" bridge present in the pyridoxamine analog in determining the reaction rate, as this seemed to dominate the enantiomeric excesses of the products in the chiral system.[4]

Solvent Isotope Effect. We have also reported that the α-proton of an amino acid produced through the nonenzymatic transamination reaction was deuteriated when methanol-*d* (MeOD) was used as the solvent.[4] This indicates that the deuterium atom comes directly from the solvent. Furthermore, the pyridoxal analog recovered after the reaction contained no deuterium atom. These results and the aforementioned fact that there was no observable electronic absorption ascribable to **5** strongly support the idea that the rate-determining step of this transamination reaction is the deprotonation of **4** (Fig. 1). In order to measure the solvent isotope effect, the reaction in MeOD was examined. The rate constant was found to be about three times smaller in MeOD than in MeOH. The obtained hydrogen isotope effects, k^H/k^D, were 3.5 for **1** and 2.9 for **2** (1.0×10^{-4} M pyridoxamine analogs, 0.5×10^{-4} M Zn^{2+}, and 6.0×10^{-4} M sodium pyruvate).

References

1) H. Kuzuhara, T. Komatsu, and S. Emoto, *Tetrahedron Lett.*, **1978**, 3563.
2) Y. Tachibana, M. Ando, and H. Kuzuhara, *Chem. Lett.*, **1982**, 1765.
3) Y. Matsushima and A. E. Martell, *J. Am. Chem. Soc.*, **89**, 1331 (1967).
4) Y. Tachibana, M. Ando, and H. Kuzuhara, *Chem. Lett.*, **1982**, 1769.
5) S. Matsumoto, Y. Karube, and Y. Matsushima, *Chem. Pharm. Bull.*, **23**, 1819 (1975).
6) M. Ando, Y. Tachibana, and H. Kuzuhara, *Bull. Chem. Soc. Jpn.*, **55**, 829 (1982).
7) H. Kuzuhara, M. Iwata, and S. Emoto, *J. Am. Chem. Soc.*, **99**, 4173 (1977).
8) The absorptions corresponding to such anions as **5** are not always observable; see Refs. 9 and 10.
9) S. Matsumoto and Y. Matsushima, *J. Am. Chem. Soc.*, **96**, 5228 (1974).
10) Y. Karube and Y. Matsushima, *J. Am. Chem. Soc.*, **99** 7356 (1977).
11) N. Y. Belokon, A. S. Melikyan, T. F. Salel'va, S. V. Vitt, and V. M. Belikov, *Tetrahedron*, **36**, 2327 (1980),.
12) L. Casella and M. Gullotti, *J. Am. Chem. Soc.*, **103**, 6339 (1981).
13) M.-D. Tsai, S. R. Byrn, C.-j. Chang, H. G. Floss, and H. J. R. Weintraub, *Biochemistry*, **17**, 3177 (1978).
14) M.-D. Tsai, H. J. R. Weintraub, S. R. Byrn, C.-j. Chang, and H. G. Floss, *Biochemistry*, **17**, 3183 (1978).

 © 1983 The Chemical Society of Japan Bull. Chem. Soc. Jpn., 56, 2267—2271 (1983)

Immunoassay Using a Metal-complex Compound as a Chemiluminescent Catalyst. I. Iron(III)phthalocyanine as a Labeling Reagent

Tadashi Hara,* Motohiro Toriyama, and Kazuhiko Tsukagoshi
Department of Chemical Engineering, Faculty of Engineering, Doshisha University, Karasuma Imadegawa, Kamigyo-ku, Kyoto 602
(Received January 10, 1983)

A synthesized metal-complex compound with catalytic activity for a chemiluminescence reaction has been used for the first time as a labeling reagent for immunoassay. Several complex compounds of iron(III) and cobalt(II) were synthesized, and their catalytic activities for the chemiluminescence reaction between 5-amino-2,3-dihydro-1,4-phthalazinedione (luminol) and hydrogen peroxide (H_2O_2) were examined. Iron(III) 4,11,18,25-tetracarboxyphthalocyanine (TCP-Fe(III)) showed the highest catalytic activity. The immunoassay of free albumin was carried out by a competitive method using albumin labeled with TCP-Fe(III) by means of the carbodiimide method; free albumin in the range of 2 to 1000 μg/tube could be determined with a coefficient of variation of from 6 to 16% in 5 analyses.

In order to determine a trace amount of component in a biological sample, various immunoassays, including radioimmunoassay (RIA), enzyme immunoassay (EIA), fluoroimmunoassay, spin immunoassay, and metalloimmunoassay, have been reported. EIA is an excellent method for the determination of a trace amount of a component in a biological sample, but it has the following defects: 1) an inhomogeneous antigen-antibody reaction caused by the steric hindrance of a large enzyme molecule as a labeling reagent, 2) the additional time necessary for the enzyme reaction, and 3) the instability of the enzyme.

Chemiluminescence immunoassay (CLIA) has also become a method of interest since the defects in EIA can be more or less overcome. Moreover, CLIA has the following characteristics: 1) high sensitivity, 2) rapid analysis after the separation of bound and free antigens, and 3) a simple and inexpensive apparatus. Various natural substances,[1-3] such as hemin, cytochrome c, vitamin B_{12}, ferritin, catalase, hemoglobin, and peroxidase, have been used as a labeling agent for CLIA. These labeling agents are limited by the kind and number of functional groups available for labeling, and by their instability and purity.

The use of a synthesized metal-complex compound instead of the above-mentioned natural substances as a catalyst in CLIA is supposed to make CLIA sensitive, inexpensive, and reproducible, and also to make labeling easy. No immunoassay has, however, been reported in which a synthesized metal-complex catalyst is used as a labeling reagent. In this connection, several metal-complex catalysts were synthesized by the authors, and their catalytic activities were examined, TCP-Fe(III) being found to be most promising. In the present study, albumin was selected as a model compound for the analysis of a protein. It was determined by CLIA using a metal-complex catalyst as follows: the free albumin as an analyte and labeled albumin with TCP-Fe(III) as a competitor were made to react competitively with an antibody immobilized on glass beads, and the TCP-Fe(III) on the bound fraction after the separation of the bound and free fractions was determined by measuring the chemiluminescence intensity between luminol and H_2O_2.

Experimental

Preparation of Labeled Albumin. TCP-Fe(III) as a labeling reagent was synthesized by the method of Shirai *et al.*[4,5] The human serum albumin (HSA) with TCP-Fe(III) was labeled by the carbodiimide method as follows. Five milligrams of TCP-Fe(III) was dissolved in 10 cm^3 of a potassium dihydrogenphosphate–disodium hydrogenphosphate buffer solution (pH 7.0)(Buffer Soln (A)); 20 mg of *N*-cyclohexyl-*N'*-(2-morpholinoethyl)carbodiimide - methyl *p*-toluenesulfonate (Fluka) was then added to the solution, and it was mixed for 20 min. Thirty milligrams of HSA (Sigma, Fraction V) was added to the above mixture, and the resulting mixture was incubated for 48 h at 4 °C. After the reaction, the mixture was centrifuged at 15000 *g*, and the precipitate was removed. To the supernatants we added 10 cm^3 of a saturated ammonium sulfate solution, after which the mixed solution was kept at 4 °C overnight. The supernatants was removed by centrifugation, and the precipitate thus obtained was dissolved in 2 cm^3 of Buffer Soln (A), after which the solution was dialyzed against Buffer Soln (A) to remove the ammonium sulfate. After dialysis, the solution was submitted to gel chromatography on a TOYOPEARL HW-50 (TOYO SODA) column (150 cm^3) by the use of Buffer Soln (A) as an eluent; a 30-cm^3 portion of an albumin fraction containing albumin labeled with TCP-Fe(III) was thus obtained.

Preparation of Glass Beads Immobilized Antibodies. One cubic centimeter of a saturated ammonium sulfate solution was added to 1 cm^3 of rabbit anti-HSA serum (Medical and Biological Laboratories), after which the mixture was kept at room temperature for 1 h. The precipitate was collected by centrifuging it at 10000 *g* for 10 min and was then dissolved in 2 cm^3 of a 0.005 mol dm^{-3} phosphate buffer solution (Buffer Soln (B), pH 7.2) consisting of sodium dihydrogenphosphate and disodium hydrogenphosphate, the resulting solution being dialysed overnight against Buffer Soln (B). The precipitate thus produced was centrifuged, and an immunoglobulin G fraction was obtained by purifying the supernatants on a DEAE-cellulose column equilibrated with a Buffer Soln (B).

On the other hand, the glass-bead surface was activated by holding 100 g of glass beads (4 mm diam.) at 100 °C for 6 h in 100 cm^3 of a 50 wt% sodium hydroxide solution. The glass beads were washed and dried; alkylamino-bonded glass beads were then prepared by holding the glass beads for 6 h under refluxing in 300 cm^3 of a 2% (3-aminopropyl)triethoxysilane toluene solution. The immobilization of antibodies onto alkylamino-bonded glass beads was done by the glu-

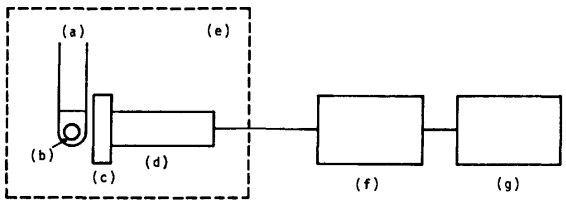

Fig. 1. Apparatus for CLIA.
a: Test tube, b: glass bead, c: shutter, d: photomultiplier, e: dark box, f: photon counter, and g: recorder.

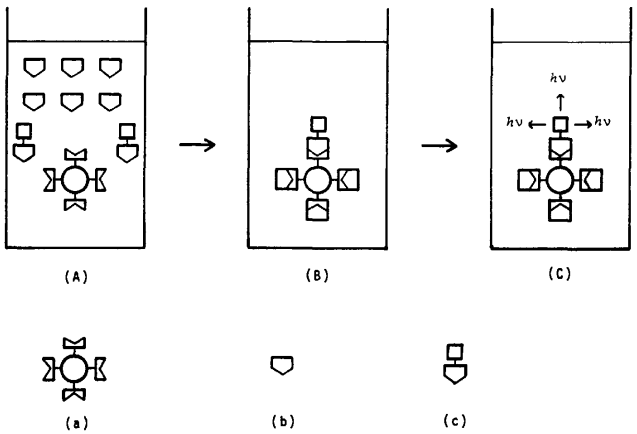

Fig. 2. Procedure for immunoassay.
A: Antigen-antibody reaction, B: separation of bound and free fractions, and C: measurement of chemiluminescence intensity. a; Glass bead immobilized with antibody, b; HSA, and c; labeled albumin.

taraldehyde method as follows. Thirty grams of the glass beads were dipped in 50 cm^3 of 5% glutaraldehyde/Buffer Soln (B) (0.01 mol dm^{-3}), and the mixture was made to react for 24 h at room temperature. After washing with Buffer Soln (B), the activated glass beads were dipped in 50 cm^3 of Buffer Soln (B) containing one-third of the antibodies which were taken out of 1 cm^3 of the antiserum; the mixture was then held at 4 °C for 48 h. The glass beads thus immobilized with antibodies were preserved at 4 °C in a Buffer Soln (B) containing 0.1% sodium azide and 0.1% bovine serum albumin.

Antigen-antibody Reaction. Twenty-five cubic millimeters of labeled albumin (containing about 0.6 μg of conjugated TCP-Fe(III)) were added to 1 cm^3 of Buffer Soln (B) containing a definite amount of albumin as an analyte, while one glass bead immobilized with an antibody was soaked in its solution. Thus the labeled albumin and the free albumin as an analyte were made to react competitively at 4 °C overnight with an antibody immobilized on the glass bead (competitive immunoassay).

Measurement of Chemiluminescence Intensity. The apparatus used for the measurement of the chemiluminescence intensity is shown in Fig. 1. One cubic centimeter of a 1.0×10^{-3} mol dm^{-3} luminol solution (pH 10.2, boric acid–potassium hydroxide buffer) and 1 cm^3 of a 2.5×10^{-3} mol dm^{-3} H_2O_2 solution were mixed in a 90×10 mm diam. test tube. The test tube was placed in front of the photomultiplier (Hamamaust TV, R464) equipped with a shutter (Copal No. 3), after which it was allowed to stand for 30 min before measurement in order to stabilize the chemiluminescence background.

After the antigen-antibody reaction, the glass beads immobilized with antibodies were washed twice with Buffer Soln (B) and then put into the above mixed solution. The shutter of the photomultiplier was immediately opened, and the chemiluminescence intensity was measured by means of a photon counter (Hamamatsu TV, C1230), the output being recorded by a Matsushita Communication Industrial apparatus (VP-6521A). Since the chemiluminescence intensity showed a maximal value about 3 min after the glass beads were put in, the maximal value was taken as the chemiluminescence intensity of a sample.

The procedure for immunoassay is shown schematically in Fig. 2.

Results and Discussion

Selection of a Labeling Reagent. The requirements for the catalyst as a labeling reagent in CLIA may be summarized as follows: 1) the catalytic activity for a chemiluminescence reaction is large enough for the sensitive detection of an analyte; 2) it has a functional group available for labeling; 3) a labeling reaction is feasible under mild conditions, 4) it is a stable compound, and 5) it can easily be prepared. Though metal ions such as cobalt(II), iron(III), copper(II), and osmium(VIII) show high catalytic activity for chemiluminescence reactions between luminol and H_2O_2, these metal ions can not satisfy all the requirements.

On the other hand, it is well known that chelate compounds, such as peroxidase, microperoxidase, hemin, hematin, and (*N,N'*-disalicylideneethylenediaminato)-cobalt(II),[6] strongly catalyze the chemiluminescence reaction between luminol and H_2O_2. Therefore, some kinds of chelate compounds may be supposed to be useful as labeling reagents. The common structure in the above-mentioned chelate compounds has the following characteristics: 1) the center of a molecule is occupied by iron(III) or cobalt(II), whose coordination number is six, 2) four coordination sites in a planar square are strongly linked with four donor atoms in a quadridentate ligand, and 3) two axial sites are weakly linked with donor atoms.

Cobalt(II) and iron(III) complex compounds were

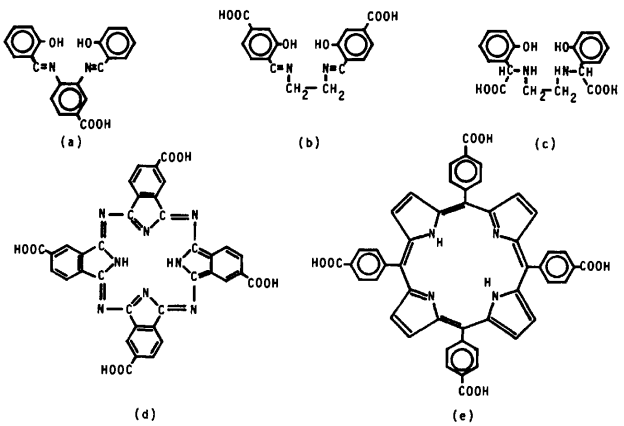

Fig. 3. Structure of ligands.
a: 3,4-Bis(salicylideneamino)benzoic acid, b: *N,N'*-bis-(4-carboxysalicylidene)ethylenediamine, c: *N,N'*-bis[2-(*o*-hydroxyphenylacetic acid)]ethylenediamine, d: 4,11, 18,25-tetracarboxyphthalocyanine, and e: 5,10,15,20-tetrakis(4-carboxyphenyl)porphine.

TABLE 1. ACTIVITY OF VARIOUS CATALYSTS IMMOBILIZED[a] ON A GLASS DISK

Catalyst		Chemiluminescence intensity/Hz	Relative activity
Ligand	Metal		
Blank		840	1.0
N,N'-Bis[2-(*o*-hydroxyphenylacetic acid)]ethylenediamine	Iron(III)	1900	2.3
	Cobalt(II)	1700	2.0
5,10,15,20-Tetrakis(4-carboxyphenyl)porphine	Cobalt(II)	1400	1.7
4,11,18,25-Tetracarboxyphthalocyanine	Iron(III)	350000	420
	Cobalt(II)	5200	6.2
N,N'-Bis(4-carboxysalicylidene)ethylenediamine	Cobalt(II)	35000	42
3,4-Bis(salicylideneamino)benzoic acid	Iron(III)	82000	98
	Cobalt(II)	7600	9.0
Hematin[b]		300000	360

a) An alkylamino-bonded glass disk was soaked in 20 cm^3 of a 1.0×10^{-3} mol dm^{-3} aqueous complex catalyst solution, and to it a 84.7-mg portion of *N*-cyclohexyl-*N'*-(2-morpholinoethyl)carbodiimide-methyl *p*-toluenesulfonate was added, the mixture then being allowed to react at room temperature for 24 h. b) Hematin was made to react with dicyclohexylcarbodiimide.

prepared by the use of the following quadridentate ligands, each of which has four donor atoms besides the carboxyl group used for the labeling reaction: 5,10,15,20-tetrakis(4-carboxyphenyl)porphine,[7,8] 4,11,18,25-tetracarboxyphthalocyanine, 3,4-bis(salicylideneamino)benzoic acid, *N,N'*-bis[2-(*o*-hydroxyphenylacetic acid)]ethylenediamine (Dojin Laboratories, EDDHA), and *N,N'*-bis(4-carboxysalicylidene)ethylenediamine[9] (Fig. 3). Their catalytic activities for the chemiluminescence reaction between luminol and H_2O_2 were measured by means of the flow-injection analysis system[10,11] and compared with each other. The flow diagram of the flow-injection analysis system and its experimental conditions are shown in Fig. 4, while the results obtained are shown in Fig. 5.

To examine the catalytic activity of a labeled complex compound, an experiment was carried out as follows: the surface of a 12-mm-diam. alkylamino-bonded glass disk was immobilized with a complex catalyst by means of the carboidimide method, and then the glass disk was placed in a stream of a mixed solution (pH 10.2, flow rate 1.96 cm^3 min^{-1}) of luminol (5.0×10^{-4} mol dm^{-3}) and H_2O_2 (1.25×10^{-3} mol dm^{-3}); after the chemiluminescence intensity was then measured with the apparatus[12] shown in Fig. 6. The results are shown in Table 1.

Figure 5 and Table 1 confirm that iron complexes generally show a higher catalytic activity and that their activities remain even after the bond formation of a carboxyl group. Especially, the catalytic activity of TCP–Fe(III) was higher than that of hematin,[13] which had been reported to be one of the most sensitive catalysts for chemiluminescence reactions. Hemin[2] has to be labeled in dimethyl sulfoxide, while TCP–Fe(III) can be labeled easily in water. Judging from these results, TCP–Fe(III) is superior to hemin.

Labeling of Albumin with TCP–Fe(III). The labeling in the immunoassay has to be carried out under mild conditions, since the analyte to be labeled is

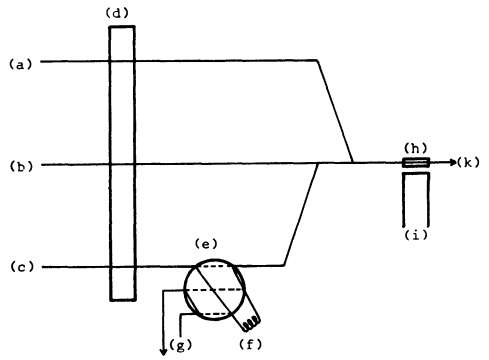

Fig. 4. Flow diagram of the flow-injection system.
a: Luminol (1.0×10^{-3} mol dm^{-3}, pH 10.2, flow rate 2.5 cm^3 min^{-1}), b: H_2O_2 (2.5×10^{-3} mol dm^{-3}, flow rate 2.5 cm^3 min^{-1}), c: buffer solution (flow rate 2.5 cm^3 min^{-1}) d: pump, e: sample inlet, h: flow-cell, i: photomultiplier, and k: waste.

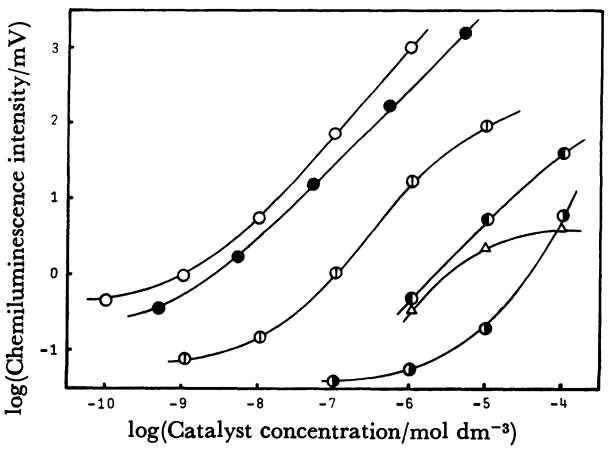

Fig. 5. Relationship between catalyst concentration and chemiluminescence intensity.
○: TCP–Fe(III), ●: hematin, ◫: Co(II) *N,N'*-bis(4-carboxysalicylidene)ethylenediamine, ◐: TCP–Co(II), △: Co(II) 5,10,15,20-tetrakis(4-carboxyphenyl)porphine, and ◑: Fe(III) 3,4-bis(salicylideneamino)benzoic acid.

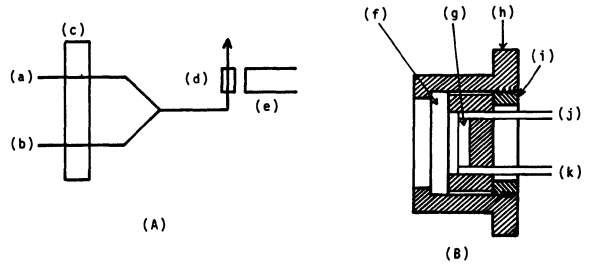

Fig. 6. Apparatus for measurement of chemiluminescence intensity based on the catalyst on the glass disk.
A: Flow diagram, a; luminol, b; H_2O_2, c; pump, d; flow-cell, and e; photomultiplier. B: Flow-cell. f; Window-glass, g; glass disk, h; cell holder, i; pressure screw, j; outlet, and k; inlet.

chemically unstable. Antigen as an analyte can be easily labeled with TCP-Fe(III) under mild conditions by the use of a water-soluble carbodiimide reagent, because water-soluble TCP-Fe(III) has carboxyl groups which are used for the formation of an amide linkage between TCP-Fe(III) and an analyte. The absorption spectrum of free TCP-Fe(III) in Buffer Soln(A) gave two peaks at 637 and 325 nm, while conjugated TCP-Fe(III) showed a peak at 630 nm and two shoulders at 576 and 338 nm. The retention volume of albumin labeled with TCP-Fe(III) in gel chromatography was slightly smaller than that of albumin alone. Judging from these results, it was concluded that albumin can be certainly labeled with TCP-Fe(III).

In addition, the precipitin arc of labeled HSA with TCP-Fe(III) in an immunodiffusion technique using rabbit anti-HSA serum was the same as that of HSA. This means that the activity of albumin for antigen-antibody reactions is not lost by its labeling.

The catalytic activities of conjugated TCP-Fe(III) and free TCP-Fe(III) for chemiluminescence reactions were also examined (Fig. 7). The concentration of conjugated TCP-Fe(III) in a labeled albumin solution was estimated from the absorption of the solution at 325 nm. As can be seen from Fig. 7, there was no marked difference between the catalytic activities of conjugated TCP-Fe(III) and free TCP-Fe(III). Thus, TCP-Fe(III) was shown to be useful as a labeling reagent for immunoassay.

Immunoassay. The relationship between the time consumed for an antigen-antibody reaction and the chemiluminescence intensity is shown in Fig. 8. The chemiluminescence intensity of a bound fraction for a certain time consumed for an antigen-antibody reaction is shown in Fig. 8 on the basis of the chemiluminescence intensity of the bound fraction which was made to react with albumin labeled with TCP-Fe(III) for 42 h. As can be seen from Fig. 8, the chemiluminescence intensity of a bound fraction was almost constant after 8 h. In all the following experiments, the antigen-antibody reaction was done overnight at 4 °C.

Figure 9 shows a calibration curve obtained by the competitive method. According to this calibration curve, albumin in the range of from 2 to 1000 μg/tube can be determined with a coefficient of variation of from 6 to 16% for 5 analyses. This calibration curve was linear, but not sigmoidal as is seen in a usual immunoas-

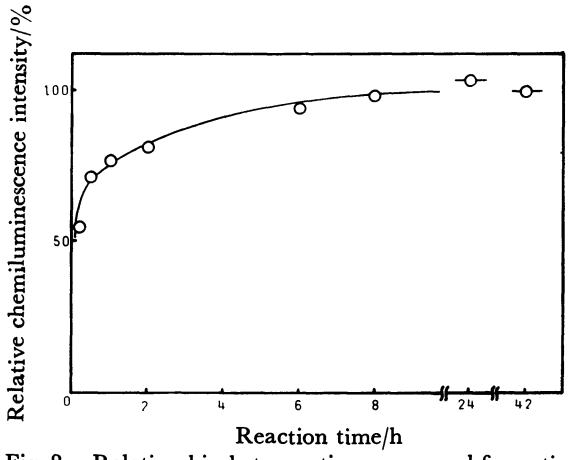

Fig. 8. Relationship between time consumed for antigen-antibody reaction and relative chemiluminescence intensity.

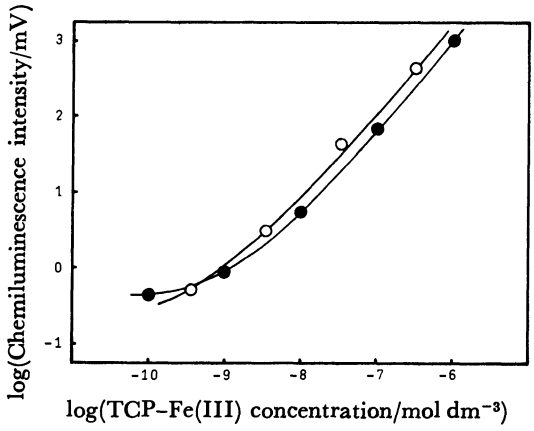

Fig. 7. Relationship between concentration of conjugated TCP-Fe(III) and chemiluminescence intensity.
○: Conjugated TCP-Fe(III) and ●: free TCP-Fe(III).

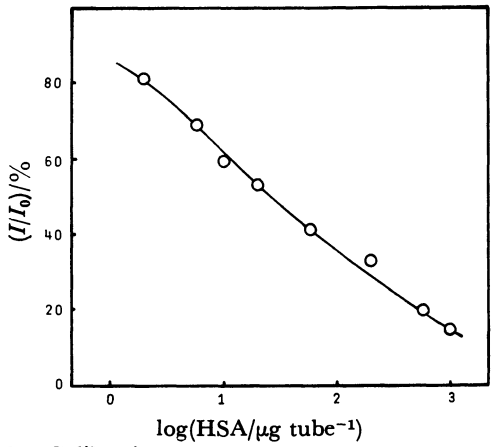

Fig. 9. Calibration curve.
I, I_0: Chemiluminescence intensity of the sample in the presence or absence of HSA.

say. This may be supposed to be due to the competitive reaction under unfavorable conditions,[14] *e.g.*, the ues of heterogeneous labeled albumin.

The present method is superior to the conventional methods of immunoassay, such as RIA and EIA, in the following points: 1) no counterplan is necessary for hazards of radioactivity in RIA; 2) the time necessary for measurement is short in comparison with EIA because the measurement is based on the chemiluminescence reaction, and 3) an analytical value is not so much influenced by contaminants[3] because the bound and free fractions are easily separated by the use of glass beads immobilized with antibodies.

It is concluded from the above-mentioned results that a synthesized metal-complex compound which works as a catalyst for a chemiluminescence reaction is useful and promising for immunoassay. Though the sensitivity and precision in the present work were not always satisfactory, they are now being improved by investigating the conditions for antigen-antibody reactions, chemiluminescence reactions, and instrumental measurements. Additional results will be reported in the near future.

References

1) Corning Glass Works, Jpn. Kokai Tokkyo Koho, 2790133 (1979); U. S. Appl. 815091 (1977); *Chem. Abstr.*, **90**, 182799f (1979).
2) Y. Ikariyama, S. Suzuki, and M. Aizawa, *Anal. Chem.*, **54**, 1126 (1982).
3) H. Arakawa, M. Maeda, and A. Tsuji, *Anal. Biochem.*, **97**, 248 (1979).
4) H. Shirai, S. Yagi, A. Suzuki, and N. Hojo, *Makuromol. Chem.*, **178**, 1889 (1977).
5) H. Shirai, A. Maruyama, K. Kobayashi, and N. Hojo, *Makuromol. Chem.*, **181**, 575 (1980).
6) I. Diehl and C. C. Hach, *Inorg. Synth.*, Vol. III, 196 (1950).
7) A. D. Alder, *J. Org. Chem.*, **32**, 476 (1967).
8) L. D. Rollmann, *J. Am. Chem. Soc.*, **97**, 2132 (1975).
9) R. H. Bailes and M. Calvin, *J. Am. Chem. Soc.*, **69**, 1886 (1947).
10) K. Tsukagoshi, M. Toriyama, and T. Hara, *Sci. Eng. Rev. Doshisha Univ.*, **23**, 119 (1982).
11) T. Hara, M. Toriyama, and K. Tsukagoshi, *Bull. Chem. Soc. Jpn.*, **56**, 1382 (1983).
12) T. Hara, M. Toriyama, and M. Imaki, *Bull. Chem. Soc. Jpn.*, **55**, 1854 (1982).
13) H. A. Neufeld, C. J. Conklin, and R. D. Towner, *Anal. Biochem.*, **12**, 303 (1965).
14) C. J. Halfman, *Anal. Chem.*, **51**, 2306 (1979).

An Improved Preparation and Characterization of Tetrahedral Co^{II} and Co^{III} Complexes with Dodecatungstate as the Tetrahedral Ligand

Kenji Nomiya, Ryoichi Kobayashi, and Makoto Miwa*
Department of Industrial Chemistry, Faculty of Engineering, Seikei University, Musashino, Tokyo 180
(Received January 28, 1983)

Tetrabutylammonium salt of the 12-tungstoheteropolyanion with central Co^{II} as the heteroatom in a tetrahedral oxygen environment, $[Co^{II}W_{12}O_{40}]^{6-}$, has been prepared by an improved manner. This manner remarkably shortens the total time needed for preparation, especially the time for purification, and gives a compound of a high purity. The corresponding Co^{III} compound has been obtained by oxidation with potassium peroxodisulfate from the potassium salt of the Co^{II} compound; its spectroscopic data (IR, near-infrared, UV-vis, and MCD) are presented.

Recently we have reported on the syntheses and the spectroscopic properties of tetrahedral transition-metal complexes of the $[MW_{12}O_{40}]$ type ($M=Cu^{II}$, Fe^{III}, Co^{II}), with dodecatungstate as the tetrahedral ligand.[1] In this paper, we wish to report on an improved method for the preparation of the cobaltate(II) ion and its subsequent conversion to the cobaltate(III) ion. The purities and absorption coefficients of the compounds obtained here were superior to those previously reported.[1-3] The cobaltate(III) ion is a d^6 high-spin complex in a tetrahedral field of the $W_{12}O_{40}$ ligand and is one of the spectrophotometrically interesting compounds. From the point of view of a reaction, the Co^{III} compound has been known to promote the oxidation of alkyl-substituted aromatic hydrocarbons[4] and to exchange an electron with the parent Co^{II} compound *via* an outer-sphere mechanism.[5] In this paper, we wish also to report the spectroscopic data (IR spectra both on a solid and in a solution and the near-infrared and UV-vis spectra and the MCD spectra in the UV-vis region) of the tetrabutylammonium cobaltate(III).

Experimental

The near-infrared and vis-UV absorption spectra were measured by means of a Hitachi 340-spectrophotometer with a computer keyboard attached. The intensity is expressed in terms of the molar absorptivity, ε, which has units of mol^{-1} dm^3 cm^{-1}. The MCD spectra were recorded by means of a JASCO J-40AS spectropolarimeter with a 10.0-kG† electromagnet mounted on it. The MCD intensity is expressed in terms of $\Delta\varepsilon=\varepsilon_l-\varepsilon_r$, which has units of mol^{-1} dm^3 m^{-1} G^{-1}. Measurements were made at room temperature. The IR spectra in acetonitrile were measured by using a KBr cell with a 0.1-mm optical path.

Preparation. $K_6[Co^{II}W_{12}O_{40}]\cdot nH_2O$: The pH of a sodium tungstate solution ($Na_2WO_4\cdot 2H_2O$ 79.2 g (0.24 mol) in 160 cm^3 water) was adjusted within 6.5—7.0 by the use of glacial acetic acid. The solution was then boiled over an open flame. $Co(CH_3COO)_2\cdot 4H_2O$ 10.0 g (0.04 mol) was dissolved in 50 cm^3 hot water, whereinto some drops of glacial acetic acid were added. This solution was then added, with continuous stirring, into a boiling sodium tungstate solution. After this addition, the solution was boiled further for about 10 min. The hot solution was then filtered, and a hot, aqueous solution saturated with KCl (52 g) was added to the boiling filtrate. The dark green solution thus obtained was allowed to stand overnight at room temperature. The green crystals of the dicobalt species, $K_8[CoCoW_{11}O_{40}H_2]$, obtained were recrystallized twice from an acid solution with the ratio of 2 cm^3 of glacial acetic acid to 400 cm^3 of water. The green compound obtained in this step was not yet pure. The crude sample was dissolved in about 150 cm^3 of water, whereinto ether was added. Into this solution, 400 cm^3 of 6 M-sulfuric acid (1 M=1 mol dm^{-3}) was continuously stirred, drop by drop. The system separated into three layers; the highest was an ether, and the second was an aqueous layer, while the lowest layer contained the ether adduct of 12-tungstocobaltic acid and metatungstic acid as impurities. The lowest layer was collected, diluted with a small amount of water, and evaporated to dryness on a steam-bath. During the process, metatungstic acid (white) was decomposed to tungsten oxide (yellow), which was insoluble in water. The residue was extracted with water and again heated on a steam-bath. This procedure was repeated until no yellow compound was formed. During the ether-extraction and the purification, the intermediate dicobalt species was changed to the monocobalt species. Free acid, $H_6[Co^{II}W_{12}O_{40}]$, obtained as blue-green crystals, was converted to the potassium salt from a concentrated aqueous solution of potassium chloride. The potassium salt was coarsely ground and thoroughly dried at 110 °C; in this procedure, the hydrogen chloride as an adduct was lost. When the compound was analyzed, it was found to be potassium tetrabutylammonium salt. Found: C, 19.91; H, 3.79; N, 1.66%. Calcd for $K_2[(C_4H_9)_4N]_4[Co^{II}W_{12}O_{40}]$: C, 19.84; H, 3.72; N, 1.75%.

$K[(C_4H_9)_4N]_4[Co^{III}W_{12}O_{40}]$: Using the potassium salt of the Co^{II} compound, the potassium salt of the Co^{III} compound was prepared by oxidation with potassium peroxodisulfate according to the method of Baker and his co-workers.[2,3] It should be noted that the free acid of the Co^{II} compound could not be directly converted into that of the Co^{III} compound because of the decomposition of the peroxodisulfate by the very strong acidity of the cobaltate(II) and/or cobaltate(III). The aqueous solution, acidified with nitric acid, with an excess of tetrabutylammonium bromide was added to the aqueous solution of potassium cobaltate(III). The precipitate thus formed was filtered, washed thoroughly with water, dried *in vacuo*, and recrystallized from acetonitrile (yield, 7.2%; golden yellow). Found: C, 19.64; H, 3.71; N, 1.43%. Calcd for $K[(C_4H_9)_4N]_4[Co^{III}W_{12}O_{40}]$: C, 19.53; H, 3.74; N, 1.48%.

Results and Discussion

The cobalt(II) compound has been obtained as potassium salt by the acid-decomposition of the intermediate dicobalt species, $K_8[Co^{II}Co^{II}W_{11}O_{40}H_2]$, which is itself formed by adding a sodium tungstate solution

† 1 G=10^{-4} T.

TABLE 1. NEAR-INFRARED AND UV-vis SPECTRA OF $K_2[(C_4H_9)_4N]_4[Co^{II}W_{12}O_{40}]$ IN AN ACETONITRILE SOLUTION

Transition	Absorption maximum $10^3\ cm^{-1}$	Molar absorptivity	
		This work	Recrystallization method[1]
$^4T_1(F) \longleftarrow {}^4A_2$	6.99	59	55
	7.72	67	61
	7.87	68	62
	8.70	67	61
	9.39[a]	17	17
$^4T_1(P) \longleftarrow {}^4A_2$	15.43[a]	194	172
	15.92	209	187
	16.56[a]	186	172
	17.73[a]	102	93
Charge transfer	38.76	3.33×10^4	3.51×10^4

a) Shoulder.

TABLE 2. IR DATA OF TETRABUTYLAMMONIUM SALTS OF $MW_{12}O_{40}$ ANIONS IN A SOLID[a]

M		Assignment
Co^{II}	Co^{III}	
1017 w	1024 w	
940 s	950 s	ν(W–O, terminal)
870 vs	876 s	ν(W–O–W, octahedral edge-sharing)
760 vs	780 vs	ν(W–O–W, octahedral corner-sharing) and ν(M–O, tetrahedral); $\nu_3(F_2)$
520—580 w(br)	490—560 w(br)	
441 m	436 m	δ(O–M–O); $\nu_4(F_2)$

a) KBr disk, cm^{-1}.

to an acidic solution of cobalt(II) acetate at 80 °C.[2] The dicobalt compound has been purified by repeated recrystallizations from an acidic aqueous solution. This process takes more than one month, however, we tried the extraction with ether and 6 M-sulfuric acid for the purification of the dicobalt compound, for such extraction has been a traditional work-up for the preparation of many other analogous tetrahedral complexes $[MW_{12}O_{40}]$ ($M=Cu^{II}$, Fe^{III}, Al^{III}, Zn^{II}, and so on), as has been described by Brown and Mair.[6-8] In this manner, free acid of the monocobalt compound, $H_6[Co^{II}W_{12}O_{40}]$, could be obtained without the procedure of acid-decomposition, although metatungstic acid is present as an impurity. The cobaltate(II) acid can be easily separated by repeatedly heating the mixture on a steam-bath, followed by extraction with water, because the metatungstic acid (white) is readily decomposed to tungsten oxide (yellow), which is insoluble in water. After the isolated free acid is converted into the potassium salt, the potassium salt of the cobalt(III) compound, $K_5[Co^{III}W_{12}O_{40}]$, is obtained by oxidation with potassium peroxodisulfate. By the use of this modified manner, the total time for preparation is shortened to within two weeks.

The analytical values of two tetrabutylammonium compounds, $K_2[(C_4H_9)_4N]_4[Co^{II}W_{12}O_{40}]$, which have been obtained with both the previous recrystallization method[1] and the present ether-extraction method agree within the allowed range (0.3%). However, the intensities of the absorption bands in the near-infrared and visible regions of the previous compound are about 10% smaller than those of the present compound, whereas the intensity in the UV region is about 10% larger. Since metatungstate has only an absorption band in the UV region, it seems that the previous compound contains metatungstate as an impurity. This cannot be completely removed only by recrystallization. A contaminating metatungstate of about 10% may not influence the analytical value because of the relatively large molecular weight of the cobalt(II) compound. This shows the essential disadvantage of the recrystallization method, for such contamination significantly influences the purity of the final product, the cobalt(III) compound. The absorption maxima and molar absorptivities of the cobalt(II) compounds obtained by two methods are presented in Table 1.

IR Spectra. The frequencies of the cobalt(III) anion in the metal-oxygen vibrational region, recorded in a KBr disk, are presented in Table 2, together with the data on the parent cobalt(II) anion. The listed bands correspond to the Keggin-structure with a $W_{12}O_{40}$ skeleton and a central tetrahedral CoO_4 moiety, as has been previously in the case of the $[MW_{12}O_{40}]$ anions ($M=Cu^{II}$, Fe^{III}, Si, P).[1,9] In the undistorted tetrahedron (T_d symmetry) of an MO_4^{n-}-type ion, there are two IR active F_2 modes: $\nu_3(F_2)$ and $\nu_4(F_2)$, both triply degenerated. The former is the mode by the M–O stretching motion, and the latter, the deformation mode by the O–M–O angle bending motion. The spectral envelopes of these bands are diagnostic, whether the central-site symmetry is a regular tetrahedron or distorted, if the effects of the crystal packing and/or the environment upon these bands are eliminated. Since the ν_3 band is overlapped with the W–O–W octahedral

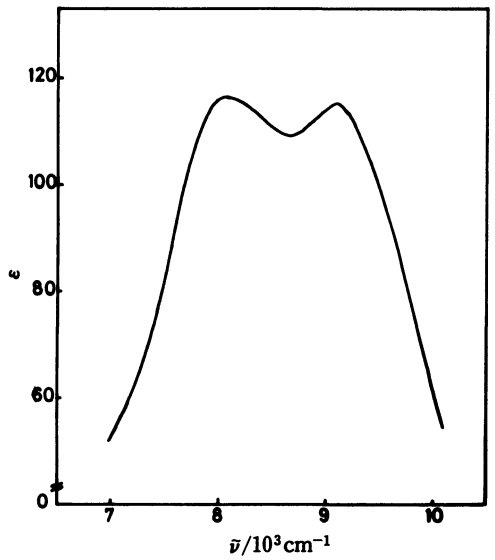

Fig. 1. Near-infrared spectrum of tetrabutylammonium salt of $[Co^{III}W_{12}O_{40}]^{5-}$ in acetonitrile solution.

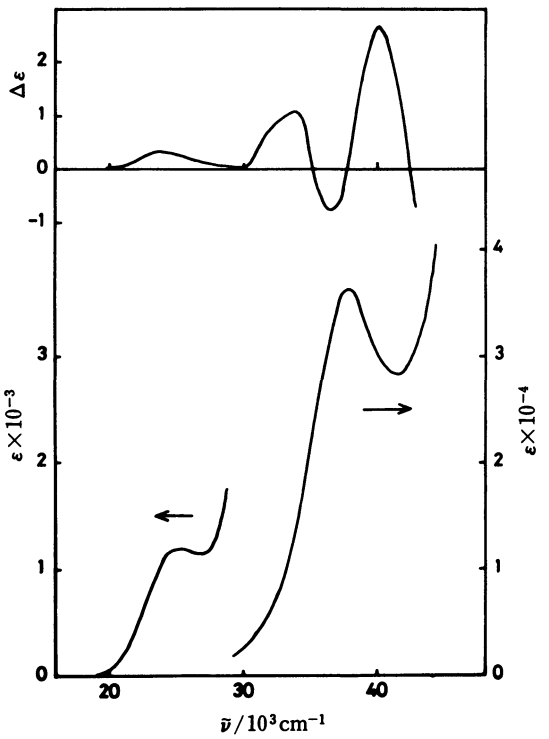

Fig. 2. Absorption and MCD spectra in UV-vis region of tetrabutylammonium salt of $[Co^{III}W_{12}O_{40}]^{5-}$ in acetonitrile solution.

corner-sharing band at *ca.* 780 cm^{-1}, the variations in the frequency and the half-width about the ν_4 band were examined in the acetonitrile solution. No splitting of the ν_4 band has been observed; a relatively symmetrical and sharp band appeared at 440 cm^{-1}, with a half-width of 25 ± 0 cm^{-1}. This fact suggests that this compound may retain an excellent T_d symmetry in the ground state, like the parent cobalt(II) compound. This is in good agreement with the crystallographical feature of $K_5[Co^{III}W_{12}O_{40}]\cdot 20H_2O$ found by Baker and his co-workers.[10]

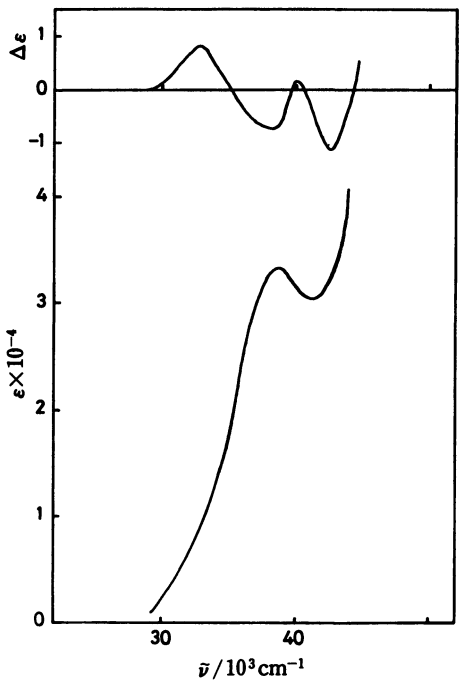

Fig. 3. UV and MCD spectra of tetrabutylammonium salt of $[Co^{II}W_{12}O_{40}]^{6-}$ in acetonitrile solution.

Absorption and MCD Spectra. The electronic spectra of the cobalt(III) compound, the absorption in the near-infrared region and the absorption and MCD in the UV-vis region, are shown in Figs. 1 and 2, respectively. The absorption in the near-infrared region with a double structure (8.06×10^3 and 9.09×10^3 cm^{-1}; ε 116 and 115 respectively; a splitting of 1.03×10^3 cm^{-1}) is due to the d-d transition. The compound is a d^6 high-spin system in a tetrahedral field. Thus, only one absorption band due to the excitation of the d shell electrons ($^5T_2\leftarrow{}^5E$) is to be expected if no account is taken of (1) the spin-orbit coupling, (2) the static and permanent distortion of the tetrahedron in the ground state, and (3) the Jahn-Teller effect in the electronically excited state.[11] In this system, the spin-orbit coupling may be discounted, for the observed splitting is 10 times the magnitude of the spin-orbit coupling constant for cobalt(III) ion. Furthermore, IR studies have inuicated that there is little distortion around the CoO_4 moiety in the ground state. It must, then, be concluded that the Jahn-Teller effect in th lectronically excited state may occur.

The large band at 37.9×10^3 cm^{-1} (ε 3.62×10^4) is due to the charge-transfer transition within the dodecatungstate lattice, such as is commonly observed in the spectra of other dodecatungstates of both central nonmetals and transition metals, and even of metatungstate. The MCD spectrum in the region clearly shows two positive and one negative components; the negative one appears near the position of the absorption maximum and exists between the two positive ones. This is characteristic of the compounds with a $W_{12}O_{40}$ skeleton, but not of the compounds with a $Mo_{12}O_{40}$ skeleton; the intensity of each component changes with the central transition metal. In Fig. 3, the absorption and MCD

in the UV region of the parent cobalt(II) compound are shown. Thus, the W–O charge-transfer band, observed as one absorption, has been found to be composed of several transitions and to be strongly influenced by the central metal.

The broad maximum at 25.4×10^3 cm^{-1} (ε 1.18×10^3) is a band unique to the cobalt(III) compound, having been first observed by Shimura and Tsuchida.[12] The MCD spectrum shows a comparably small and broad band with a positive sign. The absorption has been previously attributed to a charge transfer of the O atom, which occupies the corner of the central tetrahedral cavity, to the central Co^{III} ion.[13]

References

1) K. Nomiya, M. Miwa, R. Kobayashi, and M. Aiso, *Bull. Chem. Soc. Jpn.*, **54**, 2983 (1981).
2) L. C. W. Baker and T. P. McCutcheon, *J. Am. Chem. Soc.*, **78**, 4503 (1956).
3) L. C. W. Baker and V. E. Simmons, *J. Am. Chem. Soc.*, **81**, 4744 (1959).
4) A. W. Chester, *J. Org. Chem.*, **35**, 1797 (1970).
5) P. G. Rasmussen and C. H. Brubaker, *Inorg. Chem.*, **3**, 977 (1964).
6) J. A. Mair and J. L. T. Waugh, *J. Chem. Soc.*, **1950**, 2372.
7) D. H. Brown and J. A. Mair, *J. Chem. Soc.*, **1958**, 2597.
8) D. H. Brown, *J. Chem. Soc.*, **1962**, 3281.
9) D. H. Brown, *Spectrochim. Acta*, **19**, 585 (1963).
10) K. Eriks, N. F. Yannoni, U. C. Agarwala, V. E. Simmons, and L. C. W. Baker, *Acta Crystallogr.*, **13**, 1139 (1960).
11) F. A. Cotton and M. D. Meyers, *J. Am. Chem. Soc.*, **82**, 5023 (1960).
12) Y. Shimura and R. Tsuchida, *Bull. Chem. Soc. Jpn.*, **30**, 502 (1957).
13) V. E. Simmons, Ph. D. Thesis, Boston University, 1963.

Circular Dichroism Spectra and Stereochemistry of Dicyanotetrakis-(diamine)-tetra-μ-hydroxo-tricobalt(III)(3+) Complexes

Satoshi KAKI,* Kazuaki YAMANARI, and Yoichi SHIMURA
Department of Chemistry, Faculty of Science, Osaka University, Toyonaka, Osaka 560
(Received February 3, 1983)

The chiral tetra-μ-hydroxo-trinuclear complexes, *cis*-$[Co(CN)_2\{(OH)_2Co(NH_3)_4\}_2]^{3+}$ and *cis*-$[Co(CN)_2\{(OH)_2Co(diamine)_2\}_2]^{3+}$ have been prepared and separated into their optical isomers and/or diastereomers by column chromatography (diamine: ethylenediamine, (*R*)-1,2-propanediamine, and (*S,S*)-1,2-cyclohexanediamine). The absolute configurations of isomers have been assigned on the basis of their CD and ^{13}C NMR spectra and the characterization of mononuclear complex produced by decomposition of the trinuclear isomers of ethylenediamine ligands. It has been proved that the main CD contributions due to the two chiral $Co(OH)_4(CN)_2$ and $Co(N)_4(OH)_2$ centers are additive for the present systems.

Octaamminedicyano-tetra-μ-hydroxo-tricobalt (III) complex salts have been prepared from the reaction of "hexol" complex[1,2] $[Co\{(OH)_2Co(NH_3)_4\}_3]^{6+}$ with excess cyanide by Siebert and Schiedermaier,[3] the composition of the trinuclear(3+) ion being comfirmed by X-ray crystal structure analysis.[4] The complex ion has a chiral structure with two cyano ligands in *cis* positions. Thus the *cis*-$[Co(CN)_2\{(OH)_2Co(NH_3)_4\}_2]^{3+}$ ion should be optically resolved. However, no attempt has been reported to resolve this complex.

The present paper deals with the optical resolution of the *cis*-$[Co(CN)_2\{(OH)_2Co(NH_3)_4\}_2]^{3+}$ complex, and the preparation and the separation of isomers of the corresponding diamine complexes, *cis*-$[Co(CN)_2\{(OH)_2Co(diamine)_2\}_2]^{3+}$, where diamine stands for en (ethylenediamine), *R*-pn ((*R*)-1,2-propanediamine), or *S,S*-chxn ((*S,S*)-1,2-cyclohexanediamine). The isomers were characterized from UV-VIS absorption, circular dichroism (CD), and ^{13}C NMR spectra and from the identification of the decomposition products. The trinuclear isomers are composed of two kinds of chromophore, a *cis*-$Co(OH)_4(CN)_2$ and two *cis*-$Co(N)_4(OH)_2$, as shown in Fig. 1. The central $Co(OH)_4(CN)_2$ chromophore has a configurational chirality, Δ or Λ, due to the skew arrangement of two $Co(OH)_2Co$ four-membered rings. In the cases of the diamine complexes, each $Co(N)_4(OH)_2$ chromophore also has a configurational chirality, Δ or Λ, due to the tris-chelate type arrangement of two diamine and a $Co(OH)_2Co$ rings. Thus six optically active isomers are possible for the diamine complexes in total: $\Delta(\Delta\Delta)$, $\Delta(\Delta\Lambda)$, $\Delta(\Lambda\Lambda)$, $\Lambda(\Delta\Delta)$, $\Lambda(\Delta\Lambda)$, and $\Lambda(\Lambda\Lambda)$, where the chirality symbols in parentheses denote the configurations of the peripheral

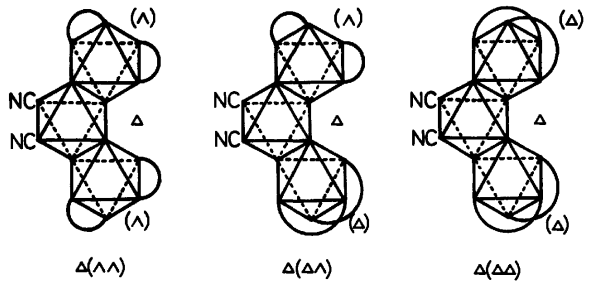

Fig. 1. Three geometrical isomers of the Δ configuration of $Co(OH)_4(CN)_2$ chromophore.

$Co(N)_4(OH)_2$ chromophores. The six optical isomers of en analogue can be classified into three geometrical isomers, since each of them finds its enantiomer in themselves. Two of these geometrical isomers, $\Delta(\Delta\Delta)$ or $\Lambda(\Lambda\Lambda)$, and $\Delta(\Lambda\Lambda)$ or $\Lambda(\Delta\Delta)$, possess a C_2 axis, whereas another one geometrical isomer $\Delta(\Delta\Lambda)$ or $\Lambda(\Delta\Lambda)$ possesses no symmetry element other than C_1 axis.

Experimental

Preparation and Optical Resolution of cis-$[Co(CN)_2\{(OH)_2Co(NH_3)_4\}_2]^{3+}$. The racemic sulfate salt was prepared by a modification of the procedure of Siebert and Schiedermaier.[3] To 5 g of "hexol" sulfate[5] $[Co\{(OH)_2Co(NH_3)_4\}_3](SO_4)_3\cdot 4H_2O$ suspended in 30 cm^3 of water was added 1.5 g of sodium cyanide dissolved in 15 cm^3 of water with stirring. A red precipitate was obtained immediately. After continued stirring for a few hours, the precipitate was filtered off and washed with water, ethanol, and ether.

Four-tenths grams of $Ba(CH_3CO_2)_2$ was added to 0.6 g of the red racemic sulfate salt suspended in 20 cm^3 of water and, after stirring for a few hours, the precipitated $BaSO_4$ was removed by filtration. To the filtrate was added 0.36 g of $Na_2(d\text{-}C_4H_4O_6)\cdot 2H_2O$. A pale-red precipitate appeared as the less-soluble diastereomer, which was filtered and purified by washing with water until the washings showed a constant CD value at *ca.* 500 nm. The less-soluble diastereomer was added to an aqueous solution containing ion exchanger resin QAE-Sephadex A-25 ($CH_3CO_2^-$ form, *ca.* 10 times excess) and stirred for a few hours. The resin was removed by filtration and $(NH_4)_2SO_4$ was added to the filtrate to give the optically active salt (Δ isomer), which was washed with water, ethanol, and ether, and dried in air. Found: C, 4.28; H, 4.92; N, 23.81%. Calcd for $[Co(CN)_2\{(OH)_2Co(NH_3)_4\}_2](SO_4)_{3/2}$: C, 4.16; H, 4.89; N, 24.27%.

Preparation and Separation of Isomers of cis-$[Co(CN)_2\{(OH)_2Co(diamine)_2\}_2]^{3+}$. *1)* cis-$[Co(CN)_2\{(OH)_2Co(en)_2\}_2]^{3+}$: A solution of the "en hexol" complex $[Co\{(OH)_2Co(en)_2\}_3]^{6+}$ prepared in the one-tenth scale of the Ref. 6 was poured onto a short column of SP-Sephadex C-25 (Na^+ form) and eluted with a NaCl solution. To the collected brown eluate of the en hexol (3.76×10^{-3} mol) was added 1.1 g of NaCN (*ca.* 6 times excess). The solution became red within a few hours. After the precipitated solid had been filtered off, the filtrate was poured onto a column (5×60 cm) of SP-Sephadex C-25 (Na^+ form). The adsorbed band was eluted with a 0.2 mol dm^{-3} $Na_2(d\text{-}C_4H_4O_6)$ solution. Succeeding a broad pink band (chemically unidentified) two red ones were eluted. The earlier- and later-eluted portions of each band showed the

opposite CD signs; that is, each band consists of a couple of enantiomers. Each of the enantiomers was named E1(−), E1(+), E2(+), or E2(−) after its sign of the CD extremum at *ca.* 500 nm. Each combined eluate E1 or E2 was diluted to about 5 times the volume with water, poured onto a short column of SP-Sephadex C-25 (Na^+ form), and eluted with a NaCl aqueous solution. The eluate was evaporated to a small volume at a temperature below 30 °C. After repeated removal of NaCl, the resulting solution was treated with an adequate amount of ethanol and kept standing in a refrigerator. Red crystals (the chloride salt) deposited in a few days were collected with suction, recrystallized from a water–ethanol solution, washed with ethanol and ether, and dried in air. The perchlorate salt was obtained in a similar way. Found for the racemic chloride of E1: C, 16.60; H, 6.06; N, 19.49%. Calcd for $[Co(CN)_2\{(OH)_2Co(en)_2\}_2]Cl_3\cdot 4.5H_2O$: C, 16.57; H, 6.26; N, 19.33%. Found for the racemic perchlorate salt of E1: C, 14.33; H, 4.40; N, 16.74%. Calcd for $[Co(CN)_2\{(OH)_2Co(en)_2\}_2](ClO_4)_3$: C, 14.37; H, 4.34; N, 16.76%. Found for the racemic chloride salt of E2: C, 16.18, H, 6.33; N, 18.88%. Calcd for $[Co(CN)_2\{(OH)_2Co(en)_2\}_2]Cl_3\cdot 5.5H_2O$: C, 16.17; H, 6.38; N, 18.86%. Found for the racemic perchlorate salt of E2: C, 13.48; H, 4.76; N, 15.77%. Calcd for $[Co(CN)_2\{(OH)_2Co(en)_2\}_2](ClO_4)_3\cdot 3H_2O$: C, 13.50; H, 4.76; N, 15.74%.

In cases in which the optically active $\Lambda(\Delta\Delta\Delta)$ isomer[6] of hexol complex $[Co\{(OH)_2Co(en)_2\}_3]^{6+}$ was used as starting material, also two red bands were characterized on the chromatographic column. The CD measurements indicated that the band eluted firstly was E1(−) and that the one eluted afterward a new isomer, which was denoted as E3(+). Each eluate was reloaded on a short column of SP-Sephadex C-25 (Na^+ form) to remove the *d*-$C_4H_4O_6^{2-}$ ion, and eluted with a NaCl aqueous solution. After repeated removal of NaCl, the E1(−) solution was poured onto a short column of QAE-Sephadex A-25 (Br^- form) and eluted with water, and the eluate was evaporated to a small volume. The resulting solution was treated with an adequate amount of ethanol and kept standing in a refrigerator. Red crystals of E1(−) deposited in a few days were collected with suction, washed with ethanol and ether, and dried in air. E3(+) isomer was obtained in a similar manner using acetone in place of ethanol. Found for E1(−): C, 14.35; H, 5.15; N, 16.40%. Calcd for $[Co(CN)_2\{(OH)_2Co(en)_2\}_2]Br_3\cdot 4H_2O$: C, 14.15; H, 5.22; N, 16.50%. Found for E3(+): C, 14.00; H, 5.06; N, 16.04%. Calcd for $[Co(CN)_2\{(OH)_2Co(en)_2\}_2]Br_3\cdot 3.5H_2O\cdot 1/5\ NaBr$: C, 13.96; H, 5.15; N, 16.28%.

The isomer E2(−) was separated as follows. The eluate E2 was diluted with water and reloaded on a column of SP-Sephadex C-25 (Na^+ form). The adsorbed band was eluted with 0.2 mol dm^{-3} Na_2(*d*-$C_4H_4O_6$) and some later fractions which showed the same CD spectrum of (−) sign at *ca.* 500 nm were collected together. This procedure was repeated until the CD values became constant and then the solution was stored for CD measurements after the chromatographic removal of *d*-$C_4H_4O_6^{2-}$ ion.

2) cis-$[Co(CN)_2\{(OH)_2Co($S,S-*chxn*$)_2\}_2]^{3+}$: The isomers were prepared and separated by the same procedure as in *1)* except for the use of *S,S*-chxn instead of en. Four red bands were observed on the chromatographic column. The CD measurements showed that the second and the third bands were each composed of two isomers. The separation of these two isomers was accomplished by the way described for E2(−). The resulting six bands were denoted as C1, C2, C3, C4, C5, and C6 in the elution order. The isolation as solid crystalline salts was successful only for the C4 and C6 eluate. Found for C4: C, 29.83; H, 6.21; N, 13.27%. Calcd for $[Co(CN)_2\{(OH)_2Co(S,S\text{-chxn})_2\}_2]Br_3\cdot 3H_2O$: C, 29.82; H, 6.35; N 13.37%. Found for C6: C, 33.51; H, 7.24; N, 14.89%. Calcd for $[Co(CN)_2\{(OH)_2Co(S,S\text{-chxn})_2\}_2]Cl_3\cdot 4H_2O$: C, 33.50; H, 7.35; N, 15.03%. The eluates C1, C2, C3, and C5 were stored for CD measurements.

3) cis-$[Co(CN)_2\{(OH)_2Co($R-*pn*$)_2\}_2]^{3+}$: The isomers were prepared and separated by the same procedure as in *1)* except for the use of *R*-pn instead of en. Three red bands were observed on the column. From the measurements of CD spectra, it turned out that the third band was composed of four isomers. Their separation was carried out by a similar procedure as described for E2(−). The resulting six bands were denoted as P1, P2, P3, P4, P5, and P6 in the elution order. No crystalline salt was isolated in this system as yet. Each eluate was stored for CD measurements after chromatographic removal of *d*-$C_4H_4O_6^{2-}$ ion.

Measurements: The visible and ultraviolet absorption spectra were measured on a Hitachi 330 spectrophotometer and CD spectra recorded on a JASCO MOE-1 spectropolarimeter. The absorption and CD measurements were made in aqueous solutions at room temperature. The ^{13}C NMR spectra were measured with a JEOL FX-90Q NMR spectrometer in D_2O containing dioxane as an internal standard.

Results and Discussion

Preparation and Characterization of Isomers. In the preparation of trinuclear complexes with diamine ligands, the purity of the starting "hexol" complex was of primary importance and therefore its separation was carried out cautiously. An unidentified brown band was observed just before the desired hexol band on the chromatographic column. If the starting hexol solution includes this unknown brown species, the reaction with NaCN gave an insoluble pale-brown precipitate as a main product. Infrared spectra of the precipitate showed two sharp bands at 2160 and 2240 cm^{-1} in the region of the CN stretching vibration mode, which indicated the coodination of CN^-. The N/C ratio was 1 for the en system and 0.8 for the *R*-pn system. These data suggest that the precipitate is a di- or polynuclear complex $Co_2(CN)_4(\mu\text{-}OH)_2(diamine)_2$, which was insoluble in most solvents.

The yields of isomers were in the order of E2>E1 for en series, P2>P4≃P6>P5>P3>P1 for the *R*-pn series, and C1≃C3≃C4≃C6>C2≃C5 for the *S,S*-chxn series. The isomers P5 and P6 underwent mutarotation during the separation by the column chromatography. In the course of attempted crystallization of C1 isomer, it was C6 isomer that appeared as crystals.

The first spin-allowed d-d absorption band of *cis*-$[Co(CN)_2\{(OH)_2Co(NH_3)_4\}_2]^{3+}$ appears at 19420 cm^{-1} and seems to be composed of those of *cis*-$CoN_4(OH)_2$ and *cis*-$Co(OH)_4(CN)_2$ chromophores, since the first absorption band of $[Co(CO_3)(NH_3)_4]^+$ appears[7] at 19100 cm^{-1} and the two components[8] of first absorption band of *cis*-$[Co(CO_3)_2(CN)_2]^{3-}$ at 18300 and 22500 cm^{-1}. In the corresponding region of CD curve there are two extrema at 16860 and 19380 cm^{-1} (Fig. 2). The absorption shoulder at 23500 cm^{-1} may be assigned to the higher wavenumber component of the split first band of $Co(OH)_4(CN)_2$ moiety. Since the second d-d transition bands of both the chromophores are expected to have about the same energies, the absorption shoulder

TABLE 1. ABSORPTION DATA of *cis*-$[Co(CN)_2\{(OH)_2Co(NH_3)_4\}_2]^{+3}$ AND *cis*-$[Co(CN)_2\{(OH)_2Co(diamine)_2\}_2]^{3+}$ IN WATER
(Position of a shoulder is presented by a rough value of wave number with a sign sh)

Complex	$\sigma_{max}/10^3$ cm^{-1} and log(ε/mol^{-1} dm^3 cm^{-1}) in parentheses			
(Ammine)	19.42 (2.36)	26.7 sh (2.63)	35.7 sh (3.61)	
	23.5 sh (2.32)			
E1(ClO_4)	19.80 (2.50)	26.3 sh (2.70)	35.7 sh (3.76)	47.00 (4.64)
E1(Cl)	19.80 (2.50)	26.3 sh (2.70)	35.1 sh (3.68)	46.00 (4.64)
E2(ClO_4)	19.80 (2.54)	26.3 sh (2.74)	35.7 sh (3.81)	46.00 (4.66)
E2(Cl)	19.80 (2.49)	26.3 sh (2.70)	35.1 sh (3.69)	46.00 (4.62)
E1(−)	19.80 (2.48)	27.0 sh (2.75)	35.7 sh (3.67)	45.5 sh (4.63)
E2(−)	19.80 (2.50[a])			
E3(+)	19.80 (2.49)	26.3 sh (2.74)	35.1 sh (3.68)	46.5 sh (4.62)
P1—P6	19.80 (2.50[a])			
C1, C2, C3, C5	19.61 (2.55[a])			
C4	19.61 (2.54)	25.6 sh (2.70)	33.9 sh (3.71)	44.6 sh (4.68)
C6	19.61 (2.55)	25.3 sh (2.68)	34.5 sh (3.72)	45.00 (4.66)

a) Estimated value (See text).

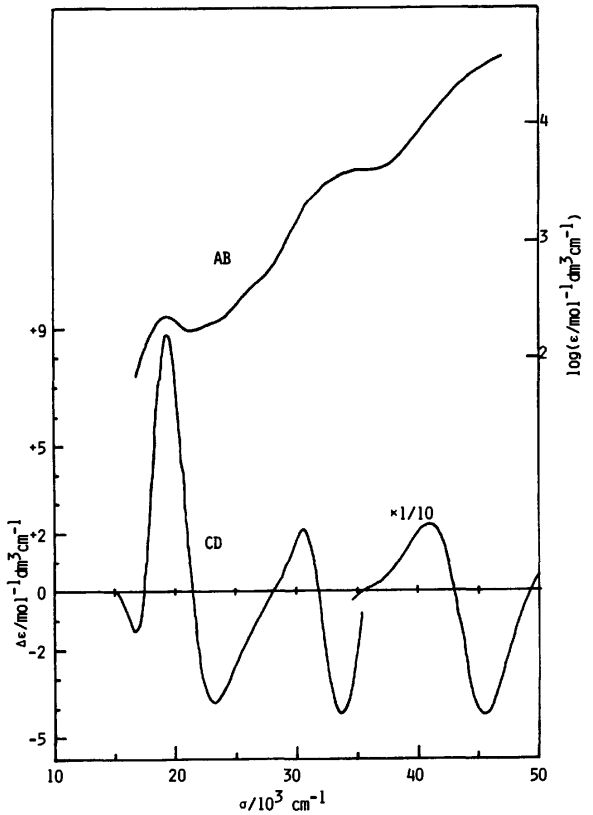

Fig. 2. The absorption (AB) and CD curves of *cis*-$[Co(CN)_2\{(OH)_2Co(NH_3)_4\}_2]^{3+}$.

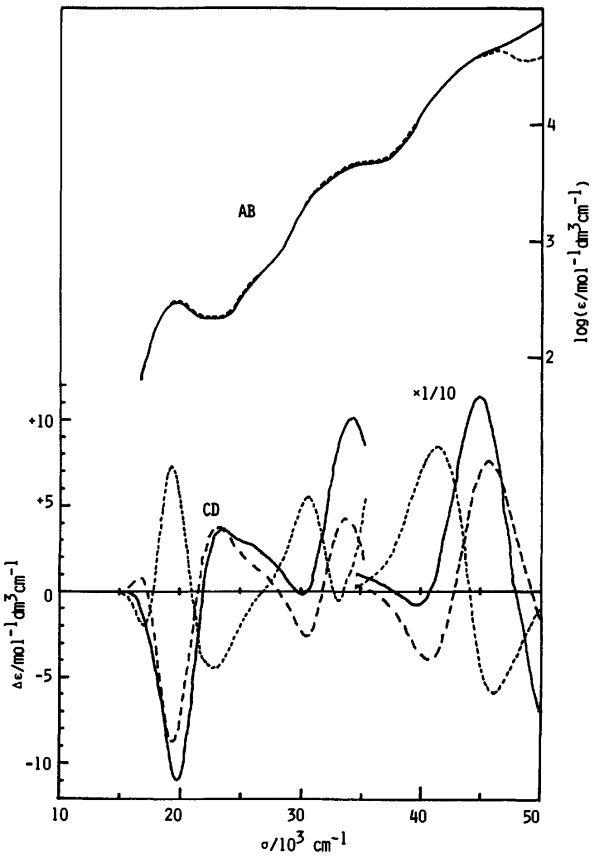

Fig. 3. The absorption (AB) and CD curves of *cis*-$[Co(CN)_2\{(OH)_2Co(en)_2\}_2]^{3+}$ isomers: E1(−) (——) and E2 (------) (AB); E1(−) (——), E2(−) (---), and E3(+) (------) (CD).

at 26700 cm^{-1} is assigned to their overlap. The intense band at 35700 cm^{-1} can be assigned to the charge-transfer transition from the OH bridging group to the central metal, $e_g(Co) \leftarrow p_\pi(O)$. The CD pattern is very similar to that of the parent "hexol" $[Co\{(OH)_2Co(NH_3)_4\}_3]^{6+}$ in the regions of around 20000 and 35000—50000 cm^{-1} (Fig. 2), and the CD intensity being about two-thirds of the "hexol."[2] Therefore, the absolute configuration of the present trinuclear complex is assigned on the basis of the CD signs in these regions: *Λ* configuration for (+) CD around 20000 cm^{-1} and for (+) and (−) bands from the lower energy side in the region of 35000—50000 cm^{-1}. Thus the isomer obtained from the less-soluble diastereomer of *d*-tartrate salt has the *Λ* absolute configuration.

All complexes containing diamine ligands showed similar absorption spectra to one another (Table 1). The first d-d absorption maxima become more intense and shift to the higher wave number than that of the corresponding ammine complex. Therefore, the CD

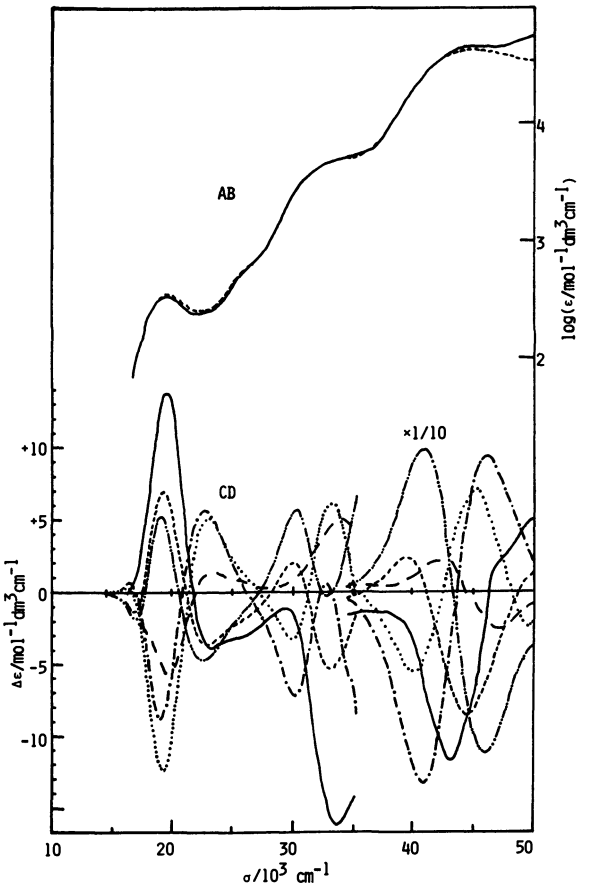

Fig. 4. The absorption (AB) and CD curves of *cis*-[Co(CN)$_2${(OH)$_2$Co(*S*,*S*-chxn)$_2$}$_2$]$^{3+}$ isomers: C4 (——) and C6 (------) (AB); C1 (——), C2 (– – –), C3 (------), C4 (·····), C5 (–·–), and C6 (—·—) (CD).

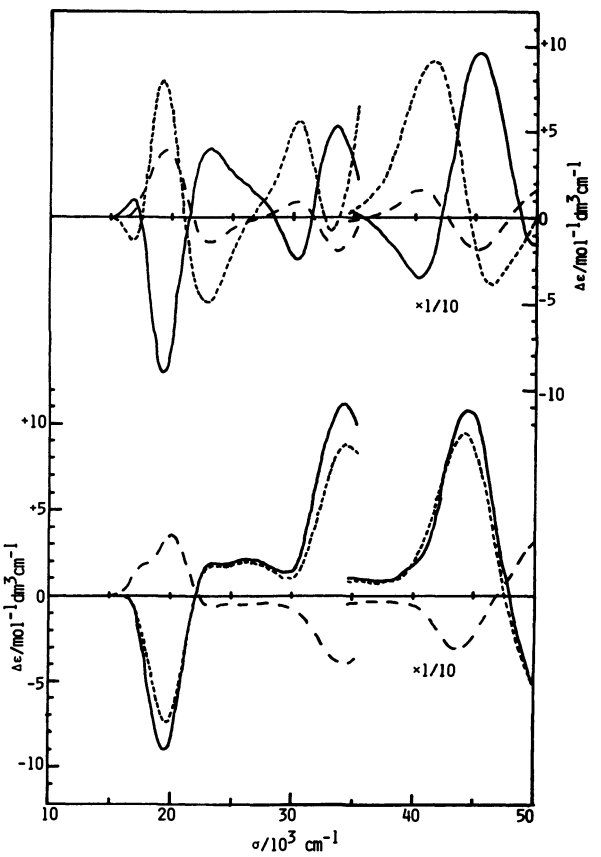

Fig. 5. The CD curves of *cis*-[Co(CN)$_2${(OH)$_2$Co(*R*-pn)$_2$}$_2$]$^{3+}$ isomers: P1 (——), P2 (------), and P3 (– – –) (lower curves); P4 (——), P5 (— —), and P6 (------) (upper curves).

intensities of the isomers which were not obtained as solid salt, were calculated on the basis of the assumption that E2(−) and all *R*-pn isomers have the molar absorption coefficient log (ε/mol^{-1} dm^3 cm^{-1})=2.50 at 19800 cm^{-1} and C1, C2, C3, and C5 isomers 2.55 at 19610 cm^{-1}. The $|\Delta\varepsilon|$ values at *ca.* 20000 cm^{-1} are in the range of 7—12 (Figs. 3, 4, and 5), being comparable with that for the ammine complex. The absolute configuration of Co(OH)$_4$(CN)$_2$ moiety can be assigned by the sign of this band; that is, *Λ* configuration for negative sign and *Δ* for positive. The CD pattern in the region of 35000—50000 cm^{-1} are also similar to that of the ammine analogue, though their intensities about 2—3 times stronger (Table 2). The intensity and sign of the CD band at *ca.* 45000 cm^{-1} of the diamine complex are comparable with those of the hexol complex of corresponding diamine.[9] The absolute configuration of Co(OH)$_4$(CN)$_2$ moiety can be assigned also on the basis of the sign of this band as was done for the Co(OH)$_6$ moiety of hexol: *Δ* configuration for a negative sign and *Λ* for positive. The assignments are in good agreement to those from the CD sign of the first d-d absorption band.

Configuration of cis-[*Co(CN)$_2${(OH)$_2$Co(en)$_2$}$_2$*]$^{3+}$. ^{13}C NMR spectra showed four signals (45.89, 45.19, 44.97, and 43.29 ppm) for E3(+), also four (46.16, 45.02, 44.64, and 43.89 ppm) for E1(rac), and six (46.27, 46.05, 45.08, 44.64, 44.00, and 42.86 ppm) for E2(rac) in the methylene region of en. This result confirms that the isomer E2(rac) has no symmetry and that the configuration of its two Co(N)$_4$(OH)$_2$ moieties are (*ΔΔ*).

Acid hydrolysis of one mole of *cis*-[Co(CN)$_2${(OH)$_2$Co(en)$_2$}$_2$]$^{3+}$ ion is expected to produce one mole of [Co(CN)$_2$(H$_2$O)$_4$]$^+$ and two moles of *cis*-[Co(en)$_2$(H$_2$O)$_2$]$^{3+}$. Since the former tetraaqua ion has no chirality, only latter bis(ethylenediamine) complex will contribute to the CD spectrum. The isomer *Δ*(*ΔΔ*) or *Λ*(*ΔΔ*) will produce two *Δ*-[Co(en)$_2$(H$_2$O)$_2$]$^{3+}$ ions, and *Δ*(*ΛΛ*) or *Λ*(*ΛΛ*) two *Λ*-[Co(en)$_2$(H$_2$O)$_2$]$^{3+}$ ions, whereas *Δ*(*ΔΔ*) or *Λ*(*ΔΔ*) will produce an equal amount of *Δ*- and *Λ*-[Co(en)$_2$(H$_2$O)$_2$]$^{3+}$, namely rac-[Co(en)$_2$(H$_2$O)$_2$]$^{3+}$. The isomer E1(−) was decomposed by adding a 6.0 mol dm^{-3} HCl solution to give a negative CD band at 483 nm ($\Delta\varepsilon$=−0.81), which corresponds to that of *Δ*-[Co(en)$_2$(H$_2$O)$_2$]$^{3+}$ ($\Delta\varepsilon_{485}$=−1.05).[10] Similarly, the isomer E3(+) also showed a negative CD band ($\Delta\varepsilon$=−0.56). These results indicate that the isomers E1(−) and E3(+) prepared from *Λ*(*ΔΔΔ*)-hexol have the *Λ*(*ΔΔ*) and *Δ*(*ΔΔ*) configurations, respectively.

Thus, from the CD and ^{13}C NMR spectra and the acid decomposition experiment it is concluded that the absolute configurations of E1(−), E1(+), E2(−), E2(+), and E3(+) isomers are *Λ*(*ΔΔ*), *Δ*(*ΛΛ*), *Λ*(*ΔΛ*),

TABLE 2. CD DATA OF *cis*-$[Co(CN)_2\{(OH)_2Co(NH_3)_4\}_2]^{3+}$ AND *cis*-$[Co(CN)_2\{(OH)_2Co(diamine)_2\}_2]^{3+}$ IN WATER (σ_{ext} value is given in 10^3 cm^{-1} and $\Delta\varepsilon$ in mol^{-1} dm^3 cm^{-1} in parentheses)

Complex	d-d transition region	charge-transfer region	Complex	d-d transition region	charge-transfer region
(Ammine, *Λ*)	16.86 (−1.41)	30.58 (+2.17)	C5[a]	17.09 (−1.92)	30.40 (+5.78)
	19.38 (+8.88)	33.67 (−4.26)		19.14 (+5.38)	32.89 (−0.34)
	23.20 (−3.87)	40.82 (+23.1)		22.62 (−4.76)	40.98 (+99.7)
		45.45 (−42.9)			45.98 (−115)
E1(−)	19.82 (−11.1)	30.21 (−0.26)	C6	16.67 (+0.64)	30.30 (−7.21)
	23.47 (+3.68)	34.31 (+10.2)		19.16 (−8.94)	32.84 (+0.62)
		39.68 (−8.12)		22.73 (+5.65)	40.82 (−134)
		45.05 (+114)			46.08 (+93.4)
E2(−)[a]	16.75 (+0.83)	30.65 (−2.61)	P1[a]	19.69 (−9.10)	34.25 (+11.1)
	19.42 (−8.79)	33.79 (+4.33)		23.7 sh (+1.87)	44.44 (+109)
	23.19 (+3.79)	40.82 (−39.3)		26.53 (+2.17)	
		45.66 (+76.6)	P2[a]	19.80 (−7.46)	34.48 (+8.78)
E3(+)	17.05 (−2.13)	30.58 (+5.57)		23.53 (+1.71)	44.25 (+94.7)
	19.29 (+7.35)	33.33 (−0.48)		26.53 (+1.96)	
	22.83 (−4.51)	41.32 (+86.4)	P3[a]	20.08 (+3.53)	34.19 (−3.97)
		46.08 (−63.0)		23.53 (−0.67)	43.48 (−30.8)
C1[a]	19.63 (+13.9)	33.90 (−16.2)		25.97 (−0.53)	
	23.36 (−3.90)	43.20 (−116)	P4[a]	16.84 (+1.09)	30.30 (−2.48)
C2[a]	19.80 (−5.66)	34.19 (+5.04)		19.38 (−9.09)	33.74 (+5.41)
	23.36 (+1.36)	42.46 (+22.0)		23.15 (+3.97)	40.32 (−34.1)
		47.17 (−25.2)			45.45 (+96.3)
C3[a]	16.95 (−1.41)	30.21 (+2.06)	P5[a]	19.57 (+3.97)	30.30 (+0.97)
	19.34 (+7.00)	33.33 (−5.33)		23.20 (−1.46)	33.67 (−1.91)
	22.99 (−3.63)	39.60 (+24.5)			40.49 (+16.3)
		44.64 (−85.9)			45.45 (−18.2)
C4	16.39 (+0.24)	30.12 (−3.30)	P6[a]	16.92 (−1.35)	30.49 (+5.64)
	19.34 (−12.5)	33.33 (+6.25)		19.23 (+8.04)	33.22 (−0.72)
	23.09 (+5.12)	40.00 (−55.9)		22.99 (−4.92)	41.15 (+93.1)
		45.35 (+70.9)			46.08 (−39.8)

a) The CD intensities were calculated by the method described in text.

TABLE 3. THE FORMATION RATIOS OF OPTICAL ISOMERS OF *cis*-$[Co(CN)_2\{(OH)_2Co(en)_2\}_2]^{3+}$ IN THE REACTION OF THE OPTICALLY ACTIVE HEXOL ISOMERS WITH EXCESS CYANIDE

(The ratio was determined from the absorbance at 505 nm.)

Absolute configuration of the starting hexol isomer[4]	Formation ratios of derivatives				
Λ(*ΔΔΔ*)	Calcd	*Λ*(*ΔΔ*) only			
	Obsd	*Λ*(*ΔΔ*)	3	*Δ*(*ΔΔ*)	1
Λ(*ΔΔΛ*)	Calcd	*Λ*(*ΔΔ*)	1	*Λ*(*ΔΛ*)	2
	Obsd	*Λ*(*ΔΔ*)	1	E2*	5

* E2: *Λ*(*ΔΛ*)+*Δ*(*ΔΔ*).

Λ(*ΔΛ*), and *Δ*(*ΔΔ*), respectively.

The preparation of en trinuclear complexes was achieved from the two optical isomers of en "hexol" instead of a mixture of several isomers. If the trinuclear complex is formed without racemization nor isomerization, that is, each of the $Co(en)_2(OH)_2$ moiety in the starting complex is replaced statistically by two cyano ligands, it is possible to predict the yields and the absolute configurations of the derivatives. However, the observed ratios are somewhat different from the estimated ones (Table 3), which are related with the partial racemization and/or isomerization.

Characterization of cis-$[Co(CN)_2\{(OH)_2Co(R\text{-}pn)_2\}_2]^{3+}$ *and* cis-$[Co(CN)_2\{(OH)_2Co(S,S\text{-}chxn)_2\}_2]^{3+}$ *Complexes.* The trinuclear complex of optically active diamine has six diastereomers. In the *R*-pn series, six isomers were found in the chromatographic separation. The isomers P1 and P2, however, showed almost the same CD spectra in all of the region measured. It appears that these isomers correspond to the geometrical ones due to the different spacial arrangements of the asymmetric carbons of four *R*-pn ligands. A similar kind of isomerism was observed for the hexol complex.[9] The six isomers of *R*-pn series are assigned in comparison of the CD spectra (Table 2) with those of the en series as follows: *Λ*(*ΔΔ*) for P1 and P2, *Δ*(*ΔΛ*) for P3, *Λ*(*ΔΔ*) for P4, *Δ*(*ΔΔ*) for P5, and *Δ*(*ΔΔ*) for P6 (Table 4).

For the *S,S*-chxn series, all the six diastereomers were completely identified. Since an *S,S*-chxn chelate ring take a *δ* conformation, the *ob* or *lel* orientation[11] should be fixed for *Δ*- or *Λ*-configuration of the $Co(N)_4(OH)_2$ moiety, respectively. It is generally accepted that the *lel* orientation is more stable than the *ob* one. The isomers C2 and C5 were less stable than the others in addition to their low yield. Therefore, their configurations of $Co(N)_4(OH)_2$ moiety are expected to be (*ΔΔ*), that is they have ob_4 form. Taking this expectationinto account, the absolute configurations of all the isomers are estimated on the CD spectra (Table 2) as follows:

TABLE 4. ABSOLUTE CONFIGURATIONS OF *cis*-$[Co(CN)_2\{(OH)_2Co(diamine)_2\}_2]^{3+}$ ISOMERS

Absolute configuration	en series	Absolute configuration	*R*-pn series	Absolute configuration	*S,S*-chxn series
$\Lambda(\Delta\Delta)$	E1(−)	$\Lambda(\Delta lel_2\cdot\Delta lel_2)$	P1, P2	$\Lambda(\Delta ob_2\cdot\Delta ob_2)$	C2
$\Delta(\Lambda\Lambda)$	E1(+)	$\Delta(\Lambda ob_2\cdot\Lambda ob_2)$	P3	$\Delta(\Lambda lel_2\cdot\Lambda lel_2)$	C1
$\Delta(\Delta\Lambda)$	E2(+)	$\Delta(\Delta lel_2\cdot\Lambda ob_2)$	P5	$\Delta(\Delta ob_2\cdot\Lambda lel_2)$	C3
$\Lambda(\Delta\Lambda)$	E2(−)	$\Lambda(\Delta lel_2\cdot\Lambda ob_2)$	P4	$\Lambda(\Delta ob_2\cdot\Lambda lel_2)$	C4
$\Delta(\Delta\Delta)$	E3(+)	$\Delta(\Delta lel_2\cdot\Delta lel_2)$	P6	$\Delta(\Delta ob_2\cdot\Delta ob_2)$	C5
$\Lambda(\Lambda\Lambda)$	—	$\Lambda(\Lambda ob_2\cdot\Lambda ob_2)$	—	$\Lambda(\Lambda lel_2\cdot\Lambda lel_2)$	C6

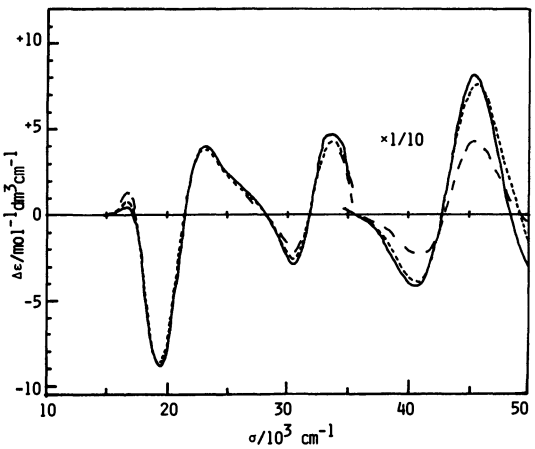

Fig. 6. Configurational CD curves of $Co(OH)_4(CN)_2$ chromophore for en.
$\Lambda=\{E1(-)-E3(+)\}/2$ (——), $\Lambda=\Lambda(\Delta\Delta)=E2(-)$ (------), and Λ configuration of ammine series (— —).

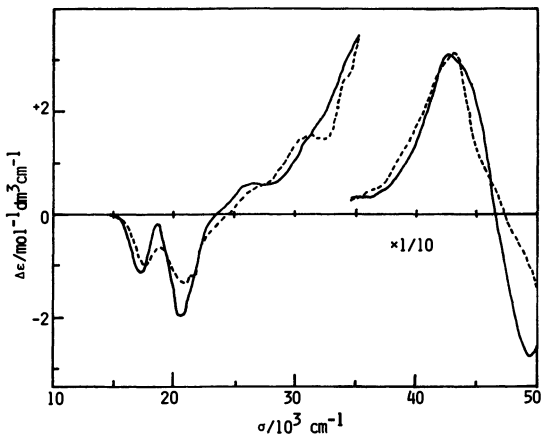

Fig. 7. Configurational CD curves of $Co(N)_4(OH)_2$ chromophore for en.
$(\Delta)=\{E1(-)-E2(-)\}/2$ (——) and $\{E2(-)+E3-(+)\}/2$ (---).

$\Delta(\Lambda\Lambda)$ for C1, $\Lambda(\Delta\Delta)$ for C2, $\Delta(\Delta\Lambda)$ for C3, $\Lambda(\Delta\Lambda)$ for C4, $\Delta(\Delta\Delta)$ for C5, and $\Lambda(\Lambda\Lambda)$ for C6. The estimation are completely confirmed by the CD curve analysis discussed below and summarized in Table 4.

Additivity of CD Contributions. If the observed CD curves of *cis*-$[Co(CN)_2\{(OH)_2Co(en)_2\}_2]^{3+}$ can be simply divided into each contribution due to $Co(OH)_4(CN)_2$ and $Co(N)_4(OH)_2$ chiralities as has been established for configurational and vicinal chiralities of many mononuclear cobalt(III) complexes,[12] the following relations are expected to hold for the observed CD curves $\Lambda(\Lambda\Lambda)$, $\Lambda(\Delta\Lambda)$, or $\Lambda(\Delta\Delta)$:

$$\Lambda(\Lambda\Lambda) = \Lambda + 2(\Lambda),$$
$$\Lambda(\Delta\Lambda) = \Lambda + (\Lambda) + (\Delta) = \Lambda,$$
$$\Lambda(\Delta\Delta) = \Lambda + 2(\Delta),$$

where Λ and Δ, and (Λ) and (Δ) are CD contributions due to the central $Co(OH)_4(CN)_2$ and the peripheral $Co(N)_4(OH)_2$ chiralities, respectively. Then the individual Λ and (Λ) contributions can be derived from the observed CD curves by the following relations:

$$\Lambda = [\Lambda(\Delta\Delta)-\Delta(\Delta\Delta)]/2,$$
$$(\Delta) = [\Lambda(\Delta\Delta)-\Lambda(\Delta\Lambda)]/2,$$
$$(\Lambda) = [\Lambda(\Delta\Lambda)+\Delta(\Delta\Delta)]/2.$$

Figure 6 shows the calculated CD contribution Λ due to the $Co(OH)_4(CN)_2$ moiety. This is quite similar to the observed CD curve $\Lambda(\Delta\Lambda)=\Lambda$ of the E2(−) isomer and also in good agreement with that of the Λ isomer of ammine series. The calculated Δ CD curves due to

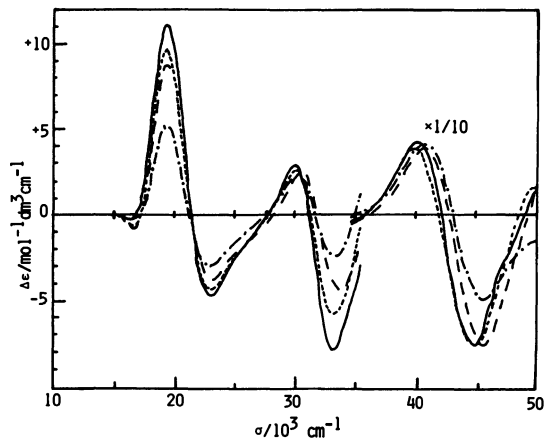

Fig. 8. Configurational CD curves of $Co(OH)_4(CN)_2$ chromophore for *S,S*-chxn. $\Delta=(C1-C6)/2$ (——), $(C5-C2)/2$ (—·—), and $(C3-C4)/2$ (------), and E2(+) (— —) for comparison.

the $Co(N)_4(OH)_2$ moiety are also similar to one another (Fig. 7) and the CD sign at *ca.* 20000 cm^{-1} is compatible with that of the main component in the region of the first d-d transition of the $[Co(en)_2(O-O)]$ complexes having the same configuration.[10] These facts mean that the simple additivity rule assumed above is adequate for the present system. It is recognized evidently that the chirality of the central $Co(OH)_4(CN)_2$ moiety induces the dominant CD contribution. In the case of the en hexol isomers, this kind of additivity of CD spectra was unsatisfactory.[6]

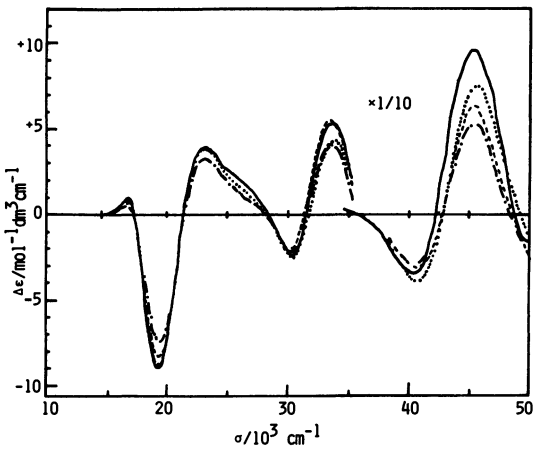

Fig. 9. Configurational CD curves of $Co(OH)_2(CN)_2$ chromophore for *R*-pn. Λ=P4 (——), (P1—P6)/2 (------), and (P2—P6)/2 (—·—), and E2(—)(·····) for comparison.

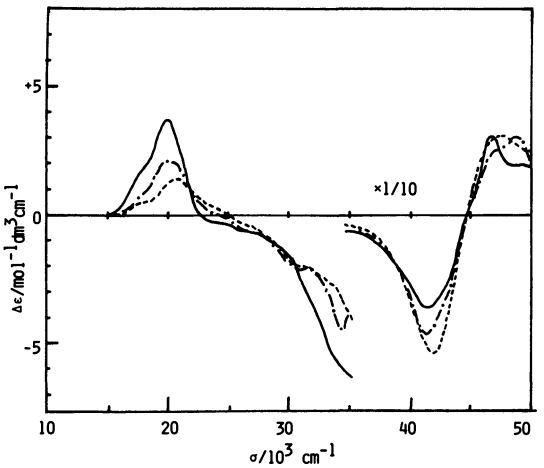

Fig. 10. Configurational CD curves of $Co(N)_4(OH)_2$ chromophore for *S,S*-chxn. (Λ)=(C1—C3)/2 (——), (C3—C5)/2 (------), and (C6—C4)/2 (—·—).

As for the *R*-pn series, we get the following relations:

$$\Delta(\Delta R_2\cdot\Delta R_2) = \Delta + 2(\Delta) + 4(R),$$

$$\Delta(\Delta R_2\cdot\Lambda R_2) = \Delta + (\Delta) + (\Lambda) + 4(R) = \Delta + 4(R),$$

$$\Lambda(\Lambda R_2\cdot\Lambda R_2) = \Lambda + 2(\Lambda) + 4(R),$$

where (R) is the vicinal contribution of an *R*-pn ligand. The individual Δ (or Λ) and (Λ) (or (Δ)) can be derived from the observed CD curves from the following relations:

$$\begin{aligned}\Delta &= [\Delta(\Lambda R_2\cdot\Lambda R_2) - \Lambda(\Lambda R_2\cdot\Lambda R_2)]/2\\ &= [\Delta(\Delta R_2\cdot\Delta R_2) - \Lambda(\Delta R_2\cdot\Delta R_2)]/2\\ &= [\Delta(\Delta R_2\cdot\Lambda R_2) - \Lambda(\Delta R_2\cdot\Lambda R_2)]/2,\\ (\Lambda) &= [\Delta(\Lambda R_2\cdot\Lambda R_2) - \Delta(\Delta R_2\cdot\Lambda R_2)]/2\\ &= [\Delta(\Delta R_2\cdot\Lambda R_2) - \Delta(\Delta R_2\cdot\Delta R_2)]/2\\ &= [\Lambda(\Lambda R_2\cdot\Lambda R_2) - \Lambda(\Delta R_2\cdot\Lambda R_2)]/2.\end{aligned}$$

Figures 8 and 9 show the calculated CD curves due to the central $Co(OH)_4(CN)_2$ moiety in the *S,S*-chxn(Δ) and *R*-pn(Λ) trinuclear complexes, respectively, as well as the observed Δ or Λ CD curves of the en isomer E2(+) or E2(—) for comparison. The vicinal contribution of *R*-pn ligands is neglected in the calculation for *R*-pn series. However, the curves are in fair agreement with one another except for that obtained from the unstable C2 and C5 isomers. Figures 10 and 11 show the calculated (Λ) and (Δ) CD curves due to the peripheral $Co(N)_4(OH)_2$ moiety. The curves are relatively in good agreement with one another. The vicinal CD contributions due to the coodinated optically active diamine (R) and (S) can not be calculated clearly because they are negligibly small compared with the CD contributions Δ, Λ, (Λ), or (Δ).

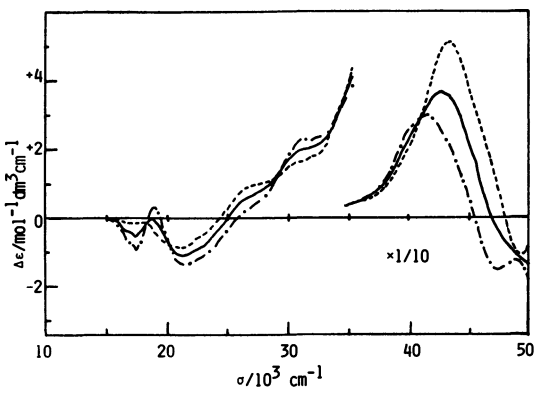

Fig. 11. Configurational CD curves of $Co(N)_4(OH)_2$ chromophore for *R*-pn. (Δ)=(P1+P6)/4 (——), (P4+P6)/2 (------), and (P1—P4)/2 (—·—).

References

1) A. Werner, *Ber.*, **47**, 308 (1914).
2) T. Kudo and Y. Shimura, *Bull. Chem. Soc. Jpn.*, **52**, 1648 (1979).
3) H. Siebert and R. Schiedermair, *Z. Anorg. Allg. Chem.*, **361**, 169 (1968).
4) K. Wieghardt, J. Weiss, and H. Siebert, *Z. Anorg. Allg. Chem.*, **383**, 151 (1971).
5) G. B. Kauffman and R. P. Pinnell, *Inorg. Synth.*, **6**, 176 (1960).
6) T. Kudo and Y. Shimura, *Bull. Chem. Soc. Jpn.*, **52**, 3553 (1979).
7) Y. Shimura and R. Tsuchida, *Bull. Chem. Soc. Jpn.*, **29**, 311 (1956).
8) S. Fujinami and M. Shibata, *Bull. Chem. Soc. Jpn.*, **46**, 3443 (1973).
9) T. Kudo and Y. Shimura, *Bull. Chem. Soc. Jpn.*, **53**, 1588 (1980).
10) A. J. McCaffery, S. F. Mason, and B. J. Norman, *J. Chem. Soc.*, **1965**, 5094.
11) J. Corey and J. C. Bailar, Jr., *J. Am. Chem. Soc.*, **81**, 2620 (1959).
12) C. T. Liu and B. E. Douglas, *Inorg. Chem.*, **3**, 1356 (1964); N. Matsuoka, J. Hidaka, and Y. Shimura, *ibid.*, **9**, 719 (1970); *Bull. Chem. Soc. Jpn.*, **48**, 458 (1975), and references therein.

 © 1983 The Chemical Society of Japan Bull. Chem. Soc. Jpn., 56, 2283—2289 (1983)

Stereoselective Formation of Rotaxanes Composed of Polymethylene-bridged Dinuclear Cobalt(III) Complexes and α- or β-Cyclodextrin

Kazuaki YAMANARI* and Yoichi SHIMURA
Department of Chemistry, Faculty of Science, Osaka University Toyonaka, Osaka 560
(Received February 5, 1983)

[2]-[[$(en)_2Co\{NH_2(CH_2)_2S(CH_2)_nS(CH_2)_2NH_2\}Co(en)_2]Cl_6$]-[α- or β-CDX]-rotaxanes were prepared with partial stereoselectivity and characterized from their absorption and ^{13}C NMR spectra, molar conductance, and elemental analysis (CDX=cyclodextrin; $n=8$, 10, and 12). The rotaxanes always showed apparently *ΔΔ*-rich CD spectra, the highest selectivity (16% *ΔΔ*-rich) being found in the case of $n=10$ and α-CDX. The results are related to the direct preparation of [2]-[*ΔΔ*-[$(en)_2Co\{NH_2(CH_2)_2S(CH_2)_nS(CH_2)_2NH_2\}Co(en)_2]Cl_6$]-[α-CDX]-rotaxanes ($n=8$, 10, and 12) in relatively higher yields than the corresponding *ΛΛ* rotaxanes: 3.5% for $n=8$, 21% for $n=10$, and 28% for $n=12$. Inclusion complexes of a new type $[Co(en)_2\{NH_2(CH_2)_2S(CH_2)_nBr\}]Cl_3\cdot 2$(α-CDX) were also isolated ($n=10$ and 12).

Cyclodextrin (CDX)[1] forms a large number of inclusion complexes with such organic compounds as benzene derivatives, carboxylic acids, alcohols, and alkane derivatives.[2] The inclusion-complex-forming property of CDX was recently applied to the synthesis of novel rotaxanes consisting of a dinuclear cobalt(III) complex $[(en)_2ClCo\{NH_2(CH_2)_{12}NH_2\}CoCl(en)_2]^{4+}$ and α- or β-CDX.[3] We have recently prepared another kind of polymethylene-bridged dinuclear complexes $[(en)_2Co\{NH_2(CH_2)_2S(CH_2)_nS(CH_2)_2NH_2\}Co(en)_2]^{6+}$ from the reaction of $[Co(aet)(en)_2]^{2+}$ with α,ω-dibromoalkane $Br(CH_2)_nBr$,[4] the complexes also being expected to form rotaxanes (aet=2-aminoethanethiolato, $NH_2CH_2CH_2S^-$).

Here we report the preparation of a series of [2]-[[$(en)_2Co\{NH_2(CH_2)_2S(CH_2)_nS(CH_2)_2NH_2\}Co(en)_2$]-$Cl_6$]-[α- or β-CDX]-rotaxanes[5] by two methods. The bridging tetradentate ligands are abbreviated to dtdd for $n=8$: 3,12-dithiatetradecane-1,14-diamine, dhdd for $n=10$: 3,14-dithiahexadecane-1,16-diamine, and dodd for $n=12$: 3,16-dithiaoctadecane-1,18-diamine. In these rotaxanes, four diastereomers are possible because of the inequality of both openings of CDX as shown in Fig. 1 (neglecting the *R* and *S* chiralities of the donor sulfur atoms). The cobalt(III) rotaxanes isolated were characterized from their elemental analyses, absorption, circular dichroism (CD) and ^{13}C NMR spectra, and molar conductance measurements. The optically active rotaxanes, [*ΔΔ*]-[α-CDX] and [*ΛΛ*]-[α-CDX], were also prepared starting from the resolved mononuclear complexes and characterized. A preliminary report has been presented.[6]

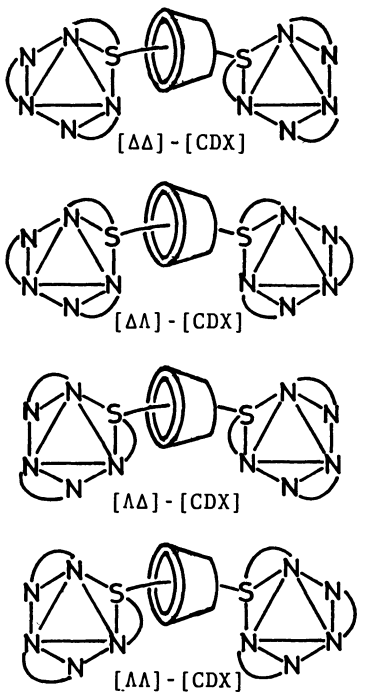

Fig. 1. Four possible diastereomers of [2]-[[$(en)_2$-$Co\{NH_2(CH_2)_2S(CH_2)_nS(CH_2)_2NH_2\}Co(en)_2]Cl_6$]-[CDX]-rotaxane.

Experimental

Preparation and Separation. *$[Co(aet)(en)_2](ClO_4)_2$*: The complex was prepared according to the literature,[7] and used as a starting material. It was found that the racemic perchlorate salt crystallizes as a conglomerate, our racemate being incidentally *Λ*-rich (*ca.* 1.5%) even when a portion of *ca.* 60 g was recrystallized in a lot. Therefore, a sample of the pure racemate was prepared by addition of an appropriate amount of *Λ*-form ($\Delta\varepsilon_{522}=-1.32$ mol^{-1} dm^3 cm^{-1}), which was obtained from optical resolution of the racemic chloride salt.[8]

To confirm the spontaneous resolution, we determined the solubilities in binary and ternary systems containing *rac*- and/or *Λ*-$[Co(aet)(en)_2](ClO_4)_2$ in water. Solubility (g/100 g H_2O): 5.39 (5 °C), 6.88 (10 °C), 8.61 (15 °C), 11.1 (20 °C), 14.0 (25 °C), 18.1 (30 °C), 23.0 (35 °C), 30.7 (40 °C), and 39.0 (45 °C) for racemic perchlorate; 3.85 (5 °C), 4.71 (10 °C), 5.98 (15 °C), 7.28 (20 °C), 9.04 (25 °C), 13.7 (35 °C), 17.0 (40 °C), and 19.0 (45 °C) for *Λ*-complex perchlorate. Solubility (mol fraction $\chi\times10^3$) in the ternary system, H_2O-*Λ*-$[Co(aet)(en)_2](ClO_4)_2$-*Δ*-$[Co(aet)(en)_2](ClO_4)_2$ at 30 °C, (χ_Λ, χ_Δ): (4.34, 0), (4.07, 1.04), (4.00, 1.20), (3.99, 1.30), (3.94, 1.61), (3.69, 2.89), (3.64, 3.29), (3.67, 3.54), and (3.65, 3.65). The solubility ratio of racemate/*Λ*-complex is 1.40 at 5 °C, 1.55 at 25 °C, and 2.05 at 45 °C. Since the ratio is larger than $2^{1/3}=1.26$ the perchlorate salt is spontaneously resolvable.[9] The ternary solubility isotherm at 30 °C showed the only one invariant point. The results confirm that the two enantiomers form a racemic mixture in the solid state.

$[Co(en)_2\{NH_2(CH_2)_2S(CH_2)_nBr\}](ClO_4)_3$ ($n=8$, 10, and 12): These complexes were also used as a starting material. Only the perchlorate salts are highly soluble in dimethyl sulfoxide (DMSO), which turned out to be the most favorable

solvent for the preparation of rotaxanes.

The chloride salts were isolated previously as a by-product in the column chromatography of the bridged complexes, $[(en)_2Co\{NH_2(CH_2)_2S(CH_2)_nS(CH_2)_2NH_2\}Co(en)_2]^{6+}$ ($n=8$ and 10).[4] They were prepared more effectively in the following way. To a 20 cm³ of DMSO solution containing $[Co(aet)(en)_2](ClO_4)_2$ (0.004 mol) was added 0.01 mol of relevant α,ω-dibromoalkane $Br(CH_2)_nBr$, and then the mixture was kept at 30 °C for 2 d. The unreactive dibromoalkane was extracted into diethyl ether for several times. The resulting dark red oil was diluted by *ca.* 20 cm³ of water, and 10 cm³ of a saturated aqueous solution of NaCl was added to it . An oily product appeared immediately and was kept standing for 2 h to give a powder precipitate of the chloride salt. The corresponding bromide (or iodide) salt could be obtained by the same procedure except for the use of NaBr (or KI) instead of NaCl. The halide salts were converted into the perchlorate salt by using QAE-Sephadex A-25 (ClO_4^- form). The eluate was concentrated on a rotary evaporator to dryness, the residue being used for the preparation of rotaxane without further purification.

[2]-[[(en)₂Co(dodd)Co(en)₂]Cl₆]-[α-CDX]-rotaxane (1). *Method [A]*: 2.2 mmol of *rac*-$[Co(aet)(en)_2](ClO_4)_2$ and 1.3 mmol of 1,12-dibromododecane (20% excess) were dissolved in 6 cm³ of DMSO containing 2.5 g of α-CDX. The mixture was kept at 30 °C for 10 d, leading to deep red solution. During this period, white crystals appeared gradually at the bottom of a reaction vessel, which were identified as the inclusion compound of $Br(CH_2)_{12}Br$ and α-CDX. The unreactive dibromoalkane was extracted into diethyl ether. The resulting dark red oil was dissolved in water, adsorbed on a cation exchange column (SP-Sephadex C-25, Na^+ form), and eluted with a 0.8 mol dm^{-3} NaCl solution. Six colored bands, f1—f6, were eluted in this order. The species, f2 (dark brown), f3 (orange), f5 (orange), and f6 (orange), were identical to the products formed by the "blank reaction" without CDX and therefore corresponded to $[Co(aet)(en)_2]^{2+}$, $[Co(en)_2\{NH_2(CH_2)_2S(CH_2)_{12}OH\}]^{3+}$, $[Co(en)_2\{NH_2(CH_2)_2S(CH_2)_{12}Br\}]^{3+}$, and the bridged complex $[(en)_2Co(dodd)Co(en)_2]^{6+}$, respectively.[4] The species isolated from the f1 eluate agreed with the composition of $[Co(en)_2\{NH_2(CH_2)_2S(CH_2)_{12}Br\}]Cl_3\cdot 2(\alpha\text{-CDX})\cdot 18H_2O$. The eluate from the orange band f4 was evaporated to a small volume and, after repeated removal of NaCl deposited out, the solution was treated with a large amount of ethanol (or acetone) to give an orange precipitate of the desired rotaxane. Analytical data are shown in Table 2. The yields based on the starting mononuclear complex *rac*-$[Co(aet)(en)_2](ClO_4)_2$ were 5±1% for f1, 4±1% for f3, 16±2% for f4, 6±1% for f5, and 34±3% for f6 (The mean for 4 preparations).

In the above preparation, pronounced stereoselectivity was observed. All eluates of each band were collected together and its optical purity was checked by CD measurements.[10] Each band showed the CD spectrum. The species f4 always showed apparently *ΔΔ*-rich CD spectra (*ca.* 8%) and f6 *ΛΛ*-rich (*ca.* 3%). The selectivities for f1, f3, and f5 species were not definitive because of their low CD values, which were also varied depending upon the preparative method ([A] or [B]) and conditions such as the molar ratio and concentrations of *rac*-$[Co(aet)(en)_2]^{2+}$ and CDX.

Method [B]: The complex $[Co(en)_2\{NH_2(CH_2)_2S(CH_2)_{12}Br\}](ClO_4)_3$ was used as a starting material. This complex (0.6 mmol), $[Co(aet)(en)_2](ClO_4)_2$ (0.72 mmol, 20% excess), and α-CDX (1.5 g) were allowed to react in 5 cm³ of DMSO and the reaction mixture was separated in a similar manner described above. The yields based on $[Co(en)_2\{NH_2(CH_2)_2S(CH_2)_{12}Br\}](ClO_4)_3$ were 1.5±0.5% for f1, 5±1% for f3, 26±1% for f4, 4±1% for f5, and 46±2% for f6 (2 preparations). The apparent selectivity was *ca.* 8% *ΔΔ*-rich for f4 and *ca.* 4% *ΛΛ*-rich for f6.

[2]-[[(en)₂Co(dhdd)Co(en)₂]Cl₆]-[α-CDX]-rotaxane (2): The complex was prepared and chromatographed by the same manner as **1** except for the use of 1,10-dibromodecane instead of 1,12-dibromododecane. In this separation, the orange band f1 was small in amount, becoming very broad during the chromatography, finally obscuring. This species is inferred as an inclusion compound of $[Co(en)_2\{NH_2(CH_2)_2S(CH_2)_{10}Br\}]Cl_3$ and α-CDX from the analogy with $[Co(en)_2\{NH_2(CH_2)_2S(CH_2)_{12}Br\}]Cl_3\cdot 2(\alpha\text{-CDX})$ described above. The yields were 5±1% for f3, 6±1% for f4, 6±1% for f5, and 54±4% for f6 (3 preparations) in method [A] and 5±1% for f3, 9±1% for f4, 3.5±1% for f5, and 63±4% for f6 (2 preparations) in method [B]. The apparent selectivity was higher in method [A] than [B]: the band f4 was *ca.* 16% *ΔΔ*-rich and f6 *ca.* 2.5% *ΛΛ*-rich in method [A], but f4 was *ca.* 8% *ΔΔ*-rich and f6 *ca.* 0.7% *ΛΛ*-rich in method [B].

[2]-[[(en)₂Co(dtdd)Co(en)₂]Cl₆]-[α-CDX]-rotaxane (3): The complex was not detectable in method [A] but prepared in a 4±1% yield (3 preparations) in method [B]. In the separation, the inclusion compound between $[Co(en)_2\{NH_2(CH_2)_2S(CH_2)_8Br\}]^{3+}$ and α-CDX, which corresponds to the f1 band in the case of **1**, was almost undetectable and five bands corresponding to f2—f6 appeared. The rotaxane was eluted as the fourth band (*ca.* 5% *ΔΔ*-rich) just before the fifth band of the bridged 6+ complex. The isolation of the rotaxane, however, was incomplete: the analytical C/N ratio (51.2/10) was low as compared with the ideal value 5.80. Satisfactory analytical data were obtained for the corresponding optically active rotaxane described below.

[2]-[ΔΔ-[(en)₂Co(dodd)Co(en)₂]Cl₆]-[α-CDX]-rotaxane (4) *and [2]-[ΛΛ-[(en)₂Co(dodd)Co(en)₂]Cl₆]-[α-CDX]-rotaxane (5)*: The rotaxane [*ΔΔ*]-[α-CDX] or [*ΛΛ*]-[α-CDX] was prepared and chromatographed in the same manner as for **1** by the use of *Δ*- or *Λ*-$[Co(aet)(en)_2](ClO_4)_2$ as a starting material, respectively. Six bands were characterized, being corresponded to the species in the separation of **1** in both cases. The yields were 2±1% for f1, 6±1% for f3, 28±1% for f4, 4±1% for f5, and 44±2% for f6 (2 preparations) in the *Δ*-system, and 0.8% for f1, 6% for f3, 14% for f5, and 49% for f6 (1 preparation) in the *Λ*-system.

[2]-[ΔΔ-[(en)₂Co(dhdd)Co(en)₂]Cl₆]-[α-CDX]-rotaxane (6): The complex was prepared by the method [A] as for **2** except for the use of *Δ*-$[Co(aet)(en)_2](ClO_4)_2$ instead of the racemate. The yields were 10±1% for f3, 22±1% for f4, 0% for f5, and 49±2% for f6 (2 preparations). It is noteworthy that the yield of rotaxane **6** (f4 band) is considerably higher than that of **2**. An attempt to prepare the corresponding [*ΛΛ*]-[α–CDX] isomer was made in the same way by using *Λ*-$[Co(aet)(en)_2](ClO_4)_2$. The yield of [*ΛΛ*]-[α-CDX], which is not isolated in solid as yet, was below 7%.

[2]-[ΔΔ-[(en)₂Co(dtdd)Co(en)₂]Cl₆]-[α-CDX]-rotaxane (7): The complex was prepared and chromatographed in the same manner as for **3** by the use of *Δ*-$[Co(aet)(en)_2](ClO_4)_2$ as a starting material. Five bands appeared and the fourth band was the desired rotaxane with a 3.5±0.5% yield, which showed the satisfactory analytical data as seen in Table 2.

[2]-[[(en)₂Co(dodd)Co(en)₂]Cl₆]-[β-CDX]-rotaxane (8): The complex was prepared by the method [A] except for the use of β-CDX instead of α-CDX. In the separation five bands f1′—f5′ were eluted in this order, though f2′ and f3′ were partly overlapped each other. The species, f1′(dark brown), f2′(orange), f3′(orange), f4′(orange), and f5′(orange), were characterized as $[Co(aet)(en)_2]^{2+}$, $[Co(en)_2\{NH_2(CH_2)_2S(CH_2)_{12}OH\}]^{3+}$, the desired rotaxane, $[Co(en)_2\{NH_2(CH_2)_2$-

$S(CH_2)_{12}Br\}]^{3+}$, and $[(en)_2Co(dodd)Co(en)_2]^{6+}$, respectively. Each band also showed a CD spectrum but the apparent selectivity was much lower than that in the corresponding system containing α-CDX: *ca.* 2% *ΔΔ*-ric for f3′ and *ca.* 0.3% *ΔΔ*-rich for f5′. The yield of f3′ rotaxane was 5±1% (3 preparations).

[2]-[[(en)$_2$Co(dhdd)Co(en)$_2$]Cl$_6$]-[β-CDX]-rotaxane (9): The complex was obtained in a 2±0.5% yield (3 preparations) by the same procedure as for **8**. The f3′ rotaxane indicated *ca.* 1% *ΔΔ*-rich CD. No β-CDX rotaxane was detectable for the corresponding dtdd case.

Measurements. The visible and ultraviolet absorption spectra were measured on a Hitachi 330 spectrophotometer and CD spectra with a JASCO MOE-1 spectropolarimeter in aqueous solutions. The ^{13}C NMR spectra were recorded with a JEOL FX-90Q NMR spectrometer in D_2O containing dioxane as an internal standard. The conductance measurements were made in water on a TOA CM-30ET conductivity apparatus. The values at room temperature were converted automatically to those at 25 °C based on the assumption that the conductance changes by 2% per one degree. The solubility in water was determined in the same way as previously reported.[9]

Results and Discussion

Preparation and Characterization. The yields of rotaxanes are collected in Table 1. The two kinds of method were used for the preparation of rotaxane. The yield was usually higher in the method [B] because the formation of inclusion compounds $Br(CH_2)_nBr\cdot m$(CDX) in DMSO lowered the yield in the method [A]. The yield of the rotaxane was higher for α-CDX than for β-CDX. This means that the annular structure of α-CDX is more suitable in size for the formation of rotaxane of the present complexes than that of β-CDX. The number of bridging methylene groups, *n*, also affected the yield in the decreasing order 12>10>8.

Table 2 shows the analytical data of the complexes containing CDX. The ratio C/N was most indicative of rotaxane formation, but somewhat higher than the ideal value (for example C/N=60/10=6.00 for the dodd rotaxane without organic solvent) because a large amount of ethanol or acetone was used for the isolation of rotaxane having high solubility. The experimental value of C/N ratio well agreed with the composition with a few molecules of the organic solvent (Table 2). In the preparation using 1,12-dibromododecane and α-CDX, the species f1 isolated from chromatography showed the C/N ratio about 18, which corresponded to $[Co(en)_2\{NH_2(CH_2)_2S(CH_2)_{12}Br\}]Cl_3\cdot 2$(α-CDX). A similar inclusion complex could be prepared directly from an aqueous solution of $[Co(en)_2\{NH_2(CH_2)_2S(CH_2)_nBr\}]Cl_3$ (*n*=10 or 12) and α-CDX (molar ratio 1 : 1). These inclusion complexes as well as the other compounds formed between $Br(CH_2)_nBr$ and α-CDX in the method [A] are considered as precursors of the rotaxanes. The direct isolation of such precursors gives strong support for the formation of rotaxanes in the reaction mixtures.

The first spin-allowed d-d absorption bands of the cobalt(III) rotaxanes locate at 20440 cm^{-1} (Fig. 2), which are characteristic of the $[Co(N)_5(S)]$ chromophore containing a thioether donor atom.[4] The absorption

Table 1. Percentage yield of rotaxanes

Bridging ligand	Co(III) component	α-CDX Method [A]	α-CDX Method [B]	β-CDX Method [A]
dtdd	*rac*	0	4(*Δ*-5)[a]	0
(*n*=8)	*Δ*	3.5		
dhdd	*rac*	6(*Δ*-16)[a]	9(*Δ*-8)[a]	2(*Δ*-1)[a]
(*n*=10)	*Δ*	21		
	Λ	<7		
dodd	*rac*	16(*Δ*-5)[a]	26(*Δ*-8)[a]	5(*Δ*-2)[a]
(*n*=12)	*Δ*	28		
	Λ	14		

a) Apparent optical purity[10] is indicated in parentheses with the configuration of the rich species.

Table 2. Analytical data of the rotaxane and other complexes

(a) [2]-[[(en)$_2$Co{NH$_2$(CH$_2$)$_2$S(CH$_2$)$_n$S(CH$_2$)$_2$NH$_2$}Co(en)$_2$]Cl$_6$]-[CDX]-rotaxane·X

n	CDX	Starting material	C/N ratio Found	C/N ratio Calcd	X	Found (Calcd) (%) C	H	N
8 (dtdd)	α	*Δ*	6.06	6.06	$2.3C_2H_5OH\cdot 8H_2O$	35.31 (35.36)	7.20 (7.34)	6.79 (6.80)
10 (dhdd)	α	*rac*	5.99	6.00	$C_2H_5OH\cdot 9.5H_2O$	35.02 (35.09)	7.08 (7.31)	6.82 (6.82)
	α	*rac*	6.11	6.10	$(CH_3)_2CO\cdot 10H_2O$	35.25 (35.32)	7.07 (7.29)	6.73 (6.75)
	α	*Δ*	6.16	6.16	$1.8C_2H_5OH\cdot 7H_2O$	36.21 (36.17)	7.29 (7.33)	6.86 (6.85)
	β	*rac*	6.84	6.80	$2C_2H_5OH\cdot 10H_2O$	36.06 (35.97)	7.09 (7.37)	6.15 (6.17)
12 (dodd)	α	*rac*	6.34	6.30	$1.5C_2H_5OH\cdot 9.5H_2O$	36.08 (35.95)	7.26 (7.47)	6.64 (6.66)
	α	*rac*	6.02	6.00	$10.5H_2O$	34.87 (35.09)	7.03 (7.31)	6.75 (6.82)
	α	*Δ*	6.49	6.50	$2.5C_2H_5OH\cdot 8H_2O$	36.74 (36.76)	7.48 (7.55)	6.60 (6.60)
	α	*Λ*	6.59	6.60	$3C_2H_5OH\cdot 7H_2O$	37.14 (37.24)	7.45 (7.58)	6.57 (6.58)
	β	*rac*	7.11	7.10	$2.5C_2H_5OH\cdot 10H_2O$	36.72 (36.73)	7.17 (7.51)	6.02 (6.03)

(b) $[Co(en)_2\{NH_2(CH_2)_2S(CH_2)_nBr\}]Cl_3\cdot 2$(α-CDX)·X

10	α	*rac*	17.80[a]	17.60	$15H_2O$	37.71 (37.78)	6.98 (6.92)	2.47 (2.50
12	α	*rac*	18.02	18.00	$18H_2O$	37.55 (37.54)	6.75 (7.07)	2.43 (2.43)
	α	*rac*	17.66[a]	18.00	$15H_2O$	38.29 (38.25)	6.82 (6.99)	2.53 (2.48)

a) These complexes were prepared directly from an aqueous solution of $[Co(en)_2\{NH_2(CH_2)_2S(CH_2)_nBr\}]Cl_3$ (*n*=10 or 12) and α-CDX (molar ratio 1:1).

TABLE 3. ABSORPTION AND CD DATA OF ROTAXANES

Bridging ligand	Co(III) component	CDX	Absorption[a]	σ_{max} (log ϵ)	CD[a] σ_{ext} ($\Delta\epsilon$)
dtdd	$\Delta\Delta$	α	20.45 (2.608) 35.35 (4.336)	28.5 (2.75)[b] 45.20 (4.552)	19.90 (−4.78), 23.53 (+0.045), 26.32 (−0,234) 29.4 (−0.94),[b] 34.90 (−27.8), 46.30 (+45.8)
dhdd	*rac*	α	20.44 (2.603) 35.25 (4.337)	28.5 (2.74)[b] 45.17 (4.556)	
	$\Delta\Delta$	α	20.43 (2.610) 35.28 (4.332)	28.5 (2.76)[b] 45.19 (4.555)	19.91 (−5.07), 26.18 (−0.195), 29.4 (−0.72)[b] 34.97 (−24.9), 45.87 (+46.2)
	rac	β	20.44 (2.599) 35.29 (4.328)	28.5 (2.74)[b] 45.15 (4.552)	
dodd	*rac*	α	20.45 (2.594) 35.32 (4.322)	28.5 (2.74)[b] 45.17 (4.547)	
	$\Delta\Delta$	α	20.45 (2.615) 35.27 (4.339)	28.5 (2.76)[b] 45.17 (4.564)	19.92 (−5.42), 26.32 (−0.180), 29.4 (−0.9)[b] 34.84 (−24.3), 45.66 (+47.9)
	$\Lambda\Lambda$	α	20.45 (2.608) 35.25 (4.330)	28.5 (2.75)[b] 45.27 (4.555)	19.96 (+5.23), 26.08 (+0.149), 29.4 (+0.7)[b] 34.97 (+20.2), 45.66 (−49.6)
	rac	β	20.44 (2.604) 35.33 (4.329)	28.5 (2.75)[b] 45.17 (4.554)	

a) Wave numbers are given in $10^3 cm^{-1}$ unit and log ϵ or $\Delta\epsilon$ values (in parentheses) in $mol^{-1}dm^3cm^{-1}$.
b) Shoulder.

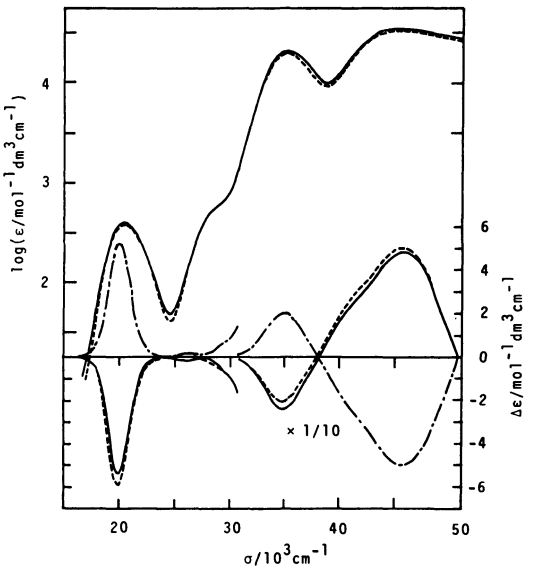

Fig. 2. Absorption and CD spectra of [2]-[$\Delta\Delta$-[(en)$_2$Co(dodd)Co(en)$_2$]Cl$_6$]-[α-CDX]-rotaxane(——), [2]-[$\Lambda\Lambda$-[(en)$_2$Co(dodd)Co(en)$_2$]Cl$_6$]-[α-CDX]-rotaxane (-----), and $\Delta\Delta$-[(en)$_2$Co(dodd)Co(en)$_2$]Cl$_6$ (------).

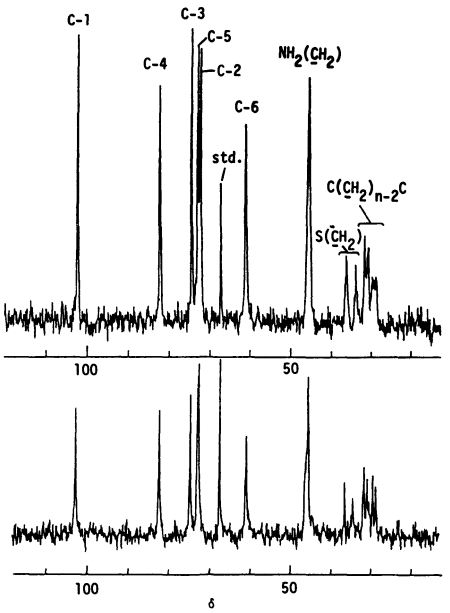

Fig. 3. ^{13}C NMR spectra of [2]-[[(en)$_2$Co(dhdd)Co(en)$_2$]Cl$_6$]-[α-CDX]-rotaxane (**2**) (upper) and [2]-[[(en)$_2$Co(dodd)Co(en)$_2$]Cl$_6$]-[α-CDX]-rotaxane (**1**) (lower). 1,4-Dioxane (δ 67.4 *vs.* Me$_4$Si) was used as the internal reference. The signals of α-CDX (C1—C6) were assigned after Ref. 12.

spectra of rotaxanes are very similar to one another irrespective of the kind of CDX (Table 3). Molar absorption coefficients of the rotaxanes are slightly higher in the thioether charge transfer (CT) band region around *ca.* 35000 cm^{-1} than those of the corresponding bridged complexes. A similar increase of CD intensity is observed in the CT band region (Fig. 2). The ratio of $\Delta\varepsilon_{287}/\Delta\ \varepsilon_{502}$is rather higher in the rotaxanes (4.48 and 3.86 for [$\Delta\Delta$]-[α-CDX] and [$\Lambda\Lambda$]-[α-CDX], respectively) than the bridged $\Delta\Delta$-complex (3.43). Interestingly, the ratio in the [$\Delta\Delta$]-[α-CDX] series increased regularly with the decrease of the methylene chain length: 4.48, 4.91, and 5.82 for the dodd-, dhdd-, and dtdd-rotaxanes, respectively. On the other hand, all the corresponding bridged complexes of $\Delta\Delta$-form showed the identical ratio *ca.* 3.5. This fact clearly shows that the steric repulsion between the cobalt(III) moiety and α-CDX becomes larger with the shortening of the methylene chain. The CD spectra of both $\Delta\Delta$ and $\Lambda\Lambda$ dodd-rotaxanes are not completely enantiomeric to each other. The deviation is eminent in the CT band region. The CD intensity ratio of $\Delta\varepsilon_{219}/\Delta\varepsilon_{287}$ is 1.97 for [$\Delta\Delta$]-[α-CDX] and 2.46 for [$\Lambda\Lambda$]-[α-CDX].

^{13}C NMR spectra offered the direct evidence of the frotaxane formation (Fig. 3). The rotaxanes **1** and **2** gave strong six signals in a lower magnetic field (60—110

ppm), which were assigned to α-CDX moiety.[11,12] Similarly, the rotaxanes of β-CDX **8** and **9** showed five signals in this region. The spectral patterns and chemical shifts of α- and β-CDX moieties are similar to those of free α- and β-CDX, respectively. The other signals in a higher field (0—60 ppm) were assigned to methylene carbons of $NH_2(CH_2)$–, –$S(CH_2)$–, and –$C(CH_2)_{n-2}C$– regions from the lower magnetic field side. These spectral patterns, however, were complicated since the present rotaxanes are a mixture consisted of four diastereomers. Figures 4 and 5 show the ^{13}C NMR spectra of the optically active rotaxanes **4**, **5**, **6**, and **7**, which are composed of a single diastereomer without symmetry element. In the –$C(CH_2)_{n-2}C$– region, the rotaxanes **4** (or **5**), **6**, and **7** showed seven (three strong and four weak), seven (one strong and six weak), and five (one strong and four weak) methylene resonances, respectively. Since it can be assumed that each of the strong signals corresponds to two methylene carbons, the total number of the methylene resonances becomes ten for **4** (or **5**), eight for **6**, and six for **7**. The results gave the direct evidence of the rotaxane formation with C_1 symmetry. Both the dodd rotaxanes, [*ΔΔ*]-[α-CDX] and [*ΛΛ*]-[α-CDX], showed seven signals in the –$C(CH_2)_{10}C$– region but the spectral patterns are obviously different from each other as expected from the fact that they are diastereomeric.

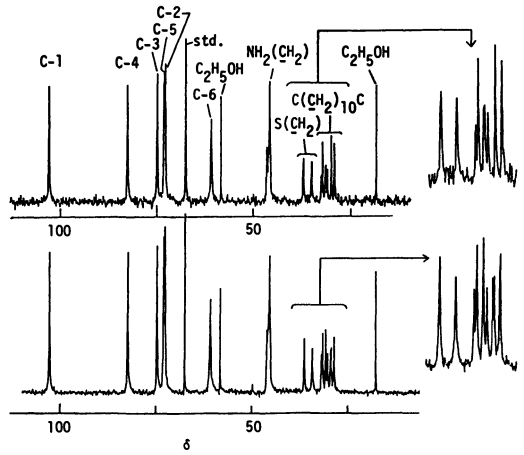

Fig. 4. ^{13}C NMR spectra of [2]-[*ΔΛ*-[$(en)_2$Co(dodd)Co-$(en)_2$]Cl_6]-[α-CDX]-rotaxane (**5**) (upper) and [2]-[*ΔΔ*-[$(en)_2$Co(dodd)Co$(en)_2$]Cl_6]-[α-CDX]-rotaxane (**4**) (lower).

The chemical shifts due to CDX in the rotaxanes were summarized in Table 4. The signals of β-CDX were assigned in the same manner by Usui *et al.*[11] and Colson *et al.*[12] but the assignment of α-CDX became reverse at C2 and C5 resonances, our assignment being after

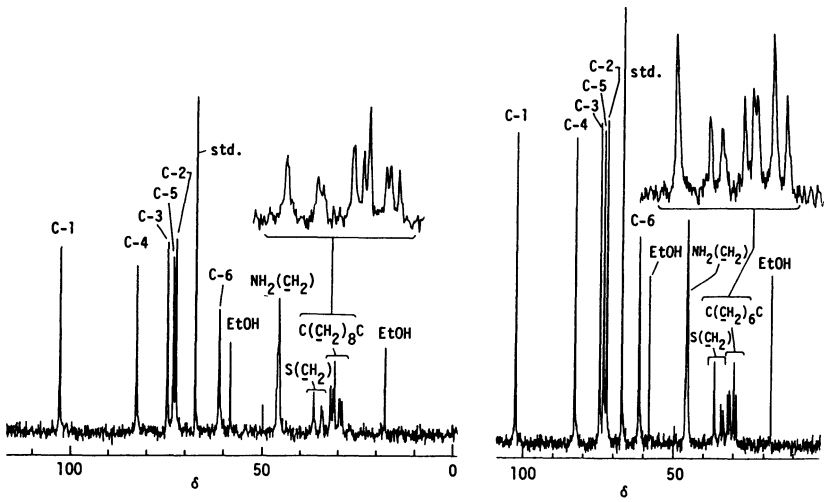

Fig. 5. ^{13}C NMR spectra of [2]-[*ΔΛ*-[$(en)_2$Co(dhdd)Co$(en)_2$]Cl_6]-[α-CDX]-rotaxane (**6**) (left) and [2]-[*ΔΛ*-[$(en)_2$Co(dtdd)Co$(en)_2$]Cl_6]-[α-CDX]-rotaxane (**7**) (right).

Table 4. ^{13}C NMR resonances due to CDX in the rotaxanes (ppm from Me_4Si)

Rotaxane	Chemical shift					
	C-1	C-4	C-3	C-5	C-2	C-6
7 (*ΔΔ*,dtdd, α)	102.64	83.06	74.71	73.47	72.44	61.66
2 (*rac*, dhdd, α)	102.78	82.68	74.72	73.15	72.50	61.23
6 (*ΔΔ*, dhdd, α)	102.73	82.62	74.69	73.11	72.46	61.20
1 (*rac*, dodd, α)	102.78	82.24	74.60	72.81	72.54	60.79
4 (*ΔΔ*, dodd, α)	102.75	82.25	74.60	72.85	72.52	60.76
5 (*ΛΛ*, dodd, α)	102.78	82.27	74.60	72.85	72.55	60.85
9 (*rac*, dhdd, β)	102.67	82.08	74.17	72.87	72.87	61.22
8 (*rac*, dodd, β)	102.72	81.92	74.17	72.87	72.87	61.00

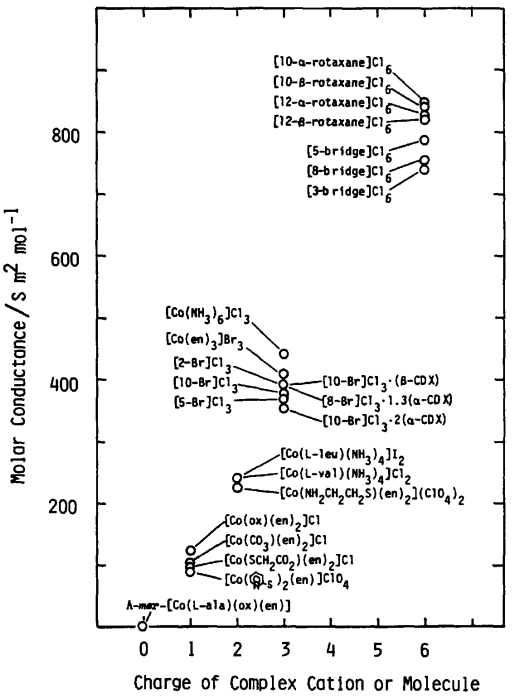

Fig. 6. Molar conductivity of the rotaxanes and other cobalt(III) complexes in water at 25 °C. Abbreviation, complex: [*n*-α-rotaxane]Cl_6=[2]-[[(en)$_2$Co{NH_2-$(CH_2)_2$S$(CH_2)_n$S$(CH_2)_2NH_2$}Co(en)$_2$]Cl_6]-[α-CDX]-rotaxane, [*n*-bridge]Cl_6=[(en)$_2$Co{$NH_2(CH_2)_2$S-$(CH_2)_n$S$(CH_2)_2NH_2$}Co(en)$_2$]Cl_6, and [*n*-Br]Cl_3=[Co(en)$_2$\{$NH_2(CH_2)_2$S$(CH_2)_n$Br\}]Cl_3; ligand: L-ala=L-alaninato, L-leu=L-leucinato, L-val=L-valinato, and ox=oxalato.

Colson *et al.*[12] The values of the dodd rotaxanes containing α-CDX are very similar to one another irrespective of the absolute configurations of the cobalt(III) moieties. The change of the bridging length affects the chemical shift. Three resonances of C4, C5, and C6 were shifted regularly to the down field with the decrease of the methylene chain length, whereas the chemical shifts of C1, C2, and C3 were hardly affected. It is well known that the intra hydrogen bonding between adjacent glucose units in α- or β-CDX is found as a stabilization factor of the cyclic structure in DMSO solution[13] as well as in solid.[14] Since the hydroxyl groups at C2 and C3 are relevant to this hydrogen bonding network, the chemical shifts of C1, C2, and C3 are almost insensitive to the change of the bridging length. On the other hand, the hydroxyl group at C6 can rotate freely and is sensitive to the steric change. Such a steric change at C6 also influences the chemical shifts of C4 and C5. Thus, our results support the assignment of the C2 and C5 resonances for α-CDX by Colson *et al.*[12] but not Usui *et al.*[11]

Chromatography and Molar Conductance. The rotaxane complex cations should have a 6+ charge, but eluted before the 3+ cations [Co(en)$_2$\{$NH_2(CH_2)_2$S-$(CH_2)_n$Br\}]$^{3+}$ (n=10 and 12). The species f1 containing α-CDX (3+) also eluted before [Co(aet)(en)$_2$]$^{2+}$. Such anomalous chromatographic behaviors as well as a similar observation reported in a similar system[3] can be ascribed to the property of SP-Sephadex ion exchangers, which have a kind of non-ionic effect in addition to the dominant ionic one. The former effect, as seen in gel filtration by Sephadex G-type, is based on the molecular size. The bulky complexes such as the rotaxanes are expected to be more rapidly eluted than the corresponding bridged complexes. The rotaxanes **3** and **7**, however, showed a normal elution order as expected from the complex charge. This fact means that the rotaxanes **3** and **7** with n=8 are relatively small in size than the other **1**, **2**, **4**, **5**, **6**, **8**, and **9** with n=10 and 12.

Molar conductances of the rotaxanes and the related complexes at 25 °C are plotted in Fig. 6. The plots for the complexes of each the same charge are distributed in a narrow range, and well separated on the other hand from those of other complexes with the different charges. The rotaxanes have slightly higher values than the corresponding bridged 6+ complexes. Mononuclear inclusion complexes with the charge 3+ showed almost the same values as the corresponding complexes [Co(en)$_2$\{$NH_2(CH_2)_2$S$(CH_2)_n$Br\}]$^{3+}$. Thus, molar conductance was not affected by the presence of CDX. The anomalous column behavior is relevant to the interaction between the SP-Sephadex resin and bulky CDX.

Stereoselectivity. The rotaxanes prepared from *rac*-[Co(aet)(en)$_2$]$^{2+}$ are each the mixture of four diastereomers, *ΔΔ*-, *ΛΛ*-, and two *ΔΛ*-forms (pseudo-*meso*) with respect to the bridged cobalt(III) moieties. Though the two pseudo-*meso* rotaxanes have no CD contribution due to the skew pairs of chelate rings around the central cobalt(III) ion, they will show the induced CD spectra owing to the chiral α- or β-CDX. This contribution is, however, considered to be relatively low and therefore the chiralities of the former two diastereomers contribute mainly to the CD spectra of the product, if an unequal distribution of them takes place. In fact, a very weak positive CD band ($\Delta\varepsilon_{545}$=+0.04) was reported as such induced CD of [2]-[[(en)$_2$ClCo {$NH_2(CH_2)_{12}NH_2$} CoCl(en)$_2$] $(ClO_4)_4$]-[β-CDX]-rotaxane.[3] In the present dodd system, the CD contribution due to α-CDX, which could be evaluated from the mean of the CD spectra of [*ΔΔ*]-[α-CDX] and [*ΛΛ*]-[α-CDX] in Fig. 2, was proved to be small. Therefore, it is reasonable that the two pseudo-*meso* type rotaxanes have a small CD contribution. The rotaxane **2** prepared by the method [A] showed a negative CD spectrum ($\Delta\varepsilon_{502}$=−0.80) in the first d-d absorption band region, which corresponded to a *ca.* 16% optical purity of *ΔΔ*-form (the highest selectivity observed). Thus the unequal distribution of [*ΔΔ*]-[α-CDX] and [*ΛΛ*]-[α-CDX] diastereomers is confirmed. This is also supported by the fact that the bridged complex formed concomitantly indicated the CD band of opposite sign ($\Delta\varepsilon_{502}$=+0.13). In general, the rotaxanes of β-CDX were less stereoselective, though they showed a positive CD band in the first d-d absorption band region. Because of the narrow cavity, α-CDX behaves more effectively to the stereoselectivity as well as to the formation of rotaxane than β-CDX. The bridging methylene chain length also influences the effectiveness of the selectivity: the order is 10>12>8 for the rotaxanes containing α-CDX.

The optically active [*ΔΔ*]-[α-CDX] rotaxane, **4** or **6**, was prepared by the method [A] in a considerably higher yield than the corresponding mixture **1** or **2**, respectively. The dtdd rotaxane with $n=8$ was not detectable in the method [A] starting from *rac*-$[Co(aet)(en)_2]^{2+}$ but could be prepared in a 3.5% yield even by the same method using *Δ*-$[Co(aet)(en)_2]^{2+}$. The stereoselectivity will be more clear by comparison between the pure *Δ*- and *Λ*-systems. In the dodd system, the yield of [*ΔΔ*]-[α-CDX] isomer is 28%, whereas that of [*ΛΛ*]-[α-CDX] one only *ca.* 14%. Similarly in the dhdd system, the yield of [*ΔΔ*]-[α-CDX] is 21% but that of [*ΛΛ*]-[α-CDX] below 7%. These results are consistent with the stereoselective formation of rotaxanes, that is, *ΔΔ*-complex being included preferentially into α-CDX.

The formation reaction of rotaxane is stepwise one as shown schematically by Ogino.[3] In the course of bridge formation process, there is the step forming an intermediate inclusion complex of $[Co(en)_2\{NH_2(CH_2)_2S(CH_2)_nBr\}]^{3+}$ and CDX. This stage is expected to be the most important for the present stereoselectivity. The expectation is confirmed by the partial optical resolution of $[Co(en)_2(NH_2CH_2CH_2SR)]^{3+}$ with a long alkyl or bromoalkyl chain ($R=(CH_2)_nBr$ and $(CH_2)_nCH_3$).[15] Interestingly, the best resolution was achieved in the case of $R=(CH_2)_{10}Br$ and α-CDX, corresponding to 61% optical purity of *Δ*-complex. The results are in fair agreement with the present selectivities.[16]

References

1) α- and β-CDX denote cyclohexaglucopyranose and cycloheptaglucopyranose, respectively.

2) M. L. Bender and M. Komiyama, "Cyclodextrin Chemistry," Springer Verlag, Berlin (1978) and references cited therein.

3) H. Ogino, *J. Am. Chem. Soc.*, **103**, 1303 (1981).

4) K. Yamanari and Y. Shimura, *Bull. Chem. Soc. Jpn.*, **53**, 3605 (1980).

5) The nomenclature for rotaxanes is based on Schill's: G. Schill, "Catenanes, Rotaxanes, and Knots," Academic Press, New York (1971).

6) K. Yamanari and Y. Shimura, *Chem. Lett.*, **1982**, 1959.

7) D. L. Nosco and E. Deutsch, *Inorg. Synth.*, **21**, 19 (1982).

8) K. Yamanari, J. Hidaka, and Y. Shimura, *Bull. Chem. Soc. Jpn.*, **50**, 2299 (1977).

9) K. Yamanari, S. Naito, and Y. Shimura, *Bull. Chem. Soc. Jpn.*, **54**, 3780 (1981); S. Kaki, K. Yamanari, and Y. Shimura, *ibid.*, **55**, 769 (1982).

10) The apparent optical purity of the rotaxane was calculated from the extremum values of the first d-d absorption band region, $\Delta\varepsilon=+2.50$ and $\varepsilon=200$ per one cobalt(III) ion, which were little affected by the kinds of complexes f3, f5, and f6 and the bridging methylene chain lengths.[4]

11) T. Usui, N. Yamaoka, K. Matsuda, K. Tuzimura, H. Sugiyama, and S. Seto, *J. Chem. Soc., Perkin Trans. 1*, **1973**, 2425.

12) P. Colson, H. J. Jennings, and Ian C. P. Smith, *J. Am. Chem. Soc.*, **96**, 8081 (1974).

13) B. Casu, M. Reggiani, G. G. Gallo, and A. Vigevani, *Tetrahedron*, **22**, 3061 (1966).

14) W. Saenger, M. Noltemeyer, P. C. Manor, B. Hingerty, and B. Klar, *Bioorg. Chem.*, **5**, 187 (1976).

15) K. Yamanari and Y. Shimura, *Chem. Lett.*, **1982**, 1957.

16) β-CDX preferentially included *Λ*-complexes in the optical resolution contrary to the present system. The difference may result from the properties of used solvents: water for the former and DMSO for the latter.

Hydration of Iodide Ions in Nitrobenzene from Charge-transfer-to-solvent Spectra and ^{1}H NMR

Kazuaki Ito, Etsuro Iwamoto, and Yuroku Yamamoto*
Department of Chemistry, Faculty of Science, Hiroshima University, Naka-ku, Hiroshima 730
(Received February 7, 1983)

The charge-transfer-to-solvent (c.t.t.s.) spectrum of the iodide ion in nitrobenzene was observed in the visible region, the intensity of the spectrum being lowered by addition of a small amount of water to the solution. From the spectral changes, the first, second, and third hydration constants, $K_1=3.5$, $K_2=2.6$, and $K_3=1.4$ (mol^{-1} dm^3) were determined. On the basis of ^{1}H NMR of water in nitrobenzene solutions in conjunction with the hydration constants obtained from the spectra, it was suggested that a fraction of the water molecules bound to the iodide ion is hydrogen bonded to each other.

The solvation of anions by a small amount of protic solvents such as water and methanol in aprotic solvents plays an important role in ionic reactions such as ligand substitution[1] and ion pair extraction,[2] and has been studied by UV,[3] NMR,[4-6] IR,[7,8] solubility,[6,9] conductance,[10,11] extraction,[12,13] and isopiestic method.[14,15] Addition of protic solvents to solutions of iodides in acetonitrile resulted in loss of a c.t.t.s. band at 40.7×10^3 cm^{-1} and growth of new bands at higher energy which were assigned to the iodide ion hydrogen bonded to a single hydroxyl proton.[3] For ethyleneglycol chelation to the iodide ion was suggested.[3]

Although nitrobenzene, dipolar aprotic and poorly basic, can not be used as a medium transparent in the ultraviolet region, it has widely been used as a useful solvent for ion pair extraction[16] and conductance studies[17] due to its solubilizing power for salts. The amount of coextracted water with anions into nitrobenzene decreases with increasing anionic radius.[12,13,15] From isopiestic measurements, hydration constants of the perchlorate ion in nitrobenzene were estimated for five hydration models.[14]

In connection with our study on solvent extraction of ion pair with tetraalkylammonium iodides (R_4NI)[2,16] it was found that when tetraalkylammonium iodides are dissolved in nitrobenzene the colour results in deep yellow from yellow and the intensity decreases as a small amount of water is added to the solution. This spectrum change which is reversible with regard to water concentrations is attributed to the formation and rupture of a charge transfer complex. On the basis of the water concentration dependence of the visible spectrum and the chemical shift of water proton, we discuss the interaction among the iodide anion, nitrobenzene and water, and the structure of hydrated species.

Experimental

Tetrapropylammonium iodide (Pr_4NI) and tetraphenylphosphonium chloride (Ph_4PCl), of the reagent grade available, were further purified by several recrystallizations from ethanol–ether (peroxide free) mixtures. Nitrobenzene was purified as previously described.[16]

Visible spectra were recorded with a Hitachi model 210-10 spectrometer, using 10 mm quartz cells at 25 °C. The absorbance for a nitrobenzene solution containing a certain concentration of $Pr_4NI$was measured as a function of water content. Nitrobenzene containing water was used as reference. ^{1}H NMR spectra were measured with a Hitachi model R-20 NMR spectrometer (60 MHz) at 25 °C, relative to tetramethylsilane in nitrobenzene as external reference. Water concentrations in nitrobenzene were determined coulometrically with a Hiranuma AQ-3 aquacounter.

Results and Discussion

(a) C.t.t.s. Spectra. Tetrapropylammonium iodide is easily dissolved in nitrobenzene and its solution gives slightly deeper yellow than that of nitrobenzene. The conductance experiment showed that no conductance change was observed in a solution at 10^{-4} mol dm^{-3} levels over the period of 1 h, suggesting that the species in nitrobenzene are stable.

The absorption spectrum of Pr_4NI (1.275×10^{-3} mol dm^{-3}) in nitrobenzene and its water concentration dependence over the range 400 to 500 nm are shown in Fig. 1 where the reference is nitrobenzene containing water of the same concentration as that in the sample cell; therefore the strong absorption due to nitrobenzene itself results in the rapid drop in absorbance below 430 nm. The addition of a small amount of water leads to a decrease in the intensity of absorption. Table 1 gives the absorbances at various concentrtions of water at 440

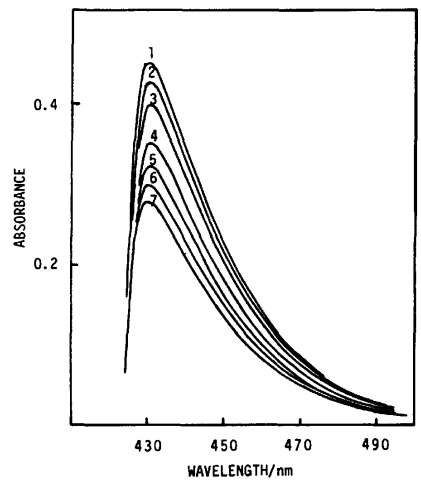

Fig. 1. Spectra of Pr_4NI (1.275×10^{-3} mol dm^{-3}) in nitrobenzene solutions using 10 mm cells as a function of water concentration in mol dm^{-3}; 1, 0.005; 2, 0.0213; 3, 0.0376; 4, 0.0702; 5, 0.103; 6, 0.135; 7, 0.168.

Table 1. Absorbances of Pr_4NI(1.275×10^{-3} mol dm^{-3}) in nitrobenzene at 440 nm as a function of water concentration at 25 °C

$[H_2O]$/mol dm^{-3}	Absorbance	$\frac{\varepsilon_{obsd}}{10\ mm^{-1}\ mol^{-1}\ dm^3}$
0.0050	0.346	271
0.0132	0.333	261
0.0213	0.325	255
0.0376	0.309	242
0.0702	0.280	220
0.103	0.255	200
0.135	0.232	182
0.152	0.221	173
0.160	0.219	172
0.168	0.215	169

nm where Lambert's law was confirmed to hold for the intensity over the range of light pass 1 to 10 mm. This water concentration dependence of the absorbance is reversible: The drying of wet nitrobenzene solutions by calcium chloride increases the absorbance again. The results mentioned above indicate that the shoulder of spectra observed above 430 nm are due to the formation of a charge transfer complex between the iodide ion and nitrobenzene or c.t.t.s. spectra. Such c.t.t.s. spectrum in the visible region is not observed for chloride, bromide, and perchlorate, which being expected on the basis of the ionization potentials of the halide ions.[18,19] The decrease in the intensity with increasing water concentration can be assigned to the hydration of the iodide ion, the iodide–nitrobenzene interaction being weakened. A similar effect of addition of a protic solvent on c.t.t.s. spectra in a aprotic solvent was also observed; addition of methanol and water results in loss of the c.t.t.s. band with a maximum at 40.7×10^3 cm^{-1} for iodide in acetonitrile and in growth of a new band at 41.8×10^3 cm^{-1} due to the iodide ion hydrogen bonded to the protic solvents.[3]

Since the ionic association constant, 33,[16] for Pr_4NI in nitrobenzene at 25 °C gives a degree of dissociation of 0.97 at 1.275×10^{-3} mol dm^{-3}, the effect of ion pairing is negligible for the following calculation. The hydration of the iodide ion is represented as

$$I^-\cdot(n-1)H_2O + H_2O \rightleftharpoons I^-\cdot nH_2O$$

with the corresponding formation constants,

$$K_n = [I^-\cdot nH_2O]/[I^-\cdot(n-1)H_2O][H_2O]. \quad (1)$$

The apparent molar extinction coefficient (ε_{app}) is written as

$$\varepsilon_{app} = [I^-](\varepsilon_0 + \varepsilon_1K_1[H_2O] + \varepsilon_2K_1K_2[H_2O]^2 + \varepsilon_3K_1K_2K_3[H_2O]^3 + \cdots)/[I^-]_{total}, \quad (2)$$

where $[I^-]_{total}$ is the total concentration of iodide ions and ε_0, ε_1, ε_2, and ε_3 the apparent absorptivity of non-hydrated, 1 : 1, 1 : 2, 1 : 3 hydrated iodide ions, respectively. Assuming $n=1$, 2, and 3, the hydration constants were calculated by use of the dependence of the absorbance at 440 nm on the water concentration (Table 1) and the monomer-dimer equilibrium constant $K_s(=[(H_2O)_2]/[H_2O]^2)$, 1.054 mol^{-1} dm^3, for water in nitrobenzene at 25 °C:[20] First, the concentrations of monomer water and nonhydrated iodide ions were obtained from the K_s value and an initial value of K_n, and then an iterative calculation was carried out to minimize the standard deviation, $[\sum(\varepsilon_{calcd}-\varepsilon_{obsd})^2/(N-1)]^{1/2}$, with a given value of ε_0 where ε_{calcd} and ε_{obsd} are apparent molar extinction coefficient calculated and observed, respectively, and N is the number of data. The best fitting values for each case are given in Table 2. For both $n=1$ and 2, ε_1 and ε_2 are nearly zero, showing that the hydration of iodide ions almost disrupts the charge-transfer transition. For $n=3$ the hydration constants were calculated, by assuming that ε_1, ε_2, and ε_3 are zero. The K_1 value, 3.5, for iodide ions is comparable to 2.4 for perchlorate ions in nitrobenzene obtained by the isopiestic method.[14]

Table 2. Hydration constants of iodide ions in nitrobenzene at 25 °C

n	1	2	3
ε_0	281	277	274
ε_1	0.0	0.4	0
ε_2		0.0	0
ε_3			0
K_1	5.0	3.9	3.5
K_2		2.1	2.6
K_3			1.4
σ[a]	3.6	1.7	1.1

a) $\sigma=\{\sum(\varepsilon_{calcd}-\varepsilon_{obsd})^2/(N-1)\}^{1/2}$, where ε_{calcd}, ε_{obsd} are apparent molar extinction coefficient calculated and observed, respectively, and N is the number of data.

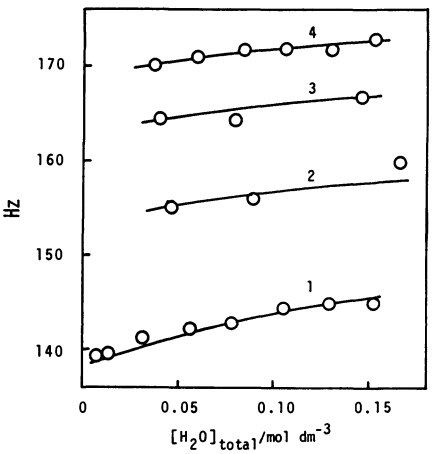

Fig. 2. Chemical shifts of water protons in the presence of Pr_4NI in nitrobenzene. Solid lines show the calculated values. Concentration of Pr_4NI in mol dm^{-3}; 1, 0.0; 2, 0.05; 3, 0.100; 4, 0.143.

(b) ^1H NMR Spectra of Water. A single resonance line for water protons in nitrobenzene was obtained irrespective of the presence of Pr_4NI and Ph_4PCl. Figures 2 and 3 show the chemical shifts of water protons as a function of water and salt concentrations. Hydrogen bonding usually leads to a down-field shift.[4,6] In Fig. 2 the increased down field shift with water concentration irrespective of the presence of salts is ascribed to the increased dimerization of water and hydration of ions, respectively.

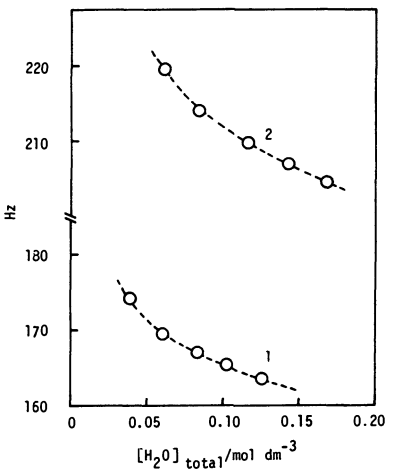

Fig. 3. Chemical shifts of water protons in the presence of Ph_4PCl in nitrobenzene. Concentration of Ph_4PCl in mol dm^{-3}; 1, 0.0109; 2, 0.0471.

In a way similar to the case for c.t.t.s. spectra, the observed chemical shift (δ_{obsd}) of water protons is represented as, in the absence of salts,

$$\delta_{obsd} = (\delta_0[H_2O]+2\delta_s K_s[H_2O]^2)/[H_2O]_{total}, \quad (3)$$

in the presence of salts,

$$\delta_{obsd} = (\delta_0[H_2O] + 2\delta_s K_s[H_2O]^2 + \delta_1 K_1[I^-][H_2O] + 2\delta_2 K_1 K_2[I^-][H_2O]^2 + 3\delta_3 K_1 K_2 K_3[I^-][H_2O]^3)/[H_2O]_{total}, \quad (4)$$

where δ_0, δ_s, δ_1, δ_2, and δ_3 are chemical shifts for non-bonded monomeric and dimeric water, 1 : 1, 1 : 2, and 1 : 3 hydrates, respectively. Although in the salt concentration range used in the NMR study the degree of ionic association for Pr_4NI is marked (0.14 for 0.01 mol dm^{-3} and 0.44 for 0.15 mol dm^{-3}), the hydration of iodide ions is not affected significantly by the association.[2,12-15] Thus, the association effect was disregarded. The chemical shifts, δ_0(138) and δ_s(175) from Eq. 3 and δ_1(232), δ_2(245), and δ_3(265) from Eq. 4 were estimated from K_s and K_1, K_2, and K_3 obtained from the c.t.t.s. spectra. It is noteworthy that the chemical shift increases stepwise with increasing degree of hydration of iodide, $\delta_1<\delta_2<\delta_3$, contrary to the behaviour for lithium ions in propylene carbonate.[4] Furthermore, the chemical shift for iodide increases with increasing the water concentration, while that for chloride decreases (Fig. 3). The increased down-field shift for iodide would be explained in terms of chelation of water molecules bound to iodide ions; models I for $n=2$ and II for $n=3$.

The chemical shift for chloride ions is much larger than that for iodide ions, showing the stronger hydration of chloride ions. It is likely that the orientation of water molecules towards chloride ions through hydrogen bonding is too strong to make a chelate ring such as the one observed for iodide ions.

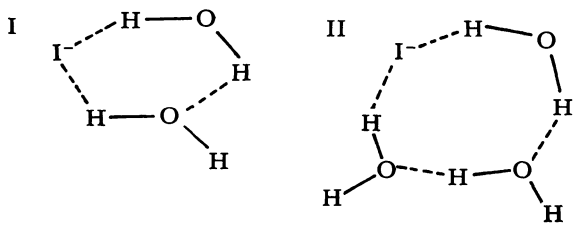

This work was supported in part by a Grant-in-Aid for Scientific Research Nos. 443013 and 454183 from the Ministry of Education, Science and Culture.

References

1) T. Fujiwara, K. Matsuda, and Y. Yamamoto, *Inorg. Nucl. Chem. Lett.*, **16**, 301 (1980).
2) K. Ito, E. Iwamoto, and Y. Yamamoto, *Bull. Chem. Soc. Jpn.*, **55**, 2143 (1982).
3) M. C. R. Symons and S. E. Jackson, *J. Chem. Soc., Faraday Trans. 1*, **75**, 1919 (1979).
4) D. R. Cogly, J. N. Butler, and E. Grunwald, *J. Phys. Chem.*, **75**, 1477 (1971).
5) M. C. R. Symons and V. K. Thomas, *J. Chem. Soc., Faraday Trans., 1*, **77**, 1891 (1981).
6) R. L. Benoit and S. Y. Lam, *J. Am. Chem. Soc.*, **96**, 7385 (1974).
7) I. D. Kuntz, Jr., and C. J. Cheng, *J. Am. Chem. Soc.*, **97**, 4852 (1975).
8) M. C. R. Symons, T. A. Shippy, and P. P. Pastogi, *J. Chem. Soc., Faraday Trans., 1*, **76**, 2251 (1980).
9) M. K. Chantooni, Jr., and I. M. Kolthoff, *J. Am. Chem. Soc.*, **89**, 1582 (1967).
10) I. M. Kolthoff and M. K. Chantooni, Jr., *J. Am. Chem. Soc.*, **91**, 4681 (1969).
11) D. J. Pirson and P. L. Huyskens, *J. Solution Chem.*, **3**, 503 (1974).
12) Y. Yamamoto, T. Tarumoto, and T. Tarui, *Bull. Chem. Soc. Jpn.*, **46**, 1466 (1973).
13) T. Kenjo and R. M. Diamond, *J. Inorg. Nucl. Chem.*, **36**, 183 (1974).
14) T. Tarui, *J. Inorg. Nucl. Chem.*, **37**, 1213 (1975).
15) C. M. Arnett, B. Chawla, and N. J. Hornung, *J. Solution Chem.*, **6**, 781 (1977).
16) a) E. Iwamoto, K. Ito, and Y. Yamamoto, *J. Phys. Chem.*, **85**, 894 (1981); b) E. Iwamoto, H. Ohmori and Y. Yamamoto, *ibid.*, **87**, 1776 (1983).
17) E. Hirsch and R. M. Fuoss, *J. Am. Chem. Soc.*, **82**, 1018 (1960).
18) M. J. Blandamer and M. F. Fox, *Chem. Rev.*, **69**, 59 (1969).
19) P. C. Dwivedi and C. N. R. Rao, *Spectrochimica Acta, Part A*, **26**, 1535 (1970).
20) S. D. Christian, A. A. Taha, and B. W. Gash, *Quart. Rev. Chem. Soc.*, **24**, 20 (1970).

Fractional Spectrophotometric Determination of Ethylenediaminetetraacetate and nitrilotriacetate as Their Iron(III) Complexes by Use of H- and Na-form Ion Exchange Resin Columns

Akihiro YAMAGUCHI, Kunio OHZEKI,* and Tomihito KAMBARA
Department of Chemistry, Faculty of Science, Hokkaido University, Sapporo 060
(Received February 21, 1983)

The fractional determination of ethylenediaminetetraacetate(EDTA) and nitrilotriacetate(NTA) was carried out by use of hydrogen- and sodium-form ion exchange resin columns. After the conversion of free and complexed EDTA and NTA to the corresponding iron(III) complexes, two aliquots of the sample solution were separately passed through the columns. The iron(III)–EDTA complex was stable in both columns but iron(III)–NTA complex was completely decomposed in the hydrogen-form resin column, therefore, both of iron(III)–EDTA and –NTA were found in the effluent of sodium form resin column but only iron(III)–EDTA was found in the effluent of hydrogen-form resin column. The complexes in the respective effluents were determined spectrophotometrically at 255 nm. The recovery tests of EDTA and NTA from the synthetic sample solutions containing various metal ions were examined and the results observed were satisfactory.

The determination of chelating agents has recently been required for the estimation of the complexing capacity and for the speciation of trace metals in water. The general method was based on the conversion of chelating agents to the corresponding copper(II) complexes with the addition of excess copper(II) ion. After the removal of excess copper(II) by means of the chelating resin column,[1] or as copper(II) oxide,[3,4] the resulting copper(II) complexes were determined by atomic absorption spectrometry[1-3] or spectrophotometry.[4] A CuO-loaded ion exchange resin column was used to determine EDTA as the copper(II) complex.[5] Chelating agents were also determined as iron(III) complexes.[6,7] The fractional determinations of chelating agents were carried out with various methods, *i.e.*, gas chromatography as methyl esters,[8] liquid chromatography as copper(II) complexes,[9] and polarography as cadmium(II) complexes.[10]

In the present paper a simple spectrophotometric method of fractional determination of EDTA and NTA is described.

Experimental

Reagents. All chemicals used were of analytical reagent grade. The stock solutions of EDTA and NTA were prepared from the Dotite reagents (Dojindo Lab.). A 10^{-2} M (1 M=1 mol dm^{-3}) EDTA solution was made by dissolving dried disodium dihydrate salt (80 °C, 2 h) in deionized water. A 10^{-2} M NTA solution was prepared by dissolving dried acid (110 °C, 2 h) in a sodium hydroxide solution, the pH of final solution being around 8. Ammonium iron(III) sulfate dodecahydrate was dissolved into acidified water (pH 1) to give a 2×10^{-2} M solution. Other metal ion solutions were made from the nitrate or chloride salts.

Ion Exchange Resin. Dowex 50W-X8 (100—200 mesh) was used in H- and Na-forms, respectively. Hydrogen-form resin was packed in a column (23 cm long, 1 cm i.d.) to make a 2-cm resin bed, and it was washed with 0.025 M sulfuric acid. Sodium-form resin was packed in another column of the same size to give a 1-cm resin height, and the column was washed with a buffer solution (pH 3.1) composed of 0.05 M formic acid and 0.01 M sodium formate.

Apparatus. A Shimadzu spectrophotometer, UV-240, was used with 1-cm quartz cells.

General Procedure. The sample solution containing EDTA and NTA was divided in two equal aliquots and placed in 50-ml volumetric flasks.

A) Procedure by the H-form Resin Column. To one of the sample aliquot were added 2.5 ml of 0.5 M sulfuric acid and 0.5 ml of 0.02 M iron(III) solution. The mixture was filled up to the mark with deionized water, the pH of final solution being 1.4. The solution was then passed through the hydrogen-form resin column at a flow rate of 2—3 ml min^{-1}. The first 10-ml portion of effluent was discarded and the next 5-ml portion was collected. The absorbance of iron(III)–EDTA complex in the effluent was measured at 255 nm against deionized water. The blank value was also determined without addition of chelating agents.

B) Procedure by the Na-form Resin Column. To another aliquot of sample solution were added 2.5 ml of 0.5 M sulfuric acid, 0.5 ml of 0.02 M iron(III) solution, and finally 3 ml of 1 M sodium formate solution. The mixture was filled up to the mark, the pH of final solution being 3.1. This solution was passed through the sodium-form resin column and the effluent was collected as described in the above procedure. The absorbance corresponding to the sum of EDTA and NTA was also determined at 255 nm.

Results and Discussion

Absorption Spectrum. Absorption spectra of iron(III)–EDTA and –NTA complexes were shown in Figs. 1 and 2. The iron(III)–NTA complex in the formate buffer solution differed from that in dilute sulfuric acid, the adduct formation of the complex with formate being suggested. The absorbance due to the excess iron(III) was successfully removed by use of the cation exchange resin column. While the photosensitivity of iron(III)–EDTA complex is known,[11,12] the complex was found to be stable at least for 3 h, when the solution was protected from the direct sunlight.

Stability of Iron(III)–NTA Complex in H- and Na-form Resin Columns. The iron(III)–NTA complex was completely dissociated during the passage of the 2-cm column packed with hydrogen-form resin, being not found in the effluent (Fig. 3). By use of a 1-cm column, however, a part of iron(III)–NTA was eluted from the column indicating that the degree of decomposition depends on the column length. On the other hand, iron(III)–NTA complex in the formate buffer solution passed safely through the sodium-form resin column.

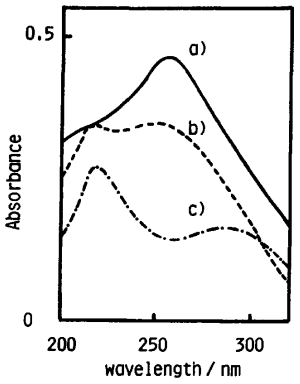

Fig. 1. Absorption spectra of iron(III) complexes in formate buffer solution (0.05 M HCOOH—0.01 M HCOONa, pH 3.1). a) 50.0 μM iron(III)–EDTA, b) 50.0 μM iron(III)–NTA, c) 50.0 μM iron(III), reference: reagent blank.

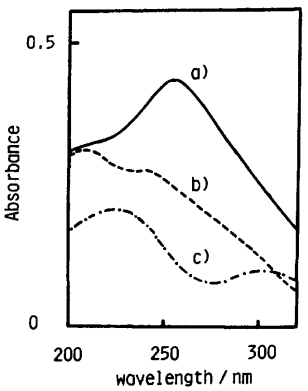

Fig. 2. Absorption spectra of iron(III) complexes in 0.025 M sulfuric acid solution (pH 1.4). The symbols have the same meanings as in Fig. 1.

The absorbance of iron(III)–NTA complex in the effluent increased with increasing pH, probably due to the adduct formation of the complex with formate.

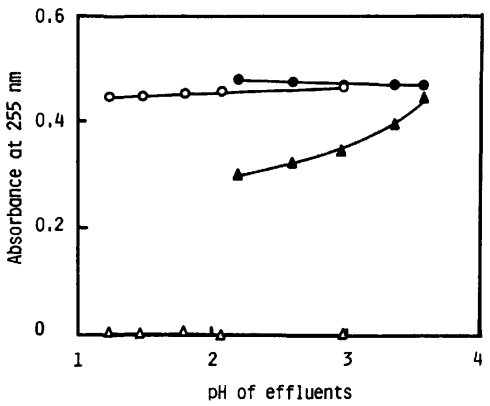

Fig. 3. Effects of pH on the stability of iron(III) complexes after passing the H- and Na-form resin columns. Iron(III)–EDTA: 51.3 μM, (○) H-form, (●) Na-form. Iron(III)–NTA: 51.0 μM, (△) H-form, (▲) Na-form.

Stability of Iron(III)–EDTA Complex in H- and Na-form Resin Column. Iron(III)–EDTA complex was stable in both columns (Fig. 3).

Calibration Curves. The calibration curves of EDTA and NTA were linear over the concentration range 20—100 μM; the regression equations were shown by

$$A_{H}^{EDTA} = 8762[EDTA] - 0.003, \quad (1)$$

$$A_{Na}^{EDTA} = 9185[EDTA] - 0.001, \quad (2)$$

$$A_{Na}^{NTA} = 6664[NTA] - 0.002, \quad (3)$$

where A denotes the absorbance and the suffixes H and Na indicate the signal obtained with the hydrogen- or sodium-form resin column. The relative standard deviations for 5.13×10^{-5} M EDTA were 0.3% (n=5) in the procedure A and 0.2% in the procedure B, respectively, and the value for 5.10×10^{-5} M NTA was 0.6% in the procedure B.

Table 1. Recovery of EDTA and NTA as their iron(III) complexes

Metal(II) added in 0.1 mM	EDTA				NTA	
	Procedure A		Procedure B		Procedure B	
	Absorbance at 255 nm	Recovery %	Absorbance at 255 nm	Recovery %	Absorbance at 255 nm	Recovery %
None	0.458		0.471		0.344	
Mg	0.462	101	0.460	98	0.345	100
Mg[a)]	0.457	100	0.471	100	0.335	97
Ca	0.459	100	0.460	98	0.346	101
Ca[a)]	0.459	100	0.469	100	0.337	98
Co	0.453	99	0.474	101	0.345	100
Cd	0.450	98	0.472	100	0.347	101
Zn	0.459	100	0.460	98	0.341	99
Pb	0.460	100	0.457	97	0.340	99
Ni	0.160	35	0.230	49	0.343	100
Ni[b)]	0.452	99	0.465	99	—	—
Cu	0.340	74	0.472	100	0.343	100
Cu[b)]	0.453	99	—	—	—	—
Mixture[b),c)]	0.455	99	0.471	100	0.344	100

a) [M]=1 mM. b) Heated for 10 min at pH 1.4. c) Mg, Ca, Co, Cd, Zn, Pb, Ni, and Cu each in 0.1 mM. [Fe(III)]=0.2 mM, [EDTA]=51.3 μM, [NTA]=51.0 μM.

Table 2. Fractional determination of EDTA and NTA in synthetic mixtures

Sample	Procedure A Absorbance	Procedure B Absorbance	EDTA			NTA		
			Taken/μM	Found/μM	Error/%	Taken/μM	Found/μM	Error/%
1	0.178	0.735	20.5	20.6	+0.5	81.6	82.3	+0.9
2	0.356	0.789	41.0	40.9	−0.2	61.2	62.4	+2.0
3[a)]	0.441	0.800	51.3	50.7	−1.2	51.0	50.7	−0.6
4	0.540	0.841	61.5	62.0	+0.8	40.8	41.3	+1.2
5	0.718	0.891	82.0	82.5	+0.6	20.4	20.8	+2.0

a) Mg(II), Ca(II), Co (II), Cd(II), Zn(II), Pb(II), Ni(II), and Cu(II), each in 0.1 mM, were added.

Table 3. Recovery of edta from toyohira river water

Sample	Volume/ml	Procedure A		Procedure B	
		Found[a)]/μM	Recovery/%	Found[a)]/μM	Recovery/%
A (upstream)	5	51.2	100	51.5	100
	25	50.4	98	51.5	100
B (midstream)	5	50.9	99	51.9	101
	25	51.0	99	50.7	99
C (downstream)	5	50.6	99	52.6	103
	25	51.2	100	51.3	100

EDTA taken: 51.3 μM. a) Mean of three determinations.

Effect of Diverse Ions. By the addition of excess iron(III), both the free and complexed NTA's were quantitatively converted to the iron(III)–NTA complex at room temperature. In the case of EDTA, however, the conversion of copper(II) and nickel(II) complexes to the iron(III) complex was first achieved by heating the acidified reaction mixture (pH 1.4) for 10 min on a water bath (Table 1).

Fractional Determination of EDTA and NTA. The determination was carried out as follows. The concentration of EDTA in the sample solution was determined by the procedure A; namely, from Eq. 1, one has

$$[\text{EDTA}] = 1.141(A_{\text{H}}^{\text{EDTA}} + 0.003) \times 10^{-4}\ \text{M}. \quad (4)$$

On the other hand, the absorbance corresponding to the sum of EDTA and NTA was determined by the procedure B; namely,

$$A_{\text{Na}} = A_{\text{Na}}^{\text{EDTA}} + A_{\text{Na}}^{\text{NTA}}. \quad (5)$$

By introducing Eqs. 2, 3, and 4 into Eq. 5, the following relationship was obtained.

$$[\text{NTA}] = [1.501(A_{\text{Na}} + 0.003) - 1.573(A_{\text{H}}^{\text{EDTA}} + 0.003)] \times 10^{-4}\ \text{M} \quad (6)$$

The results show the good accuracy, as shown in Table 2.

Recovery of EDTA from River Water Samples. The water samples were filtered through membrane filters (0.45 μm) and the various amounts of EDTA were added. After the addition of excess iron(III), the samples were heated for 10 min on a water bath and subjected to the determination according to the procedures A and B and Eqs. 1 and 2, NTA being assumed to be absent in the original sample solutions. The complete recovery of EDTA was observed in the both procedures (Table 3), which indicated that no appreciable amount of EDTA and NTA was contained in the original sample waters.

References

1) R. J. Stolzberg and D. Rosin, *Anal. Chem.*, **49**, 226 (1977).
2) S. E. Manahan and D. R. Jones IV, *Anal. Lett.*, **6**, 745 (1973).
3) R. Kunkel and S. E. Manahan, *Anal. Chem.*, **45**, 1465 (1973).
4) Y. Sasaki and M. Kawae, *Report of Fukui Tech. College*, **14**, 123 (1980).
5) A. Yamaguchi, K. Ohzeki, and T. Kambara, *Z. Anal. Chem.*, **310**, 30 (1982).
6) S. N. Bhattacharyya and K. P. Kundu, *Talanta*, **18**, 446 (1971).
7) R. M. Wallace and J. F. Hinton, *Anal. Chim. Acta*, **51**, 536 (1970).
8) M. L. Blank and F. Snyder, *J. Chromatogr.*, **170**, 379 (1979).
9) D. R. Jones IV and S. E. Manahan, *Anal. Chem.*, **48**, 502 (1976).
10) R. J. Stolzberg, *Anal. Chim. Acta*, **92**, 139 (1977).
11) B. Kratochvil and M. C. White, *Anal. Chem.*, **37**, 111 (1965).
12) R. M. Cassidy, R. Harpur, and S. Elchuk, *J. Chromatogr.*, **190**, 188 (1980).

Photochemically Induced Orthometalations. Isolation of $(PhO)_2\overline{P(OC_6H_4)}Mn(CO)_4$, $(PhO)_2\overline{P(OC_6H_4)}Mn(CO)_3P(OPh)_3$, and $(PhO)_2\overline{P(OC_6H_4)}Mn(CO)_2[P(OPh)_3]_2$ from $RMn(CO)_3[P(OPh)_3]_2$(R=CH_3 and H) and $MeMn(CO)_4P(OPh)_3$

Satoru Onaka,* Yoshinori Kondo, and Nobuhiro Furuichi
Department of Chemistry, Nagoya Institute of Technology, Gokiso-cho, Showa-ku, Nagoya 466
(Received February 25, 1983)

Photochemical reactions of $RMn(CO)_3L_2$ (R=H and CH_3; L=$P(OC_6H_5)_3$) and $CH_3Mn(CO)_4L$ in benzene gave several kinds of orthometalated products, $(PhO)_2\overline{P(OC_6H_4)}Mn(CO)_{4-x}L_x$ (x=0, 1, and 2). The reactions have been shown to proceed *via* ligand dissociation, CO and/or L, from the parent compounds and the resulting 16-electron intermediates activate a C–H bond of phenyl groups in triphenyl phosphite intramolecularly to yield orthometalated products. The results of photochemical reactions for $MeMn(CO)_3L_2$ and $MeMn(CO)_4L$ are compared with those of thermal reactions for these compounds. $HMn(CO)_4L$ was left intact by photochemical and thermal reactions.

Photochemical reactions of manganese or rhenium carbonyls with phosphines or phosphites have been a subject of recent intensive scrutiny.[1-8] The reactions have been shown to proceed *via* metal centered radicals and to terminate in intermolecular reactions by abstracting X from RX such as CCl_4 and/or by coupling of two 17-electron metal carbonyl radicals, but the importance of intramolecular reaction pathway of metal carbonyl radicals or unstable intermediates with phosphines or phosphites has not yet been well explored to our knowledge. In the previous paper, we have demonstrated that manganese carbonyl radicals with triphenyl phosphite(s) which were produced by photochemical degradation of Me_3Sn–$Mn(CO)_3L_2$ (**1**) (hereafter L denotes triphenyl phosphite) underwent intramolecular reactions by abstracting hydrogen from a benzene ring in the triphenyl phosphite moieties to afford orthometalated products[9] and the key role of 15-electron manganese carbonyl radicals with triphenyl phosphite ligand(s) was suggested to attain orthometalation. In this regard, $MeMn(CO)_3L_2$ (**2**) and $HMn(CO)_3L_2$ (**3**), which are isostructural and isoelectronic about the manganese atom with that of **1**, are attractive compounds to deepen our understanding on the intramolecular reactivity and/or orthometalation reaction mechanisms of unstable manganese carbonyl triphenyl phosphite intermediates which may be produced by photochemical excitation of these compounds. This paper reports isolation of orthometalated products from photochemical reactions of **2**, **3**, and $MeMn(CO)_4L$ (**4**) and some suggestions on the photochemically induced orthometalation mechanisms of these compounds.

Experimental

$CH_3Mn(CO)_3L_2$ (**2**),[10] $HMn(CO)_3L_2$ (**3**),[10] and $CH_3Mn(CO)_4L$ (**4**),[11] and $HMn(CO)_4L$ (**5**)[12] were prepared via reported methods under a nitrogen atmosphere. The photolysis was carried out under an argon atmosphere with a Riko 100 W high-pressure Hg lamp which was inserted in a 300 cm^3 Pyrex reaction vessel. IR spectra were obtained on a JASCO-701G infrared spectrometer with 0.1 mm NaCl windowed liquid cells or for Nujol mulls. Molecular weight was determined by a Corona 114 molecular weight apparatus with a vapor pressure osmometry; benzene was employed as a solvent.

Photolysis of 2. A 0.9 g sample of **2** was dissolved in 50 cm^3 of benzene and the solution was irradiated for 5 h. The solvent was vacuum-stripped to leave a pale yellow oil. The oil was dissolved in a minimum amount of benzene and was loaded on a Florisil column (60—100 mesh). The products were eluted with petroleum ether, cyclohexane, benzene, and chloroform successively. A colorless oil (**6**) (175 mg), three kinds of colorless crystals (**7**) (25 mg), (**8**) (50 mg), (**9**) (25 mg), and yellow crystals (**10a**) (15 mg) were obtained by carefully repeated recrystallizations of each fraction from benzene–cyclohexane. These products were characterized by IR, elemental analyses on C, H, and P, molecular weight determination and/or X-ray diffraction methods; the products **6**—**9** exhibited three IR bands (Nujol mulls) with mediumintensities at around 1100, 950, and 800 cm^{-1} which are characteristic of an orthometalated triphenyl phosphite ligand.[9] The IR spectra in ν(CO) region of **6**, **7**, and **9** are consistent with those of authentic $(PhO)_2\overline{P(OC_6H_4)}Mn(CO)_4$ (**6**), *fac-cis*-$(PhO)_2\overline{P(OC_6H_4)}Mn(CO)_3L$ (**7**), and $(PhO)_2\overline{P(OC_6H_4)}Mn(CO)_2L_2$ (**9**).[9] C, H, and P analyses on **8** suggested that this crystal has the same composition as that of **7** and molecular weight measurenents indicated a monomeric property; elemental analyses of **8**. Found C, 61.86; H, 3.79; P, 8.02%. Calcd for $C_{39}H_{29}MnO_9P_2$: C, 61.75; H, 3.85; P, 8.17%. Molecular weight: Found 787. Calcd 759. The crystal of **8** showed two ν(CO) peaks at 2055 (m) and 1975 (vs) cm^{-1}, while the isomer **7** showed three ν(CO) peaks at 2030 (vs), 1965 (s), and 1941 (vs) cm^{-1} in benzene. This result indicates that **8** has a higher symmetry than that of **7** around the manganese atom and thus a mer-trans structure is assigned to **8** (Fig. 1). The yellow crystals of **10a** are the same product as that obtained by the photolysis of **1** from all respects. The final characterization of this yellow crystal is described below.

Photolysis of 3. A 0.9 g sample of **3** was dissolved in 50 cm^3 of benzene and the solution was irradiated for 5 h. After similar work up as the case of **2**, the product were separated by column chromatography over Florisil. The first fraction was eluted with petroleum ether to afford 300 mg of the starting material after recrystallization from benzene–petroleum ether. The second fraction was eluted with cyclohexane and the third fraction was eluted with benzene. By recrystallization from benzene–petroleum ether, 60 mg of 9 and 10 mg of **7** were obtained. The final fraction was eluted with chloroform to afford 15 mg of yellow crystals **10a**.

Photolysis of 4. A 0.8 g sample of **4** was dissolved in 50 cm^3 of benzene and the solution was irradiated for 8 h. Similar work up and purification as above gave 360 mg of **6**, 40 mg of

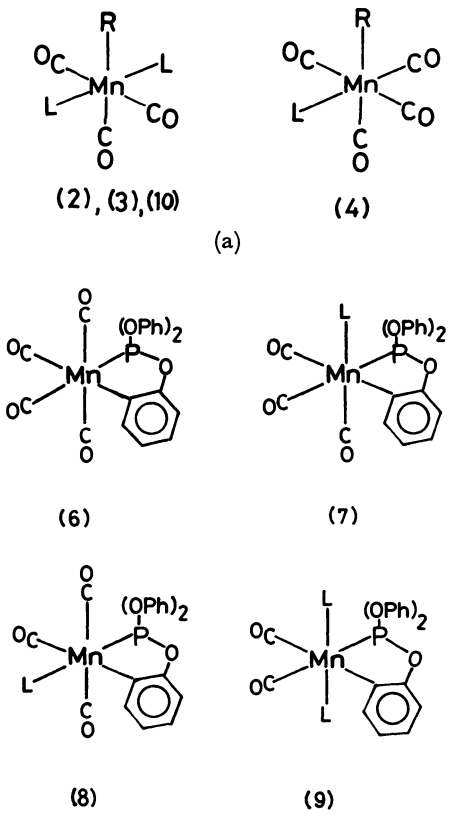

Fig. 1. Schematic pictures of starting materials (1(a)) and photochemical reaction products (1(b)).

7, 10 mg of **8**, 5 mg of **9**, and 15 mg of **10a**.

Photolysis of 5. A 0.9 g sample of **5** was dissolved in 50 cm^3 of benzene and the solution was photolyzed for 8.5 h. However, IR monitoring of the solution did not show any significant sign of reaction except slight decomposition.

Photolysis of 2 with P(OPh)$_3$. To a benzene solution (50 cm^3) containing 0.77 g (1 mmol) of **2**, 310 mg of $P(OPh)_3$ (1 mmol) was added and the solution was photolyzed for 5 h. After similar procedure of purification as above gave 20 mg of **7**, 20 mg of **8**, and 270 mg of **9**.

Photolysis of 4 with P(OPh)$_3$. A 0.88 g (1.8 mmol) of **4** and 0.83 g (2.7 mmol) of $P(OPh)_3$ were dissolved in 50 cm^3 of benzene and the mixture was photolyzed for 8 h. Through similar method of purification as above, 30 mg of **6**, 280 mg of **7**, 190 mg of **8**, 510 mg of **9**, and 15 mg of **10a** were obtained.

Photolysis of 2 in CCl_4. A carbon tetrachloride solution (40 cm^3) which contained 0.63 g of **2** was photolyzed for 1 h. With similar procedure of purification, about 200 mg of *mer-trans*-$ClMn(CO)_3L_2$ (**10**) was isolated.

Photolysis of 3 in CCl_4. A 1.0 g sample of **3** was dissolved in 50 cm^3 of carbon tetrachloride and the solution was irradiated for 1.5 h. The reaction mixture was similarly treated as above to give 200 mg of **10** and small amounts of unidentified products.

Photolysis of 4 in CCl_4. A 1.1 g sample of **4** was dissolved in 50 cm^3 of CCl_4 and the mixture was photolyzed for 3 h. Similar work up as above gave 20 mg of **2**, 50 mg of **6**, 100 mg of **7**, and 90 mg of **10**.

Thermolysis of 2 in Toluene. A 1.0 g sample of **2** was dissolved in 50 cm^3 of toluene and the mixture was refluxed for 3.5 h. The solvent was distilled off under a reduced pressure and the resulting pale brown oil was subjected to column chromatography over Florisil. By similar procedure of purification as the case of photolysis, trace amount of **6**, 280 mg of **7**, 140 mg of **8**, and 35 mg of **9** were obtained.

Table 1. Photochemical and thermal reaction products of **2**, **3**, and **4** and their proportions

Reactant	Products (Molar ratio)
Photolysis	
$CH_3Mn(CO)_3L_2$ (**2**)	**6** : **7** : **8** : **9**=10 : 1 : 2 : 1
$HMn(CO)_3L_2$ (**3**)	**7**: **9**=1 : 5
$CH_3Mn(CO)_4L$ (**4**)	**6** : **7** : **8** : **9**=160 : 10 : 4 : 1
Thermolysis	
$CH_3Mn(CO)_3L_2$ (**2**)	**6** : **7** : **8** : **9**=≈0 : 10 : 5 : 1
$CH_3Mn(CO)_4L$ (**4**)	**6** : **7**=16 : 1

Thermolysis of 3 in Toluene. A 0.4 g sample of **3** was dissolved in 30 cm^3 of toluene and the solution was refluxed for 5 h. However, no detectable change was observed by IR except decomposition.

Thermolysis of 4 in Toluene. A toluene solution (50 cm^3) which contained 0.8 g of **4** was refluxed for 3 h. Similar work up as the thermolysis of **2** afforded 400 mg of **6** and 40 mg of **7**.[13]

Thermolysis of 5. A *p*-xylene solution which contained 0.71 g of **5** was refluxed for 1 h. However, no appreciable change was observed by IR except decomposition.

The yields were averaged for several runs and molar ratios of the products are collected in Table 1.

Characterization of Yellow Crystals 10a. Attempts for characterizing this yellow crystalline compound, **10a**, was not rewarded in the previous study.[9] After publication of the paper, various experiments were added to the previous efforts; fluorescent X-ray analysis[14] revealed that chlorine atom was contained as a main component in these crystals and FD mass indicated the parent peak at m/e=795 ($ClMn(CO)_3L_2$=795). These evidences established that the crystalline compound is $ClMn(CO)_3L_2$, **10**. Next experiment was performed to clarify the origin of the chlorine atom; photolysis of relevant compounds in spectral grade benzene (Dojin Chemistry Co.) did not yield yellow crystals, **10a**. Therefore, the chlorine atom should come from HCl contained as a trace amount of impurity[15] in the benzene used as a solvent for photolysis.

Results and Discussion

As was described in the Experimental section, several kinds of orthometalated products were obtained from photodegradation of mononuclear manganese carbonyl triphenyl phosphite derivatives. Among the data on photochemically induced orthometalation reactions including those of the previous paper,[9] a few points merit description; first, the absorption spectra for **2**—**5** are essentially identical with that of **1** in the region of 230—700 nm. However, the yields of the orthometalated products and molar ratios among the products depend not only on the number of triphenyl phosphite groups of the starting materials, but also on the kind of the sixth ligand, L′, of the manganese atom for $L'Mn(CO)_xL_y$. Therefore, a comparison of the results for a series of isoelectronic and isostructural compounds, Me_3Sn–$Mn(CO)_3L_2$ (**1**), $MeMn(CO)_3L_2$ (**2**), and $HMn(CO)_3L_2$ (**3**) is interesting; **1** and **3** give the products of the same components, **7** and **9**, with somewhat different molar ratio, but **2** affords two extra products, that is **6** and a new compound **8**, in addition to **7** and **9**. In this regard,

2 is rather close to **4** which has one triphenyl phosphite group if the components of the products alone are considered. In order to get a clue on the photochemical reaction pathways of this series of compounds, following types of experiments were performed; (i) photolysis in CCl_4, (ii) photolysis with $C_6H_5CH_2Cl$ in C_6H_6, (iii) photolysis in C_6H_6 which was saturated with air, (iv) photolysis in C_6H_6 with the presence of triphenyl phosphite, and (v) photolysis in C_6H_6 with constant bubbling of argon to purge out evolved gaseous products, especially CO. The first three experiments (i), (ii), and (iii) were made to check whether a radical process, that is, homolytic cleavage of the L'–Mn bond, is a main route or not. For **2**, we obtained following results; *mer-trans*-$ClMn(CO)_3L_2$, **10** and *fac-cis*-$ClMn(CO)_3L_2$, **10'** were yielded from the experiment (i). However, bibenzyl which should be produced if the initial step is a radical process, could not be detected from the experiment (ii). The products **6**—**9** were harvested with similar total amounts, but with somewhat different molar ratios from those of the normal photolysis in the experiment (iii). For experiment (iv), **6** which contains only one triphenyl phosphite group was not isolated, instead the yield of **9** which contains three triphenyl phosphite groups was about tenfolded. For experiment (v), the yield of **9** was considerably increased, but **6** eluded isolation. The result of the second and third experiment (ii) and (iii) indicated that the radical process of homolytic cleavage of the CH_3–Mn bond is not a main process, although the result of experiment (i) suggested some contribution of the radical process (this issue will be discussed later based on the results for **4**). The experiment (iv) and (v) provided evidence that the ligand dissociation L and/or CO was photochemically induced to afford 16-electron intermediates and the dissociated ligand(s) was incorporated again into the 16-electron intermediates or orthometalated 16-electron intermediates. Before we advance our discussion on **2**, it seems appropriate to assess some results on **4** which behaved similarly to **2** in the normal photolysis; photolysis of **4** in CCl_4 produced $CH_3Mn(CO)_3L_2$ (**2**), two kinds of orthometalated products, **6** and **7**, and $ClMn(CO)_3L_2$ (**10**). As the photolysis of **10** in benzene did not yield any kind of orthometalated products, isolation of **6** and **7** indicates that these products are obtained from **4** and especially isolation of **2** is a clear evidence that the ligand dissociation is an important photochemical process for **4**. Another evidence to support this contention comes from the comparison of the result with that of $Me_2Sn[Mn(CO)_4L]_2$; according to the previous paper,[9] irradiation of this compound in benzene brought homolytic cleavage of the Sn–Mn bond to afford $\cdot Mn(CO)_4L$ radical and from this radical only one kind of orthometalated product **6** was isolated with low yield. From these observations, we are tempted to the assertion that the preponderant process of photoexcitation of **4** is ligand dissociation L or CO from the manganese atom to leave coordinatively unsaturated metal site, that is, 16-electron intermediates and these 16-electron intermediates activate a C–H bond in the phenyl groups of triphenyl phosphite(s) intramolecularly to yield orthometalated products, although some contribution of radical process to the orthometalation should not be overlooked as was described in the previous study.[9] (Schemes 1 and 2)

$$CH_3Mn(CO)_3L_2 \overset{h\nu}{\rightleftharpoons} CH_3Mn(CO)_2L_2 + CO \quad (1)$$

$$CH_3Mn(CO)_3L_2 \overset{h\nu}{\rightleftharpoons} CH_3Mn(CO)_3L + L \quad (2)$$

$$CH_3Mn(CO)_2L_2 \longrightarrow (PhO)_2\overbrace{P(OC_6H_4)}Mn(CO)_2L + CH_4 \quad (3)$$

$$CH_3Mn(CO)_3L \longrightarrow (PhO)_2\overbrace{P(OC_6H_4)}Mn(CO)_3 + CH_4 \quad (4)$$

$$(PhO)_2\overbrace{P(OC_6H_4)}Mn(CO)_2L + L \overset{h\nu}{\rightleftharpoons} (PhO)_2\overbrace{P(OC_6H_4)}Mn(CO)_2L_2 \quad (5)$$

$$(PhO)_2\overbrace{P(OC_6H_4)}Mn(CO)_2L + CO \overset{h\nu}{\rightleftharpoons} (PhO)_2\overbrace{P(OC_6H_4)}Mn(CO)_3L \quad (6)$$

$$(PhO)_2\overbrace{P(OC_6H_4)}Mn(CO)_3 + L \overset{h\nu}{\rightleftharpoons} (PhO)_2\overbrace{P(OC_6H_4)}Mn(CO)_3L \quad (7)$$

$$(PhO)_2\overbrace{P(OC_6H_4)}Mn(CO)_3 + CO \overset{h\nu}{\rightleftharpoons} (PhO)_2\overbrace{P(OC_6H_4)}Mn(CO)_4 \quad (8)$$

Scheme 1.

$$CH_3Mn(CO)_4L \overset{h\nu}{\rightleftharpoons} CH_3Mn(CO)_3L + CO \quad (9)$$

$$CH_3Mn(CO)_4L \overset{h\nu}{\rightleftharpoons} CH_3Mn(CO)_4 + L \quad (10)$$

$$CH_3Mn(CO)_3L + L \overset{h\nu}{\rightleftharpoons} CH_3Mn(CO)_3L_2 \quad (11)$$

$$CH_3Mn(CO)_4 + CO \overset{h\nu}{\rightleftharpoons} CH_3Mn(CO)_5 \quad (12)$$

$$CH_3Mn(CO)_3L \longrightarrow (PhO)_2\overbrace{P(OC_6H_4)}Mn(CO)_3 + CH_4 \quad (13)$$

$$(PhO)_2\overbrace{P(OC_6H_4)}Mn(CO)_3 + L \overset{h\nu}{\rightleftharpoons} (PhO)_2\overbrace{P(OC_6H_4)}Mn(CO)_3L \quad (14)$$

$$(PhO)_2\overbrace{P(OC_6H_4)}Mn(CO)_3 + CO \overset{h\nu}{\rightleftharpoons} (PhO)_2\overbrace{P(OC_6H_4)}Mn(CO)_4 \quad (15)$$

Scheme 2.

Scheme 2 is devoid of the mechanism for the formation of **9**. However, we would like to suggest that **9** is produced by secondary photochemical degradation of **7** and/or **8** as was clarified in the previous study[9] and the reason for low yield of **9** from **4** is also accounted for by this mechanism. $CH_3Mn(CO)_5$ eluded isolation.

For **3**, the experiment (i) afforded **10** and a few kinds of unidentified products in low yields. Although these results suggested that radical process was predominant, we could not isolate bibenzyl in the experiment (ii) and the yields of **7** and **9** were not suppressed in the

experiment (iii). In the experiment (v), the yield of **7** was suppressed, but the yield of **9** was doubled. The result of the experiment (v) indicates that the process of carbonyl dissociation and its uptake is also included in the mechanisms of the formations of **7** and **9**. Although general patterns of the photochemical reactions of **3** are quite close to those of **1**, it may be appropriate to postpone our conclusion on the orthometalation reaction mechanisms for **3** until we can get affirmative evidence in the future experiment.

Kaesz *et al.* isolated two kinds of orthometalated products, **6** and **7** by thermal reaction of $CH_3Mn(CO)_4L$ (**4**).[13] However, photochemical reaction of **4** in the present study afforded four kinds of orthometalated products instead. The ramification appeared to suggest that the intermediates produced thermally from **4** are not the same as those produced photochemically. This idea prompted us to investigate thermal reaction of **2**. As was described 'n the Experimental section, thermolysis of **2** in toluene yielded the same products as in the case of photolysis. However, the molar ratios of the orthometalated products were significantly different from those of photolysis and especially the yield of **6** was quite low. In the thermolysis, the solvent was refluxed and gaseous products such as CO should be purged out easily with this reflux. Thus, the situation is quite similar to the photolysis of **2** with constant bubbling of argon (experiment (v)); in experiment (v) of **2**, **6** was not isolated. Therefore, quite low yield of **6** in thermolysis of **2** may not be considered to imply that the intermediates produced from **2** by thermal reaction is different from those produced photochemically.

Photochemical reaction of **4** yielded extra two orthometalated products in addition to two compounds **6** and **7** which are obtained by thermolysis. The low yield of **9** in photolysis suggests that this product is generated by secondary photodegradation of orthometalated products **7** and **8**. Indeed, it was clarified in the previous study that photolysis of **7** gave **8** and **9**[9] and further, thermolysis of **7** did not yield **8** and **9**; IR monitoring of thermal reaction of **7** in refluxed toluene for 3.5 h did not exhibit significant spectral change in carbonyl stretching region. Therefore, we can suggest at present that the intermediates from **4** by thermal reaction are not essentially different from those by photochemical reaction.

The present work was partially supported by a Grant-in-Aid for Scientific Research No. 57470036 from the Ministry of Education, Science and Culture.

References

1) A. Hudson, M. F. Lappert, P. W. Lender, and B. K. Nicholson, *J. Chem. Soc., Chem. Commun.*, **1974**, 966; A. Hudson, M. F. Lappert, and B. K. Nicholson, *J. Chem. Soc., Dalton Trans.*, **1977**, 551.

2) M. S. Wrighton and D. S. Ginley, *J. Am. Chem. Soc.*, **97**, 2065 (1975); D. L. Morse and M. S. Wrighton, *ibid.*, **98**, 3931 (1976).

3) B. H. Byers and T. L. Brown, *J. Am. Chem. Soc.*, **97**, 947 (1975); D. R. Kidd and T. L. Brown, *ibid.*, **100**, 4095 (1978); B. H. Byers and T. L. Brown, *ibid.*, **97**, 3260 (1975); D. R. Kidd, C. P. Cheng, and T. L. Brown, *ibid.*, **100**, 4103 (1978); R. W. Wegman, R. J. Olsen, D. R. Grad, L. R. Faulkner, and T. L. Brown, *ibid.*, **103**, 6089 (1981).

4) D. Soonenberger and J. D. Atwood, *J. Am. Chem. Soc.*, **102**, 3484 (1980).

5) J. P. Fawcett and A. Pöe, *J. Chem. Soc., Dalton Trans.*, **1977**, 2039; A. Fox and A. Pöe, *J. Am. Chem. Soc.*, **102**, 2497 (1980).

6) W. K. Meckstroth, R. T. Walters, W. L. Waltz, A. Wojcicki, and L. M. Dorfman, *J. Am. Chem. Soc.*, **104**, 1842 (1982).

7) T. Foster, K. S. Chen, and J. K. S. Wan, *J. Organomet. Chem.*, **184**, 113 (1980).

8) R. H. Reimann and E. Singleton, *J. Chem. Soc., Dalton Trans.*, **1976**, 2109.

9) S. Onaka, Y. Kondo, N. Furuichi, and K. Toriumi, *Chem. Lett.*, **1980**, 1343; S. Onaka, Y. Kondo, N. Furuichi, K. Toriumi, and T. Ito, *Bull. Chem. Soc. Jpn.*, **56**, 87 (1983).

10) W. Hieber, M. Höfler, and J. Muschi, *Chem. Ber.*, **98**, 311 (1965).

11) W. Hieber and W. Freyer, *Chem. Ber.*, **92**, 1765 (1959).

12) W. Hieber, G. Faulhaber, and F. Theubert, *Z. Anorg. Allg. Chem.*, **314**, 125 (1962).

13) R. J. McKinney, R. Hoxmeier, and H. D. Kaesz, *J. Am. Chem. Soc.*, **97**, 3059 (1975).

14) Thanks are due to Dr. Kazuko Matsumoto of Tokyo University for fluorescent X-ray analysis.

15) The content of HCl is described to be less than 0.0004% on the label, but real content of HCl seems greater than 0.0004% judging from the yield of **10**.

 © 1983 The Chemical Society of Japan Bull. Chem. Soc. Jpn., 56, 2300—2310 (1983) [Vol. 56, No. 8

Enzymatic Oxygenation of Sulfides with Cytochrome P-450 from Rabbit Liver. Stereochemistry of Sulfoxide Formation[1)]

Toshikazu TAKATA, Mayumi YAMAZAKI,† Ken FUJIMORI, Yong Hae KIM,††
Takashi IYANAGI,** and Shigeru OAE*
Department of Chemistry, University of Tsukuba, Sakura, Ibaraki 305
***Devision of Biochemistry, School of Medicine, University of Tsukuba, Sakura, Ibaraki 305*
(Received April 19, 1983)

Stereochemistry of enzymatic oxygenations of various diaryl, dialkyl and aryl alkyl sulfides to the corresponding sulfoxides with hepatic microsomes obtained from phenobarbital pretreated rabbit was investigated in comparison with those of nonenzymatic oxidations. Relative reactivity of the sulfides in the enzymatic oxygenation, based on the yields of the sulfoxides and the amount of oxygen absorption, depends upon the steric demand of the substituent in the oxygenation of 2-substituted thiochroman derivatives. However, such a trend was not observed in the enzymatic oxygenations of various acyclic sulfides. A substantial asymmetric induction on the sulfur atom was always observed (*e.g.*, 54% *e.e.* for benzyl *t*-butyl sulfide). Formation of the sulfoxide with *R*-configuration predominated over that with *S*-configuration. The enzymatic oxygenation of all the unsymmetrical sulfides examined proceeded *via* the same steric course. Diastereomeric ratios of the sulfoxides formed in the enzymatic oxygenations of various racemic sulfides bearing alkyl substituents at α-position are markedly favoured more for the trans isomers than for the cis ones, while the ratio was nearly fifty-fifty in the nonenzymatic oxidations with both MCPBA and $NaIO_4$. These results suggest that the enzymatic oxygenation takes place at the less hindered side of the sulfide. Both enzymatic and nonenzymatic oxidations of rigid six-membered cyclic sulfides, *trans*-thiadecalins and 4-(*p*-chlorophenyl)thiane, similarly occurred at the less hindered side to give mainly equatorial sulfoxides. The yields of the four stereoisomeric sulfoxides were nicely determined in the enzymatic oxygenation of racemic 2-methyl-2,3-dihydrobenzothiophene to elucidate the steric course of the oxygenation. Dependency of this microsomal oxygenation upon cytochrome P-450 enzyme was proved by several inhibition experiments and also by the identical stereochemical results of the oxygenation of a few selected sulfides to those with a reconstituted system with purified cytochrome P-450 and co-factors.

Cytochrome P-450, a monooxygenase, is known to be present in multiple forms in mammalian tissues.[2)] Some cytochrome P-450s in adrenal grand, cytochrome $P\text{-}450_{11\beta}$ and cytochrome $P\text{-}450_{17\alpha}$, participate in the regiospecific and stereospecific hydroxylations of the steroids while cytochrome P-450s in plants carry out specific biosyntheses of biologically important substances.[2)] One major role of cytochrome P-450 in mammalian liver is known to be the oxygenation of various kinds of lipophilic xenobiotics, such as drugs, insecticides, food additives, *etc.*, to the more hydrophilic metabolites in order for these xenobiotic substances to be excreted.[2)] In such metabolic oxygenations in liver, stereospecificity may not be neccesary because the main function of the oxygenation is to convert the foreign substances to other more hydrophilic products which

$$[S] + NADPH + O_2 + H^+ \xrightarrow{\text{Cytochrome P-450}} [S\text{-}O] + NADP^+ + H_2O \quad (1)$$

can be excreted readily out of living bodies. Since the cytochrome P-450 is demonstrated to play such a role, the oxygenation with this enzyme would be less substrate selective and less stereospecific as compared to most other enzymes. However, practically no stereochemical study has appeared in the oxygenation of xenobiotic compounds by hepatic microsomal cytochrome P-450.

Meanwhile, organic sulfides are good substrates for studying the stereochemistry of the oxygenation with cytochrome P-450,[3)] since chemical and biomimetic oxidations of sulfides to the sulfoxides and their stereochemistry have been extensively studied in our laboratory,[3-5)] and hence stereochemical results obtained in the enzymatic oxygenation can be readily compared with our accumulated data.[3-5)] Thus, we have investigated the stereochemistry of the oxygenation of various sulfides to the corresponding sulfoxides with rabbit liver microsomal cytochrome P-450 in both microsomal level and reconstituted system with purified liver microsomal cytochrome P-450[1)] obtained from rabbit pretreated with phenobarbital for 5 d to induce the enzyme.

Experimental

General. Melting points and infrared spectra were taken on a Yanaco instrument and a Hitachi 215 spectrometer, respectively, and uncorrected. NMR spectra were recorded on a Hitachi Perkin-Elmer R-20 spectrometer. FT-NMR spectra were obtained by a JEOL FX-90Q spectrometer at the chemical analysis center of this university. Mass spectra were taken with a Hitachi RMU-6MG mass spectrometer. A Shimadzu GC-6A instrument was used for gas chromatography using N_2 gas as a carrier gas. Specific rotations were calculated from the values of optical rotations which were measured by a JASCO DIP-140 polarimeter using a 5 cm (length) quartz cell. CD spectra were recorded on a JASCO J-20 spectrometer. Elemental analyses were carried out by the chemical analysis center of this university.

Materials. Liver microsomes were obtained from phenobarbital pretreated (5 d) male rabbits according to the reported method.[3b,6)] Purified cytochrome P-450 was obtained from the same liver microsomes by Imai's method.[7)] NADPH-cytochrome P-450 reductase was purified by the

† Present address: Faculty of Pharmaceutical Science, University of Teikyo, Sagamiko, Kanagawa 199-01.

†† Present Address: Department of Chemistry, The Korea Advanced Institute of Science and Technology, P. O. Box 150, Chongyangni, Seoul, Korea.

method of Iyanagi *et al.* with some modification.[8] NADP+, D-glucose 6-phosphate (G-6-P), and G-6-P dehydrogenase (G-6-PDH) were obtained from Oriental Yeast Co. NMR shift reagents, $Eu(dpm)_3$ and $Eu(hfc)_3$ were of Dojin Chemical Co. and Aldrich Chemical Co., respectively. SKF 525-A ((2-*N*,*N*-diethylamino)ethyl 2,2-diphenylpentanoate) was given from Tanabe Seiyaku Co.

Sulfide and Sulfoxide. Physical and spectral data, and elemental analyses data of various sulfides and sulfoxides used here are listed in Table 1.

Most of the sulfides were either commercially available or prepared by known method described below, and some were new compounds.

Common dialkyl and aryl alkyl sulfides (**9**, **12**—**19**) were prepared by the usual method, *i.e.* the reaction of the corresponding thiols and alkyl halides in the presence of a base,[9] while *t*-butyl *p*-tolyl sulfide (**17**) was obtained by treating *p*-toluenethiol with gaseous isobutylene.[10] The genuinely pure **17** was obtained by the oxidation of the crude sulfide with H_2O_2 in AcOH followed by reduction with *O*,*O*'-diethyl hydrogenphosphodithioate[11] after purification of the sulfoxide by column chromatography (eluent: hexane and then chloroform, on silica gel). Di-*t*-butyl sulfide (**21**) and thiane (**22**) were commercially available from Tokyo Kasei Kogyo Co. and Aldrich Chemical Co., respectively. *o*-Methoxyphenyl phenyl sulfide (**20**) was prepared by the reaction of *o*-methoxybenzenediazonium salt and thiophenol as reported previously.[12] *trans*-1-Thiadecalin (**6**) was also synthesized from 1,2-epithiocyclohexane *via* several reaction steps as reported.[13] 2,3-Dihydrobenzothiophene (**11**) was obtained by the reduction of benzothiophene with metallic sodium in ethanol[14] and purified by distillation using Kugelrohr.

trans-*2-Thiadecalin* (**7**): The title sulfide, a new compound, was prepared from *trans*-1,2-cyclohexanedicarboxylic acid (**A**) through several steps as shown in Eq. 2.[15] Namely, esterification of the starting material **A**, reduction of the diester with $LiAlH_4$ and bromination of the diol with PBr_3 gave dibromide **B**. Substitution of **B** with CN^- and alkaline hydrolysis of the dicyanide thus formed afforded dicarboxylic acid **C**, which was then subjected to the Dieckmann condensation after esterification to give the cyclic keto ester that was then decarboxylated to afford ketone **D**. The Baeyer-Villiger oxidation of **D**, reduction of the lactone with $LiAlH_4$ to the diol, and bromination of the diol, yielded dibromide **E** which was then converted to desired *trans*-2-thiadecalin (**7**) by treatment with Na_2S (total yield 5%).[15]

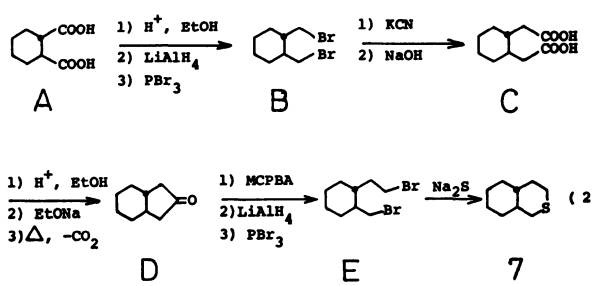

2-Methyl-2,3-dihydrobenzothiophene (5) and 1-Thiochroman (10): Cyclic sulfides **5** and **10** were obtained as an isomeric mixture in the thermal cyclization of allyl phenyl sulfide in quinoline, as reported by Anderson *et al.*[16] The mixture of **5** and **10** was separated by careful distillation, affording **10** and impure **5** containing **10**. The impure **5** was purified by oxidation with H_2O_2 in AcOH to the corresponding sulfone, followed by reduction with $LiAlH_4$, as reported.[10]

2-Alkyl Thiochroman 1-Oxides (1'—4') (Eq. 3): To a cooled solution (−70 °C) of **10'** (10 mmol) in dry THF (50—100 ml), diisopropylamine (12 mmol) and then BuLi (10% hexane solution, 10 mmol) were added under argon atmosphere. The clean colorless solution immediately turned to reddish black due to the formation of the anion of **10'**. After warming the solution up to −30 °C for several minutes the solution was cooled again to −70 °C. A dry alkyl halide (10 mmol, MeI, EtBr, *n*-BuBr, or *n*-$C_8H_{17}Br$) was added to the solution at −70 °C. The reaction mixture was gradually warmed up to 0 °C. The black color of the solution gradually faded out as the reaction proceeded, to give eventually a colorless solution. The reaction mixture was poured into cold dilute hydrochloric acid and extracted three times with chloroform. The combined organic layer was dried over anhydrous $MgSO_4$ and evaporated. The residue was subjected to column chromatography on silica gel (eluent: hexane–ethyl acetate–chloroform=4 : 1 : 1). The first fraction was a by-product. The second gave the desired alkylated product in 65—85% yield and the last fraction gave the starting material recovered. The by-product was then identified by NMR and MS spectra and elemental analysis to be butyl 3-phenylpropyl sulfoxide (**23**) which was a product by a direct reaction of **10'** with BuLi (Eq. 4).

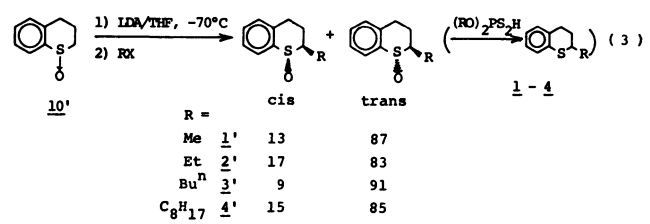

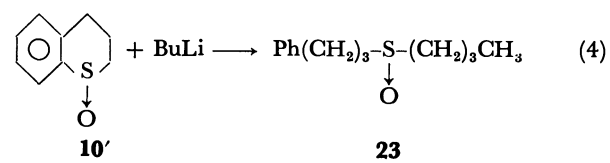

Note the predominant formation of trans 2-substituted thiochromen 1-oxides over their cis isomers in the alkylations of **10'** (Eq. 3). The cis/trans ratio was determined from the NMR spectrum using $Eu(dpm)_3$, as mentioned later. This stereochemical result can be best explained in terms of the findings[28] that the alkylation of α-sulfinyl carbanion takes place from the opposite side of the chelated ring involving Li^+ and sulfinyl oxygen to give predominantly the trans isomer, as shown in Fig. 1.

Butyl 3-Phenylpropyl Sulfoxide (23): Mp 44—47.5 °C from hexane; NMR (δ, $CDCl_3$), 0.91 (t, 3H, CH_3, J=6.8 Hz),

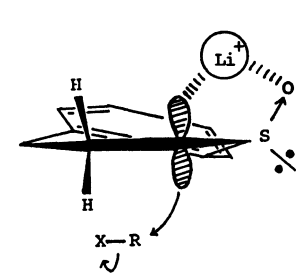

Fig. 1. Direction of alkylation of **10'** with LDA and RX (see Eq. 3). Stereospecific alkylation forms *trans*-sulfoxide predominantly.

TABLE 1. SULFIDES AND SULFOXIDES

Compound	Physical and spectral data NMR (δ, $CDCl_3$, J/Hz)	Calcd(%) C	Calcd(%) H	Found(%) C	Found(%) H
1,	bp 110 °C/3. 0 Torr (lit,[16a] 125—127 °C/9 Torr), NMR: 1.44 (d, CH_3, J=6.8), 1.66—3.10 (m, 5H), 7.14—7.90 (m, 9H).	73.11	7.36	73.45	7.36
1′,	(cis-trans mixture), oil, NMR: 1.44 66.62 (d, 3H, J=6.7), 1.69—3.38 (m, 5H), 6.96—7.87 (m,4H).	66.62	6.71	66.75	6.76
2,	oil, NMR: 1.04 (t, 3H, J=7.0), 1.40—3.45 (m, 7H), 6.83—7.08 (m, 4H).	75.10	7.91	74.07	7.91
2′,	(cis-trans mixture), oil, NMR: 1.09 (t, 3H, J=7.0), 1.73—3.10 (m, 7H), 7.00—7.60 (m, 4H).	68.00	7.58	68.16	7.97
3,	oil, NMR: 0.90 (t(br), 3H), 1.35—2.48 (m, 8H), 2.78 (m, 2H), 2.90 (m, 1H), 6.80—7.35 (m, 4H).	75.65	8.79	75.75	8.89
3′,	(cis-trans mixture), oil, NMR: 0.94 (t(br), 3H), 1.18—3.13 (m, 10H), 7.20—7.80 (m, 4H).	70.22	8.16	69.98	8.25
4,	oil, NMR: 1.03 (t(br), 3H, $-CH_3$), 1.43 (m, 12H, $-(C\underline{H}_2)_6-CH_2-$), 1.30—2.62 (m, 4H, $-C\underline{H}_2-(CH_2)-$ and $-S-\underset{}{C}H-CH_2-C\underline{H}_2-$), 2.80—3.10 (dd, 2H, $-S-\underset{}{C}H-C\underline{H}_2-$), 3.15—3.57 (bs, 1H, $-CH<$), 6.97—7.31 (m, 4H, arom).	77.79	9.98	77.89	10.14
4′,	(cis-trans mixture), oil, NMR: 0.88 (t(br), 3H), 1.10—3.10 (m, 22H), 7.24—8.10 (m, 4H).	73.32	9.14	73.28	9.58
7,	oil, MS: *m/e* 156 (M^+).	69.16	10.31	68.76	10.45
7a′,	(axial), colorless crystals, mp 98—99 °C (hexane–ethyl acetate), IR (KBr, cm^{-1}): 1029 (S=O).	62.74	9.23	62.61	9.36
7b′	(equatorial), colorless crystals, mp 53—54 °C (hexane–ethyl acetate), IR (KBr, cm^{-1}):1036 (S=O).	62.74	9.23	62.39	9.36
9,	oil, bp 89 °C/3.0 Torr, NMR: 0.89 (t, 3H, J=2.9), 1.18 (d, 3H, J=6.8), 1.41 (m, 2H), 2.46 (m, 1H), 3.60 (s, 2H, $PhC\underline{H}_2-$), 7.15—7.55 (m, 5H).	73.27	8.94	72.88	9.03
9′,	(erythro-threo mixture), oil, NMR: 0.80—1.99 (m, 8H, $-CH_3$, $-CH_2-CH_3$), 2.13—2.73(m, 1H,$-CH<$), 3.80—3.96 (m, 2H, $PhC\underline{H}_2-$) 7.30 (s, 5H, arom).	67.30	8.21	66.96	8.26
15,	oil, bp 74—76 °C/2.0 Torr.	74.17	9.34	74.01	9.45
15′,	oil, NMR: 1.16 (s, 9H), 2.38—3.23 (m, 3H, $Ph-CH_2-CH_AH_B-(H_A$ or $H_B)$), 3.63 (t,1H, H_B or H_A, J=6.3), 7.10—7.33 (br, 5H, arom.).	68.53	8.63	68.44	8.60
16,	oil, bp 106—110 °C/3.0 Torr.	74.16	9.33	73.92	9.31
16′,	oil, NMR: 1.34 (s, 9H), 2.36 (s, 3H), 3.58 (d, 1H, J=12.7), 3.90 (d, 1H, J=12.7), 7.10—7.33 (m, 4H).	68.52	8.62	68.57	8.65
19′,	oil, NMR: 1.18 (t(br), 3H), 1.90 (s, 9H, Bu^t), 1.87—2.63 (m, 12H, $-CH_2-(C\underline{H}_2)_6-CH_3$), 3.13 (t, 2H, $SO-CH_2-$, J=5.6).	65.99	12.00	65.57	11.88
19,	oil, bp 89 °C/1.5 Torr (lit,[24] 78—82 °C/0.6 Torr), NMR: 0.89 (t(br), 3H), 1.10—1.68 (m, 21H), 2.44 (t(br), 2H).				
5,	bp 85—95 °C/3.5 Torr (lit,[16] 48—50 °C/0.2 Torr).				
5a′	(cis), oil, NMR: 1.56 (d, 3H, J=6.6), 3.17—3.80 (bs, 3H), 7.91 (m, 4H) (lit,[16] 1.57 (d, 3H), 3.41 (bs, 3H), 7.55 (bs, 3H), 7.95 (m, 4H).				
5b′	(trans), mp 40 °C (lit,[16] 42—43 °C), NMR: 1.43 (d, 3H, J=6.6), 2.94 (dd, 1H, J=6.6), 3.35—4.06 (m, 2H), 7.25—7.90 (m, 4H) (lit,[16] 1.43 (d, 3H), 2.95 (dd, 1H), 3.93 (dq, 1H), 3.60 (dq, 1H), 7.54 (bs, 3H), 7.90 (m, 1H).				
6,	mp 17 °C/(lit,[17] 17—18 °C, lit,[13] 17.4 °C).				
6a′	(axial), colorless crystals, mp 87—88 °C (hexane–ethyl acetate) (lit,[18] 82.5—86 °C), IR (KBr, cm^{-1}): 1026, 1018 (sh) (S=O).				
6b′	(equatorial), colorless crystals, mp 71—72 °C (hexane–ethyl acetate) (lit,[18] 72—74 °C), IR (KBr, cm^{-1}): 1050 (sh), 1036, 1019 (sh) (S=O).				
10,	oil, bp 90—100 °C/3.5 Torr (lit,[13] 254 °C, lit,[16] 82—87 °C/1 Torr).				
10′,	oil, bp 155—165 °C/2.5 Torr (lit,[19] 117—120 °C/0.06 Torr), NMR: 1.09—3.50 (m, 6H), 7.20—7.90 (m, 4H).				
11,	oil, bp 67—69 °C/2.0 Torr (lit,[13] 253.58 °C).				
11′,	oil, 165 °C/2.0 Torr (lit,[20] 115 °C/0.09 Torr), NMR: 3.13—4.27 (m, 4H), 7.40—8.00 (m, 4H).				
12′,	oil, bp 102—103 °C/3.0 Torr (lit,[21] 114 °C/12—13 Torr), NMR: 1.28 (s, 9H), 3.90 (s, 2H), 7.16 (bs, 5H).				
12′,	mp 75—76 °C (hexane) (lit,[21] 75—76 °C), NMR: 1.46 (s, 9H), 3.56 (d, 1H, J=12.7), 3.82 (d, 1H, J=12.7), 7.30 (s, 5H).				
13,	oil, bp 92 °C/2.5 Torr (lit,[22] 123 °C/14 Torr).				

(Continued)

Compound	Physical and spectral data NMR (δ, $CDCl_3$, J/Hz)	Calcd(%) C	Calcd(%) H	Found(%) C	Found(%) H
13′,	mp 62—63 °C (lit,[23] 63—64 °C), NMR: 0.90 (t(br), 3H), 1.10—2.13 (m, 4H), 2.59 (t(br), 2H), 3.96 (s, 2H), 7.23—7.50 (m, 5H).				
14,	mp 43 °C (hexane) (lit,[21] 43—44 °C), NMR: 2.30 (s, 2H), 4.05 (s, 2H), 6.93—7.40 (m, 9H).				
14′,	mp 137—138 °C (lit,[21] 136—139 °C), NMR: 2.38 (s, 3H), 3.96 (s, 2H), 7.10—7.63 (m, 9H).				
17,	oil, bp 88 °C/4.0 Torr (lit,[21] 106 °C/10 Torr).				
17′,	mp 88—89 °C (lit,[21] 88—89 °C).				
18,	oil, bp 93 °C/2.5 Torr (lit,[21] 84 °C/0.8 Torr).				
18′,	mp 41—43 °C (lit,[23] 40—42 °C).				
20,	oil, bp 134—136 °C/4.0 Torr (lit,[25] 130—135 °C/2.0 Torr).				
20′,	mp 99 °C (lit,[26] 98—99 °C).				

1.15—2.90 (m, 12H, $-CH_2-$), 7.00—7.43 (m, 5H, arom); MS (*m/e*), 224 (M^+); Calcd for $C_{13}H_{20}SO$: C, 69.59; H, 8.98. Found: C, 69.90; H, 9.18.

*2-Alkyl Thiochromans (**1**—**4**) from Sulfoxides (**1′**—**4′**)*: The sulfoxide (**1′**, **2′**, **3′**, or **4′**, 1 mmol) obtained above, and *O,O′*-diethyl hydrogenphosphodithioate (7—9 mmol)[11] were mixed at room temperature. After keeping the mixture standing till the sulfoxide disappeared (TLC), the mixture was subjected directly to column chromatography on silica gel using hexane as an eluent. Yields were nearly quantitative in all cases.

Authentic Sulfoxides. Authentic sulfoxides were prepared by treating the corresponding sulfides with one of the following oxidation systems, *i.e.* H_2O_2/AcOH, H_2O_2/H_2SO_4/MeOH, and *m*-chloroperbenzoic acid (MCPBA)/CH_2Cl_2. Physical and spectral data, and elemental analysis data of all the sulfoxides are shown in Table 1.

Oxygenation of Sulfide with Microsomes. A mixture of hepatic microsomes (190 mg protein), 250 μmol of G-6-P and 25 μmol of $NADP^+$ in phosphate buffer (0.2 M, pH 7.4) (final volume: 17 ml) was incubated with stirring with a magnetic stirrer at 37 °C for *ca.* 10 min. The substrate. sulfide (*ca.* 0.5 mmol) and then G-6-PDH (20 units) were added to the mixture and the resulting reaction mixture was incubated at 37 °C under air or pure oxygen atmosphere. After the incubation for 1.5 h, the reaction was stopped by adding 15—20 ml of acetone and 0.5 M trichloroacetic acid (to make the solution pH *ca.* 2.0) into the reaction mixture. The resulting mixture was left in a refrigerator (at *ca.* 4 °C) for 10 min to precipitate the protein, prior to centrifugation of the mixture (3000 min^{-1} for 20 min). The supernatant collected was extracted three times with $CHCl_3$. The combined organic layer was washed with 2 M KOH and water, dried over anhydrous $MgSO_4$, and concentrated under reduced pressure. GLPC analysis of the residue showed the presence of the recovered sulfide, the product sulfoxide and some impurities derived from the protein. The sulfoxide was purified by TLC fractionation (on alumina, eluent: benzene–ethyl acetate (2 : 1)), and identified by comparison with the authentic sample. Yields and other data are listed in Tables 3 and 4.

The purified sulfoxide was subjected to the measurements of NMR, CD and optical rotation. The cis/trans ratio of the sulfoxide was determined by measuring the NMR spectrum of the mixture of the isomeric sulfoxides and a shift reagent Eu $(dpm)_3$ (0.2—0.4 equiv). The results are shown in Table 3.

Enantiomeric excess was calculated from the integration ratio in NMR spectrum of the mixture of the enantiomeric sulfoxide and an optically active shift reagent Eu $(hfc)_3$ (0.4—0.6 equiv), and/or from the value of specific rotation and reported maximum rotation of the sulfoxide (Table 4).

CD spectra were measured for **5a′**, **5b′**, **10′**, and **11′** in ethanol, though the concentrations of the compounds were not measured (Fig. 5).

Oxygen Consumption. The oxygen consumption in the oxygenation with microsomes was measured with a gas bullet attached to the two-necked reactor in a constant temperature room (24 °C). The reaction conditions were same as that in the section of "*Oxygenation of Sulfides with Microsomes.*" The measurement of the oxygen consumption was started as soon as the reaction was initiated by the addition of the substrate and G-6-PDH through a serum cap into the reactor, which contained other co-factors and was thermally pre-equilibriated. The results are shown in Fig. 2.

Control Experiments. Relative reactivities were determined by following the yields of the sulfoxides formed in a given time. As for CO inhibition test, an atmospheric mixture of CO and O_2 gas (*ca.* 1 : 1) was used as a reaction atomsphere instead of pure oxygen or air. SKF 525-A (11.3 mg, 32 μmol), 1,4-diazabicyclo[2.2.2]octane (DABCO, 120 mg, 0.61 mmol) and catalase (134 nmol) were further added to the complete system which is described in "*Oxygenation of Sulfides with Microsomes,*" at the beginning of the reaction. Boiled microsomes prepared by heating for 10 min in boiled water, was used instead of microsomes. Results obtained according to the procedure described in "*Oxygenation of Sulfides with Microsomes,*" are shown in Table 2.

*Oxidation of Racemic Sulfides (**1**—**5** and **9**) to Mixture of Diastereomeric Sulfoxides with MCPBA and $NaIO_4$.* MCPBA (1.1 mmol) was slowly added to a solution of the sulfide (1 mmol) in 5—10 ml of CH_2Cl_2 and the mixture was stirred under cooling with an ice-water bath until the spot of the sulfide disappeared (TLC). The usual work-up afforded crude diastereomeric sulfoxides which then were purified by column chromatography on silica gel using an appropriate eluent.

Oxidation with $NaIO_4$ was carried out by adding slowly an aqueous solution (5—10 ml) of $NaIO_4$ (1.1 mmol) into an acetone or methanol solution (20—25 ml) of sulfide (1 mmol) under cooling with an ice-water bath. The mixture was warmed up to room temperature and kept stirring till the sulfide was completely consumed. The usual work-up and the subsequent column chromatography (on silica gel) of the crude products gave a mixture of two pure diastereomeric sulfoxides.

In both cases, the yields of the pure sulfoxides were ranging from 70 to 85%. The mixture of diastereomeric sulfoxides thus obtained were mixed with 0.1—0.4 equiv of $Eu(dpm)_3$ in order to determine the diastereomeric ratio by NMR spectrum in which protons at peri-position (7- or 8- position of **1′**—**5′**) appeared separately in a region between 8 and 12 ppm.

Although two separable protons due to diastereomers in NMR spectrum of **9'** using $Eu(dpm)_3$ (0.4 equiv) were confirmed it was not certain which one is threo or erythro.

Both **6'** and **7'** were also prepared by the method mentioned above, and two isomeric sulfoxides (axial and equatrial) could be separated two repeated careful column chromatography in which axial one was eluted faster than the equatorial one.

Oxygenation with Reconstituted System Containing Purified Cytochrome P-450. A phosphate buffer (7 ml; 0.2 M; pH 7.7) containing 60 nmol of cytochrome P-450 and 80 nmol of cytochrome P-450 reductase was incubated for 5 min at room temperature and combined with a solution of NADPH generating system (G-6-P: 250 μmol; $NADP^+$: 25 μmol and G-6-P-DH: 36 units) containing substrate (**5** or **10**) which was finely suspended into a phosphate buffer (30 ml: 0.2 M; pH 7.7) by ultrasonic vibrator. The reaction mixture was incubated understirring with a magnetic stirrer at 37 °C for 1.5 h and subjected to the same work-up procedure described in "*Oxygenation of Sulfides with Microsomes.*" Yields of **5'** and **10'** were 5.5 and 9.0 mg, respectively. The diastereomeric ratio of **5a'** and **5b'** was similarly determined to be *ca.* 25 : 75 by measuring the FT-NMR spectrum of the mixture of **5'** and $Eu(dpm)_3$ (*ca.* 0.3 equiv) in $CDCl_3$, while *e.e.* value of **10'** was *ca.* 7.5% from the integration ratio of the FT-NMR spectrum of the mixture of **10'** and $Eu(hfc)_3$ (0.5 equiv) in $CDCl_3$.

Results and Discussion

The oxygenation of sulfides with microsomal cytochrome P-450 was carried out according to the method mentioned in Experimental section. In order to clarify co-factor requirements typical for the enzymatic oxygenation of sulfides to sulfoxides, at first control experiments were carried out.

Control Experiments. In order to examine whether or not the oxygenation of sulfides to sulfoxides with liver microsomes depends only on cytochrome P-450 enzyme, the following control experiments were carried out with thiochroman **10**. Carbon monooxide ($CO : O_2 = 1 : 1$ (v/v)) inhibited partially the oxygenation to the same extent as was found in our early study,[3b] while the reaction was not inhibited by SKF-525-A which is known to be a good inhibitor for a certain kind of dealkylation but does not inhibit the oxygenation of sulfur compounds.[27] DABCO (0.61 mmol), a singlet oxygen quencher, did not affect the oxygenation of **10**, which was either not affected by the addition of catalase (134 nmol) that catalyzes decomposition of hydrogen peroxide. Oxygenation either with boiled microsomes instead of microsomes or without NADPH generating system did not proceed, as was expected. Dependency of the oxygenation of sulfides with microsomes upon cytochrome P-450 enzyme, observed in these reactions, was also proved by the oxygenation with the reconstituted system with purified cytochrome P-450, as described later in this paper. Thus, the oxygenations of the various sulfides with liver microsomes obtained from phenobarbital pretreated rabbits are clearly due to the cytochrome P-450 enzyme.

Oxygenation of Sulfide and Oxygen Consumption. Various dialkyl, aryl alkyl, and diaryl sulfides were found to be oxygenated with the microsomal cytochrome P-450, as shown in Tables 3 and 4. However, benzothiophene was not oxygenated to the sulfoxide under the same conditions, but was recovered. Chloropromazine which is a well-known drug containing sulfur and is the first compound subjected to the oxygenation to the corresponding sulfoxide with microsomes,[3a] was also oxygenated but the yield of the sulfoxide was determined by high pressure liquid chromatography to be very small.

Table 2. Control Experiments. Relative reactivity was determined from the yield of the sulfoxide of **10** under various conditions

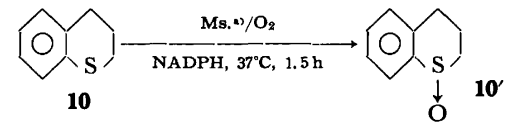

10 **10'**

System	Relative reactivity
Complete	1.00
$CO-O_2$ (1 : 1)	0.60
+SKF 525-A	0.99
+DABCO	1.09
+Catalase	0.91
−NADPH (generating sysem)	0.15
−Ms. +Boiled Ms. (100 °C, 10 min)	0.00

* The oxygenation was carried out at 37 °C for 1.5 h.
a) Ms. : Microsomes.

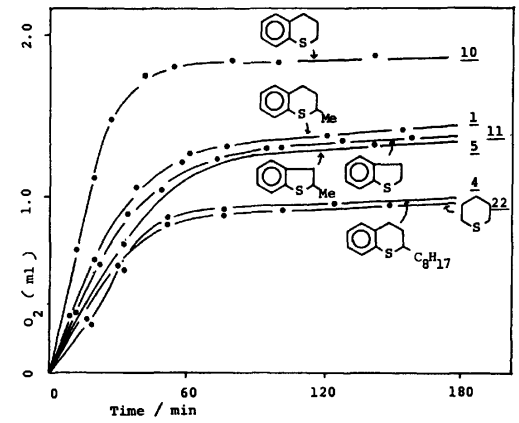

Fig. 2. Oxygen consumption in Enzymatic oxygenation of sulfides with microsomal cytochrome P-450 at 37 °C for 1.5 h was measured at a constant temperature room (24 °C).

Sulfoxides were the only products in the oxygenation. Activity of the enzyme toward various sulfides is expressed in terms of moles of product per 1.5 h per moles of cytochrome P-450, while as shown in Fig. 2, most enzymes died out after the incubation for 1 h. Since most sulfides are insoluble in water, the extent of the dispersion of the substrate into the reaction system may affect the yield of the sulfoxide. However, the yield of the sulfoxide did not change at all upon sufficient mixing of the sulfide with the buffer solution by ultrasonic vibration before the start of the oxygenation. This fact may indicate that the oxygenation takes place in a hydrophobic enzyme region.

Oxygen consumption during the reaction was measured for the compounds, **1**, **4**, **5**, **10**, **11**, and **22** at a constant temperature room (Fig. 1), and was found to follow a typical mode till 90% completion in *ca.*

Table 3. Diastereomeric ratio of sulfoxides formed in the enzymatic oxygenation of racemic sulfides with microsomal cytochrome P-450 at 37 °C for 1.5 h

Entry No.	Substrate		[Product/P-450][f]	$[\alpha]_D$/°	cis/trans ratio: Microsomal oxygenation: Microsomes	cis/trans ratio: Nonenzymatic oxidation: MCPBA	cis/trans ratio: Nonenzymatic oxidation: $NaIO_4$
1	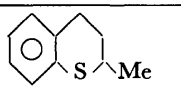	**1**	128	+4.0	18/82	56/44	55/45
2	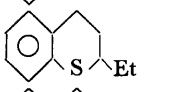	**2**	102	+1.8	18/82	43/57	—
3	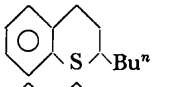	**3**	35	+14.3	16/84	44/56	—
4	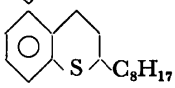	**4**	7.6	—	—	51/49	49/51
5	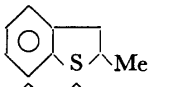	**5**	71.7	+13.1	19/81	47/53	48/52
6	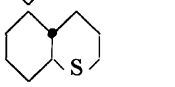	**6**	172	—	37/63[a]	30/70[a]	—
7	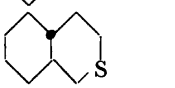	**7**	138	—	29/71[a]	30/70[a]	—
8	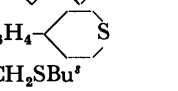	**8**	—	—	33/67[a,b]	33/67[a,b]	76/24[a,c]
9	$PhCH_2SBu^s$	**9**	108	+2.2	34/66[d]	54/46[d]	58/42[d,e]

a) Ratio of axial/equatorial isomers which was calculated from isolated yields of the isomers separated by column chromatography. b) Ref. 29. c) Ref. 30. d) Ratio of threo and erythro sulfoxides (see text). e) Ratio for the oxidation with the system of $H_2O_2/MeOH/H_2SO_4$ f) Moles of product per 1.5 h per moles of cytochrome P-450 (see text).

Table 4. Asymmetric induction in enzymatic oxygenation of sulfides with microsomal cytochrome P-450 at 37 °C for 1.5 h

Entry No.	Substrate		[Product/P-450][a]	$[\alpha]_D$/°	(*c*, solvent)	*e.e.*/%	Abs. confign. of sulfur	Max. rotation/°
1	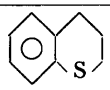	**10**	145	−21.8	(1.06, acetone)	10.7[b]	(*R*)[c]	−202 (*R*)[c]
2	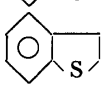	**11**	120	−7.3	(1.10, acetone)	2.6[b]	*R*	−285 (*R*)[20]
3	$PhCH_2SBu^t$	**12**	141	+129	(0.262, $CHCl_3$)	53.8[b]	*R*	+240 (*R*)[21]
4	$PhCH_2SBu^n$	**13**	112	+13.5	(0.505, $CHCl_3$)	—	(*R*)[d]	—
5	$PhCH_2STol$-*p*	**14**	44.4	−21.8	(0.248, $CHCl_3$)	22.0	*S*	+99 (*R*)[21]
6	$Ph(CH_2)_2SBu^t$	**15**	39.0	+24.5	(0.188, $CHCl_3$)	—	(*R*)[d]	—
7	$p\text{-}MeC_6H_4CH_2SBu^t$	**16**	93.0	+49.6	(0.488, $CHCl_3$)	19.8[b]	*R*	−250 (*S*)[21]
8	*p*-$TolSBu^t$	**17**	10.5	−80.0	(0.135, acetone)	46.8	*S*	+171 (*R*)[21]
9	*p*-TolSMe	**18**	188	+25.6	(0.648, $CHCl_3$)	14.1	*R*	+181 (*R*)[21]
10	$C_6H_{17}SBu^t$	**19**	26.5	+33.3	(0.102, $CHCl_3$)	—	(*R*)[d]	—
11	$C_6H_5SC_6H_4OMe$-*o*	**20**	27.8	−21.2	(0.133, EtOH)	9.6	*S*	−221 (*S*)[31]
12	Bu^tSBu^t	**21**	138	—	—	—	—	—

a) Molar ratio. b) Some of the *e.e.* values were re-confirmed by NMR spectra using $Eu(hfc)_3$. c) *R* configuration is expected by comparing signs of its specific rotation and CD spectrum with those of **11**′ (No. 2). d) *R* configuration is assumed, since most of (+)-sulfoxides like these have *R* configuration.[21] e) Calculated value from $[\alpha]_D$ and *e.e.* value.

45—60 min in all cases. This observation indicates that the lifetime of the enzyme is independent on the structure of the sulfide used. However, the amount and the rate of the oxygen consumption differed for each substrate but were parallel to the yields of the sulfoxides as shown in Tables 3 and 4. Since the rate of oxygen

Table 5. Relative reactivity of sulfides. Total turnover (product mol/cytochrome P-450 mol) and efficiency of oxygen used during the oxygenation (product mol/O_2 absorbed mol), in the oxygenation with microsomal cytochrome P-450 at 37 °C for 1.5 h

Substrate		Product (mol)[a] / P-450 (mol)	Product (mol)[a] / O_2(mol)
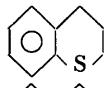	**10**	145	35
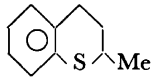	**1**	128	—[b]
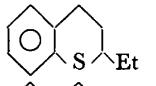	**2**	102	—[b]
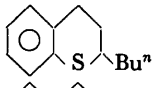	**3**	35	—[b]
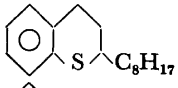	**4**	7	0
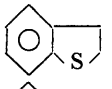	**11**	120	48
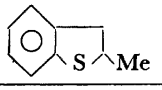	**5**	72	36

a) Product is sulfoxide. b) Not determined.

absorption into the reaction solution is sufficiently fast, the rate of oxygen consumption (initial slope) should be comparable to that of the oxygenation of each sulfide.

Meanwhile dependency of the yield of the sulfoxide on the substrate structure was confirmed with both thiochroman and 2,3-dihydrobenzothiophene derivatives. Relative reactivities of these sulfides toward cytochrome P-450 decrease with the increase of the bulkiness of the alkyl substituent (Table 5). Thus, in the oxygenations of these cyclic sulfides with microsomal cytochrome P-450, the reactivities of the sulfides seem not to depend on the hydrophobicity of the substituent but to depend largely on the steric hindrance of the substituent.

On the other hand, in the oxygenation of acyclic sulfides such clear structure-reactivity relationship was observed. Even bulky *t*-butyl group on the sulfur atom did not hinder the formation of the sulfoxide, *i.e.* *t*-butyl *p*-tolyl sulfide (**17**), di-*t*-butyl sulfide (**21**), and *t*-butyl octyl sulfide (**19**) were equally well oxygenated to the corresponding sulfoxides, although the oxygenation of 2-octylthiochroman (**4**) hardly proceeded. No good correlation between the yields of the sulfoxides and the structures of the sulfides, has also been reported for the *in vivo* oxygenations of the similar sulfides with *Aspergillus niger*.[23] This is comparable with the results obtained with *in vitro* oxygenation with microsomal cytochrome P-450 in this study. Therefore, based only on the yields of the sulfoxides in the oxygenations of both cyclic and acyclic sulfides, the steric hindrance by bulky substituents on sulfur atom may not always be crucial in the enzymatic oxygenation.

Diastereotopic Differentiating Reactions. There is always a possibility that two diastereomers are obtained in the oxidation of racemic sulfide which has an asymmetric center: for example, 2-substituted thiochromans and 2-substituted 2,3-dihydrobenzothiophene would give both cis and trans sulfoxides, while thiadecalins may give both axial and equatorial sulfoxides. In order to examine how much the diastereotopic differentiation would take place, these sulfides were oxidized enzymatically and nonenzymatically to the sulfoxides. In many cases, two diastereomeric sulfoxides were separated in pure forms, while in the others such a separation of two diastereomers was unsuccessful, and hence the ratio o the diastereomers was determined by NMR spectroscopy using an NMR shift reagent. NMR signals of the aromatic ring protons at 7-position of both cis and trans 2-methyl-2,3-dihydrobenzothiophene 1-oxides (**5a'** and **5b'**), appear in the same region. However, upon addition of an NMR shift reagent ($Eu(dpm)_3$) to the sulfoxide mixture, these signals of the cis and trans isomers shifted to down fields in different extents. Using pure authentic samples of *cis*-**5'** and *trans*-**5'** whose structures were determined by Anderson *et al.*[16] the 7-H signal of the trans isomer was found to appear at an extremely down field as compared to that of the cis isomer, so that the two signals of 7-H's of *cis*-**5'** and *trans*-**5'** can be seen separately on the NMR spectrum. Similarly, the cis/trans ratios of **1'**—**4'** obtained by both enzymatic and nonenzymatic oxidations of the corresponding sulfides were successfully determined by the relative intensities of the two NMR signals due to the protons at 8-position of the products in the presence of $Eu(dpm)_3$. The larger down field shift of the proton of the trans isomer of **1'**—**5'** than that of the cis one is presumably due to the distance between the hydrogen at 8-(or 7-) position and the europium complex bound to the oxygen of the sulfoxide. Actually, an examination with a CPK model reveals that the distance between the hydrogen of the trans sulfoxide and the shift reagent is shorter than that of the cis one. In Table 3, are summarized the results which reveal that the formation of the trans sulfoxide exceeds that of the cis isomer in the enzymatic oxygenation of the cyclic sulfides each bearing an alkyl group at α-position. However, the nonenzymatic oxidation with MCPBA and $NaIO_4$ gave nearly equal amounts of both isomers. Both *trans*-thiadecalins (**6** and **7**) gave the equatorial sulfoxides predominantly in the enzymatic and the nonenzymatic oxidations. Probably the enzyme, which has a very bulky porphyrinoxenoid at the active site,[2] would interact with the sulfide in a certain geometry, prior to the oxygenation in the enzym pocket. NMR spectroscopic analysis using the shift reagent ($Eu(dpm)_3$) of both the enzymatic and the nonenzymatic oxidations of racemic benzyl *s*-butyl sulfide (**9**), revealed that two diastereomeric sulfoxides, *threo*- and *erythro*-**9'** were formed in the both oxidations. The diastereomeric ratio of **9'** obtained by the enzymatic oxygenation was found to be considerably different from that of the MCPBA oxidation product (Table 3). Unfortunately, it could not be assigned which diastereomer was threo or erythro, since no authentic sample of the pure diastereomer was available.

Enantiotopic Differentiating Reactions. The extent of asymmetric induction in the enzymatic oxygenation of prochiral sulfides was determined, and the absolute configurations of the sulfoxides formed were also examined. The values of enantiomeric excess (*e.e.*) of the sulfoxides obtained by the enzymatic oxygenations were determined by measuring their specific rotations in comparison with the reported maximum optical rotations and/or the NMR spectroscopies using an optically active shift reagent, $Eu(hfc)_3$. Although the *e.e.* values of some of the linear acyclic sulfoxides were difficult to be determined even with the use of the shift reagent, cyclic sulfoxides such as **10'** and **11'** were easily determined by the NMR spectroscopy. For example, the doublet signals due to the aromatic proton at 8-position of **10'** of *R*-configuration appeared in the down field than that of **10'** of *S*-configuration separately in the presence of the shift reagent. The results are listed in Table 4. Inspection of the data in Table 4 reveals clearly that the asymmetric induction took place in the enzymatic oxygenation of all the sulfides. The maximum *e.e.* value of the sulfoxide obtained was 53.8% (Entry No. 3) which is unexpectedly large despite the role of the enzyme to oxidize indiscriminatingly any xenobiotic substances only to be excreted. The small *e.e.* values in the oxygenations of cyclic sulfides (**10** and **11**) may be due to the difficulty in recognition of the prochiral sulfides by the enzyme, because of the structural similarity of these prochiral sulfides, *i.e.* the two substituents attached to sulfur atom. The *e.e.* values in Table 4 should indicate that the extent of the enantiotopic differentiation in the enzymatic oxygenation of sulfides increases with the increase of the bulkiness of the substituents bound to the sulfur atom. A similar trend also has been observed in the *in vivo* oxygenations of sulfides with *Aspergillus niger*.[21]

R-Configuration was assigned to the major enantiomer of **10'** (Table 4, No. 1) obtained by the enzymatic oxygenation based on the same signs of both its specific rotation and CD spectrum (Fig. 3) as those of *R*-2,3-dihydrobenzothiophene 1-oxide (*R*-**11'**) of which the absolute configuration was already known,[20] since there is no serious structural difference between *R*-**10'** and *R*-**11'**. As for sulfoxides whose absolute configurations are not yet known (Entry Nos. 4, 6, and 10), all their configurations are considered to be of *R*-form since the configurations of most of dextro-rotatory acyclic sulfoxides of similar structures are known to be of *R*-form.[23] Thus, in the oxygenation of sulfides, **1**—**11** with cytochrome P-450 enzyme the formation of sulfoxides of *R*-configuration is prefered. When the stereospecific oxygenations of sulfides (**12**, **14**, **16**, **17**, and **18**) are compared with those of *in vivo* oxygenations with *Aspergillus niger* (for 3, 5, 7, 8, and 9 of entry in Table 4),[23] signs of the absolute configurations of these sulfoxides except for **18** are opposite (for 3, 5, 7, and 8 of entry).

Figure 4 illustrates the two directions of the oxygenations on the sulfur atom of the prochiral sulfide (R_S–*S*–R_L), when a more bulky group (R_L) is placed in a rear side, regardless of the sequence rule. Actually, the order of the bulkinesses of the substituents is not always

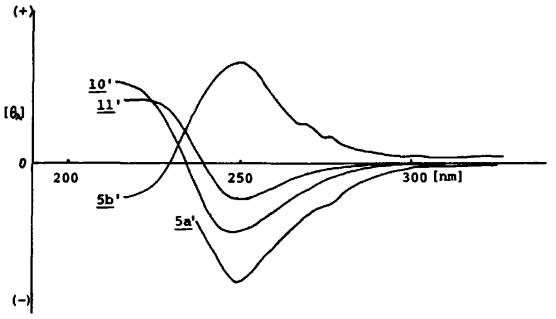

Fig. 3. CD spectra of sulfoxides obtained in the enzymatic oxygenation with microsomal cytochrome P-450 at 37 °C for 1.5 h. The spectra were recorded using EtOH as a solvent, though the concentration of the sulfoxide was not determined.

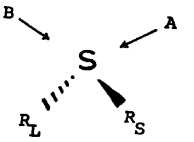

Fig. 4. Direction of the oxygenation of prochiral sulfide. More bulky substituent of the sulfide (R_L) was placed in rear side.

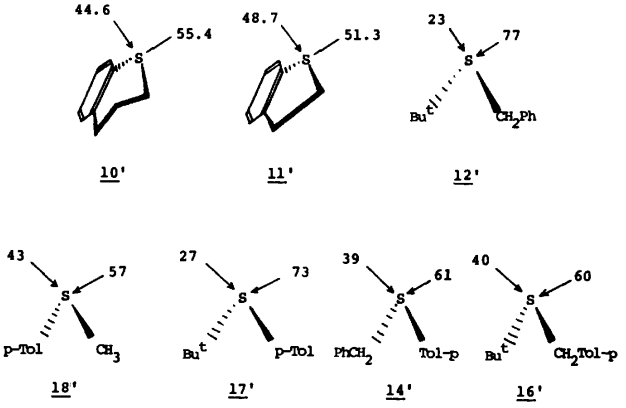

Fig. 5. Direction of the oxygenation of various prochiral sulfides with liver microsomes at 37 °C for 1.5 h. Numerical values indicate the ratios of the oxygenation at sulfur atom to produce *R* or *S*-sulfoxides.

consistent with that of the sequence rule in the *R*,*S*-nomenclature. Figure. 5 shows the actual directions of the oxygenations of various sulfides used in this study and indicates that "the direction A predominates over the direction B" in all cases (with only one exception, *i.e.* diaryl sulfide **21**), where the bulkiness is assumed to decrease in the following order: *t*-Bu>*p*-TolCH_2> $PhCH_2$>*p*-Tol>Ph>Me.

Although the enzymatic action of the hepatic cytochrome P-450 induced by phenobarbital should be sterically insensitive because of its indiscriminative nature of the metabolism of various xenobiotics, the enzyme-catalyzed reaction prefers to take the same steric course "Direction A" and this enantiotopic differentiation becomes greater as the difference of the bulkiness between the two substituents (R_S and R_L)

Table 6. Optical activity of separated diastereomers in the oxygenation with microsomal cytochrome P-450 at 37 °C for 1.5 h

Sulfoxide	$[\alpha]_D^{25}$/° (*c*, solvent)	*e.e.*/% (Abs. confign.)
cis-**5′**	−37.5 ± 7.5 (0.08, acetone)	40[a] (R_sR_c)
trans-**5′**	+15.8 ± 2.5 (0.24, acetone)	12[a] (S_sR_c)
axial-**6′**	−22.0 ± 2.5 (0.236, $CHCl_3$)	—
equatorial-**6′**	−0.5 ± 1.5 (0.398, $CHCl_3$)	—
axial-**7′**	+2.5 ± 3.8 (0.160, $CHCl_3$)	—
equatorial-**7′**	+1.5 ± 1.5 (0.400, $CHCl_3$)	—

a) Determined by NMR.

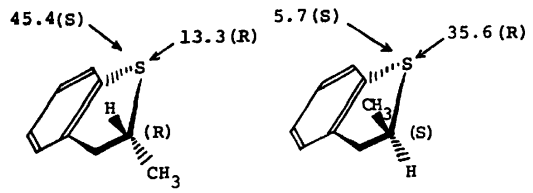

Fig. 6. Calculated ratio of the oxygenation products in the oxygenation of enantiomers of racemic sulfide **5** with microsomal cytochrome P-450 at 37 °C for 1.5 h.

bound to sulfur atom becomes larger.

Concurrent Diastereotopic and Enantiomer Differentiating Reaction. The earlier section dealt only with the ratios of the diastereomers in the enzymatic oxygenations of the racemic sulfides (**1**—**7** and **9**), despite that the mixtures of the cis and trans sulfoxides formed in this oxygenation were shown to be chiral and have some specific rotation values (Table 3). Table 6 shows the optical activities of the two separable diastereomers in the oxygenation with microsomal cytochrome P-450.

Determination of the absolute yields of the four stereoisomers was attempted in the enzymatic oxygenation of a racemic sulfide **5**. Two diastereomers of 2-methyl-2,3-dihydrobenzothiophene 1-oxides (*cis*-**5′** and *trans*-**5′**) were easily separated by TLC on alumina but diastereomeric mixtures of the other sulfoxides such as 2-substituted thiochroman 1-oxide derivatives were not separated. The values of *e.e.* of the two diastereomers were obtained from the FT-NMR spectra using $Eu(hfc)_3$. The optical activity of the *cis*-**5′** (40% *e.e.*) was relatively higher than that of the *trans*-**5′** (12% *e.e.*) (Table 6). From the CD spectra (Fig. 3) of the two diastereomers, the absolute configurations of the sulfur atoms of the enantiomerically excess sulfoxides of *cis*-**5′** and *trans*-**5′** are presumed to be of *R* for the cis form and of *S* for the trans form, respectively, on the basis of the comparison of the signs of the CD spectra with those of the other sulfoxides as shown in Fig. 3. Signs of the specific rotations also support the assignments. Thus, the extent of relative contributions of four possible steric courses in the oxygenation of racemic **5** can be shown in Fig. 6. The results shown in Fig. 6 reveal the following two features:

1) Enantiomer differentiation of racemic **5** is quite small; *i.e.* the enzymatic oxygenation of R_c-**5** is only 1.4 times greater than that of S_c-**5** (rate ratio, S_c-**5** : R_c-**5**=41 : 59 in Fig. 6).

2) In the enzymatic oxygenation of S_c-**5**, the formation of the *trans*-R_sS_c-**5**, predominates over that of the cis isomer by 6.2 folds (Course A : Course B=6.2 : 1, in Fig. 4). The formation of the *trans*-S_sR_c-**5′** predominates over that of cis isomer, however, only 3.4 folds (Course A: Course B=1 : 3.4 in Fig. 4) in the oxygenation of R_c-**5**. Apparently, the diastereotopic differentiation is more important than the enantiomer differentiation to determine the steric course in the enzymatic oxygenation of racemic **5**. Thus, the stereospecific enzymatic oxygenation of racemic **5** may be summarized at the following rules.

1) The oxidant approaches preferentially from the less hindered side, anti to α-methyl group.

2) When the sulfide **5** is placed in a manner as shown in Fig. 6, the oxygenation *via* the Course A is more favored than that *via* the Course B.

3) The rule 1 is more important than the rule 2.

As for *trans*-1- and 2-thiadecalin 1-oxides **6′** and **7′**, two diastereomers, *i.e.* axial and equatorial forms, were readily separated. All these diastereomers isolated were found to have some specific rotations (Table 6). However, unfortunately, neither the absolute configurations nor *e.e.* values of these optically active sulfoxides could be determined, because there were no authentic samples of the optically active sulfoxides.

Oxygenation with Reconstituted System with Purified Cytochrome P-450 and Co-factors.[32] In order to prove that the microsomal oxygenations depend upon the catalysis of cytochrome P-450 enzyme but not any other concomitant in the microsomes, the oxygenations of **5** and **10** with the reconstituted enzyme system containing co-factors, were carried out. The standard oxygenating system is made up with purified cytochrome P-450 (30 nmol), cytochrome reductase (80 nmol), G-6-P (250 μmol), $NADP^+$ (20 μmol), G-6-PDH (36 units), and 0.2 M phosphate buffer (pH 7.7, 30 ml) in a total volume of 37.5 ml. The oxygenation of racemic **5** with this system afforded a mixture of two diastereomeric sulfoxides (**5′**) with the ratio of cis/trans of 25/75 which is practically identical to that in the oxygenation with the microsomes (Table 7). The enantiomeric excess of the sulfoxide in the oxygenation of **10** with the reconstituted system with purified cytochrome P-450 was also identical to that with the microsomal oxygenation, and the sulfoxide of the *R*-form was produced preferentially over the *S*-form, as in the oxygenation with the microsomes (Tables 4 and 7).

Ratio of the yield of **5′** to that of **10′** (or total turnover ratio) in the oxygenation with the reconstituted system was nearly consistent with that in the microsomal oxygenation. Thus, it is concluded that cytochrome P-450 enzyme is responsible for the oxygenation of sulfide in the microsomal oxygenation in this work. Surprizing is the difference of the total turn-over

Table 7. Oxygenation of racemic **5** and **10** with reconsituted system with purified cytochrome P-450, at 37 °C for 1.5 h (see Experimental section)

Substrate	Product (sulfoxide)	Turnover[a] (min^{-1})	Total[b] turnover (−)	Total[c] turn-over with Ms. (−)
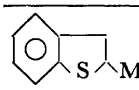 **5**	*cis*-**5′** (25%)[d] / *trans*-**5′** (75%)[d]	12	1104	72
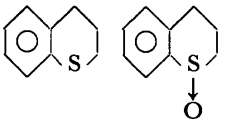 **10**	**10′**	(*R*)[e] *e.e.* 7.5%	20	1807	145

a) Product (mol)/cytochrome P-450 (mol)/min. b) Product (mol)/cytochrome P-450 (mol) with reconstituted system with purified cytochrome P-450. c) Product (mol)/cytochrome P-450 (mol) in the oxygenation with microsomes (see Tables 3 and 4). d) Ratio of *cis*-**5′** and *trans*-**5′**. e) Estimated absolute configuration.

number between the oxygenations with microsomes and with the purified cytochrome P-450. In the oxygenations with the reconstituted systems the total turn-over numbers are more than 10 times of those in the microsomal oxygenations (Tables 3, 4, and 7).

Conclusion

Various dialkyl, aryl alkyl, and diaryl sulfides were oxygenated readily with the cytochrome P-450 enzyme to the corresponding sulfoxides while the sulfone or hydroxylated product was not obtained (or too small to be detected).[33] The amount of oxygen consumed in a set period was parallel to the reactivity of the sulfide or the yield of the sulfoxide. The yield of the sulfoxide depends on the structure of the sulfide in 2-substituted thiochroman derivatives, and the bulky substituent on the thiochroman markedly decreased the reactivity. Hydrophobicity appears not to be an important factor for the reactivity of sulfides, since it has no relation with the yields of the acyclic sulfoxides, as shown in Table 4. Based on the various inhibition experiments and the stereochemical results obtained by the liver microsomal oxygenation of sulfide consistent with those obtained by the reconstituted system with the purified liver microsomal cytochrome P-450, the oxygenation of sulfides with rabbit liver microsomes is concluded to be catalyzed undoubtedly by the cytochrome P-450 enzyme. Relatively large asymmetric inductions were obtained in the oxygenations of various sulfides. Assuming the following order of the bulkiness, *t*-Bu>*p*-TolCH_2>PhCH_2>*p*-Tol>Ph>Me, the oxygenation *via* the Course A (Fig. 4) predominates significantly over that *via* the Course B. The extent of this enantiotopic differentiation in the enzymatic oxygenation of the prochiral sulfide increases with the increase of the difference of the bulkiness between the two substituents on the sulfur atom. In the enzymatic oxygenation of racemic α-substituted cyclic sulfides, the diastereotopic differentiation is more important than the enantiomer differentiation in the stereochemical course of the oxygenation. Thus, the following stereoselectivity rule may be derived.

1) The enzymatic oxygenation of the cyclic sulfide takes place predominantly at the opposite side of the alkyl substituent at α-position, to form mainly the trans sulfoxide rather than the cis one.

2) When the sulfide is represented as shown in Fig. 4, the Course A is more preferable than the Course B.

3) The rule 1 is more important than the rule 2. Thus, the stereospecificity in the oxygenation of sulfides with the aid of cytochrome P-450 clearly reveals that although the enzymatic oxygenation of xenobiotic compounds in living boides may not require any stereospecificity because the metabolic oxygenation is supposed to increase only the hydrophobicity of the oxygenated compounds, the enzyme is assymetric and hence the enzymatic oxygenation of sulfides results in the partial asymmetric induction.

This research was supported by the Toray Science and Technology Prize and Grant for 1980 and Grant-in-Aid for Scientific Research B of The Ministry of Education, Science and Culture for 1980 which are greately acknowledged.

References

1) Part of this work has been reported in T. Takata, M. Yamazaki, K. Fujimori, Y. H. Kim, S. Oae, and T. Iyanagi, *Chem. Lett.*, **1980**, 1441.

2) R. Sato, and Y. Omura, "Cytochrome P-450," Kodansha (Tokyo) and Academic Press (New York) (1978); R. E. White and M. J. Coon, *Ann. Rev. Biochem.*, **49**, 315 (1980).

3) a) The first oxygenation of a sulfide, chloromazine, was carried out with microsomes by Gillett *et al.*: J. R. Gillette and J. J. Kamm, *J. Pharmac. Exptl. Therap.*, **130**, 262 (1960); b) D. Fukushima, Y. H. Kim, T. Iyanagi, and S. Oae, *J. Biochem.*, **83**, 1019 (1978).

4) a) Y. Watanabe, T. Iyanagi, and S. Oae, *Tetrahedron Lett.*, **21**, 3685 (1980); b) Y. Watanabe, T. Numata, T. Iyanagi, and S. Oae, *Bull. Chem. Soc. Jpn.*, **54**, 1163 (1981); c) Y. Watanabe, T. Iyanagi, and S. Oae, *Tetrahedron Lett.*, **23**, 533 (1982).

5) T. Takahashi, Y. H. Kim, D. Fukushima, K. Fujimori, S. Oae, and T. Iyanagi, *Heterocycles*, **10**, 229 (1979).

6) A. H. Cooney, *Pharmcol. Rev.*, **19**, 317 (1967).

7) Y. Imai and R. Sato, *Biochem. Biophys. Res. Commun.*, **60**, 8 (1973).

8) T. Iyanagi, K. Annan, Y. Imai, and H. S. Mason, *Biochem.*, **17**, 224 (1978).

9) R. B. Wagner and H. D. Zook, "Synthetic Organic Chemistry," John-Wiley and Sons, New York (1953).

10) S. O. Jones and E. E. Reid, *J. Am. Chem. Soc.*, **60**, 2452 (1938); V. N. Ipatieff, H. Pines, and B. S. Friedman, *ibid.*, **60**, 2731 (1938).

11) A. Nakanishi and S. Oae, *Chem. and Ind. (London)*, **1971** 960.

12) E. Miller, F. S. Crossley, and M. L. Moore, *J. Am. Chem. Soc.*, **64**, 2322 (1942).

13) V. I. Dronov, V. P. Krivonogov, and V. S. Nikitina, *Khim. Geterosikl. Soedin.*, **6**, 335 (1970); *Chem. Abstr.*, **77**, 139738e (1972).

14) S. F. Birch, R. S. Dean, and E. V. Whitehead, *J. Inst. Petroleum*, **40**, 76 (1954); *Chem. Abstr.*, **47**, 10212e (1953).

15) Since the compound **7** has been prepared in our laboratory and this will be reported soon as a part of an independent study (O. Itoh, T. Numata, T. Yoshimura, and S. Oae, *Bull. Chem. Soc. Jpn.*, in contribution), only the outline of the synthesis of **7** is described here. However, the spectral and elemental analysis data of **7** and its *S*-oxides are shown in Table 1.

16) a) T. A. Danilova, T. Abdim, and E. A. Vikorova, *Neftehimiya*, **11**, 44 (1971); *Chem. Abstr.*, **75**, 76324c (1971). b) K. K. Anderson, R. L. Caret, and I. Karup-Nielson, *J. Am. Chem. Soc.*, **96**, 8026 (1974).

17) P. K. Claus, F. W. Vierhapper, and R. L. Miller, *J. Org. Chem.*, **42**, 4016 (1977).

18) R. P. Rooney and S. Evans, Jr., *J. Org. Chem.*, **45**, 180 (1980).

19) W. E. Perham and R. Koncos, *J. Am. Chem. Soc.*, **83**, 4034 (1961).

20) F. G. Yamagishi, D. R. Rayner, E. T. Zwicker, and D. J. Cram, *J. Am. Chem. Soc.*, **95**, 1916 (1973).

21) B. J. Auret, D. R. Boyd, H. B. Henbest, and S. Ross, *J. Chem. Soc., C*, **1968**, 2371.

22) I. J. Buchi, M. Prost, H. Eichenberger, and R. Lieberher *Helv. Chim. Acta*, **35**, 1527 (1952).

23) A. Cerniani, G. Modena, and P. E. Todesco, *Gazz. Chim. Ital.*, **90**, 3 (1960).

24) W. E. Truce and J. J. Breiter, *J. Am. Chem. Soc.*, **84**, 1621 (1962).

25) M. Moriyama, T. Yoshimura, N. Furukawa, T. Numata and S. Oae, *Tetrahedron*, **32**, 3003 (1976).

26) C. Y. Meyers, *Gazz. Chim. Itary.*, **93**, 1206 (1963).

27) S. Kanaoka, "Biochemistry of Drug Action (in Japanese)," Hirokawa Shoten, Tokyo (**1976**), Chap. 12; M. M. Ander, *Ann. Rev. Pharmacol.*, **11**, 37 (1971).

28) G. Chassaing, R. Lett, and A. Marquet, *Tetrahedron Lett.*, **1978**, 471; J. F. Biemann and J. J. Vicens, *ibid.*, **1978**, 467; V. Cere, S. Pollicino, E. Sandri, and A. Fava, *ibid.*, **1978**, 5239.

29) T. Numata, Y. Watanabe, and S. Oae, *Tetrahedron Lett.*, **1979**, 1411.

30) C. R. Johson and D. J. McCants, Jr., *J. Am. Chem. Soc.*, **87**, 1109 (1965).

31) D. R. Raynerm A. J. Gordon, and K. Mislow, *J. Am. Chem. Soc.*, **90**, 4854 (1968).

32) Recently, Oae *et al.* have demonstrated that FAD containing Cytochrome oxidase showed a different stereochemical result in the oxygenation of racemic **5**: A. Mikami, Y. Watanabe, K. Fujimori, S. Oae, and T. Iyanagi 45th National Meeting of the Chemical Society of Japan, Tokyo, April 1982, Abstract, p. 708 (3D07).

33) A study on the oxygenation of a sulfoxide to a sulfone with cytochrome P-450 has been reported, see Ref. 4c as an example.

Synthesis of 2-(4-Azulenyl)ethanamine Derivatives as a Nonbenzenoid Analog of Biogenic Amine

Shinji KUROKAWA

Department of Chemistry, Faculty of Education, Saga University, Honjo-machi, Saga 840

(Received October 6, 1982)

2-(4-Azulenyl)ethanamine derivatives, nonbenzenoid analogs of the biologically active amine, were synthesized by the action of methyleneammonium salts on sodium 4-methylazulenide, sodium 4,6,8-trimethylazulenide, and sodium guaiazulenide. These compounds, as well as their hydrochlorides, were characterized by UV, IR, ^{1}H NMR, ^{13}C NMR, and MS data. The reaction of sodium guaiazulenide and *N*-ethylidenemethylamine also yielded the corresponding 2-(4-azulenyl)ethanamine derivatives, but the low yield of the product showed that the electrophilicity of azomethine carbon atom to 4-methylene carbanion was insufficient. The enzyme activity for some of those products was investigated. Negligible effect was found on prostaglandin 15-hydroxydehydrogenase, and considerable inhibition to cyclic AMP-phosphodiesterase, *in vitro*.

2-Phenylethanamine derivatives, together with their indole analogs, constitute an important class of biological active compounds related to biogenic amines.[1] In studying azulene analogs of biological active amines, we previously reported the synthesis of some acyl and alkyl derivatives of 2-(1-azulenyl)ethanamine by aminoethylation of azulene or guaiazulene with *N*-acylaziridines or with aziridinium salts, as well as the effect of those compounds on enzyme activity.[2]

Our study on azulene derivatives aminoethylated in the 5-membered ring of the azulene nucleus continued with those having aminoethyl side chains in the 7-membered ring. For this type of compounds we preliminarily reported the synthesis of 2-(4-azulenyl)ethanamine derivatives by the reaction of sodium guaiazulenide and methyleneammonium salts;[3] more details are given in this paper.

The present paper also deals with the synthesis of 2-(4-azulenyl)ethanamine derivatives by the action of *N*-methylenedimethylammonium iodide on sodium 4-methylazulenide or on sodium 4,6,8-trimethylazulenide.

Results and Discussion

Sodium *N*-methylanilinide, used as the reagent, was conveniently prepared from sodium hydride and *N*-methylaniline in THF according to our modification.[4] This reagent reacted smoothly with 4-methylazulene (**1**) to form a reddish-orange solution of sodium 4-methylazulenide (**2**).[5] Next **2** was mixed with *N*-methylenedimethylammonium iodide[6] at *ca.* −80 °C, and left for 5 h to rise to room temperature.

From the hydrochloric acid extract of the reaction mixture, the intended *N*,*N*-dimethyl-2-(4-azulenyl)-ethanamine, a major product, was isolated as its hydrochloride (**7**) (44%); this was easily converted to free amine (**3**) (90%) by the usual treatment with alkali. Both compounds (**3** and **7**) were characterized by spectral data.

In this reaction, three by-products: **4** (7%), **5** (2%), and **6** (2%), were also obtained. **5** and **6** are already known to occur in the aminomethylation of **1** with *N*,*N*,*N*′,*N*′-tetramethylmethanediamine.[7] The attempted aminomethylation of **1** with *N*-methylenedimethylammonium iodide was also found to yield **5** (7%) and **6** (13%). Consequently, the formation of **5** and **6** as by-products may be reasonably explained by aminomethylation of **1**, which coexists in the solution of **2** at equilibrium and increases in its ratio after the addition of an excess of methyleneammonium salt. Quaternary salt of *N*-methylaniline might act as a proton source.

The assigned position of the dimethylaminomethyl group of the other product, **4**, was indicated by low-field shift of 8-proton (0.15 ppm) of **4** relative to **3** in ^{1}H NMR. This conclusion is consistent with the observation that a dimethylaminomethyl group gives

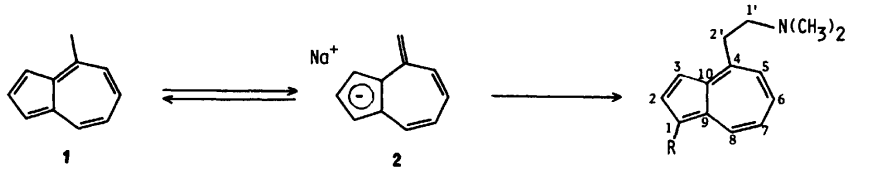

1 **2** **3** : R=H **4** : R=$CH_2N(CH_3)_2$

5 : R_1=H, R_2=$CH_2N(CH_3)_2$ **6** : R_1=R_2=$CH_2N(CH_3)_2$ **7**

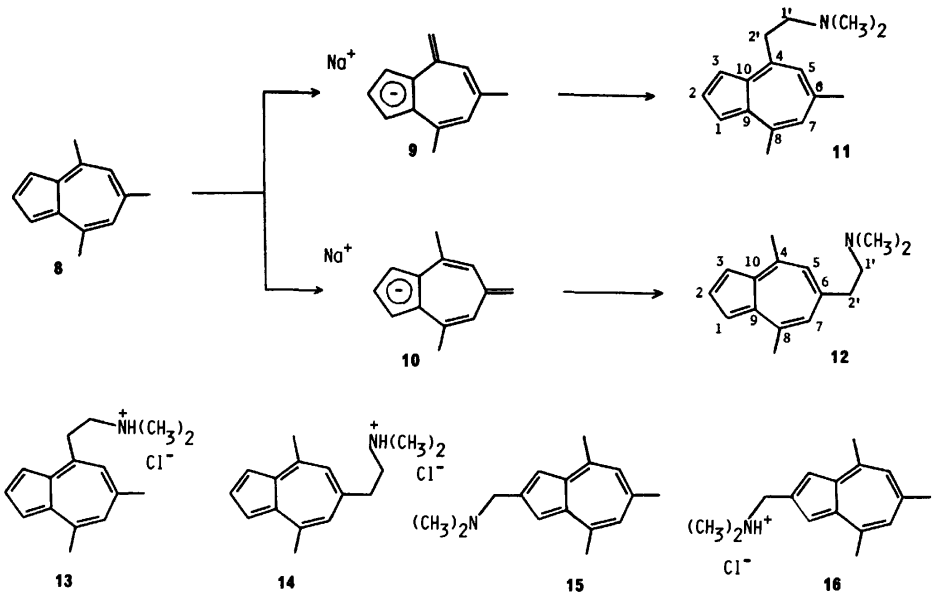

rise a considerable low-field shift at *peri*-position, as is shown in 8-proton of **5** relative to **1** (0.31 ppm) and in 2'-methylene protons of **22** relative to **21** (0.38 ppm).

Moreover, the structure of **4** was established by the action of sodium *N*-methylanilinide on **5** leading to sodium 1-dimethylaminomethyl-4-methylazulenide, followed by the reaction of it with *N*-methylenedimethylammonium iodide to yield **4** (6%). This process, even if possible, could not be a major course of formation of **4** in the reaction of **2** and methyleneammonium salt, judging from the low yields of **5** from **2** and of **4** from **5**. Thus most of **4** may be formed from the main product **3** by successive aminomethylation after aminoethylation of **2**.

Reaction of 4,6,8-trimethylazulene and sodium *N*-methylanilinide at −15 °C is known to give rise to **9** selectively, though proton abstraction from both 4(8)- and 6-methyl group is possible for this compound at higher temperatures.[5] Sodium 4,6,8-trimethylazulenide was thus prepared at −15 °C and reacted with *N*-methylenedimethylammonium iodide, at first at *ca.* −80 °C, followed by gradual completion at room temperature.

Hydrochloric acid treatment of the reaction products afforded **13** (13%), **14** (15%), and **16** (7%), all of which regenerated the corresponding 2-aminoethyl (**11** and **12**) and aminomethyl derivatives (**15**) almost quantitatively when treated with alkali.

Formation of **12** in this reaction is inconsistent with the observation in Ref. 5, but the same type of product from **10** is also noted in sodium 4,6,8-trimethylazulenide, prepared in THF at −15 °C, when it was successively treated with carbon dioxide at −10 °C.[8] The present reaction, in which the sodium 4,6,8-trimethylazulenide formed is used continuously for the next step, is thought to involve equilibrated species **8**, **9**, and **10** in the reaction mixtures, since *N*-methylaniline coexists also. Thus, **9** formed at first at −15 °C may change into **10** *via* **8** in the following reaction with *N*-methylenedimethylammonium iodide to yield **12**. Another pathway of direct conversion from **9** to **10** would require an ionic-attack of the nucleophile on anion **9** and seems improbable.[8]

The yield ratio of **11** and **12** (46 : 54) is very close to that (45 : 55) of carbonation products at 4- and 6-methylene positions in sodium 4,6,8-trimethylazulenide prepared at ordinary temperature,[8] indicating that the equilibrium between **9** and **10** is faster than the reaction of those with methyleneammonium salt.

On the other hand, product **15** cannot be formed from **8**, because the electrophilic substitution of azulene is well known to occur at 1(3)-position,[9] and in fact, aminomethylation of **8** was found to yield 1-substituted and 1,3-disubstituted products.[10] Since the substitution at 2-position, along with that at 1(3)-position, is known in carbonation of azulenide anion of Meisenheimer type,[8] this product is though to be formed from **9** and/or **10** by aminomethylation in a similar manner. So far as we know, it is the first case in methyleneazulenide-type anion that the electrophilic substitution was observed in the 5-membered ring of azulenide anion. Moreover, this fact also suggests that **5** and **6** may arise, at least in part, from **2** in the former reaction of **2** and methyleneammonium salt.

Similarly to the cases of **1** and **8**, **18** was prepared from **17** and allowed to react with some methyleneammonium salts.[3] The reaction of **18** and *N*-methylenedimethylammonium iodide was carried out as described above for **2** to give **21** (50%), **22** (7%), **19** (1%), and **20** (14%). By-products **20** and **22** may be produced by aminomethylation of **17** and/or **18**, or of **21**, as already discussed in cases of **1** and **8**. **19** is thought to be formed by nucleophilic attack of anilinide anion on the 3-methylene position of conjugate acid of **20** ($-CH_2-\overset{+}{N}H(CH_3)_2$), as described before.[3]

By virtually the same procedure as described above, the reaction of **18** with *N*-isopropylidenedimethylammonium perchlorate, *N*-isopropylidenepyrrolidinium perchlorate, or with *N*-(α-methylbenzylidene)pyrrolidinium perchlorate[11] at −20 °C or at room temperature yielded

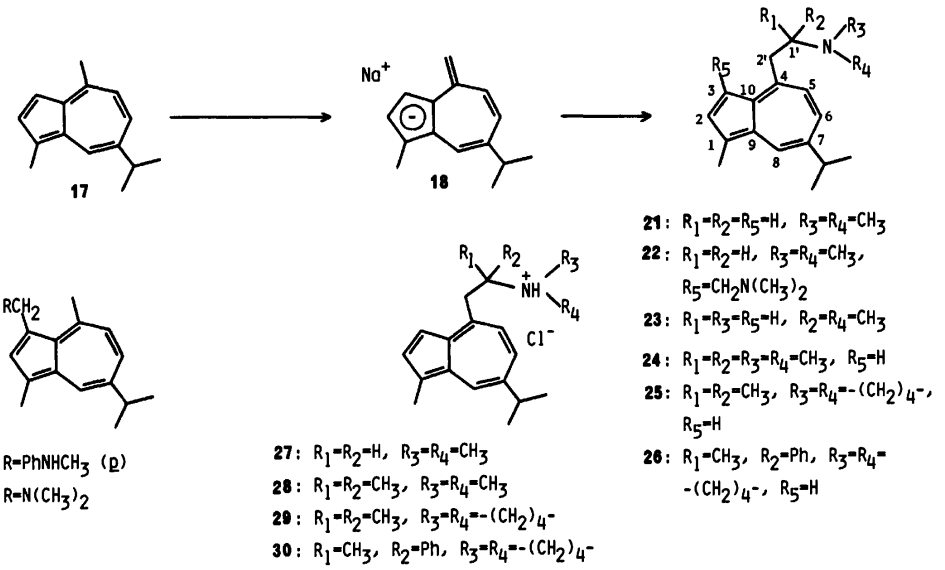

Table 1. Inhibition of cyclic AMP-phosphodiesterase (a) and prostaglandin 15-hydroxydehydrogenase (b) by 2-(4-azulenyl)ethanamine derivatives (addition of 20 μg cm^{-3} in each)

Compound	Inhibition/%	
	a	b
21	31.7	0
22	39.7	0
24	49.2	4.1
25	45.3	9.2
26	26.4	10.3

the corresponding 2-(4-azulenyl)ethanamine derivatives **24** (64%), **25** (62%), and **26** (54%). No appreciable amount of by-product was found in these cases. Of these 2-aminoethyl derivatives, **21** and **24**—**26** were converted to crystalline hydrochlorides **27** (50%), **28** (65%), **29** (51%), and **30** (28%), respectively. Both free amines and hydrochlorides were characterized by spectral data.

To clarify the reactivity of **18** further, the reaction of **18** and *N*-ethylidenemethylamine[12] was also tried and found to yield the corresponding amine, **23** (8%). However, the low yield of **23** is though to show that the electrophilicity of azomethine carbon atom is rather insufficient to allow a smooth reaction of it with the methylene carbanion of **18**.

An additional investigation was undertaken on the effect of 2-(4-azulenyl)ethanamine derivatives (**21**—**26**) for enzyme activity, *in vitro*.[13] As is observed in Table 1, considerable activities are found in inhibitions of cyclic AMP-phosphodiesterase in all compounds and especially in **24** and **25**, though less active than *N*-butyryl-2-(5-isopropyl-3,8-dimethyl-1-azulenyl)ethanamine (69.9%).[2]

Different from the amide or primary amine derivatives of 2-(1-azulenyl)ethanamine previously reported,[2] these tertiary amine derivatives (**21**—**26**) had almost a negligible effect on prostaglandin 15-hydroxydehydrogenase. This observation well accords with that about tertiary amine derivatives of 2-(1-azulenyl)ethanamine, in which no appreciable effect was found on the inhibition by prostaglandin I_2 of ADP-induced aggregation of blood platelets.[14]

Experimental

All the melting points are uncorrected. Spectral data were recorded on the following instruments: UV, Hitachi 624 digital spectrometer with a Hitachi 056 recorder; IR, Hitachi 260-10 spectrometer; ^{1}H NMR, JEOL MH-100; ^{13}C NMR, JNM-FX 100; MS, JEOL-D300 at 70 eV.

Reaction of Sodium 4-Methylazulenide (2) and N-Methylenedimethylammonium Iodide. Under dry nitrogen, a stirred solution of sodium *N*-methylanilinide, prepared from 200 mg (5.1 mmol) of 61% sodium hydride and 1.81 g (16.9 mmol) of *N*-methylaniline in 20 cm^3 of THF according to our modified procedure,[4] was mixed with another solution of 710 mg (4.99 mmol) of 4-methylazulene (**1**)[15] in 5 cm^3 of THF over a period of 15 min, and stirring was continued for 30 min more (violet color changed to reddish orange). To the stirred solution of **3** thus obtained was added, under Dry Ice–acetone cooling, 2.00 g (10.8 mmol) of *N*-methylenedimethylammonium iodide over a period of 20 min (washed in with 5 cm^3 of THF); sitrring was continued for 1 h with Dry Ice –acetone cooling and then for 5 h more, during which period the reaction mixture was gradually brought to room temperature. A facile color change from reddish orange to violet was observed at *ca.* −20 °C. The reaction mixture was taken up into 200 cm^3 of benzene, washed with 50% potassium carbonate solution (100 cm^3×2), dried on sodium sulfate, and concentrated (reduced pressure) to give a violet oil. Successive alumina chromatography (elution with 9 : 1 benzene–ethyl acetate) of the oil gave 2.15 mg (0.3%) of unchanged 4-methylazulene and 637 mg of violet oil, which was again dissolved in 200 cm^3 of benzene, extracted with 1 mol dm^{-3} hydrochloric acid (100 cm^3×3), and the hydrochloric acid solution extracted with chloroform (100 cm^3×10). The chloroform solution was dried (sodium sulfate), concentrated (reduced pressure), and chromatographed on a silica-gel column (elution with 8 : 2 chloroform–methanol) to give 521 mg (44%) of **7** as violet crystals, mp 228—230 °C: UV (C_2H_5OH) 240 (log ε 4.41), 270 (sh, 4.55), 275 (sh, 4.66), 278 (4.68), 283 (4.67), 298 (3.78), 318 (sh, 3.48), 329 (3.62), 342 (3.72), 354 (3.24), 531 (sh, 2.51), 553 (sh, 2.59), 571 (2.65), 588 (sh, 2.61), 617 (2.57), 644 (sh, 2.33), and 677 nm (2.14); IR ($CHCl_3$) 2545, 2510,

2400, 2310 (NH^+), and 1192 cm^{-1} (C–N); ^1H NMR ($CDCl_3$) δ=2.44 (6H, s, $N(CH_3)_2$), 2.90 (2H, m, 1'-H_2), 3.48 (2H, m, 2'-H_2), 6.96—7.58 (3H, m, 5-, 6-, and 7-H), 7.36 (1H, d, J=4 Hz, 1-H), 7.50 (1H, d, J=4 Hz, 3-H), 7.82 (1H, t, J=4 Hz, 2-H), and 8.28 (1H, d, J=9 Hz, 8-H).

The hydrochloric acid solution, after completion of chloroform extraction, was made alkaline by addition of ice-cooled 50% potassium carbonate solution, and extracted with benzene to give 449 mg of violet oil after removal of the solvent. Alumina chromatography of this oil with THF gave 19.6 mg (2%) of **5**, 29.7 mg (2%) of **6**, and 92.0 mg (7%) of **4** as violet oils in each case. **5** and **6** were identical with those in Ref. 7, as well as with authentic specimen obtained by the reaction of **1** and *N*-methylenedimethylammonium iodide, in UV, IR, and ^1H NMR. These compounds were also characterized with MS data. **5**: MS *m/e* (rel intensity) 199 (M^+; 18) and 155 ($M^+ - N(CH_3)_2$; 100). **6**: MS *m/e* (rel intensity) 256 (M^+; 17), 212 ($M^+ - N(CH_3)_2$; 23), and 167 ($M^+ - 2N(CH_3)_2 - H$; 100).

Product **4** was characterized as follows: UV (C_2H_5OH) 242 (log ε 4.28), 278 (sh, 4.49), 282 (4.54), 286 (4.53), 290 (sh, 4.49), 300 (sh, 3.98), 336 (3.55), 345 (3.64), 359 (3.38), 543 (sh, 2.48), 575 (2.76), 617 (2.51), and 677 nm (sh, 2.09); IR (CCl_4) 2870, 2775, 2720 ($N(CH_3)_2$), 2980, 2950, 2860, 1468, 1456, 1440, 1430, 1374 (CH_3 and CH_2), and 1040 cm^{-1} (C–N); ^1H NMR ($CDCl_3$) δ=2.25 (6H, s, $N(CH_3)_2$), 2.35 (6H, s, $N(CH_3)_2$), 2.77 (2H, m, 1'-H_2), 3.39 (2H, m, 2'-H_2), 3.86 (2H, s, 1-CH_2), 7.04 (1H, t, J=10 Hz, 7-H), 7.18 (1H, d, J=10 Hz, 5-H), 7.43 (1H, d, J=4 Hz, 3-H), 7.47 (1H, m, 6-H), 7.78 (1H, d, J=4 Hz, 2-H), and 8.47 (1H, d, J=9.5 Hz, 8-H); MS *m/e* (rel intensity) 256 (M^+; 37), 212 ($M^+ - N(CH_3)_2$; 7), 198 ($M^+ - CH_2N(CH_3)_2$; 3), 154 ($M^+ - CH_2N(CH_3)_2 - N(CH_3)_2$; 20), and 58 ($(CH_3)_2NCH_2^+$; 100).

Found: C, 79.80; H, 9.35; N, 10.46%. Calcd for $C_{17}H_{24}N_2$: C, 79.64; H, 9.44; N, 10.93%.

In order to obtain **3** from **7**, **7** was dissolved in a mixed solvent of benzene–water (100 cm^3 each) and slowly treated with 200 cm^3 of 50% potassium carbonate solution under ice-cooling and stirring. The benzene layer was separated, the aqueous layer was extracted with benzene (30 $cm^3 \times 2$), and the combined benzene extract, after being dried (sodium sulfate) and concentrated (reduced pressure), was chromatographed over alumina (elution with 98 : 2 benzene–methanol) to give 126 mg (90%) of **3** as a violet oil: UV (C_2H_5OH) 240 (log ε 4.36), 265 (sh, 4.35), 270 (sh, 4.49), 275 (sh, 4.60), 278 (4.62), 283 (4.61), 298 (3.70), 317 (sh, 3.34), 328 (3.51), 342 (3.64), 354 (3.05), 530 (sh, 2.48), 550 (sh, 2.56), 568 (2.61), 587 (sh, 2.58), 615 (2.55), 642 (sh, 2.29), and 675 nm (2.12); IR (CCl_4) 2820, 2770, 2720 (NCH_3), 2980, 2945, 2860, 1456, 1440, 1362 (CH_3 and CH_2), 1045, and 1037 cm^{-1} (C–N); ^1H NMR ($CDCl_3$) δ=2.35 (6H, s, $N(CH_3)_2$), 2.77 (2H, m, 1'-H_2), 3.40 (2H, m, 2'-H_2), 7.06 (1H, t, J=10.5 Hz, 7-H), 7.15 (1H, d, J=10.5 Hz, 5-H), 7.43 (1H, d, J=4 Hz, 1-H), 7.52 (1H, m, 6-H), 7.58 (1H, d, J=4 Hz, 3-H), 7.91 (1H, t, J=4 Hz, 2-H), and 8.33 (1H, d, J=9.5 Hz, 8-H); ^{13}C NMR ($CDCl_3$) δ=36.5 (t, 2'-C), 45.1 (q, $N(CH_3)_2$), 60.6 (t, 1'-C), 115.1 (d, 3-C), 118.8 (d, 1-C), 121.5 (d, 7-C), 125.8 (d, 5-C), 135.3 (d, 2-C), 136.3 (d, 6-C), 136.7 (d, 8-C), 137.4 (s, 10-C), 139.9 (s, 9-C), and 148.8 (s, 4-C) [*cf.* 4-methylazulene in Ref. 16][16]; MS *m/e* (rel intensity) 199 (M^+; 20), 141 ($M^+ - (CH_3)_2NCH_2$; 3), and 58 ($(CH_3)_2NCH_2^+$; 100).

Found: C, 84.34; H, 8.51; N, 7.07%. Calcd for $C_{14}H_{17}N$: C, 84.37; H, 8.60; N, 7.03%.

*Reaction of 4-Methylazulene (**1**) and N-Methylenedimethylammonium Iodide.* To a stirred solution of 300 mg (2.11 mmol) of 4-methylazulene in 5 cm^3 of dry dichloromethane was added 600 mg (3.24 mmol) of *N*-methylenedimethylammonium iodide, and the suspension was stirred for 43 h. The reaction mixture was diluted with 100 cm^3 of water, made alkaline by addition of 50% potassium carbonate solution, and extracted with chloroform (60 $cm^3 \times 3$). The chloroform extract was dried (sodium sulfate), concentrated (reduced pressure), and taken up into 100 cm^3 of benzene. This benzene solution was extracted with 1 mol dm^{-3} hydrochloric acid (35 $cm^3 \times 3$), and the hydrochloric acid solution was extracted with chloroform (50 $cm^3 \times 4$). The chloroform extract, after being dried (sodium sulfate) and concentrated (reduced pressure), was chromatographed over silica gel (elution with 8 : 2 chloroform–methanol) to give 37.0 mg (7%) of hydrochloride of **5** as dark violet crystals, mp 177—179 °C: UV (C_2H_5OH) 241 (log ε 4.42), 271 (sh, 4.47), 277 (sh, 4.62) 281 (4.67), 286 (4.66), 290 (sh, 4.57), 301 (3.98), 318 (sh, 3.45), 332 (3.60), 341 (3.68), 353 (3.40), 550 (2.70), 584 (sh, 2.66), 617 (sh, 2.45), 643 (2.28), and 680 nm (1.72); IR ($CHCl_3$) 2650, 2550, 2500, 2400, 2325 (NH^+), and 1195 cm^{-1} (C–N); ^1H NMR ($CDCl_3$) δ=2.74 (6H, s, $N(CH_3)_2$), 3.02 (3H, s, 4-CH_3), 4.70 (2H, s, CH_2), 6.54 (1H, broad s, NH), 7.48 (1H, t, J=10 Hz, 7-H), 7.53 (1H, d, J=10 Hz, 5-H), 7.68 (1H, d, J=4 Hz, 3-H), 7.92 (1H, t, J=10 Hz, 6-H), 8.34 (1H, d, J=4 Hz, 2-H), and 8.90 (1H, d, J=10 Hz, 8-H).

The hydrochloric acid layer, after completion of chloroform extraction, was made alkaline by addition of 200 cm^3 of 50% potassium carbonate solution, and extracted with benzene (50 $cm^3 \times 3$). Benzene extract, after removal of the solvent (reduced pressure), was submitted to alumina chromatography (elution with 3 : 1 benzene–THF) to afford 68.0 mg (13%) of **6**, identical with that of Ref. 7 and the authentic specimen (described above) in its UV, IR, and ^1H NMR spectra.

In order to obtain **5**, its hydrochloride was suspended in 80 cm^3 of benzene and slowly mixed with 200 cm^3 of ice-cooled 50% potassium carbonate solution. This mixture was worked up as described for **3** from **7** to give, without chromatographic separation, 17.9 mg (90%) of **5**, identical with that of Ref. 7 and the authentic specimen (described above) in its UV, IR, and ^1H NMR spectra.

Reaction of Sodium 1-Dimethylaminomethyl-4-methylazulenide and N-Methylenedimethylammonium Iodide. To a stirred solution of 0.114 mmol of sodium *N*-methylanilinide in 4 cm^3 of THF was added, under dry nitrogen, another solution of 21.8 mg (0.110 mmol) of **5** in 1 cm^3 of THF during a period of 15 min, and then, under Dry Ice–acetone cooling, 30 mg (0.162 mmol) of *N*-methylenedimethylammonium iodide (washed in with 1 cm^3 of THF). Stirring was continued at *ca.* −80 °C for 1 h and then 5 h; after the first hour the reaction mixture was gradually brought to room temperature. The reaction mixture was taken up into 20 cm^3 of benzene and extracted with 1 mol dm^{-3} hydrochloric acid (20 $cm^3 \times 3$). The hydrochloric acid extract was washed with benzene (20 $cm^3 \times 3$), made alkaline by addition of 100 cm^3 of ice-cooled 50% potassium carbonate solution, and extracted with benzene (20 $cm^3 \times 3$) to give 19.6 mg of brown oil after removal of the solvent (reduced pressure). Preparative TLC on an alumina sheet (3 : 1 benzene–THF) of the oil afforded 0.56 mg (3%) of unchanged **5** and 1.76 mg (6%) of **4**, identical with authentic specimen in TLC, UV, and IR results.

Reaction of Sodium 4,6,8-Trimethylazulenide and N-Methylenedimethylammonium Iodide. Under dry nitrogen, a stirred solution of 5.1 mmol of sodium *N*-methylanilinide in 20 cm^3 of THF was mixed at −15 °C with another solution of 850 mg (4.99 mmol) of **8** in 5 cm^3 of THF (violet color changed to orange), and then, under Dry Ice–acetone cooling, with 2.00 g (10.8 mmol) of *N*-methylenedimethylammonium iodide (washed in with 5 cm^3 of THF). The suspension was stirred for 1 h at *ca.* −80 °C and for 5 h more with a gradual rising

of the temperature. The reaction mixture was worked up as described in **2** to give a violet oil, which was taken up into 200 cm^3 of benzene, extracted with 1 mol dm^{-3} hydrochloric acid (100 $cm^3 \times 3$); the hydrochloric acid layer was extracted with chloroform (100 $cm^3 \times 6$). The benzene solution, after being dried (sodium sulfate) and concentrated (reduced pressure), was chromatographed on a silica-gel column with hexane to afford 220 mg (26%) of unchanged **8**. The chloroform extract was also dried (sodium sulfate), concentrated (reduced pressure), and submitted to silica gel chromatography (elution with 8 : 2 chloroform–methanol) to allow separation into three fractions.

From the first eluate, 174 mg (13%) of **13** was obtained as a violet oil; UV (C_2H_5OH) 244 (log ε 4.48), 270 (sh, 4.32), 275 (sh, 4.50), 281 (sh, 4.67), 285 (4.73), 294 (sh, 6.67), 305 (sh, 4.00), 328 (sh, 3.62), 334 (3.70), 343 (3.74), 348 (3.80), 359 (sh, 2.73), 547 (2.78), 565 (sh, 2.76), 580 (sh, 2.73), and 635 nm (sh, 2.31); IR ($CHCl_3$) 2500, 2400, 2360, 2325 (NH^+), and 1195 cm^{-1} (C–N); ^1H NMR ($CDCl_3$) δ=2.40 (6H, s, $N(CH_3)_2$), 2.63 (3H, s, 6-CH_3), 2.84 (2H, m, 1′-H_2), 2.86 (3H, s, 8-CH_3), 3.42 (2H, m, 2′-H_2), 7.13 (1H, s, 7-H), 7.16 (1H, s, 5-H), 7.48 (1H, q, J=4 and 1.8 Hz, 1-H), 7.58 (1H, q, J=4 and 1.8 Hz, 3-H), and 7.80 (1H, t, J=4 Hz, 2-H).

From the second eluate, 201 mg (15%) of **14** was obtained as violet crystals; these showed no certain melting point but decomposed above 200 °C: UV (C_2H_5OH) 245 (log ε 4.43), 270 (sh, 4.26), 275 (sh, 4.46), 281 (sh, 4.63), 285 (4.69), 294 (sh, 4.61), 306 (sh, 3.90), 327 (sh, 3.69), 333 (3.75), 342 (sh, 3.78), 348 (3.84), 520 (sh, 2.53), 555 (2.64), 575 (sh, 2.61), 592 (sh, 2.56), and 650 nm (sh, 2.09); IR ($CHCl_3$) 2550, 2510, 2450, 2390, 2355, 2330, 2280 (NH^+), and 1195 cm^{-1} (C–N); ^1H NMR (CD_3OD) δ=2.88 (6H, s, $N(CH_3)_2$), 2.90 (6H, s, 4- and 8-CH_3), 3.33 (4H, m, 1′- and 2′-H_2), 7.13 (2H, s, 5- and 7-H), 7.36 (2H, d, J=4 Hz, 1- and 3-H), and 7.66 (1H, t, J=4 Hz, 2-H).

From the last fraction, 85.4 mg (7%) of **16** was obtained as violet crystals, mp 41—45 °C: UV (C_2H_5OH) 246 (log ε 4.53), 287 (4.79), 293 (4.79), 335 (4.00), 351 (4.04), 536 (2.72), 560 (sh, 2.70), 615 (sh, 2.33), and 624 nm (sh, 2.27); IR ($CHCl_3$) 2500, 2400, 2350, 2330 (NH^+), and 1190 cm^{-1} (C–N); ^1H NMR ($CDCl_3$) δ=2.17 (6H, s, $N(CH_3)_2$), 2.61 (3H, s, 6-CH_3), 2.86 (6H, s, 4- and 8-CH_3), 3.83 (2H, s, CH_2), 4.48 (1H, broad s, NH^+), 7.08 (2H, s, 5- and 7-H), and 7.33 (2H, s, 1- and 3-H).

In order to obtain **11** from **13**, a solution of 51.6 mg (0.196 mmol) of **13** in 70 cm^3 of benzene–methanol (98 : 2) was mixed dropwise with 200 cm^3 of ice-cooled 50% potassium carbonate solution. After the mixture was worked up in the usual manner as described before, 44.5 mg (100%) of **11** was obtained as a violet oil: UV (C_2H_5OH) 244 (log ε 4.43), 271 (sh, 4.31), 275 (sh, 4.45), 281 (sh, 4.61), 285 (4.67), 290 (4.67), 294 (sh, 4.61), 305 (sh, 3.93), 322 (sh, 3.45), 328 (sh, 3.51), 334 (3.59), 344 (sh, 3.64), 349 (3.71), 359 (sh, 3.06), 547 (2.71), 564 (sh, 2.69), 581 (sh, 2.65), and 637 nm (sh, 2.20); IR (CCl_4) 2825, 2775, 2725 ($N(CH_3)_2$), 2980, 2950, 2860, 1467, 1458, 1438, 1372 (CH_3 and CH_2), 1045, and 1040 cm^{-1} (C–N); ^1H NMR ($CDCl_3$) δ=2.37 (6H, s, $N(CH_3)_2$), 2.60 (3H, s, 6-CH_3), 2.78 (2H, m, 1′-H_2), 2.84 (3H, s, 8-CH_3), 3.38 (2H, m, 2′-H_2), 7.06 (1H, s, 7-H), 7.09 (1H, s, 5-H), 7.40 (1H, q, J=4 and 1.5 Hz, 1-H), 7.50 (1H, q, J=4 and 1.5 Hz, 3-H), and 7.73 (1H, t, J=4 Hz, 2-H); ^{13}C NMR ($CDCl_3$) δ=25.0 (q, 8-CH_3), 28.7 (q, 6-CH_3), 37.3 (t, 2′-C), 45.2 (q, $N(CH_3)_2$), 61.1 (t, 1′-C), 115.5 (d, 3-C), 116.2 (d, 1-C), 126.7 (d, 5-C), 127.0 (d, 7-C), 132.6 (d, 2-C), 136.0 (s, 9- and 10-C), 145.4 (s, 8-C), 146.3 (s, 6-C), and 147.8 (s, 4-C) [*cf.* 4,6,8-trimethylazulene in Ref. 16][16]; MS *m/e* (rel intensity) 227 (M^+; 12), 169 ($M^+ - (CH_3)_2NCH_2$; 3), and 58 ($(CH_3)_2NCH_2^+$; 100).

Found: C, 84.23; H, 9.21; N, 6.04%. Calcd for $C_{16}H_{21}N$: C, 84.53; H, 9.31; N, 6.16%.

Similar treatment of 53.4 mg (0.202 mmol) of **14** gave 43.9 mg (0.202 mmol) of **12** as a violet oil: UV (C_2H_5OH) 244 (log ε 4.51), 275 (sh, 4.53), 281 (4.68), 284 (4.74), 289 (4.73), 294 (sh, 4.66), 304 (sh, 4.05), 322 (sh, 3.50), 328 (sh, 3.57), 333 (3.64), 343 (sh, 3.69), 348 (3.75), 548 (2.69), 562 (sh, 2.67), 584 (sh, 2.62), and 638 nm (sh, 2.18); IR (CCl_4) 2825, 2780, 2725 ($N(CH_3)_2$), 2985, 2955, 1470, 1460, 1435, 1375 (CH_3 and CH_2), 1050, and 1042 cm^{-1} (C–N); ^1H NMR ($CDCl_3$) δ=2.32 (6H, s, $N(CH_3)_2$), 2.62 (2H, m, 1′-H_2), 2.88 (6H, s, 4- and 8-CH_3), 2.94 (2H, m, 2′-H_2), 7.08 (2H, s, 5- and 7-H), 7.42 (2H, d, J=4 Hz, 1- and 3-H), and 7.74 (1H, t, J=4 Hz, 2-H); ^{13}C NMR ($CDCl_3$) δ=25.0 (q, 4- and 8-CH_3), 41.2 (t, 2′-C), 45.4 (q, $N(CH_3)_2$), 62.4 (t, 1′-C), 116.0 (d, 1- and 3-C), 126.8 (d, 5- and 7-C), 132.7 (d, 2-C), 136.2 (s, 9- and 10-C), 145.7 (s, 4- and 8-C), and 148.2 (s, 6-C); MS *m/e* (rel intensity) 227 (M^+; 5), 169 ($M^+ - (CH_3)_2NCH_2$; 1), and 58 ($(CH_3)_2NCH_2^+$; 100).

Found: C, 84.27; H, 9.03; N, 6.11%. Calcd for $C_{16}H_{21}N$: C, 84.53; H, 9.31; N, 6.16%.

Similar treatment of 37.9 mg (0.144 mmol) of **16** afforded 32.8 mg (100%) of **15** as a violet oil: UV (C_2H_5OH) 246 (log ε 5.40), 287 (5.72), 293 (5.72), 335 (4.55), 351 (4.68), 537 (2.65), 560 (sh, 2.62), and 616 nm (sh, 2.20); IR (CCl_4) 2820, 2775, 2730 ($N(CH_3)_2$), 2980, 2945, 2930, 2860, 1455, 1445, 1376, 1357 (CH_3 and CH_2), 1040, and 1030 cm^{-1} (C–N); ^1H NMR ($CDCl_3$) δ=2.35 (6H, s, $N(CH_3)_2$), 2.61 (3H, s, 6-CH_3), 2.87 (6H, s, 4- and 8-CH_3), 3.82 (2H, s, CH_2), 7.12 (2H, s, 5- and 7-H), and 7.37 (2H, s, 1- and 3-H); MS *m/e* (rel intensity) 227 (M^+; 12), 184 ($M^+ - CH_3NCH_2$; 100), 183 ($M^+ - (CH_3)_2N$; 28), 169 ($M^+ - (CH_3)_2NCH_2$; 41), and 58 ($(CH_3)_2NCH_2^+$; 13).

Found: C, 84.59; H, 9.30; N, 5.94%. Calcd for $C_{16}H_{21}N$: C, 84.53; H, 9.31; N, 6.16%.

*Reaction of Sodium Guaiazulenide (**18**) with Methyleneammonium Salts or with N-Ethylidenemethylamine. A) With N-Methylenedimethylammonium Iodide*: To a stirred solution of 10 mmol of sodium guaiazulenide (**18**) in 30 cm^3 of THF [from 440 mg (10.2 mmol) of sodium hydride, 3.62 g (33.8 mmol) of *N*-methylaniline, and 1.99 g (10.0 mmol) of guaiazulene, as described in the preparation of **2**], under dry nitrogen and with Dry Ice–acetone cooling, was added 3.70 g (20 mmol) of *N*-methylenedimethylammonium iodide over a period of 20 min (washed with 5 cm^3 of THF), and the suspension was stirred for 1 h at *ca.* −80 °C and for an additional 5 h with a gradual elevation of the temperature. The reaction mixture, after being worked up as described above for **2**, was chromatographed over alumina (elution with 9 : 1 hexane–ethyl acetate) and separated into four fractions. Further elution with ethanol afforded one more fraction.

Rechromatography of the first fraction on a silica-gel column with hexane gave 30.2 mg (2%) of unchanged guaiazulene. Successively the solvent was changed into benzene to give 32.2 mg (1%) of **19** as a blue oil: UV (C_2H_5OH) 248 (log ε 4.44), 283 (sh, 4.54), 290 (4.60), 307 (4.22), 341 (sh, 3.58), 354(3.73), 371 (3.63), 584 (sh, 2.49), 625 (2.58), 676 (sh, 2.49), and 748 (sh, 2.05); IR (CCl_4) 3440 (NH), 1375 and 1360 cm^{-1} (CH_3); ^1H NMR ($CDCl_3$)[18] δ=1.32 (6H, d, J=7 Hz, $CH(C\underline{H}_3)_2$), 2.60 (3H, s, 1-CH_3), 2.70 (3H, s, NCH_3), 2.84 (3H, s, 4-CH_3), 2.98 (1H, m, J=7 Hz, $C\underline{H}(CH_3)_2$), 3.34 (1H, broad s, NH), 4.48 (2H, s, CH_2), 6.48 (2H, d, J=8 Hz, 3″- and 5″-H), 6.76 (1H, d, J=10 Hz, 5-H), 6.88 (2H, d, J=8 Hz, 2″- and 6″-H), 7.22 (1H, q, J=10 and 2 Hz, 6-H), 7.40 (1H, s, 2-H), and 8.08 (1H, d, J=2 Hz, 8-H); MS *m/e* (rel intensity) 317 (M^+; 100), 302 ($M^+ - CH_3$; 57), and 120 ($CH_3NHC_6H_4CH_2^+$; 29).

Found: C, 86.73; H, 8.53; N, 4.30%. Calcd for $C_{23}H_{27}N$:

C, 87.02; H, 8.57; N, 4.41%.

Rechromatography of the second fraction on an alumina column (elution with 98 : 2 hexane–ethyl acetate) gave 346 mg (14%) of **20** as blue crystals, mp 37—38 °C [Ref. 10; blue oil]:[10] UV (cyclohexane) 215 (log ε 4.02), 247 (4.28), 282 (sh, 4.49), 288 (4.56), 292 (4.58), 305 (4.14), 339 (sh, 3.54), 347 (sh, 3.60), 353 (3.73), 371 (3.73), 568 (sh, 2.50), 595 (sh, 2.58), 613 (2.61), 640 (sh, 2.59), 667 (2.53), 708 (sh, 2.22), and 741 nm (2.08) [Ref. 10 (hexane); 613 (2.62), 662 (2.52), 714 (2.18), and 736 nm (2.04)]; IR (CCl_4) 2820, 2775, 2720 ($N(CH_3)_2$), 1460, 1435, and 1420 cm^{-1} (CH_2); ^1H NMR ($CDCl_3$) δ=1.30 (6H, d, J=7 Hz, $CH(C\underline{H}_3)_2$), 2.22 (6H, s, $N(CH_3)_2$), 2.60 (3H, s, 1-CH_3), 2.99 (1H, m, J=7 Hz, $C\underline{H}(CH_3)_2$) 3.12 (3H, s, 4-CH_3), 3.80 (2H, s, 3-CH_2), 6.90 (1H, d, J=11 Hz, 5-H), 7.26 (1H, q, J=11 and 2 Hz, 6-H), 7.48 (1H, s, 2-H), and 8.10 (1H, d, J=2 Hz, 8-H); MS *m/e* (rel intensity) 255 (M^+; 49) and 211 ($M^+-N(CH_3)_2$; 100).

Rechromatography of the third fraction on an alumina column (elution with 9 : 1 hexane–ethyl acetate) yielded 1.28 g (50%) of **21** as a blue oil: UV (C_2H_5OH) 217 (log ε 4.01), 245 (4.35), 280 (sh, 4.52), 284 (4.57), 288 (4.56), 302 (3.98), 327 (sh, 3.23), 338 (sh, 3.43), 350 (3.60), 367 (3.45), 563 (sh, 2.53), 585 (sh, 2.60), 607 (2.65), 632 (sh, 2.61), 654 (2.58), and 725 nm (2.16); IR (CCl_4) 2820, 2772 (NCH_3), 2964, 2864, 1468, 1445, 1424, 1391, and 1373 cm^{-1} (CH_3 and CH_2); ^1H NMR ($CDCl_3$) δ=1.31 (6H, d, J=7 Hz, $CH(C\underline{H}_3)_2$), 2.28 (6H, s, $N(CH_3)_2$), 2.66 (3H, s, 1-CH_3), 2.76 (2H, m, 1′-H_2), 2.98 (1H, m, $C\underline{H}(CH_3)_2$), 3.30 (2H, m, 2′-H_2), 6.98 (1H, d, J=10 Hz, 5-H), 7.36 (1H, q, J=10 and 1.6 Hz, 6-H), 7.40 (1H, d, J=4 Hz, 3-H), 7.68 (1H, d, J=4 Hz, 2-H), and 8.26 (1H, d, J=1.6 Hz, 8-H); ^{13}C NMR ($CDCl_3$) δ=12.9 (q, 1-CH_3), 24.7 (q, $CH(\underline{C}H_3)_2$), 36.3 (t, 2′-C), 38.1 (d, $\underline{C}H(CH_3)_2$), 45.2 (q, $N(\underline{C}H_3)_2$), 60.7 (t, 1′-C), 112.2 (d, 3-C), 124.7 (d, 5-C), 125.0 (s, 1-C), 133.0 (d, 8-C), 135.0 (d, 6-C), 136.0 (s, 10-C), 136.4 (d, 2-C), 137.3 (s, 9-C), 139.6 (s, 7-C), and 146.4 (s, 4-C) [*cf.* *S*-guaiazulene in Ref. 17][17]; MS *m/e* (rel intensity) 255 (M^+; 100), 211 ($M^+-(CH_3)_2N$; 6), and 197 ($M^+-(CH_3)_2NCH_2$; 6).

Found: C, 84.47; H, 9.61; N, 5.61%. Calcd for $C_{18}H_{25}N$: C, 84.65; H, 9.87; N, 5.48%.

The combined fourth and ethanol fractions were chromatographed on an alumina column (elution with 8 : 2 benzene–ethyl acetate) to afford 218 mg (7%) of **22** as dark blue prisms, mp 66—68 °C; UV (C_2H_5OH) 217 (sh, ε 4.09), 247 (4.34), 289 (4.56), 304 (sh, 4.12), 342 (sh, 3.61), 353 (3.72), 372 (3.69), 407 (sh, 2.09), 573 (sh, 2.55), 609 (2.64), 653 (sh, 2.57), and 727 nm (sh, 2.13); IR (CCl_4) 2820, 2770 (NCH_3), 2968, 2865, 1460, 1440, 1430, 1420, 1385, and 1370 cm^{-1} (CH_3 and CH_2); ^1H NMR ($CDCl_3$) δ=1.34 (6H, d, J=7 Hz, $CH(C\underline{H}_3)_2$), 2.23 (6H, s, $N(CH_3)_2$), 2.36 (6H, s, $N(CH_3)_2$), 2.61 (3H, s, 1-CH_3), 2.72 (2H, m, 1′-H_2), 3.02 (1H, m, J=7 Hz, $C\underline{H}(CH_3)_2$), 3.68 (2H, m, 2′-H_2), 3.84 (2H, s, 3-CH_2), 7.03 (1H, d, J=11 Hz, 5-H), 7.38 (1H, q, J=11 and 2 Hz, 6-H), 7.56 (1H, s, 2-H), and 8.16 (1H, d, J=2 Hz, 8-H); MS *m/e* (rel intensity) 312 (M^+; 3), 254 ($M^+-(CH_3)_2NCH_2$; 9), and 58 ($(CH_3)_2NCH_2^+$; 100).

Found: C, 80.35; H, 10.10; N, 8.81%. Calcd for $C_{21}H_{32}N_2$: C, 80.71; H, 10.32; N, 8.96%.

B) With N-*Isopropylidenedimethylammonium Perchlorate*: Reaction of 10 mmol of **18** and 3.71 g (20.0 mmol) of *N*-isopropylidenedimethylammonium perchlorate[11] was carried out in a manner similar to *A* except that the reagents were reacted at room temperature for 2 h. Chromatography of the reaction mixture on an alumina column (elution with 8 : 2 benzene–chloroform) gave 746 mg of blue oil, which on rechromatography over silica gel with hexane afforded 597 mg (30%) of unchanged **17**. Successive blue eluate gave 2.11 g of blue oil, which was also rechromatographed over alumina (elution with 9 : 1 hexane–ethyl acetate) to give 1.81 g (64%) of **24** as a blue oil: UV (C_2H_5OH) 247 (log ε 4.29), 282 (sh, 4.51), 285 (4.54), 289 (4.53), 305 (sh, 3.94), 340 (sh, 3.55), 351 (3.66), 368 (3.52), 566 (sh, 2.53), 588 (sh, 2.60), 609 (2.66), 634 (sh, 2.61), 659 (2.58), and 728 nm (2.14); IR (CCl_4) 2820, 2780, 2730 (NCH_3), 2960, 2925, 2870, 1460, 1385, 1365 (CH_3 and CH_2), and 1145 cm^{-1} (C–N); ^1H NMR δ=1.01 (6H, s, 1′-$C(CH_3)_2$), 1.29 (6H, d, J=7 Hz, $CH(C\underline{H}_3)_2$), 2.44 (6H, s, $N(CH_3)_2$), 2.64 (3H, s, 1-CH_3), 3.05 (1H, m, J=7 Hz, $C\underline{H}(CH_3)_2$), 3.30 (2H, s, 2′-H_2), 7.08 (1H, d, J=11 Hz, 5-H), 7.40 (1H, d, J=4 Hz, 3-H), 7.46 (1H, q, J=11 and 2 Hz, 6-H), 7.70 (1H, d, J=4 Hz, 2-H), and 8.24 (1H, d, J=2.0 Hz, 8-H); MS *m/e* (rel intensity) 283 (M^+; 0.7), 198 ($M^+-C_5H_{11}N$; 15), and 86 ($C_5H_{12}N^+$; 100).

Found: C, 84.64; H, 10.24; N, 4.41%. Calcd for $C_{20}H_{29}N$: C, 84.75; H, 10.31; N, 4.94%.

C) With N-*Isopropylidenepyrrolidinium Perchlorate*: Reaction of 10 mmol of **18** and 4.25 g (20.1 mmol) of *N*-isopropylidenepyrrolidinium perchlorate[11] was carried out in a manner similar to *A*, except that the reaction mixture was stirred for 3 h at −20 °C (ice salt mixture) and an additional 1 h at room temperature. Elution of the reaction mixture on an alumina column with hexane gave 156 mg (8%) of unchanged **17**. Then the solvent was changed into hexane–ethyl acetate (9 : 1) to give 1.93 g (62%) of **25** as a blue oil: UV (C_2H_5OH) 218 (sh, log ε 4.00), 246 (4.31), 275 (sh, 4.37), 281 (sh, 4.47), 285 (4.50), 289 (4.48), 304 (sh, 3.92), 568 (sh, 2.49), 592 (2.57), 611 (2.61), 634 (sh, 2.58), 661 (2.55), and 729 nm (2.11); IR (CCl_4) 2968, 2940, 2916, 2875, 2814, 1468, 1453, 1440, 1423, 1390, and 1370 cm^{-1} (CH_3 and CH_2); ^1H NMR ($CDCl_3$)[18] δ=1.06 (6H, s, 1′-$C(CH_3)_2$), 1.31 (6H, d, J=7 Hz, $CH(C\underline{H}_3)_2$), 1.75 (4H, m, J=6 Hz, β- and γ-H_2), 2.64 (3H, s, 1-CH_3), 2.79 (4H, m, J=6 Hz, α- and δ-H_2), 3.00 (1H, m, J=7 Hz, $C\underline{H}(CH_3)_2$), 3.32 (2H, s, 2′-H_2), 7.01 (1H, d, J=11 Hz, 5-H), 7.32 (1H, q, J=11 and 2 Hz, 6-H), 7.36 (1H, d, J=4 Hz, 3-H), 7.60 (1H, d, J=4 Hz, 2-H), and 8.16 (1H, d, J=2 Hz, 8-H); MS *m/e* (rel intensity) 309 (M^+; 3), 197 ($M^+-(CH_3)_2CNC_4H_8$; 4), 112 ($C_4H_8NC(CH_3)_2^+$; 100), and 70 ($C_4H_8N^+$; 37).

Found: C, 85.56; H, 10.09; N, 4.24%. Calcd for $C_{22}H_{31}N$: C, 85.38; H, 10.10; N, 4.53%.

D) With N-*(α-Methylbenzylidene)pyrrolidinium Perchlorate*: Reaction of 10 mmol of **18** and 5.00 g (18.3 mmol) of *N*-(α-methylbenzylidene)pyrrolidinium perchlorate was carried out in a manner similar to *C*. Elution of the reaction mixture on a silica-gel column with hexane afforded 399 mg (20%) of unchanged **17**. Then the solvent was changed into benzene–methanol (98 : 2) to give 2.02 g (54%) of **26** as a blue oil: UV (C_2H_5OH) 247 (log ε 4.32), 286 (4.51), 290 (sh, 4.49), 304 (sh, 3.93), 327 (sh, 3.40), 341 (sh, 3.51), 351 (3.61), 368 (3.50), 415 (2.27), 435 (2.26), 566 (sh, 2.49), 529 (sh, 2.62), 633 (sh, 2.58), 658 (2.55), and 730 nm (2.13); IR (CCl_4) 3110, 3090, 3070, 3035 (aromatic CH), 2975, 2880, 1465, 1450, 1440, 1423, 1390, 1380, 1370, and 1368 cm^{-1} (CH_3 and CH_2); ^1H NMR ($CDCl_3$)[18] δ=1.23 (6H, d, J=7 Hz, $CH(C\underline{H}_3)_2$), 1.24 (3H, s, 1′-$C(CH_3)$), 1.74 (4H, m, β- and γ-H_2), 2.60 (3H, s, 1-CH_3), 2.70 (4H, t, J=6 Hz, α- and δ-H_2), 2.90 (1H, m, J=7 Hz, $C\underline{H}(CH_3)_2$), 3.31 (1H, d, J=12.5 Hz, 2′-H), 4.01 (1H, d, J=12.5 Hz, 2′-H), 6.03 (1H, d, J=11 Hz, 5-H), 6.85 (1H, q, J=11 and 2 Hz, 6-H), 7.10—7.38 (6H, m, 3-H and Ph), 7.52 (1H, d, J=4 Hz, 2-H), and 8.04 (1H, d, J=2 Hz, 8-H); ^{13}C NMR ($CDCl_3$)[18] δ=13.0 (1-CH_3), 14.3 (1′-$C(\underline{C}H_3)$), 24.1 (β- and γ-C), 24.6 ($CH(\underline{C}H_3)_2$), 37.9 ($\underline{C}H(CH_3)_2$), 46.1 (α- and δ-C), 49.7 (2′-C), 63.3 (1′-C), 113.1 (3-C), 124.4 (5-C), 126.2 (1-C), 126.7 (4″-C), 127.5 (2″-, 3″-, 5″-, and 6″-C), 132.3 (8-C), 133.5 (6-C), 135.6 (2-C), 136.1 (10-C), 139.0 (9-C), 139.7 (7-C), 144.9 (1″-C), and 146.2 (4-C); MS *m/e* (rel intensi-

ty) 371 (M^+; 2), 174 ($C_6H_5C(CH_3)NC_4H_8^+$; 100), and 70 ($C_4H_8N^+$; 4).

Found: C, 87.17; H, 8.67; N, 3.35%. Calcd for $C_{27}H_{33}N$: C, 87.28; H, 8.95; N, 3.77%.

E) With N-Ethylidenemethylamine: Reaction of 10 mmol of **18** and 3.0 cm³ (40 mmol) of *N*-ethylidenemethylamine was carried out as described in *B*. Chromatography of the reaction mixture on an alumina column (elution with 8 : 2 benzene–methanol) yielded 4.08 g of blue oil, which on rechromatography (hexane–silica gel) afforded 1.74 g (88%) of unchanged **17**. The second blue eluate was rechromatographed on an alumina column (elution with 8 : 2 benzene–methanol) to afford 210 mg (8%) of **23** as a blue oil: UV (C_2H_5OH) 219 (log ε 4.02), 246 (4.36), 285 (4.58), 289 (4.58), 303 (3.99), 349 (3.62), 367 (3.49), 565 (sh, 2.55), 607 (2.66), 656 (2.59), and 725 nm (sh, 2.15); IR (CCl_4) 3330 (NH), 2790 (NCH_3), 2960, 2925, 2870, 1470, 1460, 1445, 1438, 1420, 1390, and 1370 cm⁻¹ (CH_3 and CH_2); ¹H NMR ($CDCl_3$) δ=1.12 (3H, d, J=6.3 Hz, 1′-$C(CH_3)$), 1.35 (6H, d, J=6.9 Hz, $CH(C\underline{H}_3)_2$), 1.71 (1H, broad s, NH), 2.39 (3H, s, NCH_3), 2.64 (3H, s, 1-CH_3), 2.88—3.40 (4H, m; 1′-H, 2′-H_2, and $C\underline{H}(CH_3)_2$), 6.96 (1H, d, J=10.3 Hz, 5-H), 7.28 (1H, d, J=3.4 Hz, 3-H), 7.36 (1H, q, J=10.3 and 1.7 Hz, 6-H), 7.59 (1H, d, J=3.4 Hz, 2-H), and 8.14 (1H, d, J=1.7 Hz, 8-H;) MS *m/e* (rel intensity) 255 (M^+; 7), 198 ($M^+-C_3H_7N$; 32), and 58 ($C_3H_8N^+$; 100).

Found: C, 84.70; H, 9.56; N, 5.62%. Calcd for $C_{18}H_{25}N$: C, 84.65; H, 9.87; N, 5.48%.

Preparation of Hydrochlorides from 2-(7-Isopropyl-1-methyl-4-azulenyl)ethanamine Derivatives. A) From 21: A solution of 209 mg (0.818 mmol) of **21** in 100 cm³ of benzene was extracted with 1 mol dm⁻³ hydrochloric acid (50 cm³×3); the hydrochloric acid layer was then extracted with chloroform (50 cm³×3). The chloroform solution was dried (sodium sulfate) and concentrated (reduced pressure) to leave a blue crystalline mass, which was washed with hexane (20 cm³×5) and chromatographed on a silica-gel column (elution with 9 : 1 chloroform–methanol) to give 120 mg (50%) of **27** as blue crystals, mp 200—204 °C: UV (C_2H_5OH) 218 (sh, log ε 4.05), 245 (4.29), 280 (sh, 4.46), 285 (4.52), 289 (4.51), 303 (3.95), 350 (3.58), 367 (3.41), 565 (sh, 2.51), 588 (sh, 2.57), 605 (2.61), 633 (sh, 2.56), 658 (2.53), and 730 nm (2.09); IR ($CHCl_3$) 2500, 2400, 2350, 2328 (NH^+), and 1097 cm⁻¹ (C–N); ¹H NMR ($CDCl_3$) δ=1.28 (6H, d, J=7 Hz, $CH(C\underline{H}_3)_2$), 2.32 (6H, s, $N(CH_3)_2$), 2.61 (3H, s, 1-CH_3), 2.74 (2H, m, 1′-H_2), 3.02 (1H, m, J=7 Hz, $C\underline{H}(CH_3)_2$), 3.31 (2H, m, 2′-H_2), 7.00 (1H, d, J=11 Hz, 5-H), 7.32 (1H, d, J=4 Hz, 3-H), 7.38 (1H, q, J=11 and 2 Hz, 6-H), 7.64 (1H, d, J=4 Hz, 2-H), and 8.18 (1H, d, J=2 Hz, 8-H).

B) From 24: By treating 210 mg (0.741 mmol) of **24** as described above in *A*, 153 mg (65%) of **28** was obtained as blue crystals, mp 200—204 °C: UV (C_2H_5OH) 215 (log ε 4.64), 246 (5.00), 285 (5.28), 290 (5.27), 303 (sh, 4.65), 330 (sh, 2.52), 351 (3.19), 368 (2.90), 440 (sh, 2.43), 565 (sh, 2.35), 614 (2.45), 666 (2.36), and 740 nm (1.89); IR ($CHCl_3$) 2615, 2540, 2510, 2440, 2350, 2340 (NH^+), and 1144 cm⁻¹ (C–N); ¹H NMR ($CDCl_3$) δ=1.34 (6H, s, 1′-$C(CH_3)_2$), 1.40 (6H, d, J=7 Hz, $CH(C\underline{H}_3)_2$), 2.72 (3H, s, 1-CH_3), 2.82 (6H, s, $N(CH_3)_2^+$), 3.16 (1H, m, J=7.0 Hz, $C\underline{H}(CH_3)_2$), 3.68 (2H, s, 2′-H_2), 7.12 (1H, d, J=11 Hz, 5-H), 7.54 (1H, q, J=11 and 4 Hz, 6-H), 7.60 (1H, d, J=4 Hz, 3-H), 7.84 (1H, d, J=4 Hz, 2-H), and 8.38 (1H, d, J=2 Hz, 8-H).

C) From 25: By treating 321 mg (1.04 mmol) of **25** as described in *A*, except that 6 mol dm⁻³ hydrochloric acid and a mixed solvent of chloroform–methanol (7 : 3) were used for extraction and for chromatographic separation respectively, 183 mg (51%) of **29** was obtained as blue crystals, mp 82—84 °C: UV (C_2H_5OH) 216 (log ε 3.21), 245 (3.69), 284 (4.03), 290 (4.02), 304 (sh, 2.54), 338 (sh, 3.38), 352 (3.46), 368 (3.38), 608 (2.59), 660 (2.49), and 730 nm (2.02); IR ($CHCl_3$) 2690, 2645, 2560, 2500—2400, 2360, 2340 (NH^+), and 1194 cm⁻¹ (C–N); ¹H NMR ($CDCl_3$)[18] δ=1.32 (6H, s, $C(CH_3)_2$), 1.43 (6H, d, J=7 Hz, $CH(C\underline{H}_3)_2$), 2.08 (4H, m, β- and γ-H_2), 2.24 (1H, s, NH^+), 2.76 (3H, s, 1-CH_3), 3.18 (1H, m, J=7 Hz, $C\underline{H}(CH_3)_2$), 3.32 (4H, t, J=6 Hz, α- and δ-H_2), 3.68 (2H, s, 2′-H_2), 7.19 (1H, d, J=11 Hz, 5-H), 7.58 (1H, q, J=11 and 2 Hz, 6-H), 7.64 (1H, d, J=4 Hz, 3-H), 7.84 (1H, d, J=4 Hz, 2-H), and 8.36 (1H, d, J=2 Hz, 8-H).

D) From 26: By treating 415 mg (1.12 mmol) of **26** as described in *C*, 128 mg (28%) of **30** was obtained as blue crystals, mp 80—85 °C: UV (C_2H_5OH) 246 (log ε 4.03), 286 (4.34), 291 (4.31), 303 (3.52), 329 (sh, 3.46), 335 (sh, 3.54), 351 (3.66), 368 (3.54), 416 (2.90), 436 (2.89), 560 (sh, 2.50), 602 (sh, 2.59), 611 (2.60), 660 (2.52), and 730 nm (2.08); IR ($CHCl_3$) 2670, 2560, 2490—2430, 2400, 2360, 2340 (NH^+), and 1192 cm⁻¹ (C–N); ¹H NMR ($CDCl_3$)[18] δ=1.23 (3H, s, 1′-$C(CH_3)$), 1.32 (6H, d, J=7 Hz, $CH(C\underline{H}_3)_2$), 1.88 (4H, m, β- and γ-H_2), 2.64 (3H, s, 1-CH_3), 3.02 (4H, m, α- and δ-H_2), 3.70 (1H, d, J=12.5 Hz, 2′-H), 4.15 (1H, d, J=12.5 Hz, 2′-H), 6.10 (1H, d, J=11 Hz, 5-H), 6.96 (1H, q, J=11 and 2 Hz, 6-H), 7.30 (3H, m, 3″-, 4″-, and 5″-H), 7.34 (1H, d, J=4 Hz, 3-H), 7.64 (2H, m, 2″- and 6″-H), 7.62 (1H, d, J=4 Hz, 2-H), and 8.16 (1H, d, J=2 Hz, 8-H).

We wish to thank Professor Hitoshi Takeshita of Kyushu University, for his kind measurements of ¹³C NMR, and Konan-kako Co. Ltd., for generously giving us the sample of 4,6,8-trimethylazulene.

References

1) See, for example, W. E. Coyne, "Medicinal Chemistry," 3rd ed, ed by A. Burger, Wiley Interscience, New York (1970), Part II, pp. 953—968; W. T. Comer and A. W. Gomoll, *ibid.*, pp. 1019—1056; D. J. Triggle, *ibid.*, pp. 1235—1282.

2) S. Kurokawa and A. G. Anderson, Jr., *Bull. Chem. Soc. Jpn*, **56**, 2059 (1983).

3) S. Kurokawa, *Chem. Lett.*, **1981**, 1569.

4) S. Kurokawa, *Bull. Chem. Soc. Jpn.*, **52**, 1748 (1979).

5) K. Hafner, H. Pelster, and H. Patzelt, *Justus Liebigs Ann. Chem.*, **650**, 80 (1961).

6) J. Schreiber, H. Maag, N. Hashimoto, and A. Eschenmoser, *Angew. Chem., Int. Ed. Engl.*, **10**, 330 (1971).

7) R. N. McDonald, J. M. Richmond, J. R. Curtis, H. E. Petty, and R. J. Mobley, *J. Am. Chem. Soc.*, **99**, 5739 (1977): Identifications by spectral data were performed according to N. L. Wolfe, Ph. D. Thesis, Kansas State University, Kansas, U. S. A., (1974), which was kindly sent us by Professor R. N. McDonald.

8) R. N. McDonald, H. E. Petty, N. L. Wolfe, and J. V. Paukstelis, *J. Org. Chem.*, **39**, 1877 (1974).

9) E. Heilbronner, "Non-Benzenoid Aromatic Compounds," ed by D. Ginsburg, Interscience, New York (1959), pp. 171—276.

10) K. Hafner and W. Senf, *Justus Liebigs Ann. Chem.*, **656**, 34 (1962).

11) N. J. Leonard and J. V. Paukstelis, *J. Org. Chem.*, **28**, 3021 (1963).

12) R. Tiollais, *Bull. Soc. Chim. Fr.*, **14**, 708 (1947); K. N. Campbell, A. H. Sommers, and B. K. Campbell, *J. Am. Chem. Soc.*, **66**, 82 (1944).

13) The tests for enzyme activity were performed by Masao Kidokoro at the Central Research Laboratory of Sankyo Co. Ltd., using established procedures.

14) Unpublished data available in our laboratory: These data were obtained by Cynthia H. Wilson and John B. Plastino at the University of Washington using established procedures.
15) K. Hafner and H. Weldes, *Justus Liebigs Ann. Chem.*, **606**, 90 (1957); K. Hafner, C. Berhard, and R. Müller, *ibid.*, **650**, 35 (1961).
16) S. Braun and J. Kinkeldei, *Tetrahedron*, **33**, 1827 (1977).
17) K. Sato, M. Yamaguchi, and I. Ogura, *Bunseki Kagaku*, **31**, 185 (1982).
18) This numbering was used for pyrrolidine ring and for benzene ring:

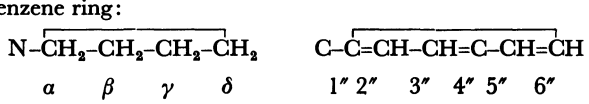

Synthetic Studies on the Validamycins. VII. Synthesis of DL-2-Deoxyhydroxyvalidamine and DL-2-Deoxyvalienamine[1,2]

Seiichiro OGAWA, Hiroyuki ITO, Takao OGAWA, Shinichi IWASAKI, and Tetsuo SUAMI*
Department of Applied Chemistry, Faculty of Science and Technology, Keio University, Hiyoshi, Kohoku-ku, Yokohama 223
(Received October 16, 1982)

Synthesis of the 2-deoxy analogs of DL-hydroxyvalidamine and DL-valienamine starting from DL-1,2-di-*O*-acetyl-(1,3,5/2)-5-bromo-3-bromomethyl-1,2-cyclohexanediol is described.

In connection with the previous paper,[3] DL-2-deoxyhydroxyvalidamine (**1**), DL-2-deoxyvalienamine (**2**), and the related cyclitol derivatives were synthesized starting from the readily available DL-1,2-di-*O*-acetyl-(1,3,5/2)-5-bromo-3-bromomethyl-1,2-cyclohexanediol (**3**),[4] following mainly the sequence previously employed for the synthesis of DL-hydroxyvalidamine.[3]

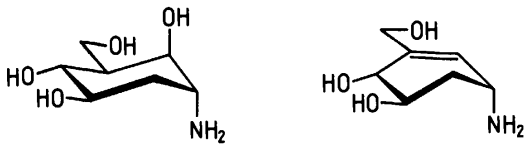

1 **2**

Scheme 1.

Treatment of **3** with 2 molar equiv. of sodium benzoate in 90% aqueous *N,N*-dimethylformamide (DMF) at 75 °C gave the monobenzoate **4** in 52% yield. When **4** reacted with 1,8-diazabicyclo[5.4.0]undec-7-ene (DBU) in toluene at reflux temperature, two olefins **7** and **8** were obtained, after chromatography on silica gel, in 48 and 25% yields, respectively. On the other hand, treatment of **3** with 3 molar equiv. of sodium benzoate and a molar equiv. of lithium bromide in DMF at 120 °C for 1 h gave, after chromatography, **7** (36%), **8** (26%), dibenzoate **9** (8%), and diolefin **10** (19%). Compound **7** was identified with an authentic sample.[5] The ^{1}H NMR spectrum of **8** showed the signals of H-1 and H-2 as a triplet of doublets (δ=5.10, J=6, 11, and 11 Hz) and a triplet (δ=5.28, J=11 Hz), supporting the structural assignment. Compound **4** was first converted, by attack of a bromide ion, into its C-5 epimer, which would readily undergo elimination to give **7** and **8**. This assumption may be supported by the formation of **9**. The ^{1}H NMR spectrum of **10** revealed the signals of H-2, H-4, and H-5 as a broad doublet (δ=6.13, J= 10 Hz), a doublet (δ=5.60, J=9 Hz) and a triplet of doublets (δ=5.53, J=3.6, 9, and 9 Hz), respectively, indicating the assigned structure. Compound **10** was characterized by conversion into the crystalline bis(*p*-nitrobenzoate).

In order to obtain desired **8** selectively, **3** was transformed into the 1,2-*O*-isopropylidene derivative **6**. Since introduction of the 1,2-*O*-isopropylidene-fused ring into the cyclohexane ring gave appreciable strain in it, the elimination reaction was expected to proceed regioselectively to give rise to either one of the two isomeric olefins.

O-Deacetylation of **3** was carried out with hydrobromic acid in aqueous ethanol at reflux temperature

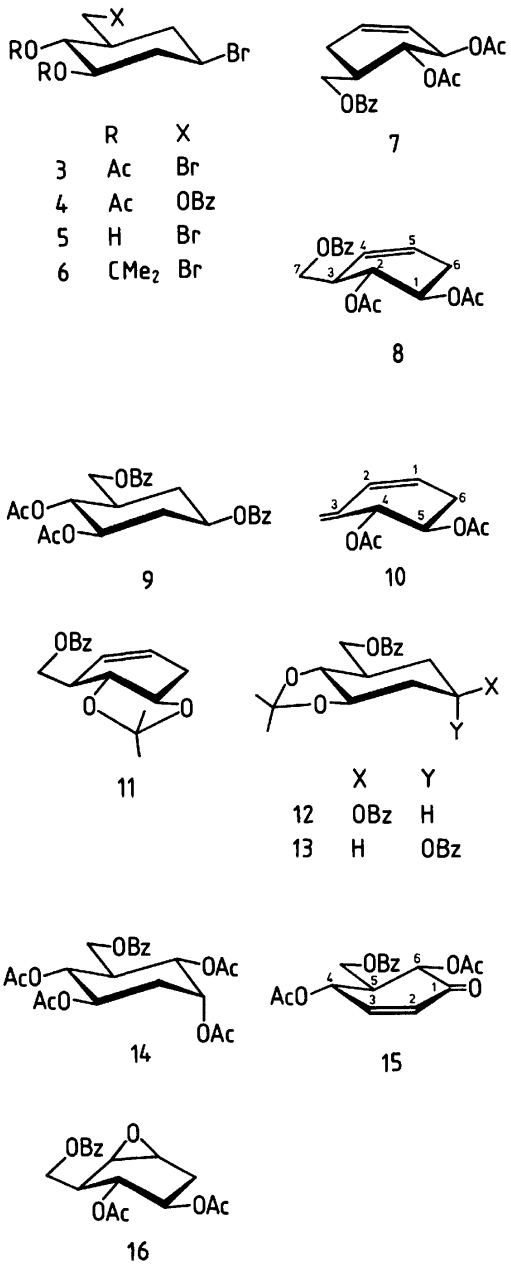

	R	X
3	Ac	Br
4	Ac	OBz
5	H	Br
6	CMe_2	Br

7 **8** **9** **10** **11**

	X	Y
12	OBz	H
13	H	OBz

14 **15** **16**

Scheme 2.

to give the dihydroxy compound **5** in 95% yield. Treatment of **5** with 2,2-dimethoxypropane in DMF in the presence of *p*-toluenesulfonic acid at 70 °C gave **6** in 97% yield. Similar treatment of **6** with sodium benzoate and lithium bromide in DMF produced a single olefin **11** in 60% yield,[6] together with the substitution products **12** (12%) and **13** (5%). The structure of

11 was confirmed by converting it into **8**. The structures of **12** and **13** were tentatively assigned by ^{1}H NMR spectroscopy. Thus, the spectra of **12** and **13** showed the signals of H-5 as a wide triplet of triplets (δ=5.20, J= 5, 5, 11, and 11 Hz) and a narrow quitet (δ=5.58, J= 3 Hz), respectively. Formation of **12** and **13** indicated that the ring bromine atom of **6** was first displaced by bromide ion as well as benzoate ion. The intermediate C-5 epimer of **6** would be converted into **11** *via* regioselective elimination and a small proportion of **12** *via* displacement reaction.

In order to see reactivity of **8** and to provide ^{1}H NMR spectral data of related cyclitol derivatives, synthesis of (hydroxymethyl)cyclohexanetetrol was carried out by oxidation with osmium tetraoxide in 2-propanol containing 5% hydrogen peroxide at room temperature. The products were subsequently acetylated with acetic anhydride in pyridine at room temperature and fractionated by silica-gel chromatography to give pentol peracylate **14** and α,β-unsaturated ketone **15** in 38 and 5.2% yields, respectively.[7] The ^{1}H NMR spectrum of **14** showed a quartet (J=3 Hz) at δ=5.40, which was attributed to the proton attached to the carbon atom bearing an axial acetoxyl group. The spectrum of **15** was interpreted assuming the first-order splitting. Formation of **15** involved facile β-elimination of the acetoxyl group at C-1.

Epoxidation of **8** with *m*-chloroperoxybenzoic acid (*m*CPBA) and sodium hydrogencarbonate in 1,2-dichloroethane at room temperature yielded almost exclusively the epoxide **16** in 80% yield, together with an isomeric epoxide (<7%). Treatment of **16** with sodium azide and ammonium chloride in aqueous 2-methoxyethanol at 75 °C gave the single azido compound **18** in 76% yield through *trans*-diaxial opening of the epoxide ring. The ^{1}H NMR spectrum of **18** exhibited a quartet (J=2.5 Hz) at δ=3.83, which was ascribed to the axial proton on the carbon atom bonding to the azido function. Treatment of **16** with sodium acetate and ammonium chloride followed by acetylation gave the chloride **17** in 58% yield. The structure of **17** was shown to correspond with that of **18** by comparison of their ^{1}H NMR spectra. Accordingly, the structure of **16** was established as shown in Scheme 2 on the basis of the above results and the ^{1}H NMR spectral data. It was thought that the peroxy acid may attack **8** from less hindered side, since there is no polar substituent on the α-carbon atom that would influence the direction of the attack of the peroxy acid.

Compound **18** was converted into the triacetate **19** or the mesylate **20** in good yield. Hydrogenation of **19** with Raney nickel in ethanol followed by the conventional acetylation afforded the peracyl derivative **21** of **1** in 60% yield. Alternatively, ammonolysis of **16** with methanolic ammonia in a sealed tube at 90 °C for 15 h followed by acetylation gave, after chromatography, three amides **21** (17%), **22** (31%), and **24** (19%). The structure of **22** was determined by comparison of the ^{1}H NMR spectrum with that of **21**. The ^{1}H NMR spectrum of **24** was in accord with that of the product derived by *trans*-diequatorial opening of the epoxide.

On the other hand, **20** was treated with DBU in toluene at reflux temperature for 6 h gave the olefin **28** in 76% yield. The ^{1}H NMR spectrum of **28** showed a broad doublet (δ=6.12, J=3 Hz) and a narrow multiplet (δ=4.10), which were assigned to H-4 and H-5, respectively. Reduction of the azido group was effected by hydrogen sulfide in aqueous pyridine at room temperature,[8] and, after acetylation, the amide **29** was obtained in 65% yield. In the ^{1}H NMR spectrum of **29**, the olefinic proton appeared as a broad doublet (J=3.5 Hz) at δ=6.03. This is indicative of the pseudo-axial conformation of the acetamido group.[9] Compound **29** was a 2-deoxy analog of valienamine.

The 5-epimer of **2** and related cyclitols were prepared according to the following sequence. Compound **8** reacted with bromine in carbon tetrachloride at room temperature to give dibromide **23** in 47% yield as the only product. The ^{1}H NMR spectrum of **23** showed the signal of C-1 proton as a triplet of doublets (J=6, 9.5, and 9.5 Hz) at δ=5.38 somewhat lower-field as compared with that (δ=4.85) of **4**. It may be attributable to the presence of the bromine atom in a 1,3-diaxial position. Treatment of **23** with sodium azide in DMF at 120 °C gave azide **30** in 91% yield as the sole product.

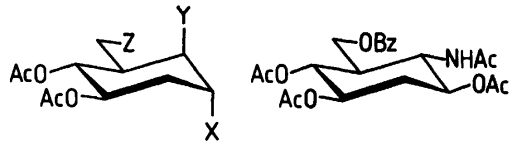

	X	Y	Z
17	Cl	OAc	OBz
18	N_3	OH	OBz
19	N_3	OAc	OBz
20	N_3	OMs	OBz
21	NHAc	OAc	OBz
22	NHAc	OAc	OAc
23	Br	Br	OBz

24

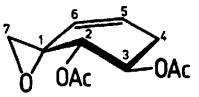

25

Scheme 3.

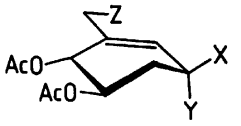

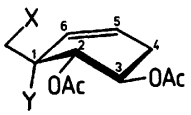

	X	Y	Z
26	H	Br	Br
27	Br	H	Br
28	H	N_3	OBz
29	H	NHAc	OBz
30	N_3	H	OBz
31	NHAc	H	OBz
32	N_3	H	OAc
33	NHAc	H	OAc
34	OBz	H	OBz
35	OAc	H	OAc
36	NPht	H	NPht
37	NHAc	H	NHAc

	X	Y
38	N_3	OAc
39	NHAc	OH

NPht = Phthalimide

Scheme 4.

The structure was assigned by comparison of its ^{1}H NMR spectrum with that of **28**. In contrast, the signal of C-4 olefinic proton appeared as a broad singlet (δ=5.99) in the case of **30**. Upon similar reduction followed by acetylation, **30** was converted into amide **31** in 58% yield. Reaction of **23** with benzoate ion in DMF similarly gave dibenzoate **34** in 62% yield. The reactions of **23** seemed to involve first the ready elimination of hydrobromic acid between C-3 and C-4. The intermediate allyl bromide was then substituted by the nucleophile *via* direct S_N2 reaction.

In addition, alternative synthetic route for deoxyvalienamine derivatives was studied starting from **10**, which could readily be prepared by treatment of **3** with DBU in toluene at reflux temperature. Reaction of **10** with bromine in carbon tetrachloride at 0 °C yielded a stereoisomeric mixture of 1,4-addition products **26** and **27** in 54% yield, together with a small amount of crystalline tetrabromide. Without further separation, the mixture of **26** and **27** was treated with an excess of sodium benzoate in 90% aqueous DMF at room temperature to give the dibenzoate **34** in 30% yield. The epimer of **34** was not isolated in pure form because of their similar mobility on TLC. Compound **34** was converted into the corresponding tetraacetate **35**. When the mixture was treated with potassium phthalimide in DMF at room temperature, a single bis(phthalimide) **36** was obtained in 58% yield selectively. Treatment of **36** with butylamine in methanol, followed by acetylation gave the bis(acetamide) **37** in 98% yield. The ^{1}H NMR spectrum was consistent with the assigned structure.

On the other hand, epoxidation of **10** with *m*CPBA in dichloromethane and phosphate buffer solution (pH 8) afforded mainly crystalline spiro epoxide **25** in 50% yield.[10] Azidolysis of **25** with sodium azide and ammonium chloride in DMF at 60 °C resulted in preferential attack at C-7 by azide ion to give only azide **38** in 92% yield. The structure of **38** was supported by ^{1}H NMR signal of the branched-chain methylene protons which appear at somewhat higher-field (AB-quartet, δ=3.60 and 3.83) than those (δ=4.15 and 4.51) of the related 1-*C*-acetoxymethyl compound.[11] Reduction of **38** with hydrogen sulfide followed by acetylation gave the amide **39** in quantitative yield. However, treatment of **25** with sodium azide and sulfuric acid in aqueous acetone at room temperature yielded, after acetylation, mainly the azide **32** in 48% yield. Similar reduction followed by acetylation gave the amide **33**, whose ^{1}H NMR spectrum showed the olefinic proton as a broad singlet (δ=4.70) and was comparable with **31** in the vicinity of the signals due to ring protons.

The branched-chain aminocyclitols and cyclitols described in this paper are not only biologically interesting compounds, but also useful model substances for structural elucidation of pseudonitrogen disaccharides reported in the accompanying paper.[12]

Experimental

Unless otherwise noted, melting points were determined on a Mitamura Riken micro hot stage apparatus and are uncorrected. ^{1}H NMR spectra were taken on a Varian EM-360 (60 MHz) or a Varian EM-390 (90 MHz) in chloroform-*d* ($CDCl_3$) with reference to tetramethylsilane as an internal standard. The peak positions are given in terms of δ-values. Values given for coupling constants are of first-order. TLC was performed on precoated silica gel 60 F-254 plates (Merck, Darmstadt; 0.25 mm thickness). The silica gel for a column chromatography was Wakogel C-300 (Wako Pure Chemical Industries, Ltd.). Organic solutions were dried over anhydrous sodium sulfate. Solutions were concentrated below 50 °C under reduced pressure.

DL-1,2-Di-O-acetyl-(1,3,5/2)-3-benzoyloxymethyl-5-bromo-1,2-cyclohexanediol (4). A mixture of DL-1,2-di-*O*-acetyl-(1,3,-5/2)-5-bromo-3-bromomethyl-1,2-cyclohexanediol (**3**)[4] (2.0 g), sodium benzoate (1.56 g, 2 molar equiv.), and 90% aqueous DMF was stirred at 75 °C for 10 h, and then concentrated. The residue was extracted with ethyl acetate and the extracts were filtered through a short column of alumina. The filtrate was concentrated and the residue was crystallized from ethanol to give 1.15 g (52%) of **4**: mp 121—123 °C.** ^{1}H NMR (90 MHz) δ=2.03 (6H, s, OAc), 4.00 (1H, tt, $J_{4eq,5}=J_{5,6eq}=4$ Hz, $J_{4ax,5}=J_{5,6ax}=12$ Hz, H-5), 4.18 (1H, dd, $J_{3,7}=5$ Hz, $J_{gem}=11.5$ Hz, H-7), 4.35 (1H, dd, $J_{3,7'}=3$ Hz, H-7′), 4.85 (1H, ddd, $J_{1,2}=9.5$ Hz, $J_{1,6eq}=4.5$ Hz, $J_{1,6ax}=11$ Hz, H-1), 5.10 (1H, t, $J_{2,3}=9.5$ Hz, H-2), 7.34—7.74 (3H, m) and 8.01—8.17 (3H, m) (phenyl).

Found: C, 52.13; H, 5.22; Br, 19.64%. Calcd for $C_{18}H_{21}BrO_6$: C, 52.31; H, 5.21; Br, 19.33%.

Reaction of 4 with DBU. A mixture of **4** (0.20 g), DBU (0.36 ml), and toluene (6 ml) was refluxed for 14 h. The reaction mixture was diluted with toluene (20 ml) and the solution was washed with 1 M hydrochloric acid (1 M=1 mol dm^{-3}), saturated sodium hydrogencarbonate, and water, and dried. Evaporation of the solvent gave an oil (0.17 g) which was chromatographed on a silica gel with ethyl acetate–hexane (1 : 5) as an eluent. The first fraction gave crystals which were recrystallized from ethanol to give 96 mg (48%) of DL-1,2-di-*O*-acetyl-(1,3/2)-3-benzoyloxymethyl-5-cyclohexene-1,2-diol (**7**) as prisms: mp 75.5—76 °C,** identical with an authentic sample (mp 75—76.5 °C).

The second fraction gave crystals which were recrystallized from ethanol to give 50 mg (25%) of DL-1,2-di-*O*-acetyl-(1,3/2)-3-benzoyloxymethyl-4-cyclohexene-1,2-diol (**8**) as prisms: mp 76—78 °C.** ^{1}H NMR (90 MHz) δ=2.03 (6H, s, OAc), 4.20 (1H, dd, $J_{3,7}=5.5$ Hz, $J_{gem}=10.5$ Hz, H-7), 4.43 (1H, dd, $J_{3,7'}=5$ Hz, H-7′), 5.10 (1H, td, $J_{1,2}=J_{1,6ax}=11$ Hz, $J_{1,6eq}=6$ Hz, H-1), 5.28 (1H, t, $J_{2,3}=11$ Hz, H-2), 5.50—5.79 (2H, m, H-4 and H-5), 7.28—7.66 (3H, m) and 7.95—8.11 (2H, m) (phenyl).

Found: C, 65.15; H, 6.07%. Calcd for $C_{18}H_{20}O_6$: C, 65.05; H, 6.07%.

Reaction of 3 with Sodium Benzoate in DMF. A mixture of **3** (0.30 g), sodium benzoate (0.35 g), lithium bromide (0.17 g), and dry DMF (10 ml) was stirred at 120—130 °C for 1 h, and then concentrated. The residue was extracted with ethyl acetate and the extracts was passed through a short column of alumina. The filtrate was concentrated to give an oil (0.27 g), which was chromatographed on a silica-gel column (15 g) with ethyl acetate–hexane (1 : 4) as an eluent. The first fraction gave 32 mg (19%) of DL-*trans*-4,5-diacetoxy-3-methylene-1-cyclohexene (**10**) as an oil. ^{1}H NMR (90 MHz) δ=2.00 (3H, s) and 2.08 (3H, s) (OAc), 2.63 (1H, br dt, $J_{1,6eq}=J_{5,6eq}=5$ Hz, $J_{gem}=16.5$ Hz, H-6eq), 4.90—5.12 (3H, m, H-5 and exocyclic methylene), 5.35—5.73 (2H, m, H-4 and H-5), 6.13

** Determined on a Büchi 510 capillary melting point apparatus.

(1H, br d, $J_{1,2}=10$ Hz, H-2). This compound was identical with a sample later derived by an unequivocal route.

The second fraction gave 97 mg (36%) of **7**. The third fraction gave 70 mg (26%) of **8**. The fourth fraction gave crystals which were recrystallized from ethanol to give 28 mg (8%) of DL-1,2-di-*O*-acetyl-5-*O*-benzoyl-(1,3,5/2)-3-benzoyloxymethyl-1,2,5-cyclohexanetriol (**9**) as needles: mp 126—128 °C. ^{1}H NMR (90 MHz) $\delta=2.02$ (3H, s) and 2.04 (3H, s) (OAc), 4.23 (1H, dd, $J_{3,7}=4.5$ Hz, $J_{gem}=11$ Hz, H-7), 4.40 (1H, dd, $J_{3,7'}=4$ Hz, H-7'), 4.86—5.30 (3H, m, H-1, H-2, and H-5), 7.32—8.18 (10H, m, phenyl).

Found: C, 66.28; H, 5.89%. Calcd for $C_{25}H_{26}O_8$: C, 66.07; H, 5.77%.

DL-(1,3,5/2)-5-Bromo-3-bromomethyl-1,2-cyclohexanediol (5). A mixture of **3** (15.0 g) and ethanol (300 ml) containing 47% hydrobromic acid (30 ml) was heated at reflux for 6 h. The reaction mixture was neutralized with 2 M sodium hydroxide (120 ml) and concentrated until precipitates appeared. The solution was extracted with chloroform (100 ml), and the extracts were washed with water thoroughly and dried. Evaporation of the solvent gave crystals which were recrystallized from chloroform to give 11.0 g (95%) of **5** as needles: mp 108—110 °C.

Found: C, 29.37; H, 4.05; Br, 55.71%. Calcd for $C_7H_{12}Br_2O_2$: C, 29.20; H, 4.20; Br, 55.49%.

DL-1,2-O-Isopropylidene-(1,3,5/2)-5-bromo-3-bromomethyl-1,2-cyclohexanediol (6). To a solution of **5** (7.0 g) in dry DMF (80 ml) was added 2,2-dimethoxypropane (30 ml) and a catalytic amount of *p*-toluenesulfonic acid, and the mixture was heated at 70—80 °C for 2 h. The reaction mixture was concentrated with a small amount of sodium hydrogencarbonate to give an oil which was dissolved in chloroform and passed through a short column of alumina. The filtrate was concentrated and the residue was crystallized from ethanol to give 7.7 g (97%) of **6** prisms: mp 59—60.5 °C.

Found: C, 36.88; H, 4.90; Br, 48.89%. Calcd for $C_{10}H_{16}Br_2O_2$: C, 36.61; H, 4.92; Br, 48.72%.

Reaction of 6 with Sodium Benzoate in DMF. A mixture of **6** (0.50 g), sodium benzoate (0.55 g), lithium bromide (0.16 g), and dry DMF (10 ml) was stirred at 105—110 °C for 2 h. The reaction mixture was processed similarly as described in the reaction of **3** and the products were fractionated by chromatography on silica gel with 2-butanone–toluene (1 : 30) as an eluent.

The first fraction gave 0.26 g (60%) of DL-1,2-*O*-isopropylidene-(1,3/2)-3-benzoyloxymethyl-4-cyclohexene-1,2-diol (**11**) as an oil. ^{1}H NMR (90 MHz) $\delta=1.44$ (6H, s, isopropylidene), 3.47 (1H, t, $J_{1,2}=J_{2,3}=9$ Hz, H-2), 3.72 (1H, td, $J_{1,6eq}=5$ Hz, $J_{1,6ax}=9$ Hz, H-1), 4.28 (1H, dd, $J_{3,7}=7$ Hz, $J_{gem}=11$ Hz, H-7), 4.57 (1H, dd, $J_{3,7'}=5$ Hz, H-7'), 5.51—5.56 (2H, m, H-4 and H-5), 7.28—7.73 (3H, m) and 8.00—8.26 (2H, m) (phenyl). Compound **11** did not give a satisfactory analytical data, and the mass spectrum was measured:[13] Found: *m/e* 194.1295. Calcd for $C_{17}H_{20}O_4$: M$^+$ 194.1307.

Compound **11** (4.6 g) was treated with 50% aqueous acetic acid (50 ml) at room temperature for 30 min. and then mixture was concentrated. The residue was treated with acetic anhydride (20 ml) and pyridine (30 ml) at room temperature overnight. The reaction mixture was concentrated and the product was recrystallized from ethanol to give 5.1 g (96%) of **8**, identical with the compound obtained before.

The second fraction gave 72 mg (12%) of DL-5-*O*-benzoyl-1,2-*O*-isopropylidene-(1,3,5/2)-3-benzoyloxymethyl-1,2,5-cyclohexanetriol (**12**) as an oil. ^{1}H NMR (90 MHz) $\delta=1.44$ (6H, s, isopropylidene), 3.32 (1H, t, $J_{1,2}=J_{2,3}=9$ Hz, H-2), 3.52 (1H, td, $J_{1,6eq}=3$ Hz, $J_{1,6ax}=9$ Hz, H-1), 4.22 (1H, dd $J_{3,7}=6.5$ Hz, $J_{gem}=11$ Hz) and 4.49 (1H, dd, $J_{3,7'}=3.5$ Hz) (C$\underline{H}_2$OBz), 5.20 (1H, tt, $J_{4eq,5}=J_{5,6eq}=5$ Hz, $J_{4ax,5}=J_{5,6ax}=11$ Hz H-5).

The third fraction gave 31 mg (6%) of DL-5-*O*-benzoyl-1,2-*O*-isopropylidene-(1,3/2,5)-3-benzoyloxymethyl-1,2,5-cyclohexanetriol (**13**) as an oil. ^{1}H NMR (90 MHz) $\delta=1.47$, (6H, s, isopropylidene), 3.35 (1H, dd, $J_{1,2}=9$ Hz, $J_{2,3}=10.5$, Hz, H-2), 3.88 (1H, ddd, $J_{1,6eq}=4$ Hz, $J_{1,6ax}=11$ Hz, H-1) 4.33 (1H, dd, $J_{3,7}=6$ Hz, $J_{gem}=11$ Hz) and 4.56 (1H, dd, $J_{3,7'}=5$ Hz) (C$\underline{H}_2$OBz), 5.58 (1H, quintet, $J=3$ Hz, H-5).

Found for **12**: *m/e* 395.1523, and for **13**: *m/e* 410.1754, 395.1475. Calcd for $C_{24}H_{26}O_6$: M$^+$, 410.1728, M$^+-15$, 395.1493.

Oxidation of 8 with Osmium Tetraoxide. To a solution of **8** (0.10 g) in *t*-butyl alcohol (2.2 ml) containing 6% hydrogen peroxide was added a solution of osmium tetraoxide (0.65 ml, 0.013 mmol), and the mixture was stirred at room temperature for 20 h. The reaction mixture was diluted with water (2 ml) and sodium sulfite was added until the peroxide was consumed. The mixture was concentrated and the residue was acetylated in the usual way. The product was chromatographed on a silica-gel column with 2-butanone–toluene (1 : 12) as an eluent. The first fraction gave crystals which were recrystallized from ethanol to give 42 mg (38%) of DL-1,2,4,5-tetra-*O*-acetyl-(1,2,4/3,5)-3-benzoyloxymethyl-1,2,4,5-cyclohexanetetrol (**14**) as prisms: mp 145—146 °C. ^{1}H NMR (90 MHz) $\delta=1.98$ (3H, s), 1.99 (3H, s), 2.02 (3H, s), and 2.10 (3H, s) (OAc), 4.28 (2H, m, C$\underline{H}_2$OBz), 4.90 (1H, dd, $J_{1,2}=3$ Hz, $J_{2,3}=11$ Hz, H-2), 5.03—5.30 (2H, m, H-4 and H-5), 5.40 (1H, q, $J=3$ Hz, H-5), 7.11—7.99 (5H, m, phenyl).

Found: C, 58.69; H, 5.89%. Calcd for $C_{22}H_{26}O_{10}$: C, 58.66; H, 5.82%.

The second fraction gave crystals which were recrystallized from ethanol to give 5.4 mg (5.2%) of DL-*r*-4,*c*-6-diacetoxy-*t*-5-benzoyloxymethyl-2-cyclohexanone (**15**) as prisms: mp 109—110 °C. ^{1}H NMR (90 MHz) $\delta=2.10$ (3H, s) and 2.15 (3H, s) (OAc), 2.75 (1H, ddd, $J_{4,5}=10$ Hz, $J_{5,6}=13$ Hz, $J_{5,7}=3$ Hz, H-5), 4.39 (2H, d, $J=3$ Hz, C$\underline{H}_2$OBz), 5.45 (1H, d, H-6), 5.77 (1H, ddd, $J_{2,4}=2$ Hz, $J_{3,4}=2.5$ Hz, H-4), 6.10 (1H, dd, $J_{2,3}=10.5$ Hz, H-3), 6.77 (1H, dd, H-2).

Found: C, 62.17; H, 5.36%. Calcd for $C_{18}H_{18}O_7$: C, 62.42; H, 5.24%.

DL-4,5-Di-O-acetyl-1,2-anhydro-(1,2,3,5/4)-3-benzoyloxymethyl-1,2,4,5-cyclohexanetetrol (16). A suspension of **8** (1.0 g), *m*CPBA (1.06 g, *ca.* 1.5 molar equiv), and sodium hydrogencarbonate (0.72 g) in 1,2-dichloroethane (20 ml) was vigorously stirred at room temperature for 18 h. The reaction mixture was diluted with water (20 ml) and sodium sulfite was added to destroy the peracid. The organic layer was washed with water thoroughly and dried. Evaporation of the solvent gave crystals which were recrystallized from ethanol to give 0.84 g (80%) of **16** as needles: mp 96—99 °C. ^{1}H NMR (90 MHz) $\delta=2.01$ (6H, s, OAc), 3.18 (1H, t, $J_{1,2}=J_{2,3}=4.5$ Hz, H-2), 3.40 (1H, ddd, $J_{1,6eq}=3.5$ Hz, $J_{1,6ax}=6.5$ Hz, H-1), 4.37 (1H, dd, $J_{3,7}=7$ Hz, $J_{gem}=11$ Hz, H-7), 4.56 (1H, dd, $J_{3,7'}=5$ Hz, H-7'), 4.82 (1H, td, $J_{4,5}=J_{5,6ax}=9.5$ Hz, $J_{5,6eq}=7.5$ Hz, H-5), 5.11 (1H, t, $J_{3,4}=9.5$ Hz H-4), 7.30—7.58 (3H, m) and 7.96—8.12 (3H, m) (phenyl).

Found: C, 61.92; H, 5.81%. Calcd for $C_{18}H_{20}O_7$: C, 62.06; H, 5.79%.

A trace of a stereoisomeric epoxide (8 mg, 7%) was obtained as an oil. ^{1}H NMR (90 MHz) $\delta=2.02$ (3H, s) and 2.07 (3H, s) (OAc), 3.07 (1H, d, $J_{1,2}=3.5$ Hz, H-2), 3.30 (1H, m, H-1), 4.35 (1H, dd, $J_{3,7}=3$ Hz, $J_{gem}=10$ Hz, H-7), 4.72 (1H, dd, $J_{3,7'}=4$ Hz, H-7'), 4.78—5.16 (2H, m, H-4 and H-5), 7.32—7.60 (3H, m) and 7.98—8.14 (2H, m) (phenyl).

DL-1,2-Di-O-acetyl-(1,3,4/2,5)-3-benzoyloxymethyl-5-chloro-1,2-

4-cyclohexanetriol (17). A mixture of **16** (0.10 g), sodium acetate (47 mg), and ammonium chloride (46 mg) in 90% aqueous 2-methoxyethanol (5 ml) was heated at 80 °C for 5 h, and then concentrated. The residue was treated with acetic anhydride and pyridine in the usual way. The product was purified by a silica-gel column with 2-butanone–toluene (1 : 10) as an eluent. The main fraction gave crystals which were recrystallized from ethanol to give 54 mg (44%) of **17**: mp 96—97 °C. ^{1}H NMR (90 MHz) δ=2.07 (3H, s) and 2.10 (6H, s) (OAc), 2.80—3.20 (1H, m, H-3), 4.25—4.70 (3H, m, H-5 and C$\underline{H}_2$OBz), 5.30—5.65 (2H, m, H-1 and H-2).

Found: C, 56.55; H, 5.40; Cl, 8.55%. Calcd for $C_{20}H_{23}ClO_8$: C, 56.28; H, 5.43; Cl, 8.31%.

DL-*1,2-Di*-O-*acetyl-(1,3,4/2,5)-5-azido-3-benzoyloxymethyl-1,2,4-cyclohexanetriol (18).* A mixture of **16** (0.20 g), sodium azide (0.11 g), ammonium chloride (0.11 g), and 90% aqueous 2-methoxyethanol (10 ml) was stirred at 75 °C for 3 h, and then concentrated. The residue was taken up in chloroform (20 ml) and the solution was filtered through a short column of alumina. The filtrate was concentrated and the residue was chromatographed on a silica-gel column (10 g) with 2-butanone–toluene (1 : 10) as an eluent. The main fraction gave crystals which were recrystallized from ethanol to give 0.17 g (76%) of **18** as needles: mp 107—109 °C. ^{1}H NMR (90 MHz) δ=2.00 (3H, s) and 2.03 (3H, s) (OAc), 3.35 (1H, d, J=4.5 Hz, OH), 3.83 (1H, q, J=2.5 Hz, H-5), 3.95 (1H, t, J=2.5 Hz, H-4), 4.20 (1H, dd, $J_{3,7}$=4.5 Hz, J_{gem}=11.5 Hz, H-7), 4.65 (1H, dd, $J_{3,7'}$=9 Hz, H-7'), 5.09 (1H, td, $J_{1,2}$=$J_{1,6ax}$=9 Hz, $J_{1,6eq}$=7.5 Hz, H-1), 5.29 (1H, t, $J_{2,3}$=9 Hz, H-2), 7.33—7.74 (3H, m) and 7.98—8.17 (2H, m) (phenyl).

Found: C, 54.97; H, 5.41; N, 10.45%. Calcd for $C_{18}H_{21}N_3O_7$: C, 55.24; H, 5.41; N, 10.74%.

DL-*1,2,4-Tri*-O-*acetyl-(1,3,4/2,5)-5-azido-3-benzoyloxymethyl-1,2,4-cyclohexanetriol (19).* Compound **18** (49 mg) was treated with acetic anhydride and pyridine in the usual way. The product was purified by passage through a short column of alumina with chloroform, giving 55 mg (100%) of **19** as an oil. ^{1}H NMR (90 MHz) δ=2.02 (3H, s) and 2.04 (6H, s) (OAc), 3.94 (1H, q, J=3.5 Hz, H-5), 4.10—4.50 (2H, m, C$\underline{H}_2$OBz), 7.36—7.73 (3H, m) and 7.98—8.17 (phenyl).

Found: C, 55.55; H, 5.43; N, 9.46%. Calcd for $C_{20}H_{23}N_3O_8$: C, 55.42; J, 5.35; N, 9.70%.

DL-*1,2-Di*-O-*acetyl-4*-O-*methylsulfonyl-(1,3,4/2,5)-5-azido-3-benzoyloxymethyl-1,2,4-cyclohexanetriol (20).* To a solution of **18** (0.17 g) in pyridine (3 ml) was added methanesulfonyl chloride (0.067 ml) dropwise under ice cooling, and then the mixture was stirred at room temperature for 16 h. Ethyl acetate (6 ml) was added to the mixture and it was washed thoroughly with saturated sodium hydrogencarbonate and water and dried. Removal of the solvent gave a crude product which was chromatographed on a silica-gel column with 2-butanone–toluene. The main fraction gave 177 mg (87%) of **21** as an oil. ^{1}H NMR (90 MHz) δ=2.03 (3H, s) and 2.06 (3H, s) (OAc), 3.07 (3H, s, OMe), 4.94 (1H, dd, $J_{3,4}$=3 Hz, $J_{4,5}$=3.5 Hz, H-4).

Found: C, 48.77; 5.05; N, 8.69; S, 6.63%. Calcd for $C_{19}H_{23}N_3O_9S$: C, 48.61; H, 4.94; N, 8.95; S, 6.83%.

DL-*1,2,4-Tri*-O-*acetyl-(1,3,4/2,5)-5-acetamido-3-benzoyloxymethyl-1,2,4-cyclohexanetriol (21).* A solution of **19** (55 mg) in ethanol (6 ml) in the presence of Raney nickel T-4[14] was hydrogenated in Parr shaker type apparatus in the initial hydrogen pressure of 3.4 kg/cm^2 at room temperature for 32 h. The product was acetylated in the usual way and purified by chromatography on silica gel with ethanol–toluene (1 : 10). The main fraction gave 35 mg (60%) of **21** as an oil. ^{1}H NMR (90 MHz) δ=1.97 (3H, s), 2.03 (6H, s), and 2.04 (3H, s) (NAc and OAc), 6.05 (1H, br d, J=7.5 Hz, NH).

Found: C, 58.50; H, 6.25; N, 2.97%. Calcd for $C_{22}H_{27}NO_9$: C, 58.79; H, 6.06; N, 3.12%.

Ammonolysis of 16. A mixture of **16** (0.10 g) and ethanol (10 ml) saturated with ammonia at 5 °C was heated in a sealed tube at 90 °C for 15 h. The reaction mixture was concentrated and the residue was treated with acetic anhydride and pyridine in the usual way. Excess reagent was removed by evaporation and the products (0.17 g) were fractionated by chromatography on silica gel (8 g) with ethanol–toluene (1 : 12) as an eluent.

The first fraction gave 25 mg (19%) of DL-1,2,5-tri-*O*-acetyl-(1,3,5/2,4)-4-acetamido-3-benzoyloxymethyl-1,2,5-cyclohexanetriol (**24**) as crystals: mp 136—140 °C. ^{1}H NMR (90 MHz) δ=2.03 (3H, s), 2.06 (6H, s), and 2.09 (3H, s) (NAc and OAc), 4.14 (1H, dd, $J_{3,7}$=6.5 Hz, J_{gem}=11 Hz, H-7), 4.32 (1H, dd, $J_{3,7'}$=7 Hz, H-7'), 4.46 (1H, 0.3 ppm width m, H-4), 4.90—5.45 (3H, m, H-1, H-2, and H-5), 6.44 (1H, br d, J=7.5 Hz, NH), 7.39—7.57 (3H, m) and 7.70—7.90 (2H, m) (phenyl).

Found: C, 58.50; H, 6.25; N, 2.97%. Calcd for $C_{22}H_{27}NO_9$: C, 58.79; H, 6.06; N, 3.12%.

The second fraction gave 22 mg (17%) of **21** as an oil, identical with the compound obtained before.

The third fraction gave 41 mg (31%) of DL-1,2,4,7-tetra-*O*-acetyl-(1,3,4/2,5)-5-acetamido-3-hydroxymethyl-1,2,4-cyclohexanetriol (**22**) as an oil. ^{1}H NMR (90 MHz) δ=2.00 (3H, s), 2.04 (9H, s), and 2.10 (3H, s) (NAc and OAc), 4.04 (1H, dd, $J_{3,7}$=6 Hz, J_{gem}=11 Hz, H-7), 4.23 (1H, dd, $J_{3,7'}$=7 Hz, H-7'), 4.02—4.31 (1H, m, H-5), 4.88—5.34 (3H, m, H-1, H-2, and H-4), 6.10 (1H, m, NH).

Found: C, 52.76; H, 6.56; N, 3.45%. Calcd for $C_{17}H_{25}NO_9$: C, 52.71; H, 6.51; N, 3.62%.

DL-*1,2-Di*-O-*acetyl-(1/2,5)-5-azido-3-benzoyloxymethyl-3-cyclohexene-1,2-diol (28).* A mixture of **20** (157 mg), DBU (0.15 ml), and toluene (9 ml) was refluxed for 6 h. The reaction mixture was washed successively with 1 M hydrochloric acid, saturated sodium hydrogencarbonate, and water, and dried. The solvent was removed and the crude product was chromatographed on a silica-gel column with 2-butanone–toluene (1 : 10) to give 95 mg (76%) as an oil. ^{1}H NMR (90 MHz) δ=2.00 (3H, s) and 2.03 (3H, s) (OAc), 4.10 (1H, m, H-5), 4.76 (2H, br s, C$\underline{H}_2$OBz), 5.12 (1H, ddd, $J_{1,2}$=5 Hz, $J_{1,6eq}$=3.5 Hz, $J_{1,6ax}$=7 Hz, H-1), 5.45 (1H, br d, H-2), 6.12 (1H, br d, $J_{4,5}$=3 Hz, H-4).

Found: C, 57.71; H, 5.18; N, 11.03%. Calcd for $C_{18}H_{19}N_3O_6$: C, 57.90; H, 5.13; N, 11.25%.

DL-*1,2-Di*-O-*acetyl-(1,2/5)-5-acetamido-3-benzoyloxymethyl-3-cyclohexene-1,2-diol (29).* To a solution of **28** (62 mg) in pyridine (1.5 ml) and water (1.5 ml) was bubbled with hydrogen sulfide for 2 h. Nitrogen was introduced to remove an excess of hydrogen sulfide for 30 min, and the mixture was concentrated. The residue was acetylated in the usual way and purified by chromatography on silica gel with ethanol–toluene (1 : 10). The main fraction gave crystals which were recrystallized from ethanol to give 43 mg (65%) of **24** as crystals: mp 135—136 °C. ^{1}H NMR (90 MHz) δ=1.96 (6H, s) and 2.00 (3H, s) (NAc and OAc), 4.72 (2H, br s, C$\underline{H}_2$OBz), 5.09 (1H, ddd, $J_{4,5}$=5 Hz, $J_{5,6eq}$=3.5 Hz, $J_{5,6ax}$=8 Hz, H-5), 5.41 (1H, br d, H-4), 6.00 (1H, d, NH), 6.03 (1H, br d, $J_{1,2}$=3.5 Hz, H-2).

Found: C, 61.87; H, 6.07; N, 3.52%. Calcd for $C_{20}H_{23}NO_7$: C, 61.69; H, 5.95; N, 3.60%.

DL-*1,2-Di*-O-*acetyl-(1,3,4/2,5)-3-benzoyloxymethyl-4,5-dibromo-1,2-cyclohexanediol (23).* To a solution of **8** (0.10 g) in carbon tetrachloride (2 ml) was added bromine (0.1 ml) in carbon tetrachloride (2 ml) and the mixture was stirred at room temperature for 2 h. The reaction mixture was treated with Amberlite IRA-400 (OH^-) (3 ml) and then concentrated

to give a crude oil which was crystallized from ethanol to give 70 mg (47%) of **23** as crystals: mp 109—110 °C. ^{1}H NMR (90 MHz) δ=2.00 (3H, s) and 2.03 (3H, s) (OAc), 4.23 (1H, dd, $J_{3,7}$=8 Hz, J_{gem}=11 Hz, H-7), 4.47 (1H, dd, $J_{3,7'}$=5.5 Hz, H-7'), 4.56—4.76 (2H, m, H-4 and H-5), 5.18—5.60 (2H, m, H-1 and H-2), 7.12—8.03 (5H, m, phenyl).

Found: C, 43.79; H, 4.09; Br, 32.15%. Calcd for $C_{18}H_{20}Br_2O_6$: C, 43.93; H, 4.10; Br, 32.47%.

DL-*1,2-Di-O-acetyl-(1,5/2)-5-azido-3-benzoyloxymethyl-3-cyclohexene-1,2-diol (30).* A mixture of **23** (0.28 g), sodium azide (91 mg), and DMF (10 ml) was stirred at 120 °C for 30 min. The reaction mixture was concentrated to give a solid residue which was suspended with chloroform and passed through a short column of silica gel. The filtrate was concentrated to give 0.19 g (91%) of **30** as an oil. ^{1}H NMR (90 MHz) δ=2.00 (3H, s) and 2.04 (3H, s) (OAc), 3.94—4.23 (1H, m, H-5), 4.75 (2H, s, C<u>H</u>$_2$OBz), 5.00 (1H, ddd, $J_{1,2}$=7 Hz, $J_{1,6eq}$=3 Hz, $J_{1,6ax}$=9.5 Hz, H-1), 5.62 (1H, br d, H-2), 5.99 (1H, br s, H-4), 7.13—8.04 (5H, m, phenyl).

Found: C, 58.03; H, 5.28; N, 11.31%. Calcd for $C_{19}H_{19}N_3O_6$: C, 57.91; H, 5.13; N, 11.25%.

DL-*1,2-Di-O-acetyl-(1,5/2)-5-acetamido-3-benzoyloxymethyl-3-cyclohexene-1,2-diol (21).* Compound **30** (0.13 g) was reduced similarly as described in the preparation of **29**. The crude amine was acetylated in the usual way and the product was purified by chromatography on silica gel with chloroform and then with ethanol–toluene (1 : 5) as an eluent . The main fraction gave crystals which were recrystallized from ethanol to give 80 mg (58%) of **31** as crystals: mp 162—163 °C. ^{1}H NMR (90 MHz) δ=1.93 (3H, s), 1.99 (3H, s), and 2.00 (3H, s) (NAc and OAc), 4.69 (2H, s, C<u>H</u>$_2$OBz), 5.50—5.76 (2H, m, H-1 and H-2), 5.90 (1H, br s, H-4), 7.11—8.01 (5H, m, phenyl).

Found: C, 61.59; H, 6.01; N, 3.80%. Calcd for $C_{20}H_{23}NO_7$: C, 61.69; H, 5.96; N, 3.60%.

DL-*1,2-Di-O-acetyl-5-O-benzoyl-(1,5/2)-3-benzoyloxymethyl-3-cyclohexene-1,2,5-triol (34).* A mixture of **23** (0.10 g), sodium benzoate (44 mg), and DMF (5 ml) was stirred at 120 °C for 30 min, and then concentrated. The residue was suspended in ethyl acetate and the mixture was passed through a short column of silica gel. The filtrate was concentrated and the residue was recrystallized from ethanol to give 57 mg (62%) of **34** as crystals: mp 107—108.5 °C. ^{1}H NMR (90 MHz) δ=2.04 (6H, s, OAc), 4.82 (2H, s, C<u>H</u>$_2$OBz), 5.15 (1H, ddd, $J_{1,2}$=6.5 Hz, $J_{1,6eq}$=3.5 Hz, $J_{1,6ax}$=9 Hz, H-1), 5.55—5.90 (2H, m, H-2 and H-5), 6.18 (1H, br s, H-4), 7.22—8.10 (10H, m, phenyl).

Found: C, 66.41; H, 5.38%. Calcd for $C_{25}H_{24}O_8$: C, 66.36; H, 5.35%.

Compound **34** was *O*-deacylated by treatment with methanolic sodium methoxide in methanol and then acetylated in the usual way to give the tetraacetate **35** as an oil. ^{1}H NMR (60 MHz) δ=1.96 (3H, s) and 1.99 (9H, s) (OAc), 4.29 (1H, d) and 4.61 (1H, d) (J_{gem}=12 Hz, C<u>H</u>$_2$OAc), 4.97 (1H, ddd, $J_{1,2}$=6 Hz, $J_{1,6eq}$=4 Hz, $J_{1,6ax}$=10 Hz, H-1), 5.53 (1H, br d, H-2), 5.20—5.50 (1H, m, H-5), 5.85 (1H, br s, H-4).

Found: C, 54.45; H, 5.95%. Calcd for $C_{15}H_{20}O_8$: C, 54.87; H, 6.14%.

*Alternative Preparation of **10** from **3**.* A mixture of **3** (3.0 g), DBU (6 ml), and toluene (6 ml) was refluxed for 90 min, and then allowed to stand in a refrigerator overnight. Precipitates were removed by filtration and the filtrate was washed successively with 1 M hydrochloric acid, saturated sodium hydrogencarbonate, and water, and dried. Evaporation of the solvent gave 1.28 g (76%) of **10** as an oil, identical with the sample obtained before by the different reaction conditions.

Compound **10** (0.80 g) was *O*-deacylated by treatment with methanolic sodium methoxide to give the dihydroxy compound: ^{1}H NMR (90 MHz, CD_3OD) δ=2.13 (1H, br dd, $J_{5,6ax}$=18 Hz, H-6ax), 2.51 (1H, dt, $J_{1,6eq}$=$J_{5,6eq}$=5.5 Hz, H-6eq), 3.60 (1H, ddd, $J_{4,5}$=9 Hz, H-5), 4.00 (1H, dt, $J_{4,7}$=$J_{4,7'}$=2.5 Hz, H-4), 4.98 (1H, br s) and 5.25 (1H, br s) (exocyclic methylene), 5.63 (1H, m, H-1), 6.12 (1H, br d, $J_{1,2}$=*ca.* 10 Hz, H-2). It was then treated with *p*-nitrobenzoyl chloride in pyridine in the usual way to give, after recrystallization from ethanol, 0.75 g of the bis(*p*-nitrobenzoate): mp 187—188 °C.

Found: C, 59.16; H, 3.95; N, 6.36%. Calcd for $C_{21}H_{16}N_2O_8$: C, 59.44; H, 3.80; N, 6.60%.

*Reaction of **10** with Bromine in Carbon Tetrachloride.* To a cooled solution of **10** (1.99 g) in carbon tetrachloride (25 ml) was added a solution (2 ml) of bromine–carbon tetrachloride (1 : 3, v/v), and the mixture was stirred at −8 °C for 30 min. The mixture was concentrated and the products were roughly fractionated by a silica-gel column with 2-butanone–toluene (1 : 6) as an eluent. The main fraction gave 1.8 g (54%) of a mixture of DL-1,2-di-*O*-acetyl-(1/2,5)- (**26**) and (1,5/2)-5-bromo-3-bromomethyl-3-cyclohexene-1,2-diol (**27**): ^{1}H NMR (90 MHz) δ=2.03 (3H, s) and 2.10 (3H, s) (OAc), 2.36 (2H, br t, $J_{1,6}$=9 Hz, $J_{5,6}$=8 Hz, H-6 and H-6'), 3.91 (2H, br s, C<u>H</u>$_2$Br), 4.75 (1H, br q, J=8 Hz, H-5), 5.23 (1H, q, J=9 Hz, H-1), 5.71 (1H, d, $J_{1,2}$=9 Hz, H-2), 6.19 (1H, d, $J_{4,5}$=8 Hz, H-4). The spectrum showed that **26** was the major product. Attempts to prepare a pure sample by chromatography failed, because of the high lability. Therefore, a crude mixture was directly used in the following experiments.

A trace of a tetrabromide was obtained: mp 158—160 °C; ^{1}H NMR (60 MHz) δ=2.05 (3H, s) and 2.15 (3H, s) (OAc), 3.65 (1H, d) and 4.15 (1H, d) (J=12 Hz, C<u>H</u>$_2$Br).

Found: C, 25.08; H, 2.70; Br, 60.49%. Calcd for $C_{11}H_{14}Br_4O_4$: C, 24.94; H, 2.66; Br, 60.32%.

*Reaction of **26** and **27** with Sodium Benzoate.* A mixture of **26** and **27** (1.29 g), sodium benzoate (2.0 g), and 90% aqueous DMF (9 ml) was stirred at room temperature overnight. Water was added and the mixture was extracted with ethyl acetate (30 ml). The extracts were dried and concentrated to give crystals which were recrystallized from ethanol to give 0.30 g (30%) of **34**: mp 100—101 °C, identical with a sample derived from **23**.

*Reaction of **26** and **27** with Potassium Phthalimide.* A mixture of **26** and **27** (0.53 g), potassium phthalimide (1.06 g), and DMF (15 ml) was stirred at room temperature overnight. The reaction mixture was diluted with ethyl acetate and washed with water thoroughly. The organic layer was dried and concentrated to give crystals. Recrystallization from ethyl acetate gave 0.42 g (58%) of DL-1,2-di-*O*-acetyl-(1,5/2)-5-phthalimido-3-phthalimidomethyl-3-cyclohexene-1,2-diol (**36**) as crystals: mp 206—207 °C. ^{1}H NMR (60 MHz) δ=1.97 (3H, s) and 2.10 (3H, s) (OAc), 4.06 (1H, d) and 4.50 (1H, d) (J=15 Hz, C<u>H</u>$_2$N), 7.76 (8H, m, phenyl).

Found: C, 64.31; H, 4.59; N, 5.65%. Calcd for $C_{27}H_{22}N_2O_8$: C, 64.55; H, 4.41; N, 5.57%.

DL-*1,2-Di-O-acetyl-(1,5/2)-5-acetamido-3-acetamidomethyl-3-cyclohexene-1,2-diol (37).* A mixture of **36** (0.50 g), butylamine (10 ml), and methanol (20 ml) was refluxed for 60 h, and then concentrated. The residue was acetylated in the usual way to give, after crystallization from ethanol, 0.32 g (98%) of **37** as crystals: mp 193—194 °C. ^{1}H NMR (60 MHz) δ=1.98 (6H, s), 2.03 (3H, s), and 2.08 (3H, s) (NAc and OAc), 3.76 (2H, d, $J_{7,NH}$=9 Hz, C<u>H</u>$_2$NHAc), 5.05 (1H, ddd, $J_{1,2}$=7 Hz, $J_{1,6eq}$=4 Hz, $J_{1,6ax}$=9.5 Hz, H-1), 5.49 (1H, d, H-2), 5.71 (1H, br s, H-4), 6.10—6.50 (2H, m, N<u>H</u>Ac).

Found: C, 54.95; H, 6.64; N, 8.37%. Calcd for $C_{15}H_{22}N_2O_6$: C, 55.20; H, 6.80; N, 8.58%.

DL-*2,3-Di-O-acetyl-1,7-anhydro-(1,2/3)-1-C-hydroxymethyl-5-cyclohexene-1,2,3-triol (25)*. A mixture of **10** (2.0 g), *m*CPBA (3.2 g), dichloromethane (60 ml), and phosphate buffer solution[15] (pH 8) (150 ml) was stirred vigorously at room temperature for 2 h. The organic layer was washed successively with aqueous sodium sulfite, sodium hydrogencarbonate, and water, and dried. The solution was concentrated to give crystals which were recrystallized from ethanol–ether to give 1.0 g (47%) of **25** as crystals: mp 91—92 °C. ^{1}H NMR (90 MHz) δ=2.01 (3H, s) and 2.09 (3H, s) (OAc), 2.37 (1H, m, H-4), 2.60 (1H, m, H-4'), 2.82 and 2.91 (AB-quartet, J=4.5 Hz, C$\underline{H}_2$O), 5.10—5.40 (3H, m, H-2, H-3, and H-6), 5.92 (1H, dt, $J_{4,5}=J_{4',5}$=3.5 Hz, $J_{5,6}$=10.5 Hz, H-5).

Found: C, 58.13; H, 6.27%. Calcd for $C_{11}H_{14}O_5$: C, 58.40; H, 6.24%.

DL-*1,2,3-Tri-O-acetyl-(1,2/3)-1-C-azidomethyl-5-cyclohexene-1,2,3-triol (38)*. A mixture of **25** (0.25 g), sodium azide (0.23 g), ammonium chloride (0.23 g), and DMF (10 ml) was stirred at 60 °C for 2 h, and then concentrated, The residual product was acetylated in the usual way in the presence of 4-diethylaminopyridine (0.20 g). An oily product was purified by chromatography on silica gel to give 0.40 g (92%) of **38** as an oil. ^{1}H NMR δ=2.00 (3H, s), 2.03 (3H, s), and 2.10 (3H, s) (OAc), 3.60 (1H, d) and 3.83 (1H, d) (J=12 Hz, C$\underline{H}_2N_3$), 5.25 (2H, br s, H-2 and H-3), 5.81 (1H, ddd, $J_{4,5}$= 3.5 Hz, $J_{4',5}$=4.5 Hz, $J_{5,6}$=10.5 Hz, H-5), 6.05 (1H, dt, $J_{4,6}$=2 Hz, H-6).

Found: C, 50.00; H, 5.47; N, 13.24%. Calcd for $C_{13}H_{17}N_3O_6$: C, 50.15; H, 5.51; N, 13.50%.

DL-*2,3-Di-O-acetyl-(1,2/3)-1-C-acetamidomethyl-5-cyclohexene-1,2,3-triol (39)*. Compound **38** (0.55 g) was reduced similarly as described in the preparation of **31**, and the product was acetylated in the usual way. The oily product was purified by a silica-gel column with 2-butanone–toluene (2 : 1) as an eluent to give 0.51 g (100%) of **39** as an oil. ^{1}H NMR (90 MHz) δ=1.93 (3H, s), 1.97 (3H, s), and 2.08 (3H, s) (NAc and OAc), 2.69 (1H, ddd, $J_{3,4}$=6 Hz, $J_{4,5}$=3 Hz, J_{gem}=18 Hz, H-4), 3.01 (1H, d) and 3.47 (1H, d) (J=13 Hz, C$\underline{H}_2$NHAc), 4.91 (1H, d, $J_{2,3}$=10.5 Hz, H-2), 5.25 (1H, td, $J_{3,4'}$=9 Hz, H-3), 5.63 (2H, br s, H-5 and H-6).

Found: C, 54.72; H, 6.32; N, 4.25%. Calcd for $C_{13}H_{19}NO_6$: C, 54.73; H, 6.71; N, 4.91%.

DL-*1,2-Di-O-acetyl-(1,5/2)-5-azido-3-acetoxymethyl-3-cyclohexene-1,2-diol (32)*. A mixture of **25** (0.46 g), sodium azide (0.9 g), acetone (20 ml), and water (12 ml) was added concd sulfuric acid (1 g), and the mixture was stirred at room temperature for 5 d. The reaction mixture was concentrated and the residue was treated with acetic anhydride and pyridine. The product was extracted with chloroform, and the extracts were washed with water, dried, and concentrated. The product was purified by chromatography on silica gel to give 0.28 g (48%) of **32** as an oil as a main product: ^{1}H NMR (90 MHz) δ=2.03 (9H, s, OAc), 4.07 (1H, m, H-5), 4.35 (1H, d) and 4.61 (1H, d) (J=13.5 Hz, C$\underline{H}_2$OAc), 4.98 (1H, ddd, $J_{1,2}$=7 Hz, $J_{1,6eq}$=4 Hz, $J_{1,6ax}$=10.5 Hz, H-1), and 5.53 (1H, d, H-2).

Found: C, 50.31; H, 5.51; N, 13.25%. Calcd for $C_{13}H_{17}N_3O_6$: C, 50.15; H, 5.51; N, 13.50%.

DL-*1,2-Di-O-acetyl-(1,5/2)-5-acetamido-3-acetoxymethyl-3-cyclohexene-1,2-diol (33)*. Compound **32** (0.42 g) was reduced with hydrogen sulfide similarly as described in the preparation of **29** and the product was acetylated in the usual way. The crude product was recrystallized from ethanol–ether to give 0.40 g (92%) of **33**: mp 148—149 °C; ^{1}H NMR (90 MHz) δ= 1.93 (3H, s) and 2.02 (9H, s) (NAc and OAc), 4.28 (1H, d) and 4.59 (1H, d) (J=13 Hz, C$\underline{H}_2$OAc), 4.70 (1H, br s, H-5), 5.00 (1H, ddd, $J_{1,2}$=7 Hz, $J_{1,6eq}$=4 Hz, $J_{1,6ax}$=10 Hz, H-1), 5.45 (1H, d, H-2), and 5.80 (2H, m, H-4 and NH).

Found: C, 54.80; H, 6.30; N, 4.42%. Calcd for $C_{15}H_{21}NO_7$: C, 55.04; H, 6.47; N, 4.28%.

The authors express their sincere thanks to Mr. Saburo Nakada for the elementary analyses. The present work was partially supported by a Grant-in-Aid for Scientific Research No. 56550617 from the Ministry of Education, Science and Culture.

References

1) Presented in part at the 44th National Meeting of the Chemical Society of Japan, Okayama, October 1981, Abstr., No. 2E23. Previous paper of this series: S. Ogawa, M. Suetsugu, T. Toyokuni, and T. Suami, *Nippon Kagaku Kaishi*, **1982**, 1721.

2) The nomenclature and numbering of cyclitols used in his paper follows IUPAC and IUB tentative rules for cyclitol nomenclature [*J. Biol. Chem.*, **243**, 5809 (1968)]. For convenience, the carbon atoms of the branched-chain substituents are numbered 7. All compounds described in this paper are racemic and the formulas depict only one of the respective enantiomers.

3) S. Ogawa, N. Chida, and T. Suami, *J. Org. Chem.*, **48**, 1203 (1983).

4) S. Ogawa, I. Kasahara, and T. Suami, *Bull. Chem. Soc. Jpn.*, **52**, 118 (1979).

5) S. Ogawa, T. Toyokuni, T. Kondoh, Y. Hattori, S. Iwasaki, M. Suetsugu, and T. Suami, *Bull. Chem. Soc. Jpn.*, **54**, 2739 (1981).

6) Alternatively, **6** was first treated with sodium benzoate in dimethyl sulfoxide (70 °C, 2 h) to give the corresponding benzoyloxymethyl derivative (mp 82—84 °C, 43%; Found: C, 55.42; H, 5.74; Br, 21.38%. Calcd for $C_{17}H_{21}BrO_4$: C, 55.30; H, 5.73; Br, 21.64%), which was then converted into **12** (98%) by treatment with DBU in toluene (reflux, 24 h).

7) β-Elimination of an acetoxyl group was also observed in the osmium tetraoxide-oxidation of DL-1,2-di-*O*-acetyl-(1,3/2)-3-bromomethyl-5-cyclohexene-1,2-diol.[5]

8) T. Adachi, Y. Yamada, and I. Inoue, *Synthesis*, **1977**, 45.

9) R. J. Abraham, H. Gottschalck, H. Paulsen, and W. A. Thomas, *J. Chem. Soc.*, **1965**, 6268.

10) The ^{1}H NMR signal for the epoxy methylene protons of the corresponding 4-acetoxy compound [(1,2,4/3)-configuration] appeared as a two-proton singlet at δ=2.88, whereas, that of its stereoisomer [(1,3/2,4)-configuration] appeared as an AB-quartet (J=6 Hz) at δ=2.73 and 3.18: T. Toyokuni, S. Ogawa, and T. Suami, *Bull. Chem. Soc. Jpn.*, **56**, 1161 (1983). These data may be in line with that of **25** used for the structural assignment. The stereoisomer of **25** was shown by TLC to be formed by the oxidation. But, during purification by use of a silica-gel column, it seemed to be converted into a branched-chain cyclitol by opening the spiro epoxide ring, catalyzed by silica gel, through an anchimeric assistance of the 2-acetoxyl group at C-1.

11) T. Toyokuni, S. Ogawa, and T. Suami, *Bull. Chem. Soc. Jpn.*, **56**, 505 (1983).

12) S. Ogawa, H. Ito, and T. Suami, *Bull. Chem. Soc. Jpn.*, **56**, 2326 (1983).

13) Mass spectra were recorded on a Hitachi M-80 mass spectrometer at 70 eV.

14) S. Nishimura, *Bull. Chem. Soc. Jpn.*, **32**, 61 (1959).

15) M. Imuta and H. Ziffer, *J. Org. Chem.*, **44**, 1351 (1979).

Synthetic Studies on the Validamycins. VIII. Synthesis of DL-2-Deoxyvalidoxylamine B and Related Compound[1,2]

Seiichiro OGAWA, Hiroyuki ITO, and Tetsuo SUAMI*
Department of Applied Chemistry, Faculty of Science and Technology, Keio University, Hiyoshi, Kohoku-ku, Yokohama 223

(Received October 16, 1982)

DL-2-Deoxyvalidoxylamine B and its diastereomer have been synthesized by the reaction of the protected DL-valienamine and the anhydro derivative of (hydroxymethyl)cyclohexanetetrol followed by removal of the protecting groups.

In connection with the previous paper,[3] the synthesis of the 2-deoxy analog (**2**) of validoxylamine B (**1**) and its related compounds is described. In the present study, a nucleophilic substitution reaction of the protected DL-valienamine and the anhydro derivative of (hydroxymethyl)cyclohexanetetrol was undertaken to build up a pseudo-disaccharide structure.

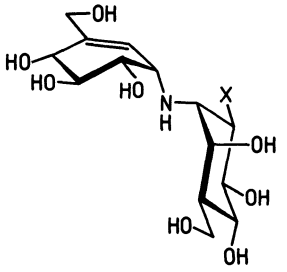

Validoxylamine B (1): X = OH
2-Deoxyvalidoxylamine B (2): X = H

Scheme 1.

DL-1,2-Anhydro-4,7-*O*-benzylidene-(1,2,3,5/4)-3-hydroxymethyl-1,2,4,5-cyclohexanetetrol (**8**) was prepared from DL-1,2-*O*-isopropylidene-(1,3/2)-3-benzoyloxymethyl-4-cyclohexene-1,2-diol (**5**)[1b] by the following sequence. *O*-Deacylation of **5** with methanolic sodium methoxide, followed by treatment with Amberlite IR-120B (H^+), gave the triol **6** in 76% yield. Treatment of **6** with α,α-dimethoxytoluene in *N*,*N*-dimethylformamide (DMF) in the presence of *p*-toluenesulfonic acid gave the benzylidene derivative **7** in 62% yield. Compound **7** was oxidized with *m*-chloroperoxybenzoic acid (*m*CPBA) to give almost specifically the β-epoxide **8** in 77% yield, together with a small proportion of the α-epoxide (9%). The mixture of the epoxides was directly treated with acetic anhydride in pyridine and the products were separated to give the acetate **9** of **8** in 88% yield. The structure of **8** was determined by the ^{1}H NMR spectrum, in which the C-4 proton resonated slightly lower field (δ 3.62) compared with that of the α-epoxide (δ 3.30), indicating that the C-4 proton which was situated close to the oxygen atom of the epoxide ring was deshielded by this moiety. The epoxidation seemed to be controlled by steric hindrance.

Reaction of an equimolar amount of the di-*O*-isopropylidene derivative (**3**)[4] of DL-validamine and **8** was carried out in 2-propanol in a sealed tube at

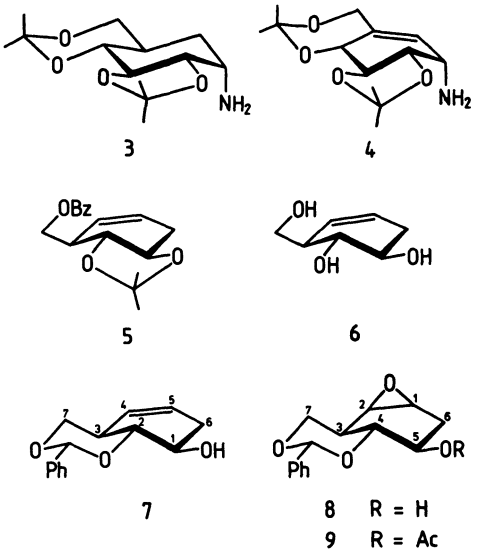

Scheme 2.

120 °C. After 44 h, the starting materials were almost consumed and the formation of two new components was observed by TLC. The products were fractionated by chromatography on silica gel with 2-butanone–toluene (1 : 30) as an eluent to give the diastereoisomeric secondary amines **10a** (42%) and **10b** (44%) as an oil. Their structures were supported by analytical data and ^{1}H NMR spectroscopy. The NMR spectral pattern was nearly identical with each other except for a small difference of the chemical shifts of the signals due to the C-1′ protons. Therefore, it was impossible to assign the exact structures to each diastereomers in this stage.

Next, the similar reaction of **3** and **9** was carried out to give an inseparable mixture of secondary amines **11a** and **11b** in 83% yield. Treatment of the mixture with acetic anhydride in pyridine gave the di-*O*-acetyl derivatives, which could clearly be separated by a silica gel column to give **12a** (31%) and **12b** (64%). The latter compound was shown to be identical with the bis(acetate) derived from **10b**. The structures of **12a** and **12b** were postulated on the basis of ^{1}H NMR spectroscopy, taking account of the data which had been observed to differentiate the diastereomers of validoxylamine A or B.[5,6] The ^{1}H NMR spectra of **12a** and **12b** revealed the signals for H-1′ as a quartet (J=3 Hz) at δ 2.94 and 3.07, and those for H-2′ as a doublet of doublets (J=2.5 and 3 Hz) at δ 4.72 and 4.93, respectively. The slight deshielding of the signals

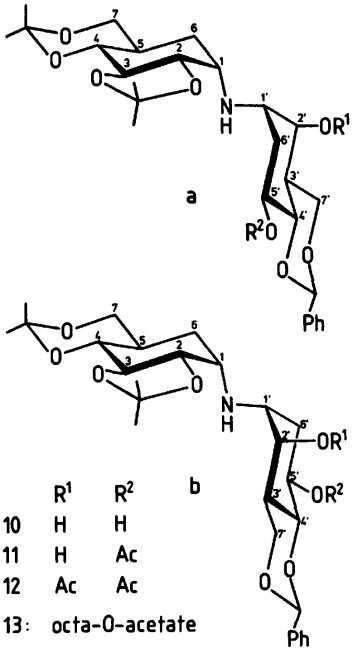

Scheme 3.

observed for **12b** might be explained by a proximity of C-2′ proton to the oxygen atoms of the 2,3-*O*-isopropylidene group. Therefore, the structures of **12a** and **12b** were tentatively assigned as shown in Scheme 3. Deprotection of **12a** and **12b** by treatment with 1 M hydrochloric acid (1 M=1 mol dm^{-3}) at reflux temperature, followed by acetylation, gave the corresponding octa-*O*-acetyl derivatives **13a** (82%) and **13b** (82%), respectively.

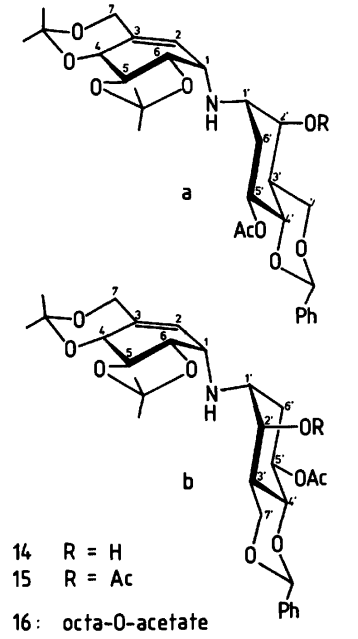

Scheme 4.

Finally, the reaction of the di-*O*-isopropylidene derivative **4**[5] of DL-valienamine and **9** was carried out by the similar way. The reaction was completed within 26 h to give 82% yield of a mixture of secondary amines **14a** and **14b** as a homogeneous oil. They were converted into the di-*O*-acetyl derivatives and separated by chromatography on silica gel to give **15a** (46%) and **15b** (54%). The ^{1}H NMR spectra of **15a** and **15b** showed the signals for H-2′ at δ 4.85 and 4.93, and those for H-3′ at δ 2.66 and 2.86, respectively. Studies of their Dreiding models indicated that the 5,6-*O*-isopropylidene group was situated close to C-2′ and C-3′ protons enough to affect, if any difference, the chemical shifts of their signals in the one diastereomer. Therefore, on the basis of the down-field shifts of H-2′ and H-3′ signals of **15b**, the relative configurations of **15a** and **15b** were tentatively assigned as shown in Scheme 4.[7] The protecting groups of **15a** and **15b** were removed to give the free bases, which were characterized by converting into the corresponding octa-*O*-acetyl derivatives **16a** (73%) and **16b** (87%), respectively.

Experimental

General Methods. The same method was used as described in the preceding paper.[1b]

DL-*(1,3/2)-3-Hydroxymethyl-4-cyclohexene-1,2-diol (6).* A mixture of DL-1,2-*O*-isopropylidene-(1,3/2)-3-benzoyloxymethyl-4-cyclohexene-1,2-diol (**5**)[1b] (2.8 g) and 1 M methanolic sodium methoxide (4 ml) in methanol (20 ml) was stirred at room temperature for 30 min. The reaction mixture was treated with Amberlite IR-120B (H$^+$) (4 ml) at room temperature for 2 h and then concentrated. The residue was crystallized from ethanol to give 1.1 g (76%) of **6**: mp 100—101 °C.

Found: C, 58.10; H, 8.17%. Calcd for $C_7H_{12}O_3$: C, 58.32; H, 8.39%.

DL-*2,7-O-Benzylidene-(1,3/2)-3-hydroxymethyl-4-cyclohexene-1,2-diol (7).* To a solution of **6** (1.08 g) in dry DMF (10 ml) was added α,α-dimethoxytoluene (1.36 ml) and a trace of *p*-toluenesulfonic acid, and the mixture was stirred at 60 °C under reduced pressure for 2 h. The reaction mixture was treated with sodium hydrogencarbonate and diluted with ethyl acetate (20 ml). The solution was washed thoroughly with water, dried, and concentrated. The residue was crystallized from ethanol to give 1.07 g (62%) of **7** as needles: mp 120—122 °C. ^{1}H NMR ($CDCl_3$) δ=3.45 (1H, dd, $J_{3.7ax}$=5 Hz, J_{gem}=10.5 Hz, H-7ax), 3.65 (1H, $J_{1.2}=J_{2.3}$=8 Hz, H-2), 4.00 (1H, td, $J_{1.6ax}$=8 Hz, $J_{1.6eq}$=6.5 Hz, H-1), 4.22 (1H, dd, $J_{3.7eq}$=4.5 Hz, H-7eq), 5.22 (1H, br d, $J_{4,5}$=*ca.* 9 Hz, H-4), 5.52—5.86 (1H, m, H-5), 5.60 (1H, s, benzylic), 7.32—7.75 (5H, m, phenyl).

Found: C, 72.39; H, 6.87%. Calcd for $C_{14}H_{16}O_3$: C, 72.39; H, 6.94%.

DL-*1,2-Anhydro-4,7-O-benzylidene-(1,2,3,5/4)-3-hydroxymethyl-1,2,4,5-cyclohexanetetrol (8).* To a solution of **7** (0.10 g) in 1,2-dichloroethane (2 ml) was added *m*CPBA (0.21 g, *ca.* 2 molar equiv.) and sodium hydrogencarbonate (0.21 g), and the mixture was vigorously stirred at room temperature for 1 h. Excess of the peroxy acid was destroyed by washing with a solution of sodium thiosulfate (0.16 g) in water (5 ml), and the organic layer was washed with water and dried. Evaporation of the solvent gave an oil (0.11 g) that was chromatographed on a silica-gel column (5 g) with 2-butanone–toluene (1 : 5) as an eluent. The major fraction (R_f 0.22) gave a crystalline product which was recrystallized from ethanol to give 82 mg (77%) of **8**: mp 111.5—112.5 °C. ^{1}H NMR ($CDCl_3$) δ=2.97 (1H, br d, J=4.5 Hz) and 3.05 (1H, br t, J=4.5 Hz) (H-1, H-2), 3.50—3.82 (2H, m, H-4, H-5), 3.95 (1H, t, $J_{3.7ax}$=10.5

Hz, J_{gem}=10.5 Hz, H-7ax), 4.30 (1H, dd, $J_{3,7eq}$=4 Hz, H-7eq), 5.52 (1H, s, benzylic), 7.30—7.65 (5H, m, phenyl).

Found: C, 67.48; H, 6.44%. Calcd for $C_{14}H_{16}O_4$: C, 67.73; H, 6.50%.

The minor fraction (R_f 0.18) gave an oily product (10 mg, 9%), which was considered by ^{1}H NMR spectrum to be a stereoisomer of **8**, but further characterization was not attempted. ^{1}H NMR ($CDCl_3$) δ=2.56—2.82 (1H, m, H-2), 2.96—3.23 (1H, m, H-1), 3.30 (1H, t, $J_{3,4}=J_{4,5}$=10 Hz, H-4), 4.34 (1H, dd, $J_{3,7eq}$=5 Hz, J_{gem}=10.5 Hz, H-7eq), 5.53 (1H, s,benzylic), 7.31—7.60 (5H, m, phenyl).

DL-*5-O-Acetyl-1, 2-anhydro-4, 7-O-benzylidene-(1,2,3,5/4)-3-hydroxymethyl-1,2,4,5-cyclohexanetetrol (9)*. Compound **7** (0.33 g) was treated with acetic anhydride (5 ml) in pyridine (5 ml) at room temperature overnight. The reaction mixture was concentrated to give the acetate as an oil. Without further purification, it was treated with *m*CPBA similarly as described in the preparation of **8**. The crude product was purified by chromatography on silica gel (25 g) with 2-butanone–toluene (1 : 20) as an eluent. The major fraction [R_f 0.45, 2-butanone–toluene (1 : 5)] gave crystals which were recrystallized from ethanol to give 0.37 g (88%) of **9** as needles: mp 126—130 °C. ^{1}H NMR ($CDCl_3$) δ=2.03 (3H, s, OAc), 2.31 (1H, td, $J_{3,4}=J_{3,7ax}$=11.5 Hz, $J_{3,7eq}$=5 Hz, H-3), 2.68 (1H, ddd, $J_{1,6eq}$=4.5 Hz, $J_{5,6eq}$=8 Hz, J_{gem}16 Hz, H-6eq), 3.04 (1H, d, J=4.5 Hz) and 3.14 (1H, t, J=4.5 Hz) (H-1, H-2), 3.95 (1H, dd, $J_{4,5}$=10 Hz, H-4), 4.02 (1H, t, J_{gem}=11.5 Hz, H-7ax), 4.38 (1H, dd, H-7eq), 4.98 (1H, br td, $J_{5,6ax}$=8 Hz, H-5), 5.56 (1H, s, benzylic), 7.30—7.59 (5H, m, phenyl).

Found: C, 66.22; H, 6.35%. Calcd for $C_{16}H_{18}O_5$: C, 66.19; H, 6.25%.

This compound was identical with a sample obtained by acetylation of **8**.

The minor fraction (R_f 0.42) gave an oily product (25 mg, 6%), whose ^{1}H NMR spectrum was in accord with that expected for a stereoisomer of **9**, but further characterization was not attempted. ^{1}H NMR ($CDCl_3$) δ=2.01 (3H, s, OAc), 2.68 (1H, d, $J_{1,2}$=4.5 Hz, H-2), 2.95—3.23 (1H, m, H-1), 3.49 (1H, t, $J_{3,7ax}$=11 Hz, J_{gem}=11 Hz, H-7ax), 3.75 (1H, dd, $J_{3,4}$=11 Hz, $J_{4,5}$=10 Hz, H-4), 4.35 (1H, dd, $J_{3,7eq}$=5 Hz, H-7eq), 4.97 (1H, td, $J_{5,6eq}$=10 Hz, $J_{5,6eq}$=6.5 Hz, H-5), 5.51 (1H, s, benzylic), 7.30—7.59 (5H, m, phenyl).

Reaction of DL-*2,3 : 4,7-Di-O-isopropylidene-(1,2,4/3,5)-2,3,4-trihydroxy-5-(hydroxymethyl)cyclohexylamine (3) and 8*. A mixture of **3**[4] (64 mg, 0.24 mmol) and **8** (59 mg, 0.24 mmol) in 2-propanol (0.5 ml) was heated in a sealed tube at 120 °C for 44 h. Formation of two components was detected by TLC [R_f 0.44 and 0.40, ethanol–toluene (1 : 5)]. The reaction mixture was concentrated and the residue was chromatographed on a silica-gel column (7 g) with ethanol–toluene (1 : 30) as an eluent. The first fraction was fractionated again by a silica-gel column (3.5 g) with 2-butanone–toluene (1 : 3) to give **3** (10 mg) and 52 mg (42%) of DL-*N*-[4,7-*O*-benzylidene-(1,4/2,3,5)-2,4,5-trihydroxy-3-(hydroxymethyl)-cyclohexyl]-2,3 : 4,7-di-*O*-isopropylidene-(1,2,4/3,5)-2,3,4-tri-hydroxy-5-(hydroxymethyl)cyclohexylamine (**10a**) as an oil. The second fraction gave 54 mg (44%) of the diastereomer **10b** as an oil. ^{1}H NMR ($CDCl_3$) for **10a**, δ=1.44 (9H, s) and 1.50 (3H, s) (isopropylidene), 2.85 (1H, q, J=3 Hz, H-1′), 5.58 (1H, s, benzylic), 7.32—7.62 (5H, m, phenyl), and for **10b**, δ=1.44 (9H, s) and 1.50 (3H, s) (isopropylidene), 2.91 (1H, q, J=3 Hz, H-1′), 5.57 (1H, s, benzylic), 7.30—7.62 (5H, m, phenyl).

Found for **10a**: C, 64.20; H, 7.73; N, 2.56%, and for **10b**, C, 64.41; H, 7.57; N, 2.75%. Calcd for $C_{27}H_{39}NO_8$: C, 64.14; H, 7.78; N, 2.77%.

Reaction of 3 and 9. A mixture of **3** (93 mg, 0.37 mmol) and **9** (100 mg, 0.34 mmol) in 2-propanol (0.7 ml) was heated in a sealed tube at 120 °C for 26 h. The reaction mixture was concentrated and the residue was chromatographed on a silica-gel column [7 g, 2-butanone–toluene (1 : 3)]. The major fraction [R_f 0.29, ethanol–toluene (1 : 8)] gave crystals which were recrystallized from ethanol to give 157 mg (83%) of a mixture of the diastereomers of DL-*N*-[5-*O*-acetyl-4,7-*O*-benzylidene-(1,4/2,3,5)-2,4,5-trihydroxy-3-(hydroxymethyl)-cyclohexyl]-2,3 : 4,7-di-*O*-isopropylidene-(1,2,4/3,5)-2,3,4-tri-hydroxy-5-(hydroxymethyl)cyclohexylamine (**11a** and **11b**) as homogeneous crystals: mp 117—119 °C. ^{1}H NMR ($CDCl_3$) δ=1.44 (9H, s) and 1.50 (3H, s) (isopropylidene), 2.03 (3H, s, OAc), 2.94 (0.5H, q) and 2.97 (0.5H, q) (J=3 Hz, H-1′), 4.96—5.30 (1H, m, H-5), 5.56 (1H, s, benzylic), 7.29—7.60 (5H, m, phenyl).

Found: C, 63.40; H, 7.43; N, 2.44%. Calcd for $C_{29}H_{41}NO_9$: C, 63.60; H, 7.55; N, 2.56%.

Diastereomers 12a and 12b of DL-N-[*2,5-Di-O-acetyl-4,7-O-benzylidene-(1,4/2,3,5)-2,4,5-trihydroxy-3-(hydroxymethyl)cyclohexyl]-2,3 : 4,7-di-O-isopropylidene-(1,2,4/3,5)-2,3,4-trihydroxy-5-(hydroxymethyl)cyclohexylamine*. A mixture of **11a** and **11b** (90 mg) was treated with acetic anhydride (1 ml) and pyridine (1 ml) at room temperature overnight. Formation of two components was detected by TLC [R_f 0.47 and 0.44, ethanol–toluene (1 : 8)]. The products were fractionated by chromatography on a silica-gel column (5 g) with 2-butanone–toluene (1 : 10) as an eluent to give in turn 30 mg (31%) of **12a** and 62 mg (64%) of **12b** as a homogeneous oil. ^{1}H NMR ($CDCl_3$) for **12a**, δ=1.45 (9H, s) and 1.50 (3H, s) (isopropylidene), 2.05 (3H, s) and 2.11 (3H, s) (OAc), 2.57 (1H, tdd, $J_{2',3'}$=2.5 Hz, $J_{3',7'eq}$=4.5 Hz, $J_{3',4'}=J_{3',7'ax}$=11 Hz, H-3′), 4.72 (1H, dd, H-2′), 5.17 (1H, ddd, $J_{4',5'}$=10 Hz, $J_{5',6'eq}$=5 Hz, $J_{5',6'ax}$=11.5 Hz, H-5′), 5.56 (1H, s, benzylic), 7.29—7.59 (5H, m, phenyl), and for **12b**, δ=1.45 (6H, s), 1.48 (3H, s), and 1.50 (3H, s) (isopropylidene), 2.04 (3H, s) and 2.10 (3H, s) (OAc), 2.57 (1H, tdd, $J_{2',3'}$=2.5 Hz, $J_{3',7'eq}$=5 Hz, $J_{3',4'}=J_{3',7'ax}$=11.5 Hz, H-3′), 3.07 (1H, q, $J_{1',2'}=J_{1',6'eq}=J_{1',6'ax}$=3 Hz, H-1′), 4.93 (1H, dd, H-2′), 5.17 (1H, ddd, $J_{4',5'}$=10 Hz, $J_{5',6'eq}$=5 Hz, $J_{5',6'ax}$=11.5 Hz, H-5′), 5.54 (1H, s, benzylic), 7.28—7.62 (5H, m, phenyl).

Found for **12a**: C, 63.12; H, 7.19; N, 2.48%, and for **12b**: C, 63.24; H, 7.36; N, 2.29%. Calcd for $C_{31}H_{43}NO_{10}$: C, 63.14; H, 7.35; H, 2.38%.

Compounds **10a** and **10b** could be correlated to **12a** and **12b**, respectively, by acetylation in the usual way.

N-[*(1SR)-(1,4/2,3,5)-2,4,5-Trihydroxy-3-(hydroxymethyl)cyclohexyl*]-*(1SR)-(1,2,4/3,5)-2,3,4-trihydroxy-5-(hydroxymethyl)cyclohexylamine Octaacetate (13a)*. A mixture of **12a** (30 mg) and 1 M hydrochloric acid (2 ml) was heated at reflux for 1 h. The reaction mixture was concentrated and the residue was acetylated in the usual way to give 28 mg (82%) of **13a** as an oil: R_f 0.21, 2-butanone–toluene (1 : 3). ^{1}H NMR ($CDCl_3$) δ=1.61 (1H, m, NH, disappears on deuteration), 1.98 (3H, s), 1.99 (3H, s), 2.02 (3H, s), 2.03 (9H, s), 2.07 (3H, s), and 2.11 (3H, s) (OAc), 2.82 (1H, q, J=3 Hz, H-1′), 3.27 (1H, q, J=3 Hz, H-1). The free base showed a single spot on TLC [R_f 0.24, chloroform–methanol (3 : 1)].

Found: C, 53.62; H, 6.50; N, 2.17%. Calcd for $C_{30}H_{43}NO_{16}$: C, 53.49; H, 6.43; N, 2.08%.

N-[*(1SR)-(1,4/2,3,5)-2,4,5-Trihydroxy-3-hydroxymethyl)cyclohexyl*]-*(1RS)-(1,2,4/3,5)-2,3,4-trihydroxy-5-(hydroxymethyl)cyclohexylamine Octaacetate (13b)*. Compound **12b** (62 mg) was deprotected and then acetylated similarly as described in the preparation of **13a** to give 58 mg (82%) of **13b** as an oil: R_f 0.23, 2-butanone–toluene (1 : 3). ^{1}H NMR ($CDCl_3$) δ=1.61 (1H, m, NH, disappears on deuteration), 1.97 (3H, s),

1.975 (3H, s), 1.99 (3H, s), 2.01 (3H, s), 2.03 (3H, s), 2.035 (3H, s), 2.06 (3H, s), 2.065 (3H, s) (OAc), 2.91 (1H, q, J=3 Hz, H-1′), 3.28 (1H, q, H-1). The free base showed a single spot on TLC [R_f 0.18, chloroform–methanol (3 : 1)].

Found: C, 53.55; H, 6.52; N, 2.19%. Calcd for $C_{30}H_{43}NO_{16}$: C, 53.49; H, 6.43; N, 2.08%.

Reaction of DL-*4,7 : 5,6-Di-*O*-isopropylidene-(1,4,6/5)-4,5,6-trihydroxy-3-hydroxymethyl-2-cyclohexylamine (**4**) with **9***. A mixture of **4**[6] (109 mg, 0.43 mmol) and **9** (124 mg, 0.43 mmol) in 2-propanol (1 ml) was heated in a sealed tube at 120 °C for 26 h. The reaction mixture was concentrated and the residue was chromatographed on a silica-gel column (13 g) with 2-butanone–toluene (1 : 6) as an eluent to give 191 mg (82%) of a mixture of the diastereomers of DL-*N*-[5-*O*-acetyl-4,7-*O*-benzylidene-(1,4/2,3,5)-2,4,5-trihydroxy-3-(hydroxymethyl)-cyclohexyl]-4, 7 : 5, 6-di-*O*-isopropylidene-(1,4,6/5)-4, 5, 6-trihydroxy-3-hydroxymethyl-2-cyclohexenylamine (**14a** and **14b**) as a homogeneous oil: R_f 0.48, ethanol–toluene (1 : 8). ^{1}H NMR ($CDCl_3$) δ=1.44 (6H, s), 1.47 (3H, s), and 1.54 (3H, s) (isopropylidene), 2.04 (3H, s, OAc), 2.45 (1H, m, H-3′), 3.17 (0.5H, q) and 3.30 (0.5H, q) (J=3 Hz, H-1′), 4.98—5.34 (1H, m, H-5′), 5.44 (0.5H, br d) and 5.61 (0.5H, br d) (J=*ca.* 4.5 Hz, H-2), 5.55 (1H, s, benzylic), 7.28—7.60 (5H, m, phenyl).

Found: C, 64.00; H, 7.25; N, 2.53%. Calcd for $C_{29}H_{39}NO_9$: C, 63.84; H, 7.20; N, 2.57%.

*Diastereomers **15a** and **15b** of* DL-N-[*2,5-Di-*O*-acetyl-4,7-O-benzylidene-(1,4/2,3,5)-2,4,5-trihydroxy-3-(hydroxymethyl)cyclohexyl]-4,7:5,6-di-*O*-isopropylidene-(1,4,6/5)-4,5,6-trihydroxy-3-hydroxymethyl-2-cyclohexenylamine*. A mixture of **14a** and **14b** (77 mg) was treated with acetic anhydride (1 ml) and pyridine (1 ml) at room temperature overnight. Formation of two components was detected by TLC [R_f 0.50 and 0.47, ethanol–toluene (1 : 8)]. The reaction mixture was concentrated and the residual products were fractionated by a silica-gel column (4.5 g) with 2-butanone–toluene (1 : 5). The first fraction (R_f 0.50) gave 38 mg (46%) of **15a** as a glass. The second fraction (R_f 0.47) gave 45 mg (54%) of **15b** as a glass. ^{1}H NMR ($CDCl_3$) for **15a**, δ=1.43 (3H, s), 1.47 (6H, s), and 1.54 (3H, s) (isopropylidene), 2.04 (3H, s) and 2.11 (3H, s) (OAc), 2.66 (1H, tdd, $J_{2',3'}$=3 Hz, $J_{3',7'eq}$=5 Hz, $J_{3',4'}=J_{3',7'ax}$=10.5 Hz, H-3′), 3.19 (1H, q, J=3 Hz, H-1′), 4.85 (1H, t, J=3 Hz, H-2′), 5.20 (1H, ddd, $J_{5',6'eq}$=6 Hz, $J_{4',5'}$=9.5 Hz, $J_{5',6'ax}$=11.5 Hz, H-5′), 5.54 (1H, s, benzylic), 5.54 (1H, br d, H-2), 7.28—7.58 (5H, m, phenyl), and for **15b**, δ=1.44 (6H, s) and 1.53 (6H, s) (isopropylidene), 2.03 (3H, s) and 2.10 (3H, s) (OAc), 2.86 (1H, tdd, $J_{2',3'}$=3 Hz, $J_{3',7'eq}$=5 Hz, $J_{3',4'}=J_{3',7'ax}$=11 Hz, H-3′), 3.21 (1H, q, J=3 Hz, H-1′), 4.93 (1H, t, J=3 Hz, H-2′), 5.19 (1H, ddd, $J_{5',6'eq}$=5.5 Hz, $J_{4',5'}$=9.5 Hz, $J_{5',6'ax}$=11 Hz, H-5′), 5.53 (1H, s, benzylic), 5.60 (1H, br d, $J_{1,2}$=5 Hz, H-2), 7.28—7.57 (5H, m, phenyl).

Found for **15a**: C, 62.52; H, 7.06; N, 2.54%, and for **15b**: C, 63.24; H, 6.94; N, 2.28%. Calcd for $C_{31}H_{41}NO_{10}$: C, 63.36; H, 7.03; N, 2.38%.

N-[(*1*SR)-(*1,4/2,3,5*)-*2,4,5-Trihydroxy-3-(hydroxymethyl)-cyclohexyl*]-(*1*SR)-(*1,4,6/5*)-*4,5,6-trihydroxy-3-hydroxymethyl-2-cyclohexenylamine Octaacetate (**16a**)*. A mixture of **15a** (24 mg) and 1 M hydrochloric acid (5 ml) was heated at reflux for 2 h. The reaction mixture was concentrated and the residue was treated with acetic anhydride and pyridine in the usual way. The product was purified by passage through a short column of active alumina with chloroform. The eluate was concentrated to give 20 mg (73%) of **16a** as a glass: R_f 0.21, 2-butanone–toluene (1 : 3). ^{1}H NMR ($CDCl_3$) δ=1.99 (3H, s), 2.03 (3H, s), 2.04 (6H, s), 2.06 (3H, s), 2.07 (6H, s), and 2.08 (3H, s) (OAc), 2.52—2.86 (1H, m, H-3′), 3.09 (1H, q, J=3 Hz, H-1′), 3.70 (1H, t, J=4 Hz, H-1), 3.96 (1H, dd, $J_{3',7'}$=5 Hz, J_{gem}=11.5 Hz) and 4.19 (1H, dd, $J_{3',7''}$=8 Hz) ($C\underline{H}_2OAc$), 4.41 (1H, d) and 4.69 (1H, d) (J_{gem}=13 Hz, C=CH_2OAc), 5.97 (1H, br d, $J_{1,2}$=4 Hz, H-2).

Found: C, 53.82; H, 6.25; N, 2.24%. Calcd for $C_{30}H_{41}NO_{16}$: C, 53.64; H, 6.15; N, 2.09%.

The free base showed a single spot on TLC [R_f 0.44, chloroform–methanol (3 : 1)].

N-[(*1*SR)-(*1,4/2,3,5*)-*2,4,5-Trihydroxy-3-(hydroxymethyl)-cyclohexyl*]-(*1*RS)-(*1,4,6/5*)-*4,5,6-trihydroxy-3-hydroxymethyl-2-cyclohexenylamine Octaacetate (**16b**)*. Compound **15b** (15 mg) was converted into **16a** similarly as described for the preparation of **16a**: yield 15 mg (87%), R_f 0.19, 2-butanone–toluene (1 : 3). ^{1}H NMR ($CDCl_3$) δ=2.00 (3H, s), 2.03 (3H, s), 2.05 (15H, s), and 2.10 (3H, s) (OAc), 2.59 (1H, m, H-3′), 3.05 (1H, q, J=3 Hz, H-1′), 3.68 (1H, m, H-1), 3.95 (1H, dd, $J_{3',7'}$=4.5 Hz, J_{gem}=11.5 Hz) and 4.20 (1H, dd, $J_{3',7''}$=9 Hz) ($C\underline{H}_2OAc$), 4.39 (1H, d) and 4.69 (J_{gem}=13 Hz, C=CCH_2OAc), 6.06 (1H, br d, $J_{1,2}$=5 Hz, H-2).

Found: C, 53.87; H, 6.28; N, 2.30%. Calcd for $C_{30}H_{41}NO_{16}$: C, 53.64; H, 6.15; N, 2.09%.

The free base showed a single spot on TLC [R_f 0.44, chloroform–methanol (3 : 1)].

The authors express their sincere thanks to Mr. Saburo Nakada for the elementary analyses. The present work was partially supported by a Grant-in-Aid for Scientific Research No. 56550617 from the Ministry of Education, Science and Culture.

References

1) a) Presented in part at the 45th National Meeting of the Chemical Society of Japan, Tokyo, April 1982, Abstr., No. 4E30; b) Previous paper of this series: S. Ogawa, H. Ito, T. Ogawa, S. Iwasaki, and T. Suami, *Bull. Chem. Soc. Jpn.*, **56**, 2319 (1983).

2) The nomenclature and numbering of cyclitols used in this paper follow IUPAC and IUB tentative rules for cyclitol nomenclature [*J. Biol. Chem.*, **243**, 5809 (1968)]. For convenience, the carbon atom of the branched-chain substituent on C-3 of the cyclohexane ring are numbered 7. All compounds described in this paper are racemic and the formulas depict only one of the respective enantiomers.

3) S. Ogawa, M. Suetsugu, T. Toyokuni, and T. Suami, *Nippon Kagaku Kaishi*, **1982**, 1721 and the references are cited therein.

4) S. Ogawa, T. Toyokuni, and T. Suami, *Chem. Lett.*, **1981**, 947; T. Toyokuni, S. Ogawa, and T. Suami, *Bull. Chem. Soc. Jpn.*, **56**, in press.

5) S. Ogawa, T. Toyokuni, Y. Iwasawa, Y. Abe, and T. Suami, *Chem. Lett.*, **1982**, 279.

6) S. Ogawa, T. Ogawa, N. Chida, T. Toyokuni, and T. Suami, *Chem. Lett.*, **1982**, 749. The similar deshielding effect was observed in the ^{1}H NMR spectrum of the corresponding 6′-acetoxy derivative.

7) Observation of chromatographic behavior of several pseudo-disaccharide derivatives obtained so far indicated that one diastereomer whose configuration corresponded to that of natural validoxylamine A moved somewhat slower than the other on TLC in several solvent systems. A similar behavior was observed in this case, correlating to the ^{1}H NMR spectral data.

 © 1983 The Chemical Society of Japan Bull. Chem. Soc. Jpn., 56, 2330—2337 (1983) [Vol. 56, No. 8

A Basic Study of the Amino Acid Residue in Protein. The Molecular Interaction Responsible for the Differentiation of Hydrocarbon Residues

Yuji Hiraki, Toshihiko Oda, and Akira Tai*
Institute for Protein Research, Osaka University, Yamada-oka, Suita, Osaka, 565
(Received October 26, 1982)

A pair of primary amines was competitively acylated with acid anhydride in water–dioxane mixed solvents. Based on the product distribution, the mode of differentiation of hydrocarbon residues in the competing substrates with a reagent was studied. In solvents with a low water content, where both reactants and products were completely soluble, no appreciable differentiation of the alkyl-chain length of alkylamines occurred. On the other hand, the differentiation of a phenyl group from an alkyl group occurred. From the dependency of the product distribution on the water content in reaction media, an attractive interaction induced by water was postulated between alkyl and phenyl groups, but no such interaction was observed between alkyl and alkyl groups. The differences in functions of the phenyl and alkyl groups in the differentiation process are discussed. In solvents with a very high water content, the acylation proceeded under heterogeneous conditions, since acid anhydrides became insoluble and provided an organic phase in the reaction mixture. In this case, the differentiation was controlled by the hydrophobicity of hydrocarbon residues of amines indexed by the partition coefficients of amines between the aqueous phase and the organic phase.

Among the various molecular interactions affecting the molecular recognition,[1–5] the interaction between hydrocarbon residues of reactant molecules is one of the essential factors in understanding the various phenomena found in the biological and organic reactions in either an aqueous or nonaqueous environment.

A systematic investigation of the competitive acylation of primary amines with an acid anhydride (Eq. 1) was carried out in order to characterize the interactions between such medium-size hydrocarbon residues as found in common amino acids in proteins.

As was briefly reported in a previous communication,[6] this reaction system had the following advantages: 1) the reaction readily proceeded in a quantitative manner in kinds of reaction media, including an aqueous one, and gave kinetically controlled products; 2) the reaction products were stable and could readily be analyzed by means of quantitative gas chromatography and; 3) the substrates and reagents substituted with many different hydrocarbon groups were readily available.

The contributions of the hydrocarbon residues to the molecular recognition in the course of the reaction (the differentiation process) were evaluated by the use of logarithmic molar ratio of products (Eq. 2):

$$\left.\begin{matrix} R^1\text{–}NH_2 \\ R_2\text{–}NH_2 \end{matrix}\right\} + (R^0\text{–}CO)_2O \longrightarrow \begin{cases} R^1\text{–}NHCO\text{–}R^0 \\ R^2\text{–}NHCO\text{–}R^0 \end{cases} \quad (1)$$

$$\ln r = \ln(R^1\text{–}NHCO\text{–}R^0/R^2\text{–}NHCO\text{–}R^0), \quad (2)$$

where R^1, R^2–, and R^0– are the hydrocarbon residues.

Experimental

Instruments. The ^{1}H-NMR and IR spectra were taken with a JEOL FX-100 spectrometer and a Shimadzu IR 27 G spectrometer respectively. The analytical GLC was carried out with a Shimadzu GC 6A gas chromatograph equipped with a Shimadzu Chromatopack C-RIA, using a 3 m-5 mm o.d. glass column packed with 2% Silicon OV-17 on Chromosorb W (OV-17) at the stated temperature. The preparative GLC was carried out with a Shimadzu 3 A instrument, using a 3 m-6 mm o.d. stainless column packed with OV-17.

Materials. All the chemical except those noted below were obtained from commercial sources and were used without further purification. The phenylacetic anhydride was prepared from the corresponding acid chloride and sodium salt of the acid by the conventional method. The needle crystals were obtained by recrystallization from ether–hexane (mp 71 °C, lit, 72 °C). The 2-phenylbutyric anhydride was prepared from the corresponding acid by refluxing with a large excess of acetic anhydride, followed by the removal of the acetic acid released by distillation. The *N*-acetyl-L-isoleucine *N*-hydroxysuccinimide ester was prepared from *N*-acetyl-L-isoleucine and *N*-hydroxysuccinimide by treatment with dicyclohexylcarbodiimide according to a conventional method; it was then purified by recrystallization from isopropyl alcohol. The authentic samples for the identification of reaction products were prepared from appropriate acid chlorides and amines by a conventional method, and were purified by preparative GLC. The NMR and IR spectra and the elemental analyses of the samples were consistent with the desired structures of the samples.

Reaction Procedure of Competitive Acylation. When the concentration of an acylating reagent was 50 mM (1 mM= 10^{-3} mol dm^{-3}), the competitive acylation was carried out by the following procedure. In a flask, a 50-μl portion of a stock solution of each amine (2 M dioxane solution) was dissolved in 0.8 ml of the solvent. A 100-μl portion of a solution of anhydride (0.5 M dioxane solution) was then added, all at once, with vigorous stirring at room temperature, after which the mixture was allowed to stand for 1 h. After a 100-μl portion of a stock solution of an internal standard (0.25 M dioxane solution), which will be described is detail, in the following section, had been added for GLC analysis, the volume of the reaction mixture was made up to 5 ml with dioxane. GLC was used for the quantitative analysis of the products of the reaction solution. When the concentration of the acylating reagent was 6.25 mM, 25-μl of each amine solution, 50-μl of the acid anhydride solution, 3.9 ml of the solvent, and 50-μl of the internal standard solution were employed instead.

Quantitative Analysis of Reaction Products. The reaction mixture prepared as has been described in the previous section was subjected to GLC analysis. The amount of the product was determined by the internal standard method. The analyses of the 2-phenylbutyramides and phenylacetamides were carried out in a column with a temperature elevated from 150 °C to 250 °C by 10 °C/min; methyl stearate was used as the internal standard. The 4-methylpentanamides were

analyzed under such GLC conditions that the column temperature was elevated from 100 °C to 260 °C by 10 °C/min, with methyl palmitate as the internal standard. The *N*-acetyl-L-isoleucinamides, isobutyramides, and isovaleramides were analyzed under such GLC conditions that the column temperature was elevated from 100 °C to 250 °C by 10 °C/min, with acetanilide as the internal standard.

Solubility of Acid Anhydrides in Aqueous Media. The solubility of an acylating reagent in water–dioxane mixed solvents was determined as follows. A 100-μl portion of a acylating reagent (0.5 M dioxane solution) was vigorously stirred into a water–dioxane mixture (0.9 ml). The resultant mixture was centrifuged at 2000 min^{-1} for 20 min to separate any undissolved acylating reagent from the solvent phase. A 50-μl portion of butylamine (2 M dioxane solution) was added to the 100-μl portion of supernatant obtained under vigorous stirring, and the mixture was allowed to stand for 1 h to complete the reaction. The quantitative GLC analysis of the *N*-butyl amides was carried out by following the procedure described in the above section.

Results

The Competitive Reaction Conditions. The competitive acylation was carried out at room temperature by using an equimolar mixture of two primary amines as substrates. The ln *r* value depends not only on the interactions between substrates and the reagent in the differentiation process, but also on the changes in the relative concentrations of the two substrates during the reaction. Thus, the reaction should be carried out in the presence of so large an excess of the substrates relative to the reagent as to eliminate the effects of the concentration changes in the substrates. To establish the appropriate reaction conditions, the ln *r* values were determined under a variety of molar ratios of substrates relative to reagent ($[R^1\text{–}NH_2+R^2\text{–}NH_2]/[(R^0\text{–}CO)_2O]$, as is shown in Fig. 1. The ln *r* value became constant when the relative molar ratio of substrates to a reagent was over four. Therefore, four molar equivalents of substrates were treated with one molar equivalent of a reagent in the following experiments. With this ratio

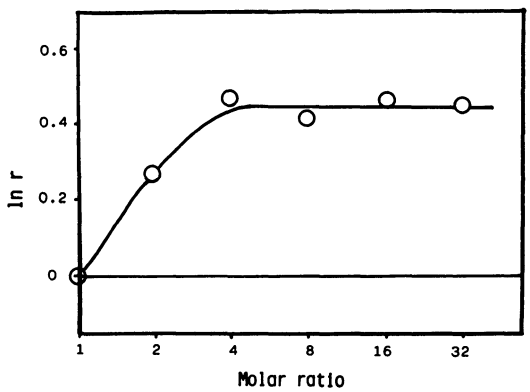

Fig. 1. The dependence of the ln *r* value on the molar ratio of substrates to a reagent ($[R^1\text{–}NH_2+R^2\text{–}NH_2]/[(R^0\text{–}CO)_2O]$).
Isovaleric anhydride, hexylamine, and propylamine were employed as $(R^0\text{–}CO)_2O$, $R^1\text{–}NH_2$, and $R^2\text{–}NH_2$, respectively. The reaction was carried out in water–dioxane mixtures of $\chi_{H_2O}=0.88$. The concentration of isovaleric anhydride was 6.25 mM.

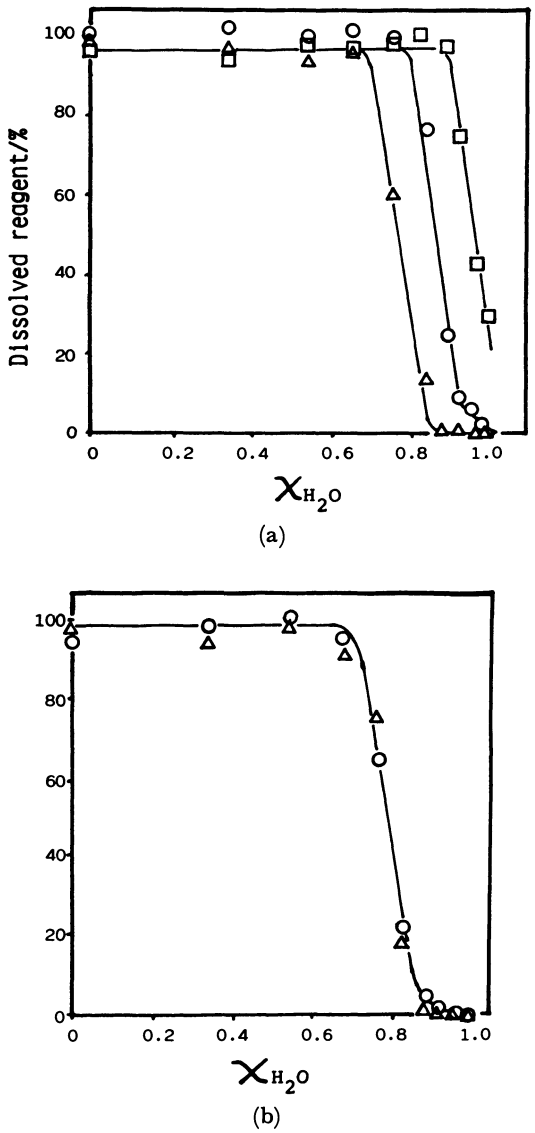

Fig. 2. The dependence of the amount of dissolved reagent (% of applied reagent) on the mole fraction of water (χ_{H_2O}) in water–dioxane mixtures.
In (a), 4-methylpentanoic anhydride (△), isovaleric anhydride (○), and isobutyric anhydride (□) were employed. Their concentration was 50 mM if all dissolved. In(b), 2-phenylbutyric anhydride (○) and phenylacetic anhydride (△) were employed. Their concentration was 12.5 mM if all dissolved.

of substrates to a reagent, it was also confirmed that the ln *r* value was not affected by the carboxylic acids liberated during the reaction: the same ln *r* values were obtained in the presence and in the absence of triethyl amine, an acid quencher.

Benzene, dioxane, and water–dioxane mixtures were employed as solvents. Figure 2 shows the relationship between the solubility of a reagent and the mole fraction of water (χ_{H_2O}) in the water–dioxane mixture. As may be found in the figure, the solubility of an acid anhydride suddenly decreased above a certain value of χ_{H_2O}. When an acid anhydride was added to a solution with a value above this critical χ_{H_2O}, the formation of a distinct organic phase was observed.

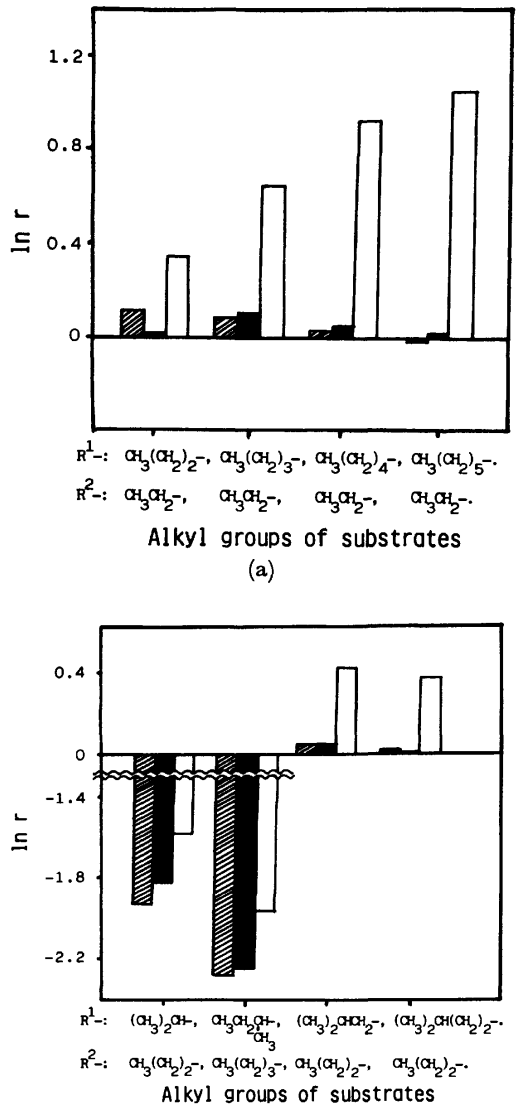

Fig. 3. (a) and (b). The competitive acylation of a pair of alkylamine with isovaleric anhydride.
The reaction was carried out in benzene (▨), dioxane (■), or water–dioxane mixtures at $\chi_{H_2O}=0.88$ (□). The concentration of a reagent was 50 mM.

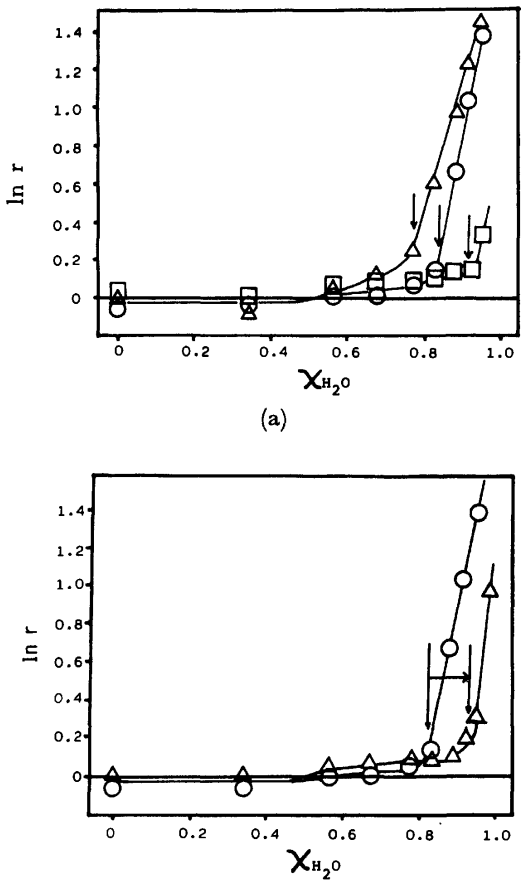

Fig. 4. The relationship between the mole fraction of water in water–dioxane mixtures (χ_{H_2O}) and the ln r value of the competitive acylation of hexylamine (R^1–NH_2) and propylamine (R^2–NH_2).
In (a), 4-methylpentanoic anhydride (△), isovaleric anhydride (○), and isobutyric anhydride (□) were employed. Their concentration was 50 mM. In (b), isovaleric anhydride was employed. Its concentration was 50 mM (○) or 6.25 mM (△).

The Competition of Alkylamines with Different Chain Lengths. A pair of alkylamine were competitively acylated with isovaleric anhydride in benzene, dioxane, or water–dioxane mixtures ($\chi_{H_2O}=0.88$). The results are shown in Fig. 3.

In dioxane or benzene, the ln r values were found to be substantially zero in every competition between unbranched alkylamines (Fig. 3(a)), and in the competition of a β- or γ-branched amine with an unbranched one (Fig. 3(b)). In the competition of an α-branched alkylamine, such as isopropylamine and *s*-butylamine, with the unbranched amines, large negative ln r values were obtained in every solvent; the formation of amides from α-branched amines was significantly suppressed, as is shown in Fig. 3(b).

In aqueous media (water–dioxane), positive ln r values were obtained except in the competition of an α-branched amine with an unbranched one (Fig. 3(a) and (b)). The ln r values obtained in the competitions of unbranched amines in water–dioxane mixtures are shown in Table 1. Thus, the reagent distinguished the longer alkylamine from the shorter one and preferentially gave the amide with the longer alkylamine.

In order to ascertain the mode of the differentiation in an aqueous solvent, the competition of hexylamine with propylamine was carried out in water–dioxane mixtures with a variety of χ_{H_2O} values. The profile of the resulting plots was apparently composed of two regions: Phase I and Phase II. For example, the plot (○) in Fig. 4(a) was composed of Phase I ($\chi_{H_2O}<0.83$) and Phase II ($\chi_{H_2O}>0.83$). In Phase I, no effective differentiation of the alkyl-chain length was observed, while considerable differentiation was observed in Phase II, and ln r remarkably increased with the increase in χ_{H_2O}.

In the acylation carried out in solvents with $\chi_{H_2O}>0.9$, it was observed that the reaction mixture became slightly turbid just after the addition of a reagent and that the turbidity disappeared instantaneously. The same ln r values were obtained in the competitive acyla-

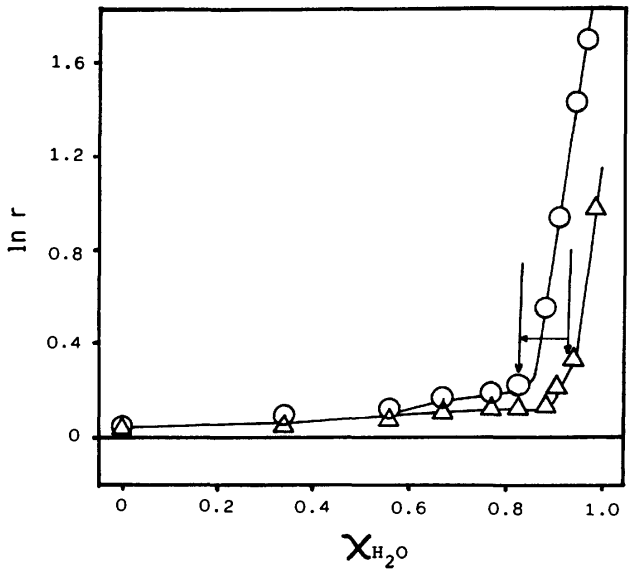

Fig. 5. The relationship between the mole fraction of water in water–dioxane mixtures (χ_{H_2O}) and the ln r value of the competitive acylation in the presence (○) or the absence (△) of CTAB.
Isovaleric anhydride, hexylamine, and propylamine were employed as $(R^0\text{–}CO)_2O$, $R^1\text{–}NH_2$, and $R^2\text{–}NH_2$, respectively. The concentration of a reagent was 6.25 mM.

tion carried out in two different manners: one was the reaction carried out by the addition of an acid anhydride to amine mixtures homogeneously dissolved in solvents the standard procedure is described in the experimental section, while the other is the reaction carried out by the addition of amine mixtures to suspensions of reagents previously prepared in solvents with large χ_{H_2O} values. These facts strongly suggested that the occurrence of two regions in the plots of ln r *vs.* χ_{H_2O} is related to the solubility of acid anhydrides in water–dioxane mixed solvents. A comparison of Figs. 4(a) and 2(a) clearly shows that the reaction took place under homogeneous conditions in Phase I, while in Phase II it took place under heterogeneous conditions. Accordingly, it can well be understood that the boundary between Phase I and Phase II shifted to a larger χ_{H_2O} value, from 0.82 to 0.9, in the eight-fold dilution of the reagent (Fig. 4(b)).

When cetyl trimethylammonium bromide (CTAB) was added to the reaction system, no apparent phase separation of the reagent occurred. However, Phase II appeared even in the presence of CTAB, as is shown in Fig. 5. The boundary between Phases I and II shifted to a smaller χ_{H_2O} value. Thus, the reagent incorporated into micelles provided by CTAB functioned much like the organic phases produced only by the aggregation of reagents.

When a water-soluble reagent such as the *N*-acetyl-L-isoleucine *N*-hydroxysuccinimide ester was used, Phase II did not appear. In this case, no effective differentiation of alkyl-chain length was observed, not even in solvents with a high χ_{H_2O} value as is shown in Table 1.

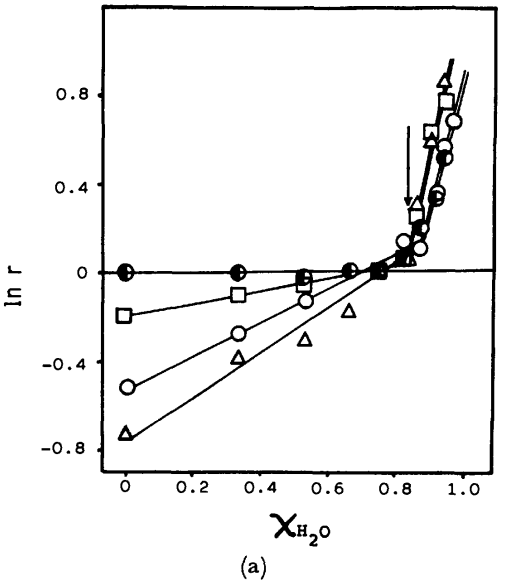

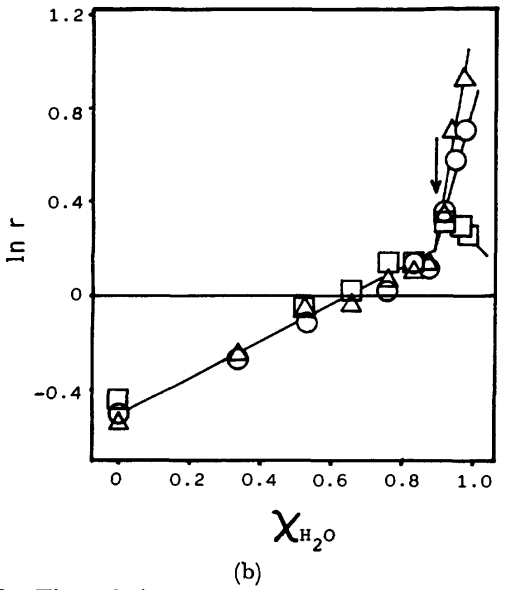

Fig. 6. The relationship between the mole fraction of water in water–dioxane mixtures (χ_{H_2O}) and the ln r value of the competitive acylation with isovaleric anhydride. In (a), benzylamine (△), phenethylamine (△), 3-phenylpropylamine (○), and pentylamine (◐) were employed as $R^1\text{–}NH_2$. Butylamine was employed as $R^2\text{–}NH_2$ in every case. The concentration of a reagent was 50 mM. In (b), phenethylamine was employed as $R^1\text{–}NH_2$. As $R^2\text{–}NH_2$, propylamine (△), butylamine (○), and hexylamine (□) were employed. The concentration of a reagent was 50 mM.

The Competition of an Alkylamine and a Phenylalkylamine. Figure 6(a) shows the results of the competitive acylation between a phenylalkylamine and an unbranched alkylamine with isovaleric acid anhydride (R^0=–$CH_2CH(CH_3)_2$). Benzylamine, phenethylamine, or 3-phenylpropylamine was employed as $R^1\text{–}NH_2$, and butylamine was employed as $R^2\text{–}NH_2$. The profile of the plots is composed of two phases: Phase I ($\chi_{H_2O}<0.83$) and Phase II ($\chi_{H_2O}>0.83$). In Phase II, the ln r values increased remarkably with the increase in χ_{H_2O}. In Phase I, the ln r value increased from negative to

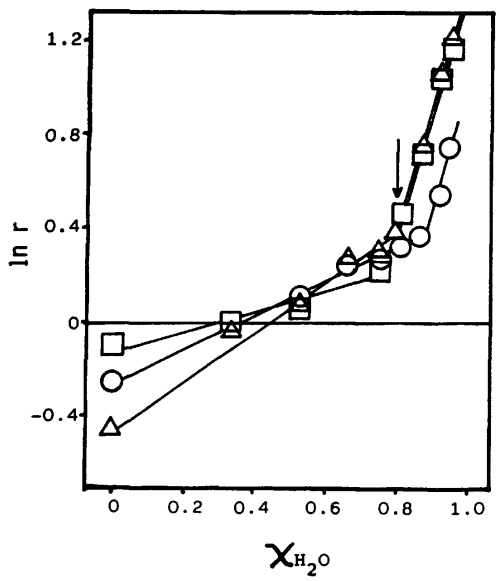

Fig. 7. The relationship between the mole fraction of water in water–dioxane mixtures (χ_{H_2O}) and the ln r value of the competitive acylation with isovaleric anhydride. Phenethylamine and butylamine were employed as R^1–NH_2 and R^2–NH_2, respectively. As a reagent, butyric anhydride (○), 2-phenylbutyric anhydride (△), and phenylacetic anhydride (□) were employed. The concentration of a reagent was 50 mM.

positive with the increase in χ_{H_2O}. This increase in ln r was more pronounced when the phenyl group was substituted near the amino group.

Figure 6(b) shows the ln r *vs.* χ_{H_2O} plots obtained by the competition of phenethylamine with propylamine, butylamine, or hexylamine. In Phase I, all the plots overlapped, even though the chain lengths of the alkylamines were different from one another. In Phase II, the slope of each plot was different. In the case of hexylamine, the ln r value decreased with the increase in χ_{H_2O} ((□) plot).

Figure 7 shows the results of the competitive acylation between phenethylamine and butylamine with several different types of reagents. In this case, the slopes of the plots in Phase I changed significantly with the change in the hydrocarbon residues of the reagents, whereas those of Phase II were similar to one another.

Figure 8 shows the results of the competitive acylation between amines with different pK_a's. The ln r value changed with χ_{H_2O} in Phase I only when benzylamine competed with others (the (○) and (□) plots). No change in the ln r value with a change in χ_{H_2O} was observed in any other combinations of amines (the (□) and (◧) plot). Thus, the changes in the ln r value with χ_{H_2O} in Phase I in the competition of phenylalkylamines with alkylamines are caused not by the difference in the pK_a's of the amines, but by the phenyl groups in the reactants.

Figure 9 shows the results of the competitive acylation in methanol–dioxane or acetonitrile–dioxane mixed solvents. At any composition of these solvents, the reaction proceeded under homogeneous conditions which corresponded to Phase I in water–dioxane solvents. As is shown by the (○) and (△) plots, the changes of

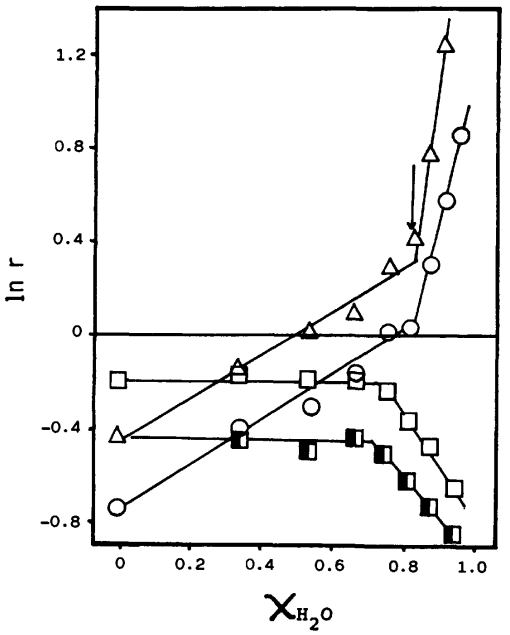

Fig. 8. The relationship between the mole fraction of water in water–dioxane mixtures (χ_{H_2O}) and the ln r value of the competitive acylation with isovaleric anhydride. The following combinations of R^1–NH_2 and R^2–NH_2 were examined: benzylamine and butyl-2-amine (○), benzylamine and 2-methoxyethylamine (△), 2-methoxyethylamine and butylamine (□), and 2-aminoethanol and butylamine (◧). The pK_a values of butylamine, benzylamine, 2-methoxyethylamine, and 2-aminoethanol were 10.64, 9.35, 9.28, and 9.5, respectively. The concentration of a reagent was 50 mM.

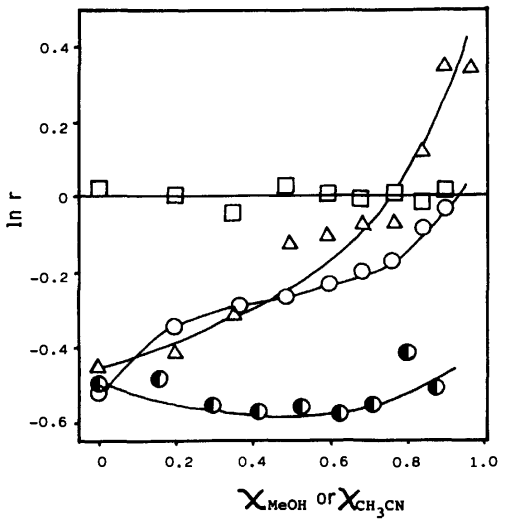

Fig. 9. The relationship between the mole fraction of methanol or acetonitrile in methanol–dioxane or acetonitrile–dioxane mixtures (χ_{MeOH} or χ_{CH_3CN}) and the ln r value.
The following combination of R^1–NH_2, R^2–NH_2, and $(R^0$–$CO)_2O$ were examined: phenethylamine, butylamine, and isovaleric anhydride in methanol–dioxane (○) and in acetonitrile–dioxane (◐), phenethylamine, butylamine, and 2-phenylbutyric anhydride in methanol–dioxane (△), hexylamine, butylamine, and isovaleric anhydride in methanol–dioxane (□). The concentration of a reagent was 50 mM.

the ln r value in Phase I were induced by either water or methanol, but no appreciable change in the ln r value was observed in acetonitrile–dioxane mixed solvents.

Discussion

In the acylation of a primary amine with an acid anhydride or an active ester, the rate-determining step is the nucleophilic attack by an amino group on a carbonyl carbon of the reagent.[7] When an excess amount of an amine ($pK_a>9$) is acylated by a reagent carrying a good leaving group such as an acid anhydride, the rate of acylation becomes insensitive to a small change in the nucleophilicity of an amino group, indexed by its pK_a value.[8] From the examination of competing reaction conditions, it was shown that the ln r value was not affected by the relative ratio of competing substrates during the reaction if the initial molar ratio of substrates to a reagent, *i.e.*, $[R^1\text{–}NH_2+R^2\text{–}NH_2]/[(R^0\text{–}CO)_2O]$, was over four (Fig. 1). Under the experimental conditions employed in the study, the ln r value is expected to represent the degree of the differentiation of substrate molecules by a reagent.

In aprotic solvents, such as dioxane and benzene, the reagent molecule could distinguish only an α-branched substrate from an unbranched one, while it could distinguish neither the difference in the alkyl-chain length of unbranched substrates nor the β- and γ-branched substrates from an unbranched one (Fig. 3). These facts show that the differentiation in a nonaqueous system was controlled by the bulkiness of the alkyl groups near the reaction center.[4]

In Phase I of water–dioxane mixed solvents, the reaction proceeded under homogeneous conditions, where the differentiation of the substrates by the reagent must be controlled by molecular interactions. As may be found in Fig. 4(a) and (b), no effective differentiation of the chain length of alkyl groups took place, even in solvents with high χ_{H_2O} value, as long as the reaction took place in Phase I. Thus, it was shown that there is no characteristic interaction contributing to the differentiation of the chain length of alkyl groups in Phase I. The absence of interaction between alkyl groups in the reagent and substrate is also supported by the fact that the slope of plots in phase I in Fig. 6(b) were not affected by the alkyl-chain length of $R^2\text{–}NH_2$.

However, the ln r value increased with the increase in χ_{H_2O} from a negative value to a positive one in the competition of a phenylalkylamine with an alkylamine in Phase I. As may be found in Fig. 6(a), the slopes of the plots depended on the structural features of the phenylalkylamines. As may be found in Fig. 6(b), the slope of the plot was determined by the sort of phenylalkylamine and was not changed by the change in the chain length of alkylamines. The results shown in Fig. 8 exculde the possibility that the slope of a plot depends on the difference in the pK_a's of the competing amines. These facts can be explained in terms of an attractive interaction between the phenyl group of a substrate and the alkyl group of a reagent (an alkyl-phenyl interaction) that was induced by the addition of water to the reaction media. Since this sort of alkyl-phenyl interaction is a molecular interaction functioning under homogeneous conditions, it can participate in the differentiation of chirality, as was reported in the previous communication.[6]

When phenylacetic anhydride is used in the competitive acylation between phenethylamine and butylamine, the slope of the ln r *vs.* χ_{H_2O} plot in Phase I will represent the difference between a phenyl-phenyl interaction (an interaction between phenyl groups of a substrate and a reagent) and an alkylphenyl interaction. The slope of the (□) plot in Fig. 7 showed a more gentle gradient than that of the (○) plot in Fig. 7 or than those of the plots in Fig. 6(b). The results show that a phenyl-phenyl interaction was induced as well as an alkyl-phenyl interaction by the addition of water to solvents. The former was a little stronger than, or comparable to, the latter.

Since the alkyl-phenyl interaction occurred not only in water, but also in methanol, which has strong intermolecular hydrogen bonds, the interaction must be solvophobic in character. No alkyl-phenyl interaction occurred in dioxane or acetonitrile ($\varepsilon=37.5$)[11] whose dielectric constant is comparable to that of methanol ($\varepsilon=32.6$)[11] (Fig. 9).

The alkyl chains of substrates were remarkably differentiated in Phase II (Fig. 4 and Table 1). These results are in clear contrast to the results in Phase I. In Phase II, the added reagents separated from the solvent phase to make fine oily droplets prior to the reaction with amines. Therefore, almost all of the reaction must proceed inside the hydrophobic domain constituted by acid anhydride. Moreover, the ln r value must be determined by the relative concentration of substrates transferred from an aqueous phase by partition. The results shown in Figs. 4 and 5 suggest that the formation of a hydrophobic domain in the aqueous phase is indispensable for the effective distinction of

Table 1. The ln r values obtained in the competitive acylation of unbranched alkylamine with isovaleric anhydride in water–dioxane mixtures ($\chi_{H_2O}=0.88$)[a]

	$R^2\text{–}NH_2$			
$R^1\text{–}NH_2$	$CH_3CH_2\text{–}NH_2$	$CH_3(CH_2)_2\text{–}NH_2$	$CH_3(CH_2)_3\text{–}NH_2$	$CH_3(CH_2)_4\text{–}NH_2$
$CH_3(CH_2)_2\text{–}NH_2$	0.330	—	—	—
$CH_3(CH_2)_3\text{–}NH_2$	0.536	0.167 (0.13)	—	—
$CH_3(CH_2)_4\text{–}NH_2$	0.863	0.418 (−0.10)	0.205	—
$CH_3(CH_2)_5\text{–}NH_2$	1.023	0.621 (0.04)	0.357	0.164

a) The concentration of a regent was 50 mM. The results of the competitions where the *N*-acetyl-L-isoleuine *N*-hydroxysuccinimide ester was used as a regent are given in parentheses.

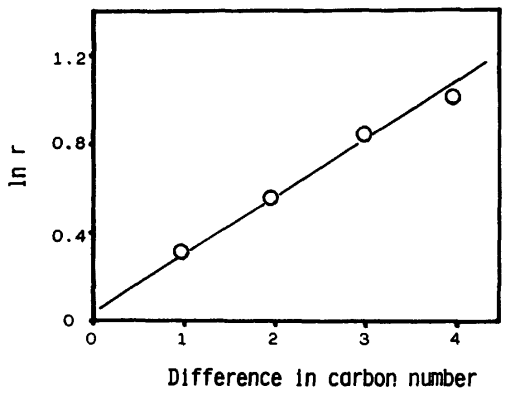

Fig. 10. The relationship between ln r and the difference in carbon number of alkyl chain of substrates in the competition of unbranched alkylamine and ethylamine.

alkyl-chain length.

In general, the hydrophobicity of a compound is evaluated from its partition constant between water and a certain organic solvent (*i.e.*, the π value).[12] Figure 10 shows the relationship between the ln r value and the difference in carbon number between alkyl groups in the competition with ethylamine. The ln r value has been linearly correlated with the difference in the carbon numbers of the hydrocarbon residues.[5a] Thus, the ln r values in Phase II can be well explained by the hydrophobicity of hydrocarbon groups.

In the competition of phenethylamine with hexylamine, the slope of the plot in Phase II showed a negative gradient, while in the competition with other, shorter alkylamines, the slopes of plots were positive (Fig. 6(b)). This result can be explained by the published finding that the phenylethyl group is more hydrophobic than the butyl group and less hydrophobic than the hexyl group.[5a]

In the results shown in Fig. 6(b), it is also worthy of note that the slopes of the plots in Phase I are all positive, regardless of their variation from positive to negative in Phase II. These results indicate that the alkyl-phenyl interaction resulting in the differentiation in Phase I has a different character from a conventionally stated hydrophobicity contributing to the differentiation in Phase II.[3,5]

In this study, we have shown that there are two different modes of the differentiation of hydrocarbon groups in the reaction in aqueous media. One is the differentiations is based on the partition of substrates between an aqueous solvent and the hydrophobic aggregates of reagents. The other is the differentiation based on characteristic molecular interactions between homogeneously dissolved substrates and reagents, such as the phenyl-phenyl and alkyl-phenyl interactions. In contrast, the molecular interaction between alkyl groups (an alkyl-alkyl interaction) is not so large as to contribute to this mode of differentiation.

The formation of a hydrophobic domain by the assembly of certain amounts of reagents is necessary for the differentiation of substrates carrying relatively short alkyl chains, since the alkyl-alkyl interaction is weak. This is an important part of understanding the role of the hydrophobic domain in macromolecules such as protein in the differentiation of the molecules carrying small-size alkyl groups. It has been reported that the rate of acylation was remarkably enhanced in an aqueous solvent when both a reagent and a substrate carried a long alkyl group.[9] This phenomenon was interpreted in terms of the "proximity effect" caused by hydrophobic bonding between hydrocarbon residues in aqueous media. However, further, critical reexaminations should be made to prove this proximity effect, as has been pointed out by Guthrie.[10] At least, the results of the present study indicate that the proximity effect is not generally applicable. Especially its contribution to the differentiation of short and medium-size alkyl groups must be negligible.

The differentiation of a phenyl group from an alkyl one could take place to a certain extent by means of a soluble reagent under homogeneous conditions. The present results suggest that aromatic hydrocarbon residues in protein not only provide a hydrophobic domain, but also have some additional functions in the differentiation of hydrocarbon residues. Several facts in the biochemical field support our results. For example, the importance of Trp or Tyr residues in the interfacial recognition site of phospholipase A_2 is well documented.[13] It has also been shown that many aromatic amino acids are neatly located along the antigen binding site of the Bence Jones protein Mcg.[14]

We wish to thank Professor Yoshiharu Izumi, Dr. Hiroshi Ozaki, and Dr. Tadao Harada of Osaka Universoty for their helpful suggestions. Thanks are also due to Mrs. Mihoko Yamamoto, Miss Masako Yamashita, and Mr. Yoichi Kuroda for their valuable assistance.

References

1) B. Giese, *Angew. Chem., Int. Ed. Engl.*, **16**, 807 (1977).

2) J. D. Morrison and H. S. Mosher, "Asymmetric Organic Reaction," Prentice-Hall, Englewood Cliffs, New Jersey (1971), Chaps. 2—9; Y. Izumi and A. Tai, "Stereo-differentiating Reaction," Kodansha, Tokyo, and Academic Press, New York (1977), Chaps. 4—7; "Stereochemistry, Fundamentals and Method," ed by H. B. Kagan, Georg Thieme, Stuttgart (1977), Vol. 3.

3) W. P. Jenks, "Catalysts in Chemistry and Enzymology," McGraw-Hill, New York (1969), Chap. 8.

4) M. S. Newman, ed., "Steric Effects in Organic Chemistry," John Wiley and Son, New York (1955), Chap. 13; M. Charton, *J. Am. Chem. Soc.*, **97**, 1552, 3691 (1975);

5) a) C. Tanford, "The Hydrophobic Effect," John Wiley and Sons, New York (1973), Chap. 2; b) A. B. Baim, "Hydrophobic Interactions," Plenum, New York (1980); c) C. Hansch A. R. Steward, J. Iwasa, and E. W. Deutsch, *Mol. Pharmacol.*, **1**, 205 (1965).

6) Y. Hiraki and A. Tai, *Chem. Lett.*, **1982**, 341.

7) J. F. Kirsch and W. P. Jenks, *J. Am. Chem. Soc.*, **86**, 837 (1964); W.P. Jenks, "Catalysis in Chemistry and Enzymology," McGraw-Hill, New York (1969), Chap. 10.

8) W. P. Jenks and M. Gilchrist, *J. Am. Chem. Soc.*, **90**, 2622 (1968).

9) J. R. Knowles and C. A. Parsons, *Nature* **221**, 53 (1969); C. A. Blyth and J. R. Knowles, *J. Am. Chem. Soc.*, **93**, 3017

(1971); C. A. Blyth and J. R. Knowles, *J. Am. Chem. Soc.*, **93**, 3021 (1971); D. G. Oskenfull, *J. Chem. Soc., Chem. Commun.*, **1655**, (1970); D. Oskenfull, *J. Chem. Soc., Perkin Trans. 2*, **1973**, 1006.

10) J. P. Guthrie, *J. Chem. Soc., Chem. Commun.*, **1972**, 897.

11) C. Reichardt, "Solvent Effects in Organic Chemistry," Verlag Chemie, New York (1979), p, 270.

12) C. Hansch and T. Fujita, *J. Am. Chem. Soc.*, **86**, 1616 (1964).

13) "Lipid-Protein Interaction," ed by P. C. Jost and O. H. Griffith, John Wiley and Sons, New York (1982), Chap. 3.

14) A. B. Edmunson, K. R. Ely, R. L. Girling, E. E. Abola, M. Schiffer, F. A. Westholm, M. D. Fausch, and H. F. Deutsch, *Biochemistry*, **13**, 3816 (1974).

Reaction of 1,8-Naphthalenediamine with Dimethyl and Diethyl Acetylenedicarboxylates

Koichi HONDA,* Hiroshi NAKANISHI, and Akira YABE
National Chemical Laboratory for Industry, Tsukuba, Yatabe, Ibaraki 305

(Received November 12, 1982)

1,8-Naphthalenediamine reacted with dimethyl and diethyl acetylenedicarboxylates, giving rise to tetrahydronaphtho[1,8-*ef*]diazepinones (**2**), dihydroperimidines (**3**) and bis(enamino)fumarates (**4**). The relative yields of **3** and **4** depended on the reaction conditions, while products **2** were always very minor. Products **4**, the yields of which increased considerably in the presence of a large excess of the acetylenes, underwent cyclization at 230 °C leading to quinolinoquinolinediones.

The reaction of amines with acetylenic esters has been investigated in detail.[1] In general, primary monoamines react with acetylenedicarboxylates, giving rise chiefly to the enaminofumarates. In the reaction of aromatic diamines such as *m*-, *p*-phenylenediamines, and 2,2'-biphenyldiamine with dimethyl acetylenedicarboxylate (DMAD), the corresponding bisenamines are formed. Aromatic *vicinal* diamines such as *o*-phenylenediamine and 2,3-naphthalenediamine, however, react with DMAD to give tetrahydroquinoxaline derivatives. On the other hand, in the reaction of 1,8-naphthalenediamine (NDA) with diethyl acetylenedicarboxylate (DEAD), it has been reported that a unique 1 : 1 adduct, 2,3-bis(ethoxycarbonyl)-1,2,3,4-tetrahydronaphtho[1,8-*ef*][1,4]diazepine (**1b**) is formed as a main product, in addition to 3-ethoxycarbonylmethylene-1,2,3,4-tetrahydronaphtho [1,8-*ef*] [1,4] diazepin-2-one (**2b**) which is a product analogous to those from the reactions of *vicinal* diamines.[2]

In connection with the study on the reaction of *peri*-substituted naphthalenes, bis(methoxycarbonyl)tetrahydronaphtho[1,8-*ef*]diazepine (**1a**) was required. Then, the synthesis of **1a** by the reaction of NDA with DMAD was attempted according to the reported method.[2] However, there was found no **1a** in the products, and **2a** was only very minor. The reaction of NDA with DEAD instead of DMAD was also attempted, but the results were similar to those for DMAD, and no **1b** was obtained. We, therefore, have studied the reactions of NAD with DMAD and DEAD in detail.

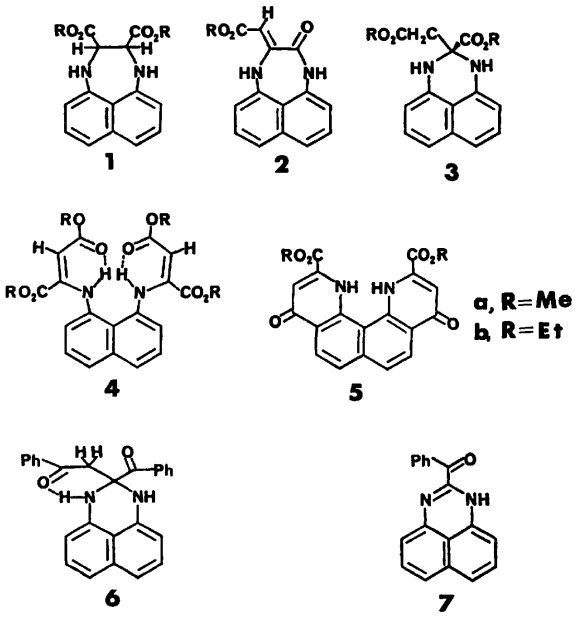

Results and Discussion

There were found two products besides **2** in the reactions. The products were identified by spectroscopic and elementary analyses as a 1 : 1 adduct, 2-methoxycarbonyl-2-methoxycarbonylmethyl-1,2,3-dihydro-1*H*-perimidine (**3a**) and a 1 : 2 adduct, 2,2'-(1,8-naphthylenediimino)difumarate (**4a**) for the reaction with DMAD, and their ethoxycarbonyl derivatives (**3b**) and (**4b**) for the reaction with DEAD. The spectroscopic data of **2a**, **3a**, and **4a** are summarized in Table 1. Identity of the IR spectrum of **3b** with that of **1b** shown in Ref. 2 indicates that **3b** was erroneously assigned as **1b**, one of the structural isomers of **3b**.

In order to elucidate the pathway of the reaction, the equimolar ethanol solutions of NDA and DMAD or DEAD were mixed under several reaction conditions. As shown in Table 2, products **2** were very minor under all the reaction conditions adopted here, while the yields of **3** and **4** depended appreciably on the conditions. Main process of the reaction is the formation of 1 : 1 adducts **3**, but the formation of 1 : 2 adducts **4** becomes efficient in the presence of a large excess of the acetylenes (Conditions **A**). The reactions probably proceed through intermediate monoenamines, although they could not be isolated under our experimental conditions. The results indicate that the intermediates undergo cyclization to **3** in preference to **2** in contrast to the analogous intermediates from *vicinal* diamines which cyclize almost exclusively to the corresponding amides like **2**.[1] At room temperature, the intramolecular cyclization of the intermediates was slow enough to compete with the formation of **4** by the reaction with the second acetylene molecule, but it became a sole process at the refluxing temperature of ethanol (Conditions **D**).

The enamine adducts formed in the reaction of primary aromatic amines with acetylenic esters were usually fumarates and underwent cyclization leading to quinolone derivatives.[1] The IR spectrum of **4a** showed two distinctive absorption bands at 1740 and 1680 cm^{-1}, corresponding to a free and a chelated ester group respectively, and a broad band at 3280 cm^{-1} due to hydrogen-bonded N–H. The IR spectrum of **4b** also showed similar bands. These bands indicate that

TABLE 1. SPECTROSCOPIC DATA OF **2a**, **3a**, AND **4a**

Product	^{1}H NMR[a] δ from TMS	^{13}C NMR[a] δ from TMS	IR (KBr) ν_{max}/cm^{-1}	MS, *m/e* (relative int.)	UV (MeOH) λ_{max}/nm (ϵ_{max})
2a	3.703 (s, 3H, OMe), 5.888 (s, 1H, =CH) 6.877 (d, *J*=7.3 Hz, 1H) 7.174 (d, *J*=7.3 Hz, 1H) 7.332 (dd, *J*=7.3 Hz, *J*=8.0 Hz, 1H) 7.350 (dd, *J*=7.3 HZ, *J*=8.0 Hz, 1H) 7.447 (d, *J*=8.0 Hz, 1H) 7.489 (d, *J*=8.0 Hz, 1H) 10.784 (s, 1H, NH), 10.981 (s, 1H, NH) (aromatic protons)	51.19 (OMe), 93.73 (=CH) 114.12, 114.53, 122.65, 123.62, 126.75 (×2) (aromatic CH) 115.28, 133.34, 136.18 (×2) (aromatic *q*.C) 146.82 (=CNH) 159.71 (amide C=O) 169.75 (ester C=O)	3200 (weak, NH) 1670, 1630 (C=O) 1430 (Me) 1280, 1230 (C-O-C) 805, 745	268 (M$^+$, 50.7) 236 (77.5) 208 (47.0) 153 (63.5) 44 (100.0)	404 (3500) 332 (26800) 324 (sh) 229 (41000)
3a	3.093 (s, 2H, CH_2), 3.547 (s, 3H, OMe) 3.687 (s, 3H, OMe), 6.202 (s, 2H, NH) 6.622 (d, *J*=7.3 Hz, 2H) 7.085 (d, *J*=7.5 Hz, 2H) 7.188 (dd, *J*=7.3 Hz, *J*=7.5 Hz, 2H) (aromatic protons)	60.11 (CH_2), 68.10 (OMe) 68.70 (OMe), 85.82 (HNCNH) 122.18, 133.64, 143.66 (aromatic CH) 129.03, 151.19, 156.47 (aromatic *q*.C) 186.77 (C=O), 188.95 (C=O)	3350 (strong, NH) 1720 (C=O), 1600, 1430, 1360 (Me) 1270, 1210 (C-O-C) 810, 760	300 (M$^+$, 14.0) 241 (91.2) 181 (74.2) 149 (100.0)	343 (10900) 330 (10800) 322 (sh) 232 (41400)
4a	3.605 (s, 6H, OMe), 3.646 (s, 6H, OMe) 5.408 (s, 2H, =CH) 6.978 (d, *J*=6.8 Hz, 2H) 7.455 (dd, *J*=6.8 Hz, *J*=8.2 Hz, 2H) 7.786 (d, *J*=8.2 Hz, 2H) 10.262 (s, broad, 2H, NH) (aromatic protons)	67.18 (OMe), 68.90 (OMe) 110.3 (=CH) 138.39, 142.80, 143.24 (aromatic CH) 139.99, 153.20, 153.83 (aromatic *q*.C) 165.10 (=CNH) 181.13 (C=O), 186.14 (C=O)	3280 (broad, NH, chelated) 1740(C=O), 1680 (C=O, chelated), 1610, 1600 (C=C), 1440, 1360 (Me), 1270, 1220 (C-O-C) 820, 760	442 (M$^+$, 6.9) 383 (100.0) 264 (29.4) 205 (53.9)	340 (sh) 329 (15200) 233(31700)

a) The solvents are DMSO-d_6 for **2a** and acetone-d_6 for **3a** and **4a**.

TABLE 2. RELATIVE YIELDS OF THE PRODUCTS IN THE REACTIONS OF NDA WITH AN EQUIMOLAR AMOUNT OF DMAD OR DEAD IN ETHANOL

Acetylenic diester	Reaction conditions[a]	Product (Relative yield/%)[b]		
DMAD	Conditions **A**	**2a** (1)	**3a** (39)	**4a** (60)
DMAD	Conditions **B**	**2a** (1)	**3a** (70)	**4a** (29)
DMAD	Conditions **C**	**2a** (3)	**3a** (86)	**4a** (11)
DMAD	Conditions **D**	**2a** (0)	**3a** (100)	**4a** (0)
DMAD	Conditions **A**	**2b** (1)	**3b** (78)	**4b** (21)
DMAD	Conditions **C**	**2b** (3)	**3b** (94)	**4b** (3)

a) The reaction conditions are as follows: Conditions **A**, dropwise addition of NDA to the acetylene over 1 h at room temperature; Conditions **B**, similar to Conditions **A** but quick addition; Conditions **C**, dropwise addition of the acetylene to NDA over 1 h at room temperature; Conditions **D**, similar to Conditions **C** but at refuxing temperature of ethanol. b) Based on the molar ratio of the isolated products.

compounds **4** have bis(enamino)fumarate structures with two intramolecular chelates between the N–H and C=O groups. The cyclization of **4a** was attempted by refluxing it in diphenyl ether, and a single product which is slightly soluble in organic solvents was isolated The structure of this product was assigned as 2,11-bis-(methoxycarbonyl) quinolino [7,8-*h*] quinoline - 4,9(1*H*,-12*H*)-dione (**5a**), on the basis of elemental analysis and spectral evidences. Therefore, it was confirmed that **4a** affords a quinolone like other bis(enamino)fumarates. The same is expected to hold for **4b**, although the cyclization was not attempted.

The reaction of NDA with acetylenic esters was found to be quite similar to that with dibenzoylacetylene (DBA). The reaction of NDA with DBA is reported to give a mixture of products consisting of 2-benzoyl-2-phenacyl-2,3-dihydro-1*H*-perimidine (**6**) (9%) and 2-benzoyl-1*H*-perimidine (**7**) (89%).[3] The formation of **7** can be rationalized in terms of loss of one acetophenone molecule from **6**. However, the corresponding perimidines were not formed from **3** under our experimental conditions. It has been reported that two methylene protons of **6** are nonequivalent because of the restricted rotation of the phenacyl group due to the hydrogen-bonding between the N–H and C=O groups.[3] On the other hand, for **3**, the singlet signal for the methylene at around 3 ppm in the ^{1}H NMR spectrum and the strong IR band of the N–H groups at around 3350 cm^{-1} indicated the free rotation of the alkoxycarbonylmethyl group without such chelation. The structural difference between **3** and **6** is very interesting in view of their facility of cyclization, and the chelation in **6** seems to play an important role for its easy conversion to **7**.

Experimental

All melting points were determined on a Mettler FP61 instrument and were uncorrected. ^{1}H NMR and ^{13}C NMR spectra were recorded on a JEOL FX-400 (400.05 MHz for ^{1}H nuclei) and a JEOL FX-90Q (22.50 MHz for ^{13}C nuclei) spectrometer respectively using TMS as an internal standard. Mass, IR and UV spectra were measured with a YHP 595A, a Hitachi 260-30 and a Shimadzu UV-300 apparatus respectively.

Materials. Commercially available NDA was purified by repeated recrystallizations from aqueous ethanol and used immediately after the purification. DMAD and DEAD were purified by distillation under reduced pressure.

Reaction of NDA with DMAD. Ethanol solutions of NDA (1.1 g, 7.0 mmol, 10 ml) and DMAD (1.0 g, 7.0 mmol, 10 ml) were mixed under stirring by the several ways described in Table 2. The mixture was left in a refrigerator (*ca.* −10 °C) overnight, from which **2a** and **4a** precipitated. On treatment of the precipitate with $CHCl_3$ at room temperature, **2a** and **4a** were separated as an undissolved product and a dissolved one respectively. Recrystallization of the undissolved product from ethanol gave pure **2a** as silky red needles; mp>300 °C. Found: C, 67.00; H, 4.55; N, 10.26%. Calcd for $C_{15}H_{12}O_3N_2$: C, 67.16; H, 4.51; N, 10.44%. Recrystallization of the dissolved product from ethanol gave pure **4a** as yellow-brown needles; mp 146 °C. Found: C, 59.66; H, 5.10; N, 6.12%. Calcd for $C_{22}H_{22}O_8N_2$: C, 59.73; H, 5.01; N, 6.33%.

From the concentrated mother liquor kept in a refrigerator for a week, **3a** was obtained as a massive precipitate. Recrystallization of the precipitate from ethanol gave pure **3a** as white needles; mp 99 °C. Found: C, 63.79; H, 5.43; N, 9.09%. Calcd for $C_{16}H_{16}O_4N_2$: C, 63.99; H, 5.37; N, 9.33%.

The spectroscopic data of **2a**, **3a**, and **4a** are shown in Table 1. The yields of **2a**, **3a**, and **4a** were as follows respectively: Conditions **A**, 0.01 g (0.53%), 0.39 g (18.6%), and 0.90 g (29.1%); Conditions **B**, 0.01 g (0.53%), 0.81 g (38.5%), and 0.51 g (16.5%); Conditions **C**, 0.05 g (2.7%), 1.35 g (64.2%), and 0.25 g (8.1%); Conditions **D**, 0 g (0%), 1.70 g (80.9%), and 0 g (0%).

Reaction of NDA with DEAD. The reaction was carried out in the same manner as that with DMAD by using 1.1 g (7.0 mmol) of NDA and 1.2 g (7.0 mmol) of DEAD. Sparingly soluble **2b** precipitated from the reaction mixture. Recrystallization of the precipitate from ethanol gave pure **2b** as red silky needles; mp>300 °C. Found: C, 67.24; H, 5.07; N, 9.59%. Calcd for $C_{16}H_{14}O_3N_2$: C, 68.08; H, 5.00; N, 9.92%. ^{13}C NMR (DMSO-d_6) 14.16 (CH_3), 59.82 (OCH_2), 94.51 (=CH), 114.14, 114.65, 122.67, 123.69, 126.77(doubled) (aromatic CH), 115.15, 133.46, 136.30, 136.34 (aromatic *q*.C), 146.89 (=CNH), 159.93 (CONH), 169.46 (CO_2Et). ^{1}H NMR (DMSO-d_6) δ 1.299 (t, J=7.0 Hz, 3H, CH_3), 4.243 (q, J=7.0 Hz, 2H, OCH_2), 6.009 (s, 1H, =CH), 6.963 (d, J=7.3 Hz, 1H), 7.239 (d, J=7.3 Hz, 1H), 7.387 (dd, J=7.8, 8.1 Hz, 1H), 7.392 (dd, J=7.3, 8.1 Hz, 1H) 7.494 (d, J=8.1 Hz, 1H), 7.546 (d, J=7.8 Hz, 1H) (aromatic protons), 10.841 (s, 1H, NH), 11.038 (s, 1H, NH).

The concentrated mother liquor left in a refrigerator for a week gave a massive precipitate of **3b**. On recrystallization from ethanol, pure **3b** was obtained as white needles; mp 80 °C. Found: C, 65.73; H, 6.11; N, 8.46%. Calcd for $C_{18}H_{20}O_4N_2$: C, 65.84; H, 6.14; N, 8.53%. ^{13}C NMR (acetone-d_6) δ 30.26 ($2CH_3$), 60.11 (CH_2CO), 77.37, 77.83 (OCH_2), 85.74 (HNCNH), 122.15, 133.58, 143.58 (aromatic CH), 129.19, 151.13, 156.58 (aromatic *q*.C), 186.24, 188.19 (C=O). ^{1}H NMR (acetone-d_6) δ 1.039 (t, J=7.1 Hz, 3H, CH_3), 1.254 (t, J=7.1 Hz, 3H, CH_3), 3.079 (s, 2H, CH_2), 4.015 (q, J=7.1 Hz, 2H, OCH_2), 4.168 (q, J=7.1 Hz, 2H, OCH_2), 6.179 (s, 2H, NH), 6.621 (d, J=7.4 Hz, 2H), 7.083 (d, J=8.3 Hz, 2H), 7.188 (dd, J=7.4, 8.3 Hz, 2H) (aromatic protons).

Removal of the solvent from the residual ethanol solution gave a mass which was chromatographed over silica gel. Elution of the column with a mixture (9 : 1) of petroleum ether (boiling range, 30—70 °C) and ether gave **4b** and **2b** as the first and the second eluted compounds respectively. Pure **4b** was obtained by recrystallization from ethanol as yellow needles; mp 92 °C. Found: C, 62.49; H, 6.03; N, 5.58%. Calcd for $C_{26}H_{30}O_8N_2$: C, 62.64; H, 6.07; N, 5.62%. ^{13}C NMR (acetone-d_6) δ 29.93, 30.80 (CH_3), 76.31, 78.37 (OCH_2), 110.28 (=CH), 138.92, 142.85, 143.33 (aromatic CH), 140.60, 153.16, 154.12 (aromatic *q*.C), 165.63 (=CNH), 180.75, 185.89 (C=O). ^{1}H NMR (acetone-d_6) δ 0.879 (t, J=7.1 Hz, 6H, $2CH_3$), 1.232 (t, J=7.1 Hz, 6H, $2CH_3$), 4.041 (q, J=7.1 Hz, 4H, $2OCH_2$), 4.111 (q, J=7.1 Hz, 4H, $2OCH_2$), 5.385 (s, 2H, 2=CH), 6.955 (d, J=6.8 Hz, 2H), 7.432 (dd, J=6.8, 8.4 Hz, 2H), 7.763 (d, J=8.4 Hz, 2H) (aromatic protons), 10.239 (s, broad, 2H, 2NH).

UV, IR, and mass spectra of **2b**, **3b**, and **4b** are similar to those of **2a**, **3a**, and **4a** respectively. The yields of **2b**, **3b**, and **4b** were as follows respectively: Conditions **A**, 0.01 g (0.51%), 0.81 g (35.2%), and 0.41 g (11.7%); Conditions **C**, 0.04 g (2.0%), 1.60 g (69.6%), and 0.08 g (2.3%).

Preparation of 5a. A mixture of **4a** (0.3 g, 0.7 mmol) and diphenyl ether (5 ml) was heated at 230 °C for 30 min. The precipitated product was filtered and treated with ether to give **5a** (0.15 g, 58% yield) as pale yellow foils, which is sparingly soluble in usual organic solvents; mp>300 °C. Found: C, 62.65; H, 3.73; N, 7.16%. Calcd for $C_{20}H_{14}O_6N_2$: C, 63.50; H, 3.73; N, 7.40%. ^{1}H NMR (DMSO-d_6) δ 4.066 (s, 6H, $2OCH_3$), 6.278 (s, broad, 2H, NH), 7.290 (s, 2H, 2=CH), 7.801 (d, J=8.2 Hz, 2H), 8.140 (d, J=8.2 Hz, 2H) (aromatic protons). IR (KBr) ν_{max} 1735 (ester C=O), 1610 (ring C=O), 1540, 1515 (C=C), 1440, 1350 (CH_3), 1215 (C–O–C) cm^{-1}. UV (methanol) λ_{max} (ε_{max}) 393 (13300), 374 (10700), 330 (sh), 322 (12700), 307 (sh), 278 (sh), 271 (sh), 249 (19700), 235 (20600), 221 (sh), 216 (37300) nm.

References

1) M. V. George, S. K. Khetan, and R. K. Gupta, "Advances in Heterocyclic Chemistry" ed by A. R. Katritzky and A. J. Boulton, Academic Press, New York (1976), Vol. 19, pp. 279—371, and the references cited therein.

2) Y. Iwanami, *Nippon Kagaku Zasshi* **83**, 597 (1962).

3) S. Lahiri, M. P. Mahajan, R. Prasad, and M. V. George, *Tetrahedron* **33**, 3159 (1977).

 © 1983 The Chemical Society of Japan Bull. Chem. Soc. Jpn., 56, 2341—2347 (1983)

Ionic Composition of Micelles and the Dissolved State of the Mixed Surfactant Solutions of Calcium and Sodium Decyl Sulfates

Masakatsu KOSHINUMA

Laboratory of Chemistry, Faculty of Education, Chiba University, Chiba 280

(Received February 20, 1982)

Single activities of the decyl sulfate (DeS^-), the calcium (Ca^{2+}), and the sodium (Na^+) ions in mixed surfactant solutions of varying mole ratios (R_m=$Ca(DeS)_2$/NaDeS) were obtained at 30±1 °C by means of three kinds of EMF cells with ion-exchange membranes or Na^+-selective electrode. The results showed that with increasing concentrations above the cmc, the activity of the DeS^- decreases gradually, while that of the Na^+ increased linearly; the activity of the Ca^{2+} remained nearly constant in the solution of $R_m=2$, but it showed a minimum in the solutions of $R_m=1$, 0.5 and 0.2. From these activities, the counterion attachments of the Ca^{2+}(r_{Ca}) and the Na^+(r_{Na}) and the degree of micellar charge ($1-2r_{Ca}-r_{Na}$) were obtained. With increasing concentration, r_{Ca} diminished gradually and approached a constant value, while r_{Na} and $1-2r_{Ca}-r_{Na}$ changed reversely except in the solution of $R_m=2$ where they were nearly constant. The Ca^{2+} was bound preferentially to the micelle surface. The Na^+, which almost diffused away for the solution of $R_m=2$, bound increasingly to lessen the electrical potential of the micelle as R_m decreased. The specific adsorption potentials and the electrical free energies of transfer of Ca^{2+} and Na^+ from solution to micelle were calculated as 1.7 and −18.4 kJ mol^{-1}, and 1.1 and −14.3 kJ mol^{-1} respectively at their cmcs. It was showed clearly that little dehydration from the counterion occured and the coulombic interaction played an important role in the counterion binding.

It is well known that valences of counterions of ionic surfactants and of added electrolytes influence markedly both the micellization and the micellar properties of surfactant solutions. A number of authors have shown that the electrical potential at the micelle surface played an important role in the formation of micelles.[1] For solutions of mixed surfactants, it has been shown that the cmc value, the ionic composition and the dissociation of micelles changed greatly depending on the valence and the concentrations of each counterion.[2,3] In explanation of the changes in the cmc, Shinoda formulated some theoretical equations,[1,4] further, Lange[5] and Moroi *et al.*[6] have independently proposed the theoretical relations.

On the other hand, the dissolved state of micellar solution containing counterions with different valences can not be clarified unless the behavior of each ion in the mixed solution is investigated separately. Recently the behavior and activities of single ions have been studied by means of the electromotive force measurements using ion-selective electrodes[7-9] or ion-exchange membranes[10-12] in the single surfactant solutions and in the solutions of the added electrolyte.[13] In the present paper, the degrees of dissociation of micelles and the ionic composition of the counterion in the micelles are studied in solutions of mixed surfactants of different valences on the basis of the single ionic activities. Furthermore, the standard free energies and the coulombic interaction energies of counterions transferring from solution to micelle surface will be calculated and discussed.

Experimental

Materials. The surfactants, calcium ($Ca(DeS)_2$) and sodium (NaDeS) decyl sulfates, were synthesized and purified in the normal way.

Electromotive Force Measurements. In order to investigate the single ionic behavior of the decyl sulfate ion (DeS^-), the calcium ion (Ca^{2+}), and the sodium ion (Na^+) in the mixed surfactant solution, three kinds of cell systems were used for the measurement of the electromotive force. For the DeS^-, a concentration cell was constructed as follows.

Saturated Ag–AgCl electrode	2 mol dm^{-3}-NH_4NO_3, 2%-Agar bridge	Sample solution $Ca(DeS)_2$+NaDeS	Anion-exchange membrane AV-4T
Standard solution NaDeS	2 mol dm^{-3}-NH_4NO_3, 2%-Agar bridge	Saturated Ag–AgCl electrode.	

The solutions of 10.0 and 2.0 mmol dm^{-3} of NaDeS were used as standards for the sample solutions having the concentrations above and below 2.0 mmol dm^{-3} of the DeS^-. The electrical potential developing across the membrane is termed E_{DeS}. For the Ca^{2+}, the multi-ionic potential was measured and the following cell was used:

Saturated Ag–AgCl electrode	2 mol dm^{-3}-NH_4NO_3, 2%-Agar bridge	Sample solution $Ca(DeS)_2$+NaDeS	Cation-exchange membrane Cl-25T
Standard solution NaDeS	2 mol dm^{-3}-NH_4NO_3, 2%-Agar bridge	Saturated Ag–AgCl electrode,	

where the solution of 10.0 mmol dm^{-3} of NaDeS was also used as the standard solution. The potential generated on the membrane is denoted as E_{Ca}. The potentials of E_{DeS} and E_{Ca} were measured at 30±1 °C by means of an electrometer (Keithly, model 610C), and were recorded as functions of time. Other experimental conditions and procedures were the same as in a previous paper.[14]

For the Na^+, the following cell was also set up:

Saturated Ag–AgCl electrode	2 mol dm^{-3}-NH_4NO_3, 2%-Agar bridge	Sample solution $Ca(DeS)_2$+NaDeS	Na^+-selective electrode

The potential, E_{Na}, of sodium-ion selective electrode (Horiba mfg. Co., model pNa-A) was measured with a pH meter (Hitachi-Horiba, model F-5) and recorded as a function of time.

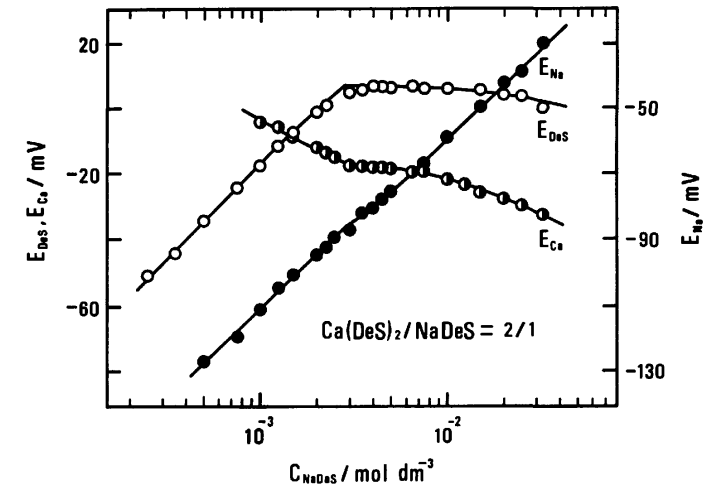

(a)

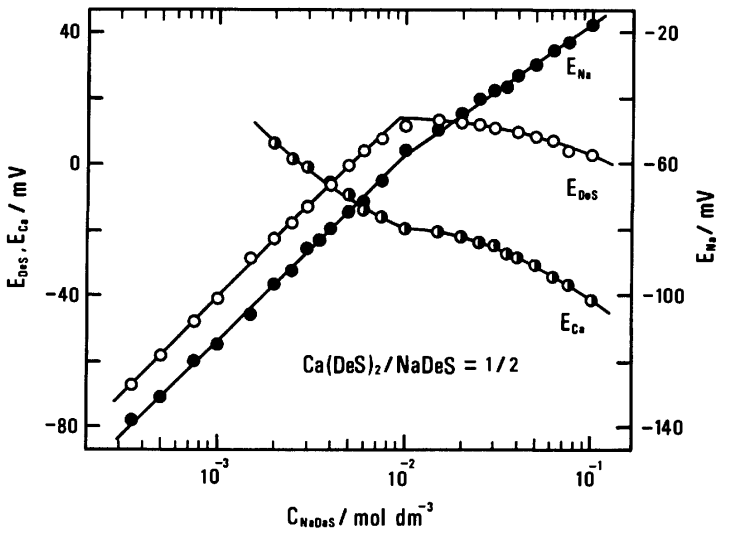

(b)

Fig. 1. The electromotive force against the concentration of NaDeS in the mixed surfactant solutions of varying mole rations (R_m=Ca(DeS)$_2$/NaDeS).

Results and Discussion

Calculation of Single Ionic Activities. The observed values of E_{DeS}, E_{Ca}, and E_{Na} in the mixed surfactant solutions of R_m=2 and 0.5 (R_m: mole ratio of Ca(DeS)$_2$ to NaDeS) are plotted against the logarithmic concentration of NaDeS in Figs. 1a and b. From these EMF, the single ionic activities, though they are conventionally defined, can be calculated in terms of the following equations. According to the Nernst equation,

$$E_{DeS} = (2.303\,RT/F)\log(a_{DeS}/a_{ODeS}), \quad (1)$$

where R, T, and F denote the gas constant, the absolute temperature, and the Faraday constant. The activities of the DeS$^-$ in the sample and in the standard solutions are represented as a_{DeS} and a_{ODeS}, respectively. Since a_{ODeS} is obtained by the same procedure as in a previous paper,[14] the values of a_{DeS} can be calculated.

The multi-ionic potential is given by[15]

$$E_{Ca} = (2.303\,RT/F)[(a_{Na}+Ua_{Ca}-a_{ONa})/(a_{Na}+2U\,a_{Ca}-a_{ONa})]\log[a_{ONa}/(a_{Na}+2Ua_{Ca})], \quad (2)$$

where U is the ratio of the mobility of Ca^{2+} to that of Na^+ in the membrane, a_{ONa}, a_{Na}, and a_{Ca} denote the activities of the Na^+ in the standard solution, of the Na^+ and of the Ca^{2+} in the sample solution, respectively. Since a_{ONa} has been obtained as 9.16 mmol dm^{-3} in the solution of 10.0 mmol dm^{-3} of single NaDeS in the previous study,[14] the value of a_{Ca} can be calculated if those of U and a_{Na} are known exactly.

For Na^+, E_{Na} is also expressed;

$$E_{Na} = (2.303\,RT/F)\log(a_{Na}+K_{NaCa}a_{Ca}^{1/2}), \quad (3)$$

where K_{NaCa} is a selective factor of the Na^+ to the Ca^{2+}. The values of U and K_{NaCa} are functions of a_{Ca} and a_{Na} and must be known in the mixed surfactant solution prior to calculation. Unfortunately we can find neither U, K_{NaCa} nor a_{Ca} and a_{Na} in the literature. Therefore we measured the values of U and K_{NaCa} by use of mixed solutions of $CaCl_2$–NaCl at various mole ratios. From these, the single ionic activities of the Ca^{2+} and the Na^+ can be calculated with the assumption of pH convention.[16] Namely, the activity coefficient of

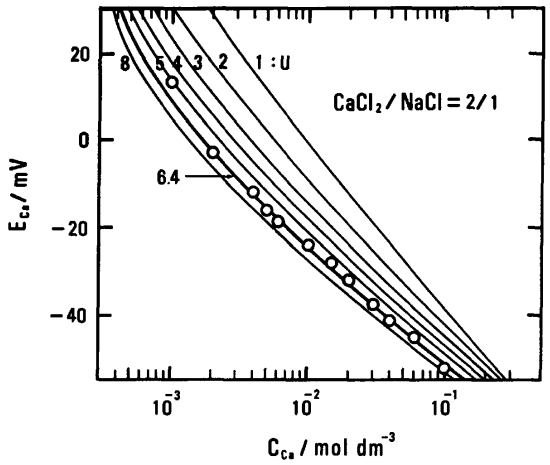

Fig. 2. Comparison of the observed E_{Ca} with the calculated E_{Ca} by use of the pH convention.
——: The calculated value. ○: the observed value.

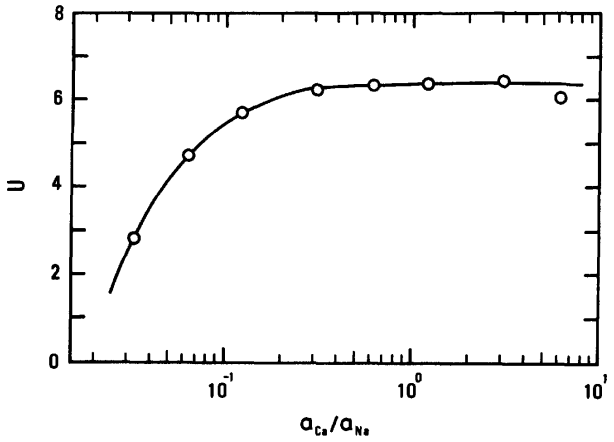

Fig. 3. The relationship between U and a_{Ca}/a_{Na}.
The activity ratio was determined at about 25 mmol dm^{-3} of total Cl^- concentration in the mixed solution.

chloride ion(f_{Cl}) is assumed,

$$\log f_{Cl} = -(0.516 \cdot I^{1/2})/(1+1.552 \cdot I^{1/2}), \quad (4)$$

where I is the total ionic strength in the solution. According to the Debye-Hückel theory, the mean activity coefficients of $CaCl_2$(f_{CaCl_2}) and of NaCl(f_{NaCl}) are given as follows;

$$\log f_{CaCl_2} = -(1.032 \cdot I^{1/2})/(1+1.552 \cdot I^{1/2}), \quad (5)$$

and

$$\log f_{NaCl} = -(0.516 \cdot I^{1/2})/(1+1.320 \cdot I^{1/2}), \quad (6)$$

where the mean radii of hydrated ions in $CaCl_2$ and NaCl are assumed as 4.7 and 4.0 Å, respectively. From the definition of the mean activity coefficient, we also have

$$3\log f_{CaCl_2} = 2\log f_{Cl} + \log f_{Ca}, \quad (7)$$

and

$$2\log f_{NaCl} = \log f_{Cl} + \log f_{Na}, \quad (8)$$

where f_{Ca} and f_{Na} denote the activity coefficients of the Ca^{2+} and the Na^+, respectively. In the mixed solution, a_{Ca} can be calculated from Eqs. 4, 5, and 7, and a_{Na} also from Eqs. 4, 6, and 8. By use of a_{Ca} and a_{Na} values obtained, U and K_{NaCa} can be determined from Eqs. 2 and 3. For example, Fig. 2 shows the curves of E_{Ca} calculated as a function of C_{Ca} with varying U and the observed values of E_{Ca}. In this calculation, the most suitable value of U was chosen as that for which the calculated E_{Ca} coincided with the experimental values. When 6.4 was adopted as U, they agreed fairly with each other except at low concentration. Figure 3 shows the U values determined in the various mixed solutions. The K_{NaCa} values, which were also determined from a_{Ca}, a_{Na}, and E_{Na} in the various mixed solutions by Srinivasan's method,[17] are shown in Fig. 4.

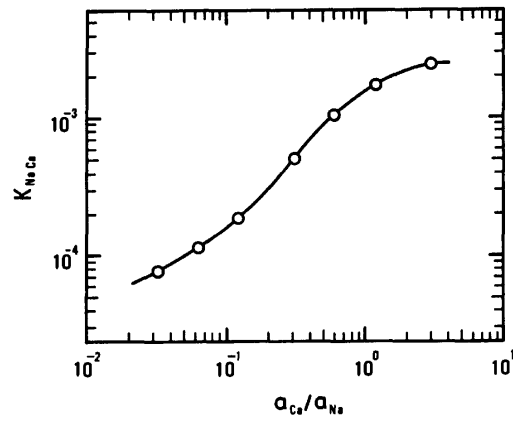

Fig. 4. The relationship between K_{NaCa} and a_{Ca}/a_{Na}.

When the values of U and K_{NaCa} are used, a_{Ca} and a_{Na} in the mixed surfactant solutions can be computed from E_{Ca} and E_{Na} through the following successive calculations. First, a_{Na} was calculated from E_{Na} by Eq. 3, where K_{NaCa} was assumed to be zero because of its small value, and then a_{Ca} could be also obtained from the value of a_{Na} calculated above and E_{Ca} by Eq. 2, where the U value was determined with the assumption that a_{Ca}/a_{Na} was equal to C_{Ca}/C_{Na} in Fig. 3. Secondly, the K_{NaCa} value was also determined from a_{Ca}/a_{Na} in Fig. 4 by use of the values of a_{Ca} and a_{Na} obtained, and then a_{Na} was recalculated by Eq. 3. Moreover, a_{Ca} could be calculated again by Eq. 2 when the values of a_{Na} obtained above and of U determined from a_{Ca}/a_{Na} in Fig. 3 were used. This successive calculation having been performed, the activities were finally obtained as the converged values.

Figures 5a and b show a_{Ca} and a_{Na} together with a_{DeS} in the mixed surfactant solutions of $R_m=2$ and 0.5. The activities of all the ions increase linearly with the surfactant concentration up to the cmc. With an increase in the concentration above the cmc, a_{DeS} decreases. This shows that the smaller the R_m value becomes, a_{DeS} decreases slightly more steeply. Contrarily, a_{Na} increases linearly giving a break point in the curve of a_{Na} against the concentration of NaDeS; the slope of the curve above the CMC reduces as the R_m value decreases. Moreover, a_{Ca} in the solution of $R_m=2$ remains almost constant, but those of $R_m=1$, 0.5 and 0.2 show minima; the sum of the activities of the three kinds of ions in the mixed solution increases gradually with the the concentration in the same manner as in the solution of each single surfactant. From the fact that a_{Na} increases linearly with the concentration without a change in the slope of the curve of a_{Na} against concentration at the

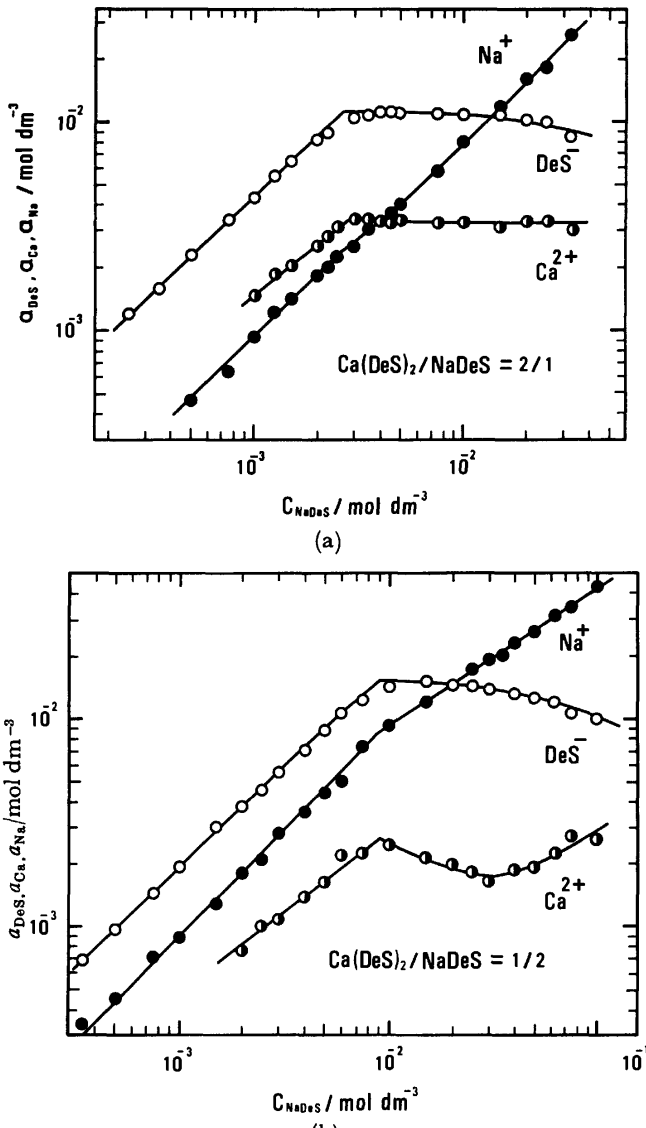

Fig. 5. The single ionic activities against the concentration of NaDeS in the mixed surfactant solutions of varying mole ratios.

TABLE 1. THE VALUES OF CMC IN THE TOTAL CONCENTRATION OF THE DeS^- AND OF K AND L IN EQ.10 IN THE MIXED SURFACTANT SOLUTIONS OF VARYING MOLE RATIO

R_m=Ca(DeS)$_2$/NaDeS	1/0	2/1	1/1	1/2	1/5	0/1
cmc / mmol dm^{-3}	12.8	13.5	14.4	18.4	22.4	32.8
K		0.052	0.049	0.046	0.039	
L		0.186	0.181	0.147	0.153	

cmc, it is suggested that most of the Na^+ in the solution of R_m=2 remains in the intermicellar solution. Further, from the decrease in the slope above the cmc with the decrease in R_m, the Na^+ may be considered to bind gradually on the micelle surface. These results can be explained by a change in the ionic composition which depends on the coulombic interaction of counterion with negatively charged micelles. Thus, the ionic composition of micelle will be determined and discussed later.

The cmcs in the mixed solutions are shown in Table 1 where these values were determined as the averages of the breaking points in the curves of activity *vs.* surfactant concentration.

Dissociation and Ionic Composition of Micelle. The valence effects of counterions on the dissociation of the micelle and on the mechanism of micelle formation have been studied in a previous paper.[14] In the mixed micellar solution of ionic surfactants, having counterions of uni and bivalence, it has been suggested that the binding of bivalent counterion occurred on the micelle surface in preference to the univalent one.[2,3] Thus the ionic composition of the micelles and the degree of micellar charge need to be investigated.

If a micelle is composed of p DeS^-, q Na^+, and s Ca^{2+} ions in equilibrium, the micelle formation is expressed by

$$p\,DeS^- + q\,Na^+ + s\,Ca^{2+} \rightleftharpoons M'$$

$$M: [D_pS_pNa_qCa_s]^{-(p-q-2s)}$$

and $$a_M/(a_{DeS}{}^p \cdot a_{Na}{}^q \cdot a_{Ca}{}^s) = K'_M,$$

where a_M is the activity of micelle and K'_M, a constant. This equation is rewritten;

$$\log a_{DeS} + r_{Na}\log a_{Na} + r_{Ca}\log a_{Ca} = (1/p)\log(a_M/K'_M) = K_M, \quad (9)$$

here, $r_{Na}(=q/p)$ and $r_{Ca}(=s/p)$ denote the counterion attachments of the Na^+ and of the Ca^{2+}, respectively. If p, q, s, a_M, and K_M are constant and independent of the surfactant concentration the phase separation theory,[18] which has described satisfactorily the formation of micelles in solutions of single NaDeS and Ca(DeS)$_2$,[14] is applicable. The solution of R_m=2 is this special cases so r_{Ca} and r_{Na} can be obtained by Eq. 9 because of the constants of a_{Ca} and K_M. But if p, q, and s change with the concentration, r_{Ca} and r_{Na}, in general, can not be calculated unless the value of K_M is given: K'_M and K_M also change.

On the other hand, we can compute r_{Ca} and r_{Na} from the intermicellar concentrations of the $DeS^-(C_{DeS})$, the $Ca^{2+}(C_{Ca})$ and the $Na^+(C_{Na})$ in the solution having the concentrations of C_{CaDeS} of Ca(DeS)$_2$ and C_{NaDeS} of NaDeS: $r_{Ca} = (C_{CaDeS} - C_{Ca})/(2C_{CaDeS} + C_{NaDeS} - C_{DeS})$ and $r_{Na} = (C_{NaDeS} - C_{Na})/(2C_{CaDeS} + C_{NaDeS} - C_{DeS})$. The values of C_{DeS}, C_{Ca}, and C_{Na} are given through the arrows illustrated schematically in Fig. 6; presence of micelle is assumed to give no effect on each activity coefficient of singly dispersed ions. Thus, C_{DeS} and C_{Ca} can be obtained provided the activity coefficient corresponding to the activity above the cmc is taken to be equal to that corresponding to the same activity below the cmc. C_{Na} is obtained with an aid of the dashed line. This is determined from the activity coefficient(f^s_{Na}) calculated with the assumption that the linear relation which holds between its activity coefficient and concentration below the cmc is also applicable to that of the Na^+ in the intermicellar solution above the cmc. Below the cmc, f^s_{Na} was successfully expressed by

$$\log f^s_{Na} = -(K\log C_{NaDeS} + L), \quad (10)$$

where K and L are the constant values which are sum-

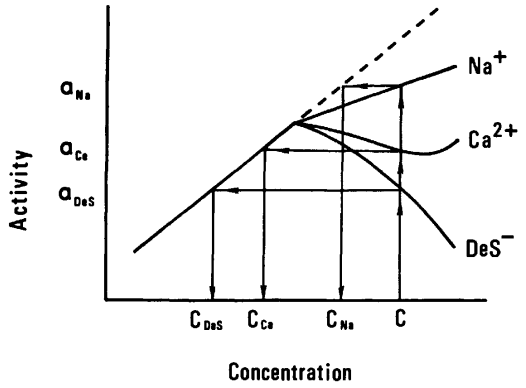

Fig. 6. Schematic description of determination of the intermicellar concentrations; C_{DeS}, C_{Ca}, and C_{Na} in the surfactant concentration of C are given through arrows. The dashed line is calculated with the assumption that the activity coefficient is given by the equation: $\log f_{Na} = -(K \log C_{NaDeS} + L)$.

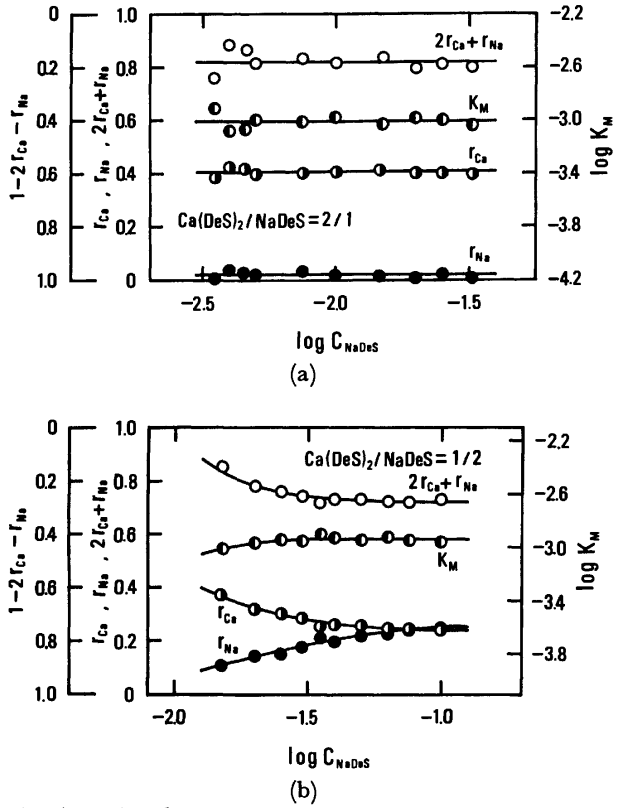

Fig. 7. The degrees of counterion attachment of the Ca^{2+} (r_{Ca}), of the Na^+ (r_{Na}), of dissociation of micelle ($1-2r_{Ca}-r_{Na}$) and the value of log K_M against the concentration of NaDeS.

marized in Table 1 for the solution of varying R_m.

Figure 7a expresses r_{Ca} and r_{Na} together with the degree of micelle charge ($1-2r_{Ca}-r_{Na}$) in the solution of $R_m=2$ showing that they are nearly constant and independent of the concentration within an experimental error. As R_m becomes smaller, r_{Ca} decreases more steeply with the concentration, and it approaches asymptopically to a constant at high concentration as shown in Fig. 7b; r_{Na} and $1-2r_{Ca}-r_{Na}$ change reversely. The assumption of Eq. 10 may be applicable just above the cmc, but it

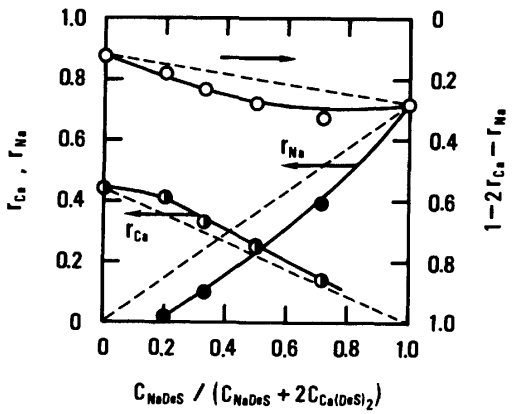

Fig. 8. The ionic composition of micelle and the degree of dissociation of micelle against the composition of the mixed surfactants.

should be tested at higher concentrations. If the assumption of Eq. 10 as well as the phase separation theory are set up, the value of K_M in Eq. 9 must be constant at the higher concentrations where r_{Ca} and r_{Na} are constant. The calculated values of K_M are shown in Figs. 7a and b, indicating that they do become constant at the high concentrations of various R_m and particularly K_M for the solution of $R_m=2$ is independent of the concentration. Therefore, the micelle formation in the mixed surfactant solution can be described by the phase separation theory at least in the solution of $R_m=2$ and in the high concentrations. The values obtained for r_{Ca}, r_{Na}, and $1-2r_{Ca}-r_{Na}$ suggest the following interpretation. Just above the cmc, the Ca^{2+} is bound on the micelle surface by the strong coulombic interaction in preference to the Na^+ from the intermicellar solution. The remaining $Na^+(C_{Na})$ increases with an increase in the surfactant concentration; the ratio of a_{Na}/a_{Ca} increases rapidly, therefore, r_{Na} increases and r_{Ca} reduces gradually. An increase in the total intermicellar concentration due to that in C_{Na} shields mainly the electrical potential at the micelle surface and consequently increases $1-2r_{Ca}-r_{Na}$.

The converged values of r_{Ca}, r_{Na}, and $1-2r_{Ca}-r_{Na}$ are plotted against the composition of mixed surfactant in Fig. 8, and these make the ionic composition of the micelle clearer. The dashed line indicates each calculated value from the assumption that r_{Ca} and r_{Na} vary proportionally to the fraction of each surfactant in the solution. The Ca^{2+} are bound preferentially on the micelle while the Na^+, which remains in the intermicellar solution of $R_m=2$, binds progressively to lessen the electical potential as R_m decreases; $1-2r_{Ca}-r_{Na}$ becomes larger mainly because of the shielding effect due to the increase in C_{Na} with the increasing content of NaDeS.

Specific Adsorption Potentials of the Ca^{2+} and the Na^+ Ions. With regard to the preferential binding of the Ca^{2+} on the micelle surface, free energies of transfer of counterions from solution to micelle surface, which have been referred to as specific adsorption potentials[19] and calculated,[3,19,20] are determined in the solution of two single surfactants for simplicity in calculation. In a solution of $Ca(DeS)_2$, we assume that a micelle consists of p DeS^- ions and $p \cdot r_{Ca} (=q)$ Ca^{2+} ions bound on the micelle surface and has $p(1-2r_{Ca})\varepsilon$ charges.

Equilibrium of the Ca^{2+} between the bulk phase and the micelle surface region is described by an equality of each electrochemical potential, $\bar{\mu}_{bCa}=\bar{\mu}_{mCa}$, in the two phases;

$$\bar{\mu}_{bCa} = \mu^{\circ}_{bCa} + kT\ln a_{Ca}, \quad (11)$$

$$\bar{\mu}_{mCa} = \mu^{\circ}_{mCa} + kT\ln C_{mCa} + \int_0^{2\varepsilon}\phi_{mCa}dQ + W_{mCa}. \quad (12)$$

Here, $\bar{\mu}_{bCa}$, $\bar{\mu}^{\circ}_{bCa}$, $\bar{\mu}_{mCa}$, and $\bar{\mu}^{\circ}_{mCa}$ are the electrochemical and the standard chemical potentials in the bulk phase and in the micelle surface region, respectively; C_{mCa} the concentration of the Ca^{2+} bound in the micellar surface region of volume V_{Ca} and W_{mCa}, a free energy related to hydration of the ion. Further, it is assumed that the electrical free energy may be given by the electrical work done, $\int_0^{2\varepsilon}\phi_{mCa}\,dQ$, when the Ca^{2+} having charge Q are brought about up to the micelle surface. The electrical potential, ϕ_{mCa}, at the micelle surface is given by[4]

$$\phi_{mCa} = -(kT/2\varepsilon)[\ln(2000\pi\cdot\sigma^2/DNkT) - \ln C_{Ca}]. \quad (13)$$

Here, D and N denote the dielectric constant of water and the Avogadro number, respectively; C_{Ca}, the intermicellar concentration of the Ca^{2+} which has been calculated theoretically in a previous paper.[14] The surface charge density of the micelle, σ, is expressed as follows;

$$\sigma = -(\varepsilon - r_{Ca}Q)/A_{CaD}, \quad (14)$$

where A_{CaD} is the molecular area occupied by the DeS^- at the surface of $Ca(DeS)_2$ micelle.

The concentration of the Ca^{2+} in the micelle surface region can be written as

$$C_{mCa} = 1000p\cdot r_{Ca}/NV_{Ca}. \quad (15)$$

If the thickness of the Stern layer can be assumed to be equal to the diameter, h_{Ca}, of the hydrated Ca^{2+}

$$V_{Ca} = pA_{CaD}h_{Ca} \quad (16)$$

is set up. From Eq. 11 to Eq. 16, we obtain the following relation,

$$\ln a_{Ca} = \Delta\mu^{\circ}_{tNa}/kT + \ln[DkTr_{Ca}A_{CaD}C_{Ca}/2\pi h_{Ca}\varepsilon^2(1-2r_{Ca})^2] + (1/r_{Ca})\ln(1-2r_{Ca}) + 2 + \Delta W_{tCa}, \quad (17)$$

where $\Delta\mu^{\circ}_{tCa}=\mu^{\circ}_{mCa}-\mu^{\circ}_{bCa}$ is a standard free energy of transfer of the Ca^{2+} from solution to micelle; similarly, ΔW_{tCa}, a hydration free energy of transfer due to changes in the state of hydration.

Similarly, in a solution of NaDeS,[3]

$$\ln a_{Na} = \Delta\mu^{\circ}_{tNa}/kT + \ln[DkTr_{Na}A_{NaD}C_{Na}/2\pi h_{Na}\varepsilon^2(1-r_{Na})^2] + 2[(1/r_{Na})\ln(1-r_{Na}) + 1] + \Delta W_{tNa} \quad (18)$$

is given, where $\Delta\mu^{\circ}_{tNa}=\mu^{\circ}_{mNa}-\mu^{\circ}_{bNa}$, A_{NaD}, h_{Na}, and ΔW_{tNa} correspond to those for the Ca^{2+}, respectively.

The specific adsorption potentials, $\Delta\mu^{\circ}_{s}+\Delta W_t$, can be calculated by Eqs. 17 and 18 if, A_{CaD}, h_{Ca}, A_{NaD}, and h_{Na} are given, because D, k, T, and ε are constant values, while a_{Ca}, a_{Na}, C_{Ca}, C_{Na}, $r_{Ca}(=0.44)$, and $r_{Na}(=0.72)$ have been obtained and reported in a previous paper.[14] Values of 4.6[3] and 6.2 Å, calculated by Stokes law based on the limiting mobility, are used for h_{Na} and h_{Ca} respectively. For A_{NaD} and A_{CaD}, values of 53.6 and 43.7 $Å^2$ molecule^{-1} have been calculated from the saturated amount of adsorption at the air/solution interfaces.[21,22] These values are employed respectively instead of those at the micelle surface. At the cmc, $\Delta\mu^{\circ}_{tNa}+\Delta W_{tNa}$ is computed as 1.1 kJ mol^{-1}, which fairly agrees with 1.3 kJ mol^{-1} expected theoretically,[19] when $a_{Ca}=25.1$ mmol dm^{-3} and $C_{Na}=32.8$ mmol dm^{-3}; $\Delta\mu^{\circ}_{tCa}+\Delta W_{tCa}$ is 1.7 kJ mol^{-1} when $a_{Ca}=3.71$ mmol dm^{-3} and $C_{Ca}=6.40$ mmol dm^{-3}, but no value to be compared has been reported for calcium alkyl sulfate. In cationic surfactant solutions, investigations have shown that for various counterions the specific adsorption potentials became progressively larger as the valence of the counterion increased.[20] This tendency is also observed in this experiment. These calculated values must be correlated to changes in the hydration of the counterions bound on the micelles on the basis not only of free energy but also of enthalpy and entropy to transfer the counterions from solution to the micelle surface, although the latter two were not determined in this experiment. However the changes may be roughly estimated, if the specific adsorption potentials can be attributed only to dehydration in binding the counterions on the micelles.

The enthalpy and the entropy of hydration[23] and the number of primary hydrated water molecule (a hydrated water molecule being adjacent to an ion)[24] of the Ca^{2+} have been reported at 25 °C as -1669 kJ mol^{-1}, -254 J deg^{-1} mol^{-1}, and 10, respectively and those of the Na^+ also as -443.9 kJ mol^{-1}, -110 J deg^{-1} mol^{-1} and 5. The value of $\Delta\mu^{\circ}_{tNa}+\Delta W_{tCa}$ corresponds to dehydration of 1.1×10^{-2} water molecule per the Ca^{2+} from the primary hydrated water and that of $\Delta\mu^{\circ}_{tNa}+\Delta W_{tNa}$ also to dehydration of 1.3×10^{-2} water molecule. From these small values, therefore, it may be considered that dehydration by counterions scarcely occurs in the binding. And if dehydration takes place, water molecules hydrated in the secondary, tertiary and outer layers, which weakly bind to the counterion, are perphaps dehydrated rather than those in the primary layer. The relation between the specific adsorption potential and the hydration entropy has been hitherto reported,[20] and importance of entropy change in the formation of ionic pair, such as the Ca^{2+} and the SO_4^{2-}, has been also studied.[25] Accordingly it would seem to be worthwhile to pay attention to such entropy changes in this study. However from the present results, it can not be clearly said what change in the hydration of the counterion is intimately correlated to the specific adsorption potential. Experimental and detailed studies are desirable on the state of the counterion near the micelle surface.

The electrical free energies, $\int\phi_m dQ$, of the Ca^{2+} and the Na^+ at the cmc were calculated as -18.4 and -14.3 kJ mol^{-1}, respectively. It is indicated that the electrical free energy dominates in the specific adsorption potential in the counterion binding. Further, the value of $\int_0^{2\varepsilon}\phi_{mCa}\,dQ$ is larger than that of $\int_0^{\varepsilon}\phi_{mNa}dQ$, then the Ca^{2+} comes to bind preferentially even in low concentrations of surfactant.

Finally, we must say that the problem of the influence of micelles on the activities of single ions remains

unconfirmed, although it has been reported that the surface tensions calculated above the cmc by use of the activities agreed satisfactorily with those observed.[11]

References

1) K. Shinoda, T. Nakagawa, B. Tamamushi, and T. Isemura, "Colloidal Surfactants," Academic Press, New York (1966), Chap. 1.

2) J. M. Corkill and J. F. Goodman, *Trans. Faraday Soc.*, **58**, 206 (1962).

3) I. Satake, T. Tahara, and R. Matuura, *Bull. Chem. Soc. Jpn.*, **42**, 319 (1969).

4) K. Shinoda, *Bull. Chem. Soc. Jpn.*, **28**, 340 (1955).

5) H. Lange, *Kolloid Z. Z. Polym.*, **131**, 96 (1953); **132**, 45 (1953).

6) Y. Moroi, K. Motomura, and R. Matuura, *J. Colloid Interface Sci.*, **46**, 111 (1970).

7) C. Gavach and P. Seta, *Anal. Chim. Acta*, **50**, 407 (1970).

8) B. J. Birch and D. E. Clarke, *Anal. Chim. Acta*, **61**, 159 (1972).

9) S. G. Cutler, P. Mears and D. G. Hall, *J. Chem. Soc., Faraday Trans., 1*, **47**, 1758 (1978).

10) K. Kaibara, T. Nakahara, I. Satake, and R. Matuura, *Mem. Fac. Sci. Kyushu Univ., Ser. C*, **7**, 1 (1970).

11) T. Sasaki, M. Hattori, J. Sasaki, and K. Nukina, *Bull. Chem. Soc. Jpn.*, **48**, 1397 (1975).

12) M. Koshinuma and T. Sasaki, *Bull. Chem. Soc. Jpn.*, **48** 2755 (1975).

13) A. Yamauchi, T. Kunisaki, T. Minematsu, Y. Tomokiyo T. Yamaguchi, and H. Kimizuka, *Bull. Chem. Soc. Jpn.*, **51**, 2791 (1978).

14) M. Koshinuma, *Bull. Chem. Soc. Jpn.*, **54**, 3128 (1981).

15) C. E. Marshall and C. A. Krinbill, *J. Am. Chem. Soc.*, **64**, 1814 (1942).

16) R. G. Bate, *Pure Appl. Chem.*, **36**, 407 (1973).

17) K. Srinivasan and G. A. Rechnitz, *Anal. Chem.*, **41**, 1208 (1969).

18) K. Shinoda and E. Hutchinson, *J. Phys. Chem.*, **66**, 942 (1962).

19) D. Stigter, *J. Phys. Chem.*, **68**, 3603 (1964).

20) C. Gamboa, L. Sepulveda, and R. Soto, *J. Phys. Chem.*, **85**, 1429 (1981).

21) K. Tajima, M. Muramatsu, and T. Sasaki, *Bull. Chem. Soc. Jpn.*, **43**, 1991 (1970).

22) J. Sasaki, K. Tajima, and T. Sasaki, *Bull. Chem. Soc. Jpn.*, **45**, 348 (1972).

23) H. L. Friedman and C. V. Krishman, "Thermodynamics of Ionic Hydration" in "Water," ed by F. Franks, Plenum, New York-London (1973), Vol. 3, Chap. 1, p. 55.

24) R. A. Robinson and R. H. Stokes, "Electrolyte Solutions," Butterworth, London (1973), p. 126.

25) R. Fujishiro, G. Wada, and R. Tamamushi, "Yoeki No Seishitsu II," Tokyo Kagaku Dojin, Tokyo (1968), p. 129.

 © 1983 The Chemical Society of Japan Bull. Chem. Soc. Jpn., 56, 2348—2354 (1983) [Vol. 56, No. 8

Reactions of NH Radicals. I. Photolysis of HN_3 Vapor at 313 nm

Sukeya KODAMA

Department of Applied Chemistry, College of Engineering, University of Osaka Prefecture, Sakai, Osaka 591

(Received September 13, 1982)

Photolysis of HN_3 vapor was studied at 313 nm as a function of HN_3 and Xe pressures, light intensity, and temperature. The photolysis of hydrazoic acid labeled with ^{15}N was also studied. The quantum yields of N_2, H_2, and NH_4N_3 as a product were 4.85, 0.494, and 0.842 at 30 °C and 6.7 kPa of HN_3, respectively. The mechanism for the main reactions was postulated as follows: $HN_3+h\nu(313\text{ nm})\rightarrow N_2+NH(a^1\Delta)$; $NH(a^1\Delta)+HN_3\rightarrow 2N_2+2H$ (2); $NH(a^1\Delta)+HN_3\rightarrow N_3+NH_2$ (3); $NH(a^1\Delta)+HN_3\rightarrow N_2+N_2H_2{}^*$ (4). The rate constant ratios of $k_3/k_2=0.746$ and $k_4/k_2=1.23$ were obtained at 30°C. $(k_3+k_4)/k_2$ decrease drastically with rising temperature. Xe is effective for the collisional deactivation, $NH(a^1\Delta)+Xe\rightarrow NH(X^3\Sigma^-)+Xe$ (15), and $k_{15}/(k_2+k_3+k_4)=0.187$ was obtained at 30 °C.

In order to study the reactions of various reactants with $NH(X^3\Sigma^-$ and $a^1\Delta)$ radicals that are in the same isoelectronic state as carbon, oxygen, and sulfur atoms and CH_2, SiH_2, and PH radicals, hydrazoic acid was chosen as a photochemical radical source.

The photolysis of HN_3 vapor at about 190 nm[1] and the mercury-photosensitized decomposition[2] were first investigated by Beckman and his co-workers. On the basis that the products are N_2, H_2, and NH_4N_3, and the quantum yield for the disappearance of HN_3 is about 3.6 in both cases, they have presented the following mechanism:

$$HN_3 + h\nu(\text{or Hg}^*) \longrightarrow NH + N_2$$
$$NH + HN_3 \longrightarrow H_2 + 2N_2 \quad (18\%)$$
$$NH + HN_3 \longrightarrow N_2H_2 + N_2 \quad (82\%)$$
$$N_2H_2 + HN_3 \longrightarrow NH_3 + 2N_2$$
$$NH_3 + HN_3 \longrightarrow NH_4N_3.$$

Thrush[3] has proposed the following mechanism from the identifications of NH, NH_2, and N_3 radicals in flash photolysis:

$$HN_3 + h\nu \longrightarrow NH + N_2$$
$$NH + HN_3 \longrightarrow NH_2 + N_3$$
$$NH_2 + HN_3 \longrightarrow NH_3 + N_3$$
$$N_3 + N_3 \longrightarrow 3N_2.$$

On the photolysis of HN_3 vapor in the vacuum-ultraviolet, Welge[4] has observed that $NH(c^1\Pi)$ and $NH(A^3\Pi_i)$ are produced below 160 nm. Okabe[5] has shown that the yield of the $NH(c^1\Pi)$ production is at most 2%, and $NH(A^3\Pi_i)$ may be formed largely by the reaction of electronically excited N_2, most probably $N_2(B^3\Pi_g)$, with HN_3.

Konar, Matsumoto, and Darwent[6] have investigated the photochemical decomposition of HN_3 at 214 nm, and reported that the primary processes are

$$HN_3 + h\nu(214\text{ nm}) \longrightarrow {}^1NH' + N_2' \quad (95—97\%)$$
$$\longrightarrow H + N_3 \quad (3—5\%)$$

and the vibrationally excited $^1NH'$ and N'_2 are capable of causig further decomposition of HN_3.

Paur and Bair[7,8] have studied the flash photolysis of HN_3 by coordinated time-resolved spectroscopic measurements of HN_3, $NH(a^1\Delta)$, $NH(X^3\Sigma^-)$, $NH(c^1\Pi)$, $NH(A^3\Pi)$, NH_2, and N_3. They have reported that the major reactive product is $NH(a^1\Delta)$ or states which quickly decay to $NH(a^1\Delta)$ above 200 nm. Disappearance of $NH(a^1\Delta)$ occurs predominantly by the process

$$NH(a^1\Delta) + HN_3 \longrightarrow NH_2 + N_3$$

with a rate constant of 9.3×10^{-11} cm^3 molecule^{-1} s^{-1}.[8]

Recently, Piper *et al.*[9] have studied the UV photolysis of HN_3 by observing the time dependent decay in the number density of the $NH(a^1\Delta)$ product following photolysis at about 290 nm. They have obtained 18×10^{-11} cm^3 molecule^{-1} s^{-1} as a rate constant for the reaction

$$NH(a^1\Delta) + HN_3 \longrightarrow NH_2(\tilde{A}^2A_1) + N_3.$$

They also obtained 9.3×10^{-11} cm^3 molecule^{-1} s^{-1} as a specific rate for the reaction of $NH_2(\tilde{A}^2A_1)$ with HN_3.

Although the photolysis of HN_3 has been investigated intensively, as cited above, the quantitative mechanism is not clear. Notably, the reaction mechanisms at short wavelengths are more complex than those at long wavelengths because of the appearance of highly excited species. On the other hand, an absorption edge on the longest absorption band of HN_3 is located at about 310 nm,[10] and the formation of the first excited singlet $NH(a^1\Delta)$ can be expected at this wavelength. Thus, the photolysis of HN_3 vapor at 313 nm had been carried out in this work, before the studies of reactions of $NH(a^1\Delta$ and $X^3\Sigma^-)$ with various reactants.

Experimental

Materials. Hydrazoic acid was prepared from the reaction of NaN_3 with sulfuric acid (H_2SO_4: H_2O=1 : 2 in volume ratio) at room temperature, dried by passing through columns packed with $CaCl_2$ and P_2O_5, and stored below a half atm in a reservoir protected from light to avoid explosion.

The UV absorption of HN_3 of 14.3 kPa at 25.7 °C was observed at wavelengths longer than 220 nm. The molecular extinction coefficients calculated from $\log_{10}(I/I_0)=-ecl$ are illustrated in Fig. 1, and are slightly higher than those measured by McDonald and co-workers.[10] In the infrared region, two absorption peaks appear at 1.54 (ε_{max}=1.79) and 2.36 μm (ε_{max}=1.34 dm^3 mol^{-1} cm^{-1}). The former peak has been found in the spectrum of frozen HN_3.[11]

To elucidate the mechanism the photolysis was also carried out with hydrazoic acid labeled with nitrogen-15. For this purpose, potassium azide labeled with ^{15}N at the third nitrogen atom to the extent of 97% was obtained from Isomet Co. The hydrazoic acid was prepared from the azide in the same way

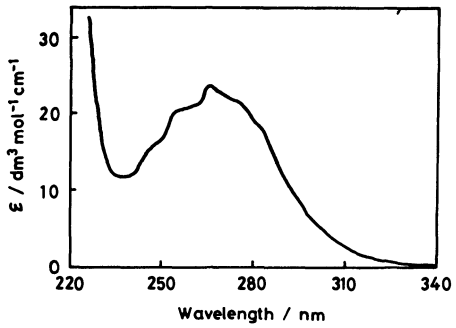

Fig. 1. UV absorption spectrum of HN_3 vapor.

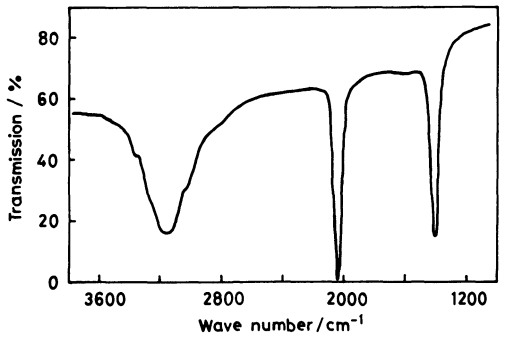

Fig. 2. Infrared spectrum of the white volatile powder condensed at the Dry Ice–acetone temperature.

as described above. It was presumably labeled at the first and third nitrogen atoms with the same probability, since the formation was due to the ionic processes:[12] $KNN^{15}N \xrightarrow{(H_2O)} K^+ + {}^{15}NNN^-$; $H^{15}NNN \longleftarrow H^+ + {}^{15}NNN^- \longrightarrow HNN^{15}N$.

Xe was obtained from Takachiho Chemical Co., and purified by vacuum distillation at liquid nitrogen temperature.

Apparatus. The photolysis was carried out at 313 nm obtained from a high pressure mercury lamp (Toshiba, SHL-100UV) of 100 W. As a filter for 313 nm, UV-D2 (Toshiba) was used. The light intensity was controlled by inserting screens between the light source and the reaction cell. The reaction cell was a quartz cylinder of 5.0 cm inner diameter and 10 cm length, with a volume of 196 cm^3. It was inserted in an electric furnace to maintain a fixed temperature.

Procedure. Hydrazoic acid was purified each time before use by condensation and evacuation at −120 °C and at Dry Ice–acetone temperature, introduced into the reaction cell, and exposed to the light. The irradiation time was usually 20 min. The degree of conversion of HN_3, calculated from the relation[13] $(2[N_2]+4[NH_4N_3])/3[HN_3]_0$, was less than 7% for all runs except 12.8% at the lowest pressure (0.787 kPa).

The reaction products were only N_2, H_2, and NH_4N_3. The formation of NH_4N_3 was first reported by Beckman and Dickenson,[1] and was further confirmed by infrared spectroscopy in this work. The spectrum observed by the KBr method for the white volatile powder condensed at Dry Ice–acetone temperature is shown in Fig. 2, and is in accord with the main three peaks in the spectrum of solid NH_4N_3 at 90 K.[14] The formation of hydrazinium azide ($N_2H_5N_3$) is ruled out judging from the infrared spectrum of hydrazine vapor.[15]

Noncondensable gases (N_2 and H_2) at the liquid nitrogen temperature were introduced into a column of silica gel[16] (for gas chromatography) at −196 °C. Hydrogen was passing through the column and collected in a Toepler gauge, and its amount was determined. Nitrogen, trapped on silica gel at −196 °C, was collected in the gauge by warming the column, and its amount was also determined.

The following method was used for the quantitative analysis of NH_4N_3: Unconverted HN_3 was removed by evacuating at Dry Ice–acetone temperature. Ammonium azide, trapped at −78 °C, was warmed, introduced into a CuO column and burnt at about 550 °C. N_2, NO, N_2O, and H_2O were separated as combustion products[17] at −210, −196, and −110 °C, respectively. The amounts of N_2, NO, and N_2O were in turn determined by the Toepler gauge. The amount of NH_4N_3 was calculated from the equation, $NH_4N_3=(N_2+N_2O)/2+NO/4$. The expectation amount of NH_4N_3 can be estimated by the equation[18] $NH_4N_3=N_2/4-3H_2/4$, and agreement between the experimental and expected amounts was very good.

The photolysis of HN_3 in the presence of Xe was also carried out by the same procedure.

Determination of Quantum Yield. Acetone was used as an actinometer, since the quantum yield of CO in photolysis of acetone at 313 nm is almost unity above 100 °C.[19] The quantum yield of nitrogen formation was 4.85 as an average value of three experiments at 30 °C, 313 nm, and 6.7 kPa of HN_3. The other quantum yields were calculated on the basis of the value for N_2.

Determination of Isotopic Composition. The isotopic composition of nitrogen formed in the photolysis of hydrazoic acid labeled by ^{15}N was analyzed by a mass spectrometer (Hitachi, RUM-5). The content of ^{15}N in NH_4N_3 was also determined by the mass spectrometric analysis of isotopic N_2, NO, and N_2O produced by the combustion.

Results

The results for photolysis of HN_3 of 6.7 kPa, measured as a function of the absorbed light intensity at 313 nm and 30 °C are shown in Fig. 3. It is found in Fig. 3 that the quantum yields, ϕ_{N_2}, ϕ_{H_2}, and $\phi_{NH_4N_3}$, are independent of the light intensity. The average values of ϕ_{N_2}, ϕ_{H_2}, and $\phi_{NH_4N_3}$ were 4.85, 0.494, and 0.842, respectively.

Figure 4 shows the results of photolysis, measured as a function of HN_3 pressure at 313 nm, 30 °C, and the incident light intensity of 2.0×10^{16} quanta s^{-1}. It is

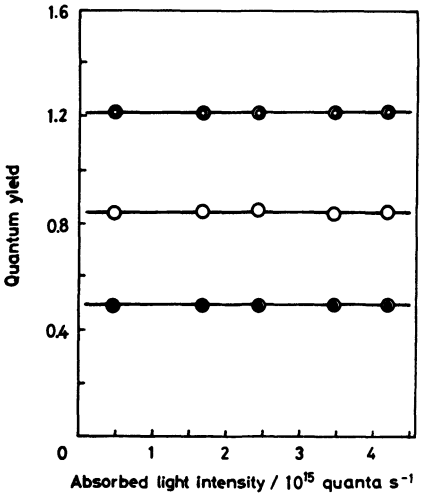

Fig. 3. Results of the photolysis of HN_3 of 6.7 kPa, measured as a function of the absorbed light intensity at 313 nm and 30 °C. ◎, $\phi_{N_2}/4$; ○, $\phi_{NH_4N_3}$; ⊙, ϕ_{H_2}.

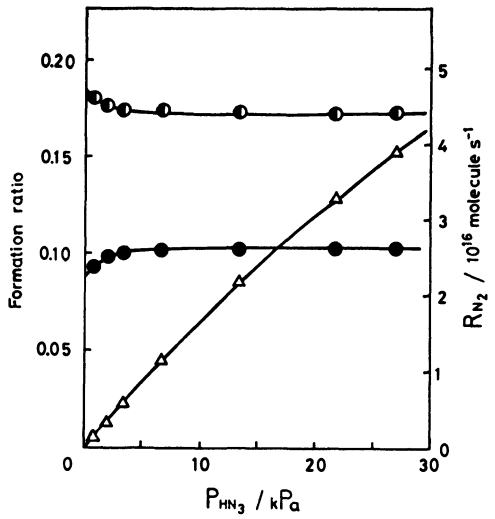

Fig. 4. Results of the photolysis, measured as a function of HN_3 pressure at 30 °C, 313 nm, and the incident light intensity of 2.0×10^{16} quanta s^{-1}. ◐, NH_4N_3/N_2; ●, H_2/N_2; △, R_{N_2}.

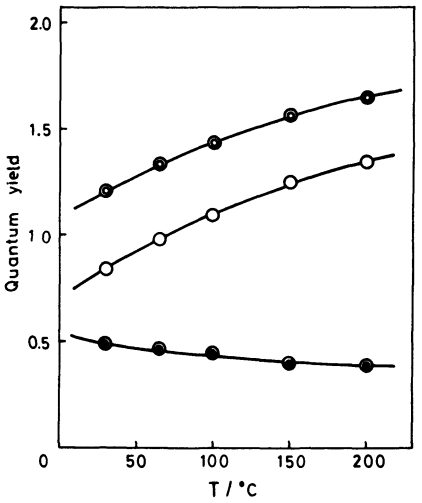

Fig. 5. Temperature dependence on the photolysis of HN_3 of 2.64 mmol dm^{-3} at 313 nm and the incident light intensity of 2.0×10^{16} quanta s^{-1}. ◎, $\phi_{N_2}/4$; ○, $\phi_{NH_4N_3}$; ⊙, ϕ_{H_2}.

seen in Fig. 4 that the relation of R_{N_2}, formation rate of N_2, *versus* P_{HN_3} changes slightly as is anticipated from Berr's law, H_2/N_2 decreases with lowering of the pressure, and NH_4N_3/N_2 increases in contrast with H_2/N_2.

The thermal decomposition of HN_3 has been studied at about 380[20] and 1000 °C,[21,22] but no decomposition was detected at least up to 200 °C in our system. Figure 5 shows the temperature dependence on the photolysis of HN_3 of 2.64×10^{-3} mol dm^{-3} (6.7 kPa at 30 °C) at 313 nm and the incident light intensity of 2.0×10^{16} quanta s^{-1}, where the quantum yields were estimated by assuming that the molecular extinction coefficient of HN_3 is independent of temperature. It is seen in Fig. 5 that ϕ_{N_2} and $\phi_{NH_4N_3}$ increase, but ϕ_{H_2} decreases with increase in temperature.

The results for the photolysis of HN_3 of 6.7 kPa,

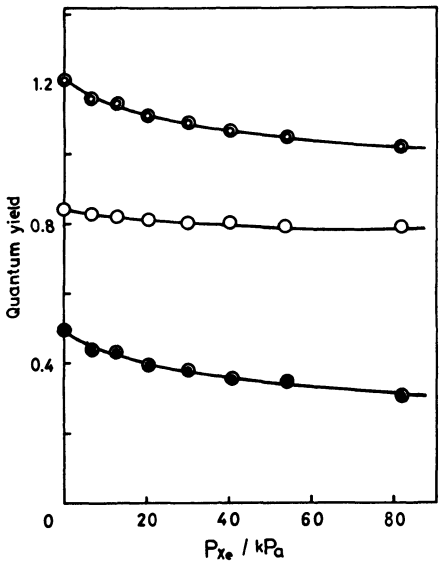

Fig. 6. Results of the photolysis of HN_3 of 6.7 kPa, measured as a function of Xe pressure at 313 nm, 30 °C, and the absorbed light intensity of 3.2×10^{15} quanta s^{-1}. ◎, $\phi_{N_2}/4$; ○, $\phi_{NH_4N_3}$; ⊙ ϕ_{H_2}.

measured as a function of Xe pressure at 313 nm, 30 °C, and an absorbed light intensity of 3.2×10^{15} quanta s^{-1}, are shown in Fig. 6. It is shown in Fig. 6 that all quantum yields decrease with an increase of Xe pressure.

On the photolysis of the labeled hydrazoic acid of 6.7 kPa at 313 nm and 30 °C, $^{14}N^{14}N/N_2$, $^{14}N^{15}N/N_2$, and $^{15}N^{15}N/N_2$ which mean the fractions of isotopic nitrogen molecules to total nitrogen molecules(N_2) were 44.5, 48.7, and 6.8%, respectively. The fraction of ^{15}N atoms to total N atoms in NH_4N_3 was 36.2%.

Discussion

Reaction Mechanism. It is difficult to determine the reaction scheme in this system, because only three kinds of products were obtained. However, we suggest the following reaction mechanism on the basis of the present results, our results in the photolysis of HN_3 in the presence of C_2H_6[23] and C_2H_4,[24] and the results obtained by previous investigators:

$$HN_3 + h\nu(313\text{ nm}) \longrightarrow N_2 + NH(a^1\Delta) \quad (1)$$

$$NH(a^1\Delta) + HN_3 \longrightarrow 2N_2 + 2H \quad (2)$$

$$NH(a^1\Delta) + HN_3 \longrightarrow N_3 + NH_2 \quad (3)$$

$$NH(a^1\Delta) + HN_3 \longrightarrow N_2 + N_2H_2^* \quad (4)$$

$$H + HN_3 \longrightarrow H_2 + N_3 \quad (5)$$

$$H + HN_3 \longrightarrow NH_2 + N_2 \quad (6)$$

$$N_2H_2^* \longrightarrow N_2H_2^{**} \quad (7)$$

$$N_2H_2^* + HN_3 \longrightarrow N_2 + H_2 + HN_3 \quad (8)$$

$$N_2H_2^* + HN_3 \longrightarrow NH_3 + 2N_2 \quad (9)$$

$$N_2H_2^{**} + HN_3 \longrightarrow NH_3 + 2N_2 \quad (10)$$

$$NH_2 + HN_3 \longrightarrow NH_3 + N_3 \quad (11)$$

$$NH_3 + HN_3 \longrightarrow NH_4N_3 \quad (12)$$

$$N_3 + HN_3 \longrightarrow HN_3\cdot N_3 \quad (13)$$

$$2HN_3\cdot N_3 \longrightarrow 3N_2 + 2HN_3. \quad (14)$$

Table 1. Selected heats of formation

	$\Delta H^\circ_{f'298}$ / kJ mol^{-1}	Ref.		$\Delta H^\circ_{f'298}$ / kJ mol^{-1}	Ref.
HN_3	299.8	a	*trans*-N_2H_2	175.7	i
$NH(X^3\Sigma^-)$	352.2	b	*cis*-N_2H_2	203.3	i
$NH(a^1\Delta)$	506.6	b,c	NH_4N_3	112.1	a
$NH(b^1\Sigma^+)$	612.8	b,d	$N(^4S_{3/2})$	474.1	e
$NH(A^3\Pi)$	711.2	b,d	$N(^2D_{5/2})$	703.7	e,j
$NH(c^1\Pi)$	873.1	b,d	HN_2	255.2	k
H	218.0	e	N_2H_3	278.9	l
N_3	468.6	f	N_2H_4	95.2	m
$NH_2(\tilde{X}^2B_1)$	171.5	g	NH_2–N=NH	274.1	n
$NH_2(\tilde{A}^2A_1)$	294.1	g,h	$N_2(A^3\Sigma_u^+)$	595.4	d
NH_3	−46.0	e	$N_2(B^3\Pi_g)$	709.2	d

a) P. Gray and T. C. Waddington, *Proc. R. Soc. London, Ser. A*, **235**, 106 (1956). b) L. G. Piper, *J. Chem. Phys.*, **70**, 3417 (1979). c) H. Okabe and M. Lenzi, *J. Chem. Phys.*, **47**, 5241 (1967). d) L. Wallace, *Astrophys. J. Suppl. Ser.*, **7**, 165 (1962). e) "JANAF Thermochemical Tables," ed by D. R. Stull, Dow Chemical Co., Midland, Mich. (1966). f) M. J. Pellerite, R. L. Jackson, and J. I. Brauman, *J. Phys. Chem.*, **85**, 1624 (1981). g) D. K. Sen Sharma and J. L. Franklin, *J. Am. Chem. Soc.*, **95**, 6562 (1973). h) K. Dressler and D. A. Ramsay, *Phil. Trans. R. Soc. London, Ser. A*, **251**, 553 (1959). i) N. W. Winter and R. M. Pitzer, *J. Chem. Phys.*, **62**, 1269 (1975). j) C. E. Moore, Natl. Bur. Std. (U. S.) Circ. No. 467 (1952). k) Ref. 25. l) A. A. Zavitsas, *J. Am. Chem. Soc.*, **94**, 2779 (1972). m) D. W. Scott, G. D. Oliver, M. E. Gross, W. N. Hubbard, and H. M. Huffman, *J. Am. Chem. Soc.*, **71**, 2293 (1949). n) L. Radom, W. J. Hehre, and J. A. Pople, *J. Am. Chem. Soc.*, **93**, 289 (1971).

In the photolysis of HN_3 in the presence of Xe, the following reactions were added to those listed above:

$$NH(a^1\Delta) + Xe \longrightarrow NH(X^3\Sigma^-) + Xe \quad (15)$$

$$NH(X^3\Sigma^-) + HN_3 \longrightarrow H_2 + 2N_2 \quad (16)$$

$$NH(X^3\Sigma^-) + HN_3 \longrightarrow NH_2 + N_3. \quad (17)$$

Thermochemical considerations were taken into account using the standard heats of formation listed in Table 1.

For HN_3 excited by absorbing light of 313 nm, the photo-decomposition processes

$$\begin{aligned} HN_3 + h\nu(313\text{ nm}) &\longrightarrow H(^2S) + N_3(X^2\Pi) \\ &\longrightarrow N_2(X^1\Sigma_g^+) + N(^4S) + H(^2S) \\ &\longrightarrow N_2(X^1\Sigma_g^+) + N(^2D) + H(^2S) \\ &\longrightarrow HN_2 + N(^2D) \end{aligned}$$

to give H and N atoms are not possible energetically.[5,25] Reaction 1 is the only photochemical process which is energetically possible and spin allowed, except the process

$$HN_3 + h\nu(313\text{ nm}) \longrightarrow N_2(X^1\Sigma_g^+) + NH(b^1\Sigma^+)$$

However, the formation of $NH(b^1\Sigma^+)$ was not detected although $NH(a^1\Delta)$ was observed as a predominant primary product.[7-9] It seems that $NH(b^1\Sigma^+)$ decays quickly to $NH(a^1\Delta)$, even if $NH(b^1\Sigma^+)$ was formed. Therefore, reactions yielding $NH(b^1\Sigma^+)$ were excluded from the reaction mechanism.

The formation of $NH(X^3\Sigma^-)$ by the collisional spin relaxation process

$$NH(a^1\Delta) + HN_3 \longrightarrow NH(X^3\Sigma^-) + HN_3$$

is negative judging from the facts that McDonald *et al.*[26] were not able to observe any triplet NH formation when helium was introduced even at pressures as high as 12 kPa, and the relation of $[NH(X^3\Sigma^-)] \ll [NH(a^1\Delta)]$ was found by Piper *et al.*[9] While, $NH(X^3\Sigma^-)$ has been observed in flash photolysis.[3,7,8,27] It seems that the formation of $NH(X^3\Sigma^-)$ is due to an emission process, $NH(A^3\Pi) \rightarrow NH(X^3\Sigma^-) + h\nu$, and the collisional quenching of $NH(a^1\Delta)$ by diluent gases such as Reaction 15.

Reactions 2, 3 and 4 are highly exothermic and their enthalpy changes are −370, −166, and −631 kJ mol^{-1}, respectively. The formation of H atoms has been found in the flash photolysis[28] and the photolysis of HN_3 in inert and reactive matrices.[29,30] Reaction 2 is also supported by the fact that the reaction, $H + C_2H_4 \rightarrow C_2H_5$, occurs during the photolysis of HN_3 with C_2H_4.[24] NH_2 radicals have been observed in the flash photolysis of HN_3 vapor.[3,7-9]

The formation of N_2H_2 has been detected in the photolysis of HN_3 in frozen matrices.[12,29,31] Reaction 4 is also supported by the facts that the similar reaction, $CH_3N + CH_3N_3 \rightarrow CH_3N_2CH_3 + N_2$, was found in the photolysis of CH_3N_3 vapor[32] and the rapid hydrogenation reaction,[33] $N_2H_2 + C_2H_4 \rightarrow C_2H_6 + N_2$, takes place in the photolysis of HN_3 with C_2H_4.[24]

On the reaction to give nitrogen atoms,

$$NH(a^1\Delta) + HN_3 \longrightarrow N(^4S \text{ or } ^2D) + N_3H_2$$

the reaction to form $N(^4S)$ is rejected because of the spin forbidden reaction. The reaction to give $N(^2D)$ may also be excluded because the heat of formation of N_3H_2 seems to be higher than 102.7 kJ mol^{-1} judging from the heat of formation of NH_2–N=NH and the bond dissociation energies of NH_2NN–H and H–NHNNH. The reaction to give H_2 molecules,

$$NH(a^1\Delta) + HN_3 \longrightarrow H_2 + 2N_2$$

is excluded because the H_2 formation decreases drastically on adding C_2H_4 in small amount.[24] Baird[25] has predicted a value of 255 kJ mol^{-1} for the heat of formation of HN_2 radicals. Therefore, the reaction

$$NH(a^1\Delta) + HN_3 \longrightarrow 2HN_2$$

is energetically possible. However, the HN_2 will decompose immediately with large excess energy even if HN_2 were formed, and it results in Reaction 2.

On the reactions of H atoms with HN_3 molecules, only Reactions 5 and 6 are energetically possible processes. The reactions

$$\begin{aligned} H + HN_3 &\longrightarrow N(^4S \text{ or } ^2D) + N_2H_2 \\ &\longrightarrow NH(X^3\Sigma^- \text{ or } a^1\Delta) + HN_2 \end{aligned}$$

are excluded energetically. Reaction 5 is the hydrogen abstraction reaction from HN_3 by H, and is supported because HN_3 is a good hydrogen donor.[34] Reaction 6 is 337 kJ mol^{-1} exothermic, and the formations of N_3 and NH_2 radicals were confirmed in the flash photolysis.[3,7,8,35] Combourieu *et al.*[36] have obtained $k = 2.54 \times 10^{-11} \exp(-2300/T)$ cm^3 molecule^{-1} s^{-1} as a rate constant of the reaction

$$H + HN_3 \longrightarrow \text{Products}.$$

Reactions 7 to 10 were introduced in order to explain the facts that NH_4N_3/N_2 increases and H_2/N_2 decreases with decrease of the HN_3 pressure, although the detail of these reactions are not clear. $N_2H_2^*$ formed by Reaction 4 is probably in an electronically excited state,[37] because Reaction 4 is very exothermic with 631 kJ mol^{-1}. If $N_2H_2^*$ is in an excited state, it may be possible that $N_2H_2^*$ transfers to a lower electronic state ($N_2H_2^{**}$) by internal conversion or intersystem crossing as Reaction 7, and $N_2H_2^{**}$ reacts to give NH_3 by Reaction 10. $N_2H_2^*$ may also possibly react with HN_3 by Reactions 8 and 9.

The bimolecular reactions as to N_2H_2,[38,39] $2N_2H_2 \rightarrow N_2H_4+N_2$ and $2N_2H_2 \rightarrow N_2+H_2+N_2H_2$, are ruled out in our system, because the formation of N_2H_4 was not observed, and the quantum yields of N_2 and H_2 were independent of the light intensity. It means that the concentration of N_2H_2 in our system is much lower than those described in Refs. 38 and 39.

Reaction 11 is the hydrogen abstraction reaction by NH_2 from HN_3 which is a good hydrogen donor.[34] Piper *et al.*[9] have presented the mechanism

$$NH(a^1\Delta) + HN_3 \longrightarrow NH_2(\tilde{A}^2A_1) + N_3$$
$$NH_2(\tilde{A}^2A_1) \longrightarrow NH_2(X^2B_1) + h\nu$$
(α bands of ammonia[40])
$$NH_2(\tilde{A}^2A_1) + HN_3 \longrightarrow NH_2(X^2B_1) + HN_3$$
$$\longrightarrow NH_3 + N_3$$

to explain the formation and disappearance of NH_2 ($\tilde{A}^2A_1$), and obtained 9.3×10^{-11} cm^3 $molecule^{-1}$ s^{-1} as a rate constant for the disappearance of $NH_2(\tilde{A}^2A_1)$ by HN_3. However, the HN_3 pressure dependence of NH_4N_3/N_2 in Fig. 4 can not be explained by their mechanism, provided that all $NH_2(X^2B_1)$ radicals disappear to give NH_3 as Reaction 11.

On the other hand, Kajimoto *et al.*[41] have observed the fluorescence from $NH_2(\tilde{A}^2A_1)$ formed by the reaction, $H+HN_3 \rightarrow N_2+NH_2(\tilde{A}^2A_1)$. Thus, Reactions 2, 3, and 6 are supported in terms of both observations for the fluorescence from $NH_2(\tilde{A}^2A_1)$. Judging from the enthalpy changes of Reactions 3 and 6, it is surmised that the emission from $NH_2(\tilde{A}^2A_1)$ formed by Reaction 6 appears at shorter wavelength than that from NH_2 ($\tilde{A}^2A_1$) formed by Reaction 3.[41]

Basic NH_3 reacts rapidly in the vapor phase with acidic HN_3 to give NH_4N_3 as a white volatile powder[42] by Reaction 12.

Paur and Bair[7,8] have observed that the disappearance rate of N_3 radicals is faster than expected for reaction with other radicals at concentrations present in their system, and concluded that this rate most likely represents reaction with HN_3. Therefore, it seems that N_3 radicals disappear to give N_2 *via* an addition intermediate ($HN_3 \cdot N_3$) as Reactions 13 and 14. Addition intermediates of N_3 with C_2H_4 and *cis*-C_4H_8 having π bond are also found in the photolysis of HN_3 with C_2H_4[24] and *cis*-C_4H_8.

Finally, all of the Reactions 1 to 14 in the photolysis of HN_3 vapor are energetically possible and spin allowed. The reaction mechanism satisfy the experimental requirements that the quantum yields of N_2, H_2, and NH_4N_3 are independent of the light intensity, and NH_4N_3/N_2 increases but H_2/N_2 decreases with lowering of HN_3 pressure. Reactions 1 to 14 are also found as a common reaction pattern in the photolysis of HN_3 in the presence of C_2H_6[23] and C_2H_4.[24]

On the photolysis of HN_3 in the presence of Xe, Reaction 15 seems to be the only process for the reaction of $NH(a^1\Delta)$ with Xe as an inert gas. For reactions of $NH(X^3\Sigma^-)$, we do not have enough experimental evidence. In any case, $NH(X^3\Sigma^-)$ will disappear to give H_2 and NH_3 by reactions with HN_3 such as Reactions 16 and 17.[43]

Recently, Kajimoto *et al.*[22] have estimated $3.0\times10^{11}\exp(-805/T)$ cm^3 mol^{-1} s^{-1} as k_{17} and 2.5×10^{13} cm^3 mol^{-1} s^{-1} as a rate constant of the reaction, $2NH(X^3\Sigma^-) \rightarrow N_2+2H$, in the thermal decomposition of HN_3 in shock waves. However, the possibility of the reaction, $2NH(X^3\Sigma^-) \rightarrow$ Products, will be negligible, because the $NH(X^3\Sigma^-)$ concentration is low in our system.

Reaction Kinetics. On the basis of the mechanism of Reactions 1 to 17, the equation

$$\frac{1}{\phi_{H_2}+\phi_{NH_4N_3}-1} = \frac{k_2+k_3+k_4}{k_2} + \frac{k_{15}[Xe]}{k_2[HN_3]}, \quad (I)$$

can be derived for the formations of H_2 and NH_4N_3. From the intercept and slope in Fig. 7 and from $k_4/k_2=1.23$ obtained in the photolysis of HN_3 with C_2H_4,[24] $k_3/k_2=0.746$, $k_{15}/k_2=0.557$ and $k_{15}/(k_2+k_3+k_4)=0.187$ are obtained.

Equation II can be derived for the formations of H_2 and N_2 in the absence of Xe.

$$\frac{1}{4/(1+R_{N_2}/R_{H_2})-\alpha} = \frac{2k_2+k_3+k_4}{k_4}\left(1+\frac{k_9}{k_8}+\frac{k_7}{k_8[HN_3]}\right), \quad (II)$$

where

$$\alpha = \frac{k_2}{2k_2+k_3+k_4}\frac{2k_5}{k_5+k_6}.$$

When α is 0.234, the best straight line is obtained as is seen in Fig. 8. From the intercept, the slope and $\alpha=0.234$, $k_6/k_5=1.15$, $k_9/k_8=1.19$, and $k_7/k_8=2.27\times10^{-7}$ mol cm^{-3} are obtained.

On the formations of H_2 and N_2 in the presence of Xe, Equation III can be derived.

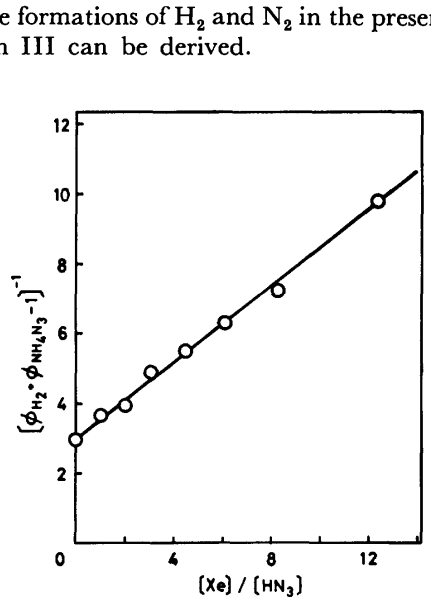

Fig. 7. Plot of $1/(\phi_{H_2}+\phi_{NH_4N_3}-1)$ *versus* $[Xe]/[HN_3]$.

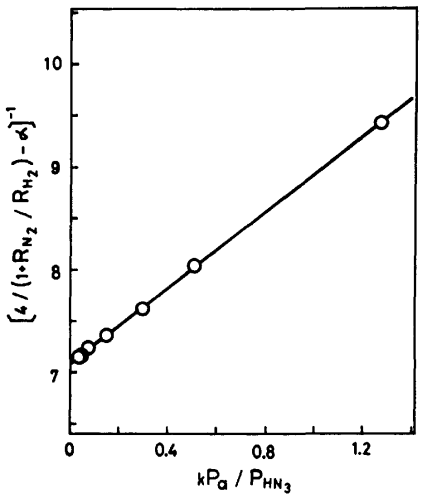

Fig. 8. Plot of $1/[4/(1+R_{N_2}/R_{H_2})-\alpha]$ against $1/P_{HN_3}$.

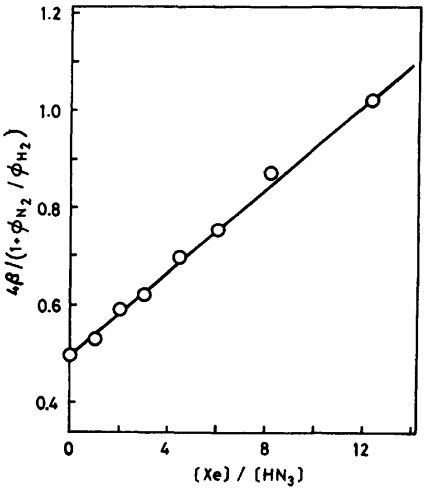

Fig. 9. Plot of $4\beta/(1+\phi_{N_2}/\phi_{H_2})$ *versus* $[Xe]/[HN_3]$.

$$\frac{4\beta}{1+\phi_{N_2}/\phi_{H_2}} = \alpha + \frac{k_4}{k_2+k_3+k_4}\frac{k_8[HN_3]}{k_7+(k_8+k_9)[HN_3]} + \frac{k_{15}}{k_2+k_3+k_4}\frac{k_{16}}{k_{16}+k_{17}}\frac{[Xe]}{[HN_3]}, \quad \text{(III)}$$

where

$$\beta = 1 + \frac{k_2}{k_2+k_3+k_4}\left(1+\frac{k_{15}}{k_2}\frac{[Xe]}{[HN_3]}\right) = 1.336 + 0.187[Xe]/[HN_3].$$

The plot of $4\beta/(1+\phi_{N_2}/\phi_{H_2})$ *versus* $[Xe]/[HN_3]$ at 6.7 kPa of HN_3 is shown in Fig. 9, and $k_{17}/k_{16}=3.22$ is obtained from the slope.

Equation I can be rewritten as

$$\frac{1}{\phi_{H_2}+\phi_{NH_4N_3}-1} - 1 = \frac{k_3+k_4}{k_2}, \quad \text{(IV)}$$

in the absence of Xe. The temperature dependence is shown in Fig. 10. It is found in Fig. 10 that $(k_3+k_4)/k_2$ decreases drastically from 1.976 at 30 °C with increasing temperature.

Isotopic Considerations. In order to confirm the reaction mechanism obtained above, the experimental values of $^{14}N^{14}N/N_2$, $^{14}N^{15}N/N_2$, $^{15}N^{15}N/N_2$, and $^{15}N/NH_4N_3$ in the absence of Xe were compared with the

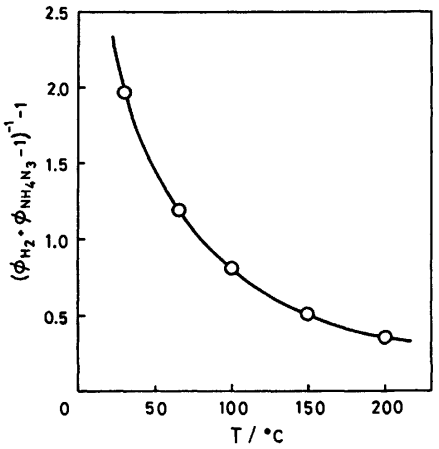

Fig. 10. Temperature dependence of $(k_3+k_4)/k_2$.

values calculated by using Eqs. V to VIII.

$$^{14}N^{14}N/N_2 = \sum_i S_i\alpha_i\phi_i/\phi_{N_2} \quad \text{(V)}$$

$$^{14}N^{15}N/N_2 = \sum_i S_i\beta_i\phi_i/\phi_{N_2} \quad \text{(VI)}$$

$$^{15}N^{15}N/N_2 = \sum_i S_i\gamma_i\phi_i/\phi_{N_2} \quad \text{(VII)}$$

$$^{15}N/NH_4N_3 = 1.5/4 \quad \text{(VIII)}$$

Here, ϕ_i is the quantum yield of i-th reaction, and can be calculated using the rate constant ratios obtained above. S_i is the stoichiometry of N_2 formed in i-th reaction. α_i, β_i and γ_i mean the fractions of $^{14}N^{14}N$, $^{14}N^{15}N$, and $^{15}N^{15}N$ including in total N_2 formed by i-th reaction, respectively. The values needed for the calculations of Eqs. V to VII are listed in Table 2, where S_i values in Reactions 3, 5, 6, and 7 include additional N_2 formations by subsequent Reactions 10, 11, 13, and 14.

The calculated values of $^{14}N^{14}N/N_2$, $^{14}N^{15}N/N_2$, $^{15}N^{15}N/N_2$, and $^{15}N/NH_4N_3$ are 43.1, 50.0, 6.89, and 37.5%, respectively. These values are consistent with the experimental values of 44.5, 48.7, 6.8, and 36.2%. Slight discrepancies may be due to incomplete isotopic enrichment (97%) of ^{15}N in the labeled hydrazoic acid. The recovery of ^{15}N calculated from the equation $3[\phi_{^{14}N^{15}N}+2\phi_{^{15}N^{15}N}+4(^{15}N/NH_4N_3)\phi_{NH_4N_3}]/(2\phi_{N_2}+4\phi_{NH_4N_3})$ is 0.974, and in accord with the original (0.97).

On the other hand, if Beckman's[1,2] and Thrush's[3] mechanisms are applied to Eq. VII, the values of $^{15}N^{15}N/N_2$ become 6.55 and 8.33%, respectively. Papazian[44] has postulated the following mechanism in outline on the photolysis of HN_3 in frozen state: $HN_3+h\nu \rightarrow NH + N_2$; $NH+HN_3 \rightarrow HN{=}N{-}N{=}NH \rightarrow 2HN_2$; $NH+HN_2+HN_3 \rightarrow H_2N{-}N{=}NH + 3/2\ N_2$; $H_2N{-}N{=}NH \rightarrow NH_3+N_2$; and $NH_3+HN_3 \rightarrow NH_4N_3$. From the mechanism, we obtain $^{15}N^{15}N/N_2=7.30\%$. The value of $^{15}N^{15}N/N_2$ calculated from the reaction scheme proposed by Konar *et al.*[6] was 2.65% in the absence of forein gases. Of the various possible mechanisms, our mechanism of Reactions 1 to 14 gives the best agreement with the isotopic measurements.

I would like to thank Emeritus Professor Osamu Toyama and Professor Shigeru Yamashita of University of Osaka Prefecture for their helpful discussions. I would also like to thank Dr. Sotaro Esho and Mr.

TABLE 2. VALUES USED TO CALCULATE THE ISOTOPIC COMPOSITIONS OF NITROGEN

Reaction No.	Quantum yield of i-th reaction	Stoichiometry of N_2 formation	Probability[a]		
			$^{14}N^{14}N$	$^{14}N^{15}N$	$^{15}N^{15}N$
i	ϕ_i	S_i	α_i	β_i	γ_i
1	1	1	1/2	1/2	0
2	0.3360	2	3/8	1/2	1/8
3	0.2505	3	5/12	1/2	1/12
4	0.4135	1	1/2	1/2	0
5	0.3128	3/2	5/12	1/2	1/12
6	0.3592	5/2	9/20	1/2	1/20
7	0.0156[b]	2	3/8	1/2	1/8
8	0.1817[b]	1	1/4	1/2	1/4
9	0.2163[b]	2	3/8	1/2	1/8

a) The probabilities (α_i, β_i, and γ_i) were estimated assuming that the enrichment of ^{15}N in the labeled hydrazoic acid is 1.00. b) Values at 6.7 kPa of HN_3.

Hidetoshi Hori for support of this work.

References

1) A. O. Beckman and R. G. Dickinson, *J. Am. Chem. Soc.*, **50**, 1870 (1928); **52**, 124 (1930).
2) A. E. Myers and A. O. Beckman, *J. Am. Chem. Soc.*, **57**, 89 (1935).
3) B. A. Thrush, *Proc. R. Soc. London, Ser. A*, **235**, 143 (1956).
4) K. H. Welge, *J. Chem. Phys.*, **45**, 4373 (1966).
5) H. Okabe, *J. Chem. Phys.*, **49**, 2726 (1968).
6) R. S. Konar, S. Matsumoto, and B. DEB. Darwent, *Trans. Faraday Soc.*, **67**, 1698 (1971).
7) R. J. Paur and E. J. Bair, *J. Photochem.*, **1**, 255 (1973).
8) R. J. Paur and E. J. Bair, *Int. J. Chem. Kinet.*, **8**, 139 (1976).
9) L. G. Piper, R. H. Krech, and R. L. Taylor, *J. Chem. Phys.*, **73**, 791 (1980).
10) J. R. McDonald, J. W. Rabalais, and S. P. McGlynn, *J. Chem. Phys.*, **52**, 1332 (1970).
11) F. O. Rice and R. B. Ingalls, *J. Am. Chem. Soc.*, **81**, 1856 (1959).
12) K. Rosengren and G. C. Pimentel, *J. Chem. Phys.*, **43**, 507 (1965).
13) The equation was derived from the material balance as to nitrogen atoms. $[HN_3]_0$ is the initial amount of HN_3.
14) D. A. Dows, E. Whittle, and G. C. Pimentel, *J. Chem. Phys.*, **23**, 1475 (1955).
15) P. A. Giguére and I. D. Liu, *J. Chem. Phys.*, **20**, 136 (1952).
16) The separation of H_2 from mixtures of H_2, O_2, N_2, CH_4, NO, and CO by this method was very favorable.
17) The formation ratio of NO to N_2 was about two-tenths, and the formation of N_2O was trace.
18) The equation was derived from the relations of $[H]=2[H_2]+3[NH_4N_3]$, $[N]=2[N_2]+[NH_4N_3]$, and $[N]/[H]=3$.
19) D. S. Herr and W. A. Noyes, *J. Am. Chem. Soc.*, **62**, 2052 (1940).
20) W. C. Richardson and D. W. Setser, *Can .J. Chem.*, **47**, 2725 (1969).
21) F. O. Rice and M. Freamo, *J. Am. Chem. Soc.*, **73**, 5529 (1951); F. O. Rice and C. Grelecki, *ibid.*, **79**, 1880 (1957); F. O. Rice and T. A. Luckenbach, *ibid.*, **82**, 2681 (1960).
22) O. Kajimoto, T. Yamamoto, and T. Fueno, *J. Phys. Chem.*, **83**, 429 (1979).
23) S. Kodama, *Bull. Chem. Soc. Jpn.*, **56**, 2355 (1983).
24) S. Kodama, *Bull. Chem. Soc. Jpn.*, **56**, 2363 (1983).
25) N. C. Baird, *J. Chem. Phys.*, **62**, 300 (1975).
26) J. R. McDonald, R. G. Miller, and A. P. Baronavski, *Chem. Phys. Lett.*, **51**, 57 (1977).
27) D. W. Cornell, R. S. Berry, and W. Lwowski, *J. Am. Chem. Soc.*, **88**, 544 (1966).
28) F. Stuhl, dissertation, The University of Bonn, Bonn, Germany (1966).
29) D. E. Milligan and M. E. Jacox, *J. Chem. Phys.*, **41**, 2838 (1964).
30) P. H. H. Fischer, S. W. Charles, and C. A. McDowell, *J. Chem. Phys.*, **46**, 2162 (1967).
31) M. V. Thiel and G. C. Pimentel, *J. Chem. Phys.*, **32**, 133 (1960).
32) C. L. Currie and B. DEB. Darwent, *Can. J. Chem.*, **41**, 1552 (1963).
33) S. K. Vidyarthi, C. Willis, R. A. Back, and R. M. McKitrick, *J. Am. Chem. Soc.*, **96**, 7647 (1974).
34) R. S. Konar and B. DEB. Darwent, *Can. J. Chem.*, **48**, 2280 (1970).
35) A. E. Douglas and W. J. Jones, *Can. J. Phys.*, **43**, 2216 (1965).
36) J. Combourieu, G. Le Bras, and J. Barassin, *Bull. Soc. Chim. Fr.*, **1970**, 1271; G. Le Bras and J. Combourieu, *Int. J. Chem. Kinet.*, **5**, 559 (1973).
37) N. C. Baird and J. R. Swenson, *Can. J. Chem.*, **51**, 3097 (1973).
38) C. Willis and R. A. Back, *Can. J. Chem.*, **51**, 3605 (1973).
39) C. Willis, R. A. Back, and J. G. Purdon, *Int. J. Chem. Kinet.*, **9**, 787 (1977).
40) W. B. Rimmer, *Proc. R. Soc. London*, **103**, 696 (1923); A. Fowler and J. S. Badami, *ibid.*, **133**, 325 (1931); G. Herzberg and D. A. Ramsay, *Discuss. Faraday Soc.*, **14**, 11 (1953); D. A. Ramsay, *Mem. Soc. R. Sci. Liege Collect.* **4**, **18**, 471 (1957); J. W. C. Johns, D. A. Ramsay, and S. C. Ross, *Can. J. Phys.*, **54**, 1804 (1976).
41) O. Kajimoto, T. Kawajiri, and T. Fueno, *Chem. Phys. Lett.*, **76**, 315 (1980).
42) E. D. Miller, Ph. D. Dissertation, Catholic University of America, Catholic University of America Press, Washington, D. C. (1961).
43) S. Tsunashima, J. Hamada, M. Hotta, and S. Sato, *Bull. Chem. Soc. Jpn.*, **53**, 2443 (1980); T. Kitamura, S. Tsunashima, and S. Sato, *ibid.*, **54**, 55 (1981).
44) H. A. Papazian, *J. Chem. Phys.*, **32**, 456 (1960).

 © 1983 The Chemical Society of Japan Bull. Chem. Soc. Jpn., 56, 2355—2362 (1983)

Reactions of NH Radicals. II. Photolysis of HN_3 in the Presence of C_2H_6 at 313 nm

Sukeya KODAMA

Department of Applied Chemistry, College of Engineering, University of Osaka Prefecture, Sakai, Osaka 591

(Received September 13, 1982)

Photolysis of HN_3 vapor with C_2H_6 was studied at 313 nm and 30 °C. The products are N_2, H_2, CH_4, NH_4N_3, $CH_3NH_2 \cdot HN_3$, $C_2H_5NH_2 \cdot HN_3$, CH_3N_3, and CH_3CN. The quantum yields of these products were measured as a function of pressures of HN_3 and C_2H_6, and the light intensity. The following mechanism for the main reactions was proposed: $HN_3+h\nu(313\text{ nm}) \rightarrow N_2+NH(a^1\Delta)$; $NH(a^1\Delta)+HN_3 \rightarrow 2N_2+2H$ (2a); $NH(a^1\Delta)+HN_3 \rightarrow NH_2+N_3$ (2b); $NH(a^1\Delta)+HN_3 \rightarrow N_2+N_2H_2^*$ (2c); $NH(a^1\Delta)+C_2H_6 \rightarrow C_2H_5NH_2^*$ (3); $NH(a^1\Delta)+C_2H_6 \rightarrow NH(X^3\Sigma^-)+C_2H_6$ (4); $C_2H_5NH_2^* \rightarrow CH_3+CH_2NH_2$ (5); $C_2H_5NH_2^* \rightarrow CH_3CN+2H_2$ (6); $C_2H_5NH_2^*+M \rightarrow C_2H_5NH_2+M$ (7). The rate constant ratios at 30 °C are: $k_3/k_2=0.334$; $k_4/k_2=0.217$; $k_6/k_5=0.038$. The values of k_7/k_5 for C_2H_6, HN_3, CO_2, and Xe are 36.5, 30.3, 29.0, and 14.5 $dm^3\ mol^{-1}$, respectively. The values of $k_5=9.8\times10^9\ s^{-1}$, $k_6=3.7\times10^8\ s^{-1}$, τ (half life of $C_2H_5NH_2^*$)$=6.8\times10^{-11}$ s, η (collisional deactivation efficiency of $C_2H_5NH_2^*$)$=1$ for C_2H_6, HN_3, and CO_2, and $\eta=0.60$ for Xe were obtained by using the collision theory.

In the previous work,[1] on the photolysis of HN_3 vapor at 313 nm, it was found that hydrazoic acid is a good radical source for the first excited singlet $NH(a^1\Delta)$. Therefore, the formation of amines by insertion of the singlet NH into the C–H bond is expected in the photolysis of HN_3 with hydrocarbons, because the insertion is a characteristic reaction of the excited singlet species as were found in the reactions of $O(^1D)$,[2] $S(^1D)$,[3] and $CH_2(^1A_1)$[4] with hydrocarbons.

Miller[5] has demonstrated the formation of amines in the photolysis of HN_3 with propane, butane, isobutane, and neopentane. Cornell *et al.*[6] have studied the flash and steady photolyses of HN_3 (DN_3) with hydrocarbons including methane and ethane. They have found that the principal nitrogen-containing products are HCN and alkanenitriles in the steady photolysis. Brash and Back[7] have investigated the photolysis of HNCO in the presence of ethane, propane, neopentane, *etc.* but no amines could be detected. Recently, Tsunashima *et al.*[8] have studied the photolysis of HN_3 in liquid ethane, propane, and isobutane at the Dry Ice–methanol temperature, and observed the formation of ethylamine from ethane, propyl- and isopropylamine from propane, and isobutyl- and *t*-butylamine from isobutane.

In the work, C_2H_6 was chosen as a reactant by the following reasons: (a) the formation of ethylamine by collisional stabilization of chemically excited $C_2H_5NH_2^*$ produced by the insertion may be expected in the vapor phase photolysis, although CH_3NH_2 could not be detected in the case of CH_4,[5] because $C_2H_5NH_2$ has more degrees of internal freedom than CH_3NH_2; and (b) the identification and the quantitative analysis of amines are easy, because C_2H_6 has only primary hydrogen as compared with higher hydrocarbons that have secondary and tertiary hydrogens. Thus, the photolysis of HN_3 with C_2H_6 in the gas phase at 313 nm and 30 °C has been carried out in the present work to obtain quantitative results.

Experimental

Reaction Procedure. Ethane obtained from Takachiho Chemical Co. was 99.8% pure. It was purified each time before use by condensation and evacuation at −160 °C and liquid nitrogen temperature. Preparation and purification of HN_3, and the reaction apparatus were the same as described previously.[1] All runs in this work were carried out at 313 nm and 30 °C. The light intensity was controlled by screens, and the irradiation time was 20 to 390 min. The degree of conversion of HN_3 was only a few per cent for all runs. The reaction products were N_2, H_2, CH_4, NH_4N_3, $CH_3NH_2 \cdot HN_3$, $C_2H_5NH_2 \cdot HN_3$, CH_3N_3, and CH_3CN. On the other side, the formation of HCN was found in addition to above products at high light intensities.

Identifications of $CH_3NH_2 \cdot HN_3$ and $C_2H_5NH_2 \cdot HN_3$. An NMR spectrum of a D_2O solution of the white volatile products, condensed at the Dry Ice–acetone temperature, was

Fig. 1. NMR spectrum of a D_2O solution of the white volatile products trapped at the Dry Ice–acetone temperature.

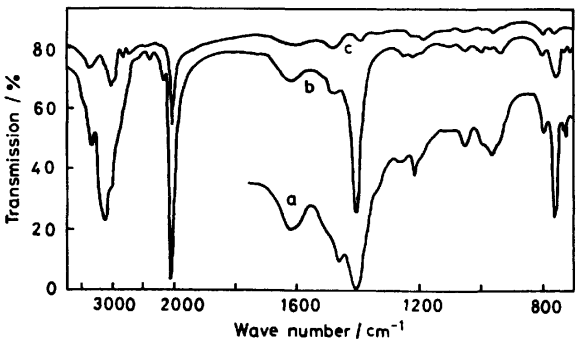

Fig. 2. IR spectra of the white volatile products (a and b) and $C_2H_5NH_2 \cdot HN_3$ sample (c).

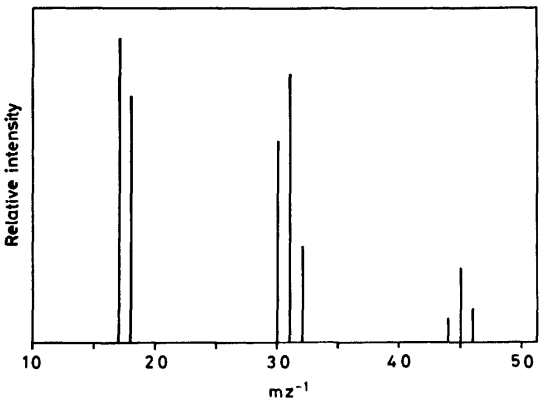

Fig. 3. Mass spectrum of the substances removed HN_3 from the white volatile products. The ionizing voltage is 15 eV.

obtained with a JNM 3H-60 (Japan Electron Optics) spectrometer, and is shown in Fig. 1. Chemical shifts are given in parts per million from $(CH_3)_4Si$. NMR spectra of known samples[9] of $CH_3NH_2 \cdot HN_3$, $C_2H_5NH_2 \cdot HN_3$, and $(CH_3)_2NH \cdot HN_3$ were also observed under the same conditions as above. From comparisons of the spectrum in Fig. 1 with the spectra of known samples, it was found that three peaks at 1.61, 1.73, and 1.85, a peak at 3.08, four peaks at 3.36, 3.48, 3.60, and 3.72, and a peak at 5.32 ppm correspond to the CH_3 group of ethylamine, CH_3 group of methylamine, CH_2 group of ethylamine, and NH_2 group of methyl- and ethylamine, respectively. Since a small peak at 3.20 ppm in Fig. 1 is in agreement with a peak of CH_3 group of $(CH_3)_2NH \cdot HN_3$ sample, the insertion of NH ($a^1\Delta$) into the C–C bond may be possible.

Infrared spectra of the white volatile products by the KBr disk method are shown in Fig. 2 together with a spectrum of a sample of $C_2H_5NH_2 \cdot HN_3$.[9] The main three peaks (1404, 2040, and 3150 cm^{-1}) in the spectra of the products are due to NH_4N_3,[1] and all peaks in the spectrum of the $C_2H_5NH_2 \cdot HN_3$ sample are found in the spectra of products as peaks or shoulders. The formation of $CH_3NH_2 \cdot HN_3$ could not be verified from the infrared spectra, because the spectrum of $CH_3NH_2 \cdot HN_3$ overlaps with the spectrum of $C_2H_5NH_2 \cdot HN_3$.

The white volatile products were introduced into a column of solid sodium hydroxide, then HN_3 molecules in the products ($RNH_2 \cdot HN_3$) were removed by the reaction,[8] $RNH_2 \cdot HN_3 + NaOH \longrightarrow RNH_2 + NaN_3 + H_2O$. A mass spectrum of the HN_3-removed products at the ionizing voltage of 15 eV is shown in Fig. 3. The existence of CH_3NH_2 and $C_2H_5NH_2$ together with NH_3 were verified from the masses of 17 (NH_3^+), 18 (NH_4^+), 30 (CH_3NH^+ or $CH_2NH_2^+$), 31 ($CH_3NH_2^+$), 32 ($CH_3NH_3^+$), 44 ($C_2H_5NH^+$ or $C_2H_4NH_2^+$), 45 ($C_2H_5NH_2^+$), and 46 ($C_2H_5NH_3^+$).

Quantitative Analysis of the Products. Noncondensable gases (N_2, H_2, and CH_4) at −210 °C were introduced into a column of silica gel (for gas chromatography) at −196 °C. Hydrogen, not trapped in the column, was collected in a Toepler gauge, and its amount determined. Nitrogen and methane, trapped on silica gel at −196 °C, were collected in the gauge by warming the column, and the total amount was also determined. The separation of N_2 and CH_4 was carried out by gas chromatography using a 5A molecular sieve column.

In the quantitative determinations of NH_4N_3, $CH_3NH_2 \cdot HN_3$, and $C_2H_5NH_2 \cdot HN_3$, the white volatile products condensed at the Dry Ice–acetone temperature were introduced on to a CuO column at about 550 °C. The combustion products were N_2, NO, CO_2, N_2O, and H_2O. The amounts of N_2 passing through a trap at −210 °C, NO trapped at −210 °C, and CO_2 and N_2O condensed at −196 °C were in turn determined by the Toepler gauge. H_2O was eliminated by trapping at −110 °C. The separation of CO_2 and N_2O was performed using a soda-lime column. The amount of CO_2 was determined by substracting the amount of N_2O from the total amount of CO_2 and N_2O.

From the stoichiometry for the combustion reactions, the relation, $[CO_2] = [CH_3NH_2 \cdot HN_3] + 2[C_2H_5NH_2 \cdot HN_3]$, is obtained for the CO_2 formation. On the other hand, the amount of $CH_3NH_2 \cdot HN_3$ can be estimated from the relation, $[CH_3NH_2 \cdot HN_3] = 0.540\ [CH_4]$, for all runs at low light intensities as discussed later. Therefore, the amount of $C_2H_5NH_2 \cdot HN_3$ can be calculated from the relation, $[C_2H_5NH_2 \cdot HN_3] = ([CO_2] - 0.540[CH_4])/2$. From the material balance of the nitrogen atoms, the amount of NH_4N_3 can be estimated by the equation, $[NH_4N_3] = (2[N_2] + 2[N_2O] + [NO])/4 - ([CO_2] + 0.540 \times [CH_4])/2$.

The quantum yields of products were measured by using HN_3 as an actinometer.[1]

Results

The results for the photolysis of HN_3 of 6.7 kPa, measured as a function of the absorbed light intensity at 313 nm, 30 °C, and 26.7 kPa of C_2H_6, are shown in Fig. 4. It is found in Fig. 4 that ϕ_{N_2}, ϕ_{CH_4}, $\phi_{CH_3NH_2 \cdot NH_3}$, and $\phi_{(CO_2)}(\phi_{CH_3NH_2 \cdot HN_3} + 2\phi_{C_2H_5NH_2 \cdot HN_3})$ decrease with an increase of the light intensity. The decrease of quantum yields seems due to radical-radical reactions, and the quantum yields converge to constant values at low light intensities. $\phi_{NH_4N_3}$, ϕ_{H_2}, and $\phi_{C_2H_5NH_2 \cdot HN_3}$ are independent of the light intensity.

Figure 5 shows the results of the photolysis measured as a function of C_2H_6 pressure at 6.7 kPa of HN_3 and low absorbed light intensity of 4.6×10^{14} quanta s^{-1} to eliminate radical-radical reactions. It is seen in Fig. 5 that ϕ_{N_2}, $\phi_{NH_4N_3}$, and ϕ_{H_2} decrease, and $\phi_{C_2H_5NH_2 \cdot HN_3}$ and $\phi_{(CO_2)}$ increase with an increase of C_2H_6 pressure, but ϕ_{CH_4} and $\phi_{CH_3NH_2 \cdot HN_3}$ decrease *via* each maximum value

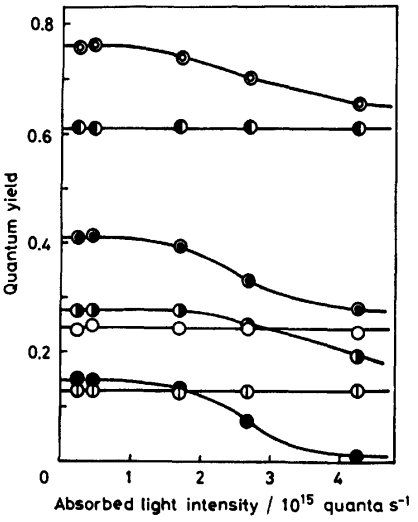

Fig. 4. Results for the photolysis of HN_3 of 6.7 kPa, measured as a function of the absorbed light intensity at 313 nm, 26.7 kPa of C_2H_6, and 30 °C. ◎, $\phi_{N_2}/5$; ◐, $\phi_{NH_4N_3}$, ⊙, $\phi_{(CO_2)}$; ◑, ϕ_{CH_4}; ○, ϕ_{H_2}; ◔, $\phi_{C_2H_5NH_2 \cdot HN_3}$; ●, $\phi_{CH_3NH_2 \cdot HN_3}$.

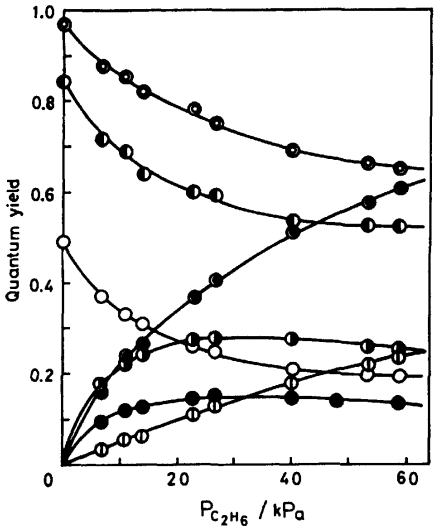

Fig. 5. Results of the photolysis of HN_3 of 6.7 kPa, measured as a function of C_2H_6 pressure at 313 nm, 30 °C, and low absorbed light intensity of 4.6×10^{14} quanta s^{-1}. The marks are the same as those in Fig. 4.

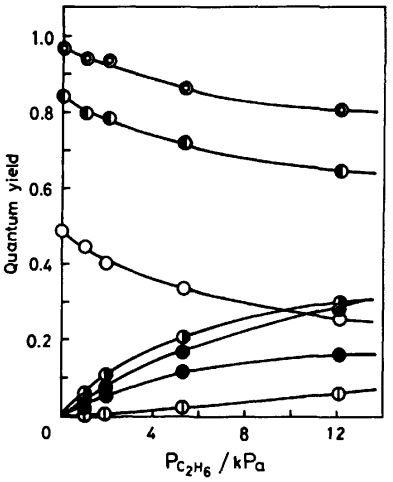

Fig. 6. Pressure dependence of C_2H_6 on the photolysis of HN_3 of 4.1 kPa at 313 nm, 30 °C, and low absorbed light intensity of 2.4×10^{14} quanta s^{-1}. The marks are the same as those in Fig. 4.

at about 27 kPa of C_2H_6.

The results for the photolysis of HN_3 at 4.1 kPa, measured as a function of C_2H_6 pressure, at low absorbed light intensity of 2.4×10^{14} quanta s^{-1} are shown in Fig. 6. In comparison with Fig. 5, it is seen from Fig. 6 that ϕ_{N_2} and ϕ_{H_2} decrease more rapidly, and ϕ_{CH_4} $\phi_{(CO_2)}$, and $\phi_{CH_3NH_2\cdot HN_3}$ increase more quickly as the C_2H_6 pressure increases.

Figure 7 shows the results of the photolysis, measured as a function of C_2H_6 pressure, at 6.7 kPa of HN_3 and high absorbed light intensity of 4.2×10^{15} quanta s^{-1}. It is seen in Fig. 7 that $\phi_{NH_4N_3}$ and ϕ_{H_2} are almost the same, but ϕ_{N_2}, $\phi_{(CO_2)}$, and ϕ_{CH_4} are lower as compared with those in Fig. 5.

Discussion

Reaction Mechanism. On the basis of the experimental results obtained above, the following reaction mechanism is postulated for the photolysis of HN_3 in the presence of C_2H_6 at low light intensities, where A, E, and M denote HN_3, C_2H_6, and deactivator molecules, respectively:

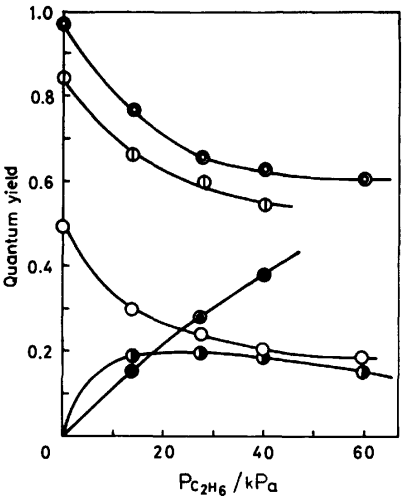

Fig. 7. Results of the photolysis of HN_3 of 6.7 kPa, measured as a function of C_2H_6 pressure at 313 nm, 30 °C, and high absorbed light intensity of 4.2×10^{15} quanta s^{-1}. The marks are the same as those in Fig. 4.

$$A + h\nu(313\text{ nm}) \longrightarrow N_2 + NH(a^1\Delta) \quad (1)$$

$$NH(a^1\Delta) + A \longrightarrow 2N_2 + 2H \quad (2a)$$

$$NH(a^1\Delta) + A \longrightarrow NH_2 + N_3 \quad (2b)$$

$$NH(a^1\Delta) + A \longrightarrow N_2 + N_2H_2^* \quad (2c)$$

$$NH(a^1\Delta) + E \longrightarrow C_2H_5NH_2^* \quad (3)$$

$$NH(a^1\Delta) + E \longrightarrow NH(X^3\Sigma^-) + E \quad (4)$$

$$C_2H_5NH_2^* \longrightarrow CH_3 + CH_2NH_2 \quad (5)$$

$$C_2H_5NH_2^* \longrightarrow 2H_2 + CH_3CN \quad (6)$$

$$C_2H_5NH_2^* + M \longrightarrow C_2H_5NH_2 + M \quad (7)$$

$$CH_2NH_2 + A \longrightarrow CH_3NH_2 + N_3 \quad (8)$$

$$CH_2NH_2 + A \longrightarrow CH_3N_3 + NH_2 \quad (9)$$

$$NH(X^3\Sigma^-) + A \longrightarrow H_2 + 2N_2 \quad (10)$$

$$NH(X^3\Sigma^-) + A \longrightarrow NH_2 + N_3 \quad (11)$$

$$H + A \longrightarrow H_2 + N_3 \quad (12)$$

$$H + A \longrightarrow NH_2 + N_2 \quad (13)$$

$$N_2H_2^* \longrightarrow N_2H_2^{**} \quad (14)$$

$$N_2H_2^* + A \longrightarrow N_2 + H_2 + A \quad (15)$$

$$N_2H_2^* + A \longrightarrow NH_3 + 2N_2 \quad (16)$$

$$N_2H_2^{**} + A \longrightarrow NH_3 + 2N_2 \quad (17)$$

$$CH_3 + A \longrightarrow CH_4 + N_3 \quad (18)$$

$$NH_2 + A \longrightarrow NH_3 + N_3 \quad (19)$$

$$N_3 + A \longrightarrow A\cdot N_3 \quad (20)$$

$$2A\cdot N_3 \longrightarrow 3N_2 + 2A \quad (21)$$

$$RNH_2(R=H,\ CH_3,\text{ and } C_2H_5) + A \longrightarrow RNH_2\cdot HN_3. \quad (22)$$

Thermochemical considerations were taken into account using the standard heats of formation listed in Table 1.

TABLE 1. SELECTED HEATS OF FORMATION*

	$\Delta H^{\circ}_{f'298}$ / kJ mol^{-1}	Ref.		$\Delta H^{\circ}_{f'298}$ / kJ mol^{-1}	Ref.
HN_3	299.8	a	C_2H_6	−84.7	e
$NH(a^1\Delta)$	506.6	b,c	CH_2CN	230.1	l
CH_3	146.9	d	CH_3CN	79.9	n
CH_4	−74.8	e	CH_3NC	150.2	o
CN	418.4	f	CH_2=C=NH	238.1	p
HCN	130.5	e	CH≡C–NH_2	222.2	p
CH_2=NH	94.6	g	CH_2CH_2N	297.5	q
CH_2NH_2	154.8	h	$C_2H_3NH_2$	48.5	p
CH_3NH	174.5	i	CH_3CH=NH	63.2	p
CH_3NH_2	−28.0	j	CH_3–N=CH_2	72.4	n
CH_3N_3	280.3	k	CH_2CH_2NH	104.6	r
C_2H_2	226.7	e	CH_3–N–CH_3	156.5	i
C_2H_3	267.8	l	CH_3CH_2NH	174	s
C_2H_4	52.3	e	$C_2H_5NH_2$	−48.5	j
C_2H_5	110.0	m	$(CH_3)_2NH$	−18.8	t

* See Table 1 in Ref. 1 for the heats of formation of NH ($X^3\Sigma^-$), N_3, NH_2, H, N_2H_2, NH_3, and NH_4N_3. a) P. Gray and T. C. Waddigton, *Proc. R. Soc. London, Ser. A*, **235**, 106 (1956). b) H. Okabe and M. Lenzi, *J. Chem. Phys.*, **47**, 5241 (1967). c) L. G. Piper, *J. Chem. Phys.*, **70**, 3417 (1979). d) M. H. Baghal-Vayjooee, A. J. Colussi, and S. W. Benson, *Int. J. Chem. Kinet.*, **11**, 147 (1979). e) "Handbook of Chemistry and Physics," 55th ed, ed by R. C. Weast, Chemical Ruffer Co. Press, Cleveland, OH (1974—1975). f) J. L. Franklin, J. G. Dillard, H. M. Rosenstock, J. T. Herron, K. Druxl, and F. H. Field, "Ionization Potentials, Appearance Potentials, and Heats of Formation of Gaseous Positive Ions," NSRDS-NBS 26, U. S. Government Printing Office, Washington D. C. (1969). g) A. J. Paine and J. Warkentin, *Can. J. Chem.*, **59**, 491 (1981). h) D. K. S. Sharma and J. L. Franklin, *J. Am. Chem. Soc.*, **95**, 6562 (1973). i) S. W. Benson and H. E. O'Neal, "Kinetic Data on Gas Phase Unimolecular Reactions," NSRDS-NBS-21, National Bureau of Standards Reference Data System, U. S. Department of Commerce, (1970). j) S. W. Benson and J. H. Buss, *J. Chem. Phys.*, **29**, 546 (1958). *k*) D. M. Golden, R. Walsh, and S. W. Benson, *J. Am. Chem. Soc.*, **87**, 4053 (1965). l) J. A. Kerr, *Chem. Rev.*, **66**, 465 (1966). m) M. Luria and S. W. Benson, *J. Am. Chem. Soc.*, **97**, 3342 (1975). n) S. W. Benson, F. R. Cruickshank, D. M. Golden, G. R. Haugen, H. E. O'Neal, A. S. Rodgers, R. Shaw, and R. Walsh, *Chem. Rev.*, **69**, 279 (1969). o) "Selected Values of Chemical Thermodynamic Properties," Circular 500, National Bureau of Standards, Washington, D. C. (1952). p) L. Radom, W. J. Hehre, and J. A. Pople, *J. Am. Chem. Soc.*, **93**, 289 (1971). q) J. W. S. Jamieson and C. A. Winkler, *J. Phys. Chem.*, **60**, 1542 (1956). r) R. A. Nelson and R. S. Jessup, *J. Res. Natl. Bur. Stand.*, **48**, 206 (1952). s) I. Tokue, M. Ikarashi, and Y. Ito, *Bull. Chem. Soc. Jpn.*, **55**, 1250 (1982). t) W. H. Johnson, E. J. Prosen, and I. Jaffé, *J. Res. Natl. Bur. Std., Sect. A* **65**, 71 (1961).

Since the formation of ethylamine has been established by the NMR, IR, and MS measurements, it is clear that the first excited singlet $NH(a^1\Delta)$ formed by the photolysis of HN_3 at 313 nm[1] reacts to give ethylamine by the insertion into a C–H bond of C_2H_6. The formation of ethylamine has also been found in the photolysis of HN_3 in liquid ethane.[8] Reaction 4 is a collisional spin relaxation process of $NH(a^1\Delta)$ by C_2H_6 as was found for Xe.[1] Similar collisional quenching processes have also been found for the other excited singlet species.[10]

Since the $C_2H_5NH_2$* formed by Reaction 3 possesses excess energy in excess of 470 kJ mol^{-1}, Reactions 5 and 6 are energetically possible. The unimolecular decomposition of $C_2H_5NH_2$* to give $C_2H_4+NH_3$, $C_2H_2+NH_3+H_2$, and $CH_4+HCN+H_2$ is possible, but these reactions are excluded, because C_2H_4, C_2H_2, and HCN were not detected in the products. The decompositions of $C_2H_5NH_2$* to give $H_2+C_2H_5N$, $C_2H_5+NH_2$, $H+C_2H_6N$, and CH_4+CH_2=NH are also possible energetically. However, the possibilities of these reactions could not be established in the reaction kinetics, although the kinetics for the formations of H_2, CH_4, and NH_4N_3 were treated with scrupulous care as mentioned later.

On the other hand, Lovas *et al.*[11] have reported that ethylamine decomposes thermally to give $NH_3+C_2H_4$, CH_2=NH+CH_4, CH_2=$CHNH_2+H_2$, and CH_3CH=NH+H_2 at about 900 °C. The difference in reaction mechanism seems to be due to the reaction conditions, that is, the thermal decomposition at high temperatures and the unimolecular decomposition of the chemically activated $C_2H_5NH_2$* at room temperature.

Reaction 7 is a collisional deactivation process of the vibrationally excited $C_2H_5NH_2$* by a third body(M). Similar collisional deactivation processes have also been found in the $O(^1D)$[2] and $CH_2(^1A_1)$[4] systems.

The CH_2NH_2 radicals formed by Reaction 5 disappear to give CH_3NH_2 and N_3 by a hydrogen abstraction reaction from HN_3, and to give CH_3N_3 and NH_2 *via* addition to a π bond of HN_3 in Reactions 8 and 9. Both reactions are supported by the formations of CH_3NH_2 and CH_3N_3. Reaction 18 is a hydrogen abstraction reaction by CH_3 from HN_3 as a strong hydrogen donor. Konar *et al.*[12] have obtained $k_{18}=8.9\times10^7$ cm^3 mol^{-1} s^{-1} in the photolysis of azomethane in the presence of HN_3 at 25 °C.

Reaction 22 was proved by the experimental fact[9] that basic ammonia and amines of CH_3NH_2 and C_2H_5-NH_2, (RNH_2), react with acidic HN_3 in the vapor phase to give the azide salts ($RNH_2\cdot HN_3$) as a white volatile powder.

In the presence of HN_3, the reactions of $NH(X^3\Sigma^-)+C_2H_6\rightarrow NH_2+C_2H_5$ and $H+C_2H_6\rightarrow H_2+C_2H_5$ could not be found in the reaction kinetics for the formations of H_2 and NH_4N_3. Reactions other than those mentioned above were discussed previously,[1] and are omitted here.

At high light intensities, the formation of HCN is observed. Moreover, as seen in Fig. 4, $\phi_{NH_4N_3}$ increases, but ϕ_{N_2}, ϕ_{CH_4}, and $\phi_{CH_3NH_2}$ decrease with an increase of the light intensity. It is clear that these facts are due to some radical-radical reactions at high light intesities. The most abundant radical in this system will be $A\cdot N_3$, because the other radicals disappear and are converted into N_3 radicals by reactions with HN_3 as Reactions 8, 11, 12, 18, and 19. The N_3 radicals then rapidly become $A\cdot N_3$, most probably by addition as Reaction

20, with HN_3.[13] Thus, the following reactions

$$CH_3 + A\cdot N_3 \longrightarrow CH_3N_3 + A, \quad (23)$$

$$CH_2NH_2 + A\cdot N_3 \longrightarrow (N_3CH_2NH_2) + A, \quad (24)$$

were added at high light intensities. By the inclusion of the above reactions, we can explain not only the formation of HCN, but also the trends shown in Fig. 4. These are also useful to ascertain the existences of CH_3, CH_2NH_2, and $A\cdot N_3(N_3)$ radicals.

Reaction Kinetics. The following reaction kinetics were formulated to confirm the mechanism of Reactions 1 to 22 and to obtain the rate constant ratios at low light intensities.

As to the formations of CH_4, $CH_3NH_2\cdot HN_3$, and $C_2H_5NH_2\cdot HN_3$, the equation

$$\frac{\phi_{(CO_2)}}{\phi_{CH_4}} = \frac{k_8}{k_8+k_9} + \frac{2k_7(HN_3)[HN_3]}{k_5} + \frac{2k_7(C_2H_6)[C_2H_6]}{k_5}, \quad (I)$$

can be derived, where $\phi_{(CO_2)}$ denotes the total formation rate of CO_2 formed by the combustions of amine salts.

$$\phi_{(CO_2)} = \phi_{CH_3NH_2\cdot HN_3} + 2\,\phi_{C_2H_5NH_2\cdot HN_3}$$

plots of $\phi_{(CH_2)}/\phi_{CO_4}$ measured as a function of C_2H_6 pressure at 4.1 and 6.7 kPa of HN_3 are shown in Fig. 8, and the values of $k_9/k_8=0.852$, $k_7(HN_3)/k_5=3.03\times10^4$ $cm^3\,mol^{-1}$, and $k_7(C_2H_6)/k_5=3.65\times10^4$ $cm^3\,mol^{-1}$ are obtained from the intercepts and the slopes. Accordingly, the quantum yield of $CH_3NH_2.HN_3$ is given by the equation, $\phi_{CH_3NH_2\cdot HN_3}=[k_8/(k_8+k_9)]\phi_{CH_4}=0.540\ \phi_{CH_4}$.

In order to obtain the collisional deactivation efficiencies of $C_2H_5NH_2$* by Xe and CO_2, the photolysis of HN_3 in the presence of C_2H_6 and Xe or CO_2 was also carried out by the same method as mentioned above. Plots of $\phi_{(CO_2)}/\phi_{CH_4}$ measured as a function of Xe or CO_2 pressure at 6.7 kPa of HN_3 and 21.6 kPa of C_2H_6 are also shown in Fig. 8. The values of $k_7(Xe)/k_5=1.45\times10^4$ and $k_7(CO_2)/k_5=2.90\times10^4$ $cm^3\,mol^{-1}$ were obtained from the relation

$$\frac{\phi_{(CO_2)}}{\phi_{CH_4}} = \left(\frac{k_8}{k_8+k_9} + \frac{2k_7(HN_3)[HN_3]+2k_7(C_2H_6)[C_2H_6]}{k_5} + \frac{2k_7(Xe)[Xe]+2k_7(CO_2)[CO_2]}{k_5}\right), \quad (II)$$

and the slopes in Fig. 8.

On the formations of H_2, CH_4, NH_4N_3, $CH_3NH_2\cdot HN_3$, and $C_2H_5NH_2\cdot HN_3$, the equation

$$\left(\frac{\phi_{(N/4)}+\phi_{H_2}}{\phi_{CH_4}} - \frac{k_6}{k_5}\right)\frac{1}{\alpha} = 1 + \frac{k_4}{k_3} + \frac{k_2+k_{2a}}{k_3}\frac{[HN_3]}{[C_2H_6]}, \quad (III)$$

can be derived, where

$$\alpha = 1 + \frac{k_6}{k_5} + \frac{k_7(HN_3)[HN_3]+k_7(C_2H_6)[C_2H_6]}{k_5},$$

and

$$k_2 = k_{2a} + k_{2b} + k_{2c},$$

and $(N/4)$ means one-quater of total nitrogen atoms found in the combustions of azide salts.

$$\phi_{(N/4)} = \phi_{NH_4N_3} + \phi_{CH_3NH_2\cdot HN_3} + \phi_{C_2H_5NH_2\cdot HN_3}$$

Equation IV can be derived as to the formations of N_2, H_2, and CH_4.

$$\left(\frac{\phi_{N_2}+\phi_{H_2}}{\phi_{CH_4}} - \frac{3k_5+2k_6}{k_5}\right)\frac{1}{\alpha} = 1 + \frac{4k_4}{k_3} + 4\left(\frac{k_2+k_{2a}}{k_3}\right)\frac{[HN_3]}{[C_2H_6]} \quad (IV)$$

By combining Eqs. III and IV, the equation

$$\frac{4\phi_{(N/4)}+3\phi_{H_2}-\phi_{N_2}}{\phi_{CH_4}} - 3\left(\frac{k_7(HN_3)[HN_3]+k_7(C_2H_6)[C_2H_6]}{k_5}\right) = \frac{5k_6}{k_5}, \quad (V)$$

can be derived. By using the experimental values of $\phi_{(N/4)}$, ϕ_{N_2}, ϕ_{H_2}, and ϕ_{CH_4}, and the values of $k_7(HN_3)/k_5$ and $k_7(C_2H_6)/k_5$ obtained above, $k_6/k_5=0.038$ was obtained as a mean value.

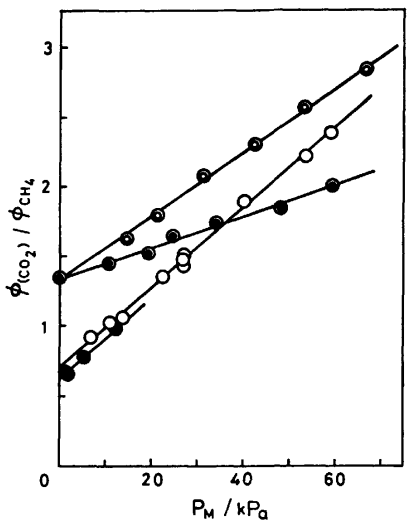

Fig. 8. Pressure dependence of $\phi_{(CO_2)}/\phi_{CH_4}$ at 313 nm and 30 °C. ◎, Measured as a function of CO_2 pressure at 6.7 kPa of HN_3 and 21.6 kPa of C_2H_6; ⊙, measured as a function of Xe pressure at 6.7 kPa of HN_3 and 21.6 kPa of C_2H_6; ○, measured as a function of C_2H_6 pressure at 6.7 kPa of HN_3; ●, measured as a function of C_2H_6 pressure at 4.1 kPa of HN_3.

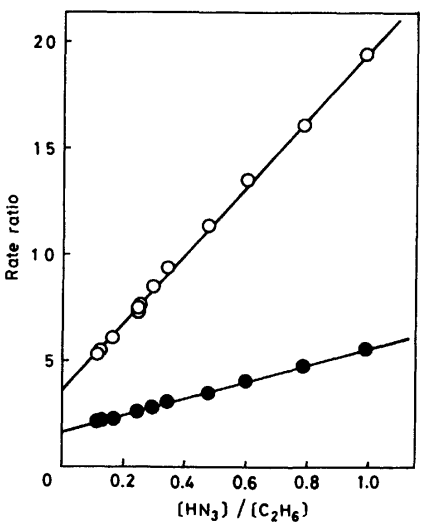

Fig. 9. Plots for Eqs. III and IV. ○, $[(\phi_{N_2}+\phi_{H_2})/\phi_{CH_4}-(3+2k_6/k_5)]/\alpha$; ●, $[(\phi_{(N/4)}+\phi_{H_2})/\phi_{CH_4}-k_6/k_5]/\alpha$. $k_6/k_5=0.038$.

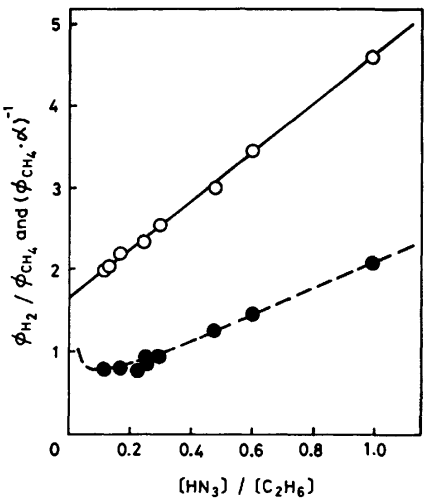

Fig. 10. Plots of $(\phi_{CH_4}\cdot\alpha)^{-1}$ and ϕ_{H_2}/ϕ_{CH_4} *versus* $[HN_3]/[C_2H_6]$. ○, $(\phi_{CH_4}\alpha)^{-1}$; ●, experimental value of ϕ_{H_2}/ϕ_{CH_4} at 6.7 kPa of HN_3; ---, calculated value of ϕ_{H_2}/ϕ_{CH_4} by Eq. VII.

The values of $[(\phi_{N_2}+\phi_{H_2})/\phi_{CH_4}-(3+2k_6/k_5)]/\alpha$ in Eq. IV were calculated using the experimental values and the rate constant ratios obtained above, and were plotted against $[HN_3]/[C_2H_6]$ as shown in Fig. 9. From the intercept and the slope, and from $k_{2b}/k_{2a}=0.746$ and $k_{2c}/k_{2a}=1.23$ obtained previously,[1] $k_3/k_2=0.334$ and $k_4/k_2=0.217$ were obtained. The relation of $[(\phi_{(N/4)}+\phi_{H_2})/\phi_{CH_4}-k_6/k_5]/\alpha$ *versus* $[HN_3]/[C_2H_6]$ in Eq. III was also plotted in Fig. 9, and the values of k_3/k_2 and k_4/k_2 obtained from the intercept and the slope were identical as those obtained from the plot for Eq. IV.

The values of k_3/k_2 and k_4/k_2 can also be obtained from the relation

$$\frac{1}{\phi_{CH_4}\alpha}=1+\frac{k_4}{k_3}+\frac{k_2}{k_3}\frac{[HN_3]}{[C_2H_6]}. \qquad \text{(VI)}$$

The values of k_3/k_2 and k_4/k_2 obtained from the straight line relation in Fig. 10 are consistent with those obtained from Eqs. III and IV.

To confirm the mechanism of succeeding reactions, the equation

$$\frac{\phi_{H_2}}{\phi_{CH_4}}=\frac{2k_6}{k_5}+\frac{k_4}{k_3}\frac{k_{10}\alpha}{k_{10}+k_{11}}+\frac{k_{2a}\alpha}{k_3}\left(\frac{2k_{12}}{k_{12}+k_{13}}+\frac{k_{2c}}{k_{2a}}\frac{k_{15}[HN_3]}{k_{14}+(k_{15}+k_{16})[HN_3]}\right)\frac{[HN_3]}{[C_2H_6]}, \qquad \text{(VII)}$$

was derived as to the formations of H_2 and CH_4. A plot of ϕ_{H_2}/ϕ_{CH_4} *versus* $[HN_3]/[C_2H_6]$ is shown in Fig. 10. The experimental values for ϕ_{H_2}/ϕ_{CH_4} are in good accord with the values calculated using the values of k_3/k_2, k_4/k_2, k_6/k_5, k_7/k_5, k_{2b}/k_{2a}, and k_{2c}/k_{2a} mentioned above, and of $k_{11}/k_{10}=3.22$, $k_{13}/k_{12}=1.15$, $k_{14}/k_{15}=2.27\times10^{-7}$ mol cm^{-3}, and $k_{16}/k_{15}=1.19$ obtained previously.[1] This means that the reaction mechanism and the rate constant ratios proposed previously[1] are also useful in the present system.

At high light intensities, the equation

$$\frac{\phi^*_{(CO_2)}-\beta\phi^\circ_{CH_4}}{\phi^*_{CH_4}}=\frac{k_8}{k_{18}}\frac{k_{23}}{k_{24}}+\left(1-\frac{k_8+k_9}{k_{18}}\frac{k_{23}}{k_{24}}\right)\left(\frac{\phi^*_{(CO_2)}}{\phi^\circ_{CH_4}}-\beta\right) \qquad \text{(VIII)}$$

can be derived for the formations of CH_4 and CO_2 by combustion, where

$$\beta=2(k_7(HN_3)[HN_3]+k_7(C_2H_6)[C_2H_6])/k_5$$

$\phi^*_{CH_4}$ and $\phi^*_{(CO_2)}$ denote the quantum yields of CH_4 and CO_2 at high light intensities. $\phi^\circ_{CH_4}$ is the estimated quantum yield of CH_4 at low light intensity, but the other experimental conditions are the same as those for $\phi^*_{CH_4}$ and $\phi^\circ_{CH_4}$. A plot of $(\phi^*_{(CO_2)}-\beta\phi^\circ_{CH_4})/\phi^*_{CH_4}$ *versus* $\phi^*_{(CO_2)}/\phi^\circ_{CH_4}-\beta$ is shown in Fig. 11. The values of $k_8k_{23}/k_{18}k_{24}=0.030$ from the intercept and $(k_8+k_9)k_{23}/k_{18}k_{24}=0.056$ from the slope were obtained. If we assumed that k_{23} is nearly equal to k_{24} because both reactions are the radical-radical combination,[14] $k_{18}/k_8=33.3$ and $k_{18}/(k_8+k_9)=18.0$ are obtained. These values imply that the reactivity of CH_2NH_2 for reaction with HN_3 is much lower than that of CH_3. It may be because CH_2NH_2 is stabilized by the interaction of an unpaired electron in CH_2 group with nonbonding electrons in NH_2 group.[15]

Comparisons of Rate Constants. The rate constant ratios for the reactions of $NH(a^1\Delta)$ are shown in Table 2, together with the values obtained by Tsunashima *et al.*[8] on the photolysis of HN_3 in liquid ethane at the Dry Ice–methanol temperature and 250 to 330 nm. The value of $k_3/(k_3+k_4)$ obtained by them is slightly higher than the value in the present work. The discrepancy may be due to the difference of the experimental conditions of phase, temperature, wavelength, *etc.*

On the other hand, their value for k_2/k_3 is extremely high as compared with our value. The most significant differences between the mechanisms are as follows: Reactions 2a, 2c, 10, and 13 were not taken into account in their mechanism; the reaction, $2NH_2\rightarrow N_2H_4$, was considered in their mechanism, although they failed to detect hydrazine.

The slope for Eq. III in Fig. 9 is steeper than the slope for Eq. VI in Fig. 10. This implies that k_{2a} is not zero.

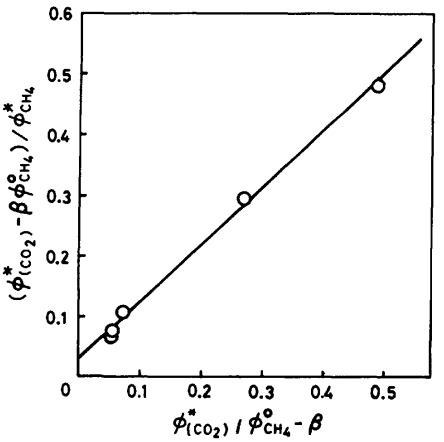

Fig. 11. Plot of $(\phi^*_{(CO_2)}-\beta\phi^\circ_{CH_4})/\phi^*_{CH_4}$ *versus* $\phi^*_{(CO_2)}/\phi^\circ_{CH_4}-\beta$.

TABLE 2. RATE CONSTANT RATIOS FOR THE REACTIONS OF $NH(a^1\Delta)$

$k_3/(k_3+k_4)$	k_2/k_3	
0.86 ± 0.04	125 ± 21	Ref. 8
0.606	2.99	This work

Moreover, if k_{2a} and k_{10} are zero, ϕ_{H_2}/ϕ_{CH_4} in Eq. VII should be reduced to 0.076 independently of $[HN_3]/[C_2H_6]$. This assumption is inconsistent with the experimental results of ϕ_{H_2}/ϕ_{CH_4} in Fig. 10. However, the large discrepancy for k_2/k_3 can not be explained by the existence of Reactions 2a, 10, and others, because the influence to k_2/k_3 on the succeeding reactions is not very large.

It seems that the reaction rate of NH($a^1\Delta$) with C_2H_6 is not very slow, judging from the specific rates of reactions of the first excited singlet species, $C(2^1D_2)$,[16] $O(2^1D_2)$,[17] and $S(3^1D_2)$,[18] with CH_4, C_2H_6, C_3H_8, and others. The main reason for the large discrepancy of k_2/k_3 seems to be due to the difference of the liquid and vapor phases.

If we assume that the arrangement of molecules in the liquid is closest-packed hexagonal, and both C_2H_6 and HN_3 molecules have the same size and a spherical shape, HN_3 molecules are mutually separated by five molecular distances at the concentration ratio of $[HN_3]/[C_2H_6]=0.0034$. When a HN_3 molecule was converted into NH($a^1\Delta$) and N_2 by the photochemical decomposition, all of 322 molecules in four molecular layers from the central NH($a^1\Delta$) are ethane. Although twelve molecules of HN_3 exist at the fifth layer, the NH($a^1\Delta$) will be lost by an insertion or quenching reaction with C_2H_6 before the NH($a^1\Delta$) encounters a HN_3 molecule, because the set-collision with C_2H_6 as a solvent molecule takes place during the diffusion process.

Since the five molecule separation was merely taken as an average value, and the mutual diffusion between NH($a^1\Delta$) and HN_3 occurs during the reaction period, the situation is not quite so simple. However, the probability that the excited singlet NH($a^1\Delta$) encounters a HN_3 molecule will be much less than that expected from the concentration. This prediction drastically reduces the appearent k_2/k_3 value. Therefore, the high value for k_2/k_3 may be due to a contribution from succeeding reactions for NH($X^3\Sigma^-$).

The high value of k_2/k_3 is also explainable if dimers and clusters of HN_3 are formed in liquid ethane at Dry Ice–methanol temperature. However, it is uncertain at present if dimers and clusters are in fact formed hydrogen bonding and molecular association.

The specific rate of Reaction 7 can be estimated from the equation

$$k_7 = \eta k_z, \qquad \text{(IX)}$$

where, k_z is the collision number of $C_2H_5NH_2$* per second, and η is the collisional stabilization efficiency. The value of k_z can be calculated from the Lennard-Jones collision frequency.[19]

$$k_z = N_A\sigma^2_{B-M}(8\pi kT/\mu_{B-M})^{1/2}\Omega^{(2,2)*}_{B-M} \qquad \text{(X)}$$

Here, N_A is Av σ_{B-M} ogadro's number,and k is Boltzmann's constant. σ_{B-M}, μ_{B-M}, and $\Omega^{(2,2)*}_{B-M}$ mean the collision diameter, the reduced mass, and the reduced collision integral for B(ethylamine) and M molecules, respectively. The values of $\Omega^{(2,2)*}_{B-M}$ are conveniently tabulated[20] as a function of kT/ε_{B-M} with the Lennard-Jones well depth $\varepsilon_{B-M}=(\varepsilon_{B-B}\cdot\varepsilon_{M-M})^{1/2}$. The σ_{B-M} is given by $\sigma_{M-B}=(\sigma_B+\sigma_M)/2$. For ethylamine, $\sigma_B=4.80$ Å and $\varepsilon_{B-B}/k=320$ K were estimated from those for C_2H_5OH,[21] C_3H_6,[22] and C_3H_8[23] molecules. The values of k_z calculated using Eq. X are shown in Table 3.

The absolute value of k_5 can be estimated from the relation

$$k_5 = \eta k_z/(k_7/k_5)_{obsd}. \qquad \text{(XI)}$$

The values of k_5 calculated by assuming $\eta=1$ are shown in Table 3, and it is found that the values for C_2H_6, HN_3, and CO_2 are almost the same. This result means that the $C_2H_5NH_2$* is deactivated with every collision in the collisions with polyatomic molecules such as C_2H_6, HN_3, and CO_2.

The value of k_5 calculated with $\eta=1$ for Xe is higher than the values for the polyatomic molecules. Therefore the collisional deactivation efficiency of Xe is less than unity, and should be reduced to 0.60 to adjust to the same value as k_5 for polyatomic molecules. The result is supported by the fact that the collisional energy transfer efficiencies by monatomic molecules are much less than those by polyatomic molecules.[24]

As a specific rate of the unimolecular decomposition of $C_2H_5NH_2$* to give CH_3 and CH_2NH_2, $k_5=9.8\times10^9$ s^{-1} is obtained by averaging the three values for polyatomic molecules. From the rate constant ratio of $k_6/k_5=0.038$, $k_6=3.7\times10^8$ s^{-1} is obtained for the unimolecular decomposition of $C_2H_5NH_2$* to give CH_3-CN and $2H_2$. By using the relation $\tau=\ln 2/(k_5+k_6)$, $\tau=6.8\times10^{-11}$ s is obtained as a half life of $C_2H_5NH_2$*.

The author is gratefully indebted to Emeritus Professor Osamu Toyama of University of Osaka Prefecture for his helpful advice and to Dr. Sotaro Esho for his cooperation.

References

1) S. Kodama, *Bull. Chem. Soc. Jpn.*, **56**, 2348 (1983).
2) H. Yamazaki and R. J. Cvetanović, *J. Chem. Phys.*, **41**, 3703 (1964); W. B. DeMore and O. F. Raper, *ibid.*, **46**, 2500

Table 3. Calculated values of k_5 and k_7 at 30 °C

M	σ_M / Å	ε_{M-M}/k / K	k_z / 10^{14} cm^3 mol^{-1} s^{-1}	$(k_7/k_5)_{obsd}$ / 10^4 cm^3 mol^{-1}	$k_5(\eta=1)$ / 10^9 s^{-1}	k_7 / 10^{14} cm^3 mol^{-1} s^{-1}
C_2H_6	4.42[a]	230[a]	3.60	3.65	9.86	3.60
HN_3	3.96[b]	240[b]	2.98	3.03	9.83	2.98
CO_2	3.75[c]	246[c]	2.83	2.90	9.76	2.83
Xe	3.97[d]	228[d]	2.39	1.45	16.48	1.42

a) J. Roberts, *Brit. Chem. Eng.*, **8**, 753 (1963). b) Estimated values. c) A. A. Clifford, P. Gray, and N. Platts, *J. Chem. Soc., Faraday Trans. 1*, **73**, 381 (1977). d) E. A. Mason and W. E. Rice, *J. Chem. Phys.*, **22**, 843 (1954).

(1967); L. M. Quick and R. J. Cvetanović, *Can. J. Chem.*, **49**, 2193 (1971); A. J. Colussi and R. J. Cvetanović, *J. Phys. Chem.*, **79**, 1891 (1975).

3) H. E. Gunning and O. P. Strausz, *Adv. Photochem.*, **4**, 143 (1966).

4) P. M. Crane and T. L. Rose, *J. Phys. Chem.*, **79**, 403 (1975); K. Shibuya, K. Obi, and I. Tanaka, *Bull. Chem. Soc. Jpn.*, **49**, 2178 (1976); H. M. Frey and G. J. Kennedy, *J. Chem. Soc., Faraday Trans. 1*, **73**, 164 (1977); A. D. Clements, H. M. Frey, and R. Walsh, *ibid.*, **73**, 1340 (1977).

5) E. D. Miller, Ph. D. Dissertation, Catholic University of America, Washington, D. C., 1961.

6) D. W. Cornell, R. S. Berry, and W. Lwoski, *J. Am. Chem. Soc.*, **88**, 544 (1966).

7) J. L. Brash and R. A. Back, *Can. J. Chem.*, **43**, 1778 (1965).

8) S. Tsunashima, J. Hamada, M. Hotta, and S. Sato, *Bull. Chem. Soc. Jpn.*, **53**, 2443 (1980).

9) These samples were prepared by the following methods: an amine was mixed with small excess of HN_3 in the vapor phase, and the salt formed was purified by evacuating excess HN_3 at the Dry Ice–acetone temperature.

10) J. A. Bell, *J. Phys. Chem.*, **75**, 1537 (1971); D. J. Little, A. Dalgleish, and R. J. Donovan, *Discuss. Faraday Soc.*, **53**, 211 (1972); S. T. Amimoto, A. P. Force, R. G. Gulotty, and J. R. Wiesenfeld, *J. Chem. Phys.*, **71**, 3640 (1979); D. Husain and D. P. Newton, *J. Chem. Soc., Faraday Trans. 2*, **78**, 51 (1982).

11) F. J. Lovas, F. O. Clark, and E. Tiemann, *J. Chem. Phys.*, **62**, 1925 (1975).

12) R. S. Konar and B. DEB. Darwent, *Can. J. Chem.*, **48**, 2280 (1970).

13) R. J. Paur and E. J. Bair, *J. Photochem.*, **1**, 255 (1973); R. J. Paur and E. J. Bair, *Int. J. Chem. Kinet.*, **8**, 139 (1976).

14) T. S. Lee, T. Ree, H. Eyring, and T. Fueno, *J. Chem. Phys.*, **36**, 281 (1962); M. J. Gibian and R. C. Corley, *Chem. Rev.*, **73**, 441 (1973).

15) C. A. Coulson and J. Jacobs, *J. Chem. Soc.*, **1949**, 1983; H. H. Jaffé, *J. Chem. Phys.*, **20**, 279 (1952); A. Pullman, *Bull. Soc. Chim. Fr.*, **1958**, 641.

16) D. Husain and L. J. Kirsch, *Trans. Faraday Soc.*, **67**, 2886, 3166 (1971).

17) P. Michaud, G. Paraskevopoulos, R. J. Cvetanović, *J. Phys. Chem.*, **78**, 1457 (1974); I. S. Fletcher and D. Husain, *Can. J. Chem.*, **54**, 1765 (1976); J. A. Davidson, H. I. Schiff, G. E. Stereit, J. R. McAfee, A. L. Schmeltekopf, and C. J. Howard, *J. Chem. Phys.*, **67**, 5021 (1977).

18) R. J. Donovan and D. Husain, *Chem. Rev.*, **70**, 489 (1970).

19) J. Troe, *J. Phys. Chem.*, **83**, 114 (1979).

20) J. O. Hirschfelder, R. B. Bird, and E. L. Spotz, *J. Chem. Phys.*, **16**, 968 (1948); J. O. Hirschfelder, C. F. Curtiss, and R. B. Bird, "Molecular Theory of Gases and Liquids," Wiley (1954), p. 1126.

21) L. Monchick and E. A. Mason, *J. Chem. Phys.*, **35**, 1676 (1961).

22) Ed. by S. Gratch, "Advances in Thermophysical Properties at Extreame Temperatures and Pressures," ASME (1965).

23) L. S. Tee, S. Gotoh, and W. E. Stwart, *Ind. Eng. Chem., Fundam.*, **5**, 356 (1966).

24) P. J. Marcoux, E. E. Siefert, and D. W. Setser, *Int. J. Chem. Kinet.*, **7**, 473 (1975); P. J. Marcoux and D. W. Setser, *J. Phys. Chem.*, **82**, 97 (1978).

 © 1983 The Chemical Society of Japan Bull. Chem. Soc. Jpn., 56, 2363—2370 (1983)

Reactions of NH Radicals. III. Photolysis of HN_3 in the Presence of C_2H_4 at 313 nm

Sukeya KODAMA

Department of Applied Chemistry, College of Engineering, University of Osaka Prefecture, Sakai, Osaka 591

(Received September 13, 1982)

Photolysis of HN_3 vapor in the presence of C_2H_4 was studied at 313 nm and 30 °C. The main products were N_2, H_2, CH_4, C_2H_6, NH_4N_3, $C_2H_5N \cdot HN_3$ (salt of C_2H_5N (azomethines) with HN_3), HCN, CH_3CN, CH_3N_3, and $C_2H_5N_3$. The quantum yields of these products were measured as a function of the light intensity and pressures of HN_3 and C_2H_4. The following mechanism for the main reactions was infered: $HN_3+h\nu(313\text{ nm})\rightarrow NH(a^1\Delta)+N_2$; $NH(a^1\Delta)+HN_3\rightarrow 2N_2+2H$ (2a); $NH(a^1\Delta)+HN_3\rightarrow NH_2+N_3$(2b); $NH(a^1\Delta)+HN_3\rightarrow N_2+N_2H_2{}^*$ (2c); $NH(a^1\Delta)+C_2H_4\rightarrow C_2H_5N^*$ (aziridine and vinylamine) (3); $C_2H_5N^*\rightarrow CH_3+CH_2N$ (4); $C_2H_5N^*\rightarrow H_2+CH_3CN$ (5); $C_2H_5N^*\rightarrow H+C_2H_4N$ (6); $C_2H_5N^*\rightarrow C_2H_3+NH_2$ (7). The rate constant ratios at 30 °C are: $k_3/k_2=1.64$; $k_5/k_4=0.102$; $k_6/k_4=0.564$; $k_7/k_4=0.734$. The collisional deactivation from $NH(a^1\Delta)$ to $NH(X^3\sum^-)$ by C_2H_4 was not found. The lifetime of $C_2H_5N^*$ is much shorter than 6.8×10^{-11} s for $C_2H_5NH_2{}^*(\leftarrow NH(a^1\Delta)+C_2H_6)$. The relative and absolute rates for the reactions of $NH(a^1\Delta)$ with HN_3, Xe, C_2H_6, and C_2H_4 are discussed.

The photolysis of HN_3 in the presence of Xe[1] and C_2H_6[2] at 313 nm has been studied previously, and it was found that HN_3 is a useful source for the first excited singlet $NH(a^1\Delta)$; ethylamine is produced by insertion of $NH(a^1\Delta)$ into a C–H bond of C_2H_6.

On the other hand, an addition reaction to a π bond as well as the insertion reaction is to be expected in the reactions of $NH(a^1\Delta)$ with unsaturated hydrocarbons, as were found in the reactions of unsaturated hydrocarbons with the isoelectronic species such as $O(^1D)$,[3] $S(^1D)$,[4] and $CH_2(^1A_1)$.[5] Therefore, it is of interest that the reactions of $NH(a^1\Delta)$ with C_2H_4 having π bond are compared with those for C_2H_6 having σ bond only.

On the photolysis of HN_3 with C_2H_4 in the vapor phase, Miller[6] has found that the reaction products are N_2, H_2, CH_4, C_2H_6, HCN, CH_3CN, NH_4N_3, and a yellowish film of polymeric material. Cornell, Berry, and Lwowski[7] have found the products of H_2, CH_4, HCN, CH_3CN, and an amorphous solid in the flash and steady photolyses. Back and his co-workers[8] have studied the reactions of C_2H_4 with NH formed by the photolysis of HNCO, and reported that no aziridine, vinylamine, nor other nitrogen-bearing products could be detected. Tidemann and Schiendler[9] have obtained $\phi_{C_2H_6}=0.56$ and $\phi_{n\text{-}C_4H_{10}}=0.03$ in the photolysis of HN_3 vapor with C_2H_4.

Jacox and Milligan[10] have observed the formation of aziridine in the photolysis of HN_3 with C_2H_4 in an argon matrix at 4 K. Recently, Kitamura, Tsunashima, and Sato[11] have found N_2, NH_3, and aziridine in the photolysis of HN_3 in liquid ethylene at the Dry Ice–methanol temperature, and obtained the relative yields of $NH_3/N_2=0.16$ and aziridine/$N_2=0.18$, independently of $[HN_3]/[C_2H_4]$.

Many results have been obtained for the reactions of NH with C_2H_4, however, they are insufficient to explain in detail the reaction mechanism and the reaction rates. Therefore, the photolysis of HN_3 vapor with C_2H_4 was reinvestigated in the present work.

Experimental

Ethylene obtained from Takachiho Chemical Co. was 99.9% in purity, and was purified each time before use by condensation and evacuation at −160 and −196 °C. Preparation and purification of HN_3, and the apparatus and procedure for reaction were the same as described previously.[1,2] All runs in this work were carried out at 313 nm at 30 °C. The light intensity was controlled with screens, and the irradiation time was varied from 10 to 120 min. The degree of conversion of HN_3 was below a few per cent for all runs.

The main reaction products were N_2, H_2, CH_4, C_2H_6, NH_4N_3, $C_2H_5N \cdot HN_3$ (salt by HN_3 with C_2H_5N(azomethines)), HCN, CH_3CN, CH_3N_3, $C_2H_5N_3$, and polymers. C_2H_2, C_3H_8, C_4H_8, and n-C_4H_{10} are also found as small amount.

For the identification of azides, CH_3N_3,[12] $C_2H_5N_3$,[13] n-$C_3H_7N_3$,[14] n-$C_4H_9N_3$,[15] and $N_3CH_2CH_2N_3$[16] were prepared as reference samples, $N_3(CH_2)_4N_3$ was prepared by heating for about 12 hours in a water bath a mixture of NaN_3 (35 g), $Br(CH_2)_4Br$ (46 g), C_2H_5OH (40 cm³), and water (100 cm³). The retention times of these azides were measured by gas chromatography using a silicone oil column (1 m) at 35 °C. The relative retention times, zero for CH_4 and unity for benzene, are shown in Table 1 together with $N_3CH_2CH_2Cl$ and $N_3(CH_2)_4Br$ formed as monosubstituted azides of $ClCH_2$-CH_2Cl and $Br(CH_2)_4Br$. The formations of CH_3N_3 and $C_2H_5N_3$ were ascertained using the data in Table 1. While, n-$C_3H_7N_3$, n-$C_4H_9N_3$, $N_3CH_2CH_2N_3$, and $N_3(CH_2)_4N_3$ could not be detected as a product.

The formation of HCN was verified by the pyridine–pyrazolone method.[17] The formation of CH_3CN was confirmed by gas chromatography using a squalene column (2 m) at 40 °C and a silicone oil column (1 m) at 35 °C.

The basic products(B) such as NH_3 and amines react with acidic HN_3 to give salts ($B \cdot HN_3$) as white volatile powders.[2] Therefore, the white volatile products trapped at the Dry Ice–acetone temperature were introduced into a solid sodium

Table 1. Relative retention times of azides by a silicone oil column (1 m) at 35 °C[a]

Azide	Relative retention time	Azide	Relative retention time
HN_3	0.187	$N_3(CH_2)_2Cl$	2.25
CH_3N_3	0.194	$N_3(CH_2)_2N_3$	5.08
$C_2H_5N_3$	0.382	$N_3(CH_2)_4Br$	22.9
n-$C_3H_7N_3$	0.846	$N_3(CH_2)_4N_3$	27.2
n-$C_4H_9N_3$	2.03		

a) The relative retention time was measured on the basis of zero for methane and unity for benzene.

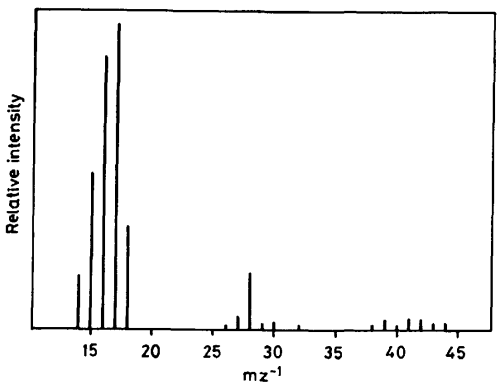

Fig. 1. Mass spectrum of a substance removed HN_3 from the white volatile products trapped at the Dry Ice–acetone temperature. The ionizing voltage is 15 eV.

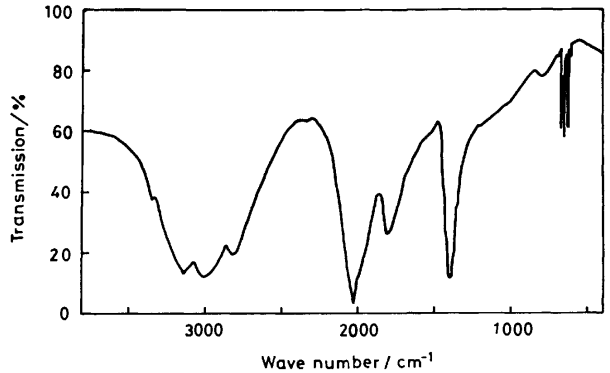

Fig. 2. Infrared spectrum of the white volatile products.

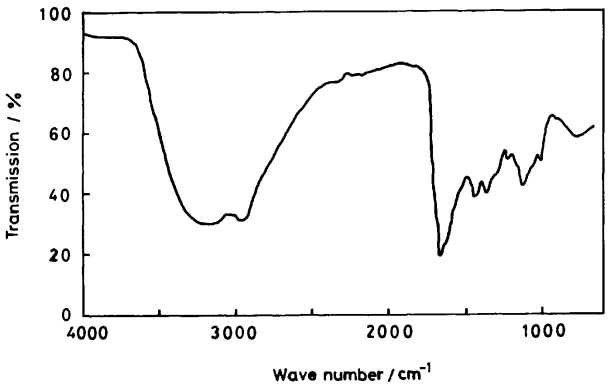

Fig. 3. Infrared spectrum of a substance prepared by removing ethanol from an ethanol solution of the yellowish polymeric material formed on the inside of the reaction cell.

hydroxide column to remove HN_3 from $B \cdot HN_3$ by the reaction $B \cdot HN_3 + NaOH \longrightarrow B + NaN_3 + H_2O$. A mass spectrum of the HN_3-free products at the ionizing voltage of 15 eV is shown in Fig. 1.

The spectrum is more complicated than the spectrum of the mixture of NH_3, CH_3NH_2, and $C_2H_5NH_2$ formed in the photolysis of HN_3 with C_2H_6.[2] It seems that $m/z=16$. 17, and 18 correspond to NH_2^+, NH_3^+, NH_4^+,[2] and the other peaks are due to $C_2H_5N^+$ ($m/z=43$) and its fragments. The large fragment peaks of $m/z=15$ and 28 may be due to the cracking reactions of $C_2H_5N \xrightarrow{e^-} CH_3^+ + CH_2{=}N$ (or $CH{=}NH$), $CH_3 + CH_2{=}N^+$ (or $CH{=}NH^+$), $C_2H_4^+ + NH$, and $C_2H_4 + NH^+$. However, the later two may be minor, because both need fission of two single bonds for aziridine and vinylamine and a double bond for CH_3–$CH{=}NH$. A mass spectrum of the HN_3-free products at the ionizing voltage of 75 V is inconsistent with that of aziridine measured at 70 V.[18] Vinylamine is not stable in the normal state. Judging from these reasons, the C_2H_5N may be CH_3–$N{=}CH_2$ or CH_3–$CH{=}NH$.

An infrared spectrum of the white volatile products trapped at Dry Ice–acetone temperature was observed by the KBr disk method, and is shown in Fig. 2. Since the spectrum is almost the same as the spectrum of solid NH_4N_3 at 90 K,[19] it was not possible to identify the structure of C_2H_5N from the spectrum in Fig. 2.

A yellowish film of polymeric material was formed on the inside of the reaction cell. The yellowish material is nonvolatile, very highly viscous, and soluble in ethanol. An infrared spectrum by the KBr disk method of a substance prepared by removing ethanol from an ethanol solution of the yellowish material is shown in Fig. 3. It is found from the spectrum that the substance includes the functional groups of NH (3200 and 1620), CH_3 (2960, 2870, 1450, 1380, and 1125), CH_2 (2950, 2850, 1450, and 1300), C=N (1670), and C–N (1230, 1175, and 1040 cm^{-1}).

A yellowish oily liquid[6] is formed by mixing aziridine and HN_3 at room temperature and the vapor phase. However, an infrared spectrum of the oily liquid is different from the spectrum in Fig. 3. Accordingly, it seems that the yellowish film of polymeric material does not result from aziridine.

N_2, H_2, CH_4, C_2H_6, NH_4N_3, and $C_2H_5N \cdot HN_3$ of the reaction products were determined quantitatively. First, these products were separated at solid nitrogen temperature (−210 °C), −160 °C, and Dry Ice–acetone temperature. Quantitative analyses of N_2, H_2, and CH_4, noncondensable gases at −210 °C, were carried out by the procedures described previously.[2] The total amount of C_2H_6 and unconverted C_2H_4, passing through a trap at −160 °C, was determined by a Toepler gauge. C_2H_6 and C_2H_4 were separated by the gas chromatography using a silica gel column (2 m) at 80 °C.

NH_4N_3 and $C_2H_5N \cdot HN_3$ condensed at Dry Ice–acetone temperature were introduced into a CuO column at about 550 °C. The amounts of N_2, NO, N_2O, and CO_2 as combustion products were determined by the method described previously.[2] The amounts of $C_2H_5N \cdot HN_3$ and NH_4N_3 can be calculated from the equations of $[C_2H_5N \cdot HN_3] = [CO_2]/2$ and $[NH_4N_3] = ([N_2] + [N_2O] - [CO_2])/2 + [NO]/4$.

The quantum yields of products were determined using HN_3 as an actinometer.[1]

Results

Results for the photolysis of HN_3 of 6.7 kPa, measured as a function of C_2H_4 pressure at 313 nm, 30 °C, and the absorbed light intensity of 2.2×10^{15} quanta s^{-1} are shown in Fig. 4. It is seen in Fig. 4 that ϕ_{H_2} and $\phi_{NH_4N_3}$ decrease drastically by adding C_2H_4 in small amount.

Figure 5 shows the results of the photolysis measured as a function of HN_3 pressure at 4.0 kPa of C_2H_4, 30 °C, 313 nm, and the incident light intensity of 1.9×10^{16} quanta s^{-1}. In Fig. 5, it is found that ϕ_{N_2} and $\phi_{C_2H_6}$ increase, but ϕ_{CH_4} decreases with an increase of HN_3 pressure. It is also found that the formation rate of N_2, R_{N_2}, increases rectilinearly as the HN_3 pressure increases.

Figure 6 shows the results of the photolysis measured as a function of the absorbed light intensity at 6.7 kPa of

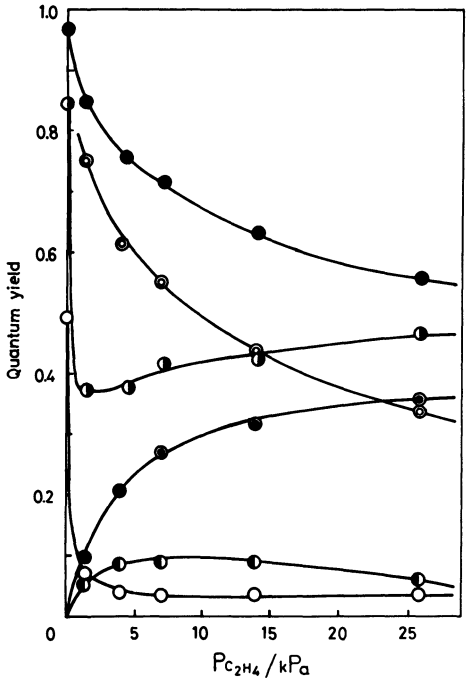

Fig. 4. Results of the photolysis of HN_3 of 6.7 kPa, measured as a function of C_2H_4 pressure at 313 nm, 30 °C, and the absorbed light intensity of 2.2×10^{15} quanta s^{-1}. ●, $\phi_{N_2}/5$; ◎, $\phi_{C_2H_6}$; ◑, $\phi_{NH_4N_3}$; ⊙, ϕ_{CH_4}; ◐, $\phi_{C_2H_5N\cdot HN_3}$; ○, ϕ_{H_2}.

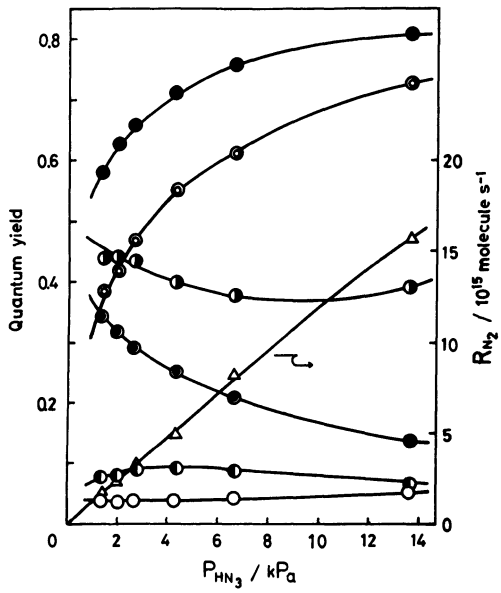

Fig. 5. Results of the photolysis measured as a function of HN_3 pressure at 4.0 kPa of C_2H_4, 30 °C, 313 nm, and the incident light intensity of 1.9×10^{16} quanta s^{-1}. △, R_{N_2}. The other marks are the same as those in Fig. 4.

HN_3, 4.0 kPa of C_2H_4, 30 °C, and 313 nm. It is shown in Fig. 6 that all quantum yields are independent of the light intensity.

Discussion

Reaction Mechanism. On the basis of the experimental results in this work and in the light of the results

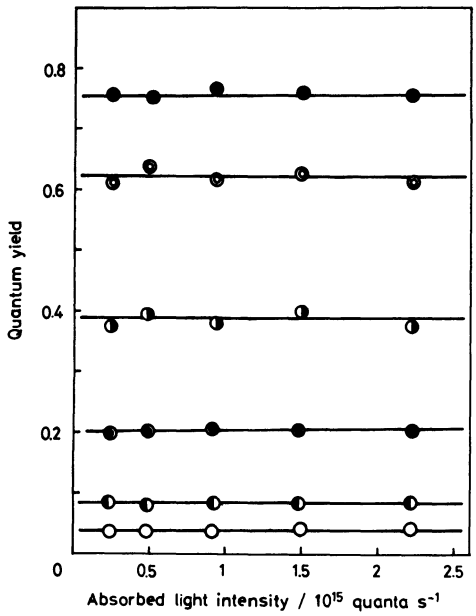

Fig. 6. Results of the photolysis measured as a function of the absorbed light intensity at 6.7 kPa of HN_3, 4.0 kPa of C_2H_4, 30 °C, and 313 nm. The marks are the same as those in Fig. 4.

achieved by previous investigators, we have postulated the following mechanism for the photolysis of HN_3 vapor in the presence of C_2H_4, where A and E mean HN_3 and C_2H_4 molecules, respectively:

$$A + h\nu(313\text{ nm}) \longrightarrow N_2 + NH(a^1\Delta) \quad (1)$$

$$NH(a^1\Delta) + A \longrightarrow 2N_2 + 2H \quad (2a)$$

$$NH(a^1\Delta) + A \longrightarrow NH_2 + N_3 \quad (2b)$$

$$NH(a^1\Delta) + A \longrightarrow N_2 + N_2H_2^* \quad (2c)$$

$$NH(a^1\Delta) + E \longrightarrow C_2H_5N^* \quad (3)$$

$$C_2H_5N^* \longrightarrow CH_3 + CH_2N \quad (4)$$

$$C_2H_5N^* \longrightarrow H_2 + CH_3CN \quad (5)$$

$$C_2H_5N^* \longrightarrow H + C_2H_4N \quad (6)$$

$$C_2H_5N^* \longrightarrow C_2H_3 + NH_2 \quad (7)$$

$$C_2H_4N + A \longrightarrow C_2H_5N + N_3 \quad (8)$$

$$C_2H_4N + E \longrightarrow C_4H_8N \quad (9)$$

$$H + A \longrightarrow H_2 + N_3 \quad (10)$$

$$H + A \longrightarrow NH_2 + N_2 \quad (11)$$

$$H + E \longrightarrow C_2H_5 \quad (12)$$

$$CH_2N + A \longrightarrow N_2 + HCN + NH_2 \quad (13)$$

$$N_2H_2^* + E \longrightarrow N_2 + C_2H_6 \quad (14)$$

$$R(CH_3, C_2H_3, C_2H_5, \text{and } NH_2) + A \longrightarrow RH + N_3 \quad (15)$$

$$NH_3 + A \longrightarrow NH_4N_3 \quad (16)$$

$$C_2H_5N + A \longrightarrow C_2H_5N\cdot HN_3 \quad (17)$$

$$C_4H_8N + E \longrightarrow \text{Polymers} \quad (18)$$

$$N_3 + A \longrightarrow A\cdot N_3 \quad (19)$$

$$N_3 + E \longrightarrow E\cdot N_3 \quad (20)$$

$$A\cdot N_3 + A\cdot N_3 \longrightarrow 2A + 3N_2 \quad (21)$$

$$A\cdot N_3 + E\cdot N_3 \longrightarrow A + CH_3N_3 + HCN + N_2 \quad (22)$$

$$E\cdot N_3 + E\cdot N_3 \longrightarrow C_2H_5N_3 + CH_3CN + N_2 \quad (23)$$

Thermochemical considerations were taken into account by using the standard heats of formation listed previously.[1,2]

Of the reactions of the first excited singlet $NH(a^1\Delta)$ with C_2H_4, the insertion reaction into the C–H bond and the addition reaction to the π bond are to be expected. Therefore, the $C_2H_5N^*$ formed by Reaction 3 are vibrationally excited vinylamine and aziridine molecules.

If the collisional spin relaxation process

$$NH(a^1\Delta) + E \longrightarrow NH(X^3\Sigma^-) + E$$

takes place, the formations of aziridine and $C_2H_5NH_2$ are expected according to the reactions

$$NH(X^3\Sigma^-) \xrightarrow{E} C_2H_5N(\text{Triplet}) \begin{cases} \nearrow \text{aziridine} \\ \xrightarrow{A} C_2H_6N(\text{doublet}) \xrightarrow{A} C_2H_5NH_2. \end{cases}$$

However, the possibility of the relaxation process seems to be negligible because neither of the products were found.

Reactions 4 to 7 are unimolecular decomposition processes of vibrationally excited $C_2H_5N^*$, and these are possible energetically. An other energetically possible reaction is

$$NH(a^1\Delta) + C_2H_4 \longrightarrow C_2H_2 + NH_3,$$

which is exothermic with 378 kJ mol^{-1}. The trace formation of C_2H_2 is probably due to this reaction. The reaction

$$NH(a^1\Delta) + C_2H_4 \longrightarrow CH_4 + HCN$$

is also exothermic with 503 kJ mol^{-1}, but the reaction to give CH_4 and HCN by this molecular mechanism could not be formulated in the reaction kinetics discussed later. Since the weakest bond in the $C_2H_3NH_2$ molecule is C–N bond,[20] the precursor for C_2H_3 and NH_2 radicals in Reaction 7 seems to be vibrationally excited vinylamine. The C_2H_4N radicals formed by Reaction 6 will be removed by hydrogen abstraction from HN_3 and addition to the π bond of C_2H_4 by such reactions as 8 and 9.

Reaction 12 is well known and very efficient.[21] Reaction 13 may proceed *via* an intramolecular hydrogen abstraction in the addition intermediate H–Ṅ–N=N–N=CH_2. Reaction 14 is the hydrogenation reaction of C_2H_4 by $N_2H_2^*$ which is an effective hydrogenation reagent.[22] The previously discussed reactions,[1,2] $N_2H_2^* \rightarrow N_2H_2^{**}$, $N_2H_2^* + HN_3 \rightarrow N_2 + H_2 + HN_3$, and $N_2H_2^* + HN_3 \rightarrow 2N_2 + NH_3$, were omitted by assuming that Reaction 14 is very fast. Reaction 15 is the hydrogen abstraction reaction by CH_3, C_2H_3, C_2H_5, or NH_2 radicals from HN_3 as a good hydrogen donor.[23] The reactions, $NH_2 + C_2H_4 \rightarrow C_2H_4NH_2$ and $C_2H_4NH_2 + HN_3 \rightarrow C_2H_5NH_2 + N_3$, are excluded because the $m/z=45$ peak ($C_2H_5NH_2^+$) was not found in the mass spectrum.

The trace formations of C_3H_8, 1-C_4H_8, and n-C_4H_{10}[9] are probably due to the reactions

$$R(CH_3, C_2H_3, C_2H_5) + C_2H_4 \longrightarrow R\text{–}C_2H_4$$
$$R\text{–}C_2H_4 + HN_3 \longrightarrow R\text{–}C_2H_5 + N_3.$$

The rate constant at 25 °C is 8.9×10^7 cm^3 mol^{-1} s^{-1} for the hydrogen abstraction from HN_3 by CH_3 radicals[23] and is about 1.2×10^6 cm^3 mol^{-1} s^{-1} for the addition of CH_3 radicals to C_2H_4.[24] The trace formation of C_3H_8 is explainable by comparing both rate constants. The same reason can also be applied for the trace formations of 1-C_4H_8 and n-C_4H_{10}. Reactions 4, 7, and 12 are supported by the existences of CH_3, C_2H_3, and C_2H_5 radicals.

The basic C_2H_5N (azomethines) formed by Reaction 8 may react to form the azide salt ($C_2H_5N \cdot HN_3$) of the white volatile powder by reaction with acidic HN_3 as Reaction 17 as well as the case of amines.[2] The C_4H_8N formed by Reaction 9 may react to produce the yellowish polymers *via* addition to C_2H_4 as Reaction 18.

Reactions 19 to 23 were introduced to explain the disappearance of N_3 radicals and the formations of HCN, CH_3CN, CH_3N_3, and $C_2H_5N_3$. It has been found in the flash photolysis of HN_3 that N_3 radicals disappear very rapidly in the presence of HN_3.[25,26] This seems due to the formation of an addition intermediate ($A \cdot N_3$), Similarly intermediate ($E \cdot N_3$) can be expected, because the addition of N_3 radicals to π bond of C_2H_4 is possible. Reactions 22 and 23 are supported by the facts that CH_3N_3 was found as a product, and $C_2H_5N_3$ of almost the same amount as CH_3CN is formed. The reactions

$$N_3 \cdot A + E \cdot N_3 \longrightarrow N_3(CH_2)_2N_3 + A$$
$$2E \cdot N_3 \longrightarrow N_3(CH_2)_4N_3$$

are excluded because $N_3(CH_2)_2N_3$ and $N_3(CH_2)_4N_3$ were not found as a product.

Reactions other than those mentioned above have been discussed previously,[1,2] and are omitted here.

Reaction Kinetics. The reaction kinetics were carried out to confirm the mechanism of Reactions 1 to 23 and to obtain the rate constant ratios.

On the quantum yield of CH_4, the equation

$$\phi_{CH_4}^{-1} = \frac{k_4 + k_5 + k_6 + k_7}{k_4}\left(1 + \frac{k_2}{k_3}\frac{[HN_3]}{[C_2H_4]}\right) \qquad \text{(I)}$$

can be derived, where

$$k_2 = k_{2a} + k_{2b} + k_{2c}.$$

The plot of $1/\phi_{CH_4}$ *versus* $[HN_3]/[C_2H_4]$ is shown in Fig. 7.

On the formations of CH_4 and $C_2H_5N \cdot HN_3$, the equation

$$\frac{\phi_{CH_4}}{\phi_{C_2H_5N \cdot HN_3}} = \frac{k_4}{k_6}\left(1 + \frac{k_9}{k_8}\frac{[C_2H_4]}{[HN_3]}\right) \qquad \text{(II)}$$

is obtained, and the linear relation is shown in Fig. 8.

Equation III was derived for the formations of CH_4, C_2H_6, H_2, and NH_4N_3, and its relation is plotted in Fig. 9.

$$\frac{\phi_{C_2H_6} + \phi_{H_2} + \phi_{NH_4N_3}}{\phi_{CH_4}} = \frac{k_4 + k_5 + k_7}{k_4} + \frac{k_2 + k_{2a}}{k_3}\frac{k_4 + k_5 + k_6 + k_7}{k_4}\frac{[HN_3]}{[C_2H_4]} \qquad \text{(III)}$$

As to the formations of H_2, CH_4, and C_2H_6, the equation

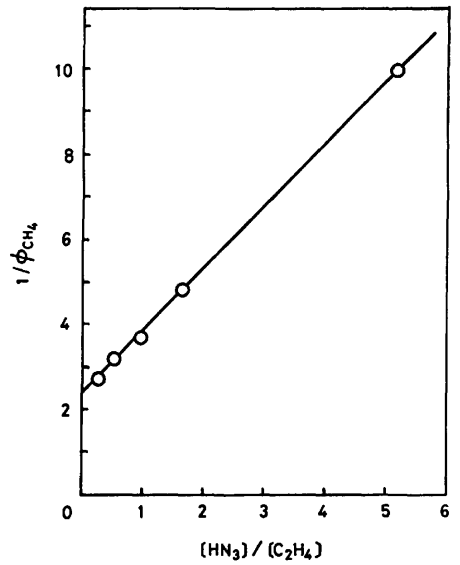

Fig. 7. Plot of $1/\phi_{CH_4}$ *versus* $[HN_3]/[C_2H_4]$.

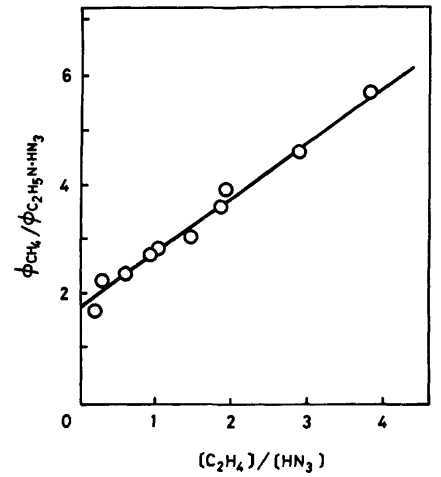

Fig. 8. Plot of $\phi_{CH_4}/\phi_{C_2H_5N\cdot HN_3}$ *versus* $[C_2H_4]/[HN_3]$.

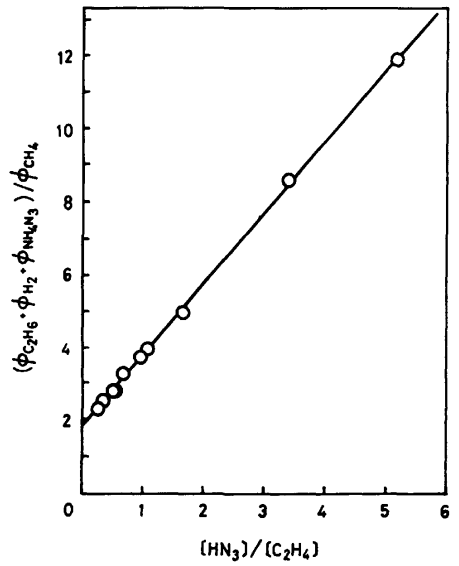

Fig. 9. Plot of $(\phi_{C_2H_6}+\phi_{H_2}+\phi_{NH_4N_3})/\phi_{CH_4}$ against $[HN_3]/[C_2H_4]$.

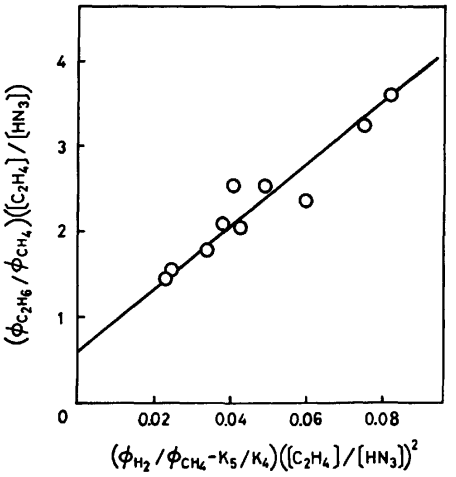

Fig. 10. Plot for Eq. IV.

$$\frac{\phi_{C_2H_6}}{\phi_{CH_4}}\frac{[C_2H_4]}{[HN_3]} = \frac{k_{2a}}{k_3}\frac{k_4+k_5+k_6+k_7}{k_4} + \frac{k_{12}}{k_{10}}\left(\frac{\phi_{H_2}}{\phi_{CH_4}}-\frac{k_5}{k_4}\right)\frac{[C_2H_4]^2}{[HN_3]^2} \quad \text{(IV)}$$

can be deerivd. Plot of $\phi_{C_2H_6}[C_2H_4]/\phi_{CH_4}[HN_3]$ *versus* $(\phi_{H_2}/\phi_{CH_4}-k_5/k_4)([C_2H_4]/[HN_3])^2$ is shown in Fig. 10, where the value of 0.102 for k_5/k_4 was selected to obtain the best straight line.

From the intercepts and the slopes in Figs. 7 to 10, and by using $k_{2b}/k_{2a}=0.746$ and $k_{11}/k_{10}=1.15$ obtained previously,[1] we obtain $k_3/k_2=1.64$, $k_5/k_4=0.102$, $k_6/k_4=0.564$, $k_7/k_4=0.734$, $k_9/k_8=0.560$, $k_{2c}/k_{2a}=1.23$, and $k_{12}/k_{10}=36.4$.

On the formations of N_2 and CH_4, the equation

$$\frac{\phi_{N_2}}{\phi_{CH_4}} = \frac{2k_4+k_5+k_6+k_7}{k_4} + \frac{(k_4+k_6+k_7)\alpha}{k_4} + \frac{k_4+k_5+k_6+k_7}{k_4}\left(\frac{k_2}{k_3}+\frac{2(k_{2a}+k_{2c})+(k_{2a}+k_{2b})\alpha}{k_3}\right)\times\frac{[HN_3]}{[C_2H_4]} + \left(\frac{k_6}{k_4}+\frac{2k_{2a}}{k_3}\frac{k_4+k_5+k_6+k_7}{k_4}\frac{[HN_3]}{[C_2H_4]}\right)\Big/\left(1+\frac{k_{10}}{k_{11}}+\frac{k_{12}}{k_{11}}\frac{[C_2H_4]}{[HN_3]}\right) \quad \text{(V)}$$

can be derived, where

$$\alpha = 1 + 2\left(1+\frac{k_{20}}{k_{19}}\frac{[C_2H_4]}{[HN_3]}\right)^{-2}.$$

Here, α was derived by assuming $k_{21}=k_{23}$ and $k_{22}=2k_{21}$, because Reactions 21 to 23 are radical-radical reactions. If $A\cdot N_3$ is non-existent ($k_{19}=0$), the stoichiometry of N_2 forming from two moles of N_3 becomes 1 by Reactions 22 and 23. The stoichiometry in the absence of $E\cdot N_3$ ($k_{20}=0$) becomes 3 by Reaction 21. Thus, α depends on the ratios of k_{20}/k_{19} and $[C_2H_4]/[HN_3]$.

The experimental values of ϕ_N/ϕ_{CH_4} *versus* $[HN_3]/[C_2H_4]$ were plotted in Fig. 11 together with the values calculated from Eq. V for two cases of $\alpha=1$ and $\alpha=3$ using the rate constant ratios obtained above. It is clear that the appropriate value for α is between 1 and 3. The values of ϕ_{N_2}/ϕ_{CH_4} calculated using $k_{19}/k_{20}=2.70$ are shown by the doted line in Fig. 11, and are in good accord with the experimental values.

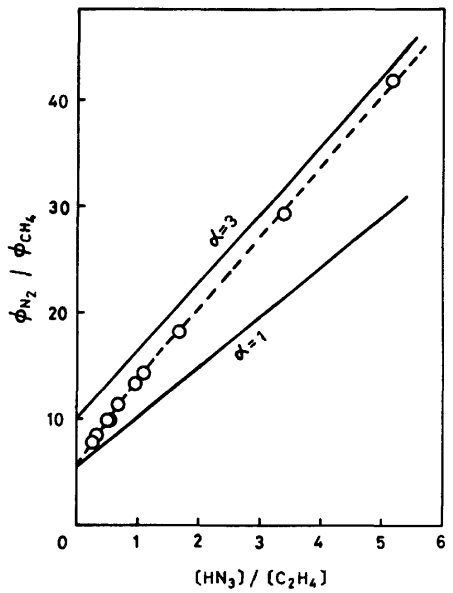

Fig. 11. Plots of ϕ_{N_2}/ϕ_{CH_4} *versus* $[HN_3]/[C_2H_4]$. ○, experimental value of ϕ_{N_2}/ϕ_{CH_4}; ---, calculated value of ϕ_{N_2}/ϕ_{CH_4} by Eq. V with $k_{19}/k_{20}=2.70$. The upper and under solid lines denote the calculated values of ϕ_{N_2}/ϕ_{CH_4} by Eq. V with $\alpha=3$ and $\alpha=1$, respectively.

Comparisons of the Rate Constants. Bras *et al.*[27] have reported that the rate constant for the reactions of hydrogen atoms with HN_3 is $2.54\times10^{-11}\exp(-4600/RT)$ cm^3 molecule^{-1} s^{-1} in the temperature range from 293 to 462 K. On the other hand, Sugawara *et al.*[21] have found that the specific rate for the addition of hydrogen atoms to C_2H_4 is $4.70\times10^{-11}\exp(-2178/RT)$ cm^3 molecule^{-1} s^{-1} in the temperature range from 206 to 461 K. From both results, it is found that the addition to C_2H_4 is 103 times faster than the reactions with HN_3 at 30 °C. In the present system, the rate constant ratio $k_{12}/(k_{10}+k_{11})$, is 17.0. The discrepancy seems to be due to "hot" hydrogen atoms because Reaction 2a is highly exothermic with 370 kJ mol^{-1}, and the hot atom effect is rather effective for reaction with high activation energy. If the value of k_{12} obtained by Sugawara *et al.*[21] is used as a basis, the absolute values of $k_{10}=2.09\times10^{10}$ and $k_{11}=2.40\times10^{10}$ cm^3 mol^{-1} s^{-1} in the present reaction conditions can be obtained from the rate constant ratios of k_{11}/k_{10} evaluated previously[1] and k_{12}/k_{10} obtained above.

Since the $C_2H_5N^*$ ($C_2H_3NH_2^*$ and aziridine*) decomposes before it is stabilized by collision with a third body M, the lifetime of $C_2H_5N^*$ is much shorter than the lifetime ($\tau=6.8\times10^{-11}$ s) of $C_2H_5NH_2^*$ formed by the insertion of $NH(a^1\Delta)$ into C–H bond of C_2H_6.[2] On the thermodynamic considerations of the reactions,

$$NH(a^1\Delta) + C_2H_4 \longrightarrow \underset{\diagdown\,N\,\diagup}{CH_2\text{–}CH_2}{}^* \quad (3a)$$
$$\qquad\qquad\qquad\quad H$$

$$NH(a^1\Delta) + C_2H_4 \longrightarrow C_2H_3NH_2^* \quad (3b)$$

$$NH(a^1\Delta) + C_2H_6 \longrightarrow C_2H_5NH_2^* \quad (3e)$$

ΔH_{3a} is almost the same as ΔH_{3e}, although Reaction 3b is 40 kJ mol^{-1} more exothermic than Reaction 3e. Therefore, the main reason for the short lifetime may be because the internal degrees of freedom of $C_2H_5N^*$ are six less than those of $C_2H_5NH_2^*$.

If we assume that all $C_2H_3NH_2^*$ molecules decompose to give C_2H_3 and NH_2 radicals as Reaction 7, and all molecules of aziridine formed by Reaction 3a decompose by Reactions 4 to 6, the reaction yield ratio of the addition to the π bond to the insertion into the C–H bond, k_{3a}/k_{3b}, is given by

$$k_{3a}/k_{3b} = (k_4+k_5+k_6)/k_7 = 2.27.$$

This ratio is similar to the result that the ratio of the addition to the insertion is 2.75 for the reactions of $NH(a^1\Delta)$ with C_3H_6 in the liquid phase.[11]

If all $C_2H_3NH_2^*$ molecules decompose to give C_2H_3 and NH_2 as assumed above, the reactivity ratio of the insertion of $NH(a^1\Delta)$ into a C–H bond of C_2H_4 to that of C_2H_6, k_{3b}/k_{3e}, is given by

$$\frac{k_{3b}}{k_{3e}} = \left(\frac{k_3}{k_2}\frac{k_7}{k_4+k_5+k_6+k_7}\right)\Big/\left(\frac{k_{3e}}{k_2}\right).$$

By using $k_{3e}/k_2=0.334$ obtained previously,[2] $k_{3b}/k_{3e}=1.50$ is obtained. The ratio per C–H bond is given by $6k_{3b}/4k_{3e}=2.25$. This means that the insertion of $NH(a^1\Delta)$ into a C–H bond which consists of a sp^2 hybrid orbital is more efficient than for the sp^3 hybrid orbital. For the photolysis of COS in the presence of both C_2H_4 and C_2H_6,[28] it has been found that the insertion rate of $S(3^1D_2)$ per C–H bond of C_2H_4 is 1.15 times faster than that of C_2H_6. This result has the same tendency as for $NH(a^1\Delta)$.

Kitamura *et al.*[11] have studied the photolysis of HN_3 in a binary solution of C_2H_6 and C_2H_4 at Dry Ice–methanol temperature, and found that the formation ratio of $C_2H_5NH_2/N_2$ decreases with an increase of the mole fraction of C_2H_4. Provided that in their experimental conditions N_2 is formed only by Reaction 1 except the high mole fraction range of C_2H_6, and that all the molecules of $C_2H_5NH_2^*$ formed by Reaction 3e are stabilized by collisions with solvent molecules, then $k_3/k_{3e}=4.4$ is obtained from the plot of $N_2/C_2H_5NH_2$ *versus* $[C_2H_4]/[C_2H_6]$. Our value for k_3/k_{3e} is $4.9((k_3/k_2)/(k_{3e}/k_2))$. The slight discrepancy seems to be due to the differences of the experimental conditions of wavelength, temperature, phase, *etc.*

When the reactions of $NH(a^1\Delta)$ with reactant (X) are presented by the general expressions,

$$NH(a^1\Delta) + X \longrightarrow \text{Products} \qquad k_r$$
$$NH(a^1\Delta) + X \longrightarrow NH(X^3\Sigma^-) + X \qquad k_d$$

the values of k_r/k_2 and k_d/k_2 for HN_3,[1] Xe,[1] C_2H_6,[2] and C_2H_4 are shown in Table 2. The following tendencies are shown in Table 2: k_r/k_2 for C_2H_6 consisting of σ bonds only is very low as compared with those for HN_3 and C_2H_4 having π bond; Xe and C_2H_6 have some

Table 2. Relative reactivity of $NH(a^1\Delta)$ with X

X	k_r/k_2	k_d/k_2
HN_3[a]	1.000	≈0
Xe[a]	0	0.187
C_2H_6[b]	0.334	0.217
C_2H_4[c]	1.637	≈0

a) Ref. 1. b) Ref. 2. c) This work.

Table 3. Comparisons of k_q (X) with k_b at about 300 K

X	$k_q(X)$ / 10^{14} cm^3 mol^{-1} s^{-1}	α / 10^{-24} cm^3	N_e	k_b / 10^{14} cm^3 mol^{-1} s^{-1}	$k_q(X)/k_b$
HN_3	1.084	3.50[a]	16	3.89	0.279
Xe	0.202	4.04[b]	8	3.23	0.063
C_2H_6	0.597	4.48[c]	14	4.03	0.148
C_2H_4	1.775	4.22[d]	12	3.97	0.447

a) Estimated from the polarizability of hydrogen atom (0.401×10^{-24} cm^3) and the polarizabilities of NO, N_2, N_2O, and NH_3 molecules. b) M. Lallemand and D. Vidal, *J. Chem. Phys.*, **66**, 4776 (1977). c) P. Sliwinski, *Z. Phys. Chem. (Frankfurt am Main)*, **63**, 263 (1969). d) N. J. Bridge and A. D. Buckingham, *Proc. R. Soc. London, Ser. A*, **295**, 334 (1966).

ability to induce collisional spin relaxation; the relaxation efficiencies by HN_3 and C_2H_4 having π bond are negligible. The relaxation efficiency by Xe, which is a monatomic molecule, is comparable to that of C_2H_6 consisting of eight atoms. It is probably due to a heavy atom effect.[29]

The absolute rate constant for the disappearance of NH($a^1\Delta$) by HN_3 was reported to be 5.6×10^{13} cm^3 mol^{-1} s^{-1} by Paur and Bair,[26] and 10.84×10^{13} cm^3 mol^{-1} s^{-1} by Piper, Krech, and Taylor.[30] If the rate constant obtained by Piper *et al.*, k_2(PKT), is used as a basis, the absolute rate constant for the quenching of NH($a^1\Delta$) by X, k_q(X), can be calculated by the equation

$$k_q(X) = \frac{(k_r+k_d)_x}{k_2}k_2(PKT).$$

The calculated values of k_q(X) are shown in Table 3.

On the other hand, the maximum rate constant of the bimolecular reaction in the gas phase, k_b, can be calculated by the equation[31]

$$k_b = \frac{2\Gamma(1-2/s)N_A}{\sigma}\left(\frac{2\pi kT}{\mu}\right)^{1/2}\left[\frac{(s-2)A}{2kT}\right]^{2/s},$$

when the intermolecular attractive potential, u, is expressed by $u=-A/r^s$. Here, A, r, Γ, N_A, σ, k, and μ mean the attractive potential constant, the intermolecular distance, the gamma function, Avogadro's number, the symmetry number, Boltzmann's constant, and the reduced mass, respectively. The attractive potential is given by

$$A = A_{dis} + \alpha_{NH}\mu_D(X)^2 + \alpha_x\mu_D(NH)^2 + 2\mu_D(NH)^2\mu_D(X)^2/3kT,$$

where α is the polarizability, and μ_D the dipole moment. The dispersion effect term of A, A_{dis}, is given by Slater and Kirkwood[32] as

$$A_{dis} = \frac{3\,h\,e\,\alpha_{NH}\alpha_X}{4\,\pi m_e^{1/2}[(\alpha/N_e)_{NH}^{1/2} + (\alpha/N_e)_X^{1/2}]}.$$

Here, h, N_e, and e and m_e are Planck's constant, the number of outer-shell electrons, and the charge and mass of an electron, respectively.

The values of k_b calculated using $s=6$ and $\sigma=1$ are shown in Table 3 together with α and N_e for X. The values of $\alpha=1.38\times10^{-24}$ cm^3,[33] $N_e=6$, and $\mu_D=1.627$ debye[34] for NH, and $\mu_D=0.847$ debye[35] for HN_3 were used for the calculation. It is shown in Table 3 that the reactivity of the first excited singlet NH($a^1\Delta$) is, in general, very high, especially $k_q(C_2H_4)$ which is close to one-half of its maximum rate constant.

The absolute and relative quenching rates of

Table 4. Comparisons of the over-all quenching rate constants at about 300 K

Quencher	Quenching rate constant / 10^{-11} cm^3 molecule^{-1} s^{-1}			
	C(2^1D_2)	O(2^1D_2)	S(3^1D_2)	NH($a^1\Delta$)
HN_3				18[h]
Xe	11[a]	7.2[e]	4.0[f]	3.4[i]
C_2H_6		26.0[d]	4.3[g]	9.9[j]
C_2H_4	≈37[b]	35.6[e]	25[g]	29.5[k]

a) Ref. 36. b) Ref. 37. c) Ref. 41. d) Estimated from $k_q^{O(^1D)}(CO_2)=10\times10^{-11}$ cm^3 molecule^{-1} s^{-1} (Ref. 40) and $k_q^{O(^1D)}(C_2H_6)/k_q^{O(^1D)}(CO_2)=2.6$ (Ref. 39). e) Estimated from $k_q^{O(^1D)}(C_2H_6)=26.0\times10^{-11}$ cm^3 molecule^{-1} s^{-1} (d)) and $k_q^{O(^1D)}(C_2H_4)/k_q^{O(^1D)}(C_2H_6)=1.37$ (Ref. 38). f) Estimated from $k_q^{S(^1D)}(C_2H_4)=25\times10^{-11}$ cm^3 molecule^{-1} s^{-1} (g)) and $k_q^{S(^1D)}(Xe)/k_q^{S(^1D)}(C_2H_4)=0.16$ (Ref. 43). g) From Refs. 4 and 42. h) Ref. 30. i) From Refs. 1 and 30. j) From Refs. 2 and 30. k) From Ref. 30 and the present work.

C(2^1D_2),[36,37] O(2^1D_2),[38-41] and S(3^1D_2)[42,43] by Xe, C_2H_6, C_2H_4, and others have been observed widely. These over-all quenching rate constants are shown in Table 4 together with those for NH($a^1\Delta$). It is found in Table 4 that the trend on the collisional quenching of NH($a^1\Delta$) is very similar to those of the first excited singlet atoms.

The author is gratefully indebted to Emeritus Professor Osamu Toyama of University of Osaka Prefecture for his helpful discussion. I would also like to thank Dr. Hideo Tabata, Mr. Akio Tomiyasu, and Katsuichi Ohta for their asistances.

References

1) S. Kodama, *Bull. Chem. Soc. Jpn.*, **56**, 2348 (1983).
2) S. Kodama, *Bull. Chem. Soc. Jpn.*, **56**, 2355 (1983).
3) R. J. Cvetanović, *Adv. Photochem.*, **1**, 115 (1963); R. E. Huie and J. T. Herron, *Prog. React. Kinet.*, **8**, 1 (1975).
4) H. E. Gunning and O. P. Strausz, *Adv. Photochem.*, **4**, 143 (1966).
5) W. B. DeMore and S. W. Benson, *Adv. Photochem.*, **2**, 219 (1964); H. M. Frey, *Prog. React. Kinet.*, **2**, 131 (1964); "Carbene Chemistry," ed by W. Kirmse, Academic Press, New York (1971); "Carbenes," ed by M. Jones, Jr., and R. A. Moss, John Wiley and Sons, New York (1973), I.
6) E. D. Miller, Ph. D. Dissertation, Catholic University of America, Washington, D. C., 1961.
7) D. W. Cornell, R. S. Berry, and W. Lwowski, *J. Am.*

Chem. Soc., **88**, 544 (1966).
8) J. L. Brash and R. A. Back, *Can. J. Chem.*, **43**, 1778 (1965); W. D. Woolley and R. A. Back, *ibid.*, **46**, 295 (1968).
9) P. Tiedemann and R. N. Schindler, Technical Report, JUL-505-PC (1968).
10) M. E. Jacox and D. E. Milligan, *J. Am. Chem. Soc.*, **85**, 278 (1963).
11) T. Kitamura, S. Tsunashima, and S. Sato, *Bull. Chem. Soc. Jpn.*, **54**, 55 (1981).
12) F. O. Rice and C. J. Grelecki, *J. Phys. Chem.*, **61**, 830 (1957); M. S. O'Dell and B. DEB. Darwent, *Can. J. Chem.*, **48**, 1140 (1970).
13) O. Dimroth and W. Wislicenus, *Ber.*, **38**, 1573 (1905).
14) E. Lieber, T. S. Chao, and C. N. R. Rao, *J. Org. Chem.*, **22**, 238 (1957).
15) J. H. Boyer and J. Hamer, *J. Am. Chem. Soc.*, **77**, 951 (1955).
16) M. O. Forster and H. F. Fierz, *J. Chem. Soc.*, **93**, 1071 (1908).
17) J. M. Kruse and M. G. Mellon, *Anal. Chem.*, **25**, 446 (1953).
18) G. Gallegos and R. W. Kiser, *J. Phys. Chem.*, **65**, 1177 (1961).
19) D. A. Dows, E. Whittle, and G. C. Pimentel, *J. Chem. Phys.*, **23**, 1475 (1955).
20) The bond dissociation energies of C–N, N–H, and C–H in $C_2H_3NH_2$ molecule are about 390, 406, and 434 kJ mol^{-1}, respectively.
21) K. Sugawara, K. Okazaki, and S. Sato, *Bull. Chem. Soc. Jpn.*, **54**, 2872 (1981).
22) S. K. Vidyarthi, C. Willis, R. A. Back, and R. M. McKitrick, *J. Am. Chem. Soc.*, **96**, 7647 (1974); C. Willis, R. A. Back, J. M. Parsons, and J. G. Purdon, *ibid.*, **99**, 4451 (1977); D. J. Pasto and D. M. Chipman, *ibid.*, **101**, 2290 (1979).
23) R. S. Konar and B. DEB. Darwent, *Can. J. Chem.*, **48**, 2280 (1970).
24) R. J. Cvetanović and R. S. Irwin, *J. Chem. Phys.*, **46**, 1694 (1967).
25) R. J. Paur and E. J. Bair, *J. Photochem.*, **1**, 255 (1973).
26) R. J. Paur and E. J. Bair, *Int. J. Chem. Kinet.*, **8**, 139 (1976).
27) G. Le Bras and J. Combourieu, *Int. J. Chem. Kinet.*, **5**, 559 (1973).
28) H. A. Wiebe, A. R. Knight, O. P. Strausz, and H. E. Gunning, *J. Am. Chem. Soc.*, **87**, 1443 (1965).
29) N. J. Turro, "Modern Molecular Photochemistry," Benjamin/Cummings Publishing Co., Menlo Park, California (1978), p. 38.
30) L. G. Piper, R. H. Krech, and R. L. Taylor, *J. Chem. Phys.*, **73**, 791 (1980).
31) K. Yang and T. Ree, *J. Chem. Phys.*, **35**, 588 (1961).
32) J. C. Slater and J. G. Kirkwood, *Phys. Rev.*, **37**, 682 (1931); J. G. Kirkwood, *Physik. Z.*, **33**, 57 (1932).
33) Estimated by assuming the atomic polarizabilities of 0.401×10^{-24} cm^3 for H and 0.975×10^{-24} cm^3 for N.
34) P. E. Cade and W. M. Huo, *J. Chem. Phys.*, **45**, 1063 (1966).
35) E. Amble and B. P. Dailey, *J. Chem. Phys.*, **18**, 1422 (1950).
36) D. Husain and L. J. Kirsch, *Trans. Faraday Soc.*, **67**, 2886 (1971).
37) D. Husain and L. J. Kirsch, *Trans. Faraday Soc.*, **67**, 3166 (1971).
38) W. B. DeMore, *J. Phys. Chem.*, **73**. 391 (1969).
39) R. J. Cvetanović, *Can. J. Chem.*, **52**, 1452 (1974).
40) G. E. Stein, C. J. Howard, A. L. Schmeltekopf, J. A. Davidson, and H. I. Schiff, *J. Chem. Phys.*, **65**, 4761 (1976).
41) J. A. Davidson, H. I. Schiff, T. J. Brown, G. E. Streit, and C. J. Howard, *J. Chem. Phys.*, **69**, 1213 (1978).
42) P. Fowles, M. deSorgo, A. J. Yarwood, O. P. Strausz, and H. E. Gunning, *J. Am. Chem. Soc.*, **89**, 1352 (1967).
43) D. L. Little, A. Dalgleish, and R. J. Donovan, *Discuss. Faraday Soc.*, **53**, 211 (1972).

 © 1983 The Chemical Society of Japan Bull. Chem. Soc. Jpn., 56, 2371—2379 (1983)

Nonequilibrium Thermodynamics of the Ion and Solvent Transports through Ion-exchange Membrane

Hideo KIMIZUKA,* Yoshihiko NAGATA, and Kozue KAIBARA
Department of Chemistry, Faculty of Science, Kyushu University, Hakozaki, Higashi-ku, Fukuoka 812
(Received November 12, 1982)

A theory for the ion and solvent transports through membrane has been developed on the basis of nonequilibrium thermodynamics. The fluxes were represented as linear functions of the effective driving potentials. The theory is reduced to that of Katchalsky when the concentration ratio of two aqueous solutions is near unity and the solutions are dilute. The effect of solvent flow on the interionic correlations was discussed. It was pointed out that Despić and Hills' theory of the electroosmotic effect on the membrane conductance is not valid with respect to both theoretical and experimental aspects. The comparison of the present theory with the previous one[1] was also made. The six independent phenomenological coefficients (elements of the conductance matrix) were experimentally determined as a function of concentration with the concentration cell consisting of the amphoteric ion-exchange membrane and aqueous calcium chloride solutions. The membrane properties were discussed in terms of the conductance matrix. The diffusional ion conductance was much greater than the electrical ion conductance, as an indication of the failure of the Nernst-Einstein relation. The cation-anion coupling coefficient was close to unity whereas the ion-water coupling coefficients were less than 0.1. The solvent effects on the interionic conductance elements were found to be small in spite of the fact that the water permeability was extremely high. The distinction between the cationic and amphoteric ion-exchange membranes was explored in terms of the elements of the conductance matrix.

A variety of transport phenomena is known to take place when a membrane system is subject to various driving forces such as the gradients of electric potential, concentration, and hydrostatic pressure. This paper is concerned with an analysis of the transport properties of an isothermal system consisting of an amphoteric ion-exchange membrane, water, and a single salt dissociating into two kinds of ions on the basis of nonequilibrium thermodynamics. Even in this simple case, there are six independent phenomenological coefficients, and hence six independent experiments are required to elucidate the transport properties.

Many papers have appeared on the application of nonequilibrium thermodynamics to the transport phenomena across the membrane, where the fundamental treatments are to determine the coefficients in the phenomenological equations. However, it is usual to make some nonthermodynamic assumptions for studying the membrane phenomena, since it is laborious to perform the detailed study for determining the six phenomenological coefficients. Nevertheless, it is important to complete the detailed study not only for elucidating the transport properties, but also for examining whether the nonthermodynamic assumptions are valid or not.

So far, only a few papers[2-4] have been published on the detailed study of the transport phenomena with the cation exchange membrane–aqueous single electrolyte system. In the preceding paper,[2] the transport phenomena with the cation-exchange membrane–aqueous barium chloride system were studied for determining the six phenomenological coefficients and the transport properties were discussed. However, the preceding theories[2-4] were essentially for the systems with the same concentrations of two external solutions and can not be suitably applied to the concentration cell. Thus a theory for the ion and solvent transports has been developed by extending the previous theory,[1] so that the solvent transport is included.

For estimating the phenomenological coefficients, the ion and solvent transports in the presence and absence of the electric current and the pressure difference should be measured in addition to the membrane potential and membrane conductance. Among these, the accurate determination of the ion transports is especially important in order to estimate the phenomenological coefficients exactly, because the transport number of an ion plays a decisive role in calculating the coefficients from the observed data. Since an accurate determination of the transport number for the co-ion is difficult with the cation- and anion-exchange membranes due to their high selectivity to the counter ions, the amphoteric ion-exchange membrane was used in the present study for the exact determination of the transport number.

In the present paper, the measurements were performed with the concentration cell consisting of the amphoteric ion-exchange membrane and the aqueous calcium chloride solutions. The six independent phenomenological coefficients (elements of a conductance matrix) were estimated from the observed data according to our theory and the membrane properties were discussed in terms of the conductance matrix.

Theory

1. Phenomenological Equation. In the previous paper,[1] the steady ion currents through the membrane have been expressed by linear functions of the effective driving potentials under the assumption of no solvent flow. Even without the assumption, it is easily seen that the flux equations including solvent flux may be written in the similar forms to those in the previous paper.[1] Thus, for the case in which the permeating species are cation α, anion β, and water w, the phenomenological equation can be written as

$$\begin{bmatrix} i_\alpha \\ i_\beta \\ Fj_w \end{bmatrix} = - \begin{bmatrix} g_{\alpha\alpha} & g_{\alpha\beta} & g_{\alpha w} \\ g_{\beta\alpha} & g_{\beta\beta} & g_{\beta w} \\ g_{w\alpha} & g_{w\beta} & g_{ww} \end{bmatrix} \begin{bmatrix} V-V_\alpha \\ V-V_\beta \\ -V_w \end{bmatrix}, \quad (1)$$

where the subscripts, α, β, and w refer to cation, anion, and water, respectively; i denotes an ion current; j_w, water flux; $g_{\gamma\delta}$ ($\gamma,\delta=\alpha,\beta$) and g_{kw} (k=α,β,w), the elements of the conductance matrix; V, the transmembrane potential; V_γ($\gamma=\alpha,\beta$), the pseudo equilibrium potential; V_w, the effective driving potential for water. V_w, V_γ, $g_{\gamma\delta}$, and g_{kw} are given by

$$FV_w = RT \ln a_w^I/a_w^{II} - \bar{v}_w \Delta P = \bar{v}_w(\Delta\pi - \Delta P) \quad (2)$$

$$Z_\gamma F V_\gamma = RT \ln a_\gamma^I/a_\gamma^{II} - \bar{v}_\gamma \Delta P \quad (3)$$

$$g_{\gamma\delta} = Z_\gamma Z_\delta F^2 |R|_{\gamma\delta}/|R| \quad (4)$$

$$g_{\gamma w} = Z_\gamma F^2 |R|_{\gamma w}/|R|, \quad (5)$$

and

$$g_{ww} = F^2 |R|_{ww}/|R|, \quad (6)$$

respectively, where the superscripts I and II refer to phases I and II separated by a membrane, respectively; R, F, and T have usual meanings; Z denotes the charge, a, the activity; v_k, the partial molar volume of a species k; $\Delta\pi$, the osmotic pressure difference; $\Delta P(=P^{II}-P^I)$, the external pressure difference; $|R|$, the determinant having R_{kl}(k,l=α,β,w) as the kl element of the generalized friction intergrated over the membrane phase, and $|R|_{kl}$, the cofactor of R_{kl}.[1] In Eq. 2, a constant molar volume is assumed for the two aqueous phases I and II. The expression such as Eq. 1 is advantageous for treating the electrical properties of the membrane.

The equation for the membrane current, I, is obtained from Eq. 1 as follows:

$$I = i_\alpha + i_\beta = - g_\alpha(V-V_\alpha) - g_\beta(V-V_\beta) + g_w V_w \quad (7)$$

$$= - G_m(V-V_0), \quad (8)$$

where g_α, g_β, and g_w denote the conductances for permeating species α, β, and w, respectively,

$$g_k = g_{k\alpha} + g_{k\beta}, \quad (9)$$

G_m, the membrane conductance

$$G_m = g_\alpha + g_\beta, \quad (10)$$

and V_0, the membrane potential at zero membrane current

$$V_0 = t_\alpha V_\alpha + t_\beta V_\beta + t_w V_w \quad (11)$$

$$t_k = g_k/G_m, \quad (12)$$

t_k, the transport number of a species k.

When the membrane current is absent, the equation for the ion current, i_γ^0, under this restriction can be written as

$$i_\gamma^0 = - g_k^0(V_0 - V_\gamma) + g_{\gamma w}^0 V_w, \quad (13)$$

where the superscript 0 refers to the absence of membrane current,

$$\frac{g_k^0}{g_k} = 1 - g_{\alpha\beta}\left(\frac{1}{g_\alpha} + \frac{1}{g_\beta}\right), \quad (14)$$

and

$$g_w^0 = g_{\alpha w}^0 + g_{\beta w}^0. \quad (15)$$

Thus, Eq. 11 is seen to be consistent with Eqs. 13—15.

2. Determination of Phenomenological Coefficient. Let us consider the way for determining the elements of the conductance matrix.

When the ion and solvent fluxes in the presence and absence of the membrane current are measured, we have from Eqs. 1, 8, and 12

$$i_\gamma - i_\gamma^0 = - g_\gamma(V-V_0) = t_\gamma I$$

$$F(j_w - j_w^0) = - g_w(V-V_0) = t_w I. \quad (16)$$

Thus, the measurements of the fluxes as a function of the potential enable to estimate g_k's and t_k's (k=α,β,w) according to Eq. 16.

When the membrane current is absent, we have from Eq. 1

$$\begin{bmatrix} i_\alpha^0 \\ Fj_w^0 \end{bmatrix} = - \begin{bmatrix} g_{\alpha\alpha} - G_m t_\alpha^2 & g_{\alpha w} - G_m t_\alpha t_w \\ g_{\alpha w} - G_m t_\alpha t_w & g_{ww} - G_m t_w^2 \end{bmatrix} \begin{bmatrix} V_\beta - V_\alpha \\ -V_w \end{bmatrix}. \quad (17)$$

Now it is assumed that the addition of nonpermeant neutral substance, *e.g.*, such as sucrose, causes no appreciable change in the phenomenological coefficients as well as the activity coefficients of salt and ions provided the salt concentrations are unaltered.[2] Then we have from Eq. 17

$$\Delta i_\alpha^0 = (g_{\alpha w} - G_m t_\alpha t_w)\Delta V_w, \quad (18)$$

$$F\Delta j_w^0 = (g_{ww} - G_m t_w^2)\Delta V_w, \quad (19)$$

where Δi_α^0 and Δj_w^0 means the changes in fluxes and ΔV_w, the change in the water potential due to the addition of sucrose. Since ΔV_w can be evaluated from the concentration of nonpermeant neutral solute, the measurements of the changes in the salt and solvent fluxes enable us to determine the coefficients $(g_{\alpha w} - G_m t_\alpha t_w)$ and $(g_{ww} - G_m t_w^2)$ according to Eqs. 18 and 19, respectively. Thus $g_{\alpha w}$ and g_{ww} can be estimated when g_k's are known. The value of $g_{\beta w}$ can be estimated according to Eq. 9 provided $g_{\alpha w}$ is known. Furthermore, $(g_{\alpha\alpha} - G_m t_\alpha^2)$ can be determined from the i_α^0 data according to Eq. 17, provided $(g_{\alpha w} - G_m t_\alpha t_w)$, V_w, and $(V_\beta - V_\alpha)$ are known. Then we can estimate $g_{\alpha\alpha}$ which serves to obtain the values of $g_{\alpha\beta}$ and $g_{\beta\beta}$ successively according to Eq. 9. Thus, the six independent phenomenological coefficients, $g_{\alpha\alpha}$, $g_{\alpha\beta}$, $g_{\beta\beta}$, $g_{\alpha w}$, $g_{\beta w}$, and g_{ww} can be determined according to the procedures mentioned above.

3. Transformation of Phenomenological Equation. Equation 1 can be rewritten as follows

$$\begin{bmatrix} i_\alpha \\ I \\ Fj_w \end{bmatrix} = - \begin{bmatrix} g_{\alpha\alpha} & g_\alpha & g_{\alpha w} \\ g_\alpha & G_m & g_w \\ g_{w\alpha} & g_w & g_{ww} \end{bmatrix} \begin{bmatrix} V_\beta - V_\alpha \\ E \\ -V_w \end{bmatrix}, \quad (20)$$

where

$$E = V - V_\beta. \quad (21)$$

Here, we introduce the osmoequilibrium potential for an ion defined as

$$Z_\gamma F V_\gamma^* = RT \ln a_\gamma^I/a_\gamma^{II} - \bar{v}_\gamma \Delta\pi$$

$$= Z_\gamma F V_\gamma - \bar{v}_\gamma(\Delta\pi - \Delta P), \quad (22)$$

then $(V_\beta - V_\alpha)$ may be expressed as

$$V_\beta - V_\alpha = V_\beta^* - V_\alpha^* - \bar{v}_s V_w/Z_\alpha \nu_\alpha \bar{v}_w, \quad (23)$$

where $\bar{v}_s$ and ν_α are the partial molar volume of the salt and the stoichiometric coefficient of cation, respectively.

Introducing the volume flow as a new flux

$$FJ_v/\bar{v}_w = Fj_w + \bar{v}_s i_\alpha/Z_\alpha\nu_\alpha\bar{v}_w, \tag{24}$$

and $(V_\beta^*-V_\alpha^*)$ as a new force, Eq. 20 can be rearranged as

$$\begin{bmatrix} i_\alpha \\ I \\ FJ_v/\bar{v}_w \end{bmatrix} = -\begin{bmatrix} g_{\alpha\alpha} & g_\alpha & g_{\alpha v} \\ g_\alpha & G_m & g_v \\ g_{v\alpha} & g_v & g_p \end{bmatrix}\begin{bmatrix} V_\beta^*-V_\alpha^* \\ E \\ -V_w \end{bmatrix}, \tag{25}$$

where

$$\begin{aligned} g_{\alpha v} &= g_{\alpha w} + g_{\alpha\alpha}\bar{v}_s/Z_\alpha\nu_\alpha\bar{v}_w \\ g_v &= g_w + g_\alpha\bar{v}_s/Z_\alpha\nu_\alpha\bar{v}_w \\ g_p &= g_{ww} + (g_{\alpha w}+g_{\alpha v})\bar{v}_s/Z_\alpha\nu_\alpha\bar{v}_w. \end{aligned} \tag{26}$$

We have from Eq. 25

$$I = -G_m(E-E_0) \tag{27}$$

$$E_0 = t_\alpha(V_\alpha^*-V_\beta^*) + t_v V_w, \tag{28}$$

where

$$t_v = g_v/G_m. \tag{28}$$

The term t_vV_w is the streaming potential referred to the anion reversible electrode, and g_v and t_v may be regarded as the conductance and transport number of volume flow, respectively.

Equation 25 can be rewritten as

$$\begin{bmatrix} J_s \\ I \\ J_v \end{bmatrix} = -\begin{bmatrix} L_{11} & L_{12} & L_{13} \\ L_{21} & L_{22} & L_{23} \\ L_{31} & L_{32} & L_{33} \end{bmatrix}\begin{bmatrix} \Delta\mu_S^* \\ E \\ \Delta P-\Delta\pi \end{bmatrix}, \tag{30}$$

where

$$\Delta\mu_s^* = Z_\alpha\nu_\alpha F(V_\beta^*-V_\alpha^*) = \bar{v}_s(\Delta\pi-\Delta\pi_s), \tag{31}$$

$$\bar{v}_s\Delta\pi_s = -(\nu_\alpha+\nu_\beta)RT\ln a_\pm^{II}/a_\pm^{I}, \tag{32}$$

$$J_s = i_\alpha/Z_\alpha\nu_\alpha F, \tag{33}$$

$$\begin{aligned} &L_{11} = g_{\alpha\alpha}/(Z_\alpha\nu_\alpha F)^2,\ L_{12} = g_\alpha/Z_\alpha\nu_\alpha F, \\ &L_{13} = \bar{v}_w g_{\alpha v}/Z_\alpha\nu_\alpha F^2, \\ &L_{22} = G_m,\ L_{23} = \bar{v}_w g_v/F,\ L_{33} = (\bar{v}_w/F)^2 g_p. \end{aligned} \tag{34}$$

When the external aqueous solutions are dilute and their concentration ratio is close to unity, the approximation given by Kachalsky[5] may be applied and $\Delta\mu_s^*$ is reduced to

$$\Delta\mu_s^* = \Delta\pi/C_s, \tag{35}$$

where C_s is the mean of the concentrations of external solutions. Thus, Eq. 30 is reduced to the phenomenological equation given by Katchalsky only when the approximation given by Eq. 35 is permitted. Krämer and Meares[6] found a new force equivalent to Eq. 23, but unfortunately they adopted this approximation to obtain the phenomenological equation equivalent to that of Katchalsky and discussed the transport phenomena. Practically, the most solvent permeation experiments were performed under the condition that Eq. 35 may not be permitted. Equation 30 should be applied in this case.

When the membrane current is absent, we have from Eq. 25

$$\begin{bmatrix} i_\alpha^0 \\ FJ_v^0/\bar{v}_w \end{bmatrix} = -\begin{bmatrix} g_{\alpha\alpha}-G_m t_\alpha^2 & g_{\alpha v}-G_m t_\alpha t_v \\ g_{\alpha v}-G_m t_\alpha t_v & g_p-G_m t_v^2 \end{bmatrix}\begin{bmatrix} V_\beta^*-V_\alpha^* \\ -V_w \end{bmatrix}, \tag{36}$$

which can be rewritten as

$$\begin{bmatrix} \bar{v}_s J_s^0 \\ J_v^0 \end{bmatrix} = -\begin{bmatrix} L_s & L_{sp} \\ L_{ps} & L_p \end{bmatrix}\begin{bmatrix} \Delta\pi-\Delta\pi_s \\ \Delta P-\Delta\pi \end{bmatrix}, \tag{37}$$

where L_s, L_{sp}, and L_p denote the thermodynamic solute permeability, the mechanical filtration coefficient, and the hydrodynamic permeability, respectively,

$$L_s = \bar{v}_s^2(g_{\alpha\alpha}-G_m t_\alpha^2)/(Z_\alpha\nu_\alpha F)^2 = -[\bar{v}_s J_s^0/(\Delta\pi-\Delta\pi_s)]_{\Delta P=\Delta\pi} \tag{38a}$$

$$\begin{aligned} L_{sp} = L_{ps} &= \bar{v}_s\bar{v}_w(g_{\alpha v}-G_m t_\alpha t_v)/Z_\alpha\nu_\alpha F^2 \\ &= -[J_v^0/(\Delta\pi-\Delta\pi_s)]_{\Delta P=\Delta\pi} \\ &= -[\bar{v}_s J_s^0/(\Delta P-\Delta\pi)]_{\Delta\pi=\Delta\pi_s}, \end{aligned} \tag{38b}$$

and

$$L_p = (\bar{v}_w/F)^2(g_p-G_m t_v^2) = -[J_v^0/(\Delta P-\Delta\pi)]_{\Delta\pi=\Delta\pi_s}. \tag{38c}$$

Eliminating $(\Delta P-\Delta\pi)$ from Eq. 37, we have

$$J_s^0 = -\omega_s(\Delta\pi-\Delta\pi_s) + (1-\sigma)J_v^0/\bar{v}_s, \tag{39}$$

where ω_s is the solute permeability coefficient

$$\omega_s = (L_s-L_{sp}^2/L_p)/\bar{v}_s = [J_s^0/(\Delta\pi-\Delta\pi_s)]_{J_v^0=0}, \tag{40}$$

and σ, the reflection coefficient

$$1-\sigma = L_{sp}/L_p = (\bar{v}_s J_s^0/J_v^0)_{\Delta\pi=\Delta\pi_s}. \tag{41}$$

According to Eq. 37, the equilibrium is established at the condition

$$\Delta P = \Delta\pi_s = \Delta\pi. \tag{42}$$

There are two cases which satisfy this condition. The one is that the two external solutions possess the same compositions and hence $\Delta P=\Delta\pi_s=\Delta\pi=0$ and the other, that a nonpermeable polyelectrolyte is present at one side and the osmotic eqilibrium such as the Donnan membrane equilibrium is established, where $\Delta P=\Delta\pi_s=\Delta\pi\neq 0$. Taking the approximation given by Eq. 35, Eqs. 37—41 are reduced to those obtained by Katchalsky.[5]

4. Electrokinetic Phenomena. It is important to examine how the electroosmosis is involved in the electrical properties of the membrane. Eliminating V_w in Eq. 25, we obtain

$$\begin{bmatrix} i_\alpha - g_{\alpha v}FJ_v/g_p\bar{v}_w \\ I - g_v FJ_v/g_p\bar{v}_w \end{bmatrix} = -\begin{bmatrix} g_{\alpha\alpha}-g_{\alpha v}^2/g_p & g_\alpha-g_{\alpha v}g_v/g_p \\ g_\alpha-g_{\alpha v}g_v/g_p & G_m-g_v^2/g_p \end{bmatrix} \times\begin{bmatrix} V_\beta^*-V_\alpha^* \\ E \end{bmatrix}, \tag{43}$$

we have from Eq. 43

$$I - g_v F(J_v-J_v^0)/g_p\bar{v}_w = -(G_m-g_v^2/g_p)(E-E_0), \tag{44}$$

which leads to

$$G_m' = -(I)_{J_v=J_v^0}/(E-E_0) = G_m - g_v^2/g_p, \tag{45}$$

where G_m' denotes the membrane conductance without volume flow. On the other hand we have from Eqs. 25 and 27

$$F(J_v-J_v^0)/\bar{v}_w = -g_v(E-E_0) = FD_e I/\bar{v}_w, \tag{46}$$

where D_e denotes the electroosmotic permeability. Since G_m' is the membrane conductance without volume flow, the L.H.S. of Eq. 44 gives the membrane current without electroomsotic current. Thus, the second term of the L.H.S. of Eq. 44 may be considered as the electroosmotic current I_v accompanied by the volume flow.

Comparing this second term with Eq. 46, we have

$$I_v = g_v F(J_v - J_v^0)/g_p \bar{v}_w = -g_v^2(E-E_0)/g_p. \quad (47)$$

Let X be the charge concentration per unit volume of pore liquid within the membrane, the elctroosmotic current I_v may be given by the relation

$$I_v = F(J_v - J_v^0)X. \quad (48)$$

Comparing Eq. 48 with Eq. 47, we find

$$X = g_v/\bar{v}_w g_p. \quad (49)$$

Combining Eq. 45 with Eqs. 38c and 49, we derive the equation for the part of the membrane conductance due to the electroosmosis as follows:

$$G_m - G'_m = g_v^2/g_p = (FX)^2 L_p + G_m(\bar{v}_w t_v X)^2. \quad (50)$$

Taking the capillary model and assuming the membrane controlling process, L_p is expressed by[5]

$$L_p = \phi_w r^2\theta/8\eta\Delta x, \quad (51)$$

where ϕ_w represents the membrane area available for permeation; r, the capillary radius; θ, the tortuosity factor; η, the viscosity of pore liquid; Δx, the membrane thickness. Substituting Eq. 51 into Eq. 50 and multiplying $\Delta x/\bar{X}$ where $\bar{X}$ is the equivalent concentration of salt per unit volume within the membrane, we have

$$\lambda - \lambda' = (FXr)^2\phi_w\theta/8\eta\bar{X} + \lambda(\bar{v}_w t_v X)^2, \quad (52)$$

where λ and λ' represent the equivalent conductances of electrolyte with and without the electroosmosis, respectively. For the cation- or anion-exchange membranes, λ and λ' respresent the equivalent conductances of counter ions with and without the electroosmosis, respectively, provided the co-ion concentration may be ignored as compared with the counter ion concentration in the membrane.

Despić and Hills[7] expressed the equation for the electroomsotic effect on the equivalent conductance of counter ions based on the kinetic approach as follows:

$$\lambda - \lambda' = (Fr)^2\bar{X}/8\eta, \quad (53)$$

which differs from Eq. 52. Ignoring the second term of the R.H.S. of Eq. 52 and putting $\phi_w\theta = 1$ and $X = \bar{X}$, Eq. 52 is reduced to Eq. 53. The replacement of X by $\bar{X}$ can not be allowed, since X is the charge concentration at the slipping plane of the pore liquid and differs from the counter ion concentration $\bar{X}$. This is experimentally recognized with the polyelectrolyte solution[8] as well as the charged membrane.[9] Furthermore, it is well known that the electroosmosis decreases with the increase in the exterior salt concentration. This implies the decrease in X of the pore liquid due to the increase in the ionic strength of the pore solution as is expected from the theory of the electrical diffuse double layer. Despić and Hills[7] also applied the Nernst-Einstein relation for evaluating λ' from the self-diffusion coefficient of the counter ion. It has been shown[10,11] that the Nernst-Einstein relation is valid only at the infinite dilution of salt solution and should not be applied to the salt solution of higher concentration[11] as well as the ion-exchange membrane.[10] Thus Despić and Hills' theory is seen to be theoretically invalid based on the above arguments. Nevertheless, several authors[12] performed the experimental studies of Eq. 53 according to Despić and Hills' treatment.[7] It is unfortunate that their studies have nothing to do with Eq. 53 because of the estimation of λ' from the self-diffusion coefficient of counter ion according to the Nernst-Einstein relation. Such experimental studies should be consulted with Eq. 14 as reported in the preceeding paper.[10]

5. Solvent Effect on the Apparent Conductance Matrix. In the preceeding paper,[10] the conductance matrix was determined from the membrane conductance, the transport number and the salt flux data according to the previous theory[1] developed by assuming no solvent flow. Thus it is of interest to examine, on the basis of the present theory, the effect of solvent flow on the apparent values of the elements of the conductance matrix estimated according to the previous theory.[1]

It is seen by comparing the present theory with the previous one[1] that the current-potential relation are the same, although the ion flux-potential relations at non membrane current are different from each other. This implies that the diffusional ion conductance estimated according to the previous theory is the apparent one, although the membrane conductance is identical. We obtain from Eq. 13

$$(g_\tau^0)_{app} = -i_\tau^0/(V_0 - V_\tau) = g_\tau^0(1+f_\tau), \quad (54)$$

where $(g_\tau^0)_{app}$ denotes the apparent diffusional conductance and f_τ, the solvent effect given by

$$f_\tau = -g_{\tau w}^0 V_w/g_\tau^0(V_0 - V_\tau)$$
$$= -[g_{\tau w} - g_{\alpha\beta}t_w/(1-t_\tau)]V_w/g_\tau^0((V_0 - V_\tau). \quad (55)$$

The expression for E_0 is obtained from Eq. 54 as follows

$$E_0 = V_0 - V_\beta = (t_\alpha)_{app}(V_\alpha - V_\beta)$$
$$= [(\nu_\alpha+\nu_\beta)(t_\alpha)_{app}RT/Z_\alpha\nu_\alpha F]\ln a_\pm^{I}/a_\pm^{II}, \quad (56)$$

and

$$(t_\tau)_{app} = (g_\tau^0)_{app}/(g_\alpha^0+g_\beta^0)_{app} = t_\tau(1+f_\tau)/(1+t_\alpha f_\alpha + t_\beta f_\beta), \quad (57)$$

provided the external pressure difference is absent. It is seen in Eq. 56 that the transport number determined from the membrane potential *vs.* salt activity relation is also the apparent one.

Thus an element of the conductance matrix estimated by the previous treatment[1] is an apparent one, too. The interionic correlation term is expressed by the relation

$$(g_{\alpha\beta})_{app} = (t_\alpha)_{app}[g_\beta - g_\beta^0]_{app}, \quad (58)$$

where $(g_\beta)_{app}$ is given by $G_m(t_\beta)_{app}$. Equation 58 has the same form as the equation for $g_{\alpha\beta}$ obtained by rewriting Eq. 14. Combining Eq. 58 with Eqs. 14, 54, and 57, we derive

$$(g_{\alpha\beta})_{app} = \frac{(1+f_\alpha)(1+f_\beta)}{1+t_\alpha f_\alpha + t_\beta f_\beta}\left\{g_{\alpha\beta} - \frac{t_\alpha t_\beta(t_\alpha f_\beta + t_\beta f_\beta)}{1+t_\alpha f_\alpha + t_\beta f_\beta}G_m\right\}, \quad (59)$$

which satisfies the reciprocal relation, accordingly we have

$$(g_{\tau\tau})_{app} = (g_\tau)_{app} - (g_{\alpha\beta})_{app}$$
$$= \frac{(1+f_\alpha)(1+f_\beta)}{1+t_\alpha f_\alpha + t_\beta f_\beta}\left\{\frac{g_{\tau\tau} - f_\tau g_{\alpha\beta}}{1+f_\tau} + \frac{t_\alpha t_\beta(t_\alpha f_\alpha + t_\beta f_\beta)}{1+t_\alpha f_\alpha + t_\beta f_\beta}G_m\right\}. \quad (60)$$

It is seen in Eqs. 57, 59, and 60 that the deviations of the apparent values from the true ones can not be evaluated unless all the matrix elements are determined. However, it will be shown later that the apparent values are close to the true ones, as an indication of small f_r's in the present experimental conditions.

It is noted here that the present theory can be applied to both the solid and liquid membranes, since the formulation is unaltered whether the membrane is solid or liquid.

Experimental

Materials. The amphoteric ion exchange membrane used in the present study is a thin crosslinked polystyrene layer with homogeneously dispersed sulfonate and quaternary ammonium groups and is tight contact with a porous support of polyvinyl chloride sheet with *ca.* 0.1 mm in thickness. The ion exchange capacity was 1 mequiv. (g-wt membrane)$^{-1}$ and the cationic/anionic capacity ratio was ranged 1.0 ± 0.2. The membrane is coded as a "1.0-PA-29" which was developed by Central Research Laboratory of Kanegafuchi Chemical Industry Co., Ltd. and kindly supplied for the present study. The details for the preparation of the membrane were described elsewhere.[13] Pure specimen of calcium chloride as well as sucrose and twice redistilled water were used for preparing salt and sucrose solutions. As to aqueous phases separated by a membrane, the salt concentration of phase II was kept at 10^{-2} mol dm^{-3} and that of phase I was varied from 10^{-3} to 10^{-1} mol dm^{-3}. The sucrose concentrations used for the osmotic flux measurement were 0.02 to 0.12 mol dm^{-3}.

Procedures of Experiments. The procedures of experiments were essentially the same as those described in the preceding paper.[2] The experiments were carried out under the regulated room temperature at 25.0 ± 1.0 °C.

The solvent flow j_w was estimated according to the relation

$$j_w = (J_v - \bar{v}_s J_s)/\bar{v}_w. \quad (61)$$

Results and Discussion

Figure 1 shows the membrane potential, E_0, at zero electric current and the membrane conductance, G_m, as a function of the logarithm of the mean electrolyte activity, $a_\pm^I$, in phase I. The apparent transport number

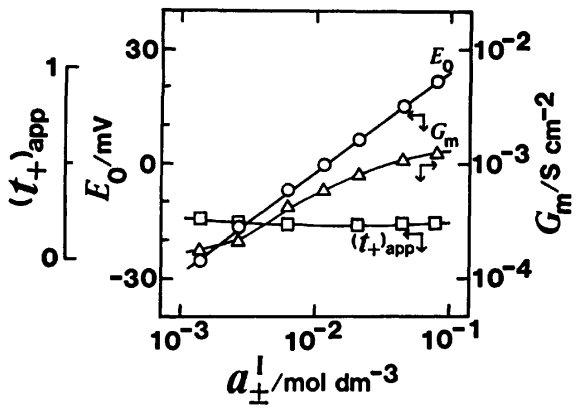

Fig. 1. Membrane potential at zero electric current, E_0, membrane conductance, G_m, and apparent cationic transport number, $(t_+)_{app}$, *vs.* mean electrolyte activity of phase I, $a_\pm^I$.
○, E_0; △, G_m; □, $(t_+)_{app}$.

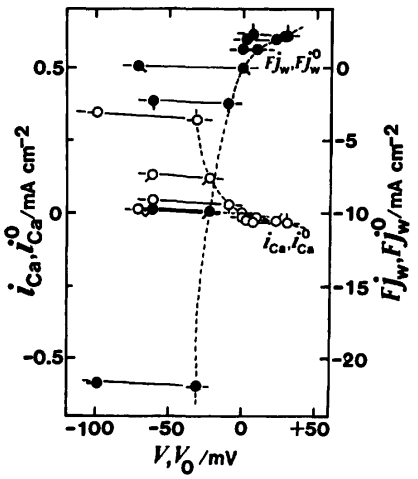

Fig. 2. Cation and water fluxes, i_{Ca} and Fj_w, *vs.* membrane potential, V.
The open and closed circles indicate i_{Ca} (i_{Ca}^0) and Fj_w (Fj_w^0), respectively. Broken lines indicate i_{Ca}^0 and Fj_w^0 at zero electric current.
○,●, 10^{-3}; ○,●, 2×10^{-3}; ○,●, 5×10^{-3}; ○,●, 10^{-2}; ○,●, 2×10^{-2}; ○,●, 5×10^{-2}; ○,●, 10^{-1}
Figures indicate the concentration of phase I in mol dm^{-3}.

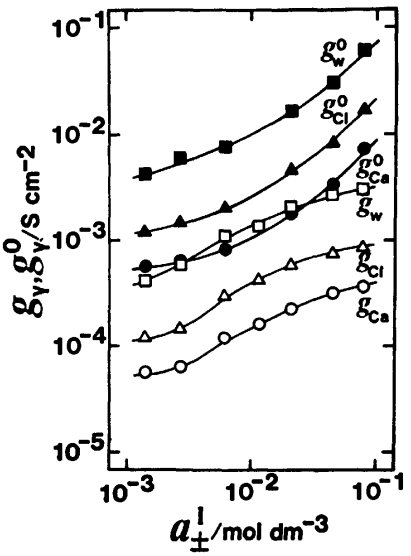

Fig. 3. Electrical ion and water conductances (g_{Ca}, g_{Cl}, g_w) and diffusional ion and water conductances (g_{Ca}^0, g_{Cl}^0, g_w^0) *vs.* mean electrolyte activity of phase I.
○, g_{Ca}; △, g_{Cl}; □, g_w; ●, g_{Ca}^0; ▲, g_{Cl}^0; ■, g_w^0.

$(t_+)_{app}$ estimated according to Eq. 56 is also shown in this figure. Figure 1 indicates that the membrane is rather selective to anion than cation. Further, G_m increases with the increase in the external salt concentration. This may indicate the increase in the concentrations of cations and anions in the membrane with the increasing external salt concentration.

Figure 2 shows the changes in i_a and Fj_w as functions of the applied potential V. All the fluxes were shown to be linear against V in this figure as an indication of the constancy of the conductances under the present experimental condition.

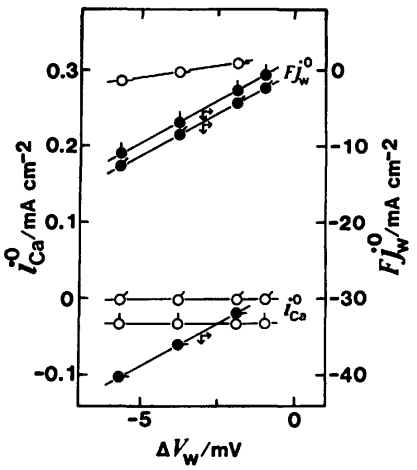

Fig. 4. Effect of osmotic pressure difference (ΔV_w) on ion and water fluxes at zero electric current. Open and closed circles are i^0_{Ca} and Fj^0_w, respectively.
○,●, 10^{-3}; ○,●, 10^{-2}; ○,●, 10^{-1}
Numericals indicate the concentration of phase I in mol dm^{-3}.

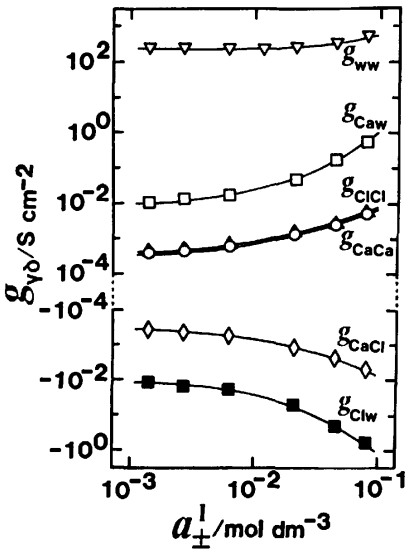

Fig. 5. Elements of conductance matrix *vs.* mean electrolyte activity of phase I.
○, g_{CaCa}; △, g_{ClCl}; ◇, g_{CaCl}; □, g_{Caw}; ■, g_{Clw}; ▽, g_{ww}.

The values of g_{Ca} and g_w can be estimated according to Eq. 16 and hence g_{Cl} can be calculated according Eq. 10. These are plotted as functions of $a^I_\pm$ in Fig. 3 together with g^0_γ calculated according to Eq. 14.

The deviation of the apparent transport number $(t_+)_{app}$ from the true one $t_{Ca}(=g_{Ca}/G_m)$ was found to be very small less than one percent and within the experimental error. This indicates that the solvent effect on the membrane potential at no membrane current, E_0, may be ignored under the present experimental conditions. This can be confirmed also by comparing E_0 with the calculated value of $t_w V_w$.

Figure 4 indicates the effect of the osmotic pressure difference ΔV_w caused by the addition of sucrose on the salt and water fluxes. The fluxes were linear against ΔV_w as shown in this figure. It is found in this figure that the slope of the i^0_a *vs.* ΔV_w relation agrees well with the intercept of the Fj^0_w *vs.* ΔV_w relation. This indicates the validity of the reciprocal relation assumed in the present theory. The membrane potential changed little by the addition of sucrose, and the change was within experimental error, probably due to the small solvent effect on the membrane potential. The phenomenological coefficients can be estimated stepwise as described in the theoretical section from the data shown in Figs. 1, 3, and 4. The estimated elements of the conductance matrix are shown in Fig. 5 as functions of the mean activity of salt in phase I.

This figure indicates that $g_{CaCa} \approx g_{ClCl} > -g_{CaCl}$ and all these coefficients are the same order of magnitude in contrast to the result in the cation-exchange membrane,[10] $g_{CaCa} \gg g_{CaCl} > g_{ClCl}$. In the preceding paper,[2] the l_{kl}(k,l=α,β,w) coefficients were determined with the cation-exchange membrane-barium chloride system. The $g_{\gamma\delta}(\gamma,\delta=\alpha,\beta)$ may be calculated according to the relation, $g_{\gamma\delta}=Z_\gamma Z_\delta F^2 l_{\gamma\delta}\Delta x$, where Δx is the membrane thickness. The order of $g_{\alpha\beta}$ is found to be $g_{BaBa} \gg g_{BaCl} > g_{ClCl}$ at the external salt concentrations less than 0.1 mol dm^{-3}. On the other hand, g_{BaCl} becomes negative at the concentrations more than 0.4 mol dm^{-3} and the order of $g_{\gamma\delta}$ is found to be $g_{BaBa} \simeq g_{ClCl} > -g_{BaCl}$ as a similar result to the amphoteric membrane. An appreciable amount of the Donnan salt may migrate in the cation-exchange membrane when the external salt concentration becomes comparable with the fixed ion concentration. Thus, the negative cross coefficients in the cation and amphoteric ion exchange-membranes may correspond to the positive $l_{\alpha\beta}(\alpha \neq \beta)$ coefficient in the salt solution.[11]

Figure 5 also indicates the positive g_{Caw} and the negative g_{Clw}. A similar result, the positive g_{Baw} and the negative g_{Clw}, may be deduced from the $l_{\gamma w}$ data observed with the cation-exchange membrane[2] at the external salt concentrations more than 0.2 mol dm^{-3}. On the other hand, both g_{Baw} and g_{Clw} are postive at the concentrations less than 0.2 mol dm^{-3}. Similar to $g_{\gamma\delta}$, the concentration dependence of $g_{\gamma w}$ in the cation-exchange membrane may be ascribed to the increase of the Donnan salt within the membrane with increasing salt concentration. Thus it may be concluded that the behaviors of the cation and amphoteric ion exchange-membranes are quite different each other at the concentrations of external salt solutions less than 0.1 mol dm^{-3} where the major migrating ionic species in the former is cations and in the latter, both cations and anions. This reflects to the relation between the diffusional and conductive membrane conductances, *i.e.*, $g_\gamma \gg g^0_\gamma$ in the cation-exchange membrane[10] and this order is reversed in the amphoteric membrane as shown in Fig. 3. The values of g_γ and g^0_γ are estimated from $g_{\gamma\delta}$'s according to Eqs. 9 and 14, and related to the electrical absolute mobility $\bar{U}_\gamma$ and the diffusion coefficient $\bar{D}_\gamma$ within the membrane, respectively, as follows:[14]

$$g_\gamma = (Z_\gamma F)^2 \bar{U}_\gamma \bar{C}_\gamma / \Delta x$$
$$g^0_\gamma = (Z_\gamma F^2) \bar{D}_\gamma \bar{C}_\gamma / RT\Delta x, \qquad (62)$$

where $\bar{U}_\gamma$ and $\bar{D}_\gamma$ denotes the mean electrical absolute

mobility and the mean diffusion coefficient of ion γ within the membrane, respectively, and $\bar{C}_\gamma$ the mean concentration of ion γ within the membrane. Comparing Eq. 14 with Eq. 62, we have

$$\lambda_\gamma - \lambda_\gamma^0 = (g_\gamma - g_\gamma^0)\Delta x/\bar{C}_\gamma = (Z_\gamma F)^2(\bar{U}_\gamma - \bar{D}_\gamma/RT) \quad (63)$$

$$= g_{\alpha\beta}\Delta x/\bar{C}_\gamma(1-t_\gamma), \quad (64)$$

where λ_γ and λ_γ^0 are the equivalent electrical and diffusional ion conductances, respectively. Despić and Hills evaluated the electroosmotic effect according to Eq. 63, although they derived Eq. 53.[7] It is evident that Despić and Hills' treatment has no relation to their theoretical expression, Eq. 53. The disagreement between g_γ and g_γ^0 implies the failure of the Nernst-Einstein relation. The order, $g_\gamma^0 \gg g_\gamma$, in the amphoteric membrane indicates that the usual dialysis is energetically more effective than the electrodialysis for removing the salt through the amphoteric membrane.

It is seen in Eq. 25 that this phenomenological equation involves $g_{\alpha v}$, g_v, and g_p as new conductance elements. These coefficients can be evaluated from the original set of conducatnce matrix elements according to Eq. 26. The deviation of the new elements from the corresponding original elements are found to be small as shown in Fig. 6. L_s, L_{sp}, L_p, and ω_s calculated according to Eqs. 38a, b, c, and 40, are plotted against $a_\pm^1$ as shown in Fig. 7. Since the value of σ calculated by Eq. 41 is almost unity over the range of concentrations studied in the present paper, it is not plotted in Fig. 7. In the phenomenological equation, a flux is given by a linear combination of forces with phenomenological coefficients and *vice versa*. This implies that the processes are more or less coupled and the coupling phenomena can be discussed in terms of the phenomenological coefficients.[5] In this respect, it is interesting to consider the phenomena in terms of the degree of coupling.[15,16] The degree of coupling can be expressed by the coupling coefficient which is an important parameter for treating the energy conversion.[15,16]

For the phenomena dealing with the two and three processes, *e.g.*, those expressed by Eqs. 37 and 1, respectively, the coupling coefficients are given by

$$q = L_{sp}/(L_s L_p)^{1/2}, \quad (65)$$

and

$$q_{kl} = -|g|_{kl}/(|g|_{kk}|g|_{ll})^{1/2}, \quad (66)$$

respectively, where $|g|_{kl}$ is the cofactor of an element g_{kl} in the conductance matrix. The coupling coefficient q_{kl} can be regarded as the extent to which the k-th flow is dragged by the l-th flow when no other flow is present and the force conjugate to the k-th flow is zero. The absolute values of q, $q_{\alpha\beta}$, $q_{\alpha w}$ and $q_{\beta w}$ calculated according to Eqs. 65 and 66, respectively are shown in Fig. 8 as functions of $a_\pm^1$. It is shown in this figure that q_{CaCl} is close to unity, although q_{Caw} and q_{Clw} are less than 0.1. This indicates that the interionic processes are strongly coupled, although the coupling between the water and ionic fluxes is weak. This might be reflected to the small solvent effects on the interionic conductance elements. Actually, deviations of the apparent interionic conductance elements, $(g_{\gamma\delta})_{app}$, estimated according to the previous treatment[10] from the true ones is within the experimental error as shown in Fig. 9. Thus it is seen that the coupling coefficient plays an important role

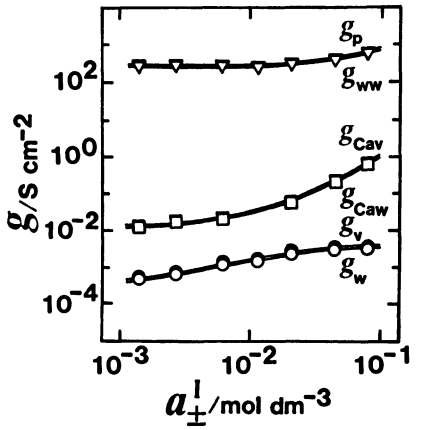

Fig. 6. Deviations of g_v, g_{Cav}, and g_p from g_w, g_{Caw}, and g_{ww}, respectively.
○, g_w; ●, g_v; □, g_{Caw}; ■, g_{Cav}; ▽, g_{ww}; ▼, g_p.

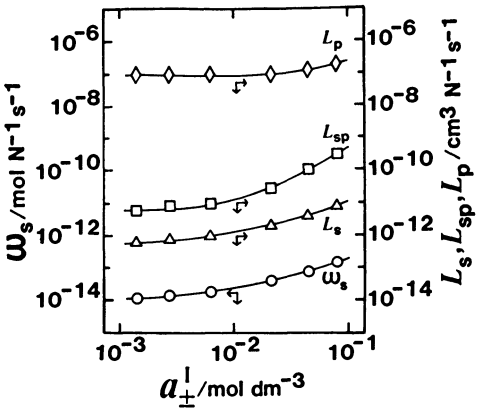

Fig. 7. Solute permeability (ω_s), thermodynamic permeability (L_s), mechanical filtration coefficient (L_{sp}) and hydrodynamic permeability (L_p) *vs.* mean electrolyte activity of phase I.
○, ω_s; △, L_s; □, L_{sp}; ◇, L_p.

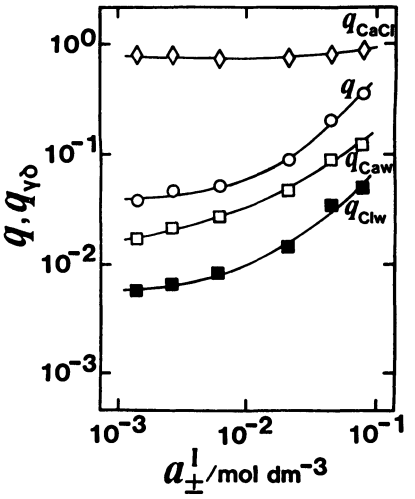

Fig. 8. Coupling coefficient *vs.* mean electrolyte activity of phase I.
○, q; ◇, q_{CaCl}; □, q_{Caw}; ■, q_{Clw}.

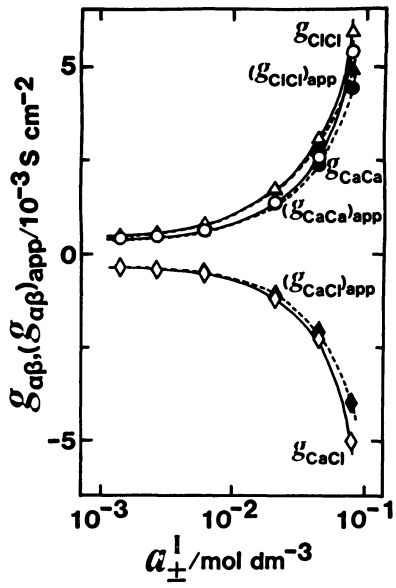

Fig. 9. Comparison of the true interionic conductance elements with the apparent ones.
○, g_{CaCa}; ●, $(g_{CaCa})_{app}$; ◇, g_{CaCl}; ◆, $(g_{CaCl})_{app}$; △, g_{ClCl}; ▲, $(g_{ClCl})_{app}$.

in the cross phenomena. The small V_w due to the small concentration difference in the concentration cell will be also responsible to little solvent effect as deduced from Eq. 55.

The electroosmosis is an example of the coupling phenomena. The electroosmotic contribution to the membrane conductance is given by g_v^2/g_pG_m as shown by Eq. 45. The factor g_v^2/g_pG_m corresponds to the square of the coupling coefficient for the membrane current-volume flow coupling in the case of no concentration difference between the two external solutions. The contribution is found to be a negligible order of 10^{-3} and the same order as that for the cation-exchange membrane.[10] This may be attributed to the low charge concentration of the flowing pore liquid X which is evaluated according to Eq. 49. In the present study, X is found to be an order of 10^{-4} mol dm^{-3} over the concentration range studied. Even for the cation-exchange membrane with the fixed ion concentration of *ca.* 2 mol dm^{-3}, the value of X evaluated from the observed phenomenological coefficient[2] is an order of 10^{-2} mol dm^{-3} and much less than the counter ion concentration within the membrane, $\bar{X}$. The strong interaction of the counter ions with the fixed charges may be the cause of the lower charge concentrations of flowing pore liquid. It is seen in Eqs. 48 and 50 that the small electroosmotic current with an appreciable volume flow may be ascribed to the low X. It is seen in the foregoing discussion that there is no appreciable contribution of the solvent effect on the interionic conductance elements, $g_{\gamma\delta}$'s, for the amphoteric and cation-exchange membranes as far as the concentrations of the external salt solutions are dilute as compared with the fixed ion concentrations. This also verifies the previous treatment[10] for estimating the $g_{\gamma\delta}$'s in the cation-exchange membrane-aqueous calcium chloride system.

It should be pointed out here that the small coupling coefficient for the coupling between solvent and ion flows is responsible to these results. It is shown in Fig. 5 that g_{ww} is extremely high and much greater than $g_{\gamma\delta}$'s by a factor of 10^5. A similar result has been observed with the cation-exchange membrane.[2] Thus, the fact that $g_{ww} \gg g_{\gamma\delta}$ suggests the small coupling coefficient. On the other hand, this fact also invalidates the assumption of no solvent flow in the previous theory.[1] The assumption should be revised as the assumption of little solvent effect on the ion transports. The small coupling coefficients may, in turn, imply no appreciable salt effect on the solvent flow.

Comparing Eq. 41 with Eq. 62, we have

$$\sigma = 1 - q(L_s/L_p)^{1/2} \tag{67}$$

which implies that the small coupling coefficient and and $L_p \gg L_s$ are the recommended conditions for the reverse osmosis.

When the external salt concentration becomes higher, the deviation of $(g_{\gamma\delta})_{app}$ from $g_{\delta\gamma}$ will be greater as can be deduced from Eq. 55. This tendency may already be seen even in Fig. 9 and in fact, a remarkable deviation occurs in the cation-exchange membrane-barium chloride system at higher salt concentrations more than 0.1 mol dm^{-3}.[2] This may be related to the increasing coupling coefficient with salt concentration.[2]

For the membrane with higher water content and lower fixed charges, the ions move as fast as the solvent molecule and hence the coupling coefficient $q_{\gamma w}$ will be greater. This may be the cause of an anormalous osmosis.[17]

Whether the water content and fixed ion concentration of a membrane is high or not, the detailed study for determining all the phenomenological coefficients should be required for describing the membrane properties precisely.

It has been shown in the present paper that the cross coefficients play an important role for elucidating the membrane properties. Thus the nonthermodynamic assumption such as ignoring the cross term should be avoided unless it is verified experimentally.

References

1) H. Kimizuka and K. Kaibara, *J. Colloid Interface Sci.*, **52**, 516 (1975).

2) E. Kumamoto and H. Kimiuzka, *J. Phys. Chem.*, **85**, 635 (1981).

3) T. Foley, J. Klinowski, and P. Meares, *Proc. R. Soc. London, Ser. A*, **336**, 327 (1974).

4) T. Foley and P. Meares, *J. Chem. Soc., Faraday Trans. I*, **72**, 1105 (1976).

5) A. Katchalsky and P. F. Curran, "Non-Equilibrium Thermodynamics in Biophysics," Harvard University Press, Cambridge, MA, (1965).

6) H. Krämer and P. Meares, *Biophys. J.*, **9**, 1006 (1969).

7) A. Despić and G. J. Hills, *Discuss. Faraday Soc.* **21**, 150 (1956).

8) B. E. Conway and R. G. Barradas "Chemical Physics in Ionic Solution," John Willey and Sons, New York, London, Sydney (1966).

9) Y. Toyoshima, Y. Kobatake, and H. Fujita, *Trans. Faraday Soc.*, **63**, 2814 (1967).

10) H. Kimizuka, K. Kaibara, E. Kumamoto, and M. Shirōzu, *J. Membr. Sci.*, **4**, 81 (1978).
11) E. Kumamoto and H. Kimizuka, *Bull. Chem. Soc. Jpn.*, **52**, 2145 (1979).
12) N. Lakshminarayanaiah "Transport Phenomena in Membranes," Academic Press, New York and London (1969).
13) A. Yamauchi, S. Tsuruyama, H. Masumori, Y. Nagata, K. Kaibara, and H. Kimizuka, *Bull. Chem. Soc. Jpn.*, **55**, 3297 (1982).
14) K. Nomura, A. Matsubara, and H. Kimizuka, *Bull. Chem. Soc. Jpn.*, **54**, 1324 (1981).
15) O. Kedem and S. R. Caplan, *Trans. Faraday Soc.*, **61**, 1897 (1965).
16) S. R. Caplan, *J. Phys. Chem.*, **69**, 3801 (1965); *J. Theor. Biol.*, **10**, 209 (1966); **11**, 346 (1966).
17) M. Tasaka, C. Wada, and M. Nagasawa, *J. Membr. Sci.*, **6**, 171 (1980).

Behavior of Trajectory with Stable and Unstable Limit Cycles in the Oregonator Model for the Belousov-Zhabotinskii Reaction

Shinji SAKANOUE,* Chiaki MURASE,† and Mitsuo ENDO

Department of Chemistry, Faculty of General Education, Tokyo University of Agriculture and Technology, Saiwaicho, Fuchu, Tokyo 183

†*Department of Physics, Faculty of General Education, Tokyo University of Agriculture and Technology, Saiwaicho, Fuchu, Tokyo 183*

(Received December 6, 1982)

Computer simulations and a theoretical analysis of the Oregonator model of the Belousov-Zhabotinskii reaction are made based on Tyson's equation. The behavior of the amplitudes of the unstable limit cycle near the transition point, p_c, can be explained theoretically fairly well by the Landau theory. The global behavior of one stable limit cycle and one unstable limit cycle is examined by means of simulations. The existence of a triple point at which three different global states coexist has been suggested.

Field and Noyes[1] have proposed a simple model (Oregonator model) for the kinetics of the Belousov-Zhabotinskii (B-Z) reaction. Tyson[2] presented this model as follows,

$$\varepsilon \frac{dx}{dt} = x + y - qx^2 - xy,$$
$$\frac{dy}{dt} = -y + fz - xy, \qquad (1)$$
$$p \frac{dz}{dt} = x - z,$$

where t, x, y, and z are the dimensionless variables corresponding to the time and the three concentrations $[HBrO_2]$, $[Br^-]$, and $[Ce^{4+}]$ respectively, and where ε, f, p, and q are the dimensionless parameters to be decided from the rate constants of the elementary reactions, the concentration of $BrCH(COOH)_2$, *etc.* The stiffly coupled approximation $dx/dt=0$ has been introduced into Eq. 1.[1,2] The meaning of this approximation has been discussed in detail by Field and Noyes[1] and by Tyson.[2] Simply speaking, this approximation is obtained by postulating that bromous acid is always present in a steady state concentration as determined by the concentration of bromide ions. Under the stiffly coupled approximation, we get:

$$\dot{\bar{y}} = -\delta\bar{y} + f\bar{z} - (\gamma+\bar{y})X(\bar{y}),$$
$$\dot{\bar{z}} = r\{X(\bar{y})-\bar{z}\}, \quad r = \frac{1}{p}, \qquad (2)$$

where $\bar{y}$ and $\bar{z}$ are the deviations of y and z from the steady state values y_0 and z_0, respectively; where the dot shows the time differentiation, and where

$$X(\bar{y}) = \{-(\alpha+\bar{y})+\sqrt{(\alpha+\bar{y})^2-4q\beta\bar{y}}\}(2q)^{-1}.$$

The detailed derivation of Eq. 2 and the definition of the constants, α, β, γ, and δ, may be seen in Ref. 3. For the sake of simplicity, we call this model (Eq. 2) the simple Oregonator model.

In a previous paper[3] we made computer simulations of Eq. 2. These simulations confirmed the coexistence of an unstable limit cycle and a stable limit cycle. Figure 1 shows a typical example of the coexistence state of the two limit cycles around a stable steady state. In the figure, the dot-dash-line denotes the trajectory. The solid line shows the stable limit cycle, and the dotted line, the unstable limit cycle, as estimated from the simulations. The steady state (y_0, z_0) is represented by the symbol "a." In order to analyze the behavior of the simple Oregonator model theoretically, we must define two quantities: the amplitude, A, of a trajectory and the amplitude-expansion rate, F. The amplitude, A, of a trajectory is defined by the distance between the steady state, "a," and the point at which the trajectory intersects the $z=z_0$ line. The amplitude-expansion rate, F, is defined by the time differentiation of the square of the amplitude, A:

$$\frac{dA^2}{dt} = F.$$

In numerical simulations, the dA^2/dt quantity is determined by $\Delta A^2/\Delta t$, where ΔA^2 and Δt are, respectively, the differences in the squares of the amplitude, A^2, and the time, t, over one turn of a trajectory. The points at which an unstable limit cycle and a stable one intersect the $z=z_0$ line are denoted by the symbols "b"

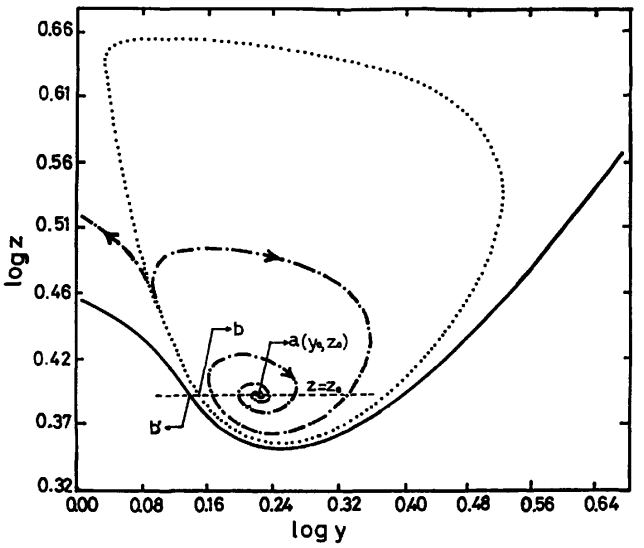

Fig. 1. Phase plane plot of $\log z$ *vs.* $\log y$ obtained numerical integrations of Eq. 1 under $dx/dt=0$ for $q=0.006$, $f=2.350$, and $p=2.0$ ($p_c=90.24$).
……: Unstable limit cycle, ——: stable limit cycle, -·-·-: trajectory, ------: $z=z_0$, a: steady state, ab: A_u (amplitude of unstable limit cycle), ab': A_s (amplitude of stable limit cycle).

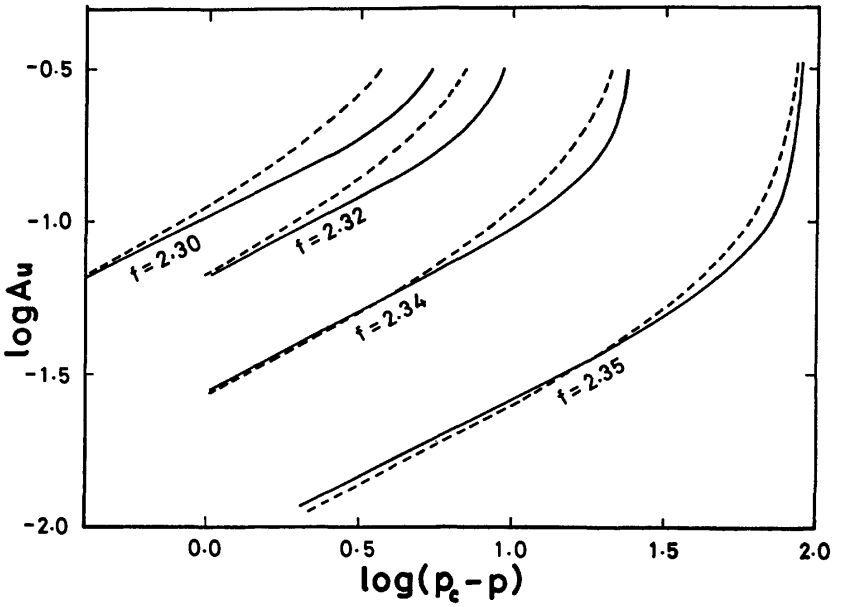

Fig. 2. Log-log plots of A_u *vs.* (p_c-p) for $q=0.006$.
——: Plots of data from computer simulations, ------: theoretical curve from Eq. 18.

and "b'" respectively, as is shown in Fig. 1. We define the A_u and A_s amplitudes (the amplitudes of an unstable limit cycle and a stable-limit one) by the ab and ab' distances, respectively.

In this paper the behavior of the trajectory and the amplitudes of two kinds of limit cycles are examined for various values of the p and f parameters by means of computer simulations. The changes in the amplitudes of the two kinds of limit cycles are obtained numerically. A quantitative explanation of these changes is made by the use of the Landau theory.[4]

Behavior of an Unstable Limit Cycle near p_c and a Perturbational Approach

Figure 2 shows the log-log plots of the amplitude, A_u, of the unstable limit cycle against (p_c-p). The solid lines represent the results from computer simulations. We will examine, on the basis of the Landau theory, how the behavior of A_u can be explained theoretically. The Landau theory elucidates the transition from a laminar flow to a turbulent one and may be represented as follows:[4]

$$\frac{dA^2}{dt} = F = \gamma_2 A^2 + \gamma_4 A^4 + \cdots. \tag{3}$$

This approach (Landau theory) is a kind of perturbation method. We will show that the behavior of the unstable limit cycle near the transition point p_c can be explained fairly well by means of Landau's equation (Eq. 3).

We determine two coefficients, γ_2 and γ_4, in Eq. 3 by the use of perturbation method. In deriving the nonlinear terms in Eq. 2, which we represent as N_y and N_z, we use the approximation $q=0$, because the q parameter is very small in a real system, of the order of 10^{-6}, as estimated by Field and Noyes.[1] Then, Eq. 2 can be presented as follows:

$$\begin{aligned} \dot{\bar{y}} &= r_c\bar{y} + f\bar{z} + N_y, \\ \dot{\bar{z}} &= ra_1\bar{y} - r\bar{z} + N_z, \end{aligned} \tag{4}$$

where the nonlinear terms, N_y and N_z, are given by:

$$\begin{aligned} N_y &= -(b_1\bar{y}^2 + b_2\bar{y}^3 + \cdots), \\ N_z &= r(a_2\bar{y}^2 + a_3\bar{y}^3 + \cdots), \end{aligned} \tag{5}$$

$$a_n = \frac{\beta}{(-\alpha)^n},\quad b_n = -\frac{2+r_c}{(-\alpha)^n}\quad (n=1,2,\cdots),$$

and where the constant, r_c, is the boundary value defined by:

$$r_c = \frac{1}{p_c} = \frac{\beta\gamma}{\alpha} - \delta.^{2,3)}$$

The linear approximation ($N_y=0$, $N_z=0$) of Eq. 4 gives two solutions, y_l and z_l (complexes), of these forms:

$$y_l = A_y \exp(\lambda t),\ z_l = A_z \exp(\lambda t), \tag{6}$$

where the eigenvalue, λ, is:

$$\begin{aligned} \lambda &= \lambda_0 + i\omega, \\ \lambda_0 &= -\frac{1}{2}(r-r_c), \\ \omega &\simeq -r\sqrt{(r_c+a_1 f)},\ (r \simeq r_c). \end{aligned} \tag{7}$$

We seek this solution:

$$\bar{y} = \mathrm{Re}(y_l+y_n),\ \bar{z} = \mathrm{Re}(z_l+z_n), \tag{8}$$

where Re denotes the real part. The contributions to y_n and z_n from nonlinear terms are determined to be of these forms:

$$\begin{aligned} y_n &= B_y \exp(2i\,\omega_c t) + C_y, \\ z_n &= B_z \exp(2i\,\omega_c t) + C_z, \end{aligned} \tag{9}$$

where ω_c is ω at $p=p_c$. The constants, B_y and C_y, are

determined to be exact up to the A_y^2 order, whereas B_z and C_z are exact to the A_z^2 order. Putting Eq. 8 into Eq. 4, we get:

$$B_y = -\frac{1}{6}cA_y^2, \quad C_y = \frac{1}{2}c|A_y|^2, \tag{10}$$

where:

$$c = \frac{b_1 - a_2 f}{r_c + a_1 f}.$$

The amplitude, A, is given by:

$$A = y_l + y_n \simeq y_l = |A_y|. \tag{11}$$

Since $\langle \bar{y}^2 \rangle \simeq (1/2)|y_l|^2 = (1/2)A^2$, the amplitude-expansion rate, F, is calculated from:

$$F = 2\frac{\mathrm{d}}{\mathrm{d}t}\langle \bar{y}^2 \rangle, \tag{12}$$

where $\langle \ldots . \rangle$ denotes the time average over one period. Using Eqs. 8 and 12, the coefficients, γ_2 and γ_4, are obtained from:

$$\gamma_2 = 4\langle \mathrm{Re}\, y_l \, \mathrm{Re}\, \dot{y}_l \rangle A^{-2},$$
$$\gamma_4 = \gamma_{41} + \gamma_{42}, \tag{13}$$

where:

$$\gamma_{41} = -4b_2\langle \mathrm{Re}\, y_l (\mathrm{Re}\, y_l)^3 \rangle A^{-4},$$
$$\gamma_{42} = -8b_1\langle \mathrm{Re}\, y_l (\mathrm{Re}\, y_l \, \mathrm{Re}\, y_n) \rangle A^{-4}.$$

Putting Eqs. 6, 9, and 10 into Eq. 13, we get:

$$\gamma_2 = -(r - r_c),$$
$$\gamma_{41} = -\frac{3}{2}b_2, \quad \gamma_{42} = -\frac{5}{3}cb_1. \tag{14}$$

For $p = p_c$ (or $r = r_c$), we can get:

$$\gamma_4 = \frac{1}{3\alpha\beta f}\left(20 - \frac{\beta}{\alpha}f\right). \tag{15}$$

Now we have determined two coefficients, γ_2 and γ_4, in Laudau's equation (Eq. 3). The properties of the two coefficients, γ_2 and γ_4, for p near p_c can easily be seen from Eqs. 14 and 15. These satisfy:

$$\gamma_2 \propto -(p_c - p) < 0, \text{ for } p < p_c,$$
$$\gamma_4 = \text{a constant independent of } p. \tag{16}$$

Figure 3 shows the plot of the amplitude-expansion rate, F, against A for $q = 0.006$, $f = 2.350$, and $p = 58.00$ ($p_c = 90.24$). The broken line shows the theoretical curve calculated from Eq. 3 using the coefficients, γ_2 and γ_4, in Eqs. 14 and 15. For the above values of q, f, and p, we get: $\gamma_2 = -0.616 \times 10^{-2}$ and $\gamma_4 = 2.132$. The solid line shows the plots of the data from the computer simulations. When p is not so far from p_c, the theoretical curve is in fairly good agreement with the results of the computer simulations. The amplitude, A_u, of the unstable limit cycle can be obtained theoretically from $F = 0$ thus:

$$\gamma_2 A_u^2 + \gamma_4 A_u^4 = 0. \tag{17}$$

For $A < A_u$, the amplitude-expansion rate, F, becomes negative and the trajectory shrinks towards $A = 0$ (steady state), whereas for $A > A_u$ the amplitude-expansion rate becomes positive and the trajectory expands. Therefore, the trajectory with A near A_u grows apart from A_u as time goes on (unstable limit cycle). From Eq. 17, the amplitude, A_u, of the unstable limit cycle becomes:

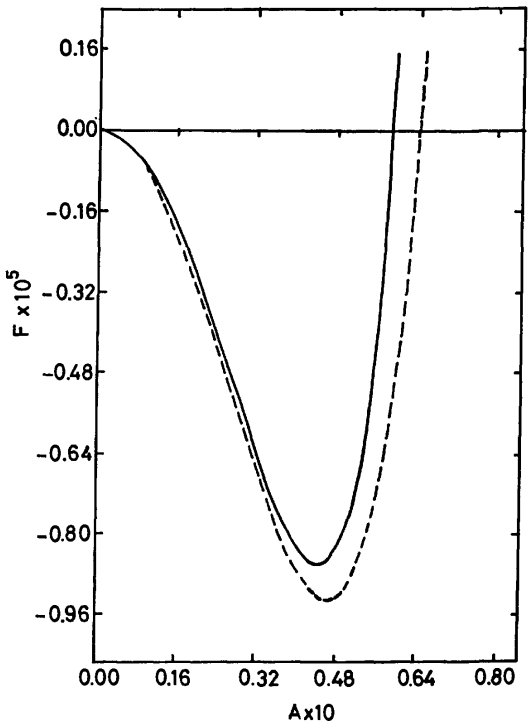

Fig. 3. Variation of amplitude expansion rate F with amplitude A of trajectory.
——: Plots of data from computer simulations, ------: theoretical curve by Landau's equation (Eq. 3) on using values of $\gamma_2 = -0.616 \times 10^{-2}$ and $\gamma_4 = 2.132$ from Eqs. 14 and 15.

$$A_u = \sqrt{-\frac{\gamma_2}{\gamma_4}}. \tag{18}$$

For $p \simeq p_c$,

$$\log A_u = \frac{1}{2}\log(p_c - p) + C, \tag{19}$$

where C is a constant independent of p. In Fig. 2 the broken line represents a theoretical curve derived from Eq. 18. For $p \simeq p_c$, the gradient of the plotted line is 1/2, which agrees well with Eq. 19. For $p \ll p_c$, however, the agreement becomes less good. The reason for this discrepancy comes from the roughness of our approximations in the perturbation method.

It has been confirmed that our perturbation method (Landau theory) can explain the behavior of the unstable limit cycle near p_c fairly well. It is insufficient, however, to explain the global behavior of the limit cycles.

Global Behavior

The global behavior of the simple Oregonator model is different from the local behavior around the steady state. The estimation of the global behavior is difficult on the basis only of the theoretical analysis (linear approximation) of the local behavior. In order to examine the global behavior of the simple Oregonator model, we have made computer simulations for various values of f and p under a fixed q (=0.05). The q parameter depends on the constants determined by the elementary reactions in the FKN model.[1] These are

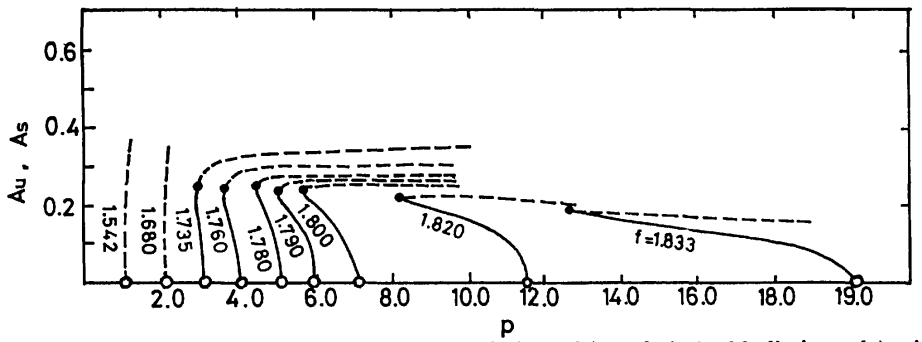

Fig. 4. Variations of amplitudes A_u (unstable limit cycle) and A_s (stable limit cycle) with parameters p and f for fixed $q=0.05$ ($f_{c_1}=0.714$, $f_{c_2}=1.850$, $f_T=1.688$).
——: Amplitude of unstable limit cycle, ------: amplitude of stable limit cycle, ○: p_c, ●: p_d.

$k_1=k_1'[H^+]^2$, $k_2=k_2'[H^+]$, $k_3=k_3'[H^+]$ and $k_4=k_4'$. The q parameter becomes:

$$q=\frac{2k_1k_4}{k_2k_3}=\frac{2k_1'k_4'}{k_2'k_3'},$$

where k_1', k_2', k_3', and k_4' are, respectively, the rate constants of the following elementary reactions in the B-Z reaction:

$$Br^- + BrO_3^- + 2H^+ \xrightarrow{k_1'} HBrO_2 + HOBr,$$

$$Br^- + HBrO_2 + H^+ \xrightarrow{k_2'} 2HOBr,$$

$$BrO_3^- + HBrO_2 + H^+ \xrightarrow{k_3'} 2BrO_2\cdot + H_2O$$

$$2HBrO_2 \xrightarrow{k_4'} HOBr + BrO_3^- + H^+.$$

As q depends only on the rate constants of the elementary reactions described above, its value can be varied by changing the temperature. Field *et al.* have determined by using known rate constants, that at 25 °C $q=8.375\times10^{-6}$. However, the dependency of every rate constant on the temperature has not been confirmed. Hence, a further examination is necessary to see whether the state of $q=0.05$ can be realized experimentally or not by changing the temperature.

We have selected such a relatively high value of q for two reasons. One is a technical reason with regard to computer simulations. In order to get the numerical value of the amplitude-expansion rate, F, continuously, we need to set q at such a high value. For a small q, for example $q=0.006$ (Fig. 1), the amplitude-expansion rate, F, becomes discontinuous near $A=A_s$. This is because the entrainment into the stable limit cycle is too strong and the trajectory does not take even one turn around the steady state. The other reason is involved with our concerns as to the qualitative property of the global behavior. As we shall see later, the global behavior of the simple Oregonator model shows a kind of phase transition as the r parameter changes.† For this purpose, the absolute value of q is not absolutely essential.

Figure 4 shows the variations in the amplitudes of the two kinds of limit cycles against p for fixed f and q values. The solid lines show the amplitudes, A_u, of the unstable limit cycles, while the broken lines show the amplitudes, A_s, of the stable limit cycles. The p_c point is the point from which a limit cycle appears. As is shown in the figure, no unstable limit cycle exists for $p>p_c$. The other transition point, p_d, is the lowest boundary value of p for the coexistence of an unstable limit cycle and a stable limit cycle. Hence, only for $p_d<p<p_c$ can two limit cycles coexist (coexistence state). Figure 5 shows the various boundary parameters on which the global behavior of the trajectory changes topologically. The f_{c_1} and f_{c_2} points are a pair of the boundary values of f inside which the steady state can be unstable; numerically, $f_{c_1}=0.714$ and $f_{c_2}=1.850$ for $q=0.05$. The T point in Fig. 5 shows the point at which three different global states coexist, where $p_d=p_c(f=f_T)$ or $r_d=r_c(f=f_T)$. We call this point, T, "a triple point"

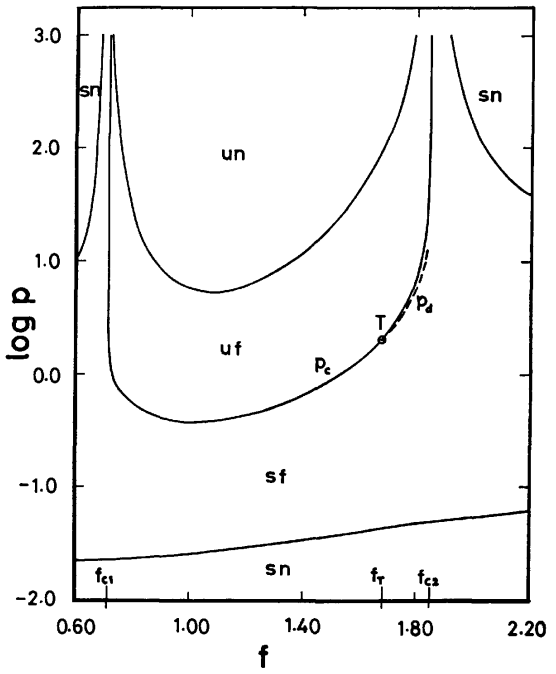

Fig. 5. Boundary parameters map for different kinds of global behavior of trajectory under $q=0.05$.
------: p_d, ⊙: triple point T, sf: stable focus, uf: unstable focus, sn: stable node, un: unstable node.

† Strictly speaking, the term phase transition is not a usual one where the system has many degrees of freedom.

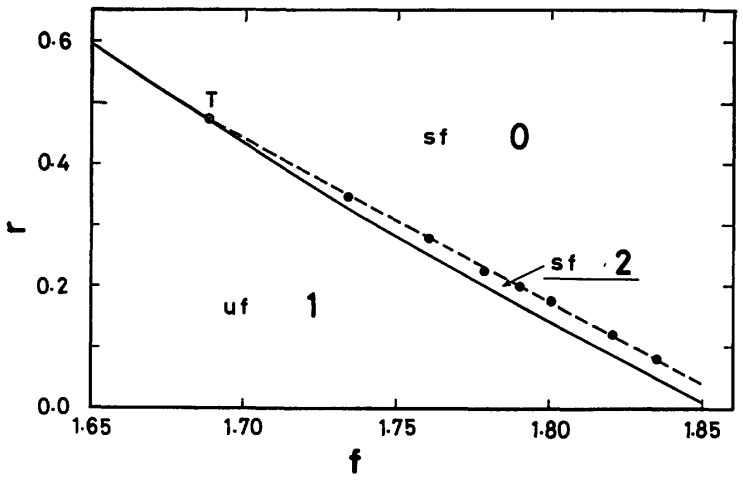

Fig. 6. Variations of $r_c \equiv 1/p_c$ and $r_d \equiv 1/p_d$ near triple point T with parameter f. (The figures in the figure represent the number of limit cycles.)
——: r_c, ●: plot point of datum from computer simulations, ⊙: triple point T, ------: line of r_d obtained by least square method, sf: stable focus, uf: unstable focus.

TABLE 1. VALUES OF BOUNDARY PARAMETERS FOR COEXISTENCE OF TWO KINDS OF LIMIT CYCLES (q=0.05)

f	r_c	r_d
1.8339	0.0500	0.0787
1.8200	0.0860	0.1215
1.8000	0.1399	0.1754
1.7900	0.1675	0.1994
1.7795	0.1969	0.2245
1.7603	0.2518	0.2793
1.7347	0.3275	0.3484
1.688 (f_T)	0.473 (r_T)	0.473 (r_T)

for the sake of simplicity. Figure 6 shows the variations in r_c and r_d near the triple point. The Arabic figures written in Fig. 6 represent the total number of limit cycles. The area specified by the Arabic figure 2 is the coexistence state (the coexistence of two kinds of limit cycles). The areas specified by the two figures 0 and 1 correspond to the states of a no-limit cycle and a one-limit cycle respectively. The solid line shows r_c. The black circles represent the points of r_d as obtained from computer simulations. The detailed values of r_c and r_d are shown in Table 1. The broken line has been obtained by the method of the least squares. The intersection of two lines, r_c and r_d, gives the triple point, T. The values of p_T, r_T, and f_T, which are defined by the values of p, r, and f respectively at the triple point, T, are obtained for q=0.05 as:

$$p_T = 2.11,\ r_T = r_c(f = f_T) = r_d(f = f_T) = 0.473,$$
$$f_T = 1.688.$$

Next we will examine the global behavior of the amplitude-expansion rate, F, under a fixed f value. The global behavior can be classified into two types: that with the coexistence state and that with no coexistence state. Our numerical simulations show that the former type can be seen for $f > f_T$, whereas the latter type can be seen for $f < f_T$. Figure 7 shows a typical example of

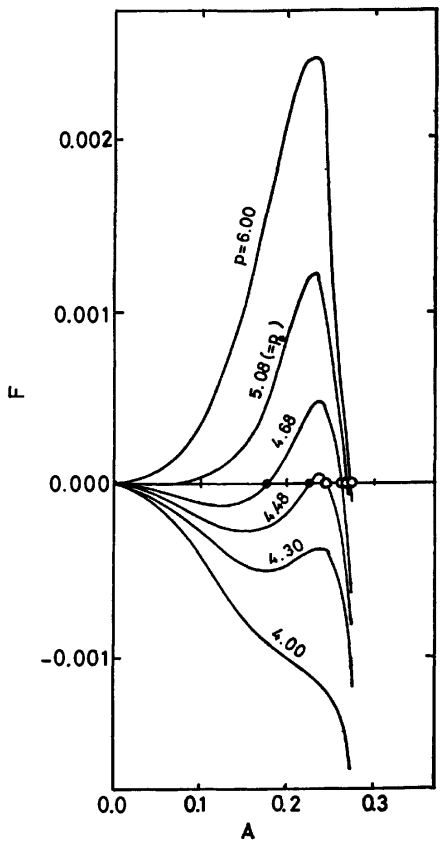

Fig. 7. Variations of amplitude expansion rate F with amplitude A of trajectory for q=0.05 and f=1.7795. (p_c=5.080, p_d=4,454, f_{c_2}=1.850, f_T=1.688) ●: Amplitude of unstable limit cycle, ○: amplitude of stable limit cycle.

the former type: f=1.7795 ($> f_T$=1.688) for q=0.05. Figure 8 shows one of the latter type: f=1.100 ($< f_T$). Here the problem arises of whether or not the coexistence

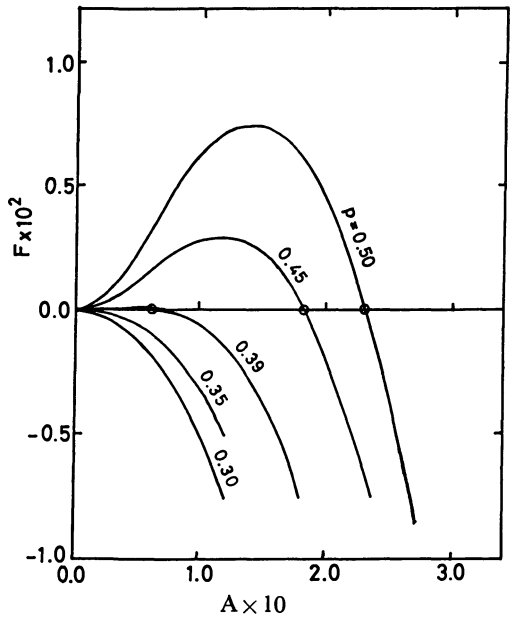

Fig. 8. Variation of amplitude expansion rate F with amplitude A of trajectory for $q=0.05$ and $f=1.100$. ($p_c=0.383$, $f_{c_1}=0.714$, $f_T=1.688$) ○: Amplitude of stable limit cycle.

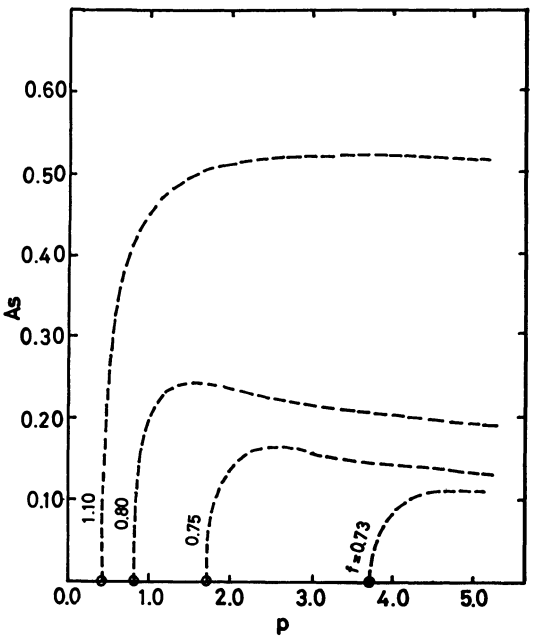

Fig. 9. Variations of amplitudes A_s (stable limit cycle) with parameters p and f for fixed $q=0.05$ ($f<1.100$, $f_T=1.688, f_{c_1}=0.714$).
------: Amplitude of stable limit cycle, ○: p_c.

state can exist for f near f_{c_1} in the range from f_{c_2} to f_{c_1} (the low-f side of the $f_{c_1}<f<f_{c_2}$ region). We conclude that there is no coexistence state on the low-f side of the region where case $q=0.05$. There are two reasons for deriving this conclusion. The first is the confirmation of the absence of an unstable limit cycle on the low-f side of the region, within the limits of accuracy of our numerical calculation by means of computer simulations. The second is the mode of the dependence of the amplitude, A_s, on p. Figures 8 and 9 show F and A_s in a no-coexistence state. In this case, the stable limit cycle (the broken line in Fig. 9) appears immediately above p_c. This kind of behavior of the amplitudes can be seen for all cases of $f<f_T$ and is quite different from the coexistence state ($f>f_T$). In the coexistence state, the unstable limit cycle (solid line) appears from p_c, and a stable limit cycle can also exist for p below p_c, as is shown in Fig. 4.

Janz *et al.*[5] have studied the steady state stability property in an attempt to investigate a coexistence state in a simple Oregonator. By simulations for $q=8.375\times 10^{-6}$, they have found two regions of the coexistence state: the low-f side and the high-f side of the region ($f_{c_1}<f<f_{c_2}$). The coexistence state investigated by us corresponds to the one on the high-f side of the region (the region of f near and below f_{c_2}). In fact, Janz *et al.* have found that the area of the coexistence state goes to zero as r exceeds a certain value††. This property is qualitatively the same as those which we have found. In our case, the boundary value of r is r_T. For $r>r_T$, the coexistence state disappears. We can not, however, find the coexistence state on the low-f side of the region for a high q ($q=5\times 10^{-2}$). The most reasonable explanation for these two inconsistent results is that the coexistence state on the low-f side disappears as q exceeds a certain value. Janz *et al.* have pointed out that the area of the coexistence state on the low-f side is about 1/10 times narrower than that on the high-f side. For example, the maximum value of Δf (the width of f for which the coexistence state has been observed) is only $\Delta f=0.038$ ($\Delta f/f_{c_1}=0.08$), whereas the maximum value of Δf on the high-f side is $\Delta f=0.38$ ($\Delta f/f_{c_2}=0.28$). This means that the area of the coexistence state on the low-f side is very small, even for a small q value ($q=8\times 10^{-6}$). This also suggests the disappearance of the coexistence state for a high q, and so the above explanation is reasonable.

Now we will show the qualitative change in the global behavior of the simple Oregonator model as determined by means of computer simulations. The global behavior can simply be expressed by the term "phase transition." The r_c (or p_c) and r_d (or p_d) quantities give the phase boundary, and the r_T point, the triple point. The phase corresponds to the number of limit cycles. The state with no limit cycle and one limit cycle is a single-phase state. The state with two limit cycles is the coexistence state of the two phases. This global behavior of the simple Oregonator model shows the type of statistical dynamic property. This property offers an important point of view from which to investigate the relations between the Oregonator model and other nonlinear, nonequilibrium systems.

References

1) R. J. Field and R. M. Noyes, *J. Chem. Phys.*, **60**, 1877

†† Janz *et al.* have used the k_5 parameter. The relation between k_5 and r is $r=k_5/(k_1A)$ (the notation of k_1, k_5, and A follows Janz *et al.*).

(1974).
2) J. J. Tyson, *J. Chem. Phys.*, **66**, 905 (1977).
3) S. Sakanoue and M. Endo, *Bull. Chem. Soc. Jpn.*, **55**, 1406 (1982).
4) L. D. Landau and E. M. Lifshitz, "Fluid Mechanics," Pergamon Press, London (1959), Chap. 27, p. 103.
5) R. D. Janz, D. J. Vanecek, and R. J. Field, *J. Chem. Phys.*, **73**, 3132 (1980).

 © 1983 The Chemical Society of Japan Bull. Chem. Soc. Jpn., 56, 2387—2389 (1983)

Kinetics of Gas Phase Addition Reactions of Trichlorosilyl Radicals. VIII. Reinvestigation of Addition to Ethylene

Takaaki DOHMARU* and Yoshio NAGATA
Radiation Center of Osaka Prefecture, Shinke-cho, Sakai, Osaka 593
(Received January 5, 1983)

The addition of $\cdot SiCl_3$ radicals to ethylene has been reinvestigated using a large conversion method. The amended values are $\log(k_3/k_5) = -0.17\pm0.05-(0.80\pm0.10)$ kcal mol^{-1}/2.303 RT and $\log\{k_{-5}/k_6$ (mol cm^{-3})$\} = 3.4\pm0.3-(22.5\pm0.7)$ kcal mol^{-1}/2.303 RT where the reactions involved are $\cdot SiCl_3 + CH_3COCH_3 \xrightarrow{3} (CH_3)_2\dot{C}OSiCl_3$, $\cdot SiCl_3 + C_2H_4 \underset{-5}{\overset{5}{\rightleftarrows}} \cdot CH_2CH_2SiCl_3$ and $\cdot CH_2CH_2SiCl_3 + HSiCl_3 \xrightarrow{6} C_2H_5SiCl_3 + \cdot SiCl_3$.

Silyl radical chemistry is now in the stage where any kinetic data leading to precise rate constants involving silyl radicals or silicon-containing compounds are in urgent need.

In the course of our kinetic study of addition of $\cdot SiCl_3$ radicals to olefins we found[1] that the A-factor of reaction (−5) for ethylene (see synopsis, $\log(A_{-5}/s^{-1}) = 12.8$) was too small compared with the ones for other 1-alkenes ($\log(A_{-5}/s^{-1}) = 14.8$—$16.3$. There is no convincing elucidation that the transition state of decomposition of the adduct radical for ethylene should be so tight while those for the other 1-alkenes are very loose. Further, transition state theory requires that $\log(A_{-5}/s^{-1}) \geq 13.4$.

In view of these facts we attempted to reinvestigate the addition to ethylene using a large conversion method (*vide infra*). In the previous study[2] there was a very small amount of impurity (possibly $(CH_3)_2CHOSiCl_2H$ by GC–MS analysis) which could not be separated completely from $C_2H_5SiCl_3$ by GLC analysis and which arised only when CH_3COCH_3 and $HSiCl_3$ were mixed. We purified CH_3COCH_3 but failed to reduce the amount of the impurity. Although we ascertained that the impurity itself did not participate in the reaction, it may have caused some systematic errors during the analytic process.

In this study we allowed the reaction to proceed to the extent that the yield of $C_2H_5SiCl_3$ is 10 times larger than the amount of the impurity.

Experimental

Materials and procedures are essentially similar to those described earlier.[2] Mixtures of CH_3COCH_3, C_2H_4, and $HSiCl_3$ were introduced into a cylindrical Pyrex cell of 137 cm^3 which was heated in an electric oven. The light source was a 50 W medium pressure mercury arc. After photolyzed, the reaction mixture was passed to a gas sampling loop and was immediately analyzed by GLC on a 2m SE 30 column.

Kinetic Equation. Photolysis of acetone in the presence of $HSiCl_3$ and C_2H_4 can be interpreted by the following chain reaction;[2] Eqs. 1 and 2, Eqs. 3 to 6, and Eqs. 7 to 9 are initiation, propagation and termination steps, respectively.

$$CH_3COCH_3(Ac) \xrightarrow{h\nu} 2\cdot CH_3 + CO \quad (1)$$

$$\cdot CH_3 + HSiCl_3(TCS) \longrightarrow CH_4 + \cdot SiCl_3 \quad (2)$$

$$\cdot SiCl_3 + CH_3COCH_3 \longrightarrow (CH_3)_2\dot{C}OSiCl_3 \quad (3)$$

$$(CH_3)_2\dot{C}OSiCl_3 + HSiCl_3 \longrightarrow (CH_3)_2CHOSiCl_3(A) + \cdot SiCl_3 \quad (4)$$

$$\cdot SiCl_3 + C_2H_4(Et) \rightleftarrows \cdot CH_2CH_2SiCl_3 \quad (5)$$

$$\cdot CH_2CH_2SiCl_3 + HSiCl_3 \longrightarrow C_2H_5SiCl_3(E) + \cdot SiCl_3 \quad (6)$$

$$2(CH_3)_2\dot{C}OSiCl_3 \longrightarrow \text{Products} \quad (7)$$

$$2\cdot CH_2CH_2SiCl_3 \longrightarrow \text{Producrs} \quad (8)$$

$$(CH_3)_2\dot{C}OSiCl_3 + \cdot CH_2CH_2SiCl_3 \longrightarrow \text{Products} \quad (9)$$

Assuming long reaction chains,[3] we obtain the following rate equation by the conventional steady state treatment of the scheme.

$$(R_A/R_E)([Et]/[Ac]) = (k_3/k_5)\{1 + (k_{-5}/k_6)[TCS]^{-1}\}, \quad (10)$$

where R, k, and [ ] have usual meanings of rate, rate constant, and concentration, respectively.

In a study where the conversion of the reactants can be kept small, we may make an approximation:

$$R_A/R_E = [A]/[E]. \quad (11)$$

Previously,[2] we used Eqs. 10 and 11 to obtain k_3/k_5 and k_{-5}/k_6.

When the conversion of the reactants can not be assumed small, however, we must find out an alternative to Eq. 11. Equation 10 itself applies at any time during the course of reaction, so the simplest solution to this problem is to obtain the initial rate ratio, *i.e.* $(R_A/R_E)_0$.

First-order approximation can be made to R_A and R_E, when reactant conversions are not very large.

Then, $$R_A/[Ac] = a_0 + a_1 t, \quad (12)$$

and $$R_E/[Et] = b_0 + b_1 t. \quad (13)$$

Here the problem is to evaluate a_0 and b_0. Integration of Eq. 12 gives

$$\ln([Ac]_0/[Ac]) = a_0 t + a_1 t^2/2. \quad (14)$$

From the mechanism we obtain

$$[\cdot SiCl_3] = (k_1/k_7)^{1/2}(k_4/k_3)[Ac]^{1/2}[TCS] \times \{[Ac]+[Et](\lambda_4/\lambda_6 p)\}^{-1}, \quad (15)$$

where λ is a kinetic chain length and p stands for $(R_A/R_E)([Et]/[Ac])$. On the other hand, $R_A/[Ac] = k_3[\cdot SiCl_3]$, so that

$$a_0 = k_4(k_1/k_7)^{1/2}[Ac]_0^{1/2}[TCS]_0 \times \{[Ac]_0 + [Et]_0(\lambda_4/\lambda_6 p)\}^{-1}, \quad (16)$$

and

$$a_1/a_0 = 1/t\left\{\frac{[Ac]^{1/2}[TCS]\{[Ac]_0+[Et]_0(\lambda_4/\lambda_6 p)\}}{[Ac]_0^{1/2}[TCS]_0\{[Ac]+[Et](\lambda_4/\lambda_6 p)\}} - 1\right\}. \quad (17)$$

Substitution of Eqs. 16 and 17 into Eq. 14 gives

$$a_0 = \frac{2}{t}\left\{\frac{[Ac]^{1/2}[TCS]\{[Ac]_0+[Et]_0(\lambda_4/\lambda_6 p)\}}{[Ac]_0^{1/2}[TCS]_0\{[Ac]+[Et](\lambda_4/\lambda_6 p)\}} + 1\right\}^{-1} \times \ln\frac{[Ac]_0}{[Ac]}. \quad (18)$$

An approximate value of p can be obtained using Eq. 11 and λ_4/λ_6 is easily calculated since $\lambda_4/\lambda_6=(k_4/k_6)(k_8/k_7)^{1/2}$, where log $(k_4/k_6)=-1.2$ kcal mol^{-1}/2.3 RT[1] and $(k_8/k_7)^{1/2}=1.04$ (calculated based upon the mass difference between the terminating radicals). Also a concentration of each reactant obeys the stoichiometric Eq. 19.

$$[\mathrm{Ac}]=[\mathrm{Ac}]_0-[\mathrm{A}]$$
$$[\mathrm{Et}]=[\mathrm{Et}]_0-[\mathrm{E}]$$
$$[\mathrm{TCS}]=[\mathrm{TCS}]_0-[\mathrm{A}]-[\mathrm{E}] \quad (19)$$

In the similar way b_0 can be derived using Eqs. 10, 12, and 13.

$$b_0=\frac{2}{t}\left[\frac{(a_0+a_1t)\{1+(k_{-5}/k_6)[\mathrm{TCS}]_0^{-1}\}}{a_0\{1+(k_{-5}/k_6)[\mathrm{TCS}]^{-1}\}}+1\right]^{-1}\ln\frac{[\mathrm{Et}]_0}{[\mathrm{Et}]} \quad (20)$$

An approximate value of k_{-5}/k_6 can be obtained from the plot of ([A]/[E])([Et]/[Ac]) *vs.* $[\mathrm{TCS}]^{-1}$. Thus we obtain a_0 and b_0. At the initial stage of reaction, Eq. 10 is expressed as

$$(R_\mathrm{A}/R_\mathrm{E})_0([\mathrm{Et}]_0/[\mathrm{Ac}]_0)=(k_3/k_5)\{1+(k_{-5}/k_6)[\mathrm{TCS}]_0^{-1}\}, \quad (21)$$

where $(R_\mathrm{A}/R_\mathrm{E})_0([\mathrm{Et}]_0/[\mathrm{Ac}]_0)=a_0/b_0$.
In this study we employed Eq. 21 to obtain k_3/k_5 and k_{-5}/k_6.

Results and Discussion

Mixtures of CH_3COCH_3, C_2H_4 and varying amounts of $HSiCl_3$ were photolyzed in the gas phase between 150 and 275 °C. Reaction conversions of C_2H_4 were *ca.* 10%. The results are shown in Table 1.

Table 1. Yields of the adducts in the photolysis[a] of mixtures of CH_3COCH_3, C_2H_4, and $HSiCl_3$

Temp °C	Time min	Reactant (μmol cm^{-3})			Product (μmol cm^{-3})	
		$[\mathrm{Ac}]_0$	$[\mathrm{Et}]_0$	$[\mathrm{TCS}]_0$	[A]	[E]
275	7	2.854	0.571	5.708	0.1410	0.0510
275	14	2.854	0.571	2.854	0.1444	0.0383
275	27	2.854	0.571	1.904	0.1828	0.0391
250	12	2.932	0.586	5.864	0.1483	0.0708
250	20	2.932	0.586	2.932	0.1208	0.0518
250	31	2.922	0.584	1.949	0.1290	0.0471
250	40	2.922	0.584	1.461	0.1212	0.0394
225	19	2.864	0.573	5.728	0.1553	0.0892
225	33	2.864	0.573	2.864	0.1311	0.0737
225	43	2.854	0.571	1.904	0.1128	0.0563
225	37	2.854	0.571	1.427	0.0714	0.0342
200	18	2.845	0.569	5.690	0.0976	0.0630
200	32	2.836	0.567	2.836	0.0853	0.0543
200	46	2.836	0.567	1.418	0.0566	0 0351
175	22	2.845	0.569	5.690	0.0714	0.0496
175	45	2.845	0.569	2.845	0.0712	0.0493
175	74	2.845	0.569	1.423	0.0577	0.0404
150	21	2.845	0.569	5.690	0.0421	0.0302
150	64	2.845	0.569	2.845	0.0643	0.0481
150	87	2.845	0.569	1.900	0.0583	0.0428

a) The volume of the cell was 137 cm^3 and the rate of absorption of light by 3 μmol cm^{-3} of acetone was *ca.* 7×10^{-12} einstein cm^{-3} min^{-1}.

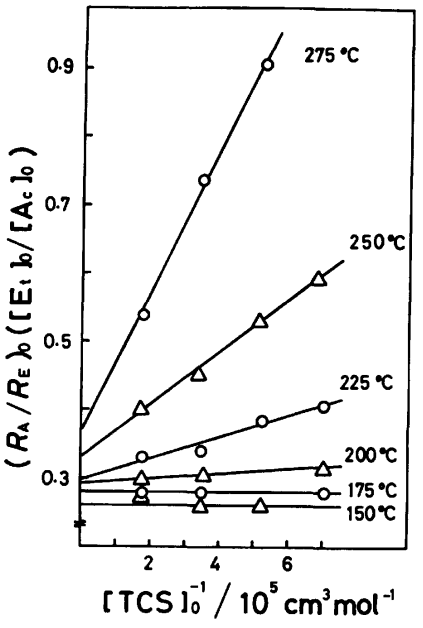

Fig. 1. Plot of Eq. 21.

The data in Table 1 were used to calculate $(R_\mathrm{A}/R_\mathrm{E})_0$, which are then plotted according to Eq. 21 (Fig. 1). The linearity of the plot at each temperature is excellent. Eq. 21 shows that the intercept of each line gives k_3/k_5 and its slope divided by the intercept value gives k_{-5}/k_6.

The least-mean-squares treatment of the Arrhenius plots of these rate constant ratios provides the Arrhenius parameters, which are shown in Table 2.

In Table 2 are compared the Arrhenius parameters obtained in this work with the previous values for 1-alkenes. The values of k_5/k_3 and k_{-5}/k_6 at 200 °C (middle temperature) in this work (3.5, 1.0×10^{-7} mol cm^{-3}) are in good agreement with those (3.2, 0.96×10^{-7} mol cm^{-3}) of the previous work.[2] Comparison of the values of log (A_{-5}/A_6) shows that the present value seems more reasonable, since there is no convincing

Table 2. Comparison of Arrhenius parameters with the previous values

	log (A_5/A_3)	$\frac{E_5-E_3}{\text{kcal mol}^{-1}}$	$\log\frac{A_{-5}/A_6}{\text{mol cm}^{-3}}$	$\frac{E_{-5}-E_6}{\text{kcal mol}^{-1}}$
Ethylene[a]	0.17 ± 0.05	−0.8 ± 0.1	3.4 ± 0.3	22.5 ± 0.7
Ethylene[b]	−0.14 ± 0.6	−1.4 ± 0.1	1.3 ± 0.4	18.0 ± 1.0
Propylene[c]	0.46 ± 0.09	−1.2 ± 0.04	3.3 ± 0.2	19.9 ± 0.4
1-Butene[c]	0.44 ± 0.05	−1.4 ± 0.1	3.8 ± 0.2	21.0 ± 0.4
1-Pentene[c]	0.51 ± 0.07	−1.4 ± 0.1	3.3 ± 0.6	19.6 ± 1.2
2-Methylpropene[c]	0.52 ± 0.41	−2.4 ± 0.8	4.8 ± 1.1	21.3 ± 2.3

a) This work. b) Ref. 2. c) Ref. 1.

elucidation that the transition state of only ethylene should be so tight while those of the other 1-alkenes are very loose.

References

1) T. Dohmaru and Y. Nagata, *J. Chem. Soc., Faraday Trans. 1*, **75**, 2617 (1979).

2) T. Dohmaru, Y. Nagata, and J. Tsurugi, *Chem. Lett.*, **1973**, 1031.

3) Since the rate of absorption of light was kept very small, *ca.* 7×10^{-12} einstein cm^{-3} min^{-1}, the kinetic chain length at the lowest temperature would exceed 50.

Electric Field Orientation of Poly(*p*-styrenesulfonate) and Its 9-Aminoacridinium Complex as Studied by Square-pulse Transient Electric Birefringence

Kiwamu YAMAOKA* and Kazuyoshi UEDA

Faculty of Science, Hiroshima University, Higashisenda-machi, Naka-ku, Hiroshima 730

(Received January 20, 1983)

Electric birefringence was measured at 20 °C and at 535 nm for sodium poly(*p*-styrenesulfonate) (NaPSS), with and without added sodium chloride, and the 9-aminoacridinium (AA) complex in aqueous solutions. The field strength dependence of both the steady-state EB ($\Delta n(\infty)$) and the field-free decay time ($\langle\tau\rangle_{EB}$) was examined. Charge suppression by added Na^+ ions or neutralization by strongly bound AA decreased both $\Delta n(\infty)$ and $\langle\tau\rangle_{EB}$ considerably, altering not only the optical factor Δg and electric moments, but also the backbone chain length. The weight-average values of chain length (l_w), pseudopermanent dipole moment (μ_w), counterion-induced electric polarizability anisotropy ($\Delta\alpha_w$), and the length-independent values of Δg were estimated by analyzing the experimental data on the basis of the "classical" orientation function which takes into account the continuous distribution of chain length for the polydisperse NaPSS sample. The electric field orientation of NaPSS and the AA-complex could be described by the interaction between an applied field and the electric moment which transforms from counterion-induced type in the extremely low field region (<1.5 kV/cm) to saturated induced permanent type at higher fields.

Among synthetic vinyl polymers, poly(*p*-styrenesulfonate) (NaPSS) has been employed as a model polyelectrolyte in many physicochemical studies.[1-12] These studies indicate that the PSS chain is stiff and may be represented by a rodlike model. A recent electric dichroism study showed that the ionized NaPSS can be oriented by an external electric field, exhibiting a negative dichroism of considerable magnitude, and that the *p*-sulfonatophenyl chromophores are arranged nearly at 60° relative to the PSS backbone chain.[10] Earlier, Yoshioka and his coworkers[2,3,7] extensively studied the electric birefringence of the potassium salt of PSS (KPSS) in aqueous solutions with various additives; they found that the field orientation of KPSS may be described as being due to the permanent dipole moment. Very recently, Tricot and Houssier[11] reported a careful work on the electric birefringence of some NaPSS fractions, finding that the birefringence (Δn) curve fits a pure induced dipole orientation. These two groups are mostly concerned with the field strength dependence of the steady-state data. We believe that the solution property of PSS polyions should also be deduced from the result obtained by transient electrooptical techniques.

The objectives of this work are (1) to show that the field orientation mechanism of the chain of NaPSS in salt-free solution can be described in terms of a transformation of the electric polarizability to a permanent-like moment, by analyzing the field strength dependence of the steady-state Δn; (2) to exemplify that the weight-average chain length (hence, the overall shape) may be estimated from the field strength dependence of the field-free relaxation times with a reasonable model by taking into account the polydispersity of the sample; (3) to demonstrate that the PSS backbone chain can be contracted significantly due to partial neutralization or suppression of the negative charge on the sulfonato group by monovalent cationic additives; (4) to simulate the rise and decay portions of a transient signal in the Kerr-law region, in order to support the notion that the field orientation is due to fast counterion-induced dipole moment.[8,12] These objectives were successfully achieved by the method of fast square-pulse transient electric birefringence.

Experimental

Materials. Sodium poly(*p*-styrenesulfonate) (NaPSS) is the same sample that was used in previous studies.[8,10,13] The original sample (KPSS) was a generous gift of Professor Koshiro Yoshioka of the University of Tokyo. The degree of polymerization was estimated to be 1360.[10] 9-Aminoacridinium chloride (denoted simply as AA), a strongly binding monocationic dye, was described elsewhere.[10,13]

Preparation of Sample Solutions. The salt-free NaPSS solution was prepared by dissolving an anhydrous sample in twice-distilled water. The NaCl-added NaPSS solution was prepared by adding an appropriate amount of NaCl to the stock NaPSS solution, the ratio of the total Na^+ ions to the counterion Na^+ being 6.00. The AA-added NaPSS solution was prepared in a similar manner. The ratio of the polymer residue to AA finally present in the mixture (denoted as P/D)[10,13] is 6.14. The concentration of NaPSS in the monomer unit is 0.66 mM (1 mM = 1×10^{-3} mol dm^{-3}) in all cases.

Measurements. Square-pulse electric birefringence was measured on an apparatus built in this Laboratory.[10,14] The pulse width was continuously variable up to 5 ms and the pulse amplitude was varied up to 11.3 kV/cm. A 1-cm long H-shaped Kerr cell made of Kel-F was used, the electrode gap being 0.207 cm. Instrumental time constants were less than 0.5 μs for the transient rise and decay signals. The phase retardation, δ, in degrees was measured at 535 nm and at 20 °C, the sign being determined with a quarter-wave plate.

Analysis of Data. The steady-state birefringence Δn and the specific Kerr constant, B/c, are defined as[14]

$$\frac{B}{c}=\lim_{E^2\to0}\frac{\Delta n}{\lambda c}\left(\frac{1}{E^2}\right)=\lim_{E^2\to0}\frac{\delta}{2\pi dc}\left(\frac{1}{E^2}\right), \quad (1)$$

where λ is the wavelength *in vacuo*, c is the mass concentration in g/cm^3, and d is the optical path length (= 1 cm). Since the theoretical treatments of the field orientation of polyelectrolytes are under development, no complete expression for the transient electric birefringence is available as yet. Under these circumstances, the "classical" theory for nonconducting rodlike macromolecules of axial symmetry should be utilized.[15] This theory is nevertheless known to be an adequate approximation for NaPSS in aqueous solutions.[2,3,7,10,11] For a polydisperse

polymer sample, the steady-state birefringence, $\Delta n(\infty)$, at an arbitrary electric field strength E is given as[16-18]

$$\Delta n(\infty) = \frac{2\pi \bar{C}_v}{n}(g_3 - g_1)\langle \Phi(\beta(l), \gamma(l))\rangle_w, \quad (2)$$

where n is the refractive index of the solution, $\bar{C}_v$ is the volume fraction of the solute, (g_3-g_1) is the optical anisotropy factor, $\langle \Phi(\beta,\gamma)\rangle_w$ is the weight-average orientation function, $\beta(l)=\mu(l)E/kT$, and $\gamma(l)=\Delta\alpha(l)E^2/2kT$. In the low electric field region where the Kerr law holds, the rise portion of the normalized transient signal is expressed by

$$\frac{\Delta n(t)}{\Delta n(\infty)} = 1 - \frac{\int_0^\infty \Delta n(\infty, l)\left\{\frac{3\beta(l)^2 e^{-2\theta_{11}(l)t} - [\beta(l)^2 - 4\gamma(l)]e^{-6\theta_{11}(l)t}}{2[\beta(l)^2+2\gamma(l)]}\right\} dl}{\int_0^\infty \Delta n(\infty, l) dl}, \quad (3)$$

where θ_{11} is the rotary diffusion coefficient of the undeformable molecule around the transverse axis, $\Delta n(\infty,l)=(2\pi\bar{C}_v/15n)(g_3-g_1)\times\phi(l)[\beta(l)^2+2\gamma(l)]$, $\phi(l)$ is the fraction of solute molecules with the length l, and $\Delta n(0)=\Delta n(\infty)$. The decay portion is expressed by

$$\frac{\Delta n(t)}{\Delta n(0)} = \frac{\int_0^\infty \Delta n(0, l)e^{-6\theta_{11}(l)t} dl}{\int_0^\infty \Delta n(0, l) dl}. \quad (4)$$

Results and Discussion

Dependence of Steady-state Birefringence on Electric Field. Figure 1 shows the dependence of phase retardation, δ, on electric field strength for NaPSS solutions with and without additives. The charge suppression of the ionized sulfonato group by added Na^+ decreases the magnitude of δ. More remarkably, the charge neutralization of the same group (one out of six) by bound AA cations diminishes the values of δ nearly tenfold. In order to ascertain if these decreases in δ are due solely to the change in the optical anisotropy factor in Eq. 2, the δ *vs.* E^2 curves of the NaPSS–AA and NaPSS–NaCl systems were multiplied by factors at an arbitrarily selected field strength ($E^2=10$ (kV/cm)^2). As indicated in Fig. 1, the NaPSS–AA and NaPSS–NaCl curves cross at this point, but otherwise they do not coincide with the salt-free NaPSS curve. This behavior suggests that the electric part in Eq. 2 is also affected; hence, the electric moment of the salt-free NaPSS chain should also be decreased by the addition of NaCl or AA.

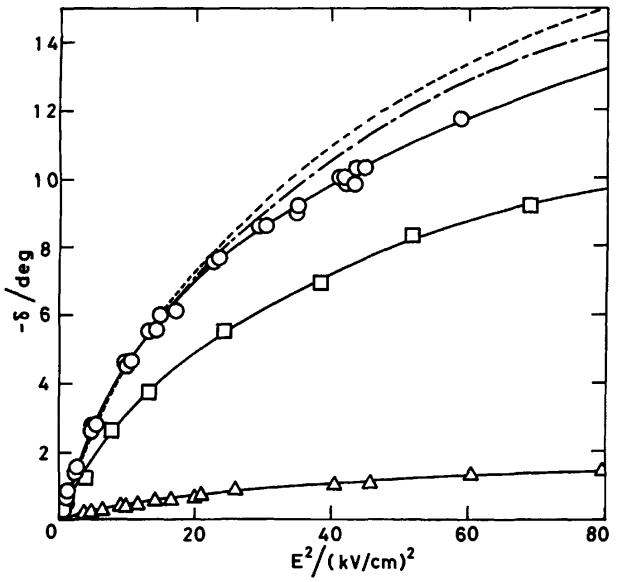

Fig. 1. The dependence of steady-state birefringence, δ, on the square of electric field strength, E^2, for the salt-free NaPSS (○), the NaPSS–NaCl (□), and the NaPSS–AA (△) solutions. The residue concentration of NaPSS is 0.66 mM in these cases. The dashed (– – –) line represents the NaPSS–AA curve which is multiplied by a factor of 10.3 at a field strength ($E^2=10$ (kV/cm)^2), while the dash-dot-dashed (—·—) line is the NaPSS–NaCl curve multiplied by 1.47.

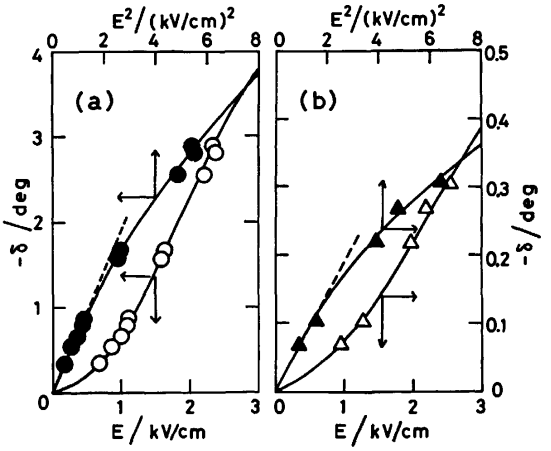

Fig. 2. The linear and quadratic dependence of δ on field strength in the low field region. (○, ●) for NaPSS and (△, ▲) for NaPSS–AA. The dashed lines indicate a linear dependence of δ on E^2 at limiting low fields.

Low Electric Field Behavior and the Kerr Constant. Figure 2 shows the values of δ in the low electric field region for the NaPSS and NaPSS–AA solutions. They

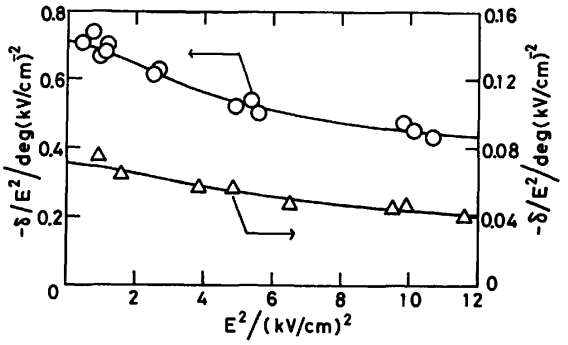

Fig. 3. Plots of the phase retardation per square of field strength, δ/E^2, against the square of field strength for NaPSS (○) and NaPSS–AA (△). The values extrapolated to zero field strength, $(-\delta/E^2)_{E\to 0}$, are 0.701 deg(cm/kV)^2 for NaPSS and 0.071 deg(cm/kV)^2 for NaPSS–AA.

TABLE 1. ELECTROOPTICAL AND HYDRODYNAMIC PROPERTIES OF NaPSS WITH AND WITHOUT IONIC ADDITIVES

Samples	B/c 10^{-6} cm^4 V^{-2} g^{-1}	$\langle\tau\rangle_w$ μs	l_w Å	μ_w 10^3 D[b]	$\Delta\alpha_w$ 10^{-15} cm^3 [c]	(g_3-g_1)[a] $\times 10^2$
NaPSS	14.2	35	1210	6.48	1.32	−1.2
NaPSS–NaCl	—	20	980	5.65	—	−0.98
NaPSS–AA	1.44	10	760	5.12	0.99	−0.16

a) A value of 0.565 was used for the partial specific volume of NaPSS in water.[11] b) 1 D$=3.336\times10^{-30}$ C m.
c) 1 cm$^3=1.113\times10^{-16}$ F m^2.

are plotted against E and also against E^2. The linear dependence of δ on the second power of the field strength is clear. It is thus evident that the Kerr law holds for the 0.66 mM NaPSS solutions with and without ionic additives.

Figure 3 shows the procedure for determining the Kerr constant. The observed values of δ/E^2 are plotted against E^2. The values extrapolated to zero field strength yield the Kerr constant B. The specific Kerr constant is given in Table 1. It should be noted that the extrapolation is inevitably associated with a small uncertainty, since the curvature of the δ/E^2 *vs.* E^2 curve depends on the electric property of a particular polymer system (*cf.* Fig. 7).[15]

Dependence of Decay Process on Electric Field. Since the field-free decay curves of the 0.66 mM NaPSS solution indicate that the sample is polydisperse,[12] the relaxation time must be the birefringence-average quantity obtained by area method[19] (*e.g.*, Eq. 6 in Ref. 17), $\langle\tau\rangle_{EB}$, which depends on the field strength of a pulse applied to orient the solute prior to the start of the decay process.[16,19] Figure 4 shows a large field dependence of $\langle\tau\rangle_{EB}$ for the salt-free NaPSS system; a clear indication of the polydispersity of molecular length.[10,16] It should be noted that the addition of NaCl or AA decreases the relaxation time considerably; unfortunately, the values of $\langle\tau\rangle_{EB}$ are scattered or undetermined at low electric fields due to low signal-to-noise ratios. The $\langle\tau\rangle_{EB}$ value at infinitely high electric field reduces to the weight-average relaxation time $\langle\tau\rangle_w$

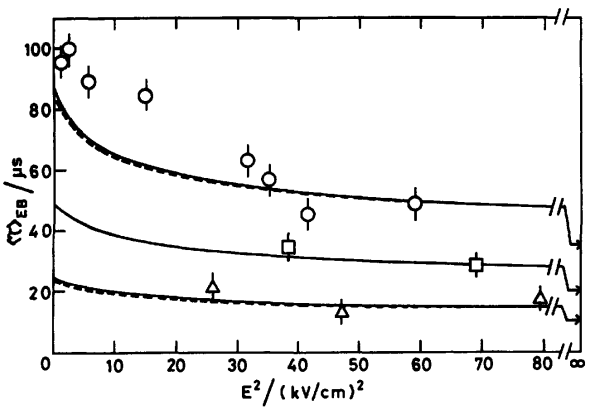

Fig. 4. The dependence of field-free relaxation time, $\langle\tau\rangle_{EB}$, on electric field strength applied prior to the start of decay process. (○) for NaPSS, (□) for NaPSS–NaCl, and (△) for NaPSS–AA. Horizontal arrows indicate the values extrapolated to infinite field strength. Points are experimental and smooth curves are theoretical.

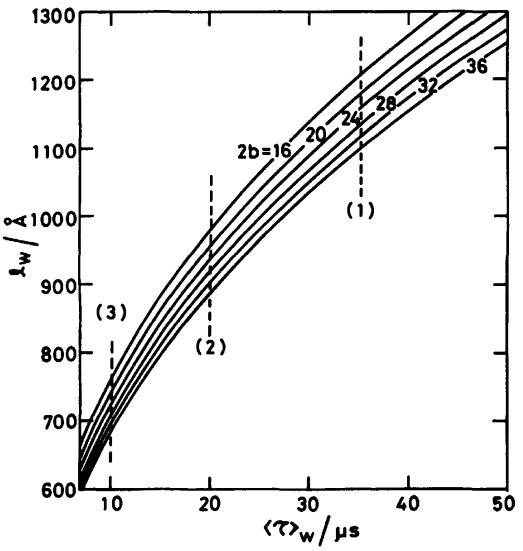

Fig. 5. Relationship between the weight-average length, l_w, and the weight-average relaxation time, $\langle\tau\rangle_w$, calculated for a polydisperse sample. The Schulz-Zimm distribution function was used to describe the polydispersity ($l_w/l_n=1.3$). The diameter of a molecule with length l was changed from 16 Å to 36 Å to calculate the value of $\langle\tau\rangle_w$ by using the Broersma equation. Vertical lines indicate the experimentally obtained values of $\langle\tau\rangle_w$ for salt-free NaPSS (1), NaCl-added NaPSS (2), and AA-added NaPSS (3).

(Eq. 9 in Ref. 17), which is independent of the electric parameters of the molecules, since the orientation function $\langle\Phi\rangle_w$ approaches unity. The values of $\langle\tau\rangle_w$ for the NaPSS, NaPSS–NaCl, and NaPSS–AA systems are given in Table 1.

Weight-average Relaxation Time and Chain Length. The overall shape of the PSS backbone chain may be assumed to be an undeformable cylinder in the sense that an applied electric field does not alter the molecular conformation. This is a reasonable approximation, when the field strength is less than 19 kV/cm for NaPSS and NaPSS–AA.[10,20] The rotational relaxation time $\tau(l)$ is related to the length l with the aid of the Broersma equation for a cylindrical model[21] (*e.g.*, Eq. 8 in Ref. 17). The diameter of the cylinder, $2b$, is not known for the present NaPSS system; therefore, it must be varied parametrically. The axial translation per residue of the most elongated PSS backbone is *ca.* 2.5 Å. It shortens to about 2.0 Å without changing the diameter appreciably; hence, the elongated chain length is in the range of 3400—2700 Å. The diameter of this rather stretched backbone is estimated to be at least 16 Å with CPK atomic models, if the *p*-sulfonatophenyl groups

wind around the backbone. If a folding of hair-pin type occurs in the backbone chain, the diameter may be widened, from 16 Å to 24 Å (radius times three) and further to 32 Å (radius times four). By varying the diameter $2b$ from 16 Å to 36 Å at intervals of 4 Å, the weight-average length l_w was calculated as a function of $\langle\tau\rangle_w$. The results are shown in Fig. 5, where the vertical dashed lines indicate the experimental values of $\langle\tau\rangle_w$ for the salt-free NaPSS (1), NaPSS–NaCl (2), and NaPSS–AA (3) solutions. The length l_w of the salt-free NaPSS ranges from 1200 Å ($2b$=16 Å) to 1100 Å ($2b$=36 Å), being affected only slightly by these diameters. These lengths are far shorter than the most extended chain length (3400 Å); hence, the folding-back of the vinyl backbone is evident. If a value of 16 Å is assumed for $2b$, the chain length l_w is 1210 Å for the salt-free NaPSS, 980 Å for the NaPSS–NaCl, and 760 Å for the NaPSS–AA. Thus, the binding of AA probably reduces the overall chain length appreciably.

An entirely different approach to the interpretation of the rotary diffusion coefficient $\theta_{11}(=(6\tau)^{-1})$ is possible. By adopting a flexible wormlike model, the persistence length of a polymer chain could be estimated from Hearst's[22] expression, which, however, introduces an additional parameter. This in turn means that to avoid ambiguities the polymer sample should be nearly monodisperse as regards the molecular weight. Thus, the flexibility of the polymer chain is an interesting subject for future studies.

Orientation Mechanism and Electric Moments. The orientation mechanism of the NaPSS in aqueous solution may be deduced from the electric field dependence of steady-state Δn (*cf.* Fig. 1). Yoshioka and his coworkers showed that the dependence can be best fitted by the permanent dipole orientation over a limited range of field strength.[2,3,7] Recently, Tricot and Houssier also studied the field dependence for NaPSS, confirming this permanent dipole orientation.[11] In addition, they believe that the induced dipole moment may also be adequate to describe the field dependence. In an electric dichroism study of NaPSS, Matsuda and Yamaoka have shown that, by taking into account a polydispersity in chain length, the field dependence can be best fitted by a mixed dipole orientation with the ratio $(\beta_w)^2/2\gamma_w$ of 8 over a very wide field strength range.[10] They also pointed out that, if the polydispersity is ignored, the dependence can be described equally well by the permanent dipole (*i.e.*, β-term only) orientation. In either case, Matsuda and Yamaoka have indicated that the fitting between the theoretical orientation function $\Phi(\beta)$ or $\langle\Phi(\beta)\rangle_w$ and the experimental points is poor in the very low field region.

With the above background, we can now analyze the field dependence of Δn. It is unrealistic to consider that the ionized PSS backbone bears a true permanent dipole moment of large magnitude. By now, ample evidence from reversing-pulse electric birefringence (PREB) indicates that the field orientation of NaPSS is not due to the permanent dipole but due to the counterion-induced dipole moment.[8,12] The redistribution of the counterions (Na^+) responsible for the induced dipole moment is faster than 10^{-6} s. We now demonstrate that the orientation of NaPSS results from the interaction between an external electric field and the ionic polarizability of the polyion in a limited, very low field region, in analogy to the pure electronic polarizability orientation for a nonconducting polymer, and that the interaction transforms gradually to a type between the field and an apparent permanent dipole moment. Theoretical treatments on this concept of induced dipole-permanent dipole transformation have lately appeared,[23,24] but further refinements are needed to fit experimental data over an entire field range.[10]

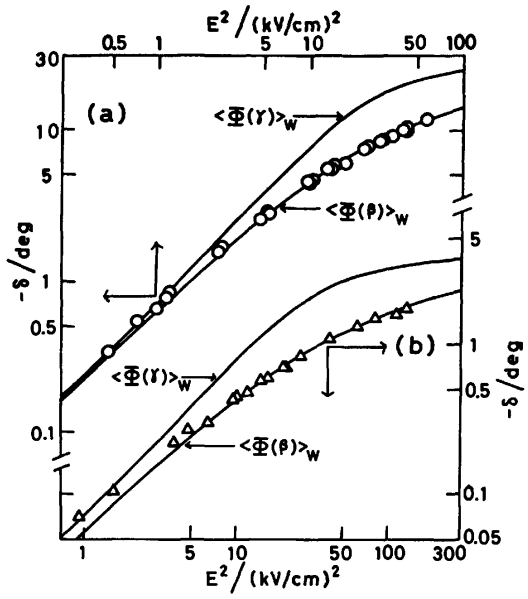

Fig. 6. Double logarithmic plots of the steady-state phase retardation *vs.* electric field strength and the theoretical orientation function, $\langle\Phi\rangle_w$. (a) Salt-free NaPSS (○) for which δ is $-29°$ at limiting high field, $\Delta a_w = 1.32\times 10^{-15}$ cm³, and μ_w=6480 D. (b) AA-added NaPSS (△) for which δ is $-3.9°$ at limiting high field, $\Delta a_w = 0.99\times 10^{-15}$ cm³, and μ_w=5120 D. $2b$=16 Å.

Experimental values of δ for NaPSS and NaPSS–AA in Fig. 1 have been replotted against E^2 on a double logarithmic scale in Fig. 6. With the parameters l_w, obtained in the preceding section, $l_w/l_n(=1.3)$, and the Schulz-Zimm distribution function[25,26] (*e.g.*, Eq. 3 in Ref. 17), the orientation functions for pure polarizability anisotropy $\langle\Phi(\gamma)\rangle_w$ and for pure permanent dipole moment $\langle\Phi(\beta)\rangle_w$ were calculated. The observed points were fitted to these functions under the assumption that the orientation mechanism transforms from the pure polarizability anisotropy γ_w in the extremely low electric field region to the pure permanent dipole moment β_w over a wide medium-to-high field range. The best-fitted orientation functions are shown with solid-lined curves in Fig. 6. In this matching procedure, both functions are adjusted to yield the same optical anisotropy factor, since this is considered to be independent of field strength.[10,18,27] The values of μ_w, Δa_w, and (g_3-g_1), all obtained from the fitting, are given in Table 1.

The pure γ_w-orientation is considered to be equivalent to the counterion-induced or ionic polarizability, while the pure β_w-orientation is equivalent to the saturated

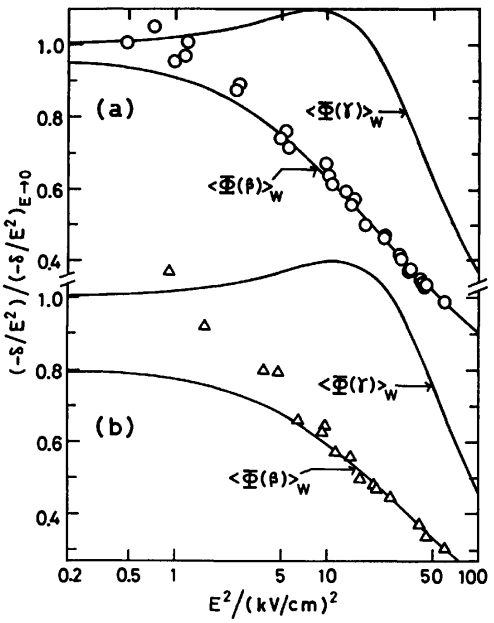

Fig. 7. Semilogarithmic plots of $(-\delta/E^2)/(-\delta/E^2)_{E\to 0}$ *vs.* E^2. Experimental values are given by circles for salt-free NaPSS (a) and by triangles for AA-added NaPSS (b), and theoretical curves by solid lines. Notations, parameters, and other conditions are all the same as those in Fig. 6.

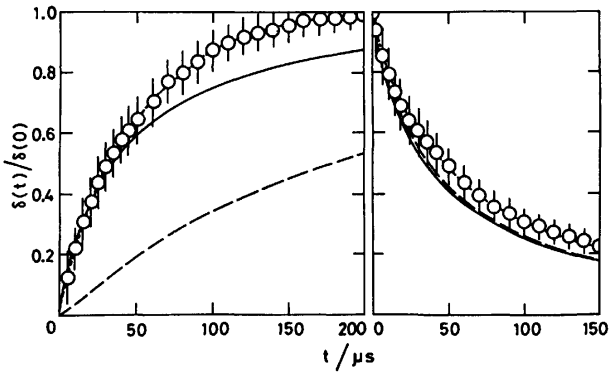

Fig. 8. Comparison of an experimental rise-and-decay signal for salt-free NaPSS with theoretically calculated transient curves. Experimental points are read from an oscillogram taken at a field strength of 1.01 kV/cm. The solid-lined curve is the theoretical one calculated on the basis of the orientation function for pure polarizability with a set of parameters ($l_w/l_n=1.3$, $l_w=1480$ Å, $2b=16$ Å) which yields the z-average relaxation time, $\langle\tau\rangle_z$, of 100 μs. The dash-lined curve is the theoretical one for pure permanent dipole orientation calculated with a set of parameters ($l_w/l_n=1.3$, $l_w=1270$ Å, $2b=16$ Å) which yields the $(z+1)$-average relaxation time, $\langle\tau\rangle_{z+1}$, of 100 μs.

induced-dipole moment. In conformity with classical theory, both the ionic polarizability and the saturated dipole moment are assumed to be proportional to the first power of the length. The dependence of these moments on the chain length remains to be explored more thoroughly in the future. In any case, it is clear that deviation from the pure γ_w-orientation appears at extremely low fields ($E<1.5$ kV/cm) for NaPSS and NaPSS–AA. This explains the previous observations that the pure permanent dipole orientation is the most appropriate one for the ionized NaPSS solution.[7,10,11]

Theoretical calculations have shown that a maximum appears in the birefringence per field strength ($\Delta n/E^2$) *vs.* E^2 curve, if the pure γ_w-orientation is the case.[15] In Fig. 7, the theoretical orientation functions, $\langle\Phi(\beta)\rangle_w$ and $\langle\Phi(\gamma)\rangle_w$, per (field strength)^2 are plotted by solid-lined curves. The observed points definitely deviate from the pure γ_w-curve, transforming to the pure β_w-curve already in the extremely low field strength region, before they reach the maximum position of the theoretical curve for the pure γ_w-orientation.

Once the values of μ_w and $\Delta\alpha_w$ are obtained from the above matching, the field strength dependence of $\langle\tau\rangle_{EB}$ shown in Fig. 4 may be examined theoretically. In this Figure are shown the theoretical curves which were calculated by assuming the pure permanent dipole moment orientation and the Schulz-Zimm distribution function. The parameters ($2b$, l_w, μ_w) are as follows: (16 Å, 1210 Å, 6480 D (1 D$=3.336\times10^{-30}$ C m)) for solid line and (32 Å, 1120 Å, 6480 D) for dashed line in the case of the salt-free NaPSS, (16 Å, 980 Å, 5650 D) for the NaCl-added NaPSS, (16 Å, 760 Å, 5120 D) for solid line and (32 Å, 700 Å, 5120 D) for dashed line in the case of the AA-added NaPSS; the viscosity of solvent is 1.009×10^{-3} Pa s. These theoretical curves are in fair agreement with experimental points, particularly, in the medium-to-high field region.

Simulation of the Rise and Decay Processes. In order to confirm the notion that the counterion-induced electric moment is fast as compared with the overall molecular rotation and that this moment can be approximated by the electronic polarizability, two theoretical transient curves for the rise and decay signal are calculated from Eqs. 3 and 4 in Fig. 8: one for the pure γ_w-orientation (solid line) and the other for the pure β_w-orientation (dashed line). In the Figure, the experimental points represent a signal of an NaPSS solution, taken at a low field strength for which the Kerr law holds. The points fit the γ_w-orientation curve better than the β_w-curve in the whole rise and decay process. This may be taken as a strong support for the notion that the orientation of NaPSS results from the fast counterion-induced dipole moment, whose induction is much faster than the overall molecular orientation. At the same time, the result in Fig. 8 indicates the limitation of the use of the classical orientation function derived for nonconducting rodlike macromolecules to an ionized polyion like NaPSS. It is clear from the present work that a further study is desirable to obtain more realistic orientation functions which can describe the electric field orientation of ionized polyelectrolytes.

Conclusion

Although the present NaPSS sample is polydisperse as regards the molecular weight, we could present a unified quantitative treatment of the ionized polyion, which possesses no permanent dipole moment, on the

framework of the classical theory for nonconducting polymers. The electric field orientation of NaPSS is due to the ionic polarization which results from the redistribution of counterions on the PSS chain surface. This counterion-induced electric moment saturates at very low electric fields and then behaves as if it was a permanent dipole moment. In conjunction with our previous work on electric dichroism[10] and reversing-pulse electric birefringence,[8,12] we believe that the solution conformation of the NaPSS and NaPSS–AA systems are now established fairly well, and that the dynamic electrooptical techniques are of great assistance in interpreting the electric properties and solution conformation of field-orientable macromolecules.

References

1) K. F. Wissbrun and A. Patterson, Jr., *J. Polym. Sci.*, **33**, 235 (1958).
2) H. Nakayama and K. Yoshioka, *Nippon Kagaku Zasshi*, **85**, 177 (1964).
3) H. Nakayama and K. Yoshioka, *J. Polym. Sci. Part A*, **3**, 813 (1965).
4) A. Takahashi, T. Kato, and M. Nagasawa, *J. Phys. Chem.*, **71**, 2001 (1967).
5) A. Minakata, *Biopolymers*, **11**, 1567 (1972).
6) M. Nagasawa, I. Noda, T. Takahashi, and N. Shimamoto, *J. Phys. Chem.*, **76**, 2286 (1972).
7) K. Kikuchi and K. Yoshioka, *J. Phys. Chem.*, **77**, 2101 (1973).
8) K. Yamaoka and K. Ueda, *J. Phys. Chem.*, **84**, 1422 (1980).
9) A. Yamagishi and F. Watanabe, *J. Phys. Chem.*, **85**, 2129 (1981).
10) K. Matsuda and K. Yamaoka, *Bull. Chem. Soc. Jpn.*, **55**, 69 (1982).
11) M. Tricot and C. Houssier, *Macromolecules*, **15**, 854 (1982).
12) K. Yamaoka and K. Ueda, *Chem. Lett.*, **1983**, 545.
13) K. Yamaoka, M. Takatsuki, and K. Nakata, *Bull. Chem. Soc. Jpn.*, **53**, 3165 (1980).
14) K. Yamaoka and K. Ueda, *J. Phys. Chem.*, **86**, 406 (1982).
15) C. T. O'Konski, K. Yoshioka, and W. H. Orttung, *J. Phys. Chem.*, **63**, 1558 (1959).
16) K. Yamaoka and K. Fukudome, *Bull. Chem. Soc. Jpn.*, **56**, 60 (1983).
17) K. Matsuda and K. Yamaoka, *Bull. Chem. Soc. Jpn.*, **55**, 1727 (1982).
18) M. Matsumoto, H. Watanabe, and K. Yoshioka, *Biopolymers*, **9**, 1307 (1970).
19) K. Yoshioka and H. Watanabe, *Nippon Kagaku Zasshi*, **84**, 626 (1963).
20) A numerical error is involved in lines below Eq. 4 in Ref. 10, where the value of 14 kV/cm should be applicable only to the 0.133 mM NaPSS solution.
21) S. Broersma, *J. Chem. Phys.*, **32**, 1626 (1960).
22) J. E. Hearst, *J. Chem. Phys.*, **38**, 1062 (1963).
23) K. Kikuchi and K. Yoshioka, *Biopolymers*, **15**, 583 (1976).
24) K. Yoshioka and K. Takakusaki, *Int. J. Biol. Macromol.*, **4**, 123 (1982).
25) G. V. Schulz, *Z. Phys. Chem.*, **B43**, 25 (1939).
26) B. H. Zimm, *J. Chem. Phys.*, **16**, 1099 (1948).
27) K. Yamaoka and K. Matsuda, *Macromolecules*, **14**, 595 (1981).

Effects of Pressure on Dielectric Relaxation in Supercooled Triphenylchloromethane-*o*-Terphenyl Solution

Motosuke NAOKI* and Manabu MATSUSHITA
Department of Textiles and Polymers, Faculty of Technology, Gunma University, Kiryu, Gunma 376
(Received February 2, 1983)

Dielectric measurements have been made as a function of frequency, temperature, and pressure on a binary mixture of triphenylchloromethane and *o*-terphenyl in its supercooled liquid region. Since the distribution of relaxation time is independent of temperature and pressure in the present experimental range, the time-temperature-pressure superposition is accurately applied. The activation parameters such as the activation enthalpy at constant pressure, H^*_P, the activation enthalpy at constant volume, H^*_V, and the activation volume V^* are obtained as a function of temperature and pressure. H^*_V is only half H^*_P unlike polymer liquids and associated liquids such as alcohols. V^* as well as the pressure coefficient of temperature at constant relaxation time τ, $(\partial T/\partial P)_\tau$, is similar in magnitude to that of polymer liquids and larger than that of associated liquids. These facts have revealed the contributions of inter- and intramolecular interactions to the molecular mobility in the supercooled liquid. $(\partial T/\partial P)_\tau$ coincides with the pressure coefficient of the glass transition temperature, dT_g/dP. This gives a statement that the glass transition temperature in simple normal liquids, as well as in polymer liquids, is an isorelaxation-time state.

The molecular mobility associated with the Brownian motion in simple liquids or with the micro-Brownian motion in polymer liquids is observed as a relaxation process at the audio- and radio-frequency range in the supercooled liquid region. The molecular mobility in the supercooled liquids is closely related to the glass transition[1,2] and the glassy state,[3-5] and the study of the relaxation process may make an important contribution to our understanding of the liquid state.

The secondary relaxation process pertaining to the local mode of motions governed by the localized energy field exists in the liquid state as well as in the glassy state,[6,7] and it merges the primary process pertaining to the Brownian motion at high frequency in elevated temperature region.[8,9] In the supercooled liquid region, however, the two processes are well separated from each other and their relaxation spectra can readily be obtainable.[6]

The introduction of pressure as a variable to the study in the molecular mobility makes primarily the role of volume in the relaxation process clear.[10] Analyses of the pressure effects on the dielectric relaxation have been reported in large numbers for associated liquids such as alcohols[11] and polymer liquids,[12-15] but a few for simple normal liquids such as short alkanes and benzene derivatives.[16] From the analysis of the viscosity of many liquids under elevated pressures above the melting temperature, MacKenzie has obtained that the activation enthalpy at constant volume, H^*_V, is only a small fraction of the activation enthalpy at constant pressure, H^*_P, in simple normal liquids, but H^*_V is almost equivalent to H^*_P in associated liquids.[17] H^*_P is given by

$$H^*_P = R\left[\frac{\partial \ln \tau}{\partial (1/T)}\right]_P, \quad (1)$$

as far as the empirical activation equation:

$$\tau = A \exp\left(\frac{G^*}{RT}\right), \quad (2)$$

is obeyed, and H^*_V is defined by

$$H^*_V = R\left[\frac{\partial \ln \tau}{\partial (1/T)}\right]_V, \quad (3)$$

Here, τ is the relaxation time, G^*, the activation Gibbs energy, R, the gas constant, and A, a constant independent of temperature T and pressure P. The ratio H^*_V/H^*_P prepresents the direct contribution of temperature to the temperature dependence of the relaxation time and gives a rough estimation of the magnitudes of the energetic or entropic contribution to the relaxation process. It may be very interesting to know H^*_V/H^*_P for simple normal liquids in the supercooled liquid region.

Many dielectric studies on the *o*-terphenyl solutions have been presented,[18,19] since *o*-terphenyl and its solutions can easily be vitrified at a relatively high temperature.[20-22] We now wish to clarify the effects of pressure on the dielectric relaxation process in the supercooled triphenylchloromethane/*o*-terphenyl solution as an example of simple normal liquids and to elucidate some intrinsic contributions to the molecular mobility in the supercooled liquid state.

Experimental

Sample. Triphenylchloromethane (TPCM) and *o*-terphenyl (oTP) were purchased from Tokyo Chemical Industry Co. and were used without further purification. In order to perform dielectric measurements without any apprehension of crystallization during the experimental period (about 3 d), crystallizability of the mixture of TPCM/oTP was preliminary tested. TPCM and oTP in various concentrations were mixed in test tubes at 130 °C. Then the mixtures were slowly cooled down to room temperature and were stored in a desiccator. Samples containing TPCM more than 50 wt% crystallized within 5 h. In samples containing TPCM less than 10 wt%, a slight crystallization peak was detected by a differential scanning calorimeter, Model DSC-1B (Perkin-Elmer Corporation) after 3 d. Any crystallization was not observed in samples containing 20—40 wt% of TPCM for one month, and we used the mixture TPCM/oTP in weight ratio of 25/75 in dielectric measurements.

Equipment. A General Radio 1620-A Capacitance Measuring Assembly, in conjunction with a General Radio 1310-B Oscillator employed to make small changes in frequency near dielectric loss peaks, was used for dielectric

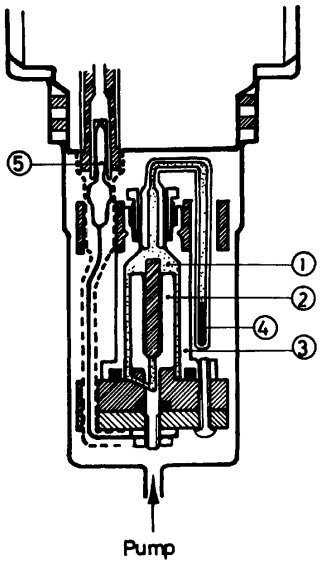

Fig. 1. Diagram of dielectric cell.
1: Sample, 2: main electrode, 3: sub electrode, 4: mercury seal, 5: electric terminal.

measurements in a frequency range of 0.03—100 kHz. The cell shown in Fig. 1 has a nominal geometric capacitance of about 15 pF with a small stray capacitance. Corrections for the stray capacitance and the change in the geometric capacitance with temperature and pressure were made by measuring the capacitance of the cell with air and with benzene (uvasol grade, Merck) in each measurement. The dielectric data of benzene were taken from those of Vij and Scaife.[23] Silicone oil (KF-94, Shin-Etsu Chemical Co.) was used to transmit the hydrostatic pressure. The pressure was measured by a Nikkiso bourdon gauge calibrated by a Heise bourdon gauge. The temperature was measured by a calibrated alumel-chromel thermocouple inserted near the sub electrode.

Experimental Procedure. The mixture (TPCM/oTP, 25/75) was prepared at 130 °C and was applied into the electrode at 70 °C. The dielectric cell was set in the pressure vessel heated previously up to 70 °C. After the pressure being increased to a desired value P_1, the temperature was lowered to the glass transition temperature T_g at P_1, $T_g(P_1)$. The dielectric measurements at P_1 were isobarically carried out at about 2 K intervals with increasing temperature to a temperature at which the frequency of dielectric loss maximum exceeded 100 kHz. This experimental operation (from the sample set to the isobaric measurements) was repeated for each pressure, *i.e.*, 1, 200, 400, 600, and 800 kg cm^{-2}. (1 kg cm^{-2}= 0.09807 MPa). The operation recurred twice for 1, 600, and 800 kg cm^{-2}.

Crystallization of the sample during the experimental period could easily be detected as a precipitous decrease in the capacitance and loss. We have excluded all the dielectric data of the experimental opetation in which the indication of the crystallization was recognized at any temperature.

Results

Some examples of the dielectric dispersion are shown in Fig. 2. The shapes of the loss curves at every temperature and pressure are all similar, being asymmetric to the high frequency side of the dispersion. The limiting low- and high-frequency dielectric constants, *i.e.*, ε_0 and ε_∞, respectively, were determined by extrapolation of

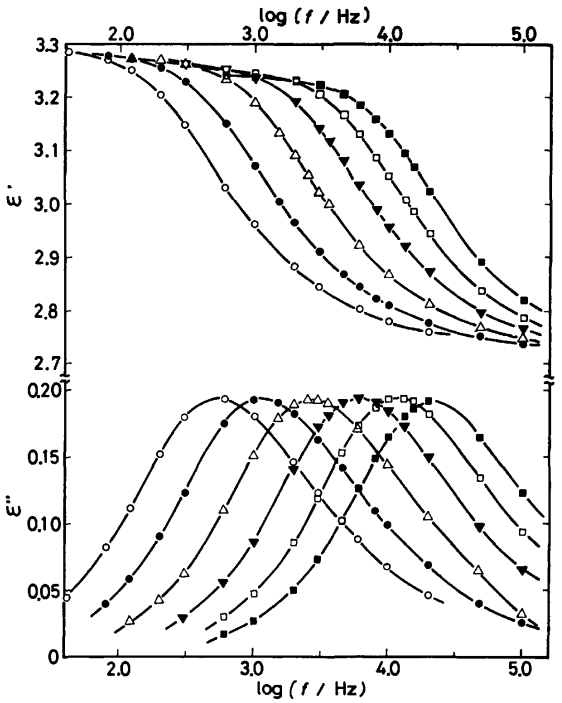

Fig. 2. Diectric dispersion at 800 kg cm^{-2}.
○: 285.92 K, ●: 288.24 K, △: 290.56 K, ▲: 293.05 K, □: 295.56 K, ■: 297.26 K.

Table 1. Static dielectric constants at log $\tau=-4$

P / kg cm^{-2}	ε_0	ε_∞	$\varepsilon_0-\varepsilon_\infty$
1	3.260 ± 0.017	2.673 ± 0.005	0.587 ± 0.019
200	3.265 ± 0.037	2.685 ± 0.008	0.580 ± 0.042
400	3.283 ± 0.010	2.698 ± 0.005	0.585 ± 0.012
600	3.279 ± 0.009	2.715 ± 0.004	0.564 ± 0.010
800	3.273 ± 0.009	2.736 ± 0.004	0.537 ± 0.010

the Cole-Cole plots. The plots appear to be well represented by the Davidson-Cole equation of a skewed-arc behavior,[24] but we do not discuss the parameter in the Davidson-Cole equation. It should be noted, however, that its asymmetric factor is independent over the present experimental range.

Values of ε_0 and ε_∞ interpolated to log $\tau=-4$ are listed in Table 1. Influences of pressure on ε_0, ε_∞, and the relaxation intensity represented by $\varepsilon_0-\varepsilon_\infty$ are very little. ε_0 is almost independent of pressure in the experimental errors, when ε_0 is plotted against $T-T_g$. ε_∞ increases with pressure in correspondence with the increase in density. Consequently, $\varepsilon_0-\varepsilon_\infty$ decreases slightly with pressure. The rather large experimental errors in ε_0 and ε_∞ values may be due to the experimental procedure that the electrode cell was reassembled for each pressure. These errors, however, exert no influence upon the following analysis, in which only the shape of the dispersion curve, the maximum loss, ε''_{max}, and the frequency of the maximum loss, f_{max}, are significant.

Figure 3 shows a master curve obtained by superposition of reduced dielectric loss, $\varepsilon''/\varepsilon''_{max}$, at every temperature and pressure to the reference one at 286.74 K and 600 kg cm^{-2}. The relaxation spectrum of the α relaxa-

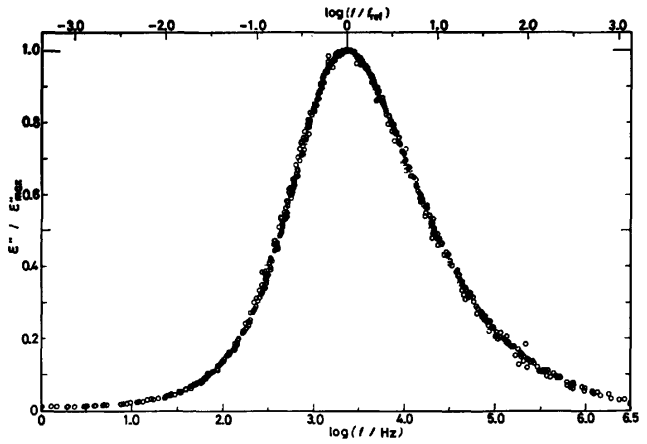

Fig. 3. Master curve of reduced dielectric loss. The reference temperature and pressure are 286.74 K and 600 kg cm^{-2}, respectively.

tion process in TPCM/oTP is typical in shape as Williams *et al.* demonstrated for oTP solutions and many polymers.[25] The value of the half width of the master curve of TPCM/oTP is 1.67 decade in frequency. This value is equal to that of anthrone/oTP solutions[18a] and smaller than those of other oTP solutions[18b] and decalin solutions.[6c]

The susperposition gives the shift factor $a_{T,P}$ at any temperature and pressure:

$$a_{T,P} = \frac{\tau}{\tau(T_r,P_r)}, \tag{4}$$

where τ is the characteristic relaxation time at T and P and $\tau(T_r,P_r)$, that at the reference temperature and pressure. The value of $\tau(T_r,P_r)$ was obtained from f_{max} at 286.74 K and 600 kg cm^{-2} by using

$$\tau(T_r,P_r) = \frac{1}{2\pi f_{max}(T_r,P_r)}, \tag{5}$$

Variations of log $a_{T,P}$ or log τ with reciprocal temperature, *i.e.*, the Arrhenius plots, are shown in Fig. 4.

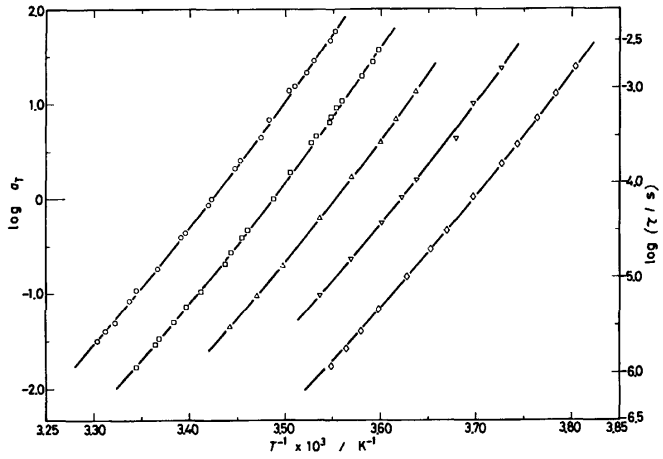

Fig. 4. Arrhenius plots of logarithmic shift factor and characteristic relaxation time. Lines: VFTH equation, Eq. 6.
◇: 1 kg cm^{-2}, ▽: 200 kg cm^{-2}, △: 400 kg cm^{-2}, □: 600 kg cm^{-2}, ○: 800 kg cm^{-2}.

The log τ isobars are well represented by the Vogel-Fulcher-Tammann-Hesse (VFTH) equation:[26]

$$\log \tau = -A + \frac{B}{T-T_0}, \tag{6}$$

which is transformable into the WLF equation for polymer liquids.[27] Values of the VFTH parameters A, B, and T_0 obtained to minimize the standard deviation σ by the least-squares regression are listed in Table 2. Since the experimental frequency range is limited, the temperature range where the dielectric loss reaches maximum is rather narrow. Consequently, long extrapolation of Eq. 6 may lead to a large uncertainty and there is no point in discussing about physical significance of B and T_0. The VFTH equation is utilized only for precise interpolation of τ to every temperature.

The T—P relations at constant τ calculated from Eq. 6 are shown in Fig. 5, in which values of the glass transition temperature T_g obtained by isobaric cooling experiments[28] are also plotted. The slope of the isochronal T—P relation is very similar to that of T_g—P relation shown in the same figure. The isothermal

Table 2. VFTH parameters

P / kg cm^{-2}	A	B / K	T_0 / K	σ
1	21.565	1803.9	166.82	0.008
200	20.494	1629.4	176.35	0.014
400	20.238	1594.0	182.29	0.024
600	20.731	1713.7	183.34	0.030
800	23.179	2372.1	167.34	0.016

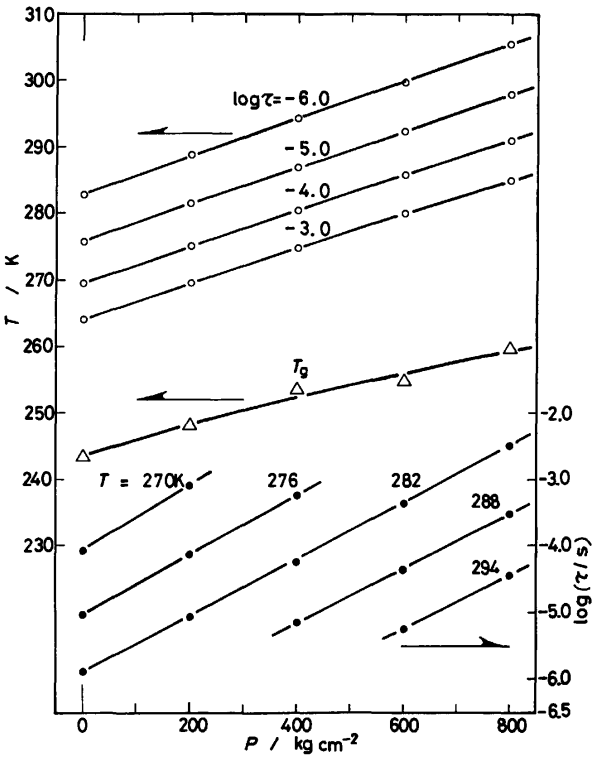

Fig. 5. Isochronal T—P relation (open circles), pressure dependence of T_g (triangles), and isothermal variations of log τ with pressure (solid circles).

dependences of τ on pressure are also shown in Fig. 5. Pressure effects on the slope of log τ—P relation are scarcely observed due to the narrowness of the experimental frequency range.

Discussion

Activation Parameters. The activation enthalpy at constant pressure, H^*_P, given by Eq. 1 was obtained by differentiating the VFTH equation, Eq. 6:

$$\frac{\partial \ln \tau}{\partial(1/T)} = \frac{BT^2}{(T-T_0)^2}, \tag{7}$$

Values of H^*_P are plotted as a function of $T-T_g$, in Fig. 6 where the value of T_g was calculated from the least-squares quadratic equation for the pressure dependence of T_g.[28] H^*_P depends on temperature and pressure. The pressure effects on H^*_P cannot be reduced by an exchange of the temperature scale from T to $T-T_g$ only. This situation remains unchanged when $T-T_g$ is replaced by T/T_g. This may be evidence for the fact that the glass transition temperature is not the corresponding point for the molecular mobility in the supercooled liquid.

The activation volume V^* given by

$$V^* = RT\left[\frac{\partial \ln \tau}{\partial P}\right]_T, \tag{8}$$

is shown in Fig. 6. The pressure effects on V^* seem to be almost reduced in the experimental errors when V^* is plotted as a function of $T-T_g$ instead of T. V^* of TPCM/oTP is equal in magnitude to that of chlorinated diphenyl,[16] similar to that of polymer liquids which ranges from 50 to 400 cm^3 mol^{-1},[14a,15] and larger than that of associated liquids.[11]

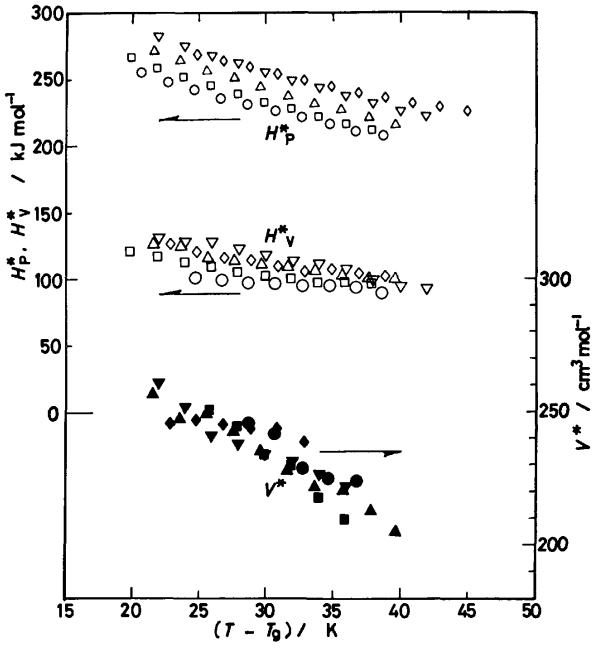

Fig. 6. Activation enthalpies at constant pressure and volume (open symbols) and activation volume (closed symbols) as a function of $T-T_g$.
○: 1 kg cm^{-2}, □: 200 kg cm^{-2}, △: 400 kg cm^{-2}, ▽: 600 kg cm^{-2}, ◇: 800 kg cm^{-2}.

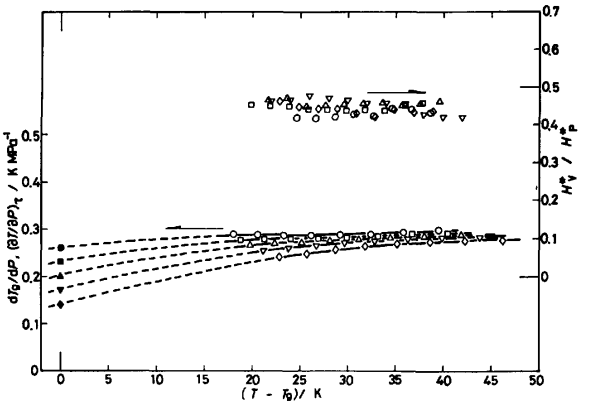

Fig. 7. Variations of H^*_V/H^*_P, $(\partial T/\partial P)_\tau$, and dT_g/dP with $T-T_g$. Symbols are the same as those in Fig. 6.

The activation enthalpy at constant volume, H^*_V, defined by Eq. 3 can be obtained from Eqs. 1 and 8 as

$$H^*_V = H^*_P - T\gamma V^*, \tag{9}$$

where γ is the thermal-pressure coefficient, $(\partial P/\partial T)_V$. From dilatometric measurements, γ of TPCM/oTP is obtained as a function of the specific volume v:[28]

$$\gamma = 11.1587 - 10.3500\,v \quad (\mathrm{K^{-1}\,MPa}). \tag{10}$$

H^*_V, which is often called as the *true* energy of activation,[29] calculated from Eqs. 9 and 10 is plotted as a function of $T-T_g$. The pressure effects on H^*_V seem not to be well-reduced by the $T-T_g$ scale. The second term in Eq. 9 is comparatively large as H^*_V and H^*_V is much smaller than H^*_P.

In Fig. 7, the ratio H^*_V/H^*_P is shown as a function of $T-T_g$. The ratio has a value of about 0.45 and is almost independent of temperature and pressure. This value is equal to those of simple normal liquids near their melting temperatures obtained by viscosity measurements,[17] and is much smaller than those of polymer liquids[30,31] and associated liquids.[17]

Pressure Coefficient of Temperature at Constant Relaxation Time. The tangent of the T—P relation at constant τ, $(\partial T/\partial P)_\tau$, is expressed by

$$\left(\frac{\partial T}{\partial P}\right)_\tau = -\left(\frac{\partial \ln \tau}{\partial P}\right)_T \Big/ \left(\frac{\partial \ln \tau}{\partial T}\right)_P. \tag{11}$$

Values of $(\partial T/\partial P)_\tau$ calculated from this equation are plotted in Fig. 7. Effects of pressure on $(\partial T/\partial P)_\tau$ diminish as the temperature increases. At lower temperature, $(\partial T/\partial P)_\tau$ approaches the pressure coefficient of the glass transition temperature, dT_g/dP, shown in the same figure, *i.e.*,

$$\left(\frac{\partial T}{\partial P}\right)_\tau \simeq \frac{dT_g}{dP}. \tag{12}$$

This supports the argument that the glass transition temperature is an isorelaxation-time state or an isoviscose state.[3-5] The argument has been proposed[32,33] and been supported[34] by the time-temperature-pressure superposition for polymer liquids. It may be stated that, irrespective of molecular weight, the T_g trace in the PVT space is identical with the isorelaxation-time trace.

$(\partial T/\partial P)_\tau$ of TPCM/oTP is equal in magnitude to

TABLE 3. REPRESENTATIVE VALUES OF H^*_V/H^*_P, $(\partial T/\partial P)_\tau$, AND dT_g/dP

Substance	H^*_V/H^*_P	$(\partial T/\partial P)_\tau$ / K MPa^{-1}	dT_g/dP / K MPa^{-1}
Simple normal liquids			
CCl_4	0.40[a]	—	—
oTP	—	—	0.26[b]
TPCM/oTP	0.42	0.288	0.26
Polymer liquids			
Poly(vinyl acetate)	0.73[c]	0.20[c]	0.212[d]
Poly(vinyl chloride)	0.86[e]	0.19[e]	0.19[e]
Associated liquids			
1-Propanol	0.86[a]	—	0.07[f]
Glycerol	0.95[g], 0.86[a]	0.029[g]	0.04[f]

a) Values near the melting temperature (Ref. 17). b) Ref. 35. c) Ref. 32. d) Ref. 4. e) Ref. 34. f) Ref. 36. g) Ref. 11d.

dT_g/dP of oTP,[35] almost the same as $(\partial T/\partial P)_\tau$ of polymer liquids,[15,30,32,36] much larger than dT_g/dP of associated liquids.[35,36] In terms of V^*, $(\partial T/\partial P)_\tau$ can be expressed as

$$\left(\frac{\partial T}{\partial P}\right)_\tau = T\frac{V^*}{H^*_P}. \tag{13}$$

The small value of associated liquids is due to the smallness of V^*. In the molecular mobilities in such liquids, the arrangements of the free space or the free volume, *i.e.*, the formation of holes, are scarcely of importance, and the rearrangements of the number of the hydrogen bonds only are significant.

It is very interesting to compare the results above on $(\partial T/\partial P)_\tau$ with that on the ratio H^*_V/H^*_P. Representative values of H^*_V/H^*_P, $(\partial T/\partial P)_\tau$, and dT_g/dP are listed in Table 3. With respect to the magnitude of H^*_V/H^*_P, liquids can be classified into two categories: the one (polymer liquids and associated liquids) whose H^*_V/H^*_P is larger than 0.7 and the other (simple normal liquids) whose H^*_V/H^*_P is smaller than 0.5. Whereas, with respect to the magnitudes of $(\partial T/\partial P)_\tau$ and dT_g/dP, the another classification applies: the one (simple normal liquids and polymer liquids) whose $(\partial T/\partial P)_\tau$ or dT_g/dP is larger than 0.15 K MPa^{-1} and the other (associated liquids) whose $(\partial T/\partial P)_\tau$ or dT_g/dP is smaller than 0.10 K MPa^{-1}.

$(\partial T/\partial P)_\tau$ is related to H^*_V/H^*_P through the following equation.

$$\frac{H^*_V}{H^*_P} = 1 - \gamma\left(\frac{\partial T}{\partial P}\right)_\tau \tag{14}$$

If one disregards differences in magnitude of γ, one finds from Eq. 14 that large(small) $(\partial T/\partial P)_\tau$ corresponds to the small(large) H^*_V/H^*_P. This is the case for simple normal liquids and associated liquids.

In polymer liquids, the contribution of the intramolecular conformational entropy is very large to the liquid entropy.[37] From the thermodynamic Maxwell relation

$$\gamma = \left(\frac{\partial P}{\partial T}\right)_V = \left(\frac{\partial S}{\partial V}\right)_T, \tag{15}$$

i.e., the thermal pressure coefficient is related to the dependence of the entropy S on volume. The intramolecular conformational entropy is regarded to be independent of volume.[37] Therefore, the magnitude of γ in polymer liquids is usually smaller than that of simple normal liquids. This is the reason for the large values of H^*_V/H^*_P in polymer liquids.

Conclusion

From the analysis on the isochronic pressure coefficient of temperature, $(\partial T/\partial P)_\tau$, we have found the fact that the glass transition temperature can be regarded as an isorelaxation-time state in the simple normal liquid as well as in polymer liquids. Therefore, the correspondence of the α relaxation process to the glass transition temperature is independent of the length of the molecules, *i.e.*, the molecular weight. The molecular mobility represented by the characteristic relaxation time, however, is significantly influenced by the molecular types such as simple normal liquids, polymer liquids, and associated liquids. The length of the molecules, regardless whether the bonds between molecules are covalent or hydrogen bonds, affects the magnitude of the ratio H^*_V/H^*_P, but not that of $(\partial T/\partial P)_\tau$. On the other hand, the kind of the intermolecular interactions such as the short range one (London potential) and long range one (coulomb potential) affects the magnitude of $(\partial T/\partial P)_\tau$ and dT_g/dP, but not that of H^*_V/H^*_P. These properties of the molecular mobilities obtained by the time-temperature-pressure superpositions of the dielectric α relaxation process are very similar to the properties of the viscosity above the melting temperature.[17] A more detailed investigation of the molecular mobility in the supercooled liquid state will be given in a succeeded paper.

References

1) J. D. Ferry, "Viscoelastic Properties of Polymers," 2nd ed, Wiley, New York (1970).
2) G. Adam and J. H. Gibbs, *J. Chem. Phys.*, **43**, 139 (1965).
3) M. Goldstein, *J. Phys. Chem.*, **77**, 667 (1973).
4) J. E. McKinney and M. Goldstein, *J. Res. Natl. Bur. Stands., Sect. A*, **78**, 331 (1974).
5) A. A. Miller, *Macromolecules*, **4**, 757 (1971).
6) a) G. P. Johari and M. Goldstein, *J. Chem. Phys.*, **53**, 2372 (1970); b) **55**, 4245 (1971); c) G. P. Johari and C. P. Smyth, *ibid.*, **56**, 4411 (1972).
7) G. Williams and P. J. Hains, *Faraday Symp. Chem. Soc.*, **6**, 14 (1972).
8) G. P. Johari, *J. Chem. Phys.*, **58**, 1766 (1973).
9) G. H. Porter and R. H. Boyd, *Macromolecules*, **4**, 589 (1971).
10) For instance: D. L. Hogenboom, W. Webb, and J. A. Dixon, *J. Chem. Phys.*, **46**, 2586 (1967).
11) a) G. E. McDuffie and M. V. Kelly, *J. Chem. Phys.*, **41**, 2666 (1964); b) Yu. A. Atanov and M. I. Shakhparanov, *Russ. J. Phys. Chem.*, **43**, 958 (1969); c) G. P. Johari and W. Dannhauser, *J. Chem. Phys.*, **50**, 1862 (1969); d) G. P. Johari and E. Whalley, *Faraday Symp. Chem. Soc.*, **6**, 23 (1972).
12) a) J. Koppelmann and J. Gielessen, *Z. Electrochem.*, **65**, 689 (1961); b) J. M. O'Reilly, *J. Polym. Sci.*, **57**, 429 (1962).
13) G. Williams, *Trans. Faraday Soc.*, **60**, 1548 (1964); **60**, 1556 (1964); **61**, 1964 (1965); G. Williams, D. C. Watts, and

P. J. Nottin, *ibid.*, **68**, 16 (1972).
14) a) S. Saito, H. Sasabe, T. Nakajima, and K. Yada, *J. Polym. Sci., Part. A-2*, **6**, 1297 (1968); b) H. Sasabe and S. Saito, *ibid.*, **6**, 1401 (1968).
15) M. Naoki, M. Motomura, T. Nose, and T. Hata, *J. Polym. Sci., Polym. Phys. Ed.*, **13**, 1737 (1975).
16) T. A. Peris and L. B. Wilner, *J. Chem. Phys.*, **53**, 753 (1960).
17) J. D. Mackenzie, *J. Chem. Phys.*, **28**, 1037 (1958).
18) a) G. Williams and P. J. Hains, *Chem. Phys. Lett.*, **10**, 585 (1971); b) M. F. Shears and G. Williams, *J. Chem. Soc., Faraday Trans. 2*, **69**, 608, 1050 (1973); c) M. S. Beevers, J. Grossley, D. C. Garrington, and G. Williams, *ibid.*, **72**, 1022 (1974).
19) M. Nakamura, H. Takahashi, and K. Higashi, *Bull. Chem. Soc. Jpn.*, **47**, 1593 (1974); T. Nagai, Y. Koga, H. Takahashi, and K. Higashi, *ibid.*, **47**, 1022 (1974).
20) J. N. Andrews and A. R. Ubbelohde, *Proc. R. Soc. London, Ser. A*, **228**, 435 (1955).
21) R. J. Greet and D. Turnbull, *J. Chem. Phys.*, **46**, 1243 (1967); **47**, 2185 (1967).
22) S. S. Chang and A. B. Bestul, *J. Chem. Phys.*, **56**, 503 (1972).
23) J. K. Vij and W. G. S. Scaife, *J. Chem. Phys.*, **64**, 2226 (1976).
24) D. W. Davidson and R. H. Cole, *J. Chem. Phys.*, **19**, 1484 (1951).
25) G. Williams and D. C. Watts, *Trans. Faraday Soc.*, **66**, 80 (1970); G. Williams, D. C. Watts, S. B. Dev, and A. M. Northe, *ibid.*, **67**, 1323 (1971); G. Williams, M. Cook, and P. J. Hains, *J. Chem. Soc., Faraday Trans. 2*, **68**, 1045 (1972).
26) H. Vogel, *Physik. Z.*, **22**, 645 (1921); G. S. Fulcher, *J. Am. Ceram. Soc.*, **8**, 339 (1925); G. Tammann and W. Hesse, *Z. Anorg. Allg. Chem.*, **156**, 245 (1926).
27) a) M. L. Williams, R. F. Landel, and J. D. Ferry, *J. Am. Chem. Soc.*, **77**, 3701 (1955); b) Ref. 1, p. 305.
28) M. Naoki, M. Matsushita, and K. Matsumoto, to be submitted to this journal.
29) A. Jobling and A. S. C. Lawrence, *Proc. R. Soc. London, Ser. A*, **206**, 257 (1951).
30) T. Nose and T. Hata, *Proc. 5th Intl. Congress on Rheology*, **3**, 215 (1970).
31) M. Naoki and T. Nose, *J. Polym. Sci., Polym. Phys. Ed.*, **13**, 1747 (1975).
32) J. M. O'Reilly, *J. Polym. Sci.*, **57**, 429 (1962).
33) J. E. McKinney and H. V. Belcher, *J. Res. Natl. Bur. Stand., Sect. A*, **67**, 43 (1963).
34) M. Naoki and A. Owada, *Polymer*, in press.
35) T. Atake and C. A. Angell, *J. Phys. Chem.*, **83**, 3218 (1979).
36) E. A. DiMarzio, J. H. Gibbs, D. D. Fleming ,and I. C. Sanchez, *Macromolecules*, **9**, 763 (1976).
37) M. Naoki and T. Tomomatsu, *Macromolecules*, **13**, 322 (1980).

Effect of Pressure on the Adsorption of 1-Octadecanol at Oil/Water Interfaces

Hidemi IYOTA,* Makoto ARATONO, Michio YAMANAKA, Kinsi MOTOMURA, and Ryohei MATUURA
Department of Chemistry, Faculty of Science, Kyushu University 33, Fukuoka 812

(Received February 4, 1983)

In order to investigate the effect of pressure on the adsorption at interfaces, the interfacial tension was measured as a function of pressure and composition for the systems of water and dilute solutions of 1-octadecanol in cyclohexane, benzene, and their equimolar mixture. The interfacial density of 1-octadecanol and the volume of interface formation were evaluated from the experimental data. Under atmospheric pressure, cyclohexane exhibits a significant adsorption of 1-octadecanol and a rapid decrease in the volume of interface formation, giving rise to the phase transition from the expanded to the condensed state in the adsorbed film, while benzene and equimolar mixture display only a small decrease in the thermodynamic quantities on the 1-octadecanol adsorption. Under high pressure, however, all the systems studied cause the phase transition. The effects of pressure and solvent on the phase transition of the adsorbed film were revealed on the basis of the thermodynamic quantities.

The adsorption of long-chain fatty alcohols at interfaces has been studied by many workers.[1-7] However, the pressure effect on the adsorption has hardly been investigated.[8-10] In the previous paper,[10] we clarified that the phase transition of the adsorbed film of 1-octadecanol takes place from an expanded to a condensed state at hexane/water interface and its interfacial tension is altered remarkably by pressure. Further, it was found that the adsorption of 1-octadecanol decreases with an increase in the affinity of oil to water.[7,11]

The object of this paper is to make clear the effect of pressure and solvent on the adsorption of 1-octadecanol, especially on the phase transition of the adsorbed film, at the organic solvent/water interface.

Experimental

Octadecanol was recrystallized five times from hexane after distillation under reduced pressure. Its purity was indicated to be better than 99.5% according to a gas-liquid chromatography test. Cyclohexane and benzene (Nakarai Chemicals Guaranteed Reagent) were refluxed with metallic sodium for 15 h and passed through a column of activated alumina(Woelm neutral activity grade I), and then distilled. Water was triply distilled, the second and third steps being done from dilute alkaline permanganate solution. Purities of organic liquid and water were checked by the equilibrium value of interfacial tension between them. Organic solvent and water were mutually saturated before measurements.

The pendant drop technique described previously[9,12] was used for the determination of interfacial tension. The pendant drops were allowed for about 45 min to attain the thermodynamic equilibrium. Densities of organic liquids, equimolar mixture of them, and water taken from literature[13-15] were used instead of those of mutually saturated oil and water because of so small solubilities. The interfacial tension was measured at 298.15 K with an accuracy of 0.05 mN m^{-1} as functions of pressure up to 150 MPa and mole fraction of 1-octadecanol. Temperature was controlled within 0.05 K at 298.15 K over the whole range of the experiments and pressure was regulated with a precision of 0.25 MPa.

Results and Discussion

The interfacial tension γ of the cyclohexane solution of 1-octadecanol against water was measured as a function of pressure p at a given mole fraction of 1-octadecanol x_1^0 in the cyclohexane solution. The γ *vs.* p curves at various concentrations are drawn in Fig. 1. In the lower concentration region, γ increases linearly with increasing p and the positive slope of γ *vs.* p curve becomes gradually smaller as the concentration increases. In the higher concentration region, on the other hand, the slope has a large negative value. It is noteworthy that a break point is observed on the γ *vs.* p curve at an intermediate concentration. This behavior resembles that of the system of hexane solution and water.[10] Therefore, we may conclude that the phase transition of the adsorbed film occurs from an expanded to a condensed state at the break point. Figure 2 shows the γ *vs.* p curves at various concentrations for the system of benzene solution and water. It is seen from this figure that the phase transition of the adsorbed film of 1-octadecanol at the benzene/water interface takes place

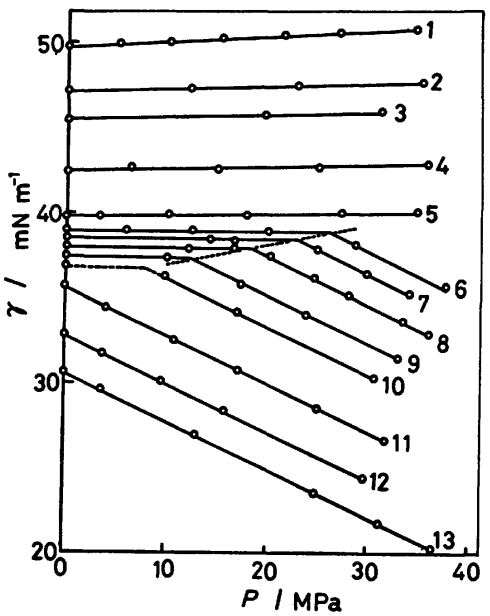

Fig. 1. Interfacial tension *vs.* pressure curves of 1-octadecanol at the cyclohexane/water interface at 298.15 K and constant mole fraction: $10^3 x_1^0 =$ (1) 0; (2) 0.199; (3) 0.404; (4) 0.910; (5) 1.543; (6) 1.881; (7) 2.030; (8) 2.189; (9) 2.499; (10) 2.729; (11) 3.354; (12) 3.965; (13) 4.560.

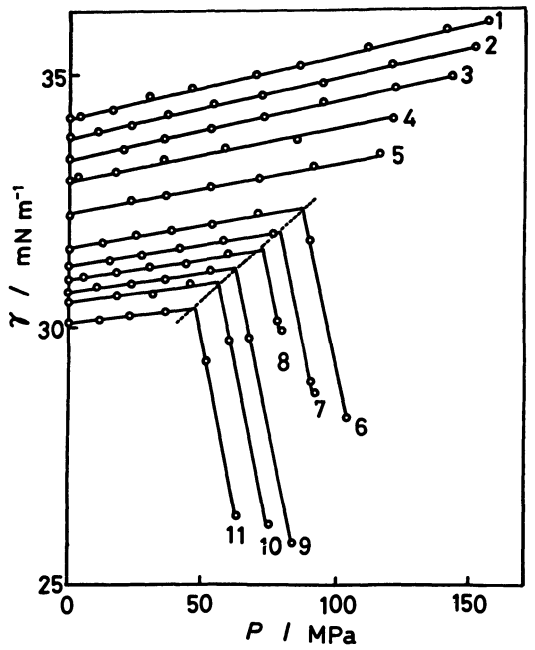

Fig. 2. Interfacial tension *vs.* pressure curves of 1-octadecanol at the benzene/water interface at 298.15 K and constant mole fraction: $10^3 x_1^0$=(1) 0; (2) 0.296; (3) 0.832; (4) 1.159; (5) 1.957; (6) 2.850; (7) 3.236; (8) 3.537; (9) 4.198; (10) 4.613; (11) 5.354.

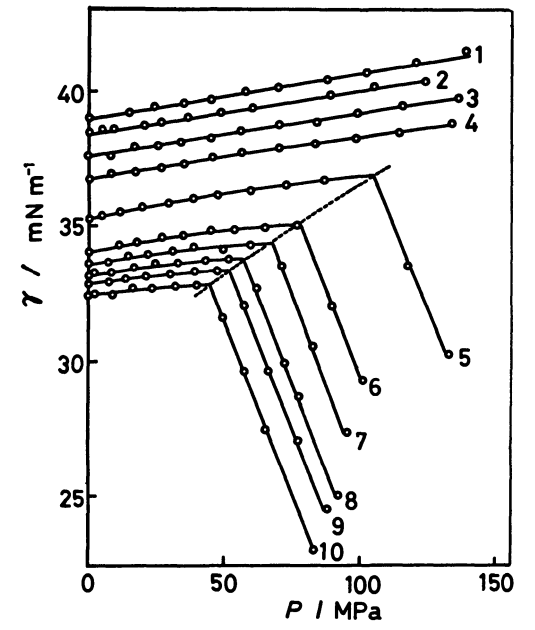

Fig. 3. Interfacial tension *vs.* pressure curves of 1-octadecanol at the X_b^0=0.503/water interface at 298.15 K and constant mole fraction: $10^3 x_1^0$=(1) 0; (2) 0.211; (3) 0.728; (4) 1.103; (5) 2.243; (6) 3.253; (7) 3.749; (8) 4.507; (9) 4.846; (10) 5.471.

only at very high pressure and concentration.

Now it is of great interest to investigate the adsorption of 1-octadecanol from the equimolar mixture of cyclohexane and benzene. Given in Fig. 3 is the γ *vs.* p curve at X_b^0=0.503, where X_b^0 is the composition of mixed solvent defined by

$$X_b^0 = x_b^0/(x_c^0 + x_b^0), \quad (1)$$

x_c^0 and x_b^0 being the mole fraction of cyclohexane and benzene, respectively. The behavior of 1-octadecanol in this interface seems to be akin to that in the benzene/water interface rather than in the cyclohexane/water interface, although the γ *vs.* p curve is slightly convex upward at higher concentrations. From Figs. 1 to 3, it is evident that higher pressure makes smaller the concentration of 1-octadecanol at which the phase transition takes place.

The adsorption behavior of 1-octadecanol is compared among the systems of cyclohexane, benzene, and their mixture in Figs. 4a and 4b where the value of interfacial tension taken up from Figs. 1 to 3 is plotted against the concentration at 0.1 and 80 MPa; the γ *vs.* x_1^0 curve at 80 MPa is not drawn for the system of cyclohexane because the cyclohexane solution freezes above about

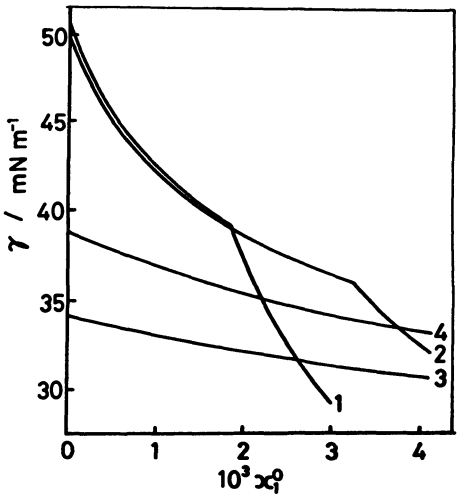

Fig. 4a. Interfaciale tension *vs.* mole fraction curves of 1-octadecanol at 298.15 K and 0.1 MPa: (1) hexane; (2) cyclohexane; (3) benzene; (4) X_b^0=0.503.

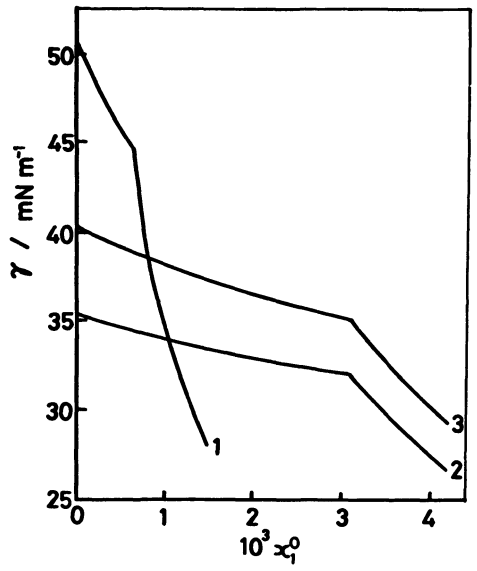

Fig. 4b. Interfacial tension *vs.* mole fraction curves of 1-octadecanol at 298.15 K and 80 MPa: (1) hexane; (2) benzene; (3) X_b^0=0.503.

40 MPa. The results for the hexane system[10] are also shown for comparison. It may be supposed from Fig. 4a that the 1-octadecanol molecule is adsorbed remarkably at the cyclohexane/water interface as at the hexane/water interface whereas it is not done so much at the benzene/water interface, and its adsorption from the mixed solvent is intermediate between the adsorptions from the pure solvents. At 80 MPa, on the other hand, the γ *vs.* x_1^0 curves are characterized by the break point.

It is now appropriate to estimate the interfacial density of 1-octadecanol Γ_1^H and the volume of interface formation Δv defined on the basis of the Hansen convention. Since the system under consideration satisfies the conditions that the two phases are actually immiscible and that the surfactant is soluble only in one of the phases, we have the following equations:[16,17]

$$\Gamma_1^H = -(x_1^0/RT)(\partial\gamma/\partial x_1^0)_{T,p} \quad (2)$$

and

$$\Delta v = (\partial\gamma/\partial p)_{T,x_1^0}, \quad (3)$$

where the ideality of the alcohol solution is assumed.

For the system in which the solvent of the oil phase is a mixture, Eqs. 2 and 3 are replaced by the equations[18]

$$\Gamma_1^H = -(x_1^0/RT)(\partial\gamma/\partial x_1^0)_{T,p,X_b^0}, \quad (4)$$

and

$$\Delta v = (\partial\gamma/\partial p)_{T,x_1^0,X_b^0}, \quad (5)$$

where the two dividing planes are chosen so as to satisfy the relations

$$\Gamma_w^H = 0, \quad (6)$$

and

$$\Gamma_b^H + \Gamma_c^H = 0. \quad (7)$$

The value of Γ_b^H is estimated by

$$\Gamma_b^H = -X_b^0 X_c^0 (\partial\gamma/\partial X_b^0)_{T,p,x_1^0} / RT[1+(\partial \ln f_b^0/\partial \ln X_b^0)_{T,p,x_1^0}], \quad (8)$$

where f_b^0 is the activity coefficient of solvent b in the oil phase.

Applying Eqs. 2 and 4 to the γ *vs.* x_1^0 curves in Figs. 4a and 4b, the value of Γ_1^H was evaluated at 0.1 and 80 MPa as a function of x_1^0. The results are illustrated in Figs. 5a and 5b, respectively. It is seen at 0.1 MPa that the Γ_1^H value of the cyclohexane system, like that of the hexane system changes discontinuously at the point of phase transition from a relatively small value of the expanded film to a very large one of the condensed film. For the benzene system, the adsorbed film remains in an expanded state of which the Γ_1^H value is significantly small. The value of the $X_b^0=0.503$ system seems to be close to that of the benzene system. On the other hand, it is found at 80 MPa that the phase transition takes place for the benzene and $X_b^0=0.503$ systems and the Γ_1^H values of condensed films are about the same irrespective of the solvent. Therefore, it may be said that the affinity of benzene molecules to water molecules affects the adsorption of 1-octadecanol in the expanded state but not in the condensed state. This can be ascribed to the intermolecular interaction between octadecanol molecules in the condensed film which is strong enough to disregard a difference in that between octadecanol and organic solvent and between organic solvent and water.

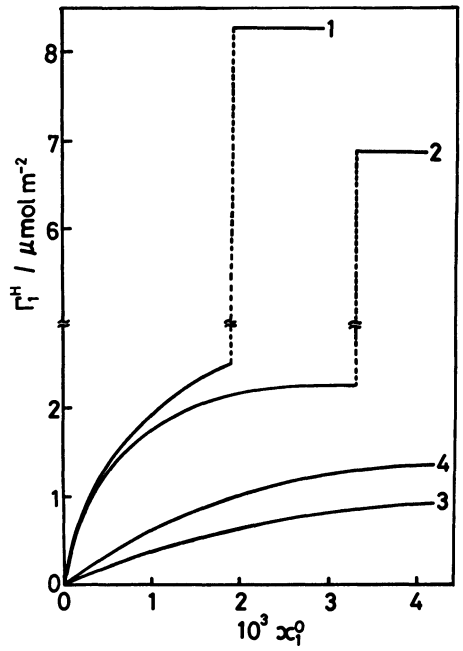

Fig. 5a. Interfacial density *vs.* mole fraction curves of 1-octadecanol at 298.15 K and 0.1 MPa: (1) hexane; (2) cyclohexane; (3) benzene; (4) $X_b^0=0.503$.

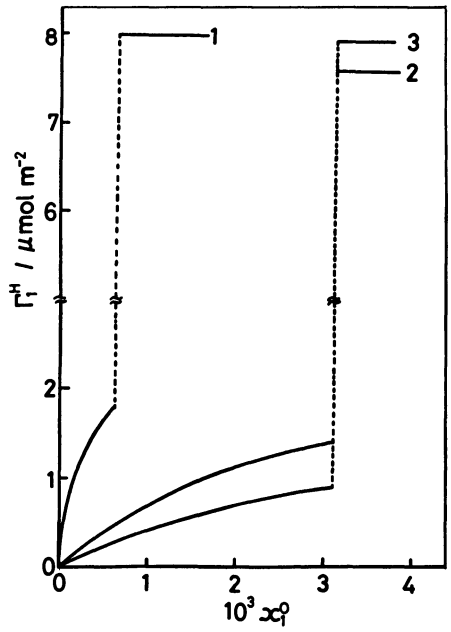

Fig. 5b. Interfacial density *vs.* mole fraction curves of 1-octadecanol at 298.15 K and 80 MPa: (1) hexane; (2) benzene; (3) $X_b^0=0.503$.

The application of Eqs. 3 and 5 to the γ *vs.* p curves in Figs. 1 to 3 enables us to calculate the value of Δv. The variation in Δv with x_1^0 at 0.1 and 80 MPa is shown in Figs. 6a and 6b. Under atmospheric pressure the Δv value for the cyclohexane system decreases rapidly with an increase in x_1^0 from the positive value of the pure

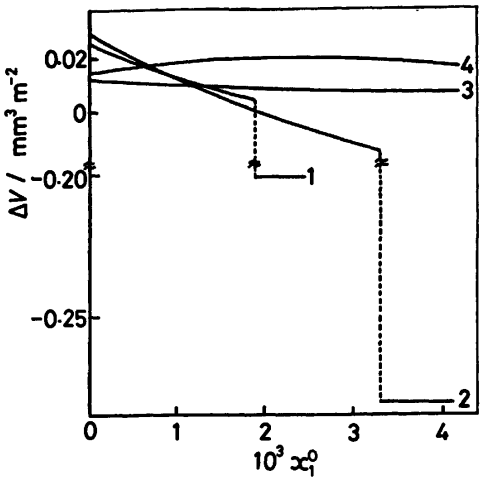

Fig. 6a. Volume change *vs.* mole fraction curves of 1-octadecanol at 298.15 K and 0.1 MPa: (1) hexane; (2) cyclohexane; (3) benzene; (4) $X_b^0=0.503$.

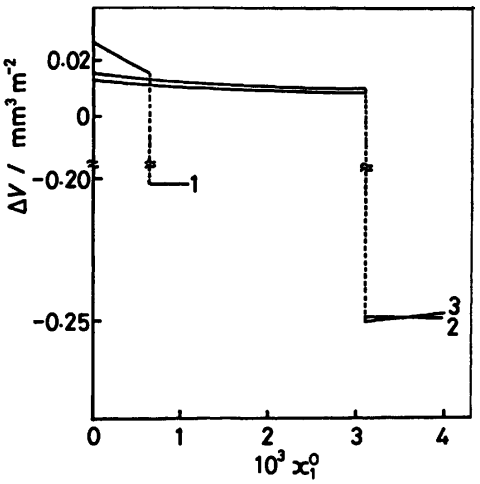

Fig. 6b. Volume change *vs.* mole fraction curves of 1-octadecanol at 298.15 K and 80 MPa: (1) hexane; (2) benzene; (3) $X_b^0=0.503$.

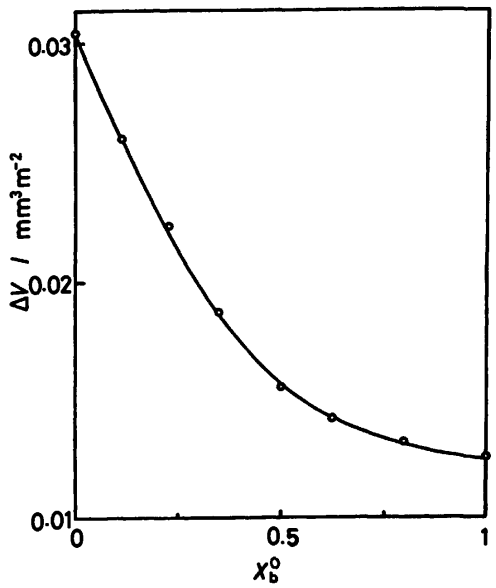

Fig. 7. Volume change *vs.* composition curve for $x_1^0=0$ at 298.15 K and 0.1 MPa.

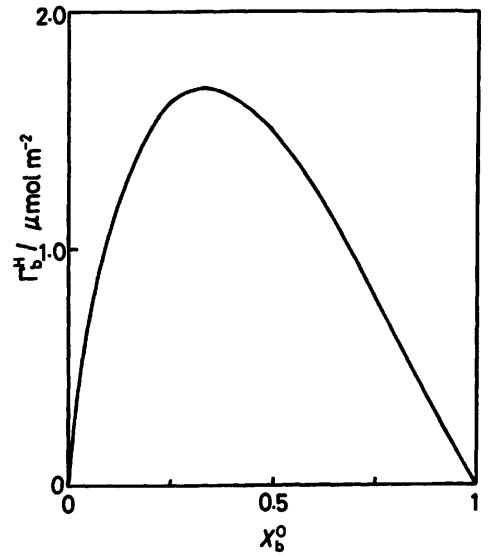

Fig. 8. Interfacial density *vs.* composition curve for $x_1^0=0$ at 298.15 K and 0.1 MPa.

interface to a large negative value of the condensed film, while the Δv values for benzene and $X_b^0=0.503$ systems vary slightly. At 80 MPa, the Δv *vs.* x_1^0 curves of the benzene and $X_b^0=0.503$ systems are quite similar in shape. It is observed that Δv has a large negative value for all the condensed films. This can be accounted for by a negative value of the partial molar volume change associated with the transfer of octadecanol molecules from the solution to the interface.[9,10] The similarity between the adsorption of 1-octadecanol from the mixture and that from benzene is presumed to be accounted for by a large concentration of benzene in the interfacial region. In Figs. 7 and 8, the values of Δv and Γ_b^H evaluated for $x_1^0=0$ are plotted against X_b^0 at 298.15 K and 0.1 MPa.[19] It is seen from Fig. 7 that the Δv *vs.* X_b^0 curve deviates greatly from the straight line connecting the values of the pure cyclohexane and benzene systems and the value of Δv at $X_b^0=0.503$ is not so different from that at $X_b^0=1$. Further, Fig. 8 shows that the value of Γ_b^H is remarkably large at the maximum. These results support the above presumption.

In order to visualize the effect of pressure on the adsorbed film of 1-octadecanol at the oil/water interfaces, let us draw its surface pressure *vs.* area curves. Since the interfacial pressure and the area per 1-octadecanol molecule are defined, respectively, by

$$\pi = \gamma^0 - \gamma, \tag{9}$$

and

$$A = 1/N_A\Gamma_1^H, \tag{10}$$

where γ^0 is the interfacial tension of pure interface and N_A is Avogadro number, the curves are obtained by making use of Figs. 4 and 5. The results are depicted in Figs. 9a and 9b. It is seen that the pressure makes the adsorbed film of 1-octadecanol condensed while the affinity of oil to water does it expanded. It should be

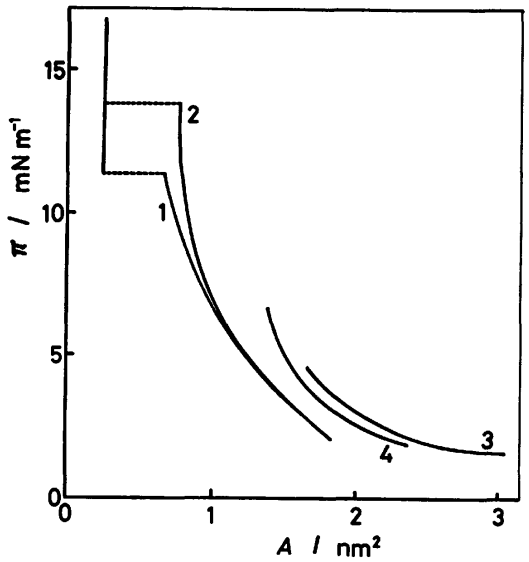

Fig. 9a. Interfacial pressure *vs.* area curves of 1-octadecanol at 298.15 K and 0.1 MPa: (1) hexane; (2) cyclohexane; (3) benzene; (4) $X_b^g=0.503$.

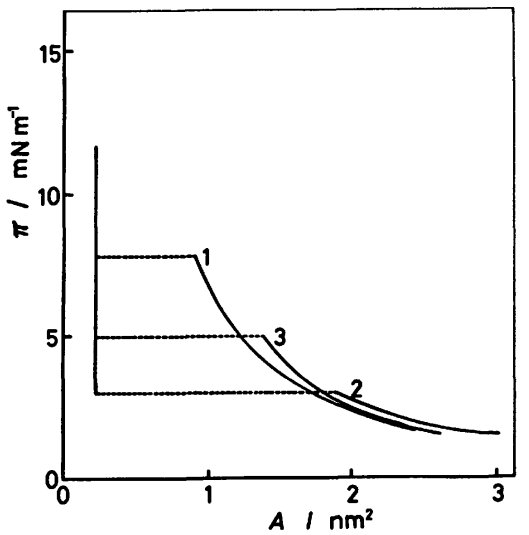

Fig. 9b. Interfacial pressure *vs.* area curves of 1-octadecanol at 298.15 K and 80 MPa: (1) hexane; (2) benzene; (3) $X_b^g=0.503$.

noted that the adsorption behavior of 1-octadecanol at the oil mixture/water interface is affected similarly by pressure.

In conclusion, we can say that the pressure has a significant effect on the phase transition of the adsorbed film to transform the expanded state produced by the affinity of benzene molecules to water molecules into the condensed one.

References

1) E. Hutchinson, *J. Colloid Interface Sci.*, **3**, 219 (1948).
2) E. Hutchinson and D. Randall, *J. Colloid Interface Sci.*, **7**, 151 (1952).
3) J. J. Jasper and B. L. Houseman, *J. Phys. Chem.* **67**, 1548 (1963).
4) E. S. Lutton, C. E. Stauffer, J. B. Martin, and A. J. Fehl, *J. Colloid Interface Sci.*, **30**, 283 (1969).
5) R. Aveyard, B. J. Briscoe, and J. Chapman, *J. Colloid Interface Sci.*, **44**, 282 (1973).
6) R. Vochten, and G. Petre, *J. Colloid Interface Sci.*, **42**, 320 (1973).
7) T. Ikenaga, N. Matubayasi, M. Aratono, and K. Motomura, and R. Matuura, *Bull. Chem. Soc. Jpn.*, **53**, 653 (1980).
8) M. Lin, *C. R. Acad. Sci., Ser. B*, **281**, 619 (1975).
9) K. Motomura, N. Matubayasi, M. Aratono, and R. Matuura, *J. Colloid Interface Sci.*, **64**, 356 (1978).
10) N. Matubayasi, K. Motomura, M. Aratono, and R. Matuura, *Bull. Chem. Soc. Jpn.*, **51**, 2800 (1978).
11) K. Motomura, H. Iyota, M. Aratono, M. Yamanaka, and R. Matuura, *J. Colloid Interface Sci.*, **93**, 264 (1983).
12) N. Matubayasi, K. Motomura, S. Kaneshina, M. Nakamura, and R. Matuura, *Bull. Chem. Soc. Jpn.*, **50**, 523 (1977).
13) G. S. Kell and E. Whally, *Phil. Trans. R. Soc. London, Ser. A*, **258**, 565 (1965).
14) T. Grindly, and J. E. Lind, Jr., *J. Chem. Phys.*, **54**, 3983 (1971).
15) H. Kashiwagi, T. Fukunaga, Y. Tanaka, H. Kubota, and T. Makita, *Rev. Phys. Chem. Jpn.*, **49**, 70 (1979).
16) K. Motomura, *J. Colloid Interface Sci.*, **64**, 348 (1978).
17) K. Motomura, *Adv. Colloid Interface Sci.*, **12**, 1 (1980).
18) K. Motomura, M. Aratono, H. Iyota, and R. Matuura, to be submitted.
19) H. Iyota, M. Aratono, K. Motomura, and R. Matuura, to be submitted.

 © 1983 The Chemical Society of Japan Bull. Chem. Soc. Jpn., 56, 2407—2410 (1983)

Acid-Base and Catalytic Properties of ZrO_2–SnO_2

Gong-Wei WANG, Hideshi HATTORI, and Kozo TANABE*
Department of Chemistry, Faculty of Science, Hokkaido University, Sapporo 060
(Received February 18, 1983)

The acid-base properties of ZrO_2–SnO_2 with different compositions have been measured by the indicator method and the adsorption with NH_3 and CO_2 and the catalytic activities studied. The ZrO_2–SnO_2 (atomic ratio=9 : 1) catalyst which was found to have the highest acid strength and the maximum acid amount exhibited the highest activities for the isomerization of cyclopropane and the dehydration of 2-butanol. The activities of the catalysts with different compositions for the two reactions correlated with the acidic properties. On the other hand, the activities for the isomerization of 1-butene and the decomposition of diacetone alcohol (4-hydroxyl-4-methyl-2-pentanone) correlated with the basic properties. The activity for the dehydrogenation of 2-butanol was found to increase with an increase of the SnO_2 content. The active sites on the ZrO_2–SnO_2 catalysts are discussed.

Recently, many kinds of mixed oxides were reported to show acidic property on the surfaces.[1] Among them, the binary oxides consisting of the oxides of the fourth group metals in the periodic table are interesting from the view-point of the acid-base property. Namely, the acid strengths of SiO_2–TiO_2[2] and SiO_2–ZrO_2[3] are very strong and that of TiO_2–SnO_2[4] is moderate, while TiO_2–ZrO_2 has not only strong acidic property,[5] but also distinct basic property.[6] These catalysts showed interesting activities for particular reactions, respectively. However, no study has been made on the acid-base and catalytic property of ZrO_2–SnO_2, another type of the binary oxides consisting of the fourth group metal oxides. Therefore, various kinds of ZrO_2–SnO_2 with different compositions calcined at different temperatures have been prepared and the acid-base property has been characterized in the present work. The catalytic activity and selectivity for the isomerizations of cyclopropane and 1-butene, and the decompositions of 2-butanol and diacetone alcohol are also studied.

Experimental

Catalysts and Reagents. Zirconium(IV) hydroxide and tin(IV) hydroxide were prepared by adding 28% aqueous ammonia to aqueous solutions of zirconium(IV) dichloride oxide ($ZrOCl_2 \cdot 8H_2O$) and anhydrous tin(IV) chloride ($SnCl_4$), respectively. The precipitates were aged at 100 °C over a water bath for 1 h, washed with deionized water until no chloride ions were detected with a silver nitrate test solution and dried at 100 °C for 24 h. The mixtures of zirconium(IV) and tin(IV) hydroxides with different atomic ratios of Zr to Sn were prepared by coprecipitation of mixed solutions of $ZrOCl_2 \cdot 8H_2O$ and $SnCl_4$ with 28% aqueous ammonia, followed by aging, washing and drying similarly as in the cases of zirconium and tin hydroxides. Zirconium oxide, tin oxide and the binary oxides with different atomic ratios of Zr to Sn were obtained by calcining the respective hydroxides at various temperatures in air for 2 h.

1-Butene and cyclopropane were purified by passage through 4A Molecular Sieves kept at Dry Ice temperature and distilled before use. 2-Butanol and diacetone alcohol were obtained from Wako Pure Chemical Industries Ltd., the latter being purified by vacuum distillation.

Measurement of Physico-chemical Properties. Specific surface areas of the samples calcined in air at various temperatures were obtained by applying the BET equation to the adsorption isotherm of nitrogen at −196 °C. Differential thermal analysis (DTA) and thermal gravimetry (TG) were carried out simultaneously with a heating rate of 10 °C/min. X-Ray diffraction patterns were measured over the range of $2\theta=20$—60 ° for the powdered samples which had been calcined in air at 500 °C for 2 h.

Acidic and basic properties of the samples calcined in the air at 500 °C for 3 h were measured by titrating with butylamine and benzoic acid in benzene, respectively, the indicators of different pK_a values being used.[7] Adsorbed amounts of CO_2 and NH_3 were measured by use of Cahn 200 electrobalance. The sample was outgassed at 500 °C for 2 h. After cooling to room temperature, it was exposed to about 10 Torr (1 Torr≈133.322 Pa) of CO_2 or NH_3 for 30 min, followed by outgassing at room temperature for 20 min.

Reaction Procedure. The isomerizations of 1-butene and cyclopropane were carried out in a closed recirculation reactor having a volume of about 789 ml. Prior to reaction, catalysts were outgassed at 500 °C for 2 h. A 100 Torr of 1-butene or cyclopropane was allowed to react at 100 °C for 1-butene or 300 °C for cyclopropane. The catalyst weights were 200 mg for the isomerization of 1-butene and 400 mg for the isomerization of cyclopropane. The reaction mixture was periodically withdrawn and analyzed by gas chromatography; VZ-7 was used for a 6 m chromatographic column of 4 mm o.d. copper tubing. For the dehydration of 2-butanol, a microcatalytic pulse reactor was employed. One μl of 2-butanol was passed over a 100 mg catalyst at 200 °C in a helium carrier whose flow rate was 20 ml/min. Products were first trapped in a liquid nitrogen trap and flash evaporated into a first gas chromatographic column in which PEG 20M was packed. Olefins which flowed out of the first column were trapped again and flash evaporated into a second gas chromatographic column in which VZ-7 was packed.

The decomposition of diacetone alcohol was carried out at 30±0.5 °C in a reactor of liquid phase suspension. Thirty ml of diacetone alcohol was allowed to react over a powdered catalyst calcined at various temperatures. The sample was taken out from the reactor at 10 min interval and analyzed by gas chromatography.

Activities for all reactions were expressed as initial mole conversion to the product per unit time per unit surface area or unit weight of catalyst.

Results and Discussion

Surface areas of ZrO_2, SnO_2, and the binary oxides with different compositions calcined in the air at different temperatures are given in Table 1. For all samples, the surface areas decreased monotonously with a rise

TABLE 1. SPECIFIC SURFACE AREAS /$m^2\ g^{-1}$

Catalyst composition	Pretreatment temperature/°C				
	500	650	750	850	1000
ZrO_2	47.8	22.8	16.7	6.35	3.06
ZrO_2–SnO_2 (9 : 1)	80.3	37.4	26.6	16.9	8.73
ZrO_2–SnO_2 (7 : 3)	72.6	—	—	—	—
ZrO_2–SnO_2 (1 : 1)	52.2	31.4	27.6	21.4	9.11
ZrO_2–SnO_2 (3 : 7)	59.9	—	—	—	—
ZrO_2–SnO_2 (1 : 9)	57.6	35.8	28.8	27.4	9.94
SnO_2	37.6	—	14.5	8.68	4.85

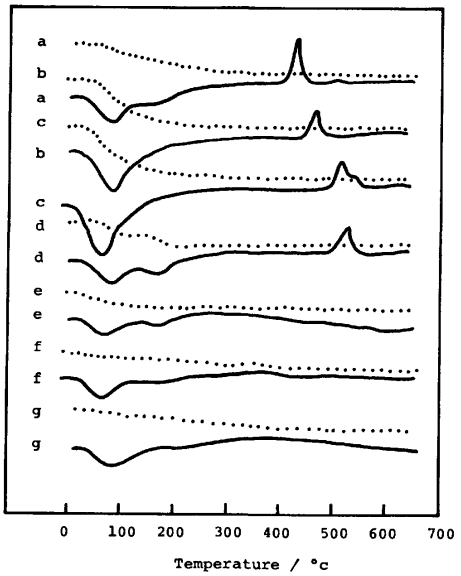

Fig. 1. DTA (——) and TG (·····) diagrams of ZrO_2, SnO_2, and the binary oxides.
a: ZrO_2, b: ZrO_2–SnO_2 (9 : 1), c: ZrO_2–SnO_2 (7 : 3), d: ZrO_2–SnO_2 (1 : 1), e: ZrO_2–SnO_2 (3 : 7), f: ZrO_2–SnO_2 (1 : 9), g: SnO_2.

of the calcination temperature. The binary oxides had larger surface areas than the single component oxides when compared at the same calcination temperature. The DTA and TG curves are shown in Fig. 1. The exothermic peak for ZrO_2 was observed at about 424 °C. The exothermic peaks for the ZrO_2–SnO_2 samples with atomic ratios (Zr/Sn) of 9 : 1, 7 : 3, and 1 : 1 shifted to 459, 508, and 516 °C, respectively. However, no exothermic peaks were observed for SnO_2 and ZrO_2–SnO_2 containing more than 50% of SnO_2. X-Ray diffraction patterns of ZrO_2–SnO_2 (9 : 1) and (7 : 3) were similar to those of monoclinic ZrO_2, while those of ZrO_2–SnO_2 (3 : 7) and (1 : 9) were similar to those of tetragonal SnO_2, though the peaks for the binary oxides were broad as compared with the single component oxides. However, ZrO_2–SnO_2 (1 : 1) showed a distinct but unidentified X-ray peak at $2\theta=29.6°$ in addition to the patterns for ZrO_2 and SnO_2. The acidity and basicity distributions of the catalysts calcined at 500 °C are summarized in Table 2. The acid sites on ZrO_2 and SnO_2 are weak; $H_0=+4.0$ and $+4.8$, respectively. Among the binary oxides, ZrO_2–SnO_2 (9 : 1) showed the highest acid strength whose H_0 value was -3. The other binary oxides were weakly acidic. The strengths were in the range of $H_0=+3.3$—$+4.0$. The amount of basic sites equal to or stronger than $H_-=9.1$ decreased with an increase in SnO_2 content. In the case of ZrO_2–SnO_2 (9 : 1), the amount of basic sites is almost comparable with the amount of acid sites having $H_0 \leqq +6.8$.

The amounts of NH_3 and CO_2 adsorbed on the catalysts outgassed at 500 °C for 2 h are shown in Fig. 2. The adsorbed amount of NH_3 was maximum on ZrO_2–SnO_2 (9 : 1) which showed the highest acid strength. The amount of CO_2 adsorbed decreased with an

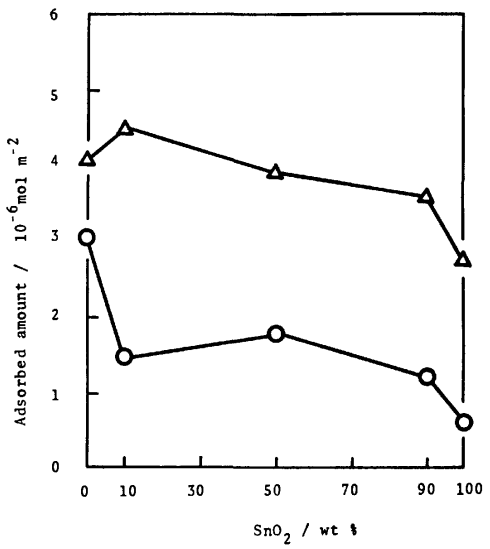

Fig. 2. Change of irreversibly adsorbed amounts of NH_3 and CO_2 with different catalyst compositions.
Temperature of adsorption and desorption: 22 °C, ○: CO_2, △: NH_3.

TABLE 2. ACIDITY AND BASICITY DISTRIBUTION OF ZrO_2–SnO_2 CALCINED AT 500 °C

Catalyst composition	Surface area / $m^2\ g^{-1}$	Acidity and basicity distribution/mmol g^{-1}						
		-3.0[a]	$+1.5$[a]	$+3.3$[a]	$+4.0$[a]	$+4.8$[a]	$+6.8$[a]	$+9.1$[b]
ZrO_2	47.9	0	0	0	0.29	—	—	0.36
ZrO_2–SnO_2 (9 : 1)	80.3	0.072	0.086	0.20	0.25	—	0.28	0.31
ZrO_2–SnO_2 (7 : 3)	72.6	0	0	0	0.17	—	0.21	0.27
ZrO_2–SnO_2 (1 : 1)	52.9	0	0	0	0.12	—	0.15	0.25
ZrO_2–SnO_2 (3 : 7)	59.9	0	0	0	0.19	—	0.12	0.19
ZrO_2–SnO_2 (1 : 9)	57.6	0	0	0.053	0.12	—	0.19	0.058
SnO_2	31.6	0	0	0	0	0.13[c]	—	—

a) H_0 value. b) H_- value. c) Cited from K. Shibata, T. Kiyoura, J. Kitagawa, T. Sumiyoshi, and K. Tanabe, *Bull. Chem. Soc. Jpn.*, **46**, 2985 (1973).

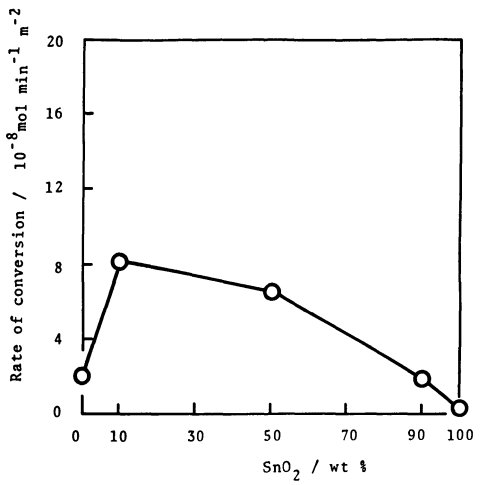

Fig. 3. Change in catalytic activity for isomerization of cyclopropane with catalyst compositions.
Reaction temperature: 300 °C.

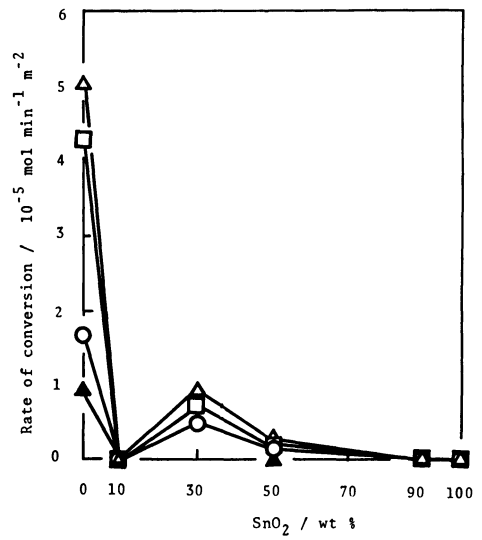

Fig. 4. Change in catalytic activity for isomerization of 1-butene with catalyst compositions.
Pretreatment temperature, ○: 500 °C, □: 750 °C, △: 850 °C, ▲: 1000 °C.

increase in SnO_2 content except ZrO_2–SnO_2 (9 : 1). The basic sites on all samples were as weak as $H_- = -9.1$.

The activities of the catalysts calcined at 500 °C for the isomerization of cyclopropane are plotted against the catalyst composition in Fig. 3. The activity change roughly correlates with the change of the acid amount measured by NH_3 adsorption shown in Fig. 2. The highest activity was observed over the ZrO_2–SnO_2 (9 : 1) catalyst which showed the maximum acid amount and the highest acid strength (*cf.* Table 2).

Table 3. Distribution of products in isomerization of 1-butene in 60 min

Catalyst composition	Products distribution/%			*cis*-/*trans*-
	cis-2-Butene	*trans*-2-Butene	1-Butene	
ZrO_2	56.2	31.6	12.2	1.78
ZrO_2–SnO_2 (9 : 1)	0	0	100	—
ZrO_2–SnO_2 (7 : 3)	43.0	14.0	43.0	3.05
ZrO_2–SnO_2 (1 ; 1)	5.74	1.25	93.0	4.59
ZrO_2–SnO_2 (3 : 7)	0.52	0	99.5	
ZrO_2–SnO_2 (1 : 9)	0.93	0	99.1	
SnO_2	1.37	0	98.6	

The variations in the activities for the isomerization of 1-butene as a function of SnO_2 content are shown in Fig. 4 for the catalysts calcined at different temperatures. For all catalysts, the activities increased with an increase in the calcination temperature and reached maxima when calcined at 850 °C. Further increase in the calcination temperature to 1000 °C resulted in a decrease in the activities. It is interesting to note that the ZrO_2–SnO_2 (9 : 1) catalyst showed no activity in spite of its acid sites being stronger than those of the other catalysts. The products distributions in the isomerization of 1-butene are summarized in Table 3. With all catalysts, *cis*-2-butene was predominantly formed. The predominant formation of *cis*-2-butene is generally observed in the base-catalyzed isomerization of 1-butene[8–11] in contrast with the formation of about equal amounts of *cis*-2-butene and *trans*-2-butene in the acid-catalyzed reaction.[8,12] Therefore, the isomerization is suggested to proceed by a carbanion mechanism over the all catalysts. Hence, no activity of the ZrO_2–SnO_2 (9 : 1) catalyst seems to be partly due to the small amount of basic sites as seen in Fig. 2, and partly due to the basic strength being weakened by the electron shift to the neighboring strong acid sites.

The results of the decomposition of 2-butanol are summarized in Table 4. As the content of SnO_2 increased, the dehydration to 1-butene decreased, whereas the dehydrogenation to ethyl methyl ketone increased. The highest activity for the formation of butenes was

Table 4. Catalytic activity and distribution of products in decomposition of 2-butanol

Catalyst composition	Distribution of products/%					$\frac{1\text{-}C_4'}{2\text{-}C_4'}$	*cis*-/*trans*-	Conversion 10^{-5} mol m^{-2}
	1-Butene	*trans*-2-Butene	*cis*-2-Butene	Ketone	2-Butanol			
ZrO_2	2.49	—	—	0.21	97.3	—	—	0.61
ZrO_2–SnO_2 (9 : 1)	1.47	0.50	2.34	4.50	91.2	0.51	4.68	1.19
ZrO_2–SnO_2 (7 : 3)	1.27	—	—	12.7	86.1	—	—	2.10
ZrO_2–SnO_2 (1 : 1)	0.46	—	—	19.4	80.1	—	—	4.15
ZrO_2–SnO_2 (3 : 7)	—	—	—	40.1	52.3	—	—	7.59
ZrO_2–SnO_2 (1 : 9)	—	—	—	41.8	57.9	—	—	7.98
SnO_2	—	—	—	33.0	66.5	—	—	11.6

$1\text{-}C_4'$: 1-Butene: $2\text{-}C_4'$: 2-butenes.

observed over ZrO_2–SnO_2 (9 : 1) which possessed the highest acidity. The dehydration activity correlates with the catalyst acidity. The butenes produced over ZrO_2, ZrO_2–SnO_2 (7 : 3) and (1 : 1) consisted exclusively of 1-butene. In the case of the ZrO_2–SnO_2 (9 : 1) catalyst, however, the formation of 2-butenes exceeded that of 1-butene. This was generally observed in the dehydrations catalyzed by strong acids.[13] It is suggested that the relatively strong acid sites which are generated on the surface of ZrO_2–SnO_2 (9 : 1) (*cf.* Table 2) are the active sites for the dehydration.

The decrease of the dehydrogenation activity with the increase of ZrO_2 content might be attributed to the decrease in the reducing property of SnO_2 on mixing of ZrO_2, since the reducing property of SnO_2 is reported to decrease on mixing of the other oxide, TiO_2.[4]

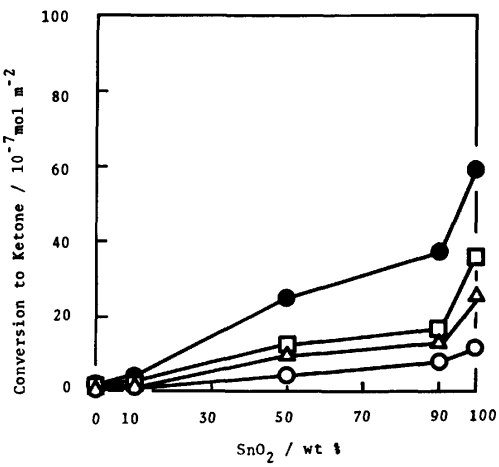

Fig. 5. Change of conversion to ketone from 2-butanol with change of pretreatment temperature of catalysts.
○: 500 °C, △: 750 °C, □: 850 °C, ●: 1000°C.

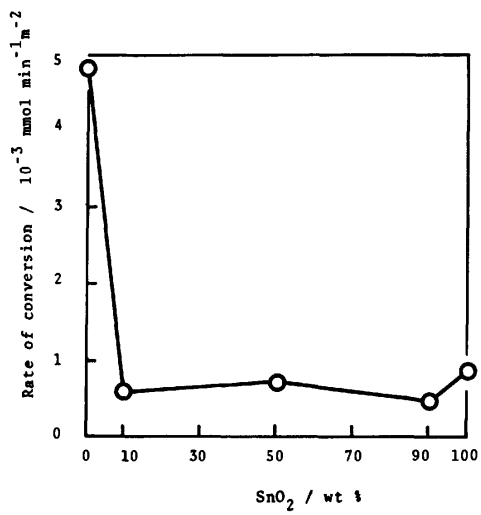

Fig. 6. Change in catalytic activity for decomposition of diacetone alcohol with catalyst compositions.

The conversion of 2-butanol to ethyl methyl ketone in the decomposition of 2-butanol over the catalysts calcined at different temperatures are plotted against the catalyst composition in Fig. 5. The formation of ethyl methyl ketone increased with a rise of the calcination temperature for all catalysts.

The activities for the decomposition of diacetone alcohol are shown in Fig. 6. The activities decreased as the content of SnO_2 increased. The activity change is roughly similar to the basicity change in Fig. 2. The little ambiguity is probably due to the difference in basic strength, though it could not be differentiated by the indicator method. Thus, the decomposition of diacetone alcohol is concluded to be controlled by both the amount and strength of the basic sites on the catalyst.

In summary, the ZrO_2–SnO_2 (9 : 1) catalyst can be classified as a solid acid catalyst having a moderate acid strength ($H_0 \leqq -3$). The acid strength is lower than that of SiO_2–TiO_2, SiO_2–ZrO_2, or TiO_2–ZrO_2 and almost equal to that of TiO_2–SnO_2. The difference in acid-base property of ZrO_2–SnO_2 from TiO_2–SnO_2 is that the ZrO_2–SnO_2 catalysts with different compositions have a definite basic property and only the ZrO_2–SnO_2 (9 : 1) showed the acid strength of $H_0 \leqq -3$. These acid-base properties reflected on the catalytic behavior.

Reference

1) K. Tanabe, "Catalysis-Science and Technology," ed by J. R. Anderson and M. Boudart, Springer-Verlag, New York (1981), Vol. 2, p. 231.
2) M. Itoh, H. Hattori, and K. Tanabe, *J. Catal.*, **35**, 225 (1974).
3) V. A. Dzisko, *Proc. Intern. Congr. Catalysis, 3rd, Amsterdam*, **I**. No. 19 (1964).
4) M. Itoh, H. Hattori, and K. Tanabe, *J. Catal.*, **43**, 192 (1976).
5) K. Shibata, T. Kiyoura, J. Kitagawa, T. Sumiyoshi, and K. Tanabe, *Bull. Chem. Soc. Jpn.*, **46**, 2985 (1973).
6) K. Arata, S. Akutagawa, and K. Tanabe, *Bull. Chem. Soc. Jpn.*, **49**, 390 (1976).
7) K. Tanabe, "Solid Acids and Bases," Kodansha, Tokyo, Academic Press, New York (1970).
8) N. F. Foster and R. J. Cvetanovic, *J. Am. Chem. Soc.*, **82** 4274 (1960).
9) C. C. Chang, W. C. Conner, and R. J. Kokes, *J. Phys. Chem.*, **77**, 1957 (1973).
10) H. Hattori, N. Yoshii, and K. Tanabe, *Proc. Intern. Congr. Catalysis, 5th*, **1972**, **10**-233 (1973).
11) S. Banks, *J. Am. Chem. Soc.*, **87**, 3245 (1965).
12) J. Hightower and W. K. Hall, *Chem. Eng. Prog.*, **63**, 122 (1967).
13) T. Yamaguchi and K. Tanabe, *Bull. Chem. Soc. Jpn.*, **47**, 424 (1974).

The Molecular Structures of (*t*-Butyl)(chloro)[(−)-sparteine]magnesium(II)† and Dichloro[(−)-sparteine]magnesium(II)††

Hiroyuki KAGEYAMA, Kunio MIKI, Yasushi KAI, Nobutami KASAI,*
Yoshio OKAMOTO, and Heimei YUKI†††
Department of Applied Chemistry, Faculty of Engineering, Osaka University, Yamadaoka, Suita, Osaka 565
Department of Chemistry, Faculty of Engineering Science, Osaka University, Machikaneyama, Toyonaka, Osaka 560

(Received March 9, 1983)

Crystals of *t*-BuMgCl–(−)-sparteine (**1**) belongs to orthorhombic system; $P2_12_12_1$, $a=25.689(6)$, $b=10.030(2)$, $c=7.942(2)$ Å, and $Z=4$; $MgCl_2$–(−)-sparteine (**2**) also crystallizes in orthorhombic system; $P2_12_12_1$, $a=11.180(4)$, $b=11.957(4)$, $c=12.573(5)$ Å, and $Z=4$. Both structures were solved by the heavy atom method, and refined by the block-diagonal least-squares procedure; (**1**) $R=0.098$ for 1199 non-zero reflections and (**2**) $R=0.091$ for 1347 observed reflections. The Mg atom in each complex has a distorted tetrahedral geometry: (**1**) Mg–N= 2.17(2) and 2.18(2), Mg–C=2.19(2), and Mg–Cl=2.332(7) Å and N–Mg–N=83.9(5)°; (**2**) Mg–N=2.150(9) and 2.160(9), and Mg–Cl=2.269(5) and 2.279(6) Å, and N–Mg–N=85.0(4)°.

The kinetics[1] and the structure and reactivity of a series of Grignard reagent–(−)-sparteine (or its derivative) complexes in the asymmetric selective polymerization of α-methylbenzyl methacrylate have been studied. The molecular structure of EtMgBr–(−)-sparteine,[2] which chooses the (*S*)-monomer out of the racemic mixture of α-methylbenzyl methacrylate (or other methacrylates) and initiates the asymmetric selective polymerization, has been determined by means of X-ray diffraction. Molecular structures of the inactive EtMgBr–(−)-α-isosparteine[3] and *t*-BuMgCl–(−)-sparteine also have been determined. This paper deals with the crystal structure determination of inactive *t*-BuMgCl–(−)-sparteine (**1**) and of related complex $MgCl_2$–(−)-sparteine (**2**).

Experimental

Many trials to prepare the complex between *t*-BuMgBr and (−)-sparteine have been unsuccessful. The *t*-BuMgCl–(−)-sparteine was then prepared by mixing a toluene solution of (−)-sparteine and an ether solution of *t*-BuMgCl under nitrogen atmosphere. Crystals obtained were recrystallized from toluene, which were used for X-ray study. All of the crystals examined did not give any sharp diffraction profiles. The other crystals, obtained from the mother liquor at room temperature, were also recrystallized from toluene, which were first considered as *t*-BuMgCl–(−)-sparteine and were later found as $MgCl_2$–(−)-sparteine. *t*-BuMgCl–(−)-sparteine was then prepared again and recrystallized from toluene. The crystals were found useful for X-ray diffraction data collection.

As both crystals were sensitive to moisture in the air, they were sealed in thin-walled glass capillary tubes, which were mounted on a Rigaku automated, four-circle diffractometer. Graphite monochromatized Mo *Kα* radiation ($\lambda=0.71069$ Å) was used. Unit-cell dimensions were determined by the least-squares fit using 2θ values of 25 strong reflections. A prismatic crystal of *t*-BuMgCl–(−)-sparteine with approximate dimensions of $0.4\times0.20\times0.18$ mm³ was used for the X-ray experiment. The $MgCl_2$–(−)-sparteine crystal used had dimensions of $0.20\times0.18\times0.50$ mm³.

Crystal Data. *t*-BuMgCl–(−)-sparteine (**1**): $C_{19}H_{35}N_2$-MgCl, M 351.3, orthorhombic, space group $P2_12_12_1$, $a=25.689(6)$, $b=10.030(2)$, $c=7.942(2)$ Å, $V=2046.3(7)$ Å³, $D_c=1.140$ g cm⁻³ for $Z=4$, μ(Mo *Kα*)=2.22 cm⁻¹. $MgCl_2$–(−)-sparteine (**2**): $C_{15}H_{26}N_2MgCl$, M 329.6, orthorhombic, space group $P2_12_12_1$, $a=11.180(4)$, $b=11.957(4)$, $c=12.573(5)$ Å, $V=1680.7(10)$ Å³, $D_c=1.303$ g cm⁻³ for $Z=4$, μ(Mo *Kα*)= 4.18 cm⁻¹.

Integrated intensities for both crystals were measured by the θ-2θ scan technique (**1**) $2\theta\leqq46.0°$; (**2**) $2\theta\leqq50.5°$: the 2θ scan rate was 4° min⁻¹ and the scan width $\Delta2\theta=(2.4+0.7\ \tan\theta)°$. The background scattering was counted for 7.5 s at both ends of a scan. Four standard reflections measured after every 60 reflections were used in order to check the crystal orientation and X-ray damage. They showed less than 5% fluctuation throughout the data collection of *t*-BuMgCl–(−)-sparteine. For $MgCl_2$–(−)-sparteine, the intensities of the four standard reflections decreased; as they did so uniformly with time, the observed intensities were corrected linearly. Usual corrections for Lorentz and polarization effects were applied but those for absorption and extinction corrections were ignored. Totals of 1678 (1199 non-zero) and 1763 (1451 non-zero) reflections were collected for *t*-BuMgCl–(−)-sparteine and $MgCl_2$–(−)-sparteine, respectively.

Structure Solution and Refinement

Both structures were solved by the heavy atom method, and refined anisotropically for non-hydrogen atoms by the block-diagonal least-squares procedure (*HBLS* V).[4] The function minimized was $\sum w(\Delta F)^2$. The H atoms were located and fixed at the calculated positions with equal isotropic thermal parameters ($B=3.3$ Å²). At the final stage of the refinement the anomalous dispersion of all the non-hydrogen atoms were considered.

t-BuMgCl–(−)-sparteine. (1) Initial positional parameters of the Cl and Mg atoms were determined by a three-dimensional Patterson function with the aid of the direct method (*MULTAN* 78).[5] The N and C atoms were located on a subsequent Fourier map. The structure was then refined. The final R factor was 0.098 for non-zero (0.206 for all) reflections and R_w was 0.124. The weighting schemes used at the final stage were

† Abbreviated as *t*-BuMgCl–(−)-sparteine.
†† Abbreviated as $MgCl_2$–(−)-sparteine.
††† Present address: Tezukayama-Gakuin Women's Junior College, Tezukayama, Sumiyoshi-ku, Osaka 558.

TABLE 1. FINAL ATOMIC POSITIONAL PARAMETERS, OF *t*-BuMgCl-(−)-SPARTEINE, WITH THEIR ESTIMATED STANDARD DEVIATIONS IN PARENTHESES

Atom	*x*	*y*	*z*	B_{eq}[a)]/Å^2
Cl	0.04219(14)	0.0720(4)	0.0861(5)	4.4
Mg	0.1037(2)	0.0490(4)	0.3000(6)	2.7
N(1)	0.1347(4)	0.2502(10)	0.3113(12)	2.7
N(2)	0.0784(4)	0.0905(10)	0.5561(12)	3.0
C(1)	0.1570(5)	−0.1191(14)	0.2685(21)	5.0
C(2)	0.0522(6)	−0.0317(14)	0.6271(17)	4.5
C(3)	−0.0009(6)	−0.0534(14)	0.5246(18)	4.9
C(4)	−0.0345(6)	0.0665(15)	0.5460(19)	5.3
C(5)	−0.0070(5)	0.1945(12)	0.4890(17)	3.7
C(6)	0.0441(5)	0.2093(12)	0.5822(16)	3.5
C(7)	0.0741(5)	0.3374(12)	0.5315(17)	3.3
C(8)	0.1187(5)	0.3553(14)	0.6599(19)	4.7
C(9)	0.1567(5)	0.2412(13)	0.6174(15)	3.3
C(10)	0.1281(5)	0.1091(12)	0.6602(17)	3.8
C(11)	0.1780(5)	0.2510(13)	0.4395(15)	3.1
C(12)	0.2152(6)	0.3681(13)	0.4197(20)	4.4
C(13)	0.2377(6)	0.3759(15)	0.2402(19)	4.8
C(14)	0.1931(6)	0.3911(13)	0.1188(18)	4.5
C(15)	0.1563(5)	0.2664(14)	0.1402(16)	4.3
C(16)	0.1599(9)	−0.1386(21)	0.0811(26)	10.4
C(17)	0.0933(5)	0.3472(13)	0.3514(16)	3.6
C(18)	0.2118(7)	−0.1074(20)	0.3303(35)	11.0
C(19)	0.1320(8)	−0.2424(16)	0.3391(30)	8.8

a) After Hamilton.[6)]

$w=\{\sigma_{cs}^2(F_o)+0.03251|F_o|+0.00231|F_o|^2\}^{-1}$ for $|F_o|>0$ and $w=0.02855$ for $|F_o|=0$.

The final atomic positional and equivalent thermal parameters[6)] are listed in Table 1.††††

$MgCl_2$-(−)-sparteine (**2**). The crystals were expected to contain *t*-BuMgCl-(−)-sparteine, but the three-dimensional Patterson function could not be interpreted satisfactorily. The *E*-map calculated by using the *MULTAN* 78 program showed a good coincidence with the interpretation of the Patterson map for $MgCl_2$-(−)-sparteine instead of *t*-BuMgCl-(−)-sparteine. The Fourier synthesis based on the phases of the Mg and two Cl atoms revealed the remaining N and C atoms of the $MgCl_2$-(−)-sparteine. The anisotropic refinement gave the final *R* as 0.091 for 1347 observed ($|F_o|\leqq 3\sigma(F_o)$) reflections ($R_w=0.104$). At the final stage the weighting scheme used was $w=\{\sigma^2(F_o)+0.10124|F_o|\}^{-1}$. The final atomic positional and equivalent thermal parameters are listed in Table 2.††††

Atomic scattering factors[7)] and anomalous dispersion coefficient[8)] used in the refinement were taken from the International Tables for X-Ray Crystallography. All the computations were done on an ACOS 700S computer at the Crystallographic Research Center, Institute for Protein Research, Osaka University.

†††† Tables of observed and calculated structure factors and anisotropic thermal parameters and calculated hydrogen positions of *t*-BuMgCl-(−)-sparteine and $MgCl_2$-(−)-sparteine are kept at the Chemical Society of Japan, Document No. 8335.

TABLE 2. FINAL ATOMIC POSITIONAL PARAMETERS, OF $MgCl_2$-(−)-SPARTEINE, WITH THEIR ESTIMATED STANDARD DEVIATIONS IN PARENTHESES

Atom	*x*	*y*	*z*	B_{eq}[a)]/Å^2
Cl(1)	0.2110(4)	0.1164(3)	0.0138(3)	4.4
Cl(2)	0.1761(4)	0.4379(3)	0.0491(3)	5.0
Mg	0.1941(4)	0.2655(3)	0.1245(3)	2.4
N(1)	0.0535(7)	0.2304(7)	0.2364(7)	2.0
N(2)	0.3045(7)	0.2883(7)	0.2637(7)	2.5
C(2)	0.4269(10)	0.3228(9)	0.2285(10)	3.1
C(3)	0.4870(10)	0.2277(12)	0.1643(12)	4.4
C(4)	0.4951(12)	0.1249(12)	0.2267(12)	4.9
C(5)	0.3706(11)	0.0927(10)	0.2696(10)	3.8
C(6)	0.3131(10)	0.1923(9)	0.3313(9)	3.0
C(7)	0.1912(10)	0.1645(10)	0.3825(9)	3.2
C(8)	0.1487(11)	0.2595(12)	0.4476(9)	4.1
C(9)	0.1321(10)	0.3544(10)	0.3769(9)	3.3
C(10)	0.2521(11)	0.3816(10)	0.3246(10)	3.8
C(11)	0.0296(10)	0.3308(9)	0.2979(8)	2.5
C(12)	−0.0933(11)	0.3261(10)	0.3540(10)	3.5
C(13)	−0.1945(10)	0.3024(10)	0.2780(10)	3.3
C(14)	−0.1689(11)	0.1950(11)	0.2237(11)	4.1
C(15)	−0.0496(10)	0.1987(11)	0.1636(11)	3.7
C(17)	0.0889(10)	0.1354(9)	0.3016(10)	3.2

a) After Hamilton.[6)]

Results and Discussion

Molecular Structure. Perspective views (*ORTEP* II)[9)] of *t*-BuMgCl-(−)-sparteine and $MgCl_2$-(−)-sparteine molecules with the numbering scheme of atoms are drawn in Figs. 1 and 2, respectively. Bond lengths and bond angles in the two complexes are given in Figs. 3 and 4, respectively.

t-*BuMgCl-(−)-sparteine* (**1**). The coordination geometry around the Mg atom is distorted tetrahedral: two N atoms of the sparteine skeleton, the C atom of the *t*-Bu group and the Cl bond to the Mg atom. Two Mg–N bond lengths are equal [2.171(12) and 2.175(12) Å] and the N(1)–Mg–N(2) angle is 83.9(5)°. The Mg–C(1) bond length of 2.19(2) Å is comparable with that in EtMgBr-(−)-sparteine [2.24(3) Å].[3)] The Mg–Cl bond length is 2.332(7) Å. The Cl–Mg–N(2) angle [117.4(4)°] is much larger than the Cl–Mg–N(1) angle [100.8(4)°]. The (−)-sparteine skeleton has a similar structure to that in EtMgBr-(−)-sparteine (an all-chair conformation). The remarkable feature of the structure is that the geometrical relation of the alkyl and halogen ligands to the (−)-sparteine skeleton in the present complex is reverse to that in EtMgBr-(−)-sparteine. The initial stage of the asymmetric selective polymerization of racemic methacrylate is considered to be coordination of the carbonyl oxygen of a substrate to the Mg atom of a Grignard reagent-(−)-sparteine complex.[1)]

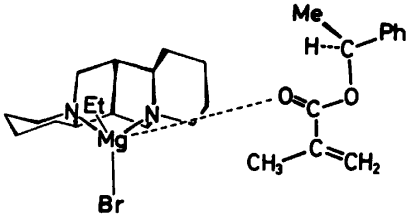

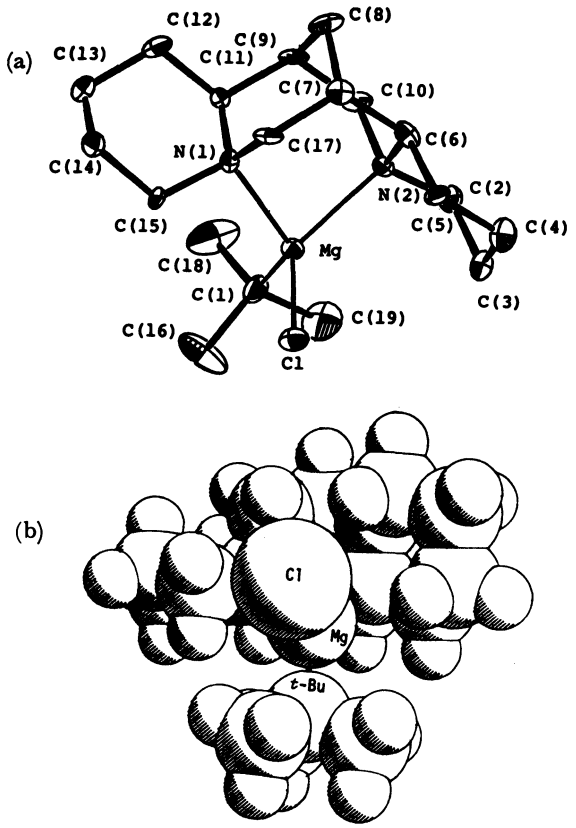

Fig. 1. (a): A perspective view[9] of the *t*-BuMgCl–(−)-sparteine molecule with the numbering scheme of atoms. Non-hydrogen atoms are drawn as thermal ellipsoids with 20% probability level. (b): A space-filling model[10] of the *t*-BuMgCl–(−)-sparteine molecule.

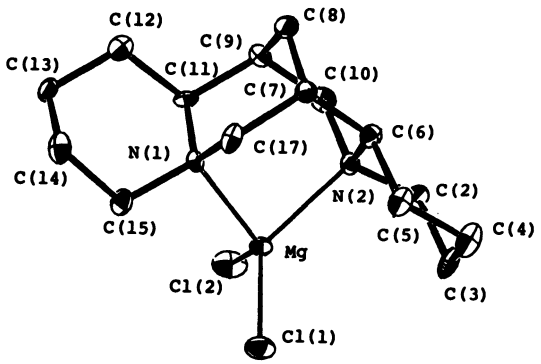

Fig. 2. A perspective view[9] of the $MgCl_2$–(−)-sparteine molecule with the numbering scheme of atoms. Non-hydrogen atoms are drawn as thermal ellipsoids with 20% probability level.

In the latter complex, the Et ligand is not so large and the Mg atom has a sufficient room to access the substrate in its neighborhood. In the former, however, the bulky *t*-Bu group blocks the central Mg atom from the substrate together with the Cl atom. This fact may explain the inactivity of the *t*-BuMgCl–(−)-sparteine on the asymmetric selective polymerization of methyl methacrylate.

$MgCl_2$–(−)-sparteine (2). As is seen in Fig. 2, the central Mg atom is tetrahedrally coordinated by

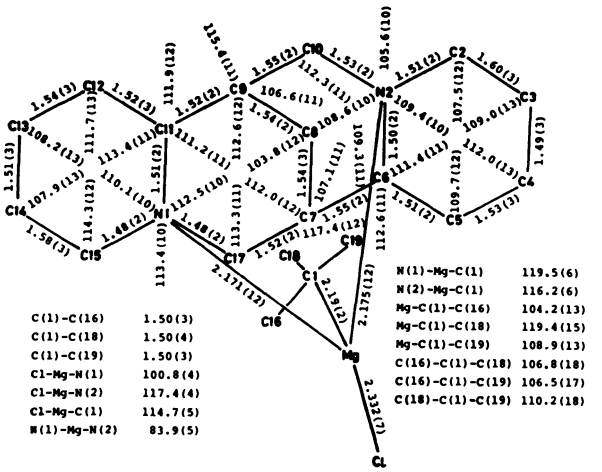

Fig. 3. Selected bond lengths [*l*/Å] and bond angles [ϕ/°] in the *t*-BuMgCl–(−)-sparteine molecule.

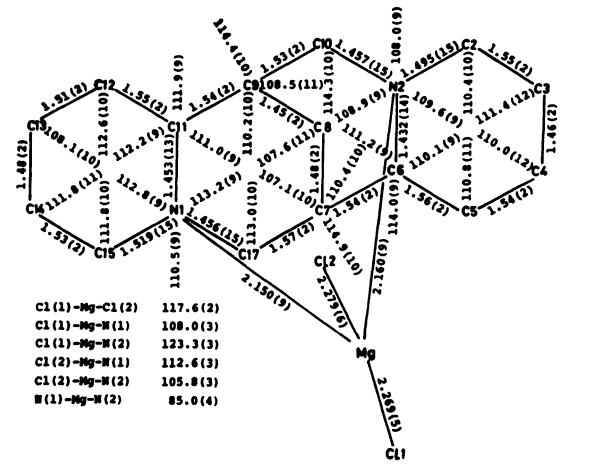

Fig. 4. Selected bond lengths [*l*/Å] and bond angles [ϕ/°] in the $MgCl_2$–(−)-sparteine molecule.

two N atoms of (−)-sparteine and two Cl ligands. Two Mg–N bond lengths [2.150(9) and 2.160(9) Å] are equal, and they are also equal to those in EtMgBr–(−)-sparteine [2.14(2) and 2.16(3) Å][2] and in *t*-BuMgCl–(−)-sparteine mentioned above. The N(1)–Mg–N(2) angle [85.0(4)°] is also equal to those in EtMgBr–(−)-sparteine [84.0(8)°] and *t*-BuMgCl–(−)-sparteine. Two Mg–Cl bonds are equal in length [2.269(5) and 2.279(6) Å], but they are significantly shorter than that in *t*-BuMgCl–(−)-sparteine. The Cl(1)–Mg–N(2) angle [123.3(3)°] is larger than the Cl(1)–Mg–N(1) [108.0(3)°] whereas the Cl(2)–Mg–N(2) [105.8(3)°] is smaller than Cl(2)–Mg–N(1) [112.6(3)°]. The (−)-sparteine skeleton in the present complex has nearly the same structure as those in EtMgBr–(−)-sparteine and *t*-BuMgCl–(−)-sparteine.

Crystal Structure. The crystal structures of *t*-BuMgCl–(−)-sparteine and $MgCl_2$–(−)-sparteine are depicted in Figs. 5 and 6, respectively. The closest intermolecular atomic contact in *t*-BuMgCl–(−)-sparteine is 3.73(3) Å (C(14) (x, y, z)···C(12) $(1/2-x, 1-y, -1/2+z)$). Molecular contacts in the crystal are rather loose, which may explain poor quality of the

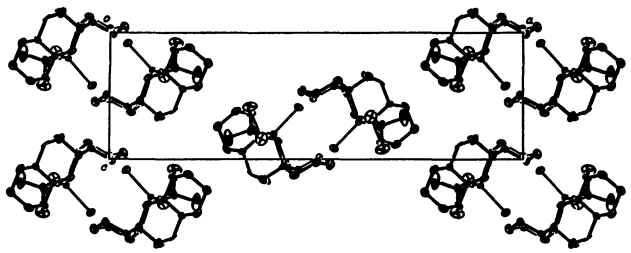

Fig. 5. The crystal structure of *t*-BuMgCl–(−)-sparteine.[9]

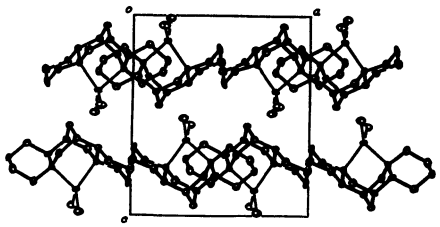

Fig. 6. The crystal structure of $MgCl_2$–(−)-sparteine.[9]

crystal. The shortest interatomic distance between molecules in contact in $MgCl_2$–(−)-sparteine is 3.64(2) Å (C(10) $(x, y, z)\cdots$C(12) $(1/2-x, 1-y, 1/2+z)$).

A part of the cost of this study was defrayed by the Grant-in-Aid for Scientific Research (No. 56470069) from the Ministry of Education, Science and Culture.

References

1) Y. Okamoto, K. Suzuki, T. Kitayama, H. Yuki, H. Kageyama, K. Miki, N. Tanaka, and N. Kasai, *J. Am. Chem. Soc.*, **104**, 4618 (1982).

2) H. Kageyama, K. Miki, N. Tanaka, N. Kasai, Y. Okamoto, and H. Yuki, *Bull. Chem. Soc. Jpn.*, **56**, 1319 (1983).

3) H. Kageyama, K. Miki, Y. Kai, N. Kasai, Y. Okamoto, and H. Yuki, *Acta Crystallogr., Sect. B.*, **38**, 2264 (1982).

4) T. Ashida, *HBLS* V, The Universal Crystallographic Computing System-Osaka, The Computation Center, Osaka Univ. (1973), pp. 55—61.

5) P. Main, S. E. Hull, L. Lessinger, G. Germain, J.-P. Declercq, and M. M. Woolfson, *MULTAN* 78, A System of Computer Programs for the Automatic Solution of Crystal Structures from X-ray Diffraction Data, University of York, England (1978).

6) W. C. Hamilton, *Acta Crystallogr.*, **12**, 609 (1959).

7) "International Tables for X-Ray Crystallography," Kynoch Press, Birmingham (1974), Vol. IV, p. 71.

8) Ref 7, p. 148.

9) C. K. Johnson, *ORTEP* II, Report ORNL-5138, Oak Ridge National Laboratory, Tennessee (1976).

10) S. Motherwell, *PLUTO*, Cambridge Crystallographic File User Mannual (1976).

 © 1983 The Chemical Society of Japan Bull. Chem. Soc. Jpn., 56, 2415—2419 (1983)

Mass-spectrometric Measurements of Thermodynamic Properties of the Molten KCl-$MnCl_2$ System

Tadashi Sasamoto,* Mitsuru Itoh,†,†† and Toshiyuki Sata†,†††
Tokyo National Technical College, 1220-2 Kunugida, Hachioji, Tokyo 193
†*Research Laboratory of Engineering Materials, Tokyo Institute of Technology, 4259 Nagatsuta, Midori-ku, Yokohama 227*
(Received September 27, 1982)

Activities and heats of mixing for the molten KCl-$MnCl_2$ system were determined mass-spectrometrically by the ion-current ratio method. Activities of components KCl and $MnCl_2$ show large negative deviations from Raoult's law, indicating a very strong interaction between KCl and $MnCl_2$. Entropies of mixing calculated from measured activities and heats of mixing have minimum values in the vicinity of 33% $MnCl_2$, and have been compared with those calculated on the basis of some molten structure models to infer possible chemical species in the molten salt.

Thermodynamic measurements on molten salts have so far been made mainly by the calorimetric or the emf method. In our previous investigation[1] we measured mass-spectrometrically activities in both solid and liquid solutions of the KCl-NaCl system, and showed that mass spectrometry had a wide range of application in the measurement of thermodynamic properties in multicomponent salt systems.

The aim of the present study is to measure activities, heats of mixing, and entropies of mixing for the KCl-$MnCl_2$ system by mass spectrometry and to discuss the relation between thermodynamic properties and molten salt structures in such binary charge-unsymmetrical molten salt mixtures as an alkali-metal halide–transition metal halide system.

There have been many reports on physical properties of the molten KCl-$MnCl_2$ system: density,[2,3] molar refractivity,[4] electrical conductivity,[2,3] magnetism,[5] liquid structure according to the X-ray diffraction analysis,[6] Raman spectra,[7] and absorption spectra.[8] Papatheodorou and Kleppa[9] and Kleppa and McCarty[10] measured enthalpies of mixing for alkali-metal chloride-MCl_2 systems (M=Mn, Co, Ni, and Mg) by using calorimeters. They found that exothermic enthalpies of mixing, ΔH^M, increase sharply with increasing ionic radius of alkali-metals and that the interaction parameter, $\lambda^M=\Delta H^M/X_1X_2$ (X_1 and X_2 are mole fractions of MCl_2 and ACl, respectively), has a minimum near $X_{MnCl_2}=1/3$ only, indicating an appreciable formation of tetrahedral complex MCl_4^{2-} in the mixture. On the other hand, the emf method also has been applied to the charge-unsymmetrical alkali-metal chloride-MCl_2 molten salts: M=Mn,[11,12] Co,[13] Ni,[14] Zn,[15] Mg,[16] Ca, Sr, and Ba.[17] These reports showed that each heat of mixing agreed roughly with each of those obtained by the variation of mixing entropy with composition was characterized by an S-shaped curve in the vicinity of $X_{MnCl_2}=0.33$. The S-shaped behavior of entropy has been explained by a few investigators[11,16,18] in terms of the partial dissociation of ionic complex species through the reaction

$$[MCl_4]^{2-} \rightleftharpoons M^{2+} + 4Cl^-, \quad (1)$$

whereas Kucharski and Flengas[12] adopted configurational terms of MCl_4^{2-}, A^+, M^{2+}, and Cl^- ions. It has been found by Φstvold and Kleppa[19] that the PbO-SiO_2 system also shows an S-shaped behavior which they attributed to formation of orthosilicate anion, $[SiO_4]^{4-}$.

Experimental

Instrument. The instrument used was a JEOL JMS-01BK doubly-focused mass spectrometer with a Knudsen cell source. As the details of the instrument were described elsewhere,[1,20] we would mention here only on the Knudsen cell which differed from the one used in our previous experiment.[1] The nickel Knudsen cell (Ni metal over 99.9% in purity) had a conical orifice, 0.005—0.006 cm in diameter, bored by electric discharge processing. In order to prevent the clogging of the cell orifice caused by wetting and crawling-up of molten salt, a fence made of thin Ni-foil was fixed in the upper part of the inside cell wall.

Sample. Vacuum-dried $MnCl_2$ and KCl powders were used as starting materials. Anhydrous $MnCl_2$ powder was obtained from $MnCl_2 \cdot 2H_2O$ by dehydration at 200 °C. Solid solution samples for the KCl-$MnCl_2$ system were prepared by the following processes: (1) preparing a mixture of KCl and $MnCl_2$ powders by weighing in dry Ar, (2) fusing the mixture in a stream of HCl gas in quartz tube to remove impurities such as alkali-metal oxides and water, and (3) replacing the HCl gas by Ar to remove the HCl dissolved in the molten salt and then cooling down the mass to room temperature. The product was pulverized just before measurement, and a sample of approximately 1 g for each run was charged in the cell in a dry box.

Calibration of Cell Temperature. As the cell temperature was measured with a W-5%Re/W-26%Re thermocouple positioned under the outside bottom of the cell, the temperature difference between the sample in the cell and the outside in contact with the thermocouple was determined by measuring some of the melting points of LiCl (883 K), $MnCl_2$ (923 K), KCl (1044 K), and NaCl (1074 K). The temperature difference was about 25 K, increasing slightly with a rise in cell temperature.

Procedure of Mass-spectrometric Measurement. Ion identification and intensity measurement for derived species were

†† Present address: Department of Metallurgy, Faculty of Engineering, Osaka University, 2-1 Yamadaoka, Suita, Osaka 565.

††† Present address: Department of Industrial Chemistry, Kumamoto Institute of Technology, 4-22-1 Ikeda, Kumamoto 860.

made by the usual mass spectrometric technique in the temperature range from melting temperature to several hundreds degrees above the melting point. Prior to starting an ion intensity measurement the constant ion intensity was examined.

The ionic species detected were K^+, KCl^+, K_2Cl^+, Cl^+, Mn^+, $MnCl^+$, and $MnCl_2^+$. Their appearance potentials, relative to H_2O^+, were 11.0, 10.5, 10.8, 15.5, 13.0, 8.5, and 7.5 eV, respectively. No other ions such as $Mn_2Cl_3^+$ (dimer ion), $KMnCl_3^+$ (mixed dimer ion), and $NiCl_n^+$ ($n=1, 2$) were detected. Both by considering appearance potentials and by using an analogy with other chlorides,[1,21-23] the molecular ions formed by simple ionization were estimated to be KCl^+, K_2Cl^+, and $MnCl_2^+$. In view of the apparent potentials for all the ions, an ionization potential of 17.5 eV was used.

Activity coefficient, γ, and heat of mixing, ΔH^M, were calculated from ion-current ratios of related ionic species by the previously outlined procedure.[1] According to Belton and Fruehan,[24] for example, the activity coefficient, γ_{MnCl_2}, and heat of mixing, $\Delta H^M_{MnCl_2}$, for the $MnCl_2$ component are given by

$$\ln \gamma_{MnCl_2} = \int_{X_{MnCl_2}=1}^{X_{MnCl_2}} \frac{X_{KCl}}{1+X_{MnCl_2}} \times d\left[\ln \frac{I_{K_2Cl^+}}{I_{MnCl_2^+}} - \ln \frac{X^2_{KCl}}{X_{MnCl_2}}\right], \quad (2)$$

$$\Delta H^M_{MnCl_2} = -R \int_{X_{MnCl_2}=1}^{X_{MnCl_2}} \frac{X_{KCl}}{1+X_{MnCl_2}} \times d\left\{\frac{d[\ln(I_{K_2Cl^+}/I_{MnCl_2^+}) - \ln(X^2_{KCl}/X_{MnCl_2})]}{d(1/T)}\right\}, \quad (3)$$

where X is mole fraction, I_i^+ the ion intensity of ion i^+, and R the gas constant.

Results and Discussion

Activity. Figure 1 shows the ion-current ratio as a function of temperature. The relationship between the ion-current ratio and the reciprocal of absolute temperature was determined by the regression analysis. In Table 1 the regression coefficients and standard deviations of error were summarized. The ion-current ratio values for the 10 mol% KCl–90 mol% $MnCl_2$ system at temperatures above 1083 K are not included in the regression analysis, since they deviated greatly from the regression line. This was probably because $MnCl_2$ gas molecules did not satisfy the Knudsen

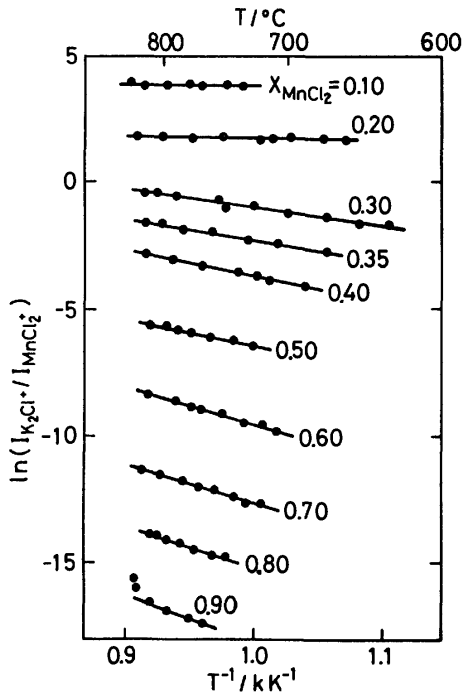

Fig. 1. Observed ion-current ratio in the molten KCl–$MnCl_2$ system.

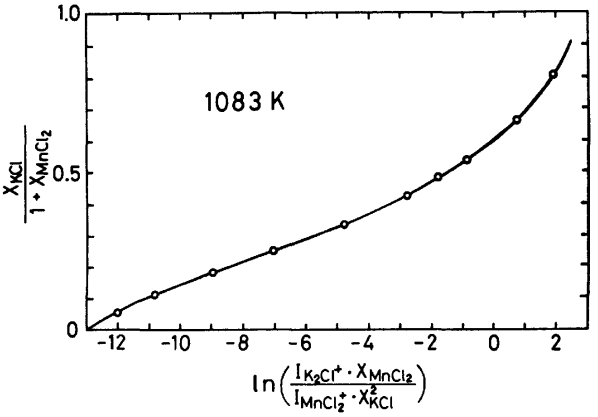

Fig. 2. Preliminary curve for the graphical integration in Eq. 2.

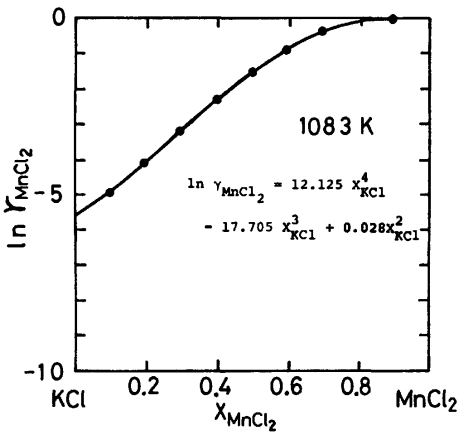

Fig. 3. Plots of $\ln \gamma_{MnCl_2}$ *vs.* X_{MnCl_2} at 1083 K.

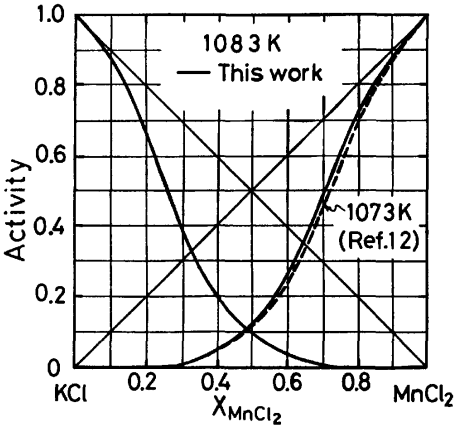

Fig. 4. Activity in the molten KCl–$MnCl_2$ system at 1083 K.

Table 1. Line-fitting parameters for lines drawn in Fig. 1.

X	0.1	0.2	0.3	0.4	0.5	0.6	0.7	0.8	0.9
$\frac{d\ln(I_{K_2Cl^+}/I_{MnCl_2^+})}{d(1/T)}$	−325	−930	−7990	−9800	−11400	−14800	−16100	−17300	−18200
b[a)]	4.169	2.651	5.876	5.686	6.176	5.439	4.772	3.543	0.06382

a) b is the constant used in the equation: $\ln(I_{K_2Cl^+}/I_{MnCl_2^+})=a(10^4/T)+b$, where a=slope.

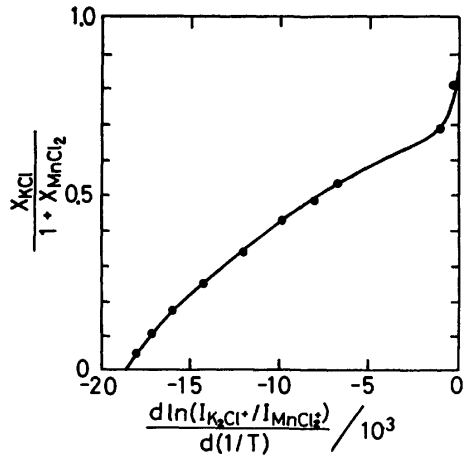

Fig. 5. Integration plots for the KCl-$MnCl_2$ system.

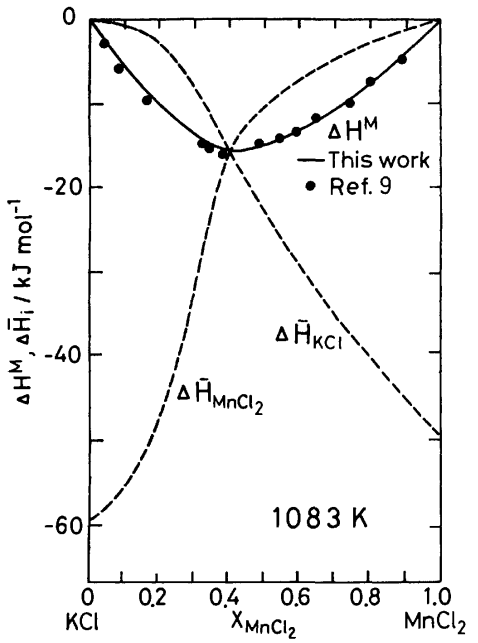

Fig. 6. Enthalpy of mixing in the molten KCl-$MnCl_2$ system.

molecular flow condition when allowed to effuse out from the orifice. In order to integrate Eq. 2 graphically and to obtain the activity coefficient, the term $[\ln(I_{K_2Cl^+}/I_{MnCl_2^+})-\ln(X/X_{KCl}^2X_{MnCl_2})]$ was plotted against the composition, X, as illustrated in Fig. 2. The solid line in Fig. 2 was given by the regression analysis. The relationships of composition *vs.* logarithmic activity coefficient and composition *vs.* activity are shown in Figs. 3 and 4. Braunstein[25] proposed a method to obtain the equilibrium constant for Reaction 1 by extrapolating the log γ *vs.* X line to $X=0$, as applicable when the excess Gibbs energy, ΔG_{XS}, is attributable to the excess entropy. His method, however, was not adopted in this case since ΔG_{XS} depends mainly on the large heat of mixing, as will be described later. It is seen from Fig. 3 that $\ln\gamma$ has an inflection point at the concentration of 30—40 mol% $MnCl_2$, which suggests a structural change in the molten salt. As shown in Fig. 4, the activity shows a great deviation from Raoult's law, suggesting a presence of strong interaction between KCl and $MnCl_2$.

Heat of Mixing and Entropy of Mixing. Figure 5 shows a preliminary curve for obtaining the heat of mixing, ΔH^M, from both Eq. 2 and the data in Table 1. An integration along the curve in Fig. 5 gives the ΔH's in Fig. 6. This result is in good agreement with the values determined by Papatheodorou and Kleppa[9] and hence the interaction parameter λ^M also agrees with them. Although the heats of mixing obtained here are considered to be average values for a wide range of temperature, they are in close agreement with those determined calorimetrically at a constant temperature. This fact suggest that the liquid structure of the KCl-$MnCl_2$ molten salt is independent of temperature, in accord with the fact that the intensity of Raman spectra in this system is independent of temperature.[7]

The partial molar entropy, $\Delta\bar{S}_i$, and the integral entropy of mixing, ΔS^M, for the molten salt were calculated from the well-known thermodynamic relations

$$\Delta\bar{G}_i = \Delta\bar{H}_i - T\Delta\bar{S}_i, \quad (4)$$

$$\Delta S^M = \sum_i X_i\Delta\bar{S}_i, \quad (5)$$

the results obtained being shown in Fig. 7.

Estimation of Chemical Species in Molten Mixture. The integrated and partial molar entropies of mixing, as shown in Fig. 7, from an S-shaped curve in the vicinity of $X_{MnCl_2}=0.33$, which suggests that some marked structural change occurs in this composition range. If anions and cations in the system behave as those in an ideal solution, the entropy of mixing should be in agreement with the values calculated from the equation $\Delta S^M_{ideal}=-R\sum X_i\ln X_i$. Obviously, this is not the case, as seen from Fig. 7. Kucharski and Flengas[12] explained the deviation from ideal entropy on the basis of possible ionic species: (1) Mn^{2+} and Cl^- ions in the pure molten $MnCl_2$; (2) A^+ (alkali-metal ion), Cl^-, and $[MnCl_4]^{2-}$ ions in the composition region of $0<X_{MnCl_2}<0.33$; (3) only $[MnCl_4]^{2-}$ and A^+ ions at $X_{MnCl_2}=0.33$; (4) A^+, Mn^{2+}, Cl^-, and $[MnCl_4]^{2-}$ ions in the region $X_{MnCl_2}>0.33$. On the basis of this model the theoretical entropy of mixing was calculated from the equations

$$\Delta S^M = -R[\sum n(i^+)\ln N(i^+) + \sum n(j^-)\ln N(j^-)]$$
$$= -R[n(K^+)\ln N(K^+) + n(Mn^{2+})\ln N(Mn^{2+})$$
$$+ n(Cl^-)\ln N(Cl^-) + n(MnCl_4^{2-})\ln N(MnCl_4^{2-})], \quad (6)$$

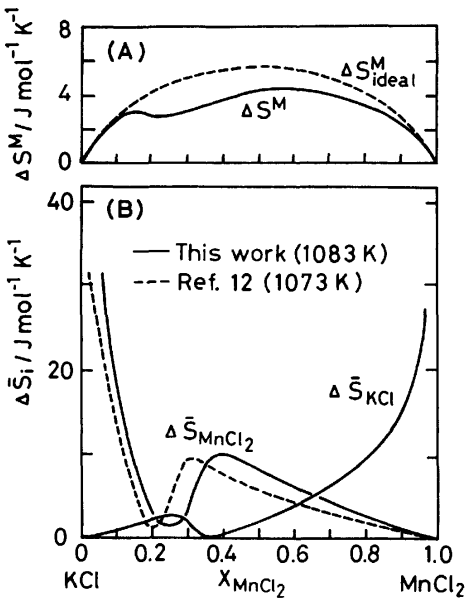

Fig. 7. Partial moral entropy of mixing and integral entropy in the molten KCl–$MnCl_2$ system.

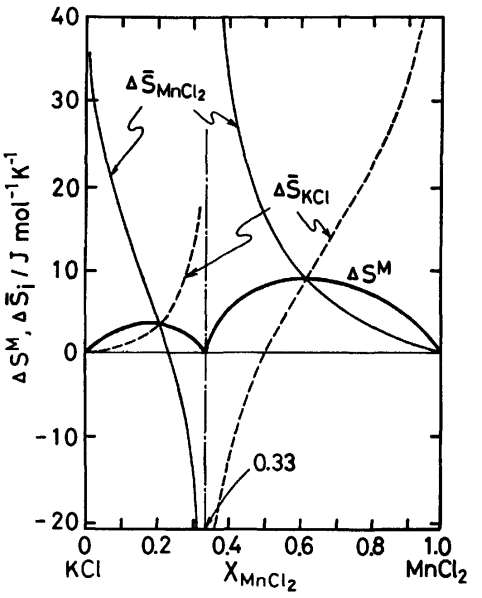

Fig. 8. Entropy of mixing in the KCl–$MnCl_2$ system calculated on the basis of Kucharski and Flengas' model.[12]

where $n(i^+ \text{ or } j^-)$ and $N(i^+ \text{ or } j^-)$ denote the mole number and ionic fraction of i^+ or j^- ion, respectively, and

$$\Delta\bar{S}_{KCl} = -\frac{R}{2}\ln\frac{X_{KCl}^3(4X_{MnCl_2}-X_{KCl})}{(1+X_{KCl})(2X_{MnCl_2}-X_{KCl})^3} \quad (7)$$

in the composition region of $X_{MnCl_2}>1/3$. Equation 6 was derived simply on statistical thermodynamics by assuming that the cations and anions will distribute randomly and that the contribution of a vibration of molecule to the entropy can be neglected. Figure 8 shows the entropies calculated from Eqs. 6 and 7. As for a comparison of Figs. 7 and 8, the model described above can explain the decrease in entropy in the vicinity of $X_{MnCl_2}=0.33$, but can not explain the value of ΔS^M at $X_{MnCl_2}=0.33$ since the ΔS^M should be 0 at $X_{MnCl_2}=0.33$ if the model is correct. Furthermore, the observed values of ΔS^M and $\Delta\bar{S}_{KCl}$ are smaller than the calculated. Therefore, we must further modify Kucharski and Flengas' model.

Takagi *et al.*[2] have concluded from electrical conductivity measurements for the KCl–$MnCl_2$ system that free Mn^{2+} ions exist in the molten salt at $X_{MnCl_2}=0.33$. Considering this fact and the proposals of Φstvold,[11] Ikeuchi and Krohn,[16] and Pelton and Thompson,[18] we take into account the following chemical equilibrium in calculating the entropy

$$[MnCl_4]^{2-} \rightleftharpoons Mn^{2+} + 4Cl^- . \quad (8)$$

Figure 9 shows the result computed for $\alpha=0.15$ and 0.50, where α is the degree of dissociation of $[MnCl_4]^{2-}$ into Mn^{2+} and Cl^- on the assumption that the dissociation constant for Eq. 8 is independent of the composition. As can be seen from Fig. 9, the disagreement near $X_{MnCl_2}=0.33$ may be solved by considering Dissociation Reaction 8. The disagreement in the high $MnCl_2$ composition side, however, remains still unsettled.

Takagi *et al.*[6] proposed the following model from an X-ray structure analysis: clusters or polymer ions (made up of $[MnCl_4]^{2-}$ exist even in the pure molten $MnCl_2$,

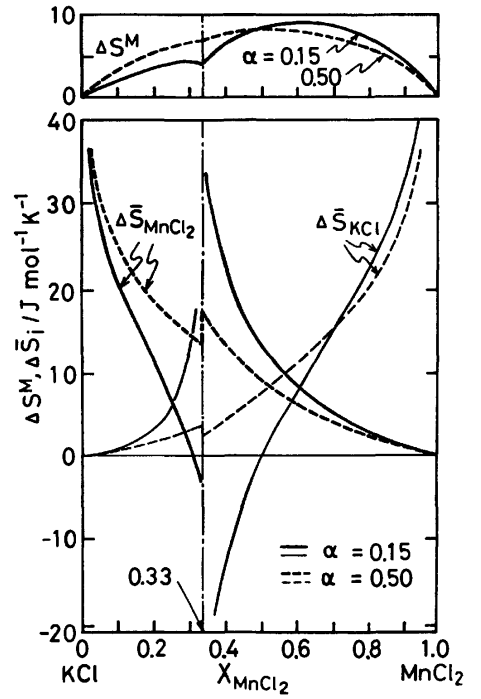

Fig. 9. Entropy of mixing in the KCl–$MnCl_2$ system calculated on the basis of the dissociation model.

and addition of component KCl will cause the polymeric ions to decompose to $[MnCl_4]^{2-}$ monomer ion through the intermediate cluster ions Mn_5Cl_{10}, $[Mn_4Cl_{10}]^{2-}$, $[Mn_3Cl_9]^{3-}$, and $[Mn_2Cl_7]^{3-}$ at compositions $X_{MnCl_2}=$ 1.0, 0.666, 0.5, and 0.4, respectively. Based on the model by Takagi *et al.*[6] we attempted again to calculate the entropy of mixing by using Eq. 6. However, we have failed in obtaining consistent results. This is probably attributable to the assumption that (1) such large cluster ions as $[Mn_3Cl_9]^{3-}$ and $[Mn_4Cl_{10}]^{2-}$ are almost negligible and the mixing of each ion is ideal,

that (2) the degree of dissociation of the complex species is independent of composition, and that (3) vibrational entropy can be neglected. A new model for the structure of a molten mixture containing polymer complex species is needed to provide an explanation for the entropy in the $MnCl_2$-rich side.

Conclusion

(1) Activities of components KCl and $MnCl_2$ in their molten mixtures show large negative deviations from Raoult's law. This suggests a very strong interaction between KCl and $MnCl_2$.

(2) The entropy of mixing has a minimum in the vicinity of $X_{MnCl_2}=1/3$ only, and the minimum has been explained in terms of the formation of complex species $[MnCl_4]^{2-}$.

The authors wish to thank Professor Tetsuro Nakamura of the Tokyo Institute of Technology for his discussion.

References

1) M. Itoh, T. Sasamoto, and T. Sata, *Bull. Chem. Soc. Jpn.*, **54**, 3319 (1981).
2) Y. Takagi, K. Tanemoto, and T. Nakamura, *Rep. Res. Lab. Eng. Matls. (Tokyo Inst. Tech.)*, **1**, 103 (1976).
3) A. S. Kucharski and S. N. Flengas, *J. Electrochem. Soc.*, **121**, 1298 (1974).
4) K. Tanemoto, Y. Takagi, and T. Nakamura, *Jpn. J. Appl. Phys.*, **15**, 1637 (1976).
5) K. Tanemoto, T. Nakamura, and T. Sata, *Chem. Lett.*, **1973**, 911.
6) Y. Takagi, T. Nakamura, T. Sata, H. Ohno, and K. Furukawa, *J. Chem. Soc., Faraday Trans. 1*, **75**, 1161 (1979).
7) K. Tanemoto and T. Nakamura, *Chem. Lett.*, **1975**, 351.
8) B. R. Sundheim and M. Kukk, *Discuss. Faraday Soc.*, **32**, 49 (1961).
9) G. N. Papatheodorou and O. J. Kleppa, *J. Inorg. Nucl. Chem.*, **32**, 889 (1961).
10) O. J. Kleppa and F. G. McCarty, *J. Phys. Chem.*, **70**, 1249 (1966).
11) T. Φstvold, *Acta Chem. Scand.*, **26**, 2778 (1972).
12) A. S. Kucharski and S. N. Flengas, *J. Electrochem. Soc.*, **119**, 1170 (1972).
13) D. C. Hamby and A. B. Scott, *J. Electrochem. Soc.*, **117**, 319 (1970).
14) D. C. Hamby and A. B. Scott, *J. Electrochem. Soc.*, **115**, 704 (1968).
15) M. Itoh and T. Nakamura, to be published.
16) H. Ikeuchi and C. Krohn, *Acta Chem. Scand.*, **23**, 2230 (1969).
17) G. D. Robbins, T. Fǿrland, and T. T. Φstvold, *Acta Chem. Scand.*, **22**, 3002 (1968).
18) A. D. Pelton and W. T. Thompson, *Can. J. Chem.*, **48**, 1585 (1970).
19) T. Φstvold and O. J. Kleppa, *Inorg. Chem.*, **8**, 78 (1969).
20) T. Sasamoto, H. Hara, and T. Sata, *Bull. Chem. Soc. Jpn.*, **54**, 3327 (1981).
21) J. Berkowitz and W. A. Chupka, *J. Chem. Phys.*, **29**, 653 (1958).
22) T. A. Milne and H. M. Klein, *J. Phys. Chem.*, **64**, 1628 (1960).
23) J. R. McCreary, S. A. Rassoul, R. J. Thorn, *High Temp. Sci.*, **1**, 412 (1969).
24) G. R. Belton and R. J. Fruehan, *Metall. Trans.*, **2**, 292 (1971).
25) J. Braunstein, *J. Chem. Phys.*, **49**, 3508 (1968).

Circular Dichroism Spectra and Absolute Configurations of *fac*(NH_3)-[Co(a)(gly)(NH_3)$_3$]$^{n+}$-type Complexes

Shuhei Fujinami,* Akihiko Hattori, and Muraji Shibata
Department of Chemistry, Faculty of Science, Kanazawa University, Kanazawa 920
(Received December 9, 1982)

Four complexes [Co(a)(gly)(NH_3)$_3$]$^+$ (a=CN^-, NO_2^-, NCS^-, and N_3^-) and a related [Co(NO_2)(β-ala)(NH_3)$_3$]$^+$ complex have been prepared; they were characterized by the absorption spectra in the ultraviolet region. The *fac*(NH_3) isomers of these complexes have been optically resolved by column chromatography. The CD spectra of *fac*(NH_3)-[Co(H_2O)(gly)(NH_3)$_3$]$^{2+}$ and *fac*(NH_3)-[Co(H_2O)(β-ala)(NH_3)$_3$]$^{2+}$ have also been measured. The absolute configurations of the *fac*(NH_3) isomers have been determined by referring to the CD spectrum of *fac*(NH_3)-(−)$_{589}$[Co(NO_2)(gly)(NH_3)$_3$]ClO_4 which had been subjected to an X-ray analysis. Each isomer has exhibited a dominant Cotton peak at *ca.* 20000 cm^{-1} in the first absorption band region. The peak has been assigned to the electronic transition component which arises in the plane containing the glycinate chelate. The CD spectra of *fac*(NH_3)-[Co(a)(gly)(NH_3)$_3$]$^+$ have been compared with those of the corresponding [Co(a)(gly)(1,4,7-triazacyclononane)]$^+$ complexes, and the sources of the optical activities in these complexes have been investigated.

We are interested in the optically active complexes whose chiralities are due to the arrangements of donor atoms around a central metal ion. In the previous papers,[1,2] the circular dichroism (CD) spectra of *fac*(*D*)-[Co(a)(BC)(DDD)]$^{n+}$ complexes have been reported. Here a represents several kinds of unidentate ligands; DDD represents a cyclic terdentate ligand: 1,4,7-triazacyclononane(=tacn), (2*R*)-2-methyl-1,4,7-triazacyclononane (Me-tacn), or 1,5,9-triazacyclododecane(=tacdd); BC denotes an amino carboxylate ion; glycinate, β-alaninate, or L-valinate. Though two helical ring-pairs exist in the complexes, the optical activities of the complexes have been mainly attributed to a chiral arrangement of four kinds of donor atoms around the central metal ion.

The *fac*(NH_3)-(−)$_{589}$[Co(NO_2)(gly)(NH_3)$_3$]$^+$ complex[3] has a chiral arrangement of donor atoms similar to the [Co(NO_2)(gly)(tacn)]$^+$ and no ring-pair is contained in the complex. The absolute configuration of the complex has been determined by X-ray analysis.[4] This paper will deal with further syntheses and optical resolutions of the *fac*(NH_3)-[Co(a)(gly)(NH_3)$_3$]$^{n+}$ (a=CN^-, NO_2^-, NCS^-, N_3^-, or H_2O) and *fac*(NH_3)-[Co(b)(β-ala)(NH_3)$_3$]$^{n+}$ (b=NO_2^- or H_2O) complexes. The CD spectra of the *fac*(NH_3) complexes will be compared with those of the corresponding tacn complexes, and the contribution of the chelate ring to the optical activities will be reported.

Experimental

Synthesis and Optical Resolution. *1)* fac(NH_3)-*Triammineglycinatonitrocobalt(III) Chloride*, fac(NH_3)-[*Co*(*NO*$_2$)(*gly*)(*NH*$_3$)$_3$]*Cl*: This complex was prepared from [Co(NO_2)(NH_3)$_5$]$^{2+}$, and optically resolved according to the literature.[3]

2) fac(NH_3)-*Triammineglycinatoisothiocyanatocobalt(III) Bromide 0.5-Hydrate*, fac(NH_3)-[*Co*(*NCS*)(*gly*)(*NH*$_3$)$_3$]*Br*·*0.5H*$_2$*O*: To an aqueous solution of [Co(NCS)(NH_3)$_5$]SO_4 (15 g in 150 cm^3 H_2O) were added glycine (3.3 g), Na_2CO_3 (2.0 g) and activated charcoal (1.0 g), and the solution was stirred for a day at room temperature. After filtering off the activated charcoal, the filtrate was adjusted to pH 7 with perchloric acid and diluted to 3 dm^3 with water. The solution was poured onto a column of Dowex 50W-X8 (Na^+ form, 100—200 mesh, ϕ4.0 cm × 40 cm). By elution with a 0.1 mol/dm^3 NaCl solution, four bands of univalent cations were discharged; they were labelled A1, A2, A3, and A4 in the order of elution. The labels are also used to designate the complex species in each band. The A3 fraction was rechromatographed with a short column of the same resin (ϕ2 cm × 10 cm) in order to convert the counter ion to bromide. The adsorbed band was eluted with 0.1 mol/dm^3 NaBr, and collected in a fraction (A3′). Each fraction was concentrated by means of a rotary evaporator with simultaneous removal of precipitated eluent. To a final filtrate was added a small amount of ethanol, and the whole was kept in a refrigerator. The crude product which precipitated was recrystallized from a minimum amount of warm water. A2 and A4 were identified to be the isomers of a known complex, [Co(gly)$_2$(NH_3)$_2$]$^+$.[5] From elemental analyses, absorption and IR spectra, A1 and A3′ were assigned to the isomers of the [Co(NCS)(gly)(NH_3)$_3$]$^+$ complex. The yields of A1 and A3′ were 0.3 g and 0.2 g respectively. Found for A1: C, 13.00; H, 4.76; N, 25.22%. Calcd for [Co(NCS)(gly)(NH_3)$_3$]Cl: C, 12.98; H, 4.72; N, 25.23%. Found for A3′: C, 11.17; H, 3.90; N, 21.02%. Calcd for [Co(NCS)(gly)(NH_3)$_3$]Br·0.5H_2O: C, 10.88; H, 4.22; N, 21.15%.

The A3′ isomer was resolved into optical antipodes by using a column of Dowex 50W-X8 (Na^+ form, 200—400 mesh, ϕ2.5 cm × 70 cm) and 0.05 mol/dm^3 Na_2[Sb_2(*d*-tart)$_2$] as eluent. This fact indicates that A3′ is a *fac*(NH_3) isomer and A1 is a *mer*(NH_3) one. When the adsorbed band descended in the neighborhood of the outlet of the column, the band was washed sufficiently with water, and collected in several fractions by eluting with 0.1 mol/dm^3 NaCl. Each fraction was concentrated and submitted to the measurement of CD spectrum, while the concentration of the complex species was evaluated from the absorption spectral data.

3) fac(NH_3)-*Triammineazidoglycinatocobalt(III) Chloride*, fac(NH_3)-[*Co*(*N*$_3$)(*gly*)(*NH*$_3$)$_3$]*Cl*: The complex was prepared in the same manner as the isothiocyanato complex, except for the use of [Co(N_3)(NH_3)$_5$]Cl_2 (13 g, 0.05 mol, in 150 cm^3 H_2O) in place of [Co(NCS)(NH_3)$_5$]SO_4. By elution with a 0.1 mol/dm^3 NaCl solution, four bands of univalent cations were discharged; they were labelled B1, B2, B3, and B4 in the order of elution. B2 and B4 were identified to be the isomers of [Co(gly)$_2$(NH_3)$_2$]$^+$.[5] B1 and B3 were assigned to the isomers of [Co(N_3)(gly)(NH_3)$_3$]$^+$. The yields of B1 and B3 were *ca.* 0.3 g. Found for B1: C, 9.48; H, 4.87; N, 37.73%. Found for B3: C, 9.41; H, 5.24; N, 37.57%. Calcd for [Co(N_3)(gly)(NH_3)$_3$]Cl: C, 9.18; H, 5.01; N, 37.49%.

The B3 isomer was optically resolved by a method similar to that described in 2). Therefore, B3 was assigned to a *fac*(NH_3)

isomer, and B1 was a *mer*(NH_3) one.

4) fac(NH_3)-*Triamminecyanoglycinatocobalt(III) Chloride 0.75-*fac(NH_3)-[*Co(CN)(gly)(NH_3)$_3$]Cl·0.75H_2O*: To a cold green solution of tricarbonatocobaltate(III) (0.042 mol scale),[6] potassium cyanide (4.1 g, 0.063 mol) was added by portions, and the mixture was stirred vigorously at room temperature for 20 min. A deep red solution was obtained. After addition of glycine (3.75 g, 0.05 mol), the solution was carefully adjusted to pH 8 with 30% perchloric acid, and stirred at room temperature for two days. The resulting red-violet solution was adjusted to pH 3 with 60% perchloric acid under an iced conditions, and stirred for 30 min. Concentrated aqueous ammonia (20 cm^3, 0.28 mol) and activated charcoal (1 g) were added to the solution and the whole was stirred at room temperature for two days. After filtration, the filtrate was neutralized with 30% perchloric acid under an iced conditions, and the precipitate was filtered out. The filtrate was diluted to 3 dm^3 with water and charged on a column of Dowex 50W-X8 (Na^+ form, 200—400 mesh, ϕ4 cm × 30 cm). By elution with a 0.1 mol/dm^3 NaCl solution, five bands of univalent cations were discharged; they were labelled C1, C2, C3, C4, and C5 in the order of elution. Each fraction was concentrated to a small volume by a rotary evaporator, with simultaneous removal of deposited NaCl. A small amount of ethanol was added to the concentrate, and the whole was kept in a refrigerator. C1 was identified to be $[Co(CN)_2(NH_3)_4]^+$,[7] and C5, to be the isomers of $[Co(gly)_2(NH_3)_2]^+$.[5] The yellow crystals obtained from C2 and the orange crystals from C3 were assigned to isomers of $[Co(CN)(gly)(NH_3)_3]^+$. Each yield was *ca.* 0.3 g. Found for C2: C, 13.04; H, 5.86; N, 25.68%. Calcd for $[Co(CN)(gly)(NH_3)_3]Cl\cdot 1.5H_2O$: C, 13.22; H, 5.92; N, 25.69%. Found for C3: C, 13.66; H, 5.76; N, 27.29%. Calcd for $[Co(CN)(gly)(NH_3)_3]Cl\cdot 0.75H_2O$: C, 13.91; H, 5.64; N, 27.03%.

The C3 isomer was optically resolved by column chromatography in the same manner as in 2). Therefore, C3 was assigned to a *fac*(NH_3) isomer and C2 to a *mer*(NH_3) one.

5) fac(NH_3)-*Triammineaquaglycinatocobalt(III) Cation,* fac-(NH_3)-[*Co(H_2O)(gly)(NH_3)$_3$*]$^{2+}$: This complex was prepared by acid-hydrolysis of the *fac*(NH_3)-[$Co(NO_2)$(gly)-(NH_3)$_3$]$^+$ complex. The nitro complex (1.0 g) was dissolved in hydrobromic acid (47%, 20 cm^3). The solution was stirred at 50—60 °C for 90 min, whereupon the corresponding aqua complex was formed. The solution was diluted to 3 dm^3 with water, and poured onto a column of SP-Sephadex C-25 (Na^+ form, ϕ4.0 cm × 30 cm). The adsorbed red band was eluted with 0.1 mol/dm^3 $HClO_4$, and collected in a fraction. The eluate was concentrated to a small volume by a rotary evaporator, and its absorption spectrum was measured. The metal concentration was evaluated from the data of the atomic absorption spectrum. This complex was unable to be crystallized because of the great solubility of the complex species in water. The chromatographic behavior of the species indicates that the species is a bivalent cation. This complex was resolved into enantiomers by using a column of SP-Sephadex C-25 (Na^+ form, ϕ2.5 cm × 140 cm) and a 0.05 mol/dm^3 $Na_2[Sb_2(d\text{-tart})_2]$ solution as eluent.

1) fac(NH_3)-*(β-Alaninato)triamminenitrocobalt(III) Chloride Monohydrate,* fac(NH_3)-[*Co(NO_2)(β-ala)(NH_3)$_3$*]Cl·H_2O: This complex was prepared in the same manner as the *fac*(NH_3)-[$Co(NO_2)$(gly)(NH_3)$_3$]Cl, except for the use of β-alanine in place of glycine. The yield was *ca.* 0.3 g. Found: C, 12.24; H, 5.69; N, 23.37%. Calcd for $[Co(NO_2)(\beta\text{-ala})(NH_3)_3]Cl\cdot H_2O$: C, 12.11; H, 5.76; N, 23.53%.

The complex was also resolved into the optical antipodes in the same manner as in 2).

7) fac(NH_3)-*(β-Alaninato)triammineaquacobalt(III) Cation,* fac(NH_3)-[*Co(H_2O)(β-ala)(NH_3)$_3$*]$^{2+}$: This complex was prepared from *fac*(NH_3)-[$Co(NO_2)$(β-ala)(NH_3)$_3$]Cl and optically resolved by the method described in 5). The values of ε and $\Delta\varepsilon$ were evaluated from the data of atomic absorption spectra. The complex species could not be isolated because of its great solubility in water.

Derivations from Optically Active Complexes. The optically active complex, *fac*(NH_3)-$(+)_{589}$[Co(NCS)(gly)(NH_3)$_3$]$^+$, was derived from the *fac*(NH_3)-$(+)_{589}$[$Co(H_2O)$(gly)(NH_3)$_3$]$^{2+}$ complex by the following procedure. To a solution of the aqua complex was added an excess amount of NaSCN, and the mixture was adjusted to pH 4 with $HClO_4$. The solution was stirred at 50—60 °C for 1 h, and then subjected to Sephadex column chromatography in a similar way to that described in 5). The eluate obtained by elution with 0.05 mol/dm^3 NaCl was concentrated by means of a rotary evaporator, and a small amount of ethanol was added to the concentrate. When the whole kept in a refrigerator, red crystals deposited.

The *fac*(NH_3)-$(-)_{589}$[$Co(N_3)$(gly)(NH_3)$_3$]$^+$ and *fac*(NH_3)-$(-)_{589}$[$Co(NO_2)$(β-ala)(NH_3)$_3$]$^+$ were also derived from *fac*-(NH_3)-$(+)_{589}$[$Co(H_2O)$(gly)(NH_3)$_3$]$^{2+}$ and *fac*(NH_3)-$(+)_{589}$-[$Co(H_2O)$(β-ala)(NH_3)$_3$]$^{2+}$ respectively, by a similar procedure to that described above. The optically active complex *fac*-,(NH_3)-$(-)_{589}$ [$Co(NO_2)$(gly)(NH_3)$_3$]$^+$, was directly converted to the optically active aqua complex, *fac*(NH_3)-$(+)_{589}$ [Co-(H_2O)(gly)(NH_3)$_3$]$^{2+}$, according to the method described in 5). When the *fac*(NH_3)-$(+)_{589}$[Co(NCS)(gly)(NH_3)$_3$]$^+$ complex was treated with aqueous H_2O_2 at *ca.* pH 3 in a similar manner to that described in the previous paper,[1] *fac*(NH_3)-$(-)_{589}$[Co(CN)(gly)(NH_3)$_3$]$^+$, *fac*(NH_3)-$(+)_{589}$[$Co(H_2O)$-(gly)(NH_3)$_3$]$^{2+}$, and optically inactive $[Co(gly)(NH_3)_4]^{2+}$ [8] were obtained by means of chromatography.

Measurements. The absorption spectra in aqueous solution were recorded with a Hitachi 323 recording spectrophotometer. The CD spectra were measured with a JASCO J-40C automatic recording spectropolarimeter equipped with a JASCO Model J-DPZ data processor for CD. For the measurements of the optical rotation, a JASCO Model DIPSL automatic polarimeter was used. In order to evaluate the metal concentrations from the data of atomic absorption spectra, a Hitachi 170-50 atomic absorption spectrophotometer was used.

Results and Discussion

Preparation and Characterization. Three *fac*(NH_3)-[Co(a)(gly)(NH_3)$_3$]$^+$ (a=NO_2^-, NCS^-, and N_3^-) complexes and the *fac*(NH_3)-[$Co(NO_2)$(β-ala)(NH_3)$_3$]$^+$ complex were derived from the corresponding pentaammineanionocobalt(III) complexes. However, the *fac*(NH_3)-[Co(CN)(gly)(NH_3)$_3$]$^+$ complex could not be derived from a $[Co(CN)(NH_3)_5]^{2+}$ complex because of the small solubility of the pentaammine complex in water. The desired cyano complex was obtained by substitution reactions starting from $[Co(CO_3)_3]^{3-}$. The aqua complexes were also not obtained from $[Co(H_2O)(NH_3)_5]^{3+}$.

There are three possible geometrical isomers in the [Co(a)(amino acidato)(NH_3)$_3$]$^{n+}$ complex: *mer*(NH_3)-*trans*(*a*,*O*), *mer*(NH_3)-*trans*(*a*,*N*), and *fac*(NH_3), where O and N represent donors of the amino acidato ligand.[3] Two *mer*(NH_3) isomers are achiral, while the *fac*(NH_3) isomer is chiral and resolvable into the optical antipodes. Except for *fac*(NH_3)-[$Co(H_2O)$(β-ala)(NH_3)$_3$]$^{2+}$, all the

fac(NH_3) isomers were separated completely into the enantiomers on columns of 200—400 mesh cation exchanger. These isomers were only partially resolved on columns of 100—200 mesh exchanger.

Absorption spectra of *fac*(NH_3)-[Co(a)(gly)$(NH_3)_3$]$^{n+}$ complexes are shown in Figs. 1—5 (a=CN^-, NO_2^-, NCS^-, N_3^-, and H_2O), along with those of the related [Co(a)(gly)(tacn)]$^{n+}$ complexes. The numerical data are summarized in Table 1. The absorption maxima of the first absorption bands of the *fac*(NH_3) complexes appear at somewhat lower frequencies than those of the corresponding tacn complexes, and the intensities of the bands of the former are weaker than those of the latter.

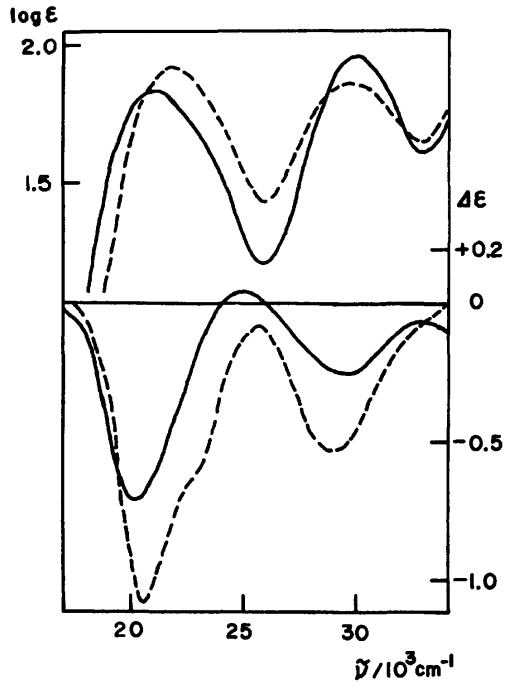

Fig. 1. Absorption and CD spectra of; ——: *fac*(NH_3)-$(-)_{589}$[Co(CN)(gly)$(NH_3)_3$]$^+$, – – –: $(-)_{589}$[Co(CN)-(gly)(tacn)]$^+$.

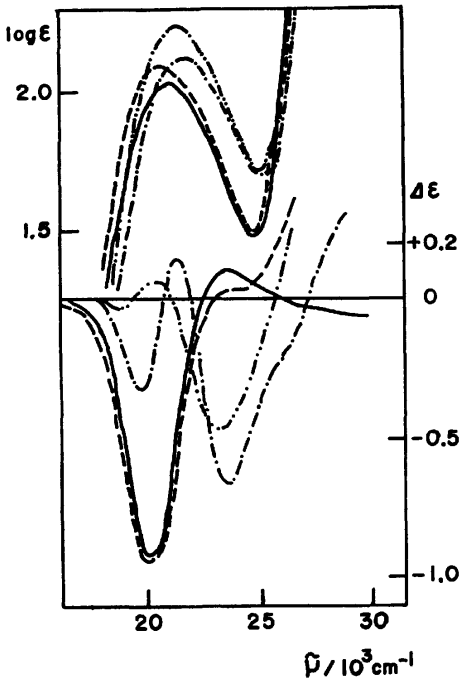

Fig. 2. Absorption and CD spectra of; ——: *fac*(NH_3)-$(-)_{589}$[Co(NO_2)(gly)$(NH_3)_3$]$^+$, – – –: *fac*(NH_3)-$(-)_{589}$-[Co(NO_2)(β-ala)$(NH_3)_3$]$^+$, –·–·–: $(-)_{589}$[Co(NO_2)(gly)-(tacn)]$^+$, –···–: $(-)_{589}$[Co(NO_2)(β-ala)(tacn)]$^+$.

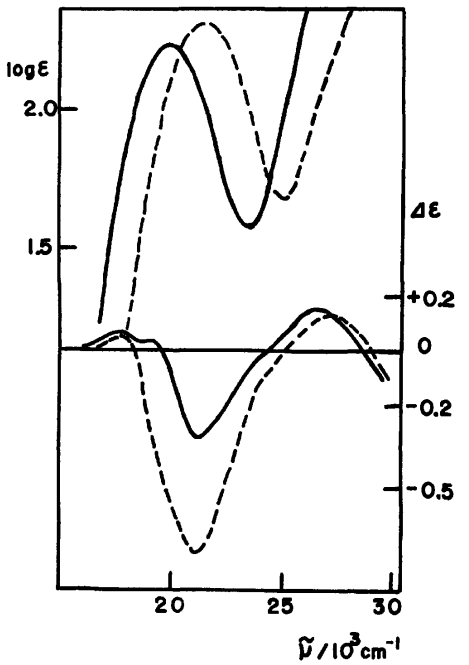

Fig. 3. Absorption and CD spectra of; ——: *fac*(NH_3)-$(+)_{589}$[Co(NCS)(gly)$(NH_3)_3$]$^+$, – – –: $(-)_{589}$[Co(NCS)-(gly)(tacn)]$^+$.

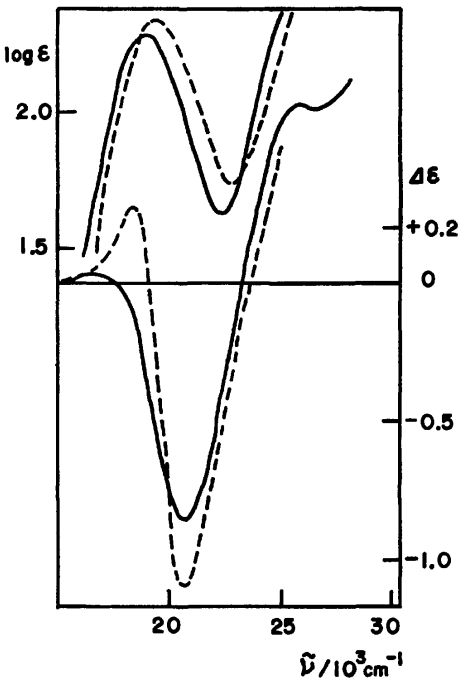

Fig. 4. Absorption and CD spectra of; ——: *fac*(NH_3)-$(-)_{589}$[Co(N_3)(gly)$(NH_3)_3$]$^+$, – – –: $(+)_{589}$[Co(N_3)-(gly)(tacn)]$^+$.

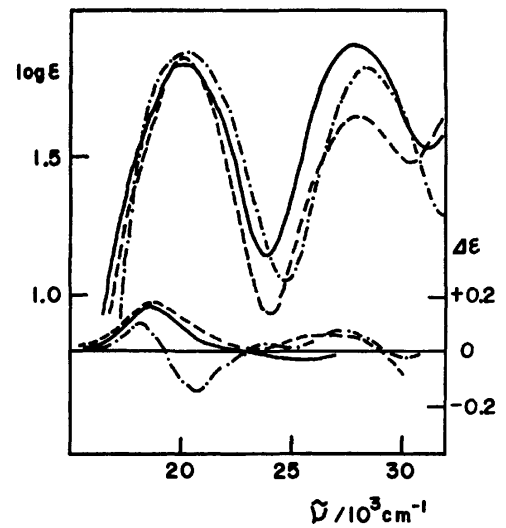

Fig. 5. Absorption and CD spectra of; ——: *fac*(NH_3)-(+)$_{589}$[Co(H_2O)(gly)(NH_3)$_3$]$^{2+}$, – – –: *fac*(NH_3)-(+)$_{589}$[Co(H_2O)(β-ala)(NH_3)$_3$]$^{2+}$, ·–·–·: (−)$_{589}$[Co(H_2O)(gly)(tacn)]$^{2+}$.

Two *mer*(NH_3) isomers were isolated for the [Co(NO_2)(gly)(NH_3)$_3$]$^+$ complex, and assigned on the basis of absorption spectra in the ultraviolet region.[3] However only one of two *mer*(NH_3) isomers was obtained for each of the [Co(CN)(gly)(NH_3)$_3$]$^+$, [Co(NCS)(gly)(NH_3)$_3$]$^+$, and [Co(N_3)(gly)(NH_3)$_3$]$^+$ complexes. As to the isothiocyanato complex, the absorption band at *ca.* 32000 cm^{-1} can be assigned to 2π(NCS)→d(z^2).[9] Since the band in the *mer*(NH_3) isomer is observed at a lower frequency than that in the corresponding *fac*(NH_3) isomer, the *mer*(NH_3)-*trans*(*NCS,O*) configuration is assignable for the *mer*(NH_3) complex in the same manner as described in the nitro complex.[3]

The absorption band at *ca.* 47000 cm^{-1} in the cyano complex can be assigned to dπ→π(CN).[9] The bands observed at *ca.* 30000 cm^{-1} in the nitro complex are assignable to dπ→π(NO_2), and the maximum of the *mer*(NH_3)-*trans*(NO_2,*O*) isomer is observed at a lower frequency than those of the *mer*(NH_3)-*trans*(NO_2,*N*) and *fac*(NH_3) isomers. Since the maximum of the *mer*(NH_3)-cyano isomer is observed at a lower frequency than that of the *fac*(NH_3) isomer, the isomer is considered to have the *mer*(NH_3)-*trans*(*CN,O*) configuration.

CD Spectra and Absolute Configurations. CD spectra of *fac*(NH_3)-[Co(a)(gly)(NH_3)$_3$]$^{n+}$ isomers, all of which were slow-moving isomers in column chromatography, are shown in Figs. 1—5, together with those of the fast-moving isomers of the corresponding tacn complexes. The (+)$_{589}$[Co(H_2O)(gly)(NH_3)$_3$]$^{2+}$ complex exhibits a single Cotton peak in the first absorption band region, and (−)$_{589}$[Co(NO_2)(gly)(NH_3)$_3$]$^+$ two peaks in this region, the CD spectra of these complexes being different from those of the corresponding tacn complexes. However, the CD spectra of (−)$_{589}$[Co(CN)(gly)-(NH_3)$_3$]$^+$, (+)$_{589}$[Co(NCS)(gly)(NH_3)$_3$]$^+$, and (−)$_{589}$-[Co(N_3)(gly)(NH_3)$_3$]$^+$ resemble those of the corresponding tacn complexes.

The *fac*(NH_3)-(+)$_{589}$[Co(H_2O)(gly)(NH_3)$_3$]$^{2+}$ complex could be converted to *fac*(NH_3)-(−)$_{589}$[Co(NO_2)-(gly)(NH_3)$_3$]$^+$, *fac*(NH_3)-(+)$_{589}$[Co(NCS)(gly)(NH_3)$_3$]$^+$, and *fac*(NH_3)-(−)$_{589}$[Co(N_3)(gly)(NH_3)$_3$]$^+$ complexes. Furthermore, the *fac*(NH_3)-(+)$_{589}$[Co(NCS)(gly)-(NH_3)$_3$]$^+$ complex was converted to *fac*(NH_3)-(+)$_{589}$-[Co(H_2O)(gly)(NH_3)$_3$]$^{2+}$ and *fac*(NH_3)-(−)$_{589}$[Co(CN)-(gly)(NH_3)$_3$]$^+$ by treatment with H_2O_2. Therefore, it is concluded that the isomers, *fac*(NH_3)-[Co(a)(gly)(NH_3)$_3$]$^{n+}$ (a=CN^-, NO_2^-, NCS^-, H_2O, or N_3^-), given in Figs. 1—5 have the same absolute configuration. The absolute configurations of the fast-moving isomers of the tacn complexes have been determined as shown in Fig. 6(a).[1,4] Since the CD spectra of (−)$_{589}$[Co(CN)-(gly)(NH_3)$_3$]$^+$, (+)$_{589}$[Co(NCS)(gly)(NH_3)$_3$]$^+$, and (−)$_{589}$[Co(N_3)(gly)(NH_3)$_3$]$^+$ resemble those of the corresponding tacn complexes, all the slow-moving isomers of the triammine complexes are predicted to have the absolute configuration illustrated in Fig. 6(b).

In order to confirm the above prediction, an X-ray analysis of *fac*(NH_3)-(−)$_{589}$[Co(NO_2)(gly)(NH_3)$_3$]ClO_4 was attempted.[4] The results of the analysis support the prediction. Since the glycinate ligand forms a chelate ring much less puckered than the 1,2-diamine chelate ring, the optical activity of *fac*(NH_3)-[Co(a)(gly)-(NH_3)$_3$]$^{n+}$ is considered to be mainly derived from a chiral arrangement of donor atoms.

Though the aqua complex exhibits a single Cotton peak in the first absorption band region, the remaining complexes exhibit two or three extrema in this region. The dominant peaks are observed at the lower frequency side of this region for the cyano and nitro complexes, and at the higher frequency side of this region for the isothiocyanato and azido complexes. However, the dominant Cotton peak is observed at *ca.* 20000 cm^{-1} in each complex.

Every complex has a rhombic ligand field in which the A_{1g}→T_{1g} transition component in octahedral parentage splits into three transition components: (xy)→(x^2—y^2), (yz)→(y^2—z^2), and (zx)→(z^2—x^2). An angular overlap model[10] predicts that the electronic transition at *ca.* 20000 cm^{-1} should be assigned to the transition component which arises in the plane containing the glycinato and two ammine ligands.[11] Therefore, it is suggested that a single chelate ring increases somewhat the rotatory strength of the Cotton peak associated with the electronic transition which arises in the plane containing a chelate ring. This finding is incompatible with the results obtained in the tris or bis(diamine) complexes such as [Co(en)(tn)(tmd)]$^{3+}$ [12] and *cis*-[Co(NH_3)$_2$(tn)$_2$]$^{3+}$.[13] In these complexes, the number of asymmetric pairs of

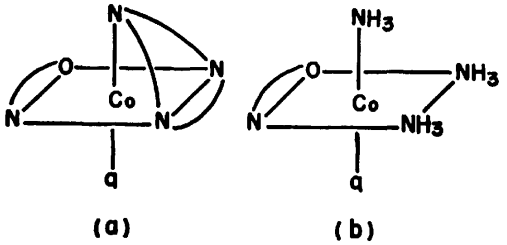

Fig. 6. Absolute configurations of; a) [Co(a)(gly)-(tacn)]$^{n+}$, b) *fac*(NH_3)-[Co(a)(gly)(NH_3)$_3$]$^{n+}$.

Table 1. Absorption and CD spectral data

Complex	Absorption		CD	
	$\tilde{\nu}/10^3$ cm^{-1}	(log ε)	$\tilde{\nu}/10^3$ cm^{-1}	($\Delta\varepsilon$)
fac(NH_3)-(−)$_{589}$[Co(CN)(gly)(NH_3)$_3$]$^+$	21.1	(1.83)	20.1	(−0.71)
			24.9	(+0.03)
	30.0	(1.95)	29.6	(−0.27)
	47.6	(4.26)		
mer(NH_3)-*trans*(*CN*,*O*)-[Co(CN)(gly)(NH_3)$_3$]$^+$	22.0	(1.94)		
	29.8	(1.93)		
	46.8	(4.27)		
fac(NH_3)-(−)$_{589}$[Co(NO_2)(gly)(NH_3)$_3$]$^+$	20.9	(2.03)	20.0	(−0.92)
			23.4	(+0.09)
	30.5	(3.18)		
	41.6	(4.14)		
mer(NH_3)-*trans*(*NO_2*,*O*)-[Co(NO_2)(gly)(NH_3)$_3$]$^+$	21.4	(2.11)		
	29.6	(3.27)		
	40.7	(4.25)		
mer(NH_3)-*trans*(*NO_2*,*N*)-[Co(NO_2)(gly)(NH_3)$_3$]$^+$	21.2	(2.02)		
	30.3	(3.33)		
	41.7	(4.21)		
fac(NH_3)-(+)$_{589}$[Co(H_2O)(gly)(NH_3)$_3$]$^{2+}$	20.0	(1.84)	18.6	(+0.15)
	27.6	(1.91)		
fac(NH_3)-(+)$_{589}$[Co(NCS)(gly)(NH_3)$_3$]$^+$	19.9	(2.23)	17.7	(+0.05)
			19.0	(+0.03)
			21.2	(−0.31)
	32.7	(3.24)	26.8	(+0.14)
mer(NH_3)-*trans*(*NCS*,*O*)-[Co(NCS)(gly)(NH_3)$_3$]$^+$	18.9	(2.25)		
	32.0	(3.22)		
fac(NH_3)-(−)$_{589}$[Co(N_3)(gly)(NH_3)$_3$]$^+$	18.9	(2.26)	16.3	(+0.02)
			20.8	(−0.86)
	32.8	(3.91)	25.6	(+0.64)
mer(NH_3)-[Co(N_3)(gly)(NH_3)$_3$]$^+$	18.4	(2.21)		
	32.7	(3.71)		
fac(NH_3)-(−)$_{589}$[Co(NO_2)(β-ala)(NH_3)$_3$]$^+$	20.5	(2.09)	20.1	(−0.95)
			24.1	(+0.03)
	30.2	(3.18)		
	41.8	(4.23)		
mer(NH_3)-*trans*(*NO_2*,*O*)-[Co(NO_2)(β-ala)(NH_3)$_3$]$^+$	21.0	(2.18)		
	29.7	(3.25)		
	40.1	(4.28)		
fac(NH_3)-(+)$_{589}$[Co(H_2O)(β-ala)(NH_3)$_3$]$^{2+}$	20.1	(1.86)	18.6	(+0.17)
	27.8	(1.63)	27.4	(+0.05)

chelate rings is more important in determining the CD intensity than the number of chelate rings.

The [Co(a)(gly)(tacn)]$^{n+}$ complexes have the same chromophore as the present complexes.[1] An intense Cotton peak was characteristically observed at the highest frequency side of the first absorption band region in the tacn complexes. Such an intense peak is not always observed in the present complexes. It is noticeable that when the unidentate ligand a in [Co(a)-(gly)(NH_3)$_3$]$^{n+}$ is planar, the CD spectrum of the complex is somewhat different from that of the corresponding [Co(a)(gly)(tacn)]$^{n+}$ complex. On the other hand, when the unidentate is a linear ligator, the CD spectrum of the complex is similar to that of the tacn complex. Since the CD spectral patterns of the [Co(a)-(gly)(NH_3)$_3$]$^{n+}$ complexes, on the whole, resemble those of the corresponding [Co(a)(gly)(tacn)]$^{n+}$ complexes, it is concluded that the chiral arrangement of donor atoms is the main source of the optical activity in [Co(a)(gly)(tacn)]$^{n+}$. This is supported by the fact that the [Co(a)(gly)(tacn)]$^{n+}$ complexes give CD spectra similar to [Co(a)(NH_3)(H_2O)(tacn)]$^{(n+1)+}$ complexes (a=CN^-, NO_2^-, NCS^-, N_3^-, and Cl^-).[14]

The *fac*(NH_3)-(−)$_{589}$[Co(NO_2)(β-ala)(NH_3)$_3$]$^+$ complex exhibits a CD spectrum similar to that of the *fac*(NH_3)-(−)$_{589}$[Co(NO_2)(gly)(NH_3)$_3$]$^+$ complex, namely, a negative dominant peak is observed at *ca.* 20000 cm^{-1} and a positive minor peak at *ca.* 24000 cm^{-1}. The CD spectrum of *fac*(NH_3)-(+)$_{589}$[Co(H_2O)(β-ala)-(NH_3)$_3$]$^{2+}$ also resembles that of *fac*(NH_3)-(+)$_{589}$[Co-(H_2O)(gly)(NH_3)$_3$]$^{2+}$, a positive extremum being observed in the complexes. Therefore, each pair of the glycinato and β-alaninato complexes is considered to have the same absolute configuration, and the change

from the five-membered chelate ring to the six-membered one has little effect on the optical activity in the complexes. A similar situation is encountered in the $(-)_{589}$[Co(NO_2)(gly)(tacn)]$^+$ and $(-)_{589}$[Co(NO_2)(β-ala)(tacn)]$^+$ complexes, the same absolute configuration being assigned to these complexes.[2)]

References

1) S. Shimba, S. Fujinami, and M. Shibata, *Bull. Chem. Soc. Jpn.*, **53**, 2523 (1980).

2) S. Fujinami, Y. Matsunami, and M. Shibata, *Bull. Chem. Soc. Jpn.*, **55**, 2101 (1982).

3) S. Fujinami and M. Shibata, *Chem. Lett.*, **1981**, 495.

4) S. Ohba, Y. Saito, S. Fujinami, and M. Shibata, *Acta Crystallogr., Sect. B*, **38**, 1305 (1982).

5) K. Kobayashi and M. Shibata, *Bull. Chem. Soc. Jpn.*, **48**, 2561 (1975).

6) M. Shibata, *Proc. Jpn. Acad.*, **50**, 779 (1974); *Nippon Kagaku Zasshi*, **87**, 771 (1966).

7) K. Konya, H. Nishikawa, and M. Shibata, *Inorg. Chem.*, **7**, 1165 (1968).

8) Y. Shimura, *Bull. Chem. Soc. Jpn.*, **31**, 173 (1958).

9) V. M. Miskowski and H. B. Gray, *Inorg. Chem.*, **14**, 401 (1975).

10) C. E. Schäffer, *Struct. Bonding*, **5**, 68 (1968); *Pure Appl. Chem.*, **24**, 361 (1970).

11) The dominant Cotton peak in the isothiocyanato complex is observed at 21200 cm^{-1}. However, the peak can be assigned to the electronic transition concerned, because the peak is observed at the highest frequency in the first absorption band region.

12) M. Kojima, M. Fujita, H. Ogino, and J. Fujita, *Bull. Chem. Soc. Jpn.*, **50**, 2325 (1977).

13) M. Sano, M. Fujita, K. Sasaki, Y. Yoshikawa, and H. Yamatera, *Bull. Chem. Soc. Jpn.*, **54**, 2823 (1981).

14) S. Fujinami, T. Hosokawa, and M. Shibata, *Bull. Chem. Soc. Jpn.*, **56**, 113 (1983).

Potentiometric and Calorimetric Studies on the Formation of Ethylenediamine Complexes of Nickel(II) Ion in Water and Dioxane-Water Mixtures

Shin-ichi Ishiguro, Yoshihiro Oka, and Hitoshi Ohtaki*
Department of Electronic Chemistry, Tokyo Institute of Technology at Nagatsuta, 4259 Nagatsuta-cho, Midori-ku, Yokohama 227
(Received December 27, 1982)

Equilibria between ethylenediamine and protons or nickel(II) ions have been investigated at 25 °C by means of potentiometric and calorimetric titrations in water and in dioxane–water mixtures (the dioxane contents are 0.1 and 0.2 mole fractions, which correspond to 35.2 and 55.0%w/w, respectively) containing 3 mol dm^{-3} $LiClO_4$ as a constant ionic medium. Thermodynamic parameters ($\Delta G°$, $\Delta H°$, and $\Delta S°$) referring to the formation of the species HL^+, H_2L^{2+}, NiL^{2+}, NiL_2^{2+}, and NiL_3^{2+} (L denotes ethylenediamine) have been determined in the solutions. All the formation constants of the nickel(II)–ethylenediamine complexes increased with increasing dioxane content in the solvent mixtures, although the formation constants of the ethylenediammonium ions remained practically unchanged. On the other hand, enthalpies referring to the formation of the nickel(II)–ethylenediamine complexes became less negative, and thus entropies for the corresponding reactions increased remarkably with increasing dioxane content in the mixtures. The solvent effects on the thermodynamic parameters of the complex formation of nickel(II) ions with ethylenediamine are discussed in terms of enhancement of solvation of the complexes due to weakening of the hydrogen-bonded structure of the bulk water by the addition of dioxane.

We have reported solvent effects on hydrolytic reactions of metal ions in water and in dioxane–water mixtures.[1-3] The thermodynamic quantities of transfer of the hydrolyzed species from water to aqueous dioxane solutions have been discussed in terms of the change in the structures of the bulk solvent and in the second coordination sphere of metal ions of the aqua and hydroxo complexes. The Gibbs energy difference divided by P (*i.e.*, $\Delta G^t_{pq}/p$) for the reaction $qM^{2+} + pOH^- = M_q(OH)_p^{(2q-p)+}$ between the aqueous solution and an aqueous dioxane mixture was approximately independent of the composition (p,q) of the complex and the kind of the metal ion, where $\Delta G^t_{pq} = \Delta G°_{pq}(\text{mix}) - \Delta G°_{pq}(\text{aq}) = -RT \ln \{\beta_{pq}(\text{mix})/\beta_{pq}(\text{aq})\}$ and β_{pq} denotes the overall formation constant of the $M_q(OH)_p^{(2q-p)+}$ complex.

On the other hand, values of $\Delta H^t_{pq}/p$ for the enthalpy difference of the reaction between in water and in dioxane–water mixtures largely depended on the species, and thus the contribution of the enthalpy term to the formation of the hydroxo complexes was practically compensated for that of the $T\Delta S^t_{pq}/p$ term.

The results are summarized in the following ways:[1-3] The hydration of the hydroxo complexes is weak relative to that of the aqua complex and depends on the fractional charge on the metal ions within the complexes. The molar enthalpy of transfer of a hydroxo complex becomes less negative compared with that of the hydrated metal ion, the fractional charge of the metal ion being lower within the former complex than within the latter.

Having a much lower donor property than water, dioxane may hardly solvate primarily to metal ions in such dioxane–water mixtures as employed here (dioxane contents are 0.1 and 0.2 mole fractions, which correspond to 35.2 and 55.0%w/w, respectively), while it may destroy the hydrogen-bonded structure of the bulk water.[4] The formation of a strong solvation shell around a metal ion stabilizes the ion in water,[5] and the weakened hydrogen-bonded structure of the bulk water might cause the hydration of metal ions more favorable.[6]

The results obtained in the determination of the partial molar enthalpies of transfer of the hydroxo complexes of metal ions in the previous investigations[1-3] suggest that a complex with a larger fractional charge on the metal ion within the complex has a stronger hydration sphere than a complex in which the metal ion has a smaller fractional charge.

It is expected that the enthalpy of transfer of a complex is closely related to the solvation structure in the second coordination sphere of the complex, if the structure of the first coordination shell of the complex remains unchanged in the course of the transfer of the complex from water to a mixed solvent.

Considering that the charge of the complexes affects significantly the structure of the second solvation sphere, we employ ethylenediamine complexes of divalent metal ions keeping the total charge at +2, and the Gibbs energies and enthalpies of transfer of the complexes with different ligand numbers are compared. In the present investigation, the ethylenediamine complexes of nickel(II) ions were chosen on considering that the structures of some of the complexes were determined by means of X-ray diffraction in aqueous solutions.[7]

Experimental

Reagents. *Lithium perchlorate*, *lithium hydroxide*, and *perchloric acid* were prepared as described previously.[8] *Dioxane* was purified by an ordinary method.[8] *Ethylenediamine* of reagent grade was first dried by adding sodium hydroxide, and then further dried by using metallic sodium with refluxing overnight under a nitrogen atmosphere, and finally distilled. *Nickel(II) perchlorate* was prepared from nickel(II) oxide and perchloric acid, and the nickel(II) oxide had been prepared by decomposition of nickel(II) nitrate under an infrared lamp, followed by heating in an electric oven at 500 °C for 12 h. The nickel(II) nitrate was of reagent grade and recrystallyzed twice from water. The nickel(II) perchlorate thus prepared

was filtered through a G4 glass filter and then recrystallyzed twice from water. In order to prevent hydrolysis of nickel(II) ions, a small amount of perchloric acid was added to the stock solution and pH of the solution was adjusted to be about 3. The concentration of the free acid in the stock solution was determined coulometrically. The concentration of nickel(II) ions was determined gravimetrically by using dimethylglyoxime.

Measurements. All potentiometric and calorimetric titrations were performed in a room thermostated at (25.0± 0.5) °C. Throughout the measurements, $LiClO_4$ of 3 mol dm^{-3} was employed as a constant ionic medium.

Potentiometric Measurement. Potentiometric measurements were performed in a liquid paraffin bath controlled at (25.00± 0.02) °C, and pH of a test solution was determined by using a glass electrode in combination with an Ag–AgCl electrode as a reference. The measurements were carried out under an atmosphere of nitrogen gas which was equilibrated with solvent vapor. In each series of titrations the constant appearing in the Nernst equation, E_0, was first determined by means of Gran plots[9] by titrating 10 cm^3 of a perchloric acid solution of a known concentration with a lithium hydroxide solution in the constant ionic medium, the concentration of the lithium hydroxide solution being also known. Then, 10 cm^3 of a solution containing metal and hydrogen ions and ethylenediamine of known concentrations was added to the solution and titrations were continued with the same lithium hydroxide solution as used for the Gran-plot procedure until pH of the test solution reached about 10. Potentials at each point of measurements were related to the concentration of free hydrogen ions, h, by the Nernst equation, $E=E_0+59.15 \log h$, in the pH region where the liquid junction potential was negligible ($3 \leq pH \leq 10$). Concentrations of nickel(II) ions and ethylenediamine in the test solutions at the initial stage of titration ranged from 8—46 mmol dm^{-3} and 32—111 mmol dm^{-3}, respectively.

Calorimetric Measurement. In the course of calorimetric measurements, a test solution of 150 cm^3 was placed in a Dewar vessel immersed in a water bath thermostated at (25.000± 0.007) °C. Initial test solutions contained nickel(II) ions and ethylenediamine, the concentration of the latter being slightly larger than three times the concentration of the former. The concentration of hydrogen ions in the solutions was kept so low that the predominant complex species in the solutions was NiL_3^{2+} at the initial stage of the titration. Then a perchloric acid solution of *ca.* 0.4 mol dm^{-3} was used for the calorimetric titrations. At each step of the calorimetric titrations was added the perchloric acid solution of 0.6—1.6 cm^3 with the certainty of ±0.001 cm^3 to the test solution by using an automatic piston buret (Dosimat E535, Metrohm, Switzerland) The on-line calorimetric system fully automatically controlled by an electronic computer JEC-6 (JEOL, Tokyo) was employed throughout the titrations, details of the procedure having been described in previous papers.[2,3]

Analysis of Potentiometric and Calorimetric Data. At each point of titrations the total concentrations of nickel(II) (C_M) and hydrogen ions (C_H) and ethylenediamine (C_L) are related to concentrations of respective free species, m, h, and l, on the basis of the mass-balance and the mass action law:

$$C_M = \sum_p \sum_q \sum_r p\beta_{pqr} m^p h^q l^r, \quad (1)$$

$$C_H = \sum_p \sum_q \sum_r q\beta_{pqr} m^p h^q l^r - K_w h^{-1}, \quad (2)$$

$$C_L = \sum_p \sum_q \sum_r r\beta_{pqr} m^p h^q l^r, \quad (3)$$

where β_{pqr} and K_w stand for the overall formation constant of the complex $M_pH_qL_r^{(2p+q)+}$ and the autoprotolysis constant of the solvent, respectively (β_{000}, β_{100}, β_{010}, and β_{001} are defined to be unity). The formation constants were determined by the least-squares method, where the error square sum, $U=\sum\{(C_M-C_{M,calcd})^2+(C_H-C_{H,calcd})^2+(C_L-C_{L,calcd})^2\}$ was minimized by using the MINIQUAD program.[10] The protonation constants of ethylenediamine had been determined in advance of the equilibrium measurements of the complexes by separate experiments, and they were kept constant in the course of the least-squares refinement of the formation constants of the nickel(II)–ethylenediamine complexes.

On the basis of the formation constants of the complexes thus obtained, the calorimetric data were analyzed by using the program KALORI.[11] Concentrations of all species involved at each point of calorimetric titrations were calculated by using the formation constants determined. The total heat accompanying the formation of species involved in a solution of the volume V is given as follows:

$$Q = -V(\sum_p \sum_q \sum_r \beta_{pqr} \Delta H^\circ_{\beta pqr} m^p h^q l^r - K_w \Delta H^\circ_{Kw} h^{-1}), \quad (4)$$

where $\Delta H^\circ_{\beta pqr}$ and ΔH°_{Kw} denote the enthalpies pertaining to the reactions, $pNi^{2+}+qH^++rL=Ni_pH_qL_r^{(2p+q)+}$ and $H^++OH^-=H_2O$, respectively. The values of K_w and ΔH°_{Kw} had been determined in the solvent mixtures in the previous works.[1,2] Heat evolved (q) at the i-th titration point was compared with the calculated one, $q_{i,calcd}=Q_{i,calcd}-Q_{i-1,calcd}$, by taking into account suitable values of $\Delta H^\circ_{\beta pqr}$ for each species. The enthalpies were optimized by minimizing the error square sum, $U=\sum(q_i-q_{i,calcd})^2$. Enthalpies for the protonation reactions of ethylenediamine were determined in advance by separate experiments.

All calculations were carried out by using an M-180 computer at the Tokyo Institute of Technology.

Results and Discussion

In all the solvents employed potentiometric titration curves for the nickel(II)–ethylenediamine system were well explained by assuming the formation of three mononuclear complexes NiL^{2+}, NiL_2^{2+}, and NiL_3^{2+}, and no protonated nickel(II)–ethylenediamine complex was detected in the present experiment. Typical titration curves obtained in the aqueous solution are shown in Fig. 1, where pH values measured are plotted against X, the degree of neutralization of ethylenediammonium ions in the solution.

All the experimental points fell on the lines calculated (X_{calcd}) by Eq. 5 over the whole range of pH examined.

$$X_{calcd} = (2C_L + K_w h^{-1} - h - \sum_p \sum_q \sum_r q\beta_{pqr} m^p h^q l^r)/C_L \quad (5)$$

The formation constants of the complexes NiL_r^{2+} ($r=1$, 2, and 3) thus obtained are listed in Table 1, together with those of the protonated ethylenediamine species H_qL^{q+} ($q=1$ and 2).

In Fig. 2, typical results for the calorimetric titrations of the nickel(II)–ethylenediamine system in the aqueous solution are depicted, where the heat evolved q_i at the addition of the i-th portion of the titrant was plotted against the average ligand number n of the nickel(II)–ethylenediamine complexes in the solution. The solid lines are drawn by using the enthalpies of formation of each species finally obtained. The values of $\Delta H^\circ_{\beta pqr}$ thus evaluated are summarized in Table 2. At each

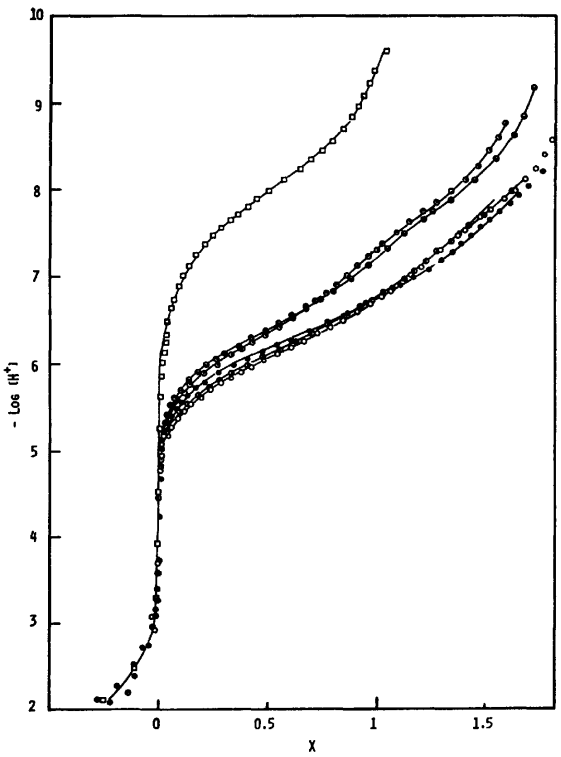

Fig. 1. Potentiometric titration curves of ethylenediamine and nickel(II)–ethylenediamine aqueous solutions.
Curve □: C_{Ni}/mmol dm^{-3}=0.0, C_L/mmol dm^{-3}= 39.47; ○: 7.78, 27.61; ⊙: 10.66, 32.13; ⊖: 18.79, 72.20; ◑: 19.45, 74.76; ◐: 8.21, 29.06; ●: 35.20, 111.13; ⓘ: 45.75, 32.30. The concentrations of the metal ion and the ligand were changed by dilution during the titrations. The solid lines show calculated curves by using the constants in Table 1.

point of the titrations, heat of 9—22 J was evolved, and the calculated heat $q_{i,\,calcd}$ agreed with the experimental one q_i within 0.3 J.

Thermodynamic parameters for the successive reactions are defined as follows:

$$H^+ + H_{q-1}L^{(q-1)+} = H_qL^+;\ \Delta G^\circ_{0q1},\ \Delta H^\circ_{0q1},\ \text{and}\ \Delta S^\circ_{0q1}, \quad (6)$$

$$NiL_{r-1}^{2+} + L = NiL_r^{2+};\qquad \Delta G^\circ_{10r},\ \Delta H^\circ_{10r},\ \text{and}\ \Delta S^\circ_{10r}. \quad (7)$$

These quantities are tabulated in Table 3.

Solvent Effects on the Formation Constants. The formation constants of the nickel(II)–ethylenediamine complexes slightly increased with the dioxane content in the solvents, although the β_{0q1} values of ethylenediammonium ions were practically independent of the solvent composition (Table 1). The stepwise formation constants or the stepwise Gibbs energies of formation of each complex ($-\Delta G^\circ_{10r}$) linearly increased with the mole fraction of dioxane in the solvent and the increment of the $-\Delta G^\circ_{10r}$ values was practically independent of the number of ethylenediamine molecules within the complexes (see Table 3). As we will discuss in later sections, the increase in $-\Delta G^\circ_{10r}$ with the dioxane content in the solvents was attributed to the contribution of the entropy term, and the enthalpy for the complex formation played a role unfavorable for stabilizing the complexes in the mixed solvents.

The $-\Delta G^\circ_{102}$ value was smaller than $-\Delta G^\circ_{101}$ by about 6.9 kJ mol^{-1} in all the solvents examined here, and $-\Delta G^\circ_{103}$ was still smaller than $-\Delta G^\circ_{102}$ by *ca.* 11.4

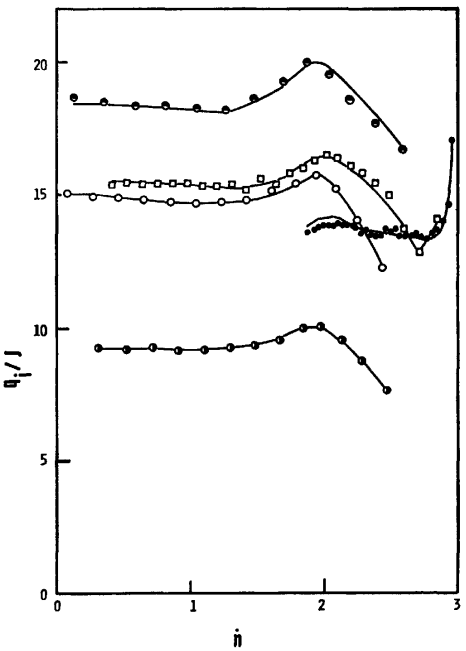

Fig. 2. Calorimetric titration curves of nickel(II)–ethylenediamine aqueous solution.
Curve ◓: C_{Ni}/mmol dm^{-3}=6.6, C_L/mmol dm^{-3}=24.4, $C_{H,tit}$/mmol dm^{-3}=288.6; ○: 6.3, 20.4, 288.6; ◑: 3.7, 13.0, 288.6; □: 11.3, 38.9, 328.2; ●: 25.0, 92.3, 310.0. $C_{H,tit}$ denotes the total concentration of hydrogen ions in the titrant used. The solid lines show calculated curve by using the constants in Table 2.

TABLE 1. THE FORMATION CONSTANTS, β_{pqr}, PERTAINING TO THE REACTIONS, $pNi^{2+}+qH^++rL=Ni_pH_qL_r^{(2p+q)+}$; $\beta_{pqr}=[Ni_pH_qL_r^{(2p+q)+}]/[Ni^{2+}]^p[H^+]^q[L]^r$ (L=ETHYLENEDIAMINE), IN SOLUTIONS CONTAINING 3 mol dm^{-3} $LiClO_4$ AT 25 °C

	Complex	Concentration of dioxane/mole fraction		
		0.0 (0.0%w/w)	0.1 (35.2%w/w)	0.2 (55.0%w/w)
log β_{011}	HL^+	10.56(0.01)	10.57(0.01)	10.66(0.01)
log β_{021}	H_2L^+	18.54(0.01)	18.51(0.01)	18.63(0.01)
log β_{101}	NiL^+	7.87(0.05)	8.18(0.05)	8.54(0.01)
log β_{102}	NiL_2^{2+}	14.53(0.07)	15.18(0.05)	15.89(0.07)
log β_{103}	NiL_3^{2+}	19.18(0.13)	20.18(0.09)	21.27(0.13)

The values in parentheses refer to the three standard deviations.

TABLE 2. THE ENTHALPIES, $\Delta H^{\circ}_{\beta pqr}$/kJ mol^{-1}, PERTAINING TO THE REACTIONS, $p\mathrm{Ni}^{2+}+q\mathrm{H}^{+}+r\mathrm{L}=[\mathrm{Ni}_p\mathrm{H}_q\mathrm{L}_r]^{(2p+q)+}$ (L=en), IN SOLUTION CONTAINING 3 mol dm^{-3} $LiClO_4$ AT 25 °C.

	Complex	Concentration of dioxane/mole fraction		
		0.0 (0.0%w/w)	0.1 (35.2%w/w)	0.2 (55.0%w/w)
$\Delta H^{\circ}_{\beta 011}$	HL^{+}	−65.2 (0.3)	−64.0 (0.3)	−62.2 (0.3)
$\Delta H^{\circ}_{\beta 021}$	H_2L^{+}	−123.7 (0.4)	−122.4 (0.3)	−119.7 (0.3)
$\Delta H^{\circ}_{\beta 101}$	NiL^{2+}	−45.4 (0.9)	−44.4 (0.8)	−42.9 (0.8)
$\Delta H^{\circ}_{\beta 102}$	NiL_2^{2+}	−95.6 (0.9)	−92.0 (0.8)	−89.1 (0.9)
$\Delta H^{\circ}_{\beta 103}$	NiL_3^{2+}	−149.1 (1.0)	−142.1 (0.9)	−137.4 (1.0)

The values in parentheses refer to three standard deviations.

TABLE 3. THE THERMODYNAMIC PARAMETERS, ΔG°_{pqr}, ΔH°_{pqr}/kJ mol^{-1} AND ΔS°_{pqr}/J K^{-1} mol^{-1}, FOR THE SUCCESSIVE FORMATION OF H_qL^{q+} AND NiL_r^{2+}

	Concentration of dioxane mole fraction		
	0.0	0.1	0.2
H^{+}–en system			
$-\Delta G^{\circ}_{011}$	60.3	60.3	60.9
$-\Delta G^{\circ}_{021}$	45.5	45.4	45.5
$-\Delta H^{\circ}_{011}$	65.2	64.0	62.2
$-\Delta H^{\circ}_{021}$	58.5	58.4	57.5
ΔS°_{011}	−16.5	−12.3	−4.5
ΔS°_{021}	−43.6	−43.7	−40.4
Ni^{2+}–en system			
$-\Delta G^{\circ}_{101}$	44.9	46.7	48.7
$-\Delta G^{\circ}_{102}$	38.0	39.9	41.9
$-\Delta G^{\circ}_{103}$	26.5	28.5	30.7
$-\Delta H^{\circ}_{101}$	45.4	44.6	42.9
$-\Delta H^{\circ}_{102}$	50.2	47.4	46.2
$-\Delta H^{\circ}_{103}$	53.6	50.1	48.3
ΔS°_{101}	−1.7	7.1	19.5
ΔS°_{102}	−40.9	−25.2	−14.3
ΔS°_{103}	−90.9	−72.5	−59.1

kJ mol^{-1}. The differences between $-\Delta G^{\circ}_{101}$ and $-\Delta G^{\circ}_{102}$ and between $-\Delta G^{\circ}_{102}$ and $-\Delta G^{\circ}_{103}$ were independent of the composition of the solvents. This fact indicated that replacement of two water molecules with one ethylenediamine within the coordination sphere of nickel(II) ion became more and more difficult with successive steps, although the replacement became more and more exothermic as will be described later.

Solvent Effects on the Enthalpies. According to the X-ray diffraction measurements of the hexaaquanickel(II) ions[12] and the nickel(II)–ethylenediamine complexes[7] in aqueous solutions, the Ni–O bond length increased from 2.04 Å within the $[Ni(H_2O)_6]^{2+}$ ion to 2.10 Å within the $[Ni(H_2O)_2L_2]^{2+}$ complex with the increase in the number of ethylenediamine molecules coordinated. The lengthening of the Ni–O bond indicated weakening of the bond due, perhaps, to the electron donation from the nitrogen atoms within the ethylenediamine molecules to the central metal ion by which the fractional charge on the nickel(II) atom might decrease. Although no structural data have been reported for the $Ni(H_2O)_4L^{2+}$ complex, we can expect such an elongation of the Ni–O bond within the Ni-$(H_2O)_4L^{2+}$ complex when an ethylenediamine molecule coordinates to an aquanickel(II) ion. Therefore, the replacement of water molecules within the $[Ni(H_2O)_{6-2r}L_r]^{2+}$ complex ($0\leq r\leq 3$) needs less and less energies with the increase in the number of ethylenediamine molecules r within the complex.

The Ni–N bond lengths are 2.10 Å and 2.20 Å within the $[Ni(H_2O)_2L_2]^{2+}$ and $[NiL_3]^{2+}$ complexes, respectively,[7] and therefore, the Ni–N bond may be weaker in the latter than in the former. Thus, we can expect that both Ni–O and Ni–N bonds more and more weaken with the introduction of ethylenediamine molecules to the coordination sphere of nickel(II) ion.

In spite of the weakening of the Ni–N bond in the $[Ni(H_2O)_{6-2r}L_r]^{2+}$ complex with increasing r, ΔH°_{10r} in the aqueous solution became more negative. This suggests that the decrease of the Ni–O bond energy within the $[Ni(H_2O)_{6-2r}L_r]^{2+}$ complex may be more enhanced than that of the Ni–N bond by the ligand substitution of two moles of H_2O with one mole of ethylenediamine.

From the enthalpic point of view, the formation of nickel(II)–ethylenediamine complexes became less favorable in a dioxane–water mixture than in water, although the decrease in the Gibbs energies at each successive complexation reaction was more pronounced in mixed solvents than in water.

We can assume that the bond lengths within the complexes are not appreciably changed when the complexes are transferred from water to a dioxane–water mixture, because no change has been observed in the UV and visible absorption spectra of the complexes in solutions with different dioxane contents. Invariable $\Delta\Delta G^{\circ}_{10r}$ and $\Delta\Delta H^{\circ}_{10r}$ values between the successive stages of formation of a given pair of complexes in two different solutions may give an indirect support for the invariable structures of the complexes concerned. Therefore, the changes in the enthalpy of the complex formation reactions in different solvents, as well as entropy changes, should be attributed to the structural changes in the second coordination sphere of the complexes, in which solvent molecules interact with the ligand molecules coordinated to the central nickel(II) ion.

It is well accepted that water molecules interact each other through hydrogen bonds in the bulk water and that the hydrogen-bonded water structure is broken by the addition of dioxane. In the ionic medium

employed here, many water molecules are hydrated to the medium salt, but still there are some water molecules having a bulk-like structure in the solution.

When nickel(II) ions are brought into the aqueous solution, the nickel(II) ions form the hexaaquanickel(II) complex which can still be solvated with water molecules in their second coordination sphere. Nickel(II)–ethylenediamine complexes, the first coordination shell of which are filled with ethylenediamine and water molecules (except for the NiL_3^{2+} complex), can be also solvated with water molecules in the aqueous solution. The second-sphere hydration of the complexes may be weak and not highly ordered, and therefore, the interaction between the ligand molecules in the first coordination sphere and water molecules in the second solvation shell may be affected rather sensitively by the change in the hydrogen-bonded structure of the bulk water. The more the hydrogen-bonded structure of the bulk water is broken by the addition of dioxane, the easier the construction of the second hydration shell is, and thus, the more negative the enthalpy of hydration in the second sphere of the complex should be, provided that the structure of the first coordination shell of the complex is not practically affected by the change in the bulk structure of water.

The enthalpies of each successive formation of the complexes became less negative with increasing dioxane content in the solvent (see Table 3). This fact suggests that the enthalpy difference of a complex $[Ni(H_2O)_{6-2r}L_r]^{2+}$ in two different solvents is larger than that of a complex $[Ni(H_2O)_{6-2(r+1)}L_{r+1}]^{2+}$.

In order to discuss the enthalpy changes of the complex formation reactions in different solvents, we estimated enthalpies of transfer of each complex ion from water to the dioxane–water mixtures employed in the present work.

Underdown *et al.*[13] have reported that the enthalpy of transfer of nickel(II) ion from water to a dioxane–water mixture was positive (endothermic) when the dioxane content in the mixture was lower than 0.04 mole fraction, but decreased to tend to be negative (exothermic) with an increase in the dioxane concentration. In an aqueous mixture with the dioxane content larger than 0.06 mole fraction, the enthalpy of transfer of nickel(II) ion from water to the mixture became negative. This fact indicates that the solvation of nickel(II) ion is enhanced in the aqueous dioxane mixtures with the dioxane content higher than 0.06 mole fraction.

The solvation of ethylenediamine does not seem to change significantly when dioxane is added to water. The heats of solution of ethylenediamine in water and in a dioxane–water mixture containing 0.2 mole fraction dioxane, both solutions having 3 mol dm^{-3} $LiClO_4$, were 34.5 kJ mol^{-1} and 34.8 kJ mol^{-1}, respectively.[14] Therefore, the enthalpy of transfer of ethylenediamine from water to the dioxane–water mixture was practically zero.

The difference $\Delta H^\circ_{\beta 10r}(\text{mix}) - \Delta H^\circ_{\beta 10r}(\text{aq})$ can be separated into contributions of each species concerned as follows:

$$\begin{aligned}
&\Delta H^\circ_{\beta 10r}(\text{mix}) - \Delta H^\circ_{\beta 10r}(\text{aq}) \\
&= \{\Delta H^\circ_{\text{sv.mix}}(NiL_r^{2+}) - \Delta H^\circ_{\text{sv.aq}}(NiL_r^{2+})\} \\
&\quad - \{\Delta H^\circ_{\text{sv.mix}}(Ni^{2+}) - \Delta H^\circ_{\text{sv.aq}}(Ni^{2+})\} \\
&\quad - r\{\Delta H^\circ_{\text{sv.mix}}(L) - \Delta H^\circ_{\text{sv.aq}}(L)\} \\
&= \Delta H^\circ_{\text{tr}}(NiL_r^{2+}) - \Delta H^\circ_{\text{tr}}(Ni^{2+}) - r\Delta H^\circ_{\text{tr}}(L), \qquad (8)
\end{aligned}$$

where $\Delta H^\circ_{\text{sv}}(j)$ and $\Delta H^\circ_{\text{tr}}(j)$ stand for the enthalpies of solvation and of transfer of species j, respectively. Here we can reasonably assume that $\Delta H^\circ_{\text{tr}}(L)$ is zero. $\Delta H^\circ_{\text{tr}}(Ni^{2+})$ can be estimated by inter- and extrapolating the values reported by Underdown *et al.*[13] to 0.1 and 0.2 mole fraction dioxane–water mixtures, respectively. Therefore, by using experimental values given in Table 2 for $\Delta H^\circ_{\beta 10r}$ of each complex formation reaction, we can evaluate the values of $\Delta H^\circ_{\text{tr}}(NiL_r^{2+})$ for the various complexes. The values thus estimated are tabulated in Table 4. The enthalpies of transfer of all the species from water to the aqueous dioxane mixtures are negative, and the values are more negative in the mixtures with the higher dioxane content. The result implies that the second-sphere solvation of the nickel(II)–ethylenediamine complexes, as well as the aquanickel(II) ion, is enhanced in the dioxane–water mixtures, but the degree of the enhancement of the second-sphere solvation is less in the complexes than in the aquanickel(II) ion.

This result indicates that the enhancement of the second-sphere solvation of the complexes and the aquanickel(II) ion may be due to a less energy needed for breaking the water structure to produce non-hydrogen-bonded water molecules which solvate the complexes, and the hydrogen-bonding of water molecules in the second-coordination sphere may be stronger in the hexaaquanickel(II) ion than in the nickel(II)–ethylenediamine complexes.

The enthalpies for the formation of ethylenediammonium ions (HL^+ and H_2L^{2+}) slightly increased with an increase in the dioxane content of the solvents, and the increment of the ΔH°_{0q1} values was practically compensated for an increase in the ΔS°_{0q1} values, which led to the ΔG°_{0q1} values practically independent of the solvent composition (see Table 3).

Solvent Effects on the Entropies. Entropies of the reaction, $[Ni(H_2O)_{6-2r}L_r]^{2+} + L = [Ni(H_2O)_{6-2(r+1)}L_{r+1}]^{2+} + 2H_2O$, decreased with an increase in the number of ethylenediamine molecules r within the complex, as reported previously by many authors. On the other hand, in the formation of a given complex, the entropies increased remarkably with increasing dioxane content

TABLE 4. ENTHALPIES OF TRANSFER, $\Delta H^\circ_{\text{tr}}$/kJ mol^{-1}, OF THE AQUANICKEL(II) ION AND NICKEL(II) –ETHYLENEDIAMINE COMPLEXES FROM WATER TO DIOXANE–WATER MIXTURES[a]

Dioxane content mole fraction	$-\Delta H^\circ_{\text{tr}}$			
	Ni^{2+}	NiL^{2+}	NiL_2^{2+}	NiL_3^{2+}
0.1	8.0[b]	7.0	4.4	1.0
0.2	24.0[c]	21.5	17.5	12.3

a) Values for NiL_r^{2+} complexes were calculated by assuming $\Delta H^\circ_{\text{tr}}(L) = 0$. b) Interporated from the values in Ref. 13. c) Extraporated from the values in Ref. 13.

in the solutions (Table 3). The increase in the entropies for the stepwise complex formations with an increase in the dioxane content in the solution is most remarkable in the formation of the highest complex NiL_3^{2+}.

The formation of the $[Ni(H_2O)_{6-2(r+1)}L_{r+1}]^{2+}$ complex is accompanied by the dehydration of two moles of water in the first coodination sphere of the $[Ni(H_2O)_{6-2r}L_r]^{2+}$ complex. The number of water molecules expelled from the whole coordination shell of the complex at the introduction of one ethylenediamine molecule may be larger than 2, because dehydration of the ethylenediamine molecule and from the second coordination sphere of the complex may also be expected in the complex formation reaction. The dehydration will cause the increase in entropy, although a part of the entropy increase in the dehydration process may be cancelled out by a decrease in entropy due to combination of an ethylenediamine molecule with the metal ion.

As we have discussed in the previous section, the hydrogen-bonded structure of water is broken by the addition of dioxane, and therefore, in the dioxane–water mixture water molecules can behave more freely compared with those in the aqueous solution.

When water molecules are liberated from the coordination sphere of a nickel(II) ion by the chelate formation with ethylenediamine molecules, the water molecules can behave more freely in the bulk phase of a dioxane–water mixed solvent than in an aqueous solution. Therefore, in the dehydration process accompanying the chelate formation with ethylenediamine, the entropy of the reaction becomes more positive in a dioxane–water mixture than in water.

The entropies for the protonation of ethylenediamine increased with increasing dioxane content in the mixture, although the increase was not remarkable compared with that for the formation of any of the nickel(II)–ethylenediamine complexes in the same solvents. In the course of the protonation reaction of ethylenediamine, $L+qH_3O^+=LH_q^{q+}+qH_2O$, the liberated water molecules might solvate the protons at the amino groups within the ethylenediammonium ion formed, so that the entropy gain by the liberation of water molecules from H_3O^+ may be cancelled out by the combination of the water molecules with the NH_3^+ groups formed.

The work has partially been supported by the Grant-in-Aid for Scientific Research No. 57470054 from the Ministry of Education, Science and Culture and by the Asahi Glass Foundation for Industrial Technology.

References

1) T. Kawai, S. Ishiguro, and H. Ohtaki, *Bull. Chem. Soc. Jpn.*, **53**, 2221 (1980).
2) S. Ishiguro and H. Ohtaki, *Bull. Chem. Soc. Jpn.*, **52**, 3198 (1979).
3) S. Ishiguro and H. Ohtaki, *Bull. Chem. Soc. Jpn.*, **54**, 335 (1981).
4) D. N. Glew, H. D. Mak, and N. H. Rath, "Hydrogen-bonded Solvent Systems," Taylor and Francis Ltd., London (1968), p. 195.
5) H. S. Frank and W.-Y. Wen, *Discuss. Faraday Soc.*, **24**, 133 (1957).
6) D. Feakins and C. T. Allan, *J. Chem. Soc., Faraday Trans. I*, **1976**, 314.
7) T. Fujita and H. Ohtaki, *Bull. Chem. Soc. Jpn.*, **55**, 455 (1982).
8) H. Ohtaki, *Inorg. Chem.*, **6**, 808 (1967).
9) G. Gran, *Analyst*, **77**, 661 (1952).
10) S. Sabatini, A. Vacca, and P. Gans, *Talanta*, **21**, 53 (1974).
11) R. Karlsson and L. Kullberg, *Chem. Scr.*, **9**, 54 (1976).
12) H. Ohtaki, T. Yamaguchi, and M. Maeda, *Bull. Chem. Soc. Jpn.*, **49**, 701 (1976); "Analytical Chemistry: Essays in Memory of Anders Ringbom," ed by E. Wänninen, Pergamon Press, New York (1977), p. 163.
13) D. R. Underdown, S. S. Yun, and J. L. Bear, *J. Inorg. Nucl. Chem.*, **36**, 2043 (1974).
14) S. Ishiguro and H. Ohtaki, unpublished data.

Reactivity of Aromatic *o*-Hydroxy Oximes. I. Synthesis and Aminolysis of Acylglycine Esters of Aromatic *o*-Hydroxy Oximes

Ikuo HAYASHI,* Keizo OGIHARA, and Kiyoshi SHIMIZU
Research and Development Laboratory of Nitto Boseki Co., Ltd., Fukuyama, Koriyama, Fukushima 963
(Received July 3, 1982)

Active esters (**1**) of glycine with *o*-hydroxybenzaldehyde oxime, *o*-hydroxyacetophenone oxime, *o*-hydroxybenzophenone oxime, and their 5-Cl and 5-NO_2 derivatives were prepared by several methods. For aminolysis with benzylamine, esters **1** show higher reactivity than similar esters containing no hydroxyl group in the ortho position. It is suggested that esters **1** forms an intramolecular hydrogen bond between the hydrogen of the hydroxyl group at the ortho position and the hydroxyimino nitrogen so as to have its carbonyl group activated for the aminolysis; this mechanism of activation seems to be a sort of "intramolecular acid-catalysis." Among the series of esters **1**, esters of *o*-hydroxybenzaldehyde oxime and its 5-Cl and 5-NO_2 derivatives are most reactive in the aminolysis. The reactivity of esters **1** is also discussed in relation to pK_a values of aromatic *o*-hydroxy oximes.

In the coupling reaction of acylamino acid with amino acid alkyl esters, various oximes are used as their alcoholic components.[1-7] As compared with esters of *p*-nitrophenol, pentachlorophenol, and *N*-hydroxysuccinimide, even the most active esters of these oximes show rather a low reactivity for the condensation with amino component.

Losse *et al.*[2] reported that esters of *m*-nitroacetophenone oxime react faster with amino acid alkyl esters than those of acetophenone oxime. But the reactivity of the former is still lower than that of *p*-nitrophenol ester for the aminolysis. Itoh[4] showed that oximes of type $HO\text{-}N{=}C\langle^{CN}_{COR}$ (R=OEt, NH_2) are effective in peptide synthesis.

A general consideration drawn from all the above cases is that an ester is activated by introduction of an electron-withdrawing substituent to its alcoholic component. According to this general consideration, it should be expected that introduction of electron-withdrawing substituent X such as NO_2 or CN to an alcoholic component (oximes **3**) is to increase the reactivity, whereas X=OH or OR is to have a deactivating effect.

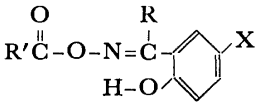

1

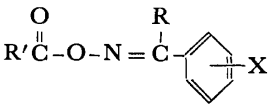

2

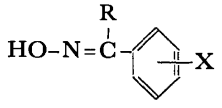

3

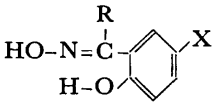

4

When oximes containing hydroxyl group at the ortho position in a benzene nucleus were used as active esters, we found that reactions with benzylamine were accelerated greatly. This unexpected result let us to conclude that the activation of **1** was a consequence of hydrogen bond formation between the phenolic hydrogen atom and the spacially adjacent unshared electron pair of the nitrogen atom in the hydroxyimino group. Such interaction induces the electron density at the nitrogen atom to decrease so that esters **1** may show a high reactivity:

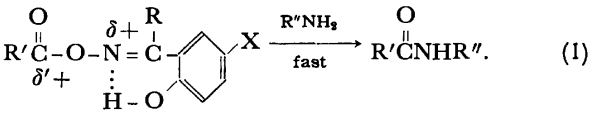

(1)

1

It is known that addition[5-8] of a weak acid (acetic or formic acid) as catalyst to oxime esters will cause rapid and smooth condensation:

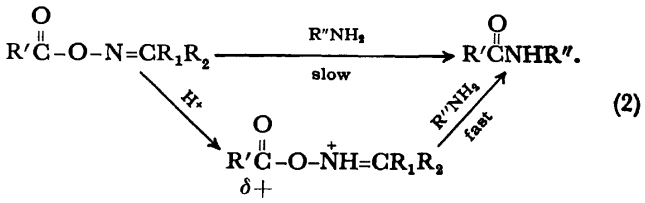

(2)

The mechanism of activation for our system corresponds to the presence of weak acids.

From the consideration descrived above, we prepared esters **1** from *N*-(benzyloxycarbonyl)glycine (Z–Gly) and various oximes of *o*-hydroxybenzaldehyde, *o*-hydroxyacetophenone, *o*-hydroxybenzophenone, and their 5-Cl and 5-NO_2 derivatives, and measured rates of aminolysis with benzylamine in order to compare reactivities of esters **1** and **2**.

We also discuss the reactivity of aminolysis of **1** in connection with pK_a values of aromatic *o*-hydroxy oximes **4**.

Results and Discussion

All aromatic *o*-hydroxy oximes **4** were of (*E*) configuration and are summarized in Table 1 together with oximes **3**.

Acylated Position of Aromatic o-*Hydroxy Oximes* **4**.
There are many papers on the aminolysis of oxime esters of acylamino acid. But there is no study on the reaction of esters of oxime **4** except for a report of Przybylski and Miecznikowska[19] on a coupling method using dicyclohexylcarbodiimide (DCC) and *o*-hydroxybenzladehyde oxime as an "Eintopf" procedure. It is of interest which position is esterified by acylamino acid, phenolic hydroxyl, or hydroxyimino group in the case of **4** with a bifunctional nature. There have been many reports[9,10,13,20-24] on the acetylation of these oximes.

Table 1. Yields and properties of oximes[a)]

Oxime of	Abbreviation (HOX)[b)]	Yield %	TLC R_f	Mp θ_m/°C Observd	Mp θ_m/°C Lit
o-Hydroxybenzaldehyde	HOHBA	84.8	0.60[c)]	55—56	57[16)]
o-Hydroxyacetophenone	HOHAP	95.0	0.68[c)]	112—114	112—112.5[16)]
o-Hydroxybenzophenone	HOHBP	62.0	0.77[d)]	139—140	142—143[15)]
5-Chloro-2-hydroxybenzaldehyde	HOHBA-5Cl	76.1	0.79[e)]	123—124	123—124[16)]
2-Hydroxy-5-nitrobenzaldehyde	HOHBA-5NO_2	83.4	0.58[e)]	212—214	220[16)]
5-Chloro-2-hydroxyacetophenone	HOHAP-5Cl	72.4	0.88[f)]	174—178	180[17)]
2-Hydroxy-5-nitroacetophenone	HOHAP-5NO_2	62.4	0.73[f)]	225—226	231[30)]
5-Chloro-2-hydroxybenzophenone	HOHBP-5Cl	77.6	0.79[d)]	139—141	144—144.5[22)]
2-Hydroxy-5-nitrobenzophenone	HOHBP-5NO_2	64.4	0.78[d)]	193—196	
p-Chlorobenzaldehyde	HOBA-pCl	73.2	0.64[c)]	100—102	106—107[16)]
m-Nitrobenzaldehyde	HOBA-mNO_2	61.9	0.58[c)]	118—120	121—123[16)]
p-Chloroacetophenone	HOAP-pCl	74.4	0.67[c)]	95—96	97[16)]
m-Nitroacetophenone	HOAP-mNO_2	57.3	0.58[g)]	130—131	133—134[16)]
Benzaldehyde	HOBA	88.7	0.84[d)]	119—120[h)]	118—119[h,16)]
Acetophenone	HOAP	87.7	0.75[d)]	56—59	59[16)]
Benzophenone	HOBP	98.1	0.78[d)]	139—140	143[16)]

a) All oximes prepared are of (*E*) configuration and were characterized by elemental analysis.

b) HOX: 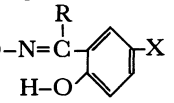 or 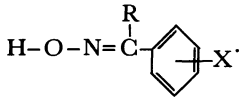

c) R_{f9}. d) R_{f8}. e) R_{f4}. f) R_{f5}. g) R_{f2}. h) Bp, °C (mmHg, 1 mmHg=133.322 Pa).

In the reaction of aromatic o-hydroxy oximes **4** with acetic anhydride under mild conditions, compounds **5** are usually obtained:

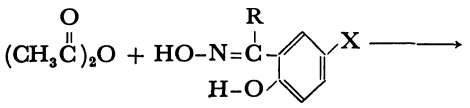

4

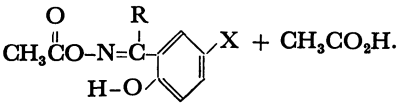

5

We tried to condense oximes **4** with acetic acid by a direct condensation using DCC and obtained the same products as in the reaction with acetic anhydride.

Esters **1** and **2** of Z-Gly with oximes **4** and **3** have been prepared (A) by direct condensation using DCC, (B) with carbonic carboxylic anhydride, or (C) with acid chloride. Representatives of them are summarized in Table 2.

Rate of Aminolysis. Effect on o-*Hydroxyl Group*: To compare reactivities of esters **1** and **2**, we measured their rates of aminolysis with benzylamine in THF at 30 °C. The results are shown in Fig. 1.

All aromatic o-hydroxy oxime esters **1** have a higher reactivity than oxime esters **2** containing no o-hydroxyl group. It is demonstrated that the existence of o-hydroxyl group greatly accelerates the rate of aminolysis.

We concluded that the activation of **1** is caused by hydrogen bond formation[9—13,25)] between the phenolic hydrogen atom and the spacially adjacent lone-pair electrons of the nitrogen atom in hydroxyimino group, and that the electron-withdrawing nature of aromatic

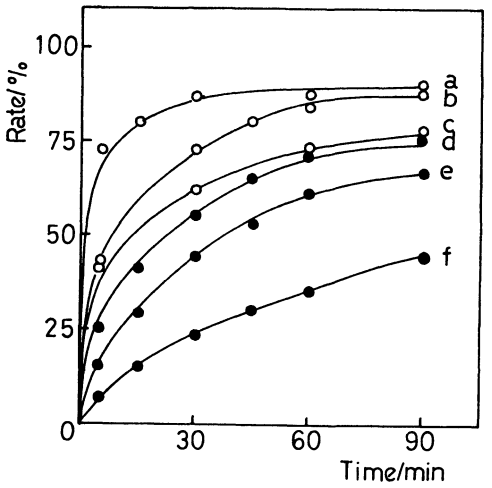

Fig. 1. Aminolysis rates of Z-Gly-OY[a)] with benzylamine. Effect on o-hydroxyl group in an alcoholic component.
a: Z-Gly-OHBA, b: Z-Gly-OHBP, c: Z-Gly-OHAP, d: Z-Gly-OBA, e: Z-Gly-OBP, f: Z-Gly-OAP.
a) -OY denotes an oxime residue such as

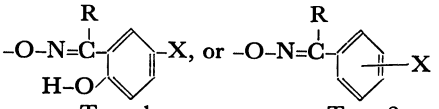

Type 1 Type 2

—○—: type 1, —●—: type 2. These abbreviations are used in Figs. 2 and 3.

o-hydroxy oximes is increased as a result of decrease in the electron density at the hydroxyimino nitrogen atom (see Eq. 1). A nonbonding interaction between the phenolic hydrogen atom and the lone-pair electrons on the hydroxyimino nitrogen would be favored by their

TABLE 2. OXIME ESTERS OF *N*-(BENZYLOXYCARBONYL) GLYCINE

Ester	Method	Yiled %	Mp θ_m/°C	Found (Calcd) (%) C	H	N
Z-Gly-OHBA	(A)	72.1	108—111	62.05 (62.19)	5.02 (4.91)	8.53 (8.53)
Z-Gly-OHBA	(B)	45.7	108—110	61.76 (62.19)	4.90 (4.91)	8.34 (8.53)
Z-Gly-OHAP	(A)	78.9	113—115	63.25 (63.15)	5.22 (5.33)	8.29 (8.18)
Z-Gly-OHAP	(B)	55.0	109—110	63.33 (63.15)	5.30 (5.33)	8.34 (8.18)
Z-Gly-OHBP	(A)	66.5	117—119	68.33 (68.31)	4.99 (4.98)	6.97 (6.93)
Z-Gly-OHBA-5Cl	(A)	78.5	129—133	56.04 (56.29)	4.15 (4.17)	7.54 (7.72)
Z-Gly-OHBA-5NO_2	(A)	30.2	133—137	54.76 (54.69)	4.04 (4.05)	11.05 (11.26)
Z-Gly-OHAP-5Cl	(A)	54.2	123—125	57.52 (57.38)	4.58 (4.55)	7.37 (7.43)
Z-Gly-OHAP-5NO_2	(A)	87.0	125—128	56.16 (55.82)	4.56 (4.42)	10.87 (10.85)
Z-Gly-OHBP-5Cl	(A)	49.2	121—123	62.95 (62.95)	4.36 (4.36)	6.39 (6.38)
Z-Gly-OHBP-5NO_2	(A)	66.3	157—159	61.64 (61.47)	4.52 (4.26)	9.39 (9.35)
Z-Gly-OBA	(C)	36.0	100—102	65.04 (65.38)	5.19 (5.16)	9.09 (8.97)
Z-Gly-OAP	(A)	75.4	71[a]	66.50 (66.25)	5.90 (5.56)	8.86 (8.58)
Z-Gly-OBP	(C)	82.9	65[b]	71.25 (71.21)	5.15 (5.19)	7.31 (7.21)
Z-Gly-OBA-*p*Cl	(B)	30.3	123—124	58.94 (58.88)	4.30 (4.36)	8.12 (8.08)
Z-Gly-OBA-*m*NO_2	(A)	52.8	132—133[c]	57.18 (57.14)	4.22 (4.23)	11.76 (11.76)
Z-Gly-OAP-*p*Cl	(B)	41.9	104—105	59.87 (59.92)	4.69 (4.75)	7.74 (7.76)
Z-Gly-OAP-*m*NO_2	(A)	56.4	76—78[d]	58.22 (58.22)	4.64 (4.61)	11.23 (11.32)

a) Lit:[1] mp 95.5—97 °C. b) Lit:[1] mp 78—79 °C. c) Lit:[1] mp 126.5—128 °C. d) Lit:[1] mp 79—80 °C.

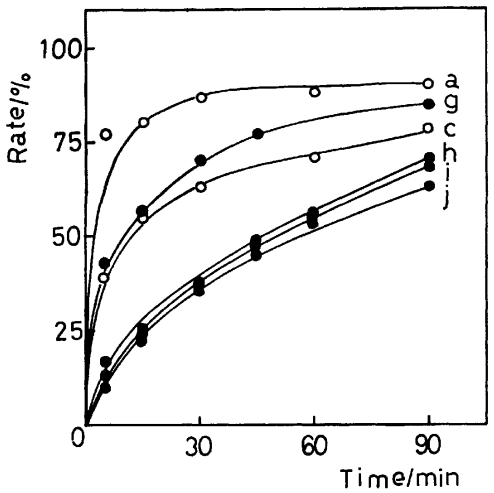

Fig. 2. Aminolysis rates of Z-Gly-OY with benzylamine. Comparison between effect on *o*-hydroxyl group and that due to an electron-withdrawing substituent X of oximes **3**.
a and c: See, Fig. 1, g: Z-Gly-OBA-*m*NO_2, h: Z-Gly-OBA-*p*Cl, i: Z-Gly-OAP-*m*NO_2, j: Z-Gly-OAP-*p*Cl.

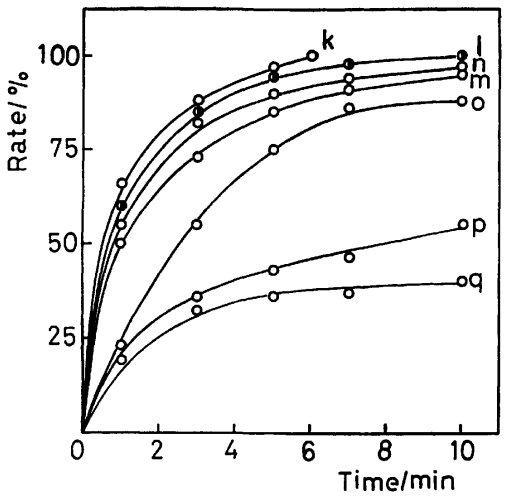

Fig. 3. Aminolysis rates of Z-Gly-OY with benzylamine. Effect on substituent X in aromatic *o*-hydroxy oximes **4**.
k: Z-Gly-OHBA-5NO_2, l: Z-Gly-ONp[a], m: Z-Gly-OHBP-5NO_2, n: Z-Gly-OHBA-5Cl, o: Z-Gly-OHAP-5NO_2, p: Z-Gly-OHBP-5Cl, q: Z-Gly-OHAP-5Cl.
a) -ONp=*p*-nitrophenol residue. —◑—: **1**.

proximity, in which **1** assumes an (*E*) configuration. Therefore, the aminolysis of **1** proceeds faster than those of **2**.

Although a considerable number of acylamino acid active esters have been prepared since the first application of *p*-nitrophenyl ester to peptide synthesis, the new method of activation adopted in this study has not so far been presented. Typical active esters comprise electron-withdrawing groups. The reason for the high reactivity of esters **1** in spite of the existence of the electron-donating hydroxyl group, is that the particular configuration of oximes **4** favors hydrogen bond formation so as to activate **1** *via* the mechanism of "intramolecular acid-catalysis."

As shown in Fig. 1, the reactivity of oxime esters having different substituents R decreases in the order;

$$H > C_6H_5 > CH_3. \quad (3)$$

The effect of phenyl group on the reactivity is less than that of hydrogen. Both the phenyl groups in this molecule can not be coplanar owing to the bulkiness of substituent $R=C_6H_5$. This noncoplanarity[10,12] of aromatic rings for HOHBP and its 5-Cl and 5-NO_2 derivatives (all abbreviations shown in Table 1) results in two "mutually independent" conjugate systems, with reduction in the electron-withdrawing effect of the phenyl substituent.

Comparison between the Effects of o*-Hydroxyl Group and of Electron-withdrawing Substituents X for Oximes 3*: Amino-

lysis rates for various substituents (X=Cl and NO_2) are shown in Fig. 2.

Z-Gly-OHBA and Z-Gly-OHAP have higher reactivity than the series of oxime esters **2**:

$$\text{Z-Gly-OHBA} > \text{Z-Gly-OBA-}m\text{NO}_2 > \text{Z-Gly-OBA-}p\text{Cl}, \quad (4)$$

$$\text{Z-Gly-OHAP} > \text{Z-Gly-OAP-}m\text{NO}_2 > \text{Z-Gly-OAP-}p\text{Cl}. \quad (5)$$

It is found that the introduction of hydroxyl group to the ortho position of aromatic oximes is superior in activating effect to the substitution of NO_2, and much more to that of Cl. It is worthwhile to point out that the activation of nonbonding interaction owing to hydrogen bonding (and thus "intramolecular acid-catalysis") is more effective than the activation through a conjugate system provided by the electron-withdrawing group such as NO_2.

Effect of Substituent X in Aromatic o-Hydroxy Oximes **4**: The effect of substituent X on the aminolysis rate is illustrated in Fig. 3, including Z-Gly-ONp for comparison. The reactivities of the active esters from HOHBA-5NO_2, HOHBA-5Cl, or HOHBP-5NO_2 are nearly equal to that of *p*-nitrophenol.

The order of reactivity is

$$NO_2 > Cl > H. \quad (6)$$

Typical examples may be provided with esters of HOHBA and its 5-NO_2 and 5-Cl derivatives. Although no series of HOHAP and HOHBP are shown in Fig. 3, the same tendency can be found to exist from a comparison with Fig. 1. This result may be understood in terms of the inductive effect that the substitution of NO_2 or Cl at the 5-position to the hydroxyimino group in an aromatic nucleus will reduce strongly the electron density on the phenolic oxygen in combination with the hydrogen bond favorable to the *o*-hydroxyl group. Therefore, the ease of the protonation of the hydroxyl group to the nitrogen atom of the hydroxyimino group increases extremely.

Relation between pK_a *values of Oximes* **3** *and* **4** *and the Reactivity for the Aminolysis of Their Active Esters.* The pK_a values of the oximes prepared are listed in Table 3.

Aromatic *o*-hydroxy oximes **4** exhibit stronger acidity than the corresponding oximes **3** containing no *o*-hydroxyl groups. Regardless of the character of R, the order of pK_a values with respect to X in **4** is

$$NO_2 < Cl < H. \quad (7)$$

The order of pK_a values with respect to R is

$$H < C_6H_5 < CH_3. \quad (8)$$

It is demonstrated that the reactivity order for the aminolysis of esters **1** is parallel to the order of pK_a values of corresponding oximes **4**.

It is well known that only the phenolic proton in **4** dissociates.[9,11,12] Therefore, the proton transfer to the hydroxyimino nitrogen has enhanced the acidity as a result of an intramolecular hydrogen bond formation between the phenolic proton and the hydroxyimino nitrogen.

When pK_a values are subject to a detailed check, no good relations are always found for **4** having X=Cl or H between the order of rate of aminolysis and that of pK_a values given by relation 8.

Patel and Patel[11] reported that the electronegative substituent Cl will reduce the electron density of HOHBP-5Cl and thus facilitate the dissociation of phenolic proton. But they[11] also postulated that the Cl would act also as a p-π donor. The irregularity found in pK_a values may be explained on their conclusion and postulate.

Experimental

All melting points were uncorrected. IR spectra were recorded on a JASCO A-102 spectrophotometer. The homogeneity of substances and the purity of isomers were checked by TLC using silica gel (Kiesel Gel 60 F254, Merck) and various developing solvent systems: R_{f2}, $CHCl_3$–MeOH–AcOH (95 : 5 : 3); R_{f4}, $CHCl_3$–MeOH–benzene (95 : 5 : 3); R_{f5}, $CHCl_3$–MeOH–ethyl acetate (95 : 5 : 3); R_{f6}, $CHCl_3$–MeOH–petroleum ether (95 : 5 : 3); R_{f8}, $CHCl_3$–MeOH–petroleum ether (95 : 3 : 3); R_{f9}, $CHCl_3$–MeOH–AcOH (95 : 2 : 3); R_{f13}, $CHCl_3$–MeOH (100 : 1). R_f spots were made visible with iodine vapor or UV light for all oximes and demonstrated by the combination of hydrobromic acid and 0.2% ninhydrin in acetone for Z-Gly derivatives.

Starting Materials. HOBA,[16] HOAP,[16] HOBP,[16] HOAP-*p*Cl,[16] HOBA-*p*Cl,[16] HOBA-*m*NO_2,[16] and HOHBA[16] were prepared in aqueous EtOH by the reaction of corresponding aldehydes or ketones with hydroxylamine hydrochloride and sodium carbonate (or sodium acetate) according to the usual method.[14] Aromatic *o*-hydroxy ketones, *o*-hydroxyacetophenone,[26] 5-chloro-2-hydroxyacetophenone,[26] *o*-hydroxybenzophenone,[27] and 5-chloro-2-hydroxybenzophenone[28] were prepared by Fries rearrangement of the corresponding phenyl esters in the presence of anhydrous aluminium chloride

Table 3. pK_a values of oximes **3** and **4**

Oxime (R=H)	pK_a	Oxime (R=C_6H_5)	pK_a	Oxime (R=CH_3)	pK_a
HOHBA	9.3	HOHBP	9.3	HOHAP	9.2
HOHBA-5Cl	8.8	HOHBP-5Cl	9.0	HOHAP-5Cl	8.8
HOHBA-5NO_2	6.7	HOHBP-5NO_2	7.3	HOHAP-5NO_2	7.4
HOBA	10.9	HOBP	11.8	HOAP	12.0
HOBA-*p*Cl	10.1			HOAP-*p*Cl	10.3
HOBA-*m*NO_2	10.1			HOAP-*m*NO_2	10.1
HONp[a]					

a) HONp : *p*-Nitrophenol.

and then their oximes were prepared according to the usual method,[14] except for HOHBP and its derivatives which were prepared as described below. 2-Hydroxy-5-nitrobenzaldehyde[29] and 2-hydroxy-5-nitroacetophenone[30] were prepared by nitration from corresponding parent compounds and their oximes were obtained according to the usual method.[14]

HOHBP: Both isomers were prepared by the method of Kohler and Bruce.[15] We obtained products of mp 139—140 °C for (*E*) and 132—133 °C for (*Z*) isomer. The mp values of the (*E*) and (*Z*) isomers of HOHBP prepared here did not agree with those given by Kohler and Bruce,[15] who reported 142—143 °C for the (*E*) and 141—142 °C for the (*Z*) isomer. We separated a mixture of (*E*) and (*Z*) isomers prepared by the usual method.[14] TLC values were as follows: $R_{f13}=0.54$ for the (*E*), 0.22 for the (*Z*), and 0.54+0.22 for the mixture. These values are identical with those obtained by the method of Kohler and Bruce. The magnitude of R_f values for the (*E*) isomer was greater than that of the (*Z*) isomer. The same tendency was also observed by Ashbrook.[32] We used the (*E*) isomer in this study.

HOHBP-5Cl: This compound was also prepared essentially as described above: mp 139—141 °C (Lit,[18] 144—144.5 °C).

HOHBP-5NO$_2$: To a suspension of 2-chloro-5-nitrobenzoic acid (50.0 g, 0.248 mol) in benzene (250 ml), phosphorus pentachloride (51.6 g, 0.248 mol) was added at room temperature with stirring. The mixture was then refluxed for 3 h. After the evolution of HCl had ceased, the excess of solvent was evaporated, leaving a viscous oil. 2-Chloro-5-nitrobenzoyl chloride was obtained from the oil: 154—155 °C (7.5 mmHg) 50.8 g (93.1%).

The acid chloride (52.9 g, 0.24 mol) was dissolved in dry benzene (300 ml) and then anhydrous aluminium chloride (48.1 g, 0.36 mol) was added. After refluxing for 1 h the mixture was cooled and poured into a mixture of cracked ice (500 ml) and concd HCl (180 ml), then the benzene layer was separated and the aqueous layer was extracted twice with benzene (200 ml). The benzene solution was washed twice with 2 mol dm^{-3} NaOH and water, and dried over magnesium sulfate. The solvent was removed by distillation, and a recrystallization of the resulting solid from EtOH gave 2-chloro-5-nitrobenzophenone: 53.7 g (85.4%), mp 83—85 °C.

Found: C, 59.70; H, 3.07; N, 5.38%. Calcd for $C_{13}H_8NO_3Cl$: C, 59.67; H, 3.08; N, 5.35%.

A mixture of 2-chloro-5-nitrobenzophenone (30.0 g, 0.115 mol), water (300 ml), and KOH (9.70 g, 0.128 mol) was charged in an autoclave. After heating at 150—160 °C with stirring for 5 h, the clear solution was cooled and then strongly acidified by adding concd HCl. The resulting solid was filtered off and washed with water. A recrystallization of the solid from EtOH gave 2-hydroxy-5-nitrobenzophenone: 15.7 g (56.1%), mp 122—123 °C (lit,[31] 124—124.5 °C).

HOHBP-5NO$_2$ was prepared essentially as described by Kohler and Bruce[15] (and, in part, Blatt and Russell[9]) for HOHBP. 2-Hydroxy-5-nitrozophenone (25.0 g, 0.103 mol) was added to 40% KOH (150 ml). To this mixture was added hydroxylamine hydrochloride (50.0 g, 0.72 mol) at room temperature with stirring. After 5 h the solution was acidified with concd HCl and the precipitated pale yellow solid was collected and washed successively with water and with a small amount of 50% MeOH. Recrystallization of the solid from benzene and a small amount of petroleum ether gave the product: 17.1 g (64.4%), mp 193—196 °C, $R_{f8}=0.78$.

Found: C, 60.38; H, 3.85; N, 10.76%. Calcd for $C_{13}H_{10}N_2O_4$: C, 60.47; H, 3.90; N, 10.85%.

Preparation of Active Esters 1 and 2. Typical example are as follows.

Method (A) Z-Gly-OHAP-5NO$_2$: Z-Gly (9.40 g, 44.9 mmol) and HOHAP-5NO$_2$ (8.80 g, 44.9 mmol) were dissolved in DMF (100 ml) and DCC (9.70 g, 47.1 mmol) was added to the solution below 0 °C with stirring. After a night the *N,N'*-dicyclohexylurea was filtered off and ethyl acetate and water were added to the filtrate. The organic layer was separated, washed with water, and dried. Evaporation of the dried solution gave a solid. This material was recrystallized from ethyl acetate–petroleum ether to give 15.1 g (87.0%), mp 125—128 °C, $R_{f6}=0.87$.

Found: C, 56.15; H, 4.56: N, 10.87%. Calcd for $C_{18}H_{17}N_3O_7$: C, 55.82; H, 4.42: N, 10.85%.

Method (B) Z-Gly-OHAP: To a solution of Z-Gly (4.18 g, 20 mmol) and triethylamine (2.8 ml, 20 mmol) in dioxane (50 ml) below −10 °C was added dropwise (over a period of 1 min) isobutyl chloroformate (2.73 g, 20 mmol) with stirring. After 5 min, HOHAP (3.02 g, 20 mmol) in dioxane (20 ml) was added. After 1 h the mixture was brought to room temperature and stirred overnight. Ethyl acetate (200 ml) and water (200 ml) was added to the mixture. The organic layer was separated, and the solution was washed with 1 mol dm^{-3} NaHCO$_3$ and water, and dried. The solvent was evaporated and the crude solid was recrystallized from ethyl acetate–petroleum ether: 3.75 g (55.0%); mp 109—110 °C; $R_{f9}=0.70$.

Found: C, 62.05; H, 5.02; N, 8.53%. Calcd for $C_{17}H_{16}N_2O_5$: C, 62.19; H, 4.91; N, 8.53%. The same material was also prepared from (Z-Gly)$_2$O and HOHAP.

Method (C) Z-Gly-OBA: To a solution of Z-Gly-Cl[33] (11.38 g, 50 mmol) in THF (120 ml) below −10 °C was added dropwise over a period of 10 min a solution of HOBA (6.06g, 50 mmol) in THF (50 ml) and triethylamine (7.0 ml, 50 mmol) with stirring. After being kept for 10 min below −10 °C, the mixture was allowed to stand overnight and then was worked up as in Method (B): 15.6 g (36.0%); mp 100—102 °C; $R_{f5}=0.76$.

Found: C, 65.04; H, 5.19: N, 9.09%. Calcd for $C_{17}H_{16}N_2O_4$: C, 65.38; H, 5.16; N, 8.97%.

Determination of the Rate of Aminolysis. In to a 50 ml volumetric flask was put a solution containing 2.0 mmol of an appropriate derivative in distilled THF. To the solution having been heated and thermostated (20±0.1 °C) was added a thermostated solution of 4.0 mmol of benzylamine in distilled THF (50 ml). At predetermined time intervals, a 10 ml aliquot of the solution was withdrawn and diluted with 40 ml of distilled water. The excess of benzylamine was back-titrated with 0.1 mol dm^{-3} HCl with Bromocresol Green solution as the indicator.[1] Blank tests showed that any presence of free oxime did not influence the accuracy of titration. Each point in Figs. 1—3 represents a mean of three to six values.

The Acetyl Derivative of HOHBA. This compound was obtained by treating the oxime with (a) an excess of acetic anhydride (Ac$_2$O) or (b) DCC. *(a)*: Ac$_2$O (75 ml) was added to the oxime. The mixture was warmed for 30 min. The solid acetyl derivative formed by stirring with an excess of cold water was collected and washed with water. Pale pink crystals (10.25 g, 57.2%) were obtained by crystallization from benzene–petroleum ether: mp 69—71 °C (lit,[20] 69 °C).

Found: C, 60.33; H, 5.11; N, 7.94%. Calcd for $C_9H_9NO_3$: C, 60.33; H, 5.06; N, 7.82%.

(b): AcOH (6.01 g, 100 mmol) and HOHBA (6.86 g, 50 mmol) were dissolved in THF (80 ml) and DCC (11.3 g, 55 mmol) was added to the solution below 0 °C with stirring. The mixture was stirred for 24 h. *N,N'*-Dicyclohexylurea was filtered off and the filtrate was diluted with ethyl acetate (200 ml) and water (200 ml). The organic layer was separated and treated as in Method (B). Recrystallization of the

residue from benzene–petroleum ether gave the acetyl ester: 5.06 g (53.8%); mp 69 °C.

Found: C, 60.38; H, 5.18; N, 7.88%. Calcd for $C_9H_9NO_3$: C, 60.33; H, 5.06; N, 7.82%.

The authors are indebted to Mr. Toshiyuki Takabayashi of our laboratory for elemental analysis. We are also grateful to the Head of our laboratory, Dr. Susumu Harada, for his helpful discussion and encouragement to this work.

Reference

1) G. Losse, A. Barth, and K. Schatz, *Justus Liebigs Ann. Chem.*, **677**, 185 (1964).
2) G. Losse, K. H. Hoffmann, and G. Hetzer, *Justus Liebigs Ann. Chem.*, **684**, 2361 (1965).
3) S. Bittner, Y. Knobler, and K. Frankel, *Tetrahedron Lett.*, **1965**, 95.
4) M. Itoh, *Bull. Chem. Soc. Jpn.*, **47**, 471 (1974).
5) M. Fujino and O. Nishimura, *Chem. Pharm. Bull.*, **17**, 1937 (1969).
6) M. Itoh, *Bull. Chem. Soc. Jpn.*, **46**, 2219 (1973).
7) M. Kruszynski and G. Kupryszewski, *Rocz. Chem.*, **50**, 1099 (1976).
8) B. O. Handford, J. H. Jones, G. T. Young, and T. F. N. Johnson, *J. Chem. Soc., C*, **1965**, 6814.
9) A. H. Blatt and L. A. Russell, *J. Am. Chem. Soc.*, **58**, 1903 (1936).
10) S. B. Hendricks, O. R. Wulf, G. E. Hibert, and U. Liddel, *J. Am. Chem. Soc.*, **58**, 1991 (1936).
11) R. P. Patel and R. D. Patel, *J. Inorg. Nucl. Chem.*, **32**, 2591 (1970).
12) A. W. Ashbrook, *Hydrometallurgy*, **1**, 5 (1975).
13) K. K. Ramaswany, C. I. Jose, and D. N. Sen, *Indian J. Chem.*, **5**, 156 (1967).
14) *E.g.*, Houben-Weyl, "Methoden der Organischen Chemie," Georg Thieme-Verlag, Stuttgart (1968), Band X(4).
15) E. P. Kohler and W. F. Bruce, *J. Am. Chem. Soc.*, **53**, 1569 (1931).
16) *E.g.*, "Beilstein Organischen Chemie," 7 and 8.
17) V. M. Gurav and U. K. Jagwani, *J. Indian Chem. Soc.*, **56**, 325 (1979).
18) G. N. Walker and R. T. Smith, *J. Org. Chem.*, **36**, 305(1971). HOHBP-5Cl was prepared from 5-chloro-2-hydroxybenzophenone, hydroxylamine hydrochloride, and pyridine in 90% EtOH.
19) J. Przybylski and H. Miecznikowska, *Pol. J. Chem.*, **52**, 1179 (1978).
20) O. L. Brady and F. P. Dunn, *J. Chem. Soc.*, **105**, 821 (1914).
21) H. Lindemann and S. Romanoff, *J. Prakt. Chem., (2)*, **122**, 214 (1929).
22) H. Lindemann and H. Thiele, *Ann.*, **449**, 63 (1926).
23) G. Mayer, *J. Org. Chem.*, **44**, 3983 (1979).
24) K. H. Gellmann and E. Tauer, *Tetrahedron Lett.*, **1974**, 3707.
25) H. H. Freedmann, *J. Am. Chem. Soc.*, **83**, 2900, (1961).
26) E. Miller and W. H. Hartung, *Org. Synth.*, Coll. Vol. II, 543 (1943).
27) F. F. Blicke and O. J. Weinkauff, *J. Am. Chem. Soc.*, **54**, 1446 (1932).
28) D. Charvararti and O. J. Bera, *J. Indian Chem. Soc.*, **21**, 109 (1944).
29) W. von Miller, *Ber.*, **20**, 1927 (1887).
30) S. S. Joshi and H. Singh, *J. Am. Chem. Soc.*, **76**, 4993 (1954).
31) F. Ullmann and E. Mallet, *Ber.*, **31**, 1694 (1898).
32) A. W. Ashbrook, *J. Chromatogr.*, **105**, 141 (1975).
33) M. Bergmann and L. Zervas, *Ber.*, **65**, 1192 (1932).

The Cycloaddition Reaction of *N*-Imidoyl Sulfoximides with Diphenylcyclopropenone to Yield Pyrimidinone or Pyrrolinone Derivatives

Hiroshi YOSHIDA,* Shingo SOGAME, Yasunori TAKISHITA, and Tsuyoshi OGATA
Department of Applied Chemistry, Faculty of Engineering, Shizuoka University, Hamamatsu 432
(Received September 29, 1982)

N-Imidoyl sulfoximide (**7**) reacted with diphenylcyclopropenone (**2**) at 130 °C to yield a mixture of 1,2-disubstituted 5,6-diphenyl-4(1*H*)-pyrimidinone (**6**) and *N*-(4-oxo-2-pyrrolin-5-yl)sulfoximide (**10**), which might be formed by [3+3] and [2+3] cycloaddition reactions between **2** and **7**. The yields of **6** and **10** depended on the electronic and steric effects of the substituents of **7**.

Diphenylcyclopropenone (**2**) and its analogs react with a variety of ylides and imides to give heterocycles.[1] *N*-Imidoyl sulfimides (**1**)[2] reacts with **2** to yield pyrimidine (**3**). In contrast, the reaction of benzo[*c*]cinnolium imide (**4**) with **2** gives the adduct (**5**),[3] which on pyrolysis yields the isomeric pyrimidine (**6**) (Scheme 1).

In a continuation of our earlier works of the chemical and physical properties of *N*-, *P*-, and *S*-ylides and imides substituted with C=S or C=N groups,[4] we have found an easy route for the preparation of the new *N*-imidoyl sulfoximide (**7**). In this paper, the reaction of **7** with **2** was carried out in order to compare it with those of **1** and **4**.

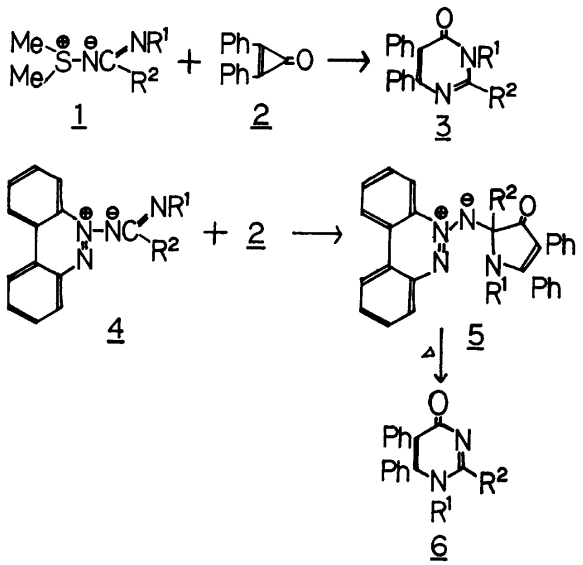

Scheme 1.

Results and Discussion

The reaction of acid chloride with unsubstituted sulfoximide (**8**) to give *N*-acylsulfoximide has been well known.[5] On the similar treatment of **8** with imidoyl chloride (**9**) in the presence of triethylamine, the sulfoximides **7** were prepared in moderate yields. The imides **7** were fairly stable at room temperature; their physical properties are collected in Table 1.

It has been reported that propenone **2** decomposes over 140 °C.[6] Thus, an equimolar mixture of **2** and **7d** in xylene was heated at 130 °C. The disappearance of **2** was checked by TLC at suitable time intervals. The subsequent purification of the product by chromatography over silica gel yielded two products: the colorless 4(1*H*)-pyrimidinone (**6d**) and the yellow sulfoximide (**10d**). The structure assignment is based on the following evidence.

The former product had the same physical properties as the previously reported compound,[3] but quite different from those of the **3a** isomer (R^1=4-MeC_6H_4, R^2=Ph) obtained from the reaction of **1a** (R^1=4-MeC_6H_4, R^2=Ph) with **2**.[2,7] The mass spectroscopic studies of **3a** and **6d** clarified the ambiguity of the structure elucidation. The **6d** isomer showed a characteristic peak corresponding to MeC_6H_4N–C(Ph)=CPh; in contrast, **3a** showed no such peak.

The latter product, **10d**, gave satisfactory elemental analysis, ^{1}H-NMR, MS, and chemical transformation. Upon treatment with ethanol in the presence of trifluoroacetic acid, **10d** yielded the pyrrolinone derivative **11b** in quantitative yield. The hydrolysis of **11b** in a mixture of aqueous sulfuric and acetic acids yielded the known furanone **12**,[8] not the isomeric acid **13**.[9]

The reaction of other sulfoximides with **2** yielded two kinds of products, corresponding to **6** and **10**. The product ratios **10**/**6** and physical properties of **6** and **10**

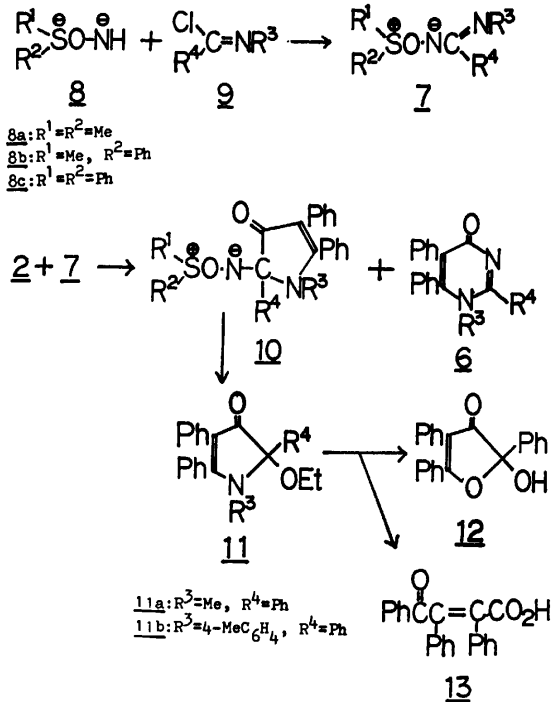

Table 1. Preparation of sulfoximide 7

	R^1	R^2	R^3	R^4	Yield %	Mp θ_m/°C	M^+	^{1}H-NMR δ in $CDCl_3$[a]	Found (Calcd) (%) C	H	N
7a	Me	Me	Me	Ph	36	84—86	210	3.03 (3H, s, NMe), 3.28 (6H, s, Me_2S)	57.02 (57.11	6.63 6.71	13.64 13.32)
7b	Me	Me	C_2H_5	Ph	67	75—78	224	1.03 (3H, t, J=7 Hz, CH_3), 3.21 (2H, q, CH_2), 3.17 (6H, s Me_2S)	58.49 (58.90	7.08 7.19	12.09 12.49)
7c	Me	Me	Ph	*t*-Bu	74	95—96	252	1.20 (9H, s, *t*-Bu), 2.65 (6H, s, Me_2S)	61.57 (61.87	8.13 7.99	11.04 11.10)
7d	Me	Me	4-MeC_6H_4	Ph	63	143—145	286	2.23 (3H, s, $\underline{Me}C_6H_4$), 3.35(6H, s, Me_2S)	67.06 (67.10	6.38 6.38	9.83 9.78)
7e	Me	Me	4-$MeOC_6H_4$	Ph	73	145—146	302	3.43 (6H, s, Me_2S), 3.75 (3H, s, MeO)	63.69 (63.55	6.05 6.00	9.34 9.26)
7f	Me	Me	2,6-$Me_2C_6H_3$	Ph	50	125—128	300	2.08(6H, s, $\underline{Me}_2C_6H_3$), 3.39 (6H, s, Me_2S)	68.07 (67.97	6.64 6.71	8.97 9.32)
7g	Me	Me	4-$NO_2C_6H_4$	Ph	72	152—153	317	3.45 (6H, s, Me_2S)	56.88 (56.77	4.73 4.76	13.06 13.24)
7h	Me	Me	Ph	4-MeC_6H_4	86	118—119	286	2.23 (3H, s, $\underline{Me}C_6H_4$), 3.31 (6H, s, Me_2S)	67.32 (67.10	6.37 6.33	10.09 9.78)
7i	Me	Me	Ph	4-$MeOC_6H_4$	82	145—146	302	3.30 (6H, s, Me_2S), 3.69 (3H, s, MeO)	63.51 (63.55	6.08 6.00	9.48 9.26)
7j	Me	Me	Ph	2,4,6-$Me_3C_6H_2$	77	94—95	314	2.15 (3H, s, Me), 2.20 (6H, s, Me_2), 3.36 (6H, s, Me_2S)	68.24 (68.76	7.14 7.05	8.82 8.91)
7k	Me	Me	Ph	4-$NO_2C_6H_4$	45	128—129	317	3.40 (6H, s, Me_2S)	56.64 (56.77	4.62 4.76	12.95 13.24)
7l	Me	Me	Ph	4-ClC_6H_4	73	114—115	306	3.35 (6H, s, Me_2S)	58.39 (58.72	4.77 4.93	9.01 9.13)
7m	Me	Ph	4-MeC_6H_4	Ph	73	138—140	348	2.20 (3H, s, $\underline{Me}C_6H_4$), 3.32 (3H, s, Me_2S)	72.46 (72.38	5.69 5.79	8.31 8.04)
7n	Ph	Ph	4-MeC_6H_4	Ph	35	139—140	410	2.32 (3H, s, Me)	75.93 (76.07	5.38 5.40	6.67 6.82)

a) Phenyl-ring protons were observed at δ 6.6—8.0.

Table 2. The reaction of 7 with 2 at 130 °C in xylene

Reactant	Time/h		Yield/%			Ratio 10/6
7a	2	—		**10a**	60	
7b	2	**6b**	1	**10b**	79	79
7c	100[a]	—		—		
7d	2	**6d**	15	**10d**	45	3.0
7e	2	**6e**	10	**10e**	50	5.0
7f	80[a]	—		—		
7g	90	**6g**	4	**10g**	11	2.8
7h	2	**6h**	19	**10h**	58	3.1
7i	2	**6i**	17	**10i**	51	3.0
7j	50[a]	—		—		
7k	27	**6k**	13	**10k**	45	3.5
7l	6	**6l**	11	**10l**	60	5.5
7m	4	**6d**	22	**10m**	63	2.9
7n	20	**6d**	1	**10n**	37	37

a) None of the products corresponding to **6** or **10** were found.

are shown in Tables 2 and 3. Since **2** decomposed slowly at the reaction temperature,[6] half a molar excess **2** was added in the course of the reaction for the cases of imides of a low reactivity: **7c**, **7f**, **7g**, and **7j**. From the reaction mixtures of such imides, none of the expected products **6** and **10** was isolated, or they were isolated only in low yields, together with an unidentifiable tarry mass. *N*-Alkylbenzimidoyl sulfoximides, **7a** and **7b**, gave **10a** and **10b** in an overwhelming majority. In contrast, the *N*-arylbenzimidoyl sulfoximides **7d**, **7e**, **7g**—**i**, and **7k**—**m** yielded the corresponding **6** and **10** in nearly similar ratios, although much rate retardation was observed for the imides substituted with the electron-withdrawing groups: **7k** and **7g**.

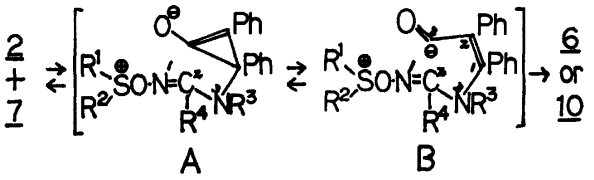

Scheme 2.

Upon heating at 140 °C for 12 h, the isolated **10b** or **10d** did not yield **6b** or **6d**, and long-time heating of the reaction mixtures of **7b** or **7d** with **2** did not improve the yields of **6b**/**10b** or **6d**/**10d**. These observations seem to indicate that **10** was not the precursor or intermediate of the production of **6**.

The ^{1}H-NMR spectroscopic studies for the sulfoximides **7** and **10** were interesting. The signal of the *S*-methyl groups of **7** appeared as a singlet at around δ 3.3, while those of the pyrrolinone-substituted sulfoximide **10** appear as two singlets at around δ 2.9 and 3.2 (Tables 1 and 3). The resolution of the two methyl groups for the *N*-alkyl substituted imides **10a** and **10b** was small. These observations seem to indicate that the free rotation around the S–N bond of **10** might be highly hindered by the bulky aryl substituents on the pyrrolinone ring.

Aldimine, ketimine, and amidine, which have C=N bonds, react with **2** to give 2-pyrrolin-4-one derivatives[8,10] *via* a [2+3] cycloaddition reaction. Considering the results obtained, the most plausible mechanism is that shown in Scheme 2. The nucleophilic attack of he terminal nitrogen (N^3) on the cyclopropenone **2**

TABLE 3. PHYSICAL PROPERTIES OF 6 AND 10

	Mp θ_m/°C	M^+	^{1}H-NMR δ in $CDCl_3$[c]	Found (Calcd) (%) C	H	N
6b	252—254[a]	352	0.83 (3H, t, J=7 Hz, CH_3), 4.82 (2H, q, CH_2)	81.78 (81.79	5.66 5.72	7.78 7.95)
6d	203—205[b]	414	2.10 (3H, s, MeC_6H_4)	83.85 (84.03	5.24 5.35	6.60 6.76)
6e	193—195	430	3.57 (3H, s, MeO)	81.19 (80.91	5.29 5.15	6.46 6.51)
6g	256—259	445		75.46 (75.49	4.14 4.30	9.45 9.43)
6h	213—214	414	2.18 (3H, s, MeC_6H_4)	84.34 (84.03	5.27 5.35	6.39 6.76)
6i	170—171	430	3.73 (3H, s, MeO)	80.97 (80.91	5.26 5.15	6.85 6.51)
6k	118—120	445		74.92 (75.49	4.18 4.30	9.54 9.43)
6l	168—169	434		77.51 (77.33	4.72 4.40	6.63 6.44)
10a	191—193	416	2.80 (3H, s, MeN), 3.17 (3H, s, MeS), 3.18 (3H, s, MeS)	71.96 (72.09	5.77 5.81	6.68 6.73)
10b	145—146	430	0.61 (3H, t, J=7 Hz, CH_3CH_2), 3.34 (2H, dq, J=3 and 7 Hz), 3.10 (3H, s, MeS), 3.18 (3H, s, MeS)	72.26 (72.53	6.05 6.09	6.55 6.51)
10d	221—222	492	2.09 (3H, s, MeC_6H_4), 2.88 (3H, s, MeS), 3.25 (3H, s, MeS)	75.38 (75.58	5.68 5.73	5.53 5.69)
10e	208—209	508	2.95 (3H, s, MeS), 3.29 (3H, s, MeS), 3.62 (3H, s, MeO)	73.14 (73.20	5.48 5.55	5.53 5.51)
10g	283—285	523	2.88 (3H, s, MeS), 3.20 (3H, s, MeS)	68.65 (68.82	4.84 4.81	7.73 8.02)
10h	161—162	492	2.15 (3H, s, MeC_6H_4), 2.74 (3H, s, MeS), 3.12 (3H, s, MeS)	75.81 (75.58	5.78 5.73	5.59 5.69)
10i	188—189	508	2.90 (3H, s, MeS), 3.26 (3H, s, MeS), 3.76 (3H, s, MeO)	73.00 (73.20	5.48 5.55	5.55 5.51)
10k	252—254	523	2.93 (3H, s, MeS), 3.22(3H, s, MeS)	69.32 (68.82	4.82 4.81	7.97 8.03)
10l	123—124	513	2.86 (3H, s, MeS), 3.21 (3H, s, MeS)	69.91 (70.23	5.10 4.91	4.82 5.46)
10m	201—203	554	2.00 (3H, s, MeC_6H_4), 3.21 (3H, s, MeS)	77.63 (77.95	5.49 5.45	4.96 5.05)
10n	233—235	616	2.10 (3H, s, Me)			

a) The reported[5] mp for the **3b** isomer (R^1=Et, R^2=Ph) was 175 °C. b) The reported[2] mp for **6d** was 204—205 °C. The isomer **3d** (R^1=MeC_6H_4, R^2=Ph) had 262—265 °C. c) Phenyl-ring protons were observed at δ 6.4—8.3.

yields the intermediate **A**, followed by the ring-opening of the cyclopropenone and the nucleophilic attack of the carbonyl carbon (C^3) on the imino nitrogen (N^1) or the imino carbon (C^2) to yield either **6** or **10** *via* [3+3] or [2+3] cycloaddition. The pyrrolinone **10** is not an intermediate for the formation of **6**.

Table 2 indicates that bulkiness and electronic nature of the substituents R^1—R^4 on **7** controlled the reactivity of **7**. The nucleophilicity of the terminal nitrogen N^3 decreased with the electron-attracting substituents on N^3 (*i.e.*, R^3) and C^2 (*i.e.*, R^4) through the C=N bond. Bulky substituents lowered the reactivity of **7** (**7c**, **7f**, and **7j**), indicating that steric hindrance might contribute not only to the initial nucleophilic attack, but also to the ring-forming step to yield **6** or **10**.

The product ratios **10**/**6** also seem greatly affected by the bulkiness of the substituents R^1—R^4. Two phenyl groups of **7n** and alkyl groups for R^3 (**7a** and **7b**) increased the product ratios. These results seem to indicate that the ring formation of **10** would be easier than the formation of **6** due to the steric crowding between the substituents.

Barr *et al.* have indicated that the nature of the cationic center of the imide can profoundly affect the character of an ambident anionic portion.[3] This finding agrees well with our present results. The free *S*,*S*-dimethylsulfimide and *S*,*S*-dimethylsulfoximide (**8a**) have pK_a values of 7.28 and 3.24 respectively.[11,12] This big difference seems to affect the imino nitrogens of **1** and **7** (N^1 in Scheme 2). The imide **1** reacts with **2** at imino nitrogen (N^1); in contrast, the sulfoximide **7** reacts with **2** at the terminal nitrogen (N^3).

Experimental

General. The melting points were not corrected. ^{1}H-NMR spectra were recorded on a Hitachi-Perkin-Elmer R-20(60 MHz) spectrometer, using TMS as the internal standard; the IR spectra, on a Japan Spectroscopic Co. Ltd., A-3 infrared spectrophotometer, and the mass spectra, on a Hitachi RMU-7M mass spectrometer.

*Preparation of Unsubstituted Sulfoximides (**8a**—**c**).* *S*,*S*-Dimethyl-, *S*-methyl-*S*-phenyl-, and *S*,*S*-diphenylsulfoximides (**8a**—**c**) were prepared according to the literature.[13-15]

*Preparation of N-Imidoyl Sulfoximides (**7**).* A solution of

unsubstituted sulfoximide **8** (10 mmol) in benzene (30 cm³) and triethylamine (11 mmol) was dried over sodium carbonate (1 g). To the stirred mixture we then added, drop by drop, imidoyl chloride **9** (10 mmol) in benzene (10—20 cm³) over a 2-h period, the temperature being kept at around 15 °C. After the reaction, the precipitate was separated by filtration and the benzene solution was washed with water, dried over sodium carbonate, and evaporated *in vacuo* to yield the crude sulfoximide **7**, which was then recrystallized from benzene–petroleum ether. The physical properties of the products **7** are shown in Table 1.

The Reaction of ***7*** *with* ***2***. An equimolar mixture of **2** and **7** (1 mmol) in a minimum amount of xylene (*ca.* 3 cm³) was heated at 130 °C. The reaction was checked by means of TLC (silica gel, ethyl acetate–petroleum ether 2 : 1) at suitable time intervals. After the reaction, the cooled mixture was chromatographed over silica gel. Elution with a mixture of chloroform and ethyl acetate (5 : 1) gave **6** and **10**. The physical properties of the products are collected in Table 3.

The Reaction of ***10a*** *and* ***10d*** *with Ethanol*. To a solution of **10a** (0.1 mmol) in dry ethanol (10 cm³) we added 3 drops of trifluoroacetic acid at room temperature. One hour later, the reaction mixture was quenched with water and extracted with chloroform. The chloroform extract was dried under reduced pressure to yield a crystalline mass, which was then recrystallized from ethanol to give **11a** in a 90% yield. **11a** (R^3=Me, R^4=Ph): mp 157—158 °C; NMR ($CDCl_3$) δ=1.37 (3H, t, J=7 Hz, $C\underline{H}_3CH_2$), 2.80 (3H, s, MeN), 3.59 (2H, q, CH_2), and 6.8—7.8 (15H, m, Ph). Found: C, 81.51; H, 6.18; N, 3.83%; M^+ 369. Calcd for $C_{25}H_{23}NO_2$: C, 81.27; H, 6.27; N, 3.79%; M 369.

When **10d** was treated similarly **11d** (R^3=4-MeC_6H_4, R^4=Ph) was obtained in a 94% yield. **11d**: mp 178—180 °C; NMR ($CDCl_3$) δ=1.27 (3H, t, J=7 Hz, $C\underline{H}_3CH_2$), 2.16 (3H, s, $\underline{Me}C_6H_4$), 3.86 (2H, q, CH_2), and 6.6—7.8 (19H, m, Ar). Found: C, 83.29; H, 6.22; H, 3.21%; M^+ 445. Calcd for $C_{31}H_{27}NO_2$: C, 83.57; H, 6.11; N, 3.14%; M 445.

Hydrolysis of ***11a*** *and* ***11d***. A solution of **11a** or **11d** (0.2 mmol) in a mixture of acetic acid, sulfuric acid, and water (50 : 2 : 25 v/v) (10 cm³) was refluxed for 24 h. The cooled mixture was quenched with water and extracted with chloroform. The extract was dried under reduced pressure to yield a colorless mass, which, on crystallization, from benzene–petroleum ether gave needles of **12**; mp 190 °C (lit,[8] mp 191 °C).

Preparation of ***3a*** *(R^1=4-MeC_6H_4, R^2=Ph)*. A solution of **1a** (R^1=4-MeC_6H_4, R^2=Ph) and **2** in benzene was refluxed for 24 h. Layer chromatography (silica gel, chloroform–ethyl acetate 1 : 1 v/v) and crystallization from ethyl acetate–petroleum ether afforded **3a** in a 21% yield. **3a**: mp 262—264 °C; NMR ($CDCl_3$) δ=2.19 (3H, s, Me) and 6.8—7.8 (19H, m, Ar). Found: C, 83.96; H, 5.64; N, 6.88%; M^+ 414. Calcd for $C_{29}H_{22}N_2O$: C, 84.03; H, 5.35; N, 6.76%; M 414.

References

1) K. T. Potts and J. S. Baum, *Chem. Rev.*, **74**, 189 (1974); M. L. Deem, *Synthesis*, **1982**, 701.

2) T. L. Gilchrist, C. J. Harris, C. J. Moody, and C. W. Rees, *J. Chem. Soc., Perkin Trans. 1*, **1975**, 1969,

3) J. J. Barr, R. Storr, and V. K. Tandon, *J. Chem. Soc., Perkin Trans. 1*, **1980**, 1147.

4) H. Yoshida, T. Ogata, and S. Inokawa, *Bull. Chem. Soc. Jpn.*, **52**, 1541 (1979).

5) P. D. Kennewell and J. B. Taylor, *Chem. Soc. Rev.*, **4**, 189 (1975).

6) R. Breslow, T. Eicher, A. Krebs, R. A. Peterson, and J. Posner, *J. Am. Chem. Soc.*, **87**, 1320 (1965).

7) L. Giammanco and F. P. Invidiata, *Ann. Chim. (Rome)*, **60**, 188 (1970).

8) T. Eicher, J. W. Weber, and G. Chatila, *Justus Liebigs Ann. Chem.*, **1978**, 1203.

9) J. Hoch and R. Teixier, *C. R. Acad. Sci., Ser. A*, **261**, 4132 (1965).

10) T. Eicher, F. Abdesaken, G. Franke, and J. L. Weber, *Tetrahedron Lett.*, **1975**, 3915; T. Eicher, G. Franke, and F. Abdesaken, *ibid.*, **1977**, 4067; T. Eicher and G. Franke, *Liebigs Ann. Chem.*, **1982**, 1337.

11) F. Knoll, J. Gronebaum, and R. Appel, *Chem. Ber.*, **102**, 848 (1969).

12) R. G. Laughlin and W. Yellin, *J. Am. Chem. Soc.*, **89**, 2435 (1967).

13) C. R. Johnson and D. E. Roger, *J. Org. Chem.*, **38**, 1793 (1973).

14) T. R. Williams and D. J. Cram, *J. Org. Chem.*, **38**, 20 (1973).

15) T. W. Fair and L. Reiver, *J. Am., Chem. Soc.*, **73**, 459 (1951).

The Electrolytic Behavior of Tetrasubstituted Iminium Salt in Acetonitrile

Atsutaka KUNAI,* Junji HARADA, Masayasu NISHIHARA, Yasuo YANAGI, and Kazuo SASAKI
Department of Applied Chemistry, Faculty of Engineering, Hiroshima University, Saijo, Higashi-Hiroshima, 724
(Received October 12, 1982)

Cathodic behavior of *N*-cyclohexylidenepyrrolidinium salt (**1**) and *N*-cyclohexylideneaniline (**2**) in acetonitrile has been studied by means of dc polarography, cyclic voltammetry and preparative electrolysis under controlled potential conditions. The compound **1** exhibits a reduction wave at about −1.8 V, which is accompanied by formation of a surface compound. The products obtained from the preparative electrolysis were neither saturated amines nor dimeric compounds but were mostly polymeric materials. However, when electrophilic olefins, such as acrylonitrile or methyl acrylate, were present in the solution, coupling products were produced. The compound **2**, which cannot be reduced by itself below −2.7 V, is reduced at about −1.8 V when benzoic acid is in the solution. The reduction product in this case was *N*-cyclohexylaniline, which was replaced by a coupling product when acrylonitrile was present in the reaction system. The formation of the coupling products is considered to occur by a radical mechanism in both cases.

The formation of C–C bonds by addition of strong nucleophilic carbanion to the carbonyl carbon atom is widely used in organic synthesis. Similar addition reaction to the imino group or particularly to the iminium group, which is the *N*-analogue of carbonyl group, is frequently utilized in alkaloid synthesis.[1] Since the carbon atom at the iminium group is strongly positively polarized, the electrolytic reduction is easier than for the corresponding carbonyl group.[2] It is considered that the product is generally a monomeric amine in protic solvents while dimeric compounds are favored in aprotic solvents.[2-4] Accordingly, it is expected that the intermediate derived from the reduction of an iminium salt will add to certain kinds of electrophiles. In fact, the electrolytic reductive coupling of some aromatic iminium salt with various benzyl bromides has been reported.[5] Except for the heterocyclic iminium salt,[3,4] however, the electrode reduction of iminium salt has not hitherto been studied extensively.[2]

In the present paper, we study the reaction of *N*-cyclohexylidenepyrrolidinium perchlorate (**1**) as a representative of an iminium salt of simple aliphatic ketones. The crossed coupling with electrophilic olefins is the main subject of our interest.[6] In addition, a similar reaction of *N*-cyclohexylideneaniline (**2**) is also studied. Polarographic studies of related compounds are available in the literature.[7] The solvent used was acetonitrile in all cases, and acrylonitrile and methyl acrylate were used as the electrophilic olefins. In some cases, methyl 3-bromopropionate was also used as the electrophile.

Experimental

General. D.c. polarography using a dropping mercury electrode and linear potential sweep experiments using a platinum, gold and hanging mercury drop electrodes were utilized for studying electrochemical properties. All measurements were made in acetonitrile solutions containing 0.1 M tetraethylammonium perchlorate (1 M = 1 mol dm^{-3}). The solution were degassed with nitrogen.

Preparative electrolyses were carried out in a divided cell with a mercury pool cathode at a constant potential.

Electrodes. The height of the dropping mercury electrode s was kept at 50 cm. The capillary constant was 578 mmHg s mg^{-1}.** Platinum and gold wires of 1 mm in dia meter and 5 mm in length were used for cyclic voltammetry. All the potential values cited are those referred to a saturated calomel electrode using acetonitrile as the solvent.[8]

Reagents. Reagent grade acetonitrile was distilled over phosphorus pentaoxide and the distillate was refluxed over calcium hydride. This was freshly distilled before use. *N*-cyclohexylidenepyrrolidinium perchrorate (**1**) was prepared by the condensation of cyclohexanone with pyrrolidinium perchlorate.[9] Similarly, *N*-cyclohexylideneaniline (**2**) was prepared from cyclohexanone and aniline, bp 87 °C/133 Pa.

Controlled Potential Electrolysis. *(a)* N-*Cyclohexylideneaniline (2)*: The base solution was acetonitrile containing 0.1 M. tetraethylammonium perchlorate. A solution (100 cm^3) containing 1 mmol of **2** and 2 mmol of benzoic acid was electrolyzed at −1.9 V under a nitrogen atmosphere. The telectrolysis was continued until the current fell to the background level. The electrolyzed solution was evaporated to remove the solvent and the residue was extracted with ether by use of a Soxhlet extractor. The extract was again concentrated and subjected to TLC separation. The amount of the starting material remaining was determined by means of the formation of cyclohexanone 2,4-dinitrophenylhydrazone. The conversion of **2** was 80% and the yield of *N*-cyclohexylaniline (**3**) was 66% on the base of the reacted imine.

(b) 2 in the Presence of Acrylonitrile: A similar procedure was applied as used in the above. The amount of acrylonitrile added was 2 millimoles. The products, **3** (R_f 0.85) and 1-anilino-1-(2-cyanoethyl)cyclohexane (**4**) (R_f 0.70), were isolated by using silica gel TLC plates (5% EtOAc in benzene). Results are shown in Table 1.

(c) N-*Cyclohexylidenepyrrolidinium Perchlorate (1) in the Presence of Acrylonitrile*: Solutions of 1 mmol of **1** and 3 mmol of acrylonitrile were electrolyzed at −1.80 V. Others were the same as *(a)*. The product, 1-(2-cyanoethyl)-1-(1-pyrrolidinyl)-cyclohexane (**6**), was isolated by preparative GLC (5% OV-17, 2 m, 215 °C). Results are shown in Table 2.

(d) 1 in the Presence of Methyl Acrylate: A mixed solvent of 10% MeOH and 90% CH_3CN was used in this case, which contained **1** (1 mmol) and methyl acrylate (3 mmol). Products obtained were 1-[2-(methoxycarbonyl)ethyl]-1-(1-pyrrolidinyl)cyclohexane (**7**) (34%) and 1,2-bis[2-(methoxycarbonyl)-ethyl]-1-(1-pyrrolidinyl)cyclohexane (**8**) (30%).

(e) 1 in the Presence of Methyl 3-Bromopropionate: Procedure

** 1 mmHg≈133.322 Pa.

was the same as (*d*). Three millimoles of 3-bromopropionate was used. Products were **7** (3%) and **8** (3%).

Product Analyses. **4**: IR (neat) 3420 (-NH-), 2950 ($-CH_2-$), 2250 (CN), 750 and 690 cm^{-1} (Ph); NMR ($CDCl_3$) δ=1.17—1.75 (10H, m), 1.75—2.60 (4H, A_2B_2), 3.37 (1H, broad), 6.53—6.95 (3H, m), and 7.00—7.30 (2H, m); MS (70 eV), *m/e* (I_{rel}), 228 (M^+, 30), 185 ($M^+-C_3H_7$, 50), 174 ($M^+-CH_2CH_2CN$, 100), and 93 ($PhNH_2$, 79). Found: C, 79.06; H, 8.82; N, 12.13%. Calcd for $C_{15}H_{20}N_2$: C, 78.90; H, 8.83; N, 12.27%.

6: IR (neat) 2950 ($-CH_2-$), 2250 (CN), and 1450 cm^{-1} ($-CH_2-$); NMR ($CDCl_3$) δ=0.83—2.10 (16H, m) and 2.10—2.70 (6H, m); MS (70 eV), *m/e* (I_{rel}), 206 (M^+, 6), 163 ($M^+-C_3H_7$, 4), and 152 ($M^+-CH_2CH_2CN$, 100). Found: C, 75.90; H, 10.70; N, 13.40%. Calcd for $C_{13}H_{22}N_2$: C, 75.68; H, 10.75; N, 13.58%.

7: IR (neat) 2940 ($-CH_2-$), 1745 and 1190 cm^{-1} ($COOCH_3$); NMR ($CDCl_3$) δ=1.22—2.05 (16H, m), 2.22—2.88 (6H, m), and 3.65 (3H, s); MS (70 eV), *m/e* (I_{rel}), 239 (M^+, 3), 208 (M^+-OCH_3, 6), 196 ($M^+-C_3H_7$, 26), and 152 ($M^+-CH_2CH_2COOCH_3$, 100). Found: C, 70.50; H, 10.56; N, 6.16%. Calcd for $C_{14}H_{25}O_2N$: C, 70.25; H, 10.53; N, 5.85%.

8: IR (neat) 2950 ($-CH_2-$) and 1745 cm^{-1} ($COOCH_3$); MS (70 eV), *m/e* (I_{rel}), 325 (M^+ for $C_{18}H_{31}O_4N$, 5), 294 (M^+-OCH_3, 8), 282 ($M^+-C_3H_7$, 18), and 238 ($M^+-CH_2-CH_2COOCH_3$, 100).

Other compounds were identified by comparison with authentic samples.

Results and Discussion

Polarography. The parent compound, cyclohexanone, does not show any reduction wave below the limit of solvent decomposition in acetonitrile (Fig. 1). Neither cyclohexanone oxime nor *N*-cyclohexylidenebenzylamine exhibits a reduction wave. *N*-cyclohexylideneaniline **2**, however, gives rise to a reduction wave with a half-wave potential at −2.8 V. The iminium salt **1** shows a wave with a characteristic maximum at about −1.8 V. On the other hand, all of electrophilic reagents such as acrylonitrile or methyl acrylate have their half-wave potentials at more negative than −2.2 V, indicating the possibility of selective reduction of the iminium salt **1**. *N*-Cyclohexylideneaniline (**2**) is also

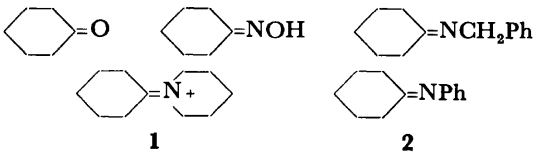

1 **2**

selectively reduced when benzoic acid is deliberately added. This is shown in Fig. 2, where the effect of benzoic acid on the polarogram of the imine **2** is studied. It is clearly evident that a marked shift of reduction wave occurs upon addition of benzoic acid. Denoting the waves of $E_{1/2}$=−1.8, −2.3, and −2.8 V as the waves I, II, and III, respectively, we analyzed the height of each wave. This is shown in Fig. 3, where

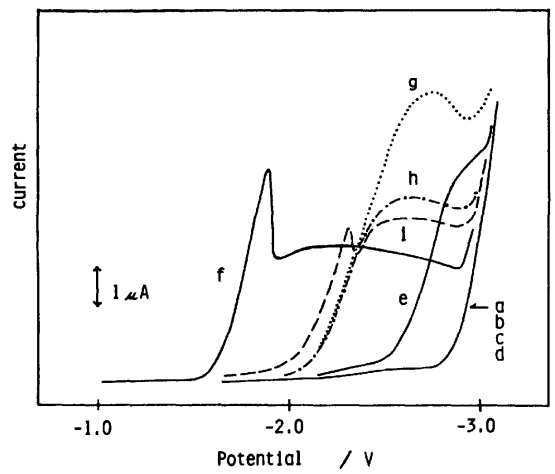

Fig. 1. Polarograms of the substrates in acetonitrile solution (1 mmol dm^{-3}).
The solution contains: a) none; b) cyclohexanone; c) cyclohexanone oxime; d) *N*-cyclohexylidenebenzylamine; e) *N*-cyclohexylideneaniline; f) *N*-cyclohexylidenepyrrolidinium perchlorate; g) acrylonitrile; h) methyl acrylate; and i) methyl 3-bromopropionate.

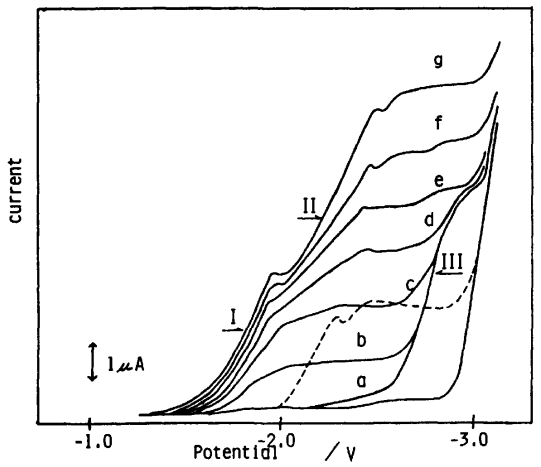

Fig. 2. Effect of benzoic acid on the polarogram of *N*-cyclohexylideneaniline (1 mmol dm^{-3}).
The concentration of benzoic acid is: a) 0; b) 0.5; c) 1; d) 1.5; e) 2; f) 2.5; and g) 3 mmol dm^{-3}. Dotted line shows the polarogram of 1 mmol dm^{-3} of benzoic acid.

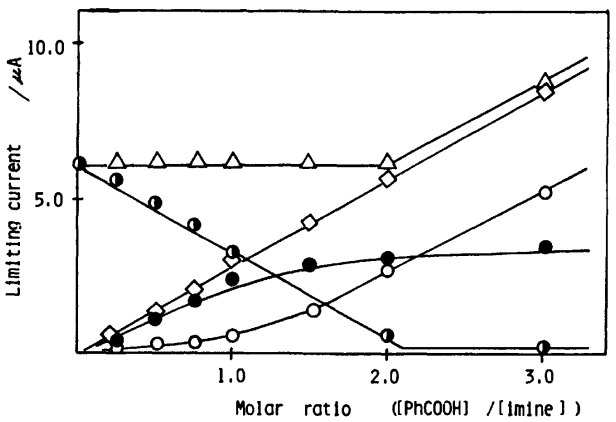

Fig. 3. Relation of the waves I through III appearing in Fig. 2.
Ordinate stands for the limiting current of: (●) wave I; (○) wave II; (◑) wave III; (◇) waves I and II; and (△) waves I, II, and III. Abscissa stands for molar ratio of benzoic acid against 1 mmol of the imine.

the scale of the abscissa indicates the molar ratio of benzoic acid to imine; R=[benzoic acid]/[imine].

The wave I increases monotonously until R becomes equal to 1 and then stops increasing. The final height is roughly one half of the original wave of the imine. Although the second wave (wave II) coincides with the wave of benzoic acid itself, a hasty interpretation seems to be misleading.

It should be noted that the second wave starts to grow appreciably after exceeding R=1 and the sum of the waves, I and II, increases exactly linearly. Moreover, the total height of waves I, II, and III remains constant until R reaches 2. In accord with the above facts, the following sequences of the reaction can be assumed, where A stands for **2** and HB is benzoic acid (Eqs. 1 through 5).

$$A + HB \rightleftharpoons AH^+ + B^- \quad (1)$$

$$AH^+ + e + \overset{\text{wave I}}{\rightleftharpoons} AH\cdot \quad (2)$$

$$2\,AH\cdot \longrightarrow AH_2 + A \quad (3)$$

$$AH\cdot + H^+ + e \overset{\text{wave II}}{\longrightarrow} AH_2 \quad (4)$$

$$A + 2e \overset{\text{wave III}}{\longrightarrow} A^= \quad (5)$$

That the final height of the wave I is one half of the original wave height of imine suggests the process occurring in the wave I to be one-electron transfer. The follow-up chemical step (3) should occur sufficiently fast to provide wave III, where free imine is reduced by two-electron transfer. At the second wave, the primary electrode product, AH·, is further reduced as far as proton is donated from benzoic acid. The reaction of wave III is undoubtedly the reduction of free imine itself, and the wave diminishes when sufficient amount of benzoic acid is present in the solution. This mechanism agrees with the result of preparative electrolysis made at a potential of wave I. As Table 1 indicates, *N*-cyclohexylaniline (**3**) is dominated in the reaction products.

Cyclic Voltammetry of ***1***. The polarogram of **1** exhibited a wave with strong maximum (see Fig. 1). It was impossible to displace this maximum by any means. Therefore we attempted to study the effect of the electrode material on the reaction of **1**. Platinum, gold and hanging mercury electrodes were chosen and cyclic voltammetry was employed. Figure 4 indicates the results. In the case of the platinum electrode (Fig. 4a), the first cathodic wave appeared at about −0.95 V, which is very positive compared with the peaks observed with gold or mercury electrodes. Because of this, we estimate the reaction at the platinum electrode to be different from that at the mercury electrode. With platinum, the peak current showed a linear dependence on the square root of the potential sweep rate. The reaction, which is consistent with the result of preparative electrolysis is as follows (Eq. 6).

$$\mathbf{1} + e \longrightarrow \mathbf{5} + 1/2\,H_2 \quad (6)$$

It should be noted that only when a platinum cathode was used hydrogen evolved appreciably. This must be related to the special affinity of hydrogen on the platinum surface.

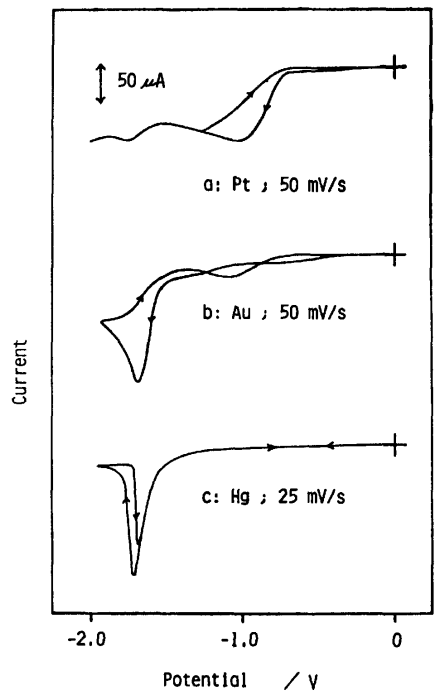

Fig. 4. Cyclic voltammograms of *N*-cyclohexylidenepyrrolidinium perchlorate in acetonitrile solution (5 mmol dm^{-3}).
Electrode is: a) platinum; b) gold; and c) hanging mercury. Sweep started from 0 V towards negative direction.

With the gold electrode (Fig. 4b), the current peak appeared at about −1.7 V. The peak current was also linear against the square root of the rate of potential sweep but did not cross the origin of the coordinate showing the contribution of some kinetic complication. The reaction at this electrode was not studied further.

At the hanging mercury drop electrode (Fig. 4c), a sharp current peak appeared at −1.72 V. The peak current, however, did not change systematically with the change of the rate of potential sweep while the peak potential value was unchanged. In addition, the current diminished rapidly after passing the peak potential, −1.72 V. When the direction of the potential sweep was reversed, the peak reappeared at a potential slightly positive to the forward sweep.

These findings lead us to assume that a surface compound was formed on the mercury surface. The surface compound would be an insulating material and the current fell steeply after it covered the mercury surface fully. A quantitative analysis of the peak current, however, failed because of the difficulty of reproducing the experiments, which was mainly caused by the poor reproducibility of the size of the hanging mercury drop.

Controlled Potential Electrolysis. *N-Cyclohexylideneaniline (**2**)*: This compound has been electrolyzed in the presence of acrylonitrile at −1.9 V, in the region of wave I, with a mercury pool electrode. In order to do this, the addition of benzoic acid was necessary as was described in the previous section. The products obtained are listed in Table 1 as a function of the molar ratio of

Table 1. Electrolysis of *N*-cyclohexylideneaniline (2)

Run[a]	Additive: Acrylonitrile (mmol)	Additive: Benzoic acid (mmol)	Electricity consumed / F mol^{-1}	2 Recovered (mmol)	3 (mmol)	4 (mmol)	Conversion of 2 / %	Yield[b]/% of 3	Yield[b]/% of 4
1	0	2.0	2.01	0.20	0.53	—	80	66	—
2	2.0	1.0	1.05	0.56	0.02	0.30	45	4	68
3	2.0	2.0	1.89	0.39	0.04	0.44	61	6	72
4	2.0	3.0	1.91	0.12	0.10	0.53	88	12	61

a) The elcctrolyses were made for the solution (100 cm^3) containing 1 mmol of **2** at −1.90 V. b) The yields were based on **2** unrecovered.

benzoic acid to the imine. In every case, the main product was the adduct **4** of acrylonitrile to the imine and the by-product was *N*-cyclohexylaniline (**3**). No dimeric product was observed. When the electrolysis was done in the absence of acrylonitrile but in the presence of 2 mmol of benzoic acid, the main product was *N*-cyclohexylaniline (**3**) (66%), which showed the sequence of Eqs. 2 and 3 is operating.

Isolation of both **3** and **4** was performed by the use of silica-gel TLC. The amount of unreacted imine was analyzed as its 2,4-dinitrophenylhydrazone. It is worth noting that the increasing amount of benzoic acid added improves the percentage conversion of imine to the adduct.

The reaction occurring in this system can be expressed by the following equations.

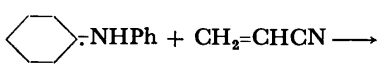

(7)

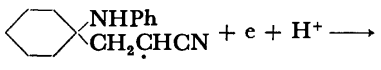

(8)

4

N-*Cyclohexylidenepyrrolidinium Perchlorate* (*1*). Referring the result of cyclic voltammetry, we electrolyzed **1** at −1.80 V in the presence of acrylonitrile with a mercury pool electrode. The results obtained are listed in Table 2. In all cases, the current reached the background level after passing about 1 F† per mole of electricity. The highest yield of the adduct **6** was 37%. No starting material remained in the electrolyzed solution. No diamine, the formation of which was suggested by Andrieux,[2] was detected. For producing **6**, an addition of methanol or 2-propanol seems to be effective.

When platinum was used as the electrode material, hydrogen evolved vigorously during the course of electrolysis. Both the GC and TLC analyses indicated that a number of compounds are produced in this case. Among these, three dominant compounds were characterized to be adiponitrile, enamine **5** (21%), and 2-(2-cyanoethyl)cyclohexanone, by comparing with the authentic samples, respectively. The amount of the adduct **6** was only 5%. These findings indicate that

† 1 F≈96480 C.

Table 2. Electrolysis of *N*-cyclohexylidene-pyrrolidinium perchlorate **1** in the presence of acrylonitrile

Run[a]	Base solution	Coulometric *n* value	Yield[b]/% of **6**
1	MeCN	0.96	26
2	MeCN–MeOH(1%)	0.98	32
3	MeCN–MeOH(5%)	0.97	33
4	MeCN–MeOH(10%)	1.11	37
5	MeCN–MeOH(10%)[c]	1.04	31
6	MeCN–*i*-PrOH(1%)	1.09	29
7	MeCN–*i*-PrOH(5%)	1.04	31
8	MeCN–*i*-PrOH(10%)	1.04	31

a) The electrolyses were made for the solution (100 cm^3) containing 1 mmol of **1** and 3 mmol of acryronitrile at −1.80 V. b) The yields were based on the amount of **1** used. c) Ten millimoles of acrylonitrile was used in this case.

the primary step occurring at the platinum electrode is the reductive decomposition (Eq. 6). The enamine **5** thus produced will further undergo the follow-up chemical reaction to give a complex mixture of the products. The cyanoethylation seems to be a suitable follow-up reaction in this case.[10]

In contrast to the platinum electrode, mercury pool electrode seems to be favored for producing **6**. This may be correlated to the difference in the primary intermediates between the two electrode systems. The formation of organomercury compounds seems plausible but their detection failed.

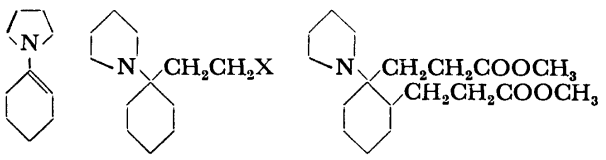

5 **6** X = CN, **7** X = $COOCH_3$ **8**

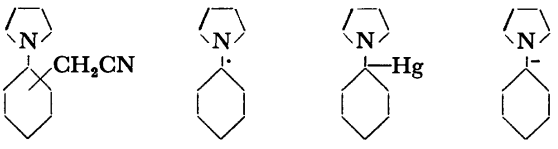

9 **10** **11** **12**

When the electrolysis was carried out in the absence of acrylonitrile, the product was mostly a polymeric substance together with a small amount of **9**, which

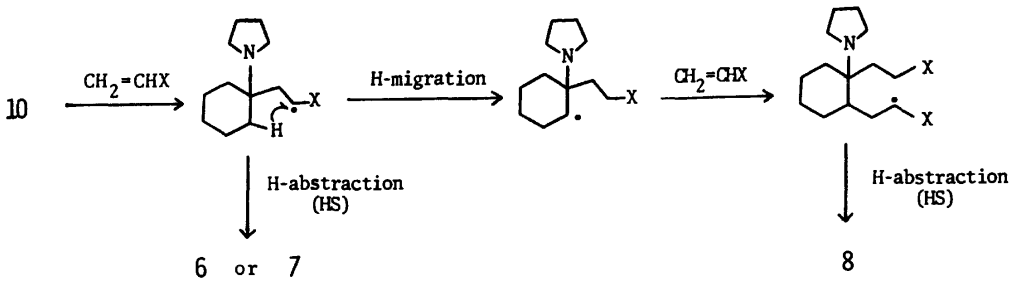

(X= -CN or $-COOCH_3$, HS= solvent)

Scheme 1.

might be derived from **10** by a radical mechanism.

When methyl acrylate was used in place of acrylonitrile, **8** was produced in 30% yield in addition to **7** (34%).

In order to account for the formation of **6** through **9**, it seems reasonable to assume the formation of the neutral radical **10** as the primary intermediate on the mercury surface. The possibility of forming either organomercury compound **11** or carbanion **12** seems unlikely in the following reasons. 1) When methyl 3-bromopropionate was used in place of methyl acrylate, the yield of **7** and **8** was less than 3%. This means that the primary species has a poor SN_2-displacement ability. 2) No organomercury compound was detected in the electrolyzed solution.

The radical **10** will react with olefins, such as acrylonitrile or methyl acrylate to form **7**, **8** or **9** as is expressed in Scheme 1. The presence of certain co-solvents such as alcohols inhibits undesirable radical polymerization.

Conclusion

The tetrasubstituted iminium salt **1** is reduced more easily than corresponding carbonyl compounds. It forms a neutral radical when it is reduced cathodically at a mercury surface. The radical thus formed is favored to polymerize rather than to dimerize. The presence of electrophilic olefins such as acrylonitrile gives rise to the formation of radical adduct as the intermediate, which gives the final products of **6** through **8**. The latter reaction is not highly selective and the polymerization always accompanies. The addition of a hydrogen donor such as methanol is effective in inhibiting the polymerization and increasing the yield of adducts.

The compound **2** is easily reduced electrolytically when it is protonated. When acrylonitrile is present in the solution, the adduct **4** is formed in more than 70% yield.

References

1) E. Wenkert and B. Wickberg, *J. Am. Chem. Soc.*, **84**, 4914 (1962); J. P. Kutney, R. T. Brown, and E. Piers, *ibid.*, **86**, 2286, 2287 (1964), **92**, 1700 (1970); G. Stork and R. N. Guthikonda, *ibid.*, **94**, 5109 (1972).

2) C. P. Andrieux and J. M. Saveant, *Bull. Soc. Chim. Fr.*, **1968**, 4671.

3) W. M. Schwarz, E. M. Kosower, and I. Shain, *J. Am. Chem. Soc.*, **83**, 3164 (1961); M. S. Spritzer, J. M. Costa, and P. J. Elving, *Anal. Chem.*, **37**, 211 (1965); L. Floch, M. S. Spritzer, and P. J. Elving, *ibid.*, **38**, 1074 (1966); J. E. Hickey, M. S. Spritzer, and P. J. Elving, *Anal. Chem. Acta*, **35**, 277 (1966); A. Cisak and P. J. Elving, *Electrochim. Acta*, **10**, 935 (1965); R. Takahashi and P. J. Elving, *ibid.*, **12**, 213 (1967).

4) 1-Alkyl-3-carbamoylpyridinium salts have also been examined as the model compounds of NAD^+/NADH system: J. N. Burnett and A. L. Anderwood, *J. Org. Chem.*, **30**, 1154 (1965); K. S. V. Santhanam and P. J. Elving, *J. Am. Chem. Soc.*, **95**, 5482 (1973); C. O. Schmakel, K. S. V. Santhanam, and P. J. Elving, *ibid.*, **97**, 5083 (1975), and references cited therein.

5) T. Shono, T. Miyamoto, M. Mizukami, and H. Hamaguchi, *Tetrahedron Lett.*, **22**, 2385 (1981), T. Shono, Y. Usui, T. Mizutani, and H. Hamaguchi, *ibid.*, **21**, 3073 (1980).

6) The crossed coupling reactions of ketones with activated olefins are known; for example, K. Sugino and T. Nonaka, *Denkikagaku*, **34**, 105 (1966); *J. Electrochem. Soc.*, **112**, 1241 (1965); *Electrochim. Acta*, **13**, 613 (1968); T. Nonaka and T. Sekine, *Denkikagaku*, **39**, 29 (1971); N. Nicholas and R. Pallaud, *C. R. Acad. Sci., Ser. C*, **265**, 1044 (1967); A. P. Tomilov, S. M. Mokarochkina, L. A. Fedorova, and G. A. Tedoradze, *Elektrokhimiya*, **9**, 525 (1973); A. Froeling, *Recl. Trav. Chim. Pays-Bas*, **93**, 47 (1974); A. P. Tomilov, B. L. Klyuer, and V. D. Nechepurnoi, *Zh. Org. Khim.*, **11**, 1984 (1975).

7) H. Lund, *Acta Chem. Scand.*, **13**, 249 (1959); J. M. W. Scott and W. H. Jura, *Can. J. Chem.*, **45**, 2375 (1967).

8) O. Bravo and R. T. Iwamoto, *J. Electroanal. Chem.*, **23**, 419 (1969).

9) N. J. Leonard and J. V. Paukstelis, *J. Org. Chem.*, **28**, 3021 (1963).

10) "Enamines: Synthesis, Structure, and Reactions," ed by A. G. Cook, Marcel Dekker, New York (1969).

 © 1983 The Chemical Society of Japan Bull. Chem. Soc. Jpn., 56, 2447—2451 (1983)

Photochemical Dehalogenation of Polyhalobenzenes. I. Survey of the Reactivity in Hexane Solution[1)]

Masahiro NAKADA,* Sachio FUKUSHI, Hideaki NISHIYAMA,† Keiji OKUBO,† Kotaro KUME,† Minoru HIROTA,*,† and Tetsuo ISHII††

Chemical Laboratory, Chiba Institute of Technology, Narashino 275

†*Department of Applied Chemistry, Faculty of Engineering, Yokohama National University, Hodogaya-ku, Yokohama 240*

††*Yokohama Research Institute for Environmental Protection, Takigashira, Isogo-ku, Yokohama 235*

(Received November 18, 1982)

Photochemical dechlorinations and debrominations of $C_6H_nX_{6-n}$ (X=Cl, Br) isomers were carried out in hexane. The products and residual reactant were determined quantitatively by means of gas chromatography. From these experiments, the relative rates of dehalogenation were obtained. The different rates among unequivalent sites in a molecule were interpreted by the effect of steric acceleration by the neighboring halogen atom(s). The reactivity of the halogen atom in polyhalobenzene towards photochemical elimination reaction is dependent both on its position in the molecule when compared among isomers and on the number of halogen atoms in a molecule when compared among polyhalobenzenes of various degrees of substitution. The latter effect is more predominant in the series of polybromobenzenes.

Physical properties of polyhalogenated aromatic compounds have been investigated rather extensively, since they were widely used as insulator, thermally stable heat-transfer medium and lubricant, and other purposes. On the other hand, reactions of these polyhaloaromatics were not known thoroughly because of their inertness towards most chemicals. Environmental contamination caused by polychlorinated biphenyls also attracted the attention to the chemical reactions of other polyhalogenated aromatics.[2)] Considerably large number of investigations concerning their metabolism, toxicity, and abundance in environment were reported[3)] together with the investigations on polychlorinated biphenyls. However, reactions of polyhalobenzenes have not been studied so extensively. In connection with the detoxication of polyhalogenated aromatic compounds, several photochemical dehalogenation procedures were reported in this decade.[4,5)] Thus some polychlorinated biphenyls were successfully dechlorinated by irradiation of ultraviolet light in aqueous alkaline media.[6)]

Pinhey and Rigby,[7)] and Ichimura and Mori[8)] have studied the mechanism of dehalogenations of several rather simple haloarenes, showing that the photochemical process is the initial absorption of light causing $^1(\pi,\pi^*)$ excitation and subsequent intersystem crossing to $^3(\sigma,\sigma^*)$ state localized on a carbon-halogen bond, which induces the fission of the bond.

$$\text{Ar–X} \xrightarrow{h\nu} \text{(Ar–X)}^* \qquad \text{X = Cl, Br}$$
$$\text{(Ar–X)}^* \longrightarrow \text{Ar}\cdot + \text{X}\cdot$$
$$\text{Ar}\cdot + \text{RH} \longrightarrow \text{Ar–H} + \text{R}\cdot$$

The abstraction of hydrogen from solvent (RH) is a thermal reaction of aryl free radical. Another explanation assuming the π-chlorobenzene intermediate, or transition state, was also proposed by Lemal[9)] and have been contradicted by Arnold.[10)]

In our previous report,[11)] relative migrating ability of halogen atom of polyhalobenzenes in the Jacobsen type rearrangement was determined and the mechanism was discussed. In this connection, the photochemical dehalogenations were carried out on all possible polychloro- and polybromobenzene isomers, as well as some polybromopolychlorobenzenes, in hexane in order to compare the reactivities of halogen (Cl or Br) atoms occupying different positions in a polyhalogenated benzene molecule. The products were analyzed quantitatively by gas chromatography, and the relative rate of dehalogenation of each dissimilar halogen atom was evaluated.

Experimental

Materials. Several tri-, tetra-, and pentabromobenzenes were prepared by the method previously reported by Furuyama *et al.*[12)] Some of other polybromo-, polychloro-, and polybromopolychlorobenzenes were prepared by combination of direct halogenation and nitration followed by reduction and Sandmeyer reaction (replacement by halogen) of appropriately halogenated benzenes and anilines. Commercially available materials were used after purification by distillation or by chromatography. All of polyhalobenzenes were identified by their melting and/or boiling points and by spectral properties.

Reactions. Photo-reactions were carried out using a 30 W low pressure Hg lamp placed at the center of concentrically surrounded quartz vessel containing the solution of reactant. In some runs, a 100 W high pressure Hg lamp was also employed. The temperature of the solution was kept at 25 °C by external cooling, though the reaction is not dependent on the temperature of the solution. The solution was sampled at an interval of definite time (usually every two hours when the reaction is not very fast) and analyzed by gas chromatography.

Spectral and Chromatographic Measurements. GC/MS measurements were carried out on a Hitachi-6L or a Shimadzu LKB-9000B mass spectrometer. Routine gas chromatographic analyses of the products were carried out on a Shimadzu GC-6A apparatus or a GC-4B-PTF apparatus equipped with a polyethylene glycol 20M, a Silicone SE 30, or an Apiezon L column (3 mm×2 m). UV/VS spectra and NMR spectra were recorded on a Shimadzu UV 365 and a JEOL FX 90Q spectrometers, respectively.

Results and Discussion

The photochemical reactions were pursued by quantitative GC analysis of the products and the starting

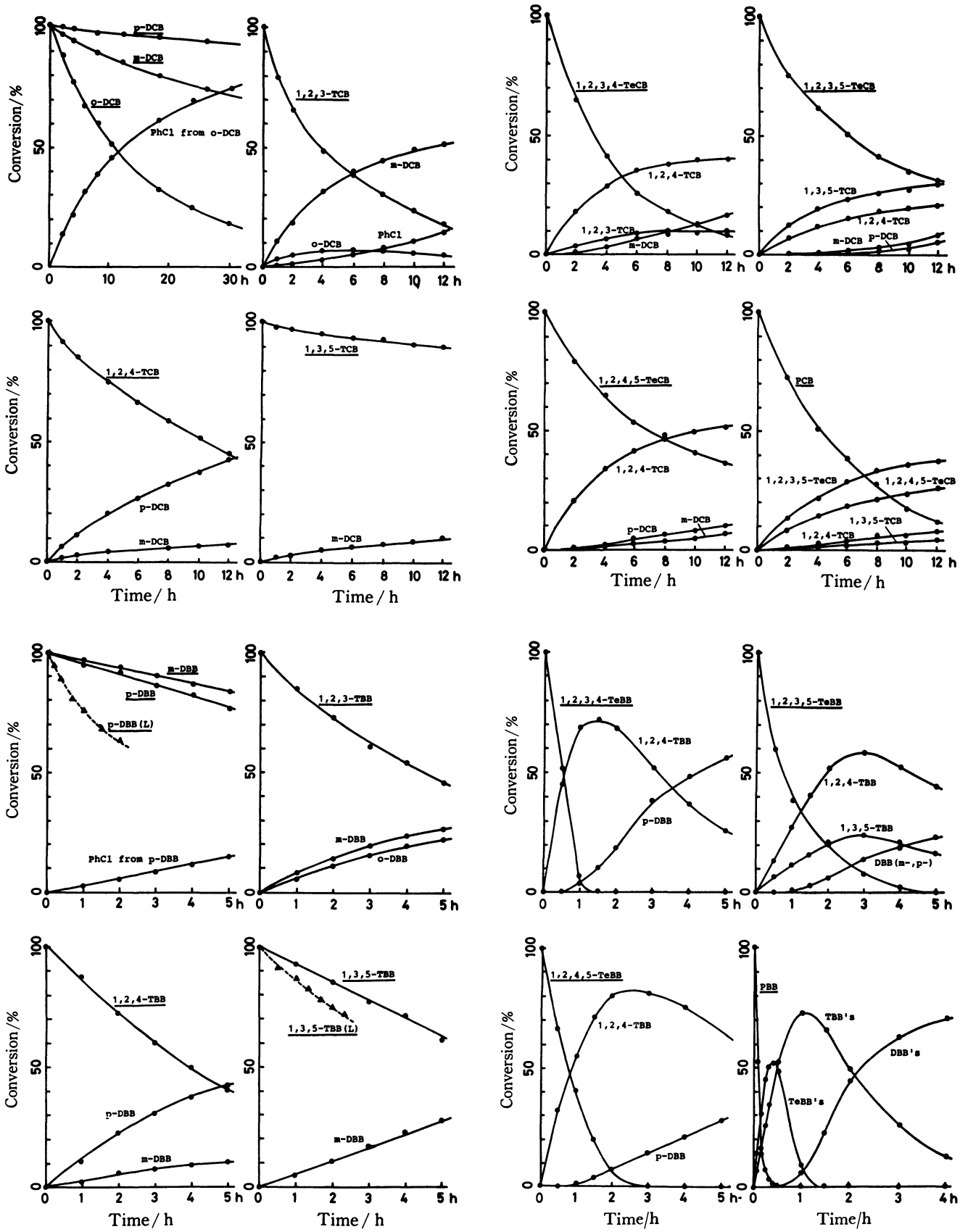

Fig. 1. Time-conversion curves for the photochemical dehalogenation of polyhalobenzenes. Experimental conditions are given in Table 1. In this figure, abbreviations such as following are used in order to name the starting materials and the products: *o*-DCB=*o*-dichlorobenzene, 1,2,3-TBB=1,2,3-tribromobenzene, 1,2,3,4-TeCB=1,2,3,4-tetrachlorobenzene, and so on. The starting material for each run is designated by underline in each diagram.

TABLE 1. RELATIVE RATES OF DEHALOGENATION (WITH REFERENCE TO THE MOST REACTIVE) IN HEXANE[13]

a) Polychlorbenzenes (concn, 0.1 mol/l; temp, 25 °C; 30 W low pressure lamp)

Substrate	No.	Position of leaving atom	Relative rate per site: Among isomers	Relative rate per site: Within molecule	No. of sites
Dichlorobenzenes					
ortho	**2a**	—	1.00		2
meta	**3a**	—	0.21		2
para	**4a**	—	0.045		2
Trichlorobenzenes					
1,2,3	**5a**	1	0.13	(0.13)	2
		2	1.00	(1.00)	1
1,2,4	**6a**	1	0.15	(0.25)	1
		2	0.60	(1.00)	1
		4	0.03	(0.05)	1
1,3,5	**7a**	—	0.05		3
Tetrachlorobenzenes					
1,2,3,4	**8a**	1	0.15	(0.15)	2
		2	1.00	(1.00)	2
1,2,3,5	**9a**	1	0.15	(0.33)	2
		2	0.46	(1.00)	1
		5	0.0	(0.0)	1
1,2,4,5	**10a**	—	0.14		4
Pentachlorobenzene					
1,2,3,4,5	**11a**	1		(0.0)	2
		2		(0.81)	2
		3		(1.00)	1

b) Polybromobenzenes (concn, 0.05 mol/l; temp, 25 °C; 100 W high pressure lamp)

Dibromobenzenes					
ortho	**2b**	—	0.87		2
meta	**3b**	—	0.61		2
para	**4b**	—	1.00		2
Tribromobenzenes					
1,2,3	**5b**	1	0.25	(0.40)	2
		2	0.62	(1.00)	1
1,2,4	**6b**	1	0.26	(0.26)	1
		2	1.00	(1.00)	1
		4	0.0	(0.0)	1
1,3,5	**7b**		0.16		3
Tetrabromobenzenes[a]					
1,2,3,4	**8b**	1	0.12	(0.12)	2
		2	1.00	(1.00)	2
1,2,3,5	**9b**	1	0.30	(0.73)	2
		2	0.41	(1.00)	1
		5	0.0	(0.0)	1
1,2,4,5	**10b**	—	0.30		4
Pentabromobenzene[b]					
1,2,3,4,5	**11b**	1		(0.0)	2
		2		(0.5)	2
				(1.0)	1

a) 0.0125 mol/l. b) 0.005 mol/l.

c) Polybromopolychlorobenzenes (concn, 0.1 mol/l; temp, 25 °C; 30 W low pressure lamp)

Substituents on substrate	Conversion/% after 4 h[a]	Position of leaving atom	Relative rate within molecule
1-Br-2, 3-Cl_2	27.6	1-Br	1
		2-Cl	0.04
		3-Cl	0.0
1-Br-2, 6-Cl_2	28.9	1-Br	1
		2-Cl	0.0
1-Br-2, 4-Cl_2	28.7	1-Br	1
		2-Cl	0.08
		4-Cl	0.0
1-Br-3, 4-Cl_2	30.0	1-Br	1
		3-Cl	0.24
		4-Cl	0.0
1-Br-3, 5-Cl_2	22.5	1-Br	1
		3-Cl	0.0
1-Br-2, 3, 4-Cl_3	18.3	1-Br	1
		2-Cl+3-Cl	0.09
		4-Cl	0.0
1-Br-2, 3, 5-Cl_3	28.9	1-Br	1
		2-Cl	0.08
		3-Cl, 5-Cl	0.0
1-Br-2, 4, 6-Cl_3	35.0	1-Br	1
		2-Cl, 4-Cl	0.0
1-Br-2, 4, 5-Cl_3	18.2	1-Br	1
		2-Cl, 4-Cl	0.0
1, 3-Br_2-4, 5-Cl_2	25.0	1-Br	0.26
		3-Br	1
		4-Cl, 5-Cl	0.0
1, 3-Br_2-2, 5-Cl_2	18.2	1-Br	1
		2-Cl, 5-Cl	0.0
1, 4-Br_2-2, 6-Cl_2	35.0	1-Br	1
		4-Br	0.09
		2-Cl	0.0
1, 2-Br_2-3, 5-Cl_2	28.9	1-Br	0.43
		2-Br	1
		3-Cl, 5-Cl	0.0
1, 2-Br_2-4, 5-Cl_2	29.0	1-Br	1
		4-Cl	0.0
1, 2, 3-Br_3-5-Cl	46.1	1-Br	0.34
		2-Br	1
		5-Cl	0.0

a) The amounts of consumed starting polyhalobenzenes after 4 h are given, since the time-conversion curves are not shown in Fig. 1.

material. Since no quantitative consideration was taken on the intensity of the light for irradiation, only the relative reactivity will be discussed here. The time-conversion curves are given in Fig. 1.

In hexane solution, dehydrogenation reaction proceeds almost exclusively. In polyhaloarenes, elimination of halogen atom from different sites proceeds competitively as initial reactions from the excited state. The relative rates of C–X (X=Cl, Br) bond fission, or the relative partial rate factors, are given in Table 1.

When the intramolecular reactivity of similar halogen atom is compared, the halogen atom flanked by two halogen atoms (at 2- and 6-positions) is the most reactive, and the one having an ortho halogen atom is the next most reactive. For example, the 2-halogen atom is the most reactive in the dehalogenations of all

1,2,3-trihalogenated benzenes investigated (**5a**, **5b**, **8a**, **8b**, **9a**, and **9b**). This might be due to the steric and electrostatic repulsion caused by the neighboring halogen atoms. Elimination of halogen atom to give the corresponding aryl free radical reduces the steric hindrance of the molecule remarkably. Electronic effect caused by non-neighbor halogen atoms are rather complicated and cannot be related quantitatively to the electron densities and bond orders from molecular orbital calculations.[14] Empirically, the halogen substituent meta to the site of reaction accelerates the dehalogenation reaction more predominantly than the para substituent when other circumstances are similar. For example, the 2-halogen atom (having one ortho and one meta halogen) of 1,2,4-trihalobenzenes (**6a** and **6b**) are more reactive than the 1-halogen atom (having one ortho- and one para-halogen). When compared intermolecularly, the 2-halogen atom of 1,2,3,4-tetrahalobenzene (having two ortho and one meta halogen) are again more reactive than the 2-halogen atom of 1,2,3,5-tetrahalobenzene (having two ortho- and one para-halogen). The same is true also for the 1-bromine atom of 1-bromo-2,3,4-trichlorobenzene and 1-bromo-2,3,5-trichlorobenzene, and other cases investigated. Since the Hammett σ-constants for *m*-chloro (+0.373) and *m*-bromo (+0.391) substituents are more positive than the corresponding constants for para substituents (*p*-Cl, +0.226; *p*-Br, +0.232), implying that meta substituents are more electron-withdrawing than the para substituents, the destabilization can be expected by the second substitution by electronegative halogen atom. This can contribute to facilitate the release of the halogeno substituent even in the homolytic fission of carbon-halogen bond.

Differences in reactivity among the positional isomers are mainly determined by the positions of halogen atoms in the molecule. In general, 1,2,3-trihalobenzene reacts most promptly and 1,3,5-trihalobenzene most slowly among isomeric trihalobenzenes. Dehalogenation of 1,2,3,4-tetrahalobenzene is the fastest among the isomeric tetrahalobenzenes.

The effect of the number and the positions of halogen substitution is considerably different when compared quantitatively between the series of polychlorobenzenes and polybromobenzenes. In the series of polybromobenzenes, the reactivity tends to increase in the following order : monobromo $<$ *o*-dibromo $<$ *m*-dibromo $<$ *p*-dibromo $<$ 1, 3, 5-tribromo $<$ 1, 2, 4-tribromo $<$ 1, 2, 3-tribromo $<$ 1,2,4,5-tetrabromo $<$ 1,2,3,5-tetrabromo $<$ 1,2,3,4-tetrabromo $<$ pentabromo $<$ hexabromo derivative. The rate of dehalogenation increases remarkably as the increase in the number of substituent halogen atoms even when statistic factor is taken into account (when the overall rate is divided by the number of halogen atoms on the benzene ring).[15] The photodehalogenation in this series of compounds were carried out using high pressure mercury arc (100 W). Two runs (with *p*-dibromo- and 1,3,5-tribromobenzenes) were carried out using low pressure mercury arc (30 W) which were used in the series of polychlorobenzenes. The overall patterns of time-conversion curves are very similar to each other.

In contrast to the reactions with polybromobenzenes, the reactivity of polychlorobenzene is very sensitive to the number of neighbor halogen atoms. As can be seen with *m*-dichloro-, *p*-dichloro-, and 1,3,5-trichlorobenzenes in Fig. 1, the rates of dechlorination of isolated chloro substituents (without ortho halogen substitution) are very low when compared with those carrying ortho halogen substituent(s). On the other hand, the rate of debromination is not so dependent on the neighboring halogen atoms. The total number of chloro-substituents on the benzene nucleus is less important than in the case of polybromobenzenes. Thus, the dehalogenations of 1,2,4-trichloro- and 1,3,5-trichlorobenzenes proceed approximately as fast as those of *o*-dichloro- and *m*-dichlorobenzenes, respectively. Increasing number of halogen substitution accelerates the reactions beyond the experimental error in polychlorobenzenes of higher degree of substitution, however.

As a consequence of the bond energy (C–Cl, 360 kJ/mol and C–Br, 297 kJ/mol) difference, the bond fission to produce the corresponding free radical proceeds more predominantly with C–Br bond than with C–Cl bond in the same molecule. Thus the debrominations take place almost exclusively in all dibromodichlorobenzenes investigated, giving corresponding bromodichlorobenzenes as primary products. No dibromochlorobenzenes were formed in detectable amounts in any runs, even if chlorobenzene (as a secondary product) was detected in some runs. In the reactions of several bromotrichlorobenzenes, dechlorination proceeds competitively with debromination. 1-Bromo-2,3,4-trichlorobenzene produces 1,2,3-trichloro- and 1-bromo-3,4-dichlorobenzenes in a 10 : 1 ratio after irradiation of 2 h. Similarly 1-bromo-2,3,5-trichlorobenzene gives 1,2,4-trichloro- and 1-bromo-3,5-dichlorobenzenes in a 12 : 1 ratio. In all cases debromination proceeds by far more promptly than dechlorination when both chloro and bromo substituents are located in the same molecule.

In order to confirm the difference in reactivity observed between polychloro- and polybromobenzenes more confidently, the photodehalogenations of some polyhalobenzenes were carried out in methanol. Methanol is another hydrogen-donating solvent from which the photochemically produced aryl free radical can abstract hydrogen atom, forming the dehalogenated product. Relative rates of dehalogenation in methanol are given in Table 2, reproducing the relative rates in hexane.

The effect of the nature of halogen (Cl or Br) on the

Table 2. Rates of dehalogenation of dihalobenzenes C_6H_4XY relative to the rate of *o*-C_6HCl_2 in methanol (0.10 mol/l)

X	Y	*o*-C_6H_4XY	*m*-C_6H_4XY	*p*-C_6H_4XY	Product
Cl	Cl	1,00	0.25	0.04	C_6H_5Cl
Cl	Br	0.73 (1.00)[a]	0.67 (0.91)	0.66 (0.89)	C_6H_5Cl
Br	Br	0.94 (1.00)	0.87 (0.92)	0.81 (0.86)	C_6H_5Br

a) Rates relative to the ortho-isomer of each series are given in parentheses.

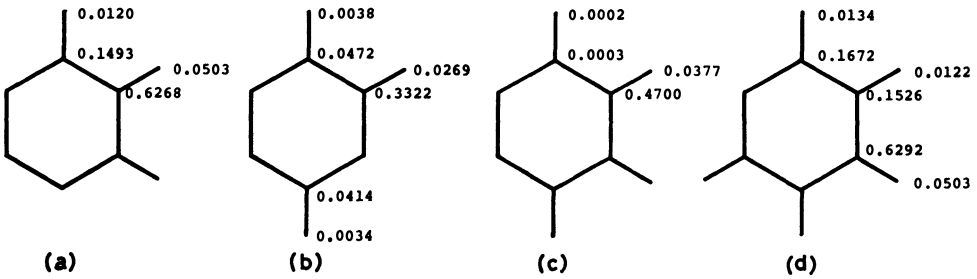

Fig. 2. π-LUMO densities of some polychlorobenzenes. (a) 1,2,3-Trichlorobenzene, (b) 1,2,4-trichlorobenzene, (c) 1,2,3,4-tetrachlorobenzene, and (d) pentachlorobenzene.

reactivity can be interpreted in the following way. In hexane, initial photolysis reaction of halobenzene to generate the corresponding aryl free radical might proceed similarly to the photolysis in gas phase. Thus the excited state leading to the photolytic cleavage of (carbon-halogen bond is expected to be the $^3(\sigma,\sigma^*)$ state localized on the breaking bond. Then the rates of dehalogenation should be determined by the probability of intersystem crossing from $^1(\pi,\pi^*)$ to $^3(\sigma,\sigma^*)$,[8] which is a function of both the energy difference of these two states and the LUMO(π^*) density on the breaking bond[14] if the wavelength and the intensity of incident light is invariable. The halogen substituent(s) ortho to the reaction site might weaken the carbon-halogen bond and lower the $^3(\sigma,\sigma^*)$ state due to the steric and electrostatic repulsive interaction. Since the energy difference between the $^1(\pi,\pi^*)$ and the $^3(\sigma,\sigma^*)$ states is supposed to be small in the case of chlorinated benzenes, the neighboring halogen effect lowering the $^3(\sigma,\sigma^*)$ state may favor the release of chlorine atom drastically under certain conditions sufficing the energetic requirement for the conversions involved. In contrast, the energy of the $^3(\sigma,\sigma^*)$ state localized on the breaking C–Br bond is considerably lower than the $^1(\pi,\pi^*)$ state in participation, and the assistance by the repulsive force does not affect their reactivities seriously. Effect of the number of substituent halogen atoms is far more predominant in the series of polybromobenzenes. This cannot be attributed to the simple steric effect due to the buttressing by the second neighbor halogen atoms. In this case, participation of direct $^3(\sigma,\sigma^*)$ or $^3(n,\sigma^*)$ excitation by irradiation is suspected owing to the contribution of heavy atom effect by bromine.[16]

The authors are grateful to Mr. Akio Kanno, former Director of Yokohama Research Institute for Environmental Protection, for his advice and support to this investigation.

References

1) Presented to the 41st National Meeting of the Chemical Society of Japan held at Osaka (April, 1980). See preprints of the 41st National Meeting of the Chemical Society of Japan, II, p. 735 (No. 3M39).

2) a) D. B. Pealal, *CRC Crit. Rev. Environ. Control*, **5**, 469 (1975); b) A. K. Ahmed, *Environment*, **18**, 6 (1976); c) W. Klein and I. Weisgerber, *Environ. Qual. Saf.*, **5**, 237 (1976).

3) H. H. Vogt, *Chem. Labor Betr.*, **29**, 136, 139 (1978).

4) L. Vollner, H. Rohleder, W. Klein, and F. Korte, *GSF–Ber.*, **205**, 71 (1975).

5) L. J. Bailin, B. L. Hertzler, and D. A. Oberacker, *Environ. Sci. Technol.*, **12**, 673 (1978).

6) T. Nishiwaki, A. Ninomiya, K. Anda, and S. Nakayama *Nippon Kagaku Kaishi*, **1972**, 2225; **1973**, 2326.

7) J. T. Pinhey and R. D. G. Rigby, *Tetrahedron Lett.*, **1969**, 1267.

8) T. Ichimura and Y. Mori, *J. Chem. Phys.*, **58**, 288 (1973).

9) M. A. Fox, W. C. Nichols, Jr., and D. M. Lemal, *J. Am. Chem. Soc.*, **95**, 8164 (1973).

10) D. R. Arnold and P. C. Wong, *J. Am. Chem. Soc.*, **99**, 3361 (1977).

11) M. Nakada, K. Ishibashi, S. Fukushi, and M. Hirota, *Bull. Chem. Soc. Jpn.*, **52**, 3761 (1979).

12) H. Furuyama and S. Fukushi, *Yuki Gosei Kagaku Kyokai Shi*, **29**, 413 (1971).

13) During the preparation of our manuscript, dehalogenation of isomeric tetrachlorobenzenes in 2-propanol was reported (M. Usui, T. Nishiwaki, K. Anda, and M. Hida, *Nippon Kagaku Kaishi*, **1982**, 638). Their results are in line with those in this Table.

14) The densities of LUMO(π^*) by simple LCAO-MO calculation could be correlated with the reactivity of polychlorobenzenes (and polybromobenzenes), however. Except the case of 1,2,3,5-tetrachlorobenzene whose LUMO has a node along the most reactive C–Cl bond because of its symmetrical property, all trichloro-, tetrachloro-, and pentachlorobenzenes have the largest LUMO density on the most reactive C–Cl bond (that is to say, the largest LUMO density of all carbon atoms and the largest LUMO density among chlorine atoms in the molecule) as given in Fig. 2. The large LUMO density will favor the intersystem crossing on the $^1(\pi, \pi^*)$ state to the $^3(\sigma, \sigma^*)$ state localized on the respective C–Cl bond.

15) Our experiment shows that the rates of conversion were related very close to the inverse of concentration, showing that the rate is controlled by the intensity of irradiated light. Substantial retarding effect by the increase of concentration was observed towards the end of reaction, which might be due to the deposit of solid or resinous secondary products on the surface of reaction vessel and also due to the coloration of the reaction mixture.

16) Possibility of the participation of direct S-T absorption has been pointed out by Soumillon and the co-worker in the photo-dechlorination of 2,4-dichloroanisole (J. Ph. Soumillon and J. Vermeulen, *Bull. Soc. Chim. Belg.*, **91**, 474 (1982).). Thus the participation of direct S-T excitation is very probable in the photo-reactions of polybromo aromatic compounds.

The Ruthenium Complex Catalyzed *N*-Heterocyclization of Aminoarenes to Quinoline Derivatives Using Allylic Alcohols and Aliphatic Aldehydes[1)]

Yoshihisa WATANABE,* Yasushi TSUJI, Yukihiro OHSUGI, and Jun SHIDA
Department of Hydrocarbon Chemistry, Faculty of Engineering, Kyoto University, Sakyo-ku, Kyoto 606
(Received December 13, 1982)

Aminoarenes reacted with 2-propen-1-ol and 2-buten-1-ol at 180 °C to give quinoline derivatives in fairly good yields in the presence of a catalytic amount of a ruthenium complex. Dichlorotris(triphenylphosphine)-ruthenium was the most effective catalyst. The aminoarenes with electron-releasing groups favored the formation of the quinolines. The *N*-heterocyclization also proceeded when aliphatic aldehydes were used in place of the allylic alcohols. The employment of allylic alcohols gave, however, higher yields in several cases. The reaction involves the isomerization of the allylic alcohols to the corresponding aldehydes. The aldehydes reacted with aminoarenes to give Schiff-base dimers which were then cyclized in the presence of the ruthenium complex to the quinolines. As a key intermediate in the reaction, the ortho-metallated species has been proposed.

Several methods have been reported using transition-metal complex catalysts for the formation of nitrogen heterocycles, such as pyrrole,[2)] indole,[3,4)] and quinoline[5,6)] derivatives. These procedures have been used to develop novel synthetic methods under non-acidic conditions.

In previous papers, we have demonstrated that rhodium, ruthenium, and palladium complexes were effective catalysts for the preparation of quinoline derivatives from aminoarenes and nitroarenes.[7-9a)] Aminoarenes were converted into quinoline derivatives in the presence of μ,μ'-dichlorobis(norbornadiene)-dirhodium(I) ($[RhCl(nbd)]_2$) by the reaction with aliphatic aldehydes.[7)] Nitroarenes were reductively converted into quinolines and (dialkylamino)arenes using aliphatic aldehydes in the presence of a rhodium–palladium binary catalyst system under carbon monoxide pressure.[8)] The quinoline derivatives were also obtained by the reductive transformation of nitroarenes using aliphatic alcohols in the presence of dichlorotris-(triphenylphosphine)ruthenium ($RuCl_2(PPh_3)_3$).[9a)] Recently, this nitroarene–aliphatic alcohol system was also adopted for the synthesis of the quinoline derivatives using a rhodium–molybdenum binary catalyst in a much larger amount (total 20 mol%).[9b)] These procedures provide a variety of synthetic methods for building up a quinoline nucleus.

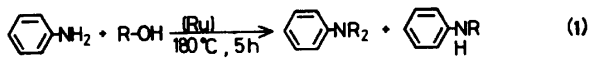
(1)

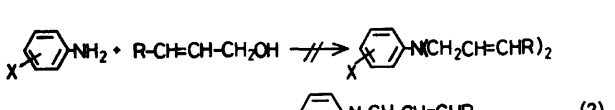
(2)

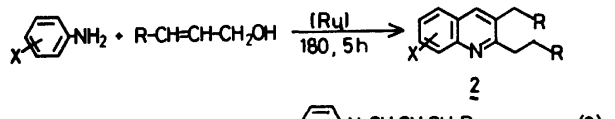
(3)

Recently, we have revealed that aniline was effectively *N*-alkylated with a primary alcohol in the presence of a ruthenium catalyst (Eq. 1).[1)] When allylic alcohols were employed in place of the primary alcohol, we first expected that *N*-alkenylated products would be obtained in the same manner as when the saturated alcohols were employed (Eq. 2). However, that was not the case. Instead, quinoline derivatives and *N*-(alkylamino)-arenes were obtained as products, and no *N*-alkenylated products were formed.

This paper deals with the ruthenium-catalyzed synthesis of the quinoline derivatives by the *N*-heterocyclization of aminoarenes using allylic alcohols. The *N*-heterocyclization also proceeds with aliphatic aldehydes in place of allylic alcohols. The results with aliphatic aldehydes are also described.

Results and Discussion

Aminoarenes reacted with allylic alcohols, such as 2-propen-1-ol and 2-buten-1-ol, at 180 °C in the presence of a catalytic amount of ruthenium and rhodium complexes to give 2,3-dialkylquinolines and *N*-alkyl-aminoarenes in good yields (Eq. 3, Table 1).

When 2-buten-1-ol was employed (Runs 1—8), the yield of 3-ethyl-2-propylquinoline depended greatly on the catalyst used. The highest yield was achieved with $RuCl_2(PPh_3)_3$ (Run 1). Ruthenium trichloride was also active, but the quinoline was obtained in a lower yield (Run 2). However, ruthenium complexes, such as $RuH_2(PPh_3)_4$, $RuHCl(PPh_3)_3$, $RuHCl(CO)(PPh_3)_3$, and $Ru(CO)_3(PPh_3)_2$, had almost no catalytic activity for the *N*-heterocyclization (Runs 3—6). On the other hand, $[RhCl(nbd)]_2$, which was the most effective catalyst for the *N*-heterocyclization of aminoarenes with *aldehydes*,[7)] showed only a low catalytic activity for this reaction (Run 7). The *N*-heterocyclization did not proceed at all without the catalyst (Run 8).

A similar trend was observed when 2-propen-1-ol was employed (Runs 9—12), although the best yield of 2-ethyl-3-methylquinoline was realized with ruthenium trichloride as a catalyst (Run 10). $RuHCl(CO)(PPh_3)_3$ had some activity (Run 11). $[RhCl(nbd)]_2$ showed also a low activity for the *N*-heterocyclization (Run 12).

The effects of other reaction variables were also

Table 1. Preparation of quinoline derivatives from aniline and allylic alcohols using ruthenium and rhodium complexes[a]

Run	Alcohol	Catalyst	Conversion/%[b]	Yield/%[b]	
				2[c]	3[c]
1	2-Buten-1-ol	$RuCl_2(PPh_3)_3$	100	54	27
2	2-Buten-1-ol	$RuCl_3 \cdot nH_2O$	96	22	22
3	2-Buten-1-ol	$RuH_2(PPh_3)_4$	77	0	Trace
4	2-Buten-1-ol	$RuHCl(PPh_3)_3$	74	Trace	Trace
5	2-Buten-1-ol	$RuHCl(CO)(PPh_3)_3$	87	Trace	Trace
6	2-Buten-1-ol	$Ru(CO)_3(PPh_3)_2$	66	0	Trace
7	2-Buten-1-ol	$[RhCl(nbd)]_2$	85	18	21
8	2-Buten-1-ol	None	0	0	0
9	2-Propen-1-ol	$RuCl_2(PPh_3)_3$	98	42	2
10	2-Propen-1-ol	$RuCl_3 \cdot nH_2O$	100	43	2
11	2-Propen-1-ol	$RuHCl(CO)(PPh_3)_3$	85	11	2
12	2-Propen-1-ol	$[RhCl(nbd)]_2$	100	29	14

a) A mixture of aniline (20 mmol), alcohol (10 ml), a catalyst (0.2 mmol, 1.0 mol% based on aniline charged), and nitrobenzene (22 mmol) was stirred at 180 °C for 5 h. b) Determined by GLC based on aniline charged. c) See Eq. 3.

Table 2. Preparation of quinoline derivatives from aniline and allylic alcohols under various reaction conditions[a]

Run	Alcohol	Catalyst[b] (mol%)	Conversion/%[b]	Yield/%[b]	
				2[c]	3[c]
1	2-Buten-1-ol	1.0	≈100	54	27
13[d]	2-Buten-1-ol	1.0	78	31	8
14	2-Buten-1-ol	0.5	65	16	Trace
15	2-Buten-1-ol	2.0	≈100	51	22
16[e]	2-Buten-1-ol	1.0	≈100	45	17
17[f]	2-Buten-1-ol	1.0	87	63	13
18[e]	2-Propen-1-ol	1.0	≈100	33	4
19[f]	2-Propen-1-ol	1.0	89	49	2

a) A mixture of aniline (20 mmol), alcohol (10 ml), $RuCl_2(PPh_3)_3$, and nitrobenzene (22 mmol) was stirred at 180 °C for 5 h. b) Based on aniline charged. c) See Eq. 3. d) Reaction temp; 150 °C. e) Without nitrobenzene. f) Benezene (10 ml) was added to the reaction mixture.

Table 3. Preparation of quinoline derivatives from aniline and aldehydes[a]

Run	Aldehyde	Conversion/%[b]	Yield/%[b]	
			2[c]	3[c]
20	Pentanal	≈100	(33)[d]	—
21	Butanal	99	59	29
22	Butanal[e]	92	55	35
23	Propanal	≈100	58	16
24	Propanal[e]	98	51	8

a) A mixture of aniline (20 mmol), aldehyde (10 ml; 94—138 mmol), $RuCl_2(PPh_3)_3$(0.2 mmol), and nitrobenzene (20 mmol) was stirred at 180 °C for 5 h. b) Based on aniline charged by GLC. c) See Eq. 3. d) Isolated yield. e) A mixture of aniline (20 mmol), aldehyde (44 mmol; 1.6—2.3 ml), benzene (10 ml), $RuCl_2(PPh_3)_3$ (0.2 mmol), and nitrobenzene (22 mmol) was stirred at 180 °C for 5 h.

examined; the results are shown in Table 2. A lower reaction temperature (150 °C) and a smaller amount of the catalyst (0.5 mol%) resulted in decreases in the conversion of aniline and in the yield of the quinoline (Runs 13 and 14). However, the yield was not improved by increasing the amount of the catalyst to 2.0 mol% (Run 15). These results indicate that an elevated temperature (180 °C) is required and that a 1.0 mol% catalyst is sufficient for a moderate yield of the quinoline. The yields of the quinolines decreased in the absence of nitrobenzene, which is considered to operate as an oxidant in the dehydrogenation step from hydroquinoline to the quinoline derivative (*vide infra*) (Runs 16 and 18). The dilution of the reaction system with benzene improved the yield of the quinoline derivatives (Runs 17 and 19).

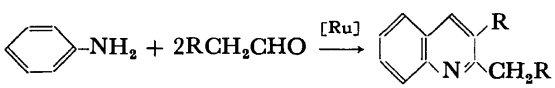

(4)

The allylic alcohols can be replaced by aliphatic aldehydes (Eq. 4). The results are listed in Table 3. Employing pentanal in excess, 2-butyl-3-propylquinoline was obtained in a 33% isolated yield (Run 20). Butanal and propanal also gave the corresponding quinolines (Runs 21 and 23). On the other hand, in the rhodium-catalyzed preparation of quinolines using aldehydes,[8]

TABLE 4. PREPARATION OF QUINOLINE DERIVATIVES FROM AMINOARENES AND ALLYLIC ALCOHOLS OR ALDEHYDE[a]

Run	Aminoarene Nitroarene (X=)	Allylic alcohol or aldehyde	Product (Yield/%)[b]
25	*p*-MeO	2-Buten-1-ol	3-Ethyl-6-methoxy-2-propylquinoline (81) *N*-Butyl-*p*-anisidine (8)
26[c]	*p*-MeO	2-Buten-1-ol	3-Ethyl-6-methoxy-2-propylquinoline (83) *N*-Butyl-*p*-anisidine (8)
27[d]	*p*-MeO	2-Buten-1-ol	3-Ethyl-6-methoxy-2-propylquinoline (63) *N*-Butyl-*p*-anisidine (17)
28	*p*-MeO	Butanal	3-Ethyl-6-methoxy-2-propylquinoline (69) *N*-Butyl-*p*-anisidine (13)
29	*p*-Me	2-Buten-1-ol	3-Ethyl-6-methyl-2-propylquinoline (82) *N*-Butyl-*p*-toluidine (36)
30[c]	*p*-Me	2-Buten-1-ol	3-Ethyl-6-methyl-2-propylquinoline (97) *N*-Butyl-*p*-toluidine (36)
31[d]	*p*-Me	2-Buten-1-ol	3-Ethyl-6-methyl-2-propylquinoline (73) *N*-Butyl-*p*-toluidine (35)
32	*p*-Me	Butanal	3-Ethyl-6-methyl-2-propylquinoline (64) *N*-Butyl-*p*-toluidine (47)
33	*p*-Cl	2-Buten-1-ol	6-chloro-3-ethyl-2-propylquinoline (17)
34	*p*-MeO	2-Propen-1-ol	2-Ethyl-6-methoxy-3-methylquinoline (56)
35	*p*-Me	2-Propen -1-ol	2-Ehtyl-6, 3-dimethylquinoline (61)
36	*o*-MeO	2-Buten-1-ol	3-Ethyl-8-methoxy-2-propylquinoline (15)
37	*o*-Me	2-Buten-1-ol	3-Ethyl-8-methyl-2-propylquinoline (23)
38	*o*-Cl	2-Buten-1-ol	8-Chloro-3-ethyl-2-propylquinoline (Trace)

a) A mixture of aminoarene (20 mmol), nitroarene (22 mmol), allylic alcohol or aldehyde (10 ml), benzene (10 ml), and $RuCl_2(PPh_3)_3$ (0.2 mmol) was stirred at 180 °C for 5 h. b) Determined by GLC based on aminoarene charged. c) Reaction time was 7.5 h. d) The reaction was carried out without nitroarene.

an excess of aliphatic aldehyde interfered with the formation of the quinolines because of side reactions, *e.g.*, aldol condensation. In the present reaction, the employment of 2.2 equivalents of aldehyde did not affect the yield essentially (Runs 22 and 24). The present results indicate that the ruthenium catalyst can be used in the preparation of the quinolines from aniline and aliphatic aldehydes, though its catalytic activity is lower than that of the rhodium catalyst described in a previous paper.[7] However, the rhodium catalyst was revealed to be less effective for the preparation of quinolines with allylic alcohols, as has been mentioned above.

This procedure is applicable to a variety of aminoarenes for the preparation of various substituted quinolines. The results for para- and ortho-substituted anilines with methyl, methoxyl, and chloro substituents are summarized in Table 4. 3-Ethyl-6-methoxy-2-propylquinoline was produced in an 81% yield by the reaction of *p*-anisidine with 2-buten-1-ol (Run 25). Prolonging the reaction time slightly improved the yield (Run 26), while the absence of the nitroarene (*p*-nitroanisole) reduced the yield (Run 27). The use of butanal in place of 2-buten-1-ol resulted in a decrease in the yield of the substituted quinoline (Run 28). *p*-Toluidine and 2-buten-1-ol gave 3-ethyl-6-methyl-2-propylquinoline in an 82% yield (Run 29). Prolonging the reaction time appreciably improved the yield to 97% (Run 30). On the other hand, the absence of nitroarene (*p*-nitrotoluene) and the use of butanal in place of 2-buten-1-ol gave poorer yields of the substituted quinoline (Runs 31 and 32). 6-Chloro-3-ethyl-2-propylquinoline was also obtained, but in a poor yield (17%), when *p*-chloroaniline was employed as an aminoarene (Run 33).

The results obtained with *p*-substituted anilines clearly indicate that aminoarenes with electron-releasing groups, *i.e.*, aminoarenes with high pK_a values, favor the *N*-heterocyclization to quinoline derivatives. Furthermore, the employment of 2-buten-1-ol in place of butanal is more favorable to the *N*-heterocyclization.

2-Propen-1-ol reacted in a similar manner with *p*-anisidine and *p*-toluidine to give 2-ethyl-6-methoxy-3-methylquinoline and 2-ethyl-3,5-dimethylquinoline in moderate yields (Runs 34 and 35).

In contrast, ortho-substituted aminoarenes gave 8-substituted quinoline derivatives only in low yields (Runs 36—38). This is presumably the result of a steric effect of the ortho-substituting groups, which interfere with the coordination of the amino group to the ruthenium catalyst.

There have been several studies concerning the ruthenium- or rhodium-catalyzed isomerization of allylic alcohols to ketones and aldehydes.[10,11] The present reaction is believed to include the isomerization of the allylic alcohols to the corresponding aldehydes. Indeed, 2-buten-1-ol and 2-propen-1-ol were isomerized to butanal and propanal in 59 and 29% yields respectively in the presence of $RuCl_2(PPh_3)_3$ under conditions similar to those for the *N*-heterocyclization (Eq. 5; see Experimental section). In the present *N*-heterocyclization, the aldehydes produced are considered to react with

$$RCH{=}CHCH_2OH \xrightarrow[180\,^\circ C,\ 5\,h]{RuCl_2(PPh_3)_3} RCH_2CH_2CHO \qquad (5)$$

	Yield/%
$R=CH_3$	59
R=H	29

aminoarenes to give the quinoline derivatives.

In this reaction *N*-alkylaminoarenes as well as the quinoline derivatives were formed. Saturated alcohols were obtained in the isomerization reaction of the allylic alcohols (see Experimental section). Therefore, we can safely say that the saturated alcohols functioned as *N*-alkylating reagents in the reaction, as has previously been reported (Eq. 1).[1] The saturated alcohols can be produced by the hydrogenation of the allylic alcohols, since $RuCl_2(PPh_3)_3$ is known to be an effective catalyst for the hydrogen-transfer reaction from alcohols.[12]

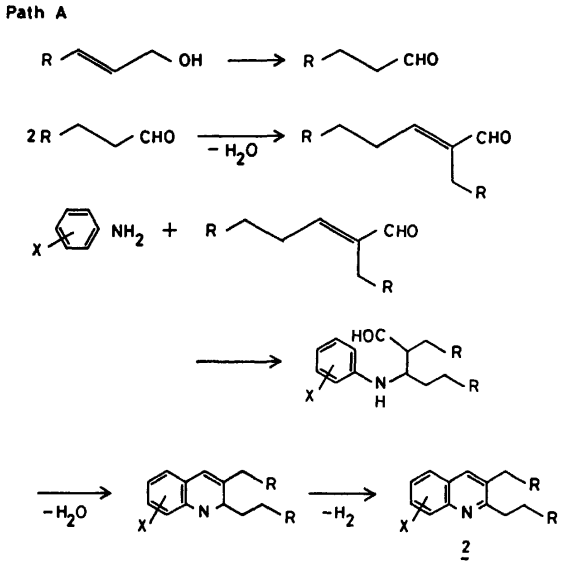

Some further studies on the mechanism of the *N*-heterocyclization to the quinolines have been carried out. Two reaction pathways are considered for the reaction. One is the path *via* aldol condensation, followed by the Michael-type addition of aminoarene (Path A). Transition metal-catalyzed aldol condensation reactions have been reported by several authors.[13] In order to examine the possibility of Path A, aniline was reacted with 2-ethyl-2-hexenal, which is an aldol condensate of butanal obtained by the method of the literature.[14] However, the corresponding quinoline, 3-ethyl-2-propylquinoline, was not obtained at all by the reaction (Eq. 6). Therefore, Path A seems not to be probable.

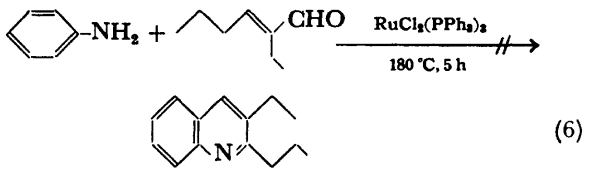

(6)

Aniline is known to react with an aldehyde to give a Schiff-base dimer.[15] The second pathway to the quinolines is one *via* the Schiff-base dimer (Path B). An equimolar mixture of aniline and butanal readily gave a Schiff-base dimer (**4**) at room temperature as white crystals (60% yield, lit, 78% yield[15b]) (Eq. 7). This Schiff-base dimer (**4**) was effectively converted to 3-ethyl-2-propylquinoline in the presence of $RuCl_2(PPh_3)_3$ (Eq. 8). Without the ruthenium complex or with 1 mol% (based on **4**) $ZnCl_2$, the corresponding quinoline was not obtained under the same reaction conditions. These results strongly suggest that the *N*-heterocyclization proceeds *via* the Schiff-base dimer and that the ruthenium catalyst operates in the cyclization stage. In Path B, the Schiff-base dimer, **4R**, forms presumably without the assistance of the ruthenium catalyst. Several transition metals have been reported to activate the aromatic *ortho*-C–H bond by oxidative addition to that bond, that is, by so-called orthometallation.[16] The ligands containing nitrogen are good ligands for maintaining such ortho-metallated species.[17] Furthermore, ruthenium is one of the most active central transition metals generating the ortho-metallated species.[18] Therefore, as one of the most plausible mechanisms of the cyclization stage, we propose the

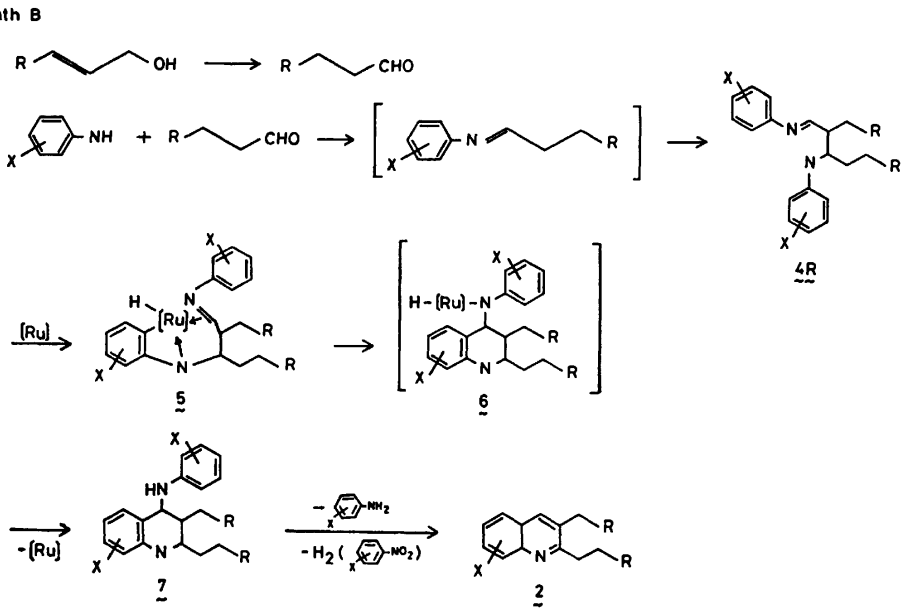

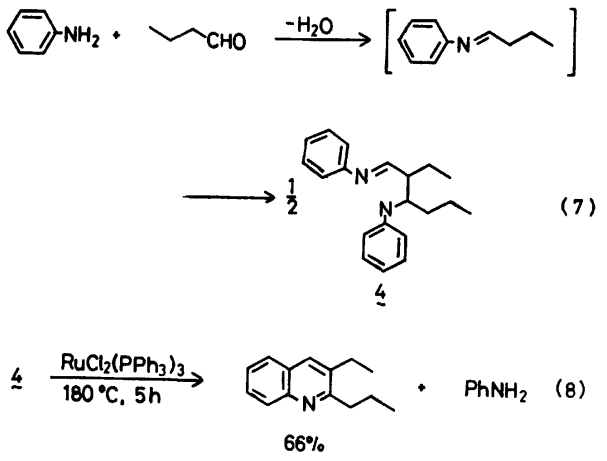

one *via* ortho-metallated species, such as **5**. This reaction is considered to proceed from **5** to **6** by an insertion of the C=N bond into the Ru–C bond.[19] The following reductive elimination of active ruthenium species will generate **7**. Finally, the quinoline is obtained by the elimination of aniline and hydrogen from **7**. The elimination of hydrogen is favored by the presence of nitroarene.

In this study, aminoarene with an electron-releasing group favored the formation of the quinoline derivatives. This might be because the more basic aminoarene facilitates a nucleophilic attack on the carbonyl carbon of the aldehyde, and so favors the formation of the Schiff-base dimer.

Experimental

Materials and Catalysts. The alcohols, aldehydes, aminoarenes, and nitroarenes were commercial products and were purified by distillation or crystallization before use. The $RuCl_3 \cdot nH_2O$ (mainly trihydrate) was purchased from Wako Chemicals and was used without further purification. The $RuCl_2(PPh_3)_3$,[21] $RuH_2(PPh_3)_4$,[22] $RuHCl(PPh_3)_3$,[23] $RuHCl(CO)(PPh_3)_3$,[24] $Ru(CO)_3(PPh_3)_2$,[25] and $[RhCl(nbd)]_2$[25] were prepared according to the methods in the literatures.

Reaction Procedure and Identification of the Products. A mixture of aminoarene (20 mmol), allylic alcohol or aliphatic aldehyde (10 ml), a ruthenium catalyst (0.20 mmol, 1.0 mol% based on aminoarene charged), nitroarene (22 mmol), and benzene (10 ml), if required, was placed in a glass liner. The glass liner was set in a 50 ml stainless steel autoclave (Taiatsu Kogyo) and the mixture was stirred with a magnetic stirrer at 180 °C for 5 h under an argon atmosphere. The GLC analysis of the reaction mixture was performed with 5% Apiezon Grease L supported on Neopak 1A 60—80 mesh (0.3 cmϕ × 3 m) by the internal-standard method. The product was isolated by fractional distillation or by medium-pressure column chromatography (silica gel, Merck No. 9385, as the absorbent and hexane–ethyl acetate as the eluent) and identified by means of ^{1}H-, ^{13}C-NMR, IR, mass spectra, and elemental analysis.

Identification of the Products. The ^{1}H-NMR spectra were obtained with a Varian HR-220(220 MHz) or JEOL JNM FX100 (100 MHz) spectrometer. The ^{13}C NMR spectra were recorded at 25.05 MHz on a JEOL JNM FX100 spectrometer. The IR spectra were measured on a Hitachi model 215 grating spectrometer, and the mass spectra were recorded on a JMS 01SG mass spectrometer. Elemental analysis was performed at the Microanalytical Center of Kyoto University.

N-*Butyl*-p-*toluidine.* ^{1}H-NMR ($CDCl_3$) δ=0.94 (t, 3H), 1.48 (m, 4H), 2.21 (s, 3H), 3.02 (t, 2H), 3.35 (s, 1H), 6.47—7.04 (m, 4H); ^{13}C-NMR ($CDCl_3$) δ=13.9(s), 20.4(s), 20.4(s), 31.8(s), 44.1(s), 112.9(s), 126.1(s), 129.6(s), 146.3(s); IR 3400 cm^{-1} (ν NH).

N-*Butyl*-p-*anisidine.* ^{1}H-NMR ($CDCl_3$) δ=0.92 (t, 3H), 1.36 (m, 2H), 1.51 (m, 2H), 2.98 (t, 2H), 3.27 (s, 1H), 3.66 (s, 3H), 6.47—6.77 (m, 4H); ^{13}C-NMR ($CDCl_3$) δ= 14.0(s), 20.4(s), 31.8(s), 44.6(s), 55.7(s), 113.9(s), 114.9(s), 142.9(s), 151.8(s); IR 3400 cm^{-1} (ν NH). The spectral data of the other products which appeared in this study were all consistent with those reported in the previous paper.[7]

Isomerization of Allylic Alcohols. In a glass liner, 2-propen-1-ol (5.0 ml, 74.6 mmol) and $RuCl_2(PPh_3)_3$ (95.9 mg, 0.10 mmol) were placed. The glass liner was then set in the autoclave, and the mixture was stirred with magnetic stirrer at 180 °C for 5 h under an argon atmosphere. The subsequent GLC analysis of the reaction mixture showed that 96% of the 2-propen-1-ol was converted and that 22 mmol (29% based on the 2-propen-1-ol used) of propanal and 7.5 mmol (10%) of propanol were obtained.

The isomerization of 2-buten-1-ol (5.0 ml, 60.5 mmol) with $RuCl_2(PPh_3)_3$ (95.9 mg, 0.10 mmol) was carried out in a similar manner. The conversion of 2-buten-1-ol was almost 100%, and 36 mmol (59% based on 2-buten-1-ol used) of butanal and 9.7 mmol (16%) of butanol) were formed.

Reaction of Aniline with 2-Ethyl-2-hexenal. A mixture of aniline (11 mmol), 2-ethyl-2-hexenal (15 mmol), nitrobenzene (12 mmol), benzene (5.0 ml), and $RuCl_2(PPh_3)_3$ (0.10 mmol) was stirred at 180 °C for 5 h under an argon atmosphere. The GLC analysis of the reaction mixture showed that no 3-ethyl-2-propylquinoline was obtained, although considerably aniline was converted.

Transformation of **4** *into 3-Ethyl-2-propylquinoline.* A solution of **4** (2.94 g, 10 mmol) in benzene (20 ml) was stirred in the presence of nitrobenzene (20 mmol) and $RuCl_2(PPh_3)_3$ (0.20 mmol) at 180 °C for 5 h. After the reaction mixture had cooled, 6.6 mmol (66% yield based on **4**) of 3-ethyl-2-propylquinoline was found by GLC analysis. When the reaction was carried out in the absence of nitrobenzene, the yield of the quinoline decreased to 3.4 mmol (34% yield).

References

1) Preliminary communication; Y. Watanabe, Y. Tsuji, and Y. Ohsugi, *Tetrahedron Lett.*, **22**, 2667 (1981).
2) S. Murahashi, T. Shimamura, and I. Moritani, *J. Chem. Soc., Chem. Commun.*, **1974**, 931.
3) L. S. Hegedus, G. F. Allen, and J. J. Bozell, *J. Am. Chem. Soc.*, **100**, 5800 (1978).
4) Y. Watanabe, M. Yamamoto, S. C. Shim, S. Miyanaga, and T. Mitsudo, *Chem. Lett.*, **1980**, 603.
5) S. E. Diamond, A. Szalkiewicz, and F. Mares, *J. Am. Chem. Soc.*, **101**, 490 (1979).
6) T. Joh and N. Hagihara, *Tetrahedron Lett.*, **1967**, 4199.
7) Y. Watanabe, S. C. Shim, and T. Mitsudo, *Bull. Chem. Soc. Jpn.*, **54**, 3460 (1981).
8) Y. Watanabe, N. Suzuki, Y. Tsuji, S. C. Shim, and T. Mitsudo, *Bull. Chem. Soc. Jpn.*, **55**, 1116 (1981).
9) a) Y. Watanabe, N. Suzuki, and Y. Tsuji, *Chem. Lett.*, **1981**, 1067; b) W. J. Boyle and F. Mares, *Organometallics*, **1**, 1003 (1982).
10) Y. Sasson and G. L. Rempel, *Tetrahedron Lett.*, **1974**, 4133.
11) W. Strohmeier and L. Weigelt, *J. Organomet. Chem.*, **86**,

C17 (1975).
12) Y. Sasson and J. Blum, *J. Org. Chem.*, **40**, 1887 (1975); G. Speier and L. Markó, *J. Organomet. Chem.*, **210**, 253 (1981).
13) K. Irie and K. Watanabe, *Bull. Chem. Soc. Jpn.*, **53**, 1366 (1980); K. Irie and K. Imagawa, *Chem. Lett.*, **1979**, 1401; M. Michman and S. Nussbaum, *J. Organomet. Chem.*, **205**, 111 (1981).
14) H. Häusermann, *Helv. Chim. Acta*, **7**, 653 (1951).
15) a) R. Tiollais, *Bull. Soc. Chim. Fr.*, **1947**, 708; b) M. S. Kharash, I. Richlin, and R. Mayo, *J. Am. Chem. Soc.*, **62**, 494 (1940).
16) G. W. Parshall, *Acc. Chem. Res.*, **3**, 139 (1970), and the references cited therein; H. D. Kaesz and R. B. Saillant, *Chem. Rev.*, **72**, 231 (1972).
17) I. Omae, *Chem. Rev.*, **79**, 287 (1979), and the references cited therein.
18) G. W. Parshall, W. H. Knoth, and R. A. Schunn, *J. Am. Chem. Soc.*, **91**, 4990 (1969); T. Itoh, S. Kitazume, A. Yamamoto, and S. Ikeda, *ibid.*, **92**, 3011 (1970); J. Chatt and J. M. Davidson, *J. Chem. Soc.*, **1965**, 843; C. A. Tolman, S. D. Itell, A. D. English, and J. P. Jesson, *J. Am. Chem. Soc.*, **100**, 4080 (1978).
19) There have been no reports concerning the insertion of the C=N bond into the orthometallated transition metal-carbon bond. However, the insertion of a C=C bond into such the orthometallated C–M bond has been reported.[20]
20) A. D. Ryabov and A. K. Yatsmirsky, *Tetrahedron Lett.*, **21**, 2757 (1980).
21) P. S. Hallman, T. A. Stephenson and G. Wilkinson, *Inorg. Synth.*, **12**, 237 (1970).
22) R. Young and G. Wilkinson, *Inorg. Synth.*, **17**, 75 (1977).
23) P. S. Hallman, B. R. McGarvey, and G. Wilkinson, *J. Chem. Soc., A*, **1968**, 3142.
24) N. Ahmad, J. J. Levison, S. D. Robinson, and M. F. Uttley, *Inorg. Synth.*, **15**, 48 (1974).
25) J. Chatt and L. M. Venanzi, *J. Chem. Soc.*, **1957**, 4735.

The Reaction of Olefins with a Mixture of Iodine and Mercury(II) Thiocyanate. Predominant Formation of *vic*-Iodo(isothiocyanato)alkanes

Nanao WATANABE,† Sakae UEMURA, and Masaya OKANO*
Institute for Chemical Research, Kyoto University, Uji, Kyoto 611
†*Koei Chemical Co. Ltd., Joto-ku, Osaka 536*
(Received December 27, 1982)

Treatment of olefins with a mixture of iodine and mercury(II) thiocyanate in benzene or diethyl ether gives *vic*-iodo(isothiocyanato)alkanes and *vic*-iodo(thiocyanato)alkanes in a high yield, the former being predominant. Similar results were obtained by using silver(I) and thallium(I) thiocyanates, though both the yield and the selectivity are slightly lower. By use of potassium thiocyanate and copper(I) isothiocyanate in place of mercury(II) thiocyanate, β-iodo thiocyanates were mainly formed. A reaction scheme involving initial formation of an iodonium ion from olefin and ISCN (formed *in situ*) and a subsequent attack of complex anion $I(SCN)_2^-$ has been proposed to account for this predominant formation of β-iodo isothiocyanates.

We reported previously that $Hg(SCN)_2$ reacts with alkyl halides in solvents of low polarity to afford alkyl isothiocyanates (RNCS) and alkyl thiocyanates (RSCN), with the former being predominant.[1] The preponderant isothiocyanate formation was explained by assuming the reaction of $XHg(SCN)_2^-$ with the alkyl cation. When a mixture of olefin and halogen is used in place of alkyl halides, selective formation of *vic*-iodo(isothiocyanato)-alkanes might be expected in a similar manner. We report here our new findings on this subject. Cambie *et al.* have recently reported that a mixture of I_2 and TlSCN reacts with cyclohexene to give the expected β-iodo isothiocyanate and β-iodo thiocyanate as the main products.[2] They have observed an unusual solvent dependence of the isothiocyanate/thiocyanate ratio: In solvents of sulfolane, dichloromethane, or diethyl ether, the ratios were around 1.5 regardless of their polarity, whereas in a suitable mixed solvent ($CHCl_3$ and sulfolane or DMSO with 1 : 1) the ratios were higher (*ca.* 3.0—4.0). Such a trend was not observed in the reaction of alkyl halides with $Hg(SCN)_2$.

Results and Discussion

First of all, we examined the reaction of cyclohexene with a mixture of I_2 and various metal thiocyanates, $M(SCN)_2$, to study the effect of metal salts on the isomer distribution in the expected products. Dry benzene was chosen as a solvent, since we previously observed the favorable formation of isothiocyanates from alkyl halides in less polar solvents. Although I_2 is soluble in benzene, all metal salts examined are only slightly soluble and thus the reaction mixture is heterogeneous in all cases. The reaction was generally carried out in the dark by adding cyclohexene to a pre-stirred (0.5 h) mixture of I_2 and $M(SCN)_2$ in benzene and by stirring the resulting mixture for 18—24 h at room temperature. The products were *trans*-1-iodo-2-isothiocyanatocyclohexane (**1**), *trans*-1-iodo-2-thiocyanatocyclohexane (**2**), and a very small amount of *trans*-1-isothiocyanato-2-thiocyanatocyclohexane (**3**) (Eq. 1). The results are shown in Table 1. $Hg(SCN)_2$ showed the

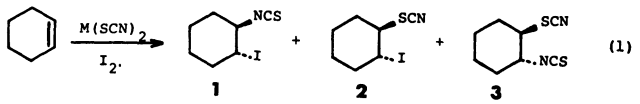

1 2 3 (1)

best results for both the total yield of **1** and **2** and the selectivity for the *N*-alkylation product **1**. Among other metal salts examined, AgSCN and TlSCN were found to be fairly effective for the formation of **1**, while almost no reaction occurred using $Ni(NCS)_2$ and $Pb(SCN)_2$, probably due to their poor reactivities toward I_2 (see below). On the contrary, the *S*-alkylation product **2** was mainly formed when KSCN (in ether), CuNCS and $Cu(NCS)_2$ were used. Cambie *et al.* also reported

Table 1. Reaction of cyclohexene with various metal thiocyanates and iodine[a]

$M(SCN)_n$	React. temp °C	React. time h	Products and Yields/%[b] 1	2	3	Ratio 1 : 2
$Hg(SCN)_2$	18—22	18	67	18	2	79 : 21
$Hg(SCN)_2$[c]	25—28	17	63	13	0	83 : 17
$Hg(SCN)_2$[d]	25—27	22	80	8	0	91 : 9
TlSCN	20—25	22	44	9	1	83 : 17
AgSCN	20—25	22	57	24	1	70 : 30
$Cu(NCS)_2$	24—27	21	Trace	16	0	
CuNCS	22—25	22	2	52	0	4 : 96
$Pb(SCN)_2$	20—22	24	0	2	0[e]	
$Ni(NCS)_2$	25—27	22	0	0	0[e]	
KSCN[f]	20—25	21	2	76	0	3 : 97

a) $M(SCN)_n$ (10/n mmol), I_2 (10 mmol), cyclohexene (10 mmol), and dry benzene (25 ml) were used. b) Isolated yield. c) $Hg(SCN)_2$ (2.5 mmol) and cyclohexene (5 mmol) were used. d) $Hg(SCN)_2$ (1 mmol) and cyclohexene (2 mmol) were used . e) *trans*-1,2-Diiodocyclohexane was formed in *ca.* 40% yield. f) Et_2O (25 ml) as solvent.

Table 2. Reaction of cyclohexene with $Hg(SCN)_2$ and I_2 under various conditions[a]

Solvent (25 ml)	React. temp °C	React. time h	Products and Yields/%[b] 1	2	3	Ratio 1 : 2
Benzene	18—20	1	53	14	1	79 : 21
Benzene	19—21	6	57	15	1	79 : 21
Benzene	18—22	18	67	18	2	79 : 21
Diethyl ether	15—20	1	51	11	1	82 : 18
Diethyl ether	19—20	4	66	14	1	83 : 17
Diethyl ether	2—4	4	52	8	1	87 : 13
Tetrahydrofuran	22—26	5	39	15	Trace	72 : 28

a) $Hg(SCN)_2$ (5 mmol), I_2 (10 mmol), and cyclohexene (10 mmol) were used. b) Determined by GLC and HPLC.

Table 3. Reaction of $Hg(SCN)_2/I_2$ or $KSCN/I_2$ with various olefins[a]

Olefin (10 mmol)	Metal salt	(mmol)	React. temp °C	React. time h	Products and Yields/%[b] -NCS	-SCN
Cyclopentene	$Hg(SCN)_2$	5	25—28	22	**4** (69)	**5** (20)
Cyclopentene	KSCN	10	20—26	20	**4** (2)	**5** (76)
Cyclohexene	$Hg(SCN)_2$	5	18—22	18	**1** (67)	**2** (18)
Cyclohexene	KSCN	10	20—25	21	**1** (2)	**2** (76)
Cycloheptene	$Hg(SCN)_2$	5	25—27	16	**6** (65)	**7** (16)
Cycloheptene	KSCN	10	26—27	22	**6** (3)	**7** (71)
trans-3-Hexene	$Hg(SCN)_2$	5	25—28	22	**8** (74)	**9** (10)
trans-3-Hexene	KSCN	10	26—29	20	**8** (3)	**9** (60)

a) I_2 (10 mmol) was used in all cases. Benzene (25 ml) was used as solvent for $Hg(SCN)_2$ and diethyl ether (25 ml) for KSCN. b) Isolated yield.

a predominant formation of β-iodo thiocyanates from some olefins in sulfolane and/or chloroform as a solvent.[2,3]

Next, the effects of the solvent and the reaction temperature and the time upon the isomer ratio in the products were studied in the reaction using $Hg(SCN)_2$. Table 2 shows that the reaction proceeds smoothly even at shorter reaction times and at a lower temperature in benzene or diethyl ether as solvent, in spite of the heterogeneous reaction system, and that the ratio of **1**/**2** is nearly constant by changing the reaction time. These results suggest that no isomerization between the two isomers occurs under these conditions.[4] As to the selectivity for the formation of **1**, diethyl ether is superior to benzene as solvent and the reaction at a lower temperature seems to be favorable. The reaction proceeded homogeneously in tetrahydrofuran, but both the product yield and the selectivity for **1** were somewhat lower. No reaction occurred in hexane as solvent.

Extension of the reaction using $Hg(SCN)_2$ to other olefins such as cyclopentene, cycloheptene, and *trans*-3-hexene resulted also in the formation of the expected β-iodo isothiocyanates (**4**, **6**, **8**) and β-iodo thiocyanates (**5**, **7**, **9**), the former being predominant in all cases as in the case of cyclohexene. Similarly, the reaction using KSCN afforded the latter highly selectively. Typical results are summarized in Table 3 together with the data of cyclohexene.

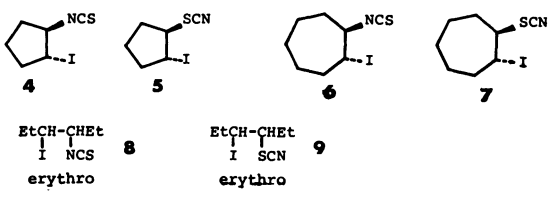

Though it is known that $Pb(SCN)_2$ effectively reacts with Br_2 to give thiocyanogen $[(SCN)_2]$[5,6] and with excess Cl_2 to afford thiocyanogen chloride (ClSCN), few similar reactions with I_2 have been reported, except for the case of the Ag salt.[7,8] Cambie *et al.*[2] recently stated that, in the reaction of 2-phenylpropene with I_2 and TlSCN in chloroform–sulfolane solvent, the total yield of the β-isothiocyanato thiocyanate and the dithiocyanate predominated over the yield of the β-iodo isothiocyanate, but no evidence was given for the generation of $(SCN)_2$ species from a mixture of I_2 and TlSCN.

We have obtained some information regarding the formation of some active species including $(SCN)_2$ from I_2 and metal thiocyanates as shown below. When an equimolar quantity of I_2 was added gradually to a stirred suspension of $Hg(SCN)_2$ in benzene and then the stirring was continued for a further 0.5 h at 25 °C, the red color of I_2 in solution almost disappeared and a red solid separated. Treatment of the filtrate, after the removal of the solid, with cyclohexene (1 equiv) for 17 h at 16—19 °C under stirring afforded **3** (19%) along with **1** (12%) and **2** (2%). In contrast to this, the use of 2 mol of I_2 in the above experiment resulted in a different product distribution: *i.e.*, **1** (57%), **2** (16%), and **3** (1%). The total yield of **1** and **2** is somewhat lower than that in the reaction without filtration of the red solid, but the ratio of **1**/**2** is nearly the same in both cases. Quite similar results were obtained in the I_2–TlSCN system as well. These observations clearly indicate that the generation of $(SCN)_2$ from an equiva-

lent mixture of I_2 and $Hg(SCN)_2$ or TlSCN (possibly the Ag(I) salt as well) is fairly rapid in spite of a heterogeneous reaction, and that under the presence of excess I_2 the *vic*-iodothiocyanation and *vic*-iodoisothiocyanation occur substantially with only a little or without any formation of the olefin–$(SCN)_2$ and olefin–I_2 adducts. Thus the most probable species for addition to olefin would be the ISCN species, which is formed by the following scheme (Eqs. 2 and 3). Here, the equilibrium shown in Eq. 3 is already known.[8]

$$Hg(SCN)_2 + I_2 \longrightarrow (SCN)_2 + HgI_2\downarrow$$

$$2TlSCN + I_2 \longrightarrow (SCN)_2 + 2TlI\downarrow \quad (2)$$

$$(SCN)_2 + I_2 \rightleftarrows 2\,ISCN \quad (3)$$

However, in the cases of $Pb(SCN)_2$ and $Ni(SCN)_2$ the generation of $(SCN)_2$ by Eq. 2 seemed to be difficult, since no appreciable decolorization of the reaction mixture was observed and no principal products other than *vic*-diiodide were found (see Table 1).

As to the product-determining step, Cambie *et al.* suggested a probable pathway for the reaction with a mixture of I_2 and $(SCN)_2$. This pathway involves the initial formation of a bridged iodonium ion, and a subsequent attack by SCN^- leading to *β*-iodo thiocyanate and the attack by ISCN or $(SCN)_2$ to *β*-iodo isothiocyanate.[3] However, we believe that a nucleophile $I(SCN)_2^-$, which is in equilibrium with SCN^- and ISCN,[9] is a more conceivable species for the latter attack. If this complex ion serves as a source of SCN^-, the reaction with cationic species would occur mainly at either of the two terminal N atoms, which are the sterically favorable and more electronegative sites (Eqs. 4 and 5). Further, when a large excess of I_2 was used in the reaction of cyclohexene, a further increase in the *N*-selectivity was observed (see Table 1). This might be attributed to the concentration of another active species $I_2(SCN)^-$, but the phenomenon was not so general for other olefins.

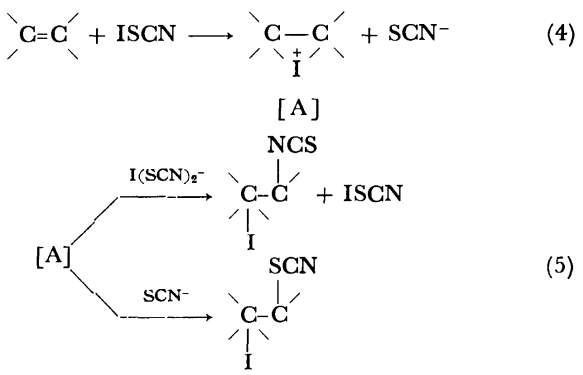

For comparison with the data using the I_2–$Hg(SCN)_2$ system, we also examined the reaction using an equimolar mixture of I_2 and $(SCN)_2$ (prepared by a known method[5] separately). The reaction in benzene at 17—24 °C for 20 h afforded the products **1** (53%), **2** (16%), and **3** (1%). A slight excess in the total yield of **1** and **2** and in the *N*-selectivity in the I_2–$Hg(SCN)_2$ cases compared to this case can be explained by assuming the competitive thiocyanation with a complex anion of $Hg(SCN)_2$ such as $IHg(SCN)_2^-$ or $Hg(SCN)_3^-$, though no direct evidence of this is available.

It is known that *vic*-iodo(isothiocyanato)alkanes react with aniline and methanol to afford 2-anilino-2-thiazoline and 2-thiazolidinone respectively.[10] By the reported methods we could prepare the corresponding new compounds such as **10** and **12** from **4** and **11** and **13** from **6** respectively.

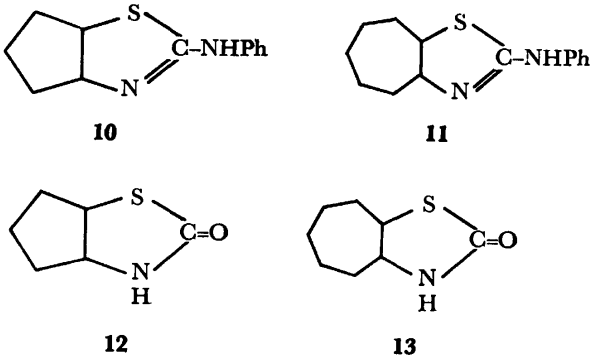

Experimental

All organic substances were distilled immediately before use. Diethyl ether and tetrahydrofuran were dried over sodium and then distilled. Commercial metal thiocyanates and isothiocyanates, HgI_2, and bromine were used without further purification.

The ^1H NMR spectra were recorded with JEOL JNM FX-100 (100 MHz) instruments on solutions in $CDCl_3$ with Me_4Si as internal standard. The ^{13}C NMR spectra were taken at 25.1 MHz with a JEOLCO ^{13}C Fourier transform NMR system and were recorded on solutions in $CDCl_3$, after 250—1000 pulses with intervals of 2.7—2.8 s. The GLC analyses were carried out with a Yanagimoto G-2800 apparatus using SE-30 (1 m) and EGSS-X (1 m) columns (H_2 as carrier gas), benzyl isothiocyanate ($PhCH_2NCS$) being used as an internal standard. The IR spectra were recorded with a Hitachi SPI-G3 spectrometer. The liquid chromatographic analyses were carried out with a Waters HPLC system equipped with a 6000A solvent delivery system and a Model 440 absorbance detector (at 254 nm) with a μ-Porasil (3.9 mm × 0.3 m) column [hexane–chloroform (3 : 1) as eluent]. The mass spectra were measured on a JEOL JMS-D300 mass spectrometer, the ionization voltage being 10 and 70 eV.

The yield of *vic*-iodo(isothiocyanato)alkanes was determined by GLC, while *vic*-iodo(thiocyanato)alkanes were decomposed at the GLC conditions. Therefore, the yield of the iodothiocyanates was evaluated by HPLC using a calibration curve between the two isomers which are stable enough for HPLC determination. The isolation of products was carried out by column chromatography using silica gel (Wakogel C-200; benzene as eluent), the isothiocyanates being eluted first.

Typical experimental procedures and analytical data of new compounds are given below.

a) The Reaction of $Hg(SCN)_2$ and I_2 with Cyclopentene in Benzene. To a suspension of $Hg(SCN)_2$ (1.58 g, 5 mmol) and benzene (5 ml) was slowly added a benzene (20 ml) solution of I_2 (2.53 g, 10 mmol) under stirring at room temperature. After 30 min, cyclopentene (0.68 g, 10 mmol) was added to the mixture by keeping the temperature within the range of 18—22 °C (a slight heat evolution was observed during the addition) and the resulting mixture was stirred for 18 h at that temperature. All operations described above were carried out in the dark by wrapping the flask with aluminium foil.

The precipitated red solid (mainly HgI_2) was filtered and the filtrate was washed with aqueous KI, aqueous $Na_2S_2O_3$, and brine successively, and then dried over $MgSO_4$. Evaporation of the solvent from the filtrate left a yellow oil, an aliquot of it being analyzed by GLC and HPLC; *trans*-1-iodo-2-isothiocyanatocyclopentane (**4**) (7.29 mmol, 73% yield) and *trans*-1-iodo-2-thiocyanatocyclopentane (**5**) (2.13 mmol, 21%). These were isolated respectively by column chromatography: **4** (1.75 g, 6.91 mmol, 69%) and **5** (0.49 g, 1.95 mmol, 20%). **4**; A colorless oil, IR 2050 (ν_{-NCS}, br) cm^{-1}. ^1H NMR δ= 1.6—2.7 (m, 6H), 4.1—4.5 (m, 2H). ^{13}C NMR δ=22.2 (t), 27.8 (d, >CHI), 31.3 (t), 36.3 (t), 66.8 (d, >CHNCS), 134.4 (s, -NCS). Mass (*m/e*) 253 (M^+), 195 (M^+—NCS), 126 (M^+—I). Found: C, 28.49; H, 3.27; N, 5.71%. Calcd for C_6H_8INS: C, 28.47; H, 3.19; N, 5.53%. **5**; A colorless oil, IR 2150 (ν_{-SCN}) cm^{-1}. ^1H NMR δ=1.6—2.7 (m, 6H), 3.93 (td. 1H, J=4.5 and 7.2 Hz, >CHSCN), 4.40 (td. 1H, J=4.5 and 6.0 Hz, >CHI). ^{13}C NMR δ=22.9 (t), 29.0 (d, >CHI), 30.6 (t), 37.0 (t), 57.1 (d, >CHSCN), 110.4 (s, -SCN). Mass (*m/e*) 254 (M^++1), 195 (M^+—SCN), 126 (M^+—I). Found: C, 28.33; H, 3.16; N, 5.84%.

The analytical data of *trans*-1-iodo-2-isothiocyanatocycloheptane (**6**) and *trans*-1-iodo-2-thiocyanatocyloheptane (**7**) are as follows. **1**, **2**, **8**, and **9** are known compounds[2,3] and the spectral and analytical data are completely the same as those of each authentic sample.

6; A colorless oil, IR 2050 (ν_{-NCS}, br) cm^{-1}. ^1H NMR δ=1.64 (br s, 6H), 1.8—2.3 (m, 4H), 4.20 (ddd 1H, J=7.5, 7.0, and 3.2 Hz, >CHNCS), 4.46 (td 1H, J=7.5 and 4.0 Hz, >CHI). ^{13}C NMR δ=22.3 (t), 26.3(t), 26.6 (t), 32.6 (t), 35.7 (d, >CHI), 36.3 (t), 67.1 (d, >CHNCS), 133.1 (-NCS). Mass (*m/e*) 281 (M^+), 233 (M^+—NCS), 154 (M^+—I). Found: C, 34.24; H, 4.49; N, 5.20%. Calcd for $C_8H_{12}INS$: C, 34.18; H, 4.30; N, 4.98%.

7; A Colorless oil, IR 2150 (ν_{-SCN}) cm^{-1}. ^1H NMR δ= 1.4—2.0 (m, 6H), 2.0—2.5 (m, 4H), 3.89 (ddd, 1H, J=7.3, 7.1, and 3.3 Hz, >CHSCN), 4.63 (dt, 1H, J=7.1 and 5.0 Hz, >CHI). ^{13}C NMR δ=24.2 (t), 25.7 (t), 26.7 (t), 32.2 (t), 36.5 (d, >CHI), 36.7 (t), 60.0 (d, >CHSCN), 110.9 (s, -SCN). Mass (*m/e*) 281 (M^+), 223 (M^+—SCN), 154 (M^+—I). Found: C, 34.14; H, 4.42; N, 5.06%.

b) The Reaction of KSCN and I_2 with Cyclopentene in Diethyl Ether. The reaction was carried out in a similar manner to that given above, using dry KSCN (0.98 g, 10 mmol), I_2 (2.53 g, 10 mmol), and cyclopentene (0.68 g, 10 mmol) in diethyl ether (25 ml) as solvent at 20—26 °C for 20 h. The products were **4** and **5**; the isolated yields of **4** and **5** were 0.04 g (0.17 mmol, 2%) and 1.91 g (7.56 mmol, 76%), respectively.

c) The Reaction of a Mixture of I_2 and Thiocyanogen with Cyclohexene. The solution of thiocyanogen (10 mmol) in benzene (20 ml) was prepared by the reported method[5] using $Pb(SCN)_2$ (3.60 g, 11 mmol) and Br_2 (1.60 g, 10 mmol). To this solution was added a benzene (20 ml) solution of I_2 (2.53 g, 10 mmol) at 10—17 °C under stirring. After 30 min, cyclohexene (0.82 g, 10 mmol) was added and the resulting mixture was stirred for 20 h at 17—24 °C in the dark and then worked up as in the case of a). The GLC and HPLC analysis revealed the presence of 1-iodo-2-isothiocyanatocyclohexane (**1**) (5.30 mmol, 53%), 1-iodo-2-thiocyanatocyclohexane (**2**) (1.90 mmol, 19%), and 1-isothiocyanato-2-thiocyanatocyclohexane (**3**) (0.10 mmol, 1%) as products. Each product was isolated by column chromatography. **3**; A colorless semisolid (lit,[11] a colorless solid), IR 2130 (ν_{-SCN}) and 2050 (ν_{-NCS}) cm^{-1}. ^1H NMR δ=1.1—2.0 (m, 6H), 2.1—2.6 (m, 2H), 3.10 (ddd, 1H, J=4.0, 10.5, and 11.5 Hz, >CHSCN), 3.76 (td, 1H, J= 10.5 and 4.0 Hz, >CHNCS). ^{13}C NMR δ=23.5 (t), 25.2 (t), 32.5 (t), 34.2 (t), 52.3 (d, >CHSCN), 59.9 (d, >CHNCS), 109.5 (>SCN), 135.5 (-NCS). Found: C, 48.24; H, 5.09; N, 14.24%. Calcd for $C_8H_{10}N_2S_2$: C, 48.46; H, 5.08; N, 14.13%.

d) The Reaction of trans*-1-Iodo-2-isothiocyanatocyclopentane (**4**) with Aniline. Preparation of* **10**: Aniline (0.76 g, 8 mmol) and (**4**) (1.02 g, 4 mmol) were dissolved in diethyl ether (25 ml) and the resulting solution was kept for 3 d at room temperature in the dark, during which period a yellow semisolid appeared at the bottom of the flask.[10] The whole mixture was washed with aqueous K_2CO_3 (in order to liberate the product from its HI salt) and brine, and then dried over $MgSO_4$. Evaporation of the solvent left a white solid of *cis*-2-anilino-4,5-trimethylenethiazoline (**10**) which was recrystallized from benzene–hexane: yield; 0.665 g, 3.05 mmol (76%). Mp 117—118 °C, IR (KBr disk) 3420 (ν_{N-H}), 1620 $\nu_{(C=N)}$ cm^{-1}. ^1H NMR δ=1.3—2.2 (m, 6H), 3.9—4.2 (m, 1H), 4.4—4.7 (m, 1H), 6.2 (br s, 1H), 6.9—7.4 (m, 5H). ^{13}C NMR δ=23.5 (t), 34.6 (t), 36.1 (t), 49.7 (d, >CH-S), 68.2 (d, >CH-N), 121.5 (d), 122.9 (d), 128.8 (d), 147.6 (s), 160.9 (s, -N=C-S). Mass (*m/e*) 218 (M^+). Found: C, 66.01; H, 6.44; N, 13.25%. Calcd for $C_{12}H_{14}N_2S$: C, 66.02; H, 6.46; N, 12.83%.

By similar treatment of **6** with aniline, *cis*-2-anilino-4,5-pentamethylenethiazoline (**11**) was obtained in an isolated yield of 84%. A colorless solid from diethyl ether–hexane (1 : 2). Mp 124.5—125.5 °C, IR (KBr disk) 3420 (ν_{NH}), 1630 ($\nu_{C=N}$) cm^{-1}. ^1H NMR δ=1.0—1.5 (m, 3H), 1.5—2.0 (m, 7H), 3.7—4.2 (m, 2H), 5.55 (br s, 1H), 6.9—7.4 (m, 5H). Mass (*m/e*) 247 (M^++1). Found: C, 68.15; H, 7.41; N, 11.68%. Calcd for $C_{14}H_{18}N_2S$: C, 68.25; H, 7.36; N, 11.37%.

*e) The Reaction of **4** with Methanol. Preparation of **12**:* The mixture of **4** (1.56 g, 6.2 mmol), methanol (10 ml), and tetrachloroethylene (20 ml) was refluxed for 3 d in the dark.[10] Evaporation of the solvent left a yellow oil which was subjected to column chromatography [silica gel, $CHCl_3$ as eluent] to give a pure *cis*-4,5-trimethylene-2-thiazolidinone (**12**) as a pale yellow oil: yield, 0.47 g, 3.3 mmol (53%). IR (neat) 3221 (ν_{NH}, br), 1660 ($\nu_{C=O}$, br) cm^{-1}. ^1H NMR δ=1.5—2.3 (m, 6H), 4.0—4.3 (m, 2H), 7.26 (br s, NH). ^{13}C NMR δ= 23.1 (t), 34.5 (t), 36.2 (t), 47.5 (d, >CH-S), 60.0 (d, >CH-N), 175.4 (>C=O). Mass (*m/e*) 143 (M^+). Found: C, 49.93; H, 6.60; N, 10.10%. Calcd for C_6H_9NOS: C, 50.32; H, 6.34; N, 9.78%.

By similar treatment of **6** with methanol, *cis*-4,5-pentamethylene-2-thiazolidinone (**13**) was obtained in an isolated yield of 42% by column chromatography as above. Mp 94—95 °C, IR (KBr disk) 3200 (ν_{NH} br), 1660 ($\nu_{C=O}$, br) cm^{-1}. ^1H NMR δ=1.0—2.1 (m, 10H), 3.9—4.1 (m, 2H), 7.18 (br s, 1H). ^{13}C NMR δ=24.8 (t), 27.3 (t), 30.4 (t), 31.2 (t), 32.5 (t), 49.5 (d, >CH-S), 59.3 (d, >CH-N), 174.5 (>C=O). Mass (*m/e*) 171 (M^+). Found: C, 56.82; H, 7.94; N, 8.29%. Calcd for $C_8H_{13}NOS$: C, 56.11; H, 7.65; N, 8.18%.

References

1) N. Watanabe, M. Okano, and S. Uemura, *Bull. Chem. Soc. Jpn.*, **47**, 2745 (1974).

2) P. D. Woodgate, H. H. Lee, P. S. Rutledge, and R. C. Cambie, *Tetrahedron Lett.*, **1976**, 1531; R. C. Cambie, H. H. Lee, P. S. Rutledge, and P. D. Woodgate, *J. Chem. Soc., Perkin Trans. 1*, **1979**, 757.

3) R. C. Cambie, D. Chambers, P. S. Rutledge, P. D. Woodgate, and S. D. Woodgate, *J. Chem. Soc., Perkin Trans. 1*, **1981**, 33.

4) We also confirmed separately that 96.1% of a mixture of **1** and **2** (**1**/**2**=4/96) could be recovered when the mixture of **1** and **2** (0.98 mmol, **1**/**2**=3/97), HgI_2 (2.5 mmol), and I_2 (5 mmol) in benzene (13 ml) was stirred at 26—27 °C for 22 h.

On the other hand, the isomerization of the thiocyanate to the thermodynamically more stable isothiocyanate is known to occur, especially by catalysis of the various acids and metal salts such as $BF_3 \cdot Et_2O$ and $ZnCl_2$: see Refs. 1 and 2 and references therein.

5) J. L. Wood, "Organic Reactions," ed by R. Adams, John Wiley and Sons, New York (1946), Vol. 3, p. 255.

6) R. G. R. Bacon and R. G. Guy, *J. Chem. Soc.*, **1960**, 318.

7) Although $(SCN)_2$ can be prepared by the action of I_2 upon an ethereal suspension of AgSCN, the reaction does not go to completion and the details are not known: E. Söderbäck, *Ann. Chem.*, **419**, 217 (1919).

8) For SCN-containing species, see R. G. Guy, "The Chemistry of Cyanates and Their Thio Derivatives," ed by S. Patai, John Wiley and Sons, New York (1977), Chap. 18, p. 854.

9) C. Long and D. A. Skoog, *Inorg. Chem.*, **5**, 206 (1966).

10) R. C. Cambie, H. H. Lee, P. S. Rutledge, and P. D. Woodgate, *J. Chem. Soc., Perkin Trans. 1*, **1979**, 765.

11) R. Bonnett, R. G. Guy, and D. Lanigan, *Tetrahedron*, **32**, 2439 (1976).

The Substituent Effects in Thiophene Compounds. I. ^{1}H NMR and IR Studies in Methyl (Substituted 2-Thiophenecarboxylate)s

Hajime SATONAKA

Industrial Research Institute of Kanagawa Prefecture, 3173, Showa-machi, Kanazawa-ku, Yokohama 236

(Received January 11, 1983)

The ^{1}H NMR spectra and the IR carbonyl stretching frequencies of methyl (3-, 4-, and 5-substituted 2-thiophenecarboxylate)s have been reported. Good linear correlations between the chemical shifts of the ring protons in methyl (4- and 5-substituted 2-thiophenecarboxylate)s and those of the corresponding protons in substituted thiophenes were observed. The coupling constants in methyl (substituted 2-thiophenecarboxylate)s gave good correlations against the corresponding ones in substituted thiophenes. The IR carbonyl stretching frequencies in methyl (5-substituted 2-thiophenecarboxylate)s were correlated reasonably well with the chemical shifts of 5-protons in 2-substituted thiophenes. The coupling constants in methyl 2-thiophenecarboxylate series were found to vary linearly with the electronegativities of the substituents.

The ^{1}H NMR spectra have been obtained for 2- and 3-substituted thiophene,[1-3] and disubstituted thiophenes,[1,4] and the effects of the substituents have been discussed.

The present study was undertaken to examine the substituent effects in methyl (3-, 4-, and 5-substituted 2-thiophenecarboxylate)s in comparison with those of 2- and 3-substituted thiophenes. The correlations of the chemical shifts and of the coupling constants between methyl (substituted 2-thiophenecarboxylate)s and substituted thiophenes have been discussed in this paper. Attempts have also been made to compare the IR carbonyl stretching frequencies in methyl (substituted 2-thiophenecarboxylate)s with the chemical shifts in substituted thiophenes, and the coupling constants in methyl (substituted 2-thiophenecarboxylate)s with the electronegativities of the substituents.

Results and Discussion

The ^{1}H NMR spectra of 2- and 3-substituted thiophenes (**1** and **2**), and methyl (3-, 4-, and 5-substituted 2-thiophenecarboxylate)s (**3**—**5**) were measured in deuteriochloroform at 25 °C. The assignments of the signals were made tentatively on the basis of the chemical shifts and the coupling constants. The refined chemical

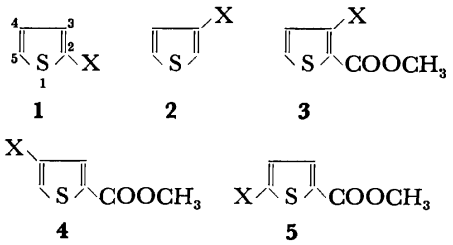

1 **2** **3**

4 **5**

TABLE 1. ^{1}H NMR CHEMICAL SHIFTS(ppm) AND COUPLING CONSTANTS(Hz) FOR 2-SUBSTITUTED THIOPHENES

No.	X	δH_3	δH_4	δH_5	Others	J_{34}	J_{35}	J_{45}	Others
1	H	7.12	7.12	7.34	7.34 (H_2)	3.50	1.05	4.95	2.85(J_{25})
2	OCH_3	6.19	6.70	6.52	3.88 (OCH_3)	3.75	1.50	5.75	
3	CH_3	6.75	6.89	7.07	2.50 (CH_3)	3.35	1.20	5.15	1.10(J_{CH_3-3}) 0.30(J_{CH_3-4}) 0.15(J_{CH_3-5})
4	Cl	6.90	6.87	7.08		3.70	1.45	5.60	
5	Br	7.04	6.86	7.22		3.70	1.35	5.60	
6	I	7.24	6.80	7.35		3.60	1.20	5.45	
7	CHO	7.79	7.22	7.77	9.95 (CHO)	3.75	1.15	4.90	1.35(J_{CHO-5})
8	$COCH_3$	7.70	7.13	7.63	2.57 ($COCH_3$)	3.80	1.20	4.90	
9	$COOCH_3$	7.80	7.10	7.55	3.89 ($COOCH_3$)	3.70	1.30	5.00	
10	NO_2	7.93	7.08	7.56		4.00	1.60	5.30	

TABLE 2. ^{1}H NMR CHEMICAL SHIFTS (ppm) AND COUPLING CONSTANTS (Hz) FOR 3-SUBSTITUTED THIOPHENES

No.	X	δH_2	δH_4	δH_5	Others	J_{24}	J_{25}	J_{45}	Others
1	H	7.34	7.12	7.34	7.12 (H_3)	1.05	2.85	4.95	3.50(J_{34})
2	OCH_3	6.24	6.74	7.17	3.81 (OCH_3)	1.60	3.10	5.20	
3	CH_3	6.88	6.89	7.20	2.27 (CH_3)	1.25	2.85	4.90	1.05(J_{CH_3-2}) 0.40(J_{CH_3-4}) 0.40(J_{CH_3-5})
4	Cl	7.10	6.96	7.27		1.35	3.30	5.10	
5	Br	7.23	7.02	7.27		1.30	3.15	5.00	
6	I	7.40	7.10	7.19		1.20	3.05	5.00	
7	CHO	8.12	7.55	7.38	9.94 (CHO)	1.20	2.85	5.10	0.35(J_{CHO-4}) 0.85(J_{CHO-5})
8	$COCH_3$	8.04	7.54	7.31	2.54 ($COCH_3$)	1.25	2.90	5.00	
9	$COOCH_3$	8.10	7.53	7.30	3.87 ($COOCH_3$)	1.15	3.05	5.05	
10	NO_2	8.31	7.66	7.37		1.40	3.35	5.30	

TABLE 3. ^{1}H NMR CHEMICAL SHIFTS(ppm) AND COUPLING CONSTANTS(Hz) FOR METHYL (3-SUBSTITUTED 2-THIOPHENECARBOXYLATE)S

No.	X	δH_4	δH_5	$\delta COOCH_3$	Others	J_{45}	Others
1	H	7.10	7.55	3.89	7.80 (H_3)	5.00	3.70(J_{34}) 1.30(J_{35})
2	OCH_3	6.86	7.41	3.83	3.97 (OCH_3)	5.55	
3	CH_3	6.90	7.36	3.85	2.55 (CH_3)	5.00	0.40(J_{CH_3-4}) 0.40(J_{CH_3-5})
4	Cl	7.01	7.46	3.90		5.25	
5	Br	7.09	7.45	3.90		5.25	
6	I	7.22	7.43	3.90		5.10	
7	CHO	7.60	7.48	3.97	10.65 (CHO)	5.20	0.40(J_{CHO-4}) 0.80(J_{CHO-5})
8	$COCH_3$	7.47	7.14	3.90	2.59 ($COCH_3$)	5.10	
9	$COOCH_3$	7.45	7.28	3.91	3.89 ($COOCH_3$)	5.15	
10	NO_2	7.59	7.54	3.94		5.40	

TABLE 4. ^{1}H NMR CHEMICAL SHIFTS (ppm) AND COUPLING CONSTANTS(Hz) FOR METHYL (4-SUBSTITUTED 2-THIOPHENECARBOXYLATE)S

No.	X	δH_3	δH_5	$\delta COOCH_3$	Others	J_{35}	Others
1	H	7.80	7.55	3.89	7.10 (H_4)	1.30	3.70(J_{34}) 5.00(J_{45})
2	OCH_3	7.42	6.50	3.86	3.80 (OCH_3)	1.85	
3	CH_3	7.60	7.12	3.86	2.27 (CH_3)	1.55	0.45(J_{CH_3-3}) 1.00(J_{CH_3-5})
4	Cl	7.63	7.32	3.89		1.60	
5	Br	7.68	7.44	3.89		1.50	
6	I	7.76	7.59	3.89		1.40	
7	CHO	8.17	8.27	3.92	9.91 (CHO)	1.40	0.30(J_{CHO-3})
8	$COCH_3$	8.17	8.20	3.91	2.54 ($COCH_3$)	1.45	
9	$COOCH_3$	8.16	8.25	3.90	3.88 ($COOCH_3$)	1.40	
10	NO_2	8.26	8.45	3.95		1.60	

TABLE 5. ^{1}H NMR CHEMICAL SHIFTS(ppm) AND COUPLING CONSTANTS(Hz) FOR METHYL (5-SUBSTITUTED 2-THIOPHENECARBOXYLATE)S

No.	X	δH_3	δH_4	$\delta COOCH_3$	Others	J_{34}	Others
1	H	7.80	7.10	3.89	7.55 (H_5)	3.70	1.35(J_{35}) 5.00(J_{45})
2	OCH_3	7.53	6.22	3.83	3.94 (OCH_3)	4.20	
3	CH_3	7.61	6.75	3.85	2.51 (CH_3)	3.70	0.45(J_{CH_3-3}) 1.05(J_{CH_3-4})
4	Cl	7.58	6.92	3.87		4.05	
5	Br	7.54	7.06	3.87		4.00	
6	I	7.43	7.25	3.87		3.90	
7	CHO	7.83	7.73	3.94	9.97 (CHO)	3.90	0.15(J_{CHO-4})
8	$COCH_3$	7.76	7.63	3.92	2.59 ($COCH_3$)	4.00	
9	$COOCH_3$	7.73	7.73	3.91	3.91($COOCH_3$)	—	
10	NO_2	7.70	7.87	3.95		4.30	

TABLE 6. FREQUENCIES(cm^{-1}) OF C=O STRETCHING VIBRATION FOR METHYL (SUBSTITUTED 2-THIOPHENECARBOXYLATE)S

No.	X	Compound **3**		Compound **4**		Compound **5**	
		anti[a]	*syn*[b]	*anti*	*syn*	*anti*	*syn*
1	H		1722		1722		1722
2	OCH_3	1700	1724		1723	1709*	1717
3	CH_3	1711*	1720		1721		1720
4	Cl	1711	1733		1727	1718*	1726
5	Br	1711	1735		1729	1719*	1726
6	I	1711	1732		1725	1719*	1724
7	CHO	1725		1725	1735	1725*	1731
8	$COCH_3$	1727		1723	1730	1725*	1728
9	NO_2	1728	1745	1728	1739	1727*	1734

a) *anti-s-trans* form. b) *syn-s-trans* form. * Shoulder.

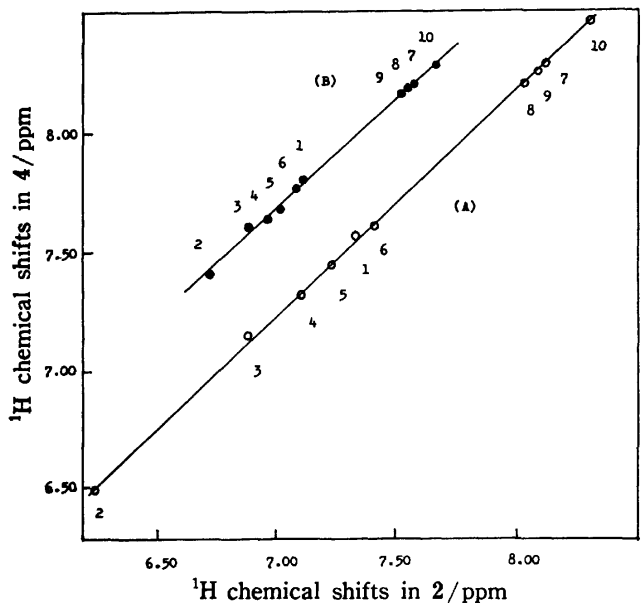

Fig. 1. Correlation between ^{1}H chemical shifts in **4** and **2**; numbering as in Table 2. A, δ_5(**4**) *vs.* δ_2(**2**); B, δ_3(**4**) *vs.* δ_4(**2**).

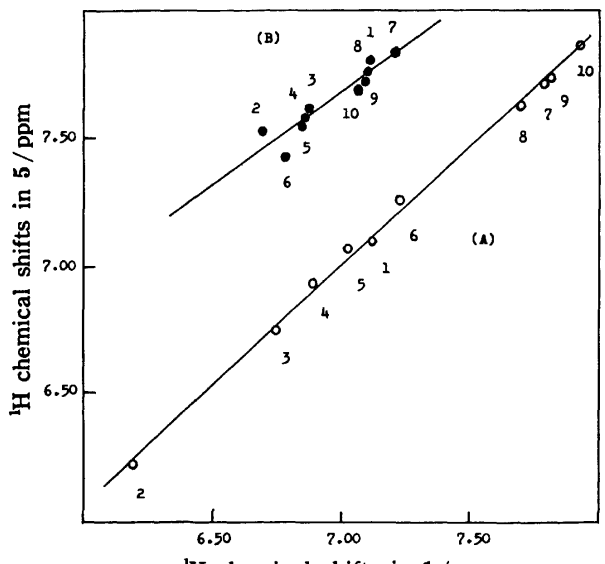

Fig. 2. Correlation between ^{1}H chemical shifts in **5** and **1**; numbering as in Table 1. A, δ_4(**5**) *vs.* δ_3(**1**). B, δ_3(**5**) *vs.* δ_4(**1**).

shifts and coupling constants were obtained iteratively using LAOCN 3.[5] The results are given in Tables 1—5. For convenience, the author uses, hereafter, the notation H_r(**N**) for the *r*-th(position)-proton on the thiophene ring of the series of compounds **N**, δ_r(**N**) for its chemical shift, and *cc*, *p*, *i*, and *s* for the correlation coefficient, slope, intercept, and standard deviation in the least-squares analysis.

The δ_5(**4**) *vs.* δ_2(**2**) (A, *cc* 1.000, *p* 0.938, *i* 0.658, *s* 0.006) and the δ_3(**4**) *vs.* δ_4(**2**) (B, *cc* 0.999, *p* 0.907, *i* 1.323, *s* 0.013) plots gave excellent correlations, as shown in Fig. 1. Line A runs almost parallel with B. The correlation coefficient between δ_3(**4**) and δ_5(**4**) is

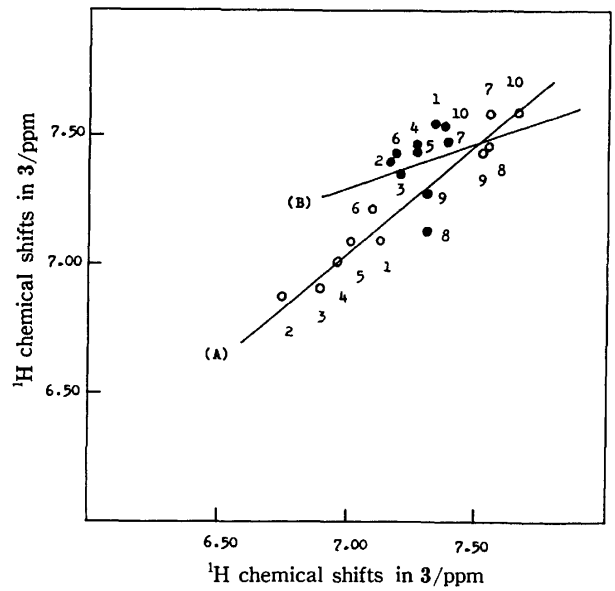

Fig. 3. Correlation between ^{1}H chemical shifts in **3** and **2**; numbering as in Table 2. A, δ_4(**3**) *vs.* δ_4(**2**); B, δ_5(**3**) *vs.* δ_5(**2**).

0.980, and this value is in accord with that between δ_2(**2**) and δ_4(**2**). These data show that the introduction of a methoxycarbonyl group into position 5 of 3-substituted thiophene is confined to the parallel transfer of the substituent effects on H_2(**2**) and H_4(**2**).

As seen in Fig. 2, good correlations were obtained with the δ_4(**5**) *vs.* δ_3(**1**) (A, *cc* 1.000, *p* 0.935, *i* 0.455, *s* 0.018) and δ_3(**5**) *vs.* δ_4(**1**) (B, *cc* 0.939, *p* 0.717, *i* 2.651, *s* 0.044) plots. The ratio of the slope of A against that of B is 0.768. Moreover, the slope of A is comparable with that of A in Fig. 1. The correlation coefficient and slope of the δ_4(**5**) *vs.* δ_5(**4**) plot are in good agreement with those between δ_3(**1**) *vs.* δ_2(**2**). These facts indicate that the methoxycarbonyl group in **5** reduces the substituent effect on the δ_3(**5**), whereas it has no effect on the δ_4(**5**).

Figure 3 shows good linearity (A, *cc* 0.982, *p* 0.835, *i* 1.207, *s* 0.051) between the effects of the substituents on δ_4(**3**) and those on δ_4(**2**), and no correlation (B, *cc* 0.215, *p* 0.357, *i* 4.806, s 0.115) between those on δ_5(**3**) and δ_5(**2**). The relationship between δ_4(**3**) and δ_3(**4**) was obtained as a linear response with a good correlation coefficient and unit slope. The correlation between δ_4(**3**) and δ_5(**4**) is almost equal to that between δ_4(**2**) and δ_2(**2**). However, apparently there is no correlation between δ_5(**3**) and δ_3(**5**), contrary to the situation between δ_5(**2**) and δ_4(**1**). Consequently, it seems that the chemical shift for the H_5 adjacent to the methoxycarbonyl group, which has a substituent on the *ortho* position, is affected considerably.

Methyl proton chemical shifts of methyl (substituted 2-thiophenecarboxylate)s, which are much less affected by the substituents on the ring, were found to have rather good correlations between proton chemical shifts of corresponding substituted thiophenes.

The chemical shifts of the ring protons of methyl (3-, 4-, and 5-substituted 2-thiophenecarboxylate)s were calculated by making use of the chemical shifts of the

protons of 2- and 3-substituted thiophenes. The calculated chemical shifts are in good agreement with the observed ones, within 0.1 ppm in the series of compounds **4** and **5** (excluding δH_4 of methoxyl derivative). For example, the calculated ring proton chemical shifts were 7.64 and 7.31 ppm for methyl 4-chloro-2-thiophenecarboxylate (**4**, X=Cl) and 7.71 and 7.91 ppm for methyl 5-nitro-2-thiophenecarboxylate (**5**, $X=NO_2$). These calculated values were in good accord with the observed ones. In methyl 5-methoxy-2-thiophenecarboxylate, the contribution of the canonical structure **a** can be presumed to become larger. Therefore, δH_3 in the compound may be shifted to lower field.

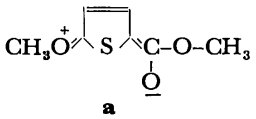

a

On the other hand, in the series of compounds **3**, there occur large deviations of the methoxyl, iodo, formyl, acetyl, and methoxycarbonyl derivatives. The two C=O stretching bands are observed in methyl 3-halo-2-thiophenecarboxylates (Table 6). These bands are considered to arise from the *syn-s-trans* and *anti-s-trans* forms as in *t*-butyl 3,4-dimethyl-2-thiophenecarboxylate.[6] Only one C=O band is observed and this is considered to be due to **b**-type isomer in methyl 2-thiophenecarboxylate. The field and magnetic

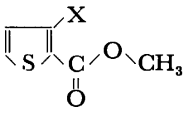

b

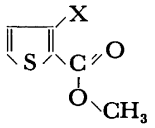

c

anisotropy effects of the C=O function may be changed by the contribution of the **c**-type isomer. The field and magnetic effects of a halogen may be also affected by the repulsion of the lone pair electrons and the steric hindrance between the halogen and the methoxycarbonyl group. The δH_4 of methyl 3-iodo-2-thiophenecarboxylate, which is greatly influenced by the effects mentioned above, thus shifts to a lower field than that calculated by the contribution of this conformational change.

The ^{1}H NMR spectrum of methyl 3-formyl-2-thiophenecarboxylate was studied by Gronowitz and coworkers.[7,8] They have reported that aldehydic hydrogen resonance in this compound occurred at a field 0.54—0.65 ppm (depending on the solvents) lower than that of the unsubstituted 2-thiophenecarbaldehyde, but that the contribution to the chemical shift of intramolecular hydrogen bonding is small. However, judging from the following experimental results, it is considered that the contribution of the rotational isomer **d**, which is capable of forming intramolecular hydrogen bonding, is a better explanation of the results

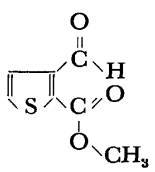

d

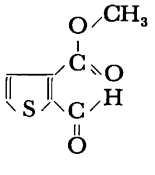

e

in methyl 3-formyl-2-thiophenecarboxylate. The resonance line of H_4 was found at 7.60 ppm, and that of H_5 at 7.48 ppm. The δH_4 was shifted towards a lower field than the values calculated, and the δH_5 towards a higher field. The chemical shift of the aldehydic hydrogen in 3-formyl derivative was 10.65 ppm, and shifted about 0.7 ppm lower than those in 4-, and 5-formyl derivatives. The chemical shift for methyl protons of methoxycarbonyl group is shifted lower than that of other compounds. The low field shift cannot be ascribed only to the effects of thiophene ring current and the substituent. The unusually low chemical shift of formyl proton might be due to the anisotropy effect of the ester carbonyl group located very close to it. If a weak hydrogen bond is persistent between the carbonyl oxygen and the formyl proton, the electric field effect lowers the chemical shift of formyl proton further. The strong ester carbonyl band in IR spectrum occurred at 1725 cm^{-1}, and could be assigned to *anti-s-trans* form **c**. The same consideration can be applied to methyl 2-formyl-3-thiophenecarboxylate. Its ^{1}H NMR spectrum exhibits the signals due to H_4 at 7.58 ppm, H_5 at 7.64 ppm, and the aldehydic proton at 10.62 ppm, indicating the presence of the preferred conformation **e**.

The chemical shifts for H_4 and H_5 in dimethyl 2,3-thiophenedicarboxylate are identical (7.51 ppm) in the calculations, but the two doublets occur at 7.45 and 7.28 ppm. Four planar conformations are considered in this ester. In methyl 3-thiophenecarboxylate, whose conformation study has not yet been reported, only one C=O stretching band is observed at 1726 cm^{-1}. It is considered that this compound exists in *syn-s-trans* form **f**, judging from the conformation of 3-thiophenecarbaldehyde.[9] From this consideration and a comparison with the chemical shifts of two ring protons in methyl 3-formyl-2-thiophenecarboxylate (conformation **d**) and methyl 2-formyl-3-thiophenecarboxylate (conformation **e**), the signal at higher field in dimethyl 2,3-thiophenedicarboxylate will be assigned to H_5, and that at lower field to H_4; the predominant conformation of this ester will lead to **g**. However, since the IR C=O stretching band occurs as a broad peak centered at 1734 cm^{-1}, other conformations are presumed to be present besides the **g** form.

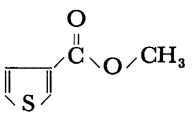

f

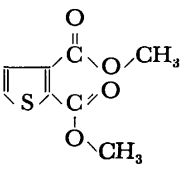

g

The correlations between the C=O stretching frequencies (*syn-s-trans* form) of methyl (substituted 2-thiophenecarboxylate)s and the proton chemical shifts of the corresponding substituted thiophenes were examined. The correlation coefficients between $\nu_{C=O}$(**4**)[10] and δ_5(**2**), between $\nu_{C=O}$(**5**) and δ_5(**1**), and between $\nu_{C=O}$(**3**) and δ_2(**2**) gave high values. As shown in Table 6, $\nu_{C=O}$(**3**), $\nu_{C=O}$(**4**), and $\nu_{C=O}$(**5**) depend strongly on the nature of the substituent. It is considered that in the series of **5** the substituent effect is mainly transmitted by the

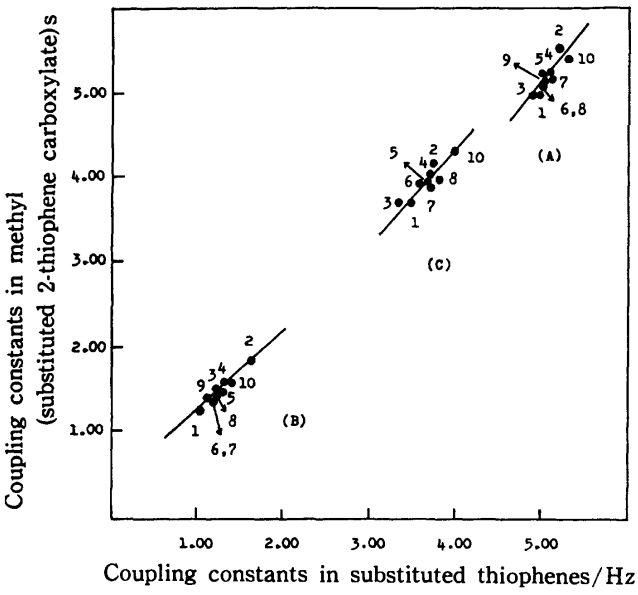

Fig. 4. Correlation between coupling constants in methyl (substituted 2-thiophenecarboxylate)s and substituted thiophenes, numbering as in Table 1. A, $J_{45}(\mathbf{3})$ *vs.* $J_{45}(\mathbf{2})$; B, $J_{35}(\mathbf{4})$ *vs.* $J_{24}(\mathbf{2})$; C, $J_{34}(\mathbf{5})$ *vs.* $J_{34}(\mathbf{1})$.

contribution of the canonical structure such as **a**, but in the series of **4** this occurs by the inductive effect. However, the correlation between $\nu_{C=O}(\mathbf{4})$ and $\nu_{C=O}(\mathbf{5})$ (*cc* 0.981, *p* 0.891) shows that the substituent effects on both frequencies have almost the same trend. It is interesting that the substituent effects in the series of **2** are almost insensitive to δH_5 but those in the series of **4** are transmitted strongly to the C=O stretching frequencies of the methoxycarbonyl groups. The slope between $\nu_{C=O}(\mathbf{4})$ and $\delta_5(\mathbf{2})$ is fivefold as steep to that between $\nu_{C=O}(\mathbf{5})$ and $\delta_5(\mathbf{1})$. The substituent effects on the C=O stretching frequencies in the series of **3**, which belong to *ortho* derivatives, are considered to become complicated due to the steric effect, in addition to the mesomeric and inductive effects, but show rather good correlations between $\delta_2(\mathbf{2})$.

The plots between the proton-proton coupling constants in methyl (substituted 2-thiophenecarboxylate)s and those in substituted thiophenes gave good correlations, as shown in Fig. 4. It is interesting that $J_{45}(\mathbf{3})$[11] gives a good correlation coefficient with $J_{45}(\mathbf{2})$ because $\delta_5(\mathbf{3})$ does not one with $\delta_5(\mathbf{2})$, in contrast to the good $\delta_4(\mathbf{3})$ *vs.* $\delta_4(\mathbf{2})$ correlation coefficient. The slopes of $J_{35}(\mathbf{4})$ *vs.* $J_{24}(\mathbf{2})$ and $J_{34}(\mathbf{5})$ *vs.* $J_{34}(\mathbf{1})$ plots are 1.00 and 0.97, respectively. This fact shows that the substituent effect is transferred equally, even though a methoxycarbonyl group is introduced into position 5 of **1** or **2**. However, the slope of $J_{45}(\mathbf{3})$ *vs.* $J_{45}(\mathbf{2})$ is 1.26, and the reason why the introduction of $COOCH_3$ into position 2 of **2** makes the substituent effect somewhat larger is not clear.

Studies on the relationships between the substituent electronegativity and the coupling constants in thiophene compounds have carried out by Bulman[12] and Galasso.[13] Bulman reported that the substituent electronegativity gave a good correlation with the sum of the coupling constants, but a rather more scattered one with the individual coupling constants in the series of compounds **1**. The relationship of the coupling constants in the series of compounds **3**, **4**, and **5** with the sum of the electronegativities of all substituents including methoxycarbonyl group was examined. Good correlations were found in all three cases. It is interesting that the three slopes are almost the same, even though the inductive and mesomeric effects of substituents on the spin-spin coupling are quite different in the three series.

Experimental

The ^1H NMR spectra of the compounds were obtained at 100 MHz on a JEOL PS-100 spectrometer. The chemical shifts were determined with an accuracy of ± 0.005 ppm relative to TMS as an internal standard and the coupling constants were determined with an accuracy of ± 0.02 Hz. The concentrations of solutions were adjusted approximately at 0.3 mol dm^{-3} with respect to substrates. The IR spectra were recorded on a Perkin–Elmer model 257 infrared spectrophotometer.

Most of materials used in this investigation were synthesized according to the methods reported,[14-25] or obtained by purification of commercially available materials.

Methyl 3-Chloro-2-thiophenecarboxylate. This material was prepared by the refluxing 3-chloro-2-thiophenecarboxylic acid[26] with methanol and H_2SO_4 for 4.5 h, mp 36 °C. Found: C, 40.92; H, 2.91; Cl, 20.07; S, 18.01%. Calcd for $C_6H_5ClO_2S$: C, 40.80; H, 2.85; Cl, 20.07; S, 18.15%. IR (KBr, cm^{-1}): 3110 (=C–H), 1719 (C=O), 1516, 1438, 1414, 730 (thiophene ring).

Methyl 3-Acetyl-2-thiophenecarboxylate. This material was prepared by the esterification of 3-acetyl-2-thiophenecarboxylic acid,[27] bp 103—105 °C/2.5 mmHg (1 mmHg≈ 133.322 Pa). Found: C, 52.02; H, 4.58; S, 17.67%. Calcd for $C_8H_8O_3S$: C, 52.16; H, 4.38; S, 17.41%. IR (neat, cm^{-1}): 3100 (=C–H); 1715, 1685 (C=O); 1510, 1438, 778 (thiophene ring).

Methyl 4-Chloro-2-thiophenecarboxylate. This material was prepared by the esterification of 4-chloro-2-thiophenecarboxylic acid,[28] bp 115—117 °C/21 mmHg. Found: C, 40.85; H, 2.78; Cl, 19.85; S, 18.28%. Calcd for $C_6H_5ClO_2S$: C, 40.80; H, 2.85; Cl, 20.07; S, 18.15%. IR (neat, cm^{-1}): 3130 (=C–H); 1718 (C=O); 1528, 1428, 1411, 749 (thiophene ring).

Methyl 4-Formyl-2-thiophenecarboxylate. This material was prepared by the esterification of 4-formyl-2-thiophenecarboxylic acid,[8] mp 63 °C. Found: C, 49.28; H, 3.63; S, 18.98%. Calcd for $C_7H_6O_3S$: C, 49.40; H, 3.55; S, 18.84%. IR (KBr, cm^{-1}): 3110, 3080 (=C–H); 1719, 1673 (C=O); 1535, 1454, 750 (thiophene ring).

Methyl 5-Methoxy-2-thiophenecarboxylate. This material was prepared by the esterification of 5-methoxy-2-thiophenecarboxylic acid,[14] mp 46 °C. Found: C, 48.98; H, 4.60; S, 18.76%. Calcd for $C_7H_8O_3S$: C, 48.82; H, 4.68; S, 18.62%. IR (KBr, cm^{-1}): 3080 (=C–H); 1699 (C=O); 1544, 1439, 1415, 748 (thiophene ring).

Methyl 4-Acetyl-2-thiophenecarboxylate. A solution of 4-acetyl-2-thiophenecarbaldehyde[29] (3.9 g, 0.025 mol) in ethanol (50 ml) was added to a shaken suspension of silver oxide, produced by adding NaOH (3.5 g) to $AgNO_3$ (9.0 g) in water (200 ml), and the mixture was shaken for 1 h. The free silver was removed by filtering, washed with water, and the filtrate was acidified with HCl. The white precipitate was recrystallized from water to give 4-acetyl-2-thiophenecarboxylic acid (3.2 g, 75%), mp 165 °C. The acid was esterified by refluxing with methanol and H_2SO_4 for 4.5 h to give methyl

4-acetyl-2-thiophenecarboxylate, mp 99—100 °C. Found: C, 52.37; H, 4.20; S, 17.51%. Calcd for $C_8H_8O_3S$: C, 52.16; H, 4.38; S, 17.41%. IR (KBr, cm^{-1}): 3110 (=C–H); 1709 (C=O); 1538, 1433, 751 (thiophene ring).

The author wishes to thank to Professor Minoru Hirota of Yokohama National University for his kind suggestions and encouragement, to Dr. Hiroshi Ozawa of Tokyo University for his permission to use the Computation Program LAOCN 3, and to Mr. Takayoshi Ozawa for the elemental analyses.

References

1) K. Takahashi, Y. Matsuki, T. Mashiko, and G. Hazato, *Bull. Chem. Soc. Jpn.*, **32**, 156 (1959).
2) R. A. Hoffman and S. Gronowitz, *Ark. Kemi*, **16**, 515 (1960).
3) S. Gronowitz and R. A. Hoffman, *Ark. Kemi*, **16**, 539 (1960).
4) R. A. Hoffman and S. Gronowitz, *Ark. Kemi*, **16**, 563 (1960).
5) S. M. Castellano and A. A. Bothner-By, *J. Chem. Phys.*, **41**, 3863 (1964).
6) D. J. Chadwick, J. Chambers, G. D. Meakins, and R. L. Snowden, *J. Chem. Soc., Chem. Commun.*, **1971**, 625.
7) S. Gronowitz, B. Gestblom, and B. Mathiasson, *Ark. Kemi.*, **20**, 407 (1962).
8) S. Gronowitz, A. Biezais, and B. Mathiasson, *Ark. Kemi*, **21**, 265 (1963).
9) G. Gacel, M. C. Fournie-Zaluski, and B. P. Roques, *Org. Magn. Reson.*, **1976**, 529.
10) The notation $\nu_{C=O}$(**N**) is hereafter used for the carbonyl stretching frequency of the series of compounds **N**.
11) The notation J_{rs}(**N**) is hereafter used for the spin-spin coupling constant between r- and s-protons on thiophene ring of the series of compounds **N**.
12) M. J. Bulman, *Tetrahedron*, **25**, 1433 (1969).
13) V. Galasso, *Chem. Phys. Lett.*, **21**, 54 (1973).
14) J. Sice, *J. Am. Chem. Soc.*, **75**, 3697 (1953).
15) B. Weinstein, *J. Am. Chem., Soc.*, **77**, 6709 (1955).
16) S. Gronowitz, *Ark. Kemi*, **8**, 441 (1955); **12**, 239, 533 (1958); S. Gronowitz, P. Moes, A. Hornfeldt, and R. Hakanssor, *ibid.*, **17**, 165 (1961); S. Gronowitz and B. Gestblom *ibid.*, **18**, 513 (1961); S. Gronowitz and V. Vilks, *ibid.*, **21**, 191 (1963).
17) S. Gronowitz and U. Rosen, *Chem. Scr.* **1**, 33 (1971).
18) I. J. Rinkes, *Recl. Trav. Chim. Pays-Bas*, **51**, 1134 (1932); I. J. Rinkes, *ibid.*, **53**, 643 (1934).
19) W. Steinkopf and W. Hanske, *Ann.*, **532**, 236 (1937).
20) R. Motoyama, K. Sato, and E. Imoto, *Nippon Kagaku Zasshi*, **78**, 779 (1957); R. Motoyama, S. Nishimura, and E. Imoto, *ibid.*, **78**, 950 (1957).
21) V. S. Babasinian, *Org. Synth.*, Coll. Vol. II, 466 (1943); H. Y. Lew and C. R. Noller, *ibid.*, IV, 545 (1963).
22) G. H. Dorofeenko, *Zh. Obshch. Khim.*, **31**, 994 (1961).
23) S. N. Godovikova and Ya. L. Gol'dfarb, *Izv. Akad. Nauk SSSR, Ser. Khim.*, **1965**, 1434.
24) P. Fournari and J. P. Chane, *Bull. Soc. Chim. Fr.*, **1963**, 479.
25) D. Spinelli, P. Noto, G. Consiglio, and A. Storace, *J. Chem. Soc., Perkin Trans. 2*, **1976**, 1805.
26) E. Frofft and G. Solf, *J. Prakt. Chem.*, **24**, 38 (1964).
27) M. Robba, B. B. Roques, and M. Bonhomme, *Bull. Soc. Chim. Fr.*, **1967**, 2495.
28) J. Iriarte, E. Martinez, and J. M. Muchowski, *J. Heterocycl. Chem.*, **13**, 393 (1976).
29) B. Decroix, J. Morel, C. Paulmier, and P. Pastour, *Bull. Soc. Chim. Fr.*, **1972**, 1848.

 © 1983 The Chemical Society of Japan Bull. Chem. Soc. Jpn., 56, 2469—2472 (1983)

Effect of Multiple Field Assistance with Reversed Micelles on the Decarboxylation of 6-Nitro-1,2-benzisoxazole-3-carboxylate

Junzo SUNAMOTO,* Kiyoshi IWAMOTO, Shinichi NAGAMATSU, and Hiroki KONDO
Department of Industrial Chemistry, Faculty of Engineering, Nagasaki University, Nagasaki 852
(Received January 22, 1983)

Decarboxylation reaction of 6-nitro-1,2-benzisoxazole-3-carboxylate (**1**) in cationic and anionic reversed micelles has been investigated with particular attention to the microenvironmental effect, such as microviscosity, micropolarity, and microactivity, in the specific and restricted reaction field as provided by reversed micelles. In 0.20 M CTAC/0.32 M $H_2O/CHCl_3$ reversed micelles, the reaction was accelerated about 1300-fold compared with that in bulk aqueous solution. Of various surfactant aggregate systems such as aqueous micelle, bilayer, and reversed micelle, the cationic reversed micelle could provide the most effective reaction field for the present decarboxylation reaction. This reaction is never accelerated in an anionic aqueous micelle. However, in the anionic AOT reversed micelle, the reaction was apparently accelerated by both lowering the micropolarity and increasing the microviscosity around the substrate. The unique rate enhancement for the decarboxylation reaction of **1** provided by reversed micelles was interpreted in terms of the "multiple field assistance."

The specific reaction field of the enzyme active site provides multiply and simultaneously different effects such as a proximity, an electronic or a structural strain, an orbital steering, an anchoring effect, and so forth. Hence, enzymes can specifically control chemical equilibria and reaction pathways or rates by *simultaneously* adjusting pH, polarity, viscosity, and activity in the microenvironment. This specific effect has been called "multiple field assistance."[1] We ourselves have presented many examples so far that reversed micelles can mimic the enzyme active site and provide a specific reaction field to afford the "multiple field assistance" for various organic[2-5] and inorganic reactions.[6-9] Because, the state and nature of water in the interior core of micelles are known to be less polar,[10,11] highly viscous,[5,10,12-14] and more active,[2,7,15-18] largely different from those of bulk water.

In the present study, as an extension of a series of our studies, the effect of the specific microenvironment, the multiple field assistance, of the water pool provided by several ionic reversed micelles on the unimolecular decarboxylation of 6-nitro-1,2-benzisoxazole-3-carboxylate (**1**) was investigated. Unimolecular reaction seems most convenient to inspect the microenvironmental effect, especially the effect of restricting the mobility of substrates on the reaction rate or path.[5,19] In addition, the decarboxylation of **1** is very insensitive to an acid-base catalysis, while extremely sensitive to solvent polarity.[20-23]

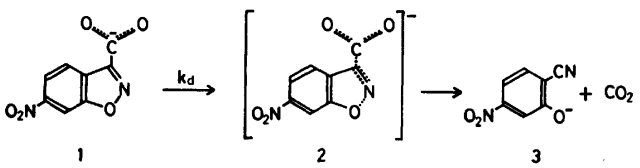

1 2 3

Scheme 1.

Experimental

Materials. 6-Nitro-1,2-benzisoxazole-3-carboxylic acid was prepared according to the method described previously.[24,25] The white and needle crystals, after drying *in vacuo* over P_2O_5 at 110 °C, showed mp 167—169 °C [lit,[25] 167—169 (monohydrate)]. Preparations and purifications of hexadecyltrimethylammonium bromide (CTAB),[9] hexadecyltrimethylammonium chloride (CTAC),[9] and sodium 1,2-bis(2-ethylhexyloxycarbonyl)ethanesulfonate (AOT)[3] were described elsewhere. Solvents employed were carefully purified, dried, and stored under prevention against moisture over molecular sieves Linde 4A.

Miscellaneous Measurements. When the *R*-value (= $[H_2O]$/[surfactant]) was changed, the water content in reversed micelles was carefully determined on a Karl-Fischer moisture automatic titration apparatus, Kyoto Electronics MFG, Model MK-AIII.

In order to examine the microscopic polarity and viscosity in the core of micelles, fluorescence spectra and steady-state fluorescence polarizations of trisodium 8-methoxy-1,3,6-pyrenetrisulfonate (Py-OMe)[10] cosolubilized in micelles were measured on a Hitachi 650-10S fluorospectrophotometer and a Union Giken FS-501S fluorescence polarization spectrophotometer using a sharp cut-off filter Y-46 (Hoya Glass Works, Tokyo).

An aqueous stock solution of the substrate **1** was freshly prepared just before the use. Reaction rates were followed by monitoring an increase in the absorbance at around 415 nm based on the release of 2-cyano-5-nitrophenolate (**3**) using a Hitachi Model 200-10 spectrophotometer equipped with a thermoregulated cell compartment. The first-order rate constants, k_d, for the decarboxylation were obtained by the Guggenheim treatment[26,27] and the correlation coefficients were always larger than 0.999. Chloroform was used as the bulk organic solvent for CTAB and CTAC micelles, while heptane was employed for AOT micelles. Surfactant concentrations were kept at 0.20 M through all the runs, while the substrate concentration was 7.2×10^{-5} M (M = mol dm^{-3}) unless otherwise stated. The reaction was initiated by injecting an aliquot (15 μl) from the stock solution of **1** into the cell containing a given amount of micellar solution (3.0 ml) with an appropriate amount of aqueous sodium hydroxide solution.

Results and Discussion

Rate constants of the decarboxylation of **1** at 30 °C in reversed micelles are summarized in Table 1 along with those in pure solvents and in a surfactant bilayer system. Clearly from Table 1, of the surfactant-aggregate systems the CTAC reversed micelle provided the most effective reaction field for the decarboxylation of **1** to be accelerated. For the decarboxylation of **1**, the dehydration

TABLE 1. RATE CONSTANTS (k_d) OF THE DECARBOXYLATION OF 6-NITRO-1,2-BENZISOXAZOLE-3-CARBOXYLATE (**1**) AT 30 °C AND FLUORESCENCE CHARACTERISTICS OF *o*-METHYLPYRANINE (Py–OMe) IN VARIOUS REACTION FIELDS

Environment	$k_d/10^{-6}$ s^{-1}	Emission maximum / nm	p[d]
Water	7.3[a]	430	0.01
MeOH	250[a]	410	0.03
EtOH	1 000[a]	407	0.04
CH_3CN	2 900 000[a]	404	0.03
Me_2CO	24 000 000[a]	401	0.03
0.2 M CTAC/H_2O/$CHCl_3$ (R=1.6)	9 600	411	0.10
0.2 M CTAB/H_2O/$CHCl_3$ (R=1.4)	6 700	415	—
0.2 M AOT/H_2O/heptane (R=1.7)	41	420	0.19
CTAB aq micelle	350[b]	410	—
$2C_{12}N^+2C_1$[c] bilayer	3 000[b]	—	—

a) From Ref. 22. b) From Ref. 35. c) Didodecyldimethylammonium bromide. d) Fluorescence depolarization (see text).

(desolvation) of the substrate is one of essential factors for the rate enhancement.[20–23] In fact, a linear relationship between log k_d and the wave number of the absorption maximum of Methyl Orange has been previously presented by Kunitake and his coworkers for the polysoap-catalyzed decarboxylation of **1**.[27] First of all, hence, we must consider the effect of micropolarity (desolvation) around the substrate on the large rate acceleration in cationic reversed micelles. Even in the reversed micellar system, the decarboxylation of **1** must proceed in an aqueous environment. Nevertheless, the decarboxylation rate in the cationic CTAC micelle was enhanced about 1300-fold compared with that in bulk water (Table 1). However, this rate enhancement seems to involve the effect of the lowered micropolarity in the reversed micellar core. Table 1 gives also the fluorescence maxima of Py–OMe to assess the micropolarity of the reaction field.[10] Py–OMe is definitely localized only in the water pool of reversed micelles owing to its highly ionic character and is considered to be a convenient probe to know the microenvironment around a water soluble substrate.[10] Results of Table 1 suggest that the micropolarity of the cationic aqueous and reversed micelles as the reaction field is almost comparable to that of methanol. Nevertheless, the reaction rate in the CTAC reversed micelle is still 40-times higher than that in methanol. As is already known, the decarboxylation of **1** is effectively accelerated by cationic aqueous micelles,[28–30] cationic polymers with a hydrophobic side chain (polysoap),[27,31,32] polymeric crown ethers complexable with cations, K^+ or Na^+,[33,34] and synthetic bilayer membranes with a positive surface charge.[35] These catalytic effects are ascribed to the stabilization of the anionic transition state (**2**) with an electrostatic assistance by the positive surface charge of these molecular assemblies. Certainly, the anionic SDS aqueous micelle can not promote this reaction.[28,29] Also in the interior core of the cationic reversed micelles, hence, the additional rate acceleration may be ascribed to the electrostatic assistance by lowering the transition state energy upon interaction of the activated complex with the cationic surface in the micellar core.

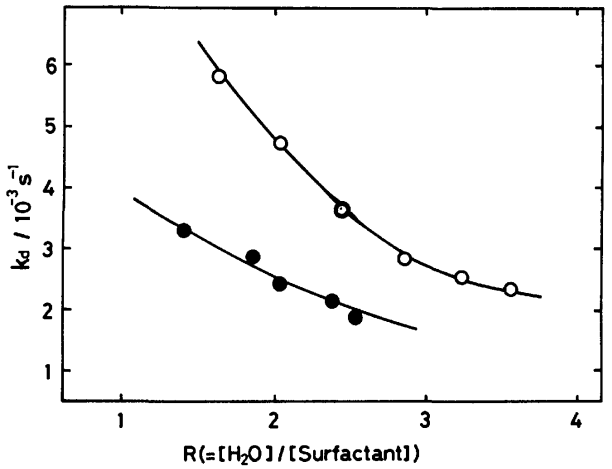

Fig. 1. The decarboxylation rates, k_d, as a function of R-value in 0.20 M CTAC/7.4×10^{-5} M aq NaOH/$CHCl_3$ (—○—) and 0.20 M CTAB/7.4×10^{-5} M aq NaOH/$CHCl_3$ (—●—) reversed micelles containing 7.2×10^{-5} M substrate **1** at 25.0 °C.

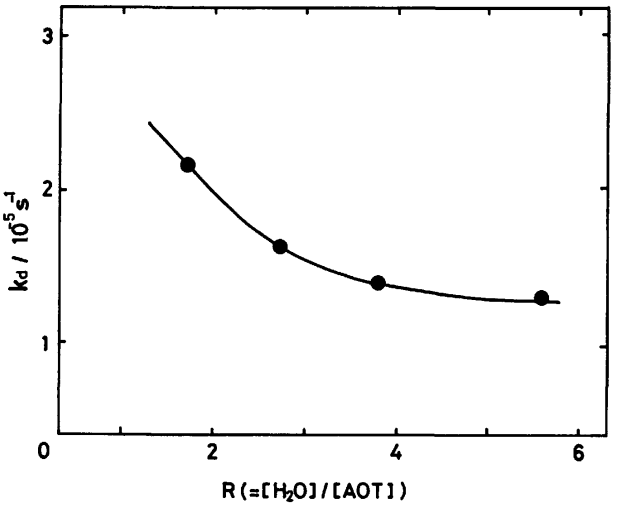

Fig. 2. The decarboxylation rate of **1** (7.2×10^{-5} M) in 0.20 M AOT/7.4×10^{-5} M aq NaOH/heptane reversed micelle as a function of R-value at 25.0 °C.

TABLE 2. THERMODYAMIC PARAMETERS OF ACTIVATION FOR THE DECARBOXYLATION OF 1 IN DIFFERENT REVERSED MICELLAR SYSTEMS AT 25.0 °C

System	R	E_a kcal mol^{-1} [b]	ΔH^* kcal mol^{-1} [b]	ΔS^* e.u.	ΔG^* kcal mol^{-1} [b]
CTAC/$CHCl_3$ reversed micelle	1.6	23.4	22.8	7.7	20.5
	2.4	23.8	23.2	8.3	20.8
	3.2	25.1	24.6	12.0	21.0
CTAB/$CHCl_3$ reversed micelle	1.4	22.7	21.1	4.4	19.8
	2.0	24.7	24.1	10.3	21.0
	2.5	24.7	24.1	10.0	21.2
AOT/heptane reversed micelle	1.9	25.2	24.6	2.6	23.8
Water[a]	—	32.6	32.0	25.4	24.4

a) From Ref. 22. b) 1 cal=4.184 J.

The CTAB reversed micelle showed lower catalytic efficiency than the CTAC one (Table 1 and Fig. 1). One reason is the slightly higher microscopic polarity in the interior core of the CTAB micelle compared with the case of CTAC micelle as suggested by the fluorescence maximum of Py-OMe (Table 1). As is well known, the hydration number for bromide ion is smaller than that for chloride ion. This means that more free water may exist in the interior core of the CTAB micelle than in the CTAC one when compared at an identical R-value, thus the former providing a more polar microenvironment. Another reason is the difference in the aggregation number between both surfactants. It has been found that for cationic reversed micelles the aggregation number decreases with an increase in the radius of the counter anion of the surfactant.[36] Assuming that one molecule of the substrate is encapsulated in a micelle, the larger aggregates (the higher aggregation number) will provide the more effective electrostatic assistance, leading to a larger rate enhancement.

Nevertheless an anionic aqueous micelle cannot accelerate this reaction,[28,29] the anionic reversed micelle shows a small, but discernible catalytic activity for the reaction. In the interior core of the AOT reversed micelle, the micropolarity is just middle between water and methanol, while the microviscosity is higher than that of the cationic reversed micelle (Table 1). Most probably, opening the benzisoxazole ring will relax the intramolecular strain upon the decarboxylation, of which effect will be more amplified in a highly viscous environment. Therefore, it appears that the release of the internal strain as well as the decreased micropolarity counteract the large destabilization of the anionic transition state with the negative surface charge of the micellar core.

Figures 1 and 2 show the rate deceleration with an increase in the R-value, or the water content, of the cationic and anionic reversed micelles, respectively. In reversed micellar systems the effect of water content on the reaction was drastic, though the rate is hardly affected by a minute amount of water in a simple organic solvent.[27] In general, an increase in the R-value leads to an increase in the micropolarity and a decrease in the microviscosity of the water pool.[11,14,18] We also observed similar phenomena for the present system employing the fluorescent probe, Py-OMe.[10] This means that in reversed micelles one can control the polarity, viscosity, and activity of the reaction field and consequently the reaction rate by changing the water content of micelles. In any event, both an increase in the micropolarity and a decrease in the microviscosity act as negative effect on the present decaboxylation (Figs. 1 and 2).

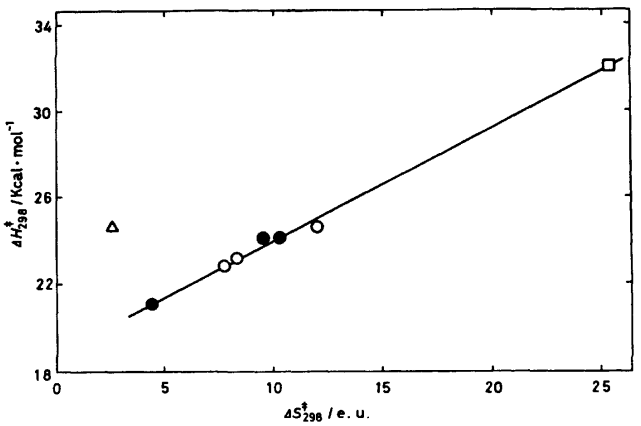

Fig. 3. Isokinetic relationship for the decarboxylation of 1 in various microenvironments, water (□), CTAC reversed micelles (○), CTAB reversed micelles (●), and AOT reversed micelle (△).

In Table 2, thermodynamic parameters of activation for the decarboxylation of 1 in reversed micelles are listed along with those in bulk aqueous solution previously reported by Kemp and Paul.[22] Its isokinetic relationship is given in Fig. 3. Except for the AOT reversed micelle, a good linear relation was obtained with the isokinetic temperature β=517 K. This means that under the reaction conditions adopted (at 298 K) the reaction is controlled enthalpically. Figure 3 supports the above argument that the low catalytic efficiency of the AOT reversed micelle in this reaction may be derived from the destabilization of the anionic transition state with the electrostatic repulsion brought about by the negative surface charge of the micellar core (ΔH^*-control). This negative effect might exceed the rate acceleration effects by the decreased polarity (ΔH^*-control) and the increased internal strain of the substrate molecule in the highly restricted reaction field (ΔS^*-

control). In any event, it is clear that in the specific and restricted reaction field as provided by reversed micelles the reaction rate is controlled simultaneously by plural factors.

Authors are grateful to Professors Toyoki Kunitake (Kyushu University) and Seiji Shinkai (Nagasaki University) for their fruitful discussion. We also thank Mr. Ichiro Miwa for his measurement of the fluorescence depolarization. This work was supported by Grants-in-Aid (No. 447068 and 56550594) for Scientific Research from the Ministry of Education, Science and Culture.

References

1) J. Sunamoto, "Solution Behavior of Surfactants: Theoretical and Applied Aspects," ed by K. L. Mittal and E. J. Fendler, Plenum Press, New York (1982), Vol. 2, p. 767.
2) J. Sunamoto and T. Hamada, "Fundamental Research in Homogeneous Catalysis," ed by M. Tsutsui, Plenum Press, New York (1978), Vol. 3, p. 809.
3) J. Sunamoto and D. Horiguchi, *Nippon Kagaku Kaishi*, **1980**, 475.
4) H. Kondo, H. Yoshinaga, and J. Sunamoto, *Chem. Lett.*, **1980**, 973.
5) J. Sunamoto, K. Iwamoto, M. Akutagawa, M. Nagase, and H. Kondo, *J. Am. Chem. Soc.*, **104**, 4904 (1982); J. Sunamoto, H. Kondo, J. Kikuchi, H. Yoshinaga, and S. Takei, *J. Org. Chem.*, **48**, (1983) in press.
6) J. Sunamoto and T. Hamada, *Bull. Chem. Soc. Jpn.*, **51**, 3130 (1978).
7) J. Sunamoto, T. Hamada, T. Seto, and S. Yamamoto, *Bull. Chem. Soc. Jpn.*, **53**, 583 (1980).
8) H. Kondo, T. Hamada, S. Yamamoto, and J. Sunamoto *Chem. Lett.*, **1980**, 809.
9) J. Sunamoto, H. Kondo, T. Hamada, S. Yamamoto, Y. Matsuda, and Y. Murakami, *Inorg. Chem.*, **19**, 3668 (1980).
10) H. Kondo, I. Miwa, and J. Sunamoto, *J. Phys. Chem.*, **86**, 4826 (1982).
11) F. M. Menger and G. Saito, *J. Am. Chem. Soc.*, **100**, 4376 (1978).
12) M. Wong, J. K. Thomas, and M. Grätzel, *J. Am. Chem. Soc.*, **98**, 2391 (1976).
13) M. Wong, J. K. Thomas, and T. Nowak, *J. Am. Chem. Soc.*, **99**, 4730 (1977).
14) F. M. Menger, G. Saito, G. V. Sanzero, and J. R. Dodd, *J. Am. Chem. Soc.*, **97**, 909 (1975).
15) J. Sunamoto, H. Kondo, and K. Akimaru, *Chem. Lett.*, **1978**, 821.
16) C. J. O'Connor, E. J. Fendler, and J. H. Fendler, *J. Am. Chem. Soc.*, **95**, 600 (1973).
17) C. J. O'Connor, E. J. Fendler, and J. H. Fendler, *J. Chem. Soc., Dalton Trans. 1*, **1974**, 625.
18) J. H. Fendler, F. Nome, and H. C. van Woert, *J. Am. Chem. Soc.*, **96**, 6745 (1974).
19) I. V. Berezin, K. Martinek, and A. K. Yatsimirski, *Russ. Chem. Rev. (Engl. Transl.)*, **42**, 787 (1973).
20) T. S. Straub and M. L. Bender, *J. Am. Chem. Soc.*, **94**, 8875 (1972).
21) D. S. Kemp and K. G. Paul, *J. Am. Chem. Soc.*, **92**, 2553 (1970).
22) D. S. Kemp and K. G. Paul, *J. Am. Chem. Soc.*, **97**, 7305 (1975).
23) D. S. Kemp, D. D. Cox, and K. G. Paul, *J. Am. Chem. Soc.*, **97**, 7312 (1975).
24) W. Borsche, *Ber.*, **42**, 1310 (1909).
25) H. Lindemann and H. Cissee, *Justus Liebigs Ann. Chem.*, **469**, 44 (1929).
26) A. A. Frost and R. G. Pearson, "Kinetics and Mechanism," John Wiley and Sons, Inc., New York (1961), p. 49.
27) T. Kunitake, S. Shinkai, and S. Hirotsu, *J. Org. Chem.*, **42**, 306 (1977).
28) C. A. Bunton and M. J. Minch, *Tetrahedron Lett.*, **1970**, 3881.
29) C. A. Bunton, M. J. Minch, J. Hidalgo, and L. Sepulveda, *J. Am. Chem. Soc.*, **95**, 3262 (1973).
30) C. A. Bunton, M. J. Minchi, and L. Sepulveda, *J. Phys. Chem.*, **75**, 2707 (1971).
31) J. Suh, I. S. Scarpa, and I. M. Klotz, *J. Am. Chem. Soc.*, **98**, 7060 (1976).
32) J. Suh and I. M. Klotz, *Bioorg. Chem.*, **8**, 283 (1979).
33) J. Smid, S. Shah, L. Wong, and J. Hurley, *J. Am. Chem. Soc.*, **97**, 5932 (1975).
34) S. Shah and J. Smid, *J. Am. Chem. Soc.*, **100**, 1426 (1978).
35) T. Kunitake, Y. Okahata, R. Ando, S. Shinkai, and S. Hirakawa, *J. Am. Chem. Soc.*, **102**, 7877 (1980).
36) K. Kon-no and A. Kitahara, *J. Colloid Interface Sci.*, **35**, 636 (1971).

 © 1983 The Chemical Society of Japan Bull. Chem. Soc. Jpn., 56, 2473—2475 (1983)

A Facile One-pot Synthesis of Hydroxy-substituted Crown Ethers

Isao IKEDA, Tetsuya KATAYAMA, Kikuo TSUCHIYA, and Mitsuo OKAHARA*

Department of Applied Chemistry, Faculty of Engineering, Osaka University, Yamadaoka 2-1, Suita, Osaka 565

(Received February 7, 1983)

Hydroxy-substituted crown ethers were prepared in one-pot synthesis by treatment of oligoethylene glycols with epichlorohydrin in the presence of alkali metals, alkali metal hydride or alkali metal hydroxides. The stability constants of complexes with sodium and potassium cations in methanol were determined.

Crown compounds having a functional group are useful for designing phase transfer catalysts, ion-selective electrodes, ion carriers or polymer supported crown compounds. Hydroxy-functionalized derivatives have recently attracted attention as one of the most promising intermediates for these purposes, and various syntheses[1-9] and applications[10-14] have been reported.

We now describe a facile one-pot synthesis of hydroxy-substituted 13-, 16-, and 19-crown ethers using epichlorohydrin and oligoethylene glycols, which are industrially available inexpensive raw materials. Although one of these crown ethers has already been prepared by Tomoi *et al.*[4] *via* several steps starting from 3-chloro-2-chloromethyl-1-propene, the improvement in preparation procedure should enhance the usefulness of these unique functional compounds. Furthermore, some trials to synthesize hydroxy crown ethers using epichlorohydrin were reported,[1,2,8] but in these cases this material was restrictively used as a coupling agent for two phenolic hydroxyl groups in a multi-step synthesis.

Results and Discussion

The reaction of oligoethylene glycols (**1**) with epichlorohydrin in the presence of base may afford oligoethylene glycol monoglycidyl ethers (**2**), which may successively cyclize to the hydroxy-substituted crown ethers (**3**) and/or (**4**) by the intramolecular attack of the alkoxide anion to the epoxy ring, as shown in the Scheme.

In practice, the reaction product showed only one peak in the expected region of the gas chromatogram. In order to confirm their formation, the possible compounds **3** and **4** were synthesized by alternative methods. The authentic compound **3b** were prepared by the coupling reaction of 2-benzyloxy-1,3-propanediol[15] and tetraethylene glycol ditosylate, and **4a**—**c** by the reported method,[7] followed by debenzylation.

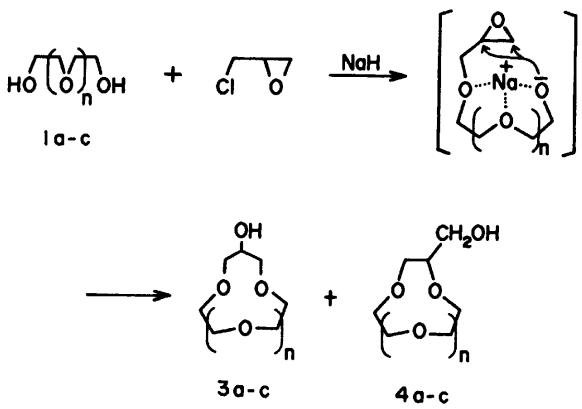

a, $n=2$ *b*, $n=3$ *c*, $n=4$

Scheme. Probable pathway of the reaction.

From GLC analysis, only **3b** was confirmed to be formed and **4b** could not be detected in the reaction product (Shimadzu GC-4CPT, Silicone OV-1 on Uniport KS 60—80 mesh, 1 m, started from 100 °C, 20 °C/min, retention time; **3b**, 4.5 min; **4b**, 4.8 min). The isolated product was characterized by spectral and elemental analyses. For the purpose of further confir-

Table 1. Spectra of hydroxy-substituted crown ethers and their acetates

Crown ether	IR ($\tilde{\nu}$/cm^{-1})	MS (*m/e*)	NMR (CCl_4, δ)
3a	1120, 3400	206(M^+), 188(M^+-H_2O), 163($M^+-C_2H_3O$)	2.75(s, 1H), 3.40—3.80(m, 17H)
5a (Acetate of **3a**)	1120, 1235, 1735	249(M^++1), 247(M^+-1), 188(M^+-CH_3COOH)	2.00(s, 3H), 3.60—3.80 (d+m, 16H), 4.96(quint, 1H)
3b	1120, 3400	250(M^+), 232(M^+-H_2O), 203($M^+-C_2H_3O$)	2.75(s, 1H), 3.40—3.80 (m, 21H)
5b (Acetate of **3b**)	1120, 1235, 1730	293(M^+-1), 232(M^+-CH_3COOH)	2.00(s, 3H), 3.50—3.80(d+m, 20H), 4.92 (quint, 1H)
3c	1120, 3400	294(M^+), 276(M^+-H_2O), 251($M^+-C_2H_3O$)	2.75(s, 1H), 3.40—3.80(m, 25H)
5c (Acetate of **3c**)	1120, 1235, 1730	337(M^++1), 335(M^+-1), 276(M^+-CH_3COOH)	2.00(s, 3H), 3.50—3.80(d+m, 24H), 4.96 (quint, 1H)

TABLE 2. THE REACTION CONDITIONS AND THE YIELDS OF **3**

Crown ether[a]	Base	(mol)	**1** (mol)	Ech[b] (mol)	Reaction temp/°C	Reaction time/h	Yield[d] %
3a	LiOH	0.10	0.02	0.02	Reflux[c]	20	40
	Li	0.04	0.024	0.02	Reflux[c]	20	23, 16[e]
3b	NaH	0.004	0.002	0.002	60	3	55, 31[e]
	NaOH	0.10	0.02	0.02	Reflux[c]	2	35
	Na	0.04	0.024	0.02	Reflux[c]	2	54
	Na	0.04	0.024	0.02	Reflux[c]	20	69
	K	0.04	0.024	0.02	Reflux[c]	2	14
3c	KOH	0.10	0.02	0.02	Reflux[c]	2	28
	K	0.0021	0.002	0.002	60	20	42[e,f]

a) Bp: **3a**; 115—120 °C/0.05 Torr, **3b**; 128—135 °C/0.02 Torr, 150 °C/0.05 Torr (Kugelrohr distillation), **3c**; 185 °C/0.04 Torr (Kugelrohr distillation). b) Epichlorohydrin. c) Dioxane was used as the solvent. d) Calculated by GLC. e) Isolated. f) KBF_4 (0.002 mol) was added in the reaction system.

mation, the product was acetylated by treatment with acetic anhydride in pyridine.

From the reactions between epichlorohydrin and tri- and pentaethylene glycol, hydroxy-13-crown-4 (**3a**, $n=2$), and hydroxy-19-crown-6 (**3c**, $n=4$) were obtained. No detectable amount of **4a** nor **4c** could be observed in any run by GLC (the same conditions as for **3b**, retention time; **3a**, 3.0 min; **4a**, 3.3 min; **3c**, 5.8 min; **4c**, 6.1 min). Spectral data of the products and their acetates are summarized in Table 1.

In the case of the reaction of tetraethylene glycol and epichlorohydrin, sodium hydroxide and metallic sodium also worked well to give the objective crown ether (**3b**), but metallic potassium gave it in a poorer yield. To obtain **3a** and **3c**, metallic lithium and potassium or their hydroxides were used and showed good yields. The reaction conditions and the yields are listed in Table 2.

The fractional distillation afforded the oligoethylene glycol-free **3**, but it is usually difficult to remove a small amount of contaminates, mainly oligoethylene glycols, from the objective compounds by Kugelrohr distillation, which is convenient in a small scale preparation. The compounds **3**, however, could be freed of the last traces of oligoethylene glycols by either of following methods: a) passing through an ion-exchange resin (metal form) column, or b) extracting from the aqueous solution with chloroform. In the case of hydroxy-16-crown-5 (**3b**), the pyrolysis of $MgBr_2$·complex also afforded the purified compound.

In order to verify the complexing property of **3**, the stability constants of the complexes with sodium and potassium cations in methanol were measured,[16] and are summarized in Table 3. The complexing ability of **3a** with both cations was too low to give reliable stability constant values. Compounds **3b** and **3c**, however, showed the good and rather selective complexing ability toward sodium and potassium cations.

TABLE 3. STABILITY CONSTANTS OF **3b** AND **3c** COMPLEXES

Crown ether	log K'[a]	
	Sodium cation	Potassium cation
3b	3.03 ± 0.01	2.53 ± 0.005
3c	2.62 ± 0.03	4.03 ± 0.03

a) Crown ether + $M^+ \overset{K'_1}{\rightleftarrows}$ (Crown ether·M)$^+$ In methanol, 25 °C. Values with the standard deviation at the 95% confidence level.

Experimental

The ^{1}H-NMR spectra were taken at 100 MHz on a JEOL JNM-PS-100 spectrometer using the tetramethylsilane internal standard. The infrared spectra were obtained on a Hitachi-260-10 spectrometer. The mass spectra were taken at an ionization potential of 70 eV on a Hitachi RMU-6E mass spectrometer.

Preparation of Hydroxy-16-crown-5 (3b). As a typical procedure for the preparation of **3**: tetraethylene glycol (**1b**, $n=3$, 3.9 g, 0.002 mol) was added dropwise to a suspension of sodium hydride (50% oil suspension, 2.0 g, 0.004 mol, washed with dioxane by decantation) in dioxane (50 ml). After the evolution of hydrogen gas had ceased, epichlorohydrin (1.9 g, 0.002 mol) was added in one quantity and the mixture was stirred for 1 h during which time the temperature was carefully regulated not to exceed 40 °C. Then the mixture was heated to 60 °C and was stirred for an additional 3 h at this temperature. The reaction mixture was neutralized with hydrochloric acid (1 : 1 ethanol), filtered and washed with dichloromethane. The solvent was removed from the filtrate combined with washings and the resultant viscous material was washed with hexane to give 4.5 g of the crude product. The hydroxy-substituted crown ether (**3b**) was obtained as a pale yellow oil by distilling a portion of the crude product (2.72 g) on a Kugelrohr distillation apparatus. Yield, 0.95 g (31%, 55% by GLC analysis).

Purification of 3b by an Ion-exchange Resin Column. Amberlite CG-120 (Type 1, Na form, 30 g) was washed 3 times with a plenty of water, and then 3 times with acetone. A little contaminated distillate (0.5 g) of **3b** dissolved in acetone was charged into the column packed with this washed resin, and eluted with 200 ml of acetone. Evaporation of the solvent afforded 0.38 g of oligoethylene glycol-free **3b**, checked by GLC.

Preparation and Pyrolysis of $MgBr_2$·Complex of 3b. The acetone solution of **3b** contaminated with a small amount of **2b** was added to acetone saturated with $MgBr_2 \cdot 6H_2O$ under stirring. White precipitates which appeared immediately were collected by filtration, washed with acetone repeatedly, and dried under reduced pressure. The white solid was heated to 200 °C in a Kugelrohr distillation apparatus at

0.015 Torr (1 Torr=133.322 Pa) to release purified **3b**, which was checked to be free of **2b** by GLC.

Synthesis of Authentic 3b. Although the synthesis of **3b** was reported,[6] from the point of availability of the starting material, an alternative method was employed to obtain the authentic compound. The starting material 2-benzyloxy-1,3-propanediol (137—140 °C/0.004 Torr, Kugelrohr distillation) was obtained by hydrolysis of *cis*-5-benzyloxy-2-phenyl-1,3-dioxane (mp 79.0—80.0 °C), which was prepared by benzylation of *cis*-2-phenyl-1,3-dioxan-5-ol (mp 84.5—85.5 °C).[15] 2-Benzyloxy-1,3-propanediol (1.8 g, 0.01 mol) was added to *t*-butyl alcohol (30 ml) containing 0.02 mol of *t*-BuONa at 60 °C under stirring. To the resulting solution was added dropwise a solution of tetraethylene glycol ditosylate (5.0 g, 0.01 mol)[17] in *t*-butyl alcohol (20 ml), and the mixture was stirred for 2 h at 60 °C. After the removal of solid salt by filtration, the *t*-butyl alcohol was evaporated off under reduced pressure to leave a viscous oil (3.5 g). An aliquot of the oil (1.6 g) was fractionated by Kugelrohr distillation. The distillate of 150 °C/0.05 Torr (0.48 g, 31%) was hydrogenated with hydrogen gas in the presence of Pd/C and *p*-toluenesulfonic acid.[7] After the work-up, the viscous oil was fractionated by Kugelrohr distillation to give a pale yellow oil (0.23 g, bp 150 °C/0.1 Torr, Kugelrohr distillation). This fraction showed the same GLC retention time and spectral data as those of **3b** shown in Table 1.

References

1) J. Ashby, R. Hull, M. J. Cooper, and E. M. Ramage, *Synth. Commun.*, **4**, 113 (1974).
2) D. G. Parsons, *J. Chem. Soc., Perkin Trans. 1*, **1978**, 451.
3) J. S. Bradshaw, R. A. Reeder, M. D. Thompson, E. D. Flanders, R. L. Carruth, R. M. Izatt, and J. J. Christensen, *J. Org. Chem.*, **41**, 134 (1976).
4) M. Tomoi, O. Abe, M. Ikeda, K. Kihara, and H. Kakiuchi, *Tetrahedron Lett.*, **1978**, 3031.
5) F. Montanari and P. Tundo, *Tetrahedron Lett.*, **1979**, 5055.
6) B. Czech, *Tetrahedron Lett.*, **21**, 4197 (1980).
7) I. Ikeda, S. Yamamura, Y. Nakatsuji, and M. Okahara, *J. Org. Chem.*, **45**, 5355 (1980).
8) G. S. Heo, R. A. Bartsch, L. L. Schlobohm, and J. G. Lee, *J. Org. Chem.*, **46**, 3574 (1981).
9) T. Miyazaki, S. Yanagida, A. Itoh, and M. Okahara, *Bull. Chem. Soc. Jpn.*, **55**, 2005 (1982).
10) I. Ikeda, T. Katayama, M. Okahara, and T. Shono, *Tetrahedron Lett.*, **22**, 3615 (1981).
11) T. Shono, M. Okahara, I. Ikeda, K. Kimura, and H. Tamura, *J. Electroanal. Chem.*, **132**, 99 (1982).
12) K. Fukunishi, B. Czeck, and S. L. Regen, *J. Org. Chem.*, **46**, 1218 (1981).
13) F. Montanari and P. Tundo, *J. Org. Chem.*, **47**, 1298 (1982).
14) J. M. Harris, N. H. Hundley, T. G. Shannon, and E. C. Struck, *J. Org. Chem.*, **47**, 4789 (1982).
15) N. Baggett, J. S. Brimacombe, A. B. Foster, M. Stacey, and D. H. Whiffen, *J. Chem. Soc.*, **1960**, 2574.
16) H. K. Frensdorff, *J. Am. Chem. Soc.*, **93**, 600 (1971).
17) J. Dale and P. O. Kristiansen, *Acta Chem. Scand.*, **26**, 1471 (1972).

Studies on the β-Turn of Peptides. IV.[1] Effect of the Chain Length on the CD Spectra of *N*-(2,4-Dinitrophenyl)-(Gly)$_n$-D-Ala-L-Pro-(Gly)$_n$ *p*-Nitroanilides (n=1—3)

Kazuki SATO,* Noriko TAKI, Ukon NAGAI, and Tsutomu HIGASHIJIMA†

Mitsubishi-Kasei Institute of Life Sciences, Minamiooya, Machida, Tokyo 194

†*Department of Biophysics and Biochemistry, Faculty of Science, The University of Tokyo, Bunkyo-ku, Tokyo 113*

(Received March 25, 1983)

N-(2,4-Dinitrophenyl)-(Gly)$_n$-D-Ala-L-Pro-(Gly)$_n$ *p*-nitroanilides (**7b**, n=2; **7c**, n=3) were synthesized in order to study the effect of chain length on their conformations. The CD spectra of both **7b** and **7c** showed similar patterns to that of **7a** (n=1), but their Cotton effects were much weaker. Therefore, both compounds seem still to have some populations of folded conformers because their Cotton effects near 350 nm were significantly larger than those of the tetrapeptide derivatives in random conformation. However, the population of the folded conformers must be quite small.

In the previous paper, we gave an outline of a new method to study the β-turn conformation of linear tetrapeptides.[2] *N*-(2,4-Dinitrophenyl)tetrapeptide *p*-nitroanilides (Dnp-tetrapeptide-pNA's)[3] exhibit characteristic CD spectra above 250 nm when they take β-turn conformations. The Cotton effects are considered to be due to exciton coupling of the transition moments in the two terminal chromophores. The magnitudes of the Cotton effects near 350 nm and 310 nm were shown to reflect well the β-turn preference of the tetrapeptides.

In this paper, we attempted to apply the method to larger peptides than tetrapeptides. CD spectrum of Dnp-Gly-D-Ala-L-Pro-Gly-pNA (**7a**) is known to show large Cotton effects at 350 nm and 310 nm, indicating that it takes β-turn conformation to a high extent.[2] So, in this work, two compounds with a general structure Dnp-(Gly)$_n$-D-Ala-L-Pro-(Gly)$_n$-pNA (**7b**, n=2; **7c**, n=3) were synthesized to study the effect of chain length on the CD spectra. If **7b** and **7c** also have high population of folded conformers with a β-turn at the D-Ala-L-Pro sequence, large Cotton effects are expected to be observed due to the approach of the Dnp and pNA chromophores (Fig. 1).

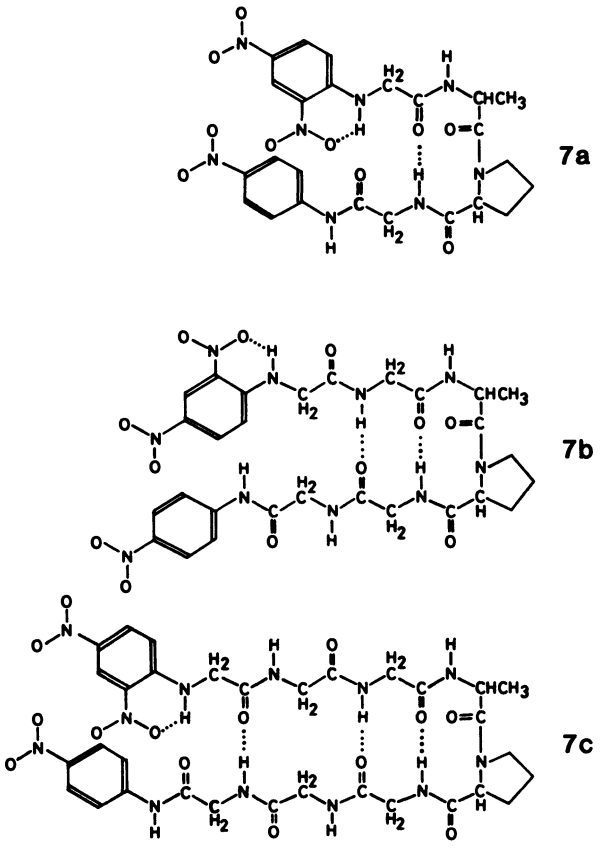

Fig. 1. Models of folded (β-sheet) conformers with a β turn at D-Ala-L-Pro sequence of Dnp-(Gly)-D-Ala-L-Pro-(Gly)$_n$-pNA (**7a**—**c**).

Results and Discussion

Syntheses of Peptides. Compounds **7b** and **7c** were synthesized by a similar manner to that described previously for **7a** (Fig. 2).[4] Boc-D-Ala-L-Pro-OH[5] and H-(Gly)$_2$-pNA·HCl (**2b**·HCl)[1] were coupled by EDC method to afford Boc-D-Ala-L-Pro-(Gly)$_2$-pNA (**3b**), which was treated with hydrogen chloride in formic acid. H-D-Ala-L-Pro-(Gly)$_2$-pNA·HCl (**4b**·HCl) obtained was coupled with Boc-(Gly)$_2$-OH[6] to afford Boc-(Gly)$_2$-D-Ala-L-Pro-(Gly)$_2$-pNA (**5b**), which was converted to the Dnp derivative, Dnp-(Gly)$_2$-D-Ala-L-Pro-(Gly)$_2$-pNA (**7b**), by deprotection and subsequent treatment with 1-fluoro-2,4-dinitrobenzene. Synthesis of **7c** was carried out similarly. Homogeneities of the peptides synthesized were confirmed by thin-layer chromatography and elemental analyses.

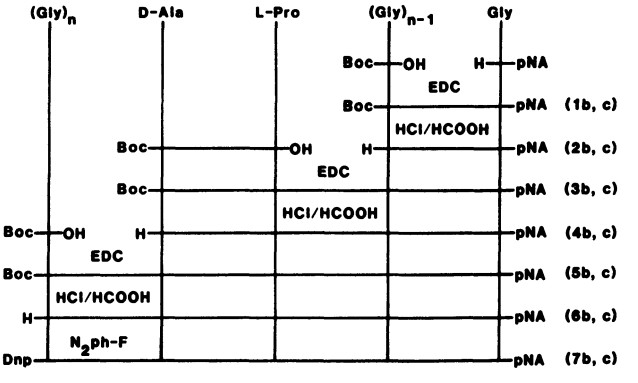

Fig. 2. Syntheses of Dnp-(Gly)$_n$-D-Ala-L-Pro-(Gly)$_n$-pNA (n=2, 3).

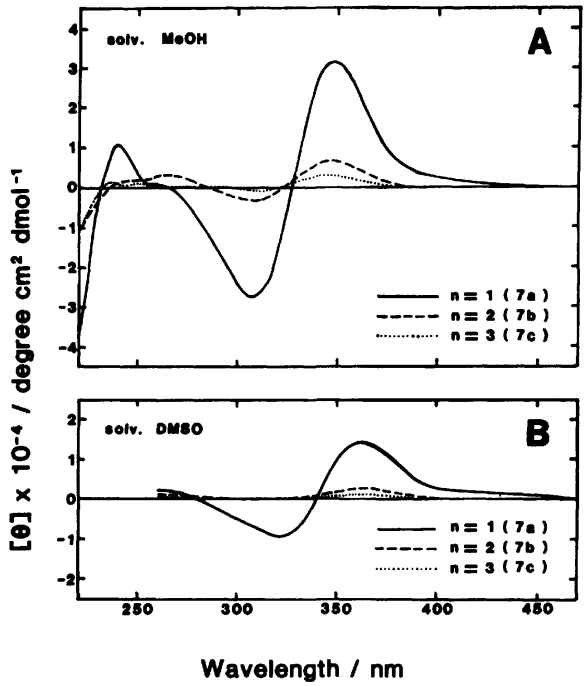

Fig. 3. CD spectra of Dnp–$(Gly)_n$–D-Ala–L-Pro–$(Gly)_n$–pNA (n=1—3).

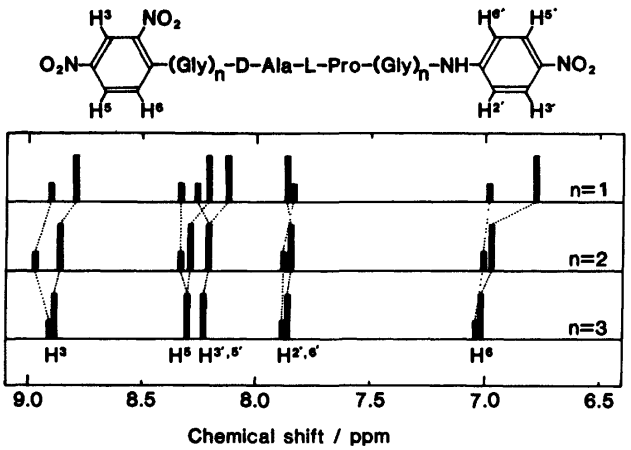

Fig. 4. Chemical shifts of aromatic protons of Dnp–$(Gly)_n$–D-Ala–L-Pro–$(Gly)_n$–pNA (n=1—3) in DMSO-d_6 at 23 °C. The large and the small bars show the major and the minor conformers with *trans* and *cis* D-Ala–L-Pro bonds, respectively.

CD Spectra Due to the Interaction between Dnp and pNA Chromophores. CD spectra of **7b** and **7c** measured in MeOH solution are represented in Fig. 3A together with that of **7a**. Both showed a similar pattern to that of **7a**, but the magnitudes were much smaller than that of **7a**. Between the two, **7b** showed a little larger Cotton effects than **7c**. Figure 3B represents the spectra measured in DMSO solution, and both showed similar spectra but of weaker strength than those in MeOH. Decrease of Cotton effects was observed also in **7a**, but the relative strengths of Cotton effects of **7b** and **7c** to those of **7a** were not so much affected by the change of solvents. Such decrease of Cotton effects as mentioned above suggested that the populations of β-turn conformer of **7a**—**c** decreased in DMSO solution as compared with those in MeOH solution, since it had been ascertained that the solvent dependence of Cotton effects were in good accordance with that of the populations of β-turn conformers using a model peptide (Dnp–L-Leu–D-Ala–L-Pro–L-Val–pNA) related to the β-turn part of gramicidin S,[2] which showed larger Cotton effects in MeOH solution than in DMSO solution as well as **7a**—**c**. MeOH is considered to be suitable for β-turn conformation of hexa- or octapeptides as well as for those of tetrapeptides. UV absorption spectra of **7a**—**c** showed maxima at 326 nm in MeOH solution and at 343 nm in DMSO solution as well as those of other peptides reported previously.[2,4] This red-shift of UV maxima corresponded well to that of CD maxima as expected from the fact that the CD spectra of Dnp–peptide–pNA's were considered to be due to the exciton coupling of the transition moments in two terminal chromophores. These results indicated that there was still a little interaction between the two terminal chromophores of **7b** and **7c**, and that they contained some populations of folded conformers, because, in the case of Dnp–L-Leu–L-Ala–L-Pro–L-Val–pNA and other tetrapeptide derivatives which take random conformation, no CD bands are observed near 350 nm. From comparison of the CD spectra, **7b** is considered to have a little higher population of β-turn conformers than **7c**, and the population was higher in MeOH solution than in DMSO.

Higher-field Shifts of Aromatic Proton Chemical Shifts Due to the Ring-current Effects. ^{1}H NMR spectra of **7a**—**c** were measured in DMSO-d_6 solution. All the spectra showed two sets of resonances for most of the protons due to *cis-trans* isomerism for the D-Ala–L-Pro bonds. In all the peptides, the populations of *trans* isomers were estimated to about 70% according to the relative peak area of the same proton. Figure 4 shows that aromatic protons of the *trans* isomer in **7a** were shifted apparently to higher field than those of the *cis* isomer because of ring-current effects, indicating the proximity of the two terminal chromophores. The *trans* isomers of **7b** and **7c** also showed similar higher-field shifts, but the shifts were much smaller than that of **7a**. Between the two, **7b** showed a little higher shift than **7c**. The *cis* isomers of **7a**—**c** are considered to take unordered conformations and consequently to have little contribution to the CD spectra of **7a**—**c**, since they showed similar chemical shifts of aromatic and some other protons for the three compounds irrespective of the chain length. In contrast, the *trans* conformers of **7a**—**c** showed large chain-length dependences of chemical shifts for many of the protons, indicating that their *trans* conformations depended on chain length. The *trans* isomers of **7b** and **7c** are considered still to have a little population of folded conformers which cause proximities of the two terminal chromophores. Between the two, **7b** is considered to have a little higher population of folded conformers than **7c**.

Intramolecular Hydrogen Bondings and β-Turn Conformations. Temperature dependences of chemical shifts of amide proton resonances are useful for distinguishing between "exposed" and "intramolecularly hydrogen-

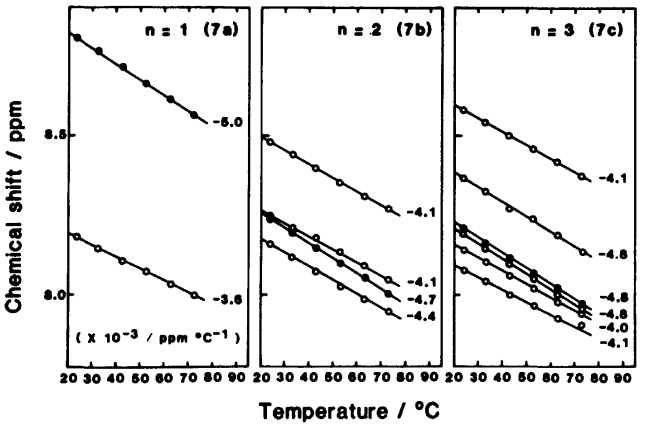

Fig. 5. Temperature dependences of chemical shifts of N^aH protons in major conformer of Dnp-$(Gly)_n$-D-Ala-L-Pro-$(Gly)_n$-pNA (n=1—3) in DMSO-d_6. The Gly^1-NH protons are omitted. ●: D-Ala-NH, ○: Gly-NH.

bonded" amide proton;[7] exposed protons exhibited larger temperature dependences than hydrogen-bonded amide protons. The temperature dependences of the chemical shifts of NH protons of **7a**—**c** were studied in DMSO-d_6 solution. Figure 5 shows the results for NH protons of the *trans* isomers in **7a**—**c**, where Gly^1-NH protons were omitted because they were not amide protons and also exhibited constantly small temperature dependence due to hydrogen bonding with the *o*-nitro group in the Dnp chromophore. The Gly^4-NH proton in **7a** showed smaller temperature dependences than the D-Ala^2-NH proton, indicating the presence of β-turn conformer with 4→1 hydrogen bond concerned by the Gly^4-NH proton as shown in Fig. 1. In the case of **7b** and **7c**, the differences in temperature dependences of Gly-NH protons and D-Ala-NH proton were quite small, but still a little differences were observed; the D-Ala-NH proton always showed the largest temperature dependence of all the NH protons, and the numbers of the Gly-NH protons with smaller dependences (-4.0——-4.1×10^{-3} ppm $°C^{-1}$) were in good accordance with the numbers of the Gly-NH protons involved in hydrogen bonding in the models of folded conformers of **7b** and **7c** shown in Fig. 1. These results suggested that both **7b** and **7c** had a little population of folded conformers, though they were quite lower levels as compared with that of **7a**. The Gly^4-NH proton of *cis* isomer in **7a**, which separated well from other resonances, showed large temperature dependence (-5.2×10^{-3} ppm $°C^{-1}$) as well as that of the D-Ala^2-NH proton (-5.3×10^{-3} ppm $°C^{-1}$), indicating that the *cis* isomer of **7a** took unordered conformation as described in the preceding section. In the case of **7b** and **7c**, the NMR spectra were too complex to study the temperature dependences of all the NH protons of minor (*cis*) isomers. Most of the protons other than amide ones of **7a**—**c** showed little temperature dependences, suggesting that the conformations of **7a**—**c** did not change significantly in the temperature range of these experiments.

Correlation between CD Spectra and β-Turn Conformations. The characteristic CD spectra of Dnp-peptide-pNA's are considered to be due to the exciton coupling of the transition moments in the two terminal chromophores. The relative strength of Cotton effects of **7a**—**c** shown in Fig. 3 were in good accordance with the populations of β-turn conformers in **7a**—**c** estimated from NMR measurements. All of the results with both CD and NMR spectra indicate that the interaction between the two chromophores decreases rapidly as length of the peptide chain increases, however, some populations of β-turn conformers are considered still to be present in both compounds (**7b** and **7c**) examined. Between the two, **7b** is considered to have a little higher population of β-turn conformers than **7c**.

Experimental

Syntheses of Peptides. All the melting points were measured on a Yanagimoto micro melting point apparatus and were uncorrected. TLC's were carried out on Merck silica gel 60 F_{254} plates with the following solvent systems: R_f^1, $CHCl_3$-MeOH (5 : 1, v/v); R_f^2, $CHCl_3$-MeOH-AcOH (95 : 5 : 1, v/v); R_f^3, *n*-BuOH-AcOH-pyridine-H_2O (4 : 1 : 1 : 2, v/v). Optical rotations were measured on an Union automatic polarimeter PM-201.

Boc-(Gly_3)-pNA (1c). To a chilled solution of Boc-$(Gly)_2$-OH[6] (465 mg, 2 mmol) and H-Gly-pNA (390 mg, 2 mmol) in DMF (8 ml) was added EDC·HCl (383 mg, 2 mmol). The mixture was stirred at 0 °C for 1 h and at room temperature overnight and evaporated *in vacuo*. Addition of water to the residue gave a solid, which was collected by filtration and washed successively with 10% citric acid, 4% $NaHCO_3$, and water. After being dried *in vacuo* over P_2O_5, the product was recrystallized from DMF-ether; yield, 562 mg (69%), mp 235—237 °C; R_f^1 0.44, R_f^2 0.10, R_f^3 0.75.

Found: C, 49.93; H, 5.71; N, 17.11%. Calcd for $C_{17}H_{23}O_7N_5$: C, 49.87; H, 5.66; N, 17.11%.

H-$(Gly)_3$-pNA·HCl (2c·HCl). Compound **1c** (491 mg, 1.2 mmol) was dissolved in 0.1 M (1 M=1 mol dm^{-3}) hydrogen chloride in formic acid (18 ml). The solution was allowed to stand at room temperature for 30 min and evaporated to leave an oil, which was crystallized by addition of ether; yield, 426 mg (100%); mp 238—240 °C; R_f^3 0.51.

Found: C, 41.47; H, 4.74; N, 20.17%. Calcd for $C_{12}H_{16}O_5N_5Cl$: C, 41.68; H, 4.66; N, 20.26%.

Boc-D-Ala-L-Pro-$(Gly)_2$-pNA (3b). To a chilled solution of Boc-D-Ala-L-Pro-OH[5] (287 mg, 1 mmol), H-$(Gly)_2$-pNA·HCl[1] (289 mg, 1 mmol), and TEA (0.14 ml, 1 mmol) in DMF (6 ml) was added EDC·HCl (192 mg, 1 mmol), and the mixture was stirred at 0 °C for 1 h and at room temperature overnight and evaporated. The residue was dissolved in EtOAc, and the solution was washed successively with 10% citric acid, 4% $NaHCO_3$, and water, dried (Na_2SO_4), and evaporated. The residue was solidified by addition of ether. The crude product dissolved in MeOH (2 ml) was applied to a column (3×170 cm) of Sephadex LH-20 and eluted with MeOH. The fractions containing the desired product detected with UV absorption and TLC were collected and evaporated, and the residue was solidified by addition of ether and recrystallized from EtOH-ether; yield, 215 mg (42%); mp 197—200 °C; $[\alpha]_D^{22}$ −2.1° (*c* 1, MeOH); R_f^1 0.77, R_f^2 0.28, R_f^3 0.75.

Found: C, 52.96; H, 5.88; N, 16.39%. Calcd for $C_{23}H_{32}O_8N_6$: C, 53.07; H, 6.20; N, 16.15%.

Boc-D-Ala-L-Pro-$(Gly)_3$-pNA (3c). This compound

was prepared from Boc-D-Ala-L-Pro-OH[5] (287 mg, 1 mmol) and **1c**·HCl (346 mg, 1 mmol) as described for **3b**; yield, 284 mg (48%); mp 112—115 °C; $[\alpha]_D^{22}$ +5.8° (*c* 1, MeOH); R_f^1 0.63, R_f^2 0.12, R_f^3 0.74.

Found: C, 51.62; H, 6.14; N, 16.77%. Calcd for $C_{25}H_{35}O_9N_7$: C, 51.98; H, 6.11; N, 16.98%.

H-D-Ala-L-Pro-(Gly)$_2$-pNA·HCl (4b·HCl). Compound **3b** (182 mg, 0.35 mmol) was dissolved in 0.1 M hydrogen chloride in formic acid (4.2 ml). The solution was allowed to stand at room temperature for 30 min and evaporated to leave an oil. The product was used for the next reaction without further treatment; the yield was quantitative; R_f^3 0.61.

H-D-Ala-L-Pro-(Gly)$_3$-pNA·HCl (4c·HCl). Compound **3c** (104 mg, 0.18 mmol) was treated with 0.1 M hydrogen chloride in formic acid (2.7 ml) as described for **4b**·HCl. The product was used for the next reaction without further treatment; the yield was quantitative; R_f^3 0.42.

Boc-(Gly)$_2$-D-Ala-L-Pro-(Gly)$_2$-pNA (5b). This compound was prepared from Boc-(Gly)$_2$-OH[6] (81 mg, 0.35 mmol) and **4b**·HCl (134 mg, 0.35 mmol) as described for **3b** except that the column chromatography with Sephadex LH-20 was not used. The crude product was recrystallized from MeOH–ether; yield, 66 mg (30%); mp 133—136 °C; $[\alpha]_D^{22}$ +0.4° (*c* 1, MeOH); R_f^1 0.52, R_f^2 0.03, R_f^3 0.73.

Found: C, 50.13; H, 5.99; N, 17.32%. Calcd for $C_{27}H_{38}O_{10}N_8 \cdot 1/2\ H_2O$: C, 50.38; H, 6.11; N, 17.41%.

Boc-(Gly)$_3$-D-Ala-L-Pro-(Gly)$_2$-pNA (5c). To a chilled solution of Boc-(Gly)$_3$-OH[8] (52 mg, 0.18 mmol), **4c**·HCl (93 mg, 0.18 mmol), and TEA (0.025 ml, 0.18 mmol) in DMF (2 ml) were added DCC (37 mg, 0.18 mmol) and HOBt (49 mg, 0.36 mmol), and the reaction mixture was stirred at 0 °C for 1 h and at room temperature overnight. Insoluble materials were removed by filtration, and the filtrate was evaporated. The residue was dissolved in MeOH (3 ml), applied to a column (3×170 cm) of Sephadex LH-20, and eluted with MeOH. The fractions containing the desired product were collected and evaporated, and the residue was crystallized from EtOH–ether, and collected by filtration. The product dissolved in a mixture (3 ml) of $CHCl_3$–MeOH (5 : 1) was applied to a column (2.5×20 cm) of silica gel 60 (Merck) and eluted with the same solvent. The fractions with the desired product were collected and evaporated, and the residue was crystallized from MeOH–ether; yield, 82 mg (61%); mp 141—143 °C; $[\alpha]_D^{22}$ +11.8° (*c* 1, MeOH); R_f^1 0.17, R_f^3 0.64.

Found: C, 48.71; H, 5.80; N, 18.44%. Calcd for $C_{13}H_{44}O_{12}N_{10} \cdot H_2O$: C, 48.56; H, 6.04; N, 18.27%.

H-(Gly)$_2$-D-Ala-L-Pro-(Gly)$_2$-pNA·HCl (6b·HCl). Compound **5b** (19 mg, 0.03 mmol) was treated with 0.1 M hydrogen chloride in formic acid (0.6 ml) as described for **4b**·HCl. The product was used for the next reaction without further treatment; the yield was quantitative; R_f^3 0.39.

H-(Gly)$_3$-D-Ala-L-Pro-(Gly)$_3$-pNA·HCl (6c·HCl). Compound **5c** (52 mg, 0.07 mmol) was treated with 0.1 M hydrogen chloride in formic acid (0.9 ml) as described for **4b**·HCl. The product was used for the next reaction without further treatment; the yield was quantitative; R_f^3 0.36.

Dnp-(Gly)$_2$-D-Ala-L-Pro-(Gly)$_2$-pNA (7b). To a solution of **6b**·HCl (17 mg, 0.03 mmol) and TEA (0.013 ml, 0.09 mmol) in DMF (1 ml) was added N_2ph–F (11 mg, 0.06 mmol), and the reaction mixture was stirred at room temperature for 3 h and evaporated. The residue dissolved in $CHCl_3$ (5 ml) was applied to a column (1.8×20 cm) of silica gel 60 (Merck), and the column was washed with $CHCl_3$. The product was eluted with the mixture of $CHCl_3$–MeOH (5 : 1, v/v). The fractions containing the desired product were evaporated to leave crystals, which were recrystallized from DMF–ether; yield, 18 mg (86%); mp 145—148 °C; $[\alpha]_D^{22}$ −15.0° (*c* 0.5, DMF); R_f^1 0.46, R_f^2 0.03, R_f^3 0.63.

Found: C, 47.48; H, 4.79; N, 19.46%. Calcd for $C_{28}H_{32}O_{12}N_{10} \cdot 1/2\ H_2O$: C, 47.39; H, 4.69; N, 19.74%.

Dnp-(Gly)$_3$-D-Ala-L-Pro-(Gly)$_3$-pNA (7c). Compound **6c**·HCl (48 mg, 0.07 mmol) was treated with N_2ph–F (26 mg, 0.14 mmol) as described for **7b**; yield, 46 mg (81%); mp 176—178 °C; $[\alpha]_D^{22}$ −1.6° (*c* 0.5, DMF); R_f^1 0.15, R_f^3 0.63.

Found: C, 44.94; H, 4.59; N, 19.72%. Calcd for $C_{32}H_{38}O_{14}N_{12} \cdot 2H_2O$: C, 45.17; H, 4.97; N, 19.76%.

CD Measurements. CD spectra were recorded on a JASCO spectropolarimeter model J-20 or J-40 in a 0.1 mM solution at room temperature (23±2 °C).

^{1}H NMR Measurements. ^{1}H NMR spectra were recorded on a Bruker WH-270 spectrometer equipped with a Nicolet-1180 computer and with a Bruker B-ST-100/700 temperature control unit. The spectra were measured at 23±0.5 °C if not mentioned otherwise. Chemical shifts were measured from the internal standard of DSS.[3] The spectra were assigned by spin-decoupling, H–D exchange, and saturation transfer methods.

The authors wish to express their thanks to Professor Tatsuo Miyazawa of The University of Tokyo for helpful discussion. Thanks are also due to the members of Analytical Department of System Engineering Laboratory, Mitsubishi-Kasei Industries Ltd., for elemental analyses.

References

1) Part III of this series: K. Sato, U. Nagai, and T. Higashijima, *Bull. Chem. Soc. Jpn.*, **56**, 1657 (1983).

2) Part I of this series: K. Sato, M. Kawai, and U. Nagai, *Biopolymers*, **20**, 1921 (1981).

3) The abbreviations used in this paper are those recommended by IUPAC-IUB: *J. Biol. Chem.*, **247**, 977 (1972). Additional abbreviations: Boc, *t*-butoxycarbonyl; Dnp, 2,4-dinitrophenyl; pNA, *p*-nitroanilide; DCC, dicyclohexylcarbodiimide; DSS, sodium 2,2-dimethyl-2-silapentane-5-sulfonate; EDC, 1-ethyl-3-(3-dimethylaminopropyl)carbodiimide; N_2ph–F, 1-fluoro-2,4-dinitrobenzene; TEA, triethylamine; DMF, *N*,*N*-dimethylformamide; DMSO, dimethyl sulfoxide; TLC, thin-layer chromatography.

4) Part II of this series: K. Sato, M. Kawai, and U. Nagai, *Bull. Chem. Soc. Jpn.*, **56**, 1527 (1983).

5) M. Kawai and U. Nagai, *Biopolymers*, **17**, 1549 (1978).

6) H. Kinoshita, K. Inomata, O. Miyano, and H. Kotake, *Bull. Chem. Soc. Jpn.*, **52**, 2619 (1979).

7) M. Ohnishi and D. W. Urry, *Biochem. Biophys. Res. Commun.*, **36**, 194 (1969); K. D. Kopple, M. Ohnishi, and A. Go, *Biochemistry*, **8**, 4087 (1969).

8) K. Channabasavaiah and K. Sivanandaiah, *Int. J. Peptide Protein Res.*, **8**, 323 (1976).

Free Radical Chain Reaction of Allylic Tin Compounds with Organic Halides Involving S_H' Process

Toshihiko MIGITA,* Kazukiyo NAGAI, and Masanori KOSUGI
Department of Chemistry, Faculty of Technology, Gunma University, Kiryu, Gunma 376
(Received March 28, 1983)

Negatively substituted halomethanes were allylated easily by allyltin compounds *via* radical chain reaction involving S_H' process. Aryl, aralkyl, and alkyl halides underwent similar chain reactions only when the tin compound was charged in excessive amounts.

Since stannyl radical has been known to add to a double bond reversibly[1] and to abstract halogen atoms from organic halides,[2] the following radical chain reaction involving S_H' process is expected to proceed.

$$\rangle Sn\cdot + R\text{-}X \longrightarrow \rangle Sn\text{-}X + R\cdot$$

$$R\cdot + CH_2{=}CHCH_2Sn\langle \longrightarrow R\text{-}CH_2CH{=}CH_2 + \rangle Sn\cdot$$

Since the first examples of the chain reaction have been presented in 1973,[3] several applications were carried out with various organic halides.[4,5] In those reports, however, experimental details are frequently not provided. In this study, in order to survey scope and limitation of the chain reaction, various organic halides were subjected to the reaction of allylic tin compounds under ordinary reaction conditions where the radical chain carrier could be produced. As a result, negatively substituted aliphatic halides such as polyhaloalkanes, α-halo esters, and α-halo nitrile were found to be good substrates, whereas aryl, benzyl, and alkyl halides were shown to be poor substrates.

Results and Discussion

Reaction of Radical Generators with Allyltin Compounds. Table 1 shows the products detected in the reaction mixtures which were obtained by decomposing the common radical generators in benzene containing allyltin compounds. With α,α'-azobisisobutyronitrile (AIBN), about 75% of 1-cyano-1-propyl radical can be explained by the products: 50% were captured by allyltin compounds giving 2,2-dimethyl-4-pentenenitrile, and 25% dimerized under these conditions. Although the fate of the stannyl groups is uncertain, the fact suggests capability of AIBN as an initiator of the reaction of the tin compounds with organic halides.

Phenyl radical derived from phenylazotriphenylmethane (PAT) was also found to react with allyltin compounds, giving allylbenzene in 50%. Formation of biphenyl indicates that some of phenyl radical (*ca.* 10%) are consumed by phenylation of the solvent benzene. The product which is expected for S_H' process between triphenylmethyl radical and allyltin compounds was not detected.

Benzoyl peroxide (BPO) reacts with allyltin compounds, giving allyl benzoate and organotin benzoate in good yield. However, these products are explained most reasonably in terms of bimolecular mechanism between BPO and allyltin, instead of S_H' involving benzoxyl radical.[6] The detailed chemistry of the reaction will be shown elsewhere.

Reaction of Allylic Tin Compounds with Negatively Substituted Halomethanes. Reaction of halides such as polyhalomethanes, α-halo carboxylic esters, α-halo ketones, and α-halo nitriles with allyltributyltin was initiated by AIBN and gave the results as shown in in Table 2. Halogen atoms in the organic halides were displaced by an allyl group in moderate yield. In all cases, tributyltin halides were produced in almost quantitatively. In the absence of AIBN the reaction occurred hardly, and the reactants were almost remained unchanged at these temperature, although at much higher temperature considerable conversion was reported to be observed.[4] The presence of galvinoxyl (10 mol%) inhibited the AIBN (3 mol%) induced reaction completely. These facts indicate that the reaction proceeds by a radical chain mechanism.

Table 3 shows the results of the reaction of these halides with crotyltributyltin under similar conditions. Halogen atoms in the substrates were displaced by 1-methyl-2-propenyl group, but not by 2-butenyl group. The observed yields were lower than those in the reaction of allyltin compound. These findings support that the radical derived by abstraction of a halogen atom reacts with allylic tin compounds by a S_H' manner.

Table 1. Reaction of radical generators with allyltin compounds[a]

$R_3SnCH_2CH{=}CH_2$		Generator		Temp	Products			
R	mmol		mmol	°C		mmol		mmol
Me	2.0	AIBN	0.1	80	$Me_2C(CN)CH_2CH{=}CH_2$	0.10	$[Me_2C(CN)\text{-}]_2$	0.02
Bu	5.0	AIBN	0.1	80	$Me_2C(CN)CH_2CH{=}CH_2$	0.10	$[Me_2C(CN)\text{-}]_2$	0.023
Me	2.0	PAT	0.1	60	$PhCH_2CH{=}CH_2$	0.05		
Bu	2.0	PAT	0.1	60	$PhCH_2CH{=}CH_2$	0.05	Ph-Ph	0.01
Me	5.0	BPO	0.25	80	$BzOCH_2CH{=}CH_2$	0.15	$BzOSnMe_3$	0.2
Bu	5.0	BPO	0.25	80	$BzOCH_2CH{=}CH_2$	0.09	$BzOSnBu_3$	0.2

a) Solvent PhH 1 ml.

Table 2. Thermal reaction of allyltributyltin with negatively substituted aliphatic halides[a)]

Halide	mmol	Additives[b)]	mmol			Solvent	ml	Product	mmol
CCl_4	1.1	None				PhH	1	CH_2=$CHCH_2$–CCl_3	Trace
CCl_4	1.1	A	0.03			PhH	1	–CCl_3	0.73
CCl_4	1.1	A	0.03	G	0.1	PhH	1	–CCl_3	Trace
CCl_4	10	None				—		–CCl_3	0.70
$CHCl_3$	1.1	A	0.03			PhH	1	–$CHCl_2$	0.40
$CHCl_3$	1.1	A	0.03	G	0.1	PhH	1	–$CHCl_2$	0
CH_3CCl_3	1.1	A	0.03			PhH	1	–CCl_2CH_3	0.42
CH_3CCl_3	1.1	A	0.03	G	0.1	PhH	1	–CCl_2CH_3	0
$BrCH_2CO_2Me$	1.1	A	0.03			PhH	1	–CH_2CO_2Me	0.60
$ClCH_2CO_2Me$	1.1	A	0.03			PhH	1	–CH_2CO_2Me	0.53
$ClCH_2COCH_3$	1.1	A	0.03			PhH	1	–CH_2COCH_3	0.43
$ClCH_2COPh$	1.1	A	0.03			PhH	1	–CH_2COPh	0.51
$ClCH_2CN$	1.1	A	0.03			PhH	1	–CH_2CN	0.40
$ClCH_2CN$	1.1	A	0.03	G	0.1	PhH	1	–CH_2CN	0

a) Using Bu_3SnCH_2CH=CH_2 1 mmol at 80 °C, 3 h. b) A: AIBN, G: galvinoxyl.

Table 3. Thermal reaction of crotyltributyltin with negatively substituted aliphatic halides[a)]

Halide	mmol	Additive	mmol	Solvent	ml	Product	mmol
CCl_4	1.1	AIBN	0.03	$PhCH_3$	1	CH_2=$CHCHMe$–CCl_3	0.26
CCl_4	10	AIBN	0.03	—		–CCl_3	0.45
$CHCl_3$	10	AIBN	0.03	—		–$CHCl_2$	0.22
$ClCH_2CN$	10	AIBN	0.03	—		–CH_2CN	0.49
$BrCH_2CO_2Me$	10	AIBN	0.03	—		–CH_2CO_2Me	0.36

a) CH_3CH=$CHCH_2SnBu_3$ 1 mmol, 80 °C, 3 h.

Table 4. Photoreaction of allyltributyltin with negatively substituted aliphatic halides[a)]

R–$SnBu_3$ R	Halide	mmol	Irradiated time/h	Product	mmol
Allyl	CCl_4	1.1	1	CH_2=$CHCH_2$–CCl_3	0.62
	$CHCl_3$	1.1	1	–$CHCl_2$	0.28
	CH_3CCl_3	1.1	3	–CCl_2CH_3	0.57
	$BrCH_2CO_2Me$	1.1	1	–CH_2CO_2Me	0.70
	$ClCH_2CO_2Me$	1.1	1		0.54
	$ClCH_2COCH_3$	1.1	1	–CH_2COCH_3	0.42
	$ClCH_2COPh$	1.1	1	–CH_2COPh	0.54
	$ClCH_2CN$	1.1	3	–CH_2CN	0.51
Crotyl	CCl_4	1.1	1	CH_2=$CHCH(CH_3)$–CCl_3	0.34
		1.1	3		0.50
		1.1	5		0.67
		1.1	24		0.65
	$CHCl_3$	1.1	5	–$CHCl_2$	0.15

a) Allylic tin compound 1 mmol, solvent: PhH 1 ml, at 21—22 °C, irradiated by high pressure Hg lamp.

$$R\cdot + CH_3CH = CHCH_2Sn\langle \longrightarrow$$
$$R\text{-}CH(CH_3)CH = CH_2 + \rangle Sn\cdot$$

Lower yields in the reactions of crotyltin may be due to crowdiness at the position being attacked by R·.

Quite similar reactions between these halides and allyl- or crotyltin compounds proceeded under irradiation by a high pressure mercury lamp. As shown in Table 4, tendencies in dependence of yield on the structure of halide are quite resembling to those in the AIBN induced reaction. This implies the nature of radical chain mechanism of the photoreactions.

Reaction of Aryl, Aralkyl, and Alkyl Halide with Allyltributyltin. Under conditions similar to those for the above reactions, AIBN- as well as photoinduced reactions of aryl, benzyl, and alkyl halides with allyltin compound were quite sluggish. Thus, as shown in Tables 5 and 6, with equimolar reactants only few % of conversion were observed, and with large excess of halide reactions did not take place almost at all. In these cases, the reactants were recovered almost quantitatively. This inactiveness of aryl halide might be surprising at a glance, since both halogen abstraction from aryl halide by stannyl radical[2)] and S_H' process involving phenyl radical have been well known.[7)]

Table 7 shows the effect of additives on the yield of

TABLE 5. THERMAL REACTION OF ALLYLTRIBUTYLTIN WITH ALKYL, ARALKYL, AND ARYL HALIDES

Allyl-$SnBu_3$ mmol	Halide	mmol	AIBN mmol	Solvent	ml	Product	mmol
1	PhI	1	0.05	PhH	1	$PhCH_2CH=CH_2$	0.05
1		10	0.05	—			Trace
2		1	0.5	PhH	1		0.35
5		0.5	0.1		1		0.29
5		0.5	0.05		1		0.10
1	PhBr	10	0.03	—			Trace
5		0.5	0.1	PhH	0.5		0.29
5	PhCl	0.5	0.1		0.5		0
1	$PhCH_2Cl$	1.1	0.03		1	$PhCH_2CH_2CH=CH_2$	Trace
1		10	0.05		1		Trace
5		0.5	0.1		1		0.34
5		0.5	0.03		1		0.09
1	$PhCH_2Br$	1.1	0.05		1		0.03
5		0.5	0.1		1		0.43
5		0.5	0.03		1		0.11
5	*n*-$C_8H_{17}Br$	0.5	0.1		1	*n*-$C_9H_{19}CH=CH_2$	0.48
5	*cyclo*-$C_6H_{11}Br$	0.5	0.1		1	*cyclo*-$C_6H_{11}CH_2CH=CH_2$	0.43

TABLE 6. PHOTOREACTION OF ALLYLTRIBUTYLTIN WITH ALKYL, ARALKYL, AND ARYL HALIDES

Halide	mmol	Tin compd mmol	Solvent	ml	Irradiated time/h	Product	mmol
PhI	1.1	1	PhH	1	1	$PhCH_2CH=CH_2$	0.08
	1.1	1		1	24		0.20
	1.5	5		1	5		0.29
PhBr	1.1	1		1	1		Trace
	1.1	1		1	24		0.18
	0.5	5	$PhCH_3$	0.5	5		0.29
PhCl	0.5	5		0.5	5		0
	0.5	5	—		25		0
$PhCH_2Cl$	1.1	1	PhH	1	24	$PhCH_2CH_2CH=CH_2$	0.10
	0.5	5		1	5		0.18
$PhCH_2Br$	1.1	1		1	24		0.24
	0.5	5		1	5		0.28
n-$C_8H_{17}Br$	0.5	5	—		5	*n*-$C_9H_{19}CH=CH_2$	0.45
cyclo-$C_6H_{11}Br$	0.5	5	—		5	*cyclo*-$C_6H_{11}CH_2CH=CH_2$	0.42

benzene produced by reduction of iodobenzene by organotin hydride for which Kuivila proposed the radical chain mechanism involving halogen abstraction by stannyl radical.[2] Even without any additive,

$$R_3SnH + PhX \longrightarrow R_3SnX + PhH$$

benzene was formed in *ca.* 30% yield by heating a mixture of iodobenzene and tributyltin hydride at 80 °C for 24 h. The yield did not diminish in the presence of radical scavengers such as galvinoxyl and *p*-benzoquinone, indicating that the reduction occurring under the conditions is not a radical chain process. However, in the presence of AIBN yield of benzene was increased up to 80%, which again fell to *ca.* 40% by the addition of a radical scavenger. This fact means that AIBN assisted reaction was suppressed almost completely by a radical scavenger. This suggests that Kuivila's chain mechanism is sound at least for the AIBN assisted reaction, and stannyl radical once formed in a medium containing iodobenzene abstracts an iodine atom quite effectively.

TABLE 7. REACTION OF IODOBENZENE BY TRIBUTYLTIN HYDRIDE[a]

Additive	mmol	Yield of PhH/%[b]
—		33
Galvinoxyl	0.04	35
p-Benzoquinone	0.04	35
AIBN	0.04	80
AIBN 0.04,	*p*-Benzoquinone 0.1	42

a) PhI 10 mmol, Bu_3SnH 1 mmol, 80 °C, 24 h. b) Based on Bu_3SnH.

On the other hand, the fact that biphenyl was formed in a considerable amount by decomposing PAT in benzene containing allyltributyltin (Table 1) suggests that S_H' reaction of phenyl radical with allyltin compound is not enough fast to construct an effective chain process. Some of phenyl radical may be consumed by non-chain by-pass such as phenylation of aryl halide

or the solvent benzene.

Employing more inert solvents, then, might be one of possible ways to enhance the efficiency of the chain reaction. However, since among the usual solvents,[8] benzene has been known to be relatively unreactive toward phenyl radical, and phenyl radical has been known to undergo S_H' with allyl sulfides 15—20 times faster than it adds to benzene,[8] increasing the relative concentration of allyltin is expected to give better results. Actually, when large excess of allyltin was employed, iodo- and bromobenzene were converted into allylbenzene in good yield, in either AIBN- or photo-induced reaction (Tables 5 and 6). However, even under these conditions, considerable amount of AIBN or prolonged irradiation is necessary to realize satisfactory yield, indicating very small kinetic chain length.

Chlorobenzene which is reduced by organotin hydride only in poor yield,[2] did not react even in the presence of large excess of allyltin, perhaps due to difficulty in chlorine abstraction by stannyl radical.

Benzyl and alkyl bromide also react under similar conditions, giving the corresponding displacement products. During the course of the study, we met the communication that the AIBN initiated reaction of cyclohexyl bromide with allyltributyltin gave allylcyclohexane in 88% yield, when 2 equiv. of tin compound was employed.[5]

Conclusion

Efficiency of free radical chain reaction between allylic tin compounds and organic halide depends on the nature of the halide, and is affected by easiness of halogen abstraction by stannyl radical and more subtly by efficiency of S_H' process. Negatively substituted halomethanes which are classified as acceptor subtrates in Huyser's sense[9] produce electron seeking radicals which will easily attack the π-bond of allyltin compound, giving S_H' product. Aralkyl and alkyl radicals, donor radicals, are less reactive toward the π-bond of allyltin. As a result, the expected chain reaction proceeds smoothly only when an excess amount of allyltin is employed. And at least concerning with the present reaction aryl radicals fall into the latter category.

Experimental

Materials. Allyltributyltin[10] was prepared by treating allylmagnesium chloride in ether. Bp 106—107 °C/1.6 mmHg (1 mmHg=133.322 Pa). Crotyltributyltin[4] was prepared by similar method or by the reaction of tributyltin-lithium with *trans*-crotyl chloride: In a three-necked flask (300 ml), tributyltin chloride (32.5 g) was placed and 7 g of metal lithium. The mixture was stirred for about 2 h. under argon atmosphere. To the mixture cooled by ice-water, was added dropwise tetrahydrofuran (100 ml) during 4 h. After the mixture turned to deep green, the mixture was stirred for one night at room temperature. After removal of unchanged lithium, a solution of *trans*-crotyl chloride (9.5 g) in tetrahydrofuran (50 ml) was added to the mixture cooled at −20 °C by means of ice–salt, during 1 h. The reaction mixture was stirred at the temperature for a half day, and for further one night, cooling by water. The mixture was treated with a saturated solution of ammonium chloride, then the product was extracted by ether. After the ethereal solution was dried over magnesium sulfate, removal of the ether and distillation under reduced pressure gave 20.9 g of the product (61%), bp 115—118 °C/2.0 mmHg. Tributyltin hydride[11] was prepared by reducing tributyltin chloride with $LiAlH_4$. Commercial organic halides were used as substrates after distillation.

Reaction Procedure. A solution containing reactants and solvent of amounts noted in the Tables is placed in a Pyrex tube and degassed. The tube was sealed and immersed in a bath kept at designated temperature for the thermal reactions. For photoinduced reaction, the tube was immersed in running water and irradiated with a high pressure mercury lamp (200 W). The products were collected by GLPC and identified NMR and IR spectroscopically. Amounts of products were determined by also GLPC.

Products. Except the well known compounds, the structures of the products were deduced based on the analytical and spectroscopic data recorded here.

4,4,4-Trichloro-1-butene: IR (neat) 1865 (C–H, out of plane), 1640 (C=C), and 645 cm^{-1} (C–Cl): ^1H NMR (CCl_4) δ=3.40 (2H, d, J=6.6 Hz) and 5.80 (3H, m). Found: C, 30.38; H, 3.08; Cl, 66.30%. Calcd for $C_4H_5Cl_3$: C, 30.13; H, 3.16; Cl, 66.71%.

4,4-Dichloro-1-butene: IR (neat) 1860 (C–H, out of plane), 1640 (C=C), 670 and 610 cm^{-1} (C–Cl): ^1H NMR (CCl_4) δ=2.87 (2H, t, J=6.4 Hz) and 5.60 (4H, m). Found: C, 38.81; H, 4.60; Cl, 56.38%. Calcd for $C_4H_6Cl_2$: C, 38.44; H, 4.84; Cl, 56.72%.

4,4-Dichloro-1-pentene: IR (neat) 1860 (C–H, out of plane), 1640 (C=C), 1380 (C–H, in plane), and 673 cm^{-1} (C–Cl): ^1H NMR (CCl_4) δ=2.17 (3H, s), 3.05 (2H, d, J=6.0 Hz), and 5.65 (3H, m). Found: C, 43.67; H, 5.45; Cl, 50.68%. Calcd for $C_5H_8Cl_2$: C, 43.20; H, 5.80; Cl, 51.00%.

4,4,4-Trichloro-3-methyl-1-butene: IR (neat) 1860 (C–H, out of plane), 1640 (C=C), and 575 cm^{-1} (C–Cl): ^1H NMR (CCl_4) δ=1.47 (3H, d, J=6.8 Hz), 3.20 (1H, m), and 5.60 (3H, m). Found: C, 34.91; H, 4.11; Cl, 61.03%. Calcd for $C_5H_7Cl_3$: C, 34.60; H, 4.02; Cl, 61.38%.

4,4-Dichloro-3-methyl-1-butene: IR (neat) 1643 (C=C) and 680 cm^{-1} (C–Cl): ^1H NMR (CCl_4) δ=1.28 (3H, d, J=7.2 Hz), 2.80 (1H, m), and 5.65 (4H, m). Found: C, 43.01; H, 5.52; Cl, 50.70%. Calcd for $C_5H_8Cl_2$: C, 43.20; H, 5.80; Cl, 51.00%.

3-Methyl-4-pentenenitrile: IR (neat) 2240 (C≡N) and 1640 cm^{-1} (C=C): ^1H NMR (CCl_4) δ=1.18 (3H, d, J=6.2 Hz), 2.49 (3H, m), and 5.60 (3H, m). Found: C, 75.49; H, 9.29; N, 15.01%. Calcd for C_6H_9N: C, 75.74; H, 9.54; N, 14.72%.

Methyl 3-Methyl-4-pentenoate: IR (neat) 1740 (C=O ester) and 1640 cm^{-1} (C=C): ^1H NMR (CCl_4) δ=1.11 (3H, d, J=6.2 Hz), 2.50 (3H, m), 3.70 (3H, s), and 5.55 (3H, m). Found: C, 65.35; H, 9.20%. Calcd for $C_7H_{12}O_2$: C, 65.60; H, 9.43%.

References

1) H. G. Kuivila and R. Sommer, *J. Am. Chem. Soc.*, **89**, 5616 (1967).

2) H. G. Kuivila, *Acc. Chem. Res.*, **1**, 299 (1968) and references cited therein.

3) M. Kosugi, K. Kurino, K. Takayama, and T. Migita, *J. Organomet. Chem.*, **56**, C11 (1973).

4) J. Grignon and M. Pereyre, *J. Organomet. Chem.*, **61**, C33 (1973); J. Grignon, C. Servens, and M. Pereyre, *ibid.*, **96**, 225 (1975).

5) G. E. Keck and J. B. Yates, *J. Am. Chem. Soc.*, **104**, 5829 (1982).
6) M. Kosugi, P. Q. Hanh, M. Nakayama, and T. Migita, *Chem. Lett.*, **1978**, 927.
7) T. Migita, M. Kosugi, K. Takayama, and Y. Nakagawa, *Tetrahedron*, **29**, 51 (1973).
8) T. Migita, K. Takayama, Y. Abe, and M. Kosugi, *J. Chem. Soc. Perkin Trans. 2*, **1979**, 1137.
9) E. S. Huyser, "Free Radical Chain Reactions," John Wiley and Sons Inc., New York (1970) p. 79.
10) D. Seyferth and M. A. Weiner, *J. Org. Chem.*, **24**, 1395 (1959); **26**, 4797 (1961).
11) H. G. Kuivila, *J. Am. Chem. Soc.*, **83**, 1249 (1961).

 © 1983 The Chemical Society of Japan Bull. Chem. Soc. Jpn., 56, 2485—2489 (1983)

N,N'-Carbonyldi[1,2-benzisoxazol-3(2*H*)-one]: New, Reactive Condensing Agent

Mitsuru UEDA,* Hideaki OIKAWA, Naomi KAWAHARASAKI, and Yoshio IMAI†

Department of Polymer Chemistry, Faculty of Engineering, Yamagata University, Yonezawa, Yamagata 992

†*Department of Textile and Polymeric Materials, Tokyo Institute of Technology, Meguro-ku, Tokyo 152*

(Received April 7, 1983)

A new condensing agent, *N,N'*-carbonyldi[1,2-benzisoxazol-3(2*H*)-one] (**6**), was readily prepared by the reaction of 1,2-benzisoxazol-3-ol and trichloromethyl chloroformate in toluene. The condensing agent **6** was shown to be very useful for the preparation of amides, esters, and dipeptides under mild conditions. A successful polyamide synthesis by one-pot polycondensation of isophthalic acid with diamines using **6** was also described.

Condensations among the most important and fundamental reactions in organic synthesis and many reagents for promoting condensations by one-pot procedures have been reported.[1-4] In particular, their full potential has been realized in conversions of carboxylic acids into amides and esters. Most such condensing agents first react with the carboxylic acids to give the intermediates, active esters or amides, which undergo subsequent nucleophilic attack by the amino or hydroxyl group. Therefore, a primary factor in determining whether or not the condensing agents are effective is their ability to activate carboxylic acids.

It is well recognized that increased reactivity of carboxylic acid derivatives toward nucleophiles may be roughly correlated with greater stability of the leaving group anions, that is, pK_a of the leaving groups. From this point of view, we previously exploited a series of good leaving groups in the syntheses of active esters and amides, demonstrating that the active ester and amide methods are useful in the preparation of high molecular weight polyamides under mild conditions.[5]

Based on the success of those studies, we continued to investigate new active condensing agents for the synthesis of amides, esters and polyamides. One requirement for improved condensing agents is that the conversion of carboxylic acids to the active intermediates should occur readily under mild conditions. In the preceding paper, we showed that 3-(2-benzothiazolythio)-1,2-benzisothiazole 1,1-dioxide and 3-(2-benzoxazolylthio)-1,2-benzisothiazole 1,1-dioxide were new reactive condensing agents for the synthesis of amides and esters.[6]

We now report that amides, esters, peptides, and polyamides can be easily obtained from carboxylic acids and nucleophiles by a one-pot procedure using the new condensing agent, *N,N'*-carbonyldi[1,2-benzisoxazol-3(2*H*)-one] (**6**).

Results and Discussion

Synthesis of N,N'-*Carbonyldi[1,2-benzisoxazol-3*(2H)*-one]* (*6*). The widely used condensing agents derived from phosgene, such as *N,N'*-carbonyldiimidazole (**1**) and *N,N'*-(carbonyldioxy)disuccinimide (**2**) have been reviewed.[7,8] The reaction of carboxylic acids with **1** and **2** lead to the intermediate imidazolides (**3**) and *N*-hydroxysuccinimide ester (**4**) respectively, both of which have been characterized by their very high reactivity in nucleophilic reactions.

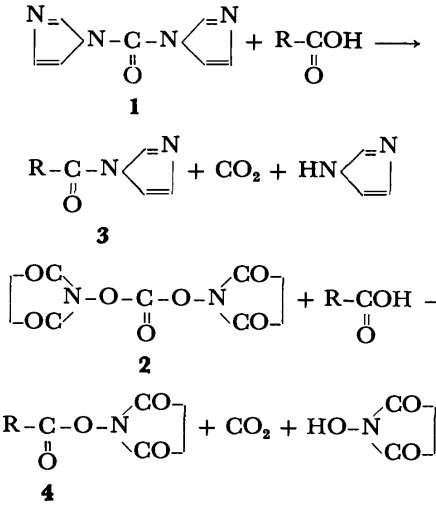

Recently, we found that the *N*- or *O*-acyl products from the acylation of 1,2-benzisoxazol-3-ol (**5**) were susceptible to aminolysis under mild conditions and the corresponding amides were produced in quantitative yields.[5i] This finding led to the synthesis of *N,N'*-carbonyldi[1,2-benzisoxazol-3(2*H*)-one] (**6**) which was expected to serve as new condensing agent with a wide range of preparative applications.

The condensing agent **6** was readily prepared in high yield by reacting **5** with trichloromethyl chloroformate (**7**) in a 4 : 1 molar ratio in toluene (Scheme 1). Recrystallization from toluene gave white needles melting point at 205—206 °C. Acylation of **5** may involve reaction at either oxygen or nitrogen. Acylations reported earlier gave *N*- or *O*-acyl products, depending on the reaction conditions employed and acylating agent used.[9] The reaction of **5** with **7** in toluene under reflux conditions gave preferentially the more thermo-

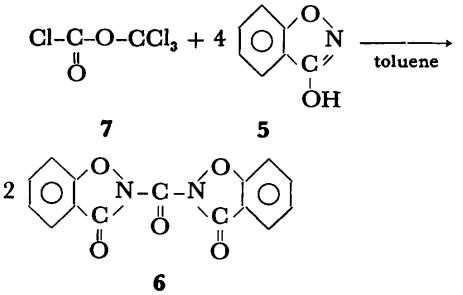

Scheme 1.

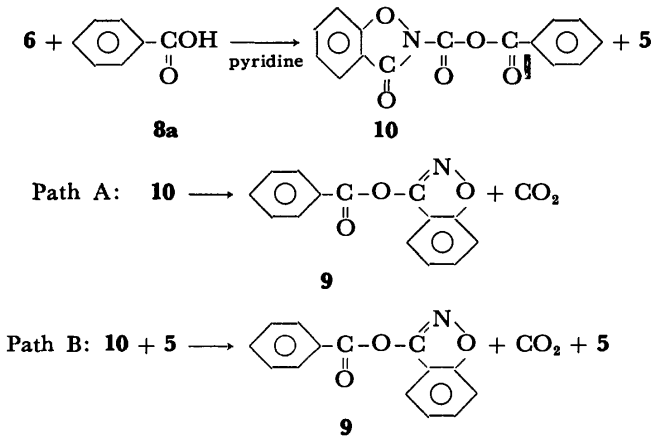

Scheme 2.

dynamically stable *N*-acyl product **6**. The structure of **6** was characterized by elemental analysis and IR spectroscopy. The IR spectrum showed carbonyl absorption bands at 1780, 1765, and 1750 cm^{-1}.

Reaction of ***6*** *with Benzoic Acid* (***8a***). To get a better picture of the course of the reaction, **6** was treated with benzoic acid (**8a**) in *N*-methyl-2-pyrrolidone (NMP) at 50 °C for 1 h in the presence of pyridine. The condensing agent **6** reacted rapidly with **8a** with liberation of CO_2, to give 3-benzoyloxy-1,2-benzisoxazole (**9**). The formation of benzoic anhydride was not observed. The intermediate **9** has been characterized by its high reactivity toward aminolysis.[5i] Consequently, the reaction pathway suggested for the formation of **9** is shown in Scheme 2.

Initially, the attack of the benzoate anion at the carbonyl carbon of **6** gives the mixed anhydride (**10**). Two pathway are possible for the further reaction of **10**. The mixed anhydride (**10**) loses CO_2 to form the intermediate **9** (Path A). Alternatively, **5** liberated in the first step of the reaction attacks the carbonyl carbon of **10**, giving the intermediate **9** (Path B). A similar mechanism has been proposed to account for the formation of imidazolide (**3**) by the reaction of **1** with carboxylic acids.[10]

Synthesis of Amides (***11***) *and Esters* (***12***). The syntheses of amides (**11**) and esters (**12**), using our new activating reagent **6**, were carried out by a one-pot procedure. This efficient procedure consists essentially of two reactions: formation of the active ester (**9**) from carboxylic acids as described above, and subsequent aminolysis or alcoholysis of the active ester (**9**) as shown in Scheme 3. The aminolysis and alcoholysis of the active ester (**9**) proceeded smoothly at room temperature to give the corresponding amides (**11**) and esters (**12**). The alcoholysis required an equimolar amount of triethylamine (TEA).

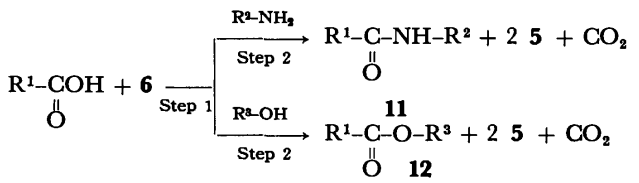

Scheme 3.

Next, the selective *N*-acylation and the *N,O*-diacylation of *p*-aminophenol (**13**) were performed in either the absence or the presence of TEA, respectively. The corresponding amide (**14**) or amide ester (**15**) were obtained in good yields (Scheme 4). These results are summarized in Table 1.

Synthesis of Dipeptides (***18***). In order to further demonstrate the preparative utility of our method, it was applied to the synthesis of dipeptides. Thus the reaction of an *N*-protected amino acid (**16**) with an amino acid ester hydrochloride (**17**) was carried out in the presence of pyridine. The *N*-protected amino acid (**16**) was reacted with equimolar amount of **6** in dichloromethane in the presence of pyridine at room temperature. After several hours, the amino acid ester hydrochloride (**17**) and TEA as an acid acceptor were added. The dipeptide product **18** was isolated in the normal manner. *N*-Protected dipeptide ester (**18**) were prepared in good yields virtually without racemization (Table 2), (Scheme 5).

Synthesis of Polyamides (***19***). Our method can be extended to the synthesis of polyamides (**19**) and it provides a novel approach to direct polycondensation. The one-pot polycondensation of isophthalic acid was carried out in solution at low temperature using three diamines (**20**): 4,4′-oxydianiline, 4,4′-methylenedianiline, and 1,6-hexanediamine. The polar aprotic solvents, NMP, hexamethylphosphoric triamide

TABLE 1. PREPARATION OF AMIDES **11** AND ESTERS **12** USING CONDENSING AGENT **6**[a]

Carboxylic acid R-COOH, **8** R-	Amine or Alcohol	Reaction time (Step 2)	Product	Yield[b] %
C_6H_5	Aniline	15 h	Benzanilide	94
C_6H_5	Benzylamine	1 h	*N*-Benzylbenzamide	80
C_6H_5	Phenol	2 d	Phenyl benzoate	86
C_6H_5	*p*-Nitrophenol	1 d	*p*-Nitrophenyl benzoate	74
C_6H_5	*p*-Nitrobenzyl alcohol	3 d	*p*-Nitrobenzyl benzoate	68
C_6H_5	*p*-Aminophenol	1 d	4′-Hydroxybenzanilide	90
C_6H_5	1/2 *p*-Aminophenol	1 d/2 d	4′-Benzoyloxybenzanilide	86
n-C_5H_{11}	Aniline	1 d	*N*-Phenylhexanamide	85
n-C_5H_{11}	Benzylamine	1 d	*N*-Benzylhexanamide	61

a) Reaction was carried out with 2 mmol of the reactants in 4 ml of NMP. Reaction temperature: Step 1, 50 °C; Step 2, room temperature. b) Isolated yields.

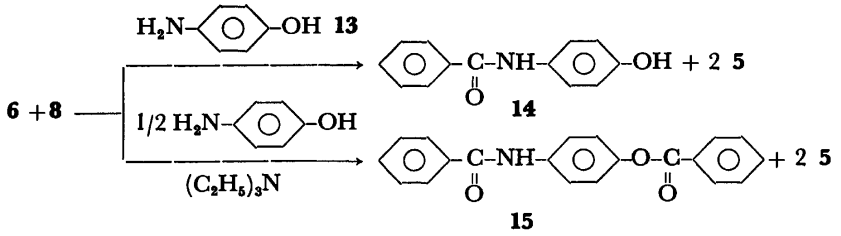

Scheme 4.

TABLE 2. PREPARATION OF DIPEPTIDE EATERS 18 USING CONDENSING AGENT 6[a)]

N-Protected α-amino acid	α-Amino acid ester	Reaction time/h		Product	Yield %	Mp θ_m/°C (Found reported)		$[\alpha]_D$/° (temp, c, solv) (reported)
		Step 1	Step 2					
Z-Val	Gly-OEt	12	24	Z-Val-Gly-OEt	87	170—171	170—171	−31.4 (22°, 1.75, dioxane)
								−32.4 (20°, 1.85, dioxane)[6)]
Z-Val	Val-OMe	3	19	Z-Val-Val-OMe	75	115	116	−24.4 (22°, 1.08, MeOH)
								−24.3 (25°, 0.3, MeOH)[12)]
Z-Ala	Gly-OEt	5	24	Z-Val-Gly-OEt	84	101	99—100	−22.3 (22°, 2.70, EtOH)
								−22.3 (3.67, EtOH)[13)]
Boc-Leu	Leu-OMe	6	17	Boc-Leu-Leu-OMe	84	138—139	141—142	−49.1 (22°, 1.75, MeOH)
								−50.0 (0.39, MeOH)[13)]
Boc-Phe	Val-OMe	3	24	Boc-Phe-Val-OMe	80	118	117—118	−11.5 (22°, 3.42, DMF)
								−11.0 (1.89, DMF)[13)]

a) Reaction was carried out with 1 mmol of the reactants in 5 ml of dichloromethane at room temperature.
b) Isolated yields.

TABLE 3. SYNTHESIS OF POLYAMIDES 19 BY A ONE-POT POLYCONDENSATION OF ISOPHTHALIC ACID WITH DIAMINES 20 USING THE CONDENSING AGENT 6[a)]

	Diamine H_2N-R-NH_2 R	Reaction conditions			Polymer		
		Base	Solvent	Time/min Step 1	Type	Yield %	η_{inh}[b)] dl·g^{-1}
20a	-C_6H_4-O-C_6H_4-	Pyridine	NMP	70	**19a**	98	0.12
20a	-C_6H_4-O-C_6H_4-	TEA	NMP	2	**19a**	99	0.10
20a	-C_6H_4-O-C_6H_4-	TEA	NMP	30	**19a**	99	0.12
20a	-C_6H_4-O-C_6H_4-	Pyridine	HMPA	70	**19a**	99	0.10
20a	-C_6H_4-O-C_6H_4-	Imidazole	HMPA	5	**19a**	99	0.17
20a	-C_6H_4-O-C_6H_4-	TEA	HMPA	5	**19a**	99	0.25
20a	-C_6H_4-O-C_6H_4-	*N*-Ethyl piperidine	HMPA	3	**19a**	99	0.18
20b	-C_6H_4-CH_2-C_6H_4-	TEA	NMP	3	**19b**	61	0.12
20b	-C_6H_4-CH_2-C_6H_4-	TEA	DMAc	3	**19b**	97	0.15
20b	-C_6H_4-CH_2-C_6H_4-	TEA	HMPA	3	**19b**	79	0.15
20b	-C_6H_4-CH_2-C_6H_4-	Pyridine	HMPA	60	**19b**	72	0.10
20c	-$(CH_2)_6$-	TEA	NMP	2	**19c**	99	0.14
20c	-$(CH_2)_6$-	TEA	DMAc	2	**19c**	99	0.18
20c	-$(CH_2)_6$-	TEA	HMPA	2	**19c**	99	0.23
20c	-$(CH_2)_6$-	Pyridine	HMPA	2	**19c**	99	0.18
20c	-$(CH_2)_6$-	Imidazole	HMPA	15	**19c**	98	0.10

a) Polymerzation was carried out with 1 mmol of the monomers using the condensing agent **6** (2 mmol) in the solvent.
b) Measured at a concentration of 0.5 g/dl in concentrated sulfuric acid at 30 °C.

(HMPA), and *N*,*N*′-dimethylacetamide (DMAc) were used as polymerization media (Scheme 6). Polycondensations in the NMP and DMAc proceeded heterogeneously which impeded the increase in molecular weight. Various tertiary amines with different base strength were also tested in these polymerizations in order to elucidate the influence of bases. TEA, with its high basicity, was found to be good base. The results are summarized in Table 3. The polyamides were produced in quantitative yields with inherent viscosities of 0.1 to 0.25 dl·g^{-1}. The polymers were identified as polyamides by comparison of their IR spectra with those of the authentic polyamides. Although this one-pot syntheses of polyamides was successful, the viscosities of polyamides were relatively low. Thus, studies of the polycondensation conditions must be continued.

In summary, our studies indicate that **6** is a very useful reagent for the formation of amides, esters and

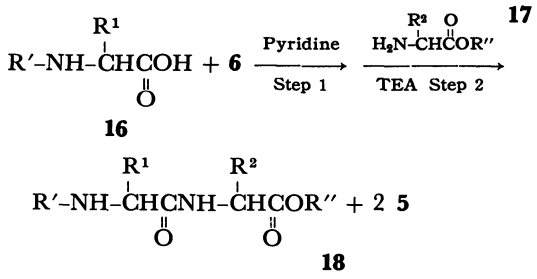

Scheme 5.

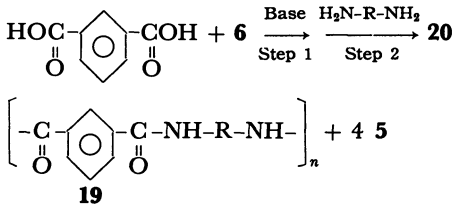

Scheme 6.

peptides. The new condensing agent **6** is a crystalline solid having excellent hydrolytic stability and therefore it is handled more easily than conventional agents. Furthermore, 1,2-benzisoxazol-3-ol (**5**), a reaction byproduct, is readily removed from the reaction products by washing the reaction mixture with 1% aqueous sodium hydrogencarbonate.

Experimental

Melting points were uncorrected. Infrared spectra were obtained using potassium bromide pellets with a JASCO IRA-1 spectrophotometer. 4,4'-Oxydianiline, and 4,4'-methylenedianiline were recrystallized from tetrahydrofuran and benzene respectively. *N*-methyl-2-pyrrolidone (supplied by Mitsubishi Chemical Industries Ltd.), hexamethylphosphoric triamide and *N,N*-dimethylacetamide were purified by vacuum distillation and stored over 4-Å Molecular Sieves. *N*-Protected amino acids and amino acid ester hydrochlorides were prepared by usual procedures. The other reagents were used without further purification.

1,2-Benzisoxazol-3-ol (5). This compound was prepared by the modified method reported by Böshangen.[11] To a ice-cold suspention of salcilohydroxamic acid (15.3 g 0.1 mol) in tetrahydrofuran (45 ml), thionyl chloride (10 ml) was added dropwise over 1 h. Then excess thionyl chloride and the solvent were removed *in vacuo* to give a white paste, which was dissolved in dioxane (10 ml). This solution was added dropwise over 1 h to a solution of triethylamine (42 ml) in dioxane (35 ml). The temperature was kept below 10 °C. The yellow mixture was poured into water (300 ml) and then was acidified with 10% HCl. The solution was allowed to crystallize overnight at 0—10 °C. The product was collected by filtration, washed with water, and dried to give 9 g of **5**. Recrystallization from 25% aqueous ethanol solution produced faint yellow needles. Mp 145—146 °C (lit,[11] 144 °C).

N,N'-*Carbonyldi*[*1,2-benzisoxazol-3(2H)-one*] (*6*). A mixture of (**5**) (4.3 g, 0.032 mol) and trichloromethyl chloroformate (0.96 ml, 0.008 mol) in toluene (30 ml) was refluxed with stirring for 1 d, then cooled. The precipitate was isolated by filtration and washed with toluene, and dried. Yield was 3.5 g (73%). Purification by recrystallization from toluene to give a white needles. Mp 205—206 °C; IR (KBr), 1780, 1765, and 1750 cm^{-1}.

Found: C, 60.8; H, 2.9; N, 9.3%. Calcd for $C_{15}H_8N_2O_5$: C, 60.82; H, 2.72; N, 9.46%.

3-Benzoyloxy-1,2-benzisoxazole (9). To a stirred solution of benzoic acid (0.244 g, 2.0 mmol), pyridine (0.16 ml, 2.0 mmol) in NMP (4 ml) was added **6** (0.592 g, 2.0 mmol), followed by stirring at 50 °C for 1 h. The reaction mixture was poured into water (100 ml). The precipitate formed was collected filtration, washed with water and dried *in vacuo*. Yield: 0.400 g (98%). Recrystallization from hexane produced white needles, mp 65—66 °C (lit,[9] 64 °C).

Amide (11). General Procedure: The condensing agent **6** (0.592 g, 2 mmol) was added to a stirred solution of the carboxylic acid (2 mmol) and pyridine (2 mmol) in NMP (4 ml) at 50 °C. After 1 h, the amine (2 mmol) was added. Stirring was continued for several hours. The mixture was poured into 1% aqueous sodium hydrogencarbonate. The precipitate was filtered and washed with water and dried.

Ester (12). General Procedure: A mixture of **6** (2 mmol), benzoic acid (2 mmol) and pyridine (2 mmol) in NMP (4 ml) was stirred at 50 °C for 1 h. To this mixture the alcohol (2 mmol) and triethylamine (2 mmol) were added. Stirring was continued for several hours. The reaction mixture was worked up as described above.

Amide Esrer (15). The condensing agent **6** (2 mmol) was added with stirring to a solution of benzoic acid (2 mmol) and pyridine (2 mmol) in NMP (4 ml) at 50 °C. After 1 h, *p*-aminophenol (**13**) (1 mmol) was added to this mixture. After stirring 1 d, triethylamine (2 mmol) was added, the mixture was stirred for 2 d and worked up as described. The compound **14** was obtained when triethylamine was omitted.

Protected Dipeptide Ester (18). General Procedure: To a solution of the *N*-protected α-amino acid (1 mmol) and pyridine (1 mmol) in dichloromethane (5 ml), **6** (1 mmol) was added under nitrogen. The solution was stirred for several hours at room temperature, then the α-amino acid ester hydrochloride (1 mmol) was added. The solution was stirred for 1 d at room temperature. After removal of the solvent *in vacuo*, the residue was dissolved in ethyl acetate, and the organic solution was washed successively with 5% aqueous sodium hydrogencarbonate, 1 M hydrochloric acid and saturated brine, and then dried ($MgSO_4$). After evaporation of ethyl acetate, the dipeptide ester was purified by crystallization.

Polyamide (19). General Procedure: The condensing agent **6** was added to a stirred solution of isophthalic acid (1 mmol) and pyridine (2 mmol) in NMP (2 ml). The mixture was stirred for a defined time, then diamine (1 mmol) was added at room temperature. Stirring was continued for 2 d. The resulting solution was poured into 1% aqueous sodium hydrogencarbonate (200 ml) and the precipitated polymer was collected and dried *in vacuo* at 60 °C for 2 d. Inherent viscosity was measured at a concentration of 0.5 $g \cdot dl^{-1}$ in concentrated sulfuric acid at 30 °C.

We are indebted to Mr. Sadao Kato for the performance of the elemental analyses.

References

1) M. A. Ogliaruso and J. F. Wolfe, "The Chemistry of Acid Derivatives," ed by S. Patai, John Wiley and Sons, New York (1979), Part I, p. 474.

2) M. Bodanszky, Y. S. Klausner, and M. A. Ondetti, "Peptide Synthesis," John Wiley and Sons, New York

(1976).

3) C. H. Stammer, "Amino Acids Peptides and Related Compounds," ed by D. H. Hey, F. R. S., and D. I. John, Butterworth and Co., London (1973), p. 135.

4) "The Peptides," ed by E. Gross and J. Meienhofer, Academic Press, New York (1979), Vol. 1.

5) a) M. Ueda, K. Okada, and Y. Imai, *J. Polym. Sci., Polym. Chem. Ed.*, **14**, 2665 (1976); b) M. Ueda, H. Hazome, and Y. Imai, *Kobunshi Ronbunshu*, **33**, 627 (1976); *Chem. Abstr.* **86**, 17023 (1977); c) M. Ueda, A. Sato, and Y. Imai, *J. Polym. Sci., Polym. Chem. Ed.*, **15**, 2731 (1977); d) M. Ueda, Y. Miyazawa, A. Sato, and Y. Imai, *Polym. J.* **8**, 609 (1976); e) M. Ueda, A. Sato, and Y. Imai, *J. Polym. Sci., Polym. Chem. Ed.*, **16**, 475 (1978); f) M. Ueda, A. Sato, and Y. Imai, *ibid.*, **17**, 2013 (1979); g) M. Ueda, A. Sato, and Y. Imai, *ibid.*, **17**, 783 (1979); h) M. Ueda, S. Aoyama, and Y. Imai, *Makromol. Chem.*, **180**, 2807 (1979); i) M. Ueda, T. Harada, S. Aoyama, and Y. Imai, *J. Polym. Sci., Polym. Chem. Ed.*, **19**, 1061 (1981); j) M. Ueda, K. Seki, and Y. Imai, *Macromolecules*, **15**, 17 (1982).

6) M. Ueda, N. Kawaharasaki, and Y. Imai, *Synthesis*, **1982**, 933.

7) H. A. Stabb and W. Rohr, "Newer Methods of Preparative Organic Chemistry," ed by W. Forest, Verlag, Weinheim (1967), Vol V, p. 64.

8) H. Ogura and K. Takeda, *Nippon Kagaku Kaishi*, **1981**, 836.

9) H. Böshangen and W. Geiger, *Chem. Ber.*, **102**, 3775 (1969).

10) J. H. Boyer, *J. Am. Chem. Soc.*, **74**, 6274 (1952).

11) H. Böshangen, *Chem. Ber.*, **100**, 954 (1967).

12) J. E. Shields, S. T. McDowell, J. Pavlos, and G. R. Gray, *J. Am. Chem. Soc.*, **90**, 3549 (1968).

13) H. Kinoshita, K. Inomata, O. Miyano, and H. Kotake, *Bull. Chem. Soc. Jpn.*, **52**, 2619 (1979).

The Recovery of Lithium from Geothermal Water in the Hatchobaru Area of Kyushu, Japan

Kenjiro YANAGASE, Tetsutaro YOSHINAGA,* Kentaro KAWANO, and Toshikazu MATSUOKA†

Department of Environmental Science, Faculty of Engineering, Kyushu Institute of Technology, Tobata-ku, Kitakyushu, Fukuoka, 804

(Received May 28, 1982)

The recovery of lithium from geothermal water at Hatchobaru in Kyushu, Japan, was investigated. A coprecipitation method using aluminium salts was employed. The lithium concentration in the geothermal water used in the present study was about 10 ppm. To make our experimental results more applicable for geothermal water, a reference lithium solution (10 ppm) was also studied as a control solution. A perfect recovery of lithium was obtained for the reference lithium solution by choosing appropriate conditions. For geothermal water, the yield of Li was not so good as in the control solution. However, an almost complete recovery of lithium was attained for geothermal water by the removal of calcium ions and polymerized silica. The mechanism of Li recovery was also considered.

The lithium industry was a minor one before World War II. In recent years, however, commercial uses of lithium and its compounds have increased in many fields, such as ceramics, glass, batteries, and metallurgy. In addition to these commercial uses, it is also anticipated that lithium can be used as blanket material in fusion reactors.[1] Still more, from the point of view of the energy problem,[2] the most important solution in the next coming century will definitely be the more basic use of lithium in the fusion energy process. A basic deuterium–tritium (D–T) reaction will release a neutron, an alpha particle, and an energy of 17.6 MeV carried by the neutron and alpha particle. Deuterium is available in seawater, but natural tritium is scarce. Bombarded by a neutron, lithium can be used as a breeder for tritium in the fusion reactor. The energy value of one gram of lithium can be increased by adding to the breeding ratio (tritons produced/tritons consumed) or by increasing the amount of energy per fusion. Lee estimated that the effective energy content of natural Li ranges from about 8.5×10^3 kW h (normal) per gram to 2.7×10^4 kW h (thermal) per gram of natural lithium.[3]

In Japan, there are practically no lithium resources. Although the concentration is very dilute (=0.18 ppm), there is a vast supply of lithium in seawater (estimated to be 2.5×10^{14} kg), probably the most reliable energy resource in the near future. At the present stage, however, the recovery of lithium from seawater in a commercially practical way is very difficult. Possible substitute for petroleum have been investigated recently in Japan. One of them is a geothermal energy. Water from the Hatchobaru power plant (50 MW), for example, gives Li values of about 140 (kg/d), (5.3×10^4 kg/Year) provided that the Li content is 10 ppm, and the fluid velocity of geothermal water, 600 t/h. Though the Li content thus obtained is small, it is equal to about one hundred million private persons' electric demand (as 1 kW·Year/Man·Year). Incidentally, the Li production in the world is about 9000 t (metric)/Year (1977), and most of lithium in the world is produced in the U.S.A. (*ca.* 70%), U.S.S.R(15—20%), Africa and china.[4] The possible lithium recovery from Hatchobaru geothermal water will contribute only 0.6% to the total world production at present. Within the next 10 years however, the ratio of geothermal energy to the total energy in Japan will become 1%. According to our calculation, lithium products in Japan in the near future will become about 50 times as large as at present. The Li concentration in seawater is about 0.2 ppm, as has been stated above, while the concentration in geothermal water from the Hatchobaru bore is about 10 ppm. Thus, the recovery from geothermal water seems relatively easy and practicable compared with that from seawater. In the present work, the recovery of lithium from geothermal water is aimed at. As techniques to recover lithium from a lithium containing solution, there have been used the inorganic ion-exchange method, the adsorption method using many adsorbents, the solvent-extraction method, the coprecipitation method, and so on. The coprecipitation method seemed to be the simplest among these and so was employed in the present study. Although the lithium recovery from low-concentration solutions has been extensively investigated,[1,5-24] the details of the mechanism for Li recovery seem not yet to have been clarified. Since the many factors concerning Li recovery are very complicated, the reported results are sometimes in conflict with each other. Thus, in the present work, a basic investigation will be made at first, then it will be applied to geothermal water.

Experimental

Geothermal Water. The geothermal water used in the present study was sampled out from bores at the Hatchobaru Power Station in Kyushu, Japan. The sampling of geothermal water was done from May 10, 1980, to January 22, 1981. Some typical constituents of geothermal water are shown in Table 1.

Reagents. *a) Precipitating Agents*: The $AlCl_3\cdot6H_2O$, $NaAlO_2$, $FeSO_4\cdot7H_2O$, $FeCl_3\cdot6H_2O$, $MgSO_4\cdot7H_2O$, $Ti(SO_4)_2$, and H_fO_2 were commercially obtained from Wako Pure Chemical Industries, Ltd.; the $ZrO\cdot nH_2O$ was from the Shinnippon Kinzoku Kagaku Co. Ltd.; the Ta_2O_5 was from Johnson, Mathey and Co., Ltd., and the $(NH_4)_6Mo_7O_{24}\cdot4H_2O$, from the Ishizu Pharmaceutical Co., Ltd.

† Present address: The Industrial Waste Guidance Division Bureau in Kitakyushu, Kokurakita-ku, Kitakyushu, Fukuoka 803.

Table 1. Typical compositions (and pHs) of geothermal waters from bores in Ohtake and Hatchobaru areas (in ppm)

Constituents	Ohtake Well Nos.		Hatchobaru Well Nos.	
	No. 9	No. 10	No. 4	No. 7
Na	1050	1030	2250	2140
K	132	124	277	266
Li	4.79	4.73	10.9	10.2
Ca	28.4	29.7	60.2	76.3
Mg	0.01	0.21	1.21	1.21
F	2.95	2.35	4.05	3.80
Cl	1774	1738	1954	1651
HCO_3	57	77	12	11
SO_4	145	193	138	95
HBO_2	84	78	191	170
SiO_2	531	433	679	746
As	2.0	2.1	3.2	3.6
pH	8.57	8.44	6.99	7.04

b) Other Reagents: The LiCl, Na_2CO_3, $(NH_4)_2CO_3$, $CaCl_2 \cdot 2H_2O$, EDTA ($C_{10}H_{14}N_2O_8Na_2 \cdot 2H_2O$), $CaCO_3$, NH_4Cl, E.B.T (indicator), and NN (indicator) were obtained from Wako Pure Chemical Industries, Ltd. All the reagents used were guaranteed reagents.

Instruments. A Toyo Kagaku Sangyo pH meter, Model Pt-3D, and Denki Kagaku Keiki pH meter, MG-7, were used with a combination electrode, HCE 101C-1T, for the measurement of the (apparent) pH's of the reference lithium solutions (abbreviated as ref. Li solutions hereafter) and geothermal water. A Nippon Jarrell-Ash AA-8200 atomic absorption spectrophotometer and flame emission were used to determine the lithium content in the sample solutions. The X-Ray diffraction patterns were measured with a Rigaku Rotor Flex RU-200 diffractometer. The DTA and TG curves were measured with a Rigaku Denki thermal analysis instrument, No. 802981.

Procedure. To examine the performance of precipitating agents, the procedure shown in Fig. 1 was employed.

Results and Discussion

No precipitating agents employed in this study, except for aluminium salts, exhibited any pronounced effect on lithium recovery. Aluminium salts have previously been employed as reagents for Li extraction,[5] and the efficiencies of Al salts were confirmed in the present investigation. Hereafter, the results will be shown and discussed only for the aluminium salts. The recovery of lithium from geothermal water is the main purpose of the present work. However, the compositions of geothermal water are different from place to place. A ref. Li solution with the same lithium concentration as in geothermal water from Hatchobaru was prepared as a control solution to make the experimental results

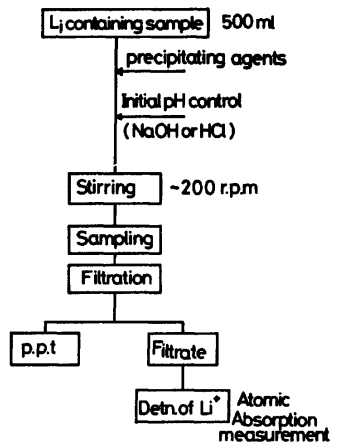

Fig. 1. Flow chart of procedure for the estimation of lithium recorvery.

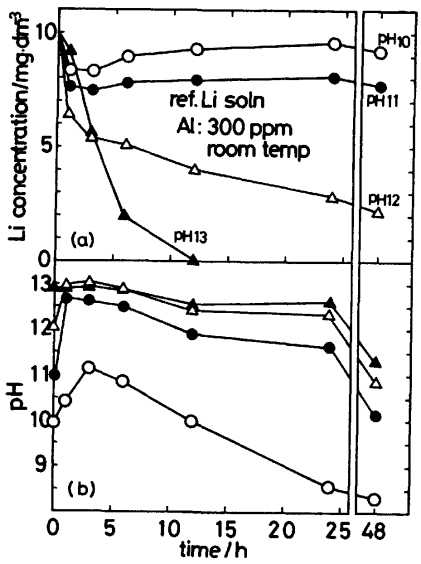

Fig. 2. The plots of residual Li concentration *vs.* time and pH *vs.* time for reference Li solution with various kinds of pH at room temperature.
Initial Li concentration: 10.0 ppm; Al concentration: 300 ppm ($AlCl_3$). (Apparent) initial pH: —○— 10.0; —●— 11.0; —△— 12.0; —▲— 13.0.

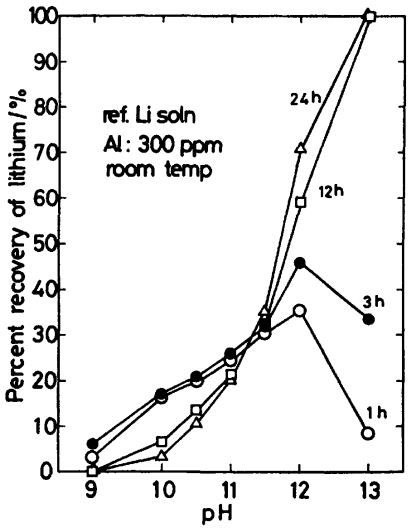

Fig. 3. The relation between percent recovery of lithium and initial pH for reference Li solution at room temperature. Initial Li concentration: 10.0 ppm; Al concentration: 300 ppm ($AlCl_3$), Stirring time: —○— 1 h; —●— 3 h; —□— 12 h; —△— 24 h.

widely applicable. In this study, LiCl was added to distilled water so that the Li concentration became 10 ppm, to be referred to hereafter as the "reference Li solution." Extensive investigations of lithium recovery have been made by many researchers. However, the conditions of Li extraction from a low-Li-content solution are influenced by many factors, such as the Li concentration, the salt constituents and their concentrations in the solution, the concentrations of the precipitating agents, the pH, the temperature, and the stirring time. Thus, the optimum conditions reported cover wide range, depending on the characteristics of the solutions, and are sometimes in conflict with each other. First, the results for the ref. Li solution will be shown. Figure 2 shows the plots of the residual Li consentration *vs.* the time, and the (apparent)pH *vs.* the time for the ref. Li solution at room temperature. The figure shows that the influence of the initial (apparent)pH is great. In this case, the experiment at an initial pH value of 12 gives the best results within about an hour. However, Fig. 2 also shows that, after 24 h, the higher the pH, the better the yield recovered. From this result, the plot of the Li recovery *vs.* pH was made, and it is shown in Fig. 3. The plot of the time dependence of pH shows a tendency, from the beginning to 1—3 h, for the values of the pH's to increase and then to decrease gradually. These changes in the pH and Li recovery with the passage of time seem to be an important key to the mechanism of Li recovery. As long as aluminium salts were used, a high Li recovery was obtained at relatively higher pH regions in this experimental study. This suggests that the use of sodium aluminate needs only a small amount of pH-control agents (acid or base) for the recovery of lithium. In Fig. 4, a pH titration curve for Al salt in an acidic solution is shown. The equilibria of Al^{3+}, $Al(OH)_3$, and AlO_2^-(or $Al(OH)_4^-$) are:

$$Al^{3+} \underset{H^+}{\overset{OH^-}{\rightleftharpoons}} Al(OH)_3 \underset{H^+}{\overset{OH^-}{\rightleftharpoons}} Al(OH)_4^-.$$

With this equilibria relation and calibration curve, the Al content in the (Li containing) solution was also determined. That is, the central region of the titration curve was used; it corresponds to the total content of the aluminium in solution. The coexistence of the Li ion did not disturb the Al analysis. At an initial pH of the 13, the Li recovery *vs.* the time, the (apparent)pH *vs.* the time, and the Li recovery *vs.* the Al concentration were examined with various kinds of Al concentrations. The results are shown in Figs. 5 and 6. Except for the Al concentrations of 50 and 1000 ppm, the percentage of the recovery of Li was about 100% after stirring for a long time. There is also a tendency that the higher the Al concentration, the quicker the recovery. For an Al concentration of 50 ppm, almost no effective recovery was observed, and for 1000 ppm, a percentage of the recovery of only 50—60% was obtained, not in accord with our expectation. This might be explained

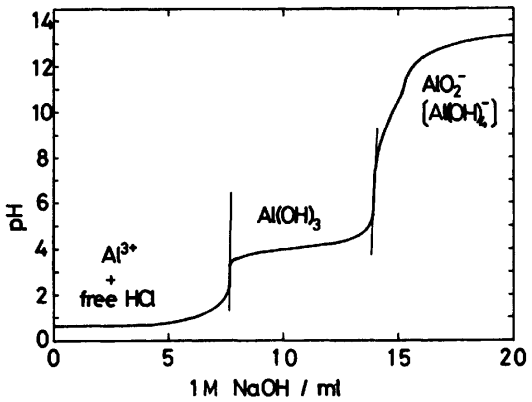

Fig. 4. pH change of aluminium salt solution during alkaline titration. [Al concentration of lithium aluminate is also determined using this potentiometric technique].

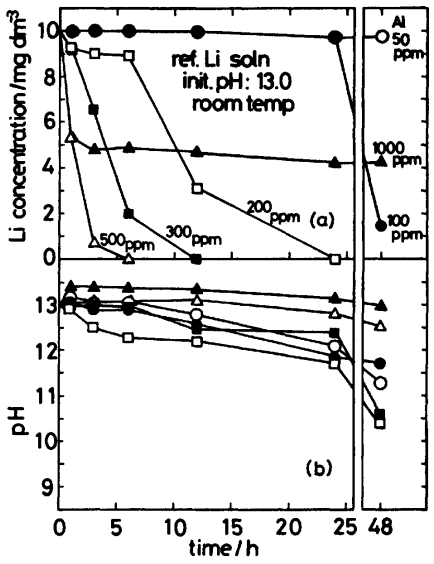

Fig. 5. The plots of residual Li concentration *vs.* time and pH *vs.* time for reference Li solution with various kinds of aluminium concentration at room temperature. Initial Li concentration: 10.0 ppm; initial pH: 13.0; Al concentrations: —○— 50 ppm; —●— 100 ppm; —□— 200 ppm; —■— 300 ppm; —△— 500 ppm; —▲— 1000 ppm.

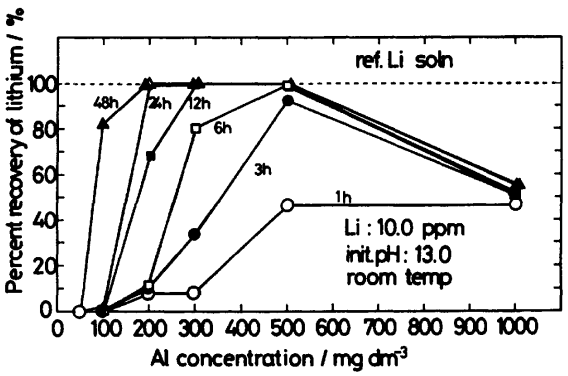

Fig. 6. The relation of percent recovery of lithium and Al concentrations for reference Li solution at room temperature.
Stirring time: —○— 1 h; —●— 3 h; —□— 6 h; —■— 12 h; —△— 24 h; —▲— 48 h.
(Apparent) initially set pH: 13.0. Al salt: $AlCl_3$.

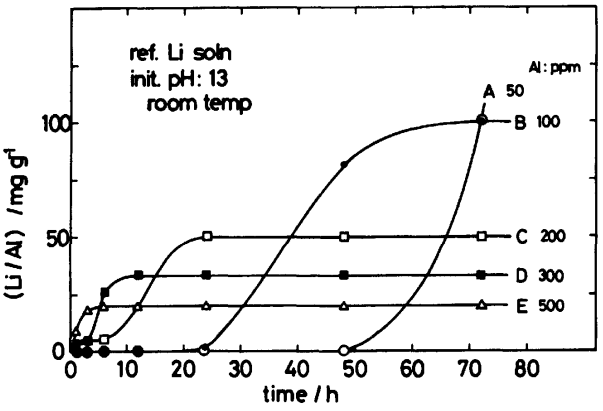

Fig. 7. The relation of (lithium/alminium) and stirring time for reference Li solution at room temperature. Al concentrations and percent recoveries of Li (in parentheses): A —○— 50 ppm (50%); B —●— 100 ppm (100%); C —□— 200 ppm (100%); D —■— 300 ppm (100%); E —△— 500 ppm (100%); [Theoretical maximum = 257 mg (Li)/g (Al), as $LiAlO_2$] (Apparent) initially set pH: 13.0.

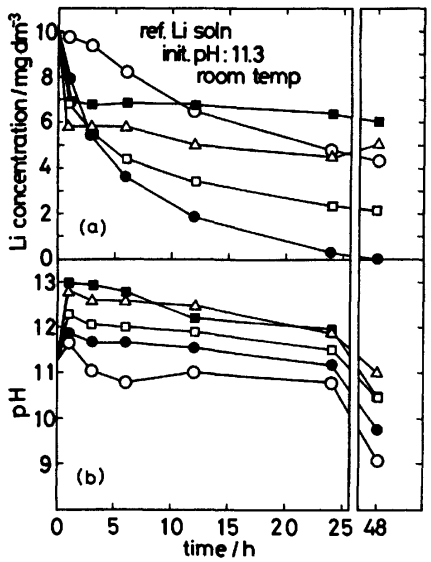

Fig. 8. The plots of residual Li concentration *vs.* time and pH *vs.* time for reference Li solution with various kinds of Al concentrations at room temperature.
Al concentrations: —○— 50 ppm; —●— 100 ppm; —□— 200 ppm; —■— 300 ppm; —▲— 500 ppm; initially set (apparent) pH: 11.3.

by the partial crystallization of the aluminium hydroxide coprecipitated. The relation of (Li(mg)/Al(g)) and the time course is shown in Fig. 7. The figure shows that, although a 100% recovery of Li for an Al concentration of 100—500 ppm is achieved after 72 h stirring, the Li yield for 1 g of aluminium decreases with the increase in the Al concentration. However, as the relation between the stirring time and the Al concentration shows, there are several cases of Li recovery [see Fig. 7]. Therefore, the stirring time is also an important factor for Li recovery from the economical point of view. Figure 8 shows the plot of the Li recovery *vs.* time for the respective Al concentration at an initial pH of 11.3.

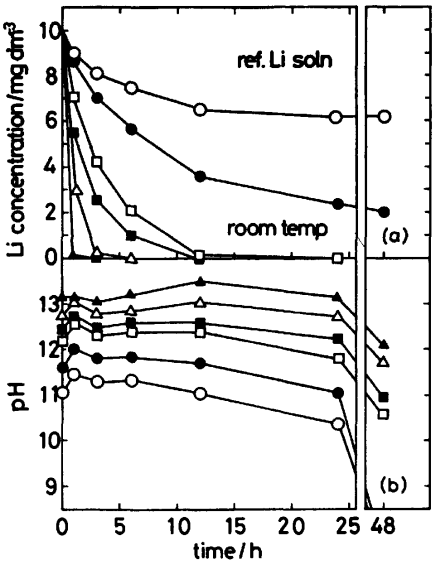

Fig. 9. The plots of residual Li concentration *vs.* time and pH *vs.* time for reference Li solution with various kinds of Al concentrations at room temperature. [Without initial pH controls]
Al concentrations ($NaAlO_2$): —○— 50 ppm; —●— 100 ppm; —□— 200 ppm; —■— 300 ppm; —△— 500 ppm; —▲— 1000 ppm.

The effects of Al concentration differ much from the results for the initial pH of 13 and a higher Li recovery is obtained in the region of relatively low Al concentrations. As has been stated above, in this experimental research, the recovery of lithium was achieved in a relatively higher pH region. This result differs considerably from the results of Goodenough *et al.*[5] In a high pH region, Al salt will exist in the state of the aluminate ion ($Al(OH)_4^-$), and the use of water-soluble aluminate might be preferable, as has been mentioned already. In Fig. 9, the results for sodium aluminate instead of aluminium chloride are shown without any pH control. This experimental result could not be compared with those for $AlCl_3$ since the initial pH control was not made. However, from the values of initial pH, the experimental results for the Al concentration of 1000 ppm by the use of $AlCl_3$ at pH 13 and the results for the Al concentration of 50 ppm at pH 11.3 can be compared with those of the corresponding Al concentration by the use of $NaAlO_2$. As far as these high and low Al concentrations are concerned, the use of sodium aluminate seems to be superior to that of aluminium chloride (see Figs. 5, 8, and 9). The difference should be small in principle, but the real difference observed cannot be explained properly at present.

On the Mechanism of Li Recovery. On the Li recovery by the coprecipitation method, two explanations are considered; one is the recovery by adsorption,[17] and the other, that by precipitation by the formation of a water-insoluble aluminate complex.[5-8] However, no satisfactory explanation has yet been given. Therefore, in the present work, attempts will be made to clarify the effects of both adsorption and precipitation by

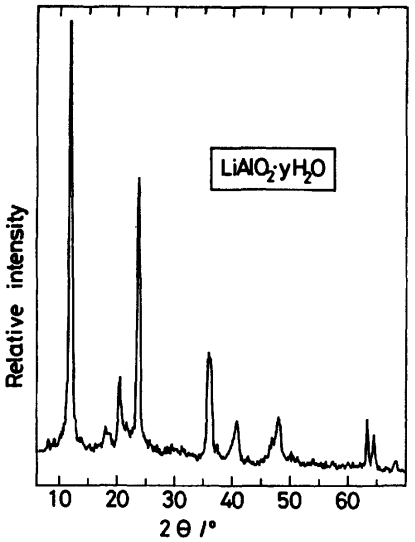

Fig. 10. X-Ray diffraction pattern of lithium alminate, $LiAlO_2 \cdot yH_2O$ (Cu $K\alpha$).

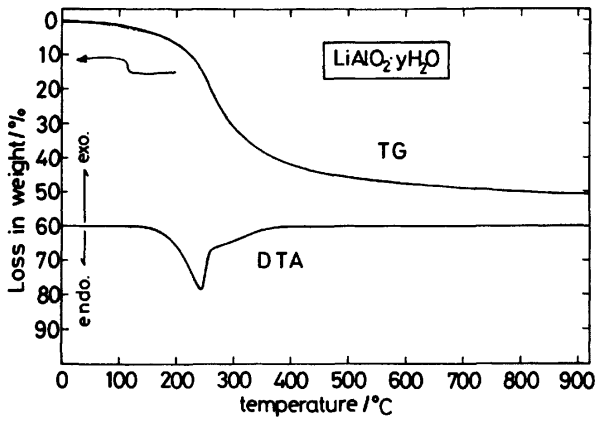

Fig. 11. Thermal analysis of lithium alminate ($LiAlO_2 \cdot yH_2O$).

means of complex formation.

(1) Formation of an Insoluble Aluminate Complex. A mixture of a $NaAlO_2$ solution and a LiCl solution causes precipitation. The precipitate is a white powder. Many kinds of precipitates were produced by the use of different mixing ratios at room temperature. After a certain time of stirring, the precipitates were filtrated with a glass filter (G-4) and then washed with water and acetone until the chloride ion was no longer detectable. Parts of the precipitates were dried in two ways: (A) by vacuum drying at room temperature, and (B) by 105 °C drying. The X-ray diffraction patterns and DTA and TG curves were measured for the A and B samples. A and B gave nearly the same patterns. In Figs. 10 and 11, the pattern and the DTA and TG curves for B (prepared under a Li-rich condition; $(Li/Al)_{mol}=5$) are shown. The X-ray diffraction patterns obtained for B were consistent with the lattice constants of lithium aluminate ($LiAlO_2 \cdot yH_2O$) listed on the ASTM card (20-618). The diffraction patterns for these compounds agreed very closely with each other, irrespective of the mixing ratio of Li to Al, although the relative intensities sometimes differed. It might be noted here that if a

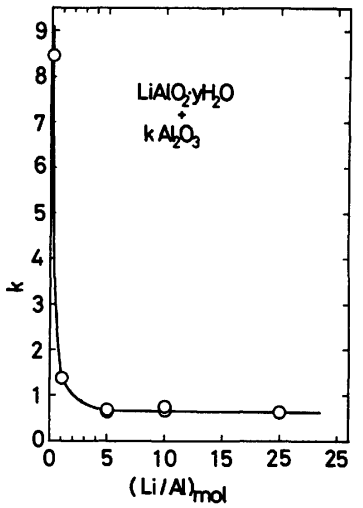

Fig. 12. Relation of $(Li/Al)_{mol}$ *vs.* k, where k represents the amount of additionally produced aluminium hydroxide.

stoichiometrically excess amount of aluminium salt for lithium was used, additional peaks of aluminium hydroxide were found. The composition of the lithium aluminate complex has been reported to be $Li_2O \cdot 2Al_2O_3$ or $Li_2O \cdot 2.5Al_2O_3$ or around $Li_2O \cdot 4.7Al_2O_3$;[5,20] this seemed somewhat in conflict with our present results obtained by means of X-ray diffraction analysis. If the aluminium complex is $LiAlO_2 \cdot yH_2O$, the ratio of Li_2O to Al_2O_3 is unity. Therefore, the precipitates obtained in our study were dissolved by hot hydrochloric acid to determine the accurate ratio of aluminium to lithium. For the analysis of aluminium, the titration method was employed (see Fig. 4). The results show that, in the synthesis of the lithium aluminate complex, the reduction of the molar ratio of LiCl to $NaAlO_2$ increases the aluminium content in the lithium aluminate complex. The DTA and TG curves for lithium aluminate complex exhibit simple patterns, as is shown in Fig. 11. However, the increase in the aluminium content in the lithium aluminate complex gives an additional endothermic DTA peak about 230 °C. The TG curve for the lithium aluminate complex (Sample B) in Fig. 11 shows a rapid decrease in weight in the range of about 200 and 300 °C; this might correspond to the dehydration of hydrated water in the lithium aluminate complex. A consideration of several data on the lithium aluminate complex leads to the following formula:

Lithium aluminate complex precipitated in the solution $\equiv LiAlO_2 \cdot yH_2O$(crystal) $+ k\, Al_2O_3 \cdot zH_2O$(amorphous).

It seems that, theoretically, in the very high pH region (about pH 13), only the lithium aluminate exsists. However, the real lithium aluminate complex precipitated contains relatively much aluminium. Aluminium hydroxide seems to be very easily formed. Figure 12 shows the relation of the k value and the lithium to aluminium ratio, $R[=(Li/Al)_{mol}]$. k decreases with an increase in R. Even if the R goes beyond 5, however, the k value does not decrease below about

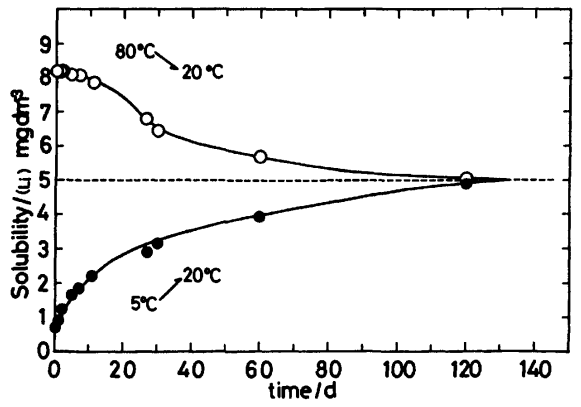

Fig. 13. Solubility of lithium alminate, $LiAlO_2 \cdot yH_2O$, represented by Li concentration (mg dm^{-3}) at 20 °C. —●—: Heated to 80 °C (1 d) and set to 20 °C. —○—: Cooled to 5 °C (1 d) and set to 20 °C.

0.6. From this value, the ratio of $(Li : Al)_{mol} = 1 : 2.2$ is obtained; this value is intermediate between 2.0 and 2.5. To diminish the k values, various conditions were introduced, such as a high pH, a high temperature (90 °C) and low temperature (5 °C) of the solutions, and high and low concentrations of LiCl and Al salts, but the results were all unsatisfactory. The use of solvents such as methanol, ethanol, acetone, and their mixture with water sometimes lowered the k values, but it was difficult to decrease the k to less than the 0.38 in the present work. [By the way, the $LiAlO_2$ listed in the ASTM card on the X-ray diffraction pattern was prepared at room temperature by the hydrolysis of γ-$LiAlO_2$ which is synthesized at a high temperature.[25]]

(2) Adsorption. A $NaAlO_2$ (500—1000 ppm as Al) solution was hydrolyzed to aluminium hydroxide by blowing CO_2 through the solution. Immediately after the $Al(OH)_3$ had been prepared, the Li ion was adsorbed, but the amount of the lithium adsorbed on hydroxide was very small. According to an experimental study by Kitamura *et al.*,[17] the value of 0.36 mg (Li)/g (adsorbent) is obtained under the best conditions. The reason for the difference between their results and ours is not clear, but, as a result of the substle difference in preparation conditions, a partial crystallization of aluminium hydroxide might have occurred in the present work. Kitamura *et al.* reported that amorphous aluminium hydroxide adsorbs much lithium, while crystallized aluminium hydroxides (beyerite, pseud böhmite *etc.*) do not adsorb lithium.

These results show that the success with lithium recovery using the coprecipitation method can not be explained by the adsorp tion only, but can be explained by the formation of a ithium aluminate complex slightly soluble in water. The formation of the lithium aluminate compound was also found in geothermal water after the removal of polymerized silica using much iron(III) hydroxide. That is, after the removal of the silica, Al salt (50—100 ppm as Al) was added to the geothermal water and the compound precipitated was measured by means of an X-ray diffractometer. In the lithium recovery using Al salt, the formation of the lithium aluminate complex is dominant. Therefore, the solubility of the lithium aluminate will be very important. The solubility of the lithium aluminate ($LiAlO_2 + (0.38Al_2O_3)$) obtained in the present study was measured by determining the Li concentration; it is shown in Fig. 13. The figure shows that the solubility of lithium aluminate is 5.0 ppm (as Li) at 20 °C.

Provided the solubility equilibrium of lithium aluminate

$$LiAlO_2 \rightleftarrows Li^+ + AlO_2^-$$

the solubility product is:

$$K_{sp} = [Li^+][AlO_2^-] = 5.2 \times 10^{-7} \text{ (at 20 °C)}.$$

If the detection limit of Li^+ by the atomic-absorption flame method is 0.02—0.05 ppm, the concentration of aluminate ions of 0.072—0.180 M; in other words, an aluminium concentration of 2000—5000 ppm is required to recover the lithium essentially to completion. The same calculation tells us that an Al concentration of about 200 ppm is required to reduce the lithium concentration to 0.5 ppm. However, when a pure LiCl solution ($[Li^+] = 10$ ppm) was used, the Al concentration of 200 ppm was enough to recover the Li completely with the optimum pH and temperature. On the basis of the above results, the following mechanism may be suggested. First, stoichiometrically excess amount of aluminium salt causes the reaction of Li^+ and the aluminate ion (AlO_2^-) to form the lithium aluminate complex, ($LiAlO_2 \cdot yH_2O$). Then, successively or simultaneously the residual Li^+ will be adsorbed by the aluminium hydroxide which is formed by the extra amount of Al salt, although the $Al(OH)_3$ is easily formed even if a stoichiometrical amount of Al salt is used. This simplified two-step mechanism can explain the major part of the lithium recovery by the coprecipitation method. The solubility of $LiAlO_2$ will depend upon the pH, the temperature, and the various kinds of polynuclear aluminium complexes and other kind of salts in solution. Thus, the values cited above may be first approximations.

Influence of Temperature on Li Recovery. It is clear that, when the Li concentration of 10 ppm is used, the formation of the lithium aluminate complex is essential and the solubility may largely depend upon the solution temperature. Geothermal water in the Hatchobaru area has a relatively high temperature (80—90 °C) at the outlet. In view of the effective utilization of the geothermal water, operations at a high temperature will be required. The experimental results on Li recovery at 80 °C are shown in Fig. 14. The figure depicts behavior fairly different from that at room temperature. That is, for all the ref. Li solutions with variously set pH's, minima are found. Within 1 to 6 h, the plot of the residual Li concentration *vs.* the time shows minima, and then shows a linear rise to the Li concentration of 9—10 ppm with the time. This phenomenon might be interpreted as follows. In the first stage, the lithium aluminate complex and aluminium hydroxide which adsorbed Li^+ are precipitated rapidly; then the aluminate dissolves linearly according to the solubility equilibrium and $Al(OH)_3$ releases the

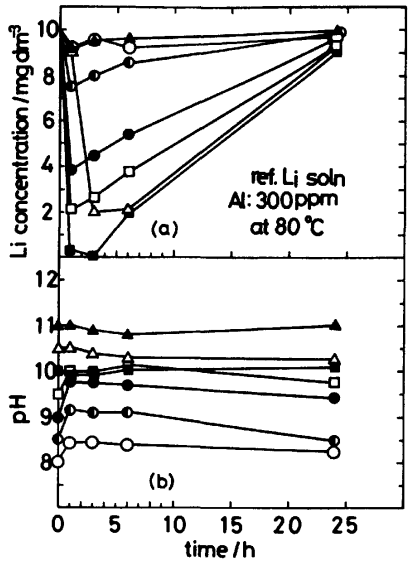

Fig. 14. The plots of residual Li concentration *vs.* time and pH *vs.* time for reference Li solution with various kinds of initially set pHs at 80 °C.
Al concentration: 300 ppm ($AlCl_3$); Apparent initial pHs: —○— 8.0; —◐— 8.5; —●— 9.0; —□— 9.5; —■— 10.0; —△— 10.5; —▲— 11.0.

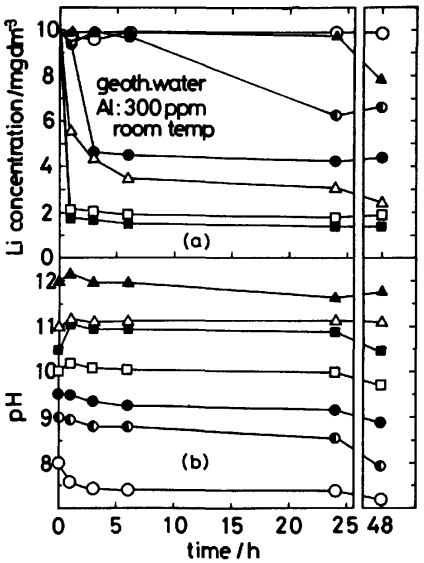

Fig. 15. The plots of residual Li concentration *vs.* time and pH *vs.* time for geothermal water with various kinds of initially set pHs at room temperature. Al concentration: 300 ppm ($AlCl_3$).
(Apparent) initial pHs: —○— 8.0; —◐— 9.0; —●— 9.5; —□— 10.0; —■— 10.5; —△— 11.0; —▲— 12.0.

Li^+ ions. Also, in this case, a high temperature seems to accelerate the precipitating speed, as is shown in Fig. 14. When the Li recovery is made at a high temperature, the pH control must be made accurately and a short recovery time is desirable.

Li Recovery Using Geothermal Water. The basic study of Li recovery has revealed several important facts, and now Li can be recovered from geothermal water.

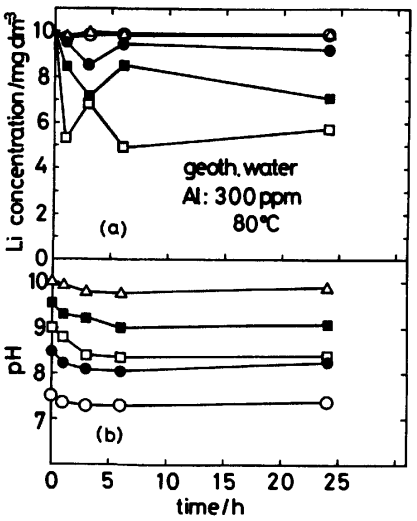

Fig. 16. The plots of residual Li concentration *vs.* time and pH *vs.* time for geothermal water with various kinds of pHs at 80 °C. Al concentration: 300 ppm ($AlCl_3$).
(Apparent) initial pHs: —○— 7.5; —●— 8.5; —□— 9.0; —■— 9.5; —△— 10.0.

Figure 15 shows the results obtained at room temperature. For geothermal water, even under the best conditions, only a recovery of 80 to 85% was attained; the optimum pH was in the range of 10—10.5. For the ref. Li solution, the percentage of recovery was 100% at the optimum pH (about 13). A relatively large difference in the behavior of Li extraction was found between the ref. Li solution and geothermal water. That is, for geothermal water, the pH dependence on the Li recovery was not large as in the case of the ref. Li solution. Geothermal water seems to have a kind of buffering action. The use of an Al concentration of 500 ppm increased the Li recovery, and the optimum pH region became wider (pH 10—11). Figure 16 shows the experimental results at 80 °C using an Al concentration of 300 ppm. The extent of Li recovery is very low, as had been expected, and the optimum pH is around 9, which is lower than that for geothermal water at room temperature. A comparison of Fig. 16 with Fig. 14 shows that, for the ref. Li solution, a high Li recovery is possible within a few hours. For geothermal water, however, no such rapid recovery of lithium is observed. In the case of the ref. Li solution, the yield of Li becomes small (within 10%) after 24 h. For geothermal water, however, the change in the Li recovery with the time is relatively small. From this fact, it can also be recognized that geothermal water has a buffering action even if the temperature rises. Next, the dependence of the Al concentration by the use of $NaAlO_2$ on the Li recovery was studied; it is shown in Figs. 17 and 18 at room temperature and at 80 °C respectively. The addition of $NaAlO_2$ to geothermal water without pH control was done just as in the case of the ref. Li solution. The yield of Li in this case was not so good as in the case of the ref. Li solution using the Al concentration of 100 ppm. In the case of geothermal water, the recovery of lithium was naught

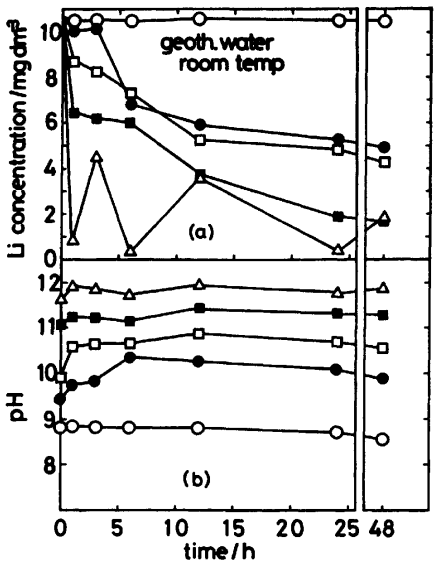

Fig. 17. The plots of residual Li concentration *vs.* time and pH *vs.* time for geothermal water with various kinds of Al concentrations at room temperature.
Al concentrations ($NaAlO_2$): —○— 100 ppm; —●— 200 ppm; —□— 300 ppm; —■— 500 ppm; —△— 1000 ppm.

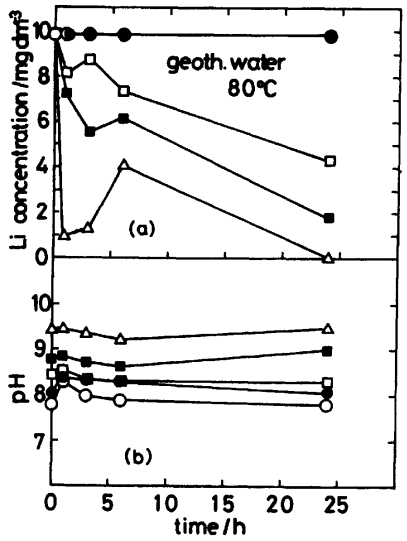

Fig. 18. The plots of residual Li concentration *vs.* time and pH *vs.* time for geothermal water with various kinds of Al concentrations at 80 °C.
Al concentrations ($NaAlO_2$): —○— 100 ppm; —●— 200 ppm; —□— 300 ppm; —■— 500 ppm; —△— 1000 ppm.

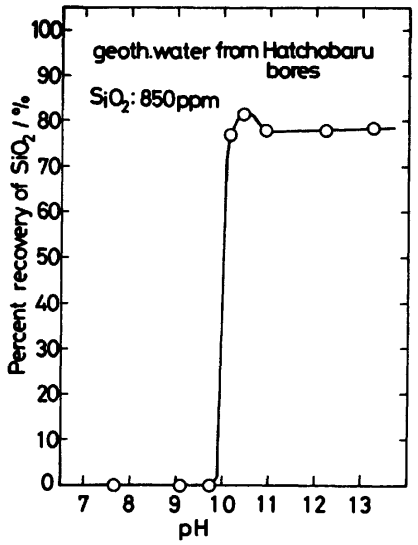

Fig. 19. The relation between precipitation of polymerized colloidal (or suspended) silica in geothermal water and pH. [The values in ordinate were determined from the silica concentrations in filtrates passed through the No. 131 filter papers.]

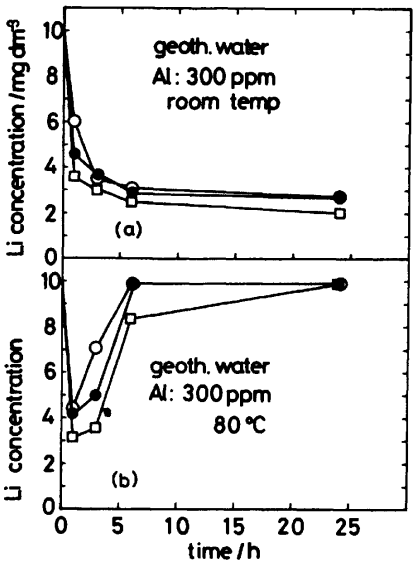

Fig. 20. The plots of Li concentration *vs.* time, for geothermal waters with three kinds of silica concentrations at room temperature (a) and at 80 °C (b).
Al concentration: 300 ppm ($AlCl_3$). [Li^+]: 9.9 ppm.
Silica concentrations: —○— 100% (=stock geothermal water; 850 ppm); —●— 20%; —□— 0%.

using the same concentration of aluminium salt. Even if the Al concentrations of 500 and 1000 ppm are used, a complete recovery is not accomplished. Strangely, the residual lithium concentration changed in a zig-zag fashion with the passage of time for the Al concentration of 1000 ppm. The results at 80 °C for Al concentrations of 300, 500, and 1000 ppm are similar to those at room temperature, although for Al concentrations of 100, or 200 ppm, practically no Li is recovered. The reasons for this are not clear. One reason may be that geothermal water contains various kinds of salts. The most probable constituents which function negatively are high-concentration sodium chloride, polymeric silicic acid, and calcium ions. The addition of much NaCl (10^4—3×10^4 ppm) to a ref. Li solution did not change the effect on the Li recovery. The polymerization of silicic acid and silicate in geothermal water is accelerated by the addition of alkali, and the particle sizes of the colloidal silica are increased. Colloidal and suspended silica in geothermal water was examined by

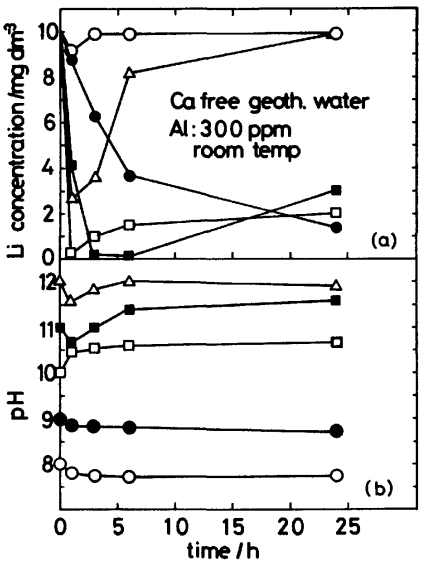

Fig. 21. The plots of residual Li concentration *vs.* time, and pH *vs.* time for Ca free geothermal water with various kinds of pHs at room temperature.
Al concentration: 300 ppm ($AlCl_3$). [Li^+]: 10.0 ppm
(Apparent) initial pHs: —○— 8.0; —●— 9.0; —□— 10.0; —■— 11.0; —△— 12.0.

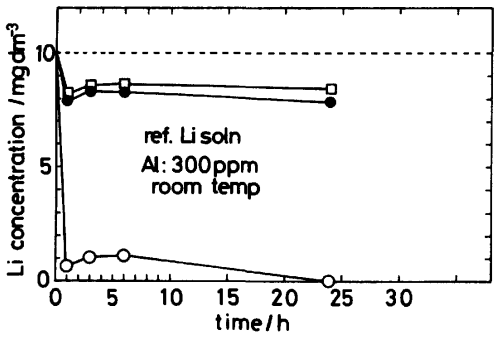

Fig. 22. The plots of residual Li concentration *vs.* time for reference Li solution with three kinds of Ca concentrations at room temperature. Al concentration: 300 ppm ($NaAlO_2$).
Ca concentrations ($CaCl_2$): —○— 0 ppm; —●— 70 ppm; —□— 400 ppm.

the molybdenum yellow method in connection with the percentage of the recovery of silica *vs.* the pH. The results are shown in Fig. 19. As is shown in this figure, a greater part of the silica in geothermal water is recovered at pH 10 or above. A perfect recovery of silica from geothermal water is accomplished by the addition of $FeCl_3$ ($[Fe^{3+}]=1000$ ppm), with the pH controlled at 10.5. The influence of silica in geothermal water was examined at room temperature and at 80 °C; the results are shown in Fig. 20. The results show that polymeric silica affects the Li recovery, but to a small extent. The influence of the calcium ions was then examined. The calcium ions (about 20 ppm) in the geothermal were eliminated in the form of calcium oxalate. The results are shown in Fig. 21. A comparison of Fig. 21 with Fig. 15 (with Ca^{2+}) shows that the Li recovery rises remarkably and that the short-time percent-recovery is relatively high in the case of calcium-free geothermal water. Experiments were also made for ref. Li solutions to which calcium chloride had been added so that the Ca concentrations were 70 and 400 ppm respectively. The effects of calcium ions are prominent, as is shown in Fig. 22.

It may be concluded, from the results obtained, that geothermal water has a kind of buffering action and that the buffer capacity may be attributed mainly to the polymeric silicic acid and/or silicate ions. The existence of polymeric silica and calcium ions leads to remarkably negative effects on the recovery of lithium from geothermal water at the Hatchobaru bores. The mechanism of lithium recovery by the coprecipitation method can be explained by the formation of lithium aluminate complex, followed by the adsorption of residual lithium by the aluminium hydroxide (amorphous) coprecipitated.

References

1) M. Steinberg and V_I-Duong Dang, *U. S. Geol. Surv. Prof. Pap.*, **1005**, 79 (1976).
2) J. P. Holden, *Lawrence Livermore Lab., UCID-15953*, (1971).
3) J. D. Lee, *Proc. NNES Conf. on Nucl. Fusion Reactors*, 471 (1969).
4) "Kisho Kinzoku To Sentan Gijutsu," ed by the Ministry of International Trade and Industry, Nikkan Kogyo Shinbun, Tokyo (1982), p. 136.
5) R. D. Goodenough, U.S. Patent 2964381 (1960).
6) R. D. Goodenough and V. A. Stenger, U.S. Patent 2980497 (1961).
7) A. M. Kennedy, *Proc. U.N. Conf.*, **3**, 502 (1961).
8) D. Kaplan, *Isr. J. Chem.*, **1**, 115 (1963).
9) S. P. Hannover and E. R. Celle, Deutches Patentamt DBP 1150055 (1964).
10) R. A. Gaska and R. D. Goodenough, U.S. Patent 3268290 (1966).
11) R. D. Goodenough and R. A. Gaska, U.S. Patent 3306712 (1967).
12) M. P. Neipert and C. K. Bon, U.S. Patent 3306700 (1967).
13) R. D. Goodenough and R. A. Gaska, U.S. Patent 3307922 (1967).
14) J. R. Nelli and T. E. Arthur, Jr., U.S. Patent 3537813 (1970).
15) D. H. Christfer *et al.*, *PB Report*, 245686 (prepared for Bureau of Mines, 12 June 1975).
16) C. E. Berthold and D. H. Baker, Jr., *U.S. Geol. Surv. Prof. Pap.*, **1005**, 61 (1976).
17) T. Kitamura and H. Wada, *Nippon Kaisui Gakkaishi*, **32**, 78 (1978).
18) J. M. Lee and W. C. Bauman, U. S. Patent 4116856 (1978).
19) W. N. Smith, U.S. Patent 4076794 (1978).
20) I. Pelly, *Soc. Chem. Ind.*, 469 (1978).
21) T. Takeuchi, Japan Kokai Tokkyo Koho, 107412 (1979).
22) S. Mercado, J. A. Löpez, and R. Angulo, *Trans. Geotherm. Resour. Counc.*, **3**, 449 (1979).
23) T. Takeuchi, *J. Nucl. Sci. Technol.*, **17**(**12**), 922 (1980).
24) J. A. Epstein, E. M. Feist, and J. Zmora, *Hydrometallurgy*, **6**, 269 (1981).
25) A-M. Lejus, *Rev. Hautes. Temp. Refract.*, **1**, 53 (1964).

 © 1983 The Chemical Society of Japan Bull. Chem. Soc. Jpn., 56, 2499—2503 (1983)

Glass-like Carbon Made from Epoxy Resin Cured with 2,4,6-Trinitrophenol

Kazuro KAWAMURA* and Shiushichi KIMURA†

Department of Chemistry, National Defense Academy, 1-10-20, Hashirimizu, Yokosuka 239

†*Research Laboratory of Engineering Materials, Tokyo Institute of Technology, Nagatsuta, Midori-ku, Yokohama 237*

(Received July 24, 1982)

It has been found that a glass-like carbon can be produced by the slow and carefully controlled pyrolysis of the epoxy resin (Epikote 828) cured with 2,4,6-trinitrophenol (TNP) with a weight of 10—15%. The most characteristic property of the glass-like carbon was seen in its change in density with the heat-treatment temperature. Under heat treatment at temperatures up to 1000 °C, a dense glass-like carbon of which density was 1.65—1.70 g/cm^3 was formed. The density of the glass-like carbon decreased, however, at heat-treatment temperatures above 1000 °C. Upon heat treatment at the temperature of 3000 °C, the density dropped to a low value of 1.04—1.11 g/cm^3. The former increase in density is connected with the large-scale dehydration reaction which may proceed between nitro groups and hydrocarbon chains in the cure resin. The latter decrease in density is caused by the progress of the graphitic orientation of carbon-layer planes in the cross-linked structure of the highest degree. If carbon fibers were present in this glass-like carbon, the graphitization of the glass-like carbon in the composite proceeded more easily than that of the glass-like carbon alone.

In general, there is a 40—50% loss in weight when carbon-rich materials are carbonized under atmospheric pressure, for pores or cracks then develop in the carbonized product as a result of the release of volatile matter and the shrinkage in volume. It is well known that some thermosetting polymer resins are converted into carbonized products resembling glass in appearance and in fractural property. The glass-like carbon is characterized by a low density, a very low gas permeability, and an isotropic disordered structure.[1-6] Phenol–formaldehyde resin and furfuryl alcohol resin are suitable as starting materials to obtain glass-like carbon in a good yield.

We have previously reported that 2,4,6-trinitrophenol (TNP) can be used as the curing agent of the liquid expoxy resin, Epikote 828. Moreover, the explanation of the curing mechanism and some applications of this cure system have been attempted.[7,8] It is a good example of the applications that the pre-heated cure resin at 150 °C turned to the glass-like carbon upon slow and carefully controlled pyrolysis. If the common curing agents such as aliphatic polyamines were used instead of TNP for the epoxy resin, the cure resin could not maintain its original shape during carbonization. In this glass-like carbon there can be seen some characteristic behavior in the process of carbonization and graphitization. In the present paper this behavior is examined by means of thermogravimetric analysis, the measurement of the density, a microindentation hardness test, an X-ray diffraction study, and optical observation, and the behavior is compared with that of the usual glass-like carbons made from phenol-formaldehyde resin and furfuryl alcohol resin. Moreover, the graphitization of the glass-like carbon containing carbon fibers is examined.

Experimental

The epoxy resin was Epikote 828 (Shell Chemical Co., diglycidyl ether of bisphenol A). The TNP used here was of a commercially guaranteed reagent grade and was dried after grinding. As furfuryl alcohol resins, Hitafuran 302 (Hitachi Kasei Co.) and its curing agent, A_3 (the same company) were used. The phenol–formaldehyde resin was of a resol type, which scarcely needed the curing agent. The carbon fibers of PAN-based Torayca T300 were chosen.

A sample containing carbon fibers was prepared in the following manner: the carbon fibers aligned in the same direction were stacked in the vessel, and then the resin was poured upon them and cured at 130 °C in air. After curing, the composite was cut in small pieces (about $10\times10\times20$ mm) by means of a diamond cutter. On the basis of a photographical survey, the carbon-fiber content in the composite was found to be in the range of 30—42% in volume.

The heat treatment was accomplished at a rate of 30 °C/h up to 500 °C, and thereafter at a rate of 120 °C/h to 1000 °C in a stream of argon. The heat treatment at temperatures from 1500 to 3000 °C was carried out in a graphite-resistance furnace in a stream of argon. Each heat treatment was achieved at a rate of 256 °C/h, after which the maximum temperature was held for 30 min.

The thermogravimetric analysis of the samples (a 100-mg portion of each sample was placed in a platinum cup) was run by heating at a rate of 2 °C/min in an argon atmosphere by using the electronbalance (Cahn 1000).

To obtain a clear indent with the Vickers hardness tester (Shimadzu Seisakusho Ltd.), the surfaces of the carbonized samples were polished as plane mirrors. The indents were marked by means of a Vickers diamond for 30 s under a load of 1000 g.

The X-ray diffraction profile of (002) line on the powdered sample was obtained with Ni-filtered Cu *Ka* radiation. The interlayer spacing, d_{002}, and the crystallite thickness, L_c, were estimated from profiles in which the corrections of the Lorentz-polarization, atomic-scattering, and absorption factors were made in a usual way.[9] The profile of the composite made from cure resin containing carbon fibers was separated into the component profiles of the matrix carbon and the fiber carbon. The separation was made as follows: the profile of fiber carbon was obtained at an individual temperature. We assumed that the profile of fiber carbon agreed with the fiber-carbon component in the composite profile at the individual temperature. The composite profile could be separated into its component profiles based on the fiber-carbon component.

Results

Carbonization. It is most proper to use 10—15%

TABLE 1. COMPARISON OF PROPERTIES OF GLASS-LIKE CARBONS MADE FROM EPOXY RESIN CURED WITH TNP, PHENOL–FORMALDEHYDE RESIN, AND FURFURYL ALCOHOL RESIN

	Epoxy resin/TNP		Phenol resin	Furfuryl resin Fur./A_3=99.7/0.3
	90/10	85/15		
Curing conditions	130 °C, 48 h ↓ 140 °C, 48 h ↓ 150 °C, 48 h	130 °C, 48 h ↓ 140 °C, 48 h ↓ 150 °C, 48 h	40 °C, 10 d ↓ 60 °C, 10 d ↓ 80 °C, 10 d	40 °C, 10 d ↓ 60 °C, 10 d ↓ 80 °C, 10 d
Bulk density of cure resin/g cm^{-3}	1.23	1.24—1.25	1.24	1.29—1.3
Shrinkage[a] $(V_1-V_2)/V_1\times 100$ (%)	75—77	74—75	50—51	50—51
Yield/wt%	29—30	32—34	56—58	56—57
Density/g cm^{-3} [b]	1.65	1.70	1.52	1.50
Vickers hardness	400—420	430—440	360—390	360—370

a) Carbonized to 1000 °C. b) Densities of finely ground samples were measured by the immersion method in 1-butanol using a pycnometer at 20 °C.

of TNP as a curing agent for the epoxy resin. The polymerization reaction of the system was dependent on the curing temperature, as has been reported previously.[7] Under the curing condition at 130 °C in air, at first a linear structure was formed, and then it was converted into a cross-linked one. The system containing 10% TNP was converted from the linear structure into the cross-linked one at 130 °C after 24 h. The converting time for the system containing 15% TNP became short (about 3 h). When carbonized at a heating rate of 30 °C/h in a stream of argon, the resin cured at 130 °C was burned with smoke by means of the rapid exothermic pyrolysis of nitro groups in the cure resin, and a porous carbonized product was formed. When the resin cured at 130 °C for 48 h in air was carefully heated at 150 °C in steps and then maintained at this temperature for about 48 h, its colour changed from yellow-orange to brown-black. When the cure resin preheated at 150 °C was heated at a rate of 30 °C/h in a stream of argon, it was gradually pyrolyzed, while keeping its shape, and was converted into a nonporous carbonized product considered to a glass-like carbon. This appearance is shown in Fig. 1. There are some cracks in the glass-like carbon, as denoted by the arrow.

The curing condition of the resins used and some properties of the glass-like carbons obtained from the cure resins heat-treated at 1000 °C are given in Table 1.

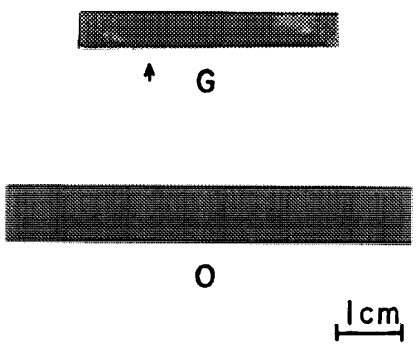

Fig. 1. Appearance of glass-like carbon made from epoxy resin cured with 10% of TNP.
O: Original resin heat-treated at 150 °C. G: Glass-like carbon obtained by heat treatment at 1000 °C.

It is worth noting that the density and the hardness of the glass-like carbon made from the epoxy resin cured with TNP are high, though its yield is low and the shrinkage in volume is larger than those of phenol–formaldehyde resin and furfuryl alcohol resin.

The pyrolysis of the epoxy resin cured with TNP was compared with that of samples heat-treated at 130 and 150 °C. The weight loss with the temperature is shown in Fig. 2. On the sample treated at 130 °C (Fig. 2, Curve 3) a rapid loss appeared at 215 °C, while on the other one, no corresponding loss could be seen (Fig. 2, Curve 4). This fact showed the difference in the appearance of the carbonized products; the former product was porous, and the latter, glass-like.

Change in Density with Heat-treatment Temperature. The changes in density on the glass-like carbons heat-treated at various temperatures up to 3000 °C are shown in Fig. 3. The density of the glass-like carbon made from the epoxy resin cured with TNP decreases as the heat-treatment temperature rises (Fig. 3, Curves 1 and 2). Although the decrease in density introduced by heat-treating glass-like carbons has previously been reported by Honda *et al.*[10] and Bose *et al.*,[11] no such large

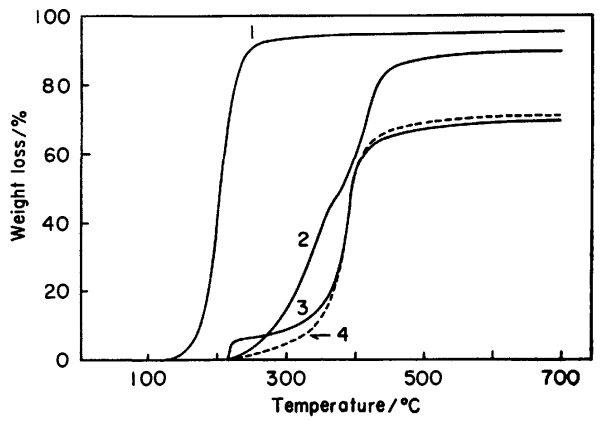

Fig. 2. Thermogravimetric analyses of TNP, epoxy resin and epoxy resin cured with 10% of TNP.
1. TNP. 2. Epoxy resin. 3. Epoxy resin cured with 10% of TNP at 130 °C for 48 h. 4. Epoxy resin cured with 10% of TNP at 130 °C for 48 h and then heat-treated at 150 °C for 48 h.

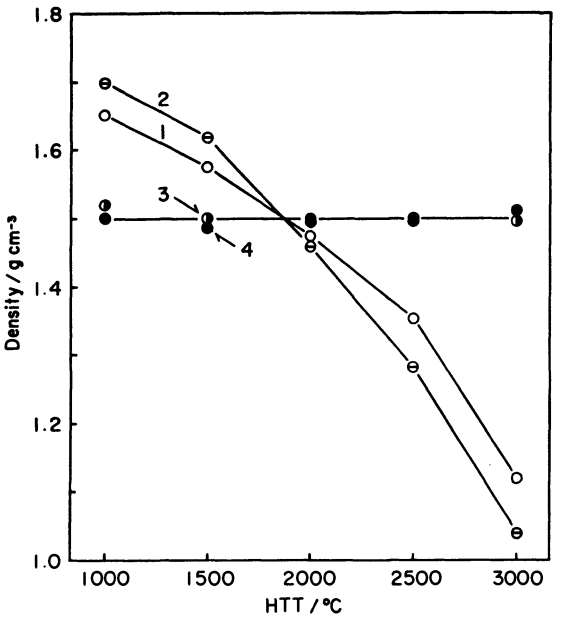

Fig. 3. Change in density of glass-like carbons with heat-treatment temperature (HTT).
1. Glass-like carbon made from epoxy resin cured with 10% of TNP. 2. Glass-like carbon made from epoxy resin cured with 15% of TNP. 3. Glass-like carbon made from phenol–formaldehyde resin. 4. Glass-like carbon made from furfuryl alcohol resin.

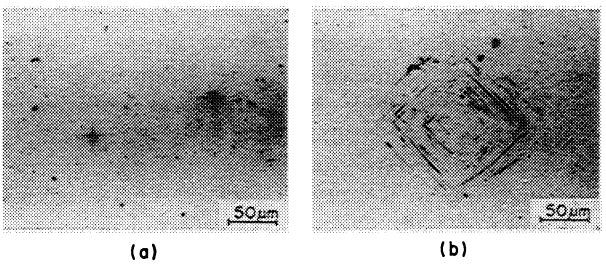

Fig. 4. Typical indent impressions obtained on polished surfaces of glass-like carbon made from epoxy resin cured with 10% of TNP.
(a) Heat-treatment temperature 1000 °C. (b) Heat-treatment temperature 3000 °C.

decrease in density as that here obtained has been known. When the glass-like carbon was made from the epoxy resin cured with 10% TNP in the heat-treatment temperature range from 1000 to 3000 °C, its density dropped from 1.65 g/cm³ to 1.11 g/cm³. On the other hand, when the glass-like carbon made from the epoxy resin was cured with 15% TNP, the density fell from 1.70 to 1.04 g/cm³. The differences in the densities of these samples are equivalent to 34 and 70% increases in the volume respectively. The change in volume is calculated by this equation; $(V_1-V_2)/V_1\times 100$, where V_1 and V_2 show the volume of the glass-like carbons heat-treated at 1000 and 3000 °C. No remarkable decrease in the density with an increase in the heat-treatment temperature can be seen on the glass-like carbons from phenol–formaldehyde resin and furfuryl alcohol resin (Fig. 3, Curves 3 and 4). They are almost constant with the heat-treatment

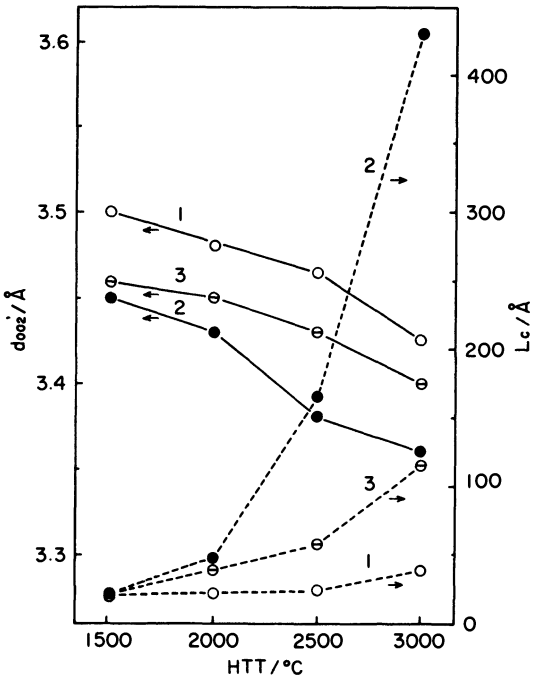

Fig. 5. Changes of interlayer spacing d_{002} and crystallite size L_c with heat-treatment temperature (HTT).
1. Glass-like carbon made from epoxy resin cured with 10% of TNP. 2. Glass-like carbon component in composite made from carbon fibers and epoxy resin–TNP (90 : 10) mixture. 3. Fiber carbon.

temperature. The change in the density of Curve 2 is larger than that of Curve 1. This shows that the large decreases in density is caused by the TNP which is used as the curing agent of the original resin.

Microindentation Hardness. Figures 4(a) and (b) show the imprints of the glass-like carbon heat-treated at 1000 and 3000 °C respectively. These photographs indicate that the imprint changes from a diagonal to a concave pattern as the heat-treatment temperature increases. This change can also be seen in the glass-like carbons made from phenol-formaldehyde resin and furfuryl alcohol resin in spite of the small change in the density, as is shown in Fig. 3, Curves 3 and 4. The concave imprint may show that the hardness of the glass-like carbon is remarkably lowered.

X-Ray Diffraction. The volume of the epoxy resin cured with TNP decreased extremely in the process of carbonization and increased largely on heat-treating above 1000 °C. If carbon fibers are contained in this cure resin, the graphitization of the matrix carbon of the composite may be influenced. This phenomenon is of interest in connection with the stress graphitization of glass-like carbon,[12-17] because the effect of a large change in the volume of the matrix carbon on the process of carbonization and graphitization has not yet been examined.

Figure 5 shows the changes in the values of d_{002} and L_c on the glass-like carbon made from the epoxy resin cured with TNP (Fig. 5, Curve 1), on the matrix carbon in the composite (Fig. 5, Curve 2), and on the fiber carbon (Fig. 5, Curve 3) heat-treated at 1500—3000 °C. Above 2000 °C, the glass-like carbon is more difficult

to graphitize than the carbon fibers. The graphitization of the matrix carbon in the composite proceeded greatly in comparison with that of the glass-like carbon only, regardless of the large increase in volume above 1000 °C.

Microscopic Observations. Micrographs of the composite made from the carbon fibers and the epoxy resin–TNP mixture are shown in Fig. 6. The matrix precursor before being carbonized had an isotropic structure (Fig. 6(a)). After heat-treatment at 1000 °C, anisotropic areas appeared in the matrix carbon around the carbon fibers and then spread out in the matrix (Fig. 6(b)). The area decreased somewhat after heat treatment at 2500 °C (Fig. 6(c)). This phenomenon is caused by the increase in the volume of the matrix carbon, which takes place upon heat treatment above 1000 °C. However, the development of a graphite-like structure was clearly recognized in the anisotropic region in the matrix, as is denoted by arrows. The carbon fibers were extremely deformed after heat treatment at 3000 °C (Figs. 6(d) and 7(b)-B). When the carbon fiber separates from the matrix carbon on heating, the shape of the carbon fiber is deformed a little (Fig. 7(b)-A). The micrograph of the cross-section parallel to the fiber axis in the composite heat-treated at 3000 °C (Fig. 7(a)) shows that the graphite-like layers are not simply aligned parallel to the fiber axis, but are zigzagged.

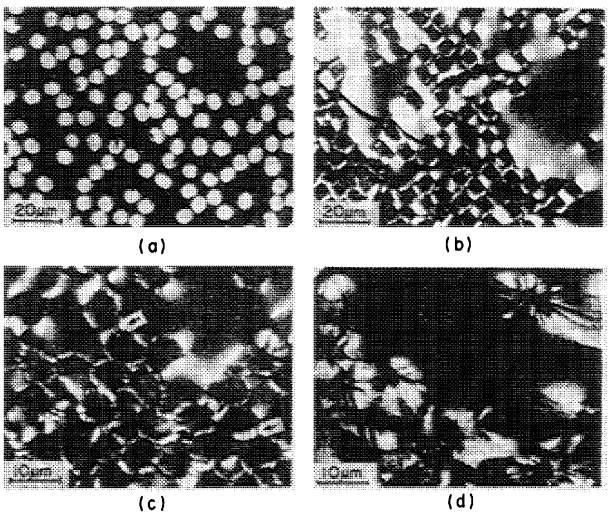

Fig. 6. Optical micrographs of composite made from carbon fibers and epoxy resin–TNP (90 : 10) mixture. (a) Original. (b) Heat-treatment temperature 1000 °C (polarized light). (c) Heat-treatment temperature 2500 °C (polarized light). (d) Heat-treatment temperature 3000 °C (polarized light).

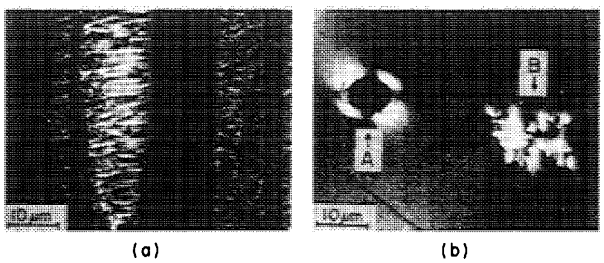

Fig. 7. Polarized light micrographs of cross section parallel (a) and perpendicular (b) to carbon fiber axis of carbon fiber–carbon composite made from carbon fibers and epoxy resin–TNP (90 : 10) mixture heat-treated at 3000 °C.

Discussion

Generally polynitro compounds are easily decomposed by heating, so it is difficult to keep the pyrolysis under control. This property does not change if they are present in cure resins.[18,19] The epoxy resin cured with 10—15% of TNP also has the property of rapidly decomposing upon heating. When the cure resin was preheated at 150 °C in air, however, the pyrolysis went on gently. It is considered that this gentle pyrolysis is brought about by the building of a highly cross-linked structure in company with the structural change in the nitro groups in the cure resin. The improvement of cross-linking formed by preheat treatment at 150 °C is proved by the insolubility in acetone. The resin cured with 10% of TNP and heat-treated at 130 °C for 48 h contained an insoluble part amounting to 70—80%. After heat treatment at 150 °C, the insoluble part increased to above 99% by weight.

Yamada, from the analytical results on gases evolved by the pyrolysis of a mixture of pitch and a nitro compound, found that the gases volatilized up to 500 °C were almost entirely occupied by water.[20] The formation of water in the present sample was suggested by the fact that the quartz window of the furnace used for carbonization was clouded by water drops at an early stage of the pyrolysis. A large-scale dehydration reaction during carbonization may lead to the formation of the highest degree of cross-linking in the structure.

The decrease in density above the heat-treatment temperature of 1000 °C can be interpreted in terms of the development of micropores and/or spaces caused by thermal swelling and structural change in the glass-like carbon. The thermal swelling may be brought by a relaxation of the rigid structure formed through the carbonization. It may be instructive to consider that nitro groups in the cured resin play an important role in pulling the carbon networks through the dehydration reaction. As a result, a rigid structure is established after carbonization. When the glass-like carbon in this state is heated at a temperature above 1000 °C, a partial bond-breaking may take place at the unstable positions of carbon networks in the glass-like carbon. The bond-breaking results in an expansion in volume. On the other hand, the structural change arises from the graphitic orientation of the carbon-layer planes in the glass-like carbon, as is shown in Fig. 5. When the values of density are plotted against those of the interlayer spacing, d_{002} (Figs. 3 and 5), along with the heat-treatment temperatures, a linear relationship is seen, as is indicated in Fig. 8. This relationship suggests that the spread of micropores and/or spaces originate in a narrowing of the interlayer spacing. This suggestion would mean that small-waved and entangled carbon-layer planes in the glass-like carbon are oriented straightly, accompanied by a combination of the carbon-

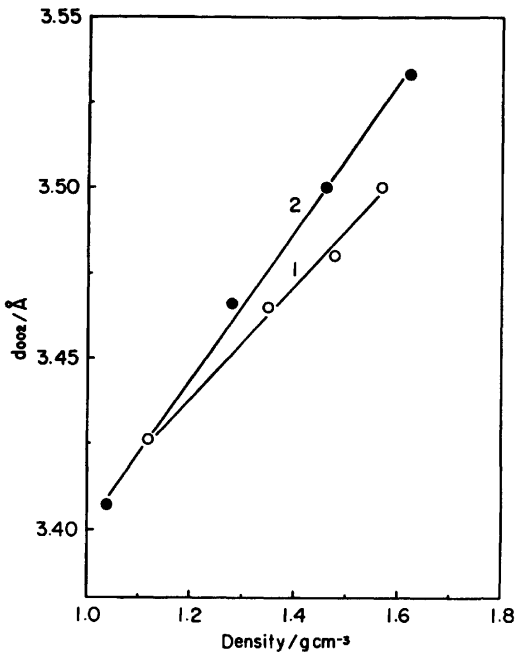

Fig. 8. Relation between interlayer spacing d_{002} and density.
1. Glass-like carbon made from epoxy resin cured with 10% of TNP. 2. Glass-like carbon made from epoxy resin cured with 15% of TNP.

layer planes, and that they jostle each other as the graphitization proceeds. The combination of carbon-layer planes and the complicated jostling may bring about the expansion in the volume of the glass-like carbon following the spread of micropores and/or spaces.

If the carbon fibers are contained in the glass-like carbon, its volumetric change will be suppressed to some degree by the stiffness of the carbon fibers. The carbon fibers in the matrix did not appear to be deformed during the carbonization (Fig. 6(b)). The expansion in volume of the matrix carbon which was caused by the high heat-treatment brought about the deformation of the carbon fibers (Figs. 6(d) and 7(b)-B). From the point of view of the stress graphitization of the matrix carbon in the carbon fiber–glassy carbon composite, the orientation of molecules (carbon-layer planes) of the matrix carbon formed in the process of carbonization is little influenced, even if a large volumetric expansion takes place in the matrix carbon of the composite after carbonization. Inagaki *et al.* have proved that the stress accumulation caused by shrinkage in the process of carbonization plays a significant role in the graphitization of matrix carbon in the carbon fiber-glassy carbon composite.[17] Our results also support their finding.

References

1) H. Honda, K. Ouchi, and Y. Hirose, *Nippon Kagaku Zasshi*, **76**, 148; H. Honda and K. Ouchi, *ibid.*, **76**, 154 (1955).
2) S. Yamada and H. Sato, *Nature*, **193**, 261 (1962).
3) H. W. Davidson, *Nucl. Eng.*, **1962**, 159.
4) S. Yamada, H. Sato, and T. Ishii, *Carbon*, **2**, 253 (1964).
5) T. Noda, M. Inagaki, and S. Yamada, *Bull. Chem. Soc. Jpn.*, **41**, 3023 (1968).
6) D. B. Fishback, *Carbon*, **9**, 193 (1971).
7) K. Kawamura, *Bull. Chem. Soc. Jpn.*, **56**, 676 (1983).
8) K. Kawamura, *Kogyo Kayaku*, **6**, 303 (1974).
9) "Tanso Zairyo Nyumon," ed by the Carbon Society of Japan, Tokyo (1972), p. 184.
10) H. Honda, Y. Sanada, T. Furuta, and H. Teranishi, *TANSO*, **46**, 2 (1966).
11) S. Bose and R. H. Bragg, *Carbon*, **19**, 289 (1981).
12) K. Tamada and S. Yamada, *J. Composite Mat.*, **7**, 119 (1973).
13) S. Yamada, K. Tamada, and M. Inagaki, *High Tem. -High Press.* **5**, 353 (1973).
14) S. Kimura, Y. Tanabe, N. Takase, and E. Yasuda, *Nippon Kagaku Kaishi*, **1981**, 1474.
15) Y. Hishiyama, M. Inagaki, S. Kimura, and S. Yamada, *Carbon*, **12**, 249 (1974).
16) S. Kimura, E. Yasuda, H. Tanaka, and S. Yamada, *Yogyo Kyokai Shi*, **82**, 26 (1975).
17) M. Inagaki, K. Tamada, and S. Yamada, *TANSO*, **90**, 85 (1977).
18) K. Kawamura, *TANSO*, **85**, 62 (1976).
19) K. Kawamura, *Kogyo Kayaku*, **38**, 31 (1977).
20) S. Yamada, *Kogyo Kagaku Zasshi*, **62**, 1200, 1533 (1959).

Decomposition of Hydrogen Bromide or Iodide by Gas Phase Electrolysis

Wakichi KONDO,* Susumu MIZUTA, Yoshinao OOSAWA, Toshiya KUMAGAI, and Kinjiro FUJII
Energy Chemistry Division, National Chemical Laboratory for Industry, Tsukuba Research Center, Yatabe, Ibaraki, 305
(Received December 10, 1982)

Gas phase electrolysis of HBr or HI was studied by using a fuel-cell-type electrolyzer provided with graphite gas diffusion electrodes and liquid film electrolyte of H_3PO_4. Current efficiency 100% may be achieved at decomposition voltages of 0.73 V (at 100 mA cm^{-2} and 150 °C) for HBr and 0.28 V (at 100 mA cm^{-2} and 145 °C) for HI. Both bromine and iodine produced may smoothly be evolved out of the anode in the gas or liquid form without being dissolved into the electrolyte H_3PO_4, causing no trouble on the separation of products. This electrolytic method may be incorporated in the bromine or iodine cycles for thermochemical hydrogen production to constitute an effective hybrid system.

The hydrogen production by a thermochemical cycle was extensively studied in 1970's. On the other hand, the hybrid system consisting of thermochemical and electrochemical processes began to be investigated when the pure thermochemical system was concluded to be extremely difficult. For the bromine and the iodine cycles,[1-6] much effort has been concentrated on the electrochemical decomposition of hydrogen bromide and iodide[4-12] since the decomposition of hydrogen halides was found to play a vital role in the cycle.

Below are listed some thermochemical values[13] associated with the decomposition of HBr and HI:

$$2HBr(g) \longrightarrow H_2(g) + Br_2(g) \quad (1)$$
$$\Delta H^\circ_{298} = 24.8 \text{ kcal mol}^{-1} \text{ (1 cal} = 4.184 \text{ J)}$$
$$\Delta S^\circ_{298} = -5.2 \text{ cal mol}^{-1} \text{ K}^{-1}$$
$$\Delta G^\circ_{298} = 26.2 \text{ kcal mol}^{-1}$$
$$\Delta G^\circ_{700} = 28.0 \text{ kcal mol}^{-1},$$
$$2HI(g) \longrightarrow H_2(g) + I_2(g) \quad (2)$$
$$\Delta H^\circ_{298} = 2.3 \text{ kcal mol}^{-1}$$
$$\Delta S^\circ_{298} = -5.3 \text{ cal mol}^{-1} \text{ K}^{-1}$$
$$\Delta G^\circ_{298} = 3.9 \text{ kcal mol}^{-1}$$
$$\Delta G^\circ_{700} = 5.6 \text{ kcal mol}^{-1}.$$

From these values one can easily understand that the thermochemical decomposition of HBr is fairly difficult[6,14,15] because of its too high a ΔG° (over 25 kcal mol^{-1}). The electrochemical decomposition of HBr in the aqueous state has extensively been studied by several investigators; according to Schuetz,[5] an HBr electrolysis, using graphite electrodes, at a cell voltage of 0.75—0.8 V and a current density of 200 mA cm^{-2} proceeds with a highly concentrated (47 wt%) HBr aqueous solution at 353—373 K and atmospheric pressure.

On the other hand, the decomposition of HI seems at first sight much easier because of its low ΔG° (5.6 kcal mol^{-1} at 700 K), but has been found more troublesome than expected since the mixed gas (H_2, I_2, HI, and H_2O) formed by direct pyrolysis requires a severe separation processing; some separation processes have been proposed[16-20] but their improvement is still required. As for the HI electrolysis no reports with detailed experimental descriptions have been published to the best of the present authors' knowledge.

The present authors have noted that the gas phase electrolysis is superior to the aqueous electrolysis in the following three respects:

1) As shown in Table 1, the theoretical decomposition voltages for the HX gases (0.58 V for HBr and 0.065 V for HI) are by far lower than those (1.08 and 0.54 V, respectively) for the aqueous HX. This is because the HX molecule in the gas phase is at a higher energy level than the one in the aqueous state ($a=1$) by the amount of free energy of hydration. For aqueous electrolyses at sufficiently low cell voltages (*e.g.*, 0.6—0.8 V for HBr) are to be achieved, an extremely concentrated HX solution is required as previously reported.[8,9,12]

2) In the case of aqueous electrolysis, it is necessary to separate product X_2 from HX solution because Br_2 or I_2 immediately dissolves into aqueous HBr or HI solution by forming polyions such as Br_3^-, Br_5^-, I_3^-, and I_5^-. Such a separation process for the aqueous products is regarded as a great burden on the whole cycle from both the viewpoints of the circulation of materials along the cycle and the suppression of excessive overvoltage. On the other hand, the gas phase electrolysis has a possibility to be provided with some proper electrolyte in which Br_2 or I_2 is insoluble.

3) In the case of actual thermochemical cycles where HBr or HI is produced mostly in the gas phase, the direct participation of HX in electrolysis with no condensation

TABLE 1. FREE ENERGY CHANGES AND THEORETICAL DECOMPOSITION VOLTAGES FOR THE DECOMPOSITION OF HBr AND HI

Reaction	Temp / K	ΔG° / kcal mol^{-1}	E° / V
$2HBr(aq\ a=1) \longrightarrow H_2(g)+Br_2(l)$	298	49.7	1.08
$2HBr(g) \longrightarrow H_2(g)+Br_2(g)$	400	26.8	0.58
$2HI(aq\ a=1) \longrightarrow H_2(g)+I_2(c)$	298	24.7	0.54
$2HI(g) \longrightarrow H_2(g)+I_2(l)$	400	3.0	0.065

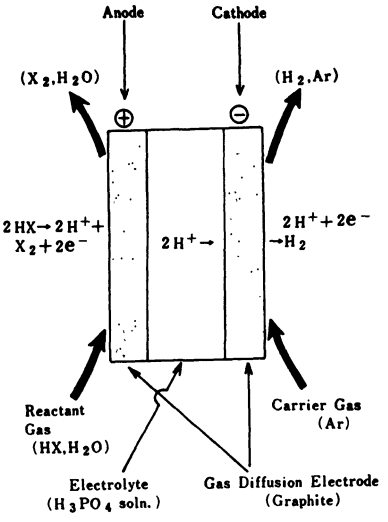

Fig. 1. Principle of the gas phase electrolysis for HX.

process is efficient and favorable.

In view of the above advantages a new process of gas phase electrolysis for hydrogen bromide or iodide has been devised and experimentally studied which makes use of a fuel-cell-type electrolyzer with electrolyte H_3PO_4 and graphite gas-diffusion electrodes.

Principle

The principle of this method is illustrated in Fig. 1. When reactant gas HX (=HBr or HI) containing some amount of water vapor is supplied into the gas diffusion type anode, the following electrochemical reaction takes place at contact points among the three phases of gas, electrolyte, and electrode:

$$2HX \longrightarrow 2H^+ + X_2 + 2e^-. \quad (3)$$

Product X_2 (=Br_2 or I_2) hardly dissolves into the electrolyte H_3PO_4 because of its intrinsic, extremely low solubility and is released from the anode in the gas or liquid form, whereas the H^+ migrates through the electrolyte to be reduced at the cathode according to the following reaction and removed by a carrier gas of Ar:

$$2H^+ + 2e^- \longrightarrow H_2. \quad (4)$$

These electrochemical processes require no cation exchanger membranes since the dissolution of HBr or HI gas into H_3PO_4 and their subsequent diffusion toward the cathode are negligible; the electrolyte H_3PO_4 is taken to serve as an ion separator.

The water vapor contained in the reactant gas does not interfere with the electrochemical reactions but has a favorable effect for the suppression of water evaporation from the electrolyte H_3PO_4.

Experimental

The fuel-cell-type electrolyzer used is illustrated in Fig. 2. The cell consists of the following parts: two stainless steel flanges of 140×120×5 t mm; two graphite holders of 95×110×22 t mm, each of which is provided with 26 ditches of 2×50×1 d mm to allow the reaction gas to pass from the inlet to outlet and with a lead terminal made of tantalum;

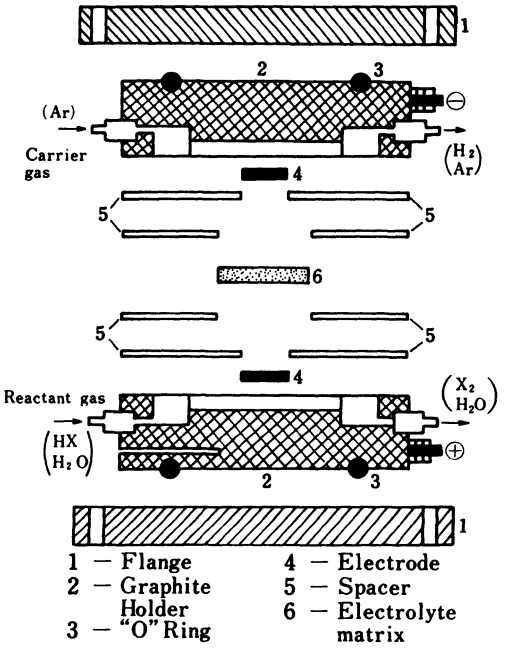

Fig. 2. Fuel-cell-type electrolyzer for HX gas.

two gas-diffusion-type graphite-cloth electrodes of 18×45×0.5 t mm, on both of which platinum was loaded by impregnation of hexachloroplatinic(IV) acid followed by H_2 reduction; four PTFE spacers 0.3—0.5 mm thick; an electrolyte-bearing matrix of 35×55×0.5 t mm, made of tantalum(V) oxide cloth with a porosity of *ca.* 90%. No trouble was experienced throughout the experiment up to temperatures as high as 170 °C. The electric resistance of the cell was about 0.12± 0.02 Ω for 85% H_3PO_4 electrolyte.

A reactant gas, prepared by mixing a commercially available anhydrous cylinder HBr or HI gas (Matheson, purity >99%) and a vaporized hydrobromic acid (aqueous HBr, 47.5 wt%) or hydriodic acid (aqueous HI, 57 wt%), respectively, was introduced into the anode side at a rate of 250 cm^3 min^{-1}. An argon carrier gas was supplied into the cathode side at a rate of about 80 cm^3 min^{-1}. The current efficiency was calculated on the basis of the hydrogen concentration in the argon as determined by gas chromatography.

To examine qualitatively the dissolution of bromine or iodine into phosphoric acid, a mixture of bromine or iodine with 85 wt% H_3PO_4 solution was heated to 150 °C, and subjected to a visual check for coloration; such a slight color change was observed that we might regard the dissolution as negligible.

Results and Discussion

Gas Phase Electrolysis for Hydrogen Bromide. The following four findings have been derived from the current-voltage results in Fig. 3 and the current efficiency results in Table 2.

(i) Current efficiency 100% is always obtained at electrolysis temperatures above 150 °C, in contrast to 75—95% at 118 °C (see Table 2). This low current efficiency at a lower temperature is possibly due to dissolution of bromine into the electrolyte H_3PO_4 followed by diffusion to the cathode. It is evident that there is no problem with respect to current efficiency above 150 °C (compare runs 1, 3, 7, and 8 with runs

Table 2. Cell voltages and current efficiencies with running conditions for HBr gas electrolysis

Run no.	Amount of catalyst / mg-Pt cm^{-2}	Temp / °C	Reactant gas constituent / atm ($HBr/H_2O/Br_2/N_2$)	Cell voltage (at 100 mA cm^{-2}) / V	Current efficiency / %
1	0.75	118	0.45/0.45/0/0.1	0.80	≈75
2	0.75	135	0.45/0.45/0/0.1	0.84	≈100
3	5.3	118	0.45/0.45/0/0.1	0.74	≈95
4	5.3	135	0.45/0.45/0/0.1	0.73	≈100
5	5.3	150	0.45/0.45/0/0.1	0.73	≈100
6	5.3	165	0.45/0.45/0/0.1	0.73	≈100
7	5.3	118	0.2/0.2/0/0.6	0.80	≈95
8	5.3	118	0.2/0.2/0.2/0.4	0.79	≈80
9	5.3	135	0.2/0.2/0.2/0.4	0.80	≈95
10	5.3	150	0.78/0.12/0/0.1	0.73	≈100
11	5.3	150	0.2/0.2/0/0.6	0.80	≈100
12	5.3	150	0.2/0.2/0.2/0.4	0.81	≈100

Table 3. Cell voltages and current efficiencies with running conditions for HI gas electrolysis

Run no.	Amount of catalyst / mg-Pt cm^{-2}	Temp / °C	Reactant gas constituent / atm ($HI/H_2O/I_2/N_2$)	Cell voltages (at 100 mA cm^{-2}) / V	Current efficiency / %
1	0.75	118	0.45/0.45/0/0.1	0.26_5	≈20
2	0.75	135	0.45/0.45/0/0.1	0.44	≈100
3	0.75	145	0.45/0.45/0/0.1	0.43	≈100
4	0.75	155	0.45/0.45/0/0.1	0.42	≈100
5	3.5	145	0.45/0.45/0/0.1	0.35	≈100
6	5.3	145	0.45/0.45/0/0.1	0.28	≈100
7	3.5	145	0.66/0.28/0/0.06	0.31_5	≈100
8	3.5	145	0.86/0.06/0/0.08	0.37	≈100
9	3.5	155	0.14/0.74/0/0.12	(0.54)[a]	≈100
10	3.5	155	0.12/0.65/0.12/0.11	(0.57)[a]	≈100

a) Extrapolated.

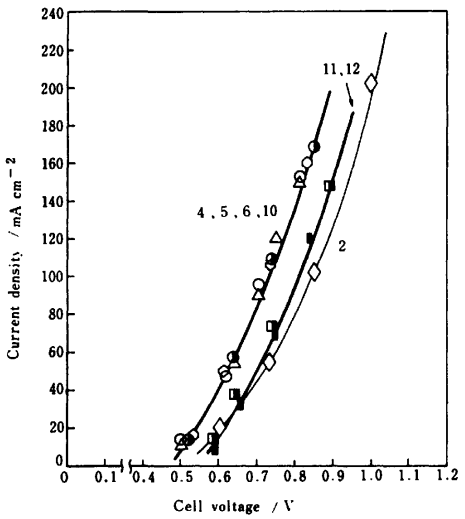

Fig. 3. Current-voltage Curves for HBr gas electrolysis.

5, 6, 10, 11, and 12).

(ii) When the reactant gas composition and the electrolysis temperature are kept $HBr/H_2O/Br_2/N_2$= 0.45/0.45/0/0.1 and 135 °C, respectively, the decomposition voltage at a current density of 100 mA cm^{-2} lowers (0.84→0.73 V) with increasing amount of the Pt catalyst loaded on the graphite electrodes (0.75→5.3 mg-Pt cm^{-2}) (compare run 2 with run 4).

Decomposition voltage 0.73 V obtained in runs 4, 5, and 6 may be considered to be low enough to be comparable with the values 0.75—0.8 V (at 200 mA cm^{-2} and 80—100 °C with 47.5 wt% HBr soln.) reported by Schuetz.[5]

(iii) When the amount of catalyst and the electrolysis temperature are kept 5.3 mg-Pt cm^{-2} and 150 °C, the decomposition voltage rises (0.73→0.80 V) with decrease in the HBr partial pressure P_{HBr} (0.78→0.2 atm) (see runs 5, 10, and 11).

(iv) Inclusion of bromine in the reactant gas decreases the current efficiency at 118 and 135 °C (runs 7, 8, and 9), and at 150 °C it causes no change in current efficiency from 100% and increases the decomposition voltage a little (0.80→0.81 V) (runs 11 and 12).

Gas Phase Electrolysis for Hydrogen Iodide. The following four findings have been derived similarly to the case of hydrogen bromide, from the current-voltage results in Figs. 4 and 5 and the current efficiency results in Table 3.

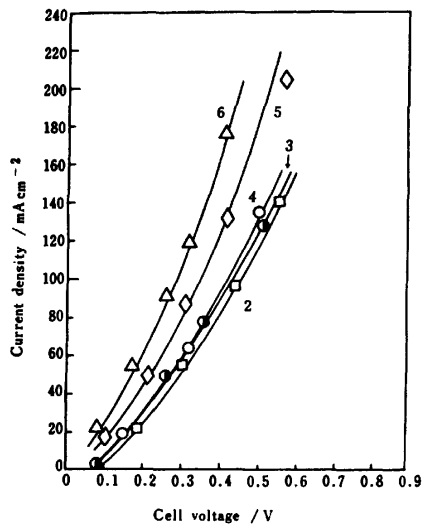

Fig. 4. Current-voltage curves for HI gas electrolysis with reactant gas constituent ($HI/H_2O/I_2/N_2$=0.45/0.45/0/0.10).

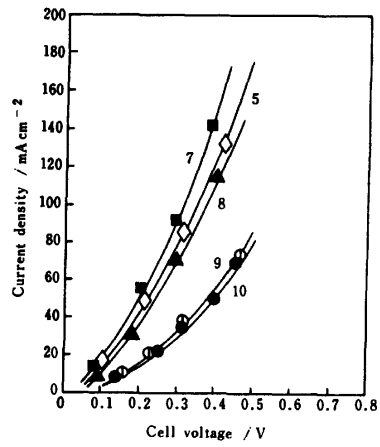

Fig. 5. Current-voltage curves for HI gas electrolysis with amount of catalyst 3.5 mg Pt/cm².

(i) Current efficiency 100% is successfully obtainable except at 118 °C (Table 3). The current efficiency drop at 118 °C is attributable to the dissolution of iodine into the electrolyte H_3PO_4 followed by the diffusion to the cathode. Above 135 °C, however, there is no trouble with the magnitude of current efficiency (compare run 1 with runs 2, 3, and 4).

(ii) When the reactant gas composition and the electrolysis temperature are kept $HI/H_2O/I_2/N_2$= 0.45/0.45/0/0.10 and 145 °C, respectively, the decomposition voltage at a current density of 100 mA cm^{-2} lowers (0.43→0.35→0.28 V) with increasing amount of the Pt catalyst loaded on the graphite electrodes (0.75→3.5→5.3 mg cm^{-2}) (see runs 3, 5, and 6).

Decomposition voltage 0.28 V obtained in run 6 may be regarded practically as sufficiently low.

(iii) When the amount of catalyst and the electrolysis temperature are fixed at 3.5 mg-Pt cm^{-2} and 145 °C, respectively, the decomposition voltage lowers (0.35→ 0.315 V) with increasing HI partial pressure P_{HI} (0.45→0.66 atm) (see runs 5 and 7). A similar lowering occurs at 155 °C (see runs 4 and 9). However, in the case of extremely low H_2O partial pressures (P_{H_2O}) such as 0.06 atm as in run 8, the decomposition voltage even rises up to 0.37 V in spite of the high P_{HI} (0.86 atm). Thus, some amount of P_{H_2O}, together with high P_{HI}, is supposed to be important for the electrochemical reaction at the anode.

(iv) Inclusion of I_2 in the reactant gas does not interfere with the electrolysis or the separation of products, although it causes the decomposition voltage to increase a little (0.54→0.57 V) (see runs 9 and 10).

No change in H_3PO_4 concentration was observed throughout the experiments and a negligible evaporation of water was observed from the cathode. No adhesion of liquid I_2 onto the anode causing an increase in overvoltage was found.

Summary. The findings described above lead us to conclude that the present gas phase electrolysis can be operated with 100% in current efficiency at a favorable decomposition voltage as low as that in the conventional electrolyses, if the electrolysis temperature, electrode catalyst, P_{HX}, and P_{H_2O} are suitably selected; for example, operating voltages available are 0.73 V at 100 mA cm^{-2}, 150 °C, 5.3 mg-Pt cm^{-2}, and 0.45 atm for HBr and 0.28 V at 100 mA cm^{-2}, 145 °C, 5.3 mg-Pt cm^{-2}, and 0.45 atm for HI.

An important advantage of the present method is the immediate separation of products Br_2 and I_2 from the electrolyte, which enables a long-term operation to run with a steady condition.

The authors would like to express their gratitude to Messrs. Kyo Fuchida, Chiaki Kawamura, and Hiroshi Yufu of Yuasa Battery Co., Ltd. for their cooperation in making the fuel-cell-type electrolyzer.

References

1) G. E. Besenbruch, K. H. McCorkle, J. H. Norman, D. R. O'Keefe, J. R. Shuster, and M. Yoshimoto, Proc. of the 3rd WHEC, Tokyo, 243 (1980).

2) H. Kameyama and K. Yoshida, Proc. of the 3rd WHEC, Tokyo, 1939 (1980).

3) S. Sato, S. Shimizu, H. Nakajima, K. Onuki, and Y. Ikezoe, Proc. of the 4th WHEC, California, USA, 533 (1982).

4) K. Fujii, W. Kondo, S. Mizuta, Y. Oosawa, and T. Kumagai, Proc. of the 4th WHEC, California, USA, 553 (1982).

5) G. H. Schuetz, Proc. of the 4th WHEC, California, USA, 493 (1982).

6) I. Uehara, E. Ishii, H. Ishikawa, and M. Nakane, Proc. of the 3rd WHEC, Tokyo, 477 (1980).

7) G. H. Schuetz, *Int. J. Hydrogen Energy*, **1**, 379 (1977).

8) G. H. Schuetz and P. J. Fiebelman, *Int. J. Hydrogen Energy*, **5**, 305 (1980).

9) D. V. Velzen and H. Langenkamp, Proc. of the 3rd WHEC, Tokyo, 423 (1980).

10) P. J. Fiebelman and G. H. Schuetz, Proc. of the 3rd WHEC. Tokyo, 1949 (1980).

11) I. Uehara, E. Ishii, H. Ishikawa, and M. Nakane, *Nippon Kagaku Kaishi*, **1981**, 221.

12) E. N. Balko, J. F. McElory, and A. B. LaConti, *Int. J. Hydrogen Energy*, **6**, 577 (1981).

13) I. Barin and O. Knacke, "Thermochemical Properties

of Inorganic Substances," Springer Verlag, Berlin, Heidelberg, New York (1973).
14) C. F. V. Mason, *Int. J. Hydrogen Energy*, **1**, 427 (1976).
15) P. Lessart, R. Benizri, and P. Courvoisier, Proc. of the 2nd WHEC, Zurich, 595 (1978).
16) Y. Shindo, K. Obata, T. Hakuta, H. Yoshitome, N. Todo, and J. Kato, Proc. of the 3rd WHEC, Tokyo, 325 (1980).
17) S. Mizuta and T. Kumagai, *Denki Kagaku*, **47**, 105 (1979).
18) Y. Oosawa, *Bull. Chem. Soc. Jpn.*, **54**, 2908 (1981).
19) D. R. O'Keefe and J. H. Nomran, Proc. of the 3rd WHEC, Tokyo, 277 (1980).
20) R. H. Wentorf, Jr., and R. E. Hanneman, *Science*, **185**, 311 (1974).

Thermal Studies of Nickel(II) Hydrazine Complexes in Solid State†

Bijoy BANERJEE, Prasanta Kumar BISWAS, and Nirmalendu RAY CHAUDHURI*
Department of Inorganic Chemistry, Indian Association for the Cultivation of Science, Calcutta 700032, India
(Received July 13, 1982)

Two bis(hydrazine)nickel(II) fluoro complexes of the type $[NiL_2F_2]\cdot H_2O$, where $L=NH_2NH_2$ have been synthesized. Besides these, $[NiL_{2.5}(H_2O)_2]F_2\cdot 0.5H_2O$ and $[NiL_{2.5}F_2]\cdot 2H_2O$ have also been synthesized. Thermal investigations of these complexes have been carried out. Four tris(hydrazine)nickel(II) chloride and four tris-(hydrazine)nickel(II) bromide complexes have been prepared and their thermal investigations have been done. Two bis(hydrazine) thiocyanato complexes have also been prepared and their thermal studies have also been carried out. These nickel(II) hydrazine complexes have been found to decompose through several complex species as intermediates. All these intermediates as well as the parent complexes have been characterized by elemental analyses, color, magnetic moment, electronic spectra (mull), and IR spectra. X-Ray powder diffraction pattern of two tris(hydrazine)nickel(II) bromide complexes have been obtained. The probable mechanistic paths for each step of decomposition have been proposed.

The formation of many inorganic compounds is generally dependent upon the conditions employed. Slight alteration in a described procedure sometimes results in an apparently identical but rather different compounds. This type of difference exhibited in the apparently similar compounds is very difficult to detect unless we characterize the compounds with X-ray crystal structure determinations. On the other hand, identification by thermal techniques may differentiate the compounds qualitatively. With this idea we have synthesized several hydrazine complexes of NiX_2, where $X=F^-$, Cl^-, Br^-, or SCN^-, considering the versatile character of hydrazine as complexing ligand[1-4] and tried to utilize the thermal techniques in differentiating apparently similar type of compounds. We wish to report the thermal investigation of hydrazine complexes of nickel(II) salts.

Experimental

Preparation of Nickel(II) Hydrazine Complexes. $[NiL_2F_2]\cdot H_2O$ $(L=NH_2NH_2)$ ***(1)***: 2 mmol†† of hydrazine hydrate (80%) was added to the 1 mmol of green hydrated nickel(II) fluoride crystals. While stirring the green crystals turned bluish pink crystals **1**. The crystals were filtered, washed thoroughly with ethanol–water mixture (1 : 1) and finally with dry ethanol.

$[NiL_2F_2]\cdot H_2O$ ***(2)***: Hydrazine hydrate (2 mmol) was added dropwise with constant stirring to the concentrated ammoniacal solution of nickel(II) fluoride crystals. Fine bluish pink shining crystals **2** separated out slowly from the solution. These shining crystals were collected and washed as mentioned in the preparation of complex **1**.

$[NiL_{2.5}(H_2O)_2]F_2\cdot 0.5H_2O$ ***(3)***: This compound was synthesized following the method adopted for the preparation of complex **1**. Here aqueous solution of nickel(II) fluoride was used instead of crystals.

$[NiL_{2.5}F_2]\cdot 2H_2O$ ***(4)***: Aqueous solution of nickel(II) fluoride afforded this compound following the method described for the preparation of complex **2**.

$[NiL_3]Cl_2$ ***(5)***: This was prepared following the method described for complex **1**.

$[NiL_3]Cl_2$ ***(6)***: This was prepared following the method described for complex **2**.

$[NiLCl_2]$ ***(7)***: This was prepared by pyrolysis of $[NiL_3]Cl_2$ (**5**) at ≈176 °C.

$[NiLCl_2]$ ***(8)***: This was synthesized by pyrolysis of $[NiL_3]Cl_2$ (**6**) at ≈170 °C.

$[NiL_3]Cl_2\cdot H_2O$ ***(9)***: This was synthesized by addition of hydrazine hydrate to the $[NiLCl_2]$ (**7**).

$[NiL_3]Cl_2\cdot H_2O$ ***(10)***: This was prepared by addition of hydrazine hydrate to the $[NiLCl_2]$ (**8**).

$[NiL_3]Br_2$ ***(11)***: This was synthesized by the corresponding procedure to the preparation of complex **1**.

$[NiL_3]Br_2$ ***(12)***: This was prepared by the corresponding procedure to the preparation of complex **2**.

$[NiL_2Br_2]$ ***(13)***: This was obtained on keeping the complex **11** in vacuum at ambient temperature. This was also prepared similarly from the complex **12**. The preparation from complex **11** required comparatively high vacuum relative to that from complex **12**.

$[NiL_2Br_2]$ ***(14)***: This was obtained from complex **11** by pyrolytic technique at ≈176 °C in nitrogen atmosphere.

$[NiL_3]Br_2$ ***(15)***: This was prepared by treatment of hydrazine hydrate on complex **13**.

$[NiL_3]Br_2$ ***(16)***: This was synthesized by treating complex **14** with hydrazine hydrate.

$[NiL_2(SCN)_2]$ ***(17)***: This was prepared by treating hydrazine hydrate (2—3 mmol) with ethanolic solution of nickel(II) thiocyanate (1 mmol).

$[NiL_2(SCN)_2]$ ***(18)***: This was prepared by the treatment of hydrazine hydrate (2—3 mmol) with ethanolic ammoniacal nickel(II) thiocyanate solution.

Thermal Measurements. The thermal analysis was carried out using a thermal analyzer (Shimadzu, Model DT-30, Japan). A constant flow of dry nitrogen (30 ml min^{-1}) was maintained. Platinum crucibles were used. Heating rate was maintained 5 °C min^{-1}. The particle size of the samples was within 150—200 mesh. Aluminium oxide was used as reference.

Elemental Analyses. Elemental analyses were carried out in the microanalytical section of the Australian Mineral Development Laboratories as well as in the microanalytical laboratory of our institute.

Spectral Measurements. Infrared spectra (KBr disk, 4000—400 cm^{-1}) and electronic spectra in mull (28570—11111 cm^{-1}) were recorded using a Beckman IR spectrophotometer, Model IR-20A and a Pye Unicam spectrophotometer, model SP8-150, respectively. Cary 17D was also used for mull

† Part of the work was presented at the third national symposium of Indian Thermal Analysis Society held at VSSC, Trivandrum, India.

†† Similar experiment was performed by using 3 mmol of hydrazine hydrate but we obtained complex $[NiL_2F_2]\cdot H_2O$.

spectra in some cases.

Magnetic Measurement. Magnetic moments of the compounds were evaluated from the magnetic susceptibilities of the samples at room temperature, corrected by applying Pascal's constants of the elements involved, using the Gouy technique where $Hg[Co(SCN)_4]$ was taken as standard.

X-Ray Powder Diffraction. X-Ray powder diffraction patterns of the compounds were obtained on a Philips powder diagram camera, using Cu *Kα* radiation.

Results

The thermal curves of two bis(hydrazine)nickel(II) fluoro complexes **1** and **2** are shown in Fig. 1. Both the species become anhydrous first and then lose hydrazine on heating. But the thermal profiles of them are distinctly different from each other.

$[NiL_{2.5}(H_2O)_2]F_2 \cdot 0.5H_2O$ (**3**) loses first its lattice water and then two molecules of coordinated water. The derived $NiL_{2.5}F_2$ is very much unstable and loses immediately hydrazine molecules in two steps as observed in TG curve (Fig. 2). The first step corresponds roughly to elimination of 0.5 molecule of hydrazine and the second corresponds to that of two molecules. But its DTA curve indicates that the elimination of hydrazine occurs in more than two steps. On the other hand, thermal curve of $[NiL_{2.5}F_2] \cdot 2H_2O$ (**4**) shown in Fig. 2 indicates that hydrazine elimination occurs here also in two steps. The first step corresponds to the elimination of one hydrazine and the second corresponds to that of the rest of hydrazine.

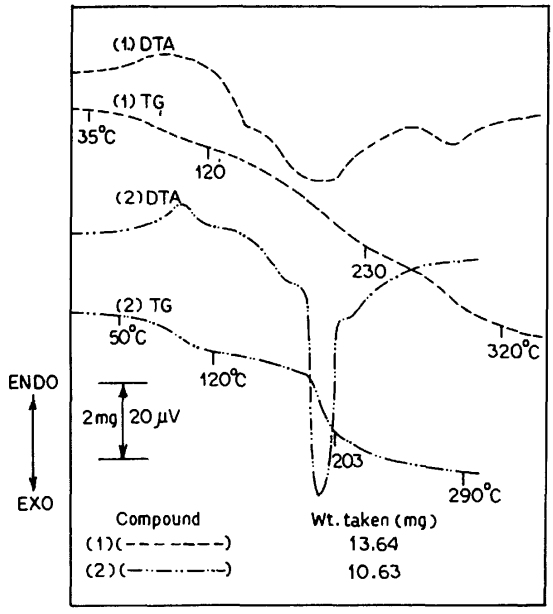

Fig. 1. Thermal curves of $[NiL_2F_2] \cdot H_2O$ (**1**) and $[NiL_2F_2] \cdot H_2O$ (**2**).

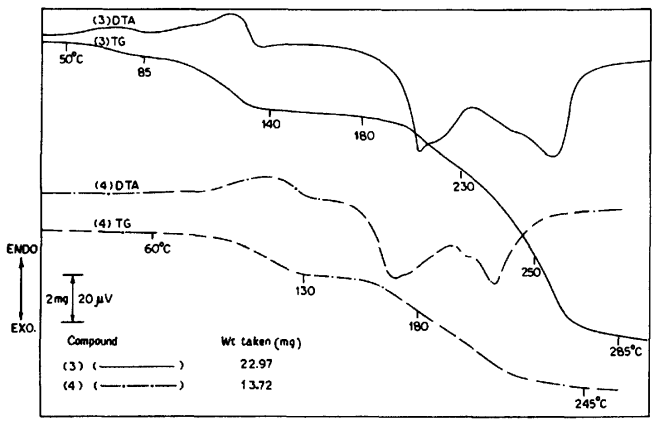

Fig. 2. Thermal curves of $[NiL_{2.5}(H_2O)_2]F_2 \cdot 0.5H_2O$ (**3**) and $[NiL_{2.5}F_2] \cdot 2H_2O$ (**4**).

Thermal curve of tris(hydrazine)nickel(II) chloride (**6**) is shown in Fig. 3. It transforms straightly to $NiLCl_2$ on heating and then to nickel(II) chloride *via* an unstable intermediate compound $NiL_{0.5}Cl_2$. Thermal curve of tris(hydrazine)nickel(II) chloride (**5**) is almost identical to that of complex **6**. Here the TG curve does not support the formation of hemi(hydrazine) species (Fig. 3).

The TG curve of $[NiL_3]Cl_2 \cdot H_2O$ (**9**) (Fig. 3) shows that it decomposes stepwise with the formation of bis as well as unis(hydrazine) chloro complex on heating. Its DTA curve hints the formation of another intermediate species in between $NiLCl_2$ and $NiCl_2$. The thermal profile of $[NiL_3]Cl_2 \cdot H_2O$ (**10**) does not differ much from that of complex **9**. In complex **10** formation of hemi(hydrazine) species, though not isolable, is evident from the TG and DTA profile (Fig. 3).

The TG curve of tris(hydrazine)nickel(II) bromide (**11**) (Fig. 4) shows that it transforms to NiL_2Br_2 in single step. But its DTA curve shows an exotherm followed by a prominent hump which indicates that the formation of isolable NiL_2Br_2 takes place *via* an unstable intermediate $[NiL_{2.5}Br]Br$. The TG curve of derived bis species shows elimination of two hydrazine molecules taking place in one step, but its DTA curve indicates the elimination taking place *via* an another unstable intermediate complex. On the other hand, tris(hydrazine)nickel(II) bromide (**12**) transforms straightly to $NiLBr_2$ in a single step as evident from its thermal curves (Fig. 4). This uni species is not isolable in pure form even by arresting temperature rising. $NiLBr_2$ on further heating transforms to $NiBr_2$ *via* probably an unstable hemi(hydrazine) complex $NiL_{0.5}Br_2$.

The TG curve of $[NiL_2Br_2]$ (**13**) (Fig. 5) shows elimination of two hydrazine molecules taking place in a single step but its DTA profile hints the elimination in two steps probably through a uni (hydrazine)species. The thermal behavior of $[NiL_2Br_2]$ (**14**) is almost identical to that of **13**.

$[NiL_3]Br_2$ (**15**) transforms straightly to $NiBr_2$ in a single step as evident from its sharp TG and DTA curves, but $[NiL_3]Br_2$ (**16**) transforms to $NiLBr_2$ in a single step (Fig. 5). The unis(hydrazine) species derived from complex **16** is not isolable in pure state even by temperature arrest technique, but transforms to $NiBr_2$ in a single step (Fig. 5).

$[NiL_2(SCN)_2]$ (**17**) begins to lose hydrazine at ≈160 °C and becomes $Ni(SCN)_2$ at ≈225 °C in a single step observed from its TG curve (Fig. 6). But the presence of two peaks overlapping with each other in the corresponding DTA curve indicates elimination of hydrazine taking place in two steps. The metal thiocyanate is not

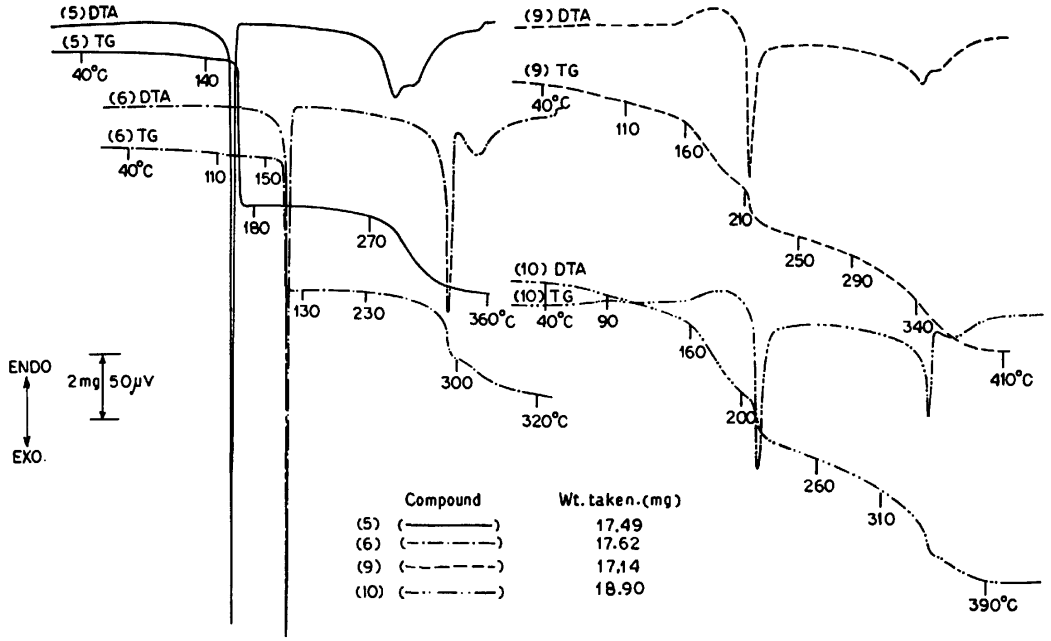

Fig. 3. Thermal curves of $[NiL_3]Cl_2$ (**5**), $[NiL_3]Cl_2$ (**6**), $[NiL_3]Cl_2 \cdot H_2O$ (**9**), and $[NiL_3]Cl_2 \cdot H_2O$ (**10**).

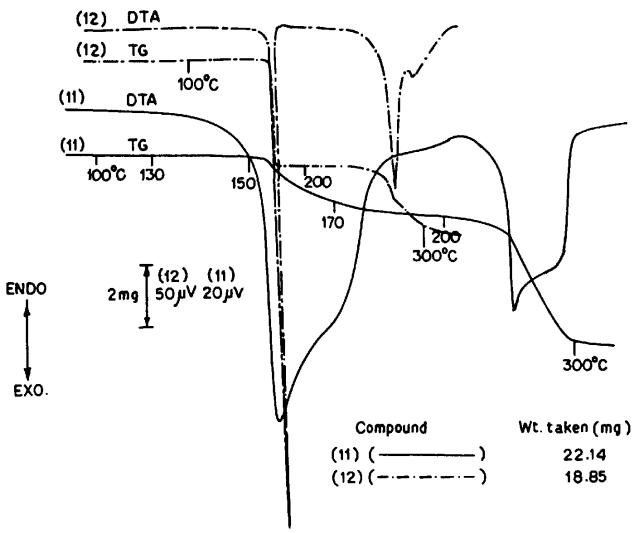

Fig. 4. Thermal curves of $[NiL_3]Br_2$ (**11**) and $[NiL_3]Br_2$ (**12**).

isolable. It immediately decomposes to metal sulfide and sulfur in two steps. On the other hand, in case of $[NiL_2(SCN)_2]$ (**18**) elimination of hydrazine and decomposition of metal thiocyanate occur simultaneously (Fig. 6).

Table 1 shows the thermal decomposition reaction in details along with temperature range and DTA peak temperature for each step of decomposition. Table 2 shows the analytical data of the hydrazine complexes and intermediate hydrazine complex species isolated by temperature arrest technique along with the color and magnetic data. IR spectra of all the hydrazine complexes are taken. Electronic mull spectra of the complexes are taken and corresponding data are shown in Table 3. X-Ray data of two complexes are shown in Table 4.

Discussion

The Complexes Derived from NiF_2 and Hydrazine Hydrate. $NiL_xF_y \cdot zH_2O$ ($x=2$, 2.5, $y=2$, $z=1$, 2, 2.5): Treatment of NiF_2 crystal with hydrazine hydrate afforded bluish pink $[NiL_2F_2] \cdot H_2O$ (**1**), whilst the samely formulated complex **2** was synthesized by reaction of hydrazine hydrate with NiF_2 crystals in concentrated ammoniacal solution. Electronic spectra (Table 3) in mull of both **1** and **2** complexes suggest O_h symmetry[5] existing in the system which is also supported by the magnetic moment (Table 2). The thermal profile for the water elimination shows existence of water molecule[6,7] as noncoordinated in both the cases. IR data also collaborate with the inference[8] drawn from thermal profile regarding the play of water molecule (Fig. 7). The medium broad band at $\approx 580\ cm^{-1}$ in IR is expected to be assigned to ν(Ni–F).[8] The bridging character of NH_2NH_2 exists in both species as ν(N–N)[9,10] appearing at $\approx 980\ cm^{-1}$. The weak intensity of this band seems to be due to the fact that the vibrational mode of N–N stretching frequency tends to be IR inactive for the strong hydrogen bonding between F and hydrogen of NH_2 group. On the other hand, the thermal decomposition patterns of both species are different which implies that they are structurally somewhat different. It is rather difficult to comment on the mechanism of decomposition pattern as no intermediate species are isolable. However, for **1** the decomposition probably follows O_h $Ni^{II} \rightarrow T_d$ Ni^{II} which ultimately affords NiF_2.

It is interesting to note that the treatment of hydrazine hydrate with concentrated solution of NiF_2 yields $[NiL_{2.5}(H_2O)_2]F_2 \cdot 0.5H_2O$ (**3**). The electronic spectrum in mull as well as magnetic moment suggests it to exist as O_h symmetry. As water molecules evolve in two steps, it seems that two types of water *i.e.* lattice water

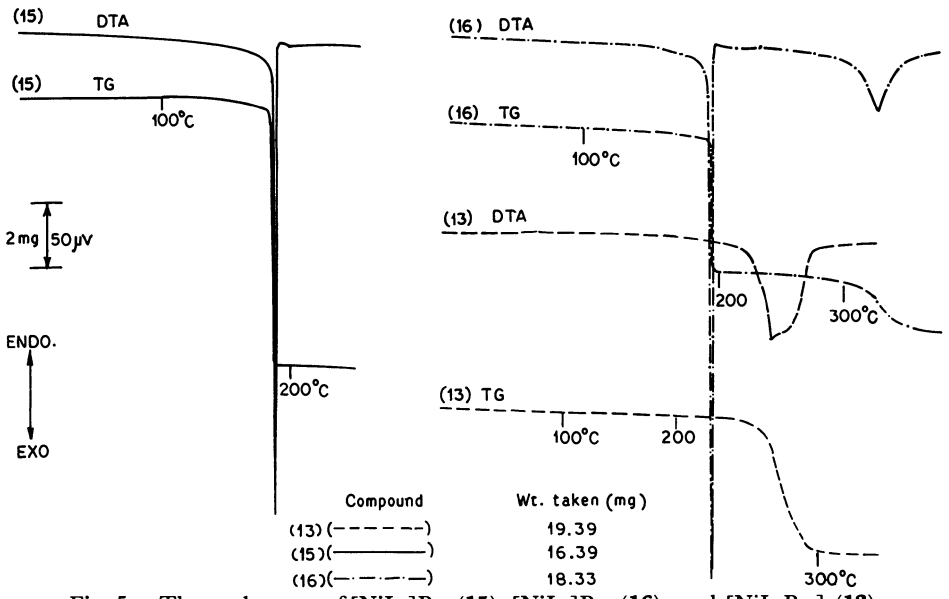

Fig. 5. Thermal curves of $[NiL_3]Br_2$ (**15**), $[NiL_3]Br_2$ (**16**), and $[NiL_2Br_2]$ (**13**).

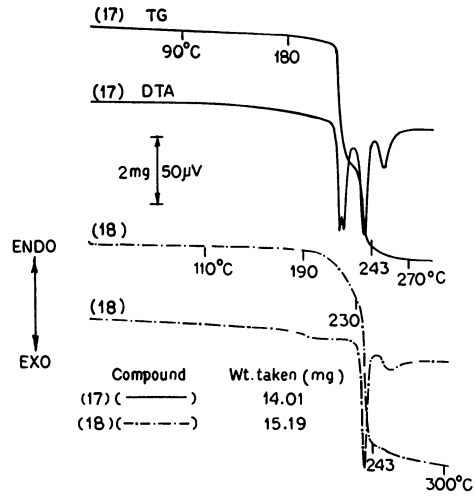

Fig. 6. Thermal curves of $[NiL_2(SCN)_2]$ (**17**) and $[NiL_2(SCN)_2]$ (**18**).

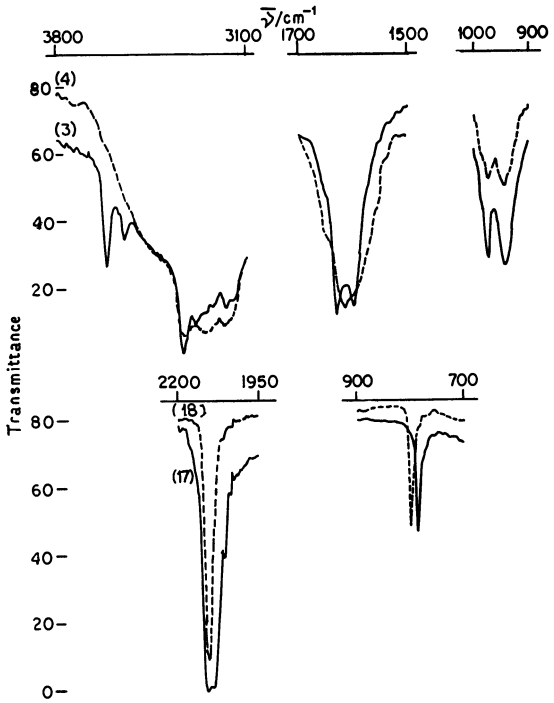

Fig. 7. IR spectra (3800—3100, 1700—1500, and 1000—900 cm^{-1}) of $[NiL_{2.5}(H_2O)_2]F_2 \cdot 0.5H_2O$ (**3**)and $[NiL_{2.5}F_2] \cdot 2H_2O$ (**4**); IR spectra (2200—1950, 900—700cm^{-1}) of $[NiL_2(SCN)_2]$ (**17**) and $[NiL_2(SCN)_2]$ (**18**).

and coordinated water exist in the system. However, the IR spectrum suggests that the two molecules of water are coordinated[11,12] to Ni^{II} as evident from the sharp bands at $\approx$3500 cm^{-1} [ν(OH)] (Fig. 7) and δ(HOH) at $\approx$1630 cm^{-1}, ρw(HOH) at 625 cm^{-1}, and [ν(MO)] at $\approx$465 cm^{-1}. The coordination of F^- to Ni^{II} is nullified by the absence of ν(MF) at $\approx$590 cm^{-1} as observed in the case of complexes **1** and **2**. Hydrazine molecules are existing in the system as both unidentate and bidentate as evident[2,4] from the presence of ν(N–N) vibrations at $\approx$935 and $\approx$975 cm^{-1} respectively (Fig. 7). The tentative structure of complex **3** is shown in Fig. 8. The elimination of water and hydrazine is complicated as the decomposition follows a number of intermediates as evident from DTA profile (Fig. 2). On the other hand, the treatment of hydrazine hydrate with concentrated solution of NiF_2 in ammoniacal medium yields $[NiL_{2.5}F_2] \cdot 2H_2O$ (**4**). O_h symmetry also exists here and the existence of hydrazine in the species is similar to complex **3**. Moreover, Ni–F bonding is also suggested by the presence of ν(MF) at $\approx$590 cm^{-1} as observed in complexes **1** and **2**. Water molecules in the complex **4** exist outside the coordination sphere as evident from its IR spectrum (Fig. 7) though temperature range for the elimination of water shown in Table 1 differs from that of complex **3**. The tentative structure of complex **4** is shown in Fig. 8. The decomposition of complex **4** appears also complicated (Fig. 2).

The Complexes Derived from $NiCl_2$ and Hydrazine Hydrate. Treatment of hydrazine hydrate with $NiCl_2$ affords

TABLE 1. THERMAL PARAMETERS OF THE NICKEL(II) COMPLEXES OF HYDRAZINE

Decomposition reactions	Temp range °C	DTA peak temp/°C
$[NiL_2F_2]\cdot H_2O$ (**1**)$\rightarrow NiL_2F_2$	40—140	85
$NiL_2F_2\rightarrow NiF_2$	140—340	150, 195, 290
$[NiL_2F_2]\cdot H_2O$ (**2**)$\rightarrow NiL_2F_2$	40—120	95
$NiL_2F_2\rightarrow NiL_{1.66}F_2$	120—188	175
$NiL_{1.66}F_2\rightarrow NiL_{0.66}F_2$	188—207	197
$NiL_{0.66}F_2\rightarrow NiF_2$	207—280	210
$[NiL_{2.5}(H_2O)_2]F_2\cdot 0.5H_2O$(**3**)$\rightarrow NiL_{2.5}(H_2O)_2F_2$	54—86	68
$NiL_{2.5}(H_2O)_2F_2\rightarrow NiL_{2.5}F_2$	87—137	125
$NiL_{2.5}F_2\rightarrow NiL_2F_2$	138—212	208
$NiL_2F_2\rightarrow NiF_2$	212—290	242, 255
$[NiL_{2.5}F_2]\cdot 2H_2O$(**4**)$\rightarrow NiL_{2.5}F_2$	86—134	114
$NiL_{2.5}F_2\rightarrow NiL_{1.5}F_2$	135—178	169
$NiL_{1.5}F_2\rightarrow NiF_2$	178—247	194, 208
$[NiL_3]Cl_2$(**5**)$\rightarrow NiLCl_2$	120—176	160
$NiLCl_2\rightarrow NiCl_2$	240—350	290, 305
$[NiL_3]Cl_2$(**6**)$\rightarrow NiLCl_2$	115—170	158
$NiLCl_2\rightarrow NiL_{0.5}Cl_2$	220—295	285
$NiL_{0.5}Cl_2\rightarrow NiCl_2$	295—360	305
$[NiL_3]Cl_2\cdot H_2O$(**9**)$\rightarrow NiL_2Cl_2$	40—215	158
$NiL_2Cl_2\rightarrow NiLCl_2$	215—320	220
$NiLCl_2\rightarrow NiCl_2$	320—400	340, 360
$[NiL_3]Cl_2\cdot H_2O$(**10**)$\rightarrow NiL_2Cl_2$	40—218	180
$NiL_2Cl_2\rightarrow NiLCl_2$	218—295	220
$NiLCl_2\rightarrow NiL_{0.5}Cl_2$	295—345	342
$NiL_{0.5}Cl_2\rightarrow NiCl_2$	345—410	364
$[NiL_3]Br_2$(**11**)$\rightarrow NiL_2Br_2$	140—176	155, 170
$NiL_2Br_2\rightarrow NiBr_2$	195—280	250, 270
$[NiL_3]Br_2$(**12**)$\rightarrow NiLBr_2$	170—180	172
$NiLBr_2\rightarrow NiL_{0.5}Br_2$	185—280	257
$NiL_{0.5}Br_2\rightarrow NiBr_2$	280—320	300
$[NiL_2Br_2]$(**13**)$\rightarrow NiBr_2$	200—310	250, 270
$[NiL_3]Br_2$(**15**)$\rightarrow NiBr_2$	130—190	175
$[NiL_3]Br_2$(**16**)$\rightarrow NiLBr_2$	160—200	185
$NiLBr_2\rightarrow NiBr_2$	205—350	320
$[NiL_2(SCN)_2]$(**17**)$\rightarrow Ni(SCN)_2$	160—225	210, 215
$Ni(SCN)_2\rightarrow NiS+S$	225—255	235, 250
$[NiL_2(SCN)_2]$(**18**)$\rightarrow NiS+S$	190—290	235, 268

$[NiL_3]Cl_2$ (**5**), while with ammoniacal medium another $[NiL_3]Cl_2$ (**6**) is formed. These two show similarity in color, magnetic moment as well as in other physical properties *e.g.*, IR and electronic spectra (mull). The spectral behavior suggests them to exist as O_h symmetry with the bridging characteristic of hydrazine. Thermal curves suggest that unis(hydrazine)nickel(II) chloride complexes $[NiLCl_2]$ (**7** and **8**), derived from the complexes **5** and **6** are slightly structurally different.

Treatment of hydrazine with complex **7** results in $[NiL_3]Cl_2\cdot H_2O$ (**9**). Similar treatment with complex **8** results in $[NiL_3]Cl_2\cdot H_2O$ (**10**). These two tris-(hydrazine) species also show similarity in color, magnetic moment and other physical properties. We expected that these two hydrated tris species, on heating, will generate anhydrous tris species, identical to complexes **5** and **6**, but the thermal behaviors of complexes **9** and **10** show that synthesis of anhydrous tris species is not feasible by pyrolytic treatment. This hints the presence of water within the coordination sphere, but both IR and electronic (mull) spectra indicate noncoordination of water molecule. No significant DTA curve is obtained (Fig. 3) at the time of evolution of first hydrazine molecule, which probably due to the simultaneous elimination of H_2O and NH_2NH_2. The exotherm for NH_2NH_2 evolution and the endotherm of H_2O probably nullify the energy with each other. This also suggests that tris species **9** and **10** are quite different

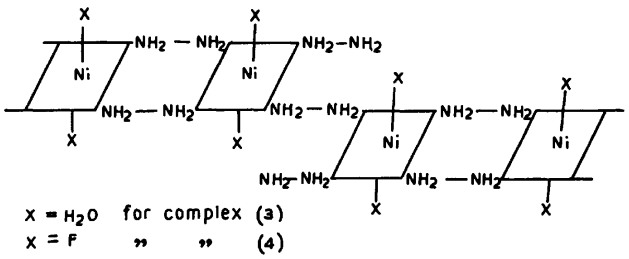

Fig. 8. Structures of $[NiL_{2.5}(H_2O)_2]F_2\cdot 0.5H_2O$ (**3**) and $[NiL_{2.5}F_2]\cdot 2H_2O$ (**4**).

TABLE 2. ANALYTICAL AND MAGNETIC DATA OF NICKEL(II) COMPLEXES DERIVED FROM THEM BY PYROLYSIS

Compound		Color	Found (Calcd) (%)			$\frac{\mu_{eff}}{BM}$
			Metal	Nitrogen	Halogen	
$[NiL_2F_2]\cdot H_2O$	(1)	Bluish pink	32.80(32.85)	31.28(31.33)	21.21(21.26)	2.95
$[NiL_2F_2]\cdot H_2O$	(2)	Bluish pink	32.82(32.85)	31.30(31.33)	21.23(21.26)	2.93
$[NiL_{2.5}(H_2O)_2]F_2\cdot 0.5H_2O$	(3)	Bluish pink	26.47(26.48)	31.54(31.57)	17.09(17.13)	2.89
$[NiL_{2.5}F_2]\cdot 2H_2O$	(4)	Bluish pink	27.57(27.60)	32.87(32.90)	17.81(17.86)	2.88
$[NiL_3]Cl_2$	(5)	Pink	25.09(26.01)	37.20(37.21)	31.43(31.45)	2.99
$[NiL_3]Cl_2$	(6)	Pink	26.00(26.01)	37.19(37.21)	31.41(31.45)	2.99
$[NiLCl_2]$	(7)	Sky blue	36.19(36.30)	17.27(17.31)	43.77(43.90)	3.38
$[NiLCl_2]$	(8)	Sky blue	36.21(36.30)	17.26(17.31)	43.89(43.90)	3.39
$[NiL_3]Cl_2\cdot H_2O$	(9)	Pink	24.01(24.09)	34.43(34.46)	29.11(29.13)	2.98
$[NiL_3]Cl_2\cdot H_2O$	(10)	Pink	24.05(24.09)	34.42(34.46)	29.09(29.13)	2.95
$[NiL_3]Br_2$	(11)	Pink	18.64(18.66)	26.62(26.70)	50.76(50.80)	3.02
$[NiL_3]Br_2$	(12)	Pink	18.63(18.66)	26.64(26.70)	50.74(50.80)	3.00
$[NiL_2Br_2]$	(13)	Sky blue	20.75(20.78)	19.76(19.82)	56.50(56.56)	3.00
$[NiL_2Br_2]$	(14)	Sky blue	20.74(20.78)	19.73(19.82)	56.52(56.56)	3.02
$[NiL_3]Br_2$	(15)	Pink	18.63(18.66)	26.64(26.70)	50.81(50.80)	3.02
$[NiL_3]Br_2$	(16)	Pink	18.63(18.66)	26.61(26.70)	50.78(50.80)	3.03
$[NiL_2(SCN)_2]$	(17)	Pink	24.55(24.59)	35.14(35.18)	26.79(26.81)*	3.10
$[NiL_2(SCN)_2]$	(18)	Pink	24.57(24.59)	35.13(35.18)	26.80(26.81)*	3.06

*denotes sulfur.

TABLE 3. ELECTRONIC (MULL) SPECTRA OF NICKEL(II) COMPLEXES OF HYDRAZINE (L)

Compound		Absorbance[a] maxima λ/nm	Compound		Absorbance[a] maxima λ/nm
$[NiL_2F_2]\cdot H_2O$	(1)	870, 550, 345, 305	$[NiL_3]Cl_2\cdot H_2O$	(10)	860, 525, 330, 290
$[NiL_2F_2]\cdot H_2O$	(2)	850, 530, 335(sh), 305	$[NiL_3]Br_2$	(11)	850, 780, 560, 500(sh), 375, 295
$[NiL_{2.5}(H_2O)_2]F_2\cdot 0.5H_2O$	(3)	850, 545, 345, 320	$[NiL_3]Br_2$	(12)	850, 780(sh), 540, 375, 300
$[NiL_{2.5}F_2]\cdot 2H_2O$	(4)	850, 560, 355, 320	$[NiL_2Br_2]$	(13)	590, 375
$[NiL_3]Cl_2$	(5)	845, 780(sh), 530, 340, 295	$[NiL_3]Br_2$	(15)	830, 530, 340(sh), 310
$[NiL_3]Cl_2$	(6)	860, 780(sh), 530, 335, 295	$[NiL_3]Br_2$	(16)	870, 545, 340(sh), 290
$[NiLCl_2]$	(7)	850, 570, 370, 295	$[NiL_2(SCN)_2]$	(17)	840, 550, 350(sh), 295
$[NiLCl_2]$	(8)	850, 530(sh), 410(sh),340(sh),310	$[NiL_2(SCN)_2]$	(18)	890, 555, 345, 300
$[NiL_3]Cl_2\cdot H_2O$	(9)	850, 520, 330, 295			

sh=shoulder. a) Arbitrary absorbance.

TABLE 4. X-RAY DIFFRACTION DATA OF $Ni(NH_2\text{–}NH_2)_3Br_2$ (11) AND $Ni(NH_2NH_2)_3Br_2$ (12)

$Ni(NH_2NH_2)_3Br_2$ (11)	$Ni(NH_2NH_2)_3Br_2$ (12)	
4.33(vs)	4.66(w)	2.28(m)
4.06(s)	4.41(w)	2.21(m)
3.46(w)	4.13(w)	2.17(s)
3.13(s)	3.97(vs)	1.99(m)
3.00(s)	3.77(w)	1.98(m)
2.90(vs)	3.38(vs)	1.94(m)
2.65(vw)	3.20(w)	1.87(s)
2.36(w)	3.06(vs)	1.75(s)
2.12(w)	2.93(s)	1.68(s)
	2.84(w)	1.64(w)
	2.77(w)	1.56(s)
	2.59(vs)	1.48(w)
	2.50(s)	1.38(w)
	2.36(m)	1.35(w)

vw=very weak, w=weak, m=medium, s=strong, vs=very strong.

from **5** and **6** complex species. It is observed that unis(hydrazine) complex could not be isolated from complexes **9** and **10** but it is true that the structure of unis(hydrazine) complexes **7** and **8** remains intact on hydrazine treatment as evident from the comparison of the nature of decomposition of either complexes **5** and **9** or **6** and **10**. Color, magnetic moment, IR and electronic (mull) spectra of complexes **9** and **10** apparently show no difference between them, suggesting O_h symmetry and bridging characteristic of hydrazine as observed in complexes **5** and **6**.

Tsuchiya *et al.*[2] investigated the thermal behaviors of $[Ni(NH_2NH_2)_6]X_2$. They noticed that hexakis(hydrazine) species becomes nickel(II) chloride *via* tris, bis and unis(hydrazine) complexes. It seems that much differences existing between the decomposition pattern of the complexes being to be reported by us and of the species reported by Tsuchiya *et al.*[2] will be due to the basic differences playing in the preparative procedures. The tentative decomposition mode of complexes **5** and **6** is probably A→B→E→F (Scheme 1), whilst the complexes **9** and **10** form $NiCl_2$ through A→D→B→E→F (Scheme 1).

The unis(hydrazine)nickel(II) chloro complexes **7** and **8** are characterized. The magnetic moments appear to be higher than those of the tris complexes (Table 2). The mull spectra suggest its O_h symmetry but the shift

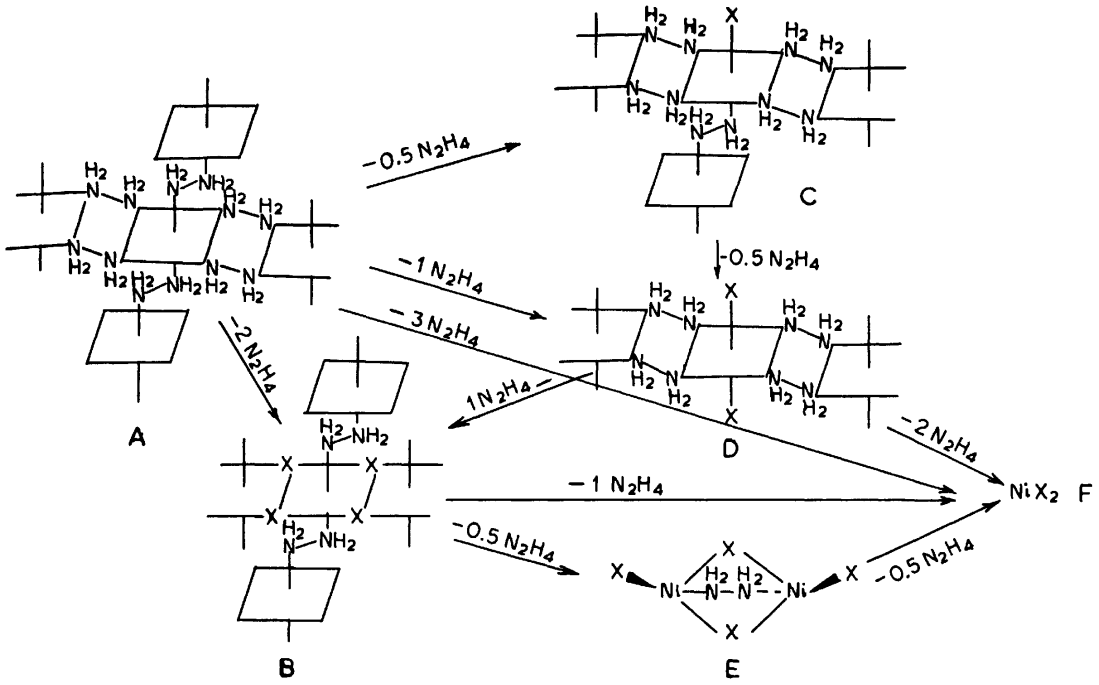

(X=Cl/Br)

Scheme 1.

of the bands (Table 3) towards lower energy region is probably due to the displacement of hydrazine molecules by chloride ions as evident from the fact that halide ions are in the lower position of the spectrochemical series. The color change, pink (tris) to sky blue (unis), also supports the halide substitution.[2,13] Moreover, this unis(hydrazine) complex further decomposes to nickel(II) chloride through unstable hemi(hydrazine) complex as evident from DTA and TG profiles (Fig. 3).

The Complexes Derived from $NiBr_2$ and Hydrazine Hydrate. Treatment of nickel(II) bromide with hydrazine hydrate yields $[NiL_3]Br_2$ (**11**) while with ammoniacal medium another tris species **12** is generated. Both of the species show no difference in color, magnetic moment and IR spectra. Electronic spectra in mull suggest O_h symmetry in them. IR spectra suggest bridging characteristics of hydrazine. But the thermal characteristics of these two species (Fig. 4, Table 1) are distinctly different from each other. It is interesting to note that both the tris species, **11** and **12** yield $[NiL_2Br_2]$ (**13**) while keeping in vacuum though the preparation from the species **11** requires high vacuum in comparison with that from the species **12**. On the contrary, complex **13** is not obtained (Table 1) as an intermediate product upon heating the complex **12**.

Treatment of hydrazine with bis(hydrazine) bromo complex **13** yields tris species **15**. Bis species **14** also yields another tris species **16** with hydrazine hydrate. These two tris species **15** and **16** possess the same color as those of complexes **11** and **12**. IR and electronic mull spectra of these two species imply here also the O_h symmetry as well as bridging characteristic of hydrazine like those of complexes **11** and **12**. But thermal profile of complex **16** is distinctly different from that of complex **15** (Fig. 5, Table 1). These observations indicate that bis species **13** is structurally different from the bis species **14** although the thermal behaviors of these two bis species **13** and **14** apparently show no difference amongst them. Moreover, these two bis complexes **13** and **14** are identical in color, magnetic moments, electronic (mull) and IR spectra suggesting here also O_h symmetry and bridging characteristic of hydrazine. DTA profile of thermal curves of complex **11** exhibits that the stable (D*** of Scheme 1) bis(hydrazine) bromo complex is formed *via* an intermediate $[NiL_{2.5}Br]Br$ (C of Scheme 1). This bis(hydrazine) bromo complex again passes through a nonisolable$[NiLBr_2]$ (B** of Scheme 1) which ultimately transforms straightly to nickel(II) bromide unlike complexes **5**, **6**, **9**, and **10**. On the other hand, the thermal curves of complex **12** suggest the decomposition to follow A→B→E→F in which B is not well characterized like complexes **5** and **6**. Moreover, the thermal curves of complex **16** suggest its decomposition pattern to follow A→B→F where B is not isolable in pure form. However, it is interesting to note that thermal curves distinctly suggest the structural differences existing in complexes **12** and **16** as an intermediate species (E) found in complex **12** is not observed in complex **16**.

The Complexes Derived from $Ni(SCN)_2$ and Hydrazine Hydrate. Treatment of nickel(II) thiocyanate in ethanol with hydrazine hydrate yields $[NiL_2(SCN)_2]$ (**17**). On the other hand, hydrazine hydrate treatment with ammoniacal nickel(II) thiocyanate in ethanolic

** B form in the general scheme is well characterized for **5** and **6**. This form is also expected for **12** as Cl/Br belongs to halide group.

*** D form is well characterissed by **11**. This suggests to follow the general scheme for the other complexes such as **9** and **10**.

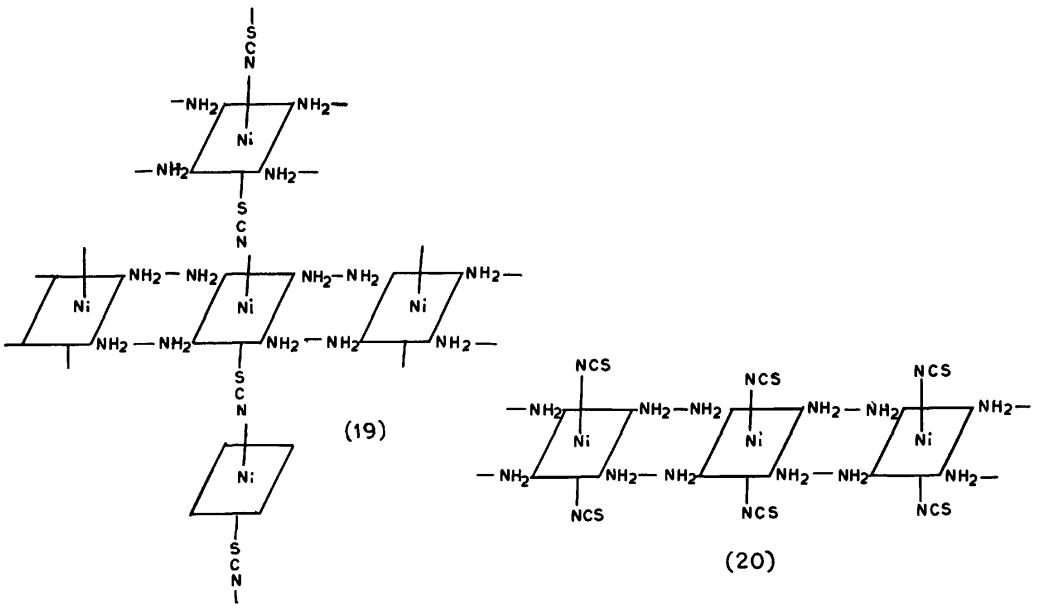

Fig. 9. Structures of $[NiL_2(SCN)_2]$ (**17**) and $[NiL_2(SCN)_2]$ (**18**).

medium yields $[NiL_2(SCN)_2]$ (**18**) which is similar in color to the species (**17**). Electronic mull spectra and magnetic data of these two thiocyanato complexes having identical chemical composition show O_h symmetry in each case. IR spectra indicate the bridging character of the hydrazine. But the thermal behaviors of these two species **17** and **18** are distinctly different from each other, indicating some structural differences. Their structural differences are evident from IR spectra of complexes **17** and **18**. The sharp band at 2085 cm^{-1} [ν(CN)] corresponds to Ni–N bonding[8] which is further supported by the sharp medium band at 800 cm^{-1} ν(CS), whilst the splitting of ν(CN) at 2085 cm^{-1} in complex **17** (Fig. 7) collaborates the bridging of SCN group.[14,15] Moreover, the negative shift of ν(CS) to 785 cm^{-1} [17] (Fig. 7) for complex **17** indicates also Ni–S bonding. The structure for compound **17** should be either $Ni(N_5S)$ or $[Ni(N_4S_2)+Ni(N_6)]$ type. However, the present limited data cannot exclusively comment on the exact chromophores of the system. Thermal data support the higher stability of compound **18** than the compound **17** as compound **18** possesses more symmetric system *i.e.*, NiN_6 chromophores whilst complex **17** possesses less symmetric system as shown in Fig. 9. Nature of the DTA curve of compound **17** suggests that the hydrazine molecules evolve successively through an unstable hydrazine complex as intermediate. On the other hand, the DTA profile for thiocyanate decomposition displays two exotherms suggesting a complicated pattern shown below:

$$Ni(SCN)_2 \longrightarrow Ni^{2+} + 2(SCN)^-$$
$$2(SCN)^- \longrightarrow S^{2-} + 1/2(CN)_2 + 1/2(SCN)_2$$

responsible for 1st DTA peak

$$Ni^{2+} + S^{2-} \longrightarrow NiS$$
$$1/2(SCN)_2 \longrightarrow S + 1/2(CN)_2$$

responsible for 2nd DTA peak

On continuation of heating it is evident that sulfur is evolved first as SO_2 followed by the decomposition of NiS which ultimately transforms to NiO.

Conclusion

In the foregoing discussion, it was observed that the presence of ammonia during the preparation of complexes **2**, **4**, **6**, **12**, and **18** probably plays an important role to form the apparently identical but structurally different complexes as explored by thermal techniques. The structural differences existing in the apparently identical compounds do not involve the change of microsymmetry (O_h) as evident from their absorption spectra taken in mull. However, this is not true for the apparently identical compounds **11** and **12** in which the spectra (Fig. 10) appearing at 540 nm as a maximum in complex **12** is split to 560 and 600 nm in complex **11**.

The X-ray diffraction patterns (Table 4) of complexes **11** and **12** are absolutely different from each other which would indicate the difference in crystal symmetry implying the bond distances being different from each

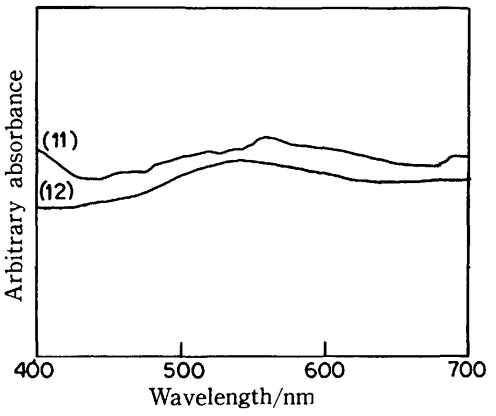

Fig. 10. Electronic spectra of $[NiL_3]Br$(**11**) and $[NiL_3]Br_2$(**12**) in mull.

other. Such concept about the structures of complexes **11** and **12** also supports the differences exhibited (high vacuum for **11** and low vacuum for **12**) in vacuum treatment. In the case of chloride, the vacuum treatment does not alter the tris variety. Since the Br^- is more labile than Cl^- in the complexes, however, the different varieties of Br^- complexes are obtained by the change of the physical and chemical environments. On the other hand, nickel fluoro complexes of hydrazine take up water molecule as F^- and H_2O possess almost similar coordinating ability.[19] Among the tested halide ions (F^-, Cl^-, Br^-)Cl^- is the most preferable one for bridging between two metal ions provided the condition for the bridging should be filled in. Br^- behaves as both bridging and unidentate ligand since the coordinating as well as briding capacity of Br^- and hydrazine may be the same. Therefore, the degree of variation in the case of bromo complexes is more than that of chloro complexes.

References

1) B. Banerjee, P. K. Biswas, and N. Ray Chaudhuri, *Thermochim. Acta*, **47**, 15 (1981).

2) R. Tsuchiya, M. Yonemura, A. Uehara, and E. Kyuno, *Bull. Chem. Soc. Jpn.*, **47**, 660 (1974).

3) P. Glavic, J. Slivnik, and A. Bole, *J. Inorg. Nucl. Chem.*, **39**, 259 (1977).

4) P. Glavic, A. Bole, and J. Slivnik, *J. Inorg. Nucl. Chem.*, **41**, 284 (1979).

5) A. B. P. Lever, "Inorganic Electronic Spectroscopy," Elsevier Publishing Company, Amsterdam (1968), p. 333.

6) R. Tsuchiya, Y. Kaji, A. Uehara, and E. Kyuno, *Bull. Chem. Soc. Jpn.*, **42**, 1881 (1969).

7) R. Tsuchiya, S. Nakagawa, A. Uehara, and E. Kyuno, *Bull. Chem. Soc. Jpn.*, **46**, 169 (1973).

8) F. A. Miller and C. H. Wilkins, *Anal. Chem.*, **24**, 1253 (1952).

9) D. Nicholls, M. Rowley, and R. Swindells, *J. Chem. Soc., A*, 950 (1966).

10) L. Sacconi and A. Sabantini, *J. Inorg. Nucl. Chem.*, **25**, 1389 (1963).

11) I. Nakagawa and T. Shimanouchi, *Spectrochim. Acta*, **20**, 429 (1964).

12) D. M. Adams and P. J. Lock, *J. Chem. Soc., A*, **1971**, 2801.

13) R. Tsuchiya, S. Joba, A. Uehara, and E. Kyuno, *Bull. Chem. Soc. Jpn.*, **46**, 1454 (1973).

14) R. J. H. Clark and C. S. Williams, *Spectrochim. Acta*, **22**, 1081 (1966).

15) S. M. Nelson and T. M. Shaphard, *J. Inorg. Nucl. Chem.*, **27**, 2123 (1965).

16) C. T. Hunt and A. L. Balch, *Inorg. Chem.*, **21**, 1242 (1982).

17) D. M. L. Goodgame, M. Goodgame, M. Hitchman, and M. Weeks, *Inorg. Chem.*, **5**, 635 (1966).

18) A. B. P. Lever, *Coord. Chem. Rev.*, **3**, 119 (1968).

19) F. Basolo and R. G. Pearson, "Mechanism of Reactions," 2nd ed, John Wiley and Sons, Inc., New York (1967), p. 170.

Emission Spectra of Toluidines by Controlled Electron Impact

Teiichiro OGAWA,* Takayuki OOMORI,† and Hirofumi KAWAZUMI
Department of Molecular Science and Technology, Kyushu University, Kasuga, Fukuoka 816
(Received March 11, 1983)

Synopsis. The spectra of *o*-, *m*-, and *p*-toluidines show an intense band of the S_1-S_0 transition of the parent molecule, and lines and bands of fragment species such as H, CH, C_2, CN, and NH.

Electron impact excitation of molecules is a revised form of the traditional electric discharge method. The aromatic molecules show intense photoemission of the parent molecules in the ultraviolet region.[1,2] These bands are similar with the fluorescence spectra and they have been assigned to the S_1-S_0 transition of the parent molecule. In the present note, the emission spectra of three isomers of toluidines have been measured and their excitation processes have been discussed.

The apparatus consists of a collision chamber, a SPEX 1269 monochromator and a photon counting system; they have been described previously.[2]

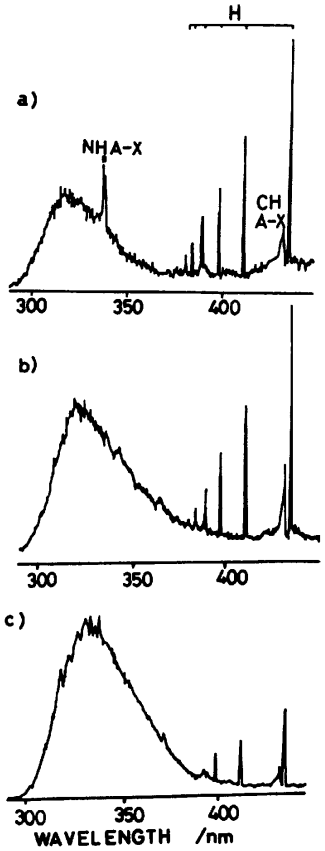

Fig. 1. Emission spectra of (a) *o*-toluidine (100 eV, 500 μA), (b) *m*-toluidine (100 eV, 100 μA), and (c) *p*-toluidine (100 eV, 70 μA) by controlled electron impact.

Typical emission spectra of toluidines by controlled electron impact are shown in Fig. 1. The intense bands observed in the 300—400 nm region are similar to those of aniline[3] and xylenes.[4] The fluorescence spectra of these molecules were measured in ethanol; they have a similar band in the identical region. Therefore, these bands have been assigned to the S_1-S_0 transition of the parent molecules.

There are also many lines and bands of fragment species. They are the Balmer series of the excited hydrogen atom, the 4300 Å system of CH (A-X), the 3360 Å system of NH (A-X) and the Swan system of C_2 (d-a). Their assignments are shown in Fig. 1.

The emission intensities of the parent molecules and such fragments as H* and CH* are proportional to the electron-beam current up to at least 600 μA; this finding indicates that these excited species are produced through a single collision between an electron and a molecule.

The S_1-S_0 band is relatively more intense at lower electron energies than lines and bands of fragments.[2] This is partly due to need of larger excitation energies for the formation of the excited fragments, as is common to most aromatic molecules.[2]

The relative intensity of this band for three toluidines can be estimated from the intensity relative to those of fragments, since the intensity of fragments is expected to be approximately independent of the molecular structure. At an identical electron energy, the band of *p*-toluidine is the most intense, as in the case of xylenes.[4] Furthermore, the band of *p*-toluidine has more vibrational structures. This is due to the higher symmetry of this molecule and, as a result, a higher quantum yield of emission.

Usually a molecule consisted of four atoms or more does not show a band of the parent molecule, unless it is fluorescent. The emission spectra of toluidines have been related with their fluorescence, as have been shown for several aromatic molecules.[1,2]

References

1) K. Hirota, M. Hatada, and T. Ogawa, *Int. J. Radiat. Phys. Chem.*, **8**, 205 (1976).
2) T. Ogawa, N. Yamami, M. Tsuji, and Y. Nishimura, *Bull. Chem. Soc. Jpn.*, **54**, 1203 (1981).
3) M. Tsuji, T. Ogawa, and N. Ishibashi, *Bull. Chem. Soc. Jpn.*, **46**, 3380 (1973).
4) T. Ogawa, M. Tsuji, M. Toyoda, and N. Ishibashi, *Bull. Chem. Soc. Jpn.*, **46**, 2637 (1973).

† Present address: Nippon Steel Co.

Carbon Monoxide Absorption by Solutions of Aluminium Copper(I) Chloride in Various Aromatic Solvents

Hidefumi HIRAI,* Masahiro NAKAMURA, and Makoto KOMIYAMA
Department of Industrial Chemistry, Faculty of Engineering, The University of Tokyo, Hongo, Bunkyo-ku, Tokyo 113
(Received December 10, 1982)

Synopsis. Carbon monoxide absorbents composed of aluminium copper(I) chloride and various aromatic solvents are prepared, and their absorbing capacities are determined. The plot of the equilibrium molar ratio of the absorbed carbon monoxide to $AlCuCl_4$ *vs.* the ionization potential of the aromatic solvent indicates that both electronic and steric factors are important in the molecular complex formation between $AlCuCl_4$ and aromatic solvent molecules.

Carbon monoxide, a valuable starting material in industry, is generally separated from gas mixtures of carbon monoxide, hydrogen, carbon dioxide, methane, nitrogen, and others.[1]

One of the recently developed carbon monoxide-separation methods takes advantage of the molecular complex formation of aluminium copper(I) chloride ($AlCuCl_4$) with carbon monoxide in a toluene solution.[2] On contact with gas mixtures, toluene interacting with aluminium copper(I) chloride is replaced by carbon monoxide. This absorbent is readily deactivated with water in the feed gas. The present authors have now exploited a water-resistant carbon monoxide absorbent by protecting aluminium copper(I) chloride with polystyrene.[3,4] Here, the water resistance has been attributed to the interactions of $AlCuCl_4$ with adjacent aromatic rings of polystyrene.

This paper will describe the preparation of carbon monoxide absorbents composed of aluminium copper(I) chloride and various aromatic solvents. The dependence of their absorbing capacities on the electronic and steric properties of the aromatic solvents will be shown.

Experimental

The aluminium chloride (guaranteed grade, Kishida Chemical Co.) was purified by sublimation. The copper(I) chloride (guaranteed grade, Koso Chemical Co.) was used without further purification. All the aromatic solvents were dried with calcium hydride immediately before use. The triethylbenzene, obtained from the Nakarai Chemical Co., was a mixture of the 1,3,5- and 1,2,4-isomers in a molar ratio of about 2 : 1. The carbon monoxide gas and nitrogen gas, which had purities of 99.95 and 99.999% respectively, were passed through the columns of a 3A molecular sieve.

The carbon monoxide absorbents were prepared by heating 35 mmol of copper(I) chloride and 35 mmol of aluminium chloride in 20 ml of an aromatic solvent in a 100 ml flask for 5 h at 100 °C (for 1,2,3,4-tetrahydronaphthalene, triethylbenzene, and triisopropylbenzene) or 40 °C (for others).

The carbon monoxide–nitrogen mixture, which had an initial volume of 1400 ml and an initial molar ratio of 0.84 : 0.16, was placed in contact with the absorbents, and then the mixture was continuously stirred with a magnetic stirrer (at 20 °C; 1 atm). The absorptions of carbon monoxide were followed by reading the uptake of carbon monoxide with a gas burette. During the first 10 min, the carbon monoxide–nitrogen mixture was made to flow over the absorbent at rate of 30 ml/s by the use of a gas pump.

Results and Discussion

Homogeneous solutions of aluminium copper(I) chloride were prepared for all the aromatic solvents investigated, *i.e.*, benzene, toluene, *o*-xylene, *m*-xylene, *p*-xylene, 1,2,3,4-tetrahydronaphthalene, mesitylene, triethylbenzene, and 1,3,5-triisopropylbenzene.

On contact with carbon monoxide-nitrogen mixtures at 20 °C, all of these solutions exhibited a rapid absorption of carbon monoxide. The molar ratios of the carbon monoxide absorbed to $AlCuCl_4$ attained equilibrium values within 1 h. By raising the temperature from 20 °C to 90 °C, almost all of the absorbed carbon monoxide was rapidly released.

Table 1 lists the equilibrium molar ratios of the absorbed carbon monoxide to $AlCuCl_4$ for all the absorbents. The molar ratio varies considerably with the aromatic solvent used; this fact seems to indicate the significant roles played by the aromatic solvents in these absorbents.

Figure 1 depicts the plot of the molar ratio *vs.* the ionization potential of the aromatic solvent.[5,6] The molar ratio decreases almost linearly with the decrease in the ionization potential from benzene to 1,2,3,4-tetrahydronaphthalene. This is attributable to the fact that the charge-transfer complex between $AlCuCl_4$ and the aromatic-solvent molecule becomes more stable with the decrease in the ionization potential. The absorption of carbon monoxide by the absorbent should be more favorable for the aromatic solvent forming the less stable molecular complex with aluminium copper(I) chloride, since it involves the substitution of the ligand on aluminium copper(I) chloride from the aromatic-solvent molecule to carbon monoxide.

As may clearly be seen from Fig. 1, the molar ratio

Table 1. Equilibrium molar ratios of the absorbed carbon monoxide to $AlCuCl_4$ in various aromatic solvents[a]

Aromatic solvent	Equilibrium molar ratio
Benzene	0.87
Toluene	0.81
o-Xylene	0.70
m-Xylene	0.74
p-Xylene	0.72
1,2,3,4-Tetrahydronaphthalene	0.63
Mesitylene	0.87
Triethylbenzene	0.85
1,3,5-Triisopropylbenzene	0.91

a) At 20 °C: total pressure, 1 atm; initial partial pressures of carbon monoxide and nitrogen, 0.84 and 0.16 atm respectively.

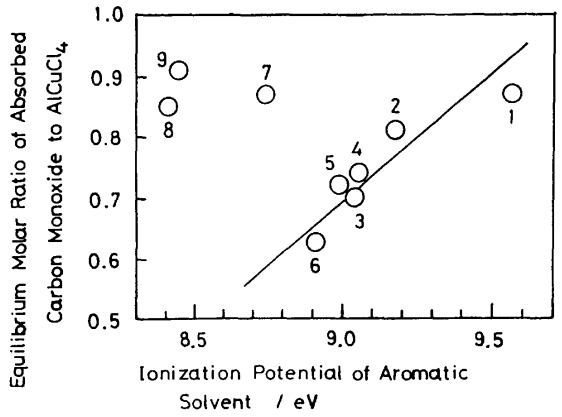

Fig. 1. Plot of equilibrium molar ratio of the absorbed carbon monoxide to $AlCuCl_4$ *vs.* ionization potential of aromatic solvent: benzene(1), toluene(2), *o*-xylene(3), *m*-xylene(4), *p*-xylene(5), 1,2,3,4-tetrahydronaphthalene (6), mesitylene (7), triethylbenzene(8), and 1,3,5-triisopropylbenzene(9).

for mesitylene, triethylbenzene, or triisopropylbenzene is much higher than the value estimated from the ionization potential alone. The molecular complex formation of these trisubstituted benzenes with aluminium copper(I) chloride in the absorbents is largely suppressed by steric hindrance, resulting in feasible ligand substitutions from the aromatic solvents to carbon monoxide. Thus, both electronic and steric factors are important in molecular-complex formation in the absorbents.

In the molecular complexes, the copper atoms, the electron-accepting centers in aluminium copper(I) chloride, are probably located on one of the six C–C bonds of the aromatic rings of the solvents. Under these circumstances, alkyl substitution at an aromatic carbon atom of the solvent molecule should hinder to a large extent the interactions of aluminium copper(I) chloride with aromatic rings at the two C–C bonds involving the substituted carbon. This is in accord with Fig. 1, which shows that the contributions of steric factors in the molecular-complex formation of trisubstituted benzenes with aluminium copper(I) chloride are larger than those for the benzenes with two, one, or no substituents. If the copper were located near the center of the aromatic ring, such large contributions of steric factors should not be observed. The proposed conformations of the molecular complexes in solutions are consistent with that of the $AlCuCl_4$–benzene complex in a solid.[7]

The above arguments are supported by the fact[8] that the equilibrium constants for the formation of molecular complexes of the silver ions with aromatic compounds, which involved silver ions located on one of the six C–C bonds of the aromatic rings,[9] were in the following order: xylenes>benzene≫mesitylene.

In conclusion, the capacities of the carbon-monoxide absorbents composed of aluminium copper(I) chloride and aromatic solvents are governed by both electronic and steric factors in the molecular-complex formation between aluminium copper(I) chloride and the aromatic compounds.

References

1) A. L. Kohl and F. C. Riesenfeld, "Gas Purification," 3rd ed, Gulf Publishing Co., Houston (1979).

2) D. J. Haase, *Chem. Eng. News*, **1975**, August 4, 52.

3) H. Hirai, M. Komiyama, and S. Hara, *Makromol. Chem., Rapid Commun.*, **2**, 495 (1981).

4) H. Hirai, M. Komiyama, and S. Hara, *Chem. Lett.*, **1982**, 1685.

5) The ionization potentials for benzene, toluene, *o*-xylene, *m*-xylene, and mesitylene were taken from G. F. Crable and G. L. Kearns, *J. Phys. Chem.*, **66**, 436 (1962).

6) The ionization potentials for 1,2,3,4-tetrahydronaphthalene was taken to be identical with that for *o*-diethylbenzene reported in "Kagaku Binran, Kiso-hen," ed by the Chemical Society of Japan, Maruzen, Tokyo (1966), p. 1127; Monograph Ser. Res. Instit. Appl. Elect. Hokkaido Univ. No. 4 (1954—1957), Appendix. The ionization potentials for triethylbenzene and triisopropylbenzene were estimated by assuming that the differences in values between these trialkylbenzenes and mesitylene were 3 times as large as the difference between toluene and ethylbenzene or that between toluene and cumene. According to J. D. Morrison and A. J. C. Nicholson (*J. Chem. Phys.*, **20**, 1021 (1952)); the difference in ionization potential between toluene and ethylbenzene is 0.11 eV, while that between toluene and cumene is 0.10 eV.

7) R. W. Turner and E. L. Amma, *J. Am. Chem. Soc.*, **88**, 1877 (1966).

8) N. Ogimachi, L. J. Andrews, and R. M. Keefer, *J. Am. Chem. Soc.*, **78**, 2210 (1956).

9) H. G. Smith and R. E. Rundle, *J. Am. Chem. Soc.*, **80**, 5075 (1958).

The Heats of Solution of Optically Active Amino Acids, the Corresponding Racemic Amino Acids, and Their Derivatives in Water

Masayuki MATSUMOTO† and Kazuo AMAYA*

National Chemical Laboratory for Industry, 1-1, Azuma, Yatabe-machi, Tsukuba, Ibaraki 305

(Received January 7, 1983)

Synopsis. The heats of solution of normal and branched α-amino acids and of their derivatives in water were measured at 298.15 K. The experimental results show that the racemates are more stable than optically active compounds, except for glycylleucine, and that the differences in the heat of solution between the two species for branched compounds are nearly constant, about 2 kJ mol^{-1}, while those for the normal compounds are dependent on the number of carbon atoms in the alkyl chains.

In the previous papers,[1,2] measurements of the heat of solution of optically active α-amino acids and their corresponding racemic compounds in water were made at 298.15 K, and that the differences in the heat of solution between the two species were appreciably larger than the heats of mixing of concentrated aqueous solutions of *d*- and *l*-isomers.

In the present work, in order to obtain further information on the difference in crystal-lattice energy between optically active amino acid and the corresponding racemic amino acid, and on that between amino acid derivatives, solution calorimetry was undertaken.

Experimental

The apparatus and procedure were the same as have been described in a previous work.[2] The alanylalanine, norvaline, and norleucine were purchased from the Sigma Chemical Company. The glycylleucine, α-amino butyric acid (ABA), *N*-formylvaline, *N*-acetylvaline, and *N*-acetylleucine were purchased from the Tokyo Kasei Company, and the other, reagents were purchased from the Takara Kohsan Company. All the samples used were the purest reagents commercially. available. The purities of the amino acid crystals were certified by the above makers and were guaranteed to be more than 98%.

The acylamino acids and dipeptides were kept in a freezer before use. The other materials were also dried as previously has been described, and then used without further purification.

Results and Discussion

At first, the measurements of the heat of solution were made at various concentrations in order to confirm the concentration dependence. No concentration dependence of the molar enthalpy of solution was found within the limits of error of measurement in the range from 10^{-3} to 10^{-2} mol kg^{-1}.

The results obtained are given in Tables 1 and 2, and they are plotted in Fig. 1 alone with two data of the previous paper.[2] The values obtained are the means of three determinations. The ΔH_s values of L-leucine and glycyl-L-leucine are in approximate agreement with those of Kresheck and Benjamin.[3] Also, the ΔH_s value of the A-form in DL-α-amino butyric acid is in good agreement with that of Abraham *et al.*[4] The difference in the ΔH_s of alanylalanine is about 1.5 times that of Alanine.

The experimental results show that the differences in ΔH_s between the two species for branched α-amino

TABLE 1. HEATS OF SOLUTION OF α-AMINO ACIDS AND THEIR DERIVATIVES IN WATER AT 298.15 K

Substance	Molality range m / mol kg^{-1}	Heat of solution ΔH_s / kJ mol^{-1}
DL-α-Amino butyric acid (A-form)	$(0.96—1.00)\times10^{-2}$	1.50±0.01
L-α-Amino butyric acid	$(0.99—1.02)\times10^{-2}$	0.65±0.02
DL-Norvaline	$(0.87—1.08)\times10^{-2}$	0.50±0.10
L-Norvaline	0.89×10^{-2}	−2.29±0.03
DL-Norleucine	$(0.84—0.92)\times10^{-3}$	6.71±0.37
L-Norleucine	$(0.92—1.43)\times10^{-3}$	2.24±0.23
DL-Leucine	$(0.92—1.43)\times10^{-3}$	5.48±0.32
L-Leucine	$(1.07—1.17)\times10^{-3}$	3.41±0.22
N-Formyl-DL-valine	$(0.73—0.75)\times10^{-2}$	16.9 ±0.2
N-Formyl-L-valine	$(0.70—0.71)\times10^{-2}$	14.9 ±0.3
N-Acetyl-DL-valine	$(0.63—0.64)\times10^{-2}$	13.3 ±0.4
N-Acetyl-L-valine	$(0.64—0.65)\times10^{-2}$	12.3 ±0.2
N-Acetyl-DL-leucine	$(0.79—0.91)\times10^{-3}$	7.49±0.30
N-Acetyl-L-leucine	$(0.89—0.91)\times10^{-3}$	6.43±0.25
DL-Alanyl-DL-alanine	$(1.43—1.72)\times10^{-3}$	−7.82±0.14
L-Alanyl-L-alanine	$(1.14—1.50)\times10^{-3}$	−11.0 ±0.4
Glycyl-DL-leucine	$(0.64—0.72)\times10^{-3}$	−3.97±0.13
Glycyl-L-leucine	$(0.76—0.77)\times10^{-3}$	−2.86±0.09

† Present address: M and A Laboratory, 428-12, Kami-asao, Asao-ku, Kawasaki 215.

Table 2. Differences in the heat of solution between optically active amino acids and their corresponding racemic compounds

Substance	Difference in the heat of solution at 298.15 K $\frac{\Delta\Delta H_s}{\text{kJ mol}^{-1}}$
α-Amino butyric acid	0.85±0.03
Norvaline	2.79±0.13
Norleucine	4.47±0.60
Leucine	2.07±0.54
N-Formylvaline	2.0 ±0.5
N-Acetylvaline	1.0 ±0.6
N-Acetylleucine	1.06±0.55
Alanylalanine	3.2 ±0.5
Glycylleucine	1.11±0.22

acids are nearly constant, about 2 kJ mol.$^{-1}$ In addition by replacing the hydrogen atom of the amino group in amino acids with an acyl group, the differences in ΔH_s for the series of acylamino acids become small.

On the other hand, the differences in ΔH_s for the normal compounds are dependent on the number of carbon atoms, n, in the alkyl chains, and they increase with the n value as is shown in Fig. 1.

It seems that, for the normal alkyl chain amino acids, the contribution of the intramolecular configuration is included in the heat of solution, whereas such contribution for the branched compounds is not included. It is known that rotational isomers exist for DL-α-amino butyric acid and DL-norleucine.[5-9] Therefore, the contribution of the intramolecular configuration is assumed to be proportional to the number of carbon-carbon bonds. Accordingly, the dependency of $\Delta\Delta H_s$ on the carbon number in the alkyl chains can reasonably be explained.

Finally, a further thermodynamic study of polymorphic forms in DL-α-amino butyric acid and DL-norleucine is now in progress.

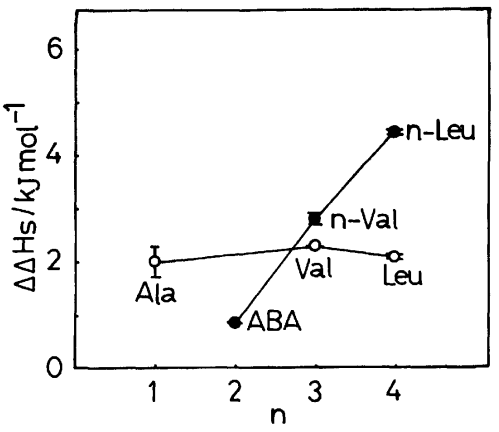

Fig. 1. The plots of the differences in the heat of solution against number of carbon atoms, n, in the alkyl chains of α-amino acids.

References

1) M. Matsumoto and K. Amaya, *Chem. Lett.*, **1978**, 87.
2) M. Matsumoto and K. Amaya, *Bull. Chem. Soc. Jpn.*, **53**, 3510 (1980).
3) G. C. Kresheck and L. Benjamin, *J. Phys. Chem.*, **68**, 2476 (1964).
4) M. H. Abraham, E. Ah-Sing, R. E. Harks, R. A. Schulz, and B. C. Stace, *J. Chem. Soc., Faraday Trans. I*, **73**, 181 (1977).
5) T. Ichikawa and Y. Iitaka, *Acta Crystallogr., Sect. B*, **24**, 1488 (1968).
6) J. Voogt and J. L. Derissen, *Acta Crystallogr., Sect. B*, **36**, 3175 (1980).
7) J. Voogt and J. B. Hulscher, *Acta Crystallogr., Sect. B*, **36**, 3178 (1980).
8) B. Dawson and A. McL. Mathieson, *Acta Crystallogr.*, **4**, 475 (1951).
9) A. McL. Mathieson, *Acta Crystallogr.*, **6**, 399 (1953).

X-Ray Structure of (10*R*)-10-Bromo-10-deoxyhexahydrolaurefucin

Akio Furusaki,* Takeshi Matsumoto, Hajime Kikuchi, Teruaki Suzuki, Minoru Suzuki, and Etsuro Kurosawa

Department of Chemistry, Faculty of Science, Hokkaido University, Kita-ku, Sapporo 060

(Received January 17, 1983)

Synopsis. The main product of the bromination of hexahydrolaurefucin with sulfinyl bromide has been established as (10*R*)-10-bromo-10-deoxyhexahydrolaurefucin by X-ray crystal structure analysis.

In a previous paper, we reported that, when treated with silica gel, the dibromo compound **1** derived from hexahydrolaurefucin (**2**) was transformed into an isomerization product **3**.[1] Although the structure of **3** was recently elucidated,[2] that of **1** remained uncertain. Therefore, in order to confirm that no skeletal change occurred during the bromination of **2** and to establish the configuration of the bromine atom at the 10-position, we have now undertaken an X-ray crystal structure analysis of **1**.

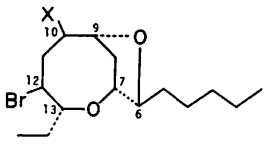

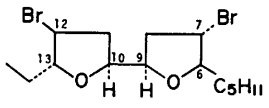

1 : X=Br 2 : X=OH 3

Experimental

A colorless, single crystal with dimensions of about 0.3×0.4×0.4 mm³ was used for the X-ray measurement. The crystal data are as follows: $C_{15}H_{26}O_2Br_2$, mp 36—37 °C, mol wt 398.18, orthorhombic, space group $P2_12_12_1$, a=10.924(4), b=17.642(7), c=9.143(3) Å, Z=4, D_c=1.501 g cm^{-3}, μ(Cu $K\alpha$)=58.6 cm^{-1}. The cell dimensions and diffraction intensities were measured on a Rigaku four-circle diffractometer at the High Energy X-Ray Diffraction Laboratory of Hokkaido University, using graphite-monochromated Cu $K\alpha$ radiation (λ=1.54178 Å). The θ-2θ scan technique was applied at a θ scan rate of 4° min^{-1}; the background was measured for 5 s at each end of the scan range. Three standard reflections, measured at intervals or every 50 reflections, showed a gradual decrease in intensity with the course of data collection; the final-intensity/initial-intensity ratios were about 0.72—0.74. The intensities were corrected for this damage of the sample as well as for the Lorentz and polarization factors, but not for the absorption or the extinction effect. In the range of 2θ values up to 120°, 1354 independent structure factors above the $3\sigma(F)$ level were selected for the structure determination.

Structure Determination

The structure was solved by the Monte Carlo direct method,[3] using the 20 reflections with the greatest $|E|$ values as the starting set. The ninth-generated random phase set led to the correct solution; an E-map based on 459 phases revealed the locations of all the non-hydrogen atoms. After the structure had been well refined by the block-diagonal least-squares method with anisotropic temperature factors, the absolute configuration was determined by taking account of the anomalous dispersion of the bromine atoms for Cu $K\alpha$ radiation. The R ratio for the two enantiomeric structures, 1.022, rejected one of them at the 99.5% confidence level.[4] Since a difference Fourier map afforded the 10 hydrogen atoms attached to the rings, further least-squares refinements were carried out including the hydrogen atoms. For these refinements, the following weighting scheme was used:

$$w = 1/\{\sigma(F)^2 \exp(AX^2+BY^2+CXY+DX+EY)\},$$

where $X=|F_o|$ and $Y=\sin\theta/\lambda$. The A, B, C, D, and E coefficients were evaluated from the $(\Delta F)^2$ distribution; $A=-0.107\times10^{-5}$, $B=-4.06$, $C=-0.757\times10^{-2}$, $D=-0.488\times10^{-3}$, and $E=1.75$. The final R value was 0.069. The final atomic parameters are listed in Table 1.[5]

The calculations were performed on a HITAC M-200H computer at the Hokkaido University Computing Center, using our own programs. The atomic scattering factors were taken from the International Tables.[6]

Results and Discussion

The molecular structure of **1** including the absolute configuration is shown in Fig. 1. This absolute configuration (6*R*, 7*R*, 9*R*, 10*R*, 12*S*, 13*R*) corresponds to that which has been already assigned to laurefucin by X-ray

Table 1. The final atomic parameters and estimated standard deviations

Atom	10^4x	10^4y	10^3z	B_{eq} a)/Å²
Br(1)	5196(1)	1550.0(7)	764.1(2)	8.41
Br(2)	9511(1)	549.7(6)	529.7(2)	7.34
O(1)	4704(5)	2310(3)	412.4(6)	4.83
O(2)	6765(5)	1477(3)	283.8(6)	4.20
C(1)	1577(11)	35(7)	−11(2)	13.31
C(2)	2389(12)	540(7)	105(2)	16.94
C(3)	2302(12)	1260(7)	62(1)	10.91
C(4)	3018(9)	1817(5)	182(1)	8.14
C(5)	4466(8)	1669(5)	183(1)	5.77
C(6)	5073(8)	2325(5)	263(1)	4.57
C(7)	6434(8)	2287(4)	264(1)	4.49
C(8)	6714(8)	2699(5)	403(1)	5.34
C(9)	5739(7)	2382(5)	508(1)	4.36
C(10)	6054(7)	1583(5)	576(1)	4.57
C(11)	7380(7)	1363(5)	593(1)	4.59
C(12)	7880(7)	935(4)	467(1)	5.13
C(13)	8019(7)	1287(5)	322(1)	4.61
C(14)	8505(8)	763(4)	198(1)	5.52
C(15)	8462(9)	1178(6)	40(1)	7.95

a) $B_{eq}=8\pi^2(u_1^2+u_2^2+u_3^2)/3$, where u_i is the root-mean-square deviation in the ith principal axis of the thermal ellipsoid.

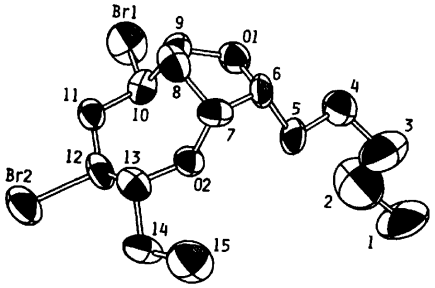

Fig. 1. A perspective view of the **1** molecule. Each non-hydrogen atom is represented as a thermal ellipsoid enclosing a 50% probability. The symbol C for carbon atoms is omitted.

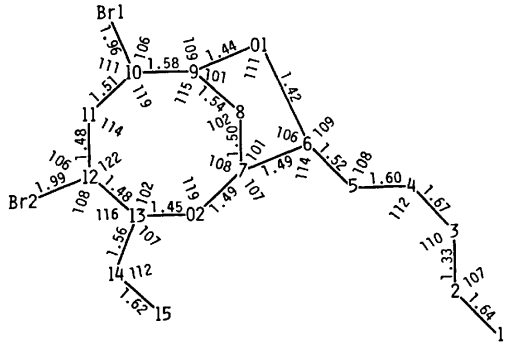

Fig. 2. The bond distances (l/Å) and angles (θ/°). The e.s.d.'s are 0.01—0.02 Å and 0.6—1.3° respectively.

methods.[1] Figure 1 demonstrates that **1** has the same skeleton as **2**, and that the Br(1) and Br(2) atoms are *cis* to each other. Thus, it has been confirmed that **2** undergoes no skeleton rearrangement during its bromination with sulfinyl bromide. It has also been revealed that this bromination proceeds with retention of the original configuration at the C(10) atom.

The bond distances and angles and the torsion angles are given in Figs. 2 and 3 respectively. If the standard deviations are considered, all the bond distances, except the C(1)–C(2), C(2)–C(3), and C(3)–C(4) distances, are normal. Of these three bond distances, the second is much shorter than the standard C–C single-bond distance, while the remaining two are considerably longer. Since the spectroscopic data show the absence of a C=C double bond in **1**, these abnormal bond distances may be due to a special and vigorous thermal

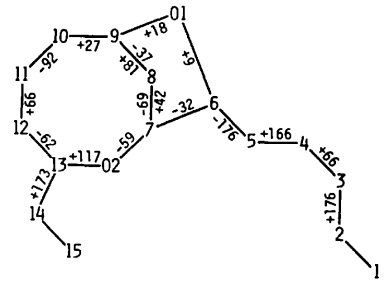

Fig. 3. The torsion angles (ϕ/°). The torsion angles relevant to atoms which form the same ring are given in the ring. The values given near the C(5)–C(6) and C(13)–C(14) bonds show the C(4)–C(5)–C(6)–C(7) and C(12)–C(13)–C(14)–C(15) torsion angles respectively.

motion or a disordering of the pentyl group. The eight-membered ether ring takes on a boat-chair conformation with an approximate mirror plane through the C(8) and C(12) atoms; the Br(1) and Br(2) atoms and the C(14)H_2–C(15)H_3 ethyl group are equatorially oriented, while the O(1) and C(6) atoms are axially placed. The five-membered ether ring adopts a conformation intermediate between the envelope form with an approximate mirror plane through the C(8) atom and the half-chair form with an approximate two-fold rotation axis through the O(1) atom. This deformation from the envelope form somewhat relieves the severe steric repulsion between the O(2) atom and the C(5)H_2 group; the O(2)···C(5) distance is 2.70(1) Å.

The molecules are held together mainly by the van der Waals interactions; there are no unusual intermolecular distances.

References

1) A. Furusaki, E. Kurosawa, A. Fukuzawa, and T. Irie, *Tetrahedron Lett.*, **1973**, 4579.

2) The details of the structure elucidation of **3** will be reported elsewhere.

3) A. Furusaki, *Acta Crystallogr., Sect. A*, **35**, 220 (1979).

4) W. C. Hamilton, *Acta Crystallogr.*, **18**, 502 (1965).

5) The tables of the anisotropic temperature factors and hydrogen parameters and the F_o-F_c table are kept at the Chemical Society of Japan (Document No. 8326).

6) "International Tables for X-Ray Crystallography," The Kynoch Press, Birmingham (1974), Vol. IV.

A New Apparatus for Surface Pressure Measurements

Makio IWAHASHI,* Steven R. MIDDLETON,†,†† Tsutomu SEIMIYA, and Brian A. PETHICA†
Department of Chemistry, Faculty of Science, Tokyo Metropolitan University, Setagaya-ku, Tokyo 158
†Clarkson College of Technology, Potsdam, N.Y. 13667, U.S.A.
(Received March 23, 1983)

Synopsis. A new type of horizontal film balance is described. The principal features of the balance are the use of lightly paraffined silk threads without the conventional floating barrier of the Langmuir surface balance and of a strain gauge as the surface pressure detector.

For the measurement of surface pressures of insoluble monolayers at the air/water interface the Wilhelmy plate and the Langmuir float methods are generally used.[1] The Wilhelmy method has the advantage that no threads are required to close off the gaps at the end of the float used in the Langmuir method, but it has the drawback that contact angle changes can occur, particularly at high surface pressures. Our experience with the Wilhelmy method will be reported elsewhere, but we note here that it is particularly sensitive to inadequate control of temperature and relative humidity. Under appropriate conditions it may be used for micromanometry or higher pressure measurements, but cross-checking with the Langmuir method is generally required to rule out contact angle changes at the plate. Although the Langmuir float method does not suffer from the contact angle problem it requires considerable care. In particular, each of the threads between the float and the sides of the trough must be set up as an arc of a circle with the points of attachment to the float and side of the trough in a line at right angles to the side.[2] If the threads are mounted in other geometries spurious results are obtained.

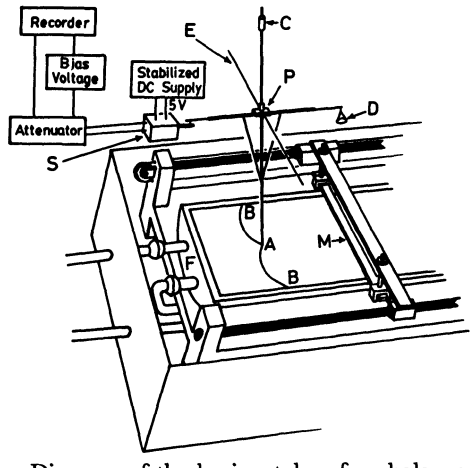

Fig. 1. Diagram of the horizontal surface balance. A is the end of the vertical arm of the frame; B, the edges of the trough; C, a counter weight; D, the calibrating pan; E, a torsion wire; P, a pivot; S, the strain gauge. The trough (F), is fitted with a glass tube for thermostatted water circulation and a driving system for the movable barrier (M) and is placed in a thermostatted box made of glass and aluminium plates. The ceiling of box is a glass plate which has a small hole for the vertical arm of the balance. The box and the balance are together installed in another thermostatted box.

The present paper describes a new apparatus adopting a strain gauge as a detector for the surface pressure and which replaces the conventional float and thread system to separate monolayer and clean surface with a simple arrangement of threads.

Figure 1 shows a schematic drawing of the surface balance. A frame made of thin stainless steel tubes (diameters 0.75 to 1.66 mm) is attached to a tungsten torsion wire (diameter 0.33 mm) with a pivot block made of aluminium. The tubes and the pivot are fixed together by spot welding. The total weight of the frame and the pivot is 4.6 g. The strain gauge (type UL-2-240, Shinko Communication Industry Co. Ltd., Zushi, Japan) is connected to the end of the horizontal arm of the frame *via* thin tungsten wire. The effect of temperature on the strain gauge output is within $\pm 0.1\%/°C$, and the total temperature effect on the calibration is *ca.* $0.2\%/°C$. The sensitivity of the strain gauge is such that surface pressures were measured down to 0.05 mN m^{-1}. This is an excellent value, though can not be compared with a sensitivity limit of 50 nN m^{-1} obtainable with the photoelectric detector described recently.[2]

The monolayer is confined between a movable hydrophobic barrier (M) and silk threads across the trough in place of the conventional float arrangement. The threads are 160 μm in diameter. A pair is knotted together, cut off in equal lengths and immersed briefly in a solution of purified paraffin[3] in distilled hexane. The threads are mounted to form to equal arcs with the vertical arm (A) in the knot and the two ends attached to the sides of the trough with paraffin wax such that the ends and knot are in a straight line at right angles to the sides of the dish. Depending on the studies intended, the dish may be of silica or Pyrex glass hydrophobed with dimethyldichlorosilane.[4] With a little experience, the hydrophobing of the thread can be judged to give excellent resistance to monolayer leakage while remaining soft and flexible to allow the threads to adopt a circular profile when a surface pressure is applied.

The use of threads without a float to confine a monolayer has been reported previously, notably by Guastalla[5] and Kim and Cannell.[6] These workers used unequal arcs of thread so arranged that the restraining arm experienced a force in a direction across the trough which was read on a torsion wire mounted in a direction along the trough. This force can be amplified by making one (short) thread in the form of a semi-circle and the other (long) in the form of a shallow arc. The geometry of the arrangement must be measured exactly to

†† Present address: Pulp and Paper Research Institute of Canada, Pointe Claire, Montreol, Quebec, Canada.

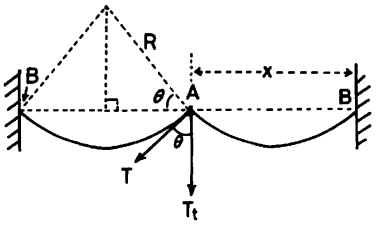

Fig. 2. Schematic drawing of the arc-shaped threads. A is the end of the arm of the frame; B, the edges of the trough; R, the radius of curvature of the threads; x, the distance A to B; T, the tension on the thread; T_t, the force on A along the direction of the trough and transverse to the torsion wire; θ, the angle between the direction of T and T_t.

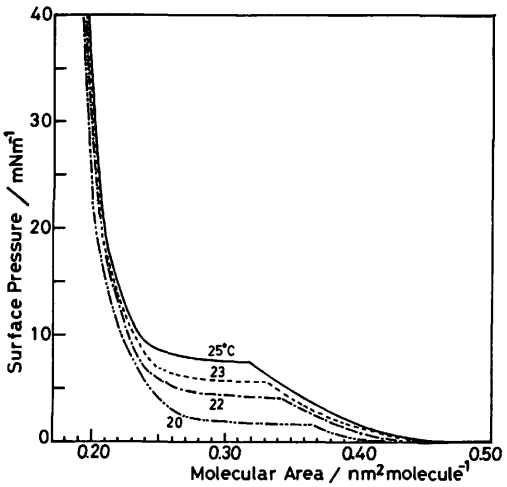

Fig. 3. Π-A diagrams for pentadecanoic acid on 0.01 mol dm^{-3} HCl at various temperatures.

convert the measured force to the surface pressure. With sensitive detectors, the use of these awkward geometried to obtain force amplification is unnecessary. The force may be read in the direction of the length of the trough and the geometry of the two equal threads used in our apparatus need not be known provided they adopt circular arc shapes with the length of each (l) conveniently in the middle of the range $\pi x > 2l > 2x$, where x is the half width of the trough and π is 3.14.

The force balance is shown in Fig. 2. For a given surface pressure Π, the tension in a flexible thread of radius of curvature R is given by the one-dimensional Laplace relation $T = \Pi R$. If each thread makes an angle θ to the direction along the trough, the force contribution in that direction (T_t) as read on the torsion balance is given by

$$T_t = 2T\cos\theta \quad (1)$$

and since $$x = 2R\cos\theta \quad (2)$$

we have $$\Pi = T_t/x. \quad (3)$$

The force read on the balance thus converts directly to surface pressure for all thread lengths in the required range. It will be obvious that if the threads are of unequal length, Eq. 3 may still be used provided that the ends and the arm (A) are again in a line at right angles to the sides of the trough. For lower pressures we have found that a single thread without a knot is convenient. The application of a surface pressure pushes the thread onto the arm, and it is sufficient to arrange the two sides approximately equal.

The surface balance was calibrated by suspending known weights from the horizontal arm of the system and measuring the voltage output of the strain gauge. The voltage output was found to be linear with applied force. Our experimental value for the surface pressure of an oleic acid (purity>99%) drop on the surface of 0.01 mol dm^{-3} HCl was good compared with that of Langmuir and Schaeffer.[7] Figure 3 shows typical Π-A diagrams for pentadecanoic acid on 0.01 mol dm^{-3} HCl; The diagrams are in agreement with reported[1] and our unpublished results which were obtained by using a conventional film balance with a float. The response of the new apparatus for a surface pressure change was superior to that of the float type film balance.

The observation of the time dependence of the surface pressure for pentadecancoic acid crystals sprinkled on the surface of 0.01 mol dm^{-3} HCl showed that the thread was resistant to film leakage at surface pressures up to 25 mN m^{-1} over a period of several days.

The authors wish to express their thanks to Miss Nobuko Maehara and Mr. Yoshihide Kaneko for their experimental assistances. The work was partially supported by a Grant-in-Aid from the National Science Foundation.

References

1) G. L. Gaines, Jr., "Insoluble Monolayers at Liquid-gas Interfaces," Wiley (Interscience), New York (1966).
2) S. R. Middleton and B. A. Pethica, *Faraday Symposium*, **16**, 109 (1981).
3) J. Mingins and J. A. G. Taylor, "A Manual for the Measurement of Interfacial Tension, Pressure and Potential at Air or Nonpolar Oil/Water Interface," (1974), p. 14.
4) *Loc. cit.*, p. 24.
5) J. Gaustalla, *Cah. Phys.*, **10**, 30 (1942).
6) W. M. Kim and D. S. Cannell, *Phys. Rev. A*, **13**, 411 (1976).
7) I. Langmuir and V. J. Schaeffer, *Chem. Rev.*, **24**, 181 (1939).

Nitrosyl(protoporphyrin IX dimethyl ester)iron(II) Complexes with Nitrogenous Bases. The Basicity Dependence of the NO Stretching Frequency

Tetsuhiko YOSHIMURA

The Environmental Science Institute of Hyogo Prefecture, Yukihira-cho, Suma-ku, Kobe 654

(Received December 25, 1982)

Synopsis. The IR spectra of nitrosyl(protoporphyrin IX dimethyl ester)iron(II) [Fe(ppdme)(NO)] complexes with various nitrogenous bases (B), such as imidazoles, pyridines, cyclic secondary amines, and aliphatic amines, were measured in benzene and 1,2-dichloroethane. The NO stretching frequencies (ν_{NO}) of these complexes and the equilibrium constants in equilibrium, [Fe(ppdme)(NO)]+B⇌[Fe(ppdme)-(NO)B], decreased and increased respectively with an increase in the basicity, $pK_a(BH^+)$, of the bases. These results are discussed in relation to the σ- and π-bonding abilities of the bases.

The investigation of (nitrosyl)(porphyrinato)iron(II) complexes as model systems for nitrosylhemoproteins have played an important role in the identification of an axial ligand *trans* to the nitrosyl group of various nitrosylhemoproteins and the elucidation of the stereochemistry of the heme environment.[1-7]

During the course of this investigation of the model complexes,[1] it has been found that the EPR and IR parameters of the (nitrosyl)(porphyrinato)iron(II) complexes are very sensitive to changes in the *trans* axial base and the solvent. The present work will report on an IR study of the system with [Fe(ppdme)-(NO)] and nitrogenous bases, such as imidazoles, pyridines, cyclic secondary amines, and aliphatic amines, in benzene and 1,2-dichloroethane.

A five-coordinate [Fe(ppdme)(NO)] reacts with a base in a solution to form a six-coordinate [Fe(ppdme)-(NO)B] according to Eq. 1:

$$[\mathrm{Fe(ppdme)(NO)}] + \mathrm{B} \overset{K}{\rightleftharpoons} [\mathrm{Fe(ppdme)(NO)B}], \quad (1)$$

Therefore, in the IR spectra of the solution, two NO bands of five- and six-coordinate species are revealed at different frequencies. It has been demonstrated that the ν_{NO} values and the equilibrium constant of Eq. 1 are markedly sensitive to the polarity and the hydrogen-bonding ability of the solvent.[1f] Accordingly, the essential differences in the *trans* effect of an axial base can be detected only in IR spectral results in the same solvent.

Table 1 lists the ν_{NO} and $\Delta\nu_{1/2}$ values (the full width in wavenumbers at a half-height in absorbance) and the equilibrium constants in benzene and 1,2-dichloroethane. The ν_{NO} values in 1,2-dichloroethane with a greater polarity are smaller than in benzene by about 10 cm^{-1}, and the equilibrium constants in 1,2-dichloro ethane with a hydrogen-bonding ability are also smaller. These trends are consistent with those reported previously.[1f]

Figures 1 and 2 show, respectively, the plots of the ν_{NO} value and the equilibrium constant in 1,2-dichloroethane against the $pK_a(BH^+)$ value. Figures similar

TABLE 1. ν_{NO} VALUE AND EQUILIBRIUM CONSTANT OF [Fe(ppdme)(NO)] COMPLEXES WITH NITROGENOUS BASES IN BENZENE AND 1,2-DICHLOROETHANE AT ROOM TEMPERATURE[a]

No.	Base	pK_a (BH^+)[b]	$\nu_{NO}(\Delta\nu_{1/2})$ / cm^{-1}		K / M^{-1}	
			C_6H_6	$C_2H_4Cl_2$	C_6H_6	$C_2H_4Cl_2$
1	1-Acetylimidazole	3.6	1636(21)	1628	2.0	1.0
2	5-Chloro-1-methylimidazole	4.75	1632(22)	1626(25)	4.8	1.6
3	Imidazole[c,d]	6.95		1620		2·7
4	1-Methylimidazole[d]	7.33	1630(21)	1621(24)	11	7.1
5	4-Methylimidazole	7.52	1629(19)	1618(22)	10	6.5
6	3-Chloropyridine	2.84	1641(22)	1635(28)	0.3	0.1
7	4-Acetylpyridine	3.51	1640(15)	1632(27)	1.1	0.2
8	Pyridine[d]	5.23	1639(15)	1631(27)	1.6	1.1
9	4-Methylpyridine	6.02	1636(21)	1628(25)	1.9	0.8
10	3,4-Dimethylpyridine	6.46	1635(18)	1627(23)	1.9	0.9
11	4-Dimethylaminopyridine	9.70	1631(21)	1618(26)	11	7.6
12	Morpholine	8.7	1639(17)	1629(30)	4.5	4.2
13	Piperazine	9.82	1638(15)	1627(28)	7.0	6.2
14	Piperidine[d]	11.22	1636(17)	1626(28)	6.9	6.8
15	Benzylamine	9.6	1637(17)	1626(24)	4.6	3.2
16	Isobutylamine	10.42	1636(17)	1625(22)	5.6	2.4
17	Butylamine[d]	10.64	1636(17)	1625(22)	7.8	3.8

a) Room temperature≈20 °C. [Fe(ppdme)(NO)]=6—8 M. [Base]/[Fe(ppdme)(NO)]=20—200. b) Imidazoles, pyridines, and cyclic secondary amines, Ref. 10; aliphatic amines, Ref. 11. c) Not sufficiently dissolved in benzene. d) Ref. 1f.

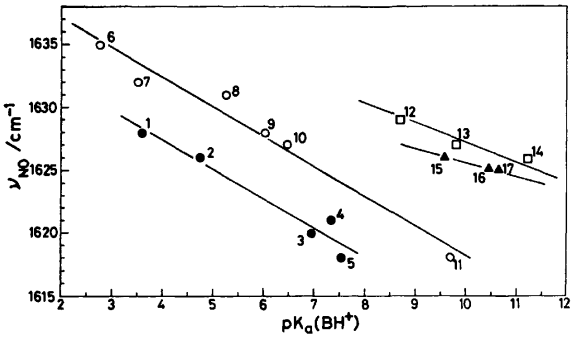

Fig. 1. A plot of ν_{NO} value against pK_a (BH^+) value for [Fe(ppdme)(NO)] complexes with nitrogenous bases in 1,2-dichloroethane. ●: Imidazoles, ○: pyridines, ▲: aliphatic amines, □: cyclic amines. Numbers refer to bases in Table 1. The Straight line was obtained by the use of least-squares method.

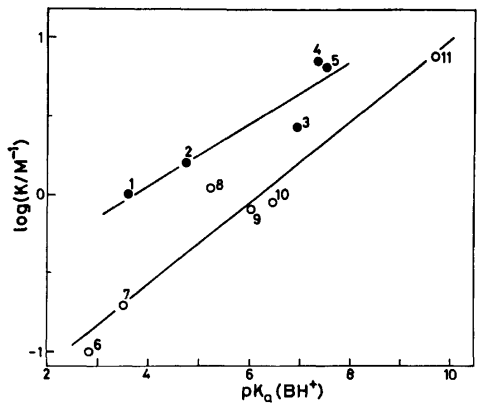

Fig. 2. A plot of log K against pK_a (BH^+) value for [Fe(ppdme)(NO)] complexes with imidazoles (●) and pyridines (○) in 1,2-dichloroethane. Numbers refer to bases in Table 1. The straight line was obtained by the use of least-squares method.

to Figs. 1 and 2 were also made by the plots in benzene against $pK_a(BH^+)$. The ν_{NO} value and the equilibrium constants, respectively, decrease and increase linearly with the basicity. The plots for imidazoles, pyridines, cyclic amines, and aliphatic amines are on separate lines.

Accordingly, the σ-electron donated from the base to the iron can increase with the basicity of the base to intensify the iron-to-base bond, resulting in an increase in the equilibrium constant. Then, since a molecular orbital consisting primarily of the d_{z^2} and the π^*(NO) orbitals is formed in the complexes with a bent Fe–N–O unit,[3,8,9] the contribution of the π^*(NO) orbital to the molecular orbital will be increased when the d_{z^2} orbital can be destabilized accompanying the σ-electron donation. Consequently, the increased antibonding character of the NO bond may induce the observed decrease in the ν_{NO} value. The concomitant increase in the energy of the d_{z^2} orbital also induces an observed decrease in EPR g values toward the free-electron value, as has been reported previously.[1c,e,7]

As is shown in Fig. 1, the ν_{NO} values decrease in the following order for bases: cyclic amines≥aliphatic amines>pyridines>imidazoles. As is shown in Fig. 2, the equilibrium constants for imidazoles are larger than those for pyridines. These tendencies have also been observed in the relation of the EPR g values for [Fe(ppdme)(NO)] complexes with various nitrogenous bases to the $pK_a(BH^+)$ values of the bases.[1c,e] These results indicate that the extra stabilization of an iron-to-base bond arises from d_π-p_π bonding formation, involving the destabilization of the π^*(NO) orbital, and that the imidazoles have a greater ability for π bonding than do the pyridines.

Experimental

The nitrosyl(protoporphyrin IX dimethyl ester)iron(II) was prepared as has been described previously.[1a] The nitrogenous bases were obtained commercially and purified by distillation, recrystallization, and sublimation as has been described previously.[1] The benzene and 1,2-dichloroethane were of a spectral grade and were used without further purification. The oxygen was removed from the solvents and the liquid bases by bubbling with pure N_2 prior to use. The samples were prepared under N_2 atmosphere.

The IR absorption spectra were recorded in the absorbance mode on a JASCO A-302 apparatus with a DP-A300 data processor. The details of the IR measurements were essentially the same as those reported in a previous paper.[1f]

The equilibrium constants were evaluated from the intensity change in the NO stretching band as has been described previously.[1f]

References

1) a) T. Yoshimura, *Bull. Chem. Soc. Jpn.*, **51**, 1237 (1978); b) T. Yoshimura, T. Ozaki, Y. Shintani, and H. Watanabe, *Arch. Biochem. Biophys.*, **193**, 301 (1979); c) T. Yoshimura, *Inorg. Chim. Acta*, **46**, 69 (1980); d) T. Yoshimura, *ibid.*, **57**, 99 (1982); e) T. Yoshimura, *Arch. Biochem. Biophys.*, **216**, 625 (1982); f) T. Yoshimura, *ibid.*, **220**, 167 (1983).

2) H. Kon and N. Kataoka, *Biochemistry*, **8**, 4757 (1969).

3) B. B. Wayland and L. W. Olson, *J. Am. Chem. Soc.*, **96**, 6037 (1974).

4) J. C. Maxwell and W. S. Caughey, *Biochemistry*, **15**, 388 (1976).

5) R. H. Morse and S. I. Chan, *J. Biol. Chem.*, **255**, 7876 (1980).

6) M. Tsubaki and N-T. Yu, *Biochemistry*, **21**, 1140 (1982).

7) K. Kobayashi, M. Tamura, and K. Hayashi, *Biochim. Biophys. Acta*, **702**, 23 (1982).

8) R. Hoffmann, M. M. L. Chen, M. Elian, A. R. Rossi, and D. M. P. Mingos, *Inorg. Chem.*, **13**, 2666 (1974).

9) A. Dedieu, M-M. Rohmer, and A. Veillard, *J. Am. Chem. Soc.*, **98**, 5789 (1976).

10) A. Albert, *Phys. Methods Heterocycl. Chem.*, **1**, 1 (1963).

11) J. A. Riddick and W. B. Bunger, "Techniques of Chemistry," ed by A. Weissberger, Wiley, New York (1974), Vol. II.

Synthesis and Magnetic, Spectral, and Electrochemical Properties of Strati-bis Cobalt(II) Complexes

Masaaki NAKAMURA

Department of Chemistry, Faculty of Science, Kyushu University 33, Hakozaki, Higashi-ku, Fukuoka 812

(Received January 13, 1983)

Synopsis. Strati-bis cobalt(II) complexes, $[Co_2(sata)]\cdot 2H_2O$ and $[Co_2(sacta)]$ have been prepared, where H_4(sata) and H_4(sacta) denote 1,2,3,4-tetrakis(salicylideneamino)-2,3-dimethylbutane and 1,2-bis(salicylideneamino)-1,2-bis(salicylideneaminomethyl) cyclohexane, respectively. Since their magnetic moments are 4.89 and 4.73 BM at room temperature, respectively, the cobalt(II) ions in $[Co_2(sata)]$ and $[Co_2(sacta)]$ have a high spin d^7 configuration. From the temperature dependence of magnetic susceptibilities of these complexes the antiferromagnetic interaction exists between the two cobalt(II) ions. The oxidation potentials for $Co^{II}\rightarrow Co^{III}$ are observed at lower potentials compared with those of corresponding mononuclear cobalt(II) complexes.

Recently there is a growing interest in chemistry of strati-bis binuclear metal complexes in which two metal coordination planes are held in juxtaposition by flexible or nonflexible linkages. In the previous papers,[1-3] it was reported the synthesis and characterization of strati-bis copper(II)–copper(II) and copper(II)–nickel(II) complexes of 1,2,3,4-tetrakis(R-salicylideneamino)-2,3-dimethylburane (H_4(R-sata)) and 1,2-bis(R-salicylideneamino)-1,2-bis(R-salicylideneaminomethyl) cyclohexane (H_4(R-sacta)), where R are the substituents on salicylaldehyde. In these complexes, the following characteristics have been recognized: 1) an "en"-chelated structure (Fig. 1a) and the existence of an equilibrium between the stacked and non-stacked forms as in the face to face manner of the MN_2O_2-planes, 2) electron delocalization over the whole molecule through the ligand π-systems, 3) one electron transfer process, Cu^{II}–$Cu^{II}\rightarrow Cu^{II}$–$Cu^{I}$, occurring at a higher potential compared with the corresponding mononuclear copper(II) complexes.

In the present study the author has prepared the strati-bis complexes, $[Co_2(sata)]$ and $[Co_2(sacta)]$ and their corresponding mononuclear cobalt(II) complexes, [Co(salpn)] and [Co(sacda)], where H_2(salpn) and H_2(sacda) denote *N,N'*-disalicylidene-1,2-propanediamine and 1-(salicylideneamino)-1-(salicylideneaminomethyl)cyclohexane, respectively. Chemical structures of $[Co_2(sata)]$, $[Co_2(sacta)]$, [Co(salpn)], and [Co(sacda)] are shown in Fig. 2.

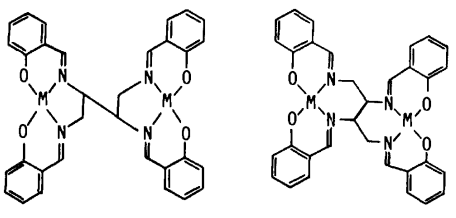

(a) (b)

Fig. 1. Possible structures for strati-bis M(II) complexes: "en"-chelated and "tn"-chelated structures.

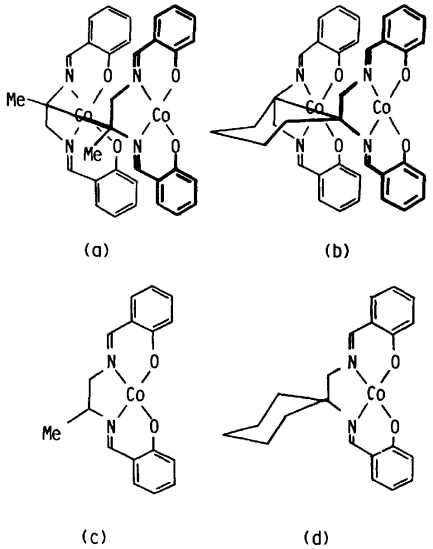

(a) (b) (c) (d)

Fig. 2. Chemical structures of a) $[Co_2(sata)]$, b) $[Co_2(sacta)]$, c) [Co(salpn)], and d) [Co(sacda)].

Experimental

Syntheses. The ligands were synthesized by the method previously reported.[1-3]

[Co(salpn)] and [Co(sacda)]: These complexes were synthesized by the literature method.[4]

$[Co_2(sata)]$: Cobalt(II) acetate tetrahydrate (0.97 g), H_4(sata) (1.1 g), and NaOH (0.3 g) were dissolved in absolute methanol, and the solution was stirred for 6 h at room temperature under nitrogen. The orange-red fine crystals were obtained. Found: C, 57.30; H, 4.58; N, 7.55%. Calcd for $C_{34}H_{30}N_4O_4Co_2\cdot 2H_2O$: C, 57.31; H, 4.81; N, 7.86%.

$[Co_2(sacta)]$: Cobalt(II) acetate tetrahydrate (0.25 g), H_4(sacta) (0.3 g), and NaOH (0.082 g) were dissolved in absolute methanol and the solution was stirred for 12 h at room temperature under nitrogen. The orange fine crystals were obtained. Found: C, 61.75; H, 4.85; N, 7.68%. Calcd for $C_{36}H_{32}N_4O_4Co_2$: C, 61.55; H, 4.59; N, 7.97%.

Measurements. Infrared spectra were measured with a Hitachi Infrared Spectrometer Model 215 on a KBr disk. Electronic spectra were recorded on a Shimadzu spectrophotometer MPS-5000 in dichloromethane. Magnetic susceptibilities were measured by Faraday method in the range from liquid nitrogen temperature to room temperature. Diamagnetic correction was made using Pascal's constants.[5] Effective magnetic moments were calculated by the equation, $\mu_{eff}=2.828(\chi_A\times T)^{1/2}$, where χ_A is the susceptibility per cobalt(II) ion. Differential pulse polarograms and cyclic voltammograms were recorded on a Yanagimoto Voltammetric Analyzer Model P-1000 in dichloromethane containing 0.1 M tetrabutylammonium perchlorate as the supporting electrolyte. A three electrode cell was used for measurements, in which the working electrode is a glassy carbon and the auxiliary electrode a platinum coil. A saturated calomel electrode (SCE)

was used as the reference electrode. In practice, instead of the reference electrode an internal standard, the ferrocene/ferricinium(1+) couple was utilized.[6]

Results and Discussion

The IR spectra of [Co_2(sata)] and [Co_2(sacta)] resemble those[1,2] of previously reported [Ni_2(sata)], [Cu_2(sata)], and [Cu_2(sacta)], and also that of mononuclear [Co(salpn)],[7] all of which have the "en" chelated structures. However, the IR spectra of the cobalt complexes do not resemble that of [Co(saltn)][8] (H_2(saltn) = *N*, *N'*-disalicylidene-1,3-propanediamine), which is the mononuclear complex of the "tn"-chelated structure. Based on these resemblance between the IR spectra, [Co_2(sata)] and [Co_2(sacta)] seem to have the "en"-chelated structure (Fig. 2).

The effective magnetic moments per cobalt(II) ions of [Co_2(sata)] and [Co_2(sacta)] are 4.89 and 4.73 BM at room temperature, respectively, and 4.48 and 4.09 BM at liquid nitrogen temperature, respectively. These results suggest that the cobalt(II) ions in [Co_2(sata)] and [Co_2(sacta)] have a high spin d^7 configuration. On the other hand, the related mononuclear cobalt(II) complex, [Co(salpn)],[9,10] has a low spin d^7 configuration. Thus, the spin states of cobalt(II) ions change to high spin on forming binuclear complexes. This may be caused by the stacking of two CoN_2O_2 moieties in the face to face manner. The magnetic moments of [Co_2(sata)] and [Co_2(sacta)] decrease with lowering of temperature. The χ_A *vs.* T^{-1} plots reveal that they obey the Curie-Weiss law $\chi_A = C/(T-\theta)$. The negative Weiss constants obtained for [Co_2(sata)] and [Co_2(sacta)], $\theta = -24$ and -42 K, respectively, imply the existence of an antiferromagnetic spin-exchange interaction.

Electronic spectra of [Co_2(sata)], [Co_2(sacta)], [Co(salpn)], and [Co(sacda)] measured in dichloromethane are shown in Fig. 3. Absorption bands in the near-infrared region of [Co(salpn)] and [Co(sacda)] are characteristic of the low spin square-planer cobalt(II) complexes,[10,11] whereas the same spectra of [Co_2(sata)] and [Co_2(sacta)] do not show sharp peaks. This difference implies that the binuclear cobalt(II) complexes have different spin states from those of mononuclear cobalt(II) complexes in solution as well.

Electrochemical properties of the cobalt(II) complexes studied by means of differential pulse polarography (D.P.P.) and cyclic voltammetry (C.V.) are given in Table 1. For mononuclear cobalt(II) complexes, [Co(salpn)] and [Co(sacda)], the one-electron oxidation from Co^{II} to Co^{III} was observed at +0.01 and +0.11 V, respectively, positive to the internal reference standard, the ferrocene/ferricinium(1+) couple.[6] In contrast, for the binuclear complexes, [Co_2(sata)] and [Co_2(sacta)] the two oxidation waves were observed at more cathodic region. These two oxidation waves may also be assigned to the oxidation from Co^{II} to Co^{III}. These electrochemical behaviors seem to reflect the presence of intramolecular spin-delocalization in the strati-bis cobalt(II) complexes.

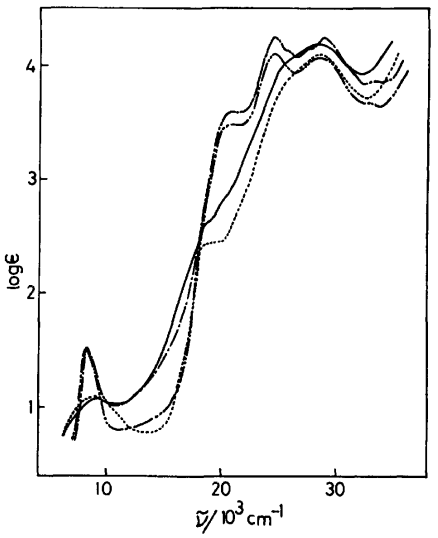

Fig. 3. Electronic absorption spectra of (——) [Co_2(sata)], (·····) [Co_2(sacta)], (·–·–·) [Co(salpn)], and (–··–) [Co(sacda)] in dichloromethane.

Table 1. Electrochemical data of the Co(II) complexes

Complex	E_{pc} [a] / V	E_{pa} [a] / V	ΔE_p / mV	$E_{1/2}$ [a] / V	(D.P.P.)
Co(salpn)	−0.08	0.02	100	0.01	
Co(sacda)·3/4 H_2O	0.02	0.10	80	0.11	
Co_2(sata)·2H_2O		−0.14		−0.18	
		0.03		0.00	
Co_2(sacta)		−0.18		−0.22	
		−0.01		−0.06	

a) V *vs.* E_{Fc/Fc^+} (E_{Fc/Fc^+}; The oxidation potential of the ferrocen/ferricinium (1+) couple as an internal reference.)

References

1) T. Izumitani, H. Ōkawa, and S. Kida, *Chem. Lett.*, **1981**, 483.
2) T. Izumitani, M. Nakamura, H. Ōkawa, and S. Kida, *Bull. Chem. Soc. Jpn.*, **55**, 2122 (1982).
3) H. Ōkawa, M. Kakimoto, T. Izumitani, M. Nakamura, and S. Kida, *Bull. Chem. Soc. Jpn.*, **56**, 149 (1983).
4) B. O. West, *J. Chem. Soc.*, **1954**, 395.
5) A. Earnshow, "Introduction to Magnetochemistry," Academic Press, London (1968), p. 4.
6) R. R. Gagné, C. A. Koval, and G. C. Lisensky, *Inorg. Chem.*, **19**, 2885 (1980).
7) M. Calligaris, G. Nardin, and L. Randaccio, *J. Chem. Soc., Dalton Trans*, **1973**, 419.
8) M. Hariharan and F. L. Urbach, *Inorg. Chem.*, **8**, 556 (1969).
9) B. N. Figgis and R. S. Nyholm, *J. Chem. Soc.*, **1959**, 338.
10) C. Busetto, F. Cariati, A. Fusi, M. Gulloti, F. Morazzoni, A. Pasini, R. Ugo, and V. Valenti, *J. Chem. Soc., Dalton Trans*, **1973**, 754.
11) H. Nishikawa and S. Yamada, *Bull. Chem. Soc. Jpn.*, **37**, 8 (1964).

Photodimerization Mechanism of *m*-Methoxystyrene *via* Its Cation Radical. Open Type Dimer Cation Radical as Its Intermediate

Masahide YAMAMOTO,* Hiroaki YOSHIKAWA, Tetsuya GOTOH, and Yasunori NISHIJIMA
Department of Polymer Chemistry, Faculty of Engineering, Kyoto University, Yoshida, Sakyo-ku, Kyoto 606
(Received July 29, 1982)

Synopsis. Two isomeric tetralin type dimers were obtained by UV excitation of *m*-methoxystyrene in the presence of an electron acceptor. Stepwise electrophilic dimerization mechanism through the dimer cation radical was confirmed. The scheme was analyzed with the aid of MO calculation.

Photodimerization of vinyl compounds conjugated to an aromatic nucleus (electron donors) has been studied extensively by direct photoexcitation,[1] or in the presence of electron acceptors.[2-10] In the presence of electron acceptors, vinyl compounds are photoionized in polar solvents to produce the cation radicals when either the ground state EDA complexes are photoexcited or the exciplexes are formed. The cation radical thus produced gives either [2+2] cyclobutane type dimers[2-6] or [2+4] tetrahydronaphthalene (tetralin) type dimers.[7-10] It has been shown that the dimerizations *via* cation radicals are nonconcerted and stepwise: the intermediates are 1,4-cation radicals.[2,10] However, the factor to determine the path to either cyclobutane type dimer or tetralin type dimer is still ambiguous: *N*-vinylcarbazole,[3] *p*-methoxystyrene,[5] *N,N*-dimethylaminostyrene,[6] *etc.* give mainly the former cyclobutanes; 1,1-diphenylethylene,[7] styrene, *α*-methylstyrene,[8] *etc.* give the latter tetralin type dimer. In this work, the reactivity of *m*-methoxystyrene cation radical was studied and this was found to give two isomers of tetralin type dimer: the one is predominant compared with the other. The mechanism is explained by the intramolecular electrophilic reaction of the 1,4-cation radical, which is supported by MO analysis.

Photoirradiation of *m*-methoxystyrene (**1**) in the presence of *m*-dicyanobenzene (**2**) in various solvents gave two isomeric tetralin type dimers:[11] 8-methoxy-1-(3-methoxyphenyl)-1,2,3,4-tetrahydronaphthalene (**3**) and 6-methoxy-1-(3-methoxyphenyl)-1,2,3,4-tetrahydronaphthalene (**4**) as shown in Table 1. Quantum yield of the dimerization in MeCN solvent (Run 1) was 0.016 with excitation wavelength of 313 nm. Effect of solvent polarity on the dimer yield and the fraction of the dimers are shown in Table 1, Runs 1, 2, and 3. In polar solvent MeCN, the rate is faster than those in less polar solvents, THF and CH_2Cl_2, and the ratio of **3**/**4** is smaller than those in less polar solvents. Runs 4, 5, and 6 show the time course of photodimerization. Dimer yields increase with irradiation time, but the ratios of **3**/**4** decrease with time. This decrease seems to be due to the variation of the partitioning between **3** and **4** with reaction time. In the limit of $t=0$, the ratio of **3**/**4** is 7.7. As for other exciplex acceptors, *p*-dicyanobenzene and dimethyl terephthalate are also effective and gave the same products with approximately the same rates and product ratios. Temperature dependence of the dimer yield was hardly observed in the range from −30 to +30 °C.

Table 1. Dimerization yields and fractions

Run	**1** / mM	**2** / mM	Solvent	Time/h	Dimer yield / %	Fraction/% **3**	Fraction/% **4**
1	37	22.4	MeCN	20	37.4	55.6	44.4
2	37	22.4	THF	20	2.2	92.1	7.9
3	37	22.4	CH_2Cl_2	20	3.0	80.9	19.1
4	149	22.4	MeCN	0.75	0.113	85.1	14.9
5	149	22.4	MeCN	1	0.378	79.9	20.1
6	149	22.4	MeCN	2	1.43	72.7	27.3

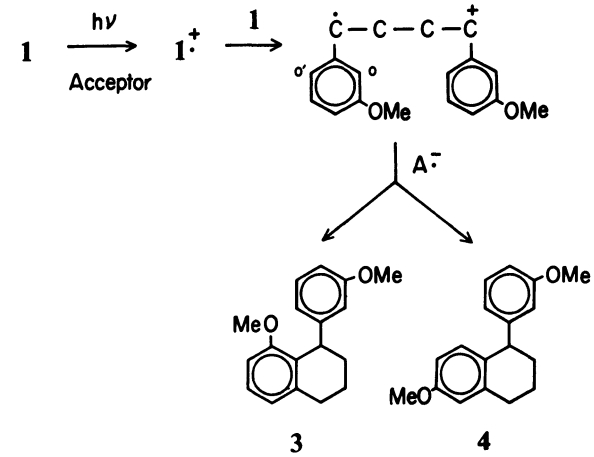

3 **4**

Fig. 1. Scheme.

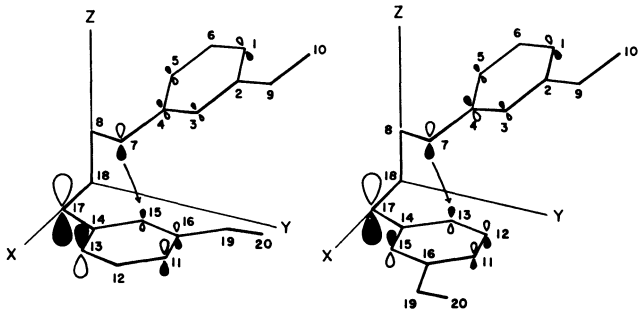

C-3 C-4

Fig. 2. 1,4-Cation radical intermediates **C-3** and **C-4** prior to $\mathbf{3}^{+}$ and $\mathbf{4}^{+}$.

The reaction scheme is shown in Fig. 1. The monomer cation radical $\mathbf{1}^{+}$ which is produced by the interaction of **1** with **2** (fluorescence quenching constant $k_q=9\times10^9\ M^{-1}\ s^{-1}$ in MeCN solvent), reacts with the monomer to form an open type dimer cation radical. Electrophilic attack of the carbenium ion to ortho-positions *o* or *o'* of phenyl ring and subsequent intramolecular proton migration give $\mathbf{3}^{+}$ and $\mathbf{4}^{+}$, respectively.[12] Back electron transfer from $\mathbf{2}^{\cdot-}$ to the dimer cation radicals gives either **3** or **4**. Yamaguchi[13] showed

Table 2. Formal charge and spin density for C-3 and C-4 conformations

Atom No.	C-3		C-4	
	Formal charge	Spin density	Formal charge	Spin density
C 7	0.158	0.182	0.140	0.183
C11	−0.065	0.061	−0.046	0.025
C12	0.072	−0.019	0.048	0.002
C13	−0.030	0.089	−0.052	0.016
C14	0.082	−0.035	0.085	−0.029
C15	−0.093	0.022	−0.070	0.084
C16	0.253	−0.006	0.268	−0.012
C17	0.010	0.647	0.019	0.635

by theoretical analysis that the dimerization of olefin cation radical with neutral olefin proceeds *via* open type cation radical.

Preferred formation of **3** to **4** can be estimated by the MO analysis. In this calculation, a reaction path to tetralin is assumed: **C-3** and **C-4** in Fig. 2 correspond to two conformations just before C7–C15 and C7–C13 bond formations, which lead to **3** and **4**, respectively. In Fig. 2, the coefficients of HOMO are also roughly shown by the size of lobes. Formal charge density, and total spin density of the dimer cation radical are given in Table 2. The carbenium ion was found to be at carbon 7, while the radical was at site C17 as can be seen from Table 2. The carbenium ion (C7) attacks *o* position (C15 in **C-3**) or *o'* position (C13 in **C-4**).[12] Electron density of *o* position (C15) for **C-3** (−0.093) is higher than that of *o'* position (C13) for **C-4** (−0.052). Formal charge at C7 for **C-3** (+0.158) is more positive than that for **C-4** (+0.140). Furthermore the AO bond population[14] between C7 and C15 in **C-3** is 0.250 and the one between C7 and C13 in **C-4** is 0.236. Therefore, it can be understood that the dimer **3** is produced more favorably than the dimer **4**. This result supports the stepwise electrophilic dimerization. In the LUMO of the styrene cation radical $\mathbf{1}^+$, the α- and β-carbons have the same sign, but in the HOMO of styrene **1** the signs of the β- and *o*-carbons are opposite, hence these do not interact in a concerted way and the products **3** and **4** are not produced by a concerted mechanism.

Experimental

^{1}H-NMR spectra were taken on a Varian HA-100 spectrometer with TMS as an internal standard. Mass spectra were taken on a Hitachi RMU-60 mass spectrometer. Photolysis was carried out through Pyrex vessel wall with a 300 W high-pressure mercury lamp (Toshiba 300H) at room temperature. Analysis of the sample solutions was performed with a Shimadzu GC-3BF with a 1 m column packed with Apiezon grease L (230 °C), using phenanthrene as an internal standard.

8-Methoxy-1-(3-methoxyphenyl)-1,2,3,4-tetrahydronaphthalene(3): After photolysis of degassed MeCN solution of **1** and **2**, the dimer fraction was collected by silica gel column eluted with dichloromethane–hexane (1 : 1) and the fraction of **3** was collected by GLPC. Recrystallization from CCl_4–dichloromethane gave an analytical sample **3**: mp 87—90 °C; IR (KBr-pellet) 1600, 1580, 1480 (phenyl), 1245 (C–O), 870 (isolated ring H atom), 790, 770 cm^{-1} (three adjacent ring H atoms); NMR (CCl_4) δ=1.44—2.86 (m, CH_2, 6H), 3.53 (s, OCH_3, 3H), 3.67 (s, OCH_3, 3H), 4.27 (m, CH, 1H), 6.36—7.10 (m, phenyl, 8H). MS (70 eV), *m/e*: 268 (M^+, main), 160 (M^+−anisole).

6-Methoxy-1-(3-methoxyphenyl)-1,2,3,4-tetrahydronaphthalene(4): In the final separation procedure of **3** from the dimer fraction, **4** was also collected. Uncrystallized. IR (neat) 1605, 1580, 1500 (phenyl), 1250 (C–O), 870, 855 (isolated ring H atom), 830 (two adjacent ring H atoms), 780 cm^{-1} (three adjacent ring H atoms); NMR (CCl_4) δ=1.20—2.90 (m, CH_2, 6H), 3.66 (s, OCH_3, 3H), 3.69 (s, OCH_3, 3H), 3.97 (m, CH, 1H), 6.40—7.20 (m, phenyl, 8H); MS (70 eV), *m/e*: 268 (M^+, main), 160 (M^+−anisole).

Method of Calculation. The calculation was carried out with the unrestricted SCF INDO method.[15] It is assumed that the effect of the contaminating spin components of the S^2 operator is negligible. The geometry of the dimer cation radical in Fig. 2 is as follows: R(C⋯C of aromatic ring)=1.40 Å, R(C4–C7)=1.47 Å, R(C7–C8)=1.51 Å, R(C8–C18)=1.54 Å, $R(C\text{–}H_{aromatic})$=1.08 Å, $R(C\text{–}H_{aliphatic})$=1.09 Å, R(C–O)=1.36 Å, ∠C17–C14–C15=110° (**C-3**), ∠C17–C14–C13=130° (**C-3**), ∠C18–C17–C14=110°, ∠C17–C18–C8=90°, ∠C18–C8–C7=100°, C7 and C17 have sp^2 shape, R(C7–C15 or C7–C13)=2.283 Å. In Fig. 2, atoms 9 and 19 are oxygen, and hydrogen atoms are not shown. The calculations were carried out on the FACOM-230-75 computer at the Computer Center of Kyoto University.

References

1) G. Kaupp, "Methoden der Organischen Chemie, Vol. IV/5a, Photochemie I (Houben-Weyl)," Georg Thieme Verlag, Stuttgart (1975), p. 278; H. F. Kauffmann, *Makromol. Chem.*, **180**, 2649, 2665, 2681, 2695 (1979).

2) S. L. Mattes and S. Farid, *Acc. Chem. Res.*, **15**, 80 (1982).

3) A. Ledwith, *Acc. Chem. Res.*, **5**, 133 (1972).

4) S. Kuwata, Y. Shigemitsu, and Y. Odaira, *J. Org. Chem.*, **38**, 3803 (1973).

5) M. Yamamoto, T. Asanuma, and Y. Nishijima, *J. Chem. Soc., Chem. Commun.*, **1975**, 53.

6) T. Asanuma, M. Yamamoto, and Y. Nishijima, *J. Chem. Soc., Chem. Commun.*, **1975**, 56.

7) R. A. Neunteufel and D. R. Arnold, *J. Am. Chem. Soc.*, **95**, 4080 (1973): T. R. Evans, R. W. Wake, and O. Jaenicke, "The Exciplex," ed by M. Gordon and W. R. Ware, Academic, New York (1975), p. 345.

8) T. Asanuma, M. Yamamoto, and Y. Nishijima, *J. Chem. Soc., Chem. Commun.*, **1975**, 608.

9) T. Asanuma, T. Gotoh, A. Tsuchida, M. Yamamoto, and Y. Nishijima, *J. Chem. Soc., Chem. Commun.*, **1977**, 485.

10) T. Gotoh, M. Yamamoto, and Y. Nishijima, *J. Polym. Sci., Polym. Lett. Ed.*, **17**, 143 (1979).

11) In the absence of **2**, the main product is *cis*-1,2-bis(3-methoxyphenyl)cyclobutane.

12) The open type cation radical could be trapped as its methoxylation product which supports electrophilic reaction. The ratio of **3**/**4** is better explained in terms of formal charge rather than spin density.

13) K. Yamaguchi, *Chem. Phys.*, **25**, 215 (1977).

14) The AO bond population proposed by Mulliken, $N_{rs}=2\sum_{j}^{occ} c_r^j c_s^j S_{rs}$ was calculated from the bond order population and the overlap integral although the overlap integral S_{rs} is not explicitly included in INDO calculation.

15) J. A. Pople, D. L. Beveridge, and P. A. Dobosh, *J. Chem. Phys.*, **47**,2026 (1967).

Thermally Derived Dimers of *o*-Vinylphenol: *trans*- and *cis*-2′-Hydroxy-4-methylflavans

Yen-Yuan CHEN, Ryuichi OSHIMA, and Ju KUMANOTANI*
Institute of Industrial Science, The University of Tokyo, 7-22-1 Roppongi, Minato-ku, Tokyo 106
(Received August 27, 1982)

Synopsis. *o*-Vinylphenol dimerizes thermally to yield quantitatively two isomers, *trans*- and *cis*-2′-hydroxy-4-methylflavans. The analysis of the dimers of *o*-vinylphenol-*O*-*d* suggests that a quinone-methide intermediate is responsible for the formation of these flavanoid compounds.

Although a number of papers have been published concerning the radical polymerization of *o*-vinylphenol,[1-5] little is known of its dimers formed in the course of the polymerization or during storage.[1] Flavanoid compounds were previously found in our laboratory to be obtained by the dimerization of *o*-vinylphenol; they were assumed to be mixtures of *cis* and *trans* isomers.[2] In this paper, we report the identification of each isomer of the dimers separated by gel-permeation chromatography (GPC) and liquid-solid chromatography (LSC).

Experimental

Thermal Dimerization. *o*-Vinylphenol (1.0 g) (bp 61 °C/3—4 mmHg (1 mmHg=133.322 Pa), made by the decarboxylation of *o*-coumaric acid)[6,7] was heated at 90 °C for 12 h in an ampoule displaced with nitrogen; the dimers were thus obtained almost quantitatively, along with a trace of higher-molecular-weight substances (less than 1%), which has been separated by GPC on a preparative TSK-gel 2000HG8 column (2.2 cm I.D.×60 cm×2), using chloroform as the eluent. The dimers were fractionated by LSC (1 : 3 in a peak-area ratio with a UV detector at 254 nm) on a semi-preparative silica column (Nomura Chemical, Develosil 60-3, 8 mm I.D.×25 cm), using hexane–ethyl acetate (95.5: 2.5 v/v) as the eluent.

The ^{1}H NMR spectra of these two isomers were recorded at 90 MHz with a Varian EM 390 spectrometer, using tetramethylsilane as the internal standard in $CDCl_3$.

The minor isomer was obtained as a white solid; mp 86 °C; mass spectrum, *m/e* 240 (M^+). Found: C, 79.61; H, 6.73%. Calcd for $C_{16}H_{16}O_2$: C, 79.97; H, 6.71%.

The major isomer was obtained as a pale yellow viscous liquid; mass spectrum, *m/e* 240 (M^+). Found: C, 79.31; H, 6.75%. Calcd for $C_{16}H_{16}O_2$: C, 79.97; H, 6.71%.

Dimerization of o-*Vinylphenol*-O-d. A mixture of 1.0 g of *o*-vinylphenol, 10 ml of carbon tetrachloride, and 1 ml of deutrium oxide was shaken vigorously for 20 min, after which the separated oily layer was again shaken with new deuterium-oxide (1 ml) for 30 min. The oily layer was separated and dried over sodium sulfate. The IR spectrum of the solution confirmed the complete H–D exchange at the hydroxyl group of *o*-vinylphenol. Then the solution was transferred into an ampoule. After the removal of carbon tetrachloride *in vacuo*, the ampoule was sealed under nitrogen and heated at 90 °C for 12 h. The dimers were then separated into two isomers by means of LSC, as has been described above. Mass spectra for both isomers: *m/e* 241 (M^+).

Results and Discussion

Each of the fractionated isomers showed the same *m/e* value (240) for the molecular ion and similar IR spectra. In the IR spectra of the isomers, the absorption bands due to a vinyl group (1630, 1420, and 910 cm^{-1}) were completely eliminated, and a new band, presumably due to an ether group, appeared at 1050 cm^{-1}. The ^{1}H NMR spectra of both isomers are shown in Fig. 1. By extensive decoupling experiments, each resonance

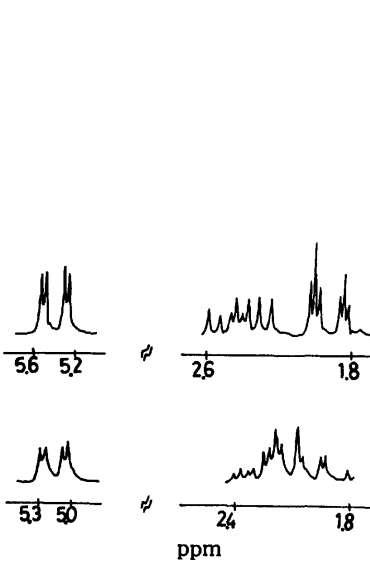

Fig. 1. ^{1}H NMR spectra of *o*-vinylphenol dimers (H_2, H_{3e}, and H_{3a}): above, *trans* and below, *cis*.

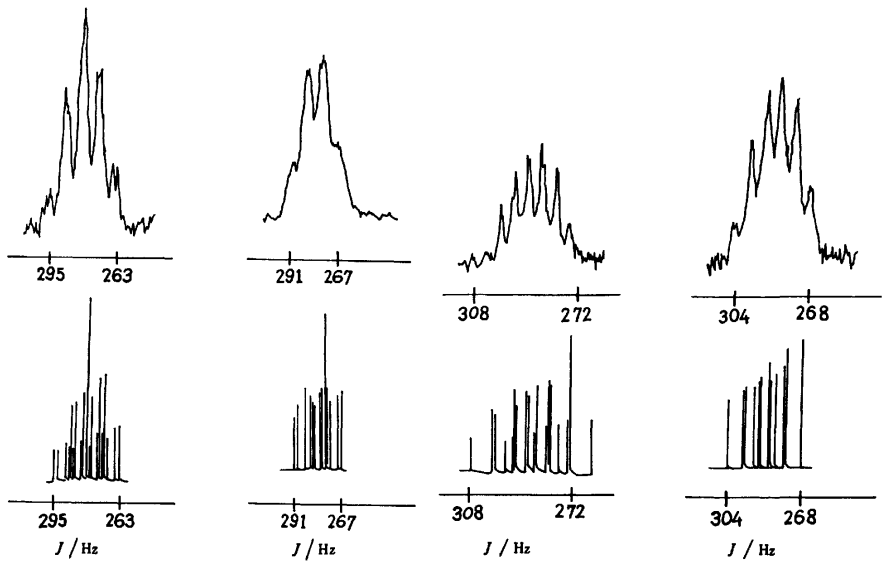

(a) (b)

Fig. 2. ^{1}H NMR spectra of H_4: (a), *trans* isomer and (b), *cis* isomer; left, undeuterated and right, deuterated; above, observed and below, calculated. The chemical shifts were expressed in Hz from TMS.

Table 1. ^{1}H NMR data of *trans*- and *cis*-2′-hydroxy-4-methylflavans

Chemical shift[a] (δ) of	*trans*	*cis*
H_2(1H)	5.30	5.25
H_{3e}(1H)	1.95	2.28
H_{3a}(1H)	2.43	1.97
H_4(1H)	3.10	3.17
H_5(3H)	1.45	1.37
Coupling constants/Hz		
3a, 3e	14	15
3e, 4	2	7
2 , 3e	3	3
3a, 4	6	13
2 , 3a	12	12
4 , 5	8	8

a) Measured at 90 MHz in $CDCl_3$. Chemical shifts (center of multiplet) are shown in δ.

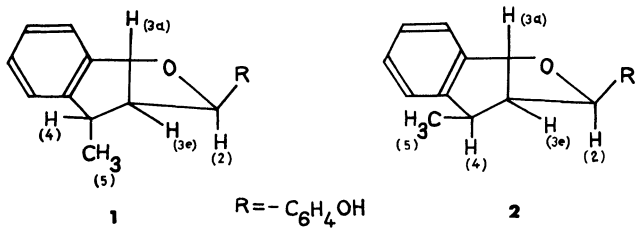

was assigned as is summarized in Table 1: in the minor product, $J_{3e,4}$ (2 Hz) corresponds to $J_{eq,eq}$, and $J_{3a,4}$ (6 Hz) to $J_{ax,eq}$, while in the major product, $J_{3e,4}$ (7 Hz) and $J_{3a,4}$ (13 Hz) stand for $J_{eq,ax}$ and $J_{ax,ax}$ respectively. From these results, it is obvious that the minor isomer has the 2,4-*trans* structure (**1**) with a quasi-axial methyl group, while the major isomer has the 2,4-*cis* structure (**2**) with a quasi-equatorial methyl group at C-4 of the flavanoid compounds. The coupling constants also indicate that the *o*-C_6H_4OH group is in the quasi-equatorial position for both isomers.[8] Accordingly, it may be concluded that the minor and major isomers are *trans*- and *cis*-2′-hydroxy-4-methylflavans, respectively.

The predominant formation of the *cis* isomer may be explained on steric effect: the *cis* isomer has both substituents at quasi-equatorial positions with less crowding than in the *trans* isomer, which has the quasi-axially oriented methyl group.

The dimers from *o*-vinylphenol-*O*-*d* showed a weak C–D absorption band at 2230 cm^{-1} and an *m/e* value of 241 for M^+. In the ^{1}H NMR spectra, no significant difference could be detected for the peaks due to H_2, H_{3a}, and H_{3e}. However, peaks from H_4 and H_5 of both isomers were obviously different from those of undeuterated dimers. The integrated intensity of the resonance of H_5 for both isomers decreased to 2/3 of that for undeuterated isomers, and the peak became a doublet of triplets with a new, small coupling (J=1.2 Hz) which can be attributed to a geminal deuterium-proton coupling.[9] The splitting of the H_4 peak is also consistent with the calculated ones.[10] (see Fig. 2)

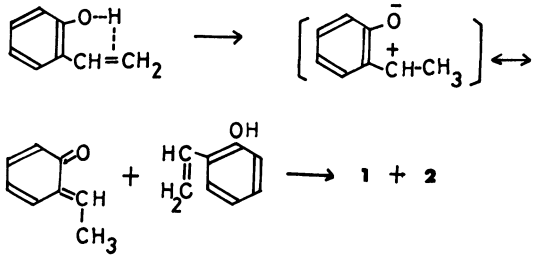

Scheme 1. A mechanism of thermal dimerization of *o*-vinylphenol.

Consequently, Scheme 1 can be taken as a mechanism of the dimerization of *o*-vinylphenol. It may be suggested that the initial migration of the proton of the phenolic hydroxyl group, making a hydrogen-bond bridge with the neighbouring vinyl group, leads to the formation of quinone methide[11] through a dipolar intermediate. Then it may react with an olefin (*o*-vinylphenol) to give the dimers by means of a Diels-Alder reaction.[12,13] This mechanism may also account for the formation of a similar type of flavanoid compound obtained from 4-isopropenyl-*m*-cresol.[14–16] When compared with styrene, which thermally gives *cis*- and *trans*-1,2-diphenylcyclobutanes as the dimers,[17] the phenolic hydroxyl group may play a significant role in the thermal dimerization of *o*-vinylphenol.

References

1) T. Tanaka, T. Yamashita, and T. Yokoyama, *Kogyo Kagaku Zasshi*, **60**, 1595 (1957).
2) J. Kumanotani and K. Oshima, paper presented at a meeting of the Society of Polymer Science, Japan, June 5th, 1964.
3) M. Kato and H. Kamogawa, *J. Polym. Sci., Part A-1*, **4**, 2771 (1966).
4) M. Kato and H. Kamogawa, *J. Polym. Sci., Part A-1*, **4**, 2771 (1966).
5) K. Hiraoka and T. Yokoyama, *Reports of the Faculty of Engineering*, Nagasaki University, **7**, 95 (1976).
6) W. J. Dale and H. E. Hennis, *J. Am. Chem. Soc.*, **80**, 3645 (1958).
7) B. B. Corson, W. J. Heintzelman, L. H. Schwartzman, H. E. Tiefenthal, R. J. Lokken, J. E. Nickels, G. R. Atwood, and F. J. Pavlik, *J. Org. Chem.*, **23**, 544 (1958).
8) B. J. Bolger, A. Hirwe, K. G. Marathe, E. M. Philbin, and M. A. Vikars, *Tetrahedron*, **22**, 621 (1966).
9) R. M. Silverstein, G. C. Bassler, and T. C. Morrill, "Spectrometric Identification of Organic Compounds," 4th ed, John Wiley and Sons, New York (1981), p. 199.
10) Spectra were calculated by means of the JEOL simulation program (JEOL, Ltd., Tokyo, Japan), using the data in Table 1.
11) A. Turner, *Quart. Rev.*, **18**, 347 (1964).
12) G. R. Sprengling, *J. Am. Chem. Soc.*, **74**, 2927 (1952).
13) K. Hultzsch, *Ber.*, **74**, 898 (1941).
14) W. Baker and D. H. Bestly, *Nature*, **144**, 865 (1939).
15) W. Baker and D. H. Bestly, *J. Chem. Soc.*, **1940**, 1103.
16) W. Baker, R. F. Curtis, and J. F. Mcomie, *J. Chem. Soc.*, **1951**, 76.
17) V. K. Kirchner and K. Bucholz, *Angew. Makromol. Chem.*, **13**, 127 (1970).

Induced Circular Dichroism in the Complex of Poly(L-arginine) Hydrochloride with Azo Dyes

Hiroyuki YAMAMOTO* and Ayako NAKAZAWA

Institute of High Polymer Research, Faculty of Textile Science and Technology, Shinshu University, Ueda 386

(Received December 13, 1982)

Synopsis. The induced circular dichroism (CD) spectra of the poly(L-arginine) hydrochloride–azo dye complexes were measured. The induced CD arose from the azo dyes bound to the polypeptide in the α-helical conformation. The configuration of the transition dipole moments of dye was examined by the exciton chirality method.

The induced optical activities of complexes of synthetic poly(L-glutamic acid) (PLG) with cationic dyes, such as Acridine Orange (AO) and pseudoisocyanine, in the pH range from 4.2 to 6.5 were first reported by Stryer and Blout.[1,2] Induced optical activities have been reported mostly on the PLG complexes. Lately, however, the complexes of poly(*S*-carboxymethyl-L-cysteine)-AO[3] and poly(L-lysine) (PLL)–azo dyes[4-6] have been reported to induce optical activity.

The first complete synthesis of poly(L-arginine) (PLA) by the *N*-carboxy anhydride method and a conformational study of the polypeptide have been reported from this laboratory.[7,8] In the course of our study of the induced CD of biopolymers, we wish to report our findings on the induced CD due to the interaction between the cationic PLA and anionic azo dyes.

Experimental

The average degree of polymerization of the PLA hydrochloride (HCl) used was 70. The three analogous azo dyes, *p*-(4-aminophenylazo)benzenesulfonic acid sodium salt (AA), *p*-(4-dimethylaminophenylazo)benzenesulfonic acid sodium salt (Methyl Orange, MO) and *p*-(4-diethylaminophenylazo)-benzenesulfonic acid sodium salt (Ethyl Orange, EO), were guaranteed reagents (Wako). The mixtures were prepared by adding the dye solutions to the PLA solution; the pH values of the solutions were then brought up to the desired pH by the addition of NaOH or HCl. The final concentrations of the dyes were 2×10^{-5} M, and the ratio of polypeptide residues to dye molecules (R/D) was less than 5. The absorption and the CD spectra were measured with JASCO UVIDEC-1 and CD J-40A instruments respectively. The ellipticity, $[\theta]$ (degree cm^2 dmol^{-1}), or molar extinction coefficient, ε (1 mol^{-1} cm^{-1}), was expressed on the basis of the dye concentration.

Results and Discussion

The CD and absorption spectra of the three azo dyes with and without polypeptide (R/D=0—5) were measured in the pH range from 2.0 to 13.6. Figure 1 shows the induced CD and absorption spectra of the PLA HCl–MO system at pH 8.7 and 10.3 for R/D=1. MO showed a single visible absorption band at 467 nm with ε_{467}=25600 (and ε_{378}=8100) at pH 7. When a complex was formed with PLA HCl, the spectrum showed an additional peak at 378 nm. The blue-shifted band at 378 nm has been considered to reflect a nearly parallel orientation of the MO molecules.[4,9] The values at R/D=1 were ε_{467}=11400 and ε_{378}=12400

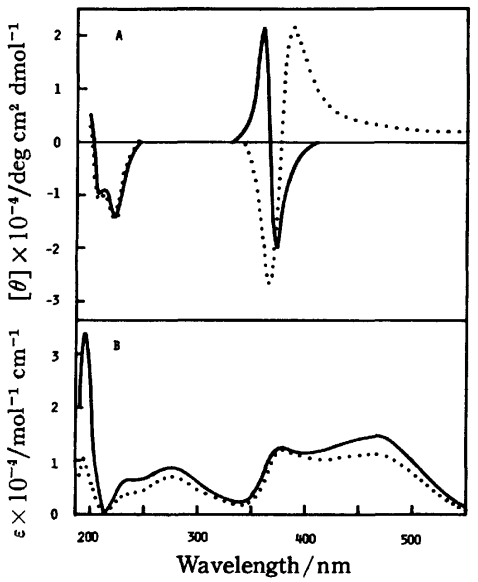

Fig. 1. Induced CD (A) and absorption (B) spectra of the PLA HCl–MO complex at R/D=1: (·····) at pH 8.7 and (——) at pH 10.3.

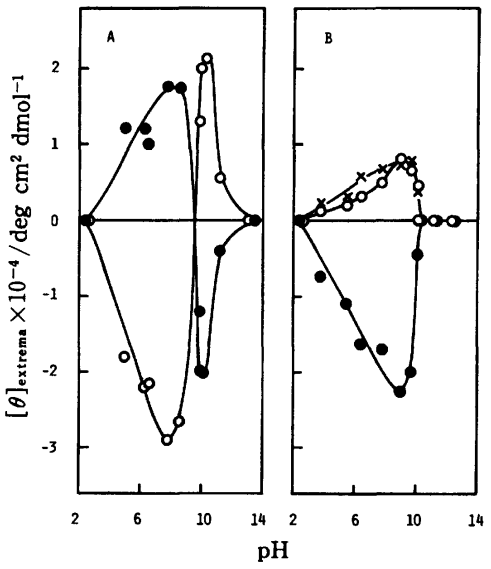

Fig. 2. Induced CD values at extrema of the PLA HCl–dye complexes as a function of pH at R/D=1. (A) PLA HCl–MO complex: ○ at 370 nm and ● at 390 nm; (B) PLA HCl–EO complex: ○ at 378 nm, ● at 400 nm, and × at 450 nm.

at pH 8.7, and ε_{467}=14600 and ε_{378}=12600 at pH 10.3. EO showed similar changes in the absorption spectra, but no change was found in AA.

Figure 2 shows the induced CD values at the extrema of the PLA HCl–azo dye complexes as a function of the pH at R/D=1. The PLA HCl–MO complex showed a

Table 1. Characteristic of CD in the PLA HCl–dye complexes

Dye	R/D	pH	ε_{max}/nm		Induced CD $[\theta]_{extrrema}$/nm		
MO	0.5	8.1	19100(467)	10900(378)		3400(390)	−4700(370)
		10.3	18500(467)	8800(378)[a]		−4200(374)	2400(361)
	1	8.7	11400(467)	12400(378)		21400(390)	−26300(370)
		10.3	14600(467)	12600(378)		−19800(374)	21500(361)
	5	8.0	9000(467)	18800(378)		35400(390)	−47200(370)
		10.4	11400(467)	10700(378)		−22100(374)	28800(361)
EO	1	9.3	17600(477)	13000(400)	7400(450)	−22600(400)	8400(378)
	5	9.0	13900(477)	17800(400)	9100(450)	−17900(400)	2500(378)

a) Shoulder.

positive CD band at 390 nm and a negative CD band at 370 nm below pH 9.6, while it showed a negative CD band at 374 nm and a positive CD band at 361 nm above pH 9.6. On the other hand, the PLA HCl–EO complex induced three CD extrema, at 450 and 378 nm (positive) and at 400 nm (negative), in the pH range of 4—10.5 (Table 1).

Both the PLA HCl–MO and EO complexes showed $[\theta]_{222}$ values of −13000—−16000 at R/D=1 in the pH range of 4—10. The positions and magnitudes of the extrema suggest that the two PLA HCl complexes are mostly in a helical conformation, since the n-π^* peptide transitions of PLA have been reported to have the ellipticity values of $[\theta]_{222}=-19000$ for a helical structure[8] and of $[\theta]_{217}=3000$—3900 for a random-coil structure.[10,11]

Many rules correlating the signs of ellipticity with the absolute configuration have been proposed including the validity of the exciton chirality method for aromatic compounds[12–15] and for polypeptide–dye complexes.[4,5] The sign of the longer wavelength CD extremum was in agreement with the sense of the handedness of the interacting transition dipole moments.[12] Since the transition of bound MO in the visible wavelength region was determined to be long-axis polarized by the stretched polyvinyl alcohol film method,[16] the CD spectra of the PLA HCl–MO complex were examined by means of the exciton chirality method. The interacting transition dipole moments of dimeric dye can be assumed to have the clockwise *R*-chirality for the PLA HCl–MO complex below pH 9.6 and the *S*-chirality for the same complex above pH 10, while the PLA HCl–EO complex showed a multiple induced CD band in the pH range of 4—10.5. When the pH was raised, the *R*-to-*S* configurational inversion of the PLA HCl–MO complex was found at pH 9.8. The reason is not clear at present, since no significant conformational differences between the two PLA HCl–MO and EO complexes were found. It is, however, conceivable that the delicate interaction of the polarized transition dipole moments affects the dihedral angle or the C_2 rotation axis of the dimeric MO molecules[17,18] accompanying the helix-to-coil conformational transition of the PLA HCl–MO complex around pH 9.8.

The authors wish to thank Professor Tadao Hayakawa of Shinshu University for his encouragement.

References

1) E. R. Blout and L. Stryer, *Proc. Natl. Acad. Sci. U. S. A.*, **45**, 1591 (1959).
2) L. Stryer and E. R. Blout, *J. Am. Chem. Soc.*, **83**, 1411 (1961).
3) S. Ikeda and T. Imae, *Biopolymers*, **10**, 1743 (1971).
4) M. Hatano, M. Yoneyama, Y. Sato, and Y. Kawamura, *Biopolymers*, **12**, 2423 (1973).
5) H. Yamamoto and A. Nakazawa, *Chem. Lett.*, **1983**, 47.
6) H. Yamamoto, A. Nakazawa, and T. Hayakawa, *J. Polym. Sci., Polym. Lett. Ed.*, **21**, 131 (1983).
7) T. Hayakawa, Y. Kondo, H. Yamamoto, and Y. Murakami, *Bull. Chem. Soc. Jpn.*, **42**, 479 (1969).
8) T. Hayakawa, Y. Kondo, and H. Yamamoto, *Bull. Chem. Soc. Jpn.*, **42**, 1937 (1969).
9) M. Kasha, H. R. Rawls, and M. A. El-Bayoumi, *Pure Appl. Chem.*, **11**, 371 (1965).
10) S. Ichimura, K. Mita, and M. Zama, *Biopolymers*, **17**, 2769 (1978).
11) H. Yamamoto and A. Nakazawa, unpublished data.
12) N. Harada and K. Nakanishi, *J. Am. Chem. Soc.*, **91**, 3989 (1969); *Acc. Chem. Res.*, **5**, 257 (1972).
13) N. Harada, S. Suzuki, H. Uda, and K. Nakanishi, *Chem. Lett.*, **1972**, 67.
14) V. Toome and M. Weigele, "The Peptide," ed by E. Gross and J. Meienhofer, Academic Press, New York (1981), Vol. 4, pp. 85—184.
15) N. Harada and K. Nakanishi, "En Nishokusei Supekutoru," Tokyo Kagakudojin, Tokyo (1982).
16) A. Yogev, L. Margulies, and Y. Mazur, *J. Am. Chem. Soc.*, **92**, 6059 (1970).
17) N. Harada, S. L. Chen, and K. Nakanishi, *J. Am. Chem. Soc.*, **97**, 5345 (1975).
18) H. Shimizu, A. Kaito, and M. Hatano, *J. Am. Chem. Soc.*, **104**, 7059 (1982).

The Lithium Diisopropylamide-induced Fragmentation of 1,3-Dithiolane Derivatives of Several Ketones Having α-Hydrogen

Hideyuki IKEHIRA,* Shigeo TANIMOTO,* and Tatsuo OIDA
Institute for Chemical Research, Kyoto University, Uji, Kyoto 611

(Received February 7, 1983)

Synopsis. The reaction of 1,3-dithiolane derivatives of ketones having α-hydrogen with lithium diisopropylamide results in fragmentation to the corresponding thioketone followed by further conversion in a few steps to the other intermediate species which, on trapping with alkyl halide, leads to a vinylic sulfide and/or a sulfide bearing a secondary alkyl group.

It has been known for a long time that 1,3-dithiolane derivatives of aldehydes are easily deprotonated at the 2-positions of the rings by strong base and the generated anions undergo facile elimination to form ethylene.[1,2] Recently, Wilson and his co-workers[3] described that the treatment of 1,3-dithiolane derivatives of saturated ketones with an excess of butyllithium in ether leads to fragmentation to the corresponding thioketones, which afforded methyl sulfides by quenching the reaction mixture with methyl iodide or underwent a subsequent reduction with butyllithium to secondary thiols. They also comment that the reaction proceeds by a mechanism involving deprotonation at the 4-position of the ring as the first step. This report prompted us to publish the results of our independent studies in which the products obtained are somewhat different from those described by the above-quoted authors. Thus, we have found that the metalation of 1,3-dithiolane derivatives of several ketones having α-hydrogen with the less nucleophilic lithium diisopropylamide (LDA) in tetrahydrofuran results in fragmentation to the corresponding thiocarbonyl compounds followed by further conversion in a few steps to the other intermediate species. These, on trapping with alkyl halide, lead to vinylic sulfides and/or sulfides bearing a secondary alky group depending on choice of the starting 1,3-dithiolane derivatives. For example, when 2-methyl-2-phenyl-1,3-dithiolane (**1a**) was treated with an excess of LDA in tetrahydrofuran solution, followed by addition of an alkyl halide, we obtained the corresponding α-(alkylthio)styrene (**6a**) in excellent yield together with alkyl vinyl sulfide (**10**). The formation of the intermediate thioacetophenone (**3a**) and ethylenethiolate anion (**4**) is certain from the analogy to the reaction mode proposed by Wilson and his co-workers.[3] Presumably, **3a** is further converted to α-styrenethiolate anion (**5a**) *via* α-proton abstraction by a second LDA molecule. On quenching with alkyl halide, this leads to **6a**.

When 2-ethyl-2-phenyl-1,3-dithiolane (**1b**) was submitted to a similar fragmentation-alkylation sequence, two products, α-alkylthio-β-methylstyrene (**6b**) and 1-alkylthio-1-phenylpropane (**9b**), were isolated. Supposedly, the mechanism of the conversion of **3b** into **9b** involves three steps. The first step is a one-electron transfer between **3b** and LDA to afford a radical anion species (**7b**). The second step is the charge neutralization by alkyl halide to generate the radical species (**8b**); the last stage is the abstraction of a hydrogen radical, in which tetrahydrofuran may be serving as a donor, eventually providing **9b**. There is no direct evidence for the intermediary presence of **7b** and **8b**. However, the feasibility of the one-electron transfer is supported by analogy to the mode of reaction of thioketones, such as thiobenzophenone and di-*t*-butyl thioketone, with organometallics proposed by Ohno and his co-workers.[4] When 2-phenyl-2-propyl-1,3-dithiolane (**1c**) was cleaved under the same conditions and further quenched with methyl iodide, two products, α-methylthio-β-ethylstyrene (**6c**) and 1-methylthio-1-phenylbutane (**9c**) were also isolated, suggesting that the intermediate propyl phenyl thioketone (**3c**) behaves similarly to **3b**. The use of 2-isopropyl-2-phenyl- (**1d**) or 2-benzyl-2-phenyl-1,3-dithiolanes (**1e**) as the starting substrate and methyl iodide as the trapping agent in this reaction resulted in the exclusive formation of **9d** and **9e**, respectively. This means that in the initially formed isopropyl phenyl thioketone (**3d**) and benzyl phenyl thioketone (**3e**) a steric hindrance at their α-position may be preventing formation of the substituted ethylenethiolate anions (**5d** and **5e**). Thus, an obvious difference in behavior among the 1,3-dithiolane derivatives (**1**) submitted to this fragmentation-alkylation sequence has been noted. These experiments are summarized in Table 1, along with the ^{1}H-NMR spectroscopic data of the products.

Several 2-alkylthio-2-bornenes (**12**) have also been made in 97—99% yields from 1,3-dithiolane derivative

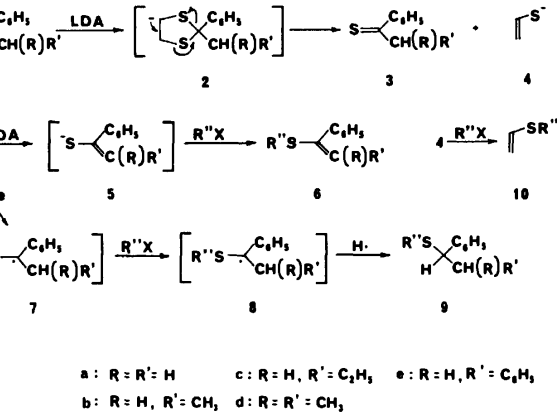

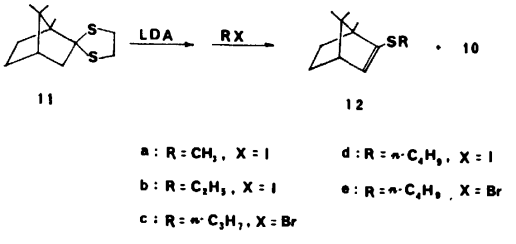

TABLE 1. THE CONVERSION OF 2-ALKYL-2-PHENYL-1, 3-DITHIOLANES (1) INTO THE COMPOUNDS 6 AND/OR THE COMPOUNDS 9

Starting substrate	RX	Product[a]	Yield/%[b]	^{1}H-NMR (δ, in CCl_4)
1a	CH_3I	**6a** (R″=CH_3)	96	2.20 (s, 3H), 4.87 (s, 1H), 5.32 (s, 1H), 7.02—7.52 (m, 5H)
1a	C_2H_5I	**6a** (R″=C_2H_5)	97	1.21 (t, 3H, J=7 Hz), 2.62 (q, 2H, J=7 Hz), 5.09 (s, 1H), 5.37 (s, 1H), 7.03—7.60 (m, 5H)
1a	n-C_4H_9I	**6a** (R″=n-C_4H_9)	99	0.67—1.12 (m, 3H), 1.12—1.82 (m, 4H), 2.61 (t, 2H, J=7 Hz), 5.09 (s, 1H), 5.35 (s, 1H), 7.03—7.57 (m, 5H)
1a	n-C_4H_9Br	**6a** (R″=n-C_4H_9)	97	
1a	$C_6H_5CH_2Br$	**6a** (R″=$C_6H_5CH_2$)	98	3.74 (s, 2H), 5.12 (s, 1H), 5.34 (s, 1H), 6.68—7.60 (m, 10H)
1b	CH_3I	**6b** (R″=CH_3)[c]	36	1.89 (s, 3H), 1.92 (d, 3H, J=7 Hz), 5.81 (q, 1H, J=7 Hz), 7.00—7.47 (m, 5H)
		9b (R″=CH_3)	39	0.88 (t, 3H, J=7 Hz), 1.72 (s, 3H), 1.83 (m, 2H), 3.43 (t, 1H, J=7 Hz), 6.99—7.30 (m, 5H)
1b	C_2H_5I	**6b** (R″=C_2H_5)[c]	42	1.03 (t, 3H, J=7 Hz), 1.81 (d, 3H, J=7 Hz), 2.20 (q, 2H, J=7 Hz), 5.83 (q, 1H, J=7 Hz), 6.93—7.40 (m, 5H)
		9b (R″=C_2H_5)	44	0.87 (t, 3H, J=7 Hz), 1.08 (t, 3H, J=7 Hz), 1.40—2.15 (m, 2H), 2.16 (q, 2H, J=7 Hz), 3.57 (t, 1H, J=7 Hz), 7.00—7.40 (m, 5H)
1c	CH_3I	**6c** (R″=CH_3)[c]	33	1.07 (t, 3H, J=7 Hz), 1.90 (s, 3H), 2.14—2.75 (m, 2H), 5.81 (t, 1H, J=7 Hz), 7.07—7.50 (m, 5H)
		9c (R″=CH_3)	50	0.95 (t, 3H, J=7 Hz), 1.13—2.08 (m, 4H), 1.80 (s, 3H), 3.61 (t, 1H, J=7 Hz), 7.07—7.40 (m, 5H)
1d	CH_3I	**9d** (R″=CH_3)	58	0.89 (d, 3H, J=7 Hz), 1.05 (d, 3H, J=7 Hz), 1.09 (s, 3H), 1.65—2.50 (m, 1H), 3.29 (d, 1H, J=7 Hz), 6.93—7.25 (m, 5H)
1d	$C_6H_5CH_2Br$	**9d** (R″=$C_6H_5CH_2$)	55	0.72 (d, 3H, J=6 Hz), 0.98 (d, 3H, J=6 Hz), 1.65—2.28 (m, 1H), 3.21 (d, 2H, J=6 Hz), 3.23 (d, 1H, J=6 Hz), 6.82—7.48 (m, 10H)
1e	CH_3I	**9e** (R″=CH_3)	77	1.75 (s, 3H), 2.95 (d, 1H, J=2 Hz), 3.07 (s, 1H), 3.75 (t, 1H, J=6 Hz), 6.68—7.50 (m, 10H)

a) The formation of alkyl vinyl sulfide **10** was observed in all the work-up procedures, but the isolation of **10** was not followed up, because it has minor importance. All products were characterized by IR, mass spectrum, elemental analysis in addition to ^{1}H-NMR and further comparison of the properties to literature data where possible. b) Yield of isolated product is based on **1**. c) The products **6b** and **6c** seem to be *E*-isomers.

TABLE 2. THE CONVERSION OF 1, 3-DITHIOALNE DERIVATIVE (11) OF (+)-CAMPHOR INTO 2-ALKYLTHIO-2-BORNENES (12)

RX	Product[a]	Yield/%[b]	^{1}H-NMR (δ, in CCl_4)
CH_3I	**12a**	99	0.61—2.40 (m, 14H), 2.10 (s, 3H), 5.30 (d, 1H, J=4 Hz)
C_2H_5I	**12b**	97	0.65—2.39 (m, 14H), 1.26 (t, 3H, J=7 Hz), 2.60 (q, 2H, J=7 Hz), 5.39 (d, 1H, J=4 Hz)
n-C_3H_7Br	**12c**	98	0.70—2.40 (m, 19H), 2.59 (t, 2H, J=7 Hz), 5.39 (d, 1H, J=4 Hz)
n-C_4H_9I	**12d**	99	0.65—2.40 (m, 21H), 2.61 (t, 2H, J=7 Hz), 5.37 (d, 1H, J=4 Hz)
n-C_4H_9Br	**12e**[c]	98	

a) All products were characterized in the same manner as described in Table 1. b) Yield of isolated product based on **11**. c) The product **12e** is identical to **12d**.

(**11**) of (+)-camphor by the present procedure. Presumably, the intermediate (+)-thiocamphor[5] in the reaction could be easily deprotonated by LDA at the 3-position. The yields as well as the ^{1}H-NMR spectroscopic data of the produced **12** are shown in Table 2.

Experimental

Reaction Summarized in Tables 1 and 2. General Procedure: A solution of diisopropylamine (0.35 g, 3.5 mmol) in tetrahydrofuran (7 ml) was cooled to −78 °C under nitrogen, treated with 1.56 molar solution (2.12 ml, 3.3 mmol) of butyllithium in hexane, and then stirred at the same temperature for 30 min and further at −15 °C for 10 min. The solution of LDA thus prepared was cooled to −78 °C and a solution of either the 2-alkyl-2-phenyl-1,3-dithiolanes (**1**) or the 1,3-dithiolane derivative (**11**) of (+)-camphor (1.3 mmol) in tetrahydrofuran (4 ml) was added. After an additional 1 h at −15 °C, the solution was cooled again to −78 °C, and an alkyl halide (3.3 mmol) was added with stirring. The stirring was continued for 1 h at −5——10 °C and for a further 24 h at room temperature. The mixture was then quenched with 100 ml of water and 20 ml of saturated aqueous solution of NH_4Cl, and extracted with ether (3×60 ml). The combined organic layer was dried over $MgSO_4$ and concentrated *in vacuo* to give a pale yellow residue, which was subjected to column chromatography.

References

1) D. Seebach and E. J. Corey, *J. Org. Chem.*, **40**, 231 (1975).
2) D. Seebach, *Angew. Chem., Int. Ed. Engl.*, **8**, 639 (1969).
3) S. R. Wilson, G. M. Georiadis, H. N. Khatri, and J. E. Bartmess, *J. Am. Chem. Soc.*, **102**, 3577 (1980).
4) A. Ohno, K. Nakamura, M. Uohama, S. Oka, T. Yamabe, and S. Nagata, *Bull. Chem. Soc. Jpn.*, **48**, 3718 (1975).
5) The conversion of thiocamphor into **12** by LDA-treatment followed by *S*-alkylation is already known: G. E. Veenstra and B. Zwanenburg, *Recl. Trav. Chim. Pays-Bas*, **95**, 37 (1976).

A Convenient Method for the Synthesis of Acyclic Ketones. Synthesis of Sex Pheromone of Douglas Fir Tussock Moth

Yasue MURATA, Katsuhiko INOMATA, Hideki KINOSHITA, and Hiroshi KOTAKE*
Department of Chemistry, Faculty of Science, Kanazawa University, Kanazawa 920
(Received February 17, 1983)

Synopsis. (α-Alkyl-α-methylthio)alkyl *p*-tolyl sulfones derived from the reaction of α-alkylated alkyl *p*-tolyl sulfones with dimethyl disulfide could be easily hydrolyzed by $CuCl_2$–SiO_2 to give the corresponding ketones in fairly good yields. This method was applied to the synthesis of Douglas Fir Tussock Moth Pheromone.

The development of the general method for the synthesis of acyclic ketone is a major point of interest in the organic synthesis and a variety of methods have been reported. In connection with our continuing interest to extend the synthetic utility of sulfones, in the preceding paper,[1] a new method for the preparation of aromatic ketones *via* chlorination of α-substituted benzyl *p*-tolyl sulfones followed by hydrolysis was described. However, the reaction was limited to the formation of aryl ketones, and drastic conditions using silver perchlorate in refluxing trifluoroacetic acid for hydrolysis were required. Recently, a convenient method for the hydrolysis of a ketone dithioacetal *S*,*S*-dioxide leading to the corresponding carbonyl group has been reported by Ogura and co-workers,[2] in which hydrochloric acid in refluxing methanol was used for hydrolysis.

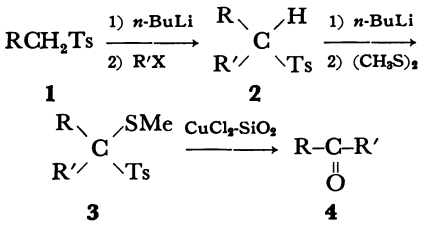

Scheme 1.

In this paper, we wish to report a more mild synthetic method of acyclic ketones (**4**) starting from alkyl *p*-tolyl sulfones (**1**), which were subjected to alkylation followed by treatment with *n*-BuLi and $(CH_3S)_2$ to afford α-(methylthio)alkyl *p*-tolyl sulfones (**3**). Subsequently, on treatment of **3** with $CuCl_2$–SiO_2 in dichloromethane at room temperature without further purification, hydrolysis to ketone compounds took place very smoothly to give the desired products (**4**) in fairly good yields as shown in Table 1.

Next, this method was applied to the synthesis of Douglas Fir Tussock Moth Pheromone[3] starting from *p*-tolyl undecyl sulfone (**5**) according to the following scheme. The reaction proceeded smoothly, and acetylenic ketone (**7**) was obtained in high yield in a similar manner above mentioned. A catalytic hydrogenation of **7** over 5% Pd–$BaSO_4$ (deactivated by quinoline) gave the desired pheromone (**8**) in an excellent yield.

Experimental

All the melting points are uncorrected. The NMR and IR spectra were recorded on JEOL/PMX-60 and JASCO IRA-1 spectrometers, respectively.

Materials. Freshly distilled THF from potassium under nitrogen was used. Thin-layer chromatography (TLC) was performed on Merck's silica gel 60 PF_{254} (Art. 7749).

A Typical Experimental Procedure for the Preparation of the Ketones. To a solution of phenethyl *p*-tolyl sulfone (123 mg, 0.5 mmol) in dry THF (5 ml) was added *n*-BuLi (0.55 mmol, hexane solution) dropwise at −20 °C under N_2. The reaction mixture was allowed to warm to room temperature in a period of 20 min and then a solution of phenethyl bromide

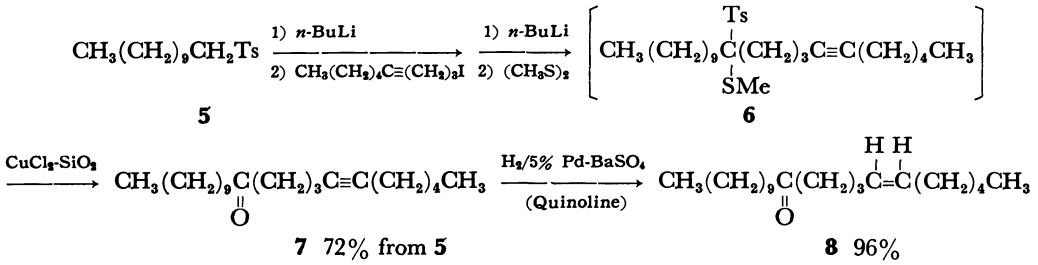

Scheme 2. Synthesis of Douglas Fir Tussock Moth Pheromone.

TABLE 1. THE SYNTHESIS OF ACYCLIC KETONES FROM ALKYL *p*-TOLYL SULFONES (**1**)

No.	R	R'X	$CuCl_2 \cdot SiO_2$	Reaction conditions	Yield of **4**[a]/%
1	$CH_3(CH_2)_9$	$C_6H_5CH_2Br$	2 equiv.	r.t., 20 min	62 (**4a**)
2	$CH_3(CH_2)_9$	$C_6H_5(CH_2)_2Br$	2 equiv.	r.t., 40 min	58 (**4b**)
3	C_6H_5	$CH_3(CH_2)_4C{\equiv}C(CH_2)_3I$	2 equiv.	r.t., 1 h	69 (**4c**)
4	C_6H_5	$C_6H_5(CH_2)_2Br$	2 equiv.	r.t., 30 min	80 (**4d**)
5	$C_6H_5CH_2$	$CH_3(CH_2)_4C{\equiv}C(CH_2)_3I$	2 equiv.	r.t., 2.5 h	67 (**4e**)
6	$C_6H_5CH_2$	$C_6H_5(CH_2)_2Br$	2 equiv.	r.t., 1 h	59 (**4f**)

a) Based on **1**.

(102 mg, 0.55 mmol) in dry THF (2 ml) was added slowly at −78 °C. The temperature of the solution was raised to room temperature, cooled down again at −20 °C, and treated with *n*-BuLi (0.55 mmol) followed by the addition of a solution of $(CH_3S)_2$ (52 mg, 0.55 mmol) in dry THF (2 ml) at −78 °C. The reaction temperature was gradually raised to room temperature, quenched with buffer solution of pH=7 ($NaOH+KH_2PO_4$) (5 ml) and HCl, extracted with AcOEt, dried over Na_2SO_4 and concentrated *in vacuo*. The resulting residue was dissolved in CH_2Cl_2 (5 ml) and treated with $CuCl_2$–SiO_2 (752 mg) for 1 h at room temperature. After filtration and concentration, the residue was subjected to preparative TLC (solvent : benzene) to give the desired ketone in 59% yield (66 mg) based on phenethyl *p*-tolyl sulfone (**1**).

The Active $CuCl_2$–SiO_2. After a mixture of $CuCl_2 \cdot 2H_2O$ (0.85 g), SiO_2 (3.5 g), and water (8 ml) was air-dried for 1 h, it was heated up at 110—130 °C for 3 h and allowed to cool to room temperature. The mixture thus obtained must be used immediately.

Preparation of 1-Iodo-4-decyne. Preparation of 1-Chloro-4-decyne: To a solution of 1-heptyne (15.8 mmol) in dry THF (15 ml) was added a solution of *n*-BuLi (15.8 mmol) in hexane (10 ml) at −78 °C under N_2. After the reaction temperature was raised to room temperature, a solution of 1-bromo-3-chloropropane (17.4 mmol) in dry THF (12 ml) was added to the reaction mixture and refluxed for 21 h. After the solvent was removed *in vacuo*, quenched with buffer solution ($NaOH+KH_2PO_4$) (20 ml) and HCl followed by extraction with AcOEt. The AcOEt extract was distilled under reduced pressure. Bp 83 °C/6 Torr, (61% yield).

Conversion of the Chloride to the Corresponding Iodide: A solution of 1-chloro-4-decyne (7.4 mmol) and NaI (7.4×4.5 mmol) in dry acetone (20 ml) was refluxed for 15 h. After the solvent was removed, AcOEt was added and the AcOEt extract was distilled under reduced pressure to give 1-iodo-4-decyne in 86% yield. Bp 73 °C/0.03 Torr; IR (neat) 2930, 1450, 1220 cm^{-1}; NMR ($CDCl_3$) δ 0.63—1.08 (distored t, 3H), 1.08—1.73 (m, 6H), 1.73—2.63 (m, 6H), 3.23 (t, 2H, J=6 Hz).

Preparation of p-*Tolyl Undecyl Sulfone*: A suspension of 1-bromoundecane (2.35 g, 10 mmol) and sodium *p*-toluenesulfinate tetrahydrate (3.75 g, 15 mmol) in EtOH (20 ml) was refluxed for 8.5 h. Then, the reaction mixture was poured into a lot of ice-water to result in precipitation of the crude product, which was collected and dried. Recrystallization from MeOH gave a pure compound. Yield 2.68 g (87%). Mp 70—71 °C. Found: C, 69.49; H, 9.98%. Calcd for $C_{18}H_{30}O_2S$: C, 69.63; H, 9.74%.

Identification of Products (4a—f). **4a**: Oil, *m/e*: 260 (M^+), IR (neat) 2930, 1710, 1600, 1495, 1450 cm^{-1}. NMR ($CDCl_3$) δ 0.73—1.04 (distored t, 3H), 1.04—1.76 (m, 16H), 2.35 (t, 2H, J=7.0 Hz), 3.55 (s, 2H), 7.08 (s, 5H).

4b: Oil, *m/e* 274 (M^+), IR (neat) 2930, 1710, 1600, 1495, 1450 cm^{-1}; NMR ($CDCl_3$) δ 0.6—1.02 (distored t, 3H), 1.02—1.73 (m, 16H), 2.33 (t, 2H, J=7 Hz), 2.50—3.07 (m, 4H), 7.10 (s, 5H).

4c: Oil, *m/e* 242 (M^+), IR (neat) 2940, 1680, 1600, 1580, 1450 cm^{-1}; NMR ($CDCl_3$) δ 0.70—1.05 (distored t, 3H), 1.05—1.68 (m, 6H), 1.68—2.48 (m, 6H), 3.05 (t, 2H, J= 7.0 Hz), 7.15—7.50 (m, 3H), 7.68—7.95 (m, 2H).

4d: Mp 70.5—71.5 °C; IR (neat) 3032, 1708, 1600, 1172, 750 cm^{-1}; NMR ($CDCl_3$) δ 2.62—2.87 (m, 4H), 3.53 (s, 2H), 6.38—7.50 (m, 10H), Found: C, 85.40; H, 6.77%. Calcd for $C_{15}H_{14}O$: C, 85.68; H, 6.71%.

4e: Oil, *m/e* 256 (M^+), IR (neat) 2920, 1710, 1600, 1495, 1450 cm^{-1}; NMR ($CDCl_3$) δ 0.70—1.05 (distored t, 3H), 1.05—1.67 (m, 8H), 1.67—2.35 (m, 4H), 2.55 (t, 2H, J= 7.0 Hz), 3.67 (s, 2H), 7.22 (s, 5H).

4f: Oil, *m/e* 224 (M^+), IR (neat) 2930, 1710, 1600, 1490, 1450 cm^{-1}; NMR ($CDCl_3$) δ 2.43—3.08 (m, 4H), 3.60 (s, 2H), 6.87—7.67 (m, 10H).

The Reaction Condition for the Synthesis of Pheromone (8).

Preparation of 6-Heneicosyn-11-one (7) from 5: A synthetic procedure was the same manner above mentioned. *p*-Tolyl undecyl sulfone (**5**) (310 mg, 1 mmol), 1-iodo-4-decyne (264 mg, 1 mmol), and dimethyl disulfide (94 mg, 1 mmol) were used for the formation of **6** (479 mg). The procedure for the conversion of **6** to **7** is as follows: To a solution of **6** (96 mg, 0.2 mmol) in CH_2Cl_2 (6 ml) was added $CuCl_2$–SiO_2 (820 mg, 1 mmol), and the suspension was stirred for 2 d at room temperature. The usual work-up gave 44 mg of **7**. Total yield of **7** was 72% based on **5**.

IR (neat) 2910, 2850, 1705, 1460, 1370, 1090 cm^{-1}; NMR ($CDCl_3$) δ 0.62—1.05 (distored t, 6H), 1.05—2.23 (m, 28H), 2.37 (t, 2H, J=7 Hz), 2.47 (t, 2H, J=7 Hz).

IR and NMR spectra of **7** were identical with those of literature.[3]

Preparation of Pheromone (8) from 7. A methanol solution (15 ml) of **7** (116 mg, 0.38 mmol) containing one drop of quinoline was hydrogenated over 5% Pd–$BaSO_4$ (20 mg) under atmospheric pressure for about 5 h. The catalyst was filtered off and the filtrate was concentrated *in vacuo* to give a residue which was taken up into AcOEt. The AcOEt solution was washed with dil-HCl, brine, dried over Na_2SO_4, and concentrated *in vacuo* to give the desired material as a single product in 96% yield (112 mg). Its IR and NMR data were identical with the reported values.[4] IR (neat) 3000, 2920, 2850, 1715, 1455, 1370, 1125, 1080 cm^{-1}; NMR ($CDCl_3$) δ 0.75—1.05 (distored t, 6H), 1.05—1.75 (m, 24H), 1.95 (m, 4H), 2.34 (t, 4H, J=7 Hz), 5.27 (m, 2H).

References

1) H. Kotake, K. Inomata, H. Kinoshita, Y. Sakamoto, and Y. Kaneto, *Bull. Chem. Soc. Jpn.*, **53**, 3027 (1980).

2) K. Ogura, M. Suzuki, J. Watanabe, M. Yamashita, H. Iida, and G. Tsuchihashi, *Chem. Lett.*, **1982**, 813.

3) R. G. Smith, G. E. Daterman, and G. D. Daves, Jr., *Science*, **1975**, 63; K. Kondo and S. Murahashi, *Tetrahedron Lett.*, **1979**, 1237; K. Mori, M. Uchida, and M. Matsui, *Tetrahedron*, **33**, 385 (1977); L. H. Smith, R. G. Smith, T. M. Loehr, G. D. Daves, Jr., G. E. Daterman, and R. H. Wohleb, *J. Org. Chem.*, **43**, 2361 (1978).

4) B. Akermark and L. Vist, *J. Org. Chem.*, **43**, 4387 (1978).

Cation Transport through Liquid Membranes Facilitated by Crown Ether-modified Poly(iminoethylene)s

Jun-ichi ANZAI, Yoko SAKATA, Yasuhiro SUZUKI, Akihiko UENO, and Tetsuo OSA*
Pharmaceutical Institute, Tohoku University, Aobayama, Sendai 980

(Received February 24, 1983)

Synopsis. Poly(iminoethylene)s containing benzo-15-crown-5 moieties as pendant groups can transport Rb^+ cation more effectively than the other alkali cations through an organic liquid membrane. The transport selectivities of the polymers diminish drastically with decreasing crown ether content in the polymer chain.

Much effort has been invested in effecting selective transport of alkali cations through artificial liquid membranes using crown-type synthetic carriers.[1-3] A desirable characteristic of crown ethers as cation carriers is their high degree of selectivity. In this connection, it may be interesting to employ polymeric crown ethers as carriers since they are endowed with high selectivities in cation binding.[4] Hence we have prepared crown ether-modified poly(iminoethylene)s (PEI-CR's **1**—**3**) and their monomer model **4** and have recently reported their cation binding properties.[5,6] The purpose of this note is to elucidate their cation transporting properties in liquid membrane systems containing a single cation species in the source aqueous phase. The results are discussed in relation to the crown ether contents in the polymer chain.

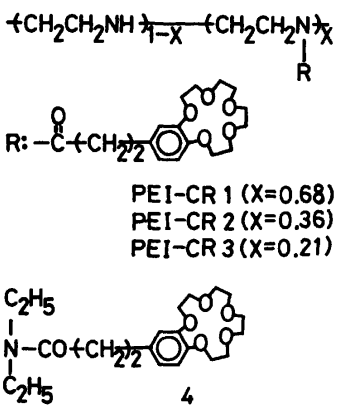

4

Experimental

Materials. The synthetic procedure of **1**—**4** was described previously.[5,6] A commercially available poly(iminoethylene) (PEI) with a molecular weight of 40000—50000 (from Tokyo Kasei) was used. The PEI has a highly branched structure and the ratio of primary, secondary, and tertiary amino groups is about 1 : 2 : 1.

Cation Transport. The transport of alkali cations was performed within a U-shaped glass tube with 17 mm diameter at 23 °C. A 20 ml of dichloromethane (CH_2Cl_2) dissolving one of the carrier compounds was put into the tube as a liquid membrane. A 5 ml of picrate solution was placed in the left arm of the tuve (source phase) and the right arm was filled with the equal volume of water (receiving phase). All three phases were stirred at a constant rate. The amount of metal picrate transported across the membrane was monitored by UV spectroscopy at 354 nm. The plots of the amount of the picrate transported *vs.* time gave good straight lines, from which the transport rates were determined. The amount of cation leakage, estimated from blank experiments, was always less than 1.25×10^{-7} mol dm^{-3} h^{-1}. At the end of the measurement the concentration of alkali picrate in the membrane was determined.

Liquid-Liqud Extraction. Liquid-liquid extractions were carried out employing a H_2O–CH_2Cl_2 system. After good agitation of two layers for 5 min at 23 °C, equilibrium was attained. The detailed procedure of extraction and subsequent analysis has been described elsewhere.[5,6]

Results and Discussion

In order to evaluate the cation binding efficiency and selectivity of **1**—**4**, liquid-liquid extractions were performed. The results are expressed as percentages of extracted picrate salts (Table 1). It is obvious that the polymers **1**—**3** extract the metal picrates more effectively than the monomer model **4**, especially in the cases of K^+ and Rb^+ cations. The selectivity sequence in extracting picrate salts with **1**—**3** is $K^+>Rb^+>Cs^+>Na^+$, while with **4** the sequence is $K^+>Na^+>Rb^+>Cs^+$. These characteristics of polymers in cation binding are believed to arise from the complex formation based on a 1 : 2 cation to crown stoichiometry intramolecularly.[4,6]

The transport rates of alkali cations through CH_2Cl_2 membranes facilitated by **1**—**4** are listed in Table 2

TABLE 1. LIQUID-LIQUID EXTRACTION OF ALKALI CATIONS

Crown ether	Extracted picrate salts (%)			
	Na	K	Rb	Cs
1	30	90	78	39
2	38	88	82	46
3	35	77	76	38
4	8.5	13	4.3	2.1

Aqueous phase: [Picrate salt]$=5\times10^{-4}$ mol dm^{-3}, [Metal hydroxide]$=1\times10^{-2}$ mol dm^{-3}; CH_2Cl_2 phase: [Crown ether]$=1\times10^{-3}$ mol dm^{-3}.

TABLE 2. ION TRANSPORT THROUGH CH_2Cl_2 MEMBRANE

Crown ether	Transport rate of alkali cations/10^{-6} mol dm^{-3} h^{-1}			
	Na	K	Rb	Cs
1	2.7	11	23	9.4
2	3.9	8.8	19	13
3	9.5	12	18	9.8
4	4.3	7.8	3.2	2.7

Source phase: 2.5×10^{-3} mol dm^{-3} of metal picrate in 5 ml of water; Receiving phase: 5 ml of water; Membrane: 1.25×10^{-4} mol dm^{-3} of crown ether in 20 ml of CH_2Cl_2.

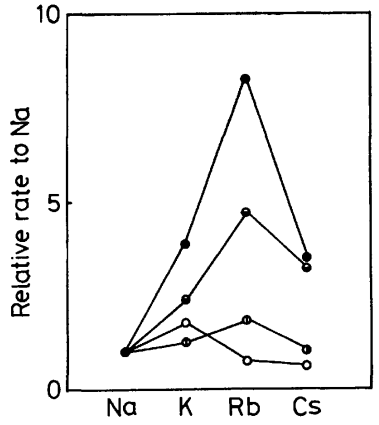

Fig. 1. Transport selectivity of **1**—**4** relative to Na cation.
—●—: **1**, —◒—: **2**, —◑—: **3**, —○—: **4**.

Table 3. Cation concentration in membrane phase[a)]

Crown ether	Concentration of alkali cations/10^{-5} mol dm^{-3}			
	Na	K	Rb	Cs
1	2.6	5.0	4.8	3.1
2	3.1	6.7	5.9	5.2
3	5.0	7.2	6.7	5.2
4	0.2	0.4	0.1	<0.1

a) These values were determined at the end of the transport rate measurements reported in Table 2.

and the transport selectivities relative to Na^+ cation are illustrated in Fig. 1. Polymers **1**—**3** transport Rb^+ cation more effectively than the other cations examined ($Rb^+ > K^+ \approx Cs^+ > Na^+$) under our experimental condition. The observed Rb^+ selectivity of **1**—**3** in cation transport is apparently incompatible with the data shown in Table 1 suggesting their K^+ selectivity. This discrepancy between the transport and extraction selectivities of polymers can interpreted reasonably based on the fact that there is an optimum range in value of the cation–carrier complex stability constant for the maximum cation transport.[7,9)] In our case, polymers **1**—**3** can transfer K^+ cation more effectively than the other cations from the source phase into the membrane but can not release it rapidly to the receiving phase owing to the high stability of polymer–K^+ complexes in the membrane. Alternatively, Rb^+ cation, which binds to polymers rather loosely, can be released rapidly at the interface from the membrane to the receiving phase. In the case of **4**, the transport selectivity is in accord with the sequence of the binding selectivity ($K^+ > Na^+ > Rb^+ > Cs^+$). In the case of the relatively low stability complexes such as **4**–cation complexes, the uptake process of cations from the source phase into the membrane seems to determine the overall transport rates. On the contrary, as for the relatively high stability complexes such as the polymer–cation complexes, the overall rates of transport are probably governed by the releasing process. The importance of the rate of release is also suggested from the data of cation concentration in the membrane (Table 3). These data indicate that K^+ cation, in all polymer systems, is transported less effectively than Rb^+ in spite of higher concentration of K^+ in the membrane. As is obvious from the above discussion, a moderately stable complex formation in the membrane is required for the effective transport of cations.

Figure 1 shows that the transport selectivity of **1**—**3** diminishes drastically with decreasing crown ether content in the polymer chains. The Rb^+/Na^+ selectivities of **1**—**3** are 8.3, 4.7, and 1.8 for **1**, **2**, and **3**, respectively. These remarkable differences in selectivity among the polymers can not be explained only from the extraction data. The unsubstituted amino groups in the polymer backbone, which were shown to bind alkali cations weakly with no selectivity,[6)] may participate in the transport process, resulting in the low selectivity of **2** and **3**. Although the reason for the remarkable dependence of the trasport selectivity on the contents of the crown ether moieties in the polymers is not obvious, it should be noted that a high degree of crown ether contents in the polymer chain is an essential requirement for the selective carriers of alkali cations. Thus it appears that PEI–CR's **1**—**3** function as Rb^+ selective carriers in liquid membrane systems containing a single cation species in the source aqueous phase.

References

1) C. F. Reusch and E. L. Cussler, *AIChE J.*, **19**, 736 (1973).
2) J. D. Lamb, R. M. Izatt, P. A. Robertson, and J. J. Christensen, *J. Am. Chem. Soc.*, **102**, 2425 (1980).
3) K. Hiratani, *Bull. Chem. Soc. Jpn.*, **55**, 1963 (1982).
4) S. Kopolow, T. W. Hogen Esch, and J. Smid, *Macromolecules*, **4**, 359 (1971).
5) J. Anzai, Y. Sakata, A. Ueno, and T. Osa, *Makromol. Chem. Rapid Commun.*, **3**, 399 (1982).
6) J. Anzai, Y. Sakata, Y. Suzuki, A. Ueno, and T. Osa, *J. Polym. Sci., Polym. Chem. Ed.*, **21**, 855 (1983).
7) M. Kirch and J. M. Lehn, *Angew. Chem., Int. Ed. Engl.*, **14**, 555 (1975).
8) Y. Kobuke, K. Hanji, K. Horiguchi, M. Asada, Y. Nakayama, and J. Furukawa, *J. Am. Chem. Soc.*, **98**, 7414 (1976).
9) J. D. Lamb, J. J. Christensen, J. L. Oscarson, J. L. Nielsen, B. W. Asay, and R. M. Izatt, *J. Am. Chem. Soc.*, **102**, 6820 (1980).

Diazomethane Ring-expansion of (−)-D_3-Trishomocubanone. Preparation and Chiroptical Properties of a Series of [*m*.1.1]Triblattanes

Masao NAKAZAKI,* Koichiro NAEMURA, and Masaki HASHIMOTO
Department of Chemistry, Faculty of Engineering Science, Osaka University, Toyonaka, Osaka 560

(Received March 31, 1983)

Synopsis. Optically active [3.1.1], [4.1.1], [5.1.1], and [6.1.1]triblattanes were prepared through the diazomethane ring-expansion of (−)-D_3-trishomocubanone. The absolute molecular rotations of [*m*.1.1]triblattanes were found to increase with *m* begining from *m*=0 till *m*=2. On going from *m*=2 to *m*=3, $[M]_{D\ abs.}$ abruptly drops, then the value remains almost constant till *m*=6.

Since our first preparation of twistane (**3**)[1] in an optically active modification, we have been interested in the preparation, stereochemistry, and biological transformations of series of cage-shaped compounds which possess the D_3-twisted bicyclo[2.2.2]octane framework **1** as a common structural feature (Fig. 1). We have classified these hydrocarbons into three categories according to the number of their diagonal bridgings, and have coined for them the generic names [*m*], [*m.n*], and [*m.n.p*]triblattanes,[2] from German, Blatt= leaf, where *m*, *n*, and *p* are the number of CH_2's in each diagonal bridge.

Figure 1[1,3] illustrates the triblattanes so far prepared in optically active forms in our laboratory and reveals the interesting chiroptical feature that all triblattanes having the D_3-twisted bicyclo[2.2.2]octane moiety with M helicity as the central core are levorotatory. Another conspicuous chiroptical property observed in [*m*.2.2], [*m*.2.1], [*m*.1.1], and [*m*]triblattanes having *m*<3 (Fig. 2), is the linear dependence of the absolute molecular rotations ($[M]_{D\ abs.}$) on the bridge span.[4] Owing to their short diagonal bridges (*m*<3), all triblattanes so far prepared in optically active forms are conformationally rigid, and this situation prompted us to prepare a series of optically active [*m*.1.1]triblattanes where *m* is greater than 2.

Results and Discussion

An obvious way for preparing optically active [3.1.1], [4.1.1], [5.1.1], and [6.1.1]triblattanes of known absolute configuration is extention of the diazomethane ring-expansion reaction which has proved successful in our synthesis of (−)-[2.1.1]triblattane (**8**) from (−)-D_3-trishomocubanone (**14**).

Our preliminary experiment utilizing (±)-**14** indicated that when kept at 0 °C an ethereal solution of (±)-**14** containing 10 equiv. of diazomethane gave a mixture of [2.1.1]triblattanone (**15**) and [3.1.1]triblattanones (**16**) with unknown location of the carbonyl group in the expanded bridge (Table 1). Addition of boron trifluoride was found to push the ring-expansion further furnishing a product consisting of higher homologs. An ethereal solution of (±)-**14** containing excess of diazomethane and 1 equiv. of BF_3–etherate was kept at 0 °C for 24 h. The reaction product was a mixture of ring-expanded ketones, again of unknown structure as to the location of the carbonyl group in the expanded bridges. To reveal composition of the mixture, the product was converted into a mixture of hydrocarbons by Wolff-Kishner reduction and the reaction product was analyzed by means of GLC. The results are summerized in Table 2.

We carried out the preparative experiment with a larger amount of (−)-**14**, $[\alpha]_D$ −26.0° (30% optical purity)[3] which was dissolved in an ethereal solution of 3 molar equiv. of diazomethane. The mixture was kept at 0 °C for 8 d, and routine workup furnished a 3 : 2 mixture of **15** and **16**, chromatography of which on alumina provided a 3.5% yield of **16**. Wolff-Kishner reduction of this [3.1.1]triblattanone (**16**) afforded [3.1.1]-triblattane (**20**), $[\alpha]_D$ −46.5°.

The major fraction obtained from the above chromatography was a 1 : 3 mixture of **15** and **16**, and this was dissolved in ether and subjected to further ring-expansion with 10 equiv. of diazomethane and 1 equiv. of BF_3–etherate. The solution was kept at 0 °C for

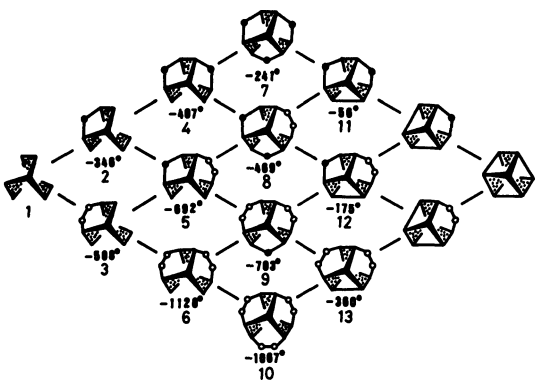

Fig. 1. Absolute configurations and absolute molecular rotations of the levorotatory tri-, tetra-, and pentacyclic hydrocarbons having D_3-twisted bicyclo[2.2.2]octane molecular framework with M helicity.

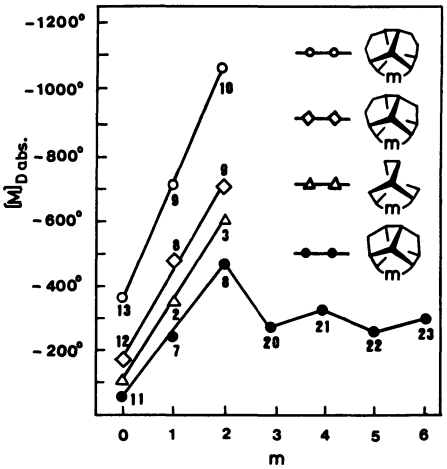

Fig. 2. Correlation between bridge span and absolute molecular rotation ($[M]_{D\ abs.}$) in four series of triblattane.

Table 1. Reaction of (±)-14 and diazomethane without catalyst

Reaction time d	Product ratio 14	15	16
1	2	98	0
3	0	81	19
5	0	73	27
8	0	65	35

Table 2. Product distribution in the ring-expansion product

CH_2N_2 (equiv.)	Product ratio 7	8	20	21	22	23
3	43	45	9	2	1	0
5	6	33	24	28	9	0
10	0	0	11	42	29	18

Scheme 1.

24 h, and routine workup gave a mixture of **16**, **17**, **18**, and **19** from which **16** was removed by alumina chromatography. Wolff-Kishner reduction of the remaining mixture of **17**, **18**, and **19** furnished a 48 : 26 : 26 mixture (by GLC analysis) of **21**, **22**, and **23**. Preparative GLC separated and purified these [*m*.1.1]-triblattanes.

The known optical purity of our starting material (−)-**14** permitted calculation of the absolute molecular rotation of these new hydrocarbons; $[M]_{D\ abs.}$ −268°, −321°, −255°, and −287° for **20**, **21**, **22**, and **23** respectively. These values are plotted in Fig. 2, inspection of which indicates that the $[M]_{D\ abs.}$ of [*m*.1.1]-triblattanes drop abruptly on going from $m=2$ to $m=3$, then remain almost constant till $m=6$. This behavior could be explained in terms of the expected conformational mobility of $(CH_2)_m$ bridge in these higher [*m*.1.1]-triblattanes which should annihilate the $[M]_D$ contribution from this part of molecule.

Experimental

Product Distribution in the Diazomethane Ring-expansion Product of (±)-D_3-Trishomocuban-4-one (14). Without Catalyst: An ethereal solution (100 mL) of diazomethane (1.5 g, 35 mmol) was added with stirring to an ice-cooled solution of (±)-**14**[5] (500 mg, 3.13 mmol) in dry ether (20 mL). The reaction mixture was allowed to stand at 0 °C, and aliquots were analyzed by GLC at 1, 3, 5, and 8 d period.

With BF_3-etherate Catalyst: The following experimental procedure is typical. An ethereal solution (100 mL) of diazomethane (1.5 g, 35 mmol) was added to a stirred and chilled (0 °C) solution of (±)-**14** (500 mg, 3.13 mmol) and freshly distilled BF_3-etherate (0.4 mL, 3.2 mmol) in dry ether (20 mL). After the resulting mixture was kept at 0 °C for 24 h, a deposited solid was removed by filtration and the filtrate was washed with aq $NaHCO_3$ and water, dried ($MgSO_4$) and concentrated to give an oily product (460 mg). The product (400 mg) was mixed with 100% hydrazine hydrate (0.35 mL), KOH (190 mg) and triethylene glycol (4 mL) and the mixture was heated for 1 h at 110—120 °C and for an additional 4 h at 190—200 °C. The product (310 mg) was analyzed by GLC.

Preparation of (−)-[3.1.1]Triblattane (20). An ethereal solution of diazomethane (11 g, 0.26 mol) was added to a stirred and chilled (0 °C) solution of (−)-**14**, $[\alpha]_D$ −26.0°[3] (13.5 g, 84.4 mmol) in dry ether (100 mL), and the mixture was kept at 0 °C for 8 d. After the remaining diazomethane was destroyed with a small amount of acetic acid, the mixture was washed with aq $NaHCO_3$ and water, and dried ($MgSO_4$). Removal of the solvent left an oily product which was analyzed by GLC and was found to be a 3 : 2 mixture of **15** and **16**. When the mixture was chromatographed on alumina, earlier pentane eluents containing **16** (≥98% estimated by GLC) (550 mg) was followed by fractions containing a 1 : 3 mixture (4.30 g) of **15** and **16** which was reserved for further ring-expansion reaction (*vide infra*). Wolff-Kishner reduction of **16** 240 mg, (1.27 mmol) was carried out by the same procedure described above. The product was chromatographed on alumina and elution with pentane provided **20** (175 mg). The analytical sample was purified by sublimation at 55 °C (15 mm); mp 73—73.5 °C (in a sealed tube); $[\alpha]_D^{22}$ −46.5° (*c* 0.212, $CHCl_3$); MS, *m/e* 174 (M^+); ^{13}C NMR ($CDCl_3$) δ 24.47 (t), 29.32 (t), 35.54 (t), 39.91 (d), 42.31 (d), 46.60 (d), 47.30 (d); GLC, *Rt.* 4′10″ (at 120 °C); Found: C, 89.65; H, 10.36%. Calcd for $C_{13}H_{18}$: C, 89.59; H, 10.41%.

Preparation of (−)-[4.1.1], (−)-[5.1.1], and (−)-[6.1.1]-Triblattanes. Ring-expansion reaction of the 1 : 3 mixture (4.00 g) of **15** and **16** obtained as described above was carried out with 1 L of ethereal solution of diazomethane (10 g, 0.23 mol) and BF_3-etherate (3.0 mL, 23 mmol) at 0 °C for 24 h. The same workup afforded a mixture (3.50 g) of **16**, **17**, **18**, and **19**. In order to remove **16**, the mixture was chromatographed on alumina, and earlier pentane eluents provided a semi-solid (630 mg) which was found to be free from **16** by GLC. Wolff-Kishner reduction of this fraction (600 mg) was carried out with 100% hydrazine hydrate (0.5 mL), KOH (260 mg), and triethylene glycol (6 mL). The same workup as described above gave a 48 : 26 : 26 mixture (232 mg) of **21**, **22**, and **23**. Preparative GLC (at 140 °C) provided specimens of (−)-**21** (80 mg), *Rt.* 8′20″, (−)-**22** (45 mg), Rt. 12′05″ and (−)-**23** (40 mg), *Rt.* 15′10″. (−)-[4.1.1]Triblattane (**21**); An oil; $[\alpha]_D^{20}$ −51.5° (*c* 0.344, $CHCl_3$); MS, *m/e* 188 (M^+); Found: C, 89.26; H, 10.70%. Calcd for $C_{14}H_{20}$: C, 89.29; H, 10.71%. (−)-[5.1.1]Triblattane (**22**); An oil; $[\alpha]_D^{24}$ −37.9° (*c* 0.796, $CHCl_3$); MS, *m/e* 202 (M^+); Found: C, 88.96; H, 10.97%. Calcd for $C_{15}H_{22}$: C, 89.04; H, 10.96%. (−)-[6.1.1]Triblattane (**23**); mp 64 °C; $[\alpha]_D^{25}$ −39.9° (*c* 1.46, $CHCl_3$); MS, *m/e* 216(M^+); Found: C, 88.67; H, 11.14%. Calcd for $C_{16}H_{24}$: C, 88.82; H, 11.18%.

References

1) K. Adachi, K. Naemura, and M. Nakazaki, *Tetrahedron Lett.*, **1968**, 5467.

2) M. Nakazaki, "Topics in Stereochemistry," Vol. 15, An Interscience Publication, John Wiley and Sons, New York, in press.

3) M. Nakazaki, K. Naemura, and N. Arashiba, *J. Org. Chem.*, **43**, 689 (1978).

4) J. A. Jenkins, R. E. Doehner, Jr., and L. A. Paquette, *J. Am. Chem. Soc.*, **102**, 2131 (1980).

5) P. E. Eaton, R. A. Hudson, and C. Giordano, *J. Chem. Soc., Chem. Commun.*, **1974**, 978.

Laser Excitation Spectrum of the $\tilde{A}^2A'(004) \leftarrow \tilde{X}^2A''(000)$ Band of HSO Radical

Masayoshi SATOH, Nobukimi OHASHI,* and Shin-ichi MATSUOKA
Institute for Spectroscopic Study of Matter, Faculty of Science, Kanazawa University, Maruno-uchi, Kanazawa 920
(Received June 21, 1982)

The dye laser excitation spectrum of the $\tilde{A}^2A'(004)\leftarrow\tilde{X}^2A''(000)$ vibronic band of HSO was observed and analyzed in the frequency range from 17132 to 17182 cm^{-1}. 414 spectral lines were assigned to an ordinary c-type transition and 21 lines to an axis-switching transition. The rotational constants of HSO in the $\tilde{A}^2A'(004)$ state were used to calculate the inertia defect of 0.518 u $Å^2$ for this state. A relatively large dependence of the centrifugal distortion constant on the vibrational quantum number was also found.

The HSO radical is expected to play an important role in various oxidations, for example, that of hydrogen sulfide. Recently, spectroscopic studies on this radical have been made by several workers[1–4] and the existence of this radical in gas phase has been established.

Schurath *et al.*[1] observed the chemical luminescence spectrum of $\tilde{A}^2A'\leftarrow\tilde{X}^2A''$ band of HSO and DSO, and deduced some vibrational frequencies: $\nu_3'(HSO)=702$, $\nu_3''(HSO)=1013$, $\nu_3'(DSO)=702$, $\nu_3''(DSO)=1030$ cm^{-1} for the SO bond stretching, and $\nu_2'(DSO)=600$ and $\nu_2''(DSO)=770$ cm^{-1} for the bending vibration.

Kakimoto *et al.*[2] observed the laser excitation spectrum of the $\tilde{A}^2A'(003)\leftarrow\tilde{X}^2A''(000)$ vibronic transition of HSO and determined the rotational constants and centrifugal distortion constants precisely.

Ohashi *et al.*[3] determined the structural parameters of HSO in the ground and the excited states by combining the rotational constants of HSO and DSO; they also estimated an approximate force field. For the $\tilde{X}^2A''$ ground state, they determined a simple valence force field by using the observed centrifugal distortion constants of HSO. The force field reproduced fairly well the fundamental frequencies obtained by Schurath *et al.*, the centrifugal distortion constants, and the inertia defects of HSO and DSO. For the $\tilde{A}^2A'$ excited state, however, they could not obtain a satisfactory force field by applying the same procedure as they had used for the ground state. The centrifugal distortion constants may depend strongly on the vibrational quantum numbers in this case. The failure in determining the force field for the excited state is considered to originate from the v-dependence of the centrifugal distortion constants.

In the present study, $\tilde{A}^2A'(004)\leftarrow\tilde{X}^2A''(000)$ band of HSO was observed and analyzed with the intention of obtaining further information on the centrifugal distortion constants and the inertia defects.

Experimental

The experimental setup for recording the laser excitation spectrum was similar to that used by Kakimoto *et al.*,[2] except that the dye laser was a ring laser (Spectra Physics, Model 380A) and the frequency scanning was in 200 MHz mode-hopping. The present measuring system for the excitation spectrum of unstable molecules has been fully described elsewhere.[5]

The wavenumber determination of spectral lines was made by using iodine lines as standard. The precision was about 0.02 cm^{-1}, which was about ten times worse than that obtained by Kakimoto *et al.*[2] because of the mode-hopping.

The generation of the HSO radical was made in the following reaction system:

$$C_2H_5SH + O_2 \text{ (MW discharge)},$$

where partial pressures measured with a Pirani gauge were 30 mTorr (1 Torr = 133.322 Pa) for C_2H_5SH and 100 mTorr for O_2. The laser output power was about 100 mW.

Results and Discussion

The excitation spectrum of the HSO radical was recorded in the spectral range of 17132 to 17182 cm^{-1}. The spectrum observed in the present work corresponds to a vibronic band of $\tilde{A}^2A'(004)\leftarrow\tilde{X}^2A''(000)$ and obeys a c-type rotational selection rule. The assignment of the spectral lines could be done easily by using a simulation spectrum calculated from the determined ground state constants[4] and the assumed upper state constants. Most of the observed lines could be assigned; 414 lines were assigned to ordinary c-type transitions. Besides these transitions, 21 lines were assigned to $\Delta K_a=0$ and $+2$ type transitions allowed by axis switching,[6] because the H–S–O angle in the excited state is smaller by about 11° than that in the ground state.

The following Hamiltonian was used in the least squares analysis:

$$H = H_{rot} + H_{cd} + H_{sr}, \tag{1}$$

$$H_{rot} = AN_a^2 + BN_b^2 + CN_c^2, \tag{2}$$

$$H_{cd} = -\Delta_N N^4 - \Delta_{NK} N^2 N_a^2 - \Delta_K N_a^4 - 2\Delta_N N^2(N_b^2 - N_c^2) - \delta_K[(N_b^2 - N_c^2)N_a^2 + N_a^2(N_b^2 - N_c^2)], \tag{3}$$

$$H_{sr} = \varepsilon_{aa} N_a S_a + \varepsilon_{bb} N_b S_b + \varepsilon_{cc} N_c S_c, \tag{4}$$

for both the upper and lower states. In the above analysis, the ground state constants were fixed to the values determined by Endo *et al.*[4] in the microwave measurements.

In Table 1, the obtained molecular constants for $\tilde{A}^2A'(004)$ of HSO are given. The rms deviation between the observed and calculated wavenumbers is

TABLE 1. MOLECULAR CONSTANTS OF HSO (MHz)

Constants	$\tilde{A}^2A'(004)$	$\tilde{A}^2A'(003)$[a]
A	293446(78)	291862(16)
B	16834.7(54)	16934.7(17)
C	15666.0(60)	15802.1(17)
Δ_N	0.0585(51)	0.0483(22)
Δ_{NK}	3.80(29)	3.318(38)
Δ_K	56.7(87)	39.9(18)
δ_N	0.0003(72)	0.00506(58)
δ_K	8.0(25)	4.01(41)
ε_{aa}	16578(869)	17854(165)
ε_{bb}	129(36)	87(32)
ε_{cc}	−345(36)	−352(32)
ν_0/cm^{-1}	17168.2116(44)	16483.0252(13)

a) Ref. 2.
Values in parentheses are 2.5 times the standard deviation and apply to the last digits.

TABLE 2. FORCE CONSTANTS, VIBRATIONAL FREQUENCIES, AND INERTIA DEFECTS FOR $\tilde{A}^2A'$ STATE

		Calculated values (1)	Calculated values (2)	Observed values
	F_{11}[a]/mdyn Å^{-1}	4.36700	4.36700	
	F_{22}/mdyn Å^{-1}	0.30437	0.25117	
	F_{33}/mdyn Å^{-1}	2.98064	3.31768	
HSO	ν_1/cm^{-1}	2754	2754	[2769][b]
HSO	ν_2/cm^{-1}	842	781	[828][b]
HSO	ν_3/cm^{-1}	679	702	702(5)[b]
HSO	$\Delta(003)$/u Å	0.203	0.410	0.407(5)[c]
HSO	$\Delta(004)$/u Å	0.241	0.514	0.518(17)[d]
DSO	ν_1/cm^{-1}	1978	1978	[1978][b]
DSO	ν_2/cm^{-1}	594	548	600(10)[b]
DSO	ν_3/cm^{-1}	707	735	702(10)[b]
DSO	$\Delta(003)$/u Å	0.131	0.131	0.388(7)[e]

a) Fixed. b) Ref. 1. c) Ref. 2. d) Present work. e) Ref. 3.
Values in brackets are estimated ones.

0.015 cm^{-1}. In Fig. 1, the observed spectrum is compared with the simulated one, which was calculated from the obtained constants. In the present calculation of the simulated spectrum, the axis-switching effect was not taken into account, because the axis-switching angle is very small(θ_T=1.65°). The good agreement between the observed and simulated spectra indicates that (1) the observed band is free from any perturbation and (2) the spectral lines attributable to other bands of HSO or to other species than HSO do not exist in the observed spectral region (17132 to 17182 cm^{-1}).

The inertia defect for the $\tilde{A}^2A'(004)$ state was obtained to be 0.518 u Å^2 from the determined rotational constants. The value for the $\tilde{A}^2A'(000)$ state was deduced to 0.074 u Å^2 by extrapolation from 0.407 u Å^2 for the (003) state[2] and 0.518 u Å^2 for the (004) state.

Using the force constants given in Table 5 of Ref. (3), values of the inertia defect for the $\tilde{A}^2A'(000)$, $\tilde{A}^2A'(003)$, and $\tilde{A}^2A'(004)$ states of HSO were calculated to be 0.088, 0.192, and 0.226 u Å, respectively. Thus, the calculated value of the (000) state agreed well with the extrapolated value, but the agreement between the calculated and observed values was poor for the (003) and (004) states.

Improvement of the force field was tried by adding the present value of inertia defect to the reported data.

(1). A valence force field was determined by using inertia defects for the (003) and (004) states of HSO and for the (003) state of DSO, and ν_3(HSO), ν_2(DSO), and ν_3(DSO). The obtained force constants, and the frequencies and inertia defects reproduced by these force constants, are summarized in column (1) of Table 2. As seen from the table, the agreement between observed and calculated values is good for vibrational frequencies of HSO and DSO, but the calculated values of inertia defects were too small, compared with the observed values. The contribution of the frequencies to the determination of the force field was thus dominant and that of the inertia defect was small. Indeed, the force field could not be determined by using data of inertia defects only.

(2). A force field was determined by using ν_3 (HSO) and $\Delta(003)$ and $\Delta(004)$ of HSO. These force constants are listed in column (2) of Table 2, together with other constants deduced from this field. In this case, close agreement between the calculated and observed values of inertia defect for HSO was obtained, but the calculated value of the inertia defect for DSO is still smaller than the observed value.

The force field, determined by data of HSO only, reproduced fairly well all the constants except $\Delta(003)$ for DSO (see column (2) in Table 2). The discrepancy of $\Delta(003)$ for DSO is considered to originate from non-diagonal components of the force field, but these can not be obtained because of lack of data. There may be some other perturbations which have an effect to this constant, but it is difficult to make these problems clear until the measurements on the (012) and (021) states are carried out.

For the centrifugal distortion constants, the obtained value in the (004) state clearly differs from that in the (003) state, in spite of the wide experimental errors (Table 1). Therefore, it can be said that the centrifugal distortion constant depends on the vibrational quantum number. This v-dependence is surely the main reason why the reasonable force field for the $\tilde{A}^2A'$ state could not be obtained from the centrifugal distortion constants. Essentially, the force field for the $\tilde{A}^2A'$ state must be determined from the centrifugal distortion constants for the vibration-free (000) state, which can be obtained by extrapolation of values of the (004) and (003) states. But the precision of obtained distortion constants is not high enough to allow us to extrapolate. The centrifugal distortion constants for the (000) state were calculated by using the force field of column (2) in Table 2, the values are Δ_N=0.0369, Δ_{NK}=1.064, Δ_K=16.592, δ_N=0.00256,

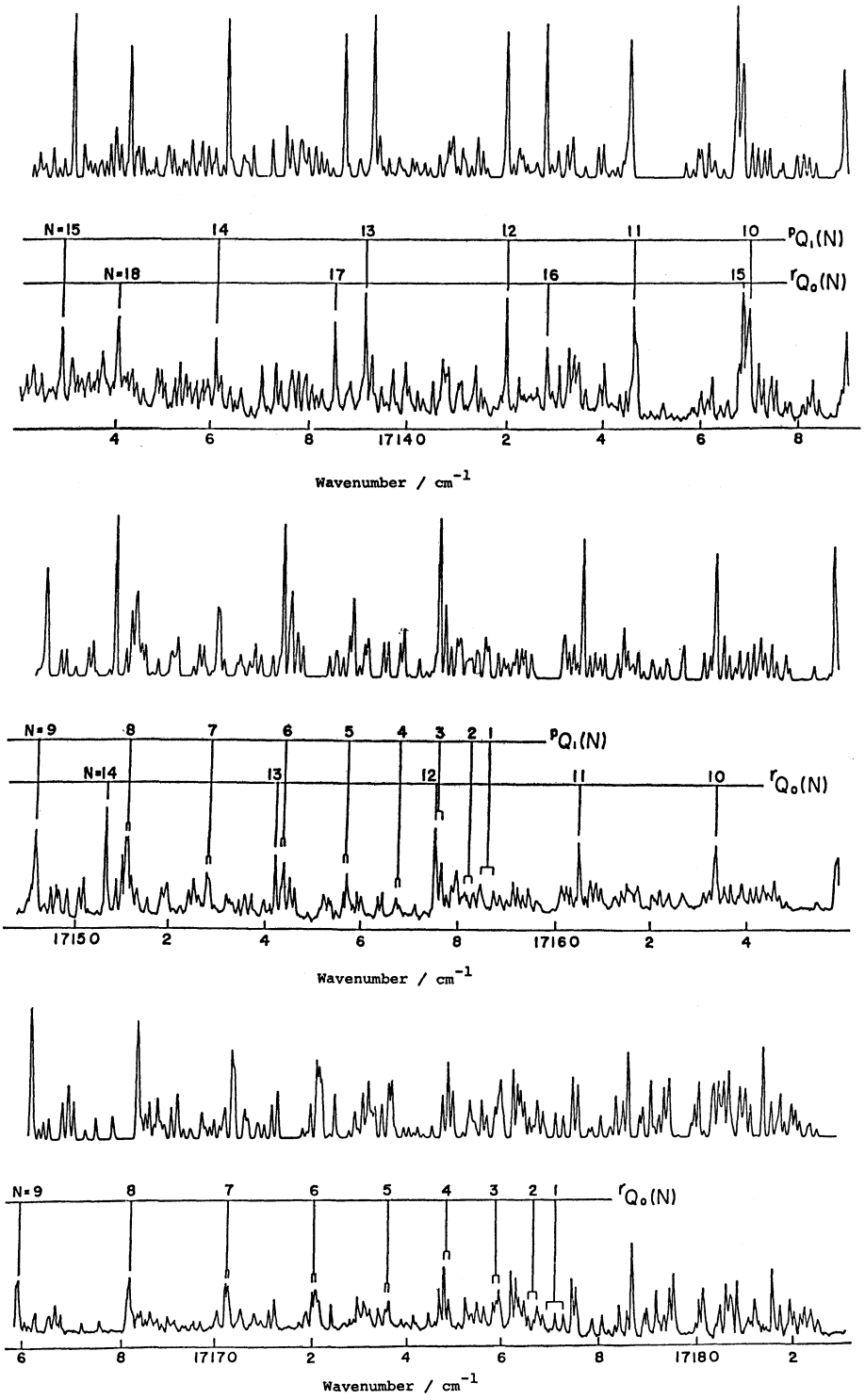

Fig. 1. Observed (bottom) and simulated (top) spectrum of the HSO $\tilde{A}^2A'(004)$ $\tilde{X}^2A''(000)$ band.

and δ_K=0.660 MHz.

The authors thank Dr. S. Saito of the Institute for Molecular Science for valuable discussions.

References

1) U. Schurath, M. Wever, and K. H. Becker, *J. Chem. Phys.* **67**, 110 (1977).
2) M. Kakimoto, S. Saito, and E. Hirota, *J. Mol. Spectrosc.* **80**, 334 (1980).
3) N. Ohashi, M. Kakimoto, S. Saito, and E. Hirota, *J. Mol. Spectrosc.* **84**, 204 (1980).
4) Y. Endo, S. Saito, and E. Hirota, *J. Chem. Phys.* **75**, 4379 (1981).
5) M. Satoh, N. Ohashi, and S. Matsuoka, *Sci. Rep. Kanazawa Univ.*, **27**, 5 (1982).
6) J. T. Hougen and J. K. G. Watson, *Can. J. Phys.* **43**, 298 (1965).

The Location and Microenvironment of Dimerizing Cationic Dyes in Lipid Membranes as Studied by Means of Their Absorption Spectra

Tetsurou HANDA, Chikako ICHIHASHI, Izumi YAMAMOTO, and Masayuki NAKAGAKI*

Faculty of Pharmaceutical Sciences, Kyoto University, Sakyo-ku, Kyoto 606

(Received October 30, 1982)

The absorption spectra of three cationic dyes, Methylene Blue (MB), 3,3′-dipropyl-2,2′-thiadicarbocyanine (diS-C_3(5)), and 9-aminoacridine (9-AA), were measured in aqueous suspensions of a phospholipid membrane and a surfactant micelle. The dyes were intensely partitioned into the membrane phase and dimerized to exhibit a remarkably large reduction in absorbance. The increase in the amount of the membrane beyond the amount where all the dye molecules were dimerized in the membrane phase resulted in a gradual increase in the absorbance due to the increase in the available membrane volume and the dilution of dye in the membrane phase. The changes in the wave lengths of the absorption maxima of the dye monomers by the partitioning into membrane thus obtained were interpreted in terms of the effective polarities of the dye surroundings (microenvironments). It was found that the rather hydrophobic diS-C_3(5) penetrates deeply into the membranes and the micelles and is located in considerably nonpolar microenvironments, while MB remains at the polar-surface regions of the membranes and the micelles. On the basis of these results, the structures of the micelles and membranes are discussed.

Membranes, micelles, and microemulsions provide wide ranges of small environments and have great effects on chemical equilibria, kinetics, and structure organizations.[1] To estimate local effective polarities in micelles and microemulsions, various spectral methods have been employed. Charge-transfer bands of pyridinium iodide and 2,6-diphenyl-4-(2,4,6-triphenyl-1-pyridino)phenoxide exhibit considerably large shifts according to the nature of the dye surroundings.[2,3] Also, the vibronic structures of aromatic hydrocarbons, such as benzene, naphthalene, and pyrene, in absorption and fluorescence spectra show strong dependencies on the solvent, micellar, and microemulsion environments.[4,5]

With respect to lipid membranes, which offer promising prospects of understanding the complex natures of biological membranes and also for pharmaceutical and industrial uses, many fluorescent dyes have been employed.[1,6] However, the fluidity-dependent shift of the fluorescence maxima associated with solvent relaxation during the lifetime of the excited state introduces potential difficulties in the estimation of the local effective polarity of the membrane, which is regarded as a small heterogeneous fluid system.[7,8]

In this study, microenvironments in phospholipid membranes (liposomes), in addition to surfactant micells, were evaluated from measurements of the visible spectra of three cationic dyes, Methylene Blue, 3,3′-dipropyl-2,2′-thiadicarbocyanine, and 9-aminoacridine. These dyes partition into the membrane phase and dimerize to exhibit remarkably large reductions in absorbance and fluorescence. The increases in the amount of membrane over the amount at which all dye molecules are dimerized in the membrane phase give rise to dilutions of the dyes in the membrane and, thereby, to restorations of the absorbance. The absorbance maxima of the dye monomer accommodated in the membranes, which are shifted from those in aqueous media, were translated into the effective polarities of the dye surroundings.

Experimental

Materials. Egg yolk phosphatidylcholine (PC) was prepared by the method of Singleton *et al.*[9] Bovine brain phosphatidylserine (PS) and L-α-dipalmitoylphosphatidic acid (PA) were obtained from the Sigma Chemical Co. The heptaethylene glycol monododecyl ether (HED) and sodium tetradecyl sulfate (STS) were purchased from the Nikko Chemicals Co., Ltd., and ICN Pharmaceuticals, Inc., respectively. The disodium hexadecyl phosphate (SHP) was synthesized by the method of Nelson.[10] The 9-aminoacridine (9-AA) and Methylene Blue (MB) were obtained from the Nakarai Chemicals Co., Ltd., and the 3,3′-dipropyl-2,2′-thiadicarbocyanine (diS-C_3(5)) was purchased from the Japanese Research Institute for Photosensitizing Dye Co., Ltd. All the solvents were distilled before use.

Preparation of Lipid Membrane (Liposome). Aliquots of phospholipid were removed from the stock solution in chloroform, after which the solvent was evaporated and dried under a vacuum for 15 h. The complete removal of the chloroform was essential. Trace amounts of the solvent remaining will introduce error in the spectroscopic measurement of dye in the membrane phase. The lipid was suspended in 1 mM (1 M = 1 mol dm^{-3}) Tris-HCl (pH 7.3) and dispersed ultrasonically for 20 min. The solvent was cooled in ice during this process. The ultrasonic device used was an UR-200P apparatus from the Tomy Seiko Co., Ltd. The ultrasonically dispersed lipid was then centrifuged for 30 min at 20000 g to remove the titanium dust from the ultrasonic tip and a small amount of untreated lipid. The lipid-membrane suspension was diluted with the 1 mM Tris-HCl buffer solution for measurement. The HED and STS micellar solutions were prepared in the 1 mM Tris-HCl buffer. For the SHP micellar solution, the pH was adjusted to 10.0 with a very dilute NaOH solution to prevent H^+ binding to the phosphate. The variation in the pH from 7.3 to 10.0 did not affect the absorption spectra of dyes in aqueous media.

Absorption Spectra. The spectra of dyes in an aqueous solution with phospholipid membranes (liposomes) or surfactant micelles were recorded with a Shimadzu UV-180 spectrophotometer. The amount of membrane composed

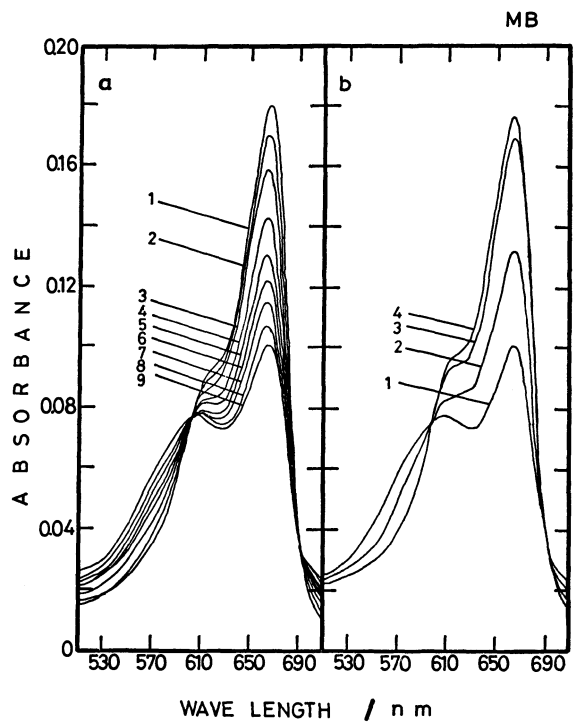

Fig. 1. (a) MB spectral change upon addition of PS membrane. The medium contains 1 mM Tris–HCl and 2 μM of MB at pH 7.3, 25 °C. The amount of (dried) lipid added (in μg/1 ml of medium): (1) 0; (2) 0.38; (3) 0.70; (4) 1.35; (5) 2.04; (6) 2.60; (7) 3.21; (8) 3.84; (9) 4.47. (1 μg PS/ml=1.4 μM PS). (b) MB spectral change upon addition of NaCl. 4.47 μg PS/ml (6.4 μM PS). The medium is the same as that on the (a) except for concentration of NaCl. [NaCl]: (1) 0; (2) 1; (3) 2; (4) 4 (in mM).

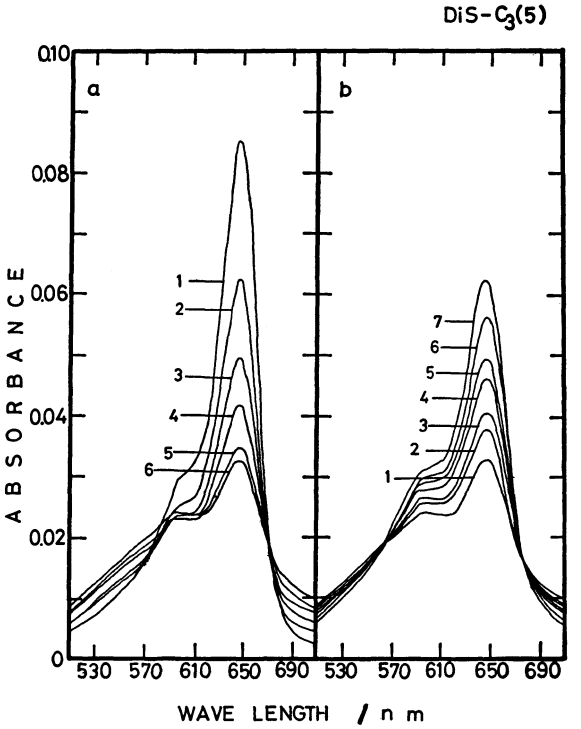

Fig. 2. (a) DiS-C_3(5) spectral change upon addition of PS membrane. The medium contains 1 mM Tris–HCl and 0.73 μM of diS-C_3(5) at pH 7.3, 25 °C. The amount of (dried) lipid added (in μg/1 ml of medium): (1) 0; (2) 0.06; (3) 0.126; (4) 0.190; (5) 0.252; (6) 0.315 (0.1 μg PS/ml=0.14 μM PS). (b) DiS-C_3(5) spectral change upon addition of NaCl. 0.315 μg PS/ml (0.45 μM PS). The medium is the same as that on the (a) except for the concentration of NaCl. [NaCl]: (1) 0; (2) 2; (3) 4; (4) 14; (5) 24; (6) 54; (7) 104 (in mM).

of an anionic phospholipid, PS or PA, in dye solutions was very small (less than 0.15 mg of the lipid in 1 ml of a medium). In the case of the PC membrane, the amout in solution went up to 8 mg in 1 ml of a medium, and the turbidity from the membrane gave rise to less accurate absorption spectra. Such data are marked in Table 1. The temperature was maintained constant at 25 °C by water circulation through the cuvet holder of the spectrophotometer. The dye concentrations of the MB, 9-AA, and diS-C_3(5) used were 2, 2, and 0.73 μM respectively, low enough for us to neglect the dimerizations in the aqueous phases.[11,12]

Results

Absorption Spectra of Cationic Dyes with Membranes and Micelles. In Figs. 1 and 2, the absorption spectra of MB (2 μM) and diS-C_3(5) (0.73 μM) in the buffer solutions with PS membranes are shown. It is shown that the monomer absorbance maxima of MB (664 nm) and diS-C_3(5) (648 nm) decrease with an increase in the amount of the lipid membrane. The dimer absorbance maxima of MB and diS-C_3(5) have been reported as 600 and 590 nm respectively.[11,12] Also, on an increase in the concentration of NaCl, the absorbances increased gradually. The 98% absorbance of MB is restored with 4 mM NaCl, while more than 100 mM NaCl recovered only 74% of the initial absorbance of diS-C_3(5). In the case of diS-C_3(5) with various amounts of PS (Fig. 2a), the small turbidity arising from the membrane (0.003 in absorption unit) disturbs the isosbestic point at 570 nm. Furthermore, the increases in the amount of the membrane beyond the amount at which the minimum absorbance was observed resulted in a gradual increase in the absorbance. The data for MB and diS-C_3(5) are shown in Fig. 3. As will be discussed later, the cationic dyes intensely bind to anionic lipid membranes or anionic surfactant micelles; the resulting enhancements in the concentrations of the dyes in the membrane phase prompt the formation of the dimer forms, which have lower extinction coefficients than the monomers. Therefore, an increase in the membrane amount beyond the amount at which almost all the dye molecules are in the membrane phase resulted in a gradual increase in the absorbance due to the decrease in the concentration of dyes in the membrane phase. The minimum absorbances of MB, diS-C_3(5), and 9-AA obtained with anionic membranes or micelles were 16, 25, and 36% of the initial absorbance values, which corresponded to the respective ratio of the extinction coefficients of a dimer to a monomeric dye and indicated that almost all the dye molecules formed dimers in the membrane or the

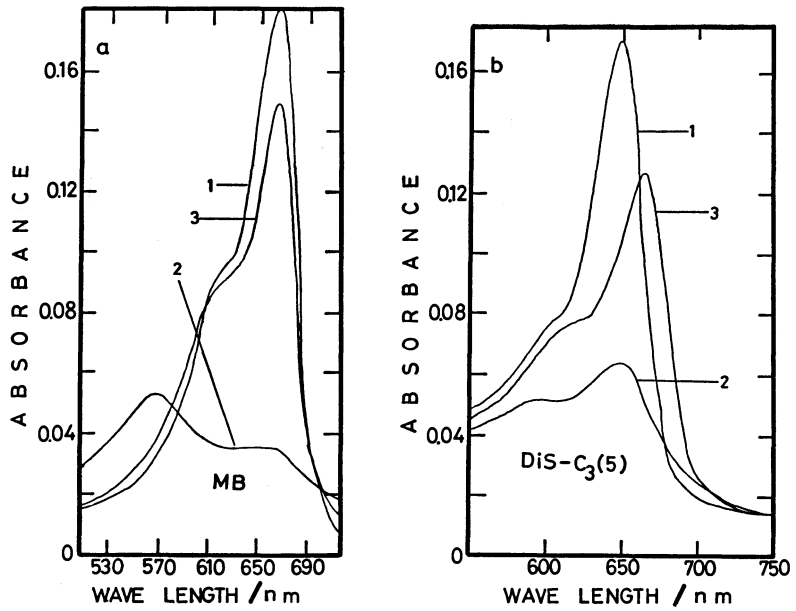

Fig. 3. Dye spectral change upon addition of PS membranes.
The medium contains 1 mM Tris–HCl at pH 7.3, 25 °C. (a) 2 μM MB with (1) 0; (2) 15; (3) 150 μg PS/ml. (b) 3 μM diS–C_3(5) with (1) 0; (2) 2.7; (3) 20 μg PS/ml. (1 μg PS/ml=1.4 μM PS).

micellar phases at the minimum points. Spectra 1 and 3 in Fig.3 are in the aqueous media and in the PS membranes respectively of MB and diS-C_3(5). In the case of MB, the wavelengths of the absorption maxima in an aqueous medium and in the membrane phase were very close, 664 and 662.8 nm. In contrast, diS-C_3(5) exhibited quite a large red shift of the absorption maximum in the membrane (648→664 nm).

In Table 1, the absorption maxima (in nm) of MB, diS-C_3(5), and 9-AA in anionic membranes and micelles (PS, PA, STS, and SHP) and in an electrically neutral membrane and micelle (PC and HED) are shown. Into the neutral membrane and micelle, the cationic dyes were not so intensely partitioned as to complete the dimerization. Therefore, we added amounts of the PC membrane and the HED micelle which were greater than the amounts at which the spectral shifts of dyes arose due to partitioning from aqueous media to the membrane or the micellar phases were complete. The accuracies of some absorption maximum values were judged to be less (±0.5 nm) than others (±0.2 nm), where appreciable turbidities from PC membranes were observed.

Solvent Effects on Absorption Spectra of the Cationic Dyes. The solvent effects on the visible spectra of MB, diS-C_3(5), and 9-AA were also studied. The absorption maxima (λ_{max}) of dyes obtained in various pure solvents and solvent mixtures are shown in Table 2. The polarities of solvents and solvent mixtures are characterized by their dielectric constants and also Reichardt-Dimorth's $E_T(30)$.[3b] The latter is empirically correlated with the solvatochromism of 2,6-diphenyl-4-(2,4,6-triphenyl-1-pyridino)phenoxide at 25 °C. The dielectric constants of methanol-water mixtures have been known to be related to the weight fraction of methanol, w_{MeOH}, as $\varepsilon=78.5-(78.5-32.6)\,w_{MeOH}$.[13] DiS-$C_3$(5) and 9-AA showed monotonous increases in λ_{max} with a reduction of the solvent polarity, while MB has a minimum value around that of methanol. It was also found that the addition of concentrated NaCl (4—5 M) to the methanol–water

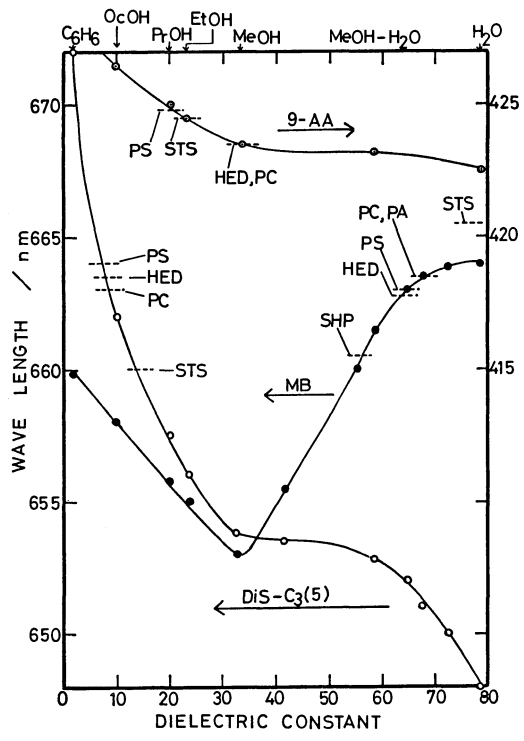

Fig. 4. Solvent effect on the wave length of absorption maximum of cationic dye monmer.
The values on the abscissa indicate dielectric constant of solvent. The wave lengths obtained in membranes and micelles are shown by the horizontal broken lines. The numerical values of effective dielectric constant estimated here are represented in Table 1.

TABLE 1. ABSORPTION MAXIMA, λ_{max}, OF CATIONIC DYE MONOMERS AND EFFECTIVE DIELECTRIC CONSTANTS, ε, IN MEMBRANES AND MICELLES

Membranes and Micelles	MB		DiS-C_3(5)		9-AA	
	λ_{max}/nm	ε	λ_{max}/nm	ε	λ_{max}/nm	ε
Phosphatidylcholine(PC) (11 mM)	663	68	663	8.5	423—424[a]	
Phosphatidylserine(PS) (0.03—0.21 mM)	662.8	65	664	7.5	424.8	20.5
Phosphatidicacid(PA) (0.03—0.21 mM)	663	68	663	8.5	424	27
Phosphatidicacid(PA) (0.21 mM, pH 10)	663	68				
Heptaethylene glycol monododecyl ether(HED) (20 mM)	663.5	63	663.5	8.0	423.6	33.5
Sodium tetradecyl sulfate(STS) (10 mM)	665.5[b]		660	13.5	424.5	23.0
Disodium hexadecyl Phosphate(SHP) (10 mM, pH 10)	661.5	56				

a) Less accurate because of appreciable turbidity. b) A close value of λ_{max} is obtained in an aqueous solution of 2 M NaCl. The concentrations of MB, diS-C_3(5), and 9-AA used are 2, 3, and 2×10^{-6} M respectively.

TABLE 2. SOLVENT EFFECTS ON THE ABSORPTION MAXIMA, λ_{max}, OF THE CATIONIC DYES

Solvent	Dielectric constant	$E_T(30)$ kcal mol^{-1} [d]	λ_{max}		
			MB	DiS-C_3(5)	9-AA
H_2O (1 mM Tris-HCl, pH 7.3)	78.5	63.1	664	648	422.5
Methanol	32.6	56.3	653	653.8	423.5
Ethanol	24.5	51.9	655	656	424.5
1-Propanol	20.1	50.7	655.8	657.5	425
1-Octanol	10.3		658	662	426.5
Benzene	2.3	34.5	659.8	672	428
Hexane	1.9	30.9	a)	675[b]	430[b]
Methanol-H_2O mixtures					
w_{MeOH}=0	78.5	63.1	664	648	422.5
0.13	72.6		663.8	650	
0.24	67.5		663.5	651	
0.30	64.8		663	652	
0.44	58.4		661.5	652.8	423.2
0.50	55.6		660		
0.56	52.8		658.5	653.3	
0.66	48.2		657.5	653.5	
0.79	41.8		655.5	653.5	
1	32.6	56.3	653	653.8	423.5
Methanol-aqueous 5 M NaCl mixtures					
w_{MeOH}=0	35		668	a)	423.5
0.13			669	653.5	424
0.24			668.5	654.5	424.2
0.30[c]			668	654.8	424.2
0.38[c]			665.5	655	424
0.44[c]			663.5	655	424

a) Insoluble. b) Rapid bleachings were observed. c) Methanol+aqueous 4 M NaCl. d) 1 cal=4.184 J.

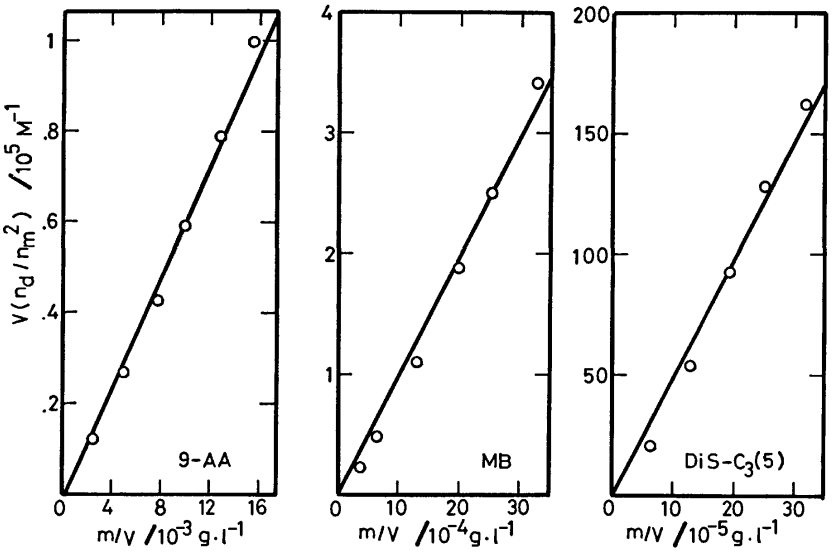

Fig. 5. Variations of $V(n_d/n_m^2)$ for 9-AA, MB, and diS-C_3(5) as a function of the concentration of PS membrane (m/V). See Eq. 9. (1×10^{-3} g PS/ml=1.4 mM PS).

mixtures gives rise to red shifts in the absorbance maxima of the cationic dyes used here. In Fig. 4, the λ_{max} values of dyes in membranes and micelles are compared with the values in solvents. The effective dielectric constants around dyes in micelles and membranes, ε, obtained in this figure are shown in Table 1.

Dimerization of Cationic Dyes in Membranes. The absorbance, A, of a cationic dye in an aqueous suspension of a lipid membrane is given by:

$$A = (\varepsilon_m n_m + 2\varepsilon_d n_d)/V, \quad (1)$$

where n_m and n_d are the moles of the dye monomer and the dimer, and where $n_m+2n_d=n_0$; here, n_0 is the total number of moles of the dye. V is the volume of the buffer solution containing the dye. The volume of the membrane phase, V_M, is very small and so can be neglected in Eq. 1. ε_m and ε_d are the extinction coefficients of the dye molecule in monomeric and dimeric forms. $\varepsilon_m/\varepsilon_d$ for MB at 664 nm has been established to be 0.157.[14] The $\varepsilon_m/\varepsilon_d$ values for diS-C_3(5) and 9-AA were estimated from the linear relations between the absorbance and fluorescence of the dyes in aqueous suspensions of anionic lipid membranes as 0.25 (at 648 nm) and 0.35 (at 422.5 nm) respectively (the dimers are nonfluorescent at the monomer fluorescence-maximum wavelength).[12] The absorbance of the same solution without a membrane, A_0, is given as:

$$A_0 = (\varepsilon_m n_0)/V. \quad (2)$$

From Eqs. 1 and 2, n_m and n_d are calculated as:

$$n_d = \frac{1}{2} n_0 (1 - A/A_0)/(1 - \varepsilon_d/\varepsilon_m), \quad (3)$$

and:

$$n_m = n_0 - 2n_d. \quad (3')$$

The equilibrium between monomeric and dimeric dyes in the membrane is represented by a dimerization constant, k_d, as:

$$C_{Md}/C_{Mm}^2 = k_d, \quad (4)$$

where C_{Md} and C_{Mm} are the concentrations of monomeric and dimeric dyes in the membrane phase. On the other hand, the partition equilibrium of a monomer between the membrane phase and the bulk phase can be written as:

$$C_{Mm}/C_{Bm} = P. \quad (5)$$

Here, P is a partition coefficient. From Eqs. 4 and 5, Eq. 6 is obtained:[15]

$$C_{Md}/C_{Bm}^2 = P^2 k_d. \quad (6)$$

Also:

$$C_{Md} = n_d/V_m = n_d/(vm). \quad (7)$$

Here, v is the partial specific volume of a phospholipid membrane, and m is the weight of a dried phospholipid in solution. Also,

$$C_{Bm} = (n_m - n_{Mm})/V \approx n_m/V. \quad (8)$$

n_{Mm} is the moles of the monomer in the membrane phase and is negligible when m is very small.[15] From Eqs. 6, 7, and 8, Eq. (9) is obtained:

$$V(n_d/n_m^2) = K(m/V), \quad \text{and } K = P^2 k_d v, \quad (9)$$

P involves the effects caused by both hydrophobic and electrostatic interactions between dye and membrane. When the pH and the ionic strength in an aqueous suspension of a PS membrane are maintained constant, P and, thereby, K can be regarded as constant for a dye.

In Fig. 5, the values of $V(n_d/n_m^2)$ calculated by means of Eq. 3 for an aqueous PS membrane suspension are plotted against the concentration of the membrane, m/V. The linear relations obtained for 9-AA, MB, and diS-C_3(5) are considered to be additional evidence for the formation of dye dimers in the membrane. Similar results were found for PA membrane and for STS, and SHP micelles.

Discussion

Microenvironments Provided by Membranes. To estimate the local effective polarities of membrane and

micelle on the basis of spectroscopic measurements with probing dyes, the data obtained for the membrane and the micelle should be interpreted in terms of some numerical indices representing the effective polarities of dye surroundings. Mainly, two factors can be proposed to account for the effective polarities in membranes and micelles: (a) the presence of a hydrocarbon environment in an aqueous medium, and (b) the presence of a high local concentration of charges arising from the head groups and the counter ions.[16] To estimate (a), alcohols and methanol–water mixtures have been considered to be better for the calibration solvents because of their hydrogen-bonding abilities with dyes.[16,22] Dipolar aprotic solvents have been found to be unsuitable for use with 2,6-diphenyl-4-(2,4,6-triphenyl-1-pyridino)phenoxide as the probing dye.[3a]

As is shown in Table 2 and Fig. 4, the simple rule for solvatochromism predicted from the change in the permanent dipole moment of the electronic transition, $\pi \rightarrow \pi^*$, cannot explain the experimental results. Alternatively, the interaction between the rapid-fluctuating transition moment of the dye molecule and the solvent is taken into account. The symmetric polymethin dyes, *e.g.*, diS-$C_3(5)$, have been known to show very little defference in the permanent dipole moments of the ground and excited (Frank-Condon) states: therefore, the dispersive effect on the transition moment due to the dye-solvent interaction seems to exert the predominant effect on the solvatochromism of diS-$C_3(5)$.[17] Thus, diS-$C_3(5)$ has a blue shift with an increase in the solvent polarity. While the solvent effects on MB and 9-AA are substantially described by similar explanations, an anomalous minimum in the λ_{max} of MB around methanol must be understood in terms of the specific solvation of water molecules, *e.g.*, hydrogen bonding with MB or solvent-cage effects on the ground-state dipole moment of MB. The deviation in the absorption maximum of MB from linearity in methanol–water mixtures also suggests the preferential solvation of water molecules.

From the results shown in Tables 1, 2, and Fig. 4, it may be found that the local effective polarities sensed by diS-$C_3(5)$ and MB are represented by those in 1-octanol and in a water–methanol mixture respectively. Therefore, diS-$C_3(5)$ penetrates deeply into membranes and micelles and is located in quite nonpolar environments. This is compatible with the fact that the dye is able to permeate through cell and lipid membranes.[18] On the other hand, MB is thought to be located at polar environments, that is, the surface regions of membranes and micelles. It is noteworthy that the λ_{max} of MB in STS is largely red-shifted and not covered by the calibration solvents used here. In the outermost regions of membranes and micelles, in addition to water molecules, electrical charges arising from the head groups and the counter ions have important effects on the microenvironments. As may be seen in Table 2, the addition of concentrated NaCl to methanol–water mixtures resulted in red-shifts of the MB adsorptions, covering the MB spectrum in the STS micelle. This indicates that the MB molecules located at the surface region, apart from the effect of alkyl chains, really experience the effect from the (b) factor. The locations of the MB molecules evaluated here are also consistent with the fact that they cannot penetrate cell and lipid membranes.[14,15]

It is also noteworthy that, even when the bulk dielectric constants are close, the dyes used here exhibit reversed spectral shifts in a methanol (dielectric constant=32.6) and in a 5 M NaCl aqueous solution (dielectric constant=35[19]). The dielectric constant reflects only the average properties of the medium, while the microenvironment evaluated spectroscopically is to be understood as the effective polarity in the close vicinity of the probing dye molecule.[16] Very often, it has been found that there is no correlation between the dielectric constant and the rate of the equilibrium constant of a solvent-dependent chemical reaction[3b]

According to the oldest chemical rule that "like dissolves like," it is concluded that the rather hydrophobic dye, diS-$C_3(5)$, and the hydrophilic dye, MB, prefer nonpolar and polar hydrophilic environments respectively, even in the same membrane or micelle.

Partition and Dimerization Equilibrium of Cationic Dye in Membrane. The cationic dyes employed in this study are intensely concentrated to dimerize in anionic membranes and micelles. Although the stacking interaction generally gives not only the dimer, but also *n*-meric forms, the isosbestic points observed in Figs. 1 and 2 suggest that the two major species, monomer and dimer, are in equilibrium and that the formation of higher aggregates is remarkably reduced in lipid membranes. Aggregations of dye ions have been known to occur much more favorably in aqueous environments than in nonaqueous environments. These facts have been interpreted in terms of water-structure promotion around the dye ions and consequent hydrophobic effects, and also in terms of the effect of the higher dielectric constant of water in reducing the repulsive force between the similarly charged dye ions in the aggregate.[11,20] These effects are more remarkable for the higher polymeric dye aggregates.

The effects of increasing amounts of NaCl on the absorbance of dyes shown in Figs. 1 and 2 suggest that the partitioning of an MB to a PS membrane is mainly attributable to electrostatic force, whereas, in the partitioning of diS-$C_3(5)$, effects other than the electrostatic one seem to play an important role. Assuming that the intrinsic partition coefficients of the dyes to membranes are independent of the lipid composition, the surface potentials of the membranes composed of PC and PA or of PC and PS were estimated from the partition equilibria of the dyes and discussed in relation to the Gouy-Chapman double-layer theory.[15] The potential obtained with MB substantially agreed with the theory, while the potential change with the NaCl concentration, as estimated with diS-$C_3(5)$, deviated greatly from the theory.[21] Also, Table 1 and Fig. 4 show that the surrounding microenvironments of MB in PC, PA, and PS membranes are similarly polar (ε=65—68). For diS-$C_3(5)$, the microenvironments in PC, PA, and PS are found to be nonpolar (ε=7.5—8.5). These results indicate that

the hydrophobic interaction may be an important factor in the partitioning of diS-C_3(5) into the lipid membranes.

Structures of Micelle and Membrane. In many other studies, the effective polarities for ionic surfactant micelles have been evaluated to be in the range between 30 and 40 in terms of the dielectric constant, ε.[1-6,22,23] These results have been interpreted on the basis of Stigter's two-state model (a modification of the Hartley model)[22,24] or explained by the use of Menger's porous model, which is inconsistent with the former model.[23] The effective polarities estimated for micelles in this study show a remarkably great variation; $\varepsilon=11\pm3$ by diS-C_3(5), 28 ± 5 by 9-AA, and 60 ± 4 by MB. These facts suggest that, in surfactant micelles, considerably nonpolar environments exist; this is in conflict with the porous model. For a nonionic micelle (Triton X-100), a micropolarity with $\varepsilon=5$—8 has been reported.[25] Table 1 and Fig. 4 also indicate that STS, SHP, and HED micelles contain various polar environments, from quite polar ($\varepsilon=60$) to moderately polar ($\varepsilon=28$), along the radial direction and, again, in contradistinction to the two-state model on which a micelle is represented as a combination of a nonpolar interior ($\varepsilon<10$) and a thin polar surface layer ($\varepsilon=30$—40).[22,24] Therefore, the following model for micelles will be proposed in this study: that micelles contain both nonpolar and polar regions, and, that the polar regions have a finite thickness with a polarity gradient.

With respect to phospholipid membranes, fairly thick polar regions have been clarified by X-ray-diffraction experiments.[26] The results on the membranes in this study show that the lipid bilayer membranes also supply a wide variety of microenvironments, from polar to nonpolar, along the normal direction to the membrane surface.

These wide varieties in environment are considered to be an important effect provided by membranes and micelles for understanding chemical equilibria, kinetics, and structure organizations in these systems. We have also found that photoinduced charge separations mediated by thiacarbocyanine dyes in lipid membranes and micelles are remarkably affected by the natures of the microenvironments around the dye.[27]

References

1) a) "Micellization, Solubilization, and Microemulsions," ed by K. L. Mittal, Plenum Press, New York (1977); b) J. H. Fendler, *J. Phys. Chem.*, **84**, 1485 (1980).

2) A. Ray and P. Mukerjee, *J. Phys. Chem.*, **70**, 2138 and 2144 (1966).

3) a) K. A. Zachariasse, N. Van Phuc, and B. Kozankiewicz, *J. Phys. Chem.* **85**, 2676 (1981); b) C. Reichardt, "Solvent Effects in Organic Chemistry," Verlag Chemie, Weinheim, New York (1979); c) F. M. Martens and J. W. Verhoeven, *J. Phys, Chem.*, **85**, 1773 (1981).

4) P. Mukerjee and J. R. Cardinal, *J. Phys. Chem.*, **82**, 1614 and 1620 (1978).

5) K. Kalyanasundaram and J. K. Thomas, *J. Am. Chem. Soc.*, **99**, 2039 (1977).

6) a) M. Grätzel and J. K. Thomas, "Modern Fluorescence Spectroscopy," ed by E. L. Wehry, Plenum Press, New York (1976), p. 196; b) G. K. Radda, "Methods in Membrane Biology," ed by E. Korn, Plenum Press, New York (1975), Vol. 4.

7) J. R. Lakowiz and D. Hogen, *Biochemistry*, **20**, 1366 (1981).

8) K. P. Ghiggino, A. G. Lee, S. R. Meech, D. V. O'Connor, and D. Phillips, *Biochemistry*, **20**, 2581 (1981).

9) W. S. Singleton, M. S. Gray, M. L. Brown, and J. L. White, *J. Am. Oil Chem. Soc.*, **42**, 53 (1965).

10) K. Nelson, *Inorg. Chem.*, **2**, 775 (1963).

11) P. Mukerjee and A. K. Ghosh, *J. Am. Chem. Soc.*, **92**, 6403 (1970); *J. Phys. Chem.*, **67**, 193 (1963).

12) S. B. Hladky and T. J. Rink, *J. Physiol.*, **263**, 287 (1976).

13) H. S. Harned and B. B. Owen, "The Physical Chemistry of Electrolyte Solutions," Reinhold Pub. Co., New York (1957).

14) S. Massari and D. Pascolini, *Biochemistry*, **16**, 1189 (1977).

15) M. Nakagaki, I. Katoh, and T. Handa, *Biochemistry*, **20**, 2208 (1981).

16) P. Mukerjee, J. R. Cardinal, and N. R. Desai, in Ref. 1a.

17) W. West and A. L. Geddes, *J. Phys. Chem.*, **68**, 837 (1964).

18) a) A. Waggoner, *J. Membr. Biol.*, **27**, 317 (1976); b) P. J. Sims, A. S. Waggoner, C, Wang, and J. F. Hoffman, *Biochemistry*, **13**, 3315 (1974).

19) R. Pottel, "Water," ed by F. Franks, Plenks, Plenum Press, New York (1973) Vol. 3.

20) W. West and S. Pearce, *J. Phys. Chem.*, **69**, 1894 (1965).

21) M. Nakagaki, I. Yamamoto, and T. Handa, unpublished work.

22) P. Mukerjee, C. Ramachandran, and A. Pyter, *J. Phys. Chem.* **86**, 3189 and 3198 (1982).

23) F. M. Menger, *Acc. Chem. Res.*, **12**, 111 (1979).

24) D. Stigter, *J. Colloid Interface Sci.*, **47**, 473 (1974); *J. Phys. Chem.*, **78**, 2480 (1974).

25) K. Kano, H. Goto, and T. Ogawa, *Chem. Lett.*, **1981**, 653.

26) a) H. Hauser, F. Paltauf, and G. Shipley, *Biochemistry*, **21**, 1061, (1982); b) D. Chapman, P. Byrne, and G. Shipley, *Proc. R. Soc. London, Ser. A*, **290**, 115 (1966); c) J. B. Finean, *Biochim. Biophys. Acta*, **10**, 371 (1953).

27) T. Handa, H. Komatsu, and M. Nakagaki, *Colloid Polym. Sci.*, accepted.

A Study of the Redistribution Reaction of Tetramethyltin with Dimethyltin Dichloride in Several Aprotic Solvents

Yukihide YAMASHITA, Koji SAITO, Akihiro YOSHINO, and Kensuke TAKAHASHI*

Department of Industrial Chemistry, Nagoya Institute of Technology, Gokiso-cho, Showa-ku, Nagoya 466

(Received December 4, 1982)

The redistribution reaction of tetramethyltin with dimethyltin dichloride was studied in eight aprotic solvents by using the ^{1}H NMR technique. The second-order rate constant of the reaction ($\ln k_2$) is proportional to the dielectric constant of the solvent. There is a weak relation between the rate constants ($\ln k_2$) and the values of ^2J(Sn-H) of Me_2SnCl_2 in several solvents, which are considered to be related to the coordination ability of the solvents. The rate constants are also related to Kosower's Z values of the solvents. The activation entropies of the reaction in four typical solvents have large negative values. This predicts that the reaction proceeds *via* a four-center transition state.

There have thus far been many reports concerning redistribution reactions (or radical exchange reactions) of organometallic compounds.[1-5]

The redistribution reaction, shown in Scheme 1, reported by Dessy *et al.*, was interpreted to proceed *via* a four-center transition state.[6] This four-center

$$R_2Hg + HgX_2 \xrightarrow{\text{solvent}} 2RHgX$$

Scheme 1.

transition state is not yet decisive in interpreting the mechanism of similar kinds of reactions, but one piece of evidence is considered to be that the reaction has a large negative activation entropy. Another typical example of the reactions is shown in Scheme 2. This

$$Me_4Sn + Me_2SnCl_2 \xrightarrow{\text{solvent}} 2Me_3SnCl$$

Scheme 2.

is the reaction between tetramethyltin and dimethyltin dichloride which forms trimethyltin chloride. The equilibrium constant between the left- and right-hand systems has been reported to be 330.[5] Plazzogna *et al.* reported the reaction in methanol and showed it to be a second-order reaction.[7]

During the course of studying the ^{1}H and ^{119}Sn NMR spectra of some organotin compounds, our attention was drawn to the large solvent effects on the NMR parameters of many organotin compounds.[8] Therefore, we have examined the reaction in Scheme 2 in several aprotic solvents and found that the reaction rates are largely dependent upon the solvents. The results have been analyzed as a second-order reaction and discussed in terms of dielectric constants, coordination ability, and Kosower's Z values of the solvents.

Experimental

The materials, the reactants, and the solvents were commercial ones and were used without further purification except for chloroform and acetone-d_6. Acetone-d_6 was dried by keeping it on a molecular sieve, while chloroform was purified by the conventional manner to remove traces of the stabilizer (ethanol). The reactants were weighed into an NMR sample tube, and then a solvent was added. The ^{1}H NMR measurement was carried out by means of a Hitachi R-20B spectrometer at 60 MHz with a variable-temperature controller. The reaction was followed by taking the methyl proton spectrum of the reaction mixture at intervals. The chemical shifts are referred to the signal of tetramethylsilane in a sealed Pyrex capillary inserted into each sample tube. The sweep width and time were 120 Hz and 200 s. The peak area of each methyl proton was measured by cutting and weighing the area under the peak on the chart, which was adjusted to have no wiggle. The temperature was measured by both a thermometer inserted into the probe and the chemical-shift difference of the two signals of ethylene glycol. The temperatures measured by the two methods were consistent within an error of ±0.5 °C.

Results and Discussion

Table 1 summarizes the equimolar second-order rate constants of the reaction as observed in eight solvents. The initial concentration of each reactant was

TABLE 1. SECOND-ORDER RATE CONSTANTS FOR THE REDISTRIBUTION REACTIONS OF TETRAMETHYLTIN WITH DIMETHYLTIN DICHLORIDE IN VARIOUS SOLVENTS[a]

Solvent	D[b]	Z[c]	T/K	k_2[d]/l mol^{-1} s^{-1}
Acetonitrile	35.95	71.3	305.5	1.0×10^{-4}
			312.2	1.9×10^{-4}
			319.2	3.1×10^{-4}
Acetone-d_6	19.8	65.7	305.5	4.5×10^{-6}
			312.5	6.0×10^{-6}
			318.3	9.5×10^{-6}
			320.5	1.1×10^{-5}
1,2-Dichloroethane	10.13	63.3	305.5	1.1×10^{-6}
			323.2	3.3×10^{-6}
			333.4	6.6×10^{-6}
			343.2	9.9×10^{-6}
Nitrobenzene	34.82	—	305.5	4.5×10^{-5}
Benzonitrile	25.20	—	305.5	1.1×10^{-5}
Chloroform	4.806	63.1	305.5	5.8×10^{-7}
Bromobenzene	5.397	59.3	305.5	3.6×10^{-7}
Benzene	2.28	54	305.5	2.0×10^{-7}
			321.0	5.0×10^{-7}
			332.4	9.2×10^{-7}
			334.2	9.4×10^{-7}
			336.2	1.4×10^{-6}

a) The initial concentration of each reactant is about 0.5 mol l^{-1}. b) Dielectric constant. c) The values are cited from Ref. 14. d) The accuracy is about 10%.

taken to be 0.5 mol l^{-1}. One example of the rate analysis is given in Fig. 1. The second-order rate constant(k_2) increases with an increase in the dielectric constant(D) of the solvent. A linear relationship between $\ln k_2$ and D has been shown in Fig. 2 at the temperature of 305.5 K. Similar relationships between the rate constants and the dielectric constants have also been reported in other organotin compounds.[9-11]

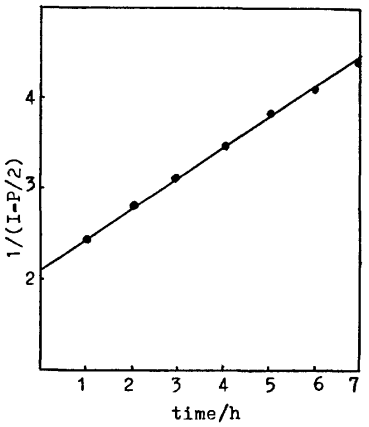

Fig. 1. An example of the concentration change of the reactant (ordinate; $1/(I-P/2)$) against time (abscissa) obtained for the reaction studied in acetonitrile at 305.5 K where I is the initial concentration of the reactant (*ca.* 0.5 mol/l) and P is the concentration of the product.

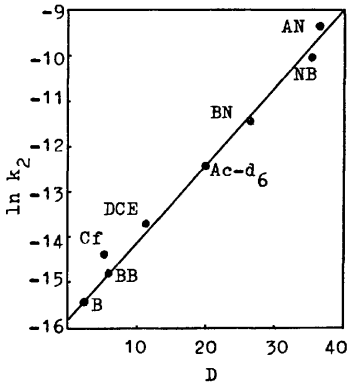

Fig. 2. Correlation between $\ln k_2$ and D for the eight solvents studied whose kinds are shown in the figure with abbreviated letters.

As is shown in Table 1, the rate observed in acetonitrile is 500 times faster than the slowest one observed in benzene. The observed thermodynamic data of the reaction are summarized in Table 2. The activation energy in acetonitrile is the largest one, but the other three values are similar in magnitude. The activation entropy change in acetonitrile is different from the other three in magnitude, although these values are negative and large, suggesting that the reaction proceeds *via* a four-center transition state, as has been suggested by Weingarten and Van Wazer.[2] The solvent used in the reaction significantly affects the activation entropy more than the activation energy.

The ^2J(H–Sn) values of the related compounds are tabulated in Table 3 as determined in several solvents. The change is small for tetramethytin, but large for dimethyltin dichloride. Similar changes in the coupling constants have been reported.[12,13] The change is interpreted by the coordination of the solvent to the tin atom and by the hybridization change. Therefore, the coupling constant change observed largely manifests the coordination power of the solvent. The value in acetone-d_6 is larger than that in acetonitrile. This tendency is consistent with that observed for trimethyltin chloride, as reported by Bolles and Drago.[12] Therefore, acetone has a larger coordination power than acetonitrile for the tin compounds in question.

As has been stated before, the activation entropies of the reaction change with the kinds of solvents with large negative values. Therefore, the transition state of the reaction may be considered to be a rather ordered state. The entropy of the reaction system is considered to be dependent upon the coordination power of the solvent used. Therefore, it is suggested

Table 2. Arrhenius and eyring parameters for the redistribution reactions of tetramethyltin with dimethyltin dichloride in various solvents

Solvent	A	E_a	$\Delta H^{\#}$	$\Delta S^{\#}$
	l mol^{-1} s^{-1}	kJ mol^{-1}	kJ mol^{-1}	J K^{-1} mol^{-1}
Acetonitrile	1.1×10^7	64	62	−28
Acetone-d_6	2.0×10^3	51	48	−45
1,2-Dichloroethane	1.1×10^3	53	50	−47
Benzene	7.5×10	50	48	−52

Table 3. Coupling constants between tin and protons of tetramethyltin and dimethyltin dichloride in various solvents in Hz[a]

Solvent	Me_2SnCl_2		Me_4Sn	
	$^2J(^1H-^{117}Sn)$	$^2J(^1H-^{119}Sn)$	$^2J(^1H-^{117}Sn)$	$^2J(^1H-^{119}Sn)$
Acetonitrile	79.4	82.8	52.8	54.9
Acetone-d_6	80.8	84.2	52.7	54.9
1,2-Dichloroethane	67.3	70.7	52.3	54.5
Nitrobenzene	71.2	74.6	52.4	54.6
Benzonitrile	75.4	78.8	52.2	54.8
Bromobenzene	66.6	69.4	51.6	54.0
Benzene	66.4	69.4	52.2	53.9

a) The accuracy is about 0.2 Hz.

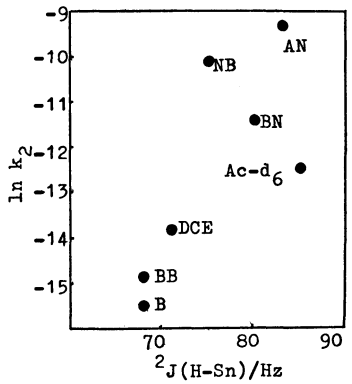

Fig. 3. Plotting of $\ln K_2$ against the ^2J(Sn–H) of Me_2SnCl_2 (the values are given in Tables 1 and 3).

Table 4. ^{1}H chemical shifts of Me_2SnCl_2, Me_3SnCl, and Me_4Sn in various solvents in ppm[a)]

Solvent	Me_2SnCl_2	Me_3SnCl	Me_4Sn
1,2-Dichloroethane	1.79	1.21	0.64
Acetonitrile	1.37	0.78	0.24
Benzonitrile	1.36	0.70	0.04
Acetone-d_6	1.12	0.52	−0.04
Bromobenzene	1.12	0.74	0.34
Benzene	0.44	0.24	0.03

a) The values are referred to the external tetramethylsilane.

that the rate will be parallel to the coordination ability of the solvent. As is plotted in Fig. 3, there is a weak relation between the rate and ^2J(Sn–H), which is a measure of the coordination ability. The correlation coefficient of the points in Fig. 3 is 0.72; this is smaller than that calculated for Fig. 2 (0.99).

The ^{1}H chemical shifts are tabulated in Table 4. The chemical shifts change in a reasonable order with the successive substitution of an electronegative chlorine atom in the molecule. Chlorination causes a downfield shift of about 0.6 ppm per chlorine atom in four solvents from the top of the table. However, benzene shows a different behaviour. The observed chemical shift values may reflect the form of coordination. In this sense, the coordination may be supposed to be different for benzene and other four solvents. Bromobenzene is intermediate between the two.

There are many parameters which express the nature of the solvent. Figure 4 shows the relation between the ln k_2 value and Kosower's Z values of the solvents.[14)] Four points fall on a straight line, but not those of benzene and bromobenzene. Such exceptions of benzenes have previously been reported in the Menschtkin reaction.[15)] The rates become larger with larger Z values of the solvents.

The reaction was also studied in the methanol solution by Plazzogna *et al.*[7)] They reported that tetramethyltin suffered an electrophilic attack by the Me_2Sn^{2+} species which is formed by the dissociation of Me_2SnCl_2. However, the ion, Me_2Sn^{2+}, is difficult to produce in acetone or acetonitrile. Therefore, they also stated that the reaction is very slow in acetone or

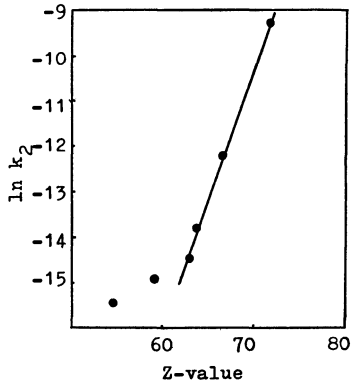

Fig. 4. Plotting of $\ln k_2$ against the Z-values.

acetonitrile. The rate observed by them in methanol is much greater than ours in Table 1, although the systems are different. The rate in methanol deviates greatly from the line plotted in Fig. 2. Therefore, it is reasonable to consider that the reaction mechanism in the aprotic solvents is different from that in the protic solvents.

We propose here a mechanism of the reaction which is dependent upon the dielectric constants of the solvents. The polarization of the reactants is important. Although one of the reactants, tetramethyltin, is nonpolar, the local polarization of the molecule occurs in the bond between the carbon and the tin atoms because of the different electronegativities of the atoms. The electrostatic attractive force leads to the four-center transition state shown in Scheme 3, which is supported by the negative activation entropies described above. The polarization of the reactants becomes larger in the polar solvents. The larger the dielectric constant of the solvent, the faster the reaction rate.

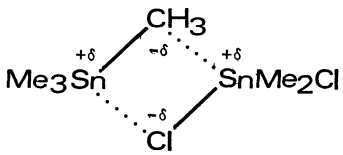

Scheme 3.

Conclusion

The redistribution reaction between tetramethyltin and dimethyltin dichloride has been studied in eight aprotic solvents. The logarithm of the rate of the reaction in the equimolar solutions is proportional to the dielectric constants of the solvents, and falls on a straight line. A weak relation is also observed between the rates and the ^2J(Sn–H) values, which are supposed to be measures of the coordination power of the solvents. The rate is almost parallel to Kosower's Z values of the solvents. The reaction has a large negative activation entropy. This is considered to be evidence of a reaction which proceeds *via* the four-center transition state.

References

1) J. C. Rockhart, *Chem. Rev.*, **65**, 131 (1965).
2) H. Weingarten and J. R. Van Wazer, *J. Am. Chem. Soc.*, **88**, 2700 (1966).
3) J. A. Ladd and B. R. Glasberg, *J. Chem. Soc., Dalton Trans.*, **1975**, 2378.
4) F. Basolo, R. G. Person, "Mechanisms of Inorganic Reactions," 2nd ed, John Wiley & Sons, New York (1967).
5) K. F. Purcell and J. C. Kotz, "Inorganic Chemistry," W. B. Saunders Co., Philadelphia (1977).
6) R. E. Dessy, Y. K. Lee, and J. Y. Kim, *J. Am. Chem. Soc.*, **83**, 1163 (1961).
7) G. Plazzogna, S. Bresadola, and G. Tagliavini, *Inog. Chim. Acta*, **1968**, 333.
8) Y. Kugimiya, Y. Hasegawa, A. Yoshino, and K. Takahashi, Preprints, 41st National Meeting of the Chemical Society of Japan, Osaka, April 1980, Vol. 1, p. 185 (1E35).
9) S. Fukuzumi and J. K. Kochi, *J. Am. Chem. Soc.*, **102**, 7290 (1980).
10) S. Fukuzumi and J. K. Kochi, *J. Phys. Chem.*, **84**, 2254 (1980).
11) E. D. Korniets, L. A. Fedorov, E. M. Rokhlia, D. N. Kravtsov, and E. I. Fedin, *Izv. Akad. Nauk. SSSR, Ser. Khim.*, **1978**, 1182.
12) T. F. Bolles, and R. S. Drago, *J. Am. Chem. Soc.*, **88**, 5730 (1966).
13) E. V. van den Berghe and G. P. van der Kelen, *J. Organomet. Chem.*, **11**, 479 (1968).
14) E. M. Kosower, *J. Am. Chem. Soc.*, **80**, 3253 (1958).
15) J. D. Reinheimer, J. D. Harley, and W. W. Meyers, *J. Org. Chem.*, **28**, 1575 (1963).

ESR Studies of Bunsen-type Methane-Air Flames. I. Effects of the Entrainment and Diffusion of Secondary Air on the Chemical Reactions in the Flame

Ola Claesson,† Shoji Noda,†† and Hiroshi Yoshida*

Faculty of Engineering, Hokkaido University, Kita-ku, Sapporo 060

(Received January 5, 1983)

H atoms in a Bunsen-type methane-air flame have been studied by observing their ESR signals at different flow rates of O_2 and N_2 in a synthetic secondary air. The optical emissions from excited CH, C_2, and OH radicals in the same flame have been also studied. It has been found that an increased O_2 flow rate produces changes in the intensity of the ESR and emission signals, and that it also increases the burning velocity in the inner-cone flame. An increased N_2 flow rate, on the other hand, has almost no effect on the flame. The inner-cone of a Bunsen-type flame is, therefore, not a completely premixed flame; it is affected chemically by the secondary air.

A Bunsen flame is roughly characterized as a double flame: an inner, premixed flame propagating through the combustible gas mixture(usually fuel-rich) against the gas stream, and an outer, diffusion flame where further combustion of the gas mixture is assisted by the surrounding secondary air. Secondary air plays an important role in stabilizing a Bunsen flame.[1] Its entrainment and diffusion into the flame have great effects on the flame characteristics and flame chemistry, but these effects have not yet been elucidated.

Electron spin resonance(ESR) has been proved to be a convenient means for observing atomic and free radical intermediates in combustion reactions.[2-5] Recently we ourselves have reported an ESR study of methane combustion where the nature of the H atom ESR signal and the spatial distribution of H atoms were studied by inserting a flame burning under ambient pressure directly into the resonant cavity.[3] Although such a flame-in-cavity method allows neither the detection of species other than H atoms(because of the collisional broadening of the resonance lines) nor a detailed examination of the distribution of the H atoms, it is a convenient and useful method for studying the chemical aspects of flames by observing the dependence of the total H-atom concentration on the burning conditions. Our previous investigation has, therefore, now been extended to get a picture of the chemical effects of the entrainment and diffusion of secondary air by examining the H-atom concentrations at different flow rates and compositions of a mixture of O_2 and N_2 acting as the secondary air. Some excited radicals were also detected in the flame by using optical-emission spectrophotometry.

Experimental

A burner with three concentric quartz tubes, one outside the other, was constructed. In the innermost tube (4 mmϕ) the premixed combustible gas was allowed to flow. The flame was anchored on top of this tube. The second tube (18 mmϕ) was the combustion room, and the secondary air was let flow through it. The outermost tube (22 mmϕ) was for the flowing of the coolant air. All gas-flow rates were regulated by flow meters with precision needle valves. The premixed combustible gas consisted of a mixture of methane (99.0% purity), 90 cm^3/min, and air, 500 cm^3/min. The secondary air was a mixture of O_2 and N_2. Its composition and flow rate were varied by keeping the rate of one component in the mixture constant while varying the other. Thus, for an O_2 flow of 65 cm^3/min, N_2 was varied between 50 and 260 cm^3/min, and for a N_2 flow of 170 cm^3/min, O_2 was varied from 58 to 95 cm^3/min. These constant flows were chosen because an O_2/N_2 mixture with these flow rates maximized the ESR signal of the H atoms.

The flame height was estimated from close-up color photographs taken of the flame under different burning conditions. The scale of the pictures was determined by comparing the diameter of the innermost tube as measured on the photographs with its real size.

The H atoms present in the flame were detected by means of ESR (a Varian E-109 spectrometer, X-band with 100 kHz modulation) using the flame-in-cavity method, which has been described elsewhere.[3] A recent improvement of the experimental method was the use of a cylindrical TE_{011} large-access cavity (Varian, Model E-235), which accepts a large burner. A large burner was needed for the flame to be stabilized under a variety of burning conditions.

The excited radicals in the flame were studied from their optical emission spectra. These were recorded by inserting the burner into the detection chember of a conventional fluorescence spectrophotometer (Hitachi, Model, MPF-2A).

Results and Discussion

Apparent Burning Velocity. The flame showed a bright blue inner-cone flame and a faint bluish outer flame. The height of the inner flame decreased with an increase in the O_2 content in the secondary air, as is shown in Fig. 1A. At an O_2 flow rate of less than 55 cm^3/min, the flame was not stably anchored at the top of the burner, but started to lift off. Under the present experimental conditions, the apparent burning velocity in the inner flame can be roughly approximated as inversely proportional to the inner-flame height.[6] The apparent burning velocity thus increases with an increase in the O_2 flow rate in the secondary air. At an increasing N_2 flow, the tip of

† On leave from the Studsvik Research Laboratory, S-611 82 Nyköping, Sweden.

†† Present Address: Toyota Central Research & Development Labs., Inc., Nagakute-cho, Aichi 480-11.

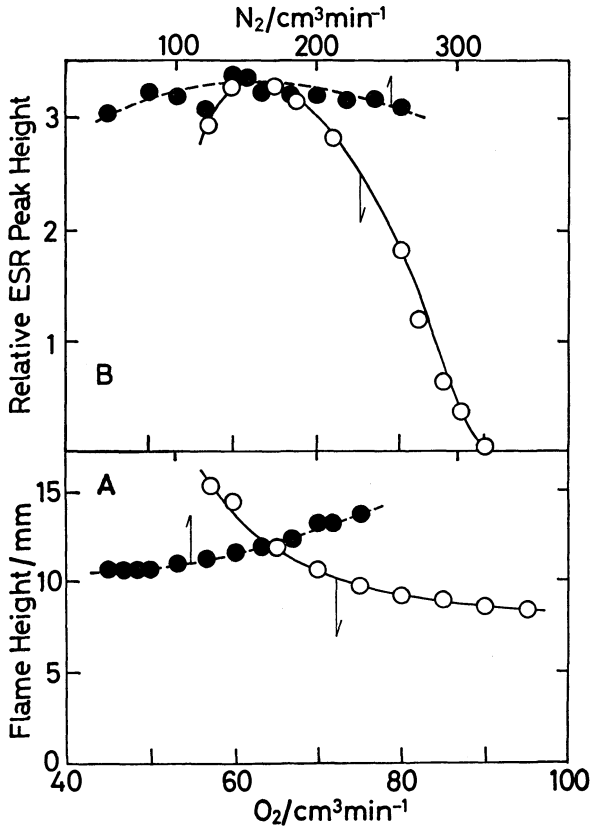

Fig. 1. Dependence of (A) the height of the inner cone flame and (B) the ESR intensity of the H atoms in a Bunsen-type methane-air flame on the composition of the secondary air. Data shown by open circles were obtained for a constant N_2 flow of 170 cm^3/min. Data shown by closed circles were for a constant O_2 flow of 65 cm^3/min.

the inner flame became less and less luminous, and the outer flame disappeared. The inner cone height increased, as is shown in Fig. 1A, indicating a decrease in the apparent burning velocity.

These observations agree well with Kimura and Ukawa's results obtained from a propane/air flame where an increased $O_2/(O_2+N_2)$ ratio raised the burning velocity.[7] Apparently the secondary air affects the combustion characteristics in the inner flame.

H Atoms in the Flame. The ESR spectrum observed from the flame consisted of two sharp lines with a hyperfine separation of 51.0 mT centered at 330 mT. It is assigned to H atoms. The sensitivity of the ESR measurements depends on the position in the resonant cavity. As a matter of fact, the spectral intensity varied depending on the location of the burner in the cavity along the cavity axis. This dependece was more pronounced in the present study than in the previous study.[3] The difference is attributed to the fact that, in the present study, the H atoms are confined in a more limited region of the flame burning in a wider combustion room. This is consistent with our previous result, obtained by the point-to-point probe-sampling method,[4] that the H atoms are mostly located within 1 cm downstream from the flat inner flame of a free-burning methane-air Bunsen flame.

The spectral intensity of the H atoms in the flame under different burning conditions was examined by locating the burner so as to maximize the intensity. It was found to depend drastically on the flow of O_2 in the secondary air, as can be seen in Fig. 1B. The O_2 content in the secondary air apparently affects the chemical reaction in the inner cone. The N_2 flow, however, can be changed over a wide interval, thereby changing the total flow of the secondary air, without having much effect on the H-atom signal. As an increase in the N_2 flow is accompanied by a decrease in the apparent burning velocity, it seems that even though the reaction zone is broadened (diluent effect), the chemical reactions are essentially unaffected.

Neither the concentration profile in the flame nor the absolute concentration was determined in the present study. However, the observed ESR intensity can be regarded as a measure of the H-atom steady-state concentration averaged over the whole flame. The confinement of the H atoms in a narrow region excludes the possibility that the change in the ESR intensity with the varying O_2 flow may be primarily due to the change in the flame shape. Actually, the intensity changed little, though the reaction zone was apparently broadened with the increase in the N_2 flow. The temperature in the flame monitored with a fine Pt–Rh thermocouple was the highest in or close to the inner-cone flame and changed from 1620 to 1760 K, depending on the burning conditions. The ESR intensity shown in Fig. 1B has not been corrected with the flame temperature, because the temperature effect is of no significance.

It has previously been demonstrated by probe-sampling a Bunsen flame and ESR detection that H atoms are abundant in the fuel-rich inner flame and that they are consumed by reacting with O_2, probably coming from the secondary air:[4]

$$H + O_2 \rightarrow O + OH. \quad (1)$$

Here we have found that the apparent burning velocity in the inner flame increases at higher O_2 flow rates, while the H-atom steady-state concentration is tremendously reduced(see Fig. 1). This results from Reaction 1, effectuated by the involvement of O_2 from the secodary air even in the inner flame. The overall combustion reactions are accelerated, the lifetime of the H atoms being reduced. The chain-carrying intermediates which support the flame at a low O_2 content in the atmosphere surrounding the flame are H atoms, while at a high O_2 content O atoms and OH radicals are chain carriers. These observations are consistent with Pickering and Linnett's analysis of the relations among the O_2%, the burning velocity, and the calculated equilibrium concentrations of H, O, and OH for a premixed ethylene/air flame.[8]

Excited Free Radicals in the Flame. An example of the optical emission spectra recorded from the flame is shown in Fig. 2. According to the literature data,[9] the observed spectrum is composed of emission lines due to OH, CH, and C_2 radicals and a broad continuum due to CO_2. Weak emission lines due to CHO radicals are also discernible. It is known that

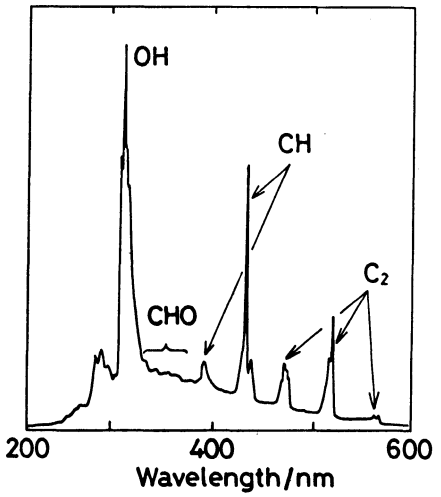

Fig. 2. An example of optical emission spectra recorded from the luminous inner cone flame of a Bunsen-type methane-air flame. No correction of the photometer sensitivity was made.

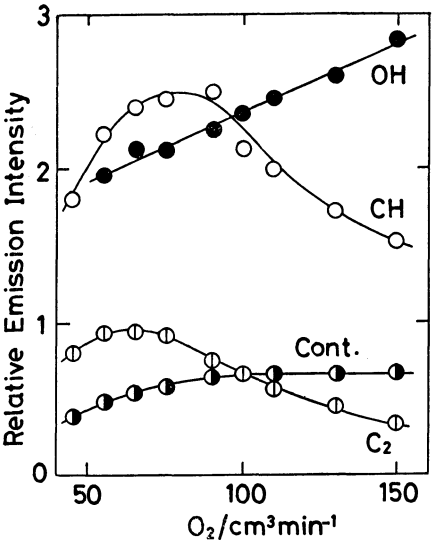

Fig. 3. Dependence of the optical emission from excited free radicals (and continuum spectrum due to CO_2) on the flow rate of O_2 in the secondary air. The N_2 flow rate was kept constant at 170 cm³/min. The emission comes mostly from the luminous inner cone.

the emissions of Bunsen flames almost exclusively originate from the inner premixed flame and that they are chemiluminescence in nature.[9] The exception is the OH emission, which comes from the outer flame as well.

The effects of the composition of the secondary air on those chemiluminescences are pictured in Fig. 3. The emission intensities are sensitively dependent on the O_2 flow rate in the secondary air. The OH emission intensity increases steadily with an increase in the O_2 flow rate. The CH and C_2 emissions have maximum intensities at the O_2 flow rates of 90 and 60 cm³/min respectively. These emissions come from the corresponding electronically excited radicals, which are generated through side-reactions in the overall process of combustion.[9] However, the dependence of these intensities on the O_2 flow rate indicates the far-reaching involvement of O_2 from the secondary air in the chemical reactions in the inner flame. Similar intensity variations have been reported for the CH and C_2 emissions in low-pressure premixed hydrocarbon flames with a varied fuel-to-air ratio.[9]

Conclusions. Bunsen-type burners are now incorporated in many gas appliances, yet the combustion chemistry of these burners has been but little elucidated because of their complexity as chemical reaction systems. The present investigation has been focussed on one of the principal reaction intermediates of combustion, the H atoms, in the methane-air Bunsen-type flame. It has been found that the H-atom ESR spectrum is significantly affected by the O_2 content in the secondary air. These results, combined with those of the optical-emission study of the excited free radicals, indicate that the inner cone of the Bunsen-type flame is not a wholly premixed flame, but that it is affected by the entrainment and diffusion of the secondary air. This provides a convenient experimental method to study the chemical reactions in combustion by simply mixing an additive in the secondary air.

The present authors are grateful of the Toyota Foundation for the financial support (1977—1979) needed to initiate the present investigation. One of the authors (O. C.) also acknowledges the support of the Yamada Foundation and the Swedish Natural Science Research Council for his stay at Hokkaido University.

References

1) For example, A. G. Gaydon and H. G. Wolfhard, "Flames, Their Structure, Radiation, and Temperature," 4th ed, Chapman and Hall, London (1979).

2) R. M. Fristrom, and A. A. Westenberg, "Flame Structure," McGraw-Hill, New York (1965), and the literature cited in Ref. 3.

3) S. Noda, M. Miura, and H. Yoshida, *Bull. Chem. Soc. Jpn.*, **53**, 841 (1980).

4) S. Noda, M. Miura, and H. Yoshida, *J. Phys. Chem.*, **81**, 3143 (1980).

5) J. F. Pawels, M. Carller, and L. R. Sochet, *J. Phys. Chem.*, **86**, 4330 (1982).

6) R. A. Strehlow, "Fundamentals of Combustion," International Textbook Co., Scranton (1968).

7) I. Kimura and H. Ukawa, *Eighth Symposium (International) on Combustion*, Williams & Wilkins Co., Baltimore (1962), p. 521.

8) H. S. Pickering and J. W. Linnett, *Trans. Farady Soc.*, **47**, 1101 (1951).

9) A. G. Gaydon, "The Spectroscopy of Flames," 2nd ed, Chapman and Hall, London (1974).

ESR Studies of Bunsen-type Methane-Air Flames. II. The Effects of the Addition of Halogenated Compounds to the Secondary Air on the Hadrogen Atoms in the Flame

Shoji NODA,† Susumu FUJIMOTO, Ola CLAESSON,†† and Hiroshi YOSHIDA*

Faculty of Engineering, Hokkaido University, Kita-ku, Sapporo 060

(Received January 5, 1983)

Hydrogen atoms in a methane-air Bunsen-type flame were detected by the flame-in-cavity ESR method. The addition of a halogenated compound to the secondary air was found to reduce the H-atom concentration linearly with an increase in the additive concentration. The eight halogenated compounds examined showed an increased effectiveness in scavenging H atoms in this order; $HCl < CF_2Cl_2 < CHCl_3 < CH_3Cl < CH_2Cl_2 < CFCl_3 < CCl_4 < CH_3Br$. This chemical effect of the halogenated compounds on the combustion reactions agrees well with the inhibitor index for these compounds.

Extensive studies have been carried out on the effects of additives such as halogenated compounds on the inhibition of premixed flames.[1-6] The relative effectiveness of a flame inhibitor has been evaluated from the change in the burning velocity of the flame upon the addition of the inhibitor, according to this equation:

$$\phi_v = ([O_2]/[In])(\delta V/V_0), \quad (1)$$

where $[O_2]$ and [In] are the initial concentrations of O_2 and the inhibitor respectively, where V_0 is the burning velocity in the absence of the inhibitor, and where δV is the decrease in the burning velocity due to the presence of the inhibitor.[1,7] There has been few reports on the inhibition of diffusion flames.[8,9] The addition of hydrogen halides to the surrounding air has been found to quench diffusion flames more effectively than direct addition to the fuel.[8] It has been suggested that CH_3Br quenches diffusion flames chemically, though no mechanism for this has been discussed.[9]

Flame inhibition is a combination of the chemical and physical effects of an inhibitor. The chemical effects are mostly the scavenging of the carriers of the chain reactions in the combustion, like H, O, and OH. There have, however, been no reports showing the correlation between flame inhibition and radical scavenging.

In a preceeding paper (Part I of this study)[10] we found, by using the flame-in-cavity electron-spin-resonance (ESR) method, that the concentration of H atoms in the Bunsen-type methane-air flame is reduced when the O_2 content in the secondary air is increased. This indicates that O_2 diffuses from the secondary air into the inner zone of the flame, as the H atoms are most abundant in the fuel-rich inner reaction zone.[11] This also shows that the flame-inhibition effect can be studied by adding inhibitors to the secondary air around Bunsen-type flames and by detecting the H atoms in the flame by means of ESR. Because of the collisional broadening of the resonance lines, the reaction intermediates observable by the flame-in-cavity ESR method from a flame at atmospheric pressure are atoms whose electronic ground state is a S-state like $H(^2S)$ or $N(^4S)$. In spite of this limitation, the flame-in-cavity ESR method is a useful method for studying H atoms under a variety of burning conditions.

Experimental

The Bunsen-type burner used consisted of three concentric quartz tubes and was the same as that reported previously.[10] The premixed combustible gas consisted of a mixture of methane (99.0% purity), 88 cm^3/min, and air, 380 cm^3/min. The flow rate of the secondary air was 430 cm^3/min. These flow rates were chosen to maximize the ESR signal of the H atoms. The added inhibitor was injected into the secondary air using a 200-cm^3 glass syringe and a microfeeder. Five different flow rates of an added inhibitor, ranging from 0.067 to 0.33 cm^3/min, could be attained by using different combinations of driving gears on the microfeeder. The halogenated compounds used as inhibitors were HCl (purity 99%, Takachiho), CH_3Cl (99%, Takachiho), CH_2Cl_2 (Spectrograde, Eastman Kodak), $CHCl_3$, CCl_4, CF_2Cl_2, $CFCl_3$, and CH_3Br (all reagent grade, Tokyo Kasei). As they were liquid at room temperature, they were evaporated in a heated chamber, while the syringe and secondary air were preheated to keep them from condensing.

The H atoms in the flame were detected by ESR using a flam-in-cavity method which has been described elsewhere.[10,12] The spectrometer (Varian, Model E-109) was operated in the X-band with a magnetic-field modulation of 100 kHz.

Results

ESR Spectra of the Flame Gases. H atoms were detected in both the presence and absence of a halogenated compound in the secondary air. The H-atom spectrum showed two lines with a hyperfine separation of 51.0 mT, the same as has been reported previously.[10-12] O_2 molecules have been demonstrated to cause a broadening of the H-atom lines in the ESR spectrum from a flame.[12] We found that the spectral linewidth of the H-atom signal was independent of the concentration of all the halogenated compounds added except for the case of CH_3Br. On the addition of CH_3Br, the linewidth increases with an increase in the CH_3Br concentration in the secondary air, as can be seen in Fig. 1.

An ESR linewidth is inversely proportional to the

† Present Address: Toyota Central Research & Development Labs., Inc., Nagakute-cho, Aichi 480-11.

†† On leave from the Studsvik Research Laboratory, S-611 82 Nyköping, Sweden.

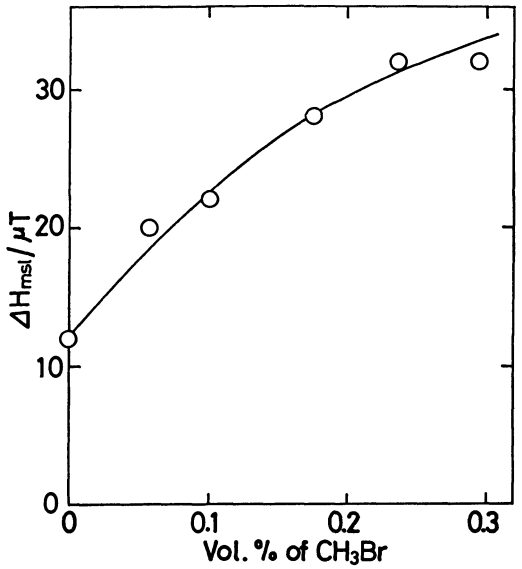

Fig. 1. Dependence of the peak-to-peak width of the derivative ESR spectrum of H atoms in a Bunsen-type methane-air flame on the concentration of CH_3Br added into the secondary air. 1 G=0.1 mT.

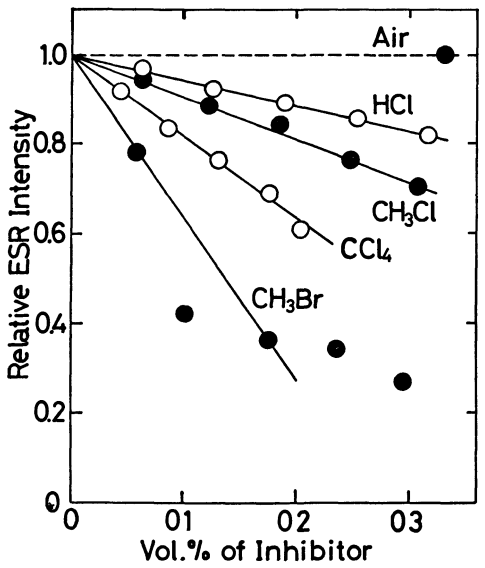

Fig. 2. Dependence of the ESR intensity of the H atoms in a Bunsen-type methane-air flame on the concentration of halogenated compounds added into the secondary air. For simplicity, the data for CH_2Cl_2, $CHCl_3$, CF_2Cl_2, and $CFCl_3$ were omitted.

spin-spin relaxation time, T_2, which can be expressed as:

$$\frac{1}{T_2} = \frac{1}{T_2'} + \frac{1}{2T_1}, \tag{2}$$

where T_2' is the spin-dephasing time and where T_1 is the spin-lattice relaxation time. The latter is related to the lifetime of the spin sublevels.[13] The most important intermolecular process in the gas phase is collision broadening; on each collision, the phase memory of the spin precession is lost. This will make the first term on the right-hand side of Eq. 2 comparatively important and will determine the ESR linewidth. The presence of halogenated compounds is expected to produce paramagnetic halogen atoms, like Cl and Br.[4,7] The Br atoms have a rapid spin-lattice relaxation which makes them an efficient sink of the spin energy of the H atoms. The presence of Br atoms will thus shorten the T_1 of the H atoms and cause a line-broadening due to the second term. The H-atom concentration in the flame as deduced from ESR was corrected for this variation in linewidth.

Effect of Inhibitors on H-atom Concentration. The amount of H atoms in a Bunsen flame has been found to depend on the concentration of O_2 in the secondary air.[10] It has also been demonstrated that H atoms react with O_2 molecules which diffuse into the flame from the surrounding air.[11]

The introduction of halogenated compounds into the secondary air reduced the amount of H atoms in the flame to a varying extent, depending on the inhibitor. The observed results are shown in Fig. 2 for some of the inhibitors. As a blank test, excess air was added to the secondary air in place of an inhibitor, but no appreciable reduction in the amount of the H atoms was observed. This indicates that the change in the H-atom concentration arises from the chemical reactions of the added inhibitors, and not from any physical modification of the flame caused by the addition of the inhibitors.

The observed ESR signal intensity of the H atoms decreases linearly with the concentration of the halogenated compound added, as is shown in Fig. 2. This linearity comes fortuitously through the complex combustion reactions in the flame. However, the negative slope of the straight lines in Fig. 2 serves to determine the chemical effectiveness of the inhibitors, as

$$\phi_\tau = \frac{[H]_0 - [H]}{[H]_0} \cdot \frac{1}{[In]}, \tag{3}$$

where [H] and $[H]_0$ are the amounts of H atoms in the presence and in the absence of an inhibitor respectively. The ϕ_τ values thus obtained are shown in Fig. 3 for all the halogenated compounds examined.

Discussion

For halogenated compounds, Fristrom and Van Tiggelen[1] derived an inhibitor index, ϕ_ν, as:

$$\phi_\nu = n_C\phi_C + n_H\phi_H + \Sigma n_X\phi_X, \tag{4}$$

where n_C, n_H, and n_X are the numbers of carbon, hydrogen, and halogen atoms in a halogenated compound and where ϕ_C, ϕ_H, and ϕ_X are the atomic-inhibitor indices for the corresponding atoms. The atomic-inhibitor indices have been derived from the observed change in the burning velocity of a premixed flame caused by the inhibitors based on kinetic considerations of combustion reactions.[1] They have also been shown to depend on the fuel and also on equivalence ratio, though not strongly. Although the equivalence ratio can not be defined for a Bunsen-type flame, one can obtain a good linear relationship between ϕ_τ and ϕ_ν, as can be seen in Fig. 3, by using a typical set of values:[1] $\phi_C=1.0$, $\phi_H=0.25$, $\phi_F=1.0$, $\phi_{Cl}=1.5$, and $\phi_{Br}=12.3$. The general trend is that

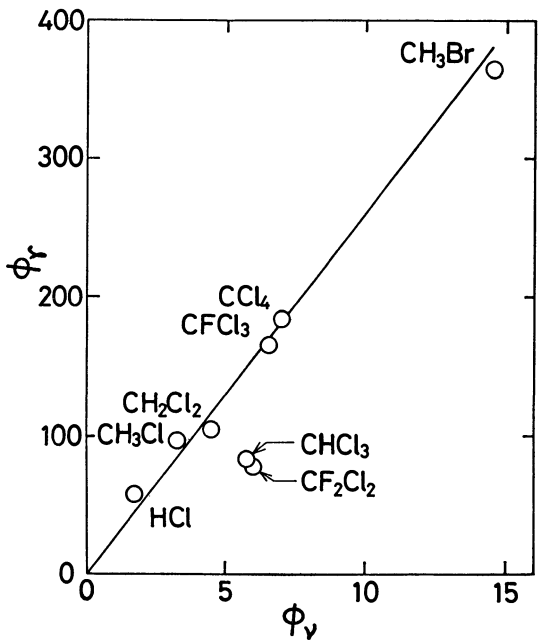

Fig. 3. Correlation between the effectiveness, ϕ_r, of halogenated compounds in scavenging H atoms in a methane-air flame determined by the ESR method and the inhibitor index, ϕ_v, determined from their effect on the burning velocity.[1]

an increase in the number of Cl atoms in the inhibitor molecule results in a more pronounced reduction in the amount of H atoms in the flame. The halogen atoms reduce the amount of H atoms in this increasing order: F<Cl<Br.

A halogenated compound inhibits flame reactions by scavenging H atoms, which are the principal reactive intermediates in hydrocarbon combustion. The reduction in the amount of H atoms observed above is not necessarily due to the direct scavenging of H atoms by the inhibitors; it can also be an indirect result of the scavenging of other reactive intermediates, like O atoms and OH radicals. However, because, in a fuel-rich hydrocarbon flame, H atoms are the most abundant reactive intermediates,[7] we will focus our discussion on the scavenging of H atoms.

Halogenated compounds can scavenge H atoms and convert them into stable molecules and unreactive radicals by reactions like:

$$H + RX = HX + R, \quad (5)$$

$$H + HX = H_2 + X. \quad (6)$$

In addition, halogen atoms can assist the cyclic recombination of H atoms in reaction sequences where the halogen atom is rapidly regenerated:[1]

$$H + X + M \rightarrow HX + M, \quad (7)$$

followed by Reaction 6. The equilibrium of Reaction 6 tends to be shifted far to the right in a high-temperature flame when X is Br and I.[5,6] As a matter of fact, about 70% of the bromine has been shown to exist in the atomic form in a HBr-inhibited methane-air flame.[14] From the ϕ_v data, the rate constant of the forward reaction, 7, for Br (and I) has been evaluated to be about nine times larger than that for Cl.[1] Thus, the efficient decrease in the amount of H atoms caused by CH_3Br compared to the chlorinated and fluorinated methane found in this study is consistent.

An inhibitor molecule containing more than one halogen atom (*e.g.*, CCl_4) can be stripped of its halogen atoms by successive reactions with H atoms:

$$CCl_4 + H \rightarrow CCl_3 + HCl, \quad (8)$$

$$CCl_3 + H \rightarrow CCl_2 + HCl, \quad (9)$$

and so forth.[5] Therefore, HCl can be expected to scavenge one H atom by means of Reaction 6, while CH_3Cl scavenges two H atoms by the combined reactions of 5 and 6, and CCl_4 even more by successive reactions of the 9 type. The observed ϕ_r values agree qualitatively with what can be expected, except for the cases of $CHCl_3$ and CF_2Cl_2.

The authors are grateful to the Toyota Foundation for its financial support (1977—1979) in initiating the study. One of the present authors (O. C.) acknowledges the support of the Yamada Foundation and the Swedish National Science Council for his stay at Hokkaido University.

References

1) R. M. Fristrom and P. Van Tiggelen, *Seventeenth Symposium (International) on Combustion*, The Combustion Institute, Pittsburgh (1978), p. 773.
2) W. E. Wilson, Jr., *Tenth Symposium (International) on Combustion*, The Combustion Institute, Pittsburgh (1965), p. 47.
3) J. C. Biordi, C. P. Lazzara, and J. F. Papp, *Combst. Flame*, **24**, 401 (1975).
4) G. Dixon-Lewis and R. J. Simpson, *Sixteenth Symposium (International) on Combustion*, The Combustion Institute, Pittsburgh (1977), p. 1111.
5) G. LeBras and J. Combourieu, *J. Chim. phys.*, **71**, 465 (1974).
6) C. K. Westbrook, *Combust. Sci. Tech.*, **23**, 191 (1980).
7) J. W. Hastie, *J. Res. Nat. Bur. Stand. (U. S.)*, **77A**, 733 (1973).
8) N. R. Lerner and D. E. Cagliostro, *Combust. Flame*, **21**, 315 (1973).
9) D. M. Tucker, D. D. Drysdale, and D. J. Rasbach, *Combust. Flame*, **41**, 293 (1981).
10) O. Claesson, S. Noda, and H. Yoshida, *Bull. Chem. Soc. Jpn.*, **56**, 2559 (1983).
11) S. Noda, M. Miura, and H. Yoshida, *J. Phys. Chem.*, **84**, 3143 (1980).
12) S. Noda, M. Miura, and H Yoshida, *Bull. Chem. Soc. Jpn.*, **53**, 841 (1980).
13) C. P. Slichter, "Principles of Magnetic Resonance," 2nd ed, Springer-Verlag, Berlin (1978), Chap. 5.
14) S. Noda, H. Demise, O. Claesson, and H. Yoshida, *J. Phys. Chem.*, in press.

 © 1983 The Chemical Society of Japan Bull. Chem. Soc. Jpn., 56, 2565—2568 (1983)

Ultraviolet Photoelectron Spectra of α- and β-Polymorphs of Copper Phthalocyanine

Chen Shang Xian,† Kazuhiko Seki, Hiroo Inokuchi,* Shi Zurong,†† and Qian Renyuan††

Institute for Molecular Science, Myodaiji, Okazaki 444

†† *Institute of Chemistry, Academia Sinica, Beijing, China*

(Received January 14, 1983)

The ultraviolet photoelectron spectra have been measured for α- and β-forms of copper phthalocyanine at 183 °C, to investigate the correlation of photoemissive behavior with crystal structure. Their threshold ionization potentials were 4.8_8 and 4.6_2 eV,** with polarization energy of 1.2_7 and 1.5_3 eV, respectively. This difference could not be explained by calculation with point charge-point dipole approximation, but calculation with distributed charge on the cation and distributed induced dipoles on the nearest neighbor two molecules gave semi-quantitative agreement with the experimental findings.

The phthalocyanines are used as pigments or photoreceptors, and their structures are similar to those of porphyrins such as chlorophyll and hemoglobin; accordingly they have been extensively studied.[1–5] Copper phthalocyanine (CuPc) is representative. In 1963, Vilesov *et al.*[6] measured its photoelectron spectrum. In 1968, Schechtman and Spicer[7] reexamined this and compared the density of the occupied states of CuPc from experimental results with that derived from theoretical calculations. This revealed a good agreement between them. In 1978, Berkowitz[8] measured the photoelectron spectra of various phthalocyanine compounds in the gas phase.

As is well known,[9–10] CuPc exists in different crystal structures as α-, β-, and x-forms. The β-form is the most stable and the others are metastable at room temperature. It is interesting to study the dependence of photoemissive behaviors on their polymorphism. From these measurements we could establish a correlation between the molecular packing and the electronic structure.

In this paper, we report the threshold ionization potential of α- and β-CuPc by means of ultraviolet photoelectron spectroscopy (UPS). There is 0.2_6 eV difference in the threshold ionization potentials between them. We believe this to be the first UPS study of polymorphs of organic crystal with known structures, which permit a detailed analysis of the origin of the difference between the two forms.

Experimental

Two samples of CuPc were used and gave the same results. One of them was prepared and purified as described previously.[11] The other was supplied by Dainihon Ink Co. Ltd., and was used without further purification. The sample film was prepared on a Cu-substrate by evaporation and measured *in situ* in vacuum of 10^{-5} to 10^{-6} Pa; the film thickness was controlled around 50 nm and measured with a quartz thickness monitor. The α- and β-polymorphs were prepared by evaporation on the substrate at room temperature and 250 °C, respectively. The resultant structures were examined by X-ray diffraction, and the data agreed with those in the literature.[9,10]

The light source of the photoemission machine was a Hinteregger-type hydrogen-discharge lamp used in conjunction with a 0.5 m Seya-Namioka-type monochromator. The energy of the photoelectron was analyzed with a retarding-potential-type energy analyzer as reported previously.[12] The energy resolution was about 0.2 eV. All the observed values were reproducible within ±0.05 eV.

Results and Discussion

Initially, we tried to measure the photoelectron spectra of α- and β-CuPc at room temperature. The measurement of the α-form was not difficult, but for the β-form there was a severe charging of the sample. This is probably due to the low conductivity of the β-form at room temperature. As reported by Wihksne, dark conductivity of β-metal free phthalocyanine is 10^5 times lower than that of α-form at 180 °C, and further, this difference is expected to increase at room temperature.[11] It is reasonable to assume similar relations for the α- and β-CuPc. This experimental difficulty was revolved by elevating the temperature to increase the conductivity of the β-form. We found that the α-form does not change to β-form below 200 °C, then both forms could be measured at the same temperature (183±2 °C).

The photoeletron spectra of the β- and α-forms at this temperature, 183±2 °C, and that of α-form at room temperature using a photon energy of 7.8 eV are shown in Fig. 1 as curve a, b, and c, respectively. Table 1 lists the photoemission threshold values I_s^{th} obtained from these curves using the Einstein relation $I_s^{th}=h\nu-E_k^{max}$, where E_k^{max} is the maximum kinetic energy of the photoeletrons.

From Table 1, we see that I_s^{th} of the α-form at 183 °C is a little lower than that at room temperature. Most of this we can ascribe to the coupling of ionizing electronic excitation with low-energy modes of lattice phonon which satisfy $\hbar\omega \ll kT$, where $\hbar\omega$ is the phonon energy quantum, k the Boltzmann factor, and T the temperature. Using the theory of Duke,[13] a lowering of I_s^{th} proportional to $T^{1/2}$ is expected. With a theoretical value of proportional constant for benzene with all lattice phonon modes taken into account,[13] we can estimate a lowering of ≈0.18 eV, which is comparable with the observed value for α-CuPc. Since all the lattice phonon modes of phthalocyanines

† On leave from the Institute of Chemistry, Academia Sinica, Beijin, China.

** 1 eV≅0.1602 aJ.

TABLE 1. THE THRESHOLD IONIZATION POTENTIALS AND POLARIZATION ENERGIES OF α- AND β-COPPER PHTHALOCYANINE

Crystal form	Threshold ionization potential / eV			Polarization energy / eV	
	Crystal at RT	Crystal at 183 °C	Gas	Crystal at RT	Crystal at 183 °C
α	$5.0_9\pm0.05$	$4.8_8\pm0.05$	6.15[a]	1.0_6	1.2_7
β	—	$4.6_2\pm0.05$	6.15[a]	—	1.5_3

a) Estimated from Berkowitz's data (Ref. 8).

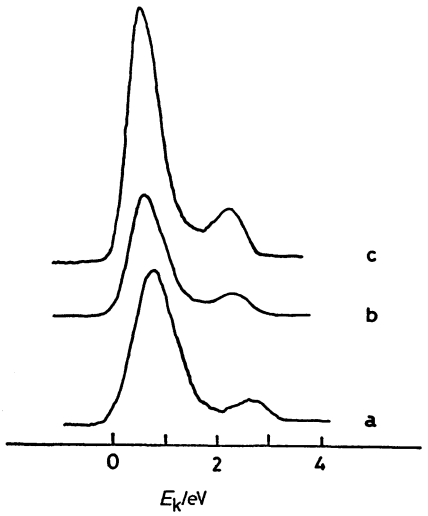

Fig. 1. Photoelectron spectra of copper phthalocyanine at $h\nu=7.8$ eV in kinetic energy (E_k) scale. a: β-form at 183 °C, b: α-form at 183 °C, and c: α-form at room temperature.

will appear in the region $\hbar\omega \ll 100$ cm^{-1},[14] all modes will contribute to the temperature dependence in both the α- and β-forms. Therefore we can expect that the temperature dependence of I_s^{th} is almost common in the two phases, and its difference will not play an important role in discussing the I_s^{th} difference of α- and β-forms at the same temperature.

From Table 1, it can be seen that there is a small but distinct difference 0.2_6 eV in threshold ionization potentials between the two crystal forms. According to Lyons,[15] the ionization potential of solid is determined by gas phase ionization potential and its lowering due to the electric polarization of the molecules surrounding the cation, which is called polarization energy. In Table 1, the polarization energies obtained by using gas phase threshold ionization potential of 6.15 eV[8] are also listed.

The present results indicate that the polarization energies of the two crystalline forms are different. Our work offers the first experimental evidence for the dependence of photoelectron spectra on polymorphs of known strucure. In 1978, Nielsen[16] reported the substrate dependent ionization and polarization energies of dibenzotetrathiafulvalene and explained the experimental results as due to the formation of different structure or orientations. However, he did not show the direct evidence to demonstrate the existence of different crystalline forms.[17]

The polarization energy of molecular solid constructed with nonpolar molecules can be considered as the interaction energy of the charge of the cation and electric multipoles induced on surrounding molecules.[15] For simplicty, we will neglect multipoles higher than dipole and the interaction among dipoles.

In general, the charge on the cation and the dipole for the neutral molecules are distributed over each molecule. If we represent them by a point charge and a point dipole at the center of the molecule, the polarization energy can be expressed as[15]

$$P_s = \sum_i \frac{e^2}{2r_i^6} \boldsymbol{r}_i \alpha \boldsymbol{r}_i, \tag{1}$$

where $\boldsymbol{r}_i$ is the distance vector of i-th molecule from the cation, r_i, its absolute value, e, electronic charge, α, the molecular polarizability tensor, and summation is taken over all the molecules in the crystal except the ionized molecule.

To obtain a roughly correct order of P_s, calculations with more simplified forms[18,19]

$$P_s = ke^2\bar{\alpha}d^{-4/3}, \tag{2a}$$

or

$$P_s = (e^2/2\rho)(1-1/\varepsilon), \tag{2b}$$

are known to be useful, where k is a constant, $\bar{\alpha}$, the averaged molecular polarizability, d, the density, ρ, half of r_i of the nearest neighbor molecule, ε, the optical permissivity which can be estimated from $\bar{\alpha}$ and k. In the present case of CuPc, $\bar{\alpha}$ is common to the α- and β-forms, and d is also almost the same (1.62 and 1.61) for α- and β-forms, respectively.[20-22] Therefore, such simple formulae cannot be used to explain the difference in P_s in these forms.

We calculated P_s of both forms using Eq. 1. Since there seems to be no experimental data of α, we expressed the polarizability perpendicular and parallel to the molecular plane as α_0 and $b\alpha_0$, respectively. The data for other molecules suggest that $\alpha_0 \approx 30\times 10^{-27}$ m^3 [23] and b is between 2 and 3.[23,24] The crystal structures of α- and β-forms[4] are shown in Fig. 2. The summation in Eq. 1 was taken for molecules within cubes of edge length of $l=60$, 80, 120, and 200 Å. They showed good linear relationships with $1/l$, and the extrapolation to $l=\infty$ gave the values P_1 in Table 2. The values for the α-form are larger than those of the β-form, which does not agree with the observed results. Further, the calculated values are too large.

In order to improve this situation, we took account of the distribution of charges and dipoles on the cation

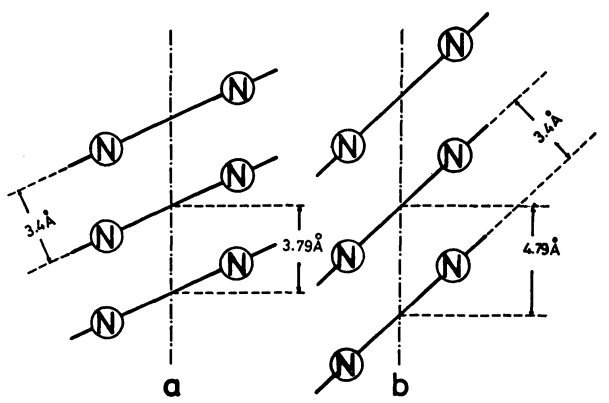

Fig. 2. Molecular arrangements in copper phthalocyanine crystals of (a) α- and (b) β-forms.[18] —·—·—: b-Axis, N-N: Molecular plan. The angle between the b-axis and the molecular plane for the α- and β-forms are 65.2° and 45.7°, respectively.

Table 2. Calculated polariztion energies

Anisotropy parameter b	Form	P_1/eV	B/eV	P_2/eV
2	α	3.35	0.85	1.45
	β	2.24	1.01	1.53
3	α	4.06	1.15	1.86
	β	3.05	1.41	2.05

and the nearest neighboring two molecules. As seen in Fig. 2, the overlap of the cation and nearest neighbors is large in both forms of CuPc, and the validity of the point-charge and point-dipole is dubious for the interaction among these molecules. When we divide P_1 into the contribution from the nearest neighbors A_1 and that from the other molecules B ($P_1=A_1+B$), A_1 is overwhelmingly large as shown in Table 3. Thus the examination of A_1 is important.

The highest occupied orbital of CuPc is known to be the π-orbital shown by the bold line in Fig. 3.[7,8,25] We approximated this with a dotted square in Fig.3, and assumed a uniform charge distribution of total amount of e. As for the dipole distribution, we adopted the "submolecular concept," [26,27] where we regard a large aromatic molecule as an aggregate of independently polarizable aromatic rings. This treatment is known to give reasonable dielectric properties for large molecules.[26,27] We treated CuPc as 12 aggregated rings in Fig. 3, with each ring represented by a dipole at its center. The polarizability of each ring was assumed to be 1/12 of α_0 and $b\alpha_0$.

Initially, we calculated the electric field at the center of each ring by the distribution charge on the cation, and calculated the induced dipole and the dipole-electric field interaction energy. These were summed for the twelve rings to give the total contribution A_4 from the nearest neighboring two molecules. For comparison, we also calculated the values for point charge-distributed dipole(A_2) and distributed charge-point dipole (A_3) approximations. Table 3 lists these values. We see that the values of both forms decrease by the consideration of distributions, but the change of α-form is much more than that of β-form. As a result, the difference between the two forms becomes

Table 3. Contributions of Nearest neighbor two molecules to polarization energy calculated with various approximation for $b=2$.

Form	A_1/eV[a]	A_2/eV[b]	A_3/eV[c]	A_4/eV[d]
α	2.50	1.28	0.75	0.60
β	1.23	0.96	0.72	0.52

a) Point charge-point dipole, b) Point charge-distributed dipole, c) Distributed charge-point dipole, d) Distributed charge-distributed dipole.

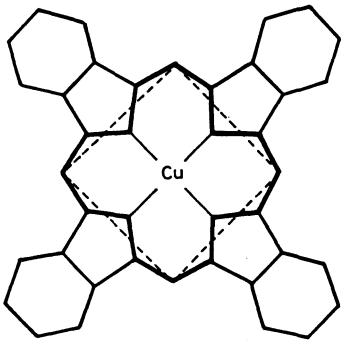

Fig. 3. Molecular structure and the highest occupied π-orbital (bold line) of copper phthalocyanine. The dotted line indicates the approximated charge arrangement.

very small, in particular for the distribution of the positive charge in the cation.

The values of P_s reevaluated as $P_2=A_4+B$ is shown in Table 2. The values of α-form become larger than those of β-form, in agreement with the experimental findings. Further, the absolute magnitude of P_2 is comparable with the observed values, although the estimation of α_0 may include considerable error. We should note that the ratio of P_2 values of α- and β-forms does not depend on α_0 but only on b.

Although the above estimation of P_s is very approximate, we may safely say that the extended distrubution of charges on the cation(and maybe the distribution of dipoles on neutral molecules and the anisotropy of polarizability) results in a very small difference for the contribution of the nearest neighbor. This made the total P_s difference to be determined by a larger difference of B. This is instructive about the role of the charge distribution, since at first glance of Fig. 2 we may expect a larger P_s of α-form because of the smaller center-to-center distance and a larger overlap of molecules than in the β-form. Studies of the P_s of aromatic hydrocarbon crystals using a similar formulation will be interesting, since those molecules are not stacked as in CuPc, and the effect of charge distribution may be not so important as in the present case. The validity of simplified formulae Eq. 2a and 2b can be also examined.

Finally we wish to stress the usefulness of studying polymorphs for a detailed examination of the theory of polarization energy. If the theory is satisfactory, it should explain the data of two or more polymorphs using the same molecular parameter α, and this will restrict the degree of freedom in adjusting the theore-

tical parameters much more than in studying different compounds. Further future studies of various polymorphs with known structures are therefore desired.

The authors would like to express their sincere thank to Prof. I. Koyano and Dr. N. Sato for their helpful discussion, and to Dr. T. Kobayashi for the information of far-infrared spectral data. One of the authors (Chen Shang Xian) is indebted to Yamada Science Foundation for the financial support.

References

1) K. Wihksne and A. E. Newkirk, *J. Chem. Phys.*, **34**, 2184 (1961).
2) C. Y. Liang and E. G. Scalco, *J. Electrochem. Soc.*, **110**, 779 (1963).
3) F. W. Karasek and J. C. Decius, *J. Am. Chem. Soc.*, **74**, 4716 (1952).
4) M. Ashida, N. Uyeda, and E. Suito, *J. Cryst. Growth*, **8**, 45 (1971).
5) J. H. Sharp and R. L. Miller, *J. Phys. Chem.*, **72**, 3335 (1968).
6) F. I. Vilesov, A. A. Zagrubskii, and D. Garbuzov, *Sov. Phys.-Solid State*, **5**, 1460 (1964).
7) B. H. Schechtman and W. E. Spicer, *Chem. Phys. Lett.*, **2**, 207 (1968).
8) J. Berkowitz, *J. Chem. Phys.*, **70**, 2819 (1979).
9) J. H. Sharp and M. Abkowitz, *J. Phys. Chem.*, **77**, 477 (1973).
10) F. A. Hamm and E. Van Norman, *J. Appl. Phys.*, **19**, 1097 (1948).
11) 1st group, 4th Lab., Inst. Chem., Acad. Sinica, *Huaxue Xuebao*, **34**, 262 (1976).
12) T. Hirooka, K. Tanaka, K. Kuchitsu, M. Fujihira, H. Inokuchi, and Y. Harada, *Chem. Phys. Lett.*, **18**, 390 (1973).
13) C. B. Duke, J. S. Miller, "Extended Linear Chain Compounds," Plenum, New York (1982), Chap. 2.
14) T. Kobayashi, *Spectrochim. Acta, Part A*, **26**, 1313 (1970).
15) F. Gutmann and L. E. Lyons, "Organic Semiconductors," John Wiley and Sons, New York (1967); M. Batley, L. J. Johnstone, and L. E. Lyons, *Aust. J. Chem.*, **23**, 2397 (1970).
16) P. Nielsen, *Solid Siate Commun.*, **26**, 835 (1978).
17) Recently Sato found that the UPS and also the X-ray diffraction patterns of this compound evaporated on Cu and In substrates are different (N. Sato, private communication).
18) N. Sato, K. Seki, and H. Inokuchi, *J. Chem. Soc., Faraday, Trans. 2*, **77**, 1621 (1981).
19) M. Born, *Z. Phys.*, **1**, 45 (1920).
20) M. Ashida, N. Uyeda, and E. Suito, *Bull. Chem. Soc. Jpn.*, **39**, 2616 (1966).
21) C. Hamann, *Phys. Status Solidi*, **20**, 481 (1967).
22) C. J. Brown, *J. Chem. Soc., A*, **1968**, 2488.
23) R. J. W. Le Fevre and K. M. S. Sundaram, *J. Chem. Soc.*, **1963**, 4442.
24) W. Liptay and H.-J. Schlosser, *Z. Naturforsch., A*, **27**, 1336 (1972).
25) M. Iwan, E. E. Koch, T, C. Chiang, D. E. Eastman, and F.-J. Himpsel, *Solid State Commun.*, **34**, 57 (1980).
26) T. Lüty, *Chem. Phys. Lett.*, **44**, 335 (1976).
27) P. J. Bounds and R. W. Munn, *Chem. Phys.*, **24**, 343 (1977).

 © 1983 The Chemical Society of Japan Bull. Chem. Soc. Jpn., 56, 2569—2571 (1983)

Surface Treatment of Inorganic Pigments by N^{ε}-Acyllysine

Kunio Esumi,* Shigeki Yoshida, and Kenjiro Meguro

Department of Applied Chemistry, Institute of Colloid and Interface Science, Science University of Tokyo, Kagurazaka 1-3, Shinjuku-ku, Tokyo 162

(Received February 2, 1983)

Inorganic pigments(calcium carbonate, iron oxide, and titanium dioxide) were treated with N^{ε}-lauroyl-L-lysine, which is almost insoluble in both polar and nonpolar solvents. Two methods were employed for the treatment: (1) grinding of various weight proportional mixtures of pigment and the *N*-acyllysine; (2) adsorption of the *N*-acyllysine from its calcium ethylate solution on pigment. In method(1), the sufficient hydrophobic treatment was made when the weight percent of the *N*-acyllysine in the mixture was above about 30%. On the other hand, in method(2), although the amount adsorbed of the *N*-acyllysine was about in the range of 10^{-6} mol/g, the treated pigment showed a hydrophobicity. The critical surface tension of the treated samples estimated by using various mixtures of methanol and water was in the range from 23 to 39 dyn/cm.†

The surface treatment of solids[1-3], especially pigments, by surface active agents, polymers, and coupling agents are very important for preparing a good dispersion in the paint and printing industries. However, the above methods are not always suitable due to the detachment of the treating agents from the pigments in suspensions.

In general, it is known that amino acids and their derivatives[4,5] show surface activities for modifying wettability of solids. Especially, N^{ε}-Acyllysine is an interesting material because it is insoluble in both ordinary polar and nonpolar solvents due to its strong hydrogen bonding within the molecules. If the *N*-acyllysine could be applied to treat surface of pigments, a strong coating would be expected without detaching the *N*-acyllysine from the treated surfaces.

In this work, surface treatment of inorganic pigments by an *N*-acyllysine such as N^{ε}-lauroyl-L-lysine is described.

Experimental

Materials. The pigments used in this study were calcium carbonate (calcite) supplied by Kokusan Chemicals Co., Ltd., and iron oxide (R-110-A) and titanium dioxide (rutile) supplied by Titan Kogyo Co., Ltd.

N^{ε}-Lauroyl-L-lysine prepared from lauric acid and L-lysine[6] was kindly supplied by Ajinomoto Co., Ltd. This structural formula is shown as follows:

$$n\text{-}C_{11}H_{23}CONH(CH_2)_4CH(NH_2)COOH.$$

Calcium ethylate[7] was prepared by heating calcium chloride and ethyl alcohol together until calcium chloride completely dissolved.

Apparatus and Procedure. Two methods were employed for the surface treatment of pigments by N^{ε}-lauroyl-L-lysine.

(1) The Coating by Grinding: Calcium carbonate and N^{ε}-lauroyl-L-lysine were ground together in various proportions (total weight, 20 g) by a grinder (Type AOA of Ishikawa Kojo Co.). The various proportions of calcium carbonate to N^{ε}-lauroyl-L-lysine were as follows: sample No. 1, 1:10; No. 2, 1:5; No. 3, 1:3; No. 4, 1:2; No. 5, 1:1; No. 6, 2:1; No. 7, 3:1; No. 8, 5:1; No. 9, 10:1. The change of crystal form of the ground samples was measured by X-ray diffraction consisting of a Geigerflex diffractometer with nickel filtered copper radiation. The specific surface areas of the ground samples were measured by a Sorptograph Model ADS-1B (Shimadzu Seisakusho Co., Ltd.). To measure the sedimentation volume of the ground samples, water was added to 1 g of the ground sample in a 30 ml graduated cylinder to adjust a total volume of 30 ml.

(2) The Coating by Adsorption of N^{ε}*-Lauroyl-L-lysine from Its Calcium Ethylate Solution*: One gram of pigment was placed in a L-shaped test tube and N^{ε}-lauroyl-L-lysine solution of calcium ethylate was added. Then the L-shaped test tube was shaken at 25 °C. After at leat 2 h, having reached adsorption equilibrium, the sample was separated by centrifuging and dried *in vacuo*. The amount of N^{ε}-lauroyl-L-lysine adsorbed was determined from the difference of the concentrations of N^{ε}-lauroyl-L-lysine before and after the adsorption, by means of an UV spectrophotometer (Type ESP-3T of Hitachi).

The critical surface tension of the pigment coated with N^{ε}-lauroyl-L-lysine was estimated by using various mixtures of methyl alcohol and water at 20 °C.[8]

Results and Discussion

(1) The Coating by Grinding. The intensities of all the reflections of calcium carbonate alone in the X-ray diffraction diagrams decreased and became weaker during the grinding process. Similarly, all the reflections of N^{ε}-lauroyl-L-lysine alone decreased with the grinding time. Further, although the X-ray diffraction measurement was carried out on the ground samples of calcium carbonate and N^{ε}-lauroyl-L-lysine, the change of crystal forms of the ground samples was difficult to estimate due to a remarkable difference of their intensities. Since the original crystal forms of calcium carbonate and N^{ε}-lauroyl-L-lysine were not changed by up to 1 h grinding, the grinding time was taken as 1 h to study an effect of coating without considering any crystal transformation.

The specific surface areas of all the ground samples are plotted against the weight percent of N^{ε}-lauroyl-L-lysine, as shown in Fig. 1. The specific surface areas of the ground samples had a minimum value and increased gradually with an increase of content of N^{ε}-lauroyl-L-lysine in the mixture; finally they reached the value of N^{ε}-lauroyl-L-lysine alone. This might be interpreted by assuming that the grinding of calcium carbonate is interfered with by the addition of N^{ε}-lauroyl-L-lysine and the calcium carbonate becomes

† 1 dyn = 10^{-5} N.

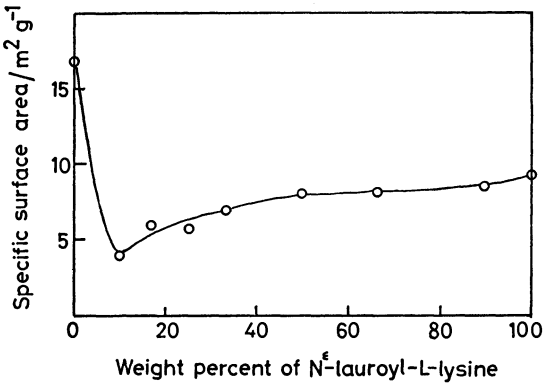

Fig. 1. Specific surface areas of ground samples as a function of weight percent of *N*$^{\varepsilon}$-lauroyl-L-lysine.

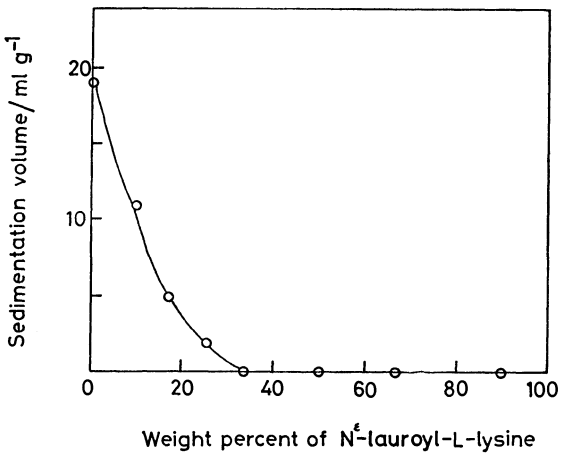

Fig. 2. Sedimentation volumes of ground samples as a function of weight percent of *N*$^{\varepsilon}$-lauroyl-L-lysine.

covered with *N*$^{\varepsilon}$-lauroyl-L-lysine with an increase of the amount of *N*$^{\varepsilon}$-lauroyl-L-lysine.

Figure 2 gives the sedimentation volume of all the ground samples in water *vs.* the weight percent of *N*$^{\varepsilon}$-lauroyl-L-lysine in the mixtures. Calcium carbonate alone completely sedimented, while *N*$^{\varepsilon}$-lauroyl-L-lysine formed a compact layer at the air/water interface. In the mixtures from No. 1 to No. 6, the particles were attached to the air/water interface like *N*$^{\varepsilon}$-lauroyl-L-lysine alone. The sedimentation of particles was observed distinctly in mixture No. 7, and further the volume ratio of the floating particles to the sedimented ones was nearly unity in mixture No. 9. Here, all the sedimented particles were confirmed to be calcium carbonate by the X-ray diffraction measurement. Thus, the above results indicate that when the weight percent of *N*$^{\varepsilon}$-lauroyl-L-lysine in the mixture is above about 30%, the efficient coating for calcium carbonate can be obtained which will show a strong hydrophobicity like *N*$^{\varepsilon}$-lauroyl-L-lysine alone.

(2) The Coating by Adsorption of N$^{\varepsilon}$*-Lauroyl-L-lysine from Its Calcium Ethylate Solution.* Figure 3 shows the adsorption isotherms of *N*$^{\varepsilon}$-lauroyl-L-lysine on pigments at 25 °C. It can be seen from Fig. 3 that, except for iron oxide, the amount of *N*$^{\varepsilon}$-lauroyl-L-lysine adsorbed increases with an increase of the concentration of *N*$^{\varepsilon}$-lauroyl-L-lysine. In the case of

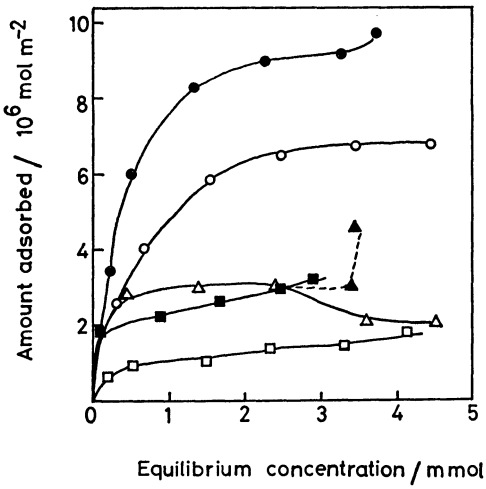

Fig. 3. Adsorption isotherms of *N*$^{\varepsilon}$-lauroyl-L-lysine on pigments: no addition of water; ○ $CaCO_3$, △ α-Fe_2O_3, □ TiO_2, addition of water (5 vol%); ● $CaCO_3$, ▲ α-Fe_2O_3, ■ TiO_2.

Table 1. The area occupied per *N*$^{\varepsilon}$-lauroyl-L-lysine molecule on pigments

Pigment	Area occupied/Å^2	
	(I)	(II)
Calcium carbonate	24.6	18.0
Iron oxide	67.0	53.2
Titanium dioxide	125.8	51.9

(II) lists the values obtained by the addition of water.

calcium carbonate, the adsorption isotherm follows a Langmuir type. Also, Fig. 3 gives the adsorption isotherms of *N*$^{\varepsilon}$-lauroyl-L-lysine on each pigment by the addition of water(5 vol%) into the solution. In all cases, the amount of *N*$^{\varepsilon}$-lauroyl-L-lysine adsorbed was enhanced compared with that for no addition of water. This result can be explained as a lowering of the solubility of *N*$^{\varepsilon}$-lauroyl-L-lysine in calcium ethylate solution by the addition of water. Further, the area occupied per molecule of *N*$^{\varepsilon}$-lauroyl-L-lysine on the pigment at the equilibrium concentration of 3 mmol dm^{-3} is obtained and their values are listed in Table 1. It is found that the area occupied for calcium carbonate is smaller than that for the other pigments, indicating that *N*$^{\varepsilon}$-lauroyl-L-lysine molecules on calcium carbonate are much more "collapsed" than that for the others. This difference might be interpreted by the acid-base property of pigments.

Generally, it is known[9] that calcium carbonate is a basic pigment, while the others(iron oxide and titanium dioxide) are neutral or acidic. As the pH of the *N*$^{\varepsilon}$-lauroyl-L-lysine solution in this study ranges between 4.5—5.0, it is anticipated that the adsorption capacity of *N*$^{\varepsilon}$-lauroyl-L-lysine on calcium carbonate can be enhanced by the acid-basic interaction.

(3) Wettability of the Pigment Coated by N$^{\varepsilon}$*-Lauroyl-L-lysine.* The results of wettability experiments for the pigment coated by the adsorption of *N*$^{\varepsilon}$-lauroyl-L-lysine are given in Fig. 4. The critical surface

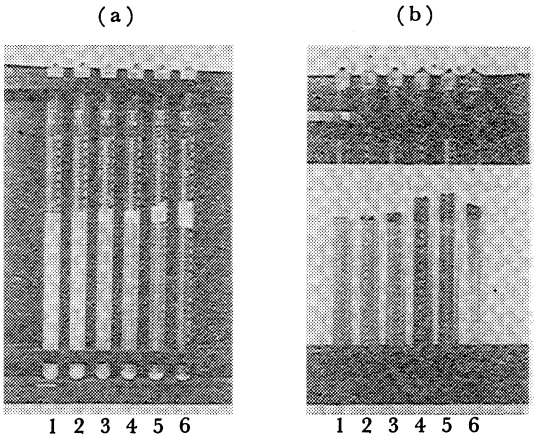

Fig. 4. Results of wettability experiments in aqueous methanol solutions: (a) calcium carbonate, (b) iron oxide; surface tension(dyn/cm), 1=23, 2=30, 3=39, 4=50, 5=60, 6=71.

tension of the pigment coated by N^{ϵ}-lauroyl-L-lysine was determined by using a series of aqueous methanol solutions. The pigment coated by N^{ϵ}-lauroyl-L-lysine became completely wet in solutions with surface tension below its critical surface tension. The critical surface tension of calcium carbonate coated with N^{ϵ}-lauroyl-L-lysine (No. 1—6) by grinding and by the adsorption had almost the same value, ranging between 30 and 39 dyn/cm. Also, the critical surface tension of iron oxide coated with N^{ϵ}-lauroyl-L-lysine by the adsorption was in the range between 23 and 30 dyn/cm.

Although the wettability of calcium carbonate coated with N^{ϵ}-lauroyl-L-lysine is not so different for the two methods, there is an extraordinary difference of the amount of N^{ϵ}-lauroyl-L-lysine required to render the surface hydrophobic sufficiently; the amount required by grinding is about 1.3 mmol/g, while that by the adsorption ranges as low as 10^{-3} mmol/g.

It is very important to elucidate how strong the attachment of N^{ϵ}-lauroyl-L-lysine is against organic solvents, to determine the stability of coating. So, the following test was carried out to estimate the strength of coating of N^{ϵ}-lauroyl-L-lysine on the pigment; the iron oxide coated with N^{ϵ}-lauroyl-L-lysine by the adsorption was treated in toluene at its boiling point for 10 min and then the sample was dried in a vacuum oven to eliminate toluene. The critical surface tension of the treated sample was then determined by the previous method. If N^{ϵ}-lauroyl-L-lysine is removed from the coated sample by the above treatment, the critical surface tension of the treated sample would show a higher value compared with that for the untreated sample. In this experiment, the critical surface tension of the treated sample showed almost the same value as that without the treatment. This result shows that the attachment of N^{ϵ}-lauroyl-L-lysine on the iron oxide is strong enough against the toluene treatment.

References

1) K. Meguro, *Kogyo Kagaku*, **58**, 905 (1955).
2) R. Kroker, M. Schnoeider, and K. Hamman, *Prog. Org. Coat.*, **1**, 23 (1972).
3) K. Esumi and K. Meguro, *Bull. Chem. Soc. Jpn.*, **56**, 331 (1983).
4) H. Shimada, M. Ueno, and K. Meguro, *Colloid Polym. Sci.*, **258**, 864 (1980).
5) H. Shimada, K. Yamazaki, M. Ueno, and K. Meguro, *J. Am. Oil Chem. Soc.*, **57**, 318 (1980).
6) K. Sakamoto, K. Takizawa, S. Inazuka, and R. Yoshida, *Yukagaku*, **26**, 110 (1977).
7) M. Homma, Japan Patent Tokkyo, **56-35**, 179 (1981).
8) D. T. Hornsby and J. Leja, *Colloids and Surfaces*, **1**, 425 (1980).
9) K. Tanabe, "Solid Acids and Bases," Kodansha, Tokyo, Academic Press, New York (1970).

The Long-wavelength nπ* Phosphorescence Spectra of *p*-Quinones in Polycrystalline Solutions at 77 K

Akira KUBOYAMA,* Yoshikuni KOJIMA,† and Sanae Y. MATSUZAKI

National Chemical Laboratory for Industry, Tsukuba Research Center, Yatabe, Ibaraki 305

† *The Tokyo Metropolitan Industrial Technology Center, Kita-ku, Tokyo 115*

(Received February 10, 1983)

Besides the usual nπ* phosphorescence spectra, broad, long-wavelength nπ* phosphorescence spectra are observed in normal paraffine solutions, such as a heptane solution, of 1,4-naphthoquinone, and in a benzene solution of 5,14 : 7,12-pentacenediquinone at 77 K. The energy difference between the two spectra are *ca.* 750 and 980 cm^{-1} respectively. The intensity of the long-wavelength spectra relative to the short-wavelength spectra becomes weaker with decreases in the concentrations of the quinones, and the lifetimes of the long-wavelength spectra are shorter than those of the short-wavelength spectra. These long-wavelength spectra are assigned to those of the quinone aggregates. The excitation spectra of these phosphorescences have also been obtained. An explanation of the above red-shift of the nπ* phosphorescence spectra of the aggregates is presented; in it, the phosphorescence state of the aggregates corresponds to the nπ* triplet excimer state.

Heretofore, we have studied the phosphorescence spectra of quinones in solutions at 77 K.[1] normal paraffin polycrystalline solutions, such as a heptane solution, of 1,4-naphthoquinone(NQ)[1e] at 77 K show a regular broad phosphorescence spectrum besides a sharp nπ* phosphorescence spectrum; the broad spectrum is at considerably longer wavelengths than the sharp spectrum. A similar, broad, long-wavelength phosphorescence spectrum is also found in a benzene crystalline solution of 5,14 : 7,12-pentacenediquinone (PDQ)[2] at 77 K. In this work, these broad, long-wavelength phosphorescene spectra of the *p*-quinones have been studied.

Experimental

Measurements. The phosphorescence spectra in solutions at 77 K were measured using an Aminco-Bowman spectrofluorometer (Instrument I, PM tube R105UH) and an SPF-500 spectrofluorometer (Instrument II, PM tube R777) in the manner described in previous papers.[1a,1c,1e] The phosphorescence excitation spectra were obtained using Instrument II, equipped with a photon counter (PM tube 1P28). The energy distribution of the exciting light (a 250-W Xenon arc lamp) and the spectral transmittance of the monochromator have not been taken into account. The temperature dependence of the phosphorescence spectra was measured by means of the Instrument II equipped with a cryostat (Model CF 204, Oxford Electric Instrument, Ltd.). Two kinds of cooling speeds, fast and slow, were used.[1b] normal paraffin and benzene solutions, and methylcyclohexane and toluene solutions, formed polycrystalline and glassy states respectively at 77 K.

Materials. Commercially-available NQ was purified in the same manner as has been described in a previous work.[1e] PDQ of the Tojin Gosei Kogyo Co. was purified by means of vacuum sublimation, and its purity was checked by the TLC method. The solvents used were all of spectro-grade except for dodecane. Dodecane of GR grade of the Tokyo Kasei Kogyo Co. was used.

Results. The phosphorescence spectra and their excitation spectra obtained are shown in Figs. 1, 2, 4, and 5, and Figs. 3 and 6, respectively. The peak wavelengths of the phosphorescence spectra obtained are shown in Table 1. The broad, long-wavelength phosphorescence spectra observed in the heptane and octane solutions of NQ (Figs. 1 and 2) and the benzene solution of PDQ (Figs. 4 and 5) can not be observed using the phosphoroscope (10600 min^{-1}) because of their short lifetimes. They are weaker in slow-cooling than in rapid-cooling, as in the

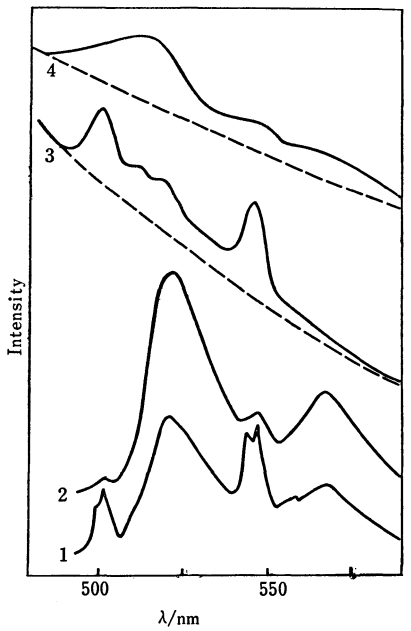

Fig. 1. Phosphorescence spectra of NQ in the heptane solution at 77 K.
1: 3×10^{-3} M, 313 nm ex., 2: 3×10^{-3} M, 365 nm ex., 3: 10^{-5} M, 313 nm ex., 4: 10^{-5} M, 365 nm ex. (In Figs. 1 and 5, ex. denotes excitation.)

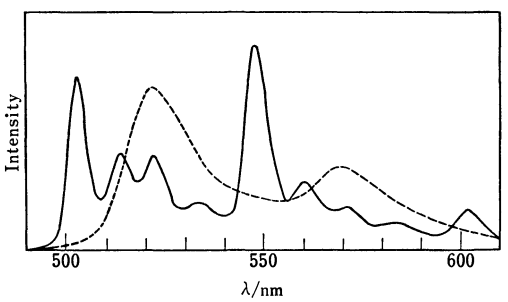

Fig. 2. Phosphorescence spectra of NQ in solutions at 77 K.
——: Methylcyclohexane, 1.6×10^{-3} M, ----: octane, 1.9×10^{-3} M.

case of the short-wavelength spectra. In NQ, the short-wavelength spectrum of the heptane solution also can not be observed using the phosphoroscope, but the corresponding phosphorescence spectrum of the hexane solution is barely observable using the phosphoroscope. The phosphorescence spectra of the hexane and toluene solutions of PDQ (Fig. 4) can be observed using the phosphoroscope; the observed lifetimes are 1.8 and 3.2 ms respectively. The observed lifetime of the short-wavelength phosphorescence spectrum of the benzene solution of PDQ (Fig. 5) is *ca.* 2 ms. The phosphorescence spectrum of PDQ crystals (Fig. 4) can not be observed using the phosphoroscope.

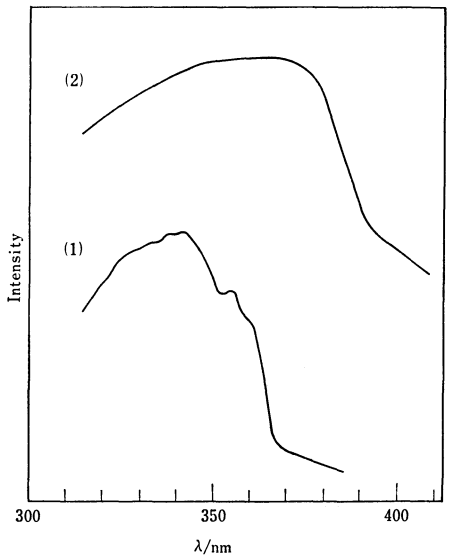

Fig. 3. Phosphorescence excitation spectra of NQ in solutions at 77 K.
(1) Methylcyclohexane, 1.6×10^{-3} M, 548 nm mon., (2) heptane, 1.5×10^{-3} M, 522 nm mon. (In Figs. 3 and 6, mon. denotes monitor.)

Table 1. Peak wavelengths, λ, of the phosphorescence spectra

	Solvent	λ/nm	
		I[a]	II[a]
NQ	Heptane	498, 501.5	521
		544, 547.5	569
	Methyl-cyclohexane	501	
		547	
		602	
	Octane		521
			569
PDQ	Hexane	472	
		477	
		481	
		488	
		492	
		502	
		504.5	
		513	
		517.5	
		523	
		545	
		560.5	
	Benzene	472	495
		511.5	539.5
		558	591.5
	Toluene	461	
		497	
		540	

a) I and II denote the short- and long-wavelength spectra respectively.

Discussion

In normal paraffine solutions, such as pentane, hexane, and heptane solutions, a regular, broad phosphorescence spectrum appears at wavelengths longer by *ca.* 750 cm^{-1} than the sharp nπ* phosphorescence spectrum,[1e] and the intensity of the former spectrum relative to the latter becomes weaker with decreases in the concentrations of the solutions, as may be seen from a comparison of the 1 and 3 spectra in Fig. 1.[3] The long-wavelength spectrum appears most strongly in the heptane solution, though it is relatively weak. In the heptane solution, it is observed even at the low concentration of NQ (10^{-5} mol/l), as may be seen in Fig. 1. In the octane solution, it appears alone, as may be seen in Fig. 2. The long-wavelength spectrum is clearly different from that of the NQ crystals.[5] Therefore, the long-wavelength spectrum is thought to be due to NQ aggregates. Since the lifetime of the short-wavelength spectrum of the heptane solution is thought to be close to that of the hexane solution, it may be longer than that of the long-wavelength spectrum. As the long-wavelength spectrum shows the C–O stretching vibrational structre and its lifetime is short, it may be assigned to the nπ* phosphorescence spectrum. No such broad, long-wavelength spectrum has been observed in the other solutions of NQ studied.

In the phosphorescence excitation spectra of NQ in Fig. 3, the main broad spectra are assigned to the low-energy ππ* absorption spectrum.[6] The correspondence between these excitation spectra and the ππ* absorption spectra is qualitative, because the absorption in this wavelength region is very strong in the light of the NQ concentrations of the solutions used. Figure 3, however, proves that the ππ* absorption spectrum in the heptane solution is at considerably longer wavelengths than that in the methylcyclohexane solution.[7] The spectra corresponding to the S–S nπ* absorption spectra at the long wavelengths could not be accurately observed. However, the corresponding spectrum in the heptane solution is qualitatively observed to be at shorter wavelengths than that in the methylcyclohexane solution. As may be seen in Fig. 1, the intensity of the broad spectrum relative to that of the sharp spectrum is far larger at the 365 nm excitation than at the 313 nm excitation. This fact can reasonably be explained by the above results.

In Fig. 4, the phosphorescence spectra of the hexane and toluene solutions of PDQ are reasonably assigned to the nπ* spectrum because of their C–O stretching vibrational structure and short lifetime. The spectrum of the toluene solution is at shorter wavelengths than that of the hexane solution; this is a result of the

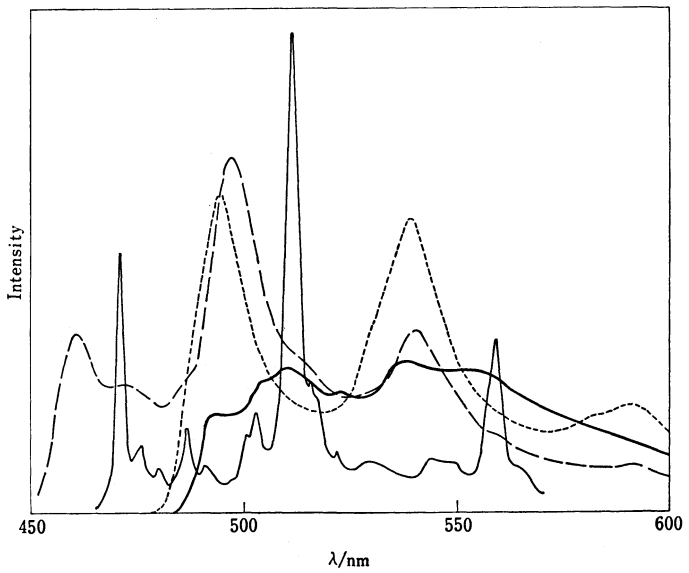

Fig. 4. Phosphorescence spectra of PDQ in solutions and the crystalline phase at 77 K.
——: Hexane, 2×10^{-5} M, ----: benzene, 10^{-3} M, — —: toluene, 10^{-3} M, ——: crystalline phase.

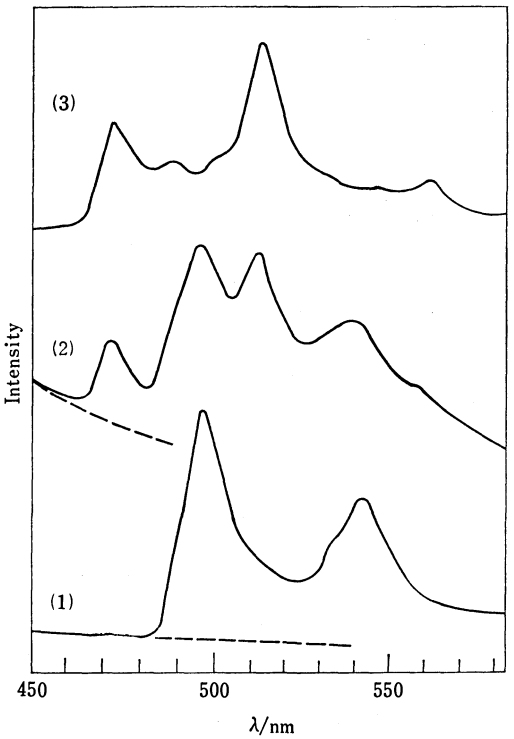

Fig. 5. Phosphorescence spectra of PDQ in the benzene solution at 77 K.
(1) 10^{-3} M, 365 nm ex., (2) 5×10^{-5} M, 365 nm ex., (3) 5×10^{-5} M, 365 nm ex.

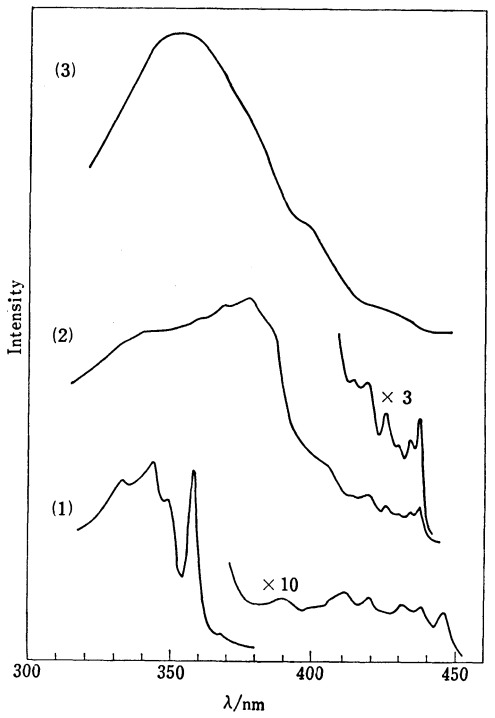

Fig. 6. Phosphorescence excitation spectra of PDQ in solutions at 77 K.
(1) Dodecane, 2×10^{-4} M, 513 nm mon., (2) benzene, 10^{-3} M, 540 nm mon., (3) toluene, 10^{-3} M, 498 nm mon.

charge-transfer interaction between toluene and PDQ, as in the cases of other quinones.[1e,1f] As may be seen in Fig. 4, PDQ[2] also shows a broad, long-wavelength phosphorescence spectrum, with the C–O stretching vibrational structure, in the benzene solution at 77 K. This spectrum is also different from that of the PDQ crystals. A similar phosphorescence spectrum has not been observed in other solutions. In the benzene solution, as may be seen in Fig. 5, a new phosphorescene spectrum appears at the wavelengths shorter by *ca.* 980 cm^{-1} than the above long-wavelength spectrum as the concentration of PDQ decreases; the former can be observed through the phosphoroscope. This short-wavelength spectrum is situated close to the phosphorescence spectrum of the hexane solution and is similar in shape to that of the toluene

solution. From these results, the long- and short-wavelength spectra in the benzene solution are also assigned to the nπ* phosphorescence spectra of the quinone aggregates and isolated molecules respectively, as in the case of NQ.

In the phosphorescence excitation spectra[8] of PDQ in Fig. 6, the long-wavelength weak and structured spectra and the short-wavelength strong spectra are assigned to the S–S nπ* and ππ* absorption spectra respectively.[2,9] In the benzene and toluene solutions, the correspondence between the short-wavelength spectra and the ππ* absorption spectra is also thought to be qualitative, as in the case of NQ in Fig. 3. In the benzene solution, the ππ* absorption spectrum is at considerably longer wavelengths than those in other solutions studied, while the nπ* absorption spectrum is at shorter wavelengths than that in the dodecane solution as in the case of the heptane solution of NQ. At 77 K, since the S–S nπ* absorption spectrum in the benzene solution is, as has been mentioned above, at shorter wavelengths than that in the dodecane solution, the T–S nπ* absorption spectrum[10] in the benzene solution is also thought to be at shorter wavelengths than that in the dodecane solution, while the nπ* phosphorescence spectrum in the benzene solution is at considerably longer wavelengths than that in the hexane solution. A similar situation is also found in the case of NQ. It can, therefore, be concluded that, in the phosphorescence state, the geometry of the NQ and PDQ aggregates changes from that at the ground state in such a manner that the phosphorescent nπ* level of the aggregates becomes considerably lower than that of the isolated quinone molecules.

In the long-wavelength phosphorescence spectrum of the benzene solution of PDQ in Fig. 4, a very weak shoulder on the shorter-wavelength side of each peak is observed. This shoulder may be due to aggregates of another form, different from the aggregates showing the peaks. As for the temperature dependence of the long-wavelength phosphorescence spectrum in the benzene solution, it almost disappears at 100 K, while the phosphorescence spectrum in the dodecane solution can still be clearly observed at 200 K.

The shorter lifetimes of the phosphorescence spectra of these quinone aggregates relative to those of the isolated quinone molecules are thought to be due to the intermolecular interaction between the components of the aggregates. The aggregates of NQ and PDQ are thought to be favorably formed in the heptane and benzene crystals respectively. These host-guest combinations may correspond to that of key and keyhole. As for the structure of the aggregates of these quinones, it is thought probable that the aggregates consist of two quinone molecules, because large-sized aggregates can not be favorably formed in the solvent crystals, and that they take the form of a slipped sandwich-type dimer,[11] since the π-electronic exchange interaction between the component molecules of these quinone aggregates may not be very small, in view of the aforementioned large red-shift of the low-energy ππ* absorption spectrum.

The aforementioned large red-shift of the nπ* phosphorescence spectra of these aggregates may be explained as follows. The three kinds of intermolecular interaction in the aggregates, the electrostatic, dispersion-force, and π-electronic exchange interactions, may affect the shift of the nπ* spectra. The electrostatic interaction usually brings about the blue-shift for the nπ* transition spectra. On the other hand, the dispersion-force interaction is thought to be too weak to bring about such a large red-shift as that. Therefore, the exchange interaction is thought to raise the above red-shift. In the ground-state geometry of the aggregates, the eletrostatic interaction, which is a long-range interaction, may be the predominant factor in the shift of the nπ* absorption spectra, resulting in the aforementioned blue-shift of the nπ* absorption spectrum of the PDQ aggregates. On the other hand, in the nπ* phosphorescent-state geometry of the aggregates, the exchange interaction, which is a short-range interaction, may become the predominant factor in the shift of the nπ* phosphorescence spectra, resulting from a decrease in the distance between the components of the aggregates, accompanied by the formation of a state corresponding to the nπ* triplet excimer state.[13] In this explanation, therefore, the phosphorescent state of the aggregates corresponds to the nπ* triplet excimer state.

This red-shift of the nπ* phosphorescence spectra which is brought about by the π-electronic exchange interaction may be explained using a simple one-electron model as follows. In the nπ* phosphorescent state of the aggregates, in comparison with the case of the isolated quinone molecules, the degenerate π*-levels will split to some extent through the intermolecular π-electronic exchange interaction, while the degenerate n-levels will remain almost unchanged, because the overlap between the π*-orbitals of the component molecules may not be small, while that between the n-orbitals is very small. Threfore, the nπ* phosphorescence spectra of the aggregates may shift considerably to the red in comparison with that of the isolated quinone molecules. Such a long-wavelength nπ* phosphorescence spectrum as is studied in this work can be expected to be found in other p-quinones.

References

1) a) A. Kuboyama and S. Yabe, *Bull. Chem. Soc. Jpn.*, **40**, 2475 (1967); b) A. Kuboyama, *ibid.*, **43**, 3373 (1970); c) A. Kuboyama and M. Anze, *Nippon Kagaku Kaishi*, **1972**, 229; d) A. Kuboyama and S. Matsuzaki, *ibid.*, **1973**, 2249; e) A. Kuboyama, *Bull. Chem. Soc. Jpn.*, **51**, 2771 (1978); f) A. Kuboyama and S. Y. Matsuzaki, *ibid.*, **54**, 3635 (1981).

2) N. A. Shcheglova, D. N. Shigorin, D. S. Dokunikhin, and G. T. Khachaturova, *Russ. J. Phys. Chem.*, **45**, 287 (1971).

3) In Fig. 1, in the sharp phosphorescence spectrum two nπ* phosphorescence spectra overlap as a result of the Shpol'skii effect.[4]

4) E. V. Shpol'skii, *Sov. Phys. Usp.*, **3**, 372 (1960); **5**, 522 (1962).

5) The NQ crystals show a weak, broad ππ*-type phosphorescence spectrum in the range from 560 to 600 nm at 77 K.[1a]

6) A. Kuboyama, S. Matsuzaki, M. Takagi, and H. Arano, *Bull. Chem. Soc. Jpn.*, **47**, 1604 (1974).

7) In the *syn*-[2.2](5,8)-1,4-naphthoquinonophane and the anti isomer, the low-energy $\pi\pi^*$ absorption spectra show large red-shifts relative to that of NQ (H. A. Staab and C. P. Herz, *Angew. Chem., Int. Ed. Engl.*, **16**, 392 (1977).

8) The concentration of the dodecane solution is near to that of the saturated solution. The phosphorescence spectrum of the dodecane solution is, briefly speaking, similar to that of the hexane solution, but it is complex because of the effect of the Shpol'skii multiplet.[1b] The phosphorescence excitation spectrum of the dodecane solution is similar to that of the hexane solution, but the former has been observed in a higher S/N ratio than the latter.

9) A. Kuboyama, Y. Kojima, and J. Maeda, *Bull. Chem. Soc. Jpn.*, **55**, 3635 (1982).

10) A. Kuboyama, *Bull. Chem. Soc. Jpn.*, **35**, 295 (1962).

11) The manner of overlap of the molecules observed in a NQ crystal[12] may be suggestive.

12) J. Gaultier and C. Hauw, *Acta Crystallogr.*, **18**, 179 (1965).

13) E. C. Lim and S. K. Chakrabarti, *Mol. Phys.*, **13**, 293 (1967); R. W. Chambers and D. R. Kearns, *J. Phys. Chem.*, **72**, 4718 (1968); G. A. George and G. C. Morris, *Mol. Cryst. Liq. Cryst.*, **15**, 65 (1971).

 © 1983 The Chemical Society of Japan Bull. Chem. Soc. Jpn., 56, 2577—2580 (1983)

Laser-induced Fluorescence of the NaCs Molecule

Kyoko Onomichi and Hajime Katô*,†

Department of Chemistry, Faculty of Science, Kobe University, Nada-ku, Kobe 657

(Received February 18, 1983)

Laser-induced fluorescence of NaCs is observed when a mixture of sodium and cesium is irradiated by the 5682 Å laser line. The spectroscopic constants of the ground state $X\,^1\Sigma^+$ have been determined and the potential energy curve was calculated by the RKR method. The excited state was identified as $D\,^1\Pi$, and the potential curve was estimated from the analysis of the fluorescence intensities.

The alkali heteronuclear diatomic molecule NaCs coexists with sodium and cesium atoms and Na_2 and Cs_2 molecules in the vapor of a mixture of sodium and cesium metals. Liveing and Dewar[1] referred an absorption in the yellow-green either to Cs_2 or to NaCs. Walter and Barratt[2] concluded that this absorption is due to the NaCs molecule, and they found another band of NaCs molecule in the violet region between 4315 and 3930 Å. Weizel and Kulp[3] assigned the lines observed by Walter and Barratt. According to their study, the vibrational constants ω_e are 98 ± 1, 65 ± 2, and 60 ± 3 cm^{-1} for the ground state, the yellow-green band, and the violet band, respectively.

The absorption of NaCs in the yellow-green region is overlapped with that of Cs_2, and spectroscopic analysis of the absorption spectrum is very difficult. However, a suitably chosen laser line may excite the NaCs molecule to only one specific rotational-vibrational level of the excited state. The resulting fluorescence will be simple, and it will be superior for studying such mixed alkali metal molecules. Nevertheless, no study of the laser-induced fluorescence of NaCs has been reported. We have succeeded in observing the fluorescence spectrum of the NaCs molecule; the results will be reported in this article.

As in the case for NaK,[4] we denote the ground and low-lying molecular states resulting from ground and excited atoms of Na and Cs as follows: $X\,^1\Sigma^+$ and $a\,^3\Sigma^+$ (from Na 3 ^{2}S+Cs 6 ^{2}S); $A\,^1\Sigma^+$, $b\,^3\Pi$, $B\,^1\Pi$, and $c\,^3\Sigma^+$ (from Na 3 ^{2}S+Cs 6 ^{2}P); $C\,^1\Sigma^+$, $d\,^3\Pi$, $D\,^1\Pi$, and $e\,^3\Sigma^+$ (from Na 3 ^{2}P+Cs 6 ^{2}S);···. In addition to these, there are molecular states resulting from Na 3 ^{2}S and Cs 5 ^{2}D. The states will have a shallow potential minimum at long internuclear distance, but the excited state of the yellow-green band is known to have a potential curve of $\omega_e=65\pm2$ cm^{-1} and the anharmonicity is not so large.[3] Therefore we will not take account of these states in the present analysis.

Experimental

Cesium metal, which was 99.9% pure and contained sodium as 0.1% impurity, was enclosed in an optical cell and heated to a temperature of about 570 K. The vapor pressure of Na, Na_2, Cs, and Cs_2 at 570 K are 1.3×10^{-2}, 1.2×10^{-4}, 2.2, and 1.3×10^{-2} Torr (1 Torr=133.322 Pa), respectively,[5] and that of NaCs is estimated to be 2.6×10^{-3} Torr by means of the Gibson-Heitler equation.[6] The experimental arrangement to observe the fluorescence spectrum is the same as our previous report.[7] A polarization scrambler was placed in front of the entrance slit of the spectrometer. Polarization of the fluorescence line was observed by placing a polarization analyser between the sample and the polarization scrambler. The intensity of the fluorescence line polarized parallel to the polarization of the laser line, $I_{//}$, and the one polarized perpendicular to the direction of polarization of laser line, $I_\perp$, were observed.

† Adjunct Associate Professor of Institute for Molecular Science (April 1981—March 1983).

Results and Discussion

When the cell which contained a mixture of sodium and cesium was irradiated by the 5682 Å Kr^+ laser line, several series of fluorescence lines with a vibrational spacing of about 99 cm^{-1} at the high energy end were observed in the region between 17000 and 18400 cm^{-1}. The vibrational spacing is close to that of NaCs, which was assigned by Weizel and Kulp.[3] The vibrational constants ω_e of the coexisting molecules Cs_2 and Na_2 are known to be about 42 and 159 cm^{-1}, respectively.[8] Therefore the observed lines can be identified as those of the NaCs molecule. One of the fluorescence spectra is shown in Fig. 1. The predominant lines are a series of P and R doublets of a large rotational quantum number J. When the frequency of the laser line was changed slightly by changing the angle of the etalon installed within the laser cavity, another series of fluorescence lines, as shown in Fig. 2, was observed. Whether an observed series of line is formed by a Q-branch or closely spaced P- and R-branches of small J has been distinguished by measuring the degree of polarization. The degree of polarization[9]

$$P_l = \frac{I_{//}-I_\perp}{I_{//}+I_\perp}, \tag{1}$$

of the lines of singlet bands in resonance fluorescence excited by linearly polarized light are given by[10]

$$P_l[P \text{ branch excited by } P(J) \text{ line}] = \frac{2J^2-5J+3}{14J^2+5J+1}, \tag{2}$$

$$P_l[R \text{ branch excited by } P(J) \text{ line}] = \frac{1}{7}, \tag{3}$$

$$P_l[P \text{ branch excited by } R(J) \text{ line}] = \frac{1}{7}, \tag{4}$$

$$P_l[R \text{ branch excited by } R(J) \text{ line}] = \frac{2J^2+9J+10}{14J^2+23J+10}, \tag{5}$$

$$P_l[Q \text{ branch excited by } Q(J) \text{ line}] = \frac{4J^2+4J-3}{8J^2+8J-1}. \tag{6}$$

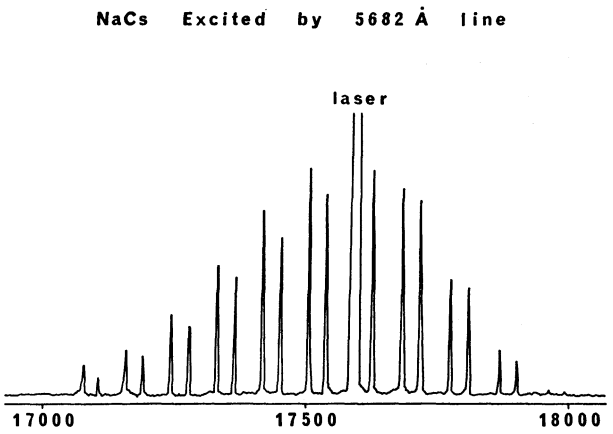

Fig. 1. Fluorescence spectrum of NaCs excited by a single mode 5682 Å line of Kr^+ laser. This P and R doublet series is assigned as the $D\,^1\Pi(v'=0,\ J'=109)\rightarrow X\,^1\Sigma^+(v'', J''=108$ and $110)$ transitions.

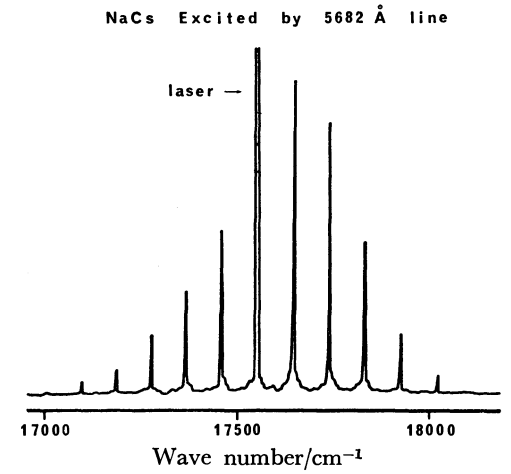

Fig. 2. Fluorescence spectrum of NaCs excited by another single mode 5682 Å line of Kr^+ laser. This fluorescence is assigned as a Q-line series of $D\,^1\Pi(0,\ J)\rightarrow X\,^1\Sigma^+(v'',\ J)$ transition. The value of J could not be assigned.

The fluorescence lines in Fig. 2 are identified as a Q line from the polarization measurement, since the degree of polarization was observed to be 0.5 The intensity decreases monotonically on either side of a single intensity maximum, and this is the same for fluorescence in Fig. 1. This result suggests that the fluorescence in Figs. 1 and 2 originates from the $v'=0$ level.

After the same procedure of changing the laser line, another series of fluorescence lines, shown in Fig. 3, was observed. This spectrum exhibits three intensity maxima. Therefore, it is reasonable to suppose that the fluorescence originates from the $v'=2$ level. Each fluorescence line in a low resolution spectrum was found to be composed of doublet lines of different intensities in a high resolution spectrum (See Fig. 3). If the doublet lines are P and R doublets from the same upper state(v', J') level, the rotational quantum number J' is estimated to be about 18 from the spacing

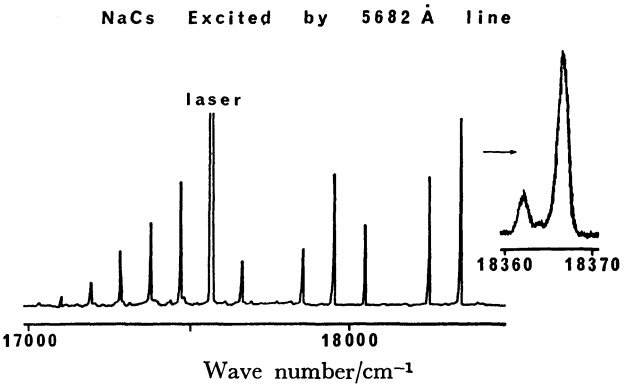

Fig. 3. Fluorescence spectrum of NaCs excited by another single mode 5682 Å line of Kr^+ laser. Each line at low resolution is composed of doublet lines of different intensities at high resolution as shown on the right. These lines are assigned as a series of $D\,^1\Pi(2,\ 18)\rightarrow X\,^1\Sigma^+(v'', J''=17$ and $19)$ transitions and a series of $D\,^1\Pi(2,\ 12)\rightarrow X\,^1\Sigma^+(v'',\ 12)$ transitions. The transitions $D\,^1\Pi(2,\ 18)\rightarrow X\,^1\Sigma^+(v'',\ 17)$ and $D\,^1\Pi(2,\ 12)\rightarrow X\,^1\Sigma^+(v'',\ 12)$ could not be resolved in the present resolution limit.

between the P line and the R line. The line strengths of P and R doublets of such J' are expected to have almost the same magnitude.[9] The degree of polarization was 0.1 for the line on the low-energy side and 0.3 for the line on the high-energy side. Thus we identified a fluorescence series of P and R lines and another fluorescence series of a Q line for the spectrum in Fig. 3, where an R line of a P and R doublets fluorescence series is overlapped with a Q line of another fluorescence series.

For a $^1\Pi$–$^1\Sigma$ transition, only Q lines appear in fluorescence for excitation by a Q line and both P and R lines appear for excitation by a P or R line. On the other hand, only $\Delta J=\pm 1$ transitions are allowed for $^1\Sigma$–$^1\Sigma$ transition and $\Delta J=0$ is forbidden.[9] We observed both Q-line series and P- and R-lines series for the yellow-green band of NaCs, but not P, Q, and R triplets from the same upper state(v', J') level. This band system is thus identified as a $^1\Pi$–$^1\Sigma$ transition.

Since the vibrational quantum numbers v' of the excited levels are small in the present case, it is easy to assign the v'' and v' quantum numbers to each line. The rotational numbering is more difficult, especially for Q-line series. It is necessary to know the rotational constant B_e in order to assign J, but the value is not known yet. We assumed therefore a tentative constant B_e which was estimated by additivity of atomic radii,[11] and we estimated the rotational numbering for a P and R doublet series. The rotational constants are determined by making a least-squares fit of the spacing between the two doublet members (v'', $J'+1$) and (v'', $J'-1$) of fluorescence series against v''. Then the members of another series are identified and assigned. This procedure is repeated until all the observed series can be assigned consistently. The spectroscopic constants of the ground state are improved by making a least-squares fit to all the lines in different series. The resulting spectroscopic constants of the $X\,^1\Sigma^+$ ground state are listed in Table

Table 1. Spectroscopic constants for the $X\,^1\Sigma^+$ and $D\,^1\Pi$ states of the NaCs molecule (cm^{-1})

	$X\,^1\Sigma^+$	$D\,^1\Pi$
ω_e	99.389	65.0
$\omega_e x_e$	0.380	0.293
$\omega_e y_e$	1.804×10^{-3}	
B_e	5.732×10^{-2}	4.69×10^{-2}
α_e	5.824×10^{-4}	3.05×10^{-4}
D_e	-8.598×10^{-7}	
β_e	-6.646×10^{-9}	
T_{00}	0	18250
D^e	4800[a]	3600[a]
R_e/Å	3.874	4.28

a) Estimated value. See text.

1, and the assignment of each fluorescence series is described in the caption of each spectrum.

Since the excited state is found to be $^1\Pi$, the state is either the $B\,^1\Pi$ state, which decomposes into Na(3 ^{2}S) and Cs(6 ^{2}P), or the $D\,^1\Pi$ state, which decomposes into Na(3 ^{2}P) and Cs(6 ^{2}S). The dissociation energy of the $X\,^1\Sigma^+$ ground state is roughly estimated as 4800 cm^{-1}, which is the average value of dissociation energies of Na_2 and Cs_2. The dissociation limit of the $B\,^1\Pi$ state will be then 16532 cm^{-1} from the bottom of the potential curve of the $X\,^1\Sigma^+$ state, where 16532 cm^{-1} is the sum of the dissociation energy of the $X\,^1\Sigma^+$ state and the energy of the atomic line Cs($6\,^2P_{3/2}\rightarrow 6\,^2S_{1/2}$). The excitation energy of the 5682 Å (17595 cm^{-1}) laser line exceeds the dissociation limit. The excited state is therefore identified as the $D\,^1\Pi$ state. Although there will be some error in the estimation of the dissociation energy of the $X\,^1\Sigma^+$ state, we are convinced this identification to be correct because the 5682 Å laser line excited to the levels of small vibrational quantum numbers v'; hence the excited level should be close to the potential minimum.

Since the number of excitations is small in the present study, we could not determine the spectroscopic constant of the excited state from the analysis of energies of the excited levels alone. Since the vibrational quantum number of the excited level is small, we would be able to estimate the equilibrium internuclear distance with a reasonable accuracy from the analysis of the intensity distribution of the fluorescence lines.

The intensity for the emission of a light quantum $h\nu$ in an electric dipole transition can be written as

$$I(e'v'J' \rightarrow e''v''J'') \propto \mu_e^2 \nu^4 |\langle v'|v''\rangle|^2, \quad (7)$$

where μ_e is the electronic transition moment and $|v'>$ and $|v''>$ are the vibrational wave functions of the initial and final state. Here the electronic transition moment is assumed to be independent of the internuclear distance in the range of vibration, since the vibrational quantum number of the excited level is small. The vibrational wave functions appropriate to any one-dimensional potential are obtained by solving the radial Schrödinger equation,[12] and the Franck-Condon factor $|\langle v'|v''\rangle|^2$ can be calculated.

The potential curve of the $X\,^1\Sigma^+$ state is calculated

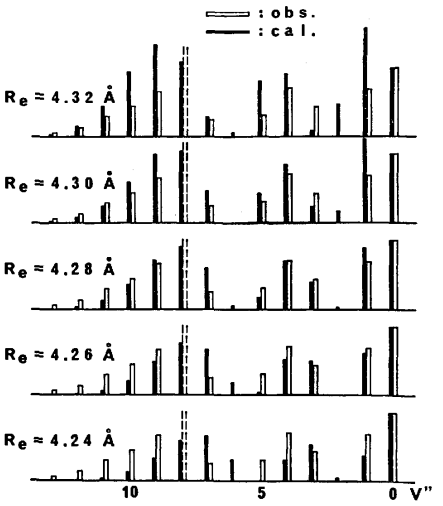

Fig. 4. Comparison of the observed (open bars) and calculated (full bars) intensity distribution $\nu^4|\langle v'|v''\rangle|^2$ of the $D\,^1\Pi(v'=2)\rightarrow X\,^1\Sigma^+(v'')$ transitions for five different values of equilibrium internuclear distance of the $D\,^1\Pi$ state.

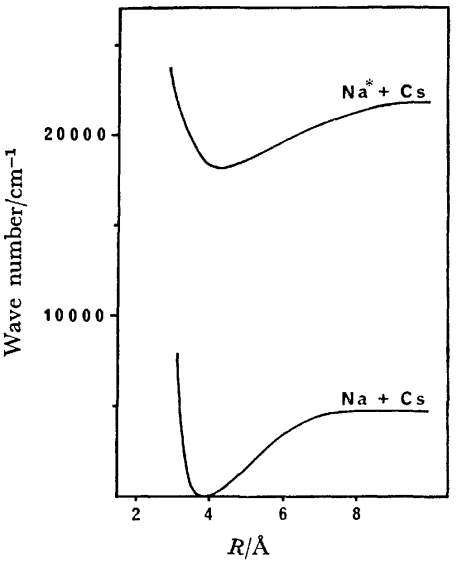

Fig. 5. Potential energy curves for NaCs. The potential curve of the $X\,^1\Sigma^+$ state is calculated by the RKR method. The potential curve of the $D\,^1\Pi$ state is approximated by a Morse function. The spectroscopic constants of these are listed in Table 1.

by the RKR method[13] from the molecular constants listed in Table 1. The potential curve of the $D\,^1\Pi$ state is approximated by a Morse function. The vibrational constant ω_e is assumed to be 65 cm^{-1}. The dissociation limit will be at 16956 cm^{-1} above the dissociation limit of the $X\,^1\Sigma^+$ state, where 16956 cm^{-1} is the energy of the atomic line Na($3\,^2P_{1/2}\rightarrow 3\,^2S_{1/2}$). The energy of the excited vibrational level is known from the assignment. The Morse function is therefore fixed if the equilibrium internuclear distance R_e is determined.

We have calculated the intensity distribution of the fluorescence lines as a function of R_e. The results are schematically shown in Fig. 4. The equilibrium

internuclear distance of the $D\,^1\Pi$ state is determined to be 4.28 ± 0.01 Å. The resulting molecular constants are listed in Table 1, and the potential curves of the $X\,^1\Sigma^+$ and $D\,^1\Pi$ states are schematically shown in Fig. 5.

H. K. thanks the Ministry of Education, Science and Culture for Grant-in-Aid for Scientific Researchs of Nos. 56540278 and No.58490020. The calculations were carried out at the computer center of IMS.

References

1) G. D. Liveing and J. Dewar, *Proc. R. Soc. London*, **27**, 350 (1878).
2) J. M. Walter and S. Barratt, *Proc. R. Soc. London, Ser. A*, **119**, 257 (1928).
3) W. Weizel and M. Kulp, *Ann. Phys. (Leipzig)*, **4**, 971 (1930).
4) H. Katô and C. Noda, *J. Chem. Phys.*, **73**, 4940 (1980).
5) A. N. Nesmeyanov, "Vapor Pressure of the Chemical Elements," Elsevier, New York (1963).
6) G. E. Gibson and W. Heitler, *Z. Phys.*, **49**, 465 (1928).
7) H. Katô, T. Matsui, and C. Noda, *J. Chem. Phys.*, **76**, 5678 (1982).
8) K. P. Huber and G. Herzberg, "Constants of Diatomic Molecules," Van Nostrand Reinhold, New York (1979), pp. 188 and 432.
9) G. Herzberg, "Spectra of Diatomic Molecules," Van Nostrand Reinhold, New York (1950), pp. 305 and 208.
10) P. P. Feofilov, "The Physical Basis of Polarised Emission," Consultants Bureau, New York (1961), p. 101.
11) P. J. Dagdigian and L. Wharton, *J. Chem. Phys.*, **57**, 1487 (1972).
12) R. N. Zare, *J. Chem. Phys.*, **40**, 1934 (1964).
13) R. Rydberg, *Z. Phys.*, **73**, 376 (1931); O. Klein, *ibid.*, **76**, 226 (1932); A. L. G. Rees, *Proc. Phys, Soc., Ser. A*, **59**, 998 (1947).

 © 1983 The Chemical Society of Japan Bull. Chem. Soc. Jpn., 56, 2581—2583 (1983)

The Selectivity Characteristics of Surfactant Ion-sensitive Nitrobenzene-membrane Electrode

Iwao SATAKE,* Shun-ichi NODA, and Tamaki MAEDA

Department of Chemistry, Faculty of Science, Kagoshima University, Korimoto, Kagoshima 890

(Received February 28, 1983)

The selectivity coefficients of nitrobenzene-membrane electrode containing dodecyltrimethylammonium dodecyl sulfate as an ion exchanger were determined. For a homologous series of surfactant ions, the logarithm of the selectivity coefficient was found to increase linearly with increasing hydrocarbon chain length. The selectivity sequence for anionic surfactant ions with the same alkyl chain length became alkylbenzenesulfonate ion > alkyl sulfate ion ≫ alkanesulfonate ion, while that for cationic ones became alkyltrimethylammonium ion ≈ 1-alkylpyridinium ion ≫ alkylammonium ion. These results can reasonably be interpreted in terms of the partition coefficient of surfactant ion between aqueous and membrane phases. A tentative estimation based on the theory of liquid-membrane electrode led to $-2900\ \mathrm{J\ mol^{-1}}$ for the standard free energy of transfer of a methylene group from water to nitrobenzene.

The utility of the liquid-membrane electrode sensitive to a surfactant ion both in analytical and physicochemical studies of ionic surfactant solutions is now well recognized. However, only a few works[1-4] have been concerned with the determination of the selectivity coefficients of these electrodes for various interferents. It has been found that *o*-dichlorobenzene-membrane electrodes[1-3] with an appropriate ion exchanger are highly selective for a surfactant ion over common inorganic ions but subject to serious interference from surfactant ions with longer alkyl chain length than the measuring ion. For a homologous series of surfactant such as sodium alkyl sulfates[1-3] and sodium alkanoates,[2,3] the selectivity coefficient was found to increase regularly with increasing hydrocarbon chain length. A similar result, though confined to sodium alkyl sulfates, was also obtained for a nitrobenzene-membrane electrode[4] which is an another typical liquid-membrane electrode sensitive to the surfactant ion. So far as we know, however, the selectivity characteristics of nitrobenzene-membrane electrode have yet not been fully elucidated. In this work, we investigated the effects of the nature of ionic head group as well as the alkyl chain length of interfering surfactant ion on the selectivity coefficient of nitrobenzene-membrane electrode which contains dodecyltrimethylammonium dodecyl sulfate as an ion exchanger.

Experimental

Materials. Sodium alkyl sulfates with 8, 10, and 12 carbon atoms were synthesized by esterification of the corresponding long-chain alcohols which had been purified by vacuum distillation. Sodium alkanesulfonates with 9, 11, and 13 carbon atoms (Tokyo Kasei Kogyo Co. Ltd.) were further extracted with petroleum ether for 40 h and recrystallized twice from ethanol. Dodecylammonium chloride was prepared from dodecylamine according to the method of Kolthoff and Stricks.[5] 1-Dodecylpyridinium chloride (Wako Pure Chemical Industry Co. Ltd.) was dissolved in ethanol and refluxed overnight with active carbon. After removal of the active carbon, the precipitate was purified further by repeated recrystallization from acetone. Dodecyltrimethylammonium chloride (DTAC, Tokyo Kasei Kogyo Co. Ltd.) was recrystallized twice from acetone. Sodium dodecylbenzenesulfonate (purity >99%, Wako Pure Chemical Industry Co. Ltd.) and tetraalkylammonium chlorides of guaranteed grade were used without further purifications. An ion exchanger, dodecyltrimethylammonium dodecyl sulfate (DTADS) was prepared by mixing the dilute solutions of DTAC and sodium dodecyl sulfate (SDS). The resulting complex was recrystallized twice from acetone and dissolved in nitrobenzene in a concentration of about $5\times10^{-4}\ \mathrm{mol\ dm^{-3}}$.

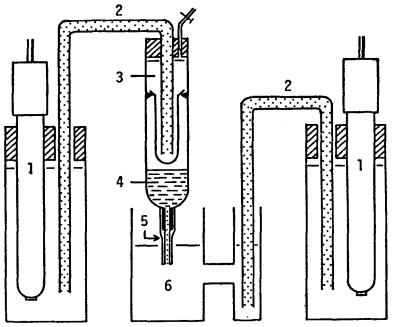

Fig. 1. The experimental setup of the nitrobenzene membrane electrode.
1; Reference electrode, 2; agar bridge, 3; reference solution, 4; nitrobenzene, 5; Teflon tube, 6; sample solution.

Membrane Potential Measurements. Since the nitrobenzene-membrane electrode containing DTADS as an ion exchanger responds both to anionic and cationic surfactant ions, the measurements were made with the following cells which have the experimental setup shown in Fig. 1.

Reference electrode (Ag-AgCl) | 1 mol $\mathrm{dm^{-3}}$ NH_4Cl agar bridge | Reference solution (SDS or DTAC, 5×10^{-4} mol $\mathrm{dm^{-3}}$) | Nitrobenzene (5×10^{-4} mol $\mathrm{dm^{-3}}$ DTADS) | Sample solution (SDS or DTAC, C_1; Interferent, C_J) | 1 mol $\mathrm{dm^{-3}}$ NH_4Cl agar bridge | Reference electrode (Ag-AgCl).

The electromotive force (E) of the cell was measured with an accuracy of ±0.1 mV at 25 °C, by using a digital voltmeter connected to a voltage follower amplifier (input impedance $\approx10^{13}\ \Omega$). The selectivity coefficient was determined by the mixed solution method,[6] *i.e.*, E was followed as a function of the measuring ion concentration, C_1, under the conditions of a constant interferent concentration, C_J.

Results and Discussion

In Fig. 2 is shown the typical semilogarithmic plots of E *vs.* SDS concentration in the presence and

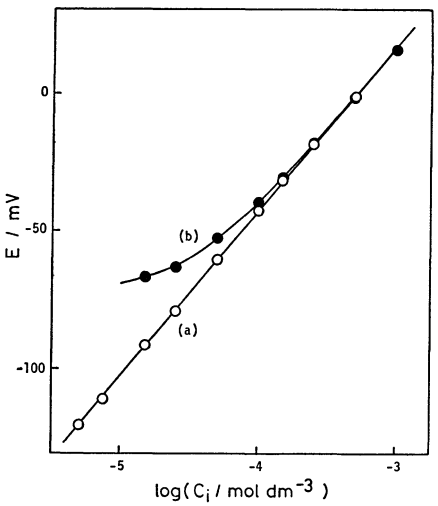

Fig. 2. Plots of the electromotive force (E) of the cell *vs.* the logarithm of SDS concentration (C_i) at 25 °C.
(a); In the absence of interferent, (b); in the presence of 1.5×10^{-4} mol dm^{-3} SDeS.

absence of sodium decyl sulfate(SDeS). In the absence of interfering ion, the electrode responds to the dodecyl sulfate ion down to 5×10^{-6} mol dm^{-3} with a slope of 59.7 mV per decade change in SDS concentration. This is also the case for the cationic surfactant ion sensitive electrode in which SDS is replaced by DTAC. An excellent agreement between the observed slope and an ideal Nernst slope (59.2 mV at 25 °C) suggests that the inorganic counterions such as Na^+ and Cl^- do not interfere appreciably with the electrode response to the surfactant ion. As is shown in Fig. 2 by the curve(b), however, the presence of a surfactant ion other than the dodecyl sulfate ion causes a remarkable interference. Under constant concentration of SDeS, the deviation from Nernstian response becomes progressively greater as SDS concentration decreases. Similar results were also obtained for all the interferents studied.

On the basis of these experimental results, we estimated the selectivity coefficient, K_{ij}, defined by

$$E = E_a + (RT/F)\ln[(C_i+K_{ij}C_j)/C_i^\circ], \quad (1)$$

where the subscript i refers to the measuring ion, *i.e.*, dodecyl sulfate ion or dodecyltrimethylammonium ion, j to the interfering ion, superscript ° to the reference solution, and E_a to the asymmetric potential of overall cell system, respectively; other symbols have their usual meanings. Under our experimental conditions, the activity coefficients can be ignored without loss of accuracy. The calculation was made by applying the graphical curve-fitting method described elsewhere.[7] The selectivity coefficients for various interferents, taken with respect to the dodecyl sulfate ion or the dodecyltrimethylammonium ion, are summarized in Table 1. In conformity with the results obtained both for liquid[1-4] and plastic[7,8] membrane electrodes, the selectivity coefficient for a homologous series of surfactant ions increases quite regularly with increasing alkyl chain length. As is shown in Fig. 3, the semilogarithmic plot of K_{ij} *versus* the number

TABLE 1. THE SELECTIVITY COEFFICIENTS OF NITROBENZENE MEMBRANE ELECTRODE FOR VARIOUS INTERFERENTS AT 25 °C

Measuring ion (i)	Interferent (j)	K_{ij}
Dodecyl sulfate ion	$C_nH_{2n+1}SO_4Na$	
	$n=10$	9.0×10^{-2}
	$n=8$	9.3×10^{-3}
	$C_nH_{2n+1}SO_3Na$	
	$n=13$	6.3×10^{-2}
	$n=12$	(1.8×10^{-2})[a]
	$n=11$	5.3×10^{-3}
	$n=9$	5.9×10^{-4}
	$C_{12}H_{25}C_6H_4SO_3Na$	8.9
Dodecyltrimethyl ammonium ion	$C_{12}H_{25}C_5H_5N^+Cl^-$	9.3×10^{-1}
	$C_{12}H_{25}NH_3^+Cl^-$	2.5×10^{-2}
	$(C_nH_{2n+1})_4N^+Cl^-$	
	$n=1$	2.0×10^{-5}
	$n=2$	2.0×10^{-4}
	$n=3$	1.0×10^{-2}

a) Estimated from Fig. 3.

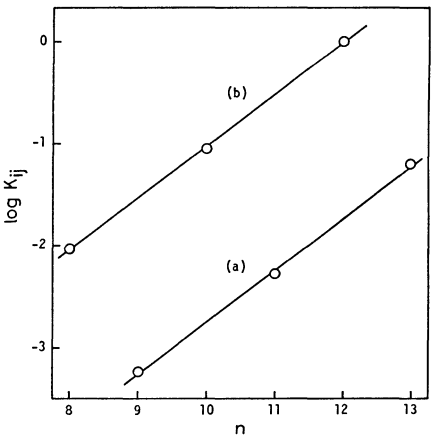

Fig. 3. The semilogarithmic plots of the selectivity coefficients for the homologous series surfactant ions *vs.* the number of carbon atoms in the alkyl chain at 25 °C.
(a); Sodium alkanesulfonate, (b); sodium alkyl sulfate.

of carbon atoms, n, in the alkyl chain gives the straight line with a slope virtually independent of the nature of ionic head group. This fact leads immediately to the selectivity coefficient of 1.8×10^{-2} for sodium dodecanesulfonate. Thus the present electrode gives the selective sequence for anionic surfactant ions with the same alkyl chain length as alkylbenzenesulfonate ion > alkyl sulfate ion ≫ alkanesulfonate ion. In the case of cationic surfactant ions, the selective sequence becomes alkyltrimethylammonium ion ≈ 1-alkylpyridinium ion ≫ alkylammonium ion. The interference of the tetraalkyl ammonium ion with shorter chain length is negligibly small.

According to the theory[9] of liquid-membrane electrode in which the dissolved ion exchanger is completely dissociated, the selectivity coefficient is described in terms of the mobility, u^*, in the membrane phase and the partition coefficient, k, as

$$K_{ij} = u_j^* k_j / u_i^* k_i. \quad (2)$$

It is somewhat doubtful whether DTADS is completely dissociated in such medium as nitrobenzene having comparatively low relative permittivity of 34.8 at 25 °C. However, the use of Eq. 2 still shed light on the fundamental factors which determine the selectivity sequence shown in Table 1. Substituting the thermodynamic expression for the partition coefficient in Eq. 2, we have

$$RT\ln K_{ij} = RT\ln(u_j^*/u_i^*) + (\Delta\mu_i^\oplus - \Delta\mu_j^\oplus), \quad (3)$$

where, $\Delta\mu^\oplus$ denotes the standard free energy of transfer of surfactant ion from aqueous medium to membrane phase. If, therefore, the mobilities of surfactant ions of similar size are comparable to each other in nitrobenzene phase, $\ln K_{ij}$ for a homologous series of the surfactant ions should be linearly dependent on n, since $\Delta\mu_j^\oplus$ is known to be a linear function of n.[10] This is exactly what was found with sodium alkyl sulfates and alkanesulfonates. We can thus expect that the slope of the straight lines in Fig. 3 represents the increment of $\Delta\mu_j^\oplus$ per methylene group, *i.e.*, the free energy change, w, for transfering a methylene group from aqueous medium to organic phase. A tentative estimation based on the result in Fig. 3 leads to -2900 J mol^{-1} for w from water to nitrobenzene at 25 °C. This figure is in good agreement with the value of -3100 J mol^{-1} for w from water to *bis*(2-ethylhexyl) phthalate estimated in a previous study of cationic surfactant ion-sensitive poly(vinyl chloride)-membrane electrode containing a neutral carrier[7]. It is also worth noting that the value of w estimated above is close to the free energy change of about -2700 J mol^{-1} associated with the transfer process of a methylene group from water to the hydrophobic interior of surfactant micelle at 25 °C.[11] Apart from the underlying assumptions, therefore, Eq. 2 seems to explain reasonably the observed selectivity characteristics of nitrobenzene-membrane electrode. It has already been pointed out by several authors[1-4,7,8] that the partition coefficient plays the most important role in determining the selectivity sequence of liquid and plastic membrane electrodes for the homologous series surfactant ions.

An interesting comparison may also be made between the selectivity coefficients for surfactant ions with the same alkyl chain length. If we denote the contribution of the head group to the transfer free energy of the surfactant ion by w^h, Eq. 3 can be rewritten as follows.

$$RT\ln(K_{ij}/K_{ii}) \approx w_i^h - w_j^h \quad (4)$$

In Table 2 are given the values of $w_i^h - w_j^h$ estimated for various combinations of surfactant ions with dodecyl chain at 25 °C. Since dodecanesulfonate and dodecylbenzenesulfonate have the same ionic group, the estimated value for these ions is presumed to be close to the transfer free energy of phenylene group from water to nitrobenzene. Indeed, the numerical value in Table 2 is comparable with the free energy change of -1.9×10^4 J mol^{-1} for transfering benzene molecule from water to pure liquid benzene.[12] This fact not only supports the validity of Eq. 4 but suggests that the marked difference in the selectivity coefficients for dodecylbenzenesulfonate and dodecanesulfonate comes virtually from the difference in their partition coefficients. In view of the fact that the value of $w_i^h - w_j^h$ for dodecyltrimethylammonium ion and 1-dodecylpyridinium ion is negligibly small, the hydrophobicity of trimethylammonium group is considered to be nearly identical with that of pyridinium ring. The lack of the hydrophobic part in the ionic head group will probably be responsible for the pronounced decrease in the selectivity coefficient for dodecylammonium ion. Unfortunately, we are unable to give any reasonable account of the observed value of $w_i^h - w_j^h$ for dodecyl sulfate and dodecanesulfonate, since an information about the free energy change associated with the dehydration process of ionic group in nitrobenzene phase is unavailable at the present stage.

Table 2. The calculated values of $w_i^h - w_j^h$ for various surfactant ions with a dodecyl chain at 25 °C

Surfactant ion i	Surfactant ion j	$(w_i^h - w_j^h)$/J mol^{-1}
$-C_6H_4SO_3^-$	$-SO_3^-$	-1.5×10^4
$-SO_3^-$	$-SO_4^-$	9.9×10^3
$-N^+C_5H_5$	$-N^+(CH_3)_3$	180
$-NH_3^+$	$-N^+(CH_3)_3$	9.1×10^3

The present work was partially supported by a Grant-in-Aid for Scientific Research No. 57540254 from the Ministry of Education, Science and Culture.

References

1) B. J. Birch and D. E. Clarke, *Anal. Chim. Acta*, **67**, 387 (1973).
2) D. F. Anghel, G. Popescu, and N. Ciocan, *Mikrochimica Acta*, **1977** II, 639.
3) N. Ciocan and D. F. Anghel, *Fresenius' Z. Anal. Chem.*, **290**, 237 (1978).
4) A. Yamauchi, T. Kunisaki, T. Minematsu, Y. Tomokiyo, T. Yamaguchi, and H. Kimizuka, *Bull. Chem. Soc. Jpn.*, **51**, 2791 (1978).
5) I. M. Kolthoff and W. Stricks, *J. Phys. Colloid Chem.*, **52**, 915 (1948).
6) N. Lakshminarayanaiah, "Membrane Electrodes," Academic Press, New York (1976), p. 124.
7) T. Maeda, M. Ikeda, M. Shibahara, T. Haruta, and I. Satake, *Bull. Chem. Soc. Jpn.*, **54**, 94 (1981).
8) S. G. Cutler, P. Mears, and D. G. Hall, *J. Electroanal. Chem.*, **85**, 145 (1977).
9) Ref. 6, p. 77.
10) C. Tanford, "The Hydrophobic Effect: Formation of Micelles and Biological Membranes," John Wiley & Sons, New York (1973), Chaps. 2 and 3.
11) K. Shinoda, *Bull. Chem. Soc. Jpn.*, **26**, 101 (1953); *J. Phys. Chem.*, **59**, 432 (1955).
12) Ref. 10, p. 9.

Stereochemical Studies of the Electrolytic Reactions of Organic Compounds. Part 18. Comparative Study of Hydrogenation on Metal-black Cathodes and Catalysts

Tsutomu NONAKA,* Masahiko TAKAHASHI, and Toshio FUCHIGAMI
Department of Electronic Chemistry, Tokyo Institute of Technology, 4259 Nagatsuta, Midori-ku, Yokohama, 227
(Received March 10, 1983)

Stereoselective hydrogenation on metal-black cathodes and catalysts, which were prepared by electrodeposition under the same conditions, was comparatively investigated. Stereoisomeric ratios of alcohols formed from the ketones on the Pd- and Pt-black cathodes seemed to be almost equal to those on the corresponding metal-black catalysts, while the yields were quite different between the cathodic and catalytic hydrogenations. On the other hand, results of the hydrogenation of the acetylenes on the cathodes were also different, in not only the yield but also the isomeric ratio, from those on the catalysts. In addition to stereoselectivity, relative hydrogenation rates between *cis*- and *trans*-olefins were compared in both the cathodic and catalytic hydrogenations. It was also found that a mercury pool cathode gave quite different stereochemical results in the hydrogenation of the unsaturated compounds from those obtained with either the metal-black cathodes or the catalysts.

A variety of studies on stereoselective and stereospecific hydrogenations of unsaturated compounds on metal catalysts has been extensively reported, while such studies using catalytically-active metal cathodes have been more rarely reported. Campbell[1] and Sakuma[2] reported that some acetylenic compounds could be hydrogenated on spongy nickel and Pd-black cathodes, respectively, to give the corresponding *cis*-olefins as major products. Kita *et al.*[3] have recently indicated the ratio of *cis*-2-butene to *trans*-2-butene formed as minor products in the cathodic hydrogenation of 1,3-butadiene on a Pt-black cathode. However, these results were not compared with the hydrogenation on catalysts consisting of the same metal components and/or might be incomplete in isomeric analysis of the products. In this work, the hydrogenation of unsaturated compounds to the corresponding stereoisomeric product mixtures on metal-black cathodes and catalysts was comparatively investigated. In addition to this, results obtained were compared with those of the reductive hydrogenation on a mercury cathode which induces a typical cathodic reaction by direct electron-transfer between the cathode and substrates.

In an earlier work,[4] we supposed that the hydrogenation of nitriles on a Pd-black cathode may resemble that on Pd-black catalysts in view of substituent effect. Moreover, it may be consentient that the cathodic hydrogenation on the active metal cathodes resembles the catalytic hydrogenation in gross natures, since the general course of the cathodic hydrogenation is seemed to be very similar to that of the catalytic hydrogenation, as illustrated in Fig. 1. However, it should be difficult to exclude completely that there may be some differences between the both hydrogenations, because of few comparative studies reported. In this viewpoint, it is interesting to compare the cathodic hydrogenation with the catalytic hydrogenation on the same metal: If the both hydrogenations give the same result, the cathodic hydrogenation may be able to be an excellent method, instead of catalytic one in some cases, without any gaseous hydrogen sources, air-tight reactors and efficient stirring equipments, while it can be used as a characteristic method in a case where the both give otherwise results. In addition, comparative studies of the both hydrogenations may result in some new informations available for a mechanistic discussion on the hydrogenations.

A metal catalyst surface is electrically neutral or slightly positive.[5] On the catalyst surface, hydrogen molecules dissociate and the resulting atomic hydrogen adsorbs. An unsaturated compound molecule contacts with the catalyst surface and its π-electron is donated to the unoccupied d-band of the catalyst to form a π-adsorption state. This is an oxidized state rather than reduced one. An active adsorbing species, which is a π-complex-adsorption or σ-adsorption state, is formed by the back-donation of an electron from the catalyst, and the hydrogenation is completed *via* a partially hydrogenated state resulted by the attack of the adsorbing atomic hydrogen and the consequent fission of a bond between the catalyst and the substrate. In Fig. 1, the general course of the hydrogenation on metal catalysts and also cathodes is illustrated.[5]

In the case of hydrogenation on catalytic cathodes, hydrogen is formed by the discharge of protons on the cathode surface. Since the cathode surface should be more negative than the catalyst surface, some differences between the cathodic and catalytic hydrogenations on the same kind of metal may be found.

In a previous work,[6] it was found that the stereoisomeric ratio cis/trans of 4-*t*-butylcyclohexanol formed in the cathodic and catalytic hydrogenation of 4-*t*-butylcyclohexanone on Pt-black in a strongly acidic solution was greatly affected by the preparative method of Pt-black: The ratio cis/trans varied in the ranges of 0.9—4.3 and 0.9—2.7 in the cathodic and catalytic hydrogenation, respectively.

In this work, similar stereochemical comparison was made under a variety of reaction conditions, extending the substrate compounds to an open-chain ketone and also acetylenic and olefinic compounds. For a successful investigation, following situations should be required: (a) The cathode and the catalyst prepared

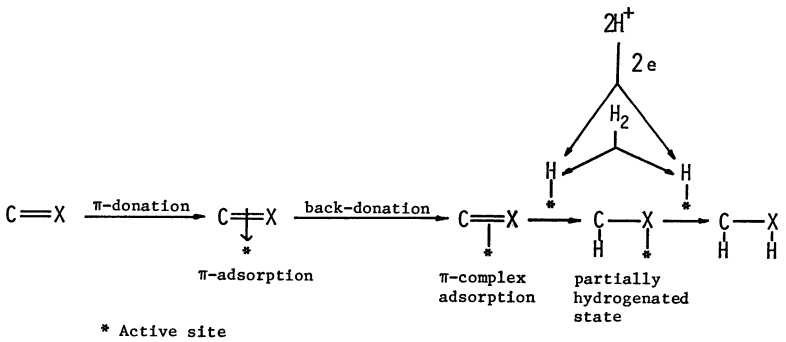

Fig. 1. General course of hydrogenation of unsaturated bond on active metal cathode and catalyst.

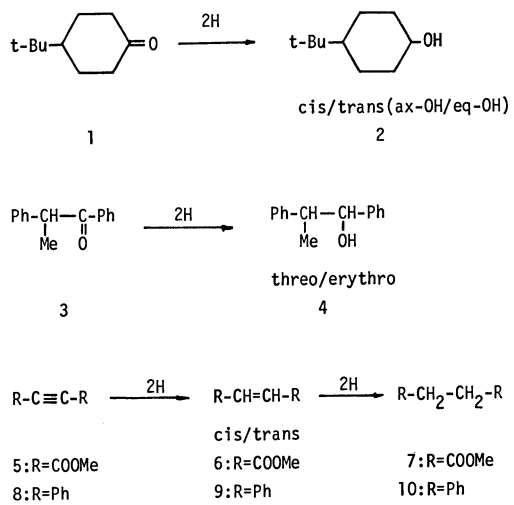

Fig. 2. Hydrogenation of unsaturated compounds.

Table 1. Hydrogenation of 4-*t*-butylcyclohexanone (**1**) on Pt- and Pd-black cathodes and catalysts

Cathode or catalyst	Solution	4-*t*-Butylcyclohexanol (**2**) Cathodic Yield/%	cis/trans	Catalytic Yield/%	cis/trans
Pt-black	A[a]	46 63[d]	0.9 1.1	48	0.9
Pt-black	WA[b]	3	0.2	16	0.2
Pt-black	B[c]	5	1.0	100	1.0
Pd-black	A[a]	30	0.1	0	—
Pd-black	B[c]	0	—	0	—
Hg-pool	A[a]	30	0.2	—	—
Hg-pool	B[c]	16	0.4	—	—

a) Strongly acidic. b) Weakly acidic. c) Strongly basic. d) Electrolyzed at 2.0 A dm^{-2} (at 0.5 A dm^{-2} unless stated otherwise).

from the same kind of metal by the same method can be used. (b) The same type of reaction of the same substrate compound can occur on the cathode and the catalyst prepared thus. (c) The cathodic and catalytic reactions can proceed under the same conditions to give detectable stereochemical results. Items (a) and (b) could be almost completely satisfied, while it seemed to be difficult to give the strictly same reaction conditions(Item (c)) for the cathodic and catalytic hydrogenation because of no catalytic reaction factors corresponding to current density and amount of charge passed in the electrolytic reaction.

Results and Discussion

In this work, the hydrogenation of ketones(*t*-butylcyclohexanone (**1**) and 1,2-diphenyl-1-propanone (**3**)), acetylenes (dimethyl acetylenedicarboxylate (**5**) and diphenylacetylene (**8**)) and olefins (dimethyl maleate (cis-**6**), dimethyl fumarate (*trans*-**6**), *cis*-stilbene (*cis*-**9**), and *trans*-stilbene (*trans*-**9**)) on metal (Pt and/or Pd)-black cathodes and catalysts were comparatively investigated under the same reaction conditions. Results on a mercury cathode were also given for comparison with the above hydrogenation.

Metal-black Cathodes and Catalysts. Generally, hydrogenation is greatly affected by the preparative procedure of catalysts. Therefore, in comparative studies of cathodic and catalytic hydrogenation on metal-blacks, the preparative procedure should be strictly controlled. Pt-black electrodeposited on Pt-plates from a chloroplatinic acid solution containing a small amount of lead(II) acetate was used in this work, because Pt-black prepared thus gave more reproducible results in both the cathodic and catalytic hydrogenations than others.[6] Pd-black was also electrodeposited on Pd-plates from a palladium chloride solution without lead(II) acetate.

One of the metal-black plates prepared at the same time, under the same conditions and by the same procedure was used as a cathode in an electrolytic cell, and another one was placed in a margen-flask for catalytic hydrogenation.

Stereoselective Hydrogenation of Ketones. As shown in Table 1, 4-*t*-butylcyclohexanone (**1**) was hydrogenated on both Pt-black cathode and catalyst in a wide pH range to give 4-*t*-butylcyclohexanol (**2**). Although the isomeric ratio of **2** formed in the cathodic hydrogenation was slightly influenced by current density, the ratio seemed almost equal to that in the catalytic hydrogenation.

On the other hand, **1** could not be hydrogenated on the Pd-black catalyst in both strongly acidic(A-solution) and basic(B-solution) media. In contrast, **1** could be hydrogenated on the Pd-black cathode in the A-solution to give **2** in 30% yield. This result

may suggest that an oxygen-Pd bonding(Fig. 1) on the cathode in a partially hydrogenated state is weakened by its negative polarization and consequently that the hydrogenation can proceed more easily.

The hydrogenation of methylcyclohexanones on the Pd-black cathode in the A-solution hardly proceeded to result in only 1—2% yields. Comparison of this fact with the result obtained in the hydrogenation of **1** suggests that steric hindrance between the cathode surface and the *t*-butyl group weakens the oxygen-Pd bonding in the partially hydrogenated state and promotes the progress of the hydrogenation to the final state.

In the B- and weakly acidic (WA) solutions, the isomeric ratios of **2** formed on the Pt-black cathode were equal to those on the Pt-black catalyst, as described above, but the yields were extremely lower. The cathode should be more negetively polarized in the B- and WA-solutions than the A-solution. Therefore, the lower yields may be due to such a more negative polarization of the Pt-black cathode.

As a conclusion, the yield of **2** is influenced by the polarization of cathode and catalyst, while the isomeric ratio is not. More exactly describing, the negative polarization of the Pt-black suppresses the adsorption of substrate on it and decreases the yield, while on the Pd-black the polarization assists to cleave the oxygen-Pd bonding in the partially hydrogenated state and increases the yield. Such a difference between the Pt- and Pd-blacks may be caused by the stronger adsorption[7] and bonding[8] in the latter.

A mercury-pool cathode, which is a typical high hydrogen overvoltage one, resulted in the isomeric ratio smaller than the thermodynamic equilibrium value(0.25[9]) in the A-solution, while larger in the B-solution. Different stereochemical results between the metal-black and mercury-pool cathodes should be due to different reaction mechanism between the both cathodes.

At the next stage of the investigation, the stereoselective hydrogenation of open-chain ketones was attempted: Among 1,2-diphenyl-1-propanone (**3**), 3-phenyl-2-butanone, and 4-phenyl-2-pentanone, only **3** could be hydrogenated on either the Pd-black cathode or catalyst, and others could not.

As shown in Table 2, **3** could be hydrogenated on Pt- and Pd-black cathodes and catalysts to give 1,2-diphenyl-1-propanol (**4**) in good yields. The isomeric ratio threo/erythro of **4** formed in the cathodic hydrogenation seemed almost equal to that in the catalytic hydrogenation, except for the result obtained on the Pd-black in the WA-solution. It seems difficult to rationalize this exceptional result. An Hg-cathode gave some different isomeric ratios from those on the metal-black cathodes.

Table 2. Hydrogenation of 1,2-diphenyl-1-propanone (**3**) on Pt- and Pd-black cathodes and catalysts

Cathode or catalyst	Solution	1,2-Diphenyl-1-propanol (**4**)			
		Cathodic		Catalytic	
		Yield %	threo/erythro	Yield %	threo/erythro
Pt-black	A[a]	72	0.0	27	0.0
Pt-black	WA[b]	100	0.1	30	0.0
Pt-black	B[c]	11	0.0	14	0.0
Pd-black	A[a]	72 19[d]	0.5 0.45	23	0.5
Pd-black	WA[b]	78	1.0	100	0.6
Pd-black	B[c]	0	—	0	—
Hg-pool	A[a]	11	0.5	—	—
Hg-pool	WA[b]	94	0.4	—	—
Hg-pool	B[c]	98	0.3	—	—

a) Strongly acidic. b) Weakly acidic. c) Strongly basic. d) Electrolyzed at 2.0 A dm^{-2} (at 0.5 A dm^{-2} unless stated otherwise).

Stereoselective Hydrogenation of Acetylenes. Dimethyl acetylenedicarboxylate (**5**) was hydrogenated on the Pd-black cathode and catalyst to give the corresponding olefin(dimethyl maleate; *cis*-**6** and fumarate; *trans*-**6**), as shown in Table 3. In this hydrogenation, a part of **6** formed seemed to be hydrogeanated further to dimethyl succinate (**7**). Therefore, in order to discuss strictly stereochemical results obtained, some correction should be made for the estimation of isomeric ratio cis/trans of **6**. For the correction, the relative hydrogenation rate ratio k_c/k_t of *cis*-**6** to *trans*-**6** was used. The detailed description of k_c/k_t is given in the following item.

Both the uncorrected and corrected isomeric ratios of **6** obtained in the cathodic hydrogenation were smaller than those in the catalytic hydrogenation in

Table 3. Hydrogenation of dimethyl acetylenedicarboxylate (**5**) on Pd-black cathode[a] and catalyst

Cathode or catalyst	Solution	Dimethyl 2-butenedioate (**6**)				Dimethyl succinate (**7**)	
		Cathodic		Catalytic		Catalytic	
		Yield/%	cis/trans[b]	Yield/%	cis/trans[b]	yield/%	Catalytic yield/%
Pd-black	A[c]	13	12(1.4)	40	32(3.9)	35	21
Pd-black	WA[d]	10	12(1.2)	12	19(1.7)	40	29
Pd-black	B[e]	Trace	—(0.9)	3	∞(1.1)	13	9
Hg-pool	A[c]	32	0.0	—	—	30	—
Hg-pool	B[e]	27	0.0	—	—	Trace	—

a) Electrolyzed at 0.5 A dm^{-2}. b) Figures in parentheses show the corrected values. c) Strongly acidic. d) Weakly acidic. e) Strongly basic.

Table 4. Hydrogenation of 1,2-diphenylacetylene (**8**) on Pd- and Pt-black cathods[a] and catalysts

Cathod or catalyst	Solution	Stilbene (**9**)				1,2-Diphenylethane (**10**)	
		Cathodic		Catalytic			
		Yield/%	cis/trans[b]	Yield/%	cis/trans[b]	Cathodic yield/%	Catalytic yield/%
Pd-black	A[c]	68	46(6.1)	77	24(6.4)	20	10
Pd-black	B[d]	60	7(4.8)	82	7(5.8)	9	7
Pt-black	A[c]	27	9	36	7	32	30
Pt-black	B[d]	82	16	20	4	2	Trace
Hg-pool	A[c]	1	0.6	—	—	Trace	—
Hg-pool	B[d]	8	0.2	—	—	Trace	—

a) Electrolyzed at 0.5 A dm^{-2}. b) Figures in parentheses show the corrected values. c) Strongly acidic. d) Strongly basic.

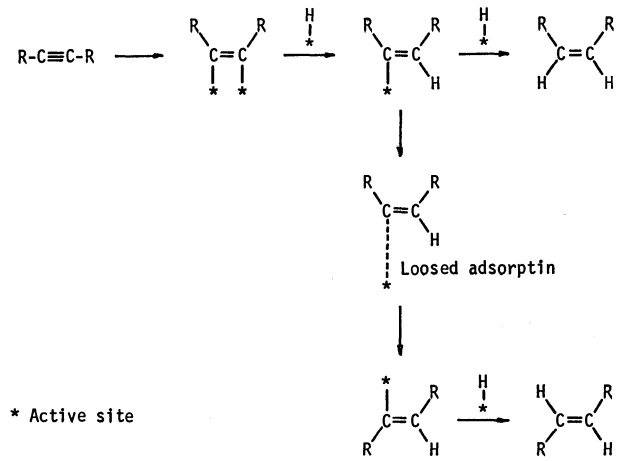

Fig. 3. Stereochemical course of hydrogenation of acetylenes.

Table 5. Hydrogenation rate ratio(k_c/k_t) of *cis*-olefins to the *trans*-olefins on Pd-black cathode[a] and catalyst

Olefin	Solution	k_c/k_t[b]	
		Cathodic	Catalytic
Dimethyl 2-butenedioate (**6**)	A[c]	0.81	0.87
	WA[d]	0.86	1.01
	B[e]	0.96	1.11
Stilbene (**9**)	A[c]	0.84	0.28
	WA[d]	0.84	0.82
	B[e]	0.99	1.39

a) Electrolyzed at 0.5 A dm^{-2}. b) Equimolar mixtures of *cis*- and *trans*-olefins were incompletely hydrogenated and the ratio k_c/k_t was calculated from amounts of unreacted olefins. c) Strongly acidic. d) Weakly acidic. e) Strongly basic.

the same solution. The cathodic hydrogenation of diphenylacetylene (**8**) on the Pd-black also gave smaller cis/trans ratios of stilbene (**9**) than the catalytic hydrogenation, as shown in Table 4.

Generally, disubstituted acetylenes are hydrogenated on metal catalysts to give the *cis*-olefins, which are thermodynamically less stable than the corresponding *trans*-olefins, in excess.[10] As illustrated in Fig. 3, an acetylene molecule adsorbs in the *cis*-olefin form(sp^2) on the catalyst[11] and hydrogenated *via* the partially hydrogenated state.[12] If the adsorption is loosed by steric hindrance between the adsorbing species and the catalyst, so-called the catalyst hindrance, the formation of the *cis*-olefin is suppressed in some extent.[13] The stronger adsorption reasonably causes the higher catalyst hindrance. Therefore, the more negative polarization of the Pd-black also causes the weaker adsorption and the lower hindrance, and cosequently the supression of the *cis*-olefin formation. This is a rationalization for the smaller cis/trans ratio in the cathodic hydrogenation than the catalytic hydrogenation.

The cis/trans ratio decreased in the B-solution in both the cathodic and catalytic hydrogenations. This may be rationalized as due to weak adsorption in basic solution[14,15] or the isomerization of olefin formed,[16] though the hydrogenation was not carried out under so drastic that the isomerization occurs easily.

It is noticeable that the hydrogenation of **8** on the Pt-black resulted in a reversed situation, comparing with that on the Pd-black, though any corrected isomeric ratios of **9** could not be given. It may be also interesting to note that the Hg-pool cathode afforded the completely reversed isomeric ratios of **9** to the metal-blacks.

Hydrogenation Rate Ratio of cis-*Olefins to the* trans-*Olefins.* Mixtures of *cis*- and *trans*-olefins (**6** and **9**) were hydrogenated with insufficient amounts of electricity and hydrogen on the Pd-black cathode and catalyst, respectively. The hydrogenation rate ratio (k_c/k_t) of the *cis*-olefin to the *trans*-olefin was calculated from amounts of the unreacted olefin isomers, considering their average concentrations during the hydrogenation:

$$k_c/k_t = \frac{(c_1-c_2)}{(t_1-t_2)} \cdot \frac{(t_1+t_2)/2}{(c_1+c_2)/2} = \frac{(c_1-c_2)(t_1+t_2)}{(t_1-t_2)(c_1+c_2)},$$

where c_1 and c_2 are the initial and final concentrations of the *cis*-olefin, and t_1 and t_2 are those of the *trans*-olefin. Table 5 shows k_c/k_t values obtained in the hydrogenation of the equimolar mixtures of the isomers ($c_1=t_1$).

Results for each olefin are apparently clear and interesting, as shown in Table 5. However, it seems difficult to rationalize comprehensively these kinetic data, because (a) the hydrogenation course involves several activation steps,[17] and (b) the rate-determining step can not be specified.[18]

Experimental

Materials. *Ketones*: Cyclic ketones (**1** and three methylcyclohexanones) were commercially supplied from Tokyo Kasei Co., while open-chain ketones (**3**, 3-phenyl-2-butanone and 4-phenyl-2-pentanone) were prepared by methods of our earlier works.[19,20]

Acetylenes and Olefins: All the compounds (**5**, **6**, **8**, and **9**) were commercially supplied.

Standard Samples of Products: The compounds **2**, **6**, **7**, and **10** were commercially supplied, while *threo*- and *erythro*-**4** were prepared by the method of earlier work.[19]

Metal-blacks: Pt-black was electrodeposited on a Pt plate (Area, 7.7 cm^2) from 33 ml of an aqueous solution containing chloroplatinic acid (1.0 g as $H_2[PtCl_6]\cdot 6H_2O$) and lead(II) acetate (7 mg) by passing electricity at 2 $A\cdot dm^{-2}$ of current density for 10 min. Pd-black was also deposited on a Pd plate (area, 7.7 cm^2) from 33 ml of 1 M (1 M= 1 mol dm^{-3}) HCl containing palladium chloride (0.2 g) by the same procedure as the above. The Pt- and Pd-blacks prepared thus were repeatedly washed with cold water, and then cathodically treated at 2 A dm^{-2} in 1 M H_2SO_4 for 30 min and sulfuric acid was rinsed out with warm water.

Usually, two pieces of the metal-blacks were prepared for the cathodic and catalytic hydrogenations at same time.

Reaction Solutions: Three kinds of solutions were used: A-solution, 1 M H_2SO_4-CH_3OH (1:1, v/v); WA-solution, 3 M AcONa-3 M AcOH-CH_3OH (1:1:2, v/v); B-solution, 2 M NaOH-CH_3OH (1:1, v/v). 100 ml of the solution containing the substrate in 10—50 mM was used for each experiment.

Hydrogenation. *Cathodic Hydrogenation*: 2 F/mol was passed for each electrolysis at 0.5 A dm^{-2} and room temperature, except for the case of **3** where 20 F/mol was passed.

Catalytic Hydrogenation: The hydrogenation was carried out in a margen-flask, in which the metal-black plate was placed, at atmospheric pressure and room temperature. The concentration of substrate was same as that in the corresponding cathodic hydrogenation. The margen-flask was continuously shaken till 1 mol H_2/1 mol substrate was taken up.

Product Analysis. After the hydrogenation, the reaction solution was neutralized with aqueous sulfuric acid or sodium hydroxide and then extracted repeatedly with ether. The combined ethereal extract was dried over anhydrous sodium sulfate. The solution concentrated by evaporation was subjected to gas-chromatographic analysis under following conditions: A 2.25 m PEG 20 M column at 90 °C for **1**, **2**, and **5**—**7**; a 4 m PEG 20 M column at 200 °C for **8**—**10**; a 4 m Apiezon Grease L column at 200 °C for **3** and **4**.

In the hydrogenation of **1** and **3**, the corresponding alkanes and hydrodimers were also formed as by-products, but these were not analyzed quatitatively.

The authors wish to thank professor Taro Sekine for his helpful suggestions and discussions. This work was partly supported by a Grant-in-Aid for Scientific Research No. 0055320 from the Ministry of Education, Science and Culture.

References

1) K. N. Campbell, *J. Am. Chem. Soc.*, **65**, 965 (1943).
2) M. Sakuma, *J. Electrochem. Soc. Jpn.*, **28**, 164 (1960).
3) H. Kita and N. Kubota, *Electrochim. Acta*, **27**, 861 (1982).
4) Y. Hatta, N. Yui, T. Nonaka, and K. Odo, *Nippon Kagaku Kaishi*, **1974**, 2277.
5) S. Mitsui and M. Imaizumi, *Nippon Kagaku Zasshi*, **77**, 1516 (1956).
6) T. Nonaka, M. Takahashi, and T. Fuchigami, *J. Electrochem. Soc. Jpn.*, **51**, 129 (1983).
7) Since Pd-catalysts are more sensitive to "catalyst hindrance" than Pt-catalysts, the absorption on the Pd-catalysts may be stronger.
8) E. Breitner, E. Roginski, and P. N. Rylander, *J. Org. Chem.*, **24**, 1855 (1959).
9) S. Mitsui, H. Saito, and K. Hebiguchi, The 24th National Meeting of the Chem. Soc. of Jpn., 1967, Abstract III, p. 88.
10) W. Orshnik, G. Karmas, and A. D. Mebane, *J. Am. Chem. Soc.*, **74**, 295 (1952).
11) F. J. McQuillin, W. O. Ord, and P. L. Simpson, *J. Chem. Soc.*, **1963**, 5995.
12) J. Sheridan, *J. Chem. Soc.*, **1945**, 133.
13) W. Surber, *Helv. Chim. Acta*, **39**, 1299 (1956).
14) S. Pietra and C. B. Riolo, *Gazz. Chim. Ital.*, **86**, 1129 (1956); *Chem. Abstr.*, **52**, 269d (1958).
15) F. J. McQuillin and W. O. Ord, *J. Chem. Soc.*, **1959**, 2902.
16) R. Romanet, *Compt. Rend.*, **236**, 1044, 1176, 1677 (1953).
17) S. Siegel, *Adv. Catal.* **16**, 123 (1966).
18) S. Mitsui, "Organic Reaction Mechanism (Yuki Han-no Kiko," ed by M. Imoto, Tokyo Kagaku Dojin, Tokyo (1970), Vol. 13, Part 1, p. 11.
19) T. Nonaka, Y. Kusayanagi, and T. Fuchigami, *Electrochim. Acta*, **25**, 1679 (1980).
20) T. Nonaka and Y. Kusayanagi, *Electrochim. Acta*, **26**, 893 (1981).

 © 1983 The Chemical Society of Japan Bull. Chem. Soc. Jpn., 56, 2589—2590 (1983)

Synergistic Solvent Extraction of Crown Ether Complexes with Alkali Metal Picrates by Neutral Donor Solvents

Yasuyuki TAKEDA

Department of Chemistry, Faculty of Science, Chiba University, Yayoi-chō, Chiba 260

(Received March 25, 1983)

The solvent extraction of rubidium and caesium picrates has been studied at 25 °C with mixtures of crown ether and tributyl phosphate (TBP) or trioctylphosphine oxide (TOPO) in benzene, and the adduct-formation constants in the benzene solution have been calculated. The crown ethers used in this work were 12-crown-4 (12C4), 15-crown-5 (15C5), and benzo-15-crown-5 (B15C5). The stoichiometric composition of any extracted complex under the present experimental conditions is alkali metal ion : crown ether : TBP or TOPO : picrate ion = 1 : 1 : 1 : 1. The TOPO complex is more extractable than the corresponding TBP complex. The extractability of the Rb^+ complex is larger than that of the corresponding Cs^+ complex. For both TBP and TOPO, the adduct-formation constant value sequences of Rb^+ and Cs^+ are B15C5 > 12C4 > 15C5 and 12C4 > B15C5 > 15C5, respectively.

Extractions of crown ether complexes with metal picrates are enhanced by the addition of a neutral donor solvent such as tributyl phosphate (TBP) and trioctylphosphine oxide (TOPO).[1-3] This enhancement is attributed to the fact that the crown ether complexes with the metal picrates form adducts with the neutral donor solvents. The crown ether complex (metal ion : crown ether : picrate ion = 1 : 1 : 1) accepts one or two neutral donor solvents. The magnitude of the adduct-formation constant in the organic phase reflects the chemical nature of the metal ion trapped in the crown ether cavity.

At present, only a few quantitative data have been reported on the synergistic solvent extraction study for crown ethers.

In the present study, the solvent extraction of rubidium and caesium picrates has been investigated at 25 °C with mixtures of crown ether and TBP or TOPO in benzene. The compositions of the extracted complexes have been determined and the adduct-formation constants in a benzene solution have been calculated. The crown ethers used in this work were 12-crown-4 (12C4), 15-crown-5 (15C5), and benzo-15-crown-5 (B15C5). Since it is known that TOPO forms more stable adducts than TBP, TOPO was chosen in the hope that the higher extractabilities for alkali metal ions compared with TBP could be obtained.

Experimental

Materials. 12-Crown-4 and TBP were obtained from Wako-Pure Chemicals, Ltd., 15C5 from Nisso Co., Ltd., and TOPO from Dojin-Do Co., Ltd. They were used without further purification. The method of the purification of B15C5 (Merck Japan Ltd.) was described elsewhere.[1] Analytical-grade benzene was washed three times with distilled water.

Procedure. An aqueous phase contained alkali metal hydroxide ($(2.0—6.5)\times10^{-3}$ M; 1 M = 1 mol dm^{-3}) and picric acid ($(1.0—8.9)\times10^{-3}$ M). A benzene phase contained one of the extractants (TBP: 9.0×10^{-2}—6.5×10^{-1} M, TOPO: 2.4×10^{-2}—1.8×10^{-1} M, crown ether: 1.4×10^{-3}—1.3×10^{-1} M), or both TBP (8.8×10^{-2}—6.6×10^{-1} M) or TOPO (2.4×10^{-2}—1.8×10^{-1} M) and crown ether (1.4×10^{-3}—1.3×10^{-1} M). The two phases in stoppered glass tubes (30 ml) were shaken in a thermostated water bath for 45 min at 25±0.2 °C and then centrifuged. The initial valume of each phase was 10 ml in all cases. The extractions were carried out at pH 5.8—6.2. The alkali metal in the benzene phase was back-extracted into 8 ml of a 0.1 M HNO_3 aqueous solution, and the alkali metal concentration was determined by atomic absorption spectrometry.

Results

The equilibrium constants for this solvent extraction system can be defined by the following equations:

$$K\mathrm{ex(MLL'A)} = [\mathrm{MLL'A}]_o[\mathrm{H^+}]/[\mathrm{M^+}][\mathrm{L}]_o[\mathrm{L'}]_o[\mathrm{HA}]_o, \quad (1)$$

$$K_{\mathrm{D,L}} = [\mathrm{L}]_o/[\mathrm{L}], \quad (2)$$

$$K\mathrm{ex(HA)} = [\mathrm{HA}]_o/[\mathrm{H^+}][\mathrm{A^-}], \quad (3)$$

$$K_{\mathrm{MLL'A,o}} = [\mathrm{MLL'A}]_o/[\mathrm{MLA}]_o[\mathrm{L'}]_o, \quad (4)$$

where the subscript "o" and the lack of a subscript denote the organic and the aqueous phase, respectively; M^+, A^-, L, and L′ refer to an alkali metal ion, a picrate ion, crown ether, and another neutral ligand, respectively. The all activity coefficients of the chemical species in this study have been assumed as unity. The Kex(HA) value was spectrophotometrically determined to be 247.

When the benzene phase contains both L and L′, the distribution ratio is represented by

$$D = [\mathrm{MLL'A}]_o/[\mathrm{M^+}]. \quad (5)$$

The substitution of Eqs. 1 and 3 into Eq. 5 gives

$$D = K\mathrm{ex(MLL'A)}K\mathrm{ex(HA)}[\mathrm{L}]_o[\mathrm{L'}]_o[\mathrm{A^-}]. \quad (6)$$

The log $(D/[A^-])$ *vs.* log $[L]_o$ plots for the 15C5-TOPO system are given in Fig. 1. The log$(D/[A^-])$ *vs.* log$[L']_o$ plots for the 15C5-TOPO system are illustrated in Fig. 2. The plots of the other systems (12C4-TBP, 12C4-TOPO, and B15C5-TOPO) were similar, and so have been omitted. For each system, the plots of both Rb and Cs have a slope of 1 (*e.g.*, Figs. 1 and 2). Thus, the Kex(MLL′A) in this study can be described by Eq. 1. The value of $[L']_o$ in Eq. 6 was presumed to be nearly equal to that of $[L']_t$, and those of $[L]_o$ and $[A^-]$ were calculated from Eqs. 7 and 8 respectively:

$$[\mathrm{L}]_o = ([\mathrm{L}]_t - [\mathrm{MLL'A}]_o)/(1 + K_{\mathrm{D,L}}{}^{-1}), \quad (7)$$

$$[\mathrm{A^-}] = [\mathrm{HA}]_t - [\mathrm{MLL'A}]_o, \quad (8)$$

where the subscript "t" denotes the total concentration. The equilibrium constants obtained from these data

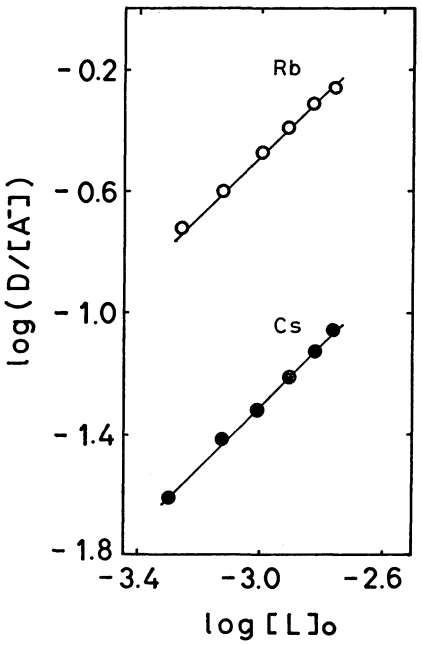

Fig. 1. Plots of log (D/[A$^-$]) *vs.* log [L]$_o$ for the 15C5-TOPO system (L=15C5).

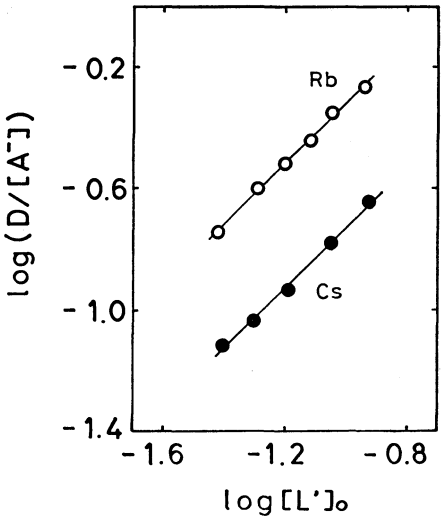

Fig. 2. Plots of log (D/[A$^-$]) *vs.* log [L']$_o$ for the 15C5-TOPO system (L'=TOPO).

are listed in Table 1.

Discussion

In the case of the same crown ether, the extractability of the same alkali metal ion increases in the order TBP<TOPO<crown ether except Cs(12C4)$_2$A (Table 1). For the same L and L' system, Rb$^+$ is more extractable than Cs$^+$, and extraction-selectivity for Rb$^+$ compared to Cs$^+$ is enhanced in the order TBP< TOPO<crown ether (Table 1).

$K_{MLL'A,o}$ represents the formation constant for the MLL'A complex in a benzene solution. For each of Rb$^+$ and Cs$^+$, the log $K_{MLL'A,o}$ value of the same crown ether increases in the order TBP<TOPO< crown ether except for the case of Cs(12C4)$_2$A. The reason why the TOPO complex is more stable than the TBP complex may be attributed to the higher basicity of TOPO compared with that of TBP. It is interesting that, although the number of donor oxygen atoms is much larger for 12C4 than for TOPO, the Cs(12C4)$_2$A complex is slightly less stable than the Cs(12C4)(TOPO)A complex. The fact that the other sandwich complexes with two crown ethers are more stable than the corresponding TOPO complexes may reflect the larger number of donor oxygen atoms of the crown ether compared to that of TOPO.

For both TBP and TOPO, the log $K_{MLL'A,o}$ value sequences of Rb$^+$ and Cs$^+$ are B15C5>12C4>15C5 and 12C4>B15C5>15C5, respectively. It thus appears that the electron density in the crown ether cavity is one of the most important factors in determining the stabilities of the TBP- and TOPO-adducts.[1] In each case of the ML(TOPO)A and ML(TBP)A complexes, the stability for Rb$^+$ is larger than that for Cs$^+$. This is probably due to the higher charge density of Rb$^+$ compared to Cs$^+$.

The MLA complex in the series of our synergistic solvent extraction studies[1,2] accepts a TBP or a TOPO molecule in a benzene solution, while, a dibenzo-18-crown-6 complex with silver picrate accepts two TOPO molecules in a $CHCl_3$ solution.[3]

TABLE 1. EQUILIBRIUM CONSTANTS AT 25 °C

$K_{D,L}$	12C4 0.15[4]	15C5 0.15$_6$[5]	B15C5 20[1]	
	L	L'	Rb$^+$	Cs$^+$
log Kex(MLL'A)	12C4	TBP	−0.84	−0.99
		TOPO	−0.34	−0.57
		12C4	−0.29[2]	−0.64[2]
	15C5	TBP	0.56[2]	0.19[2]
		TOPO	1.25	0.78
		15C5	2.15[2]	1.48[2]
	B15C5	TBP	0.37[1]	−0.15[1]
		TOPO	0.88	0.21
		B15C5	1.22[1]	0.41[1]
log $K_{MLL'A,o}$	12C4	TBP	1.26	1.19
		TOPO	1.76	1.61
		12C4	1.81[2]	1.54[2]
	15C5	TBP	0.81[2]	0.68[2]
		TOPO	1.50	1.27
		15C5	2.40[2]	1.97[2]
	B15C5	TBP	1.32[1]	1.16[1]
		TOPO	1.83	1.52
		B15C5	2.17[1]	1.72[1]

References

1) Y. Takeda, Y. Wada, and S. Fugiwara, *Bull. Chem. Soc. Jpn.*, **54**, 3727 (1981).
2) Y. Takeda, *Bull. Chem. Soc. Jpn.*, **54**, 526 (1981).
3) Y. Hasegawa, K. Suzuki, and T. Sekine, *Chem. Lett.*, **1981**, 1075.
4) Y. Takeda, *Bull. Chem. Soc. Jpn.*, **53**, 2393 (1980).
5) Y. Takeda and H. Katō, *Bull. Chem. Soc. Jpn.*, **52**, 1027 (1979).

Phosphorescence Spectra of *p*-Dichlorobenzene in Various Matrices at 1.4 K

Minoru KINOSHITA,* Narito GOTO,† and Noriko IWASAKI

The Institute for Solid State Physics, The University of Tokyo, Roppongi, Minato-ku, Tokyo 106

(Received April 1, 1983)

The phosphorescence spectra of *p*-dichlorobenzene have been obtained at 1.4 K in various hosts; benzene, *p*-xylene, *p*-dichlorobenzene, *p*-dichlorobenzene-d_4, and *p*-dibromobenzene. The long progressions in the b_{2g}, C–Cl bending vibration are indicative of a molecular distortion in the out-of-plane direction. With the aid of the technique of optical detection of zero-field magnetic resonance, the intense 1580 cm^{-1} band previously ascribed to the a_g, ν_{8a} vibration is found to be due to the b_{3g}, ν_{8b} vibration. The appearance of the b_{3g} band with strong intensity suggests a possibility of an additional in-plane distortion of phosphorescent *p*-dichlorobenzene.

The electronic structure and the molecular geometry of phosphorescent *p*-dichlorobenzene (DCB) have been the subjects of extensive studies in these years. It was first proposed from polarized T←S absorption spectra that the orbital symmetry of the lowest triplet state of DCB is B_{2u}.[1] However, optically detected magnetic resonance (ODMR) experiments[2–6] performed afterwards have shown that the symmetry is most probably described by B_{1u}.

The phosphorescence spectra of the exciton[7,8] and the traps[3,8] in a neat DCB crystal exhibit long progressions in the b_{2g}, C–Cl bending vibration. This suggests that the DCB molecule is distorted in the phosphorescent state. The out-of-plane position of the two chlorine atoms has been proposed by Buckley and Harris[2] from the observation of somewhat large (≈8%) reductions in the ^{35}Cl quadrupolar coupling constant from −69.662 MHz in the ground state to −64.5 MHz in the triplet state. Furthermore, recent ODENDOR experiments[6] also indicate that the C–H fragments are not positioned in the moleculalr plane.

The phosphorescence spectrum of the 23 cm^{-1} trap-(x-trap) in a neat DCB crystal shows a strong vibrational band at 1579 cm^{-1} from the electronic origin.[3,8] This band corresponds to the extremely strong band due to the e_{2g}, ν_8 skeletal vibration in the phosphorescence spectrum of benzene. In benzene, it has been shown that the appearance of this band with remarkable intensity is due to a strong vibronic coupling or the pseudo Jahn-Teller interaction between the lowest $^3B_{1u}$ state and the second lowest $^3E_{1u}$ state.[9–11] This interaction causes potential curve distortions along the coordinate of the ν_8 mode in the interacting electronic states and a deviation of the triplet electron distribution from the hexagonal symmetry.

It is quite natural to expect that the strong 1579 cm^{-1} band in the DCB phosphorescence also results from a similar cause. In DCB, the ν_8 vibration splits into the a_g, ν_{8a} and the b_{3g}, ν_{8b} vibration. In most works, however, the band at approximately 1580 cm^{-1} was assigned as being due to the a_g vibration,[7,8] but Buckley *et al.*[3] ascribed it to a superposition of the a_g and the b_{3g} vibration. The PMDR(phosphorescence microwave double resonance) spectra by these authors clearly indicate a marked difference in the behaviour of this band and that of other a_g bands; this suggests a b_{3g} possibility. However, the relative radiative decay rates of the T_y and T_z spin sublevels are found to be $k_y^r/k_z^r=1.4$ in this band, which is unfavorable for the b_{3g} assignment.

The main purpose of this paper is to demonstrate that the band is superposed by the a_g and b_{3g} vibrations with vibrational frequencies slightly different from each other and that the b_{3g} band appears more strongly in most cases. The latter relates to a possibility of an in-plane distortion in the triplet spin distribution in addition to the out-of-plane distortion of the molecule proposed.[2]

Experimental

p-Dichlorobenzene was purchased from Wako Pure Chemical Industries, Ltd. and purified by recrystallizations from ethanol and then by zone-refining (more than 150 passes). *p*-Dichlorobenzene-d_4 was purchased from Merck, Sharp & Dohme, Canada Ltd. and purified by zone-refining (more than 150 passes). Commercially available zone-refined *p*-dibromobenzene was used without further purification. Crystals were grown by the Bridgman method. Benzene and *p*-xylene were used after purification by vacuum distillation.

The samples were excited with light of 313 nm from a super-high pressure mercury arc lamp (Orc CH-612, 1 kW) through a saturated $NiSO_4$ aqueous solution filter and a Toshiba UV-D33S filter. The phosphorescence emission from a sample was isolated by a Spex 1700-III 3/4 m spectrometer in conjunction with a pair of rotating disk choppers and detected by an EMI-9789SB photomultiplier tube and a PAR-128A lock-in amplifier.

ODMR experiments were carried out at 1.4 K with an HP-8620A sweep oscillator equipped with appropriate plug-ins and a Weinschell model 221 sweep oscillator with an H-408 plug-in. Details of the ODMR experiments were described in previous papers.[12,13]

Phosphorescence Spectra

The phosphorescence spectra of DCB in various hosts were detected at 1.4 K. The spectra obtained in *p*-dibromobenzene (DBB) and in DCB-d_4 are shown in Fig. 1. It is to be noted that the position of the 0,0 band in the spectrum of DCB in DCB-d_4 coincides with that of the exciton phosphorescence origin[7] and the T←S absorption origin[1] of crystalline DCB. The phosphorescence spectra of DCB in *p*-xylene and 23 cm^{-1} trap in the neat crystal are found to be essentially

† Present address: Konishiroku Photo Industry Co., Ltd., Sakura-cho, Hino, Tokyo 191.

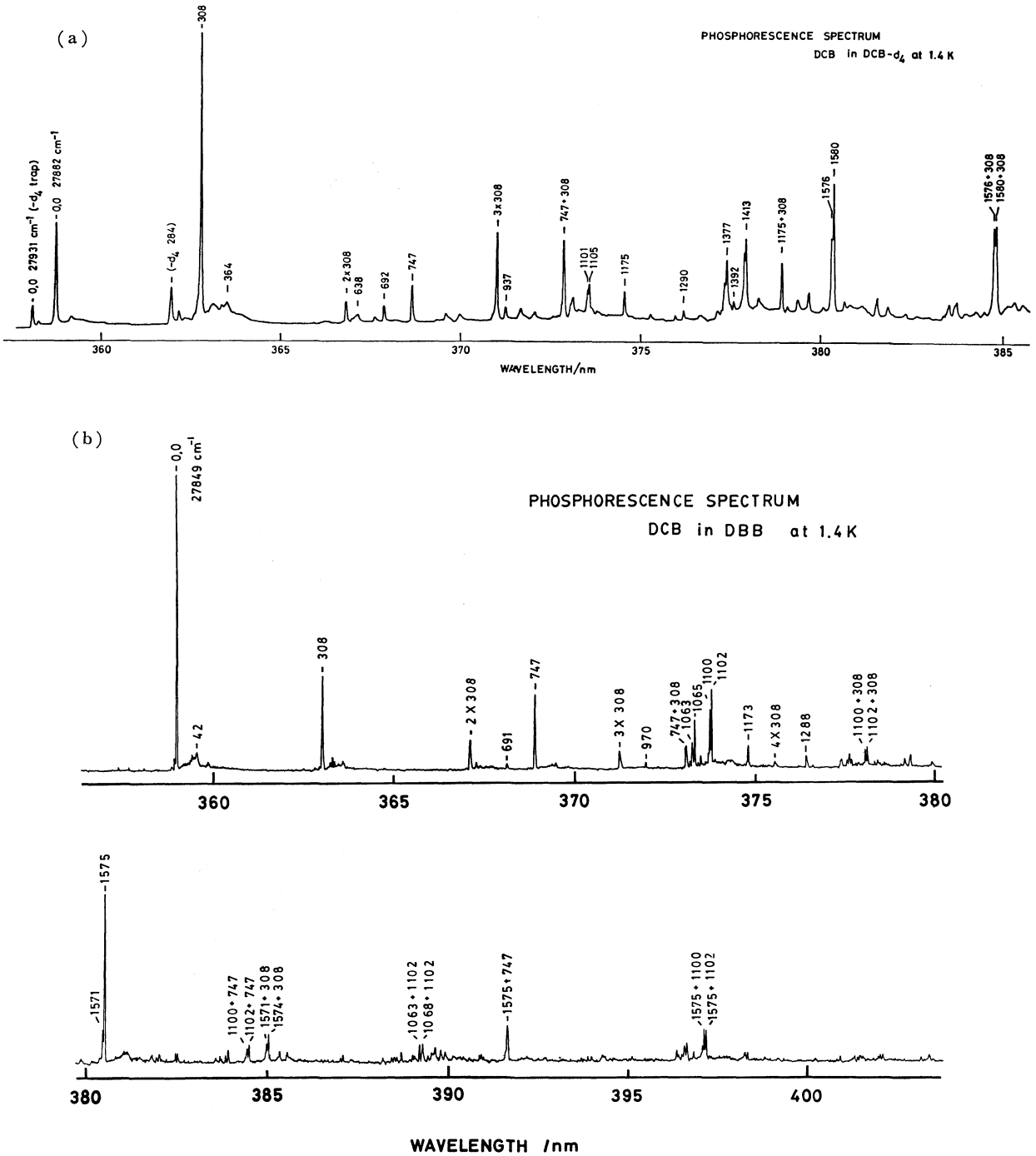

Fig. 1. The phosphorescence spectra of *p*-dichlorobenzene in (a) *p*-dichlorobenzene-d_4 and in (b) *p*-dibromobenzene at 1.4 K.

the same as those reported previously.[3,4,8] The spectrum in benzene shows a multi-site emission consisting of broad vibrational bands.

The band at about 310 cm^{-1} from the electronic origin has been assigned as being due to the progression-forming b_{2g}, C–Cl out-of-plane bending vibration. The progression can be followed through the fifth member in all the spectra obtained but in benzene. The spectra shown in Fig. 1 display a marked contrast in the intensity of the fundamental band of this mode. The band at 0—308 cm^{-1} is the strongest band in the spectrum of DCB in DCB-d_4. A similar feature is observed in the spectra of DCB in *p*-xylene and in benzene. In the spectrum of DCB in DBB, on the other hand, the corresponding band is weaker than the 0,0 band. The spectrum of the x-trap in the neat crystal also exhibits a similar trend.

Zero-field Splitting and Decay Rates

The zero-field splitting and the molecular symmetry axes are shown in Fig. 2. The zero-field splittings and the decay rates of the individual spin states of

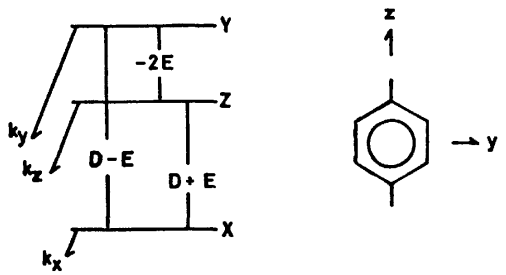

Fig. 2. The definition of the molecular symmetry axes and the zero-field splitting of *p*-dichlorobenzene.

Table 1. The positions of phosphorescence origin bands, zero-field splittings and phosphorescence decay rates of the individual spin sublevels of *p*-dichlorobenzene in various matrices at 1.4 K

	p-Xylene	Benzene (site II)	DBB	Neat cryst.	DCB-d_4
$\nu_{0,0}$/cm^{-1}	27415	27786	27849	27859	27882
D/GHz	4.324	4.421	4.472	4.483	4.505
$-2E$/GHz	1.369	(1.634)	(1.778)	1.758	1.849
k_y/s^{-1}	73.5	56.5	71.4	73.6	55.6
k_z/s^{-1}	7.0	21.7	57.1	35.6	18.8
k_x/s^{-1}	0.65	1.6	11.9	2.1	1.1

DCB in these matrices are determined by the MIDP (microwave-induced delayed phosphorescence) method. The results are listed in Table 1. The sublevel ordering has been determined to be $T_y > T_z > T_x$ in the *p*-xylene and neat crystal systems.[3,4] The same ordering is deduced for the other systems from the similarity in the splitting and from the relation of $k_y > k_z > k_x$. This relation has been commonly observed in various mono- and 1,4-dihalobenzenes.[4,13]

The zero-field splitting parameters, D and E, vary slightly depending on the matrix used. It may be pertinent to point out that the variation of the zero-field splitting parameters exhibits a good correlation with the shift of the phosphorescence origin band as shown in Table 1, although a slight discrepancy is seen between the neat crystal system and the DBB host system. A similar correlation has also been observed in the case of pyrazine.[14]

The values of k_z and k_x are small in the *p*-xylene system, but become large in the other systems, even in benzene. The increase in k_z and k_x in the DCB and DBB crystalline systems are related to the external heavy atom effect. However, the k_z and k_x values for the trap in the neat crystal seem to have an influence from other sources in addition to the external heavy atom effect, because these values are about twice those for DCB in DCB-d_4. As a possible cause for this, we presently consider a distortion or a rotation of the trap molecules from the results of T←S excitation experiments.[15] The values for DCB in benzene seem to be affected by spin-lattice relaxation.

Table 2. Relative radiative decay rate constants of *p*-dichlorobenzene at 1.4 K

System	Band	Symmetry	k_y^r	k_z^r	k_x^r
In *p*-xylene	0, 0		1	0.008	0.008
	303 cm^{-1}	b_{2g}	1	0.04	0.01
	1573	b_{3g}	1	1.82	0.44
	1577	a_g	1	0.03	0.03
In benzene	0, 0		1	0.16	0.026
	307	b_{2g}	1	0.34	0.033
Neat crystal	0, 0		1	0.15	0.038
	314	b_{2g}	1	0.29	0.015
	1578	a_g	1	0.17	0.032
	1581	b_{3g}	1	1.0	0.045
In DCB-d_4	0, 0		1	0.04	0.01
	308	b_{2g}	1	0.17	0.04
	1576	a_g	1	0.16	0.10
	1580	b_{3g}	1	6.67	0.13
In DBB	0, 0		1	0.82	0.14
	308	b_{2g}	1	0.35	0.05
	1571	a_g	1	0.73	0.19
	1575	b_{3g}	1	1.54	0.33

Relative Radiative Decay Rates

The relative radiative decay rate constants of the three spin sublevels of DCB in the hosts used are determined at 1.4 K in some of the main vibrational bands. The results are summarized in Table 2. The values for the 0,0 and b_{2g} bands in the spectrum of DCB in *p*-xylene are essentially in agreement with the results reported previously.[4] The assignments of the bands appearing at approximately 0—1580 cm^{-1} will be discussed in detail below.

If the electron distribution in DCB is retained in the D_{2h} symmetry in the triplet state, the transition from the T_z sublevel in the 0,0 band and the transitions from the T_x sublevel in the b_{2g} bands are strictly forbidden as shown in Table 3. The fact that these bands originate from all the spin sublevels suggests that the electron distribution is deformed from

Table 3. Polarizations of radiative transitions from the triplet state sublevels in four bands of the phosphorescence spectrum of *p*-dichlorobenzene as expected from group theoretical considerations

Orbital symmetry	Magnetc sublevel	Spin-orbit symmetry	Vibrationl band polarization			
			a_g	b_{1g}	b_{2g}	b_{3g}
$^3B_{1u}(\pi,\pi^*)$	T_y	B_{3u}	x	y	z	f [a]
	T_z	A_u	f	z	y	x
	T_x	B_{2u}	y	x	f	z

a) f = forbidden.

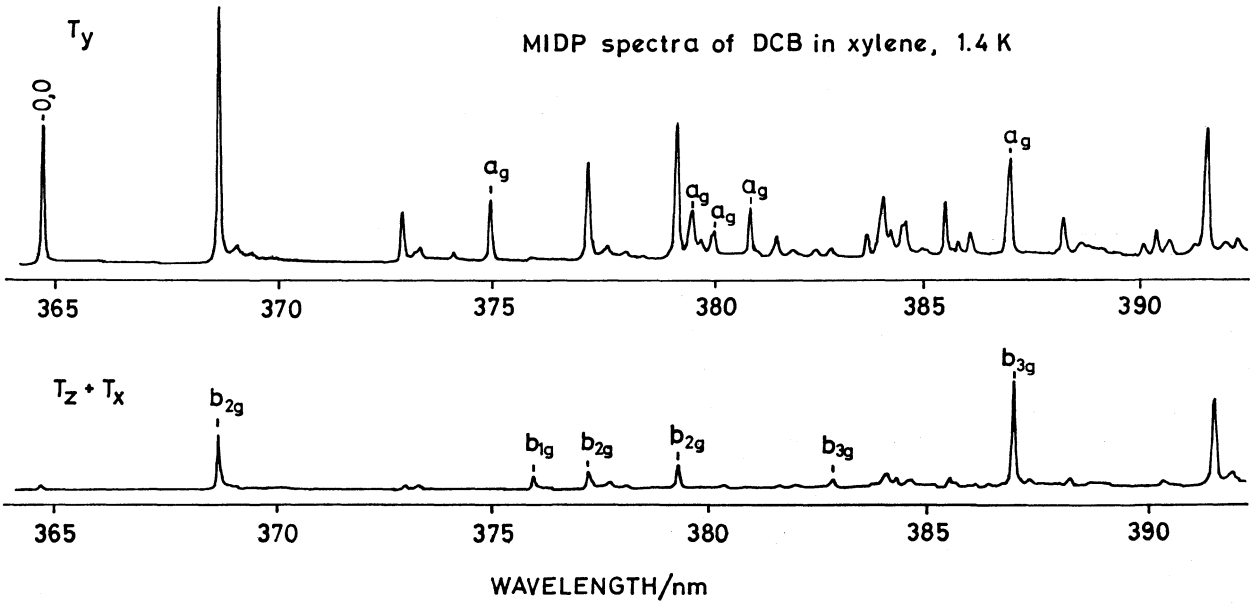

Fig. 3. The sublevel phosphorescence spectra of *p*-dichlorobenzene in *p*-xylene at 1.4 K.

TABLE 4. FUNDAMENTAL VIBRATIONS IDENTIFIED IN THE PHOSPHORESCENCE SPECTRUM OF *p*-DICHLOROBENZENE IN cm^{-1}

Symmetry	Raman (crystal)	In *p*-xylene	In benzene		x-Trap neat crystal	In DCB-d_4	In DBB	x-Trap neat crystal[a]	Exciton[b]
			site I	site II					
a_g	327		313	307	333	337	330	327	330
								331	
	744	751	751	749	746	747	747	749	746
	1103	1098	1106	1105	1108	1101	1100	1103	1103
						1105	1102	1106	
	1174	1171			1180	1175	1173	1178	1173
	1577	1577	(1584)[c]	(1581)	1578	1576	1571	1576	1578
								1579	
	3071								
b_{1g}	814	821			818	815	816	816	
b_{2g}	306	303			314	308	308	309	310
	689	694			691	692	691	690	
	976	(938)			(938)	(937)	970		
b_{3g}	350				(355)	(364)	(326)		(355)
	628	637			636	638	628		(635)
	1293	1297			1292	1290	1288		
	1577	1573	(1584)	(1581)	1581	1580	1575		
	3064								

a) From Ref. 8. b) From Ref. 7. c) The assignment of the band in the parentheses is not certain.

D_{2h} to C_{2h} or a lower symmetry by small perturbations. In particular, the b_{2g} progression alternates in intensity with the members of odd quanta being the strongest. Therefore, a distortion along the out-of-plane direction is most probable. Possible perturbations for this have already been discussed by Buckley *et al.*[3]

Sublevel Spectra and Vibrational Analysis

The phosphorescence spectrum of DCB in *p*-xylene is resolved into two sublevel spectra as shown in Fig. 3. The T_y spectrum recorded by phase-sensitively detecting the MIDP signals produced 100 ms after the excitation cutoff by irradiating the microwaves resonant with the $T_y \leftrightarrow T_z$ transition. The T_z+T_x spectrum was taken by sampling the tail portions(100—150 ms) of the phosphorescence decay. As the contribution from the T_x emission is small, the T_z+T_x spectrum can be regarded as consisting mainly of the emission from T_z.

The 0,0 band and the band at 0—303 cm^{-1} appear very strongly in the T_y spectrum, but weakly in the T_z+T_x spectrum. Therefore, the bands appearing strongly in the T_y spectrum and weakly in the other can be ascribed to a_g or b_{2g} vibrations. Referring to the results of the Raman studies[16] and the previous phosphorescence works,[3,4,7,8] we assigned the bands

at 0—751, 0—1112, 0—1171, and 0—1577 cm^{-1} as being due to the a_g fundamentals and the bands at 0—303 and 0—694 cm^{-1} as being due to the b_{2g} fundamentals. The assignment of the 1577 cm^{-1} band will be described in the following section. One of the bands at 0—938 and 0—965 cm^{-1} may also be ascribed to b_{2g}. Although the latter is consistent with the Raman results, we tentatively assign the former to the band due to the b_{2g} vibration, because the former band appears relatively strongly in all the spectra studied. In addition to the bands assigned above, there are many overtone and combination bands of a_g and b_{2g} symmetries. Of these, the band at 0—1078 cm^{-1} ($2\times b_{1u}$) is in Fermi resonance with the 1112 cm^{-1} a_g vibration.

The bands at 0—821, 0—1297, and 0—1573 cm^{-1} differ in behavior in the sublevel spectra from the bands due to a_g and b_{2g} vibrations. These bands appear relatively strongly in the T_z+T_x spectrum. The band at 0—637 cm^{-1} is also stronger than the 0,0 band in the T_z+T_x spectrum, but is much weaker than the 0,0 band in the T_y spectrum. Therefore, these bands may be attributed to either b_{1g} or b_{3g} vibration.

The MIDP sublevel spectra for the x-trap were also obtained in a similar manner. The MIDP signals due to the $T_y\leftrightarrow T_x$ and $T_z\leftrightarrow T_x$ transitions were sampled in this case to obtain the T_y and T_z spectra. The spectra showed essentially the same feature as the am-PMDR subspectra obtained by Buckley *et al.*[3] The results of the vibrational analysis are given in Table 4 for the fundamentals identified. The results for the x-trap and DCB in *p*-xylene are used for the analyses of the other systems.

The 1580 cm^{-1} Vibrations

In this work, a particular attention is paid to the assignment of the band appearing at approximately 0—1580 cm^{-1} in all the systems studied. In Fig. 4(a), the 1573 cm^{-1} band in the spectrum of DCB in *p*-xylene is shown under magnification. The band seems to have a shoulder at 0—1577 cm^{-1}. The same band recorded under different conditions are shown in Figs. 4(b) and 4(c). The band in Fig. 4(b) was taken by sampling the emission between 100 and 150 ms after the excitation cutoff. The intensity of the shoulder band is diminished. As the population in T_y has been almost completely exhausted before the sampling time, the shoulder band is regarded as the band originating mainly from T_y. The band shown in Fig. 4(c) was recorded in the same sampling time but with the microwave pulses which initiate the $T_y\leftrightarrow T_z$ transition 100 ms after the excitation cutoff. The peak decreases in intensity, but the shoulder increases. This can be seen clearly in Figs. 4(d) and 4(e), where the MIDP signals produced by the microwave pulses($T_y\leftrightarrow T_z$) at about 190 ms for the peak and for the shoulder position are shown, respectively. The changes in intensity result from the population transfer from T_z to T_y. Thus the peak emission has its origin in the T_z sublevel, whereas the shoulder emission in the T_y sublevel.

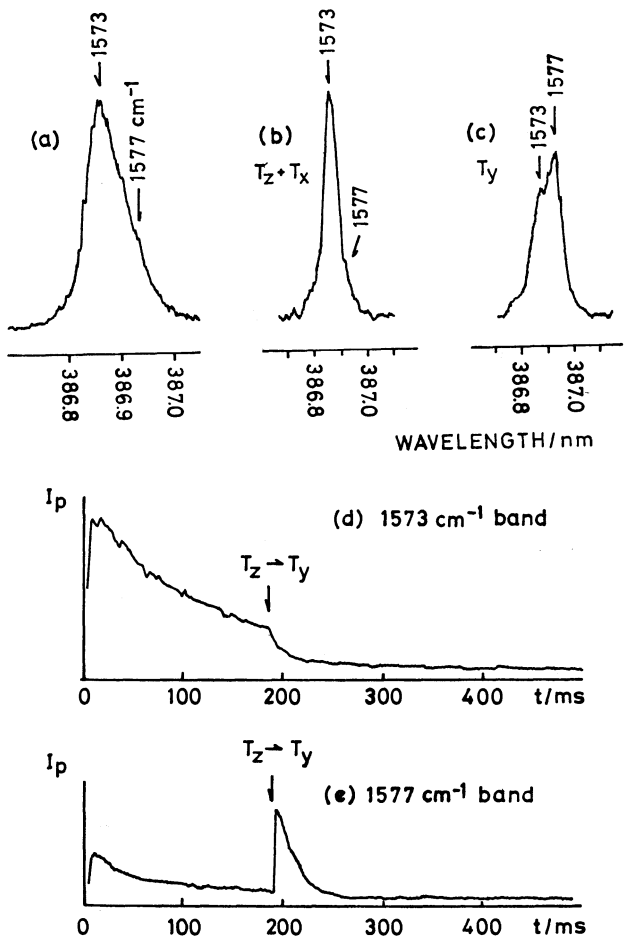

Fig. 4. The 1573 cm^{-1} band in the phosphorescence spectrum of *p*-dichlorobenzene in *p*-xylene at 1.4 K under various conditions(a—c; see the text) and the MIDP signals obtained by monitoring the emission at slightly different wavelengths (d and e).

Similar results have also been obtained in all the other systems but in benzene. As another example, the 1581 cm^{-1} band observed in the spectrum of the x-trap is shown in Fig. 5. In this case, the T_y and T_z spectra were taken by applying the microwaves resonant with the $T_y\leftrightarrow T_x$ and the $T_z\leftrightarrow T_x$ transitions, respectively. It is clear from the figure that the peak band originates mainly from T_z while the shoulder from T_y.

In the system of DCB in DCB-d_4, a splitting of the band is recognized even in the phosphorescence spectrum in Fig. 1. The MIDP experiments on this system and the system of DCB in DBB also showed that the peak band originates mainly from T_z. The spectrum in benzene is too broad to obtain conclusive results.

As discussed above, the shoulder band originating from T_y has to be assigned as being due to the a_g, ν_{8a} vibration. The vibration involved in the peak band is therefore unambiguously assigned to the b_{3g}, ν_{8b} vibration. It is to be noted that in all these systems the peak positions correspond to the band due to the b_{3g} vibration. In this regard, the previous assignment[7,8] to the a_g vibration should be revised. In the high resolution spectrum of the x-trap reported

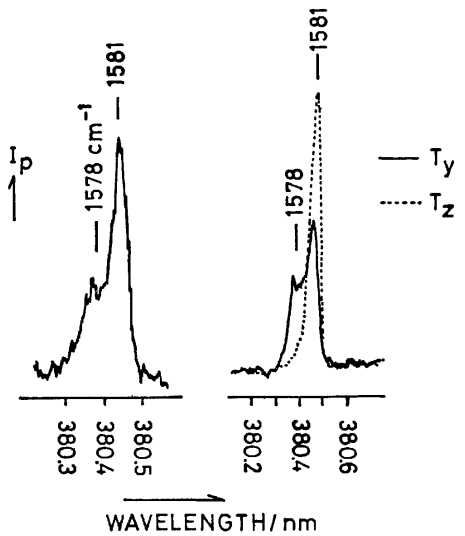

Fig. 5. The 1581 cm^{-1} band in the phosphorescence spectrum of the x-trap (23 cm^{-1}) in the neat *p*-dichlorobenzene crystal(left) and the same band observed with microwave perturbations (right; see the text).

by Gash *et al.*,[8] the band of present interest is clearly split, but they ascribed the both components to the a_g vibration, since they observed some of other a_g bands as doublets. However, they also observed the 749 and 1178 cm^{-1}, a_g bands without splitting. In view of this and our present results, the band at 0—1579.0 cm^{-1} in their spectrum is to be attributed to the b_{3g} vibration.

In the case of benzene, the ν_8 band in the phosphorescence spectrum appears with remarkable intensity, because of the strong vibronic coupling between the $^3B_{1u}$ and $^3E_{1u}$ states through the ν_8 mode. It seems that a similar situation is retained in DCB. Therefore, the main mechanism by which the ν_{8b}, b_{3g} band acquires the dipole activity is described by the second order spin-orbit vibronic coupling scheme of $^3B_{1u} \leftarrow b_{3g} \rightarrow {}^3B_{2u} \leftarrow H_{so}(T_z) \rightarrow {}^1B_{3u}$. The emission to the b_{3g} vibrational levels steals its intensity mainly from the $^1B_{3u} \rightarrow {}^1A_g$ transition as the emission to the a_g vibrational level does. The differentiation of a_g and b_{3g} vibrations are therefore not feasible from the phosphorescence polarization measurements. A similar situation has also been found in *p*-chloroaniline.[13]

As mentioned above, the coupling between the $^3B_{1u}$ and $^3E_{1u}$ states through the ν_8, e_{2g} mode in benzene results in pseudo Jahn-Teller instability, which combined with the crystal field of lower symmetry causes a distortion of the hexagonal symmetry of both the nuclei and the electronic structure. Indeed, various experiments[17-25] have shown that the lowest triplet state of benzene has a non-hexagonal electronic structure; *i.e.*, the in-plane distortion along the e_{2g} mode. Therefore, it is very probable that the DCB molecule is also subject to a similar distortion along the b_{3g} mode.

This kind of distortion would result in a deviation of the in-plane principal axes of the fine structure tensor from the molecular symmetry axes. Vergragt *et al.*[26,27] have demonstrated that the in-plane principal axes of toluene and *p*-xylene are skew in the triplet state by approximately $70(\pi/180)$ rad with respect to the axes expected for an undistorted molecule. In DCB, such a large deviation of the principal axes may not be expected, because the radiative decay rate ratio, k_z^x/k_y^x, for the 0,0 band is small in *p*-xylene and in DCB-d_4 as shown in Table 2. Recently, it has been shown from NQR experiments for DCB in DBB[28,29] that the in-plane principal axes are rotated by about 10 $(\pi/180)$—$12(\pi/180)$ rad about the axis normal to the molecular plane. Furthermore, an out-of-plane deviation of the principal axis, y, by about $20(\pi/180)$ rad is also deduced from the NQR experiments.[28] These results, though somewhat large in the DBB host, are consistent with our present expectations.

The present work is partly supported by a Grant-in-Aid for Scientific Research from the Ministry of Education, Science and Culture.

References

1) G. Castro and R. M. Hochstrasser, *J. Chem. Phys.*, **46**, 3617 (1967).
2) M. J. Buckley and C. B. Harris, *J. Chem. Phys.*, **56**, 137 (1972).
3) M. J. Buckley, C. B. Harris, and R. M. Panos, *J. Am. Chem. Soc.*, **94**, 3692 (1972).
4) G. Kothandaraman and D. S. Tinti, *Chem. Phys. Lett.*, **19**, 225 (1973).
5) D. S. Tinti, G. Kothandaraman, and C. B. Harris, *J. Chem. Phys.*, **59**, 190 (1973).
6) C. von Borczyskowski. M. Plato, K. P. Dinse, and K. Mobius, *Chem. Phys.*, **35**, 355 (1978).
7) G. A. George and G. C. Morris, *Mol. Cryst. Liq. Cryst.*, **11**, 61 (1970).
8) B. W. Gash, D. B. Hellman, and S. D. Colson, *Chem. Phys.*, **1**, 191 (1973).
9) J. H. van der Waals, A. M. P. Berghuis, and M. S. de Groot, *Mol. Phys.*, **13**, 301 (1967).
10) J. van Egmond and J. H. van der Waals, *Mol. Phys.*, **26**, 1147 (1973).
11) J. van Egmond and J. H. van der Waals, *Mol. Phys.*, **28**, 457 (1974).
12) N. Nishi and M. Kinoshita, *Chem. Phys. Lett.*, **27**, 342 (1974).
13) E. Kanezaki, N. Nishi, M. Kinoshita, and K. Niimori, *Chem. Phys. Lett.*, **29**, 529 (1974).
14) N. Nishi, M. Kinoshita, T. Nakashima, R. Shimada and Y. Kanda, *Mol. Phys.*, **33**, 31 (1977).
15) N. Iwasaki, N. Goto, and M. Kinoshita, *Chem. Phys.*, in press.
16) M. Suzuki and M. Ito, *Spectrochim. Acta, Part A*, **25**, 1017 (1969).
17) G. C. Nieman and D. S. Tinti, *J. Chem. Phys.*, **46**, 1432 (1967).
18) G. C. Nieman, *J. Chem. Phys.*, **50**, 1674 (1969).
19) A. M. Ponte Goncalves and C. A. Hutchson, Jr., *J. Chem. Phys.* **49**, 4235 (1968).
20) D. M. Burland, G. Castro, and G. W. Robinson, *J. Chem. Phys.*, **52**, 4100 (1970).
21) A. A. Gwaiz, M. A. El-Sayed, and D. S. Tinti, *Chem. Phys. Lett.*, **9**, 454 (1971).
22) M. S. de Groot, I. M. A. Hesselmann, and J. H. van der Waals, *Mol. Phys.*, **13**, 583 (1967).
23) M. S. de Groot, I. M. A. Hesselmann, and J. H.

van der Waals, *Mol. Phys.*, **16**, 45 (1969).
24) Ph. J. Vergragt and J. H. van der Waals, *Chem. Phys., Lett.*, **36**, 283 (1975).
25) Ph. J. Vergragt and J. H. van der Waals, *Chem. Phys. Lett.*, **42**, 193 (1977).
26) Ph. J. Vergragt and J. H. van der Waals, *Mol. Phys.*, **33**, 1507 (1977).
27) Ph. J. Vergragt, J. A. Kooter, and J. H. van der Waals, *Mol. Phys.*, **33**, 1523 (1977).
28) M. Deiling and K. P. Dinse, *Chem. Phys. Lett.*, **69**, 587 (1980).
29) C. von Borczyskowski, *Chem. Phys. Lett.*, **85**, 293 (1982).

Kinetic Pressure and Substituent Effects on the Thermal Isomerization of Triphenylformazans

Yoshimi Sueishi* and Norio Nishimura

Department of Chemistry, Faculty of Science, Okayama University, Tsushima, Okayama 700

(Received April 2, 1983)

The rates of the thermal isomerizations around N=N (Process A) and C=N (Process B) of substituted triphenylformazans were followed spectrophotometrically at various temperatures and under high pressures, and the activation parameters were determined. The values of the activation energy, entropy, and volume were found to be *ca.* 70 kJ mol^{-1}, *ca.* -20 J K^{-1} mol^{-1}, and *ca.* -5.0 cm^3 mol^{-1} respectively for Process A, and *ca.* 40 kJ mol^{-1}, *ca.* -200 J K^{-1} mol^{-1}, and *ca.* -10 cm^3 mol^{-1} respectively for Process B. It was suggested that the thermal isomerizations both for Processes A and B proceed by the inversion mechanism. Furthermore, in the transition state of Process B, a quasi six-membered ring was assumed to form. The very large negative entropy of Process B was discussed in terms of the restricted internal rotations, and others.

Formazans have two double bonds. There are some reports with regard to their conformations and electronic and IR spectra.[1,2] However, there are very few reports regarding its isomerization mechanism. Kuhn and Weitz[3] suggested the following isomerization scheme.

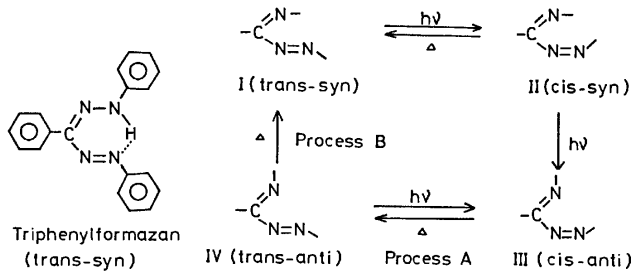

Scheme 1.

But they did not give a full detail of mechanism of the thermal isomerization.

In the preliminary communication,[4] it was shown that the kinetic substituent effects really reverse above and below the isokinetic temperature. In spite of the low activation energy,[3] the rate of the thermal isomerization for Process B is so slow that it seems to us worth while investigating the reaction mechanism in some detail.

In analogy with the isomerizations of azobenzenes and azomethines, there are two possible mechanisms for the thermal isomerizations of triphenylformazans, one *via* a rotation around the double bonds and involves a π-bond rupture, the other *via* an inversion on the nitrogen atom, the π-bond remaining intact.[5,6]

This paper presents the substituent and pressure effects on the rate of the thermal isomerization of several formazans and their mechanistic implications are discussed.

Experimental

Reagents. Substituted triphenylformazans were prepared according to the method by Kuhn and Weitz[3] and recrystallized from a chloroform–ethanol mixture. Melting point and IR spectra were used for identification.

1,3,5-Triphenylformazan: mp 173 °C (lit, 173.5 °C), 3-(*p*-methoxyphenyl)-1,5-diphenylformazan: mp 157—158 °C (lit, 156—158 °C), 3-(*p*-methylphenyl)-1,5-diphenylformazan: mp 171—172 °C, 3-(*p*-chlorophenyl)-1,5-diphenylformazan: mp 199—200 °C (lit, 178—179 °C), 3-(*p*-bromophenyl)-1,5-diphenylformazan: mp 209—210 °C, 3-(*p*-cyanophenyl)-1,5-diphenylformazan: mp 221—222 °C, 3-(*p*-nitrophenyl)-1,5-diphenylformazan: mp 230—231 °C (lit, 204 °C), 3-(*m*-nitrophenyl)-1,5-diphenylformazan: mp 185.7 °C (lit, 185 °C), 1,5-bis(*o*-methylphenyl)-3-phenylformazan: mp 129—130 °C (lit, 130 °C, 1,5-bis(*p*-methylphenyl)-3-phenylformazan: mp 164—165 °C), 1,5-bis(*p*-chlorophenyl)-3-phenylformazan: mp 184—185 °C (lit, 183—184 °C).

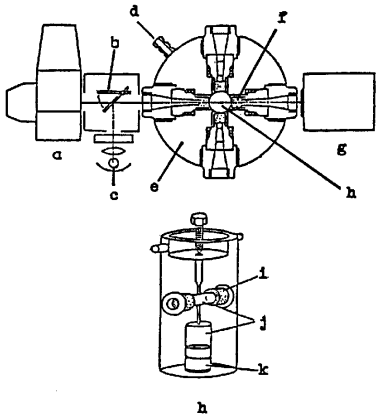

Fig. 1. Schematic diagram for spectrophotomeric measurement (top view) and inner cell.
a, Monochromator; b, turn mirror; c, tungsten lamp for excitation; d, water inlet; e, high pressure vessel; f, sapphire window; g, photomultiplier; h, teflon inner cell; i, sapphire window; j, sample cell; k, liquid separation piston.

Solvents. Toluene was dried over metallic sodium and distilled. Hexane of reagent grade was used as received.

Measurements under Atmospheric Pressure. An appropriate concentration of the sample solution was irradiated for 1 h with a 100W tungsten lamp to produce a *cis-anti* isomer (III). In the dark, the *cis-anti* isomer (III) isomerizes to a *trans-anti* isomer (IV) and the *trans-anti* isomer (IV) turns back to a *trans-syn* isomer (I) (Scheme 1), both in accordance with the first-order kinetics. The reaction rates for Processes A and B were estimated spectrophotometrically, by following the maximum absorbance at *ca.* 400 nm for the former by a Union 401 spectrophotometer, and the maximum absorbance at *ca.* 500 nm for the latter

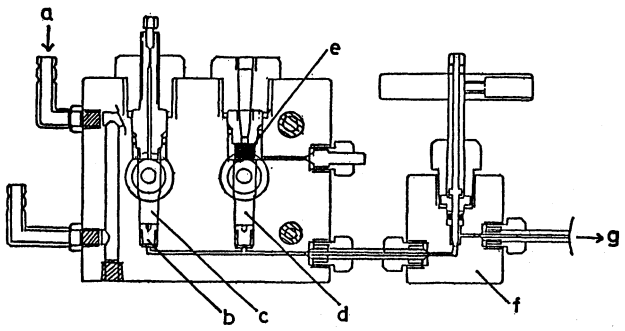

Fig. 2. High pressure vessel for spectral measurement (side view).
a, Water inlet; b, liquid separation piston; c, reference cell; d, sample cell; e, sapphire window for excitation light; f, stop valve; g, to pump system.

by a Hitachi 101 spectrophotometer. These are checked by several runs.

Measurements under High Pressures. The thermal *cis*-to-*trans* isomerization (Process A) was followed by using a pressure vessel made of SNCM-8 stainless steel and equipped with an inner cell, optical windows, and a water jacket (Fig. 1.). The pressure was generated by means of a plunger-pump. The pressure was measured by a Haise Bourdon gauge. The reaction temperature was controlled by circulating the thermostated water through the water jacket. Sample solutions were charged in the inner cell which is made of teflon and consists of two parts connected with a narrow tube, in order that an irradiated part of the solution for optical measurements does not mix with an unirradiated part of the solution. The solution was compressed, and then irradiated with a 650 W tungsten projection lamp for 1 min. After irradiation, the mirror b was turned by 45° and the change in the absorbance with time was followed with a Hitachi 139 spectrophotometer.

The rate of the thermal *anti*-to-*syn* isomerization (Process B) was so slow that this process was followed by using a high pressure vessel made of 17-4PH stainless steel (Fig. 2). The pressure vessel have two cells for sample and reference solutions, equipped with sapphire windows in horizontal direction for spectral measurements and one window in vertical direction for irradiation. The reaction solution in the pressure vessel was brought up to the required pressure, and then the stop valve was closed. The vessel was separated at the stop valve from the pump system. After the reaction solution had been irradiated with a 650 W tungsten projection lamp for 2 min, the pressure vessel was set in a Hitachi 100-50 double-beam spectrophotometer and the absorbance was recorded.

Results and Discussion

The thermal *cis*-to-*trans* and *anti*-to-*syn* isomerizations of substituted triphenylformazans were carried out at various temperatures. The rate constants estimated

Table 1. Substituent effects on rate constants, activation energies, and activation entropies for the thermal isomerization of Process A in toluene (probable errors in parentheses)

Compd No.	$10^2\,k/s^{-1}$					E_a	$\Delta S^{\ddagger}_{298}$
	−5 °C	5 °C	15 °C	20 °C	30 °C	kJ mol^{-1}	J K^{-1} mol^{-1}
1	0.264(0.003)	0.926(0.007)	2.62(0.04)	4.57(0.06)	12.1(0.1)	74.9(1.7)	−22.6(6.7)
2	0.283(0.008)	0.914(0.009)	2.48(0.03)	4.12(0.13)	9.63(0.05)	64.5(1.7)	−59.8(6.3)
3	0.279(0.010)	0.902(0.002)		4.19(0.09)	11.0(0.8)	69.9(1.3)	−39.8(4.6)
4	0.261(0.002)	0.969(0.017)	2.01(0.07)	4.91(0.07)	15.2(0.5)	76.6(1.7)	−16.7(5.9)
5	0.256(0.004)	0.915(0.003)		5.09(0.07)	15.7(0.1)	78.7(1.3)	−8.8(4.2)
6	0.362(0.007)	1.10 (0.02)		5.79(0.08)		74.9(2.1)	−20.5(6.7)
7	0.376(0.004)	1.22 (0.02)		6.69(0.14)		74.1(0.8)	−22.6(2.9)
8	0.458(0.005)		3.53(0.04)	6.42(0.01)		71.5(2.1)	−33.5(6.7)
9	0.206(0.010)[a]	0.548(0.008)[b]	2.13(0.05)	3.60(0.05)	12.8(0.1)	80.8(1.3)	−5.0(4.6)
10	0.943(0.011)	3.65 (0.08)[c]		16.1 (0.3)		73.7(0.8)	−17.2(2.1)
11	0.417(0.004)	1.91 (0.07)[c]		8.11 (0.01)		77.4(2.5)	−10.0(9.6)

a) At −4.4 °C. b) At 4 °C. c) At 6.3 °C.

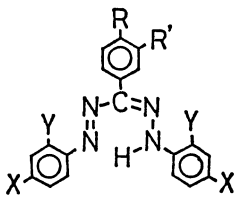

Compd No.	Substituent			
	R	R′	X	Y
1	H	H	H	H
2	OCH_3	H	H	H
3	CH_3	H	H	H
4	Cl	H	H	H
5	Br	H	H	H
6	CN	H	H	H
7	NO_2	H	H	H
8	H	NO_2	H	H
9	H	H	H	CH_3
10	H	H	CH_3	H
11	H	H	Cl	H

Table 2. Substituent effects on rate constants, activation energies, and activation entropies for the thermal isomerization of Process B in toluene (probable errors in parentheses)

Compd No.	$10^6\ k/s^{-1}$ 25 °C	35 °C	40 °C	E_a / kJ mol^{-1}	$\Delta S^{\ddagger}_{298}$ / J K^{-1} mol^{-1}
1	4.33(0.01)	6.39(0.49)	9.08(0.37)	36.9(4.3)	−231(14)
2	21.0 (0.3)	36.5 (0.7)	47.6 (3.2)	42.2(0.3)	−201(2)
3	14.8 (1.6)	26.1 (0.2)	27.5 (0.1)	33.7(5.7)	−232(19)
4	4.34(0.11)	9.94(0.04)	12.8 (2.1)	57.0(3.7)	−164(12)
5	5.38(0.37)	8.01(0.16)	11.5 (0.3)	37.9(4.5)	−227(15)
6	12.1 (1.2)	15.6 (0.4)	19.5 (1.3)	23.8(2.7)	−267(9)
7	10.8 (0.8)	23.8 (0.3)	41.8 (3.5)	68.5(4.9)	−119(16)
8	28.1 (0.6)	65.1 (8.1)	66.9 (2.8)	47.8(9.8)	−179(32)
9	2.44(0.06)	9.34(0.79)	13.9 (1.6)	91.8(6.3)	−52(21)
10	19.3 (0.9)	40.2 (3.7)	51.2 (0.5)	51.2(2.8)	−171(9)
11	3.92(0.35)	5.07(0.50)	6.02(0.40)	21.8(1.3)	−283(4)

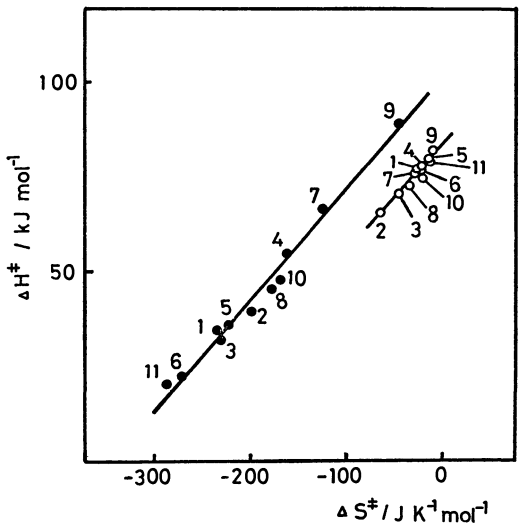

Fig. 3. $\Delta H^* - \Delta S^*$ relationships for Processes A (○) and B (●).

from the first-order plots and the activation parameters are listed in Tables 1 and 2. It is interesting to note that the activation entropies for Process B are surprisingly small except **9**. Therefore, the rate constants for Process B are about 10^4 smaller than those for Process A, in spite of the very low activation energies. In **9**, the steric effect by the *ortho*-CH_3 substituent may be severe in the transition state and this may be responsible for both the increased activation energy and entropy. Figure 3 shows the linear relationships between the activation enthalpy and entropy. This linear enthalpy-entropy relationship suggests that in Process B as well as A, a single mechanism is operating.[7] Similarly, a linear relationship between ΔH^* and ΔS^* has been reported for the thermal *cis*-to-*trans* isomerization of substituted azobenzenes.[8]

Arrhenius Parameters. It has been shown theoretically that the activation energies for the *syn*-to-*anti* isomerization of oximes[9–12] by the inversion mechanism are lower than those by the rotation mechanism. Moreover, Warren *et al.*[13] calculated the energy barrier for the isomerization of *N*-benzylideneaniline *via* the inversion to be 88.8 kJ mol^{-1} and the barrier to the rotation around the C=N double bond was calculated to be 252 kJ mol^{-1} by means of the CNDO/2 method. Experimental values of various kinds of azobenzenes and azomethines are about 80 kJ mol^{-1}. Most of the activation entropies for the thermal isomerizations of azobenzenes and azomethines fall in the range of about −60 to 0 J K^{-1} mol^{-1}. Judging from these, our results for Process A (Table 1) seem to be compatible with the inversion mechanism.

Recently, Bach and Wolber[9] reported that electron-withdrawing substituents at nitrogen markedly increase the inversion barrier and that an allyl type molecular orbital containing the nitrogen lone pair contributes most significantly to the activation energy. On the other hand, it has been suggested that if substituents at carbon strongly polarize the π-electron of the C=N bond, the rotation mechanism accompanying the charge separation might be possible.[10,14] Moreover, Bauer *et al.*[15] and Taylor and Bartulin have reported that the activation energies for the rotational isomerizations of guanidine salts around the C=N bond and of some olefines around the C=C bond are as low as 80 kJ mol^{-1} or even less. Therefore, the activation energy less than 80 kJ mol^{-1} may not necessarily afford a conclusive evidence for the inversion mechanism.

The extraordinarily small values of the Arrhenius parameters for Process B (Table 2) are noteworthy. There are some examples of such small values of the activation entropy for second-order reactions. As far as we are aware, however, the values of the activation entropy for first-order reactions are much larger than this. The above findings have lead us to the idea that the transition state might be much more product-like and hence its molecular conformation is similar to that of *trans-syn* for which a quasi six-membered ring is formed, internal rotations being severely restricted.

Since an internal rotation interacts with other modes of rotations and vibrations, it is difficult to calculate the exact contribution of the internal rotation to entropy. However, if we use a proper model, the rotational entropy can approximately be estimated. Figure 4 shows a model of the cyclic transition state of triphenylformazan. If a quasi six-membered ring for-

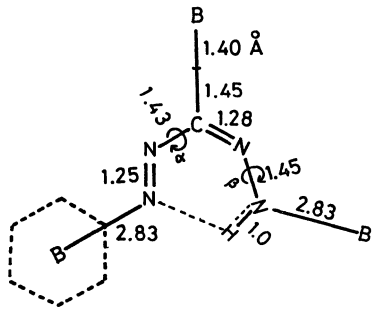

Fig. 4. Model of the cyclic transition state of triphenylformazan. The bond lengths (Å) of azobenzene derivative[17] and *N*-benzylideneaniline[13] were used. B, Phenyl group; C, carbon; N, nitrogen; H, hydrogen.

mation occurs in the transition state, rotations around the C–N and N–N bonds as depicted become impossible. Now, for brevity, we assume that the two possible internal rotation axes agree with these bond-axes. The entropy of an internal rotation can be calculated by

$$S_{\mathrm{rot}} = NkT(\mathrm{d}\ln q_{\mathrm{rot}}/\mathrm{d}T) + Nk\ln q_{\mathrm{rot}}, \quad (1)$$

where q_{rot} is the one-dimensional rotational partition function and is given by

$$q_{\mathrm{rot}} = (8\pi^2 IkT/h^2)^{1/2}\pi^{1/2}/\sigma, \quad (2)$$

for which σ is the symmetry number and the reduced moment of inertia I is given by $I=I_1I_2/(I_1+I_2)$ in which I_1 and I_2 are the moment of inertia around the common axis. Therefore, S_{rot} is expressed as follows.

$$S_{\mathrm{rot}} = Nk\left[\frac{1}{2}+\frac{1}{2}\ln(8\pi^3 IkT/h^2)-\ln\sigma\right]$$
$$= R\left[\frac{1}{2}\ln(I/\mathrm{amu\ Å^2})+\frac{1}{2}\ln(T/\mathrm{K})-\ln\sigma-0.522\right]. \quad (3)$$

Substituting the numerical values into these equations, the entropies for the internal rotations around the C–N and N–N bonds at 25 °C are calculated to be S_{rot}(C–N)=38.6 J K^{-1} mol^{-1} and S_{rot}(N–N)=44.1 J K^{-1} mol^{-1}. Therefore, the total entropy loss due to these restricted rotations may be about 80 J K^{-1} mol^{-1} on going from the initial to the transition state.

It may be instructive to compare the entropy loss with those of similar reactions. For example, some Claisen and Cope rearrangements[18,19] have been reported to proceed *via* a cyclic transition state. The entropies of activation for the Claisen rearrangement of allyl ethers have been reported as −50——120 J K^{-1} mol^{-1}.[18] Assuming that only two rotations around the O–CH_2 and CH_2–CH bonds become forbidden upon activation, the total entropy losses for the corresponding species can be estimated as −50——90 J K^{-1} mol^{-1}. For 3-phenyl-2-propenyl phenyl ether, the discrepancy is *ca.* 30 J K^{-1} mol^{-1} probably owing to the restriction of other modes of internal rotations involving two phenyl rings upon activation.

Now, in our case, the steric hindrance in the transition state may become less severe than in the ground state, and hence one might imagine that the free rotations involving the benzene rings become possible (see Scheme 2). However, as we have advocated in the case of the thermal isomerization of azobenzenes,[5] the most important factor for determining the conformation of such a "soft" species involving aromatic rings connected by single bonds is mesomeric one. Therefore, the mesomeric effects which tend to keep the three benzene rings coplanar would overwhelm the tendency for them to rotate freely, resulting in the net loss of entropy upon activation. Indeed, the absorption maxima of the conjugation band are 495 nm for the *trans-syn* isomer (I) and 405 nm for the *trans-anti* isomer (IV), suggesting a drastic change in the molecular conformation (coplanality).

There is a vast of reports for hydrogen bond formation.[20] The reported values of ΔH and ΔS for the H-bond formation vary depending on the type of bonding and others, but ΔH is generally *ca.* −20 kJ per H-bond per mol, and ΔS is *ca.* −50 J K^{-1} mol^{-1}. If the H-bond formation takes place in the transition state for Process B, further entropy loss of *ca.* 50 J K^{-1} mol^{-1} could be expected. The contribution from the solvation may be responsible for at least a part of the remaining entropy loss.

The very low values of the activation energy for Process B (Table 2) seem to be worth to pay attention. According to the Hammond postulate, among a group of similar reactions, the less exothermic ones have the later transition states and *vice versa*. Since Process B involves a formation of the hydrogen bond, it must be exothermic ($\Delta H \approx -20$ kJ mol^{-1}, *vide supra*). At first sight, it seems that the reaction may have the earlier transition state compared with similar types of isomerizations, and this is apparently against the

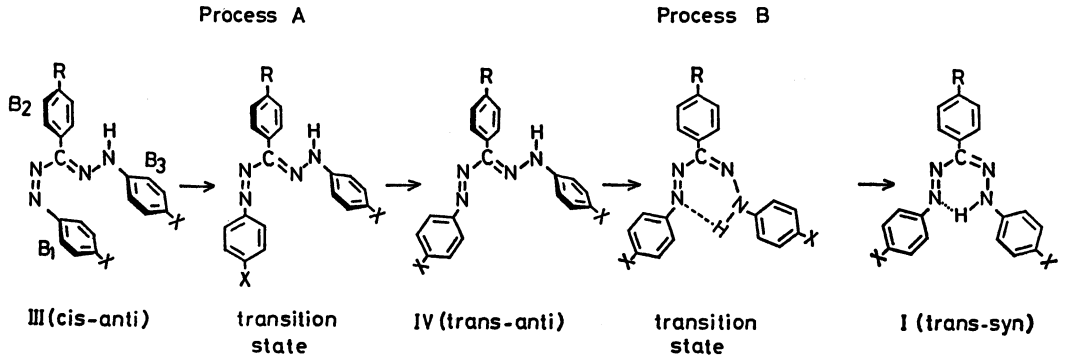

Scheme 2.

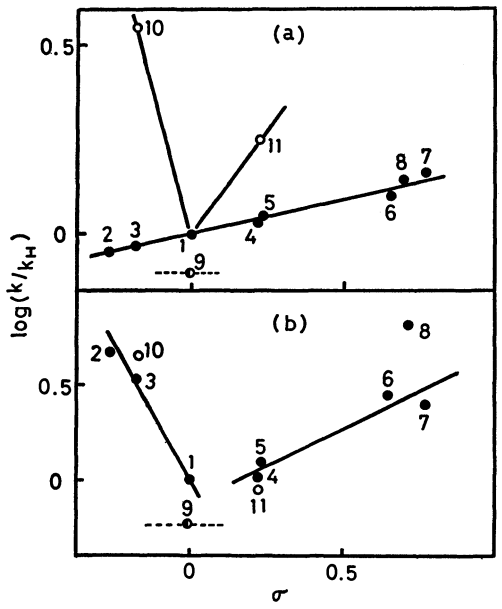

Fig. 5. Plots of log (k/k_H) against the Hammett σ for (a) Process A at 20 °C and (b) Process B at 25 °C. ●: Substituents R, ○: substituents X, ◐: **9**.

above assumption that the conformation of the transition state is similar to I. However, as seen above, the entropy factor plays a very important role in this process, and the reaction is controlled by the activation energy as well as the activation entropy. The isokinetic temperature (*ca.* 300 K) estimated from the slope of the linear ΔH^* *vs.* ΔS^* plot in Fig. 3 is very near the experimental temperatures. In such a case as this, the Hammond postulate must be invalidated, since the postulate tacitly assumes that reactions in question are energy-controlled. It is noted that the true reaction coordinate must be drawn in terms of the free energy. Therefore, in spite of the low activation energy, the barrier of the free energy will be at the later stage of reaction coordinate.

Substituent Effects. In the preliminary communication,[4] we reported that the strictly linear ΔH^*–ΔS^* relationship holds for a limited series of substituted triphenylformazans and the isokinetic temperature at which substituent effects should vanish does exist (Process A). Figure 5(a) shows the substituent effect for the thermal isomerizations of 11 kinds of triphenylformazans. The Hammett plots of **1**, **10**, and **11** show a V-line. Moreover, the *ortho*-substituent retards the isomerization rate (**9**). On the other hand, a linear Hammett relationship approximately holds for **1**—**8**. The above findings are considered as follows. In the *cis-anti* conformation, the three benzene rings (B_1, B_2, and B_3 in Scheme 2) must be twisted to one another owing to the steric repulsion (III in Scheme 2). In the inversion transition state, however, a conjugation between the reaction center (the N=N bond) and the substituent X in B_1 becomes possible, thus resulting in the extra free energy depression in analogy with the case of azobenzene derivatives,[5] as depicted in Scheme 3:

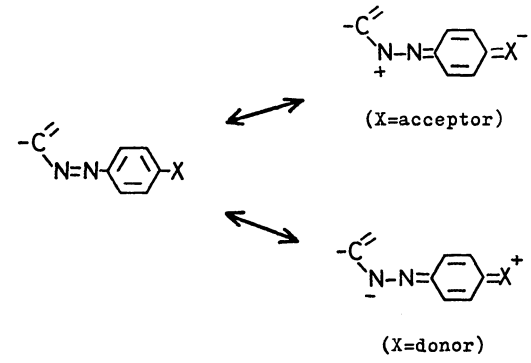

Scheme 3.

The acceleration effect irrespective of the nature of substituents is accounted for by this reason. On the contrary, in **1**—**8**, a conjugation of the reaction center (the N=N bond) and the substituent R in B_2 is impossible. Therefore, the substituent R would exhibit a mild inductive effect, thus accounting for the usual Hammett relationship. In the rotational mechanism, these substituent effects can be explained in no way.

There are two possible routes also for Process B (Scheme 4).

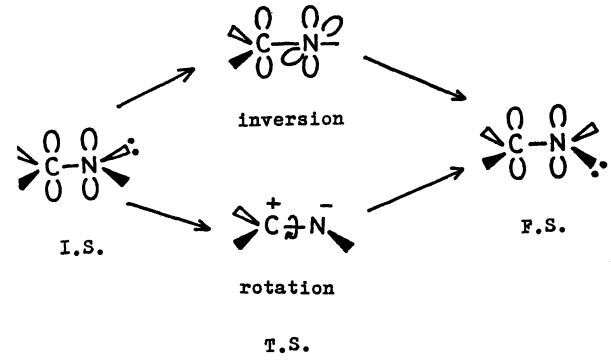

Scheme 4.

The isomerizations of azomethines[20,21] are also characterized by a V line. Herkstroeter[21] and Hall *et al.*[22] explained the V plot in terms of the change in mechanism. As explained earlier,[4] we have a different idea. If the inversion transition state is assumed for Process B, B_2, B_3, and the connecting C=N–N group would become coplanar. This makes the conjugation between the substituent R and the C=N–N group possible, but the conjugation between the substituent X and the C=N group is impossible. Therefore, the kinetic behavior of a series of the substituents R (the V plot in Fig. 5(b)) and of X can well be accounted for by the same way as explained for Process A. On the contrary, if the rotational transition state is assumed, the introduction of the electron-donating groups (R) would help the polarization (Scheme 4) and hence the isomerization rate is accelerated and *vice versa*. Thus we may expect the linear Hammett plot. This is against the experimental observations. The detail of the discussion on this problem has been reported elsewhere.[5]

Pressure Effects. The entropy of activation often affords important informations about the manner of

Table 3. Pressure effects (k_p/k_1) and activation volumes for Processes A and B

	Compd No.	Solvent	Temp °C	k_p/k_1							ΔV^* cm^3 mol^{-1}
				$P/10^5$ Pa	1	230	390	540	770	790	1180	
Process A	**1**	Toluene	15		1		1.09			1.17	1.29	−5.0±0.1
	2	Toluene	15		1		1.08			1.17	1.25	−4.5±0.1
	7	Toluene	15		1		1.07			1.16	1.26	−4.7±0.1
Process B	**1**	Toluene	20		1	1.17	1.13	1.17	1.39			−8.7±1.4
	1	Hexane	45		1		1.18			1.47	1.66	−11.7±0.6
	3	Hexane	45		1		1.13			1.36	1.61	−10.9±0.5
	7	Hexane	45		1		1.14			1.23	1.50	−8.6±0.7

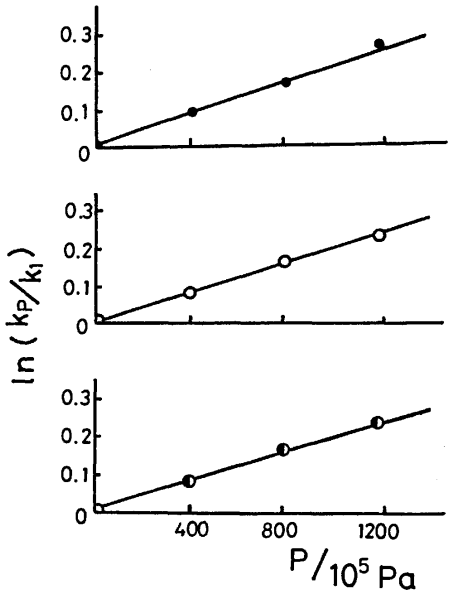

Fig. 6. Pressure effects on the thermal isomerization for Process A in toluene at 15 °C.
●: **1**, ○: **2**, ◐: **7**.

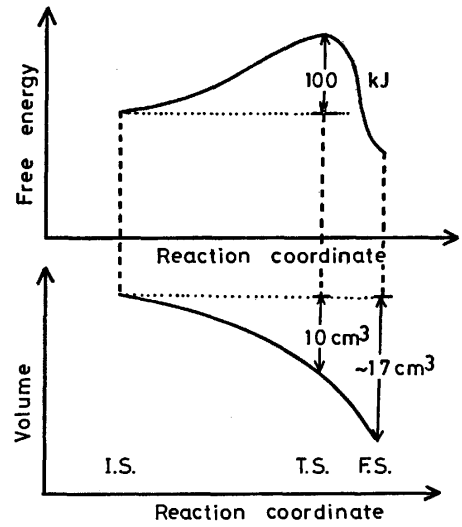

Fig. 7. Free energy and volume profiles for Process B.

bonding, the change in freedom, the extent of solvation, *etc.* However, since ΔH^* and ΔS^* can be obtained as a set from the Arrhenius plot, inevitable errors are often involved in ΔS^*, which, as pointed out by Petersen,[23] might lead to the misunderstanding for the existence of the isokinetic temperature. On the other hand, the volume of activation can be estimated from the slope of $\ln k$ *versus* P plot, in accordance with Eq. 4,

$$(\partial \ln k/\partial P)_T = -\Delta V^*/RT, \quad (4)$$

and the concept of volume is more straightforward than that of entropy. The activation volume is usually divided into two terms:

$$\Delta V^* = \Delta V_1^* + \Delta V_2^*, \quad (5)$$

where ΔV_1^* represents the difference in the intrinsic volume of reacting molecules between the initial and the transition state, and ΔV_2^* is the change in volume of surrounding solvents. Therefore, if no substantial intrinsic volume change is expected as may be so for Process A, ΔV^* obtained experimentally may be ascribed to ΔV_2^*.

Pressure effects on the thermal isomerizations for Processes A and B are given in Table 3. The rate constants in logarithmic scale were plotted against P (Fig. 6), and the estimated activation volumes are given in Table 3.

The small negative values of the activation volume for Process A indicate that the polarity change is, if any, not so large as suggested for the rotational transition state.[24] These values are, together with the values of E_a and ΔS^*, very similar to those for the isomerization of azobenzene derivatives for which the inversion mechanism has been advocated.[5,8]

Judging from the very small activation entropy for Process B, the transition state might be highly polar. However, the activation volume indicates that it is not so. If the isomerization for Process B proceeds *via* a cyclic transition state, the activation volume may be similar to those of the Claisen and Cope rearrangements.[25,26] The activation volumes reported are −9—−18 cm^3 mol^{-1} for these reactions, and are −9.5 ($\alpha\rightarrow\gamma$) and −7.9 ($\gamma\rightarrow\alpha$) cm^3 mol^{-1} for the equilibration of α- and γ-methylallylazide[27] respectively. It has been considered that these reactions proceed *via* moderately polar cyclic transition states. Judging from the values in Table 3, the isomerization for Process B will proceed *via* a moderately polar and cyclic transition state. It may safely be considered that the difference in the molar volumes between the *trans-syn* isomer (I) and the *trans-anti* isomer (IV) is similar to that between 1-hexene and cyclohexane (−17 cm^3 mol^{-1}).[26] On the basis of the activation parameters and on the assumptions stated above, the presumed free energy and volume profiles for Process B could be sketched as shown in Fig. 7.

In conclusion, the kinetic substituent and pressure effects, together with the activation parameters, are in favor of the inversion mechanism *via* the moderately polar transition states both for Processes A and B, and against the rotational mechanism *via* the very polar transition states.

References

1) W. Otting and F. A. Neugebauer, *Chem. Ber.*, **102**, 2520 (1969).
2) W. Otting and F. A. Neugebauer, *Z. Naturforsch., B*, **23**, 1064 (1968).
3) R. Kuhn and H. M. Weitz, *Chem. Ber.*, **86**, 1199 (1953).
4) N. Nishimura, Y. Sueishi, and S. Yamanoto, *Chem. Lett.*, **1979**, 429.
5) N. Nishimura, T. Sueyoshi, S. Yamanoto, and S. Hasegawa, *Bull. Chem. Soc. Jpn.*, **49**, 1381 (1976) and references therein.
6) G. Wettermark, J. Weinstein, J. Sousa, and L. Dogliott, *J. Phys. Chem.*, **69**, 1584 (1964). D. Y. Curtin, E. J. Grubbs, and C. G. McCarty, *J. Am. Chem. Soc.*, **88**, 2775 (1966).
7) J. E. Leffler, *J. Org. Chem.*, **31**, 533 (1966).
8) T. Asano, T. Okada, S. Shinkai, K. Shigematsu, Y. Kusano, and O. Manabe, *J. Am. Chem. Soc.*, **103**, 5161 (1981).
9) R. D. Bach and G. J. Wolber, *J. Org. Chem.*, **47**, 245 (1982).
10) F. Kerek and G. Ostrogovich, *J. Chem. Soc., B*, **13**, 541 (1971).
11) D. Liotard, A. Dargelos, and M. Chaillet, *M. Theor. Chim. Acta*, **31**, 325 (1973).
12) W. F. Hwang and H. A. Kusano, *J. Phys. Chem.*, **82**, 2126 (1978).
13) C, H. Warren, G. Wettermark, and K. Weiss, *J. Am. Chem. Soc.*, **93**, 4658 (1971).
14) M. Raban and E. Carlson, *J. Am. Chem. Soc.*, **93**, 685 (1971).
15) V. J. Bauer, W. Fulmor, G. O. Morton, and S. R. Safir, *J. Am. Chem. Soc.*, **90**, 6846 (1968).
16) E. C. Taylor and J. Bartulin, *Tetrahedron Lett.*, **34**, 3259 (1967).
17) M. Komeyama, S. Yamanoto, N. Nishimura, and S. Hasegawa, *Bull. Chem. Soc. Jpn.*, **46**, 2606 (1973).
18) L. D. Huestis and L. J. Andrews, *J. Am. Chem. Soc.*, **83**, 1963 (1961).
19) W. N. White, D. G. Wynn, R. Scharles, C, Girard, and W. Fife, *J. Am. Chem. Soc.*, **80**, 3271 (1958); H. L. Goering and R. R. Tacobson, *ibid.*, **80**, 3277 (1958); S. J. Rhoads and R. E. Michel, *ibid.*, **85**, 585 (1963).
20) G. C. Pimentel and A. L. McClellan, "The Hydrogen Bond," ed by L. Pauling, W. H. Freeman and Company, San Francisco and London (1960).
21) W. G. Herkstroeter, *J. Am. Chem. Soc.*, **95**, 8686 (1973).
22) G. E. Hall, W. J. Middleton, and T. D. Roberts, *J. Am. Chem. Soc.*, **93**, 4778 (1971).
23) R. C. Petersen, *J. Org. Chem.*, **29**, 3133 (1964).
24) T. Asano, T. Yano, and T. Okada, *J. Am. Chem. Soc.*, **104**, 4900 (1982).
25) C. Walling and M. Naiman, *J. Am. Chem. Soc.*, **84**, 2628 (1962).
26) E. Whally, *Adv. Phys. Org. Chem.*, **2**, 93 (1964).
27) W. J. Noble, *J. Phys. Chem.*, **67**, 2451 (1963).

The Synthesis, Properties, and Structure of Bis(*N,N*-dimethylacetamide)-tris(*O,O'*-diisopropyl dithiophosphato)lanthanum(III)

Kiyofumi NAGAI,* Yoshiyuki SATO, Satoshi KONDO, and Akira OUCHI

Department of Chemistry, College of General Education, The University of Tokyo, Komaba 3-8-1, Meguro-ku, Tokyo 153

(Received January 11, 1983)

The new complex indicated in the title has been synthesized, and its crystal and molecular structure has been determined by the X-ray diffraction method. The crystal was triclinic; space group $P\bar{1}$, $Z=2$, $a=23.071(9)$, $b=11.060(11)$, $c=10.793(13)$ Å, $\alpha=120.0(1)$, $\beta=97.2(2)$, $\gamma=88.9(2)°$. The final R value for 5969 reflections is 0.047. The central lanthanum(III) atom is an octa-coordination and in a dodecahedron geometry, being coordinated with six sulfur atoms of three *O,O'*-diisopropyl dithiophosphate ligands (iPr_2dtp), which span at three *m* edges, and with two oxygen atoms of both the *N,N*-dimethylacetamide ligands (dma) at both ends of the remaining *m* edge. The other $[Ln(iPr_2dtp)_3L_2]$-type complexes, where Ln=La or Nd; L=dma or *N,N*-dimethylformamide, have also been obtained. The P=S double bond of the iPr_2dtp ligand in the title complex is almost completely delocalized.

Some lanthanoid metal compexes, where sulfur atoms are coordinated to metal, such as their dialkyldithiocarbamates,[1–6] dialkyldithiophosphinates,[7–10] and *O,O'*-dialkyl dithiophosphates(R_2dtp),[8,11,12] had previously been synthesized and investigated, though the lanthanoid elements are known as "hard acid" according to the HSAB theory.[13] The structures of a number of these complexes were also clarified; the octa-coordination of the central metal is common for the complexes of light lanthanoid elements,[5,6,11,12] except for those where voluminous ligands are coordinated.[7,10]

The authors had previously found that some amine adducts of cobalt(II) *O,O'*-dialkyl dithiophosphates are more stable than the original complexes.[14,15] Although triphenylphosphine oxide–*O,O'*-diethyl dithiophosphate(Et_2dtp) mixed complexes of lanthanoid (III) elements had already been investigated,[11b] almost no other such type of mixed complex was known yet. Therefore, the syntheses and the structure determination of the adducts of lanthanoid(III) *O,O'*-dialkyl dithiophosphates was started in our laboratory. Thus far, the title complex and some related ones have been obtained; their structure and properties will be shown below.

Experimental

*Synthesis of Bis(*N,N*-dimethylacetamide)tris(*O,O'*-diisopropyldithiophosphato)lanthanum(III).* Sodium *O,O'*-diisopropyl dithiophosphate ($Na(iPr_2dtp)$) was obtained from diphosphorus pentasulfide and 2-propanol (sodium carbonate was used for the neutralization of the free acid), by applying the method used for synthesizing the sodium *O,O'*-diethyl dithiophosphate ($Na(Et_2dtp)$).[16] Sodium tetrakis(*O,O'*-diisopropyl dithiophosphato)lanthanate(III) ($Na[La(iPr_2dtp)_4]$) was obtained by a reaction between lanthanum(III) chloride and $Na(iPr_2dtp)$ in a 2-propanol medium, using the method of synthesizing $Na[La(Et_2dtp)_4]$, written by Pinkerton.[8]

The sodium salt (0.83 g, 0.82 mmol) and *N,N*-dimethylacetamide (dma) (0.14 g, 2.2 mmol) were refluxed in 20 cm^3 of diisopropyl ether for 20 minutes; then it was filtered off to remove a turbid white mass and the residue while warm, and the filtrate was left standing for several hours. The product was precipitated as white crystals. The crude product was dissolved in 20 cm^3 of diisopropyl ether (60—65 °C), a turbid white mass was filtered off, the solution was left standing in a silica-gel desiccator overnight, and the complex was precipitated. Yield: 0.63 g (81%). The crystals thus obtained were submitted to X-ray diffraction after having been checked by means of Weissenberg photography. Found: La, 14.45; C, 32.68; H, 6.35; N, 2.89%. Calcd for $LaC_{26}H_{60}N_2O_8S_6P_3$: La, 14.58; C, 32.77; H, 6.35; N, 2.94%.

Syntheses of Other $Ln(iPr_2dtp)_3L_2$-type Complexes, Where Ln=La, Nd; L=Amides. These mixed complexes were obtained by almost the same technique as that used for the title complex. The neodymium(III) complexes were obtained via sodium tetrakis(*O,O'*-diisopropyl dithiophosphato)neodymate(III), which has been synthesized similarly. To synthesize the *N,N*-dimethylformamide (dmf) adducts, the optimum ratio of the starting materials was: the sodium salt:dmf=1:3 (in mol/mol).

$Nd(iPr_2dtp)_3(dma)_2$: Found, Nd, 15.68; C, 32.08; H, 6.26; N, 2.63%. Calcd for $NdC_{26}H_{60}N_2O_8S_6P_3$: Nd, 15.05; C, 32.59; H, 6.13; N, 2.92%. Yield, 73%. Magnetic moment of the solid, 3.4_2 BM† (22 °C). $La(iPr_2dtp)_3(dmf)_2$: Found, La, 14.82; C, 30.54; H, 6.12; N, 2.99%. Calcd for $CaC_{24}H_{56}N_2O_8S_6P_3$: La, 15.03; C, 31.18; H, 6.11; N, 3.03%. Yield, 62%. $Nd(iPr_2dtp)_3(dmf)_2$: Found, Nd, 15.77; C, 30.55; H, 6.07; N, 2.93%. Calcd for $NdC_{24}H_{56}N_2O_8S_6P_3$: Nd, 15.51; C, 31.00; H, 6.07; N, 3.01%. Yield, 76%. Magnetic moment of the solid, 3.4_1BM (22 °C).

Single-crystal X-Ray Analysis. A crystal with dimensions of $0.3\times0.3\times0.2$ mm^3 was used for the measurement. All its edges were ground off, but it was not shaped into a sphere.

The crystallographic data are: $LaC_{26}H_{60}N_2O_8S_6P_3$: F.W. =952.91, triclinic, space group $P\bar{1}$, $Z=2$, $a=23.071(9)$, $b=11.060(11)$, $c=10.793(13)$ Å, $\alpha=120.00(11)$, $\beta=97.17(16)$, $\gamma=88.92(24)°$, $D_x=1.34$, $D_m=1.37(3)$ Mg m^{-3}, μ(Mo $K\alpha$)=1.08 mm^{-1}. The reflections within the range of $2\theta<50°$ were collected on a Philips PW 1100 automated four-circle diffractometer with Mo $K\alpha$ radiation, the $\theta-2\theta$ scan technique being employed. Due to the limitation of our computation program (upper limit of the numbers of reflections=6000), 5969 $|F_o|>5.5\sigma(|F_o|)$ reflections from the 6753 independent ones measured were used for the calculation. The intensities were corrected for Lorentz and polarization factors, but no correction was made for absorption or extinction.

All the calculations were carried out on a HITAC M-

† 1 BM=$9.274078(36)\times10^{-24}$ J T^{-1}.

Table 1. Final atomic coordinates ($\times 10^4$) and equivalent isotropic temperature factors, with estimated standard deviations in parentheses

Atom	x	y	y	B_{eq}/Å^2 a)	Atom	x	y	z	B_{eq}/Å^2 a)
La	2320.8(1)	1148.5(3)	99.7(4)	4.8	S(5)	2415(1)	1348(2)	3021(2)	7.1
S(1)	3616(1)	827(2)	530(2)	7.5	S(6)	2531(1)	4091(2)	2608(2)	6.8
S(2)	3040(1)	2377(2)	-1227(2)	7.1	P(3)	2625(1)	3373(2)	3964(2)	6.2
P(1)	3763(1)	1834(2)	-503(2)	6.8	O(5)	2275(2)	4253(5)	5304(4)	7.1
O(1)	4225(2)	3099(5)	474(6)	9.3	O(6)	3277(2)	3756(5)	4776(5)	7.8
O(2)	4107(2)	956(5)	-1844(6)	9.0	C(51)	1629(3)	4203(8)	5084(8)	8.4
C(11)	4095(4)	4327(8)	1865(10)	10.1	C(52)	1462(4)	5689(9)	5581(11)	11.3
C(12)	4272(7)	5580(11)	1746(16)	19.5	C(53)	1419(4)	3595(10)	5973(11)	12.3
C(13)	4448(6)	4337(12)	3125(12)	15.4	C(61)	3472(4)	3258(9)	5791(8)	10.0
C(21)	4680(3)	442(9)	-1669(10)	10.6	C(62)	3935(5)	2287(14)	5209(13)	16.6
C(22)	5135(4)	1223(13)	-1875(16)	17.8	C(63)	3695(6)	4563(13)	7184(11)	14.7
C(23)	4663(5)	-1065(13)	-2658(16)	17.2	O(100)	2303(2)	-1144(4)	-106(4)	7.6
S(3)	1544(1)	2748(2)	-968(2)	7.6	C(101)	2239(5)	-2136(7)	61(8)	10.8
S(4)	1066(1)	979(2)	452(2)	8.4	C(102)	1525(4)	-2586(10)	-21(11)	12.0
P(2)	857(1)	1969(2)	-638(2)	6.9	N(100)	2494(5)	-2839(6)	308(8)	14.7
O(3)	399(2)	3123(5)	138(5)	7.7	C(103)	3187(4)	-2255(10)	558(13)	13.3
O(4)	483(2)	1004(5)	-2173(5)	8.2	C(104)	2421(5)	-4124(9)	381(12)	14.0
C(31)	527(3)	4198(8)	1670(8)	8.3	O(200)	2173(2)	-568(4)	-2440(4)	7.1
C(32)	-19(5)	4371(13)	2317(14)	16.8	C(201)	2275(4)	-829(8)	-3668(10)	10.6
C(33)	732(6)	5554(9)	1776(12)	13.0	C(202)	1867(5)	-181(11)	-4491(10)	13.5
C(41)	16(3)	19(8)	-2411(9)	9.2	N(200)	2656(4)	-1522(8)	-4276(9)	13.9
C(42)	221(6)	-1420(10)	-3422(15)	15.8	C(203)	3023(5)	-2231(10)	-3497(10)	11.6
C(43)	-529(4)	357(10)	-3043(11)	12.1	C(204)	2842(8)	-1759(14)	-5676(13)	19.8

a) The equivalent isotropic temperature factors were computed using the following expressing: $B_{eq}=(4/3)(B_{11}a^2+B_{22}b^2+B_{33}c^2+B_{12}ab\cos\gamma+B_{13}ac\cos\beta+B_{23}bc\cos\alpha)$. The B_{ij}'s are defined by: $\exp[-(h^2B_{11}+k^2B_{22}+l^2B_{33}+2klB_{23}+2hlB_{13}+2hkB_{12})]$.

200H computer at the Computer Center of The University of Tokyo, using the local version of the UNICS program.[17] The atomic-scattering factors were taken from the tables.[19]

Structure Determination. The structure was solved by the heavy-atom method. The positions of the lanthanum, phosphorus, and sulfur atoms were deduced from a three-dimensional Patterson map, while all the other non-hydrogen atoms were located by means of successive Fourier syntheses. Their positional and thermal parameters were refined by the block-diagonal least-squares method. All attempts to determine hydrogen-atom positions were unsuccessful, and so they were not included in the calculation. In the last cycle of the refinement with anisotropic temperature factors for all atoms, almost all the parameter shifts were less than one-third of the corresponding standard deviations; the exceptions were only slightly higher than one-third of the corresponding standard deviations. The final R value obtained was 0.047.[19]

Other Measurements. The X-ray powder patterns of these complexes were obtained by the use of a diffractometer, Model DX-GO-F JEOL, using Cu $K\alpha$ radiation, in the range from 6° to 50° in 2θ. The magnetic moments of the solid samples were measured using a Gouy balance at an ambient temperature. The infrared absorption spectra of the samples were obtained by means of a JASCO A-202 grating infrared spectrophotometer, using Nujol and hexachloro-1,3-butadiene mull. The visible absorption spectra of the solutions, as well as the diffuse reflectance spectra of the solid samples, were measured by means of a Hitachi 124 spectrophotometer. The ^{1}H-NMR spectra were measured by means of a Varian EM-390 NMR-spectrometer, using tetramethylsilane (TMS) as the internal standard.

Results and Discussion

The final atomic parameters of the title complex are listed in Table 1,[20] while the bond lengths as well as the bond angles are tabulated in Table 2. The perspective drawing of the complex around the central lanthanum atom, together with the numbering scheme, is shown in Fig. 1, and the crystal packing diagram, in Fig. 2.

The complex molecules in the crystal are discrete, and neither bridges nor hydrogen bonds are recognized between different molecules. As is shown in Fig. 3, the central lanthanum(III) atom is in an octa-coordination and in a distorted dodecahedron geometry, coordinated to six sulfur atoms of three iPr_2dtp ligands, which span at m edges of the dodecahedron, and to two oxygen atoms of two dma ligands, which bond at both the ends of its remaining m edge. The plane equations of the two trapezia of the dodecahedron are shown as follows.

(x, y, and z in the equations are taken in the a, b, and c directions of the unit cell respectively, and are shown in Å units):

TABLE 2. BOND LENGTHS AND BOND ANGLES, WITH ESTIMATED STANDARD DEVIATIONS IN PARENTHESES

Bond length	l/Å	Bond length	l/Å
La-S(1)	3.009(3)	La-S(2)	3.046(7)
La-S(3)	3.012(9)	La-S(4)	2.988(3)
La-S(5)	3.029(4)	La-S(6)	3.013(10)
La-O(100)	2.432(5)	La-O(200)	2.413(10)
S(1)-P(1)	1.986(6)	S(2)-P(1)	1.964(6)
P(1)-O(1)	1.583(10)	P(1)-O(2)	1.588(10)
O(1)-C(11)	1.499(13)	O(2)-C(21)	1.458(12)
C(11)-C(12)	1.522(22)	C(11)-C(13)	1.490(23)
C(21)-C(22)	1.477(23)	C(21)-C(23)	1.460(16)
S(3)-P(2)	1.971(7)	S(4)-P(2)	1.986(6)
P(2)-O(3)	1.595(9)	P(2)-O(4)	1.593(9)
O(3)-C(31)	1.470(12)	O(4)-C(41)	1.452(14)
C(31)-C(32)	1.478(19)	C(31)-C(33)	1.526(18)
C(41)-C(42)	1.478(19)	C(41)-C(43)	1.485(17)
S(5)-P(3)	1.981(7)	S(6)-P(3)	1.973(5)
P(3)-O(5)	1.594(9)	P(3)-O(6)	1.593(7)
O(5)-C(51)	1.477(8)	O(6)-C(61)	1.475(17)
C(51)-C(52)	1.512(15)	C(51)-C(53)	1.543(22)
C(61)-C(62)	1.463(19)	C(61)-C(63)	1.508(17)
O(100)-C(101)	1.212(13)	C(101)-C(102)	1.707(18)
C(101)-N(100)	1.083(17)	N(100)-C(103)	1.675(17)
N(100)-C(104)	1.476(17)	O(200)-C(201)	1.260(16)
C(201)-C(202)	1.610(22)	C(201)-N(200)	1.187(16)
N(200)-C(203)	1.579(21)	N(200)-C(104)	1.516(26)

Bond angle	θ/°	Bond angle	θ/°
S(1)-La-S(2)	65.88(5)	S(1)-La-S(3)	135.74(5)
S(1)-La-S(4)	156.80(5)	S(1)-La-S(5)	81.37(5)
S(1)-La-S(6)	87.26(4)	S(1)-La-O(100)	80.79(12)
S(1)-La-O(200)	95.74(9)	S(2)-La-S(3)	70.54(6)
S(2)-La-S(4)	137.16(6)	S(2)-La-S(5)	134.29(6)
S(2)-La-S(6)	81.95(5)	S(2)-La-O(100)	131.39(13)
S(2)-La-)(200)	76.43(10)	S(3)-La-S(4)	66.75(5)
S(3)-La-S(5)	127.54(6)	S(3)-La-S(6)	79.38(5)
S(3)-La-O(100)	137.39(12)	S(3)-La-O(200)	81.02(9)
S(4)-La-S(5)	77.89(5)	S(4)-La-S(6)	93.20(4)
S(4)-La-O(100)	81.87(12)	S(4)-La-O(200)	93.70(9)
S(5)-La-S(6)	64.81(5)	S(5)-La-O(100)	67.96(12)
S(5)-La-O(200)	140.55(9)	S(6)-La-O(100)	132.47(12)
S(6)-La-O(200)	154.64(9)	O(100)-La-O(200)	72.73(14)
La-S(1)-P(1)	90.91(10)	La-S(2)-P(1)	90.26(10)

Bond angle	θ/°	Bond angle	θ/°
S(1)-P(1)-S(2)	112.9(2)	S(1)-P(1)-O(1)	109.9(2)
S(1)-P(1)-O(2)	113.3(3)	S(2)-P(1)-O(2)	106.8(3)
O(1)-P(1)-O(2)	99.7(3)	P(1)-O(1)-C(11)	122.0(5)
O(1)-C(11)-C(12)	103.5(1)	O(1)-C(11)-C(13)	111.0(9)
C(12)-C(11)-C(13)	110.7(11)	P(1)-O(2)-C(21)	121.1(6)
O(2)-C(21)-C(22)	109.9(11)	O(2)-C(21)-C(23)	108.7(7)
C(22)-C(21)-C(23)	113.6(11)	La-S(3)-P(2)	89.26(11)
La-S(4)-P(2)	89.70(13)	S(3)-P(2)-S(4)	113.1(1)
S(3)-P(2)-O(3)	112.4(2)	S(3)-P(2)-O(4)	107.2(3)
S(4)-P(2)-O(3)	109.9(2)	S(4)-P(2)-O(4)	113.1(2)
O(3)-P(2)-O(4)	100.5(3)	P(2)-O(3)-C(31)	121.0(5)
O(3)-C(31)-C(32)	107.3(8)	O(3)-C(31)-C(33)	108.7(10)
C(22)-C(31)-C(33)	111.4(9)	P(2)-O(4)-C(41)	123.2(6)
O(4)-C(41)-C(42)	105.7(7)	O(4)-C(41)-C(43)	108.4(9)
C(42)-C(41)-C(43)	112.8(8)	La-S(5)-P(3)	89.58(10)
La-S(6)-P(3)	90.20(9)	S(5)-P(3)-S(6)	113.1(1)
S(5)-P(3)-O(5)	111.1(2)	S(5)-P(3)-O(6)	112.2(2)
S(6)-P(3)-O(5)	111.6(2)	S(6)-P(3)-O(6)	108.4(2)
O(5)-P(3)-O(6)	99.8(3)	P(3)-O(5)-C(51)	120.1(4)
O(5)-C(51)-C(52)	105.8(6)	O(5)-C(51)-C(53)	106.9(9)
C(52)-C(51)-C(53)	113.9(9)	P(3)-O(6)-C(61)	119.2(7)
O(6)-C(61)-C(62)	108.1(10)	O(6)-C(61)-C(63)	104.6(8)
C(62)-C(61)-C(63)	111.9(9)	La-O(100)-C(101)	165.9(6)
O(100)-C(101)-C(102)	114.1(9)	O(100)-C(101)-N(100)	140.4(12)
C(102)-C(101)-N(100)	105.5(10)	C(101)-N(100)-C(103)	104.0(10)
C(101)-N(100)-C(104)	140.5(12)	C(103)-N(100)-C(104)	115.2(9)
La-O(200)-C(201)	144.21(7)	O(200)-C(201)-C(202)	118.7(9)
O(200)-C(201)-N(200)	124.7(12)	C(202)-C(201)-N(200)	116.6(13)
C(201)-N(200)-C(203)	115.6(12)	C(201)-N(200)-C(204)	127.5(14)
C(203)-N(200)-C(204)	116.8(11)		

a) La, S(1), S(2), S(3), and S(4) plane:
$-0.040x-0.480y-0.876z+0.960=0.0$.
Deviations (in Å): La, 0.080; S(1), −0.105; S(2), 0.088; S(3), −0.113; S(4), 0.093.

b) La, S(5), S(6), O(100), and O(200) plane:
$-0.997x+0.076y-0.008z+5.288=0.0$.
Deviations (in Å): La, 0.030; S(5), 0.077; S(6), −0.053; O(100), −0.092; O(200), 0.043 Å.

The dihedral angle of both the planes is 89.4 °.

As is shown in Table 2, all the La–S bond lengths are in the range of 3.046(7)—2.988(3) Å; they are almost equal. All the P–S bond lengths are also almost the same; 1.986(6)—1.964(6) Å. Therefore, it is likely that the P=S double bond of the ligand is almost completely delocalized in the complex. The oxygen atom of iPr_2dtp, and the nitrogen atom of the dma ligand are not coordinated to the central metal atom.

The La–S bond length of this complex is comparable with those of $La(Et_2dtp)_3\{(C_6H_5)_3PO\}_2$ (2.98—3.07

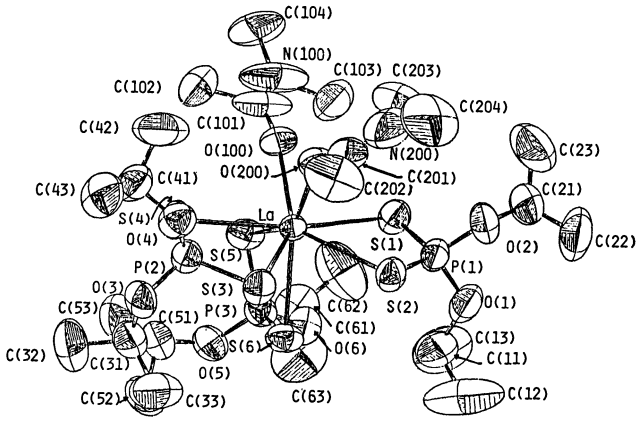

Fig. 1. A perspective drawing of the title complex with the numbering scheme.

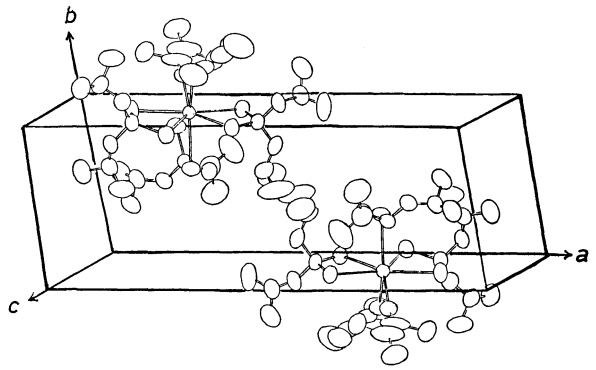

Fig. 2. Crystal packing diagram of the title complex.

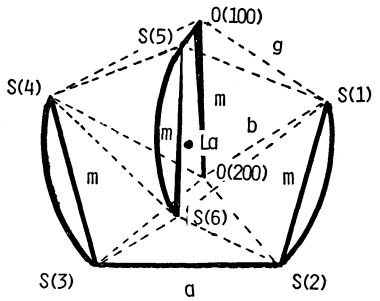

Fig. 3. Dodecahedron geometry around La^{III}.

Å),[11a] and $[As(C_6H_5)_4][La(Et_2dtp)_4]$ (2.96—3.01 Å).[12] The La–O bond lengths of this complex(2.41, 2.43 Å) are also almost equal to those of $La(Et_2dtp)_3\{(C_6H_5)_3PO\}_2$(2.42, 2.46 Å).[11a] The bond lengths are slightly shorter than those of the common lanthanum(III) complexes in which the oxygen atoms of the ligands are coordinated(about 2.5 Å).[21–24] Consequently, the bond between La^{III} and dma in this complex can be expected to be very strong.

The configuration of the central metal of the title complex is different from that of $La(Et_2dtp)_3\{(C_6H_5)_3PO\}_2$, which is in the square-antiprism geometry, and the two triphenylphosphine oxide ligands are located on opposite sides of the molecule.[11a] The discrepancy between them is probably due to the bulkiness of the triphenylphosphine oxide ligands in the latter complex, for the ligands cannot be located side by side on the coordination sphere due to the steric hindrance.

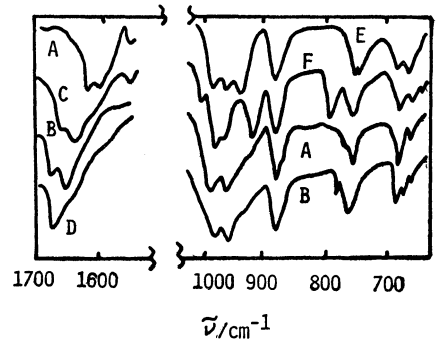

Fig. 4. Infrared absorption spectra of the title complex and the related compounds. A: $La(iPr_2dtp)_3(dma)_2$; B: $La(iPr_2dtp)_3(dmf)_2$; C: dma; D: dmf; E: $Na(iPr_2dtp)$; F: $Na[La(iPr_2dtp)_4]$.

In tetrakis(4-thioxo-2-pentanonato)zirconium(IV), where the central metal is in a square-antiprism geometry, four sulfur atoms and four oxygen atoms of the ligands are located side by side.[25] Similarly, it is expected that, in the comlpexes with high-coordination-number geometry, if two kinds of ligating atoms exist, the same kind of atoms may be apt to be located side by side on the coordination polyhedron if their "hardness" (in the HSAB concept) is different from that of the others, unless no steric interference exists.

Although the positions and thermal parameters of the lanthanum(III) atom and the atoms near it are exactly determined, those of the isopropyl carbon atoms have relatively large standard deviations; the hydrocarbon chains are not tightly fixed.

From the powder X-ray diffraction patterns of $Ln(iPr_2dtp)_3L_2$, where Ln=La or Nd; L=dma or dmf, both of the dma complexes, as well as both of the dmf complexes, may be said to be isostructural with each other.

The infrared absorption spectral patterns of the dma adducts of the lanthanum(III) and neodymium (III) complexes, as well as of their dmf adducts, resemble each other. The infrared spectra of the title complex and of some related compounds are shown in Fig. 4. The ν(CO) of dma shifts to the lower-wave number side when it is coordinated with the lanthanoid metal; *i.e.* 1657, 1640→1620, 1597 cm^{-1}. On the other hand, the ν(CO) of dmf makes only a small shift, but splits into two peaks, 1668→1680, 1643 cm^{-1}, when it is coordinated to La^{III} or Nd^{III} in this type of complex.

In the infrared spectra of these metal R_2dtp complexes, the characteristic strong peak, which is probably to be assigned as a mixed band of ν(P–S) and ν(P–O), appears near 750 cm^{-1}.[26] In the case of $Na[La(iPr_2dtp)_4]$, the band is split into two peaks; 760 and 741 cm^{-1}. On the other hand, in the case of the title adduct, the peak appears as a single one at 760 cm^{-1}. The X-ray diffraction data shows that, in the $[La(Et_2dtp)_4]^-$ ion, the La–S pair as well as the P–S bond lengths of a Et_2dtp ligand are a little different from each other,[11a] probably because of the partial localization of the P=S double bond of the ligand. In the title complex, as was shown above, the P=S double bond is delocalized almost completely. There-

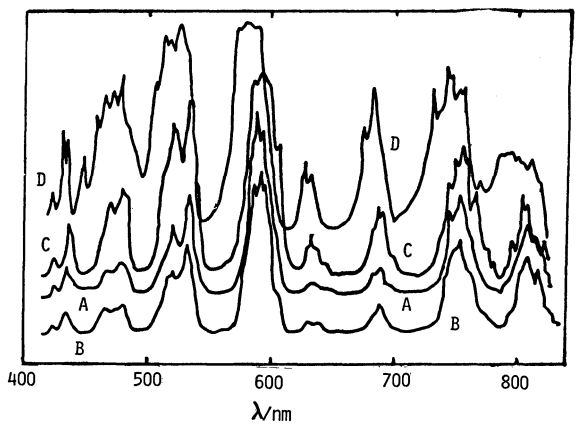

Fig. 5. Diffuse reflectance spectra of the neodymium-(III) complexes and its chloride hexahydrate. A: $Nd(iPr_2dtp)_3(dma)_2$; B: $Nd(iPr_2dtp)_2(dmf)_2$; C: $Na[(iPr_2dtp)_4]$; D: $NdCl_3 \cdot 6H_2O$.

fore, some relation between the splitting of the peak and the delocalization degree of the P=S double bond of the ligand is to be expected. In the infrared spectra of the dmf adduct, the main, strong peak is found at 766 cm^{-1}, although a small additional one appears at 788 cm^{-1}.

The diffuse reflectance spectra of $Nd(iPr_2dtp)_3(dma)_2$ and of the related compounds are shown in Fig. 5. The general features of the spectra resemble each other; however, all the bands of the R_2dtp-containing complexes, $Na[Nd(iPr_2dtp)_4]$ and $Nd(iPr_2dtp)_3L_2$(where L=dma or dmf), make red shift compared with the corresponding peaks of $NdCl_3 \cdot 6H_2O$. The $Nd(iPr_2dtp)_3(dma)_2$ complex is soluble in chloroform, and the visible absorption spectra of the solution show the maxima which are also found in the reflection spectra of its solid. The absorption maxima are as follows:

808(1.2); 754(0.9_5); 590(1.5); 532, 518(0.9_5, 0.8_2) (concentration of the samples: 8×10^{-3} mol dm^{-3}; figures are shown by λ/nm; log ε in parentheses).

When dma is added to the solution, these peaks make a blue shift; their intensities decrease a little at the same time, and its spectral pattern tends to become the same as that of the $NdCl_3$ dissolved in chloroform containing dma. Although the quantitative study has not yet been completed, the change in the spectra is likely to be due to the displacement of the iPr_2dtp ligand with dma in the solution when the concentration of dma increases.

The ^{1}H-NMR spectra of the title complex and some related compounds are shown in Table 3. The samples were dissolved in chloroform-*d*(about 5 wt%). As is shown in the table, the methyl proton signals of dma or dmf in the complexes appeared in a lower-magnetic-field region compared with those of the respective free amides. This shows that such amide ligands are coordinated to the lanthanoid metal, acting as donors even in a solution.

The authors wish to thank Professor Yoichi Iitaka, The Faculty of Pharmaceutical Sciences, The University of Tokyo, for the collection of the intensity data. They are also greatly obliged to The Shin-Etsu Chemical Co., Ltd., for aiding in this study by presenting the highly pure lanthanoid oxides. The present work was partially supported by a Grant-in-Aid for Scientific Research No. 57430011 from the Ministry of Education, Science and Culture.

Table 3. ^{1}H-NMR spectra of the title complex and some related compounds

	$-N(CH_3)_2$ (2 singlets)	CH_3CO-	CH_3 in iPr_2dtp (doublet)
$La(iPr_2dtp)_3(dma)_2$	3.12, 3.05	2.30	1.30(J=6)
$La(iPr_2dtp)_3(dmf)_2$	3.05, 3.00		1.30(J=6)
dma	3.05, 2.94	2.11	
dmf	2.99, 2.87		

Chemical shift, δ ppm, TMS=0; J in Hz.

References

1) D. Brown and D. G. Holm, *Chem. Commun.*, **1968**, 1545.
2) M. Delepine, *Bull. Soc. Chim. Fr.*, **3**, 643 (1908); T. Moeller, D. F. Martin, L. C. Thompson, R. Ferris, G. R. Feister, and W. J. Randell, *Chem. Rev.*, **65**, 1 (1965).
4) T. H. Siddall, III, and W. E. Stewart, *J. Inorg. Nucl. Chem.*, **32**, 1147 (1970).
5) D. Brown, D. G. Holah, and C. E. F. Rickard, *J. Chem. Soc., A*, **1970**, 786.
6) M. Ciampolini, N. Nardi, P. Colamario, and P. Orioli, *J. Chem. Soc., Dalton Trans.*, **1977**, 379.
7) Y. Meseri, A. A. Pinkerton, and G. Chapius, *J. Chem. Soc. Dalton Trans.*, **1977**, 725.
8) A. A. Pinkerton, Y. Meseri, and C. Rieder, *J. Chem. Soc., Dalton Trans.*, **1978**, 85.
9) A. A. Pinkerton and W. L. Earl, *J. Chem. Soc., Dalton Trans.*, **1979**, 1347.
10) A. A. Pinkerton and D. Schwarzenbach, *J. Chem. Soc., Dalton Trans.*, **1980**, 1300.
11) a) A. A. Pinkerton and D. Schwarzenbach, *J. Chem. Soc., Dalton Trans.*, **1976**, 2464; b) **1976**, 2466.
12) A. A. Pinkerton and D. Schwarzenbach, *J. Chem. Soc., Dalton Trans.*, **1981**, 1470.
13) R. G. Pearson, *J. Chem. Educ.*, **45**, 581, 643 (1968).
14) Y. Yamada, M. Shimoi, and A. Ouchi, *Chem. Lett.*, **1978**, 867.
15) M. Shimoi, A. Ouchi, T. Uehiro, Y. Yoshino, S. Sato, and Y. Saito, *Bull. Chem. Soc. Jpn.*, **55**, 2371 (1982).
16) S. E. Livingstone and A. E. Mihkelson, *Inorg. Chem.*, **9**, 2545 (1970).
17) "The Universal Crystallographic Computation Program System (UNICS)," ed by, T. Sakurai, Crystallographic Society of Japan, Tokyo (1967).
18) "International Tables for X-Ray Crystallography," Kynoch Press, Birmingham (1974), Vol. IV.
19) $R=\Sigma||F_o|-|F_c||/\Sigma|F_o|$
20) The final thermal parameters and the final F_o-F_c table are deposited as Document No. 8329 at the Office of the Editor of Bull. Chem. Soc. Jpn.
21) J. L. Hoard, B. Lee, and M. D. Lind, *J. Am. Chem. Soc.*, **87**, 1613 (1965).
22) H. B. Kerfoot, G. R. Choppin, and T. J. Kistenmacher, *Inorg. Chem.*, **18**, 787 (1979).
23) A. R. Al-Karaghouli and J. S. Wood, *Inorg. Chem.*, **18**, 1177 (1979).
24) T. Phillips, II, D. E. Sands, and W. F. Wagner, *Inorg. Chem.*, **7**, 2295 (1968).
25) M. E. Silver, H. K. Chun, and R. C. Fay, *Inorg. Chem.*, **21**, 3765 (1982).
26) W. Rudzinski, G. T. Behenke, and Q. Fernando, *Inorg. Chem.*, **16**, 1206 (1977).

Raman Spectra in the Skeletal Vibration Region of $[Co(gly)_x(ox)_y(en)_z]^{(3-x-2y)+}$ Complexes ($x+y+z=3$)

Toshihide F. MARUYAMA, Ken-ichi OKAMOTO,† Jinsai HIDAKA,† and Hisahiko EINAGA*

Institute of Materials Science, University of Tsukuba, Sakura, Ibaraki 305

† *Department of Chemistry, University of Tsukuba, Sakura, Ibaraki 305*

(Received January 26, 1983)

The Raman spectra were measured for the complete series of cobalt(III) complexes, $[Co(gly)_x(ox)_y(en)_z]^{(3-x-2y)+}$, where gly, ox, and en denote glycinate, oxalate, and ethylenediamine, respectively, and $x+y+z$ is equal to 3, in aqueous solution in the skeletal vibration region to deduce their structure-spectra relation. The spectra could be classified into four categories: polarized bands in the 610—520 cm^{-1} region due to a totally symmetric stretching vibration mode, depolarized bands in the 520—400 cm^{-1} region due to Co-O and Co-N stretching vibration modes, depolarized bands in the 400—300 cm^{-1} region due to the metal-ligand skeletal bending deformation mode, and polarized bands in the 300—200 cm^{-1} region due to the chelate ring deformation mode. The depolarized bands due to the stretching vibration mode could be used for the differentiation of C_2-*cis* and C_1-*cis* isomers of $[Co(N)_4(O)_2]$ and $[Co(N)_2(O)_4]$ type complexes.

Elucidation of the spectra-structure relations of coordination compounds is of practical importance for the study of their stereochemistry. The Raman spectroscopy in the skeletal vibration region of cobalt(III) complexes has produced several studies on their spectral characteristics,[1–13] which were found to be available for differentiation of some of their geometrical isomers, such as *cis* and *trans* ones of $[Co(a)(b)(NH_3)_4]$,[12] $[Co(a)(b)(en)_2]$,[10] and $[Co(a)(b)(tn)_2]$[13] type complexes, where a and b stand for unidentate ligands and en and tn denote ethylenediamine and trimethylenediamine, respectively.

The present study was attempted to deduce more general information on the relation between geometrical structure and the Raman spectra in the skeletal vibration region of cobalt(III) complexes. A series of $[Co(gly)_x(ox)_y(en)_z]^{(3-x-2y)+}$ complexes, where gly and ox denote glycinate and oxalate and $x+y+z$ is equal to 3, were chosen as a typical example and their Raman spectra were measured in the 610—200 cm^{-1} region in aqueous solution in order to avoid contribution of lattice vibrations observed in the solid state.

Experimental

Complexes. The complete series of $[Co(gly)_x(ox)_y(en)_z]^{(3-x-2y)+}$ complexes were prepared and characterized according to standard literature procedures; $[Co(en)_3]Cl_3\cdot 3H_2O$,[14] $[Co(gly)(en)_2]I_2\cdot H_2O$,[15] $[Co(ox)(en)_2]Cl\cdot H_2O$,[16] C_1-*cis(O)*-$[Co(gly)_2(en)]Cl\cdot 3H_2O$,[17] C_2-*cis(O)*-$[Co(gly)_2(en)]Cl\cdot 0.5H_2O$,[17] *trans(O)*-$[Co(gly)_2(en)]Cl\cdot H_2O$,[18] *mer(N)*-$[Co(gly)(ox)(en)]$,[18] *mer(N)*-$[Co(gly)_3]\cdot 1.5H_2O$,[19] *fac(N)*-$[Co(gly)_3]\cdot H_2O$,[19] *fac(N)*-$[Co(gly)(ox)(en)]$,[18] *trans(N)*-$K[Co(gly)_2(ox)]$,[17] C_2-*cis(N)*-$Na[Co(gly)_2(ox)]$,[17] C_1-*cis(N)*-$Na[Co(gly)_2(ox)]$,[17] $Na[Co(ox)_2(en)]\cdot 2.5H_2O$,[16] $Na_2[Co(gly)(ox)_2]\cdot 2H_2O$,[20,21] and $K_3[Co(ox)_3]\cdot 2H_2O$.[22] $[Co(NH_3)_6]Cl_3$ was also prepared according to the literature procedure.[23]

Measurements. The Raman spectra were recorded on a JASCO Laser Raman Spectrometer, which was constructed specially from a double monochromator, model CT-25, a He-Ne laser, model NEC GLS-8500, and a data processor, model DP-500 as the main components. The sample solution was excited at 632.8 nm and the Raman spectra were calibrated with indene.

Results and Discussion

General Aspect. Raman spectral data of $[Co(gly)_x(ox)_y(en)_z]^{(3-x-2y)+}$ complexes are summarized in Table 1. The Raman spectra of $[Co(NH_3)_6]^{3+}$, $[Co(en)_3]^{3+}$, and $[Co(ox)_3]^{3-}$ shown in Fig. 1 clearly demonstrate that $[Co(en)_3]^{3+}$ and $[Co(ox)_3]^{3-}$ give the same spectral characteristics; a polarized band in the 610—520 cm^{-1} region(depolarization ratio: ≈ 0), two

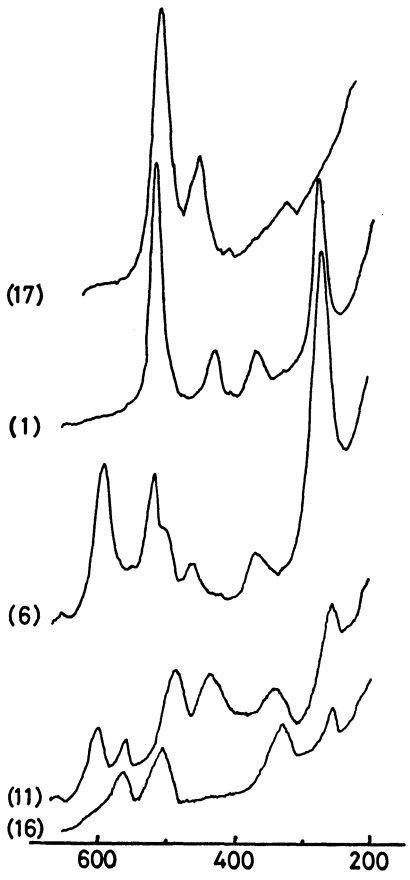

Fig. 1. Raman spectra of $[Co(NH_3)_6]^{3+}$, $[Co(en)_3]^{3+}$, $[Co(ox)_3]^{3-}$, *trans(O)*-$[Co(gly)_2(en)]^+$, and *trans(N)*-$[Co(gly)_2(ox)]^-$. Numbers in parentheses correspond to those in Table 1.

Table 1. Observed Raman bands and their assignments for $[Co(gly)_x(ox)_y(en)_z]^{(3-x-2y)+}$ complexes ($x+y+z=3$)

No.	Complex	Raman frequency/cm^{-1} [a,b]						
1	$[Co(en)_3]^{3+}$			525 (501) s, p 526 ($A_{1g}(O_h)$)[9]		440 (422) w, dp 444 ($E_g(O_h)$)[9]	378 (350) w, dp 376 ($T_{2g}(O_h)$)[9]	283 (274) s, p 280 (δ_{crd})[9]
2	$[Co(gly)(en)_2]^{2+}$	584 (583) w, p		521 (493) s, p	471 (439) vw, dp	447 (427) w, dp	374 (344) w, dp	279 (265) s, p
3	$[Co(ox)(en)_2]^{+}$		565 (555) m, p	528 (496) s, p	480 (454) vw, dp	456 (430) w, dp	374 (344) w, dp 358 vw, dp	278 (265) s, p
4	*cis*(*O*)-$[Co(gly)_2(en)]^{+}$	593 (577) m, p		526 (495) m, p	494 (466) w, dp 469 (449) w, dp	430 (422) vw, dp 422 (409) vw, dp	358 (343) w, dp	276 (269) s, p
5	*cis*(*O*)-$[Co(gly)_2(en)]^{+}$	598 (580) m, p		538 (506) s, p	486 (458) w, dp	433 (425) w, dp	360 (340) w, dp	276 (269) s, p
6	*trans*(*O*)-$[Co(gly)_2(en)]^{+}$	596 (571) m, p		523 (486) m, p	504 (486) w(sh), dp	458 (442) w, dp	368 (347) w, dp	275 (264) s, p
7	*mer*(*N*)-[Co(gly)(ox)(en)]	602 w, p	567 m, p	532 m, p	498 vw, dp[c]	466 w, dp[c] 436 vw, dp[c]	362 w, dp	275 s, p
8	*mer*(*N*)-$[Co(gly)_3]$	602 s, p			540 vw, dp[c]	496 w, dp[c] 440 vw, dp[c]	356 w, dp	272 s, p
9	*fac*(*N*)-$[Co(gly)_3]$	603 s, p			487 w, dp	438 w, dp	364 w, dp	270 s, p
10	*fac*(*N*)-[Co(gly)(ox)(en)]	603 m, p	566 m, p	531 s, p	488 w, dp	426 w, dp	358 w, dp	270 s, p
11	*trans*(*N*)-$[Co(gly)_2(ox)]^{-}$	608 vw, p	565 vw, p		494 w, dp	440 w, dp	348 w, dp	260 w, p
12	*cis*(*N*)-$[Co(gly)_2(ox)]^{-}$	602 m, p	564 m, p		510 w, dp	432 w, dp	348 w, dp	260 s, p
13	*cis*(*N*)-$[Co(gly)_2(ox)]^{-}$	604 m, p	564 m, p		512 w, dp 504 w, dp	432 w, dp 419 w, dp	342 w, dp	262 s, p
14	$[Co(ox)_2(en)]^{-}$		567 s, p	542 m, p	492 w, dp	432 w, dp	354 w, dp 340 vw, dp	268 s, p
15	$[Co(gly)(ox)_2]^{2-}$	605 w, p	567 w, p		505 w, dp	446 w, dp	340 w, dp	260 w, p
16	$[Co(ox)_3]^{3-}$		570 w, p		506 w, dp		335 w, dp	257 w, p
17	$[Co(NH_3)_6]^{3+}$			495 s, p		440 m, dp	320 w, dp	—
				495 ($A_{1g}(O_h)$)[3]		440 ($E_g(O_h)$)[3]	—	
				490 ($A_{1g}(O_h)$)[4]		440 ($E_g(O_h)$)[4]	317 ($T_{2g}(O_h)$)[4]	
				494 ($A_{1g}(O_h)$)[6]		442 ($E_g(O_h)$)[6]	322 ($T_{2g}(O_h)$)[6]	
Assignment[b]		ν_{ts}(Co-L) for gly	ν_{ts}(Co-L) for ox	ν_{ts}(Co-L) for en	ν(Co-O)	ν(Co-N)	δ_{sbd}(L-Co-L)	δ_{crd}(Co$\langle^{L}_{L}$)

a) Numerical data in the parentheses are for the N-deuterated complexes. b) The following abbreviations were used: s, strong; m, medium; w, weak; vw; very weak; sh, shoulder; p, polarized; dp, depolarized; ν_{ts}, totally symmetric stretching vibration mode; ν, stretching vibration mode, excluding the totally symmetric one; δ_{sbd}, metal-ligand skeletal bending deformation mode; δ_{crd}, chelate ring deformation mode; and L, donor atom(N and/or O). c) Consult the text.

depolarized bands in the 520—400 cm^{-1} and 400—300 cm^{-1} regions(depolarization ratio: $\approx$0.75), and a polarized one in the 300—200 cm^{-1} region(depolarization ratio: 0.12—0.16). Furthermore, it is evident that the Raman bands of $[Co(en)_3]^{3+}$ can well be correlated to those of $[Co(NH_3)_6]^{3+}$ having an O_h symmetry[9] except the polarized one in the 300—200 cm^{-1} region, which relates to the en chelate ring.

It has been pointed out that, based on the depolarization characteristics and the comparison with $[Co(NH_3)_6]^{3+}$, $[Co(en)_3]^{3+}$ has an effective symmetry[9] of O_h for the skeletal vibrations. This simplified treatment can be supported by two depolarized bands in the 520—400 cm^{-1} region of *trans(O)*-$[Co(gly)_2(en)]^+$ and of *trans(N)*-$[Co(gly)_2(ox)]^-$ (*cf.* Fig. 1) having the effective symmetry of D_{4h}(Co–O and Co–N stretching vibration modes(except totally symmetric one): $A_{1g}+B_{1g}$) rather than the true symmetry of C_2. (Polarized bands in the 610—520 cm^{-1} region show a peculiar aspect(*cf.* Table 1) and will be treated separately.) Hence we may expect that, so far as the skeletal vibrations of the octahedral tris(bidentate)cobalt(III) complexes with five-membered chelate rings are concerned, the Raman spectra are treated in terms of the effective symmetry which is mainly specified by arrangement of coordinated atoms around the central metal atom. Accordingly, the polarized band in the 610—520 cm^{-1} region, the depolarized bands in the 520—400 cm^{-1} region, and the depolarized band in the 400—300 cm^{-1} region can be assigned to totally symmetric metal-ligand stretching, Co–O and Co–N stretching, and metal-ligand skeletal bending deformation modes,[1-4,6,8,9] respectively. The polarized band in the 300—200 cm^{-1} region with the depolarization ratio of 0.12—0.16 can be assigned to the chelate ring deformation mode which is totally symmetric.[9,10] The contribution of the totally symmetric stretching character of the metal-ligand to this has been pointed out by Flint and Matthews[24] based on vibronic spectra in the d-d transition region($^1A_{1g}$—$^1T_{1g}(O_h)$) of $[Co(en)_3]^{3+}$.

It is interesting to note that the intensities of the polarized bands of $[Co(ox)_3]^{3-}$, $[Co(gly)(ox)_2]^{2-}$, and *trans(N)*-$[Co(gly)_2(ox)]^-$ decreased when the first absorption band($^1A_{1g}$—$^1T_{1g}(O_h)$) of the complexes is in the proximity of the excitation wavelength (632.8 nm) (*cf.* Table 1). This de-enhancement of the Raman intensities may be due to a sort of anti-resonance Raman effect.[9]

Polarized Bands in the 610—520 cm^{-1} Region.
Figure 2 depicts the spectra-structure relation of $[Co(gly)_x(ox)_y(en)_z]^{(3-x-2y)+}$ complexes in the totally symmetric stretching vibration region. It is noteworthy that *mer(N)*- and *fac(N)*-$[Co(gly)_3]$ show only one Raman band and that the Raman bands of $[Co(en)_3]^{3+}$ and $[Co(ox)_3]^{3-}$ as well as *mer(N)*- and *fac(N)*-$[Co(gly)_3]$ become doublets for $[Co(gly)_x(ox)_y]^{(3-x-2y)+}$, $[Co(gly)_x(en)_z]^{(3-x)+}$, and $[Co(ox)_x(en)_z]^{(3-2y)+}$ and triplets for [Co(gly)(ox)(en)] irrespective of the geometry. These splittings of the Raman bands may be caused by relaxation of the selection rule with respect to the effective symmetry of the complexes. It is evident from Table 1 that the coordinated en, ox, and gly ligands have characteristic bands in the regions 542—521 cm^{-1}, 570—564 cm^{-1}, and 608—584 cm^{-1}, respectively. Inconsistency in metal-coordinated atom bond strengths and totally symmetric stretching frequencies of coordinated en relative to gly and ox reflects the contribution of rigidity of the framework of the chelate ring. These results demonstrate that the coordinated bidentate ligands with five-membered chelate rings behave, for the totally symmetric stretching vibration, as a unit, owing to restrictions by the chelate rings. The Raman bands in this region are characteristic of coordinated ligands for the tris(bidentate)cobalt(III) complexes with five-membered chelate rings.

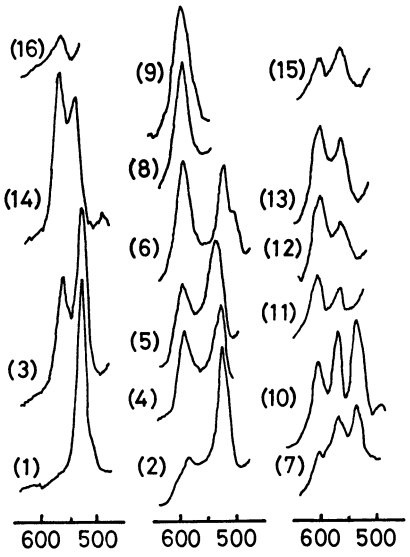

Fig. 2. Raman spectra of $[Co(gly)_x(ox)_y(en)_z]^{(3-x-2y)+}$ complexes in the totally symmetric stretching vibration region. Numbers in parentheses correspond to those in Table 1.

Depolarized Bands in the 520—400 cm^{-1} Region.
Unlike those in the 610—520 cm^{-1} region, the Raman bands in this region show some unique aspects: the Co–N stretching mode lies as a general rule in the region below 460 cm^{-1} and the Co–O stretching mode above 470 cm^{-1}, respectively,[25] and numbers of the Raman bands reflect the effective symmetry of $[Co(gly)_x(ox)_y(en)_z]^{(3-x-2y)+}$ complexes. $[Co(N)_6]$ and $[Co(O)_6]$ type complexes with the effective symmetry of O_h give only one band, which becomes a doublet for *trans(O)*-$[Co(N)_4(O)_2]$ and *trans(N)*-$[Co(N)_2(O)_4]$ complexes with that of D_{4h}. The doublet for $[Co(N)_5(O)]$ and $[Co(N)(O)_5]$ type complexes, $[Co(gly)(en)_2]^{2+}$ and $[Co(gly)(ox)_2]^{2-}$, with that of C_{4v}(Co–O and Co–N stretching vibration modes(except totally symmetric one): A_1+B_1+E) may be explained by correlation of the E mode to the Raman inactive E_u mode of the D_{4h} symmetry, whereas the A_1 and B_1 modes of the former correspond to the A_{1g} and B_{1g} modes of the latter, respectively. Thus the E mode may be almost undetectable[12] in the Raman spectra of the complexes with the effective symmetry of C_{4v}.

Figures 3 and 4 show the spectra-structure relations of $[Co(N)_4(O)_2]$ and $[Co(N)_2(O)_4]$ type complexes and

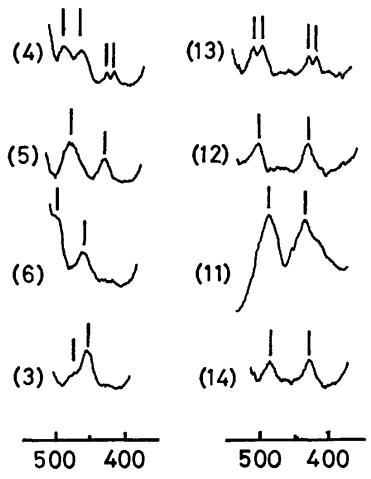

Fig. 3. Raman spectra of *trans*, C_2-*cis*, and C_1-*cis* isomers of $[Co(gly)_2(en)]^+$ and $[Co(gly)_2(ox)]^-$ and of $[Co(ox)(en)_2]^+$ and $[Co(ox)_2(en)]^-$ in the Co–O and Co–N stretching vibration region. Numbers in parentheses correspond to those in Table 1.

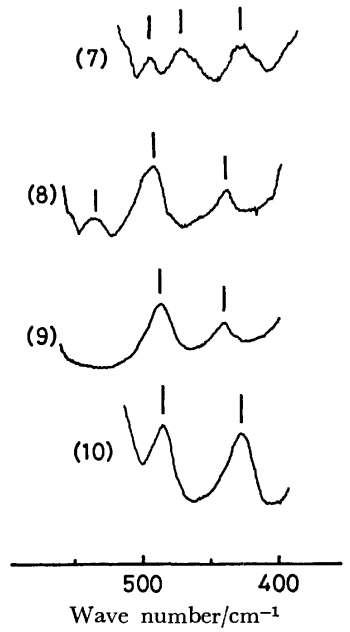

Fig. 4. Raman spectra of *mer* and *fac* isomers of $[Co(gly)_3]$ and $[Co(gly)(ox)(en)]$ in the Co–O and Co–N stretching vibration region. Numbers in parentheses correspond to those in Table 1.

of $[Co(N)_3(O)_3]$ type complexes, respectively. C_2-*cis(O)* and C_2-*cis(N)* isomers of $[Co(gly)_2(en)]^+$ and $[Co(gly)_2(ox)]^-$ give doublets, which however split into quartets on going from the C_2-*cis* to C_1-*cis* isomers. Here, the configuration of the chelate rings comes to play a role in the effective symmetry because both of the isomers belong to C_{2v} symmetry for the arrangement of the coordinated atoms. $[Co(ox)(en)_2]^+$ and $[Co(ox)_2(en)]^-$ with the effective symmetry of C_{2v} also give doublet in this region. Analogously, the *fac* isomers of $[Co(gly)_3]$ and $[Co(gly)(ox)(en)]$ with the higher effective symmetry give doublets, whereas the *mer* isomers with the lower symmetry give triplets. In the latter isomers, the middle bands of 476 cm^{-1} for *mer(N)*-$[Co(gly)(ox)(en)]$ and 496 cm^{-1} for *mer(N)*-$[Co(gly)_3]$ (*cf.* Table 1) may have a largely Co–O stretching character.

These results, together with considerations on numbers of the Raman active stretching vibrations for $[Co(a)_{6-n}(b)_n]$ and $[Co(AB)_3]$ type complexes, reveal that the effective symmetry of the $[Co(gly)_x(ox)_y(en)_z]^{(3-x-2y)+}$ complexes is higher than the true symmetry. In fact, the *fac(N)* isomers of $[Co(gly)_3]$ and $[Co(gly)(ox)(en)]$ can be treated uniformly as *fac(N)*-$[Co(N)_3(O)_3]$ type with the effective symmetry of C_{3v} and likewise the *mer(N)* isomers can be treated as having C_{2v}-type effective symmetry.

In summary, the Raman bands in this region are characteristic of the geometry of the $[Co(N)_4(O)_2]$ and $[Co(N)_2(O)_4]$ type complexes and of $[Co(N)_3(O)_3]$ type complexes. They can be used for the differentiation of the *fac* and *mer* isomers of the latter and of the C_2-*cis* and C_1-*cis* isomers of the former. This is considered to be of practical importance, although the differentiation by comparison of the d-d transition energies and the molar absorptivities in the first ($^1A_{1g}$—$^1T_{1g}$-(O_h)) and the second absorption band($^1A_{1g}$—$^2T_{1g}$-(O_h)) may also be possible.[17]

Depolarized Bands in the 400—300 cm^{-1} Region. The Raman spectra in the metal-ligand skeletal bending deformation region show only one band, except for $[Co(ox)_x(en)_z]^{(3-2y)+}$, which gives a major band accompanied with a very weak one in its lower wavelength side. Numbers of the Raman bands depend neither on the composition nor on the geometry of the complexes, indicating that N–Co–N, N–Co–O, and O–Co–O bending deformation modes are mostly degenerate. However, correlation was noticed between an increase in the Raman shift and an increase in the d-d transition energies in the first and the second absorption bands, as is readily deduced from Table 1. This means that the bending deformation mode reflects coordinate bond strength.

Polarized Bands in the 300—200 cm^{-1} Region. A polarized Raman band is observed in this region for $[Co(en)_3]^{3+}$, $[Co(ox)_3]^{3-}$, and $[Co(gly)_3]$, and for all the mixed-ligand complexes as well. Hence, the totally symmetric chelate ring deformation modes of en, ox, and gly are considered to be degenerate. The same correlation as that found in the skeletal bending deformation was noticed for the chelate ring deformation.

References

1) K. Nakamoto, "Infrared and Raman Spectra of Inorganic and Coordination Compounds," 3rd ed, Wiley-Interscience, New York (1977), Part III.
2) H. Block, *Trans. Faraday Soc.*, **55**, 867 (1959).
3) T. E. Haas and J. R. Hall, *Spectrochim. Acta*, **22**, 988 (1966).
4) H. Siebert and H. H. Eysel, *J. Mol. Struct.*, **4**, 29 (1969).
5) T. V. Long, II, A. W. Herlinger, E. F. Epstein, and I, Bernal, *Inorg. Chem.*, **9**, 459 (1970).
6) T. W. Swaddle, P. J. Craig, and P. M. Boorman, *Spectrochim. Acta, Part A*, **26**, 1559 (1970).

7) J. Gouteron-Vaissermann, *C. R. Acad. Sci., Ser. B*, **275**, 149 (1972); *ibid., Ser. C*, **276**, 555 (1973).
8) K. H. Schmidt and A. Müller, *Inorg. Chem.*, **14**, 2183 (1975).
9) P. Stein, V. Miskowski, W. H. Woodruff, J. P. Griffin, K. G. Werner, B. P. Gaber, and T. G. Spiro, *J. Chem. Phys.*, **64**, 2159 (1976).
10) K. Kanamori and K. Kawai, *Bull. Chem. Soc. Jpn.*, **53**, 2520 (1980).
11) K. Kanamori, T. Morikawa, and K. Kawai, *Bull. Chem. Soc. Jpn.*, **53**, 2787 (1980).
12) K. Kanamori and K. Kawai, *Bull. Chem. Soc. Jpn.*, **55**, 764 (1982).
13) K. Kanamori, H. Ichinose, and K. Kawai, *Bull. Chem. Soc. Jpn.*, **55**, 1315 (1982).
14) J. B. Work, *Inorg. Synth.*, **2**, 221 (1946).
15) C. T. Liu and B. E. Douglas, *Inorg. Chem.*, **3**, 1356 (1964).
16) F. P. Dwyer, I. K. Reid, and F. L. Garvan, *J. Am. Chem. Soc.*, **83**, 1285 (1961).
17) N. Matsuoka, J. Hidaka, and Y. Shimura, *Bull. Chem. Soc. Jpn.*, **40**, 1868 (1967).
18) N. Matsuoka, J. Hidaka, and Y. Shimura, *Bull. Chem. Soc. Jpn.*, **39**, 1257 (1966).
19) M. Mori, M. Shibata, E. Kyuno, and M. Kanaya, *Bull. Chem. Soc. Jpn.*, **34**, 1837 (1961).
20) F. P. Dwyer, I. K. Reid, and A. M. Sargeson, *Aust. J. Chem.*, **18**, 1919 (1965).
21) K. Yamasaki, J. Hidaka, and Y. Shimura, *Bull. Chem. Soc. Jpn.*, **42**, 119 (1969).
22) J. C. Bailar, Jr., and E. M. Jones, *Inorg. Synth.*, **1**, 37 (1939).
23) J. Bjerrum and J. P. McReynolds, *Inorg. Synth.*, **2**, 216 (1946).
24) C. D. Flint and A. P. Matthews, *Inorg. Chem.*, **14**, 1219 (1975).
25) Shift of the Raman bands on N-deuteration above 470 cm^{-1} region implies a partial contribution of the Co–N stretching vibration through the chelate ring to the Co–O stretching one.

 © 1983 The Chemical Society of Japan Bull. Chem. Soc. Jpn., 56, 2615—2617 (1983)

Studies on Lanthanoids-Antimony-Chalcogenides. I. Synthesis and Crystal Data of Three New Lanthanum Antimony Chalcogenides

Jin-zhang GAO,† Izumi NAKAI, and Kozo NAGASHIMA*

Department of Chemistry, The University of Tsukuba, Sakura-mura, Ibaraki 305

(Received February 2, 1983)

Three new La-Sb chalcogenides were synthesized by hydrothermal or evacuated silica tube methods. (1) $LaSbO_2S_2$: a bright-red needle crystal; crystal system, hexagonal; space group, $P6_3/m$; lattice constants, $a=14.954(3)$, $c=3.898(2)$ Å, and $Z=6$. (2) $La_6Sb_8S_{21}$: a blackish-red columnar crystal with metallic luster, orthorhombic, $P222$, $a=14.317(2)$, $b=15.239(4)$, $c=8.685(1)$ Å, and $Z=2$. (3) $La_3Sb_3S_{10}$: a bright-red plate-like crystal, monoclinic, $a=13.209(6)$, $b=14.229(6)$, $c=5.583(1)$ Å, $\beta=94.54(3)°$, and $Z=2$.

There has been much attention in rare earth chalcogenides because of their interesting electric, magnetic, and optical properties. However, so far very few investigations have been made concerning the preparation of single crystals of rare earth antimony chalcogenides. Lemoine *et al.*,[1] reported the synthesis and the structure analysis of $Eu_3Sb_4S_9$, yet it has been mentioned that the oxidation number of europium is +2, not the general oxidation number for rare-earth elements. The only well characterized rare-earth antimony sulfide containing Ln^{3+} is $Pr_8Sb_2S_{15}$[2].

This work has been done as a part of our study on the crystal chemistry of sulfosalt compounds having a general chemical formula $A_mB_nX_p$, where A=metal, B=As,Sb, and X=O,S,Se.[3,4] These compounds have been characterized by the chemical nature of the element A.[5] The purpose of this study is to elucidate the crystal chemical behavior of rare-earth elements in sulfosalt compounds. This paper reports the methods of preparation of single crystals and the crystal data of three new lanthanum antimony chalcogenides.

Experimental

Two methods of syntheses were employed for the preparation of the three compounds. One is an evacuated silica tube method. A double silica tube method was adopted to protect against explosion, because a silica tube was easily attacked at high temperature. The other is a hydrothermal method, which was applied to the single crystal growth of $LaSbO_2S_2$. The reagents used were lanthanum metal chips (99.9%), sulfur powder (99.99%), and antimony trisulfide (99.99%).

Syntheses of La-Sb-S ternary compounds by the silica tube method were carried out as follows. Weighed quantities of La, Sb, S, and Sb_2S_3 were mixed and placed in a double silica tube, and then sealed under vacuum (less than 10^{-3} Torr, 1 Torr≈133.322 Pa). The reaction tube was placed in an electric furnace. The synthesis was usually continued over a week, in which the tube was first maintained at the reaction temperature of 1200 °C or 1000 °C, then kept at 1000 °C or 900 °C for three days at least, and finally the temperature was slowly lowered to room temperature.

The hydrothermal synthesis was made using a stellite bomb of the test-tube type. A starting material was a polycrystalline material obtained by the silica tube method. About 70 mg of the starting material and 0.07 ml of solvent (H_2O, 3%NaOH or 5%Na_2S) were sealed in a gold tube (length: 35 mm, inner diameter: 2.8 mm). Conditions employed were: the temperature range 350—500 °C; the pressure 800—1000 kg/cm² for 5—10 d.

The products were examined by the X-ray powder diffraction method, Weissenberg and precession cameras, SEM-XMA, and an automatic four-circle diffractometer. Chemical analyses were made by an electron microprobe analyzer using an operating voltage of 20 kV and a probe current of 0.015 μA. Synthetic Sb_2S_3 and La_2TiO_5 were used as the standards.

Results and Discussion

Three new compounds have been obtained from our synthesis. Their chemical compositions are given in Table 1.

Characterization of Crystals. $LaSbO_2S_2$ is a needle crystal and bright-red in color. The maximum size of the single crystal is $0.3\times0.03\times0.03$ mm³. The presence of oxygen in $LaSbO_2S_2$ was determined by the appearance of Sb–O absorption in the IR spectra (see *Infrared Spectroscopy*). The starting material did not contain any oxygen. The source of oxygen is considered to be the silica tube used as a container, since it was easily attacked at high temperature. The melting point of $LaSbO_2S_2$ is higher than 1000 °C.

$La_6Sb_8S_{21}$ is a columnar crystal of $0.4\times0.1\times0.05$ mm³ in maximum size. It is blackish-red with metallic luster. Thermal analysis showed that it melted incongruently at 985 °C into $La_3Sb_3S_{10}$ and liquid Sb_2S_3. The crystal is stable in air at room temperature and dissolved in diluted HNO_3 solution.

$La_3Sb_3S_{10}$ is a plate-like crystal of $0.3\times0.3\times0.01$ mm³. The crystal is bright-red and transparent. The melting point is higher than 1000 °C. Unfortunately,

Table 1. Electron microprobe chemical analysis of the three compounds

	$LaSbO_2S_2$		$La_6Sb_8S_{21}$		$La_3Sb_3S_{10}$	
	wt%	Atomic ratio	wt%	Atomic ratio	wt%	Atomic ratio
La	38.26	1.01	31.85	5.95	37.26	2.97
Sb	33.21	1	37.54	8	32.93	3
S	17.39	1.99	25.89	20.95	29.60	10.23
O	8.85	2.03				
Total	97.71		95.28		99.79	

† On leave from Department of Chemistry, Northwestern Teachers College, Lanchow, China.

the chemical formula of $La_3Sb_3S_{10}$ remains in question. The formula appears not to hold the electrical neutrality, if La and Sb are considered to be trivalant and S is divalent. Moreover, as mentioned later in this paper, $La_3Sb_3S_{10}$ has a superstructure. The limited amount of the specimen available precluded a precise wet chemical analysis. At the present stage, it is difficult to conclude whether it is $La_3^{3+}Sb_3^{3+}S_8(S_2)^{2-}$, or a mixed valence compound $La_3^{3+}Sb_2^{3+}Sb^{5+}S_{10}$ or a nonstoichiometric compound from the electron microprobe data.

Conditions of Formation. The experimental results of the silica tube method are summarized in Table 2. The purpose of maintaining the tube at the growth temperature is to obtain large crystals. However, in the case of $LaSbO_2S_2$, the crystal growth rate was slow and only polycrystalline materials were obtained. The results show that the appearance of a phase largely depends upon the temperature, but not on the ratio of the starting materials. For example, we could not obtain $La_3Sb_3S_{10}$ from the synthesis under conditions of the reaction temperature 1100 °C and the growth temperature 900 °C. Contrariwise, when the reaction temperature was 1200 °C and the growth temperature was 1000 °C, the crystals of $La_6Sb_8S_{21}$

TABLE 2. EXPERIMENTAL CONDITIONS AND RESULTS OF SYNTHESES BY SILICA TUBE METHOD

Run No.	Starting material/mol	Time / d	T/°C: Reaction	T/°C: Growth	Main product
1	$La:S:Sb_2S_3=2:3:2$	10	1200	1000	$La_3Sb_3S_{10}$
2	LaS_2[a]$:Sb_2S_3=1:2$	7	1200	1000	$La_3Sb_3S_{10}$
3	$La:S:Sb_2S_3=1:2:2$	10	1000	900	$La_6Sb_8S_{21}$
4	LaS_2[a]$:Sb_2S_3=1:2$	6	1000	900	$La_6Sb_8S_{21}$
5	$La:S:Sb_2S_3=2:3:2$	7	1000	900	$La_6Sb_8S_{21}$

a) LaS_2 was obtained by the silica tube method at 900 °C using a stoichiometric mixture of the elements.

TABLE 3. EXPERIMENTAL CONDITIONS AND RESULTS OF SYNTHESES BY HYDROTHERMAL METHOD

Run No.	Solvent	T / °C	Pressure / kg cm^{-2}	Time / d	Main product
1	H_2O	500	1000	6	$LaSbO_2S_2$
2	H_2O	400	1000	9	$LaSbO_2S_2$
3	H_2O	350	900	7	$LaSbO_2S_2$
4	3% NaOH	500	1000	6	Sb_2S_3
5	5% Na_2S	350	800	8	Sb_2S_3

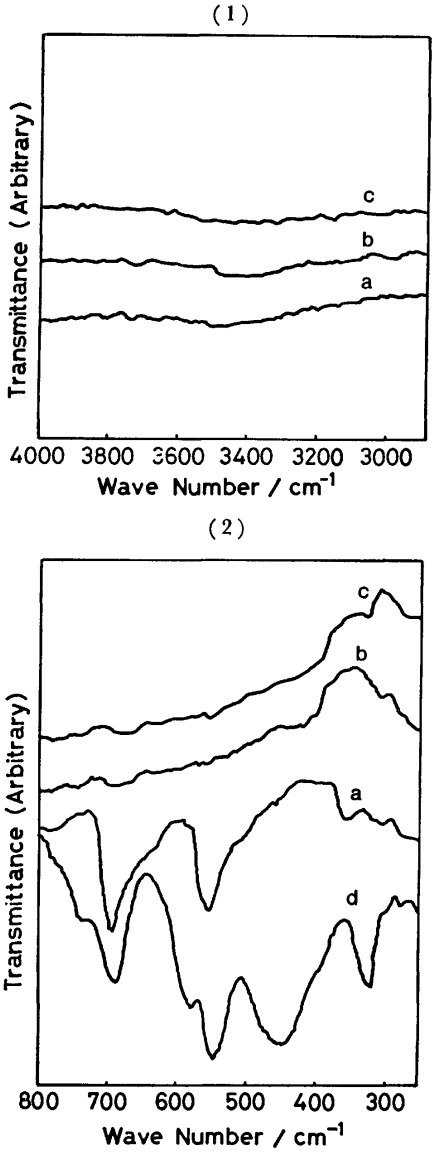

Fig. 1. Infrared spectra; a: $LaSbO_2S_2$, b: $La_6Sb_8S_{21}$, c: $La_3Sb_3S_{10}$, d: Sb_2O_3.

TABLE 4. CRYSTALLOGRAPHIC DATA

Compound	Crystal system	Space group	Lattice constants	Z	d_{obsd} / g cm^{-3}	d_{calcd} / g cm^{-3}
$LaSbO_2S_2$	hexagonal	$P6_3/m$	$a=14.954(3)$Å $c=3.898(2)$	6	4.84	4.71
$La_6Sb_8S_{21}$	orthorhombic	$P222$	$a=14.317(2)$ $b=15.239(4)$ $c=8.685(1)$	2	4.45	4.35
$La_3Sb_3S_{10}$	monoclinic		$a=13.209(6)$ $b=14.229(6)$ $c=5.583(1)$ $\beta=94.54(3)°$	2	3.70	3.61

Table 5. X-Ray powder diffraction data obtained using a 114.6 mm diameter Gandolfi camera. Cu/Ni radiation, intensities estimated visually

$LaSbO_2S_2$			$La_6Sb_8S_{21}$			$La_3Sb_3S_{10}$		
d/Å	I_{obsd}	$h\ k\ l$	d/Å	I_{obsd}	$h\ k\ l$	d/Å	I_{obsd}	$h\ k\ l$
7.51	vw	1 1 0	4.04	vw	3 2 0	3.76	s	$\bar{2}$ 2 1
4.92	s	2 1 0	3.69	w	1 4 0	3.56	s	0 4 0
3.61	s	1 3 0	3.63	w	2 1 2	3.29	m	4 0 0
3.35	w	2 0 1	3.48	s	3 3 0	3.03	vw	3 2 1
3.06	vs	2 1 1	3.34	m	2 2 2	2.780	s	0 0 2
2.983	w	2 3 0	3.24	m	4 2 0	2.732	w	0 1 2
2.902	w	3 0 1	2.962	w	3 2 2	2.679	m	1 0 2
2.836	w	4 1 0	2.811	s	1 4 2	2.629	w	5 0 0
2.653	m	3 1 1	2.716	w	3 3 2	2.439	vw	$\bar{3}$ 0 2
2.498	m	4 0 1	2.661	w	2 4 2	2.386	vw	3 5 0
2.371	m	3 2 1	2.459	w	1 5 2	2.271	m	3 0 2
2.229	s	4 1 1	2.365	m	5 1 2	2.232	w	2 6 0
2.139	w	3 4 0	2.178	m	0 0 4	2.196	m	5 2 1
2.084	w	5 2 0	2.074	w	4 6 0	2.078	w	5 3 1
1.952	w	0 0 2	1.998	vw	3 6 2	1.993	w	$\bar{5}$ 0 2
1.890	m	1 1 2	1.938	w	6 3 2	1.774	w	4 4 2
1.876	m	4 3 1				1.699	w	2 2 3
1.717	m	3 1 2				1.639	w	3 6 2

were not observed.

The results of hydrothermal experiments are given in Table 3. Single crystals of $LaSbO_2S_2$ have been obtained from the synthesis. $La_6Sb_8S_{21}$ and $La_3Sb_3S_{10}$ were found to be unstable under the hydrothermal conditions. Three kinds of liquids, *i.e.* H_2O, 3% NaOH, 5% Na_2S solutions, were examined as solvents. In the case of 3% NaOH or 5% Na_2S solutions, only La_2O_3 and Sb_2S_3 were observed as the products.

Crystallographic Data. Crystallographic data for the three compounds are summarized in Table 4. The crystal systems and space groups were determined by Weissenberg and precession photographs. X-Ray diffraction spots of $La_3Sb_3S_{10}$ were very diffuse, probably due to the thermal strain and very thin thickness of the crystal. Oscillation photographs (rotation axis =c) exhibited very weak super structure reflections with c=3c'. However, the super lattice could not be determined because of the diffuse nature and the weakness of the diffraction spot intensities. The average lattice is given in Table 4.

Unit cell dimensions were first determined from the photographs. The final cell parameters were calculated by a least-squares treatment of 2θ values centered automatically on the automatic four-circle diffractometer using monochromated Mo $K\alpha$ radiation (λ=0.70926Å). X-Ray powder diffraction data were obtained with the Gandolfi camera using Ni filtered Cu $K\alpha$ radiation and are given in Table 5.

Morphology of the single crystal of $LaSbO_2S_2$ is a hexagonal column elongated along c axis. $La_6Sb_8S_{21}$ is a plate crystal having well developed (010) faces. The elongation axis is c. $La_3Sb_3S_{10}$ is a very thin plate with well developed (100) faces and the elongation axis is c.

Infrared Spectroscopy. IR spectra were measured by the conventional KBr method in the region from 4000 to 250 cm^{-1} to examine the absorption bands of H_2O, OH, and Sb–O bonds. Figure 1-(1) shows the spectra of the three compounds in the region from 4000 to 2900 cm^{-1}, in which these spectra indicate the absence of any hydroxide ion or water of hydration. Figure 1-(2) shows the spectra of the three compounds and Sb_2O_3 for comparison. Two rather strong absorption bands at 695 and 555cm^{-1} were observed in $LaSbO_2S_2$. These bands are attributed to the Sb–O vibration from analogy with the spectrum of Sb_2O_3. From these results, $LaSbO_2S_2$ is considered to be oxide-sulfide but not to be hydrated sulfide nor sulfate of La and Sb. Both $La_6Sb_8S_{21}$ and $La_3Sb_3S_{10}$ exhibit featureless spectra even in the low wave number regions.

The authors wish to express their thanks to Mr. Ritsuro Miyawaki for his help in the electron microprobe analysis.

References

1) P. Lemoine, D. Carré, and M. Guittard, *Acta Crystallogr., Sect. B*, **37**, 1281 (1981).

2) G. G. Guseinov, F. Kh. Mamedov, I. R. Amiraslanov, and Kh. S. Mamedov, *Sov. Phys. Crystallogr.*, **26**, 470 (1981).

3) K. Nagashima, M. Ogino, and I. Nakai, *Bull. Chem. Soc. Jpn.*, **51**, 1761 (1978).

4) I. Nakai and D. E. Appleman, *Chem. Lett.*, **1981**, 1327.

5) I. Nakai, S. Katsura, and K. Nagashima, Proceedings of the International Symposium on Hydrothermal Reactions, March 22—26, 1982, Yokohama, Japan.

Note added in proof: The crystal structure of $LaSbO_2S_2$ has been determined from Patterson and Fourier syntheses using intensity data collected on the four-circle diffractometer. The structure was refined by a full-matrix least-square method to a conventional R of 0.065 for 738 observed reflections. The structure consists of the $[La_3O_6]_\infty$ hexagonal prism and $[Sb_2S_4]_\infty$ double chain. They are parallel to the c-axis and linked each other by the weak La–S bonds.

Enrichment and Determination of Trace Amounts of Iron as the Colored Complex on the Thin Layer of Ion-exchange Resins

Kunio Ohzeki,* Yuhko Satoh, Yoshito Kawamura, and Tomihito Kambara
Department of Chemistry, Faculty of Science, Hokkaido University, Sapporo 060

(Received February 28, 1983)

A trace amount of iron was extracted as the complex with 4,7-diphenyl-1,10-phenanthrolinedisulfonic acid from aqueous solution using finely divided anion and cation exchange resins. The mixed resins were collected on a filter paper as the disk of thin layer. The colored complex in the resin phase was determined with the use of a densitometer at 540 nm. The calibration graph was linear over the range 0.1—0.5 μg of iron(II). The relative standard deviation for 0.5 μg of iron(II) in 50 ml of the test solution was 2.1% (n= 5). The method was applied to the trace determination of total iron in water samples.

The concentration procedure is usually required for the spectrophotometric determination of trace amounts of ions in water samples. Although the most popular method is the extraction of colored species into a nonaqueous solvent, the utilization of solid adsorbents is of interest. For example, Wills and Sangster[1] used Amberlite XAD-2 for the extraction of iron(II)–1,10-phenanthroline complex. The complex fixed on the resin was then eluted by a small amount of organic solvent and determined. It was possible to concentrate the iron by a factor greater than 200. Nigo *et al.*[2] used the cation exchanger, Dowex 50W-X4, to collect the iron(II)-complex. The determination was made by the direct measurement of the resin phase absorbance using a 1-mm cell.

The combined use of finely divided anion and cation exchange resins have been reported.[3,4,5] The colored species were collected in the thin layer of mixed resins and determined spectrophotometrically[3,4] or densitometrically.[5] The volume of resin phase is about 0.07 cm^3, and so it is possible to concentrate the colored species in a 50-ml sample solution by a factor greater than 700. In the present paper, the rapid extraction of iron(II)–4,7-diphenyl-1,10-phenanthrolinedisulfonate into the resin phase is studied and the results are applied to the determination of trace amounts of iron in water samples.

Experimental

Reagents. Hydrochloric acid used was of super special grade (SSG reagent, Wako). All other chemicals used were of analytical reagent grade. Deionized redistilled water was used.

Standard stock solutions (1000 ppm) of iron(II) and iron(III) were prepared by dissolving 7.021 g of ammonium iron(II) sulfate hexahydrate and 8.634 g ammonium iron(III) sulfate dodecahydrate, respectively, in 1 dm^3 of water containing hydrochloric acid. The pH of both solutions was around 1.5. Respective working solutions, 10 ppm in iron(II) and iron(III), were prepared fresh daily by dilution with diluted hydrochloric acid solution (pH *ca.* 1.5).

The reagent, 4,7-diphenyl-1,10-phenanthroline (Bathophenanthroline, abbreviated as BP; Dotite), was used as received. A 1 mM (1 M=1 mol dm^{-3}) solution was made by dissolving 33 mg of the reagent in 50 ml of ethanol and then diluting with water to 100 ml.

Disodium salt of 4,7-diphenyl-1,10-phenanthrolinedisulfonic acid (Bathophenanthroline disulfonic acid, Na_2 salt, abbreviated as BPS; Dotite) was used as received. An aqueous 1 mM solution was prepared.

An aqueous 10 w/v% solution of hydroxylammonium chloride was prepared and purified by extracting the impurity iron as the BP complex into isopentyl alcohol.

Sodium acetate was dissolved in water to give 10 w/v% solution. The impurity iron was removed extraction as the BP complex in the presence of purified hydroxylammonium chloride.

Ion-exchange Resin Suspension. The macroreticular type ion-exchangers, Amberlyst 15 and A-27 (Rohm and Haas), were used in RSO_3H and $RN(CH_3)_3Cl$ forms, respectively. The cation exchange resin suspension (CRS) and the anion exchange resin suspension (ARS) were prepared according to the method already reported.[6] The ion-exchange capacities of CRS and ARS were determined by conductometric titration with standard sodium hydroxide and silver nitrate solutions, respectively. The capacities were 11.8 μequiv. ml^{-1} for CRS and 7.00 μequiv. ml^{-1} for ARS. When a 2-ml portion of CRS is mixed with 3 ml of ARS, both resins were almost completely coagulated and quantitatively collected on a filter paper on a holder. For masking any iron present as impurity, 10 ml of 0.01 M EDTA were added to 240 ml of CRS and ARS, respectively.

Apparatus. A Toyo KG-25 filter holder was used with filter paper of No. 5B (Toyo Roshi) for preparing thin layer of the mixed resins by filtration.

The densitometer used was a Shimadzu Chromatoscanner CS-920. Numerical values corresponding to the integrated absorbance were printed out automatically. Experimental conditions were as follows; *i.e.*, wavelength 540 nm, scanparameter, x=24 mm and y=30 mm, linearizer 1. A Shimadzu spectrophotometer UV-240 was also used.

Micropipets (Finnpipett) were used for pipetting out the working solution and hydrochloric acid.

A Corning hot plate, PC-100, was used. The 100-ml beakers containing sample solutions were placed on the hot plate and covered with a 5-dm^3 beaker. Nitrogen gas was introduced in the covering beaker and samples were heated.

All glasswares were immersed overnight in 6 M nitric acid, and then rinsed thoroughly with deionized water.

Procedure. Place a sample solution, containing usually less than 0.5 μg of iron, in a 100-ml beaker. Add 100 μl of 20% hydrochloric acid and 2.0 ml of 10% hydroxylammonium chloride. Heat on the hot plate for 15 min under nitrogen atmosphere, and cool the sample to room temperature. Add 1.0 ml of 1 mM BPS solution and 2.0 ml of sodium acetate solution. Adjust the volume to 50 ml with water. The pH of final solution is 4.5. Allow the mixture to stand for 20 min and then add 2.0 ml of CRS and 3.0 ml of ARS. Stir the mixture for 5 min. Collect the resulting coagulated resins on a filter paper strip placed on the holder by suction. A disk of thin layer, 17 mm in

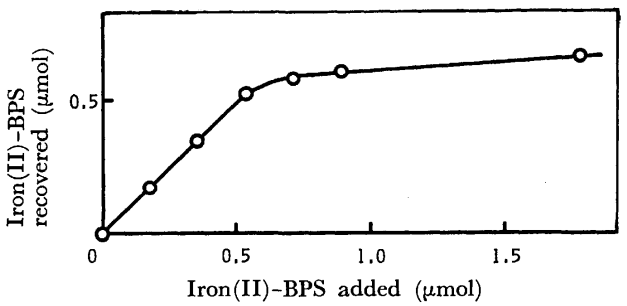

Fig. 1. Recovery of iron(II)–BPS complex on the resin mixture of 3.0 ml of ARS and 2.0 ml of CRS. Test solution 50 ml, ionic strength 0.01.

diameter and about 0.3 mm in thickness, is obtained. Keep the filter strip wet in water for 10 min, and place it on a white plastic plate fixed on a scanning board in the chromatoscanner. Measure the absorbance twice and determine the mean of duplicate values, which coincided each other within less than 0.1%.

The calibration graph was prepared using the iron(II) standard solution, the heating step being omitted. There was no significant difference between the blank values obtained with and without heating step.

Results and Discussion

Masking of Impurity Iron in CRS and ARS. The impurity in hydroxylammonium chloride, as well as in sodium acetate solution, was removed successfully by extraction as iron(II)–BP complex, but the extraction procedure could not be applied to the purification of ion-exchange resins. The use of EDTA was found to be efficient. When EDTA was previously added to ARS and CRS, the formation of iron(II)–BPS complex from the impurity in the resins was masked effectively, while the complex once formed was stable in the presence of EDTA.

Preparation of Thin Layer of Mixed Resins. In the course of 5-min stirring, the iron(II)–BPS complex was fixed on the anion exchange resin and the resin was coagulated with the cation exchanger. The resin mixture was collected on a filter paper by filtration with suction within 5 min. The stable coloration was kept for at least 3 h, when the thin layer was stored in wet in water. The absorption spectrum of the iron(II)–BPS complex was compared with that in the solution. A small shift of the maximum wavelength was observed, *i.e.*, from 533 nm in the solution to 540 nm in the resin phase.

Recovery of Iron(II)–BPS Complex. The extraction of the complex into the resin mixture of 3.0 ml of ARS and 2.0 ml of CRS was examined in the presence of 0.01 M sodium chloride to keep a constant ionic strength. Up to 0.54 μmol, the complex was quantitatively fixed on the mixed resins (Fig. 1). The recovery of 0.5 μg of iron(II) as the BPS complex on the mixed resins was also studied by varying added amounts of BPS from 0.5 to 3.5 μmol. A constant recovery was obtained over the range studied.

Calibration Graph. The least-squares regression equation for iron(II) over the range 0.1—0.5 μg was $y=5.79\times10^4x+2.58\times10^4$, where y is the integrated absorbance of the resin phase, as measured against the filter paper, and x is the amount of iron(II) in μg. The intercept at $x=0$ is due to the background absorbance of the thin layer prepared from the test solution without addition of iron(II). The mean value with the standard deviation was $(2.60\pm0.05)\times10^4$ ($n=5$) for the blank and $(5.48\pm0.03)\times10^4$ ($n=5$) for 0.5 μg of iron(II). Thus, the net value for 0.5 μg of iron(II) was $(2.88\pm0.06)\times10^4$, and the relative standard deviation was 2.1%.

Effect of Copper. As well known, 1,10-phenanthroline and the analogous compounds are selective colorimetric reagents for iron.[7] Among cations likely to be present, only the interference of a large amount of copper is reported. The recovery of 0.5 μg of iron(III) as the iron(II)–BPS complex was examined in the presence of varying amounts of copper(II).

Table 1. Effect of copper(II) on determination of iron(III)[a]

Cu(II) added (μg)	Net value of chromatoscanner absorbance for iron(II)-BPS $\times10^{-4}$	Recovery (%)
0	2.94	100
5	2.95	100
10	2.92	99
20	3.00	102
50	0.66	22

a) Iron(III) taken: 0.5 μg.

Table 2. Determination of total iron in water samples

Sample	Sample amount (ml)	Iron(II) added (μg)	Iron found (μg)	Iron in sample (μg)	Iron in sample (ng ml^{-1})
Tap water					
Sep. 17, 1981	50	0.00	0.20_4	0.20_4	4.1
	50	0.10	0.30_0	0.20_0	4.0
	50	0.20	0.40_1	0.20_1	4.0
Nov. 17, 1981	50	0.00	0.07_6	0.07_6	1.5
	50	0.10	0.18_1	0.08_1	1.6
	50	0.20	0.27_9	0.07_9	1.6
Mineral	5	0.00	0.20_2	0.20_2	40.4
	5	0.10	0.30_4	0.20_4	40.8
	5	0.20	0.39_0	0.19_0	38.0

The recovery was quantitative in the presence of 20 μg of copper (Table 1). In the presence of 50 μg of copper, however, copper(I)–BPS complex is predominantly formed and the recovery of iron was suppressed.

Determination of Total Iron in Water Samples. The total iron in the tap water supplied to our laboratory from the well in our University campus was determined. After the running of water longer than 20 min, the 50-ml portions were taken. The recovery of added amounts of iron(II) was quantitative (Table 2). The iron content in a commercially available mineral water was also determined successfully.

The present method is very sensitive and only a small sample amount is required, which is especially advantageous to the determination of total iron, since the sample is easily heated without contamination from the vessel and atmosphere.

The solvent extraction method[8] requires a 200-ml sample solution and a 4-cm cuvette for the determination of iron in the ppb range as the iron(II)–BP complex. The solvent extraction process using a large volume of sample water is tedious.

References

1) R. B. Wills and D. Sangster, *Anal. Chem.*, **48**, 59 (1976).
2) S. Nigo, K. Yoshimura, and T. Tarutani, *Talanta*, **28**, 669 (1981).
3) K. Ohzeki, T. Sakuma, and T. Kambara, *Bull. Chem. Soc. Jpn.* **53**, 2878 (1980).
4) K. Matsuhisa, K. Ohzeki, and T. Kambara, *Bull. Chem. Soc. Jpn.*, **54**, 2675 (1981).
5) K. Suzuki, G-D. Park, K. Ohzeki, and T. Kambara, *Bull. Chem. Soc. Jpn.*, **55**, 3335 (1982).
6) M. Abe, K. Ohzeki, and T. Kambara, *Bull. Chem. Soc. Jpn.*, **51**, 1090 (1978).
7) O. G. Koch and G. A. Koh-Dedic, "Handbuch der Spurenanalyse 2," Auflage, Springer-Verlag, (1974), p. 696.
8) A. L. Willson, *Analyst*, **89**, 389 (1964).

Determination of Ethylenediaminetetraacetic Acid and Nitrilotriacetic Acid as Their Iron(III)-Complexes by Reversed Phase High Performance Liquid Chromatography

Akihiro YAMAGUCHI, Allah Rakha RAJPUT,** Kunio OHZEKI,* and Tomihito KAMBARA

Department of Chemistry, Faculty of Science, Hokkaido University, Sapporo 060

(Received March 10, 1983)

The iron(III) complexes with ethylenediaminetetraacetic acid (EDTA, H_4edta) and nitrilotriacetic acid (NTA, H_3nta) were separated by the ion-association reversed phase high performance liquid chromatography. The retention behavior of iron(III)-nta complex on the column (4.6 mm i.d., 25 cm long) packed with ZORBAX-ODS was seriously affected by the pH of eluent composed of phosphate buffer solution containing tetrabutylammonium bromide and acetonitrile. A mixture of edta and nta in a synthetic sample solution containing the commonly present metal ions was converted to the corresponding iron(III) complexes and determined successfully by the present method.

The importance of analysis of naturally occurring and pollutant chelating agents has been claimed[1] and a method was proposed in which the copper(II) complexes of amine-*N*-carboxylic acids, such as EDTA and NTA, were separated by liquid chromatography and detected by atomic absorption spectrometry. The detection sensitivity was enough, but the separation of the chelates on a weak anion exchange resin column was insufficient. Recently, reversed phase high performance liquid chromatography (RPLC) was successfully applied to the separation of edta complexes of bismuth(III), iron(III), and copper(II).[2]

This paper describes a simple RPLC method for determining iron(III)–edta and –nta complexes. The conversion of free and complexed edta and nta to iron(III) complexes is made quantitatively by heating a sample solution in the presence of excess iron(III).[3] The excess iron(III) is removed by a cation exchange resin column and the effluent is directly subjected to the analysis by RPLC.

Experimental

Apparatus. The liquid chromatograph employed was a Shimadzu product, type LC-3A, equipped with a UV-detector, model SPD-2A (195—350 nm), and a data processor Chromatopac C-R1A. A prepacked ODS column (ZORBAX, Du Pont) was consisted of a stainless steel tube, 4.6 mm i.d. and 25 cm long. A Shimadzu spectrophotometer, UV-240, was used for measurements of absorption spectra.

Reagents. All chemicals used were of analytical reagent grade. Dotite reagents, Na_2H_2edta·$2H_2O$ and H_3nta were used. A 10^{-2} M (1 M = 1 mol dm^{-3}) edta stock solution was prepared by dissolving dried reagent (80 °C, 2 h) in deionized water. A 10^{-2} M nta stock solution was prepared by dissolving dried acid (110 °C, 2 h) in sodium hydroxide solution, the pH of the final solution being around 8. Ammonium iron(III) sulfate dodecahydrate was dissolved into acidified water to give 10^{-2} M solution (pH = 1). Tetrabutylammonium bromide (TBAB) was obtained from Wako Pure Chemicals.

Ion Exchange Resin. The sodium-form Dowex 50W-X8 (100—200 mesh) resin was packed in a column, 1 cm i.d., 23 cm long, in a 1-cm bed.

Preparation of Mobile Phase. To a one-liter flask containing 500 ml of redistilled water, were added 1.15 g of ammonium dihydrogenphosphate, 17.5 ml of 10^{-2} M TBAB solution, 50 ml of acetonitrile, and 6 ml of 1.67 M phosphoric acid. The mixture was filled up to the mark with redistilled water. The pH of the final solution was 2.5. The solution was then filtered through a membrane filter of 0.45 μm pore size.

Procedure. The sample solution containing edta and nta was taken into a 50-ml volumetric flask and 2.5 ml of 0.05 M sulfuric acid, 1 ml of 0.01 M iron(III) solution, and 3 ml of sodium formate were added successively. When the sample contained metal ions, it was heated in the presence of excess iron(III) before the addition of formate. The mixture was made up to the volume with water, the pH of the final solution being around 3. A part of the solution was passed through the sodium-form resin column at the flow rate of 2—3 ml min^{-1}. The first 10-ml portion of effluent was discarded and the next 5-ml portion was collected. The test solution thus obtained was filtered with the use of MILLEX-SR (Millipore Co.) unit with 0.5 μm membrane filter. A 10-μl portion of the filtrate was injected with a 25-μl syringe to the column. Ion-assosiation chromatography with organic modifier was applied. Tetrabutylammonium (TBA) ion was used as the counter ion and acetonitrile as the organic modifier in the phosphate buffer solution. Chromatographic conditions were summerised in Table 1. The wavelength was fixed to the absorption maximum of iron(III)-edta complex.

Table 1. Chromatographic conditions

Column:	ZORBAX-ODS (4.6×250 mm)
Mobile phase:	0.02 M phosphate buffer solution (pH 2.5)
	0.175 mM TBAB
	5% acetonitrile
Flow rate:	1 ml min^{-1}
Pressure:	95 kg cm^{-2}
UV-detection:	255 nm
Injection size:	10 μl

Results and Discussion

Effect of pH. The pH of mobile phase was adjusted with the use of phosphate buffer solution. The retention time and peak area of iron(III)–nta complex were drastically influenced by the pH values,

** Present address: Abbott Laboratories (Pak.) Ltd. P.O. Box No. 7229, Landhi, Karachi, Pakistan.

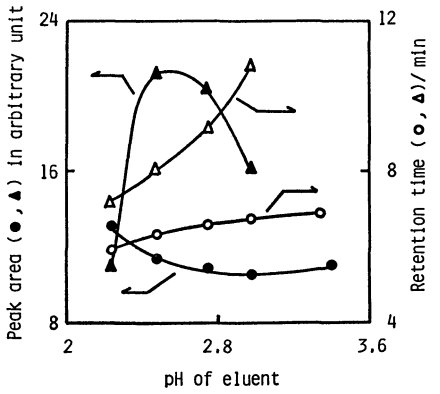

Fig. 1. Effects of pH on retention time (○, △) and peak area (●, ▲).
(○, ●): 20.1 μM iron(III)–edta, (△, ▲): 81.3 μM iron(III)–nta. Conditions except pH of eluent are the same as in Table 1.

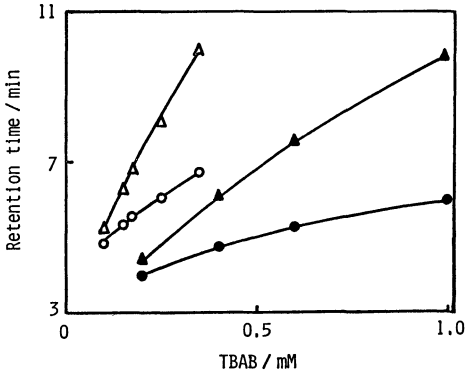

Fig. 2. Effect of concentrations of TBAB and acetonitrile.
Retention time of 20.1 μM iron(III)–edta: (○) 5% acetonitrile, (●) 10% acetonitrile; retention time of 81.3 μM iron(III)–nta: (△) 5% acetonitrile, (▲) 10% acetonitrile. The conditions are the same as in Table 1.

compared with those of iron(III)–edta complex (Fig. 1). The peak width of iron(III)–nta complex broadened with increasing pH, and pH>3.5, the peak was no longer detectable.

Effect of Tetrabutylammonium Ion and Acetonitrile. The retention time of both compounds increased with increasing concentration of TBA ion and decreased with increasing concentration of acetonitrile (Fig. 2). The peak shape of iron(III)–nta complex was also extremely affected by the concentrations of TBA ion and acetonitrile. The distorted peak was observed when the phosphate buffer mobile phase contained 0.35 mM TBA ion and 5% acetonitrile, or 1.0 mM TBA ion and 10% acetonitrile. The combained use of 0.175 mM TBA ion and 5% acetonitrile were pertinent. A typical chromatogram was shown in Fig. 3.

Calibration Curve. The calibration curves of edta and nta were linear over the concentration range 2—20 μM and 6—50 μM, respectively, while the curve for nta did not pass through the origin. The relative standard deviations (n=5) were in the range of 2.0 to 1.7% for edta and 7.3 to 3.1% for nta, respectively.

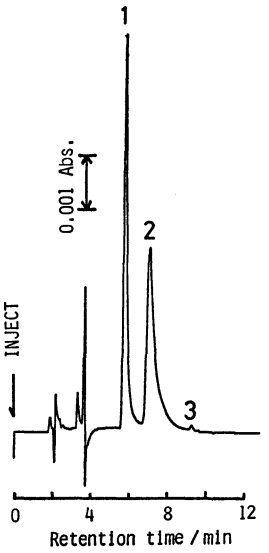

Fig. 3. Typical chromatogram.
(1) 20.1 μM iron(III)–edta, (2) 50.8 μM iron(III)–nta, (3) unknown peak, column: ZORBAX-ODS, Eluent: 0.02 M phosphate buffer solution containing 0.175 mM TBAB and 5% acetonitrile (pH 2.5). Flow rate: 1 ml min^{-1}, temperature: ambient, injection size: 10 μl, UV-detection: 255 nm

TABLE 2. EFFECT OF METAL(II) IONS

[edta]/μM			[nta]/μM		
Taken	Found	Error(%)	Taken	Found	Error(%)
10.1	9.9	−2.0	25.4	25.5	+0.4
12.1	12.1	0	30.5	30.2	−1.0
14.1	14.1	0	35.6	35.0	−1.7

Mg, Ca each in 1 mM, Co, Cd, Zn, Ni, and Cu each in 0.1 mM.

Effect of Diverse Ions. The quantitative conversion of free edta and nta or the complexes with metal ions commonly present was carried out by heating sample solution in the presence of excess iron(III).[3] The excess iron(III) and metal ions were removed by the cation exchange resin column, and hence the present method was essentially free from interference of metal ions (Table 2).

Among the anions studied, a high concentration of nitrate ion gave the peak which had almost the same retention time as iron(III)–nta and caused the positive error (Table 3). In the presence of considerable amounts of phosphate, white precipitate formed by the addition of excess iron(III). However, the precipitate being removed by the sodium form resin column, no interference was observed. The anionic surfactant, dodecylbenzenesulfonate is expected to block TBA cation in the mobile phase, but no effect was found.

Absorption Spectra of Iron(III)–edta and –nta. The spectrum of iron(III)–nta complex in the formate buffer solution was different from that in the phosphate buffer solution, and both spectra were different from that in the dilute sulfuric acid solution (Fig. 4). The mixed ligand complexes of iron(III)–nta with formate or phosphate were postulated. The spectra of iron-

Table 3. Effect of foreign anions

Anions		12.1 μM edta		30.5 μM nta	
added as	Concn(mM)	Found(μM)	Error(%)	Found(μM)	Error(%)
$NaNO_3$	0.1	12.3	+1.7	30.3	−0.7
	0.5	12.0	−0.8	30.1	−1.3
	1.0	12.4	+2.5	31.6	+3.6
	2.0	12.2	+0.8	37.0	+21.3
NaCl	2.0	11.9	−1.7	31.0	+1.6
$NH_4H_2PO_4$	2.0	11.9	−1.7	29.7	−2.6
DBS[a)]	0.4	12.0	−0.8	30.9	+1.3

a) Sodium dodecylbenzenesulfonate.

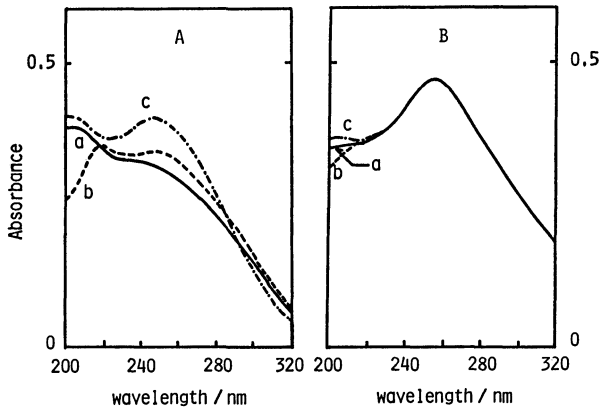

Fig. 4. Absorption spectra of iron(III)–nta and iron(III)–edta.
Spectra of (A) 50 μM iron(III)–nta and (B) 50 μM iron(III)–edta: (a) in dilute sulfuric acid, pH 3.0; (b) in 0.05 M HCOOH–0.01 M HCOONa, pH 2.9; (c) in 0.02 M phosphate buffer solution, pH 2.5.

(III)–edta complex in the varying media coincided each other (Fig. 4). The TBA ion and acetonitrile gave no effect on the absorption spectra. The absorption profiles of iron(III)–edta and –nta in the mobile phase were obtained by plotting each peak area against wavelength, the peak areas having been determined at different wavelength. The profiles were in close agreement with the absorption spectra in the phosphate buffer solution.

Separation of Iron(III)–edta and –nta by Means of an Open Column. Both complexes were found to be retained by the anion exchange resin and eluted with formate buffer solution. The chromatogram obtained on a 1-cm open column packed with sulfate-form Dowex 1-X4 (100—200 mesh) was shown in Fig. 5. The eluate was fractionated and analysed by the present method. Evidently both chelates are negatively charged.

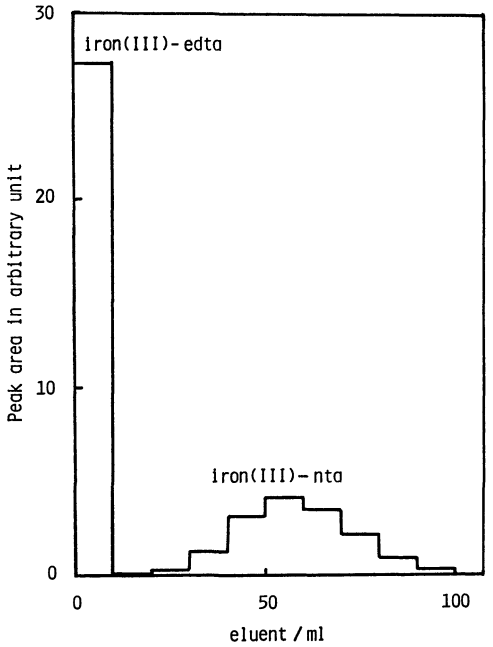

Fig. 5. Separation of iron(III)–nta and –edta by use of a sulfate-form anion exchange resin column.
The mixture of 0.5 μmole iron(III)–edta and 1.0 μmole iron(III)–nta was retained on the column from aqueous solution and eluted by formate buffer solution (0.05 M HCOOH–0.01 M HCOONa).

References

1) D. R. Jones IV, and S. E. Manahan, *Anal. Chem.*, **48**, 502 (1976).
2) K. Hirowatari, Y. Koumura, K. Kumamoto, K. Hattori, and S. Aoshima, *Bunseki Kagaku*, **30**, 534 (1981).
3) A. Yamaguchi, K. Ohzeki, and T. Kambara, *Bull. Chem. Soc. Jpn.*, **56**, 2293 (1983).

The Coagulated Ion-exchanger Colorimetry of Cobalt(II)–Thiocyanate Complex

Kin-ya Suzuki, Kunio Ohzeki, and Tomihito Kambara*
Department of Chemistry, Faculty of Science, Hokkaido University, Sapporo 060
(Received March 14, 1983)

The coagulated ion-exchanger colorimetry was applied to the determination of a trace amount of cobalt(II). Cobalt(II)–thiocyanate complex was fixed by a batch method on the coagulated material composed of fine particles of anion and cation exchangers. The coagulated material was collected on a filter paper and a colored thin layer was prepared. The coloration of the compound was further intensified by dipping the thin layer in a concentrated thiocyanate solution, and the absorbance was determined by a densitometer. The calibration curve showed a good linearity in the range of 1—15 μg of cobalt(II). Iron(III) and copper(II) showed interfering coloration, but these ions were effectively masked by the addition of fluoride and egta, respectively. Zinc(II) gave seriously negative error.

The blue coloration of cobalt(II)–thiocyanate complex is specific for cobalt(II) and is applied to the spot test.[1] The coloration is intensified in the presence of organic solvents such as acetone and ethanol. The increase in the coloration is also observed when the complex is fixed on an anion exchange resin. Therefore, for cobalt(II), the spot test on the resin phase developed by Fujimoto[2] showed higher sensitivity than that for the ordinary solution method. The ion-exchanger colorimetry[3] was applied to the determination of cobalt(II) in which the thiocyanate complex fixed on the anion exchange resin was determined in a 1-mm cell. The combined use of finely divided anion and cation exchange resins was introduced to the colorimetric determinations of chromium(VI),[4] phosphate,[5,6] and hexacyanoferrate(III).[7] The mixed resins fixing the colored complex were collected on a filter paper as a thin layer and the coloration was determined by spectrophotometry[4,5,6] or densitometry.[7]

In the present study, cobalt(II)–thiocyanate complex is rapidly concentrated on the mixed resins and determined by densitometry. The sensitivity of the method and the effects of foreign ions are discussed.

Experimental

Reagents. All chemicals used were of analytical reagent grade.

Standard cobalt(II) solution, 1 mg Co dm^{-3}, was prepared by dissolving cobalt(II) chloride hexahydrate in 1 dm^3 of deionized water containing 10 ml (1 ml = 1 cm^3) of concentrated hydrochloric acid. More dilute standard solutions were prepared as required by diluting the stock solution.

The 0.5 M (1 M = 1 mol dm^{-3}) sodium fluoride and 8 M potassium thiocyanate solutions were prepared.

The dipping aqueous solution was composed of 80 w/v% potassium thiocyanate and 0.2% sodium fluoride.

Ion Exchange Resin Suspensions. The ion-exchangers used were macroreticular type Amberlyst 15 and A-27 (both Rohm and Haas Co.) in RSO_3H and $RN(CH_3)_3Cl$ forms, respectively. The anion exchange resin suspension (ARS) and the cation-exchange resin suspension (CRS) were prepared according to the reported method.[8] The stock suspensions were stored in 5-dm^3 polyethylene bottles, respectively, and were well shaken before being pipetted out. The exchange capacities, as determined by conductometric titration, were 4.40 μequiv. ml^{-1} for ARS and 8.02 μequiv. ml^{-1} for CRS. The resins in 4—6 ml of ARS were almost completely coagulated with those in 2 ml of CRS.[8] The combination of 4 ml of ARS and 2 ml of CRS was used throughout the following experiments.

Apparatus. A Shimadzu Chromatoscanner CS-920 was used for measurement of reflecting absorbance of colored complex in the thin layer of mixed resins. A Shimadzu UV-visible recording spectrophotometer, type UV-240, was used for measuring absorpion spectra. A Hitachi-Horiba pH meter, type F-7_{LC}, was employed. A Toyo KG-25 filter holder was served for the preparation of thin layer of the coagulated material by filtration with suction. Filter papers of No. 5B (Tokyo Roshi) were used. Micropipets were used for pipetting out the standard solution.

Procedure. An aliquot of sample solution containing more than 1 μg of cobalt(II) is placed in a 100-ml beaker. A 2-ml portion of 0.5 M of sodium fluoride is added for masking iron(III) ion in the sample. A 1 ml portion of 8 M of potassium thiocyanate is added. After the volume is adjusted to 40 ml with deionized water, 2 ml of CRS and 4 ml of ARS are added. The mixture is stirred by means of a magnetic stirrer for 10 min. The resulting coagulated material is collected on the filter paper, placed between cylindrical filter holder, by suction. A disk of thin layer of colored resin is formed, which is 17 mm in diameter and about 0.3 mm in thickness. It it then dipped into the dipping solution for 30 min, then the color becomes more intense. The wet filter paper holding the colored resin is placed on a white plastic plate fixed on a scanning board in the densitometer. A light beam (1.2 × 1.2 mm) scans the disk of thin layer in a range of 24 mm wide and 30 mm long and the integrated absorbance is printed out on the chart paper. The measurement is performed using linearizer in mode 1 at 625 nm against the filter paper substrate. All procedures were carried out at room temperature.

Results and Discussion

Absorption Spectra. Absorption spectra of cobalt(II)–thiocyanate complex in the resin phase are shown in Fig. 1. The spectrum against the blank thin layer was the same as that of the complex in acetone having an absorption maximum at 625 nm, which was prepared as described by Snell's.[9]

Effect of Dipping Solution. The coloration in the thin layer of mixed resins faded gradually during the strage in water. Therefore, for the stabilization of color, the resin phase was dipped in the thiocyanate solution together with filter paper before absorption

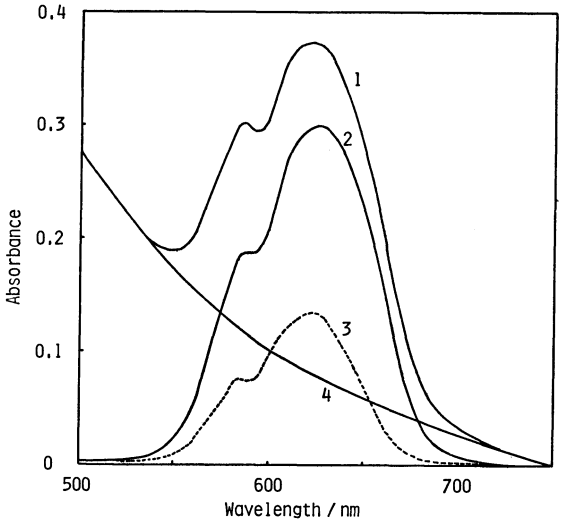

Fig. 1. Absorption spectra of cobalt(II)–thiocyanate complex.
——: Thin layer of mixed resin, ----: acetone solution; (1) and (2) 10 μg of cobalt(II), (3) 200 μg of cobalt(II), (4) blank; (1) and (4) *vs.* wet filter paper, (2) *vs.* blank thin layer, (3) *vs.* blank solution.

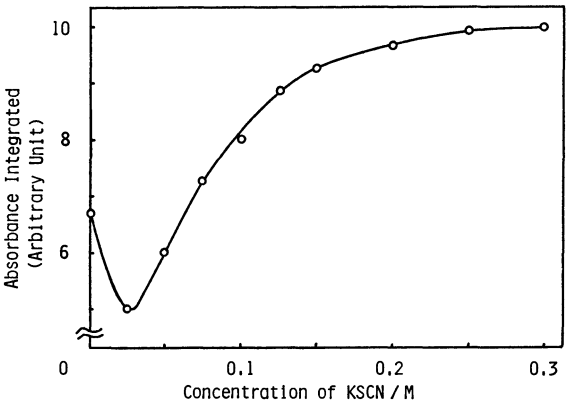

Fig. 2. Recovery of cobalt(II).
Cobalt(II) taken 10 μg; sodium fluoride 1 mmol; sample volume 40 ml; wavelength 625 nm.

measurement. The dipping solution containing 0.2% sodium fluoride was used for masking impurity iron(III). The coloration was intensified with increasing thiocyanate concentration. However, for the concentration over 85%, the solubility of sodium fluoride decreased. Consequently, 80% potassium thiocyanate solution was used throughout the experiments. About 15 min were necessary for obtaining a constant coloration, which was stable at least for 24 h.

Recovery of Cobalt(II). The effect of thiocyanate concentration on the recovery of cobalt(II) was investigated. The amount of cobalt(II) fixed on the mixed resin was first decreased with the addition of thiocyanate and then increased with increasing thiocyanate concentration (Fig. 2). The minimum recovery is probably due to the formation of neutral cobalt(II)–thiocyanate complex. The subsequent experiments were carried out in 0.2 M thiocyanate solution, since the longer filtration time was required with increasing thiocyanate concentration.

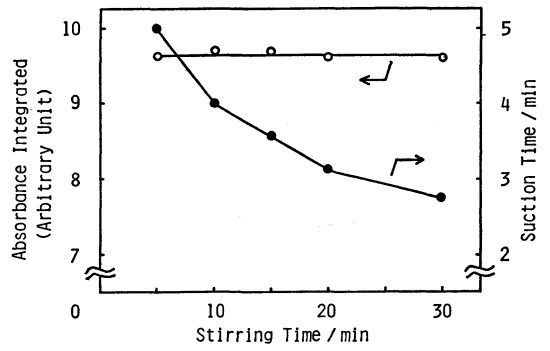

Fig. 3. Effect of stirring time.
Cobalt(II) taken 10 μg; sample volume 40 ml; wavelength 625 nm.

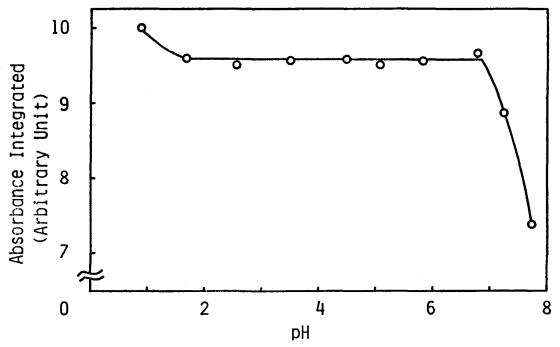

Fig. 4. Effect of pH of sample solution.
Cobalt(II) taken 10 μg; sample volume 40 ml; wavelength 625 nm.

Effect of Stirring Time. During the course of stirring, cobalt(II)–thiocyanate complex is fixed on the anion exchanger in the coagulated mixed resins. The rate of adsorption is very fast and a constant coloration was obserbed in the range of 5 to 30 min studied. On the other hand, the suction time for collecting the mixed resins decreased with increasing stirring time (Fig. 3), since the mixed resins coagulated to form a bulky material during the longer stirring time.

Effect of pH. The effect of pH on the absorbance of complex at 625 nm is shown in Fig. 4. The pH was adjusted by the addition of hydrochloric acid or phosphate buffer solution. A constant absorbance was observed in the range of pH 1.7 to 6.7. The higher value was found at pH 0.9. This is due to the red coloration of iron(III)–thiocyanate complex, the masking of iron(III) by fluoride ion being impossible in this pH region. Above pH 7, cobalt hydroxide being formed, the absorbance decreased.

Calibration Curve. The calibration curve showed a good linearity in the range of 1—15 μg of cobalt(II). The relative standard deviation was 0.89% (n=6) for 10 μg of cobalt(II). The lowest determinable concentration was 25 μg dm^{-3} in 80 ml of sample volume.

Effect of Sample Volume. The effect of sample volume was studied, the thiocyanate concentration being kept to 0.2 M. A constant absorbance was obtained in the range of 30 to 80 ml. For the volume above 80 ml, the filtration time increased seriously. Moreover, the surface of the resulting thin layer did not become uniform and the absorbance decreased.

Effect of Foreign Ions. Most anions studied did

Table 1. Effect of foreign anions on the determination of cobalt(II)[a]

Anion	Anion added(mg)	Cobalt(II) found(μg)	Error (%)
Chloride	350	10.17	+1.7
Fluoride	50	10.05	+0.5
Iodide	60	9.99	−0.1
Nitrate	10	9.91	−0.9
Sulfate	10	10.09	+0.9
Phosphate	10	10.06	+0.6
Pyrophosphate	10	9.80	−2.0
Thiosulfate	10	10.25	+2.5
Acetate	10	9.96	−0.4
Citrate	10	10.00	0
Tartrate	10	9.57	−4.3
Borate	10	10.44	+4.4
Oxalate	10	9.48	−5.2
Hexacyanoferrate(II)	1	5.05	−49.5
Hexacyanoferrate(II)	0.1	9.77	−2.3

a) Cobalt(II) taken: 10 μg.

Table 2. Effect of foreign cations on the determination of cobalt(II)[a]

Cation[b]	Cobalt(II) found(μg)	Error (%)	Cation[b]	Cobalt(II) found(μg)	Error (%)
Mg	9.97	−0.3	Cu^{II}	9.25	−7.5
Ca	9.84	−1.6	Cu^{II}	10.35[c]	+3.5
Ba	10.22	+2.2	Zn^{II}	4.13	−58.7
Si^{IV}	10.18	+1.8	Zn^{II}	10.08[d]	+0.8
Al^{III}	10.16	+1.6	Cd^{II}	9.88	−1.2
Cr^{III}	10.64	+6.4	Hg^{II}	9.32	−6.8
Mn^{II}	10.32	+3.2	Mo^{VI}	10.03	+0.3
Fe^{II}	10.41	+4.1	Pb^{II}	10.37	+3.7
Fe^{III}	10.39	+3.9	Ag^{I}	9.90	−1.0
Ni^{II}	10.68	+6.8			

a) Cobalt(II) taken: 10 μg. b) Foreign cations added: 100 μg. c) The pH of sample solution was adjusted to 4 and 5 μmol of egta were added. d) The sample solution was passed through a column packed with anion exchange resin, Dowex 1-X8 (100—200 mesh, Cl-form). Eluting agent: 0.1 M HCl containing 5% NaCl.

Table 3. Analysis of cobalt(II) in synthetic sample solution

Sample[a] number	Concentration/μg ml^{-1}							Cobalt(II) found(μg)[b]	Error (%)
	Co^{II}	Ca	Mg	Zn^{II}	Fe^{III}	Cu^{II}	Ni^{II}		
I	0.4	4.0	4.0	—	—	—	—	10.00	0
II	0.4	4.0	4.0	4.0	—	—	—	9.96	−0.4
III	0.4	4.0	4.0	4.0	4.0	—	—	10.18	+1.8
IV[c]	0.4	4.0	4.0	4.0	4.0	4.0	—	10.36	+3.6
V[c]	0.4	4.0	4.0	4.0	4.0	4.0	4.0	10.50	+5.0

a) All solutions contained HCl in 0.1 M and NaCl in 5%. b) Effluent taken: 25 ml, mean value of duplicate analyses. c) The pH of effluent was adjusted to 4 and 5 μmol of edta were added.

not interfere with the determination of 10 μg of cobalt(II) (Table 1). However, 100-fold hexacyanoferrate(II) gave negative error, since cobalt(II)–hexacyanoferrate(II) is more stable than the thiocyanato complex. The effect of divers cations was summarized in Table 2. Interference by iron(III) was eliminated with sodium fluoride, as stated before. Copper(II) salts, giving a red-brown coloration with thiocyanate, were masked by the addition of egta (3,6-dioxaoctane-1,8-diamine-*N*,*N*,*N*′-*N*′-tetraacetic acid). The 10-fold amount of chromium(III) and nickel(II) gave positive errors, while mercury(II) a negative one. Zinc(II) gave a serious negative error. No interference being found in the solution method, an additional reaction would occur between thiocyanate complexes of cobalt(II) and zinc(II) on the resin phase. Zinc(II) ions were easily removed from the sample solution as their chlorocomplex by use of an anion exchange resin of strong base type.[10]

Analysis of Synthetic Sample Solution. The synthetic sample solutions containing 0.4 μg ml^{-1} of cobalt(II) and 4 μg ml^{-1} of various foreign ions were analyzed (Table 3). An anion exchange resin column was prepared to remove zinc(II). The column (25 cm × 1 cm i.d.) was packed with 1.5 g of Dowex 1-X8 (100—200 mesh) in the chloride form and washed with 50 ml of 2 M hydrochloric acid solution. The sample solution containing 0.1 M hydrochloric acid and 5% sodium chloride was passed through the column. The first 10 ml were discarded and the next 25 ml of effluent were taken and neutralized with sodium hydroxide. Then, the solution was submitted to the analysis according to the above method. The results obtained were satisfactory.

References

1) F. Feigl and V. Anger, "Spot Tests in Inorganic Analysis," 6th ed, Elsevier Publ. Co., New York (1972), p. 200.
2) M. Fujimoto, *Bull. Chem. Soc. Jpn.*, **27**, 48 (1954).
3) K. Yoshimura, H. Waki, and S. Ohashi, *Talanta*, **23**, 449 (1976).
4) K. Ohzeki, T. Sakuma, and T. Kambara, *Bull. Chem. Chem. Soc. Jpn.*, **53**, 2878 (1980).
5) K. Matsuhisa, K. Ohzeki, and T. Kambara, *Bull. Chem. Soc. Jpn.*, **54**, 2675 (1981).
6) K. Matsuhisa, K. Ohzeki, and T. Kambara, *Bull. Chem. Soc. Jpn.*, **55**, 3335 (1982).
7) K. Suzuki, G. D. Park, K. Ohzeki, and T. Kambara, *Bull. Chem. Soc. Jpn.*, **55**, 2851 (1982).
8) M. Abe, K. Ohzeki, and T. Kambara, *Bull. Chem. Soc. Jpn.*, **51**, 1090 (1978).
9) F. D. Snell, C. T. Snell, and C. A. Snell, "Colorimetric methods of Analysis," D. Van Nostrand Co., Princeton, New Jersey (1959), Vol. IIA, p. 285.
10) K. A. Kraus and G. E. Moore, *J. Am. Chem. Soc.*, **75**, 1460 (1953).

The Formation of Tetrasulfur Dinitride during the Mild Pyrolysis of Tetrasulfur Tetranitride

Yoshiyuki KUDO and Shuichi HAMADA*

Department of Chemistry, Faculty of Science, Science University of Tokyo, Kagurazaka, Shinjuku-ku, Tokyo 162

(Received March 1, 1983)

Tetrasulfur dinitride was formed by the mild pyrolysis of tetrasulfur tetranitride in the presence of a large amount of sulfur. The stoichiometric correlations of the pyrolytic products indicated a step-by-step degradation of the tetrasulfur tetranitride. Differential scanning calorimetry of an interrupted pyrolysis and determinations of the products gave the enthalpy of the formation of gaseous tetrasulfur dinitride as 351 ± 3 kJ mol^{-1}, which was reasonable judging from the bond enengies calculated by Sanderson's method and those deduced from known bond energies. The obtained standard enthalpy of the formation of tetrasulfur tetranitride was 469 ± 1 kJ mol^{-1}, which agreed with the value reported by Barker *et al.*

Heal[1] mentiond that tetrasulfur tetranitride, S_4N_4, decomposed slowly above 120 °C in the presence of a large amount of sulfur, whereas the pure crystals broke down explosively to sulfur and nitrogen upon heating at 190 °C.[1,2] Backens[3] pointed out that tetrasulfur dinitride, S_4N_2, appeared on the mild pyrolysis of tetrasulfur tetranitride mixed with sulfur above 125 °C. Little information on the pyrolysis of tetrasulfur dinitride is available because of its thermal instability.[1,4] In this work, the formation of tetrasulfur dinitride during mild pyrolysis was studied quantitatively. Furthermore, the enthalpy of the formation of tetrasulfur dinitride was estimated and discussed.

Experimental

Materials. The tetrasulfur tetranitride was prepared using the method described by Jolly and Becke-Goehring[5] as follows. Disulfur dichloride vapor was reacted with ammonium chloride pellets at 200 °C for 48 h. The crude product was purified by column chromatography and then recrystallized repeatedly from a benzene solution. Thin-layer chromatograph (TLC) analysis showed that the tetrasulfur tetranitride thus obtained was pure enough to be used in this work. The sulfur was recrystallized several times from a carbon disulfide solution. A homogeneous mixture of sulfur and tetrasulfur tetranitride powder was obtained by a thorough grinding of the compounds at molar ratios ranging from 0.20 to 0.80.

Procedures. Differential thermal analysis (DTA) and thermal gravimetry (TG) were carried out on samples heated at a rate of 3 °C min^{-1} in an argon atmosphere with a Rigaku Denki Thermoflex, model 8002, differential thermal analyzer.

The mixed sample (100—220 mg), placed in a reaction tube, was pyrolyzed at specified temperatures, which were kept constant to ±0.1 °C using a thermostated aluminium block. Volatile pyrolytic products were removed from the reaction tube by the use of a carbon dioxide carrier gas at a flow rate of 30 cm^3 min^{-1} and finally trapped at -30 °C. The trapped product and the solid that remained in the reaction tube were dissolved in small volumes of carbon tetrachloride and used for the identification and determination of the constituent species. The concentrations of tetrasulfur tetranitride, tetrasulfur dinitride, and sulfur in the solution were obtained from a spectrum over the wave-length region from 320 to 480 nm based on the corresponding molar absorption coefficients previously determined (Fig. 1). A freshly prepared pure tetrasulfur dinitride[6] was used to determine its own spectrum. The amount of nitrogen resulting from the decomposition of tetrasulfur tetranitride was estimated with an azotometer after trapping the volatile products.

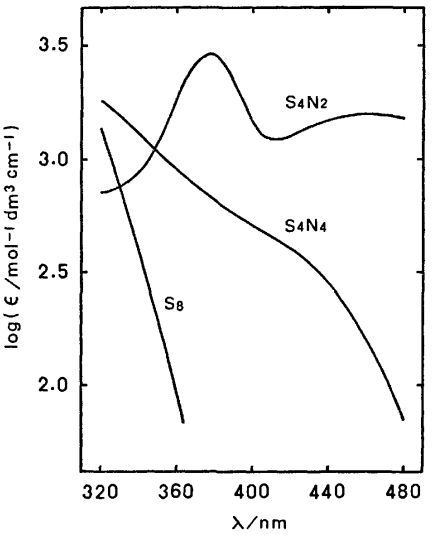

Fig. 1. Absorption spectra of S_4N_2, S_4N_4, and S_8 in CCl_4 solutions.

The heat of decomposition of the sample was measured with a Perkin-Elmer model DSC-1B differential scanning calorimeter at the heating rate of 4 °C min^{-1}. The sample was tightly sealed in an aluminium container under an argon atmosphere, and the equipment was calibrated with indium of a 99.999% purity under the same conditions.

Results

Differential Thermal Analysis of Tetrasulfur Tetranitride Mixd with Sulfur and Its Pyrolytic Products. The pure tetrasulfur tetranitride decomposed abruptly at 190 °C in the argon atmosphere, as is shown in Fig. 2a. The DTA of the mixed sample showed a broad exothermic peak in addition to the endothermic peaks resulting from the fusion of sulfur. The exothermic-peak temperature became lower as the sulfur content increased(Figs. 2b and 2c). The TG also indicated an enhanced decomposition of the mixed sample, while a decrease in the weight of the pure sample resulted from its sublimation.[7] Judging from these results, it is obvious that the pyrolysis of tetrasulfur tetranitride is accelerated in the presence of sulfur.

The tetrasulfur dinitride and the sulfur were con-

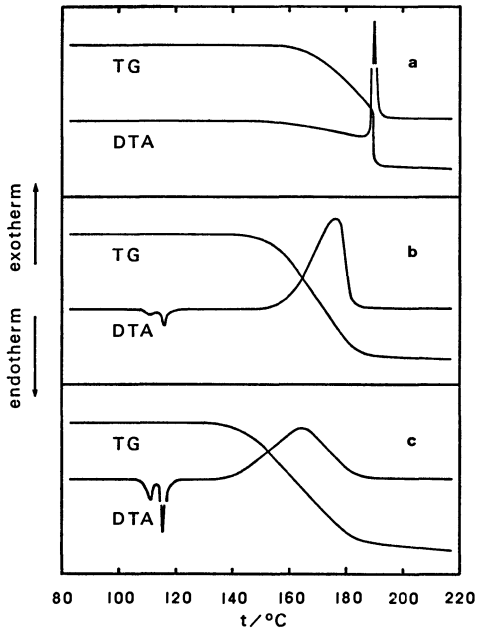

Fig. 2. DTA and TG patterns of pure and mixed S_4N_4.
a: pure, b: $n(S_4N_4)/n(S_8)=0.80$, c: $n(S_4N_4)/n(S_8)=0.20$

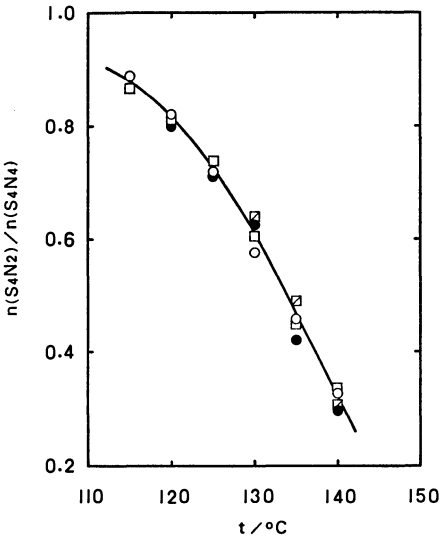

Fig. 3. Molar ratios of produced S_4N_2 at different temperatures.
Molar ratios of original samples, $n(S_4N_4)/n(S_8)$, are 0.65 (▨), 0.50 (●), 0.35 (□), and 0.20 (○), respectively.

firmed as solid products during the pyrolysis of the mixed sample under an atmosphere of either argon or carbon dioxide by IR spectrophotometry[8] and by TLC.[9] Only nitrogen was identified as a gaseous product of the mixed sample by gas chromatography.

Stoichiometry of Products during Mild Pyrolysis of Tetrasulfur Tetraniride. The molar ratios of the pyrolysis products, $n(S_4N_2)/n(S_4N_4)$ and $n(N_2)/n(S_4N_4)$, were determined in order to elucidate the degradation process of tetrasulfur tetranitride mixed with sulfur. The symbols $n(S_4N_2)$ and $n(N_2)$ designate the moles of tetrasulfur dinitride and nitrogen produced, and $n(S_4N_4)$, the moles of pyrolyzed tetrasulfur tetranitride. The amount of the sample used in the experiment did not affect these molar ratios under the specified conditions; for instance, samples ranging from 102 to 221 mg(molar ratio of S_4N_4=0.20), when pyrolyzed at 130 °C for 60 min, gave essentially constant values of $n(S_4N_2)/n(S_4N_4)=0.58\pm0.01$ and $n(N_2)/n(S_4N_4)=1.36\pm0.01$. The values of $n(N_2)/n(S_4N_4)$ were slightly smaller than those calculated from the mass balance because some nitrogen bubbles remained in the molten sample. Reaction times between 40 and 120 min at 125 °C also had little effect on the above molar ratios.

Figure 3 shows that the $n(S_4N_2)/n(S_4N_4)$ ratio remained nearly constant for a given temperature of pyrolysis regardless of the variation in the original composition of the sample, whereas the amount of tetrasulfur dinitride produced increased at high contents of sulfur. The value of $n(S_4N_2)/n(S_4N_4)$ approached unity with a lowering of the temperature of pyrolysis. A decrease in this ratio at higher temperatures arose from the thermal instability of tetrasulfur dinitride.[4] A predominant decomposition of tetrasulfur tetranitride to its elements in the presence of sulfur should yield a value of $n(S_4N_2)/n(S_4N_4)$ much smaller than unity, even at low temperatures of pyrolysis. Based on these observations, the dominant pyrolytic process of tetrasulfur tetranitride mixed with sulfur can be expressed as:[10]

$$S_4N_4 = S_4N_2 + N_2 \text{ (in the presence of sulfur)}, \quad (1)$$

$$S_4N_2 = \frac{1}{2}S_8 + N_2. \quad (2)$$

Enthalpy Change during Pyrolysis of Tetrasulfur Tetranitride. The final products of either pure tetrasulfur tetranitride or of samples containing sulfur were identfied as sulfur and nitrogen when the pyrolysis was carried out in a closed system. Therefore, assuming the temperature dependence of the heat of decomposition to be negligible, the heat of decomposition (q) during the complete pyrolysis yields the standard enthalpy of the formation of tetrasulfur tetranitride, $\Delta H_f^\circ(S_4N_4)$, according to:

$$\Delta H_f^\circ(S_4N_4) = \frac{q}{a} + 2RT + \frac{1}{2}\Delta H_{trans}(S_\mu) + \frac{1}{2}\Delta H_{fus}(S_\lambda), \quad (3)$$

where a are the moles of the tetrasulfur tetranitride, and $\Delta H_{trans}(S_\mu)$ and ΔH_{fus} (S_λ) are the enthalpies of the transition from S_λ to S_μ [13.3 kJ mol^{-1} (as S_8 unit)][11] and of the fusion of S_α [17.0 kJ mol^{-1} (as S_8 unit)][11] respectively. Table 1 shows the results obtained according to Eq. 3 for the decomposition of tetrasulfur tetranitride in a closed system over the temperature range from 115 to 220 °C. The $\Delta H_f^\circ(S_4N_4)$ was estimated to be 469 ± 1 kJ mol^{-1}, which agreed well with the value reported by Barker *et al.*,[12] 460 ±8 kJ mol^{-1}.

When the pyrolysis of the mixed sample is interrupted, Eqs. 1 and 2 show that a moles of tetrasulfur tetranitride will change to $(a-x)$ moles of tetrasulfur dinitride, $(a+x)$ moles of nitrogen, and $x/2$ mol of sulfur (as S_8 units). Assuming that the tetrasulfur dinitride

Table 1. Standard enthalpy of formation of tetrasulfur tetranitride

Molar ratio of S_4N_4	$a=n(S_4N_4)\times10^7$ / mol	$q\times10^3$ / J	$\Delta H_f^\circ(S_4N_4)$ / kJ mol^{-1}
1.00	12.1	546	472
1.00	7.87	355	471
0.80	8.52	381	467
0.80	8.52	381	467
0.80	9.33	420	470
0.65	8.95	403	470
0.65	10.4	472	474
0.65	11.3	502	464
		Average	469±1

Table 2. Enthalpy of formation of gaseous tetrasulfur dinitride

Molar ratio of S_4N_4	$a=n(S_4N_4)\times10^7$ / mol	$(a-x)=n(S_4N_2)\times10^7$ / mol	$q\times10^3$ / J	$\Delta H_f(S_4N_2)$ / kJ mol^{-1}
0.80	6.64	1.50	249	349
0.80	4.78	1.17	175	360
0.80	8.40	1.65	322	354
0.65	5.44	1.31	201	353
0.65	6.67	1.15	262	343
0.65	14.7	3.80	537	344
			Average	351±3

thus produced is in the gaseous state under the present experimental conditions, the enthalpy of the formation of gaseous tetrasulfur dinitride, $\Delta H_f(S_4N_2)$, is given by:

$$\Delta H_f(S_4N_2) = \left[a\Delta H_f^\circ(S_4N_4) - q - (a+x)RT - \frac{x}{2}\Delta H_{trans}(S_\mu) - \frac{x}{2}\Delta H_{fus}(S_\lambda)\right] \Big/ (a-x), \quad (4)$$

where q is the heat of decomposition observed on the interrupted pyrolysis during the DSC measurement. On reaching≈175 °C, which is the approximate peak temperature of the exothermic change, the sample container was immediately removed from the DSC equipment to stop the pyrolysis, and then the solid quickly dissolved in a small volume of carbon tetrachloride, followed by the spectrophotometric determination of species.

Table 2 shows the results obtained according to Eq. 4. The $\Delta H_f(S_4N_2)$ was estimated to be 351±3 kJ mol^{-1}, which was nearly constant regardless of the difference in the composition of the samples.

Discussion

Tetrasulfur dinitride can be prepared by several processes,[13–15] including the pyrolysis of tetrasulfur tetraimide.[9] Tetrasulfur tetranitride degrades easily to tetrasulfur dinitride in the presence of sulfur, whereas the vapor at a low pressure in the absence of sulfur dissociates to disulfur dinitride, S_2N_2, around 250 °C.[16,17] For example, the degree of decomposition of a sample kept at 130 °C for 60 min increased from 18 to 53% when the molar ratio of sulfur was raised from 0.20 to 0.80, while the $n(S_4N_2)/n(S_4N_4)$ ratio remained constant(0.59—0.61). A step-by-step degradation was confirmed by the quantitative relationship of the pyrolysis products of the mixed sample as a function of the temperature.

Table 3. Bond lengths and bond energies in tetrasulfur dinitride

Bond	Bond length[21] r/pm	Bond energy, E/kJ mol^{-1}	
		Calcd(1)[a]	Deducd(2)
S-S	206.1	262	257[22]
S-N	167.1	250	247[b]
S=N	156.1	339	352[b]
$\Delta H_f[S_4N_2(1)]$/kJ mol^{-1}			361
$\Delta H_f[S_4N_2(2)]$/kJ mol^{-1}			350
$\Delta H_f[S_4N_2$(This work)]/kJ mol^{-1}			351±3

a) Calculated according to Sanderson's method.[20] b) Deduced from the linear correlation between the bond lengths and bond energies of the S≈N bonds.

Using the standard enthalpy of the formation of tetrasulfur tetranitride, $\Delta H_f^\circ(S_4N_4)$, of 469±1 kJ mol^{-1}, the standard enthalpies of the formation of atomic nitrogen and sulfur (473 and 279 kJ mol^{-1} respectively),[18] and the enthalpy of sublimation (89 kJ mol^{-1}),[7] the S–N bond energy (nominal bond order, n=1.5) in tetrasulfur tetranitride was calculated to be 306 kJ mol^{-1}, which is close to the values reported by Barker *et al.* (308 kJ mol^{-1})[12] and by Fleig and Becke-Goehring (301 kJ mol^{-1}).[19]

The calculations described by Sanderson[20] gave the S–S, S–N, and S=N bond energies in the six-membered ring molecule of tetrasulfur dinitride as 262, 250, and 339 kJ mol^{-1} respectively, as is shown in Table 3. Based on these bond energies and the standard enthalpies of the formation of atomic nitrogen and sulfur,[18] the enthalpy of the formation of gaseous tetrasulfur dinitride, $\Delta H_f[S_4N_2$ (1)], was calculated to be 361 kJ mol^{-1}.

The bond energies can also be deduced from other known parameters. The S–S bond length and the S–S–S bond angle (206.1 pm and 102.9°)[21] in tetrasulfur dinitride are very close to those in cyclohexasulfur, S_6, (205.7 pm and 102.2°),[22] so that the S–S bond energy in tetrasulfur dinitride can assumed to be the same as in cyclohexasulfur (257 kJ mol^{-1}).[23] From the linear relationships between the bond lengths and the bond energies of the S≈N bond [158 pm[24] and 335 kJ mol^{-1} [19] for $S_3N_2O_2$ (n=2), 161.6 pm[25,26] and 306 kJ mol^{-1} for S_4N_4 (n=1.5), and 167.4 pm[27,28] and 249 kJ mol^{-1} [19] for $S_4(NH)_4$ (n=1)], the S–N and S=N bond energies in tetrasulfur dinitride were deduced to be 247 and 352 kJ mol^{-1} respectively, as is shown in Table 3. These latter values, combined with the deduced S–S bond energy and the standard enthalpies of the formation of atomic nitrogen and sulfur,[18] gave the enthalpy of the formation of gaseous tetrasulfur dinitride, $\Delta H_f[S_4N_2$ (2)], of 350 kJ mol^{-1}. The corresponding value obtained in this work (351±3 kJ

mol^{-1}) agrees exceedingly well with those calculated above and by Sanderson.[20]

Tetrasulfur dinitride has a melting point of 23.5 °C,[29] and it gives a viscous liquid on melting. The vapor pressure of the latter and the enthalpy of vaporization have not been reported. Heal[1] mentioned that tetrasulfur dinitride evaporated easily at 30—40 °C under a pressure of 670 Pa. Sato[30] showed that the enthalpy of vaporization for a normal liquid, ΔH_{vap}, could be calculated (to within an error of 5%) from the following equation, which was derived from Hildebrand's rule:

$$\frac{\Delta H_{vap}}{T} = 176.8\left(\frac{p}{T}\right)^{-0.119}, \quad (5)$$

where p is the vapor pressure and T, the absolute temperature. Assuming that Eq. 5 is applicable to liquid tetrasulfur dinitride and that its vapor pressure is 670 Pa at 35 °C, the enthalpy of vaporization was calculated to be 50 kJ mol^{-1}. Consequently, the standard enthalpy of the formation of tetrasulfur dinitride, $\Delta H_f^\circ(S_4N_2)$, was estimated to be 301 kJ mol^{-1}, involving an uncertainty caused by the lack of a reliable value of the enthalpy of vaporization.

References

1) H. G. Heal, "Advances in Inorganic Chemistry and Radiochemistry," ed by H. J. Emeléus and A. G. Sharpe, Academic Press, New York (1972), Vol. 15, p. 384.

2) M. Goehring and D. Voigt, *Z. Anorg. Allg. Chem.*, **285**, 181 (1956).

3) A. Backens, Doctoral Thesis, University of Heidelberg, Heidelberg, West Germany, 1957.

4) M. Becke-Goehring, *Prog. Inorg. Chem.*, **1**, 207 (1959).

5) W. L. Jolly and M. Becke-Goehring, *Inorg. Chem.*, **1**, 76 (1962).

6) On the pyrolysis of tetrasulfur tetranitride mixed with sulfur, the pure tetrasulfur dinitride was trapped at −30 °C after the vapors of the reaction products had been passed through a glass tube (30 cm in length), with temperature gradients from 130 to 40 °C, to remove any contaminants. Its purity was confirmed by TLC.

7) S. Hamada, *Bull. Chem. Soc. Jpn.*, **46**, 3598 (1973).

8) S. Apter, M. Carruthers, and L. H. Sutcliffe, *Inorg. Chim. Acta*, **31**, L-455 (1978).

9) S. Hamada and Y. Kudo, *Bull. Chem. Soc. Jpn.*, **52**, 1063 (1979).

10) It is assumed that the sulfur produced in this decomposition process exists as cyclooctasulfur, S_8.

11) B. Meyer, "Elemental Sulfur," ed by B. Meyer, Interscience Publishers, New York (1965), p. 71.

12) C. K. Barker, A. W. Cordes, and J. L. Margrave, *J. Phys. Chem.*, **69**, 334 (1965).

13) M. Becke-Goehring, "Inorgonic Synthesis," ed by E. G. Rochow, McGraw-Hill, New York (1960), Vol. 6, p. 128.

14) H. G. Heal and R. J. Ramsay, *J. Inorg. Nucl. Chem.*, **37**, 286 (1975).

15) L. Niinistö and R. Laitinen, *Inorg. Nucl. Chem. Lett.*, **12**, 191 (1976).

16) R. D. Smith, *J. Chem. Phys. Lett.*, **55**, 590 (1978).

17) M. M. Labes, P. Love, and L. F. Nichols, *Chem. Rev.*, **79**, 1 (1979).

18) L. Brewer and G. M. Rosenblatt, *Adv. High Temp. Chem.*, **2**, 1 (1969).

19) H. Fleig and M. Becke-Goehring, *Z. Anorg. Allg. Chem.*, **375**, 8 (1970).

20) R. T. Sanderson, *J. Inorg. Nucl. Chem.*, **28**, 1553 (1966).

21) T. Chivers, P. W. Codding, and R. T. Oakley, *J. Chem. Soc., Chem. Commun.*, **1981**, 584.

22) J. Donohue, A. Caron, and E. Goldish, *J. Am. Chem. Soc.*, **83**, 3748 (1961).

23) B. Meyer, "Inorganic Sulfur Chemistry," ed by G. Nickless, Elsevier, Amsterdam (1968), p. 241.

24) J. Weiss, *Z. Naturforsch., B*, **16**, 477 (1962).

25) D. Clark, *J. Chem. Soc.*, **1952**, 1615.

26) B. D. Sharma and J. Donohue, *Acta Crystallogr.*, **16**, 891 (1963).

27) R. L. Sass and J. Donohue, *Acta Crystallogr.*, **11**, 497 (1958).

28) E. W. Lund and S. R. Svendsen, *Acta Chem. Scand.*, **11**, 940 (1957).

29) J. Nelson and H. G. Heal, *J. Chem. Soc., A*, **1971**, 131.

30) K. Sato, *Kagaku Kikai*, **14**, 270 (1950).

Preparation and Stereochemistry of Cobalt(III) Complexes with *S*-Alkyl-L-cysteinate, *N,N'*-Trimethylenebis(*S*-methyl-L-cysteinate), and *S,S'*-Ethylene(or -Trimethylene)bis(L-cysteinate)

Takumi KONNO,* Ken-ichi OKAMOTO, and Jinsai HIDAKA
Department of Chemistry, University of Tsukuba, Sakura, Ibaraki 305

(Received March 8, 1983)

Five cobalt(III) complexes of [Co(terdentate-$N,S,O)_2$] and [Co(sexidentate-N_2,S_2,O_2)] types were prepared; here terdentate-*N,S,O* denotes *S*-ethyl-L-cysteinate (L-sec) and *S*-benzyl-L-cysteinate (L-sbc), and sexidentate-N_2,S_2,O_2 denotes *N,N'*-trimethylenebis(*S*-methyl-L-cysteinate) (L,L-tbsmc), *S,S'*-ethylenebis(L-cysteinate) (L,L-ebc), and *S,S'*-trimethylenebis(L-cysteinate) (L,L-tbc). Three isomers, *trans(S)*, *trans(N)*, and *trans(O)*, were chromatographically isolated for each of the bis L-sec and L-sbc complexes, while only the *trans(O)* isomer was isolated for each of the L,L-tbsmc, L,L-ebc, and L,L-tbc complexes. These isomers were characterized from their absorption, CD, and ^1H and ^{13}C NMR spectra. The *trans(O)* isomers of the bis type and L,L-tbsmc complexes, which were assigned to a mixture of *R(S),R(S)*, *R(S),S(S)*, and *S(S),S(S)* configurations concerning the coordinated sulfur atoms, showed a similar CD spectral behavior to each other in the whole region. The *trans(O)-R(S),R(S)* L,L-ebc isomer and *trans(O)-S(S),S(S)* L,L-tbc one showed characteristic absorption and CD spectral behavior in the sulfur-to-metal charge transfer band region.

Cobalt(III) complexes with multidentate thioether type ligands such as *S*-methyl-L-cysteine, L-methionine, and their derivatives exhibited an extreme specificity concerning the formation of geometrical isomers.[1–12] The causes for the specificity were mostly related to the stereochemical property of the coordinated sulfur atoms of the thioether ligands.[8,9,11] The stereochemical behavior of the chiral sulfur donor atoms was reflected in the CD spectra of the complexes.[5,8,11] However, it is difficult to specify directly the contribution due to the chiral sulfur donor atoms to the CD spectra of the complexes, because of the overlap with the CD contribution due to other optically active sources in the complexes and an apprehension of sulfur inversion.[7,9] The present work was attempted to investigate the contribution of the chiral sulfur donor atoms of the thioether ligands such as *S*-alkyl-L-cysteine and its derivatives to the CD spectra of the cobalt(III) complexes, especially in the sulfur-to-metal charge transfer band region.

Cobalt(III) complexes with thioether type terdentate-*N,S,O* ligands, $[Co(L\text{-sec})_2]^+$ and $[Co(L\text{-sbc})_2]^+$, were prepared and chromatographically separated into three geometrical isomers: *trans(S)*, *trans(N)*, and *trans(O)*. For cobalt(III) complexes with a thioether type sexidentate-N_2,S_2,O_2 ligand, $[Co(L,L\text{-tbsmc})]^+$, where two nitrogen donor atoms were bridged by trimethylene (*N,N*-bridge), and $[Co(L,L\text{-ebc})]^+$ and $[Co(L,L\text{-tbc})]^+$, where two sulfur donor atoms were bridged by ethylene and trimethylene (*S,S*-bridge), only *trans(O)* isomers were selectively obtained. All isomers were characterized from their absorption and CD spectra in comparison with those of the three isomers of bis(*S*-methyl-L-cysteinato)cobalt(III) complex, $[Co(L\text{-smc})_2]^+$,[10] and the configurations of the coordinated sulfur atoms of the isomers were suggested on the basis of the ^1H and ^{13}C NMR spectra. The CD spectral change due to the substitution of the *S*-alkyl group in the L-terdentate-*N,S,O* ligands was investigated for each of the three isomers of the bis type complexes. The CD spectral differences among the *trans(O)* isomers of the bis type, the *N,N*-bridge and the *S,S*-bridge complexes are discussed in relation to the configurations of the chiral sulfur donor atoms of the thioether ligands.

Experimental

Preparation of Ligands. *1)*: *S*-Ethyl-L-cysteine was prepared from L-cysteine and ethyl iodide according to the method of Frankel *et al.*[13] Found: C, 40.18; H, 7.39; N, 9.44%. Calcd for L-Hsec = $C_5H_{11}NO_2S$: C, 40.24; H, 7.43; N, 9.38%.

2): *N,N'*-Trimethylenebis(*S*-methyl-L-cysteine) was prepared by the same procedure as that for *N,N'*-ethylenebis(*S*-methyl-L-cysteine),[9] using 1,3-dibromopropane instead of 1,2-dibromoethane. Found: C, 39.29; H, 7.07; N, 8.37%. Calcd for L,L-H_2tbsmc·1.5H_2O = $C_{11}H_{22}N_2O_4S_2$·1.5H_2O: C, 39.15; H, 7.46; N, 8.30%.

3): *S,S'*-Ethylenebis(L-cysteine) was prepared from L-cysteine and 1,2-dibromoethane according to the method of Magee *et al.*[2] Found: C, 35.72; H, 5.96; N, 10.47%. Calcd for L,L-H_2ebc = $C_8H_{16}N_2O_4S_2$: C, 35.80; H, 6.01; N, 10.43%.

4): *S,S'*-Trimethylenebis(L-cysteine) was prepared by the same procedure as in 3), using 1,3-dibromopropane instead of 1,2-dibromoethane. Found: C, 38.04; H, 6.35; N, 9.73%. Calcd for L,L-H_2tbc = $C_9H_{18}N_2O_4S_2$: C, 38.28; H, 6.42; N, 9.92%.

Preparation of Complexes. *5) Bis(S-methyl-L-cysteinato)cobalt(III) Perchlorate*: $[Co(L\text{-}smc)_2]ClO_4$. This complex was prepared and separated into three geometrical isomers: *trans(S)*, *trans(N)*, and *trans(O)*, by the method described in a previous paper.[10]

6) Bis(S-ethyl-L-cysteinato)cobalt(III) Bromide: $[Co(L\text{-}sec)_2]Br$. This complex was prepared by the same procedure as that for $[Co(L\text{-}smc)_2]ClO_4$ described in 5), using L-Hsec instead of L-Hsmc. The reaction mixture was poured onto a column (3 cm × 50 cm) containing Dowex 50W-X8 resin (200—400 mesh, NH_4^+ form). After sweeping the column with water, the adsorbed band was eluted with 0.3 mol dm^{-3} aqueous solution of NH_4Br. Three bands: violet (A-1), red (A-2), and blue-violet (A-3), were eluted in this order. Their absorption and CD spectra of the fractions showed that A-1 contained the *trans(S)* isomer, A-2 the *trans(O)* one, and A-3 the *trans(N)* one. The formation ratio of the isomers, *trans(S)* : *trans(O)* : *trans(N)*, was about 3 : 2 : 1. The three eluates were separately concentrated to a small volume in a rotary evaporator. The deposit, NH_4Br, was filtered off and to each of the filtrates was

added a large amount of ethanol. The crude isomers, A-1, A-2, and A-3, were recrystallized from as little water as possible by cooling in an ice bath after adding an appropriate amount of ethanol. Found for *trans(S)* isomer (A-1): C, 27.57; H, 4.57; N, 6.59%. Found for *trans(O)* isomer (A-2): C, 27.33; H, 4.40; N, 6.60%. Calcd for $[Co(L\text{-sec})_2]Br = CoC_{10}H_{20}N_2O_4S_2Br$: C, 27.59; H, 4.63; N, 6.43%. Found for *trans(N)* isomer (A-3): C, 26.44; H, 4.84; N, 6.17%. Calcd for $[Co(L\text{-sec})_2]Br \cdot H_2O$: C, 26.50; H, 4.89; N, 6.18%.

7) Bis(S-benzyl-L-cysteinato)cobalt(III) Chloride: *[Co(L-sbc)$_2$]Cl*. To a solution of L-Hsbc (5.0 g) in 400 cm^3 of hot water–ethanol (1 : 1.4) mixture were added a solution of $Co(CH_3COO)_2 \cdot 4H_2O$ (4.0 g) in 60 cm^3 of water and lead dioxide (10 g). The mixture was stirred at 65 °C for 10 min, whereupon the solution became violet. The reaction mixture was cooled to room temperature and filtered to remove insoluble materials. The filtrate was concentrated to *ca.* 200 cm^3 in a rotary evaporator and then poured onto a column (4 cm × 100 cm) containing SP-Sephadex C-25 resin (Na^+ form). After sweeping the column with water, the adsorbed band was eluted with 0.03 mol dm^{-3} aqueous solution of NaCl. Three bands: red-violet (B-1), violet (B-2), and dark violet (B-3), were eluted in this order. The absorption and CD spectra of the fractions showed that B-1 contained the *trans(O)* isomer, B-2 the *trans(S)* one, and B-3 the *trans(N)* one. The formation ratio of the isomers, *trans(S)* : *trans(O)* : *trans(N)*, was about 6 : 3 : 1. The three eluates were separately concentrated to a small volume in a rotary evaporator. To each solution was added a large amount of ethanol. The deposit, NaCl, was filtered off and the filtrates were again separately concentrated almost to dryness in a rotary evaporator. The resultant crystals of the three isomers, B-1, B-2, and B-3, were collected by filtration and washed with acetone and ether, and then dried in a vacuum desiccator. Found for *trans(O)* isomer (B-1): C, 45.42; H, 4.63; N, 5.38%. Calcd for $[Co(L\text{-sbc})_2]Cl \cdot 0.5H_2O = CoC_{20}H_{24}N_2O_4S_2Cl \cdot 0.5H_2O$: C, 45.85; H, 4.81; N, 5.35%. Found for *trans(S)* isomer (B-2): C, 40.07; H, 4.46; N, 5.02%. Calcd for $[Co(L\text{-sbc})_2]Cl \cdot H_2O \cdot NaCl$: C, 40.62; H, 4.43; N, 4.74%. Found for *trans(N)* isomer (B-3): C, 44.03; H, 4.90; N, 5.24%. Calcd for $[Co(L\text{-sbc})_2]Cl \cdot 1.5H_2O$: C, 44.32; H, 5.02; N, 5.17%.

8) N,N'-Ethylenebis(S-methyl-L-cysteinato)cobalt(III) Perchlorate: *[Co(L,L-ebsmc)]ClO$_4$*. This complex was prepared by the method described in a previous paper,[9] and only *trans(O)* isomer was isolated.

9) N,N'-Trimethylenebis(S-methyl-L-cysteinato)cobalt(III) Perchlorate: *[Co(L,L-tbsmc)]ClO$_4$*. This complex was prepared by the same procedure as that for $[Co(L,L\text{-ebsmc})]ClO_4$ described in 8), using L,L-H_2tbsmc instead of L,L-H_2ebsmc. The reaction mixture was filtered to remove the excess of lead dioxide. The filtrate was poured onto a column (3 cm × 35 cm) containing Dowex 50W-X8 resin (200—400 mesh, Na^+ form). After sweeping the column with water, the adsorbed band was eluted with 0.2 mol dm^{-3} aqueous solution of $NaClO_4$. Two bands, pink-violet and violet, were eluted in this order. It was found, from their absorption and CD spectra of the fractions, that the earlier eluate contained the *trans(S)* isomer and the later eluate the *trans(O)* one. The formation ratio of the isomers, *trans(S)* : *trans(O)*, was about 3 : 7. The two eluates were separately concentrated to a small volume in a rotary evaporator below 30 °C and the deposit, NaCl, was filtered off. To each of the filtrates was added an appropriate amount of ethanol and then kept in a refrigerator. Dark-red crystals appeared for each of the filtrates. The absorption and CD spectra showed that both crystals were *trans(O)* isomer. Namely, the *trans(S)* isomer in the earlier eluate isomerized to the *trans(O)* one during the procedure after elution. Found: C, 27.54; H, 4.35; N, 5.87%. Calcd for $[Co(L,L\text{-tbsmc})]ClO_4 \cdot H_2O = CoC_{11}H_{20}N_2O_8S_2Cl \cdot H_2O$: C, 27.25; H, 4.57; N, 5.78%.

10) N,N'-Ethylenebis(L-methioninato)cobalt(III) Perchloride: *[Co(L,L-ebm)]ClO$_4$*. This complex was prepared and isolated by the same procedure as that for $[Co(L,L\text{-ebsmc})]ClO_4$ described in 8), using L,L-H_2ebm.[2] The only isomer obtained showed the identical absorption and CD spectra with those of *trans(O)*-$[Co(L,L\text{-ebm})]^+$ prepared by Magee *et al.*[2] Found: C, 29.64; H, 4.63; N, 5.70%. Calcd for $[Co(L,L\text{-ebm})]ClO_4 = CoC_{12}H_{22}N_2O_8S_2Cl$: C, 29.98; H, 4.61; N, 5.83%.

11) S,S'-Ethylenebis(L-cysteinato)cobalt(III) Chloride and Nitrate: *[Co(L,L-ebc)]X*; *X$^-$ = Cl$^-$, NO$_3^-$*. A suspension of L,L-H_2ebc (4.1 g) in 250 cm^3 of water was adjusted to pH 8 by the addition of an aqueous solution of NaOH (1 mol dm^{-3}). To this were added a solution of $CoCl_2 \cdot 6H_2O$ (4.1 g) in 50 cm^3 of water and lead dioxide (10 g). The mixture was stirred at 60 °C for 20 min, whereupon the solution became purple. The reaction mixture was cooled to room temperature and filtered to remove insoluble materials. The filtrate was poured onto a column (4 cm × 60 cm) containing SP-Sephadex C-25 resin (Na^+ form). After sweeping the column with water, the adsorbed band was eluted with a 0.1 mol dm^{-3} aqueous solution of NaCl. Only one purple band was eluted and fractionated. The absorption and CD spectra of the fractions showed that the eluate contained only *trans(O)* isomer. The eluate was concentrated to a small volume in a rotary evaporator and the deposit, NaCl, was filtered off. To the filtrate was added an appropriate amount of ethanol and then ether. The resultant violet complex was recrystallized from water by adding ethanol. Found: C, 24.90; H, 4.31; N, 7.51%. Calcd for $[Co(L,L\text{-ebc})]Cl \cdot H_2O = CoC_8H_{14}N_2O_4S_2Cl \cdot H_2O$: C, 25.37; H, 4.27; N, 7.40%. This chloride salt was converted to the nitrate salt by use of an anion-exchange column containing QAE-Sephadex A-25 resin (NO_3^- form). The nitrate salt showed the identical absorption and CD spectra to those of the chloride salt. Found: C, 23.26; H, 3.97; N, 10.28%. Calcd for $[Co(L,L\text{-ebc})]NO_3 \cdot H_2O = CoC_8H_{14}N_3O_7S_2 \cdot H_2O$: C, 23.71; H, 3.98; N, 10.37%.

12) S,S'-Trimethylenebis(L-cysteinato)cobalt(III) Chloride and Nitrate: *[Co(L,L-tbc)]X*; *X$^-$ = Cl$^-$, NO$_3^-$*. This complex was prepared by the same procedure as that for $[Co(L,L\text{-ebc})]X$ described in 11), using L,L-H_2tbc instead of L,L-H_2ebc. The absorption and CD spectra of the chloride and nitrate salts were identical. Found for chloride salt: C, 26.31; H, 4.80; N, 6.42%. Calcd for $[Co(L,L\text{-tbc})]Cl \cdot 2H_2O = CoC_9H_{16}N_2O_4S_2Cl \cdot 2H_2O$: C, 26.31; H, 4.92; N, 6.82%. Found for nitrate salt: C, 25.18; H, 4.43; N, 9.92%. Calcd for $[Co(L,L\text{-tbc})]NO_3 \cdot 1.5H_2O = CoC_9H_{16}N_3O_7S_2 \cdot 1.5H_2O$: C, 25.24; H, 4.47; N, 9.81%.

Measurements. The electronic absorption spectra were recorded with a JASCO UVIDEC-1 spectrophotometer, and the CD spectra with a JASCO J-20 spectropolarimeter. All measurements were carried out in aqueous solution at room temperature.

The ^1H and ^{13}C NMR spectra were recorded in deuterium oxide on a JEOL JNM-MH-100 or FX-100 NMR spectrometer at the probe temperature. Sodium 2,2-dimethyl-2-silapentane-5-sulfonate (DSS) was used as an internal reference.

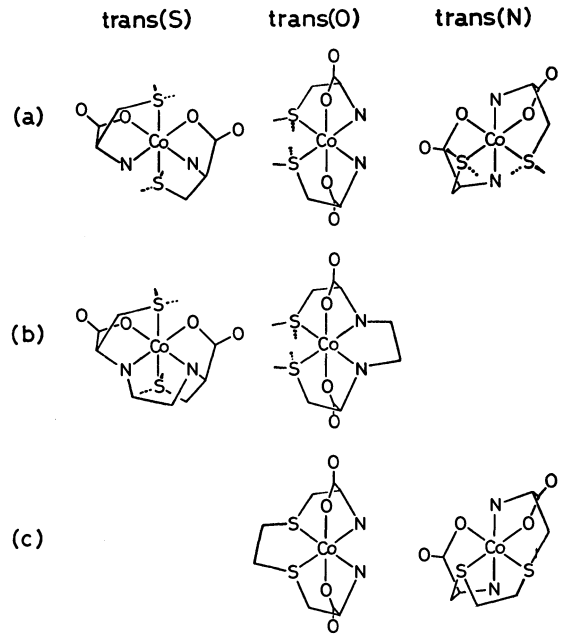

Fig. 1. The possible geometrical isomers of [Co(L-sec)$_2$]$^+$ and [Co(L-sbc)$_2$]$^+$ (a), [Co(L,L-ebsmc)]$^+$ (b), and [Co(L,L-ebc)]$^+$ (c).

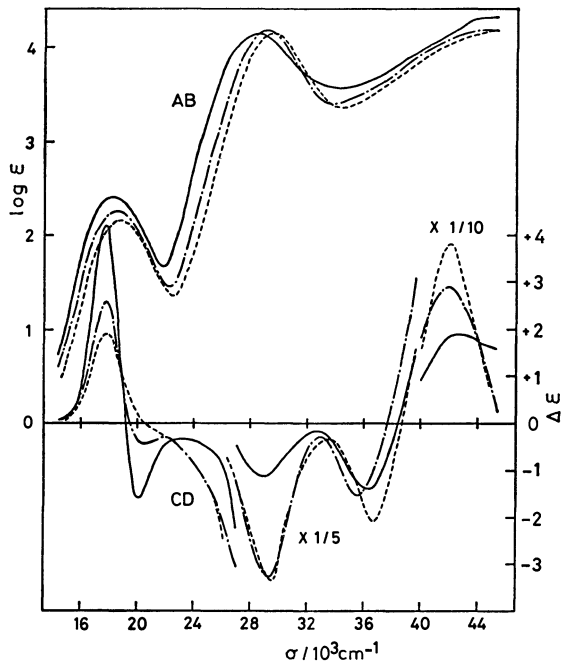

Fig. 2. Absorption and CD spectra of *trans(S)* isomers: [Co(L-sbc)$_2$]$^+$ (——), [Co(L-sec)$_2$]$^+$ (—·—·—), and [Co(L-smc)$_2$]$^+$ (-----).

Results and Discussion

*Structural Assignments. Bis(L-terdentate-*N,S,O*) Type Complexes*: For the [Co(L-sec)$_2$]$^+$ and [Co(L-sbc)$_2$]$^+$ complexes which belong to a [Co(N)$_2$(S)$_2$(O)$_2$] type, three geometrical isomers, *trans(S)*, *trans(N)*, and *trans(O)*, are possible (Fig. 1(a)). Their absorption and CD spectra are shown in Figs. 2—4, together with those of the [Co(L-smc)$_2$]$^+$ isomers; the data are summarized in Tables 1 and 2. Splitting patterns of

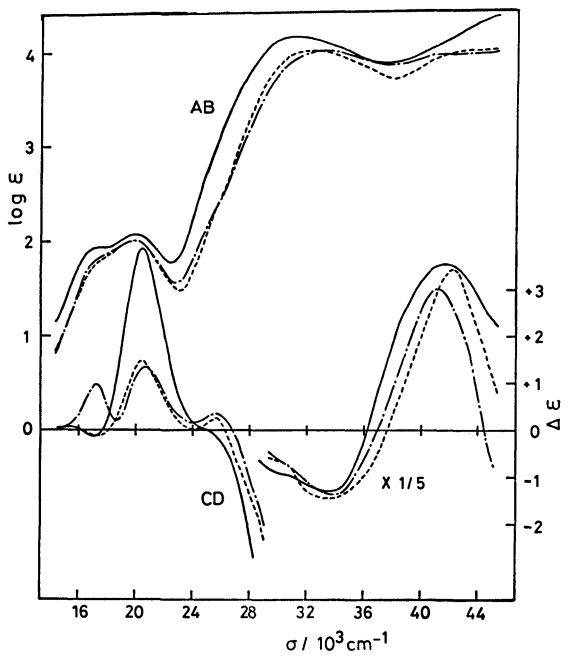

Fig. 3. Absorption and CD spectra of *trans(N)* isomers: [Co(L-sbc)$_2$]$^+$ (——), [Co(L-sec)$_2$]$^+$ (—·—·—), and [Co(L-smc)$_2$]$^+$ (-----).

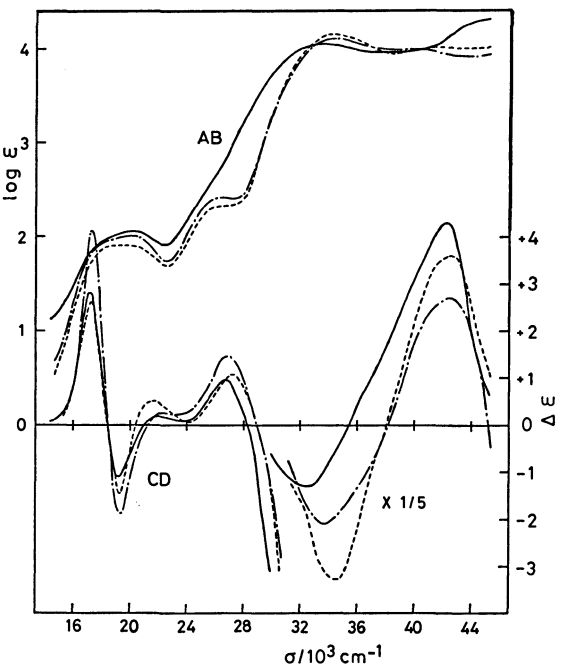

Fig. 4. Absorption and CD spectra of *trans(O)* isomers: [Co(L-sbc)$_2$]$^+$ (——), [Co(L-sec)$_2$]$^+$ (—·—·—), and [Co(L-smc)$_2$]$^+$ (-----).

the first absorption bands and maximum positions of the sulfur-to-metal charge transfer bands of the present isomers correspond well with those of the three isomers of [Co(L-smc)$_2$]$^+$.[10] Their CD spectral behavior could be classified into CD patterns of the three L-smc isomers (Figs. 2—4). Accordingly, A-1 and B-2 isomers can be assigned confidently as *trans(S)*, A-2 and B-1 isomers as *trans(O)*, and A-3 and B-3 isomers as *trans(N)*. The formation of the three geometrical isomers de-

TABLE 1. ABSORPTION DATA OF [Co(terdentate-$N,S,O)_2$] AND [Co(sexidentate-N_2,S_2,O_2] TYPE COMPLEXES

Complex	First band	Second band	Charge transfer band
trans(S)-[Co(L-smc)$_2$]$^+$ a)	18.73 (2.18)		29.47 (4.16)
trans(N)-[Co(L-smc)$_2$]$^+$ a)	17.5 (1.81 sh) 19.87 (2.01)		32.13 (4.03)
trans(O)-[Co(L-smc)$_2$]$^+$ a)	19.40 (1.93)	26.48 (2.34)	34.47 (4.16)
trans(S)-[Co(L-sec)$_2$]$^+$	18.42 (2.22)		29.15 (4.17)
trans(N)-[Co(L-sec)$_2$]$^+$	17.7 (1.85 sh) 19.88 (2.01)		33.00 (4.03)
trans(O)-[Co(L-sec)$_2$]$^+$	18.0 (1.92 sh) 20.00 (2.01)	26.39 (2.42)	34.60 (4.11)
trans(S)-[Co(L-sbc)$_2$]$^+$	18.25 (2.41)		28.41 (4.16)
trans(N)-[Co(L-sbc)$_2$]$^+$	17.2 (1.93 sh) 19.96 (2.07)		31.06 (4.18)
trans(O)-[Co(L-sbc)$_2$]$^+$	18.2 (1.96 sh) 20.20 (2.05)		33.67 (4.05)
trans(O)-[Co(L,L-ebsmc)]$^+$ b)	18.4 (2.10 sh) 20.83 (2.37)	26.7 (2.49 sh)	34.01 (4.07)
trans(O)-[Co(L,L-tbsmc)]$^+$	18.69 (1.97) 20.0 (1.94 sh)	26.0 (2.48 sh)	33.61 (4.09)
trans(O)-[Co(L,L-ebc)]$^+$	17.61 (2.48)	27.9 (2.27 sh)	35.21 (4.06)
trans(O)-[Co(L,L-tbc)]$^+$	17.76 (2.29)		32.3 (3.86 sh) 35.59 (4.08)

a) Ref. 10. b) Ref. 9. Wave numbers and log ε values (in parentheses) are given in 10^3 cm^{-1} and mol^{-1} dm^3 cm^{-1}, respectively. Sh denotes a shoulder.

creases with the order of *trans(S)*, *trans(O)*, and *trans(N)* for both of [Co(L-sec)$_2$]$^+$ and [Co(L-sbc)$_2$]$^+$. This order runs parallel to the crowdedness of the *S*-alkyl groups of the ligands in each isomer.

Another type of three isomers arising from the chiralities of the coordinated sulfur atoms of the ligands, *R(S),R(S)*, *R(S),S(S)*, and *S(S),S(S)*, are possible for each of the three geometrical isomers. The ^{1}H NMR spectrum of the *trans(S)* L-sec isomer exhibits only one set of triplet peaks in the methyl proton region (1.48 ppm from DSS), while the spectra of the *trans(O)* and *trans(N)* L-sec isomers show two sets of triplet peaks, respectively (1.39 and 1.52 ppm for the *trans(O)*, and 1.39 and 1.43 ppm for the *trans(N)*). The *trans(S)* L-sbc isomer shows a single peak due to the aromatic protons (7.36 ppm), while the *trans(O)* and *trans(N)* isomers show a peak with a shoulder at the higher magnetic field (7.44 ppm for the *trans(O)* and 7.43 ppm for the *trans(N)*). Furthermore, the ^{13}C NMR spectrum of the *trans(S)* isomer shows four peaks due to the aromatic carbons (128.4, 129.9, 130.5 and 139.6 ppm), while the *trans(O)* and *trans(N)* isomers show multiple peaks in the corresponding region. These NMR spectral behaviors of the L-sec and L-sbc isomers are quite similar to those of the three isomers of [Co(L-smc)$_2$]$^+$.[10] Inspection of models suggests that the *trans(S)* isomers take the *S(S),S(S)* configuration, the *trans(N)* isomers a mixture of *R(S),S(S)* and *S(S),S(S)* ones, and the *trans(O)* isomers a mixture of *R(S),R(S)*, *R(S),S(S)*, and *S(S),S(S)* ones, as in the case of the three isomers of the L-smc complex.[10]

N,N- *and* S,S-*Bridge(*L,L-*sexidentate*-N_2,S_2,O_2*) Type Complexes*: The possible geometrical isomers for [Co(L,L-ebsmc)]$^+$ [9] and [Co(L,L-tbsmc)]$^+$ are limited to two: *trans(S)* and *trans(O)*, because the two nitrogen donor atoms of the ligands were bridged by ethylene (L,L-ebsmc) and trimethylene (L,L-tbsmc) (Fig. 1(b)). Of the two isomers, only the *trans(O)* isomer was selectively formed and isolated for the L,L-ebsmc complex.[9] For the L,L-tbsmc complex, the *trans(S)* and *trans(O)* isomers were formed, but only the *trans(O)* isomer could be isolated, because the *trans(S)* L,L-tbsmc isomer isomerized to the *trans(O)* one during the procedure after elution. Two geometrical isomers, *trans(O)* and *trans(N)*, are possible for [Co(L,L-ebc)]$^+$ and [Co(L,L-tbc)]$^+$, where the two sulfur donor atoms of the ligands were bridged by ethylene (L,L-ebc) and trimethylene (L,L-tbc) (Fig. 1(c)). For each of the two *S,S*-bridge complexes, only the *trans(O)* isomer was selectively formed and isolated. The four isomers of the *N,N*- and *S,S*-bridge complexes which belong to a [Co$(N)_2(S)_2(O)_2$] type were assigned to *trans(O)* from the comparison of the absorption and CD spectra with the isomers of the bis type complexes mentioned above (Figs. 5 and 6 and Tables 1 and 2).

The *N,N*-bridge complexes, [Co(L,L-ebsmc)]$^+$ and [Co(L,L-tbsmc)]$^+$, have another chirality arising from the two nitrogen donor atoms. Of the two complexes, [Co(L,L-ebsmc)]$^+$ was confirmed to be *trans(O)-R(N),R(N)* isomer by the X-ray diffraction study.[9] Taking the rigid framework of the parental isomer, *trans(O)*-[Co(L-smc)$_2$]$^+$, into consideration, it is certain that the *trans(O)* L,L-tbsmc isomer prefers the *R(N),R(N)* configuration. The ^{1}H NMR spectrum of the *trans(O)* L,L-ebsmc isomer indicated that the two sulfur donor atoms took a mixture of *R(S),R(S)*, *R(S),S(S)*, and *S(S),S(S)* configurations,[9] as in the case of *trans(O)*-[Co(L-smc)$_2$]$^+$. The ^{1}H NMR spectrum of the *trans(O)* L,L-tbsmc isomer shows multiple peaks in the *S*-methyl proton region, suggesting that the

TABLE 2. CD DATA OF [Co(terdentate-$N,S,O)_2$] AND [Co(sexidentate-N_2,S_2,O_2)] TYPE COMPLEXES

Complex	First band region	Second band region	Charge transfer band region
trans(*S*)-[Co(L-smc)$_2$]$^+$ a)	17.87 (+1.92)		29.63 (−16.5)
			36.80 (−11.1)
			42.27 (+40.1)
trans(*N*)-[Co(L-smc)$_2$]$^+$ a)	15.47 (+0.06)	25.60 (+0.23)	33.54 (−7.8)
	17.33 (−0.11)		42.27 (+17.3)
	20.43 (+1.44)		
trans(*O*)-[Co(L-smc)$_2$]$^+$ a)	17.23 (+2.70)	27.20 (+1.08)	34.47 (−18.3)
	19.25 (−1.44)		42.80 (+18.3)
	21.60 (+0.57)		
trans(*S*)-[Co(L-sec)$_2$]$^+$	17.70 (+2.59)		29.41 (−16.4)
	20.53 (−0.44)		35.71 (−7.6)
			41.32 (+28.9)
trans(*N*)-[Co(L-sec)$_2$]$^+$	17.21 (+0.98)	25.64 (+0.35)	33.90 (−6.8)
	20.70 (+1.34)		41.15 (+14.8)
trans(*O*)-Co(L-sec)$_2$]$^+$	17.18 (+4.16)	26.95 (+1.47)	33.67 (−10.6)
	19.38 (−1.91)		42.55 (+13.4)
	22.22 (+0.23)		
trans(*S*)-[Co(L-sbc)$_2$]$^+$	18.32 (+4.21)		28.82 (−5.6)
	20.08 (−1.24)		36.23 (−7.0)
			42.19 (+18.9)
trans(*N*)-[Co(L-sbc)$_2$]$^+$	15.27 (+0.08)		33.33 (−6.5)
	17.04 (−0.35)		41.67 (+17.9)
	20.37 (+3.88)		
trans(*O*)-[Co(L-sbc)$_2$]$^+$	17.12 (+2.84)	26.67 (+1.00)	32.68 (−6.4)
	19.18 (−1.10)		42.37 (+21.5)
	21.98 (+0.19)		
trans(*O*)-[Co(L,L-ebsmc)]$^+$ b)	17.33 (+2.82)	24.57 (−0.17)	33.67 (−10.8)
	19.27 (−2.68)	27.47 (+2.64)	43.48 (+19.2)
	21.93 (+1.38)		
trans(*O*)-[Co(L,L-tbsmc)]$^+$	16.78 (+2.09)	23.52 (−0.02)	33.30 (−10.8)
	18.62 (−2.79)	26.04 (+0.63)	42.60 (+29.9)
	21.28 (+0.29)		
trans(*O*)-[Co(L,L-ebc)]$^+$	17.76 (+10.26)	27.93 (+6.80)	32.00 (+6.9)
	20.45 (−6.59)		35.71 (−29.3)
			40.32 (+21.3)
trans(*O*)-[Co(L,L-tbc)]$^+$	17.79 (+8.66)		31.35 (+19.7)
	20.28 (−5.29)		35.37 (−30.6)
			40.00 (+10.2)

a) Ref. 10. b) Ref. 9. Wave numbers and $\Delta\varepsilon$ values (in parentheses) are given in 10^3 cm^{-1} and dm^3 cm^{-1}, respectively. Sh denotes a shoulder.

chiral sulfur atoms take a mixture of *R*(*S*),*R*(*S*), *R*(*S*),*S*(*S*), and *S*(*S*),*S*(*S*) configurations, like the *trans*-*(O)* L,L-tbsmc isomer does.

For each of the two *S*,*S*-bridge isomers, *trans(O)*-[Co(L,L-ebc)]$^+$ and *trans(O)*-[Co(L,L-tbc)]$^+$, the possible configurations of the sulfur donor atoms are limited to two: *R*(*S*),*R*(*S*) (C_2 symmetry) and *R*(*S*),*S*(*S*) (C_1 symmetry) for the L,L-ebc isomer, and *S*(*S*),*S*(*S*) (C_2 symmetry) and *R*(*S*),*S*(*S*) (C_1 symmetry) for the L,L-tbc isomer. As shown in Fig. 7(a), the ^{13}C NMR spectrum of the *trans(O)* L,L-ebc isomer shows four peaks for the eight carbons of the ligand. This means that the L,L-ebc isomer takes the *R*(*S*),*R*(*S*) configuration having C_2 symmetry, where the backbone five-membered chelate ring takes an asymmetric gauche form with δ conformation. Similarly, the *trans(O)* L,L-tbc isomer takes *S*(*S*),*S*(*S*) configuration having a skew-boat form with δ conformation for the backbone six-membered chelate ring, because the ^{13}C NMR spectrum shows five peaks for the nine carbons of the ligand (C_2 symmetry) (Fig. 7(b)).

Absorption and CD Spectra. As shown in Figs. 2—4, the absorption spectra in each group of the three geometrical isomers of the bis L-smc, L-sec, and L-sbc complexes are similar to each other except that the sulfur-to-metal charge transfer bands of the L-sbc isomers shift to somewhat lower energies in comparison with those of the L-smc and L-sec isomers. The overall CD pattern is similar in each group. However, some notable differences due to the substitution of the *S*-alkyl group can be observed in more minute detail. In the first absorption band region, the *trans(S)*-

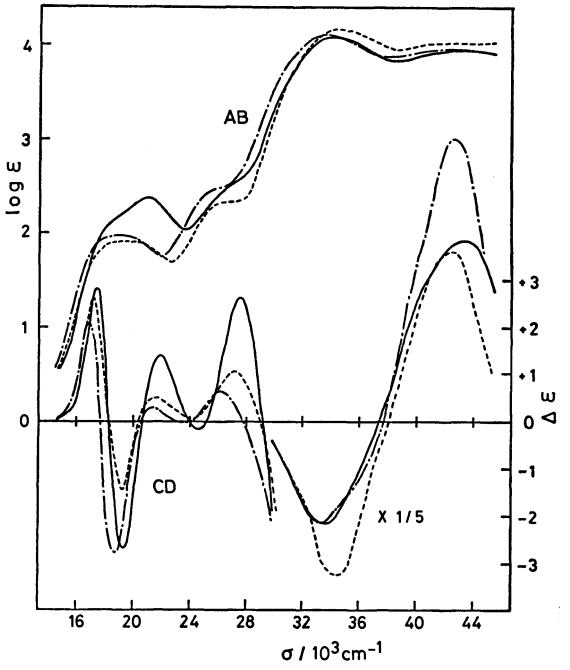

Fig. 5. Absorption and CD spectra of *trans(O)* isomers: [Co(L,L-ebsmc)]$^+$ (——), [Co(L,L-tbsmc)]$^+$ (—·—·—), and [Co(L-smc)$_2$]$^+$ (-----).

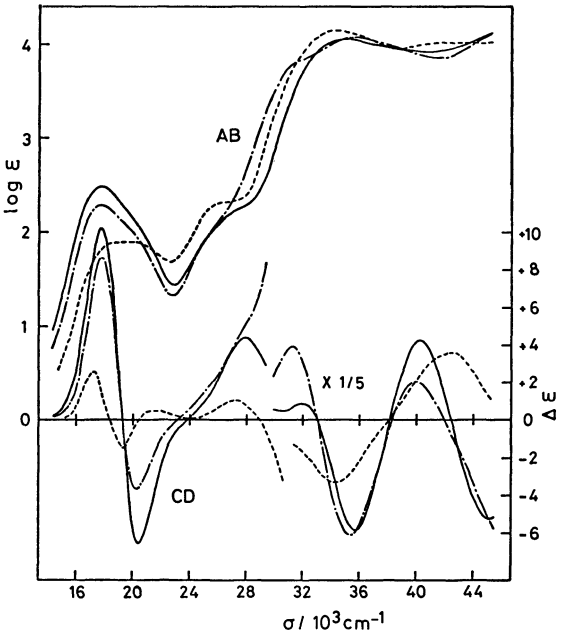

Fig. 6. Absorption and CD spectra of *trans(O)* isomers: [Co(L,L-ebc)]$^+$ (——), [Co(L,L-tbc)]$^+$ (—·—·—), and [Co(L-smc)$_2$]$^+$ (-----).

S(S),S(S) isomers commonly show a positive CD band (at *ca.* 18.0×10^3 cm^{-1}) whose intensity decreases with the order of the L-sbc, L-sec, and L-smc isomers, and a negative band at higher energy disappears in the L-smc isomer (Fig. 2). The *trans(N)* isomers assigned to the mixture of *R(S),S(S)* and *S(S),S(S)* configurations commonly show a positive CD band at 20.5×10^3 cm^{-1}. The L-smc and L-sbc isomers show two additional weak CD bands ((+) and (−) from lower energy), while the L-sec isomer shows one positive band

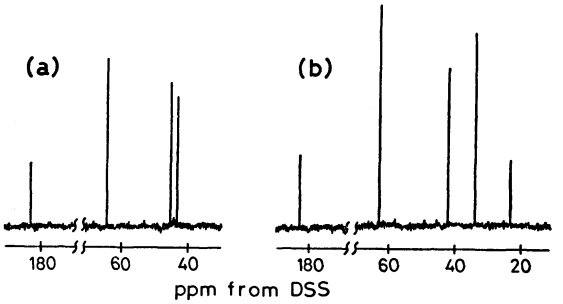

Fig. 7. ^{13}C NMR spectra of *trans(O)*-[Co(L,L-ebc)]$^+$ (a) and *trans(O)*-[Co(L,L-tbc)]$^+$ (b).

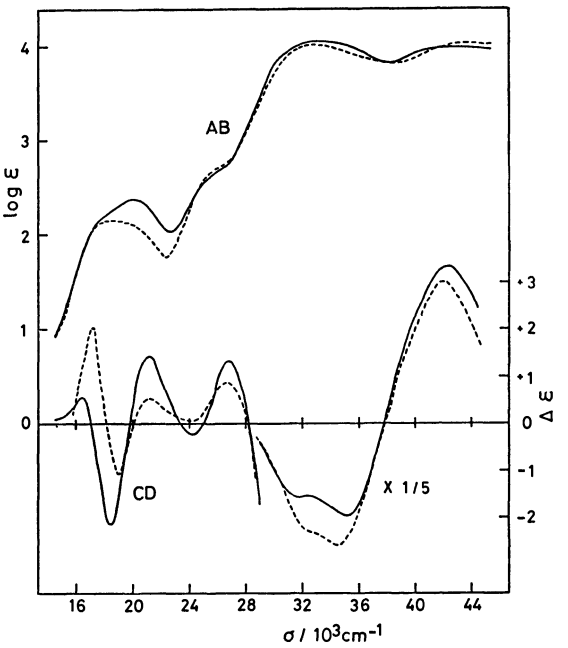

Fig. 8. Absorption and CD spectra of *trans(O)* isomers: [Co(L,L-ebm)]$^+$ (——) and [Co(L-met)$_2$]$^+$ (-----).

in the corresponding region (Fig. 3). In contrast to the *trans(S)* and *trans(N)* isomers, the *trans(O)* isomers assigned to the mixture of *R(S),R(S)*, *R(S),S(S)*, and *S(S),S(S)* configurations show quite similar CD spectral behavior in the whole region, with no significant differences. This good agreement in CD spectra seems to suggest that the CD contribution due to the coordinated sulfur atoms in the *trans(O)* isomers was almost cancelled out because of the mixture of *R(S),R(S)*, *R(S),S(S)*, and *S(S),S(S)* configurations.

The absorption and CD spectra of the *N,N*-bridge complexes are shown in Fig. 5, together with those of *trans(O)*-[Co(L-smc)$_2$]$^+$. The *trans(O)* L,L-ebsmc and L,L-tbsmc isomers show a CD pattern quite similar to that of *trans(O)*-[Co(L-smc)$_2$]$^+$ in the whole region, though the former two have an additional chilarity, *R(N),R(N)*, due to the bridged nitrogen donor atoms of the ligands. This result suggests that the CD contribution due to the chiral nitrogen atoms of the *N,N*-bridge *trans(O)* isomers is inconspicuous except for some increase in CD intensity. This trend is also valid for the CD spectra of *trans(O)*-[Co(L-met)$_2$]$^+$ [1] and *trans(O)*-[Co(L,L-ebm)]$^+$, where the two nitrogen donor atoms were bridged by ethylene (Fig. 8), though two

conformations, chair and skew-boat, are probable for the six-membered N–S ring of the coordinated L-met. A similar CD spectral behavior was observed for a series of *cis*-$[Co(ida)_2]^-$, $[Co(edta)]^-$, and $[Co(1,3\text{-pdta})]^-$.[14] In contrast to the *N,N*-bridge isomers, the CD spectral behaviors of the *S,S*-bridge *trans(O)* isomers differ significantly from that of *trans(O)*-$[Co(L\text{-smc})_2]^+$ (Fig. 6 and Table 2). In the first absorption band region, the CD spectra of the *trans(O)* L,L-ebc and L,L-tbc isomers are remarkedly intensified in comparison with that of *trans(O)*-$[Co(L\text{-smc})_2]^+$. Of the three CD bands in the first absorption band region of *trans(O)*-$[Co(L\text{-smc})_2]^+$, the two CD bands in the higher energy side change to one negative band, though the positive band at the lowest energy side remains unchanged. A remarkable deviation in absorption and CD spectra from *trans(O)*-$[Co(L\text{-smc})_2]^+$ are observed in the region of $(28\text{—}38)\times10^3$ cm^{-1}. Especially, it is noteworthy that the *trans(O)* L,L-tbc isomer shows another intense absorption component (at *ca.* 32.3×10^3 cm^{-1}) in addition to the charge transfer band (at 35.59×10^3 cm^{-1}) which commonly appears for the other *trans(O)* isomers. In this absorption band region, a new positive CD band appears for each of the two *S,S*-bridge isomers, namely, $\Delta\varepsilon=+19.7$ at 31.35×10^3 cm^{-1} for the L,L-tbc isomer and $\Delta\varepsilon=+6.9$ at 32.00×10^3 cm^{-1} for the L,L-ebc one. This positive CD band for the L,L-ebc isomer suggests that the isomer also has an absorption component in the corresponding region, as in the L,L-tbc isomer. This absorption component seems to arise from the splitting of the multiple thioether charge transfer band.[15] The appearance of the new positive CD band (at *ca.* 31.5×10^3 cm^{-1}) for the two *S,S*-bridge isomers suggests that *R(S),R(S)*, *R(S),S(S)*, and *S(S),S(S)* configurations in the *trans(O)*-$[Co(L\text{-smc})_2]^+$ were unified to only one configuration (*R(S),R(S)* for the *trans(O)* L,L-ebc isomer and *S(S),S(S)* for the L,L-tbc one) by bridging the sulfur atoms of the two cysteinates.

References

1) J. Hidaka, S. Yamada, and Y. Shimura, *Chem. Lett.*, **1974**, 1487.
2) R. J. Magee, W. Mazurec, M. J. O'Conner, and A. T. Phillip, *Aust. J. Chem.*, **27**, 1629 (1974).
3) P. D. Meester and D. J. Hodgson, *J. Chem. Soc., Dalton Trans.*, **1976**, 618.
4) K. Yamanari, J. Hidaka, and Y. Shimura, *Bull. Chem. Soc. Jpn.*, **50**, 2299 (1977).
5) K. Yamanari, J. Hidaka, and Y. Shimura, *Bull. Chem. Soc. Jpn.*, **50**, 2451 (1977).
6) R. J. Gune and M. R. Snow, *Acta Crystallogr., Sect. B*, **33**, 70 (1977).
7) W. G. Jackson and A. M. Sargeson, *Inorg. Chem.*, **17**, 2165 (1978).
8) T. Isago, K. Igi, and J. Hidaka, *Bull. Chem. Soc. Jpn.*, **52**, 407 (1979).
9) K. Okamoto, T. Isago, M. Ohmasa, and J. Hidaka, *Bull. Chem. Soc. Jpn.*, **55**, 1077 (1982).
10) K. Okamoto, K. Wakayama, H. Einaga, S. Yamada, and J. Hidaka, *Bull. Chem. Soc. Jpn.*, **56**, 165 (1983).
11) M. Suzuki, K. Okamoto, H. Einaga, and J. Hidaka, *Bull. Chem. Soc. Jpn.*, **55**, 3929 (1982).
12) K. Okamoto, M. Suzuki, and J. Hidaka, *Chem. Lett.*, **1983**, 401.
13) M. Frankel, D. Gertner, H. Jacobson, and A. Zilkha, *J. Chem. Soc.*, **1960**, 1390.
14) C. W. Van Saun and B. E. Douglas, *Inorg. Chem.*, **8**, 1145 (1969).
15) R. C. Elder, G. J. Kennard, M. D. Payne, and E. Deutsch, *Inorg. Chem.*, **17**, 1296 (1978).

Reaction Process of Zirconium Tetrachloride with Ammonia in the Vapor Phase and Properties of the Zirconium Nitride Formed

Akimasa YAJIMA, Yutaka SEGAWA, Ryoko MATSUZAKI, and Yuzo SAEKI*

Research Laboratory of Resources Utilization, Tokyo Institute of Technology, 4259, Nagatsuta-cho, Midori-ku, Yokohama 227

(Received March 24, 1983)

The reaction products of gaseous $ZrCl_4$ with ammonia were $ZrCl_4 \cdot 2NH_3$ at 300 °C; $ZrCl_4 \cdot 2NH_3$, ZrClN, and NH_4Cl at 350—700 °C; $ZrCl_4 \cdot 2NH_3$, ZrClN, ZrN_x, Zr_3N_4, and NH_4Cl at 750 °C; ZrClN, ZrN_x, Zr_3N_4, and NH_4Cl at 800—950 °C; ZrN_x, Zr_3N_4, and NH_4Cl at 1000—1050 °C; and ZrN_x, NH_4Cl, and HCl at 1100—1400 °C. The N/Zr atomic ratios, x, of the ZrN_x formed was 1.28 at 1100 °C, 1.24 at 1200 °C, 1.18 at 1300 °C, and 1.12 at 1400 °C. The lattice constants of the ZrN_x formed were shown. The reaction process of gaseous $ZrCl_4$ with ammonia can be represented as follows: The reaction of gaseous $ZrCl_4$ with ammonia to form $ZrCl_4 \cdot 2NH_3$ occurs first. Above *ca.* 330 °C, the $ZrCl_4 \cdot 2NH_3$ reacts with ammonia to form ZrClN. Above *ca.* 750 °C, the ZrClN reacts with ammonia to form ZrN_x and Zr_3N_4. Above *ca.* 1000 °C, ZrN_x was also formed by the thermal decomposition of the Zr_3N_4. On heating the $ZrN_{x(x=1.28)}$, formed by the vapor-phase reaction, at temperatures higher than 700 °C in an argon atmosphere, the value of x decreased and became close to that of the stoichiometric nitride, being 1.03 at 1100—1300 °C.

The vapor-phase reaction of transition metal chlorides with ammonia has recently become important for the preparation of fine powders of transition metal nitrides, which are aquiring importance as new industrial materials. Concerning the formation of zirconium nitride from zirconium tetrachloride ($ZrCl_4$) by the vapor-phase reaction, Okabe *et al.*[1] have reported the preparation of zirconium nitride powders by a vapor-phase reaction of the $ZrCl_4$–NH_3–N_2–H_2 system at 1000—1500 °C with emphasis on the effect of reaction conditions on the conversion of the $ZrCl_4$ to zirconium nitride. However, no information is at present available on the reaction process of $ZrCl_4$ with ammonia in the vapor phase.

In this paper, the reaction products of gaseous $ZrCl_4$ with ammonia at 300—1400 °C were examined in detail. The possible reactions which were considered to occur during the reaction process on the basis of the above experiments were examined. The N/Zr atomic ratios, lattice constants, and thermal stability of the zirconium nitrides formed were also examined. The zirconium nitrides which formed were also examined by electron microscopy.

Experimental

Materials. The $ZrCl_4$ used was prepared by the reaction of zirconium sponge (Reactor grade, Nippon Mining Co., Ltd.) with chlorine at 330 °C and purified by fractional sublimation. The chemical analysis gave Zr, 39.1; Cl, 60.8% (calcd for $ZrCl_4$: Zr, 39.14; Cl, 60.86%). The ammonia was dried by passing it over sodium hydroxide granules and barium oxide powders.

Experimental Procedures. A transparent quartz or alumina tube (1000 mm length) was used for examining the reaction products of gaseous $ZrCl_4$ with ammonia. Gaseous $ZrCl_4$ was formed by heating solid $ZrCl_4$ (14 g) at 280 °C and was carried by a stream of argon (50 cm³/min) into the reaction zone (28 mm i.d., 250 mm length) held at a specified temperature. The $ZrCl_4$ inlet tube consisted of two concentric tubes. Gaseous $ZrCl_4$ carried by argon was introduced through the inner tube and the outer tube was utilized for introducing argon (50 cm³/min) as a sheath gas to prevent formation of the product deposits at the chloride inlet tube. Ammonia was simultaneously introduced at a flow-rate of 100 cm³/min into the reaction zone through a separate tube. The mean flow-rate of gaseous $ZrCl_4$ was 6.0 cm³/min. A quartz or alumina tube was inserted inside the reaction tube to make the removal of the reaction product easier. The reaction was allowed to proceed for 2 h.

The by-product ammonium chloride (NH_4Cl) which deposited outside the reaction zone together with the zirconium nitride formed was separated by heating the mixture *in vacuo* at 400 °C.

Analytical. Chemical analyses of the reaction products were performed as follows: The zirconium content of the $ZrCl_4$–NH_3 adduct was gravimetrically determined as ZrO_2 using mandelic acid as a precipitating agent, after dissolving the sample in water. The chlorine and ammonia contents were determined by a gravimetric method as AgCl and by the Kjeldahl method from the aqueous solution. The zirconium content of zirconium chloride nitride (ZrClN) was gravimetrically determined as ZrO_2 after hydrolyzing the sample in water. The chlorine and nitrogen contents were determined by the gravimetric method and by the Kjeldahl method, respectively, from the filtrate.

X-Ray analysis of the product was performed with an X-ray powder diffractometer equipped with a proportional counter using Ni filtered Cu radiation. The sample chamber of the diffractometer was maintained under a dry nitrogen atmosphere, if necessary, to prevent any contamination of the sample with atmospheric moisture during the irradiation.

The sensitivity of the quartz helix used for thermogravimetry (TG) was approximately 113 mm/g. The sample (0.2 g) was heated at a rate of 2.5 °C/min and the flow-rate of ammonia was maintained at 50 cm³/min.

The N/Zr atomic ratio of the zirconium nitride formed was evaluated as follows: The sample zirconium nitride was oxidized to ZrO_2 by heating in an oxygen atmosphere to 700 °C, using a Shimadzu high-sensitive thermal balance, Model TGA31. The zirconium content of the sample was calculated from the amount of ZrO_2 formed. The amount of nitrogen was determined as the difference between the amount of the initial sample and that of the zirconium. The value of the N/Zr atomic ratio was evaluated with an accuracy within ±0.01.

The lattice constant of the zirconium nitride was calculated based on the X-ray diffraction data obtained by using silicon powders as an internal standard and under the scanning speed of 1/2—1/4° min^{-1}.

Throughout this work, the $ZrCl_4$ and the reaction products were handled in an argon atmosphere or *in vacuo* to prevent contamination by atmospheric moisture.

Results and Discussion

Reaction Products of Gaseous Zirconium Tetrachloride with Ammonia. The products formed by heating gaseous $ZrCl_4$ in an ammonia stream at various temperatures were examined by both X-ray analysis[2-5] and chemical analysis. Reaction temperatures above 300 °C were employed, because gaseous $ZrCl_4$ was generated at 280 °C.

The product formed at 300 °C showed a hitherto unknown X-ray diffraction pattern which was clearly different from those of known zirconium compounds. The chemical analysis of the product gave Zr, 34.1; Cl, 53.0; NH_3, 12.8%. The ratio of Zr : Cl : NH_3 was calculated to be 1:4.00:2.01. This was considered to indicate that the product formed at 300 °C had a composition of $ZrCl_4 \cdot 2NH_3$ (calcd for $ZrCl_4 \cdot 2NH_3$: Zr, 34.15; Cl, 53.10; NH_3, 12.75%). The X-ray diffraction data of the $ZrCl_4 \cdot 2NH_3$ formed are shown in Table 1. Based on these data, $ZrCl_4 \cdot 2NH_3$ could be indexed on cubic lattice with $a_0=10.13$Å, as shown in Table 1.

Table 1. X-Ray diffraction data of $ZrCl_4 \cdot 2NH_3$

d/Å	I/I_0	$h\,k\,l$	d_{calcd}/Å
5.83	100	1 1 1	5.849
5.07	80	2 0 0	5.065
3.58	10	2 2 0	3.581
3.06	50	3 1 1	3.054
2.92	60	2 2 2	2.924
2.53	90	4 0 0	2.532
2.33	15	3 3 1	2.324
2.27	45	4 2 0	2.265
1.949	20	3 3 3	1.950
1.791	45	4 4 0	1.791
1.713	12	5 3 1	1.712
1.689	20	6 0 0, 4 4 2	1.688
1.461	12	4 4 4	1.462

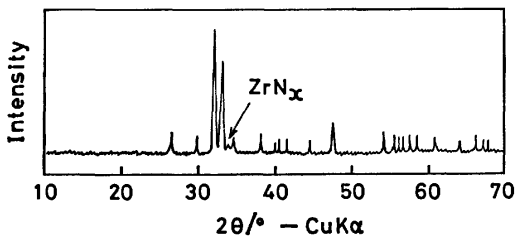

Fig. 1. X-Ray diffraction pattern of the product obtained inside the reaction zone at 950 °C.

X-Ray analysis of the product formed at 750—1050 °C showed a hitherto unknown X-ray diffraction pattern in addition to those of the known α-ZrClN,[2] β-ZrClN,[3] ZrN_x,[4] NH_4Cl,[5] and the above $ZrCl_4 \cdot 2NH_3$. As shown in Fig. 1, the product obtained at 950 °C inside the reaction zone showed an X-ray diffraction pattern consisting of the unknown pattern and a very weak diffraction line corresponding to the strongest line of ZrN_x ($2\theta=34.0°$). The product was thus examined by chemical analysis. The chlorine content of the product was first checked after heating the sample in molten sodium carbonate. The result showed that the product contained no chlorine. This indicated that the product was zirconium nitride. The N/Zr atomic ratio of the product was found to be 1.33. As described above, this product contained a slight amount of ZrN_x. As seen from the results shown in Table 5 described later, the N/Zr atomic ratio of ZrN_x formed by the vapor-phase reaction increased with the decrease in the reaction temperature, the N/Zr atomic ratio of ZrN_x formed at 1100 °C being 1.28. Considering these facts and the accuracy of the measurement of the N/Zr atomic ratio (±0.01), the presence of a slight amount of ZrN_x caused no significant error in the measurement of the N/Zr atomic ratio of the product showing the unknown X-ray diffraction pattern. From these results and the fact that the presence of Zr_3N_4 in addition to ZrN_x had been reported[6-8] as zirconium nitride, the product showing the unknown X-ray pattern, formed at 750—1050 °C, was found to be Zr_3N_4.

Table 2. Reaction products of gaseous $ZrCl_4$ with ammonia at various temperatures

Temp/°C	Products	
	In the reaction zone	Outside the reaction zone
300	$ZrCl_4 \cdot 2NH_3$	$ZrCl_4 \cdot 2NH_3$
350—400	$ZrCl_4 \cdot 2NH_3 \gg ZrClN[\alpha]$	$ZrCl_4 \cdot 2NH_3$; NH_4Cl
500—550	$ZrClN[\alpha]$	$ZrCl_4 \cdot 2NH_3$; NH_4Cl
600	$ZrClN[\alpha \gg \beta]$	$ZrCl_4 \cdot 2NH_3 \gg ZrClN[\alpha]$; NH_4Cl
650	$ZrClN[\alpha > \beta]$	$ZrCl_4 \cdot 2NH_3 \gg ZrClN[\alpha]$; NH_4Cl
700	$ZrClN[\beta > \alpha]$	$ZrCl_4 \cdot 2NH_3 \gg ZrClN[\alpha]$; NH_4Cl
750	$ZrClN[\beta > \alpha] \gg ZrN_x$, Zr_3N_4	$ZrCl_4 \cdot 2NH_3 > ZrClN[\alpha]$; NH_4Cl
800	$ZrClN[\beta > \alpha] \gg ZrN_x$, Zr_3N_4	$ZrClN[\alpha > \beta]$; NH_4Cl
850	$ZrClN[\beta > \alpha] \gg ZrN_x$, Zr_3N_4	$ZrClN[\alpha, \beta]$; NH_4Cl
900	$ZrClN[\beta] > Zr_3N_4 \gg ZrN_x$	$ZrClN[\alpha, \beta]$; NH_4Cl
950	$Zr_3N_4 \gg ZrN_x$	$ZrClN[\alpha, \beta] \gg ZrN_x$, Zr_3N_4; NH_4Cl
1000—1050	$Zr_3N_4 > ZrN_x$	$ZrN_x \gg Zr_3N_4$; NH_4Cl
1100—1400	—	ZrN_x; NH_4Cl, HCl

TABLE 3. EXPERIMENTAL RESULTS FOR $ZrCl_4 \cdot 2NH_3$ ON HEATING IN AN AMMONIA STREAM

Heating temp/°C	Products		Unreacted $ZrCl_4 \cdot 2NH_3$/%
	In the boat	Outside the boat	
350	ZrClN[α](25)	ZrClN(3), $ZrCl_4 \cdot 2NH_3$(6), NH_4Cl	66
400	ZrClN[α](60)	ZrClN(25), $ZrCl_4 \cdot 2NH_3$(15), NH_4Cl	—

The value in parentheses is mole percentage of $ZrCl_4 \cdot 2NH_3$ converted to the product.

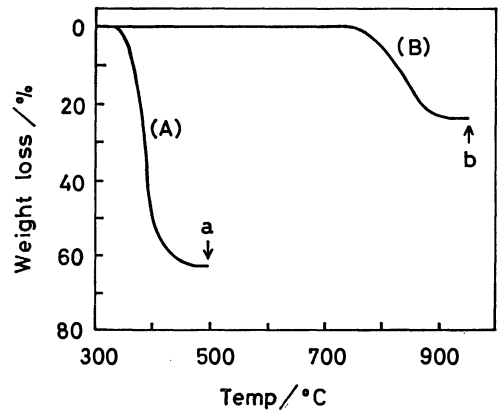

Fig. 2. TG curves of $ZrCl_4 \cdot 2NH_3$ and ZrClN in an ammonia stream.
(A): $ZrCl_4 \cdot 2NH_3$, (B): ZrClN.

The reaction products of gaseous $ZrCl_4$ with ammonia at various temperatures above 300 °C are summarized in Table 2. The symbols α and β in the parentheses represent the modifications of ZrClN.

Unreacted $ZrCl_4$ was not observed throughout the temperature range of this work. The products which formed below 750 °C were obtained inside and outside the reaction zone. Above 800 °C, a large portion of the products were obtained outside the reaction zone, and above 1100 °C, all the products were obtained outside the reaction zone. Above 1100 °C, HCl was formed in addition to by-product NH_4Cl. The percentage of HCl formed to the total amount of chlorine introduced as $ZrCl_4$ was <1% at 1100 °C, 10% at 1200 °C, 25% at 1300 °C, and 60% at 1400 °C. The value is nearly the same as that of the HCl formed by the thermal decomposition of NH_4Cl at each temperature under the experimental conditions in this work.[9] This was considered to indicate that the HCl formed was due to the decomposition of the by-product NH_4Cl.

Reaction Process of Gaseous Zirconium Tetrachloride with Ammonia. To elucidate the reaction process of gaseous $ZrCl_4$ with ammonia, the behavior of the $ZrCl_4 \cdot 2NH_3$, the ZrClN, and the Zr_3N_4, which had been formed during the reaction process, on heating in an ammonia stream were examined.

Behavior of $ZrCl_4 \cdot 2NH_3$ on Heating in an Ammonia Stream: The TG curve of $ZrCl_4 \cdot 2NH_3$ in an ammonia stream is shown in Fig. 2 (A).

$ZrCl_4 \cdot 2NH_3$ lost weight above 330 °C. It was observed that NH_4Cl and a small amount of $ZrCl_4 \cdot 2NH_3$ deposited outside the heating zone during the weight loss. The sample after the heating to point a was found to be α-ZrClN by X-ray analysis. The final weight loss was 62.8%. This value was considerably larger than the calculated value, 47.33%, based on the reaction, $ZrCl_4 \cdot 2NH_3 + 2NH_3 \rightarrow ZrClN + 3NH_4Cl$. This was considered to be due to the vaporization of a part of the $ZrCl_4 \cdot 2NH_3$.

In order to obtain more detailed information on the behavior of $ZrCl_4 \cdot 2NH_3$ on heating in an ammonia stream, $ZrCl_4 \cdot 2NH_3$ (1.0 g) in a quartz boat (70 mm length, 15 mm width, 7 mm depth) was placed in a straight reaction tube (28 mm i.d., 1000 mm length). Ammonia was introduced into the reaction tube at a flow-rate of 100 cm^3/min. The sample part was then placed in the centre of an electric furnace (300 mm heating length) maintained at a specified temperature for 1 h. The products obtained inside and outside the boat were examined by X-ray analysis and chemical analysis. The results are shown in Table 3.

From these results, it was found that on heating $ZrCl_4 \cdot 2NH_3$ in an ammonia stream, $ZrCl_4 \cdot 2NH_3$ reacted with ammonia above about 330 °C to form ZrClN and NH_4Cl and that the reaction was accompanied by the vaporization of a part of $ZrCl_4 \cdot 2NH_3$. The formation of ZrClN outside the boat was considered to indicate that the reaction of gaseous $ZrCl_4 \cdot 2NH_3$ with ammonia to form ZrClN also occurred.

Behavior of ZrClN on Heating in an Ammonia Stream: The TG curve of ZrClN in an ammonia stream is shown in Fig. 2(B). α-ZrClN obtained inside the reaction zone by the reaction of gaseous $ZrCl_4$ with ammonia at 500 °C was used. ZrClN lost weight above 750 °C. The sample after the heating to point b was found to be a mixture of ZrN_x and a small amount of Zr_3N_4 by X-ray analysis. It was observed that NH_4Cl alone was deposited outside the heating zone during the weight loss.

In order to obtain more detailed information on the behavior of ZrClN on heating in an ammonia stream, the products obtained by heating ZrClN(α) (0.5 g) in a quartz boat in an ammonia stream (100 cm^3/min) for 1 h at a specified temperature were examined by X-ray analysis and chemical analysis. The results are shown in Table 4.

These results showed that, on heating ZrClN(α) in an ammonia stream, the transition of α-ZrClN to β-ZrClN occurred above about 600 °C and that the reaction of ZrClN with ammonia occurred above about 750 °C to form ZrN_x, Zr_3N_4, and NH_4Cl at 750—1000 °C and ZrN_x and NH_4Cl at 1100 °C.

Behavior of Zr_3N_4 on Heating in an Ammonia Stream: The products obtained by heating Zr_3N_4 (0.2 g) in an ammonia stream (100 cm^3/min) for 1 h at various temperatures were examined. The sample Zr_3N_4 used was the Zr_3N_4 containing a slight amount of ZrN_x,

Table 4. Experimental results for ZrClN on heating in an ammonia stream

Heating temp/°C	Products		Unreacted ZrClN/%
	In the boat	Outside the boat	
550	ZrClN[α]	—	100
600—700	ZrClN[$\alpha > \beta$]	—	100
750	ZrClN[$\alpha > \beta$], $ZrN_x > Zr_3N_4$	NH_4Cl	64
800	$ZrN_x >$ ZrClN[β], Zr_3N_4	NH_4Cl	25
850	$ZrN_x > Zr_3N_4 >$ ZrClN[β]	NH_4Cl	10
900	$ZrN_x > Zr_3N_4$	NH_4Cl	—
1000	$ZrN_x \gg Zr_3N_4$	NH_4Cl	—
1100	ZrN_x	NH_4Cl	—

Table 5. N/Zr atomic ratios and lattice constants of the ZrN_x formed

Formation temp/°C	x in ZrN_x	a_0/Å
1100	1.28	4.560
1200	1.24	4.564
1300	1.18	4.568
1400	1.12	4.571

which was formed by the reaction of qaseous $ZrCl_4$ with ammonia at 950 °C, because Zr_3N_4 alone was not obtained throughout the experiments in this work. X-Ray analysis of the sample after the heating at each temperature showed it to be $Zr_3N_4 \gg ZrN_x$ (unchanged) at 900 °C, Zr_3N_4, ZrN_x at 1000 °C, and $ZrN_x > Zr_3N_4$ at 1100 °C. The results showed that Zr_3N_4 decomposed to ZrN_x above about 1000 °C in an ammonia stream.

From the results, it was considered that ZrN_x formed by heating ZrClN in an ammonia stream at temperatures lower than 1000 °C (Table 4) was formed without passing through Zr_3N_4. Consequently, it may be concluded that on heating ZrClN in an ammonia stream, it reacts with ammonia above about 750 °C to from ZrN_x and Zr_3N_4. Above about 1000 °C, ZrN_x was also formed by the thermal decomposition of the Zr_3N_4 formed.

Based on the above experimental results, the reaction process of gaseous $ZrCl_4$ with ammonia was discussed. As shown in Table 2, $ZrCl_4 \cdot 2NH_3$ alone was formed at 300 °C. This fact indicates that the reaction of gaseous $ZrCl_4$ with ammonia to form $ZrCl_4 \cdot 2NH_3$ occurs first. The ZrClN formed at 350—950 °C is considered to be due to the reaction of $ZrCl_4 \cdot 2NH_3$ with ammonia, because the $ZrCl_4 \cdot 2NH_3$ reacts with ammonia above about 330 °C to form ZrClN, as described above. The ZrN_x and Zr_3N_4 formed above 750 °C are considered to be due to the reaction of ZrClN with ammonia, because the ZrClN reacts with ammonia to form ZrN_x and Zr_3N_4 above about 750 °C. Above about 1000 °C, ZrN_x is considered to be formed also by the thermal decomposition of Zr_3N_4, because Zr_3N_4 decomposes to ZrN_x in an ammonia stream above about 1000 °C.

From the above-mentioned results, the reaction process of $ZrCl_4$ with ammonia in the vapor phase can be represented as follows: The reaction of gaseous

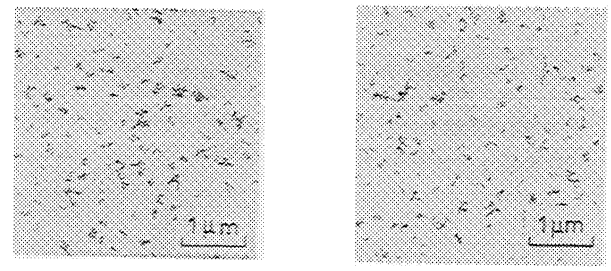

(a) 1200 °C (b) 1400 °C

Fig. 3. Electron micrographs of the ZrN_x formed at various temperatures.

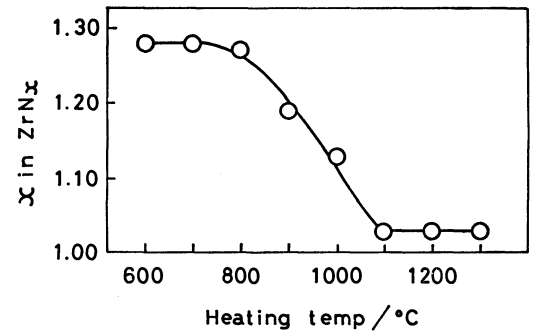

Fig. 4. N/Zr atomic ratios of ZrN_x obtained after heating $ZrN_{1.28}$ at various temperatures in an argon atmosphere.

$ZrCl_4$ with ammonia to form $ZrCl_4 \cdot 2NH_3$ occurs first. Above about 330 °C, the $ZrCl_4 \cdot 2NH_3$ reacts with ammonia to form ZrClN. Above about 750 °C, the ZrClN reacts with ammonia to form ZrN_x and Zr_3N_4. Above about 1000 °C, ZrN_x is also formed by the thermal decomposition of the Zr_3N_4.

Properties of the ZrN_x Formed. The N/Zr atomic ratios of ZrN_x formed outside the reaction zone by the reaction of geseous $ZrCl_4$ with ammonia at 1100—1400 °C are shown in Table 5. Prior to this examination, the presence of residual NH_4Cl in the ZrN_x, obtained after the removal of NH_4Cl at 400 °C *in vacuo*, was checked by chemical analysis,[10] after the heating of the ZrN_x sample in molten sodium carbonate. The NH_4Cl content in the ZrN_x was 1.5% for the ZrN_x formed at 1100 °C, 0.9% at 1200 °C, 0.4% at 1300 °C, and <0.1% at 1400 °C. For the evaluation of the N/Zr atomic ratio of the ZrN_x formed, the initial weight of the sample was corrected by subtracting the amount of NH_4Cl contained, because the NH_4Cl was

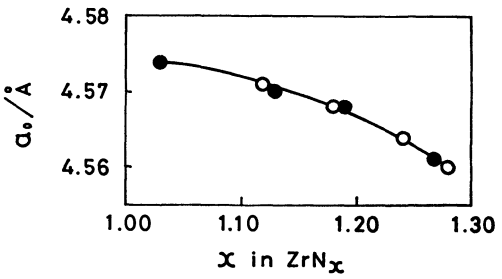

Fig. 5. Lattice constants of the ZrN_x with various x values.
○: From ZrN_x formed by the reaction of gaseous $ZrCl_4$ with ammonia, ●: From ZrN_x obtained after the heating of $ZrN_{1.28}$.

vaporized during the oxidation.[9]

It has been known that the ZrN_x phase has a NaCl structure.[4] The lattice constant of ZrN_x formed at each temperature is also shown in Table 5.

The ZrN_x formed by the reaction of gaseous $ZrCl_4$ with ammonia above 1100 °C were examined by electron microscopy. Typical micrographs of the ZrN_x are shown in Fig. 3.

As seen from Fig. 3, the ZrN_x formed is uniform, ultrafine powders with the particle diameters of the order of 1/100 μm.

Finally, to obtain knowledge of the thermal stablilty of the ZrN_x formed, the N/Zr atomic ratios of the samples obtained by heating $ZrN_{x(x=1.28)}$ at various temperatures in an argon atmosphere for 1 h were examined. The results are shown in Fig. 4. In addition, it was found that the residual NH_4Cl in the ZrN_x was completely removed by the heating above 900 °C.

The results indicated that when the ZrN_x formed was heated in an argon atmosphere at temperatures higher than 700 °C, the N/Zr atomic ratio decreased and became close to that of the stoichiometric nitride. The value of x was 1.03 at the heating temperatures of 1100—1300 °C.

The lattice constants of the ZrN_x with various x values, obtained in this work, are shown in Fig. 5.

The present work was partially supported by a Grant-in-Aid for Scientific Research No.56470058 from the Ministry of Education, Science and Culture.

References

1) Y. Okabe, J. Hojo, and A. Kato, *Yogyo Kyokai Shi*, **85**, 173 (1977).
2) R. Juza and J. Heners, *Z. Anorg. Allg. Chem.*, **332**, 159 (1964).
3) JCPDS, Powder Diffraction File 18-1493.
4) ASTM, X-Ray Powder Data File 2-956.
5) ASTM, Powder Diffraction File 7-7.
6) R. Juza, A. Gabel, H. Rabenau, and W. Klose, *Z. Anorg. Allg. Chem.*, **329**, 136 (1964).
7) R. Juza, A. Rabenau, and I. Nitschke, *Z. Anorg. Allg. Chem.*, **332**, 1 (1964).
8) V. P. Orlovskii, N. V. Rudenko, and B. V. Ivanov-Emin, *Russ. J. Inorg. Chem.*, **12**, 1217 (1967).
9) Y. Saeki, R. Matsuzaki, A. Yajima, and M. Akiyama, *Bull. Chem. Soc. Jpn.*, **55**, 3193 (1982).
10) JIS H 1615 (1973), p. 2.

 © 1983 The Chemical Society of Japan Bull. Chem. Soc. Jpn., 56, 2643—2646 (1983)

Cooperativity in the Binding of Sodium Dodecyl Sulfate to Amylose

Masako YAMAMOTO,† Takayuki SANO, Shoji HARADA, and Tatsuya YASUNAGA*

Department of Chemistry, Faculty of Science, Hiroshima University, Hiroshima 730

† *Department of Home Economics, Hiroshima Women's University, Hiroshima 734*

(Received November 8, 1982)

The binding isotherm of sodium dodecyl sulfate to amylose was potentiometrically investigated by using amyloses of various degrees of polymerization from 32 to 1100. From the Scatchard plots, the binding was found to be cooperative for the amyloses of DP≧76 and Langmuir type for those of DP≦57. By analogous experiments using a series of sodium alkyl sulfates, it was clarified that (1) eight carbon atoms of surfactant are required for the complexation and (2) more than twelve carbon atoms of surfactant are required for the cooperative binding. Thus, the amylose has an interrupted helical structure in solution and the cooperativity arises from the hydrophobic interaction between the surfactants included partly in the helic of amylose.

A number of investigations[1-7] have been performed on the complex formation of amylose with various reagents, in connection with the biological significance of the amylose structure in solution. Three representative models have been proposed, *i.e.*, an interrupted helix,[8,9] an entirely random coil,[10] and a deformed helix.[11,12] In previous papers,[13,14] we have proposed the interrupted helical structure as the most adequate model for amylose conformation in solution from the kinetic and static investigations on the amylose–iodine complex formation by using the amyloses of various degrees of polymerization, DP.

In extension of our studies on the structure of amylose, the binding isotherm of sodium dodecyl sulfate, SDS, to amylose was investigated with use of amyloses of various DPs. Further, the same experiment was performed for the homologue of SDS using the amylose of DP 1100, and the effect of the chain length of alkyl group of surfactant on the binding isotherm was examined.

Experimental

Materials. Potato amylose, purchased from Pierce Chemical, was purified by precipitation three times from 1-butanol. Amyloses of various DPs were prepared as described in a previous paper.[13] The molecular weight, $\bar{M}_w$, of the amylose was estimated from the elution profile of the gel chromatography on a Sepharose 4B column (2.5×62 cm), using the following relationship obtained by Dextran T10, T20, T70, T150, and T500.

$$\log \bar{M}_w = 7.05 - 3.19 K_{av}, \quad (1)$$

with

$$K_{av} = \frac{V_e - V_v}{V_t - V_v}, \quad (2)$$

where K_{av} is the partition coefficient;[15] V_v, V_t, and V_e are the void volume, total volume, and elution volume, respectively. The amylose was used in the form of the wet 1-butanol complex.[10] Sodium alkyl sulfates, $CH_3(CH_2)_{n-1}SO_4Na$ with n=6, 8, 10, 12, and 14, were synthesized according to the method of Dreger.[16] Dodecyltrimethylammonium dodecyl sulfate was prepared according to the method of Satake and Yang.[17]

Measurements. The concentration of bound SDS was determined by its electromotive force (emf) using a cell constructed as follows:[17,18]

|reference electrode|agar bridge|reference solution; 0.6×10^{-4} M** SDS|nitrobenzene; 1×10^{-4} M $(C_{12}H_{25}(CH_3)_3N)^+(SO_4C_{12}H_{25})^-$|sample solution; 5×10^{-3} M amylose in AGU, SDS|agar bridge|reference electrode|.

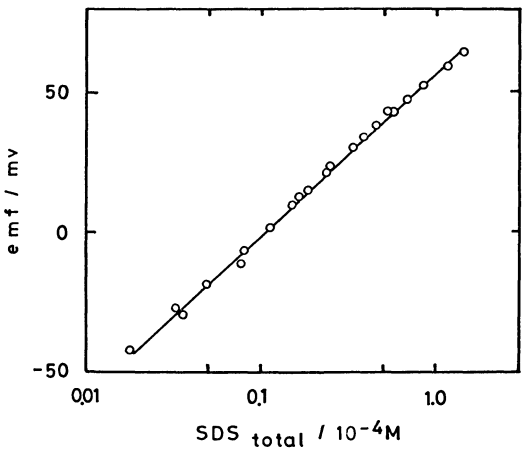

Fig. 1. Plot of emf *vs.* the logarithm of the concentration of SDS at 30 °C.

Calibration of the apparatus was performed by measuring the emf of the SDS solution without amylose. To attain a stable and accurate responce of the liquid membrane, 21.3 mM of sodium chloride was added to each solution. Figure 1 shows the semilogarithmic plot of the emf *vs.* SDS concentration. The slope of the line, 59 mV at 30 °C, agrees well with the ideal Nernst slope (60 mV at 30 °C), which implies that the liquid membrane responds exclusively to a surfactant ion.[19] The pH of the solutions ranged from 5.5 to 6.2, since no buffer solution was used. Amylose solution was freshly prepared immediately before the measurements and the concentration in anhydroglucose residue unit was determined by the phenol-sulfuric acid method.[20] To rule out any effect due to the micellization, the concentration of surfactant was kept below the critical micelle concentration. All measurements were carried out at 30 °C.

Results and Discussion

Typical potentiometric titration curves obtained with SDS in the presence and absence of amylose are shown in Fig. 2. Since the SDS bound to amylose can not contribute to the emf, the concentration of the bound SDS is equal to the difference in the SDS concentrations required to give the same emf on curves a and b in Fig. 2. The concentration of the bound SDS estimated for the various DPs of amylose is plotted against the free SDS concentration in Fig. 3. As seen

** 1 M=1 mol dm^{-3}.

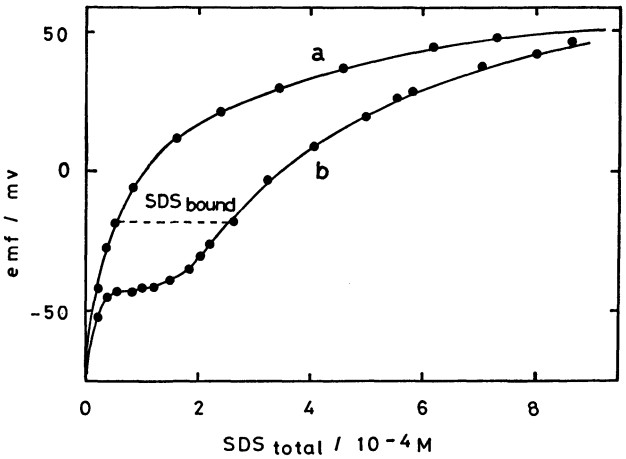

Fig. 2. Potentiometric titration curves of amylose (DP 1100) with SDS. (a); Without amylose, (b); with amylose of 5 mM in anhydroglucose residue unit.

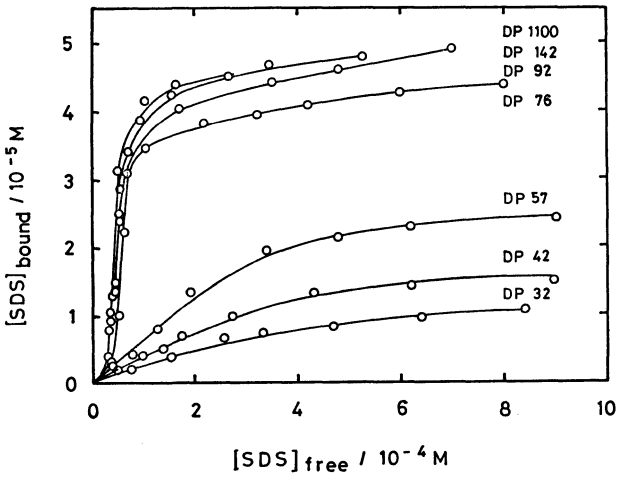

Fig. 3. Binding isotherms of SDS for a series of amyloses at 30 °C.

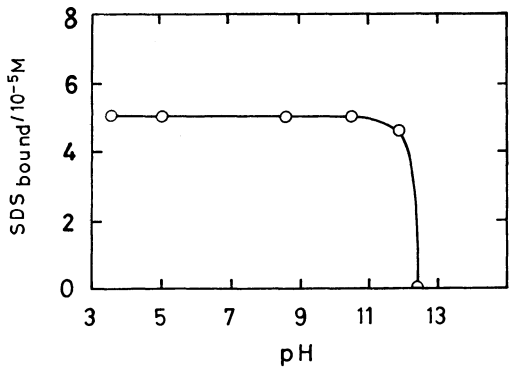

Fig. 4. pH dependence of the total amount of bound SDS to amylose (DP 1100, 1 mM) at 30 °C.

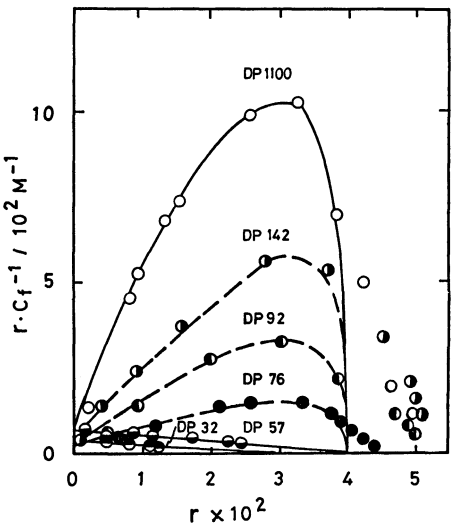

Fig. 5. Representative Scatchard plots of binding isotherms of SDS to amyloses. Solid lines show theoretical curves obtained by Eqs. 2 and 3. The dotted lines have no theoretical meaning. (○); DP 1100, (◑); DP 142, (◐); DP 92, (●); DP 76, (◒); DP 57, (◓); DP 32.

in this figure, the total amount of the bound SDS increases with the DP of amylose.

As for the pH dependence of the concentration of bound SDS, no alteration takes place up to pH 10.6, but a sudden decrease appears at around pH 12, as shown in Fig. 4. A similar drastic change in the conformation of amylose with pH has been reported; this was ascribed to the break-down of the helical structure.[4] From a consideration of these two experimental results, it can be deduced that the SDS molecule binds to the helical part of amylose.

The binding equilibrium of amylose–SDS system is written as

$$A + SDS_f \rightleftharpoons SDS_b, \quad (3)$$

where A is the binding site of amylose and SDS_f and SDS_b are the free and bound SDS, respectively. The Scatchard equation for Reaction 3 is given by

$$r/C_f = K(n-r), \quad (4)$$

where r is the ratio of bound SDS to total amylose in anhydroglucose residue units, n is the maximum amount of bound SDS per anhydroglucose residue, C_f is the concentration of free SDS, and K is the apparent equilibrium constant. The representative Scatchard plots for the amyloses of various DPs are shown in Fig. 5. At first glance, an obvious difference can be seen in the plots, *i.e.*, straight lines with negative slope for the amyloses of DP≦57, and curvature with upward convex for those of DP≧76. The straight lines indicate the Langmuir type binding of SDS to amylose, while the curvature indicates the cooperative binding. A similar change in the binding profile around DP 60 has been also recognized in the amylose–iodine complex formations, as previously reported.[13] These facts give support for the interrupted helix model of the conformation of amylose in solution.

For the Langmuir type binding, n and K_L (the subscript L means the Langmuir type binding) were evaluated from the intercept and the slope of the straight line, respectively. These values are listed in Table 1 together with the number of binding sites of SDS on one amylose molecule, m. The value of m increases with DP of amylose, whereas the equilibrium constant, K_L, remains constant.

As for the cooperative binding, the equilibrium con-

Table 1. The binding parameters of the complex formation

DP	m	$n\times10^2$	Langmuir type binding	Cooperative binding	
			K_L / $10^3\ M^{-1}$	K_0 / $10^3\ M^{-1}$	K_c
32	0.94	2.95	1.7±0.3	—	—
42	1.22	2.90	1.4±0.6	—	—
57	2.30	4.00	2.0±0.2	—	—
1100	59	4.00	—	2.0±0.7	22±2

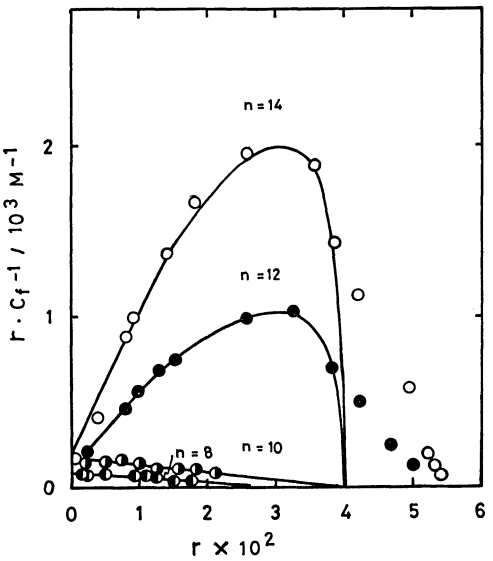

Fig. 6. Scatchard plots of binding isotherms of surfactants to amylose (DP 1100). Solid lines show theoretical curves obtained by Eqs. 2 and 3. (○); $n=14$, (●); $n=12$, (◑); $n=10$, (◐); $n=8$.

stant K in Eq. 4 can be rewritten according to the one-dimensional Ising model by McGhee and von Hippel;[22]

$$K = K_0\left\{\frac{n-2r+R}{2(n-r)}\right\}^2, \quad (5)$$

with

$$R = [(n-2r)^2 + 4K_c r(n-r)]^{1/2}, \quad (6)$$

where K_0 is the equilibrium constant for the intrinsic binding of SDS to amylose (intrinsic equilibrium constant) and K_c is the cooperative parameter. The values of K_0 and K_c were determined for the amylose of DP 1100 so as to give the best fit of the data to the Scatchard equation, and are listed in Table 1. As can be seen in Fig. 5, experimental points deviate from the theoretical curve in the region of $r\geqq0.04$ for DP 1100. These data were disregarded for analysis because of their low reliability. A good agreement between values of K_0 for DP 1100 and K_L for DP$\leqq$57 in Table 1 implies the similarity in the mechanism of the isolated binding and the Langmuir binding. Meanwhile, the value of K_c for the amylose of DP 1100 means positive cooperativity, *i.e.*, the cooperative interaction contributes to the stabilization of the complex. In the cases of amyloses of DP 76 to 142, the Scatchard plots are also indicative of the cooperativity, as seen in Fig. 5. Further quantitative analysis of these plots, however, was not carried out because Eq. 5 can not be applied to these small amyloses.[22]

Table 2. Effect of the chain length of alkyl group of surfactants on the binding parameters of the complex formation

Alkyl group	$n\times10^2$	Langmuir type binding	Cooperative binding	
		K_L / $10^3\ M^{-1}$	K_0 / $10^3\ M^{-1}$	K_c
n-C_8H_{17}	2.1	2.1±0.2		
n-$C_{10}H_{21}$	4.0	2.2±0.2		
n-$C_{12}H_{25}$	4.0		2.0±0.7	22±2
n-$C_{14}H_{29}$	4.0		2.2±0.9	36±8

In order to clarify the effect of the chain length of alkyl group of surfactant on the complexation, the binding isotherms of a series of sodium alkyl sulfates $CH_3(CH_2)_{n-1}SO_4Na$ with n=8, 10, 12, and 14 to amylose of DP 1100 were investigated. The Scatchard plots for these surfactants are shown in Fig. 6. These plots showed large differences in the binding profiles; the binding of surfactants of n=8 and 10 is Langmuir type, whereas that of n=12 and 14 is cooperative. These results suggest that a certain length of the alkyl chain of surfactant ($n\geqq12$) is necessary for the cooperative binding. Meanwhile, sodium alkyl sulfate with n=6 did not bind to amylose. Consequently at least eight carbon atoms of surfactant molecule should be required for the complex formation. Table 2 summarizes the binding parameters obtained for each surfactant system. As can be seen from this table, the values of K_L for surfactants of n=8 and 10 are in good agreement with that of K_0 for n=12 and 14, which implies that the alkyl chain length included in a helix of amylose is approximately equal for each surfactant system.

The binding parameters of SDS to the amylose of DP 1100 were obtained at various temperatures; their temperature dependences are shown in Fig. 7. From these, thermodynamic parameters were obtained and are listed in Table 3. It is seen that the intrinsic complex formation is enthalpy-determined while the cooperative interaction between bound SDS is entropy-determined.

Finally, the possibility of two other models for amylose structure was examined. Three experimental facts already noted above: noncooperative binding of two SDS molecules to an amylose of DP 57, sudden appearance of the cooperative binding of SDS to the amylose of DP 76, and noncooperative binding of

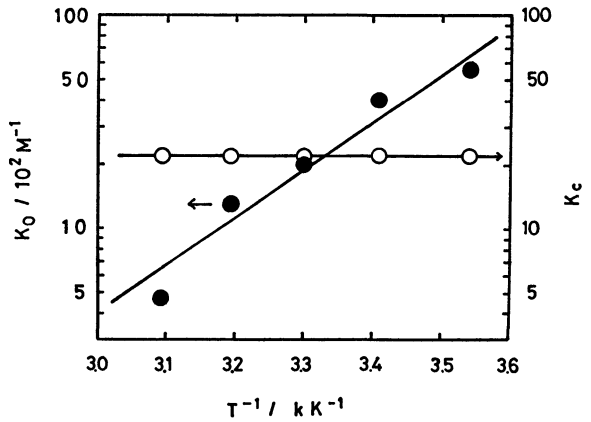

Fig. 7. The temperature dependence of the binding parameters of SDS to the amylose of DP 1100.

TABLE 3. THERMODYNAMIC PARAMETERS OF THE COMPLEX FORMATION

ΔH_0/kJ mol^{-1}	−40.5
ΔG_0/kJ mol^{-1}	−19.1
ΔS_0/J K^{-1} mol^{-1}	−70.5
ΔH_c/kJ mol^{-1}	0
ΔG_c/kJ mol^{-1}	−7.8
ΔS_c/J K^{-1} mol^{-1}	26

alkyl sulfates of n=8 and 10 to the amylose of DP 1100, exclude the possibility of two models: that of the entirely random coil and that of the deformed helix, for the structure of amylose in solution.

We have revealed the existence of two types of binding of SDS to amylose, as shown schematically in Fig. 8. One was ascribed to the Langmuir type binding due to an inclusion of SDS at the end of a helical segment of amylose, and the other to the cooperative binding due to the interaction of the outer part of alkyl chain of SDS bound to the interrupted helix of amylose. Furthermore, on the basis of the present work, the binding isotherms of fatty acids and alcohols with amylose, which have been hitherto reported as showing only Langmuir adsorption, should be reinvestigated from the standpoint of the cooperative binding with use of amylose of various DPs.

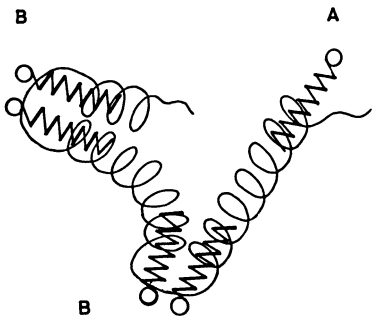

Fig. 8. Schematic picture of the structure of amylose–SDS complex. A; Langmuir type binding, B; cooperative binding.

References

1) R. E. Rundle and F. C. Edwards, *J. Am. Chem. Soc.*, **65**, 2200 (1943).
2) F. F. Mikus, R. M. Hixon and R. E. Rundle, *J. Am. Chem. Soc.*, **68**, 1115 (1946).
3) T. Takagi and T. Isemura, *Bull. Chem. Soc. Jpn.*, **33**, 437 (1960).
4) V. S. R. Rao and J. F. Foster, *Biopolymers*, **1**, 527 (1963).
5) F. Osman-Ismail and J. Solms, *Staerke*, **24**, 213 (1972).
6) N. Nishimura and M. Janado, *J. Biochem.*, **77**, 421 (1975).
7) T. Handa and H. Yajima, *Biopolymers*, **20**, 2051 (1981).
8) J. Hóllo and J. Szejtli, *Staerke*, **10**, 49 (1958).
9) M. B. Senior and E. Hamori, *Biopolymers*, **12**, 65 (1973).
10) W. Banks and C. T. Greenwood, *Staerke*, **23**, 300 (1971).
11) O. Kratky and G. Porod, *Recl. Trav. Chim. Pays-Bas*, **68**, 1106 (1949).
12) Q. T. Nguyen, P. Aptel, and J. Neel, *Biopolymers*, **15**, 2097 (1976).
13) M. Yamamoto, T. Sano, and T. Yasunaga, *Bull. Chem. Soc. Jpn.*, **55**, 1886 (1982).
14) M. Yamamoto, T. Sano, S. Harada, and T. Yasunaga, *Bull. Chem. Soc. Jpn.*, **55**, 3702 (1982).
15) T. C. Laurent and J. Killander, *J. Chromatogr*, **14**, 317 (1964).
16) E. E. Dreger, G. I. Keim, and G. D. Milles, *Ind. Eng. Chem.*, **36**, 610 (1944).
17) I. Satake and J. T. Yang, *Biopolymers*, **15**, 2263 (1976).
18) The ion-exchanger $(C_{12}H_{25}(CH_3)_3N)^+(SO_4R)^-$ corresponding to each R was used for the measurements of RSO_4Na. For the measurement of these surfactants of R=n-C_6H_{13} and n-C_8H_{17}, the ion-exchanger of R=n-$C_{10}H_{21}$ was used.
19) From the slope of the line, the values in the range from 59 to 60 mV were obtained for these surfactants of $n \geqq 10$, but those in the cases of R=n-C_6H_{13} and n-C_8H_{17} decreased.
20) M. Dubois, K. A. Gilles, J. K. Hamilton, R. A. Rebers, and F. Smith, *Anal. Chem.*, **28**, 350 (1956).
21) G. Schwarz, *Biophys. Chem.*, **6**, 65 (1977).
22) J. D. McGhee and P. H. von Hippel, *J. Mol. Biol.*, **86**, 469 (1974).

The Ruthenium Catalyzed *N*-Alkylation of Amides with Alcohols

Yoshihisa WATANABE,* Tetsuo OHTA, and Yasushi TSUJI
Department of Hydrocarbon Chemistry, Kyoto University, Sakyo-ku, Kyoto 606

(Received December 23, 1982)

Amides reacted with primary alcohols in the presence of a catalytic amount of $RuCl_2(PPh_3)_3$ at 180 °C to give the corresponding *N*-monoalkyl amides in fairly good yields. Thus, benzamide reacted with 1-octanol to give *N*-octylbenzamide in 76% yield with excellent product selectivity. Little esterification of amides with alcohols occurred and selectivity to the *N*-alkylation was high. Most of the amides gave *N*-monoalkyl amides but no *N,N*-dialkyl amides. But formamide reacted with 1-butanol to give *N,N*-dibutylformamide, as well as *N*-butylformamide, in low yield. $RuCl_2(PPh_3)_3$ was the most effective catalyst for this reaction and $RuHCl(PPh_3)_3$ also had some catalytic activity.

N-Alkylation is important for selective synthesis of substituted amines; various methods have been developed. A conventional alkylating reagent is alkyl halide. On the other hand, *N*- and *C*-alkylation using alcohols as the alkylating reagent in the presence of Ni catalyst[1] have been reported and recently in the presence of Rh and Ru catalysts.[2-4]

We have previously demonstrated that ruthenium complexes were effective for the activation of alcohols and that they were excellent catalysts for *N*-alkylation and *N*-heterocyclization of aminoarenes and nitroarenes using alcohols.[3,4] This paper describes the alkylation

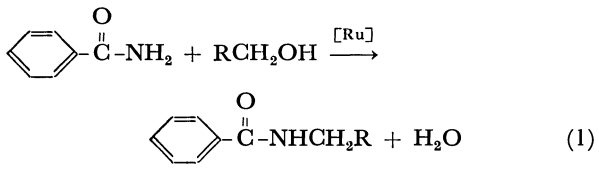

$$\text{PhCONH}_2 + \text{RCH}_2\text{OH} \xrightarrow{[\text{Ru}]} \text{PhCONHCH}_2\text{R} + \text{H}_2\text{O} \qquad (1)$$

of amides with alcohols in the presence of ruthenium catalyst (Eq. 1).

Results and Discussion

Benzamide was *N*-alkylated with various alcohols in the presence of $RuCl_2(PPh_3)_3$. The results are summarized in Table 1. Ethanol, 1-propanol, 1-hexanol, 1-octanol, and 1-dodecanol are employed as alkylating reagents to give *N*-ethyl-, *N*-propyl-, *N*-hexyl-, *N*-octyl-, and *N*-dodecylbenzamide, respectively. The selectivities of the products were high. The conversions of benzamide increased with elongating a carbon chain of the alcohols; 1-octanol gave the best result. Benzyl alcohol gave *N*-benzylbenzamide with 94% selectivity(Run 8), but prolonging the reaction time induced a decrease in its selectivity. However, methanol and secondary alcohol, 2-propanol, gave almost no *N*-alkylbenzamides in this procedure. A similar tendency was observed in the ruthenium-catalyzed *N*-alkylation of aminoarenes using alcohols,[3] where methanol and secondary alcohols were much less reactive as alkylating reagents than primary alcohols were.

By the present procedure, benzamide was converted to *N*-alkylbenzamide selectively, *N,N*-dialkylbenzamide was not obtained as the product, even in the presence of excess alcohol. This result is in striking contrast to that of the *N*-alkylation of aniline,[3] where *N,N*-dialkylanilines were the major products under similar reaction conditions. The *N,N*-dialkylation of aniline appears to proceed stepwise *via* *N*-monoalkylation. The reaction is not controlled at the *N*-monoalkylation stage and proceed readily to the *N,N*-dialkylation step. Thus, these observations reveal that the amides are less reactive than aminoarenes in the *N*-alkylation by alcohols, presumably owing to a neighboring carbonyl group.

The results of the *N*-alkylation of other amides are listed in Table 2. *p*-Chlorobenzamide reacted with 1-butanol to give *N*-butyl-*p*-chlorobenzamide with high selectivity. The conversion of the amide slightly decreased as compared with that of benzamide. Furthermore, acetamide, phenylacetamide, and butanamide were also *N*-alkylated with alcohols. However,

TABLE 1. THE RUTHENIUM-CATALYZED *N*-ALKYLATION OF BENZAMIDE WITH ALCOHOL[a]

Run	Alcohol	Product	Benzamide[b] conversion/%	Product[c] selectivity/%
1[d]	Methanol	*N*-Methylbenzamide	4	—[e]
2	Ethanol	*N*-Ethylbenzamide	57	97
3	1-Propanol	*N*-Propylbenzamide	54	93
4[d]	2-Propanol	*N*-Isopropylbenzamide	14	—[e]
5	1-Hexanol	*N*-Hexylbenzamide	73	93
6	1-Octanol	*N*-Octylbenzamide	78	97
7[f]	1-Dodecanol	*N*-Dodecylbenzamide	61	96
8	Benzyl alcohol	*N*-Benzylbenzamide	34	94
9[g]	Benzyl alcohol	*N*-Benzylbenzamide	74	66

a) A mixture of benzamide(10 mmol), alcohol(5 ml), and $RuCl_2(PPh_3)_3$ (0.2 mmol) was heated at 180 °C for 4 h. b) Determined by GLC based on an amount of benzamide used. c) Determined by GLC based on the conversion of benzamide. d) $RuCl_2(PPh_3)_3$(0.1 mmol) was used. e) Product selectivities could not be estimated since the products gave only trace yields. f) The reaction time: 7 h. g) The reaction time: 12 h.

TABLE 2. *N*-ALKYLATION OF AMIDES BY $RuCl_2(PPh_3)_3$-ALCOHOL

Run	Amide	Alcohol	Product	Reaction time/h	Amide[b] conversion/%	Product[c] selectivity/%
10	*p*-Chlorobenzamide	1-Butanol	*N*-Butyl-*p*-chlorobenzamide	6	49	96
11	Acetamide	Ethanol	*N*-Ethylacetamide	4	9	100
12	Acetamide	Ethanol	*N*-Ethylacetamide	10	69	30
13	Acetamide	1-Octanol	*N*-Octylacetamide	4	30	80
14	Phenylacetamide	Ethanol	*N*-Ethylphenylacetamide	4	25	60
15	Butanamide	1-Butanol	*N*-Butylbutanamide	12	32	88
16	Butanamide	1-Octanol	*N*-Octylbutanamide	4	26	62
17	6-Hexanelactam	Ethanol		4	0	0
18	3-Pyridinecarboxamide	Ethanol		4	0	0
19	Acrylamide	Ethanol	(Propanamide)	4	58	64

a) A mixture of amide(10 mmol), alcohol(5 ml), and $RuCl_2(PPh_3)_3$ (0.2 mmol) was heated at 180 °C. b) Determined by GLC based on an amount of the amide used. c) Determined by GLC based on the conversion of amide.

TABLE 3. RUTHENIUM CATALYZED *N*-ALKYLATION OF BENZAMIDE. EFFECT OF CATALYST[a]

Run	Catalyst	Benzamide[b] conversion/%	*N*-Ethylbenzamide[c] selectivity/%
20	$RuCl_2(PPh_3)_3$	53	85
21	$RuHCl(PPh_3)_3$	33	67
22	$RuHCl(CO)(PPh_3)_3$	29	66
23	$Ru(CO)_3(PPh_3)_2$	8	Trace
24[d]	$RuH_2(PPh_3)_4$	4	Trace
25	$RuCl_3 \cdot nH_2O$	0	0
26[d]	$RhCl(PPh_3)_3$	0	0
27[d]	$RhH(PPh_3)_4$	9	Trace

a) A mixture of benzamide(10 mmol), ethanol(5 ml), and a catalyst(0.1 mmol) was heated at 180 °C for 4 h. b) Determined by GLC based on an amount of benzamide used. c) Determined by GLC based on the conversion of benzamide. d) Catalyst(0.2 mmol) was used.

in these cases the conversions of the amides decreased considerably and the selectivities were not high. 6-Hexanelactam and 3-pyridinecarboxamide were not converted at all. Secondary amides cannot be alkylated by the present systems as indicated by the result that no *N*,*N*-dialkyl amides were obtained while the *N*-alkyl amides formed. From the reaction solution of 3-pyridinecarboxamide, red crystals were obtained. These crystals had no catalytic activity in the *N*-alkylation of benzamide with ethanol.

Acrylamide reacted with ethanol in the presence of $RuCl_2(PPh_3)_3$ to give propanamide. Since $RuCl_2(PPh_3)_3$ is known as an effective catalyst for hydrogen transfer form alcohol,[5] propanamide was obtained by the transfer hydrogenation of acrylamide by ethanol.

Catalytic Activity. Several ruthenium and rhodium compounds were examined as catalysts for this reaction (Table 3). The catalytic activities decreased in the order of $RuCl_2(PPh_3)_3$, $RuHCl(PPh_3)_3$, and $RuHCl(CO)(PPh_3)_3$. $Ru(CO)_3(PPh_3)_2$ and $RuCl_3 \cdot nH_2O$ showed little catalytic activities. $RuH_2(PPh_3)_4$, $RuCl(PPh_3)_3$, and $RhH(PPh_3)_4$ also had no catalytic activities, though these complexes were reported to have the catalytic activities of the *N*-alkylation of aliphatic amines by alcohols.[2]

Reaction Conditions. The reaction of benzamide with ethanol was carried out at 150, 180, and 220 °C. The highest yield of *N*-ethylbenzamide was obtained at 180 °C. The conversion of benzamide was low at 150 °C. The selectivity of *N*-ethylbenzamide was low at 220 °C, although the conversion was high. Prolonging the reaction time and an increase in an amount of a catalyst did not improve the yield of *N*-ethylbenzamide appreciably.

In conventional *N*-alkylation of amides, alkyl halides or esters of sulfuric or sulfonic acids can be employed as the alkylating reagent.[6] Amides are very weak bases, far too weak to attack alkyl halides. Therefore, the amides must first be converted to their salts. There was no example of the transition-metal-catalyzed alkylation of amides using alcohols. Reid[7] reported

TABLE 4. *N*-ALKYLATION OF BENZAMIDE BY $RuCl_2(PPh_3)_3$-ALCOHOL. EFFECT OF REACTION CONDITIONS[a]

Run	Catalyst (mmol)	Reaction temp/°C	Reaction time/h	Benzamide[b] cnnversion/%	*N*-Ethylbenzamide[c] selectivity/%
28	0.1	150	4	24	58
20	0.1	180	4	53	85
29	0.1	220	4	88	51
30	0.1	180	5.5	57	90
31	0.1	180	6.5	62	80
2	0.2	180	4	57	97

a) A mixture of benzamide(10 mmol), ethanol(5 ml), and $RuCl_2(PPh_3)_3$ was heated. b) Determined by GLC based on the amount of benzamide used. c) Determined by GLC based on the conversion of benzamide.

that benzamide reacted with alcohols without catalyst at 220 °C for more than 60 h to give *N*-alkylbenzamides with low selectivities(30—70%) and a considerable amount of by-products by solvolysis.

This $RuCl_2(PPh_3)_3$–alcohol system has several advantages. The reaction proceeds under neutral conditions. The amides do not need to be activated to their salts. In comparison with the results of Reid, the ruthenium-catalyzed reaction is performed in shorter reaction time at lower reaction temperature. Furthermore the selectivities of the *N*-alkyl amides are high and no *N*,*N*-dialkyl amides are obtained except formamide(*vide infra*).

Two reaction paths, path A and path B, are possible for this reaction. In path A, alcohol is oxidized to aldehyde by a ruthenium complex and then the aldehyde reacts with amide to give *N*-acyl amino alcohol which undergoes dehydration; the dehydrated product is hydrogenated by hydride on the ruthenium complex or by ruthenium catalyzed transfer hydrogenation from alcohol.

Path A

$$R'CH_2OH \xrightarrow{[Ru]} R'CHO$$

$$R'CHO + RC(=O)-NH_2 \longrightarrow RC(=O)-N(H)-CH(OH)R'$$

1

$$\xrightarrow[-H_2O]{} RC(=O)-N=CHR' \xrightarrow{[Ru]} RC(=O)NHCH_2R'$$

2

The oxidation of alcohol by a ruthenium complex[8] has been reported by several authors and this step was assumed in the *N*-alkylation of aliphatic and aromatic amines with alcohols.[2,3] In the reaction of amide with aldehyde, the formation of *N*-acyl amino alcohol(**1**)[9] and its dehydrated product(**2**)[10] was ascertained.

Path B

$$RCNH_2 + R'CH_2OH \longrightarrow RCOCH_2R' + NH_3$$

$$NH_3 + R'CH_2OH \longrightarrow NH_2CH_2R' + H_2O$$

$$RCOCH_2R' + NH_2CH_2R' \longrightarrow RCNHCH_2R' + R'CH_2OH$$

In path B, alcoholysis of amide partially occurs, to give ester and ammonia. Then ammonia is alkylated with alcohol to alkylamine. The ester reacts with the alkylamine to produce *N*-alkyl amide.

The *N*-alkyl amides seem to be formed *via* path A, since ammonia, alkylamine, and ester were not produced substantially. Furthermore, addition of aldehyde gave a better yield of *N*-alkyl amides.[11] In a separate experiment ammonia reacted with alcohol to give trialkylamine, and monoalkylamine was not obtained.[12] These results indicate that path A is more plausible.

Formamide showed different results. Formamide reacted with 1-butanol for 24 h at 180 °C in the presence of $RuCl_2(PPh_3)_3$ to give *N*-butylformamide and *N*,*N*-dibutylformamide in 9 and 18% isolated yields, respectively (Eq. 2). Tributylamine was detected in 14% yield (based on formamide charged) in the reaction mixture after 8 h reaction time. *N*,*N*-Dialkyl amides were not obtained from other amides but only from formamide. Therefore, *N*,*N*-dibutylformamide seems to be produced from a different mechanism (path B'). Ammonia or alkylamine produced by Path B'

$$HCNH_2 + 1\text{-Butanol} \xrightarrow[180\,^\circ C,\ 24\,h]{RuCl_2(PPh_3)_3} HCN(Bu)_2 + HCNH(Bu) \quad (2)$$

18% 9%

$$HCNH_2 + R'CH_2OH \xrightarrow{\text{path A}} HCNHCH_2R'$$

$$HCNHR + R'CH_2OH \longrightarrow HCOCH_2R' + NH_2R$$

$$NH_2R + R'CH_2OH \longrightarrow N(CH_2R')_2R$$

$$HCNHR + N(CH_2R')_2R \longrightarrow HCN(CH_2R')_2$$

R: H or CH_2R'

the alcoholysis of amide is alkylated to di- or trialkylamine. The di- or trialkylamine formed reacts with the amide, not with the ester, since butyl formate did not react with tributylamine (Eq. 3).[13] The exchange of amine was reported in the reaction of formamide with amine.[14] Path B' is also supported by the result that formamide reacted with tributylamine in 1-butanol to give *N*,*N*-dibutylformamide and no *N*-butylformamide (Eq. 4).[15]

$$HCOBu + N(Bu)_3 \xrightarrow[n\text{-BuOH},\ 180\,^\circ C,\ 24\,h]{RuCl_2(PPh_3)_3} \text{no reaction} \quad (3)$$

$$HCNH_2 + N(Bu)_3 \xrightarrow[n\text{-BuOH},\ 180\,^\circ C,\ 24\,h]{RuCl_2(PPh_3)_3} HCN(Bu)_2 + N(Bu)_3 \quad (4)$$

48% 130%

Experimental

Analytical Procedure. GLC analysis was performed on a Shimadzu GC-3BT. The ^1H NMR spectra were obtained at 60 MHz with a JEOL JNM-60 NMR spectrometer or 100 MHz with a JEOL pulsed Fourier Transform spectrometer, model FX-100, and the ^{13}C NMR spectra were recorded at 25.05 MHz with a JEOL pulsed Fourier Transform spectrometer, model FX-100, using tetrametylsilane as an internal standard. IR spectra were measured on a Hitachi model 215 grating spectrophotometer. Elemental analysis were performed at the Microanalytical Center of Kyoto University. The mass spectra were recorded on a JMS 01SG mass spectrometer.

Materials. All substrates used were commercial products. The amides and alcohols were distilled or recrystallized before use. $RuCl_3 \cdot nH_2O$, $RhCl_3 \cdot nH_2O$, and PPh_3 were commercial products. $RuCl_2(PPh_3)_3$,[16] RuHCl-

$(PPh_3)_3$,[17] $RuHCl(CO)(PPh_3)_3$,[18] $Ru(CO)_3(PPh_3)_2$,[18] $RuH_2(PPh_3)_4$,[19] $RhCl(PPh_3)_3$,[20] and $RhH(PPh_3)_4$[18] were prepared according to the methods in the literature.

General Procedure. A stainless steel autoclave(50 ml) containing a glass liner was used in the reaction. Alcohol (5 ml), amide(10 mmol), and $RuCl_2(PPh_3)_3$ (0.2 mmol) were put into it with a magnetic stirring bar under argon flow. The reactor was sealed and degassed by three 15 atm pressurization-depressurization cycles with argon. The autoclave was heated at 180 °C in an oil bath for 4 h. The conversion of the amide and the selectivity of the product were determined with GLC(3 mmϕ×2.9 m column packed with 20% DEGA on Uniport B 80—100 mesh or with 10% Silicone SE-30 on Chromosorb W AW DMCS 80—100 mesh) by the internal standard method. The products were isolated by medium pressure column chromatography (silica gel 60, 40—64 μm, Merck). *N*-Ethylbenzamide,[21] *N*-propylbenzamide,[22] *N*-benzylbenzamide,[23] *N*-ethylacetamide,[24] *N*-butyl-*p*-chlorobenzamide,[25] *N*-butylformamide,[26] and *N*,*N*-dibutylformamide[27] were identified by comparison of their ^1H NMR spectral data with those in the literature. The identifications were confirmed with their ^{13}C NMR spectra. *N*-Ethylphenylacetamide was identified by comparison of ^{13}C and ^1H NMR spectra of authentic sample (mp 69 °C, lit, 69.5 °C) which was synthesized by the literature method.[28] The identities of other compounds were confirmed by IR, ^1H NMR, ^{13}C NMR, mass spectra, and elemental analysis.

The analytical data of the products are described below.

N-*Ethylbenzamide.* ^{13}C NMR($CDCl_3$) δ=14.7(q), 34.9 (t), 127.1(d,2C), 128.2(d,2C), 131.0(d), 134.7(s), 167.8(s). ^1H NMR (100 MHz)($CDCl_3$) δ=1.17(t, 3H), 3.41(d of q, 2H), 7.36(m, 4H), 7.80(m, 2H).

N-*Propylbenzamide.* ^{13}C NMR($CDCl_3$) δ=11.4(q), 22.9 (t), 41.7(t), 126.6(d,2C), 128.1(d,2C), 130.9(d), 134.5(s), 167.3(s). ^1H NMR (60 MHz) ($CDCl_3$) δ=0.95(t, 3H), 1.63 (Hex,2H), 3.38(q, 2H), 6.38(s, 1H), 7.18—7.88(m, 5H).

N-*Benzylbenzamide.* ^{13}C NMR($CDCl_3$) δ=43.7(t), 127.1(d,2C), 127.4(d,3C), 128.2(d,2C), 128.4(d,2C), 131.2 (d), 134.2(s), 138.4(s), 167.6(s). ^1H NMR(100 MHz) ($CDCl_3$) δ=4.44(d,2H), 7.18(s, 5H), 7.10—7.50(m, 3H), 7.71(m, 3H).

N-*Ethylacetamide.* ^{13}C NMR($CDCl_3$) δ=14.8(q), 23.2 (q), 34.4(t), 170.0(s). ^1H NMR(60 MHz)($CDCl_3$) δ=1.13 (t, 3H), 1.98(s, 3H), 3.27(d of q, 2H), 7.00(s, 1H).

N-*Butyl*-p-*chlorobenzamide.* ^{13}C NMR($CDCl_3$) δ=13.7 (q), 20.1(t), 31.6(t), 39.9(t), 128.4(d,2C), 128.5(d,2C), 133.2 (s), 137.3(3), 166.7(s). ^1H NMR(60 MHz)($CDCl_3$) δ=0.88 (t, 3H), 1.07—1.83(m, 4H), 3.49(q, 2H), 7.10—7.92(m, 5H).

N-*Butylformamide.* ^1H NMR(60 MHz)($CDCl_3$) δ=0.93 (t, 3H), 1.17—1.67(m, 4H), 3.26(q, 2H), 6.40(s, 1H), 8.12 (s, 1H).

N,N-*Dibutylformamide.* ^{13}C NMR($CDCl_3$) δ=13.6(q), 13.8(q), 19.6(t), 20.2(t), 29.4(t), 30.7(t), 41.9(t), 47.2(t), 162.6(d). ^1H NMR(60 MHz)($CDCl_3$) δ=0.93(t, 6H), 1.13—1.77(m, 8H), 3.22(q, 2H), 3.25(q, 2H), 8.00(s, 1H).

N-*Ethylphenylacetamide.* ^{13}C NMR($CDCl_3$) δ=14.4(q), 34.5(t), 43.4(t), 126.9(d), 128.8(d,2C), 129.3(d,2C), 135.6 (s), 171.8(s). ^1H NMR(60 MHz)($CDCl_3$) δ=1.03(t, 3H), 3.22(q, 2H), 3.51(s, 2H), 7.27(s, 6H).

N-*Hexylbenzamide.* ^{13}C NMR($CDCl_3$) δ=14.0(q), 22.5 (t), 26.7(t), 29.6(t), 31.5(t), 40.2(t), 127.0(d,2C), 128.2(d, 2C), 131.0(d), 134.8(s), 167.7(s). ^1H NMR(100 MHz) ($CDCl_3$) δ=0.86(t, 3H), 1.04—1.70(m, 8H), 3.37(q, 2H), 7.36(m, 4H), 7.82(m, 2H). IR(KBr disk) 3335(NH), 1625 (amide I), and 1525 cm^{-1}(amide II). MS, *m/e* 205(M^+). Calcd for $C_{13}H_{19}NO$: C, 76.06; H, 9.33; N, 6.82. Found: C, 76.31; H, 9.19; N, 6.62.

N-*Octylbenzamide.* ^{13}C NMR($CDCl_3$) δ=14.1(q), 22.7 (t), 27.1(t), 29.3(t), 29.4(t), 29.7(t), 31.8(t), 40.2(t), 127.1 (d,2C), 128.2(d,2C), 131.0(d), 134.8(s), 167.7(s). ^1H NMR (60 MHz)($CDCl_3$) δ=0.87(t, 3H), 1.08—1.87(m, 12H), 3.38 (q, 2H), 7.35(m, 4H), 7.85(m, 2H). IR(KBr disk) 3335 (NH), 1625(amide I), and 1525 cm^{-1}(amide II). MS, *m/e* 233(M^+). Calcd for $C_{15}H_{23}NO$: C, 77.21; H, 9.94; N, 6.00. Found: C, 77.08; H, 9.95; N, 5.96.

N-*Dodecylbenzamide.* ^{13}C NMR($CDCl_3$) δ=14.1(q), 22.7(t), 27.1(t), 29.4(t,2C), 29.7(t,5C), 31.9(t), 40.2(t), 127.1(d,2C), 128.2(d,2C), 131.0(d), 134.9(s), 167.7(s). ^1H NMR(60 MHz)($CDCl_3$) δ=0.89(t, 3H), 1.10—1.77(m, 20H), 3.37(q, 2H), 7.31(m, 4H), 7.80(m, 2H). IR(KBr disk) 3335(NH), 1625(amide I), and 1530 cm^{-1}(amide II). MS, *m/e* 289(M^+). Calcd for $C_{19}H_{31}NO$: C, 78.84; H, 10.80; N, 4.84. Found: C, 78.73; H, 10.95; N, 4.71.

N-*Octylacetamide.* ^{13}C NMR($CDCl_3$) δ=14.1(q), 22.8 (t and q, 2C), 27.2(t), 29.4(t), 29.5(t), 29.6(t), 32.0(t), 39.8(t), 170.8(s). ^1H NMR(100 MHz)($CDCl_3$) δ=0.88(t, 3H), 1.29(m, 12H), 1.96(s, 3H), 3.18(q, 2H), 8.04(t, 1H). IR(neat) 3290(NH), 1650(amide I), and 1560 cm^{-1}(amide II). MS, *m/e* 171(M^+). Calcd for $C_{10}H_{21}NO$: C, 70.12; H, 12.36; N, 8.18. Found: C, 70.41; H, 12.56; N, 8.48.

N-*Butylbutanamide.* ^{13}C NMR($CDCl_3$) δ=13.8(q, 2C), 19.4(t), 20.2(t), 31.8(t), 38.5(t), 39.3(t), 173.5(s). ^1H NMR (60 MHz)($CDCl_3$) δ=0.91(t, 3H), 0.93(t, 3H), 1.17—1.91 (m, 6H), 2.17(t, 2H), 3.18(q, 2H), 6.93(s, 1H). IR(neat) 3290(NH), 1640(amide I), and 1550 cm^{-1}(amide II). MS, *m/e* 143(M^+). Calcd for $C_8H_{17}NO$: C, 67.09; H, 11.96; N, 9.78. Found: C, 67.35; H, 12.25; N, 10.02.

N-*Octylbutanamide.* ^{13}C NMR($CDCl_3$) δ=13.8(q), 14.1 (q), 19.4(t), 22.7(t), 26.8(t), 27.1(t), 29.4(t, 2C), 29.8(t), 31.6(t), 31.9(t), 38.6(t), 39.6(t), 173.5(s). ^1H NMR(100 MHz)($CDCl_3$) δ=0.87(t, 3H), 0.94(t, 3H), 1.05—1.82(m, 14H), 2.18(t, 2H), 3.21(q, 2H), 7.12(t, 1H). IR(neat) 3275(NH), 1640(amide I), and 1550 cm^{-1} (amide II). MS, *m/e* 199(M^+). Calcd for $C_{12}H_{25}NO$: C, 72.31; H, 12.64; N, 7.03. Found: C, 72.55; H, 12.81; N, 7.08.

References

1) R. G. Rice and E. J. Kohn, *J. Am. Chem. Soc.*, **77**, 4052 (1955); Y. Sprinzak, *ibid.*, **78**, 3207 (1956).

2) R. Grigg, T. R. B. Mitchell, S. Sutthivaiyakit, and N. Tongpenyai, *J. Chem. Soc., Chem. Commun.*, **1981**, 611; *Tetrahedron Lett.*, **22**, 4107 (1981); S. Murahashi, K. Kondo, and T. Hakata, *ibid.*, **23**, 229 (1982).

3) Y. Watanabe, Y. Tsuji, and Y. Ohsugi, *Tetrahedron Lett.*, **22**, 2667 (1981).

4) Y. Watanabe, Y. Tsuji, and N. Suzuki, *Chem. Lett.*, **1981**, 1067.

5) Y. Sasson and J. Blum, *J. Org. Chem.*, **40**, 1887 (1975); H. Imai, T. Nishiguchi, and K. Fukuzumi, *ibid.*, **41**, 2688 (1976).

6) J. Zabicky, "The Chemistry of Amides," Interscience Publishers, New York (1970), pp. 731—857.

7) E. E. Reid, *Am. Chem. J.*, **45**, 43 (1911).

8) K. Oshima and H. Nozaki, *Tetrahedron Lett.*, **22**, 1605 (1981); K. B. Sharpless, K. Akashi, and K. Oshima, *ibid.*, **1976**, 2503.

9) P. E. Newallis and E. J. Rumannwski, *J. Org. Chem.*, **29**, 3114 (1964).

10) H. E. Zaugg and W. B. Martin, *Org. React.*, **14**, 52 (1965).

11) Butanal(2.3 mmol) was added to the reaction of butanamide (10 mmol) with 1-butanol(5 ml) in the presence

of $RuCl_2(PPh_3)_3$ (0.2 mmol) at 180 °C for 4 h. The conversion of butanamide was 38% and the selectivity of *N*-butylbutanamide was 87%.

12) The mixture of ammonia(20 mmol), 1-butanol(5 ml), and $RuCl_2(PPh_3)_3$(0.2 mmol) was heated at 180 °C for 4 h in a 50 ml stainless steel autoclave. Tributylamine was produced in 16% yield(based on ammonia); dibutylamine was detected in only 1% yield and butylamine was not obtained.

13) The mixture of butyl formate(10 mmol), tributylamine (10 mmol), 1-butanol(5 ml), $RuCl_2(PPh_3)_3$(0.2 mmol), and H_2O(10 mmol) was heated at 180 °C for 24 h. The reaction did not proceed.

14) M. A. Kraus, *Synthesis*, **1973**, 361.

15) The reaction of formamide(10 mmol), with tributylamine(10 mmol) in 1-butanol(5 ml) in the presence of $RuCl_2(PPh_3)_3$(0.2 mmol) was carried out at 180 °C for 24 h under argon in a 50 ml stainless steel autoclave. *N*,*N*-Dibutylformamide(4.0 mmol) and tributylamine(13 mmol) were detected after reaction.

16) P. S. Hallman, T. A. Stephenson, and G. Wilkinson, *Inorg. Synth.*, **12**, 237 (1970).

17) P. S. Hallman, B. R. McGarvey, and G. Wilkinson, *J. Chem. Soc., A*, **1968**, 3142.

18) N. Ahmad, J. J. Levison, S. D. Robinson, and M. F. Uttley, *Inorg. Synth.*, **15**, 45 (1974).

19) R. Young and G. Wilkinson, *Inorg. Synth.*, **17**, 75 (1977).

20) J. A. Osborn and G. Wilkinson, *Inorg. Synth.*, **10**, 67 (1967).

21) V. I. Stenberg, S. P. Singh, and N. K. Narain, *J. Org. Chem.*, **42**, 2244 (1977).

22) M. Nojima, S. Hasegawa, and N. Tokura, *Bull. Chem. Soc. Jpn.*, **46**, 1254 (1973).

23) Sadtler Standard NMR Spectra, Spectral number 17948 M.

24) Sadtler Standard NMR Spectra, Spectral number 146 M.

25) D. J. Calvert and C. J. O'Connor, *Aust. J. Chem.*, **32**, 337 (1979).

26) I. Ojima and S. Inaba, *J. Organomet. Chem.*, **140**, 97 (1977).

27) Sadtler Standard NMR Spectra, Spectral number 21466 M.

28) R. Delaby, P. Reynaud, and F. Lilly, *Bull. Soc. Chim. Fr.*, **1961**, 2067.

The Synthesis and Reaction of Spiro[oxolane-2,2′-piperazine]-3′,6′-diones with *N*-Bromosuccinimide in the Presence or Absence of Water

Chung-gi Shin,* Yoshiaki Sato, Seiji Honda, and Juji Yoshimura†

Laboratory of Organic Chemistry, Faculty of Technology, Kanagawa University, Rokkakubashi, Kanagawa-ku, Yokohama 221

† *Laboratory of Chemistry for Natural Products, Faculty of Science, Tokyo Institute of Technology, Nagatsuta, Midori-ku, Yokohama 227*

(Received January 26, 1983)

The compound 3-(3-hydroxy)propylidene-piperazine-2,5-dione, derived from ethyl 4-ethoxycarbonyl-2-chloroacetylamino-2-butenoate, was treated with *N*-bromosuccinimide (NBS) in chloroform to give the spiro-[oxolane-2,2′-piperazine]-3′,6′-dione derivative. The spiro compound was further treated with NBS in water to give the corresponding spiro[oxolane-2,2′-piperazine]-3′,5′,6′-trione and -3′,6′-dione-5′-ol. The latter compound and a new spiro-5′,6′-dione-3′-ol derivative were also obtained by the reduction of the spiro-3′,5′,6′-trione. The structural confirmation of all the new products is discussed.

Bicyclomycin, which has been produced by *Streptomyces (St.) sapporonensis*[1] and *St. aizunenensis*,[2] was degraded with various acids by heating to give the dispiropiperazinedione derivatives.[3] Although the total synthesis of bicyclomycin is very attractive and much attention has by now been devoted to the bioactivity, the chemistry of the degradation products, spiro- or dispiro-piperazinedione derivatives, are also very interesting. There have been a few reports on the synthesis of the spiro derivatives by three routes,[3–5] but the synthesis and the reaction have not been investigated in detail.

Previously, we reported briefly the synthesis of 3-(3-hydroxy)propylidene-piperazine-2,5-dione (**3a**) and its conversion into the corresponding spiro[oxolane-2,2′-piperazine]-3′,6′-dione {[oxolane-2,2′-piperazine]-3′,6′-dione=PDO} derivatives.[6] Here, we wish to report in detail the synthesis of the various spiro-PDO derivatives by the reaction of **3a** with NBS, followed by the hydrogenolysis and further reaction with NBS, in water. Moreover, the structural confirmation of the spiro-PDO is discussed.

Results and Discussion

Synthesis of 3-Alkylidene-piperazine-2,5-dione. According to the method reported previously,[7] ethyl 4-ethoxycarbonyl-2-oxobutanoate was condensed with chloroacetamide in benzene in the presence of a mixture of $POCl_3$ and concentrated H_2SO_4 under reflux to give the starting ethyl 4-ethoxycarbonyl-(*Z*)-2-chloroacetylamino-2-butenoate (**1**) in a 57% yield. After the halogen-exchange reaction of **1** with potassium iodide,[8,9] the resulting 2-iodoacetylamino derivative was immediately cyclized with benzylamine to give 1-benzyl-3-(2-ethoxycarbonyl)ethylidene-piperazine-2,5-dione (**2**) in an 80% yield. By the usual method, the subsequent selective reduction of exocyclic 2-ethoxycarbonyl group of **2** with $LiAlH_4$ in THF was achieved to give the expected **3a** in a 60% yield.

In order to ascertain and to protect the 3-hydroxyl group, the **3a** compound was subjected to acylation and alkylation, followed by the addition of methanol to the exocyclic carbon-carbon double bond. The acetylation and the benzoylation of **3a** with acetic anhydride and with benzoyl chloride, in the usual ways, gave 1-benzyl-3-(3-acetoxy)- and -(3-benzoyloxy) propylidene-piperazine-2,5-diones (**3b** and **3c**) in 82 and 86% yields respectively. On the other hand, the alkylation of **3a** with 2,3-dihydropyrane gave 1-benzyl-3-(3-tetrahydropyrane-2-yloxy)propylidene-piperazine-2,5-dione (**3d**) in an 82% yield. Furthermore, the **3a,b,d** compounds thus obtained were treated with methanol in the presence of NBS to give the corresponding 1-benzyl-3-(1-bromo)alkyl-3-methoxy-piperazine-2,5-dione derivatives (**4a,b,d**) in *ca.* an 88% yield. Subsequently, the catalytic hydrogenolysis of **4b,d** with 10% Pd/C in the presence of triethylamine was carried out to give the corresponding 1-benzyl-3-alkyl-3-methyl-piperazine-2,5-dione derivatives (**5b,d**) in *ca.* a 78% yield.

The characteristic absorption of the IR spectra, the chemical shifts, and the coupling constants of **2** and **3** were assigned as is shown in Table 1. In the NMR spectra, the signals of the olefinic protons appeared in the δ 6.30 and δ 6.18—6.26 regions as a triplet, while the β-alkyl protons were shifted to the δ 3.26 and δ 2.40—2.64 regions. From the comparison of the NMR spectral data of **2** and **3** with that of the *E*-isomer of the α-dehydroamino acid ester and its cyclic dipeptide derivative prepared by us,[10] Compounds **1**, **2**, and **3** could be readily confirmed to have a *(Z)*- geometric structure. In addition, the IR and NMR spectral data of **4** and **5** are summarized in Table 2.

Synthesis of Spiro-PDO Derivatives. In order to synthesize the desired spiro-PDO derivatives, Compound **3a** was led to cyclization by the intramolecular addition of the 3-hydroxylpropylidene group to the exocyclic carbon-carbon double bond. The treatment of **3a** with NBS in chloroform gave a viscous syrup, which was found to consist of two stereoisomers. From the spectral data and the satisfactory elemental analysis of the two kinds of crystals separated, the new products were identified as 4′-benzyl-3-bromospiro-PDO (**6a** and **6b**) as diastereomers in an 86% total yield. The catalytic hydrogenolysis of each isomer with 10% Pd/C in methanol gave exactly the same crystals as these identified as 4′-benzyl-spiro-PDO (**7**) in a 91% yield from **6a** and in a 90% yield from **6b**. Subsequently, the prolonged catalytic redution of **7** for 24 h was found to give 1-benzyl-3-(3-hydroxy) propyl-

Table 1. 4-Benzyl-3-alkylidene-piperazine-2,5-dione derivatives (**2** and **3**)

Compd No.	Yield %	Mp θ_m/°C	Formula	Found (Calcd) (%) C	H	N	IR, $\tilde{\nu}$/cm^{-1} in KBr NH	C=C	NMR, δ in $CDCl_3$ -CH= (J_{Hz})	NH
2	79	131—132[a]	$C_{16}H_{18}N_2O_4$	63.74 (63.56	5.88 6.00	9.05 9.26)	3200,	1635	6.30 (7.5),	9.76
3a	60	130—131[b]	$C_{14}H_{16}N_2O_3$	64.66 (64.60	6.14 6.20	10.68 10.76)	3200,	1630	6.25 (8.0),	9.62
3b	82	127—128[c]	$C_{16}H_{18}N_2O_4$	63.56 (63.56	5.99 6.00	9.21 9.26)	3190,	1640	6.18 (8.0),	9.56
3c	86	146—147[c]	$C_{21}H_{20}N_2O_4$	69.32 (69.21	5.57 5.53	7.46 7.69)	3180,	1640	6.26 (8.0),	9.76
3d	83	90— 91[d]	$C_{19}H_{24}N_2O_4$	66.20 (66.26	7.14 7.02	8.13 8.13)	3230,	1620	6.25 (8.0),	9.22

a) Colorless needles from ethanol. b) Colorless prisms from ethyl acetate. c) Colorless needles from ethyl acetate. d) Colorless needles from dibutyl ether.

Table 2. 3-Alkyl-4-benzyl-piperazine-2,5-dione derivatives (**4** and **5**)

Compd No.	Yield %	Mp θ_m/°C	Formula	Found (Calcd) (%) C	H	N	IR, $\tilde{\nu}$/cm^{-1} [d] NH (OH)	NMR, δ in $CDCl_3$ -CH- (-CH_2-) (J_{Hz})	NH
4a	85	173—174[a]	$C_{15}H_{19}N_2O_4Br$	48.63 (48.53	5.06 5.16	7.61 7.55)	3170 (3380)	4.70 dd (2.0, 11.0)	9.05
4b	96	syrup	$C_{17}H_{21}N_2O_5Br$	49.71 (49.40	4.98 5.12	6.89 6.78)	3200	4.60 m	8.24
4d	81	syrup	$C_{20}H_{27}N_2O_5Br$	52.98 (52.75	6.11 5.98	6.35 6.15)	3200	4.82 m	8.04 8.11
5b	94	syrup	$C_{17}H_{22}N_2O_5$	61.32 (61.06	6.85 6·63	8.13 8.38)	3200	(1.6—2.3)[b]	8.00
5c	87	syrup	$C_{20}H_{28}N_2O_5$	64.02 (63.81	7.38 7.50	7.74 7.44)	3200	(1.4—2.3)[c]	7.90

a) Colorless needles from methanol. b) 4H. c) 10H. d) Measured in KBr.

Table 3. 4′-Benzylspiro[oxolane-2,2′-piperazine]-3′,6′-dione derivatives (**6—14**)

Compd No.	Yield %	Mp θ_m/°C	Formula	Found (Calcd) (%) C	H	N	IR, $\tilde{\nu}$/cm^{-1} [e] NH OH	NMR, δ in $CDCl_3$ -CHBr- [-CHOH-] (J_{Hz})	OH
6a	61	142—143	$C_{14}H_{15}N_2O_3Br$	49.49 (49.57	4.39 4.46	8.24 8.26)	3270	5.05 dd (7.5, 8.0)	
6b	25	150—151	$C_{14}H_{15}N_2O_3Br$	49.56 (49.57	4.50 4.46	8.17 8.26)	3180	4.28 dd (3.0, 9.5)	
7	91[a] 90[b]	94—95	$C_{14}H_{16}N_2O_3$	64.51 (64.60	6.25 6.20	10.59 10.76)	3200	—	
8	80	68—69	$C_{15}H_{18}N_2O_3$	65.74 (65.67	6.62 6.61	10.12 10.21)	—	—	
9a	56	139—140	$C_{14}H_{16}N_2O_3$	60.69 (60.86	5.79 5.84	10.03 10.14)	3230	[4.86 dd] (1.0, 11.0)	4.50 d
9b	9	135—136	$C_{14}H_{16}N_2O_4$	60.98 (60.86	5.88 5.84	9.92 10.14)	3220	[5.07 d] (4.0)	5.15 d
10a	20[c] 19[d]	134—135	$C_{15}H_{18}N_2O_4$	62.02 (62.05	6.28 6.25	9.68 9.65)	3130	[4.93 d] (9.0)	4.83 d
10b	28	123—124	$C_{15}H_{18}N_2O_4$	62.03 (62.05	6.25 6.25	9.42 9.65)	3270	[4.98 d] (5.0)	6.41 d
11	34	156—157	$C_{14}H_{14}N_2O_4$	61.22 (61.31	5.13 5.15	9.93 10.21)	3230	—	
12	40	129—130	$C_{15}H_{16}N_2O_4$	62.70 (62.49	5.61 5.59	9.73 9.72)	—	—	
13	86	209—210	$C_{14}H_{16}N_2O_4$	60.52 (60.86	5.80 5.84	10.07 10.14)	3350	[4.58 d] (7.0)	7.00 d
14	68	222—223	$C_{15}H_{18}N_2O_4$	62.17 (62.05	6.24 6.25	9.48 9.65)	3300	[4.60 d] (6.0)	6.63 d

a) Yield from **6a**. b) Yield from **6b**. c) Yield from **8**. d) Yield from **12**. e) Measured in KBr.

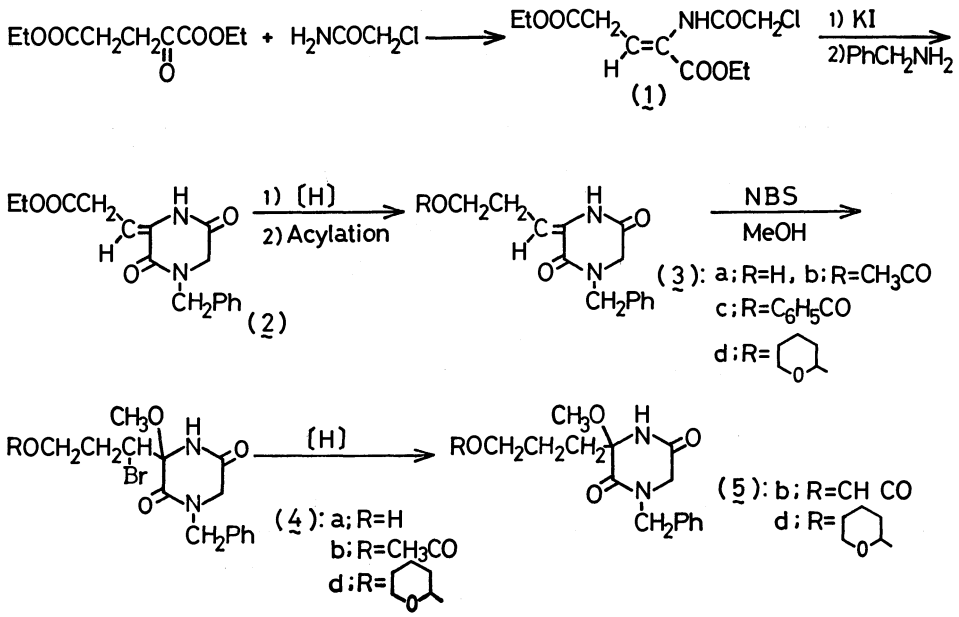

Scheme 1.

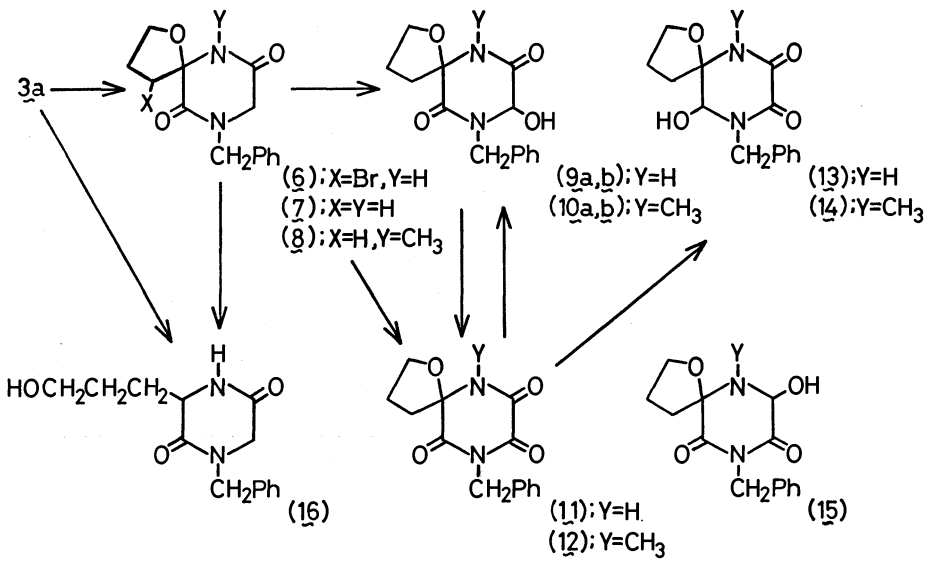

Scheme 2.

piperazine-2,5-dione (**16**) in a 64% yield, by the carbon-oxygen bond fission of the spiro ring. Compound **16** was entirely in agreement with the product prepared independently by the hydrogenation of **3a** with 10% Pd/C.

When Compound **7** was further treated with NBS in a mixture of water and chloroform, three kinds of products were obtained in fairly good yields. Based on the NMR spectral data, the compound from the first fraction was confirmed to be 4′-benzyl-spiro [oxolane-2,2′-piperazine]-3′,5′,6′-trione (**11**) in a 31% yield; the other two kinds of compounds, which were stereoisomers with each other, were obtained from the second and the final fractions in 51% and 10% yields respectively. The two stereoisomers separated were also characterized as 4′-benzyl-spiro[oxolane-2,2′-piperazine]-3′,6′-dione-5′-ol (**9a** and **9b**).

In order to generalize the above reactions, after the methylation of the 1′-position of **7** with methyl iodide, according to a method previously reported by us,[9] the resulting 4′-benzyl-1′-methylspiro-PDO (**8**) was similarly treated with NBS in water. The expected corresponding 1′-methylspiro-3′,5′,6′-trione derivative (**12**) was obtained in a 40% yield, while 1′-methylspiro-3′,6′-dione-5′-ol derivatives (**10a** and **10b**) as diastereomers were also obtained in 20 and 28% yields respectively. The subsequent reduction of the 1′-methyl trione derivative (**12**) with $NaBH_4$ in methanol was carried out to give another new compound (**14**) with **10a** in a 19% yield. Moreover, the similar reduction of **11** was worked up to also give a new compound (**13**) alone.

The structural assignment and the conformational analysis of **6**—**13** and **14** have also been elucidated

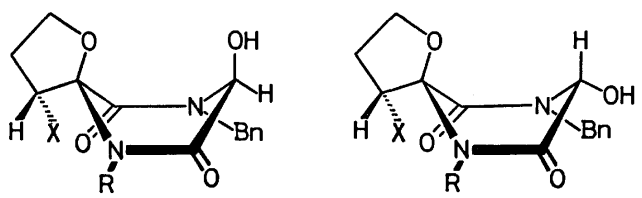

Fig. 1.

from their spectroscopic data and satisfactory elemental analyses (see Table 3). Consequently, the two new compounds could be readily identified as 4′-benzyl- and 4′-benzyl-1′-methylspiro[oxolane-2,2′-piperazine]-5′,6′-dione-3′-ol (**13** and **14**) in 86 and 68% yields respectively, not the spiro[oxolane-2,2′-piperazine]-3′,5′-dione-6′-ol derivative (**15**).

In the NMR spectrum of **6**, the chemical shift of the 3-proton on the spiro ring is in the δ 5.05 (**6a**; J=7.5 Hz) and δ 4.28 (**6b**; J=3.0 Hz, J=7.5 Hz) regions as a double doublet. On the other hand, the 3-proton signals on the spiro ring of **7**, derived from both **6a** and **6b**, also appeared in the δ 2.7—3.1 and δ 1.7—2.3 regions as splitting multiplets. This fact indicates that the spiro-PDO structure is maintained during the hydrogenolysis. From the above results, it may be supposed that one proton of the 3-position on the spiro ring of **6a** and **7** resonating in the lower magnetic field is due to the coplanar interaction between the 3-proton and the 3′-carbonyl groups on the boat structural piperazine-2,5-dione ring. Accordingly, it is assumed that all the spiro compounds obtained here have the boat structure, as is illustrated in Fig. 1. In fact, the Dreiding model of the spiro-PDO structure and the following facts further support the above presumption. In addition, the NMR spectrum of **9a** showed a long-range coupling at δ 4.86 (6-H, $J_{4,6}$=1.0 Hz, $J_{6,OH}$=11.0 Hz) as a double doublet, due to the *W*-letter relationship between two protons at the 3- and 5′-positions. On the other hand, in the NMR spectrum of **9b**, the signal at δ 5.05 (6-H, $J_{6,OH}$= 4.0Hz), appearing as only a doublet, is attributable to the two protons between 5′-H and the hydroxyl group. By a comparison of the chemical shifts and the coupling constants, the orientation of the hydroxyl group of **9a** appearing at an upper magnetic field was determined to be axial and that of **9b** at a lower field, to be equatorial, as is illustrated in Fig. 1. Similarly, based on the above results, the orientation of the hydroxyl group of **10a** appearing at a comparatively high field (δ 4.93, d, J=9.0 Hz) was also confirmed to be axial, and that of **10b** at a lower field (δ 4.94, d, J=6.0 Hz and J=7.0 Hz), to be equatorial. Furthermore, since the NMR spectrum of **13** showed a long-range coupling (J=1.0Hz) at δ 4.58 between 3′- and 1′-protons, the orientation of the hydroxyl group at the 3′-position could be unambiguously inferred to be axial.

Consequently, even if the spiro-PDO derivatives were transformed to the piperazine-3′,5′,6′-trione and -3′,6′-dione-5′-ol, the spiro and the boat conformational structures were found to be maintained.

Experimental

All the melting and boiling points are uncorrected. The IR spectra were recorded with a Hitachi EPI-G3 Spectrometer. The NMR spectra were measured with a JNM-PS-100 Spectrometer (Japan Electron Optics Laboratory Co., Ltd.,), using tetramethylsilane as the internal standard.

Starting Material. Compound **1** was prepared by the condensation of ethyl 4-ethoxycarbonyl-2-oxobutanoate (70 g, 347 mmol) with chloroacetamide (36 g, 385 mmol) in the presence of $POCl_3$ (7 ml) and concentrated H_2SO_4 (3 ml), according to the method reported previously.[7] Yield, 57%; bp 162—164 °C/2 mmHg (1 mmHg≈133.322 Pa). IR (KBr): 3280, 1730, 1690, 1515 cm^{-1}. NMR ($CDCl_3$): δ 6.94 t, 7.36 t (-CH=, J=7.0 Hz), 8.28 and 8.68 (NH), Found: C, 47.78; H, 6.02; N, 4.88%. Calcd for $C_{11}H_{16}NO_5Cl$: C, 47.57; H, 5.81; N, 5.04%.

Preparation of 2. After the halogen exchange of **1** (3.0 g, 10.81 mmol) with potassium iodide,[8,9] into the resulting solution in ethanol (40 ml), we stirred benzylamine (2.9 g, 27.03 mmol) in, drop by drop, at room temperature for 2 h. The crystals thus precipitated were collected and recrystallized from ethanol to give **2** as colorless needles.

Preparation of 3a. Into a mixture of $LiAlH_4$ (200 mg, 5.3 mmol) in THF (30 ml), we stirred a solution of **2** (1.0 g, 3.3 mmol) in THF (30 ml) at −10 °C. After treating the excess $LiAlH_4$ in the solution with 1 M HCl (1M= 1 mol dm^{-3}), the insoluble substance was filtered off, and then the filtrate was concentrated. The crude residual syrup was purified on a silica-gel column, using a mixture of $CHCl_3$ and ethanol (30 : 1 v/v) as the eluent. After the eluted fraction had been concentrated, the crystalline residue was recrystallized from ethyl acetate to give **3a** as colorless prisms.

Preparation of 3b—d. Into a solution of **3a** (200 mg, 0.769 mmol) in pyridine (3 ml), we stirred acetic anhydride (100 mg, 0.980 mmol) at room temperature for 3 h. The resulting solution was poured into CH_2Cl_2 (30 ml) and washed successively with 3 M HCl and water, and then dried over anhydrous Na_2SO_4. The removal of the solvent gave crude crystals, which were recrystallized from ethyl acetate to give **3b** as colorless needles.

In a similar manner, a solution of **3a** (1.0 g, 3.85 mmol) and benzoyl chloride (650 mg, 4.62 mmol) in pyridine (3 ml) was worked up under cooling for 1 h to give crystals. The subsequent recrystallization of the crystals from ethyl acetate gave **3c** as colorless needles.

Similarly, a mixture of **3a** (520 mg, 2.0 mmol), 3,4-dihydro-2*H*-pyran (346 mg, 4.0 ml), and *p*-toluenesulfonic acid (4 mg) in CH_2Cl_2 (10 ml) was worked up at room temperature for 6 h to give crystals. Recrystallization from dibutyl ether gave **3d** as colorless needles.

Preparation of 4a, 4b, and 4d. Into a solution of **3d** (770 mg, 2.23 mmol) in methanol (30 ml), we stirred NBS (438 mg, 2.46 mmol) at room temperature for 10 min. The subsequent removal of the solvent gave crude crystals, which were collected and then washed with water. The recrystallization of the crystals from methanol gave **4a** as colorless needles.

In a similar manner, a mixture of **3b** (1.6 g, 5.30 mmol) and NBS (943 mg, 530 mmol) in methanol (40 ml) was worked up to give a syrupy residue. The residue was dissolved in $CHCl_3$ (30 ml), and the resulting solution was washed twice with water and then dried over anhydrous Na_2SO_4. The removal of the solvent gave a viscous oil,

which was purified on a silica-gel column, using a mixture of $CHCl_3$ and acetone (20 : 1 v/v), to give **4b** as a viscous syrup.

Similarly, a mixture of **3d** (600 mg, 1.74 mmol) and NBS (310 mg, 1.74 mmol) in methanol (30 ml) gave **4c** as a viscous syrup.

*Preparation of **5b** and **5c**.* A solution of **4b** (1.9 g, 4.60 mmol) in methanol (50 ml) in the presence of triethylamine (500 mg, 4.95 mmol) was hydrogenolyzed with 10% Pd/C (200 mg) at room temperature for 15 min. After the Pd/C had been filtered off, the resulting solution was concentrated to give residual syrupy crystals, which were dissolved in CH_2Cl_2 (50 ml). The solution was washed twice with water and then dried over anhydrous Na_2SO_4. After the removal of the solvent, the residual oil was purified on a silica-gel column, using a mixture of $CHCl_3$ and acetone (15 : 1 v/v) as the eluent. The fraction thus obtained was concentrated to give **5b** as a viscous syrup.

In a similar manner, a solution of **4d** (900 mg, 1.98 mmol) and potassium *t*-butoxide (244 mg, 2.18 mmol) in methanol (50 ml) was worked up to give **5d** as a viscous syrup.

*Preparation of **6**.* Into a solution of **3a** (800 mg, 3.08 mmol) in $CHCl_3$ (20 ml), we stirred NBS (548 mg, 3.08 mmol) at room temperature for 10 min. The resulting solution was washed twice with water, dried over anhydrous Na_2SO_4, and then concentrated. The residual syrup thus obtained was chromatographed on a silica-gel column, using a mixture of $CHCl_3$ and acetone (25 : 1 v/v) as the eluent. From the two fractions thus separated, two diastereomeric isomers, **6a**,**b**, were obtained. The first fraction was concentrated to give crude crystals, which were then recrystallized from ethanol to give **6a** as colorless needles. Similarly, the second fraction gave **6b** as colorless needles from benzene.

*Preparation of **7**.* A solution of **6a** and **6b** (560 mg, 1.65 mmol) in methanol (50 ml) in the presence of triethylamine (170 mg, 1.68 mmol) was hydrogenolyzed with 10% Pd/C (60 mg) at room temperature for 20 min. After the removal of the Pd/C, the reaction solution was concentrated and the residue thus obtained was dissolved in CH_2Cl_2 (20 ml). The resulting solution was washed twice with water and then dried over anhydrous Na_2SO_4. The evaporation of CH_2Cl_2 gave crystals, which were subsequently recrystallized from diethyl ether to give **7** as colorless needles.

*Preparation of **8**.* Into a solution of **7** (500 mg, 1.92 mmol) in THF (20 ml), we stirred 55% NaH (84 mg, 1.92 mmol) at room temperature. After the evolution of hydrogen had ceased in a few minutes, we stirred methyl iodide into the resulting solution at room temperature for 6 h. The reaction solution was neutralized with acetic acid and then concentrated. The residue thus obtained was dissolved in $CHCl_3$ (30 ml), and the resulting solution was washed with water and then dried over anhydrous Na_2SO_4. After the removal of the $CHCl_3$, the residue was purified on a silica-gel column, using a mixture of $CHCl_3$ and acetone (15 : 1 v/v) as the eluent. The concentration of the fraction gave crystals, which were subsequently recrystallized from diethyl ether to give **8** as colorless needles.

*Preparation of **9** and **11**.* Into a solution of **7** (1.0 g, 3.85 mmol) in $CHCl_3$ (30 ml) and water (3 ml), we stirred NBS (690 mg, 3.85 mmol) at room temperature for 3 h. The $CHCl_3$ layer was separated, washed with water, and finally dried over anhydrous Na_2SO_4. After the removal of the $CHCl_3$, the residue was chromatographed on a silica-gel column, using a mixture of $CHCl_3$ and acetone (15 : 1 v/v) as the eluent. Three fractions were obtained, and then each fraction was concentrated. The first fraction gave **11** as colorless prisms from a mixture of benzene and hexane, while the second and third fractions gave **9a** as colorless needles from CCl_4 and **9b** as colorless prisms from benzene respectively.

*Preparation of **10** and **12**.* In a similar manner, the treatment of **8** (820 mg, 2.99 mmol) in a mixture of $CHCl_3$ (30 ml) and water (5 ml) with bromine (580 mg, 3.62mmol) was worked up for 6 h to give three fractions. The first fraction gave colorless needles **12** from a mixture of benzene and hexane. The second and the third fractions gave colorless needles **10a** and **10b** from benzene-hexane.

Moreover, similarly, in the case of the reaction of **8** (1.35 g, 4.93 mmol) with *ca.* two moles of NBS (1.8 g). Compound **12** alone was obtained in *ca.* a 92% yield.

*Reduction of **11**.* Into a mixture of **11** (1.2 g, 4.17 mmol) in methanol (50 ml), we stirred $NaBH_4$ (160 mg, 4.21 mmol), portion by portion, under cooling for 10 min. After a few drops of acetic acid had been added and the methanol evaporated, the residue thus obtained was chromatographed on a silica-gel column, using a mixture of $CHCl_3$ and ethanol (15 : 1 v/v) as the eluent. From the first fraction, Compound **9a** was obtained, while the second fraction gave **13** as colorless prisms from ethanol.

*Reduction of **12**.* A similar hydrogenation of **12** was worked up to give **10a** and **14**.

*Preparation of **16**.* *From **7***: The catalytic reduction of **7** (360 mg, 1.38 mmol) with 10% Pd/C (70 mg) in methanol (50 ml) at room temperature overnight, and the concentration of the resulting solution, gave **16** as colorless needles from ethyl acetate. Yield, 64%; mp 103—104 °C. IR (KBr): 3500, 3200, 1670, 1640 cm^{-1}. NMR ($CDCl_3$): δ 1.4—1.2 m (-CH_2-, 4H), 4.10 m (3-H), 3.82 (OH), 8.12 (NH). Found: C, 64.20; H, 6.99; N, 10.58%. Calcd for $C_{14}H_{18}N_2O_3$: C, 64.10; H, 6.92; N, 10.68%.

*From **3a***: In a similar manner, the reduction of **3a** (500 mg, 1.93 mmol) with 10% Pd/C (50 mg) in methanol (50 mg) was worked up for 20 min to give **16** in a 93% yield.

References

1) T. Miyoshi, N. Miyairi, H. Aoki, M. Kohsaka, H. Sakai, and H. Imanaka, *J. Antibiot.*, **25**, 569 (1972).

2) S. Miyamura, N. Ogasawara, H. Otsuka, S. Niwayama, H. Tanaka, T. Take, T. Uchiyama, H. Ochiai, K. Abe, K. Koizumi, K. Asao, K. Mitsuki, and T. Hoshino, *J. Antibiot.*, **25**, 610 (1972); S. Miyamura, N. Ogasawara, H. Otsuka, S. Niwayama, H. Tanaka, T. Take, T. Uchiyama, and H. Ochiai, *ibid.*, **26**, 479 (1973).

3) H. Maag, J. F. Blount, D. L. Coffen, T. V. Steppe, and F. Wong, *J. Am. Chem. Soc.*, **100**, 6786 (1978).

4) S. Nakatsuka, K. Yoshida, and T. Goto, *Tetrahedron Lett.*, **22**, 2009 (1981).

5) T. Fukuyama, B. D. Robins, and R. A. Sachleben, *Tetrahedron Lett.*, **22**, 4155 (1981).

6) C. Shin, Y. Sato, and J. Yoshimura, *Tetrahedron Lett.*, **22**, 2401 (1981).

7) C. Shin, M. Fujii, and J. Yoshimura, *Tetrahedron Lett.*, **1971**, 2499; C. Shin, K. Sato, A. Ohtsuka, K. Mikami, and J. Yoshimura, *Bull. Chem. Soc. Jpn.*, **46**, 3876 (1973).

8) C. Shin, Y. Sato, H. Ohmatsu, and J. Yoshimura, *Bull. Chem. Soc. Jpn.*, **54**, 1137 (1981).

9) C. Shin, Y. Sato, M. Hayakawa, M. Kondo, and J. Yoshimura, *Heterocycles*, **16**, 1573 (1981).

10) C. Shin, M. Hayakawa, T. Suzuki, A. Ohtsuka, and J. Yoshimura, *Bull. Chem. Soc. Jpn.*, **51**, 550 (1978).

The Reaction of Sulfur Dioxide with Thiols Catalyzed by Boron Trifluoride Etherate. Evidence for a Possible Intervention of Dithiosulfite as a Reaction Intermediate

Fuminori Akiyama

Chemical Research Institute of Non-Aqueous Solutions, Tohoku University, Sendai 980

(Received February 21, 1983)

The reaction of sulfur dioxide (SO_2) with 1-propanethiol (NPT), 2-propanethiol (IPT), or 2-methyl-2-propanethiol (TBT) catalyzed by boron trifluoride ethrate (BF_3OEt_2) was investigated. The ratios of dialkyl trisulfide to dialkyl disulfide obtained (RSSSR/RSSR) at an early stage of the reaction were larger than 1 for the reaction of TBT and less than 1 for the reaction of NPT or IPT. The reaction of dithiosulfites with BF_3OEt_2 in the presence or absence of thiol was investigated. From a consideration of the similarity of the composition of the sulfides formed in the reaction of dithiosulfites with BF_3OEt_2 to those in the reaction of SO_2 with thiol in the presence of BF_3OEt_2, the possibility of the intervention of dithiosulfite as a reaction intermediate in the reaction of SO_2 with thiol was discussed.

In previous papers it was reported that the reaction of SO_2 with 1-alkanethiols took place in the presence of tertiary amine or acids.[1] The reaction of SO_2 with thiols catalyzed by triethylamine or pyridine proceeded to only a small extent for the reaction of thiols with a secondary alkyl group adjacent to the SH group, and scarcely occurred for the reaction of thiols with a tertiary alkyl group.[2] The reaction mechanism of the reaction of SO_2 with thiols has not yet been elucidated, although a mechanism including dithiosulfite as one of the reaction intermediates has been proposed in previous papers.[1a,c] In the present report it is reported that the reaction of SO_2 with not only 1-alkanethiols, but also with thiols having a secondary or tertiary alkyl group, occurs in the presence of BF_3OEt_2. Also, evidence which suggests the possible intervention of dithiosulfite as one of the reaction intermediates is presented.

Results and Discussion

The yields of the products of the reaction of SO_2 with NPT, IPT, or TBT in the presence of BF_3OEt_2 are shown in Table 1. In this table the ratios of trisulfide to disulfide are calculated, and the decrease in the proportion of trisulfide and the increase in the proportion of disulfide as the reaction proceeds are shown. Since the reason for these changes was considered to be the disproportionation of the trisulfide formed, the reactions of dialkyl trisulfides with BF_3OEt_2 were carried out; the change in the composition with the reaction time is shown in Fig. 1. Contrary to the reported result in the literature that the homolitical disproportionation reaction of dialkyl trisulfide gave equal amounts of dialkyl di- and tetrasulfide,[3] Fig. 1 shows that the value of RSSSSR/RSSR given in the disproportionation by BF_3OEt_2 is in the order of R= *t*-Bu (0.7)>*i*-Pr (0.6)>*n*-Pr (0.3). In the reaction of dialkyl trisulfide with BF_3OEt_2, presumably not only the disproportionation of trisulfide to give di- and tetrasulfide, but also the removal of the sulfur atom from trisulfide to give disulfide preferentially, occurs. It is well known that the removal of sulfur atom from trisulfide to give disulfide occurs in the reaction of trisulfide with triphenylphosphine.[4] Table 1 indicates that the yields of tetrasulfide for the reactions of three sorts of thiols with SO_2 for a prolonged reaction time are in the order of R=*t*-Bu>*i*-Pr>*n*-Pr, which is same as that of the reaction shown in Fig. 1, although, the absolute amount of tetrasulfide is larger in Fig. 1 than in Table 1 because the reactions in Fig. 1 are carried out using pure trisulfide, while in the reactions in Table 1 trisulfide increases as the reaction proceeds. Therefore, the change in the composition of three sulfides during the reaction of SO_2 with thiol may be attributed to the disproportionation reaction of the

Table 1. Yields of the dialkyl sulfides from the reaction of SO_2 with alkanethiols in the presence of BF_3OEt_2 at 25 °C[a]

RSH	BF_3OEt_2 (mmol)	Reaction time / h	RSH (residual) (%)	Sulfides formed[b] RSSR (%)	RSSSR (%)	RSSSSR (%)	Total (%)	RSSSR/RSSR
n-PrSH	2	72	70.5	15.8	14.4	0	101	0.87
	20	0.4	36.2	33.7	29.5	0	99	0.87
	20	24	4.0	55.1	32.6	2.0	94	0.59
i-Pr	2	72	74.8	13.5	13.5	0	102	1.0
	20	0.4	84.1	7.7	6.0	0	98	0.78
	20	24	8.4	50.5	33.1	3.7	96	0.65
t-BuSH	2	72	79.0	1.0	1.8	6.8	89	1.80
	20	2.2	70.3	7.7	14.7	Trace	93	1.90
	20	48	5.7	39.6	32.2	10.2	88	0.81

a) 40 mmol of thiol and 20 mmol of SO_2 were used. b) 100× (mol of product)/0.5× (mol of thiol used).

Table 2. Yields of the dialkyl sulfides in the reaction of dialkyl dithiosulfites with BF_3OEt_2 in the presence or absence of thiol at 25 °C[a]

Entry	O RSSSR (mmol)	RSH (mmol)	BF_3OEt_2 (mmol)	Sulfides formed[b] RSSR (mmol)	RSSSR (mmol)	RSSSSR (mmol)
1	R=Pr^i, 1	2	1	0.95	0.98	Trace
2	Pr^i, 1	0	1	0.44	0.21	0.09
3	R=Bu^t, 1	2	1	0.68	0.96	Trace
4[c]	Bu^t, 1	0	1	0.056	0.28	0.15[d]

a) Average values of two runs for each experiment are listed. The reactions were carried out in 2.9 ml of the CH_2Cl_2 solution. Although all of the dithiosulfite was consumed immediately after the addition of BF_3OEt_2, analyses were done 3 min after the addition of BF_3OEt_2 (The compositions did not depend on when analyses were done for several minutes after addition). b) No polysulfides higher than tetrasulfide were observed. c) Isobutene was identified in the gas over the reaction mixture. d) A explanation of the formation of the considerable amount of tetrasulfide is presented in Ref. 8.

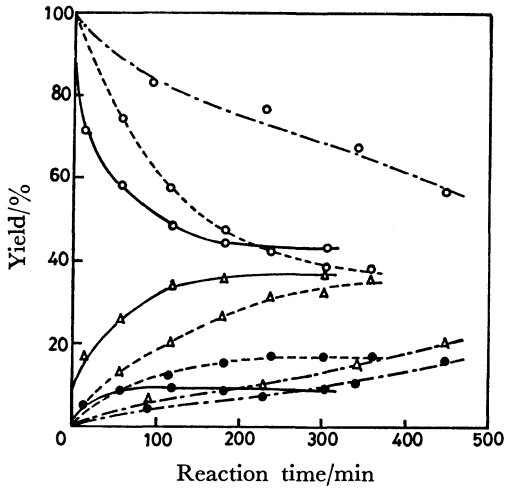

Fig. 1. Disproportionation reaction of dialkyl trisulfides catalyzed by BF_3OEt_2 to give disulfides and tetrasulfides in CH_2Cl_2 at 25 °C. $[RS_3R]=0.33$ mol/l, $[BF_3OEt_2]=0.33$ mol/l. ○: Decrease of RSSSR; △: increase of RSSR; ●: increase of RSSSSR. ——: R=*n*-Pr; -----: R=*i*-Pr; ————: R=*t*-Bu. Reactions were carried out in 3.0 ml of CH_2Cl_2 solution. Higher polysulfides than tetrasulfide were scarcely observed.

trisulfide formed. Therefore, the compositions of the products obtained at early stage of the reaction reflect the reaction mechanism of SO_2 with thiol.

The kinetics of the reaction of SO_2 with thiols is hampered by the acceleration of the reaction rate as the reaction proceeds, which disturbs the reaction and prevents it from fitting the first- or second-order rate law.[5] Although, in hope of seeing a signal of the reaction intermediates, the proton NMR of the reaction mixture was measured, there were no paticular signal other than those of the reactant, products, and catalyst. Kice *et al.* have reported that signals of the intermediates of the reaction of selenite with thiols were not observed.[6] Probably the concentration of the intermediates does not build up to a level sufficient to be detected because of the instability (*vide infra*) of the intermediates.

In a previous paper[1a] three sorts of reaction intermediates, I, II, and III, were proposed:

I II III

Although there is no way to synthesize I or II, dithiosulfite(III), which seems to indicate the most stable compounds of the three structures, can be synthesized (dithiosulfite, having a primary alkyl group, can not be synthesized).[7] Since direct proofs (kinetic or spectroscopic observation of the reaction intermediates in the reaction mixture) were impossible, as has been mentioned above, indirect proof of the reaction intermediate, especially dithiosulfite(III), was attempted as follows. If dithiosulfite intervenes as a reaction intermediate, dithiosulfite may react with BF_3OEt_2 and/or thiol. Therefore, the reaction of dithiosulfites with BF_3OEt_2 in the presence or absence of thiol was tried; the results are shown in Table 2. This table indicates that the compositions of the products of the reaction of dithiosulfite with BF_3OEt_2 are similar to the composition at an early stage of the reaction of SO_2 with thiols (see Table 1) in the sense that the value of RSSSR/RSSR is larger than 1 for R=*t*-Bu and close to 1 or a little less than 1 for R=*i*-Pr. This fact suggests the possibility that one of the reaction intermediates is dithiosulfite.

Field and Lacefield have assumed that the lower decomposition velocity of dithiosulfites with a tertiary alkyl group than that of dithiosulfites with a secondary alkyl group could be attributed to a bimolecular decomposition mechanism.[7] Since the reaction of di-*t*-butyl dithiosulfite (TBDS) with TBT or another molecule of TBDS suffers steric hindrance, TBDS would have chance to react with BF_3OEt_2 without being attacked by TBT or another molecule of TBDS. The reduction of sulfoxide by acids such as hydrogen iodide,[9,10] phosphorus trichloride,[11] or phosphorus pentachloride,[12] has been reported to give monosulfide. If a similar reduction mechanism works also for the reaction of this dithiosulfite with BF_3OEt_2, the preferential formation of trisulfide in the reaction of TBDS

with BF_3OEt_2 may be explained (Entries 3 and 4 in Table 2):

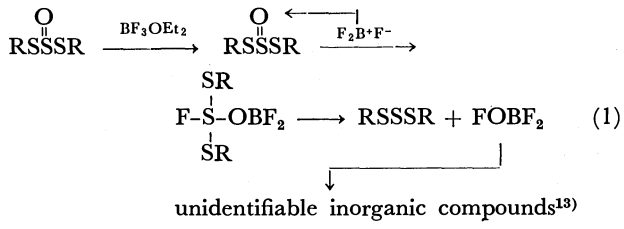

$$RSSSR \xrightarrow{BF_3OEt_2} RSSSR \xrightarrow{F_2B^+F^-} F\text{-}S\text{-}OBF_2 \longrightarrow RSSSR + FOBF_2 \quad (1)$$

unidentifiable inorganic compounds[13]

The reaction of IPDS (Entry 1) or TBDS (Entry 3 in Table 2) in the presence of IPT or TBT, respectively, occurs by reaction paths other than Eq. 1 (a part of the TBDS would react with BF_3OEt_2 without being attacked by TBT even in the presence of TBT). The reaction schemes proposed by Kice *et al.* for the reaction of RSSe(O)SR with thiol[6] are reasonable (2a—c):

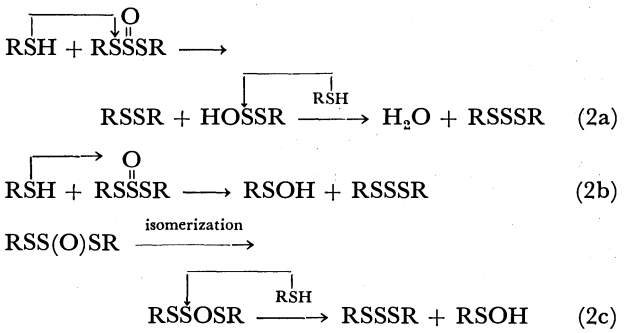

$$RSH + RSSSR \longrightarrow RSSR + HOSSR \xrightarrow{RSH} H_2O + RSSSR \quad (2a)$$

$$RSH + RSSSR \longrightarrow RSOH + RSSSR \quad (2b)$$

$$RSS(O)SR \xrightarrow{\text{isomerization}} RSSOSR \xrightarrow{RSH} RSSSR + RSOH \quad (2c)$$

Kice *et al.* considered that the reaction of thiol with RSSe(O)SR proceeded by a reaction of type 2b or 2c in order to interpret the formation of the thiosulfonic *S*-ester (RSO_2SR), which was considered to be formed from the reaction of RSOH. In the present reaction of SO_2 with thiol, the formation of the thiosulfonic *S*-ester was not observed at all.[14] Therefore, dithiosulfite probably disappears by means of the process shown in Eq. 2a in the reaction in the presence of thiol. The reaction of TBDS most likely occurs by means of both Eqs. 1 and 2a: It gives a ratio of RSSSR/RSSR larger than 1. For the reaction of IPDS, Eq. 1 would not contribute so much: Instead, Eq 2a would contribute to a large extent.

If, in the reaction of NPT or IPT with SO_2, sulfides form through only the reaction of dithiosulfite (Eq. 2a), an equal amount of di- and trisulfide must form. However, a little larger amount of disulfide than trisulfide forms at an early stage of the reaction of NPT or IPT with SO_2. This fact suggests that a reaction path giving disulfide preferentially also most likely contributes to some extent. One possible reaction path is shown in Eq. 3:

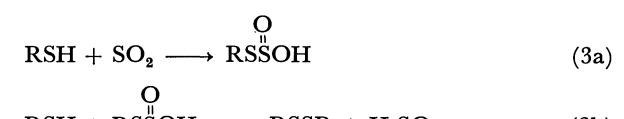

$$RSH + SO_2 \longrightarrow RSSOH \quad (3a)$$

$$RSH + RSSOH \longrightarrow RSSR + H_2SO_2. \quad (3b)$$

The reduction of SO_2 with 1-alkanethiol in the presence of an equal amount of triethylamine to give disulfide and thiosulfuric acid preferentially[15] can be explained by means of Eq. 3 (Thiosulfuric acid forms by the reaction of H_2SO_2). A part of the reaction of NPT or IPT with SO_2 most likely passes through Eq. 3, even in the case of a reaction catalyzed by BF_3OEt_2. On the other hand, the reaction of TBT with SO_2 would not pass through Eq. 3, since the attack of TBT on the sulfenyl sulfur of RSS(O)OH (R=*t*-Bu) is suppressed because of steric hindrance between *t*-Bu groups of TBT and RSS(O)OH.

Finally, the aspects of the reaction of thiols with SO_2 catalyzed by BF_3OEt_2 may be summarized as follows. In the reaction of NPT or IPT with SO_2 the dithiosulfite formed decomposes through Eq. 2a, which gives equal amounts of di- and trisulfide. In addition to this reaction path, Eqs. 3a and 3b occur to some extent. Therefore, the value of RSSSR/RSSR at an early stage of the reaction of NPT or IPT with SO_2 is little less than 1. On the other hand, in the reaction of TBT with SO_2, the dithiosulfite formed decomposes through both Eqs. 1 and 2a. In this case, the reactions in Eq. 3 scarcely occur. Therefore, the value of RSSSR/RSSR at an early stage of the reaction of TBT with SO_2 is considerably larger than 1. In the reactions of three sorts of thiols with SO_2 the disproportionation reaction of trisulfide formed to give di- and tetrasulfide takes place as the reaction proceeds, giving a lesser value than 1 of RSSSR/RSSR at a prolonged reaction time.

Experimental

Procedure for the Reaction of SO_2 with Thiols Catalyzed by BF_3OEt_2. The reagents were introduced and the reaction was started by the same method reported in a preceding paper.[1c] At an appropriate time, 20 ml of dichloromethane, appropriate amounts of hexamethylbenzene (an internal standard for sulfides), and cyclohexane (an internal standard for residual thiol) were added to make a uniform solution, which was then analyzed by means of GLC using SE-30, 15%, on a chromosorb W column.

Separation and Identification of Dialkyl Sulfides. Two mixtures, each of which contains thiol (80 mmol), BF_3OEt_2 (40 mmol), and SO_2 (40 mmol), were allowed to stand for 2 d. The upper layers of the two reaction mixtures thus obtained were combined and washed with water, a dilute alkaline aqueous solution, and water again: They were then dried over anhydrous magnesium sulfate and distilled to give pure di- and trisulfide. The structures of the disulfides and trisulfides isolated were established on the basis of the following data (the date for dipropyl di- and trisulfide were reported in Ref. 3):

Diisopropyl Disulfide: Bp 50—51 °C/6.5 mmHg (1 mmHg≈133.322 Pa) (lit,[16] 54—55 °C/7.5 mmHg). $\delta(CDCl_3)=1.33$ (6H, d, $J=6.5$ Hz, 2Me), 3.05 (1H, septet, $J=6.5$ Hz, $SC\underline{H}(CH_3)_2$). Found: C, 47.70; H, 8.99; S, 42.25%. Calcd for $C_6H_{14}S_2$: C, 47.95; H, 9.39; S, 42.66%.

Diisopropyl Trisulfide: Bp 78—79 °C/6.5 mmHg (lit,[16] 75—76 °C/5 mmHg). $\delta(CDCl_3)=1.41$ (6H, d, $J=6.5$ Hz, 2Me), 3.28 (1H, septet, $J=6.5$ Hz, $SC\underline{H}(CH_3)_2$), ν_{max} 500 cm^{-1} (S-S). Found: C, 39.23; H, 7.70; S, 52.30%. Calcd for $C_6H_{14}S_3$: C, 39,52; H, 7.74; S, 52.74%.

Di-t-butyl Disulfide: Bp 47 °C/1 mmHg (lit,[16] 64 °C/5.5 mmHg). $\delta(CDCl_3)=1.30$ (s). Found C, 54.24; H, 10.07; S, 35.76%. Calcd for $C_8H_{18}S_2$: C, 53.87; H, 10.17; S, 35.95%.

Di-t-butyl Trisulfide: Bp 70—71 °C/1 mmHg (lit,[16] 86 °C/

4 mmHg). $\delta(CDCl_3)=1.38$ (s), ν_{max} 500 cm^{-1}. Found: C, 45.59; H, 8.41; S, 45.33%. Calcd for $C_8H_{18}S_3$: C, 45.66; H, 8.62; S, 45.71%.

Isolation of dialkyl tetrasulfides was not attempted, because the yields of tetrasulfide were quite low. Instead, the retention time in the glc of the compounds obtained in this study was compared with that of dialkyl tetrasulfides synthesized by literature method:[17,18] The results showed a good coincidence.

Preparation and Purification of Dithiosulfites. TBDS was synthesized and purified by the method of Field *et al.*[7] The compound purified by chromatography (on Florisil), which had a mp of 48.5—49.5 °C (lit,[7] 48—49.5 °C), NMR $\delta(CDCl_3)=1.56$ (singlet) (lit,[7] 1.50) and IR 1105 cm^{-1} (lit,[7] 1110 cm^{-1}) was used for the reaction with BF_3OEt_2 without further recrystallization. IPDS was also synthesized by the same method.[7] Although Field *et al.* using crude IPDS without purification for their decomposition experiment,[7] their purification method using Florigil for TBDS was found to be also effective for IPDS. Purified IPDS (liq) showed NMR signals at $\delta(CDCl_3)=1.51$ (doublet, 6H, $J=6.5$ Hz) and at 3.66 (septet, 1H, $J=6.5$ Hz), IR absorption at 1110 cm^{-1} (lit,[7] 1110 cm^{-1}). The preservation of purified IPDS as a $CDCl_3$ solution (10%) at room temperature for 10 d and at −20 °C for 4 months gave about 50% and only a slight decomposition respectively. Therefore, purified IPDS was used for the reaction with BF_3OEt_2 after preservation in a refrigerator (−20 °C) for a few days.

The author wishes to thank Professor Minoru Matsuda of this Institute for his comments and suggestions.

References

1) a) F. Akiyama, *J. Chem. Soc., Perkin Trans. 1*, **1978**, 1046; b) F. Akiyama, R. Tatsuta, and M. Matsuda, *J. Polym. Sci., Polym. Lett. Ed.*, **17**, 23 (1979); c) F. Akiyama, *ibid.*, **18**, 401 (1980).

2) F. Akiyama, unpublished results.

3) T. L. Pickerring, K. T. Saunders, and A. V. Tobolsky, *J. Am. Chem. Soc.*, **89**, 2364 (1967).

4) D. N. Harpp, and R. A. Smith, *J. Am. Chem. Soc.*, **104**, 6045 (1982), and the references cited therein.

5) Several authors have described decompositinn reactions of boron trifluoride with water, such as $2BF_3+3H_2O \rightarrow HBF_4+2HF+B(OH)_3$ (see A. V. Topchiev, S. V. Zavgorondnii, and Ya. M. Paushikin, "Boron Trifluoride and its Compounds as Catalysts in Organic Chemistry," International Series of Monographs on Organic Chemistry, ed by W. Doering and H. R. Barton, Pergamon Press, London (1957), Vol. 2, p. 46) and the decomposition of BF_3OEt_2 with water to give BF_3 and diethyl ether (see Y. Kawashima, H. Takeo, and C. Matsumura, *Chem. Phys. Lett.*, **57**, 145 (1978); *J. Mol. Spectrosc.*, **78**, 493 (1979)). Presumably water formed by the reduction of SO_2 decomposes BF_3OEt_2, thus resulting in the acceleration of the reaction rate.

6) J. L. Kice, T. W. S. Lee, and S-T Pan, *J. Am. Chem. Soc.*, **102**, 4448 (1980).

7) L. Field and W. B. Lacefield, *J. Org. Chem.*, **31**, 3555 (1966).

8) Although the origin of the formation of a considerable amount of tetrasulfide in the case of Entry 4 in Table 2 can not be explained on the basis of experimental proof, sulfoxide-sulfenate rearrangement (see E. G. Miller, O. R. Rayner, H. T. Thomas, and K. Mislow, *J. Am. Chem. Soc.*, **90**, 4861 (1968) and H. Mizuno, M. Matsuda, and M. Iino, *J. Org. Chem.*, **46**, 520 (1981)) or α-di-sulfoxide-sulfenyl sulfinate rearrangement (see M. M. Chau and J. L. Kice, *J. Am. Chem. Soc.*, **98**, 7711 (1976) and F. Freeman and C. N. Anglestakis, *ibid.*, **103**, 6232 (1981)) suggests the possibility that the following reaction occurs in the reaction of TBDS with BF_3OEt_2 in the absence of TBT:

$RSS(O)SR \rightleftharpoons RSSOSR$ or

$RSSS(O)R \rightarrow RSS\cdot + \cdot OSR$ or $\cdot S(O)R$

$RSS\cdot \rightarrow 0.5RSSSSR$

9) E. N. Karaulova and G. D. Gal'pern, *Zh. Obshch. Khim*, **29**, 3033 (1959).

10) D. Landini, F. Montanari, H. Hogeveen, and G. Maccagnami, *Tetrahedron Lett.*, **1964**, 2691; D. Landini, F. Montanari, G. Modena, and G. Scorano, *Chem. Commun.*, **1968**, 86; *J. Am. Chem. Soc.*, **92**, 7168 (1970).

11) I. Granoth and A. Kalir, *J. Chem. Soc., C*, **1967**, 2424.

12) A. Michaelis and E. Godchaux, *Chem. Ber.*, **24**, 763 (1891).

13) The treatment of the reaction mixture of TBDS with BF_3OEt_2 with a dilute aqueous sodium hydroxide solution, followed by the separation of aqueous layer and the evaporation of the layer, gave a white solid. IR spectra of this solid showed no contamination of organic compounds. The separation and identification of the inorganic boron compounds formed was unsuccessful.

14) One might suspect that the thiosulfonic *S*-ester was formed in the reaction of SO_2 with thiols, but decomposed after formation. When a mixture of 1 mmol of authentic *S*-*t*-butyl 2-methyl-2-propanethiosulfonate (for synthetic method: see Ref. 6), 2 mmol of TBT, 1 mmol of BF_3OEt_2, and 25 ml of CH_2Cl_2 was allowed to stand for 2 d at 25 °C, a decrease of only 10% of the concentration of the thiosulfonic *S*-ester was observed. This fact excludes the possibility of the formation of the thiosulfonic *S*-ester.

15) F. Akiyama, Japan Kokai Tokkyo Koho, 82, 106 505; *Chem. Abstr.*, **97**, 111970 p (1982).

16) E. E. Reid, "Organic Chemistry of Bivalent Sulfur," Chemical Publishing Co, New York (1960), Vol. III, p. 395.

17) G. C. Chakravarti, *J. Chem. Soc.*, **1923**, 964.

18) S. F. Birch, T. V. Cullumn, and R. A. Dean, *J. Inst. Pet.*, **39**, 206 (1953).

The Baeyer-Villiger Oxidation of 8-Oxabicyclo[3.2.1]octan-3-ones. Substituent Effects on the Regioselectivity[1,2]

Ryoji Noyori,* Tsuneo Sato, and Hiroshi Kobayashi

Department of Chemistry, Nagoya University, Chikusa-ku, Nagoya 464

(Received February 23, 1983)

8-Oxabicyclo[3.2.1]octan-3-one derivatives serve as excellent models that elucidate factors controlling the reactivities and selectivities in the Baeyer-Villiger oxidation. The regioselectivity of the oxidation with trifluoroperacetic acid is markedly affected by the electronic properties of substituents at position α or β to the carbonyl function. Remote effects of the γ-substituents are also of significance. This study has disclosed yet unrecognized through-bond electronic influence and regioselection based on chiral orientation of hydroxyl group in the transient tetrahedral intermediate.

Oxidation of ketones by peroxy acids (Baeyer-Villiger reaction)[3] proceeds by way of transient tetrahedral intermediates,[4] which undergo fragmentation to give esters and carboxylic acids. Migration of R_m (sp^3)

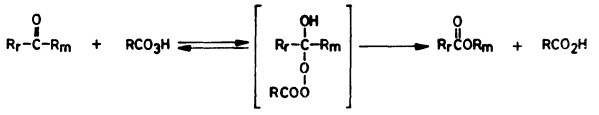

R_m=migrating group
R_r=remaining group

group to the adjacent electron-deficient oxygen atom occurs in a concerted manner with retention of configuration. The migratory aptitude appears to be related to the ability of a group to support a positive charge developing in the transition state.[5] Besides such electronic effects, conformational factors are also important in determining the regiochemistry.[6] 8-Oxabicyclo[3.2.1]octan-3-one structures serve as excellent models for examining factors which control the reactivity and selectivity in the reaction, because the C_s symmetry incorporated in the basic skeleton is not distorted to any great extent by introduction of substituents. In connection with our program of *C*-nucleoside synthesis,[7] we had an opportunity of examining the oxidation of a series of the substituted oxabicyclic ketones and found several unique substituent effects.

Results and Discussion

The oxidation of the ketonic substrates was carried out in dichloromethane at 15—25 °C by using three- to seven-fold excess of trifluoroperacetic acid in the presence of anhydrous disodium hydrogenphosphate. Most reaction proceeded smoothly, but the reaction mixture was routinely stirred for 10—36 h to ensure the completion. The structures of the products were elucidated by spectroscopic methods, particularly ^{1}H NMR measurement. The isomeric ratio of the products was conveniently determined by ^{1}H NMR or high-performance liquid chromatography (HPLC) analysis.

Reaction of the α-Substituted Ketones. The Baeyer-Villiger oxidation of the α-substituted ketones, **1**—**3**, proceeded rapidly and, as expected,[3] only single lactonic isomers, **5**—**7**, were obtained in high yield.[8] In a like manner, oxidation of the dimethylated ketone **4** afforded the lactone **8** as a sole product. The complete regioselectivity is based on the positive charge-stabilizing ability of the alkyl or phenyl group at position α to the carbonyl function.

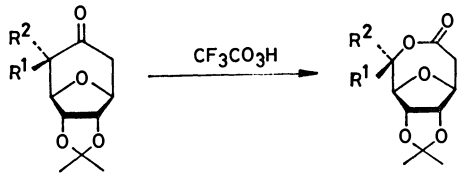

1, $R^1=CH_3$; $R^2=H$
2, $R^1=n\text{-}C_5H_{11}$; $R^2=H$
3, $R^1=C_6H_5$; $R^2=H$
4, $R^1=R^2=CH_3$

5, $R^1=CH_3$; $R^2=H$
6, $R^1=n\text{-}C_5H_{11}$; $R^2=H$
7, $R^1=C_6H_5$; $R^2=H$
8, $R^1=R^2=CH_3$

Reaction of the β-Substituted Ketones. This class of compounds afforded a mixture of the regioisomeric lactones.[9] ^{1}H NMR spectra of the products arising from α-carbon migration exhibited an AB quartet due to the CH_2OCO protons, whereas the spectra of the α'-migrated isomers showed the same pattern of signals at higher field due to the CH_2COO protons. β-Alkyl substituents appear to direct the regiochemistry to only slight extent, giving the α- and α'-migration products in nearly equal amounts (Table 1). However, introduction of phenyl group which possesses ability of stabilizing positive charge partially developing at the α-methylene group resulted in greater α/α' ratio, **14a**/**14b**=88:12.[10,11]

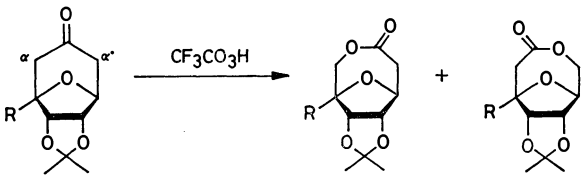

9, $R=CH_3$
10, $R=n\text{-}C_5H_{11}$
11, $R=C_6H_5$

12a, $R=CH_3$ **12b**, $R=CH_3$
13a, $R=n\text{-}C_5H_{11}$ **13b**, $R=n\text{-}C_5H_{11}$
14a, $R=C_6H_5$ **14b**, $R=C_6H_5$

Reaction of the γ-Substituted Ketones. In the course of study of oxidation of a variety of the γ-substituted bicyclo ketones, we observed yet unrecognized remote substituent effects.

A. Remote Electronic Effects. Reaction of the ketones, **15**—**22**, and trifluoroperacetic acid gave mixtures of the corresponding α-and α'-migration products

Table 1. Reaction of the β-substituted ketones[a]

Ketone No.	Ketone β-Substituent, R	CF_3CO_3H (equiv)	Temp °C	Time h	Lactone product Yield/%[b]	Lactone product **a**/**b** ratio[c]
9	CH_3	3	20	10	90	53 : 47
10	n-C_5H_{11}	7	20	15	91	50 : 50
11	C_6H_5	5	25	12	93	88 : 12

a) Reaction with CF_3CO_3H in CH_2Cl_2. b) Isolated yield. c) Determined by ^1H NMR analysis.

Table 2. Reaction of the γ-substituted ketones.[a] Remote electronic effects on the regioselectivity

Ketone No.	Ketone β-Substituent, R	^{13}C NMR shift of C=O[b]	Lactone product Yield/%[c]	Lactone product **a**/**b** ratio[d]
15	$OSi(CH_3)_2$-t-C_4H_9	205.85	100	55 : 45
9	H	205.59	90	53 : 47
10	n-C_4H_9	205.88	91	50 : 50
16	$OCH_2C_6H_5$	205.41	83	48 : 52
17	$OCOCH_3$	204.19	80	35 : 65
18	OCO-t-C_4H_9	204.44	91	31 : 69
19	$OCOC_6H_5$	204.49	100	28 : 72
20	$OCOCF_3$	203.34	98	23 : 77
21	OSO_2CH_3	203.62	93	19 : 81
22	OSO_2CF_3	202.74	89	14 : 86
8-Oxabicyclo[3.2.1]octan-3-one		206.67	—	—
33	$OCH_2C_6H_5$	205.66	81	30 : 70
34	$OSi(CH_3)_2$-t-C_4H_9	205.76	93	30 : 70
35	$OCOCH_3$	204.78	78	46 : 54
36	OCO-t-C_4H_9	204.77	89	35 : 65
37	$OCOC_6H_5$	204.86	95	35 : 65

a) Reaction with 3 equiv of CF_3CO_3H in CH_2Cl_2 at 25 °C (for **15**—**22**) or at 15 °C (for **33**—**37**) for 12 h. For **9**, 3 equiv of CF_3CO_3H at 20 °C for 10 h. For **10**, 7 equiv of CF_3CO_3H at 20 °C for 15 h. b) In $CDCl_3$ with $(CH_3)_4Si$ as internal standard. c) Isolated yield. d) ^1H NMR determination for the reaction with **15**—**22**. HPLC analysis for the reaction with **33**—**37**.

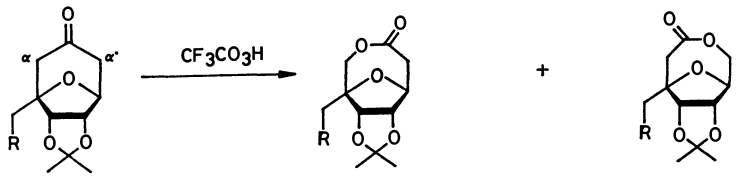

15, R=$OSi(CH_3)_2$-t-C_4H_9 **23a**, R=$OSi(CH_3)_2$-t-C_4H_9 **23b**, R=$OSi(CH_3)_2$-t-C_4H_9
16, R=$OCH_2C_6H_5$ **24a**, R=$OCH_2C_6H_5$ **24b**, R=$OCH_2C_6H_5$
17, R=$OCOCH_3$ **25a**, R=$OCOCH_3$ **25b**, R=$OCOCH_3$
18, R=OCO-t-C_4H_9 **26a**, R=OCO-t-C_4H_9 **26b**, R=OCO-t-C_4H_9
19, R=$OCOC_6H_5$ **27a**, R=$OCOC_6H_5$ **27b**, R=$OCOC_6H_5$
20, R=$OCOCF_3$ **28a**, R=$OCOCF_3$ **28b**, R=$OCOCF_3$
21, R=OSO_2CH_3 **29a**, R=OSO_2CH_3 **29b**, R=OSO_2CH_3
22, R=OSO_2CF_3 **30a**, R=OSO_2CF_3 **30b**, R=OSO_2CF_3

in 80—100% yield. As is seen from Table 2, the isomeric ratio is highly dependent on the nature of γ-substituent R. The general trend indicates that the regioselectivity is determined by remote electronic effects of R group. Model inspection provides no indication for significance of steric or conformational factors. Notably electron-accepting substituents favor the α'-carbon migration over the α-carbon rearrangement. The relative α'-directing capabilities decrease in the order of OSO_2R > OCOR > OR > alkyl or H; OSO_2CF_3 > OSO_2CH_3; $OCOCF_3$ > $OCOC_6H_5$ > $OCOCH_3$; $OCH_2C_6H_5$>$OSi(CH_3)_2$-t-C_4H_9. By contrast, electron-donating groups exhibited slight preference for the α-migration. The feeble but definite α-selection observed with **9** is to be noted. The well-known Si^+O^- polarization[12] also resulted in some α-regioselection. These findings can be rationalized by considering the mode of transmission of through-

bond electronic effects.[13] The C(γ)–R bond polarization caused by an electronegative R group decreases electron density of the γ-and α-positions in the tetrahedral intermediate **31**, whereas an electron-donating R group makes these two carbon atoms more eletropositive. The α-position is unaffected through such electronic perturbation. As a consequence, the observed regiochemical bias is resulted.

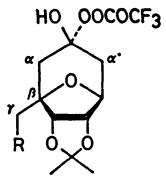

31

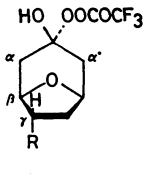

32

This type of induced electronic directing effect was noticed also in the oxidation of the ketones **33**—**37** which proceeds *via* the intermediate **32** (Table 2). The structures, **38a**—**42a** and **38b**—**42b**, were readily differentiated by ^{1}H NMR; the isomers of **a** series gave the C*H*R signal at a lower field than the **b** regioisomers owing to the anisotropic effect of the lactone oxygen atom. Thus electron-withdrawing groups attached to the γ-carbon atom showed a moderate degree of α'-regioselection. Here the substituent effects would be less straightforward, because (1) R group in **32** is accommodated in the seven-membered ring and exerts electronic influence not only the α-carbon but also the α'-position, though less effectively, and (2) the R–C(γ)–C(β)–C(α) backbone is distorted to some extent from normal zig-zag arrangement. Nevertheless the observed regioselectivity is compatible qualitatively with the above described interpretation.

These unprecedented remote interactions between the directing substituent and the migrating group should be a reflection of the regidity of the σ framework that facilitates the through-bond electronic influence. Some indication for the efficiency of electronic transmission in these systems may be offered by ^{13}C NMR measurement of the parent ketones; the carbonyl carbon signal appears to move *upfield* considerably with an increase in electron-withdrawing ability of γ-substituents (Table 2).

B. Steric Effects. Oxidation of the oxabicyclic ketones **43**—**50** with trifluoroperacetic acid was examined, and the structures of the regioisomeric lactone products were verified again easily by ^{1}H NMR as the case with the reaction of **33**—**37**. Here ease with which the oxidation takes place was found to be influenced profoundly by bulkiness of the substituent having endo configuration. The parent ketone (R= H) was readily transformed to the lactone, but introduction of methyl group, for instance, reduced the reaction rate by a factor of 4, as revealed by a competition experiment. The *t*-butyl derivative **45** was totally inert to the peroxy acid oxidation. This is obviously ascribable to steric screening effect of R group. Nucleophilic addition of trifluoroperacetic acid to the bicyclic ketones is expected to occur stereoselectively from the less hindered side[14] and, therefore, formation of the tetrahedral adducts of type **58** would be retarded by the presence of a bulky R group which introduces substantial steric repulsion with the hydroxyl.

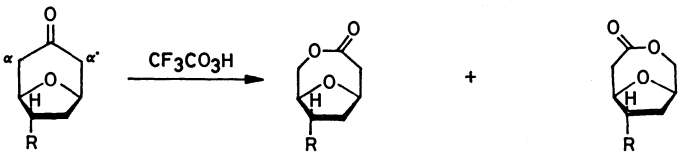

33, R=$OCH_2C_6H_5$	**38a**, R=$OCH_2C_6H_5$	**38b**, R=$OCH_2C_6H_5$
34, R=$OSi(CH_3)_2$-*t*-C_4H_9	**39a**, R=$OSi(CH_3)_2$-*t*-C_4H_9	**39b**, R=$OSi(CH_3)_2$-*t*-C_4H_9
35, R=$OCOCH_3$	**40a**, R=$OCOCH_3$	**40b**, R=$OCOCH_3$
36, R=OCO-*t*-C_4H_9	**41a**, R=OCO-*t*-C_4H_9	**41b**, R=OCO-*t*-C_4H_9
37, R=$OCOC_6H_5$	**42a**, R=$OCOC_6H_5$	**42b**, R=$OCOC_6H_5$

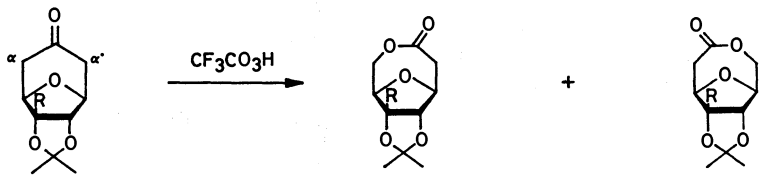

43, R=CH_3	**51a**, R=CH_3	**51b**, R=CH_3
44, R=*n*-C_5H_{11}	**52a**, R=*n*-C_5H_{11}	**52b**, R=*n*-C_5H_{11}
45, R=*t*-C_4H_9	—	—
46, R=C_6H_5	**53a**, R=C_6H_5	**53b**, R=C_6H_5
47, R=$CH_2OSi(CH_3)_2$-*t*-C_4H_9	**54a**, R=$CH_2OSi(CH_3)_2$-*t*-C_4H_9	**54b**, R=$CH_2OSi(CH_3)_2$-*t*-C_4H_9
48, R=$CH_2OCH_2C_6H_5$	**55a**, R=$CH_2OCH_2C_6H_5$	**55b**, R=$CH_2OCH_2C_6H_5$
49, R=CH_2OCO-*t*-C_4H_9	**56a**, R=CH_2OCO-*t*-C_4H_9	**56b**, R=CH_2OCO-*t*-C_4H_9
50, R=$CH_2OCOC_6H_5$	**57a**, R=$CH_2OCOC_6H_5$	**57b**, R=$CH_2OCOC_6H_5$

Table 3. Reaction of the γ-substituted ketones.[a] Steric effects on the regioselectivity

Ketone		Conversion/%	Lactone product	
No.	β-Substituent, R		Yield/%[b]	**a**/**b** ratio[c]
43	CH_3	62	84	33 : 67[d]
44	n-C_5H_{11}	48	85	25 : 75[d]
45	t-C_4H_9	0	—	—
46	C_6H_5	19	82	39 : 61[d]
47	$CH_2OSi(CH_3)_2$-t-C_4H_9	38	94	26 : 74
48	$CH_2OCH_2C_6H_5$	32	76	23 : 77
49	CH_2OCO-t-C_4H_9	46	82	34 : 66
50	$CH_2OCOC_6H_5$	28	75	40 : 60

a) Reaction with 3 equiv of CF_3CO_3H in CH_2Cl_2 at 20 °C for 36 h (for **43**, at 25 °C for 36 h). b) Isolated yield. Based on consumed starting material. c) Determined by HPLC analysis. d) Obtained by ^1H NMR analysis.

In usual, rate-determining step of the Baeyer-Villiger oxidation has been considered to be the fragmentation of the tetrahedral intermediate,[15] but in the present case equilibrium concentration of the intermediate **58** is also important.[16]

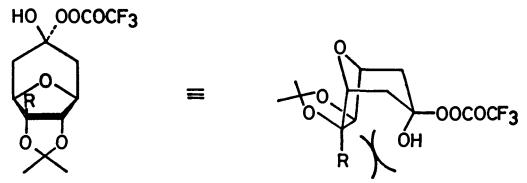

58

Regioselectivity is also affected by the γ-substituents. Presence of the substituent groups, regardless of the electronic properties, provided a marked bias toward the α′-methylene migration (Table 3). We would postulate that this regioselection relies primarily on a yet unreported controlling factor, chiral orientation of the hydroxyl group in the transient tetrahedral intermediate. *A priori* three types of transition states, **59**—**61**, are conceivable for the concerted fragmentation. The cyclic structures, however, can hardly explain the preference of R_m migration. The five-membered ring **59** is rather rigid and, when an oxabicyclic ketone is employed as starting material, this has basically C_s symmetry. The seven-membered structure **60** is more flexible but the fragmentation *via* such transition state is symmetry-forbidden in nature. On the other hand, the acyclic, extended transition state **61** has a chiral basic geometry; R_m and R_r are clearly diastereotopic each other and are to be differentiated during the concerted fragmentation process.[17] In order for R_m to migrate to O(1) atom with concomitant carboxylic acid ejection, two prerequisites must be satisfied. Firstly, R_m–C–O(1)–O(2) should lie in an antiperiplanar manner. Secondly, since the electron release from the hydroxyl oxygen to the migration origin attached to it is crucial to promote the shift of R_m,[18] one of the hydroxyl nonbonding electron pairs has to be anti to R_m. On the basis of such stereoelectronic requirements, only **61A** and **61B** are the reactive conformers. Conformer **61C** is unreactive. When this consideration is applied to the reaction of the oxabicyclic ketones **43**—**50**, four structures, **58A**, **58B**, **58A′**, and **58B′**, emerge as reactive conformers; **58A** and **58B** lead to the α-methylene migration product, whereas **58A′** and **58B′** result in α′-carbon rearrangement. Here when the nonbonded repulsion between R and the hydroxyl hydrogen is taken into consideration, the relative stabilities are estimated to be **58A′**>**58A**≫**58B**≈**58B′**, consistent with the observed α′-regioselection.[19] Thus chiral arrangement of the hydroxy group in the tetrahedral intermediate seems quite significant in controlling the regiochemical outcome. In this system, through-bond electronic effects of the γ substituents are less important compared with the above described series, because of the stereochemical arrangement is not appropriate for the transmission.[20]

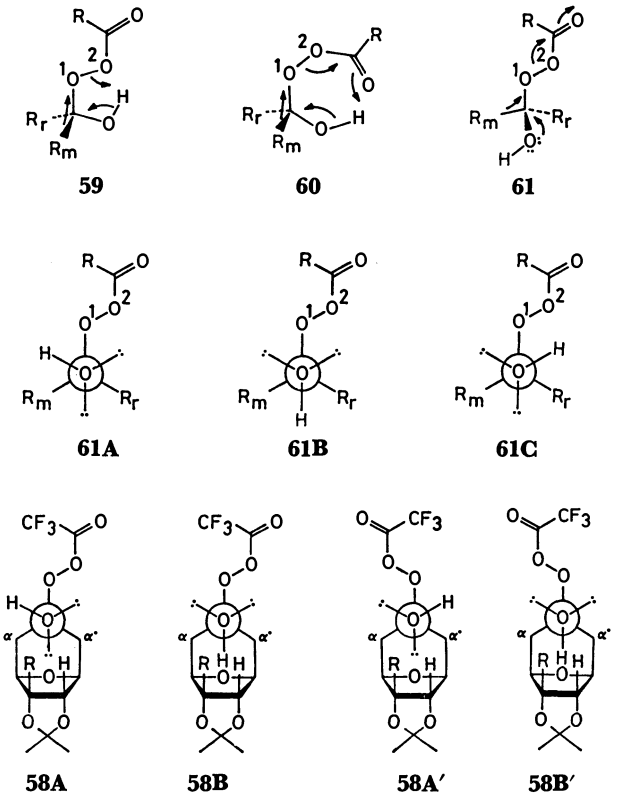

59 **60** **61**

61A **61B** **61C**

58A **58B** **58A′** **58B′**

Experimental

General. All melting and boiling points are uncorrected. IR spectra were recorded on a JASCO IRA-1 spectrometer in $CHCl_3$ solution unless otherwise stated. ^1H NMR spectra were obtained using a Varian NV-21 or HA-100 spectrometer, and ^{13}C NMR spectra were recorded at 20 MHz on a Varian CFT-20 spectrometer or at 25 MHz on a JEOL FX-100 spectrometer. The chemical shifts are recorded in parts per million relative to tetramethylsilane as an internal standard. Singlet, doublet, triplet, and multiplet were abbreviated to s, d, t, and m, respectively. Low-resolution mass spectra were measured on a JEOL D 100 instrument and only a parent peak or prominent fragment peaks are described. Exact mass spectra were obtained at Center Research Laboratory of Ono Pharmaceutical Co. Elemental analyses were performed at the Research Laboratory of Fujisawa Pharmaceutical Co., Faculty of Engineering of Nagoya University, and Institute of Pharmaceutical Sciences of Meijo University. Drying of organic extracts was done over anhyd Na_2SO_4. For concentration of organic solvents, a vacuum (50—100 mmHg)** rotary evaporator was used. Bulb-to-bulb short-path distillation was performed by using a Büchi Kugelrohrofen. The cited temperatures for these distillations refer to the maximum temperature attained by the oven during the distillation and are thus not true boiling points.

Chromatography. Thin-layer chromatography (TLC) was done using 0.25-mm layers of silica gel 60 PF_{254} obtained from E. Merck and preparative TLC using 20×20-cm glass plates coated with a 1.0-mm layer of silica gel 60 PF_{254}. Analytical plates were visualized by spraying with a solution of 2% $Ce(SO_4)_2$ in 5% H_2SO_4 or 2% *p*-anisaldehyde in 5% ethanolic H_2SO_4 followed by heating on a hot plate. The position of spots is shown by R_f values. For column chromatography, E. Merck Kieselgel 60 (70—230 mesh) was used. High-performance liquid chromatography (HPLC) was performed with a Waters Model 6000A liquid chromatograph equipped with a Radial Pak B column (4.0ϕ×250) and a refractive index detector or a UV index detector. The position of peaks is shown by V_R (retention volume) values.

Solvents and Materials. DMF, pyridine, *t*-C_4H_9OH, and furan were used after distillation from CaH_2. Acetone and CH_2Cl_2 were distilled from P_2O_5. THF and ether were distilled from sodium benzophenone ketyl. CH_3OH was distilled over magnesium ribbons. Preparation of Zn/Ag couple,[21] Zn/Cu couple,[22] pyridinium *p*-toluenesulfonate,[23] polybromo ketones,[24] pyridinium chlorochromate,[25] trimethylsilyl triflate,[26] 3-pentylfuran,[27] 3-*t*-butylfuran,[28] 3-phenylfuran,[29] 2-phenylfuran,[30] trifluoromethanesulfonic anhydride,[31] *N*-methylmorpholine *N*-oxide monohydrate,[32] 8-oxabicyclo[3.2.1]oct-6-en-3-one,[21b] (1*S**, 2*R**, 5*S**)-2-methyl-8-oxabicyclo[3.2.1]oct-6-en-3-one,[21b] and 2,2-dimethyl-8-oxabicyclo[3.2.1]oct-6-en-3-one[21b] was performed according to the known procedures. Other commercially supplied materials and solvents were used as received.

Preparation of 2-Pentylfuran.[33] To a solution of *n*-C_4H_9Li, prepared from THF (200 ml)*** and *n*-C_4H_9Li in hexane (1.5 mol dm^{-3} solution, 293 ml, 0.44 mol), was added furan (29.1 ml, 0.40 mol) at −10 °C under argon. After stirring for 6 h at the same temperature, 1-bromopentane (54.5 ml, 0.44 mol) was added to this mixture. The resulting mixture was stirred at 25 °C for 12 h and then poured into ice water (300 ml). The organic layer was separated and the aqueous layer was extracted with ether (150 ml×2). The combined extracts were dried and evaporated. The residue was distilled under reduced pressure (64—65 °C/40 mmHg) to give 2-pentylfuran (31.5 g, 57%). ^1H NMR ($CDCl_3$) δ 0.90 (t, J=6.2 Hz, 3H), 1.1—1.9 (m, 6H), 2.62 (t, J=7.0 Hz, 2H), 5.99 (m, 1H), 6.27 (m, 1H), 7.30 (m, 1H).

Preparation of 3-(Benzyloxymethyl)furan. To a mixture of $LiAlH_4$ (760 mg, 20 mmol) in THF (10 ml) was added ethyl 3-furoate (2.80 g, 20 mmol) in THF (5 ml) at 0 °C under argon. After stirring for 1 h at the same temperature, the reaction mixture was diluted with ether (15 ml). To this was added carefully 1 mol dm^{-3} NaOH (1 ml) and the insoluble material was removed by filtration. The filtrate was evaporated to give a colorless oil. To a suspension of NaH (50% oil dispersion, 1.25 g, 26 mmol) in DMF (10 ml) was added the oil in DMF (5 ml) at room temperature. After stirring for 1 h at 50 °C, the mixture was cooled to room temperature. To this was added benzyl chloride (4.62 ml, 40 mmol) and the reaction mixture was stirred for 12 h and poured into ice water (40 ml) and extracted with ether (50 ml×2, 30 ml×1). The ether layer was dried and evaporated to give an oil. Chromatography of this oil on a silica-gel column (10:1 hexane–ethyl acetate) afforded 3-(benzyloxymethyl)furan (3.86 g, 100%). R_f= 0.39 (4:1 hexane–ethyl acetate); ^1H NMR ($CDCl_3$) δ 4.42 (s, $C\underline{H}_2OCH_2C_6H_5$), 4.52 (s, $CH_2\underline{H}_2C_6H_5$), 6.44 (s, H_4), 7.32 (s, C_6H_5), 7.40 (s, H_2 and H_5).

Preparation of 3-(Tetrahydropyran-2-yloxymethyl)furan. A mixture of ethyl 3-furoate (28.0 g, 0.20 mol) and $LiAlH_4$ (7.60 g, 0.20 mol) in THF (300 ml) was stirred for 1 h at 0 °C under argon. To this was added slowly 1 mol dm^{-3} NaOH (20 ml) and the resulting white precipitate was filtered off. The filtrate was evaporated to afford a colorless oil. A solution of this oil, 3,4-dihydro-2*H*-pyran (23.7 ml, 0.26 mol), and pyridinium *p*-toluenesulfonate (5.0 g) in CH_2Cl_2 (150 ml) was stirred for 12 h at 20 °C under argon. The mixture was washed with brine (50 ml×3), dried ($MgSO_4$), and evaporated to give a colorless oil. Chromatography of this oil on a silica-gel column using a 3:1 hexane–ethyl acetate mixture to afford 3-(tetrahydropyran-2-yloxymethyl) furan (29.3 g, 80%) as a colorless oil. R_f=0.19 (3:1 hexane–ethyl acetate); ^1H NMR ($CDCl_3$) δ 1.1—2.2 (m, CH_2), 3.4—4.1 (m, $CH_2C\underline{H}_2O$), 4.41 (d, J=12.4 Hz, $C\underline{H}_aH_b$-OTHP), 4.65 (d, J=12.4 Hz, $CH_a\underline{H}_b$OTHP), 4.69 (m, $CH_2OC\underline{H}OCH_2$), 6.43 and 7.42 (m, H_1, H_2, and H_4).

Preparation of 8-Oxabicyclo[3.2.1]octan-3-one. A mixture of 8-oxabicyclo[3.2.1]oct-6-en-3-one (133 mg, 1.07 mmol), 10% Pd/C (20 mg), and ether (4 ml) was stirred for 16 h at 25 °C under hydrogen and the insoluble material was removed by filtration and the filtrate was evaporated to afford the title compound (129 mg, 95%). ^1H NMR ($CDCl_3$) δ 1.70—2.20 (m, H_6 and H_7), 2.32 (dd, J=1.0, 15.5 Hz, H_{2a} and H_{4a}), 2.77 (dd, J=5.0, 15.5 Hz, H_{2b} and H_{4b}), 4.75 (m, H_1 and H_5); ^{13}C NMR ($CDCl_3$) δ 29.66, 49.75, 74.84, 206.67.

Preparation of 8-Oxabicyclo[3.2.1]oct-6-en-3-one Derivatives. *(1S*,2R*,5S*)-2-Pentyl-8-oxabicyclo[3.2.1]oct-6-en-3-one*: To a mixture of Zn/Ag couple (68.7 g, 1.05 g-atom), furan (240 ml, 3.5 mol), and THF (600 ml) was added 1,1,3,3-tetrabromo-2-octanone (310 g, 0.7 mol) in THF (600 ml) over 1 h at −10 °C under argon. The reaction mixture was stirred at the same temperature for 1 h and then at 25 °C for 39 h. The insoluble material was filtered off and the filtrate was concentrated to dryness. The residue was dissolved in 1.2 l of CH_3OH saturated with NH_4Cl and to this was added Zn/Cu couple (240 g, 3.6 g-atom). The mixture was stirred for 1 h at 25 °C and the insoluble material

** 1 mmHg≈133.322 Pa.

*** 1 ml=0.001 dm^3.

was removed by filtration. The filtrate was diluted with H_2O (300 ml) and saturated disodium dihydrogen ethylenediaminetetraacetate (Na_2H_2edta) (300 ml) and then extracted with CH_2Cl_2 (500 ml×1, 200 ml×2), dried (Na_2SO_4), evaporated to afford a yellow oil. This oil was chromatographed on a silica-gel column using a 10:1 to 3:1 hexane–ethyl acetate mixture to give the title compound (63.2 g, 47%). Analytically pure sample was obtained by bulb-to-bulb distillation (130 °C/0.01 mmHg). R_f=0.31 (3:1 hexane–ethyl acetate); IR 1715 cm^{-1} (C=O); ^1H NMR ($CDCl_3$) δ 0.90 (t, J=6.0 Hz, CH_3), 1.30 (m, CH_2), 1.26 (d, J=5.0 Hz, H_{4a}), 1.70 (m, H_2), 1.74 (dd, J=5.0, 15.0 Hz, H_{4b}), 4.96 (d, J=5.0 Hz, H_1), 5.02 (d, J=5.0 Hz, H_5), 6.27 (s, H_6 and H_7); MS m/z 194 (M^+). Found: C, 74.32; H, 9.02%. Calcd for $C_{12}H_{18}O_2$: C, 74.19; H, 9.34%.

(1S,2S*,5S*)-2-Phenyl-8-oxabicyclo[3.2.1]oct-6-en-3-one*: A mixture of 1-phenyl-1,1,3,3-tetrabromo-2-propanone (90 g, 0.20 mol), Zn/Ag couple (19.5 g, 0.30 g-atom), furan (72.7 ml, 1.0 mol), and THF (250 ml) was stirred for 12 h at 25 °C. Reduction with Zn/Cu couple (65 g, 1.0 g-atom) in NH_4Cl/CH_3OH (700 ml) followed by ordinary extractive workup gave a dark oil. Chromatography of this oil on a silica-gel column using a 3:1 to 1:1 hexane–ethyl acetate mixture afforded 19.2 g (48%) of the title compound. Analytically pure sample was obtained by recrystallization from hexane. Mp 112.8—113.1 °C; R_f=0.35 (1:1 hexane–ethyl acetate); IR 1715 cm^{-1} (C=O); ^1H NMR ($CDCl_3$) δ 2.23 (dd, J=2.5, 16.4 Hz, H_{4a}), 2.88 (dd, J=4.7, 16.4 Hz, H_{4b}), 4.42 (d, J=4.9 Hz, H_2), 5.00 (dd, J=1.5, 4.9 Hz, H_1), 5.13 (ddd, J=1.5, 2.5, 4.7 Hz, H_5), 6.31 (dd, J=1.5, 7.0 Hz, H_6), 6.45 (dd, J=1.5, 7.0 Hz, H_7), 7.10 and 7.30 (m, C_6H_5); MS m/z 200 (M^+). Found: C, 78.05; H, 6.09%. Calcd for $C_{13}H_{12}O_2$: C, 77.98; H, 6.04%.

(1R,5S*)-1-Methyl-8-oxabicyclo[3.2.1]oct-6-en-3-one*: A solution of $\alpha,\alpha,\alpha',\alpha'$-tetrabromoacetone (212 g, 0.60 mol) in THF (200 ml) was added to a mixture of Zn/Ag couple (39.0 g, 0.60 g-atom), 2-methylfuran (30.0 ml, 0.30 mol), and THF (200 ml) over 1 h at −10 °C. The resulting mixture was stirred for 1 h at the same temperature and then for 24 h at 25 °C. Reductive workup with Zn/Cu couple (130 g, 2.0 g-atom) in NH_4Cl/CH_3OH (400 ml) followed by ordinary extractive workup gave a brown oil. Purification of this oil by chromatography on a silica-gel column (4:1 hexane–ethyl acetate) afforded the title compound (25.0 g, 60%) as an oil. R_f=0.22 (4:1 hexane–ethyl acetate); IR (neat) 1718 cm^{-1} (C=O); ^1H NMR ($CDCl_3$) δ 1.50 (s, CH_3), 2.1—2.9 (m, H_2 and H_4), 5.06 (ddd, J=1.2, 1.8, 5.0 Hz, H_5), 6.05 (d, J=5.8 Hz, H_7), 6.20 (dd, J=1.8, 5.8 Hz, H_6); MS m/z 138 (M^+). Found: m/z 138.0682. Calcd for $C_8H_{10}O_2$: M, 138.0681.

(1R,5S*)-1-Pentyl-8-oxabicyclo[3.2.1]oct-6-en-3-one*: A mixture of $\alpha,\alpha,\alpha',\alpha'$-tetrabromoacetone (112 g, 0.30 mol), Zn/Ag couple (13.0 g, 0.20 g-atom), 2-pentylfuran (15.0 g, 0.10 mol), and THF (250 ml) was stirred for 12 h at 25 °C. Reduction with Zn/Cu couple (100 g, 1.54 g-atom) in NH_4Cl/CH_3OH (300 ml) followed by extractive workup gave a brown oil. This oil was purified on a silica-gel column (4:1 hexane–ethyl acetate) to afford the title compound (9.70 g, 50%) as an oil. R_f=0.37 (4:1 hexane–ethyl acetate); IR (neat) 1718 cm^{-1} (C=O); ^1H NMR ($CDCl_3$) δ 0.91 (t, J=6.5 Hz, CH_3), 1.1—1.9 (m, CH_2), 2.1—2.8 (m, H_2 and H_4), 5.06 (ddd, J=1.1, 1.9, 5.0 Hz, H_5), 6.05 (d, J=6.0 Hz, H_7), 6.19 (dd, J=1.9, 6.0 Hz, H_6); MS m/z 194 (M^+). Found: m/z 194.1328. Calcd for $C_{12}H_{18}O_2$: M, 194.1307.

(1R,5S*)-1-Phenyl-8-oxabicyclo[3.2.1]oct-6-en-3-one*: A mixture of $\alpha,\alpha,\alpha',\alpha'$-tetrabromoacetone (77.8 g, 0.208 mol), Zn/Ag couple (9.0 g, 0.139 g-atom), 2-phenylfuran (10 g, 69.4 mmol), and THF (170 ml) was stirred for 48 h at 25 °C. Reduction with Zn/Cu couple (70 g, 1.08 g-atom) in NH_4Cl/CH_3OH (200 ml) followed by ordinary extractive workup gave a brown oil. Purification of this oil on a silica-gel column using a 4:1 hexane–ethyl acetate mixture afforded the title compound (8.60 g, 62%). Mp 94—96 °C (hexane–chloroform); R_f=0.29 (4:1 hexane–ethyl acetate); IR (neat) 1720 cm^{-1} (C=O); ^1H NMR ($CDCl_3$) δ 2.39 (dd, J=1.0, 16.0 Hz, H_{4a}), 2.82 (s, H_2), 2.83 (dd, J=5.0, 16.0 Hz, H_{4b}), 5.26 (dd, J=1.0, 5.0 Hz, H_5), 6.30 (s, H_6 and H_7), 7.42 (m, C_6H_5); MS m/z 200(M^+). Found: C, 78.24; H, 6.06%. Calcd for $C_{13}H_{12}O_2$: C, 77.98; H, 6.04%.

(1S,5S*)-1-Acetoxymethyl-8-oxabicyclo[3.2.1]oct-6-en-3-one*: A mixture of $\alpha,\alpha,\alpha',\alpha'$-tetrabromoacetone (3.74 g, 10 mmol), Zn/Ag couple (981 mg, 15.0 mg-atom), furfuryl acetate (7.0 g, 50 mmol), and THF (35 ml) was stirred for 12 h at 20 °C and worked up in a usual manner to give a dark oil. Chromatography on a silica-gel column using a 7:1 to 3:1 hexane–ethyl acetate mixture afforded 1.73 g (52%) of (1*S**, 2*R**,4*S**,5*R**)-1-acetoxymethyl-2,4-dibromo-8-oxabicyclo-[3.2.1]oct-6-en-3-one as a yellow solid. Pure sample was obtained by recrystallization from hexane–ethyl acetate. Mp 115—116.5 °C; R_f=0.14 (7:1 hexane–ethyl acetate); IR 1745 cm^{-1} (C=O); ^1H NMR ($CDCl_3$) δ 2.18 (s, CH_3CO), 4.54 (d, J=13.5 Hz, $\underline{H}_a\underline{H}_bCOC{=}O$), 4.67 (d, J=13.5 Hz, $H_a\underline{H}_bCOC{=}O$), 4.90 (d, J=4.5 Hz, H_4), 4.95 (s, H_2), 5.12 (dd, J=2.0, 4.5 Hz, H_5), 6.32 (d, J=6.5 Hz, H_7), 6.60 (dd, J=2.0, 6.5 Hz, H_6). Found: C, 33.95; H, 2.71; Br, 44.99%. Calcd for $C_{10}H_{10}O_4Br_2$: C, 33.93, H, 2.85; Br, 45.15%.

Treatment of this dibromo ketone (1.50 g, 4.44 mmol) with Zn/Cu couple (6.0 g, 92.3 mg-atom) in CH_3OH–CH_3COCH_3 (5:1, 30 ml) saturated with NH_4Cl at 20 °C for 1 h followed by extractive workup afforded the title compound (776 mg, 89%) as a yellow oil. Analytical sample was obtained by bulb-to-bulb distillation (bp 120 °C/0.01 mmHg). R_f=0.22 (2:1 hexane–ethyl acetate); IR 1722 cm^{-1} (C=O); ^1H NMR ($CDCl_3$) δ 2.12 (s, CH_3CO), 2.2—2.9 (m, H_2 and H_4), 4.34 (s, $CH_2OC{=}O$), 5.13 (m, H_5), 6.09 (d, J=6.0 Hz, H_7), 6.30 (dd, J=2.0, 6.0 Hz, H_6); ^{13}C NMR ($CDCl_3$) δ 45.07, 47.57, 65.25, 77.73, 84.83, 132.73, 134.54, 170.18, 204.00. Found: C, 61.10; H, 6.28%. Calcd for $C_{10}H_{12}O_4$: C, 61.24; H, 6.17%.

(1S,5S*)-1-Benzyloxymethyl-8-oxabicyclo[3.2.1]oct-6-en-3-one*: A mixture of $\alpha,\alpha,\alpha',\alpha'$-tetrabromoacetone (113 g, 0.3 mol), Zn/Ag couple (13.0 g, 0.2 g-atom), 2-(benzyloxymethyl)-furan (18.0 g, 95.7 mmol), and THF (300 ml) was stirred for 48 h at 30 °C and worked up in a usual manner to give a dark oil. Treatment of this oil with Zn/Cu couple (98 g, 1.5 g-atom) in NH_4Cl/CH_3OH (250 ml) at 25 °C for 1 h followed by silica-gel column chromotography using a 3:1 hexane–ethyl acetate mixture to afford 8.17 g (35%) of the title compound as a yellow oil. R_f=0.50 (1:1 hexane–ethyl acetate); IR (neat) 1720 cm^{-1} (C=O); ^1H NMR ($CDCl_3$) δ 2.1—2.9 (m, H_2 and H_4), 3.65 (s, $C\underline{H}_2OC\underline{H}_2C_6H_5$), 4.62 (s, $C\underline{H}_2C_6H_5$), 6.08 (d, J=6.0 Hz, H_7), 6.23 (dd, J=2.0, 6.0 Hz, H_6), 7.33 (s, C_6H_5).

(1R,5R*,6S*)-6-Benzoyloxy-8-oxabicyclo[3.2.1]octan-3-one* (**37**): To a solution of 8-oxabicyclo[3.2.1]oct-6-en-3-one (5.70 g, 50 mmol)[21b] in dry toluene (50 ml) was added diisobutylaluminium hydride in toluene (1.5 mol dm^{-3} solution, 44 ml, 65 mmol) at −78 °C under argon. After stirring for 3 h, the mixture was diluted with ether (50 ml) and to this was added slowly saturated NH_4Cl (10 ml). The mixture was warmed up to room temperature and stirred for 1 h. The insoluble material was removed by a Celite 545

pad and the filtrate was evaporated to give 8-oxabicyclo-[3.2.1]oct-6-en-3-ol (4.73 g, 82%) as a white semi-solid. This material was used in the next step without further purification. R_f=0.17 (1:1 hexane–ethyl acetate); IR (neat) 3380 cm^{-1} (OH); ^1H NMR ($CDCl_3$) δ 1.6—2.5 (m, H_2 and H_4), 4.0 (m, H_3), 4.74 (m, H_1 and H_5), 6.10 and 6.44 (s, 28:72 ratio).

A mixture of this alcohol (4.30 g, 37.1 mmol), pyridinium *p*-toluenesulfonate (931 mg, 3.71 mmol), 3,4-dihydro-2*H*-pyran (4.06 ml, 44.5 mmol), and CH_2Cl_2 (30 ml) was stirred for 48 h at 20 °C. The mixture was washed with brine (30 ml), dried, and evaporated to give a dark oil. Chromatography of the residue on a silica-gel column using a 4:1 hexane–ethyl acetate mixture afforded 3-(tetrahydropyran-2-yloxy)-8-oxabicyclo[3.2.1]oct-6-ene (6.68 g, 86%) as a colorless oil. R_f=0.39 (4:1 hexane–ethyl acetate); ^1H NMR ($CDCl_3$) δ 1.4—2.4 (m, 10H), 3.5 (m, 1H), 4.0 (m, 2H), 4.7 (m, 3H), 6.22 (m, 2H).

To a solution of this THP ether (3.30 g, 15.7 mmol) in dry THF (10 ml) was added BH_3 in THF (1.0 mol dm^{-3} solution, 6.8 ml, 6.8 mmol) at 0 °C under argon. The mixture was stirred for 1.5 h at 20 °C and to this was added H_2O (1 ml). After stirring for 10 min, 3 mol dm^{-3} NaOH (2.5 ml, 7.5 mmol) and 30% H_2O_2 (2.24 ml, 20.4 mmol) were added. The mixture was stirred for 1 h at 50 °C, cooled to room temperature, and diluted with ether (20 ml). The organic layer was separated, washed with brine, dried, and evaporated to give a colorless oil. To this oil in pyridine (10 ml) was added benzoyl chloride (2.39 ml, 20.4 mmol) under argon. The mixture was stirred for 12 h at 20 °C and evaporated. The residue was diluted with ether (50 ml), washed with brine, neutralized with 1 mol dm^{-3} HCl, dried, and evaporated to give a yellow oil. Chromatography of this oil on a silica-gel column using a 3:1 hexane–ethyl acetate mixture afforded (1*S**,5*R**,6*S**)-6-benzoyloxy-3-(tetrahydropyran-2-yloxy)-8-oxabicyclo[3.2.1]-oct-6-ene (4.64 g, 89%) as a colorless oil. R_f=0.31 (2:1 hexane–ethyl acetate); IR 1720 cm^{-1} (C=O); ^1H NMR ($CDCl_3$) δ 1.5—2.4 (m, 8H), 2.70—3.14 (m, 1H), 3.40—3.66 (m, 1H), 3.76—4.22 (m, 2H), 4.30—4.82 (m, 3H), 5.37 (m, 1H), 5.76 (dd, J=3.0, 7.1 Hz) and 5.93 (dd, J=2.2, 7.1 Hz) (total 1H), 7.30 and 8.06 (m, C_6H_5).

A mixture of this benzoate (4.60 g, 13.9 mmol), pyridinium *p*-toluenesulfonate (349 mg, 1.39 mmol), and CH_3OH (30 ml) was stirred for 20 h at 20 °C. The mixture was evaporated and the residue was diluted with ether (50 ml). The ether layer was washed with brine, dried, and evaporated to give a colorless oil. To a mixture of pyridinium chlorochromate (5.89 g, 27.8 mmol), sodium acetate (658 mg, 8.34 mmol), and CH_2Cl_2 (30 ml) was added the oil, obtained above, in CH_2Cl_2 (15 ml). The mixture was stirred for 2 h at 20 °C and diluted with hexane (20 ml). The insoluble material was removed by filtration and the filtrate was evaporated and chromatographed on a silica-gel column (1:1 hexane–ethyl acetate) to afford 2.20 g (58%) of **37** as a white solid. Mp 142—143 °C (hexane–chloroform); R_f=0.49 (1:2 hexane–ethyl acetate); IR 1720 cm^{-1} (C=O); ^1H NMR ($CDCl_3$) δ 2.2—2.9 (m, H_2, H_4, and H_7), 4.75 (d-like, J=5.2 Hz, H_5), 4.92 (m, H_1), 5.29 (dd, J=4.7, 5.2 Hz, H_6), 7.30 and 8.04 (m, C_6H_5); ^{13}C NMR ($CDCl_3$) δ 38.13, 46.26, 49.10, 74.69, 78.14, 80.18, 128.44, 129.69, 133.22, 133.57, 166.23, 204.86. Found: C, 68.45; H, 5.69%. Calcd for $C_{14}H_{14}O_4$: C, 68.28; H, 5.73%.

*(1*R*,5R*,6S*)-6-Benzyloxy-8-oxabicyclo[3.2.1]octan-3-one* (**33**): To a mixture of **37** (492 mg, 2 mmol), 1,2-bis(trimethylsiloxy)ethane (492 mg, 2.4 mmol), and dry CH_2Cl_2 (5 ml) was added trimethylsilyl triflate in CH_2Cl_2 (0.05 mol dm^{-3} solution, 4 ml, 0.2 mmol) at 0 °C under argon. The mixture was stirred for 30 min at 20 °C and to this was added pyridine (0.1 ml). The reaction mixture was washed with brine, dried, and evaporated to afford ethylene acetal of **37** (580 mg, 100%) as white crystals. Mp 92—93 °C; R_f=0.47 (1:1 hexane–ethyl acetate); IR 1718 cm^{-1} (C=O); ^1H NMR ($CDCl_3$) δ 1.70 (d-like, J=14.7 Hz, 1H), 1.95—2.23 (m, 4H), 2.80 (dd, J=7.8, 14.7 Hz, 1H), 3.92 (m, OCH_2CH_2O), 4.45 (m, H_5), 4.66 (m, H_1), 5.69 (dd, J=2.7, 7.3 Hz, H_6), 7.45 and 8.02 (m, C_6H_5).

A mixture of this ethylene acetal (2.03 g, 7 mmol), lithium hydroxide (40 mg), and CH_3OH (25 ml) was stirred for 48 h at 15 °C under argon. The mixture was evaporated and the residue was diluted with ether (50 ml). The organic layer was washed with saturated NH_4Cl (10 ml), brine, dried, and evaporated to give a yellow oil. To a suspension of NaH (50% oil dispersion, 323 mg, 6.72 mmol) in DMF (10 ml) was added the above obtained oil in DMF (5 ml). The mixture was stirred for 1 h at 50 °C under argon. After the mixture was cooled to 0 °C, benzyl chloride (1.19 ml, 10.3 mmol) was added. The reaction mixture was stirred for 12 h at 15 °C and evaporated. The residue was diluted with ether (20 ml) and the ether layer was washed with brine, dried, and evaporated to give a yellow oil. Chromatography of this oil on a silica-gel column using a 1:1 hexane–ethyl acetate mixture afforded a colorless oil (1.14 g, 80%). ^1H NMR ($CDCl_3$) δ 1.55—2.19 (m, 5H), 2.59 (dd, J=7.0, 12.7 Hz, 1H), 3.89 (m, OCH_2CH_2O), 4.41 (m, 1H), 4.49 (s, $C\underline{H}_2C_6H_5$), 4.61 (m, 1H), 7.34 (s, C_6H_5).

A mixture of this oil (1.14 g, 4.14 mmol), oxalic acid (100 mg), THF (10 ml), and H_2O (10 ml) was stirred for 8 h at 50 °C. The mixture was evaporated, extracted with chloroform (30 ml), washed with brine, dried, and concentrated to give 872 mg (91%) of **33** as a white solid. Mp 55—57 °C (ether–hexane); R_f=0.35 (1:1 hexane–ethyl acetate); IR (neat) 1719 cm^{-1} (C=O); ^1H NMR ($CDCl_3$) δ 2.02—2.80 (m, H_2, H_4, and H_7), 3.94 (dd, J=3.2, 6.0 Hz, H_6), 4.46 (s, $C\underline{H}_2C_6H_5$), 4.64 (d-like, J=5.0 Hz, H_5), 4.80 (m, H_1), 7.30 (s, C_6H_5); ^{13}C NMR ($CDCl_3$) δ 38.50, 46.80, 49.24, 71.23, 74.71, 79.55, 82.36, 127.72, 128.45, 137.85, 205.66. Found: C, 72.13; H, 6.90%. Calcd for $C_{14}H_{16}O_3$: C, 72.39; H, 6.94%.

*(1*R*,5R*,6S*)-6-Hydroxy-8-oxabicyclo[3.2.1]octan-3-one*: A mixture of **37** (10.0 g, 40.7 mmol), lithium hydroxide (293 mg, 12.2 mmol), and dry CH_3OH (100 ml) was stirred for 15 h at 20 °C under argon. The mixture was evaporated and the residue was chromatographed on a silica-gel column using 3:1 hexane–ethyl acetate to pure ethyl acetate afforded 9.39 g (98%) of the title compound as a colorless oil. R_f=0.18 (3:1 ethyl acetate–hexane); IR (neat) 3380 (OH), 1720 cm^{-1} (C=O); ^1H NMR ($CDCl_3$) δ 2.0—2.8 (m, H_2, H_4, and H_7), 3.15 (s, OH), 4.27 (dd, J=3.2, 6.0 Hz, H_6), 4.51 (d-like, J=6.0 Hz, H_5), 4.84 (m, H_1); ^{13}C NMR ($CDCl_3$) δ 41.27, 46.14, 49.47, 74.70, 75.45, 82.69, 206.09.

*(1*R*,5R*,6S*)-6-t-Butyldimethylsiloxy-8-oxabicyclo[3.2.1]-octan-3-one* (**34**): A mixture of **37** (2.00 g, 8.13 mmol), lithium hydroxide (60 mg, 2.5 mmol), and CH_3OH (10 ml) was stirred for 12 h at 20 °C. The reaction mixture was evaporated to dryness and coevaporated with benzene (5 ml × 3). To the residue in DMF (10 ml) were added *t*-butyldimethylsilyl chloride (1.83 g, 12.2 mmol) and imidazole (1.66 g, 24.4 mmol) in DMF (15 ml).[34] The mixture was stirred for 12 h at 20 °C and evaporated. The residue was diluted with ethyl acetate, washed with brine, dried, and evaporated to give a pale yellow oil. This oil was chromatographed on a silica-gel column using a 2:1 hexane–ethyl acetate mixture to afford 1.83 g (90%) of **34** as a colorless oil. R_f=

0.45 (2:1 hexane–ethyl acetate); IR (neat) 1720 cm^{-1} (C=O); ^1H NMR ($CDCl_3$) δ 0.02 (s, t-$C_4H_9(C\underline{H}_3)_2Si$), 0.85 (s, t-$C_4\underline{H}_9(CH_3)_2Si$), 1.94—2.79 (m, H_2, H_4, and H_7), 4.20 (dd, J=3.8, 6.0 Hz, H_6), 4.41 (d-like, J=5.2 Hz, H_5), 4.80 (m, H_1); ^{13}C NMR ($CDCl_3$) δ 18.01, 25.78, 42.02, 46.78, 49.28, 74.93, 76.08, 83.02, 205.76.

(1R,5R*,6S*)-6-Acetoxy-8-oxabicyclo[3.2.1]octan-3-one (**35**)*: A mixture of (1*R**,5*R**,6*S**)-6-hydroxy-8-oxabicyclo[3.2.1]-octan-3-one (426 mg, 3 mmol), pyridine (2 ml), and acetic anhydride (2 ml) was stirred for 12 h at 20 °C under argon. The reaction mixture was evaporated and the residue was chromatographed on a silica-gel column using a 2:1 ethyl acetate–hexane mixture to afford 564 mg (100%) of **35** as a white solid. Mp 57—58 °C (hexane–chloroform); R_f= 0.40 (2:1 ethyl acetate–hexane); IR 1732 and 1723 cm^{-1} (C=O); ^1H NMR ($CDCl_3$) δ 2.07 (s, CH_3CO), 2.14—2.88 (m, H_2, H_4, and H_7), 4.62 (d-like, J=5.2 Hz, H_5), 4.88 (m, H_1), 5.06 (dd, J=4.7, 6.0 Hz, H_6); ^{13}C NMR ($CDCl_3$) δ 20.81, 38.02, 46.15, 49.05, 74.58, 77.32, 80.06, 170.40, 204.78. Found: C, 58.58; H, 6.63%. Calcd for $C_9H_{12}O_4$: C, 58.69; H, 6.57%.

(1R,5R*,6S*)-6-Pivaloyloxy-8-oxabicyclo[3.2.1]octan-3-one (**36**)*: To a solution of (1*R**,5*R**,6*S**)-6-hydroxy-8-oxabicyclo[3.2.1]octan-3-one (426 mg, 3 mmol) in dry pyridine (7 ml) was added pivaloyl chloride (0.75 ml, 6 mmol) at 0 °C under argon. After stirring for 12 h at 20 °C, the mixture was concentrated. The residue was chromatographed on a silica-gel column using a 1:1 hexane–ethyl acetate mixture to give **36** (687 mg, 100%) as a white solid. Mp 57—58 °C (ether–hexane); R_f=0.50 (1:1 hexane–ethyl acetate); IR 1723 cm^{-1} (C=O); ^1H NMR ($CDCl_3$) δ 1.19 (s, t-C_4H_9), 2.08—2.86 (m, H_2, H_4, and H_7), 4.55 (d-like, J=5.5 Hz, H_5), 4.86 (m, H_1), 5.01 (dd, J=4.0, 6.0 Hz, H_6); ^{13}C NMR ($CDCl_3$) δ 27.04, 38.02, 38.51, 46.32, 49.04, 74.64, 77.42, 80.14, 178.04, 204.77. Found: C, 63.40; H, 8.11%. Calcd for $C_{12}H_{18}O_4$: C, 63.70; H, 8.02%.

6-Methyl-8-oxabicyclo[3.2.1]oct-6-en-3-one: To a mixture of Zn/Ag couple (39.0 g, 0.60 g-atom), 3-methylfuran (4.6 g, 0.3 mol), and THF (300 ml) was added a solution of α,α,α′,α′-tetrabromoacetone (337 g, 0.9 mol) in THF (150 ml) over 1 h at 0 °C. After stirring for 14 h at 25 °C, the mixture was concentrated. Reduction with Zn/Cu couple (293 g, 4.5 g-atom) in NH_4Cl/CH_3OH (500 ml) followed by ordinary extractive workup afforded a brown oil. Chromatography of this oil on a silica-gel column using a 5:1 hexane–ethyl acetate mixture afforded the title compound (35.8 g, 86%) as an oil. R_f=0.26 (5:1 hexane–ethyl acetate); IR (neat) 1718 cm^{-1} (C=O); ^1H NMR ($CDCl_3$) δ 1.78 (s, CH_3), 2.16—2.82 (m, H_2 and H_4), 4.70 (d, J=5.0 Hz, H_5), 4.94 (m, H_1), 5.78 (m, H_7); ^{13}C NMR ($CDCl_3$) δ 11.75, 45.04, 45.44, 77.08, 79.94, 126.24, 142.96, 204.25; MS m/z 138 (M^+).

6-Pentyl-8-oxabicyclo[3.2.1]oct-6-en-3-one: A mixture of 3-pentylfuran (3.59 g, 26 mmol), Zn/Ag couple (3.36 g, 52 mg-atom), α,α,α′,α′-tetrabromoacetone (29.2 g, 78 mmol), and THF (66 ml) was stirred for 48 h at 30 °C under argon. Reduction with Zn/Cu couple (26 g, 0.39 g-atom) in NH_4Cl/CH_3OH (100 ml) followed by ordinary extractive workup gave a brown oil. Purification of this oil on a silica gel column using a 6:1 hexane–ethyl acetate mixture afforded 984 mg (20%) of the title compound as an oil. R_f=0.43 (3:1 hexane–ethyl acetate); IR (neat) 1718 cm^{-1} (C=O); ^1H NMR ($CDCl_3$) δ 0.90 (m, CH_3), 1.1—1.7 (m, CH_2), 2.0—2.9 (m, CH_2, H_2, and H_4), 4.79 (d, J=4.8 Hz, H_5), 4.99 (m, H_1), 5.81 (m, H_7); ^{13}C NMR ($CDCl_3$) δ 13.96, 20.50, 27.22, 31.67, 46.37, 77.81, 79.46, 125.56, 148.81, 205.37.

6-t-Butyl-8-oxabicyclo[3.2.1]oct-6-en-3-one: A mixture of 3-*t*-butylfuran (9.18 g, 74 mmol), Zn/Ag couple (9.56 g, 148 mg-atom), α,α,α′,α′-tetrabromoacetone (83.2 g, 222 mmol), and THF (177 ml) was stirred for 60 h at 20 °C under argon. Reduction with Zn/Cu couple (73 g, 1.11 g-atom) in NH_4Cl/CH_3OH (300 ml) followed by ordinary extractive workup gave a brown oil. Chromatography of this oil on a silica-gel column using a 5:1 to 1:1 hexane–ethyl acetate afforded the title compound (3.06 g, 23%) as an oil. R_f=0.50 (2:1 hexane–ethyl acetate); IR (neat) 1716 cm^{-1} (C=O); ^1H NMR ($CDCl_3$) δ 1.10 (s, t-C_4H_9), 2.1—3.0 (m, H_2 and H_4), 4.96 (m, H_1 and H_5), 5.82 (m, H_7); ^{13}C NMR ($CDCl_3$) δ 29.55, 31.73, 46.42, 48.13, 77.16, 77.56, 124.17, 128.34, 204.96.

6-Phenyl-8-oxabicyclo[3.2.1]oct-6-en-3-one: A mixture of 3-phenylfuran (5.51 g, 38.3 mmol), Zn/Ag couple (4.97 g, 76.6 mg-atom), α,α,α′,α′-tetrabromoacetone (42.9 g, 115 mmol), and THF (100 ml) was stirred for 48 h at 19 °C. Reduction with Zn/Cu couple (49.8 g, 766 mg-atom) in NH_4Cl/CH_3OH (100 ml) followed by ordinary extractive workup afforded 1.69 g (22%) of the title compound as a solid. Mp 94.0—96.5 °C (ether–hexane); R_f=0.69 (2:1 ethyl acetate–hexane); IR 1715 cm^{-1} (C=O); ^1H NMR ($CDCl_3$) δ 2.3—3.0 (m, H_2 and H_4), 5.16 (m, H_1), 5.40 (m, H_5), 6.48 (d, J=2.2 Hz, H_7), 7.34 (s, C_6H_5); ^{13}C NMR ($CDCl_3$) δ 45.87, 46.56, 77.97, 78.54, 125.90, 126.26, 128.85, 128.96, 131.45, 204.53.

6-(Tetrahydropyran-2-yloxymethyl)-8-oxabicyclo[3.2.1]oct-6-en-3-one: A mixture of 3-(tetrahydropyran-2-yloxymethyl)furan (17.0 g, 43.3 mmol), Zn/Ag couple (12.2 g, 0.187 g-atom), α,α,α′,α′-tetrabromoacetone (105 g, 280 mmol), and THF (224 ml) was stirred for 60 h at 20 °C. Reduction with Zn/Cu couple (91 g, 1.4 g-atom) in NH_4Cl/CH_3OH (500 ml) followed by ordinary extractive workup gave the title compound (6.93 g, 31%) as a brown oil. R_f=0.44 (1:1 hexane–ethyl acetate); IR (neat) 1715 cm^{-1} (C=O), ^1H NMR ($CDCl_3$) δ 1.4—1.9 (m, 6H), 2.19—2.92 (m, H_2 and H_4), 3.32—3.95 (m, 2H), 4.14 (d, J=13.6 Hz, $\underline{H}_a\underline{H}_b$COTHP), 4.36 (d, J=13.6 Hz, $H_a\underline{H}_b$COTHP), 4.60 (br, OCHO), 4.98 (m, H_1 and H_5), 6.08 (m, H_7).

Preparation of 6,7-Isopropylidenedioxy-8-oxabicyclo[3.2.1]octan-3-one Derivatives. (1R,2R*,5S*,6S*,7R*)-6,7-Isopropylidenedioxy-2-methyl-8-oxabicyclo[3.2.1]octan-3-one (**1**)*: To a mixture of (1*S**,2*R**,5*S**)-2-methyl-8-oxabicyclo[3.2.1]oct-6-en-3-one (8.0 g, 57.9 mmol), acetone (60 ml), t-C_4H_9OH (6 ml), ether (6 ml), and OsO_4 (30 mg) was added 30% H_2O_2 (19.0 ml, 174 mmol) over 10 min at 0 °C. After stirring for 12 h at 25 °C, the mixture was cooled to 0 °C. To this was added slowly $Na_2S_2O_3 \cdot 5H_2O$ (30 g) and the reaction mixture was stirred for 3 h at 0 °C and concentrated. The residue was extracted with ethyl acetate (60 ml×4) and the organic extracts were dried and evaporated to give a dark solid. To a solution of this solid in acetone (100 ml) was added $CuSO_4$ (13 g) and p-toluenesulfonic acid (15 mg) and the mixture was stirred for 18 h at 25 °C. The insoluble material was removed by filtration and the filtrate was evaporated to give a yellow oil. Chromatography of this oil on a silica-gel column using a 2:1 to 1:1 hexane–ethyl acetate mixture afforded **1** (6.82 g, 56%). Mp 126.1—127.5 °C (ether); R_f=0.46 (1:1 hexane–ethyl acetate); IR 1710 cm^{-1} (C=O); ^1H NMR ($CDCl_3$) δ 1.28 (d, J=7.0 Hz, CH_3), 1.29 and 1.50 (s, isopropylidene CH_3), 2.34 (d, J=16.0 Hz, H_{4a}), 2.73 (dd, J=6.0, 16.0 Hz, H_{4b}), 2.80 (m, H_2), 4.39 (d, J=5.5 Hz, H_1), 4.46 (s, H_6 and H_7), 4.60 (d, J=6.0 Hz, H_5); MS m/z 197 (M^+—15). Found: C, 61.85; H, 7.72%. Calcd for $C_{11}H_{16}O_4$: C, 62.25; H, 7.60%.

(1R,2R*,5S*,6S*,7R*)-6,7-Isopropylidenedioxy-2-pentyl-8-oxabicyclo[3.2.1]octan-3-one (**2**)*: To a mixture of (1*S**,2*R**,5*S**)-2-pentyl-8-oxabicyclo[3.2.1]oct-6-en-3-one (26.8 g, 138

mmol), acetone (250 ml), ether (20 ml), t-C_4H_9OH (20 ml), and OsO_4 (200 mg) was added 30% H_2O_2 (75.9 ml, 691 mmol) over period of 1 h. After stirring for 24 h at 25 °C, OsO_4 (100 mg) and 30% H_2O_2 (50 ml) were further added. The mixture was stirred for 12 h and worked up in a usual manner to afford a pale green oil. This oil was dissolved in 150 ml of dry acetone and to this was added $CuSO_4$ (40 g) and p-toluenesulfonic acid (300 mg). The resulting mixture was stirred for 12 h at 25 °C and worked up in a usual manner to give a yellow oil. Chromatography of this oil on a silica-gel column using a 3:1 hexane–ethyl acetate mixture afforded 18.5 g (50%) of **2**. Analytically pure sample was obtained by bulb-to-bulb distillation (160 °C/0.03 mmHg). Mp 45—47 °C; R_f=0.54 (1:1 hexane–ethyl acetate); IR 1719 cm^{-1} (C=O); ^1H NMR (C_6D_6) δ 0.84 (t-like, J=6.0 Hz, CH_3), 1.09 and 1.51 (s, isopropylidene CH_3), 1.20 (m, CH_2), 1.83 (d, J=15.0 Hz, H_{4a}), 2.16 (dd, J=6.0, 15.0 Hz, H_{4b}), 2.20 (m, H_2), 4.08 (d, J=6.0 Hz, H_6), 4.27 (d, J=6.0 Hz, H_7), 4.40 (m, H_1 and H_5); MS m/z 253 (M^+-15). Found: C, 67.34; H, 9.01%. Calcd for $C_{15}H_{24}O_4$: C, 67.13; H, 9.02%.

(1S,5S*,6S*,7S*)-2,2-Dimethyl-6,7-isopropylidenedioxy-8-oxabicyclo[3.2.1]octan-3-one (**4**)*: A mixture of 2,2-dimethyl-8-oxabicyclo[3.2.1]oct-6-en-3-one (12.8 g, 84.2 mmol), acetone (240 ml), t-C_4H_9OH (24 ml), ether (24 ml), OsO_4 (100 mg), and 30% H_2O_2 (28 ml, 253 mmol) was stirred for 12 h at 25 °C and worked up in a usual manner to afford a white solid. To a solution of this solid in acetone (150 ml) was added $CuSO_4$ (20 g) and p-toluenesulfonic acid (100 mg) and the mixture was stirred for 12 h at 25 °C. Usual workup left a yellow oil. Chromatography of the residue on a silica-gel column using a 3:1 hexane–ethyl acetate mixture afforded **4** (11.2 g, 59%). Mp 109.5—110 °C (ether); R_f=0.34 (2:1 hexane–ethyl acetate); IR 1709 cm^{-1} (C=O); ^1H NMR ($CDCl_3$) δ 1.11 and 1.34 (s, CH_3), 1.31 and 1.50 (s, isopropylidene CH_3), 2.20 (d, J=16.0 Hz, H_{4a}), 2.91 (dd, J=6.0, 16.0 Hz, H_{4b}), 4.02 (s, H_1), 4.44 (d, J=5.5 Hz, H_6), 4.52 (d, J=6.0 Hz, H_5), 4.60 (d, J=5.5 Hz, H_7); MS m/z 226 (M^+). Found: C, 63.74; H, 8.07%. Calcd for $C_{12}H_{18}O_4$: C, 63.70; H, 8.02%.

(1R,2S*,5S*,6S*,7R*)-6,7-Isopropylidenedioxy-2-phenyl-8-oxabicyclo[3.2.1]octan-3-one (**3**)*: A mixture of (1*S**,2*S**,5*S**)-2-phenyl-8-oxabicyclo[3.2.1]oct-6-en-3-one (5.10 g, 25.5 mmol), acetone (50 ml), ether (5 ml), t-C_4H_9OH (5 ml), and OsO_4 (30 mg) was added 30% H_2O_2 (7 ml, 63 mmol) at 0 °C. The resulting mixture was stirred for 24 h at 25 °C and worked up in a usual manner to give a yellow solid. To a solution of this solid in 30 ml of dry acetone was added $CuSO_4$ (5 g) and p-toluenesulfonic acid (10 mg) and the mixture was stirred for 20 h at 25 °C. Usual workup in a usual manner followed by purification on a silica-gel column using a 2:1 hexane–ethyl acetate mixture afforded **3** (3.55 g, 51%). Mp 162.3—162.8 °C (hexane–ethyl acetate); R_f=0.42 (1:1 hexane–ethyl acetate); IR 1710 cm^{-1} (C=O); ^1H NMR ($CDCl_3$) δ 1.28 and 1.50 (s, isopropylidene CH_3), 2.48 (d, J=16.0 Hz, H_{4a}), 2.88 (dd, J=6.0, 16.0 Hz, H_{4b}), 4.02 (d, J=5.0 Hz, H_2), 4.61 (d, J=5.7 Hz, H_6), 4.65 (m, H_1 and H_5), 4.78 (d, J=5.7 Hz, H_7); MS m/z 274 (M^+). Found: C, 70.17; H, 6.46%. Calcd for $C_{16}H_{18}O_4$: C, 70.05; H, 6.61%.

(1R,5S*,6S*,7S*)-6,7-Isopropylidenedioxy-1-methyl-8-oxabicyclo[3.2.1]octan-3-one (**9**)*: To a solution of (1*R**,5*S**)-1-methyl-8-oxabicyclo[3.2.1]oct-6-en-3-one (25.0 g, 181 mmol), acetone (181 ml), t-C_4H_9OH (18 ml), ether (18 ml), and OsO_4 (400 mg) was added 30% H_2O_2 (39.3 ml, 362 mmol) and the resulting mixture was stirred for 12 h at 25 °C. The mixture was subjected to usual workup to give oily residue. A mixture of the resulting oil, $CuSO_4$ (50 g), p-toluenesulfonic acid (170 mg), and acetone (180 ml) was stirred for 12 h at 25 °C. The mixture was usually worked up to give a black oil, which was purified on a silica-gel column using a 5:1 to 3:1 hexane–ethyl acetate to afford **9** (20.3 g, 53%). Mp 76—77 °C (hexane–chloroform); R_f=0.40 (2:1 hexane–ethyl acetate); IR 1719 cm^{-1} (C=O); ^1H NMR ($CDCl_3$) δ 1.30 and 1.52 (s, isopropylidene CH_3), 1.42 (s, CH_3), 2.2—2.8 (m, H_2 and H_5), 4.30 (d, J=5.7 Hz, H_7), 4.51 (d, J=5.7 Hz, H_6), 4.55 (dd, J=1.8, 5.2 Hz, H_5); ^{13}C NMR ($CDCl_3$) δ 20.11, 24.99, 26.15, 45.12, 52.70, 78.99, 83.72, 84.45, 84.68, 112.39, 205.59; MS m/z 197 (M^+-15). Found: C, 61.97; H, 7.84%. Calcd for $C_{11}H_{16}O_4$: C, 62.25, H, 7.60%.

(1R,5S*,6S*,7S*)-6,7-Isopropylidenedioxy-1-pentyl-8-oxabicyclo[3.2.1]octan-3-one (**10**)*: A mixture of (1*R**,5*S**)-1-pentyl-8-oxabicyclo[3.2.1]oct-6-en-3-one (9.70 g, 50.0 mmol), OsO_4 (100 mg), 30% H_2O_2 (11 ml, 100 mmol), acetone (150 ml), t-C_4H_9OH (15 ml), and ether (15 ml) was stirred for 24 h at 25 °C. The resulting mixture was worked up in a usual manner to produce a brown oil. A mixture of this oil, $CuSO_4$ (10 g), p-toluenesulfonic acid (100 mg), and acetone (100 ml) was stirred for 48 h at 25 °C and then worked up in a usual manner to give a brown oil. Chromatography of this oil using a 7:1 to 4:1 hexane–ethyl acetate mixture afforded **10** (7.0 g, 56%) as an oil. R_f=0.50 (4:1 hexane–ethyl acetate); IR 1719 cm^{-1} (C=O); ^1H NMR ($CDCl_3$) δ 0.91 (t, J=7.0 Hz, CH_3), 1.2—2.0 (m, CH_2), 1.29 and 1.50 (s, isopropylidene CH_3), 2.2—2.8 (m, H_2 and H_4), 4.33 (d, J=5.8 Hz, H_7), 4.49 (d, J=5.8 Hz, H_6), 4.55 (dd, J=1.7, 6.0 Hz, H_5); ^{13}C NMR ($CDCl_3$) δ 13.95, 22.55, 23.40, 25.05, 26.17, 32.39, 33.68, 45.52, 50.10, 78.88, 84.14, 84.44, 86.39, 112.29, 205.88; MS m/z 253 (M^+-15).

(1R,5S*,6S*,7S*)-6,7-Isopropylidenedioxy-1-phenyl-8-oxabicyclo[3.2.1]octan-3-one (**11**)*: A mixture of (1*R**,5*S**)-1-phenyl-8-oxabicyclo[3.2.1]oct-6-en-3-one (14.7 g, 73.1 mmol), acetone (150 ml), t-C_4H_9OH (15 ml), ether (15 ml), OsO_4 (200 mg), and 30% H_2O_2 (16.2 ml, 146 mmol) was stirred at 25 °C. After stirring for 12 h, 30% H_2O_2 (8.1 ml, 73.1 mmol) was further added. After further stirring for 12 h, the reaction mixture was worked up in a usual manner to afford a black oil. A mixture of this oil, $CuSO_4$ (35 g), p-toluenesulfonic acid (200 mg), and acetone (100 ml) was stirred for 24 h at 25 °C and worked up in a usual manner to afford a brown solid. Chromatography of this solid using a silica-gel column (7:1 to 4:1 hexane–ethyl acetate) afforded **11** (10.1 g, 51%). Mp 166—168 °C (hexane–chloroform); R_f=0.48 (4:1 hexane–ethyl acetate); IR 1720 cm^{-1} (C=O); ^1H NMR ($CDCl_3$) δ 1.24 and 1.34 (s, isopropylidene CH_3), 2.3—3.0 (m, H_2 and H_4), 4.61 (d, J=5.5 Hz, H_7), 4.69 (d, J=5.5 Hz, H_6), 4.77 (dd, J=1.5, 5.5 Hz, H_5), 7.2—7.6 (m, C_6H_5); ^{13}C NMR ($CDCl_3$) δ 24.93, 26.00, 45.30, 53.01, 78.94, 84.48, 85.33, 87.48, 112.63, 125.51, 127.59, 128.26, 139.55, 205.50; MS m/z 259 (M^+-15). Found: C, 69.58, H, 6.76%. Calcd for $C_{16}H_{18}O_4$: C, 70.05; H, 6.61%.

(1S,5S*,6S*,7S*)-1-Acetoxymethyl-6,7-isopropylidenedioxy-8-oxabicyclo[3.2.1]octan-3-one (**17**)*: A mixture of (1*R**,5*S**)-1-acetoxymethyl-8-oxabicyclo[3.2.1]oct-6-en-one (13.1 g, 66.7 mmol), acetone (150 ml), t-C_4H_9OH (15 ml), ether (15 ml), OsO_4 (200 mg), and 30% H_2O_2 (14.7 ml, 133 mmol) was stirred for 20 h at 25 °C and worked up as usual. The residual oil was dissolved in acetone (150 ml) and to this was added $CuSO_4$ (20 g) and p-toluenesulfonic acid (100 mg). The resulting mixture was stirred for 12 h at 25 °C and worked up usual. Purification on a silica-gel column using a 3:1 to 1:1 hexane–ethyl mixture afforded 11.2 g

(62%) of **17** as a yellow oil. Analytically pure sample was obtained by recrystallization from hexane–chloroform. Mp 84—86 °C; R_f=0.40 (1:1 hexane–ethyl acetate); IR 1732 and 1720 cm^{-1} (C=O); ^{1}H NMR ($CDCl_3$) δ 1.30 and 1.50 (s, isopropylidene CH_3), 2.12 (s, CH_3CO), 2.2—2.9 (m, H_2 and H_4), 4.36 (s, CH_2OC=O), 4.46 (d, J=6.0 Hz, H_7), 4.56 (d, J=6.0 Hz, H_6), 4.63 (m, H_5); ^{13}C NMR ($CDCl_3$) δ 20.44, 24.69, 25.85, 44.78, 47.57, 64.25, 79.45, 83.66, 84.01, 112.69, 170.02, 204.19. Found: C, 57.39; H, 6.66%. Calcd for $C_{13}H_{18}O_6$: C, 57.77; H, 6.71%.

(1S,5S*,6S*,7S*)-1-Benzyloxymethyl-6,7-isopropylidenedioxy-8-oxabicyclo[3.2.1]octan-3-one (**16**)*: A mixture of (1*R**,5*S**)-1-benzyloxymethyl-8-oxabicyclo[3.2.1]oct-6-en-3-one (1.50 g, 6.14 mmol), acetone (20 ml), ether (2 ml), *t*-C_4H_9OH (2 ml), OsO_4 (30 mg), and 30% H_2O_2 (1.35 ml, 12.3 mmol) was stirred for 12 h at 25 °C. Usual workup left a brown oil, which was mixed with acetone (20 ml), $CuSO_4$ (5 g), and *p*-toluenesulfonic acid (10 mg), and kept for 12 h at 25 °C. Usual workup left a brown oil. Purification of this oil on a silica-gel column using a 4:1 hexane–ethyl acetate mixture afford **16** (1.07 g, 55%) as a yellow oil. R_f=0.23 (4:1 hexane–ethyl acetate); IR (neat) 1721 cm^{-1} (C=O); ^{1}H NMR ($CDCl_3$) δ 1.24 and 1.45 (s, isopropylidene CH_3), 2.1—3.0 (m, H_2 and H_4), 3.63 (d, J=11.0 Hz, H_aH_b-$COCH_2C_6H_5$), 3.78 (d, J=11.0 Hz, $H_aH_bCOCH_2C_6H_5$), 4.40 (d, J=6.0 Hz, H_6), 4.50 (d, J=6.0 Hz, H_7), 4.58 (d, J=4.2 Hz, $H_aH_bCC_6H_5$), 4.68 (d, J=4.2 Hz, $H_aH_bCC_6H_5$), 4.72 (m, H_5), 7.33 (s, C_6H_5); ^{13}C NMR ($CDCl_3$) δ 24.88, 26.04, 45.16, 48.13, 70.46, 73.71, 79.50, 84.03, 85.36, 112.52, 127.71, 128.39, 138.21, 205.41.

(1S,5S*,6S*,7S*)-1-Hydroxymethyl-6,7-isopropylidenedioxy-8-oxabicyclo[3.2.1]octan-3-one*: A mixture of **17** (113 mg, 0.419 mmol) and lithium hydroxide (5 mg) in CH_3OH (2.5 ml) was stirred for 12 h at 20 °C under argon. The mixture was evaporated and the residue was triturated with CH_2Cl_2 (10 ml). Evaporation of the organic solvent afforded the title compound (96 mg, 96%) as a yellow oil. Analytically pure sample was obtained by recrystallization from ether–ethyl acetate–hexane. Mp 89—91 °C; R_f=0.31 (1:1 hexane–ethyl acetate); IR 3500 (OH), 1720 cm^{-1} (C=O); ^{1}H NMR ($CDCl_3$) δ 1.28 and 1.50 (s, isopropylidene CH_3), 1.97 (br, OH), 2.2—2.9 (m, H_2 and H_4), 3.79 (d, J=11.5 Hz, H_aH_bCOH), 3.97 (d, J=11.5 Hz, H_aH_bCOH), 4.47 (d, J=5.5 Hz, H_7), 4.56 (d, J=5.5 Hz, H_6), 4.62 (m, H_5). Found: C, 57.84; H, 7.07%. Calcd for $C_{11}H_{16}O_5$: C, 57.88; H, 7.07%.

(1S,5S*,6S*,7S*)-6,7-Isopropylidenedioxy-1-pivaloyloxymethyl-8-oxabicyclo[3.2.1]octan-3-one (**18**)*: To a mixture of (1*S**, 5*S**,6*S**,7*S**)-1-hydroxymethyl-6,7-isopropylidenedioxy-8-oxabicyclo[3.2.1]octan-3-one (500 mg, 2.1 mmol) in pyridine (10 ml) was added pivaloyl chloride (0.52 ml, 4.1 mmol) at 0 °C under argon. The mixture was stirred for 30 min at the same temperature and for 12 h at 25 °C. The mixture was evaporated and the residue was partitioned between ethyl acetate and brine. The organic layer was dried and evaporated. The residue was chromatographed on a silica-gel column using a 4:1 hexane–ethyl acetate mixture to afford 639 mg (98%) of **18** as a colorless oil. Analytical sample was obtained by recrystallization from ether–hexane. Mp 88—90 °C, R_f=0.64 (1:1 hexane–ethyl acetate); IR 1724 cm^{-1} (C=O); ^{1}H NMR ($CDCl_3$) δ 1.24 (s, *t*-C_4H_9), 1.29 and 1.50 (s, isopropylidene CH_3), 2.2—2.9 (m, H_2 and H_4), 4.35 (s, CH_2OC=O), 4.45 (d, J=6.0 Hz, H_7), 4.55 (d, J=6.0 Hz, H_6), 4.63 (m, H_5); ^{13}C NMR ($CDCl_3$) δ 24.82, 25.98, 27.19, 38.89, 45.03, 47.87, 64.37, 79.57, 83.83, 84.07, 84.27, 112.78, 117.59, 204.44. Found: C, 61.54; H, 7.80%. Calcd for $C_{16}H_{24}O_6$: C, 61.52; H, 7.75%.

(1S,5S*,6S*,7S*)-1-Benzoyloxymethyl-6,7-isopropylidenedioxy-8-oxabicyclo[3.2.1]octan-3-one (**19**)*: To a solution of (1*S**, 5*S**,6*S**,7*S**)-1-hydroxymethyl-6,7-isopropylidenedioxy-8-oxabicyclo[3.2.1]octan-3-one (500 mg, 2.10 mmol) in pyridine (10 ml) was added benzoyl chloride (0.49 ml, 4.2 mmol) at 0 °C. The mixture was stirred for 30 min at 0 °C and then 12 h at 25 °C. The mixture was evaporated and the residue was diluted with benzene. The organic layer was washed with brine, 1 mol dm^{-3} HCl, saturated $NaHCO_3$, and then dried, and evaporated to give a yellow oil. Chromatography of this oil on a silica-gel column using a 3:1 hexane–ethyl acetate mixture afforded 615 mg (88%) of **19** as a white solid. Mp 152—153 °C (hexane–chloroform); R_f=0.55 (1:1 hexane–ethyl acetate); IR 1722 cm^{-1} (C=O); ^{1}H NMR ($CDCl_3$) δ 1.30 and 1.52 (s, isopropylidene CH_3), 2.2—2.9 (m, H_2 and H_4), 4.56 (s, CH_2OC=O), 4.62 (s, H_6 and H_7), 4.66 (m, H_5), 7.3—7.6 and 8.0—8.1 (m, C_6H_5); ^{13}C NMR ($CDCl_3$) δ 24.93, 26.05, 45.09, 48.02, 64.86, 79.69, 83.90, 84.17, 113.01, 128.48, 129.74, 133.21, 204.49. Found: C, 64.76; H, 6.01%. Calcd for $C_{18}H_{20}O_6$: C, 65.05; H, 6.07%.

(1S,5S*,6S*,7S*)-6,7-Isopropylidenedioxy-1-trifluoroacetoxymethyl-8-oxabicyclo[3.2.1]octan-3-one (**20**)*: To a solution of (1*S**,5*S**,6*S**,7*S**)-1-hydroxymethyl-6,7-isopropylidenedioxy-8-oxabicyclo[3.2.1]octan-3-one (100 mg, 0.420 mmol) in CH_2Cl_2 (2 ml) was added trifluoroacetic anhydride (135 μl, 0.840 mmol) at 0 °C. The mixture was stirred for 50 min at the same temperature and evaporated. Chromatography of the residue on a silica-gel column using a 4:1 hexane–ethyl acetate mixture afforded 103 mg (76%) of **20** as a colorless oil. Mp 84—85 °C (ether–hexane); R =0.57 (1:1 hexane–ethyl acetate); IR 1785 and 1725 cm^{-1} (C=O); ^{1}H NMR ($CDCl_3$) δ 1.28 and 1.50 (s, isopropylidene CH_3), 2.2—2.9 (m, H_2 and H_4), 4.4—4.8 (m, H_5, H_6, H_7, and H_2COC=O); ^{13}C NMR ($CDCl_3$) δ 24.65, 25.86, 44.80, 47.35, 67.64, 79.84, 83.41, 83.66, 84.19, 113.24, 158.04, 203.34. Found: C, 47.77; H, 4.80%. Calcd for $C_{13}H_{15}O_6F_3$: C, 48.15; H, 4.66%.

(1S,5S*,6S*,7S*)-6,7-Isopropylidenedioxy-1-mesyloxymethyl-8-oxabicyclo[3.2.1]octan-3-one (**21**)*: To a mixture of (1*S**, 5*S**,6*S**,7*S**)-1-hydroxymethyl-6,7-isopropylidenedioxy-8-oxabicyclo[3.2.1]octan-3-one (500 mg, 2.1 mmol), triethylamine (0.59 ml, 4.2 mmol), and CH_2Cl_2 (10 ml) was added methanesulfonyl chloride (0.33 ml, 4.2 mmol). The mixture was stirred for 30 min at 0 °C and then 12 h at 28 °C. The mixture was diluted with CH_2Cl_2 (10 ml) and the organic layer was washed with brine, dried, and evaporated. Chromatography of the residue on a silica-gel column using a 1:1 hexane–ethyl acetate mixture afforded 635 mg (99%) of **21** as a white solid. Mp 149—151 °C (hexane–chloroform); R_f=0.31 (1:1 hexane–ethyl acetate); IR 1726 cm^{-1} (C=O); ^{1}H NMR ($CDCl_3$) δ 1.28 and 1.51 (s, isopropylidene CH_3), 2.2—2.9 (m, H_2 and H_4), 3.08 (s, CH_3), 4.4—4.7 (m, H_5, H_6, H_7, and CH_2OC=O); ^{13}C NMR ($CDCl_3$) δ 24.71, 25.98, 37.53, 44.85, 47.42, 69.57, 79.81, 83.60, 84.15, 113.13, 203.62. Found: C, 46.73; H, 5.74; S, 10.40%. Calcd for $C_{12}H_{18}O_7S$: C, 47.05; H, 5.92; S, 10.47%.

(1S,5S*,6S*,7S*)-1-t-Butyldimethylsiloxymethyl-6,7-isopropylidenedioxy-8-oxabicyclo[3.2.1]octan-3-one (**15**)*: A mixture of (1*S**,5*S**,6*S**,7*S**)-1-hydroxymethyl-6,7-isopropylidenedioxy-8-oxabicyclo[3.2.1]octan-3-one (500 mg, 2.10 mmol), *t*-butyldimethylsilyl chloride (479 mg, 3.15 mmol), and imidazole (428 mg, 6.30 mmol) in dry DMF (8 ml) was stirred for 12 h at 25 °C and then evaporated. The residue was partitioned between ethyl acetate and brine, and organic layer was separated, dried, and evaporated, leaving a colorless oil. Chromatography of this oil on a silica-gel column

using a 5:1 hexane–ethyl acetate mixture afforded 715 mg (100%) of **15** as a colorless oil. R_f=0.67 (1:1 hexane–ethyl acetate); IR (neat) 1724 cm^{-1} (C=O); ^1H NMR ($CDCl_3$) δ 0.08 (s, *t*-$C_4H_9(C\underline{H}_3)_2Si$), 0.92 (s, *t*-$C_4\underline{H}_9(CH_3)_2Si$), 1.28 and 1.50 (s, isopropylidene CH_3), 2.1—3.0 (m, H_2 and H_4), 3.86 (s, H_2COSi), 4.41 (d, J=5.7 Hz, H_7), 4.51 (d, J=5.7 Hz, H_6), 4.57 (m, H_5); ^{13}C NMR ($CDCl_3$) δ 18.35, 24.90, 25.92, 36.22, 45.31, 47.99, 63.94, 79.45, 83.68, 84.08, 86.09, 112.35, 205.85.

(1S,5S*,6S*,7S*)-6,7-Isopropylidenedioxy-1-trifluoromesyloxymethyl-8-oxabicyclo[3.2.1]octan-3-one (**22**)*: To a mixture of (1*S**,5*S**,6*S**,7*S**)-1-hydroxymethyl-6,7-isopropylidenedioxy-8-oxabicyclo[3.2.1]octan-3-one (100 mg, 0.438 mmol), pyridine (70 μl, 0.876 mmol) in CH_2Cl_2 (3 ml) was added trifluoromethanesulfonic anhydride (111 μl, 0.657 mmol). The mixture was stirred for 15 min at 0 °C and diluted with CH_2Cl_2 (7 ml). To this was added saturated NaCl (1 ml) and the organic layer was dried and evaporated to give a yellow solid. Chromatography of this solid on a silica-gel column using a 2:1 hexane–ethyl acetate mixture afforded 138 mg (88%) of **22** as a white solid. Mp 103—104 °C (ether–hexane); R_f=0.65 (2:1 ethyl acetate–hexane); IR 1725 cm^{-1} (C=O); ^1H NMR ($CDCl_3$) δ 1.26 and 1.49 (s, isopropylidene CH_3), 2.22—2.91 (m, H_2 and H_4), 4.40—4.84 (m, H_5, H_6, H_7, and CH_2OSO_2); ^{13}C NMR ($CDCl_3$) δ 24.64, 25.81, 44.71, 47.03, 75.55, 80.81, 83.06, 83.60, 84.28, 113.50, 202.74. Found: C, 40.20; H, 4.33; S, 9.36%. Calcd for $C_{12}H_{15}O_7SF_3$: C, 40.00; H, 4.20; S, 8.90%.

(1S,5R*,6R*,7S*)-6,7-Isopropylidenedioxy-6-methyl-8-oxabicyclo[3.2.1]octan-3-one (**43**)*: *Method A.*[35] To a solution of 20% aqueous $(C_2H_5)_4NOH$ (0.59 ml, 0.80 mmol) and 6-methyl-8-oxabicyclo[3.2.1]oct-6-en-3-one (1.00 g, 7.25 mmol) in *t*-C_4H_9OH (13 ml) were added 70% *t*-C_4H_9OOH (2.24 ml, 17.4 mmol) and OsO_4 in *t*-C_4H_9OH (0.02 mol dm^{-3} solution, 3.62 ml, 0.0725 mmol) at 0 °C. After stirring for 1 h at 0 °C and for 12 h at room temperature, the mixture was cooled to 0 °C. To this were added renewedly 70% *t*-C_4H_9OOH (0.45 ml, 3.84 mmol) and OsO_4 in *t*-C_4H_9OH (0.02 mol dm^{-3} solution, 0.72 ml, 0.0144 mmol) and the mixture was further stirred for 24 h at room temperature. After the mixture was cooled to 0 °C, 20% aqueous $NaHSO_3$ (10 ml) was added. The mixture was stirred for 1 h and evaporated. The residue was dissolved in acetone (40 ml) and the insoluble material was removed by filtration. The filtrate was concentrated and the residue was dissolved in ethyl acetate (40 ml), dried, and evaporated to give a white solid. A mixture of this solid, $CuSO_4$ (3 g), *p*-toluenesulfonic acid (30 mg) and acetone (50 ml) was stirred for 1 h at room temperature. Usual workup left a pale yellow solid. Chromatography of this solid on a silica-gel column using a 3:1 to 1:1 hexane–ethyl acetate mixture afforded **43** (962 mg, 63%) as a white solid. Analytical sample was obtained by recrystallization from chloroform–hexane. Mp 72.0—73.0 °C; R_f=0.58 (1:1 hexane–ethyl acetate); IR 1720 cm^{-1} (C=O); ^1H NMR ($CDCl_3$) δ 1.41 (s, CH_3), 1.41 and 1.50 (s, isopropylidene CH_3), 2.2—2.9 (m, H_2 and H_4), 4.15 (s, H_7), 4.45 (t-like, J=5.0 Hz, H_1 and H_5); ^{13}C NMR ($CDCl_3$) δ 21.09, 27.62, 28.26, 45.21, 45.39, 80.85, 83.23, 89.76, 91.17, 112.83, 204.86. Found: C, 62.28; H, 7.72%. Calcd for $C_{11}H_{16}O_4$: C, 62.25; H, 7.60%.

Method B.[32] To a solution of *N*-methylmorpholine *N*-oxide monohydrate (172 mg, 1.27 mmol) in H_2O (0.4 ml) and acetone (0.2 ml) were added a solution of OsO_4 in *t*-C_4H_9OH (0.02 mol dm^{-3} solution, 0.41 ml, 0.81×10^{-2} mmol) and 6-methyl-8-oxabicyclo[3.2.1]oct-6-en-3-one (138 mg, 1 mmol) at 20 °C. After stirring for 10 h, *N*-methylmorpholine *N*-oxide monohydrate (70 mg, 0.52 mmol) and OsO_4 in *t*-C_4H_9OH (0.02 mol dm^{-3} solution, 0.41 ml, 8.1×10^{-3} mmol) were added. The reaction mixture was stirred for an additional 12 h at 20 °C and to this was added a suspension of $Na_2S_2O_4$ (30 mg) and magnesol (300 mg) in H_2O (1.2 ml). After stirring for 10 min, the mixture was diluted with acetone (10 ml). The insoluble material was removed by filtration and the filtrate was evaporated. The residue was coevaporated with C_2H_5OH (10 ml×2). The crude material was dissolved in acetone (20 ml) and to this were added $CuSO_4$ (1.5 g) and *p*-toluenesulfonic acid (25 mg). The mixture was stirred for 2 h at 20 °C and worked up in a usual manner to give a yellow solid. Chromatography of this solid on a column of silica gel using a 3:1 hexane–ethyl acetate mixture afforded **43** (165 mg, 78%).

(1S,6R*,5R*,7S*)-6,7-Isopropylidenedioxy-6-pentyl-8-oxabicyclo[3.2.1]octan-3-one (**44**)*: To a solution of *N*-methylmorpholine *N*-oxide monohydrate (1.00 g, 7.14 mmol) in H_2O (2.0 ml) and acetone (1 ml) were added OsO_4 in *t*-C_4H_9OH (2.0×10^{-5} mol dm^{-3} solution, 2.38 ml, 47.6 μmol) and 6-pentyl-8-oxabicyclo[3.2.1]oct-6-en-3-one (924 mg, 4.76 mmol). The mixture was stirred for 96 h at 15 °C and to this were added $Na_2S_2O_3\cdot5H_2O$ (242 mg) and magnesol (2.42 g) in H_2O (5 ml). Usual workup left a yellow oil. The mixture of this oil, dissolved in acetone (30 ml), $CuSO_4$ (2 g), and *p*-toluenesulfonic acid (500 mg) was stirred at 15 °C. After stirring for 1 h, *p*-toluenesulfonic acid (100 mg) was further added. The reaction mixture was stirred for 1 h and worked up in a usual way to afford a yellow solid. Chromatography of this solid on a silica-gel column using a 3:1 ethyl acetate–hexane mixture afforded **44** (718 mg, 56%). Mp 82—84 °C (hexane); R_f=0.84 (2:1 ethyl acetate–hexane); IR 1720 cm^{-1} (C=O); ^1H NMR ($CDCl_3$) δ 0.89 (m, CH_3), 1.2—1.7 (m, CH_2), 1.41 and 1.53 (s, isopropylidene CH_3), 2.3—2.8 (m, H_2 and H_4), 4.14 (s, H_7), 4.50 (d-like, J=5.8 Hz, H_1 and H_5); ^{13}C NMR ($CDCl_3$) δ 13.88, 22.45, 24.31, 27.90, 28.68, 32.13, 34.45, 45.29, 45.78, 80.79, 82.44, 89.50, 94.77, 113.33, 205.07. Found: C, 66.95; H, 9.20%. Calcd for $C_{15}H_{24}O_4$: C, 67.13; H, 9.02%.

(1S,5R*,6R*,7S*)-6-t-Butyl-6,7-isopropylidenedioxy-8-oxabicyclo[3.2.1]octan-3-one (**45**)*: To a solution of 6-*t*-butyl-8-oxabicyclo[3.2.1]oct-6-en-3-one (1.00 g, 5.56 mmol) in THF (10 ml) was added OsO_4 (1.69 g, 6.65 mmol) in pyridine (7 ml). The mixture was stirred for 60 h at 30 °C in the dark and washed with ether (30 ml×3). The residue was dissolved in C_2H_5OH (10 ml) and H_2O (10 ml) and to this was added Na_2SO_3 (7.0 g). The mixture was heated at reflux for 6 h and the insoluble material was removed by filtration and the filtrate was evaporated to give a black solid. After this solid was coevaporated with C_2H_5OH, the residue was acetonized by standard method, as described above, to give 218 mg (15%) of **45**. Mp 121—123 °C (hexane–ether–ethyl acetate); R_f=0.71 (1:1 hexane–ethyl acetate); IR 1722 cm^{-1} (C=O); ^1H NMR ($CDCl_3$) δ 1.00 (s, *t*-C_4H_9), 1.46 and 1.62 (s, isopropylidene CH_3), 2.0—2.9 (m, H_2 and H_4), 4.38 (s, H_7), 4.3—4.6 (m, H_1 and H_5); ^{13}C NMR ($CDCl_3$) δ 27.79, 28.14, 34.68, 44.20, 46.13, 80.53, 82.41, 85.82, 100.97, 113.48, 204.66. Found: C, 66.04; H, 8.76%. Calcd for $C_{14}H_{22}O_4$: C, 66.11; H, 8.72%.

(1S,5R*,6R*,7S*)-6,7-Isopropylidenedioxy-6-phenyl-8-oxabicyclo[3.2.1]octan-3-one (**46**)*: To a solution of *N*-methylmorpholine *N*-oxide monohydrate (1.69 g, 12.1 mmol) in H_2O (3.24 ml) and acetone (1.67 ml) were added OsO_4 in *t*-C_4H_9OH (2.0×10^{-5} mol dm^{-3} solution, 4.03 ml, 80.5 μ mol) and 6-phenyl-8-oxabicyclo[3.2.1]oct-6-en-3-one (1.61 g, 8.05 mmol). After stirring for 72 h at 20 °C, *N*-methylmorpholine *N*-oxide monohydrate (0.56 g, 4.03 mmol) was further added. The mixture was further stirred for 72 h

and to this were added $Na_2S_2O_3 \cdot 5H_2O$ (410 mg) and magnesol (4.1 g) in H_2O. This mixture was worked up in a usual way to give a yellow solid. The solid was mixed acetone (40 ml) with $CuSO_4$ (5 g), and *p*-toluenesulfonic acid (0.2 g), and stirred at room temperature. After stirring for 1 h, *p*-toluenesulfonic acid (0.2 g) was further added. The resulting mixture was stirred for 3 h and worked up in a usual manner. Chromatography of the residue on a silica-gel column using a 4:1 to 1:1 hexane–ethyl acetate mixture afforded **46** (1.26 g, 57%). Mp 134—135 °C (hexane–ether–ethyl acetate); R_f=0.76 (2:1 ethyl acetate–hexane); IR 1720 cm^{-1} (C=O); ^1H NMR ($CDCl_3$) δ 1.02 and 1.56 (s, isopropylidene CH_3), 1.7—3.0 (m, H_2 and H_4), 4.61 (d-like, J=6.5 Hz, H_1 and H_5), 4.92 (s, H_7), 7.34 (s, C_6H_5); ^{13}C NMR ($CDCl_3$) δ 27.18, 36.29, 44.30, 45.45, 81.08, 83.31, 86.88, 95.92, 112.50, 126.14, 128.53, 128.83, 139.01, 204.54. Found: C, 69.77; H, 6.67%. Calcd for $C_{16}H_{18}O_4$: C, 70.05; H, 6.61%.

(1S,5R*,6R*,7S*)-6-Hydroxymethyl-6,7-isopropylidenedioxy-8-oxabicyclo[3.2.1]octan-3-one*: To a solution of *N*-methylmorpholine *N*-oxide monohydrate (4.41 g, 32.7 mmol) in H_2O (8.5 ml) and acetone (4.3 ml) was added OsO_4 in *t*-C_4H_9OH (0.02 mol dm^{-3} solution, 11.7 ml, 0.21 mmol). 6-(Tetrahydropyran-2-yloxymethyl)-8-oxabicyclo[3.2.1]oct-6-en-3-one (5.00 g, 21.0 mmol) was subjectedly added. The reaction mixture was stirred for 36 h at 20 °C and to this were added $Na_2S_2O_3$ (630 mg) and magnesol (6.3 g) in H_2O (25 ml). Usual workup left a yellow oil. A mixture of this oil, $CuSO_4$ (8 g), *p*-toluenesulfonic acid (300 mg), and acetone (50 ml) was stirred at the room temperature. After stirring for 3 h, *p*-toluenesulfonic acid (300 mg) was further added. The resulting mixture was stirred for 1 h and worked up in a usual way. Chromatography of the residue on a silica-gel column using a 4:1 to 1:1 hexane–ethyl acetate mixture afforded (1*S**,5*R**,6*R**,7*S**)-6,7-isopropylidenedioxy-6-(tetrahydropyran-2-yloxymethyl)-8-oxabicyclo[3.2.1]octan-3-one (1.07 g, 16%), mp 126—130 °C (ether–hexane); R_f=0.68 (2:1 ethyl acetate–hexane); IR 1721 cm^{-1} (C=O); ^1H NMR ($CDCl_3$) δ 1.42 and 1.54 (s, isopropylidene CH_3), 1.62 (m, 6H), 2.2—2.9 (m, H_2 and H_4), 3.3—4.1 (m, CH_2O), 4.3—4.7 (m, H_1, H_5, H_7, and OCHO). Found: C, 61.40; H, 7.87%. Calcd for $C_{16}H_{24}O_6$: C, 61.52; H, 7.75%, and the title compound (1.92 g, 40%). Mp 138—140 °C; R_f=0.35 (2:1 ethyl acetate–hexane); IR 3590 (OH), 1721 cm^{-1} (C=O); ^1H NMR ($CDCl_3$) δ 1.40 and 1.52 (s, isopropylidene CH_3), 2.2—2.9 (m, H_2 and H_4), 3.65 (d, J=12.0 Hz, $\underline{H}_aH_bCOH$), 3.85 (d, J=12.0 Hz, $H_a\underline{H}_bCOH$), 4.24 (s, H_7), 4.58 (m, H_1 and H_5); ^{13}C NMR ($CDCl_3$) δ 27.77, 28.57, 44.90, 45.27, 63.90, 80.87, 81.82, 86.60, 95.20, 114.07, 205.11. Found: C, 58.04; H, 7.22%. Calcd for $C_{11}H_{16}O_5$: C, 57.88; H, 7.07%.

Deprotection of (1S,5R*,6R*,7S*)-6,7-Isopropylidenedioxy-6-(tetrahydropyran-2-yloxymethyl)-8-oxabicyclo[3,2,1]octan-3-one.* A mixture of (1*S**, 5*R**, 6*R**,7*S*)-6,7-isopropylidenedioxy-6-(tetrahydropyran-2-yloxymethyl)-8-oxabicyclo[3.2.1]octan-3-one (6.13 g, 19.6 mmol) and oxalic acid dihydrate (819 mg, 6.5 mmol) in THF (19.6 ml) and H_2O (6 ml) was stirred at 50 °C. After stirring for 2 h, oxalic acid dihydrate (819 mg, 6.5 mmol) in H_2O (5 ml) was further added. After stirring for 4 h, the reaction mixture was evaporated. The residue was extracted with chloroform (40 ml×4) and the organic layer was dried and evaporated to give a yellow solid which was washed with ether. (1*S**,5*R**,6*R**,7*S**)-6-Hydroxymethyl-6,7-isopropylidenedioxy-8-oxabicyclo[3.2.1]-octan-3-one was obtained as a white solid, 3.50 g (78%). The mother liquid was concentrated and the residue was chromatographed to afford the same compound (0.18 g, 4%). Total amount was 3.68 g (82%).

(1S,5R*,6R*,7S*)-6-t-Butyldimethylsiloxymethyl-6,7-isopropylidenedioxy-8-oxabicyclo[3.2.1]octan-3-one (47)*: To a solution of (1*S**,5*R**,6*R**,7*S**)-6-hydroxymethyl-6,7-isopropylidenedioxy-8-oxabicyclo[3.2.1]octan-3-one (1.86 g, 8.16 mmol) in dry DMF (25 ml) was added a solution of *t*-butyldimethylsilyl chloride (1.88 g, 12.5 mmol) and imidazole (1.70 g, 25 mmol) in dry DMF (25 ml).[34] The mixture was stirred for 30 min at 0 °C and for 20 h at 20 °C. The reaction mixture was evaporated and the residue was diluted with ether (250 ml). The organic layer was washed with brine, dried, and evaporated. The residual oil was chromatographed on a silica-gel column using a 4:1 hexane–ethyl acetate mixture to afford **47** (2.52 g, 90%) as a colorless oil. R_f=0.50 (3:1 hexane–ethyl acetate); IR (neat) 1725 cm^{-1} (C=O); ^1H NMR ($CDCl_3$) δ 0.08 (s, *t*-$C_4H_9(C\underline{H}_3)_2Si$) 0.90 (s, *t*-$C_4\underline{H}_9(CH_3)_2Si$), 1.40 and 1.52 (s, isopropylidene CH_3), 2.2—2.9 (m, H_2 and H_4), 3.66 (d, J=11.5 Hz, $\underline{H}_aH_bCOSi$), 3.86 (d, J=11.5 Hz, $H_a\underline{H}_bCOSi$), 4.24 (s, H_7), 4.50 (m, H_1 and H_5); ^{13}C NMR ($CDCl_3$) δ 18.41, 25.93, 27.87, 28.42, 44.53, 45.01, 65.10, 80.85, 82.08, 86.40, 95.15, 113.76, 204.60.

(1S,5R*,6R*,7S*)-6-Benzyloxymethyl-6,7-isopropylidenedioxy-8-oxabicyclo[3.2.1]octan-3-one (48)*: To a solution of *N*-methylmorpholine *N*-oxide monohydrate (210 mg, 1.5 mmol) in H_2O (0.4 ml) and acetone (0.2 ml) were added OsO_4 in *t*-C_4H_9OH (2.0×10^{-5} mol dm^{-3} solution, 0.5 ml, 0.01 mmol) and 6-benzyloxymethyl-8-oxabicyclo[3.2.1]oct-6-en-3-one (244 mg, 1 mmol). The reaction mixture was stirred for 84 h at 20 °C and to this were added $Na_2S_2O_3$ (31 mg) and magnesol (310 mg) in H_2O (1.2 ml). Usual workup left a yellow oil. The mixture of this oil, dissolved in acetone (20 ml), $CuSO_4$ (1.5 g), and *p*-toluenesulfonic acid (50 mg) was stirred at 20 °C. After stirring for 30 min, *p*-toluenesulfonic acid (50 mg) was further added. The mixture was stirred for 2 h and worked up in a usual way. The residue was purified on a silica-gel column using a 4:1 hexane–ethyl acetate mixture to afford **48** (206 mg, 65%). Mp 90.5—91.5 °C (hexane–ethyl acetate); R_f=0.71 (2:1 ethyl acetate–hexane); ^1H NMR ($CDCl_3$) δ 1.34 and 1.50 (s, isopropylidene CH_3), 2.2—2.8 (m, H_2 and H_4), 3.48 (d, J=10.5 Hz, $\underline{H}_aH_bCOCH_2C_6H_5$), 3.66 (d, J=10.5 Hz, $H_a\underline{H}_bCOCH_2C_6H_5$), 4.26 (s, H_7), 4.4—4.6 (m, H_1 and H_5), 4.54 (s, $C\underline{H}_2C_6H_5$), 7.32 (s, C_6H_5); ^{13}C NMR ($CDCl_3$) δ 27.82, 28.30, 44.72, 45.01, 71.33, 73.85, 80.73, 82.09, 86.88, 93.98, 114.05, 127.99, 128.52, 137.50, 204.56. Found: C, 68.19; H, 7.20%. Calcd for $C_{18}H_{22}O_5$: C, 67.91; H, 6.97%.

(1S,5R*,6R*,7S*)-6,7-Isopropylidenedioxy-6-pivaloyloxymethyl-8-oxabicyclo[3.2.1]octan-3-one (49)*: To a solution of (1*S**,5*R**,6*R**,7*S**)-6-hydroxymethyl-6,7-isopropylidenedioxy-8-oxabicyclo[3.2.1]octan-3-one (456 mg, 2.00 mmol) in pyridine (10 ml) was added pivaloyl chloride (0.5 ml, 4.0 mmol) at 0 °C. The mixture was stirred for 30 min at 0 °C and for 12 h at 20 °C. After the mixture was evaporated, the residue was dissolved in ethyl acetate (50 ml). The ethyl acetate layer was washed with brine, dried, and evaporated. Chromatography of the residue on a silica-gel column using a 4:1 hexane–ethyl acetate mixture afforded 468 mg (75%) of **49**. Mp 97.0—98.5 °C (hexane–ether); R_f=0.55 (1:1 hexane–ethyl acetate); IR 1730 cm^{-1} (C=O); ^1H NMR ($CDCl_3$) δ 1.20 (s, *t*-C_4H_9), 1.40 and 1.51 (s, isopropylidene CH_3), 2.40 (dd, J=6.4, 17.0 Hz, H_{4a}), 2.76 (dd, J=3.0, 17.0 Hz, H_{4b}), 3.94 (d, J=12.5 Hz, $\underline{H}_aH_bCOC$=O), 4.38 (s, H_7), 4.54 (d, J=12.5 Hz, $H_a\underline{H}_bCOC$=O), 4.45—4.55 (m, H_1 and H_5); ^{13}C NMR ($CDCl_3$) δ 27.22, 27.77, 28.27, 39.00, 44.92, 45.53, 65.13, 81.09, 81.93, 86.43, 93.20, 114.39, 177.80, 204.23. Found: C, 61.22; H, 7.70%. Calcd

for $C_{16}H_{24}O_6$: C, 61.52; H, 7.75%.

(1S,5R*,6R*,7S*)-6-Benzoyloxymethyl-6,7-isopropylidenedioxy-8-oxabicyclo[3.2.1]octan-3-one (**50**)*: To a solution of (1*S**, 5*R**,6*R**,7*S**)-6-hydroxymethyl-6,7-isopropylidenedioxy-8-oxabicyclo[3.2.1]octan-3-one (456 mg, 2.0 mmol) in pyridine (10 ml) was added benzoyl chloride (0.47 ml, 4.0 mmol) at 0 °C. The reaction mixture was stirred for 30 min at 0 °C and for 12 h at 20 °C and evaporated. The residue was dissolved in benzene (10 ml) and washed with brine, 1 mol dm^{-3} HCl, saturated $NaHCO_3$, dried, and the benzene layer was evaporated. The residue was purified on a silica-gel column using a 3:1 hexane–ethyl acetate mixture to afford **50** (586 mg, 88%). Mp 164—168 °C (hexane–ether–ethyl acetate); R_f=0.59 (1:1 hexane–ethyl acetate); IR 1728 cm^{-1} (C=O); ^{1}H NMR ($CDCl_3$) δ 1.41 and 1.54 (s, isopropylidene CH_3), 2.3—3.0 (m, H_2 and H_4), 4.35 (d, J=12.2 Hz, $\underline{H}_a H_b COC{=}O$), 4.44 (s, H_7), 4.5—4.8 (m, H_1 and H_5), 4.70 (d, J=12.2 Hz, $H_a \underline{H}_b COC{=}O$), 7.3—7.8 (m, C_6H_5); ^{13}C NMR ($CDCl_3$) δ 27.82, 28.32, 45.00, 45.59, 65.33, 81.22, 81.97, 86.86, 93.21, 114.68, 128.58, 128.97, 129.90, 130.67, 133.36, 134.51, 166.03, 204.20. Found: C, 65.18; H, 5.79%. Calcd for $C_{18}H_{20}O_6$: C, 65.05; H, 6.07%.

*Baeyer-Villiger Oxidation of α-Substituted Ketones. Oxidation of **1***: A mixture of **1** (6.80 g, 32.1 mmol) and Na_2HPO_4 (82.4 g, 580 mmol) in CH_2Cl_2 (100 ml) was cooled in an ice bath and stirred magnetically. To this was added dropwise over 15 min trifluoroperacetic acid, which had been prepared from 90% H_2O_2 (3.70 ml, 96.3 mmol) and trifluoroacetic anhydride (16.4 ml, 116 mmol) in CH_2Cl_2 (50 ml). The reaction mixture was stirred for 16 h at 25 °C under argon and to this was added $NaHSO_3$ (79 g) and $NaHCO_3$ (15 g). After stirring for 1 h, the insoluble material was removed by filtration. The filtrate was evaporated and the resulting yellow residue was chromatographed on a silica-gel column using a 1:1 to 1:2 hexane–ethyl acetate mixture to afford (1*R**,2*R**,6*S**,7*S**,8*R**)-7,8-isopropylidenedioxy-2-methyl-3,9-dioxabicyclo[4.2.1]nonan-4-one (**5**) (6.20 g, 85%). Mp 126.2—127.8 °C(chloroform–hexane); R_f= 0.34 (2:1 hexane–ethyl acetate); IR 1732 cm^{-1} (C=O); ^{1}H NMR ($CDCl_3$) δ 1.26 and 1.42 (s, isopropylidene CH_3), 1.31 (d, J=7.0 Hz, CH_3), 2.92 (m, H_5), 4.14 (s, H_1), 4.28 (t-like, J=4.0 Hz, H_6), 4.58 (q, J=7.0 Hz, H_2), 4.61 (d, J=6.0 Hz, H_7), 4.87 (d, J=6.0 Hz, H_8); MS m/z 213 (M^+—15). Found: C, 57.82; H, 6.91%. Calcd for $C_{11}H_{16}O_5$: C, 57.88, H, 7.07%.

*Oxidation of **2***: To a mixture of **2** (12.0 g, 44.7 mmol), Na_2HPO_4 (115 g, 0.807 mol), and CH_2Cl_2 (150 ml) was added slowly trifluoroperacetic acid in CH_2Cl_2 (1.53 mol dm^{-3} solution, 146 ml, 0.224 mol) under argon. After stirring for 8 h at 25 °C, solid $NaHCO_3$ (50 g) was added to the mixture. Usual workup left an oil, chromatography of which on a silica-gel column using a 5:1 hexane–ethyl acetate mixture afforded (1*R**,2*R**,6*S**,7*S**,8*R**)-7,8-isopropylidenedioxy-2-pentyl-3,9-dioxabicyclo[4.2.1]nonan-4-one (**6**) (9.80 g, 78%). Mp 64—65 °C (hexane); R_f=0.24 (3:1 hexane–ethyl acetate); IR 1732 cm^{-1} (C=O); ^{1}H NMR ($CDCl_3$) δ 0.90 (t, J=6.0 Hz, CH_3), 1.30 and 1.49 (s, isopropylidene CH_3), 1.50 (m, CH_2), 2.90 (dd, J=4.5, 16.5 Hz, H_{5a}), 3.07 (dd, J=3.0, 16.5 Hz, H_{5b}), 4.26 (s, H_1), 4.40 (m, H_6 and H_2), 4.65 (d, J=5.8 Hz, H_7), 4.93 (d, J= 5.8 Hz, H_8); MS m/z 269 (M^+—15). Found: C, 63.07; H, 8.67%. Calcd for $C_{15}H_{24}O_5$: C, 63.36; H, 8.51%.

*Oxidation of **3***: Trifluoroperacetic acid in CH_2Cl_2 (1.37 mol dm^{-3} solution, 28 ml, 38.3 mmol) was added slowly to a mixture of **3** (3.50 g, 12.7 mmol), Na_2HPO_4 (19.6 g, 138 mmol), and CH_2Cl_2 (30 ml) at 0 °C. After stirring for 11 h at 25 °C, solid $NaHCO_3$ (10 g) and $NaHSO_3$ (6 g) were added. The mixture was worked up in a usual manner to give a solid. Purification of this solid on a silica-gel column using a 2:1 to 1:1 hexane–ethyl acetate mixture afforded (1*S**,2*S**,6*S**,7*S**,8*S**)-7,8-isopropylidenedioxy-2-phenyl-3,9-dioxabicyclo[4.2.1]nonan-4-one (**7**) (2.45 g, 67%). Mp 160.8—161.2 °C (ether); R_f=0.30 (1:1 hexane–ethyl acetate); IR 1739 cm^{-1} (C=O); ^{1}H NMR ($CDCl_3$) δ 1.31 and 1.46 (s, isopropylidene CH_3); 3.00 (dd, J=2.5, 16.0 Hz, H_{5a}), 3.20 (dd, J=4.5, 16.0 Hz, H_{5b}), 4.41 (dd, J= 2.5, 4.5 Hz, H_6), 4.50 (s, H_1), 4.77 (d, J=6.0 Hz, H_7), 5.07 (d, J=6.0 Hz, H_8), 5.57 (s, H_2), 7.42 (br s, C_6H_5); MS m/z 290 (M^+). Found: C, 65.98; H, 6.23%. Calcd for $C_{16}H_{18}O_5$: C, 66.19; H, 6.25%.

*Oxidation of **4***: To a mixture of **4** (11.2 g, 49.6 mmol), Na_2HPO_4 (127 g, 0.895 mol), and CH_2Cl_2 (150 ml) was added trifluoroperacetic acid in CH_2Cl_2 (1.14 mol dm^{-3} solution, 131 ml, 149 mmol) at 0 °C. After stirring for 6 h at 25 °C, solid $NaHCO_3$ (15 g) and $NaHSO_3$ (7 g) were added. Usual workup left a yellow oil. Chromatography of the residue on a silica-gel column using a 2:1 hexane–ethyl acetate mixture afforded (1*S**,6*S**,7*S**,8*S**)-2,2-dimethyl-7,8-isopropylidenedioxy-3,9-dioxabicyclo[4.2.1]nonan-4-one (**8**) (9.70 g, 81%). Mp 158.5—159.2 °C (ether); R_f=0.35 (2:1 hexane–ethyl acetate); IR 1730 cm^{-1} (C=O); ^{1}H NMR ($CDCl_3$) δ 1.34 and 1.56 (s, isopropylidene CH_3), 1.46 and 1.50 (s, CH_3), 2.88 (dd, J=3.0, 17.0 Hz, H_{5a}), 3.12 (dd, J=4.0, 17.0 Hz, H_{5b}), 4.10 (s, H_1), 4.33 (dd, J=3.0, 4.0 Hz, H_6), 4.64 (d, J=6.0 Hz, H_7), 4.97 (d, J=6.0 Hz, H_8); MS m/z 227 (M^+—15). Found: C, 59.20; H, 7.46%. Calcd for $C_{12}H_{18}O_5$: C, 59.49; H, 7.49%.

*The Baeyer-Villiger Oxidation of β-Substituted Ketones. Oxidation of **9***: To a mixture of **9** (9.35 g, 44.1 mmol), Na_2HPO_4 (61.8 g, 0.435 mol), Na_2H_2edta (3 g), and CH_2Cl_2 (150 ml) was added trifluoroperacetic acid in CH_2Cl_2 (1.74 mol dm^{-3} solution, 76 ml, 132 mmol) at 0 °C. The mixture was stirred for 10 h at 20 °C and usual workup left a white solid. ^{1}H NMR analysis of this material indicated that (1*R**,6*S**,7*S**,8*S**)-7,8-isopropylidenedioxy-1-methyl-3,9-dioxabicyclo[4.2.1]nonan-4-one (**12a**) and (1*S**,6*R**,7*S**,8*S**)-7,8-isopropylidenedioxy-6-methyl-3,9-dioxabicyclo[4.2.1]-nonan-4-one (**12b**) were produced in 53:47 ratio. Chromatography of this solid on a silica-gel column using a 3:1 ether–petroleum ether mixture afforded **12a** (5.5 g, containing 15% of **12b** determined by ^{1}H NMR) and **12b** (4.0 g, containing 10% of **12a** determined by ^{1}H NMR). Total yield was 90% (9.5 g). Pure samples of **12a** and **12b** were obtained by rechromatography and recrystallization from chloroform–hexane. **12a**: Mp 100—102 °C; R_f=0.35 (2:1 ether–petroleum ether); IR 1735 cm^{-1} (C=O); ^{1}H NMR (C_6D_6) δ 1.01 (s, CH_3), 1.07 and 1.40 (s, isopropylidene CH_3), 2.25 (dd, J=2.9, 15.5 Hz, H_{5a}), 2.45 (dd, J=4.1, 15.5 Hz, H_{5b}), 3.38 (d, J=14.0 Hz, H_{2a}), 3.56 (d, J=14.0 Hz, H_{2b}), 3.93 (dd, J=2.9, 4.1 Hz, H_6), 4.41 (d, J=6.0 Hz, H_7), 4.48 (d, J=6.0 Hz, H_8); MS m/z 213 (M^+—15). Found: C, 57.30; H, 7.05%. Calcd for $C_{11}H_{16}O_5$: C, 57.88; H, 7.07%. **12b**: Mp 100—101 °C; R_f=0.30 (2:1 ether–petroleum ether); IR 1735 cm^{-1} (C=O); ^{1}H NMR (C_6D_6) δ 1.05 and 1.38 (s, isopropylidene CH_3), 1.16 (s, CH_3), 2.34 (d, J=16.0 Hz, H_{5a}), 2.54 (d, J=16.0 Hz, H_{5b}), 3.36 (dd, J=4.0, 13.8 Hz, H_{2a}), 3.60 (d, J=13.8 Hz, H_{2b}), 3.91 (d, J=4.0 Hz, H_1), 4.33 (d, J=6.0 Hz, H_7), 4.67 (d, J=6.0 Hz, H_8); MS m/z 228 (M^+). Found: C, 57.90; H, 7.12%. Calcd for $C_{11}H_{16}O_5$: C, 57.88; H, 7.07%.

*Oxidation of **10***: Trifluoroperacetic acid in CH_2Cl_2 (1.54 mol dm^{-3} solution, 14.2 ml, 21.8 mmol) was added to a mixture of **10** (835 mg, 3.12 mmol), Na_2HPO_4 (10.2 g, 72.0

mmol), Na_2H_2edta (500 mg), and CH_2Cl_2 (20 ml) at 0 °C. The mixture was stirred for 15 h at 20 °C and the usual workup gave a white solid. ^1H NMR analysis of this solid indicated that (1*R**,6*S**,7*S**,8*S**)-7,8-isopropylidenedioxy-1-pentyl-3,9-dioxabicyclo[4.2.1]nonan-4-one (**13a**) and (1*S**,6*R**,7*S**,8*S**)-7,8-isopropylidenedioxy-6-pentyl-3,9-dioxabicyclo[4.2.1]nonan-4-one (**13b**) were produced in 50:50 ratio. Chromatographic separation (silica gel, 1:1 ether–petroleum ether) yielded 400 mg (45%) of **13a** and 406 mg (46%) of **13b**. Total yield was 91% (806 mg). **13a**: Mp 60—61 °C (chloroform–hexane); R_f=0.46 (2:1 ether–petroleum ether); IR 1734 cm^{-1} (C=O); ^1H NMR (C_6D_6) δ 0.85 (t, J=6.0 Hz, CH_3), 1.0—1.8 (m, CH_2), 1.07 and 1.42 (s, isopropylidene CH_3), 2.40 (m, H_5), 3.67 (s, H_2), 3.99 (dd, J=3.0, 4.7 Hz, H_6), 4.51 (s, H_7 and H_8); MS *m/z* 284 (M^+). Found: C, 63.19; H, 8.71%. Calcd for $C_{15}H_{24}O_5$: C, 63.36; H, 8.51%. **13b**: Mp 106—107 °C (chloroform–hexane); R_f=0.38 (2:1 ether–petroleum ether); IR 1735 cm^{-1} (C=O); ^1H NMR (C_6D_6) δ 0.86 (t, J=6.0 Hz, CH_3), 1.07 and 1.40 (s, isopropylidene CH_3), 1.2—1.9 (m, CH_2), 2.41 (d, J=15.5 Hz, H_{5a}), 2.72 (d, J=15.5 Hz, H_{5b}), 3.43 (dd, J=4.1, 13.2 Hz, H_{2a}), 3.66 (d, J=13.2 Hz, H_{2b}), 3.98 (d, J=4.1 Hz, H_1), 4.45 (d, J=5.9 Hz, H_7), 4.73 (d, J=5.9 Hz, H_8); MS *m/z* 284 (M^+). Found: C, 63.25; H, 8.62%. Calcd for $C_{15}H_{24}O_5$: C, 63.36; H, 8.51%.

Oxidation of ***11***: A mixture of **11** (12.0 g, 43.8 mmol), Na_2HPO_4 (103 g, 723 mmol), Na_2H_2edta (5 g), and CH_2Cl_2 (150 ml) was stirred at 0 °C and to this was added a CH_2Cl_2 solution of trifluoroperacetic acid (1.86 mol dm^{-3}, 118 ml, 219 mmol). After stirring for 12 h at 25 °C, the usual workup afforded a yellow residue. ^1H NMR analysis of this residue indicated that (1*R**,6*S**,7*S**,8*S**)-7,8-isopropylidenedioxy-1-phenyl-3,9-dioxabicyclo[4.2.1]nonan-4-one (**14a**) and (1*S**,6*R**,7*S**,8*S**)-7,8-isopropylidenedioxy-6-phenyl-3,9-dioxabicyclo[4.2.1]nonan-4-one (**14b**) were in 88:12 ratio. Purification of the residue on a silica-gel column using a 1:1 ether–petroleum ether mixture afforded **14a** (10.6 g, 84%) and **14b** (1.2 g, 9%). Total yield was 93% (11.8 g). **14a**: Mp 156—158 °C (chloroform–hexane); R_f=0.27 (1:1 ether–petroleum ether); IR 1735 cm^{-1} (C=O); ^1H NMR (C_6D_6) δ 1.13 and 1.30 (s, isopropylidene CH_3), 2.45 (m, H_5), 3.75 (d, J=13.5 Hz, H_{2a}), 4.01 (d, J=13.5 Hz, H_{2b}), 4.13 (m, H_6), 4.61 (d, J=6.0 Hz, H_7), 4.95 (d, J=6.0 Hz, H_8), 7.0—7.5 (m, C_6H_5); MS *m/z* 290 (M^+). Found: C, 66.09; H, 6.22%. Calcd for $C_{16}H_{18}O_5$: C, 66.19; H, 6.25%. **14b**: Mp 153—154 °C (chloroform–hexane); R_f=0.19 (1:1 ether–petroleum ether); IR 1733 cm^{-1} (C=O); ^1H NMR (C_6D_6) δ 0.99 and 1.10 (s, isopropylidene CH_3), 2.62 (d, J=15.5 Hz, H_{5a}), 3.15 (d, J=15.5 Hz, H_{5b}), 3.44 (dd, J=4.1, 13.5 Hz, H_{2a}), 3.69 (d, J=13.5 Hz, H_{2b}), 4.11 (d, J=4.1 Hz, H_1), 4.79 (d, J=5.8 Hz, H_7), 4.85 (d, J=5.8 Hz, H_8), 7.0—7.5 (m, C_6H_5); MS *m/z* 290 (M^+). Found: C, 65.54; H, 6.10%. Calcd for $C_{16}H_{18}O_5$: C, 66.19; H, 6.25%.

Baeyer-Villiger Oxidation of γ-Substituted Ketones. A. Results in Table 2: General. Unless otherwise stated, the Baeyer-Villiger oxidation was performed as follows. A mixture of a ketonic substrate (1 equiv), Na_2HPO_4 (9 equiv), and CH_2Cl_2 (3 ml/1 equiv of ketone) was cooled in an ice bath and stirred magnetically. To this was added dropwise a 1.0 mol dm^{-3} CH_2Cl_2 solution of trifluoroperacetic acid (3 equiv). The resulting mixture was stirred for 12 h at 25 °C and diluted with CH_2Cl_2 (5—10 ml/1 equiv of ketone). To this was added $Na_2S_2O_3\cdot5H_2O$ (0.8—1.6 g/1 equiv of ketone) at 0 °C and the mixture was stirred for 3 h at 25 °C. The insoluble material was removed by filtration and the filtrate was evaporated to give a crude product. The corresponding lactonic products were obtained as a mixture of two regioisomers. The isomeric ratio was determined by ^1H NMR and listed in Table 2. The regioisomers were separated by the silica-gel column chromatography and HPLC progress. The progress of elution of column chromatography was monitored by analytical TLC and fractions containing the desired product were combined and evaporated. Samples for elemental analysis were obtained by recrystallizations of the chromatographed products.

Typical Procedure. Oxidation of ***15***: Trifluoroperacetic acid in CH_2Cl_2 solution (1.0 mol dm^{-3}, 2.8 ml, 2.8 mmol) was added to a stirred, ice-cooled mixture of Na_2HPO_4 (1.20 g, 8.42 mmol) and **15** (320 mg, 0.936 mmol) in CH_2Cl_2 (2.8 ml). The mixture was stirred for 12 h at 25 °C and diluted with CH_2Cl_2 (10 ml). To this was added $Na_2S_2O_3\cdot5H_2O$ (1.5 g) at 0 °C and the resulting mixture was stirred for 3 h at 25 °C. The insoluble material was removed by filtration and the filtrate was evaporated. The residue (343 mg, 100%) consisted of (1*S**,6*S**,7*S**,8*S**)-1-*t*-butyldimethylsiloxymethyl-7,8-isopropylidenedioxy-3,9-dioxabicyclo[4.2.1]-nonan-4-one (**23a**) and (1*S**,6*S**,7*S**,8*S**)-6-*t*-butyldimethylsiloxymethyl-7,8-isopropylidenedioxy-3,9-dioxabicyclo[4.2.1]-nonan-4-one (**23b**) (55:45 ratio as determined by ^1H NMR analysis). Silica-gel column chromatography (1:1 ether–hexane) gave samples of **23a** and **23b**. **23a**: Mp 75—76 °C (ether–hexane); R_f=0.50 (3:1 ether–petroleum ether); IR 1735 cm^{-1} (C=O); ^1H NMR ($CDCl_3$) δ 0.08 (s, *t*-$C_4H_9(C\underline{H}_3)_2Si$), 0.91 (s, *t*-$C_4\underline{H}_9(CH_3)_2Si$), 1.32 and 1.49 (s, isopropylidene CH_3), 2.99 (m, H_5), 3.61 (d, J=10.5 Hz, $\underline{H}_aH_bCOSi$), 3.95 (d, J=10.5 Hz, $H_a\underline{H}_bCOSi$), 4.30 (d, J=13.2 Hz, H_{2a}), 4.31 (t-like, J=3.8 Hz, H_6), 4.58 (d, J=13.2 Hz, H_{2b}), 4.68 (d, J=6.0 Hz, H_7), 4.86 (d, J=6.0 Hz, H_8). Found: *m/z* 343.1601. Calcd for $C_{16}H_{27}O_6Si$: (M−CH_3), 343.1575. **23b**: Mp 64—65 °C (ether–hexane); R_f=0.38 (3:1 ether–petroleum ether); IR 1738 cm^{-1} (C=O); ^1H NMR ($CDCl_3$) δ 0.09 (s, *t*-$C_4H_9(C\underline{H}_3)_2Si$), 0.92 (s, *t*-$C_4\underline{H}_9(CH_3)_2Si$), 1.32 and 1.49 (s, isopropylidene CH_3), 2.92 (d, J=16.0 Hz, H_{5a}), 3.23 (d, J=16.0 Hz, H_{5b}), 3.65 (d, J=10.5 Hz, $\underline{H}_aH_bCOSi$), 3.90 (d, J=10.5 Hz, $H_a\underline{H}_bCOSi$), 4.29—4.53 (m, H_1 and H_2), 4.60 (d, J=5.9 Hz, H_7), 5.00 (d, J=5.9 Hz, H_8). Found: *m/z* 343.1573. Calcd for $C_{16}H_{27}O_6Si$: (M−CH_3), 343.1575.

Oxidation of ***16***: Oxidation of **16** under the standard conditions afforded (1*R**,6*S**,7*S**,8*S**)-1-benzyloxymethyl-7,8-isopropylidenedioxy-3,9-dioxabicyclo[4.2.1]nonan-4-one (**24a**) and (1*S**,6*S**,7*S**,8*S**)-6-benzyloxymethyl-7,8-isopropylidenedioxy-3,9-dioxabicyclo[4.2.1]nonan-4-one (**24b**). **24a**: Mp 107—108 °C (ether–hexane); R_f=0.39 (3:1 ether–petroleum ether); IR 1736 cm^{-1} (C=O); ^1H NMR ($CDCl_3$) δ 1.33 and 1.48 (s, isopropylidene CH_3), 3.00 (m, H_5), 3.57 (d, J=10.0 Hz, $\underline{H}_aH_bCOCH_2C_6H_5$), 3.80 (d, J=10.0 Hz, $H_a\underline{H}_bCOCH_2C_6H_5$), 4.34 (m, H_6), 4.44 (d-like, J=3.2 Hz, H_2), 4.62 (d-like, J=2.0 Hz, $C\underline{H}_2C_6H_5$), 4.68 (d, J=6.0 Hz, H_7), 4.90 (d, J=6.0 Hz, H_8), 7.34 (s, C_6H_5). Found: C, 64.74; H, 6.69%. Calcd for $C_{18}H_{22}O_6$: C, 64.65; H, 6.63%. **24b**: Colorless oil; R_f=0.29 (3:1 ether–petroleum ether); IR 1736 cm^{-1} (C=O); ^1H NMR ($CDCl_3$) δ 1.36 and 1.52 (s, isopropylidene CH_3), 3.07 (d, J=16.0 Hz, H_{5a}), 3.25 (d, J=16.0 Hz, H_{5b}), 3.62 (d, J=10.0 Hz, $\underline{H}_aH_bCOCH_2C_6H_5$), 3.76 (d, J=10.0 Hz, $H_a\underline{H}_bCOCH_2C_6H_5$), 4.19—4.57 (m, H_1 and H_2), 4.59 (d, J=12.0 Hz, $H_a\underline{H}_bCC_6H_5$), 4.68 (d, J=6.0 Hz, H_7), 4.77 (d, J=12.0 Hz, $H_a\underline{H}_bCC_6H_5$), 5.05 (d, J=6.0 Hz, H_8), 7.39 (s, C_6H_5). Found: *m/z* 334.1415. Calcd for $C_{18}H_{22}O_6$: M, 334.1415.

Oxidation of ***17***: Oxidation of **17** afforded (1*R**,6*S**,7*S**,8*S**)-1-acetoxymethyl-7,8-isopropylidenedioxy-3,9-dioxabicyclo[4.2.1]nonan-4-one (**25a**) and (1*S**,6*S**,7*S**,8*S**)-6-acetoxymethyl-7,8-isopropylidenedioxy-3,9-dioxabicyclo[4.2.1]-

nonan-4-one (**25b**). **25a**: Mp 131—132 °C (ether–hexane); R_f=0.18 (3:1 ether–petroleum ether); IR 1739 cm^{-1} (C=O); ^1H NMR ($CDCl_3$) δ 1.33 and 1.50 (s, isopropylidene CH_3), 2.12 (s, CH_3CO), 3.02 (m, H_5), 4.10—4.50 (m, H_6, H_2, and CH_2OC=O), 4.72 (d, J=5.8 Hz, H_7), 4.91 (d, J=5.8 Hz, H_8); (C_6D_6) δ 1.00 and 1.32 (s, isopropylidene CH_3), 1.59 (s, CH_3CO), 2.32 (m, H_5), 3.71 (d, J=13.5 Hz, H_{2a}), 2.91 (d, J=13.5 Hz, H_{2b}), 3.97 (m, H_6), 4.14 (d, J=11.8 Hz, $\underline{H}_aH_bCOC$=O), 4.36 (d, J=11.8 Hz, $H_a\underline{H}_bCOC$=O), 4.43 (d, J=6.0 Hz, H_7), 4.61 (d, J=6.0 Hz, H_8). Found: C, 54.46; H, 6.32%. Calcd for $C_{13}H_{18}O_7$: C, 54.54; H, 6.34%. **25b**: Mp 151—153 °C (ether–hexane); R_f=0.16 (3:1 ether–petroleum ether); IR 1738 cm^{-1} (C=O); ^1H NMR ($CDCl_3$) δ 1.32 and 1.49 (s, isopropylidene CH_3), 2.11 (s, CH_3CO), 3.03 (s, H_5), 4.09—4.57 (m, H_1, H_2, and CH_2OC=O), 4.65 (d, J=5.7 Hz, H_7), 5.01 (d, J=5.7 Hz, H_8); (C_6D_6) δ 1.01 and 1.33 (s, isopropylidene CH_3), 1.63 (s, CH_3CO), 2.51 (d, J=13.8 Hz, H_{5a}), 2.91 (d, J=13.8 Hz, H_{5b}), 3.34 (dd, J=4.0, 13.8 Hz, H_{2a}), 3.60 (d, J=13.8 Hz, H_{2b}), 3.95 (d, J=4.0 Hz, H_1), 4.22 (d, J=11.5 Hz, $\underline{H}_aH_bCOC$=O), 4.40 (d, J=11.5 Hz, $H_a\underline{H}_bCOC$=O), 4.50 (d, J=5.8 Hz, H_7), 4.64 (d, J=5.8 Hz, H_8). Found: C, 54.57; H, 6.43%. Calcd for $C_{13}H_{18}O_7$: C, 54.54; H, 6.34%.

Oxidation of ***18***: Oxidation of **18** gave (1*S**,6*S**,7*S**,8*S**)-7,8-isopropylidenedioxy-1-pivaloyloxymethyl-3,9-dioxabicyclo-[4.2.1]nonan-4-one (**26a**) and (1*S**,6*S**,7*S**,8*S**)-7,8-isopropylidenedioxy-6-pivaloyloxymethyl-3,9-dioxabicyclo-[4.2.1]nonan-4-one (**26b**). **26a**: Mp 113—114 °C (ether–hexane); R_f=0.41 (3:1 ether–petroleum ether); IR 1732 cm^{-1} (C=O); ^1H NMR ($CDCl_3$) δ 1.20 (s, t-C_4H_9), 1.30 and 1.45 (s, isopropylidene CH_3), 2.98 (d-like, J=4.0 Hz, H_5), 4.00—4.51 (m, H_2, H_6, and CH_2OC=O), 4.70 (d, J=6.0 Hz, H_7), 4.90 (d, J=6.0 Hz, H_8); (C_6D_6) δ 0.98 and 1.30 (s, isopropylidene CH_3), 1.09 (s, t-C_4H_9), 2.29 (m, H_5), 3.76 (d, J=14.0 Hz, H_{2a}), 3.92 (m, H_6), 3.94 (d, J=14.0 Hz, H_{2b}), 4.14 (d, J=11.9 Hz, $\underline{H}_aH_bCOC$=O), 4.38 (d, J=11.9 Hz, $H_a\underline{H}_bCOC$=O), 4.43 (d, J=6.0 Hz, H_7), 4.58 (d, J=6.0 Hz, H_8). Found: C, 58.30; H, 7.34%. Calcd for $C_{16}H_{24}O_7$: C, 58.52; H, 7.37%. **26b**: Mp 121—122 °C (ether–hexane); R_f=0.32 (3:1 ether–petroleum ether); IR 1732 cm^{-1} (C=O); ^1H NMR ($CDCl_3$) δ 1.22 (s, t-C_4H_9), 1.30 and 1.48 (s, isopropylidene CH_3), 3.00 (s, H_5), 4.04—4.50 (m, H_1, H_2, and CH_2OC=O), 4.63 (d, J=5.5 Hz, H_7), 5.00 (d, J=5.5 Hz, H_8); (C_6D_6) δ 1.00 and 1.31 (s, isopropylidene CH_3), 1.14 (s, t-C_4H_9), 2.56 (d, J=15.7 Hz, H_{5a}), 2.92 (d, J=15.7 Hz, H_{5b}), 3.34 (dd, J=4.0, 13.5 Hz, H_{2a}), 3.58 (d, J=13.5 Hz, H_{2b}), 3.94 (d, J=4.0 Hz, H_1), 4.24 (d, J=11.5 Hz, $\underline{H}_aH_bCOC$=O), 4.40 (d, J=11.5 Hz, $H_a\underline{H}_bCOC$=O), 4.48 (d, J=6.0 Hz, H_7), 4.64 (d, J=6.0 Hz, H_8). Found: C, 58.68; H, 7.52%. Calcd for $C_{16}H_{24}O_7$: C, 58.52; H, 7.37%.

Oxidation of ***19***: The reaction of **19** afforded (1*S**,6*S**,7*S**,8*S**)-1-benzoyloxymethyl-7,8-isopropylidenedioxy-3,9-dioxabicyclo[4.2.1]nonan-4-one (**27a**) and (1*S**,6*S**,7*S**,8*S**)-6-benzoyloxymethyl-7,8-isopropylidenedioxy-3,9-dioxabicyclo-[4.2.1]nonan-4-one (**27b**). **27a**: Mp 171—173 °C (chloroform–hexane); R_f=0.34 (3:1 ether–petroleum ether); IR 1728 cm^{-1} (C=O); ^1H NMR ($CDCl_3$) δ 1.34 and 1.50 (s, isopropylidene CH_3), 3.03 (m, H_5), 4.30—4.60 (m, H_2, H_6, and CH_2OC=O), 4.71 (d, J=5.9 Hz, H_7), 4.99 (d, J=5.9 Hz, H_8), 7.48—8.03 (m, C_6H_5); (C_6D_6) δ 0.99 and 1.31 (s, isopropylidene CH_3), 2.30 (m, H_5), 3.78 (d, J=13.5 Hz, H_{2a}), 3.92 (m, H_6), 3.99 (d, J=13.5 Hz, H_{2b}), 4.37 (d, J=6.0 Hz, $\underline{H}_aH_bCOC$=O), 4.50 (d, J=6.0 Hz, H_7 and $H_a\underline{H}_bCOC$=O), 4.65 (d, J=6.0 Hz, H_8), 7.16 and 8.08 (m, C_6H_5); ^{13}C NMR ($CDCl_3$) δ 24.70, 26.07, 42.37, 64.35, 73.46, 78.60, 82.23, 84.52, 85.88, 113.16, 128.55, 129.76, 133.32, 165.79, 171.80. Found: C, 62.30; H, 5.79%. Calcd for $C_{18}H_{20}O_7$: C, 62.06; H, 5.79%. **27b**: Mp 162—163 °C (chloroform–hexane); R_f=0.27 (3:1 ether–hexane); IR 1727 cm^{-1} (C=O); ^1H NMR ($CDCl_3$) δ 1.34 and 1.52 (s, isopropylidene CH_3), 3.14 (s, H_5), 4.18—4.69 (m, H_1, H_2, and CH_2OC=O), 4.73 (d, J=6.0 Hz, H_7), 5.06 (d, J=6.0 Hz, H_8), 7.50 and 8.08 (m, C_6H_5); (C_6D_6) δ 0.94 and 1.27 (s, isopropylidene CH_3), 2.54 (d, J=15.6 Hz, H_{5a}), 2.95 (d, J=15.6 Hz, H_{5b}), 3.28 (dd, J=4.0, 14.0 Hz, H_{2a}), 3.54 (d, J=14.0 Hz, H_{2b}), 4.92 (d, J=4.0 Hz, H_1), 4.27—4.74 (m, H_7, H_8, and CH_2OC=O), 7.09 and 8.09 (m, C_6H_5); ^{13}C NMR ($CDCl_3$) δ 24.55, 25.98, 55.23, 65.98, 71.24, 82.27, 82.88, 83.93, 113.32, 128.52, 129.77, 133.27, 165.89, 171.39. Found: C, 61.84; H, 5.76%. Calcd for $C_{18}H_{20}O_7$: C, 62.06; H, 5.79%.

Oxidation of ***20***: The reaction of **20** produced (1*S**,6*S**,7*S**,8*S**)-7,8-isopropylidenedioxy-1-trifluoroacetoxymethyl-3,9-dioxabicyclo[4.2.1]nonan-4-one (**28a**) and (1*S**,6*S**,7*S**,8*S**)-7,8-isopropylidenedioxy-6-trifluoroacetoxymethyl-3,9-dioxabicyclo[4.2.1]nonan-4-one (**28b**). **28a**: Mp 139—141 °C (ether–hexane); R_f=0.41 (3:1 ether–petroleum ether); IR 1781 and 1737 cm^{-1} (C=O); ^1H NMR ($CDCl_3$) δ 1.31 and 1.48 (s, isopropylidene CH_3), 3.00 (d-like, J=3.7 Hz, H_5), 4.37 (s, CH_2OC=O), 4.37 (m, H_6), 4.40 (d, J=12.0 Hz, H_{2a}), 4.63 (d, J=12.0 Hz, H_{2b}), 4.71 (d, J=5.9 Hz, H_7), 4.92 (d, J=5.9 Hz, H_8); (C_6D_6) δ 0.96 and 1.28 (s, isopropylidene CH_3), 2.24 (m, H_5), 3.64 (s, H_2), 3.89 (m, H_6), 4.09 (d, J=12.0 Hz, $\underline{H}_aH_bCOC$=O), 4.24 (d, J=12.0 Hz, $H_a\underline{H}_bCOC$=O), 4.33 (d, J=6.0 Hz, H_7), 4.48 (d, J=6.0 Hz, H_8). Found: C, 45.70; H, 4.30%. Calcd for $C_{13}H_{15}O_7F_3$: C, 45.89; H, 4.44%. **28b**: Mp 130—132 °C (ether–hexane); R_f=0.34 (3:1 ether–petroleum ether); IR 1781 and 1738 cm^{-1} (C=O); ^1H NMR ($CDCl_3$) δ 1.32 and 1.50 (s, isopropylidene CH_3), 3.06 (s, H_5), 4.18—4.58 (m, H_1, H_2, and CH_2OC=O), 4.68 (d, J=5.3 Hz, H_7), 5.04 (d, J=5.3 Hz, H_8); (C_6D_6) δ 0.92 and 1.26 (s, isopropylidene CH_3), 2.41 (d, J=15.1 Hz, H_{5a}), 2.64 (d, J=15.1 Hz, H_{5b}), 3.20 (dd, J=4.0, 13.0 Hz, H_{2a}), 3.42 (d, J=13.0 Hz, H_{2b}), 3.82 (d, J=4.0 Hz, H_1), 4.07 (d, J=11.8 Hz, $\underline{H}_aH_bCOC$=O), 4.27 (d, J=11.8 Hz, $H_a\underline{H}_bCOC$=O), 4.31 (d, J=5.9 Hz, H_7), 4.51 (d, J=5.9 Hz, H_8). Found: C, 46.01; H, 4.30%. Calcd for $C_{13}H_{15}O_7F_3$: C, 45.89; H, 4.44%.

Oxidation of ***21***: Oxidation of **21** afforded (1*S**,6*S**,7*S**,8*S**)-7,8-isopropylidenedioxy-1-mesyloxymethyl-3,9-dioxabicyclo[4.2.1]nonan-4-one (**29a**) and (1*S**,6*S**,7*S**,8*S**)-7,8-isopropylidenedioxy-6-mesyloxymethyl-3,9-dioxabicyclo-[4.2.1]nonan-4-one (**29b**). **29a**: Mp 134—135 °C (chloroform–hexane); R_f=0.39 (2:1 ethyl acetate–hexane); IR 1738 cm^{-1} (C=O); ^1H NMR ($CDCl_3$) δ 1.30 and 1.49 (s, isopropylidene CH_3), 2.92—3.18 (m, H_5), 3.06 (s, CH_3SO_2), 4.18—4.53 (m, H_2, H_6, and CH_2OSO_2), 4.70 (d, J=5.9 Hz, H_7), 4.90 (d, J=5.9 Hz, H_8); (C_6D_6) δ 0.90 and 1.24 (s, isopropylidene CH_3), 2.18 (s, CH_3SO_2), 2.12—2.28 (m, H_5), 3.61 (d, J=13.8 Hz, H_{2a}), 3.74 (m, H_6), 4.78 (d, J=13.8 Hz, H_{2b}), 4.11 (s, CH_2OSO_2), 4.31 (d, J=5.9 Hz, H_7), 4.39 (d, J=5.9 Hz, H_8). Found: C, 44.61; H, 5.56; S, 10.21%. Calcd for $C_{12}H_{18}O_8S$: C, 44.72; H, 5.63; S, 9.95%. **29b**: Mp 137—138 °C (chloroform–hexane); R_f=0.33 (2:1 ethyl acetate–hexane); IR 1739 cm^{-1} (C=O); ^1H NMR ($CDCl_3$) δ 1.31 and 1.50 (s, isopropylidene CH_3), 3.07 (s, CH_3SO_2 and H_5), 4.20—4.53 (m, H_1, H_2, and CH_2OSO_2), 4.65 (d, J=6.0 Hz, H_7), 5.01 (d, J=6.0 Hz, H_8); (C_6D_6) δ 0.90 and 1.25 (s, isopropylidene CH_3), 2.21 (s, CH_3SO_2), 2.42 (d, J=16.0 Hz, H_{5a}), 2.85 (d, J=16.0 Hz, H_{5b}), 3.20 (dd, J=4.0, 13.1 Hz, H_{2a}), 3.44 (d, J=13.1 Hz, H_{2b}), 3.84 (d, J=4.0 Hz, H_1), 4.02 (d, J=11.0 Hz, $\underline{H}_aH_bCOSO_2$), 4.20

(d, J=11.0 Hz, $H_a\underline{H}_bCOSO_2$), 4.28 (d, J=6.0 Hz, H_7), 4.51 (d, J=6.0 Hz, H_8). Found: C, 44.35; H, 5.52%; S, 10.11%. Calcd for $C_{12}H_{18}O_8S$: C, 44.72; H, 5.63; S, 9.95%.

Oxidation of ***22***: Oxidation of **22** produced (1*S**,6*S**,7*S**,8*S**)-7,8-isopropylidenedioxy-1-trifluoromesyloxymethyl-3,9-dioxabicyclo[4.2.1]nonan-4-one (**30a**) and (1*S**,6*S**,7*S**,8*S**)-7,8-isopropylidenedioxy-6-trifluoromesyloxymethyl-3,9-dioxabicyclo[4.2.1]nonan-4-one (**30b**). **30a**: colorless oil; R_f=0.32 (3:1 ether–hexane); IR 1740 cm^{-1} (C=O); ^{1}H NMR ($CDCl_3$) δ 1.29 and 1.48 (s, isopropylidene CH_3), 3.01 (d-like, J=3.5 Hz, H_5), 4.38 (s, H_2), 4.53 (d, J=10.3 Hz, $\underline{H}_aH_bCOSO_2$), 4.70 (d, J=10.3 Hz, $H_a\underline{H}_bCOSO_2$), 4.71 (d, J=5.6 Hz, H_7), 4.91 (d, J=5.6 Hz, H_8); (C_6D_6) δ 0.87 and 1.20 (s, isopropylidene CH_3), 2.04 (dd, J=3.0, 16.1 Hz, H_{5a}), 2.21 (dd, J=5.9, 16.1 Hz, H_{5b}), 3.51 (s, H_2), 4.79 (dd, J=3.0, 5.9 Hz, H_6), 4.04—4.44 (m, H_7, H_8, and CH_2OSO_2). Found: m/z 376.0436. Calcd for $C_{12}H_{15}O_8SF_3$: M, 376.0440. **30b**: Mp 80—83 °C (ether–hexane); R_f=0.27 (3:1 ether–hexane); IR 1740 cm^{-1} (C=O); ^{1}H NMR ($CDCl_3$) δ 1.30 and 1.48 (s, isopropylidene CH_3), 2.99 (d, J=16.0 Hz, H_{5a}), 3.17 (d, J=16.0 Hz, H_{5b}), 4.33—4.62 (m, H_1, H_2, and CH_2OSO_2), 4.67 (d, J=5.8 Hz, H_7), 5.03 (d, J=5.8 Hz, H_8); (C_6D_6) δ 0.93 and 1.23 (s, isopropylidene CH_3), 2.42 (d, J=16.0 Hz, H_{5a}), 2.67 (d, J=16.0 Hz, H_{5b}), 3.28 (dd, J=3.7, 13.9 Hz, H_{2a}), 3.49 (d, J=13.9 Hz, H_{2b}), 3.87 (d, J=3.7 Hz, H_1), 4.28 (d, J=5.8 Hz, H_7), 4.42 (s, CH_2OSO_2), 4.53 (d, J=5.8 Hz, H_8). Found: m/z 376.0423. Calcd for $C_{12}H_{15}O_3SF_3$: M, 376.0440.

Oxidation of ***37***: Oxidation of **37** gave (1*R**,6*R**,8*S**)-8-benzoyloxy-3,9-dioxabicyclo[4.2.1]nonan-4-one (**42a**) and (1*R**,6*R**,7*S**)-7-benzoyloxy-3,9-dioxabicyclo[4.2.1]nonan-4-one (**42b**). **42a**: Mp 137—138 °C (chloroform–hexane); R_f=0.34 (3:1 ether–benzene); V_R=6.4 ml (9:1 ether–petroleum ether); IR 1738 and 1719 cm^{-1} (C=O); ^{1}H NMR ($CDCl_3$) δ 2.44 (t-like, J=5.8 Hz, H_7), 2.91 (dd, J=4.6, 16.0 Hz, H_{5a}), 3.13 (dd, J=2.7, 16.0 Hz, H_{5b}), 4.28—4.62 (m, H_1 and H_2), 4.69 (m, H_6), 5.73 (dd, J=5.0, 5.5 Hz, H_8), 7.51 and 8.04 (m, C_6H_5); ^{13}C NMR ($CDCl_3$) δ 37.54, 45.19, 71.57, 72.77, 75.87, 82.47, 128.35, 129.56, 133.20, 166.29, 172.48. Found: C, 64.41; H, 5.40%. Calcd for $C_{14}H_{15}O_5$: C, 64.11; H, 5.38%. **42b**: Mp 128—130 °C (chloroform–hexane); R_f=0.29 (3:1 ether–benzene); V_R=7.8 ml (9:1 ether–petroleum ether); IR 1735 and 1719 cm^{-1} (C=O); ^{1}H NMR ($CDCl_3$) δ 2.32 (ddd, J=3.1, 8.5, 14.0 Hz, H_{8a}), 2.78 (ddd, J=1.2, 7.3, 14.0 Hz, H_{8b}), 2.95 (dd, J=2.2, 15.9 Hz, H_{5a}), 3.21 (dd, J=5.0, 15.9 Hz, H_{5b}), 4.12 (dd, J=4.0, 15.9 Hz, H_{2a}), 4.44 (m, H_6), 4.47 (d, J=15.9 Hz, H_{2b}), 4.76 (m, H_1), 5.38 (dd, J=3.1, 7.3 Hz, H_7), 7.47 and 8.02 (m, C_6H_5); ^{13}C NMR ($CDCl_3$) δ 33.68, 43.06, 73.05, 77.85, 78.12, 78.27, 128.50, 129.74, 133.35, 166.25, 172.15. Found: C, 64.01; H, 5.40%. Calcd for $C_{14}H_{14}O_5$: C, 64.11; H, 5.38%.

Oxidation of ***34***: Oxidation of **34** led to (1*R**,6*R**,8*S**)-8-*t*-butyldimethylsiloxy-3,9-dioxabicyclo[4.2.1]nonan-4-one (**39a**) and (1*R**,6*R**,7*S**)-7-*t*-butyldimethylsiloxy-3,9-dioxabicyclo[4.2.1]nonan-4-one (**39b**). **39a**: Mp 70—72 °C (ether–hexane); R_f=0.18 (1:1 ether–hexane); V_R=20.0 ml (5:1 hexane–ethyl acetate); IR 1738 cm^{-1} (C=O); ^{1}H NMR ($CDCl_3$) δ 0.03 (s, *t*-$C_4H_9(C\underline{H}_3)_2Si$), 0.90 (s, *t*-$C_4\underline{H}_9(CH_3)_2Si$), 1.4—2.5 (m, H_7), 2.81 (dd, J=5.0, 16.0 Hz, H_{5a}), 3.06 (dd, J=2.3, 16.0 Hz, H_{5b}), 4.18—4.43 (m, H_1 and H_2), 4.63 (m, H_6), 4.75 (dd, J=3.4, 6.9 Hz, H_8). **39b**: Mp 48—51 °C (ether–hexane); R_f=0.18 (1:1 ether–hexane); V_R=23.6 ml (5:1 hexane–ethyl acetate); IR 1735 cm^{-1} (C=O); ^{1}H NMR ($CDCl_3$) δ 0.02 (s, *t*-$C_4H_9(C\underline{H}_3)_2Si$), 0.87 (s, *t*-$C_4\underline{H}_9(CH_3)_2Si$), 2.30—2.69 (m, H_8), 2.92 (m, H_5), 4.06 (dd, J=4.1, 13.8 Hz, H_{2a}), 4.12 (m, H_6), 4.40 (dd, J=3.0, 7.0 Hz, H_7), 4.42 (d, J=13.8 Hz, H_{2b}), 4.68 (m, H_1).

Regioisomeric ratio of **39a** and **39b** was determined as follows. To a solution of the lactones (53 mg, 0.195 mmol) in THF (1.0 ml) was added (n-$C_4H_9)_4NF$ in THF (0.822 mol dm^{-3} solution, 0.356 ml, 0.293 mmol) at 15 °C under argon. After stirring for 20 min, the reaction mixture was worked up to give a yellow oil. To this oil dissolved in pyridine (1 ml) was added benzoyl chloride (0.048 ml, 0.39 mmol) at 0 °C under argon. After stirring for 12 h at 15 °C, the reaction mixture was worked up to give a mixture of **42a** and **42b** (50 mg) as an oil. This oil was analyzed by HPLC.

Oxidation of ***33***: Oxidation of **33** afforded (1*R**,6*R**,8*S**)-8-benzyloxy-3,9-dioxabicyclo[4.2.1]nonan-4-one (**38a**) and (1*R**,6*R**,7*S**)-7-benzyloxy-3,9-dioxabicyclo[4.2.1]nonan-4-one (**38b**). This mixture was subjected to elemental analysis. Found: C, 67.38; H, 6.51%. Calcd for $C_{14}H_{16}O_4$: C, 67.73; H, 6.50%. **38a**: colorless oil; R_f=0.19 (6:1 ether–hexane); V_R=19.0 ml (2:1 hexane–ethyl acetate); IR 1738 cm^{-1} (C=O); ^{1}H NMR ($CDCl_3$) δ 2.75 (t-like, J=5.0 Hz, H_7), 2.94 (m, H_5), 4.1—4.7 (m, H_1, H_2, H_6, and H_8), 7.29 (s, C_6H_5). **38b**: Mp 103—104 °C (ether–hexane); R_f=0.19 (6:1 ether–hexane); V_R=20.4 ml (2:1 hexane–ethyl acetate); IR 1739 cm^{-1} (C=O); ^{1}H NMR ($CDCl_3$) δ 2.0—2.7 (m, H_8), 2.88 (d-like, J=3.5 Hz, H_5), 4.02 (dd, J=4.0, 13.9 Hz, H_{2a}), 4.19 (dd, J=4.1, 7.8 Hz, H_7), 4.30 (m, H_6), 4.40 (d, J=13.9 Hz, H_{2b}), 4.48 (s, $C\underline{H}_2C_6H_5$), 4.64 (m, H_1), 7.32 (s, C_6H_5).

Ratio of **38a** and **38b** was determined as follows. The mixture of lactones (20 mg, 0.0862 mmol), 10% Pd/C (2 mg), and ethyl acetate (1 ml) was stirred for 12 h at 15 °C under atmospheric pressure of hydrogen. The insoluble material was removed by filtration and the filtrate was evaporated to give a colorless oil. To this oil dissolved in pyridine (0.44 ml) was added benzoyl chloride (0.021 ml, 0.172 mmol) at 0 °C under argon. After stirring for 10 h at 15 °C, the reaction mixture was worked up to give a mixture of **42a** and **42b** (22 mg) as a yellow oil, which was analyzed by HPLC.

Oxidation of ***35***: The reaction of **35** led to (1*R**,6*R**,8*S**)-8-acetoxy-3,9-dioxabicyclo[4.2.1]nonan-4-one (**40a**) and (1*R**,6*R**,7*S**)-7-acetoxy-3,9-dioxabicyclo[4.2.1]nonan-4-one (**40b**). This mixture was subjected to elemental analysis. Found: C, 54.01; H, 6.20%. Calcd for $C_9H_{12}O_5$: C, 53.99; H, 6.04%. **40a**: colorless oil; R_f=0.19 (7:1 ether–hexane); V_R=12.5 ml (1:1 hexane–ethyl acetate); IR 1735 cm^{-1} (C=O); ^{1}H NMR ($CDCl_3$) δ 2.08 (s, CH_3CO), 2.22—2.38 (m, H_7), 2.88 (dd, J=4.5, 15.1 Hz, H_{5a}), 3.12 (dd, J=2.7, 15.1 Hz, H_{5b}), 4.40 (s, H_2), 4.42 (m, H_1), 4.62 (m, H_6), 5.47 (dd, J=4.0, 6.5 Hz, H_8). **40b**: Mp 80—82 °C (ether–hexane); R_f=0.14 (7:1 ether–hexane); V_R=14.0 ml (1:1 hexane–ethyl acetate); IR 1738 cm^{-1} (C=O); ^{1}H NMR ($CDCl_3$) δ 2.07 (s, CH_3CO), 2.10—2.34 (m, H_{8a}), 2.64 (dd, J=7.9, 14.2 Hz, H_{8b}), 2.89 (dd, J=2.9, 15.1 Hz, H_{5a}), 3.14 (dd, J=4.5, 15.1 Hz, H_{5b}), 4.10 (dd, J=4.1, 13.6 Hz, H_{2a}), 4.31 (m, H_6), 4.44 (d, J=13.6 Hz, H_{2b}), 4.70 (m, H_1), 5.13 (dd, J=3.0, 7.9 Hz, H_7).

Oxidation of ***36***: Oxidation of **36** gave (1*R**,6*R**,8*S**)-8-pivaloyloxy-3,9-dioxabicyclo[4.2.1]nonan-4-one (**41a**) and (1*R**,6*R**,7*S**)-7-pivaloyloxy-3,9-dioxabicyclo[4.2.1]nonan-4-one (**41b**). Elemental analyses of this mixture were: Found: C, 59.54; H, 7.78%. Calcd for $C_{12}H_{18}O_5$: C, 59.49; H, 7.49%. **41a**: Colorless oil; R_f=0.24 (3:1 ether–hexane); V_R=12.2 ml (2:1 hexane–ethyl acetate); IR 1732 cm^{-1} (C=O); ^{1}H NMR ($CDCl_3$) δ 1.18 (s, *t*-C_4H_9), 2.0—2.7 (m, H_7),

2.85 (dd, J=5.0, 16.5 Hz, H_{5a}), 3.06 (dd, J=2.0, 16.5 Hz, H_{5b}), 4.32 (m, H_1), 4.36 (s, H_2), 4.58 (m, H_6), 5.45 (dd, J=3.7, 6.8 Hz, H_8). **41b**: Mp 82—83 °C (ether–hexane); R_f=0.22 (3:1 ether–hexane); V_R=15.3 ml (2:1 hexane–ethyl acetate); IR 1735 cm^{-1} (C=O); ^1H NMR ($CDCl_3$) δ 1.18 (s, t-C_4H_9), 2.08 (ddd, J=3.2, 8.0, 13.8 Hz, H_{8a}), 2.63 (dd, J=7.8, 13.8 Hz, H_{8b}), 2.87 (dd, J=3.0, 16.0 Hz, H_{5a}), 3.15 (dd, J=4.8, 16.0 Hz, H_{5b}), 4.08 (dd, J=4.0, 13.1 Hz, H_{2a}), 4.25 (m, H_6), 4.43 (d, J=13.1 Hz, H_{2b}), 4.67 (m, H_1), 5.10 (dd, J=3.2, 7.8 Hz, H_7).

B. Results of Table 3. General: The Baeyer-Villiger oxidation and workup were generally performed as follows. To a mixture of a ketone (1 equiv), Na_2HPO_4 (11.9—12.8 g/l equiv of ketone), and CH_2Cl_2 (2.0—2.5 ml/l equiv of ketone; for **43**, 60 mg/(1 equiv of the ketone) of Na_2H_2edta was used) was added 1.0 mol dm^{-3} CH_2Cl_2 solution of trifluoroperacetic acid (3 equiv) at 0 °C. After stirring for 36 h at 20 °C (at 25 °C for **43**), the mixture was diluted with CH_2Cl_2 (1.5—5.5 ml/l equiv of ketone). To this was added $Na_2S_2O_3\cdot5H_2O$ (0.66—1.6 g/l equiv of ketone) at 0 °C and the resulting mixture was stirred for 2 h at 20 °C (for 4 h at 25 °C for **43**). The insoluble material was removed by filtration and the filtrate was evaporated to give a solid. The residue was subjected to silica-gel column chromatography to afford the desired lactones and an unreached starting material. Elution course of the column chromatography was monitored by TLC. The lactone was obtained as a mixture of two regioisomers. The product ratio was determined by ^1H NMR (for **43**, **44**, and **46**) or HPLC (for **47**, **48**, **49**, and **50**) and given in Table 3. The isomers were separated by rechromatography on silica gel (except for **43**). Samples for elemental analysis were obtained by recrystallizations of chromatographed products.

Typical Procedure. Oxidation of 43: Trifluoroperacetic acid in CH_2Cl_2 (1.0 mol dm^{-3} solution, 141 ml, 141 mmol) was added dropwise to a stirred, ice-cooled mixture of Na_2HPO_4 (64.8 g, 569 mmol), Na_2H_2edta (3 g), **43** (10.0 g, 47.4 mmol), and CH_2Cl_2 (200 ml). The mixture was stirred for 36 h at 25 °C and diluted with CH_2Cl_2 (200 ml). To this was added $Na_2S_2O_3\cdot5H_2O$ (75 g) at 0 °C and the resulting mixture was stirred for 4 h at 25 °C. The insoluble material was removed by filtration and the filtrate was evaporated. Chromatography of the residue on a silica gel column using a 9:1 mixture of hexane and ethyl acetate to pure ethyl acetate afforded a 33:67 mixture (determined by ^1H NMR) of (1*R**,6*S**,7*R**,8*R**)-7,8-isopropylidenedioxy-8-methyl-3,9-dioxabicyclo[4.2.1]nonan-4-one (**51a**) and (1*S**,6*R**,7*R**,8*S**)-7,8-isopropylidenedioxy-7-methyl-3,9-dioxabicyclo[4.2.1]nonan-4-one (**51b**) (5.59 g, 52%, 84% based on consumed **43**). In addition, unreacted **43** was obtained (3.80 g). Compounds **51a** and **51b** were separated by fractional recrystallizations from hexane–chloroform. **51a**: Mp 129.5—130 °C; R_f=0.46 (1:1 hexane–ethyl acetate); IR 1736 cm^{-1} (C=O); ^1H NMR (C_6D_6) δ 1.32 (s, CH_3), 1.34 and 1.48 (s, isopropylidene CH_3), 2.24 (dd, J=3.0, 16.0 Hz, H_{5a}), 2.52 (dd, J=4.8, 16.0 Hz, H_{5b}), 3.38 (dd, J=3.2, 14.0 Hz, H_{2a}), 3.62 (d, J=14.0 Hz, H_{2b}), 3.78 (m, H_1 and H_6), 4.14 (s, H_7); ^{13}C NMR ($CDCl_3$) δ 20.24, 27.87, 29.07, 42.94, 70.51, 79.69, 85.62, 91.47, 113.19, 171.70. Found: C, 58.14; H, 7.22%. Calcd for $C_{11}H_{16}O_5$: C, 57.88; H, 7.07%. **51b**: Mp 132—133 °C; R_f=0.46 (1:1 hexane–ethyl acetate); IR 1731 cm^{-1} (C=O); ^1H NMR (C_6D_6) δ 1.28 (s, CH_3), 1.28 and 1.48 (s, isopropylidene CH_3), 2.26 (dd, J=3.2, 17.0 Hz, H_{5a}), 2.52 (dd, J=4.2, 17.0 Hz, H_{5b}), 3.38 (dd, J=3.3, 14.6 Hz, H_{2a}), 3.58 (d, J=14.6 Hz, H_{2b}), 3.82 (m, H_1 and H_6), 4.34 (s, H_8); ^{13}C NMR ($CDCl_3$) δ 19.62, 27.68, 28.68, 42.02, 71.88, 82.01, 84.44, 86.82, 92.19, 113.12, 172.83. Found: C, 57.93; H, 7.05%. Calcd for $C_{11}H_{16}O_5$: C, 57.88; H, 7.07%.

Oxidation of 44: The reaction of **44** formed (1*R**,6*S**,7*R**,8*R**)-7,8-isopropylidenedioxy-8-pentyl-3,9-dioxabicyclo[4.2.1]nonan-4-one (**52a**) and (1*S**,6*R**,7*R**,8*S**)-7,8-isopropylidenedioxy-7-pentyl-3,9-dioxabicyclo[4.2.1]nonan-4-one (**52b**). Elemental analysis was performed as a mixture of **52a** and **52b**. Found: C, 63.13; H, 8.56%. Calcd for $C_{15}H_{24}O_5$: C, 63.36; H, 8.51%. **52a**: R_f=0.56 (3:1 ether–petroleum ether); IR 1736 cm^{-1} (C=O); ^1H NMR ($CDCl_3$) δ 0.8—1.8 (m, n-C_5H_{11}), 1.36 and 1.50 (s, isopropylidene CH_3), 2.28 (dd, J=2.6, 16.2 Hz, H_{5a}), 2.52 (dd, J=5.0, 16.2 Hz, H_{5b}), 3.3—4.0 (m, H_1, H_2, and H_6), 4.20 (s, H_7). **52b**: R_f=0.50 (3:1 ether–petroleum ether); IR 1732 cm^{-1} (C=O); ^1H NMR ($CDCl_3$) δ 0.8—1.8 (m, n-C_5H_{11}), 1.30 and 1.49 (s, isopropylidene CH_3), 2.34 (dd, J=3.2, 16.8 Hz, H_{5a}), 2.62 (dd, J=4.0, 16.8 Hz, H_{5b}), 3.42 (dd, J=3.8, 13.6 Hz, H_{2a}), 3.64 (dd, J=1.2, 13.6 Hz, H_{2b}), 3.80 (d-like, J=3.2 Hz, H_6), 3.96 (t-like, J=3.2 Hz, H_1), 4.44 (s, H_8).

Oxidation of 45: To a mixture of **45** (252 mg, 0.992 mmol), Na_2HPO_4 (1.81 g, 12.7 mmol), and CH_2Cl_2 (2.0 ml) was added dropwise trifluoroperacetic acid in CH_2Cl_2 (1.0 mol dm^{-3} solution, 3.0 ml, 3.0 mmol) at 0 °C. After stirring for 36 h at 20 °C, the reaction mixture was worked up as usual to give 220 mg of a white solid. TLC and NMR analysis of this solid indicated complete recovery of the starting material.

Oxidation of 46: Oxidation of **46** afforded (1*R**,6*S**,7*R**,8*S**)-7,8-isopropylidenedioxy-8-phenyl-3,9-dioxabicyclo[4.2.1]nonan-4-one (**53a**) and (1*S**,6*R**,7*R**,8*S**)-7,8-isopropylidenedioxy-7-phenyl-3,9-dioxabicyclo[4.2.1]nonan-4-one (**53b**). **53a**: Mp 148—149 °C (chloroform–hexane); R_f=0.42 (3:1 ether–petroleum ether); IR 1738 cm^{-1} (C=O); ^1H NMR ($CDCl_3$) δ 1.02 and 1.50 (s, isopropylidene CH_3), 3.10 (m, H_5), 3.80 (dd, J=3.6, 13.8 Hz, H_{2a}), 4.28 (d, J=13.8 Hz, H_{2b}), 4.38 (m, H_6), 4.60 (d-like, J=3.2 Hz, H_1), 5.16 (s, H_7), 7.3—7.6 (m, C_6H_5). Found: C, 65.80; H, 6.31%. Calcd for $C_{16}H_{18}O_5$: C, 66.19; H, 6.25%. **53b**: Mp 142—143 °C (chloroform–hexane); R_f=0.28 (3:1 ether–petroleum ether); IR 1741 cm^{-1} (C=O); ^1H NMR ($CDCl_3$) δ 1.04 and 1.52 (s, isopropylidene CH_3), 2.44 (dd, J=4.2, 17.4 Hz, H_{5a}), 2.88 (dd, J=3.0, 17.4 Hz, H_{5b}), 4.4—4.6 (m, H_1, H_2, and H_6), 5.52 (s, H_8), 7.3—7.6 (m, C_6H_5). Found: C, 65.58; H, 6.29%. Calcd for $C_{16}H_{18}O_5$: C, 66.19; H, 6.25%.

Oxidation of 47: Oxidation of **47** gave (1*R**,6*S**,7*R**,8*S**)-8-*t*-butyldimethylsiloxymethyl-7,8-isopropylidenedioxy-3,9-dioxabicyclo[4.2.1]nonan-4-one (**54a**) and (1*S**,6*R**,7*R**,8*S**)-7-*t*-butyldimethylsiloxymethyl-7,8-isopropylidenedioxy-3,9-dioxabicyclo[4.2.1]nonan-4-one (**54b**). **54a**: Mp 99.0—100 °C (ether–hexane); R_f=0.48 (2:1 hexane–ethyl acetate); V_R=11.2 ml (4:1 hexane–ethyl acetate); IR 1732 cm^{-1} (C=O); ^1H NMR (C_6D_6) δ 0.08 (s, t-$C_4H_9(C\underline{H}_3)_2Si$), 0.96 (s, t-$C_4\underline{H}_9(CH_3)_2Si$), 1.38 and 1.54 (s, isopropylidene CH_3), 2.29 (dd, J=2.8, 16.2 Hz, H_{5a}), 2.54 (dd, J=5.0, 16.2 Hz, H_{5b}), 3.6—4.2 (m, H_1, H_2, and H_6), 4.00 (s, H_7), 4.20 (s, CH_2OSi); ^{13}C NMR ($CDCl_3$) δ 18.37, 25.93, 27.98, 28.92, 42.88, 65.83, 70.78, 79.98, 84.58, 85.85, 96.04, 113.96, 171.77. Found: C, 56.52; H, 8.30%. Calcd for $C_{17}H_{30}O_6Si$: C, 56.96; H, 8.44%. **54b**: Mp 79.0—80.0 °C (ether–hexane); R_f=0.40 (2:1 hexane–ethyl acetate); V_R=14.7 ml (4:1 hexane–ethyl acetate); IR 1735 cm^{-1} (C=O); ^1H NMR (C_6D_6) δ 0.08 (s, t-$C_4H_9(C\underline{H}_3)_2Si$), 0.95 (s, t-$C_4\underline{H}_9(CH_3)_2Si$), 1.39 and 1.56 (s, isopropylidene CH_3), 2.44 (dd, J=3.0, 16.8 Hz, H_{5a}), 3.02 (dd, J=4.2, 16.8 Hz, H_{5b}), 3.42 (dd, J=3.4, 13.6 Hz, H_{2a}), 3.62 (dd, J=1.0, 13.6 Hz, H_{2b}), 3.84 (d, J=3.0

Hz, CH_2OSi), 3.84 (m, H_6), 4.15 (m, H_1), 4.44 (s, H_8); ^{13}C NMR ($CDCl_3$) δ 18.40, 25.96, 27.90, 28.76, 41.53, 64.40, 71.70, 80.96, 83.48, 84.58, 96.54, 113.95, 172.93. Found: C, 56.88; H, 8.47%. Calcd for $C_{17}H_{30}O_6Si$: C, 56.96; H, 8.44%.

Oxidation of ***48***: Oxidation of **48** afforded (1*R**,6*S**,7*R**,8*S**)-8-benzyloxymethyl-7,8-isopropylidenedioxy-3,9-dioxabicyclo[4.2.1]nonan-4-one (**55a**) and (1*S**,6*R**,7*R**,8*S**)-7-benzyloxymethyl-7,8-isopropylidenedioxy-3,9-dioxabicyclo[4.2.1]nonan-4-one (**55b**). **55a**: oil; R_f=0.50 (6:1 ether–petroleum ether); V_R=7.6 ml (3:2 petroleum ether–ethyl acetate); IR 1740 cm^{-1} (C=O); ^1H NMR (C_6D_6) δ 1.30 and 1.50 (s, isopropylidene CH_3), 2.24 (dd, J=2.5, 16.0 Hz, H_{5a}), 2.50 (dd, J=5.0, 16.0 Hz, H_{5b}), 3.52 (d, J=10.4 Hz, $\underline{H_a}H_bCOCH_2C_6H_5$), 3.84 (d, J=10.4 Hz, $H_a\underline{H_b}CO$-$CH_2C_6H_5$), 3.6—4.2 (m, H_1, H_2, and H_6), 4.18 (s, H_7), 4.36 (s, $C\underline{H_2}C_6H_5$), 7.20 (s, C_6H_5). Found: *m/z* 334.1418. Calcd for $C_{18}H_{22}O_6$: M, 334.1416. **55b**: Mp 116—117 °C (chloroform–hexane); R_f=0.45 (6:1 ether–petroleum ether); V_R=8.67 ml (3:2 petroleum ether–ethyl acetate); IR 1740 cm^{-1} (C=O); ^1H NMR (C_6D_6) δ 1.29 and 1.50 (s, isopropylidene CH_3), 2.36 (dd, J=3.0, 16.6 Hz, H_{5a}), 2.98 (dd, J=4.2, 16.6 Hz, H_{5b}), 3.36 (dd, J=3.0, 14.0 Hz, H_{2a}), 3.56 (dd, J=1.4, 14.0 Hz, H_{2b}), 3.61 (s, $\underline{H_2}CO$-$CH_2C_6H_5$), 3.81 (d-like, J=3.0 Hz, H_6), 4.21 (m, H_1), 4.38 (s, H_8), 4.42 (s, $C\underline{H_2}C_6H_5$), 7.18 (s, C_6H_5). Found: C, 64.70; H, 6.68%. Calcd for $C_{18}H_{22}O_6$: C, 64.65; H, 6.63%.

Oxidation of ***49***: Oxidation of **49** led to (1*R**,6*S**,7*R**,8*S**)-7,8-isopropylidenedioxy-8-pivaloyloxymethyl-3,9-dioxabicyclo[4.2.1]nonan-4-one (**56a**) and (1*S**,6*R**,7*R**,8*S**)-7,8-isopropylidenedioxy-7-pivaloyloxymethyl-3,9-dioxabicyclo[4.2.1]nonan-4-one (**56b**). **56a**: Mp 137—138 °C (hexane–ethyl acetate); R_f=0.54 (6:1 ether–petroleum ether); V_R=12.2 ml (7:3 hexane–ethyl acetate); IR 1740 cm^{-1} (C=O); ^1H NMR ($CDCl_3$) δ 1.24 (t-C_4H_9), 1.44 and 1.50 (s, isopropylidene CH_3), 3.04 (d-like, J=3.5 Hz, H_5), 4.2—4.4 (m, H_1 and H_6), 4.32 (d, J=11.5 Hz, $\underline{H_a}H_bCOC$=O), 4.41 (s, H_2), 4.46 (s, H_7), 4.74 (d, J=11.5 Hz, $H_a\underline{H_b}COC$=O). Found: C, 58.40; H, 7.44%. Calcd for $C_{16}H_{24}O_7$: C, 58.52; H, 7.37%. **56b**: Mp 131—132 °C (hexane–ethyl acetate); R_f=0.46 (6:1 ether–petroleum ether); V_R=15.0 ml (7:3 hexane–ethyl acetate); IR 1740 cm^{-1} (C=O); ^1H NMR ($CDCl_3$) δ 1.24 (s, t-C_4H_9), 1.44 and 1.50 (s, isopropylidene CH_3), 3.08 (d-like, J=3.6 Hz, H_5), 4.08 (d, J=12.5 Hz, $\underline{H_a}H_bCOC$=O), 4.2—4.5 (m, H_1 and H_6), 4.37 (s, H_2), 4.72 (d, J=12.5 Hz, $H_a\underline{H_b}COC$=O), 4.80 (s, H_8). Found: C, 58.52; H, 7.30%. Calcd for $C_{16}H_{24}O_7$: C, 58.52; H, 7.37%.

Oxidation of ***50***: Oxidation of **50** afforded (1*R**,6*S**,7*R**,8*S**)-8-benzoyloxymethyl-7,8-isopropylidenedioxy-3,9-dioxabicyclo[4.2.1]nonan-4-one (**57a**) and (1*S**,6*R**,7*R**,8*S**)-7-benzoyloxymethyl-7,8-isopropylidenedioxy-3,9-dioxabicyclo[4.2.1]nonan-4-one (**57b**). **57a**: Mp 196—197 °C (hexane–ethyl acetate); R_f=0.46 (6:1 ether–petroleum ether); V_R=9.54 ml (3:2 petroleum ether–ethyl acetate); IR 1730 cm^{-1} (C=O); ^1H NMR ($CDCl_3$) δ 1.42 and 1.50 (s, isopropylidene CH_3), 3.08 (d-like, J=4.0 Hz, H_5), 4.30 (t-like, J=3.6 Hz, H_6), 4.46 (s, H_2), 4.52 (m, H_1), 4.62 (s, H_7), 4.70 (d, J=12.6 Hz, $\underline{H_a}H_bCOC$=O), 4.86 (d, J=12.6 Hz, $H_a\underline{H_b}COC$=O), 7.3—7.6 (m, C_6H_5). Found: *m/z*, 333.0923. Calcd for $C_{17}H_{17}O_7$: ($M-CH_3$), 333.0873. **57b**: Mp 189—190 °C (hexane–ethyl acetate); R_f=0.39 (6:1 ether–petroleum ether); V_R=11.2 ml (3:2 petroleum ether–ethyl acetate); IR 1734 cm^{-1} (C=O); ^1H NMR ($CDCl_3$) δ 1.42 and 1.50 (s, isopropylidene CH_3), 3.12 (d-like, J=4.0 Hz, H_5), 4.38 (s, H_2), 4.2—4.5 (m, H_1, H_6, and $\underline{H_a}H_bCOC$=O) 4.80 (d, J=12.8 Hz, $H_a\underline{H_b}COC$=O), 4.94 (s, H_8), 7.3—7.6 (m, C_6H_5). Found: C, 60.68; H, 5.35%. Calcd for $C_{18}H_{20}O_7\cdot 0.3H_2O$: C, 61.11; H, 5.86%.

Competitive reaction of ***43*** *and (1*R**,5*S**,6*S**,7*R**)-6,7-isopropylidenedioxy-8-oxabicyclo[3.2.1]octan-3-one.* To a mixture of (1*R**,5*S**,6*S**,7*R**)-6,7-isopropylidenedioxy-8-oxabicyclo[3.2.1]octan-3-one (1.07 g, 5 mmol),[21b] **43** (1.14 g, 5 mmol), Na_2HPO_4 (212 mg, 1.5 mmol), and CH_2Cl_2 (20 ml) was added CH_2Cl_2 solution of trifluoroperacetic acid (1.0 mol dm^{-3}, 1.0 ml, 1.0 mmol) at 0 °C. After stirring for 5 h at 20 °C, the mixture was diluted with CH_2Cl_2 (20 ml). To this was added $Na_2S_2O_3\cdot 5H_2O$ (300 mg) at 0 °C and the mixture was stirred for 1 h at 20 °C. The reaction mixture was worked up in a usual way to give a white solid. HPLC analysis of the residue indicated that **51** (two regioisomers) and (1*R**,6*S**,7*S**,8*R**)-7,8-isopropylidenedioxy-3,9-dioxabicyclo[4.2.1]nonan-4-one were produced in 22:78 ratio. V_R (3:2 ethyl acetate–hexane): 9.3 ml (**51**), 10.7 ml (1*R**,6*S**,7*S**,8*R**)-7,8-isopropylidenedioxy-3,9-dioxabicyclo[4.2.1]nonan-4-one.

References

1) *C*-Nucleoside Synthesis. 18. Part 17: T. Sato, Y. Hayakawa, and R. Noyori, submitted for publication.

2) For preliminary accounts of this work see: R. Noyori, T. Sato, and H. Kobayashi, *Tetrahedron Lett.*, **21**, 2569 (1980); R. Noyori, H. Kobayashi, and T. Sato, *ibid.*, **21**, 2573 (1980).

3) Reviews: C. H. Hassall, *Org. React.*, **9**, 73 (1957); P. A. S. Smith, "Molecular Rearrangements," ed by P. de Mayo, Interscience, New York Vol. 1, (1963), p. 577; L. B. Lee and B. C. Uff, *Q. Rev., Chem. Soc.*, **21**, 429 (1967); H. O. House, "Modern Synthetic Reactions," 2nd ed, Benjamin, Menlo Park (1972), pp. 321—329.

4) R. Criegee, *Justus Liebigs Ann. Chem.*, **560**, 127 (1948); W. von E. Doering and E. Dorfman, *J. Am. Chem. Soc.*, **75**, 5595 (1953); B. Phillips, F. C. Frostick, Jr., and P. S. Starcher, *ibid.*, **79**, 5982 (1957).

5) W. von E. Doering and L. Speers, *J. Am. Chem. Soc.*, **72**, 5515 (1950); Y. Yukawa and T. Yokoyama, *Mem. Inst. Sci. Ind. Res. Osaka Univ.*, **13**, 171 (1956); M. F. Hawthorne, W. D. Emmons, and K. S. McCallum, *J. Am. Chem. Soc.*, **80**, 6393 (1958).

6) R. R. Sauers, *J. Am. Chem. Soc.*, **81**, 925 (1959); J. Meinwald and E. Frauenglass, *ibid.*, **82**, 5235 (1960); R. R. Sauers and G. P. Ahearn, *ibid.*, **83**, 2759 (1961); R. R. Sauers and J. A. Beisler, *J. Org. Chem.*, **29**, 210 (1964).

7) For instance, see: R. Noyori, T. Sato, and Y. Hayakawa, *J. Am. Chem. Soc.*, **100**, 2561 (1978).

8) T. Sato, M. Watanabe, and R. Noyori, *Tetrahedron Lett.*, **1978**, 4403.

9) T. Sato, M. Watanabe, and R. Noyori, *Tetrahedron Lett.*, **1979**, 2897.

10) T. Sato, M. Watanabe, and R. Noyori, *Heterocycles*, **14**, 761 (1980).

11) Powerful directing effect of β-trimethylsilyl group was reported: P. F. Hudrlik, A. M. Hudrlik, G. Nagendrappa, T. Yimenu, E. T. Zellers, and E. Chin, *J. Am. Chem. Soc.*, **102**, 6894 (1980).

12) H. Oberhammer and J. E. Boggs, *J. Am. Chem. Soc.*, **102**, 7241 (1980), and references cited therein. We thank Professor H. Sakurai for his valuable comments on this matter. See also: M. Suzuki, H. Takada, and R. Noyori, *J. Org. Chem.*, **47**, 902 (1982).

13) J. A. Pople and M. Gordon, *J. Am. Chem. Soc.*, **89**, 4253 (1967).

14) For the stereoselective reaction of bicyclo[3.2.1]octan-3-one and related systems, see A. H. Beckett, N. J. Harper, A. D. J. Balon, and T. H. E. Wattz, *Tetrahedron*, **6**, 319

(1959); Y. Hayakawa and R. Noyori, *Bull. Chem. Soc. Jpn.*, **47**, 2617 (1974); G. Büchi, H. Fliri, and R. Shapiro, *J. Org. Chem.*, **42**, 2192 (1977); Y. Hayakawa, Y. Baba, S. Makino, and R. Noyori, *J. Am. Chem. Soc.*, **100**, 1986 (1978), and references cited therein. Attempted reaction of **45** and methyllithium resulted in recovery of the ketone.

15) M. F. Hawthorne and W. D. Emmons, *J. Am. Chem. Soc.*, **80**, 6398 (1958); B. W. Palmer and A. Fry, *ibid.*, **92**, 2580 (1970); T. Mitsuhashi, H. Miyadera, and O. Simamura, *Chem. Commun.*, **1970**, 1301; Y. Ogata and Y. Sawaki *J. Am. Chem. Soc.*, **94**, 4189 (1972); *J. Org. Chem.*, **37**, 2953 (1972).

16) For the related phenomenon, see T. Momose, S. Atarashi, and Muraoka, *Tetrahedron Lett.*, **1974**, 3697.

17) Protonation of hydrogen bonding to the leaving group facilitate the fragmentation.

18) V. A. Stoute, M. A. Winnik, and I. G. Csizmadia, *J. Am. Chem. Soc.*, **96**, 6388 (1974).

19) Possible hydrogen bonding between the hydroxyl group and oxygen atom of R group would not affect the regioselectivity, because (1) alkyl groups and ether- or ester-containing substituents exhibit the same directing effect and (2) the hydrogen-bonded conformer does not satisfy the stereoelectronic prerequisite described in the text (model inspection).

20) ^{13}C NMR shift of carbonyl carbon of the ketones is little affected by the nature of R. Typical substituents and the chemical shifts ($CDCl_3$, ppm downfield from $(CH_3)_4Si$ internal standard) follow: H, 204.32; *n*-C_5H_{11}, 205.07; C_6H_5, 204.54; $CH_2OSi(CH_3)_2$-*t*-C_4H_9, 204.60; $CH_2OCH_2C_6H_5$, 204.56; CH_2OCO-*t*-C_4H_9, 204.23; $CH_2OCOC_6H_5$, 204.20.

21) a) R. D. Clark and C. H. Heathcock, *J. Org. Chem.*, **41**, 636 (1976); b) T. Sato and R. Noyori, *Bull. Chem. Soc. Jpn.*, **51**, 2745 (1978).

22) E. LeGoff, *J. Org. Chem.*, **29**, 2048 (1964).

23) M. Miyashita, A. Yoshikoshi, and P. A. Grieco, *J. Org. Chem.*, **42**, 3772 (1977).

24) C. Rappe, *Acta Chem. Scand.*, **16**, 2467 (1962).

25) E. J. Corey and J. W. Suggs, *Tetrahedron Lett.*, **1975**, 2647.

26) H. C. Marsmann and H.-G. Horn, *Z. Naturfosch., B*, **27**, 1448 (1972).

27) K. Inomata, S.-I. Aoyama, and H. Kotake, *Bull. Chem. Soc. Jpn.*, **51**, 930 (1978).

28) D. Miller, *J. Chem. Soc., C*, **1969**, 12.

29) H. Wynberg, *J. Am. Chem. Soc.*, **80**, 364 (1958).

30) D. C. Ayres and J. R. Smith, *J. Chem. Soc., C*, **1968**, 2737.

31) J. Burdon, I. Farazmand, M. Stacey, and J. C. Tatlow, *J. Chem. Soc.*, **1957**, 2574.

32) V. VanRheenen, R. C. Kelly, and D. Y. Cha, *Tetrahedron Lett.*, **1976**, 1973; V. VanRheenen, D. Y. Cha, and W. M. Hartley, *Org. Synth.*, **58**, 43 (1978).

33) M. J. Arco, M. H. Trammell, and J. D. White, *J. Org. Chem.*, **41**, 2075 (1976).

34) E. J. Corey and A. Venkateswarlu, *J. Am. Chem. Soc.*, **94**, 6190 (1972).

35) K. B. Sharpless and K. Akashi, *J. Am. Chem. Soc.*, **98**, 1986 (1976).

Stereocontrolled General Synthesis of Pyrimidine *C*-Nucleosides Having Branched-chain Sugar Moieties[1]

Tsuneo SATO, Makoto WATANABE, Hiroshi KOBAYASHI, and Ryoji NOYORI*

Department of Chemistry, Nagoya University, Chikusa-ku, Nagoya 464

(Received February 23, 1983)

A variety of pyrimidine *C*-nucleosides bearing branched-chain sugars can be synthesized starting from adequately substituted (1*R**,6*S**,7*S**,8*R**)-7,8-isopropylidenedioxy-3,9-dioxabicyclo[4.2.1]nonan-4-ones. The general procedure consists of condensation with *t*-butoxybis(dimethylamino)methane, giving the corresponding α-dimethylaminomethylene lactones, base-catalyzed heterocycle formation with urea, thiourea, or guanidine, and acid-promoted removal of the isopropylidene protective group. The overall transformation proceeds with retention of the stereochemistry to afford only *C*-β-glycosyl nucleoside structures.

We have recently developed a novel method[2] for the synthesis of pseudouridine (**1**), a component of tRNA, and its analogues such as 2-thiopseudouridine (**2**) and pseudoisocytidine (**3**)[3] *via* a common intermediate, (1*R*,6*S*,7*S*,8*R*)-7,8-isopropylidenedioxy-3,9-dioxabicyclo[4.2.1]nonan-4-one (**4**), which possesses a rigid *C*-β-glycoside structure. Realization of this method relies on the efficiency of the transition metal aided [3+4] annulation using polybromo ketones and furans[4] and the stereoregulation of the subsequent oxidative transformation. The great flexibility of this new procedure prompted us to prepare a variety of the synthetic analogues. So far interest in the synthesis of *C*-nucleoside analogues has centered around the compounds having an arabionsyl or deoxyribosyl residue.[5] Being stimulated by the discovery of the antibiotics, angustomycin A and C[6] and nucleosidin,[7] which exhibit cytostatic or virostatic activity, we were particularly interested in *C*-nucleosides bearing a branched-chain ribofuranosyl moiety. Although a number of routes to branched-chain sugars have been developed during the past few years,[8] there were reported no efficient total syntheses which gave directly and stereospecifically such sugar derivatives. The present paper describes a completely stereocontrolled entry to pyrimidine *C*-nucleosides containing branched-chain sugar moieties.

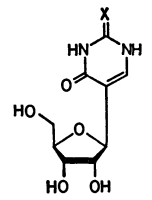

1, X=O
2, X=S

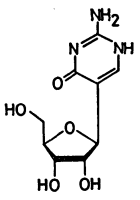

3

4

Results and Discussion

Synthesis of 5′-Modified Pyrimidine C-*Nucleosides.*[9] The iron carbonyl- or Zn/Ag couple-promoted cyclocoupling of polybromo ketones and furan provides a general way to give the adducts of type **5**.[4] The bicyclic ketone **5a** thus obtained can be transformed oxidatively to **6a** under perfect stereo- and regiochemical control.[1] Heating of a mixture of the lactone **6a** and a Bredereck reagent, t-$C_4H_9OCH[N(CH_3)_2]_2$[10] (excess), in DMF at 50 °C afforded the dimethylaminomethylene lactone **7a** (*Z*:*E*=70:30) in a good yield. Condensation of **7a** and urea with ethanolic sodium ethoxide formed the uracil derivative **8a** in 48% yield. The β stereochemistry at the anomeric 1′ position was confirmed by the ^{1}H NMR analysis in pyridine-d_5. The isopropylidene methyl signals appeared at δ 1.41 and 1.67 (Δδ=0.26 ppm), in accord with the Imbach's empirical rule.[11] The spin-spin coupling constant, $J_{4',5'}$=3.7 Hz, also supported this assignment.[12] Subsequent treatment of **8a** with 10% HCl in methanol at 25 °C furnished (±)-5′,5′-dimethylpseudouridine (**9a**). No pyranose derivatives were formed by this deprotection procedure.

When **7a** was treated with thiourea in refluxing ethanolic sodium ethoxide, the thiouracil derivative **10a** was obtained. The glycol protective group was then removed by 10% HCl in methanol to give (±)-5′,5′-dimethyl-2-thiopseudouridine (**11a**).

The base-catalyzed condensation of **7a** with guanidine furnished the pseudoisocytidine derivative **12a**, which, by treatment with 10% HCl in methanol, afforded (±)-5′,5′-dimethylpseudoisocytidine (**13a**) in quantitative yield.

In a similar manner, the 5′-monoalkylated or -phenylated pseudouridines **9b—d**, the 5′-monosubstituted 2-thiopseudouridines **11b—d**, and 5′-monosubstituted pseudoisocytidines **13b—d** were prepared from the corresponding ketones **5b—d**. In addition to the complete stereochemical control achieved in this synthesis, the configurational relationship between the carbonyl α position in **5** and the 5′ carbon of the resulting nucleosides, **9**, **11**, and **13**, is noteworthy. Since the chiral center created in the initial reductive [3+4] cyclocoupling of polybromo ketones and furan remains intact during the subsequent transformation, the stereochemistry inherent in **5b**, for example, leads to the 6′-deoxyallofuranosyl structure, **9b**, **11b**, and **13b**. Thus this approach allows a general entry to pyrimidine *C*-nucleosides possessing various carbon substituents at the 5′ position.[13]

Synthesis of 1′- and 4′-Modified Pyrimidine C-*Nucleosides. A. 4′-Alkylated Pyrimidine* C-*Nucleosides*:[14,15] The readily available lactone **14a**[1] was condensed with t-$C_4H_9OCH[N(CH_3)_2]_2$ to afford the dimethylaminomethylene derivative **15a** in 70% yield. Conversion of **15a** to a uracil derivative **16a** was accomplished by heating **15a** with urea (10 equiv) in ethanolic sodium ethoxide in a fair yield. The assignment of

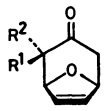

5

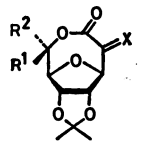

6, X=H_2
7, X=$CHN(CH_3)_2$

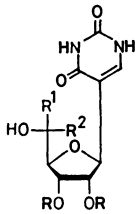

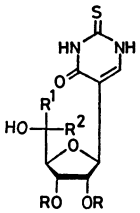

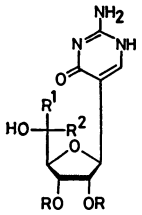

8, R-R=$C(CH_3)_2$ **10**, R-R=$C(CH_{,2}$ **12**, R-R=$C(CH_3)_2$
9, R=H **11**, R=H **13**, R=H (HCl salt)
a, $R^1=R^2=CH_3$ **b**, $R^1=CH_3$; $R^2=H$ **c**, $R^1=(CH_2)_4CH_3$; $R^2=H$
d, $R^1=C_6H_5$; $R^2=H$

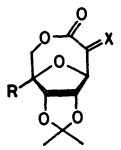

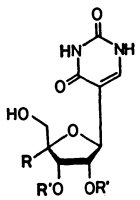

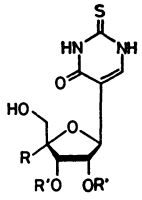

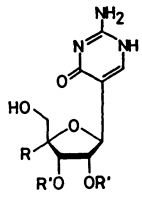

14, X=H_2 **16**, R′-R′=$C(CH_3)_2$ **18**, R′-R′=$C(CH_3)_2$ **20**, R′-R′=$C(CH_3)_2$
15, X=$CHN(CH_3)_2$ **17**, R′=H **19**, R′=H **21**, R′=H (HCl salt)
a, R=CH_3 **b**, R=$(CH_2)_4CH_3$ **c**, R=C_6H_5

β configuration of the uracil base was made on the basis of the ^1H NMR chemical shifts of the isopropylidene methyls (δ 1.40 and 1.66, $\Delta\delta$=0.26 ppm).[11] Exposure of **16a** to 10% HCl in methanol formed (±)-4′-methylpseudouridine (**17a**) in quantitative yield. Preparation of (±)-4′-methyl-2-thiopseudouridine (**19a**) was effected by heating **15a** with thiourea in ethanolic sodium ethoxide, followed by acidic removal of the isopropylidene group. Condensation of **15a** with guanidine followed by removal of the isopropylidene protective group produced (±)-4′-methylpseudoisocytidine (**21a**) in 64% yield.

When an alkylated lactone **14b**[1] was used as the starting material, the 4′-pentyl pyrimidine *C*-nucleosides, **17b**, **19b**, and **21b**, were obtained according to similar synthetic procedures.

The otherwise unaccessible 4′-arylated pyrimidine *C*-nucleoside analogues, **17c**, **19c**, and **21c**, have been prepared by this completely stereocontrolled recipe starting from the phenylated lactone **14c**, derived from 2-phenylfuran and $\alpha,\alpha,\alpha',\alpha'$-tetrabromoacetone.[18]

B. 1′-Alkylated Pyrimidine C-*Nucleosides*:[14] When the methylated lactone **22a**[1] was treated with *t*-$C_4H_9OCH[N(CH_3)_2]_2$ (neat, 90 °C), there was obtained the dimethylaminomethylene lactone **23a**, displaying IR absorptions at 1670 (C=O) and 1590 cm^{-1} (C=C). This was subjected immediately to the condensation with urea in ethanolic sodium ethoxide to afford **24a**. The reaction proceeded only sluggishly and the yield was only 7% based on **22a**. The ^1H NMR spectrum of **24a** indicated that the product has β configuation at C-1′ position; the singlets due to the isopropylidene methyls occurred at δ 1.39 and 1.65 ($\Delta\delta$=0.26 ppm).[11] Removal of the isopropylidene block with 10% HCl in methanol yielded (±)-1′-methylpseudouridine (**25a**). The lactone **23a** underwent the sodium ethoxide-promoted condensation with thiourea in refluxing ethanol to produce the acetonide **26a**. Subsequent deprotection with 10% HCl in methanol liberated (±)-1′-methyl-2-thiopseudouridine (**27a**). Construction of the heterocyclic nucleus with guanidine gave rise to **28a**, methanolysis of which catalyzed by HCl afforded hydrochloride salt of **29a**. In a like manner, 1′-pentyl pyrimidine *C*-nucleosides, **25b**, **27b**, and **29b**, were obtained by employing the lactone **22b**.[1] Elaboration of heterocycles onto **22** was achieved less effectively because of the severe steric hindrance caused by the C-1′ alkyl substitution. Nevertheless, this method realized the first synthesis of 1′-alkylated *C*-nucleosides.[22]

C. 1′- and 4′-Hydroxymethylated Pyrimidine C-*Nucleosides*:[23] Condensation of the lactone **30**[1] with *t*-$C_4H_9OCH[N(CH_3)_2]_2$ in DMF at 90 °C provided the dimethylaminomethylene compound **31** in 91% yield.

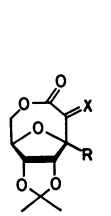

22, X=H_2
23, X=CHN$(CH_3)_2$
a, R=CH_3 **b**, R=$(CH_2)_4CH_3$

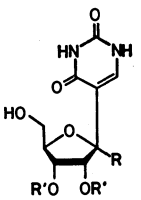

24, R′-R′=$C(CH_3)_2$
25, R′=H

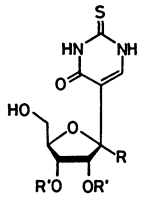

26, R′-R′=$C(CH_3)_2$
27, R′=H

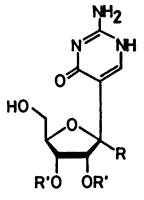

28, R′-R′=$C(CH_3)_2$
29, R′=H (HCl salt)

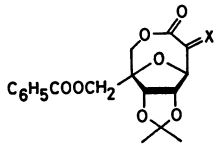

30, X=H_2
31, X=CHN$(CH_3)_2$

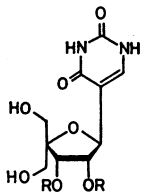

32, R-R=$C(CH_3)_2$
33, R=H

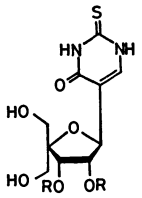

34, R-R=$C(CH_3)_2$
35, R=H

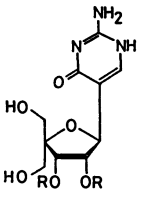

36, R-R=$C(CH_3)_2$
37, R=H (HCl salt)

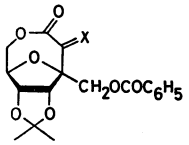

38, X=H_2
39, X=CHN$(CH_3)_2$

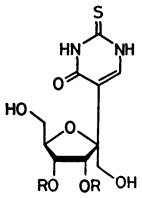

40, R-R=$C(CH_3)_2$
41, R=H

Treatment of **31** with urea in the presence of sodium ethoxide constructed the uracil skeleton and simultaneous removal of the benzoyl moiety gave **32** in a moderate yield. Deprotection of the isopropylidene group by 10% HCl in methanol formed (±)-4′-hydroxymethylpseudouridine (**33**) in 89% yield. Similarly, treatment of **31** with thiourea under the basic conditions, giving **34**, followed by deprotection afforded (±)-4′-hydroxymethyl-2-thiopseudouridine (**35**). The base-catalyzed cyclization of **31** with guanidine, giving **36**, followed by removal of the isopropylidene block furnished (±)-4′-hydroxymethylpseudoisocytidine (**37**) as hydrochloride salt.

In a parallel fashion, the lactone **39**, derived from **38** by the reaction with *t*-$C_4H_9OCH[N(CH_3)_2]_2$, was convertible to 1′-hydroxymethylated pyrimidine *C*-nucleosides such as (±)-1′-hydroxymethyl-2-thiopseudouridine (**41**). Thus the base-promoted condensation of **39** and thiourea affording the acetonide **40** and subsequent removal of the protective group gave the *C*-nucleoside **41** which consists of psicose and a pyrimidine base.[22]

D. 1′,4′-Dialkylated Pyrimidine C-*Nucleosides*:[24] Bishydroxylation of **42a**[25] using hydrogen peroxide (3 equiv) in the presence of a catalytic amount of osmium tetraoxide in a 10:1:1 mixture of acetone, *t*-butyl alcohol, and ether, followed by acetonidation with $CuSO_4$ and *p*-toluenesulfonic acid in acetone gave **43a**. The α stereochemical assignment was made on the basis of the ^1H NMR spectrum which exhibited the H_6 and H_7 signal as a singlet at δ 4.30.[26] Then exposure of **43a** to trifluoroperacetic acid gave the lactone **44a** in 77% yield. Subsequent reaction with neat tris(dimethylamino)methane[27] at 90 °C afforded the (*Z*)-dimethylaminomethylene lactone **45a** in 38% yield (88% based on consumed **44a**) as a single isomer. Condensation of **45a** with urea with ethanolic sodium ethoxide formed **46a** in 28% yield, which was then treated with 10% methanolic HCl to give (±)-1′,4′-dimethylpseudouridine (**47a**). The ^1H NMR spectrum giving the isopropylidene methyl signals at δ 1.28 and 1.50 ($\Delta\delta$=0.22 ppm) confirmed the β heterocycle stereochemistry assigned for **46a**.[11,28] When thiourea was employed for the analogous cyclization, there was obtained in 60% yield the 2-thiouracil derivative **48a**, leading to **49a** after deprotection. Use of guanidine in place of urea gave rise to **51a** as HCl salt *via* **50a** in 75% yield.

In a usual manner, the 1′,4′-dipentyl analogues, **47b**, **49b**, and **51b**, have also been prepared starting with **42b**.

Thus present way appears to provide a facile, general entry to 1′,4′-disubstituted pyrimidine *C*-nucleosides which are not available by the conventional approaches

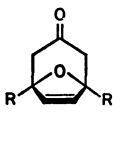

42

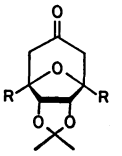

43

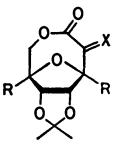

44, X=H_2
45, X=$CHN(CH_3)_2$

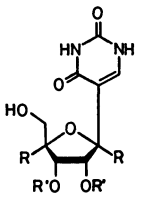

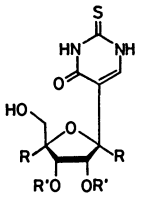

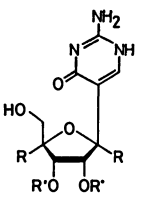

46, R′-R′=$C(CH_3)_2$
47, R′=H
a, R=CH_3 **b**, R=$(CH_2)_4CH_3$

48, R′-R′=$C(CH_3)_2$
49, R′=H

50, R′-R′=$C(CH_3)_2$
51, R′=H (HCl salt)

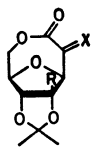

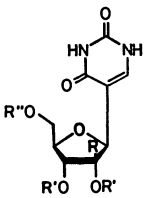

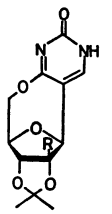

52a, R=CH_2OTBDMS; X=H_2
52b, R=CH_3; X=H_2
53a, R=CH_2OTBDMS; X=$CHN(CH_3)_2$
53b, R=CH_3; X=$CHN(CH_3)_2$

54a, R=CH_2OTBDMS; R′-R′=$C(CH_3)_2$; R″=H
54b, R=CH_3; R′-R′=$C(CH_3)_2$; R″=H
55a, R=CH_2OH; R′=R″=H
55b, R=CH_3; R′=R″=H
56a, R=CH_2OTBDMS; R′-R′=$C(CH_3)_2$; R″=SO_2CH_3
56b, R=CH_3; R′-R′=$C(CH_3)_2$; R″=SO_2CH_3

57a, R=CH_2OTBDMS
57b, R=CH_3

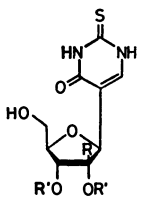

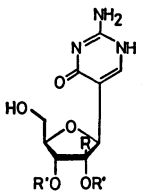

58a, R=CH_2OTBDMS; R′-R′=$C(CH_3)_2$
58b, R=CH_3; R′-R′=$C(CH_3)_2$
59a, R=CH_2OH; R′=H
59b, R=CH_3; R′=H
TBDMS=$Si(CH_3)_2$-*t*-C_4H_9

60a, R=CH_2OTBDMS; R′-R′=$C(CH_3)_2$
60b, R=CH_3; R′-R′=$C(CH_3)_2$
61a, R=CH_2OH; R′=H (HCl salt)
61b, R=CH_3; R′=H (HCl salt)

reported to date.

Synthesis of 2′-Alkylated Pyrimidine C-*Nucleosides*:[29] Treatment of **52a**[1] with excess *t*-$C_4H_9OCH[N(CH_3)_2]_2$ at 70 °C afforded the corresponding condensation product **53a** in 52% yield. The base-aided reaction with excess urea led to the uracil derivative **54a** in 20% yield, deprotection of which by methanolic HCl gave (±)-2′-hydroxymethylpseudouridine (**55a**) in 95% yield. The β stereochemistry at the anomeric position was established chemically by converting the acetonide **54a** to the cyclo-*C*-nucleoside **57a**. Thus reaction of **54a** and methanesulfonyl chloride in pyridine and subsequent treatment with 1,8-diazabicyclo[5.4.0]-undec-7-ene (DBU) in acetonitrile gave **57a** in *ca.* 60% yield.[30] Formation of the expected product was substantiated by comparison of the UV spectrum in methanol (λ_{max} 295 nm, ε 3720) showing a well-known, characteristic bathochromic shift, with that of the starting open-form **54a** (λ_{max} 266 nm, ε 7150).[21]

When the lactone **53a** was annulated with thiourea,

the protected nucleoside **58a** was obtained in high yield. Brief treatment of **58a** with methanolic HCl afforded (±)-2′-hydroxymethyl-2-thiopseudouridine (**59a**). Similarly, treatment of **53a** with guanidine, giving **60a**, and acid-assisted deprotection under the standard conditions led to (±)-2′-hydroxymethylpseudoisocytidine (**61a**) as HCl salt.

In a like fashion, 2′-methylated pyrimidine *C*-nucleosides, **55b**, **59b**, and **61b**, were synthesized by use of **52b**.[1)]

This method allows ready construction of the difficult-to-make hamamelose and 2′-methylribofuranose skeletons and introduction of pyrimidine rings at the 1′-position.[31)]

As has been outlined above, this approach is synthetically very flexible and a variety of *C*-nucleoside analogues can be made by parallel routes. The possibility was examined only with achiral or racemic precursors, but the optical resolution of the intermediates, leading to the "natural" configurations, could be done most conveniently at the stage of the lactones of type **4**.[2)]

Experimental

General. All melting and boiling points are uncorrected. IR spectra were recorded on a JASCO IRA-1 spectrometer in $CHCl_3$ solution unless otherwise stated. ^1H NMR spectra were obtained using a Varian NV-21 or HA-100 spectrometer, and ^{13}C NMR spectra were recorded at 20 MHz on a Varian CFT-20 spectrometer or at 25 MHz on a JEOL FX-100 spectrometer. The chemical shifts are recorded in parts per million relative to tetramethylsilane as an internal standard. Singlet, doublet, triplet, and multiplet are abbreviated to s, d, t, and m, respectively. Exact mass spectra were obtained at Central Research Laboratory of Ono Pharmaceutical Co. Elemental analyses were performed at the Research Laboratory of Fujisawa Pharmaceutical Co. and Faculty of Engineering of Nagoya University. Drying of organic extracts was done over anhydrous Na_2SO_4. For concentration of organic solvents, a vacuum (50—100 mmHg)** rotary evaporator was used.

Chromatography. Thin-layer chromatography (TLC) was done using a glass plate coated with 0.25-mm layers of silica gel 60 PF_{254} obtained from E. Merck and for preparative TLC, 20×20-cm glass plates coated with a 1.0-mm layer of silica gel 60 PF_{254} were employed. Analytical plates were visualized by spraying with a solution of 2% $Ce(SO_4)_2$ in 5% H_2SO_4 or 2% *p*-anisaldehyde in 5% ethanolic H_2SO_4 followed by heating on a hot plate. The position of spots are shown by R_f values. For column chromatography, E. Merck Kieselgel 60 (70—230 mesh) was used. For separation of the dimethylaminomethylene lactones, silica gel treated with diluted aqueous ammonia was used.[33)]

Solvents and Materials. DMF, acetonitrile, *t*-C_4H_9OH, and 1,8-diazabicyclo[5.4.0]undec-7-ene (DBU) were used after distillation from CaH_2. Acetone and CH_2Cl_2 were distilled from P_2O_5. Ethanol was distilled over magnesium ribbons. THF and ether were distilled from sodium benzophenone ketyl. Preparations of Zn/Ag couple,[34)] Zn/Cu couple,[35)] 2-pentylfuran,[1)] α,α,α′,α′-tetrabromoacetone,[36)] *t*-butoxybis(dimethylamino)methane,[10)] and tris(dimethylamino)methane[27)] were performed according to the known procedures. Other commercially supplied materials and solvents were used as received.

Preparation of Methyl [(2S,3S*,4S*,5R*)-5-Hydroxymethyl-3,4-isopropylidenedioxy-5-phenyltetrahydrofuran-2-yl]acetate.* A mixture of **14c** (111 mg, 0.383 mmol),[1)] sodium methoxide (31.0 mg, 0.574 mmol), and CH_3OH (3 ml)*** was stirred at 0 °C for 1 h under argon and to this was added oxalic acid (100 mg). Evaporation followed by extraction with chloroform afforded the title compound (115 mg, 91%) as a white solid. R_f=0.28 (1:1 hexane–ethyl acetate); IR 3580 (OH), 1732 cm^{-1} (C=O); ^1H NMR ($CDCl_3$) δ 1.04 and 1.28 (s, isopropylidene CH_3), 2.74 (dd, J=6.0, 14.5 Hz, $\underline{H}_aH_bCC{=}O$), 2.96 (dd, J=4.8, 14.5 Hz, $H_a\underline{H}_bCC{=}O$), 3.62 (d, J=12.5 Hz, $\underline{H}_aH_bCOH$), 3.77 (s, OCH_3), 3.86 (d, J=12.5 Hz, $H_a\underline{H}_bCOH$), 4.40 (m, H_2), 4.56 (t-like, J=6.0 Hz, H_3), 5.02 (br, OH), 5.16 (d, J=6.0 Hz, H_4), 7.35 (m, C_6H_5); ^{13}C NMR ($CDCl_3$) δ 25.80, 26.70, 37.21, 51.94, 69.33, 79.65, 83.86, 84.06, 90.23, 114.44, 126.50, 127.27, 127.82, 138.12, 171.69. Found: *m/z*, 291.1231. Calcd for $C_{16}H_{19}O_5$: (M−OCH_3), 291.1232.

Preparation of 2,5-Dipentylfuran. To a mixture of *n*-C_4H_9Li (1.6 mol dm^{-3} hexane solution, 288 ml, 0.461 mol) and THF (350 ml) was added 2-pentylfuran (60.6 g, 0.439 mol) at −10 °C under argon. After the mixture was stirred at the same temperature for 6 h, pentyl iodide (91.3 g, 0.461 mol) was added. The reaction mixture was stirred at 20 °C for 12 h and then poured into ice-water (200 ml). The organic layer was separated and the aqueous layer was extracted with ether (150 ml×3). The combined organic extracts were dried ($MgSO_4$) and evaporated to leave a yellow oil, which was distilled under reduced pressure to give 2,5-dipentylfuran (68.2 g, 75%, bp 103—108 °C/9 mmHg (lit,[37)] 99—100 °C/5 mmHg)) as a colorless oil. ^1H NMR ($CDCl_3$) δ 0.91 (t, J=6.3 Hz), 1.1—1.8 (m), 2.57 (t, J=7.0 Hz), 5.84 (s); MS *m/z* 208 (M^+).

*1,5-Dimethyl-8-oxabicyclo[3.2.1]oct-6-en-3-one (**42a**).* To a mixture of Zn/Ag couple (26.0 g, 0.40 g-atom) and 2,5-dimethylfuran (21.3 ml, 0.20 mol) in THF (150 ml) was added a solution of α,α,α′,α′-tetrabromoacetone (224 g, 0.60 mol) in THF (200 ml) over 30 min at −10 °C under argon. The mixture was allowed to warm up to 20 °C and stirred at the same temperature for 12 h. The mixture was evaporated and the residue was dissolved in CH_3OH saturated with NH_4Cl (400 ml). To this was added portionwise Zn/Cu couple (130 g, 2.0 g-atom) over 2 h at 0 °C. The mixture was stirred at 20 °C for an additional 1 h and diluted with water (400 ml) and saturated disodium dihydrogen ethylenediaminetetraacetate (Na_2H_2edta) solution (400 ml). The insoluble material was removed by filtration and the filtrate was extracted with CH_2Cl_2 (300 ml×3). The combined organic layers were dried (Na_2SO_4) and concentrated. Chromatography of the residue on a silica-gel column using a 3:1 hexane–ethyl acetate mixture afforded **42a** (20.0 g, 66%) as a white solid. Mp 64—66 °C (hexane–chloroform); R_f=0.47 (3:1 hexane–ethyl acetate); IR 1715 cm^{-1} (C=O); ^1H NMR ($CDCl_3$) δ 1.50 (s, CH_3), 2.32 (d, J=16.1 Hz, H_{2a} and H_{4a}), 2.51 (d, J=16.1 Hz, H_{2b} and H_{4b}), 5.97 (s, H_6 and H_7); ^{13}C NMR ($CDCl_3$) δ 23.30, 51.12, 83.83, 136.42, 207.07. Found: C, 71.55, H, 8.06%. Calcd for $C_9H_{12}O_2$: C, 71.02; H, 7.95%.

*1,5-Dipentyl-8-oxabicyclo[3.2.1]oct-6-en-3-one (**42b**).* A mixture of Zn/Ag couple (39.0 g, 0.60 g-atom), 2,5-dipentylfuran (62.4 g, 0.30 mol), α,α,α′,α′-tetrabromoacetone (337 g, 0.9 mol), and THF (400 ml) was stirred at 20 °C for 24 h. Reduction of the reaction mixture with Zn/Cu couple (292 g, 4.50 g-atom) in CH_3OH (500 ml) saturated with NH_4Cl

** 1 mmHg≈133.322 Pa.

*** 1 ml=0.001 dm^3.

followed by extractive workup with CH_2Cl_2 gave a brown oil. Chromatography of the residue on a silica-gel column using a 10:1 hexane–ethyl acetate mixture afforded **42b** (32.5 g, 41%) as a colorless oil. R_f=0.35 (10:1 hexane–ethyl acetate); IR (neat) 1720 cm^{-1} (C=O); ^1H NMR ($CDCl_3$) δ 0.90 (t, J=6.5 Hz, CH_3), 1.1—1.9 (m, CH_2), 2.28 (d, J=16.0 Hz, H_{2a} and H_{4a}), 2.48 (d, J=16.0 Hz, H_{2b} and H_{4b}), 5.95 (s, H_6 and H_7); ^{13}C NMR ($CDCl_3$) δ 14.00, 22.59, 23.65, 32.18, 36.65, 50.53, 86.59, 135.42, 207.25. Found: *m/z*, 264.2092. Calcd for $C_{17}H_{28}O_2$: M, 264.2089. In addition, unreacted 2,5-dipentylfuran (12.9 g) was recovered.

(1S,5R*,6S*,7R*)-1,5-Dimethyl-6,7-isopropylidenedioxy-8-oxabicyclo[3.2.1]octan-3-one (**43a**).* To a mixture of **42a** (25.0 g, 0.164 mol) and OsO_4 (300 mg, 1.18 mmol) in acetone (200 ml), t-C_4H_9OH (20 ml), and ether (20 ml) was added 30% H_2O_2 (36.2 ml, 0.329 mol). The mixture was stirred at 19 °C for 15 h and to this was added renewedly 30% H_2O_2 (18.1 ml, 0.165 mol). The mixture was stirred for an additional 12 h and cooled to 0 °C. To this was added powder of $Na_2S_2O_3 \cdot 5H_2O$ (77 g) and stirring was continued at 20 °C for 3 h. The residue obtained by evaporation was extracted with ethyl acetate (250 ml×3). The combined organic layers were dried (Na_2SO_4) and evaporated. The residue was dissolved in acetone (250 ml) and to this was added $CuSO_4$ (30 g) and p-toluenesulfonic acid (250 mg). The resulting mixture was stirred at 20 °C for 12 h. The insoluble material was removed by filtration and the filtrate was concentrated to afford a dark oil, which was chromatographed on a silica-gel column using a 3:1 hexane–ethyl acetate mixture to afford **43a** (22.5 g, 61%). Mp 67—68 °C (hexane–chloroform); R_f=0.32 (3:1 hexane–ethyl acetate); IR 1720 cm^{-1} (C=O); ^1H NMR ($CDCl_3$) δ 1.30 and 1.52 (s, isopropylidene CH_3), 1.41 (s, CH_3), 2.28 (d, J=15.0 Hz, H_{2a} and H_{4a}), 2.50 (d, J=15.0 Hz, H_{2b} and H_{4b}), 4.30 (s, H_6 and H_7); ^{13}C NMR ($CDCl_3$) δ 20.12, 25.00, 26.12, 51.71, 82.59, 85.30, 112.42, 206.90. Found: *m/z*, 211.0971. Calcd for $C_{11}H_{15}O_4$: (M−CH_3), 221.0970.

(1S,5R*,6S*,7R*)-1,5-Dipentyl-6,7-isopropylidenedioxy-8-oxabicyclo[3.2.1]octan-3-one (**43b**).* A mixture of **42b** (11.8 g, 44.7 mmol), acetone (70 ml), t-C_4H_9OH (7 ml), ether (7 ml), OsO_4 (100 mg), and 30% H_2O_2 (14.7 ml, 134 mmol) was stirred at 20 °C for 12 h and to this was added $Na_2S_2O_3 \cdot 5H_2O$ (33.5 g) at 0 °C. The resulting mixture was stirred at 20 °C for 3 h. After the usual workup, the residue was dissolved in acetone (150 ml). To this was added $CuSO_4$ (15 g) and p-toluenesulfonic acid (100 mg). After stirring at 20 °C for 24 h, the usual workup and chromatographic isolation (silica gel, 10:1 hexane–ethyl acetate) yielded **43b** (6.50 g, 43%) as a colorless oil. R_f=0.36 (10:1 hexane–ethyl acetate); IR 1720 cm^{-1} (C=O); ^1H NMR ($CDCl_3$) δ 0.90 (t, J=6.0 Hz, CH_3), 1.28 and 1.50 (s, isopropylidene CH_3), 1.1—1.9 (m, CH_2), 2.30 (d, J=14.5 Hz, H_{2a} and H_{4a}), 2.48 (d, J=14.5 Hz, H_{2b} and H_{4b}), 4.30 (s, H_6 and H_7); ^{13}C NMR ($CDCl_3$) δ 16.64, 25.19, 26.12, 27.78, 28.80, 35.03, 36.43, 52.18, 87.39, 87.59, 114.78, 210.07.

(1R,6S*,7R*,8S*)-1,6-Dimethyl-7,8-isopropylidenedioxy-3,9-dioxabicyclo[4.2.1]nonan-4-one (**44a**).* Trifluoroperacetic acid prepared from trifluoroacetic anhydride (46.5 ml, 0.328 mol) and 90% H_2O_2 (11.8 ml, 0.312 mol) in CH_2Cl_2 (150 ml) was added dropwise to a stirred, ice-cooled mixture of Na_2HPO_4 (140 g, 0.984 mol), Na_2H_2edta (1 g), and **43a** (35.2 g, 0.156 mol) in CH_2Cl_2 (200 ml). The mixture was stirred at 20 °C for 13 h and diluted with CH_2Cl_2 (200 ml). To this was added $Na_2S_2O_3 \cdot 5H_2O$ (78 g) at 0 °C and the resulting mixture was stirred at 20 °C for 3 h. The insoluble material was removed by filtration and the filtrate was evaporated. Chromatography of the residue on a silica-gel column using a 3:1 to 2:1 hexane–ethyl acetate mixture afforded **44a** (28.9 g, 77%). Mp 123—124 °C (hexane–chloroform); R_f=0.15 (3:1 hexane–ethyl acetate); IR 1735 cm^{-1} (C=O); ^1H NMR ($CDCl_3$) δ 1.27 and 1.35 (s, CH_3), 1.35 and 1.51 (s, isopropylidene CH_3), 2.83 (d, J=16.0 Hz, H_{5a}), 3.07 (d, J=16.0 Hz, H_{5b}), 4.11 (d, J=13.5 Hz, H_{2a}), 4.33 (d, J=13.5 Hz, H_{2b}), 4.56 (d, J=6.0 Hz, H_7), 4.88 (d, J=6.0 Hz, H_8); ^{13}C NMR ($CDCl_3$) δ 17.95, 22.16, 24.73, 26.01, 49.44, 75.96, 81.12, 83.63, 85.52, 112.57, 172.09. Found: C, 59.47; H, 7.60%. Calcd for $C_{12}H_{18}O_5$: C, 59.49, H, 7.49%.

(1R,6S*,7R*,8S*)-1,6-Dipentyl-7,8-isopropylidenedioxy-3,9-dioxabicyclo[4.2.1]nonan-4-one (**44b**).* To a mixture of **43b** (15.5 g, 45.9 mmol), Na_2HPO_4 (64.8 g, 0.456 mol), and CH_2Cl_2 (100 ml) was added trifluoroperacetic acid in CH_2Cl_2 (1.08 mol dm^{-3} solution, 128 ml, 0.138 mol) at 0 °C. After stirring at 20 °C for 12 h, the reaction mixture was worked up to give a white solid, which was purified on a silica-gel column (10:1 hexane–ethyl acetate) to give **44b** (12.2 g, 77%) as a white solid. Mp 60—62 °C (chloroform–hexane); R_f=0.37 (5:1 hexane–ethyl acetate); IR 1736 cm^{-1} (C=O); ^1H NMR ($CDCl_3$) δ 0.89 (t, J=6.0 Hz, CH_3), 1.31 and 1.49 (s, isopropylidene CH_3), 1.1—1.9 (m, CH_2), 2.28 (d, J=15.5 Hz, H_{5a}), 2.99 (d, J=15.5 Hz, H_{5b}), 4.17 (d, J=13.9 Hz, H_{2a}), 4.32 (d, J=13.9 Hz, H_{2b}), 4.52 (d, J=5.9 Hz, H_7), 4.98 (d, J=5.9 Hz, H_8); ^{13}C NMR ($CDCl_3$) δ 13.96, 22.41, 23.52, 24.57, 25.92, 32.26, 32.86, 35.56, 46.74, 75.06, 83.17, 85.11, 85.30, 112.12, 173.12. Found: C, 67.79; H, 9.76%. Calcd for $C_{20}H_{34}O_5$: C, 67.76; H, 9.67%. In addition, unreacted ketone **43b** (1.90 g) was recovered.

Preparation of the α-Dimethylaminomethylene Lactones. *General Procedure*: Unless otherwise stated, the dimethylaminomethylenation was performed as follows. A mixture of a lactone, t-butoxybis(dimethylamino)methane or tris(dimethylamino)methane, and DMF (in some reactions, DMF was not used) was magnetically stirred at the stated temperature under argon. After stirring for the stated period, the mixture was concentrated under reduced pressure (0.01 mmHg) at 25—50 °C. Chromatography was done on a silica-gel column using the described solvent system as eluent. Elution course of the column chromatography was monitored by TLC and fractions including the desired product were combined and evaporated. A sample for elemental analysis was obtained by recrystallizations of the chromatographed product.

(1S,6R*7R*,8S*)-2,2-Dimethyl-5-(dimethylaminomethylene)-7,8-isopropylidenedioxy-3,9-dioxabicyclo[4.2.1]nonan-4-one (**7a**).* A mixture of **6a**[1] (520 mg, 1.75 mmol), DMF (5 ml), and t-butoxybis(dimethylamino)methane (2.5 ml) was heated at 50 °C for 3 h. The reaction mixture was subjected to the usual workup. Pure **7a** (442 mg, 85%) was obtained by silica-gel column chromatography (5:1 to 1:1 hexane–ethyl acetate). Mp 136.5—137.2 °C (ether); R_f=0.35 (ethyl acetate); IR 1670 (C=O), 1590 cm^{-1} (C=C); ^1H NMR ($CDCl_3$) δ 1.33 and 1.51 (s, isopropylidene CH_3), 1.44 and 1.47 (s, CH_3), 2.93 and 3.14 (s, $N(CH_3)_2$, 3:7 ratio), 6.58 and 7.39 (s, =C<u>H</u>N$(CH_3)_2$, 3:7 ratio); MS *m/z* 297 (M^+); UV λ_{max} (CH_3OH) 300 nm (ε 15850). Found: C, 60.24; H, 7.79; N, 4.55%. Calcd for $C_{15}H_{23}O_5N$: C, 60.59; H, 7.80; N, 4.71%.

(1R,2R*,6R*,7R*,8R*)-5-(Dimethylaminomethylene)-7,8-isopropylidenedioxy-2-methyl-3,9-dioxabicyclo[4.2.1]nonan-4-one (**7b**).* A mixture of **6b**[1] (35 mg, 0.15 mmol), t-butoxybis(dimethylamino)methane (0.3 ml), and DMF (1 ml) was stirred at 50 °C for 1 h. After the usual workup, the crude product was purified by preparative TLC (ethyl acetate) to give

7b (20 mg, 47%). Mp 120.1—121.3 °C (ether–hexane); R_f=0.33 (ethyl acetate); IR 1680 (C=O), 1590 cm^{-1} (C=C); ^{1}H NMR ($CDCl_3$) δ 1.34 and 1.53 (s, isopropylidene CH_3), 1.38 (d, J=7.3 Hz, CH_3), 2.94 and 3.14 (s, $N(CH_3)_2$, 35:65 ratio), 6.66 and 7.34 (s, =C<u>H</u>N$(CH_3)_2$, 35:65 ratio); MS m/z 283 (M^+); UV λ_{max} (CH_3OH) 298 nm (ε 16590). Found: C, 59.42; H, 7.64; N, 4.85%. Calcd for $C_{14}H_{21}O_5N$: C, 59.35; H, 7.47; N, 4.94%.

(1R,2R*,6R*,7R*,8R*)-5-(Dimethylaminomethylene)-7,8-isopropylidenedioxy-2-pentyl-3,9-dioxabicyclo[4.2.1]nonan-4-one* (**7c**). A mixture of **6c**[1] (2.37 g, 8.36 mmol), *t*-butoxybis(dimethylamino)methane (12.0 ml), and DMF (15 ml) was stirred at 50 °C for 5 h. After the usual workup, the crude product was chromatographed on silica gel using ethyl acetate as the eluent to give **7c** (2.45 g, 86%). Mp 86.2—87.8 °C (ether–hexane); R_f=0.53 (ethyl acetate); IR 1680 (C=O), 1595 cm^{-1} (C=C); ^{1}H NMR ($CDCl_3$) δ 0.89 (t-like, J=6.0 Hz, CH_3), 1.32 and 1.50 (s, isopropylidene CH_3), 2.94 and 3.12 (s, $N(CH_3)_2$, 37:63 ratio), 6.65 and 7.32 (s =C<u>H</u>N$(CH_3)_2$, 37:63 ratio); MS m/z 339 (M^+); UV λ_{max} (CH_3OH) 298 nm (ε 23980). Found: C, 63.62; H, 8.75; N, 4.01%. Calcd for $C_{18}H_{29}O_5N$: C, 63.69; H, 8.61; N, 4.13%.

(1S,2S*,6R*,7R*,8R*)-5-(Dimethylaminomethylene)-7,8-isopropylidenedioxy-2-phenyl-3,9-dioxabicyclo[4.2.1]nonan-4-one* (**7d**). A mixture of **6d**[1] (98 mg, 0.338 mmol), *t*-butoxybis(dimethylamino)methane (0.5 ml), and DMF (2 ml) was stirred at 50 °C for 3.5 h. The usual workup and preparative TLC (2:1 ethyl acetate–hexane) yielded **7d** (74.0 mg, 64%) as a foam. R_f=0.51 (ethyl acetate); IR 1680 (C=O), 1590 cm^{-1} (C=C); ^{1}H NMR ($CDCl_3$) δ 1.28 and 1.47 (s, isopropylidene CH_3), 2.94 and 3.15 (s, $N(CH_3)_2$, 38:62 ratio), 6.73 (s, =C<u>H</u>N$(CH_3)_2$, *E*-isomer); MS m/z 345 (M^+); UV λ_{max} (CH_3OH) 299 nm (ε 13810).

(1R,6R*,7S*,8S*)-5-(Dimethylaminomethylene)-7,8-isopropylidenedioxy-1-methyl-3,9-dioxabicyclo[4.2.1]nonan-4-one* (**15a**). A mixture of **14a**[1] (952 mg, 4.18 mmol), tris(dimethylamino)methane (4.5 ml), and DMF (1 ml) was stirred at 70 °C for 1 h. To this was renewedly added tris(dimethylamino)methane (1.2 ml). After 2 h, tris(dimethylamino)methane (0.5 ml) was added again and stirring was continued for 3 h. The usual workup and chromatography on silica gel with a 1:1 hexane–ethyl acetate mixture to pure ethyl acetate afforded **15a** (831 mg, 70%). Mp 118—120 °C (ether); R_f=0.37 (ethyl acetate); IR 1680 (C=O), 1590 cm^{-1} (C=C); ^{1}H NMR ($CDCl_3$) δ 1.26 and 1.51 (s, isopropylidene CH_3), 1.33 (s, CH_3), 2.94 and 3.11 (s, $N(CH_3)_2$, 33:67 ratio), 6.67 and 7.34 (s, =C<u>H</u>N$(CH_3)_2$, 33:67 ratio); MS m/z 297 (M^+); UV λ_{max} (CH_3OH) 297 nm (ε 19800). Found: C, 59.18; H, 7.79; N, 4.92%. Calcd for $C_{14}H_{21}O_5N$: C, 59.35; H, 7.47; N, 4.92%.

(1R,6R*,7S*,8S*)-5-(Dimethylaminomethylene)-7,8-isopropylidenedioxy-1-pentyl-3,9-dioxabicyclo[4.2.1]nonan-4-one* (**15b**). A mixture of **14b**[1] (754 mg, 2.23 mmol), tris(dimethylamino)methane (2.6 ml) was stirred at 70 °C for 1 h. The reaction mixture was worked up and purified by silica gel column chromatography (1:1 hexane–ethyl acetate to ethyl acetate) to give **15b** (683 mg, 91%). Mp 117—118 °C (ether); R_f=0.46 (ethyl acetate); IR 1680 (C=O), 1595 cm^{-1} (C=C); ^{1}H NMR ($CDCl_3$) δ 0.89 (t-like, J=6.0 Hz, CH_3), 1.30 and 1.50 (s, isopropylidene CH_3), 2.94 and 3.13 (s, $N(CH_3)_2$, 31:69 ratio), 6.67 and 7.34 (s, =C<u>H</u>N$(CH_3)_2$, 31:69 ratio); MS m/z 339 (M^+); UV λ_{max} (CH_3OH) 297 nm (ε 18500). Found: C, 63.38; H, 8.94; N, 4.09%. Calcd for $C_{18}H_{29}O_5N$: C, 63.69; H, 8.61; N, 4.09%.

(1R,6R*,7S*,8S*)-5-(Dimethylaminomethylene)-7,8-isopropylidenedioxy-1-phenyl-3,9-dioxabicyclo[4.2.1]nonan-4-one* (**15c**). A mixture of **14c**[1] (987 mg, 3.40 mmol), tris(dimethylamino)methane (3.5 ml), and DMF (2 ml) was stirred at 70 °C for 1 h. Purification of the reaction mixture by silica-gel column chromatography (1:1 hexane–ethyl acetate to ethyl acetate) gave **15c** (1.08 g, 92%). Mp 233—235 °C (acetone); R_f=0.48 (ethyl acetate); IR 1680 (C=O), 1598 cm^{-1} (C=C); ^{1}H NMR ($CDCl_3$) δ 1.30 and 1.33 (s, isopropylidene CH_3), 2.98 and 3.20 (s, $N(CH_3)_2$, 37:63 ratio), 6.80 (s, =C<u>H</u>N$(CH_3)_2$, *E*-isomer); MS m/z 345 (M^+); UV λ_{max} (CH_3OH) 298 nm (ε 18300). Found: C, 66.21; H, 6.68, N, 4.02%. Calcd for $C_{19}H_{23}O_5N$: C, 66.07; H, 6.71, N, 4.06%.

(1R,6R*,7S*,8S*)-1-Benzoyloxymethyl-5-(dimethylaminomethylene)-7,8-isopropylidenedioxy-3,9-dioxabicyclo[4.2.1]nonan-4-one* (**31**). A mixture of **30**[1] (350 mg, 1.00 mmol) and *t*-butoxybis(dimethylamino)methane (1 ml) in DMF (1 ml) was stirred at 90 °C for 30 min. Workup followed by column chromatography (1:1 hexane–ethyl acetate to pure ethyl acetate) afforded **31** (368 mg, 91%) as a white foam. R_f=0.28 (1:2 hexane–ethyl acetate); IR 1725 and 1683 (C=O), 1590 cm^{-1} (C=C); ^{1}H NMR ($CDCl_3$) δ 1.31 and 1.50 (s, isopropylidene CH_3), 2.94 and 3.11 (s, $N(CH_3)_2$, 37:63 ratio), 6.70 (s, =C<u>H</u>N$(CH_3)_2$, *E*-isomer).

(1R,6R*,7R*,8R*)-6-Benzoyloxymethyl-5-(dimethylaminomethylene)-7,8-isopropylidenedioxy-3,9-dioxabicyclo[4.2.1]nonan-4-one* (**39**). A mixture of **38**[1] (696 mg, 2.0 mmol), *t*-butoxybis(dimethylamino)methane (2 ml), and DMF (1.5 ml) was stirred at 60 °C for 4 h. Chromatography on a silica-gel column using a 1:1 to 3:1 ethyl acetate–hexane mixture gave **39** (223 mg, 29%, 57% based on consumed starting material) as a white foam. R_f=0.46 (ethyl acetate); IR 1722 and 1690 (C=O), 1600 cm^{-1} (C=C); ^{1}H NMR ($CDCl_3$) δ 1.32 and 1.51 (s, isopropylidene CH_3), 2.84 and 3.16 (s, $N(CH_3)_2$, 80:20 ratio), 6.75 (s, =C<u>H</u>N$(CH_3)_2$, *E*-isomer). In addition, unreacted **38** was recovered (340 mg).

(1R,5Z,6R*,7R*,8S*)-5-(Dimethylaminomethylene)-1,6-dimethyl-7,8-isopropylidenedioxy-3,9-dioxabicyclo[4.2.1]nonan-4-one* (**45a**). A mixture of **44a** (7.92 g, 32.7 mmol) and tris(dimethylamino)methane (30 ml) was stirred at 90 °C for 8 h. Workup gave a solid, which was purified on a silica-gel column (1:1 hexane–ethyl acetate to pure ethyl acetate) to give **45a** (3.70 g, 38%). Mp 116—118 °C (ether); R_f=0.41 (ethyl acetate); IR 1680 (C=O), 1595 cm^{-1} (C=C); ^{1}H NMR ($CDCl_3$) δ 1.25 and 1.47 (s, CH_3), 1.33 and 1.53 (s, isopropylidene CH_3), 2.87 (s, $N(CH_3)_2$), 3.97 (d, J=13.0 Hz, H_{2a}), 4.16 (d, J=13.0 Hz, H_{2b}), 4.59 (d, J=5.9 Hz, H_7), 4.72 (d, J=5.9 Hz, H_8), 6.79 (s, =C<u>H</u>N$(CH_3)_2$); ^{13}C NMR ($CDCl_3$) δ 17.48, 20.41, 24.69, 26.04, 44.22, 75.17, 82.15, 84.26, 84.87, 88.33, 100.57, 112.10, 149.13, 170.40. Found: C, 60.25; H, 7.87; N, 4.57%. Calcd for $C_{15}H_{23}O_5N$: C, 60.59; H, 7.80; N, 4.71%. In addition, unreacted **44a** (4.51 g) was recovered.

(1R,5Z,6R*,7R*,8S*)-5-(Dimethylaminomethylene)-1,6-dipentyl-7,8-isopropylidenedioxy-3,9-dioxabicyclo[4.2.1]nonan-4-one* (**45b**). A mixture of **44b** (1.76 g, 4.97 mmol) and tris(dimethylamino)methane (5 ml) was stirred at 90 °C for 4 h. The usual workup of the reaction mixture gave an oily product, which was subjected to silica-gel chromatography with a 1:1 hexane–ethyl acetate mixture to pure ethyl acetate to afford **45b** (1.23 g, 61%) as a yellow oil. R_f=0.39 (1:1 hexane–ethyl acetate); IR 1688 (C=O), 1601 cm^{-1} (C=C); ^{1}H NMR ($CDCl_3$) δ 0.88 (t, J=6.0 Hz, CH_3), 1.33 and 1.51 (s, isopropylidene CH_3), 1.1—1.9 (m, CH_2), 2.84 (s, $N(CH_3)_2$), 3.88 (d, J=13.1 Hz, H_{2a}), 4.15 (d, J=13.1 Hz, H_{2b}), 4.52 (s, H_7 and H_8), 6.39 (s, =C<u>H</u>N$(CH_3)_2$); ^{13}C NMR ($CDCl_3$) δ 14.03, 22.41, 23.37, 24.87, 26.09, 32.44, 33.00, 35.19, 43.61, 71.50, 83.22, 85.29, 86.45, 88.98, 99.58, 112.03, 146.50, 171.43.

(1R,6S*,7R*,8R*)-5-(Dimethylaminomethylene)-7,8-isopropylidenedioxy-7-methyl-3,9-dioxabicyclo[4.2.1]nonan-4-one (**53b**).* A mixture of **52b**[1] (1.00 g, 4.41 mmol), *t*-butoxybis(dimethylamino)methane (11 ml), and DMF (1 ml) was stirred at 70 °C for 1 h. Purification of the crude product by silica-gel chromatography (1:1 hexane–ethyl acetate to pure ethyl acetate) afforded **53b** (789 mg, 63%). Mp 137—138 °C (hexane–ethyl acetate); R_f=0.45 (ethyl acetate); IR 1672 (C=O), 1592 cm^{-1} (C=C); ^1H NMR ($CDCl_3$) δ 3.44 and 3.52 (s, $N(CH_3)_2$, 3:2 ratio), 6.64 and 7.46 (s, =C<u>H</u>N-$(CH_3)_2$, 3:2 ratio); UV λ_{max} (CH_3OH) 300 nm (ε 16400). Found: C, 59.18; H, 7.41; N, 4.86%. Calcd for $C_{14}H_{21}O_5N$: C, 59.35; H, 7.47; N, 4.94%.

(1R,6S*,7R*,8R*)-7-t-Butyldimethylsiloxymethyl-5-(dimethylaminomethylene)-7,8-isopropylidenedioxy-3,9-dioxabicyclo-[4.2.1]nonan-4-one (**53a**).* A mixture of **52a**[1] (1.86 g, 5.20 mmol), *t*-butoxybis(dimethylamino)methane (14.7 ml), and DMF (1.2 ml) was stirred at 70 °C for 1 h. Usual workup followed by silica-gel chromatography (2:1 to 1:2 hexane–ethyl acetate) afforded **53a** (1.12 g, 52%). Mp 139—142 °C (hexane–ethyl acetate); R_f=0.37 (1:2 hexane–ethyl acetate); IR 1675 (C=O), 1581 cm^{-1} (C=C); ^1H NMR ($CDCl_3$) δ 2.95 and 3.14 (s, $N(CH_3)_2$, 1:2 ratio), 6.68 and 7.50 (s, =C<u>H</u>N$(CH_3)_2$, 1:2 ratio). Found: C, 57.64; H, 8.57; N, 3.21%. Calcd for $C_{20}H_{35}O_6NSi$: C, 58.08; H, 8.53; N, 3.39%.

Reaction of Dimethylaminomethylene Lactones with Urea, Thiourea, and Guanidine. General Procedure: Method A: A mixture of a dimethylaminomethylene lactone, urea, and a C_2H_5ONa in C_2H_5OH solution was heated at reflux under argon until the reaction completed. The mixture was cooled to room temperature and evaporated to dryness. The resulting residue was dissolved in H_2O. After careful neutralization with diluted hydrochloric acid, the aqueous solution was extracted with ethyl acetate. The organic layer was dried over anhydrous Na_2SO_4. The organic solution was concentrated under reduced pressure (50—90 mmHg), giving a crude material. The residue was subjected to preparative TLC. In TLC separation, silica-gel layer of the product area absorbing the 254-nm light was collected and extracted with a 1:1 chloroform–CH_3OH mixture. A sample for elemental analysis was obtained by repeated preparative TLC or recrystallization of the chromatographed product.

Method B: The reaction was carried out according to Method A. After the reaction was complete, the mixture was cooled to room temperature. The reaction mixture was evaporated and the resulting residue was taken up in water. To this was carefully added diluted hydrochloric acid until the solution was neutralized by monitoring with a pH test paper. The aqueous solution was concentrated and the resulting residue was diluted with ethanol. The insoluble material was removed by the filtration through a short column of Celite 545 and concentrated with a rotary evaporator under reduced pressure (50—90 mmHg) at 25—50 °C. The residue was subjected to preparative TLC and worked up as described above.

The same procedure was applied for the reaction using thiourea and guanidine hydrochloride instead of urea.

With Urea. 5-[(2R,3R*,4S*,5S*)-5-(1-Hydroxy-1-methylethyl)-3,4-isopropylidenedioxytetrahydrofuran-2-yl]uracil (**8a**)*: A mixture of **7a** (906 mg, 3.05 mmol), urea (1.90 g, 30.5 mmol), and 2.3 mol dm^{-3} C_2H_5ONa in C_2H_5OH solution (13 ml) was stirred for 5 h. The reaction mixture was subjected to the usual workup according to Method A. Pure **8a** (438 mg, 48%) was obtained by preparative TLC (5:1 chloroform–CH_3OH). Mp 153.1—156.8 °C (CH_3OH); R_f=0.42 (7:1 chloroform–CH_3OH); ^1H NMR (C_5D_5N) δ 1.41 and 1.67 (s, isopropylidene CH_3), 1.48 and 1.53 (s, CH_3), 4.12 (d, J=3.7 Hz, H_5), 5.08 (d, J=3.7 Hz, H_2), 5.30 (m, H_3 and H_4), 7.93 (s, =CH); UV λ_{max} (CH_3OH) 263 nm (ε 3890), λ_{max} (0.1 mol dm^{-3} NaOH) 286 nm (ε 5370). Found: C, 53.96; H, 6.40; N, 9.05%. Calcd for $C_{14}H_{20}O_6N_2$: C, 53.84; H, 6.45; N, 8.97%.

5-[(2R,3R*,4R*,5R*)-5-[(R*)-1-Hydroxyethyl]-3,4-isopropylidenedioxytetrahydrofuran-2-yl]uracil (**8b**)*: A mixture of **7b** (975 mg, 3.45 mmol), urea (2.10 g, 34.5 mmol), and 2.30 mol dm^{-3} C_2H_5ONa in C_2H_5OH (15 ml) was stirred for 5 h. After the usual workup according to Method A, the crude product was purified by preparative TLC (5:1 chloroform–CH_3OH) to afford **8b** (464 mg, 47%). Mp 264.5—266 °C (CH_3OH); R_f=0.37 (7:1 chloroform–CH_3OH); ^1H NMR (C_5D_5N) δ 1.40 and 1.66 (s, isopropylidene CH_3), 1.43 (d, J=5.2 Hz, CH_3), 4.27 (dd, J=3.0, 3.5 Hz, H_5), 4.30 (m, C<u>H</u>OH), 4.90 (br, OH), 5.10 (d, J=3.6 Hz, H_2), 5.30 (m, H_3 and H_4), 7.90 (s, =CH); UV λ_{max} (CH_3OH) 262 nm (ε 8310), λ_{max} (0.1 mol dm^{-3} NaOH) 285 nm (ε 7410). Found: C, 52.10; H, 5.97; N, 9.40%. Calcd for $C_{13}H_{18}O_6N_2$: C, 52.34; H, 6.08; N, 9.39%.

5-[(2R,3R*,4R*,5R*)-5-[(R*)-1-Hydroxyhexyl]-3,4-isopropylidenedioxytetrahydrofuran-2-yl]uracil (**8c**)*: A mixture of **7c** (546 mg, 1.61 mmol), urea (981 mg, 16.1 mmol), and 1.6 mol dm^{-3} C_2H_5ONa in C_2H_5OH (10 ml) was stirred for 5 h. The usual workup according to Method A and preparative TLC (5:1 chloroform–CH_3OH) gave **8c** (197 mg, 35%). Mp 209.5—212.0 °C (acetone); R_f=0.44 (7:1 chloroform–CH_3OH); ^1H NMR (C_5D_5N) δ 0.83 (t-like, J=6.0 Hz, CH_3), 1.10—1.90 (m, CH_2), 1.42 and 1.67 (s, isopropylidene CH_3), 4.19 (m, C<u>H</u>OH), 4.37 (t, J=3.0 Hz, H_5), 5.10 (d, J=4.5 Hz, H_2), 5.34 (m, H_3 and H_4), 7.91 (s, =CH); UV λ_{max} (CH_3OH) 263 nm (ε 6760), λ_{max} (0.1 mol dm^{-3} NaOH) 286 nm (ε 7400). Found: C, 57.47; H, 7.35; N, 7.98%. Calcd for $C_{17}H_{26}O_6N_2$: C, 57.61; H, 7.40; N, 7.91%.

5-[(2R,3R*,4R*,5S*)-5-[(S*)-α-Hydroxybenzyl]-3,4-isopropylidenedioxytetrahydrofuran-2-yl]uracil (**8d**)*: A mixture of **7d** (205 mg, 0.594 mmol), urea (361 mg, 5.94 mmol), and 2.0 mol dm^{-3} C_2H_5ONa in C_2H_5OH (3 ml) was stirred for 4 h. The reaction mixture was worked up according to Method A and separated by preparative TLC (5:1 ethyl acetate–hexane) to afford **8d** (90 mg, 42%). Mp 250.4—251.5 °C (CH_3OH); R_f=0.48 (7:1 chloroform–CH_3OH); ^1H NMR (C_5D_5N) δ 1.27 and 1.55 (s, isopropylidene CH_3), 4.75 (dd, J=2.2, 4.2 Hz, H_5), 5.08 (dd, J=1.9, 4.0 Hz, H_3), 5.40 (m, H_2, H_4, and C<u>H</u>OH), 7.30—7.80 (m, C_6H_5), 7.88 (s, =CH); UV λ_{max} (CH_3OH) 263 nm (ε 2390), λ_{max} (0.1 mol dm^{-3} NaOH) 285 nm (ε 7580). Found: C, 60.09; H, 6.02; N, 7.90%. Calcd for $C_{18}H_{20}O_6N_2$: C, 59.99; H, 5.59; N, 7.77%.

5-[(2R,3S*,4S*,5R*)-5-Hydroxymethyl-3,4-isopropylidenedioxy-5-methyltetrahydrofuran-2-yl]uracil (**16a**)*: A mixture of **15a** (537 mg, 1.90 mmol), urea (1.14 g, 19.0 mmol), and 1.58 mol dm^{-3} C_2H_5ONa in C_2H_5OH (12 ml) was stirred for 2 h. The reaction mixture was worked up according to Method A and purified by preparative TLC (10:1 chloroform–CH_3OH) to give **16a** (175 mg, 31%). Mp 200—205 °C (CH_3OH); R_f=0.60 (5:1 chloroform–CH_3OH); ^1H NMR (dimethyl-d_6 sulfoxide) δ 1.16 (s, CH_3), 1.24 and 1.51 (s, isopropylidene CH_3), 3.55 (br s, C<u>H</u>$_2$OH), 4.48—4.86 (m, H_2, H_3, and H_4), 7.56 (s, =CH), 10.94 (br, NH); (C_5D_5N) δ 1.40 and 1.66 (s, isopropylidene CH_3), 1.50 (s, CH_3), 3.79 (d, J=11.0 Hz, <u>H</u>$_a$H$_b$COH), 3.95 (d, J=11.0 Hz, H$_a$<u>H</u>$_b$COH), 5.07 (d, J=5.5 Hz, H_4), 5.15 (d, J=6.5 Hz, H_2), 5.44 (dd, J=5.5, 6.5 Hz, H_3), 7.92 (s, =CH); ^{13}C NMR (dimethyl-d_6 sulfoxide) δ 18.18, 25.22, 26.80, 67.19, 79.12,

82.99, 84.28, 85.13, 110.38, 112.70, 140.27, 151.07, 163.61; UV λ_{max} (CH_3OH) 266 nm (ε 7230), λ_{max} (0.1 mol dm^{-3} NaOH) 285 nm (ε 7510). Found: C, 52.03; H, 6.14; N, 9.22%. Calcd for $C_{13}H_{18}O_6N_2$: C, 52.34; H, 6.08; N, 9.39%.

5-[(2R,3S*,4S*,5R*)-5-Hydroxymethyl-3,4-isopropylidenedioxy-5-pentyltetrahydrofuran-2-yl]uracil (**16b**)*: A mixture of **15b** (571 mg, 1.68 mmol), urea (1.01 g, 16.8 mmol), and 1.4 mol dm^{-3} C_2H_5ONa in C_2H_5OH (12 ml) was stirred for 2 h. Workup according to Method A followed by preparative TLC (10:1 chloroform–CH_3OH) gave **16b** (169 mg, 28%). Mp 219—221 °C (CH_3OH); R_f=0.72 (5:1 chloroform–CH_3OH); ^{1}H NMR (dimethyl-d_6 sulfoxide) δ 0.88 (t, J=5.7 Hz, CH_3), 1.27 and 1.49 (s, isopropylidene CH_3), 1.2—1.9 (m, CH_2), 3.36 (br s, C$\underline{H}_2$OH), 4.55 (d, J=5.0 Hz, H_4), 4.63 (d, J=6.2 Hz, H_2), 4.78 (dd, J=5.0, 6.2 Hz, H_3), 7.55 (s, =CH), 11.03 (br, NH); (C_5D_5N) δ 0.84 (t, J=6.0 Hz, CH_3), 1.1—2.2 (m, CH_2), 1.41 and 1.67 (s, isopropylidene CH_3), 3.86 (d, J=11.3 Hz, $\underline{H}_aH_bCOH$), 4.07 (d, J=11.3 Hz, $H_a\underline{H}_bCOH$), 5.03 (d, J=6.0 Hz, H_4), 5.20 (d, J=6.0 Hz, H_2) 5.51 (t, J=6.0 Hz, H_3), 7.96 (s, =CH); ^{13}C NMR (dimethyl-d_6 sulfoxide) δ 13.71, 21.92, 22.66, 25.30, 26.95, 31.31, 32.15, 64.77, 79.66, 83.68, 86.74, 90.03, 110.30, 112.41, 140.37, 151.00, 163.52; UV λ_{max} (CH_3OH) 264 nm (ε 7830), λ_{max} (0.1 mol dm^{-3} NaOH) 285 nm (ε 7930). Found: C, 54.75; H, 7.32; N, 7.45%. Calcd for $C_{17}H_{26}O_6N_2\cdot H_2O$: C, 54.82; H, 7.58; N, 7.52%.

5-[(2R,3S*,4S*,5R*)-5-Hydroxymethyl-3,4-isopropylidenedioxy-5-phenyltetrahydrofuran-2-yl]uracil (**16c**)*: A mixture of **15c** (43.2 mg, 0.125 mmol), urea (75 mg, 1.25 mmol), and 0.83 mol dm^{-3} C_2H_5ONa in C_2H_5OH (1.5 ml, 1.25 mmol) was stirred for 2 h. Workup according to Method A gave an oil, which was purified by preparative TLC (5:1 chloroform–CH_3OH) to give **16c** (13.0 mg, 29%). Mp 282—285 °C (CH_3OH); R_f=0.62 (5:1 chloroform–CH_3OH); ^{1}H NMR (dimethyl-d_6 sulfoxide) δ 1.02 and 1.21 (s, isopropylidene CH_3), 3.50 (m, C$\underline{H}_2$OH), 4.78 (d, J=5.1 Hz, H_2), 4.84 (m, H_3), 5.08 (d, J=5.1 Hz, H_4), 7.32 (m, C_6H_5), 7.77 (s, =CH), 11.20 (br, NH); (C_5D_5N) δ 1.24 and 1.35 (s, isopropylidene CH_3), 4.01 (d, J=6.8 Hz, $\underline{H}_aH_bCOH$), 4.24 (d, J=6.8 Hz, $H_a\underline{H}_bCOH$), 5.20 (m, H_3), 5.62 (m, H_2 and H_4), 7.2—7.8 (m, C_6H_5), 8.13 (s, =CH); ^{13}C NMR (dimethyl-d_6 sulfoxide) δ 25.59, 26.72, 68.29, 80.40, 83.38, 83.81, 89.50, 109.64, 112.51, 126.43, 127.24, 139.90, 141.34, 151.01, 164.00; UV λ_{max} (CH_3OH) 263 nm (ε 7990), λ_{max} (0.1 mol dm^{-3} NaOH) 285 nm (ε 7640). Found: C, 59.62; H, 5.50; N, 7.64%. Calcd for $C_{18}H_{20}O_6N_2$: C, 59.99; H, 5.59; N, 7.77%.

5-[(2R,3R*,4R*,5R*)-5-Hydroxymethyl-3,4-isopropylidenedioxy-2-methyltetrahydrofuran-2-yl]uracil (**24a**)*: A mixture of **22a** (619 mg, 2.72 mmol), and *t*-butoxybis(dimethylamino)-methane (2.8 ml) was stirred at 90 °C for 5 h under argon. The resulting solution was evaporated to give (1*R**,6*S**,7*R**,8*R**)-5-(dimethylaminomethylene)-7,8-isopropylidenedioxy-6-methyl-3,9-dioxabicyclo[4.2.1]nonan-4-one (**23a**) as a brown oil, which was used to the next step without purification. A mixture of crude **23a**, urea (2.45 g, 40.9 mmol), and 2 mol dm^{-3} C_2H_5ONa in C_2H_5OH (20 ml) was stirred. After 2 h, the reaction mixture was worked up according to Method A to give a brown solid, which was purified by preparative TLC (10:1 chloroform–CH_3OH) to give **24a** (54.2 mg, 7% based on **22a**) as a yellow foam. R_f=0.42 (5:1 chloroform–CH_3OH); ^{1}H NMR (C_5D_5N) δ 1.39 and 1.65 (s, isopropylidene CH_3), 1.94 (s, CH_3), 4.02 (m, C$\underline{H}_2$OH), 4.56 (m, H_5), 5.00 (dd, J=4.1, 6.2 Hz, H_4), 5.31 (d, J=6.2 Hz, H_3), 8.19 (s, =CH); UV λ_{max} (CH_3OH) 263 nm (ε 8450), λ_{max} (0.1 mol dm^{-3} NaOH) 288 nm (ε 10790). Found: *m/z*, 298.1156. Calcd for $C_{13}H_{18}O_6N_2$: M, 298.1149.

5-[(2R,3R*,4R*,5R*)-5-Hydroxymethyl-3,4-isopropylidenedioxy-2-pentyltetrahydrofuran-2-yl]uracil (**24b**)*: A mixture of **23b** prepared from **22b** (963 mg, 3.39 mmol) and *t*-butoxybis(dimethylamino)methane (3.4 ml), urea (2.03 g, 33.9 mmol), and 2.26 mol dm^{-3} C_2H_5ONa in C_2H_5OH (15 ml) was stirred for 2 h. Workup according to Method A and preparative TLC (7:1 chloroform–CH_3OH) afforded **24b** (45.8 mg, 4% based on **22b**) as a yellow foam. R_f=0.43 (5:1 chloroform–CH_3OH); ^{1}H NMR (dimethyl-d_6 sulfoxide) δ 0.81 (t, J=6.0 Hz, CH_3), 1.0—1.7 (m, CH_2), 1.28 and 1.46 (s, isopropylidene CH_3), 3.44 (m, C$\underline{H}_2$OH), 3.89 (m, H_5), 4.50 (dd, J=4.3, 5.8 Hz, H_4), 4.72 (d, J=5.8 Hz, H_3), 7.44 (s, =CH); UV λ_{max} (CH_3OH) 264 nm (ε 7930), λ_{max} (0.1 mol dm^{-3} NaOH) 289 nm (ε 5670). Found: *m/z*, 336.1731. Calcd for $C_{17}H_{24}O_5N_2$: ($M-H_2O$), 336.1777.

5-[(2R,3S*,4S*)-5,5-Bis(hydroxymethyl)-3,4-isopropylidenedioxytetrahydrofuran-2-yl]uracil (**32**)*: A mixture of **31** (594 mg, 1.47 mmol), urea (442 mg, 7.37 mmol), and 1 mol dm^{-3} C_2H_5ONa in C_2H_5OH (7 ml) was stirred for 5 h. After workup according to Method B, the residue was subjected to preparative TLC (5:1 chloroform–CH_3OH) to afford **32** (164 mg, 39%) as a white foam. R_f=0.37 (3:1 chloroform–CH_3OH); ^{1}H NMR (dimethyl-d_6 sulfoxide) δ 1.23 and 1.46 (s, isopropylidene CH_3), 3.50 (m, C$\underline{H}_2$OH), 4.53—4.86 (m, H_2, H_3, and H_4), 7.51 (s, =CH); ^{13}C NMR (dimethyl-d_6 sulfoxide) δ 25.11 26.86, 60.39, 63.19, 79.81, 82.87, 84.00, 86.76, 110.19, 112.54, 140.54, 151.05, 163.55; UV λ_{max} (CH_3OH) 263 nm (ε 4910), λ_{max} (0.1 mol dm^{-3} NaOH) 284 nm (ε 4670). Found: *m/z*, 299.0879. Calcd for $C_{12}H_{15}O_7N_2$: ($M-CH_3$), 299.0880.

5-[(2R,3R*,4S*,5R*)-2,5-Dimethyl-5-hydroxymethyl-3,4-isopropylidenedioxytetrahydrofuran-2-yl]uracil (**46a**)*: A mixture of **45a** (118 mg, 0.397 mmol), urea (119 mg, 1.99 mmol), and 1 mol dm^{-3} C_2H_5ONa in C_2H_5OH (2 ml) was stirred for 24 h. The workup of the reaction product according to Method A gave an oil, which was subjected to preparative TLC (8:1 chloroform–CH_3OH) to afford **46a** (35.1 mg, 28%) as a white foam. Mp 126—134 °C (CH_3OH); R_f=0.51 (5:1 chloroform–CH_3OH); ^{1}H NMR (dimethyl-d_6 sulfoxide) δ 1.18 and 1.28 (s, CH_3), 1.28 and 1.50 (s, isopropylidene CH_3), 3.19 (m, C$\underline{H}_2$OH), 4.45 (d, J=6.2 Hz, H_3), 4.82 (d, J=6.2 Hz, H_4), 4.95 (br, OH), 7.47 (s, =CH), 10.80 (br, NH); (C_5D_5N) δ 1.42 and 1.70 (s, isopropylidene CH_3), 1.70 and 1.92 (s, CH_3), 3.78 (s, C$\underline{H}_2$OH), 4.85 (d, J=6.2 Hz, H_3), 5.46 (d, J=6.2 Hz, H_4), 8.32 (br s, =CH), 12.45 (br, NH), 13.04 (br, NH); ^{13}C NMR (dimethyl-d_6 sulfoxide) δ 19.65, 24.41, 24.94, 25.59, 66.30, 82.95, 83.12, 84.71, 85.18, 111.36, 117.30, 138.01, 151.48, 163.18; UV λ_{max} (CH_3OH) 264 nm (ε 6680), λ_{max} (0.1 mol dm^{-3} NaOH) 217 nm (ε 10070), 287 (7610). Found: C, 53.29; H, 6.61; N, 8.24%. Calcd for $C_{14}H_{20}O_6N_2$: C, 53.84; H, 6.45; N, 8.97%.

5-[(2R,3R*,4S*,5R*)-2,5-Dipentyl-5-hydroxymethyl-3,4-isopropylidenedioxytetrahydrofuran-2-yl]uracil (**46b**)*: A mixture of **45b** (2.00 g, 4.89 mmol), urea (2.93 g, 48.9 mmol), and 1 mol dm^{-3} C_2H_5ONa in C_2H_5OH (49 ml) was stirred for 5 h. The reaction mixture was worked up according to Method A and the crude product was purified by preparative TLC (8:1 chloroform–CH_3OH) to give **46b** (472 mg, 23%) as a white foam. Mp>250 °C (CH_3OH); R_f=0.53 (10:1 chloroform–CH_3OH); ^{1}H NMR (dimethyl-d_6 sulfoxide) δ 0.84 (m, CH_3), 1.0—1.7 (m, CH_2), 1.26 and 1.46 (s, isopropylidene CH_3), 3.22 (m, C$\underline{H}_2$OH), 4.47 (d, J=6.6 Hz, H_3), 4.63 (br, OH), 4.77 (d, J=6.6 Hz, H_4), 7.37 (s, =CH),

10.82 (br, NH); ^{13}C NMR (dimethyl-d_6 sulfoxide) δ 13.66, 21.96, 22.93, 31.73, 32.15, 24.44, 25.35, 63.89, 83.49, 84.90, 86.17, 111.16, 114.96, 138.88, 151.47, 162.89; UV λ_{max} (CH_3OH) 265 nm (ε 5820), λ_{max} (0.1 mol dm^{-3} NaOH) 289 nm (ε 4240). Found: C, 62.02; H, 8.57; N, 6.33%. Calcd for $C_{22}H_{36}O_6N_2$: C, 62.24; H, 8.55; N, 6.60%.

5-[(2S,3R*,4R*,5R*)-3-t-Butyldimethylsiloxymethyl-5-hydroxymethyl-3,4-isopropylidenedioxytetrahydrofuran-2-yl]uracil (**54a**)*: A mixture of **53a** (1.18 g, 2.86 mmol), urea (1.20 g, 8.58 mmol), and 0.41 mol dm^{-3} C_2H_5ONa in C_2H_5OH (21 ml) was stirred for 3 h. Workup according to Method B and preparative TLC (10:1 chloroform–CH_3OH) afforded **54a** (246 mg, 20%). Mp 238—242 °C (CH_3OH–acetone–petroleum ether); R_f=0.27 (10:1 chloroform–CH_3OH); ^{1}H NMR (dimethyl-d_6 sulfoxide) δ 0.06 (s, t-$C_4H_9(C\underline{H}_3)_2Si$), 0.84 (s, t-$C_4\underline{H}_9(CH_3)_2Si$), 1.33 and 1.51 (s, isopropylidene CH_3), 3.49 (s, CH_2OSi), 3.57 (m, $C\underline{H}_2OH$), 3.96 (m, H_5), 4.52 (d, J=2.8 Hz, H_4), 4.82 (s, H_2), 7.34 (br, =CH), 10.86 (br, NH), 11.02 (br s, NH); ^{13}C NMR (dimethyl-d_6 sulfoxide) δ 17.74, 25.49, 26.84, 28.31, 61.01, 61.60, 80.44, 82.73, 83.02, 91.54, 107.86, 113.08, 138.68, 150.78, 162.56; UV λ_{max} (CH_3OH) 266 nm (ε 7150), λ_{max} (0.1 mol dm^{-3} NaOH) 289 nm (ε 6150). Found: C, 53.40; H, 7.54; N, 6.78%. Calcd for $C_{19}H_{32}N_2O_7Si$: C, 53.25; H, 7.53; N, 6.54%.

5-[(2S,3R*,4R*,5R*)-5-Hydroxymethyl-3,4-isopropylidenedioxy-3-methyltetrahydrofuran-2-yl]uracil (**54b**)*: A mixture of **53b** (730 mg, 2.58 mmol), urea (1.08 g, 18.1 mmol), and 0.9 mol dm^{-3} C_2H_5ONa in C_2H_5OH (20 ml, 18 mmol) was stirred for 3 h. Workup according to Method B followed by preparative TLC (4:1 chloroform–CH_3OH) gave **54b** (245 mg, 32%). Mp 126—128 °C; R_f=0.50 (4:1 chloroform–CH_3OH); ^{1}H NMR (dimethyl-d_6 sulfoxide) δ 1.12 (s, CH_3), 1.32 and 1.51 (s, isopropylidene CH_3), 3.52 (d-like, J=4.0 Hz, $C\underline{H}_2OH$) 3.92 (m, H_5), 4.30 (d, J=3.0 Hz, H_4), 4.80 (s, H_2), 7.34 (s, =CH); ^{13}C NMR (dimethyl-d_6 sulfoxide) δ 20.37, 27.16, 28.38, 61.53, 81.39, 82.68, 87.28, 89.36, 109.17, 112.79, 139.33, 151.13, 162.89; UV λ_{max} (CH_3OH) 265 nm (ε 7430), λ_{max} (0.1 mol dm^{-3} NaOH) 289 nm (ε 7750). Found: m/z, 283.0939. Calcd for $C_{12}H_{15}N_2O_6$: (M−CH_3), 283.0930.

With Thiourea. *5-[(2R*,3R*,4S*,5S*)-5-(1-Hydroxy-1-methylethyl)-3,4-isopropylidenedioxytetrahydrofuran-2-yl]-2-thiouracil (**10a**)*: A mixture of **7a** (423 mg, 1.42 mmol), thiourea (868 mg, 9.94 mmol), and 1.14 mol dm^{-3} C_2H_5ONa in C_2H_5OH (10 ml) was stirred for 5 h. The reaction mixture was worked up according to Method A. Pure **10a** (332 mg, 71%) was obtained by preparative TLC (5:1 chloroform–CH_3OH). Mp 161.0—162.0 °C (ethyl acetate); ^{1}H NMR (acetone-d_6) δ 1.20 (s, CH_3), 1.32 and 1.51 (s, isopropylidene CH_3), 3.79 (d, J=3.1 Hz, H_5), 4.68 (dd, J=3.3, 4.5 Hz, H_3), 4.80 (d, J=3.3 Hz, H_2), 4.82 (dd, J=3.1, 4.5 Hz, H_4), 7.71 (s, =CH); UV λ_{max} (CH_3OH) 213 nm (ε 11100), 276 (13800), 290 (13000), λ_{max} (0.1 mol dm^{-3} NaOH) 222 nm (ε 14700), 264 (12000), 285 (9490). Found: C, 48.07; H, 6.29; N, 8.00%. Calcd for $C_{14}H_{20}O_5N_2S\cdot 1.2H_2O$: C, 48.04; H, 6.45; N, 8.00%.

5-[(2R,3R*,4R*,5R*)-5-[(R*)-1-Hydroxyethyl]-3,4-isopropylidenedioxytetrahydrofuran-2-yl]-2-thiouracil (**10b**)*: A mixture of **7b** (305 mg, 1.08 mmol), thiourea (660 mg, 8.64 mmol), and 1.23 mol dm^{-3} C_2H_5ONa in C_2H_5OH (7 ml) was stirred for 5 h. The reaction mixture was subjected to the Method A workup and preparative TLC (7:1 chloroform–CH_3OH) afforded **10b** (277 mg, 82%). Mp 201.2—202.5 °C (ether–CH_3OH); ^{1}H NMR (acetone-d_6) δ 1.19 (d, J=7.0 Hz, CH_3), 1.32 and 1.52 (s, isopropylidene CH_3), 3.87 (m, H_5 and $\underline{H}COH$), 4.66 (d, J=4.2 Hz, H_2), 4.82 (m, H_3 and H_4), 7.66 (s, =CH); UV λ_{max} (CH_3OH) 213 nm (ε 12500), 274 (14400), 286 (13100), λ_{max} (0.1 mol dm^{-3} NaOH) 223 nm (ε 16220), 264 (15140), 284 (11480). Found: C, 49.06; H, 5.85; N, 8.44%. Calcd for $C_{13}H_{18}O_5N_2S$: C, 49.67; H, 5.77; N, 8.91%.

5-[(2R,3R*,4R*,5R*)-5-[(R*)-1-Hydroxyhexyl]-3,4-isopropylidenedioxytetrahydrofuran-2-yl]-2-thiouracil (**10c**)*: A mixture of **7c** (491 mg, 1.45 mmol), thiourea (776 mg, 10.2 mmol), and 1.16 mol dm^{-3} C_2H_5ONa in C_2H_5OH (10 ml) was stirred for 5 h. After the Method A workup, the crude product was purified by preparative TLC (7:1 chloroform–CH_3OH) to give **10c** (365 mg, 68%). Mp 203.0—204.5 °C (ether); ^{1}H NMR (acetone-d_6) δ 0.91 (t, J=6.0 Hz, CH_3), 1.10—1.70 (m, CH_2), 1.31 and 1.51 (s, isopropylidene CH_3), 3.76 (m, $\underline{H}COH$), 3.95 (dd, J=3.1, 6.1 Hz, H_5), 4.65 (d, J=4.1 Hz, H_2), 4.86 (m, H_3 and H_4), 7.67 (s, =CH), 11.23 (br, NH); UV λ_{max} (CH_3OH) 214 nm (ε 12880), 276 (15850), 291 (14800), λ_{max} (0.1 mol dm^{-3} NaOH) 222 nm (ε 16990), 264 (13490), 283 (10960). Found: C, 54.56; H, 7.04; N, 7.39; S, 8.68%. Calcd for $C_{17}H_{26}O_5N_2S\cdot 0.25H_2O$: C, 54.45; H, 7.12; N, 7.46; S, 8.55%.

5-[(2R,3R*,4R*,5S*)-5-[(S*)-α-Hydroxybenzyl]-3,4-isopropylidenedioxytetrahydrofuran-2-yl]-2-thiouracil (**10d**)*: A mixture of **7d** (74 mg, 0.214 mmol), thiourea (115 mg, 1.50 mmol), and 0.85 mol dm^{-3} C_2H_5ONa in C_2H_5OH (2 ml) was stirred. After stirring for 5 h, the workup according to Method A and preparative TLC (5:1 chloroform–CH_3OH) afforded **10d** (59 mg, 73%). Mp 240—241 °C; ^{1}H NMR (C_5D_5N) δ 1.29 and 1.55 (s, isopropylidene CH_3), 4.75 (dd, J=3.9, 5.0 Hz, H_5), 5.17 (d, J=4.0 Hz, H_2), 5.38 (m, H_3, H_4, and $\underline{H}COH$), 7.3—7.9 (m, C_6H_5), 7.94 (s, =CH); UV λ_{max} (CH_3OH) 276 nm (ε 7940), 289 (7240), λ_{max} (0.1 mol dm^{-3} NaOH) 264 nm (ε 10970), 280 (8510). Found: C, 50.29; H, 5.57; N, 6.36%. Calcd for $C_{18}H_{20}O_5N_2S\cdot 3H_2O$: C, 50.22; H, 6.09; N, 6.51%.

5-[(2R,3S*,4S*,5R*)-5-Hydroxymethyl-3,4-isopropylidenedioxy-5-methyltetrahydrofuran-2-yl]-2-thiouracil (**18a**)*: A mixture of **15a** (284 mg, 1.00 mmol), thiourea (532 mg, 7.0 mmol), and 1.4 mol dm^{-3} C_2H_5ONa in C_2H_5OH (5 ml) was stirred for 2 h. The Method A workup and preparative TLC (5:1 chloroform–CH_3OH) gave **18a** (248 mg, 79%) as a yellow foam. R_f=0.67 (5:1 chloroform–CH_3OH); ^{1}H NMR (dimethyl-d_6 sulfoxide) δ 1.17 (s, CH_3), 1.28 and 1.50 (s, isopropylidene CH_3), 3.35 (br s, $C\underline{H}_2OH$), 4.54—4.86 (m, H_2, H_3, and H_4), 7.56 (s, =CH); (C_5D_5N) δ 1.40 and 1.65 (s, isopropylidene CH_3), 1.55 (s, CH_3), 3.77 (d, J=11.5 Hz, $\underline{H}_aH_bCOH$), 3.93 (d, J=11.5 Hz, $H_a\underline{H}_bCOH$), 5.09 (d, J=6.0 Hz, H_4), 5.17 (d, J=5.0 Hz, H_2), 5.36 (dd, J=5.0, 6.0 Hz, H_3), 8.05 (s, =CH); ^{13}C NMR (dimethyl-d_6 sulfoxide) δ 18.20, 25.21, 26.70, 67.06, 78.93, 82.97, 84.56, 85.64, 112.69, 116.16, 139.44, 160.57, 175.38; UV λ_{max} (CH_3OH) 215 nm (ε 9490), 276 (14390), 290 (13190), λ_{max} (0.1 mol dm^{-3} NaOH) 223 nm (ε 9640), 264 (8700), 289 (6740). Found: C, 47.89; H, 5.67; N, 8.40%. Calcd for $C_{13}H_{18}O_5N_2S\cdot 0.7H_2O$: C, 47.75; H, 5.98; N, 8.57%.

5-[(2R,3S*,4S*,5R*)-5-Hydroxymethyl-3,4-isopropylidenedioxy-5-pentyltetrahydrofuran-2-yl]-2-thiouracil (**18b**)*: A mixture of **15b** (330 mg, 0.973 mmol), thiourea (517 mg, 6.81 mmol), and 0.85 mol dm^{-3} C_2H_5ONa in C_2H_5OH (8 ml) was stirred for 2 h. The reaction mixture was worked up according to Method A. Preparative TLC (10:1 chloroform–CH_3OH) gave **18b** (247 mg, 69%). Mp 181—183 °C (ether); R_f=0.64 (5:1 chloroform–CH_3OH); ^{1}H NMR (dimethyl-d_6 sulfoxide) δ 0.89 (t, J=5.7 Hz, CH_3), 1.28 and 1.50 (s, isopropylidene CH_3), 1.1—1.7 (m, CH_2), 3.38 (br s, $C\underline{H}_2OH$), 4.56—4.94 (m, H_2, H_3, and H_4), 7.55 (s, =CH), 12.40 (br, NH); (C_5D_5N) δ 0.89 (t, J=6.0 Hz, CH_3),

1.2—2.2 (m, CH_2), 1.45 and 1.70 (s, isopropylidene CH_3), 3.90 (d, J=11.2 Hz, $\underline{H}_aH_bCOH$), 4.06 (d, J=11.2 Hz, $H_a\underline{H}_bCOH$), 5.16 (d, J=6.0 Hz, H_4), 5.18 (d, J=5.0 Hz, H_2), 5.46 (dd, J=5.0, 6.0 Hz, H_3), 8.14 (s, =CH); ^{13}C NMR (dimethyl-d_6 sulfoxide) δ 13.80, 21.93, 22.78, 25.42, 27.30, 31.67, 32.15, 65.62, 81.68, 82.99, 83.87, 86.52, 111.67, 112.39, 154.54, 156.20, 163.03; UV λ_{max} (CH_3OH) 213 nm (ε 13640), 276 (17330), 290 (sh, 15820), λ_{max} (0.1 mol dm^{-3} NaOH) 220 nm (ε 17230), 264 (13530), 282 (sh, 10910). Found: C, 55.06; H, 7.24; N, 7.56; S, 8.70%. Calcd for $C_{17}H_{26}O_5N_2S$: C, 55.12; H, 7.07; N, 7.56; S, 8.65%.

5-[(2R,3S*,4S*,5R*)-5-Hydroxymethyl-3,4-isopropylidenedioxy-5-phenyltetrahydrofuran-2-yl]-2-thiouracil (**18c**)*: A mixture of **15c** (36.8 mg, 0.107 mmol), thiourea (57 mg, 0.749 mmol), and 0.38 mol dm^{-3} C_2H_5ONa in C_2H_5OH (2 ml) was stirred for 2 h. The reaction mixture was worked up according to Method A. Preparative TLC (5:1 chloroform–CH_3OH) afforded **18c** (23.5 mg, 58%). Mp 210—213 °C; R_f=0.64 (5:1 chloroform–CH_3OH); ^{1}H NMR (dimethyl-d_6 sulfoxide) δ 1.01 and 1.21 (s, isopropylidene CH_3), 3.45 (d, J=11.1 Hz, $\underline{H}_aH_bCOH$), 3.72 (d, J=11.1 Hz, $H_a\underline{H}_bCOH$), 4.86 (m, H_2 and H_3), 5.05 (m, H_4), 7.33 (m, C_6H_5), 7.76 (s, =CH); (C_5D_5N) δ 1.20 and 1.34 (s, isopropylidene CH_3), 4.04 (d, J=12.0 Hz, $\underline{H}_aH_bCOH$), 4.25 (d, J=12.0 Hz, $H_a\underline{H}_bCOH$), 5.36 (m, H_3), 5.60 (m, H_2 and H_4), 7.2—7.9 (m, C_6H_5), 8.30 (s, =CH); ^{13}C NMR (dimethyl-d_6 sulfoxide) δ 25.42, 26.47, 67.94, 80.05, 83.23, 83.92, 89.72, 112.35, 114.97, 126.31, 126.65, 127.09, 139.62, 141.23, 160.83, 175.59; UV λ_{max} (CH_3OH) 275 nm (ε 12780), 291 (sh, 11250), λ_{max} (0.1 mol dm^{-3} NaOH) 264 nm (ε 11530), 281 (sh, 9880). Found: C, 53.98; H, 5.78; N, 6.62; S, 7.70%. Calcd for $C_{18}H_{20}O_5N_2S\cdot 1.2H_2O$: C, 54.31; H, 5.67; N, 7.04; S, 8.06%.

5-[(2R,3R*,4R*,5R*)-5-Hydroxymethyl-3,4-isopropylidenedioxy-2-methyltetrahydrofuran-2-yl]-2-thiouracil (**26a**)*: A mixture of **23a** obtained from 1.03 g (4.50 mmol) of **22a** and *t*-butoxybis(dimethylamino)methane (4.5 ml) as described above and thiourea (2.39 g, 31.5 mmol) in 1 mol dm^{-3} C_2H_5ONa in C_2H_5OH (31.5 ml) was stirred for 2 h. Workup according to Method A followed by column chromatography (20:1 to 15:1 chloroform–CH_3OH) afforded **26a** (268 mg, 20% based on **22a**) as a yellow foam. R_f=0.60 (5:1 chloroform–CH_3OH); ^{1}H NMR (C_5D_5N) δ 1.95 (s, CH_3), 1.42 and 1.66 (s, isopropylidene CH_3), 3.90 (dd, J=5.0, 11.0 Hz, $\underline{H}_aH_bCOH$), 4.07 (dd, J=4.0, 11.0 Hz, $H_a\underline{H}_bCOH$) 4.59 (ddd, J=4.0, 4.0, 5.0 Hz, H_5), 4.99 (dd, J=4.0, 6.0 Hz, H_4), 5.27 (d, J=6.0 Hz, H_3), 8.29 (s, =CH); UV λ_{max} (CH_3OH) 214 nm (ε 9540), 275 (12850), 290 (11920), λ_{max} (0.1 mol dm^{-3} NaOH) 223 nm (ε 11880), 261 (11680), 292 (6800). Found: *m/z*, 314.0930. Calcd for $C_{13}H_{18}N_2O_5S$: M, 314.0936.

5-[(2R,3R*,4R*,5R*)-5-Hydroxymethyl-3,4-isopropylidenedioxy-2-pentyltetrahydrofuran-2-yl]-2-thiouracil (**26b**)*: A mixture of **23b** obtained from **22b** (577 mg, 2.03 mmol) and *t*-butoxybis(dimethylamino)methane (3 ml), thiourea (1.08 g, 14.2 mmol), and 2.0 mol dm^{-3} C_2H_5ONa in C_2H_5OH (7 ml) was stirred for 2 h. Workup according to Method A followed by column chromatography (30:1 to 20:1 chloroform–CH_3OH) gave **26b** (88.1 mg, 12% based on **22b**) as a foam. R_f=0.62 (5:1 chloroform–CH_3OH); ^{1}H NMR (dimethyl-d_6 sulfoxide) δ 0.80 (t, J=6.5 Hz, CH_3), 1.0—1.8 (m, CH_2), 1.25 and 1.45 (s, isopropylidene CH_3), 3.91 (m, H_5), 4.50 (dd, J=4.5, 6.0 Hz, H_4), 4.70 (d, J=6.0 Hz, H_3), 7.40 (s, =CH), $C\underline{H}_2OH$ peaks obscured by H_2O peak; UV λ_{max} (CH_3OH) 214 nm (ε 9430), 276 (13690), 289 (12700), λ_{max} (0.1 mol dm^{-3} NaOH) 232 nm (ε 13400), 261 (16840), 303 (8480). Found: C, 53.19; H, 6.90; N, 7.50%. Calcd for $C_{17}H_{26}O_5N_2S\cdot H_2O$: C, 52.56; H, 7.26; N, 7.21%.

5-[(2R,3S*,4S*)-5,5-Bis(hydroxymethyl)-3,4-isopropylidenedioxytetrahydrofuran-2-yl]-2-thiouracil (**34**)*. A mixture of **31** (337 mg, 0.84 mmol), thiourea (447 mg, 5.88 mmol), and 1 mol dm^{-3} C_2H_5ONa in C_2H_5OH (6 ml) was stirred for 3 h. The Method B workup gave a solid, which was purified by preparative TLC (5:1 chloroform–CH_3OH) to give **34** (160 mg, 63%) as a white foam. R_f=0.39 (5:1 chloroform–CH_3OH); ^{1}H NMR (dimethyl-d_6 sulfoxide) δ 1.24 and 1.46 (s, isopropylidene CH_3), 3.50 (d-like, J=7.5 Hz, $C\underline{H}_2OH$), 4.67 (m, H_2, H_3, and H_4), 5.5—8.0 (br, HN and OH), 7.56 (s, =CH); ^{13}C NMR (dimethyl-d_6 sulfoxide) δ 25.11, 26.84, 60.42, 63.07, 79.80, 82.85, 84.25, 87.23, 127.89, 140.77, 160.68; UV λ_{max} (CH_3OH) 276 nm (ε 12770), 297 (11540), λ_{max} (0.1 mol dm^{-3} NaOH) 213 nm (ε 11320), 265 (9060), 292 (7320). Found: *m/z*, 330.0890. Calcd for $C_{13}H_{18}O_6N_2S$: M, 330.0884.

5-[(2R,3R*,4R*,5R*)-2,5-Bis(hydroxymethyl)-3,4-isopropylidenedioxytetrahydrofuran-2-yl]-2-thiouracil (**40**)*: A mixture of **39** (220 mg, 0.57 mmol), thiourea (303 mg, 3.99 mmol), and 1 mol dm^{-3} C_2H_5ONa in C_2H_5OH (5 ml) was stirred for 3 h. The reaction mixture was worked up according to Method B to give a yellow solid, which was purified by preparative TLC (5:1 chloroform–CH_3OH) to afford **40** (93.0 mg, 51%) as a white foam. R_f=0.50 (5:1 chloroform–CH_3OH); ^{1}H NMR (dimethyl-d_6 sulfoxide) δ 1.26 and 1.48 (s, isopropylidene CH_3), 3.3—3.8 (br, OH), 3.52 (d-like, J=7.5 Hz, $C\underline{H}_2OH$), 4.56—4.88 (m, H_3, H_4, and H_5), 7.52 (s, =CH); UV λ_{max} (CH_3OH) 214 nm (ε 8780), 276 (11350), 293 (10040), λ_{max} (0.1 mol dm^{-3} NaOH) 223 nm (ε 12910), 264 (8430), 289 (7080). Found: C, 44.63; H, 5.54; N, 8.00%. Calcd for $C_{13}H_{18}O_7N_2S$: C, 45.08; H, 5.24; N, 8.09%.

5-[(2R,3R*,4S*,5R*)-2,5-Dimethyl-5-hydroxymethyl-3,4-isopropylidenedioxytetrahydrofuran-2-yl]-2-thiouracil (**48a**)*: A mixture of **45a** (621 mg, 2.09 mmol), thiourea (1.11 g, 14.6 mmol), and 1 mol dm^{-3} C_2H_5ONa in C_2H_5OH (14 ml) was stirred for 5 h. After workup according to Method A, the residue was subjected to preparative TLC (8:1 chloroform–CH_3OH) to give **48a** (426 mg, 61%). Mp 90—95 °C (CH_3OH); R_f=0.67 (5:1 chloroform–CH_3OH); ^{1}H NMR (dimethyl-d_6 sulfoxide) δ 1.20 and 1.30 (s, CH_3), 1.30 and 1.50 (s, isopropylidene CH_3), 3.22 (m, $C\underline{H}_2OH$), 4.46 (d, J=6.2 Hz, H_3), 4.83 (d, J=6.2 Hz, H_4), 4.96 (t-like, J=4.2 Hz, OH), 7.49 (s, =CH), 12.16 and 12.34 (br, NH); (C_5D_5N) δ 1.42 and 1.70 (s, isopropylidene CH_3), 1.70 and 1.84 (s, CH_3), 3.72 (br s, $C\underline{H}_2OH$), 4.77 (d, J=6.2 Hz, H_3), 5.37 (d, J=6.2 Hz, H_4), 8.41 (s, =CH); ^{13}C NMR (dimethyl-d_6 sulfoxide) δ 19.47, 24.41, 24.59, 25.59, 66.18, 83.00, 83.12, 84.89, 111.36, 122.89, 137.78, 160.25, 175.13; UV λ_{max} (CH_3OH) 215 nm (ε 12560), 276 (16180), 290 (14820), λ_{max} (0.1 mol dm^{-3} NaOH) 223 nm (ε 14860), 261 (14270), 292 (8650). Found: C, 51.02; H, 6.24; N, 8.67; S, 9.60%. Calcd for $C_{14}H_{20}O_5N_2S$: C, 51.21; H, 6.14; N, 8.53; S, 9.76%.

5-[(2R,3R*,4S*,5R*)-2,5-Dipentyl-5-hydroxymethyl-3,4-isopropylidenedioxytetrahydrofuran-2-yl]-2-thiouracil (**48b**)*: A mixture of **45b** (1.23 g, 2.80 mmol), thiourea (1.49 g, 19.6 mmol), and 1 mol dm^{-3} C_2H_5ONa in C_2H_5OH (20 ml) was stirred. After 5 h, the reaction mixture was worked up according to Method A and the crude product was purified by preparative TLC (10:1 chloroform–CH_3OH) to give **48b** (798 mg, 64%). Mp 207—210 °C (CH_3OH); R_f=0.47 (10:1 chloroform–CH_3OH); ^{1}H NMR (C_5D_5N) δ 0.84 (m, CH_3), 1.1—1.7 (m, CH_2, 14H), 1.44 and 1.74 (s, isopropylidene CH_3), 2.1—2.3 (m, CH_2, 2H), 3.73 (d, J=12.2 Hz, $\underline{H}_aH_bCOH$), 3.94 (d, J=12.2 Hz, $H_a\underline{H}_bCOH$), 4.81

(d, J=6.5 Hz, H_3), 5.37 (d, J=6.5 Hz, H_4), 8.51 (s, =CH); ^{13}C NMR (dimethyl-d_6 sulfoxide) δ 13.82, 22.06, 23.12, 24.41, 25.35, 31.71, 32.18, 63.59, 83.36, 84.95, 85.71, 86.36, 111.24, 120.77, 138.77, 160.13, 175.18; UV λ_{max} (CH_3OH) 215 nm (ε 12820), 276 (16450), 290 (sh, 15290), λ_{max} (0.1 mol dm^{-3} NaOH) 227 nm (ε 9570), 261 (10640), 305 (6030). Found: C, 59.03; H, 8.06; N, 5.93%. Calcd for $C_{22}H_{36}O_5N_2S\cdot 0.5H_2O$: C, 58.76; H, 8.29; N, 6.23%.

5-[(2S,3R*,4R*,5R*)-3-t-Butyldimethylsiloxymethyl-5-hydroxymethyl-3,4-isopropylidenedioxytetrahydrofuran-2-yl]-2-thiouracil (**58a**)*: A mixture of **53a** (500 mg, 1.21 mmol), thiourea (645 mg, 8.47 mmol), and 0.94 mol dm^{-3} C_2H_5ONa in C_2H_5OH (9 ml) was stirred for 3 h. The Method B workup gave a crude product which was subjected to preparative TLC (10:1 chloroform–CH_3OH) to afford **58a** (333 mg, 62%). Mp 208—210 °C (acetone–hexane); R_f=0.27 (10:1 chloroform–CH_3OH); ^{1}H NMR (dimethyl-d_6 sulfoxide) δ 0.06 (s, t-$C_4H_9(C\underline{H}_3)_2Si$), 0.84 (s, t-$C_4\underline{H}_9(CH_3)_2Si$), 1.34 and 1.51 (s, isopropylidene CH_3), 3.30 (br, OH), 3.4—3.7 (m, C$\underline{H}_2$OH and CH_2OSi), 4.00 (m, H_5), 4.51 (d, J=3.0 Hz, H_4), 4.82 (s, H_2), 7.34 (s, =CH), 12.30 (br, NH); ^{13}C NMR (dimethyl-d_6 sulfoxide) δ 17.74, 25.49, 26.90, 28.25, 60.95, 61.65, 80.21, 82.91, 83.14, 91.65, 113.26, 113.61, 138.22, 159.52, 174.61; UV λ_{max} (CH_3OH) 216 nm (ε 9160), 275 (11800), 299 (11200), λ_{max} (0.1 mol dm^{-3} NaOH) 224 nm (ε 9990), 262 (9110), 296 (6780). Found: C, 50.74; H, 7.55; N, 6.53%. Calcd for $C_{19}H_{32}O_6N_2SSi\cdot 0.5H_2O$: C, 50.30; H, 7.33; N, 6.18%.

5-[(2S,3R*,4R*,5R*)-5-Hydroxymethyl-3,4-isopropylidenedioxy-3-methyltetrahydrofuran-2-yl]-2-thiouracil (**58b**)*: A mixture of **53b** (200 mg, 0.707 mmol), thiourea (377 mg, 4.95 mmol), and 0.92 mol dm^{-3} C_2H_5ONa in C_2H_5OH (5.4 ml) was stirred for 3 h. The Method B workup and preparative TLC (4:1 chloroform–CH_3OH) afforded **58b** (155 mg, 70%). Mp 142—144 °C (CH_3OH); R_f=0.62 (5:1 chloroform–CH_3OH); ^{1}H NMR (dimethyl-d_6 sulfoxide) δ 1.14 (s, CH_3), 1.32 and 1.50 (s, isopropylidene CH_3), 3.56 (d-like, J=4.0 Hz, C$\underline{H}_2$OH), 3.96 (m, H_5), 4.31 (d, J=2.8 Hz, H_4), 4.80 (s, H_2), 7.38 (s, =CH), ^{13}C NMR (dimethyl-d_6 sulfoxide) δ 20.26, 27.07, 28.32, 61.47, 81.21, 82.91, 87.30, 89.36, 112.84, 114.74, 138.92, 159.82, 175.16; UV λ_{max} (CH_3OH) 215 nm (ε 12600), 275 (15800), 297 (14900), λ_{max} (0.1 mol dm^{-3} NaOH) 221 nm (ε 13700), 262 (12100), 298 (8110). Found: *m/z*, 314.0949. Calcd for $C_{13}H_{18}O_5N_2S$: M, 314.0936.

With Guanidine Hydrochloride. 5-[(2R,3R*,4S*,5S*)-5-(1-Hydroxy-1-methylethyl)-3,4-isopropylidenedioxytetrahydrofuran-2-yl]isocytosine (**12a**)*: Guanidine hydrochloride (1.11 g, 11.8 mmol) was dissolved in 1.69 mol dm^{-3} C_2H_5ONa in C_2H_5OH (7 ml). To this was added **7a** (436 mg, 1.47 mmol) and the mixture was stirred for 5 h. The Method A workup followed by trituration of the residue with ether afforded **12a** (334 mg, 73%). Mp 242.0—243.1 °C (CH_3OH); ^{1}H NMR (dimethyl-d_6 sulfoxide) δ 1.10 (s, CH_3), 1.28 and 1.49 (s, isopropylidene CH_3), 3.67 (d, J=3.0 Hz, H_5), 4.51 (m, H_3), 4.68 (m, H_2 and H_4), 6.64 (br, NH_2), 7.66 (s, =CH); UV λ_{max} (CH_3OH) 227 nm (ε 5330), 290 (5370), λ_{max} (0.1 mol dm^{-3} NaOH) 233 nm (ε 7420), 276 (5940). Found: C, 54.16; H, 6.67; N, 13.30%. Calcd for $C_{14}H_{21}O_5N_3$: C, 54.01; H, 6.80; N, 13.50%.

5-[(2R,3R*,4R*,5R*)-5-[(R*)-1-Hydroxyethyl]-3,4-isopropylidenedioxytetrahydrofuran-2-yl]isocytosine (**12b**)*: A mixture of **7b** (952 mg, 3.36 mmol), guanidine hydrochloride (2.54 g, 26.9 mmol), and 2.69 mol dm^{-3} C_2H_5ONa in C_2H_5OH (10 ml) was stirred for 5 h. The reaction mixture was worked up according to Method A, and the product was subjected to trituration with ethyl acetate to give **12b** (665 mg, 67%). Mp 219.8—220.9 °C (CH_3OH); ^{1}H NMR (dimethyl-d_6 sulfoxide) δ 1.06 (d, J=6.0 Hz, CH_3), 1.27 and 1.48 (s, isopropylidene CH_3), 3.71 (m, H_5 and C$\underline{H}_2$OH), 4.71 (m, H_3), 4.74 (m, H_2 and H_4), 6.66 (br, NH_2), 7.64 (s, =CH); UV λ_{max} (CH_3OH) 226 nm (ε 7240), 290 (7240), λ_{max} (0.1 mol dm^{-3} NaOH) 232 nm (ε 9120), 276 (6920). Found: C, 52.50; H, 6.50; N, 13.97%. Calcd for $C_{13}H_{19}O_5N_3$: C, 52.51; H, 6.44; N, 14.13%.

5-[(2R,3R*,4R*,5R*)-5-[(R*)-1-Hydroxyhexyl]-3,4-isopropylidenedioxytetrahydrofuran-2-yl]isocytosine (**12c**)*: A mixture of **7c** (428 mg, 1.26 mmol), guanidine hydrochloride (951 mg, 10.1 mmol), and 1 mol dm^{-3} C_2H_5ONa in C_2H_5OH (10 ml) was stirred for 5 h. Workup according to Method A followed by trituration (ether) of the crude product gave pure **12c** (327 mg, 74%). Mp 212.0—213.9 °C (CH_3OH); ^{1}H NMR (C_5D_5N) δ 0.81 (t, J=6.0 Hz, CH_3), 1.2—1.8 (m, CH_2), 1.40 and 1.68 (s, isopropylidene CH_3), 4.18 (m, C$\underline{H}_2$OH), 4.42 (t-like, J=4.1 Hz, H_5), 5.06 (d, J=4.2 Hz, H_2), 5.38 (m, H_3 and H_4), 8.04 (s, =CH), 8.10 (br, NH_2); UV λ_{max} (CH_3OH) 227 nm (ε 10720), 290 (10720), λ_{max} (0.1 mol dm^{-3} NaOH) 233 nm (ε 11480), 277 (9330). Found: C, 57.05; H, 7.50; N, 11.91%. Calcd for $C_{17}H_{27}O_5N_3$: C, 57.77; H, 7.70; N, 11.89%.

5-[(2R,3R*,4R*,5S*)-5-[(S*)-α-Hydroxybenzyl]-3,4-isopropylidenedioxytetrahydrofuran-2-yl]isocytosine (**12d**)*: A mixture of **7d** (206 mg, 0.597 mmol), guanidine hydrochloride (394 mg, 4.18 mmol), and 3.2 mol dm^{-3} C_2H_5ONa in C_2H_5OH (1.5 ml) was stirred for 5 h. After workup according to Method A, the crude product was purified by trituration with ether to give **12d** (44 mg, 21%). Mp 273.8—275.0 °C (CH_3OH); ^{1}H NMR (dimethyl-d_6 sulfoxide) δ 1.18 and 1.42 (s, isopropylidene CH_3), 4.10 (dd, J=2.0, 4.0 Hz, H_5), 4.50 (d, J=4.3 Hz, H_2), 4.90 (m, H_3 and H_4) 5.82 (dd, J=2.0, 4.0 Hz, C$\underline{H}$OH), 6.60 (br, NH_2), 7.30 (m, C_6H_5), 7.64 (s, =CH), 11.0 (br, NH); UV λ_{max} (CH_3OH) 227 nm (ε 12310), 290 (13180), λ_{max} (0.1 mol dm^{-3} NaOH) 233 nm (ε 5490), 277 (4360). Found: C, 59.98; H, 6.05; N, 11.38%. Calcd for $C_{18}H_{21}O_5N_3$: C, 60.16; H, 5.89; N, 11.69%.

5-[(2R,3S*,4S*,5R*)-5-Hydroxymethyl-3,4-isopropylidenedioxy-5-methyltetrahydrofuran-2-yl]isocytosine (**20a**)*: A mixture of **15a** (705 mg, 2.49 mmol), guanidine hydrochloride (1.89 g, 19.9 mmol), and 1.4 mol dm^{-3} C_2H_5ONa in C_2H_5OH (14 ml) was stirred for 2 h. The workup according to Method A and trituration with ethyl acetate gave **20a** (434 mg, 64%). Mp 252—254 °C (CH_3OH); R_f=0.44 (5:1 chloroform–CH_3OH); ^{1}H NMR (dimethyl-d_6 sulfoxide) δ 1.14 (s, CH_3), 1.27 and 1.50 (s, isopropylidene CH_3), 3.34 (br s, C$\underline{H}_2$OH), 4.53 (d, J=5.2 Hz, H_4), 4.64 (d, J=6.0 Hz, H_2), 4.85 (dd, J=5.2, 6.0 Hz, H_3), 5.08 (br, OH), 6.82 (br, NH_2), 7.64 (s, =CH), 11.14 (br, NH); ^{13}C NMR (dimethyl-d_6 sulfoxide) δ 18.14, 25.31, 27.10, 67.70, 80.83, 83.29, 83.50, 84.72, 111.88, 112.56, 154.10, 156.09, 163.00; UV λ_{max} (CH_3OH) 225 nm (ε 13890), 289 (11220), λ_{max} (0.1 mol dm^{-3} NaOH) 233 nm (ε 10320), 276 (7930). Found: C, 52.60; H, 6.27; N, 13.85%. Calcd for $C_{13}H_{19}O_5N_3$: C, 52.51; H, 6.44; N, 14.13%.

5-[(2R,3S*,4S*,5R*)-5-Hydroxymethyl-3,4-isopropylidenedioxy-5-pentyltetrahydrofuran-2-yl]isocytosine (**20b**)*. A mixture of **15b** (471 mg, 1.39 mmol), guanidine hydrochloride (1.06 g, 11.1 mmol), and 0.93 mol dm^{-3} C_2H_5ONa in C_2H_5OH (12 ml) was stirred for 2 h. The reaction mixture was worked up according to Method A. Trituration with ethyl acetate afforded pure **20b** (356 mg, 73%). Mp 228—230 °C (CH_3OH); R_f=0.51 (5:1 chloroform–CH_3OH); ^{1}H NMR (dimethyl-d_6 sulfoxide) δ 0.88 (t, J=6.0 Hz, CH_3), 1.28 and 1.51 (s, isopropylidene CH_3), 1.1—1.7 (m, CH_2), 3.39 (br s, C$\underline{H}_2$OH), 4.46 (d, J=6.0 Hz, H_4), 4.68 (d, J=6.0 Hz, H_2), 4.87 (t, J=6.0 Hz, H_3), 5.14 (br, OH), 6.81

(br, NH_2), 7.64 (s, =CH); (C_5D_5N) δ 0.83 (t, J=6.0 Hz, CH_3), 1.2—2.1 (m, CH_2), 1.38 and 1.68 (s, isopropylidene CH_3), 3.85 (d, J=11.5 Hz, H_aH_bCOH), 4.01 (d, J=11.5 Hz, H_aH_bCOH), 4.99 (d, J=5.5 Hz, H_4), 5.20 (d, J=5.5 Hz, H_2), 5.59 (t, J=5.5 Hz, H_3), 8.06 (s, =CH), 8.06 (br, NH_2); UV λ_{max} (CH_3OH) 227 nm (ε 9510), 290 (9540), λ_{max} (0.1 mol dm^{-3} NaOH) 216 nm (ε 9210), 233 (9750), 276 (7740). Found: C, 57.98; H, 7.78; N, 11.36%. Calcd for $C_{17}H_{27}O_5N_3$: C, 57.77; H, 7.70; N, 11.89%.

5-[(2R,3S*,4S*,5R*)-5-Hydroxymethyl-3,4-isopropylidenedioxy-5-phenyltetrahydrofuran-2-yl]isocytosine (**20c**)*: A mixture of **15c** (537 mg, 1.56 mmol), guanidine hydrochloride (1.19 g, 12.5 mmol), and 0.78 mol dm^{-3} C_2H_5ONa in C_2H_5OH (16 ml) was stirred for 2 h. Trituration with ethyl acetate gave **20c** (436 mg, 78%). Mp 270—272 °C (CH_3OH); R_f=0.53 (5:1 chloroform–CH_3OH); ^{1}H NMR (dimethyl-d_6 sulfoxide) δ 1.14 and 1.24 (s, isopropylidene CH_3), 4.63 (d, J=6.0 Hz, H_4), 5.01 (dd, J=5.8, 6.0 Hz, H_3), 5.13 (d, J=5.8 Hz, H_2), 6.75 (br, NH_2), 7.40 (m, C_6H_5), 7.67 (s, =CH), 11.50 (br, NH), CH_2OH peaks obscured by H_2O peaks; ^{13}C NMR (dimethyl-d_6 sulfoxide) δ 25.66, 27.21, 68.71, 82.89, 83.84, 89.40, 111.99, 112.35, 126.22, 126.54, 127.37, 140.02, 154.47, 156.77, 164.22; UV λ_{max} (CH_3OH) 226 nm (ε 12330), 289 (10390), λ_{max} (0.1 mol dm^{-3} NaOH) 211 nm (ε 15210), 234 (11940), 276 (9020). Found: C, 60.00; H, 5.88; N, 11.69%. Calcd for $C_{18}H_{21}O_5N_3$: C, 60.16; H, 5.89; N, 11.69%.

5-[(2R,3R*,4R*,5R*)-5-Hydroxymethyl-3,4-isopropylidenedioxy-2-methyltetrahydrofuran-2-yl]isocytosine (**28a**)*: A mixture of crude **23a** [prepared from **22a** (248 mg, 1.09 mmol) and *t*-butoxybis(dimethylamino)methane (2 ml)], guanidine hydrochloride (1.06 g, 8.72 mmol), and 1.25 mol dm^{-3} C_2H_5ONa in C_2H_5OH (7 ml) was stirred for 2 h. Workup according to Method A followed by preparative TLC (5:1 chloroform–CH_3OH) afforded **28a** (53.4 mg, 17% based on **22a**) as a yellow foam. R_f=0.40 (5:1 chloroform–CH_3OH), ^{1}H NMR (C_5D_5N) δ 1.36 and 1.62 (s, isopropylidene CH_3), 1.91 (s, CH_3), 4.00 (d, J=5.2 Hz, CH_2OH), 4.54 (m, H_5), 5.01 (dd, J=4.1, 6.0 Hz, H_4), 5.39 (d, J=6.0 Hz, H_3), 8.04 (br, NH_2), 8.33 (s, =CH); UV λ_{max} (CH_3OH) 224 nm (ε 10400), 290 (8450), λ_{max} (0.1 mol dm^{-3} NaOH) 231 nm (ε 7710), 278 (5950). Found: *m/z*, 297.1312. Calcd for $C_{13}H_{19}N_3O_5$: M, 297.1325.

5-[(2R,3R*,4R*,5R*)-5-Hydroxymethyl-3,4-isopropylidenedioxy-2-pentyltetrahydrofuran-2-yl]isocytosine (**28b**)*: A mixture of crude **23b** [prepared from **22b** (632 mg, 2.23 mmol) and *t*-butoxybis(dimethylamino)methane (3 ml)], guanidine hydrochloride (1.69 g, 17.8 mmol), and 1 mol dm^{-3} C_2H_5ONa in C_2H_5OH (18 ml) was stirred for 2 h. Workup according to Method A and column chromatography (20:1 to 10:1 chloroform–CH_3OH) afforded **28b** (31.6 mg, 4% based on **22b**) as a yellow foam. R_f=0.42 (5:1 chloroform–CH_3OH); ^{1}H NMR (dimethyl-d_6 sulfoxide) δ 0.77 (t, J=6.0 Hz, CH_3), 1.0—2.0 (m, CH_2), 1.22 and 1.42 (s, isopropylidene CH_3), 3.38 (d, J=2.7 Hz, CH_2OH), 3.82 (m, H_5), 4.43 (dd, J=2.0, 6.0 Hz, H_4), 4.81 (d, J=6.0 Hz, H_3), 6.78 (br, NH_2), 7.61 (s, =CH); UV λ_{max} (CH_3OH) 225 nm (ε 5770), 292 (3680), λ_{max} (0.1 mol dm^{-3} NaOH) 230 nm (ε 6720), 278 (4770). Found: *m/z*, 335.1842. Calcd for $C_{17}H_{25}O_4N_3$: (M−H_2O), 335.1840.

5-[(2R,3S*,4S*)-5,5-Bis(hydroxymethyl)-3,4-isopropylidenedioxytetrahydrofuran-2-yl]isocytosine (**36**)*: A mixture of **31** (368 mg, 0.91 mmol), guanidine hydrochloride (608 mg, 6.37 mmol), and 1 mol dm^{-3} C_2H_5ONa in C_2H_5OH (7 ml) was stirred for 5 h. Workup according to Method B gave a yellow solid, which was purified by preparative TLC (3:1 chloroform–CH_3OH) to give **36** (128 mg, 45%). Mp 245—247 °C (CH_3OH); R_f=0.39 (3:1 chloroform–CH_3OH); ^{1}H NMR (dimethyl-d_6 sulfoxide) δ 1.25 and 1.46 (s, isopropylidene CH_3), 3.53 (m, CH_2OH), 4.0—5.0 (br, OH), 4.47 (d, J=5.5 Hz, H_4), 4.70 (d, J=5.5 Hz, H_2), 4.82 (t, J=5.5 Hz, H_3), 6.85 (br, NH_2), 7.63 (s, =CH); ^{13}C NMR (dimethyl-d_6 sulfoxide) δ 25.24, 27.16, 60.71, 64.01, 81.74, 83.09, 86.44, 111.44, 112.46, 154.41, 156.45, 163.18, UV λ_{max} (CH_3OH) 227 nm (ε 5960), 290 (5720), λ_{max} (0.1 mol dm^{-3} NaOH) 233 nm (ε 10250), 277 (7770). Found: C, 49.54; H, 6.10; N, 13.40%. Calcd for $C_{13}H_{19}O_6N_3$: C, 49.83; H, 6.11; N, 13.41%.

5-[(2R,3R*,4S*,5R*)-2,5-Dimethyl-5-hydroxymethyl-3,4-isopropylidenedioxytetrahydrofuran-2-yl]isocytosine (**50a**)*: A mixture of **45a** (1.07 g, 3.60 mmol), guanidine hydrochloride (2.74 g, 28.8 mmol), and 1 mol dm^{-3} C_2H_5ONa in C_2H_5OH (30 ml) was stirred for 5 h. Workup according to Method A followed by trituration with ethyl acetate afforded **50a** (878 mg, 77%). Mp 255—257 °C (CH_3OH), R =0.43 (5:1 chloroform–CH_3OH); ^{1}H NMR (dimethyl-d_6 sulfoxide) δ 1.19 and 1.32 (s, CH_3), 1.32 and 1.49 (s, isopropylidene CH_3), 3.18 (d-like, J=4.8 Hz, CH_2OH), 4.48 (d, J=6.3 Hz, H_3), 4.91 (d, J=6.3 Hz, H_4), 6.46 (br, NH_2), 7.72 (s, =CH), 10.90 (br, NH); ^{13}C NMR (dimethyl-d_6 sulfoxide) δ 19.82, 24.59, 24.94, 25.71, 66.71, 83.24, 83.30, 83.42, 84.59, 111.30, 119.42, 156.01; UV λ_{max} (CH_3OH) 225 nm (ε 9930), 292 (8160), λ_{max} (0.1 mol dm^{-3} NaOH) 231 nm (ε 8750), 278 (6930). Found: C, 52.90; H, 6.75; N, 12.89%. Calcd for $C_{14}H_{21}O_5N_3\cdot0.5H_2O$: C, 52.49; H, 6.92; N, 13.12%.

5-[(2R,3R*,4S*,5R*)-2,5-Dipentyl-5-hydroxymethyl-3,4-isopropylidenedioxytetrahydrofuran-2-yl]isocytosine (**50b**)*: A mixture of **45b** (1.31 g, 3.20 mmol), guanidine hydrochloride (2.43 g, 25.6 mmol), and 1 mol dm^{-3} C_2H_5ONa in C_2H_5OH (25 ml) was stirred. After 5 h, the mixture was worked up according to Method A to give an oil, which was triturated with ethyl acetate to give **50b** (528 mg, 39%). Mp 168—170 °C (CH_3OH); R_f=0.54 (5:1 chloroform–CH_3OH); ^{1}H NMR (dimethyl-d_6 sulfoxide) δ 0.86 (m, CH_3), 1.0—2.0 (m, CH_2), 1.26 and 1.46 (s, isopropylidene CH_3), 3.34 (m, CH_2OH), 4.49 (d, J=6.2 Hz, H_3), 4.74 (br, OH) 4.87 (d, J=6.2 Hz, H_4), 6.60 (br, NH_2), 7.62 (s, =CH), 11.10 (br, NH); ^{13}C NMR (dimethyl-d_6 sulfoxide) δ 13.80, 22.02, 22.66, 23.13, 24.36, 25.42, 31.76, 32.11, 34.70, 63.58, 83.34, 85.01, 85.66, 85.95, 110.78, 116.83, 155.52; UV λ_{max} (CH_3OH) 225 nm (ε 7530), 292 (5810), λ_{max} (0.1 mol dm^{-3} NaOH) 231 nm (ε 5440), 279 (3980). Found: C, 61.28; H, 8.79; N, 9.39%. Calcd for $C_{22}H_{37}O_5N_3\cdot0.5H_2O$; C, 61.09, H, 8.86; N, 9.71%.

5-[(2S,3R*,4R*,5R*)-3-t-Butyldimethylsiloxymethyl-5-hydroxymethyl-3,4-isopropylidenedioxytetrahydrofuran-2-yl]isocytosine (**60a**)*: A mixture of **53a** (500 mg, 1.21 mmol), guanidine hydrochloride (809 mg, 8.47 mmol), and 0.94 mol dm^{-3} C_2H_5ONa in C_2H_5OH (9 ml) was stirred for 3 h. After the Method B workup, the residue was subjected to preparative TLC (10:1 chloroform–CH_3OH) to give **60a** (339 mg, 67%). Mp 231—233 °C (CH_3OH–acetone–hexane); R_f=0.25 (10:1 chloroform–CH_3OH); ^{1}H NMR (dimethyl-d_6 sulfoxide) δ 0.06 (s, *t*-$C_4H_9(CH_3)_2Si$), 0.85 (s, *t*-$C_4H_9(CH_3)_2Si$), 1.34 and 1.51 (s, isopropylidene CH_3), 3.4—3.7 (m, CH_2OH and CH_2OSi), 3.97 (m, H_5), 4.54 (d, J=3.0 Hz, H_4), 4.89 (s, H_2), 6.67 (br, NH_2), 7.59 (s, =CH), 11.00 (br, NH); ^{13}C NMR (dimethyl-d_6 sulfoxide) δ 17.62, 25.37, 26.72, 28.31, 61.42, 81.03, 82.50, 82.73, 91.59, 108.92, 112.79, 128.29, 153.70, 155.18; UV λ_{max} (CH_3OH) 228 nm (ε 9500), 294 (8840), λ_{max} (0.1 mol dm^{-3} NaOH) 233 nm (ε 5090), 280 (3910). Found: C, 52.15; H, 7.67; N, 9.58%. Calcd for $C_{19}H_{33}O_6N_3Si\cdot0.5H_2O$: C, 52.27; H, 7.85; N, 9.62%.

5-[(2S,3R*,4R*,5R*)-5-Hydroxymethyl-3,4-isopropylidenedioxy-3-methyltetrahydrofuran-2-yl]isocytosine (**60b**)*: A mixture

of **53b** (200 mg, 0.707 mmol), guanidine hydrochloride (473 mg, 4.95 mmol), and 0.92 mol dm^{-3} C_2H_5ONa in C_2H_5OH (5.4 ml) was stirred for 3 h. The Method B workup of the reaction mixture gave a crude product which was subjected to preparative TLC (4:1 chloroform–CH_3OH) to afford **60b** (132 mg, 63%). Mp 178—180 °C (CH_3OH); R_f=0.45 (5:1 chloroform–CH_3OH); ^{1}H NMR (dimethyl-d_6 sulfoxide) δ 1.14 (s, CH_3), 1.34 and 1.51 (s, isopropylidene CH_3), 3.56 (d-like, J=5.0 Hz, C$\underline{H}_2$OH), 3.93 (m, H_5), 4.32 (d, J=2.8 Hz, H_4), 4.88 (s, H_2), 6.80 (br, NH_2), 7.58 (s, =CH); ^{13}C NMR (dimethyl-d_6 sulfoxide) δ 20.55, 27.23, 28.44, 61.72, 82.22, 82.50, 87.37, 89.47, 110.76, 112.62, 152.83, 155.77, 162.22; UV λ_{max} (CH_3OH) 226 nm (ε 6830), 293 (6290), λ_{max} (0.1 mol dm^{-3} NaOH) 233 nm (ε 11000), 280 (8690). Found: C, 50.11; H, 6.51; N, 13.30%. Calcd for $C_{13}H_{19}O_5N_3\cdot 0.8H_2O$: C, 50.09; H, 6.66; N, 13.48%.

Deprotection of the 5-(5-Hydroxymethyl-3,4-isopropylidenedioxytetrahydrofuran-2-yl)pyrimidine C-Nucleosides by Methanolic Hydrogen Chloride. General Procedure: Unless otherwise stated, removal of the isopropylidene group was performed as follows. A mixture of a 5-(5-hydroxymethyl-3,4-isopropylidenedioxytetrahydrofuran-2-yl)pyrimidine *C*-nucleoside and 10% methanolic hydrogen chloride solution was stirred at the room temperature until the reaction was complete (TLC analysis). The reaction mixture was concentrated under reduced pressure (50—90 mmHg), giving a crude material, which was coevaporated with C_2H_5OH. The resulting solid was triturated with ether or ethyl acetate to give the desired deprotection product. A pure sample was collected by recrystallization.

5-[(2R,3R*,4R*,5R*)-3,4-Dihydroxy-5-[(R*)-1-hydroxyethyl]tetrahydrofuran-2-yl]uracil ((±)-5′-Methylpseudouridine)* (***9b***): To a solution of **8b** (51.2 mg, 0.172 mmol) in CH_3OH (2 ml) was added 10% HCl in CH_3OH (2 ml) and the mixture was stirred for 10 min. The above described workup gave **9b** (42.8 mg, 96%). Mp 237.2—239.1 °C (aqueous C_2H_5OH); ^{1}H NMR (dimethyl-d_6 sulfoxide) δ 1.06 (d, J=6.0 Hz, CH_3), 3.50 (m, H_5 and C$\underline{H}$OH), 4.0 (m, H_3 and H_4), 4.37 (d, J=6.0 Hz, H_2), 7.70 (d, J=6.0 Hz, =CH), 10.87 (d, J=6.0 Hz, NH), 11.08 (s, NH); UV λ_{max} (CH_3OH) 264 nm (ε 5620), λ_{max} (0.1 mol dm^{-3} HCl) 263 nm (ε 8130), λ_{max}(0.1 mol dm^{-3} NaOH) 287 nm (ε 8510). Found: C, 46.67; H, 5.39; N, 10.71%. Calcd for $C_{10}H_{14}O_6N_2$: C, 46.51; H, 5.47; N, 10.85%.

5-[(2R,3R*,4S*,5S*)-3,4-Dihydroxy-5-(1-hydroxy-1-methylethyl)tetrahydrofuran-2-yl]uracil ((±)-5′,5′-Dimethylpseudouridine)* (***9a***): To a solution of **8a** (218 mg, 0.699 mmol) in CH_3OH (4 ml) was added 10% HCl in CH_3OH (3 ml) and the resulting mixture was stirred for 10 min. Workup in a usual manner left pure **9a** (185 mg, 97%). Mp 221.4—224.8 °C; ^{1}H NMR (C_5D_5N) δ 1.53 and 1.57 (s, CH_3), 4.32 (dd, J=3.0, 5.0 Hz, H_4), 4.34 (d, J=3.0 Hz, H_5), 5.12 (dd, J=5.0, 6.5 Hz, H_3), 5.25 (d, J=6.5 Hz, H_2), 5.75 (br, OH and NH), 8.00 (s, =CH); UV λ_{max} (CH_3OH) 212 nm (ε 7940), 263 (6600), λ_{max} (0.1 mol dm^{-3} HCl) 264 nm (ε 8310), λ_{max} (0.1 mol dm^{-3} NaOH) 218 nm (ε 8310), 287 (10960). Found: C, 48.42; H, 6.02; N, 10.11%. Calcd for $C_{11}H_{16}O_6N_2$: C, 48.52; H, 5.92; N, 10.29%.

5-[(2R,3R*,4R*,5R*)-3,4-Dihydroxy-5-[(R*)-1-hydroxyhexyl]tetrahydrofuran-2-yl]uracil ((±)-5′-Pentylpseudouridine)* (***9c***): A mixture of **8c** (134 mg, 0.379 mmol) in CH_3OH (3 ml) and 10% HCl in CH_3OH (3 ml) was stirred for 10 min. The usual workup gave **9c** (71 mg, 60%). Mp 193.3—197.7 °C; ^{1}H NMR (C_5D_5N) δ 0.81 (t, J=6.0 Hz, CH_3), 1.10—1.90 (m, CH_2), 4.24 (m, C$\underline{H}$OH), 4.54 (t, J=2.8 Hz, H_5), 4.94 (dd, J=2.8, 4.3 Hz, H_4), 5.15 (m, H_2 and H_3), 5.50 (br, OH and NH), 7.95 (s, =CH); UV λ_{max} (CH_3OH) 212 nm (ε 8510), 265 (6910), λ_{max} (0.1 mol dm^{-3} HCl) 264 nm (ε 3540), λ_{max} (0.1 mol dm^{-3} NaOH) 217 nm (ε 10960), 286 (7240). Found: C, 53.38; H, 7.21; N, 8.78%. Calcd for $C_{14}H_{22}O_6N_2$: C, 53.49; H, 7.05; N, 8.91%.

5-[(2R,3R*,4R*,5S*)-3,4-Dihydroxy-5-[(S*)-α-hydroxybenzyl]tetrahydrofuran-2-yl]uracil ((±)-5′-Phenylpseudouridine)* (***9d***): To a solution of **8d** (39.0 mg, 0.108 mmol) in CH_3OH (1 ml) was added 10% HCl in CH_3OH (1.5 ml). The resulting mixture was stirred for 5 min and worked up to yield **9d** (36.3 mg, 100%) as a wax. ^{1}H NMR (C_5D_5N) δ 4.90 (m, H_5 and C$\underline{H}$OH), 5.24 (m, H_3 and H_4), 5.47 (d, J=4.0 Hz, H_2), 7.20—7.50 (m, C_6H_5), 7.83 (s, =CH); UV λ_{max} (CH_3OH) 265 nm (ε 7410), λ_{max} (0.1 mol dm^{-3} HCl) 264 nm (ε 7250), λ_{max} (0.1 mol dm^{-3} NaOH) 285 nm (ε 9330). Found: C, 56.31; H, 5.23; N, 8.61%. Calcd for $C_{15}H_{16}O_6N_2$: C, 56.25; H, 5.04; N, 8.75%.

5-[(2R,3S*,4S*,5R*)-3,4-Dihydroxy-5-hydroxymethyl-5-methyltetrahydrofuran-2-yl]uracil ((±)-4′-Methylpseudouridine)* (***17a***): To a solution of **16a** (14.0 mg, 0.0392 mmol) in CH_3OH (1 ml) was added 10% HCl in CH_3OH (1 ml). After stirring for 15 min, usual workup afforded **17a** (11.6 mg, 100%). Mp 226—228 °C (CH_3OH); R_f=0.37 (3:1 chloroform–CH_3OH); ^{1}H NMR (C_5D_5N) δ 1.69 (s, CH_3), 3.90 (d, J=11.5 Hz, $\underline{H}_aH_bCOH$), 4.08 (d, J=11.5 Hz, $H_a\underline{H}_bCOH$), 4.87 (m, H_4), 5.26 (m, H_2 and H_3), 6.32 (br, OH), 7.98 (s, =CH), 12.50 and 13.20 (br, NH); UV λ_{max} (CH_3OH) 264 nm (ε 7760), λ_{max} (0.1 mol dm^{-3} HCl) 264 nm (ε 7510), λ_{max} (0.1 mol dm^{-3} NaOH) 286 nm (ε 7540). Found: *m/z*, 258.0855. Calcd for $C_{10}H_{14}O_6N_2$: M, 258.0852.

5-[(2R,3S*,4S*,5R*)-3,4-Dihydroxy-5-hydroxymethyl-5-pentyltetrahydrofuran-2-yl]uracil ((±)-4′-Pentylpseudouridine)* (***17b***): To a mixture of **16b** (16.0 mg, 0.0452 mmol) in CH_3OH (1 ml) was added 10% HCl in CH_3OH (1 ml), and the resulting mixture was stirred for 10 min. Workup afforded **17b** (15.7 mg, 100%). Mp 205—209 °C (CH_3OH); R_f=0.60 (3:1 chloroform–CH_3OH); ^{1}H NMR (C_5D_5N) δ 0.84 (t, J=6.0 Hz, CH_3), 1.2—2.3 (m, CH_2), 3.98 (d, J=11.8 Hz, $\underline{H}_aH_bCOH$) 4.14 (d, J=11.8 Hz, $H_a\underline{H}_bCOH$) 4.88 (d, J=4.5 Hz, H_4), 5.14 (d, J=8.0 Hz, H_2), 5.34 (dd, J=4.5, 8.0 Hz, H_3), 5.91 (br, OH), 7.89 (s, =CH), 12.50 and 13.20 (br, NH); UV λ_{max} (CH_3OH) 264 nm (ε 9530), λ_{max} (0.1 mol dm^{-3} HCl) 264 nm (ε 9210), λ_{max} (0.1 mol dm^{-3} NaOH) 287 nm (ε 8390). Found: C, 50.54; H, 6.68; N, 7.68%. Calcd for $C_{14}H_{22}O_6N_2\cdot H_2O$: C, 50.59; H, 7.28; N, 8.43%.

5-[(2R,3S*,4S*,5R*)-3,4-Dihydroxy-5-hydroxymethyl-5-phenyltetrahydrofuran-2-yl]uracil ((±)-4′-Phenylpseudouridine)* (***17c***): To a solution of **16c** (34.2 mg, 0.095 mmol) in CH_3OH (2 ml) was added 10% HCl in CH_3OH (2 ml). After stirring for 15 min, the mixture was worked up to give **17c** (32.0 mg, 100%). Mp 245—249 °C (CH_3OH); R_f=0.55 (3:1 chloroform–CH_3OH); ^{1}H NMR (C_5D_5N) δ 4.07 (d, J=11.9 Hz, $\underline{H}_aH_bCOH$), 4.17 (d, J=11.9 Hz, $H_a\underline{H}_bCOH$), 5.28 (d, J=5.2 Hz, H_4), 5.35 (d, J=7.5 Hz, H_2), 5.62 (dd, J=5.2, 7.5 Hz, H_3), 5.92 (br, OH), 7.2—8.0 (m, C_6H_5), 8.08 (s, =CH), 13.30 (br, NH); UV λ_{max} (CH_3OH) 264 nm (ε 5380), λ_{max} (0.1 mol dm^{-3} HCl) 263 nm (ε 8790), λ_{max} (0.1 mol dm^{-3} NaOH) 288 nm (ε 5150).[38]

5-[(2R,3R*,4R*,5R*)-3,4-Dihydroxy-5-hydroxymethyl-2-methyltetrahydrofuran-2-yl]uracil ((±)-1′-Methylpseudouridine)* (***25a***): A mixture of a solution of **24a** (16.9 mg, 0.128 mmol) in CH_3OH (1 ml) and 10% HCl in CH_3OH (1 ml) was stirred for 30 min. Usual workup gave **25a** (15.9 mg, 100%) as a palc green foam. R_f=0.40 (3:1 chloroform–CH_3OH); ^{1}H NMR (C_5D_5N) δ 2.16 (s, CH_3), 4.22 (dd, J=3.1, 11.2 Hz, $\underline{H}_aH_bCOH$), 4.38 (dd, J=2.5, 11.2 Hz,

H_aH_bCOH), 4.61 (ddd, J=2.5, 3.1, 7.5 Hz, H_5), 4.84 (dd, J=4.7, 7.5 Hz, H_4), 5.00 (d, J=7.5 Hz, H_3), 6.26 (br, OH), 8.52 (s, =CH), 12.42 and 12.96 (br, NH); UV λ_{max} (CH_3OH) 263 nm, λ_{max} (0.1 mol dm^{-3} HCl) 263 nm, λ_{max} (0.1 mol dm^{-3} NaOH) 265 nm (sh), 289, molar extinction coefficient has not been measured because of the extreme hygroscopicity.[38]

5-[(2R,3R*,4R*,4R*)-3,4-Dihydroxy-5-hydroxymethyl-2-pentyltetrahydrofuran-2-yl]uracil ((±)-1'-Pentylpseudouridine)* (**25b**): To a solution of **24b** (30.0 mg, 0.0847 mmol) in CH_3OH (1 ml) was added 10% HCl in CH_3OH (1 ml). After stirring for 30 min, usual workup and preparative TLC (3:1 chloroform–CH_3OH) afforded **25b** (9.6 mg, 36%) as a yellow foam. R_f=0.44 (3:1 chloroform–CH_3OH); ^1H NMR (C_5D_5N) δ 0.80 (t, J=7.0 Hz, CH_3), 1.1—2.0 (m, CH_2), 2.3—3.1 (m, CH_2, 2H), 4.36 (m, $C\underline{H}_2OH$), 4.58 (m, H_5), 4.84 (m, H_4), 5.00 (m, H_3), 8.62 (s, =CH); UV λ_{max} (CH_3OH) 265 nm (ε 5960), λ_{max} (0.1 mol dm^{-3} HCl) 265 nm (ε 6610), λ_{max} (0.1 mol dm^{-3} NaOH) 266 nm (sh, ε 3260), 289 (4840).[38]

5-[(2R,3S*,4S*)-3,4-Dihydroxy-5,5-bis(hydroxymethyl)-tetrahydrofuran-2-yl]uracil ((±)-4'-Hydroxymethylpseudouridine)* (**33**): A mixture of **32** (50 mg, 0.175 mmol) and 10% HCl in CH_3OH (1.5 ml) was stirred for 10 min. Workup afforded **33** (38.3 mg, 89%) as a white powder. Mp 76—79 °C; ^1H NMR (dimethyl-d_6 sulfoxide) δ 3.46 (d-like, J=6.0 Hz, $C\underline{H}_2OH$), 4.33 (m, H_2, H_3, and H_4), 4.0—5.0 (br, OH), 7.43 (d, J=5.8 Hz, =CH), 10.87 (d, J=5.8 Hz, NH), 11.05 (br s, NH); ^{13}C NMR (dimethyl-d_6 sulfoxide) δ 61.63, 63.88, 72.40, 74.06, 78.33, 86.47, 110.59, 140.44, 150.91, 163.94; UV λ_{max} (CH_3OH) 264 nm (ε 6580), λ_{max} (0.1 mol dm^{-3} HCl) 264 nm (ε 6090), λ_{max} (0.1 mol dm^{-3} NaOH) 287 nm (ε 6780).[38]

5-[(2R,3R*,4S*,5R*)-3,4-Dihydroxy-2,5-dimethyl-5-hydroxymethyltetrahydrofuran-2-yl]uracil ((±)-1',4'-Dimethylpseudouridine)* (**47a**): To a solution of **46a** (313 mg, 0.911 mmol) in CH_3OH (2 ml)was added 10% HCl in CH_3OH (3 ml). The resulting mixture was stirred for 1 h. Usual workup afforded **47a** (274 mg, 100%). Mp 134—138 °C (CH_3OH); R_f=0.45 (3:1 chloroform–CH_3OH); ^1H NMR (C_5D_5N) δ 1.78 and 2.14 (s, CH_3), 3.96 (s, $C\underline{H}_2OH$), 4.87 (d, J=5.5 Hz, H_3), 5.05 (d, J=5.5 Hz, H_4), 6.24 (br, OH), 8.48 (br s, =CH), 12.50 (br, NH), 13.04 (br, NH); ^{13}C NMR (dimethyl-d_6 sulfoxide) δ 19.74, 23.46, 67.24, 72.11, 75.80, 82.23, 84.53, 117.80, 139.04, 151.60, 164.15; UV λ_{max} (CH_3OH) 265 nm (ε 6190), λ_{max} (0.1 mol dm^{-3} NaOH) 287 nm (ε 4760). Found: C, 46.52; H, 5.87; N, 8.98%. Calcd for $C_{11}H_{16}O_6N_2 \cdot 0.8H_2O$: C, 46.08; H, 6.19; N, 9.77%.

5-[(2R,3R*,4S*,5R*)-3,4-Dihydroxy-2,5-dipentyl-5-hydroxymethyltetrahydrofuran-2-yl]uracil ((±)-1',4'-Dipentylpseudouridine)* (**47b**): To a solution of **46b** (100 mg, 0.236 mmol) in CH_3OH (1 ml) was added 10% HCl in CH_3OH (3 ml). After stirring for 1.5 h, the mixture was worked up to give **47b** (82.5 mg, 91%). Mp 232—236 °C (CH_3OH); ^1H NMR (dimethyl-d_6 sulfoxide) δ 0.86 (m, CH_3), 1.0—2.1 (m, CH_2), 3.51 (br s, $C\underline{H}_2OH$), 4.03 (m, H_3 and H_4), 4.81 (br, OH), 7.51 (m, =CH), 10.88 (m, NH), 11.00 (br s, NH); ^{13}C NMR (dimethyl-d_6 sulfoxide) δ 13.73, 21.98, 22.40, 22.58, 31.62, 31.77, 32.35, 32.77, 63.93, 72.11, 76.65, 83.80, 85.65, 115.67, 138.98, 151.07, 163.94; UV λ_{max} (CH_3OH) 265 nm (ε 7240), λ_{max} (0.1 mol dm^{-3} HCl) 265 nm (ε 2300), λ_{max} (0.1 mol dm^{-3} NaOH) 290 nm (ε 7200).[38]

5-[(2R,3S*,4R*,5R*)-3,4-Dihydroxy-3,5-bis(hydroxymethyl)-tetrahydrofuran-2-yl]uracil ((±)-2'-Hydroxymethylpseudouridine)* (**55a**): To a solution of **54a** (94 mg, 0.219 mmol) in CH_3OH (0.1 ml) was added 10% HCl in CH_3OH (0.2 ml). After stirring for 30 min, the mixture was worked up to give **55a** (57 mg, 95%) as a white foam. Mp 125—130 °C; R_f= 0.29 (10:10:1 chloroform–CH_3OH–Water); ^1H NMR (dimethyl-d_6 sulfoxide) δ 3.28 (s, C(OH)$C\underline{H}_2OH$), 3.4—3.9 (m, H_4, H_5, and $C\underline{H}_2OH$), 4.68 (s, H_2), 7.50 (d, J=4.8 Hz, =CH), 12.28 (d, J=4.8 Hz, NH), 12.40 (br, NH); ^{13}C NMR (dimethyl-d_6 sulfoxide) δ 60.56, 63.21, 70.58, 79.62, 80.42, 82.06, 110.75, 139.17, 150.96, 164.18; UV λ_{max} (CH_3OH) 267 nm (ε 5710), λ_{max} (0.1 mol dm^{-3} HCl) 266 nm (ε 5140), λ_{max} (0.1 mol dm^{-3} NaOH) 285 nm (ε 3780).[38]

5-[(2R,3S*,4R*,5R*)-3,4-Dihydroxy-5-hydroxymethyl-3-methyltetrahydrofuran-2-yl]uracil ((±)-2'-Methylpseudouridine)* (**55b**): To a solution of **54b** (30 mg, 0.101 mmol) in CH_3OH (0.5 ml) was added 10% HCl in CH_3OH (0.5 ml) and the resulting mixture was stirred for 1 h. Workup afforded **54b** (25 mg, 96%). Mp 138—142 °C; R_f=0.40 (2:1 chloroform–CH_3OH); ^1H NMR (dimethyl-d_6 sulfoxide) δ 0.99 (s, CH_3), 3.60 (m, H_4, H_5, and $C\underline{H}_2OH$), 4.00 (br, OH), 4.68 (s, H_2), 7.60 (d, J=5.0 Hz, =CH), 10.78 (d, J=5.0 Hz, NH), 10.99 (br, NH); ^{13}C NMR (dimethyl-d_6 sulfoxide) δ 20.95, 60.31, 73.57, 77.99, 81.31, 81.53, 112.13, 138.92, 150.90, 163.68; UV λ_{max} (CH_3OH) 264 nm (ε 6420), λ_{max} (0.1 mol dm^{-3} HCl) 263 nm (ε 8760), λ_{max} (0.1 mol dm^{-3} NaOH) 285 nm (ε 8020).[38]

5-[(2R,3R*,4S*,5S*)-3,4-Dihydroxy-5-(1-hydroxy-1-methylethyl)tetrahydrofuran-2-yl]-2-thiouracil ((±)-5',5'-Dimethyl-2-thiopseudouridine)* (**11a**): A mixture of **10a** (158 mg, 0.549 mmol) and 10% HCl in CH_3OH (5 mol) was stirred for 10 min. Usual workup afforded **11a** (135 mg, 97%) as a white powder. Mp 109—115 °C; ^1H NMR (C_5D_5N) δ 1.58 and 1.60 (s, CH_3), 4.34 (d, J=3.8 Hz, H_5), 4.96 (m, H_3 and H_4), 5.31 (d, J=5.0 Hz, H_2), 5.70 (br, OH and NH), 8.19 (s, =CH); UV λ_{max} (CH_3OH) 214 nm (ε 5780), 276 (6660), 292 (5990), λ_{max} (0.1 mol dm^{-3} HCl) 214 nm (ε 7560), 274 (8810), 289 (8890), λ_{max} (0.1 mol dm^{-3} NaOH) 222 nm (ε 7910), 263 (6670), 284 (5020).[38]

5-[(2R,3R*,4R*,5R*)-3,4-Dihydroxy-5-[(R*)-1-hydroxyethyl]tetrahydrofuran-2-yl]-2-thiouracil ((±)-5'-Methyl-2-thiopseudouridine)* (**11b**): To a solution of **10a** (52.1 mg, 0.155 mmol) in CH_3OH (2 ml) was added 10% HCl in CH_3OH (2 ml). The resulting mixture was stirred for 5 min and worked up to give **11b** (48.6 mg, 100%) as a wax. ^1H NMR (C_5D_5N) δ 1.51 (d, J=6.0 Hz, CH_3), 4.67 (m, H_5 and $\underline{H}COH$), 4.96 (m, H_3 and H_4), 5.35 (d, J=5.2 Hz, H_2), 6.0 (br, OH and NH), 8.16 (s, =CH); UV λ_{max} (CH_3OH) 215 nm (ε 6610), 277 (8350), 291 (7590), λ_{max} (0.1 mol dm^{-3} HCl) 213 nm (ε 6080), 280 (4630), 295 (5630), λ_{max} (0.1 mol dm^{-3} NaOH) 221 nm (ε 11400), 264 (10200), 285 (7730).[38]

5-[(2R,3R*,4R*,5R*)-3,4-Dihydroxy-5-[(R*)-1-hydroxyhexyl]tetrahydrofuran-2-yl]-2-thiouracil ((±)-5'-Pentyl-2-thiopseudouridine* (**11c**): To a solution of **10c** (62.8 mg, 0.170 mmol) in CH_3OH (1 ml) was added 10% HCl in CH_3OH (2 ml). After stirring for 10 min, the mixture was worked up to afford **11c** (32.5 mg, 58%). Mp 164—170 °C; ^1H NMR (C_5D_5N) δ 0.81 (t, J=7.0 Hz, CH_3), 1.1—2.0 (m, CH_2), 4.30 (m, $\underline{H}COH$) 4.57 (t-like, J=3.0 Hz, H_5), 5.00 (m, H_3 and H_4), 5.35 (d, J=5.2 Hz, H_2), 5.4—6.8 (br, OH and NH), 8.14 (s, =CH); UV λ_{max} (CH_3OH) 214 nm (ε 4310), 276 (5160), 291 (4670), λ_{max} (0.1 mol dm^{-3} HCl) 215 nm (ε 7090), 276 (8230), 290 (8230), λ_{max} (0.1 mol dm^{-3} NaOH) 222 nm (ε 5300), 264 (4340), 285 (3420).[38]

5-[(2R,3R*,4R*,5S*)-3,4-Dihydroxy-5-[(S*)-α-hydroxybenzyl]tetrahydrofuran-2-yl]-2-thiouracil ((±)-5'-Phenyl-2-thiopseudouridine)* (**11d**): To a suspension of **10d** (26.6 mg, 0.071 mmol) in CH_3OH (1 ml) was added 10% HCl in CH_3OH (1 ml). The resulting mixture was stirred for 10

min and worked up to give **11d** (24.9 mg, 100%). Mp 126—130 °C; ^{1}H NMR (dimethyl-d_6 sulfoxide) δ 3.95 (d-like, J=3.1 Hz, H_5), 4.46 (d, J=3.0 Hz, H_4), 4.70 (m, H_3), 4.90 (m, H_2), 5.59 (d, J=3.0 Hz, HCOH), 7.2—7.5 (m, C_6H_5), 7.44 (s, =CH); UV λ_{max} (CH_3OH) 212 nm (ε 4380), 277 (3620), 290 (3240), λ_{max} (0.1 mol dm^{-3} HCl) 275 nm (ε 6900), 290 (6440), λ_{max} (0.1 mol dm^{-3} NaOH) 264 nm (ε 6510), 285 (5030).[38]

5-[(2R,3S*,4S*,5R*)-3,4-Dihydroxy-5-hydroxymethyl-5-methyltetrahydrofuran-2-yl]-2-thiouracil ((±)-4′-Methyl-2-thiopseudouridine) (**19a**)*: To a solution of **18a** (22.1 mg, 0.0704 mmol) in CH_3OH (1.5 ml) was added 10% HCl in CH_3OH (1.5 ml) and the resulting mixture was stirred for 20 min. Usual workup afforded **19a** (18.4 mg, 95%). Mp 157—162 °C (CH_3OH); R_f=0.55 (3:1 chloroform–CH_3OH); ^{1}H NMR (C_5D_5N) δ 1.69 (s, CH_3), 3.93 (d, J=11.5 Hz, H_aH_bCOH), 4.07 (d, J=11.5 Hz, H_aH_bCOH), 4.88 (d, J=5.5 Hz, H_4), 5.10 (t, J=5.5 Hz, H_3), 5.35 (d, J=5.5 Hz, H_2), 8.16 (s, =CH); UV λ_{max} (CH_3OH) 215 nm (ε 10920), 276 (15550), 291 (14070), λ_{max} (0.1 mol dm^{-3} HCl) 214 nm (ε 13150), 276—290 (flat, 15570), λ_{max} (0.1 mol dm^{-3} NaOH) 223 nm (ε 12640), 264 (11240), 286 (8570). Found: *m/z*, 274.0613. Calcd for $C_{10}H_{14}O_5N_2S$: M, 274.0623.

5-[(2R,3S*,4S*,5R*)-3,4-Dihydroxy-5-hydroxymethyl-5-pentyltetrahydrofuran-2-yl]-2-thiouracil ((±)-4′-Pentyl-2-thiopseudouridine) (**19b**)*. To a suspension of **18b** (17.7 mg, 0.048 mmol) in CH_3OH (1.5 ml) was added 10% HCl in CH_3OH (1.5 ml). After stirring for 30 min, the mixture was worked up in a usual manner to give **19b** (16.9 mg, 100%). Mp 203—205 °C (CH_3OH); R_f=0.74 (3:1 chloroform–CH_3OH); ^{1}H NMR (C_5D_5N) δ 0.81 (t, J=6.0 Hz, CH_3), 1.2—2.0 (m, CH_2), 3.96 (d, J=11.8 Hz, H_aH_bCOH), 4.12 (d, J=11.8 Hz, H_aH_bCOH), 4.87 (br s, H_4), 5.20 (m, H_2 and H_3), 6.0 (br, OH), 8.02 (s, =CH); UV λ_{max} (CH_3OH) 215 nm (ε 13320), 276 (18690), 291 (16950), λ_{max} (0.1 mol dm^{-3} HCl) 214 nm (ε 14310), 275—290 (flat, 16500), λ_{max} (0.1 mol dm^{-3} NaOH) 223 nm (ε 13790), 264 (12100), 286 (9340).[38]

5-[(2R,3S*,4S*,5R*)-3,4-Dihydroxy-5-hydroxymethyl-5-phenyltetrahydrofuran-2-yl]-2-thiouracil ((±)-4′-Phenyl-2-thiopseudouridine) (**19c**)*: A mixture of **18c** (106 mg, 0.282 mmol) and 9:1 CF_3COOH–H_2O (4 ml) was stirred for 10 min. Usual workup afforded **19c** (84.1 mg, 89%). Mp 249—250 °C (CH_3OH); R_f=0.70 (3:1 chloroform–CH_3OH); ^{1}H NMR (dimethyl-d_6 sulfoxide) δ 3.34 (m, CH_2OH), 4.57 (m, H_3), 5.10 (m, H_2 and H_4), 7.30 (m, C_6H_5), 7.66 (d, J=5.5 Hz, =CH), 12.43 (d, J=5.5 Hz, NH), 12.57 (br s, NH); UV λ_{max} (CH_3OH) 276 nm (ε 16620), 290 (14970), λ_{max} (0.1 mol dm^{-3} HCl) 276 nm (ε 13620), 289 (13790), λ_{max} (0.1 mol dm^{-3} NaOH) 216 nm (ε 19540), 264 (13910), 289 (13790). Found: C, 52.75; H, 4.70; N, 8.12; S, 9.68%. Calcd for $C_{15}H_{16}O_5N_2S$: C, 53.36; H, 4.80; N, 8.33; S, 9.53%.

5-[(2R,3R*,4R*,5R*)-3,4-Dihydroxy-5-hydroxymethyl-2-methyltetrahydrofuran-2-yl]-2-thiouracil ((±)-1′-Methyl-2-thiopseudouridine) (**27a**)*: To a solution of **26a** (54.7 mg, 0.175 mmol) in CH_3OH (1 ml) was added 10% HCl in CH_3OH (1 ml). After stirring for 30 min, the mixture was worked up to give **27a** (50.3 mg, 100%) as a yellow foam. R_f=0.60 (3:1 chloroform–CH_3OH); ^{1}H NMR (C_5D_5N) δ 2.16 (s, CH_3), 4.21 (dd, J=2.0, 11.9 Hz, H_aH_bCOH), 4.38 (dd, J=3.1, 11.9 Hz, H_aH_bCOH), 4.60 (ddd, J=2.0, 3.1, 6.1 Hz, H_5), 4.82 (dd, J=4.6, 6.1 Hz, H_4), 4.96 (d, J=6.1 Hz, H_3), 6.0—6.9 (br, OH and NH), 8.71 (s, =CH); UV λ_{max} (CH_3OH) 215 nm (ε 10940), 276 (14430), 290 (13270), λ_{max} (0.1 mol dm^{-3} HCl) 215 nm (ε 11000), 275 (14330), 290 (sh, 13320), λ_{max} (0.1 mol dm^{-3} NaOH) 221 nm (sh, ε 12680), 262 (12310), 295 (sh, 6620).[38]

5-[(2R,3R*,4R*,5R*)-3,4-Dihydroxy-5-hydroxymethyl-2-pentyltetrahydrofuran-2-yl]-2-thiouracil ((±)-1′-Pentyl-2-thiopseudouridine) (**27b**)*: To a solution of **26b** (52.6 mg, 0.142 mmol) in CH_3OH (1 ml) was added 10% HCl in CH_3OH (1 ml). The mixture was stirred for 30 min and worked up to give **27b** (41.6 mg, 89%) as a yellow foam. R_f=0.72 (3:1 chloroform–CH_3OH); ^{1}H NMR (C_5D_5N) δ 0.76 (t, J=7.0 Hz, CH_3), 1.0—1.9 (m, CH_2), 2.2—3.1 (m, CH_2, 2H), 4.27 (dd, J=2.2, 11.9 Hz, H_aH_bCOH), 4.44 (dd, J=2.3, 11.9 Hz, H_aH_bCOH), 4.56 (ddd, J=2.2, 2.3, 7.0 Hz, H_5), 4.86 (dd, J=5.0, 7.0 Hz, H_4), 4.95 (d, J=5.0 Hz, H_3), 6.0—7.2 (br, OH and NH), 8.78 (s, =CH); UV λ_{max} (CH_3OH) 215 nm (ε 10910), 277 (14540), 291 (13190), λ_{max} (0.1 mol dm^{-3} HCl) 213 nm (sh, ε 7280), 273 (8440), 295 (sh, 6160), λ_{max} (0.1 mol dm^{-3} NaOH) 220 nm (sh, ε 9340), 262 (9420), 297 (sh, 4590). Found: *m/z*, 330.1244. Calcd for $C_{14}H_{22}O_5N_2S$: M, 330.1249.

5-[(2R,3S*,4S*)-3,4-Dihydroxy-5,5-bis(hydroxymethyl)tetrahydrofuran-2-yl]-2-thiouracil ((±)-4′-Hydroxymethyl-2-thiopseudouridine) (**35**)*: A mixture of **34** (35.8 mg, 0.119 mmol) and 10% HCl in CH_3OH (1 ml) was stirred for 10 min. Usual workup afforded **35** (32.3 mg, 90%) as a white powder. Mp 84—87 °C; ^{1}H NMR (dimethyl-d_6 sulfoxide) δ 3.48 (d-like, J=5.9 Hz, CH_2OH), 4.06 (m, H_3), 4.61 (m, H_2 and H_4), 4.3—5.0 (br, OH), 7.52 (d, J=5.9 Hz, =CH), 11.84 (d, J=5.9 Hz, NH), 11.98 (br s, NH); ^{13}C NMR (dimethyl-d_6 sulfoxide) δ 61.68, 63.94, 72.45, 74.09, 78.41, 86.51, 110.62, 140.43, 150.92, 163.95; UV λ_{max} (CH_3OH) 213 nm (ε 14110), 275 (15840), 296 (sh, 13120), λ_{max} (0.1 mol dm^{-3} HCl) 214 nm (ε 13500), 273 (13500), 292 (sh, 12080), λ_{max} (0.1 mol dm^{-3} NaOH) 265 nm (ε 13620), 285 (12920).[38]

5-[(2R,3R*,4R*,5R*)-3,4-Dihydroxy-2,5-bis(hydroxymethyl)-tetrahydrofuran-2-yl]-2-thiouracil ((±)-1′-Hydroxymethyl-2-thiopseudouridine) (**41**)*: To a solution of **40** (50 mg, 0.156 mmol) in CH_3OH (1 ml) was added 10% HCl in CH_3OH (0.5 ml). After stirring for 10 min, the mixture was worked up in a usual manner to give **41** (39 mg, 87%) as a white powder. Mp 130—135 °C; ^{1}H NMR (dimethyl-d_6 sulfoxide) δ 3.49 (d-like, J=6.5 Hz, CH_2OH), 3.9—4.3 (m, H_3, H_4, H_5, and OH), 7.53 (m, =CH), 12.30 (br, NH), 12.44 (br s, NH); UV λ_{max} (CH_3OH) 213 nm (ε 12360), 275 (12540), 299 (sh, 10300), λ_{max} (0.1 mol dm^{-3} HCl) 213 nm (ε 13820), 274 (13340), 297 (sh, 11200), λ_{max} (0.1 mol dm^{-3} NaOH) 265 nm (ε 12580), 284 (10440).[38]

5-[(2R,3R*,4S*,5R*)-3,4-Dihydroxy-2,5-dimethyl-5-hydroxymethyltetrahydrofuran-2-yl]-2-thiouracil ((±)-1′,4′-Dimethyl-2-thiopseudouridine) (**49a**)*: To a solution of **48a** (229 mg, 0.670 mmol) in CH_3OH (2 ml) was added 10% HCl in CH_3OH (3 ml). The resulting mixture was stirred for 1 h and worked up to afford **49a** (192 mg, 98%). Mp 182—186 °C (CH_3OH); ^{1}H NMR (C_5D_5N) δ 1.75 and 2.13 (s, CH_3), 3.98 (s, CH_2OH), 4.86 (d, J=5.2 Hz, H_3), 4.97 (d, J=5.2 Hz, H_4), 6.50 (br, OH), 8.65 (s, =CH); ^{13}C NMR (dimethyl-d_6 sulfoxide) δ 19.59, 22.88, 66.42, 71.24, 75.06, 81.95, 84.30, 123.01, 138.83, 160.89, 175.01; UV λ_{max} (CH_3OH) 216 nm (ε 13430), 277 (18980), 290 (17230), λ_{max} (0.1 mol dm^{-3} HCl) 216 nm (ε 12870), 277 (16560), 285 (16370), λ_{max} (0.1 mol dm^{-3} NaOH) 222 nm (ε 15860), 262 (14800), 290 (9650). Found: C, 45.76; H, 5.74; N, 9.47; S, 10.86%. Calcd for $C_{11}H_{16}O_5N_2S$: C, 45.83; H, 5.59; N, 9.72, S, 11.12%.

5-[(2R,3R*,4S*,5R*)-3,4-Dihydroxy-2,5-dipentyl-5-hydroxymethyltetrahydrofuran-2-yl]-2-thiouracil ((±)-1′,4′-Dipentyl-2-thiopseudouridine) (**49b**)*: To a solution of **48b** (404 mg, 0.910 mmol) in CH_3OH (3 ml) was added 10% HCl in CH_3OH

(3 ml). The mixture was stirred for 1 h and worked up in a usual manner to afford **49b** (392 mg, 100%). Mp 105—110 °C (CH_3OH); ^1H NMR (dimethyl-d_6 sulfoxide) δ 0.84 (m, CH_3), 1.0—2.1 (m, CH_2), 3.34 (m, $C\underline{H}_2OH$), 3.8—5.0 (br, OH), 4.04 (m, H_3 and H_4), 7.57 (m, =CH), 12.26 (m, NH), 12.35 (br s, NH); ^{13}C NMR (dimethyl-d_6 sulfoxide) δ 13.73, 21.99, 22.50, 31.71, 32.37, 63.71, 71.89, 76.25, 83.89, 85.78, 121.27, 138.93, 160.73, 174.68; UV λ_{max} (CH_3OH) 215 nm (ε 9330), 277 (13170), 290 (sh, 11690), λ_{max} (0.1 mol dm^{-3} HCl) 217 nm (ε 6280), 275 (9980), 289 (9460), λ_{max} (0.1 mol dm^{-3} NaOH) 225 nm (ε 10110), 262 (10790).[38]

5-[(2S,3R*,4R*,5R*)-3,4-Dihydroxy-3,5-bis(hydroxymethyl)-tetrahydrofuran-2-yl]-2-thiouracil ((±)-2′-Hydroxymethyl-2-thiopseudouridine) (**59a**)*: To a solution of **58a** (237 mg, 0.534 mmol) in CH_3OH (2.8 ml) was added 10% HCl in CH_3OH (5 ml). After stirring for 30 min, the mixture was worked up as usual to afford **59a** (148 mg, 96%). Mp 140—145 °C; R_f=0.48 (10:10:1 chloroform–CH_3OH–water); ^1H NMR (dimethyl-d_6 sulfoxide) δ 3.27 (s, C(OH)$C\underline{H}_2OH$), 3.4—3.7 (m, H_4 and H_5), 3.64 (d, J=8.0 Hz, $\underline{H}_aH_bCOH$), 3.85 (d, J=8.0 Hz, $H_a\underline{H}_bCOH$), 4.25 (br, OH), 4.68 (s, H_2), 7.50 (d, J=5.5 Hz, =CH), 12.26 (d, J=5.5 Hz, NH), 12.38 (br, NH); ^{13}C NMR (dimethyl-d_6 sulfoxide) δ 60.54, 62.70, 70.17, 79.88, 80.16, 82.05, 116.58, 138.54, 160.90, 174.63; UV λ_{max} (CH_3OH) 215 nm (ε 9080), 277 (11700), λ_{max} (0.1 mol dm^{-3} HCl) 215 nm (ε 9400), 276 (11000), λ_{max} (0.1 mol dm^{-3} NaOH) 220 nm (ε 11700), 264 (9060). Found: C, 37.22; H, 5.06; N, 7.42%. Calcd for $C_{10}H_{14}O_6N_2S\cdot 2.3H_2O$: C, 36.21; H, 5.64; N, 8.45%.

5-[(2S,3R*,4R*,5R*)-3,4-Dihydroxy-5-hydroxymethyl-3-methyltetrahydrofuran-2-yl]-2-thiouracil ((±)-2′-Methyl-2-thiopseudouridine) (**59b**)*: To a solution of **58b** (194 mg, 0.618 mmol) in CH_3OH (3 ml) was added 10% HCl in CH_3OH (5 ml). The mixture was stirred for 30 min and worked up to give **59b** (164 mg, 97%). Mp 132—136 °C (CH_3OH–ether); R_f=0.61 (2:1 chloroform–CH_3OH); ^1H NMR (dimethyl-d_6 sulfoxide) δ 0.98 (s, CH_3), 3.6 (m, H_4, H_5, and $C\underline{H}_2OH$), 4.22 (br, OH), 4.70 (s, H_2), 7.68 (d, J=5.5 Hz, =CH), 12.26 (d, J=5.5 Hz, NH), 12.38 (br, NH); ^{13}C NMR (dimethyl-d_6 sulfoxide) δ 20.87, 60.18, 73.46, 78.06, 81.05, 81.59, 117.70, 138.51, 160.53, 174.75; UV λ_{max} (CH_3OH) 215 nm (ε 9470), 276 (11600), λ_{max} (0.1 mol dm^{-3} HCl) 215 nm (ε 10200), 275 (11000), λ_{max} (0.1 mol dm^{-3} NaOH) 220 nm (ε 17300), 263 (14500). Found: C, 40.81; H, 5.19; N, 9.44; S, 10.58%. Calcd for $C_{10}H_{14}O_5N_2S\cdot 1.1H_2O$: C, 40.84; H, 5.55; N, 9.53; S, 10.90%.

5-[(2R,3R*,4S*,5S*)-3,4-Dihydroxy-5-(1-hydroxy-1-methylethyl)tetrahydrofuran-2-yl]isocytosine Hydrochloride ((±)-5′,5′-Dimethylpseudoisocytidine Hydrochloride) (**13a**)*: To a suspension of **12a** (35.2 mg, 0.113 mmol) in CH_3OH (2 ml) was added 10% HCl in CH_3OH (1 ml). The reaction mixture was stirred for 10 min and worked up in a usual way to afford **13a** (40.1 mg, 100%) as a wax. ^1H NMR (dimethyl-d_6 sulfoxide) δ 1.14 (s, CH_3), 3.52 (d, J=4.1 Hz, H_5), 3.97 (m, H_3 and H_4), 4.49 (d, J=5.0 Hz, H_2), 4.6—6.4 (br, OH), 7.91 (s, =CH), 8.53 (br, NH_2); UV λ_{max} (CH_3OH) 223 nm (ε 10500), 265 (7160), 290 (3910), λ_{max} (0.1 mol dm^{-3} HCl) 221 nm (ε 8950), 262 (6890), λ_{max} (0.1 mol dm^{-3} NaOH 233 nm (ε 8670), 276 (6870).[38]

5-[(2R,3R*,4R*,5R*)-3,4-Dihydroxy-5-[(R*)-1-hydroxyethyl]tetrahydrofuran-2-yl]isocytosine Hydrochloride ((±)-5′-Methylpseudoisocytidine Hydrochloride) (**13b**)*: To a suspension of **12b** (57.4 mg, 0.193 mmol) in CH_3OH (2 ml) was added 10% HCl in CH_3OH (2 ml). After stirring for 10 min, the mixture was worked up to afford **13b** (53.1 mg, 94%). Mp 198.0—202.0 °C; ^1H NMR (C_5D_5N) δ 1.58 (d, J=5.8 Hz, CH_3), 4.35 (m, H_5 and $\underline{H}COH$), 4.92 (m, H_4), 5.18 (m, H_2 and H_3), 6.50 (br, OH and NH), 8.12 (s, =CH); UV λ_{max} (CH_3OH) 223 nm (ε 10500), 265 (7160), 290 (3910), λ_{max} (0.1 mol dm^{-3} HCl) 221 nm (ε 8950), 262 (6890), λ_{max} (0.1 mol dm^{-3} NaOH) 233 nm (ε 8670), 276 (6870).[38]

5-[(2R,3R*,4R*,5R*)-3,4-Dihydroxy-5-[(R*)-1-hydroxyhexyl]tetrahydrofuran-2-yl]isocytosine Hydrochloride ((±)-5′-Pentylpseudoisocytidine Hydrochloride (**13c**)*: To a suspension of **12c** (106 mg, 0.30 mmol) in CH_3OH (3 ml) was added 10% HCl in CH_3OH (2 ml) and the resulting mixture was stirred for 15 min. Usual workup afforded **13c** (95.1 mg, 91%). Mp 168.0—172.0 °C (CH_3OH); ^1H NMR (dimethyl-d_6 sulfoxide) δ 0.88 (t, J=6.0 Hz, CH_3), 1.1—1.6 (m, CH_2), 3.60 (m, H_5 and $\underline{H}COH$), 4.00 (m, H_3 and H_4), 4.47 (d, J=4.9 Hz, H_2), 7.80 (s, =CH), 8.45 (br, NH_2); UV λ_{max} (CH_3OH) 224 nm (ε 9630), 266 (6220), 290 (4180), λ_{max} (0.1 mol dm^{-3} HCl) 220 nm (ε 11800), 262 (9070), λ_{max} (0.1 mol dm^{-3} NaOH) 233 nm (ε 7340), 276 (5840). Found: C, 47.83; H, 6.90; N, 12.04%. Calcd for $C_{14}H_{23}O_5N_3Cl$: C, 48.21; H, 6.65; N, 12.05%.

5-[(2R,3R*,4R*,5S*)-3,4-Dihydroxy-5-[(S*)-α-hydroxybenzyl]tetrahydrofuran-2-yl]isocytosine Hydrochloride ((±)-5′-Phenylpseudoisocytidine Hydrochloride) (**13d**)*: To a suspension of **12d** (29.3 mg, 0.082 mmol) in CH_3OH (1 ml) was added 10% HCl in CH_3OH (1 ml). After stirring for 15 min, the mixture was worked up in a usual manner to give **13d** (33.4 mg, 100%) as a wax. ^1H NMR (dimethyl-d_6 sulfoxide) δ 3.98 (m, H_3, H_4, and H_5), 4.4—5.7 (br, OH), 4.48 (d, J=6.0 Hz, H_2), 4.70 (m, $\underline{H}COH$), 7.35 (m, C_6H_5), 7.61 (s, =CH), 8.57 (br, NH_2); UV λ_{max} (CH_3OH) 225 nm (ε 12700), 264 (8240), 290 (3960), λ_{max} (0.1 mol dm^{-3} HCl) 263 (ε 10300), λ_{max} (0.1 mol dm^{-3} NaOH) 233 nm (ε 13200), 277 (10100).[38]

5-[(2R,3S*,4S*,5R*)-3,4-Dihydroxy-5-hydroxymethyl-5-methyltetrahydrofuran-2-yl]isocytosine Hydrochloride ((±)-4′-Methylpseudoisocytidine Hydrochloride) (**21a**)*: To a solution of **20a** (14.9 mg, 0.05 mmol) in CH_3OH (3 ml) was added 10% HCl in CH_3OH (2 ml) and the resulting mixture was stirred for 30 min. After usual workup, pure **21a** (17.9 mg, 100%) was obtained. Mp 212—215 °C (CH_3OH); ^1H NMR (dimethyl-d_6 sulfoxide) δ 1.10 (s, CH_3), 3.25 (d, J=11.5 Hz, $\underline{H}_aH_bCOH$), 3.41 (d, J=11.5 Hz, $H_a\underline{H}_bCOH$), 3.93 (d, J=5.8 Hz, H_4), 4.10 (dd, J=5.8, 6.0 Hz, H_3), 4.52 (d, J=6.0 Hz, H_2), 7.80 (s, =CH), 8.38 (br, NH_2); UV λ_{max} (CH_3OH) 223 nm (ε 12360), 263 (8050), 290 (5530), λ_{max} (0.1 mol dm^{-3} HCl) 220 nm (ε 14820), 262 (10940), λ_{max} (0.1 mol dm^{-3} NaOH) 238 nm (ε 11760), 280 (4530). Found: C, 40.45, H, 5.30; N, 14.10%. Calcd for $C_{10}H_{15}O_5N_3Cl$: C, 40.89; H, 5.49; N, 14.31%.

5-[(2R,3S*,4S*,5R*)-3,4-Dihydroxy-5-hydroxymethyl-5-pentyltetrahydrofuran-2-yl]isocytosine Hydrochloride ((±)-4′-Pentylpseudoisocytidine Hydrochloride) (**21b**)*: To a solution of **20b** (20.3 mg, 0.0575 mmol) in CH_3OH (2 ml) was added 10% HCl in CH_3OH (2 ml). After stirring for 30 min, the mixture was worked up in a usual manner to give **21b** (12.9 mg, 58%). Mp 188—190 °C CH_3OH); ^1H NMR (dimethyl-d_6 sulfoxide) δ 0.92 (t, J=6.0 Hz, CH_3), 1.1—1.7 (m, CH_2), 3.42 (br s, $C\underline{H}_2OH$), 4.01 (d, J=5.0 Hz, H_4), 4.23 (dd, J=5.0, 7.0 Hz, H_3), 4.50 (d, J=7.0 Hz, H_2), 7.80 (s, =CH), 8.38 (br, NH_2); UV λ_{max} (CH_3OH) 225 nm (ε 7520), 266 (4910), 290 (3020), λ_{max} (0.1 mol dm^{-3} HCl) 220 nm (ε 10840), 262 (8200), λ_{max} (0.1 mol dm^{-3} NaOH) 231 nm (ε 12550), 276 (8620). Found: C, 46.64; H, 6.65; N, 11.60%. Calcd for $C_{14}H_{23}O_5N_3Cl\cdot 0.5H_2O$: C, 46.99; H, 6.76; N, 11.74%.

5-[(2R,3S*,4S*,5R*)-3,4-Dihydroxy-5-hydroxymethyl-5-phenyl-*

*tetrahydrofuran-2-yl]isocytosine Hydrochloride ((±)-4′-Phenylpseudoisocytidine Hydrochloride) (**21c**)*: To a solution of **20c** (35.7 mg, 0.0994 mmol) in CH_3OH (1 ml) was added 10% HCl in CH_3OH (1 ml) and the resulting mixture was stirred for 10 min. Usual workup gave **21c** (35.0 mg, 99%). Mp 218—221 °C (CH_3OH); ^1H NMR (dimethyl-d_6 sulfoxide) δ 3.40 (d, J=11.9 Hz, $\underline{H}_aH_bCOH$), 3.69 (d, J=11.9 Hz, $H_a\underline{H}_bCOH$), 4.35 (m, H_2 and H_3), 4.69 (d, J=6.0 Hz, H_4), 7.30 (m, C_6H_5), 7.98 (s, =CH), 8.48 (br, NH_2); UV λ_{max} (CH_3OH) 217 nm (ε 17630), 262 (9530), λ_{max} (0.1 mol dm^{-3} HCl) 263 nm (ε 7880), λ_{max} (0.1 mol dm^{-3} NaOH) 231 nm (ε 14130), 276 (9740).[38]

5-[(2R,3R*,4R*,5R*)-3,4-Dihydroxy-5-hydroxymethyl-2-methyltetrahydrofuran-2-yl]isocytosine Hydrochloride ((±)-1′-Methylpseudoisocytidine Hydrochloride) (**29a**)*: To a suspension of **28a** (52.4 mg, 0.178 mmol) in CH_3OH (1 ml) was added 10% HCl in CH_3OH (1 ml). After stirring for 30 min, the mixture was worked up as usual to afford **29a** (48.4 mg, 93%) as a yellow foam. ^1H NMR (dimethyl-d_6 sulfoxide) δ 1.38 (s, CH_3), 3.5—3.9 (m, H_4, H_5, and $C\underline{H}_2OH$), 4.02 (d, J=3.5 Hz, H_3), 7.90 (s, =CH), 8.48 (br, NH_2); UV λ_{max} (CH_3OH) 222 nm (ε 9490), 262 (6290), 300 (sh, 1030), λ_{max} (0.1 mol dm^{-3} HCl) 221 nm (ε 8680), 262 (6450), λ_{max} (0.1 mol dm^{-3} NaOH) 230 nm (ε 11030), 278 (8250).[38]

5-[(2R,3R*,4R*,5R*)-3,4-Dihydroxy-5-hydroxymethyl-2-pentyltetrahydrofuran-2-yl]isocytosine Hydrochloride ((±)-1′-Pentylpseudoisocytidine Hydrochloride) (**29b**)*: To a solution of **28b** (28.2 mg, 0.0799 mmol) in CH_3OH (1 ml) was added 10% HCl in CH_3OH (1 ml) and the resulting mixture was stirred for 30 min. Usual workup afforded **29b** (25.7 mg, 92%) as a yellow foam. ^1H NMR (dimethyl-d_6 sulfoxide) δ 0.81 (t, J=6.0 Hz, CH_3), 1.0—2.0 (m, CH_2), 3.5—3.9 (m, H_4, H_5, and $C\underline{H}_2OH$), 4.04 (d, J=4.0 Hz, H_3), 7.86 (s, =CH), 8.2—8.8 (br, NH_2); UV λ_{max} (CH_3OH) 210 nm (sh, ε 12180), 225 (7940), 261 (4380), 300 (sh, 1170), λ_{max} (0.1 mol dm^{-3} HCl) 210 nm (ε 12310), 225 (sh, 8660), 262 (4780), λ_{max} (0.1 mol dm^{-3} NaOH) 230 nm (sh, ε 7120), 277 (4780).[38]

5-[(2R,3S*,4S*)-3,4-Dihydroxy-5,5-bis(hydroxymethyl)tetrahydrofuran-2-yl]isocytosine Hydrochloride ((±)-4′-Hydroxymethylpseudoisocytidine Hydrochloride) (**37**)*: A mixture of **36** (56.0 mg, 0.179 mmol) and 10% HCl in CH_3OH (1.5 ml) was stirred for 15 min. Usual workup gave **37** (50.3 mg, 91%) as a white powder. Mp 177—182 °C; ^1H NMR (dimethyl-d_6 sulfoxide) δ 3.51 (d-like, J=6.1 Hz, $C\underline{H}_2OH$), 4.08 (m, H_3 and H_4), 4.57 (m, H_2), 5.0—6.4 (br, OH), 7.82 (br s, =CH), 8.50 (br, NH_2); UV λ_{max} (CH_3OH) 224 nm (ε 9250), 263 (7870), λ_{max} (0.1 mol dm^{-3} HCl) 222 nm (ε 9580), 263 (7520), λ_{max} (0.1 mol dm^{-3} NaOH) 233 nm (ε 10870), 278 (8510).[38]

5-[(2R,3R*,4S*,5R*)-3,4-Dihydroxy-2,5-dimethyl-5-hydroxymethyltetrahydrofuran-2-yl]isocytosine Hydrochloride ((±)-1′,4′-Dimethylpseudoisocytidine Hydrochloride) (**51a**)*: To a suspension of **50a** (202 mg, 0.641 mmol) in CH_3OH (3 ml) was added 10% HCl in CH_3OH (3 ml). After stirring for 1 h, the mixture was worked up to afford **51a** (193 mg, 97%) as a white powder. Mp 215—220 °C; ^1H NMR (dimethyl-d_6 sulfoxide) δ 1.12 and 1.39 (s, CH_3), 3.29 (s, $C\underline{H}_2OH$), 3.90 (d, J=5.7 Hz, H_3), 4.11 (d, J=5.7 Hz, H_4), 7.94 (s, =CH), 8.37 (br, NH_2); ^{13}C NMR (dimethyl-d_6 sulfoxide) δ 19.47, 22.77, 66.07, 70.95, 74.83, 81.77, 84.24, 122.18, 137.78, 152.54, 159.42; UV λ_{max} (CH_3OH) 223 nm (ε 18460), 263 (12580), 292 (sh, 3300), λ_{max} (0.1 mol dm^{-3} HCl) 222 nm (ε 9550), 263 (6930), λ_{max} (0.1 mol dm^{-3} NaOH) 231 nm (ε 9080), 278 (6860). Found: C, 41.86; H, 5.72; N, 13.33%. Calcd for $C_{11}H_{18}O_5N_3Cl\cdot0.5H_2O$: C, 41.94, H, 6.01; N, 13.34%.

5-[(2R,3R*,4S*,5R*)-3,4-Dihydroxy-2,5-dipentyl-5-hydroxymethyltetrahydrofuran-2-yl]isocytosine Hydrochloride ((±)-1′,4′-Dipentylpseudoisocytidine Hydrochloride) (**51b**)*: To a suspension of **50b** (269 mg, 0.63 mmol) in CH_3OH (5 ml) was added 10% HCl in CH_3OH (5 ml) and the resulting mixture was stirred for 1 h. Usual workup afforded **51b** (260 mg, 100%). Mp 245—250 °C; ^1H NMR (dimethyl-d_6 sulfoxide) δ 0.87 (m, CH_3), 1.0—2.0 (m, CH_2), 3.19 (d, J=7.1 Hz, $\underline{H}_aH_bCOH$), 3.33 (d, J=7.1 Hz, $H_a\underline{H}_bCOH$), 4.04 (m, H_3 and H_4), 4.0—5.2 (br, OH), 7.82 (s, =CH), 8.30 (br, NH_2); ^{13}C NMR (dimethyl-d_6 sulfoxide) δ 14.02, 22.28, 22.59, 32.20, 32.64, 63.95, 72.06, 76.55, 84.14, 86.08, 120.55, 139.68, 153.32, 160.33; UV λ_{max} (CH_3OH) 263 nm (ε 5230), λ_{max} (0.1 mol dm^{-3} HCl) 265 nm (ε 3720), λ_{max} (0.1 mol dm^{-3} NaOH) 230 nm (ε 6780), 278 (3920).[38]

5-[(2S,3R*,4R*,5R*)-3,4-Dihydroxy-3,5-bis(hydroxymethyl)-tetrahydrofuran-2-yl]isocytosine Hydrochloride ((±)-2′-Hydroxymethylpseudoisocytidine Hydrochloride) (**61a**)*: To a solution of **60a** (200 mg, 0.468 mmol) in CH_3OH (2.3 ml) was added 10% HCl in CH_3OH (5 ml). After stirring for 15 min, the mixture was worked up to afford **61a** (139 mg, 96%). Mp 215—217 °C; ^1H NMR (dimethyl-d_6 sulfoxide) δ 3.30 (s, $C(OH)C\underline{H}_2OH$), 3.4—3.9 (m, H_4 and H_5), 3.67 (d, J=8.8 Hz, $\underline{H}_aH_bCOH$), 3.92 (d, J=8.8 Hz, $H_a\underline{H}_bCOH$), 4.71 (s, H_2), 7.76 (s, =CH), 8.48 (br, NH_2); ^{13}C NMR (dimethyl-d_6 sulfoxide) δ 60.70, 62.50, 70.01, 80.20, 82.00, 116.48, 137.80, 152.49, 159.18; UV λ_{max} (CH_3OH) 224 nm (ε 12500), 265 (7770), λ_{max} (0.1 mol dm^{-3} NaOH) 232 nm (ε 8800), 280 (6420). Found: C, 37.81; H, 5.16; N, 13.08%. Calcd for $C_{10}H_{16}O_6N_3Cl\cdot0.5H_2O$: C, 37.68; H, 5.38; N, 13.19%.

5-[(2S,3R*,4R*,5R*)-3,4-Dihydroxy-5-hydroxymethyl-3-methyltetrahydrofuran-2-yl]isocytosine Hydrochloride ((±)-2′-Methylpseudoisocytidine Hydrochloride) (**61b**)*: To a solution of **60b** (263 mg, 0.886 mmol) in CH_3OH (3 ml) was added 10% HCl in CH_3OH (5 ml) and the resulting mixture was stirred for 30 min. Usual workup gave **61b** (253 mg, 97%). Mp 222—225 °C (CH_3OH–ether); ^1H NMR (dimethyl-d_6 sulfoxide) δ 1.02 (s, CH_3), 3.62 (m, H_4, H_5, and $C\underline{H}_2OH$), 4.70 (s, H_2), 7.88 (s, =CH), 8.48 (br, NH_2); ^{13}C NMR (dimethyl-d_6 sulfoxide) δ 20.84, 60.20, 73.35, 78.28, 80.97, 81.64, 117.18, 138.33, 152.50, 159.53; UV λ_{max} (CH_3OH) 244 nm (ε 10700), 265 (6890), λ_{max} (0.1 mol dm^{-3} HCl) 222 nm (ε 5800), 264 (4250), λ_{max} (0.1 mol dm^{-3} NaOH) 233 nm (ε 9010), 280 (6750). Found: C, 40.46; H, 5.52; N, 14.00; Cl, 12.32%. Calcd for $C_{10}H_{16}O_5N_3Cl$: C, 40.89; H, 5.49; N, 14.31; Cl, 12.07%.

5-[(2S,3R*,4R*,5R*)-3-t-Butyldimethylsiloxymethyl-3,4-isopropylidenedioxy-5-mesyloxymethyltetrahydrofuran-2-yl]uracil (**56a**)*: To a solution of **54a** (50 mg, 0.117 mmol) in pyridine (0.8 ml) was added methanesulfonyl chloride (28 μl, 0.351 mmol) at 0 °C under argon, and then this mixture was stirred at the same temperature for 30 min and at 15 °C for 12 h. The reaction mixture was concentrated and the resulting residue was coevaporated with C_2H_5OH (2ml×2). Purification of the residue on preparative TLC (10:1 chloroform–CH_3OH) afforded **56a** (40 mg, 67%). Mp 195—197 °C (acetone–hexane); R_f=0.42 (10:1 chloroform–CH_3OH); ^1H NMR (dimethyl-d_6 sulfoxide) δ 0.06 (s, t-$C_4H_9(C\underline{H}_3)_2Si$), 0.84 (s, t-$C_4\underline{H}_9(CH_3)_2Si$), 1.36 and 1.52 (s, isopropylidene CH_3), 3.28 (s, CH_3SO_2), 3.52 (s, CH_2OSi), 4.2—4.6 (m, H_4, H_5, and CH_2OMs), 4.88 (s, H_2), 7.22 (d, J=5.0 Hz, =CH), 10.92 (d, J=5.0 Hz, NH), 11.12 (br, NH); ^{13}C NMR (dimethyl-d_6 sulfoxide) δ 17.74, 25.49, 26.84, 28.31, 61.01, 61.60, 80.44, 82.73, 83.02, 91.54, 107.80, 113.08, 138.68, 150.78, 162.56; UV λ_{max} (CH_3OH) 266 nm (ε 7150), λ_{max} (0.1 mol dm^{-3} NaOH) 289 nm (ε 6150). Found: C,

45.11, H, 6.44, N, 4.91%. Calcd for $C_{20}H_{34}O_9N_2SSi \cdot 1.5H_2O$: C, 45.01, H, 6.98; N, 5.25%.

5-[(2S,3R*,4R*,4R*)-3,4-Isopropylidenedioxy-3-methyl-5-mesyloxymethyltetrahydrofuran-2-yl]uracil (**56b**)*: A mixture of **54b** (20 mg, 0.067 mmol), methanesulfonyl chloride (26 μl, 0.335 mmol), and pyridine (0.4 ml) was stirred at room temperature for 14 h and worked up as described above. Subsequent preparative TLC (5:1 chloroform–CH_3OH) afforded **56b** (21 mg, 83%). Mp 199—202 °C; R_f=0.47 (1:1 chloroform–CH_3OH); ^{1}H NMR (dimethyl-d_6 sulfoxide) δ 1.15 (s, CH_3), 1.34 and 1.50 (s, isopropylidene CH_3), 3.22 (s, CH_3SO_2), 4.1—4.5 (m, H_3, H_4, and CH_2OMs), 4.86 (s, H_2), 7.22 (s, =CH), 11.00 (br, NH); UV λ_{max} (CH_3OH) 261 nm (ε 7000).

*2'-t-Butyldimethylsiloxymethyl-2',3'-O-isopropylidene-4,5'-cyclopseudouridine (**57a**)*: To a solution of **56a** (30 mg, 52.9 μmol) in acetonitrile (1.2 ml) was added DBU (9.8 μl, 65.1 μmol) under argon and the mixture was stirred at 80 °C. After stirring for 2 h, DBU (4.9 μl, 32.6 μmol) was renewedly added. The resulting mixture was stirred for an additional 2 h and evaporated to give a yellow solid, which was purified by preparative TLC (10:1 chloroform–CH_3OH) to afford **57a** (22 mg, 90%). Mp 240—241 °C (acetone–hexane); R_f=0.34 (10:1 chloroform–CH_3OH); ^{1}H NMR (dimethyl-d_6 sulfoxide) δ 0.06 (s, t-$C_4H_9(C\underline{H}_3)_2Si$), 0.80 (s, t-$C_4\underline{H}_9(CH_3)_2Si$), 1.38 and 1.45 (s, isopropylidene CH_3), 3.38 (d, J=11.5 Hz, $C\underline{H}_aH_bOSi$), 3.62 (d, J=11.5 Hz, $CH_a\underline{H}_bOSi$), 3.98 (d, J=13.0 Hz, $\underline{H}_aH_bCO$), 4.32 (br s, H_5), 4.52 (d, J=13.0 Hz, $H_a\underline{H}_bCO$), 4.70 (s, H_2), 4.90 (s, H_4), 7.96 (s, =CH); UV λ_{max} (CH_3OH) 295 nm (ε 3720). Found: C, 50.82; H, 7.77; N, 5.94%. Calcd for $C_{19}H_{30}O_6N_2Si \cdot 2H_2O$: C, 51.10; H, 7.67; N, 6.27%.

*2',3'-O-Isopropylidene-2'-methyl-4,5'-cyclopseudouridine (**57b**)*: A mixture of **54b** (20 mg, 0.053 mmol), DBU (8.8 μl, 0.059 mmol), and acetonitrile (1.1 ml) was stirred at 80 °C for 3 h and the resulting mixture was worked up as described above. Subsequent preparative TLC (5:1 chloroform–CH_3OH) gave **57b** (12 mg, 81%). Mp 225—229 °C(CH_3OH–acetone–hexane); R_f=0.47 (1:1 chloroform–CH_3OH); ^{1}H NMR (dimethyl-d_6 sulfoxide) δ 1.10 (s, CH_3), 1.40 and 1.43 (s, isopropylidene CH_3), 3.96 (d, J=6.5 Hz, $\underline{H}_aH_bCO$) 4.2—4.5 (m, H_5 and $H_a\underline{H}_bCO$), 4.62 (s, H_2), 4.78 (s, H_4), 8.02 (br s, =CH); UV λ_{max} (CH_3OH) 293 nm (ε 3080). Found: *m/z*, 280.1049. Calcd for $C_{13}H_{16}O_5N_2$: M, 280.1059.

References

1) *C*-Nucleoside Synthesis. 19. Part 18: R. Noyori, T. Sato, and H. Kobayashi, *Bull. Chem. Soc. Jpn.*, **56**, 2661 (1983).

2) R. Noyori, T. Sato, and Y. Hayakawa, *J. Am. Chem. Soc.*, **100**, 2561 (1978); T. Sato, Y. Hayakawa, and R. Noyori, submitted for publication.

3) Pseudoisocytidine was found to be active toward various mouse leukemias. J. H. Burchenal, K. Ciovacco, K. Kalaher, T. O'Toole, R. Kiefner, M. D. Dowling, C. K. Chu, K. A. Watanabe, I. Wempen, and J. J. Fox, *Cancer Res.*, **36**, 1520 (1976).

4) Reviews: R. Noyori, *Ann. N. Y. Acad. Sci.*, **295**, 225 (1977); *Acc. Chem. Res.*, **12**, 61 (1979); R. Noyori and Y. Hayakawa, *Org. React.*, **29**, 163 (1983).

5) U. Reichman, C. K. Chu, I. Wempen, K. A. Watanabe, and J. J. Fox, *J. Heterocycl. Chem.*, **13**, 933 (1976); C. K. Chu, U. Reichman, K. A. Watanabe, and J. J. Fox, *ibid.*, **14**, 1119 (1977); *J. Med. Chem.*, **21**, 96 (1978); M. J. Robins and W. H. Muhn, *J. Chem. Soc., Chem. Commun.*, **1978**, 677; A. Matsuda, K. Pankiewicz, B. K. Marcus, K. A. Watanabe, and J. J. Fox, *Carbohydr. Res.*, **100**, 297 (1982).

6) Isolation: H. Yüntsen, H. Yonehara, and H. Ui, *J. Antibiot., Ser. A*, **7**, 113 (1954); H. Yüntsen, K. Ohkuma, Y. Ishii, and H. Yonehara, *ibid.*, **9**, 195 (1956); W. Schroeder and H. Hoeksema, *J. Am. Chem. Soc.*, **81**, 1767 (1959); H. Hoeksema, G. Slomp, and E. E. van Tamelen, *Tetrahedron Lett.*, **1964**, 1787. Review: R. J. Suhadolnik, "Nucleoside Antibiotics," Wiley-Interscience, New York, N. Y. (1970), pp. 96—122.

7) Isolation: R. I. Hewitt, A. R. Gumble, L. H. Taylor, and W. S. Wallace, *Antibiot. Annu.*, **1956/57**, 722; S. O. Thomas, V. L. Singleton, J. A. Lowery, R. W. Sharpe, L. M. Pruess, J. N. Porter, J. H. Mowat, and N. Bohonos, *ibid.*, **1956/57**, 716; E. J. Backus, H. D. Tresner, and T. H. Campbell, *Antibiot. Chemother.*, **7**, 532 (1957). Review: Ref. 6, pp. 246—256.

8) F. Shafizadeh, *Adv. Carbohydr. Chem.*, **11**, 263 (1956); W. G. Overend, *Chem. Ind. (London)*, **1963**, 342; H. Grisebach, "Biosynthetic Patterns in Microorganisms and Higher Plants," Wiley-Interscience, New York, N. Y. (1967); *Helv. Chim. Acta*, **51**, 928 (1968); J. S. Brimacombe, *Angew. Chem., Int. Ed. Engl.*, **8**, 401 (1969); **10**, 236 (1971); H. Grisebach and R. Schmid, *ibid.*, **11**, 159 (1972); H. Paulsen, *Pure Appl. Chem.*, **49**, 1169 (1977); J. Yoshimura, *Yuki Gosei Kagaku Kyokai Shi*, **40**, 778 (1982).

9) For preliminary accounts of this work see: T. Sato, M. Watanabe, and R. Noyori, *Tetrahedron Lett.*, **1978**, 4403; *Chem. Lett.*, **1978**, 1297.

10) H. Bredereck, G. Simchen, S. Rebsdat, W. Kantlehner, P. Horn, R. Wahl, H. Hoffmann, and P. Gieshaber, *Chem. Ber.*, **101**, 41 (1968).

11) J. L. Imbach, *Ann. N. Y. Acad. Sci.*, **255**, 177 (1975).

12) H. Ohrui and S. Emoto, *J. Org. Chem.*, **42**, 1951 (1977).

13) 5',5'-Dimethyladenosine, a branched-chain sugar *N*-nucleoside having a tertiary 5'-hydroxyl group, was synthesized by Walton *et al.*, and its interesting biological activities were reported. R. F. Nutt and E. Walton, *J. Med. Chem.*, **11**, 151 (1968). See also: H. T. Shigeura and S. D. Sampton, *Nature*, **215**, 419 (1967).

14) For preliminary accounts of this work see: T. Sato, M. Watanabe, and R. Noyori, *Tetrahedron Lett.*, **1979**, 2897; *Heterocycles*, **14**, 761 (1980).

15) Powerful *anti*-trypanosomal property of nucleocidin[7] has stimulated interest in devising efficient methods allowing substituent incorporation at the C-4' position,[16] only very few modifications at this position have been reported.[17] To date, no reports describing 4'-arylated nucleosides have appeared.

16) I. D. Jenkins, J. P. H. Verheyden, and J. G. Moffatt, *J. Am. Chem. Soc.*, **93**, 4323 (1971).

17) J. P. H. Verheyden, I. D. Jenkins, G. R. Owen, S. D. Dimitrijevich, C. M. Richards, P. C. Srivastava, N. Le-Hong, and J. G. Moffatt, *Ann. N. Y. Acad. Sci.*, **255**, 151 (1975); G. R. Owen, J. P. H. Verheyden, and J. G. Moffatt, *J. Org. Chem.*, **41**, 3010 (1976); R. Youssefyeh, D. Tegg, J. P. H. Verheyden, G. H. Jones, and J. G. Moffatt, *Tetrahedron Lett.*, **1977**, 435; J. A. Secrist III and W. J. Winter, *J. Am. Chem. Soc.*, **100**, 2554 (1978); C. M. Richards, J. P. H. Verheyden, and J. G. Moffatt, *Carbohydr. Res.*, **100**, 315 (1982).

18) Feature of the NMR (^{1}H and ^{13}C) signal shift observed in going from 5-[(2*R*,3*R*,4*R*,5*R*)-3,4-isopropylidenedioxy-5-hydroxymethyltetrahydrofuran-2-yl]uracil[19] to the phenyl derivative **16c** are quite similar to those induced by the struc-

tural change, methyl [(2*S*,3*S*,4*R*,5*R*)-3,4-isopropylidenedioxy-5-hydroxymethyltetrahydrofuran-2-yl]acetate[20] to methyl [(2*S**,3*S**,4*S**,5*R**)-3,4-isopropylidenedioxy-5-hydroxymethyl-5-phenyltetrahydrofuran-2-yl]acetate, compatible with the assigned β stereochemistry at the anomeric carbon.

19) Prepared from pseudouridine according to the reported procedure:[21] ^{1}H NMR (dimethyl-d_6 sulfoxide) δ 1.27 and 1.49 (s, isopropylidene CH_3), 3.53 (m, CH_2OH), 3.91 (q-like, J=4.0 Hz, H_5), 4.6—5.0 (m, H_2, H_3, and H_4), 7.55 (s, =CH), 10.93 and 11.14 (br, NH); ^{13}C NMR (dimethyl-d_6 sulfoxide) δ 25.45, 27.42, 61.74, 80.30, 81.55, 83.91, 84.83, 110.40, 112.81, 140.03, 151.05, 163.27.

20) For ^{1}H and ^{13}C NMR data, see H. Ohrui, G. H. Jones, J. G. Moffatt, M. L. Maddox, A. T. Christensen, and S. K. Byram, *J. Am. Chem. Soc.*, **97**, 4602 (1975).

21) A. M. Michelson and W. E. Cohn, *Biochem.*, **1**, 490 (1962).

22) For 1′-hydroxymethylated ribonucleosides such as angustmycin A and C, see Ref. 6.

23) For a preliminary account of this work see: T. Sato and R. Noyori, *Tetrahedron Lett.*, **21**, 2535 (1980).

24) For a preliminary account of this work see: T. Sato, M. Watanabe, and R. Noyori, *Chem. Lett.*, **1980**, 679.

25) Prepared from α,α,α′,α′-tetrabromoacetone and 2,5-dimethylfuran by the aid of Zn/Ag couple in 66% yield. see T. Sato and R. Noyori, *Bull. Chem. Soc. Jpn.*, **51**, 2745 (1978).

26) Typical H_6 and H_7 chemical shifts ($CDCl_3$, δ) are: **43** (R=H), 4.53; **43** (R=H and CH_3), 4.30 and 4.51; **43** (R=H and n-C_5H_{11}), 4.33 and 4.49; **43** (R=n-C_5H_{11}), 4.30.

27) H. Bredereck, F. Effenberger, and T. Brendle, *Angew. Chem., Int. Ed. Engl.*, **5**, 132 (1966); H. H. Wasserman and J. L. Ives, *J. Org. Chem.*, **43**, 3238 (1978).

28) In the ^{1}H NMR spectrum of 5′-*O*-trityl derivatives of **46** (R=H) in $CDCl_3$, the isopropylidene methyls exhibited singlets at δ 1.32 and 1.56 ($\Delta\delta$=0.24 ppm). Its α isomer afforded the methyl signals at δ 1.27 and 1.39 ($\Delta\delta$=0.12 ppm). See C. K. Chu, I. Wempen, K. A. Watanabe, and J. J. Fox, *J. Org. Chem.*, **41**, 2793 (1976).

29) For preliminary accounts of this work see: T. Sato, H. Kobayashi, and R. Noyori, *Tetrahedron Lett.*, **21**, 1971 (1980); *Heterocycles*, **15**, 321 (1981).

30) The cyclization was carried out according to the method of Watanabe: K. A. Watanabe, U. Reichman, C. K. Chu, and J. J. Fox, "Nucleic Acid Chemistry," ed by L. B. Townsend and R. S. Tipson, Wiley-Interscience, New York, N.Y. (1978), Part 1, p. 273.

31) Introduction of methyl group to the C-2′ or C-3′ position of certain nucleosides is known to retard the enzymatic destruction, thereby increasing the biological activities markedly.[32] In addition, 2′-methylated nucleosides might be expected to minic 2′-deoxy nucleosides either by lowing the chemical activity of the 2′-hydroxy function[13] or by changing conformation of normal ribofuranosyl skeleton.

32) E. Walton, S. R. Jenkins, R. F. Nutt, M. Zimmermann, and F. W. Holly, *J. Am. Chem. Soc.*, **88**, 4524 (1966); S. R. Jenkins, B. Arison, and E. Walton, *J. Org. Chem.*, **33**, 2490 (1968).

33) J. G. Buchanan and J. C. P. Schwarz, *J. Chem. Soc.*, **1962**, 4770; J. Lehrfeld, *J. Org. Chem.*, **32**, 2544 (1967).

34) R. D. Clark and C. H. Heathcock, *J. Org. Chem.*, **41**, 636 (1976); Ref. 25.

35) E. LeGoff, *J. Org. Chem.*, **29**, 2048 (1964).

36) C. Rappe, *Acta Chem. Scand.*, **16**, 2467 (1962).

37) K. Y. Novitskiy, V. P. Volkov, L. P. Shayderova, and Y. K. Yurev, *Zh. Obshch. Khim.*, **31**, 136 (1961).

38) For this new compound, correct analytical data were not obtained. However, the spectral properties, together with the generality and straightforwardness of the synthetic route, fully support the assigned structure.

General Synthesis of Homo-*C*-nucleosides[1]

Tsuneo SATO and Ryoji NOYORI*

Department of Chemistry, Nagoya University, Chikusa-ku, Nagoya 464

(Received February 23, 1983)

Lithium aluminium hydride reduction of methyl (2,3-*O*-isopropylidene-5-*O*-trityl-β-D-ribofuranosyl)acetate gives 2-(2,3-*O*-isopropylidene-5-*O*-trityl-β-D-ribofuranosyl)ethanol. Subsequent tosylation, displacement by cyanide ion, nitrile hydrolysis, and diazomethane methylation afford methyl 3-(2,3-*O*-isopropylidene-5-*O*-trityl-β-D-ribofuranosyl)propionate. The base-promoted formylation followed by methylation with methyl iodide forms methyl 2-[(2,3-*O*-isopropylidene-5-*O*-trityl-β-D-ribofuranosyl)methyl]-3-methoxyacrylate. Base-catalyzed condensation of the methoxyacrylate and urea followed by deprotection produces 5-[(β-D-ribofuranosyl)methyl]-uracil. In a like manner, condensation of the methoxyacrylate with thiourea or guanidine gives, after deblocking, 5-[(β-D-ribofuranosyl)methyl]-2-thiouracil and 5-[(β-D-ribofuranosyl)methyl]isocytosine, respectively. Ozonolysis of the methoxyacrylate yields methyl 3-(2,3-*O*-isopropylidene-5-*O*-trityl-β-D-ribofuranosyl)pyruvate, which undergoes condensation with carbamoylmethylenetriphenylphosphorane to furnish a mixture of methyl 2-[(2,3-*O*-isopropylidene-5-*O*-trityl-β-D-ribofuranosyl)methyl]fumaramate and 2-[(2,3-*O*-isopropylidene-5-*O*-trityl-β-D-ribofuranosyl)methyl]maleimide. Deprotection of the latter leads to 2-[(β-D-ribofuranosyl)methyl]maleimide. Condensation of the keto ester with ethyl hydrazinoacetate followed by cyclization affords 3-[(2,3,*O*-isopropylidene-5-*O*-trityl-β-D-ribofuranosyl)methyl]-5-methoxycarbonyl-4-hydroxypyrazole. Ammonolysis of the methyl ester and deprotection furnishes 3-[(β-D-ribofuranosyl)methyl]-5-carbamoyl-4-hydroxypyrazole.

The naturally occurring *C*-nucleosides such as pseudouridine (**1**), showdomycin (**2**), pyrazomycin (**3**), *etc.*, have received considerable attention because of their unique structures and remarkable biological activities.[2] Derivatives of certain homonucleosides such as **4** and **5**[3] are also of importance from a biological point of view. As such we have been intrigued by the synthesis of homo-*C*-nucleosides, in which a carbon atom of the nitrogen base and C-1 atom of D-ribose are linked by a methylene unit.[4] This paper discloses an efficient method for the synthesis of this class of compounds, as exemplified by preparation of the *C*-nucleoside analogues, **6**—**8**.[5]

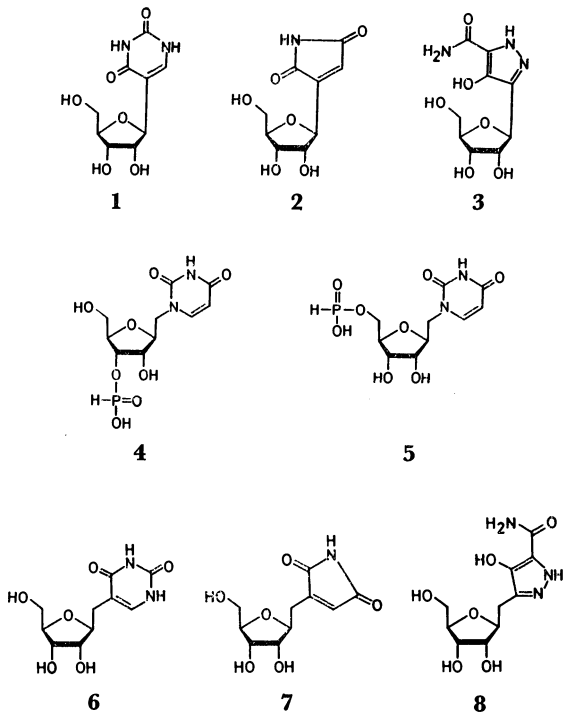

1 **2** **3** **4** **5** **6** **7** **8**

Results and Discussion

*Synthesis of Pyrimidine Homo-*C*-nucleosides.* The synthesis started from the chiral hydroxy ester **9**, which was readily obtainable from D-ribose[6] or by using the transition metal-promoted 3+4 annulation between α, α,α′,α′-tetrabromoacetone and furan as the key step.[7,8] Reduction of the tritylated derivative **10**[6] with lithium aluminum hydride in THF at −20 °C gave the alcohol **11** in 83% yield. Treatment of **11** with *p*-toluenesulfonyl chloride in pyridine gave the tosylate **12**, which was then transformed in 67% yield to the nitrile **13** by the reaction with 3 equiv of potassium cyanide and 0.1 equiv of perhydrodibenzo-18-crown-6 in acetonitrile.[9] Hydrolysis of **13** in ethylene glycol containing potassium hydroxide[10] was followed by methylation with diazomethane in ether to afford the methyl ester **14** in 32% overall yield (or 74% yield based on consumed **13**). This compound was then treated with lithium diisopropylamide in THF and methyl formate, leading to **15**, which without isolation was quenched with methyl iodide in DMF to give the *(E)*-enol ether **16**. The IR spectrum showed absorptions at 1696 and 1634 cm^{-1} characteristic of the carbonyl and olefinic functions, respectively. In the ^1H NMR spectrum, two methoxyl proton signals were observed at δ 3.69 ($COOCH_3$) and 3.75 ($=CHOCH_3$). Condensation of **16** with urea promoted by ethanolic sodium ethoxide gave the 5′-substituted uracil derivative **17** in 35% yield. The ^{13}C NMR signals of the isopropylidene methyl groups observed at δ 25.79 and 27.58 (Δδ 1.79 ppm) were consistent with the β configuration.[4c] Brief treatment of **17** with 10% methanolic hydrogen chloride furnished homopseudouridine (5-[(β-D-ribofuranosyl)methyl]uracil) (**6**).

The versatility of the intermediate **16** was demonstrated by the preparation of homo-2-thiopseudouridine (5-[(β-D-ribofuranosyl)methyl]-2-thiouracil) (**19**) and homopseudoisocytidine (5-[(β-D-ribofuranosyl)methyl]-isocytosine) (**21**). When a 1:7 mixture of **16** and thiourea was heated at reflux in ethanol containing so-

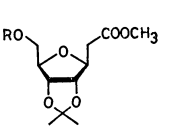

9, R=H
10, R=C(C_6H_5)$_3$

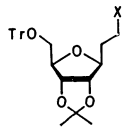

11, X=OH
12, X=OSO$_2$$C_6H_4$-*p*-$CH_3$
13, X=CN
14, X=$COOCH_3$

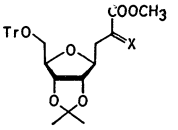

15, X=CHOLi
16, X=$CHOCH_3$-(*E*)
22, X=O
24, X=$CHCONH_2$-(*E*)
25, X=$NNHCH_2COOC_2H$

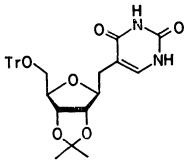

17

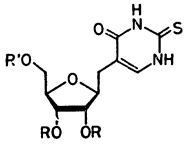

18, R-R=C(CH_3)$_2$; R′=C(C_6H_5)$_3$
19, R=R′=H

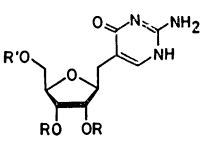

20, R-R=C(CH_3)$_2$; R′=C(C_6H_5)$_3$
21, R=R′=H (HCl salt)

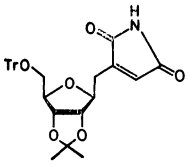

23

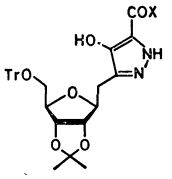

26, X=OCH_3
27, X=NH_2

dium ethoxide, the protected homo-2-thiopseudouridine **18** was produced in 68% yield. Deprotection of **18** with methanolic hydrogen chloride afforded **19**. In a like manner, cyclization of **16** with guanidine, giving **20**, followed by treatment with 10% hydrogen chloride in methanol formed the HCl salt of **21**.

Synthesis of Homoshowdomycin and Homopyrazomycin. Homoshowdomycin (2-[(β-D-ribofuranosyl)methyl]-maleimide) (**7**) and homopyrazomycin (3-[(β-D-ribofuranosyl)methyl]-5-carbamoyl-4-hydroxypyrazole) (**8**) were also prepared starting from the key intermediate **16**.

Ozonolysis of **16** in dry ethyl acetate, followed by reductive workup with dimethyl sulfide,[11] afforded the labile keto ester **22**. This compound was then subjected to the Wittig reaction with carbamoylmethylenetriphenylphosphorane[12] in dry chloroform to give a 23:77 mixture of the maleimide derivative **23** and uncyclized compound **24** having an *E* double bond (66% yield based on **16**). In the ^{13}C NMR spectrum of the β structure **23** ($CDCl_3$), signals of the isopropylidene methyl groups appeared at δ 25.53 and 27.44 ($\Delta\delta$ 1.91 ppm).[4c] The IR spectrum of **23** showed absorptions due to carbonyl functions at 1781 and 1728 cm^{-1}, and for NH at 3440 cm^{-1}. The UV spectrum revealed the presence of a typical maleimide chromophore giving an absorption at 221 nm (sh, ε 13500). The compound **24** displayed the IR absorptions at 1708 (ester carbonyl) and 1668 cm^{-1} (amide carbonyl), and 3470 and 3310 cm^{-1} (NH). The ^1H NMR spectrum of **24** showed a singlet at δ 6.97 assigned to the vinylic proton. Direct conversion of **24** to **23** was not successful. However, **24** could be subjected to recycle use, since upon ozonolysis it reverted to the keto ester **22**. Treatment of **23** with a 9:1 trifluoroacetic acid–water mixture resulted in simultaneous removal of both trityl and isopropylidene protective groups to give crystalline homoshowdomycin (**7**) in 90% yield.

When the keto ester **22** was treated with ethyl hydrazinoacetate hydrochloride and sodium acetate in a 15:20:7 mixture of methanol, THF, and water, the hydrazone **25** was obtained in 47% yield based on **16**. Cyclization of **25** using sodium methoxide in methanol gave **26** in 37% yield.[13] The UV spectrum revealed the presence of a 4-hydroxypyrazole chromophore having absorption maxima at 228 (sh, ε 14200) and 268 nm (ε 4830). Treatment of **26** with ammonia at 25 °C in methanol giving the amide **27** (59%, or 79% based on consumed starting material), followed by deprotection with a 9:1 CF_3COOH–H_2O mixture gave crystalline homopyrazomycin (**8**) in 87% yield.

Thus straightforward construction of homo-*C*-nucleosides was realized. This method is quite general and stereochemically unambiguous. Since the starting materials of type **9** can be prepared from a variety of dibromo or further brominated ketones and furan derivatives,[7,8] this procedure finds wide flexibility in the synthesis of the analogues containing a branched-chain sugar moiety.

Preliminary *in vivo* testing indicated that homoshowdomycin (**7**) has moderate inhibitory activity against S-180 in mouse (T/C=152.8%, at 20 mg/kg) and L-1210 in mouse (T/C=113%, at 20 mg/kg).

Experimental

General. All melting points are uncorrected. The IR spectra were recorded on a JASCO IRA-1 spectrometer in chloroform. The ^1H NMR spectra were obtained using a Varian HA-100D spectrometer and the ^{13}C NMR spectra

*Methyl 2-(2,3-O-Isopropylidene-5-O-trityl-β-D-ribofuranosyl)-3-methoxyacrylate (**16**).* To a solution of lithium diisopropylamide freshly prepared from diisopropylamine (1.4 ml, 10 mmol) and *n*-C_4H_9Li (1.5 mol dm^{-3} hexane solution, 7.5 ml, 11 mmol) in THF (10 ml) under argon was added a solution of **14** (2.5 g, 5 mmol) in THF (20 ml) at −78 °C. The reaction mixture was stirred at the same temperature for 30 min and to this was added methyl formate (1.5 ml, 25 mmol). After stirring at −78 °C for an additional 30 min, the mixture was warmed up to 0 °C and allowed to stand for 4 h. The resulting mixture was evaporated to dryness. The resulting residue was dissolved in 15 ml of dry DMF and treated with methyl iodide (1.5 ml, 25 mmol) at 20 °C under argon. The mixture was stirred at 20 °C for 12 h and concentration, giving a residue. This was triturated with benzene (30 ml) and washed with brine (10 ml). The aqueous layer was extracted with benzene (15 ml). The organic layer was dried (Na_2SO_4) and evaporated to give rise to a residual oil, which was subjected to chromatography on silica gel. Elution with a 30:1 benzene–ethyl acetate mixture afforded 2.41 g (90%) of **16** as a colorless syrup: R_f=0.40 (9:1 benzene–ethyl acetate); IR 1634 (C=C), 1696 cm^{-1} (C=O); ^{1}H NMR ($CDCl_3$) δ 1.30 and 1.49 (s, isopropylidene CH_3), 2.57 (m, CH_2C=), 3.15 (dd, J=5.0, 10.3 Hz, $H_{5'a}$), 3.29 (dd, J=4.8, 10.3 Hz, $H_{5'b}$), 3.69 and 3.75 (s, OCH_3), 4.11 (m, $H_{1'}$ and $H_{4'}$), 4.41 (dd, J=3.5, 6.2 Hz, $H_{2'}$), 4.42 (dd, J=4.0, 6.2 Hz, $H_{3'}$), 7.30 (m, Tr and a vinyl proton); ^{13}C NMR ($CDCl_3$) δ 25.87, 27.64, 28.75, 51.19, 61.35, 64.62, 82.75, 83.19, 83.49, 84.78, 86.79, 106.74, 113.64, 126.78, 127.00, 127.81, 128.96, 144.21, 160.32, 168.50.

*5-[(2,3-O-Isopropylidene-5-O-trityl-β-D-ribofuranosyl)methyl]uracil (**17**).* A mixture of **16** (883 mg, 1.66 mmol), urea (720 mg, 11.6 mmol), and 1 mol dm^{-3} ethanolic sodium ethoxide solution (12 ml, 12 mmol) was refluxed for 24 h under argon and evaporated under reduced pressure. The residue was taken up in 5 ml of water, neutralized with 1 mol dm^{-3} HCl, and then immediately extracted with ethyl acetate (7 ml×3). The ethyl acetate solution was dried over Na_2SO_4 and evaporated to dryness. The resulting oil was chromatographed on silica-gel plates using a 5:1 benzene–methanol mixture as an eluent. The compound **17** was obtained as a white foam. Yield was 312 mg (35%): $[\alpha]_D^{20}$ −13.7° (*c* 0.205, $CHCl_3$); R_f=0.26 (7:1 benzene–methanol); ^{1}H NMR ($CDCl_3$) δ 1.30 and 1.50 (s, isopropylidene CH_3), 2.66 (m, CH_2–uracil), 3.26 (m, $H_{5'}$), 4.13 (m, $H_{1'}$ and $H_{4'}$), 4.44 (dd, J=4.1, 6.3 Hz, $H_{2'}$), 4.62 (dd, J=3.5, 6.3 Hz, $H_{3'}$), 7.30 (m, Tr); ^{13}C NMR ($CDCl_3$) δ 25.79, 27.58, 30.26, 64.40, 82.41, 82.56, 82.91, 83.56, 84.65, 110.76, 114.42, 127.22, 127.91, 128.87, 138.72, 143.97, 152.57, 164.27; UV λ_{max} (CH_3OH) 264 nm (ε 6850). Found: C, 70.23; H, 6.23; N, 4.61%. Calcd for $C_{32}H_{32}O_6N_2$: C, 71.09; H, 5.97; N, 5.18%.

*5-[(2,3-O-Isopropylidene-5-O-trityl-β-D-ribofuranosyl)methyl]-2-thiouracil (**18**).* A mixture of **16** (535 mg, 1 mmol) and thiourea (532 mg, 7 mmol) in ethanol containing sodium ethoxide (7 ml, 7 mmol as ethoxide) was refluxed for 12 h under argon and evaporation under reduced pressure gave a residue, which was taken up in 10 ml of water, neutralized with 1 mol dm^{-3} HCl, and then extracted with ethyl acetate (20 ml, 10 ml×2). The ethyl acetate solution was dried over Na_2SO_4. Evaporation followed by chromatography on silica-gel plates using a 15:1 chloroform–methanol mixture as an eluent produced the compound **18** as a white foam (378 mg, 68%): $[\alpha]_D^{20}$ −14.1° (*c* 0.255, $CHCl_3$); R_f=0.43 (15:1 benzene–methanol); ^{1}H NMR ($CDCl_3$) δ 1.32 and 1.52 (s, isopropylidene CH_3), 2.63 (m, CH_2–2-thiouracil), 3.24 (m, $H_{5'}$), 4.16 (m, $H_{1'}$ and $H_{4'}$), 4.40 (dd, J=3.2, 6.0 Hz, $H_{2'}$), 4.60 (dd, J=3.0, 6.0 Hz, $H_{3'}$), 7.35 (m, Tr), 10.50 (br, NH); ^{13}C NMR ($CDCl_3$) δ 25.66, 27.68, 30.13, 64.33, 82.61, 82.71, 83.64, 84.50, 87.06, 114.60, 115.28, 127.11, 127.31, 127.94, 128.87, 138.63, 143.83, 144.06, 161.21, 174.93; UV λ_{max} (CH_3OH) 274 nm (ε 11400), 293 (9950). Found: *m/z*, 414.1845. Calcd for $C_{27}H_{26}O_4$: (M−(B+CH_2+H)), 414.1859.

*5-[(2,3-O-Isopropylidene-5-O-trityl-β-D-ribofuranosyl)methyl]isocytosine (**20**).* A mixture of **16** (535 mg, 1 mmol), guanidine hydrochloride (669 mg, 7 mmol), and 1 mol dm^{-3} ethanolic sodium ethoxide solution (7 ml) was refluxed for 19 h under argon. Removal of ethanol under reduced pressure left a viscous residue, which was taken up in 5 ml of water, neutralized with 1 mol dm^{-3} HCl, and then extracted with ethyl acetate (20 ml×3). After drying over Na_2SO_4, the organic solution was evaporated and subjected to preparative TLC on silica gel using a 15:1 benzene–methanol mixture as an eluent, giving the compound **20** as a white foam (350 mg, 65%): $[\alpha]_D^{20}$ −2.08° (*c* 0.24, CH_3OH); R_f=0.26 (7:1 benzene–methanol); ^{1}H NMR (dimethyl-d_6 sulfoxide) δ 1.20 and 1.37 (s, isopropylidene CH_3), 2.41 (m, CH_2–isocytosine), 3.06 (m, $H_{5'}$), 3.95 (m, $H_{1'}$ and $H_{4'}$), 4.47 (m, $H_{2'}$ and $H_{3'}$), 6.57 (br, NH_2), 7.40 (m, Tr), 11.00 (br, NH); ^{13}C NMR (dimethyl-d_6 sulfoxide) δ 25.45, 27.28, 31.10, 64.40, 81.66, 82.70, 83.91, 86.13, 110.24, 113.11, 126.95, 127.80, 128.28, 143.65, 155.22, 163.02; UV λ_{max} (CH_3OH) 293 nm (ε 10300). Found: C, 71.85; H, 6.12; N, 7.06%. Calcd for $C_{32}H_{33}O_5N_3$: C, 71.22; H, 6.16; N, 7.79%.

*5-[(β-D-Ribofuranosyl)methyl]uracil (Homopseudouridine) (**6**).* A mixture of **17** (100 mg, 0.185 mmol) and 10% methanolic hydrogen chloride solution (3 ml) was stirred at 20 °C for 40 min. The solvent was evaporated *in vacuo* to give a syrup which was triturated with 2 ml of ether three times. The title compound **6** (44.4 mg, 93%) was obtained as a white powder: mp 184—186 °C; $[\alpha]_D^{20}$ −8.15° (*c* 0.135, CH_3OH); ^{1}H NMR (dimethyl-d_6 sulfoxide) δ 2.36 (m, CH_2–uracil), 3.43 (m, $H_{5'}$), 3.62 (m, $H_{1'}$ and $H_{4'}$), 3.74 (m, $H_{2'}$ and $H_{3'}$), 3.1—4.9 (br, OH), 7.27 (m, H_6), 10.69 and 11.00 (br, NH); ^{13}C NMR (dimethyl-d_6 sulfoxide) δ 30.06 (CH_2–uracil), 62.00 ($C_{5'}$), 71.11, 74.33, 81.10, 84.09 ($C_{1'}$—$C_{4'}$ of ribose), 127.79, 139.14, 151.23, 164.60; UV λ_{max} (CH_3OH) 265 nm (ε 7130), λ_{max} (1 mol dm^{-3} HCl) 266 nm (ε 7080), λ_{max} (1 mol dm^{-3} NaOH) 285 nm (ε 7100).[15]

*5-[(β-D-Ribofuranosyl)methyl]-2-thiouracil (Homo-2-thiopseudouridine) (**19**).* A mixture of **18** (300 mg, 0.539 mmol) and 10% methanolic hydrogen chloride solution (3 ml) was stirred at 20 °C for 40 min. The solvent was evaporated *in vacuo* to give a syrup which was triturated with 3 ml of ether three times. The compound **19** was obtained as a white powder (133 mg, 90%). ^{1}H NMR (dimethyl-d_6 sulfoxide) δ 2.41 (m, CH_2–2-thiouracil), 3.42 (m, $H_{5'}$), 3.61 (m, $H_{1'}$ and $H_{4'}$), 3.76 (m, $H_{2'}$ and $H_{3'}$), 4.03 (br, OH), 7.31 (m, H_6), 12.17 and 12.36 (br, NH); ^{13}C NMR (dimethyl-d_6 sulfoxide) δ 30.12 (CH_2–2-thiouracil), 61.65 ($C_{5'}$), 70.86, 74.15, 80.14, 83.96 ($C_{1'}$—$C_{4'}$ of ribose), 114.49, 139.08, 161.45, 174.42; UV λ_{max} (CH_3OH) 216, 277, 290 nm (sh), λ_{max} (1 mol dm^{-3} HCl) 216, 277, 290 nm (sh), λ_{max} (1 mol dm^{-3} NaOH) 222, 261, 290 nm. This compound was so hygroscopic that optical extinction (ε value) could not be obtained.[15]

*5-[(β-D-Ribofuranosyl)methyl]isocytosine Hydrochloride (Homopseudoisocytidine Hydrochloride) (**21**).* A mixture of **20** (125 mg, 0.232 mmol) and 10% methanoli chydrogen chloride solution (3 ml) was stirred at 20 °C for 50 min. Concentration *in vacuo* gave a white solid which was coeva-

porated with ethanol (2 ml×3). The residue was triturated three times with 5 ml of ether. The compound **21** was obtained as a white powder (62 mg, 91%): mp 185—188 °C; $[\alpha]_D^{20}$ −48.9° (*c* 0.37, CH_3OH); ^1H NMR (dimethyl-d_6 sulfoxide) δ 2.47 (m, CH_2–isocytosine), 3.44 (m, $H_{5'}$), 3.64 (m, $H_{1'}$ and $H_{4'}$), 3.80 (m, $H_{2'}$ and $H_{3'}$), 3.8—5.0 (br, OH), 7.59 (s, H_6), 8.49 (br, NH_2); ^{13}C NMR (dimethyl-d_6 sulfoxide) δ 29.85 (CH_2–isocytosine), 61.79 ($C_{5'}$), 71.00, 74.23, 80.07, 84.30 ($C_{1'}$—$C_{4'}$ of ribose), 113.82, 138.05, 152.28, 160.27; UV λ_{max} (CH_3OH) 224 (ε 11500), 263 nm (7830), λ_{max} (1 mol dm^{-3} HCl) 223 (ε 12300), 264 nm (9420), λ_{max} (1 mol dm^{-3} NaOH) 232 (ε 11300), 281 nm (9100). Found: C, 40.27; H, 5.46; N, 13.60%. Calcd for $C_{10}H_{16}O_5N_3Cl\cdot 0.5H_2O$: C, 39.91; H, 5.63, N, 13.96%.

*2-[(2,3-O-Isopropylidene-5-O-trityl-β-D-ribofuranosyl)methyl]-maleimide (**23**).* A solution of olefinic ester **16** (1.07 g, 2 mmol) in 20 ml of dry ethyl acetate was treated with ozone at −78 °C. After dry nitrogen was blown through the solution to remove excess ozone, dimethyl sulfide (1.47 ml, 20 mmol) was added.[11] The mixture was stirred at −78 °C for 1 h, then at 0 °C for 1 h, finally at 25 °C for 1 h. The mixture was evaporated to give methyl 3-(2,3-*O*-isopropylidene-5-*O*-trityl-β-D-ribofuranosyl)pyruvate (**22**) as a colorless syrup. This material displayed no olefinic absorption in the IR spectrum. To a solution of the crude product in 15 ml of dry chloroform was added a solution of 829 mg (2.6 mmol) of carbamoylmethylenetriphenylphosphorane[12] in 10 ml of dry chloroform. The yellow solution was stirred at 25 °C for 30 min. Evaporation followed by chromatography on a silica-gel column with a 10:1 benzene–ethyl acetate mixture as an eluent gave **23** (162 mg, 15%). Elution with a 3:1 benzene–ethyl acetate mixture gave methyl 2-[(2,3-*O*-isopropylidene-5-*O*-trityl-β-D-ribofuranosyl)-methyl]fumaramate (**24**) (564 mg, 51%). **23**: $[\alpha]_D^{20}$ −7.1° (*c* 0.14, $CHCl_3$); R_f=0.46 (3:1 benzene–ethyl acetate); IR 3440 (NH), 1781 and 1728 cm^{-1} (C=O); ^1H NMR ($CDCl_3$) δ 1.34 and 1.54 (s, isopropylidene CH_3), 2.79 (m, CH_2–maleimide), 3.20 (dd, J=4.8, 10.5 Hz, $H_{5'a}$), 3.35 (dd, J=4.0, 10.5 Hz, $H_{5'b}$), 4.18 (m, $H_{1'}$ and $H_{4'}$), 4.45 (dd, J=4.9, 6.1 Hz, $H_{2'}$), 4.67 (dd, J=3.5, 6.1 Hz, $H_{3'}$), 6.51 (m, H_3), 7.30 (m, Tr), 7.94 (br, NH); ^{13}C NMR ($CDCl_3$) δ 25.53, 27.44, 29.34, 64.03, 81.96, 82.26, 83.47, 84.55, 86.74, 114.56, 127.09, 127.81, 128.59, 129.32, 143.63, 146.39, 171.09; UV λ_{max} (CH_3OH) 221 nm (sh, ε 13500). Found: C, 73.42; H, 6.17; N, 2.67%. Calcd for $C_{32}H_{31}O_6N$; C, 73.12; H, 5.95; N, 2.67%. **24**: $[\alpha]_D^{20}$ −1.6° (*c* 0.32, $CHCl_3$); R_f= 0.24 (3:1 benzene–ethyl acetate); IR 3470 and 3310 (NH), 1708 and 1668 cm^{-1} (C=O); ^1H NMR ($CDCl_3$) δ 1.32 and 1.52 (s, isopropylidene CH_3), 2.87 (dd, J=9.1, 13.1 Hz, $H_aH_bCC{=}C$), 3.11 (dd, J=5.0, 13.1 Hz, $H_aH_bCC{=}C$), 3.24 (dd, J=3.6, 12.8 Hz, $H_{5'a}$), 3.38 (dd, J=4.2, 12.8 Hz, $H_{5'b}$), 3.74 (s, OCH_3), 4.07 (m, $H_{1'}$ and $H_{4'}$), 4.45 (dd, J=5.0, 6.2 Hz, $H_{2'}$), 4.64 (dd, J=4.8, 5.0 Hz, $H_{3'}$), 6.44 (br, NH), 6.97 (s, $=CHCONH_2$), 7.30 (m, Tr); ^{13}C NMR ($CDCl_3$) δ 25.69, 27.57, 32.24, 51.34, 63.39, 81.64, 82.59, 83.17, 84.25, 87.03, 114.91, 127.29, 127.94, 128.72, 134.00, 135.03, 143.56, 167.08, 167.14. Found: C, 71.34; H, 6.13; N, 2.40%. Calcd for $C_{33}H_{35}O_7N$: C, 71.06; H, 6.33; N, 2.51%.

*2-[(β-D-Ribofuranosyl)methyl]maleimide (Homoshowdomycin) (**7**).* A mixture of **23** (203 mg, 0.387 mmol) and 9:1 CF_3COOH–H_2O (2 ml) was stirred at 25 °C for 45 min. Evaporation followed by chromatography on silica-gel plates with a 1:1 ethyl acetate–acetone mixture as an eluent afforded 85 mg (90%) of **7** as a white powder which was recrystallized from acetone–benzene: mp 150—154 °C; $[\alpha]_D^{20}$ −24° (*c* 0.20, CH_3OH); R_f=0.38 (1:1 acetone–ethyl acetate); ^1H NMR (acetone-d_6) δ 2.70 (m, CH_2–maleimide), 3.36 (m, $H_{5'}$), 3.82 (m, $H_{1'}$ and $H_{4'}$), 4.16 (m, $H_{2'}$ and $H_{3'}$), 4.0—5.0 (br, OH), 6.56 (m, H_3), 9.52 (br, NH); ^{13}C NMR (acetone-d_6) δ 61.36 ($C_{5'}$), 70.68, 74.39, 80.10, 84.30 ($C_{1'}$—$C_{4'}$ of ribose), 146.41, 173.32, CH_2–maleimide obscured by acetone peaks; UV λ_{max} (CH_3OH) 221 nm (ε 10200).[15]

*Preparation of **25**.* A mixture of **22** (from 2 mmol of **16**), ethyl hydrazinoacetate hydrochloride (620 mg, 4 mmol), and sodium acetate (328 mg, 4 mmol) in THF–CH_3OH–H_2O (15 ml, 20 ml, and 7 ml, respectively) was stirred at 25 °C for 12 h. After removal of the solvent, 50 ml of chloroform was added. The solution was dried over Na_2SO_4 and evaporated to dryness. The crude product was purified by chromatography on a column of silica gel using a 9:1 benzene–ethyl acetate mixture. Yield was 585 mg (47% based on **16**): R_f=0.24 (9:1 benzene–ethyl acetate); IR 3270 (NH), 1740 and 1703 cm^{-1} (C=O); ^1H NMR ($CDCl_3$) δ 1.12—1.50 (m, 3H), 1.29 and 1.51 (s, isopropylidene CH_3), 2.6—3.4 (m, 4H), 3.46 and 3.71 (s, OCH_3, 1:3 ratio), 3.9—4.7 (m, 8H), 7.4 (m, Tr).

*3-[(2,3-O-Isopropylidene-5-O-trityl-β-D-ribofuranosyl)methyl]-5-methoxycarbonyl-4-hydroxypyrazole (**26**).* To a solution of **25** (616 mg, 1 mmol) in 10 ml of methanol was added a 1 mol dm^{-3} methanolic sodium methoxide solution (4 ml). The solution was refluxed for 4.5 h and evaporated under reduced pressure.[13] The residue was taken up in 3 ml of water, neutralized with 1 mol dm^{-3} HCl, and then extracted with ethyl acetate (30 ml×3). The organic solution was dried (Na_2SO_4) and evaporated to dryness. The residue was purified by chromatography on a column of silica gel using a 3:1 benzene–ethyl acetate mixture. Compound **26** was obtained as a white foam (210 mg, 37%): $[\alpha]_D^{19}$ −24° (*c* 0.23, $CHCl_3$); R_f=0.31 (3:1 benzene–ethyl acetate); IR 3580—3200 (NH and OH), 1698 cm^{-1} (C=O); ^1H NMR ($CDCl_3$) δ 1.35 and 1.54 (s, isopropylidene CH_3), 2.92 (dd, J=7.3, 15.9 Hz, CH_aH_b–pyrazole), 3.15 (dd, J=4.6, 15.9 Hz, CH_aH_b–pyrazole), 3.25 (dd, J=5.0, 10.5 Hz, $H_{5'a}$), 3.41 (dd, J=4.0, 10.5 Hz, $H_{5'b}$), 3.95 (s, OCH_3), 4.12 (m, $H_{1'}$ and $H_{4'}$), 4.56 (m, $H_{2'}$ and $H_{3'}$), 7.32 (m, Tr); ^{13}C NMR ($CDCl_3$) δ 25.71, 27.56, 28.24, 51.74, 64.26, 82.39, 83.55, 83.87, 84.06, 87.14, 114.63, 127.21, 127.94, 128.82, 143.39, 143.84, 163.29; UV λ_{max} (CH_3OH) 228 nm (sh, ε 14200), 268 (4830). Found: C, 69.76; H, 6.18; N, 4.62%. Calcd for $C_{33}H_{34}O_7N_2$: C, 69.46; H, 6.01; N, 4.91%.

*3-[(2,3-O-Isopropylidene-5-O-trityl-β-D-ribofuranosyl)methyl]-5-carbamoyl-4-hydroxypyrazole (**27**).* A solution of the pyrazole **26** (320 mg, 0.575 mmol) in dry methanol (10 ml) was saturated with ammonia by passing the gas at 0 °C. The mixture was stirred at 25 °C for 4 d. The solvent was evaporated and the crude product was purified by chromatography on a column of silica gel using a 3:1 to 1:1 benzene–ethyl acetate mixture as an eluent to give a foam (184 mg, 59%): $[\alpha]_D^{19}$ −25° (*c* 0.20, $CHCl_3$); R_f=0.25 (1:1 benzene–ethyl acetate); IR 3580—3200 (NH and OH), 1675 cm^{-1} (C=O); ^1H NMR ($CDCl_3$) δ 1.30 and 1.50 (s, isopropylidene CH_3), 2.87 (dd, J=7.9, 15.1 Hz, CH_aH_b–pyrazole), 3.19 (dd, J=3.5, 15.1 Hz, CH_aH_b–pyrazole), 3.21 (dd, J=5.5, 10.3 Hz, $H_{5'a}$), 3.46 (dd, J=3.2, 10.3 Hz, $H_{5'b}$), 4.22 (m, $H_{1'}$ and $H_{4'}$), 4.49 (m, $H_{2'}$ and $H_{3'}$), 5.97 and 6.67 (br, NH_2), 7.30 (m, Tr), 8.03 (br, NH and OH); ^{13}C NMR ($CDCl_3$) δ 25.52, 27.43, 28.22, 64.13, 82.05, 83.68, 83.86, 84.08, 87.24, 114.90, 127.21, 127.82, 128.75, 141.40, 143.66, 164.29; UV λ_{max} (CH_3OH) 227 nm (sh, ε 14300), 268 (5100). Found: C, 69.37; H, 6.20; N, 7.57%. Calcd for $C_{32}H_{33}O_6N_3$: C, 69.17; H, 5.98; N, 7.56%. In addition, the unreacted **26** was recovered (77 mg, 25%).

3-[(β-D-Ribofuranosyl)methyl]-5-carbamoyl-4-hydroxypyrazole

(Homopyrazomycin) (8). A mixture of **27** (220 mg, 0.407 mmol) and 9:1 CF_3COOH–H_2O (4 ml) was stirred at 25 °C for 20 min. Concentration and subsequent chromatography on silica-gel plates using a 6:1:2:1 ethyl acetate–acetone–methanol–water mixture as an eluent yielded compound **8** as a white powder (128 mg, 87%) which was recrystallized from methanol–ethyl ether: mp 109—113 °C; $[\alpha]_D^{21}$ −22° (*c* 0.23, CH_3OH); R_f=0.24 (6:1:1:1 ethyl acetate–acetone–methanol–water); ^{1}H NMR (D_2O)[16] δ 3.01 (m, CH_2–pyrazole), 3.73 (m, $H_{5'}$), 3.90—4.30 (m, $H_{1'}$, $H_{2'}$, $H_{3'}$, and $H_{4'}$); ^{13}C NMR (D_2O)[16] δ 30.38 (CH_2–pyrazole), 64.82 ($C_{5'}$), 74.25, 77.20, 84.80, 86.78 ($C_{1'}$—$C_{4'}$ of ribose), 132.31, 169.22; UV λ_{max} (H_2O) 223 (ε 8630), 266 nm (5150), λ_{max} (0.1 mol dm^{-3} NaOH) 235 (ε 4330), 311 nm (5460).[15]

*Conversion of **24** to **23**.* To a solution of the unsaturated amide **24** (557 mg, 1 mmol) in 15 ml of dry ethyl acetate was passed ozone at −78 °C. Dry nitrogen was bubbled through the solution to remove excess ozone, and dimethyl sulfide (0.73 ml, 10 mmol) was added.[11] The mixture was stirred at −78 °C for 1 h, then at 0 °C for 1 h, finally at 25 °C for 1 h. Evaporation left a crude product, which was dissolved in 7 ml of dry chloroform and to this was added a solution of 415 mg (1.30 mmol) of carbamoylmethylenetriphenylphosphorane[12] in 3 ml of dry chloroform. The reaction mixture was stirred at 25 °C for 30 min and evaporated to dryness. The oily residue was chromatographed on a column of silica gel. Elution with a 3:1 benzene–ethyl acetate mixture gave **23** (67 mg, 13%). Continued elution with a 3:1 benzene–ethyl acetate mixture gave **24** (276 mg, 50%). Compounds **23** and **24** were identical in all respects with the authentic samples.

We thank Miss Keiko Marunouchi for her valuable contribution in some preliminary experiments. We are also indebted to Ajinomoto Co., Ltd. for a generous offer of D-ribose and for biological assay.

References

1) *C*-Nucleoside Synthesis. 20. For part 19 see: T. Sato, M. Watanabe, H. Kobayashi, and R. Noyori, *Bull. Chem. Soc. Jpn.*, **56**, 2680 (1983).

2) Showdomycin (**2**) shows quite significant antibacterial and antitumor activities. Pyrazomycin (**3**) is a potent antiviral agent. Pseudouridine (**1**) is a component of tRNA. Reviews: R. J. Suhadolnik, "Nucleoside Antibiotics," Wiley-Interscience, New York, N.Y. (1970), Chaps 9 and 10; P. Roy-Burman, "Analogues of Nucleic Acid Components," Springer-Verlag, New York, N.Y. (1970); S. Nakamura and H. Kondo, *Heterocycles*, **8**, 583 (1977); L. Goodman, "Basic Principles in Nucleic Acid Chemistry," ed by P. O. P. Ts'o, Academic Press, New York (1974), Vol. 1, p. 93; G. D. Daves, Jr. and C. C. Cheng, *Prog. Med. Chem.*, **13**, 303 (1976); S. Hanessian and A. G. Pernet, *Adv. Carbohydr. Chem. Biochem.*, **33**, 111 (1976); S. D. Gero, J. Cleophax, D. Mercier, and A. Olesker, "Synthetic Methods for Carbohydrates," ed by H. S. Khadem, American Chemical Society, Washington, D.C. (1976), p. 64; Y. Mizuno, O. Mitsunobu, and T. Hata, "Synthesis of Nucleosides and Nucleotides," Maruzen, Tokyo (1977), pp. 16—32; T. Sato and R. Noyori, *Kagaku (Chemistry)*, **33**, 74 (1978); K. Galankievicz, *Khim. Geterotsikl. Soedin.*, **1978**, 723; S. R. James, *J. Carbohydr. Nucleosides, Nucleotides*, **6**, 417 (1979); H. Ogura and H. Takahashi, *Yuki Gosei Kagaku Kyokai Shi.*, **38**, 756 (1980); T. Sato and R. Noyori, *ibid.*, **38**, 862, 947 (1980); M. Ohno, "Anticancer Agents Based on Natural Product Models," ed by J. M. Cassady and J. D. Douros, Academic Press, New York, N.Y. (1980), p. 73.

3) M. Bobek, J. Farkas, and F. Sorm, *Collect. Czech. Chem. Commun.*, **34**, 1684 (1969); A. Holy, *ibid.*, **35**, 81 (1970).

4) The term, homo-*C*-nucleoside, was first suggested by Gensler.[4a] Only two investigations dealt with the synthesis of these nucleosides. a) W. J. Gensler, S. Chan, and D. B. Bell, *J. Am. Chem. Soc.*, **97**, 436 (1976); b) *J. Org. Chem.*, **46**, 3407 (1981); c) J. A. Secrist III, *ibid.*, **43**, 2925 (1978).

5) A part of this work was reported in preliminary forms: T. Sato, K. Marunouchi, and R. Noyori, *Tetrahedron Lett.*, **1979**, 3669; T. Sato and R. Noyori, *Heterocycles*, **13**, 141 (1979).

6) H. Ohrui, G. H. Jones, J. G. Moffatt, M. L. Maddox, A. T. Christensen, and S. K. Byram, *J. Am. Chem. Soc.*, **97**, 4602 (1975).

7) Reviews: R. Noyori, *Ann. N.Y. Acad. Sci.*, **295**, 225 (1977); *Acc. Chem. Res.*, **12**, 61 (1979); R. Noyori and Y. Hayakawa, *Org. React.*, **29**, 163 (1983).

8) a) R. Noyori, T. Sato, and Y. Hayakawa, *J. Am. Chem. Soc.*, **100**, 2561 (1978); b) T. Sato, R. Ito, Y. Hayakawa, and R. Noyori, *Tetrahedron Lett.*, **1978**, 1829.

9) J. W. Zubrick, B. I. Dunbar, and H. D. Durst, *Tetrahedron Lett.*, **1975**, 71.

10) C.-T. Peng and T. C. Daniel, *J. Am. Chem. Soc.*, **77**, 6682 (1955).

11) J. J. Pappas, W. P. Keaverey, E. Gancher, and M. Berger, *Tetrahedron Lett.*, **1966**, 4273.

12) S. Trippett and D. M. Walker, *J. Chem. Soc.*, **1959**, 3874; G. Trummlitz, D. B. Repke, and J. G. Moffatt., *J. Org. Chem.*, **40**, 3352 (1975).

13) The cyclization was carried out according to the method of G. Just and S. Kim, *Can. J. Chem.*, **55**, 427 (1977).

14) J. G. Buchanan and J. C. P. Schwarz, *J. Chem. Soc.*, **1962**, 4770; J. Lehrfeld, *J. Org. Chem.*, **32**, 2544 (1967).

15) Correct analytical data were not obtained for this nucleoside. However, the secure structural proof was gained at the stage of the precursory acetonide.

16) Sodium 3-(trimethylsilyl)propionate-d_4 (TSP) was used as an internal standard.

Electron Microscope Studies on Radiography. III.[1,2] Formation of Lumpish Developed Silver in Radiography

Hiroshi HARA

Tokyo Metropolitan Isotope Research Center, Fukazawa, Setagaya-ku, Tokyo 158

(Received October 27, 1982)

The shape of developed silver in industrial X-ray films exposed to a high energy radiation has been found mainly lumpish, which differs from the filamentary shape observed in ordinarily-developed photographic films. The formation process and crystalline states of lumpish silver were studied with an electron microscope in comparison with those of filamentary silver. Lumpish silver cannot be in a single uniform crystalline state under a kind of hindrance due to too active a development for regular crystal growth, the thickness of emulsion layer and the concentration of silver halide also have some effects.

It has been thought[3] that the developed silver of photographic film has a filamentary structure (Fig. 1) in normal development and that the reduced silver grows on development nuclei. However, according to the author's observation, the develoed silver in industrial X-ray film has a shape to be called "lumpish" (Fig. 2) and grows at sites apart from development nuclei. On the shape and the formation process for such silver, no paper has been reported with discrimination from ordinary ones.[3] To make clear the development characteristics of industrial X-ray film, the difference between the structures of lumpish and filamentary silvers and their formation conditions were studied.

Many electron microscopic studies on developed silver have been reported, and a lot of morphologic knowledge on developed silver is available. We also applied a transmission type electron microscope for this stuby. This equipment was also applied for an electron diffraction study to analyze the crystal structure and crystalline state of developed silver.

Fig. 1. An electron micrograph of developed silver in FUJI NEOPAN SS film developed with FUJIDOL. Crystalline state of the silver correspond to Figs. 4B—D.

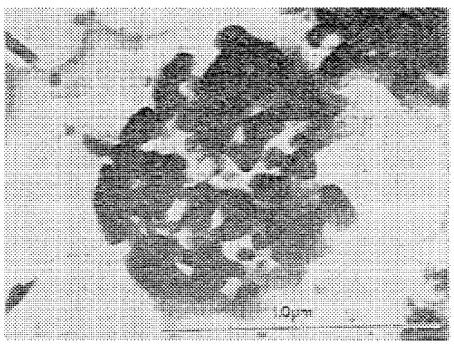

Fig. 2. An electron micrograph of developed silver in SAKURA RR industrial X-ray film developed with KONIDOL-X. Crystalline state of the silver correspond to Figs. 4B—G.

Many experimental methods which appeared in the past were carried out mostly under special conditions, *i.e.*, by using diluted monodispersed emulsion or by using partial development with a particular developer. These experiments disclosed that the tubic, Mueller's type developed silver[5] is formed in the dilute monodispersed emulsion layer and very thick filamentary silver[4] is formed via a particular physical development. These developed silvers are not observed in the conventional development. Therefore, in this study, the author has carried out an experiment by using commercial films under the ordinary conditions, *i.e.*, by exposing and developing them according to manufacturer's instruction, and the morphological variation of silver has been systematically observed in course of development.

Although the crystal structure of developed silver has already been determined by some workers, no information has been supplied of the structure of developed silver in course of development. In this study, therefore, the variation of the crystalline state of silver during development has also been traced systematically by the electron diffraction method.

Experimental

Specimens for electron micrscopic observation were prepared from several strips of Sakura RR industrial X-ray film in the following procedure. Test film strips were exposed uniformly to 150 kVp X-ray beam of optimum dose, 0.2 R (5.16×10^{-5} C/kg), and developed for 10, 30, 60, 90, 120, 150, 180, 240, or 300 s with Konidol-X, the commercial developer for Sakura industrial X-ray film. The specimens were prepared[6] from developed and stop-bathed, but not fixed, film strips. The degree of the degradation of gelatin in emulsion layer with enzyme which allows silver halide particles to be isolated, was controlled so that deformation of developed silver might be prevented. The rotation speed of the centrifuge used for washing silver and silver halide particles was also controlled so as to be kept as low as 800 rpm for the same purpose. The finished specimens were observed with a JEM Type-100 transmission electron micrscope, and morphological and crystallographical variations of silver in every step of development were studied. Magnifying powers of 5000—60 000 were applied according to the size of silver and silver halide particles

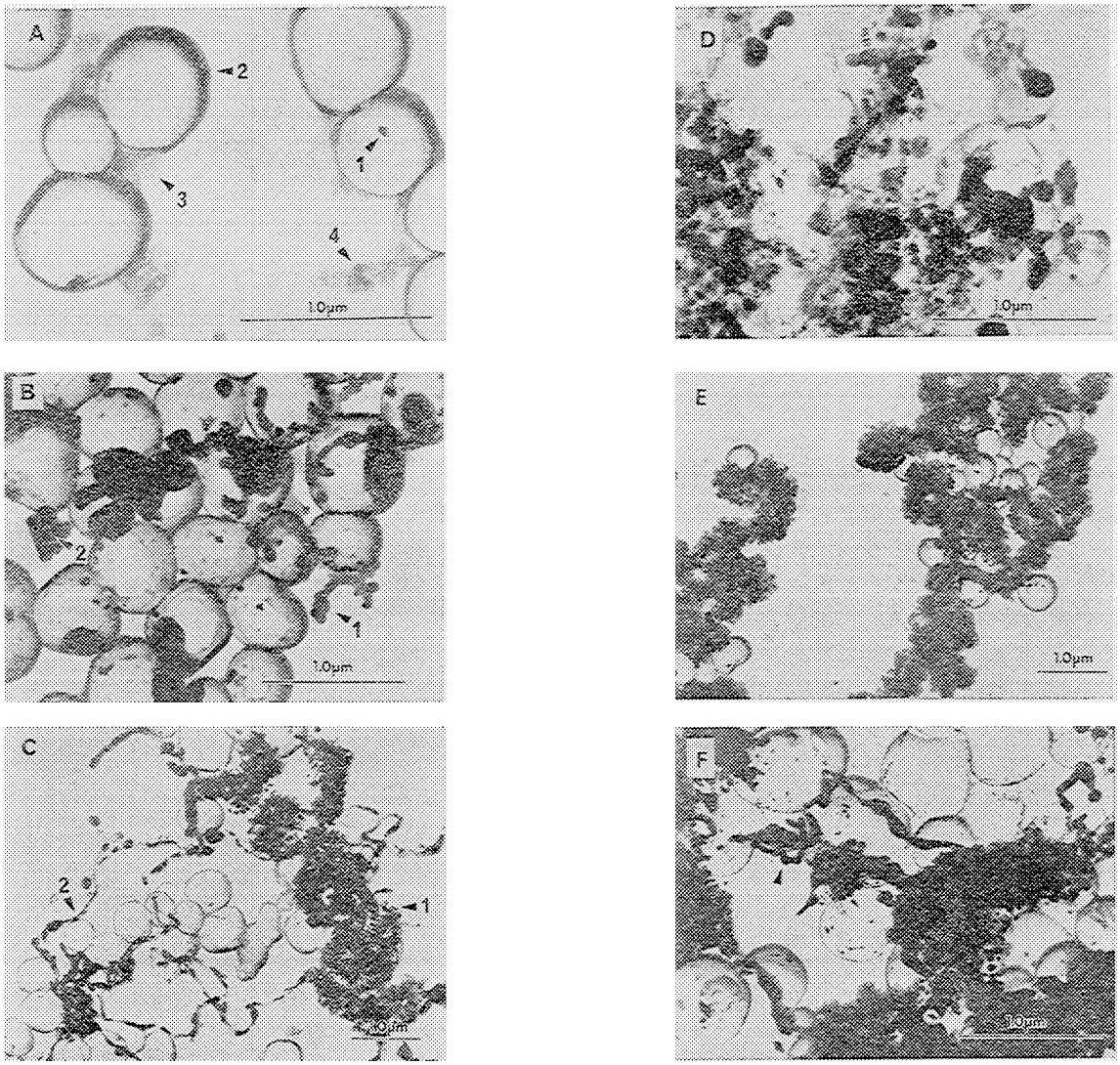

Fig. 3A—F. Variation of shape and crystalline state of the developed silver in SAKURA RR industrial X-ray film exposed to 150 kVp X-ray is developed for various times with KONIDOL-X.
Figs. A and B are for developed 30 s, Fig. C for 60 s, and Figs. D—F for 150 s respectively. Figs. A and B correspond to Figs. 4A and 4B, Fig. C to Figs. 4B—D, and Figs. D—F to Figs. 4B—G respectively.

and the electron diffraction apparatus equipped with the JEM Type-100 electron microscope was used for the measurement[7] of crystalline states of silver.

The formation process of filamentary silver, whose shape is well known as a general one, was also studied by the same method as used for lumpish silver, and the difference between these processes has been studied. The specimens for filamentary silver were prepared from Fuji Neopan SS (fine grain panchromatic negative film), uniformly exposed to sunlight, and developed for 30, 60, 90, 120, 150, 180, 240, 300, or 420 s with Fujidol, the commercial developer for Fuji Neopan SS.

Furthermore, factors influencing the shape of silver were also studied on other types of photographing materials by changing exposure and development conditions. These materials include Fuji 150 industrial X-ray, Sakura Konipan SS, Fuji Minicopy HR II, Sakura Color III, and Sakura NR-M2 nuclear liquid emulsion. For Sakura RR, Fuji Neopan SS, and Sakura NR-M2, some special materials were also prepared for which the concentration of silver halide and the thickness of emulsion layer were modified after decomposing film emulsion with enzyme. These materials were used for studying the relation between the shape of silver and the physical constitution of film material. All the materials were exposed to 150 kVp X-ray or to sunlight for studying the influence of radiation. Two type of developers, Konidol-X as an active developer and Fujidol as a moderate one, were used. Each developer was diluted so as to have a concentration of 100, 50, 25, 10, 5, 2, or 1% with water for studying the influence of developing conditions. The microscopic procedures used for these materials were the same as those for Sakura RR film used to observe lumpish silver, and the shape and crystalline state of silver on each material were studied at various stages of development.

Results and Discussion

The change in the shape of silver observed in the conventional development process of Sakura RR film is shown in Figs. 3A—F, and the change in the crystalline state of silver accompanying that in the shape is shown in Figs. 4A—H by electron diffraction patterns. The pattern of Fig. 4A indicates that the silver is in an amorphous state since it has no diffraction dot. Ac-

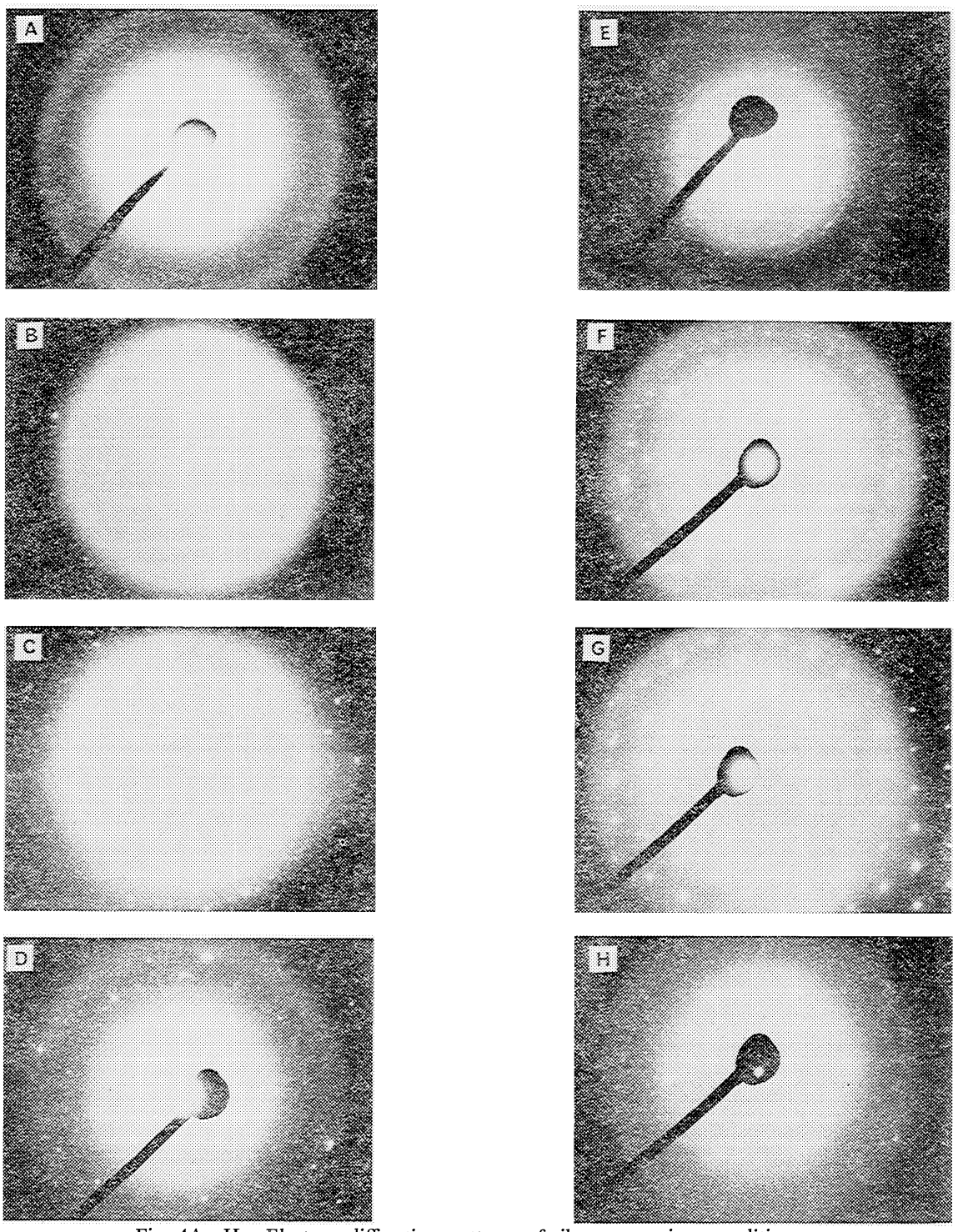

Fig. 4A—H. Electron diffraction patterns of silver on various conditions.
A: Amorphous, B—G: Progress of crystallization, H: Big crystal.

cording to the patterns of Figs. 4B—D, some crystallites are generated in the amorphous silver because some dots are found in the field. The increase in the number of dots means the increase in the amount of crystallites to be due to the progress of the crystallization of silver. The patterns of "Debye-Scherrer ring" in Figs. 4E and F indicate that almost all silver is finely crystallized in crystallites. The pattern in Fig. 4 G indicates a crystal growth of silver from a fine to coarse state. The pattern of "Laue" in Fig. 4 H indicates that the silver takes a structure of single crystal, and the Laue pattern of hexagon indicates that the crystal structure of developed silver is a face-centered cubic lattice.[7]

Several different shapes of developed silver are found in the early stage of development, *i,e.*, at 30 s development time, pointlike (Fig. 3A-1), bandlike (3A-2), and mistlike (3A-3) which are amorphous (Fig. 4A), and dendrite (3B-1). It seems that the mistlike silver will emerge from the silver-gelatin (complex) envelope[8] which is covering the silver halide particles (Fig. 3A-3

and -4). The mistlike silver thus having emerged then aggregates (Fig. 3B-2) as the amount of reduced silver increases and the crystallization progresses slightly (Fig. 4B). A further crystallization of aggregate silver was observed in the middle stage of development, *i.e.*, at 60 s, (Figs. 3C-1 and 4B—D). In the later stage of development, *i.e.*, at 150—300 s, the developed silver turned lumpish because of rapid progresses of aggregation and crystallization (Figs. 3D and 3E). The crystalline state of lumpish silver is complicated because the electron diffraction patterns obtained for several parts of the same lumpish silver are not the same (Figs. 4B—G). This means that the lumpish silver is produced as the result of a disorderly progress of crystallization.

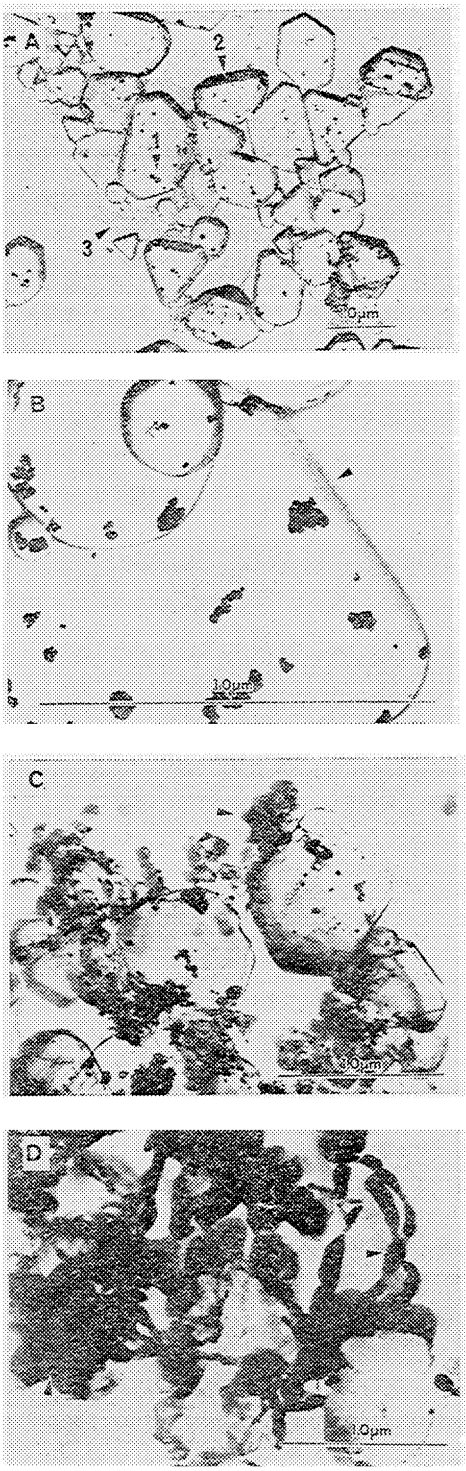

Fig. 5A—D. Variation of shape and crystalline state of the developed silver in FUJI NEOPAN SS film exposed to sunlight and developed for various times with FUJIDOL.
Figs. A and B are for developed 30 s, Fig. C for 60 s, and Fig. D for 150 s respectively. Figs. A and B correspond to Fig. 4A, Fig. C to Figs. 4A and 4B, Fig. D to Figs. 4B—D respectively.

Silver particles other than lumpish shape, such as dendritic, tubular, filamentary and pointlike ones, have also been found in a slight amount on Sakura RR film fully developed. The tubular silver generated in and after the middle stage of development is similar in shape to the silver which has been found by Mueller[5] (Fig. 3C-2), and their crystallization degrees are almost the same as that of the aggregate silver (Figs. 4B—D). A filamentary silver was also found in a somewhat unusual shape (Figs. 3F and 4B—D). The size and number of pointlike silver particles produced in the early stage of development change little, though the development progresses to the final stage (Figs. 3A and 3E). It has been clarified that the development process in radiography is complicated because of the existense of silvers having various shapes and being in various states of crystallization.

On the other hand, the shapes of silver observed in the process of ordinary development of Fuji Neopan SS film are shown in Figs. 5A—D and 1, and their crystalline states are shown in Figs. 4A—D. The silver reduced in the early stage of development, at 30 s, has a pointlike (Fig. 5A-1), bandlike (A-2), mistlike (A-3), or dendrite (in a rare case) shape, which are amorphous (Fig. 4A) except for dendrite. These results are the same as those obtained with Sakura RR (Fig. 3A). The mistlike silver was found to emerge from the silver–gelatin (complex) envelope (Figs. 5B and 4A) in the early stage and to aggregate in the next process (Figs. 5C, 4A, and 4B). However, the aggregate silver does not take a lumpish shape in the middle stage of development, at 150 s, but the filamentary silver grows up there (Fig. 5D). The crystallization of aggregate and filamentary silvers at this stage scarcely progresses (Figs. 4B and 4C). The greater parts of aggregate silver change to filamentary silver in the later stage of development, at 300—420 s (Fig. 1). The crystallization of filamentary silver in the final stage shows only a slight progress, in contrast with the lumpish silver (Figs. 4B—D). The crystalline state of filamentary silver is almost the same at any parts in a filament. The shapes of silver other than the filamentary one, such as tubular, lumpish, and dendritic, were seldem been found in this experiment. No growth or increase in number of pointlike silver are found in the later stage, nor any formation process of lumpish silver. There seem to be little information on the shape of lumpish silver or its formation process, and then the new results obtained here on the formation process of filamentary silver, in comparison with that of lumpish silver, cannot entirely be explained on the basis of the formation mechanism[3] for developed silver widely accepted at present. It is thus pointed out

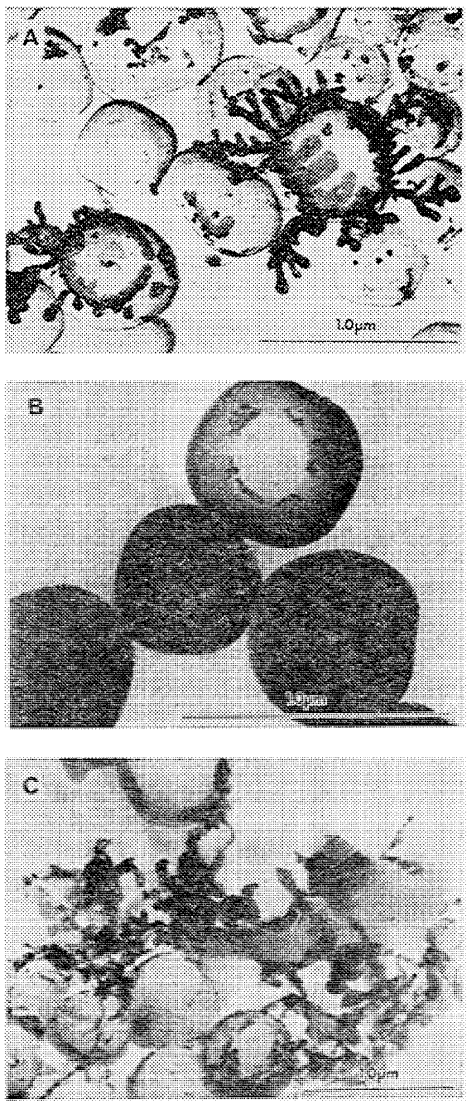

Figs. 6A—C. Electron micrographs of developed silver obtained from modified SAKURA RR industrial X-ray film at various treatment conditions.
A: Gelation free silver halide particles are isolated perfectly from the gelatin layer. B: Extremely thick emulsion layer with silver halide of low concentration. C: Thin emulsion layer with silver halide of medium concentration.

that any appropriate development mechanisms should consider not only the reduction process of silver halide but also the crystallization process of reduced silver.

The factor determining the shape of silver has been studied more widely from the above point of view.

The popular shape of silver observed at a sufficient depth of ordinary development is either filamentary or lumpish. Neither the difference in film manufacturers nor the difference in exposure conditions is a dominating factor determining the shape of silver. Lumpish silver has been found to be formed only when industrial X-ray film is caused to be developed ordinarily and when other types of film materials are developed with higher-activity developers. However, the shape of developed silver of Sakura RR film which is lumpish, has been found to change variously according to the modification of the emulsion layer of film. For instance, gelatin-free silver halide particles

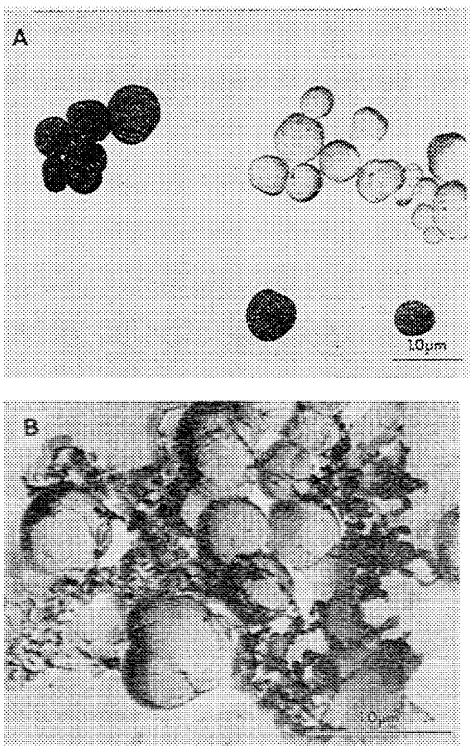

Fig. 7A—B. Electron micrographs of developed silver in SAKURA RR industrial X-ray film developed with KONIDOL-X of various dilution.
A: 1/25, B: 1/5.

obtained by an enzyme processing of Sakura RR film gave the dendritic silver after development (Figs. 6A and 4H). These gelatin-free silver halide particles were redispersed in gelatin solution and coated so as to have a thick emulsion layer with a low concentration of silver halide particles. This modified Sakura RR film gave spherical silver after development (Figs. 6B, 4A, and 4B). In the case of another type of film having extremely thin layer with a low concentration of silver halide particles gave the filamentary shape (Figs. 6C and 4B—D). Therefore, the constitution of emulsion layer, the concentration of silver halide, and the thickness of emulsion layer are effective factors determining the shape of silver.

On the other hand, another important factor determining the shape of silver is the activity of developer depending on the composition and development temperature. The shape of developed silver in Sakura RR film can easily be changed by varying the activity of the developer used; the spherical shape (Figs. 7A, 4A, and 4B) has been found at the lowest activity, the filamentary shape (Figs. 7B and 4B—D) at the medium activity, and the lumpish shape (Figs. 2 and 4B—G) at the highest activity.

Therefore, it has been clarified that the constitution of silver halide emulsion layers and the activity of developers are the most important factors that determine the shape of silver during the crystallization process of silver.

Conclusion

Most of developed silvers in industrial X-ray films

formed with ordinary X-ray film developers have a lumpish shape, which differs from the filamentary silver formed in negative films not only in shape but also in crystalline state.

When lumpish silver is formed, some dendrite, tubular, and filamentary silvers are also formed. Lumpish silver consists of amorphous and crystalline parts, and the latter is composed of fine crystallites with various degrees of crystallization. Therefore, in the formation process of lumpish silver, the progress of crystallization of developed silver is highly influenced by the constitution of emulsion layer and the conditions of development as compared with the case of filamentary silver.

At the early stage of development with ordinary developers, developed silvers of both negative type films and industrial X-ray films exist in amorphous and formless states. Furthermore, the following processes occur: (1) amorphous and formless silvers emerge in the gelatin matrix around silver halide particles, (2) aggregate there, and (3) crystallize.

In this process, the developed silver shows several shapes resulting from the asymmetrical progress of crystallization governed by the above-mentioned factors.

References

1) H. Hara, *J. Soc. Photogr. Sci. Tech. Jpn.*, **42**, 263 (1979).

2) H. Hara, *J. Soc. Photogr. Sci. Tech. Jpn.*, **43**, 102 (1980).

3) T. H. James, "The Theory of Photographic Process," 4th ed, ed by T. H. James, Macmillan, New York (1977), p. 373; Y. Hamano and T. Suga, "Shashin Kogaku No Kiso-Gin-en Shashin Hen," ed by the Society of Photographic Society and Technology of Japan, Koronasha, Tokyo (1978), p. 299.

4) R. B. Pontius, R. G. Willis, and R. J. Newmiller, *Photogr. Sci. Eng.*, **16**, 406 (1972); H. J. Metz, *J. Photogr. Sci.*, **20**, 111 (1972); R. W. Hone, M. N. Mcmorris, and R. H. Ottewill, *ibid.*, **10**, 235 (1962); C. R. Berry, *Photogr. Sci. Eng.*, **15**, 65 (1969).

5) W. E. Mueller, *Photogr. Sci. Eng.*, **15**, 369 (1971); *J. Photogr. Sci.*, **19**, 132 (1971); *Photogr. Sci. Eng.*, **17**, 94 (1973); W. Gross, *J. Photogr. Sci.*, **19**, 207 (1971).

6) T. Sakaguchi and T. Shiozawa, "Denshikenbikyo Shiryo Gijustu Shu," ed by the Japanese Society of Electron Microscopy Kanto Branch, Seibundo Shinko Sha, Tokyo (1970), pp. 121, 123.

7) R. Ueda, "Denshikenbikyo No Riron To Oyo (1)," ed by the Japanese Society of Electron Microscopy, Maruzen, Tokyo (1959), Chap. 5; A. Mizuwatari and K. Takiyama, "Denshikenbikyo Bunseki-Bunseki Library 15," ed by the Japan Society for Analytical Chemistry, Tokyo Kagaku Dozin, Tokyo (1971), Chap. 4; N. Kitamura and T. Hibi, "Denshikenbikyo No Riron To Oyo (3)," ed by the Japanese Society of Electron Microscopy, Maruzen, Tokyo (1959), Chap. 2.

8) Y. Shimizu, E. Mizuki, and S. Fujisawa, *J. Soc. Photogr. Jpn.*, **21**, 160 (1958); F. A. Hamm and J. J. Comer, *J. Appl. Phys.*, **24**, 1495 (1953).

Static and Kinetic Studies of the Interaction of Tryptophan with Fluorescein Mercury(II) Acetate by Fluorescence and Absorption Spectrophotometry and by Fluorescence Stopped-flow Method[1)]

Masatake Ohnishi, Michio Taniguchi, and Keitaro Hiromi*

Department of Food Science and Technology, Kyoto University, Kitashirakawa, Sakyo-ku, Kyoto 606

(Received March 14, 1983)

Fluorescein mercury(II) acetate (FMA) was found to combine with tryptophan (Trp) to form the FMA-Trp complex. The interaction was interpreted in terms of a reversible single-step binding mechanism. The dissociation constant of the complex estimated kinetically by means of the stopped-flow method using the forward and backward rate constants was in good agreement with that obtained by the static method. From comparison with several derivatives of tryptophan, it was found that the protonated amino group and the indole moiety of tryptophan are essential for the complex formation.

Fluorescein mercury(II) acetate (FMA), a highly fluorescent dye, is known to react with a mercapto group, accompanied by a decrease in its fluorescence intensity as well as a change in its absorption spectrum[2)]. Because it has these characteristics, FMA is used for the chemical modification of cysteine(Cys) residues of protein[3,4)]. Recently, Takeuchi and Maeda have reported that the fluorescent dye binds to some kinds of nucleic acids at the nitrogen sites of thymine and guanine residues[5)]. The fluorescent dye FMA, therefore, is useful for the discrimination of the constituent residue(s) and the conformation of proteins and nucleic acids.

Kinetic studies of the reaction of FMA with Cys by the stopped-flow method have already been made in order to discriminate[6)] the fast-reacting Cys residues in proteins.[7)] However, the authors have noticed, in the case of amylases, that even certain other residues could react with FMA.[8)] In fact, Watt and Voss found that fluorescein, which has the same aromatic rings as FMA, interacts with Trp, leading to a decrease in its fluorescence intensity.[9)] Because of these findings, the interactions between Trp and FMA have to be examined in detail before FMA can be applied to the modification of proteins including both Cys and Trp residues.

In this work, the fast complex formation between Trp and FMA was studied statically and kinetically through the decrease in the fluorescence intensity and the change in the difference absorption spectrum. The complex formation was consistent with a single-step association mechanism.

Results and Discussion

Interaction between FMA and Trp as Studied by Static Fluorescence Spectrophotometery. Figure 1 shows the fluorescence emission spectrum of FMA, which has a peak at 525 nm when excited at 495 nm (Fig. 1, 0). The fluorescence intensity at 525 nm was found to decrease with an increase in the concentration of Trp (Fig. 1, 1 and 2). The interaction of Trp with FMA also shows a difference absorption spectrum, which has a trough at 492 nm, a peak at 516 nm, and an isosbestic point at 505 nm (Fig. 2). Thus, the interaction between Trp and FMA can be followed either through the absorption or by the fluorescence change. The fluorescence measurement is preferable because of its high sensitivity.

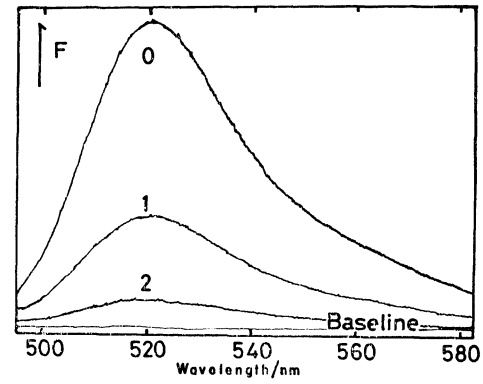

Fig. 1. Fluorescence emission spectra of FMA in the presence and absence of tryptophan.
[FMA]; 1.0 μM, [Trp]; 0; 0 M, 1; 5 μM, 2; 80 μM. Baseline means buffer solution. Excitation at 495 nm, pH 9.0, 25 °C.

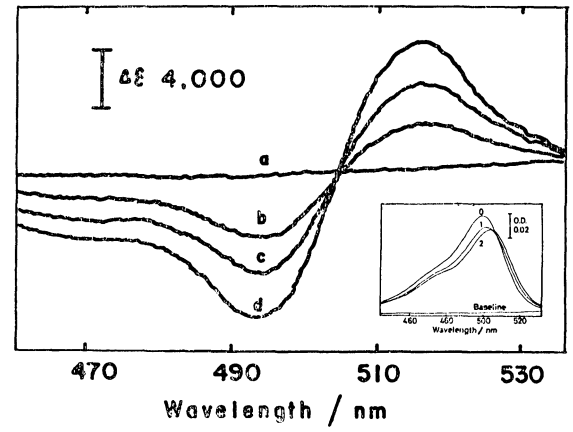

Fig. 2. Difference absorption-spectra of FMA produced by the addition of tryptophan.
[FMA]; 10.0 μM, [Trp]; a; 0 μM, b; 10 μM, c; 20 μM, d; 50 μM. Inset means the absorption spectra of FMA in the presence and absence of tryptophan. [Trp]; 0; 0 M, 1; 5 μM, 2; 80 μM, Baseline; buffer. [FMA]; 1.0 μM.

Figure 3 shows the dependence of the fluorescence intensity change (decrease), ΔF, on the initial concentration of Trp, where ΔF is expressed as the percentage of the change in the fluorescence intensity

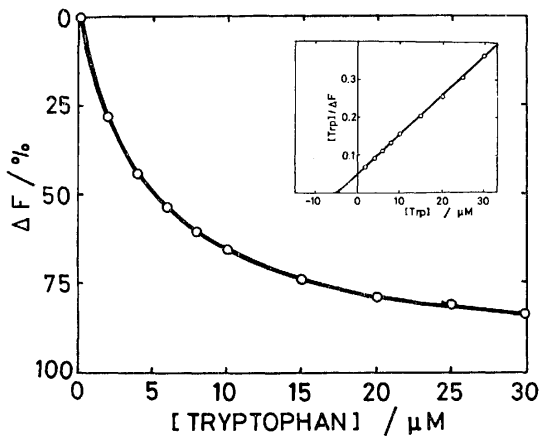

Fig. 3. Dependency of the fluorescence decrease of FMA, ΔF, upon the concentration of tryptophan. [FMA]; 1.0 μM, pH 9.0, 25 °C. Inset is the plots of [Trp]/ΔF *vs.* [Trp].

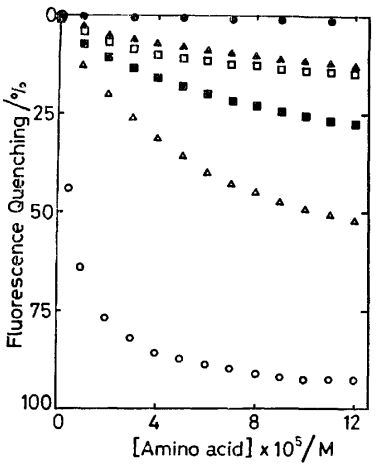

Fig. 4. Dependency of the fluorescence decrease of FMA upon the concentrations of amino acids. [FMA]; 0.2 μM, pH 9.0, 25 °C. ●; His, ▲; N^{α}-acetyl-Lys, □; Asp, ■; Phe, △; Tyr, ○; Trp.

relative to that of free FMA. The experimental points fit the characteristic hyperbolic curve, indicating a reversible complex formation between Trp and FMA:

$$\text{Trp} + \text{FMA} \rightleftharpoons \text{Trp-FMA}, \quad (1)$$

where Trp–FMA represents the Trp–FMA complex. The dissociation constant of the Trp–FMA complex, K_d, is defined as follows:

$$K_d = [\text{Trp}][\text{FMA}]/[\text{Trp-FMA}]. \quad (2)$$

A linear plot, [Trp]/ΔF against [Trp], is shown in the inset of Fig. 3, according to:

$$[\text{Trp}]/\Delta F = [\text{Trp}]/\Delta F_{max} + K_d/\Delta F_{max} \quad (3)$$

$$[\text{Trp}] \gg [\text{FMA}],$$

where ΔF_{max} is the maximum fluorescence decrease when FMA is saturated with Trp and where [Trp] is the initial concentration of Trp ([Trp]≫[FMA]). The experimental points fit a straight line, from which the K_d and ΔF_{max} values were obtained as 5.0×10^{-6} M (1 M=1 mol dm^{-3}) and 98% respectively. The solid lines in Fig. 3 (including the inset) are the theoretical ones drawn according to Eq. 3 with the obtained values of K_d and ΔF_{max}. The statically obtained experimental results are thus consistent with the mechanism represented by Eq. 1.

Complex Formation of FMA with Other Amino Acids. Tyrosine, phenylalanine, and three other amino acids besides Trp were examined for the complex formation with FMA in the manner described above. The fluorescence-intensity changes caused by the addition of each of the amino acids were measured at various concentrations. As is shown in Fig. 4, the decrease in the fluorescence intensity could be observed with all the amino acids examined, except for His. The degree of the decrease in the fluorescence intensity is strongly dependent on the nature of the amino acid. The values of K_d and ΔF_{max}, evaluated in the same way as for Trp, are summarized in Table 1. Tryptophan has the smallest K_d value and the largest ΔF_{max} value among the amino acids examined. Thus, it seems worthwhile to investigate the interaction of FMA with Trp in detail.

Table 1. The K_d and ΔF_{max} values of the FMA–amino acid complex formation

Amino acid	$K_d/10^{-6}$ M	ΔF_{max}/%
Asp	66	20
Arg	100	11
Gly	180	19
N^{α}-acetyl-Lys	95	12
Ser	25	22
Phe	87	36
Tyr	48	65
Trp	5.0	98

Excitation at 495 nm, emission at 525 nm, pH 9.0, 25 °C.

Some derivatives of Trp were also examined in order to ascertain what part of the Trp molecule contributes to the Trp–FMA complex formation. In this case, the difference absorption was used as a probe for measurement, since it is more suitable for quantitative analysis than the fluorescence measurement. The difference-absorption change measured at 492 nm, ΔA_{492}, was plotted against the concentration of the derivatives, as is shown in Fig. 5. The tryptophan methyl ester as well as tryptophan can form a complex with FMA to produce the difference absorption change, whereas neither *N*-acetyltryptophan nor the acetyltryptophan ethyl ester show any evidence of forming such a complex. These findings indicate that the amino group of the derivatives plays an essential role in the complex formation. Thus, both the indole and the amino group seem to be essential to the complex formation, whereas the carboxyl group is not essential.

Effect of pH on the Complex Formation of FMA with Trp. The dependence of ΔF on the concentration of Trp was studied at various pH's above 8, since FMA is not fluorescent at lower pH's. Figure 6 shows a part of the data showing the variation in the plots of ΔF *vs.* [Trp] at various pH's. The values of K_d and ΔF_{max} for the Trp–FMA complex at every pH were evaluated in the manner described above. The

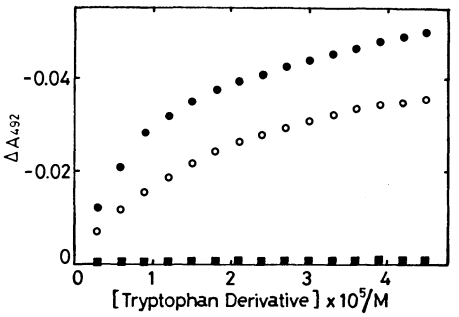

Fig. 5. Difference absorption change (ΔA) of FMA at 492 nm induced by tryptophan and its derivatives.
[FMA]; 10.0 μM, pH 9.0, 25 °C. ●; H_2N-Trp-COOH, ○; H_2N-Trp-$COOCH_3$, ■; *N*-acetyl-Trp-COOH and *N*-acetyl-Trp-$COOC_2H_5$

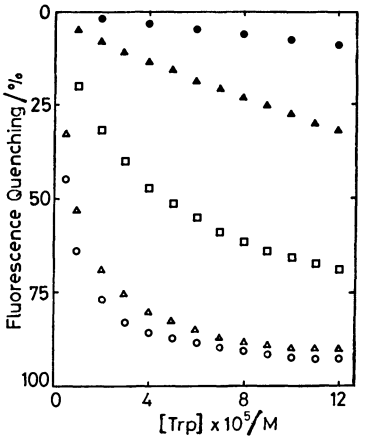

Fig. 6. Dependence of the fluorescence decrease of FMA upon the concentration of tryptophan at various pH's.
[FMA]; 0.2 μM, 25 °C. ●; pH 12.5, ▲; pH 11.7, □; pH 10.8, △; pH 9.9, ○; pH 9.0.

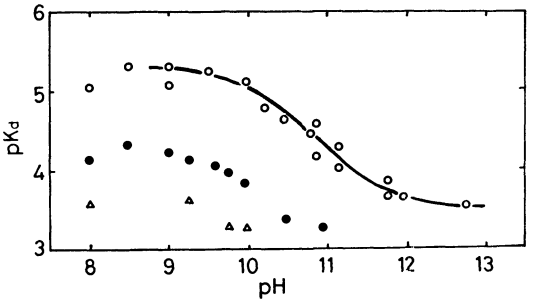

Fig. 7. pH dependency of K_d for Trp, Tyr, and Phe.
Solid line was obtained by the calculation with $pK_a = 10.8$ according to the scheme, $Trp\text{-}NH_2 + H \rightleftharpoons Trp\text{-}NH_3^+$. ○; Trp, ●; Tyr, △; Phe.

pH-dependence of pK_d ($= -\log K_d$) is shown in Fig. 7, together with those obtained with Tyr and Phe. The slope of the pK_d *vs.* pH plot is nearly unity; thus, one proton, which could be Trp ($pK \simeq 10.8$), contributes to the complex formation. The pK_d value of the Trp–FMA complex is appreciably larger than those of the two other amino acids, Tyr and Phe, over the pH range examined (pH 8—11).

Kinetics of the Trp–FMA Complex Formation. The formation of the Trp–FMA complex was studied kinetically by means of the fluorescence stopped-flow method in order to evaluate the nechamism by observing the rapid decrease in the fluorescence intensity. Figure 8 shows a typical example of the reaction curves obtained in an excess of Trp over FMA. The reaction obeys first-order kinetics, as may be seen from the straight line in the Guggenheim plot (the inserted figure in Fig. 8).[10,11] The apparent first-order rate constant, k_{app}, for the interaction was evaluated at variuos Trp concentrations. The results are shown in Fig. 9. The linearity of the plot is consistent with the following single-step binding mechanism, where k_{+1} and k_{-1} are the rate constants for the forward and backward processes respectively:

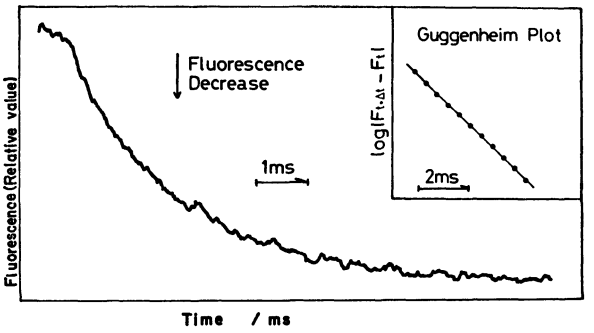

Fig. 8. A typical example of the reaction curves observed by a fluorescence stopped-flow spectrophotometer.
[FMA]; 0.2 μM, [Trp]; 12.5 μM, pH 8.5, 25 °C. Inset is the Guggenheim plot ($k_{app} = 499\ s^{-1}$).

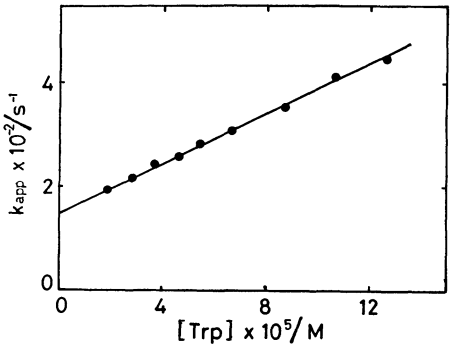

Fig. 9. Dependency of k_{app} upon the concentration of tryptophan.
The straight line was obtained by the given values, $k_{+1} = 2.37 \times 10^7\ M^{-1}\ s^{-1}$ and $k_{-1} = 149\ s^{-1}$ according to the scheme, Eq. 4 and $k_{app} = k_{+1}[Trp] + k_{-1}$, where [Trp] is the tryptophan concentration. [FMA]; 0.2 μM, pH 8.5, 25 °C.

$$Trp + FMA \underset{k_{-1}}{\overset{k_{+1}}{\rightleftharpoons}} Trp\text{-}FMA, \quad (4)$$

Based on the mechanism, k_{app} is expressed, when [FMA]≪[Trp], as follows:[12]

$$k_{app} = k_{+1}[Trp] + k_{-1}. \quad (5)$$

From the plot of k_{app} against [Trp], the rate constants, k_{+1} and k_{-1}, were evaluated by the use of the least-squares method to be $2.4 \times 10^7\ M^{-1}\ s^{-1}$ and $150\ s^{-1}$ respectively (pH 8.5). The solid line in Fig. 9 is the

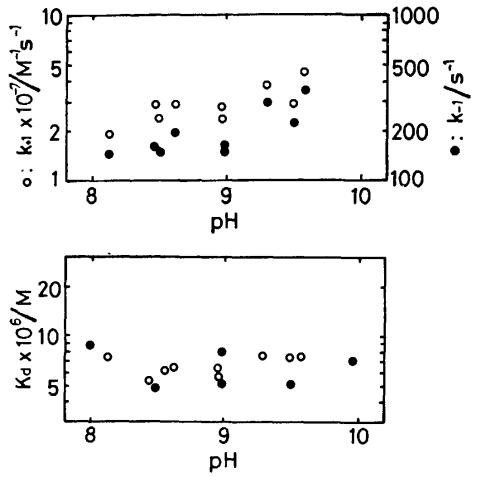

Fig. 10. pH dependencies of the rate constants, k_{+1} (open circle) and k_{-1} (closed circle) and the dissociation constant, K_d (Open circles were obtained by the kinetic observation with the stopped-flow method and closed circles were by the static observation).

theoretical one drawn according to Eq. 5, using the given rate constants. Thus, the interaction between FMA and Trp can reasonably be accounted for by a single-step binding mechanism, as has been described in Eq. 4, at least in the concentration range studied. The dissociation constant, K_d ($=k_{-1}/k_{+1}$), was evaluated from the rate constants to be 6.3×10^{-6} M (pH 8.5).

Figure 10 shows the two rate constants, k_{+1} and k_{-1} and the K_d values evaluated at various pH's in the range from 8 to 10. The K_d values obtained from the kinetic study are reasonably consistent with the values from the static measurements described above; they are nearly constant between pH 8 and 9.5, in spite of the fact that both k_{+1} and k_{-1} increase with an increase in the pH.

Experimental

Chemicals. Fluorescein mercury(II) acetate (FMA) was synthesized from uranine (fluorescein sodium salt) and mercuric acetate by the method of Karush *et al.*[2] and was purified by Sephadex G-15 column chromatography using a 20 mM aqueous ammonia solution as the eluent. The main fraction was shown by dithizone titration[5] to contain two mercury atoms per molecule; it is in agreement with the chemical structure assigned to FMA by Karush *et al.*[2] The concentration of FMA was determined spectrophotometrically using the molar absorption of 78000 at 499 nm.[2] Tryptophan (Trp) and its derivatives, tyrosine (Tyr), phenylalanine (Phe), and the other amino acids, and the chemicals used were all of a guaranteed grade, purchased from Kanto Chemical Industries Co. Ltd., Tokyo.

Measurements of Difference Absorption and Fluorescence Spectra. The difference-absorption spectrum (450—540 nm) of FMA caused by amino acid was measured in a 50 mM borate buffer, pH 9.0 at 25 °C, by means of a Union Giken SM-401 spectrophotometer. The fluorescence measurements were made with a Union Giken FS-401 fluorescence spectrophotometer. The excitation wavelength was 495 nm unless otherwise stated.

Kinetic Observation of the Interaction between FMA and Trp by the Fluorescence Stopped-flow Method. The time course of the change in the fluorescence intensity caused by the interaction of FMA with Trp was observed with a Union Giken SF-70 (piston driven type) or RA-1300 (gas-pressure driven type) stopped-flow spectrophotometer, with a 50-W tungsten lamp as the light source and a cylindrical cell with a 2 mm bore. The excitation wavelength was 495 nm, and the fluorescence emission was observed from a right angle through a cut-off filter (50% transmission at 530 nm). The reaction signals were usually accumulated 9 times to improve the signal-to-noise ratio, using a Union Giken RA-450 kinetic-data-averaging processer. All the reactions were carried out in a 50-mM borate buffer, pH 8—10, at 25 °C.

This study was supported in part by a Grant-in-Aid for Scientific Research from the Ministry of Education, Science and Culture.

References

1) Reported in part at the Kansai (Middle west)/Nishi Nippon (West Japan) Regional Meeting of the Agricultural Chemical Society of Japan, Okayama, Oct. 14, 1978.
2) F. Karush, N. R. Klinman, and R. Marks, *Anal. Biochem.*, **9**, 100 (1964).
3) J. R. Heitz and B. M. Anderson, *Arch. Biochem. Biophys.* **127**, 637 (1968).
4) J. R. Heitz, *J. Biol. Chem.*, **246**, 5790 (1973).
5) S. Takeuchi and A. Maeda, *Biochim. Biophys. Acta*, **454**, 309 (1976).
6) K. Hiromi, T. Kawagishi, and M. Ohnishi, *J. Biochem.* **81**, 1583 (1977).
7) S. Takeuchi and A. Maeda, *J. Biochem.*, **81**, 971 (1977).
8) Unpublished data, (M. Taniguchi, Bachelor's Thesis (1978) and Master's Thesis (1980), Kyoto University, College of Agriculture).
9) R. M. Watt and E. W. Voss, Jr., *Immunochemistry*, **14**, 533 (1977).
10) H. A. Guggenheim, *Philos. Mag.*, **3**, 538 (1926).
11) Hiromi, "Kinetics of Fast Enzyme Reactions," Kodansha-Halsted Press, Tokyo and New York (1979).
12) M. Eigen and L. DeMaeyer, "Techniques of Chemistry," ed by S. Weissberger, John Wiley & Sons, New York (1974), Vol. 6.

The Catalytic Cracking of Slack Wax with Molten Mixtures Containing Aluminum Chloride and Bromide

Yasuo Ohtsuka,* Kazutoshi Oizumi, and Yasukatsu Tamai

Chemical Research Institute of Non-Aqueous Solutions, Tohoku University, 2-1-1 Katahira, Sendai 980

(Received March 16, 1983)

The catalytic cracking of slack wax with molten mixtures of $AlCl_3$ and $AlBr_3$ was investigated in an atmospheric semi-batch reactor at low temperatures of 100—160 °C. The cracking rate was proportional to the amount of unreacted wax. The conversion at 135 °C reached 25 wt% under typical reaction conditions. About 95 wt% of the cracking products consisted of isobutane, 2-methylbutane, and methylpentanes, *ca.* 50% of these isoparaffins being isobutane. The difference in cracking activity between this catalyst and a solid acid catalyst is discussed based on the product distribution. Hardly any reaction took place without HCl, which shows that the presence of HCl is essential for this cracking. The cracking rate increased sharply with an increase in the amount of the catalyst. The rate did not depend on the composition of the $AlCl_3$–$AlBr_3$ catalyst, but the product distribution did depend on it and the content of the gasoline fraction in the products increased with an increase in the concentration of $AlBr_3$. The cracking residue was characterized by IR and NMR spectroscopy. The results show that the cracking reaction probably occurs heterogeneously at the interface between the liquid wax and the molten catalyst.

Petroleum waxes are present in all crude oils, the content depending on the source. Among imported oils, the value is high in Minas and Taching crude, reaching 15—20 wt%. In such waxy crude oils, the upgrading of the waxes may be needed in the future.

Several works on the hydrocracking or hydroisomerization of paraffin wax have been carried out for the purpose of obtaining valuable lighter products.[1,2] Since such reactions are conducted over solid acid catalysts at high temperatures, the high isoparaffin yield attainable at low temperatures is sacrificed and expensive hydrogen is consumed. The use of Lewis acid catalysts, which are very active at low temperatures and without hydrogen, may be preferable for the cracking of paraffin wax. However, little work has been published in this connection. About thirty years ago, however, Potolovsky and Spektor shortly reported the cracking of paraffin wax with the $AlCl_3$ catalyst at temperatures of 200—250 °C.[3]

We now wish to report the cracking of slack wax, the wax obtained in the process of dewaxing lubricating oils, at low temperatures of 100—160 °C. We employed molten salt mixtures containing $AlCl_3$ and $AlBr_3$ as cracking catalysts, because they had been found in preliminary experiments to have low melting points (*ca.* 90 °C) and to show a high activity toward the conversion of lower normal paraffins. In this paper, the effect of some parameters on the cracking rate and the product distribution will be investigated, and the reaction process will be discussed.

Experimental

Materials. The slack wax used in this study was supplied by Idemitsu Kosan Co., Ltd. The properties were as follows: melting point, 53.0 °C; specific gravity at 100 °C, 0.770; kinematic viscosity at 98.9 °C, 4.38×10^{-6} $m^2 s^{-1}$; oil content, 6.0 wt%; average molecular weight, 400. The weight fractions of the normal alkanes, isoalkanes, cycloalkanes and aromatics in the wax were 57.5, 30.6, 10.8, and 1.1% respectively. The carbon numbers of the normal alkanes range mainly from 26 to 30. Anhydrous aluminum chloride and bromide, and sodium chloride were of a reagent grade, and they were used as received. Helium and hydrogen chloride were of a research grade.

Apparatus. The cracking of slack wax was carried out in a semi-batch reaction system. The reactor consisted of a Pyrex test tube onto which a water-cooling jacket was glassblown. This test tube was connected to a vacuum system, a carrier gas line, and a gas-chromatographic unit through three separate metal-glass joints. The reactor was heated electrically by nichrome wire wound onto it and insulated thermally by an annular Pyrex tube. This assembly made it possible to observe the appearance of the reaction process with the naked eye. The reaction temperature was measured with a chromel-alumel thermocouple located in a well embedded in a liquid mixture of slack wax and the catalyst melt.

Procedure and Analysis. In most runs, molten salt mixtures of $AlCl_3$ and $AlBr_3$ were used as cracking catalysts. First, the catalyst was prepared in the reactor by melting a powdery mixture of the two salts at *ca.* 100 °C. The details of the preparation have been described elsewhere.[4] Care was taken throughout the preparation to avoid contact between the catalyst and moisture. After the completion of the preparation, the reactor was kept at 60 °C under flowing He. At this temperature, the catalyst was solid.

Then, a fixed amount of liquid slack wax was quickly poured onto the catalyst and the reactor was rapidly heated up to a predetermined reaction temperature. Finally, HCl diluted with the He carrier, at a total flow rate of 76 cm^3 (STP)/min, was bubbled into the mixture of slack wax and the catalyst melt, and simultaneously the mixture was stirred magnetically. This time was taken as the start of the reaction. Typical cracking conditions were as follows: amount of catalyst, 18 g; its composition, 35 mol% $AlCl_3$–65 mol% $AlBr_3$; amount of slack wax, 54 g; volume fraction of HCl, 0.21; reaction time, 3 h.

The effluent from the reactor outlet was led to a gas-chromatographic unit; all the cracking products were analyzed periodically and separated by means of a 9-m column with 30 wt% propylene carbonate on C-22.

After a constant reaction time, the flow of HCl was stopped and the reactor was cooled to room temperature. The contents of the reactor were separated into two layers by allowing it to stand. The separated materials were then analyzed by IR and NMR spectroscopy method. The IR spectra were measured by sandwiching the sample between two KBr plates. The NMR spectra were deter-

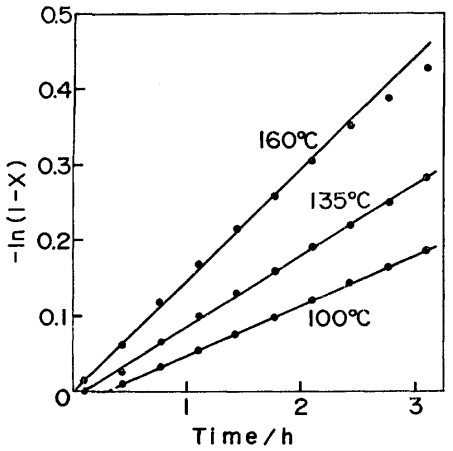

Fig. 1. First-order rate plots for the cracking of slack wax at different reaction temperatures.

mined as solutions in CCl_4 using TMS as a reference.

Results and Discussion

Cracking Rate. Figure 1 illustrates the first-order rate plots for the cracking of slack wax. The fractional conversion, X, is expressed as a weight fraction of the summation of all the cracking products in the effluent to the feed wax. In all runs, about 95 wt% of the products consisted of isobutane, 2-methylbutane, and methylpentanes. The detailed product distribution will be given later.

As is shown in the figure, a linear relationship between $-\ln(1-X)$ and time was observed at all reaction temperatures, except for the induction period at low temperatures. This result means that the cracking rate is proportional apparently to the amount of the unreacted wax. The rate constant of cracking is obtained from the slope of the straight line in Fig. 1; the values at 100, 135, and 160 °C were 1.1×10^{-3}, 1.6×10^{-3}, and 2.5×10^{-3} min^{-1} respectively. When the temperature was raised from 100 to 160 °C, the rate increased by a factor of 2.3.

The induction period was observed at low temperatures of 100 and 135 °C. The period may arise from the small contact area between wax and catalyst, because, at the beginning of the reaction, especially at 100 °C, the liquid wax and the molten catalyst were immiscible with each other, and thus there existed two separated layers. Such an incomplete mixing may be ascribed to the difference in viscosity between the two. As the cracking proceeded, the mixture apparently became homogeneous.

At high conversions at 160 °C, a little deviation from linearity was observed. The catalyst deterioration may be considered as one reason for this. It is possible that the catalyst reacts with olefinic or aromatic hydrocarbons which may be formed during the cracking, and thus loses its activity.[5]

Distribution of Cracking Products. The results are given in Table 1. The main products were isobutane, 2-methylbutane, and 2- and 3-methylpentane. The product yield increased with an increase in the cracking temperature, but the selectivity to each product depended hardly at all on the temperature. The selectivities to the above main products were 46—47, 32—33, and 14—15 wt% respectively. Thus, about 95% of the products consisted of such lower isoparaffins, which were all monomethylalkanes. The content of the gasoline fraction in the products was 51—53 wt%. No formation of olefinic and aromatic hydrocarbons was found in the products. H_2 and CH_4 were not formed, either.

Table 1. Product distribution at different reaction temperatures[a]

Temperature/°C	100	135	160
Conversion/wt%	16	24	34
Product yield/wt%			
C_3H_8	t[b]	0.2	0.6
n-C_4H_{10}	0.1	0.1	0.2
i-C_4H_{10}	7.7	11	16
n-C_5H_{12}	t	t	0.1
i-C_5H_{12}[c]	5.4	7.8	11
i-C_6H_{14}[d]	2.4	3.6	4.8
i-C_7H_{16}[e]	0.8	1.1	1.6

a) Under typical conditions. b) Trace (<0.05 wt%). c) 2-Methylbutane. d) 2-Methyl- and 3-methylpentane. e) Mixture of methylhexanes.

Table 2. Comparison of carbon-number distribution of cracking products between this molten catalyst and a solid-acid catalyst

Catalyst	$AlCl_3$–$AlBr_3$	SiO_2–ZrO_2–Al_2O_3[a]
Temperature/°C	135	500
Conversion/wt%	24	24
Selectivity/mol%		
C_1+C_2	0	5(5)[b]
C_3	1	27(29)
C_4	54	28(30)
C_5	30	18(19)
C_6	12	14(15)
C_7	3	2(2)
C_8^+	—	6

a) Ref. 6. b) Values in parentheses denote the selectivity calculated by excluding the C_8^+ fraction.

It is interesting to examine the difference in cracking activity between this catalyst and the solid-acid one. For this purpose we compared our carbon-number distribution of cracking products with that for the cracking of cetane over the SiO_2–ZrO_2–Al_2O_3 catalyst at 500 °C.[6] These two examples differ in feed stock, but this point is insignificant, because it has been reported that the products from centane are similar to those from paraffin wax (approximately n-$C_{24}H_{50}$) over the above solid catalyst.[7] A comparison at the same conversion is made in Table 2. The charateristics of this cracking is that the selectivity to C_3 hydrocarbons is extremely low, while the selectivity to C_4 and C_5 hydrocarbons is considerably high. Furthermore, although it is not shown in the table, another point to be noted is that the iso-to-normal ratio in total paraffins with this catalyst is significantly high,

Table 3. Effect of hydrogen chloride on cracking at 135 °C[a]

HCl/vol%	0	10	21
k[b]/10^{-3} min^{-1}	—	1.3	1.6
Conversion/wt%	0.1	19	24

a) Under typical conditions. b) First-order rate constant.

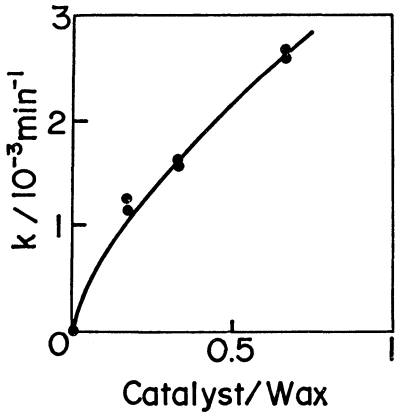

Fig. 2. Effect of amount of catalyst on the cracking of slack wax at 135 °C.

more than twenty times the ratio (*ca.* 3) with the solid-acid catalyst.[6] The low cracking temperatures in this work are one reason for the high iso-to-normal ratio. Since the catalytic cracking of slack wax with molten salts would proceed through the same carbonium-ion mechanism as the Lewis acid-catalyzed cracking,[5] the results shown in Table 2 may characterize this cracking as follows: normal secondary carbonium ions hardly break down into fragments of small molecules such as C_3 fragments, and such normal ions easily undergo skeletal isomerization to form tertiary carbonium ions, which then break down by β fission into fragments of C_4 or larger.

Effect of Hydrogen Chloride. As is generally accepted, hydrogen halide or an equivalent proton source is essential for the isomerization and cracking of paraffins by aluminum halide catalyst.[5] However, such reactions also take place even in the absence of these materials at around 150 °C.[4,8] Thus, the effect of HCl on the cracking of the slack wax was examined. The results are given in Table 3.

In the absence of HCl, a very small amount of the products was formed, and that only at the beginning of the reaction; thereafter, no appreciable cracking was observed. Consequently, the conversion was no more than 0.1 wt%. A trace amount of water present in the slack wax or catalyst probably serves as a proton source for the cracking at the initial reaction time. The addition of 10 vol% of HCl to the carrier gas increased the cracking rate considerably; the conversion reached about 20% in a reaction time of 3 h. An additional two-fold increase in the volume fraction of HCl further increased the cracking rate, but the increase in the rate seemed to level off. The presence of an optimum amount may be considered. It is evident from these results that the presence of HCl is essential for the cracking of slack wax with molten catalysts.

Table 4. Effect of catalyst composition on cracking conversion and product distribution at 135 °C[a]

Catalyst composition[b] (mole ratio)	$AlCl_3$–$AlBr_3$ (35:65)	$AlCl_3$–$AlBr_3$ (61:39)	$AlCl_3$–NaCl (61:39)
k[c]/10^{-3} min^{-1}	1.6	1.6	0.50
Conversion/wt%	24	24	8.7
Selectivity/wt%			
C_3H_8	1	1	6
n-C_4H_{10}	t	1	3
i-C_4H_{10}	47	54	64
n-C_5H_{12}	t	t	1
i-C_5H_{12}	33	30	22
i-C_6H_{14}	15	10	4
i-C_7H_{16}	5	4	t

a) Under typical conditions. b) Catalyst amounts were 18, 15, and 14 g, in the order shown. c) First-order rate constant.

Effect of Amount of Catalyst. Figure 2 illustrates the effect of the catalyst amount on cracking at 135 °C. In this experiment, the weight of the molten catalyst (35 mol% $AlCl_3$–65 mol% $AlBr_3$) was varied from 9.0 to 36 g, while the weight of the wax was kept constant (54 g). In the figure, the first-order rate constants are plotted as a function of the weight ratio of the catalyst to the wax.

Without a catalyst, of course, no pyrolysis of wax was observed at temperatures of 100—160 °C. The catalyst promoted the cracking of the wax considerably, and the rate increased sharply with an increase in the amount of the catalyst. The plots of $\log k$ against log (catalyst/wax) gave a straight line, and from the slope of the line the order with respect to the amount of the catalyst was found to be about 0.6. A similar value has been reported for the liquid-phase isomerization of ethylcyclohexane in the presence of $AlCl_3$.[9]

Such a dependence of rate on the catalyst amount suggests that a stoichiometric reaction between catalyst and wax may occur or that the extent of contact between the two may be a key factor in determining the cracking rate. If the stoichiometric reaction between AlX_3 and paraffins in the wax in the presence of HCl is predominant, the rate will not vary against the catalyst weight above an equimolar amount with paraffins. As is shown in Fig. 2, however, the rate constant increased further even against the weight ratio above 0.50, the value which corresponds to the equimolar ratio of AlX_3 to paraffins. This discussion shows that such the reaction is a minor possibility.

As is shown in Fig. 1, the induction period appears at the beginning of the reaction; it may be ascribed to the small contact area between catalyst and wax. The length of the period decreased with an increase in the amount of the catalyst, and the period disappeared at the highest amount in Fig. 2. These results also suggest that the degree of the contact between the molten catalyst and the liquid wax determines

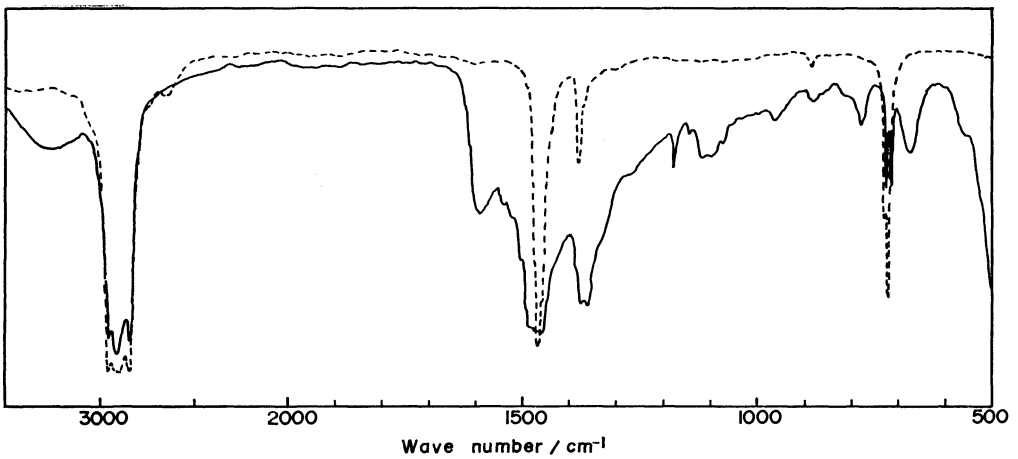

Fig. 3. IR spectra of feed wax (---) and tarry material (——).

the cracking rate to a considerable extent.

Effect of Catalyst Composition. The results are given in Table 4; three molten catalysts with different compositions were employed. The weight of each catalyst is somewhat different, as is shown in the footnote in Table 4, but the three catalysts are equal in the molar content of aluminum halide. For the $AlCl_3$–$AlBr_3$ catalyst, the cracking rate depended scarcely at all on the molar ratio of $AlCl_3$ to $AlBr_3$ within our experimental conditions, but the product distribution obviously did so depend. The selectivity to the C_4 components increased with an increase in the content of $AlCl_3$ in the catalyst, and instead the selectivity to the components above C_5 decreased. It is noteworthy that $AlCl_3$ has a higher activity to crack to lower molecules than $AlBr_3$, although the reason for this is not clear. In our unpublished work, a quite similar result was found for the catalytic conversion of lower paraffins, such as butane and pentane, on molten mixtures containing $AlCl_3$ or $AlBr_3$.

As is shown in the last two columns in the table, the substitution of NaCl for $AlBr_3$ in the $AlCl_3$–$AlBr_3$ catalyst affected both the cracking rate and the product distribution. The rate decreased by a factor of 0.3, and the selectivity to the gasoline fraction above the C_5 components decreased from 44 to 27 wt%. Therefore, the $AlCl_3$–NaCl catalyst is unsuitable for the production of a gasoline fraction by cracking slack wax. The low activity of this catalyst must be due to the decreased amount of free $AlCl_3$, which is the active species for the isomerization or cracking of lower paraffins by a molten $AlCl_3$–NaCl catalyst.[4] It is well accepted that $AlCl_3$ reacts with NaCl to form $Na^+AlCl_4^-$ in molten mixtures.[10,11] Thus, the addition of NaCl decreases the concentration of free $AlCl_3$.

Charaterization of Reaction Residue and Cracking Process.

As has been described in the Experimental section, the contents remaining in the reactor after the stop of the cracking were easily separated into two layers. The upper layer consisted of a white waxy material. No ash was found to be present in it, which shows that the waxy material contains no catalyst. Its NMR and IR spectra were identical with those of feed wax, and the two were equal in the ratio of methylene-to-methyl protons obtained by the NMR spectrum. These findings indicate that the white waxy material is the feed wax itself.

The lower of the two separated layers consisted of a black tarry material including the catalyst. The IR spectrum obviously differed from that of the feed wax. Figure 3 shows this. The spectrum of the feed wax is a typical one for paraffin wax, and every peak can be attributed to aliphatic absorption bands, in which the splitting peak at 720—730 cm^{-1} is assigned to methylene chains having four or more units.

With the spectrum for the tarry material, the intensity of the peak due to the chains decreased considerably. This indicates a decrease in the chain length of paraffins upon cracking. In addition, the major aliphatic absorptions at 2840—2950 cm^{-1} and 1450—1480 cm^{-1} decreased in intensity. The increase in the intensity of the peak for methyl groups at 1370 cm^{-1} and the splitting of this peak show the presence of branched paraffins; besides, the appearance of two new peaks at 1180 and 1155 cm^{-1} enables us to assign them to isopropyl groups. Judging from the absence of any appreciable absorptions in the range of 1200—1260 cm^{-1}, *t*-butyl groups and quarternary carbons seem to be absent. The presence of isopropyl groups in the catalyst layer corresponds to the evolution of a large quantity of monomethylalkanes (shown in Table 1).

Aromatic compounds are also present in the tarry material, because the absorption bands at 1500, 1590, and 3030 cm^{-1} appeared; the former two absorptions are assigned to aromatic-ring vibrations. Thus, the peaks at 680, 780, and 880 cm^{-1} may be attributed to substituted aromatic-ring structures. Evidently the aromatization takes place concurrently with the cracking. It has been suggested that the aromatization process of a normal paraffin, such as that of *n*-dodecane by an $AlCl_3$ catalyst without HCl, takes place predominantly *via* the dehydrogenation of the cycloparaffins formed.[12] However, no evolution of H_2 in this cracking of the wax suggests a mechanism other than the above. Since carbonium ions formed in acidic systems such as $AlCl_3$–HCl are in equilibrium with the corresponding olefins,[13,14] such olefins may undergo polymerization and aromatization reactions. The aromatic compounds may react with the catalyst, which may result in catalyst deactivation.

As has been mentioned above, the catalyst layer including the cracked fragments can be easily separated from the layer of unreacted wax by allowing the reaction mixture to stand. This means that the two layers are essentially immiscible. The cracking of the wax would occur at the interface between the molten catalyst and the liquid wax in the presence of HCl. Since little formation of normal paraffins was found in the cracking products, normal paraffins in the wax may first undergo skeletal isomerization and then the cracking reaction. Part of the cracked fragments may be carried with the carrier gas to the gas phase and observed as products. The rest of the fragments may dissolve in the catalyst phase, undergo further miscellaneous reactions, and finally be converted into lower paraffins and an asphaltene-like material. In conclusion, the catalytic cracking of slack wax by molten mixtures in the presence of HCl probably occurs heterogeneously at the interface between the molten catalyst and the liquid wax.

References

1) F. Breimer, H. I. Waterman, and A. B. R. Weber, *J. Inst. Pet.*, **43**, 297 (1957).
2) T. M. John and B. W. Wojciechowski, *Can. J. Chem. Eng.*, **54**, 584 (1976).
3) L. A. Potolovsky and G. S. Spektor, *J. Appl. Chem. USSR (Engl. Transl.)*, **28**, 729 (1955).
4) Y. Ohtsuka and Y. Tamai, *J. Catal.*, **67**, 316 (1981).
5) F. E. Condon, "Catalysis," ed by P. H. Emmett, Reinhold, New York (1958), Vol. 6, p. 43.
6) B. S. Greensfelder, H. H. Voge, and G. M. Good, *Ind. Eng. Chem.* **41**, 2573 (1949).
7) B. S. Greensfelder and H. H. Voge, *Ind. Eng. Chem.*, **37**, 514 (1945).
8) H. Pines and R. C. Wackher, *J. Am. Chem. Soc.*, **68**, 595 (1946).
9) H. Segawa, Y. Kurata, A. Amano, and H. Tokuhisa, *Sekiyu Gakkai Shi*, **13**, 350 (1970).
10) G. Torsi, G. Mamantov, and G. M. Begun, *Inorg. Nucl. Chem. Lett.* **6**, 553 (1970).
11) E. Rytter, H. A. Oye, S. J. Cyvin, B. N. Cyvin, and P. Klaeboe, *J. Inorg. Nucl. Chem.*, **35**, 1185 (1973).
12) T. Miyagawa, I. Fujishima, Y. Takegami, and T. Suzuki, *Nippon Kagaku Kaishi*, **1974**, 1269.
13) D. A. McCaulay, *J. Am. Chem. Soc.*, **81**, 6437 (1959).
14) W. C. Van Zijll Langhout, Preprint, 9th World Petroleum Congress, PD20(5), 197 (1975).

 © 1983 The Chemical Society of Japan Bull. Chem. Soc. Jpn., 56, 2721—2726 (1983)

Cobalt(III) Complexes with Quadridentate Ligands. IV.[1] The Preparation and Properties of "*cis*-β_1 and β_2" Isomers of the 2-Methyl-8-quinolinolato(triethylenetetramine)-cobalt(III) and Related Complexes

Yoshihisa YAMAMOTO,* Eiko TOYOTA, and Yutaka YAMAMOTO†

Faculty of Pharmaceutical Sciences, Higashi Nippon Gakuen University, Ishikari-Tobetsu, Hokkaido 061-02

† *Tohoku College of Pharmacy, Komatsushima, Sendai 983*

(Received January 13, 1983)

cis-β_1- and β_2-8-Quinolinolato or 2-methyl-8-quinolinolato(triethylenetetramine)cobalt(III) complexes, [Co(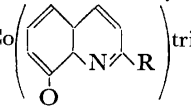)trien]$X_2 \cdot nH_2O$ (R: H, Me; X: Cl, NO_3), have been isolated from a reaction mixture of *cis*-α-dichloro(triethylenetetramine)cobalt(III) chloride, Ag_2O, and 8-quinolinol or 2-methyl-8-quinolinol. The separation of their *cis*-β_1 and β_2 isomers was achieved by the use of ion-exchange resin. The IR spectra of these complexes showed five or six absorption bands in the 990—1100 cm^{-1} region and four or five absorption bands in the 3000—3300 cm^{-1} region. This indicates that these complexes assume the β form. In *cis*-β_1-2-methyl-8-quinolinolato(triethylenetetramine)cobalt(III) complexes, the methyl group of the coordinated 2-methyl-8-quinolinolato ligand has a steric hindrance for the NH-side methylene protons of the coordinated trien ligand. On the other hand, no methyl group of the corresponding *cis*-β_2 form has steric hindrance for the methylene protons of the coordinated trien ligand. Therefore, the distinction of the *cis*-β_1 form and the β_2 form of these complexes has been clarified on the basis of their ^1H NMR spectra. Also, the ^{13}C NMR spectra of these complexes have shown two different configurations of the "*cis*-β_1 and β_2" forms.

In an octahedral configuration, the isomers of bis(8-quinolinolato)metal complexes with dialkyl,[2] dichloro,[3] dicarbonyl,[4] chloro and nitrosyl,[5] diammine,[6] or ethylenediamine ligands[7] have been reported in recent years, but those of (8-quinolinolato)metal complex have not yet been described, except for the *cis*-β_1 and *cis*-β_2-8-quinolinolato(triethyleneteramine) cobalt(III) complexes.[8]

Previously, we have been concerned with the isomers (*cis*-β_1 and β_2) of salicylato(quadridentate amine) cobalt(III)chloride[9] and of 8-quinolinolato(triethylenetetramine)cobalt(III) chloride.[8] The X-ray studies of both the isomers of the above complexes and related complexes[10] have also never been described yet, because their crystals could not be obtained. Now, we have found that the methyl group of the coordinated 2-methyl-8-quinolinolato ligand in the *cis*-β_1-2-methyl-8-quinolinolato(triethylenetetramine)cobalt (III) complexes has a steric hindrance for the NH-side methylene protons of the coordinated trien ligand, though no methyl group of the corresponding *cis*-β_2 form has the steric hindrance. The present paper will, then, deal with the preparation and properties of *cis*-β_1 and β_2-2-methyl-8-quinolinolato(triethylenetetramine)cobalt(III) complexes and with the assignment of the *cis*-β_1 and β_2 isomers of their NMR spectra.

Results and Discussion

Complexes. *cis*-2-Methyl-8-quinolinolato(triethylenetetramine)cobalt(III) chloride hydrates have three isomeric forms–*cis*-β_1, *cis*-β_2, and *cis*-α, as is shown in Fig. 1. In the *cis*-β_1 form, the methyl group of the coordinated 2-methyl-8-quinolinolato ligand has a position very near the N(3)H-side methylene protons of the coordinated trien ligand, so the methyl group can show a steric hindrance for the N(3)H-side methylene protons. Thus, in the ^1H NMR spectra, the methylene proton signals of the coordinated trien ligand must be different from those of the corresponding 8-quinolinolato complexes. However, the methyl group in the *cis*-β_2 or *cis*-α form does not show the steric hindrance, because the methyl group has a position far from the methylene protons of the coordinated trien ligand; *i.e.*, the methylene proton signals of the coordinated trien ligand differ little from those of the corresponding 8-quinolinolato complexes in the ^1H NMR spectra. Then, the distinction of the *cis*-β_1 form and *cis*-β_2 form or *cis*-α form can be expected to be clarified on the basis of their NMR spectra. Thus, we have isolated the *cis*-β_1-2-methyl-8-quinolinolato(trien)cobalt(III) chloride dihydrate and the corresponding *cis*-β_2 form.

TABLE 1. THE ABBREVIATIONS OF THE 8-QUINOLINOLATO-(TRIEN)COBALT(III) COMPLEXES

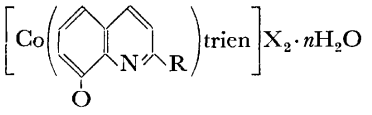

No.	1	2	3	4	5	6	7	8
Form	β_1	β_1	β_2	β_2	β_1	β_1	β_2	β_2
R	H	Me	H	Me	H	Me	H	Me
X	Cl	Cl	Cl	Cl	NO_3	NO_3	NO_3	NO_3
n	2	2	2	2	1	1	1	1

The abbreviations of the 8-quinolinolato- or 2-methyl-8-quinolinolato(trien)cobalt(III) complexes studied in this paper are listed in Table 1. A mixture of *cis*-β_1 and β_2-8-quinolinolato or 2-methyl-8-quinolinolato(trien)cobalt(III) chloride dihydrate was obtained from a reaction mixture of *cis*-α-dichloro(trien) cobalt(III) chloride,[11] Ag_2O, and 8-quinolinol or 2-

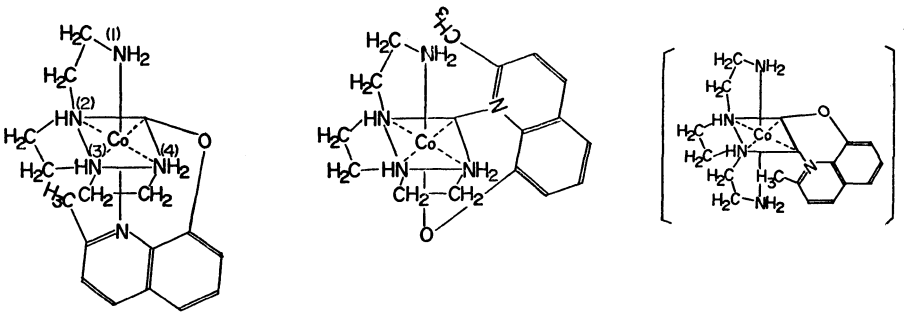

β_1 β_2 α

Fig. 1. The *cis*-α, β_1 and β_2 configurations of 2-methyl-8-quinolinolato(trien)cobalt(III) chloride.

TABLE 2. IR AND ABSORPTION SPECTRA OF COMPLEXES

Complex No.	IR spectra $\tilde{\nu}$/cm^{-1}				Absorption bands[1]	
	3000—3300		990—1100		λ/nm	ε
1	3040(sh)	3070	1005(w)	1030	326	970
	3120(sh)	3180	1040	1060	340	1200
	3220(sh)		1070	1085	410	2590
2	3000(sh)	3020	995	1035	325	940
	3080	3200(sh)	1050	1060	342	900
			1080(sh)	1090	403	2560
3	3020(sh)	3060	1010	1035(sh)	325	1050
	3150	3200(sh)	1040	1055	339	1280
			1060(sh)		407	2690
4	3050(sh)	3090	1010(w)	1020	325	1010
	3170	3220(sh)	1040	1060	343	970
			1075(w)		409	2620
5	3050(sh)	3080	1005(w)	1030	326	1030
	3140(sh)	3200	1040	1060	340	1260
	3250(sh)		1070	1085	410	2750
6	3020(sh)	3040	1000	1040	325	1030
	3100	3210	1055	1060	342	970
			1085(sh)	1090	401	2755
7	3020(sh)	3070	1010	1040(sh)	325	1050
	3150	3200(sh)	1045	1060	339	1290
			1070(sh)		407	2755
8	3020(sh)	3070	1010	1035	324	1030
	3150	3200(sh)	1050(sh)	1060	342	990
			1075(w)		400	2690

Solvent: 1) methanol.

methyl-8-quinolinol. The separation of the *cis*-β_1 and β_2 isomers was achieved by the use of ion-exchange resin. The *cis*-α form could not be isolated from the reaction mixture at pH 2—8.[12] From the reaction mixture of the *cis*-β_1 and β_2-8-quinolinolato or 2-methyl-8-quinolinolato(trien)cobalt(III) chloride dihydrate (**1**—**4**) and silver nitrate, the corresponding nitrate hydrates (**5**—**8**) have been prepared.

All the complexes are soluble in dimethyl sulfoxide, methanol, water, and acidic solvents, such as nitric acid, hydrochloric acid, but they are insoluble in the common organic solvents. Their β_1 forms are soluble in ethanol, though their β_2 forms are somewhat soluble in ethanol. The color in the solid state of **1** is reddish brown, **3** is yellowish brown, **2** and **5**—**7** are brown, and **4** and **8** are greyish black.

Their IR spectra showed five or six absorption bands in the 990—1100 cm^{-1} region and four or five absorption bands in the 3000—3300 cm^{-1} region, as is shown in Table 2. This indicates that they assumed the β form.[13]

NMR Spectra. The ^{1}H NMR spectra of **1**—**8** were measured in 1.8 mol dm^{-3} D_2SO_4. The signals of the methylene and amine protons of the coordinated trien ligands in **1**—**8** were assigned on the basis of the results in the previous papers.[9,10] The methylene protons of the coordinated trien ligand in **1** showed one signal, though those of the coordinated trien ligand in **3** showed two signals, in the 2.4—4.0 ppm region, as is shown in Table 3 and Fig. 2. The differences between **1** and **3** are similar to those between *cis*-β_1 and β_2-salicylato(trien)cobalt(III) chloride hydrate,[10] *cis*-β_1- and β_2-[Co(sal)trien]Cl·H_2O (**9**); therefore, the **1** and **3** complexes can be assigned to the *cis*-β_1 form

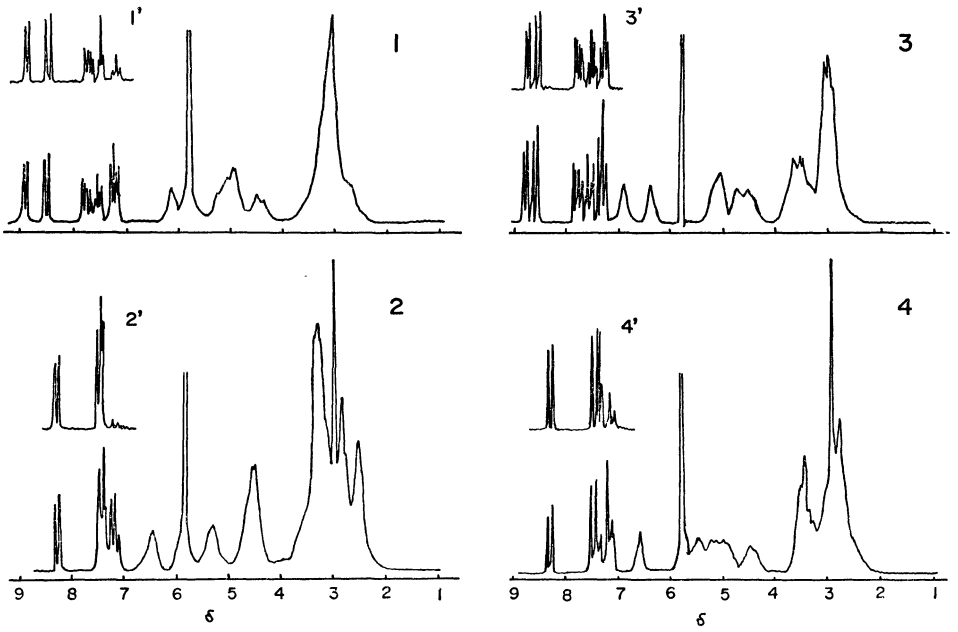

Fig. 2. The ^{1}H NMR spectra of **1**—**4** complexes.
1: *cis*-β_1-[Co(8-quinolinolato)trien]$Cl_2 \cdot 2H_2O$; 2: *cis*-β_1-[Co(2-methyl-8-quinolinolato)trien]$Cl_2 \cdot 2H_2O$; 3: *cis*-β_2-[Co(8-quinolinolato)trien)$Cl_2 \cdot 2H_2O$; 4: *cis*-β_2-[Co(2-methyl-8-quinolinolato)-trien]$Cl_2 \cdot 2H_2O$ in 1.8 mol dm^{-3} D_2SO_4.
The signals of **1**′—**4**′ are those in the 1.8 mol dm^{-3} D_2SO_4 solution after 25 min.

and *cis*-β_2 form respectively. In the ^{1}H NMR spectra of the **2** and **4** complexes, the methylene protons of **2** show three signals, and the intensity ratios are 2:2:8 in the 2.5—3.8 ppm region. These signals are different from those (one signal) of **1**, as is shown in Fig. 2. On the other hand, the methylene proton signals of **4** are little different from those of **3**. Therefore, the isomeric forms of **2** and **4** have been assigned to the *cis*-β_1 and *cis*-β_2 forms respectively.

In the **3** and **4** complexes, the signals at 2.2—3.2 ppm (8H) and 3.2—4.0 ppm (4H) have been assigned to the NH-side methylene protons and the NH_2-side methylene protons of the coordinated trien ligand respectively. The chemical shift of the NH-side methylene protons of the **3** and **4** complexes is at a higher field than that of the NH_2-side methylene protons. This property is different from that of **9**.[9] This can be attributed to the electronic and structural effects of the coordinated 8-quinolinolato and salicylato ligands. On the other hand, the signals of the amine protons of the coordinated trien ligand in **2** and **4** are different from those of **1** and **3**. This can be based on the electronic effect of the methyl group of the coordinated 2-methyl-8-quinolinolato ligand in the **2** and **4** complexes. The NMR spectral data of the nitrate complexes (**5**—**8**) are similar to those of the chloride complexes (**1**—**4**), as is shown in Table 3.

In the ^{1}H NMR spectra of **1**—**4**, both the ring proton signals (H-5 and H-7) of the coordinated 8-quinolinolato or 2-methyl-8-quinolinolato ligand changed to the proton signals of **1**′, **2**′, **3**′, and **4**′ after 25 min, as is shown in Fig. 2. Then, both the ring protons were replaced at deuterium in a 1.8 mol dm^{-3} D_2SO_4 solution. The order of the replacement is: **3**<**1**<**4**<**2**. Thus, the deuterium replacement of the *cis*-β_1

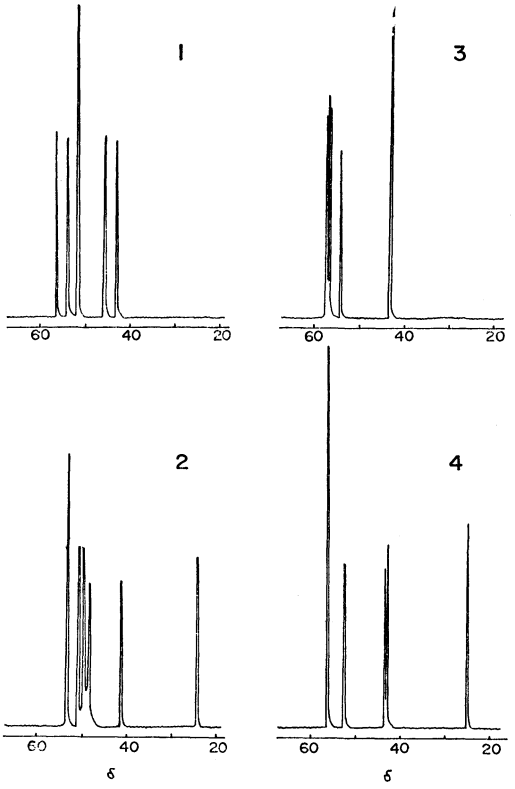

Fig. 3. The ^{13}C NMR spectra of **1**—**4** complexes in D_2O.
1: *cis*-β_1-[Co(8-quinolinolato)trien]$Cl_2 \cdot 2H_2O$; 2: *cis*-β_1-[Co(2-methyl-8-quinolinolato)trien]$Cl_2 \cdot 2H_2O$; 3: *cis*-β_2-[Co(8-quinolinolato)trien]$Cl_2 \cdot 2H_2O$; 4: *cis*-β_2-[Co(2-methyl-8-quinolinolato)trien]$Cl_2 \cdot 2H_2O$.

TABLE 3. ^{1}H AND ^{13}C NMR

^{1}H	$NH_2CH_2CH_2NHCH_2CH_2NHCH_2CH_2NH_2$ δ					
Complex (Form)	$-CH_2NHCH_2CH_2NH_2$	$NHCH_2CH_2NH_2$	$N(1)H_2$	$N(4)H_2$	N(3)H	N(2)H
1 (β_1)	2.42—3.76(12H)		4.48(1H) 4.69—5.37(3H)		a)	6.14(1H)
2 (β_1)	2.51(2H) 2.81(2H)	3.03—3.80(8H)	4.52(3H)	5.31(1H)	a)	6.45(1H)
3 (β_2)	2.39—3.24(8H)	3.24—4.01(4H)	4.43(1H) 4.64(1H)	5.06(2H)	6.37(1H)	6.87(1H)
4 (β_2)	2.27—3.22(8H)	3.22—3.78(4H)	4.47(1H) 4.70—5.36(2H)	5.50(1H)	a)	6.60(1H)
5 (β_1)	2.43—3.76(12H)		4.44(1H) 4.72—5.36(3H)		a)	6.13(1H)
6 (β_1)	2.51(2H) 2.82(2H)	3.03—3.91(8H)	4.53(3H)	5.29(1H)	5.93(1H)	6.39(1H)
7 (β_2)	2.42—3.27(8H)	3.27—4.03(4H)	4.46(1H) 4.68(1H)	5.02(2H)	6.31(1H)	6.82(1H)
8 (β_2)	2.20—3.22(8H)	3.22—3.82(4H)	4.47(1H) 4.75—5.32(2H)	5.49(1H)	a)	6.61(1H)

^{13}C	$NH_2CH_2CH_2NHCH_2CH_2NHCH_2CH_2NH_2$ δ						(2-Methyl-)			
	$NHCH_2CH_2NH_2$		$-CH_2NHCH_2CH_2NH_2$				C-2	C-3	C-4	C-5
1 (β_1)	43.4	46.1	52.1	54.5	56.5		150.1	114.9	141.3	124.0
2 (β_1)	41.5	48.4	49.5	50.9	53.5		164.3	114.7	140.8	127.8
3 (β_2)	43.3		54.1	56.7	56.8	57.2	151.5	115.1	141.0	124.2
4 (β_2)	43.1	43.6	52.4	56.3			163.9	115.2	141.0	127.0
L							156.9	109.8	136.1	122.7

Solvent and standard: 1) 1.8 mol dm^{-3} D_2SO_4, internal DSS, 2) D_2O, internal dioxane (δ=67.4), 3) $CDCl_3$, internal $CDCl_3$ (δ=77.1). a): This signal overlapped with each solvent. **L**: 2-methyl-8-quinolinol.

form is faster than that of the *cis*-β_2 form. In both *cis*-β_1 and β_2 complexes, that of the 2-methyl-8-quinolinolato complexes is faster than that of the 8-quinolinolato complexes.

In the ^{13}C NMR spectra of the **1**—**4** complexes in D_2O, there have been observed four or five signals for the coordinated trien ligand and nine or ten signals for the coordinated 8-quinolinolato or 2-methyl-8-quinolinolato ligands. From Fig. 3, it can be seem that the spectrum of **4** is very similar to that of **3**, but the spectrum of **2** is different from that of **1** because of the steric hindrance of the methyl group. These results also suggest that the **3** and **4** complexes are *cis*-β_2 form, while the **1** and **2** complexes are *cis*-β_1 form. The chemical shifts of the coordinated 8-quinolinolato or 2-methyl-8-quinolinolato ligands[7] in **1**—**4** are assigned; they are collected in Table **3**. The carbon signals of C-2 of the coordinated 2-methyl-8-quinolinolato ligands in the **2** and **4** complexes shift to a low field. This is the effect of the methyl group[14] of the coordinated 2-methyl-8-quinolinolato ligand. The chemical shifts of the coordinated trien ligand in **1**—**4** are difficult to assign to the individual carbon atom, though they are collected in the two groups[9] of the NH-side methylene carbons and the NH_2-side methylene carbons.

Other Properties. The absorption spectra of **1**—**8** have three absorption bands around 325, 340, and 400 nm in methanol as is shown in Table 2. The absorption bands at 340 nm of the **1**, **3**, **5**, and **7** complexes are stronger than those at 325 nm, though the absorption bands at 340 nm of the **2**, **4**, **6**, and **8** complexes are weaker than those at 325 nm, as is shown in Table 2. This property is based on the substituted methyl group in the coordinated 8-quinolinolato ligand. The absorption bands around 400 nm are charge-transfer bands.[6,7] All the complexes are diamagnetic, and their electric conductivities in an aqueous solution are 225—250 S cm^2 equiv.$^{-1}$

Experimental

Measurements. The NMR spectra were recorded with an FX-60 spectrometer (JEOL) for ^{13}C NMR and with an R-40 apparatus (Hitachi) for ^{1}H NMR. The IR spectra were recorded over potassium bromide disks with a IR-27G spectrophotometer (Shimadzu). The visible absorption spectra were recorded with a Shimadzu MPS-5000 recording spectrophotometer. The electric conductivities of an aqueous solution were determined by the use of a conductmetric meter, CM-30 (Shimadzu), at room temperature. The pH was measured with a Corning pH-meter M-125. The magnetic susceptibilities were measured by Faraday's method using a magnetic balance (Shimadzu) at room temperature.

Preparation of Complexes. *cis-β-8-Quinolinolato(trien)-cobalt(III) Chloride Dihydrate (**A**) and cis-β-2-Methyl-8-quinolinolato(trien)cobalt(III) Chloride Dihydrate (**B**)*: A methanol solution (100 cm^3) of 8-quinolinol (4.35 g, 30 mmol) (or 2-methyl-8-quinolinol (4.78 g, 30 mmol)) was added, drop by drop, to an aqueous solution (100 cm^3) of $[CoCl(OH)-trien]^+$,[15] which had been prepared from *cis*-α-dichloro-(trien)cobalt(III) chloride[11] (9.35 g, 30 mmol), and Ag_2O, which had been prepared from $AgNO_3$ (5.1 g, 30 mmol) and KOH (1.69 g, 30.1 mmol). The mixture was then stirred for 30 h at 50 °C. In the reaction, *cis*-α-dichloro-(trien)cobalt(III) chloride isomerized to the corresponding β form. The reaction mixture was then concentrated on a rotary evaporater and dried over silica gel. Complex **A** (or **B**) was extracted with methanol from the dried mixture and was recrystallized from water. Yields: 6.10 g (44.6%) for **A**; 6.51 g (46.1%) for **B**.

*Separation of cis-β$_1$-8-Quinolinolato(trien)cobalt(III) Chloride Dihydrate (**1**), cis-β$_1$-2-Methyl-8-quinolinolato(trien)cobalt(III)*

SPECTRA OF COMPLEXES

(2-Methyl-)8-quinolinolato δ							
H-5	H-7	H-6	H-3	H-4	H-2	CH_3	Solvent
7.22 d	7.26 d	7.51 dd	7.75 dd	8.52 d	8.92 d	—	1
7.00—7.27 (2H)		7.27—7.51 (2H)		8.24 d	—	2.98 (s, 3H)	1
7.16—7.36 (2H)		7.51 dd	7.74 dd	8.54 d	8.73 d	—	1
7.05—7.28 (2H)		7.28—7.60 (2H)		8.30 d	—	2.96 (s, 3H)	1
7.21 d	7.23 d	7.49 dd	7.74 dd	8.52 d	8.91 d	—	1
7.00—7.30 (2H)		7.31—7.52 (2H)		8.25 d	—	2.96 (s, 3H)	1
7.15—7.36 (2H)		7.50 dd	7.72 dd	8.52 d	8.70 d	—	1
7.07—7.30 (2H)		7.30—7.58 (2H)		8.30 d	—	2.98 (s, 3H)	1

8-quinolinolato δ						
C-6	C-7	C-8	C-9	C-10	CH_3	
115.9	131.2	146.5	165.1	131.4	—	2
116.3	129.9	146.2	164.6	129.4	24.7	2
116.5	131.4	145.9	164.6	131.4	—	2
116.6	129.8	145.3	164.5	129.9	25.1	2
117.6	126.7	137.7	151.8	126.7	24.9	3

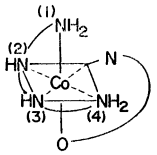

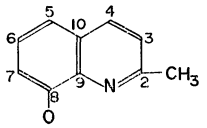

Chloride Dihydrate (2), cis-β_2-*8-Quinolinolato(trien)cobalt(III) Chloride Dihydrate (3)*, *and* cis-β_2-*2-Methyl-8-quinolinolato-(trien)cobalt(III) Chloride Dihydrate (4)*: Five-tenths of a gram of *cis-β*-[Co(oxine-R)trien]$Cl_2 \cdot 2H_2O$ (R: H, CH_3) was dissolved in 1.5 cm^3 of water, after which the solution was passed through a large column of cation-exchange resin (2.5×30 cm, SP-Sephadex C-25, Na^+ form). Two bands separated on subsequent elution with a 0.2 mol dm^{-3} Na_2SO_4 solution. Solutions of the first band (β_2 complex) and of the second band (β_1 complex) were concentrated in a rotary evaporator, and the Na_2SO_4 was removed by filtration. The *cis-*β_1 and β_2 complexes were recrystallized from water-acetone twice. Yields: 0.05 g (10.0%) for **1**; 0.04 g (8.0%) for **2**; 0.42 g (84.0%) for **3**; 0.41 g (82.0%) for **4**. Found **1**: C, 39.78; H, 6.48; N, 15.20; Cl, 15.50%. **2**: 40.48; H, 6.72; N, 14.84; Cl, 14.86%. **3**:C, 39.47; H, 6.29; N, 15.13; Cl, 15.30%. **4**: C, 40.79; H, 6.33; N, 14.87; Cl, 15.12%. Calcd for **1** and **3**: $CoC_{15}H_{28}N_5O_3Cl_2$ (MW 456.26), C, 39.49; H, 6.19; N, 15.35; Cl, 15.54%. **2** and **4**: $CoC_{16}H_{30}N_5O_3Cl_2$ (MW 470.29) C, 40.86; H, 6.43; N, 14.89; Cl, 15.08%. Mp (or Decomp) **1**: (237—238 °C), **2**: 211—213 °C, **3**: (241—243 °C), **4**: 213—215 °C. Λ=250 for **1**, 230 for **2**, 240 for **3**, and 225 S cm^2 equiv.$^{-1}$ for **4** in water.

cis-β_1-*8-Quinolinolato(trien)cobalt(III) Nitrate Hydrate (5) and* cis-β_2-*8-Quinolinolato(trien)cobalt(III) Nitrate Hydrate (7)*: To an aqueous solution of Complex **1** or **3** (0.5 g, 1.10 mmol) we added an aqueous solution of silver nitrate (0.38 g, 2.24 mmol). The mixture was then stirred, and the silver chloride thus precipitated was filtered. The filtrate was concentrated. Complexes **5** and **7** were recrystallized from water twice. Yields: 0.46 g (85.2%) for **5**, 0.48 g (88.9%) for **7**. Found **5**: C, 36.96; H, 5.04; N, 20.25%. **7**: C, 37.23; H, 5.22; N, 19.72%. Calcd for $CoC_{15}H_{26}N_7O_8$ (MW 491.35) C, 36.67; H, 5.33; N, 19.95%.

cis-β_1-*2-Methyl-8-quinolinolato(trien)cobalt(III) Nitrate Hydrate (6) and* cis-β_2-*2-Methyl-8-quinolinolato(trien)cobalt(III) Nitrate Hydrate (8)*: These complexes were prepared from Complex **2** or **4** (0.5 g, 1.06 mmol) and silver nitrate (0.36 g, 2.12 mmol) according to the method used for Complexes **5** and **7**. Yields: 0.4 g (74.6%) for **6**, 0.42 g (78.4%) for **8**. Found **6**: C, 38.71; H, 5.18; N, 19.49%. **8**: C, 37.67; H, 5.38; N, 19.91%. Calcd for $CoC_{16}H_{28}N_7O_8$ (MW 505.38) C, 38.03; H, 5.58; N, 19.40%.

References

1) Part III: Ref. 9.
2) a) E. O. Schlemper, *Inorg. Chem.*, **6**, 2012 (1967); b) T. Tanaka, M. Komura, Y. Kawasaki and R. Okawara, *J. Organomet. Chem.*, **1**, 484 (1964).
3) B. F. Studd and A. G. Swallow, *J. Chem. Soc., A.*, **1968**, 1961.
4) J. A. Van Doorn and P. W. N. M. Van Leeuwen, *J. Organomet. Chem.*, **222**, 299 (1981).
5) Y. Wada, R. Hirota, E. Miki, K. Mizumachi, T. Ishimori, and T. Kimura, The 32nd Symposium on Coordination Chemistry of the Chemical Society of Japan, 1A13, 44 (1982).
6) Y. Yamamoto, *Chem. Lett.* **1980**, 1555.
7) Y. Yamamoto, R. Kataoka, S. Imahara, and T. Amano, *Bull. Chem. Soc. Jpn.*, **54**, 2972 (1981).
8) Y. Yamamoto and E. Toyota, *Chem. Pharm. Bull.*, **28**, 3153 (1980).
9) Y. Yamamoto, H. Kudo, and E. Toyota, *Bull. Chem. Soc. Jpn.*, **56**, 1051 (1983).
10) a) Y. Yamamoto, E. Toyota, and N. Mitsudera, *Bull. Chem. Soc. Jpn.*, **53**, 3517 (1980); b) Y. Yamamoto

and E. Toyota, *Bull. Chem. Soc. Jpn.*, **52**, 2540 (1979); c) Y. Yamamoto and E. Toyota, *Chem. Pharm. Bull.*, **26**, 2275 (1978).

11) A. M. Sargeson and G. H. Searle, *Inorg. Chem.*, **6**, 787 (1967).

12) B. F. Anderson, J. D. Bell, D. A. Bukingham, P. J. Cresswell, G. J. Gainsford, L. G. Marzilli, G. B. Robertson, and A. M. Sargeson, *Inorg. Chem.* **16**, 3233 (1977).

13) D. A. Buckingham and D. Jones, *Inorg. Chem.*, **4**, 1387 (1965).

14) a) G. C. Levy, G. L. Nelson, and J. D. Cargioli, *J. Am. Chem. Soc.*, **94**, 3089 (1972); *J. Chem. Soc., Chem. Commun.*, **1971**, 506; b) G. C. Levy and G. L. Nelson, "Carbon-13 NMR for Organic Chemist," Wiley-Interscience, New York (1972), p. 81.

15) E. Kyuno, L. J. Boucher, and J. C. Bailar, *J. Am. Chem. Soc.*, **87**, 4458 (1965).

 © 1983 The Chemical Society of Japan Bull. Chem. Soc. Jpn., 56, 2727—2732 (1983)

Synthesis, Characterization, and Crystal-structure Analysis of the 2:1 Molecular Complexes between 1,3,5-Trinitrobenzene and Copper(II), Nickel(II), or Palladium(II) Complexes with the Schiff Base Ligands Derived from *o*-Hydroxynaphthaldehydes and Monoamines

Naohide Matsumoto,* Tadanori Hara, Akira Hirano, and Akira Ohyoshi

Department of Industrial Chemistry, Faculty of Engineering, Kumamoto University, Kurokami 2-39-1, Kumamoto 860

(Received January 25, 1983)

The molecular complexes between 1,3,5-trinitrobenzene(TNB) and copper(II), nickel(II), or palladium(II) complexes with the Schiff base ligands derived from 1-hydoxy-2-naphthaldehyde or 2-hydroxy-1-naphthaldehyde and monoamines (RNH_2: R=CH_3, C_2H_5, *n*-C_3H_7, *i*-C_3H_7, *n*-C_4H_9) have been prepared and characterized. One of the molecular complexes bis(1-(isopropyliminomethyl)-2-naphtholato)palladium(II)-bis(1,3,5-trinitrobenzene) (Pd(2,1-*i*-$C_3H_7)_2\cdot$2TNB) has been subjected to the single-crystal X-ray analysis. Its crystal structure consists of alternately stacked donor (naphthalene moiety of the metal complex) and acceptor (TNB) molecules. The coordination geometry is a square planar with a markedly stepped chair-like shape, where the seat and the rests are formed by the coordination plane (PdO_2N_2) and two naphthalene moieties. The Pd atom is deviated by 0.62 Å from the least-squares plane of the naphthalene ring and the dihedral angle between the coordination plane and the naphthalene ring is 25.1°. When the crystal structure was viewed perpendicular to the donor or acceptor plane, the center of the TNB molecule coincides approximately the center of terminal benzene ring of the naphthalene moiety. Electronic spectra of the molecular complexes in Nujol mull showed a new band at about 18×10^3 cm^{-1}, which was not observed in solution spectra.

Previously[1,2] we have studied the 2:1 molecular complexes between TCNQ and the Schiff base metal complexes **1** or **2**, in order to investigate the structure of the molecular complex in which both the π–π type donor-acceptor interaction and the steric hindrance of the *N*-substituted alkyl group causing a tetrahedral distortion of the coordination geometry are operating simultaneously, where the abbreviations of the compounds are shown in Fig. 1. The results indicated that the donor-acceptor interaction can affect the coordination geometry and the steric hindrance between two neighboring acceptor molecules lied on the naphthalene moieties of the complex as well as the overlapping mode between donor and acceptor molecules is important for the formation of the molecular complex. TNB molecule takes C_{3v} symmetry, while TCNQ takes D_{2h} symmetry. Based on preliminary molecular model consideration, TNB molecule seems to be sterically much favorable for the formation of the molecular complex with **1** or **2** than TCNQ, although TNB is a weaker π-electron acceptor than TCNQ. In this study, TNB instead of TCNQ was used to examine whether the complexes **1** or **2** can form the molecular complexes with TNB. One of the molecular complexes with TNB, Pd(2,1-*i*-$C_3H_7)_2\cdot$2TNB has been subjected to the single-crystal X-ray analysis, in order to confirm the basic structure for a series of the molecular complexes with TNB and compare the overlapping mode of TNB adduct with that of TCNQ adduct.

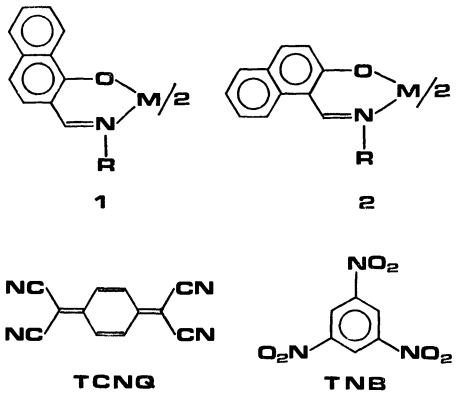

Fig. 1. Structures of Schiff base metal complexes **1** and **2**, and 7,7,8,8-tetracyanoquinodimethane (TCNQ), and 1,3,5-trinitrobenzene (TNB). Bis(2-(alkyliminomethyl)-1-naphtholato)metal(II) (**1**) and bis(1-(alkyliminomethyl)-2-naphtholato)metal(II) (**2**) are abbreviated as M(1,2-R)$_2$ and M(2,1-R)$_2$, respectively, where M and R denote metal ion and alkyl group, respectively.

Experimental

Physical Measurements. Elemental analyses were performed by Mr. Shinichi Miyazaki at the Technical Service Center of Kumamoto University. Electronic spectra were measured on a Shimadzu UV-200 spectrometer in Nujol mull and on a Hitachi recording spectrophotometer 323 in acetone-chloroform solution. Thermogravimetric analysis (TGA) was carried out on a Shimadzu TGC-20 type microthermobalance at the heating rate of 5 °C min^{-1}. Differential scanning calorimetry (DSC) was carried out on a Shimadzu DT-20Bs and DSC-20 and the calibration was made by the use of Indium metal.

Syntheses. 1-Hydroxy-2-naphthaldehyde was prepared by the method of Weil and Ostermeier.[3] 2-Hydroxy-1-naphthaldehyde was purchased from Tokyo Chemical Industry Co., Ltd.

*Parent Complexes **1** and **2**.* Bis(1-(alkyliminomethyl)-2-naphtholato)copper(II), -nickel(II), and -palladium(II) were prepared by the method of Chakravorty and Holm[4] from the Schiff base reaction of bis(1-formyl-2-phtholato)-coppor(II), -nickel(II), and -palladium(II) with monoamines, where the complexes are abbreviated as M(2,1-R)$_2$ (M=Cu^{2+}, Ni^{2+}, Pd^{2+}; R=CH_3, C_2H_5, *n*-C_3H_7, *i*-C_3H_7, *n*-C_4H_9, *i*-C_4H_9, *s*-C_4H_9, *t*-C_4H_9). Bis(2-(alkyliminomethyl)-1-naphtholato)copper(II) was also prepared according to the literature[4] and abbreviated as Cu(1,2-R)$_2$ (R=CH_3, C_2H_5,

TABLE 1. FINAL ATOMIC PARAMETERS OF Pd(2,1-*i*-$C_3H_7)_2$·2TNB. THE ATOMIC PARAMETERS HAVE BEEN MULTIPLIED BY 10^4

Atom	*x*	*y*	*z*	B_{eq}/Å^2
Pd	0	0	0	1.5
O(1)	853(3)	581(9)	1603(5)	2.2
N(1)	405(4)	1992(10)	−453(6)	1.8
C(1)	1692(5)	2207(13)	1401(7)	1.8
C(2)	1517(5)	1340(13)	2037(7)	1.9
C(3)	2070(5)	1302(15)	3203(7)	2.4
C(4)	2797(6)	1998(15)	3739(8)	2.7
C(5)	3031(5)	2734(13)	3133(8)	2.4
C(6)	3841(5)	3303(15)	3713(8)	3.0
C(7)	4064(6)	3934(14)	3128(9)	3.1
C(8)	3513(6)	4052(15)	1971(8)	2.8
C(9)	2738(5)	3522(14)	1385(8)	2.6
C(10)	2480(5)	2872(13)	1961(7)	2.0
C(11)	1123(5)	2606(13)	244(7)	1.9
C(12)	−145(5)	2786(14)	−1584(7)	2.1
C(13)	−623(6)	4264(16)	−1576(9)	3.6
C(14)	256(6)	3508(16)	−2012(8)	2.8
O(2)	2654(6)	−3078(16)	3895(8)	7.8
O(3)	3922(5)	−2953(15)	5070(7)	6.7
O(4)	5290(4)	−580(14)	3859(7)	6.3
O(5)	4648(4)	506(12)	2187(7)	5.0
O(6)	1817(4)	−266(14)	−431(6)	5.1
O(7)	1384(5)	−2505(14)	−43(7)	6.7
N(2)	3285(6)	−2753(14)	4162(8)	4.6
N(3)	4699(5)	−269(15)	2925(8)	4.2
N(4)	1872(5)	−1421(14)	169(7)	3.9
C(15)	3284(6)	−2128(15)	3237(8)	3.1
C(16)	3987(6)	−1527(14)	3508(8)	2.9
C(17)	3957(6)	−941(15)	2656(9)	2.9
C(18)	3276(6)	−843(15)	1554(8)	2.9
C(19)	2601(6)	−1496(15)	1331(8)	2.9
C(20)	2586(6)	−2122(14)	2149(8)	2.8

n-C_3H_7, *i*-C_3H_7, *n*-C_4H_9, *i*-C_4H_9, *s*-C_4H_9, *t*-C_4H_9). The parent complexes are identified by their elemental analyses and melting points.[5]

Molecular Complexes with TNB. The method for the preparation of the molecular complexes is practically the same and exemplified by the synthesis of Pd(2,1-*i*-$C_3H_7)_2$·2TNB. A solution of Pd(2,1-*i*-$C_3H_7)_2$ (5 mmol) in 20 cm^3 of dichloromethane is added to a solution of TNB (10 mmol) in 20 cm^3 of acetone. The solution was warmed at 40 °C for 5 min in a water bath, which on standing overnight in a refrigerator precipitated red needle crystals. They were collected and dried *in vacuo*. The other molecular complexes were prepared under the same reaction condition described above.

*X-Ray Analysis of Pd(2,1-*i*-$C_3H_7)_2$·2TNB.* Red needle crystals were prepared by slow precipitation of an equivolume solution of dichloromethane and acetone at room temperature. A crystal with approximate dimensions of $0.2\times0.3\times0.5$ mm^3 was used for the X-ray diffraction study. The unit cell parameters and intensity data were measured on a Rigaku Denki AFC-5 automated four-circle diffractometer with a graphite monochromatized Mo $K\alpha$ radiation at 20±1 °C. The unit cell parameters were determined by the least-squares method based on 20 reflections in the range of $18°<2\theta<28°$. Crystal data: $PdO_{14}N_8C_{40}H_{34}$, F.W.=957.2, monoclinic, space group $P2_1/c$, $a=22.236(7)$, $b=7.255(1)$, $c=15.584(4)$ Å, $\beta=129.66(1)°$, $V=1935.2(10)$ Å^3, $D_m=1.63$ (by flotation method in aqueous KI solution), $D_x=1.643$ g cm^{-3} ($Z=2$), and $\mu=3.8$ cm^{-1} (Mo $K\alpha$).

Intensity data were collected by the $\theta-2\theta$ scan technique with a scan rate of 8° min^{-1}. For weak reflections the peak scan was repeated up to three times depending on their intensities. Three check reflections were monitored every 100 reflections throughout the set and displayed no decay of intensities. A total of 3392 independent reflections with $1.5°<2\theta<48°$ were collected, of which 2601 reflections with $|F_o|>3\sigma(|F_o|)$ were used for the structure analysis. Lorentz and polarization corrections were applied, but no correction for absorption was made because of the crystal size and low absorption coefficient.

TABLE 2. ELEMENTAL ANALYSES OF MOLECULAR COMPLEXES

Complex	Found (Calcd) (%)		
	C	H	N
Cu(2,1-$CH_3)_2$·2TNB	50.14(50.38)	3.03(3.05)	12.89(13.06)
Cu(2,1-$C_2H_5)_2$·2TNB	51.43(51.50)	3.41(3.41)	12.70(12.64)
Cu(2,1-*n*-$C_3H_7)_2$·2TNB	52.33(52.55)	3.66(3.75)	12.28(12.26)
Cu(2,1-*i*-$C_3H_7)_2$·2TNB	52.55(52.55)	3.66(3.75)	12.18(12.26)
Cu(2,1-*n*-$C_4H_9)_2$·2TNB	53.43(53.53)	4.03(4.06)	11.75(11.89)
Ni(2,1-$CH_3)_2$·2TNB	50.65(50.67)	3.08(3.07)	13.10(13.13)
Ni(2,1-$C_2H_5)_2$·2TNB	51.86(51.78)	3.43(3.43)	12.75(12.71)
Ni(2,1-*n*-$C_3H_7)_2$·2TNB	52.56(52.83)	3.77(3.77)	12.36(12.32)
Ni(2,1-*i*-$C_3H_7)_2$·2TNB	52.81(52.83)	3.69(3.77)	12.33(12.32)
Ni(2,1-*n*-$C_4H_9)_2$·2TNB	53.83(53.81)	4.09(4.09)	11.94(11.95)
Pd(2,1-*n*-$C_3H_7)_2$·2TNB	50.20(50.19)	3.51(3.58)	11.76(11.71)
Pd(2,1-*i*-$C_3H_7)_2$·2TNB	50.17(50.19)	3.50(3.58)	11.76(11.71)
Pd(2,1-*n*-$C_4H_9)_2$·2TNB	51.17(51.20)	3.83(3.89)	11.34(11.37)
Cu(1,2-*n*-$C_3H_7)_2$·2TNB	52.44(52.55)	3.70(3.75)	12.25(12.26)
Cu(1,2-*i*-$C_3H_7)_2$·2TNB	52.32(52.55)	3.69(3.75)	12.27(12.26)
Cu(1,2-*n*-$C_4H_9)_2$·2TNB	53.12(53.53)	3.91(4.06)	11.93(11.89)

TABLE 3. BOND DISTANCES AND ANGLES WITH THEIR ESTIMATED STANDARD DEVIATIONS FOR 1:2 MOLECULAR ADDUCT BETWEEN BIS(1-(ISOPROPYLIMINOMETHYL)-2-NAPHTHOLATO)PALLADIUM(II) AND 1,3,5-TRINITROBENZENE

Bond distance	l/Å	Bond distance	l/Å	Bond distance	l/Å	Bond distance	l/Å
Bis(1-(isopropyliminomethyl)-2-naphtholato)-palladium(II)				1,3,5-Trinitrobenzene			
Pd-O(1)	1.991(8)	C(7)-C(8)	1.39(1)	N(2)-O(2)	1.20(1)	C(17)-C(18)	1.38(1)
Pd-N(1)	2.054(9)	C(8)-C(9)	1.39(1)	N(2)-O(3)	1.21(1)	C(18)-C(19)	1.39(1)
O(1)-C(2)	1.29(1)	C(9)-C(10)	1.41(1)	N(2)-C(15)	1.51(1)	C(19)-N(4)	1.47(1)
C(2)-C(1)	1.42(1)	C(10)-C(1)	1.45(1)	C(15)-C(16)	1.40(1)	N(4)-O(6)	1.20(1)
C(2)-C(3)	1.40(1)	C(1)-C(11)	1.42(1)	C(16)-C(17)	1.35(1)	N(4)-O(7)	1.20(1)
C(3)-C(4)	1.36(1)	C(11)-N(1)	1.30(1)	C(17)-N(3)	1.50(1)	C(19)-C(20)	1.37(1)
C(4)-C(5)	1.44(1)	N(1)-C(12)	1.47(1)	N(3)-O(4)	1.20(1)	C(20)-C(15)	1.38(1)
C(5)-C(6)	1.46(1)	C(12)-C(13)	1.51(1)	N(3)-O(5)	1.21(1)		
C(5)-C(10)	1.41(1)	C(12)-C(14)	1.50(1)				
C(6)-C(7)	1.36(1)						

Bond angle	ϕ/°	Bond angle	ϕ/°
Bis(1-(isopropyliminomethyl)-2-naphtholato)palladium(II)			
N(1)-Pd-O(1)	90.3(3)	C(9)-C(10)-C(1)	123(1)
Pd-O(1)-C(2)	127.1(7)	C(9)-C(10)-C(5)	118(1)
O(1)-C(2)-C(3)	115(1)	C(5)-C(10)-C(1)	118(1)
O(1)-C(2)-C(1)	123(1)	C(10)-C(1)-C(11)	116.6(9)
C(1)-C(2)-C(3)	120(1)	C(10)-C(1)-C(12)	119(1)
C(2)-C(3)-C(4)	120(1)	C(2)-C(1)-C(11)	123(1)
C(3)-C(4)-C(5)	121(1)	C(1)-C(11)-N(1)	127(1)
C(4)-C(5)-C(6)	121(1)	C(11)-N(1)-C(12)	119.9(9)
C(4)-C(5)-C(10)	119(1)	C(11)-N(1)-Pd	121.6(7)
C(10)-C(5)-C(6)	119(1)	Pd-N(1)-C(12)	118.3(7)
C(5)-C(6)-C(7)	120(1)	N(1)-C(12)-C(13)	108.4(9)
C(6)-C(7)-C(8)	119(1)	N(1)-C(12)-C(14)	113.0(9)
C(7)-C(8)-C(9)	121(1)	C(13)-C(12)-C(14)	111(1)
C(8)-C(9)-C(10)	120(1)		
1,3,5-Trinitrobenzene			
C(20)-C(15)-C(16)	121(1)	C(17)-N(3)-O(5)	117(1)
C(20)-C(15)-N(2)	119(1)	O(4)-N(3)-O(5)	126(1)
N(2)-C(15)-C(16)	118(1)	C(17)-C(18)-C(19)	116(1)
C(15)-N(2)-O(2)	115(1)	C(18)-C(19)-C(20)	122(1)
C(15)-N(2)-O(3)	115(1)	C(18)-C(19)-N(4)	117(1)
O(2)-N(2)-O(3)	127(1)	N(4)-C(19)-C(20)	119(1)
C(15)-C(16)-C(17)	117(1)	C(19)-N(4)-O(6)	117(1)
C(16)-C(17)-C(18)	124(1)	C(19)-N(4)-O(7)	113(1)
C(16)-C(17)-N(3)	118(1)	O(6)-N(4)-O(7)	128(1)
N(3)-C(17)-C(18)	117(1)	C(19)-C(20)-C(15)	117(1)
C(17)-N(3)-O(4)	115(1)		

Structure Determination. The Pd atom is required to lie at an inversion center from the consideration of the space group and the number of the formula unit in the unit cell. A Fourier synthesis based on the Pd atom revealed all the nonhydrogen atoms. Block-diagonal least-squares refinement was calculated by initially isotropic thermal parameters and the anisotropic ones, where the function minimized was $\sum w(|F_o|-k|F_c|)^2$ and $w=1/\sigma(|F_o|)^2$. At this stage, a difference Fourier synthesis was calculated and located all the hydrogen atoms at the chemically reasonable positions. Further refinement including the hydrogen atoms with anisotropic thermal parameters for nonhydrogen atoms and isotropic ones for hydrogen atoms was calculated to give final discrepancy indices of 6.26 and 6.95% for $R=\sum||F_o|-|F_c||/\sum|F_o|$ and $R_w=[\sum w(|F_o|-|F_c|)^2/\sum w|F_o|^2]^{1/2}$, respectively. A final difference Fourier synthesis showed no regions of significant electron density (less than 0.5 e Å^{-3}).

The neutral atomic scattering factors for H, C_{cov}, N, O, and Pd were taken from International Tables for X-Ray Crystallography, Vol. IV.[6] Anomalous dispersion corrections $\Delta f'$ and $\Delta f''$ for all the component atoms were also taken from the literature.[6] All the calculations were carried out on a FACOM M-200 computer at the Computer Center of Kyushu University by the use of local version[7] of the UNICS II Crystallographic Computing System.[8] Final positional parameters with their estimated standard deviations are given in Table 1. Lists of struc-

ture factors and anisotropic thermal parameters have been deposited as the supplementary data at the Chemical Society of Japan as Document No. 8338.

Results and Discussion

Preparations of Molecular Complexes with TNB. In this study, the 2:1 molecular complexes between TNB and Schiff base copper(II), nickel(II), or palladium (II) complexes with the structure of **1** or **2** have been isolated by mixing a dichloromethane solution of **1** or **2** and an acetone solution of TNB under the reaction conditions noted in the experimental section. Their elemental analytical data are given in Table 2. It seems that the parent complex **1** or **2** forms the molecular complex preferably with TNB rather than with TCNQ, because all the parent complexes which formed the molecular complexes with TCNQ[1] formed the molecular complexes with TNB and some of other **1** or **2** formed the molecular complexes with TNB.

Crystal and Molecular Structure of Pd(2,1-i-C_3H_7)$_2$·2TNB. Crystal structure projected along the b- and c-axis is presented in Figs. 2 and 3, respectively, showing the overlapping mode and the stacking of Pd (2,1-*i*-C_3H_7)$_2$ and TNB molecules. Bond distances and angles with their estimated standard deviations in parentheses are given in Table 3. Some selected least-squares planes with the deviations of atoms from the plane and the dihedral angles between them are given in Table 4. Donor-acceptor intermolecular distances are given in Table 5.

TABLE 4. EQUATIONS OF LEAST-SQUARES PLANES AND DISTANCES (Å) OF ATOMS FROM THE PLANE (IN BRACKETS)

Plane 1:	napthalene ring C(1)-C(10) $-0.3902x+0.9181y+0.0696z=0.6239$ [O(2)−3.14, O(3)−3.60, O(4)−3.77, O(5)−3.28, O(6)−2.57, O(7)−3.51, C(15)−3.36, C(16)−3.44, C(17)−3.42, C(18)−3.28, C(19)−3.24, C(20)−3.26, Pd−0.62]
Plane 2:	TNB O(2)-O(6), N(2)-N(4), C(15)-C(20) $-0.3549x+0.9255y+0.1518z=-2.2024$ [O(2)0.22, O(3)−0.06, O(4)−0.19, O(5)0.14, O(6)0.46, O(7)−0.49, N(2)0.08, N(3)−0.02, N(4)−0.04]
Plane 3:	Pd, O(1), N(1) $-0.7362x+0.6760y-0.0318z=0.0000$
Dihedral angle between the planes	Plane 1-Plane 2 5.1° Plane 1-Plane 3 25.1°

As shown in Figs. 2 and 3, the crystal structure consists of π-π type molecular structure in which the donor (naphthalene ring of Pd(2,1-*i*-C_3H_7)$_2$) and the acceptor (TNB) molecules stack alternately. The structure has a center of symmetry and the Pd atom lies at an inversion center. Therefore the Pd atom has a square planar coordination geometry. As shown in Fig. 3, the complex assumes a markedly stepped chair-like shape, where the seat and the rests are formed by the coordination plane (PdO_2N_2) and two 1-(imonomethyl)-2-naphtholato moieties. The Pd atom is deviated by 0.62 Å from the least-squares plane of the naphthalene ring, and the dihedral angle between the coordination plane and the mean plane of the naphthalene ring is 25.1°. The plane of TNB molecule is approximately parallel to the naphthalene ring and the dihedral angle between them is 5.1°. If there was a difference of the molecular structure between the parent palladium(II) and the molecular complex, it should be the degree of the stepped structure, that is, the deviation of Pd atom from the mean plane of the naphthalene moiety, because palladium(II) demands strongly square planar coordination geometry.[9]

The structural feature of the present molecular complex is quite similar to that of Cu(2,1-*i*-C_3H_7)$_2$·2TCNQ,[1] suggesting the generality of the structure with a chair-like shape and the alternately stacking of the donor and acceptor molecules for a series of 2:1 molecular complexes between TCNQ or TNB and **1** or **2**. However, there is a significant difference between Cu(2,1-*i*-C_3H_7)$_2$·2TCNQ and Pd(2,1-*i*-C_3H_7)$_2$·2TNB. When the crystal structure was viewed perpendicular to the donor or acceptor plane, for Cu (2,1-*i*-C_3H_7)$_2$·2TCNQ, the center of TCNQ molecule coincides approximately the center of the naphthalene ring of the complex. On the other hand, for Pd(2,1-*i*-C_3H_7)$_2$·2TNB, the center of TNB molecule coincides approximately the center of terminal benzene ring.

The crystal structure of the 2:1 molecular complex between TNB and bis(*N*-methylsalicylideneaminato)-copper(II) (Cu(Sal-CH_3)$_2$·2TNB) has been determined by the single-crystal X-ray analysis.[10] The crystal structure consists of rather discrete Cu(Sal-CH_3)$_2$·

TABLE 5. DONOR-ACCEPTOR INTERMOLECULAR DISTANCES LESS THAN 3.5 Å OF Pd(2,1-*i*-C_3H_7)$_2$·2TNB

Intermolecular distance		*l*/Å	Intermolecular distance		*l*/Å
C(1)-N(4)	1	3.43	C(1)-C(19)	1	3.40
C(1)-C(20)	1	3.50	C(2)-C(20)	1	3.38
C(3)-O(2)	1	3.34	C(4)-C(15)	1	3.44
C(7)-N(3)	1	3.46	C(8)-O(5)	1	3.46
C(9)-C(18)	1	3.34	C(10)-C(18)	1	3.50
C(10)-C(19)	1	3.38	C(11)-O(6)	1	3.14
C(11)-N(4)	1	3.40	C(6)-O(3)	2	3.37
O(5)-C(7)	3	3.40	C(7)-C(15)	2	3.40
C(7)-C(16)	2	3.37	C(9)-C(20)	2	3.47

1: x, y, z; 2: x, $y+1$, z; 3: $1-x$, $y-1/2$, $-z+1/2$.

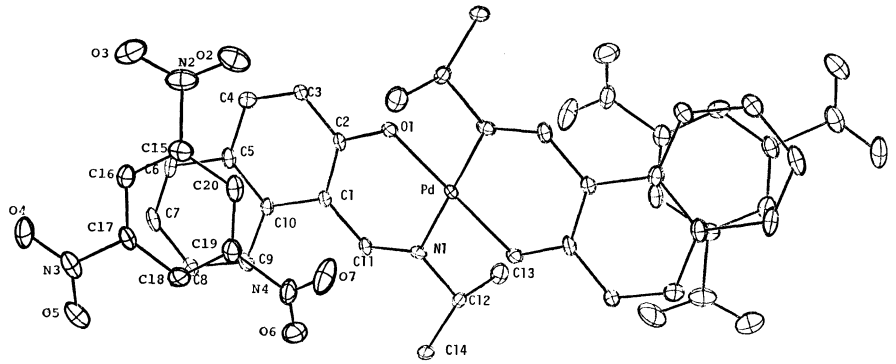

Fig. 2. Crystal structure of Pd(2,1-*i*-$C_3H_7)_2$·2TNB projected onto the TNB plane and the atom numbering scheme.

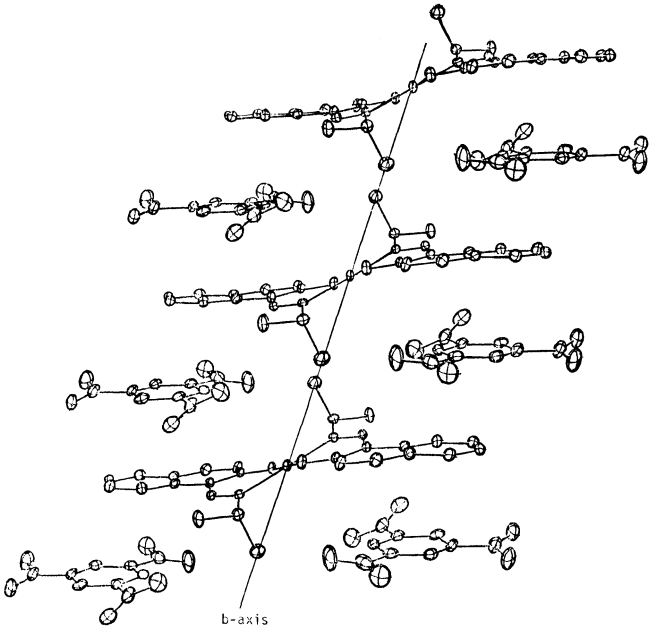

Fig. 3. Crystal structure of Pd(2,1-*i*-$C_3H_7)_2$·2TNB projected onto the ab plane.

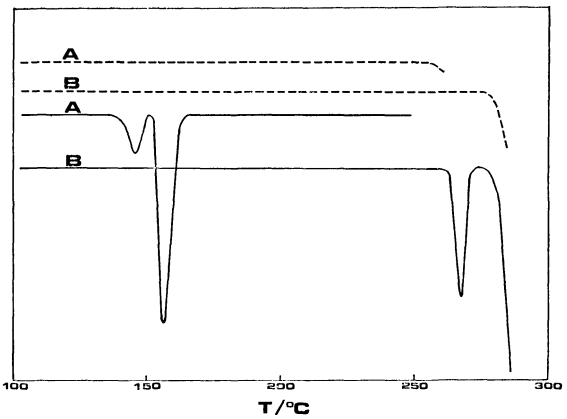

Fig. 4. Thermogravimetric and differential scanning calorimetric curves for Cu(2,1-*n*-$C_4H_9)_2$ (A) and Ni(2,1-$CH_3)_2$ (B).

2TNB unit, because the TNB molecule is approximately parallel to the nearest salicylideneaminato moiety but is tilted to the another neighboring moiety with a tilt angle of 26.4°.

Thermal Analysis. It is well known that some of the bis(*N*-alkylsalicylideneaminato)metal(II) complexes exhibit the isomerization from a square planar form to tetrahedral or polymeric octahedral form in solid state by heating.[11–13] Then the thermal analysis (TGA and DSC) was carried out for the parent complexes Cu(2,1-R)$_2$ (R=C_2H_5, *n*-C_3H_7, *n*-C_4H_9, *i*-C_4H_9, *s*-C_4H_9, *t*-C_4H_9), Ni(2,1-R)$_2$ (R=CH_3, C_2H_5, *n*-C_3H_7), and Pd(2,1-R)$_2$ (R=*n*-C_4H_9, *t*-C_4H_9). Of which Cu(2,1-*n*-$C_4H_9)_2$ and Ni(2,1-$CH_3)_2$ showed isomerization peak in solid state by heating, as shown in Fig. 4. The DSC curve of Cu(2,1-*n*-$C_4H_9)_2$ posseses two endothermic peaks without weight loss, of which the second peak corresponds to phase transformation from solid to liquid. The endothermic peaks in the solid state can be attributed to the change of the coordination geometry, and the values of 1.80 kcal mol^{-1} for Cu(2,1-*n*-$C_4H_9)_2$ and 1.77 kcal mol^{-1} for Ni(2,1-$CH_3)_2$ are of the same order of the π-π type donor-acceptor interaction.[14] (1 cal=4.184 J) The palladium(II) complexes showed no isomerization peak, being consistent that palladium(II) strongly demands the square planar geometry.[9] It should be noted that their molecular complexes with TCNQ show no peaks corresponding to the isomerization.[15]

Electronic Spectra. Electronic spectra were measured in Nujol mull and in equivolume solution of acetone and chloroform. The solution spectra of the parent complex and its molecular complex with TNB are quite similar to each other in absorption coefficient and band maxima in the region of $(14-22)\times10^3$ cm^{-1}, in which TNB molecule shows no absorption. On the other hand, in Nujol mull, an intense band appeared at about 18×10^3 cm^{-1}. As a typical example, the electronic spectra of Ni(2,1-*i*-$C_3H_7)_2$ and Ni(2,1-*i*-$C_3H_7)_2$·2TNB in Nujol mull and in solution are shown in Fig. 5. Since all the molecular complexes of nickel(II), copper(II), and palladium(II) exhibit this band at about same wave number, this band may be attributable to a charge transfer band between TNB and naphthalene moiety. In the case of the palladium(II) complexes, it is well known that palladium(II) demands strongly square planar configuration[11–13] so that the coordination geometrical change associated with the formation of the molecular complex (at least from

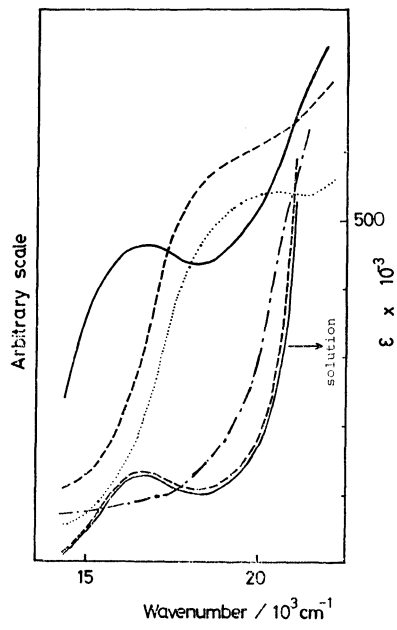

Fig. 5. Electronic spectra of Ni(2,1-n-C_3H_7)$_2$ (——) and Ni(2,1-n-C_3H_7)$_2$·2TNB (— — —) measured in Nujol mull and in a acetone-chloroform solution, and Nujol mull spectra of Pd(2,1-i-C_3H_7)$_2$ (—·—) and Pd(2,1-i-C_3H_7)$_2$·2TNB (·····).

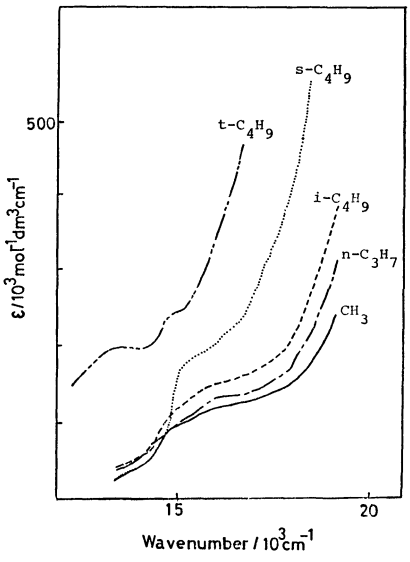

Fig. 6. Electronic spectra of Cu(2,1-R)$_2$ (R=CH_3, n-C_3H_7, i-C_4H_9, s-C_4H_9, t-C_4H_9) in chloroform solution.

tetrahedral to square planar) can be deleted. In addition, the electronic spectra of the parent complexes for a series of Pd(2,1-R)$_2$ (R=CH_3, C_2H_5, n-C_3H_7, i-C_3H_7, n-C_4H_9) are quite similar to each other and show no absorption band around 18×10^3 cm^{-1}. So this band can be arised from donor-acceptor interaction between TNB and terminal benzene ring. It must be noted that 1:1 molecular complex between naphthalene and TNB (Nap·TNB) did not exhibit the band at the wave number, where the center of Nap coincides the center of TNB so that the overlapping mode[16] is different from that of the present complex. In the case of the copper(II) complexes, the spectra of the parent complexes exhibit d-d transition bands in the region of $(12-18)\times10^3$ cm^{-1} which can provide the information of the coordination geometry, as shown in Fig. 6. Red shift and intensity enchancement of d-d bands are recognized indicators of the transformation from square planar to tetrahedral stereochemistry, as known by the well-established complexes.[17] However, the information with respect to the coordination geometrical change associated with the formation of the molecular complex with TNB is hidden by the intense band at 18×10^3 cm^{-1}.

We are grateful to Prof. Sigeo Kida at the Faculty of Science, Kyushu University, for allowing us to use the X-ray diffractometer. Thanks are also due to Mr. Yasuhiro Sagara and Mr. Toshiro Miyazaki for the assistance of the experiment.

References

1) N. Matsumoto, Y. Nonaka, S. Kida, S. Kawano, and I. Ueda, *Inorg. Chim. Acta*, **37**, 27 (1979).
2) N. Matsumoto, T. Miyazaki, Y. Sagara, and A. Ohyoshi, *Inorg. Chim. Acta*, **63**, 249 (1982).
3) H. Weil and H. Ostermeier, *Ber.*, **54**, 3217 (1921).
4) A. Chakravorty and R. H. Holm, *Inorg. Chem.*, **3**, 1010 (1964).
5) The elemental analytical data and the melting points of 27 parent complexes have been deposited as supplementary data.
6) "International Tables for X-Ray Crystallography," Kynoch Press, Birmingham (1974), Vol. IV.
7) S. Kawano, *Rep. Comp. Cent. Kyushu Univ.*, **13**, 39 (1980).
8) T. Sakurai, H. Iwasaki, Y. Watanabe, K. Kobayashi, Y. Bando, and Y. Nakamichi, *Rikagaku Kenkyusho Hokoku*, **50**, 75 (1974).
9) S. Yamada, H. Nishikawa, and K. Yamasaki, *Bull. Chem. Soc. Jpn.*, **36**, 483 (1963); S. Yamada and K. Yamanouchi, *ibid.*, **42**, 2543 (1969).
10) A. W. King, D. A. Swann, and T. N. Waters, *J. Chem. Soc., Dalton Trans.*, **1973**, 1819.
11) A. Takeuchi and S. Yamada, *Bull. Chem. Soc. Jpn.*, **42**, 3046 (1969).
12) N. Arai, M. Sorai, and S. Seki, *Bull. Chem. Soc. Jpn.*, **45**, 2398 (1972).
13) K. Miyokawa, H. Hirashima, and I. Masuda, *Bull. Chem. Soc. Jpn.*, **54**, 3361 (1981).
14) G. Briegleb, J. Czekalla, and G. Reuss, *Z. Phys. Chem. N. F.*, **30**, 333 (1961); A. Kabayama, and S. Nagakura, *J. Am. Chem. Soc.*, **77**, 2644 (1955).
15) The thermal analysis of the molecular complex with TNB was not carried out due to the potentially explosive of TNB.
16) "Charge Transfer Complex," Kagaku Zokan, Kagaku Dozin, Kyoto (1971), Vol. 48, p. 104.
17) H. Yokoi and A. W. Addison, *Inorg. Chem.*, **16**, 1341 (1977), and references therein.

 © 1983 The Chemical Society of Japan Bull. Chem. Soc. Jpn., 56, 2733—2738 (1983)

Electrochemical Reduction of Some Tris(β-diketonato)ruthenium(III) Complexes in Acetonitrile and Interaction of the Reduced Anions with Lithium and Sodium Ions

Akira Endo

Department of Chemistry, Faculty of Science and Technology, Sophia University, 7-1 Kioicho, Chiyoda-ku, Tokyo 102

(Received February 21, 1983)

In tetraethylammonium perchlorate–acetonitrile solution, $[Ru(R_1\text{-}CO\text{-}CR_2\text{-}CO\text{-}R_3)_3]$ (R_1,R_3=$-CH_3$, $-CF_3$, $-C_6H_5$, $-C(CH_3)_3$; R_2=$-H$, $-C_6H_5$) was reversibly reduced at a dropping mercury electrode to the corresponding univalent anion. A linear relationship was found between the half-wave potential and the sum of the Hammett constants of the substituents of ligands. In some cases, the polarogram and the cyclic voltammogram were shifted to more positive potentials in the presence of lithium or sodium ions. This effect was explained quantitatively by the two-step association between the reduction product, $[Ru(R_1\text{-}CO\text{-}CR_2\text{-}CO\text{-}R_3)_3]^-$, and alkali metal ions. The association constants were calculated. The K_2 values were appreciable and the K_1 values were much larger than expected for a simple electrostatic interaction. Furthermore, the K_1 values were linearly related to the sum of the Hammett constants of the substituents of the ligands. These results suggest the importance of the local charge distribution on the complex anions. In the presence of lithium ion, $[Ru(acac)_3]^-$ forms $Li[Ru(acac)_3]$ which is insoluble in acetonirile.

The polarographic behavior of acetylacetonato complexes is affected by the properties of solvents and by the addition of perchlorate of alkali metal or alkaline earth metal. Murray and Hiller[1] first studied in detail the mechanism of polarographic reduction of $[Fe(acac)_3]$ in lithium perchlorate–acetonitrile solutions. They found that the reduction potential of $[Fe(acac)_3]$ was shifted to more positive potentials by the addition of $LiClO_4$. They have shown that the effect is caused by a coordinative relaxation reaction of the reduction product, $[Fe(acac)_3]^-$, in which an acetylacetonato ligand becomes transferred to lithium ion. Heineman *et al.*[2] have confirmed this interaction by means of the optically transparent thin-layer electrode. Misumi *et al.*[3] also examined this effect in *N*,*N*-dimethylformamide (DMF) and obtained similar results. Recently, Kalinowski and Ćmiel[4] investigated solvent effects on the interaction between $[Fe(acac)_3]^-$ and Li^+, Na^+, or K^+ and discussed them in terms of the donor-acceptor concept. The coordinative relaxation reaction was also observed in the systems of $[Cu(acac)_2]^-$–Li^+ (in acetonitrile)[5] and $[Eu(acac)_3]^-$–Li^+, Mg^{2+} (in DMF).[3] In the reduction of $[Mn(acac)_3]$,[6] the potential shifts were also observed on the addition of perchlorate of Li^+, Na^+, or K^+ in many nonaqueous solvents. These effects were qualitatively explained in terms of the ion-pair formation between $[Mn(acac)_3]^-$ and alkali metal ions. This explanation, however, appears to lack quantitative corroboration.

In the course of a polarographic study of tris(acetylacetonato)ruthenium(III) in aqueous and acetonitrile solutions,[7] we came to notice that the reduction step in acetonitrile is shifted to more positive potentials in the presence of sodium ions.

The present paper deals with the interaction of lithium and sodium ions with eight kinds of tris(β-diketonato)ruthenate(II) ions which are produced by the polarographic reduction of the corresponding Ru^{III} complexes. Effects of the substituents of the ligands are also discussed.

Experimental

Preparation of the Complexes.† Among the eight complexes, $[Ru(pfm)_3]$ and $[Ru(paa)_3]$ are new compounds. They were synthesized as described below. $[Ru(bzac)_3]$ and $[Ru(acac)_3]$ were prepared according to the published methods (Refs. 8 and 7, respectively). For the other complexes, see the appendix.

[Ru(pfm)$_3$]: Hydrated ruthenium trichloride (1 g, *ca.* 4 mmol as Ru), 3.3 g (17 mmol) of Hpfm and 0.5 g (5 mmol) of potassium hydrogencarbonate were refluxed at 120 °C for 10 h. An additional 1.2 g (12 mmol) of potassium hydrogencarbonate was added, and the reflux was continued at 150 °C for 20 h. The mixture was then extracted with dichloromethane several times. The extracts were combined and this mixture was washed in a separatory funnel successively with 2% potassium hydrogencarbonate solution, 2% HCl solution, and water. Removal of the solvent from extracts left an oily red material, which was steam-distilled. The first 5 cm^3 portion of the distillate being discarded, the distillate containing drops of red liquid was collected and left to stand overnight, during which the drops solidified. The solid was dried under vacuum and then ground to powder, which was again vacuum-dried at room temperature. Found: C, 42.5; H, 4.5%. Calcd for $RuC_{24}H_{30}O_6F_9$: C, 42.0; H, 4.40%.

[Ru(paa)$_3$]: A portion of ruthenium(III) chloride solution (5 mmol as Ru, dissolved in 40 cm^3 of 1 mol dm^{-3} HCl) was reduced with ethanol to the bivalent state, and the mixture was evaporated nearly to dryness on a water bath. The blue residue was dissolved in 50 cm^3 of water and the pH of the solution was adjusted to about 2 with 1 mol dm^{-3} NaOH solution. The solution was then refluxed on a water bath with 4 g (23 mmol) of Hpaa and 200 cm^3 of ethanol under nitrogen atmosphere. After 4 h, the pH

† The following ligand abbreviations will be used in this paper (in the order of Table 1): Hbzfa, 1,1,1-trifluoro-4-phenyl-2,4-butanedione; Hfac, 1,1,1-trifluoro-2,4-hexanedione; Hpfm, 1,1,1-trifluoro-5,5-dimethyl-2,4-pentanedione; Hdbm, 1,3-diphenyl-1,3-propanedione; Hbzac, 1-phenyl-1,3-butanedione; Hacac, 2,4-pentanedione; Hpaa, 3-phenyl-2,4-pentanedione; Hdpm, 2,2,6,6-tetramethyl-3,5-heptanedione.

Table 1. Polarographic data for RuL_3 ($L=R_1$-CO-CR_2-CO-R_3^-) in 0.1 mol dm^{-3} TEAP acetonitrile solution at 25 °C

	Complex	$[R_1\text{-CO-}CR_2\text{-CO-}R_3]^-$			$E^\circ_{1/2}$/V[a]	Reciprocal slope/mV
		R_1	R_2	R_3		
1	$[Ru(bzfa)_3]$	$-CF_3$	-H	$-C_6H_5$	−0.29	−64.5
2	$[Ru(fac)_3]$	$-CF_3$	-H	$-CH_3$	−0.36	−57.0
3	$[Ru(pfm)_3]$	$-CF_3$	-H	$-C(CH_3)_3$	−0.47	−61.7
4	$[Ru(dbm)_3]$	$-C_6H_5$	-H	$-C_6H_5$	−0.86	−65.0
5	$[Ru(bzac)_3]$	$-C_6H_5$	-H	$-CH_3$	−0.96	−64.0
6	$[Ru(acac)_3]$	$-CH_3$	-H	$-CH_3$	−1.08	−61.0
7	$[Ru(paa)_3]$	$-CH_3$	$-C_6H_5$	$-CH_3$	−1.17	−65.8
8	$[Ru(dpm)_3]$	$-C(CH_3)_3$	-H	$-C(CH_3)_3$	−1.39	−64.0

a) Against a silver-silver ion electrode (0.01 mol dm^{-3} $AgNO_3$ in acetonitrile).

of the solution was readjusted to about 2, and the reflux was continued for *ca.* 10 h, when the color of the solution turned to reddish purple. The pH of the solution was then adjusted to about 6, and further refluxing was continued for 5 h. After removal of the solvent, the residue was extracted into several portions of benzene. The combined benzene solution was passed through a column of Merck Alminiumoxid 90 (Aktivitätsstufe II—III). The eluent was concentrated, and the complex was precipitated by adding ethanol. A red powdery material was obtained, which was dried under vacuum at room temperature. Found: C, 63.3; H, 5.5%. Calcd for $RuC_{33}H_{33}O_6$: C, 63.3; H, 5.3%.

Complexes **1**, **2**, **3**, and **5** have geometrical isomers, and each of the complexes has optical isomers. The isomeric mixtures were used, since the precision of the present method seemed too low to detect any difference among the isomers. Indeed, in the case of $[Ru(bzac)_3]$, the half-wave potentials of the *mer*- and *fac*-isomers were identical in both TEAP and $NaClO_4$ solutions.[9]

Other Chemicals: Tetraethylammonium perchlorate (TEAP) and tetrabutylammonium perchlorate (TBAP) were of special polarographic grade purchased from Nakarai Chemicals, Ltd. Anhydrous $LiClO_4$ of ICN Pharmaceutical, Inc., was dried under vacuum at 130 °C. Anhydrous $NaClO_4$ of guaranteed reagent grade of Kanto Chemical Co., Inc., was dried under vacuum at 120 °C. Purification of acetonitrile has been described previously.[7]

Measurement. All the potentials were measured against a silver-silver ion electrode (Ag/0.01 mol dm^{-3} $AgNO_3$ in acetonitrile), and all the electrochemical measurements were carried out at (25.0±0.1) °C. Deoxygenation of solutions was carried out with argon gas which had been passed through two wash bottles containing acetonitrile kept at 25 °C. Electrochemical measurement was carried out mainly by using a Fuso Polarograph Model 312 with a Fuso Potential Scanning Unit Model 321 and a Riken Denshi X-Y Recorder Model F-42CP. An H-type electrolytic cell with a glass frit was used. A dropping mercury electrode (DME) and a counter electrode of spiral platinum wire were both placed in one compartment and the reference electrode was connected to the other compartment through a bridge filled with 0.1 mol dm^{-3} TEAP solution. The DME had a flow rate of mercury of 1.38 mg s^{-1} under a mercury head of 50 cm. Cyclic voltammetry was carried out as previously described,[7] except that the silver-silver ion reference electrode was used and both compartments were filled with the supporting electrolyte solution. A Hitachi Model 200-20 Spectrophotometer was used for recording absorption spectra. An NEC PC 8001 Personal Computer was used for data processing. Elemental analyses of C, H, and N were carried out by means of a Shimadzu Seisakusho Ltd. CHN Analyzer CHN-1A. Lithium was determined by means of a Seiko SAS 740 Atomic Absorption/Flame Spectrophotometer. Ruthenium was determined spectrophotometrically according to the ruthenate method.[10]

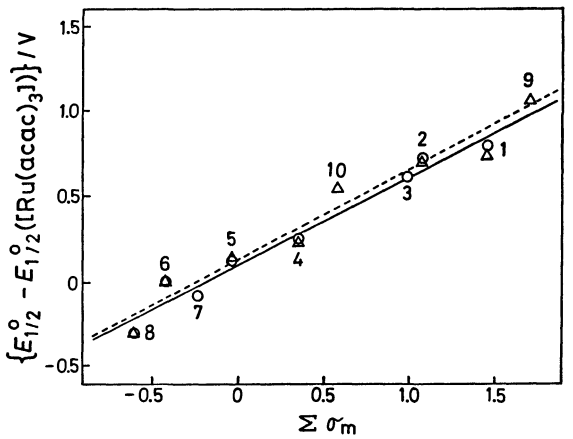

Fig. 1. Relationship between relative half-wave potential and the sum of the Hammett constants in 0.1 mol dm^{-3} TEAP at 25 °C. —○—, this work (in acetonitrile); ---△---, Patterson and Holm[11] (in DMF). Complexes are numbered as in Table 1 except for **9** ($[Ru(acac)(hfac)_2]$ and **10** ($[Ru(acac)_2(hfac)]$) (Hhfac, 1,1,1,5,5,5-hexafluoro-2,4-pentanedione).

Results and Discussion

TEAP Systems. In 0.1 mol dm^{-3} TEAP solution, every complex listed in Table 1 showed a reduction step with diffusion-controlled limiting current, which corresponded to Nernstian one-electron reduction to the univalent anion. The half-wave potentials ($E^\circ_{1/2}$) and the reciprocal slopes of the logarithmic plots of the reduction steps are presented in Table 1.

Patterson and Holm[11] investigated in DMF the substituent effect on the $E^\circ_{1/2}$ of a series of tris(β-diketonato)ruthenium(III) complexes including six of the present ones. In the present case, too, the plot of $E^\circ_{1/2}$ *vs.* the sum of the Hammett constant ($\Sigma\sigma_m$ or $\Sigma\sigma_p$) was a straight line. In Fig. 1, this relationship

is represented in terms of the half-wave potentials relative to that of $[Ru(acac)_3]$ and along with these authors' data, where $\Sigma\sigma_m$ is calculated by using the values given by Murov.[12] The agreement between the two sets of data is remarkable. This is not surprising since the relative permittivities of the two solvents are almost the same (ε_r(acetonitrile)=38 and ε_r(DMF)=37 at 25 °C[13]), if there is little specific solute-solvent interaction. Patterson and Holm[11] explained this linear relationship qualitatively as follows. Since Ru^{III} has the low spin, d^5 electronic configuration, the d electrons are localized in the t_{2g} metal orbital. The t_{2g} metal orbital which is a $d\pi$ orbital, forms a π molecular orbital with a π ligand orbital, and in the redox process the electron will be added to or subtracted from this molecular orbital. The substituents affect the eletron density of σ and π molecular orbitals. The Hammett constant is a measure of the electron-accepting character of the substituent. The more electron-accepting is the substituent, the more stabilized is the reduced form with respect to the oxidized form, hence the more positive is $E^\circ_{1/2}$.

A linear correlation between $E^\circ_{1/2}$ and the Hammett constant is known in many systems of organic substances.[14-16] For benzene derivatives, azo dyes,[16] and some heterocylic compound derivatives,[15] slopes ranging from +0.02 V to +0.37 V were observed. The slope of *ca.* +0.5 V obtained in the present case is somewhat larger, probably reflecting the more immediate influence of the substituents on the orbital energies of the metal chelate.

$LiClO_4$ and $NaClO_4$ Systems. In the presence of $LiClO_4$, the polarogram and cyclic voltammogram of $[Ru(acac)_3]$ were shifted to more positive potentials; but their shapes were so distorted by the presence of maxima, apparently owing to the formation of insoluble film, that no quantitative analyses of the waves were possible. When the large scale reduction at a mercury pool electrode was carried out in 0.1 mol dm^{-3} $LiClO_4$ with enforced stirring of the mercury surface, a brown precipitate was obtained. The precipitate was collected by the filtration and washed with deoxygenated acetonitrile under argon atmosphere. In the presence of atmospheric oxygen, the precipitate redissolved instantly to give the tervalent species. It was fairly stable when dry and was subjected to elemental analysis. The results were in good agreement with the calculated values for $Li[Ru(acac)_3]$. Found: Ru, 24.0; C, 44.2; H, 5.2; Li, 1.6%. Calcd for $Li[Ru(acac)_3]$: Ru, 24.9; C, 44.4; H, 5.2; Li, 1.7%. On reduction in the presence of lithium ions, therefore, the reduction product, $[Ru(acac)_3]^-$, forms the lithium salt, which is insoluble in acetonitrile.

In the presence of $NaClO_4$, the polarogram and the cyclic voltammogram of $[Ru(acac)_3]$ were also shifted to more positive potentials, as shown in Fig. 2, without changing the Nernstian characteristics (Table 2). The $E_{1/2}$ was independent of the depolarizer concentration at a given sodium perchlorate concentration. The addition of small amounts of water did not affect the $E_{1/2}$. When the $[Ru(acac)_3]$ was partially reduced at a mercury pool electrode in 0.1 mol dm^{-3} $NaClO_4$, a single redox step appeared at the same $E_{1/2}$. When

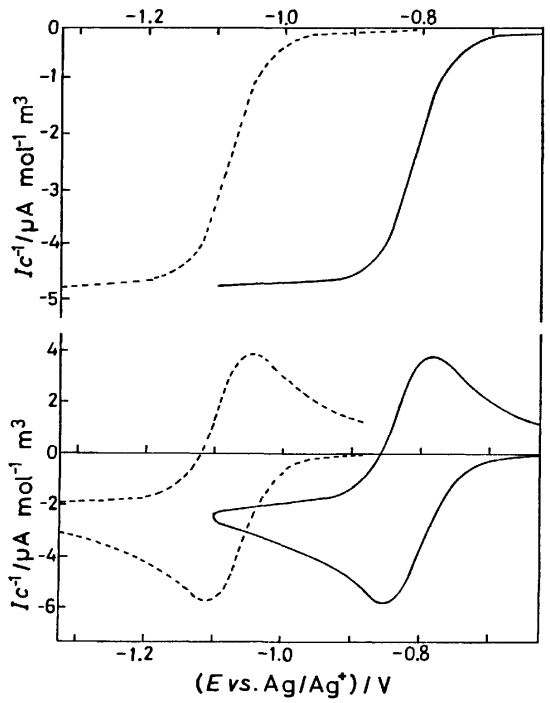

Fig. 2. DC polarograms and cyclic voltammograms of $[Ru(acac)_3]$ in acetonitrile. ----, in 0.1 mol dm^{-3} TEAP; ——, in 0.1 mol dm^{-3} $NaClO_4$; scan rate for CV=0.1 V s^{-1}, 25 °C.

Table 2. The dependence of $\Delta E_{1/2}$ of $[Ru(acac)_3]$ on the concentration of dissociated sodium ions in acetonitrile at 25 °C

$[Na^+]$/mol m^{-3}	$\Delta E_{1/2}$/mV[a]	Reciprocal slope/mV
0	(0)	−61.0
6.9	151	−60.7
13.7	187	−62.5
20.6	207	−60.1
34.3	232	−59.7
48.0	246	−61.5
68.4	269	−59.6

a) Against a silver-silver ion electeode (0.01 mol dm^{-3} $AgNO_3$ in acetonitrile). Concentration of $[Ru(acac)_3]$ is 1 mol m^{-3}.

the cathodic diffusion currents recorded intermittently in the course of the electrolytic reduction were plotted against the quantity of electricity, the magnitude of the former decreased and that of the latter increased linearly. The plots indicate that the process is a one-electron reduction, without any complication owing to subsequent chemical reactions. The UV-visible spectra of $[Ru(acac)_3]$ were the same in both 0.1 mol dm^{-3} $NaClO_4$ and 0.1 mol dm^{-3} TEAP. It follows that the shift of $E_{1/2}$ is attributable to a specific interaction of sodium ions with $[Ru(acac)_3]^-$, not with $[Ru(acac)_3]$. The spectra of the reduced forms, in fact, were different in the two media.

Consequently, the shift of $E_{1/2}$ is interpreted in terms of the association equilibria between sodium or lithium ion (M^+) and $[Ru(acac)_3]^-$ subsequent to the electron transfer:

$$[Ru(acac)_3] + e^- \rightleftharpoons [Ru(acac)_3]^- \quad (1)$$

$$[Ru(acac)_3]^- + M^+ \rightleftharpoons M[Ru(acac)_3]$$

$$M[Ru(acac)_3] + M^+ \rightleftharpoons \{M_2[Ru(acac)_3]\}^+ \quad (2)$$

$$\cdots\cdots$$

$$\{M_{n-1}[Ru(acac)_3]\}^{(n-2)+} + M^+ \rightleftharpoons \{M_n[Ru(acac)_3]\}^{(n-1)+}.$$

When the electron transfer is Nernstian and the subsequent reactions are reversible and the large excess of M^+ is present, this relation holds:[17]

$$E = E^{o'} + (RT/F) \ln (\bar{D}_R/D_O)^{1/2} + (RT/F) \ln (1 + \sum_{i=1}^{n} \beta_i [M^+]^i) + (RT/F) \ln [(I_d - I)/I], \quad (3)$$

with

$$\beta_i = \prod_{j=1}^{i} K_j, \quad (4)$$

where D_O is the diffusion coefficient of $[Ru(acac)_3]$, and $\bar{D}_R$ is the mean diffusion coefficient of the reduced form, the other symbols having the usual meanings. K_j is the conditional stepwise formation constant of the jth associate in terms of amount-of-substance concentration:

$$K_j = C_j/[M^+]C_{j-1}, \quad (5)$$

where C_j is the concentration of $\{M_j[Ru(acac)_3]\}^{(j-1)+}$. Hence the half-wave potential is given by

$$E_{1/2} = E^{\circ}_{1/2} + (RT/F) \ln (\bar{D}_R/D_R)^{1/2} + (RT/F) \ln (1 + \sum_{i=1}^{n} \beta_i [M^+]^i), \quad (6)$$

where D_R is the diffusion coefficient of $[Ru(acac)_3]^-$ and $E^{\circ}_{1/2}$ is the half-wave potential at $[M^+]=0$. Since $\bar{D}_R$ and D_R are expected to be almost the same,

$$\Delta E_{1/2} = E_{1/2} - E^{\circ}_{1/2} = (RT/F) \ln (1 + \sum_{i=1}^{n} \beta_i [M^+]^i). \quad (7)$$

The β_i values were calculated by analysing the dependence of $\Delta E_{1/2}$ on $[M^+]$ according to the method presented by Momoki *et al.*[18] For this purpose the values of $[M^+]$ were calculated from the analytical concentration of the perchlorate by using the association constants of TEAP (7.3 mol^{-1} dm^3) and $MClO_4$ (4.0 mol^{-1} dm^3 for M=Li and 6.8 mol^{-1} dm^3 for M=Na at 25 °C) reported by Fujinaga *et al.*[19] Although those values are thermodynamic association constants, they were used in the present calculation without correction for the ionic strength, because their values were found to have little effect on the results of the following numerical analysis. It is assumed that the association between $[Ru(acac)_3]^-$ and tetraethylammonium ions is negligible; this assumption seems legitimate in view of the fact that the $E^{\circ}_{1/2}$ remained unchanged when the concentration of TEAP was changed from 0.05 mol dm^{-3} to 0.1 mol dm^{-3} or TEAP was replaced by TBAP. The total electrolyte concentration was, therefore, kept constant at 0.1 mol dm^{-3} with TEAP.

The maximum number of the bound cations, n, has to be known to carry out the calculation. For $n=1$, no reasonable fitting was obtained (Fig. 3); for $n=3$, β_3 resulted in a negative value. It was therefore decided that the association of up to two sodium ions per complex anion was meaningful under the experimental conditions. The $\Delta E_{1/2}$ values calculated on the basis of the β values for $n=2$ are in very good agreement with the experiment (Fig. 3).

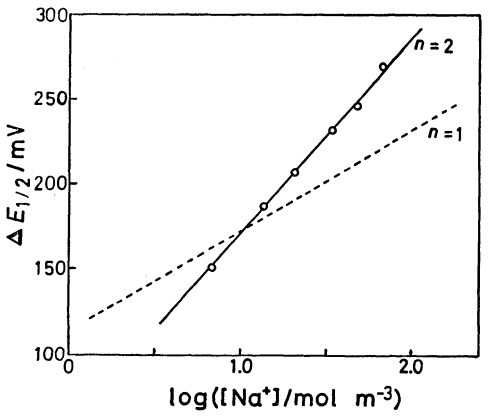

Fig. 3. $\Delta E_{1/2}$ *vs.* log ($[Na^+]$/mol m^{-3}) plot for $[Ru(acac)_3]^-$–Na^+ system in acetonitrile. ○, observed values; ----, calculated line for $n=1$; ——, calculated line for $n=2$. Total concentration of $NaClO_4$ = 0.01–0.1 mol dm^{-3}, 25 °C.

Table 3. The conditional stepwise formation constants of tris(β-diketonato)ruthenate(II) ions with Li^+ and Na^+ in acetonitrile at 25 °C, electrolyte concentration = 0.1 mol dm^{-3}

	Complex anion	log (K_1/mol^{-1} dm^3)		log (K_2/mol^{-1} dm^3)	
		Li^+	Na^+	Li^+	Na^+
1	$[Ru(bzfa)_3]^-$	—	—	—	—
2	$[Ru(fac)_3]^-$	—	—	—	—
3	$[Ru(pfm)_3]^-$	—	—	—	—
4	$[Ru(dbm)_3]^-$	1.7	2.6	1.2	1.1
5	$[Ru(bzac)_3]^-$	2.3	2.8	1.0	1.6
6	$[Ru(acac)_3]^-$	#	3.8	#	3.1
7	$[Ru(paa)_3]^-$	#	#	#	#
8	$[Ru(dpm)_3]^-$	4.7	4.1	1.4	1.2

—, not detectable ($\log(K/mol^{-1}\,dm^3) < ca.\ 0.5$); #, not measurable.

The other tris(β-diketonato)ruthenate(II)–Li^+, Na^+ systems were analyzed in the same way, since the electrochemical behavior was quite similar except for $[Ru(paa)_3]^-$, of which the polarograms were distorted in the presence of Na^+ or Li^+ and the analysis was impossible.

In Table 3, the results are presented in terms of K_1 and K_2; for the first three cases, no shift of $E_{1/2}$ was detectable. These formation constants reveal that the interaction is not simply electrostatic ion-pairing.

First, the K_2 values are appreciable. It is reported that the anion radicals of a number of *p*-quinones produced by the one-electron reduction in DMF react with lithium or barium cations to form 2-cations-to-1-anion associates.[20,21] To the author's knowledge, the present systems are the first examples of 2 to 1 association for univalent anions of a metal complex.

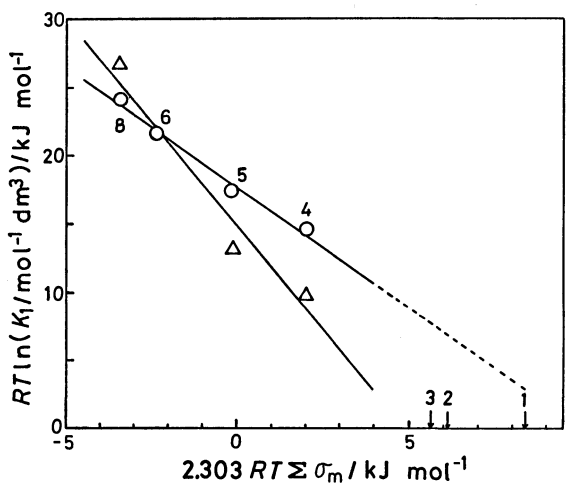

Fig. 4. Relationships between K_1 and the sum of the Hammett constants. —○—, Na^+ system; —△—, Li^+ system. Complex anions are numbered as in Table 3.

Second, the K_1 values are much larger than expected for simple ion-ion electrostatic attraction. For example, the Fuoss theory,[22] which can well explain the association constants of $LiClO_4$ and $NaClO_4$, predicts about 7 mol^{-1} dm^3 when the ion-ion distance is assumed to be 0.6 nm in the case of $[Ru(acac)_3]^-$–Na^+ system (crystallographic radius of $[Ru(acac)_3]$ molecule is *ca.* 0.5 nm[23]). Inversely, an unreasonably small value (*ca.* 0.1 nm) for the ion-ion distance would be required for a formation constant of 5.8×10^3 mol^{-1} dm^3 (experimental value in $[Ru(acac)_3]^-$–Na^+ system). Examination of the K_1 values indicates that the local charge distribution on the complex anion plays an important role. The K_1 seems to be independent of the bulkiness of the complex anion, since the diffusion current constants ($I_d/c\,m^{2/3}\,t^{1/6}$) of the complex were experimentally in the order of **4**, **5**, **8**, **6**. However, the value of K_1 depends on $E^\circ_{1/2}$: the more negative is $E^\circ_{1/2}$, the larger becomes K_1. $E^\circ_{1/2}$ is in turn linearly dependent on the sum of the Hammett constants of the substituents of the ligand, as mentioned earlier. The relationships between K_1 and $\Sigma\sigma_m$ for Li^+ and Na^+ systems are presented in Fig. 4, where the two quantities are expressed in energetic terms. The two straight lines can be explained as follows. When the substituents on the ligand are stronger electron acceptors, the electron density on the chelate rings will decrease. This decrease in the electron density, on one hand, will make the reduction of the neutral complex molecule easier (more positive $E^\circ_{1/2}$) and on the other hand will make it less easy for the cation to attach to the reduced complex anion. This picture implies that the association is attributable mainly to the chelate rings. There are similar cases: Kalinowski and Galazka[24] pointed out the possibility of interaction between Li^+ and the π electron system of the ligands of $[Cu(acac)_2]$ in some aprotic solvents, and Steinbach and Burns[25] found that $[M(acac)_3]$ ($M=Fe^{III}$, Al^{III}, or Cr^{III}), when recrystallized from chloroform, in corporated two solvent molecules to form the chloroformate and inferred that the hydrogen atom of chloroform was possibly attracted to the oxygens of the acetylacetonate. If the association accompanies desolvation of the cation, the stability will be determined by the balance of two antagonistic factors: the energy loss in desolvation and the energy gain in association. The former depends mainly on the cation size, and the latter on both the cation size and the density of the local negative charge on the ligand system. A high local negative charge will favor the association with a smaller cation, since the energy gain in association offsets the larger desolvation energy. When the local negative charge is low, however, the desolvation energy becomes predominant and a small cation will associate less easily. The two straight lines in Fig. 4 seem to reflect qualitatively this situation, although the examples are too few to allow a quantitative interpretation.

In connection with the present study only the effects of magnesium ion were studied, for potassium, rubidium, and caesium perchlorates were too sparingly soluble in acetonitrile. Magnesium ion does react with the complex anions. But the electrode process was complicated by rapid decomposition subsequent to the association. Besides, a small amount of water had a pronounced effect, making the situation more complicated experimentally. Some results of this study will be reported separately.

Appendix

Preparation of the Complex. *[Ru(bzfa)$_3$]*: "Hydrated ruthenium trichloride" (0.5 g, ca. 2 mmol as Ru), 0.4 g (4 mmol) of potassium hydrogencarbonate, 3.9 g (18 mmol) of Hbzfa were ground together in an agate motar. The resulting muddy solid was extracted with a few portions of carbon tetrachloride. After removal of the solvent, the residue was dissolved in ethanol, and the solution was passed through a column of Merck Alminiumoxid 90 (Aktivitätsstufe II—III). A red material obtained after removal of the solvent from the eluent was dried under vacuum at room temperature. Found: C, 49.3; H, 3.0%. Calcd for $RuC_{30}H_{18}O_6F_9$: C, 48.7; H, 2.6%.

[Ru(fac)$_3$]: A blue residue was obtained, as in the case of $[Ru(paa)_3]$, starting from 0.5 g of ruthenium(III) chloride (2.4 mmol as Ru, dissolved in 40 cm^3 of 1 mol dm^{-3} HCl); it was dissolved in 50 cm^3 of water. The pH was adjusted to about 3 with 1 mol dm^{-3} KOH solution, and then the solution was refluxed on a water bath with 5 g (33 mmol) of Hfac and 20 cm^3 of ethanol for 8 h. After being cooled, the solution was filtered, and the residue was extracted with ethanol. The ethanol solution was concentrated until small crystals began to appear on the surface. Crude $[Ru(fac)_3]$ was obtained on cooling. The product, after being washed with water, was recrystallized from ethanol and dried under a vacuum at room temperature. Found: C, 33.0; H, 2.1%. Calcd for $RuC_{15}H_{12}O_6F_9$: C, 33.8; H, 2.3%.

$[Ru(dbm)_3]$: This complex was prepared by the method of Wolf *et al.*[26] with slight modifications. $[Ru(acac)_3]$ (1.6 g, 4 mmol) and 5.4 g (24 mmol) of Hdbm were dissolved in 50 cm^3 of ethyl benzoate. The solution was refluxed at 160 °C for 12 h under nitrogen atmosphere. Then, 1.2 g of potassium hydrogencarbonate was added to the solution and the reflux was continued for 6 h. After removal of solvent, the residue was extracted with methanol. The

black crystalline material obtained by concentration of the extract was recrystallized from benzene and dried under vacuum at room temperature. Found: C, 70.6; H, 4.5%. Calcd for $RuC_{45}H_{33}O_6$: C, 70.1; H, 4.3%.

[*Ru(dpm)*$_3$]: "Hydrated ruthenium trichloride" (1.5 g, 7 mmol as Ru), 1.0 g (10 mmol) of sodium hydrogencarbonate, and 10 g (54 mmol) of Hdpm were refluxed for 6 h at 160 °C on an oil bath. An additional amount (2.0 g) of sodium hydrogencarbonate was introduced, and the reflux was continued for 18 h at 210 °C. Excess Hdpm and water were removed under reduced pressure, and the residue was extracted into carbon tetrachloride. After removal of the solvent, the residue was dissolved in benzene. This solution was passed through a column of Merck Alminiumoxid 90 (Aktivitätsstufe II—III) and the eluent was concentrated to about 5 cm^3. Acetonitrile and a small amount of water were added to the solution to precipitate the complex. Orange crystals collected by filtration were dried under vacuum. Found: C, 61.0; H, 8.6%. Calcd for $RuC_{33}H_{57}O_6$: C, 60.9; H, 8.8%.

The author wishes to express his thanks to professor Gen P. Satô and Asst. Professor Kunio Shimizu, Sophia University, for their invaluable discussions and encouragement. He thanks Hiroyuki Moriya, Yasuko Sakura, Ayako Shimazaki, and Yasushi Takeuchi for their helpful experimental assistance. The present work was partially supported by a Grant-in-Aid for Scientific Research No. 547045 from the Ministry of Education, Science and Culture. The financial support by Saneyoshi Scholarship Foundation is gratefully acknowledged. Thanks are also due to Dr. F. Scott Howell, Sophia University, for correcting the manuscript.

References

1) R. W. Murray and L. K. Hiller, Jr., *Anal. Chem.*, **39**, 1221 (1967).
2) W. R. Heineman, J. N. Burnett, and R. W. Murray, *Anal. Chem.*, **40**, 1970 (1968).
3) S. Misumi, M. Aihara, and Y. Nonaka, *Bull. Chem. Soc. Jpn.*, **43**, 774 (1970).
4) M. K. Kalinowski and A. Ćmiel, *Inorg. Chim. Acta*, **49**, 179 (1981).
5) J. N. Burnett, L. K. Hiller, Jr., and R. W. Murray, *J. Electrochem. Soc.*, **117**, 1028 (1970).
6) G. Gritzner, H. Murauer, and V. Gutmann, *J. Electroanal. Chem.*, **101**, 185 (1979).
7) A. Endo, M. Watanabe, S. Hayashi, K. Shimizu, and G. P. Satô, *Bull. Chem. Soc. Jpn.*, **51**, 800 (1978).
8) J. G. Gordon, II, M. J. O'Connor, and R. H. Holm, *Inorg. Chim. Acta*, **5**, 381 (1971).
8) T. Kobayashi, Master's Thesis, Sophia University, Tokyo, Japan, 1981.
10) G. A. Stoner, *Anal. Chem.*, **27**, 1186 (1955).
11) G. S. Patterson and R. H. Holm, *Inorg. Chem.*, **11**, 2285 (1972).
12) S. L. Murov, "Handbook of Photochemistry", Marcel Dekker, Inc., New York (1973), Section 26.
13) J. N. Butlar, "Reference Electrodes in Aprotic Organic Solvents," in "Advances in electrochemistry and Electrochemical Engineering," ed by P. Delahay and C. W. Tobias, Interscience Publishers, New York (1970), Vol. 7, p. 82.
14) P. Zuman, "Current Trends in the Study of the Influence of Structure on the Polarographic Behavior of Organic Substances," in "Progress in Ploarography," ed by P. Zuman, I. M. Kolthoff, Interscience Publishers, New York (1962), Vol. 1, p. 319.
15) P. Zuman, "Influence of Substituents in Aliphatic and Heterocyclic Series," in "Advances in Polarography," ed by I. S. Longmuir, Pergamon Press, New York (1960), Vol. 3, p. 812.
16) P. N. Gupta and S. A. Bhat, *J. Electrochem. Soc. India*, **30**, 209 (1981).
17) J. Heyrovský and Kůta, "Principle of Polarography," Academic Press, New York and London (1966), Chap. VIII.
18) K. Momoki, H. Sato, and H. Ogawa, *Anal. Chem.*, **39**, 1072 (1967).
19) T. Fujinaga and I. Sakamoto, *J. Electroanal. Chem.*, **67**, 201 (1976).
20) T. Nagaoka, S. Okazaki, and T. Fujinaga, *J. Electroanal. Chem.*, **133**, 89 (1982).
21) T. Nagaoka, S. Okazaki, and T. Fujinaga, *Bull. Chem. Soc. Jpn.*, **55**, 1967 (1982).
22) R. M. Fuoss, *J. Am. Chem. Soc.*, **80**, 5059 (1958).
23) G. K. Chao, R. L. Sime, and R. J. Sime, *Acta Crystallogr., Sect. B*, 2845 (1973).
24) M. K. Kalinowski and A. Galazka, *Electrochim. Acta*, **25**, 1205 (1980).
25) J. F. Steinbach and J. H. Burns, *J. Am. Chem. Soc.*, **80**, 1839 (1958).
26) L. Wolf, E. Butter, and H. Weinelt, *Z. Anorg. Allg. Chem.*, **306**, 87 (1960).

Spectrophotometric Determination of Iron(II) after Extraction of Its 4′-(*p*-Methoxyphenyl)-2,2′ : 6′,2″-terpyridine Complex with Tetraphenylborate Anion into Molten Naphthalene

Jenn-Lin Lin, Lih-Fen Chang, and Masatada Satake*,†

Nat onal Taiwan College of Education, Changhwa, Taiwan, Republic of China

† *Faculty of Engineering, Fukui University, Fukui 910*

(Received February 24, 1983)

A new method is described for the extraction of ion-associated complex of iron(II) 4′-(*p*-methoxyphenyl)-2,2′ : 6′,2″-terpyridine (abbreviated as MPTP) cation with tetraphenylborate (TPB) anion into molten naphthalene. The solid mixture containing the colored complex is dissolved in *N*,*N*-dimethylformamide (DMF) and the absorbance was measured at 576 nm. The other factors such as pH, amounts of reagents and naphthalene, shaking time and diverse ions are studied. The method has been applied for the determination of iron in reference materials and practical samples and the results was compared with the conventional 2,4,6-tri(2-pyridyl)-1,3,5-triazine (TPTZ) procedure.

Extractive spectrophotometry has been widely employed for the analysis of trace amounts of metal ions. However, this method is not applicable when the solubility of metal complexes in solvents is small. By the aid of the extraction with molten naphthalene, such complexes have successfully been applied to the separation and concentration of metal ions.[1–4]

In the present paper, 4′-(*p*-methoxyphenyl)-2,2′:6′, 2″-terpyridine (MPTP) was recommended as a new extraction reagent for the spectrophotometric determination of iron(II) with naphthalene. MPTP reacts with iron(II) to form a water-soluble red complex cation.[5–7] In the presence of tetraphenylborate(TPB) anion, iron(II)–MPTP cation forms a water-insoluble, thermally stable ion-associated complex. This com plex can hardly be extracted into nonaqueous organic solvents because of the poor solubility of the complex in solvents and the incomplete phase separation, but easily extracted into molten naphthalene at temperatures above 81 °C. Compared with the ordinary solvent extraction method, the method is characterized by the greater extraction rate and the higher solubility of the complex into molten naphthalene.

Experimental

Reagents. Standard iron(III) solution, 100 ppm. Prepared by dissolving 0.8635 g of ammonium iron(III) sulfate dodecahydrate in 100 cm³ of 0.5 M (1 M = 1 mol dm⁻³) H_2SO_4 and by diluting to 500 cm³ with water.

4′-(*p*-Methoxyphenyl)-2,2′:6′,2″-terpyridine solution, 0.02%. Prepared by dissolving 0.02 g of this reagent in a few drops of concentrated hydrochloric acid and by diluting to 100 cm³ with water.

Hydroxylammonium chloride solution, 2% in water.

Sodium tetraphenylborate solution, 1% in water.

Buffer solutions were prepared by mixing 1 M acetic acid and 1 M ammonium acetate solution for pH 3—6, and 1 M aqueous ammonia and 1 M ammonium acetate solution for pH 8—11.

Naphthalene, acetone, *N*,*N*-dimethylformamide and all other reagents were of analytical-reagent grade, and used without further purification.

Apparatus. The absorbance measurements were made with a Hitachi Model 200-20 double beam spectrophotometer with 10-mm glass cells.

All the pH measurements were done with a Toa-Dempa HM-5A pH meter.

General Procedure. To about 25 cm³ of sample solution containing 1—19 μg of iron(III) in a 80-cm³ tightly stoppered Erlenmeyer flask, add 1.0 cm³ of 2% hydroxylammonium chloride solution, 2.0 cm³ of buffer solution (pH 5.0) and 3.0 cm³ of 0.02% MPTP solution. Mix the solution well and add 1.5 cm³ of 1% TPB solution. After warming on a water bath (50—60 °C) for 15 min, add 1.5 g of naphthalene and warm the mixture on a water bath at 90 °C to melt naphthalene completely. Shake it vigorously until the naphthalene solidifies forming many fine crystals. Filter the naphthalene mixture on a filter paper (No. 5A). Wash with water, blot the excess water with a dry filter paper and dry in an oven at 50—60 °C. Dissolve the naphthalene in *N*,*N*-dimethylformamide, dilute to 10 cm³, and measure the absorbance at 576 nm against a reagent blank prepared similarly.

Results and discussion

Absorption Spectra. Absorption spectrum of the ternary complex iron(II)–MPTP–TPB in naphthalene–*N*,*N*-dimethylformamide solution is shown in Fig. 1, together with that of the reagent blank. The complex has an absorption maximum at 576 nm, while the reagent blank showed no significant absorption at this wavelength.

Effect of pH. The effect of pH on the absorbance of the ternary complex was studied at 576 nm (Fig. 2). The pH of aqueous solution after extraction was measured at room temperature. The pH range 4.0—6.8 seems to be suitable for the extraction of the complex.

Effect of Hydroxylammonium Chloride Concentration. Varying volumes of 2% hydroxylammonium chloride solution were added to the sample containing 10 μg of iron(III). Iron(III) was completely reduced to iron (II) by the addition of 0.1—8 cm³ of 2% solution. Thus 1.0 cm³ of 2% solution was taken for the further work.

Effect of MPTP and TPB Concentration. Different amounts of MPTP were added to the sample containing 10 μg of iron(III). It was observed that the extraction was quantitative for 0.8—8.0 cm³ of 0.02% MPTP solution (Fig. 3). Thus 3.0 cm³ of 0.02% solution was added. Similar studies with sodium tetraphenylborate showed that the absorbance remained

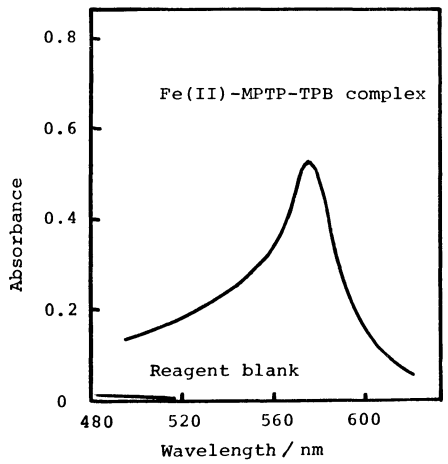

Fig. 1. Absorption spectra of MPTP-TPB and iron(II)-MPTP-TPB complex in naphthalene-*N*,*N*-dimethylformamide solution.
Iron(III): 10 μg; pH: 5.0; 2% $NH_2OH \cdot HCl$: 1.0 cm^3; 0.02% MPTP: 3.0 cm^3; 1% TPB: 1.5 cm^3. Naphthalene: 1.5 g. Reference: water.

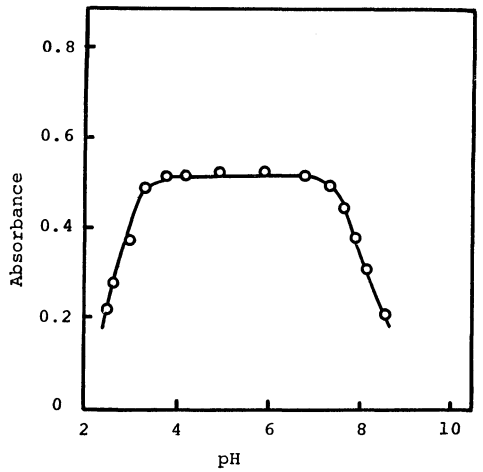

Fig. 2. Effect of pH.
Iron(III): 10 μg; Wavelength: 576 nm; pH: 5.0. Conditions were the same as in Fig. 1. Reference: reagent blank.

constant over the range of 0.1—4.0 cm^3 of 1% TPB solution. Therefore, 1.5 cm^3 of 1% TPB solution was used.

Effect of Buffer Solution and Digestion Time. Varying volumes of buffer solution were added to the sample containing 10 μg of iron(III), other variables being kept constant. When the volumes between 1.0 and 4.0 cm^3 were added, the absorbance did not show any change. The solution containing iron(II)–MPTP–TPB complex at pH 5.0 was digested at 50—60 °C. The digestion time is not critical and only one minute was sufficient for the completion of the complex formation.

Effect of Addition of Naphthalene and of Shaking Time. The extraction of the complex into molten naphthalene was carried out by varying amounts of naphthalene from 0.5 to 3.0 g. In all cases the amount of naphthalene had no influence on the absorbance of the system. Thus 1.5 g of naphthalene was used as a

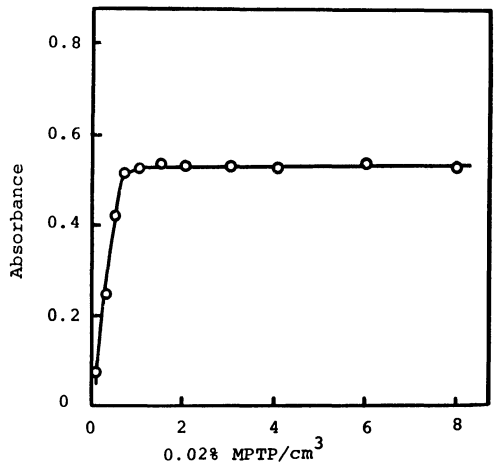

Fig. 3. Effect of reagent concentration.
Iron(III): 10 μg; Wavelength: 576 nm. Conditions were the same as in Fig. 2.

TABLE 1. EFFECT OF DIVERSE IONS

Diverse ion	Tolerance limit	Diverse ion	Tolerance limit
I^-	17 g	Ca^{2+}	200 mg
NO_3^-	6 g	Mn^{2+}	150 mg
SO_4^{2-}	4 g	Cr^{6+}	10 mg
CH_3COO^-	2.2 g	Hg^{2+}	8 mg
Cl^-	2.4 g	Pb^{2+}	4000 μg
SCN^-	1.8 g	Pt^{4+}	1000 μg
Cit^{3-}	0.5 g	Ni^{2+}	500 μg
$Tart^{2-}$	0.3 g	Cd^{2+}	200 μg
ClO_4^-	0.2 g	Sn^{2+}	100 μg
$H_2PO_4^-$	36 mg	Al^{3+}	70 μg
$C_2O_4^{2-}$	20 mg	Zn^{2+}	50 μg
CN^-	1.2 mg	Cu^{2+}	50 μg
H_2edta^{2-}	6.2 μg	Co^{2+}	15 μg
		Bi^{3+}	2 μg

Iron(III): 10 μg; pH: 5.0; 0.02% MPTP: 3.0 cm^3

suitable amount. Naphthalene(1.5 g) was added to the solution containing the complex and the mixture was shaken vigorously for periods ranging 3 to 90 s. The experimental results showed that the complex is extracted quantitatively into molten naphthalene by vigorous shaking for about a few seconds. Consequently, 30 s of shaking time was selected for convenience.

Effect of Aqueous Phase Volume. Since the organic/aqueous phase ratio is important factor in such procedures, the effect of aqueous phase volume on the extraction of the complex was studied. The extraction was quantitative when the volume of aqueous phase did not exceed 70 cm^3. Above this volume of aqueous phase the extractability decreased gradually.

Effect of Standing Time. The mixture of the ternary complex and naphthalene was dissolved in *N*, *N*-dimethylformamide, and the effect of standing time on the absorbance was examined between 1 and 20 h. It was observed that the absorbance remained constant for these periods. Consequently, 20 min of standing time was selected for all absorbance measurements.

Calibration Curve. The absorbances for varying concentration of iron(III) were measured at 576 nm against a reagent blank under the optimum conditions

Table 2. Analysis of iron in metals

Sample	Composition of alloy (%)	Iron, certified value/%	Iron content[a]/%	
			Present method	TPTZ method
N.B.S. SRM-85b Al alloy	Cu: 3.99, Cr: 0.21 Mn: 0.61, Ni: 0.089 Si: 0.18, Ti: 0.022 Zn: 0.03, Ga: 0.019 V: 0.006, Pb: 0.021	0.24	0.242±0.003	0.253±0.002
N.B.S. SRM-158a Silicon-Bronze alloy	Cu: 90.93, Si: 3.03 Zn: 2.08, Mn: 1.11 Ti: 0.96, Al: 0.46 Pb: 0.097, Ni: 0.001 P: 0.026	1.23	1.21±0.02	1.24±0.02
Metallic magnesium (powder)	—	—	0.0021±0.0001	0.0023±0.0001
Metallic aluminum (powder)	—	—	0.149±0.002	0.151±0.002

a) Average of five determinations.

described above. The results followed Beer's law over the concentration range of 1—19 μg of iron(III) in 10 cm^3 of *N,N*-dimethylformamide. The molar absorptivity of the complex was calculated to be 2.9×10^4 $dm^3\ mol^{-1}\ cm^{-1}$, and the sensitivity was 0.00192 μg of iron(III) per cm^3 for 0.001 absorbance. Ten determinations of a sample containing 10 μg of iron(III) gave a mean absorbance of 0.522 with relative standard deviation of 1.34%.

Choice of Solvent. Various organic solvents were tested to dissolve the extracted mixture of the complex and naphthalene. The mixture is soluble in *N,N*-dimethylformamide, dimethyl sulfoxide, propylene carbonate and acetonitrile. *N,N*-dimethylformamide is sensitive and cheaper than other solvents mentioned above.

Effect of Diverse Ions. Various amounts of diverse ions were added to the sample containing 10 μg of iron(III). The tolerance limit (Table 1) was listed at the amounts required to cause 5% error. Among anions examined, only Na_2H_2 edta interfered even at the concentration equivalent to that of iron(III). The cations Bi^+ and Co^{2+} interfered seriously.

Iron Analysis in Reference Materials and Metallic Samples. This method has been successfully employed for the analysis of iron in reference materials and other metallic samples. The results are in reasonably good agreement with those obtained by the conventional spectrophotometric method employing 2, 4,6-tri(2-pyridyl)-1,3,5-triazine(TPTZ)[8–10], as shown in Table 2. The analytical procedures were as follows: a 1 g portion of reference aluminum alloy(N.B.S., SRM-85b) was gently dissolved in 40 cm^3 of hydrochloric acid(1+1) and 2 cm^3 of 30% hydrogen peroxide. The excess of hydrogen peroxide was decomposed by heating the mixture gently on a boiling-water bath. After cooling, the volume of the sample was adjusted to 500 cm^3 with water. A 2 cm^3 aliquot was transferred to a 100 cm^3 separatory funnel, and 40 cm^3 of hydrochloric acid (1+1) was added. The iron(III) in this sample was extracted by vigorous shaking for 5 min with 20 cm^3 of isobutyl methyl ketone(MIBK).[11] The iron(III) was then back-extracted from the organic phase with 25 cm^3 of water, and the proposed method and TPTZ procedure were applied.

A 100 mg portion of reference silicon bronze alloy (N.B.S., SRM-158a) was dissolved in the mixed solution of 10 cm^3 of hydrochloric acid(1+1), 1 cm^3 of concentrated nitric acid and 3 cm^3 of concentrated sulfuric acid. The mixture was gently heated on a boiling-water bath. The excess of the acids was evaporated and then the solution was diluted to 1000 cm^3 with water. This solution was used for both methods.

Metallic magnesium powder (10 g) and aluminum powder(2 g) were analyzed in the same way as in the case of the aluminum alloy.

In the present study, the extraction of the ternary complex into molten naphthalene is easily attained merely by contact with molten naphthalene or by vigorous shaking for a few seconds. Since a small amount (1.5 g) of organic phase (naphthalene) is required for the complete extraction of the complex, the method is useful for the concentration of trace iron ion from a large volume of aqueous solution, and proved to be more excellent in the sensitivity snd precision than the MPTP procedure[5–7] in aqueous medium.

References

1) T. Fujinaga, M. Satake, and T. Yonekubo, *Bull. Chem. Soc. Jpn.*, **48**, 899 (1975).
2) M. Satake and Y. Takagi, *Bunseki Kagaku*, **26**, 386 (1977).
3) M. Satake, *Anal. Chim. Acta*, **92**, 423 (1977).
4) A. Kumar, M. F. Hussain, M. Satake, and B. K. Puri, *Bull. Chem. Soc. Jpn.*, **55**, 3455 (1982).
5) E. Deggau, F. Kroehnke, K. E. Schalke, Hj. Staudinger, and W. Weis, *J. Clin. Chem.*, **3**, 102 (1965).
6) D. Stamm, Hj. Staudinger, and W. Weis, *Z. Klin. Chem.*, **4**, 222 (1966).
7) R. Schmidt, W. Weis, V. Klingmueller, and Hj. Staudinger, *Z. Klin. Chem.*, **5**, 304 (1967).
8) P. F. Collins and H. Diehl, *Anal. Chem.*, **31**, 1862 (1959).
9) P. F. Collins and H. Diehl, *Anal. Chim. Acta*, **22**, 125 (1960).
10) S. Maekawa and K. Kato, *Jpn. Anal.*, **16**, 482 (1967).
11) JIS H1353 (1972).

Structural Study of Optical Resolution. XII. The Crystal and Molecular Structure of $(-)_{589}$-*trans*-*SS*-Bis(isothiocyanato)(triethylenetetramine)-cobalt(III) μ-(+)-Tartrato(4−)-μ-(+)-hydrogentartrato(3−)-diantimonate(III) Tetrahydrate

Yoshihiko KUSHI,* Masahiro KURAMOTO, Shunji UTSUNO,† and Hayami YONEDA

Department of Chemistry, Faculty of Science, Hiroshima University, Higashi-senda-machi, Naka-ku, Hiroshima 730

† *Department of Chemistry, Faculty of Science, Shizuoka University, Oya, Shizuoka 422*

(Received March 19, 1983)

The crystal and molecular structure of the diastereoisomeric salt, $(-)_{589}$-*trans*-$[Co(NCS)_2(trien)][Sb_2((+)\text{-tart})((+)\text{-tartH})]\cdot 4H_2O$, has been determined by the X-ray diffraction method. The red crystals were monoclinic, with the space group $P2_1$, $a=8.987(1)$, $b=15.949(2)$, $c=10.726(1)$ Å, $\beta=102.57(2)°$, and $Z=2$. The structure was solved by the heavy-atom method and refined by the block-diagonal least-squares method, using 2976 independent reflections, to the final R-value of 0.033. In the complex cation, the conformations of the three five-membered chelate rings are ($\delta\lambda\delta$), while the absolute configurations of the two asymmetric nitrogen atoms are both *S*. The mononegative anion has a dimeric structure of $[Sb_2((+)\text{-}C_4H_2O_6)((+)\text{-}C_4H_3O_6)]^-$, in which $(+)\text{-}C_4H_2O_6^{4-}$ and $(+)\text{-}C_4H_3O_6^{3-}$ coordinate to two Sb^{III} atoms. The extra hydrogen atom in $(+)\text{-}C_4H_3O_6^{3-}$ bonds to the free oxygen atom(OTB5) of the carboxylato group, and a short contact is formed between this oxygen atom and a water molecule(OW2); OTB5···OW2 2.43(1) Å. Though six N-H hydrogen atoms are present in the complex cation, three of them form N-H···O hydrogen bonds to the oxygen atoms of the dimeric anion; NTR3···OTA1 2.86(1), NTR4···OTA6 2.86(1), and NTR1···OTB4 3.19(1) Å.

Potassium bis(μ-(+)-tartrato(4−))diantimonate(III), tartar emetic, is a familiar resolving reagent for metal complexes.[1] From the X-ray structure analyses, the presence of a unique dinegative dimeric structure in which two tetranegative (*R*,*R*)-tartrate anions, $(C_4H_2O_6)^{4-}$ abbreviated (+)-tart, coordinate to two Sb^{III} atoms was proved.[2] Recently, *trans*-$[Co(NCS)_2(trien)]^+$ complexes were newly prepared and resolved by using this anion.[3] Under acidic conditions, red crystals of the optically active diastereoisomeric salt with the chemical formula of $[Co(NCS)_2(trien)][Sb_2((+)\text{-tart})((+)\text{-tartH})]\cdot 4H_2O$ were precipitated.[4] Since the ratio of cation *vs.* anion in this crystal is 1:1, the presence of a mononegative bis(μ-(+)-tartrato)diantimonate (III) anion is strongly suggested.

As a part of our structural studies of optical resolution, we recently determined several diastereoisomeric salts including the mononegative hydrogen (+)-tartrate anion, $d\text{-}C_4H_5O_6^-$, as the resolving reagent,[5] and compared their structures with those found in the diastereoisomeric salts with the dinegative (+)-tartrate anion, $d\text{-}C_4H_4O_6^{2-}$.[6] Thus, in order to determine the molecular structure of the mononegative bis(μ-(+)-tartrato)diantimonate(III) anion and the absolute configuration of $(-)_{589}$-*trans*-$[Co(NCS)_2(trien)]^+$ and in order to compare the crystal-packing mode with those found in diastereoisomeric salts including the $[Sb_2((+)\text{-tart})_2]^{2-}$ anion, we have undertaken the single-crystal X-ray structure analysis of the title compound.

Experimental

Preparation of Compound. Racemic *trans-RR,SS*-$[Co(NCS)_2(trien)]ClO_4$ was prepared by the method given in the literature.[3] The less-soluble diastereoisomeric salt, $(-)_{589}$-*trans*-$[Co(NCS)_2(trien)][Sb_2((+)\text{-tart})((+)\text{-tartH})]\cdot 4H_2O$, was prepared by the following procedure.[4] A solution of racemic *trans-RR,SS*-$[Co(NCS)_2(trien)]ClO_4$ (3×10^{-3} mol) was adsorbed on a column of SP-Sephadex C-25 (the total exchange capacity: 2.7 mequiv) and then eluted with an aqeous solution of $Ca[Sb_2((+)\text{-tart})_2]$ (1.3×10^{-3} mol). The eluent was concentrated to about 10 ml, and the diastereoisomeric salt was precipitated by the addition of 1.3 ml of 1 M HCl (1 M = 1 mol dm^{-3}). When the red precipitate thus obtained was recrystallized from a hot aqueous solution, red rectangular crystals were deposited. Found: C, 20.82; H, 3.42; N, 9.05%. Calcd for $C_{16}H_{31}O_{16}N_6S_2CoSb_2$: C, 20.66; H, 3.36; N, 9.04%.

Crystallographic Data Collection. The intensities and cell dimensions were measured on a SYNTEX-R3 diffractometer with Mo $K\alpha$ radiation ($\lambda=0.7107$ Å), monochromated by a graphite plate. The size of the crystal used for the X-ray measurement was $0.22\times0.20\times0.18$ mm^3. The systematic absences for $0k0$ ($k=2n+1$) suggested $P2_1$ or $P2_1/m$ as the possible space groups, but the latter was eliminated because of the optical activity of the compound. The unit cell dimensions were refined by a least-squares treatment of the setting angles of 25 reflections. The crystal data were as follows: monoclinic, space group $P2_1$, $a=8.987(1)$, $b=15.949(2)$, $c=10.726(1)$ Å, $\beta=102.57(2)°$, $D_m=2.04$ g cm^{-3} (by flotation in a chloroform-bromoform mixture), $Z=2$, and $D_c=2.06$ g cm^{-3}. The intensity data were collected in the ω-scan mode up to $2\theta=55°$. Of the 3128 unique observed reflections, 2976 reflections with $|F_o|>3\sigma(F_o)$ were used for the structure determination. Corrections for absorption effect were neglected (μ(Mo $K\alpha$) = 25.9 cm^{-1}).

Determination and Refinement of Crystal Structure. The coordinates of the Sb and Co atoms could be deduced from a Patterson map. The positions of the other lighter atoms, except for the hydrogen atoms, were revealed by the Fourier synthesis. Several cycles of the block-diagonal least-squares refinement with anisotropic temperature factors reduced the R-value ($R=\{\Sigma(|F_o|-|F_c|)/\Sigma|F_o|\}$) to 0.050. At this stage, a difference map was examined for the hydrogen-atom positions with reference to the calculated ones (1.0 Å for N-H and C-H bond distances and tetrahedral angle). There were clear indications for most of the hydrogen atoms. The final refinement including these H atoms with isotropic temperature factors caused the R-

value to converge to 0.033. In the refinement, the quantity minimized was $w(|F_o|-k|F_c|)^2$. The weighting scheme used was $w=(\sigma_{cs}^2+a|F_o|+b|F_o|^2)^{-1}$, where σ_{cs} is the standard deviation obtained from the counting statistics for each reflection; the a and b values were 0.2 and 0.0009 respectively.

All the atomic scattering factors, with corrections for the anomalous dispersion of Sb, Co, and S atoms, were taken from the International Tables for X-ray Crystallography, Vol. IV.[7] All the computations were carried out by a HITAC M-180 computer at the Hiroshima University Information Processing Center. The computer programs used were FOURP21[8] and HBLS-IV, with a slight modification.[9] An ORTEP drawing was carried out by the use of a computer system, XTL, in a SYNTEX-R3 diffractometer.[10] The final atomic parameters are listed in Table 1. The anisotropic thermal parameters and complete lists of the $|F_o|$ and $|F_c|$ values have been preserved by the Chemical Society of Japan (Document No. 8337).

Results and Discussion

The projections of the crystal structure along the a- and b-axes are shown in Figs. 1 and 2 respectively. The thermal ellipsoids in these figures are illustrated with a 50% probability.

Cation Geometry. Figure 3 shows a perspective drawing of the complex cation, which has an approximate two-fold axis through the midpoint of the CTR3-CTR4 bond and the central Co atom. The absolute structure of the crystal could be deduced, since the absolute configuration of (*R,R*)-tartrate was known.[11] Figure. 3 represents the absolute configuration of the complex cation correctly. The conformations of the three chelate rings of the triethylenetetramine ligand are of a $\delta\lambda\delta$ form, and the absolute configurations of the two asymmetric nitrogen atoms, NTR2 and NTR3, are both *S*.[12] Thus, the absolute configuration of the present $(-)_{589}$-*trans*-[Co(NCS)$_2$(trien)]$^+$ can be denoted as *trans-SS*-$\delta\lambda\delta$.

The bond lengths and angles within the complex cation are listed in Table 2. The Co–N(NCS) distances are 1.901(7) and 1.884(7) Å, while the Co–N–C angles are 162.0(7) and 161.4(7)°. The bond distances of the Co–N(trien) are 1.964(8) and 1.961(7) Å for the

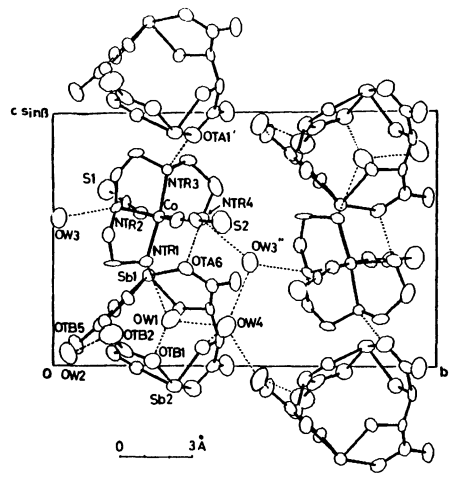

Fig. 1. A perspective drawing of the contents of the unit cell viewed down the a-axis. Possible hydrogen bonds are indicated by bloken lines. Hydrogen atoms are omitted for clarity.

Table 1. Positional parameters ($\times 10^4$) and thermal parameters

Atom	x	y	z	B_{eq} or B/Å^2
Sb(1)	257(1)	2500(1)	3613(1)	2.15(2)
Sb(2)	1102(1)	3183(1)	-803(1)	2.88(2)
C(TA1)	-1283(10)	4173(5)	-22(7)	2.57(31)
C(TA2)	194(9)	4339(5)	978(7)	2.34(30)
C(TA3)	-98(9)	4094(4)	2300(7)	2.21(28)
C(TA4)	1441(10)	4143(5)	3219(7)	2.62(32)
C(TB1)	3068(9)	1875(6)	649(7)	2.86(34)
C(TB2)	1444(9)	1568(5)	495(7)	2.49(31)
C(TB3)	1166(9)	1337(5)	1787(7)	2.39(31)
C(TB4)	-523(9)	1161(5)	1667(7)	2.47(31)
O(TA1)	-1128(7)	3633(4)	-893(5)	3.08(25)
O(TA2)	-2451(8)	4529(4)	23(7)	4.05(31)
O(TA3)	1434(7)	3905(4)	733(5)	2.66(23)
O(TA4)	-747(6)	3291(3)	2281(5)	2.28(20)
O(TA5)	2234(8)	4761(4)	3342(6)	3.69(30)
O(TA6)	1879(6)	3454(4)	3869(5)	2.46(22)
O(TB1)	3227(7)	2620(5)	198(6)	3.58(28)
O(TB2)	4145(8)	1454(6)	1164(7)	4.46(35)
O(TB3)	367(6)	2176(4)	-79(5)	2.64(23)
O(TB4)	1693(6)	1950(3)	2710(5)	2.43(22)
O(TB5)	-1139(7)	603(4)	885(6)	3.63(29)
O(TB6)	-1246(6)	1594(3)	2298(5)	2.64(23)
Co	5433(1)	2768(1)	5938(1)	1.84(3)
S(1)	1331(3)	1413(2)	6977(3)	4.55(12)
S(2)	9563(4)	4413(2)	5710(3)	5.68(15)
N(1)	3534(8)	2300(4)	6087(6)	2.52(28)
N(2)	7293(7)	3262(4)	5794(6)	2.46(26)
N(TR1)	5074(7)	2436(5)	4134(5)	2.27(24)
N(TR2)	6301(7)	1670(4)	6307(5)	1.95(23)
N(TR3)	6017(8)	2981(4)	7747(5)	2.27(25)
N(TR4)	4494(8)	3884(4)	5807(6)	2.56(27)
C(1)	2616(8)	1934(5)	6471(7)	2.16(28)
C(2)	8235(11)	3760(6)	5776(8)	3.11(36)
C(TR1)	5741(11)	1600(5)	4048(7)	3.06(35)
C(TR2)	6993(10)	1426(5)	5219(8)	2.88(34)
C(TR3)	7244(10)	1662(5)	7615(7)	2.69(32)
C(TR4)	6356(10)	2165(5)	8407(7)	2.79(32)
C(TR5)	4879(10)	3550(6)	8095(7)	2.88(33)
C(TR6)	4706(11)	4257(6)	7128(8)	3.22(37)
O(W1)	6153(7)	3113(5)	1902(6)	3.74(28)
O(W2)	6130(8)	385(5)	533(7)	4.21(33)
O(W3)	4274(8)	147(4)	5900(7)	4.20(33)
O(W4)	4454(9)	4523(5)	1566(8)	4.97(38)
H(CB2)	129(14)	107(8)	-9(12)	3.2(27)
H(CB3)	177(14)	82(8)	207(12)	3.5(29)
H(CA2)	-24(18)	491(11)	87(14)	5.5(38)
H(CA3)	-84(14)	450(8)	258(12)	3.5(29)
H(N2)	553(13)	124(8)	633(11)	3.2(27)
H(N3)	699(14)	329(9)	800(12)	3.7(28)
H(N1A)	554(14)	285(9)	364(11)	4.0(31)
H(N1B)	396(14)	240(9)	375(12)	3.9(29)
H(N4A)	341(15)	382(9)	542(13)	3.7(29)
H(N4B)	495(15)	424(8)	526(12)	3.3(27)
H(C1A)	614(13)	156(8)	325(11)	2.6(25)
H(C1B)	492(15)	117(10)	400(13)	4.5(33)
H(C2A)	795(14)	180(8)	522(11)	3.3(28)
H(C2B)	734(15)	82(9)	529(13)	4.5(34)
H(C3A)	827(12)	192(7)	763(10)	2.5(24)
H(C3B)	743(15)	107(9)	795(13)	4.3(32)
H(C4A)	697(13)	225(8)	930(11)	2.7(25)
H(C4B)	539(14)	187(8)	845(12)	3.6(29)
H(C5A)	390(12)	324(7)	804(9)	1.9(21)
H(C5B)	526(13)	377(8)	897(11)	3.1(27)
H(C6A)	563(17)	463(10)	730(15)	5.7(39)
H(C6B)	379(14)	460(8)	719(11)	3.0(26)
H(OB5)	-228(19)	53(11)	75(16)	6.6(43)
H(W2A)	589(15)	6(9)	-28(12)	3.9(30)
H(W2B)	540(16)	77(10)	77(13)	4.8(35)
H(W4A)	339(17)	431(10)	128(14)	5.4(37)
H(W4B)	509(17)	399(10)	169(13)	5.2(37)
H(W1A)	729(17)	319(11)	209(14)	5.8(37)
H(W1B)	555(15)	279(9)	125(13)	4.4(31)
H(W3A)	471(16)	-7(10)	678(14)	5.1(36)
H(W3B)	320(16)	24(9)	558(14)	5.0(36)

$B_{eq}=8\pi^2(U_{11}+U_{22}+U_{33})/3$. The anisotropic thermal parameters have been preserved by the Chemical Society of Japan. The positional parameters of the hydrogen atoms are represented on the scale of $\times 10^3$.

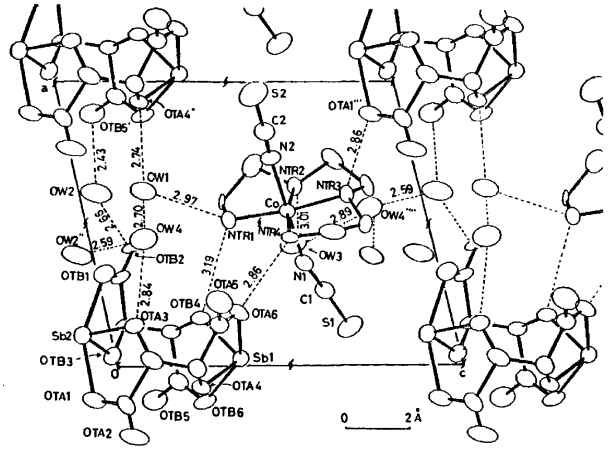

Fig. 2. A boundary projection of the contents of the unit cell viewed down the b-axis (from $y=0.54$ to $y=-0.06$) with the numbering scheme.

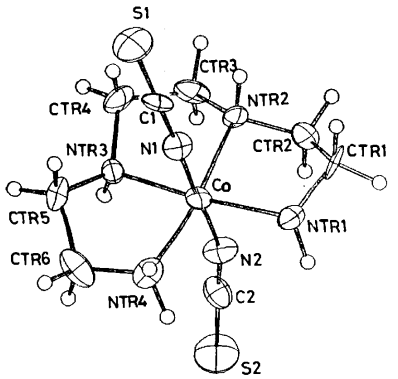

Fig. 3. An ORTEP drawing of the complex cation. All atoms are drawn with the 50% probability ellipsoids.

terminal nitrogen atoms and 1.923(7) and 1.927(6) Å for the middle nitrogen atoms respectively. The N–Co–N angles of the outer chelate rings are 86.0(3) and 86.0(3)°, while that of the central one is 86.8(3)°. These values are in good agreement with the values obtained for *trans-meso*-$[Co(CN)_2(trien)]ClO_4$.[13]

The two outer chelate rings have an unsymmetrical envelope conformation. The ring carbon atoms, CTR1 and CTR2, lie at -0.105 and -0.736 Å from the plane formed by NTR1, Co, and NTR2. The corresponding deviations of CTR5 and CTR6 from the plane of NTR3, Co, and NTR4 are 0.677 and 0.034 Å respectively. In the central chelate ring, CTR3 and CTR4 lie 0.347 below and 0.386 Å above the plane of NTR2, Co, and NTR3. These values are in good agreement with the values obtained for $(-)_{589}$-*trans*-$[Co(NO_2)_2$(L-3,8-dimetrien)$]ClO_4$.[14]

Anion Geometry. Figure 4 shows a perspective drawing of the dimeric anion with the water molecule OW2. The geometry of the mononegative dimeric anion, whose interatomic distances and angles are listed in Table 2, resembles the structure found for a number of dinegative bis(μ-(+)-tartrato(4−))-diantimonate(III).[2] The coordination geometry is pseudotrigonal bipyramidal, with average axial and equatrial angles of 150.8(2) and 99.3(2)° respectively

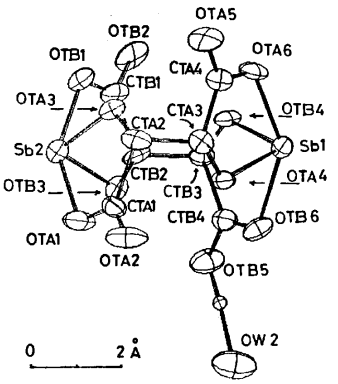

Fig. 4. Structure of the mononegative dimeric anion with including the water molecule OW2.

(compared with 150(2) and 100(4)° for $[Sb_2((+)$-tart$)_2]^{2-}$).[15]

Of great interest are the bond distances and angles given in Table 2 for the (+)-$C_4H_3O_6$(TB-tart) group. Though four –COO groups are present in this anion, only one –COO group in TB-tart has a symmetrical structure; CTB4–OTB5 1.266(11) and CTB4–OTB6 1.245(10) Å and CTB3–CTB4–OTB5 118.1(7), CTB3–CTB4–OTB6 118.8(7), and OTB5–CTB4–OTB6 123.1 (8)°, respectively. The other –COO group in TB-tart and two –COO groups in TA-tart have the usual unsymmetrical form, as is summarized in Table 2; the averaged C–O distances are 1.207(12) Å for free oxygen atoms and 1.306(12) Å for oxygen atoms bonded to Sb^{III}. Additionally, the Sb1–OTB6 distance, 2.252(6) Å, is longer than the other Sb–O(–COO distance); 2.084(6), 2.111(6), and 2.171(6) Å. Moreover, a short contact is found between OTB5 and the water molecule OW2; OTB5···OW2 2.43(1) Å. Thus, we can safely conclude that the extra hydrogen atom (proton) of the (+)-$C_4H_3O_6$ group bonds to the OTB5 carboxyl oxygen atom. It is noteworthy that the present short O(–COOH)···O(H_2O) contact, 2.43 Å, is nearly equal to the O(H_2O)···H···O(H_2O) 2.431 Å in $(H_5O_2)^+$ included in *trans*-$[CoCl_2(en)_2]Cl\cdot(H_5O_2)\cdot Cl$[16] and to the O(–COOH)···O(OOC–) 2.44 Å observed in $(+)_{589}$-[Co(ox)(en)$_2$]H-*d*-tart$\cdot H_2O$.[17]

Tapscott *et al.* recently determined the crystal structure of sodium hydrogen bis(μ-*meso*-tartrato)-bis(2,2′-bipyridyl) dichromate(III) heptahydrate.[18] They found that this mononegative Cr^{III} complex anion has a dimeric structure and that the extra hydrogen atom (proton) bridges the gap between the two hydroxyl oxygen atoms which belong to the *meso*-tartrate groups within the dimeric unit. This marked difference in the position of the extra hydrogen atom(proton) between the Sb^{III} and the Cr^{III} mononegative dimeric anions probably comes from the different structural features of these anions. The former, the present Sb^{III} complex anion, has two (+)-tartrate anions in the trigonal bipyramidal configuration, but the latter, the Cr^{III} complex, has two *meso*-tartrate anions in the distorted octahedral configuration. The O(hydroxyl)···O(hydroxyl) interatomic distances of the former, OTA3··· OTB3 2.986(8) and OTA4···OTB4 3.026(8) Å, are considerably longer than that in the latter, O(hydroxyl)···

TABLE 2. BOND DISTANCES AND ANGLES (e.s.d.'s IN PARENTHESES)

Bond distance	l/Å	Bond distance	l/Å	Bond distance	l/Å
Co - N1	1.901(7)	CTR4 - NTR3	1.481(11)	CTA1 - OTA1	1.301(11)
Co - N2	1.884(7)	NTR3 - CTR5	1.475(12)	CTA1 - OTA2	1.203(11)
Co - NTR1	1.964(8)	CTR5 - CTR6	1.517(13)	CTA2 - OTA3	1.384(10)
Co - NTR2	1.923(6)	CTR6 - NTR4	1.509(12)	CTA3 - OTA4	1.406(10)
Co - NTR3	1.927(7)	Sb1 - OTA4	1.971(5)	CTA4 - OTA5	1.208(11)
Co - NTR4	1.961(7)	Sb1 - OTB4	1.979(6)	CTA4 - OTA6	1.314(10)
N1 - C1	1.157(10)	Sb1 - OTA6	2.084(6)	CTB1 - CTB2	1.513(12)
C1 - S1	1.610(8)	Sb1 - OTB6	2.252(6)	CTB2 - CTB3	1.507(12)
N2 - C2	1.165(12)	Sb2 - OTA3	1.979(6)	CTB3 - CTB4	1.521(12)
C2 - S2	1.596(10)	Sb2 - OTB3	1.960(6)	CTB1 - OTB1	1.303(12)
NTR1 - CTR1	1.474(13)	Sb2 - OTA1	2.111(6)	CTB1 - OTB2	1.209(13)
CTR1 - CTR2	1.519(14)	Sb2 - OTB1	2.171(7)	CTB2 - OTB3	1.413(10)
CTR2 - NTR2	1.488(11)	CTA1 - CTA2	1.537(12)	CTB3 - OTB4	1.399(10)
NTR2 - CTR3	1.473(11)	CTA2 - CTA3	1.547(12)	CTB4 - OTB5	1.266(11)
CTR3 - CTR4	1.516(13)	CTA3 - CTA4	1.516(12)	CTB4 - OTB6	1.245(10)
Bond angle	**ϕ/°**	**Bond angle**	**ϕ/°**	**Bond angle**	**ϕ/°**
N1-Co-N2	178.5(3)	Co-NTR2-CTR2	107.3(5)	OTA3-Sb2-OTB3	98.6(2)
Co-N1-C1	162.0(7)	Co-NTR2-CTR3	109.1(5)	CTA2-CTA1-OTA1	113.8(7)
Co-N2-C2	161.4(7)	NTR2-CTR3-CTR4	105.4(7)	CTA2-CTA1-OTA2	121.3(8)
N1-C1-S1	178.8(7)	CTR3-CTR4-NTR3	106.0(7)	OTA1-CTA1-OTA2	124.9(8)
N2-C2-S2	177.2(9)	CTR4-NTR3-CTR5	120.0(7)	CTA1-CTA2-OTA3	113.0(7)
NTR1-Co-NTR2	86.0(3)	Co-NTR3-CTR4	108.0(5)	CTA1-CTA2-CTA3	107.6(7)
NTR2-Co-NTR3	86.8(3)	Co-NTR3-CTR5	108.2(5)	CTA3-CTA2-OTA3	110.6(7)
NTR3-Co-NTR4	86.0(3)	NTR3-CTR5-CTR6	104.9(7)	CTA2-CTA3-OTA4	111.7(7)
NTR4-Co-NTR1	101.5(3)	CTR5-CTR6-NTR4	108.8(7)	CTA2-CTA3-CTA4	105.7(7)
Co-NTR1-CTR1	108.9(6)	Co-NTR4-CTR6	109.0(5)	CTA4-CTA3-OTA4	111.9(7)
NTR1-CTR1-CTR2	110.6(8)	OTA4-Sb1-OTB4	100.0(2)	CTA3-CTA4-OTA5	123.1(8)
CTR1-CTR2-NYR2	103.9(7)	OTA6-Sb1-OTB6	149.1(2)	CTA3-CTA4-OTA6	115.3(7)
CTR2-NTR2-CTR3	119.5(7)	OTA1-Sb2-OTB1	152.6(3)	OTA5-CTA4-OTA6	121.5(8)
CTB2-CTB1-OTB1	115.8(8)	CTB1-CTB2-CTB3	109.1(7)	CTB4-CTB3-OTB4	111.5(7)
CTB2-CTB1-OTB2	121.9(9)	CTB3-CTB2-OTB3	109.4(7)	CTB3-CTB4-OTB5	118.1(7)
OTB1-CTB1-OTB2	122.3(9)	CTB2-CTB3-OTB4	112.4(7)	CTB3-CTB4-OTB6	118.8(7)
CTB1-CTB2-OTB3	112.2(7)	CTB2-CTB3-CTB4	109.3(7)	OTB5-CTB4-OTB6	123.0(8)

TABLE 3. DISTANCES OF ATOMS FROM LEAST-SQUARES PLANES IN Å

Least-squares planes							
Plane(1)		Plane(2)		Plane(3)			
Co	−0.001	CTA1	0.054	CTB1	−0.058		
NTR1	−0.048	CTA2	−0.055	CTB2	0.063		
NTR2	0.064	CTA3	−0.049	CTB3	0.051		
NTR3	−0.066	CTA4	0.052	CTB4	−0.051		
NTR4	0.054						
Plane(4)		Plane(5)		Plane(6)		Plane(7)	
CTA1	0.006	CTB1	0.005	CTA3	−0.025	CTB3	−0.021
CTA2	0.023	CTB2	0.023	CTA4	−0.010	CTB4	0.014
OTA1	0.008	OTB1	0.006	OTA4	0.023	OTB4	0.016
OTA2	−0.017	OTB2	−0.015	OTA5	0.019	OTB5	0.018
OTA3	−0.020	OTB3	−0.019	OTA6	−0.008	OTB6	−0.020

Dihedral angles between the planes

Plane(2)—Plane(3)	0.9°	Plane(3)—Plane(5)	54.4
Plane(2)—Plane(4)	58.4	Plane(3)—Plane(7)	56.6
Plane(2)—Plane(6)	55.1	Plane(5)—Plane(7)	69.0
Plane(4)—Plane(6)	66.5		

Plane equations: each plane is represented by $lx'+my'+nz'+p=0$ with respect to the orthogonal axes, where x', y', and z' are coordinates in Å.

Plane	(1)	(2)	(3)	(4)	(5)	(6)	(7)
l	−0.920	0.273	0.262	−0.351	0.226	0.624	0.046
m	−0.383	−0.950	−0.952	−0.743	−0.399	−0.309	−0.689
n	0.084	−0.151	−0.161	0.570	−0.889	−0.717	0.723
p	4.383	6.688	2.217	4.565	1.215	4.111	0.067

O(hydroxyl) 2.418(6) Å.[18]

The relevant least-squares planes are listed in Table 3. The two planes of the C–C–C–C skeletons of TA-tart and TB-tart are quite parallel. The planes including five non-hydrogen atoms of each α-hydroxycarboxylate moiety are approximately coplanar. The angles between the two planes, 66.5° for TA-tart and 69.0° for TB-tart, are normal.[2]

Crystal-packing Mode and Waters of Crystallization. The packing features of the complex cations and dimeric anions are shown in Figs. 1 and 2. There are four waters of crystallization associated with the ionic species contained in the structural unit. The selected intermolecular distances, including the hydrogen-

Table 4. Intermolecular distances and angles

Hydrogen-bond distances and bonding modes			
D-H···A	D···A l/Å	H···A l/Å	D-H···A ϕ/°
OTB5-HOB5···OW2^{i}	2.43(1)	1.42(18)	177(18)
OW2-HW2A···OW4^{ii}	2.59(1)	1.60(14)	178(13)
OW2-HW2B···OTB2	2.66(1)	1.69(15)	179(14)
OW4-HW4B···OW1	2.70(1)	1.69(16)	179(14)
OW4-HW4A···OTA3	2.84(1)	1.44(16)	179(14)
OW1-HW1A···OTA4^{iii}	2.74(1)	1.74(17)	175(15)
OW1-HW1B···OTB1	2.96(1)	2.16(15)	143(12)
OW3-HW3A···OW4^{iv}	2.89(1)	1.88(16)	179(14)
NTR1-HN1A···OW1	2.97(1)	2.10(14)	146(11)
NTR2-HN2···OW3	3.01(1)	2.08(13)	160(11)
NTR4-HN4B···OW3^{v}	3.09(1)	2.12(13)	179(13)
NTR4-HN4A···OTA6	2.86(1)	2.00(14)	145(15)
NTR3-HN3···OTA1^{vi}	2.86(1)	1.92(14)	159(15)
NTR1-HN1B···OTB4	3.19(1)	2.22(14)	175(15)

Selected intermolecular distances (l/Å)			
Sb1···Cl	3.446(8)	OTA6···N1	3.12(1)
Sb1···N1	3.524(7)	OTA6···NTR1	3.26(1)
Sb1···S1	3.930(3)	OTA5···OW4	3.07(1)
Sb1···S2^{i}	3.920(4)	N2···OTA1^{vi}	3.58(1)
Sb2···S1^{vii}	3.727(3)	C2···OTA1^{vi}	3.50(1)

Roman numerals as superscripts refer to the following equivalent positions, relative to the reference atom at (x, y, z): i ($-1+x$, y, z), ii ($1-x$, $-1/2+y$, $-z$), iii ($1+x$, y, z), iv ($1-x$, $-1/2+y$, $1-z$), v ($1-x$, $1/2+y$, $1-z$), vi ($1+x$, y, $1+z$), vii (x, y, $-1+z$).
D; Hydrogen donor, A; Hydrogen acceptor.

bonding modes, are summarized in Table 4.

The hydrogen-bonding features in this crystal are as follows:

(1) Along the a-axis, there are strong hydrogen bondings, OTB5···OW2···OTB2^{i}, and the dimeric anions are joined to each other by the water molecule OW2; OTB5···OW2 2.43(1) and OW2···OTB2^{i} 2.66 (1) Å. (2) Along the c-axis, there are bonds from the tartrate oxygens of (+)-$C_4H_2O_6$(TA-tart) to triethylenetetramine nitrogens, with distances of OTA6···NTR4 2.86(1) and NTR3···OTA1^{vi} 2.86(1) Å respectively. (3) Along the b-axis, near the $y=0$ and $y=1/2$ there are sheets of the waters of crystallization, as shown in Fig. 1. (4) The planes of C–C–C–C skeleton of the two (+)-tart groups(TA and TB-tart) are approximately perpendicular to the crystallographic b-axis(within 4°), and the cell length of the b-axis is probably determined by the size of the dimeric anion. (5) As a result, the *trans-SS* complex cation is surrounded by the four dimeric anions on the ac-plane, and they are piled up along the b-axis by the two-fold screw operations. The short contacts around the complex cation along the b-axis are NTR2···OW3 3.01(1) and NTR4···OW3^{v} 3.09(1) Å.

It is interesting to note that, though there are two tartrate groups in the present [Sb_2((+)-$C_4H_2O_6$)((+)-$C_4H_3O_6$)]$^-$ complex, only the (+)-$C_4H_2O_6$ group(TA-tart) has short contacts to the nitrogen atoms of the triethylenetetramine ligand. The other group, (+)-$C_4H_3O_6$ (TB-tart), has short contacts to the water molecules and forms the hydrogen-bonding chain mentioned above along the a-axis. If the absolute configurations of the two nitrogen atoms of the trien ligand (NTR2 and NTR3) change from *S* to *R*, the hydrogen-bonding modes around these nitrogen atoms change completely. Thus, the optical discrimination between the $(+)_{589}$-*RR*- and $(-)_{589}$-*SS*-*trans*-[Co(NCS)$_2$(trien)]$^+$ probably comes from the different contact modes between the (+)-$C_4H_2O_6$ (TA-tart) of the dimeric anion and the corresponding optically active complex cations.

In contrast, in diastereoisomeric salts containing [Sb_2((+)-tart)$_2$]$^{2-}$ as the resolving reagent, for example *cis*-[Co(NCS)$_2$(tn)$_2$]$_2$[Sb_2((+)-tart)$_2$]·$2H_2O$ and its Cr^{III} analogue, the dimeric anions lie exactly on a crystallographic two-fold axis and the two (+)-tart groups are equivalent.[19] In [Fe(phen)$_3$][Sb_2((+)-tart)$_2$]·$8H_2O$, the dimeric anion has a crystallographic two-fold axis again, and only the halves of the two (+)-tart groups are crystallographically independent.[20] Thus, the crystal-packing modes in these salts are different from the present one.

Another interesting point in this crystal is in the averaged O···O distances around the water molecules: 2.80 Å for OW1, 2.56 Å for OW2, 2.89 Å for OW3, and 2.76 Å for OW4. The oxygen atom (OTB5) of the (+)-$C_4H_3O_6$(TB-tart) group is linked by hydrogen bonding to OW2 with the following sequence of the water molecules, as is shown in Fig. 2: OTB5···OW2···OW4···OW1 or ···OW3. The averaged distances around the water molecules reflect the positive charges which spread from the OTB5 to the water molecules through the hydrogen bodings: these results confirm the presence of an extra hydrogen atom(proton) between the OTB5 and water molecule OW2.

We wish to acknowledge a Grant-in-Aid for Scientific Research No. B547043 from the Ministry of Education, Science and Culture.

References

1) K. Garbett and R. D. Gillard, *J. Chem. Soc., A*, **1966**, 802; I. J. Kindred and D. A. House, *J. Inorg. Nucl. Chem.*, **37**, 1359 (1975).
2) R. E. Tapscott, R. L. Belford, and I. C. Paul, *Coord. Chem. Rev.*, **4**, 323 (1969).
3) Y. Sakai, Y. Nokami, H. Kanno, and S. Utsuno, *Chem. Lett.*, **1981**, 371.
4) Y. Nokami, M. Irimichi, Y. Tahata, and S. Utsuno, *Proc. Meet. Jpn. Coordination Chemistry, 31st*, 1981, Sendai, Abstr., 3B14.
5) M. Kuramoto, Y. Kushi, and H. Yoneda, *Bull. Chem. Soc. Jpn.*, **53**, 125 (1980).
6) T. Tada, Y. Kushi, and H. Yoneda, *Bull. Chem. Soc. Jpn.*, **55**, 1063 (1982).
7) "International Tables for X-ray Crystallography," Kynoch Press, Birmingham (1974), Vol. IV.
8) Y. Kushi, unpublished work.
9) T. Ashida, "The Universal Crystallographic Computation Program System," ed by T. Sakurai, The Crystallographic Society of Japan (1967).
10) C. K. Johnson, ORTEP, Report ORNL-3794, Oak Ridge National Laboratory, Oak Ridge, Tennessee, U.S.A., 1965.
11) J. M. Bijvoet, A. F. Peerdeman, and A. J. van

Bommel, *Nature*, **168**, 271 (1951).
12) This configuration is in accordance with the assignment based on the hexadecadal regional rule; S. F. Mason, *J. Chem. Soc., A*, **1971**, 667.
13) R. K. Wismer and R. A. Jacobson, *Inorg. Chim. Acta*, **7**, 477 (1973).
14) M. Ito, F. Marumo, and Y. Saito, *Acta Crystallogr., Sect. B*, **28**, 463 (1972).
15) D. Marcovich, E. N. Duesler, R. E. Tapscott, and T. F. Them, *Inorg. Chem.*, **21**, 3336 (1982).
16) J. Roziere and J. M. Williams, *Inorg. Chem.*, **15**, 1174 (1976).
17) M. Kuramoto, Y. Kushi, and H. Yoneda, *Bull. Chem. Soc. Jpn.*, **51**, 3251 (1978).
18) R. B. Ortega, R. E. Tapscott, and C. F. Campana, *Inorg. Chem.*, **21**, 2517 (1982).
19) K. Matsumoto, S. Ooi, H. Kawaguchi, M. Nakano, and S. Kawaguchi, *Bull. Chem. Soc. Jpn.*, **55**, 1840 (1982).
20) A. Zalkin, D. H. Templeton, and T. Ueki, *Inorg. Chem.*, **12**, 1641 (1973).

Thiolate-bridged Metal Complexes. Nickel(II), Palladium(II), and Cobalt(III) Binuclear Complexes of 1,5-Diamino-3-pentanethiol

Ichiro MURASE*, Shigehiro UENO,† and Sigeo KIDA†

Laboratory of Chemistry, College of General Education, Kyushu University, 01, Chuo-ku, Fukuoka 810

† *Department of Chemistry, Faculty of Science, Kyushu University, 33, Hakozaki, Higashi-ku, Fukuoka 812*

(Received April 16, 1983)

A binucleating ligand with thiolate sulfur as a bridging atom, 1,5-diamino-3-pentanethiol (Hdpet) and its metal complexes, $Ni_2(dpet)_2X_2$ (X=Br, ClO_4, NO_3, BPh_4, and NCS) were synthesized. All the complexes are diamagnetic at room temperature. The Ni(II) and Pd(II) complexes assume binuclear thiolate-bridged square planar coordination. This structure is maintained even in aqueous solution. The electronic spectra of the Ni(II) complexes showed a band at 27.3×10^3 cm^{-1} corresponding to the 29.8×10^3 cm^{-1} band of $[Ni_2(dpl)_2]^{2+}$ which is characteristic of oxo-bridged Cu(II) and Ni(II) complexes and was assigned to the $p\pi(O)\rightarrow d\sigma$(metal) transition. Several trials by different methods only resulted in the separation of a single species of Co(III) complex, $Co_2(dpet)_3(ClO_4)_3$. This was characterized as a bioctahedron facially joined at the three thiolate sulfur atoms.

In contrast to a great number of alkoxo- and phenoxo-oxygen-bridged complexes, only few thiolate-sulfur-bridged complexes have been reported,[1] though thiolate coordination is important in bioinorganic chemistry. In this paper we report the synthesis of binucleating ligand, 1,5-diamino-3-pentanethiol (Hdpet), and its nickel(II), palladium(II), and cobalt (III) complexes. This ligand has no unsaturated bond, hence no absorption in the visible and the near-ultraviolet region ($<35\times10^3$ cm^{-1}). Thus, in the spectra of complexes with this ligand the d-d and CT bands would be easily identified in that region. This ligand is an analogue of 1,5-diamino-3-pentanol (Hdpl) whose copper(II) and nickel(II) complexes were previously reported.[2,3] The palladium(II) complex of dpl was newly prepared in this study. Thus, we can clearly see the effect of substitution of sulfur for bridging alkoxo-oxygen by comparing the properties of the dpet complexes with those of dpl analogs. The copper(II) and nickel(II) dpl complexes showed a band in the ultraviolet region which is characteristic of oxo-bridged structure and was assigned to the $p\pi$ (O)$\rightarrow d\sigma$(metal) transition.[2,4] It is interesting to see whether such a band is also observed in the dpet complexes.

Results and Discussion

$[Ni_2(dpet)_2]X_2$ (X=Br, ClO_4, NO_3, BPh_4, NCS). The elemental analysis data accord with the values calculated as the 1:1 complex for all the nickel complexes. The planar and binuclear structure as depicted in Fig. 1 was supposed for this series of complexes on the bases of the binucleating nature of the ligand and the analogy of the dpl complexes.[2,3] The square planar coordination was confirmed by the spectral and magnetic measurements; *i.e.*, all these complexes are diamagnetic at room temperature, and the electronic spectra show only one band in the visible region in solution (20.6×10^3 cm^{-1}, ε=360 in methanol) and in Nujol mull (21.1×10^3 cm^{-1} for the perchlorate). All the $[Ni_2(dpet)_2]^{2+}$ complexes except for the tetraphenylborate are soluble and stable in water forming an orange-red solution whose spectrum is almost identical with that of the methanol solution (*cf.* Figs. 2 and 3). This fact implies that the axial coordination of water molecule is very weak and the planar binuclear structure is maintained in aqueous solution.

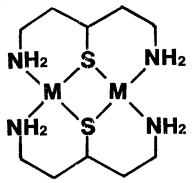

Fig. 1. $[M_2(dpet)_2]^{2+}$.

Nujol mull and powder reflectance spectra of the perchlorate, tetraphenylborate, and bromide showed the d-d band at almost the same position ((20.9—21)$\times10^3$ cm^{-1}), but in the case of the thiocyanate the d-d band shifts to 20.0×10^3 cm^{-1}. These facts imply that practically no axial coordination is present except for the thiocyanate, where a weak axial interaction with NCS^- may exist.

In the IR spectrum of $Ni_2(dpet)_2(ClO_4)_2$ there is also no indication of perchlorate coordination, either, since the splitting of the ν(Cl–O) band at about 1100 cm^{-1} is small (less than 70 cm^{-1}). The thiocyanate showed the band due to NCS^- at 2050 and 2075 cm^{-1}. This may be interpreted in terms of the assumption that one of the NCS^- ions weakly coordinates to the nickel ion while the other one is free, thus, the 2050 and 2075 cm^{-1} bands being assigned to the coordinated and the free NCS^-, respectively.[6] All these views deduced from IR data are quite consistent with those from the electronic spectra.

The band at 27.3×10^3 cm^{-1} (in methanol) should correspond to the near-ultraviolet band (29.8×10^3 cm^{-1}) of $Ni_2(dpl)_2(BPh_4)_2$ which is characteristic of alkoxo-bridged planar copper(II) and nickel(II) complexes, and was assigned to the $p\pi(O)\rightarrow d\sigma$(metal) transition.[2,4] Thus, the 27.3×10^3 cm^{-1} band is attributable to the CT transition from $p\pi$(S) to $d\sigma$(Ni). Here, it is to be noted that this is the first observation of the S→Ni CT transition which corresponds to the band characteristic of alkoxo-oxygen-bridged copper (II) and nickel(II) complexes.[4] The band at 33.2×10^3 cm^{-1} (in methanol) may be assigned to the σ(S)→$d\sigma$(Ni) transition. Similar sequence of the bands was observed for Ni_2LX_2 ($L=NH_2CH_2CH_2NH(CH_2)_nS^-$,

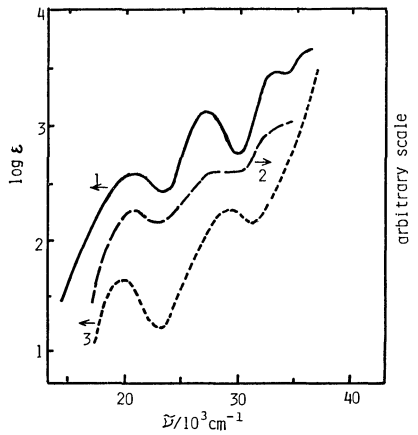

Fig. 2. Absorption spectra of $Ni_2(dpet)_2Br_2$ in methanol (1) and in Nujol mull (2), and $Ni_2(dpl)_2(Bph_4)_2$ in methanol (3).

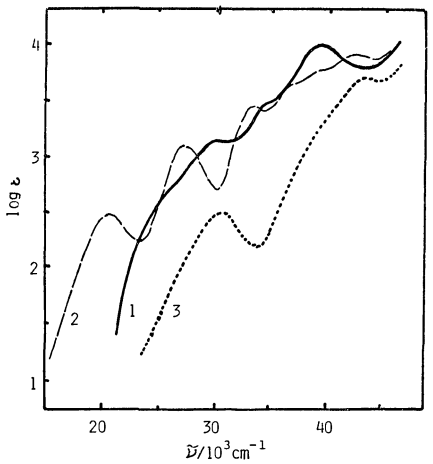

Fig. 3. Absorption spectra of $Pd_2(dpet)_2(ClO_4)_2$ (1), $Ni_2(dpet)_2(ClO_4)_2$ (2), and $Pd_2(dpl)_2(ClO_4)_2$ (3) in water.

X=Cl, Br); *e.g.*, 19.8 (ε=593), 28.2 (1510), and 32.9×10^3 cm^{-1} (5290) for n=2, X=Cl in methanol,[5] hence similar transitions can be assigned to these bands.

$Pd_2(dpet)_2(ClO_4)_2$. Infrared spectrum of this compound is nearly identical with that of the corresponding nickel analogue, indicating that the compound has a similar structure.

The electronic spectrum is, in general, much higher in intensity compared with that of $Pd_2(dpl)_2(ClO_4)_2$ and shifted to a higher frequency region compared with that of $Ni_2(dpet)_2(ClO_4)_2$ as shown in Fig. 3. The bands observed at ≈26 (shoulder), 30.3, and 35×10^3 cm^{-1} (shoulder) seem to correspond to the 20.8, 27.3, and 33.2×10^3 cm^{-1} bands of $Ni_2(dpet)_2^{2+}$ (*cf.* Fig. 3).

$Co_2(dpet)_3(ClO_4)_3$. Applying several different methods, and eluting the reaction products on a SP-Sephadex column, we have obtained only a single species of well defined cobalt(III) complex. The elemental analysis revealed that the crystals were formulated as $Co_2(dpet)_3(ClO_4)_3$. Since this compound is diamagnetic at room temperature, it is most likely to be a cobalt(III) complex. For the reasonable structure of this compound only the binuclear structure as depicted in Fig. 4 can be figured. It is to be remarked here that in the case of 1,3-diamino-2-propanethiol the mononuclear cis and trans 1:2 cobalt(III) complexes were obtained.[7]

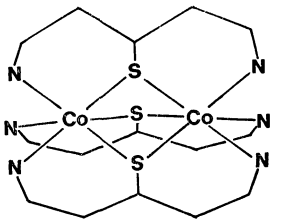

Fig. 4. The proposed structure of $[Co_2(dpet)_3]^{3+}$.

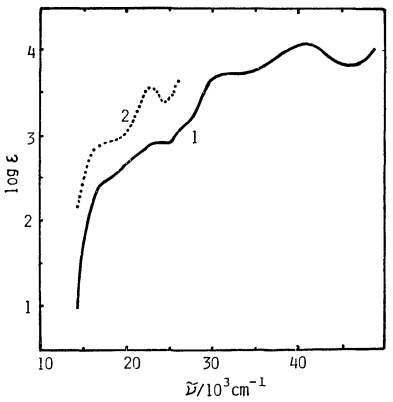

Fig. 5. Absorption spectra of $Co_2(dpet)_3(ClO_4)_3$ (1) and $[CdCo_2(mea)_6]^{2+}$ [8] (2).

The electronic spectrum of $[Co_2(dpet)_3](ClO_4)_3$ is shown in Fig. 5. This closely resembles the spectrum of $[CdCo_2(mea)_6]^{2+}$ (mea=2-aminoethanethiol) where the two *fac*-$[CoN_3S_3]$ chromophores are joined with the $[CdS_6]$ octahedron at the opposite faces.[8] The bands at 17.3×10^3 cm^{-1} (ε=280) and 23.3 (ε=791) are attributable to the spin-allowed d-d transitions, $^1A_{1g}\rightarrow{}^1T_{1g}$ and $^1A_{1g}\rightarrow{}^1T_{2g}$, respectively, in an approximation of O_h symmetry. It is known that the energy difference between the two spin-allowed bands can be a measure of the "nephelauxetic effect" of cobalt(III) complexes.[9] The value (6.3×10^3 cm^{-1}) for $[Co_2(dpet)_3]^{3+}$ is in between those for $[Co(en)_3]^{3+}$ (8.1×10^3 cm^{-1}) and $[Co(dtc)_3]$ (5.5×10^3 cm^{-1}), where dtc^- denotes diethyldithiocarbamate ion. This is consistent with the proposed structure and the assignment of the bands.

Experimental

Ligand Synthesis. 1,5-Diamino-3-pentanethiol was prepared as illustrated in the following scheme:

$$H_2NCH_2CH_2\underset{\underset{OH}{|}}{CH}CH_2CH_2NH_2\cdot2HCl \xrightarrow{HBr}$$

Hdpl

$$H_2NCH_2CH_2\underset{\underset{Br}{|}}{CH}CH_2CH_2NH_2\cdot2HBr \xrightarrow{Na_3SPO_3}$$

1

$$H_2NCH_2CH_2\underset{\underset{SPO_2H_2}{|}}{CH}CH_2CH_2NH_2 \xrightarrow[(HCl)]{H_2O}$$

2

$H_2NCH_2CH_2CHCH_2CH_2NH_2 \cdot 2HCl$
SH
3

1,5-Diamino-3-pentanol[2] (Hdpl) was converted to 3-bromo-1,5-pentanediamine (**1**) according to the standard method.[10] Conversion of (**1**) to the corresponding thiol (**3**) was best proceeded via the phosphorothioate (**2**), which was obtained by the reaction of **1** with trisodium phosphorothioate.[11]

3-Bromo-1,5-pentanediamine Dihydrobromide. A mixture of 1,5-diamino-3-pentanol dihydrochloride (50 g, 0.26 mol) and 47% hydrobromic acid (500 g, 2.9 mol) was heated in an oil bath with keeping the temperature of the bath at 145—150 °C, and 85 cm³ of hydrobromic acid was slowly distilled at bp 125 °C. The residual solution was refluxed for 1 h and then hydrobromic acid (45 cm³) was distilled off. This procedure was repeated additional two times and 37 cm³ and 28 cm³ of hydrobromic acid were recovered respectively. After refluxing the residual solution for 1 h, the bath temperature was raised to 155—160 °C and hydrobromic acid was distilled off so far as possible. In total 315 cm³ of hydrobromic acid has been recovered. The warm residue was poured into 500 cm³ of acetone and the resulting crystalline material was collected by filtration and dried in a vacuum desiccator. Crude yield was 83 g (92%). The sample was recrystallized from ethanol. Found: C, 18.00; H, 4.54; N, 8.32%. Calcd for $C_5H_{13}N_2Br \cdot 2HBr$: C, 17.51; H, 4.42; N. 8.17%.

1,5-Diaminopentane-3-phosphorothioic Acid. Trisodium phosphorothioate (21.6 g, 0.12 mol) was dissolved in 140 cm³ of water under nitrogen atmosphere at room temperature and diluted with 100 cm³ of water. To this was added 3-bromo-1,5-diaminopentane dihydrobromide (40.8 g, 0.12 mol) by portions, then *N,N*-dimethylformamide (120 cm³) was added dropwise during 30 minutes at 30 °C. The mixture was further stirred for 2 h at 30 °C and the resulting light brown solution was concentrated to a small volume under reduced pressure. Addition of ethanol (800 cm³) to the residual solution resulted white crystalline product, which was collected by filtration and washed with ethanol. The material (30 g) which contained appreciable amount of inorganic salts was used for the next reaction without purification.

1,5-Diamino-3-pentanethiol Dihydrochloride. A mixture of crude *S*-[3-amino-1-(2-aminoethyl)propyl] dihydrogenphosphorothioate (30 g) and 20% hydrochloric acid (180 g) was heated for 1 h in an oil bath at 100—110 °C under nitrogen atmosphere. The resulting clear solution was concentrated under reduced pressure and methanol (300 cm³) was added. The precipitates yielded were filtered off and the filtrate was concentrated. Acetone (500 cm³) was added to the residue and the mixture was kept in a refrigerator overnight. The crystalline powder was collected by filtration, washed with acetone, and dried under vacuum over P_2O_5. This highly hygroscopic material (18 g) contained inorganic salts, but it was used for complex synthesis without further purification. The pure sample was isolated as a tetraphenylborate which was recrystallized from methanol–water, mp 92 °C. Found: C, 80.08; H, 7.57; N, 3.49%. Calcd for $(C_5H_{16}N_2S)\ [B(C_6H_5)_4]_2 \cdot H_2O$: C, 80.29; H, 7.39; N, 3.53%.

Complex Synthesis. *$Ni_2(dpet)_2(ClO_4)_2$*: Crude 1,5-diamino-3-pentanethiol (Hdpet·2HCl, 0.8 g, ≈4 mmol) and nickel(II) perchlorate hexahydrate (1.5 g, 4 mmol) were dissolved in 20 cm³ of water and the pH of the solution was adjusted to ≈9 by the addition of triethylamine. The resulting deep red solution was heated on a water bath for ten minutes and undissolved material was filtered off. Addition of excess sodium perchlorate to the filtrate resulted orange-red crystals, which were collected by filtration, washed with methanol, recrystallized from water, and dried over P_2O_5 under vacuum at room temperature. Found: C, 20.55; H, 4.59; N, 9.57; Ni, 19.9%. Calcd for $Ni_2(C_5H_{13}N_2S)_2$: C, 20.61; H, 4.50; N, 9.61; Ni, 20.1%.

The bromide, thiocyanate, nitrate, and tetraphenylborate were also obtained from a warm concentrated aqueous solution of the perchlorate (above) by adding a sodium salt of the corresponding anion in excess and cooling to room temperature. The tetraphenylborate complex was recrystallized from acetone–methanol mixture and others were done from water and all dried over P_2O_5 under vacuum at room temperature.

$Ni_2(dpet)_2Br_2$: C, 21.99; H, 4.86; N, 10.18; Ni, 21.3%. Calcd for $Ni_2(C_5H_{13}N_2S)_2Br_2$: C, 22.09; H, 4.81; N, 10.30; Ni, 21.6%.

$Ni_2(dpet)_2(NCS)_2$: C, 28.82; H, 5.33; N, 16.72; Ni, 23.4%. Calcd for $Ni_2(C_5H_{13}N_2S)_2(SCN)_2$: C, 28.82; H, 5.24; N, 16.81; Ni, 23.5%.

$Ni_2(dpet)_2(NO_3)_2$: C, 23.71; H, 5.22; N, 16.43; Ni, 23.3%. Calcd for $Ni_2(C_5H_{13}N_2S)_2(NO_3)_2$: C, 23.65; H, 5.16; N, 16.55; Ni, 23.1%.

$Ni_2(dpet)_2(BPh_4)_2 \cdot C_2H_5OH$: C, 67.31; H, 6.70; N, 5.16%. Calcd for $Ni_2(C_5H_{13}N_2S)_2(C_{24}H_{20}B)_2 \cdot C_2H_6O$: C, 67.45; H, 6.79; N, 5.24%.

$Pd_2(dpet)_2(ClO_4)_2$ Potassium tetrachloropalladate(II) (0.48 g, 1.5 mmol) in 10 cm³ of water was mixed with Hdpet·2HCl (0.3 g, ≈1.5 mmol) in 10 cm³ of water and the pH of the mixture was brought to ≈9 by the addition of triethylamine at room temperature. The resulting yellow-orange precipitates were filtered off, and an excess of sodium perchlorate was added to the filtrate. The complex was obtained as pale yellow crystals, which were recrystalized from water. Found: C, 17.45; H, 3.77; N, 8.18%. Calcd for $Pd_2(C_5H_{13}N_2S_2)_2(ClO_4)_2$: C, 17.71; H, 3.86; N, 8.26%.

$Co_2(dpet)_3(ClO_4)_3$. A mixture of Hdpet·2HCl (0.6 g, ≈3 mmol) aud trisodium tricarbonatocobaltate(III) trihydrate (0.8 g, 2 mmol) in 10 cm³ of water was heated at 70 °C for ten minutes. The initial green solution turned deep red-brown with evolution of CO_2. The solution was cooled to room temperature, filtered, and an excess of sodium perchlorate was added to the warmed filtrate. Deep red crystals which were deposited on cooling was recrystallized from water, and dried over P_2O_5 under vacuum. Found: C, 22.09; H, 4.81; N, 10.29; Co, 14.6%. Calcd for $Co_2(C_5H_{13}N_2S)_3(ClO_4)_3$: C, 22.08; H, 4.82; N, 10.30; Co, 14.4%.

$Pd_2(dpl)_2(ClO_4)_2$. To a mixture of potassium tetrachloropalladate(II) (0.9 g, 2.7 mmol) and 1,5-diamino-3-pentanol dihydrochloride (Hdpl·2HCl, 0.5 g, 2.7 mmol) in 40 cm³ of water was added sodium carbonate (0.84 g, 8.1 mmol) by portions. The mixture was heated on a water bath until the resulting precipitates were dissolved to give a yellow solution. The hot solution was filtered and an excess of sodium perchlorate was added to the filtrate. The pale yellow precipitates were collected by filtration, washed with methanol, and recrystallized from water. Found: C, 18.65; H, 4.07; N, 8.57%. Calcd for $Pd_2(C_5H_{13}N_2O)_2(ClO_4)_2$: C, 18.59; H, 4.06; N, 8.67%.

The reaction of Hdpet·2HCl with copper(II) ion resulted in ligand oxidation, and any kind of copper complex could not be obtained so far.

References

1) J. G. Hughes and R. Robson, *Inorg. Chim. Acta*, **36**, 237 (1979); R. Kelson and R. Robson, *J. Coord. Chem.*, **6**, 235 (1979); P. Krautil and R. Robson, *ibid.*, **10**, 7 (1980).

2) I. Murase, M. Hatano, M. Tanaka, S. Ueno, H. Okawa, and S. Kida, *Bull. Chem. Soc. Jpn.*, **55**, 2404 (1982).

3) Y. Nishida and S. Kida, *Mom. Fac. Sci. Kyushu Univ., Ser. C*, **13**, 35 (1981).

4) Y. Ishimura, Y. Nonaka, Y. Nishida, and S. Kida, *Bull. Chem. Soc. Jpn.*, **46**, 3728 (1973); S. Kida, Y. Nishida, and M. Sakamoto, *ibid.*, **46**, 2428 (1973); Y. Nishida, F. Numata, and S. Kida, *Inorg. Chim. Acta*, **11**, 189 (1974); Y. Nishida and S. Kida, *J. Inorg. Nucl. Chem.*, **38**, 451 (1976).

5) S. L. Rose, R. E. Hoskin, J. E. Cavaugh, C. J. Smith, and E. L. Blim, *Inorg. Chim. Acta*, **40**, 7 (1980).

6) K. Nakamoto, "Infrared and Raman Spectra of Inorganic and Coordination Compounds," 3rd ed Wiley-Interscience, New York (1978) pp. 270—274.

7) K. Yamanari, N. Takeshita, T. Komorita, and Y. Shimura, *Chem. Lett.*, **1981**, 861.

8) E. L. Blinn, P. Butler, K. M. Chapman, and S. Harris, *Inorg. Chim. Acta*, **24**, 139 (1977).

9) C. K. Jørgensen, *Prog. Inorg. Chem.* **4**, 73 (1962).

10) *Cf.* F. Cortese, *Org. Synth.* Coll. Vol. II, 91 (1948).

11) J. R. Piper and T. P. Johnson, *J. Org. Chem.*, **33**, 636 (1968).

Aromatic Nucleophilic Substitution. XVIII.[1] Kinetics of Reactions of 2-(Acetylamino)ethyl 2,6-Dinitrophenyl Ether and *N*-Acetyl-*N*-(2-hydroxyethyl)-2,6-dinitroaniline with Sodium Isopropoxide

Shizen Sekiguchi,* Motohiko Hirai, and Noboru Tomoto†

Department of Synthetic Chemistry, Gunma University, Kiryu, Gunma 376

† *Department of Industrial Chemistry, Miyazaki University, 1-1-1 Kirishima, Miyazaki, Miyazaki 880*

(Received September 30, 1982)

The kinetics of the reactions of 2-(acetylamino)ethyl 2,6-dinitrophenyl ether (Smiles rearrangement) and *N*-acetyl-*N*-(2-hydroxyethyl)-2,6-dinitroaniline with sodium isopropoxide in the DMSO-2-propanol mixture (20 : 80 v/v) was studied. Both reactions were found to rapidly produce the same spiro anionic σ complex, giving *N*-(2-acetoxyethyl)-2,6-dinitroaniline. Although the rates for formation of the complex were different in both reactions, the rates for rearrangement were the same.

Previously we reported the OH^--catalyzed Smiles rearrangement of 2-(acetylamino)ethyl 2-X-4-nitrophenyl ether (**1a** X=Y=NO_2, Z=H; **1b** X=Br, Y=NO_2, Z=H; **1c** X=CN, Y=NO_2, Z=H), where the process **1**⇄**2**⇄**3** was very fast and the one **3**⇄**4**→**5** relatively slow (Scheme 1).[2-5]

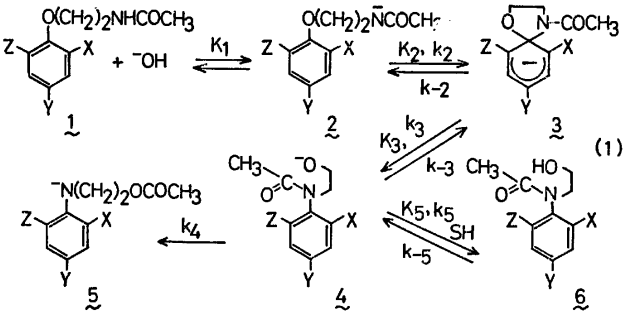

Scheme 1.

Hence, the former process (hereafter called Stage I) can be followed by stopped-flow technique, whereas the latter (hereafter called Stage II) can be done by usual spectrophotometry.

As shown in previous work,[1] no information on the K_3 and K_5 processes was obtained in the kinetics of rearrangement of **1**.[3,5]

Although the kinetics of the reaction of **6** with bases should give such detailed information, the synthesis of **6a**, **6b**, and **6c** has been unsuccessful. More recently *N*-acetyl-*N*-(2-hydroxyethyl)-2,6-dinitroaniline [**6d** (X=Z=NO_2; Y=H)] has been synthesized.[1]

As the UV-VIS and NMR time-dependent spectra of the base-catalyzed rearrangements of 2-(acetylamino)ethyl 2,6-dinitrophenyl ether (**1d**, X=Z=NO_2, Y=H) and **6d** showed the reaction path shown in Scheme 1,[1] this paper reports the kinetics of the reactions of **1d** and **6d** with $NaOCH(CH_3)_2$ in the DMSO–2-propanol mixture (20:80 v/v) in order to elucidate the detailed reaction processes.

Results

*Stage I. Rearrangement of 2-(Acetylamino)ethyl 2,6-Dinitrophenyl Ether (**1d**)*: In carrying out the kinetic measurement of Stage I, one can neglect Stage II reaction. Accordingly, in the presence of excess $NaOCH(CH_3)_2$ the apparent first-order rate constant

Table 1. Rate constants for formation and decomposition of spiro anionic σ complex formed from 2-(acetylamino)ethyl 2,6-dinitrophenyl ether (**1d**) and sodium isopropoxide in the DMSO–2-propanol mixture (20:89 v/v)[a]

Temp / °C	10^3[$NaOCH(CH_3)_2$] / M	k_ψ^o [b] / s^{-1}
15	1.77	0.490±0.081
	3.54	0.851±0.023
	5.90	1.91 ±0.04
	8.85	2.50 ±0.05
	11.8	3.80 ±0.13
	18.9	5.99 ±0.11
25	2.63	1.61 ±0.01
	5.25	3.82 ±0.07
	7.88	6.36 ±0.42
	10.5	8.16 ±0.09
	15.8	13.8 ±0.2
	20.3	15.0 ±0.4
	24.6	18.7 ±0.8
35	2.63	3.07 ±0.18
	5.25	7.70 ±0.2
	7.88	11.8 ±0.5
	9.40	14.0 ±0.6
	10.5	16.0 ±0.6
	15.8	22.6 ±0.8
	18.9	27.1 ±1.4

a) $[\mathbf{1d}]_0$ 3.67×10^{-5} M (≡mol dm^{-3}); μ 0.04 M ($NaClO_4$). b) Measured at 580 nm (λ_{max} for **3d**) with a stopped-flow method.

(k_ψ^o) for formation of **3d** is expressed in Eq. 2. If K_1[$NaOCH(CH_3)_2$]≪1, Eq. 3 is derived. Table 1

$$k_\psi^o = k_{-2} + \frac{k_2K_1[NaOCH(CH_3)_2]}{1+K_1[NaOCH(CH_3)_2]} \quad (2)$$

$$k_\psi^o = k_{-2} + k_2K_1[NaOCH(CH_3)_2] \quad (3)$$

shows the dependence of k_ψ^o on [$NaOCH(CH_3)_2$], which is illustrated in Fig. 1. The results in Fig. 1 are compatible with Eq. 3. As a result, the k_{-2} and k_2K_1 values can be estimated from the intercept and slope in the linear plots, respectively (Table 3).

*Rearrangement of N-Acetyl-N-(2-hydroxyethyl)-2,6-dinitroaniline (**6d**)*: In the reaction of **6d** with $NaOCH(CH_3)_2$ the fast process **6d**⇄**4d**⇄**3d** occurs first, followed by the comparatively slow one **3d**⇄**4d**⇄**5d**.[1] Accordingly the similar kinetic procedure applies aptly

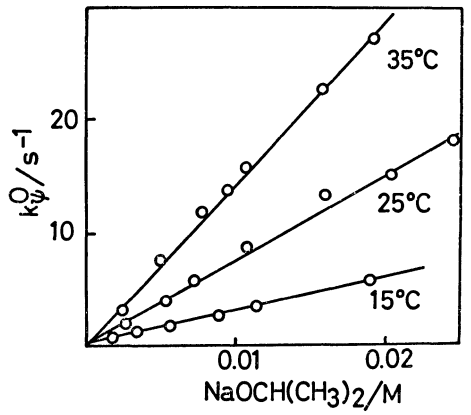

Fig. 1. Relationship between k_ψ^o and $[NaOCH(CH_3)_2]$ in the reaction of 2-(acetylamino)ethyl 2,6-dinitrophenyl ether (**1d**) with $NaOCH(CH_3)_2$ in the DMSO-2-propanol mixture (20:80 v/v) [μ 0.04 M ($NaClO_4$)].

Table 2. Rate constants for formation and decomposition of spiro anionic σ complex formed from *N*-acetyl-*N*-(2-hydroxyethyl)-2,6-dinitroaniline (**6d**) in the DMSO-2-propanol mixture (20:80 v/v)[a]

Temp °C	$10^3[NaOCH(CH_3)_2]$ M	k_ψ^N [b] s^{-1}
20	4.40	293± 7
	6.75	444±11
	9.38	695±17
	11.3	844±21
	15.2	1204±30
	20.2	1514±38
	27.4	1947±49
	33.0	2393±84
30	4.30	630±19
	5.50	841±25
	6.75	931±28
	9.38	1468±51
	10.8	1559±55
	12.9	1896±76
	17.2	2399±84
40	4.30	1063±43
	6.75	1627±65
	9.38	2175±87
	10.8	2479±109

a) $[\mathbf{6d}]_0$ 3.71×10^{-5} M; μ 0.04 M ($NaClO_4$). b) Measured at 580 nm (λ_{max} for **3d**) with a stopped-flow method.

in this case, too. As a result, the following expression can be derived as to the apparent first-order rate constant (k_ψ^N) for formation of **3d** in the presence of excess $NaOCH(CH_3)_2$ (note the relationship between the directions of reactions and rate or equilibrium constants).

$$k_\psi^N = k_3 + \frac{\frac{k_{-3}}{K_5}[NaOCH(CH_3)_2]}{1+\frac{1}{K_5}[NaOCH(CH_3)_2]} \quad (4)$$

Therefore, the plot of k_ψ^N against $[NaOCH(CH_3)_2]$ would show the curvilinear dependence asymptotically approaching the fixed value unless $[NaOCH(CH_3)_2]/K_5 \gg 1$. If $[NaOCH(CH_3)_2]/K_5 \ll 1$, however, the linear dependence should be obtained (Eq. 5). Table 2

$$k_\psi^N = k_3 + \frac{k_{-3}}{K_5}[NaOCH(CH_3)_2] \quad (5)$$

shows the linear dependence of k_ψ^N on $[NaOCH(CH_3)_2]$ (not shown), giving the k_3 and k_{-3}/K_5 values from the intercept and slope in the linear plots (Table 3).

Table 3 shows the temperature dependence of k_2K_1, k_{-2}, $k_{-3}K_5^{-1}$, k_3, $K_3^{-1}K_5^{-1}$ for formation and decomposition of **3d**. Comparison of k_{-2} with k_3 shows that **3d** proceeds to **4d** faster than reverts to **2d**, which is compatible with the fact that alkoxyl groups of activated aromatics are easily displaced with amines.[6-8]

*Stage II. Rearrangement of 2-(Acetylamino)ethyl 2,6-Dinitrophenyl Ether (**1d**)*: In treatment of the kinetics of Stage II, Stage I reaction can be regarded as a fast mobile equilibrium lying almost entirely on the right (Table 3). Accordingly, as to the rate of Stage II reaction (k_{obsd}^o apparent first-order rate constant for rearrangement of **1d**) the following expression is obtained in the presence of excess $NaOCH(CH_3)_2$, provided that the k_4 stage is rate-determining and the K_5 and K_3 stages are fast mobile equilibria (Table 4).

$$k_{obsd}^o = \frac{k_4K_1K_2K_3[NaOCH(CH_3)_2]}{\left(1+K_1K_2K_3K_5+(K_1+K_1K_2+K_1K_2K_3)[NaOCH(CH_3)_2]\right)} \quad (6)$$

Although the relationship between k_{obsd}^o and $[NaOCH(CH_3)_2]$ is curvilinear (asymptotically approaching the fixed value), Eq. 7 would hold, if $(K_1+K_1K_2+K_1K_2K_3)\times[NaOCH(CH_3)_2] \gg 1+K_1K_2K_3K_5$. Therefore, k_{obsd}^o is independent of $[NaOCH(CH_3)_2]$ (Fig. 2). The re-

Table 3. Temperature dependence of k_2K_1, k_{-2}, K_1K_2, $k_{-3}K_5^{-1}$, k_3, and $K_5^{-1}K_3^{-1}$ for formation and decomposition or spiro anionic σ complexes formed from 2-(acetylamino)ethyl 2,6-dinitrophenyl ether (**1d**) or *N*-acetyl-*N*-(2-hydroxyethyl)-2,6-dinitroaniline (**6d**) and sodium isopropoxide in the DMSO-2-propanol mixture (20:80 v/v)[a]

Temp °C	k_2K $M^{-1}s^{-1}$	k_{-2} s^{-1}	$10^3K_1K_2$ [b] M^{-1}
		1d	
15	326±17	—	—
25	774±43	0.12±3.86	6.4
35	1460±90	0.60±1.31	2.4
	$10^{-4}k_{-3}K_5^{-1}$ $M^{-1}s^{-1}$	k_3 s^{-1}	$10^{-3}K_5^{-1}K_3^{-1}$ [b] M^{-1}
		6d	
15	5.66±0.06	7.86±4.43	7.2
20	7.10±0.12	25.8±13.2	2.8
30	13.6±0.2	62.8±10.7	2.2
40	11.8±0.1	135±40	—

a) $[\mathbf{1d}]_0$ 3.67×10^{-5} M; $[\mathbf{6d}]_0$ 3.71×10^{-5} M; μ 0.04 M ($NaClO_4$). b) Calculated from $K_1K_2=k_2K_1/k_{-2}$ and $K_3^{-1}K_5^{-1}=k_{-3}K_5^{-1}/k_3$ by using the mean values, respectively.

Table 4. Rate constants for rearrangement of 2-(acetylamino)ethyl 2,6-dinitrophenyl ether (**1d**) in the DMSO–2-propanol mixture (20:80 v/v)[a]

Temp °C	10^3[NaOCH$(CH_3)_2$] M	$10^4 k^O_{obsd}$[b] s^{-1}
20	3.42	1.30
	5.13	1.31
	6.84	1.13
	19.5	1.17
	34.2	1.11
	39.0	1.13
30	4.20	4.16
	5.13	3.91
	8.40	4.08
	12.6	3.90
	19.3	4.09
40	3.42	10.7
	5.13	11.8
	6.84	11.4
	19.3	10.5
	34.3	11.0

a) $[\mathbf{1d}]_0$ 5.88×10^{-5} M; μ 0.04 M ($NaClO_4$). b) Estimated limit of error ±1.5%; measured at 580 nm (λ_{max} for **3d**).

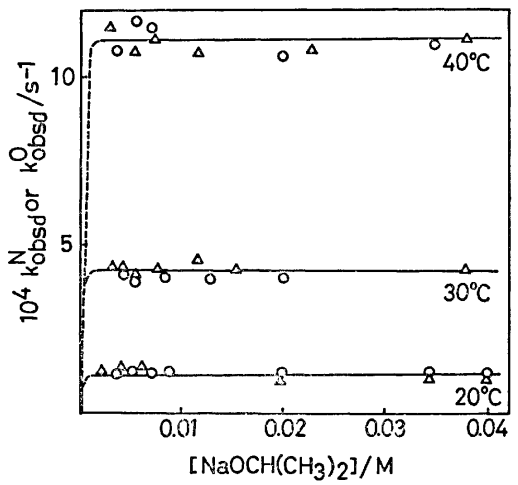

Fig. 2. Relationship between k^O_{obsd} or k^N_{obsd} and [NaOCH$(CH_3)_2$] in the reaction of 2-(acetylamino)-ethyl 2,6-dinitrophenyl ether (**1d**) or *N*-acetyl-*N*-(2-hydroxyethyl)-2,6-dinitroaniline (**6d**) with NaOCH-$(CH_3)_2$ in the DMSO–2-propanol mixture (20:80 v/v) [μ 0.04 M ($NaClO_4$)]: ○ k^O_{obsd}; △ k^N_{obsd}.

sults in Table 4 are compatible with Eq. 7.

$$k^O_{obsd} = \frac{k_4K_2K_3}{1+K_2+K_2K_3} \quad (7)$$

Rearrangement of N-*Acetyl*-N-*(2-hydroxyethyl)-2,6-dinitroaniline (6d)*: In the rearrangement of **6d**, the process **6d**⇄**4d**⇄**3d** is very fast, and the one **3d**⇄**4d**→**5d** relatively slow.[1] Therefore, in the kinetics of Stage II the K_3 and K_5 stages can be regarded as fast mobile equilibria. Accordingly, as to the rate of Stage II (k^N_{obsd} apparent first-order rate constant for rearrangement of **6d**) Eq. 8 is obtained in the presence of excess

Table 5. Rate constants for rearrangement of *N*-acetyl-*N*-(2-hydroxyethyl)-2,6-dinitroaniline [**6d**] in the DMSO–2-propanol mixture (20:80 v/v)[a]

Temp °C	10^3[NaOCH$(CH_3)_2$] M	$10^4 k^N_{obsd}$[b] s^{-1}
20	1.78	1.46
	3.56	1.46
	5.34	1.42
	8.90	1.40
	19.7	1.13
	34.3	1.12
	39.0	1.12
30	3.68	4.46
	3.80	4.40
	5.52	4.05
	7.60	4.30
	11.4	4.72
	15.2	4.30
	38.6	4.14
40	2.97	11.6
	5.57	10.7
	7.00	11.1
	11.4	10.7
	22.8	10.8
	38.6	11.3

a) $[\mathbf{6d}]_0$ 1.32×10^{-5} M; μ 0.04 M ($NaClO_4$). b) Estimated limit of error ±1.5%; measured at 580 nm (λ_{max} for **3d**).

$$k^N_{obsd} = \frac{\frac{k_4}{K_5}[\mathrm{NaOCH(CH_3)_2}]}{1+\frac{1}{K_5}\left(1+\frac{1}{K_3}\right)[\mathrm{NaOCH(CH_3)_2}]} \quad (8)$$

NaOCH$(CH_3)_2$, indicating the curvilinear dependence of k^N_{obsd} on [NaOCH$(CH_3)_2$] (asymptotically approaching the fixed value). Under the condition $1/K_5(1+1/K_3)$[NaOCH$(CH_3)_2$]$\gg$1, Eq. 9 is obtained, indicating that k^N_{obsd} is independent of [NaOCH$(CH_3)_2$]. Equation 9 is compatible with the results in Table 5.

$$k^N_{obsd} = \frac{k_4K_3}{1+K_3} \quad (9)$$

Most interestingly the k^N_{obsd} values are nearly equal to the k^O_{obsd} ones at each [NaOCH$(CH_3)_2$] (Fig. 2), which shows that either **1d** or **6d** is catalyzed with [NaOCH-$(CH_3)_2$] to substantially change into **3d** at first, and then undergoes the rearrangement, giving **5d**.

Discussion

Stage I. With **1d** and **6d** the k_2, K_1, k_{-3}, and K_5 values can not be estimated separately from Eqs. 3 and 5. With **6d**, however, the k_3, k_{-3}, and K_5 values at 15 °C could be determined as follows: when the rate measurement was carried out at higher [NaOCH-$(CH_3)_2$], the relationship between k^N_ϕ and [NaOCH-$(CH_3)_2$] was found to be curvilinear (asymptotically approaching the fixed value), in which the different ionic strengths did not affect the rate (Fig. 3). The result is compatible with Eq. 4. If the k_3 value (7.86 s^{-1}) can be obtained by extrapolation of [NaOCH-$(CH_3)_2$]→0 in Eq. 4, one can derive the following

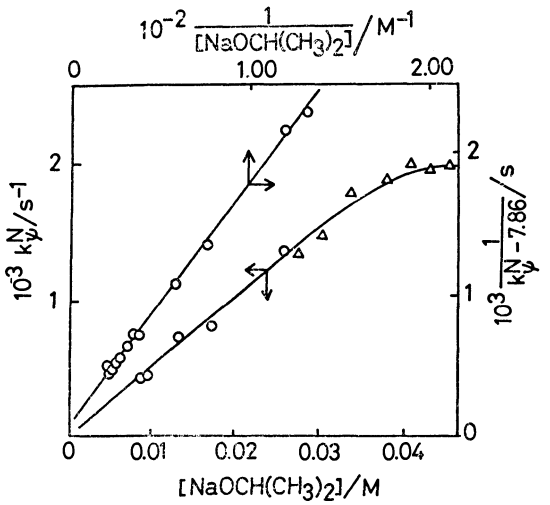

Fig. 3. Relationships between k_ψ^N and $[NaOCH(CH_3)_2]$ and between $1/(k_\psi^N-7.86)$ between $1/[NaOCH(CH_3)_2]$ in the reaction of *N*-acetyl-*N*-(2-hydroxyethyl-2,6-dinitroaniline (**6d**) with $NaOCH(CH_3)_2$ in the DMSO-2-propanol mixture (80:20 v/v at 15 °C): ○ at μ=0.04 M ($NaClO_4$); △ at μ=0.05 M ($NaClO_4$); $[\mathbf{6d}]_0$ 3.71×10^{-5} M.

equation (Eq. 10) by substituting this value into Eq. 4 and rearranging. Thus, k_{-3} and K_5 can be obtained from the slope and intercept in the plot of $1/(k_\psi^N-7.86)$ against $[NaOCH(CH_3)_2]$. The k_{-3}, K_5^{-1} (equilibrium constant for **6d**⇄**4d**), and K_3^{-1} (equilibrium constant for **4d**⇄**3d**) values were found to be 1.82×10^4 s^{-1}, 3.1 M^{-1}, and 2.3×10^3, respectively (all the values are average ones). As a result, the $K_3^{-1}K_5^{-1}$ value is calculated by using these values to be $7.1_3\times10^3$ M^{-1}, which is fairly in agreement with the value (7.2×10^3 M^{-1}) shown in Table 3. Furthermore, the K_5 value (0.32 M) is considered to be reasonable, compared with those by Hine and Hine[9] and Bowden,[10] although the solvents used are different. From these values, the equilibrium **3d**⇄**4d** lies almost on the side of **3d**, indicating that such anionic σ complexes as **3d** having activating substituents at 2- and 6-positions are extermely stable.[2-5,11,12] The equilibrium **6d**⇄**4d** was reasonably found to lie almost on the side of **4d**. Therefore, in the rearrangement of **1d**, the K_5 stage is considered to scarcely contribute to the process.

$$\frac{1}{k_\psi^N-7.86}=\frac{1}{k_{-3}}+\frac{K_5}{k_{-3}[NaOCH(CH_3)_2]} \qquad (10)$$

With **1d** such results as shown in Fig. 3 were not obtained. The K_1, k_2, and k_{-2} values, however, can be estimated with some accuracy. In a previous work on the rearrangement of 2-(acetylamino)ethyl 2-X-4-nitrophenyl ether (**1**),[3] those values were determined (for **1b**, k_2 1.18×10^2 s^{-1}, k_{-2} 1.10×10 s^{-1}, K_1 1.31×10^2 M^{-1}:; for the pyridyl derivative,[3] k_2 5.99×10^2 s^{-1}, k_{-2} 1.20×10 s^{-1}, K_1 9.33×10 M^{-1}).

2,6-Dinitrophenyl group is expected to be inferior in electron-withdrawing character to 2-X-4-nitrophenyl one owing to the steric hindrance. Accordingly the k_2 value is expected to be at least two orders or one in magnitude. Anyhow, the k_2 value is clearly smaller than the k_{-3} one, indicating that an alkoxide ion is superior in nucleophilicity to an acetamide ion, in which the negative charge on the nigrogen is reduced by the resonance effect of an acetyl group.

Stage II. Tables 4 and 5 interestingly show that k_{obsd}^O and k_{obsd}^N are almost the same within the experimental error.

The reason for this equality is as follows: the K_2 value is rationally expected to be far larger than one, based on the above discussion. Then, Eq. 7 is reduced to Eq. 11. As a result, k_{obsd}^O is equal to k_{obsd}^N (Eq. 9).

$$k_{obsd}^O=\frac{k_4K_3}{1+K_3}(=k_{obsd}^N) \qquad (11)$$

In conclusion, almost **1d** or **6d** is base-catalyzed to change into **3d** (K_1K_2 and $K_3^{-1}K_5^{-1}$ in Table 3), which, then, slowly rearranges to **5d** at the same rate as if the process **1d**⇄**2d**⇄**3d** were irreversible.[7]

At the end, one remark should be added: since there are two isomers ([*Z*] and [*E*]) for **6d**,[1] the equilibrium and rate constants might be the results from the composite effect of each isomer. The above-mentioned discussion, however, would not be affected by this fact.

Experimental

Meterials. The compounds (**1d** and **6d**) were prepared according to the methods described in the literature.[1]

Rate Measurement. As regards the kinetics of formation and decomposition of the spiro anionic σ complex (**3d**), the transmittance of complex was measured in order to estimate the apparent pseudo-first-order rate constants (k_ψ^O and k_ψ^N) with a thermostatted Union RA-1300 Stopped-Flow Analyzer (Union Giken). The kinetic measurements for decomposition of the complex (rearrangement (k_{obsd}^O and k_{obsd}^N) were made on a thermostatted Hitachi Model 200-10 Spectrophotometer for following the decrease in the absorbance due to **3d**.

This work was partially supported by a Grant-in-Aid for Scientific Research from the Ministry of Education, Science and Culture, to which the author (S.S.) is due.

References

1) Part XVII, S. Sekiguchi, O. Hoshino, M. Hirai, K. Okada, and N. Tomoto, *Bull. Chem. Soc. Jpn.*, **56**, 2173 (1983).
2) S. Sekiguchi and K. Okada, *J. Org. Chem.*, **40**, 2782 (1975).
3) K. Okada and S. Sekiguchi, *J. Org. Chem.*, **43**, 441 (1978).
4) K. Okada, K. Matsui, and S. Sekiguchi, *Bull. Chem. Soc. Jpn.* **51**, 2601 (1978).
5) S. Sekiguchi, I. Otsuka, and K. Okada, *J. Org. Chem.*, **44**, 2601 (1978).
6) J. Miller, "Aromatic Nucleophilic Substitution," Elsevier Publishing Co., New York (1968), Chap. 5.
7) J. A. Orvik and J. F. Bunnett, *J. Am. Chem. Soc.*, **92**, 2417 (1970).
8) J. F. Bunnett, S. Sekiguchi, and L. A. Smith, *J. Am. Chem. Soc.*, **103**, 4865 (1981).
9) J. Hine and M. Hine, *J. Am. Chem. Soc.*, **74**, 5266 (1952).
10) K. Bowden, *Chem. Rev.*, **66**, 119 (1966).
11) M. J. Strauss, *Chem. Rev.*, **70**, 667 (1970).
12) S. Sekiguchi, *Yuki Gosei Kagaku Kyokai Shi*, **36**, 633 (1978).

Reactive Troponoids and *o*-Aminophenol. V. The Reaction of 3-Bromo-2-methoxytropone and *o*-Aminophenol[1]

Taichi Someya, Harue Okai,† Hidetsugu Wakabayashi,† and Tetsuo Nozoe*

Central Research Laboratory of Takasago Perfumery Co., Ltd., Kamata, Ohta-ku, Tokyo 144

† *Tokyo Research Laboratory of Kao Soap Co., Ltd., Bunka, Sumida-ku, Tokyo 131*

(Received December 3, 1982)

The reaction products of the title substances in hot acetic acid were separated by preparative TLC into compounds **A**—**L** according to the R_f-values, and the structural assignments for these products were now made as follows: **A**, 14*H*-[1,4]benzoxazino[3′,2′ : 3,4]cyclohepta[1,2-*b*][1,4]benzoxazine; **B**, 1-formylphenoxazine; **F**, cyclohepta[2,1-*b* : 2,3-*b*′]di[1,4]benzoxazine; **G**, cyclohepta[*b*][1,4]benzoxazin-10(11*H*)-one or its enolic form; **J**, cyclohepta[*b*][1,4]benzoxazin-6(11*H*)-one; **L**, 6-(*o*-hydroxyanilino)cyclohepta[*b*][1,4]benzoxazine hydrobromide. A small amount of 2-methylamino-3*H*-phenoxazin-3-one was also produced. Possible reaction pathways for the formation of these products are also discussed.

We reported in a previous paper[2] that the condensation of 2-bromo-7-methoxytropone (**1**) and *o*-aminophenol (**2**) in refluxing acetic acid mainly gave 2-bromo-7-(*o*-hydroxyanilino)tropone (**3**). In addition to this substitution product, a 4.7% yield of orange yellow needles and 0.5% of a dark violet pigment were isolated, to which the tentative structures **4** and **5** were respectively assigned on the basis of the elemental analyses and spectral data. These minor products were considered to be derived from a common intermediate **7** according to the pathways shown in Scheme 1,[2] since both compounds were produced upon treatment of the ring-closed product **6** with another equivalent of **2** in acetic acid.

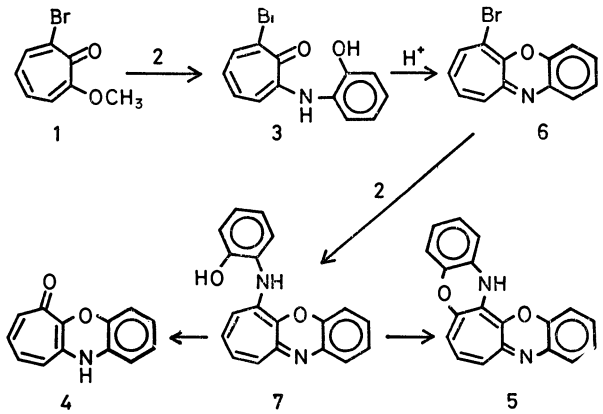

Scheme 1.

The formation of such minor products prompted us to examine the condensation of an isomeric tropone **8** (3-bromo-2-methoxytropone) with **2**. Separation of the reaction products by preparative TLC on silica gel gave at least twelve, colorful bands, which were referred to as **A**—**L** according to their R_f-values.[3] This paper describes the structures of these products, together with the possible reaction mechanism of the formation of these compounds.[4]

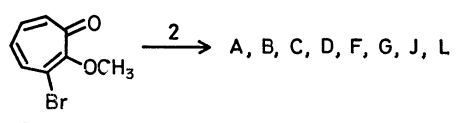

Results and Discussion

Compounds A and D. Compound **A** ($C_{19}H_{12}N_2O_2$), separated from the fastest-eluting fraction, was found to be identical with the dark violet pigment obtained previously from **1** or **6**.[2] However, the 360 MHz ^{1}H- and 47.3 MHz ^{13}C-NMR spectral analyses[5] performed later on this product clearly showed the presence of a nearly C_{2v} symmetry in the molecule on the grounds that: 1) the ^{13}C-NMR spectrum consisted of 10 signals, 2) the proton signals (in DMSO-d_6) of the seven-membered ring consisted of a slightly broadened doublet at δ 5.79 (2H; J=10.8 Hz) and a slightly broadened triplet at δ 6.00 (1H; J=10.8 Hz), and 3) the two benzene rings showed four-proton signals well-resolved at δ 6.5—6.9. Compound **A** showed an IR absorption at 3250 cm^{-1} due to a NH group, and the UV spectrum closely resembled that of **10** prepared from 3,7-dibromotropolone (**9**) and *o*-aminobenzenethiol.[6] These results, along with the mode of formation (see below), led us to revise the structure of compound **A** to 14*H*-[1,4]benzoxazino[3′,2′:3,4]cyclohepta[1,2-*b*][1,4]benzoxazine (**11**),[7] instead of the previously assigned structure **5**[2] or another isomeric structure **11a**, since these compounds (**5** and **11a**) are not likely to show a C_{2v} symmetry in the ^{1}H- and ^{13}C-NMR spectra, or to exhibit similar UV absorption to that of **10**. The assignments for the NMR signals of compound **A** are given in the Experimental section.

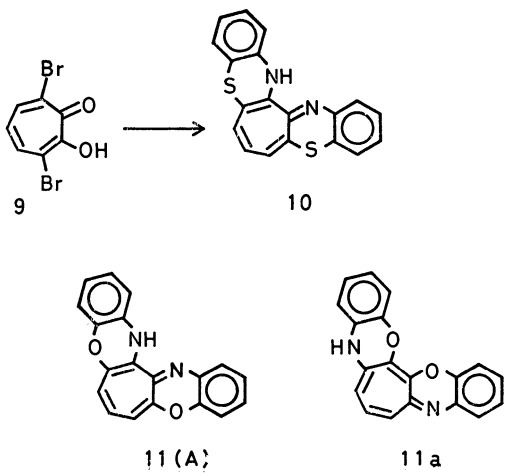

Compound **D** was shown to change readily to compound **A** by re-chromatography on silica gel, suggesting that compound **D** was most likely an air-sensitive dihydro form, such as **34**, of compound **A** as shown below (Scheme 3). However, compound **D** could not be isolated as a pure material

*Compounds **B** and **C**.* Compound **C** gradually degraded into compounds **2** and **B** ($C_{13}H_9NO_2$) on heating in methanol, and rapidly in the presence of a trace of dilute sulfuric acid. The latter compound **B** was identical with the orange-yellow needles, obtained previously from **1** or **6**[2] and assigned to **4** by the comparison of its IR and UV spectra with those of cyclohepta[*b*][1,4]benzothiazin-6(11*H*)-one (**13**), which had been prepared from 2-chloro-3-methoxytropone (**12**) and *o*-aminobenzenethiol.[6] However, as the ^{1}H- and ^{13}C-NMR spectra of compound **B** later indicated the presence of a formyl group, its structure was examined, and the compound **B** is now proved to be 1-formylphenoxazine (**14**)[8] by comparing the spectra and other data with those of other three, isomeric formylphenoxazines which are now available.[9] Thus, the previous formulations **4**[2] and **15**,[4] tentatively assigned to compound **B**, should now be replaced by **14**. The assignments of the NMR signals of compound **B** are shown in the Experimental section. The structure of compound **C**, together with those of other isomeric formylphenoxazines, will be published elsewhere.[9,10]

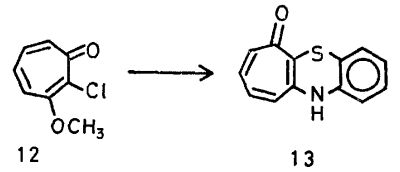

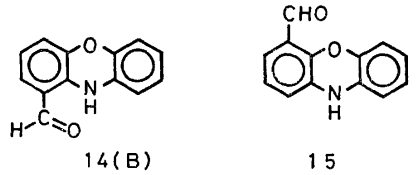

*Compounds **F** and **L**.* The compound **L** obtained from the slowest-eluting fraction was shown to have a composition $C_{19}H_{15}N_2O_2Br$ by elemental analysis and the mass spectrum. The structure of 6-(*o*-hydroxyanilino)cyclohepta[*b*][1,4]benzoxazine hydrobromide (**7a**) was assigned to compound **L** from the spectral data: see the Experimental section.

Compound **F** was isolated as yellow needles, when the uneluted fractions (with benzene) of the reaction mixture of **8** and **2** were re-chromatographed on silica gel TLC using acetone as the eluant, or, in better yields, when compound **L** was allowed to stand in methanol containing a slight excess of alkali or simply purified by alumina column chromatography. The structure cyclohepta[2,1-*b*:2,3-*b*']di[1,4]benzoxazine (**16**) was established for compound **F** by elemental analysis ($C_{19}H_{12}N_2O_2$) and the spectral data.

Compound **F** possessed only a moderately conjugated

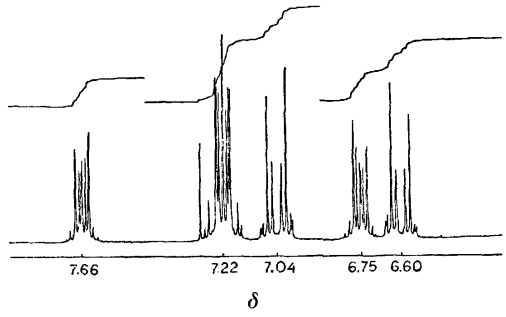

Fig. 1. The ^{1}H-NMR (200 MHz) spectrum of compound **F** in $CDCl_3$.

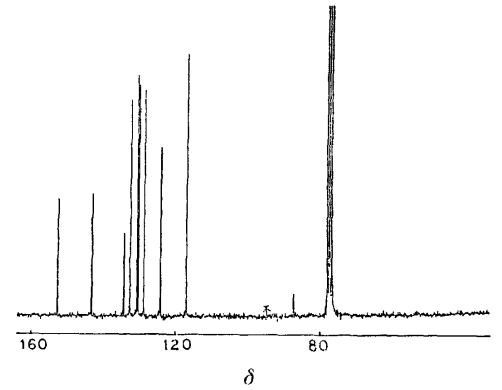

Fig. 2. The ^{13}C-NMR (50.3 MHz) spectrum of compound **F** in $CDCl_3$.

system (λ_{max} 378 nm). The IR spectrum showed that neither an OH nor an NH group was present in the molecule. The 200 MHz ^{1}H- and ^{13}C-NMR spectra[11] of compound **F** (Figs. 1 and 2) indicated the presence of a C_{2v} symmetry, as in the case of compound **A**, but of a different type. The singlet signal at δ 86.87 in the ^{13}C-NMR off-resonance spectrum was assignable to a sp^3 acetal carbon (see the Experimental section for the assignments of the NMR signals). It should be noted that compound **F** contains an interesting chiral center.[12] The salt **L** (**7a** as acetate) was regenerated from compound **F** by zinc dust reduction in acetic acid, further supporting the structure **7a** for compound **L**, which is considered to be derived from **6** by the normal substitution with **2**.

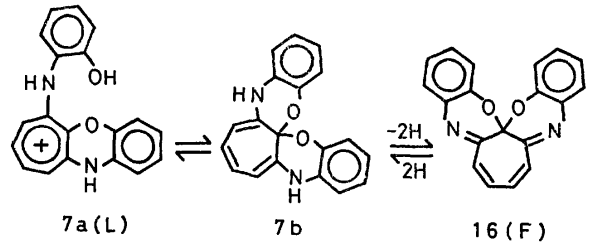

*Compounds **G** and **J**.* The structures of compounds **G** (red needles) and **J** (reddish brown needles) were now assigned to cyclohepta[*b*][1,4]benzoxazin-10(11*H*)-one (**17**) and cyclohepta[*b*][1,4]benzoxazin-6(11*H*)-one (**4**) respectively on the basis of the elemental analyses (both $C_{13}H_9NO_2$) and the spectral data,

Compound **G** showed NH and C=O absorptions at 3230 and 1605 cm^{-1}, and its UV spectrum resembled those of isopropylcyclohepta[*b*][1,4]benzoxazin-10-(11*H*)-ones (**19a**—**c**)[13] and the S-analog, cyclohepta-[*b*][1,4]benzothiazin-10(11*H*)-one (**20**).[14] The longest wavelength absorption (λ_{max} 483 nm) showed a considerable bathochromic shift compared with those of the normal tropones, suggesting that compound **G** may exist predominantly as the 10-hydroxy form (**17a**). The complete assignment for the ^{1}H-NMR signals was made by using a decoupling technique, and the result is shown in the Experimental section.

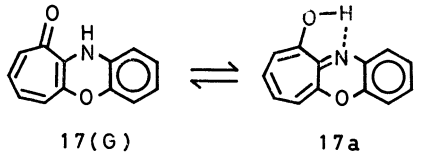

17(G) 17a

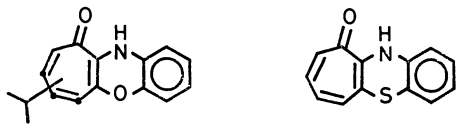

19a-c 20

Compound **J** showed NH and C=O absorptions at 3240 and 1640 cm^{-1}; the latter is slightly higher than that of compound **G**. Although the singlet at δ 7.68 was apparently due to NH, the rest of the proton signals of compound **J** were not well resolved at 90 MHz in acetone-d_6. However, a sufficiently resolved ^{1}H-NMR spectrum of **J** was available at 250 MHz in CF_3COOD,[15] and the signals at δ 7.45, 7.24, 7.40, and 7.03 were best assignable respectively to H-7, 8, 9, and 10 of structure **4**; the structure **18** proposed previously,[4] was thus revised to **4** on the ground of these NMR data. The relatively slow elution on TLC and the short retention time in the reversed phase HPLC[9] suggested a considerable contribution of the zwitterion form (**4a**) to the actual structure of compound **J**. However, neither methyl nor acetyl derivatives of compounds **G** and **J** were available upon treatment with diazomethane (or alkaline dimethyl sulfate) or acetic anhydride.

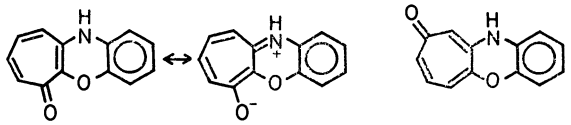

4 (J) 4a 18

Other Products. From the relatively slow-eluting fraction were further isolated small amounts of brown needles (**21**) and reddish violet needles (**22**). The structure 2-methylamino-3*H*-phenoxazin-3-one (**21**) was established for the former product by the elemental analysis and the spectral data; the UV spectrum of **21** closely resembled that of the known oxidative dimer 2-amino-3*H*-phenoxazin-3-one (**23**) of **2**, and the IR, ^{1}H-NMR, and the mass spectra supported the structure **21**. The origin of the methyl group in **21** is obscure at the moment. Although the violet-colored product (**22**) showed the molecular ion peak at *m/z* 502 and the longest wavelength absorption at 540 nm, its structure remained to be established. From fractions **E** and **I** were recovered small amounts of starting materials **8** and **2**, respectively.

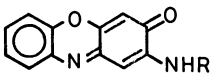

21 : R = CH_3
23 : R = H

Possible Reaction Pathways for the Formation of the Products from 8 and 2. Nucleophilic reactions of troponoids bearing more than two leaving groups have attracted considerable notice in view of the regioselectivities.[16] Dipole moment[17] and X-ray[18] studies indicated that the 2-methoxyl group of **8** was forced to stay out of the plane of the seven-membered ring because of the steric congestion by the bulky bromine and carbonyl groups. Therefore, the nucleophilic displacement at C-2 of **8** is expected to be retarded or slow. Indeed, Takase *et al.*[19] recently found that the treatment of **1** with a monofunctional nucleophile such as morpholine or pyrrolidine first gave the monosubstituted product (**24**), then the 2,7-disubstituted tropone (**25**), whereas **8** first afforded a mixture of the normal and cine-substitution products (**26** and **27**), which eventually yielded 2,7- and 2,3-disubstituted tropones (**25** and **28**), respectively.

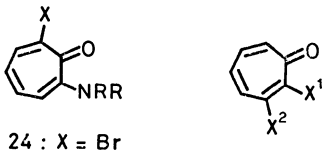

24 : X = Br
25 : X = NRR
27 : X = OCH_3
26 : X^1 = OCH_3, X^2 = NRR
28 : X^1 = X^2 = NRR

Similar reactivities are anticipated, at least in the initial stage, for **8** with nucleophile **2**. Thus the normal and cine-substitution of the bromine atom of **8** with the amino group of **2** should give the unstable intermediates **29** and **30**, which subsequently produce the 1:1 condensation products **4** (**J**) and **17** (**G**), respectively, after the ring-closure and hydrogen shift, followed by the removal of a molecule of methanol as illustrated in Scheme 2.[4]

Substitution of the 2-methoxyl group of **30** with another molecule of **2**, followed by the ring-closure at C-1, or substitution of 6-methoxy group of **32** with **2**, should afford **7** as the hydrobromide (**L**).

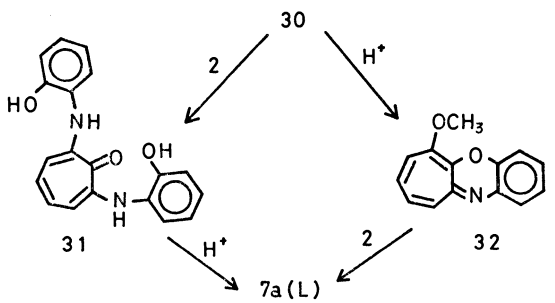

31 32 7a(L)

Compound **F** (**16**) is obviously derived from the

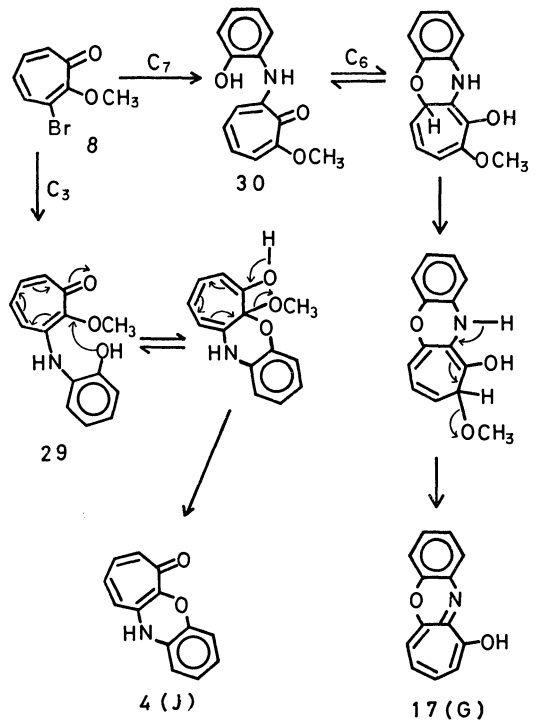

Scheme 2.

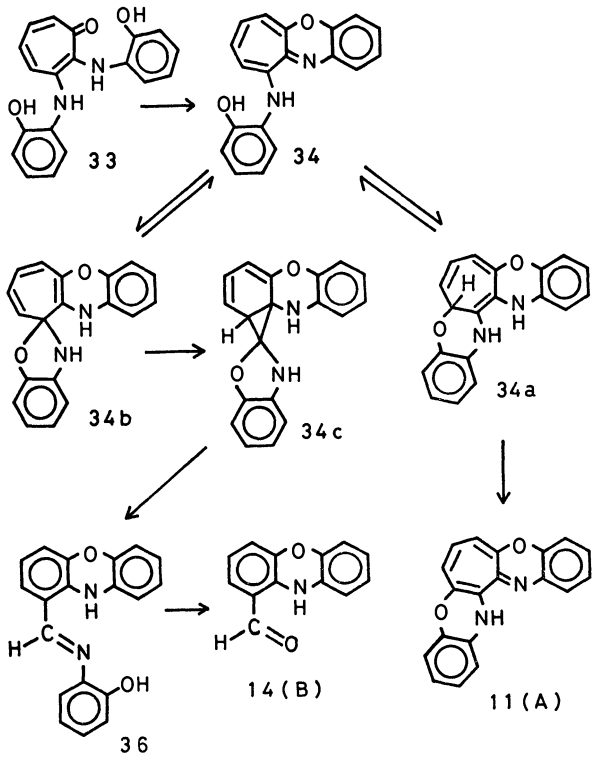

Scheme 3.

ring-closed tautomer (**7b**) of **7** through the air-oxidation as shown previously.

On the other hand, compounds **A**, **D**, **B**, and **C**[9,10] are presumably formed through the isomeric, common intermediate (**34**) derived from **29** *via* **33**, followed by the sequential steps illustrated in Scheme 3. The exact mechanism of this unusual substitution and the interesting ring closures accompanied by the rearrangement are currently under investigation in detail.[9,10] Nevertheless, the present experimental results clearly demonstrate a part of the diversity of the chemical reactions and the intricate character of troponoid compounds.

Experimental

Melting points are uncorrected. The IR and UV spectra were taken on a Hitachi EPI-G2 and a Hitachi 124 spectrometer, respectively; the UV spectra in acid and alkali were taken after adding three drops of 1 M HCl or 1 M NaOH (1 M = 1 mol dm^{-3}) to the sample solution. The NMR spectra were measured in $CDCl_3$ (unless otherwise specified) on a JEOL FX-90Q NMR spectrometer using TMS as the internal standard. The mass spectra were taken on a Hitachi RMU-6M mass spectrometer at 75 eV. The HPLC was carried out with Hitachi gel #3011 with MeOH–hexane (9:1) as solvent.

Reaction of 3-Bromo-2-methoxytropone (8) and o-Aminophenol (2). A solution of 4.9 g (22.8 mmol) of **8** and 3.7 g (34.2 mmol) of **2** in 20 ml of acetic acid was refluxed for 2 h. The solvent was removed *in vacuo*. The residue was separated by means of preparative TLC on silica gel (Merck, 20×40 cm, 2 mm thickness, 6 plates) using benzene as the eluant, thus affording crude compounds **A**, **B**, **C**, **D**, **G**, and the rest, according to the R_f values. The last fraction was eluted with methanol and re-chromatographed using acetone as the eluant, thus giving compounds **F**, **J**, **21**, **22**, and **L**.

Compound A: 14*H*[1,4]Benzoxazino[3′,2′:3,4]cyclohepta[1,2-*b*][1,4]benzoxazine (**11**); dark violet needles (240 mg, 3.9%); mp 246 °C (from hexane); UV_{max} (MeOH) 207, 254, 360, and 500 nm (log ε 4.10, 3.99, 3.43, and 3.68), (MeOH+HCl) 207, 223, 275, 325^{sh}, 410, and 535 nm (log ε 4.08, 4.02, 4.00, 3.57, 3.68, and 3.54); IR (KBr) 3250 cm^{-1} (NH); ^{1}H-NMR (360 MHz in $CDCl_3$)[5] δ=5.68 (2H, m, *J*=10.68 Hz, H-6,8), 5.84 (1H, m, *J*=10.68 Hz, H-7), the signals of H-7,6,8 were shown to be AB_2 spin system at $J/\Delta\delta$=0.177. 6.45 (2H, dd, *J*=7.2, 1.3 Hz, H-4,10), 6.62 (2H, dd, *J*=7.2, 1.3 Hz, H-1,13), 6.68 (2H, td, *J*=7.2, 1.3 Hz, H-2,12 or H-3,11), 6.72 (2H, td, *J*=7.2, 1.3 Hz, H-3,11 or H-2,12), and 7.55 (1H, s, NH), (360 MHz in DMSO-d_6)[5] δ=5.79 (2H, d, *J*=10.8 Hz, H-6,8), 6.00 (1H, t, *J*=10.8 Hz, H-7), 6.53 (2H, dd, *J*=7.2, 1.3 Hz, H-4,10), 6.75 (4H, m, H-2,3,11,12), and 6.88 (2H, dd, *J*=7.2, 1.3 Hz, H-1,13); ^{13}C-NMR (47.3 MHz)[5] δ=150.36, 145.16, 139.28, 132.69, 125.56, 124.56, 124.42, 119.30, 117.40, and 114.35.

Found: C, 76.25; H, 4.09; N, 9.38%; M$^+$, 300. Calcd for $C_{19}H_{12}N_2O_2$: C, 75.99; H, 4.03; N, 9.33%; M, 300.

Compound B: 1-Formylphenoxazine (**14**); orange yellow needles (140 mg, 3.1%); mp 115 °C (from hexane after TLC purification; lit,[8] mp 105—110 °C); UV_{max} (MeOH) 207, 227, 275, 310, and 435 nm (log ε 4.28, 4.43, 3.88, 3.48, and 3.74); IR (KBr) 3300 (NH) and 1650 cm^{-1} (C=O); ^{1}H-NMR (100 MHz) δ=9.74 (1H, s, CHO), 9.08 (1H, s, NH), 6.99 (1H, dd, *J*=7.0, 2.5 Hz, H-2), 6.55—6.80 (5H, m, H-3,4,6,7,8), and 6.46 (1H, m, H-9); ^{13}C-NMR (33.3 MHz) δ(off resonance)=193.59 (d, CHO), 144.89 (s), 135.99 (s), 128.41 (d), 124.08 (d), 122.88 (d), 119.36 (d), 118.38 (s), 115.67 (d), and 114.48 (d).

Found: C, 73.64; H, 4.27; N, 6.70%; M$^+$, 211. Calcd for $C_{13}H_9NO_2$: C, 73.92; H, 4.30; N, 6.63%; M, 211.

Compound D: Purification of the crude compound **D** by column chromatography on silica gel produced only **11** (13 mg), thus the pure compound **D** was not isolated.

Compound ***F***: Cyclohepta[2,1-*b*:2,3-*b'*]di[1,4]benzoxazine (**16**); yellow needles (275 mg, 4.1%); mp 191 °C (from ether after silica gel column purification); UV_{max} (MeOH) 208, 235, 287, and 378 nm (log ε 4.45, 4.29, 4.30, and 3.86); ^{1}H-NMR (200 MHz)[11] δ=7.66 (2H, m, H-4,11), 7.22 (4H, m, H-2,3,12,13), 7.04 (2H, m, H-6,9), 6.75 (2H, m, H-1,14), and 6.60 (2H, m, H-7,8); ^{13}C-NMR (50.309 MHz)[11] δ (off resonance)=86.87 (s, acetal carbon C-15a), 116.49 (d, C-1), 123.65 (d, C-4), 128.12 (d), 129.67 (d), 130.08 (d), 131.95 (d), 133.60 (s, C-5a, 9a), 142.48 (s, C-4a,10a), and 151.85 (s, C-14a,16a).

Found: C, 75.84; H, 3.79; N, 9.28%; M^+, 300. Calcd for $C_{19}H_{12}N_2O_2$: C, 75.99; H, 4.03; N, 9.33%; M, 300.

Compound ***G***: Cyclohepta[*b*][1,4]benzoxazin-10(11*H*)-one (**17**); red needles (830 mg, 18.1%); mp 175 °C from ethyl acetate after purification as the picrate, which was recrystallized from ethanol, decomposed with 1M NaOH, and finally extracted with benzene); UV_{max} (MeOH) 205, 227, 259, 270, 284, 305,^{sh} 320,^{sh} 415,^{sh} and 483 nm (log ε 4.24, 4.28, 4.21, 4.21, 4.05, 3.72, 3.59, 3.62, and 3.88); (MeOH+HCl) 205, 227, 260,^{sh} 271, 284, 320,^{sh} 420,^{sh} and 480 nm (log ε 4.15, 4.29, 4.14, 4.20, 4.19, 3.59, 3.68, and 3.83); (MeOH+NaOH) 213, 259, 270, 284,^{sh} 305,^{sh} 320,^{sh} 415,^{sh} and 483 nm (log ε 4.41, 4.17, 4.18, 4.05, 3.72, 3.59, 3.60, and 3.83); IR (KBr) 3230 (NH) and 1605 cm^{-1} (C=O); ^{1}H-NMR (200 MHz)[11] δ=7.53 (1H, s, NH), 7.09 (1H, br d, *J*=12.0 Hz, H-9), 6.95 (1H, ddd, *J*=12.0, 8.5, 1.5 Hz, H-8), 6.74 (1H, br d, *J*=12.0 Hz, H-6), 6.71 (2H, m, H-2,3), 6.59 (1H, ddd, *J*=12.0, 8.5, 1.5 Hz, H-7), and 6.49 (2H, m, H-1,4).

Found: C, 73.70; H, 4.28; N, 6.68%; M^+, 211. Calcd for $C_{13}H_9NO_2$: C, 73.92: H, 4.30; N, 6.63%: M, 211.

Compound ***J***: Cyclohepta[*b*][1,4]benzoxazin-6(11*H*)-one (**4**); red brown needles (290 mg, 6.3%); mp 270 °C (from ethanol); UV_{max} (MeOH) 205, 228, 260, 270,^{sh} 292, 310,^{sh} 323,^{sh} and 400 nm (log ε 4.40, 4.34, 4.20, 4.15, 4.10, 4.04, 3.91, and 3.88); (MeOH+HCl) 205, 228, 281, and 418 nm (log ε 4.35, 4.40, 4.28, and 3.93); (MeOH+NaOH) 260, 290, and 418 nm (log ε 4.20, 4.10, and 3.88); IR (KBr) 3240 (NH) and 1640 cm^{-1} (C=O); ^{1}H-NMR (250 MHz in CF_3COOD)[15] δ=7.45 (1H, dd, *J*=11.5, 1.5 Hz, H-7), 7.40 (1H, ddd, *J*=11.5, 9.0, 1.5 Hz, H-9), 7.24 (1H, ddd, *J*=11.5, 9.0, 1.0 Hz, H-8), 7.03 (1H, br d, *J*=11.5 Hz, H-10), 6.99 (2H, m, H-2,3), 6.84 (1H, m, H-1), 6.68 (1H, m, H-4).

Found: C, 73.91; H, 4.48; N, 6.47%; M^+, 211. Calcd for $C_{13}H_9NO_2$: C, 73.92; H, 4.30; N, 6.63%; M, 211.

*2-Methylamino-3*H*-phenoxazin-3-one (**21**).* The extract of the band between compounds **F** and **J** during the TLC purification using acetone (see above) was further purified by the silica gel column chromatography, thus affording 110 mg (2.2%) of **21** as brown needles, mp 225 °C (from chloroform); UV_{max} (MeOH) 205, 238, 270,^{sh} 420, and 435 nm (log ε 4.56, 4.57, 4.26, 4.40, and 4.41); (MeOH+HCl) 238, 465, and 520 nm (log ε 4.57, 4.02, and 3.90); IR (KBr) 3370 (NH) and 1580 cm^{-1} (C=O); ^{1}H-NMR (100 MHz) δ=7.70—7.35 (4H, m, H-6,7,8,9), 6.41 (1H, s, H-1), 6.19 (1H, s, H-4), 3.48 (1H, q, *J*=6.0 Hz, NH), and 2.99 (3H, d, *J*=6.0 Hz, N-CH_3).

Found: *m/z* 226.0722.[20] Calcd for $C_{13}H_{10}N_2O_2$: M, 226.0742.

22: The extract of the band between compounds **J** and **L** during the TLC purification using acetone was recrystallized from ethanol, thus affording 20 mg of **22** as reddish violet crystals, mp 235 °C decomp; UV_{max} (MeOH) 211, 235, 265,^{sh} 275, 303, 420,^{sh} and 540 nm (log ε 4.63, 4.34, 4.13, 4.07, 3.92, 3.68, and 3.75); (MeOH+NaOH) 235, 275, 300, 540, and 575 nm (log ε 4.58, 3.99, 3.95, 3.70, and 3.70). Found: C, 51.69; H, 3.64; N, 4.47%; M^+, 502.

Compound ***L***: 6-(*o*-Hydroxyanilino)cyclohepta[*b*][1,4]-benzoxazine hydrobromide (**7a**); a) A solution of 1.00 mg (4.65×10^{-3} mmol) of **8** and 0.91 mg (8.34×10^{-3} mmol) of **2** in 8 ml of acetic acid was heated at 100 °C for 2.5 h. After the removal of the solvent *in vacuo*, the residue was chromatographed on a column of silica gel first using benzene–methanol (10:1), then methanol as the eluant. The latter fraction was concentrated and allowed to stand in the refrigerator, thus depositing **7a** as dark brown needles. Recrystallization from methanol gave an analytical sample: mp >300 °C decomp; UV_{max} (MeOH) 265, 309, and 435 nm (log ε 4.32, 4.08, 4.05); (MeOH+0.1 M NaOH) 271, 463, and 485 nm (log ε 4.33, 4.12, and 4.07); Found: C, 61.35; H, 3.95; N, 7.67; Br, 18.98%. Calcd for $C_{19}H_{14}N_2O_2\cdot$HBr: C, 59.55; H, 3.95; N, 7.31; Br, 20.85%.

Found: *m/z* 302.1069.[20] Calcd for $C_{19}H_{14}N_2O_2$: M 302.1055.

The dark brown solution of **7a** in methanol and 0.1 M NaOH turned pale yellow after being set aside overnight at 20 °C, and the solution was found to contain compound **F** by means of TLC, reversed phase HPLC, and UV absorption.

b) From compound **F**: Zinc dust was added to a solution of compound **F** in acetic acid at room temp. The solution turned to reddish brown in a short period and was found to contain mainly compound **L** on the evidence of the reversed phase HPLC and UV absorption.

We thank Professors K. Takase, M. Yasunami (Tohoku Univ.), I. Murata (Osaka Univ.), H. Yamamoto (Okayama Univ.), Drs. Y. Naya, S. Imajo, H. Naoki (Suntory Inst. Bioorg. Res.), H. Tsuruta (Takasago Perfumery Co.), T. Takita (Institute of Microbial Chemistry), and Mr. K. Fujimori (Shinshu Univ.) for their helpful discussions and spectral measurements. We also thank Professor S. Ishikawa (Josai Univ.) for allowing his assistant (H. W.) to carry out the present research at Kao Soap Co.

References

1) T. Nozoe, Presented at the 14th Japanese Symposium on the Chemistry of Nonbenzenoid Aromatic Compounds, Okayama, October 1981.

2) T. Nozoe, T. Someya, and H. Okai, *Bull. Chem. Soc. Jpn.*, **52**, 1156 (1979).

3) T. Nozoe, H. Okai, and H. Wakabayashi, Presented at National Meeting of Chem. Soc. Jpn., Fukuoka, October 1979, Abstr. II, p. 805. and Higashi-Osaka, April 1980, Abstr. II, p. 887.

4) T. Nozoe, *Pure Appl. Chem.*, **54**, 975 (1982).

5) Kindly measured at Suntory Institute of Bioorganic Research, Osaka, with a Nicolet NT-360 spectrometer.

6) T. Nozoe, T. Asao, and K. Takahashi, *Bull. Chem. Soc. Jpn.*, **39**, 1980 (1966).

7) Recently, structure **11** was confirmed by X-ray crystallographic analysis of compound **A**, and the results will be reported elsewhere by Professor Y. Iitaka and Mrs. H. Nakamura.

8) M. Haeferist, *J. Org. Chem.*, **27**, 4326 (1962); spectral data of **14** were not reported.

9) T. Nozoe, H. Okai, and H. Wakabayashi, to be published.

10) T. Nozoe, H. Okai, H. Wakabayashi, K. Shindo,

and S. Ishikawa, to be published.

11) Kindly measured by Prof. M. Yasunami at Tohoku Univ., Sendai, with a Varian FX-200 for ^{1}H-NMR at 200 MHz and for ^{13}C-NMR at 50.309 MHz.

12) The two enantiomers were successfully separated using a optical active poly(triphenylmethyl methacrylate) (Chiralpak OT (+)) by Y. Okamoto (Osaka Univ.); the result will be published elsewhere.

13) T. Nozoe and T. Someya, *Bull. Chem. Soc. Jpn.*, **51**, 3316 (1978).

14) T. Nozoe, T. Asao, and K. Takahashi, *Bull. Chem. Soc. Jpn.*, **34**, 146 (1961).

15) Kindly measured by Dr. T. Miyake (Institute of Bioorg. Chem.) with a Bruker WM-250 spectrometer.

16) T. Nozoe *et al.*, "Nonbenzenoid Aromatic Compounds," in "Dai Yuki Kagaku (Comprehensive Organic Chemistry)," ed by M. Kotake, Asakura Shoten, Tokyo (1960), Vol. 13, pp. 214—261.

17) Y. Kurita, S. Seto, T. Nozoe, and M. Kubo, *Bull. Chem. Soc. Jpn.*, **26**, 272 (1953); T. Nozoe, Y. Kitahara, and S. Masamune, *Proc. Jpn. Acad.*, **27**, 649 (1951).

18) K. Furukawa, Y. Sasada, A. Shimada, and T. Watanabe, *Bull. Chem. Soc. Jpn.*, **37**, 1871 (1964).

19) Y. Sasakawa, M. Yasunami, and K. Takase, 37th National Meeting of Chem. Soc. of Jpn., Kanagawa, April 1978, Abstr. II, p. 805.

20) Kindly measured by Mr. S. Sugiura (Kao Soap Co.) with a JMS-D300 (JEOL) mass spectrometer.

Benzofuran Derivatives. I. On the Effects of Substituents in Benzofuran Syntheses

Tsuneo Suzuki,* Takaaki Horaguchi,† Takahachi Shimizu,† and Teishiro Abe††

Nippon Dental University, Niigata, 1-8, Hamaura-cho, Niigata 951

† *Department of Chemistry, Faculty of Science, Niigata University, Ikarashi, Niigata 950-21*

†† *Department of General Education, Niigata University, Ikarashi, Niigata 950-21*

(Received January 24, 1983)

The Rössing's reaction of 4-substituted 2-acylphenoxyacetic acids give a mixture of benzofurans and 2-benzofurancarboxylic acids. The relative yields of benzofurans and 2-benzofurancarboxylic acids depend on the substituents on the benzene ring of the 2-acylphenoxyacetic acids. Electron-withdrawing substituents such as nitro groups favor the formation of 2-benzofurancarboxylic acids. On the other hand, the formation of benzofurans is favored by the steric hindrance of 2-acyl groups in the reaction of 2-acyl-4-nitrophenoxyacetic acids with anhydrous sodium acetate and acetic anhydride.

Benzofurans are well-known heterocyclic compounds and have been prepared by Rössing's method.[1] This is a general procedure to obtain benzofurans from 2-acylphenoxyacetic acids by heating them with anhydrous sodium acetate and acetic anhydride. In this method 2-benzofurancarboxylic acids were obtained as minor products. The formation of 2-benzofurancarboxylic acids has not been noted because of their poor yields.[2] Burgstahler and Worden, however, reported that 2-benzofurancarboxylic acid was obtained in high yield (45%) by the reaction of 2-formylphenoxyacetic acid with anhydrous sodium acetate and acetic anhydride.[3] Recently, we reported that 2-acetyl-5-nitrophenoxyacetic acid gave 3-methyl-6-nitrobenzofuran and 3-methyl-6-nitro-2-benzofurancarboxylic acid in 58 and 42% yields, respectively.[4] Thus, substituents in 2-acylphenoxyacetic acids influence the relative yields of benzofurans and 2-benzofurancarboxylic acids. In the present paper, we examined the electronic and steric effects on the relative yields of benzofurans (**2**) and 2-benzofurancarboxylic acids (**3**) in the Rössing's method.

Results and Discussion

Some 2-acylphenoxyacetic acid derivatives (**1a**—**j**) were prepared in order to investigate substituent effects (R^1 and R^2) on the syntheses of benzofurans (**2a**—**j**) and 2-benzofurancarboxylic acids (**3a**—**j**). The syntheses of **1a**,[5] **1c**,[6] **1d**,[7] **1g**,[8] and **1h**[9], were carried out according to reported methods. The synthetic methods of **1b**, **1e**, **1f**, **1i**, and **1j**, are summarized in Scheme 1.

When 4-substituted 2-acylphenoxyacetic acids (**1a**—**j**) were heated with anhydrous sodium acetate and acetic anhydride at 110±1 °C for 3 h, benzofurans (**2a**—**j**) and 2-benzofurancarboxylic acids (**3a**—**j**) were obtained. The isolated and relative yields of **2a**—**j** and **3a**—**j** are summarized in Table 1.

Initially, the effects of R^2 were examined for $R^1=NO_2$ by changing R^2 from hydrogen to methyl, ethyl, or isopropyl groups. In the case of $R^2=H$, the relative yields of benzofuran (**2h**) and 2-benzofurancarboxylic acid (**3h**) were 25.5 and 74.5%, respectively. Therefore, the latter was the major product, whereas the yield (86.2%) of benzofuran (**2j**) exceeded that (13.8%) of 2-benzofurancarboxylic acid (**3j**) when R^2 was an isopropyl group. When R^2 were methyl or ethyl groups, the yields of **2e** and **3e** were 62.5 and 37.5%, and those of **2i** and **3i** were 66.4 and 33.6%, respectively. Thus, the formation of benzofurans (**2**) was favored as the steric bulk of R^2 increased. The results are explained in terms of steric effects of R^2, since the electronic effects of methyl, ethyl, and isopropyl groups are similar.

Table 1. The reaction of 4-substituted 2-acylphenoxyacetic acids with anhydrous sodium acetate and acetic anhydride

a) $R^1=CH_3O$, $R^2=CH_3$
b) $R^1=CH_3$, $R^2=CH_3$
c) $R^1=H$, $R^2=CH_3$
d) $R^1=Cl$, $R^2=CH_3$
e) $R^1=NO_2$, $R^2=CH_3$
f) $R^1=CH_3$, $R_2=H$
g) $R^1=H$, $R^2=H$
h) $R^1=NO_2$, $R^2=H$
i) $R^1=NO_2$, $R^2=CH_2CH_3$
j) $R^1=NO_2$, $R^2=CH(CH_3)_2$

Starting materials	Isolated yields[a]/%		Relative yields/%	
	2	**3**	**2**	**3**
1a	96.6	3.2	96.8	3.2
1b	96.0	1.7	98.3	1.7
1c	93.8	1.4	98.5	1.5
1d	91.3	7.4	92.5	7.5
1e	56.9[b]	34.2[b]	62.5	37.5
1f	27.2[c]	55.5	44.5[d]	55.5
1g	22.2[c]	53.0	47.0[d]	53.0
1h	25.3[b]	73.9[b]	25.5	74.5
1i	64.7[b]	32.8[b]	66.4	33.6
1j	84.8[b]	13.6[b]	86.2	13.8

a) Benzofuran **2** and methyl ester of **3** were analyzed by GLPC and the yields of **3** were calculated from those of methyl esters. b) Analyzed by usual method. c) The yields are low because of the high volatility. d) Calculated in equation 100-**3f**, **g** (%).

Although little information[10] is available concerning reaction mechanisms of formation of the furan ring, 3-hydroxy-2,3-dihydro-2-benzofurancarboxylate ion (**4**)

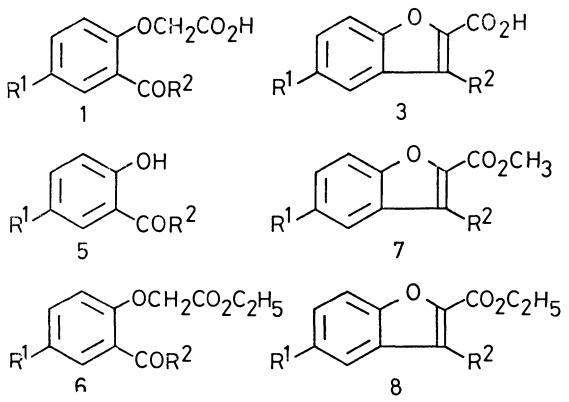

b) $R^1=CH_3$, $R^2=CH_3$ f) $R^1=CH_3$, $R^2=H$
c) $R^1=H$, $R^2=CH_3$ g) $R^1=H$, $R^2=H$
d) $R^1=Cl$, $R^2=CH_3$ i) $R^1=NO_2$, $R^2=CH_2CH_3$
e) $R^1=NO_2$, $R^2=CH_3$ j) $R^1=NO_2$, $R^2=CH(CH_3)_2$

5b ⟶ 1b

5e,f ⟶ 6e,f ⟶ 1e,f

p-Nitrophenol ⟶ 5i,j ⟶ 6i,j ⟶ 1i,j

3b,c,d ⟶ 7b,c,d

5f ⟶ 8f ⟶ 3f ⟶ 7f

5g ⟶ 3g ⟶ 7g

Scheme 1. The synthetic pathways of 4-substituted 2-acylphenoxyacetic acids (**1**) and methyl 2-benzofurancarboxylates (**7**).

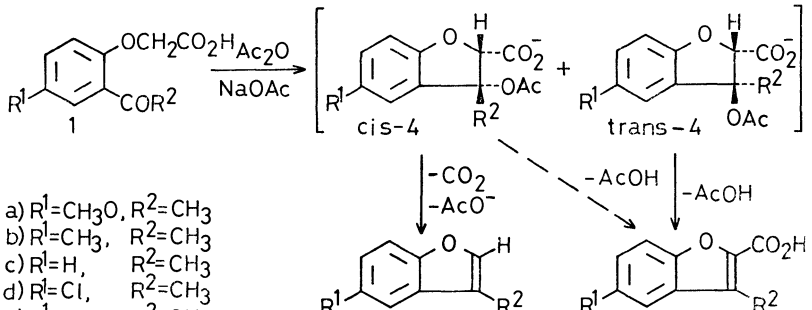

a) $R^1=CH_3O$, $R^2=CH_3$
b) $R^1=CH_3$, $R^2=CH_3$
c) $R^1=H$, $R^2=CH_3$
d) $R^1=Cl$, $R^2=CH_3$
e) $R^1=NO_2$, $R^2=CH_3$
f) $R^1=CH_3$, $R^2=H$
g) $R^1=H$, $R^2=H$
h) $R^1=NO_2$, $R^2=H$
i) $R^1=NO_2$, $R^2=CH_2CH_3$
j) $R^1=NO_2$, $R^2=CH(CH_3)_2$

Scheme 2. The reaction pathways for the production of benzofurans (**2**) and 2-benzofurancarboxylic acids (**3**).

was assumed as an intermediate in the formation of benzofurans.[11] A similar intermediate was isolated recently in the syntheses of 4,5-dihydro-3*H*-naphtho-[1,8-*bc*]furan.[12]

A proposed reaction mechanism is depicted in Scheme 2. The reaction of 2-acylphenoxyacetic acids (**1**) with anhydrous sodium acetate and acetic anhydride will afford two intermediates (*cis*-**4** and *trans*-**4**). The relative ratio of *cis*-**4** to *trans*-**4** will be varied by changing R^2. In the case of **1h** ($R^2=H$), *trans*-**4h** will be preferentially produced because the steric repulsion between the acetoxyl group and the carboxylate ion of *cis*-**4h** is larger than that of *trans*-**4h**. On the other hand, **1j** ($R^2=CH(CH_3)_2$) will preferentially

give *cis*-**4j** because of the steric repulsion between the isopropyl group and the carboxylate ion. Preferential formation of benzofuran (**2j**) suggests that **2j** must be produced mainly through *cis*-**4j** by *syn* elimination of carbon dioxide and acetate ion, while 2-benzofurancarboxylic acid (**3h**) must be produced exclusively through *trans*-**4h** by *syn* elimination of acetic acid.[13]

Secondly, the effects of R^1 were examined. In the first case, R^2 was fixed as a methyl group, and R^1 was varied from hydrogen to methoxyl, methyl, nitro groups, or a chlorine atom. The reaction of **1a—d** with anhydrous sodium acetate and acetic anhydride gave a mixture of 3-methylbenzofurans (**2a—d**) and 3-methyl-2-benzofurancarboxylic acid (**3a—d**) in relative yields of 98.5—92.5 and 1.5—7.5%, respectively. Electronic effects of substituents R^1 did not influence the relative yields of **2a—d** and **3a—d**, while compound **1e** ($R^1=NO_2$) gave benzofuran (**2e**) and 2-benzofurancarboxylic acid (**3e**) in relative yields of 62.5 and 37.5%, respectively. The strongly electron-withdrawing nitro group makes the hydrogen atom attached at the C_2 carbon atom of *cis*-**4e** more acidic than that of *cis*-**4a—d** as illustrated in Scheme 2, and facile *anti* elimination of acetic acid gives 2-benzofurancarboxylic acid (**3e**).

In the second case, R^2 was fixed as hydrogen and R^1 was varied from hydrogen to methyl or nitro groups. The reaction of **1f** ($R^1=CH_3$) with anhydrous sodium acetate and acetic anhydride gave benzofuran (**2f**) and 2-benzofurancarboxylic acid (**3f**) in 44.5 and 55.5 % relative yields, respectively. Compound **1g** also afforded **2g** and **3g** in similar relative yields. On the other hand, compound **1h** ($R^1=NO_2$) gave benzofuran (**2h**) and 2-benzofurancarboxylic acid (**3h**) in relative yields of 25.5 and 74.5%, respectively. Therefore, nitro group of **1h** also favored the formation of 2-benzofurancarboxylic acid (**3h**) by its electron-withdrawing nature.

We wish to try to trap intermediates, *cis*-**4** and *trans*-**4**, and are continuing further research on the mechanism of furan ring formation.

Experimental

All melting points are uncorrected. The infrared absorption spectra were determined on a JASCO Model DS402G infrared spectrometer and a HITACHI EP1-G grating infrared spectrometer. Nuclear magnetic resonance spectra were determined at 100 MHz on a JEOL Model 4H-100 NMR spectrometer, using tetramethylsilane as an internal standard. GLC analyses were performed on a YANACO Gas Chromatograph Model G 80-FP equipped with a glass column (1.5 m; $\phi=4$ mm) packed with 5% Silicone Gum SE-30 on Chromosorb W AW-DMCS (80—100 mesh) at 110—200 °C for each case. The column chromatography was performed on silica gel (Wakogel C-200).

General Procedure for Determination of the Ratio of ***3*** *to* ***2*** *in the Reaction of* ***1***. A typical procedure will be described for the reaction of **1b**. A mixture of **1b** (1.04 g, 0.5 mmol), anhydrous sodium acetate (2.6 g, 31.6 mmol), and acetic anhydride (17 ml) was heated at 110±1 °C for 3 h. After cooling, the reaction mixture was poured into 100 ml of water and stirred for 1 h. This mixture was extracted with 250 ml of ether, and the ethereal solution was washed with water (40 ml×5). The ethereal solution was concentrated by evaporation to approximately 50 ml. An ethereal solution of diazomethane was added dropwise to the residue until the color of the solution turned yellow. The resulting solution was diluted with ether exactly to a total volume of 200 ml (sample 1). Five ml of the sample 1 was pipetted and was diluted with ether exactly to a total volume of 50 ml (sample 2). The quantity of **2b** in the sample 2 and that of **7b** in the sample 1 were determined by gas chromatography and the yield of **3b** was calculated from the quantity of **7b**. The resulting chromatograms were compared by measuring the areas of peaks by triangulation with those of the standard sample for which the concentration was known. The yield of **2b** was 96.0% and that of **3b** was 1.7%. The results of the reaction of **1a,c,d,f** and **1g** with anhydrous sodium acetate and acetic anhydride were obtained similarly and are listed in Table 1. Nitro compounds (**1e**, **1h—j**) were run in the same manner as described above. The separation and quantitative analyses of the products were carried out in the usual manner and the results are summarized in Table 1. Compounds **2h**[14] and **3h**[14] were identified by comparison of their IR and NMR spectra with those of authentic samples.

2e: Mp 89—90 °C. IR(KBr): ν_{max} 3088, 2920, 1625, 1586, 1516 (NO_2), 1442 (C=C), 1334 (NO_2), 887 (furan ring), 804 cm^{-1} (two adjacent aromatic hydrogen atoms). Found: C, 61.02; H, 4.04%. Calcd for $C_9H_7NO_3$: C, 61.02; H, 3.98%.

3e: Mp 285—286 °C (decomp). IR(KBr): ν_{max} 3100, 2800—2400, 1692 (CO_2H), 1620, 1580, 1525 and 1329 (NO_2), 903 (CO_2H), 832 cm^{-1} (two adjacent aromatic hydrogen atoms). Found: C, 54.32; H, 3.23%. Calcd for $C_{10}H_7NO_5$: C, 54.30; H, 3.19%.

2i: Mp 89—90 °C. IR (KBr): ν_{max} 3095, 2960, 1578, 1515 (NO_2), 1445 (C=C), 1342 (NO_2), 887 (furan ring), 830 cm^{-1} (two adjacent aromatic hydrogen atoms). Found: C, 62.72; H, 4.76%. Calcd for $C_{10}H_9NO_3$: C, 62.82; H, 4.74%.

3i: Mp 240—243 °C. IR (KBr): ν_{max} 3100, 2970, 2800—2400, 1678 (CO_2H), 1617, 1584, 1520 (NO_2), 1447, 1340 (NO_2), 924 (CO_2H), 831 cm^{-1} (two adjacent aromatic hydrogen atoms). Found: C, 56.12; H, 3.99%. Calcd for $C_{11}H_9NO_5$: C, 56.17; H, 3.85%.

2j: Mp 110.5—111.0 °C. IR (KBr): ν_{max} 3105, 2960, 2875, 1623, 1585, 1508 (NO_2), 1444 (C=C), 1335 (NO_2), 885 (furan ring), 818 cm^{-1} (two adjacent aromatic hydrogen atoms). Found: C, 64.34; H, 5.40%. Calcd for $C_{11}H_{11}NO_3$: C, 64.38; H, 5.40%.

3j: Mp 249—250 °C. IR (KBr): ν_{max} 3080, 2960, 2800—2400, 1674 (CO_2H), 1608, 1585, 1515 and 1340 (NO_2), 908 (CO_2H), 832 cm^{-1} (two adjacent aromatic hydrogen atoms). Found: C, 57.89; H, 4·48%. Calcd for $C_{12}H_{11}NO_5$: C, 57.83; H, 4.44%.

*Preparation of Materials (****1a—j****).* 2-Acetyl-4-methoxyphenoxyacetic acid (**1a**) was prepared by Whalley's method,[5] 2-acetylphenoxyacetic acid (**1c**) by Rosseels' method,[6] and 2-acetyl-4-chlorophenoxyacetic acid (**1d**) by Deorha's method.[7] 2-Formylphenoxyacetic acid (**1g**) was prepared by Dumont's method,[8] and 2-formyl-4-nitrophenoxyacetic acid (**1h**) by Jacobs' method.[9]

*2-Acetyl-4-methylphenoxyacetic Acid (****1b****).* A mixture of 2-hydroxy-5-methylacetophenone[15] (**5b**) (10 g), ethyl bromoacetate (16.5 g), anhydrous potassium carbonate (40 g), and acetone (200 ml) was refluxed at 70 °C for 6 h. After cooling, the insoluble salts were removed by filtration and the filtrate was concentrated under evaporation. The

residue was treated with ethanol (50 ml) and 3 M (1 M= 1 mol dm^{-3}) sodium hydroxide solution (50 ml) at room temperature for 30 min. The reaction mixture was poured into cold water (100 ml) and acidified with 6 M hydrochloric acid. The precipitates were filtered, washed with cold water, and dried under vacuum to give 12.9 g (92%) of **1b** as crystals. Recrystallization from aqueous methanol gave colorless plates, mp 156—157 °C. IR (KBr): ν_{max} 1773 (CO_2H), 1654 cm^{-1} (CO). NMR (CD_3COCD_3): δ= 2.29 (3H, s, $PhCH_3$), 2.67 (3H, s, $COCH_3$), 4.76 (2H, s, CH_2), 6.88 (1H, d, J=8.5 Hz, C_6-H), 7.28 (1H, dd, J= 8.5 and 2.5 Hz, C_5-H), 7.47 (1H, J=2.5 Hz, C_3-H). Found: C, 63.21; H, 5.89%. Calcd for $C_{11}H_{12}O_4$: C, 63.45; H, 5.81%.

*Ethyl 2-Acetyl-4-nitrophenoxyacetate (**6e**).* 2-Hydroxy-5-nitroacetophenone (**5e**) was prepared by Joshi's method.[16] A mixture of **5e** (10 g), ethyl bromoacetate (11 g), anhydrous potassium carbonate (30.4 g), and acetone (200 ml) was refluxed at 70 °C for 3 h. After cooling, insoluble salts were removed by filtration. The residue obtained upon evaporation of the acetone was purified by recrystallization from hexane-ethanol to give 12.4 g (84.3%) of **6e** as pale yellow short needles, mp 88.0—89.5 °C. IR (KBr): ν_{max} 1760 (-CO_2-), 1674 (CO), 1507 and 1338 (NO_2), 836 cm^{-1} (two adjacent aromatic hydrogen atoms). Found: C, 53.97; H, 4.97%. Calcd for $C_{12}H_{13}NO_6$: C, 53.93; H, 4.90%.

*2-Acetyl-4-nitrophenoxyacetic Acid (**1e**).* A mixture of **6e** (1 g), anhydrous potassium carbonate (0.5 g), and water (10 ml) was refluxed for 40 min. Insoluble material in the reaction mixture was filtered while hot, and the filtrate was acidified after cooling with 6 M hydrochloric acid. The precipitates were filtered, washed with cold water, and dried under vacuum to give 0.8 g (90%) of **1e** as crystals. Recrystallization from aqueous ethanol gave pale yellow short needles, mp 198—200 °C (decomp). IR (KBr): ν_{max} 1739 (CO_2H), 1675 (CO), 1516 and 1340 cm^{-1} (NO_2). NMR (CD_3OD): δ=2.72 (3H, s, $COCH_3$), 4.99 (2H, s, CH_2), 7.24 (1H, d, J=8.7 Hz, C_6-H), 8.35 (1H, dd, J=8.7 and 3.7 Hz, C_5-H), 8.51 (1H, d, J=3.7 Hz, C_3-H). Found: C, 50.31; H, 3.86%. Calcd for $C_{10}H_9NO_6$: C, 50.21; H, 3.79%.

*Ethyl 2-Formyl-4-methylphenoxyacetate (**6f**).* From 5-methylsalicylaldehyde[17] (**5f**) (3 g), **6f** (4 g, 81.6%) was obtained in the same manner as has been described for **6e** except that tetrahydrofuran was used as solvent instead of acetone. Recrystallization from aqueous ethanol gave colorless short needles, mp 51.5—52.5 °C. IR (KBr): ν_{max} 1767 (-CO_2-), 1671 (CHO), 837 cm^{-1} (two adjacent aromatic hydrogen atoms). Found: C, 65.01; H, 6.39%. Calcd for $C_{12}H_{14}O_4$: C, 64.85; H, 6.34%.

*2-Formyl-4-methylphenoxyacetic Acid (**1f**).* A mixture of **6f** (2.61 g), 20% potassium hydroxide solution (10 ml) and ethanol (12 ml) was warmed at 60 °C for 30 min. After cooling, 150 ml of water was poured into the reaction mixture and the mixture was acidified with 6 M hydrochloric acid. Resulting precipitates were filtered, washed with cold water, and dried under vacuum to give 1.9 g (83.3%) of **1f** as crystals. Recrystallization from aqueous acetone gave colorless plates, mp 147—148 °C (lit,[18] mp 151 °C). IR (KBr): ν_{max} 1745 and 1720 (CO_2H), 1690 (CHO), 927 (CO_2H), 822 cm^{-1} (two adjacent aromatic hydrogen atoms), (Found: C, 61.83; H, 5.29%).

*2'-Hydroxy-5'-nitropropiophenone (**5i**).* By the modified method of Joshi[16], **5i** (7.5 g, 35.7%) was prepared from the reaction of *p*-nitrophenol (15 g) with propionyl chloride (18.6 g) in nitrobenzene (150 ml) in the presence of anhydrous aluminium chloride (41 g) as catalyst. Recrystallization from methanol gave colorless short needles, mp 94.5—95.0 °C. IR (KBr): ν_{max} 3070, 1640 (CO), 1615, 1576, 1510 and 1338 (NO_2), 825 cm^{-1} (two adjacent aromatic hydrogen atoms). Found: C, 55.38; H, 4.71%. Calcd for $C_9H_9NO_4$: C, 55.38; H, 4.64%.

*Ethyl 4-Nitro-2-propionylphenoxyacetate (**6i**).* In the same manner as has been described for **6e**, **6i** (12.3 g, 63.4%) was prepared from **5i** (13.5 g). Recrystallization from aqueous ethanol gave colorless short needles, mp 58—59 °C. IR (KBr): ν_{max} 1730 (-CO_2-), 1682 (CO), 1510 and 1334 (NO_2), 833 cm^{-1} (two adjacent aromatic hydrogen atoms). Found: C, 55.59; H, 5.37%. Calcd for $C_{13}H_{15}NO_6$: C, 55.51; H, 5.38%.

*4-Nitro-2-propionylphenoxyacetic Acid (**1i**).* Acid **1i** (8.1 g, 90%) was obtained from **6i** (10 g) in the same way as described for the preparation of **1e**. Recrystallization of **1i** from benzene-acetone gave colorless plates, mp 128—129 °C. IR (KBr): ν_{max} 1752 and 1720 (CO_2H), 1663 (CO), 1522 and 1345 (NO_2), 834 cm^{-1} (two adjacent aromatic hydrogen atoms). Found: C, 52.27; H, 4.41%. Calcd for $C_{11}H_{11}NO_6$: C, 52.17; H, 4.37%.

*2'-Hydroxy-5'-nitroisobutyrophenone (**5j**).* By the modified method of Joshi[16], **5j** (2.7 g, 8.6%) was prepared from the reaction of *p*-nitrophenol (15 g) with isobutyryl chloride (21.3 g) in nitrobenzene (170 ml) in the presence of anhydrous aluminium chloride (41 g) as a catalyst. Recrystallization from methanol gave pale yellow short needles, mp 74.0—74.5 °C. IR (KBr): ν_{max} 3080, 1636 (CO), 1615, 1575, 1506 and 1334 (NO_2), 821 cm^{-1} (two adjacent aromatic hydrogen atoms). NMR (CD_3COCD_3): δ=1.28 (6H, d, J=7.5 Hz, -$CH(C\underline{H}_3)_2$), 3.95 (1H, m, J= 7.5 Hz, -$C\underline{H}(CH_3)_2$), 7.20 (1H, d, J=10 Hz, C_3-H), 8.42 (1H, dd, J=10 and 2.5 Hz, C_4-H), 8.86 (1H, d, J=2.5 Hz, C_6-H). Found: C, 57.37; H, 5.34%. Calcd for $C_{10}H_{11}NO_4$: C, 57.41; H, 5.29%.

*Ethyl 2-Isobutyryl-4-nitrophenoxyacetate (**6j**).* In the same manner as has been described for **6e**, **6j** (4.5 g, 77.7%) was prepared from **5j** (4.1 g). Recrystallization of **6j** from ethanol gave colorless short needles, mp 58—60 °C. IR (KBr): ν_{max} 1730 (-CO_2-), 1667 (CO), 1510 and 1334 cm^{-1} (NO_2). Found: C, 57.01; H, 5.87%. Calcd for $C_{14}H_{17}NO_6$: C, 56.94; H, 5.80%.

*2-Isobutyryl-4-nitrophenoxyacetic Acid (**1j**).* Acid **1j** (5.8 g, 95%) was obtained from **6j** (6.8 g) in the same way as described for the preparation of **1e**. Recrystallization of **1j** from benzene gave colorless short needles, mp 108—109 °C. IR (KBr): ν_{max} 1739 (CO_2H), 1667 (CO), 1515 and 1334 (NO_2), 910 (CO_2H), 826 cm^{-1} (two adjacent aromatic hydrogen atoms). Found: C, 53.86; H, 4.96%. Calcd for $C_{12}H_{13}NO_6$: C, 53.93; H, 4.90%.

*Preparation of Standard Compounds (**2a—d**, **2f,g**, **7a—d**, and **7f,g**) for Gas Chromatography Analyses.* 5-Methoxy-3-methylbenzofuran (**2a**) was prepared by Whalley's method,[5] **2c** by Rosseels' method,[6] **2d** by Deorha's method,[7] **2f** by Auwer's method,[19] and **2g** by Tanaka's method.[20] methyl ester **7a** was prepared by methylation of **3a** with diazomethane in ether.[5]

*3,5-Dimethylbenzofuran (**2b**).* A mixture of **1b** (5.0 g), anhydrous sodium acetate (13.0 g), and acetic anhydride (85.0 ml) was heated at 110±1 °C for 3 h. After cooling, the reaction mixture was poured into 200 ml of water and stirred for 1 h and then extracted with 300 ml of ether. The ethereal solution was washed with 3% potassium carbonate solution (40 ml×3), with water (40 ml×3), and dried over anhydrous sodium sulfate. Ether was removed by evaporation and the residue was distilled under reduced

pressure to give 2.74 g (72%) of **2b** as colorless oil, bp 83 °C at 12 Torr.† IR (neat): ν_{max} 3120, 3022, 2950, 2923, 1580, 1450, 1289, 868 (furan ring), 804 cm^{-1} (two adjacent aromatic hydrogen atoms). Found: C, 82.03; H, 6.96%. Calcd for $C_{10}H_{10}O$: C, 82.16; H, 6.89%.

*Methyl 3,5-Dimethyl-2-benzofurancarboxylate (**7b**).* Diazomethane in ether was added to an ethereal solution of **3b**[21] (1 g) until the reaction mixture turned yellow and the solution was allowed to stand at room temperature for 20 min. The residue (1.2 g) obtained upon evaporation of ether was recrystallized from aqueous methanol to give 0.7 g (84%) of **7b** as colorless short needles, mp 50—51 °C. IR (KBr): ν_{max} 1713 ($-CO_2-$), 844 (furan ring), 808 cm^{-1} (two adjacent aromatic hydrogen atoms). Found: C, 70.45; H, 5.94%. Calcd for $C_{12}H_{12}O_3$: C, 70.57; H, 5.92%.

*Methyl 3-Methyl-2-benzofurancarboxylate (**7c**).* In the same manner as has been described for **7b**, **7c** (3.82 g, 93%) was prepared from **3c**[22] (3.34 g). Recrystallization of **7c** from methanol gave colorless short needles, mp 69—70 °C. IR (KBr): ν_{max} 1705 ($-CO_2-$), 837 (furan ring), 763 cm^{-1} (four adjacent aromatic hydrogen atoms). Found: C, 69.41; H, 5.38%. Calcd for $C_{11}H_{10}O_3$: C, 69.46; H, 5.29%.

*Methyl 5-Chloro-3-methyl-2-benzofurancarboxylate (**7d**).* In the same procedure as the preparation of **7b**, ester **7d** (1 g, 94%) was obtained from **3d**[7] (1 g). Recrystallization of **7d** from methanol gave colorless short needles, mp 95.0—95.8 °C. IR (KBr): ν_{max} 1708 ($-CO_2-$), 813 cm^{-1} (two adjacent aromatic hydrogen atoms). Found: C, 58.89; H, 4.15%. Calcd for $C_{11}H_9ClO_3$: C, 58.81; H, 4.03%.

*Ethyl 5-Methyl-2-benzofurancarboxylate (**8f**).* A mixture of 5-methylsalicylaldehyde[17] (**5f**) (3 g), ethyl bromoacetate (10 g), and anhydrous potassium carbonate (12 g) was heated at 140 °C for 6 h. After cooling, acetone (100 ml) was added to the reaction mixture and the insoluble salts were removed by filtration. The residue obtained upon evaporation of acetone was purified by column chromatography and eluted with benzene to give crude **8f** (3.6 g, 80%). Recrystallization from hexane gave colorless short needles, mp 41—42 °C. IR (KBr): ν_{max} 3003, 2950, 2880, 1728 ($-CO_2-$), 1297, 1214, 820 cm^{-1} (two adjacent aromatic hydrogen atoms). Found: C, 70.52; H, 5.92%. Calcd for $C_{12}H_{12}O_3$: C, 70.57; H, 5.92%.

*5-Methyl-2-benzofurancarboxylic Acid (**3f**).* A mixture of **8f** (2.2 g) and 20% potassium hydroxide solution (25 ml) was refluxed for 1 h. After cooling, the reaction mixture was acidified with 6 M hydrochloric acid and the precipitates were filtered, washed with cold water, and dried under vacuum to give crude **3f** (1.8 g, 94.8%). Recrystallization from acetone gave colorless plates, mp 237—238 °C (lit,[23] mp 237 °C). IR (KBr): ν_{max} 1693 (CO_2H), 1623, 1585, 921 (CO_2H), 827 cm^{-1} (two adjacent aromatic hydrogen atoms), (Found: C, 68.29; H, 4.67%).

*Methyl 5-Methyl-2-benzofurancarboxylate (**7f**).* In the same procedure as the preparation of **7b**, ester **7f** (1.4 g, 87.5%) was obtained from **3f** (1.5 g). Recrystallization of **7f** from aqueous methanol gave colorless short needles, mp 58.5—59.5 °C. IR (KBr): ν_{max} 1723 ($-CO_2-$), 808 cm^{-1} (two adjacent aromatic hydrogen atoms). Found: C, 69.38; H, 5.34%. Calcd for $C_{11}H_{10}O_3$: C, 69.47; H, 5.29%.

*2-Benzofurancarboxylic Acid (**3g**).* A mixture of salicylaldehyde (**5g**) (10 g), ethyl bromoacetate (54.7 g), and anhydrous potassium carbonate (45 g) was heated at 100 °C for 1.5 h then at 140 °C for 4.5 h. After cooling, water (300 ml) was added to the reaction mixture, which was extracted with ether. The ethereal solution was washed with water, dried over anhydrous sodium sulfate, and concentrated by evaporation. The residue was hydrolyzed without purification as has been described for **3f** to give 7.4 g of **3g** in a 55.7% yield. Recrystallization from aqueous acetone gave colorless plates, mp 193.0—193.5 °C (lit,[20] mp 192—193 °C). IR (KBr): ν_{max} 1680 and 943 (CO_2H), 745 cm^{-1} (four adjacent aromatic hydrogen atoms), (Found: C, 66.77; H, 3.93%).

*Methyl 2-Benzofurancarboxylate (**7g**).* By the same procedure as the preparation of **7b**, ester **7g** (0.8 g, 82%) was prepared from **3g** (0.9 g). Recrystallization from aqueous methanol gave colorless short needles, mp 52—53 °C. IR (KBr): ν_{max} 1732 ($-CO_2-$), 758 cm^{-1} (four adjacent aromatic hydrogen atoms). Found: C, 68.36; H, 4.64%. Calcd for $C_{10}H_8O_3$: C, 68.17; H, 4.57%.

The authors wish to thank to Mr. Hideo Saisu for infrared analyses, to Mr. Takao Ohno for nuclear magnetic resonance analyses, and to Mr. Yoshiaki Takahashi for the elemental analyses.

† 1 Torr = 133.322 Pa.

References

1) A. Rössing, *Ber.*, **17**, 2998 (1884).
2) F. M. Dean, P. Halewood, S. Mongkolsuk, A. Robertson, *J. Chem. Soc.*, **1953**, 1250; L. R. Worden, K. D. Kaufman, J. A. Weise, and T. K. Schuof, *J. Org. Chem.*, **34**, 2311 (1969).
3) A. W. Burgstahler and L. R. Worden, *Org. Synth.* Coll. Vol. V, 251 (1973).
4) T. Suzuki, T. Horaguchi, and T. Shimizu, *Bull. of Nippon Dental University General Education*, **11**, 232 (1982).
5) W. B. Whalley, *J. Chem. Soc.*, **1953**, 3479.
6) G. Rosseels, J. Matteazzi, M. Claret, and M. Prost, *Ing. Chim. (Brusseles)*, **53**, 37 (1971); *Chem. Abstr.*, **77**, 5258q (1972).
7) D. S. Deorha and P. Gupta, *Indian J. Chem.*, **2**, 459 (1964).
8) H. Dumont and St. v. Kostanecki, *Ber.*, **42**, 912 (1909).
9) W. A. Jacobs and M. Heiderberger, *J. Am. Chem. Soc.*, **39**, 2212 (1917).
10) P. Cagniant and D. Cagniant, "Advances in Heterocyclic Chemistry," ed by A. R. Katritzky, A. J. Boulton, Academic Press, London (1975), Vol. 18, p. 337; T. Matsumoto and K. Fukui, *Bull. Chem. Soc. Jpn.*, **30**, 3 (1957); G. N. Walker and R. T. Smith, *J. Org. Chem.*, **36**, 305 (1971); S. Tanaka, *Nippon Kagaku Zasshi*, **72**, 307 (1951).
11) S. Kawai, T. Nakamura, and N. Sugiyama, *Proc. Imp. Acad. (Tokyo)*, **15**, 45 (1939); S. Kawai, T. Nakamura, and M. Yoshida, *Ber.*, **73B**, 581 (1940).
12) T. Horaguchi, H. Narita, and T. Suzuki, *Bull. Chem. Soc. Jpn.*, **56**, 184 (1983).
13) F. G. Bordwell and R. J. Kern, *J. Am. Chem. Soc.*, **77**, 1141 (1955); C. H. Depuy and R. W. King, *Chem. Rev.*, **60**, 431 (1960); H. R. Nace, "Organic Reaction," ed by A. C. Cope, R. Adams, T. L. Cairns, A. H. Blatt, D. Y. Curtin, V. Boekelheide, and C. Niemann, John Wiley & Sons, New York (1962), Vol. 12, p. 57; M. P. Cooke, Jr., and J. L. Coke, *J. Am. Chem. Soc.* **90**, 5556 (1968).
14) H. Erlenmeyer, *Helv. Chim. Acta.*, **31**, 75 (1948).
15) K. W. Rosenmund and W. Schnurr, *Justus Liebigs*

Ann. Chem., **460**, 56 (1928).
16) S. S. Joshi and H. Singh, *J. Am. Chem. Soc.*, **76**, 4993 (1954).
17) F. Tiemann and C. Schotten, *Ber.*, **11**, 767 (1878).
18) K. v. Auwers, *Justus Liebigs Ann. Chem.*, **393**, 365 (1912).
19) K. v. Auwers, *Justus Liebigs Ann. Chem.*, **408**, 274 (1915).
20) S. Tanaka, *J. Am. Chem. Soc.*, **73**, 872 (1951).
21) T. Horaguchi, T. Shimizu, and T. Suzuki, *Bull. Chem. Soc. Jpn.*, **48**, 1249 (1975).
22) W. R. Boehme, *Org. Synth.* Coll. Vol. IV, 590 (1963).
23) G. Pappalardo, F. Duro, *Boll. Sci. Chim. Ind. Bologna.*, **10**, 168 (1952); *Chem. Abstr.*, **49**, 1000f (1955).

Product Distribution in Degradation of Polypropylene over Silica-Alumina and CaX Zeolite Catalysts

Yoshio UEMICHI,* Yasunori KASHIWAYA, Masaya TSUKIDATE, Akimi AYAME, and Hisao KANOH

Department of Industrial Chemistry, Muroran Institute of Technology, Mizumoto-cho, Muroran 050

(Received March 14, 1983)

The composition of degradation products of polypropylene, especially liquid fraction, formed over silica-alumina and CaX zeolite catalysts was investigated extensively. The catalysts gave almost the same product distribution as a function of carbon number at the initial stages of the reaction. The liquid fractions were rich in the same isoalkanes and aromatics as those contained in the gasoline fraction. Most of the isoalkanes were methyl-branched, while the aromatics consisted mainly of those with one or more methyl groups. The catalytic degradations involved extensive aromatization, isomerization and hydrogen transfer as secondary reactions. The difference in catalytic behaviors between silica-alumina and CaX was most remarkable in coke deposition on the catalysts and more deposition on CaX led to greater saturation of the products. The H/C ratio of the products was regarded as a good measure for the degree of coke formation on the catalyst surfaces.

In recent years attention has been paid to the reuse of plastic wastes from the viewpoint of energy diversification, necessitating the development of processes capable of recovery as chemical resources or fuel. As the thermal degradation products of polypropylene are distributed in a wide range of carbon numbers,[1,2] the utility value of the products recovered is low, so that upgrading will be required for efficient utilization of them. On the other hand, a selective recovery of useful fractions is possible in catalytic degradation and further the product distribution is controlled more readily than the case of thermal degradation. Thus, the catalytic procedures are superior to thermal methods provided that the products are intended for resources. However, only a few investigation have been reported on catalytic degradation of polypropylene.[3-5] A great deal of emphasis is placed on the identification of the products in thermal degradation of polypropylene.[6-9] Similarly, a detailed analysis of the products is undoubted to be important also in catalytic degradation, but there has been no report on an extensive analysis of degradation products of polypropylene in the presence of acid catalysts because of complexity of the product composition. The authors have already reported the catalytic degradations of polypropylene over silica-alumina and CaX zeolite,[3] which were aimed at the formation of gaseous fractions so that the liquid fractions were characterized by gross properties such as average molecular weight, iodine number and infrared spectrum. However, it is expected that a survey of the composition of liquid fractions is very informative for clarifying the degradation mechanism, and further the survey will be a significant research for efficient utilization of the products.

From the point of view described above, the purpose of this study is to identify the degradation products, especially liquid fractions, of polypropylene over silica-alumina and CaX zeolite catalysts and to discuss the catalytic degradation mechanism.

Experimental

Apparatus and Procedures. The experiments were conducted in the same fixed-bed flow system, except that a water-cooler was connected at the outlet of a separator, as in the previous study.[3] Polypropylene sample was melted in a melter at 240 °C under an atmosphere of nitrogen. The melt of polypropylene was introduced into a reactor through a capillary of inside diameter of 2 mm. The feed rate of polypropylene was controlled by both the temperature of the capillary and the pressure of the nitrogen in the melter. They were kept constant through a run at given levels in the range of 280—320 °C and 0.3—0.4 kg/cm^2 G, respectively. Liquid products were collected in the separator at 20 min intervals. Because of high activities of the catalysts, the relatively low temperature of 477 °C was employed for catalytic degradation, rather than 526 °C which was used for the thermal degradation.

Materials. Isotactic polypropylene and silica-alumina and CaX catalysts were the same as those used in the previous study.[3] The average molecular weight of the polypropylene was 1.6×10^5 and its tacticity was characterized by pyrolysis-gas chromatographic method.[10] The catalysts were calcined before use in the air at 550 °C for 3 h and 3.0 g of each catalyst was used in a run. A reactor packed with glass beads of 3.5 mm in diameter was used in thermal degradation.

Analysis. The degradation products were analyzed by gas chromatography. Three columns, VZ-7 (5 m×3 mm i.d.), active carbon (1 m×3 mm i.d.) and OV-101 (50 m×0.28 mm i.d.), were used for the separation of components. Two methods were employed as supplementary techniques for the identification of the products. One was hydrogenation of alkenes using a column of supported palladium catalyst. The other was selective absorption of alkenes and aromatics using an absorbent column of supported mercury(II) perchlorate. The details of the two methods have been described elsewhere.[11] A splitter was independently held at 250 °C to attain reproducible splitting for the degradation products with a wide range of volatility. The peaks in a chromatogram were identified by co-injection of the products with standard materials. When pure materials were not available, the identification was based on a linear relation between boiling point and retention index. From a quantitative analysis using methylcyclohexane as internal standard, the products were found to contain nondetectable fractions under the gas chromatographic condition, and so they were summarized as high-boiling-point products (H.B.P).

Results and Discussion

The composition of the degradation products of

Table 1. Distribution of catalytic degradation products[a]

Carbon No.	Silica-Alumina					CaX				
	Normal alkanes	Iso-alkanes	Alkenes	Aromatics	Total	Normal alkanes	Iso-alkanes	Alkenes	Aromatics	Total
H_2					0.1 (tr)[c]					tr (tr)[d]
1	0.8				0.8 (0.4)	0.9				0.9 (0.9)
2	0.4		0.5		0.9 (0.5)	0.9		0.5		1.4 (0.8)
3	1.6		9.6		11.2 (7.8)	2.6		8.3		10.9 (2.8)
4	1.8	13.6	13.1		28.5 (20.1)	3.6	19.1	8.0		30.7 (5.0)
5	1.0	10.0	10.7		21.7 (19.6)	2.1	17.1	3.9		23.1 (7.5)
6	0.4	6.7	6.5	0.3	13.9 (18.7)	1.1	11.4	1.3	0.2	14.0 (6.8)
7	0.1	2.3	2.7	2.9	8.0 (7.9)	0.4	6.0	0.2	1.1	7.7 (7.3)
8	tr[b]	1.3	0.7	3.5	5.5 (4.7)	0.2	2.5		2.3	5.0 (8.3)
9		0.6	0.2	2.0	2.8 (2.6)	0.1	0.9		1.8	2.8 (8.2)
10		0.2		1.4	1.6 (1.4)	tr	0.2		0.6	0.8 (2.0)
11		0.1		0.2	0.3 (0.1)		0.1		0.1	0.2 (1.4)
12		tr		0.3	0.3 (tr)		tr		tr	tr (0.9)
13—16					0.5 (tr)					(2.0)
H.B.P					3.8 (16.1)					2.6 (46.2)
Total	6.1	34.8	44.0	10.6	99.9 (99.9)	11.9	57.3	22.2	6.1	100.1 (99.9)

a) Distribution (wt%) obtained at the initial stages of the reaction. Reaction temperature: 477 °C, catalyst weight (W): 3.0 g, feed rate (F): 0.150 g-PP min^{-1} (PP) polypropylene. b) Trace amount of less than 0.05%. c) Distribution at 165 min after starting reaction. d) Distribution at 130 min.

polypropylene was simplified by the selective absorption of alkenes and aromatics, which resulted in a chromatogram consisting of saturated hydrocarbons only. The absorbed alkenes and aromatics were distinguished each other by the hydrogenation over palladium catalyst. The hydrogenation caused a transformation of alkenes to corresponding alkanes, although aromatics except for naphthalenes were not hydrogenated. Thus, the degradation products were classified into five groups of hydrogen, normal alkanes, isoalkanes, alkenes and aromatics. However, most of the alkenes were difficult to identify because of many possible isomers. The product distributions as a function of carbon number at the initial stages of the reaction are shown in Table 1. Both catalysts gave essentially the same distribution and the relative yield of C_3—C_6 fractions was very high. Isoalkanes were preferentially produced in C_4—C_6 fractions. The selectivity to aromatics became higher, while that to alkenes decreased, as carbon number increased. The products formed over CaX were more saturated than those over silica-alumina. The difference in the degree of saturation would be attributed to the extent of hydrogen transfer reaction. This will be described later. The normal alkane content was always smaller than that of isoalkanes and, as carbon number increased, the content of multibranched alkanes increased in proportion to the number of possible isomers. Figure 1 well illustrates these facts for the products formed over silica-alumina. Here, most of the branchings were methyl groups. CaX catalyst also gave the same distribution of alkane isomers. Further, detailed compositions of aromatics are shown in Table 2. Toluene, xylenes and trimethylbenzenes were the main aromatics. The aromatics with ethyl group were minor products and those with C_3 or C_4 alkyl group were little produced. Therefore, C_{10} aromatics in Table 2 would correspond

Table 2. Composition of aromatics[a]

Component	Silica-Alumina	CaX
Benzene	3.5	5.3
Toluene	31.6	27.0
Ethylbenzene	2.1	2.8
Xylenes	32.0	36.5
Ethyltoluenes	3.6	7.1
Trimethylbenzenes	13.5	15.0
Tetramethylbenzenes	3.8	1.8
C_{10} Aromatics	6.7	4.0
Methylnaphthalenes	1.5	0.3
Dimethylnaphthalenes	1.8	0.3

a) Composition: mol%, reaction conditions: See Table 1.

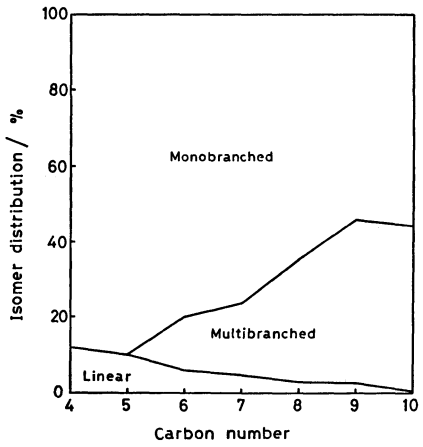

Fig. 1. Distribution of alkane isomers formed over silica-alumina.
Reaction conditions: See Table 1.

Table 3. Comparison between isomer distribution and thermodynamic equilibrium

Type	Component	Isomer distribution[a]/%		Equilibrium[b]/%
		Silica-Alumina	CaX	
Alkanes	2,2-Dimethylbutane	0	0	21
	2,3-Dimethylbutane	14	12	10
	2-Methylpentane	47	49	28
	3-Methylpentane	33	30	17
	Hexane	6	9	24
Alkenes	3-Methyl-1-butene	4	4	4
	1-Pentene	5	5	5
	2-Methyl-1-butene	22	22	27
	trans-2-Pentene	15	14	14
	cis-2-Pentene	8	8	9
	2-Methyl-2-butene	46	47	41
Aromatics	1,3,5-Trimethylbenzene	24	24	23
	1,2,4-Trimethylbenzene	64	64	66
	1,2,3-Trimethylbenzene	12	12	11

a) Reaction conditions: See Table 1. b) 470 °C

Table 4. Distribution of thermal degradation products[a]

Carbon No.	Normal alkanes	Isoalkanes	Alkenes	Total	Main components
H_2				tr[b]	
1	1.0			1.0	Methane
2	2.1		1.0	3.1	Ethane
3	0.4		8.3	8.7	Propylene
4			3.5	3.5	Isobutylene
5	4.0		1.5	5.5	Pentane
6		0.3	4.8	5.1	2-Methyl-1-pentene
7			2.5	2.5	2,4-Dimethyl-1-pentene
8		0.8	1.3	2.1	4-Methylheptane
9		0.5	11.4	11.9	2,4-Dimethyl-1-heptene
10			1.0	1.0	2,4,6-Trimethyl-1-heptene
11		0.4	0.5	0.9	4,6-Dimethylnonanes (2)[c]
12			1.7	1.7	2,4,6-Trimethyl-1-nonenes (2)
13			0.8	0.8	2,4,6,8-Tetramethyl-1-nonenes (2)
14		0.2	0.2	0.4	4,6,8-Trimethylundecanes (3)
15			3.0	3.0	2,4,6,8-Tetramethyl-1-undecenes (4)
16			1.1	1.1	2,4,6,8,10-Pentamethyl-1-undecenes (3)
17—24			5.1	5.1	
H.B.P				42.9	
Total	7.5	2.2	47.7	100.3	

a) Distribution: wt%, reaction temperature: 526 °C, feed rate: 0.116 g-PP min^{-1}. b) Trace amount of less than 0.05%. c) The number of diastereomeric isomer.

to those with methyl and/or ethyl groups.

In general, isomer distribution is strongly dependent on thermodynamics. Table 3 shows the comparison between isomer distribution and thermodynamic equilibrium.[12–14] Alkene and aromatic isomers were distributed approximately in accord with the corresponding thermodynamic equilibria, whereas the distribution of alkane isomers was entirely different and the content of branched alkanes exceeded the possible thermodynamic equilibrium concentration. These results indicate that equilibria of alkene and aromatic isomers are more rapidly attained than an equilibrium among alkanes. Although each component of alkenes larger than C_5 fraction was not identified, it is expected that alkenes show a higher ratio of linear to branched hydrocarbons than do the alkanes of the same carbon number. This is because of faster saturation of branched alkenes than linear alkenes.[15]

As mentioned above, the liquid products from catalytic degradation of polypropylene contained large amount of isoalkanes and aromatics which constitute the gasoline fraction.[16] The formation of a gasoline fraction seems to be advantageous for a utilization of the products. Further, the composition of the catalytic degradation products of polypropylene over silica-alumina resembled that of polyethylene.[11] A

TABLE 5. EFFECTS OF CONTACT TIME AND REACTION TIME ON COMPOSITION OF THE PRODUCTS FORMED OVER SILICA-ALUMINA[a]

Component	Contact time/g-cat min g-PP^{-1}						
	20.0				26.2	34.7	82.5
	10 min[b]	45	126	165	10 min	10 min	10 min
Hydrogen	3.2	2.6	2.2	2.1	5.1	4.4	5.6
Normal alkanes	9.8	7.8	6.4	6.2	11.7	16.1	20.9
Isoalkanes	32.0	19.4	13.4	11.9	32.2	38.2	47.2
Alkenes	48.4	67.3	76.1	77.4	46.5	35.8	19.9
Aromatics	6.6	2.9	2.0	1.7	4.5	5.0	6.5
H/C ratio of products	2.12	2.07	2.05	2.03	2.18	2.21	2.27
Molar ratio of aromatics to aliphatics (C_6-C_{12} fractions)	0.41				0.49	0.47	0.84

a) Composition: mol%, reaction temperature: 477 °C. b) Reaction time.

similar result is probably available over CaX.

Since polypropylene is presumably decomposed thermally to some extent under conditions of catalytic degradation, the characterization of the products in thermal degradation is of great significance to clarify the catalytic degradation mechanism. The product distribution in thermal degradation is shown in Table 4. The composition of the liquid fractions was very complicated consisting of about ninety components of C_5—C_{24} fractions. The identification of each component was further complicated because of many diastereomeric isomers derived from methyl branchings along the polymer chain. However, the chromatogram was simplified after hydrogenation, because three peaks of alkane, alkamonoene and alkadiene with the same carbon skeleton became a single peak of alkane. So, the liquid products were identified from the analysis of the hydrogenated products according to the method by Sugimura *et al.*[10] Main products were propylene, 2-methyl-1-pentene (propylene dimer), 2,4-dimethyl-1-heptene (trimer), 2,4,6-trimethyl-1-nonenes (tetramers consisting of two diastereomeric isomers), and 2,4,6,8-tetramethyl-1-undecenes (pentamers of four diastereomeric isomers), the formations of which have been explained in terms of a radical mechanism involving intramolecular radical transfer to the tertiary carbon atoms in the secondary radicals and subsequent β-scission.[8] This product distribution was approximately in line with the results by other investigators.[6-8] The saturated hydrocarbons in the liquid fractions were pentane, 2-methylpentane, 4-methylheptane, and 4,6-dimethylnonanes (two diastereomeric isomers), but these hydrocarbons except for pentane were minor products. From the results obtained here, the thermal degradation of polypropylene is characterized as follows: The C–C bonds of the chain are preferentially broken and structual isomerization or demethylation of branchings hardly occurs. Most of the products are 1-alkenes. Monomethyl-branched hydrocarbons are limited to isobutylene, 2-methylpentane, 2-methyl-1-pentene and 4-methylheptane. The products of carbon number greater than 8 are branched hydrocarbons with two or more methyl branchings at the even-numbered carbons. Linear hydrocarbon except for C_1—C_3 fragments is pentane only.

As evident from the comparison between catalytic and thermal degradation products, the formation in a large quantity of aromatics and monomethyl-branched hydrocarbons, especially with branchings at the odd-numbered carbons, and higher degree of saturation of the products are remarkable in catalytic degradations. From these characteristics, the catalytic degradation of polypropylene can be considered to proceed to a large extent through aromatization, isomerization and hydrogen transfer reactions together with the C–C bond scission of the chain, and the tertiary carbonium ions which are readily formed because of methyl branchings along the polymer chain would be predominant intermediates.[4] If isomerization or aromatization hardly occurs, the hydrocarbons produced by β-scission of the tertiary carbonium ions should be the same types as those by β-scission of the tertiary radicals in thermal degradation, and further if no hydrogen transfer reaction occurs, most of the products should be alkenes. However, the difference in product distribution of catalytic and thermal degradations would indicate that such fragments listed in Table 4 as main components further isomerize, cyclize or are saturated in catalytic degradation, resulting in the formation of aromatics and monomethyl alkanes. At the present stage of this study, however, a detailed mechanism is not clear.

The effects of contact time and reaction time on the composition of the products obtained over silica-alumina are shown in Table 5. A longer contact time promoted further degradations of liquid fractions to give the increase in the relative yield of gaseous products. The further degradations would be attributed to those of aliphatic hydrocarbons, and aromatics would hardly undergo further degradation, because the amount of aromatics and their composition changed very little with contact time. This low reactivity of aromatics with methyl groups is readily expected from

their great stability. Therefore, the increase in the ratio of aromatics to aliphatics in C_6—C_{12} fractions with contact time is a reasonable result.

The product composition was also dependent on reaction time. More alkenes were produced (Table 5) and the distribution of the products shifted to higher carbon numbers (Table 1) as increasing reaction time, *i.e.*, progressing deactivation of silica-alumina catalyst. Even after 3 h, however, the products were concentrated on smaller carbon numbers compared to those obtained by thermal degradation. Similar results were obtained over CaX, but the catalyst deactivated with reaction time more rapidly than silica-alumina, as can be seen from the larger shift in product distribution shown in Table 1. Over both catalysts, high-boiling-point products were formed in increasing amount as reaction time lengthened, but the fractions of carbon number from 16 to 24 were absent in significant amounts. The gas chromatographic conditions used in the present study were enough to detect quantitatively the fractions of carbon number up to about 24. Therefore, the high-boiling-point products were estimated to be hydrocarbons with carbon number of at least greater than 24. Further, high viscous products showing wax-like aspect at room temperature were obtained when CaX catalyst was largely deactivated, suggesting the presence of such hydrocarbons with high molecular weight as estimated above. Although there is no evidence in the results obtained here for determining whether the degradation of polypropylene in the presence of the catalysts is initiated catalytically or thermally, the thermal initiation reaction would undoubtedly occur at reaction temperature of 477 °C and the catalytic initiation is also likely to occur. Kodaira *et al.*[4] showed by thermogravimetric analysis that polypropylene was decomposed at lower temperature by 50—100 °C in the presence of natural zeolite than that in the absence of the catalyst. This would suggest the participation of the zeolite catalyst in the initiation reaction and probably the catalytic initiation reaction takes place at external surface or neighborhood of pore mouth of the catalyst. In this study, therefore, it seems reasonable to assume that polypropylene is first decomposed thermally or catalytically to produce fragments of various sizes and then smaller fragments, which are able to diffuse into pores of the catalysts, selectively proceed to catalytic degradation, whereas larger fragments which can not diffuse into catalyst pores turn out as high-boiling-point products.

As described above, contact time and reaction time had large effects on alkene content, which was expected to be closely associated with coke deposition, and so the amount of coke deposited on catalyst was determined in each series of experiments by measuring the increase in catalyst weight. As is known commonly in catalytic cracking reaction, the relation between the weight percent of coke on catalyst, C, and reaction time, t,[17] is given as follows:

$$C = at^n,$$

where a and n are constant. The results of the present experiments using silica-alumina and CaX catalysts are shown in Fig. 2. The deposition of coke on silica-alumina followed the above relation. On the other hand, the relation in the case of CaX was satisfied only during the first 50 min on stream and after about 100 min the coke formation was substantially stopped. Figure 3 shows the dependence of the rate of coke formation on reaction time. Coke formation was extremely rapid in the initial reaction stages, at which CaX had nearly twice the rate of coke formation compared with silica-alumina, but the rate showed a severe decline with reaction time, while the decline was much less severe on silica-alumina. The amount of coke deposited during 3 h was nearly independent of feed rate over both catalysts. This observation means that the weight percent of coke on feed increases with contact time, that is, coke is more susceptible to deposition under a condition of longer contact time to produce less amount of alkenes.

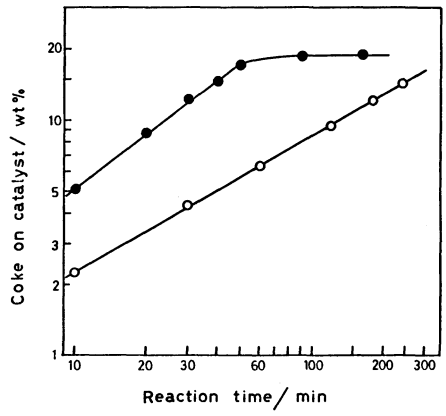

Fig. 2. Relation between coke deposition and reaction time at 477 °C.
○: Silica-alumina at $F=0.116$ g-PP min^{-1}, ●: CaX at $F=0.122$ g-PP min^{-1}.

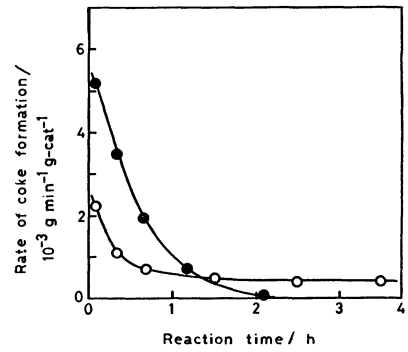

Fig. 3. Variation in rate of coke formation with reaction time.
Reaction conditions: See Fig. 2. ○: Silica-alumina, ●: CaX.

In this study, it was possible to evaluate the H/C ratio of the products. As the H/C ratio of polypropylene, $(C_3H_6)_n$, is 2, it should be also 2 for total degradation products provided that coke deposition is negligibly small. The ratio, in fact, was 2.03 in the thermal degradation. A slight deviation from the theoretical value of 2 would be due to the assumption that all of alkenes and high-boiling-point products were alkamonoenes. If some alkadienes are contained in

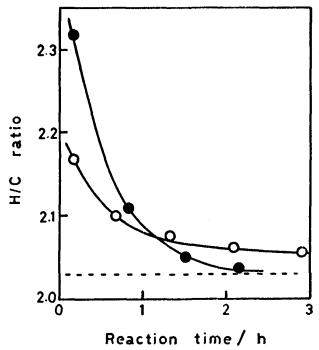

Fig. 4. Dependence of H/C ratio of products on reaction time.
Reaction conditions: See Fig. 2. ○: Silica-alumina, ●: CaX. ----: Level in thermal degradation under the same conditions as Table 4.

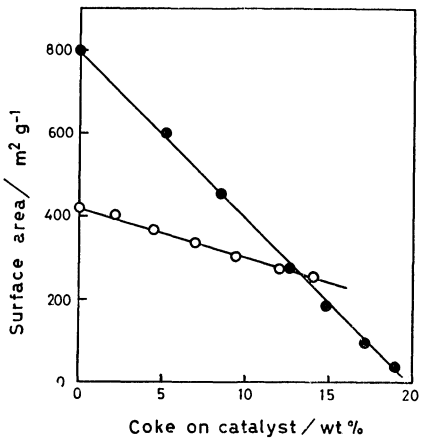

Fig. 5. Effect of coke on surface area of catalyst.
Reaction conditions: See Fig. 2. ○: Silica-alumina, ●: CaX.

the thermal degradation products, and this can probably be so, the ratio approaches 2. On the other hand, the H/C ratios of catalytic degradation products were greater than 2 and reduced with reaction time as shown in Fig.4. The curves in the figure resembled those of the rate of coke deposition (Fig. 3) in shape. When the rate over CaX became nearly zero in about 2 h, the ratio reached to the level of the products by thermal degradation. Therefore, the reduction of the H/C ratio with increasing reaction time is concluded to result from the decrease in coke deposition since the supply of hydrogen from a coke precursor to unsaturated molecules, *i.e.*, hydrogen transfer, leads the H/C ratio greater than 2. The hydrogen transfer occurs also in aromatization process, but it has no effect on the ratio. Thus, the H/C ratio of products will be a good and qualitative indicator for expressing the degree of formation of coke. By taking into account the coke deposition, the effects of contact time and reaction time on alkene content were reasonably explained. As aromatics are much more strongly adsorbed on acid catalysts than more saturated hydrocarbons, it seems reasonable to assume that aromatics, particularly of condensed rings such as naphthalenes, most closely relate to coke deposition.[18,19]

Figure 5 shows that the accumulation of coke exerts its effect by reducing surface area of the catalysts. About 95% loss in surface area was observed at 19 wt% of coke on CaX catalyst. This level of coke deposition would be close to a limiting degree in the reaction conditions. More pronounced reduction in surface area of CaX compared with silica-alumina makes possible to assume that CaX catalyst with smaller pores is susceptible to clogging of its pore structure by coke and consequent elimination of accessible surface. As the clogging disturbs the diffusion of reactants or products, coke itself is a diffusion barrier. This pore clogging may occur more or less on silica-alumina, but apparently it does not occur to the same extent as on CaX. The coke deposition, of course, is dependent on acidic properties of catalyst, but depends also on pore structure. Therefore, it seems clear that the formation of coke has large effect on catalyst diffusivity.

References

1) K. Murata and T. Makino, *Nippon Kagaku Kaishi*, **1975**, 192.
2) H. Nishizaki, M. Sakakibara, K. Yoshida, and K. Endoh, *Nippon Kagaku Kaishi*, **1977**, 1899.
3) Y. Uemichi, A. Ayame, and H. Kanoh, *Nippon Kagaku Kaishi*, **1980**, 1741.
4) I. Kodaira, Z. Osawa, and H. Ando, *Nippon Kagaku Kaishi*, **1977**, 1892.
5) T. Yamaguchi, T. Kamiguchi, T. Ito, S. Ohkita, and T. Goto, *Nippon Kagaku Kaishi*, **1976**, 1171.
6) T. A. Iida, T. Iida, H. Nozaki, and M. Sukigara, *Nippon Kagaku Kaishi*, **1976**, 837.
7) Y. Tsuchiya and K. Sumi, *J. Polym. Sci., Part A-1*, **7**, 1599 (1969).
8) E. Kiran and J. K. Gillham, *J. Appl. Polym. Sci.*, **20**, 2045 (1976).
9) M. Seeger and H. J. Cantow, *Makromol. Chem.*, **176**, 2059 (1975).
10) Y. Sugimura, T. Nagaya, S. Tsuge, T. Murata, and T. Takeda, *Macromolecules*, **13**, 928 (1980).
11) Y. Uemichi, A. Ayame, Y. Kashiwaya, and H. Kanoh, *J. Chromatogr.*, **259**, 69 (1983).
12) F. D. Rossini, E. J. Prosen, and K. S. Pitzer, *J. Res. Nat. Bur. Stand.*, **27**, 529 (1941).
13) J. E. Kilpatrick, E. J. Prosen, K. S. Pitzer, and F. D. Rossini, *J. Res. Nat. Bur. Stand.*, **36**, 559 (1946).
14) S. H. Hastings and D. E. Nicholson, *J. Chem. Eng. Data*, **6**, 1 (1961).
15) H. H. Voge, G. M. Good, and B. S. Greensfelder, *Ind. Eng. Chem.*, **38**, 1033 (1946).
16) M. Nakamura, *J. Jpn. Petrol. Inst.*, **16**, 51 (1973).
17) A. Voorhies, Jr., *Ind. Eng. Chem.*, **37**, 318 (1945).
18) W. G. Appleby, J. W. Gibson, and G. M. Good, *Ind. Eng. Chem., Process Des. Dev.*, **1**, 102 (1962).
19) P. E. Eberly, Jr., C. N. Kimberlin, Jr., W. H. Miller, and H. V. Drushel, *Ind. Eng. Chem., Process Des. Dev.*, **5**, 193 (1966).

Electro-organic Reactions on Organic Electrodes. Part 2.[1] Electrochemical Asymmetric Reduction of Citraconic and Mesaconic Acids on Optically-active Poly(amino acid)-coated Electrodes[2]

Tsutomu NONAKA,* Shigemitsu ABE, and Toshio FUCHIGAMI

Department of Electronic Chemistry, Graduate School at Nagatsuta, Tokyo Institute of Technology, 4259 Nagatsuta, Midori-ku, Yokohama, 222

(Received March 23, 1983)

Influence of a number of electrolytic conditions on the asymmetric yield of methylsuccinic acid (**2**) formed in the electrochemical reduction of citraconic acid (**1**) on poly(amino acid)-coated electrodes was examined. The asymmetric yield was greatly affected by the conditions, while the absolute configuration of an excess enantiomer((*S*)-(−)-**2**) remained unchanged even when a polymer with the reversed configuration of the monomer unit was used. The configuration of the excess enantiomer was also unchanged in the asymmetric reduction of mesaconic acid which is the geometrical isomer of **1**.

Some methods for electrochemical asymmetric reduction of prochiral compounds had been reported, as summarized by Tilborg and Smit.[3] Among the methods, only the use of optically-active alkaloids as an asymmetry-inductor had resulted in high asymmetric yields over 40%.[4,5] Recently, Osa *et al.*[6] have reported a new method for the electrochemical asymmetric reduction: They obtained (*S*)-(+)-2-hexanol in 2—6% asymmetric yields from 2-hexanone using Raney-nickel powder electrodes modified with (*S,S*)-(−)-tartaric acid. More recently, we have found another new method[1]: 43 and 25% asymmetric yields were obtained in the reduction of 2-methylcoumarin and citraconic acid (**1**), respectively, on a poly(L-valine)-coated graphite cathode.

Although a number of studies on polymer-coated electrodes have been recently reported, few papers[7-9] dealing with their electrosynthetic utilization have been published.

In this work, as a part of studies on electrosyntheses of organic compounds using electrodes modified with organic materials, influences of a number of electrolytic conditions on the asymmetric reduction of **1**, its dimethyl ester (**4**), and mesaconic acid (**3**) on optically-active poly(amino acid)-coated electrodes were examined in detail.

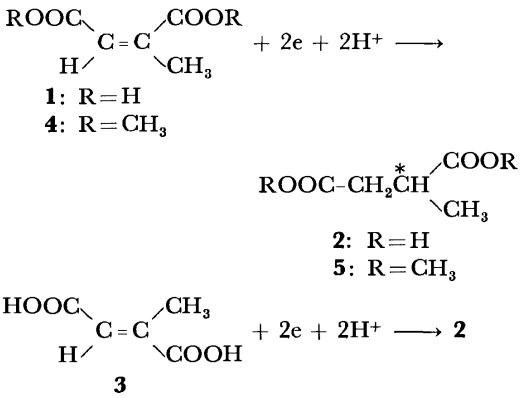

Results and Discussion

*Reduction of Citraconic Acid (**1**) on Graphite Coated with Various Poly(amino acid)s.* Poly(amino acid)s (**6**—**11**) prepared from the corresponding optically-pure amino acids were coated on graphite base electrodes by a dipping method in their solutions. Molecular weights of the poly-amino acids except for poly(L-valine) (**6**) (*ca.* 2000[1]) were unknown.

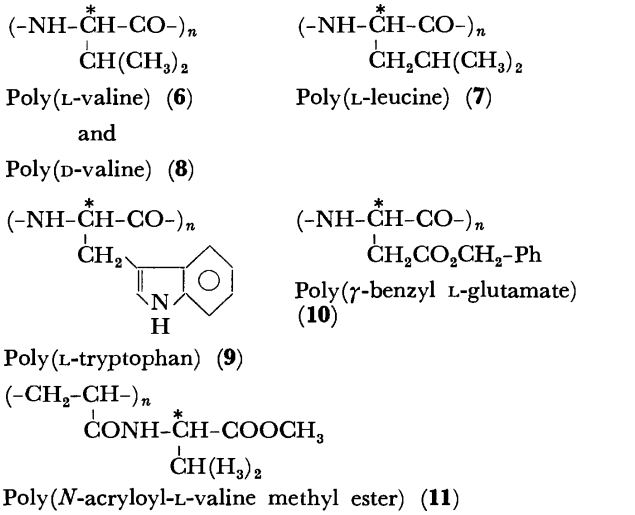

As shown in Fig. 1, the asymmetric yield of methylsuccinic acid (**2**) has a clear relationship to optical rotating powers of the poly(amino acid)s (**6**—**11**), and poly(L-valine) gave the highest asymmetric yield oı 25%. The relationship of the secondary structure(α- and β-forms) of the poly(amino acid)s to the asymmetric yield does not seem to be clear.

Generally, if an asymmetry-inducing reagent with an absolute configuration results in the excess formation of an enantiomer of a compound in an asymmetry-induction reaction, the reagent with the inverted configuration should give another enantiomer inverted configurationaly in the same asymmetric yield under the same conditions. In this viewpoint of the asymmetry induction, it is interesting that both poly(L-valine) (**6**) and poly(D-valine) (**8**), which have the reverse optical rotations and consist of the valine units with the inverted configurations, resulted in the excess formation of the *S*-enantiomer of **2** in different asymmetric yields. This fact suggests that the asymmetry of **2** is induced by the chirality of not only the valine monomer units but also the whole structures of the poly-valines. More generally this should be regarded as one of polymer effects.[10] Electrochemical asymmetric reduction using optically-active polymer-coated

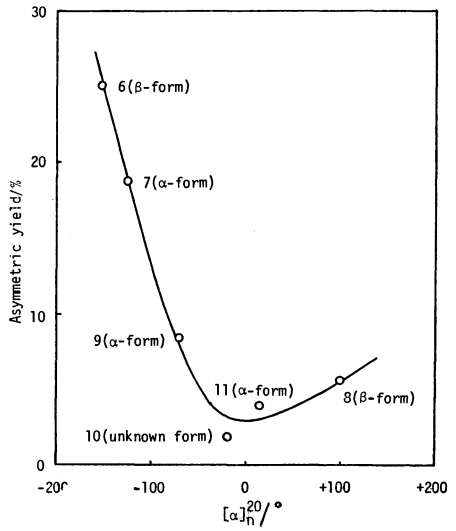

Fig. 1. Relation between optical rotation of poly-(amino acid)s (**6**—**11**) and asymmetric yield of methylsuccinic acid (**2**) formed on poly(mino acid)-coated graphite electrodes.
Electrolytic conditions: pH, 6.0; cathodic potential, −1.0 V *vs.* SCE; charge passed, 96500×0.2 C mol^{-1}; temperature, 0—5 °C; concentration of **1**, 0.145 M. Coating solution: 0.5%(w/v). Current efficiency for **2**: 10—80%. Configuration of excess enantiomer of **2**: *S*.

Table 1. Influence of base electrode materials coated[a] with poly(L-valine) (**6**) on asymmetric yield of methylsuccinic acid (**2**)[b] formed in reduction[c] of citraconic acid (**1**)

Base electrode material	Asymmetric yield/%
Graphite	8.1
Lead	6.0
Zinc	1.2

a) Coated in 0.5% (w/v) poly(L-valine) trifluoroacetic acid solution. b) Yield and current efficiency: 18—32%. Configuration of excess enantiomer: *S*. c) Electrolytic conditions: pH, 4.7; current density, 1.2 A dm^{-2}; charge passed, 96500×2.0 C mol^{-1}; concentration of **1**, 0.145 M (mol dm^{-3}); temperature, 20 °C.

electrodes may be also characterized by this polymer effect.

*Reduction of Citraconic Acid (**1**) on Some Base Electrodes Coated with Poly(L-valine).* As shown in Table 1, graphite was better as a base electrode material than metals such as lead and zinc.

A poly(L-valine) (**6**) film may be fixed on a graphite surface by hydrogen bonding of the amido groups of **6** with oxygen functions such as COOH, CO and OH, while such a hydrogen bonding can not be formed on the metal surface. Even if the hydrogen bonding with surface oxides of the metals might be formed, it should be exhausively disappeared by reduction of the oxides during electrolysis. The adsorptivity of **6** on the base electrodes seems to be one of important factors in the asymmetric reduction.

*Reduction of Citraconic Acid (**1**) on Poly(L-valine) (**6**)-coated Graphite Electrode. Influence of Coating Thickness*: Because the thickness of coating films could not be directly measured, the relation between the number of chirality centers on the electrode and the asymmetric yield was examined. As shown in Fig. 2, the highest asymmetric yield was obtained using an electrode with 0.25×10^{22} cm^{-2} of the number of chirality centers. If the density of **6** is in the range of 0.8—1.4 similarly to ordinary organic polymers,[11] the thickness of the film is estimated as $(2.8—1.6)\times10^{-4}$ cm.

Increase of the thickness resulted in remarkable de-

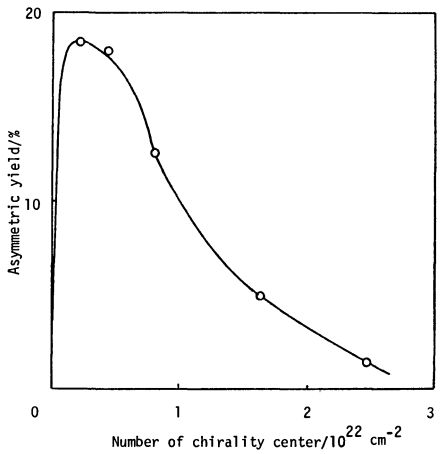

Fig. 2. Influence of number of chirality centers on poly(L-valine)-coated graphite electrode on symmetric yield of methylsuccinic acid (**2**).
Electrolytic conditions: pH, 6.0; current density, 1.2 A dm^{-2}; temperature, 0—5 °C; concentration of **1**, 0.145 M; charge passed, 96500×2.0 C mol^{-1}.
Current efficiency and yield: 10—23%. Configuration of excess enantiomer of **2**: *S*.

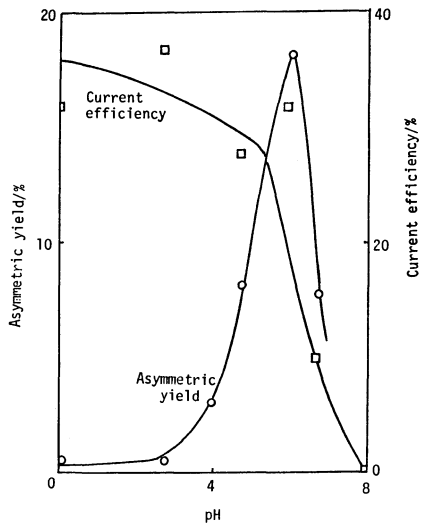

Fig. 3. Influence of pH on asymmetric yield of methylsuccinic acid (**2**) formed in reduction of citraconic acid (**1**) on poly(L-valine)-coated graphite electrode (number of chirality centers, 0.25×10^{22} cm^{-2}).
Electrolytic conditions: current density, 1.2 A dm^{-2}; temperature, 0—5 °C; concentration of **1**, 0.145 M; charge passed, 96500×2.0 C mol^{-2}.
Configuration of excess enantiomer of **2**: *S*.

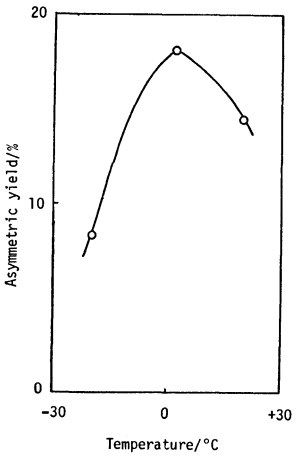

Fig. 4. Influence of temperature on asymmetric yield of methylsuccinic acid (**2**) formed in reduction of citraconic acid (**1**) on poly(L-valine)-coated graphite electrode (number of chirality centers, 0.25×10^{22} cm^{-2}).
Electrolytic conditions: pH, 6.0; current density, 1.2 A dm^{-2}; concentration of **1**, 0.145 M; charge passed, 96500×2.0 C mol^{-1}.
Current efficiency and yield: 10—26%. Configuration of excess enantiomer of **2**: *S*.

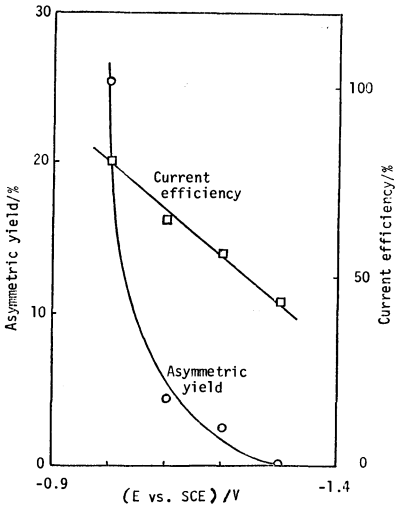

Fig. 5. Influence of cathode potential on asymmetric reduction of citraconic acid (**1**) to methylsuccinic acid(**2**) on poly(L-valine)-coated graphite electrode (number of chirality centers, 0.25×10^{22} cm^{-2}).
Electrolytic conditions: pH, 6.0; temperature, 0—5 °C; concentration of **1**, 0.145 M; charge passed, 96500×0.2 C mol^{-1}.
Configuration of excess enantiomer of **2**: *S*.

crease of the asymmetric yield. This may be suggest that a key step for the asymmetry induction does not occur inside the film. The induction may occur in an interface between the film and the graphite.

Influence of pH: As shown in Fig. 3, the highest asymmetric yield was obtained at pH 6.0, while the cuurent efficiency decreased at pHs higher than 6.0 and **2** was not formed in alkaline solutions. Although such a pH dependence is interesting from an aspect of the asymmetry induction mechanism of this reaction,

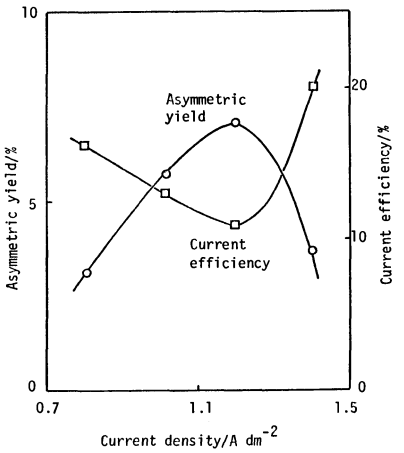

Fig. 6. Influence of current density on reduction of citraconic acid (**1**) to methylsuccinic acid (**2**) on poly(L-valine)-coated graphite electrode (number of chirality centers, 0.25×10^{22} cm^{-2}).
Electrolytic conditions: pH, 4.7; temperature, 20 °C; concentration of **1**, 0.145 M; charge passed, 96500×2.0 C mol^{-1}.
Configuration of excess enantiomer of **2**: *S*.

it is difficult to rationalize clearly the dependence. The asymmetry induction mechanism will be discussed from another aspect in a little more details in the final item of the text.

Influence of Temperature: As shown in Fig. 4, the highest asmmetric yield was obtained at *ca.* 0 °C. In most cases of asymmetric reactions, lower temperature is more favorable. A lower asmmetric yield at −20 °C in this work may be due to an undesirable change in film properties of **6** at such a low temperature, which may be close to its glass transition temperature.

Influence of Cathode Potential: Figure 5 indicates that lower potentials resulted in higher asymmetric yields and current efficiencies. This fact may suggest that hydrogen evolution on the graphite surface decreased the adsorptivity of the **6** film, because hydrogen bubbles might not smoothly go through the film, and consequently the asymmetry-inducing power of the coated electrode was decreased.

Influence of Current Density: The highest asymmetric yield and the lowest current efficiency were obtained at 1.2 A dm^{-2} of current density, as shown in Fig. 6.

Influence of Charge Passed: Influence of charge passed on the asymmetric yield and current efficiency was examined in controlled-potential electrolyses at −1.0 V *vs.* SCE. As shown in Fig. 7, passing of larger amounts of charge, in another word longer time of the electrolyses, resulted in decrease of both the asymmetric yield and current efficiency. The decrease of the former may be caused by the decrease of the asymmetry-inducing power of the **6** film due to contamination of the film-graphite interface during the electrolysis.

Reuse of Electrode: An electrode was repeatedly reused at 1.2 A dm^{-2} of current density passing 96500×2.0 C mol^{-1} of charge for each electrolysis. As shown in Fig. 8, the asymmetry inducing power of **6** was lost at the fifth electrolysis, the film of **6** remained

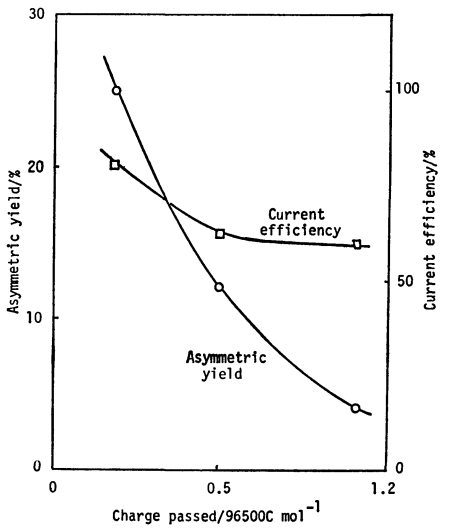

Fig. 7. Influence of charge passed on asymmetric reduction of citraconic acid (**1**) to methylsuccinic acid (**2**) on poly(L-valine)-coated graphite electrode (number of chirality centers, 0.25×10^{22} cm^{-2}).
Electrolytic conditions: pH, 6.0; cathodic potential, -1.0 V *vs.* SCE; temperature 0—5 °C; concentration of **1**, 0.145 M.
Configuration of excess enantiomer of **2**: *S*.

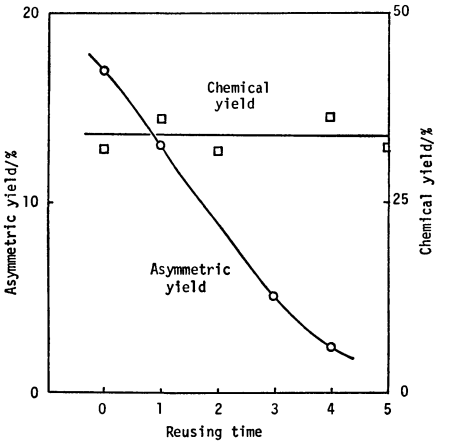

Fig. 8. Asymmetric reduction of citraconic acid (**1**) to methylsuccinic acid (**2**) on reused poly(L-valine)-coated graphite electrode (number of chirality centers, 0.5×10^{22} cm^{-2}).
Electrolytic conditions: pH, 6.0; current density, 1.2 A dm^{-2}; temperature, 0—5 °C; charge passed for each electrolysis, 96500×2.0 C mol^{-1}; concentration of **1**, 0.145 M.
Configuration of excess enantiomer of **2**: *S*,

on the electrode surface. The chemical yield did not change.

Optimization of Asymmetric Reduction of Citraconic Acid (1). The asymmetric reduction of **1** on the poly (L-valine)-coated graphite electrode is optimized under the conditions given in Table 2. From a synthetic aspect, it is undesirable that small amounts of charge passed and/or short electrolysis time are needed to obtain high asymmetric yields. To dissolve this problem, a high current concentration electrolysis using a high surface electrode may be recommended.

Table 2. Optimization of electrochemical asymmetric reduction of citraconic acid (**1**) to methylsuccinic acid (**2**) on poly(amino acid)-coated electrode

Condition	Optimum
Optically-active poly-amino acid	poly(L-valine)
Base eleactrode material	Graphite
Number of chirality centers on electrode	0.25×10^{22} cm^{-2}
pH	6.0
Cathode potential	-1.00 *vs.* SCE (Low as possibe)
Current density	1.2 A dm^{-2}
Temperature	0—5 °C
Charge passed	Small as possible
Reusing time of electrode	First use
Electrolysis time	Short as possible

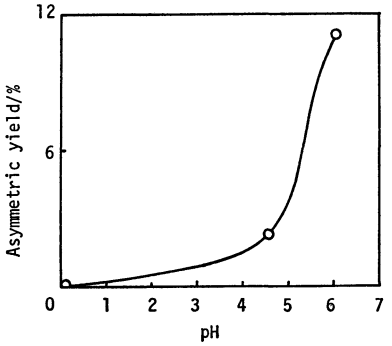

Fig. 9. Asymmetric reduction of mesaconic acid (**3**) to methylsuccinic acid (**2**) on poly(L-valine)-coated graphite electrode (number of chirality centers, 0.25 $\times10^{22}$ cm^{-2}).
Electrolytic conditions: current density, 1.2 A dm^{-2}; temperature, 0—5 °C; charge passed, 96500×2.2 C mol^{-1}; concentration of **1**, 0.145 M.
Current efficiency and yield: 33—45%. Configuration of excess enantiomer of **2**: *S*.

Asymmetric Reduction of Dimethyl Citraconate (4) to Dimethyl Methylsuccinate (5). As shown in Table 3, the asymmetric yield of **5** was extremely low compared with those of **2** formed under the same conditions. This fact suggests that hydrogen bonding of carboxyl groups of **1** contributes to the asymmetry induction.

Asymmetric Reduction of Mesaconic Acid (3) to Methylsuccinic Acid (2). As shown in Fig. 9, **3** gave **2** in lower asymmetric yields than **1**, while both **3** and **1** gave the enantiomer with the *S*-configuration in excess. These results seem to be important for the discussion of the asymmetry induction mechanism.

Asymmetry Induction Mechanism. The poly(amino acid) film coated on base electrode surface is not electroconductive and does not include any electron-carrier, and also is so thick that any electron can not go through the film. Protons and substrate molecules may go through the film, because electrolyses proceeded smoothly without any remarkable cell-voltage increase. Therefore, electron-transfer to the substrate seems to occur in the interface of the film and the base electrode.

Although the mechanism of electrochemical asym-

TABLE 3. ELECTROCHEMICAL ASYMMETRIC REDUCTION[a] OF DIMETHYL CITRACONATE (4) TO DIMETHYL METHYLSUCCINATE (5) ON POLY(L-VALINE)-COATED GRAPHITE ELECTRODE (NUMBER OF CHIRALITY CENTERS, 0.5×10^{22} cm^{-2})

Cathode potential *vs.* SCE / V	Current density / A dm^{-2}	Charge passed / 96500 C mol^{-1}	5		
			Chemical yield/%	Asymmetric yield/%	Configuration of excess enantiomer
−1.25	—[b]	2.0	33	0.0	—
−1.15	—[b]	2.0	65	2.3	*S*
—[c]	1.2	4.0	14	0.0	—
—[c]	1.0	4.0	21	0.0	—

a) Electrolytic conditions: pH, 4.7; temperature, 0—5 °C; concentration of 4, 0.145 M. b) Controlled potential electrolysis. c) Constant current electrolysis.

metry induction was discussed on the basis of steric interaction between prochiral substrate and chiral supporting salt molecules by Horner and Skaletz,[12] any essential conclusion has not been reported. Generally, it may be possible to suppose two types of the asymmetry induction mechanisms, as indicated below: (a) Asymmetric electron-transfer and (b) asymmetric protonation. As described above, **4** was not asymmetrically reduced. This fact may be as due to no interaction between S and I* (in the (a)-mechanism) by hydrogen bonding and thus support the (a)-mechanism. In addition, it may also support the (a)-mechanism that **1** and **3** gave **2** with the same configuration in different asymmetric yields: In the (b)-mechanism, **1** and **3** should give **2** in the same asymmetric yield, because an intermediate $H\bar{S}$ formed via no enantiodifferentiating step from either of **1** and **3** should be racemic. On the other hand, the (a)-mechanism is not in conflict with the above experimental results: Since *cis*- and *trans*-carboxylic groups interact with I*(**6**), **1** and **3** in somewhat different ways give the different asymmetric yields. Although it is difficult to give a concrete conclusion for the asymmetry induction mechanism, the (a)-mechanism is tentatively proposed for the asymmetry induction mechanism.

(a) $S + I^* \rightleftharpoons SI^* \overset{2e+H^+}{\rightleftharpoons} H\bar{S}^* + I^* \xrightarrow{H^+} HS^*H + I^*$

$H^+ + I^*$

(b) $S \overset{2e+H^+}{\rightleftharpoons} H\bar{S} \xrightarrow{H^+I^*} HS^*HI^* \longrightarrow HS^*H + I^*$

S: Prochiral substrate.
I: Chiral asymmetry-inducing reagent.
HSH: Product.
*: Chiral species.

Experimental

Materials. Citraconic acid (**1**) and mesaconic acid (**3**) were supplied from Tokyo Kasei Chemical Co., while dimethyl citraconate (**4**) was prepared by the esterification of **3** with diazomethane in ether and purified by silica-gel column chromatography (bp, 98 °C/15 Torr (lit,[13] 92.8 °C/10 Torr, 1 Torr≈133.322 Pa)).

Poly(L-valine) (**6**), poly(L-leucine) (**7**), poly(D-valine) (**8**), and poly(L-tryptophan) (**9**) were prepared from the corresponding optically pure amino acids by the NCA method.[1] Poly(γ-benzyl-L-glutamate) (**10**) was supplied from Dr. K. Komoto of Tokyo Institute of Technology and poly(*N*-acryloyl-L-valine methyl ester) (**11**) was prepared by a following method. To 10 ml of an aqueous solution containing 3.1 g (0.03 mol) of triethylamine and 5.0 g (0.03 mol) of L-valine methyl ester were dropwise added 3.0 g (0.033 mol) of acryloyl chloride and 11 ml (0.033 mol) of 3 mol dm^{-3} NaOH for 5 h under ice-cooling. After the the reaction mixture was acidified (pH 2—3) with 5 mol dm^{-3} HCl, it was extracted with ethyl acetate. By distillation of the extract in the presence of a small amount of hydroquinone, 3.4 g (62%) of *N*-acryloyl-L-valine methyl ester was obtained: bp, 128 °C/10 Torr (lit,[14] 102 °C/3 Torr); MS, *m/e* 185 (M^+); IR (film), 3300, 1760, 1660, and 1630 cm^{-1}. The ester (2.0 g, 0.011 mol) obtained thus was polymerized in 12 ml of dry methanol in the presence of 0.02 g of 2,2′-azobisisobutyronitrile at 50 °C for 2 h. The reaction mixture was poured into 100 ml of water and 0.72 g (36%) of **11** was obtained as precipitates: IR (KBr), 3350, 1750, and 1670 cm^{-1}. Found: C, 58.31; H, 8.27; N, 7.35%. Calcd for $(C_9H_{15}NO_3)_n$: C, 58.36; H, 8.16; 7.56%. The optical rotating powers of all the poly(amino acd)s (**6**—**11**) are given in Fig. 1. The secondary structures confirmed by IR spectra are also given in Fig. 1. The molecular weight (*ca.* 2000) of **6** only could be known.[1] As polymer properties (molecular weight distribution and secondary structure) of poly(amino acid)s are generally affected by their preparative methods and procedures, the same lot products were used for each set of experiments in this work.

Poly(amino acid)-coated Electrodes. The coated electrodes were prepared by the dipping method described in the previous work.[1] Amounts of **6** coated were estimated from its recovery which was made by washing repeatedly the electrode with trifluoroacetic acid or by shaving off the film of **6**: **6** recovered thus was weighed or its nitrogen content was was analyzed.

Electrolysis and Product Analysis. Electrolytic solutions were aqueous ethanol (50—80%) buffered: 1 M (1 M=1 mol dm^{-3}) H_2SO_4 (pH *ca.* 0); 0.5 M $ClCH_2COOH$-0.5 M $ClCH_2COONa$ (pH 2.8); 4 M CH_3COOH-4 M CH_3COONa (pH 4.0); 0.5 M CH_3COOH-0.5 M CH_3COONa (pH 4.7); 0.17 M KH_2PO_4-0.03 M Na_2HPO_4 (pH 6.0); 0.5 M CH_3COONH_4 (pH 6.7, unbuffered); 0.5 M $NaClO_4$ (pH 7.0, unbuffered; 0.05 M $NaHCO_3$-0.1 M Na_2CO_3 (pH *ca.* 10); 0.5 M NaOH (pH *ca.* 14). Procedures for the electrolysis and product analysis were similar to those in the previous work.[1] The asymmetric yields were calculated with reference to optical rotating powers reported for the optically-pure enantiomers: $[\alpha]_D^{20}$ +17.9° (*c* 4.4 in ethanol)[15] for *R*-**2** and $[\alpha]_D^{25}$ +6.1° (neat)[15] for *R*-**5**.

This work was performed as a preliminary investigation for a project supported financially by the Grant-

in-Aid for Scientific Research from the Ministry of Education, Science and Culture.

References

1) Part 1. S. Abe, T. Nonaka, and T. Fuchigami, *J. Am. Chem. Soc.*, **105**, 3630 (1983).
2) Stereochemical Studies of the Electrolytic Reactions of Organic Compounds. Part 21.
3) W. J. M. Tilborg and C. J. Smit, *Recl. Trav. Chim. Pay-Bas*, **97**, 89 (1978).
4) J. Kopilov, E. Kaliv, and L. L. Miller, *J. Am. Chem. Soc.*, **99**, 3450 (1977).
5) R. Hazard, S. Jaouannet, and A. Tallec, *Tetrahedron*, **38**, 93 (1982).
6) M. Fujihira, A. Yokozawa, H. Kinoshita, and T. Osa, *Chem. Lett.*, **1982**, 1089.
7) J. B. Kerr, L. L. Miller, and M. R. V. D. Mark, *J. Am. Chem. Soc.*, **102**, 3383 (1980).
8) J. F. Rubinson, T. D. Behymer, and H. B. Mark, Jr., *J. Am. Chem. Soc.*, **104**, 1224 (1982).
9) Private communication from S. Nakahama: Product-selective reduction of benzaldehyde on a silicon polymer-coated lead cathode.
10) It is well known as an asymmetric polymer effect that optical rotating powers of polymers have no simple relation (additivity) to the optical rotating powers of their monomer units.
11) F. W. Billmeyer, Jr., "Textbook of Polymer Science," 2nd ed, John-Wiley & Sons, New York (1971), p. 503.
12) L. Horner and D. H. Skaletz, *Justus Libigs Ann. Chem.*, **1977**, 1365.
13) L. Straete, *Bull. Sci. Akad. R. Berg.*, **21**, 226 (1935).
14) N. Oida and N. Koine, *Nippon Kagaku Zasshi*, **88**, 1087 (1967).
15) R. Rossi, *Gass. Chim. Ital.*, **98**, 139 (1968).

Preparation, Characterization and Stereochemistry of 2-Methyl-2-silabicyclo[2.2.1]heptane Derivatives[1)]

Akira Hosomi, Masashi Mikami, and Hideki Sakurai*
Department of Chemistry, Faculty of Science, Tohoku University, Sendai 980
(Received March 24, 1983)

A new class of bicyclic compounds containing a single silicon atom at the bridge, 2-exo- and endo-substituted 2-methyl-2-silabicyclo[2.2.1]heptanes, have been prepared from the corresponding 3-cyclopentenylmethylhydrosilane by the intramolecular hydrosilylation catalyzed by chloroplatinic acid, and their structures were unquivocally assigned by ^1H and ^{13}C NMR spectra. Dramatic crossover from inversion to retention was found in the phenylation of chlorosilanes with phenyllithium and phenylmagnesium bromide in ether. Regio- and stereoselective insertion of dichlorocarbene generated from phenyl(bromodichloromethyl)mercury, or from chloroform and sodium hydroxide in the presence of a phase transfer catalyst, into $C_{(6)}$–$H_{(exo)}$ bond of 2-silanorbornanes has been observed.

In spite of a large number of publications relating to silacycloalkanes, little attention has been paid to a class of bicyclic organosilicon compounds, except for bridgehead silicon compounds. We have prepared 2-silabicyclo[2.2.1]heptanes (**1**—**5**) by the intramolecular hydrosilylation of (3-cyclopentenylmethyl)hydrosilanes. Very recently Cremer and Blankenship have also reported the preparation of 2-silanorbornanes (**2** and **5**).[2)] Now we report our own results with respect to their characterizations by spectroscopic methods, some interesting stereochemical behaviors on the silicon atom and a remarkably regio- and stereoselective insertion of dichlorocarbene into the $C_{(6)}$ carbon–hydrogen bond.

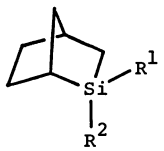

1, $R^1=R^2=CH_3$
2a, $R^1=CH_3$, $R^2=H$: **2b**, $R^1=H$, $R^2=CH_3$
3a, $R^1=CH_3$, $R^2=C_6H_5$: **3b**, $R^1=C_6H_5$, $R^2=CH_3$
4a, $R^1=CH_3$, $R^2=i\text{-PrO}$: **4b**, $R^1=i\text{-PrO}$, $R^2=CH_3$
5a, $R^1=CH_3$, $R^2=Cl$: **5b**, $R^1=Cl$, $R^2=CH_3$

Hitherto optically active silicon compounds have been used almost exclusively in order to investigate the stereochemical behavior of reactions on a silicon atom.[4)] We have felt frequently, however, that these compounds give rise to rather limitations for exploring the stereochemistry of some reactions, *e.g.*, arylations or dearylations, since substituents in the case of optically active silicon compounds are mostly restricted in their kinds. After desiring to produce a quite new system involving geometrical isomers in organosilicon chemistry for several years,[3)] we recently realized this vision by means of the synthesis of 4-*t*-butylsilacyclohexane derivatives.[5)]

The present system possesses a similar molecular structure to the parent norbornane which shows a lot of unique reactivities in ionic[6)] and free radical process,[7)] and at the same time indicates practically the following merits to investigate the stereochemistry: (a) preparation of objective compounds is easily attained in good yield if we use the intramolecular hydrosilylation catalyzed by a transition metal, the procedure of which was already established;[9,10)] (b) resolution of exo and endo isomers is easy by GLC; (c) two isomers are determined by ^1H NMR because the chemical shift of Si–CH_3 protons is characteristic for each isomer; (d) hence it is possible to discuss the stereochemistry of reactions by using both of the geometrical isomers without optical resolution; (e) accordingly a small amount of substrate is sufficient to study the stereochemical behavior by NMR spectroscopy.

Results and Discussion

Preparation and Characterization. First 3-cyclopentenylmethyl chloride(**11**), the starting alkyl chloride, was prepared from *trans*-1,4-dichloro-2-butene and diethyl malonate in the presence of two equivalents of sodium ethoxide by a six-step synthesis through diethyl 2-vinyl-1,1-cyclopropanedicarboxylate (**6**), diethyl 3-cyclopentene-1,1-dicarboxylate (**7**), 3-cyclopentene-1,1-dicarboxylic acid (**8**), 3-cyclopentenecarboxylic acid (**9**), 3-cyclopentenylmethanol (**10**), as follows (Scheme 1).

The Grignard reagent from **11** in ether as well as (3-cyclopentenylethyl)magnesium bromide[8)] was quite stable, and did not cause any intramolecular cyclization due to the participation of a carbanionic carbon in the olefinic double bond. The addition of bromodimethylsilane and chloromethylphenylsilane to this solution afforded (3-cyclopentenylmethyl)dimethylsilane (**13**) and (3-cyclopentenylmethyl)methylphenylsilane (**14**), respectively, which were the precursors of 2-silanorbornanes, in good yields. (3-Cyclopentenylmethyl)chloromethylsilane (**16**) was prepared by the inverse addition of the Grignard reagent to excess dichloromethylsilane. Analogously (3-cyclopentenylmethyl)dimethyldeuteriosilane (**17**) was derived by the lithium aluminum deuteride reduction of (3-cyclopentenylmethyl)chlorodimethylsilane (**15**) which was conveniently obtained by the inverse addition of the Grignard reagent to dichloromethylsilane. (Scheme 2)

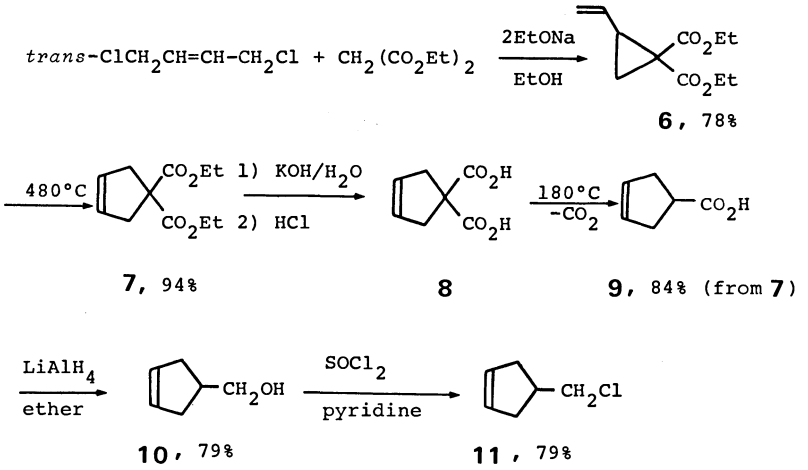

Scheme 1. Synthesis of 3-cyclopentenylmethyl chloride (**11**).

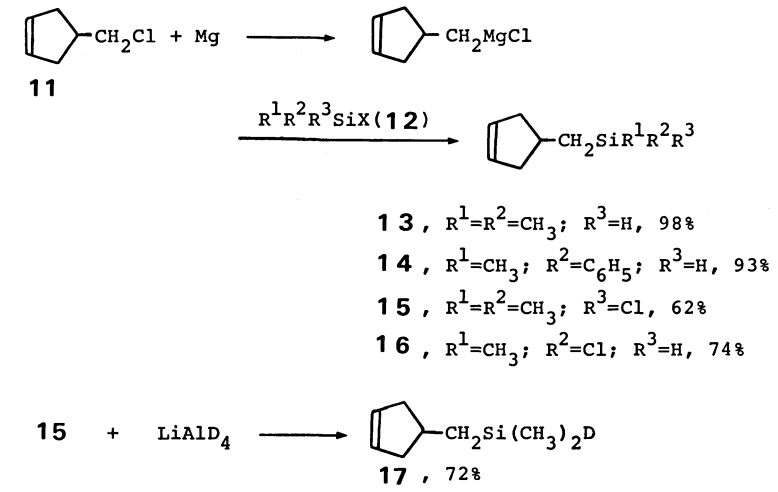

Scheme 2. Synthesis of (3-cyclopentenylmethyl)hydrosilanes (**13**—**17**).

During the investigation of transition metal-[9,10] or free radical-[9]catalyzed hydrosilylation, we[9] and Swicher *et al.*[10] had found that the intramolecular hydrosilylation took place more favorably and easily rather than the intermolecular reaction, provided that a double bond and a silicon–hydrogen bond were separated by three methylene groups, so that this should offer a general and good method to prepare a five or six membered ring compound. Accordingly it will be quite reasonable to consider that the bicyclic compounds involving a silicon atom could be derived intramolecularly from the hydrosilane which involves a cyclic olefin separated by three carbon atoms.

When a neat solution of (3-cyclopentenylmethyl)-dimethylsilane (**13**) was heated in the presence of a catalytic amount of chloroplatinic acid at 130 °C for 100 h in a sealed tube, 2,2-dimethyl-2-silabicyclo[2.2.1]-heptane (**1**) was obtained in 82% yield. Analogously, in the case of R^1=Me and R^2=Ph or Cl, the products **3** and **5** consisting of a mixture of two geometrical isomers at the ratio of *exo*-Me:*endo*-Me=65:35 or 63:37, respectively, were prepared in good yields (Eq. 1). More elevated temperature was required for the cyclization to bicyclic compounds than for that to a monocyclic compound as reported earlier.[9,10] Palladium on charcoal was also effective as a catalyst but free radical initiators not so good.

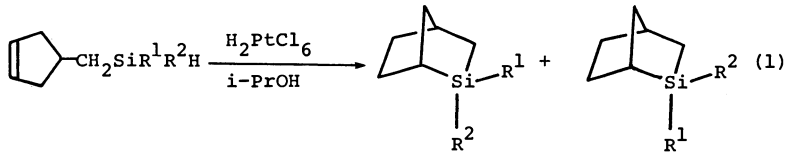

13, $R^1=R^2=CH_3$ — **1**, $R^1=R^2=CH_3$

14, $R^1=CH_3$; $R^2=C_6H_5$ — **3a**, $R^1=CH_3$; $R^2=C_6H_5$ — **3b**, $R^1=CH_3$; $R^2=C_6H_5$

16, $R^1=CH_3$; $R^2=Cl$ — **5a**, $R^1=CH_3$; $R^2=Cl$ — **5b**, $R^1=CH_3$; $R^2=Cl$

Table 1. ^{13}C NMR chemical shifts[a] of 2-silanorbornanes

	C_1	C_3	C_4	C_5	C_6	C_7	2-*exo*-CH_3	2-*endo*-CH_3
(2a)	22.0	18.0	35.9	30.5	24.9	37.4	−4.9	
(2b)	22.0	17.0	36.8	30.9	23.2	38.9		−7.8
(1)	23.5	21.0	36.5	30.6	23.5	38.1	−2.3	−4.9
(3a)[b]	24.0	19.0	36.7	30.8	23.4	38.9	−2.8	
(3b)[c]	23.6	19.9	36.8	30.9	23.6	39.1		−5.2
(4a)[d]	21.7	19.6	35.9	30.3	23.9	36.6	1.4	
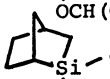 (4b)[e]	21.7	21.7	34.8	29.7	23.2	37.5		−1.0

a) δ (ppm), downfield from TMS (0.00 ppm) in $CDCl_3$–$CHCl_3$ (2:1). b) The aromatic carbons resonated at 134.8, 128.0, 129.3 and 137.1 ppm (*o*, *m*, *p*, and *ipso* carbon, respectively). c) The aromatic carbons resonated at 134.1, 127.8, 128.9 and 138.6 ppm (*o*, *m*, *p*, and *ipso* carbon, respectively). d) The methine and methyl carbon of the isopropyl group resonated at 65.6 and 25.0 ppm, respectively. e) 65.3 and 25.0 ppm for the methine and methyl carbon.

Compounds **2** and **4** were mutually prepared from the chlorosilane **5** by the following transformations. (Scheme 3)

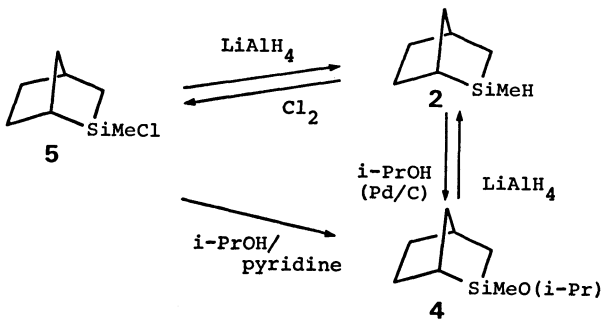

Scheme 3. Mutual transformations between **2**, **4**, and **5**.

Each of stereoisomer of **3** and **4** was readily isolated by fractional distillation and subsequent preparative GLC (Apiezon L, 20% 5 m) collection. In all the compounds investigated in this report the silicon atom has beared at least one methyl group, so that the exo and endo isomers were defined with respect to the methyl group throughout the paper for avoiding confusion. Thus, the exo means that the methyl group orients to exo direction and suffix a is given. Analogously the endo means its geometrical isomer and suffix b is given.

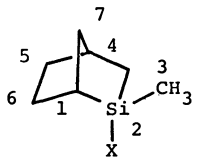

exo: a

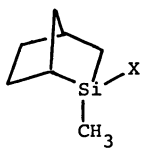

endo: b

The unequivocal assignment of the stereochemistry of 2-silanorbornanes could be achieved on the basis of the ^1H and ^{13}C NMR spectroscopic studies where **2a** and **2b** were used. Although neither isomer of **2** could be isolated by GLC collection, a 200 MHz ^1H NMR spectrum of approximately 1:2 mixture of **2a** and **2b** shows that the characteristic signals due to Si–CH_3 and Si–H appear at δ 0.03 (d, J=4.0 Hz) and 0.12 (d, J=4.0 Hz) (3H as a total), and δ 3.72 (m) and 3.87 (m) (1H as a total), respectively. The signals due to 3-exo and 3-endo protons of **2a** and **2b** appear at δ 0.48 (m) as an unseparable multiplet peak, and at δ 0.07 (m) and 0.80 (m), respectively, in a integral ratio of approximately 4:1:1 (2H as a total). $H_{(1)}$, $H_{(4)}$, and $H_{(5),(6),(7)}$ signals of **2a** and **2b** are obtained as peaks which resonate at δ 1.4 (m), 2.5 (m) and 0.9—1.8 (m), respectively, in a ratio of 1:1:6. Irradiation of the higher field Si–CH_3 signal reveals a quartet of the Si–H proton, since the coupling constants due to three vicinal protons, $H_{(1)}$, $H_{(3exo)}$ and $H_{(3endo)}$, become equal (J=2.5 Hz) fortuitously. Thus, small $J_{(2),(3endo)}$ and $J_{(2),(3exo)}$ suggest that this isomer should be the exo (**2a**). On the other hand

Table 2. Si-CH_3 Proton chemical shifts of 2-silanorbornanes[a]

Compound	*exo*-CH_3	*endo*-CH_3	Δ[b]
1	0.03	0.09	0.06
2	0.03	0.12	0.09
3	0.35	0.40	0.05
4	0.17	0.22	0.05
5	0.50	0.55	0.05

a) δ (ppm) from TMS in CCl_4. b) Difference in exo-endo methyl proton (ppm).

decoupling of Si–H signal in a lower field reveals that $J_{(2),(3exo)}$ is 5.5 Hz. Therefore this compound should be identified as the endo isomer (**2**b).

2-Silanorbornanes have a similar trend, though in a smaller extent, not only in the coupling constants but also in the chemical shifts originating in the exo and endo Si–H protons as is generally observed for the ^1H NMR spectra of norbornane derivatives.[11] The absorption of the 2-exo proton attached to a silicon appeared as a somewhat broad peak at 0.15 ppm lower field than the corresponding endo proton. Clearly it has been found that NMR spectra are most convenient and effective to investigate the stereochemistry in these systems.

These assignments were further supported by the ^{13}C NMR spectra shown in Table 1. The chemical shifts were decided relatively by their comparison with those of the norbornane systems, using both wide-band ^1H decoupled and off-resonance decoupling experiments. The $^{13}C_{(6)}$ carbon chemical shift is distinctly assigned by the complete decoupling of the $C_{(6)}$-deuterium labelled compound.

Depending upon the stereochemistry of a silicon bearing a methyl group, the $C_{(7)}$ carbon in **2**a and the $C_{(6)}$ carbon in **2**b revealed slightly up-field shifts by 1.5 ppm and 1.7 ppm, compared with the corresponding carbons in **2**b and **2**a, respectively. In general, it is well established that both of ^{13}C chemical shifts of two carbons which approach spatially each other cause up-field shift.[12] This phenomenon is called the steric compression shift.[13] Therefore, the upfield shifts associated with $C_{(6)}$- and $C_{(7)}$-carbons in each isomer could be reasonably explained by the steric shift.

The stereochemistry of **3**a and **3**b, and **4**a and **4**b is analgously determined by the results arising from ^{13}C NMR steric shift. Supporting evidence of the assignment with respect to the stereochemistry was further obtained from the results that the methyl group on the silicon atom in all these bicyclic systems exhibited configurationally dependent shieldings[13c] with endo groups more shielded than their exo counterparts (See Table 2). Thus the structures determined by the ^{13}C NMR spectra are in doubtless consistent with those assigned by ^1H NMR spectra. The relationship and some characteristics in ^1H and ^{13}C NMR spectra between 2-silanorbornane and norbornane derivatives[13c] are shown in Table 3.

Throughout these series, the exo isomers have shorter retention times on GLC (Apiezon L and SE 30) than do the endo ones, and in the IR spectra, although only groups of absorption bands characteristic of C–H and Si–CH_3 stretching were observed, any characteristic bands to be attributed to the bicyclic structure did not appear. The IR spectra therefore could not be effectively applied for the structural analysis so much.

Stereochemistry on a Silicon Atom. There have been extensively systematized studies with respect to the stereochemistry on an asymmetric silicon atom in a number of different chiral organosilane systems.[4] As results, it is known that the predominant stereochemistry depends largely on the nature of leaving groups and entering groups and frequently the solvent but not usually on the nature of substituents, even if the cis and trans geometrical isomers such as a series of 4-*t*-butylsilacyclohexanes were used.[5] However dramatic crossover from inversion to retention has been recently reported on the stereochemistry of some optical and geometrical isomers in which strained carbon-silicon bonds were substantially involved.[14–16]

Our new stereochemical systems may be suitable for the tests of the effect of angle strain at the silicon because of their longer Si–C bond length than C–C bond length in norbornanes.[17]

An interesting example of stereochemical behavior can be found in the case of phenylation of the chlorosilanes with both the Grignard reagent and the lithium reagent in ether. The results are shown in Table 4 along with some other stereochemical reactions (Scheme 4). Thus the result in which the chlorine atom in **5**a and **5**b was displaced in highly retentive way (>92% predominant stereochemistry) with both phen-

Table 3. Relationship and characteristics between 2-silanorbornanes and norbornanes in ^1H and ^{13}C NMR spectra

	2-Silanorbornanes	Norbornanes[11]
Coupling constants	$Si_{(2)}H_{(exo)}$-$C_{(3)}H_{(exo)}$ 5.5 Hz $Si_{(2)}H_{(endo)}$-$C_{(3)}H_{(exo)}$ 2.5 Hz $Si_{(2)}H_{(endo)}$-$C_{(3)}H_{(endo)}$ 2.5 Hz	$C_{(2)}H_{(exo)}$-$C_{(3)}H_{(exo)}$ 9—10 Hz $C_{(2)}H_{(endo)}$-$C_{(3)}H_{(exo)}$ 2.5—5.0 Hz $C_{(2)}H_{(endo)}$-$C_{(3)}H_{(endo)}$ 6.7 Hz
Chemical shift (^1H)	Si-H; endo upfield Si-CH_3; exo upfield	C-H; endo upfield
Chemical shifts (^{13}C)	Si-CH_3; endo upfield	C-CH_3; endo upfield

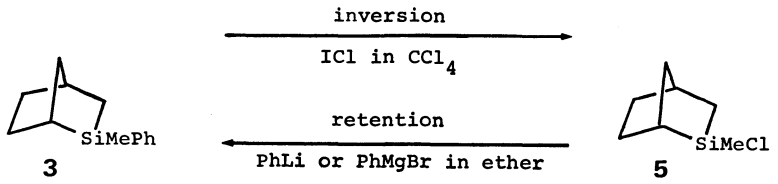

Scheme 4. Stereochemistry on a silicon atom.

Table 4. Stereochemistry on silicon atom

Reaction	Substrate	Proedominant Stereochemistry (%)[a]
Chlorodephenylation with ICl in CCl_4 at r.t.	3a	Inversion 86.0
	3b	Inversion 77.5
Phenylation with PhLi in Et_2O at r.t.	5a	Retention 95.6
	5b	Retention 92.9
Phenylation with PhMgBr in Et_2O at r.t.	5a	Retention 97.4
	5b	Retention 96.5
Chlorination with Cl_2 in CCl_4	2a:2b =71:29	Retention 5a:5b=71:29

a) 90% retention means that the product was 90% retained and 10% inverted, if the pure starting material was used.

yllithium and phenylmagnesium bromide might be attributed to the angle strain.[16] In sharp contrast, however, Sommer et al. have observed that the inversive reaction *via* S_N2-Si mechanism took place in the reaction of the asymmetric chlorosilane with both organolithium and Grignard reagents[4,18] and we have also found the similar configuration inversion in 4-*t*-butylsilacyclohexane system,[19] in which the strained angle with the silicon will not be large in size so much.

On the other hand, the phenyl group was displaced by a chlorine atom with configuration inversion in the chlorodephenylation of **3**a and **3**b with iodine monochloride, in a manner analogous to that noted in our previous report.[19]

Reduction of **5** (**5**a:**5**b=83:17) with lithium aluminum hydride in ether gave the corresponding hydrosilane **2** (**2**a:**2**b=86:14) in quantitative yield. Interestingly the reduction of **5** (**5**a:**5**b=17:83) which was enriched by **5**b also led to a mixture of the similar composition of **2** (**2**a:**2**b=85:15). Apparently the equilibration to the thermodynamic controlled mixture of **2** occurred during the LAH reduction.[20]

Regio- and Stereoselective Dichlorocarbene Insertion into $C_{(6)}$–$H_{(6exo)}$ Bond of 2-Silabicyclo[2.2.1]heptanes. The problem of the high exo:endo rate ratio in the solvolysis of 2-norbornyl system is a topic in physical organic chemistry during a few decades.[6,21–23] 2-Silabicyclo[2.2.1]heptanes might be favorable to investigate a hyperconjugating ability of a silicon-carbon bond to an incipient positive charge at $C_{(6)}$-carbon, because they provide not only a polarized but also highly strained carbon-metal σ bonds which could afford significantly large stabilization of neighboring cation.[22]

We have found an interesting dichlorocarbene insertion into 6-carbon–hydrogen exo bond of 2-silanorbornanes (Eq. 2). Important features of this reaction are (a) regiospecific β-CH bond insertion at $C_{(6)}$ position, although there are three kinds of β-CH bond in **1**, (b) the overwhelmingly predominant insertion into the exo CH bond.

2,2-Dimethyl-2-silabicyclo[2.2.1]heptane (**1**) reacts

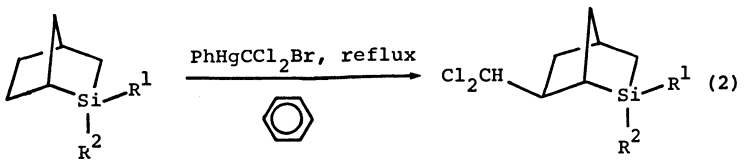

1 , R^1= R^2= CH_3
3a , R^1= CH_3; R^2= C_6H_5
3b , R^1= C_6H_5; R^2= CH_3

18 , R^1= R^2= CH_3
19a , R^1= CH_3; R^2= C_6H_5
19b , R^1= C_6H_5; R^2= CH_3

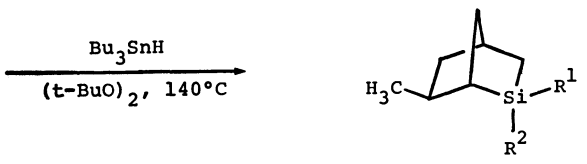

20, R^1= R^2= CH_3

with phenyl(bromodichloromethyl)mercury in benzene at reflux to give a corresponding dichlorocarbene insertion product **18** in 22% yield, along with the recovered **1**. Quite similarly, only **18** was obtained in 71% yield by the reaction of **1** with the dichlorocarbene *in situ* generated from chloroform and sodium hydroxide in benzene-water medium in the presence of benzyltrimethylammonium chloride at room temperature.[24] From the 200 MHz NMR spectrum, the presence of both doublet proton resonance at δ 5.43 (J=9.0 Hz) assigned as the dichloromethyl proton and triply doublet resonance at δ 2.43 (J=9.0 Hz, 9.0 Hz, 6.0 Hz) assigned as the $C_{(6)}$ proton bearing dichloromethyl group clearly led to the suggestion that this compound could be identified as 6-*exo*-dichloromethyl-2,2-dimethyl-2-silabicyclo[2.2.1]heptane (**18**). It was found that the insertion product **18** was derived to 2,2,6-*exo*-trimethyl-2-silabicyclo[2.2.1]heptane (**20**) by the reduction with tributyltin hydride in the presence of free radical initiator (Eq. 2). Analogously 2-*exo*- and 2-*endo*-phenyl derivatives (**3a** and **3b**) afforded exclusively regio- and stereoselective dichlorocarbene insertion products, **19a** and **19b**, respectively, by the reaction with phenyl(bromodichloromethyl)mercury.

The characteristic cracking patterns of the mass spectra have appeared in all of insertion products. Namely the cation in which a dichloromethyl group was removed from the molecular ion peak was strikingly strong, resulting in a base peak.

The stereochemistry and the position at which the insertion of dichlorocarbene occurred were further unambiguously established by the structural analysis of the reaction product when 6-*endo*-deuterium labelled compound (**21**) was utilized as a substrate (Eq. 3).

Thus 6-*endo*-deuterio-2,2-dimethyl-2-silabicyclo[2.2.1]-heptane (**21**), which was derived intramolecularly by the cis addition[25] of (3-cyclopentenylmethyl)-dimethyldeuteriosilane (**17**) catalyzed by chloroplatinic acid, gave exclusively the $C_{(6)}$–H but not $C_{(6)}$–D insertion product (**22**) whose proton NMR spectrum revealed singlet resonance at δ 5.43 and no signals at δ 2.43 in (**18**) (Eq. 3).

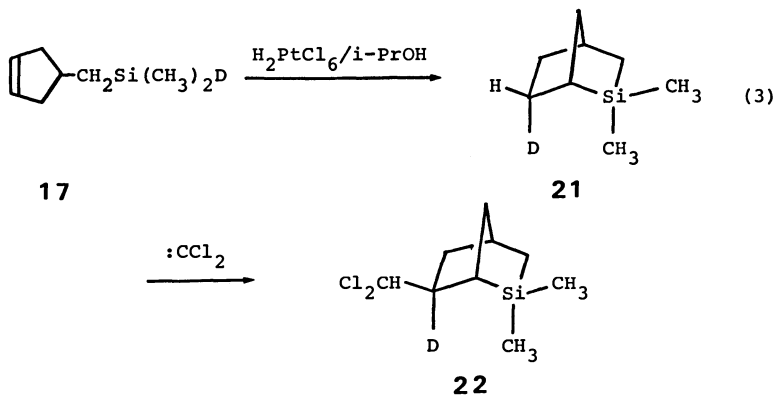

(3)

In its mass spectrum, that the cation $[C_6H_{14}DSi]^+$ (m/e=140) appeared as a base peak would reveal the further evidence to demonstrate that the dichlorocarbene insertion was regio- and stereoselective.

Although the mechanism of insertion of the dichlorocarbene generated from phenyl(bromodichloromethyl)-mercury into C–H bonds has been investigated in details,[26] two distinct and important features should be instructive to discuss the present results. One is that the dichlorocarbene insertion takes place with retention with respect to the carbon configuration,[27] and the other is that only the activated C–H bonds such as α–CH bond of ethers,[28] β–CH bond of organometallic compounds[29] or tertiary CH bond,[30] show the enhanced reactivity due to the mildly electrophilic nature of free dichlorocarbene.[31] It is worth to note that, in our cases, the insertion of CCl_2 not only into the bridgehead tertiary C–H bond at $C_{(4)}$ but also into bridge methylene C–H bonds at $C_{(7)}$ could not compete at all with the insertion at $C_{(6)}$ position, although all of them were also located in β-position from the metal.

We suggest that the regio- and stereoselectivity in the present system, therefore, may be best understood in terms of the stabilization of the partial positive charge in exo direction in the transition state due to σ-π hyperconjugation using the strained carbon$_{(1)}$–silicon$_{(2)}$ σ bond. This represents a remarkably interesting example in which the existence of the stereoelectronic effect in σ-π hyperconjugation[32] was clearly demonstrated in chemical reactivity. The steric origin, leading to the high stereoselectivity, of course, should be appreciably considered, although it is hard to estimate precisely the steric effect in its extent. Studies on kinetics as well as products of hydride abstraction by trityl cation are presently in progress.

Experimental

General. All reactions were carried out under nitrogen. ^{1}H NMR spectra were recorded with Varian Associates T-60, HA-100 and XL-200 spectrometers. ^{13}C NMR spectra were taken with a Hitachi Perkin-Elmer R-26 spectrometer. GLC was used extensively in the analysis of reaction mixtures and for the isolation of products. Hitachi 063 for the analysis and Varian 90-P gas chromatographs for the collection were used. The columns packed with SE-30 silicone rubber gum or Apiezon L grease on Celite 545 were used. Mass spectra were taken with Hitachi RMU-6D and JEOL JMS-300D Mass spectrometers. Thin layer chromatography (TLC) was used to monitor the organomercurial reactions and to isolate the insertion products. Boiling points are uncorrected.

Bromodimethylsilane. According to the procedure of the S_H2 reaction of organodisilane with 1,2-dibromoethane,[33a] 1,2-dibromoethane (52.6 g, 0.28 mol) was added slowly to 1,1,2,2-tetramethyldisilane (33 g, 0.28 mol) in the presence a catalytic amount of dibenzoyl peroxide. During the addition, ethylene was evolved vigorously. The reaction mixture was distilled to give pure bromodimethylsilane[33b] (52.9 g, 68% yield). Bp 58 °C; NMR (CCl_4) δ 0.59 (6H, d, J=3.5 Hz, Si-CH_3), 4.80 (1H, septet, J=3.5 Hz, Si-H).

*Synthesis of Diethyl 2-Vinyl-1,1-cyclopropanedicarboxylate (**6**).* According to the procedure described in the literature,[34] the ester (**6**) (165 g) was obtained from sodium ethoxide (2.1 mol), diethyl malonate (160 g, 1.0 mol), and *trans*-1,4-dichloro-2-butene (125 g, 1.0 mol) in ethanol (1.5 l) in 78% yield. Bp 85 °C (2 mm) (lit,[34] 116—119 °C (16 mm)); NMR (CCl_4) δ 1.13 (3H, t, J=7.5 Hz, CH_3), 1.15 (3H, t, 7.5 Hz, CH_3), 1.33—1.59 (2H, m, cyclopropane-CH_2), 2.15—2.56 (1H, m, cyclopropane-CH), 4.07 (2H, q, J=7.5 Hz, CH_2), 4.08 (2H, q, J=7.5 Hz, CH_2), 4.85—5.47 (3H, m, CH=CH_2); IR (TF) 3100 (w), 2990 (s), 2850 (m), 1730 (s), 1640 (m), 1450 (m), 1375 (m), 1320 (m), 1275 (s), 1200 (s), 1130 (s), 1030 (m), 990 (w), 960 (w), 920 (m), 865 (s), 855 (m) cm^{-1}.

*Synthesis of 3-Cyclopentenecarboxylic Acid (**9**).*[34] The ester (**6**) (130 g, 0.61 mol) was pyrolyzed through a quartz tube at 480 °C to give diethyl 3-cyclopentene-1,1-dicarboxylate (**7**) (122 g, 94% yield). NMR (CCl_4) δ 1.21 (6H, t, J=7.5 Hz, CH_3), 2.91 (4H, s, cyclopentene-CH_2), 4.12 (4H, q, J=7.5 Hz, CH_2), 5.52 (2H, s, CH=). For the saponification, **7** (121 g, 0.57 mol), thus obtained, was heated with stirring with potassium hydroxide (100 g, 1.7 mol) in 80% ethanol (1 l) for 6 h. After evaporation of ethanol and water, the mixture was acidified with 6 M (1 M= 1 mmol dm^{-3}) hydrochloric acid and extracted with ether. The solvent was evaporated, and the residue was decarboxylated by heating at 180 °C and distilled to give pure 3-cyclopentenecarboxylic acid (**9**) 37.8 g (0.34 mol) in 84% yield. Bp 110 °C (22 mm) (lit,[34] 118—121 °C (20 mm)); NMR (CCl_4) δ 2.53—3.20 (5H, m, CH, CH_2), 5.61 (2H, s, CH=), 11.77 (1H, s, CO_2H); IR (TF) 3200 (s), 3050 (s), 2940 (s), 2850 (m), 1700 (s), 1640 (w), 1420 (m), 1340 (w), 1300 (m), 1230 (m), 1180 (m), 950 (m), 930 (m) cm^{-1}.

*Synthesis of 3-Cyclopentenylmethanol (**10**).*[35] The alcohol (**10**) (25 g, 0.255 mol) was obtained by the reduction of the carboxylic acid (**9**) (36.3 g, 0.324 mol) with lithium aluminum hydride (13.3 g, 0.35 mol) in ether (150 ml) in 79% yield. Bp 90 °C (50 mm) (lit,[35] 98—99 °C (57 mm)); NMR (CCl_4) δ 1.49—2.63 (5H, m), 3.39 (2H, d, J=6 Hz), 4.22 (1H, s), 5.57 (2H, s); IR (TF) 3400 (s), 3050 (m), 2930 (s), 2850 (m), 1650 (m), 1080 (m), 1040 (s), 950 (m), 940 (w), 900 (w) cm^{-1}.

*3-Cyclopentenylmethyl Chloride (**11**).* The alcohol (**10**) (31.9 g, 0.33 mol) was treated with thionyl chloride (42.9 g, 0.36 mol) in pyridine (28.2 g, 0.36 mol) under ice-cooling. After the mixture was heated moderately for an hour, the oily material was separated and immediately distilled under reduced pressure to give **11** (30.1 g, 79% yield). Bp 70 °C (94 mm); n_D^{20} 1.4698; NMR (CCl_4) δ 1.91—2.84 (5H, m, -CH_2-CH(CH_2Cl)CH_2-) 3.47 (2H, d, J=6 Hz, -CH_2Cl), 5.65 (2H, s, =CH-); IR (TF) 3075 (m), 2950 (s), 2850 (s), 1620 (w), 1580 (w) 1440 (s), 1340 (m), 1290 (m), 1210 (m), 1130 (m), 1060 (w), 1040 (w) cm^{-1}. Calcd for C_6H_9Cl: C, 61.81; H, 7.78%. Found: C, 61.98; H, 7.62%.

*(3-Cyclopentenylmethyl)dimethylsilane (**13**) and (3-Cyclopentenylmethyl)methylphenylsilane (**14**).* To the Grignard reagent prepared from 4.7 g (0.04 mol) of the chloride and 1.2 g (0.05 g-atom) of magnesium in 20 ml of dry ether was added 5.6 g (0.04 mol) of bromodimethylsilane. The mixture was stirred for 10 h and hydrolyzed. After work up as usual, distillation of the organic layer under reduced pressure gave 5.5 g (0.039 mol, 98% yield) of **13**. Bp 76 °C (74 mm); n_D^{20} 1.4504; NMR (CCl_4) δ 0.09 (6H, J=4 Hz, Si-CH_3) 0.71—1.04 (2H, m, Si-CH_2), 1.61—2.94 (5H, m, CH_2-CH-CH_2) 5.61 (2H, s, -HC=CH-); IR (TF) 3050 (m), 2900 (m), 2800 (s), 2100 (s), 1610 (w), 1440 (m), 1350 (m), 1250 (s), 1220 (s), 1110 (m), 1070 (m), 1040 (m), 940 (m), 850 (s) cm^{-1}; Mass *m/e* (rel intensity) 140 (11), 125 (11), 99 (60), 97 (78), 59 (100). Calcd for $C_8H_{16}Si$: C, 68.49; H, 11.50%. Found: C, 68.71; H, 11.50%. **14** (7.5 g, 0.037 mol) was analogously prepared from the Grignard reagent (from **11** (5.3 g) and magnesium (1.22 g)) and chloromethylphenylsilane[36] (6.25 mol, 0.04 mol) in 93% yield. Bp 102 °C (7 mm); n_D^{20} 1.5306; NMR (CCl_4) δ 0.29 (3H, d, J=3.5 Hz, Si-CH_3), 0.91—1.11 (2H, m, Si-CH_2), 1.61—2.68 (5H, m, CH_2-CH-CH_2), 4.37 (1H, m, J=3.5 Hz, Si-H), 5.51 (2H, s, -HC=CH-), 7.21—7.61 (5H, m, C_6H_5); IR (TF) 3050 (s), 2100 (s), 1950 (w), 1880 (w), 1820 (w), 1760 (w), 1590 (w), 1490 (w), 1430 (s), 1330 (w), 1260 (s), 1120 (s), 880 (s), 840 (s) cm^{-1}. Calcd for $C_{13}H_{18}Si$: C, 77.61; H, 8.97%. Found: C, 77.29; H, 9.34%.

*(3-Cyclopentenylmethyl)dimethylchlorosilane (**15**) and (3-Cyclopentenylmethyl)chloromethylsilane (**16**).* The Grignard reagent prepared from 5.9 g (0.05 mol) of the chloride (**11**) and 1.5 g (0.06 g-atom) of magnesium in dry ether was added to a dilute ether solution of 10.4 g (0.08 mol) of dichlorodimethylsilane and the mixture was stirred for 10 h with refluxing. Filtration and fractionation of the organic layer gave 5.5 g (0.031 mol, 62% yield) of pure **15**. Bp 70 °C (19 mm); n_D^{20} 1.4626; NMR (CCl_4) δ 0.42 (6H, s, Si-CH_3); 1.05 (2H, d, J=6 Hz, Si-CH_2), 1.60—2.85 (5H, m, $(CH_2)_2C$ 1.05 (2H, d, J=6 Hz, Si-CH_2), 1.60—2.85 (5H, m, $(CH_2)_2CH$), 5.65 (2H, s, =CH-); IR (TF) 3020 (s), 2900 (s), 2820 (s), 2115 (s), 1610 (m), 1440 (m), 1345 (m), 1335 (m), 1240 (s), 1195 (m), 1105 (m), 1065 (m), 930 (s), 925 (s), 890 (s), 825 (s), 790 (m), 765 (m) cm^{-1}. Calcd for $C_8H_{15}ClSi$: C, 54.99; H, 8.65%. Found: C, 55.16; H, 8.64%.

From **11** (2.9 g, 0.025 mol), magnesium (0.73 g, 0.03 g-atom), and methyldichlorosilane (5.75 g, 0.050 mol), **16** (3.0 g, 0.019 mol) was obtained in 74% yield. Bp 73 °C (38 mm); NMR (CCl_4) δ 0.45 (3H, d, J=3.5 Hz, Si-CH_3), 0.94—1.24 (2H, m, Si-CH_2), 1.71—2.81 (5H, m, CH_2-CH-CH_2), 4.79 (1H, m J=3.5 Hz, Si-H), 5.62 (2H, s, -HC=CH-); IR (TF) 3050 (m), 2950 (s), 2900 (s), 2850 (s), 2160 (s), 1615 (m), 1440 (m), 1350 (m), 1250 (s), 1210 (m), 1110 (m br), 940 (m) cm^{-1}. Calcd for $C_7H_{13}ClSi$: C, 52.31; H, 8.15%. Found: C, 52.29; H, 8.24%.

*(3-Cyclopentenylmethyl)dimethyldeuteriosilane (**17**).* A 6.0 g (0.034 mol) of **15** was reduced with lithium aluminum deuteride (>99% D) (0.42 g, 0.01 mol) in ether. After work up as usual, distillation gave 3.5 g (0.0248 mol) of **17** in 72% yield. Bp 62 °C (34 mm); n_D^{20} 1.4513. The GLC retention time of the product on Silicone gum SE-30, Apiezon L or PEG 20M column was identical with that of the undeuterated material (**13**). NMR (CCl_4) δ 0.07 (6H, s, Si-CH_3) 0.80 (2H, d, J=6 Hz, Si-CH_2), 1.70—2.78 (5H, m, -CH_2-CH-CH_2), 7.64 (2H, s, =CH-) and no Si-D chemical shift. The infrared spectra showed Si-D band at 1532 cm^{-1} and Si-CH_3 band at 1234 cm^{-1}. IR (TF) 3000 (m), 2930 (s), 2870 (s), 2800 (s), 1610 (w), 1540 (m), 1532 (s), 1440 (w), 1350 (w), 1234 (s), 1190 (w), 1100 (w), 1065 (m), 930 (s), 890 (w), 830 (s), 790 (m) cm^{-1}; MS *m/e* (rel intensity) 141 (M^+, 16.5), 126 (M^+-CH_3, 43.5), 100 (54), 99 (64), 98 (79.5), 97 (64), 60 (100), 59

(55.5). A deuterium analysis by the peak ratio at M^+-15 (126/125) by mass stectrum showed 94% replacement of one hydrogen by deuterium. Calcd for $C_8H_{15}DSi$ (d content 94%): C, 68.03; H (D), 12.09%. Found: C, 67.46; H (D), 11.97%.

*Preparation of 2-Silanorbornanes (**1**, **3**, and **5**) by Intramolecular Hydrosilylation. 2,2-Dimethyl-2-silabicyclo[2.2.1]heptane (**1**)*: **13** (2.5 g, 0.018 mol) was placed together with a catalytic amount of chloroplatinic acid in isopropyl alcohol (10^{-2} M, 2 μl) in a glass tube. The tube was sealed and immerced in an oil bath kept constant temperature at 130 °C for 100 h, and then opened. Distillation gave the product (**1**) (2.2 g, 82% yield). Bp 60 °C (38 mm); n_D^{20} 1.4735; NMR (CCl_4) δ 0.03 (3H, s, $Si-CH_{3(exo)}$), 0.09 (3H, s, $Si-CH_{3(endo)}$), 0.20 (1H, d, $J_{(3exo),(3endo)}=14$ Hz, $H_{(3endo)}$), 0.56 (1H, ddd, $J_{(3exo),(3endo)}=14$ Hz, $J_{(3exo),(4)}=5$ Hz, $J_{(3exo),(5exo)}=2$ Hz, $H_{(3exo)}$), 0.85—1.73 (7H, m, $H_{(1),(5),(6),(7)}$), 2.43 (1H, m, $H_{(4)}$); IR (TF) 2925 (s), 2875 (s), 1440 (w), 1400 (w), 1310 (w), 1250 (s), 1150 (w), 1090 (w), 1050 (m), 1020 (w), 1000 (w), 940 (m), 880 (m), 850 (s), 830 (s), 810 (s), 750 (s), 720 (s), 700 (w) cm^{-1}. Calcd for $C_8H_{16}Si$: C, 68.49; H, 11.50%. Found: C, 68.64; H, 11.66%.

*6-Deuterio-2,2-dimethyl-2-silabicyclo[2.2.1]heptane (**21**).* Analogously, from the deuteriosilane (**17**) (1.5 g, 0.11 mol) was obtained **21** (1.0 g, 67% yield). Bp 64 °C (40 mm); n_D^{20} 1.4738; NMR (CCl_4) δ 0.03 (3H, s, $Si-CH_{3(exo)}$), 0.09 (3H, s, $Si-CH_{3(endo)}$), 0.20 (1H, dm, $J_{(3endo),(3exo)}=14$ Hz, $H_{(3exo)}$), 0.56 (1H, ddm, $J_{(3exo),(3endo)}=14$ Hz, $J_{(3exo),(4)}=5$ Hz, $H_{(3exo)}$), 0.85—1.73 (6H, m, $H_{(1),(5),(6),(7)}$), 2.43 (1H, m, $H_{(4)}$); IR (TF) 2950 (s), 2870 (s), 2185 (m), 1470 (m), 1460 (m), 1410 (w), 1300 (m), 1255 (s), 1190 (m), 1095 (m), 1050 (s), 990 (m), 950 (m), 920 (w), 880 (s), 860 (s), 845 (s), 830 (s), 800 (w), 765 (w), 730 (w), 710 (m) cm^{-1}. IR showed only one C–D band at 2185 cm^{-1}. MS *m/e* (rel intensity) 141 (M^+, 40), 126 (24), 99 (100). A deuterium analysis by M^+-15 peaks of mass spectrum showed 72.5% replacement of one hydrogen by deuterium. Assuming that the addition has proceeded *via* cis stereochemistry,[25] it appears reasonable to conclude that the deuterium is located almost exclusively in the $C_{(6\text{-endo})}$ position, *i.e.*, the product is 2,2-dimethyl-6-endo-deuterio-2-silabicyclo-[2.2.1]heptane (**21**). The retention time on GLC was identical with that of **1**. Calcd for $C_8H_{15}DSi$ (d content 72.5%): C, 68.13; H (D), 11.95%. Found: C, 67.73; H (D), 11.92%.

*2-exo- and endo-Methyl-2-phenyl-2-silabicyclo[2.2.1]heptane (**3a** and **3b**).* According to the procedure described above, a mixture of compounds **3a** and **3b** (**3a**:**3b**=68:32) (4.0 g, 20 mmol) boiling over the range of 106—108 °C (5 mm) was obtained from **14**. (5.5 g, 27 mmol). Total yield of **3a** and **3b** was 73%. Either of isomers was readily isolated by preparative GLC (250 °C) equipped with a column packed with Apiezon L 20% (5m) on Celite 545. The retention time on GLC of the exo (**3a**) was shorter than that of the endo isomer (**3b**). **3a**: n_D^{20} 1.5504; NMR (CCl_4) δ 0.35 (3H, s, $Si-CH_{3(exo)}$), 0.78 (2H, m, $J_{(3exo),(4)}=J_{(3endo),(4)}=3$ Hz, $H_{(3endo),(3exo)}$), 1.30—1.77 (7H, m, $H_{(1),(5),(6),(7)}$), 2.61 (1H, m, $H_{(4)}$), 7.23—7.59 (5H, m, C_6H_5); IR (TF) 3090 (w), 3045 (w), 2940 (s), 2870 (m), 1450 (w), 1425 (m), 1400 (w), 1300 (w), 1255 (m), 1190 (w), 1120 (w), 1050 (m), 1000 (w), 940 (m), 880 (m), 860 (m), 820 (m), 800 (m), 780 (m), 740 (m), 700 (s), 680 (w), 640 (w), 600 (w) cm^{-1}. Calcd for $C_{13}H_{18}Si$: C, 77.16; H, 8.97%. Found: C, 77.43; H, 8.92%.

3b: n_D^{20} 1.5512; NMR (CCl_4) δ 0.40 (3H, s, $Si-CH_{3(endo)}$), 0.48 (1H, dm, $J_{(3endo),(3exo)}=14.5$ Hz, $H_{(3endo)}$), 1.08 (1H, dd, $J_{(3endo),(3exo)}=14.5$ Hz, $J_{(3exo),(4)}=6.5$ Hz, $H_{(3exo)}$), 1.22—1.88 (7H, m, $H_{(1)(5)(6)(7)}$), 7.23—7.57 (5H, m, C_6H_5). Calcd for $C_{13}H_{18}Si$: C, 77.16; H, 8.97%. Found: C, 76.90; H, 9.00%.

*2-exo- and endo-Methyl-2-chloro-2-silabicyclo[2.2.1]heptane (**5a** and **5b**).* A mixture of **5a** and **5b** (**5a**:**5b**=63:37) (1.47 g, 9.1 mmol) boiling over the range of 63—65 °C (17 mm) was obtained from **16** (1.61 g, 10 mmol) by the chloroplatinic acid catalyzed hydrosilylation, total yield being 91%. The mixture was used for the following derivatizations without the isolation of each isomer. NMR as a mixture of **5a** and **5b** (63:37) (CCl_4) δ 0.50 (s, $Si-CH_{3(exo)}$), 0.55 (s, $Si-CH_{3(endo)}$), 0.72 (2H, m, $H_{(3)}$), 1.00—1.85 (7H, m, $H_{(1),(5),(6),(7)}$), 2.62 (1H, m, $H_{(4)}$); IR (TF) 2900 (s), 2850 (s), 1454 (m), 1403 (m), 1300 (m), 1253 (s), 1215 (s), 1190 (m), 1140 (w), 1085 (m), 1048 (s), 1022 (w), 1000 (w), 930 (m), 880 (m), 850 (m) cm^{-1}. Calcd for $C_7H_{13}ClSi$: C, 52.31; H, 8.15%. Found: C, 52.59; H, 8.33%.

*Preparation of 2-Silanorbornanes (**2**, **3**, **4**, **5**) by Mutual Transformations. 2-exo- and endo-Methyl-2-silabicyclo[2.2.1]heptane (**2a** and **2b**)*: A mixture (1.29 g, 8.0 mmol) of **5a** and **5b** (**5a**:**5b**=63:37) was reduced with lithium aluminum hydride (LAH) (0.15 g) in dry ether (10 ml). Hydrolysis of the reaction mixture and drying and distillation of the organic layer gave **2** (1.02 g, 98% yield), as an isomeric mixture of **2a**:**2b**=74:26. Bp 142 °C; n_D^{20} 1.4796.

A mixture of **2a** and **2b** (**2a**:**2b**=70:30) was also derived from a mixture of **4a** and **4b** (**4a**:**4b**=70:30) by LAH reduction. NMR (200 MHz) as a mixture of **2a** and **2b** (CCl_4) δ 0.03 (3H, d, $J_{(CH_3),(2endo)}=4.0$ Hz, *exo*-CH_3), 0.48 (2H, m, $J_{(2endo),(3exo)}=J_{(2endo),(3endo)}=2.5$ Hz, $H_{(3exo)}$ and $H_{(3endo)}$), and 3.72 (1H, m, $J_{(2endo),(CH_3)}=4.0$ Hz, $J_{(2endo),(1)}=J_{(2endo),(3exo)}=J_{(2endo),(3endo)}=2.5$ Hz, $H_{(2endo)}$) which are attributed to **2a**, and δ 0.07 (1H, m, $J_{(3exo),(3endo)}=15.5$ Hz, $H_{(3endo)}$), 0.12 (3H, d, $J_{(CH_3),(2exo)}=4.0$ Hz, *endo*-CH_3), 0.80 (1H, m, $J_{(3exo),(3endo)}=15.5$ Hz, $J_{(3exo),(4)}=J_{(3exo),(2exo)}=5.5$ Hz, 3.87 (1H, m, $J_{(2exo),(3exo)}=5.5$ Hz, $J_{(2exo),(CH_3)}=4.0$ Hz, $H_{(2exo)}$) which belong to **2b**. Besides, the following complex multiplet signals are obtained from a mixture of **2a** and **2b**: δ 1.4 (1H, m, $H_{(1)}$), 2.5 (1H, m, $H_{(4)}$), 0.9—1.8 (6H, m, $H_{(5)}$, $H_{(6)}$ and $H_{(7)}$). IR (TF) 2910 (s), 2850 (s), 2130 (s), 1455 (w), 1410 (w), 1300 (w), 1250 (m), 1215 (s), 1188 (m), 1140 (w), 1087 (w), 1050 (m), 1028 (w), 1000 (w), 938 (s), 890 (s, br) cm^{-1}. Calcd for $C_7H_{14}Si$: C, 66.58; H, 11.18%. Found: C, 65.92; H, 10.93%.

*2-exo- and endo-Methyl-2-isopropoxy-2-silabicyclo[2.2.1]heptane (**4a** and **4b**).* A mixture of **5** (exo:endo=60:40) (3.2 g, 0.02 mol), isopropyl alcohol (1.8 g, 0.03 mol) and pyridine (2.4 g, 0.03 mol) was heated with stirring for 20 h in dry ether. After filtration of the salt and evaporation of the solvent, ditillation gave 3.1 g (0.017 mol, 84% yield) of the isopropoxy derivative (**4**), as an isomeric mixture of the ratio of **4a**:**4b**=82:18, boiling over the range of 72—76 °C (16 mm).

Alternatively 0.42 g (33% yield) of the compound **4**, as an isomeric mixture of **4a**:**4b**=53:47, boiling over the range of 72—14°/17 mm, was obtained from 0.91 g (7 mmol) **2** (**2a**:**2b**=74:26) and isopropyl alcohol (1 ml) in the presence of Pd–C (10%) (25 mg) in petroleum ether (10 ml) according to the procedure described previously.[37] Either of isomers was readily isolated by preparative GLC (220 °C) using a column packed with Apiezon L 20% (5 m) on Celite 545. The retention time of GLC of **4a** was shorter than that of the endo isomer (**4b**).

4a: n_D^{20} 1.4579; NMR (CCl_4) δ 0.17 (3H, s, $Si-CH_{3(exo)}$), 0.28 (1H, dd, $J_{(3endo),(3exo)}=14.6$ Hz, $J_{(3endo),(4)}=2.1$ Hz, $H_{(3endo)}$), 0.53 (1H, dd, $J_{(3exo),(3endo)}=14.6$ Hz, $J_{(3exo),(4)}=$

5.7 Hz, $H_{(3exo)}$), 1.16 (6H, d, J=6.3 Hz, -CH-$(CH_3)_2$), 1.25—1.90 (7H, m, $H_{(1),(5),(6),(7)}$), 2.43 (1H, m, $H_{(4)}$), 3.96 (1H, septet, J=6.3 Hz, OCH).

4b: n_D^{20} 1.4586; NMR (CCl_4) δ 0.22 (3H, s, Si-$CH_{3(endo)}$), 0.27 (1H, dd, $J_{(3endo),(3exo)}$=14.8 Hz, $J_{(3endo),(4)}$=2.1 Hz, $H_{(endo)}$), 0.72 (1H, dd, $J_{(3exo),(3endo)}$=14.8 Hz, $J_{(3exo),(4)}$=5.0 Hz, $H_{(3exo)}$), 1.13 (6H, d, J=5.9 Hz, -CH-$(CH_3)_2$), 0.97—1.80 (7H, m, $H_{(1),(5),(6),(7)}$), 2.54 (1H, m, $H_{(4)}$), 3.96 (1H, sept, J=5.9 Hz, OCH). Calcd for $C_{10}H_{20}OSi$: C, 65.15; H, 10.93%. Found: C, 65.15; H, 11.16%.

Chlorination of Compound **2**. Into a carbon tetrachloride solution of **2** (**2a**:**2b**=71:29) dry chlorine gas was passed through until the yellowish color was left in nmr tube. The yield of the chloride **5** was almost quantitative by GLC determination. The ratio of **5a**:**5b** was 71:29 by nmr determination.

Chlorodephenylation of **3** *and Phenylation of* **5**. The exo isomer **3a** (0.1 g), freshly isolated, was treated with iodine monochloride in carbon tetrachloride. Predominant formation of endo isomer **5b** (**5a**:**5b**=14.0:86.0) was observed by NMR determination. After carbon tetrachloride was substituted for dry ether, the mixture was treated with phenyllithium or phenylmagnesium bromide at ether refluxing temperature. After work up, the phenylated compound **3** as an isomeric mixture of **3a**:**3b**=19.5:80.5 or 19.4:80.6, respectively, was isolated by GLC in the pure state. In repeated runs, essentially the same result was obtained.

Analogously, the compound **3b** was chlorodephenylated, resulting in the predominant stereochemistry of the isomer **5a**, where **5a**:**5b**=77.5:22.5. Phenylation of the products with phenyllithium or phenylmagnesium bromide in ether gave the compound **3**, as an isomeric mixture of **3a**:**3b**=77.0:23.0. From the combination of the above reactions, the predominant stereochemistry in the phenylation with phenyllithium was 95.6% for **5a** and 92.9% for **5b**, and with phenylmagnesium bromide was 97.4% for **5a** and 96.5% for **5b**.

Reactions of 2-Silanorbornanes with Dichlorocarbene. Method A: The following general procedure was used. A mixture of 880 mg (2.0 ml) of phenyl(bromodichloromethyl)mercury, prepared by the reported procedure,[38] and 2.0 mmol of 2-silanorbornane in 3 ml of dry benzene was displaced into a 50 ml two necked flask equipped with a reflux condenser topped with a nitrogen inlet tube and magnetic stirring unit. The flask then was immersed into an oil bath kept at 90 °C. The solution was stirred and heated at reflux for 10 h. Filtration gave phenylmercury(II) bromide, yielding usually above 90% in good purity (mp 275 °C). The filtrate was free from the solvent, the remaining material subsequently was analyzed by NMR and GLC and the product was isolated by preparative TLC. The yields of the insertion product were 1) 22% for 6-*exo*-dichloromethyl-2,2-dimethyl-2-silabicyclo[2.2.1]heptane (**18**), 2) 11% for 6-*exo*-dichloromethyl-2-*exo*-methyl-2-*endo*-phenyl-2-silabicyclo-[2.2.1]heptane (**19a**), 3) 13% for 6-*exo*-dichloromethyl-2-*endo*-methyl-2-*exo*-phenyl-2-silabicyclo[2.2.1]heptane (**19b**). In each reaction, the starting material was almost recovered.

Method B: To a solution of 2,2-dimethyl-2-silabicyclo-[2.2.1]heptane (**1**) (10 g, 0.07 mol), 50% aqueous sodium hydroxide (145 ml), benzene (14.5 ml) and benzyltrimethylammonium chloride (0.29 g, 28 mmol), chloroform (43.5 ml, 0.25 mol) was added slowly with vigorous stirring for a period of 7.5 h at 60 °C. After additional stirring for 2 h, diethyl ether (50 ml) was added and the organic layer was centrifuged. After similar operation was carried out 10 times, the ethereal layer was dried over sodium sulfate and the solvent was removed by distillation. The residue was distilled under reduced pressure to give 6-*exo*-dichloromethyl-2,2-dimethyl-2-silabicyclo[2.2.1]heptane (**18**) (11.4 g, 0.05 mol) in 71.3% yield. Bp 117 °C (9 mmHg, 1 mmHg≈133.322 Pa); n_D^{20} 1.5116.

18: NMR (CCl_4) δ 0.12 (3H, s, Si-$CH_{3(exo)}$), 0.23 (3H, s, Si-$CH_{3(endo)}$), 0.32 (1H, d, J=14.5 Hz, $H_{3(endo)}$), 0.66 (1H, dd, $J_{(3exo),(3endo)}$=14.5 Hz, $J_{(3exo),(4)}$=6.0 Hz, $H_{(3exo)}$), 1.20—1.72 (5H, m, $H_{(1),(5),(7)}$), 2.43 (1H, ddd, $J_{(6endo),(6\text{-}exo\text{-}CH)}$=9.0 Hz, J=9.0 Hz, J=6.0 Hz, $H_{(6endo)}$), 2.57 (1H, m, $H_{(4)}$), 5.43 (1H, d, $J_{(6\text{-}exo\text{-}CH),(6endo)}$=9.0 Hz, $CHCl_2$); IR (TF) 2930 (s), 2830 (s), 1460 (w), 1440 (m), 1400 (m), 1300 (s), 1290 (m), 1280 (w), 1250 (s), 1210 (s), 1120 (s), 1050 (s), 1000 (w), 970 (m), 900 (m), 840 (s) cm^{-1}; MS *m/e* (rel intensity) 224 (M^++2, 0.1), 222 (M^+, 0.3) 140 (14), 139 (M^+-CHCl_2, 100), 95 (29), 93 (81), 79 (72), 59 (48); High resolution MS, $C_8H_{15}Si$ (M^+-CHCl_2), obsd *m/e* 139.0943 (calcd 139.0943). Calcd for $C_9H_{16}Cl_2Si$: C, 48.73; H, 7.23%. Found: C, 48.22; H, 7.08%.

19a: NMR (CCl_4) δ 0.32 (3H, s, Si-$CH_{3(exo)}$), 0.74—0.84 (2H, m, $H_{(3)}$), 1.25—1.82 (5H, m, $H_{(1),(5),(7)}$), 2.27 (1H, ddd, $J_{(6endo),(6\text{-}exo\text{-}CH)}$=8.5 Hz, J=8.5 Hz, J=6.0 Hz, $H_{(6endo)}$), 2.60—2.75 (1H, m, $H_{(4)}$), 5.39 (1H, d, $J_{(6endo),(6\text{-}exo\text{-}CH)}$=8.5 Hz, $CHCl_2$), 7.20—7.59 (5H, m, C_6H_5); MS *m/e* (rel intensity) 286 (M^++2, 0.1), 284 (M^+, 0.2), 201 (M^+-CHCl_2, 100), 157 (38), 155 (99), 123 (12), 121 (62), 105 (19), 93 (21), 91 (32), 79 (dd), 74 (10), 59 (19); High resolution MS, $C_{13}H_{17}Si$ (M^+-CHCl_2), obsd *m/e* 201.1095 (calcd 201.1098).

19b: NMR (CCl_4) δ 0.44 (3H, s, Si-$CH_{3(endo)}$), 0.49 (1H, dd, $J_{(3exo),(3endo)}$=14.2 Hz, $J_{(3endo),(4)}$=3.2 Hz, $H_{(3endo)}$), 1.10 (1H, dd, $J_{(3exo),(3endo)}$=14.2 Hz, $J_{(3exo),(4)}$=6.0 Hz, $H_{(3exo)}$), 1.23—1.92 (5H, m, $H_{(1),(5),(7)}$), 2.55 (1H, ddd, $J_{(6endo),(6\text{-}exo\text{-}CH)}$=9.0 Hz, J=9.0 Hz, J=6.0 Hz, $H_{(6endo)}$), 2.55—2.76 (1H, m, $H_{(4)}$), 5.47 (1H, d, $J_{(6\text{-}exo\text{-}CH),(6endo)}$=9.0 Hz, $CHCl_2$), 7.20—7.59 (5H, m, C_6H_5); MS *m/e* (rel intensity) 286 (M^++2, 0.1), 284 (M^+, 0.1), 201 (M^+-CHCl_2, 47), 157 (37), 155 (100), 121 (64), 105 (18), 93 (25), 91 (24), 79 (58); High resolution MS, $C_{13}H_{17}Si$ (M^+-CHCl_2), obsd *m/e* 201.1086 (calcd 201.1098).

*Reduction of the Insertion Product (***18***) with Tributyltin Hydride.* **18** (80 mg) was heated tributylin hydride (500 mg) in the presence of di-*t*-butyl peroxide (20 mg) at 140 °C for 15 h in a sealed tube. By a GLC collection (Apiezon L 30%, 3m, 190 °C) of the reaction mixture, 6-*exo*-methyl-2,2-dimethyl-2-silabicyclo[2.2.1]heptane (**20**) was obtained. NMR (CCl_4) δ 0.01 (3H, s, Si-$CH_{3(exo)}$), 0.09 (3H, s, Si-$CH_{3(endo)}$), 0.15 (1H, d, $J_{(3endo),(3exo)}$=14.5 Hz, $H_{(3endo)}$), 0.52 (1H, ddd, $J_{(3exo),(3endo)}$=14.5 Hz, $J_{(3exo),(4)}$=6.5 Hz, $J_{(3exo),(5exo)}$=2.8 Hz, $H_{(3exo)}$), 0.91 (3H, d, $J_{(6\text{-}exo\text{-}CH),(6endo)}$=6.8 Hz, 6-$CH_{3(exo)}$), 0.82—2.03 (6H, m, $H_{(1)(5),(6endo),(7)}$). Calcd for $C_9H_{18}Si$: C, 70.05; H, 11.76%. Found: C, 70.28; H, 11.84%.

*Reaction of 2,2-Dimethyl-6-*endo*-deuterio-2-silabicyclo[2.2.1]-heptane (***21***) with Phenyl(bromodichloromethyl)mercury.* The reaction of $PhHgCCl_2Br$ with the deuterio compound (**21**) (72.5% enriched by derterium) was carried out in a similar manner as described above. The product **22** was obtained in 17.4% yield. The retention time on GLC was identical with that of **18**. Deuterium analysis by NMR and mass spectrum showed 71% excess deuterium at 6-endo position in the product. IR spectrum showed 2160 cm^{-1} characteristic of C-D streching.

22: NMR (CCl_4) δ 0.12 (3H, s, Si-$CH_{3(exo)}$), 0.23 (3H, s, Si-$CH_{3(endo)}$), 0.32 (1H, d, $J_{(3endo),(3exo)}$=14.5 Hz, $H_{(3endo)}$), 0.66 (1H, dd, $J_{(3exo),(3endo)}$=14.5 Hz, $J_{(3exo),(4)}$=6.0 Hz, $H_{(3exo)}$), 1.20—1.72 (5H, m, $H_{(1),(5),(7)}$), 2.57 (1H, m, $H_{(4)}$), 5.44 (1H, s, $CHCl_2$); IR (TF) 2920 (s), 2850 (s), 2160 (w),

1470 (w), 1450 (m), 1410 (m), 1300 (m), 1290 (m), 1280 (w), 1250 (s), 1210 (s), 1120 (w), 1050 (s), 985 (s), 900 (m), 840 (s) cm^{-1}; MS *m/e* (rel intensity) 225 (M^++2, 0.2), 223 (M^+, 0.2), 141 (15), 140 (M^+-CHCl_2, 100), 139 (45), 95 (36), 93 (97), 80 (46), 79 (44), 59 (51); High resolution MS, $C_8H_{14}DSi$ (M^+-CHCl_2), obsd *m/e* 140.1002 (calcd 140.1004).

References

1) a) Chemistry of Organosilicon Compounds. 177. b) Presented in part at the 23rd Symposium of Organometallic Compounds, Tokyo, Japan, Oct. 6, 1975, Abstracts p. 11. At the time when our work had been almost over, Cremer and Blankenship have recently reported the preparation of 2-silanorbornanes.[2)]

2) S. E. Cremer and C. Blankenship, *J. Org. Chem.*, **47**, 1626 (1982).

3) 1-Silabicyclo[2.2.1]heptanes and 1-silabicyclo[2.2.2]-octanes: L. H. Sommer and O. F. Bennett, *J. Am. Chem. Soc.*, **79**, 1008 (1957); **81**, 251 (1959); L. H. Sommer, O. F. Bennett, P. G. Campbell, and D. R. Weyenberg, *ibid.*, **79**, 3295 (1957); G. D. Homer and L. H. Sommer, *J. Organomet. Chem.*, **84**, 297 (1975); **49**, C13 (1973); *J. Am. Chem. Soc.*, **95**, 7700 (1973); R. L. Hilderbrandt, G. D. Homer, and P. Boudjouk, *ibid.*, **98**, 7486 (1976); Y. Nagai, H. Inaba, H. Matsumoto, and H. Watanabe, *Bull. Chem. Soc. Jpn.*, **45**, 3224 (1972); T. Ikeura, K. Tanaka, E. Hirota, S. Inaba, and Y. Nagai, *ibid.*, **50**, 1309 (1977); H. Sakurai, K. Ogi, A. Hosomi, and M. Kira, *Chem. Lett.*, **1974**, 891.

2-Silabicyclo[2.2.1]hept-1-enes and 7-Silabicyclo[2.2.1]-heptanes; P. R. Jones, T. F. O. Lim, and R. A. Pierce, *J. Am. Chem. Soc.*, **102**, 4970 (1980); R. A. Benkerser, E. C. Mozden, W. C. Muench, R. T. Roche, and M. R. Siklosi, *J. Org. Chem.*, **44**, 1370 (1979).

3-Silabicyclo[3.2.1]octanes: S. E. Cremer and C. Blankenship, *Tetrahedron Lett.*, **21**, 3979 (1980); Q. Shen, R. L. Hilderbrandt, C. Blankenship, and S. E. Cremer, *J. Organomet. Chem.*, **214**, 155 (1981); R. Carleer, N. Hosten, and M. J. O. Anteunis, *Bull. Soc. Chim. Belg.*, **87**, 109 (1978); R. Carleer and M. J. O. Anteunis, *Org. Magn. Reson.*, **12**, 673 (1979).

4) L. H. Sommer, "Stereochemistry, Mechanism and Silicon," McGraw-Hill, New York (1965); R. Corriu and J. Masse, *Bull. Soc. Chim. Fr.*, **1969**, 349.

5) H. Sakurai and M. Murakami, *J. Am. Chem. Soc.*, **94**, 5081 (1972).

6) D. G. Sargent "Carbonium Ions," ed by G. Olah and P. v. R. Schleyer, John Wiley Sons, New York, N.Y. (1972), Vol. III, Chap. 24; H. C. Brown, *Acc. Chem. Res.*, **6**, 377 (1973); J. A. Berson in "Molecular Rearrangements," P. de Mayo, Interscience, New York, M.Y. (1963), Vol. 1, Chap. 3.

7) P. B. Bartlett, G. N. Fickes, F. C. Haupt, and R. Helgeson, *Acc. Chem. Res.*, **3**, 177 (1970).

8) F. A. Hill, R. J. Thiessen, A. Doughty, and R. Miller, *J. Org. Chem.*, **34**, 3681 (1969).

9) H. Sakurai, T. Hirose, and A. Hosomi, *J. Organomet. Chem.*, **86**, 197 (1975).

10) J. V. Swicher and H. H. Chen, *J. Organomet. Chem.*, **69**, 83 (1974).

11) L. M. Jackman and S. Sternhell, "Application of Nuclear Magnetic Resonance Spectroscopy in Organic Chemistry," 2nd ed, Pergamon Press, Elmsford, New York (1969).

12) G. C. Leny and G. L. Nelson, "Carbon-13 Nuclear Magnetic Resonance for Organic Chemists," John Wiley & Sons, New York (1972); N. K. Wilson and J. B. Stothers, "Topics in Stereochemistry," ed by E. L. Eliel and N. L. Allinger, John Wiley & Sons, (1974), Vol. 8, p. 1.

13) a) D. M. Grant and B. V. Cheney, *J. Am. Chem. Soc.*, **89**, 5315 (1967); b) J. J. Reich, M. Jantelat, M. T. Messe, F. J. Weigert, and J. D. Roberts, *ibid.*, **91**, 7445 (1969); c) J. B. Grutzner, M. Jantelat, J. B. Dence, R. A. Smith, and J. D. Roberts, *ibid.*, **92**, 7107 (1970).

14) D. N. Roark and L. H. Sommer, *J. Am. Chem. Soc.*, **95**, 969 (1973).

15) B. G. McKinnie, N. S. Bhacca, F. K. Cartledge, and J. Foyssoux, *J. Am. Chem. Soc.*, **96**, 2637 (1974).

16) R. Corriu and J. Masse, *J. Organomet. Chem.*, **34**, 221 (1972); R. Corriu, J. Masse, and G. Royo, *J. Chem. Soc., Chem. Commun.*, **1971**, 252.

17) Norbornanes have large angle strain at 2-carbon ($C_1C_2C_3$=104°), see, J. F. Chiang, C. F. Wilcox, Jr., and S. Bauer, *J. Am. Chem. Soc.*, **90**, 3149 (1968); Y. Morino, K. Kuchitsu, and A. Yokozeki, *Bull. Chem. Soc. Jpn.*, **40**, 1552 (1967).

18) L. H. Sommer, C. L. Frye, C. A. Parker, and K. W. Michael, *J. Am. Chem. Soc.*, **86**, 3271 (1964); L. H. Sommer, W. D. Korte, and P. S. Podcwald, *ibid.*, **89**, 862 (1967).

19) M. Murakami, Ph. D. Theses, Tohoku University, 1972; C. Eaborn and O. W. Steward, *Proc. Chem. Soc.*, 59 (1963).

20) F. Meganem, A. Jean, and M. Lequan, *J. Organomet. Chem.*, **74**, 43 (1974).

21) S. Winstein and D. Trifan, *J. Am. Chem. Soc.*, **74**, 1147, 1154 (1952).

22) T. G. Traylor, W. Hanstein, J. J. Berwin, N. A. Clinton, and R. S. Brown, *J. Am. Chem. Soc.*, **93**, 5715 (1971) and references cited therein.

23) H. C. Brown, B. G. Gredin, K. Takeuchi, and E. N. Peters, *J. Am. Chem. Soc.*, **96**, 610 (1975).

24) M. Makosza and M. Wawrzyniewicz, *Tetrahedron Lett.*, **1969**, 4659.

25) J. L. Speier, J. A. Webster, and G. H. Barnes, *J. Am. Chem. Soc.*, **79**, 974 (1957); R. A. Benkeser and R. A. Hickner, *ibid.*, **80**, 5298 (1958); **83**, 4585 (1961); A. J. Chalk and J. F. Harrod, *ibid.*, **87**, 16 (1965).

26) D. Seyferth, *Acc. Chem. Res.*, **5**, 65 (1972).

27) D. Seyferth and Y. M. Cheng, *J. Am. Chem. Soc.*, **93**, 4072 (1971); D. Seyferth, H. M. Shih, J. Dubac, P. Mazerdles, and B. Serres, *J. Organomet. Chem.*, **50**, 39 (1973). The insertion into Si–H bond also took place at retention on a silicon atom, see, D. Seyferth and E. M. Hanson, *J. Am. Chem. Soc.*, **90**, 2438 (1968).

28) D. Seyferth, V. A. Mai, and M. E. Gorden, *J. Org. Chem.*, **35**, 1993 (1970).

29) D. Seyferth, S. S. Washburne, C. J. Attridge, and K. Yamamoto, *J. Am. Chem. Soc.*, **92**, 4405 (1970).

30) D. Seyferth, J. M. Burlitch, K. Yamamoto, S. S. Washburne, and C. J. Attridge, *J. Org. Chem.*, **35**, 1989 (1970).

31) D. Seyferth and Y. M. Cheng, *J. Am. Chem. Soc.*, **95** 6763 (1973); D. Seyferth, R. Damrauer, Y. P. Mui, and T. F. Jula, *ibid.*, **90**, 2944 (1968).

32) W. Hanstein, H. J. Berwin, and T. G. Traylor, *J. Am. Chem. Soc.*, **92**, 7476 (1970); C. G. Pitt, *J. Organomet. Chem.*, **23**, C35 (1970); V. A. Petrukov, V. F. Mironov, and P. P. Shorygin, *Izv. Acad. Nauk, SSSR, Ser. Khim*, **12**, 2203 (1964); H. Sakurai, S. Tasaka, and M. Kira, *J. Am. Chem. Soc.*, **94**, 9285 (1972).

33) a) A. Hosomi and H. Sakurai, *J. Am. Chem. Soc.*, **95**, 1384 (1972); b) M. Kumada and H. Hattori, *Kogyo*

Kagaku Zasshi, **56**, 269 (1953); *Chem. Abstr.*, **48**, 10543 (1954).
34) G. H. Schmidt and A. W. Wolkoff, *J. Org. Chem.*, **32**, 254 (1967).
35) J. W. Wilt, S. N. Massle, and R. B. Dabek, *J. Org. Chem.*, **35**, 2803 (1970).
36) V. A. Ponomarenko, G. V. Odabashyan, and A. D. Petrov, *Dokl. Akad. Nauk SSSR*, **130**, 333 (1960); *Chem. Abstr.*, **54**, 10914 (1960).
37) L. A. Sommer and J. E. Lyons, *J. Am. Chem. Soc.*, **91**, 7061 (1969).
38) M. Fedrynski and M. Makosza, *J. Organomet. Chem.*, **51**, 89 (1973).

Silicon-Carbon Unsaturated Compounds. XVI.[1] Photorearrangement of an Adduct Derived from Reaction of a Silicon-Carbon Unsaturated Compound with *t*-Butyl Alcohol

Mitsuo Ishikawa,* Michio Oda, Kunio Nishimura, and Makoto Kumada

Department of Synthetic Chemistry, Faculty of Engineering, Kyoto University, Yoshida, Sakyo-ku, Kyoto 606

(Received April 14, 1983)

Photolysis of pentamethylphenyldisilane in the presence of *t*-butyl alcohol gave a mixture of adducts which were readily oxidized to 1-(*t*-butoxydimethylsilyl)-2-(trimethylsilyl)benzene by oxygen. Photolysis of *p*-tolylpentamethyldisilane in the presence of *t*-butyl alcohol afforded 4-(*t*-butoxydimethylsilyl)-1-methyl-5-trimethylsilyl-1,3-cyclohexadiene (**4**) as a primary photoproduct. The UV-irradiation of **4** gave ring opened products, 2-(*t*-butoxydimethylsilyl)-5-methyl-1-trimethylsilyl-1,3,5-hexatriene and 2-(*t*-butoxydimethylsilyl)-5-methyl-3-trimethylsilyl-1,3,5-hexatriene in a ratio of 1.8/1.

Previous studies in our laboratory have shown that the photolysis of aryldisilanes causes their rearrangement to isomeric silicon–carbon unsaturated compounds, which can react with many types of trapping agent.[2-4] As reported previously, the silicon-carbon unsaturated intermediate generated photochemically from pentamethyl(*p*-tolyl)disilane in a benzene solution reacts with methyl alcohol to give 1-(methoxydimethylsilyl)-4-methyl-6-trimethylsilyl-1,3- and 1,4-cyclohexadiene in the ratio of approximately 1/1 in high yield.[5] We now wish to report the reaction of this intermediate with *t*-butyl alcohol and the photochemistry of the resulting adduct.

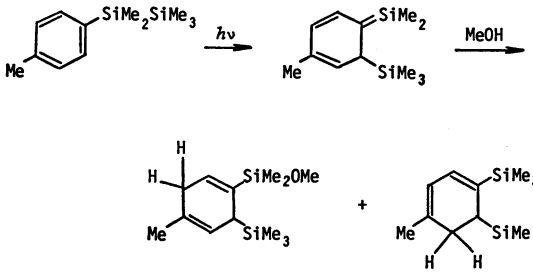

Results and Discussion

Photolysis of Aryldisilanes in the Presence of t-*Butyl Alcohol.* The photochemical studies were carried out with a low-pressure immersion mercury lamp having a Vycor filter.

First, we investigated the photolysis of pentamethylphenyldisilane (**1**) in the presence of *t*-butyl alcohol in benzene. In this case, a mixture of two isomers was obtained in 38% yield as reaction products; the ^{1}H NMR spectrum of the mixture showed two resonances in a ratio of 1/3 for *t*-butoxyl protons. Preparative GLC and column chromatography were used to isolate each isomer from the mixture, but they could not be separated under any of the conditions used. The mass spectrum of the mixture showed a parent peak at *m/e* 282, corresponding to the calculated molecular weight for $C_{15}H_{30}OSi_2$. The alcohol adducts can readily be oxidized by atmospheric oxygen. Thus, when the mixture of the adducts was allowed to stand for a week at room temperature in an oxygen atmosphere, 1-(*t*-butoxydimethylsilyl)-2-(trimethylsilyl)-benzene (**2**) was obtained in 65% yield, in addition to 17% of the starting adducts.

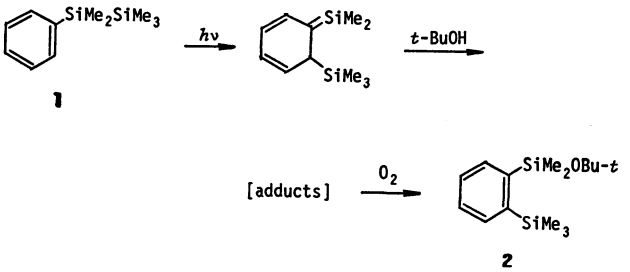

We then turned our attention to pentamethyl(*p*-tolyl)disilane (**3**) as a source of the silicon–carbon double-bonded intermediate. As we reported earlier, the photolysis of **3** in the presence of methyl alcohol afforded two addition products which could easily be separated by preparative GLC.[5] Interestingly, the photolysis of **3** in the presence of *t*-butyl alcohol in benzene at room temperature gave 4-(*t*-butoxydimethylsilyl)-1-methyl-5-trimethylsilyl-1,3-cyclohexadiene (**4**) as a primary photoproduct in 27% yield, when 70% of the starting disilane was photolyzed. At this stage, 2-(*t*-butoxydimethylsilyl)-5-methyl-1-trimethylsilyl-1,3,5-hexatriene (**5**) (6% yield) and 2-(*t*-butoxydimethylsilyl)-5-methyl-3-trimethylsilyl-1,3,5-hexatriene (**6**) (6% yield) were formed as secondary photoproducts. Small amounts of *t*-butoxydimethyl(*p*-tolyl)silane (**7**)

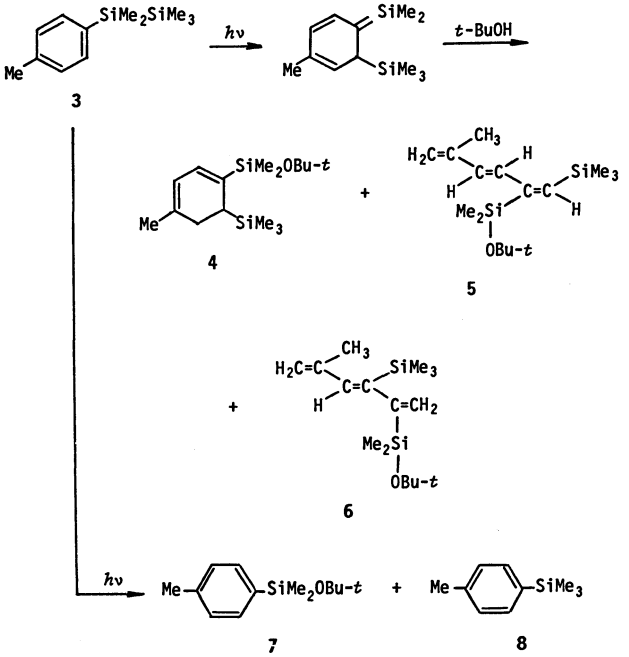

(3% yield) and *p*-tolyltrimethylsilane (**8**) (2% yield) were also produced. However, no isolable amount of the disilyl-substituted 1,4-cyclohexadiene isomer was obtained, whereas under similar conditions but using a lower primary alcohol such as methyl alcohol[5] and ethyl alcohol (see Experimental section) as a quencher, both the analogous 1,3- and 1,4-cyclohexadiene isomers were found to be produced.

At present, no convincing explanation for the absence of the 1,4-cyclohexadiene in the product is available, but steric interactions arising from an approach of the alcohol to the silicon–carbon unsaturated compound would be important for the product distribution. We found that the adducts to the less hindered alcohols are photochemically more stable than those to the hindered alcohols under the used conditions. Thus, the photolysis of **3** in the presence of methyl alcohol afforded no isolable amounts of the ring opened products when 80% of **3** was photolyzed. On the other hand, compound **4** decomposed slowly to give photoproducts, **5** and **6**, under prolonged irradiation.

Compound **4** was identified by mass and NMR spectroscopic methods. Compound **4** exhibited proton absorptions at δ 0.01 (CH_3–$SiMe_2$, s, 9H), 0.23 (CH_3–SiOBu-*t*, s, 6H), 1.28 (*t*-BuO–Si, s, 9H), 1.6—2.0 (H–$CSiMe_3$, m, 1H), 1.76 (CH_3–C, broad s, 3H), 2.3—2.6 (H_2C–$CSiMe_3$, m, 2H), 5.59 (H–C=CMe, m, 1H) and 6.07 (H–C=CSiOBu-*t*, broad d, 1H, J=5 Hz).

Photochemical Isomerization of 4. In order to learn more about the photoisomerization of **4** to **5** and **6**, we investigated the photochemistry of **4**. When a solution of **4** in benzene was photolyzed at room temperature for 13.5 h, **5** and **6** were obtained in 43 and 24% yield, respectively, in addition to 24% of the starting substance. No other isomer such as a bicyclo[3.1.0]hexene derivative (**11**), which might be expected to be formed from formal intramolecular [2+4] cycloaddition of 1,3,5-triene (**10**), could be detected by spectroscopic analysis.[6–8] Furthermore, it was shown that compound **5**, which could easily be isolated by preparative GLC, did not undergo isomerization at all when irradiated under similar conditions. These results indicate that both the products, **5**, and **6**, must come independently from the photoisomerization of **4**. The *trans* triene structure for **5** is based on its NMR spectrum: δ=0.17 (CH_3–$SiMe_2$, s, 9H), 0.25 (CH_3–SiOBu-*t*, s, 6H), 1.25 (*t*-Bu–O, s, 9H), 1.87 (CH_3–C=C, broad s, 3H), 4.98 (H_2C=CMe, broad s, 2H), 6.17 (H–$CSiMe_3$, broad s, 1H), 6.48 (H–C–CMe, d, 1H, J=16 Hz), and 6.72 (H–C–CSi, d, 1H, J=16 Hz). The magnitude of the coupling constant requires that the geometrical configuration of **5** is *trans*.

Compound **6** can also be shown unambiguously to have the proposed structure by proton NMR spectroscopy: (δ) 0.17 (CH_3–$SiMe_2$, s, 9H), 0.29 (CH_3–SiOBu-*t*, s, 6H), 1.28 (*t*-Bu–O, s, 9H), 1.84 (CH_3–C=C, broad s, 3H), 4.91 (H_2C=CMe, broad, s, 2H), 6.30 (H_2C=CSi, s, 2H), and 6.64 (H–C=C, s, 1H).

Two modes of conrotatory motion are possible in the ring opening of **4**.[9,10] One involves the formation of the triene **9**, in which the two silyl groups are brought into a *cis* relationship, and the other comprises the production of the triene **10** having *E*-configuration for the two silyl groups. Unfortunately both compounds **9** and **10** could not be detected either by GLC or spectroscopic analysis. However, the former process seems to be unlikely, because *Z*-configuration of the two bulky silyl groups about the carbon-carbon double bond is sterically very unfavorable. Compound **10** thus formed would undergo rapid isomerization to afford the observed product **5**. The formation of **6** can be explained in terms of successive 1,3-sigmatropic hydrogen shifts in the compound **4**, followed by rapid ring opening and rearrangement of the resulting product (**12**).

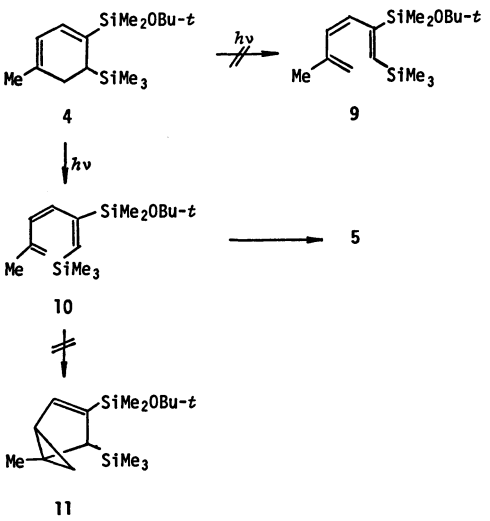

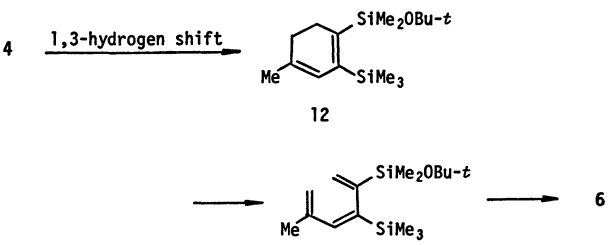

Experimental

^{1}H NMR spectra were determined with a JEOL JNM-MH-100 spectrometer in carbon tetrachloride. Mass spectra were measured on a JEOL JMS-300 mass spectrometer equipped with a JMA-2000 data processing system. Ionization voltage was 24 eV for all compounds. A Shimazu Model GC-4B gas chromatograph with a column containing 30% methylsilicon polymer (5 mm×1.5 m) was used for analysis of the products. An Aerograph Model 90 gas chromatograph with a thermal conductivity detector was used for separation of the products reported here.

Materials. Pentamethylphenyldisilane[11] and pentamethyl(*p*-tolyl)disilane[12] were prepared as described in the literature. *t*-Butyl alcohol was purified fractional distillation. Benzene was dried over lithium aluminum hydride and distilled just before use.

Photolysis of Pentamethylphenyldisilane (1) in the Presence of t-Butyl Alcohol. A solution of 1.00 g (4.8 mmol) of **1** and 20 ml of *t*-butyl alcohol in 80 ml of dry benzene was photolyzed for 3 h at room temperature under bubbling nitrogen. The solvent benzene and unchanged *t*-butyl al-

cohol were evaporated, and the residue was distilled under reduced pressure. GLC analysis of the distillate showed that 37% yield of the adduct consisting of two isomers was produced in addition to phenyltrimethylsilane (2%), 1-(*t*-butoxydimethylsilyl)-2-(trimethylsilyl)benzene (**2**) (2.5%) and the starting compound (11.5%). The adduct was isolated by preparative GLC as a mixture. MS *m/e* 282; Found: C, 63.77; H, 10.54%. Calcd for $C_{15}H_{30}OSi_2$: C, 63.90; H, 10.70%.

Oxidation of the Adduct. The photolysis mixture containing 1.6 mmol of the adduct was concentrated and the residue was allowed to stand in an oxygen atmosphere for a week at room temperature. GLC analysis of the resulting mixture showed that 64% yield of **2** was produced, and 17% of the starting adduct was recovered. Pure **2** was isolated by preparative GLC; MS *m/e* 280; ^{1}H NMR δ=0.37 (CH_3–$SiMe_2$, s, 9H); 0.43 (CH_3–SiMeOBu-*t*, s, 6H), 1.30 (CH_3–CMe_2OSi, s, 9H) and 7.15—7.63(ring protons, m, 4H); Found: C, 64.62; H, 10.1%. Calcd for $C_{15}H_{28}OSi_2$: C, 64.42; H, 10.06%.

Photolysis of p-*Tolylpentamethyldisilane (**3**) in the Presence of Ethyl Alcohol.* A solution of 0.9896 g (4.45 mmol) of **3** and 10 ml of ethyl alcohol in 90 ml of benzene was photolyzed for 3 h at room temperature. The solvent benzene was evaporated and the residue was distilled under reduced pressure to give volatile products. GLC analysis showed the presence of 4-(ethoxydimethylsilyl)-1-methyl-5-trimethylsilyl-1,3-cyclohexadiene (**13**) and 4-(ethoxydimethylsilyl)-1-methyl-3-trimethylsilyl-1,4-cyclohexadiene (**14**) in 27 and 18% yield, respectively, along with 7% of ethoxydimethyl(*p*-tolyl)silane[13] and 27% of the starting **3**. A small amount of unidentified compounds (less than 5%) was also detected. For, **13**: MS *m/e* 268; ^{1}H NMR δ=-0.04 (CH_3–$SiMe_2$, s, 9H), 0.14 (CH_3–SiMeOEt, s, 6H), 1.16 (CH_3–CH_2O, t, 3H, J=6 Hz), 1.76 (CH_3–C, broad s, 3H), 1.85—2.47 (H_2C–CH, m, 3H), 3.65 (CH_2–O, q, 2H, J=6 Hz), 5.64 (H–C=CMe, m, 1H); 6.15 (H–C=CSi, d, 1H); Found: C, 62.89; H, 10.66%. Calcd for $C_{14}H_{28}OSi_2$: C, 62.62; H, 10.51%. For **14**: MS *m/e* 268; ^{1}H NMR δ=−0.03 (CH_3–$SiMe_2$, s, 9H), 0.17 (CH_3–SiMeOEt, s, 6H), 1.15 (CH_3–CH_2O, t, 3H, J=6 Hz), 1.70 (CH_3–C, broad s, 3H), 2.37—2.65 (H_2C and HC, m, 3H), 3.62 (CH_2–O, q, 2H, J=6 Hz), 5.45 (H–C=CMe, m, 1H), 6.00 (H–C=CSi, t, 1H); Found: C, 62.32; H, 10.75%. Calcd for $C_{14}H_{28}OSi_2$: C, 62.62; H, 10.51%.

*Photolysis of **3** in the Presence of* t-*Butyl Alcohol.* A solution of 1.0170 g (4.57 mmol) of **3** and 20 ml of *t*-butyl alcohol in 80 ml of benzene was irradiated for 4 h. The solvent benzene was evaporated and the residue was distilled under reduced pressure to give volatile products. GLC analysis showed that the distillate contained **4** (28%), **5** (6%), and **6** (6%), together with *t*-butoxydimethyl(*p*-tolyl)silane **7** (2%), *p*-tolyltrimethylsilane (**8**) (trace) and the starting disilane (30%). Compound **4** was isolated by preparative GLC. MS *m/e* 296; Found: C, 65.09; H, 11.01%. Calcd for $C_{16}H_{32}OSi_2$: C, 64.79; H, 10.87%. Compounds **7** and **8** were identified by comparison of their retention times on GLC with those of the authentic samples.

*Photoisomerization of **4**.* A solution of 472 mg (1.59 mmol) of **4** in 80 ml of dry benzene was irradiated for 13.5 h at room temperature. Distillation of the reaction mixture afforded **5** and **6** in 43 and 24% yield, respectively, together with 24% of the starting compound. Both **5** and **6** were isolated by preparative GLC. For **5**: MS *m/e* 296; Found: C, 64.59; H, 10.79%. Calcd for $C_{16}H_{32}OSi_2$: C, 64.79; H, 10.87%. For **6**: MS *m/e* 296; Found: C, 64.55; H, 10.64%. Calcd for $C_{16}H_{32}OSi_2$: C, 64.79; H, 10.87%.

The cost of this research defrayed by a Grant-in-Aid for Scientific Research by the Ministry of Education, Science and Culture and Toray Science and Technology Grant to which our thanks are due. We also express our appreciation to Toshiba Silicone Co., Ltd., Shinetsu Chemical Co., Ltd., and Toray Silicone Co., Ltd., for gift of organochlorosilanes.

References

1) For part 15, see M. Ishikawa, H. Sugisawa, M. Kumada, T. Higuchi, K. Matsui, K. Hirotsu, and J. Iyoda, *Organometallics*, **2**, 174 (1983).
2) M. Ishikawa, T. Fuchikami, T. Sugaya, and M. Kumada, *J. Am. Chem. Soc.*, **97**, 5924 (1975).
3) M. Ishikawa, *Pure Appl. Chem.*, **50**, 11 (1978).
4) M. Ishikawa and M. Kumada, *Adv. Organomet. Chem.*, **19**, 51 (1981).
5) M. Ishikawa, T. Fuchikami, and M. Kumada, *J. Organomet. Chem.*, **118**, 155 (1976).
6) W. G. Dauben, M. S. Kellogg, J. I. Seeman, N. D. Vietmeyer, and P. H. Wendschuh, *Pure Appl. Chem.*, **33**, 197 (1973).
7) A. Padwa, L. Brodsky, and S. Clough, *J. Am. Chem. Soc.*, **94**, 6767 (1972).
8) Y. Nakadaira, S. Kanouchi, and H. Sakurai, *J. Am. Chem. Soc.*, **96**, 5621 (1974).
9) P. Courtot and R. Rumin, *Tetrahedron Lett.*, **1970**, 1849.
10) C. W. Spangler and R. P. Hennis, *J. Chem. Soc., Chem. Commun.*, **1972**, 24.
12) M. Ishikawa, T. Fuchikami, and M. Kumada, *J. Organomet. Chem.*, **118**, 139 (1976).
13) D. W. Levis and G. C. Gainer, *J. Am. Chem. Soc.*, **74**, 2931 (1952).

Cyclotrimerization and Polymerization of 1-Hexyne Catalyzed by Group 5, 6 Transition Metal Chlorides[1)]

Toshio MASUDA, Yun-Xiang DENG,† and Toshinobu HIGASHIMURA*

Department of Polymer Chemistry, Faculty of Engineering, Kyoto University, Sakyo-ku, Kyoto 606

(Received April 20, 1983)

1-Hexyne could be cyclotrimerized selectively and quantitatively by $NbCl_5$ and $TaCl_5$. The cyclotrimer formed consisted of 1,2,4- and 1,3,5-isomers. The 1,2,4/1,3,5 isomer ratio of the product was about 70/30—80/20 with $NbCl_5$, and about 55/45—70/30 with $TaCl_5$. The polymerization of 1-hexyne by $MoCl_5$- and WCl_6-based catalysts afforded a methanol-insoluble polymer and methanol-soluble products in comparable amounts. The polymer (mol wt 3000—5000) was an orange-yellow viscous material with structure $\{CH=C(n\text{-Bu})\}_n$. For comparison, the cyclotrimerization and polymerization using Ziegler catalysts were also examined.

1-Hexyne can be cyclotrimerized by transition metal catalysts [$TiCl_4$–Et_3Al,[3)] $(Ph_3P)_2Ni(CO)_2$,[4)] and $(\eta^5\text{-}C_5H_5)_2V$[5)]]. The polymer and linear oligomer of 1-hexyne, however, are often formed as by-products in the cyclotrimerization. Further, the cyclotrimer formed (tributylbenzene) is usually a mixture of 1,2,4- and 1,3,5-isomers. The selectivity of the cyclotrimerization and the 1,2,4/1,3,5 isomer ratio of cyclotrimer have hardly been clarified.

1-Hexyne can be polymerized by transition metal catalysts [$TiCl_3$–Et_3Al,[6,7)] Fe(III) naphthenate-$(i\text{-Bu})_3Al$,[8)] and $PhCH_3\cdot Mo(CO)_3$[9)]]. High molecular weight poly(1-hexyne) ($[\eta]=2$—6 dl/g) is obtained with a Ziegler catalysts, Fe(III) naphthenate-$(i\text{-Bu})_3Al$. The yield of cyclotrimer as by-product and the geometric structure of the polymer, however, have not been studied.

Acetylene[10)] and phenylacetylene[11)] are cyclotrimerized by $NbCl_5$ and $TaCl_5$. Various acetylenes are polymerized by $MoCl_5$- and WCl_6-based catalysts.[12)] Therefore, it is interesting to examine the selectivity and product structure in the cyclotrimerization of 1-hexyne by $NbCl_5$ and $TaCl_5$, and in the polymerization of the monomer by $MoCl_5$ and WCl_6.

This paper deals with the cyclotrimerization and polymerization of 1-hexyne. It has been found that the cyclotrimerization by $NbCl_5$ and $TaCl_5$ selectively yields cyclotrimer, while not only polymer but also cyclotrimer is formed in the polymerization by $MoCl_5$ and WCl_6. For comparison, the cyclotrimerization and polymerization by Ziegler catalysts were also carried out.

Experimental

1-Hexyne was purchased from Farchan Labs, USA, and distilled twice from calcium hydride under nitrogen before use. Commercially available transition metal and organometallic compounds were used without further purification. Polymerization solvents were washed with acid and/or alkaline solutions and distilled from appropriate drying agents; care was exercised to dry and deaerate them sufficiently.

Two-component catalysts were aged in solution at 30 °C for 15 min before use. Reactions of 1-hexyne were carried out under nitrogen and terminated by adding ammoniacal methanol. Monomer consumptions (conversions) were determined by ges chromatography.

Cyclotrimerization was worked up by washing reaction mixtures with dilute hydrochloric acid and water and then evaporating the solvent. The ratio of cyclotrimer to linear oligomer was determined by liquid chromatography (JASCO Triroter II chromatograph; Shodex A802, A804 polystyrene gel columns). Two isomers of cyclotrimer (1,2,4- and 1,3,5-tributylbenzenes) could be separated by gas chromatography (Shimadzu GC3B chromatograph; Silicone DC550 supported on Chromosorb W (10%) 5 m, 195 °C). The isomer with a shorter retention time was identified as 1,3,5-tributylbenzene because it showed a singlet ($\delta=6.80$) in the aromatic region in ^1H NMR (a multiplet was observed for the other isomer). Therefore the ratio of the two isomers was determined by gas chromatography.

The polymeric product in polymerization was recovered by precipitation in a large amount of methanol, and its yield was determined by gravimetry. The oligomeric product was dealt with similarly to the cyclotrimerization product. Number-average molecular weights, $\overline{M}_n$, of polymers were obtained by vapor pressure osmometry (Hitachi 117 molecular weight apparatus). Differential thermal analysis (DTA) was performed under nitrogen with a Shimadzu 20B analyzer.

Results and Discussion

Cyclotrimerization. The cyclotrimerization of 1-hexyne by $NbCl_5$ and $TaCl_5$ proceeded quantitatively under the conditions shown in Table 1. Hydrocarbons and halogenated hydrocarbons were useful solvents, whereas ethers, esters and ketones were not. The products consisted exclusively of cyclotrimer, which was a mixture of two isomers, that is, 1,2,4- and 1,3,5-tributylbenzenes. The 1,2,4/1,3,5 isomer ratio of the product was about 70/30—80/20 with $NbCl_5$, and about 55/45—70/30 with $TaCl_5$; the former catalyst generally yielded more 1,2,4-isomer. The ratio was affected only slightly by the solvents used.

The effect of temperature on the cyclotrimerization was examined between 0 and 60 °C (Table 2). The reaction rate greatly reduced with decreasing temperature. The 1,2,4/1,3,5 isomer ratio of product somewhat decreased with both $NbCl_5$ and $TaCl_5$, as the reaction temperature was lowered.

Thus $NbCl_5$ and $TaCl_5$ effected highly selective cyclotrimerization of 1-hexyne similarly to the case of phenylacetylene.[11)] The 1,2,4/1,3,5 isomer ratio varied only in a range of 54/46—78/22 with reaction con-

† Present address: Zhongshen (Sun Yatsen) University, China.

Table 1. 1,2,4/1,3,5 Isomer ratios of products in the cyclotrimerization of 1-hexyne by NbCls and TaCls[a]

Cat	Benzene	Toluene	Hexane	Cyclohexane	CCl_4	$CHCl_3$	$(CH_2Cl)_2$
$NbCl_5$	78/22	78/22	75/25	76/24	78/22	74/26	72/28
$TaCl_5$	72/28	68/32	54/46	56/44	72/28	57/43	62/38

a) $[1\text{-Hexyne}]_0=1.0$ mol dm^{-3}, $[cat]=10$ mmol dm^{-3}, 60 °C (50 °C for $CHCl_3$), 2 h: cyclotrimer (1,2,4- and 1,3,5-isomers) was selectively and quantitatively obtained.

Table 2. Temperature dependence of the cyclotrimerization of 1-hexyne by $NbCl_5$ and $TaCl_5$[a]

Cat	1,2,4/1,3,5 ratio		
	60 °C	30 °C	0 °C
$NbCl_5$	78/22	76/24	73/27
$TaCl_5$	68/32	60/40	55/45

a) $[1\text{-Hexyne}]_0=1.0$ mol dm^{-3}. $[cat]=10$ (60 °C) or 30 (30°, 0 °C) mmol dm^{-3}, in toluene, 2 (60 °C), 24 (30 °C) or 120 (0 °C) h: cyclotrimer (1,2,4- and 1,3,5-isomers) was selectively and quanitatively obtained.

Table 3. Cyclotrimerization of 1-hexyne by Ziegler catalysts[a]

Cat	Cocat	Conversion %	Yield/%		
			Cyclotrimer		Linear oligomer
			1,2,4	1,3,5	
$TiCl_4$	Et_2AlCl	100	53	47	0
$TiCl_4$	Et_3Al	85	33	37	15
VCl_4	Et_2AlCl	96	21	50	25
VCl_4	Et_3Al	95	26	26	43
$VOCl_3$	Et_2AlCl	90	52	38	0
$VOCl_3$	Et_3Al	95	13	11	71

a) $[1\text{-Hexyne}]_0=1.0$ mol dm^{-3}, $[cat]=30$ mmol dm^{-3}, $[cocat]=45$ mmol dm^{-3}, in toluene, 30 °C, 24 h; catalyst aging 30 °C, 15 min.

ditions (catalyst, solvent and temperature). This contrast with a larger variance of the ratio (17/83—94/6) in the cyclotrimerization of phenylacetylene with similar changes in reaction conditions. Metallacyclopentadienes should be involved as intermediates in the cyclotrimerizaton of acetylenes with transition metal catalysts.[13] Since the phenyl group is bulkier than the butyl group, it is reasonable that the orientation of two acetylene molecules during the formation of a metallacyclopentadiene is more dependent on reaction conditions in phenylacetylene than in 1-hexyne.

The cyclotrimerization of 1-hexyne by Ziegler catalysts was investigated for comparison. Though various combinations of transition metal chlorides and organoaluminums were employed as catalysts, most of them yielded not only cyclotrimer but also linear oligomer. Chlorides of Ti and V were most effective among various transition metal chlorides. $EtAlCl_2$ possessed a high Lewis acidity to give linear oligomer by the cationic mechanism. The catalyst systems that showed relatively high selectivity for cyclotrimerization are given in Table 3. The 1,2,4/1,3,5 isomer ratios were usually close to unity.

Polymerization. Table 4 shows results for the polymerization of 1-hexyne by $MoCl_5$- and WCl_6-based catalysts. Both $MoCl_5$- and WCl_6-based catalysts worked effectively, the latter being somewhat more active. Methanol-insoluble polymers were about half the whole products in quantity. The polymers had relatively low molecular weights (3000—5000). Methanol-soluble oligomers consisted of linear oligomer and cyclotrimer (both 1,2,4- and 1,3,5-isomers involved). The observed cocatalyst effect shows that both or either of methanol and Ph_4Sn is useful to increase conversion and polymer yield. Nonpolar solvents such as benzene, cyclohexane and carbon tetrachloride were preferable.

Table 4. Polymerization of 1-hexyne by $MoCl_5$ and WCl_6[a]

Cat	Coat	Solvent	Conversion %	Polymer[b]	
				Yield %	$\overline{M}_n$
$MoCl_5$	None	Benzene	41	13	—
$MoCl_5$	CH_3OH	Benzene	75[c]	38	3200
$MoCl_5$	Ph_4Sn	Benzene	20	8	—
$MoCl_5$	CH_3OH	Cyclohexane	91	35	3200
$MoCl_5$	CH_3OH	CCl_4	95	47	4900
WCl_6	None	Benzene	62	9	—
WCl_6	CH_3OH	Benzene	83	51	3500
WCl_6	Ph_4Sn	Benzene	90[d]	62	4300
WCl_6	Ph_4Sn	Cyclohexane	100	58	3100
WCl_6	Ph_4Sn	CCl_4	100	63	3900

a) $[1\text{-Hexyne}]_0=1.0$ mol dm^{-3}, $[cocat]=10$ (CH_3OH) or 20 (Ph_4Sn) mmol dm^{-3}, 30 °C, 3 h. b) The methanol-insoluble product. c) Yields of methanol-soluble products: linear oligomer 19%, 1,2,4-cyclotrimer 7%, 1,3,5-cyclotrimer 11%. d) Yields of methanol-soluble products: limear oligomer 15%, 1,2,4-cyclotrimer 3%, 1,3,5-cyclotrimer 10%.

For comparison, the polymerization by Ziegler catalysts was examined. In acetylene polymerization, polymer is selectively formed only when both transition metal and organoaluminum compounds have low Lewis acidities.[14] Therefore, we chose combinations of transition metal acetylacetonates and Et_3Al as catalyst systems. A high polymer yield was achieved in the polymerization using $Fe(acac)_3$ in cyclohexane solution (Table 5). Though $VO(acac)_3$ and $Co(acac)_3$ were also effective, the polymer yields were rather low. The main products were methanol-insoluble polymers; small amounts of linear oligomer and cyclotrimer were also formed. Polymer molecular weights were 5000—13000, higher than those with $MoCl_5$- and WCl_6-based catalysts. Aliphatic and aromatic hydrocarbons were

Table 5. Polymerization of 1-hexyne by Ziegler catalysts[a]

Cat	Solvent	Conversion %	Polymer[b] Yield %	Polymer[b] $\overline{M}_n$
$Fe(acac)_3$	Cyclohexane	100[c]	85	6000
$Fe(acac)_3$	Toluene	0	0	—
$VO(acac)_3$	Cyclohexane	40	27	7900
$VO(acac)_3$	Toluene	60	39	13200
$Co(acac)_3$	Cyclohexane	44	19	5000
$Co(acac)_3$	Toluene	35	22	11300

a) $[1\text{-Hexyne}]_0=1.0$ mol dm^{-3}, [cat]=20 mmol dm^{-3}, cocatalyst: Et_3Al (60 mmol dm^{-3}), 30 °C, 3 h; catalyst aging 30 °C, 15 min. b) The methanol-insoluble product. c) Yields of methanol-soluble products: linear oligomer 9%, 1,2,4-cyclotrimer 3%, 1,3,5-cyclotrimer 3%.

Table 6. Relationship between monomer structure and product in the polymerization of monosubstituted acetylenes by $MoCl_5$ and WCl_6

Monomer: Steric effect[a]	Monomer: Example	Ref	Product: Mol wt of polymer	Product: Cyclotrimer[b]
	HC≡C(*n*-Bu)	This work		
Small	HC≡C(*n*-C_6H_{11})	15	10^3—10^4	Comparable
	HC≡C(*i*-Bu)	15		
	HC≡C(*s*-Bu)	15		
Medium	HC≡C(*c*-C_6H_{11})	15	10^4—10^5	<1/10
	HC≡CPh	16		
Large	HC≡C(*t*-Bu)	17	10^5—10^6	0

a) Steric effect of the substituent in monomer. b) Relative yields of cyclotrimer to polymer.

useful polymerization solvents. It is not clear why the polymerization using the $Fe(acac)_3$ system did not occur in toluene.

Table 6 summarizes polymer molecular weights and cyclotrimer(by-product) yields in the $MoCl_5$- and WCl_6-catalyzed polymerization of monosubstituted acetylenes. As the substituent in the monomer becomes bulkier and shows a greater steric effect, polymer molecular weight clearly increases and cyclotrimer yield approaches zero. As an extreme case, *t*-butylacetylene affords a very high polymer and does not form cyclotrimer; on the contrary, Ziegler catalysts cannot polymerize this monomer.[17] It does not appear an important factor whether the substituent is an alkyl or an aryl group. Table 6 leads to the conclusion that $MoCl_5$- and WCl_6-based catalysts are particularly effective towards sterically hindered acetylenes [*e.g.*, HC≡C(*t*-Bu)], while not so effective to sterically unhindered acetylenes [*e.g.*, HC≡C(*n*-Bu)]. It has been inferred that two acetylene molecules coordinate to a transition metal to form the intermediate in cyclotrimerization,[13] while one acetylene molecule in polymerization.[12]

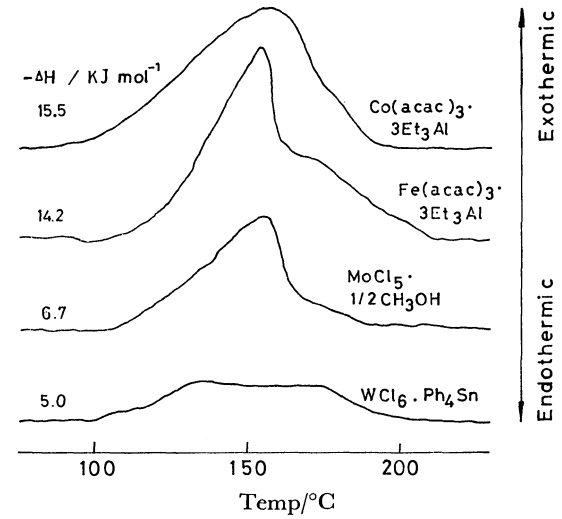

Fig. 1. DTA thermograms of poly(1-hexyne)s.

Therefore, polymerization will not suffer the steric effect so greatly as cyclotrimerization, which seems responsible for the selective polymerization of *t*-butylacetylene.

Spectral data of the poly(1-hexyne) obtained with $WCl_6\cdot Ph_4Sn$ in toluene are as follows: IR 1650—1600 cm^{-1} (w; conjugated C=C). ^{1}H NMR ($CDCl_3$) δ 5.87 (s, 1, –CH=), 2.21 (s, 2, $=CCH_2-$), 1.30 (s, 4, $-CH_2CH_2Me$), 0.90 (s, 3, CH_3). ^{13}C NMR ($CDCl_3$) δ 140.0 (C_2), 126.1 (C_1), 31.0 (C_3), 23.0, 22.6 (C_4, C_5), 14.0 (C_6). UV (hexane) λ_{max} 285 nm (ε 1600); the absorption continued as far as 450 nm. All the poly(1-hexyne)s obtained in the present study showed practically the same spectra. These data lead to the conclusion that the polymer has the conjugated polyene structure –[–CH=C(*n*-Bu)–]–.

In general, poly(1-hexyne) was an orange-yellow viscous material soluble in hydrocarbons and halogenated hydrocarbons. This polymer was gradually oxidized by air at room temperature, as confirmed by a carbonyl band at 1710 cm^{-1} in the IR spectrum. This contrasts with the fact that poly(*t*-butylacetylene), which cannot take a planar conformation, is very stable.[17]

Poly(1-hexyne)s obtained with several catalysts showed exothermic peaks of different magnitudes in the same temperature range in the DTA thermograms (Fig. 1). It is known that polyacetylene[18] and poly(phenylacetylene)[19] show exothermic peaks in DTA due to their isomerization from cis to more stable trans form. The cis content of poly(phenylacetylene) has been qualitatively estimated by the isomerization exotherm. Based on a similar discussion, one can conclude from Fig. 1 that the cis content of poly(1-hexyne) decreases in the following order of catalyst: $Co(acac)_3\cdot 3Et_3Al > Fe(acac)_3\cdot 3Et_3Al > MoCl_5\cdot(1/2)CH_3OH > WCl_6\cdot Ph_4Sn$. A similar order has been observed with poly(phenylacetylene): $Fe(acac)_3\cdot 3Et_3Al > MoCl_5\cdot(1/2)CH_3OH > WCl_6\cdot Ph_4Sn$.[19b] Thus $MoCl_5$- and WCl_6-based catalysts tend to give polymers with higher trans contents than do Ziegler catalysts.

This work was partly supported by a Grant-in-Aid

for Scientific Research No. 565299 from the Ministry of Education, Science and Culture.

References

1) Part VI of "Polymerization of Aliphatic Acetylenes," For part V, see Ref. 2.
2) Y. Okano, T. Masuda, and T. Higashimura, *Polym. J.*, **14**, 477 (1982).
3) E. F. Lutz, *J. Am. Chem. Soc.*, **83,** 2551 (1961).
4) L. S. Meriwether, E. C. Colthup, G. W. Kennerly, and R. N. Reusch, *J. Org. Chem.*, **26,** 5155 (1961).
5) R. Tsumura and N. Hagihara, *Bull. Chem. Soc. Jpn.*, **37**, 1889 (1964).
6) Natta, G. Mazzanti, and P. Pino, *Angew. Chem.*, **69**, 685 (1957).
7) A. A. Berlin, E. F. Vainshtein, M. I. Cherkashin, and Yu. Sh. Moshkovskii, *Vysokomol. Soedin.*, **5**, 1354 (1963).
8) W. J. Trepka and R. J. Sonnenfeld, *J. Polym. Sci., Part A-1*, **8**, 2721 (1970).
9) P. S. Woon and M. F. Farona, *J. Polym. Sci., Polym. Chem. Ed.*, **12,** 1749 (1974).
10) G. Dändliker, *Helv. Chim. Acta*, **52,** 1482 (1969).
11) T. Masuda, T. Mouri, and T. Higashimura, *Bull. Chem. Soc. Jpn.*, **53,** 1152 (1980).
12) For a review, T. Masuda, *Kagaku*, **37,** 570 (1982).
13) D. R. McAlister, J. E. Bercaw, and R. G. Bergman, *J. Am. Chem. Soc.*, **99,** 1666 (1977); H. Yamazaki and Y. Wakatsuki, *J. Organomet. Chem.*, **139,** 157 (1977); Y. Wakatsuki and H. Yamazaki, *ibid.*, **139,** 169 (1977).
14) T. Ito, H. Shirakawa, and S. Ikeda, *J. Polym. Sci., Polym. Chem. Ed.*, **12,** 11 (1974); H. Shirakawa and S. Ikeda, *J. Polym. Sci., Polym. Chem. Ed.*, **12,** 929 (1974).
15) T. Masuda, M. Kawasaki, T. Takahashi, Y. Okano, and T. Higashimura, *Polym. Preprints, Jpn.*, **31**, 1197 (1982); T. Masuda, M. Kawasaki, Y. Okano, and T. Higashimura, *Polym. J.*, **14,** 371 (1982).
16) T. Masuda, T. Takahashi, K. Yamamoto, and T. Higashimura, *J. Polym. Sci., Polym. Chem. Ed.*, **20,** 2603 (1982).
17) T. Masuda, Y. Okano, Y. Kuwane, and T. Higashimura, *Polym. J.*, **12,** 907 (1980).
18) T. Ito, H. Shirakawa, and S. Ikeda, *J. Polym. Sci., Polym. Chem. Ed.*, **13,** 1943 (1975).
19) C. I. Simionescu, S. Dumitrescu, and V. Percec, *J. Polym. Sci., Polym. Symp.*, **64,** 209 (1978); T. Masuda, T. Ohtori, and T. Higashimura, *Polym. Preprints*, **20**, 731 (1979).

Assignment of a Characteristic Infrared Absorption Band at 810 cm^{-1} in Heat-treated Polyacrylonitrile

Masao Okamoto

Department of Fiber and Polymer Engineering, Faculty of Engineering, Yamagata University, Jonan, Yonezawa 992

(Received August 10, 1982)

When polyacrylonitrile (PAN) was heat-treated at about 250 °C under nitrogen, a violent exothermic reaction took place. PAN lost weight and the infrared absorption at 2240 cm^{-1} disappeared, but there was little change in the atomic ratios of carbon, hydrogen, and nitrogen. This indicates that fragmentation is accompanied by rapid polymerization of cyano groups. The sample obtained after the completion of the exothermic reaction seems to be liable to oxidation, because a strong exothermic reaction and weight gain occur immediately if air is admitted to enter. During the oxidation the percentages of carbon and nitrogen did not change, but that of hydrogen largely decreased, indicating the occurrence of oxidation and subsequent dehydration in the moieties subjected to polymerization of cyano groups. Therefore, the tri-substituted carbon-carbon double bonds are formed in the six-membered ring systems. A new infrared absorption band which appears at 810 cm^{-1} is assigned to the C–H out-of-plane bending vibration in such a double bond.

Polyacrylonitrile (PAN) fiber is changed into flame-proof fiber by heat treatment in air at 200—300 °C.[1] Carbon fiber is produced by heating the flame-proof fiber in an inert atmosphere at 1000—1500 °C.[2] Thus a prior oxidative treatment is necessary in the preparation of carbon fiber from PAN fiber. In infrared absorption spectrum of PAN subjected to such an oxidative treatment, a strong absorption appears at 810 cm^{-1}. This was assigned to C–H out-of-plane bending vibration in –CH=C(C≡N)–,[3–8] but no absorption appeared at 810 cm^{-1} in the spectra of the products obtained by dehydrochlorination of poly(α-chloroacrylonitrile).[9] This fact is not consistent with the assignment.

Experimental

Preparation of PAN. The preparative method was reported in a previous work.[10]

Isothermal Heat Treatment. Heat treatment of PAN was carried out in a differential thermal analyzer (Rigaku CAT. No. 8001 Thermoflex) to observe the change of the sample temperature. The rate of the temperature rise is 20 °C/min.

Infrared Absorption Spectra. A Hitachi EPI-G_2 diffraction grating infrared spectrophotometer was used. Samples were examined as KBr disks. Normalized absorbance (A) of an absorption band was calculated by the equation:

$$A = \frac{a}{w} \times \frac{W}{W_0},$$

where a is the observed absorbance for w mg of the sample, and W (mg) is the amount left after heating W_0 (mg) of PAN. The yield given in Table 1 was calculated by

$$\text{Yield} = \frac{W}{W_0} \times 100 \ (\%).$$

Results and Discussion

Observation of an Exotherm in the Course of Heat Treatment. Change of the sample temperature was measured during the isothermal heat treatment (Fig. 1). Under nitrogen an exotherm due to polymerization of cyano groups was always observed when the heat-treatment temperature was above 230 °C. The

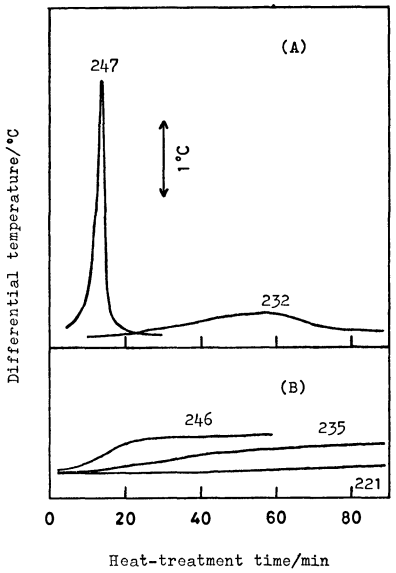

Fig. 1. Observation of an exotherm during isothermal heat treatment of 50 mg of PAN (A) under nitrogen and (B) in air. The heat-treatment temperature (°C) is given in the figure.

differential temperature increases with the treatment temperature. Especially, generation of heat was very sharp for the heat treatment at *ca.* 250 °C. In air an exotherm due to both polymerization of cyano groups and oxidation was observed at *ca.* 220 °C, but the peak was broad and weak even at 250 °C. This indicates that oxygen can retard a rapid polymerization of cyano groups at *ca.* 250 °C.

Compositions of Samples Heat-treated under Different Conditions. Samples 1, 2, 3, and 4 were heat-treated at 250 °C under the conditions given in Fig. 2. The yields and compositions are shown in Table 1. The percentage changes in carbon, hydrogen, and nitrogen due to the heat treatment are given in Table 2.

When PAN was heat-treated for 29 min under nitrogen, and for additional 10 min under reduced pressure, there was little change in the atomic ratios of carbon, hydrogen, and nitrogen although the weight loss was 6.3 wt%. This indicates fragmentation accompanied

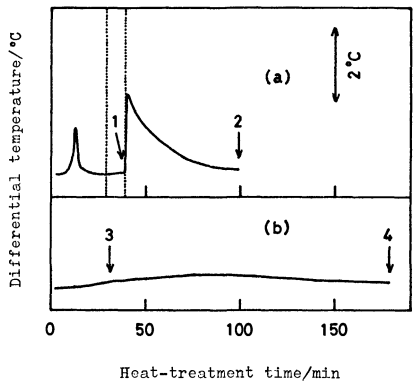

Fig. 2. Preparation of samples 1, 2, 3, and 4 by the isothermal heat treatment of 30 mg of PAN at 250 °C. The arrows indicate the end of heat treatment. Sample 1 was cooled by admitting nitrogen. Samples 2, 3, and 4 were cooled in a desiccator.
Atmosphere for heat treatment: (a) Nitrogen (0—29 min), reduced pressure (29—39 min), and air (39—99 min). (b) Air.

Table 1. Yields and analytical data of samples 1, 2, 3, and 4

Sample	Yield/%	Chemical compositions (%)				
		C	H	N	Ash	O (+Errors)
PAN	100	67.6	5.9	25.7	0.3	0.5
1	93.7	65.9	5.5	24.4	0.5	3.7
2	98.3	62.9	3.2	22.5	0.9	10.5
3	98.7	—	—	—	—	—
4	94.3	60.1	3.4	22.1	1.0	13.4

Table 2. Changes in weights of carbon, hydrogen, and nitrogen by heat-treating PAN

Sample	Residual weights (%)		
	C	H	N
PAN	100	100	100
1	91.3	87.3	88.9
2	91.5	53.4	86.1
4	83.8	54.4	81.1

by rapid polymerization of cyano groups. Sample 1 seems to be liable to oxidation, because a strong exothermic reaction and weight gain occur immediately if air is admitted to enter. Since weight loss of sample 2 obtained by heat-treating sample 1 in air for 60 min was 1.7 wt%, it is clear that oxygen combined with sample 1 to give weight gain of at least 4.6 wt%. During the oxidation the percentages of carbon and nitrogen did not change, but that of hydrogen decreased remarkably. This indicates that sample 1 was easily oxidized and subsequently dehydrated.

Sample 4 obtained by heat-treating PAN in air for 179 min resembles sample 2 and flame-proof fibers[1,11] in composition. Further there was no difference between the weight losses of hydrogen for a flame-proof fiber[11] and samples 2 and 4. The weight losses of

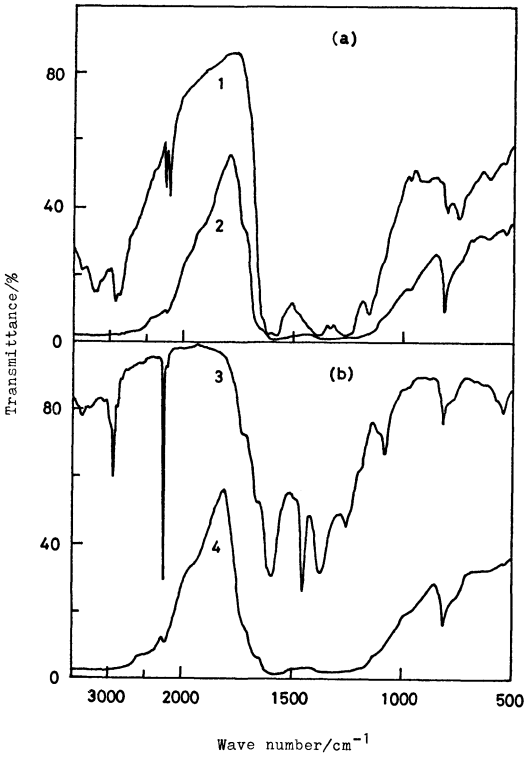

Fig. 3. Infrared absorption spectra of samples 1, 2, 3, and 4.

Table 3. Normalized absorbances at 2240, 2220, 2200, and 810 cm^{-1} in infrared absorption spectra of samples 1, 2, 3, and 4

Sample	Normalized absorbances			
	2240 cm^{-1}	2220 cm^{-1}	2200 cm^{-1}	810 cm^{-1}
PAN	0.300			
1	0.054		0.072	—[a]
2		0.034		0.221
3	0.254		0.010	0.036
4		0.050		0.121

a) Only observed as a shoulder of the band at 800 cm^{-1}.

carbon and nitrogen for a flame-proof fiber[11] and sample 4, however, were much higher than those for sample 2. This indicates that the degree of degradation for a flame-proof fiber[11] and sample 4 is much higher than that for sample 2.

Infrared Spectra of Samples Heat-treated under Different Conditions. Infrared spectra of samples 1, 2, 3, and 4 are shown in Fig. 3. The normalized absorbances at 2240, 2220, 2200, and 810 cm^{-1} are given in Table 3.

Since sample 1 had rapid polymerization of cyano groups, the absorbance of the C≡N stretching vibration band at 2240 cm^{-1} was below 1/5 of the value for PAN. However, there is no reason why 4/5 of cyano groups are lost only by polymerization, because it is accompanied by the elimination of volatile fragments and the appearance of a band at 2200 cm^{-1}. The following reactions[12,13] will be related with the appearance of this band:

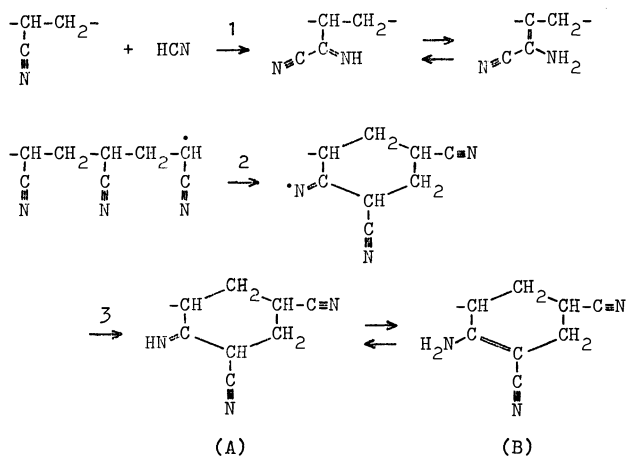

(A) (B)

In these reactions the atomic ratios do not change. The band at 2240 cm^{-1} disappears with reaction 1, but moieties A and B formed by six-membered ring formation 2 and subsequent hydrogen abstraction 3 have cyano groups which absorb at 2240 cm^{-1}. This explains why sample 1 obtained after the completion of rapid polymerization of cyano groups shows the band at 2240 cm^{-1}.

Sample 2 shows a strong absorption at 810 cm^{-1}, which is the characteristic band appearing in the spectra of PAN samples heat-treated in the presence of oxygen.[3-8,14] If this band is due to –CH=C(C≡N)– formed by the oxidation and subsequent dehydration in acrylonitrile repeating units,[4] its absorbance for sample 4 must be higher than that for sample 2, because the amount of acrylonitrile repeating units for sample 1 is below 1/5 of that for PAN. Since the reverse is the case, the band at 810 cm^{-1} cannot be assigned to the C–H out-of-plane bending vibration in –CH=C(C≡N)–. A band at 2220 cm^{-1} can be assigned to the C≡N stretching vibration in such a moiety. As stated above, the moieties subjected to polymerization of cyano groups are readily liable to oxidation followed by dehydration. Therefore, when sample 1 is heat-treated in air, 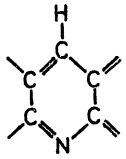 should be easily formed. Since sample 2 should have such a moiety and shows a strong band at 810 cm^{-1}, this band is assigned to the C–H out-of-plane bending vibration in this moiety.

When PAN is subjected to slow polymerization of cyano groups in air, a band at 810 cm^{-1} will appear after completion of the exothermic reaction caused by polymerization and oxidation. Consequently sample 4 is expected to show such a strong band at 810 cm^{-1}. However, the normalized absorbance observed was only 0.121, much lower value than that for sample 2. This seems to be related with a higher degree of degradation for sample 4 than for sample 2.

References

1) W. G. Vosburgh, *Text. Res. J.*, **30**, 882 (1960).
2) A. Shindo, *Kobunshi*, **11**, 11 (1962).
3) R. T. Conley and J. F. Bieron, *J. Appl. Polym. Sci.*, **7**, 1757 (1963).
4) K. Miyamichi, M. Okamoto, O. Ishizuka, and M. Katayama, *Sen'i Gakkai Shi*, **22**, 538 (1966).
5) J. E. Bailey and A. J. Clarke, *Nature*, **234**, 529 (1971).
6) A. J. Clarke and J. E. Bailey, *Nature*, **243**, 146 (1973).
7) M. Minagawa, M. Okamoto, and O. Ishizuka, *Nippon Kagaku Kaishi*, **1976**, 825.
8) M. M. Coleman and P. J. Petcavich, *J. Polym. Sci., Polym. Phys. Ed.*, **16**, 821 (1978).
9) M. Okamoto, C. Aoki, and O. Ishizuka, *Nippon Kagaku Kaishi*, **1978**, 433. Preparation of samples was explained: M. Okamoto, C. Aoki, and O. Ishizuka, *Nippon Kagaku Kaishi*, **1977**, 103.
10) M. Okamoto, R. Yamada, and O. Ishizuka, *Bull. Chem. Soc. Jpn.*, **54**, 1227 (1981).
11) K. Miyamichi, N. Kikuchi, M. Anzai, and M. Katayama, *Sen'i Gakkai Shi*, **21**, 640 (1965).
12) N. Grassie and R. McGuchan, *Eur. Polym. J.*, **6**, 1277 (1970).
13) T. Shimomura, E. Tsuchida, and I. Shinohara, *Kogyo Kagaku Zasshi*, **70**, 980 (1967).
14) W. J. Burlant and J. L. Parsons, *J. Polym. Sci.*, **22**, 249 (1956).

New Industrial Synthesis of Squalane

Takashi NISHIDA,* Yoichi NINAGAWA, Kazuo ITOI, and Yoshiji FUJITA
Central Research Laboratories, Kuraray Co., Ltd., Sakazu, Kurashiki, Okayama 710

(Received January 13, 1983)

Squalane is synthesized by the ethynylation reaction of geranylacetone with a complex of 1,3-butadiyne : *N*-methylpyrrolidone (=1 : 1) in the presence of a KOH catalyst and by hydrogenation with a Raney nickel catalyst, followed by hydrogenation hydrogenolysis with a mixed catalyst of nickel/diatomaceous earth and silica-alumina. An alternative synthesis of squalane from dehydronerolidol is also achieved by oxidative coupling reaction with a copper(II) catalyst under a helium atmosphere.

Squalane (**1**), a useful base oil for cosmetic formulations, has been commercially produced in large quantities by the hydrogenation of squalene (**2**) obtained from shark liver oil.[1] In spite of numerous studies of the stereoselective synthesis of **2**,[2] there have been few investigations directed toward an efficient total synthesis of **1**.[3] Among the various possible key intermediates for constructing this symmetrical structure, attention was focused on diol (**3**), which could be synthesized by the Grignard reaction of 1,4-dibromobutane and geranylacetone (**5**).[4] Compound **5** is available as a precursor of isophytol on the scale of several thousand tons/year. Thus, we examined the ethynylation of **5**, using 1,3-butadiyne as a key building block, instead of the Grignard reaction of 1,4-dibromobutane to obtain an analogous diol (**4a**) [Path A]. The industrial synthesis of pure squalane is now achieved by the hydrogenation of the unsaturated bonds of **4a**, followed by hydrogenation hydrogenolysis. Then, two alternative methods for deriving **4a** and **4b** from dehydronerolidol (**6**) *via* an oxidative coupling reaction in the presence of a copper(II) ion catalyts [Path B] or via dimerization with a rhodium catalyst under a helium atmosphere [Path C] are also described.

1,3-Butadiyne, one of the major by products of acetylene synthesis by the cracking of natural gas, can be separated from a mixture of other acetylenic compounds (vinylacetylene, 1-propyne, *etc.*) as a complex of 1,3-butadiyne:*N*-methylpyrrolidone (NMP) (=1:1) by passing the mixed gas through a NMP solution.[5] 1,3-Butadiyne is liberated from the complex by heating at *ca.* 40 °C under reduced pressure.

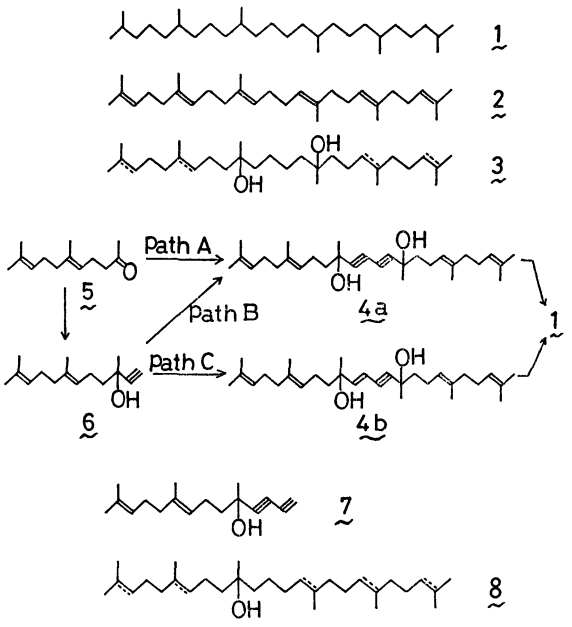

Scheme 1.

The ethylnyation of ketones with 1,3-butadiyne on both terminal sides gives good yields when a stoichiometric amount of sodium amide[6] or the Grignard reagent[7] is used and also, more economically, by means of a semicatalytic reaction with potassium or sodium hydroxide.[8] In this report a 1,3-butadiyne: NMP complex in an NMP solution was employed instead of explosive 1,3-butadiyne, and the reaction was carried out in liquid ammonia at 15 °C in the presence of a potassium hydroxide catalyst (7 mol% *vs.* **5**) [Favorskii conditions].[8] As is shown in Fig. 1, the maximum yield of **4a** (80%) was obtained at the theoretical molar ratio of 1,3-butadiyne:**5** of 0.5:1. However, the undesired alcohol (**7**) was also generated in *ca.* a 10% yields, and the selectivity of **4a** (=yield of **4a**/conversion of **5**×100) is *ca.* 85% under these conditions. On the other hand, the optimum condition of industrial operation was a molar ratio of *ca.* 0.4:1 at which the selectivity of **4a** was 92%, with *ca.* a 75% conversion of **5**. It is better to use **5** in an excess for the complete consumption of 1,3-butadiyne, and the unreacted **5** can be recycled by distillation after the hydrogenation of the ethynylation mixture. The distillation of **5** directly from the ethynylation mixture is dangerous. It was confirmed by gel-permeation chromatography (GPC) that the yield of **7** was less than *ca.* 3% at this molar ratio.

The direct synthesis of squalane from **4a** via hydro-

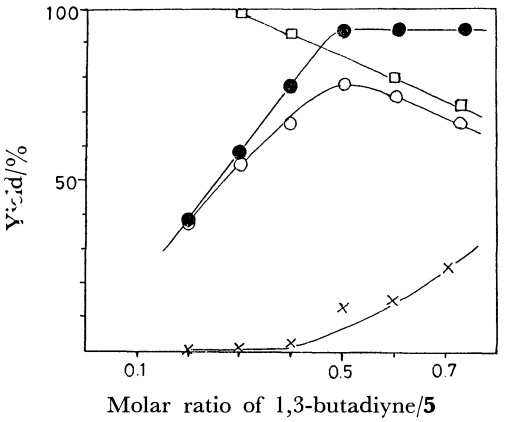

Fig. 1. Ethynylation of **5** with 1,3-butadiyne in ammonia (KOH 7 mol%; reac. temp, 15 °C; reac. time, 20 min). ●: Conversion of **5**; □: selectivity **4a**; ○: yield of **4a**; ×: yield of **7**.

Table 1. Hydrogenation hydrogenolysis of 4[a1)]

Expt No.	Catalyst (wt% *vs.* 4a)	Solvent	Reaction conditions		H_2-Pressure	Product ratio (%)			
			Temp/°C	Time/h	kg cm^{-2}	4a	3	8	1
1	5%-Pd/C (10)	Heptane	100	100 min	5	—	95	5	—
2	5%-Pd/C (10)	EtOAc	100	54 min	5	—	95.3	4.2	0.5
3	5%-Pd/C (10)	EtOH	100	210 min	5	—	84.9	14.6	0.5
4	5%-Pd/C (10)	$(CH_3)_2CHCO_2H$	100	12	5	—	56.1	30.3	13.6
5	5%-Pd/C (10)	CH_3CO_2H	100	12	5	—	9.3	30.9	57.8
6	5%-Pd/C (10)	CH_3CO_2H	150	12	5	—	—	7.0	93
7[2)]	5%-Pd/C (10) +3 M-HCl (0.2 ml)	CH_3CO_2H	100	12	0	—	—	—	100
8[2)]	Ni/Si-Al (4/4)	Hexane	230	2	110—112	—	—	—	100
9[2)]	Ni/Si-Al (8/2)	Hexane	230	2	115—125	—	—	—	100
10[2)]	Ni/Si-Al (8/1)	Hexane	230	2	100	—	—	10	90

1) A 10-g sample of **4a** in 100 ml of a solvent was treated under various conditions. 2) The GC analyses of **1** are exhibited in Fig. 2.

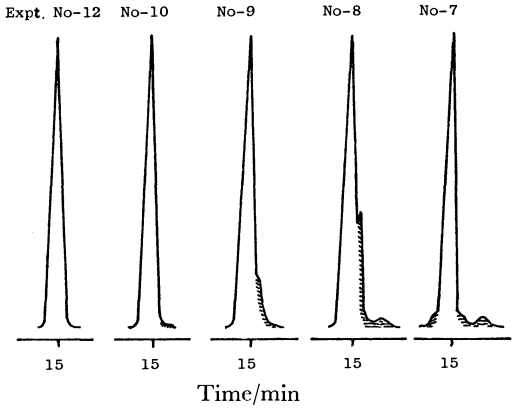

Fig. 2. GC-analyses of **1** prepared by hydrogenation hydrogenolysis of **4a** or **3**.
PEG-20M (2%), 2m, inject. temp, 350 °C, column temp. 150—240 °C (10 °C/min).

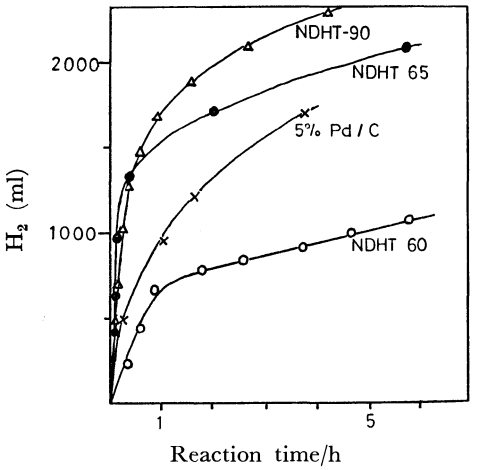

Fig. 3. Hydrogen absorption curve of **4a** with various Raney nickel or Pd/C catalyst. 10 g sample of **4a** in hexane (40 ml) at 100 °C; H_2 pressure 15—20 kg/cm^2; Raney nickel (5 wt%); Pd/C (2.5 wt%).

genation hydrogenolysis was carried out by using Pd/C or a mixed catalyst of Ni/diatomaceous earth and silica-alumina (Ni/Si–Al) under various conditions (Table 1). In the case of the Pd/C catalyst (Expt Nos. 1—7), the use of an acidic solvent such as acetic acid or isobutylic acid was indispensable to convert the diol (**3**) and monool (**8**) into **1** under a low hydrogen pressure and at a relatively low temperature. The addition of a catalytic amount of 3 M-hydrochloric acid (1 M=1 mol cm^{-3}) was effective in completing the conversion of **3** and **8**. The treatment of **4a** with a mixed catalyst of Ni/Si–Al under various conditions (high hydrogen pressure at high temperature) also yielded **1** almost quantitatively (Expt Nos. 8—10). In this reaction, the ratio of silica-alumina was critical to obtain **1** of a good quality. However, as is shown in Fig. 2, squalane synthesized by these procedures contained unknown impurities inseparable from **1** by rectification when **4a** was used as the starting material of the hydrogenation hydrogenolysis.

Consequently, as an industrial method we chose this three-step process: (i) the hydrogenation of the unsaturated triple (and partially some double) bonds of **4a** by means of a Raney nickel catalyst, (ii) the recovery of **5** by distillation, and (iii) the hydrogenation hydrogenolysis of the saturated diol (**3**) by means of a mixed catalyst of Ni/Si–Al. The hydrogenation of **4a** proceeded in the presence of *ca.* 5 wt% of the Raney Ni catalyst (NDH: trade name of Kawaken Fine Chem. Co.) in hexane at 100 °C, with a hydrogen-pressure range of 15—20 kg/cm^2 (Fig. 3).[9)]

After the separation of the catalyst, the unreacted **5** was recovered by distillation to obtain **3** as a residue. The results of the hydrogenation hydrogenolysis of **3** under various conditions are listed in Table 2. Expt Nos. 11—13 show the influence of the temperature, and Expt Nos. 14—17, the effect of the amount of the catalyst on the product distribution. Contrary to the previous direct synthesis of **1** from **4a**, good results were obtained in this case using much of the silica-alumina catalyst in order to complete the reaction without the formation of impurities (Fig. 2; Expt No. 12). This process is now employed for the industrial production of squalane in quantities amounting to several hundred tons a year.

An alernative method for the synthesis of the key

Table 2. Results of hydrogenation hydrogenolysis of 3[1]

Expt No.	Ni/Si-Al (wt% *vs.* 3)	Reaction conditions		H_2-Pressure	Product ratio (%)		
		Temp/°C	Time/h	kg cm^{-2}	3	8	1
11	2/4	230	1	100—110	—	8.7	91.3
			2	100—110	—	0.4	99.6
12	2/4	260	0.5	105—112	—	3.9	96.1
			1	105—112	—	1.9	98.1
			2	105—112	—	—	100
13[2]	2/4	290	1	110—115	—	—	100
14	2/6	290	1	100	—	1.1	98.9
15	1/6	230	1	100	—	1.6	98.4
16	0.6/6	230	1	100	—	9.0	91.0

1) A 10-g sample of 3 in 100 ml of hexane was treated under various conditions. 2) The GC analysis of 1 is exhibited in Fig. 2.

Table 3. Results of oxidative coupling reaction of 6

6 (mmol)	Cu-catalyst (mmol)	Pyridine (mmol)	Solvent (g)	Reaction conditions		Conversion of 6/%[a]	Yield of 4a/%[b]
				Temp/°C	Time/h		
10	$CuCl_2$ (1.0)	136.4	Xylene (20)	65	2	21	0
10	CuCl (1.0)	136.4	Xylene (20)	65	3	93	[87]
10	$Cu(OAc)_2$ (1.0)	136.4	—	60	1	88	—
10	$Cu(OAc)_2$ (0.5)	136.4	—	40	1	64	—
10	$Cu(OAc)_2$ (0.3)	68.2	—	80	1	92	83
37.6	$Cu(OAc)_2 \cdot H_2O$ (1:2)	24.8	$C_{13}H_{28}$ (14)	72	0.5	44	—
					1	80	—
					3	94	85.6 [86.2]
1000	$Cu(OAc)_2$ (30)	600	Hexane	75	3	95	[87]

a) Determined by GC (PEG-20 M, 3 m, 190 °C), using eicosane as the internal standard. b) Determined by HPLC (butyl acetate/hexane=10/90), using solanesol as the internal standard; [ ]: isolated yield after silica gel column chromatography.

intermediate **4a** was also described in order to expand the production of squalane because of the limitation of the amount of 1,3-butadiyne obtained as a by product of the acetylene industry. The oxidative coupling reaction, which has been actively studied not only for its synthetic utility, but also for its mechanistic interest, seemed to be suitable for this purpose [Path B].[10] The reaction, which has been thought to need an excess amount of a copper catalyst,[11—13] was modified by Hay for practical usage as follows[14]: oxygen (air) was bubbled into a mixture of **6** and the copper catalyst (3 mol% *vs.* **6**) in hexane/pyridine in the temperature range of *ca.* 40—80 °C for 3 h to afford **4a** in a high yield. It is recommended to dissolve the catalyst before the introduction of the oxygen. If the catalyst was not completely dissolved, the reaction usually stopped before completion, particularly when the reaction was carried out under a lower temperature (room temperature to *ca.* 60 °C). According to our reinvestigation of the copper catalyst, copper(I) chloride and copper(II) acetate gave good results. Copper (II) acetylacetonate, copper(II) chloride, copper(II) sulfate, *etc.* were ineffective. Pyridine, which has been known to be a good solvent (ligand) in this reaction, has a strong effect on the reaction rate and the conversion of **6**. A pyridine/copper catalyst molar ratio of at least 10, and better, 20—30, is required to complete the reaction (Table 3).

Kinetic studies of this reaction showed that the consumption rate of **6** was proportional to the amount of the pyridine and the copper catalyst, and the activation energy (E_a) was calculated to be approximately 10.8 kcal/mol (Fig. 4) in the presence of an excess amount of oxygen. The order of the reaction was estimated to be zero in the initial stage (0—60% conversion of **6**), first at a 60—90% conversion, and second in the final stage (90% conversion). The reaction usually stopped when the conversion of **6** reached *ca.* 94—97%. The reverse ethynylation of **6** and **4a**, which has never before been reported, was observed in a large-scale experiment: The purification of the reaction mixture by column chromatography (ethyl acetate/hexane=10/90—25/75) yielded **5** (*ca.* 2%) and **7** (*ca.* 3—4%), which might be derived from **6** (or **4a**) and **4a** respectively. Acetylene was also trapped as a white precipitate of silver acetylide by passing the outlet gas of the reaction into a silver nitrate/ethanol solution; the amount of silver acetylide increased when the supply of oxygen was decreased. The amount of the higher-boiling products was relatively small (*ca.* 3%),

Table 4. Dimerization of 6 with Wilkinson catalyst

6 (mmol)	$RhX(PPh_3)_3$ (mmol)	Solvent (ml)	Reaction conditions: Temp/°C	Reaction conditions: Time/h	Conversion of 6/%[a]	Yield of 4b/% [isolated]
70	X=Cl (1)	Toluene (100)	110	8	96	[77]
50	X=Cl (1)	Benzene (100)	85	12	93	86
50	X=Cl (0.5)	Benzene (100)	85	12	84	72
50	X=Cl (0.3)	Toluene (100)	110	8	76	60
50	X=Cl (0.5)	Toluene (100)	110	8	97	83 [78]

a) Determined by GC (PEG-20 M, 3 m, 190 °C), using eicosane as the internal standard. b) Determined by HPLC (butyl acetate/hexane=10/90), using solanesol as the internal standard.

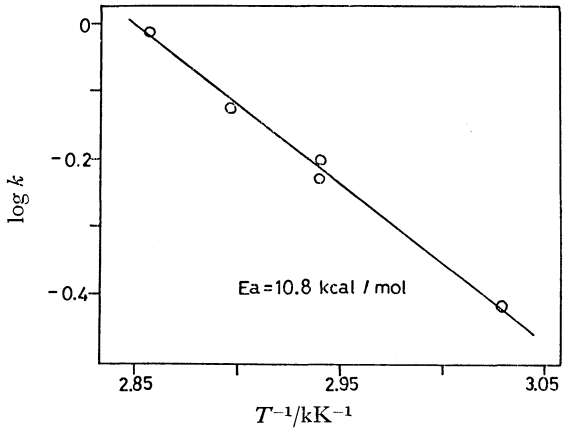

Fig. 4. Effect of temperature on rate constant (K) of disappearance of **6** in oxidative coupling reaction: **6** (37.6 mmol), $Cu(OAc)_2 \cdot H_2O$ (1.2 mmol), pyridine (24.8 mmol) in $C_{13}H_{28}$ (14.0 g); air 5.5 l/h.

and the yield of **4a** was approximately 87%, with a 95% conversion of **6**.

The dimerization of **6** to **4b** with the Wilkinson catalyst (Path C)[15] was also investigated. The treatment of **6** with $RhCl(PPh_3)_3$ (1—5 wt% *vs.* **6**) in dry benzene (toluene), sufficiently degassed with helium at 80—110 °C for 7 h, gave **4b** in a good yield (Table 4). If oxygen was contained in this reaction system, the reaction often stopped before completion and *ca.* 10% of the catalyst was required for completion. The almost pure product, **4b**, obtained by short-column chromatography on silica gel was converted to **1**, as has been mentioned in connection with the oxidative coupling process (total yield from **6**=77%). The di-substituted double bond of **4b** was identified as having an *E*-form. The economical recycling of this expensive catalyst, however, still remains open as a significant problem; it is now under investigation in our laboratories.[16]

In conclusion, we first employed the 1,3-butadiyne process (Path A) as an industrial squalane synthesis and are now also investigating the oxidative coupling process (Path B) as an alternative. The dimerization process with the Wilkinson catalyst (Path C) can not now be employed as a practical method unless the economical recycling of the catalyst can be achieved.

Experimental

The boiling points are uncorrected. The IR spectra were recorded with a Digilab FTS-20 C/D spectrometer. The NMR spectra were taken with a Varian EM 390 apparatus (with hexamethyldisiloxane as an internal standard), and the mass spectra, with a Finnigan 9500 or JEOL JMS-D 300 instrument. GC analyses were made by means of a Shimadzu GC-7AG gas chromatograph using a 3 mm×200 cm column of 10% Silicone DC-550, 10% PEG-20M, or OV-1 on Celite 545 with He as the carrier gas, and HPLC analyses, with a Waters Associates liquid chromatograph using a μ-Porasil P/N 27477 S/N column.

Geranylacetone (**5**) and dehydronerolidol (**6**), commercially available from the Kuraray Co., Ltd., NIC-division, are used as (*Z*)- and (*E*)-forms or as *Z*/*E*=4/6 mixture.

*2,6,10,15,19,23-Hexamethyl-2,6,18,22-tetracosatetraene-11,13-diyne-10,15-diol (**4a**). Ethynylation of Geranylacetone (**5**) with 1,3-Butadiyne*: In a 500-ml autoclave was placed a *Z*/*E*=4/6 mixture of 6,10-dimethyl-5,9-undecadien-2-one (**5**) [38.8 g; 0.2 mol], 40 g of a 10% solution of 1,3-butadiyne (0.08 mol) in NMP, and 3.92 g of a 20 wt% aqueous KOH catalyst in 200 ml of liquid ammonia to react at 15—20 °C for 3 h. The autoclave was then cooled to *ca.* −35 °C, and the reaction mixture was neutralized with ammonium chloride. After the ammonia had then been purged, 200 ml of hexane was added to the residue and the mixture was washed with water and dried over magnesium sulfate. The evaporation of hexane afforded crude **4a** (42.1 g), which was then analyzed by means of HPLC (butyl acetate/hexane=1/9; solanesol as the internal standard) and found to contain **5** (24%), **4a** (70%), and **7** (3%). **4a** was composed of three stereoisomers of (6*Z*,18*Z*)[HPLC retention time 14.2 min], (6*Z*,18*E*) [15.9 min], and (6*E*,18*E*) [18.0 min] in a ratio of *ca.* 1:3:2. The analytical sample of **4a** was purified by means of silica gel column chromatography (ethyl acetate/hexane=10/90—25/75): IR (neat) 3360, 2962, 2920, 2850, 1446, 1375, 1118 cm^{-1}. NMR ($CDCl_3$) δ=1.46 (s, 6H, CH_3COH), 1.57, 1.63, 1.64 (each s, 18H, CH_3), 2.23 (s, 2H, OH), 5.07 5.10 (each t, 4H, =CH, J=7.5 Hz). Found: C, 81.86; H; 10.33, O; 7.58. Calcd for $C_{30}H_{46}O_2$: C; 82.14, H; 10.57, O; 7.29.

Compound **7** was confirmed by the following data: GC-mass (OV-1, 2 m, 100—290 °C) *m*/*e*=229 (M^+-CH_3), 142, 127, 69. The hydrogenation of the ethynylation mixture with Pd/C afforded 5,9,13-trimethyl-5-tetradecanol, whose GC retention time agreed completely with that of the authentic sample prepared by the Grignard reaction of 1-bromobutane and 6,9-dimethyl-2-undecanone.

*Oxidative Coupling of Dehydronerolidol (**6**).* In a four-

necked flask fitted with a thermometer, a gas-inlet tube, and a condenser (−20 °C) was placed 400 ml of hexane, pyridine (95 g; 1.2 mol), and copper(II) acetate (5.45 g; 0.03 mol) to dissolve at room temp. After the addition of **6** (220 g; 1 mol), the reaction temp was elevated to 70 °C by introducing air at the rate of 5.5 l/h for 3 h. The reaction mixture was then successively washed with water (100 ml × 3), 5% sulfuric acid (100 ml × 3), and 5% sodium hydroxide (50 ml)/15% sodium sulfate (100 ml). Quantitative analyses of the product with HPLC showed that the conversion of **6** was 94% and that the yield of **4a** was 85.6%, containing 4% of **7**. The subsequent purification of the product by means of silica gel column chromatography gave 188.8 g of **4a** (yield, 86.2%).

A kinetic study of this reaction was carried out at various temperature ranges by using 8.27 g (37.6 mmol) of **6**, 0.12 g (0.6 mmol)—0.36 g (1.8 mmol) of copper(II) acetate monohydrate, 0.5—4 ml of pyridine, and 2.0 g of elicosane as an internal standard in 14.0 g of a tridecane solvent by bubbling an air at the rate of 5.5 l/h. The rate of the disappearance of **6** was monitored by means of GC (PEG-20 M, 3 m, 190 °C).

*2,6,10,15,19,23-Hexamethyl-2,6,11,18,22-tetracosapentaen-13-yne-10,15-diol (**4b**).* *Dimerization of 6 with Rhodium Catalyst*: A mixture of a chlorotris(triphenylphosphine)rhodium catalyst (0.925 g; 1 mmol) in dry toluene (100 ml) was sufficiently degassed under a helium atmosphere to make possible the addition of **6** (15.4 g; 70 mmol) in one portion. A reaction at 110 °C for 8 h, the evaporation of the solvent, and the purification of the residue by means of silica-gel column chromatography (ethyl acetate/hexane=10/90—25/75) afforded **4b** (11.8 g; 77%) as a dark red oil: IR (neat) 3380, 2960, 2920, 2850, 1450, 1375, 1105, 960 cm^{-1}. NMR ($CDCl_3$) δ=1.23, 1.45 (s, 6H, CH_3COH), 1.58, 1.66 (s, 18H, CH_3), *ca.* 5.10 (m, 4H, =CH), 5.72 (d, 1H, =CH, J=16 Hz), 6.15 (d, 1H, =CH, J=16 Hz). Found: C, 81.58, H; 10.62, O; 7.07. Calcd for $C_{30}H_{48}O_2$: C, 81.76, 10.98, O; 7.26.

*2,6,10,15,19,23-Hexamethyltetracosane (**1**).* *Direct Synthesis from **4a** with Pd/C catalyst*: Hydrogen was bubbled vigorously into a mixture of **4a** (10 g; 22.8 mmol), 3 M-hydrochloric acid (0.2 ml), and 5% Pd/C (1 g) in acetic acid (100 ml) at 100 °C for 12 h. After the filtration of the catalyst, the filtrate was poured into water and extracted with hexane. The organic layer was washed with 5% sodium carbonate and dried over magnesium sulfate. The evaporation of the solvent and subsequent distillation of the residue afforded **1** (9.04 g; 94%): bp 202—208 °C/0.3—0.4 mmHg.† The analyses of **1** by means of ^{13}C-NMR, IR, mass, and GC-retention time agreed with those of an authentic sample prepared by the hydrogenation of squalene.

*Direct Synthesis from **4a** with Mixed Catalyst of Nickel/Diatomaceous Earth and Silica-alumina.* In a 300-ml stainless steel autoclave was placed **4a** (10 g; 22.8 mmol), nickel/diatomaceous earth (0.4 g), and a silica-alumina (0.4 g) catalyst in hexane (100 ml). After the atmosphere had been sufficiently replaced with hydrogen, further hydrogen was introduced into the system until a pressure of *ca.* 30 kg/cm² was reached. The reaction temperature was then rapidly elevated to 230 °C, while carefully controlling the pressure range of 110—112 kg/cm²; stirring was then continued for 2 h. The subsequent filtration of the catalyst, evaporation of solvent, and distillation of the residue afforded **1** in a 95% yield.

*Step-by-step Synthesis from **4a** via **3**.* In a 300-ml autoclave, 50 g (114 mmol) of **4a**, 3.6 ml of Raney nickel (about 2.5 g), and 100 ml of hexane were placed, after which the mixture was hydrogenated at 100 °C under a hydrogen pressure of 15—20 kg/cm² for 6 h. After the reaction, the catalyst was filtered off and the hexane was removed under reduced pressure to give 49.5 g of a viscous brown liquid, **3**. Investigation by means of the ^{13}C-NMR spectra confirmed qualitatively that this liquid has no triple bond and that some parts of the double bonds were hydrogenated, but a considerable amount of the double bonds remained. The liquid in hexane (500 ml) with the nickel/diatomaceous earth (1 g)/silica-alumina (2 g) catalyst was reacted in an autoclave at 260 °C for 2 h under a hydrogen pressure of 105—115 kg/cm² to obtain 41.6 g of **1** (total yield from **4a** after distillation, 86%).

The authers wish to thank Mr. Masahisa Tanomura and Mr. Takuo Kawaguchi for their useful discussions throughout this research, Mr. Michihiro Ishiguro for the technical assistance with the kinetic studies of the oxidative coupling process, and Mr. Yoshin Tamai for an engineering studies. We also grateful to Dr. Shigetoshi Amiya for obtaining the NMR spectra, to Mr. Masanari Oka for the mass spectra, and to Mr. Isao Akuta for the HPLC and GPC analyses.

† 1 mmHg≈133.322 Pa.

References

1) M. Tsujimoto, *Ind. Eng. Chem.*, **8**, 889 (1916); K. J. Sax and F. H. Stross, *Anal. Chem.*, **29**, 1700 (1957).

2) For example; a) P. Karrer and A. Helfenstein, *Helv. Chim. Acta*, **14**, 78 (1931); b) O. Isler, R. Ruegg, L. Chopard-dit-Jean, H. Wagner, and K. Bernhard, *ibid.*, **39**, 897 (1956); c) J. W. Cornforth, R. H. Cornforth, and K. K. Mathew, *J. Chem. Soc.*, **1959**, 2539; d) W. S. Johnson, L. Werthermann, R. Bartlett, T. J. Brocksom, and T-T. Li, *J. Am. Chem. Soc.*, **92**, 741 (1970); e) E. H. Axelrod, G. M. Milne, and E. E. van Tamelen, *ibid.*, **92**, 2139 (1970).

3) K. J. Sax and F. H. Stross, *J. Org. Chem.*, **22**, 1251 (1957).

4) W. G. Dauben and H. L. Bradlow, *J. Am. Chem. Soc.*, **74**, 5204 (1952).

5) N. Shachat, *J. Org. Chem.*, **27**, 2928 (1962).

6) J. B. Armitage, E. R. H. Jones, and M. C. Whiting, *J. Chem. Soc.*, **1951**, 44; T. Herbertz, *Chem. Ber.*, **85**, 475 (1952).

7) H. H. Inhoffen, F. Bohlmann, H. J. Aldag, S. Bork, and G. Leibner, *Ann.*, **573**, 1 (1951); H. H. Achlubach and V. Franzen, *ibid.*, **573**, 105 (1951).

8) For example; a) W. Chodkiewicz, P. Cadiot, and A. Willemart, *Compt. Rend.*, **239**, 885 (1954); b) A. V. Bogdanova, G. P. K. Shemyakina, A. N. Volkov, and V. G. Arakelyan, *Izv. Akad. Nauk SSSR, Ser. Khim.*, **1964**, 174: *Chem. Abstr.*, **60**, 9133 (1964); c) W. Franke, German Patent 895 596 (1958); *Chem. Abstr.*, **52**, 7344 (1958).

9) NDHT-90, for example, means that the Raney nickel catalyst (NDH) is prepared at 90 °C.

10) T. F. Rutledge, "Acetylenic Compounds. Preparation and Substitution Reaction," Reinhold Book Corporation, New York (1968).

11) G. Eglinton and W. McCrae, "Advances in Organic Chemistry. Methods and Results," Interscience Publishers, New York (1963); G. Eglinton and A. R. Galbraith, *J. Chem. Soc.*, **1959**, 889.

12) A. L. Klebanskii, I. V. Grachev, and O. M. Kuznetsova, *Zh. Obsch. Khim.*, **27**, 2977 (1957); *Chem. Abstr.*,

52, 8034 (1958).
13) J. B. Armitage, C. L. Cock, N. Entwistle, E. R. H. Jones, and M. C. Whiting, *J. Chem. Soc.*, **1952**, 1998.
14) A. S. Hay, *J. Org. Chem.*, **25**, 1275 (1960); **27**, 3320 (1962).
15) H. Singer and G. Wilkinson, *J. Chem. Soc., A*, **1968**, 849. H. J. Schmitt and H. Singer, *J. Organomet. Chem.*, **153**, 165 (1978).
16) Recently a modification and reexamination of our process [Path B; T. Nishida *et al.*, U.S. Patent 3 923 918 (1975) and 3 981 930 (1976); Path C; Y. Fujita *et al.*, *ibid*, 3 975 451 (1975)] has been reported by J. W. Scott and D. Valentine, Jr., *Org. Prep. Proced. Int.*, **12**, 7 (1980). They replaced the ligand of the rhodium complex to tris(4-dimethylaminophenyl)phosphine and recovered the catalyst by extraction with water.

 © 1983 The Chemical Society of Japan Bull. Chem. Soc. Jpn., 56, 2811—2813 (1983)

Extraction-Spectrophotometric Determination of Molybdenum(V) with Imidoyl Derivatives and Thiocyanate

Khageshwar Singh PATEL*,† and Rajendra Kumar MISHRA
Department of Chemistry, Ravishankar University, Raipur-496 010 M.P., India
(Received January 29, 1982)

Three new organic reagents derived from *N*-phenylbenzimidoyl chloride and thiourea, phenylthiourea or thiosemicarbazide react with Mo(V) in strongly acidic media in the presence of thiocyanate ions to give rise red-orange complexes, insoluble in water but soluble in benzene. The nature of the ligands has been described to be as univalent, bidentate chelating agents which may coordinate to Mo(V) to form complexes with the composition of Mo 0.2SCN·SR (SCN denotes thiocyanate ion and SR, deprotonated form of the reagents). The molar absorptivity of the complexes was found to be in the range of $(0.8—1.4)\times10^4$ l mol^{-1} cm^{-1} at λ_{max}, 465 nm. The method is simple, rapid and highly selective for Mo. The ferroalloy elements which are associated with the metal do not interfere with the determination. The method was applied to the analysis of ore and alloy steel samples for Mo.

Many methods have been reported for the spectrophotometric determination of molybdenum in soils, ferroalloys, *etc.*[1-8] However, they suffered from many practical difficulties such as interference of cations including Mn^{2+}, Ni^{2+}, Co^{2+}, Cr^{3+}, Ti^{4+}, Zr^{4+}, V^{5+}, Nb^{5+}, Ta^{5+}, and W^{6+}; variation of color intensity of the complex with respect to amount of reagents and standing time; prolonged extraction of the metal with rigid control of some analytical variables; requirement of Fe^{2+} or Ti^{3+} for full color development.[1-2,5,8] In the present paper, a simple, convenient and highly selective extractive-spectrophotometric method is described for the determination of micro amounts of the metal with newly synthesized imidoyl derivatives, namely, (*N*-phenylbenzimidoyl)thiourea (PBTU), *N*-(*N*-phenylbenzimidoyl)-*N*-phenylthiourea (PBPTU) and 1-(*N*-phenylbenzimidoyl)thiosemicarbazide (PBTSC) in the presence of thicyanate ions. Of these, PBPTU has been preferred for detail study owing to wide acidity range for the extraction of the metal and high distribution coefficient of the reagent. They are stable towards heat, light and air, and their solutions can be stored for a long time without deterioration. Each compound may exist as the tautomers **1** and **2**, in the fashion similar to esters and amides and the species containing a SH group would react with Mb(V)–SCN^- to form benzene-extractable complexes.

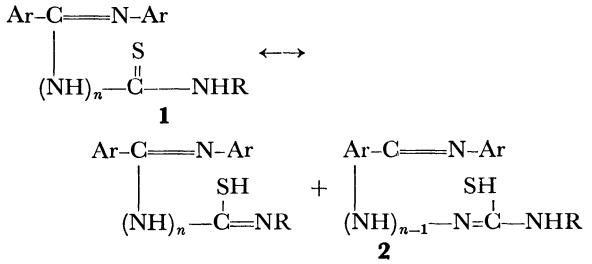

1

2

$n=1$ or 2; Ar = phenyl; R = H or phenyl

Experimental

Apparatus, Reagents, and Solutions. The absorbances were read with an ECIL UV-VIS spectrophotometer model GS-865 matched 1-cm cells and recorded with a Carl-Zeiss Specord UV-VIS spectrophotometer.

All chemicals and reagents used were of Analytical grade. A stock solution of molybdenum(VI) was prepared by dissolving 2.01 g of ammonium molybdate in 1 l of distilled water and standardized gravimetrically.[9]

Imidoyl derivatives were prepared by the condensation of equimolar amount of *N*-phenylbenzimidoyl chloride with the respective substances like thiourea, phenylthiourea and thiosemicarbazide at 120 °C. The products were recrystallized from ethanol and characterized in terms of melting point, elemental analysis and ultraviolet and infrared spectra.[10]

About 0.2—0.4% (W/V) solutions of the reagents in benzene, 20% (W/V) solutions of L-ascorbic acid and ammonium thiocyanate and 10 M hydrochloric acid or sulfuric acid (1 M = 1 mol dm^{-3}) were used.

All the solutions employed were presaturated with benzene.

Procedure. A sample solution containing upto 100 μg of Mo was transferred to a 100-ml separatory funnel. Into this was added 3 ml each of L-ascorbic acid and ammonium thiocyanate solution in a final volume of 25 ml at desired acidity. The solution was equilibrated with 25 ml benzene solution of the relevant reagent for 2 min. After seperation of the two phases, the organic phase was dried with 2 g of anhydrous sodium sulfate in a 50-ml beaker. The absorbance of the benzene extract was measured at λ_{max} against a suitable reference.

Results and Discussion

Spectral Characteristics. The absorption spectra of PBPTU and its Mo(V)–SCN^- complex are shown in Fig. 1. The imidoyl derivative complexes showed a sharp λ_{max} around 465 nm and its position was intact with respect to variation of the amount of reagents and the acidity of the aqueous phase. The molar absorptivity of the complex was evidently affected by the type of functional grouping or substituent, as shown in Table 1.

Choice of Solvents and Reducing Agents. The Mo(V)-complexes are extracted into many organic solvents such as benzene, toluene, chloroform, carbon tetrachloride, acetophenone and 1-pentanol. Benzene was selected as the solvent beacuse of the highest extractability as well as the highest stability of the complex. L-Ascorbic acid and tin(II) chloride were tested for the reduction of Mo(VI) to Mo(V). Variation of the amount of L-ascorbic acid was insensitive to the absorbance of the complex. Tin(II) chloride is too strong as a reducing agent for Mo(VI); it did not

† Present address: Department of Chemistry, K. Govt. Arts and Science College, Raigarh-496 001, M.P., India.

Table 1. Spectral data of Mo(V)–SCN⁻–PBTU–PBPTU–PBTSC complexes in benzene at 2.0 M HCl

Compound	Acidity range M HCl	Molar absorptivity at λ_{max}, 465 nm $l\ mol^{-1}\ cm^{-1}$	Sandell's sensitivity $\mu g\ cm^{-2}$ of Mo
(*N*-Phenylbenzimidoyl)thiourea	1.2—2.5	8000	0.0120
N-(*N*-Phenylbenzimidoyl)-*N*-phenylthiourea	1.0—5.0	13000	0.00738
1-(*N*-Phenylbenzimidoyl)thiosemicarbazide	1.2—3.5	14000	0.00685

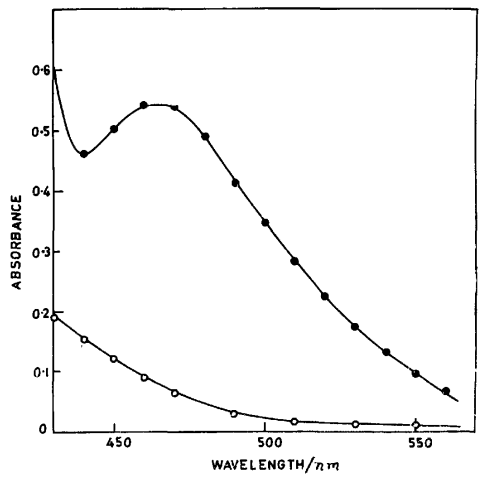

Fig. 1. Absorption spectra of PBPTU and its complex in benzene.
[HCl]: 4.0 M, [SCN]: 0.3 M, [PBPTU]: 0.006 M, [Mo]: 95 μg. —●—: Mo(V)–SCN⁻–PBPTU, —○—: 0.2%, W/V (0.006 M) PBPTU.

produce color as much as L-ascorbic acid and the color intensity of the complex gradually decreased as its concentration increased. The color can also be developed in the presence of thiocyanate ions which serve not only as a weak reducing agent for Mo(VI) but also as a ligand for Mo(V). In this case, however, a prolonged time was required for the full color development. Therefore, L-ascorbic acid was preferred for the experimental work.

Effect of Acidity. The effect of acidity on the extraction of Mo(V) with imidoyl derivatives in the presence of thiocyanate ions was studied with various acids like HCl, H_2SO_4, HNO_3, and CH_3COOH. Of these, only HCl and H_2SO_4 were found to be adequate for the extraction purpose. The optimum acidity ranges for the extraction of the metal with SCN^- and PBPTU lie between 1.0—5.0 M HCl/0.8—6.0 M H_2SO_4. The optimum acidity ranges for PBTU and PBTSC were examined in a similar way and shown in Table 1. The later experimental work was performed with PBPTU at 4 M HCl.

Effect of Other Variables. At least 130-fold molar excess of PBPTU was necessary for the complete extraction of the metal. Similarly, at least 0.05—1.0 M ammonium thiocyanate was required for the full color reaction. The order of addition of reagents was not critical. Variation of temperature from 15 to 35 °C and volume of the aqueous phase from 15 to 60 ml did not affect the color intensity of the complex. A period of 2 min was sufficient for the complete extraction of the complex and more extraction up to 30 min produced no measureable change in the absorbance. The metal complex was stable for at least 10 h at room temperature. The effect of salting out agents like NaCl, KCl, or $(NH_4)_2SO_4$ was studied and no remarkable change in the extraction of the metal was noticed up to 2 M.

N-Phenylbenzimidoyl Derivatives as Analytical Reagents. All the derivatives react with Mo(V) in hydrochloric acid solution in the presence of thiocyanate ions to give benzene-extractable red-orange complexes, the optimum acidity ranges being tabulated in Table 1. The colored systems obeyed Beer's law. When PBPTU was used as the reagent, Beer's law is obeyed over the range 0.5—7.0 ppm of Mo, the optimum concentration range for the determination being 0.8—6.5 ppm. The precision of the method was evaluated by determining 75 μg of Mo/25 ml and the relative standard deviation was found to be ±0.81% for 10 measurements. As shown in Table 1, the phenyl substitution on the thioureido group of PBTU improved the molar absorptivity of the complex and the optimum acidity for the extraction of the metal to a considerable extent. The high extractability of the complex may be attributed to the highly organophilic nature of PBPTU molecule. At least 2—3 times molar excess of PBTU and PBTSC to PBPTU was required for the complete extraction of Mo. Therefore, PBPTU was found to be the most convenient reagent for the spectrophotometric determination of Mo(V) in the present investigation.

Composition of the Complex. The composition of the complex was determined by curve-fitting method[11] using the relationship between log *D* (distribution ratio of the metal) and log [Reagent concentration]. The results obtained indicates the formation of a 1 : 2 : 1 (Mo : SCN^- : RS^-) red-orange ternary complex in benzene. The overall reaction can be expressed as follows:

$$MoO^{3+} + 2\,SCN^- + HSR_o \rightleftharpoons Mo\,0.2\,SCN{\cdot}SR_o + H^+.$$

Where, subscript o denotes organic phase.

Effect of Diverse Ions. The effect of diverse ions in the solvent-extraction and subsequent spectrophotometric determination of 3 ppm of Mo at 4 M HCl with

Table 2. Determination of molybdenum in ore and alloy steels with PBPTU

Sample	Mo found[a] (%)	Mo certified (%)	Relative standard deviation ±%
Ore[b]	2.086	2.091	0.62
BCS 64	4.092	4.11	0.78
BCS 219/3	0.595	0.60	0.86
BCS 225/2	0.340	0.34	0.84

a) Average of six determinations. b) Obtained from Indian Bureau of Mines, Nagpur, India. BCS, British Chemical Standard.

thiocyanate ions (0.3 M) and PBPTU (0.006 M) in benzene was examined. The following metal ions did not interfere up to 2 M Cl^-, Br^-, SO_4^{2-}, or alkali metals; up to 1 M Mn^{2+}, Ni^{2+}, Cr^{3+}, or U^{6+}; up to 0.5 M alkaline earth elements, lanthanoid, Zn^{2+}, Cd^{2+}, Fe^{2+}, Al^{3+}, $C_2O_4^{2-}$, citrate, tartrate, or phosphate. The tolerated amounts of other ions (in ppm) causing an error $<2\%$ are shown in parentheses: Fe^{3+}, Bi^{3+}, Sb^{3+}, Tl^{3+}, Th^{4+} (1500); Hg^{2+}, F^-, $S_2O_3^{2-}$ (1000); Pb^{2+}, Zr^{4+} (2000); I^-, AsO_4^{3-} (3000); Co^{2+}, Pd^{2+}, V^{5+}, Ta^{5+} (400); Nb^{5+}, or W^{6+} (200).

Application of the Method. The method was satisfactory applied to the determination of Mo in ore and some alloy steels, the results being tabulated in Table 2. A weighed sample containing about 2 mg of Mo was decomposed first with aqua regia (10 ml), and then with concentrated H_2SO_4 (3 ml). The sulfuric acid solution was heated to fumes of SO_2, cooled, dissolved with 0.5 M HCl and made up with water to a desired volume. The metal content of the solution was determined as described in the recommended procedure using a suitable reference.

References

1) Z. Marczenko, "Spectrophotometric Determination of Elements," Horwood, Chichester (1976), p. 361.
2) C. P. Savariar, M. K. Arunachalam, and T. R. Hariharan, *Anal. Chim. Acta*, **69**, 305 (1974).
3) D. A. Willian, I. J. Holomb, and D. F. Boltz, *Anal. Chem.*, **47**, 2025 (1975).
4) B. Tamhina, M. J. Herak, and V. Jagodic, *Anal. Chim. Acta*, **76**, 417 (1975).
5) A. G. Fogg, J. L. Kumar, and D. T. Burns, *Analyst*, **100**, 311 (1975).
6) M. Mitra and B. K. Mitra, *Talanta*, **24**, 698 (1977).
7) H. P. Tarasiewicz, A. Grudniewska, and M. Tarasiewicz, *Anal. Chim. Acta*, **94**, 435 (1977).
8) T. J. Koralewski and G. A. Parker, *Anal. Chim. Acta*, **113**, 389 (1980).
9) A. I. Vogel, "A Text Book of Quantitative Inorganic Analysis," 3rd ed, Longmans Green and Co. Ltd., London (1961), p. 508.
10) K. S. Patel and R. K. Mishra, to be communicated.
11) L. G. Sillen, *Acta Chem. Scand.*, **10**, 185 (1956).

Studies in Nickel(IV) Chemistry. V.** Kinetics of Electron Transfer in Redox Systems Containing Tris(dimethylglyoximato)-nickelate(IV), Hydroxylamine, and Catalytic Amounts of Copper(II) in Aqueous Alkaline Media

Sridhara ACHARYA, Gautam NEOGI, Rama Krushna PANDA,* and Dorai RAMASWAMY††
Department of Chemistry, Berhampur University, Berhampur 760 007, India
††*Chemical Laboratories, Central Leather Research Institute, Madras 600 020, India*
(Received March 2, 1982)

Kinetics of electron transfer in the redox system containing hydroxylamine and tris(dimethylglyoximato)-nickelate(IV) ($[Ni(dmg)_3]^{2-}$), in the presence of catalytic amounts of added copper(II) ions, have been studied in aqueous medium in the pH range 8.04—11.81. The kinetics exhibit pseudo-zero-order disappearance of $[Ni(dmg)_3]^{2-}$ when excess $[NH_2OH]_0$ is present, in the presence and absence of added metal ions. While addition of Cu(II) results in significant catalysis, that of Co(II)/Co(III), Fe(II)/Fe(III), Ni(II) or Zn(II) does not. The pseudo-zero-order rate constants (k_0) are found to be linearly dependent on $[NH_2OH]_0$ and on added [Cu(II)]. The k_0 values register a decrease as $[OH^-]$ is increased in the pH range 8.04—*ca.*9.42, attaining a limiting value in the pH range *ca.* 9.8—*ca.*11.81. Results are interpreted in terms of a probable mechanism involving formation of precursor complexes from hydroxylamine and Cu(II) species, followed by rate-determining breakdown of the precursors with concomitant electron transfer. The Cu(II)·aq species reacts several orders of magnitude faster than the $Cu(OH)_2$·aq species. The Ni(IV) does not appear to have any kinetic role in the redox system and is involved only in rapid product formation steps. The stoichiometric ratios $(\Delta[Ni(IV)]/\Delta[NH_2OH])$ of *ca.* 1.0 in the lower pH region (7.8—8.6) and *ca.* 0.5 in the higher pH region (9.1—11.6) are explained in terms of differential product formation.

Hydroxylamine and its derivatives are versatile reducing agents and numerous reports are available on kinetics of their oxidation by various metal ions.[1–15] The electron transfer kinetics, as well as products of oxidation of hydroxylamine and their distribution and stoichiometry, are, among other factors, strongly pH-dependent, but most of these studies are restricted to reaction media of "acidic" pH conditions. A few studies[7,8,16] were, however, reported on metal ion-catalyzed reactions of hydroxylamine in aqueous alkaline media. Bridgart *et al.*[8] reported that the oxidation of hydroxylamine by alkaline hexacyanoferrate(III) exhibits first-order kinetics with respect to the initial stage of disappearance of hexacyanoferrate(III) and that the reaction is strongly catalyzed by copper(II). We have currently been interested[17–20] in the chemistry of tris-(dimethylglyoximato)nickelate(IV), $[Ni(dmg)_3]^{2-}$ (dmg^{2-} =dimethylglyoximate dianion) and came across an early qualitative mention by Simek[21] that hydroxylamine and hydrazine effectively reduce Ni(IV)[22] by two-electron transfer. While studying the kinetics of oxidation of hydroxylamine by Ni(IV), we observed that the disappearance of Ni(IV) was always zero-order irrespective of the source of samples employed, and that the reactions were tremendously retarded in the presence of added edta.[23] To substantiate the suspected extensive metal ion-catalysis in the redox cycle, we have collected results of investigations on metal ion-catalyzed electron transfers involving hydroxylamine and Ni(IV) in aqueous media and are reporting them in this communication.

Experimental

Materials and Methods. Freshly prepared doubly distilled water, distilled from an all-glass apparatus containing a dilute solution (*ca.* 1×10^{-4} M) (1 M=1 mol dm^{-3}) of edta, was exclusively used for preparation of solutions and in kinetic runs. Characterization of $[Ni(dmg)_3]^{2-}$ and preparation of its aqueous solutions were performed as described earlier.[17,18] Hydroxylammonium chloride (Poole, England) was of guaranteed reagent grade, was recrystallized twice before use, and its solutions were freshly prepared; the solutions were standardized by the acid bromate method.[24] The substrate solutions were appropriately diluted and their pH adjusted, as required, when they were employed for kinetic runs. Fresh stock solutions of BDH AnalaR grade samples of MCl_2 (M= Cu, Fe, Ni, Co, or Zn) were prepared and standardized;[24] requisite amounts from the stock were taken to prepare M(II) solutions for kinetic runs. Other reagents were of analytical grade and were used as such. Standard buffer solutions were prepared in water using potassium salts (BO_3^{3-}—H^+/OH^-, acetate—OH^-, $H_2PO_4^-$—H^+/OH^-, and CO_3^{2-}—HCO_3^-).

The reactions were monitored for disappearance of Ni(IV) at 460 nm (ε_{460}=9,600 M^{-1} cm^{-1}), continuously as a function of time, in a VSU 2-P or Pye Unicam SP 1800 UV-VIS spectrophotometer or in an Aminco stopped-flow assembly as described previously.[17–19] In a typical run, an aqueous solution of Ni(IV) containing the metal ion at its requisite catalytic concentration was rapidly mixed[25] with the hydroxylamine solution at the appropriate temperature (±0.1 °C), ionic strength (μ, supporting electrolyte being KCl), and pH; the decrease in absorbance of Ni(IV) was monitored. The pH values of the reaction medium were maintained with standard buffers; they were determined by a Systronics 335 digital pH meter both before and after the reaction and the average (which did not differ by more than ±0.01 unit from the measured values) was taken into record. Correction for ionic strength contribution[26] was applied in calculating $[OH^-]$ from the average pH value. The pseudo-zero-order rate constants were calculated from least-squares fits of absorbance and time data in accordance with the following function which was found valid for the range over 90% of the disappearance of Ni(IV):

** Parts I—IV are Refs. 17—20.

$$(A_t - A_\infty) = (A_0 - A_\infty) - \varepsilon_{460} k_0 t, \quad (1)$$

where A_t, A_0, and A_∞, refer respectively to the absorbance at time t, the initial absorbance of Ni(IV) before commencement of reaction, and the absorbance at effective infinite time. $Ni(dmgH)_2$, a product from reduction of Ni(IV), was found to have a negligible absorbance at 460 nm. For the major part of Ni(IV) disappearance, the reaction medium was found to be homogeneous; slow precipitation of $Ni(dmgH)_2$ towards the later stage did not significantly influence the kinetics at least for three half-lives of reaction. The proton-assisted[17,19] and metal ion-mediated acid-decomposition[20] of Ni(IV) was negligible under the conditions of investigation. The k_0 values, calculated from data obtained through monitoring the disappearance of Ni(IV) at other wavelengths (440—480 nm), matched well those calculated similarly through monitoring the disappearance at 460 nm. Replicate runs (2 to 7) were reproducible to ±5%. Reproducibility (within ±10%) in zero-order rate constants in the uncatalyzed system was also observed when different freshly prepared stock solutions of the same samples were used and intercomparisons were made.

Computations were done using a DCM Data Products Minicomputer Microsystem 1121.

Results

Stoichiometry. The stoichiometric experiments were conducted in an inert atmosphere in the pH range 7.75—11.6. In experiments employing $[Ni(IV)]_0 \gtrsim [NH_2OH]_0$, the unreacted [Ni(IV)] was estimated spectrophotometrically (Table 1); 4×10^{-6} M of added Cu(II) was present in all the experiments. In experiments employing $[NH_2OH]_0 > [Ni(IV)]_0$, the reaction mixture was acidified with HCl after completion of reaction and the left-over $[NH_2OH]$ was estimated by rapid bromatometric titration.[24] (Under acidic conditions, the oxidation of $dmgH_2$ was found to be so slow as to be negligible.) The observed stoichiometric ratios, $\Delta[Ni(IV)]/\Delta[NH_2OH]$, of *ca.* 1.0 and *ca.* 0.5, would conform to the following equations:

$$2[Ni(dmg)_3]^{2-} + 2NH_2OH \xrightarrow{Cu(II)} 2[Ni(dmgH)_2] + 2\,dmg^{2-} + H_2O + N_2O, \quad (2)$$

$$[Ni(dmg)_3]^{2-} + 2\,NH_2OH \xrightarrow{Cu(II)} [Ni(dmgH)_2] + dmg^{2-} + 2\,H_2O + N_2. \quad (3)$$

In another set of experiments at pH 8.0, 8.6, 9.1, 10.4, and 11.5, a solution of Ni(IV) (0.2 M, 50 mL) was allowed to react with a solution of hydroxylamine (0.2 M, 50 mL) in the presence of 4×10^{-6} M of added Cu(II), and the produced gases were qualitatively identified by a gas chromatographic procedure[27] using a Packard 377 instrument. $Ni(dmgH)_2$ was identified by IR after being filtered from the reaction mixture, recrystallized, and dried.

Kinetics. Even though a pseudo-first-order excess of $[NH_2OH]_0$ over $[Ni(IV)]_0$ was maintained, the disappearance of Ni(IV) in the Ni(IV)–NH_2OH reaction never followed a first-order pattern as evidenced from nonlinearity of log $(A_t - A_\infty)$ *vs.* time plots. Instead, plots of A_t *vs.* time were perfectly linear for several half-lives of disappearance. The zero-order disappearance of Ni(IV) was observed irrespective of the source of the samples employed, and in the absence of any added

Table 1. Stoichiometry data[a] for the oxidation of hydroxylamine

(Addded[Cu(Ni(II)]=(4—5)×10^{-6}, μ=0.25[b], and 35 °C)

pH	$10^5[Ni(IV)]_0$[c]	$10^5[NH_2OH]_0$[d]	$\frac{\Delta[Ni(IV)]}{\Delta[NH_2OH]}$[e]
7.75	2.6	2	1.04
7.8	14.1	4	1.02
7.85	3.8	2	1.01
8.0	10.0	50	0.9
8.24	14.1	4	0.85
8.3	2.6	2	0.88
8.6	5.3	4	1.04
8.6	10.0	50	0.8
9.1	14.1	4	0.53
9.5	10	50	0.55
10.43	2.6	2	0.65
10.5	10	50	0.55
11.4	3.8	4	0.50
11.4	14.1	4	0.52
11.5	2.6	2	0.51
11.61	5.3	6	0.50
11.6	14.1	4	0.51
11·6	10	50	0.51

a) Average of three determinations for each entry. b) All concentration units are expressed in M. c) Initial analytical concentration fixed by spectrophotometry. d) Initial analytical concentration fixed by the bromatometric titration. stoichiometric ratio of the [Ni(IV)] reacted to $[NH_2OH]$ reacted.

Table 2. Average[a] pseudo-zero-order rate constant for the oxidation of hydoxylamine

pH[c]	$10^2[NH_2OH]_0$	$\frac{10^8 k_0'}{M\,s^{-1}}$	pH[c]	$10^2[NH_2OH]_0$	$\frac{10^8 k_0'}{M\,s^{-1}}$
7.7	(1—1.2)	14.8	7.44	2	25.8
8.3		7.6	9.3	2	5.0
8.32		(7.3)[d]	9.3	2	4.5[e]
8.7		4.2	9.3	2	4.3[f]
8.75		3.6	9.3	2	2.5[g]
8.95		(3.5)	9.3	2	0.7[h]
9.05		3.3	9.35	0.4	1.1
9.1		(3.2)	9.35	1	2.6
9.2		3.1	9.35	1	(2.6)
9.25		(3.0)	9.35	2	(4.7)
10.6		2.4	9.35	3	6.8
11.3		2.3	9.35	10	24.9
11.7		2.3	9.83	2	4.6
11.7		(2.6)	12.25	3	5.8
11.9		2.3	12.6	3	4.1
11.9		(2.6)	12.77	3	4.6
12.0		2.4	12.78	3	(4.6)
13.0		2.0	12.85	3	5.0

a) Deviations from the average value of 2 to 4 replicates are within ±10%. b) All concentration units are expressed in M. c) Corrected pH. Buffers used (pH range): $H_2PO_4^-$—OH^- (7.4—7.7), BO_3^{3-}—H^+/OH^- (8.3—10.6), and HPO_4^{2-}— OH^- (11.3—13.0). d) Values in parentheses were obtained by employing different batches of solutions of the same samples. e—h) In the presence of 2×10^{-6}, 4×10^{-6}, 8×10^{-6}, and 20×10^{-6} M of added edta, respectively.

metal ion. There was progressive retardation of the pseudo-first-order rate constants (k_0', in the absence of any added metal ion) in the presence of added edta (Table 2) and this conformed to the empirical equation:

$$k_0' = p[\text{edta}]^{-1}/(1+q[\text{edta}]^{-1}), \quad (4)$$

where p and q are functions of NH_2OH, OH^-, and M^{n+} concentrations. (M^{n+} refers to metal ion impurities present in the reaction system). Thus there is significant metal ion-catalysis in the redox reaction.

Zero-order disappearance of Ni(IV) was also observed in the presence of a metal ion (M=Cu(II), Fe(II)/Fe(III), Ni(II), Co(II)/Co(III), or Zn(II)) added in small concentrations. Some representative plots are shown in Fig. 1. The pseudo-zero-order rate constants (k_0) were found to remain almost constant in the range $1\times10^{-5}\leq[\text{Ni(IV)}]_0\leq1.9\times10^{-4}$ M ($k_0\gg k_0'$). The k_0 values were linearly dependent on $[NH_2OH]_0$ (Table 3) as well as on added [Cu(II)] (Table 4). The pH dependence of k_0 is presented in Table 5 and that of k_2 ($=k_0/([NH_2OH]_0\,[\text{Cu(II)}])$) in Fig. 2. In the range $11.81\gtrsim\text{pH}\gtrsim9.8$, k_0 registered a marginal increase by only *ca.* 7% for a hundred-fold decrease in [OH^-], but the increase was more prominent below pH *ca.* 8.9.

The k_0 values were found to remain almost constant when different buffers were employed at the same pH

Table 3. Average[a] pseudo-zero-order rate constants for the oxidation of hydroxylamine
($[\text{Ni(IV)}]_0=(4\text{—}6)\times10^{-5}$, added$[\text{Cu(II)}]=(5\text{—}6)\times10^{-7}$, $\mu=0.25$[b], and 35 °C)

pH[c]	$10^4[NH_2OH]_0$	10^8k_0[d]	pH[c]	$10^4[NH_2OH]_0$	10^8k_0[d]
8.5	5	21.7	9.0	5	5.2
	10	37.4		10	10.0
	10	90.8[e]		10	19.9[e]
	10	251[f]		10	40.2[f]
	10	33.8[g]		10	10.3[g]
	10	34.5[h]		10	10.1[h]
	10	35.1[i]		10	10.5[i]
	10	35.8[j]		10	9.8[j]
	15	50.3		20	19.5
	20	69.5		50	49.2
	30	106		100	95.4
	50	175		200	198
	100	350		400	400
	200	743		600	578
10.2[c]	1	0.5	10.2[c]	10	5.4[j]
	5	2.6		20	10.3
	7	3.6		50	25.6
	10	5.2		90	46.0
	10	10.0[e]		120	62.0
	10	18.7[f]		160	82.1
	10	5.5[g]		200	103
	10	5.1[h]		400	202
	10	5·2[i]		800	410

a) Deviations from the average value of 2 to 7 replicates are within ±5%. b) All concentration units are expressed in M. c) Corrected pH. Buffers used: BO_3^{3-}—H^+/OH^-. d) Units are M s^{-1}. e, f) At 40 and 45 °C, respectively. g) In the presence of 1×10^{-4} M of added acrylonitrile. h—j) At 0.1, 0.5, and 1.0 M of ionic strength, respectively.

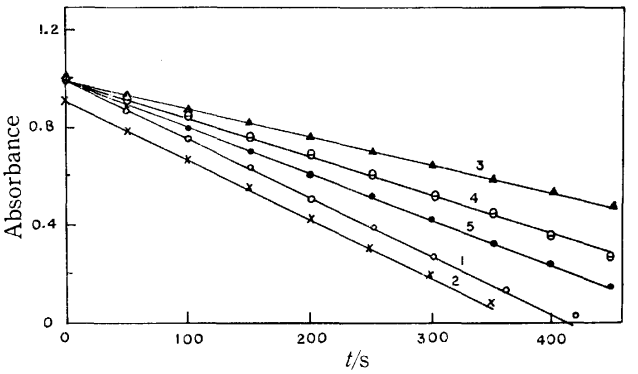

Fig. 1. Absorbance *vs.* time plots.
$[NH_2OH]_0=2\times10^{-3}$ M, $\mu=0.25$ M, 35 °C, Aqueous medium, $[M^{n+}]=2\times10^{-6}$ M.
1): Without added metal ion, pH=7.44; 2): Zn(II), pH=7.2; 3): Fe(II)/Fe(III), pH=7.6; 4): Co(II)/Co(III), pH=7.2; 5): Ni(II), pH=7.4.

Table 4. Average[a] pseudo-zero-order rate constants for the oxidation of hydroxylamine
($[\text{Ni(IV)}]_0=(4\text{—}6)\times10^{-5}$, $[NH_2OH]_0=(1\text{—}1.1)\times10^{-3}$, $\mu=0.25$[b], 35 °C, and pH=10.2)

10^7[Cu(II)] (added)	10^8k_0 / M s^{-1}
5	5.2
6	5.4
7	7.0
10	9.9
11	10.2
15	14.3
21	20.2
30	29.0
45	45.0
74	71.0

a) Deviations from the average value of 2 to 7 replicates are within ±5%. b) All concentration units are expressed in M.

(Table 5). The k_0 values were also insensitive to variation of ionic strength of the medium (Table 3), indicating that at least one of the reactants might be neutral in charge.

The temperature dependence of k_0 was studied in the range 35—45 °C. The average values of the activation parameters $\Delta H^{\neq}$ (in kJ mol^{-1}) and $\Delta S^{\neq}$ (in J K^{-1} mol^{-1}) were calculated, respectively, to be 69 and −83 at pH=8.5, 47 and −165 at pH=9.0, and 43 and −184 at pH=10.2.

Table 6 compares the rate constants for the Ni(IV)–NH_2OH reaction in the presence of various added metal ions Ni(II), Fe(II)/Fe(III), Co(II)/Co(III), and Zn(II)). Cu(II) only appears to have a catalytic effect on the redox system.

Discussion

Mechanism and Rate Law. One scheme consistent with the observed kinetics can be given by Scheme 1. In the pH range of the study, hydroxylamine would

Table 5. Average rate constants for the oxidation of hydroxylamine
($[Ni(IV)]_0=(4—6)\times10^{-5}$, $[NH_2OH]_0=(1—1.1)\times10^{-3}$, added$[Cu(II)]=(5—6)\times10^{-7}$, $\mu=0.25$[b], and 35 °C)

pH[c]	10^8k_0[d] / M s^{-1}	$10^{-2}k_2$[e] / M^{-1} s^{-1}	$10^{-2}k_2$ (calcd)[f] / M^{-1} s^{-1}
8.04	103	20.6	22.1
8.15	83.3	16.7	15.6
8.23	69.4	13.9	12.2
8.31	59.5	10.9	9.8
8.32[g]	52.1	10.4	9.5
8.35	41.7	8.3	8.7
8.50	37.4	6.9	6.3
8.65	20.2	4.0	4.3
8.84	13.2	2.7	3.0
9.00	10.0	2.0	2.3
9.15	8.7	1.7	1.9
9.24	7.4	1.5	1.7
9.31	6.7	1.4	1.6
9.42	6.4	1.3	1.5
9.81	5.2	1.0	1.2
9.98[h]	5.2	1.0	1.1
10.06[i]	5.7	1.1	1.1
10.11	5.1	1.0	1.1
10.20	5.1	1.0	1.1
10.47[i]	5.4	1.1	1.1
11.04[j]	5.1	1.0	1.0
11.41[j]	5.1	1.0	1.0
11.81[j]	5.5	1.1	1.0

a) Deviations from the average value of 2 to 7 replicates are within ±5%. b) All concentration units are expressed in M. c) Corrected pH. Buffers used: BO_3^{3-}-H^+/OH^- (unless otherwise mentioned). d) Observed pseudo-zero-order rate constants. e) $k_2=k_0/([NH_2OH]_0[Cu(II)])$. f) Calculated from a least-square fit of data to Eq. 10. g—j) Refer to buffers of acetate-OH^-, HCO_3^--CO_3^{2-}, HCO_3^--OH^-, and HPO_4^{2-}-OH^-, respectively.

$$Cu^{2+} + L \overset{K_{1c}}{\rightleftharpoons} [CuL]^{2+} \xrightarrow{k_{1x}} \text{Intermediate products}$$
$$\uparrow\downarrow OH^-,\ K_1$$
$$Cu(OH)^+ + L \overset{K_{2c}}{\rightleftharpoons} [HOCuL]^+ \xrightarrow{k_{2x}} \text{Intermediate products}$$
$$\uparrow\downarrow OH^-,\ K_2$$
$$Cu(OH)_2 + L \overset{K_{3c}}{\rightleftharpoons} [(HO)_2CuL] \overset{k_{3x}}{\rightleftharpoons} \text{Intermediate products}$$
$$\text{Intermediate products} + Ni(IV) \xrightarrow[\text{fast}]{k_p} \text{products}$$

(L = NH_2OH; aqua ligands are omitted for convenience.)

Scheme 1.

exist almost totally in the form of NH_2OH species since the proton-dissociation constant of NH_3OH^+ is $10^{-5.8}$ M at 35 °C.[28] The values of K_1 and K_2 employed for the calculation in the present study are 1.6×10^7 M^{-1} and 3.9×10^{11} M^{-1}, respectively, assuming enthalpy changes with temperature for the steps of Eqs. 5 and 6 to be minimal. The K_1 value was calculated using the reported[29] constant K_5 for Eq. 5 and the ionic product

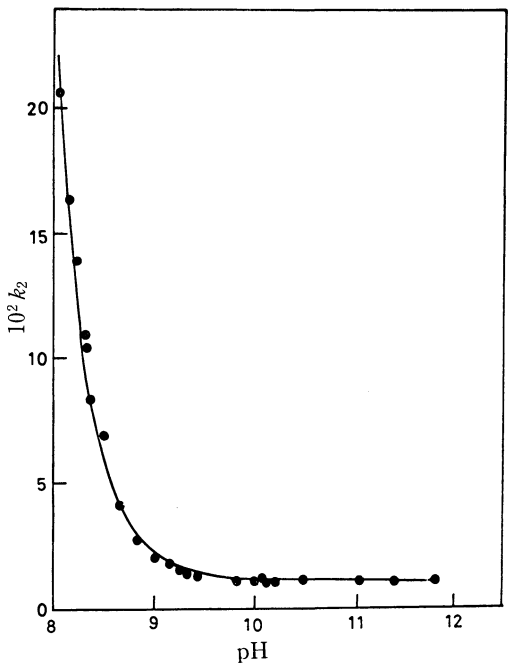

Fig. 2. The k_2 *vs.* pH Plot.
$k_2=k_0/([Cu(II)]\ [NH_2OH]_0)$.
Point and line respectively refer to experimental and calculated k_2.

Table 6. Average pseudo-zero-order rate constants for the oxidation of hydroxylamine
($[Ni(IV)]_0=(4—6)\times10^{-5}$, $[NH_2OH]_0=2\times10^{-2}$, $\mu=0.25$, and 35 °C)

Added metal Ion (M^{n+})	$10^6[M^{n+}]$	pH	10^8k_0/M s^{-1}
Co(II)/Co(III)	2	7.2	17.0
Fe(II)/Fe(III)	2	7.6	12.1
	2	8.6	7.0
	10	8.7	8.0
Ni(II)	2	6.6	40.0
	2	7.4	20.0
	2	9.7	4.1
	10	9.7	3.6
Zn(II)	2	7.2	25.0
	10	7.2	24.0

a) Deviations from the average value of 2 to 4 replicates are within ±5%. b) All concentration units are expressed in M.

of water K_w, and the K_2 value was calculated from Eq. 6 and the value of K_1:

$$Cu^{2+} + H_2O \rightleftharpoons [CuOH]^+ + H^+,\ K_5 = 10^{-6.8}\ M, \quad (5)$$
$$Cu(OH)_2 \rightleftharpoons Cu^{2+} + 2OH^-,\ K_6 = (K_1K_2)^{-1} = 1.6\times10^{-10}\ M^2. \quad (6)$$

The operation of other equilibria,[29] Eqs. 7 and 8, related to this system was considered negligible in the experimental concentration ranges of Cu(II) and OH^- employed in the present investigation:

$$Cu(OH)_2 + 2OH^- \rightleftharpoons CuO_2^{2-} + 2OH_2,\quad K_7 = 1.2\times10^{-3}\ M^{-2}, \quad (7)$$

$$2\,Cu^{2+} + 2\,H_2O \rightleftharpoons [Cu_2(OH)_2]^{2+} + 2H^+, \quad K_8 = 1.38 \times 10^{-11}\,M. \tag{8}$$

If it is assumed that $k_{nx} \gg k_{-nc}$ (where k_{-nc} is defined by $K_{nc}=k_{nc}/k_{-nc}$), a rate law can be derived from Scheme 1 as follows:

$$\frac{k_0}{[Cu(II)]_T[NH_2OH} = \frac{k_{1x}K_{1c}+k_{2x}K_{2c}K_1[OH^-]+k_{3x}K_{3c}K_1K_2[OH^-]^2}{1+K_1[OH^-]+K_1K_2[OH^-]^2}, \tag{9}$$

which on rearrangement becomes

$$\frac{k_0(1+K_1[OH^-]+K_1K_2[OH^-]^2)}{[Cu(II)]_T[NH_2OH]} = k_{1x}K_{1c} + k_{2x}K_{2c}K_1[OH^-] + k_{3x}K_{3c}K_1K_2[OH^-]^2. \tag{10}$$

A least-squares fit of the data of Table 5 results in the values of $k_{1x}K_{1c}$, $k_{2x}K_{2c}$, and $k_{3x}K_{3c}$ as $(7.8\pm0.4)\times10^9$ $M^{-1}\,s^{-1}$, $(4.6\pm0.2)\times10^8$ $M^{-1}\,s^{-1}$, and $(1.0\pm0.4)\times10^2$ $M^{-1}\,s^{-1}$, respectively. The calculated values of rate constants are found to match well those obtained experimentally, lending credence to the proposed rate law.

The envisaged mechanism in Scheme 1 depicts the reaction to proceed through equilibrium precursor complex formation involving the various species of Cu(II) and NH_2OH prior to rate-determining breakdown of the precursor complex(es) with concomitant electron transfer. The intermediate products containing Cu(I) species and $NH_2O\cdot$ radical[15] are rapidly oxidized by Ni(IV) in subsequent kinetically insignificant step(s) (*i.e.*, the composite reaction constant $k_p \gg k_{nx}$), thus resulting in zero-order disappearance kinetics of Ni(IV).

The overall picture of product formation can be formulated as

$$2Cu(I) + [Ni(dmg)_3]^{2-} + 2H_2O \longrightarrow 2Cu(II) + [Ni(dmgH)_2] + dmg^{2-} + 2OH^-, \tag{11}$$

$$NH_2O\cdot - e \longrightarrow HNO + H^+, \tag{12}$$

$$2HNO \longrightarrow N_2O + H_2O, \tag{13}$$

$$HNO + NH_2OH \longrightarrow N_2 + 2H_2O, \tag{14}$$

$$2NH_2O\cdot \longrightarrow N_2 + 2H_2O. \tag{15}$$

The Cu(I) in Eq. 11 may either be a Cu(I) hydroxo species or a Cu(I)–NH_2OH complex. Equations 11—15 will be very rapid and the magnitudes of their rates relative to the rates of the reaction are such that the present redox system in a nitrogen atmosphere does not initiate polymerization of a radical-trapping agent, *viz.*, acrylonitrile, nor was there any significant influence of added acrylonitrile on rates of the reaction (Table 3). Nevertheless, the formation of radicals is not precluded on the basis of this negative finding, because if k_{12}, k_{13}, k_{14}, or $k_{15} \gg k_{(\text{induced polymerization})}$, which is quite probable, the extent of the induced change may lie well below the limit of detectability, even under conditions favorable for this induced reaction, and also because that the absence of polymerization is not connected with a lack of radicals since measurements[30] show that in an acidic medium in the presence of dissolved oxygen, acrylonitrile does not polymerize even if the process is initiated by gamma-radiolysis or by thermal decomposition of peroxodisulfate.

It can be inferred from the stoichiometric experiments of Table 1 that the molar ratios of the reactants (and the product distribution) depend to a great extent on the ratio of the initial concentration of Ni(IV) to NH_2OH (at constant [Cu(II)]) and the pH of the reaction medium. The stoichiometric ratio of *ca.* 1.0 in the lower pH range (*ca.* 7.8—8.6) decreases to *ca.* 0.5 in the higher pH range (*ca.* 9.1—11.6) of the study. While N_2O appears to be the predominant product in the lower pH region, N_2 is predominantly formed in the higher pH region. When $[NH_2OH]_0$ is in excess over $[Ni(IV)]_0$, there is a tendency to form more N_2 in the lower pH region than is observed when $[Ni(IV)]_0 \geq [NH_2OH]_0$. The stoichiometric observations of the present study are in line with those predicted in several earlier reports.[15,16]

The values of $\Delta H^{\neq}$ and $\Delta S^{\neq}$ at different pH values give some indication to the nature of the transition states formed in the reaction; the larger negative $\Delta S^{\neq}$ values at pH 9.0 and 10.2 are presumed to reflect an increased restriction in the transition state imposed by the formation of the (unstable) intermediate complex.

In deriving the rate law (Eq. 9), it was assumed that $k_{nc} \gg k_{-nc}$, *i.e.*, the precursor complex(es) would have only a limited stability under the conditions employed. In that event, the product of the equilibrium formation constant and the decomposition rate constant of the precursor complex, $K_{nc}k_{nx}$, is identifiable as a bimolecular second-order rate constant k'_{nx}. This assumption finds support from the observed kinetics which demonstrate that even over a wide range of $[NH_2OH]_0$ (*viz.*, 800-fold at pH 10.2), the k_0 values do not show any tendency to saturate at high relative $[NH_2OH]_0$.

The ligating properties of hydroxylamine have been shown earlier[31] and the formation of $[Cu(NH_2OH)_n]^{2+}$ ($n=1$, 2, or 4) complexes is firmly established in many reaction systems such as the Cu(II)-catalyzed $[Fe(CN)_6]^{3-}$–NH_2OH reaction,[8] the metal ion-catalyzed decomposition of hydroxylamine in strongly alkaline aqueous media,[16] and in oxidation reactions[9,10] of NH_2OH by Cu(II). However, the reported equilibrium constants[32] for the complexes of $[Cu(NH_2OH)_n]^{2+}$ ($n=1$ or 2) should be strongly pH-dependent. In a recent report, the state of Cu(II) in solutions containing hydroxylamine has been well documented;[10] while in ethanolic solution the $[Cu(NH_2OH)_n]^{2+}$ complexes appear to be stable, in aqueous solutions they decompose instantaneously with a tendency towards stabilization of Cu(I)–NH_2OH complexes.

Unfortunately, the Cu(II)–NH_2OH redox system could not independently be studied (to compare the results with those observed in the present study) due to the low molar absorptivity of Cu(II) and the precipitation of Cu_2O if high concentration of Cu(II) was employed. However, if the values of the (intercept)/(slope) of the plots of $[Cu(II)]/k_0$ *vs.* $1/[NH_2OH]_0$ are thought as representing the formation constants of the precursor in the medium, then the approximate values are ≤ 2, 40, and 220 (all expressed in M^{-1}) at pH 10.2, 9.05, and 8.35, respectively. Even though much importance cannot be attached to these values (which have been obtained from small values of intercepts of the plots), their magnitudes show the relative order

of stability of the precursors with respect to the pH of the medium. Incidentally, the formation constant of $[Cu(NH_2OH)]^{2+}$ has been reported as $10^{2.4}$ at 20 °C and $\mu=0.5$ M ($NaNO_3$) in aqueous medium.[32]

The reaction rate remains almost constant when different buffers are employed at the same pH and hence the reaction is subject to general acid catalysis. General acid catalysis should be observed when $k_{17} \gg k_{-16}$ [A^-] with respect to

$$[CuLOH]^{(n-1)+} + HA \underset{k_{-16}}{\overset{k_{16}}{\rightleftharpoons}} [CuLOH_2]^{n+} + A^-, \quad (16)$$

$$[CuLOH_2]^{n+} \xrightarrow{k_{17}} \text{products}. \quad (17)$$

This inference also draws its testimony from the fact that in the present reaction system, the rate is accompanied by an increase when the pH is lowered. The magnitudes of the resolved rate constants ($k_{1x}K_{1c} > k_{2x}K_{2c} \gg k_{3x}K_{3c}$) do follow the trend predicted by the electrostatic theory and are much below the rate constant for the exchange of water from the first coordination sphere of Cu^{2+}·aq ion (*ca.* 8×10^9 s^{-1} at 25 °C),[33] showing that the Cu(II)–NH_2OH precursors are indeed formed in the redox system.

In the reaction scheme presented, the Cu(II) species represent the aqua species. The dimethylglyoxime complexes of Cu(II) might be thought as being produced from a trace dimethylglyoxime impurity (which might have been produced due to proton-assisted decomposition[17,19] or Cu(II)-mediated acid-decomposition[20] of $[Ni(dmg)_3]^{2-}$). However, since the rates of the latter two reactions are insignificant in comparison with those of the present redox system, such a possibility, if at all exists, does not alter the discussion presented here. (The rate constants for proton-assisted decomposition of the $[Ni(dmg)_3]^{2-}$ range from 1.3×10^{-5} s^{-1} to 2.6×10^{-7} s^{-1} in the pH range 8.3—12.3 at 35 °C and $\mu=0.25$ M;[17,19] the rate constant for Cu(II)-mediated acid-decomposition[20] of Ni(IV) is 2.2×10^{-3} s^{-1} at 35 °C, $\mu=0.57$ M, pH=6.15, and $[Cu(II)]=4\times10^{-5}$ M).

The possibility of involvement of Cu(III) as an intermediate in the present system is also ruled out since strict zero-order kinetics in Ni(IV) have been observed. Moreover, the redox potential of Ni(IV)/Ni(III) (*ca.* 0.4 V)[34] is not sufficient to oxidize Cu(II)·aq to Cu(III)·aq.

It may be pertinent to remark here that in previous studies involving Cu(II)-catalyzed oxidation of hydroxylamine, the authors[6,8] were either not interested in considering the pH dependence of rate or were silent on this aspect. Another aspect which needs mention is that, while the Cu(II)-catalyzed oxidation of hydroxylamine by hexacyanoferrate(III) in aqueous alkaline media[8] exhibited first-order kinetics on $[Fe(CN)_6]^{3-}$ (with respect to the initial stage of disappearance of $[Fe(CN)_6]^{3-}$), the present system shows perfect zero-order kinetics with respect to several half-lives of disappearance of Ni(IV). Inasmuch as the oxidation potentials for the couples ($[Fe(CN)_6]^{3-}/[Fe(CN)_6]^{4-}$ = 0.36 V[29] and $[Ni(dmg)_3]^{2-}/[Ni(dmgH)_2]=0.7$ V[35,36] in aqueous alkaline solutions are comparable, the reason for the above behavior is not clear. Some probable explanation may lie in the different methods of analysis of the experimental rate data and/or in the fact that, whereas in the former system $[Fe(CN)_6]^{3-}$ (d^5 low-spin O_h) is capable of forming with Cu(II) (a d^9 system) a heteronuclear intermediate[37] before the electron transfer process occurs, the $[Ni(dmg)_3]^{2-}$ (d^6 low-spin D_3) will participate only in rapid outer sphere oxidation of Cu(I) species and NH_2O· radicals formed. However, further probe appears necessary to authenticate the argument.

In sum, (1) the main course of the redox reaction involving $[Ni(dmg)_3]^{2-}$ and hydroxylamine is mediated by trace metal ion impurities present in solution and is strongly catalyzed by Cu(II); (2) the mechanism of the Cu(II)-catalyzed reaction proceeds through equilibrium formation of precursor complex and its rate-determining decomposition with concomitant electron transfer; (3) Ni(IV) does not have any kinetic role in the mechanism and is involved only in rapid product formation steps; (4) the hydroxo species of Cu(II) are less effective in catalysis of the redox system than the aqua species of Cu(II).

We thank the CSIR for award of fellowships (to SA and GN) and the UGC for award of National Associate Scheme and Scheme No. F. 23-930/79 (SR-II). We also thank the Director of CLRI for some facilities and Professor P. S. Radhakrishna Murti for helpful discussions.

References

1) D. S. Honig, K. Kustin, and J. F. Martin, *Inorg. Chem.*, **11**, 1895 (1972).
2) G. Davies and K. Kustin, *Inorg. Chem.*, **8**, 484 (1969).
3) C. P. Lloyd and W. F. Pickering, *J. Inorg. Nucl. Chem.*, **19**, 1907 (1967).
4) R. A. Scott, G. P. Haight, Jr., and N. J. Copper, *J. Am. Chem. Soc.*, **96**, 4136 (1974) and references therein.
5) K. Jijee and M. Santappa, *Proc. Indian Acad. Sci.* (*A*), **69**, 117 (1969); B. Sramkova, J. Zyka, and J. Dolezal, *J. Electroanal. Chem.*, **30**, 169 (1971); **31**, 125 (1972); *Anal. Chim. Acta*, **62**, 113 (1972).
6) A. K. Banerjee, A. K. Basak, and D. Banerjea, *Indian J. Chem.*, **18A**, 332 (1979) and references therein.
7) V. K. Jindal, M. C. Agrawal, and S. P. Mushran, *J. Chem. Soc., A*, **1970**, 2060.
8) G. J. Bridgart, W. A. Waters, and I. R. Wilson, *J. Chem. Soc., Dalton Trans.*, **1973**, 1582 and references therein.
9) H. T. S. Britton and M. Konigstein, *J. Chem. Soc.*, **1940**, 673.
10) E. M. Ivashvoich and G. D. Tort, *Russ. J. Inorg. Chem.*, **23**, 237 (1978).
11) B. M. Thakuria and Y. K. Gupta, *J. Chem. Soc., Dalton Trans.*, **1975**, 77.
12) G. Bengtsson, *Acta Chem. Scand.*, **27**, 1717 (1973).
13) T. D. Smith, C. H. Tan, D. J. Cookson, and J. R. Pilbrow, *J. Chem. Soc., Dalton Trans.*, **1980**, 1297.
14) N. Hlasivcova, J. Novak, and J. Zyka, *Collect. Czech. Chem. Commun.*, **32**, 4410 (1967) and references therein.
15) A. F. M. Nazer and C. F. Wells, *J. Chem. Soc., Dalton Trans.*, **1980**, 1532 and references therein.
16) S. Lunak and J. Veprek-Siska, *Collect. Czech. Chem. Commun.*, **39**, 391 (1974) and references therein.
17) S. Acharya, G. Neogi, R. K. Panda, and D. Ramaswamy, *J. Chem. Soc., Dalton Trans.*, in press.

18) R.K. Panda, S. Acharya, G. Neogi, and D.Ramaswamy, *J. Chem. Soc., Dalton Trans.*, **1983**, in press.
19) G. Neogi, S. Acharya, R.K. Panda, and D.Ramaswamy, *J. Chem. Soc., Dalton Trans.*, **1983**, in press.
20) G. Neogi, S. Acharya, R.K. Panda, and D.Ramaswamy, *J. Chem. Soc., Dalton Trans.*, **1983**, in press.
21) M. Simek, *Collect. Czech. Chem. Commun.*, **27**, 220 (1967).
22) Ni(IV) is the abbreviated form for tris(dimethylglyoximato)nickelate(IV) throughout the text.
23) "edta" represents ethylenediaminetetraacetate with varying degrees of protonation; the disodium salt was used in the experiments.
24) A. I. Vogel, "Text Book of Quantitative Inorganic Analysis," ELBS, London (1978).
25) Since the pH of the reaction mixture at the beginning and end of the reaction remained almost constant ($\pm$0.01 unit), the pH-temperature jump effect was considered negligible.
26) R. P. Frankenthal, "Handbook of Analytical Chemistry," ed by L. Meites, McGraw-Hill, New York (1963), Sect. 1, p. 8.
27) J. Veprek-Siska and S. Lunak, *Collect. Czech. Chem. Commun.*, **39**, 272 (1974).
28) V. E. Bower and R. G. Bates, "Handbook of Analytical Chemistry," ed by L. Meites, McGraw-Hill, New York (1963)' Sect. 1, p. 24.
29) W. M. Latimer, "The Oxidation States of the Elements and Their Potentials in Aqueous Solutions," 2nd ed, Prentice-Hall, Inc., Englewood Cliffs, N. J. (1961), p. 187.
30) R. K. Panda, G. Neogi, and D. Ramaswamy, *Bull. Chem. Soc. Jpn.*, **55**, 587 (1982).
31) I. Szilard, *Acta Chem. Scand.*, **17**, 2674 (1963).
32) L. G. Sillen and A. E. Martell, "Stability Constants of Metal-ion Complexes," Suppl. No. 1, The Chemical Society Special Publ. No. 25 (1971); R. M. Smith and A. E. Martell, "Critical Stability Constants," Inorganic Complexes, Plenum Press, New York (1976), Vol. 4.
33) F. Basolo and R. G. Pearson, "Mechanisms of Inorganic Reactions," 2nd ed, John Wiley, New York (1967), p. 152.
34) K. Nag and A. Chakravorty, *Coord. Chem. Rev.*, **31**, 87 (1980) and references therein.
35) Value obtained from a quasi-reversible cyclic voltammogramme of $[Ni(dmg)_3]^{2-}$ in alkaline solutions (unpublished results).
36) D. J. Davis and E. A. Boudreaux, *J. Electroanal. Chem.*, **8**, 434 (1964).
37) I. Bertini, C. Luchinat, F. Mani, and A. Scozzafava, *Inorg. Chem.*, **19**, 1333 (1980).

Studies in Nickel(IV) Chemistry. Kinetics of Electron Transfer from Hydrazine to Tris(dimethylglyoximato)nickelate(IV) in Aqueous Medium

Sridhara ACHARYA, Gautam NEOGI, Rama Krushna PANDA,* and Dorai RAMASWAMY†

Department of Chemistry, Berhampur University, Berhampur 760 007, Orissa, India

†*Chemical Laboratories, Central Leather Research Institute, Madras 600 020, India*

(Received August 27, 1982)

Kinetics of electron transfer from hydrazine(L) to tris(dimethylglyoximato)nickelate(IV), $[Ni(dmg)_3]^{2-}$, follow pseudo-first-order disappearance in the Ni(IV) in aqueous medium in the range $5.0 \leqslant pH \leqslant 7.0$. The pseudo-first-order rate constants (k_{obsd}) increase with increasing $[L]_0$ and attain limiting values at higher relative $[L]_0$. The k_{obsd}-pH profiles at various $[L]_0$ show that the k_{obsd} values register steep decrease with increasing pH till $pH \approx 6.5$ tending to level off at higher relative pH. Results are consistent with probable interactions of the one-protonated and two-protonated Ni(IV) species with the protonated substrate, or with the metal ion-substrate complex that might have been formed from trace metal ion and the substrate. The two-protonated Ni(IV) complex apparently reacts several orders of magnitude faster than the one-protonated species.

Several important reports are available on kinetics of electron transfer from hydrazine to various oxidants.[1-6] While two-electron transfer[7] from hydrazine resulted, almost exclusively and often quantitatively, in water and nitrogen as products, the products of one-electron change[4,8,9] were nitrogen and/or ammonia. We have been currently interested in the chemistry of tris(dimethylglyoximato)nickelate(IV), $[Ni(dmg)_3]^{2-}$ (dmg^{2-}=dimethylglyoximate dianion) and reported its preparation (in part) and reaction with 1-phenylhydrazine[10a] and with hydroxylamine.[10b] The details of the preparative methods and characterization studies were also described.[10c] An early qualitative report mentioned that hydroxylamine or hydrazine effectively reduced the Ni(IV) complex, prepared by Simek[11], by a two-electron transfer. In the kinetics of oxidation of hydroxylamine by $[Ni(dmg)_3]^{2-}$, we observed that the disappearance of the nickel(IV) was always pseudo-zero-order irrespective of the source of the samples employed and that the zero-order reactions were tremendously catalyzed by added aquacopper(II).[10b] in contrast, the disappearance kinetics of the Ni(IV) follow a pseudo-first-order pattern in the Ni(IV)-hydrazine reaction. The preliminary results on kinetics of this reaction are presented in this communication.

Experimental

Materials and Methods. Freshly prepared doubly distilled water (distilled from an all-glass apparatus containing *ca.* 1×10^{-4} M†† of EDTA) were used throughout. Characterization of $[Ni(dmg)_3]^{2-}$ and preparation of its aqueous solutions were performed as described earlier.[10] Hydrazinium chloride (BDH, AnalaR) reagent was recrystallized twice before use, its solutions were freshly prepared, and standardized by acid bromate method.[12a] The substrate solutions were appropriately diluted and their pH adjusted, as required, when they were employed for kinetic runs. Fresh stock solutions of a BDH(AnalaR) grade sample of $CuCl_2$ were prepared and standardized;[12b] requisite amounts from the stock were taken to prepare Cu(II) solutions for kinetic runs. Other reagents were of analytical grade. Standard buffer solutions were prepared in water using potassium salts. KCl was used to maintain the ionic strength (μ) of the medium.

†† 1 M=1 mol dm^{-3}.

The reactions were monitored for the disappearance of the Ni(IV) at 460 nm (ε_{460}=9 600 M^{-1} cm^{-1}). In a typical experiment, an aqueous solution of the freshly prepared Ni(IV) complex[10a] was rapidly mixed with an equal volume of the substrate solution at the desired pH, μ and temperature ($\pm$0.1 °C), and the progress of the reaction was monitored, continuously as a function of time, on a Pye Unicam SP 1800, a Zeiss VSU 2-P UV-visible spectrophotometer or on an Aminco stopped-flow assembly, as described earlier.[10] The pH values of the solutions were measured before and after the reactions and the mean value (which did not differ by more than $\pm$0.01 units from the measured values) was taken into record after allowing due corrections for ionic strength effect. In experiments carried out in the presence of small amounts of added aquacopper(II), the Cu(II) was either taken along with the oxidant solution or with the substrate solution; in both the cases, the results obtained were practically the same. Pseudo-first-order rate constants were calculated from the usual expression and were found to remain practically constant for at least three half-lives of Ni(IV) disapperance in the 440—480 nm range or when the reactions were conducted in a nitrogen atmosphere in representative runs. Replicate runs (2 to 7) were reproducible to $\pm$5%.

Stoichiometry and Products. The stoichiometry experiments were conducted at pH values of 5.3, 6.2, and 7.0. In a set of experiments at each of the pH and with $[Ni(IV)]_0 > [hydrazine]_0$ ($[Ni(IV)]_0 = 0.8 \times 10^{-4} - 1.6 \times 10^{-4}$ M, $[hydrazine]_0 = 0.1 \times 10^{-4} - 0.6 \times 10^{-4}$ M), the unreacted Ni(IV) was spectrophotometrically estimated at the end of the reaction. Keeping $[hydrazine]_0 > [Ni(IV)]_0$ ($[hydrazine]_0 = 1 \times 10^{-3} - 4 \times 10^{-3}$ M, $[Ni(IV)]_0 = 0.4 \times 10^{-3} - 1 \times 10^{-3}$ M), the left-over [hydrazine] was estimated by acid bromate method.[12a] One mol equivalent of the substrate was found to have reacted with 2 ± 0.1 mol equivalents of Ni(IV) conforming to Eq. 1.

$$N_2H_5^+ + 2[Ni(dmg)_3]^{2-} + 3H^+ \longrightarrow N_2 + 2[Ni(dmgH)_2] + 2\,dmgH_2 \quad (1)$$

The products were identified by a procedure similar to the one described earlier.[10b] Nitrogen was qualitatively identified by a gas chromatographic procedure. Tests for ammonia by Nessler's reagent method[13a] gave negative results.

Potentiometric Measurements. The first proton-dissociation constant (K_a) of hydrazinium ion (LH^+) was determined potentiometrically in an atmosphere of nitrogen gas with a Systronics 335 digital pH-meter equipped with glass and saturated calomel electrodes. The concentration of H^+ was calculated from the measured pH values after applying due corrections for ionic strength effect.[13b] The value of pK_a was

Table 1. Average[a] pseudo-first-order rate constants for the oxidation of hydrazine by Ni(IV) complex (Aqueous medium, $\mu=0.25$,[b] 35 °C, $[N(IV)]_0=(3—5)\times10^{-5}$ M)

pH[c]	$10^3 k_{obsd}/s^{-1}$ $10^3[N_2H_4]_0$				
	1	4	10	20	40
5.0	27.0	40.5	46.0	47.5	48.6
5.0[b]	48.3	129	257		
5.15	18.9	28.4	32.5	33.8	34.7
5.15[e]	0.8		1.30		
5.3	13.6	20.3	23.5	24.2	24.8
5.3[d]	24.3	65.0	130		
5.52	8.2	12.2	14.5	14.9	15.3
6.0	2.8	4.2	5.5	5.5	5.7
6.0[d]	5.1	13.7	28.8		
6.15	2.0	3.0	4.5	4.5	4.5
6.15[e]	0.1		0.2		
6.3	1.3	2.2	3.2	3.2	3.2
6.52	0.9	1.4	2.3	2.3	2.4
6.52[e]		0.06	0.09		
7.0	0.4	0.6	1.4	1.4	1.4
7.0[d]	0.8	2.2	6.0		

a) Deviations from the average value are within ±5%; $[N_2H_4]_0$ refers to the initial analytical concentration of hydrazine. b) All concentration units are expressed in M (1 M=1 mol dm^{-3}). c) Corrected pH (±0.01 units). Buffer used (pH range): hydrogen phthalate-OH^- (5.0—6.0); $H_2PO_4^-$—OH^- (6.0—7.0). Potassium salts were used. d) In presence of 2×10^{-6} M of added aquacopper (II). e) In presence of 6×10^{-5} M of added EDTA.

Table 2. Average[a] pseudo-first-order rate constants for the oxidation of hydrazine by Ni(IV) complex (Aqueous medium, 35 °C, $[Ni(IV)]_0=(3—5)\times10^{-5}$ M, $[hydrazine]_0=4\times10^{-3}$ M)

pH	μ/M	$10^3 k_{obsd}/s^{-1}$
5.62	0.25	9.9 (9.7)[b]
	0.50	10.1
	1.00	9.7
5.70	0.25	8.3 (8.2)[b]
	0.50	8.2
	1.00	8.4
6.23	0.25	2.6 (2.4)[b]
	0.50	2.5
	1.00	2.5
6.43	0.25	1.7 (1.8)[b]
	0.50	1.8
	1.00	1.7

a) Deviations from the average value are within ±5%. b) In the presence of 1×10^{-4} M of acrylonitrile (N_2 atmosphere).

found to be 8.1±0.2 at 35 °C and $\mu=0.25$ M (KCl), which agreed with earlier reported values.[2,14]

Results

In order to examine possible pathways for electron transfer from hydrazine to the Ni(IV), a series of experiments was designed maintaining pseudo-first-order excess of $[L]_0$ over $[Ni(IV)]_0$. The pseudo-first-order rate constants for the Ni(IV) disappearance (k_{obsd}) were found to remain almost constant in the range of $1\times10^{-5}\leq[Ni(IV)]_0\leq1.4\times10^{-4}$ M at constant $[L]_0$, temperature, μ and pH. In presence of added Cu(II)·aq, the pseudo-first-order disappearance of Ni(IV) was still maintained, but the pseudo-first-order rate constants were found to have enhanced values.

Table 1 presents the values of the k_{obsd} for varying $[L]_0$ and pH of the medium at 35 °C and $\mu=0.25$ M. The k_{obsd} values were found to increase with increasing $[L]_0$, showing a tendency to attain limiting values at higher relative $[L]_0$. The k_{obsd} values were found to decrease steeply with increasing pH, tending to level off at higher relative pH (Fig. 1). While the log k_{obsd} *vs.* pH plots were almost linear up to pH ≈6.5 with slopes of *ca.* −1, the corresponding slopes were nearly equal to zero beyond this pH. These observations pointed to probable involvement of different orders of $[H^+]$.

The retarding effect of added EDTA (ethylenediaminetetraacetate added in the form of the disodium salt of the tetrabasic acid) on the k_{obsd}, shown in Table 1, suggested that the present reaction might be subject to influence of metal ions. It may be mentioned that the kinetics of the Ni(IV)-hydroxylamine reaction[10b] was influenced in the presence of metal ions, significantly retarded by added EDTA and tremendously catalyzed by aquacopper(II).

The values of the k_{obsd} were found to be almost insensitive to varying ionic strengths of the medium (Table 2). Added acrylonitrile also did not practically influence the values of the k_{obsd} (Table 2), nor was there

Table 3. Average[a] pseudo-first-order rate constants and average values of the activation parameters for the oxidation of hydrazine by Ni(IV) complex (Aqueous medium, $\mu=0.25$,[b] $[Ni(IV)]_0=(3—5)\times10^{-5}$, $[hydrazine]_0=4\times10^{-3}$)

pH	$10^3 k_{obsd}/s^{-1}$				
	30 °C	35 °C	40 °C	45 °C	50 °C
5.83	3.3	6.2	11.7	21.0	37.2
6.15	1.8	3.0	6.7	12.6	21.1
6.45	0.87	1.6	2.9	5.9	10.6
6.88	0.38	0.7	1.3	2.7	5.3
$10^{-3} k_{2z}K_{2H}$	2.13	4.04	7.68	13.4	23.6
$10^4 k_{2y}$	1.29	2.80	5.96	12.3	25.1
pH	$\Delta H^{\neq}$/kJ mol^{-1} [c]			$\Delta S^{\neq}$/J K^{-1} mol^{-1} [c]	
5.83	96			29	
6.10	113			71	
6.45	100			33	
6.88	105			33	
$k_{2z}K_{2H}$	95[d]			133[d]	
k_{2y}	118[e]			71[e]	

a) Deviations from the average value are within ±5%. b) All concentrations are in M. c) The net activation parameters. d, e) Respectively associated with the constants $k_{2z}K_{2H}$ and k_{2y} (The temperature dependence of K_{1H} K_{2H}, and K_a are assumed to be negligible).

any detectable polymerization (in a nitrogen atmosphere) observed, implying that radical-trapping agents might not have significant effect on the kinetics of the oxidation.

From the temperature dependence of the k_{obsd} in the range 30—50 °C and at different pH values (Table 3), the activation parameters were evaluated.

Discussion

It was shown earlier[10a,d] that in alkaline solutions (pH $\gtrsim$11.5) the Ni(IV) complex was in the form of pseudooctahedral $[Ni(dmg)_3]^{2-}$ which underwent two successive protonations; the subsequent protonations were much below pH 1.23 and were not detectable kinetically. The potentiometrically determined values (at 35 °C in aqueous medium) of the first and second protonation constants, K_{1H} and K_{2H}, were 8.07×10^{10} M^{-1} and 2.24 M^{-1} at μ=0.57 M, and 7.08×10^{10} M^{-1} and 4.46 M^{-1} at μ=0.25 M; the K_{1H} value as determined from spectrophotometric pH titrations was 8.33×10^{10} M^{-1} at 35 °C and μ=0.57 M. It was also shown earlier that protonations of the complex assisted its decomposition (with concomitant intramolecular electron transfer). The first (outside-) protonation was at a dioximate oxygen, forming a hydrogen bonded structure O—H···O between the dioximate oxygens, without much alteration of c.f.s.e. of the original pseudooctahedral $[Ni(dmg)_3]^{2-}$, and the second protonation most probably occurred *via* a direct proton-transfer to a ring-opened (ligand) nitrogen site. The values of the solvent-assisted, first proton-assisted and second proton-assisted rate constants (k_{0d}, k_{1d}, and k_{2d}) were respectively 2.6×10^{-7} s^{-1}, 1.2×10^{-5} s^{-1} and 44.3 s^{-1} at 35 °C and μ=0.25 M in aqueous medium. However, since the proton-assisted decomposition reaction was much too slow compared to the rates of the present redox system, it would not enter into the rate picture in the present investigation.

One general scheme which is consistent with the observed kinetic behaviour of the redox system can be presented as in Scheme 1.

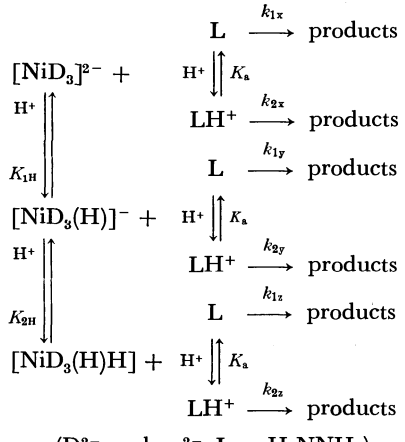

(D^{2-} = dmg^{2-}, L = H_2NNH_2)

Scheme 1.

The rate law derivable from this scheme with all the possible reacting species is as in Eq. 2.

$$k_{obsd}=\frac{\{k_{1x}K_a+(k_{2x}k_{1y}K_{1H}K_a)[H^+]+(k_{2y}K_{1H}+k_{1z}K_{1H}K_{2H}K_a)[H^+]^2+k_{2z}K_{1H}K_{2H}[H^+]^3\}}{(1+K_{1H}[H^+]+K_{1H}K_{2H}[H^+]^2)([H^+]+K_a)}, \quad (2)$$

where k_{nx}, k_{ny}, and k_{nz} are functions of $[L]_0$. Expressing the denominator terms as Y_1Y_2 and the coefficients of the $[H^+]$-independent, $[H^+]$, $[H^+]^2$, and $[H^+]^3$ terms in the numerator as a, b, p, and q respectively, Eq. 2 can be written in the form of Eq. 3 or 4.

$$k_{obsd}\,Y_1Y_2 = a + b[H^+] + p[H^+]^2 + q[H^+]^3 \quad (3)$$

$$\text{or } \frac{k_{obsd}\,Y_1Y_2}{[H^+]^2} = \frac{a}{[H^+]^2} + \frac{b}{[H^+]} + p + q[H^+] \quad (4)$$

It was seen that plots of $k_{obsd}\,Y_1Y_2/[H^+]^2$ *vs.* $[H^+]$ were linear (Fig. 2), implying that the terms containing the coefficients "*a*" and "*b*" were negligible in comparison with those containing the coefficients "*p*" and "*q*". In that event if the contributions of the $[NiD_3]^{2-}$ and the L species to the overall reactivity are assumed to be negligible under the conditions employed, Eq. 4 takes the form of Eq. 5.

$$\frac{k_{obsd}\,Y_1Y_2}{K_{1H}[H^+]^2} = k_{2y} + k_{2z}\,K_{2H}[H^+] \quad (5)$$

The values of k_{2y} and k_{2z} at varying $[L]_0$, as obtained from a least-squares fit of the data of Table 1 in accordance with Eq. 5, are listed in Table 4.

The limiting kinetics observed for varying $[L]_0$ can be explained in terms of Eqs. 6 and 7.

$$[Ni\,D_3(H)]^- + LH^+ \underset{}{\overset{K_{2C}}{\rightleftharpoons}} \underset{(C_1)}{[Ni\,D_3(H)LH]} \xrightarrow{k'_{2y}} \text{products} \quad (6)$$

$$[Ni\,D_3(H)H] + LH^+ \overset{K_{2D}}{\rightleftharpoons} \underset{(C_2)}{[Ni\,D_3(H)H\,LH]^+} \xrightarrow{k'_{2z}} \text{products} \quad (7)$$

whence it follows that

$$k_{2y} = \frac{k'_{2y}K_{2C}[L]_0}{1+K_{2C}[L]_0}, \quad (8)$$

and

$$k_{2z} = \frac{k'_{2z}K_{2D}[L]_0}{1+K_{2D}[L]_0}. \quad (9)$$

From plots of $1/k_{2y}$ *vs.* $1/[L]_0$ and $1/k_{2z}$ *vs.* $1/[L]_0$, the values of the constants of Eqs. 8 and 9 have been resolved (Table 4). The values of k_{calcd}, estimated using these resolved constants, match well the k_{obsd} values (Fig. 1).

The two-protonated oxidant species appears to react several orders of magnitude faster than the one-protonated one even though the abundance of the former species is very much lesser than the latter in the conditions employed. One probable reason for this reactivity order may be the structural difference in the protonated species. Whereas the one-protonated species continues to be almost pseudooctahedral, the two-protonated Ni(IV) complex is an unstable "kinetic intermediate" with a ring-opened structure.[10a,d] The latter species is, therefore, more prone to react either by a substitution-controlled mechanism or by an outer-sphere route, resulting in a higher reactivity. This is also borne out of the fact that the magnitudes of k_{2y} and k_{2z} almost

Table 4. Average values of the various constants (Aqueous medium, 35 °C, μ=0.25 M)

10^3[Hydrazine]$_0$/M	$10^4 k_{2y}$/s^{-1}	$10^{-2} k_{2z}$/s^{-1}
1	1.0	6
4	2.8	9
10	7.5	10
20	8.1	10.5
40	10.1	10.7
K_{1H}/M^{-1}	7.08×10^{10}	
K_{2H}/M^{-1}	4.46	
K_a/M	$10^{-8.1}$	
k'_{2y}/s^{-1}	1.3×10^{-3}	
K_{2C}/M^{-1}	$77(\approx10^{1.9})$	
k'_{2z}/s^{-1}	1.1×10^{3}	
K_{2D}/M^{-1}	1.2×10^{3} ($\approx10^{3.1}$)	

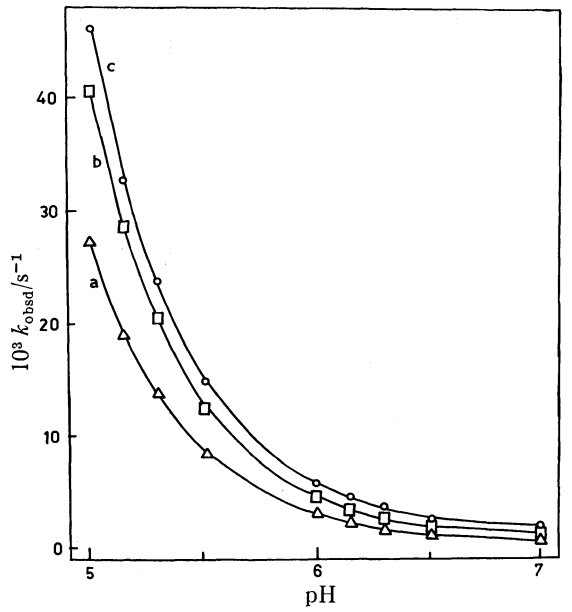

Fig. 1. The k_{obsd} *vs.* pH plots.
Aqueous medium, μ=0.25 M, 35 °C, [Ni(IV)]$_0$=(3—5)$\times10^{-5}$ M, 10^3 [Hydrazine]$_0$/M : 1 (a), 4 (b), 10 (c) (representative). (The solid lines are drawn through the calculated values).

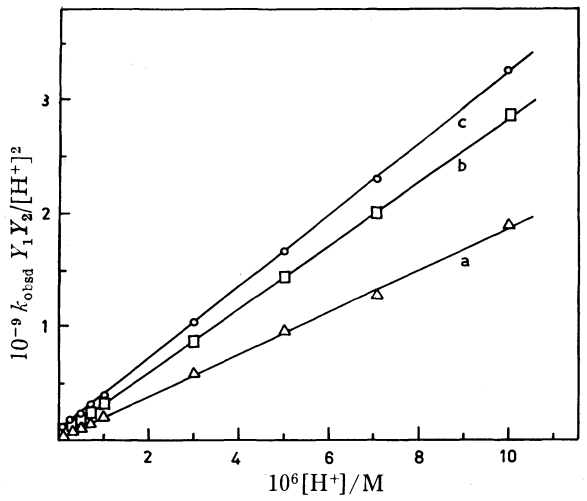

Fig. 2. The plots of k_{obsd} Y_1Y_2/[H$^+$]^2 *vs.* [H$^+$]. (*cf.*, text)
Aqueous medium, μ=0.25 M, 35 °C, [Ni(IV)]$_0$=(3—5)$\times10^{-5}$ M, 10^3 [Hydrazine]$_0$/M : 1 (a), 4 (b), 10 (c) (representative).

parallel (but are higher than) the k_{1d} and k_{2d} values pertaining to the one-protonated and two-protonated Ni(IV) complex respectively.

It is well established[15] that hydrazine transfers two electrons to an oxidant to form the diimide intermediate which on further very rapid two-electron loss gives nitrogen; the overall stoichiometry for this process would be e/[N_2H_4]=4. On the other hand, the loss of one electron (hydrogen atom) from hydrazine results in the incumbent hydrazyl radical,[8] two units of which give nitrogen and ammonia as products with a stoichiometric ratio of e/[N_2H_4]=1. The observed stoichiometry ratio

$$N_2H_4 - 2e \longrightarrow N_2H_2 + 2H^+ \quad (10)$$

$$N_2H_2 - 2e \longrightarrow N_2 + 2H^+ \quad (10a)$$

$$N_2H_4 - e \longrightarrow N_2H_4^{\cdot+} \longrightarrow N_2H_3 + H^+ \quad (11)$$

$$2N_2H_3 \longrightarrow 2NH_3 + N_2 \quad (11a)$$

(Δ[Ni(IV)]/Δ[hydrazine]) of $\approx$2 and nitrogen as the product of oxidation of hydrazine suggest that two-electron transfers might have taken place. If there would have been a discernible one-electron loss, two reactive species, Ni(III) and hydrazyl radical, would have been produced in the rate-limiting step for which the activation enthalpy would have been much too higher than what has been observed here.

Even though the kinetic observations have been most plausibly explained in terms of the rate equations (Eqs. 5—9), and the mechanism of an analogous redox reaction of Ni(IV) with phenylhydrazine was definitely established to be outer-sphere in nature,[10a] the actual mechanistic routes in the present redox system are complicated by several factors.

1. Whether C_1 and C_2 of Eqs. 6 and 7 represent (a) precursor complexes with inner-sphere substitution by the substrate unit at a ring-opened site of the Ni(IV) complex species (followed by rate-determining decomposition of the precursors with electron transfer), or (b) structures in which the Ni(IV) species and the substrate are held together (in an outer-sphere manner) by means of hydrogen bonding between a dioximate oxygen and a substrate unit, cannot be easily distinguished. Both routes (a) and (b) will exhibit almost negligible ionic strength effect and limiting kinetics at higher relative [L]$_0$, as have been observed.

2. Since the k_{obsd} values are tremendously retarded when the reactions are carried out in the presence of added EDTA (Table 1) and are enhanced in the presence of catalytic amounts of added aquacopper(II), an alternative to Scheme 1 can be written as in Scheme 2.

$$M^{n+} + LH^+ \overset{K_C}{\rightleftharpoons} [MLH]^{(n+1)+}$$

$$[MLH]^{(n+1)+} + [NiD_3(H)]^- \xrightarrow{k''_{2y}} \text{Intermediate products}$$

$$[MLH]^{(n+1)+} + [NiD_3(H)H] \xrightarrow{k''_{2z}} \text{Intermediate products}$$

$$\text{Intermediate products} + \text{Ni(IV)} \xrightarrow{\text{fast}} \text{products}$$

(M^{n+} represents the trace metal ion impurities present or Cu(II) added in catalytic concentrations).

Scheme 2.

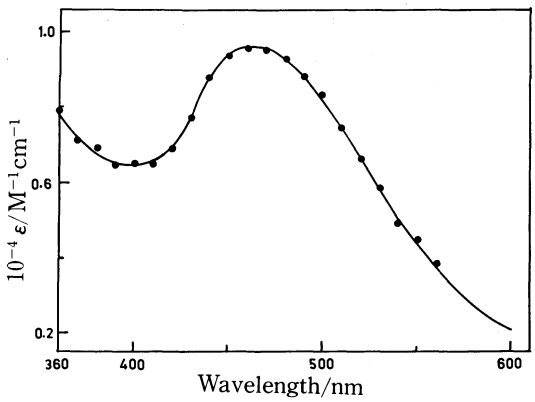

Fig. 3. Spectra of the nickel(IV) complex and reaction mixture.
Line: The Ni(IV) complex (1×10^{-4} M), points: the reaction mixture. ($[Ni(IV)]_0=1\times10^{-4}$ M, $[Hydrazine]_0=1\times10^{-3}$ M)
Aqueous medium, $\mu=0.25$ M, 35 °C, pH=7 (50 ms mode).

From the rate law of Scheme 2 it can be easily written that

$$k_{2y}=\frac{k''_{2y}K_C[L]_0}{1+K_C[L]_0} \quad (12)$$

and

$$k_{2z}=\frac{k''_{2z}K_C[L]_0}{1+K_C[L]_0}, \quad (13)$$

where k''_{2y} and k''_{2z} are the reaction constants of the metal ion-hydrazine complex with the one-protonated and two-protonated Ni(IV) complex under limiting (or trace impurity) concentrations of M^{n+}, and K_c is the formation constant of a 1 : 1 complex of metal ion and hydrazine. If the [L]-dependence of small quantities of k_{2y} (Eq. 12) is neglected, the K_c value from Eq. 3 is obtained as $\approx10^{3.1}$ M^{-1} at 35 °C and $\mu=0.25$ M (K_c and K_{2D} being identical). The 1 : 1 complex of Cu(II)-N_2H_4 has a reported value[14] of $10^{3.18}$ at 30 °C and $\mu=1.0$ M of ClO_4^-. Since the presence of Cu(II) in the reaction at an impurity level of 10^{-8}—10^{-7} M cannot be ruled out, these two values appear to be in excellent agreement.

3. Point-by-point spectra of reaction mixtures on the stopped-flow apparatus (in the 380—550 nm range) at pH 5.2, 6.3 and 7.0 are not different from those of the original Ni(IV) under the same pH conditions. For example, Fig. 3 presents representative spectra of the original Ni(IV) complex and a reaction mixture containing the Ni(IV) complex and hydrazine at pH= 7, 35 °C and $\mu=0.25$ M in aqueous medium. The Aminco stopped-flow assembly used[10] has a nominal mixing time of 2 ms and the point-by-point absorbance values were recorded at 10 nm wavelength intervals using a time scale on 50 ms mode.

4. Many apparently "uncatalyzed" redox systems have actually been found to be metal ion-catalyzed.[16]

5. The reactivity of $[Ni(dmg)_3(H)H]$ being several order higher than that of $[Ni(dmg)_3(H)]^-$ is also compatible with Scheme 2.

The inherent complexities of the redox system studied and the kinetics observed make unambiguous assignment of the reaction scheme difficult. Schemes 1(a) or (b) and 2 appear equally probable. Since the formation of Cu(II)–hydrazine complexes are well established,[17] Scheme 2 appears more likely in the presence of catalytic concentrations of Cu(II). However, further probes are needed for a definite choice.

We thank the CSIR and UGC, New Delhi for award of fellowships (to SA and GN) and National Associate Scheme and Scheme No. F. 23-930/79 (SR II). We also thank the Director of CLRI for some facilities and Prof. P. S. Radhakrishnamurti for helpful discussions.

References

1) G. P. Haight Jr., T. J. Huang, and H. Platt, *J. Am. Chem. Soc.*, **96**, 3137 (1974); K. K. Sengupta, S. S. Gupta, and H. R. Chatterjee, *J. Inorg. Nucl. Chem.*, **38**, 549 (1976).
2) K. K. Sengupta, P. K. Sen, and S. S. Gupta, *Inorg. Chem.*, **16**, 1396 (1977).
3) K. S. Gupta and Y. K. Gupta, *Ind. J. Chem.*, **11**, 1285 (1973); S. S. Gupta and Y. K. Gupta, *Inorg. Chem.*, **20**, 1748 (1981).
4) J. I. Morrow and G. W. Sheeres, *Inorg. Chem.*, **11**, 2606 (1972).
5) K. K. Sengupta and P. K. Sengupta, *Inorg. Chem.*, **18**, 979 (1979).
6) C. W. Wellman, J. R. Ward, and L. P. Kuhn, *J. Am. Chem. Soc.*, **98**, 1683 (1976); H. Erlenmeyer, C. Fleirl, and H. Siegel, *Chimia*, **22**, 433 (1968); H. Erlenmeyer, C. Flierl, and H. Siegel, *J. Am. Chem. Soc.*, **91**, 1065 (1969).
7) V. K. Jindal, M. C. Agarwal, and S. P. Mushran, *J. Inorg. Nucl. Chem.*, **32**, 2325 (1970); M. T. Beck and D. A. Durham, *ibid.*, **32**, 1971 (1970).
8) E. Hayon and M. Simik, *J. Am. Chem. Soc.*, **92**, 42 (1972); J. W. Cahn and R. E. Powel, *J. Am. Chem. Soc.*, **76**, 2568 (1954); P. Wrights and J. C. E. Higginson, *J. Chem. Soc.*, **1955**, 1551; G. Davies and K. Kustin, *J. Phys. Chem.*, **73**, 2248 (1969); W. L. Jolly, "The Inorganic Chemistry of Nitrogen," W. A. Benjamin, New York, N. Y. (1964), p. 61.
9) J. C. E. Higginson, D. Sutton, and P. Wright, *J. Chem. Soc.*, **1953**, 1380; H. C. Mishra and R. N. P. Sinha, *Ind. J. Chem.*, **9**, 1300 (1971).
10) a) S. Acharya, G. Neogi, R. K. Panda, and D. Ramaswamy, *Int. J. Chem. Kinet.*, **14**, 1253 (1982); b) S. Acharya, G. Neogi, R. K. Panda, and D. Ramaswamy, *Bull, Chem. Soc. Jpn.*, **56**, 2814 (1983); c) R. K. Panda, S. Acharya. G. Neogi, and D. Ramaswamy, *J. Chem. Soc., Dalton Trans.*, **1983**, in press; d) G. Neogi, S. Acharya, R. K. Panda, and D. Ramaswamy, *J. Chem. Soc., Dalton Trans.*, **1983**, in press.
11) M. Simek, *Collect. Czech. Chem. Commun.*, **27**, 220 (1962).
12) a) "Comprehesive Inorganic Chemistry," ed by J. C. Bailar *et al.*, Pergamon Press (1973), p. 264. b) A. I. Vogel, 'A Text Book of Quantitative Inorganic Analysis," ELBS, London (1971), pp. 358, 380, 441, and 445.
13) "Hand Book of Analytical Chemistry," ed by L. Meites, McGraw Hill, New York (1963), a) Sec. 6, p. 37; b) Sec. 1, p. 8.
14) J. W. Sutherland, *J. Phys. Chem.*, **83**, 789 (1979); L. G. Sillen and A. E. Martell, "Stability Constants of Metal-ion Complexes," Suppl. No. 1, Spl. Publ. No. 25, The Chemical Society, London (1971).
15) E. J. Corey, W. L. Mock, and D. J. Pasto, *Tetrahedron lett.*, **1961**, 347, 353; *J. Am. Chem. Soc.*, **83**, 2957 (1961); E. J. Corey and W. L. Mock, *ibid.*, **84**, 685 (1962).
16) a) J. H. Anderson, *Analyst*, **89**, 357 (1964); b) A. Huss

Jr., P. K. Lim, and C. A. Eckert, *J. Am. Chem. Soc.*, **100**, 6252 (1978); J. G. Bridgart, M. W. Fuller, and I. R. Wilson, *J. Chem. Soc., Dalton Trans.*, **1973**, 1274; J.G. Bridgart and I.R. Wilson, *ibid.*, **1973**, 1281; J. G. Bridgart, W. A. Waters, and I.R. Wilson, *ibid.*, **1973**, 1582; L. M. Bharadwaj, D.N. Sharma, and Y. K. Gupta, *ibid.*, **1980**, 1527.

17) D. B. Brown, J. A. Donner, J. W. Hall, S. R. Wilson, R. B. Wilson, D. J. Hodgson, and W. E. Hatfield, *Inorg. Chem.*, **18**, 2635 (1979).

 © 1983 The Chemical Society of Japan Bull. Chem. Soc. Jpn., 56, 2827—2830 (1983)

A New Series of Heptamolybdonickelate(IV) and Manganate(IV). Investigation of the Unusual Magnetic and Electronic Spectral Behavior of the Nickel(IV) Compound

Ajoy Roy[1] and Muktimoy Chaudhury*

Department of Inorganic Chemistry, Indian Association for the Cultivation of Science, Calcutta 700 032, India

(Received July 9, 1982)

Two new heteropolymolybdates of nickel(IV) and manganese(IV) of composition $K_2H_8NiMo_7O_{28}\cdot 6H_2O$ and $K_2H_8MnMo_7O_{28}\cdot 4H_2O$ with a hitherto unknown 1 : 7 (Ni/Mn : Mo) stoichiometry are reported. X-Ray powder patterns show that they are isomorphous. The electronic spectrum of the nickel(IV) compound exhibits four absorption bands at 16.4, 17.5, 18.3, and 24×10^3 cm^{-1}, and the room temperature magnetic moment of the compound is abnormally high, 1.78 μB. The rationale for these observations is that there are Ni^{3+} impurity which occupy interstitial positions in the crystal lattice and as a consequence of dynamic Jahn-Teller distortion the high-spin $^4A_{2g}(^4T_{1g})$ state of the Ni^{3+} ion lies close to the low-spin ground state $^2A_{1g}(^2E_g)$ to get thermally populated to an appreciable extent leading to significant triplet state contribution.

Stabilization of higher oxidation states of nickel and manganese is a topic of current interest.[2,3] Most of the coordinating agents that stabilize the higher oxidation states of metal ions are organic molecules. Among the few inorganic ligands which are capable of forming higher valent metal complexes, isopolyanions are the prominent examples. Metal complexes of isopolymolybdates deserve special interest because of the diversity of their structural features. Crystal structure determinations have established their structures as hexa-, ennea-, deca-, and dodecamolybdometalates.[4-7]

Following the early discovery of nickel(IV) enneamolybdate by Hall,[8] several studies[5,9-11] have been reported on this and the analogous manganese(IV) species. However, to our knowledge, so far no hetero heptamolybdate has been reported in literature. This paper reports the preparation and characterization of nickel(IV) and manganese(IV) heptamolybdates.

Experimental

All chemicals were analytical grade and used without further purification.

Preparation of Dipotassium Octahydrogen Heptamolybdonickelate(IV), $K_2H_8NiMo_7O_{28}\cdot 6H_2O$. An aqueous solution (350 cm^3) of ammonium heptamolybdate (24.75 g, 20 mmol) was mixed with a solution (30 cm^3) of nickel(II) sulfate hexahydrate (2.65 g, 10 mmol). The solution was filtered, and to the filtrate 5.4 g (20 mmol) of potassium peroxodisulfate in small portions (addition required about 30 min) was added with constant stirring. During this addition the solution was maintained at 80 °C and stirred continuously. After $\approx$1 h a dark brown solution resulted which on standing overnight yielded dark brown shining crystals. The crystals were collected by filtration, washed several times with an aqueous solution of 0.1% $K_2S_2O_8$ followed by ice cooled water and finally dried over $CaCl_2$. Yield 6.3 g.

Dipotassium Octahydrogen Heptamolybdomanganate(IV), $K_2H_8MnMo_7O_{28}\cdot 4H_2O$. An aqueous solution (50 cm^3) of manganese(II) sulfate tetrahydrate (2.25 g, 10 mmol) was added to an aqueous solution (300 cm^3) of ammonium heptamolybdate (24.75 g, 20 mmol) with constant stirring. The solution turned yellowish in colour which was then filtered. The filtrate was heated on a steam bath and 5.4 g (20 mmol) of potassium peroxodisulfate was added in small portions (addition continued for 30 min) while stirring the solution vigorously. The colour of the solution gradually changed to orangeyellow. On standing at room temperature for $\approx$2 h, orangered shining crystals deposited. The product was collected on a glass frit and washed several times with 0.1% $K_2S_2O_8$ followed by ice cooled water and finally dried over $CaCl_2$. Yield 10.4 g.

Analyses. Chemical analyses were performed at least in triplicate. Manganese was estimated volumetrically by redox titration. Nickel and molybdenum were estimated gravimetrically using dimethylglyoxime and 8-quinolinol respectively as the reagents.[12] Water contents were determined thermogravimetrically.

Oxidation States†. About 30 mg of the compound was suspended in 25 cm^3 of water taken in an iodine flask. To this was added 2 g of iodate free potassium iodide and 10 ml of 2 mol dm^{-3} hydrochloric acid. 400 mg of sodium hydrogencarbonate was then added in small portions. The flask was stoppered immediately and the solution was stirred continuously for 2 h in dark with a magnetic stirrer. The solution was diluted to about 200 cm^3 and the liberated iodine was titrated with a standardized solution of sodium thiosulfate.

Measurements. The diffuse reflectance spectra were recorded (780—300 nm) on a Cary 14D spectrophotometer using magnesium oxide as the reference. Electronic spectra in solution were measured (800—200 nm) with a Pye Unicam SP8-150 spectrophotometer. Magnetic susceptibility measurements were made at room temperature on a Gouy balance with $Co[Hg(SCN)_4]$ as calibrant. X-Ray powder data were recorded with a Philips X-ray generator PW 1130 coupled with a Counter Diffractometer PW 1050,51 with nickel filtered Cu *Ka* radiation. Thermal analyses were carried out on a Shimadzu DT-30 thermal analysis system in an atmosphere of nitrogen at a heating rate of 5 °C min^{-1}.

Results and Discussion

The analytical results of the compounds shown in Table 1 are compatible with the assigned formulations. Both manganese and nickel are shown by the analytical data to possess the +4 oxidation state. The equivalent weight measurements as shown in Table 1 also support the 7 : 1 stoichiometry. In solid state, both the heptamolybdo compounds are indefinitely stable. The manganese(IV) compound is insoluble in water but the

† All solutions used in these measurements were prepared with deaerated water.

Table 1. Elemental analysis and equivalent weight of the compounds

Compound		M[a]	Mo	H_2O	Mo/M	Equivalent[b] weight
$K_2H_8NiMo_7O_{28}\cdot 6H_2O$	Found(%)	4.18	48.29	7.51	7.06	676 ± 4[d]
(1372.7)[c]	Calcd (%)	4.28	48.95	7.57		
$K_2H_8MnMo_7O_{28}\cdot 4H_2O$	Found(%)	4.13	50.30	5.50	6.98	663 ± 5[d]
((1333)[c]	Calcd (%)	4.12	50.41	5.40		

a) M=Ni or Mn. b) With respect to reduction of the hetero atom to the +2 oxidation state. c) Molecular weight of the compound. d) Experimental mean of four determinations.

Table 2. Observed *d*-spacings and intensities of $K_2H_8NiMo_7O_{28}\cdot 6H_2O$ and K_2H_8 $MnMo_7O_{28}\cdot 4H_2O$

$K_2H_8NiMo_7O_{28}\cdot 6H_2O$		$K_2H_8MnMo_7O_{28}\cdot 4H_2O$	
d	Intensities	*d*	Intensities
5.63	9	5.57	10
4.70	16	4.76	14
3.92	44	3.93	43
3.60	72	3.61	70
3.22	100	3.25	100
3.00	43	2.99	41
2.82	43	2.82	42
2.49	10	2.51	10
2.40	61	2.41	65
2.03	42	2.04	42
1.97	25	1.99	24
1.79	20	1.69	19
1.63	13	1.65	15
1.42	30	1.42	31
1.41	20	1.41	19

nickel(IV) compound is sparingly soluble in hot water (≈40 °C).

Table 2 summarizes the powder diffraction data of both $K_2H_8MnMo_7O_{28}\cdot 4H_2O$ and $K_2H_8NiMo_7O_{28}\cdot 6H_2O$. The identical *d*-spacings as well as intensities confirm that they are isomorphous. Similar isomorphism in other heteropolymetalates of Ni(IV) and Mn(IV) is well documented in literature.[11,13,14]

The number of water molecules present in the nickel(IV) and manganese(IV) compounds were determined from TGA and DTA. $K_2H_8NiMo_7O_{28}\cdot 6H_2O$ loses the six water molecules between 60 and 190 °C. The DTA shows that the water molecules are lost in two overlapping steps having the endothermic peaks at 105 and 135 °C. The observed weight loss, 7.51% agrees well with the calculated value, 7.58%. The thermolysis product arrested at 190 °C have the composition $K_2H_8NiMo_7O_{28}$ and the iodometric assay shows +4 oxidation state of nickel. On further heating, $K_2H_8NiMo_7O_{28}$ decomposes between 240—500 °C in a complicated way with the evolution of water along with oxygen as indicated by the appearance of two consecutive exotherms in the DTA. In $K_2H_8MnMo_7O_{28}\cdot 4H_2O$ the four water molecules are lost between 50 and 200 °C in a single step (DTA peak temperature, 120 °C). Above 230 °C further decomposition takes place in a way similar to the nickel(IV) compound. From the thermal analysis it may be stated that both the compounds contain two types of water, *viz.* the water of crystallization and the constitutional water which evolve at a considerably higher temperature (between 230—500 °C) compared to the water of crystallization.

Table 3. The diffuse reflectance spectra of $K_2H_8NiMo_7O_{28}\cdot 6H_2O$ and $K_2H_8MnMo_7O_{28}\cdot 4H_2O$

$K_2H_8NiMo_7O_{28}\cdot 6H_2O$		$K_2H_8MnMo_7O_{28}\cdot 4H_2O$	
Band position $\tilde{\nu}/10^3$ cm^{-1}	Assignments	Band position $\tilde{\nu}/10^3$ cm^{-1}	Assignments
16.4	$^1A_{1g}\rightarrow{}^1T_{1g}$[a] or $^2A_{1g}\rightarrow{}^4A_{2g}$[b]	14.3	$^4A_{2g}\rightarrow{}^2E_g$
17.5	$^1A_{1g}\rightarrow{}^1T_{2g}$[a]	15.0	$^4A_{2g}\rightarrow{}^2T_{2g}$
18.3	$^2A_{1g}\rightarrow{}^4E_g$[b]	20.4	$^4A_{2g}\rightarrow{}^4T_{2g}$
24.0	$^2A_{1g}\rightarrow{}^2B_{1g}$[b]	27.9	$^4A_{2g}\rightarrow{}^4T_{1g}$(F)

a) Due to Ni(IV). b) Due to Ni(III).

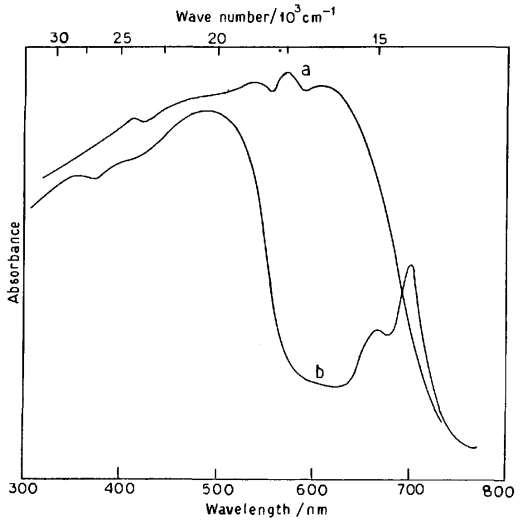

Fig. 1. Diffuse reflectance spectra of (a) $K_2H_8NiMo_7O_{28}\cdot 6H_2O$ and (b) $K_2H_8MnMo_7O_{28}\cdot 4H_2O$.

Electronic Spectra and Magnetic Moments. The electronic spectrum of $K_2H_8NiMo_7O_{28}\cdot 6H_2O$ in saturated aqueous solution contains two bands at 17.8 and 47.4×10^3 cm^{-1}. The first one has also been observed in enneamolybdonickelate(IV)[11] and is assigned to nickel(IV) d-d ($^1A_{1g}\rightarrow{}^1T_{2g}$) transition. The other band at 47.4×10^3 cm^{-1} is most likely due to a charge transfer transition.

The diffuse reflectance spectra of the compounds with probable assignments are listed in Table 3. The electronic spectrum of the nickel(IV) compound in solid state as shown in Fig. 1 exhibits four bands at 16.4, 17.5, 18.3, and 24×10^3 cm^{-1}. The band at 17.5×10^3 cm^{-1} which is also observed in solution is the most

intense one, while the other three are of comparable intensities. It seems likely that due to their lower intensities they were not observed in the spectrum obtained with saturated aqueous solution.

In interpreting the electronic spectra of the nickel(IV) and manganese(IV) compounds we have considered that these metal ions are present in an octahedral array of oxygen atoms which is consistent with the structural information available for the heteropolymolybdates.

A common feature for most of the spin paired octahedral d^6 metal ions like nickel(IV) is that they give rise to two allowed ($^1A_{1g}\rightarrow{}^1T_{1g}$ and $^1A_{1g}\rightarrow{}^1T_{2g}$) and two spin forbidden ($^1A_{1g}\rightarrow{}^3T_{1g}$ and $^1A_{1g}\rightarrow{}^3T_{2g}$) ligand field transitions of which the $^1A_{1g}\rightarrow{}^1T_{2g}$ transition is of highest energy and maximum intensity.[15] Thus the most intense ligand field band observed at 17.5×10^3 cm^{-1} in the solid state spectrum of $K_2H_8NiMo_7O_{28}\cdot6H_2O$ can safely be assigned to $^1A_{1g}\rightarrow{}^1T_{2g}$ nickel(IV) transition. Since of the remaining three bands, two appear at still higher energies relative to the one at 17.5×10^3 cm^{-1}, their origin cannot be due to d-d transition of nickel(IV). However, the band at 16.4×10^3 cm^{-1} can tentatively be assigned to the second spin allowed nickel(IV) d-d transition, *viz.* $^1A_{1g}\rightarrow{}^1T_{1g}$.

In order to explain the appearance of two higher energy bands at 18.3 and 24×10^3 cm^{-1}, we invoke the presence of Ni^{3+} ion in the crystal lattice of $K_2H_8NiMo_7O_{28}\cdot6H_2O$. This assumption is based on the observation made from magnetic moment measurements (see later). It is conjectured that during the preparation of $K_2H_8NiMo_7O_{28}\cdot6H_2O$, some of the nickel(IV) sites are occupied by nickel(III) in the crystal lattice. These Ni^{3+} ions present in an octahedral array of oxygen should ordinarily have a low-spin ^2E_g ground state. It is well known[16] that for a ground state of E symmetry the octahedral environment undergoes tetragonal distortion by interaction with the ε_g vibrational mode leading to either elongation or compression along the four fold axis together with appreciable ground-state splitting. Reinen *et al.*[17,18] have shown from EPR and ligand field data that for a Ni^{3+} ion in an octahedral site, Jahn-Teller distortion sharply splits ^2E_g into $^2B_{1g}+{}^2A_{1g}$ while $^4T_{1g}$ undergoes a much smaller splitting into ^4E_g and $^4A_{2g}$. In effect, $^2A_{1g}$ becomes the ground state with $^4A_{2g}$ lying only slightly above it. The result is the equilibrium $^2A_{1g}\rightleftharpoons{}^4A_{2g}$. Similar tetragonal ground state splitting has also been considered by Warren *et al.*[19] during their attempt to explain the electronic spectrum of $[NiF_6]^{3-}$ ion.

Thus following the energy level diagram as proposed by Reinen,[18] the bands at 18.3 and 24×10^3 cm^{-1} can be assigned to ($^2A_{1g}\rightarrow{}^4E_g$) and ($^2A_{1g}\rightarrow{}^2B_{1g}$) transitions respectively. The lowest energy band at 16.4×10^3 cm^{-1} which has been previously indicated as due to $^1A_{1g}\rightarrow{}^1T_{1g}$ of nickel(IV) can alternatively be assigned to $^2A_{1g}\rightarrow{}^4A_{2g}$ nickel(III) d-d transition.

Table 3 shows that the spectrum of Mn(IV) compound contains four bands (also shown in Fig. 1). The ruby band observed at 14.3×10^3 cm^{-1} was also observed by Baker *et al.*[11] in enneamolybdomanganate(IV) and was assigned to $^4A_{2g}\rightarrow{}^2E_g$ transition. The next higher energy band at 15×10^3 cm^{-1} was also observed in the spectrum of hexamolybdochromate(III) and was interpreted as due to $^4A_{2g}\rightarrow{}^2T_{2g}$ transition.[11] The remaining two higher energy bands appeared at 20.4 and 27.9×10^3 cm^{-1} are considered to be due to first and second spin allowed transitions to excited $^4T_{2g}$ and $^4T_{1g}(F)$ states respectively following the arguements made by Jørgensen.[20]

The room temperature magnetic moment of the Mn(IV) compound is 3.95 BM which is in agreement with the value 3.88 BM calculated for a high-spin d^3 Mn(IV) configuration. Although on the basis of analytical and X-ray powder data one would expect that $K_2H_8NiMo_7O_{28}\cdot6H_2O$ should be diamagnetic; however, it is paramagnetic having a room temperature magnetic moment of 1.78 BM. This unusually high magnetic moment for a nickel(IV) compound can not be explained on the basis of its temperature independent paramagnetism which at the most can have a contribution of ≈0.6 BM.[21] Such unusual paramagnetic behavior was also observed in nickel(IV) periodate[22] and was explained from EPR studies as due to nickel(III) impurities.[23] The presence of nickel(III) impurity has been already considered in order to explain the electronic spectrum of $K_2H_8NiMo_7O_{28}\cdot6H_2O$. Obviously the concentration of nickel(III) is very low as the chemical composition indicates and literature[2] shows that nickel(III) species are almost invariably low-spin with one unpaired electron. Thus a small concentration of nickel(III) ion with a low-spin ground state (^2E_g) having no orbital contribution can not alone explain such a high room temperature magnetic moment. Hoppe *et al.*[24,25] in order to explain the unusually high magnetic moments of Ni^{3+} ion in alkali metal hexafluoronickelates considered thermal equilibrium between the high and low-spin forms. We also propose that because of the dynamic Jahn-Teller effect, the high-spin $^4A_{2g}$ ($^4T_{1g}$) state of the nickel(III) lies close enough to the low-spin ground state $^2A_{1g}(^2E_g)$ to get thermally populated to an appreciable extent leading to significant triplet state contribution towards the room temperature magnetic moment.

In conclusion we emphasize that the Ni^{3+} ion that is present as impurity in $K_2H_8NiMo_7O_{28}\cdot6H_2O$ provides a rare example of spin state equilibrium of nickel(III). To our knowledge such example is restricted only to alkalimetal hexafluoronickelates(III).

The authors are grateful to Dr. K. Nag of this department for many helpful discussions during the course of this investigation.

References

1) Present address: Department of Electrical Engineering, University of Colorado, Boulder, U. S. A.

2) K. Nag and A. Chakravorty, *Coord. Chem. Rev.*, **33**, 187 (1980).

3) W. Levason and C. A. McCauliffe, *Coord. Chem. Rev.*, **12**, 151 (1974).

4) H. T. Evans, Jr., *J. Am. Chem. Soc.*, **90**, 3275 (1968).

5) J. L. T. Waugh, D. P. Shoemaker, and L. Pauling, *Acta Crystallogr.*, **7**, 438 (1954).

6) H. T. Evans, Jr., and J. S. Showell, *J. Am. Chem. Soc.*,

91, 6881 (1969).
7) D. D. Dexter and J. V. Silverton, *J. Am. Chem. Soc.*, **90**, 3589 (1968).
8) R. D. Hall, *J. Am. Chem. Soc.*, **29**, 692 (1907).
9) P. Souchay and R. Schaal, *Anal. Chim, Acta*, **3**, 1 (1949).
10) P. Ray, A. Bhaduri, and B. Sharma, *J. Ind. Chem. Soc.*, **25**, 51 (1948).
11) L. C. W. Baker and T. J. R. Weakley, *J. Inorg. Nucl. Chem.*, **28**, 447 (1966).
12) A. I. Vogel, "A Text-Book of Quantitative Inorganic Analysis," 2nd ed, Longmans, Green and Co., London (1955).
13) C. M. Flynn, Jr., and G. D. Stucky, *Inorg. Chem.*, **8**, 332 (1969).
14) C. M. Flynn, Jr., and M. T. Pope, *J. Am. Chem. Soc.*, **92**, 85 (1970).
15) A. B. P. Lever, "Inorganic Electronic Spectroscopy," Elsevier Publishing Company (1968), p. 302.
16) H. A. Jahn and E. Teller, *Proc. R. Soc. London, Ser. A*, **161**, 220 (1937).
17) D. Reinen, C. Friebel, and V. Propach, *Z. Anorg. Allg. Chem.*, **408**, 187 (1974).
18) D. Reinen, *J. Solid State Chem.*, **27**, 71 (1979).
19) G. C. Allen and K. D. Warren, *Inorg. Chem.*, **8**, 1895 (1969).
20) C. K. Jørgensen, *Acta Chem. Scand.*, **12**, 1539 (1958).
21) R. L. Carlin and A. J. Duyneveldt, "Magnetic Properties of Transition Metal Compounds," Springer-Verlag, New York (1977), p. 20.
22) P. Ray and B. Das Sarma, *J. Ind. Chem. Soc.*, **25**, 204 (1948).
23) M. Chaudhury, A. Roy, B. P. Ghosh, and K. Nag, *Z. Naturforsch., B*, **35**, 1201 (1980).
24) E. Alter and R. Hoppe, *Z. Anorg. Allg. Chem.*, **405**, 167 (1974).
25) H. Henkel and R. Hoppe, *Z. Anorg. Allg. Chem.*, **364**, 253 (1969).

© 1983 The Chemical Society of Japan

NOTES

Bull. Chem. Soc. Jpn., 56, 2831—2832 (1983)

Heats of Solutions of Bolaform Electrolytes in Water

Kunio TAMAKI* and Kaoru IRIE

Department of Chemistry, Yokohama City University, Kanazawa-ku, Yokohama 236

(Received March 12, 1983)

Synopsis. The heats of solutions of polymethylenediammonium dichlorides $[H_3N(CH_2)_nNH_3]Cl_2$ (n=2—8, 10, and 12) and disodium polymethylene disulfates $Na_2[O_3SO(CH_2)_nOSO_3]$ (n=2—6, 8, and 10) in water were measured at 15, 25, and 35 °C. The changes in the heat capacity for dissolution, $\Delta C_p°$, were obtained from the relation between the heats of soultion and the temperature, and the results were compared with the $\Delta C_p°$ values for alkylammonium chlorides and sodium alkyl sulfates previously reported.

The physical properties of amphiphilic electrolytes in water have been discussed in terms of the resultant change in the water structure upon the introduction of ions into water. Nonpolar groups, such as alkyl groups and polymethylene groups, act as water-structure makers in water; that is, the water molecules form an icelike structure around the nonpolar groups. The study of the heat capacities of aqueous electrolyte solutions provides a useful method of obtaining information about the influence of ions on the structure of solvent water. In previous papers,[1,2] the results on the changes in the heat capacity for the dissolution in water, $\Delta C_p°$ for a series of alkylammonium chlorides ($C_nH_{2n+1}NH_3Cl$, which will be abbreviated as C_nCl) and sodium alkyl sulfates ($C_nH_{2n+1}OSO_3Na$, which will be abbreviated as, NaC_n) were reported. In this paper, the experimental results regarding the heats of solution and the $\Delta C_p°$ values for polymethylenediammonium dichlorides ($[H_3N(CH_2)_nNH_3]Cl_2$, which will be abbreviated as, C_nCl_2) and disodium polymethylene disulfated ($Na_2[O_3SO(CH_2)_nOSO_3]$, which will be abbreviated as, Na_2C_n) will be reported. This type of electrolyte, in which an ionic part is attached at each end of the chain, is called a bolaform eletrolyte. The main object of this paper is to compare the hydrophobic character of the polymethylene group in a bolaform electrolyte with that of the alkyl group for a monovalent electrolyte.

Experimental

Materials. The organic chemicals used were obtained from the Tokyo Kasei Kogyo Co., Ltd. C_7Cl_2, C_8Cl_2, $C_{10}Cl_2$, and $C_{12}Cl_2$ were prepared by the neutralization of the corresponding diamines in methanol with hydrochloric acid, and the solvents were evaporated to dryness. All the C_nCl_2 salts were recrystallizaed twice from ethanol–water solutions and dried *in vacuo* at room temperature. Na_2C_n salts were synthesized by the esterification of the corresponding alcohols by the use of concentrated sulfuric acid in cabon tetrachloride or chloroform below 15 °C. After removing the carbon tetrachloride or chloroform, the solutuions were neutralized with a concentrated solution of sodium hydroxide. The reaction mixtures were dried in air and extracted with ethanol–water solutions (about 60% ethanol). The products were further purified several times by recrystallizing them from ethanol–water solutions (about 80% ethanol) and then dried *in vacuo* at 100 °C. Water was triply distilled.

Table 1. Heats of solution and heat-capacity changes

n	$\Delta H_s°$/kJ mol^{-1} 15 °C	25 °C	35 °C	$\Delta C_p°$/J K^{-1} mol^{-1} 25 °C
		$[H_3N(CH_2)_nNH_3]Cl_2$		
2	31.21	28.24	25.48	−287
3	27.53	25.19	22.97	−228
4	26.69	24.98	23.30	−170
5	9.62	8.45	7.53	−105
6	22.84	22.51	22.26	−29
7	20.63	20.84	21.17	27
8	22.89	23.89	24.89	100
10	29.58	32.01	34.31	237
12	40.88	44.31	47.91	352
		$Na_2[O_3SO(CH_2)_nOSO_3]$		
2	27.93	25.69	23.60	−217
3	10.70	8.87	7.35	−167
4	30.49	29.51	28.63	−93
5	22.36	21.92	21.50	−43
6	20.60	20.94	21.08	24
8	23.36	24.80	25.99	132
10	37.09	39.76	42.61	276

Calorimetry. The heats of solution in water were measured at 15, 25, and 35 °C with a twin isoperibol calorimeter TIC-2C, manufactured by the Tokyo Riko Co., Ltd. The sample and blank ampoules were, respectively, set in the measuring and reference Dewar vessels, each containing 200 cm^3 of water, resting in depressions in an aluminum block controlled to ±0.01 °C. After thermal equilibrium had been attained, the sample and blank ampoules were broken simultaneously. The difference in temperature measured by a pair of thermistors was recorded on a chart recorder. The calorimeter was checked by measuring the heat of solution of potassium chloride at 25 °C. The value obtained was within 1% of that reported in the literature.[3]

Results and Discussion

Heat-of-solution measurements have been carried out in the concentration range of 6×10^{-4}—2.5×10^{-3} mol dm^{-3}. In this concentration range, any dependence of the heat of solution on the concentration is within the limits of experimental error, so the average of three or more measurements has been taken as the heat of solution at an infinite dilution, $\Delta H_s°$. The $\Delta H_s°$ values of C_nCl_2 and Na_2C_n are listed in Table 1. Results from the $\Delta H_s°$ values were used to calculate the change in the heat capacity in going from the pure compounds to an aqueous solution at an infinite

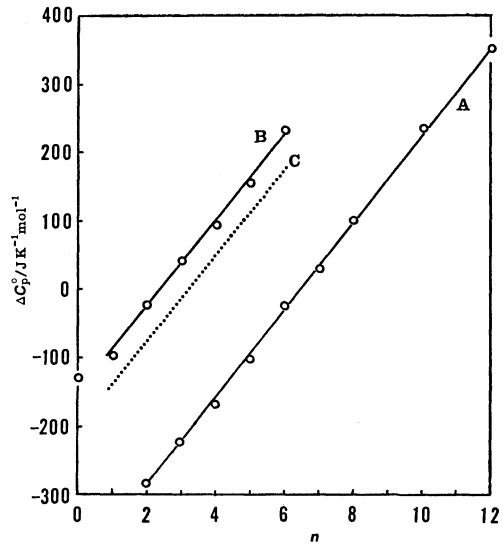

Fig. 1. Plot of ΔC_p° against n. A, $[H_3N(CH_2)_nNH_3]$-Cl_2; B, $C_nH_{2n+1}NH_3Cl$; C, $-(CH_2)_nNH_3Cl$.

dilution, ΔC_p°;

$$\Delta C_p^\circ = d\Delta H_s^\circ/dT,$$

where T is the temperature. The ΔC_p° values obtained at 25 °C are also listed in Table 1. The magnitude and sign of ΔC_p° can be taken as relative measures of the structural effect upon the solvent water.[1,4,5] The ΔC_p° values of simple salts indicate negative values, whereas the ΔC_p° values of hydrophobic solutes indicate positive values.

As may be seen in Table 1, the ΔC_p° values for C_2Cl_2, C_3Cl_2, C_4Cl_2, C_5Cl_2, and C_6Cl_2 are negative, while the ΔC_p° values become positive in the case of C_7Cl_2 and higher homologs. In an earlier work[1] on C_nCl series, C_1Cl and C_2Cl showed negative values of ΔC_p°, while C_3Cl and higher homologs showed positive values of ΔC_p°. Figure 1 shows the ΔC_p° values as a function of the number of carbon atoms, n, in the polymethylene or alkyl group for C_nCl_2 and C_nCl. If we take one-half the ΔC_p° values for C_nCl_2, the ΔC_p° values for a series of $-(CH_2)_nNH_3Cl$ can be estimated. The ΔC_p° *vs.* n relation thus obtained is plotted as a dotted line in Fig. 1. It is found that, for the same number of carbon atoms, the ΔC_p° values for $-(CH_2)_nNH_3Cl$ are lower than those for C_nCl. With the same ΔC_p° values, the difference in n between the two ΔC_p°-*vs.*-n lines for C_nCl and $-(CH_2)_nNH_3Cl$ corresponds to about 0.8.

Table 1 indicates that the ΔC_p° values for Na_2C_2, Na_2C_3, Na_2C_4, and Na_2C_5 are negative, while the ΔC_p° values for Na_2C_6 and higher homologs are positive. In a previous paper[2] on a NaC_n series, NaC_1 showed a negative value of ΔC_p°, while NaC_3 and higher homologs showed positive ΔC_p° values. Figure 2 shows the ΔC_p° values as a function of n for Na_2C_n and NaC_n. The dotted line in Fig. 2 represents the data for a $-(CH_2)_nOSO_3Na$ series. With the same ΔC_p° values, the differnce in n between the two ΔC_p°-*vs.*-n relations for NaC_n and $-(CH_2)_nOSO_3Na$ corresponds to about 0.7.

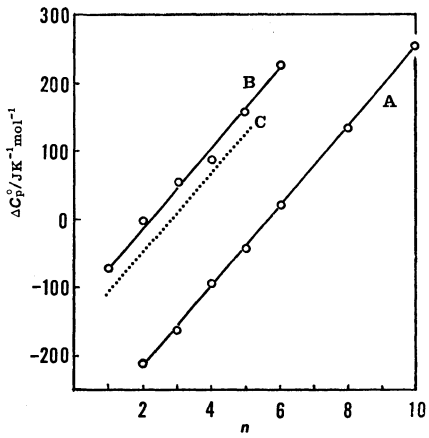

Fig. 2. Plot of ΔC_p° against n. A, $Na_2[O_3SO(CH_2)_n$-$OSO_3]$; B, $C_nH_{2n+1}OSO_3Na$; C, $-(CH_2)_nOSO_3Na$.

With bolaform electrolytes, the electrostrictive hydration due to the two ionic parts situated at opposite ends of a chain may interfere with the interaction of the hydrophobic polymethylene chain with water, and the smaller members of both series of C_nCl_2 and Na_2C_n are water-structure-breaking ions. When the charged groups are sufficiently far apart, the solvent-structuring effect of the hydrophobic polymethyene chain becomes important. However, the hydrophobic character of the polymethylene chain in bolaform electrolytes is considerably diminished as compared with that of the alkyl chain in monovalent electrolytes.

Thanks are due to Mr. Akihide Kudo, Mr. Shinichi Hata, and Ms. Izumi Makino for the preliminary experiments.

References

1) K. Tamaki, S. Yoshikawa, and M. Kushida, *Bull. Chem.Soc.Jpn.*, **48**, 3018 (1975).
2) K. Tamaki, Y. Isomura, and Y. Ōhara, *Bull. Chem. Soc. Jpn.*, **45**, 2939 (1972).
3) G. Somsen, J. Coops, and M. W. Tolk, *Recl. Trav. Chim. Pays-Bas*, **82**, 231 (1963).
4) E. M. Arnett and J. J. Campion, *J. Am. Chem. Soc.*, **92**, 7097 (1970).
5) B. Chawla and J. C. Ahluwalia, *J. Solution Chem.*, **4**, 383 (1975).

Colloidal Rhodium Dispersions Protected by Cyclodextrins

Makoto KOMIYAMA* and Hidefumi HIRAI

Department of Industrial Chemistry, Faculty of Engineering, The University of Tokyo, Hongo, Bunkyo-ku, Tokyo 113

(Received March 30, 1983)

Synopsis. Refluxing of an aqueous solution of rhodium(III) chloride and α- or β-cyclodextrin, followed by further refluxing in the presence of ethanol, gives a colloidal dispersion of rhodium particles of 28 Å in diameter. The colloidal dispersion exhibits effective catalyses in hydrogenation of olefins at 30 °C under an atmospheric pressure.

Interests in colloidal dispersions of metals have been rapidly increasing especially in this decade.[1,2]

Previously,[2-5] the present authors succeeded in the preparation of colloidal dispersions of noble metals by reducing their salts with alcohols such as ethanol and 1-propanol in the presence of various polymers. The polymers used were poly(vinyl alcohol), poly(*N*-vinylpyrrolidone), and poly(methyl vinyl ketone). The resulting colloidal dispersions were characterized both by quite small particle sizes and by narrow distributions in particle sizes.

This paper describes the preparation of colloidal rhodium dispersions through the reduction of rhodium(III) chloride with ethanol using cyclodextrins, cyclic oligomers of 6—8 glucose units, as protective colloids. The catalytic activities of these colloidal dispersions in the hydrogenation of olefins will be shown.

Experimental

Colloidal rhodium dispersions were prepared as follows. First, 7.0 mg (2.7×10^{-5} mol) of rhodium(III) chloride trihydrate (Nippon Engelhard, Ltd.) and various amounts of α-, β-, or γ-cyclodextrin (Nakarai Chemical Co.) were dissolved in 30 ml of water, and the solution was refluxed for 30 min. Then, 10 ml of ethanol was added and the solution was further refluxed for 10 min, resulting in the formation of colloidal rhodium dispersion as a dark brown solution.

Sample films of colloidal dispersions for electron microscopy were prepared by evaporating the solvent to dryness on a collodion film coated with a carbon layer. Electron micrographs were measured by a Hitachi Model H 500 electron microscope operated at 125 kV at the magnification of 100000.

Hydrogenation of olefins catalyzed by colloidal rhodium dispersions was carried out at 30.0 °C under an atmospheric hydrogen pressure, and was followed by reading the uptake of hydrogen.

Results and Discussion

Homogeneous colloidal rhodium dispersion was obtained using α- or β-cyclodextrin. The minimal molar ratios of cyclodextrin to rhodium(III) chloride, required for the preparation of the colloidal dispersions, were 0.5 for α-cyclodextrin and 0.1 for β-cyclodextrin. These results were markedly in contrast with the rapid formation of black precipitates in the absence of cyclodextrin. The precipitation took place immediately after the refluxing of the water-ethanol mixture started.

When γ-cyclodextrin was used in place of α- or β-cyclodextrin, rapid precipitation took place and colloidal dispersion was not obtained, even at the molar ratio unity of γ-cyclodextrin to rhodium(III) chloride.

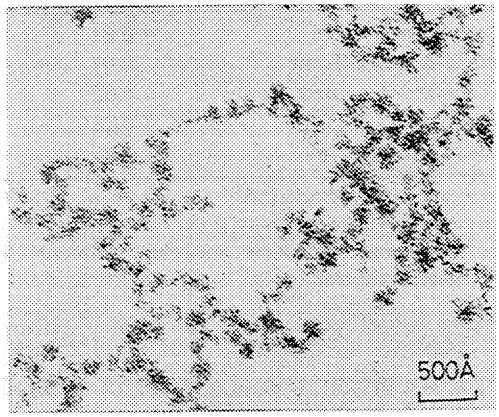

Fig. 1. Electron micrograph of colloidal rhodium dispersion prepared by using β-cyclodextrin equimolar to rhodium(III) chloride; ×100000.

From these results, it is concluded that the protecting abilities of cyclodextrins are in the following order:

β-cyclodextrin > α-cyclodextrin ≫ γ-cyclodextrin ≈ 0.

Figure 1 shows the electron micrograph of rhodium colloidal dispersion prepared in the presence of β-cyclodextrin equimolar to rhodium(III) chloride. Highly dispersed fine rhodium particles are observed. The average diameter of the particles is 28 Å.

In aqueous solutions, apolar particles of rhodium metal should be bound to the apolar cavities of cyclodextrins. Since the particles are too large to be totally included in the cavity of α- or β-cyclodextrin, they sit on the top of the cavity. Thus, the surface of the rhodium particles is mostly covered with several cyclodextrin molecules, which prevent aggregation of particles.

The proposed structures of the present colloidal particles are consistent with the larger protecting ability of β-cyclodextrin than that of α-cyclodextrin, since almost all of the guest compounds previously investigated showed stronger binding with β-cyclodextrin than with α-cyclodextrin.[6] Minimal protecting ability of γ-cyclodextrin is associated with less apolar property of the cavity. The order for the three kinds of cyclodextrins in the protecting abilities is also identical with the decreasing order in their solubilities in water.

The above arguments are supported by the fact that dextran (degree of polymerization, 360), which has no cavities, shows no measurable protecting ability at the molar ratio 7 to rhodium(III) chloride. Here, a glucose residue of dextran is taken as a unit. Furthermore, both poly(ethylene oxide) and poly(*N*-vinylpyrrolidone)(degree of polymerization, 110 and 90, respectively) exhibit no effective protection at the residual molar ratio unity with respect to rhodium(III) chloride.

Table 1. Catalytic activities of colloidal dispersion of rhodium prepared by using β-cyclodextrin in the hydrogenation of olefins[a)]

Substrate	Initial rate of hydrogen uptake (H_2 mol/Rh g-atoms·s)
3-Buten-2-one	0.24
3-Methyl-3-buten-2-one	0.07
3,4-Dimethyl-3-penten-2-one	0.32
Acrylonitrile	0.22
Methacrylonitrile	0.06

a) Hydrogenation conditions: temperature, 30.0 °C; total pressure, 1 atm; [Rh]=[β-cyclodextrin]=4×10^{-5} mol·dm^{-3}; [substrate]=2.5×10^{-2} mol·dm^{-3}; solvent, 19.5: 0.5 (v/v) water-ethanol.

The refluxing of aqueous solution of rhodium(III) chloride prior to the addition of ethanol is definitely required for the preparation of a homogeneous colloidal dispersion. When rhodium(III) chloride was directly dissolved in the 3:1 water–ethanol mixture and the solution was refluxed for 10 min, considerable amounts of precipitates were formed together with a homogeneous dark brown colloidal dispersion.

On refluxing an aqueous solution of rhodium(III) chloride and β-cyclodextrin for 30 min, the absorbance in the 200—350 nm region decreased and a shoulder appeared at 260 nm. These changes are attributable to complex formation of rhodium(III) chloride with β-cyclodextrin. Rhodium ions in the complexes were then reduced by the ethanol added, and the resulting colloidal dispersion showed a monotonic absorption without peaks.[4)]

As shown in Table 1, the rhodium colloidal dispersion prepared with β-cyclodextrin effectively catalyzed hydrogenation of water-soluble olefins at 30.0 °C under an atmospheric hydrogen pressure.

Methyl substitutions in the substrate at the β-position with respect to the carbonyl group enhance catalytic hydrogenation. The hydrogenation of 3,4-dimethyl-3-penten-2-one is about 4.6 times as fast as that of 3-methyl-3-buten-2-one. In contrast, methyl substitution at the α-position with respect to the carbonyl or cyano group suppresses the reaction. The rates for 3-methyl-3-buten-2-one and methacrylonitrile are 3 fold smaller than the values for the corresponding substrates without a methyl group at the α-position.

These results indicate the inclusion complex formation of the substrates with one of the β-cyclodextrins, located on the surface of the rhodium particles, prior to the catalytic functions of the particles. In order to make the catalyses effective, the penetration of the substrate in the cavity should be from the side involving the C–C double bond rather than from the side involving the polar groups. The alkyl substitution at the β-position enhances the inclusion of the substrate into the apolar cavity from the side involving the C–C double bond due to increase in the apolar character of this side. On the other hand, alkyl substitution at the α-position decreases the polar character in the side involving the polar group, resulting in the suppression of the inclusion from the side involving the C–C double bond.

The participation of β-cyclodextrin, located on the surface of rhodium particles, in the catalyses is further supported by the fact that the hydrogenation of 3-buten-2-one is almost totally inhibited by the addition of 10^{-2} mol dm^{-3} of cyclohexanol. In contrast, methanol exhibits no effect on the hydrogenation at the same concentration. The inhibition by cyclohexanol, which forms inclusion complex with β-cyclodextrin, is attributable to its competition with the substrate for the cavity of β-cyclodextrin.

In conclusion, complex formation of rhodium(III) chloride with α- or β-cyclodextrin, followed by the reduction of them with ethanol, gives a colloidal rhodium dispersion. The dispersion exhibits specific catalyses in the hydrogenation of olefins.

The authors would like to thank Mr. Hidehiko Wakabayashi in our laboratory for his help in electron micrograph measurements.

References

1) R. H. Grubbs, *Chem. Technol.*, **1977**, 512.
2) H. Hirai, *J. Macromol. Sci. Chem.*, **A13**, 633 (1979).
3) H. Hirai, Y. Nakao, N. Toshima, and K. Adachi, *Chem. Lett.*, **1976**, 905.
4) H. Hirai, Y. Nakao, and N. Toshima, *J. Macromol. Sci. Chem.*, **A12**, 1117 (1978).
5) H. Hirai, Y. Nakao, and N. Toshima, *J. Macromol. Sci. Chem.*, **A13**, 727 (1979).
6) M. L. Bender and M. Komiyama, "Cyclodextrin Chemistry," Springer-Verlag, Berlin (1978).

The Dissolution of Heat-treated Acenaphthylene Pitch

Yoshio YAMADA,* Minoru SHIRAISHI, Takeshi FURUTA, and Toshio YAMAKAWA
National Research Institute for Pollution and Resources, Yatabe, Ibaraki 305

(Received April 8, 1983)

Synopsis. About half of the pyridine insolubles in heat-treated acenaphthylene pitch was dissolved into hydrogenated pitch. Observation with optical and scanning electron microscopes showed that the components dissolved consisted of small mesophase spherules with an optically isotropic texture.

An optically anisotropic mesophase texture appears from isotropic pitch when the pitch is carbonized. Once the mesophase texture is formed, most of the anisotropic structures are insoluble, even in such powerful solvents as pyridine and quinoline.[1-3] In this study we attempt to dissolve the mesophase texture formed at an early stage of carbonization by using a hydrogenated pitch and a pyridine-soluble fraction containing molecular species near the mesophase constituent.

Experimental

A pitch (683-4) containing 15.2 wt% of pyridine insolubles (PI) and 8.6 wt% of quinoline insolubles (QI) was obtained by heat-treating acenaphthylene at 683 K for 4 h in a nitrogen atmosphere. The process of preparing the additives used for dissolution is shown in Fig. 1. Acenaphthylene was heated at 703 K for 2 h in a nitrogen stream and then evacuated at 623 K for 2 h to remove any volatile materials. The pitch (703-2) was hydrogenated with Li-ethylenediamine,[4] *i.e.*, by BenKeser reduction, and the product thus obtained was treated under a vacuum at 623 (703-2BK(623)) or 648 K (703-2BK(648)) for 2 h. On the other hand, the pyridine-soluble fraction from the pitch of 703-2 was evacuated at 623 (703-2PS(623)) or 648 K (703-2PS(648)) for 2 h.

The pitch of 683-4 was mixed with an equal portion of each additive, and the mixture was transferred into an ampule connected to a vacuum line to degas and seal it. After the sealed ampule had been heat-treated at 623 K for 1 h in a fluidized sand bath, all the product in the ampule was used to estimate the solubility. The amounts of PI and QI were determined by soxhlet extraction and the JIS-K2425 method respectively.

Results and Discussion

The infrared spectra of 703-2BK and 703-2PS are shown in Fig. 2. The peaks at 2850 and 2900 cm^{-1} due to aliphatic CH symmetric and antisymmetric stretching are largely enhanced by the hydrogenation of the pitch of 703-2. Since condensed aromatic hydrocarbons are mainly converted to saturated or partially saturated ring compounds by BenKeser reduction,[4] in this case also some naphthenic hydrocarbons are considered to be present in 703-2BK. The results of elemental analyses and the hydrogen-to-carbon atomic ratio of the additives are given in Table 1, along with that of 703-2. The hydrogen content increases with the BenKeser reduction, but some of the hydrogens added are eliminated by treatment *in vacuo* at these temperature ranges. The extent of dehydrogenation for 703-2BK is much higher than that for 703-2PS. This was confirmed by the analysis of the gas evolved on the heat-treatment of these samples. This suggests that the hydrogens in naphthenic rings formed by the saturation of the aromatic molecules are unstable. The average molecular weight for 430-2BK is comparable to that for 703-2PS at the same treatment temperature (Table 2). However, an increase in the temperature tends to raise the molecular weight and, at the same time, to form PI, although the QI are negligibly small for all the samples except for 703-2. The formation of PI may be considered to

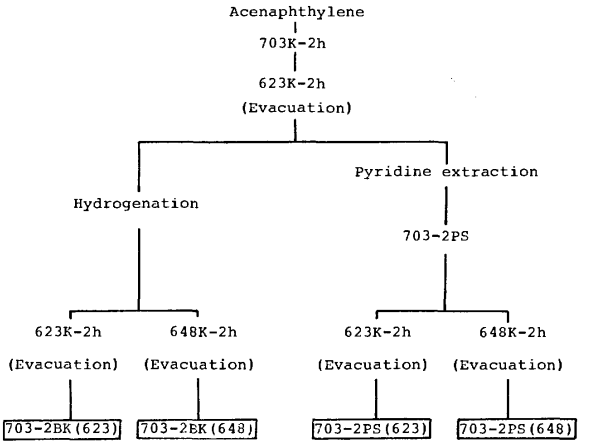

Fig. 1. Preparation of additives.

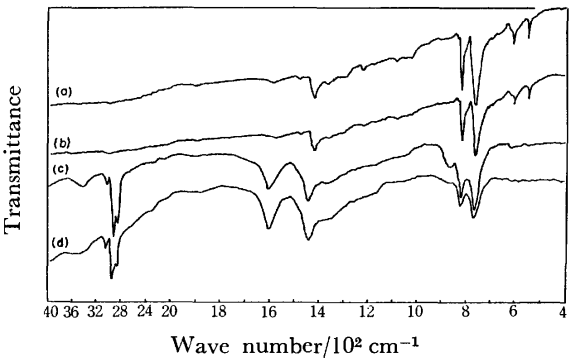

Fig. 2. Infrared spectra of additives, (a): 703-2PS (623), (b): 703-2PS(648), (c): 703-2BK(623), (d): 703-2BK(648).

TABLE 1. ELEMENTAL ANALYSIS OF ADDITIVES

Additive	C (wt%)	H (wt%)	H/C (atomic ratio)
703-2	96.68	4.27	0.526
703-2BK (623)	92.63	6.67	0.858
703-2BK (648)	93.44	5.92	0.745
703-2PS (623)	95.49	4.37	0.545
703-2PS (648)	95.66	4.30	0.536

Table 2. Molecular weight, PI, and QI of additives

Additive	Average molecular weight[a)]	PI (wt%)	QI (wt%)
703-2	—	18.6	10.3
703-2BK (623)	780	0.0	0.0
703-2BK (648)	1005[b)]	2.6	0.1
703-2PS (623)	670[b)]	4.7	0.4
703-2PS (648)	1025[b)]	5.6	0.4

a) Measured in pyridine by means of a vapor-pressure osmometer. b) Obtained on the sample without PI.

Table 3. Effect of addirives on PI and QI contents of 683-4

Additive	PI (wt%)	QI (wt%)
—	15.2	8.6
703-2BK (623)	8.1	7.1
703-2BK (648)	9.4	8.1
703-2PS (623)	14.0	8.0
703-2PS (648)	15.4	8.9

result from the condensation of large molecules and from a decrease in the fluidity due to the elimination of the molecules with comparatively low molecular weight on evacuation. No appreciable amount of PI could be detected when these additives were treated in a sealed ampule at 623 K for 1h.

Table 3 show the data for pyridine and quinoline insolubility when the mixture of the pitch of 683-4 and additives was treated at 623 K for 1 h. Since the insoluble fractions are already involved in 703-2BK (648), 703-2PS(623), and 703-2PS(648) (Table 2), the values of PI were corrected for the mixture with these additives. When the pitch hydrogenated was used as an additive, about half of the PI in the pitch of 683-4 was dissolved and converted to a component soluble in pyridine. On the contrary, when 703-2PS(623) and (648) were added and treated, no effect could be observed on the values of PI and QI. It can be presumed, on the basis of these results, that hydrogen transfer is needed to dissolve the pyridine-insoluble component, for the additives of 703-2BK contain the labile naphthenic hydrogens described above.

A microscopic observation of the whole sample of the 683-4 alone shows that the pitch contains both mesophase spherules with a wide range of distribution in terms of diameter and a flow texture which settles at the bottom of the sample tube. Also, the pyridine-insoluble fraction of this pitch consists of isotropic and anisotropic phases, whereas the QI fraction is composed of almost anisotropic textures where both large mesophase spherules and a partially coalesced flow domain are present. In the case of the mixture of 683-4 and 703-2BK, anisotropic components were predominantly observed in the PI of the mixture treated. These observations may indicate that the isotropic part and the small spheres in the PI of 683-4 are dissolved upon the addition of 703-2BK. The rough agreement between PI and QI values upon the addition of 703-2BK in Table 3 might be qualitatively consistent with the optical observations; both PI and QI are mainly composed of anisotropic textures with large spheres and flow domain.

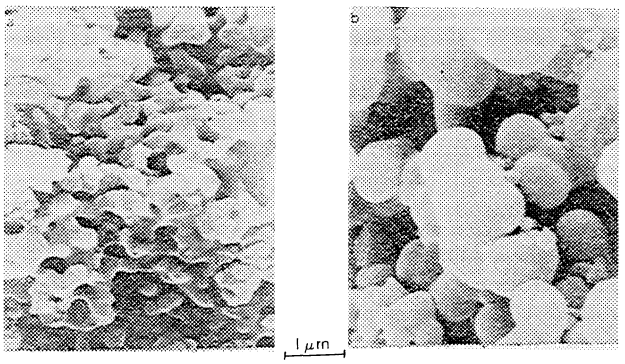

Fig. 3. Scanning electron microphotographs. (a): pyridine insoluble component from 683-4, (b): pyridine insoluble component from the mixture of 683-4 and 703-2BK(623).

The size and the shape of particles in PI were observed with a scanning electron microscope. While in the PI from the 683-4 pitch small spheres (0.3 μm) are partially fused and linked with each other in spherules of about 1 μm, spherical bodies of about 1 μm in size are agglomerated, and each body has round shape near a true sphere, in the case of the PI from the mixture of 683-4 and 703-2BK(623), as can be seen in Fig. 3.

It can be considered, therefore, that the hydrogenated pitch used as an additive dissolves small spherules and the optically isotropic texture connecting these spherules.

References

1) M. Ihnatowicz, P. Chiche, J. Deduit, S. Pregermain, and R. Tounant, *Carbon*, **4**, 41 (1966).
2) H. Honda, H. Kimura, Y. Sanada, S. Sugawara, and T. Furuta, *Carbon*, **8**, 181 (1970).
3) Chwastiak and I. C. Lewis, *Carbon*, **16**, 156 (1978).
4) J. D. Brooks and H. Silberman, *Fuel*, **41**, 67 (1962).

The Chemical Preparation of Tin Organosol

Sumio Ichiba,* Hiroaki Ono, Shunji Kawasaki, Sakae Nakagawa, and Masaaki Yamada
Department of Chemistry, Faculty of Science, Hiroshima University, Higashisenda-machi, Naka-ku, Hiroshima 730
(Received January, 8, 1983)

Synopsis. A stable colloidal tin suspension in an organic solvent was prepared by the chemical reduction of tin(II) chloride with sodium tetrahydridoborate in the presence of a protective agent. The tin organosol was examined by means of the Mössbauer absorption spectra of ^{119}Sn in the frozen solution and by means of an electron microscope.

Vernon *et al.* have extensively studied the chemical preparation of colloidal metal suspensions in non-aqueous solvents.[1,2] They have reported the preparation of a stable tin organosol of a very dilute concentration by reducing tin(II) chloride with phosphorus-hydrazine. We have tried to obtain tin organosols in concentrations higher than 0.2% by Vernon's method. However, it was difficult because tin(II) chloride was not reduced sufficiently, even at the raised temperature of 70 °C.

In this study, we have tried to prepare a colloidal tin suspension in ethanol by chemical reduction with the reducing agent of $NaBH_4$ in the presence of a protective agent.

Experimental

Freshly prepared anhydrous stannous chloride (0.17—1.36 mmol) was dissolved in dry ethanol (20 ml). Three times as much poly(vinylpyrrolidone) (PVP) as $SnCl_2$ was added to the solution as a protective agent. Then three times as much $NaBH_4$ as $SnCl_2$ was added at 3 °C under a nitrogen atmosphere, while the solution was stirred by means of ultrasonic waves. The solution became red-brown immediately, and after a few minutes it gave a homogenous black solution forming a stable tin suspension.

The tin microcrystals in the suspension were examined by means of the Mössbauer absorption spectra of ^{119}Sn in the frozen solution and by means of an electron microscope.

Results and Discussion

Stannous chloride is reduced to tin by $NaBH_4$ in ethanol according to this reaction:

$$SnCl_2 + 2NaBH_4 \xrightarrow[3\,°C]{\text{ethanol}} Sn + B_2H_6 + H_2 + 2NaCl$$

In confirmation of this reaction, the fine powder filtered out of the suspension were identified by means of X-ray diffraction as a mixture of β-tin and NaCl. Observation of the electron micrograph of the microcrystals in a suspension with a tin concentration of 1 mg cm^{-3} revealed that the particle size of the microcrystals was about 300 Å and that the microcrystals aggregated to a size of 1000 Å or more.

The Mössbauer absorption spectra of ^{119}Sn in frozen solutions with various tin concentrations at 90 K are shown in Fig. 1. The values of the isomer shift (δ) and the total area under the absorption peak derived from the spectra are shown in Table 1. The values of the isomer shift at the higher concentrations coincide with the value of the bulk of β-tin, 2.56 mm s^{-1}. However, at the lower concentrations the values turned out to be more negative.

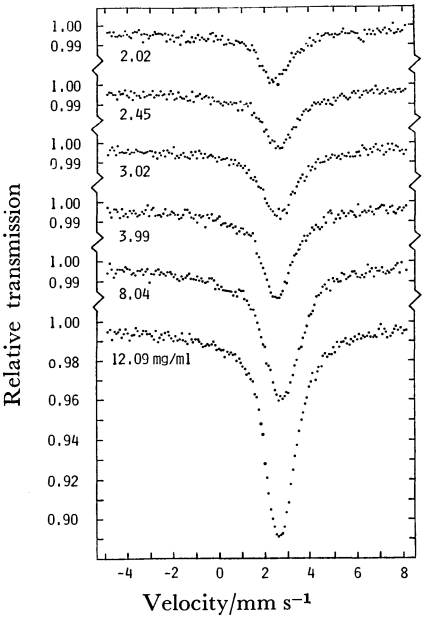

Fig. 1. Mössbuer absorption spectra of ^{119}Sn in the frozen solutions of tin suspension in ethanol at 90 K.

Table 1. ^{119}Sn Mössbauer data of tin organosol

Concentration / mg cm^{-3}	δ / mm s^{-1}	Area
1.01	2.22	0.035
2.02	2.42	0.056
2.45	2.59	0.075
3.02	2.53	0.049
3.99	2.47	0.114
8.04	2.69	0.186
12.09	2.60	0.258

The plots of the total area against the tin concentration are shown in Fig. 2. The area decreases linearly with the decreasing concentration, but it deviates from the line to the lower value at lower concentrations.

Suzdalev *et al.* have investigated, in an aerosol, tin particles with diameters of 250, 370, and 600 Å; they reported that the probability of the Mössbauer effect diminishes as the particle diameter decreases and that this result is associated with the influence of the surface.[3] With reference to their findings, it seems likely that the size of the mycrocrystals formed in the organic suspensions will be reduced with the decreasing tin concentration and that the surface effects will become manifest at concentrations lower than 3 mg cm^{-3}.

A few cases of isomer-shift differences between bulk and microcrystals have been reported and their origins

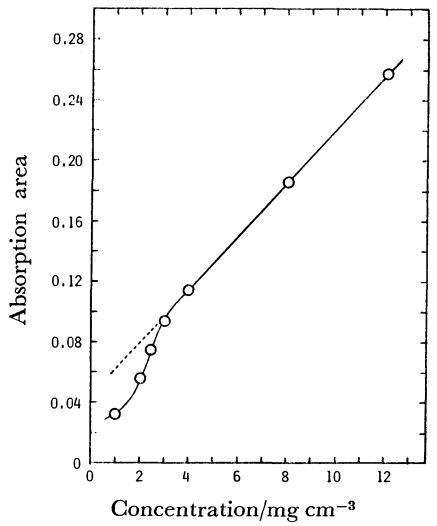

Fig. 2. Total area under the absorption peak *vs.* concentration of tin in suspension.

discussed by Schroeer.[4] The isomer-shift difference, *i.e.*, the decrease in the microcrystals formed at the lower concentration, is also observed in our study. In tin microcrystals, the negative isomer shift to a bulk value may occur through the second-order Doppler shift, surface bonding, and the conversion of β-tin to α-tin. However, it is difficult to make the origin clear.

The authors wish to express their thanks to Professor Yukitomo Komura and Dr. Seiji Takeda of Hiroshima University for obtaining electron micrographs. This work was partially supported by a Grant-in-Aid for Scientific Research from the Ministry of Education, Science and Culture.

References

1) A. A. Vernon and H. A. Nelson, *J. Phys. Chem.*, **44**, 12 (1940).
2) A. A. Vernon and H. A. Nelson, *J. Phys. Chem.*, **44**, 21 (1940).
3) I. P. Suzdalev, M. Y. Gen, V. I. Goldanskii, and E. F. Makarov, *Sov. Phys. JETP*, **24**, 79 (1967).
4) D. Schroeer, "The Mössbauer Effect in Microcrystals," in "Mössbauer Effect Methodology," ed by I. J. Gruverman, Plenum Press, New York (1970), Vol. 5, p. 141.

Studies of the Cobalt(III) Complexes of 8-Amino-3,6-diazaoctanate Ion. V.[1] Optical Resolutions and Circular Dichroism Spectra of 8-Amino-3,6-diazaoctanato(glycinato)cobalt(III) Perchlorates

Kiyokatsu WATANABE

Department of Chemistry, Faculty of Science, Ehime University, Matsuyama, Ehime 790

(Received January 31, 1983)

Synopsis. Three optically active isomers, $(+)_{589}$-, $(-)_{589}$-*cis(O)*-, and $(-)_{589}$-*trans(O)*-[Co(adao)(gly)]ClO_4, where adao and gly stand for 8-amino-3,6-diazaoctanate and glycinate, have been obtained. The structures have been determined on the basis of the absorption, circular dichroism, and proton NMR spectra.

All cobalt(III) complexes with 8-amino-3,6-diazaoctanate (adao)[2] are chiral, but the resolution has not been reported except for $[Co(adao)(en)]Cl_2$.[2,3] Therefore, it is significant to obtain the optically active isomers to clarify the relationship between the structures and circular dichroism (CD) spectra.

Experimental

Resolutions. *(1)* $(+)_{589}$- *and* $(-)_{589}$-cis(O)-[*Co(adao)(gly)*]ClO_4: *cis(O)*-[Co(adao)(gly)]ClO_4[4] was transformed into the chloride form by passing the solution through a column of an anion exchanger (Dowex 1-X8, Cl^- form). Orange red crystals pptd. by adding ethanol to the eluate were collected on a filter and washed with ethanol, ether in turn.

The *cis(O)*-[Co(adao)(gly)]Cl (3.28 g) was dissolved in 10 cm^3 of water and then NH_4bcs (1.64 g)[2] was added. The mixture was warmed at 45 °C for 5 min. Orange red crystals appeared were collected, and washed with an ethanol–ether mixture (1 : 1), and ether. The yield of diastereoisomeric salt was 2.07 g. The filtrate (named as F-A) was reserved for the isolation of the antipodal isomer.

The diastereoisomeric salt (2.0 g) was suspended in 20 cm^3 of water, and after adding 5 cm^3 of 6 M (1 M=1 mol dm^{-3}) $HClO_4$, the suspension was heated at 65 °C for 5 min. Orange red crystals appeared were filtered and washed with ethanol. The yield was 1.1 g. After the crystals were extracted with two 10 cm^3 portions of hot water (70 °C), the third extract with 20 cm^3 of hot water was cooled. The crystals deposited from the third extract were collected and washed with ethanol. The optically active isomer showed positive optical rotation at 589 nm. The yield of $(+)_{589}$-*cis(O)*-[Co(adao)(gly)]$ClO_4 \cdot H_2O$ (named as **1a**) was about 0.5 g. Found: C, 23.24; H, 5.10; N, 13.77%. Calcd for [Co(adao)(gly)]$ClO_4 \cdot H_2O = CoC_8H_{20}N_4O_9Cl$: C, 23.40; H, 4.91; N, 13.64%.

The F-A was concentrated to 5 cm^3 at 40 °C. After cooling, the precipitate was filtered off. To the filtrate was added 2 cm^3 of 6 M $HClO_4$, and the mixture was cooled. The crystals deposited were collected and washed with ethanol. The yield was 1.7 g. Recrystallization was carried out with the same method mentioned above. This enantiomer showed negative optical rotation at 589 nm. The yield of $(-)_{589}$-*cis(O)* enantiomer (named as **1b**) was 0.7 g.

(2) $(-)_{589}$-trans(O)-[*Co(adao)(gly)*]ClO_4: By using a similar method mentioned in *(1)*, *trans(O)*-[Co(adao)(gly)]-Cl was obtained from *trans(O)*-[Co(adao)(gly)]ClO_4.[4]

Silver oxide obtained from $AgNO_3$ (0.84 g) and 5 cm^3 of 1 M NaOH was added to a solution of $(+)_{589}$-tartaric acid (0.75 g) in 5 cm^3 of water, and the mixture was stirred at 65 °C for 5 min. To the suspension was added a solution of *trans(O)*-[Co(adao)(gly)]Cl (1.64 g) in 10 cm^3 of water. The mixture was heated at 65 °C for 5 min and cooled.

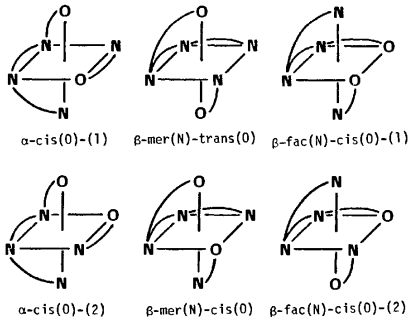

Fig. 1. The possible *Λ* enantiomers of $[Co(adao)(gly)]^+$.

After the removal of AgCl, the filtrate was concentrated to 3 cm^3. The solution was kept in a refrigerator overnight and the precipitate was filtered off. After the addition of a small amount of ethanol, the mixture was left in a refrigerator again for two months, whereupon one large red crystal deposited out. The crystal was separated from the mother liquor, and then washed with ethanol, and ether. The yield of diastereoisomeric salt was 0.8 g.

After the diastereoisomeric salt (0.8 g) was dissolved in 1 cm^3 of water, two drops of 6 M $HClO_4$ were added. Red crystals appeared. After cooling, the crystals were collected and washed with ethanol–ether (1 : 1). The optically active isomer showed negative optical rotation at 589 nm. Furthermore, its absorption (AB) spectrum was exactly the same as that of the racemic *trans(O)*-[Co(adao)(gly)]ClO_4.[4] The yield of $(-)_{589}$-*trans(O)*-[Co(adao)(gly)]ClO_4 (named as **2**) was 0.5 g.

Measurements. The AB and ^1H NMR spectra were recorded with similar methods reported in the previous paper.[1] The optical rotations and CD spectra were measured by a JASCO DIP-180 polarimeter and JASCO MOE-1 spectropolarimeter, respectively.

Results and Discussion

The Structures of [*Co(adao)(gly)*]ClO_4. As glycinate is an unsymmetrical N–O type ligand, $[Co(adao)(gly)]^+$ belongs to a type of $[CoN_4O_2]$. Without consideration of the adao's secondary amine (*s*-N) configurations, $[Co(adao)(gly)]^+$ has twelve optically active isomers (Fig. 1).

In Fig. 2 the AB spectra of **1a**, **1b**, and **2** are shown along with their CD ones. It is known that the first AB band of *trans(O)* isomer is more split than that of *cis(O)* in a type of $[CoN_4O_2]$.[4–6] On the basis of their first AB band shapes, **1a** and **1b** can be assigned to the *cis(O)* structure, and **2**, to the *trans(O)*. From Fig. 1 it is apparent that the adao coordination mode in **2** is the *β-mer(N)*. However, it is difficult to determine the adao coordination modes in **1a** and **1b** from the AB spectra alone. The ^1H NMR spectra of **1a** and **2** showed similar quartet patterns: for **1a**, (1.76, 1.93, 2.69, 2.86 ppm), and for **2**, (1.86, 2.03, 2.83, 3.00 ppm). This indicates that the adao's glycinate ring takes the apical disposition in these isomers,[1,4,7] and that **1a** takes the *α* or the *β-mer(N)* structure,

Table 1. AB and CD spectral data of $[Co(adao)(gly)]ClO_4$

	AB $\tilde{\nu}_{max}/cm^{-1}$ ($\varepsilon/mol^{-1}\,dm^3\,cm^{-1}$)		CD $\tilde{\nu}_{ext}/cm^{-1}$ ($\Delta\varepsilon/mol^{-1}\,dm^3\,cm^{-1}$)	
Λ-(+)$_{589}$-*β-mer(N)-cis(O)*-[Co(adao)(gly)]ClO_4	20000	(172)	19000	(+1.18)
			21600	(+0.51)
(orange red)	27860	(142)	25500	(+0.14)
			28170	(−0.33)
Δ-(−)$_{589}$-*β-mer(N)-cis(O)*-[Co(adao)(gly)]ClO_4	20000	(172)	19000	(−1.35)
			21360	(−0.59)
(orange red)	27860	(142)	25500	(−0.17)
			28170	(+0.36)
Δ-(−)$_{589}$-*β-mer(N)-trans(O)*-[Co(adao)(gly)]ClO_4	18940	(102)	18600	(−0.09)
	20300	(—)	22000	(−0.36)
(red)[a]	27870	(153)	28000	(+0.19)

a) Partial resolution.

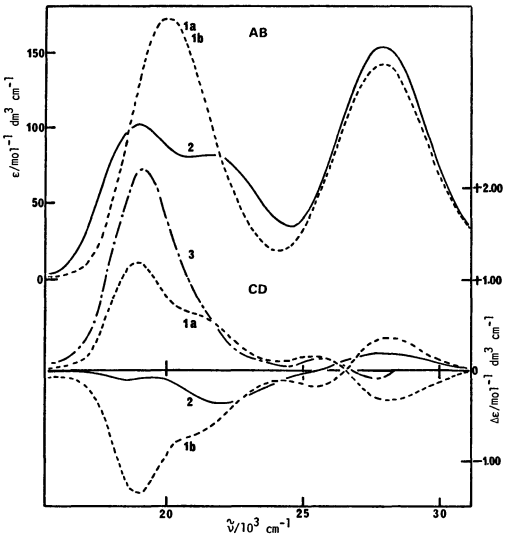

Fig. 2. The absorption (AB) and circular dichroism (CD) spectra.
----: *Λ-β-mer(N)-cis(O)*-$[Co(adao)(gly)]ClO_4$ (**1a**),
----: *Δ-β-mer(N)-cis(O)*-$[Co(adao)(gly)]ClO_4$ (**1b**),
——: *Λ-β-mer(N)-trans(O)*-$[Co(adao)(gly)]ClO_4$ (**2**),
————: *Λ-C$_1$-cis(O)*-$[Co(gly)_2(en)]I$ (**3**).

The CD curve of **1a** in the first AB band region shows two positive peaks (Fig. 2). The CD curve of **1b** is the mirror image to that of **1a**. The fact suggests that **1a** and **1b** are enantiomers. It is well known that the absolute configuration of a cobalt(III) complex with three bidentate ligands, in which each bidentate ligand forms a five membered chelate ring, can be assigned from the sign of major CD peak in the first AB band region, *i.e.*, the *Λ* complex has (+) major CD peak, and the *Δ* complex has (−) one.[8–12] By applying this empirical rule, **1a** and **1b** can be assigned to *Λ* and *Δ* structure, respectively.

The chelate ring pairs of *Λ-α-cis(O)-(1)-* and *Λ-β-mer(N)-cis(O)*-$[Co(adao)(gly)]^+$ are compared with those of *Λ-C$_1$-cis(O)*-$[Co(gly)_2(en)]I$ (named as **3**)[11] having the same *cis(O)*-$[CoN_4O_2]$ chromophore (Fig. 3). **3** and *Λ-α-cis(O)-(1)*-$[Co(adao)(gly)]^+$ have *ΛΛΛ* chelate ring pairs and *Λ-β-mer(N)-cis(O)*-$[Co(adao)(gly)]^+$ has *ΛΔΛΔ* (net **2***Λ*). When **1a** takes the *Λ(ΔΛΔ)-α* structure, its CD strength is expected to be similar to that of **3**. When **1a** takes the *Λ(ΔΛΔΛ)-β-mer(N)* structure, its CD strength is expected to be smaller than that of **3**. The CD strength of **3** is stronger than that of **1a**, as seen in Fig. 2. Therefore, it is appropriate to assign tentatively **1a** to the *Λ(ΔΛΔΛ)-β-mer(N)-cis(O)* structure, and **1b** to the *Δ(ΔΔΔΛ)-β-mer(N)-cis(O)* one.

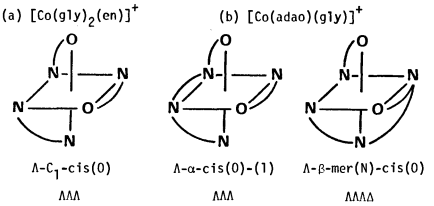

Fig. 3. The comparison of chelate ring pairs among *Λ*-C$_1$-*cis(O)*-$[Co(gly)_2(en)]^+$, *Λ-α-cis(O)-(1)*-$[Co(adao)(gly)]^+$, and *Λ-β-mer(N)-cis(O)*-$[Co(adao)(gly)]^+$.

In the chromatographic separation of reaction product of *β-mer(N)*-$[Co(adao)(Cl)(H_2O)]ClO_4$ and gly,[2] one *trans(O)* (red) and two *cis(O)* (orange red, pink red) racemic isomers were detected. The yield of the orange red isomer was higher than that of the pink red. It was reported that under weak alkaline conditions using *β-mer(N)*-$[Co(adao)(Cl)(H_2O)]ClO_4$ as the starting material, the yield of *α* isomer is lower than that of *β-mer(N)*.[1,7,13] Thus, the orange red *cis(O)* isomer can be assigned to the *β-mer(N)* structure. This chromatographic behavior supports the above assignments for the optically active *cis(O)* isomers.

The CD spectrum of **2** is shown in Fig. 2. From the two negative CD peaks in the first AB band region,[9–12] **2** is assignable to the *Δ(ΔΔΔΛ)* structure. Because of the weak CD strength, however, **2** seems to have been obtained as the partially resolved isomer. These AB and CD spectral data are summarized in Table 1.

The author is indebted to Professor Yoichi Shimura and Professor Kashiro Kuroda for useful suggestions.

References

1) K. Watanabe, Part IV of this series: *Bull. Chem. Soc. Jpn.*, **55**, 2866 (1982).
2) The following abbreviations are used for the ligands: adao, 8-amino-3,6-diazaoctanate; gly, glycinate; bcs, (+)$_{589}$-(1*R*, 3*S*, 4*S*, 7*R*)-3-bromocamphor-9-sulfonate; en, ethylenediamine.
3) M. Fujita, Y. Yoshikawa, and H. Yamatera, the 28th Symposium on Coordination Chemistry of Japan, Matsuyama, 1978, Abstract, p.323.
4) P. W. Schneider and J. P. Collman, *Inorg. Chem.*, **7**, 2010 (1968); K. Watanabe and K. Kuroda, *Nippon Kagaku Kaishi*, **1972**, 1409.
5) M. Ogawa, Y. Shimura, and R. Tsuchida, *Nippon Kagaku Zasshi*, **81**, 72 (1960).
6) N. Matsuoka, J. Hidaka, and Y. Shimura, *Bull. Chem. Soc. Jpn.*, **39**, 1257 (1966).
7) K. Watanabe, *Bull. Chem. Soc. Jpn.*, **49**, 3068 (1976).
8) IUPAC, "Nomenclature of Inorganic Chemistry," 2nd ed, Definitive Rules (1970), Butterworth, London (1971); *Inorg. Chem.*, **9**, 1 (1970).
9) B. E. Douglas, R. A. Haines, and J. G. Brushmillar, *Inorg. Chem.*, **2**, 1194 (1963); C. T. Liu and B. E. Douglas, *ibid.*, **3**, 1356 (1964).
10) M. Shibata, H. Nishikawa, and Y. Nishida, *Bull. Chem. Soc. Jpn.*, **39**, 2310 (1966).
11) N. Matsuoka, J. Hidaka, and Y. Shimura, *Inorg. Chem.*, **9**, 719 (1970); *Bull. Chem. Soc. Jpn.*, **45**, 2491 (1972).
12) R. D. Gillard, J. R. Lyons, and C. Thorpe, *J. Chem. Soc., Dalton. Trans.*, **1972**, 1584.
13) K. Watanabe. *Bull. Chem. Soc. Jpn.*, **55**, 427 (1982).

The Thermal Decomposition of Manganese(III) Phosphate Monohydrate

Eiichi NARITA* and Taijiro OKABE

Department of Applied Chemistry, Faculty of Engineering, Tohoku University, Aramaki, Sendai 980

(Received February 16, 1983)

Synopsis. Manganese(III) phosphate monohydrate begins to decompose at 200 °C by the dehydration accompanying the reduction of manganese(III) and changes completely to manganese(II) pyrophosphate at 500 °C. The reaction order and activation energy for the reduction process are 1.3 and 176.8 kJ mol^{-1}, respectively.

Manganese(III) phosphate monohydrate was just synthesized by Christensen[1] and is prepared conveniently by the reaction of manganese(III) acetate with phosphoric acid or by the oxidation of manganese(II) nitrate with nitric acid in the presence of phosphoric acid.[1,2] Although manganese(III) phosphate monohydrate is one of the few manganese(III) salts, no information is at present available concerning its properties. It has been reported that manganese(III) phosphate monohydrate loses water of crystallization slowly at 300 to 400 °C and rapidly at a red-heat with the simultaneous loss of oxygen.[2,3] However, this is doubtful. The present authors have shown that manganese(III) phosphate monohydrate precipitates *via.* $[Mn(PO_4)_2]^{3-}$ complex ion by the reduction of manganate(VII) ion in the presence of phosphoric acid and changes to manganese(II) pyrophosphate at 500 °C.[4]

In this study the thermal decomposition of manganese(III) phosphate monohydrate has been investigated by TG and DTA techniques.

Experimental

Material.[1] To a warm solution of 34.2 g of manganese(II) chloride tetrahydrate in 50 cm^3 of water, 30 g of concentrated phosphoric acid (87%) and 10 g of concentrated nitric acid (61%) were added. On concentrating slowly to near dryness, this mixture deposited a green-grey precipitate. After cooling, water was added and the precipitate filtered off, washed and dried overnight in an electric oven in air at 110 °C. According to chemical analyses,[4] the composition of the precipitate was: $Mn^{3+}:PO_4^{3-}:H_2O = 1:1.03:1.13$.

Decomposition Procedure. The thermal decomposition of manganese(III) phosphate monohydrate (32—36 mg) was carried out using a Rigaku Denki Thermoflex high temperature type TG-DTA instrument in air. Ignited α-Al_2O_3 was used as a reference material in the DTA sample block. The heating rate of the furnace was 5—20 deg/min.

Measurement. The X-ray diffraction patterns of the heated products were obtained using a Rigaku Denki Geigerflex 2013 with Ni filtered Cu $K\alpha$ radiation, with 30 kV and 10 mA. The IR absorption spectra were obtained using a Shimadzu I-430 spectrometer with the KBr pellet technique.

Results and Discussion

Thermal Decomposition Process. The TG and DTA curves for manganese(III) phosphate monohydrate are shown in Fig. 1. The weight loss in the heating process was indicated on the TG curve in three steps which corresponded to the endothermic peaks of the DTA curve at 263, 377, and 476 °C, respectively. The X-ray diffraction patterns of four samples obtained at A(110 °C), B(320 °C), C(420 °C), and D(520 °C) in Fig. 1 are shown in Fig. 2. Sample A was typical manganese(III) phosphate monohydrate. Although the pattern of sample B, which was obtained just after the first weight loss, indicated the partial disintegration of the crystal structure and the formation of a small amount of manganese(II) pyrophosphate,[5] it still was similar to that of sample A. Sample C obtained just after the second weight loss was manganese(II) pyrophosphate. The IR spectrum also indicated that it had lost the PO_4^{3-} structure and still contained a large amount of water. In spite of the largest third weight loss, the pattern of sample D was hardly changed in comparison with that of

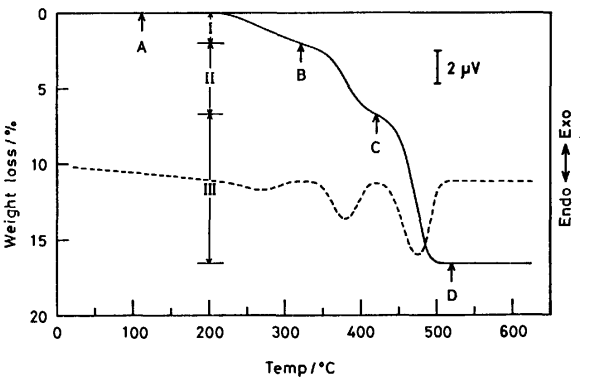

Fig. 1. TG and DTA curves of manganese(III) phosphate monohydrate under an air atmosphere. Heating rate of furnace: 10 (deg/min), sample weight: 32.6 (mg), ——: TG, ----: DTA.

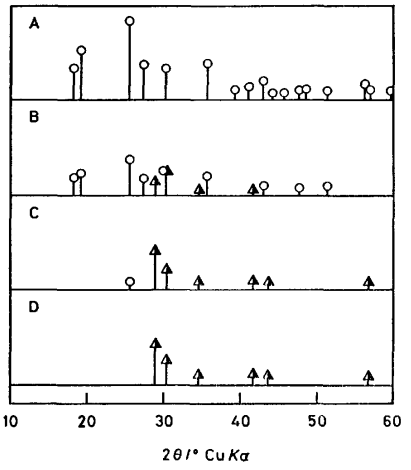

Fig. 2. X-Ray diffraction patterns of the heating products of manganese(III) phosphate monohyrate. A: 110 °C, B: 320 °C, C: 420 °C, D: 520 °C, ○; $MnPO_4 \cdot H_2O$, △: $Mn_2P_2O_7$.

sample C. On the basis of these results, manganese(III) phosphate monohydrate appears to decompose in three steps as follows:

$$MnPO_4 \cdot H_2O \longrightarrow MnPO_4 \cdot (1-x)H_2O + xH_2O\uparrow \quad \text{(Step I)}$$

$$2[MnPO_4 \cdot (1-x)H_2O] \longrightarrow Mn_2P_2O_7 \cdot 2(1-x)H_2O + 1/2\,O_2\uparrow \quad \text{(Step II)}$$

$$Mn_2P_2O_7 \cdot 2(1-x)H_2O \longrightarrow Mn_2P_2O_7 + 2(1-x)H_2O\uparrow. \quad \text{(Step III)}$$

The value of x was 0.25 from the TG curve in Fig. 1. The important feature in this process is that the reduction of manganese(III) phosphate monohydrate occurred even at 400 °C.

Kinetics. On the second weight loss (Step II), *i.e.*, the reduction of manganese(III) to manganese(II), the methods of Freeman-Carroll,[6] Coats-Redfern,[7] and Kissinger[8] were used to study the kinetics. The methods are generally used only when the reaction is a single elementary reaction.

The formula of the Freeman-Carroll method is written as

$$\Delta\log(dW/dt)/\Delta\log Wr = n - E\Delta(1/T)/2.303R(\Delta\log Wr), \quad (1)$$

where dW/dt is the weight change in mg per minute, n the order of the reaction, T the absolute temperature and $Wr = W - Wc$, where W is the weight(mg) at time t and Wc the weight(mg) of the sample at the end of the reaction, E the energy of activation. If the plot of the ratio $\Delta\log(dW/dt)/\Delta\log Wr$ values *vs.* $\Delta(1/T)/\Delta\log Wr$ lie on a straight line, the activation energy and the reaction order will be given by its slope and intercept, respectively. This is illustrated in Fig. 3. As given in Table 1, the reaction order and activation energy obtained by the Freeman-Carroll method were 1.3 and 184.9 kJ mol^{-1}, respectively.

When the reaction order is not 1.0, the formula of the Coats-Redfern method is written as

$$\log\{1-(1-x)^{1-n}/(1-n)T^2\} = \log(AR/\phi E)(1 - 2RT/E) - E/2.303RT, \quad (2)$$

where x is the fraction of reaction, ϕ the heating rate of furnace and A the frequency factor. Graphic representation of the $\log\{1-(1-x)^{1-n}/(1-n)T^2\}$ values as a function of $1/T$ gives a straight line of slope $-E/2.303R$ for the correct value of n. As also illustrated in Fig. 3, a good linear relationship was obtained when the value of n was postulated as 1.3. The activation energy was calculated as 169.4 kJ mol^{-1}.

According to the Kissinger method, the activation energy of the reaction is obtained from the change in peak temperature on the DTA curve when the heating rate of furnace, ϕ, was altered. The formula of the Kissinger method is written as

$$d\{\log(\phi/T_m^2)/d(1/T_m)\} = -E/2.303R, \quad (3)$$

where T_m is the sample temperature, $T_m = T_p - T_h$, where T_p is the absolute temperature of peak, T_h the height of peak(deg). Graphic representation of $\log(\phi/T_m^2)$ as a function of $1/T_m$ gives a straight line of slope $-E/2.303R$. In this experiment ϕ was altered as 5, 10, and 20 °C/min. A straight line of slope 9.20 was obtained and the activation energy was calculated as 176.1 kJ mol^{-1}.

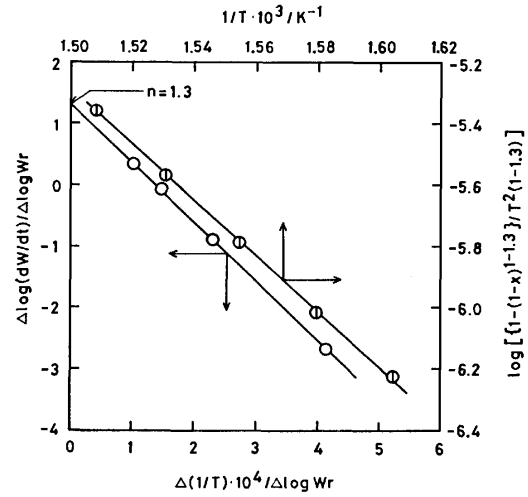

Fig. 3. Freeman-Carroll and Coats-Redfern straight lines for the thermal decomposition (reduction: Step II) of manganese(III) phosphate monohydrate.
○: Freeman-Carroll plots, ⓘ: Coats-Redfern plots.

Table 1. Reaction order and activation energy of the thermal decomposition (reduction: Step II) of manganese(III) phosphate monohydrate

Method	Activation energy / kJ mol^{-1}	Reaction order
Freeman-Carroll (TG)	184.9	1.3
Coats-Redfern (TG)	169.4	1.3
Kissinger (DTA)	176.1	—
Average	176.8	1.3

As can be seen in Table 1, the kinetics parameters obtained by the three methods agreed well with each other and the average reaction order and activation energy were 1.3 and 176.8 kJ mol^{-1}, respectively. On the first and third weight losses (Steps I and III), *i.e.*, the dehydration, the above analytical methods could not be used. However, it was found that a large part of the water of crystallization was lost after the reduction of manganese(III) to manganese(II) and the dehydration was completed at about 500 °C.

References

1) O. T. Christensen, *J. Prakt. Chem.*, **28**, 1 (1883).
2) J. C. Bailar, "Comprehensive Inorganic Chemistry," Pergamon Press, Oxford (1973), Vol. 2, p. 829.
3) J. W. Mellor, "A Comprehensive Treatise on Inorganic and Theoretical Chemistry," Longmans, Green and Co. Ltd., London (1932), Vol. 12, p. 460.
4) E. Narita and T. Okabe, *Ind. Eng. Chem. Prod. Res. Dev.*, **21**, 662 (1982).
5) X-Ray Powder Data File (ASTM Card 3-555).
6) E. S. Freeman and B. Carroll, *J. Phys. Chem.*, **62**, 394 (1958).
7) A. W. Coats and J. P. Redfern, *Nature*, **201**, 68 (1964).
8) H. E. Kissinger, *Anal. Chem.*, **29**, 1702 (1957).

Halogenation of Mixed Ligand Cobalt(III) Complexes with 12- or 13-Membered Tetraaza Macrocycle and Acetylacetone, $[Co[Z]aneN_4(acac)](ClO_4)_2$ ($Z=12$, 13)

Akira HIRANO, Naohide MATSUMOTO,* and Akira OHYOSHI

Department of Industrial Chemistry Faculty of Engineering, Kumamoto University, Kurokami 2-39-1, Kumamoto 860

(Received March 11, 1983)

Synopsis. The parent cobalt(III) complex $[Co[12]aneN_4(acac)](ClO_4)_2$, $[Co[12]aneN_4(bzac)](ClO_4)_2$, or $[Co[13]aneN_4(acac)](ClO_4)_2$ reacts with *N*-halogenosuccinimide to give the substituted complex $[Co[12]aneN_4(Xacac)](ClO_4)_2$, $[Co[12]aneN_4(Xbzac)](ClO_4)_2$, or $[Co[13]aneN_4(Xacac)](ClO_4)_2$, where $[12]aneN_4$=1,4,7,10-tetraazacyclododecane, $[13]aneN_4$=1,4,7,10-tetraazacyclotridecane, acac=acetylacetonato, bzac=benzoylacetonato, X=Cl, Br.

Kuroda and coworkers[1,2] have studied the halogenation and nitration of $[CoA_4(acac)]^{2+}$ and succeeded to prepare the halogenated and nitrated complexes $[CoA_4(Xacac)]^{2+}$, where $A_4=(NH_3)_4$, (ethylenediamine)$_2$, 3,6-diazaoctane-1,8-diamine. Previously we reported the synthesis, spectral characterization, and X-ray analysis of $[Co[12]aneN_4(acac)](ClO_4)_2$ and its brominated complex $[Co[12]aneN_4(Bracac)](ClO_4)_2$, in which the cobalt ion is coordinated in a distorted octahedral fashion to four nitrogen atoms of $[12]aneN_4$ and two oxygen atoms of the acetylacetonato moiety in a cis position.[3] As an extension of the study, we wish to report the synthesis and spectral characterization of the halogenated complexes $[Co[Z]aneN_4(Xacac)](ClO_4)_2$ and $[Co[12]aneN_4(Xbzac)](ClO_4)_2$ ($Z=12$, 13; X=Cl, Br).

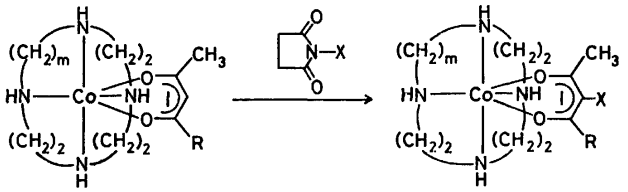

Fig. 1. Synthetic scheme and abbreviations of complexes $[Co[Z]aneN_4(Xacac)]^{2+}$: $Z=12$ ($m=2$), $Z=13$ ($m=3$), X=H, C, Br, R=CH_3; $[Co[12]aneN_4(Xbzac)]^{2+}$: X=H, Cl, Br, R=$C_6H_5$.

Experimental

Measurements. Infrared spectra were recorded as KBr disks on a Shimadzu IR-410, while visible and ultraviolet spectra were measured in aqueous solutions on a Hitachi recording spectrophotometer 323. Conductivity measurements were carried out by a Denki Kagaku AOC-10 at *ca.* 10^{-3} mol dm^{-3} in aqueous solutions at room temperature. The 100 MHz ^{1}H NMR spectra were recorded by a JEOL MH 100 spectrometer at room temperature. The solvent used was deuterium oxide and shift measurements were made relative to 3-(trimethylsilyl)-1-propanesulfonic acid sodium salt.

Syntheses. The macrocyclic ligands, 1,4,7,10-tetraazacyclododecane ($[12]aneN_4$) and 1,4,7,10-tetraazacyclotridecane ($[13]aneN_4$) were prepared according to the high yield synthetic method of Raymond *et al.*[4] which was applied for the synthesis of $[16]aneN_4$. The unsubstituted (parent) complexes $[Co[12]aneN_4(acac)](ClO_4)_2$ and $[Co[12]aneN_4(bzac)](ClO_4)_2$ were prepared by the reaction of $[Co[12]aneN_4CO_3]ClO_4$ and acetylacetone or benzoylacetone according to a similar method described previously.[3] The complex $[Co[13]aneN_4(acac)](ClO_4)_2$ was prepared by the reaction of cis/trans mixture of $[Co[13]aneN_4Cl_2]ClO_4$[5] and acetylacetone. To a solution of 2.0 g of cis/trans mixture of $[Co[13]aneN_4Cl_2]ClO_4$ in 10 cm^3 of water is added a solution of 1.5 cm^3 of acetylacetone in 10 cm^3 of 1 M NaOH. The solution was stirred at *ca.* 50 °C for 2 h. After the addition of several drops of 6 M $HClO_4$, the solution was left at room temperature to precipitate red crystals. They were collected and recrystallized from a dilute $HClO_4$ solution. The substituted complexes $[Co[Z]aneN_4(Xacac)](ClO_4)_2$ and $[Co[12]aneN_4(Xbzac)](ClO_4)_2$ ($Z=12$, 13; X=Cl, Br) were prepared according to a similar method of Kuroda *et al.* which was used for the preparation of $[CoA_4(Xacac)](ClO_4)_2$.[1,2]

Results and Discussion

The elemental analytical data for C, H, and N, along with the molar electrical conductances are given in Table 1. The molar electrical conductances are in the range of 197—236 S cm^2 mol^{-1} and these values are in the expected range for the 1:2 electrolytes,[6] and consistent with the formula of $[Co[Z]aneN_4(Xacac)]^{2+}$.

Spectral data of infrared, ^{1}H NMR, and electronic spectra are summerized in Table 2. The infrared spectra of unsubstituted complexes exhibit two strong bands in the region of 1500—1600 cm^{-1}, which are assignable to ν(C=O) and ν(C=C). On the other hand, the substituted complexes have only one band in the region. This spectral feature has been found in the well-characterized complexes such as $[M(Xacac)_3]$ (M=Cr^{3+}, Co^{3+}; X=H, Cl, Br, I),[7] providing an evidence of the substitution. Busch *et al.*[5] have shown that the infrared bands in the CH_2 rocking region (800—910 cm^{-1}) can be used to distinguish cis from trans isomers of $[Co[13—16]aneN_4CO_3]^+$. The infrared spectra of the present complexes $[Co[13]aneN_4(Xacac)](ClO_4)_2$ (X=H, Cl, Br) are in accord with the formation of the cis complexes.

The ^{1}H NMR spectra were measured to verify the substitution on the γ-carbon of the acetylacetonato residue. The methine proton resonance about 6.5 ppm of the unsubstituted complexes disappeared in the halogenated complexes, providing further evidence of the substitution on the γ-position. The methyl proton resonance around 2.3 ppm of the unsubstituted complexes shifted to lower magnetic field upon the substitution.

Some of the electronic spectra are shown in Fig. 2. Electronic spectra are quite similar to each other

Table 1. Elemental analytical data for C, H, and N, along with the molar electrical conductances

	Complex	C (%) Found (Calcd)	H (%) Found (Calcd)	N (%) Found (Calcd)	Conductance $S^{-1}\,mol^{-1}\,cm^2$
1	$[Co[12]aneN_4(Clacac)](ClO_4)_2\cdot H_2O$	26.51 (26.84)	4.59 (4.84)	9.74 (9.63)	236
2	$[Co[12]aneN_4(bzac)](ClO_4)_2$	36.36 (36.56)	4.92 (4.94)	9.54 (9.47)	197
3	$[Co[12]aneN_4(Clbzac)](ClO_4)_2\cdot 0.5H_2O$	34.06 (34.00)	4.56 (4.45)	8.80 (8.83)	217
4	$[Co[12]aneN_4(Brbzac)](ClO_4)_2\cdot 0.5H_2O$	31.83 (31.83)	4.28 (4.30)	8.26 (8.25)	217
5	$[Co[13]aneN_4(acac)](ClO_4)_2\cdot 0.5H_2O$	30.50 (30.45)	5.50 (5.48)	10.35 (10.15)	206
6	$[Co[13]aneN_4(Clacac)](ClO_4)_2$	29.14 (29.11)	4.86 (4.89)	9.81 (9.70)	204
7	$[Co[13]aneN_4(Bracac)](ClO_4)_2$	27.11 (27.03)	4.51 (4.54)	9.08 (9.01)	206

Table 2. Spectral data of infrared, ^1H NMR, and electronic spectra

	ν(C=O, C=C) cm^{-1}	Methine (ppm)	Methyl (ppm)	First band of d-d $\tilde{\nu}/10^3\,cm^{-1}$ (ε)	Specific band $\tilde{\nu}/10^3\,cm^{-1}$ (ε)	Dq^{av} a) cm^{-1}
1	1558	—	2.54, 2.57	18.7 (310)	28.8 (3200)	2250
2	1558, 1515	6.57	2.34	18.7 (340)	28.1 (6800)	2250
3	1543	—	2.72	18.8 (340)	27.8 (4400)	2260
4	1549	—	2.66	18.7 (350)	27.5 (4700)	2250
5	1570, 1524	6.36	2.21	19.8 (240)	30.5 (3400)	2360
6	1556	—	2.46	19.7 (240)	29.0 (3500)	2350
7	1557	—	2.56	19.7 (270)	29.0 (3300)	2350

a) Evaluated by $10Dq^{av}=\nu^1T_{1g}\leftarrow{}^1A_{1g}+3800$.[5]

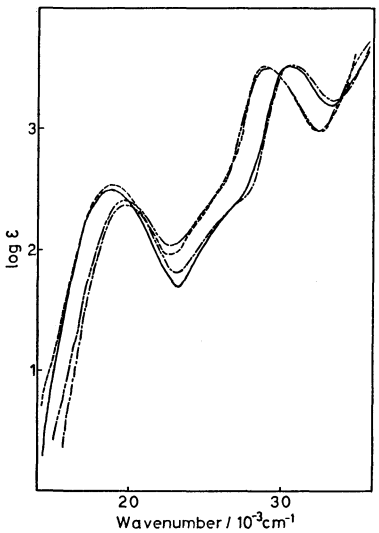

Fig. 2. Electronic spectra of $[Co[12]aneN_4(acac)](ClO_4)_2\cdot H_2O$ (——), $[Co[12]aneN_4(Bracac)](ClO_4)_2\cdot 0.5H_2O$ (·····), $[Co[13]aneN_4(acac)](ClO_4)_2\cdot 0.5H_2O$ (—·—), and $[Co[13]aneN_4(Bracac)](ClO_4)_2$ (—··—).

and to the related low-spin six-coordinated cobalt(III) complexes, such as $[CoA_4(Xacac)]^{2+}$.[1,2] The spectra exhibit two bands attributable to the d-d transitions, $^1T_{1g}\leftarrow{}^1A_{1g}$ and $^1T_{2g}\leftarrow{}^1A_{1g}$, in which the latter band appeared as shoulder. The average ligand field strength Dq^{av} can be evaluated to be 2250 and 2350 cm^{-1} for the 12- and 13-membered complexes, respectively. The data indicated that the ligand $[13]aneN_4$ provides a stronger ligand field than $[12]aneN_4$ does, being consistent with the result of $[Co[12—13]-aneN_4CO_3]^+$.[5] The spectra exhibit also a specific band attributable to the charge-transfer band from metal t_{2g} to ligand π^* orbital.[8] The specific band shifted to lower wave number upon the substitution, while the d-d transitions showed no shift.

References

1) K. Kuroda and Y. Kamiiba, *Chem. Lett.*, **1975**, 1027.
2) K. Kuroda, K. Yoshitani, K. Kunigida, Y. Kamiiba, and K. Watanabe, *Bull. Chem. Soc. Jpn.*, **49**, 2445 (1976).
3) N. Matsumoto, A. Hirano, T. Hara, and A. Ohyoshi, *J. Chem. Soc., Dalton Trans.*, in press.
4) W. L. Smith, J. P. Ekstrand, and K. N. Raymond, *J. Am. Chem. Soc.*, **100**, 3539 (1978).
5) Y. Hung, L. Y. Martin, S. C. Jackels, A. M. Tait, and D. H. Busch, *J. Am. Chem. Soc.*, **99**, 4029 (1977), and references therein.
6) R. G. Hayter, *J. Am. Chem. Soc.*, **84**, 3046 (1962).
7) J. P. Collman, R. A. Moss, H. Maltz, and C. C. Heindel, *J. Am. Chem. Soc.*, **83**, 531 (1961).
8) I. Hanazaki, F. Hanazaki, and S. Nagakura, *J. Chem. Phys.*, **50**, 265 (1969).

The Crystal and Molecular Structure of Potassium *u-fac*-Bis(*N*-methyliminodiacetato)cobaltate(III) Sesquihydrate

Yoshihiko KUSHI,* Toshio IDENO, Takaji YASUI,† and Hayami YONEDA

Department of Chemistry, Faculty of Science, Hiroshima University, Higashi-senda-machi, Naka-ku, Hiroshima 730

†*Department of Chemistry, Faculty of Science, Kochi University, Akebono-cho, Kochi 780*

(Received March 26, 1983)

Synopsis. The crystal and molecular structure of the title complex has been determined by X-ray analysis. It has been found that the *cis*-N_2O_4 octahedron about the cobalt(III) has a large distortion caused by the steric compression between the two adjacent *N*-methyl groups.

Recently, the *u-fac* bis(*N*-methyliminodiacetato)cobaltate(III) complex, *u-fac*-$[Co(mida)_2]^-$, was newly prepared and characterized.[1] It was expected that the steric repulsion between the two adjacent *N*-methyl groups would result in the large distortion into the *cis*-N_2O_4 coordination geometry about the Co atom. Indeed, the first absorption-band maximum of the complex was observed at a considerably lower energy than those of the *u-fac*-$[Co(ida)_2]^-$,[2] $[Co(edta)]^-$, and $[Co(1,3\text{-pdta})]^-$.[3] The *u-fac*-$[Co(mida)_2]^-$ decomposes easily in a basic aqueous solution, and the ligand decomposes.[1] In this note, we wish to report the results of the determination of the crystal and the molecular structure of the title compound. The highly strained *cis*-N_2O_4 geometry is compared with those related ones reported previously.

Experimental

Blue crystals were grown from an aqueous solution by adding methanol.[1] The cell dimensions and reflection intensities were measured on a SYNTEX-R3 diffractometer using Mo $K\alpha$ radiation(λ=0.7107 Å). The crystal data are as follows: $C_{10}H_{17}O_{9.5}N_2KCo$, M=415.3, monoclinic, a=29.057(3), b=7.144(1), c=15.783(2) Å, β=111.67(4)°, space group C2/c, D_m=1.80 g cm^{-3}, Z=8, D_c=1.81 g cm^{-3}. The intensity data were collected by the ω-scan technique up to 2θ=55°. The crystal used had approximate dimensions of 0.3×0.3×0.3 mm^3. A total of 2370 reflections were obtained, of which 2127 were non-zero reflections($|F_o| > 3\sigma(F_o)$). No corrections for absorption and extinction were made(μ(Mo $K\alpha$)=15.0 cm^{-1}).

Structure Determination and Refinement

The structure was solved by the heavy-atom method and refined by the block-diagonal least-squares method. The R-value was finally reduced to 0.038 for 2127 reflections. The weighting scheme used was $w=(\sigma_{cs}^2+a|F_o|+b|F_o|^2)^{-1}$, where σ_{cs} is the standard deviation for each reflection; the a and b values were 0.2 and 0.0009. The final positional parameters and equivalent isotropic temperature factors for non-hydrogen atoms are listed in Table 1.[4]

Results and Discussion

The structure viewed down the pseudo-two-fold axis of the complex molecule is shown in Fig. 1 (ORTEP program[5]), while that projected on the N_2O_2 plane is shown in Fig. 2, along with the selected bond distances and angles.[6] In the complex molecule, both *N*-methyliminodiacetato groups act as terdentate ligands and form a distorted *cis*-N_2O_4-type octahedron about the cobalt atom. The nonbonded short contact between the two adjacent methyl groups is 3.438(7) Å. This value is comparable with the intramolecular nonbonded $-CH_3\cdots H_3C-$ contact, 3.466(8) Å, observed in $[Co(NH_2CH_3)_5Cl](NO_3)_2$.[7] Recently, the nonbonded short contact of the $-CH_3$ group has aroused some interest in relation to the CH/π interactions.[8] The present result indicates that the minimum radius

TABLE 1. POSITIONAL (×10^4) AND THERMAL PARAMETERS

ATOM	X	Y	Z	B_{eq}/Å^2	WG
O(W1)	5000(0)	-2435(6)	2500(0)	2.96(18)	0.50
O(W2)	2528(2)	-2852(8)	-1052(4)	11.86(58)	1.00
K	5199(0)	2463(1)	5854(1)	2.11(3)	1.00
CO	3853(0)	1245(1)	2035(0)	1.31(2)	1.00
O(1)	3301(1)	208(3)	1102(2)	2.13(11)	1.00
O(2)	4256(1)	122(3)	1476(2)	2.52(11)	1.00
O(3)	4391(1)	2397(4)	2935(2)	2.36(11)	1.00
O(4)	3969(1)	-944(3)	2745(2)	2.18(11)	1.00
N(1)	3803(1)	3381(4)	1185(2)	1.52(11)	1.00
N(2)	3439(1)	1945(4)	2737(2)	1.58(11)	1.00
C(ME1)	3818(2)	5340(5)	1515(3)	2.95(18)	1.00
C(ET1)	3340(1)	3084(5)	381(2)	2.10(15)	1.00
C(BX1)	3130(1)	1157(5)	366(2)	2.07(15)	1.00
O(XY1)	2795(1)	628(4)	-320(2)	3.00(13)	1.00
C(ET2)	4240(1)	3153(5)	925(3)	2.47(16)	1.00
C(BX2)	4361(1)	1104(5)	894(2)	2.11(16)	1.00
O(XY2)	4553(1)	497(4)	387(2)	3.29(13)	1.00
C(ME2)	3005(2)	3190(6)	2329(3)	3.28(19)	1.00
C(ET3)	3792(2)	2767(5)	3612(2)	2.55(17)	1.00
C(BX3)	4298(1)	3050(5)	3609(2)	2.00(15)	1.00
O(XY3)	4601(1)	3884(4)	4248(2)	2.95(13)	1.00
C(ET4)	3250(1)	127(5)	2931(2)	2.24(16)	1.00
C(BX4)	3652(1)	-1320(5)	3109(2)	2.07(15)	1.00
O(XY4)	3671(1)	-2724(4)	3559(2)	3.71(14)	1.00

$B_{eq}=8\pi^2(U_{11}+U_{22}+U_{33})/3$. The anisotropic thermal parameters have been preserved by the Chemical Society of Japan.

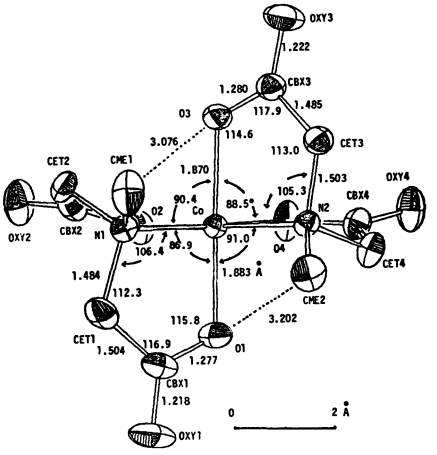

Fig. 1. The projected structure viewed down the pseudo two-fold axis of the complex molecule. Hydrogen atoms are omitted for clarity.

Table 2. The geometrical parameters and absorption maxima of the first band for *cis*-$[CoN_2O_4]$-type complexes with (edta)-like ligands

Complex	Bond distance Co-N(av)	*l*/Å Co-O(av)	Bond angle N-Co-N	*φ*/° O-Co-O	*λ*/nm
$NH_4[Co(edta)]\cdot 2H_2O$[a]	1.93(1)	1.92(3)	89.7(7)	104.0(6)	537[e]
$K[Co(1,3\text{-pdta})]\cdot 2H_2O$[b]	1.966(9)	1.904(9)	99.0(3)	92.6(3)	553[f]
$K[Co(ida)_2]\cdot 2.5H_2O$[c]	1.942(4)	1.899(4)	98.5(2)	90.0(2)	561.5[g]
$K[Co(mida)_2]\cdot 1.5H_2O$[d]	1.990(4)	1.880(4)	105.9(2)	88.5(2)	580.0[h]

a) Ref. 9. b) Ref. 10. c) Ref. 11. d) This work. e) Ref. 3. f) Ref. 3. g) Ref. 2. h) Ref. 1.

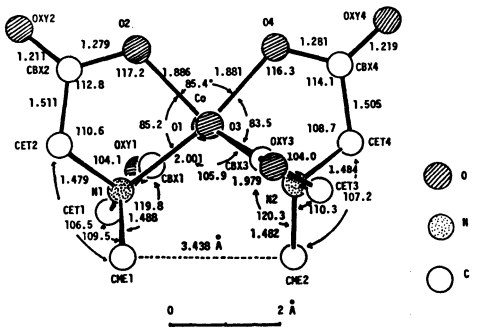

Fig. 2. The molecular structure projected on the N_2O_2 plane.

of the $-CH_3$ group in side contact is 1.72 Å. The Co–N–C(methyl) angles, 119.8(3)° for N1 and 120.3 (3)° for N2, are considerably larger than the tetrahedral value. If the tetrahedral angle around the nitrogen atoms is assumed (109.5°), the CME1···CME2 contact falls at 3.16 Å. Therefore, the relaxation of CME1···CME2 steric repulsion comes from three factors: (1) the elongation of the Co–N bonds, (2) the increase in the N–Co–N angle, and (3) the increase in the Co–N–C(methyl) angles.

The geometrical parameters of the N_2O_2 plane(N1, N2, O2, and O4) are listed in Table 2, along with the previously reported values of the related complexes: $NH_4[Co(edta)]\cdot 2H_2O$,[9] $K[Co(1,3\text{-pdta})]\cdot 2H_2O$,[10] and *u-fac*-$K[Co(ida)_2]\cdot 2.5H_2O$.[11] The values of the first absorption maxima of these complexes are also listed in Table 2. In the equatorial N_2O_2 plane, a gradual increase in the N–Co–N angle and a gradual decrease in the O–Co–O angle are observed in these *cis*-N_2O_4-type structures. The observed red shift in the first absorption maximum from $[Co(edta)]^-$ to *u-fac*-$[Co(mida)_2]^-$ reflects the distortion about the cobalt atom.

References

1) T. Ama, H. Kawaguchi, and T. Yasui, *Chem. Lett.*, **1981**, 323; T. Yasui, H. Kawaguchi, N. Koine, and T. Ama, *Bull. Chem. Soc. Jpn.*, **56**, 127 (1983).

2) J. Hidaka, Y. Shimura, and R. Tuchida, *Bull. Chem. Soc. Jpn.*, **35**, 567 (1962).

3) C. W. Van Saun and B. E. Douglas, *Inorg. Chem.*, **8**, 1145 (1969). The following abbreviations are used: ida=iminodiacetato^{2-}, edta=ethylenediaminetetraacetato^{4-}, 1,3-pdta=1,3-propanediaminetetraacetato^{4-} ligands.

4) Tables of the atomic parameters for the hydrogen atoms, the anisotropic temperature factors, the structure factors, and the projected figure of the crystal structure are kept in the Office of the Chemical Society of Japan (Document No. 8334).

5) All computations were carried out using a HITAC-M-180 computer at the Hiroshima University Information Processing Center, using UNICS programs of The Crystallographic Society of Japan with slight modifications.

6) The estimated standard deviations are as follows: Co–N 0.003; Co–O 0.003; C–O, C–N, and C–C 0.006~7 Å; N–Co–N, O–Co–O, and N–Co–O 0.2°; Co–O–C and Co–N–C 0.3°; N–C–C, O–C–C, and O–C–O 0.4°, respectively.

7) B. M. Foxman, *Inorg. Chem.*, **17**, 1932 (1978).

8) Y. Kodama, K. Nishihata, M. Nishino, and N. Nakagawa, *Tetrahedron Lett.*, **1977**, 2105.

9) H. A. Weakliem and J. L. Hoard, *J. Am. Chem. Soc.*, **81**, 549 (1959).

10) R. Nagao, F. Marumo, and Y. Saito, *Acta Crystallogr., Sect. B*, **28**, 1852 (1972).

11) A. B. Corradi, C. G. Palmieri, M. Nardelli, M. A. Pellinghelli, and M. E. V. Tani, *J. Chem. Soc., Dalton Trans.*, **1973**, 655.

Oxidation of 9-Xanthenones with Lead(IV) Acetate. Formation of Di-γ-lactones

Hiroshi NISHINO* and Kazu KUROSAWA

Department of Chemistry, Faculty of Science, Kumamoto University, Kurokami 2-39-1, Kumamoto 860

(Received October 2, 1982)

Synopsis. The oxidation of 9-xanthenones with lead (IV) acetate afforded 3a,3b,6a,12b-tetrahydro-2*H*-difuro[3,2-*a*:3′,2′-*c*]xanthene-2,5,7(3*H*,6*H*)-triones in addition to other products. Characterization of the di-γ-lactones and the difference between the oxidation reaction of lead(IV) and manganese(III) acetates in the 9-xanthenone system are discussed.

Recently, we have reported that the oxidation of 9-xanthenones with manganese(III) acetate (MTA) affords carboxy-, carboxymethyl-, acetoxymethyl-, and diacetoxymethyl-9-xanthenones, and that carboxyl groups are preferentially introduced at the peri positions of the 9-xanthenones.[1] This regioselectivity was explained in terms of complexation between substrate and MTA.[1] In connection with the MTA oxidation, we have investigated the oxidation of 9-xanthenones with lead(IV) acetate (LTA)[2] to give di-γ-lactones, carboxymethyl, acetoxymethyl, and methyl derivatives.

When 9-xanthenone (**1a**) was oxidized with LTA for 3.2 h, di-γ-lactone (**2a**; 22%), 1-carboxymethyl-9-xanthenone (**3a**; 3%), 4-carboxymethyl-9-xanthenone (**4a**; 8%), 4-carboxymethyl-1-methyl-9-xanthenone (**5a**; 1%), 1-acetoxymethyl-9-xanthenone (**7a**; 1%), 4-acetoxymethyl-9-xanthenone (**8a**; 1%),[1] and 1-methyl-9-xanthenone (**10a**; 2%) were obtained. The com-

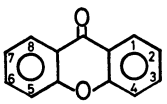

1a

1b : 1-CH_3O-3-CH_3

3a : 1-HO_2CCH_2

4a : 4-HO_2CCH_2

4b : 1-CH_3O-3-CH_3-4-HO_2CCH_2

4b′: 1-CH_3O-3-CH_3-5-HO_2CCH_2

5a : 1-CH_3-4-HO_2CCH_2

6b : 1-CH_3O-3-CH_3-4-$HOCH_2$-5-HO_2CCH_2

7a : 1-$AcOCH_2$

8a : 4-$AcOCH_2$

8b : 1-CH_3O-3-CH_3-4-$AcOCH_2$

9b : 1-CH_3O-3,8-$(CH_3)_2$-4-$AcOCH_2$

10a : 1-CH_3

10b : 1-CH_3O-3,8-$(CH_3)_2$

11a : 1,3-$(CH_3O_2CCH_2)_2$-4-CH_3O

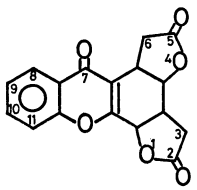

2a

2b: 8-CH_3O-10-CH_3-11-$AcOCH_2$

Fig. 1. 9-Xanthenones (**1a, b**) and the oxidation products.

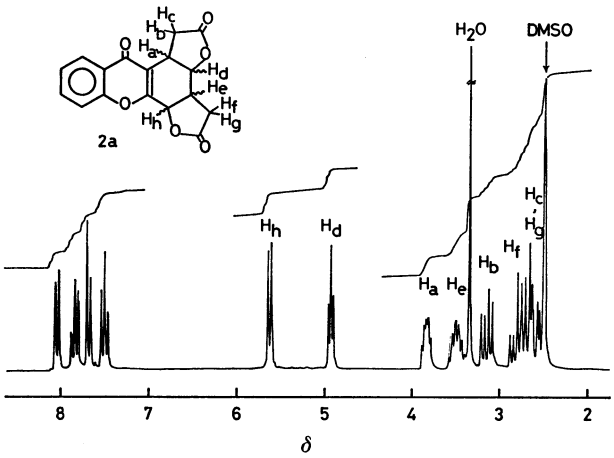

Fig. 2. ^{1}H-NMR spectrum of di-γ-lactone (**2a**) in DMSO-d_6 (δ ppm, 200 MHz).

pound (**2a**) showed a parent ion peak at *m/e* 312 in the MS spectrum, and strong IR absorption bands at 1775 and 1640 cm^{-1} in KBr. The ^{1}H-NMR spectrum (200 MHz) of **2a** in DMSO-d_6 is shown in Fig. 2. Decoupling the triplet at δ=4.95 (H_d) collapsed the multiplet at δ=3.85 (H_a) to four peaks. Decoupling the H_a collapsed the triplet of H_d and two double doublets at δ=3.15 (H_b) and 2.64 (H_c) to three doublets. When the multiplet at δ=3.50 (H_e) was decoupled, the doublet at δ=5.64 (H_h), the triplet (H_d), the double doublets at δ=2.82 (H_f) and 2.64 (H_g) were collapsed to a sharp singlet and three doublets, respectively. The coupling constants are as follows: J_{ab}=8.8, J_{ac}=4.4, J_{bc}=17.8, J_{ad}=5.9, J_{de}=4.9, J_{ef}=8.3, J_{eg}=4.4, J_{fg}=17.3, and J_{eh}=7.3 Hz. In the ^{13}C-NMR spectrum of **2a** seventeen peaks appeared. In addition, **2a** (44 mg) was hydrolyzed with 50% KOH–ethanol, then treated with 3 M (1 M= 1 mol dm^{-3}) sulfuric acid, followed by methylation to give 1,3-bis(methoxycarbonylmethyl)-4-methoxy-9-xanthenone (**11a**; 16 mg, 31%). It is known that the addition of a $\cdot CH_2COOH$ radical to olefins occurs by cis-addition.[3] Therefore, the γ-lactone rings of **2a** may add cis to the cyclohexene ring. From the results described above the structure of **2a** was deduced to be 3a,3b,6a,12b-tetrahydro-2*H*-difuro[3,2-*a*:3′,2′-*c*]-xanthene-2,5,7(3*H*,6*H*)-trione, though the configurations at C-3a, 3b, 6a, and 12b could not be determined.

The oxidation of 1-methoxy-3-methyl-9-xanthenone (**1b**) with LTA for 2.5 h gave 11-acetoxymethyl-8-methoxy-10-methyl-3a,3b,6a,12b-tetrahydro-2*H*-difuro-[3,2-*a*:3′,2′-*c*]xanthene-2,5,7(3*H*,6*H*)-trione (**2b**; 6%), 4-carboxymethyl-1-methoxy-3-methyl-9-xanthenone (**4b**; 3%), 5-carboxymethyl-1-methoxy-3-methyl-9-xanthenone (**4b′**; 1%),[1] 5-carboxymethyl-4-hydroxymethyl-1-methoxy-3-methyl-9-xanthenone (**6b**; 5%), 4-acetoxymethyl-1-methoxy-3-methyl-9-xanthenone (**8b**; 12%),[1] 4-acetoxymethyl-1-methoxy-3,8-dimethyl-9-xanthenone (**9b**; 1%), and 1-methoxy-3,8-dimethyl-9-

xanthenone (**10b**; 1%).

It is known that LTA decomposes in acetic acid to yield $\cdot CH_3$ radicals[4] which react with acetic acid to afford $\cdot CH_2COOH$ radicals.[5] The $\cdot CH_2COOH$ radicals attack aromatic compounds and the CH_2-COOH group is then introduced; this is also converted into a CH_2OAc group.[5] Therefore, these groups are substituted at the positions ortho or para to electron-donating groups because of the electrophilic nature of $\cdot CH_2COOH$ radicals.[6] $\cdot CH_3$ radicals also attack 9-xanthenones to yield methylated products, which can be further oxidized with LTA to give acetoxymethyl-9-xanthenones.[5] In MTA oxidation, on the other hand, $\cdot CH_2COOH$ radicals predominantly attack the peri positions regardless of the effect of the electron-donating groups.[1] However, in the present LTA oxidation such a tendency was not observed and the yields of products were not so good as those in MTA oxidation. Consequently, the interaction between the substrate and oxidant which was assumed in MTA oxidation is not important in LTA oxidation.[1] It is known that the reaction of olefins with LTA gives γ-lactones.[3] The present reaction is, however, the first example that $\cdot CH_2COOH$ radicals add to the aromatic rings to give di-γ-lactones.

Experimental

Measurements. The ^{1}H-NMR spectra were recorded on a Hitachi Perkin-Elmer R-24 spectrometer (60 MHz) in $CDCl_3$ and a JEOL FX-200 spectrometer (200 MHz), while the ^{13}C-NMR spectrum was measured on a JEOL FX-90Q spectrometer. The IR spectra were taken on a JASCO IRA-1 grating spectrometer in $CHCl_3$. The Mass spectra were measured on a JEOL DX-300 mass spectrometer. The UV spectra were recorded for methanol solution with a Hitachi EPS-3T spectrophotometer. The melting points were determined with a Yanagimoto micromelting point apparatus and were not corrected.

Oxidation of 9-Xanthenones. A mixture of 9-xanthenone (**1a** or **1b**; 1 mmol), LTA (5 mmol), and acetic acid (25 ml) was heated under reflux. The work-up procedure including the esterification of the acidic products was the same as described elsewhere.[1] The yields are based on the amount of substrate consumed.

2a: Mp 281—283 °C (EtOH); λ_{max} nm (log ε), 231 (4.28), 253^{sh} (3.95), 268^{sh} (3.73), 307 (3.80); ^{1}H-NMR δ= 2.64 (1H, dd, J=17.3, 4.4 Hz, H_c or H_g), 2.65 (1H, dd, J=17.8, 4.4 Hz, H_c or H_g), 2.82 (1H, dd, J=17.3, 8.3 Hz, H_f), 3.15 (1H, dd, J=17.8, 8.8 Hz, H_b), 3.50 (1H, m, H_e), 3.85 (1H, m, H_a), 4.95 (1H, t, H_d), 5.46 (1H, d, J=7.3 Hz, H_h), 7.5—8.1 (4H, m, ArH); ^{13}C-NMR δ=30.2 (t, CH_2), 31.4 (d, CH), 34.3 (t, CH_2), 36.1 (d, CH), 72.5 (d, H–C–O), 75.7 (d, H–C–O), 117.3 (d, ArC), 118.3 (s, ArC), 122.5 (s, ArC), 125.0 (d, ArC), 125.7 (d, ArC), 134.8 (d, ArC), 155.5 (s, C=), 156.0 (s, C=), 174.6 (s, C=O), 175.3 (s, C=O), 176.3 (s, C=O); *m/e* 312 (96), 268 (100), 226 (64), 197 (43). Found: C, 65.23; H, 4.05%. Calcd for $C_{17}H_{12}O_6$: C, 65.38; H, 3.87%.

*Methyl Esters of **3a** and **4a***: The methyl ester of **3a** was not separated from the methyl ester of **4a** because they have the same R_f values on TLC; mp 148—150 °C (MeOH); IR ($CHCl_3$) 1670, 1745 cm^{-1} (C=O); **3a** ($CDCl_3$) δ=3.69 (3H, s, CO_2CH_3), 4.25 (2H, s, CH_2), 6.95—8.35 (7H, m, ArH); **4a** δ=3.69 (3H, s, CO_2CH_3), 3.93 (2H, s, CH_2), 6.95—8.35 (7H, m, ArH). Found: C, 71.34; H, 4.55%. Calcd for $C_{16}H_{12}O_4$: C, 71.63; H, 4.51%.

*Methyl Ester of **5a***: Mp 149—150 °C (MeOH); IR 1665, 1740 cm^{-1} (C=O); δ=2.89 (3H, s, CH_3), 3.70 (3H, s, CO_2CH_3), 3.91 (3H, s, CH_2), 7.04 (1H, d, J=7.8 Hz, $H_{(2)}$), 7.44 (1H, d, J=7.8 Hz, $H_{(3)}$), 7.15—8.40 (4H, m, ArH); *m/e* 282.0798 (52, M$^+$), 223 (100), 194 (20). Calcd for $C_{17}H_{14}O_4$: M, 282.0892.

7a: Mp 132—133 °C (EtOH); IR 1665, 1745 cm^{-1} (C=O); δ=2.20 (3H, s, OAc), 5.87 (2H, s, CH_2), 7.19—8.42 (7H, m, ArH); *m/e* 268.0711 (8, M$^+$), 225 (100), 197 (28). Calcd for $C_{16}H_{12}O_4$: M, 268.0736.

10a: Mp 113 °C (MeOH) (lit,[7] mp 114 °C).

11a: Mp 137 °C (MeOH); IR 1660, 1740 cm^{-1} (C=O); δ=3.71 (6H, s, 2×CO_2CH_3), 3.77 (2H, s, CH_2), 4.03 (3H, s, OCH_3), 4.19 (2H, s, CH_2), 7.00 (1H, s, $H_{(2)}$), 7.25—8.34 (4H, m, ArH); *m/e* 370.1080 (20, M$^+$), 338 (66), 323 (100), 311 (38), 295 (38), 237 (50). Calcd for $C_{20}H_{18}O_7$: M, 370.1051.

2b: Mp 199—204 °C (EtOH); λ_{max} nm (log ε), 237 (4.33), 265^{sh} (4.07), 285^{sh} (3.62), 324 (3.73); IR 1645, 1745, 1785 cm^{-1} (C=O); δ=2.07 (3H, s, OAc), 2.46—3.88 (6H, m, 2×CH_2, 2×CH), 2.52 (3H, s, CH_3), 3.95 (3H, s, OCH_3), 4.80 (1H, t, J=6.0 Hz, $H_{(3b)}$), 5.30 (2H, s, CH_2), 5.38 (1H, d, J=6.6 Hz, $H_{(12b)}$), 6.70 (1H, s, $H_{(9)}$); *m/e* 428.1113 (2, M$^+$), 384 (19), 326 (23), 325 (100), 253 (63). Calcd for $C_{22}H_{20}O_9$: M, 428.1107.

*Methyl Ester of **4b***: Mp 160—161 °C (MeOH); IR 1655, 1740 cm^{-1} (C=O); δ=2.41 (3H, s, CH_3), 3.71 (3H, s, CO_2CH_3), 3.88 (2H, s, CH_2), 3.97 (3H, s, OCH_3), 6.66 (1H, s, $H_{(2)}$), 7.20—8.37 (4H, m, ArH). Found: C, 69.01; H, 5.12%. Calcd for $C_{18}H_{16}O_5$: C, 69.22; H, 5.16%.

*Methyl Ester of **6b***: Mp 224—225 °C (MeOH); IR 1655, 1740 (C=O), 3250—3600 cm^{-1} (OH); δ=2.45 (3H, s, CH_3), 3.08 (1H, br. s, OH), 3.70 (3H, s, CO_2CH_3), 3.89 (2H, s, CH_2CO_2), 3.91 (3H, s, OCH_3), 4.86 (2H, s, CH_2O), 6.47 (1H, s, $H_{(2)}$), 7.10—8.20 (3H, m, ArH). Found: C, 66.57; H, 5.28%. Calcd for $C_{19}H_{18}O_6$: C, 66.66; H, 5.30%.

9b: Mp 184—186 °C (EtOH); IR 1655, 1740 cm^{-1} (C=O); δ=2.06 (3H, s, OAc), 2.50 (3H, s, CH_3), 2.91 (3H, s, CH_3), 4.00 (3H, s, OCH_3), 5.42 (2H, s, CH_2), 6.63 (1H, s, $H_{(2)}$), 6.98—7.69 (3H, m, ArH); *m/e* 326.1165 (100, M$^+$), 297 (31), 267 (89), 250 (25), 249 (95), 238 (26). Calcd for $C_{19}H_{18}O_5$: M, 326.1154.

10b: Mp 168—170 °C (MeOH); IR 1655 cm^{-1} (C=O); δ=2.43 (3H, s, CH_3), 2.89 (3H, s, CH_3), 4.00 (3H, s, OCH_3), 6.56 (1H, d, J=1.8 Hz, $H_{(2)}$), 6.79 (1H, d, J=1.8 Hz, $H_{(4)}$), 6.94—7.59 (3H, m, ArH); *m/e* 254.0942 (55, M$^+$), 236 (100). Calcd for $C_{16}H_{14}O_3$: M, 254.0943.

The authors wish to thank Dr. John F. W. McOmie, Dr. Martin Murray, and Dr. K. MacNeil of Bristol University, England, for their measurements of the ^{1}H-NMR (200 MHz), ^{13}C-NMR, and MS spectra, and for their helpful discussion.

References

1) H. Nishino and K. Kurosawa, *Bull. Chem. Soc. Jpn.*, **56**, 474 (1983).

2) S. Ueda and K. Kurosawa, *Bull. Chem. Soc. Jpn.*, **50**, 193 (1977).

3) E. I. Heiba, R. M. Dessau, and W. J. Koehl, Jr., *J. Am. Chem. Soc.*, **90**, 2706 (1968).

4) J. M. Davidson and C. Triggs, *J. Chem. Soc., A*, **1968**, 1331.

5) E. I. Heiba, R. M. Dessau, and W. J. Koehl, Jr., *J. Am. Chem. Soc.*, **90**, 1082 (1968).

6) E. I. Heiba, R. M. Dessau, and W. J. Koehl, Jr., *J. Am. Chem. Soc.*, **91**, 138 (1969).

7) A. A. Goldberg and A. H. Wragg, *J. Chem. Soc.*, **1958**, 4227.

Partial Benzylation of Methyl α- and β-D-Galactopyranosides

Naohiko MORISHIMA, Shinkiti KOTO,* Megumi OSHIMA, Akiko SUGIMOTO, and Shonosuke ZEN
School of Pharmaceutical Sciences, Kitasato University, Shirokane, Minato-ku, Tokyo 108

(Received December 23, 1982)

Synopsis. Partial benzylation of methyl α-D-galactopyranoside with benzyl chloride and LiOH selectively gave the 2,3,6-tribenzyl ether, while that using KOH or RbOH gave the 2,4,6-isomer as the main product. Methyl β-D-galactopyranoside afforded the 3,4,6-tribenzyl ether predominantly, irrespective of the alkali used.

Synthetic studies of oligosaccharides require the preparation of partially benzylated carbohydrates.[1] Such compounds have often been prepared by kinetic benzylation[2] of unprotected glycosides.[3,4b] This paper will deal with a direct partial benzylation of methyl α- and β-D-galactopyranosides (**1** and **6**) and the dependence of the selectivity upon the alkali used and the anomeric configuration of the substrates.

The kinetic tribenzylation of **1** was carried out using benzyl chloride and a variety of alkalis (Table 1). The benzylation using excess LiOH (8 equiv.) for 9 h at 140 °C gave methyl 2,3,6-tri-*O*-benzyl-α-D-galactopyranoside (**3**) in a 52% yield, together with small amounts of the other tribenzyl ethers (**4** and **5**). This result contrasts with the observation that the reactivity

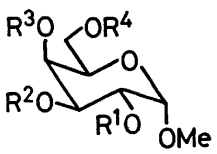

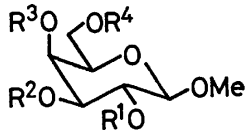

	R¹	R²	R³	R⁴		R¹	R²	R³	R⁴
1	H	H	H	H	**6**	H	H	H	H
2	Bn	Bn	Bn	Bn	**7**	Bn	Bn	Bn	Bn
3	Bn	Bn	H	Bn	**8**	Bn	Bn	H	Bn
4	Bn	H	Bn	Bn	**9**	Bn	H	Bn	Bn
5	H	Bn	Bn	Bn	**10**	Bn	Bn	Bn	Bn
11	Bn	H	H	Bn	**14**	Bn	H	H	Bn
12	H	Bn	H	Bn	**15**	H	Bn	H	Bn
13	H	H	Bn	Bn	**16**	H	H	Bn	Bn
17	All	All	H	H	**19**	All	All	H	H
18	All	H	All	H					

TABLE 1. PARTIAL BENZYLATION OF METHYL α- AND β-D-GALACTOPYRANOSIDES (**1** AND **6**) AND THEIR DIBENZYL ETHERS WITH BENZYL CHLORIDE[a] AND ALKALI

Galactoside	Alkali (equiv.)	Temp °C	Time h	Yields of tetra- and tri-benzyl ether of **1** or **6**/%			
				2	**3**	**4**	**5**
1	LiOH (8.0)	140	9.0	8	52	10	3
	NaOH (4.0)	140	1.5	7	16	23	12
	KOH (4.5)	100	1.5	18	5	28	10
	RbOH (4.5)	70	3.0	13	6	42	14
	CsOH (4.5)	70	1.5	11	3	14	5
11[b]	LiOH (2.0)	140	6.0	3	48	12	—
	RbOH (1.3)	70	3.0	6	29	41	—
12[b]	LiOH (2.0)	140	6.0	5	41	—	5
	RbOH (1.3)	70	3.0	5	19	—	34
13[b]	LiOH (2.0)	140	6.0	7	—	27	13
	RbOH (1.3)	70	3.0	0	—	25	13
				7	**8**	**9**	**10**
6	LiOH (8.0)	140	6.0	4	12	5	13
	NaOH (4.5)	100	4.5	6	11	13	26
	KOH (4.5)	100	1.5	9	10	19	34
	RbOH (4.5)	100	1.5	21	8	24	32
14[b]	KOH (1.3)	100	3.0	5	27	41	—
15[b]	KOH (1.3)	100	3.0	10	18	—	48
16[b]	KOH (1.3)	100	3.0	7	—	25	45

a) Twenty parts of benzyl chloride was used. b) The reactions were conducted in 0.2—0.3 mmol scale.

of the axial OH-4 is higher than the equatorial OH-3 in the partial benzylation of methyl 2,6-di-*O*-benzyl-α-D-galactopyranoside (**11**) and methyl 6-deoxy-α-L-galactopyranoside with benzyl bromide and NaH in *N*,*N*-dimethylformamide.[4] The use of NaOH, KOH, or RbOH, however, changed the selectivity of the reaction to produce the 2,4,6-tribenzyl ether **4** predominantly. Its maximized yield was 42% for the reaction using RbOH (4.5 equiv.) for 3 h at 70 °C. Controlled benzylation with a limited amount of alkali formed the 2,6-, the 3,6-, and the 4,6-dibenzyl ethers (**11**, **12**, and **13**), whose yields depended on the alkali used: 10, 9, and 1% for LiOH (4.0 equiv.) and 4, 6, and 8% for RbOH (2.5 equiv.) Furthermore, the selectivity in the monobenzylation of these dibenzyl ethers was also dependent upon the alkali used (Table 1). Thus, the equatorial OH-3 of **11** and the OH-2 of **12** were selectively benzylated with LiOH, while the axial OH-4 of **11** and **12** were selectively benzylated with RbOH.

Partial benzylation of **6** gave the 3,4,6-tribenzyl ether (**10**) as the main product, irrespective of the alkali used; the best of the alkalis was KOH (Table 1). The controlled benzylation of **6** using KOH (2.0 equiv.) afforded the 2,6- 3,6-, and 4,6-dibenzyl ethers (**14**, **15**, and **16**) in 5, 15, and 12% yields: the lower reactivity of OH-2 of **6** is similar to that of OH-3 of the α-gluco- and the α-xylopyranosides,[3] both of which are located at the center of three contiguous equatorial hydroxyl groups. The OH-2 of **15** and **16** were also less susceptible to benzylation.

The structure of the tri- and the dibenzyl ethers were determined by examining ^{1}H NMR spectra of their acetates (Table 3). The new dibenzyl ethers were synthesized *via* alternative routes.

Experimental

General. See the previous papers.[3] LiOH·H_2O and **1**·H_2O (Pfanstiehl) were dehydrated *in vacuo* at 105 and

TABLE 2. PHYSICAL AND ANALYTICAL DATA OF TRI- AND DIBENZYL ETHERS OF METHYL D-GALACTOPYRANOSIDES

Compound	Mp θ_m °C	$[\alpha]_D^{25}$ ° (*c*, $CHCl_3$)	R_f (Toluene / 2-Butanone)		Found(%) C	Found(%) H
Tribenzyl ether					72.39[a]	6.94[a]
3	—	+34(3.0)[b]	0.43		72.07	6.89
4	—	+44(3.7)[c]	0.34		72.20	6.93
5	85—88.5[f]	+94(0.7)	0.26		72.07	6.90
8	—	+3.4(3.6)[d]	0.40	(7/1)	72.30	6.88
9	—	+0.7(1.6)[e]	0.49		72.41	6.87
10	99—99.5	−4.2(1.0)[f]	0.20		72.61	6.91
Dibenzyl ether					67.36[g]	7.00[g]
11	—	+76(2.2)[h]	0.37		66.93	7.01
12	—	+109(1.9)	0.33		66.90	6.92
13	—	+77(3.5)	0.22		67.65	6.99
14	—	+9.5(3.4)[i]	0.45	(3/2)	67.55	7.11
15	—	+1.0(4.1)[j]	0.37		66.92	7.05
16	116—117	−29(1.0)	0.20		67.59	7.09

a) Calcd for $C_{28}H_{32}O_6$. b) Lit,[4b] $[\alpha]_D^{25}$ +39.5° (*c* 2.38, $CHCl_3$). c) Lit,[4b] $[\alpha]_D^{25}$ +46.6° (*c* 1.04, $CHCl_3$). d) Lit,[9] $[\alpha]_D$ +3° ($CHCl_3$). e) Lit,[4b] $[\alpha]_D^{25}$ 3.1° (*c* 2.58, $CHCl_3$). f) Lit,[10] mp 99—99.5 °C, $[\alpha]_D^{25}$ −5.4° (*c* 1, $CHCl_3$). g) Calcd for $C_{21}H_{28}O_6$. h) Lit,[11] $[\alpha]_D^{11}$ +74.9° (*c* 1.68, $CHCl_3$). i) Lit,[4a] mp 83—85 °C, $[\alpha]_D^{25}$ +8.6° (*c* 1.08, $CHCl_3$). j) Lit,[12] $[\alpha]_D^{25}$ −1.9° (*c* 1.575, $CHCl_3$).

Table 3. ^{1}H NMR data for the acetates of the tri- and dibenzyl ethers and diallyl ethers of methyl α- and β-D-galctopyranosides[a)]

Compound	δ / J/Hz	H-1	H-2	H-3	H-4		MeO	Ac-2	Ac-3	Ac-4	Ac-6
			$J_{1,2}$	$J_{2,3}$	$J_{3,4}$	$J_{4,5}$					
Acetate of:											
3	δ	4.58	3.58	3.83	5.48		3.33	—	—	1.99	—
	J	3.5	9.7	3.2		1.2					
4	δ	4.60	3.87	5.13	3.90		3.30	—	1.89	—	—
	J	3.6	10.7	3.2		1.4					
5	δ	4.86	5.15	3.81	n.d.		3.30	1.99	—	—	—
	J	3.5	10.5	3.9		n.d.					
11	δ	4.61	3.65	5.17	5.33		3.34	—	1.87	1.94	—
	J	3.6	10.5	3.3		1.2					
12	δ	4.81	4.85	3.75	5.49		3.31	1.99	—	1.99	—
	J	3.6	9.8	3.6		1.0					
13[b)]	δ	4.90	5.21	4.36	4.10		3.35	2.01 (1.99)	1.99 (1.98)	—	—
	J	2.9	11.2	2.3		n.d.					
17[c)]	δ	4.81	3.63	3.78	5.40		3.39	—	—	2.11	2.04
	J	3.3	10.1	3.0		0.6					
18[c)]	δ	4.83	3.88	5.15	4.03		3.38	—	2.09	—	2.05
	J	3.7	10.7	3.1		1.0					
8	δ	4.13	n.d.	n.d.	5.43		3.44	—	—	1.99	—
	J	7.8	n.d.	2.1		1.3					
9	δ	4.19	3.57	4.71	3.84		3.45	—	1.81	—	—
	J	8.1	10.2	3.3		1.1					
10	δ	4.19	5.22	3.40	3.86		3.34	1.93	—	—	—
	J	7.9	10.0	3.0		0.9					
14	δ	4.24	3.36	4.82	5.27		3.48	—	1.84	1.94	—
	J	7.8	10.2	3.4		1.1					
15	δ	4.17	4.91	3.38	5.47		3.36	1.93	—	2.02	—
	J	8.0	10.1	3.3		0.7					
16	δ	4.27	5.16	4.79	3.88		3.37	1.98	1.90	—	—
	J	7.8	10.4	3.2		0.6					
19[c)]	δ	4.12	3.63	3.75	5.33		3.52	—	—	2.10	2.04
	J	8.4	7.3	1.2		0.8					

a) Measured in CCl_4 with Me_4Si at 90 MHz. b) Measured in $(CD_3)_2CO$ with Me_4Si. The δ values for Ac group in CCl_4 are shown in parentheses. c) Measured in $CDCl_3$ with Me_4Si.

80 °C over P_2O_5.

*Procedure for the Partial Benzylation of Methyl α- and β-D-Galactopyranosides (**1** and **6**).* A mixture of **1** or **6** (1.0 g, 5.2 mmol) freshly crushed alkali, and $PhCH_2Cl$ (20 ml) was stirred under anhydrous conditions. After the usual work-up,[3)] chromatography (toluene:2-butanone=100:1→1:1, gradient) of the reaction mixture gave the totally and the partially benzylated derivatives of **1** or **6** (Table 1). Physical and analytical data of the tribenzyl ethers (**3**—**5** and **8**—**10**) and dibenzyl ethers (**11**—**16**) are listed in Table 2. The ^{1}H NMR data for the acetylated compounds derived from the tri- and dibenzyl ethers as well as the diallyl ethers desctibed below through the treatment with acetic anhydride in pyridine are given in Table 3.

*Methyl 2,6-Di-O-benzyl-α-D-galactopyranoside (**12**).* Methyl 3,6-di-*O*-trityl-α-D-galactopyranoside[5)] (0.75 g, 1.1 mmol) was refluxed in allyl bromide (7.5 ml) containing NaH (≈60% disp., 0.52 g) for 4 h. The filtrate of the reaction mixture was evaporated and heated in aq. AcOH (80%) at 100 °C for 1 h. After evaporation, chromatography (toluene:2-butanone=2:1) and recrystallization from toluene containing diisopropyl ether gave methyl 2,4-di-*O*-allyl-α-D-galactopyranoside (**18**), (0.22 g, 73%): mp 129.5—130 °C; $[\alpha]_D^{20}$ +123° (*c* 0.7, $CHCl_3$). Found: C, 57.03; H, 8.16%. Calcd for $C_{13}H_{22}O_6$: C, 56.92; H, 8.08%. Benzylation of **18** (0.22 g, 0.80 mmol) with $PhCH_2Cl$ (4.4 ml) and KOH (0.90 g) at 100 °C for 4.5 h, followed by chromatography (toluene:2-butanone=30:1), yielded the 2,3-diallyl-4,6-dibenzyl ether. This was then treated with chlorotris(triphenylphosphine)rhodium(I)[6)] (214 mg) in a mixed solvent (EtOH:benzene:H_2O=7:3:1, 22 ml) for 26 h, followed by refluxing in a mixture of aq HCl (1 mol dm^{-3}, 0.8 ml) and acetone (20 ml) for 30 min. After evaporation, chromatography (diisopropyl ether:ethyl acetate=7:1) afforded **12** (0.24 g, 80%).

*Methyl 4,6-Di-O-benzyl-α-D-galactopyranoside (**13**).* Methyl 4,6-*O*-benzylidene-α-D-galactopyranoside[7)] (1.4 g, 5 mmol) was refluxed in allyl bromide (35 ml) containing NaH (≈60% disp., 1.6 g) for 2 h. The filtrate of the reaction mixture was evaporated and heated in aq AcOH (80%) at 100 °C for 30 min. After evaporation, chromatography ($CHCl_3$:MeOH=50:1) gave methyl 2,3-di-*O*-allyl-α-D-galactopyranoside (**17**), (0.70 g, 51%): $[\alpha]_D^{20}$ +119° (*c* 4.4, $CHCl_3$). Found: C, 56.51; H, 8.14%. Calcd for $C_{13}H_{22}O_6$: C, 56.92; H, 8.08%. Compound **17** (0.45 g, 1.64 mmol) was benzylated with $PhCH_2Cl$ and KOH, and subsequently deallylated as described above to give **13** (0.36 g, 59%).

*Methyl 4,6-Di-O-benzyl-β-D-galactopyranoside (**16**).* Methyl 4,6-di-*O*-benzylidene-β-D-galactopyranoside[8)] (80 mg, 0.28 mmol) was similarly converted into methyl 2,3-di-*O*-allyl-β-D-galactopyranoside (**19**), (70 mg, 91%): $[\alpha]_D^{20}$ +1.7° (*c* 1.1, $CHCl_3$). Found: C, 56.50; H, 8.14%. Calcd for $C_{13}H_{22}O_6$: C, 56.92; H, 8.08%. Benzylation of **19** (70 mg, 0.26 mmol) and subsequent deallylation gave **16** (65 mg, 68%).

References

1) A. F. Bochkov and G. E. Zaikov, "Chemistry of the *O*-Glycosidic Bond. Formation and Cleavage," Pergamon Press, London (1979), Chap. 2.

2) A. H. Haines, *Adv. Carbohydr. Chem. Biochem.*, **33**, 11 (1976).

3) a) S. Koto, Y. Takebe, and S. Zen, *Bull. Chem. Soc. Jpn.*, **45**, 291 (1971); b) N. Morishima, S. Koto, C. Kusuhara, and S. Zen, *ibid.*, **55**, 631 (1982).

4) a) H. M. Flowers, *Carbohydr. Res.*, **39**, 245 (1975); b) H. M. Flowers, *ibid.*, **99**, 170 (1982).

5) S. Koto, N. Morishima, T. Yoshida, M. Uchino, and S. Zen, *Bull. Chem. Soc. Jpn.*, **56**, 1171 (1983).

6) P. A. Gent and R. Gigg, *J. Chem. Soc., Chem. Commun.*, **1974**, 277.

7) G. J. Robertson and R. A. Lamb, *J. Chem. Soc.*, **1934**, 1321.

8) J. W. H. Oldham and D. H. Bell, *J. Am. Chem. Soc.*, **60**, 323 (1938).

9) H. B. Borén, P. J. Garegg, L. Kenne, Å. Pilotii, S. Svensson, and C.-G. Swahn, *Acta Chem. Scand.*, **27**, 2740 (1973).

10) H. F. Vernay E. S. Rachman, R. Eby, and C. Schuerch, *Carbohydr. Res.*, **78**, 267 (1980).

11) J. Schneider, Y. C. Lee, and H. M. Flowers, *Carbohydr. Res.*, **36**, 159 (1974).

12) T. Ogawa, T. Nukada, and M. Matsui, *Carbohydr. Res.*, **101**, 263 (1982).

The Laser-flash Photolysis of 2-Hexanone and 5-Methyl-2-hexane for the Direct Detection of the Triplet 1,4-Biradical

Ikuo NAITO

Department of Photography Kyushu Sangyo University, Matsugadai, Higashi-ku, Fukuoka 813

(Received December 23, 1982)

Synopsis. In the laser-flash photolysis of 2-hexanone and 5-methyl-2-hexanone (265 nm, 15 ns pulse), triplet 1,4-biradicals were detected directly. The absorption spectrum exhibits absorption maxima at $\lambda=250$ nm and at $\lambda=320$ nm. The decay-rate constant of the 1,4-biradical increases as follows: in methanol < in acetonitrile < in hexane < in dichloromethane [$(2—4)\times10^7$ s^{-1} (2-hexanone), $(3—6)\times10^7$ s^{-1} (5-methyl-2-hexanone)].

There have been many reports on the laser-flash photolysis of aromatic carbonyl compounds, and some transient species, *i.e.*, triplet-state and triplet 1,4-biradical intermediates on the Norrish Type-II reaction, have been identified. In the case of aliphatic caybonyl compounds, triplet 1,4-biradicals formed from 2-pentanone,[1] pentanal,[2] and 2-substituted cyclohexanone,[3] were trapped by HBr (gas phase)[1] and paraquat ions.[2,3]

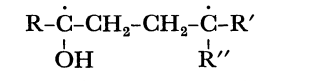

(Triplet 1,4-biradical)

Recently, the triplet states of propanone,[4,5] butanone,[5] and 2-pentanone[5] and the triplet 1,4-biradical formed from poly(3-buten-2-one)[5] were detected. The photolysis of 2-hexanone and 5-methyl-2-hexanone are accepted as proceeding predominantly through the Norrish Type-II mechanism.[6] The laser-flash photolysis of these compounds were carried out in order to detect the triplet 1,4-biradical, directly.

Experimental

Materials. The 2-hexanone and 5-methyl-2-hexanone were dried on anhydrous sodium sulfate and distilled three times by using a splitting-tube column.

The dichloromethane (for fluorescence spectroscopy) was washed five times with a 5% sodium carbonate solution and five times with distilled water. After drying on calcium chloride, the dichloromethane was distilled twice by using the splittingtube column.

The acetonitrile (for spectroscopy) was purified by refluxing it five times on diphosphrus pentaoxide for ten hours and was then distilled twice by using the splitting-tube column.

The hexane (for fluorescence spectroscopy) was washed five times with sulfuric acid and five times with distilled water. After drying on calcium chloride and calcium hydride, the hexane was distilled twice by using the splitting-tube column.

The methanol (for spectroscopy) was purified by refluxing on a magnesium metal for one night and distilled twice by using the splitting-tube column.

The *cis*-1,3-pentadiene was used after two distillations.

Apparatus. The Nd laser apparatus has been described before (265 nm, 15 ns pulse).[7] The output of this laser apparatus was about 100 mJ. The intensity of the laser light was determined by means of the cycloreversion reaction of *r*-1,*t*-2,*t*-3,*c*-4-tetraphenylcyclobutane in 1-chlorobutane ($\phi=0.34$). Normal flashed photons: 2.0×10^{-8} einstein per flash. By choosing an appropriate solute concentration, the optical density was kept at 0.5 (*ca.* 3.0×10^{-2} mol dm^{-3}). The measured emission and absorption spectra were calibrated by the normal number of photons per flash.

Results and Discussion

The Nd laser-flash photolysis of 2-hexanone and 5-methyl-2-hexanone were carried out in dichloromethane in order to detect the triplet 1,4-biradical intermediate. Immediately after the flash, emission (fluorescence) and transient absorption spectra were monitored in the wavelength ranges from 300 nm to 540 nm and from 230 nm to 400 nm respectively. The transient absorption spectrum exhibits absorption maxima at $\lambda=250$ nm and at $\lambda=320$ nm, as it shows in Fig. 1. The triplet absorption spectra of propanone, butanone, and 2-pentanone do not exhibit a minor absorption maximum at $\lambda=320$ nm.[4,5] The acetyl radical absorbed the light in the wavelength range from 500 nm to 600 nm.[5,8] The measured spectra do not agree with those of the triplet state and acetyl radical. The transient absorption decay obeys first order kinetics, and its decay rate (k) is constant over all the wavelength ranges monitored [$k=3.9\times10^7$s^{-1} (2-hexanone), 6.0×10^7 s^{-1} (5-methyl-2-hexanone)]. Figure 2 shows the effect of absorbed photons on the transient absorption in methanol. Although the transient absorbance increases with the quantity of absorbed photons, k is independent of the quantity of absorbed photons.

The laser-flash photolysis were carried out in the presence of a triplet quencher, *cis*-1, 3-pentadiene[$(0.2-1.0)\times10^{-2}$ mol dm^{-3}]. The transient absorbance of 2-hexanone decreased with the quencher concentration. The quenching rate ($k_g\tau_T$) of 2-hexanone was de-

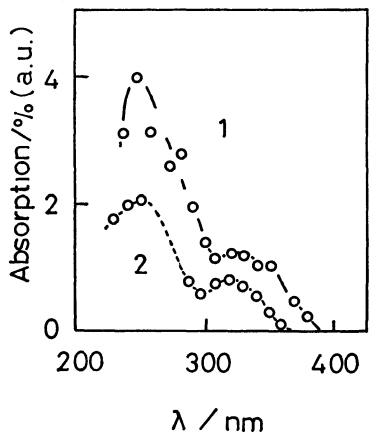

Fig. 1. Transient absorption spectra monitored in the laser flash photolysis of 2-hexanone (1) and 5-methyl-2-hexanone (2) in dichloromethane immediately at the end of the flash. Absorbed photons were normalized to 1.1×10^{-8} einstein per flash. Concentration: 3×10^{-2} mol dm^{-3}.

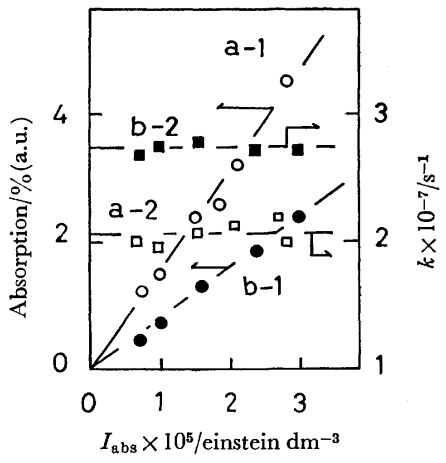

Fig. 2. Effect of absorbed photons on the transient absorption. The absorbance (1) and the decay rate (2) were plotted against the absorbed photons on the laser flash photolysis of 2-hexanone (a) and 5-methyl-2-hexanone (b) in methanol (3×10^{-2} mol dm^{-3}).

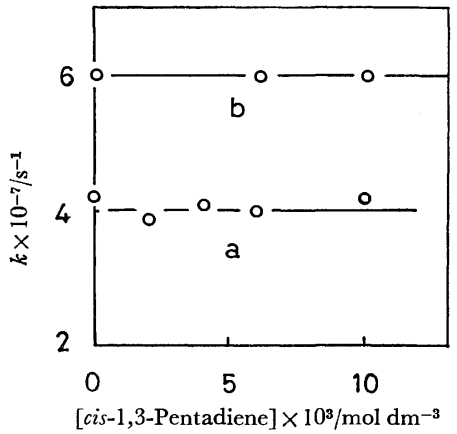

Fig. 3. Change of the decay rate (k) of the transient species in the concentration of *cis*-1,3-pentadiene on the laser flash photolysis of 2-hexanone (a) and 5-methyl-2-hexanone (b) in dichloromethane (3×10^{-2} dm^{-3}).

termined to be *ca.* 3×10 dm^3 mol^{-1} by means of the transient absorbance but the rate of 5-methyl-2-hexanone could not be determined because the results were scattered. Figure 3 shows the plots of k *vs.* the quencher concentration. The decay rates, k, did not increase with the quencher concentration. The quenching rate constant of *cis*-1,3-pentadiene in acetonitrile has been reported to be 4.4×10^9 dm^3 mol^{-1} s^{-1}.[9] If the transient species monitored were the triplet states, the k values were increased to *ca.* 8×10^7 s^{-1} (2-hexanone) and *ca.* 1×10^8 s^{-1} (5-methyl-2-hexanone) in the presence of 1×10^{-2} mol dm^{-3} of the quencher. The triplet decay rate (k_T) of 2-hexanone has been reported to be 1×10^9 s^{-1},[6] and the k_T values have been estimated to be 1×10^8 s^{-1} (2-hexanone) and 3×10^8 s^{-1} (5-methyl-2-hexanone) by means of the $K_g\tau_T$ values reported.[10] These k_T values are much larger than the k values. It can be stated that the transient species monitored is the triplet 1,4-biradical and that k is its decay-rate constant.

These laser-flash photolyses were carried out in acetonitrile, in hexane, and in methanol. The results are listed in Table 1. The k value increased as follows:

in dichloromethane < in hexane < in acetonitrile < in methanol.

Table 1. Decay-rate constants of the transient species formed from 2-hexanone and 5-methyl-2-hexanone in various solvents and the reaction-rate constant of oxygen

Compound	Solvent	$k\times10^{-7}$ a) / s^{-1}	$k'\times10^{-7}$ b) / s^{-1}	$[O_2]\times10^3$ / mol dm^{-3}	$k_{O_2}\times10^{-10}$ / dm^3 mol^{-1} s^{-1}
2-Hexanone	Dichloromethane	3.0	6.8	2c)	1.5
	Hexane	3.3	7.8	3.9d)	1.5
	Acetonitrile	2.4	7.8	1.3e)	4.2?
	Methanol	2.06	5.1	2.12d)	1.4
5-Methyl-2-hexanone	Dichloromethane	6.0	8.8	2c)	1.4
	Hexane	5.4	9.6	3.09d)	1.6?
	Acetonitrile	2.9	8.0	1.3e)	3.9
	Methanol	2.75	6.0	2.12d)	1.5

a) Error limit, ±10%. b) Error limit, ±20%. c) Ref. 5. d) Ref. 12. e) Ref. 13.

Small and Scaiano reported that the 1,4-biradical formed from the aromatic carbonyl compound was stabilized in a polar solvent for the formation of hydrogen bonding with the solvent and a heavy-atom effect was also detected.[11] The characteristics of the triplet 1,4-biradical from the aliphatic carbonyl compounds agree with the results reported by Small and Scaiano.[11] The decay rates of the 1,4-biradical in the presence of oxygen (k') were determined by means of pseudo-first-order kinetics to be as one listed in Table 1. The rate, k', can be written in the form of the following equation;

$$k' = k + k_{O_2}[O_2]$$

where k_{O_2} is the reaction-rate constant of oxygen with the 1,4-biradical. Although the k' rate contains a relatively large error, k_{O_2} is a constant for every solvent ($k_{O_2}=ca.\ 1.5\times10^{10}$ dm^3 mol^{-1} s^{-1}).

I am grateful to Prof. Wolfram Schnabel of Hahn-Meitner-Institut for many supports and useful discussions and to Prof. Setuo Takamuku of Osaka University for his discussions.

References

1) H. E. O'Neal, R. G. Miller, and E. Gunderson, *J. Am. Chem. Soc.*, **96,** 3351 (1974).
2) M. V. Encinas and J. C. Scaiano, *J. Am. Chem. Soc.*, **100** 7108 (1978).
3) M. V. Encinas and J. C. Scaiano, *J. Chem. Soc., Perkin Trans. 1*, **1980,** 56.
4) G. Porter, R. W. Yip, J. M. Duston, A. J. Cessna, and S. E. Sugamori, *Trans. Faraday Soc.*, **67** 3149 (1971).
5) I. Naito and W. Schnabel, in preparation.
6) P. J. Wagner and G. S. Hammond, *J. Am. Chem. Soc.*, **88,** 1245 (1966).
7) S. Takamuku, G. Beck, and W. Schnabel, *J. Photochem.*, **11,** 49 (1979).
8) S. Noda, K. Fueki, and Z. Kuri, *J. Chem. Phys.*, **49,** 3287 (1968).
9) N. J. Turro and Y. Tanimoto, *J. Photochem.*, **14,** 199 (1980).
10) P. J. Wagner, *Acc. Chem. Res.*, **4,** 168 (1971).
11) R. D. Small and J. C. Scaiano, *Chem. Phys. Lett.*, **59,** 246 (1978).
12) S. L. Murov, "Handbook of Photochemistry," Marcel Dekker, New York (1973), p. 89.
13) U. Grollman and W. Schnabel, private communication.

Synthesis of 3-(4-Piperidylidene)-1,3-dihydro-2*H*-indol-2-one Derivatives

Hiroyuki OBASE,* Nobuhiro NAKAMIZO, Haruki TAKAI, and Masayuki TERANISHI

Tokyo Research Laboratory, Kyowa Hakko Co., Ltd., Asahimachi 3-6-6, Machida, Tokyo 194

(Received January 11, 1983)

Synopsis. 3-[1-(2-Aryl-2-hydroxyethyl)-4-piperidylidene]-1,3-dihydro-2*H*-indol-2-one with structure **II**, as potential antihypertensive agent was synthesized. The intermediates, 3-[1-(2-aryl-2-oxoethyl)-4-piperidylidene]-1,3-dihydro-2*H*-indol-2-one (**5**) were prepared from 4-piperidone *via* 4 steps. Selective reduction of carbonyl group in **5** was realized using diisobutyl aluminium hydride to afford compound **II**.

As part of a research program aimed at the development of new antihypertensive agents we have investigated compounds showing a selective inhibitory activity against α-adrenoreceptor, and reported recently syntheses of 4-piperidylbenzimidazolinones (**I**), and their antihypertensive activities.[1-2] As an extension of our studies, we have attempted to modify I by replacing the benzimidazol-2-one group with other heterocycles. This paper describes the synthesis of compounds **II**, in which benzimidazole nitrogen is replaced by an sp^2 carbon atom.

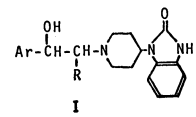

I

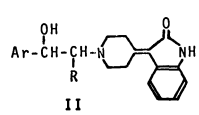

II

The target compounds were synthesized by the route indicated in the following chart. 4-Piperidone hydrate hydrochloride (**1**) reacted with *t*-butyl *s*-(4,6-dimethylpyrimidin-2-yl)thiocarbonate (Boc–S) in the presence of triethylamine (TEA) in dioxane to give 1-t-butoxycarbonyl-4-piperidone (**2**) in 81% yield.

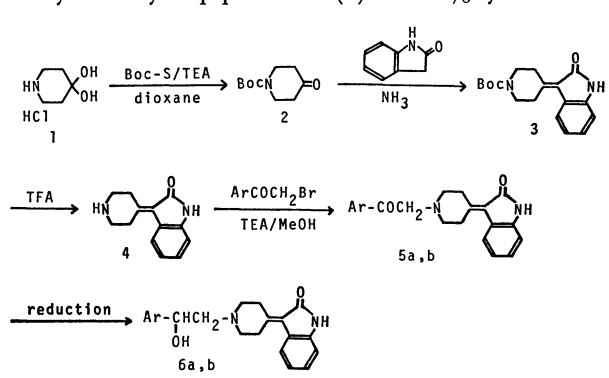

Boc : t-butoxycarbonyl
Ar : a=3,4-dimethoxyphenyl, b=3,4-methylenedioxyphenyl

Base-catalyzed condensation[3] of **2** with 2-oxindole afforded 68% of 3-(1-*t*-butoxycarbonyl-4-piperidylidene)-1,3-dihydro-2*H*-indol-2-one (**3**), which was treated with trifluoroacetic acid to produce 3-(4-piperidylidene)-1,3-dihydro-2*H*-indol-2-one (**4**) in an excellent yield. Bromoacetophenone derivatives were condensed with **4** in a similar manner as previously reported[1] to yield aminoketones **5**. It has been observed that the 3-exo double bond in 2-oxindole is reducible by several reducing agents.[3-6] Therefore, some studies were made on the selective reduction of carbonyl group in **5a**. Aminoketone **5a** was reduced with sodium cyanoborohydride in the presence of acetic acid in MeOH to afford 3-[1-[2-(3,4-dimethoxyphenyl)-2-oxoethyl]piperidin-4-yl]-1,3-dihydro-2*H*-indol-2-one (**7**) in 68% yield. [free **7**: oil, IR($CHCl_3$) 1705, 1680 (sh) cm^{-1}; **7** ·fumarate: mp 190—192 °C

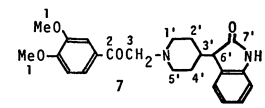

7

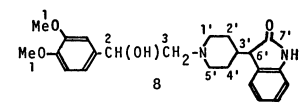

8

(EtOH)]. The structure of **7** is based on its ^{13}C NMR spectrum,[7] in which **7** exhibited peaks at δ 195.0 (C-2 carbon), δ 140.6 (C-3′ carbon) and 156.6 (C-6′ carbon). Starting material **5a** was recovered in the Meerwein-Pondorf-Verley reduction despite of extensive examination of reducting conditions. Although certain compounds such as enolizable β-keto esters, β-diketones and sterically hindered ketones are known to be resistant to aluminium isopropoxide reduction,[8] no reduction of β-amino-ketones by this method has been reported yet. Since aluminium hydride (AlH_3) was found to be the most selective reagent for the reduction of α,β-unsaturated carbonyl group,[9] this reagent was tried. When **5a** was reduced with 3 mol equiv. of AlH_3, it afforded 3-[1-[2-(3,4-dimethoxyphenyl)-2-hydroxyethyl]piperdin-4-yl]-1-,3-dihydro-2*H*-indol-2-one (**8**) [free **8**: oil, IR ($CHCl_3$) 1705 cm^{-1}, ^1H NMR (DMSO-d_6) δ 4.60 (t, 1H, ArCHOH); **8** ·succinate: mp 166—167 °C (from EtOH)]. The structure of **8** is based on its ^{13}C NMR spectrum (δ 38.3 for C-3′ carbon, δ 50.0 for C-6′ carbon and δ 69.4 for C-2 carbon) and elemental analyses. Reduction with 1.5 mol equiv. of AlH_3 afforded a mixture of four products which were separated by preparative TLC to give **6a** (15%), **7** (7%), and **8** (26%) together with starting material **5a** (35%). In the ^1H NMR spectrum of **6a**, the C-2 proton signal was observed at δ 4.72 as a triplet, and the C-3′ and C-6′ carbon signals at δ 140.6 and 157.3, respectively in the ^{13}C NMR spectrum. In the infrared spectra, **6a** absorbed strongly at 1697 cm^{-1} due to a conjugated CONH group, while **8** absorbed at 1705 cm^{-1} due to an isolated CONH group. Although **6a** was obtained by this procedure, the yield was low and the isolation of the product was troublesome. Consequently, reduction using diisobutyl aluminium hydride ((DIBAH)[10]) was further studied. The reaction with 3.5 mol equiv. of DIBAH at room temperature in CH_2Cl_2 gave a 6:4 mixture of **6a** and **8**. However, the reaction carried out at low temperatures (−10—−20 °C) afforded **6a** almost exclusively. In this manner we succeeded in the practical synthesis of **6a** in a fairly good yield. Compound **6b** was also obtained by this procedure from **5b** in 56.3% yield.

Experimental

Infrared spectra were recorded on a Hitachi 215 grating infrared spectrometer. ^{1}H NMR spectra were measured on a JNM-PFT-100 spectrometer. ^{13}C NMR spectra were obtained at 25.1 MHz on a JNM-FX-100 spectrometer, operating in the Fourier transform mode with Me_4Si as an internal standard.

1-t-Butoxycarbonyl-4-piperidone (2). A solution of 4-piperidone hydrate hydrochloride (**1**, 9.3 g, 0.061 mol), triethylamine (12.5 g, 0.124 mol), and Boc–S (14.8 g, 0.062 mol) in 100 ml of dioxane and 30 ml of water was stirred at 20 °C for 6 h and concentrated under reduced pressure. The residue was extracted with AcOEt. The extract was worked up as usual to give crude crystals, which were recrystallized from petroleum ether to give 9.8 g (81.3%) of **2** ; mp 70—72 °C. IR (KBr) 1730 (sh), 1720, 1695 cm^{-1}. Found: C, 60.38; H, 8,78; N, 6.92%. Calcd for $C_{10}H_{17}NO_3$: C, 60.28; H, 8.60; N, 7.03%.

3-[1-(t-Butoxycarbonyl)-4-piperidylidene]-1,3-dihydro-2H-indol-2-one (3). NH_3 (2.4 g, 0.14 mol), **2** (1.51 g, 7,58 mmol), and oxindole (1.01 g, 7.59 mmol) in 25 ml of EtOH were made to react according to the reported procedure[3] to afford 1.62 g (67.9%) of **3**; mp 204—205 °C (EtOH). IR (KBr) 1700, 1690 (sh), 1670 cm^{-1}. Found: C, 68.66; H, 7.05; N, 8.82%. Calcd for $C_{18}H_{22}N_2O_3$: C, 68.77; H, 7.05; N, 8.91%.

3-(4-Piperidylidene)-1,3-dihydro-2H-indol-2-one (4). Compound **3** (7.5 g, 23,9 mmol) was treated with 25 ml of trifluoroacetic acid (TFA) at 0 °C. After stirring the solution for 2 h at 0 °C, TFA was removed *in vacuo* and the residue was made alkaline with 1 M NaOH. The crystals separated were collected and recrystallized from AcOEt to yield 4.4 g (85.9%) of **4**; mp 234—238 °C (decomp), IR (KBr) 1697, 1680 (sh) cm^{-1}. Found: C, 72.59; H, 6.60; N, 12,81%. Calcd for $C_{23}H_{14}N_2O$: C, 72.87; H, 6.59; N, 13.08%.

3-[1-[2-(3,4-Dimethyoxyphenyl)-2-oxoethyl]-4-piperidylidene]-1,3-dihydro-2H-indol-2-one (5a). Compound **5a** was obtained by the previously reported procedure[1] in 89.5% yield from **4** and 3,4-dimethoxybromoacetophenone; mp 145—146 °C (EtOH). IR (KBr) 1690 (br) cm^{-1}. ^{1}H NMR (DMSO-d_6) δ=3.9 (s, 2H, $COCH_2N$), 10.5 (NH). ^{13}C NMR (DMSO-d_6 δ=28.0, 31.2 (C-2′, C-4′), 53.1, 53.6 (C-1′, C-5′), 55.5, 55.7 (C-1), 62.8 (C-3), 140.6 (C-3′), 156.6 (C-6′), 168.7 (C-7′), 195.0 (C-2). Found: C, 70.20; H, 6.04; N, 7.04%. Calcd for $C_{23}H_{24}N_2O_4$: C, 70.39; H, 6.16; N, 7.14%. Compound **5b** was prepared in a similar manner as **5a** in 82.2% yield; mp 167.5—171 °C decomp. IR (KBr) 1698—1680 (br) cm^{-1}. NMR (DMSO-d_6) δ=3.80 ($COCH_2N$), 6.12 (OCH_2O), 10.3 (NH). Found: C, 69.96; H, 5.29; N, 7.33%. Calcd for $C_{22}H_{20}N_2O_4$: C, 70.20; H, 5.36; N, 7.44%.

Reduction of 5a with DIBAH. To a cooled solution of **5a** (2.73 g, 6.96 mmol) in 160 ml of CH_2Cl_2 was added DIBAH (5.0 g, 35.2 mmol) in 70 ml of CH_2Cl_2 at −20 °C over 2 h. The solution was stirred for additional 5 h at the same temperature. Then, 60 ml of MeOH and 200 ml of water were successively added to the solution. The organic layer was separated, washed with water, dried over $MgSO_4$, and concentrated. The residue was recrystallized from AcOEt to afford 1.3 g (47.4%) of **6a**; mp 98—99 °C. IR (KBr) 1697 cm^{-1}. ^{1}H NMR (DMSO-d_6) δ=4.72 (t, 1H, ArCHOH), 10.4 (NH). ^{13}C NMR (DMSO-d_6) δ 28.1, 31.3 (C-2′, C-4′), 53.7, 54.0 (C-1′, C-5′), 55.4, 55.5, (C-1), 65.4 (C-3), 69.7 (C-2), 14.06 (C-3′), 157.3 (C-6′), 168.8 (C-7′). Found: C, 69.89; H, 6.82; N, 6.59%. Calcd for $C_{23}H_{26}N_2O_4$; C, 70.03; H, 6.64; H, 7.10%.

Similar treatment of **5b** with DIBAH gave 56.3% of **6b**; mp 176—178 °C (from MeOH–CH_2Cl_2). IR (KBr) 1692 cm^{-1}. ^{1}H NMR (DMSO-d_6) δ=4.72 (t, 1H, ArCHOH), 5.95 (s, 2H, OCH_2O), 10.35 (br, 1H, NH). Found: C, 69.97; H, 5.84; N, 7.33%. Calcd for $C_{22}H_{22}N_2O_4$: C, 69.82; H, 5.86; N, 7.40%.

References

1) H. Obase, N. Nakamizo, H. Takai, M. Teranishi, K. Kubo, K. Shuto, Y. Kasuya, H. Kato, and K. Shigenobu, *Chem. Pharm. Bull.*, **30**, 462 (1982).

2) Y. Kasuya, K. Shigenobu, M. Hashikami, N. Karashima, H. Obase, H. Takai, M. Teranishi, A. Karasawa, and K. Kubo, *J. Med. Chem.*, in press.

3) I. W. Elliott and P. Rivers, *J. Org. Chem.*, **29**, 2438 (1964).

4) M. Mori and Y. Ban, *Tetrahedron Lett.*, **1979,** 1133.

5) H. G. Lindwall and J. S. Maclennan, *J. Am. Chem. Soc.*, **54**, 4739 (1932).

6) M. J. Kornet, A. P. Thio, and J. H. Thorstenson, *J. Pharm. Sci.*, **66**, 1022 (1977).

7) In the ^{1}H NMR spectra of **7** and **8** the signals assignable to C-3′ and C-6′ protons overlapped with those of piperidine ring protons. Therefore the structures were confirmed by ^{13}C NMR spectroscopy.

8) A. L. Wilds, "Organic Reactions," ed by R. Adams, W. E. Bachmann, L. F. Fieser, J. R. Johnson, and H. R. Snyder, John Wiley & Sons, New York (1957), Vol. 2, Chap. 5, pp. 178—223.

9) H. C. Brown and H. M. Hess, *J. Org. Chem.*, **34,** 2206 (1969).

10) E. Winterfeldt, *Synthesis*, **1972**, 27; **1975**, 617 and the references cited therein.

11) H. C. Brown and N. M. Yoon, *J. Am. Chem. Soc.*, **88**, 1464 (1966).

Bis(acetylacetonato)copper Catalyzed Cross-coupling Reaction of Alkenyldicyclohexylborane with 1-Bromo-1-alkyne or 3-Bromo-1-propene

Masayuki Hoshi, Yuzuru Masuda, and Akira Arase*
Department of Applied Chemistry, Kitami Institute of Technology, Kitami 090
(Received January 22, 1983)

Synopsis. Bis(acetylacetonato)copper is capable of catalyzing cross-coupling reaction of alkenyldicyclohexylborane with 1-bromo-1-alkyne or 3-bromo-1-propene to give conjugated (*E*)-enyne or (*E*)-1,4-diene in a highly stereoselective manner, respectively.

Caporusso *et al.*[1] reported that trialkylaluminium reacted with 1-alkyne in the presence of tris(acetylacetonato)manganese to give a mixture of some unsaturated compounds:

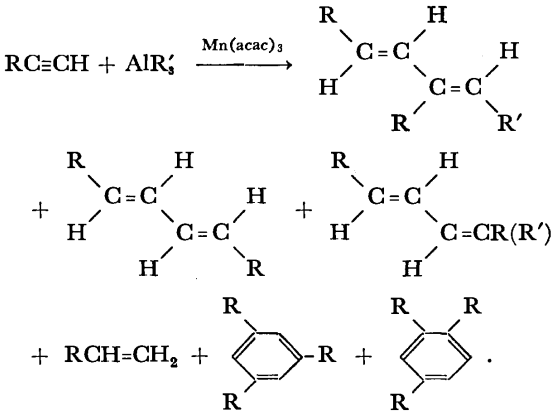

The present authors, on the other hand, have reported of coupling reactions of the alkyl groups of trialkylborane with such groups as SCN,[2,3] SeCN,[3,4] and $OCOCH_3$[5] bonded to some metals. They[6] also reported that trialkylborane reacted with 1-alkyne in the presence of lead(IV) acetate to give an internal alkyne together with an internal enol acetate:

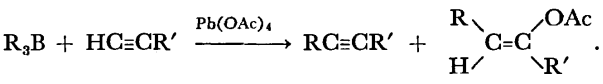

In the course of our investigation on reactions of organoborane with metal complexes, we have come to get interested in the behavior of organoborane in the presence of metal acetylacetonate.

The reaction of trihexylborane with 1-hexyne was first examined in the presence of several metal acetylacetonates. However, such compounds as had been detected in the reaction of trialkylaluminium could not be found at temperatures ranging from −20 to 40 °C; thus 1-bromo-1-hexyne was used instead of 1-hexyne. In this case a considerably clean cross-coupling reaction occurred between trihexylborane and 1-bromo-1-hexyne in the presence of bis(acetylacetonato)copper to give 5-dodecyne in a yield above 60% as based on trihexylborane used.[7] A higher yield of cross-coupling product was obtained when 1-hexenyldicyclohexylborane was treated with aqueous sodium hydroxide and 1-bromo-1-hexyne in the presence of a catalytic amount of bis(acetylacetonato)copper (5%). Thus, 5-dodecene-7-yne, a coupling product of the hexenyl and the hexynyl group, was provided in 75% yield with a high isomeric purity (above 99%):

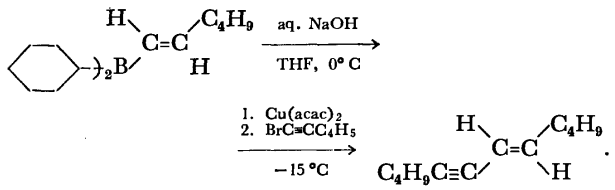

E-configuration of this enyne was assigned from the coupling constant between olefinic protons (J=16 Hz) in ^{1}H NMR spectrum and the absorption band at 965 cm^{-1} in IR spectrum. To obtain a highly pure (*E*)-5-dodecene-7-yne, it is necessary to keep the temperature below −15 °C during the addition of 1-bromo-1-hexyne. Otherwise, some by-products will appear and prevent easy isolation of the enyne from the reaction mixture.[8]

As shown in Table 1, a similar reaction also proceeded without any difficulty which produced the corresponding (*E*)-enyne when an internal alkenyldicyclohexylborane was used as the starting material. Similar results were also obtained when 1-bromo-2-phenylethyne was employed instead of 1-bromo-1-hexyne. High isomeric purities of (*E*)-enyne (above 99%) were obtained in all cases examined. These results suggest that the present reaction may provide a general method for the synthesis of conjugated (*E*)-enyne.

Miyaura *et al.*[9] reported of excellent cross-coupling reactions of alkenyldialkylborane with 1-bromo-1-alkyne; they obtained high yields (72—100%) of conjugated (*E*)-enyne in the presence of a catalytic amount of tetrakis(triphenylphosphine)palladium. The present reaction, though inferior to theirs in yield, is comparable in stereoselectivity of reaction.

The present reaction is also applicable to cross-coupling reaction of alkenyldicyclohexylborane with 3-bromo-1-propene; (*E*)-1,4-diene was afforded in a highly stereoselective manner:

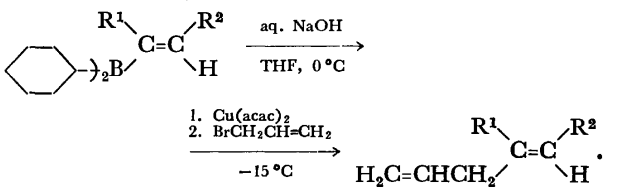

Since the cross-coupling reaction of alkenyldialkylborane with 3-bromo-1-propene has already been studied extensively by several workers,[10] any investigation of this coupling reaction was not made with a variety of substrates.

The present bis(acetylacetonato)copper-catalyzed cross-coupling reaction is a new application of this reagent as a catalyst in the reaction of organoborane and seems to be an easy and inexpensive method for the synthesis of conjugated (*E*)-enyne or (*E*)-1,4-diene.

Table 1. $Cu(acac)_2$-catalyzed cross-coupling reaction of alkenyldicyclohexylborane with 1-bromo-1-alkyne or 3-bromo-1-propene

R^1	R^2	R^3	Compound No.	Product and yield/%[a] $R^3C{\equiv}CR^3$ A	B	$H_2C{=}CHCH_2$ A	B
H	Butyl	Butyl	**1**	75	67		
Ethyl	Ethyl	Butyl	**2**	83	77		
H	Phenyl	Butyl	**3**	85	80		
H	Butyl	Phenyl	**4**	66	55		
Ethyl	Ethyl	Phenyl	**5**	63	55		
H	Phenyl	Phenyl	**6**	65	57		
H	Octyl	$BrCH_2C{\equiv}CH$	**7**			78	63
H	Phenyl	$BrCH_2C{\equiv}CH$	**8**			95	86

a) Based on alkenyldicyclohexylborane employed: A, yield determined by GLC; B, yield determined via isolation by column chromatography.

Experimental

Instruments. IR spectra (film) were recorded with a Hitachi-285 spectrometer. ^1H NMR (60 MHz) spectra (CCl_4) were recorded on a Hitachi R-20A spectrometer. Mass spectra were recorded with a Hitachi M-52 mass spectrometer.

Reagents. Cyclohexene and THF were dried over lithium aluminium hydride and distilled before use. 1-Bromo-1-hexyne and 1-bromo-2-phenylethyne were prepared as described in the literature.[11] 1-Hexyne, 1-octyne, phenylacetylene, and 3-bromo-1-propene were dried over molecular sieves 5A. THF solution of BH_3 was prepared by the method described in the literature.[12]

General procedure. A 50 ml round bottomed flask, equipped with a gas inlet for argon, a sample inlet with serum cap, and a magnetic stirring bar, was flushed with argon, and used to prepare dicyclohexylborane by adding 40 mmol of cyclohexene to 20 mmol BH_3 in THF. To the solution, 20 mmol of alkyne was slowly added at 0 °C and the solution was stirred for 3 h at the same temperature. Then, 20 mmol of aqueous sodium hydroxide (2 mol dm^{-3}) was added at 0 °C and stirring was continued for 0.5 h at room temperature. The solution was cooled again to −15 °C, 1 mmol of $Cu(acac)_2$ was introduced into the reaction mixture under a slow argon flow, and then 20 mmol of 1-bromo-1-alkyne or 3-bromo-1-propene was added at the same temperature. After 1 h reaction at −15 °C, the reaction mixture was warmed to room temperature and kept stirred for 20 h, and then the residual organoborane was oxidized with alkaline hydrogen peroxide. The reaction mixture was extracted twice with 30 ml of hexane. The combined extracts were washed twice with NaCl-saturated water and dried over anhydrous calcium chloride. After removal of the solvents under reduced pressure, the reaction mixture was passed through a column packed with silica-gel (Wako-gel Q-50). The products were isolated by elution with hexane.

Analytical data for the products are as follows:

(E)-*5-Dodecen-7-yne (**1**)*: n_D^{20} 1.4732; ^1H NMR (CCl_4) δ= 0.88 (6H, t, J=7 Hz), 1.11 (8H, m), 1.83—2.40 (4H, m), 5.27 (1H, d, J=16 Hz), and 5.62—6.13 (1H, m); IR (film) 2230 and 965 cm^{-1}; MS *m/e* 164 (M^+). Found: C, 87.70; H, 12.15%. Calcd for $C_{12}H_{20}$: C, 87.73; H, 12.27%.

(E)-*4-Ethyl-3-decen-5-yne (**2**)*: n_D^{20} 1.4677; ^1H NMR (CCl_4) δ=0.70—1.30 (9H, m), 1.30—1.65 (4H, m), 1.65—2.40 (6H, m), and 5.55 (1H, t, J=7 Hz); IR (film) 2210 cm^{-1}; MS *m/e* 164 (M^+). Found: C, 87.68; H, 12.20%. Calcd for $C_{12}H_{20}$: C, 87.73; H, 12.27%.

(E)-*1-Phenyl-1-octen-3-yne (**3**)*: n_D^{20} 1.5873; ^1H NMR (CCl_4) δ=0.88 (3H, t, J=7 Hz), 1.10—1.70 (4H, m), 2.13 —2.45 (2H, m), 5.99 (1H, dt, J_t=16 Hz and J_d=2 Hz), 6.70 (1H, d, J=16 Hz), and 7.12 (5H, m); IR (film) 2190 and 960 cm^{-1}; MS *m/e* 184 (M^+). Found: C, 91.20; H, 8.72%. Calcd for $C_{14}H_{16}$: C, 91.25; H, 8.75%.

(E)-*1-Phenyl-3-octen-1-yne (**4**)*: n_D^{20} 1.5674; ^1H NMR (CCl_4) δ=0.88 (3H, t, J=Hz), 1.10—1.60 (4H, m), 1.87—2.31 (2H, m), 5.50 (1H, d, J=16 Hz), 5.87—6.40 (1H, m), and 7.05—7.50 (5H, m), IR (film) 2190 and 955 cm^{-1}; MS *m/e* 184 (M^+). Found: C, 91.24; H, 8.69%. Calcd for $C_{14}H_{16}$: C, 91.25; H, 8.75%.

(E)-*3-Ethyl-1-phenyl-3-hexen-1-yne (**5**)*: n_D^{20} 1.5620; ^1H NMR (CCl_4) δ=0.70—1.60 (6H, m), 1.90—2.20 (4H, m), 5.79 (1H, t, J=7 Hz), and 7.05—7.55 (5H, m), IR (film) 2190 cm^{-1}; MS *m/e* 184 (M^+). Found: C, 91.27; H, 8.78%. Calcd for $C_{14}H_{16}$: C, 91.25; H, 8.75%.

(E)-*1,4-Diphenyl-1-buten-3-yne (**6**)*: mp 87 °C; ^1H NMR (CCl_4) δ=6.20 (1H, d, J=16 Hz), 6.92 (1H, d, J=16 Hz), and 7.10—7.50 (10H, m); MS *m/e* 204 (M^+). Found: C, 94.01; H, 5.94%. Calcd for $C_{16}H_{12}$: C, 94.08; H, 5.92%.

(E)-*1,4-Undecadiene (**7**)*: n_D^{20} 1.4385; ^1H NMR (CCl_4) δ= 0.84 (3H, t, J=7 Hz), 1.10—1.70 (8H, m), 1.80—2.18 (2H, m), 2.50—2.80 (2H, m), and 4.70—6.10 (5H, m),; IR (film) 970 cm^{-1}; MS *m/e* 152 (M^+). Found: C, 86.73; H, 13.23%. Calcd for $C_{11}H_{20}$: C, 86.76; H, 13.24%.

(E)-*1-Phenyl-1,4-pentadiene (**8**)*: n_D^{20} 1.5513; ^1H NMR (CCl_4) δ=2.83 (2H, t, J=7 Hz), 4.98 (2H, m), 5.45—6.30 (3H, m), and 7.10 (5H, m); IR (film) 965 cm^{-1}; MS *m/e* 144 (M^+). Found: C, 91.55; H, 8.34%. Calcd for $C_{11}H_{12}$: C, 91.61; H, 8.93%.

References

1) A. M. Caporusso, G. Giacomelli, and L. Lardicci, *J. Org. Chem.*, **44**, 1496 (1979).

2) A. Arase, Y. Masuda, and A. Suzuki, *Bull. Chem. Soc. Jpn.*, **47**, 2511 (1974).

3) A. Arase and Y. Masuda, *Chem. Lett.*, **1976**, 1115.

4) A. Arase and Y. Masuda, *Chem. Lett.*, **1976**, 785.

5) Y. Masuda and A. Arase, *Bull. Chem. Soc. Jpn.*, **51**, 901 (1978).

6) Y. Masuda, M. Hoshi, and A. Arase, *Chem. Lett.*, **1980**, 413.

7) The result of metalacetylacetonate-catalyzed cross-coupling reaction of trialkylborane with 1-alkyne will be reported elsewhere.

8) 1-Cyclohexyl-1-hexyne is a major by-product, which cannot be removed from (*E*)-5-dodecen-7-yne by any simple procedures such as column chromatography and distillation.

9) N. Miyaura, K. Yamada, and A. Suzuki, *Tetrahedron Lett.*, **1979**, 3437; N. Miyaura, H. Suginome, and A. Suzuki, *ibid.*, **1981**, 127.

10) T. Yano, N. Miyaura, and A. Suzuki, *Bull. Chem. Soc. Jpn.*, **53**, 1471 (1980); H. C. Brown and J. B. Campbell, Jr., *J. Org. Chem.*, **45**, 552 (1980); H. Yatagai, *ibid.*, **45**, 1649 (1980); N. Miyaura, T. Yano, and A. Suzuki, *Tetrahedron Lett.*, **1980**, 2865.

11) K. E. Schulte and M. Goes, *Arch. Pharm. Weinheim, Ger.*, **29**, 118 (1959).

12) G. Zweifel and H. C. Brown, *Org. React.*, **13**, 1 (1963).

Reaction of Some Compounds Having Both Endo and Exo Olefinic Bonds with 1,2,4-Triazoline-3,5-diones

Tatsuo OSHIKAWA* and Mitsuji YAMASHITA

Department of Applied Chemistry, Faculty of Engineering, Shizuoka University, Hamamatsu 432

(Received January 29, 1983)

Synopsis. Reaction of piperitenone, (+)-limonene, or styrene with 1,2,4-triazoline-3,5-dione (TAD) produces adducts by ene reaction. The reaction of (+)-limonene gives a 2:1 adduct which results from further addition of TAD to an intermediary ene reaction product. The reaction of styrene gives 2:1 adducts *via* further addition of TAD to the Diels-Alder reaction product.

1,2,4-Triazoline-3,5-dione (TAD) and its 4-phenyl (PTAD) and 4-methyl (MTAD) derivatives have widely been used as dienophiles or enophiles.[1] An extensive mechanistic study[1] revealed that derivatives of TAD were the most reactive dienophiles or enophiles. In the present study, we are interested in reactions of PTAD with two monoterpenoid ring compounds, *i.e.*, 3-methyl-6-isopropylidene-2-cyclohexen-1-one (piperitenone)[2] and (+)-limonene, and with styrene.

(+)-Pulegone and mesityl oxide are known to be reactive enophiles with PTAD,[3] however no studies have been reported on reactions with PTAD of such compounds as contain both endo and exo olefins, *e.g.*, piperitenone and (+)-limonene.

Results and Discussion

A reaction of equimolar amounts of PTAD and piperitenone (**1**) in ethyl acetate or dichloromethane for 12 h at ambient temperature gave, on work up, compound **2** in 64% yield. Under the same conditions (+)-limonene (**3**) gave adduct **5** in 64% yield.

The structures of products **2** and **5** were determined from ^{1}H NMR, mass, and IR spectra by identifying the olefin protons of the isopropenyl groups, the molecular ion peaks, and the absorption of the vinylidene olefin groups, respectively.

Adduct **2** is exactly of the same type as the compound afforded by the reaction of (+)-pulegone or mesityl oxide, which gives an isopropenyl group on the 6-position *via* a hydrogen abstraction from the methyl group. Product **5** is a 2:1 adduct, which we can easily infer to have been formed *via* an addition of PTAD to the isopropenyl group through ene reaction to give intermediate **4**, which is successively subject to an ene reaction on the 4-position with the second PTAD to generate product **5**. Formation *via* 1:1 adduct **6** of 2:1 adduct **7**, which should have no isopropenyl proton, is denied on the basis of ^{1}H NMR spectra.

Under the same conditions styrene (**8**) gave 2:1 adduct **10** in quantitative yield. The above results indicate that the ene reaction[4] of a reactive enophile of TAD derivative with the exo cyclic olefin in compound **4** or **9** takes place by involving a proton transfer, thus leading to a 2:1 adduct in the reaction of **3** or **8** with TAD. Diels-Alder adduct **9** possesses the structure of conjugated endo cyclic diene, however it gave 2:1 adduct **10**, as a result of ene reaction with the second MTAD, rather than the Diels-Alder reaction product.

The above results, have first revealed that the reaction of a compound having both endo and exo olefinic bonds with TAD proceeds predominantly *via* addition to the exo olefin. The reaction of 2,3-dimethyl-1-butene (**11**) with MTAD has clearly demonstrated that MTAD first attacks the isopropenyl group, with a subsequent reaction with another molecule of enophile leading to a 2:1 adduct.

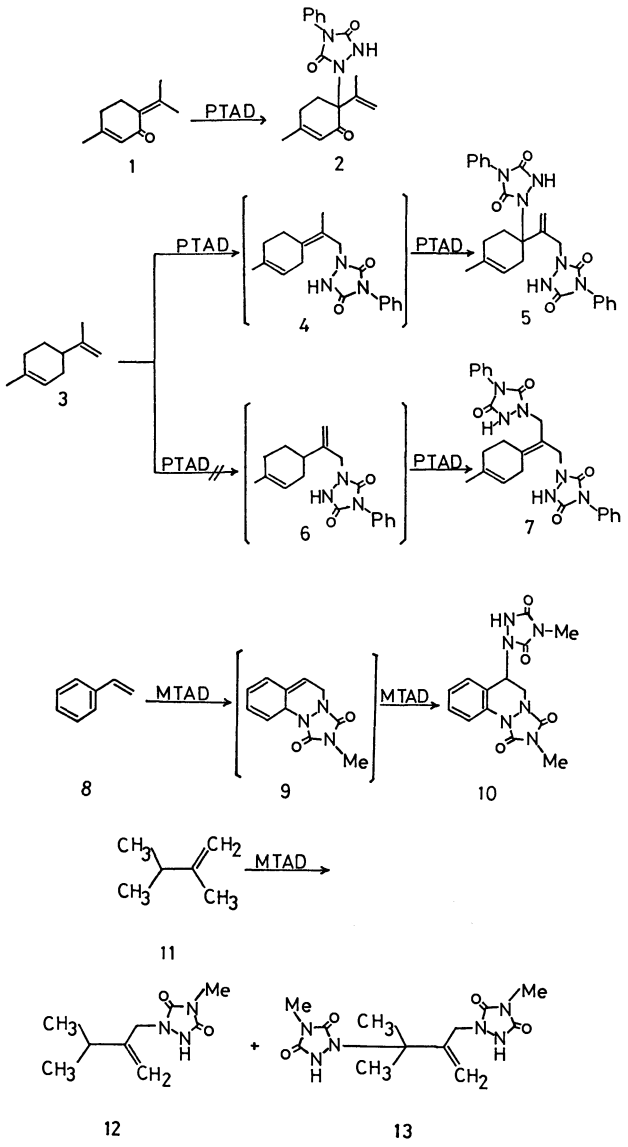

Experimental

Measurements. Melting points were measured on a Yanagimoto Seisakusho micro melting point apparatus. ^{1}H

NMR spectra were recorded on a Hitachi R-24 (60 MHz) spectrometer with TMS as an internal standard, IR spectra on a JASCO A-3 infrared spectrophotometer, and mass spectra on a Hitachi RMU 7MG GC-MS spectrometer.

*Reaction of **1** with PTAD.* *Typical Procedure*: To a solution of 0.5 g (3.33 mmol) of **1** in 10 ml of ethyl acetate or dichloromethane, 0.6 g (3.33 mmol) of PTAD was added all at once. The mixture was stirred magnetically at room temperature with light excluded for protection until the red color of PTAD had faded completely (12 h) and a light yellow solution had appeared. The solution was poured into petroleum ether to precipitate colorless crystalline product **2** (0.7 g, 64% yield): mp 194—196 °C (needles from ethanol ethyl acetate); ^{1}H NMR ($CDCl_3$) δ=1.88 (s, 3H, CH_3), 1.95 (s, 3H, CH_3), 2.33 (br d, J=4.55 Hz, 2H, CH_2), 2.65 (br d, J=4.5 Hz, 2H, CH_2), 4.87 (s, 1H, 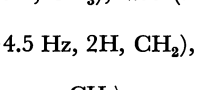), 5.19 (s, 1H, 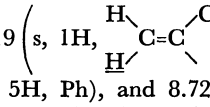), 5.93 (s, 1H, endo olefin), 7.44 (s, 5H, Ph), and 8.72 (br, 1H, NH); IR ν_{max}^{KBr} 3360, 1780, 1700, and 1620 cm^{-1}; MS *m/e* 325 (M^+) and 149 (M^+—PTADH).

Found: C, 66.26; H, 5.83; N, 13.05%. Calcd for $C_{18}H_{19}N_3O_3$: C, 66.46; H, 5.85; N, 12.92%.

*Reaction of **3** with PTAD.* A reaction of **3** with PTAD in the same procedure as described above gave 2:1 adduct **5** in 64% yield: mp 150—151 °C; ^{1}H NMR ($CDCl_3$) δ= 1.97 (s, 3H, CH_2), 1.48 2.40 (br m, 6H, ring CH_2), 4.31 (br, 2H, N CH_3), 6.35 (br s, 2H, NH), 7.43 (s, 10H, Ph); IR ν_{max}^{KBr} 3460, 1785, 1725, and 1600 cm^{-1}; MS *m/e* 482 (M^+), and 130 (M^+—2PTADH).

Found: C, 64.78: H, 4.71; N, 17.46%. Calcd for $C_{26}H_{24}N_6O_4$: C, 64.46; H, 4.96; N, 17.36%.

*Reaction of **8** with MTAD.* As soon as MTAD was added all at once to **8** under the same condition as above, white crystals precipitated. After stirring for 15 min, the white precipitate, which is 2:1 adduct **10**, was collected by filtration in quantative yield: mp 270—273 °C; ^{1}H NMR (DMSO-d_6) δ=3.15 (s, 3H, N CH_3), 3.23 (s, 3H, N CH_3), 3.85 (d, J=12.5 Hz, 2H, CH_2), 5.76 (s, 1H, N CH), 7.33 (m, 4H, aryl), and 8.33 (br, 1H, NH); MS *m/e* 330 (M^+).

Found: C, 50.95; H, 4.21; N, 25.28%. Calcd for $C_{14}H_{14}N_6O_4$: C, 50.99; H, 4.24; N, 25.46%.

*Reaction of **11** with MTAD.* A reaction of **11** with MTAD gave 1:1 **12** and 2:1 **13** adducts in 73 and 15% yields, respectively. Major product **12**: oil; ^{1}H NMR (CCl_4) δ=1.46 (s, 3H, CH_3), 1.67 (s, 3H, CH_3), 2.17 (m, 1H, CH), 3.01 (s, 3H, N CH_3), 4.16 (s, 2H, CH_2), 4.96 ((s, 2H,), and 8.92 (br, 1H, NH). Minor product **13**: Colorless needles; mp 160—161 °C; ^{1}H NMR (DMSO-d_6) δ=1.46 (s, 3H, CH_3), 1.96 (s, 3H, CH_3), 3.04 (s, 6H, N CH_3), 4.30 (s, 2H, N CH_2), 4.87 (s, 1H,), 5.08 (s, 1H,), and 8.99 (br, 2H, NH); MS *m/e* 310 (M^+).

Found: C, 46.48; H, 5.88; N, 27.04%. Calcd for $C_{12}H_{18}N_6O_4$: C, 46.45; H, 5.81; N, 27.10%.

References

1) R. C. Cookson, S. S. Gupe, I. D. Stevens, and C. T. Watts, *Org. Synth.*, **51**, 121 (1971); W. Adam and O. DeLucchi, *Angew. Chem., Int. Ed. Engl.*, **19**, 762 (1980).

2) H. Ueda, K. Takeo, P. Tsai, and C. Tatsumi, *Agric. Biol. Chem.*, **29**, 374 (1965).

3) J. D. Shiloff and N. R. Hunter, *Tetrahedron Lett.*, **1976**, 3773.

4) D. J. Pasto and A. Fu-Taichen, *Tetrahedron Lett.*, **1973**, 713.

Synthesis of 3a,8a-Dihydrocyclopent[*a*]inden-3(8*H*)-one[1]

Yoshikazu SUGIHARA,* Takashi SUGIMURA, and Ichiro MURATA*

Department of Chemistry, Faculty of Science, Osaka University, Toyonaka, Osaka 560

(Received February 7, 1983)

Synopsis. 3a,8a-Dihydrocyclopent[*a*]inden-3(8*H*)-one (**6**) was prepared from a known compound, 2,2-dichloro-2,2a,7,7a-tetrahydro-1*H*-cyclobut[*a*]inden-1-one, by a simple ketone 1,2-transposition followed by introduction of a double bond. The photochemical behavior of **6** was also examined.

The reaction sequence which involves the preparation of the appropriate enone (step-A), its photoannelation with acetylene (or its equivalents) (step-B), and photochemical construction of bicyclobutane (step-C), is our strategy for the synthesis of valene-type isomers of cyclic conjugated systems.[2]

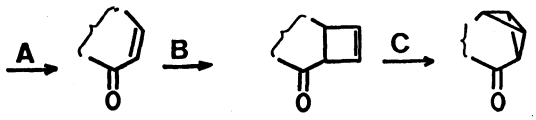

As already reported, enones **5** and **4** proved to be useful intermediates for our synthesis of **1**[2c] and **2**,[2d] respectively. 3a,8a-Dihydrocyclopent[*a*]inden-3(8*H*)-one (**6**) corresponds to the precursor for the synthesis of a benzazulvalene derivative **3** on the line of our methodology. Although the β,γ-unsaturated ketone chromophore in **6** is presumed to disturb the desired photochemical transformations,[3] synthesis and efficiency of photocycloaddition of **6** were pursued.

Enone **6** was prepared from the known compound **7**[4] by a simple ketone 1,2-transposition[5] followed by introduction of a double bond. Thus cyclobutanone

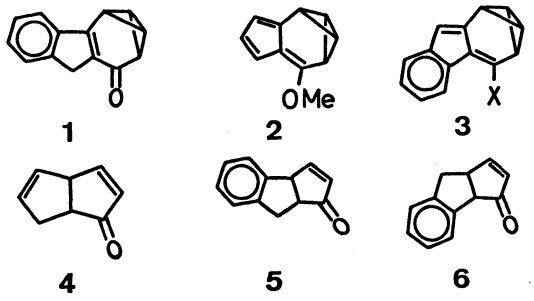

7 was subjected to ring enlargement[6] with diazomethane to afford **8** (87%), which was reduced with sodium borohydride in methanol to yield epimeric alcohols **9** as a colorless solid. Vinyl chloride **10** obtained from **9** through reduction with zinc dust in acetic acid was transformed to cyclopentanone **11** by hydrolysis with 90% sulfuric acid at room temperature for 30 min, in 40.6% yield based on **8**. Alcohol **9** and vinyl chloride **10** could be used without purification during the above transformations.

Because of the easy deprotonation at angular position α to carbonyl group of **11**, routine sulfenylation[7] (LDA 2 equiv., diphenyl disulfide 2 equiv.) afforded bissulfenylated ketone **14** as a sole product. However, a similar method used in the synthesis of **5**[2c,8] was applicable to regiospecific introduction of a double

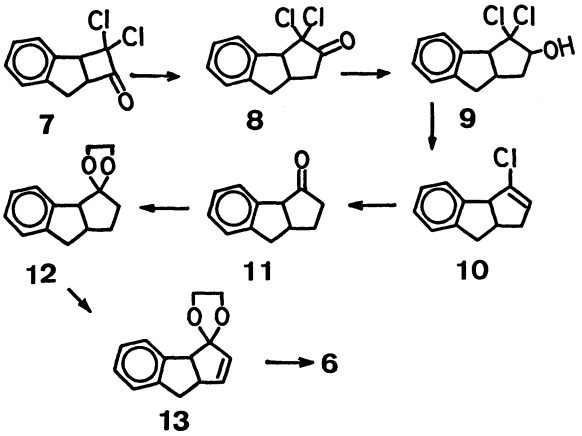

bond to **11** in a yield of 80.4%. While the formation of enone **5** was accompanied with the formation of **15** (15%), none of the isomeric enone was produced during the formation of **6**.

Photoannelations of **6** with acetylene, 1,2-dichloroethylene or bis(trimethylsilyl)acetylene were unsatisfactory. In all cases, the yields of the desired adducts were less than 5% and reaction mixtures showed several spots on TLC and strong absorption band at 1820 cm^{-1} in their IR spectra. Upon photolysis in KBr disk, **6** showed infrared absorption band characteristic of a ketene at 2120 cm^{-1}. Furthermore, irradiation of **6** in a mixture of acetone–methanol afforded methyl ester **16** in 80% yield. Apparently, a Norrish-type I reaction of **6**, followed by formation of ketene **17**, overcomes photocycloaddition.

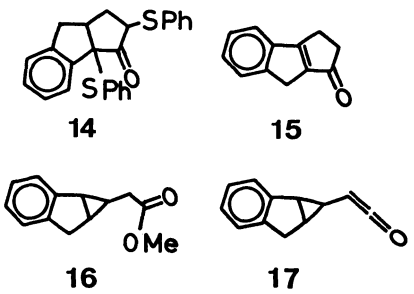

In conclusion, the synthetic method involving ketone 1,2-transposition is useful for the preparation of related cyclopentenones. Enone **6** is not appropriate to our purpose. The benzene ring must be masked. Studies in this line are in progress.

Experimental

^{1}H NMR (100 MHz) spectra were recorded on a Varian XL-100 spectrometer. Chemical shifts are reported in ppm (δ) downfield from TMS as internal standard and coupling constants are given in Hz. IR spectra were recorded on a JASCO A-100 instrument and mass spectra were obtained on a JEOL JMS-01SG-2 spectrometer.

3,3-Dichloro-3,3a,8,8a-tetrahydrocyclopent[a]*inden-2(1H)-one (8).* Ring expansion of **7** with diazomethane was carried out as described in the literature.[6] Yield: 87%; mp: 70—73 °C from ether: IR (KBr): 1761 cm^{-1}; ^1H NMR ($CDCl_3$): δ=2.44 (1H, dd, J=19.5 and 5.1 Hz), 2.72—3.44 (4H, m), 4.24 (1H, d, J=7.8 Hz), 7.15—7.35 (3H, m), 7.6 (1H, m). Found: C, 59.77; H, 4.20%. Calcd for $C_{12}H_{10}OCl_2$: C, 59.78; H, 4.18%.

3,3-Dichloro-1,2,3,3a,8,8a-hexahydrocyclopent[a]*inden-2-ol (9).* To a solution of 1.862 g of **8** in 40 ml of methanol was added 302.6 mg of sodium borohydride. After one hour stirring, 250 ml of ether was added. The mixture was washed (H_2O and then brine), dried ($MgSO_4$), and concentrated to yield 1.886 g of crude alcohol **9** as a colorless solid, which was used in a next step without purification.

3-Chloro-1,3a,8,8a-tetrahydrocyclopent[a]*indene (10).* 1.886 g of alcohol **9** was treated with 1.530 g of zinc in 20 ml of acetic acid at 90 °C for 1 h. After cooling, 100 ml of hexane was added. The mixture was washed (H_2O and then brine) and dried ($MgSO_4$). Removal of the solvent afforded an oil which was passed through a short plug of deactivated silica gel (10% water) with hexane to yield 884 mg of **10** as yellow oil, which was used in the next step without further purification.

1,2,8,8a-Tetrahydrocyclopent[a]*inden-3(3aH)-one (11).* Sulfuric acid (90%, 3 ml) was slowly added to 884 mg of **10** with stirring at 0 °C. After 30 min the mixture was poured onto ice. After routine treatment, chromatography over 8 g of deactivated silica gel (10% water), eluted with a mixture of hexane–benzene (9:1 v/v) afforded 540 mg of **11** as a colorless oil; bp: 65 °C/0.3 mmHg; IR (neat): 1740 cm^{-1}; ^1H NMR ($CDCl_3$): δ=1.58 (1H, m), 2.10—2.40 (3H, m), 3.20 (1H, m), 2.80, 3.24 (2H, AB-part of an ABX_n, J=14.0), 3.73 (1H, dm, J=8.0), 7.10—7.26 (3H, m), 7.43 (1H, m). Found: C, 83.81; H, 7.03%. Calcd for $C_{12}H_{12}O$: C, 83.94; H, 7.00%.

3a,8a-Dihydrocyclopent[a]*inden-3(8H)-one (6).* This material was obtained from the ketone **11** by using the general procedure (acetalization, bromination, dehydrobromination and deacetalization) of Eaton *et al.*[8] Yield: 80.4%; mp: 85.5—86.0 °C from hexane–ether, colorless needles; IR (KBr): 1695 cm^{-1}; ^1H NMR ($CDCl_3$): δ=2.92 (1H, d, J=16.5 Hz), 3.35 (1H, dd, J=16.5 and 9.0 Hz), 3.82 (1H, m), 3.87 (1H, m), 6.03 (1H, dd, J=5.7 and 1.6 Hz), 7.10—7.25 (3H, m), 7.50 (1H, m), 7.59 (1H, dd, J=5.7 and 2.5 Hz). Found: C, 84.32; H, 5.93%. Calcd for $C_{12}H_{10}O$: C, 84.68; H, 5.92%.

Attempted Photoannelation of 6. In a typical run, 222 mg of **6** was dissolved in 80 ml of dichloroethylene. After nitrogen was bubbled through for 1 h, the solution was irradiated at 0 °C. After **6** was disappeared on TLC examination, the solvent was removed under reduced pressure and the residue was checked by IR and NMR spectra for product analysis. Other conditions examined were: acetylene in acetone at −78 °C and bis(trimethylsilyl)acetylene in acetone or acetonitrile at 0 °C. In all cases, irradiations were conducted with a 100 W high pressure mercury lamp through Pyrex filter.

Photolysis of 6 in KBr Disk. 3 mg of **6** was placed in a KBr disk. The disk was irradiated using a 100 W high pressure mercury lamp through a Pyrex filter. The photolysis was followed by measuring the IR spectrum every 10 min. After 50 min, the absorption band attributable to ketene at 2120 cm^{-1} reached its maximum and then gradually decreased on further irradiation.

Photolysis of 6 in the Presence of Methanol. 100 mg of **6** was dissolved in a mixture (50 ml) of acetone–methanol (2:1 v/v). After nitrogen was bubbled through for 30 min, the solution was irradiated using 100 W high pressure mercury lamp through Pyrex filter. After 1 h, the solvent was removed under reduced pressure and the residue was chromatographed over deactivated silica gel (6% water) with benzene. An epimeric mixture of the methyl ester **16** (94 mg) was obtained as a colorless oil. IR (neat): 1720 cm^{-1}; MS: 202 (M^+, 10%), 143 ($M^+-C_2H_3O_2$, 23%), 142 ($M^+-C_2H_4O_2$, 46%), 141 ($M^+-C_2H_5O_2$, 40%), 129 ($M^+-C_3H_5O_2$, 42%), 128 (naphthalene cation, 100%), 115 (indenium ion, 60%); ^1H NMR ($CDCl_3$): δ=0.7 (0.6 H, m), 1.2—2.05 (2.4 H, m), 2.10—2.60 (2H, m), 2.70—3.50 (2H, m), 3.55 (1.2 H, s), 3.65 (1.8 H, s), 6.6—7.4 (4H, m).

References

1) This work was announced at the 13th Symposium on Nonbenzenoid Aromatic Compounds, Nagoya, October 1980, Abstr., No. Cl-05, p. 176.

2) a) Y. Sugihara, N. Morokoshi, and I. Murata, *Tetrahedron Lett.*, **1977**, 3887; b) Y. Sugihara, N. Morokoshi, and I. Murata, *Chem. Lett.*, **1979**, 745; c) Y. Sugihara, T. Sugimura, and I. Murata, *ibid.*, **1980**, 1103; d) Y. Sugihara, T. Sugimura, and I. Murata, *J. Am. Chem. Soc.*, **103**, 6738 (1981); e) Y. Sugihara, A. Yamato, and I. Murata, *Tetrahedron Lett.*, **22**, 3257 (1981).

3) K. N. Houk, *Chem. Rev.*, **76**, 1 (1976).

4) L. R. Krepski and A. Hassner, *J. Org. Chem.*, **42**, 2879 (1978).

5) For a related transposition, see A. E. Greene, *Tetrahedron Lett.*, **21**, 3059 (1980).

6) A. E. Greene and J.-P. Depres, *J. Am. Chem. Soc.*, **101**, 4003 (1979).

7) B. M. Trost, T. N. Salzman, and K. Hiroi, *J. Am. Chem. Soc.*, **98**, 4887 (1976).

8) P. E. Eaton, R. H. Mueller, G. R. Carlson, D. A. Cullison, G. F. Cooper, J.-C. Chou, and E. P. Krebs, *J. Am. Chem. Soc.*, **99**, 2751 (1977).

The η^5-$C_9H_{11}Fe(CO)_2$(isobutylene)$^+BF_4^-$ Complex as a Protecting Group of Carbon-Carbon Double Bonds

Yasutaka Ishii,* Takashi Kagayama, Akihiro Inada, and Masaya Ogawa*

Department of Applied Chemistry, Faculty of Engineering, Kansai University, Senriyama, Suita, Osaka 564

(Received February 12, 1983)

Synopsis. η^5-$C_9H_{11}Fe(CO)_2$(isobutylene)$^+BF_4^-$ (**6**), [Fpi(isobutylene)]$^+BF_4^-$, was prepared and used as a protecting group of carbon–carbon double bonds. The complex **6** undergoes ligand exchange with a variety of diolefins to give Fpi(diolefin)$^+BF_4^-$ complexes, whose subsequent hydrogenations on Pd/C give olefins hydrogenated regioselectively.

The dicarbonyl η^5-cyclopentadienyliron cation moiety, η^5-$C_5H_5Fe(CO)_2^+$ (Fp$^+$), serves as a good protecting group for the carbon–carbon double bond of olefins.[1,2] The Fp(isobutylene)$^+BF_4^-$ complex (**1**), which is readily available from the Fp dimer, undergoes ligand exchange with olefins under mild conditions to give Fp(olefin)$^+$-BF_4^- (**2**) (Eq. 1).

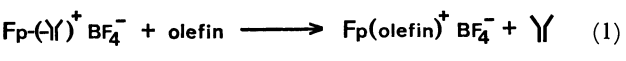

1 2 (1)

In a previous paper, we have reported the $Fe(CO)_5$ catalyzed disproportionation of *cis*-bicyclo[4.3.0]nona-3,7-diene (**3**) to bicyclo[4.3.0]non-1(6)-ene (**4**) and indan (Eq. 2).[3] In the course of the reaction, it was found that tetracarbonylbis(η^5-4,5,6,7-tetrahydroindenyl)diiron (**5**) (Fpi dimer), which is structurally analogous to the Fp dimer, was formed. The stoichiometric reaction of **3** and $Fe(CO)_5$ gave **5** in a moderate yield (35—46%).[4]

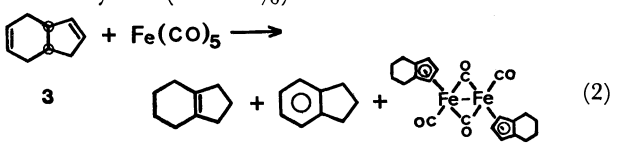

3 4 5 (2)

The Fpi moiety, which is more bulky than the Fp moiety, can be expected to provide a method for protecting the carbon–carbon double bonds. Thus, the Fpi(isobutylene)$^+BF_4^-$ complex (**6**) was prepared and used as a protecting group of the double bonds for various diolefins.

The preparation of **6** from **5** was achieved in 60—65% yields by a modification of the Rosenblum method[5] for the synthesis of **1**. Complex **6** reacted with a variety of diolefin **3**, **7**—**11** in 1,2-dichloroethane to afford Fpi(diolefin)$^+BF_4^-$ complexes **12**—**18** (Scheme 1). The yields of the Fpi(diolefin)$^+BF_4^-$ complexes were preferable to those of the ligand exchange between Fp(isobutylene)$^+BF_4^-$ and diolefins[1] (Scheme 1). The ^{13}C NMR chemical shifts of these complexes are listed in Tables 1 and 2.

The ligand exchange of **6** with bicyclo[2.2.1]hepta-2,5-diene **7** gave **12** in a 91% yield. In the ^{13}C NMR spectrum of **12**, the signal of the α-carbons (C-2 and C-3) shifted about 55 ppm upfield compared with those of **7**.[6] The *exo*-configuration of the Fpi$^+$ moiety in **12** was confirmed on the basis of the upfield shift (*ca.* 18 ppm) of the bridge carbon (C-7) attributable to the steric compression effect. The exchange of **6** with *endo*-tricyclo[5.2.1.$0^{2,6}$]deca-3,8-diene **8** proceeded

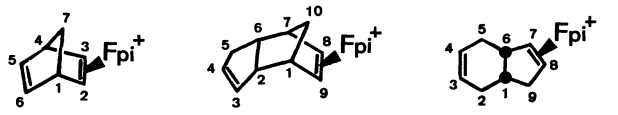

12 (91%) 13 (83%) 14 (60%)

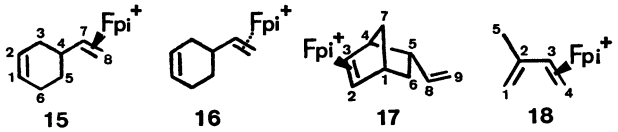

15 (31%) 16 (31%) 17 (60%) 18 (95%)

Scheme 1.

regio- and stereoselectively, affording **13** in an 83% yield. A similar steric effect by the Fpi$^+$ moiety was observed at the bridge carbon (C-10) of **13**. This shows that the configuration of the Fpi$^+$ group in **13** has the *exo*-orientation.

The reaction of **6** with **3** gave exclusively complex **14**, in which the Fpi$^+$ group is probably located in an anti-direction. If the Fpi$^+$ moiety in **14** is situated in a sterically more crowded *syn*-geometry, obvious upfield shifts due to the steric compression effect must be observed in ^{13}C resonances of the fused cyclohexene ring.

The hydrogenation of **14** on Pd/C, followed by treatment with NaI, gave olefin (**19**) (Eq. 3).

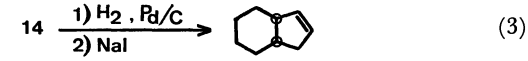

19 (3)

The regiospecific formation of **14** is noteworthy, since the reactivities of the two double bonds in **3** closely resemble each other.

In the exchange of **6** with 4-vinyl-1-cyclohexene (**9**), the ^{13}C NMR spectra of resulting Fpi$^+$ complexes showed two pairs of signals having approximately equal intensities. Although the complexes could not be separated into components, from a consideration of their NMR spectra it was found that the exchange occurred regioselectively, but not stereoselectively, at the vinyl-double bond to give a stereoisomeric mixture of **15** and **16** whose subsequent hydrogenations led to the same olefin (**20**) (Eq. 4).

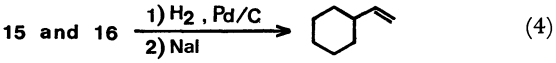

20 (4)

Previously, Nicholas[1] has reported that the exchange of **1** with 5-vinylbicyclo[2.2.1]hept-2-ene (**10**)[8] affords two regioisomers in which the Fp$^+$ group is coordinated to the vinyl- and bicyclo[2.2.1]heptenyl double bonds in a ratio of 65:35. However, the ligand exchange of **6** with **10** occurred preferentially at the bicyclo-[2.2.1]heptenyl double bond to give the Fpi complex **17**.[9]

Table 1. ^{13}C NMR chemical shifts of Fpi(diolefin)$^+BF_4^-$ complexes

Complex	C-1	C-2	C-3	C-4	C-5	C-6	C-7	C-8	C-9	C-10
12	47.9	86.3	86.3	47.9	143.8	143.8	56.2			
13	43.4[a]	54.3	129.6	132.5	31.1	41.1	44.5[a]	75.8	81.0	38.6
14	30.0	23.9	124.8[a]	125.1[a]	27.2	38.6	85.5	80.8	35.9	
15 and **16**	126.5	124.8	32.8	39.2	30.7	24.2	94.0	52.0		
	126.5	124.8	32.8	39.2	29.7	24.2	93.4	52.0		
17	46.2	75.8	79.0	40.9	31.5	42.8	37.1	139.0	114.8	
18	123.1	140.9	89.1	49.2	15.5					

a) An alternative assignment is also possible in each line.

Table 2. ^{13}C NMR chemical shifts of the Fpi-moiety[a]

Complex	C-1	C-2	C-3	C-4	C-5	C-6	C-7	C-8	C-9	C-10 or C-11	
12	108.0	21.2[b]	20.8[b]	20.8[b]	21.2[b]	108.0	84.4	90.6	84.4	211.7	211.7
13	108.0	21.1[b]	20.7[b]	20.7[b]	21.1[b]	108.0	83.9[c]	90.4	84.3[c]	212.0	211.7
14	108.1	21.3[b]	20.9[b]	20.9[b]	21.3[b]	108.1	83.8[c]	91.1	84.1[c]	212.0	211.8
15 and **16**	108.7	21.6[b]	20.7[b]	20.7[b]	21.6[b]	108.7	85.3	90.1	85.3	211.5	209.2
	107.4	20.7	20.7	20.7	20.7	107.4	81.6[b]	90.1	82.3[b]	211.5	209.2
17	107.9	21.2[b]	20.8[b]	20.8[b]	21.2[b]	107.9	84.2[c]	90.9	84.2[c]	211.7	211.6
18	108.2	21.3[b]	20.7[b]	20.7[b]	21.3[b]	107.8	83.6[c]	90.4	84.0[c]	210.9	210.6

a) 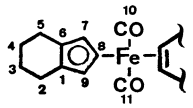

b, c) An alternative assignment is also possible in each line.

The reaction of **6** with acyclic diene, isoprene **11**, took place regioselectively at the less hindered double bond to form Complex **18** in a 95% yield.

These results suggest that Complex **6**, which was readily prepared from the Fpi-dimer, serves as a good protecting group of carbon-carbon double bonds, especially toward the diolefins with a closely analogous reactivity. Furthermore, **6** shows a higher regioselectivity than Complex **1** in the exchange with certain diolefins.

Experimental

The IR spectra were taken with a JASCO-A202 spectrometer. The ^1H and ^{13}C NMR spectra were recorded with a JEOL PMX-60 and a JNM-PS-100 FT-NMR spectrometer respectively. The chemical shifts were obtained in a nitromethane-d_3 solution, containing TMS as the internal standard.

Materials. The Fpi dimer (**5**) was obtained in a manner similar to that described above.[3]

Fpi(isobutylene)$^+BF_4^-$ (**6**) was prepared by a modification of Rosenblum procedure.[5] To a solution of Fpi(η^1-2-methyl-2-propenyl) (33 mmol), which has been prepared from FpiNa and 2-methyl-2-propenyl chloride,[10] we added, drop by drop, 1 equiv of 42% HBF_4 in acetone (1:1) at 0 °C. Stirring was continued at 0 °C for 1 h. At the end of this time, 20 cm^3 of acetone was added, and then the solution was poured to a large amount of ether (500 cm^3). The orange crystals thus precipitated were collected and recrystallized from dichloromethane to give pure **6** in 60—65% overall yields; ^1H NMR (CD_3NO_2) δ=1.9 (m, 10H), 2.5 (m, 4H), 3.7 (s, 2H), 5.2 (s, 3H); ^{13}C NMR (CD_3NO_2) δ=21.4(t), 21.9(t), 27.7(q), 55.1(t), 84.0(d), 91.3(d), 110.1 (s), 122.7(s), 211.0(s); IR(Nujol) 3400, 2050, 1990, 1060, 1010 cm^{-1}.

*Ligand Exchange of **6** with Diolefins.* To a solution of diolefin (60 mmol) in 1,2-dichloroethane (200 cm^3) we added **6** (6 mmol) in 1,2-dichloroethane (80 cm^3). Stirring was continued at 65—70 °C for 10—15 min. After the subsequent removal of the solvent and unreacted diolefin *in vacuo*, the residue was dissolved in a minimum amount of acetone and filtered off. The filtrate was poured into 500 cm^3 of ether to precipitate Fpi(diolefin)$^+BF_4^-$ complexes in 60—95% yields.

Hydrogenation of Fpi(diolefin)$^+BF_4^-$ Complexes and Liberation of the Fpi Moiety from Complexes. The hydrogenations of **14**—**16** were accomplished according to the Nicholas procedure.[2] The hydrogenated complexes (0.8 mmol) were dissolved in nitromethane-d_3 (2 cm^3) containing sodium iodide (1.0 mmol), after with the mixture was refluxed for 3 h. After centrifugation, the supernatant was subjected to NMR measurements.

References

1) P. R. Boyle and K. M. Nicholas, *J. Org. Chem.*, **40**, 2682 (1975).
2) K. M. Nicholas, *J. Am. Chem. Soc.*, **97**, 3254 (1975).
3) T. Kagayama, S. Okabayashi, Y. Amaike, Y. Matsukawa, Y. Ishii, and M. Ogawa, *Bull. Chem. Soc. Jpn.*, **55**, 2297 (1982).
4) Complex **5** was synthesized from spirononadiene and $Fe(CO)_5$ in a 30% yield: B. F. Hallam and P. L. Pauson, *J. Chem. Soc.*, **1958**, 646.
5) W. P. Giering and M. Rosenblum, *J. Chem. Soc., Chem. Commun.*, **1971**, 441.
6) A similar upfield shift was observed in the ethylene-ligand carbons of Fp(ethylene)$^+BF_4^-$: J. M. Fallor and B. Y. Johnson, *J. Organomet. Chem.*, **88**, 101 (1975).
7) The ligand exchange of **1** with **9** has been attempted by Nicholas,[1] but the formation of stereoisomeric Fp-(diolefin)$^+BF_4^-$ complexes has not been described.
8) Compound **10** was a mixture of *endo* and *exo* vinyl derivatives (75:25).
9) A small amount of some other Fpi(diolefin)$^+BF_4^-$ complexes were produced together with **17**, but no components other than **17** could be identified.
10) W. P. Giering and M. Rosenblum, *J. Organomet. Chem.*, **25**, C71 (1970).

Hydrocyanation of α,ω-Diynes Catalyzed by Tetracyanonickelate. Regiospecific Synthesis of a New Series of Acyclic Dinitriles

Takuzo FUNABIKI,* Yoshihiro SATO, and Satohiro YOSHIDA

Department of Hydrocarbon Chemistry, Faculty of Engineering, Kyoto University, Sakyo-ku, Kyoto 606

(Received February 17, 1983)

Synopsis. Hydrocyanation of α,ω-diynes without the use of HCN has been described. Cyanonickelate, prepared by reducing $[Ni(CN)_4]^{2-}$ with $NaBH_4$ or Zn in the presence of excess KCN in water or ethylene glycol, catalyzes hydrocyanation of α,ω-diynes, $HC{\equiv}C(CH_2)_nC{\equiv}CH$ to give quantitatively $CH_3CH(CN)(CH_2)_nCH(CN)CH_3$, a new series of acyclic dinitriles. Importance of the preliminary formation of a (π-acetylene)nickel(0) complex for the hydrocyanation has been suggested.

Previously we have reported the hydrocyanation of acetylenes, without the use of hydrogen cyanide, catalyzed by cyanocobaltate[1] and cyanonickelate.[2] The reaction is useful not only for synthesis of secondary saturated nitriles from acetylenes, but also for elucidation of mechanisms of hydrocyanation with the use of hydrogen cyanide, which have been little clarified. To extend the utility of this new method of synthesis of nitriles, we have studied the reaction of α,ω-diynes, $HC{\equiv}C(CH_2)_nC{\equiv}CH$ ($n=3$—6). The diynes were hardly hydrocyanated by cyanocobaltate. However, they were readily hydrocyanated by cyanonickelate to form $CH_3CH(CN)(CH_2)_nCH(CN)CH_3$ selectively. The nitriles synthesized here are new compounds except for the case $n=3$, in which the nitrile has been obtained by a complicated procedure, *i.e.*, by hydrogenation of $CH_3CH(CN)(CH_2)_2CH{=}C(CN)CH_3$ derived from 3,7-dicyano-3,7-dimethylperhydro-1,2-diazepine.[3] The chemistry of these dinitriles has not been studied, but it is well expected that the present method is applicable to the diynes irrespective to its chain length and that they are useful as starting materials for organic and polymer synthesis.

Results and Discussion

Hydrocyanation was performed under three different conditions, *i.e.*, $[Ni(CN)_4]^{2-}$ was reduced 1) by $NaBH_4$ in water, 2)by $NaBH_4$ in ethylene glycol (EG), or 3)by Zn in water, in the presence of excess cyanide ion. The results of hydrocyanation and the data for identification of products are shown in Tables 1 and 2, respectively. The reactivity of the diynes under the condition (1) ($NaBH_4$–H_2O) was low in contrast to the high reactivity of terminal monoacetylenes under the same condition.[2] The reactivity and selectivity for formation of dinitriles decreased with increasing chain length of the diyne. The reaction under the condition (2) ($NaBH_4$–EG) gave good yields of dinitriles regardless of the chain length, but the selectivity for the dinitrile synthesis decreased slightly with increasing chain length. The reactivity under the condition (3) (Zn–H_2O) was as high as that under the condition (2), but 1,6-heptadiyne formed mainly unsaturated mononitrile, $CH_2{=}C(CN)(CH_2)_4CH_3$. The reason for this peculiar reactivity is not clear at present.

Recently,[4] hydrocyanation of monoacetylenes has been performed by $Ni[P(OPh)_3]_4$ in the presence of hydrogen cyanide, but the hydrocyanation of terminal acetylenes forms not only the internal but also terminal nitriles, indicating that the regioselectivity is not so high as that in the present case. In addition, our procedure does not require the use of HCN. The yields of dinitriles in Table 1 indicate that the hydrocyanation proceeds catalytically. Because of good yields, very high regioselectivity, and experimental simplicity, the present hydrocyanation procedure is more useful for synthesis of internal dinitriles from α,ω-diynes than the conventional method.[4]

Table 1. Hydrocyanation of $HC{\equiv}C(CH_2)_nC{\equiv}CH$ by cyanonickelate[a]

α,ω-Diyne n	Conditions[b]	Conv.[c] %	Yield[d] %	Composition of products (mol%) $CH_3CH(CN)(CH_2)_n$-$CH(CN)CH_3$	$CH_2{=}C(CN)$-$(CH_2)_{n+1}CH_3$	$CH_3CH(CN)$-$(CH_2)_{n+1}CH_3$
3	$NaBH_4$-H_2O	46	28	86	0	16
4		46	28	50	0	50
5		21	8	13	0	83
6		11	2	0	0	100
3	$NaBH_4$-EG	100	96(81)	94	0	6
4		100	86(80)	93	0	7
5		97	76(75)	88	0	12
6		89	78(76)	77	0	23
3	Zn-H_2O	100	85(81)	35	52	13
4		100	98(92)	92	0	8
5		100	90(89)	96	0	4
6		100	99(91)	95	0	5

a) $K_3[Ni(CN)_4]$ (0.8 mmol), KCN (1.6 mmol), diyne (0.8 mmol), at 45 °C, reaction time 6 h. b) $NaBH_4$ (4 mmol) or Zn (4 mmol) in 4 cm³ H_2O or ethylene glycol (EG). c) Determined by GLC analysis, based on added acetylenes. d) GLC and isolated (in parentheses, the reactions were performed in 20 cm³ of solvents) yields, based on added acetylenes.

It is known that in the presence of hydrogen cyanide $K_4[Ni(CN)_4]$ catalyzes hydrocyanation of activated olefins, and nonactivated olefins are hydrocyanated by other zero-valent nickel complexes such as $Ni[P(OR)_3]_4$.[5] In the absence of hydrogen cyanide, cyanonickelate catalyzes hydrogenation of olefins,[6] but not hydrocyanation. It has been proposed that in the hydrocyanation of olefins catalyzed by low-valent transition metal complexes (M) in the presence of HCN, H–M–CN is formed as an active species and olefins react with H–M–CN to form a σ-alkyl–M–CN complex (Eqs. 1 and 2).[5] Previously,[2] we have proposed a mechanism for hydrocyanation of acetylene, in which acetylene reacts directly with $[Ni(CN)_3H]^{2-}$ to form $[Ni(CN)_3(\sigma\text{-vinyl})]^{2-}$ in a similar way as shown in reactions (1) and (2). However, the mechanism cannot explain why olefins are not hydrocyanated in the absence of HCN. The peculiar reactivity of the complex with acetylene seems to be explained by assuming that the hydrocyanation proceeds *via* a (π-acetylene)nickel(0) complex. It is known that low-valent transition metal complexes form fairly stable

$$M + HCN \rightleftharpoons H\text{-}M\text{-}CN \quad (1)$$

$$H\text{-}M\text{-}CN + \rangle C{=}C\langle \longrightarrow \rangle CH\text{-}\underset{|}{C}\text{-}M\text{-}CN \quad (2)$$

Table 2. Characterization of dinitriles

Dinitriles[a] n	Bp θ_b/°C[b]	Ret. time[c] min	IR[d] $\tilde{\nu}$/cm^{-1}	^{1}H NMR[e] δ	^{13}C NMR[e] δ	Analysis Found (%) C	H	N	Calcd (%) C	H	N
3	110/0.3	4.88	2230	1.34 (d, J=7.08 Hz) 1.67 (m) 2.65 (m)	17.9 (q)[f] 24.5 (t) 24.7 (t) 25.3 (d) 25.4 (d) 33.3 (t) 33.5 (t) 122.6 (s, CN)	71.84	9.67	18.36	71.96	9.39	18.65
4	115/0.3	7.33	2230	1.33 (d, J=7.08 Hz) 1.56 (m) 2.64 (m)	18.0 (q) 25.4 (d) 26.5 (t) 33.7 (t) 122.8 (s, CN)	73.38	9.99	16.80	73.26	9.81	17.06
5	140/0.3	11.02	2232	1.32 (d, J=7.08 Hz) 1.54 (m) 2.62 (m)	18.0 (q) 25.4 (d) 26.7 (t) 28.5 (t) 33.8 (t) 122.7 (s, CN)	73.87	10.45	15.95	74.11	10.18	15.71
6	155/0.3	14.97	2230	1.32 (d, J=7.08 Hz) 1.51 (m) 2.62 (m)	18.0 (q) 25.5 (d) 26.9 (t) 28.8 (t) 34.0 (t) 123.0 (s, CN)	74.82	10.64	14.53	74.95	10.48	14.57

a) $CH_3CH(CN)CH_2)_nCH(CN)CH_3$. b) Oven temperature of Kugelrohr apparatus in the vaccum distillation (1 mmHg=133.322 Pa). c) A 3 m column of Silicone SE-30 (10% on Uniport B (60-80 mesh)), carrier gas flow 40 cm^3 min^{-1}, column temp 180 °C. A Shimadzu GC-4CM gas chromatograph was used, and data were analyzed by a Shimadzu Chromatopac E1A. d) ν_{CN}, observed with the neat film. e) Observed in $CDCl_3$, using TMS as an internal reference. JEOL FX-100 NMR spectroscopy was used. f) A mixture of two stereoisomers (the ratio is 2:3).

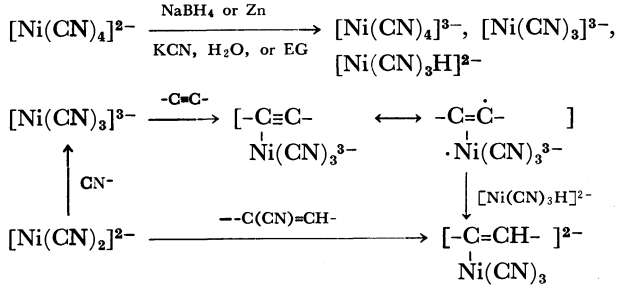

Scheme 1.

π-acetylene complexes.[7] The reaction solution may involve both zero- and univalent cyanonickelate,[6] but formation of the π-acetylene complex with Ni(0) seems more probable than with Ni(I). The coordinated acetylene may have some radical character,[7] and react with $[Ni(CN)_3H]^{2-}$ to form a (σ-vinyl)nickel(II) complex as shown in Scheme 1.

Experimental

The reaction was performed in a three-necked flask equipped with a cold finger at 45 °C under an atmosphere of nitrogen. $K_2[Ni(CN)_4]$ (0.8 mmol, 0.193 g), KCN (1.6 mmol, 0.101 g), $NaBH_4$ (4 mmol, 0.151 g), or Zn (4 mmol, 0.262 g) were placed in the flask. After purging the reaction vessel thoroughly with nitrogen, diyne, $HC{\equiv}C(CH_2)_nC{\equiv}CH$, (0.8 mmol, 0.09 cm^3 ($n$=3), 0.10 cm^3 ($n$=4), 0.12 cm^3 ($n$=5), 0.13 cm^3 ($n$=6), purchased from Tokyo Kasei Co. LTD) and 4 cm^3 of solvent (water or ethylene glycol) were added with syringes through a rubber serum cap, and the solution was stirred magnetically. The yellow reaction solution became dark red when the reaction was complete. The products were extracted with dichloromethane and analyzed by GLC, using a 3 m column of Silicone SE-30, with carrier gas flow of 40 cm^3 min^{-1}, at 180 °C. A larger scale reaction was also performed in a 20 cm^3 solvent, and the products were distilled by using Kugelrohr apparatus (Büchi's Glass Tube Oven KGR-50). Pure products were obtained by a preparative GLC. They gave satisfactory elemental analyses. Their structures were characterized by IR, ^{1}H, and ^{13}C NMR spectroscopy.

References

1) T. Funabiki, Y. Yamazaki, and K. Tarama, *J. Chem. Soc., Chem. Commun.*, **1978**, 63.
2) T. Funabiki and Y. Yamazaki, *J. Chem. Soc., Chem. Commun.*, **1979**, 1110.
3) C. G. Oberberger, P-T. Huang, and T. B. Gibb, Jr., *J. Am. Chem. Soc.*, **75**, 2082 (1953).
4) W. R. Jackson and C. G. Lovel, *J. Chem. Soc., Chem. Commun.*, **1982**, 1231.
5) E. S. Brown, "Aspects of Homogeneous Catalysis," ed by R. Ugo, Reidel, Dordrecht (1974), Vol. 2, p. 57; "Organic Syntheses via Metal Carbonyls," ed by I. Wender and P. Pino, John Wiley & Sons, New York (1977), Vol. 2, p. 655 and refs. therein.
6) B. R. James, "Homogeneous Hydrogenation," John Wiley & Sons, New York (1973), pp. 314—319.
7) S. Otsuka and A. Nakamura, *Adv. Organomet. Chem.*, **14**, 245 (1976).

Synthesis of 2,9,23,30-Tetraoxa[2]paracyclo[2](1,1′)ferroceno[2]paracyclo-[2](1,1′)ferrocenophane-1,10,22,31-tetraone

Akira KASAHARA,* Taeko IZUMI, and Katsuo SAITO

Department of Applied Chemistry, Faculty of Engineering, Yamagata University, Yonezawa 992

(Received February 28, 1983)

Synopsis. Ferrocenophane, in which the two ferrocene rings are linked by ester bonds and *p*-substituted benzene rings, has been synthesized by the reaction of hydroquinone with 1,1′-bis(chloroformyl)ferrocene. The structure of the compound has been studied on the basis of the NMR and electronic spectra.

Although a considerable number of [*m*]ferrocenophanes with one or more bridges joining the two rings of ferrocene nucleus are known, the [*m.n*]ferrocenophane system in which two ferrocene nuclei are joined through two or more bridges has received little attention.[1] However, it has recently been reported that the [2.2]-,[2] [3.3]-,[3] and [5.5]ferrocenophanes[3] showed transannular π-electronic interactions owing to the relative proximity of the two bridging elements. In this report we wish to describe the synthesis of 2,9,23,30-tetraoxa[2]paracyclo[2](1,1′)ferroceno[2]paracyclo[2]-(1,1′)ferrocenophane-1,10,22,31-tetraone (**1**), in which the two ferrocene moieties are linked by ester linkages and *p*-substituted benzene rings.

The reaction of 1,1′-bis(chloroformyl)ferrocene (**2**) with an excess amount of hydroquinone (**3**) led to the formation of 1,1′-bis(*p*-hydroxyphenoxycarbonyl)-ferrocene (**4**), accompanied by a small amount of **1**. The reaction of **2** with **4** afforded **1** in 6% yield. Furthermore, in the presence of trifluoroacetic anhydride, the reaction of ferrocene-1,1′-dicarboxylic acid (**5**) with **3** afforded a mixture of **1** and **4**.

The reference compound, *p*-phenylene bis(ferrocenecarboxylate) (**6**), was prepared by the reaction of (chloroformyl)ferrocene (**7**) with **3**, accompanied by the formation of *p*-hydroxyphenyl ferrocenecarboxylate (**8**).

In the ferrocenophane **1**, the IR spectrum revealed the presence of 1,1′-disubstituted ferrocene and *p*-substituted benzene rings and ester linkage. In ferrocene, the distance between the two cyclopentadienyl rings is 3.32 Å,[4] while the van der Waals separation between the parallel π-systems is 3.345 Å.[5] The molecule of **1** probably exists in the conformation with the phenyl rings approximately parallel to each other and approximately coplanar to the plane of the cyclopentadienyl ring. Structural evidence for the structure of **1** mainly came from its ^{1}H NMR spectrum, which shows two peaks at δ 4.62 (m) and 5.01 (m) for the cyclopentadienyl protons and two peaks at δ 6.70 (d) and 6.99 (d) for the aromatic protons. The aromatic protons in **1** are shifted to higher field than the corresponding protons of the reference compound, *p*-phenylene bis(ferrocenecarboxylate) (**6**) (δ, 7.21 (s)). It has previously been reported that [2]paracyclo[2]-paracyclo[2](1,1′)ferrocenophane-1,9,17-triene, which has the parallel stacked configuration, shows an upfield shift of aromatic protons which lie in close proximity to opposed aromatic moiety.[6] So, the remarkable upfield shift of aromatic protons in **1** is probably due to a diamagnetic shielding effect to the opposed aromatic ring and clearly indicates a pallalel stacked configuration (**1**) rather than a cross-stacked one (**1a**).

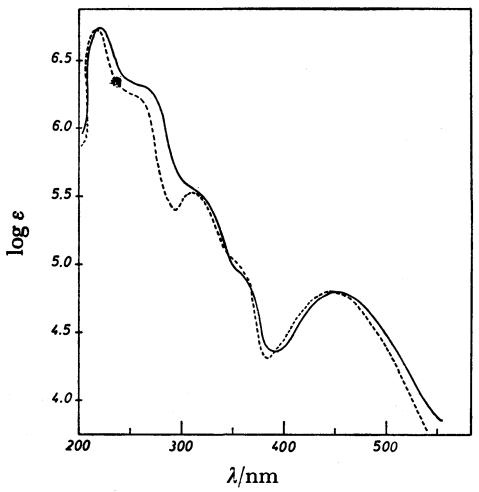

Fig. 1. Electronic spectra of **1** and **6** in tetrahydrofuran.
——: **1**, ----: **6**.

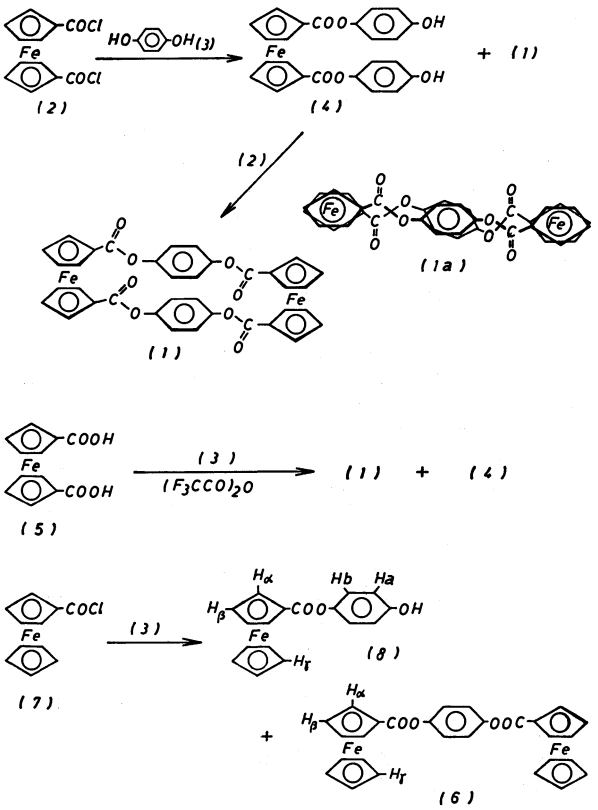

Scheme 1.

The electronic spectra of the ferrocenophane **1** and

the reference compound **6** are shown in Fig. 1. It is well known that the transannular electronic interactions in cyclophanes result in the bathochromic and hyperchromic shifts of absorption bands in electronic spectra.[7] The electronic spectrum of **1** showed somewhat bathochromic and hyperchromic shifts and an unambiguous broadening in a range 220—300 nm, compared with those of the reference compound **6**. This result may be due to transannular π-electronic interactions between the two aromatic chromophores in **1**. On the other hand, the electronic spectrum of ferrocene has two main absorptions at 325 and 440 nm, and it has been found that it is the 440 nm band which is most affected by the ferrocene ring tilt.[8] The electronic spectrum of **1**, in 330—450 nm region, is closely similar to those of open chain model **6**. This suggests that, in **1**, no ferrocene ring tilt distortion occurs.

Experimental

Measurements and Materials. All melting points are uncorrected. All reactions were performed under nitrogen. IR spectra were measured using a Hitachi 260-10 spectrophotometer. ^{1}H NMR spectra were obtained at 90 MHz with a Hitachi R-22 spectrometer using TMS as the internal standard. Mass spectra were recorded with a Hitachi RMU-6M spectrometer and electronic spectra with a Hitachi 200-10 spectrophotometer.

1,1′-Bis(chloroformyl)ferrocene (**2**)[9] and chloroformylferrocene (**7**)[10] were prepared by the methods described in the literature.

*The Reaction of 1,1′-Bis(chloroformyl)ferrocene (**2**) with Hydroquinone (**3**).* To a solution of **3** (6.93 g, 63 mmol) in dry acetonitrile (50 cm^3) was added dropwise a solution of **2** (6.52 g, 21 mmol) in dry benzene over 24 h under refluxing. After an additional 70 h period of reflux, the mixture was evaporated under reduced pressure. The reddish residue was chromatographed on silica gel.

The first fraction, eluted with chloroform–acetone (5:1) and followed by evaporation and recrystallization from ethanol, afforded orange crystals (3.65 g, 38% yield). These were determined to be **4** (mp 226—228 °C (decomp). IR (KBr): 3370 (–OH), 1690 (ester), 3100, 805 (1,1′-disubstituted ferrocene ring), and 865 cm^{-1} (*p*-substituted benzene ring). ^{1}H NMR (acetone-d_6): δ=4.68 (t, 4H, Hβ), 5.01 (t, 4H, Hα), 6.83 (d, J=9 Hz, 4H, Ha), 7.05 (d, J=9 Hz, 4H, Hb), and 8.49 (b-s, 2H, –OH). Found: C, 62.68; H, 3.81%; M$^+$, 458. Calcd for $C_{24}H_{18}FeO_6$: C, 62.90; H, 3.95%; M, 458.

The second fraction, eluted with chloroform-acetone (5:1) and followed by evaporation and recrystallization from benzene, afforded reddish orange crystals, mp 222—224 °C (decomp) (0.12 g, 0.82% yield). These were determined to be **1**. IR (KBr): 1720 (ester), 3100, 800 (1,1′-disubstiuted ferrocene ring), and 850 cm^{-1} (*p*-substituted benzene ring). ^{1}H NMR (tetrahydrofuran-d_8): δ=4.62 (m, 8H, Hβ), 5.01 (m, 8H, Hα), 6.70 (d, J=9 Hz, 4H, Ar–H), and 6.99 (d, J=9 Hz, 4H, Ar–H). Found: C, 61.93; H, 3.35%; M$^+$, 696. Calcd for $C_{36}H_{24}Fe_2O_8$: C, 62.09; H, 3.47%; M, 696.

*The Reaction of 1,1′-Bis(chloroformyl)ferrocene (**2**) with* 1,1′-*Bis(*p*-hydroxyphenoxycarbonyl)ferrocene (**4**).* The reaction of **2** (3.19 g, 10.3 mmol) with **2** (4.39 g, 9.6 mmol) was carried out in the same way as described above, and the ferrocenophane **1** was obtained in 6% yield.

*The Reaction of Hydroquinone (**3**) with Ferrocene-1,1′dicarboxylic Acid (**5**).* At room temperature, the solution of **3** (2.20 g, 20 mmol) in dry acetonitrile (25 cm^3) was added to the mixture of **5** (2.75 g, 10 mmol) and trifluoroacetic anhydride (5 cm^3) in dry benzene (30 cm^3). After an additional 30 h period of stirring, the solution was evaporated *in vacuo* and the residue was extracted with chloroform. The extracts were washed with 5% sodium hydrogencarbonate solution and then with brine, and the solvent was removed. The residue was purified by column chromatography on silica gel (chloroform–acetone (5:1)) to give **2** (25% yield) and 1 (11% yield).

*p-Phenylene Bis(ferrocenecarboxylate) (**6**).* The reaction of chloroformylferrocene (**7**) (9.92 g, 40 mmol) with **3** (1.84 g, 16.7 mmol) was carried out in the same way as has been described for the reaction of **2** with **3**, and the products were separated by chromatography on silica gel.

The first fraction, eluted with chloroform gave *p*-hydroxyphenyl ferrocenecarboxylate (**8**) as orange crystals, mp 179—180 °C, in 20% yield. IR (KBr): 3400 (–OH), 1690 (ester), 3100, 1100, 1000, 800 (monosubstituted ferrocene ring), and 850 cm^{-1} (*p*-substituted benzene ring). ^{1}H NMR (acetone-d_6): δ=4.30 (s, 5H, Hγ), 4.54 (t, 2H, Hβ), 4.92 (t, 2H, Hα), 6.87 (d, J=8 Hz, 2H, Ha), 7.05 (d, J=8 Hz, 2H, Hb), and 8.48 (b-s, 1H, –OH). Found: C, 63.30; H, 4.29%; M$^+$, 322. Calcd for $C_{17}H_{14}FeO_3$: C, 63.38; H, 4.38%; M, 322.

The second fraction, eluted with chloroform gave **6** as reddish orange crystals (mp 183—184 °C (decomp) in 40% yield. IR (KBr): 1725 (ester), 3100, 1100, 1000, and 800 (monosubstituted ferrocene ring). ^{1}H NMR ($CDCl_3$): δ= 4.29 (s, 10H, Hγ), 4.51 (t, 4H, Hβ), 4.97 (t, 4H, Hα), and 7.21 (s, 4H, Ar–H). Found: C, 62.83; H, 2.58%; M$^+$ 534. Calcd for $C_{28}H_{22}Fe_2O_4$: C, 62.95; H, 2.64%; M, 534.

References

1) G. B. Shul'pin and M. I. Rybinskaya, *Usp. Khim.*, **43**, 1524 (1974).

2) A. Kasahara and T. Izumi, *Chem. Lett.*, **1978**, 21.

3) A. Kasahara, T. Izumi, and I. Shimizu, *Chem. Lett.*, **1979**, 1317.

4) J. D. Dunitz, L. E. Orgel, and A. Rich, *Acta Crystallogr.*, **9**, 373 (1956).

5) G. E. Bacon, *Acta Crystallogr.*, **4**, 558 (1951).

6) A. Kasahara, T. Izumi, I. Shimizu, T. Oikawa, H. Umezawa, and I. Hoshino, *Bull. Chem. Soc. Jpn.*, **56**, 1143 (1983).

7) D. J. Cram, N. L. Alliger, and H. Steinberg, *J. Am. Chem. Soc.*, **76**, 6132 (1963).

8) T. H. Barr and W. E. Watts, *Tetrahedron*, **24**, 6111 (1968).

9) F. W. Knobloch and W. H. Rauscher, *J. Polym. Sci.*, **54**, 651 (1961).

10) E. M. Acton and R. M. Silverstein, *J. Org. Chem.*, **24**, 1487 (1959).

2-(4-Chlorophenylseleno)-2-butenal as a New Dienophile for Diels-Alder Reaction

Kenji UNEYAMA, Kunikazu TAKANO, and Sigeru TORII*
Department of Industrial Chemistry, School of Engineering, Okayama University, Okayama 700
(Received April 18, 1983)

Synopsis. Diels-Alder reaction of 2-(4-chlorophenylseleno)-2-butenal with butadiene, isoprene, *trans*-1,3-pentadiene, and cyclopentadiene provided the corresponding adducts in 80—90% yields, which were subsequently transformed into cyclohexadienal derivatives.

Diels-Alder reactions of α,β-unsaturated carbonyl compounds have been extensively studied and well reviewed.[1] In the transition state a carbonyl group interacts significantly with π-bond of a diene giving an endo-product in preference to the exo-product.[1,2] Meanwhile, an α-substituent of α,β-unsaturated carbonyl compounds affects the reaction rate and regio- and stereoselectivity in both steric and electronic senses.[3] However, no report on the effect of selenium group has appeared. We describe here a prominent reactivity of 2-(4-chlorophenylseleno)-2-butenal (**1**) in Diels-Alder reaction with dienes.

Results and Discussion

The seleno enal **1** was prepared by the electrochemical hydroxyselenenylation of 3-butyn-2-ol in acetonitrile–water in 87% yield.[4] The Diels-Alder reaction of **1** with butadiene proceeded at 115 °C, affording a normal cycloadduct **4** (81%) along with 1,4-cycloadduct **5** (9%).[5] The aluminum chloride-catalyzed reaction of **1** in dichloromethane proceeded smoothly at room temperature to give **4** (80%) as a sole product. In contrast to the successful cycloaddition of **1**, crotonaldehyde provided the desired adduct in 40% yield in similar reaction conditions (120 °C, 40 h), demonstrating that arylseleno group promotes the cycloaddition despite of the steric bulkyness. The usual oxidative deselenenylation of **4** provided the corresponding dienal **6** (89%).[6] Likewise, the reaction of **1** with isoprene provided a mixture of regioisomers in 92% yield (**7**:**8**=70:30). The structures of **7** and **8** were confirmed by the transformation into dienals **9** and **10**, respectively. The aluminum chloride-catalyzed reaction preferentially led to the formation of **7** (**7**:**8**=96:4). Oxidative deselenenylation of **7** provided **9** (95%, purity 99% by VPC). The apparent catalytic effect for the product selectivity with Lewis acids was consistent with those observed in the Diels-Alder reaction with acrylaldehyde and methyl vinyl ketone.[7] The reaction of **1** with *trans*-1,3-pentadiene gave two stereoisomers **11** and **12**.[8] Oxidative deselenenylation of a mixture of **11** and **12** gave dienal **13** (75%) which was subsequently dehydrogenated by the action of DDQ in a refluxing benzene, affording 2,6-dimethylbenzaldehyde in 66% yield.[9]

The selenide **1** added to cyclopentadiene, affording exo adduct **14** as a major product along with endo adduct **15** (**14**:**15**=62:38). The stereochemistry of **14** was elucidated by the examination of ^{1}H and ^{13}C NMR chemical shifts (Scheme 2). Consequently, methyl

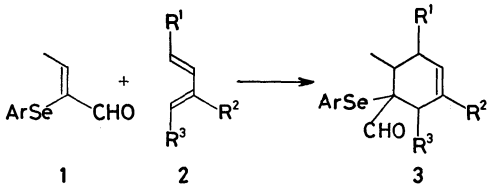

1 2 3

Scheme 1.

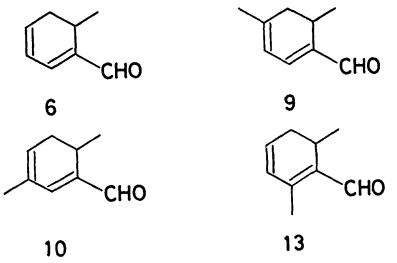

6 9 10 13

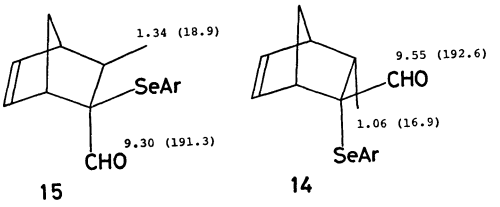

15 14

Scheme 2.

proton on C-3 of **15** was deshielded and in turn that of **14** was shielded. Taking into account of the endo preference in cycloaddition of cyclopentadiene with acrylaldehyde[2] and methyl acrylate,[10] the observed exo preference is quite unexpected. However, it is plausible that divalent selenide group would interact with π-bond of dienes as an electron accepting moiety.

Experimental

2-(4-Chlorophenylseleno)-2-butenal (1). A mixture of 3-butyn-2-ol (55% in water, 1.66 g, 13.0 mmol), bis(4-chlorophenyl) diselenide (495 mg, 1.3 mmol), Et_4NClO_4 (27 mg, 0.11 mmol), and concd H_2SO_4 (90 mg, 0.9 mmol) dissolved in MeCN (18 ml) and H_2O (3 ml) was electrolyzed at 65 °C under a constant current (3.3 mA/cm^2) for 58.5 h (16.8 F/mol) using platinum foils as electrodes in an undivided cell. Sat. $NaHCO_3$ (3 ml) was added. The organic layer was extracted with AcOEt. The extracts were washed with brine, dried over Na_2SO_4, and concentrated *in vacuo*. The residue was chromatographed (SiO_2) to give **1** as a pale yellow oil (585 mg, 87%): bp 90 °C/0.02 mmHg; ^{13}C NMR δ 190.3 (d), 158.6 (d), 136.9 (s), 133.0 (d), 132.7 (s), 129.2 (d), 127.7 (s), 19.0 (q); ^{1}H NMR δ 9.42 (s, 1H), 7.53—7.11 (m, 5H), 2.21 (d, J=4.6 Hz, 3H); IR (neat) 2720, 2675 (CHO), 1698 (C=O), 1617 cm^{-1} Found: C, 46.36; H, 3.48%. Calcd for $C_{10}H_9OClSe$: C, 46.27; H, 3.49%.

Thermal Diels-Alder Reaction of 1 with Dienes. A mixture of **1** (300 mg, 0.385 mmol), diene **2** (7.7 mmol) and

Table 1. Thermal and aluminum-catalyzed Diels-Alder reaction of 1[a]

Entry	Diene	Conditions			Products
		Temp/°C	Time/h	Solvent	Yield/% (Isomer ratio)
1		115	42.5	none	90(90 : 10)
		r. t.	42	CH_2Cl_2[b]	4 5 80(100 : 0)*
2		115—125	39	none	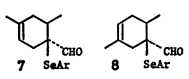 92(70 : 30)
		r. t.	13	CH_2Cl_2[c]	7 8 87(96 : 4)*
3		125—130	39	toluene	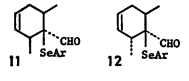 92(74 : 26)
					11 12
4		115—125	32.5	none	14 15 83(62 : 38)
		r. t.	17	CH_2Cl_2[b]	76(53 : 47)*

a) The results of aluminum chloride-catalyzed reaction were described on the bottom line of each entry (*). Ar=4-chlorophenyl. b) 0.4 equiv of $AlCl_3$ to **1**. c) 0.2 equiv of $AlCl_3$ to **1**.

2,5-di-*t*-butylhydroquinone (30 mg, 0.135 mmol) in a sealed glass tube was heated in an oil bath. After evaporating the volatiles the residue was chromatographed (SiO_2).

*6-Methyl-1-(4-chlorophenylseleno)-3-cyclohenecarbaldehyde (**4**).* Bp 95 °C/0.015 mmHg; ^{1}H NMR δ 9.24 (s, 1H), 7.54—7.23 (m, 4H), 5.78—5.46 (m, 2H), 2.41—1.70 (m, 5H), 1.28 (d, J=6.9 Hz, 3H); IR (neat) 3020, 2795, 2695, 1705, 1645 cm^{-1}. Found; C, 53.72; H, 4.86%. Calcd for $C_{14}H_{15}$OClSe; C, 53.61; H, 4.82%.

*3,4-Dihydro-4-methyl-5-(4-chlorophenylseleno)-2-vinyl-2H-pyran (**5**).* Bp 98 °C/0.01 mmHg; ^{1}H NMR δ 7.46—7.07 (m, 4H), 6.96 (d, J=2.0 Hz, 1H), 6.81 (o, J_1=16.0 Hz, J_2=10.0 Hz, J_3=6.0 Hz, 1H), 6.32 (d, J=16.0 Hz, 1H), 6.18 (d, J=10.0 Hz, 1H), 4.56—4.30 (m, 1H), 2.62—2.26 (m, 1H), 2.26—1.34 (m, 2H), 1.05 (d, J=6.6 Hz, 3H): IR (neat) 3075, 1640, 1610, 1465, 1150 cm^{-1}. Found: C, 53.72; H, 4.84%. Calcd for $C_{14}H_{15}$OClSe: C, 53.61; H, 4.82%.

*4,6-Dimethyl-1-(4-chlorophenylseleno)-3-cyclohexenecarbaldehyde (**7**).* Bp 96—102 °C/0.02 mmHg; ^{1}H NMR δ 9.21 (s, 1H), 7.63—7.17 (m, 4H), 5.43—5.21 (m, 1H), 2.39—1.48 (m, 5H), 1.61 (br s, 3H), 1.25 (d, J=6.8 Hz, 3H); IR ($CHCl_3$) 2790, 1698, 1379 cm^{-1}. Found: C, 55.00; H, 5.25%. Calcd for $C_{15}H_{17}$OClSe: C, 54.98; H, 5.23%.

*3,6-Dimethyl-1-(4-chlorophenylseleno)-3-cyclohexenecarbaldehyde (**8**).* Bp 96—102 °C/0.02 mmHg; ^{1}H NMR δ 9.23 (s, 1H), 7.55—7.07 (m, 4H), 5.41—5.15 (m, 1H), 2.39—1.46 (m, 5H), 1.66 (br s, 3H), 1.24 (d, J=6.8 Hz, 3H); IR ($CHCl_3$) 2710, 1700, 1382 cm^{-1}. Found: C, 55.00; H, 5.25%. Calcd for $C_{15}H_{17}$OClSe: C, 54.98; H, 5.23%.

*4,6-Dimethyl-1,3-cyclohexadienecarbaldehyde (**9**).* Bp 93 °C/10 mmHg; ^{1}H NMR δ 9.51 (s, 1H), 6.73 (d, J=5.6 Hz, 1H), 6.08—5.91 (m, 1H), 2.90 (quint, J=8 Hz, 1H), 2.52 (q, J_1=17 Hz, J_2=9 Hz, 1H), 2.02 (d, J=17 Hz, 1H), 1.94 (br s, 3H), 0.95 (s, 3H); IR (neat) 2700, 1668, 1638 cm^{-1}. Found: C, 79.24; H, 8.91%. Calcd for $C_9H_{12}O$; C, 79.37; H, 8.88%.

*3,6-Dimethyl-1,3-cyclohexadienecarbaldehyde (**10**).* Bp 92 °C/10 mmHg; ^{1}H NMR δ 9.55 (s, 1H), 6.61 (br s, 1H), 5.99—5.79 (m, 1H), 3.00—1.79 (m, 3H), 1.89 (br s, 3H), 0.94 (d, J=6.8 Hz, 3H); IR (neat) 2695, 1675, 1646 cm^{-1}. Found: C, 79.24; H, 8.91%. Calcd for $C_9H_{12}O$: C, 79.37; H, 8.88%.

*(1RS,2SR,6RS)-2,6-Dimethyl-1-(4-chlorophenylseleno)-3-cyclohexenecarbaldehyde (**11**).* Bp 100—110 °C/0.02 mmHg: ^{1}H NMR δ 9.61 (s, 1H), 7.54—7.24 (m, 4H), 5.76—5.46 (m, 2H), 2.70—1.45 (m, 4H), 1.24 (d, J=8.0 Hz, 3H), 1.21 (d, J=7.0 Hz, 3H); IR ($CHCl_3$) 2710, 1700, 1387, 1337, 1365 cm^{-1}. Found: C, 55.02; H, 5.24%. Calcd for $C_{15}H_{17}$OClSe: C, 54.98; H, 5.23%.

*(1RS,2RS,6RS)-2,6-Dimethyl-1-(4-chlorophenylseleno)-3-cyclohexenecarbaldehyde (**12**).* Bp 100—110 °C/0.02 mmHg; ^{1}H NMR δ 9.14 (s, 1H), 7.54—7.19 (m, 4H), 5.81—5.40 (m, 2H), 2.78—1.46 (m, 4H), 1.36 (d, J=7.8 Hz, 3H), 1.34 (d, J=7.4 Hz, 3H); IR ($CHCl_3$) 2710, 1705, 1694, 1386, 1374, 1363 cm^{-1}. Found: C, 55.02; H, 5.24%. Calcd for $C_{15}H_{17}$OClSe: C, 54.98; H, 5.23%. The stereochemical assignment of **11** and **12** may be reversed.

*2,6-Dimethyl-1,3-cyclohexadienecarbaldehyde (**13**).* Bp 95 °C/10 mmHg; ^{1}H NMR δ 10.12 (s, 1H), 6.24 (o, J_1=10.0 Hz, J_2=6.0 Hz, J_3=3.0 Hz, 1H), 5.96 (q, J_1=10.0 Hz, J_2=3.0 Hz, 1H), 3.11—2.71 (m, 1H), 2.66—1.60 (m, 2H), 2.21 (s, 3H), 0.91 (d, J=7.0 Hz, 3H); IR (neat) 2740, 1663, 1640 cm^{-1}; Found: C, 79.25; H, 8.90%. Calcd for $C_9H_{12}O$: C, 79.37; H, 8.88%.

*(1RS,2RS,3RS,4RS)-3-Methyl-2-(4-chlorophenylseleno)bicyclo[2.2.1]hept-5-ene-2-carbaldehyde (**14**).* Bp 101—108 °C/0.02 mmHg; ^{13}C NMR δ 192.6 (d), 139.1(s), 138.3 (d), 137.6 (d), 135.6 (d), 129.3 (d), 124.1 (s), 70.9 (s), 48.4 (d), 47.7 (t), 47.7 (d), 37.7 (d), 16.9 (q); ^{1}H NMR δ 9.55 (s, 1H), 7.60—7.22 (m, 4H), 6.53—6.27 (m, 2H), 3.14—3.00 (m, 1H), 2.96—2.77 (m, 1H), 2.68—2.36 (m, 1H), 1.74—1.53 (m, 1H), 1.38—1.17 (m, 1H), 1.06 (d, J=7.1 Hz, 3H): IR ($CHCl_3$) 2715, 1698, 1389, 1378 cm^{-1}; Found: C, 55.37; H, 4.66%. Calcd for $C_{15}H_{15}$OClSe: C, 55.32; H, 4.64%.

*(1RS,2RS,3RS,4RS)-3-Methyl-2-(4-chlorophenylseleno)bicyclo[2.2.1]hept-5-ene-2-carbaldehyde (**15**).* Bp 101—108/0.02 mmHg; ^{13}C NMR δ 191.3 (d), 139.1 (d), 139.1 (d), 136.1 (s), 134.0 (d), 129.4 (d), 124.3 (s), 70.4 (s), 50.3 (d), 48.1 (d), 44.8 (t), 38.3 (d), 18.9 (q);^{1}H NMR δ 9.30 (s, 1H), 7.65—7.20 (m, 4H), 6.38—6.17 (m, 1H), 6.12—5.90 (m, 1H), 2.99—2.76 (m, 1H), 2.75—2.54 (m, 1H), 2.50—2.24 (m, 1H), 2.30—1.97 (m, 1H), 1.80—1.51 (m, 1H), 1.34 (d, J=7.1 Hz, 3H); IR ($CHCl_3$) 2715, 1699, 1390, 1380 cm^{-1}. Found: C, 55.37; H, 4.66%. Calcd for $C_{15}H_{15}$OClSe: C, 55.32; H, 4.64%.

The authors are grateful to the Ministry of Education, Science and Culture for a financial support by a Grant-in-Aid (No. 57118002).

References

1) H. L. Holmes, *Org. React.*, Vol. IV, 60 (1965); Vol. IV, 1 (1965); M. C. Kloetzel, M. Petrzilka, and J. I. Grayson, *Synthesis*, **1981**, 753; W. Oppolzer, *Angew. Chem., Int. Ed. Engl.*, **16**, 10 (1977).

2) K. Alder, G. Stein, M. Liebmann, and E. Rolland, *Ann. Chem.*, **514**, 197 (1934).

3) 2-Alkylpropenal, I. Yamamoto and T. Tsuruta, *Kogyo Kagaku Zasshi*, **69**, 928 (1966); 2-Phenylthio-2-cyclopentenone, S. Knapp, R. Lis, and P. Michna, *J. Org. Chem.*, **46**, 624 (1981); 3-(phenylthio)-3-buten-2-one, K. Takagi, M. Yamada, and K. Negoro, *ibid.*, **47**, 5246 (1982).

4) K. Uneyama, K. Takano, and S. Torii, *Tetrahedron Lett.*, **23**, 1161 (1982).

5) A similar 1,4-cycloaddition was observed in the thermal reactions of 3-(phenylthio)-3-buten-2-one (Ref. 3) and acrylaldehyde. R. E. Ireland and D. Häbich, *Tetrahedron Lett.*, **21**, 1389 (1980).

6) J. M. McIntosh, H. Khalil, and D. W. Pillon, *J. Org. Chem.*, **45**, 3436 (1980).

7) P. Yate and P. Eaton, *J. Am. Chem. Soc.*, **82**, 4436 (1960); E. F. Lutz and G. M. Bailey, *ibid.*, **86**, 3899 (1964).

8) The stereochemistry was tentatively assigned.

9) M. Ryang, I. Rhee, and S. Tsutsumi, *Bull. Chem. Soc. Jpn.*, **37**, 341 (1964).

10) J. Sauer and J. Kredel, *Tetrahedron Lett.*, **1966**, 731

Convenient Preparation of Tetraarylphosphonium Halides

Toshihiko MIGITA,* Tohru NAGAI, Kazuhiko KIUCHI, and Masanori KOSUGI
Department of Chemistry, Faculty of Technology, Gunma University, Kiryu, Gunma 376

(Received May 6, 1983)

Synopsis. Tetraarylphosphonium halides, particularly iodides, can be conveniently prepared by the Pd-catalyzed reaction of aryl halides and triarylphosphines in good yields.

There have been known a few reactions which can be used for preparation of tetraarylphosphonium salts:

$$PhI + PPh_3 \xrightarrow[65\,°C,\ 46\,h]{h\nu} Ph_4P^+I^- \qquad 23\%^{1)}$$

$$PhN(NO)COCH_3 + PPh_3 \xrightarrow[PhH]{\text{aq. HBr}} Ph_4P^+Br^- \qquad 32\%^{2)}$$

$$PhMgBr + PhBr + PPh_3 \xrightarrow{CoCl_2} Ph_4P^+Br^- \qquad 55\%^{2)}$$

These reactions, which belong to a reaction of aryl radical with triarylphosphine, give relatively low yields, and the experimental procedures are not simple.

Previously aryl iodide and bromide activated by zero-valent palladium were shown to undergo nucleophilic substitution with soft nucleophiles such as thiolate and triphenylphosphine.[3] Here we wish to note utility of the Pd-catalyzed reaction of aryl halide with triarylphosphine for the preparation of tetraarylphosphonium halides.

$$Ar'X + PAr_3 \xrightarrow{[Pd]} Ar'P^+Ar_3X^-$$

The reaction takes place by heating a mixture of equimolar reactants, 1 mol% of $Pd(PPh_3)_4$ or more conveniently $Pd(OAc)_2$, and the solvent (aromatic hydrocarbon) at 120 °C for 25 h. The product, tetraarylphosphonium salt insoluble in the solvent, deposites as fine crystals, which can be easily collected and purified by recrystallization. Table shows a number of phosphonium salt obtained by using $Pd(OAc)_2$ as a catalyst.

The following tendencies about scope and limitation of the present method can be seen. Among halides, the best results were obtained by using aryl iodides as substrates. The reactions of aryl bromides gave only low yields and aryl chlorides hardly reacted with triarylphosphine under the conditions. Electron releasing substituents appear to enhance the reactivities of aryl halides. For example, *p*-methoxyiodobenzene reacts smoothly with triphenylphosphine even at lower temperature (100 °C), giving the corresponding quaternary salt in 96% yield. Reaction of negatively substituted iodobenzenes afforded poor yields such as given without the catalyst.

Perhaps due to steric hindrance, ortho substituents on aryl halide as well as triarylphosphine retard the reaction, giving quite low yields of phosphonium salts. Triarylphosphines bearing substituents which enhance the nucleophilicities of the phosphines gave better results.

TABLE 1. TETRAARYLPHOSPHOONIUM HALIDE, $YC_6H_4P^+(C_6H_4Z)_3X^-$ PREPARED FROM HALDE, YC_6H_4X AND TRIARYLPHOSPHINE, $P(C_6H_4Z)_3$

X	Y	Z	Yield %	Mp θ_m/°C	C (%) Calcd	C (%) Obsd	H (%) Calcd	H (%) Obsd
Cl	H	H	0					
Br	H	H	Trace	288	68.75	68.51	4.81	4.75
	p-CH_3	H	19	177	69.30	68.98	5.12	5.15
	p-NO_2	*p*-CH_3	16[b)]	224d	64.04	64.57	4.98	5.10
I	H	H	98	346 (337)[a)]	61.82	61.80	4.32	4.21
	H	*p*-CH_3	81	197	63.79	63.72	5.15	5.37
	H	*p*-Cl	32	298	50.60	50.73	3.01	3.09
	o-CH_3	H	Trace					
	m-CH_3	H	95	201 (199—201)[a)]	62.52	62.88	4.62	4.49
	p-CH_3	H	100	214 (207—209)[a)]	62.52	62.16	4.62	4.52
	p-CH_3	*p*-CH_3O	100	199	58.96	59.28	4.95	4.87
	o-CH_3O	H	27	168	60.50	60.86	4.47	4.67
	m-CH_3O	H	70	206	60.50	60.40	4.47	4.21
	m-CH_3O	*p*-CH_3	97	161	62.46	62.66	5.24	4.99
	p-CH_3O	H	99	219	60.50	60.22	4.47	4.50
	p-CH_3O	*p*-Cl	76	Very high	50.19	50.07	3.19	3.20
	p-Cl	H	28	212 (216—217)[a)]	57.57	57.47	3.82	3.80

a) Known salts, in Ref. 2. b) N: calcd (%), 2.77; obsd (%), 3.03.

Experimental

Material. Triarylphosphines were prepared by the known method from the corresponding arylmagnesium bromides and trichlorophosphine.[4] Commercially available products of palladium acetates and aryl halides were used without purification.

Procedure. A mixture of aryl halide (2 mmol), triarylphosphine (2 mmol), palladium acetate (0.02 mmol), and 3 cm^3 of a solvent (benzene or toluene) was placed in a tube. The tube was evacuated and sealed, then immersed in a bath kept at 120 °C for 25 h. In the course of the period the catalyst was dissolved and phosphonium salt separated from the solution. The salts were filtered, washed with benzene, and recrystallized from chloroform–benzene. The yield and analytical data of the products obtained by this procedure are listed in Table 1.

In the above procedure, the mixture was heated in an evacuated sealed tube to avoid Pd-catalysed oxidation of the phosphine by air,[5] but refluxing a solution of the reactants and the catalyst in xylene gave similar results. Thus from iodobenzene and triphenylphosphine, tetraarylphosphonium iodide was obtained in 80% yield by the refluxing method.

References

1) J. B. Plumb and C. E. Griffin, *J. Org. Chem.*, **27**, 4711 (1962).
2) L. Horner and H. Hoffmann, *Chem. Ber.*, **91**, 45 (1958).
3) T. Migita, T. Shimizu, Y. Asami, J. Shiobara, Y. Kato, and M. Kosugi, *Bull. Chem. Soc. Jpn.*, **53**, 1385 (1980).
4) F. G. Mann and E. J. Chepine, *J. Chem. Soc.*, **1937**, 527.
5) S. Takahashi, K. Sonogashira, and N. Hagihara, *Nippon Kagaku Zasshi*, **87**, 610 (1966).

Nitrite Substitution on *cis*-Tetraamminediaquacobalt(III) Ion in HNO_2-NO_2^- Buffer Media

Manik Chandra GHOSH and Pradyot BANERJEE*
Department of Inorganic Chemistry, Indian Association for the Cultivation of Science, Jadavpur, Calcutta 700 032, India
(Received July 30, 1982)

Synopsis. The anation of the title complex by NO_2^- was followed spectrophotometrically. The anation proceeds in two steps. A simple second-order rate law applies to each step. No evidence has been furnished for the formation of any nitrito intermeidates.

Studies previously reported by Pearson *et al.*[1] showed that nitrite substitution reactions for pentaammineaquacobalt(III) and *cis*-aquabis(ethylenediamine)nitrocobalt(III) ions involve a nitrosation step followed by an intramolecular rearrangement to give stable nitro derivatives. Rates of the rearrangement reaction were found independent of the concentration of added nitrite. We report here some results from kinetic studies on reactions of *cis*-tetraamminediaquacobalt(III) ion with NO_2^-, which however has provided no evidence for *O*-nitrosation.

The formation of the dinitro complex was followed with a Pye-Unicam spectrophotometer SP8-150 by measuring the growth of its absorption maximum at 440 nm. Spectra of solutions which had ceased reacting were identical at nitrite concentrations exceeding *ca.* 0.04 M (1 M=1 mol dm^{-3}) at a given complex concentration (10^{-3} M) and agreed well with the spectrum of *cis*-tetraamminedinitrocobalt(III),[2] ensuring complete conversion to the product. Conventional pseudo-first-order plots of log $(A_\infty - A_t)$ *vs.* time (where A_t and A_∞ denote the absorbances at time=t and ∞ respectively) gave curved plots, suggestive of a biphasic nature of the reaction (Fig. 1) based on replacement of two coordinated water molecules, and were resolved following Weyh and Hamm.[3] At a constant pH the reaction was first-order dependent on $[NO_2^-]$ in each of the steps (Table 1). Variation of pH in the region 4.0—6.04 had no measurable effect on the first-step reaction rate ($k^{I}_{obsd}=(1.43\pm0.04)\times10^{-3}$ s^{-1} at $[NO_2^-]=0.1$ M, temp =40 °C, and $I=0.2$ M). The rate of the second-step reaction also remained constant upto pH *ca.* 5.6 ($k^{II}_{obsd}=(1.17\pm0.02)\times10^{-4}$ s^{-1} under the identical conditions), but on going above this pH, k^{II}_{obsd} dropped by as much as 30%. Experimental runs above pH 6.04 could not be conducted since the complex was found to decompose to form a brown precipitate.

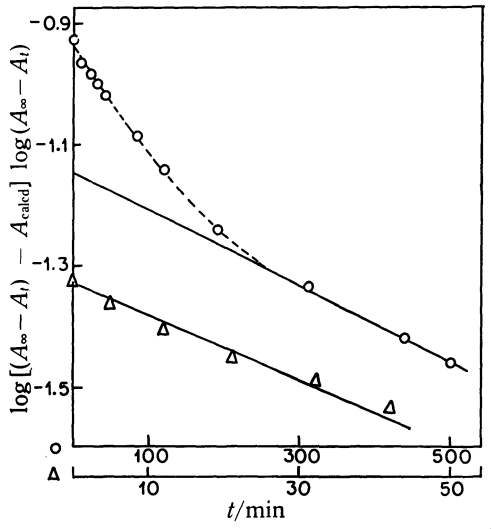

Fig. 1. A typical kinetic plot for the nitrite substitution of *cis*-$[Co(NH_3)_4(H_2O)_2]^{3+}$·[complex], 10^{-3} M; $[NO_2^-]$, 0.1 M; pH, (5.07±0.03); temp, 20 °C; I, 0.2 M ($NaClO_4$).
A_{calcd} at different times are extracted from the linear portion of the curve after extrapolation to zero time.

Except a few runs above pH 5.6, the anion and pH variation results are consistent with the rate law: rate= k[complex]$[NO_2^-]$. This simple rate law for the replacement of H_2O by NO_2^- is of some significance. In many $R_5Co(OH_2)^{3+}$–NO_2^- reactions[1,4] where R is an ammine, a nitrito intermediate is observed and the rate law assumes the form $-d[R_5Co(OH_2)^{3+}]/dt=k$[complex]$[NO_2^-]^2[H^+]$. This is generally the case when the water exchange rate is low and the second-order rate dependence on $[NO_2^-]$ arises from the involvement of N_2O_3. In the present system no nitrito intermediate could be detected and the NO_2^- dependence caused no measurable deviation from the first-order dependence. It may be that under the conditions adopted no formation of nitrito intermediate actually occurs. This points to a different mechanism operating here which involves rupture of the cobalt-oxygen bond. The pK_1[5] of the diaqua species under investigation is 5.69 at 20 °C. On going above pH 4.4, formation of aquahydroxo species starts. The absence of any pH effect on the first-step reaction suggests that both the

TABLE 1. RATE CONSTANTS IN THE NITRITE SUBSTITUTION REACTION OF *cis*-TETRAAMMINEDIAQUACOBALT(III) ION AT 20 °C

$10^2[NO_2^-]$ / M[a]	$10^4 k^{I}_{obsd}$ / s^{-1}	$10^3 k^{I}$ / $M^{-1}s^{-1}$[b]	$10^5 k^{II}_{(obsd)}$ / s^{-1}	$10^4 k^{II}$ / $M^{-1}s^{-1}$
5	1.08	2.16	1.23	2.46
7	1.53	2.19	1.70	2.43
9	1.92	2.13	2.07	2.30
10	2.12	2.12	2.30	2.30
12.5	2.77	2.22	2.90	2.32
15	3.27	2.18	3.30	2.20
17.5	3.77	2.15	3.92	2.24
20	4.13	2.06	4.60	2.30

a) pH=(5.07±0.03) held constant with $[NaNO_2]/[HClO_4]=100$; [complex]=1×10^{-3} M; ionic strength= 0.2 M ($NaClO_4$). b) Under the identical conditions, the second-order rate constants evaluated at 40 °C are $k^{I}=(1.35\pm0.10)\times10^{-2}$ $M^{-1}s^{-1}$ and $k^{II}=(1.19\pm0.04)\times10^{-3}$ $M^{-1}s^{-1}$.

diaqua and aquahydroxo species are kinetically indistinguishable with respect to the NO_2^- substitution. In the anation reaction of *trans*-$[Co(dmgH)_2(NO_2)(OH_2)]$ by NO_2^- ($dmgH^-$=dimethylglyoximate ion), Hague and Halpern[6] have shown two paths, one of which is pH independent (predominant at high pH) and the other pH dependent. The pH-independent path was shown to be first-order in $[NO_2^-]$. The pH-dependent path, though not studied in detail by the authors, has been presumed to be arising from attack of HNO_2 which apparently has stronger nucleophilicity than NO_2^-. The pH dependence on rate obtained for the mononitro species above pH 5.6 in our study may be attributed to the lower reactivity of the corresponding hydroxo species. The pK[5] (25 °C) of the second coordinated water in *cis*-$[Co(NH_3)_4(H_2O)_2]^{3+}$ is 8.0 and coordinated NO_2^- could have some effect for lowering this value significantly. This view is supported by known pK values[7] (25 °C) for closely comparable systems: 8.19 as the pK_2 of *cis*-$[Co(en)_2(H_2O)_2]^{3+}$ and 6.34 as the pK of *cis*-$[Co(en)_2(NO_2)(H_2O)]^{2+}$ (en=ethylenediamine).

Experimental

cis-Tetraamminediaquacobalt(III) perchlorate was prepared by the method described in the literature[8] and spectra of this compound matched well with those reported. Recrystallized sodium nitrite (AR grade) was used. Ionic strength was maintained with sodium perchlorate. Buffering was achieved by adding perchloric acid to sodium nitrite to a constant ratio.

Thanks are due to Dr. Mahesh Prasad Pujari for some technical assistance.

References

1) R. G. Pearson, P. M. Henry, J. G. Bergmann, and F. Basolo, *J. Am. Chem. Soc.*, **76**, 5920 (1954).
2) G. B. Kauffman, S. F. Abbott, S. E. Clark, J. M. Gibson, and R. D. Meyers, *Inorg. Synth.*, **18**, 69 (1978).
3) J. A. Weyn and R. E. Hamm, *Inorg. Chem.*, **8**, 2298 (1969).
4) R. K. Murmann and H. Taube, *J. Am. Chem. Soc.*, **78**, 4886 (1956).
5) G. Schwarzenbach, J. Boesch, and H. Egli, *J. Inorg. Nucl. Chem.*, **33**, 2141 (1971).
6) D. N. Hague and J. Halpern, *Inorg. Chem.*, **6**, 2059 (1967).
7) "Stability Constants of Metal-ion Complexes," ed by L. G. Sillen and A. E. Martell, The Chemical Society, London (1964), Special Publication No. 17, pp. 55, 56.
8) J. Springborg and C. E. Schaffer, *Inorg. Synth.*, **18**, 83 (1978).

 © 1983 The Chemical Society of Japan Bull. Chem. Soc. Jpn., 56, 2873—2876 (1983)

A Photochemical Storage Battery with an *n*-GaP Photoelectrode

Yoshiro YONEZAWA,* Makoto OKAI, Masato ISHINO, and Hiroshi HADA
Department of Industrial Chemistry, Faculty of Engineering, Kyoto University, Yoshida, Sakyo-ku, Kyoto 606
(Received December 27, 1982)

We have constructed a photochemical storage battery with an *n*-GaP Photoelectrode. A two-compartment cell, *n*-GaP|aqueous $K_3[Fe(CN_6]$–$K_4[Fe(CN)_6]$||aqueous $NiSO_4$|Pt, is capable of being charged by the irradiation of the photoelectrode. The current efficiency of nickel deposition on the storage electrode was 80%. When we drew electrical energy out of the dattery, the deposited nickel could act as a Ni electrode in the Ni^{2+} solution. The power efficiency of the storage battery amounted to about 2%. We could recharge the battery more than five times after discharge.

In an earlier paper, we proposed a concept of a solid-state photogalvanic cell.[1] We would now like to introduce a new term; a "photochemical storage battery," as a substitute, because it is less abstract and so less likely to cause unnecessary confusion regarding the concept. Active materials stored photoelectrochemically on the electrode surface can yield electrical energy whenever necessary. We have actually made up four kinds of batteries and found that the TiO_2|aqueous $Ce(SO_4)_2$–$Ce_2(SO_4)_3$||aqueous $AgNO_3$|Pt cell has especially excellent characteristics. Such a regenerative storage of light energy is one of the most remarkable advantages of photochemical storage batteries in contrast to usual photovoltatic cells. This aspect has been pointed out by several investigators recently.[2,3]

Two methods for storing light energy as solid materials on the electrode surface have been reported thus far. One of them, proposed by us,[1] is to use a half-cell of metal ion/metal, such as Ag^+/Ag and Cu^{2+}/Cu, while the other is to use a half-cell of either metal sulfide or metal hydroxide, such as $Ag_2S/Ag,S^{2-}$, $Ni(OH)_2/Ni$, OH^-, and $Cd(OH)_2/Cd,OH^-$, as introduced by Hodes *et al.*[2] and Ang and Sammells.[3] Though the *n*-TiO_2 photoanode is photochemically stable, the band-gap energy (3.05 eV, 405 nm) is rather large; therefore, the incident light available for energy storage is limited to the near-ultraviolet region. In contrast, *n*-GaP has a smaller band-gap energy (2.25 eV, 550 nm), but a photoanode made of it might suffer irreversible decomposition in an electrolyte solution. Recently, Memming has stressed that the anodic dissolution of the illuminated *n*-GaP electrode can be suppressed by adding the $[Fe(CN)_6]^{3-}/[Fe(CN)_6]^{4-}$ couple to the electrolyte at pH=6.5—9.5.[4] As the flat-band potential of *n*-GaP is *ca.* −1.0 V at pH=1 and the standard redox potential of this couple is +0.36 V *versus* a normal hydrogen electrode (NHE), various kinds of metal ion/metal combinations can be used as active materials for the storage electrode in the battery. In this report, we have chosen the Ni^{2+}/Ni couple (−0.25 V *versus* NHE) and tried to improve the power efficiency of the battery by using the *n*-GaP photoanode.

Experimental

The experimental setup of a photochemical storage battery and the procedure were almost the same as those reported previously.[1] A schematic representation of the battery was given in a figure of that paper. Single crystals of *n*-GaP, in the form of wafers 0.2—0.3 mm thick, were provided by the Sanyo Electric Co., Ltd. They were of a 99.999% purity, doped with S at the concentration of $(2—3)\times10^{17}$ cm^{-3}. The *n*-GaP photoelectrode(P) was prepared according to the method of Nakato *et al.*[5] The surface area to be exposed to the electrolyte solution was 1 cm^2. A storage electrode(A) was made of a platinum-black disk 3 cm^2 in area, while the counter electrode(C) was made of platinum and had a 5-cm^2 area. The two compartments were separated by three sheets of ion-exchange membrane(M). Each membrane was 1.7 cm^2 in area and *ca.* 0.2 mm thick. They were CSV (proton-permeable membrane), ACH-45 T (anion-specific membrane), and CSV, provided by the Tokuyama Soda Co., Ltd. Tne electrolyte solution in the compartment of the P- and C-electrodes consisted of aqueous solutions of 0.2 M-K_2SO_4, 0.05 M $K_3[Fe(CN)_6]$, and 0.05 M $K_4[Fe(CN)_6]$, while tnat in the A-electrode compartment consisted of aqueous solutions of 0.05 M K_2SO_4, 0.2 M $NiSO_4$, and 0.06 M $NiCl_2$. In order to keep the pH of the solutions between 6.5—7.0, it was sometimes necessary to add either H_3BO_3 or NH_4Cl to the electrolyte soulution in the A-electrode compartment. All the potentials given in this peper were measured *versus* NHE.

As the light source, a high-pressure 500 W mercury lamp (Ushio Denki Co., Ltd.) was used in combination with a cut-off filter VY-45 (Toshiba Co., Ltd.) and a water filter to select a longer-wavelength light of more than 450 nm. The incidentlight intensity between 450—540 nm was 3.1 mW cm^{-2} according to both ferric oxalate actinometry[6] and photoelectronic measurement by means of a photometer IL-600 (International Light Co., Ltd.). The amount of the Ni atom deposited on the storage electrode was determined by the aid of a Jarrel-Ash AA-780 atomic-absorption spectrophotometer.

Results and Discussion

The polarization curves of the *n*-GaP electrode were measured by using a potentiostat/galvanostat HA-104 (Hokuto Denko Co., Ltd.). The electrolyte solution was composed of K_2SO_4, $K_3[Fe(CN)_6]$, and $K_4[Fe(CN)_6]$, whose concentrations were the same as those used for the photochemical charging of the battery. The typical behavior of the *n*-type semiconductor electrode was observed: the dark current was not evident at an electrode potential more positive than −0.4 V, but it then increased steeply with the cathodic polarization. The anodic photocurrent flowed at an electrode potential more positive than −0.8 V, and

† 1 M=1 mol dm^{-3}.

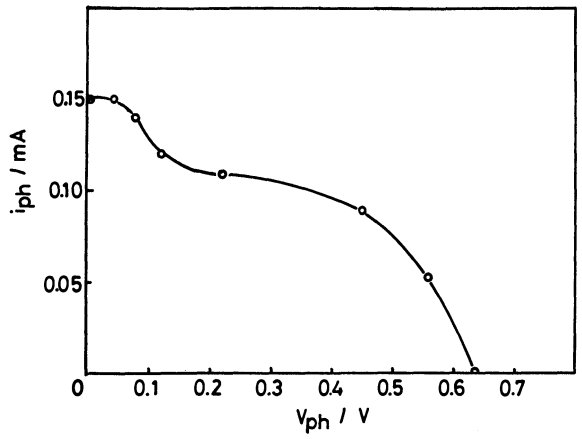

Fig. 1. Curve of photocurrent, i_{ph}, against photovoltage, V_{ph}, for the *n*-GaP battery: *n*-GaP|$K_3[Fe(CN)_6]$–$K_4[Fe(CN)_6]$||Ni^{2+}|Pt.

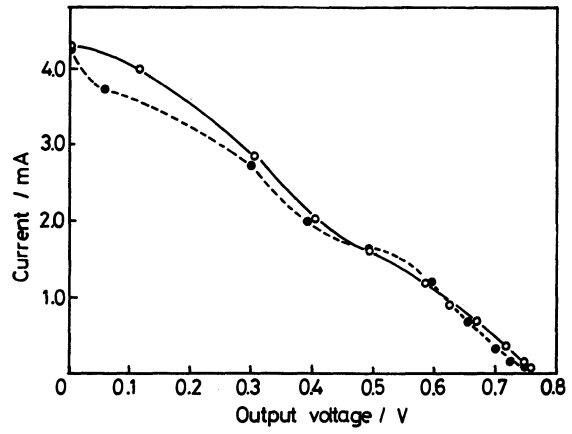

Fig. 2. The current-voltage characteristics of the battery: Pt|$K_3[Fe(CN)_6]$–$K_4[Fe(CN)_6]$||Ni^{2+}|Pt.
○; Photochemical charging, ●; electrochemical charging.

its saturated value was 155 μA cm^{-2}.

Figure 1 shows a curve of the photocurrent against the photovoltage during irradiation. The photocurrent flowed from a storage electrode to the GaP electrode. The net electrochemical reactions are as follows:

$$n\text{-GaP} + h\nu \longrightarrow e^- + p^+, \quad (1)$$

$$Ni^{2+} + 2e^- \longrightarrow Ni, \quad (2)$$

$$K_4[Fe(CN)_6] + p^+ \longrightarrow K_3[Fe(CN)_6], \quad (3)$$

where e^- and p^+ denote an electron and a positive hole respectively. The photocurrent under the short-circuit condition was 0.15 mA; the apparent quantum efficiency (the number of electrons passed per s divided by the number of incident photons for the 450—540 nm region per s) was *ca.* 13%. The photovoltage under the open-circuit condition was 0.63 V. On illuminating the battery for photochemical charging, the potential of the A-electrode shifted from +0.4 V to −0.2 V within 900 s, but after that it remained constant. After the cell had been illuminated for 7200 s (the quantity of electricity flowing was 1.08 C), the A-electrode was switched off from the P-electrode. Stored energy was stable in the dark for more than 24 h under the open-circuit condition. Electrical energy was drawn out by connecting the A- and C-electrodes through the external load resistance(L). We also tried to deposit the Ni atom on the A-electrode by using a galvanostat (electrochemical charging). Under a constant charging current of 2 mA, the potential of the A-electrode shifted from +0.4 to −0.3 V within 60 s, and after that remained constant. The current-voltage curve of the battery charged by 1.0 C in this manner was measured by changing the load resistance and was then compared with that charged photochemically (Fig. 2). The two cells show almost the same features: a short-circuit current of 4.3 mA and an open-circuit voltage of 0.75 V. The observed open-circuit voltage is somewhat larger than the difference in the standard electrode potential between Ni^{2+}/Ni and $[Fe(CN)_6]^{3-}$/$[Fe(CN)_6]^{4-}$. The discharge current with the load resistance was initially constant, but it gradually decreased with the discharge time. We could hardly draw any electrical energy out of the battery either before charging or after a nearly

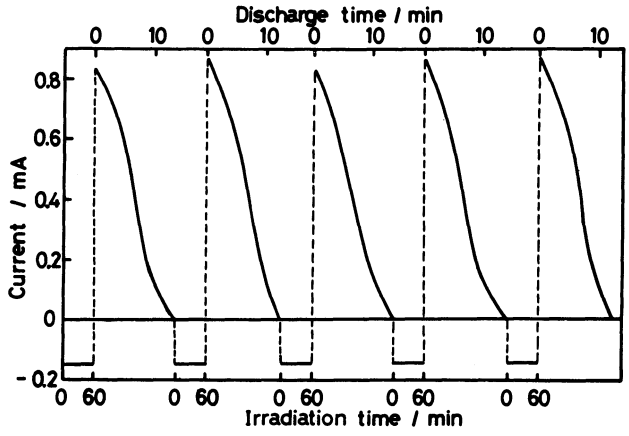

Fig. 3. Current of the battery during photochemical charging upon illumination of the *n*-GaP electrode and during discharge through A- and C-electrodes. The current of negative value corresponds to charging current when 2 Ω external resistance is inserted between P- and A-electrodes and that of positive value corresponds to discharge current with 700 Ω load.

complete discharge. The change in the performance of the battery during the cycle of photochemical charging and discharge has been examined (Fig. 3). The battery was capable of being recharged more than five times after discharge.

We have also examined the dependence of the amount of deposited Ni, Q_{Ni}, on the quantity of electricity passed through while charging the battery, Q_{ch}. The quantity of electricity flowing during irradiation was determined by integrating the total photocurrent. Figure 4 shows the linear relation observed for both photochemical and electrochemical charging. It is shown that the Ni deposition proceeds in this battery with a current efficiency of 80%. It should be noted, however, that the efficiency was considerably lowered when we used a platinum disk instead of the platinum-black disk as the A-electrode.

We have also investigated the behavior of the battery

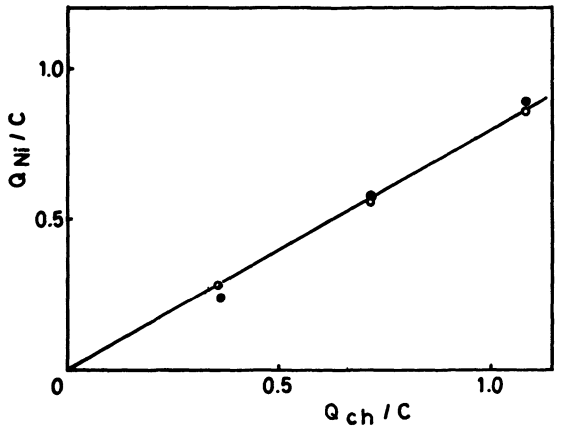

Fig. 4. Relation between the quantity of electricity flowed during charging, Q_{ch}, and the amount of Ni deposited on a platinum-black electrode, Q_{Ni}.
○; Photochemical charging, ●; electrochemical charging.

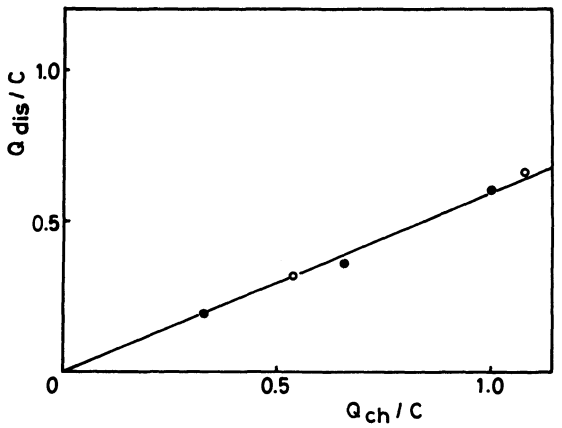

Fig. 5. Dependence of the quantity of electricity flowed during discharge, Q_{dis}, on Q_{ch}.
○; Photochemical charging, ●; electrochemical charging.

during discharge. After photochemical charging, the battery was discharged for an appropriate period, and the quantity of electricity flowing during that period, as determined from the discharge current, was compared with the amount of dissolved Ni. The latter value was evaluated approximately by subtracting the amount of Ni left on the A-electrode after discharge from the hypothetical amount of Ni deposited while charging the battery, *i.e.*, 80% of the quantity of electricity flowing during charging. Under such an approximation, it was deduced that the amount of Ni dissolved was almost the same as the quantity of electricity flowing during discharge; *i.e.*, Ni in quantities of about 0.0, 0.20, and 0.45 C was dissolved during the discharge of the battery by amounts of 0.0, 0.22, and 0.42 C respectively. We could thus determine that the deposited Ni at the A-electrode acts as a Ni electrode in the Ni^{2+} solution. Figure 5 shows the linear relation between the quantity of electricity flowing during discharge, Q_{dis}, and that during charging, Q_{ch}. In this case, Q_{dis} was determined by integrating the total current over the discharge time until the current fell off to *ca.* 1% of its initial value. Though the conversion efficiency of Q_{ch} to Q_{dis} seems to be sensitive to the discharge condition,[1] about 55% of the Q_{dis} could be drawn out of the battery as an effective discharge current. We suppose that the discrepancy between the efficiencies of conversion from Q_{ch} to Q_{Ni} and from Q_{ch} to Q_{dis} is due to the somewhat poor discharge condition; *i.e.*, some of the active materials stored during charging are still left on the A-electrode surface after discharge. We can also not overlook the possibility that the imperfect selectivity of on permeation of the separator(M) allows the self-discharge reaction to proceed to some extent during the prolonged discharge. According to a study of the electrochemical behavior of Ni in aqueous solutions,[7] it is likely that a passive film is formed in neutral and alkaline solutions under suitable conditions. However, judging from the fairly fine features, the formation of such a film seems not to be very likely in this battery. Nevertheless, it is possible that the electrode reaction

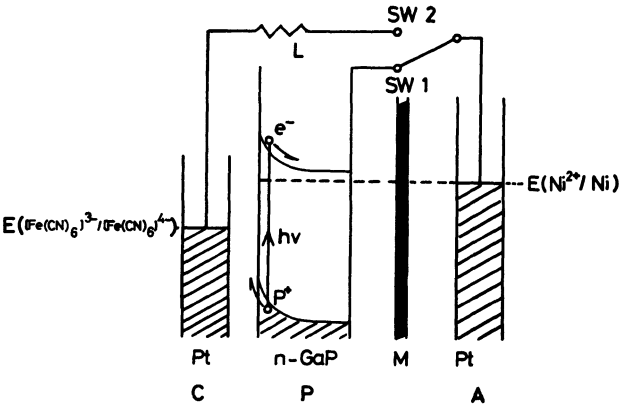

Fig. 6. Energy-level diagram of an illuminated battery.

of the $Ni(OH)_2/Ni,OH^-$ couple plays some role at the Ni electrode surface, resulting in a larger open-circuit voltage than that expected solely from the standard electrode potential of the Ni^{2+}/Ni couple. We may also note that the pH of the electrolyte solutions in this battery should be carefully controlled in view of two restrictions: the photodissolution of *n*-GaP and the passivity of Ni.

We could thus establish the photochemical charging of the storage battery with an *n*-GaP photoelectrode. An energy-level diagram of the battery during irradiation is shown in Fig. 6. In this battery, the storage of light energy is possible because of the existence of both the space-charge layer at the semiconductor surface and the separator between the cell compartments. The former assures the occurrence of charging reactions according to Eqs. 1—3, while the latter avoids the mixing of the $Fe(CN)_6]^{3-}$ and $[Fe(CN)_6]^{4-}$ in the compartment of the P- and C-electrodes and the Ni^{2+} in the compartment of the A-electrode. We could not dispense with the three-membrane system of the separator, as it was difficult to assemble a useful battery having only either an ACH-45T or CSV membrane. It seems that the existence of these three membranes has some effect upon the output voltage of the battery, as

the open-circuit voltage was slightly dependent on the combination of the membranes. We may try to define the power efficiency of the storage battery, η, in the following way:

$$\eta = \Phi_i \Phi_m \frac{q|E(\mathrm{Ox/Red}) - E(\mathrm{N}^{n+}/\mathrm{N})|}{E_g}, \quad (4)$$

where Φ_i and Φ_m denote the apparent quantum efficiency of the charging current and the efficiency of conversion from Q_{ch} to Q_{dis} respectively. E_g is the band-gap energy of the photoelectrode; $E(\mathrm{Ox/Red})$ and $E(\mathrm{N}^{n+}/\mathrm{N})$ are the standard electrode potentials of the redox couple and metal ion/metal respectively. q is the electron charge. As Φ_i and Φ_m are 13 and 55% respectively in this battery, η amounts to 1.9%. This value is considerably larger than the $\eta = 0.14\%$ evaluated for the storage battery with the n-TiO_2 photoelectrode.[1]

Hodes *et al.*[2] and Ang and Sammells[3] have used n-CdSe, n-GaAs, and n-$MoSe_2$ as the photoelectrodes of the photoelectrochemical systems with energy storage. In their cells, they have chosen various kinds of half-cells which demonstrate a good electrochemical cyclic performance in conventional batteries. However, the exact amount of light energy stored in the form of solid materials seems to be ambiguous in their cells, such as n-CdSe|S/S^{2-}|Ag_2S–Ag[2] and n-GaAs|Se/Se^{2-}|Cd[3], because they have employed metal electrodes themselves as the storage electrodes, *i.e.*, the Ag electrode in the former cell and the Cd electrode in the latter cell.

Of all the photoelectrolysis cells which can store light energy as chemical energy, light-energy storage as solid materials on the electrode surface seems to have two striking features; it enables the cell size to be compact, and the electrical energy can easily by drawn out of the cell by switching the junction of the electrodes.

This work was carried out with financial support from the Ministry of Education, Science and Culture (Grant-in-Aid for Scientific Research, No. 57040014).

References

1) H. Hada, K. Takaoka, M. Saikawa, and Y. Yonezawa, *Bull. Chem. Soc. Jpn.*, **54**, 1640 (1981).

2) G. Hodes, J. Manassen, and D. Cahen, *Nature*, **261**, 403 (1976); J. Manassen, G. Hodes, and D. Cahen, *J. Electrochem. Soc.*, **124**, 532 (1977).

3) P. G. P. Ang and A. F. Sammells, *Faraday Discuss. Chem. Soc.*, **70**, 207 (1980).

4) R. Memming, *J. Electrochem. Soc.*, **125**, 117 (1978).

5) Y. Nakato, K. Abe, and H. Tsubomura, *Ber. Bunsenges. Phys. Chem.*, **80**, 1002 (1976).

6) C. G. Hatchard and C. A. Parker, *Proc. R. Soc. London, Ser. A*, **235**, 518 (1956).

7) M. Pourbaix, "Atlas of Electrochemical Equilibria in Agueous Solutions," translated by J. A. Franklin, Pergamon Press, Oxford (1966), pp. 330—342.

Ab Initio SCF-SDCI Prediction of Type II Spectra and Geometry of $(ClHCl)^-$ Hydrogen Bond Complex. I. One Dimensional Vibrational Analysis

Toshikazu SAITOH,* Kazuhide MORI, Kotoku SASAGANE, and Reikichi ITOH
Department of Chemistry, School of Science and Engineering, Waseda University, Shinjuku-ku, Tokyo 160
(Received January 17, 1983)

Ab initio SCF(self-consistent field)-SDCI(single and double configuration interaction) calculations are presented on HCl_2^-. Applied basis sets are 4-31G, 4-31G(**) (no 3d-polarization functions on Cl atoms and 2p-polarization functions on H atom), 4-31G** (addition of polarization functions both on Cl and H atoms) and the split basis by Dunning (Cl/12s9p)(H/4s)→[Cl/6s5p][H/2s] with the addition of diffuse functions and/or polarization functions. Vibrational and geometrical analyses are performed on the Cl–Cl potential surface under symmetry conservation, and then on the proton potential surface at optimized R_{Cl-Cl} position. After potential interpolation by the continuous quadratic functions which reconstruct the calculated potential values on all mesh points, the quantal vibrational analysis is perfomed by the Störmer-Levy difference method. Discussion is made on the experimental confusion about the assignment of type II spectra of HCl_2^- as ν_3 mode in an argon matrix by the selection of basis set and of CI matrix expansion. Whereas the calculations in a primitive size proposes the double minimum potential surface of proton and type II spectra in $\approx$700 cm^{-1} region as ν_3 (which corresponds to the experimental data by Evans and Lo (1966) and Ault (1975)), the extended calculations (*i.e.* the large basis sets and the great number of CI matrix expansion) reduce the central barrier of the proton potential and then conclude the IR absorption in 1000—1100 cm^{-1} region as ν_3 in the type II spectra (which corresponds to the experimental results of $CsCl \cdot 1/3\ [H_3O^+HCl_2^-]$ by Schröder (1970) and Smith (1973)).

It is the well known fact that the hydrogen bonded hydrogen dihalide ions $(XHX)^-$ and $(XHY)^-$ provide the useful informations about the symmetric and the asymmetric hydrogen bonds. Earlier investigations on this kind of molecules are focusd on $(FHF)^-$, which is one of the strongest hydrogen bonds (Hydrogen bond energy is 58 ± 5 kcal mol^{-1}).[1,2] Neutron diffraction,[3,4] neutron inelastic scattering,[5] and IR-Raman studies[6-8] predicted that HF_2^- ions in $NaHF_2$ and KHF_2 crystals have symmetric linear triatomic structure ($D_{\infty h}$ symmetry) with single minimum proton potential. Singh ans Wood (1968, 1969)[9] estimated the vibrational structure of this ion using the variational method for the empirical potential surface. Almlöf (1972)[10] calculated the *ab initio* SCF-MO potential surface of linear $(FHF)^-$ ion in the two vibrational degrees of freedom and succeeded in the assignment of the vibrational spectra with high accuracy. Jiang and Anderson (1973)[11] and Barton and Thorson (1979)[12] also performed the vibrational studies on $(FHF)^-$ by one-dimensional approach and adiabatic approximation respectively on the semi-empirical (Lippincott-Schröder) potential which was fitted to the MO potential by Almlöf. They also gave supports to the experimental accounts on the structure and properties of $(FHF)^-$ ion. Though the anions in KHF_2 and $NaHF_2$ have symmetric structures, $(FHF)^-$ in *p-toluidinium hydrogen difluoride* has an asymmetric structure affected by an enviroment. R_{F-F} is 2.26 Å in both symmetric salts and asymmetric salt. R_{H-F} distances in asymmetric $(FHF)^-$ ion are 1.025 and 1.235 Å.[13]

The hydrogen bond energies of $(ClHCl)^-$, $(BrHBr)^-$, $(IHI)^-$, and $(ClHBr)^-$ are 18.9,[14] 11.6, 7.3, and 9.1[15] kcal mol^{-1} respectively. This implies that the structures and spectra of those ions are readily influenced by the molecular enviroment. Waddington (1958)[16] reported the IR spectra of $(CH_3)_4N^+HCl_2^-$ and suggested that $(ClHCl)^-$ has the linear symmetric structure on the basis of the similarity of the spectra with that of $(FHF)^-$. Evans and Lo (1966)[17] obtained two different types of spectra for salts of HCl_2^- and $(ClHBr)^-$. They reported the IR spectra of $Cs^+HCl_2^-$ in solid phase and a series of $R_4N^+HCl_2^-$ type solutions. Type I spectra are observed for $Cs^+HCl_2^-$, $(CH_3)_4N^+HCl_2^-$, and n-$(C_3H_7)_4N^+HCl_2^-$. There are two intense broad peaks at 1520—1670 cm^{-1} and near 1200 cm^{-1} and weak band near 220 cm^{-1} in the type I spectra. Type II spectra are obtained for $(C_2H_5)_4N^+HCl_2^-$, n-$(C_3H_7)_4N^+HCl_2^-$, and n-$(C_5H_{11})_4N^+HCl_2^-$. Type II salts indicate intense and broad band at 700—800 cm^{-1} which is extending from 600 to 1300 cm^{-1} region and consecuted to another weak and broad peak at 1000—1050 cm^{-1}. Evans and Lo predicted that $(ClHCl)^-$ ions in type I salts are in the asymmetric ($C_{\infty h}$ or C_s) structures and type II salts are in the symmetric ($D_{\infty h}$ or C_{2v}) structures. Isotope frequency ratio of ν_3 suggests that the proton potentials are single minimum both in type I and type II salts. Nibler and Pimentel (1967)[18] also predicted that type I HCl_2^- ion in $Cs^+HCl_2^-$ salt is not in the symmetric structure by the group theory consideration on the infrared activities and by the analogy of IR spectra between Cs^+ClHBr^- and $Cs^+HCl_2^-$. Neutron scattering studies on $Cs^+HCl_2^-$ by Stirling *et al.* (1970),[19] Smith *et al.* (1973),[20] and Howard *et al.* (1979)[21] also gave supports to the prediction of the noncentrosymmetric structure of type I salts. The definitive structural data on a dichloride salt is obtained for $CsCl \cdot 1/3\ [H_3O^+HCl_2^-]$ by X-ray diffraction experiment (Schröder and Ibers (1966)[22]). The dichloride ions occur as strings$\cdots(ClHCl)^-\cdots(ClHCl)^-\cdots$, parallel to the hexagonal axis in the structure. R_{Cl-Cl} distance is 3.14 ± 0.02 Å. Schröder (1970)[23] also obtained type II spectra of this crystal. IR and Raman data predict the centrosymmetric structure for $(ClHCl)^-$ ion. ^{35}Cl Neutron Quadrupole Resonance (NQR) spectroscopy of $(ClHCl)^-$ salts show two different ^{35}Cl frequencies for

type I and type II salts. Ludman *et al.* (1970)[24] obtained ^{35}Cl NQR spectra on $(CH_3)_4N^+HCl_2^-$, $Cs^+HCl_2^-$ (type I salts) and on $(C_2H_5)_4N^+HCl_2^-$, $CsCl\cdot 1/3\,[H_3O^+HCl_2^-]$ (type II salts). ^{35}Cl frequencies of type I salt are classified into the group which indicate about 20 MHz and type II are about 12 MHz. Dixon *et al.* (1975)[25] obtained the theoretical value of ^{35}Cl NQR frequency by *ab initio* SCF-MO calculation with the use of minimal STO basis functions. Calculated values are 12.6 MHz for $(FHCl)^-$ and 37.5 MHz for $(ClHCl)^-$. Thomson *et al.* (1975)[14] also calculated the potential surface and ^{35}Cl NQR frequency for $(ClHCl)^-$ by *ab initio* SCF-MO applying STO double zeta+polarization basis functions. Their results are that;

(i) proton potential surface is flat (nearly single minimum) at $R_{Cl-Cl}=3.14$ Å (which corresponds to the experimental R_{Cl-Cl} distance of $CsCl\cdot 1/3\,[H_3O^+HCl_2^-]$), the proton localizes in the center of mass and then ^{35}Cl NQR frequency is 13.11 MHz,

(ii) proton potential has two equivalent minima at $R_{Cl-Cl}=3.22$ Å (which corresponds to the experimental R_{Cl-Cl} distance in $Cs^+HCl_2^-$), the proton localizes in either minimum and ^{35}Cl NQR frequency is 21.0 MHz in the two equivalent minima at $R_{HCl}=1.365$ Å.

It is assured by these experimental and theoretical results that HCl_2^- ions in type I salts are in the noncentrosymmetric structures and type II are in the centrosymmetric ones.

However on the assignments of ν_2 and ν_3 modes in type II spectra there are some disagreements among the experimental results. Evans and Lo assigned the ν_2 and ν_3 modes of $n\text{-}(C_5H_{11})_4N^+HCl_2^-$ as 1050 and 780 cm^{-1} respectively. Whereas Schröder (1970)[23] predicted $\nu_2=500$—$1200\ cm^{-1}$ and $\nu_3=1050$—$1200\ cm^{-1}$ for $CsCl\cdot 1/3\,[H_3O^+HCl_2^-]$. (The overlap with the ν_2 mode of H_3O^+, 1150 cm^{-1}, prevented the detailed assignments of ν_2 and ν_3 modes of $(ClHCl)^-$.) Neutroninelastic scattering studies of types II salts[20] predicted $\nu_2=795\ cm^{-1}$, $\nu_3=1275\ cm^{-1}$ for $(C_2D_5)N^+(CD_3)_3HCl_2^-$ and $\nu_2=795\ cm^{-1}$ for $CsCl\cdot 1/3\,[H_3O^+HCl_2^-]$. The ν_1 mode of centrosymmetric anion should be Raman active and IR inactive. Though type II spectra by Evans and Lo indicate the weak ν_1 absorption peak in the far-IR region (250 cm^{-1}), Schröder observed ν_1 mode as Raman active and far-IR inactive. The ν_1 mode by neutron inelastic scattering spectra[20] were 218 cm^{-1} for $(C_2D_5)N^+(CD_3)_3HCl_2^-$ and 275 cm^{-1} for $CsCl\cdot 1/3\,[H_3O^+HCl_2^-]$. Recently Ault and Andrews (1975)[26] reported a series of IR and Raman spectra of $M^+HCl_2^-$ (M=alkali metal) in the argon matrix. For example the results for $Rb^+HCl_2^-$ are $\nu_1=250\ cm^{-1}$ (Raman), $\nu_2=600\ cm^{-1}$ (IR), and $\nu_3=729\ cm^{-1}$ (IR). This encourage the assignments by Evans and Lo. ν_3 spectra of this type had been explained as those of HCl_2^- radical. Noble and Pimentel (1968)[27] obtained the IR spectra of $HCl/Cl_2/Ar$ matrix which indicate absorption peaks at 696.4 cm^{-1} (ν_3) and 955.6 cm^{-1} ($\nu_1+\nu_3$). However the later study (Milligan and Jacox (1970)[20]) by vacuum ultraviolet photolysis of HCl/Ar matrix provided the same spectra; $\nu_3=696\ cm^{-1}$ and $\nu_1+\nu_3=956\ cm^{-1}$, which were accounted as those of HCl_2^- ion. Type II spectra of alkali halide salts are consistent with those by Milligan and Jacox, and by Evans and Lo. The isotope frequency ratios ν_3^H/ν_3^D by Ault are almost the same those of harmonic oscillators. This is indicative of the single minimum potential for the vibration of proton. Since ν_1 is only Raman active, the structure of $ClHCl^-$ line is expected to have $D_{\infty h}$ symmetry.

The purpose of this paper is to determine the assignments of type II spectra of $(ClHCl)^-$ ion in the centrosymmetric structure by the theoretical consideration. We calculate the vibrational potential surfaces of Cl–Cl and proton by the *ab initio* SCF-SDCI method applying Gaussian basis sets. We still calculated the quantal vibrational eigenvalues for ν_1 and ν_3 modes by one dimensional Störmer-Levy difference method. In the next section we review the computational details, *i.e.* the selection of the basis sets, single and double excitations from the single reference state configuration interaction (SDCI) method, interpolation method of potential surface and quantal vibrational analysis (Störmer-Levy method). In the result section the calculated results are presented. In the final section we shall consider in the level of discussion the assignment of ν_3 in the type II spectra of centrosymmetric $(ClHCl)^-$ anion.

Computational Details

The AO basis sets employed in the present calculation are seven types of split valence ones. To clarify the types of basis sets we employ the following expressions,

(i) the well known 4-31G basis sets,[29]

(ii) 4-31G(**) *i.e.* we denote the addition of 2p polarization functions on H atom to 4-31G basis sets,

(iii) 4-31G** *i.e.* the addition of 3d polarization functions on Cl atoms and of 2p polarization functions on H atom,

(iv) [6s5p](**) basis for chlorine in a (6,3,1,1,1,1/5,1,1,1,1) contraction (*i.e.* [Cl/6s5p])[30] and hydrogen in a (3,1/1) contraction (*i.e.* [H/2slp]),[31]

(v) [6s5p](**)+diff basis sets with the addition of diffuse functions on Cl atoms to [6s5p](**) basis sets,

(vi) [6s5p]** basis sets with the addition of 3d polarization functions on Cl atoms to [6s5p](**) basis sets, and

(vii) [6s5p]**+diff basis sets with the addition of 3d polarization functions and diffuse functions on Cl atoms to [6s5p](**) basis sets.

The orbital exponents of 2p polarization functions of hydrogen are $\zeta_p=1.0$ (in 4-31G(**) and 4-31G**),[32] $\zeta_p=0.75$ (in Dunning basis sets)[33] which is optimized for HCl molecule. The exponents of 3d polarization functions are $\zeta_d=0.6$ for all basis sets, which is optimized for [Cl/6s4p] basis sets of HCl molecule.[33] Literature cited ζ_d value for Cl atom is 0.619 which is obtained by Ahlrichs equation, $\zeta_d=0.77\cdot Z-0.69$ (for $11\leqq Z\leqq 18$).[34] The employed ζ_d value will be a reasonable selection. The exponent of 3p diffuse function has the value $\zeta_{3p}=0.049$ for all Cl atoms.[35] SCF calculations are carried out with the use of GAUSSIAN 70 program[36] for 4-31G basis set calculations and with GAUSSIAN 76 program[32] for other basis sets in a double precision on IMS HITAC M-200H computers.

The CI calculations are in a single and double excitations from single reference state configuration interaction (SDCI) type[37] for 4-31G and 4-31G(**) calculations and in a direct SDCI (CIMI) type[38] for other calculations. All configuration state functions (CSF's)are treated with a common sets of MO's from the SCF solution. The valence occupied MO's of the SCF solution consist of $(\sigma_g)^2(\sigma_u)^2(\sigma'_g)^2(\pi_g)^4(\pi_u)^4(\sigma'_u)^2$ MO's. CSF's are generated from the pair of single and double excitations from the occupied MO's to the virtual MO's. For all calculations the size of CI matrix is selected so that the occupied MO's are restricted to the valence MO's only and the virtual MO's are from the lower state to a required state in consideration of the results. Another corrections to the CI energies are generated using Davidson's formula[39] for estimating the contribution of quadrupole excitations. Standard SDCI program is linked both to GAUSSIAN 70 and 76 SCF program and direct SDCI program is linked only to the latter.

The coordinates of the system are taken as to make two dimensional potential surface in which the vibration of Cl–Cl and proton on Cl–Cl axis occur. The origin of the potential is taken at the center of Cl–Cl. The interpolation of the MO potential is inevitable for the quantal vibrational analysis for the lack of mesh points. We employed the continuous quadratic functions interpolation method that is to interpolate the required potential values for the difference method. The procedure of the calculation starts with the computation of the MO potential value P_n at $N+1$ points S_n $(0 \leqq n \leqq N)$. Three pairs of potential data (S_{n-1}, P_{n-1}), (S_n, P_n), and (S_{n+1}, P_{n+1}) in a series provide one approximate potential function $f_n(x)=a_nx^2+b_nx+c_n$ which generates a series of mesh point values in a region $S_n \leqq x \leqq S_{n+1}$. The coefficients a_n, b_n, and c_n are given by,

$$a_n = \frac{P_{n-1}(S_{n+1}-S_n)-P_n(S_{n+1}-S_{n-1})+P_{n+1}(S_n-S_{n-1})}{(S_{n+1}-S_n)(S_{n+1}-S_{n-1})(S_n-S_{n-1})}, \quad (1)$$

$$b_n = \frac{P_n-P_{n-1}}{S_n-S_{n-1}} + a_n(S_{n-1}+S_n), \quad (2)$$

and

$$c_n = \frac{P_nS_{n-1}-P_{n-1}S_n}{S_{n-1}-S_n} + a_nS_{n-1}S_n (\text{for } 1 \leqq n \leqq N-1). \quad (3)$$

The potential value $h(x)$ (where $S_n \leqq x \leqq S_{n+1}$) are evaluated by the average of $f_n(x)$ and $f_{n+1}(x)$, which are generated succesively by the following equation,

$$h(x) = \frac{(S_{n+1}-x)f_n(x)+(x-S_n)f_{n+1}(x)}{S_{n+1}-S_n}$$
$$(\text{for } S_n \leqq x \leqq S_{n+1} \text{ and } 1 \leqq n \leqq N-1). \quad (4)$$

The potential values for $x<S_1$ and $x>S_{N-1}$ are extrapolated by the start and the final functions $f_1(x)$ and $f_N(x)$ respectively. The coordinates of the system are taken as the same ones by Almlöf[10] and Janoschek *et al.*[40] That is, the origin is centered on the $(Cl(1)–H–Cl(2))^-$ ion and the symmetry coordinates $R_{Cl-Cl}=R_{Cl(1)-H}+R_{Cl(2)-H}$ and $r_H=1/2\ (R_{Cl(1)-H}-R_{Cl(2)-H})$ are employed. This is one of the molecular Jacobi coordinates for symmetric linear triatomic system and is called as "molecular coordinates".[12] The reduced masses of two vibrational degrees of freedom are taken as $\mu_1=M_{Cl}/2$ and $\mu_3=2M_HM_{Cl}/(2M_{Cl}+M_H)$.

The quantal vibrational analysis is given by the Störmer–Levy difference method.[43] This method gives an accurate solution even in the case of discrete potential values in a numerical form with the great number of mesh points and with the proper selection of the position to start the initial guess at outside enough of the potential well. Vibrational analysis is performed on R_{Cl-Cl} surface and r_H surface. Initial point, final point, and the mesh width ΔR are taken as (2.7 Å, 3.8 Å, 0.001 Å) in R_{Cl-Cl} direction and (−0.914 Å, +0.886 Å, 0.001 Å) in r_H direction. The number of calculated MO potential values are 8 points in R_{Cl-Cl} direction and 11 points (21 points up to total by the symmetry) in r_H direction at optimized R_{Cl-Cl} distance.

Results

Figure 1 illustrates the correction energy variation in R_{Cl-Cl} direction. The effect of basis set extension is in the order 4-31G**>4-31G(**) both in magnitude and in R_{Cl-Cl} dependence of the shift value. This implies that the "steepness" of Cl–Cl potential curve is in the order 4-31G>4-31G**>4-31G(**) and the equilibrium

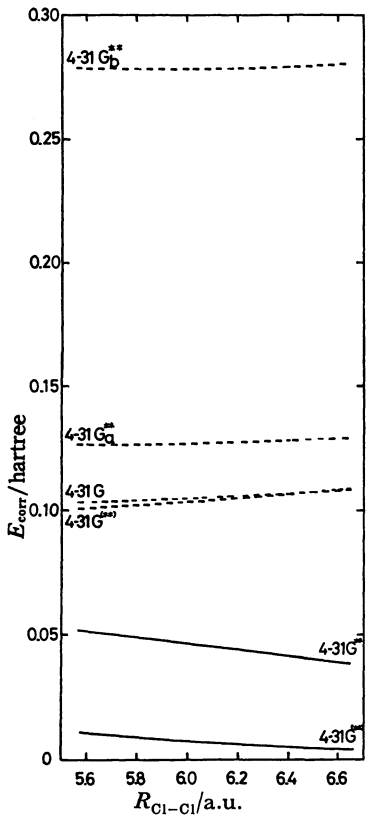

Fig. 1. Correction energy values of Cl–Cl direction on basis set expansion for 4-31G basis sets and on CI. $E_{corr}=E_T$(4-31G SCF)$-E_T$ for SCF calculation and $E_{corr}=E_T$(SCF)$-E_T$(CI) (in the same basis set) for CI calculation. ——: SCF calculation and ------: CI calculation. 4-31G$_a^{**}$ denotes that the number of CI matrix expansion is 4005 and 4-31G$_b^{**}$ denotes that the expansion is 13041. (1 a.u.$=5.291677\times10^{-11}$ m, 1 hartree$=4.359814\times10^{-18}$ J).

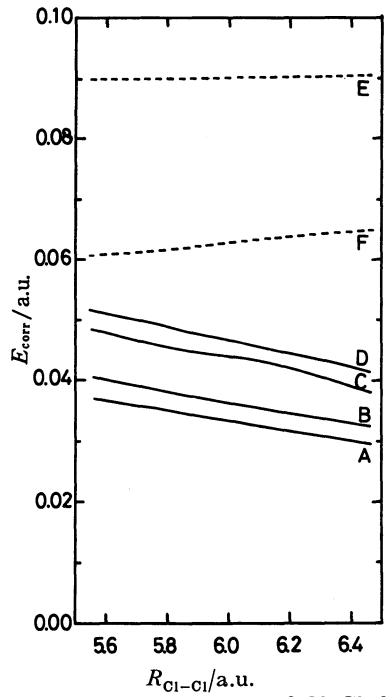

Fig. 2. Correction energy values of Cl–Cl direction on basis set expansion and CI for [6s5p] basis sets. $E_{corr}=-1.0+E_T$(4-31G SCF)$-E_T$ for SCF calculations and $E_{corr}=E_T$(SCF)$-E_T$(CI) for CI calculations. ——: SCF calculation and ------: CI calculation. A: [6s5p]$^{(**)}$ SCF, B: [6s5p]$^{(**)+diff}$ SCF, C: [6s5p]** SCF, D: [6s5p]$^{**+diff}$ SCF, E: [6s5p]$^{(**)}$ CI (the number of CI matrix expansion is 5565), and F: [6s5p]$^{**+diff}$ CI (CI expans.=5565).

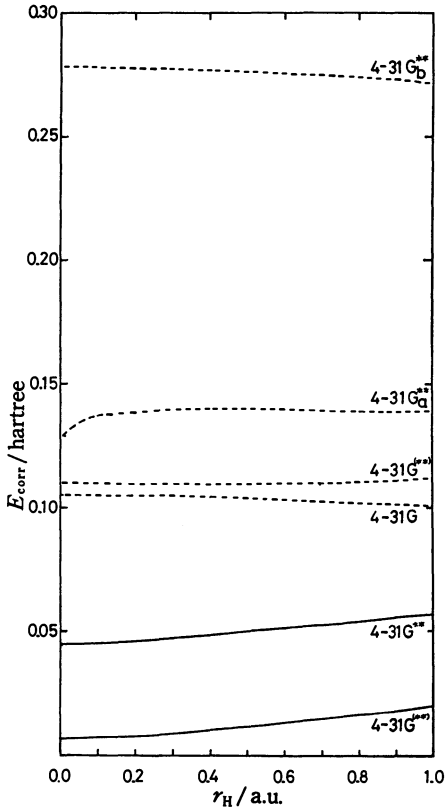

Fig. 3. Correction energy values on proton displacement from the symmetric position. $E_{corr}=E_T$(4-31G SCF)$-E_T$ for SCF calculations and $E_{corr}=E_T$(SCF)$-E_T$(CI) for CI calculations (in the same basis set). ——: SCF calculation and ------: CI calculation. 4-31G$_a^{**}$ denotes that the number of CI matrix expansion is 4005 and 4-31G$_b^{**}$ denotes that the expansion is 13041.

distance for Cl-Cl is in the order 4-31G>4-31G$^{(**)}$>4-31G**. Though the effect of CI is greater than that of basis set extension, R_{Cl-Cl} dependence of CI correction energy for the same basis set is rather small and in increase with the increase of R_{Cl-Cl}. This also implies that R_{Cl-Cl} potential become "gentle-sloping" in the long Cl–Cl distance and then lengthen the equilibrium Cl—Cl distance. The slope of CI potential curve is expected to be in the order 4-31G**>4-31G>4-31G$^{(**)}$. The effect of basis set extension cancel the effect of CI on the sloping of the potential. Thus the

TABLE 1. CALCULATED VIBRATIONAL FREQUENCIES AND OPTIMIZED GEOMETRY OF HCl_2^- (4-31 G, 4-31 G$^{(**)}$, and 4-31 G** basis sets)

Basis set	Method	ν_1 / cm^{-1}	ν_3		ν_H/ν_D	R_{Cl-Cl} / Å	Min.pos.[a] / Å	Barrier height / cm^{-1}
			ν_H / cm^{-1}	ν_D / cm^{-1}				
4-31 G	SCF	274.0	1044	688.0	1.56	3.222	0.0	0.0
	CI[b]	289.6	1089	726.5	1.50	3.264	0.0	0.0
	SDQ	288.9	1112	745.4	1.49	3.274	0.0	0.0
4-31 G$^{(**)}$	SCF	266.3	553.0	278.6	1.99	3.158	±0.228	404.4
	CI[c]	257.4	686.2	387.1	1.77	3.227	±0.194	205.5
	SDQ	269.8	711.5	408.7	1.74	3.234	±0.189	115.9
4-31 G**	SCF	350.2	867.7	521.3	1.66	3.132	±0.145	88.6
	CI(1)[d]	337.9	485.9	196.6	2.47	3.143	±0.194	2826
	(2)[e]	352.3	1050	672.2	1.56	3.134	0.0	0.0
	SDQ(1)	334.2	444.4	156.4	2.84	3.149	±0.195	3058
	(2)	340.6	1094	709.1	1.54	3.140	0.0	0.0

a) Minimum position of the proton displacement potential at optimized R_{Cl-Cl} distance (displacement value from the central position). b) CI matrix expansion is 3321. R_{Cl-Cl}=3.228 Å. c) CI matrix expansion is 3321. R_{Cl-Cl}=3.228 Å. d) CI matrix expansion is 4005. R_{Cl-Cl}=3.149 Å. e) CI matrix expansion is 13041. R_{Cl-Cl}=3.140 Å.

TABLE 2. CALCULATED VIBRATIONAL FREQUENCIES AND OPTIMIZED GEOMETRY OF HCl_2^- ([6s5p]$^{(**)}$, [6s5p]$^{(**)+diff}$, [6s5p]**, and [6s5p]$^{**+diff}$ basis sets)

Basis set	Method	ν_1 / cm^{-1}	ν_3		ν_H/ν_D	R_{Cl-Cl} / Å	Min. pos.[a] / Å	Barrier height / cm^{-1}
			ν_H / cm^{-1}	ν_D / cm^{-1}				
[6s5p]$^{(**)}$	SCF	342.3	723.3	401.6	1.80	3.157	±0.190	254.9
	CI[b]	334.2	826.4	493.0	1.68	3.161	±0.152	92.4
	SDQ	323.9	849.7	513.2	1.66	3.193	±0.147	66.9
[6s5p]$^{(**)+diff}$	SCF	342.9	688.3	371.9	1.85	3.155	±0.197	351.2
	CI[c]	326.8	1177	789.7	1.49	3.188	0.0	0.0
	SDQ	323.9	1214	821.1	1.48	3.193	0.0	0.0
[6s5p]**	SCF	351.4	892.4	538.2	1.66	3.143	±0.142	84.2
[6s5p]$^{**+diff}$	SCF	352.1	860.4	510.7	1.69	3.141	±0.150	118.2
Jiang and Anderson(1974)	Semiempirical	—	762	455	1.67	3.133	±0.20	81
Exptl	($Na^+(HCl_2)^-$)	302	658	436	1.51	(3.22)[d]	—	—
	($K^+(HCl_2)^-$)	250	736	498	1.48	—	—	—
	($Rb^+(HCl_2)^-$)	250	729	512	1.42	—	—	—
	($Cs^+(HCl_2)^-$)	250	723	507	1.42	(3.14)[e]	—	—

a) Minimum position of the proton displacement potential at optimized R_{Cl-Cl} distance. b) CI matrix expansion is 5565. $R_{Cl-Cl} = 3.157$ Å. c) CI matrix expansion is 5565. $R_{Cl-Cl} = 3.155$ Å. d) For $(CH_3)_4N^+HCl_2^-$. e) For CsCl·1/3 [$H_3O^+HCl_2^-$].

basis set extension is expected to play an important role on the spacing of the vibrational energy to the extent of CI expansion terms.

Figure 2 shows the correction energies on Dunning basis sets. SCF results suggest that Dunning basis sets make the Cl–Cl potential "steeper" and make the equilibrium distance shorter in comparison with 4-31G SCF potential. The relation between SCF and CI among the SCF results for different basis sets are the same in 4-31G system. The CI correction value in the same number of CI expansion terms become smaller for the basis set extension from [6s5p]$^{(**)}$ to [6s5p]$^{(**)+diff}$. This indicates that the greater number of CI matrix expansion for the smaller basis set is the better selection to obtain the potential surface which involves the greater CI correction energy. Since R_{Cl-Cl} dependence of CI correction energy is relatively small, it is expected that the greater ν_1 value and shorter R_{Cl-Cl} distance appear in every calculation on Dunning basis sets in comparison with 4-31G results.

Tables 1 and 2 show calculated vibrational frequencies and optimized geometry of HCl_2^- for the basis sets (i)—(iii) and (iv)—(vii). In Tables 1 and 2 the above-mentioned tendencies are veirfied numerically. In Table 1 ν_1 values are in the order 4-31G** >4-31G $\gtrsim$4-31G$^{(**)}$ in SCF calculation. Since ν_1 values from CI potential are the sum of basis set contribution and CI contribution to the potential curvature around the equilibrium distance, the ν_1 variation become the complicated order. ν_1 values by CI are greater than those by SCF in 4-31G and 4-31G** CI(2). But the reverse relations are detected in 4-31G$^{(**)}$ and 4-31G** CI(1). In every calculation SDQ potentials provide no considerable shift in ν_1 values. R_{Cl-Cl} distances are also in the order 4-31G>4-31G$^{(**)}$>4-31G** in SCF calculations. In all basis sets in Table 1 R_{Cl-Cl} distances are in the order SCF>CI>SDQ. The competing contributions from basis set extension and CI and/or SDQ are indicated characteristically in Table 1. In Table 2 the effect of basis set extension makes ν_1 value greater The addition of diffuse function gives no significant shift on ν_1 value. Whereas the addition of 3d polarization functions on Cl atoms provides the greater ν_1 values. ν_1 values in all calculations correspond with the results for 4-31G**. Even in the case of [6s5p]$^{(**)}$ basis set ν_1 value is 37% greater than the experimental value 250 cm^{-1}. Whereas ν_1 values by 4-31G and 4-31G$^{(**)}$ SCF are only about 10% greater than the experimental value. Thus the basis set extension in every calculation seems to make the poorer fits of calculated ν_1 values to the experimental ones. Calculated equilibrium R_{Cl-Cl} distances show the same tendency as in 4-31G in the basis set extension. R_{Cl-Cl} distances are in the order [6s5p]$^{**+diff}$<[6s5p]**< [6s5p]$^{(**)+diff}$<[6s5p]$^{(**)}$ in SCF calculation. And the order SDQ>CI>SCF are detected for the R_{Cl-Cl} equilibrium distances by [6s5p]$^{(**)}$ and [6s5p]$^{(**)+}$< basis sets. Diffuse functions also make no significant effect on the equilibrium R_{Cl-Cl} distance. The competing relations between basis set extension and CI are also recognized in the calculations by Dunning basis sets. Both 4-31G**SDQ(2) and [6s5p]$^{**+diff}$ SCF calculations provide the best fits to the experimental R_{Cl-Cl} distance for CsCl·1/3 [$H_3O^+HCl_2^-$]. These results imply that the best calculation may be attained either by the small basis set and large scale CI calculation or by the large basis SCF calculation.

Figure 3 indicates the variation of correction energy in the direction of r_H. In the central region the potential is mainly depressed by CI correction energy in comparison with the SCF potential. Thus CI reduces the central barrier. But the 4-31G$_a$** result shows the anomalous depression of correction energy around the central position. This increases the anomalous barrier

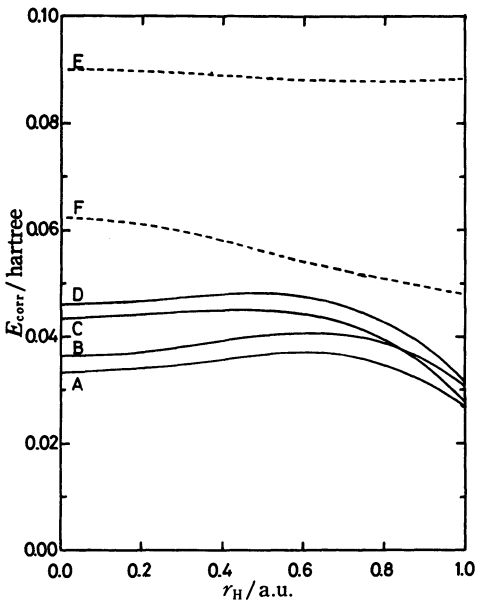

Fig. 4. Correction energy values (for Dunning's basis sets) on proton displacement from the central position. $E_{corr}=E_T(\text{4-31G SCF})-E_T$ for SCF calculation and $E_{corr}=E_T(\text{SCF})-E_T(\text{CI})$ for CI calculation (in the same basis set). The effects of basis set expansion are shown by —— and those of CI are shown by -------. A: [6s5p]$^{(**)}$ SCF, B: [6s5p]$^{(**)+diff}$ SCF, C: [6s5p]** SCF, D: [6s5p]$^{**+diff}$ SCF, E: [6s5p]$^{(**)}$ CI (the number of CI matrix expansion is 5565), F: [6s5p]$^{(**)+diff}$ CI (CI expans.=5565).

height. The reason for this will be discussed in the next section. In comparison with the relatively small change of CI correction energies on proton displacement, the correction to 4-31G SCF potential by the introduction of polarization function indicate the greater change on proton displacement. Slope of SCF correction curve is in the order 4-31G$^{(**)}$>4-31G**. Since the correction values by polarization functions are in the minimum at the symmetric position, SCF potentials for 4-31G$^{(**)}$ and 4-31G** are lowered in the asymmetric regions. This makes the central barrier greater and then makes ν_1 value smaller. Table 1 shows the numerical supports of these tendencies. The barriers come to be 404.4 and 88.6 cm^{-1} at 4-31G$^{(**)}$ SCF and 4-31G** SCF potentials respectively. The barrier height of 4-31G$^{(**)}$ SCF potential is reduced to be 205.5 and 115.9 cm^{-1} by introducing CI and SDQ respectively. In 4-31G calculation the barrier vanishes by CI(2) and SDQ(2) calculations. Though ν_3 values are about 1050 cm^{-1} in cases of single minimum potential, they decreased to be 550—870 cm^{-1} in double minimum potentials. The shift of ν_3 value for the basis set extension is in the order 4-31G>4-31G**>4-31G$^{(**)}$ and for the methods is in the order SDQ>CI>SCF. Exception is detected in the calculation of 4-31G** CI(1) and SDQ(1), in which the anomalous central barriers exist because of small number of CI matrix expansion.

Figure 4 shows the correction energy values on proton displacement from the symmetric position for the group of Dunning basis sets. The contribution from 3d polarization functions on the correction energy show the maximum at $r_H=0.5$ a.u. and is reduced in the highly asymmetric region. Whereas the contribution from the diffuse functions seems to be in nearly constant value in all regions. CI correction values are diminished in the asymmetric region and the value for [6s5p]$^{(**)+diff}$ (curve F) is smaller than that for [6s5p]$^{(**)}$ (curve E) in the same number of CI expansion terms and the curve E decreases in the asymmetric region. This implies the size of CI is not sufficient in [6s5p]$^{(**)+diff}$ CI calculation. These trends are also verified by the numerical results in Table 2. All of SCF potentials indicate double minimum shapes. The barrier heights by the SCF calculations are in the order [6s5p]$^{(**)+diff}\gtrsim$[6s5p]$^{(**)}$ >[6s5p]$^{**+diff}\gtrsim$[6s5p]**. The barrier heights for the methods are in the order SCF>CI>SDQ for [6s5p]$^{(**)}$ calculation. The barrier height for [6s5p]** or [6s5p]$^{**+diff}$ is nearly the same for 4-31G**.

ν_3 varies from 688.3 cm^{-1} to 892.4 cm^{-1} in SCF calculations. The contribution of 3d polarization functions adds about 100 cm^{-1} to the ν_3 values without 3d polarization functions. Single minimum potentials for [6s5p]$^{(**)+diff}$ CI and SDQ make ν_3 greater than 1100 cm^{-1}. The effect of diffuse functions on ν_3 is not significant. Whereas CI and SDQ contributions make ν_3 slightly greater than that by SCF value in [6s5p]$^{(**)}$ calculation. The experimental ν_3 values for $M^+HCl_2^-$ (M=alkali metal) varies from 658 to 736 cm^{-1}. Theoretical results by Jiang and Anderson[11] are $\nu_3=762$ cm^{-1} and $R_{Cl-Cl}=3.133$ Å, which are well corresponding with the experimental results. The value of barrier height 81 cm^{-1} by Jiang and Anderson corresponds well with our results by 4-31G** SDQ, 4-31G** SCF [6s5p]$^{(**)}$ CI, [6s5p]** SCF, and [6s5p]$^{**+diff}$ SCF. R_{Cl-Cl} value by 4-31G$^{(**)}$ is greater than the experimental ones. Results by above-mentioned basis sets except for 4-31G$^{(**)}$ seem to show good agreements with the experimental values not only in R_{Cl-Cl} but also in ν_3 value and the barrier height. However the isotope frequency ratios ν_3^H/ν_3^D are in poorer agreements with the experimental values. The experimental ones show nearly the harmonic values. But the above-mentioned values show the greater isotope frequency ratios about 1.7—1.9. Though the values for the single minimum potential show better fits to the experimental ν_3^H/ν_3^D values, ν_3^H is about 300 cm^{-1} greater than the experimental ones. The calculated results have lead us to the complicated situation in which the alternative relations exist between the small ν_3 value and the fit of ν_3^H/ν_3^D. This is the critical point for the explanation of the state of isolated HCl_2^- ion; *i.e.* whether isolated HCl_2^- has double minimum potential or single minimum one along r_H axis. Experimental R_{Cl-Cl} values of HCl_2^- are obtained for $(CH_3)_4N^+HCl_2^-$ and CsCl·1/3 [H_3O^+ HCl_2^-] crystals. The longer experimental R_{Cl-Cl} value is 3.22 Å for $(CH_3)_4N^+HCl_2^-$ which corresponds with the asymmetric bond. And the shorter experimental R_{Cl-Cl} value is 3.14 Å for CsCl·1/3 [$H_3O^+HCl_2^-$], which agrees well with the results by 4-31G**, [6s5p]**, and [6s5p]$^{**+diff}$. Experimental ν_3 value of type II spectra for n-$(C_5H_{11})_4N^+HCl_2^-$ is obtained by Evans and Lo as 780 cm^{-1} and for CsCl·1/3 [$H_3O^+HCl_2^-$] is predicted as 1050—1200 cm^{-1} by Schröder. Calculated

TABLE 3. CALCULATED HYDROGEN BOND ENERGY of HCl_2^- (SCF CALCULATION)
(1 kcal mol^{-1} = 4.184 × 10^3 J mol^{-1})

Basis set	E_{min} / hartree	E_{400}[a] / hartree	ΔE / kcal mol^{-1}	Vibrational correction / cm^{-1}	ΔE_{coor} / kcal mol^{-1}
4-31 G	−918.647540	−918.591285[b]	35.30	930.3	37.96
4-31 G(**)	−918.649382	−918.604737	28.02	918.9	30.65
4-31 G**	−918.687646	−918.645779	26.27	869.6	28.76
[6s5p](**)	−919.674645	−919.644168	19.13	910.9	21.73
[6s5p]**	−919.684183	−919.654063	18.90	885.8	21.43
[6s5p](**)+diff	−919.677933	−919.650648	17.12	943.2	19.82
[6s5p]**+diff	−919.687388	−919.660463	16.90	848.9	19.33

a) Total energy at R_{Cl-H} = 2.4087 a.u. and R_{H-Cl^-} = 400 a.u. b) Total energy at R_{Cl-H} = 2.4087 a.u. and R_{H-Cl^-} = 20 a.u.

TABLE 4. CALCULATED HYDROGEN BOND ENERGY OF HCl_2^- (CI CALCULATION)
(1 kcal mol^{-1}=4.184× 10^3 J mol^{-1})

Basis set[a]		E_{min} / hartree	E_{400}[b] / hartree	ΔE / kcal mol^{-1}	Vibrational correction / cm^{-1}	ΔE_{corr} / kcal mol^{-1}
4-31 G	(3321)	−918.746132	−918.695165[c]	31.98	865.0	34.45
4-31 G(**)	(3321)	−918.752865	−918.707077	28.73	1002	31.59
	(5565)	−918.759847	−918.714882	28.22	960.1	30.97
4-31 G**	(4005)	−918.828444	−918.785176	27.15	508.1	28.60
	(13041)	−918.965735	−918.917897	30.02	897.3	32.59
[6s5p](**)	(5565)	−919.763769	−919.731633	20.17	786.8	22.42
[6s5p](**)+diff	(5565)	−919.738943	−919.702381	22.94	860.4	25.40

a) Numbers in parentheses denote CI matrix expansion. b) E_{400} denotes the total energy at R_{Cl-H} = 2.4087 a.u. and R_{H-Cl^-} = 400 a.u. c) The total energy at R_{Cl-H} = 2.4087 a.u. and R_{H-Cl^-} = 20 a.u.

ν_3 value for 4-31G(**) SDQ is 711.5 cm^{-1} and for 4-31G** SDQ (2) is 1094 cm^{-1}. Since SCF results for [6s5p](**), [6s5p]**, and [6s5p]**+diff give the counterpart of 4-31G** SCF results, 4-31G** represents the large basis sets. The shift of basis sets from 4-31G(**) to 4-31G** may represents the change from double minima to single minimum in the large CI and SDQ calculations. The experimental values of isotope frequency ratio ν_3^H/ν_3^D are near the harmonic value 1.42 for $(C_2H_5)_4N^+HCl_2^-$, 1.37 for n-$(C_3H_7)_4N^+HCl_2^-$, and 1.48 for n-$(C_5H_{11})_4N^+$-HCl_2^- in solution. In Table 2 the isotope frequency ratios for $M^+HCl_2^-$ (M=alkali metal) in argon matrix are given and ν_3^H/ν_3^D values vary from 1.42 to 1.51. The calculated results to provide lower ν_3 values (*i.e.* in the case of double minimum potential) show greater ν_3^H/ν_3^D values than the harmonic ones. ν_3^H/ν_3^D values close to harmonic ones are attained in the cases of single minimum potential. Introduction of CI reduces ν_3^H/ν_3^D value to the extent of the decrease of the central barrier in every case, but increase ν_3 value to be greater than 1000 cm^{-1}.

Tables 3 and 4 show the calculated hydrogen bond energies of HCl_2^- for SCF and CI calculations. Vibrationally corrected hydrogen bond energy ΔE_{corr} is obtained as follows;

$$\Delta E_{corr} = (E_{\infty}^{ClHCl^-} - E_{min}^{ClHCl^-}) + (E_{vib}^{HCl} - E_{vib}^{ClHCl^-}), \quad (5)$$

where $E_{\infty}^{ClHCl^-}$ denotes the total engy at $R_{H\cdots Cl}=\infty$ which is replaced by the value at R_{Cl-H}=2.4087 a.u. and $R_{H\cdots Cl}$=400 a.u., $E_{min}^{ClHCl^-}$ denotes the minimum energy in the total potential surface, E_{vib}^{HCl} denotes the vibrational zero point enrgy of HCl molecule and $E_{vib}^{ClHCl^-}$ denotes the vibrational ground state energy of $ClHCl^-$. The former parenthesis in Eq. 5 means the contribution of electronic energy difference between Cl–H···Cl^- and $ClHCl^-$. And the latter means the vibrational correction part. ΔE value is also estimated by the difference between the energies of HCl+Cl^- and $ClHCl^-$ (*i.e.* $\Delta E'=E_{Cl^-+HCl}-E_{min}^{ClHCl^-}$). In the case of 4-31G ΔE become 31.70 kcal mol^{-1} for SCF and 30.96 kcal mol^{-1} for CI, where the number of CI matrix expansion is employed the value 325 for HCl and 153 for Cl^-. Though ΔE values are greater than $\Delta E'$ in the case of 4-31G, we employ the ΔE value for simplicity of the estimation of CI energy. Orbital crossings to make significant change of CI correction value have not occured in every calculation between the equilibrium point and near dissociation limit. We also employed the correction by the experimental value of the vibrational zero point energy of HCl. The experimental vibrational constants of HCl are ω_e=2990.9 cm^{-1} and $\chi_e\omega_e$=52.8 cm^{-1}.[43] Thus the zero point energy of HCl is 1482.3 cm^{-1}. The vibrational correction terms are evaluated by the difference between the zero point energy of free HCl and the sum of zero point energy of ν_1 and ν_3. In comparison with the experimental value of hydrogen bond energy of HCl_2^- (18.9 kcal mol^{-1}), calculated values by 4-31G and its extended basis sets are fairly overestimated both in SCF and CI calculations. Though introduction of polarization functions reduce

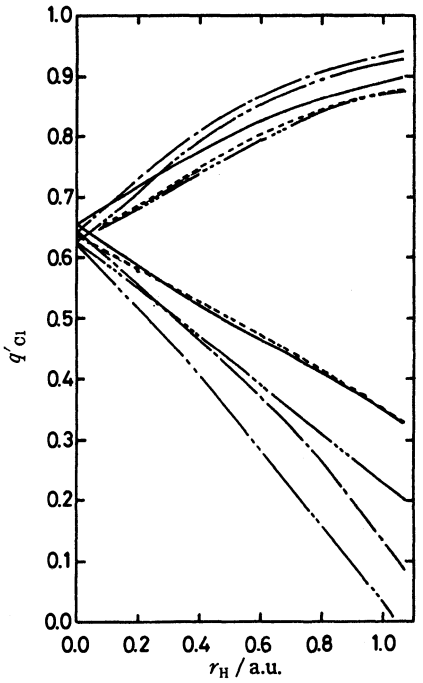

Fig. 5. Shift value of atomic charge on Cl ($q'_{Cl}=q_{Cl}-17.0$) with the proton displacement from the symmetric position at $R_{Cl-Cl}=3.228$ Å for 4-31G, 4-31G(**), and 4-31G**, at $R_{Cl-Cl}=3.157$ Å for [6s5p](**) and at $R_{Cl-Cl}=3.143$ Å for [6s5p]**. ------: 4-31G SCF, -----: 4-31G(**) SCF, ——: 4-31G** SCF, —·—: [6s5p](**) SCF, and ·—·—·: [6s5p]** SCF. CI results are not shown because the shifts on CI from SCF values are not so remarkable.

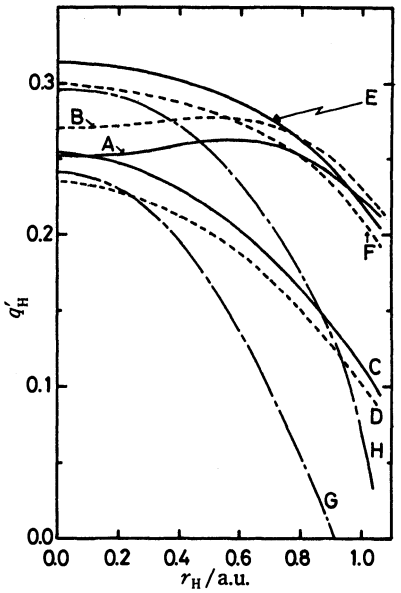

Fig. 6. Shift value of atomic charge on H ($q'_H=1.0-q_H$) with the proton displacement from the symmetric position at $R_{Cl-Cl}=3.228$ Å. R_{Cl-Cl} values are the same as that of Fig. 5. A: 4-31G SCF, B: 4-31G(**) CI (the number of CI matrix expansion is 3321), C: 4-31G(**) SCF, D: 4-31G(**) CI (CI expans.=5565), E: 4-31G** SCF, F: 4-31G** CI (CI expans.=13041), G: [6s5p](**) SCF, and H: [6s5p]** SCF.

both ΔE value and vibrational correction value and then reduce ΔE_{corr}, ΔE is rather greater than the experimental one in the best approximation. CI results are greater than SCF ones except for 4-31G. This is attributed to the difference of the weight of CI estimation in the total energy between $(Cl-H-Cl)^-$ and $Cl-H\cdots Cl^-$. Since SCF energy for 4-31G is obtained at $R_{H\cdots Cl^-}=20$ a.u. by the computational restriction, CI correction value is taken much more than in other cases. The SCF energy difference between the point at $R_{H\cdots Cl^-}=$ 200 a.u. and 400 a.u. is in the order 10^{-6} Hartree which approaches to the threshold of SCF convergence 10^{-7} hartree. The ΔE_{corr} values for [6s5p](**) and its extended basis sets are close to the experimental value. The extension of the basis set reduce the calculated hydrogen bond energy ΔE_{corr}. The effect by diffuse function is greater than that by 3d polarization functions. Though CI increase ΔE_{corr}, the weight of CI is greater in [6s5p](**) than in [6s5p](**)+diff. ΔE_{corr} value (SCF) for [6s5p]**+diff (19.33 kcal mol^{-1}) closes to the experimental one.[14] This is better than the SCF value, 28.96 kcal mol^{-1}, by Thomson *et al.*[14] $\Delta E'$ value for 4-31G SCF, 31.7 kcal mol^{-1}, is in agreement with the result by Alagona.[42] Our results give support to the experimental prediction of hydrogen bond energy of isolated HCl_2^- ion by Ault and Andrews[26] as 18—20 kcal mol^{-1}.

To verify the propriety of the basis sets we also estimated the shift of atomic charge on Cl and H with the proton displacement from the central position in Figs. 5 and 6 respectively. The shifts of atomic charge on Cl indicate no significant variation between SCF and CI, and among small basis set and extended ones. The curve for CI are not shown in Fig. 5. In Fig. 5 it is shown that there is little difference on the charge of Cl^- between the curves for 4-31G and 4-31G**, but significant difference on the charge of Cl at HCl side in the process $ClHCl^- \longrightarrow ClH+Cl^-$. The shift of Cl charge on HCl molecule is the same for 4-31G and 4-31G** and is also the same for [6s5p]** and 4-31G(**). The shift of Cl^- charge is in similar curves for [6s5p]** and [6s5p](**). These results provide the fact that the effect of 3d polarization function appears mainly on the HCl molecule rather than Cl^- and calculated hydrogen bond energy is fairly improved as the difference between the charges on Cl^- and Cl become greater with the extension of basis set. The improvement by the extension of basis sets appears considerably on Cl atom of HCl. Figure 6 shows the shift of atomic charge on H with the proton displacement from the central position. For every basis set SCF and CI curves are nearly in pararrel but slightly close with each other in an asymmetric region. The anomalous variations of q'_H are detected for 4-31G results. 4-31G(**) and [6s5p](**) curves are close to 4-31G curve at $r_H=0$ a.u. and q'_H decrease monotonically in asymmetric region. The reason of the anomalous shift of q'_H is attributed to the lack of 2p polarization functions on H atom. The q'_H values for extended basis sets (*i.e.* 4-31G** and [6s5p]**) are almost the same and are about 0.3 at $r_H=0$ a.u., but the shift along r_H is the greatest for [6s5p]**. The great variations of

q'_H are detected for Dunning basis sets. The shift values for 4-31G and its extended basis sets are rather small. It is summarized that,

(i) the effect of 3d polarization functions on Cl appears to be the increace of q'_H at $r_H=0$ a.u.,

(ii) the effect of 2p polarization functions on H atom reduces the anomalous change of q'_H,

(iii) the effect of basis set extension 4-31G→[6s5p] results in a great shift of q'_H along r_H.

The check on R_{Cl-Cl}, the hydrogen bond energy and (q'_{Cl}, q'_H) indicate that the addition of 2p polarization functions on the basis functions of hydrogen bonding H atom makes remarkable improvement for the calculation and that even in the calculation by small basis set such as 4-31G** the potential function around the equilibrium distance may provide the reliable vibrational constants of HCl_2^-.

Discussion

As mentioned in the previous section, in type II spectra of $ClHCl^-$ anion the experimental values of ν_3 are classified into the two series of data. One is predicted to take the value about 1050 cm^{-1} in $CsCl\cdot 1/3$ [H_3O^+-HCl_2^-] crystal.[23] And another is about 700 cm^{-1} in $M^+HCl_2^-$ (M=alkali metal) in argon matrix.[17,26] One of our results by the use of 4-31G** basis set and CI calculation seems to correspond to the experimental value. However the results by 4-31G(**) and [6s5p](**) seems to correspond to the latter experimental value. Our results of R_{Cl-Cl} by the use of 4-31G** CI correspond to the former experimental one ($R_{Cl-Cl}=3.14$ Å). Whereas the calculated results $R_{Cl-Cl}=3.22$ Å and $\nu_3=700$ cm^{-1} are obtained by the use of 4-31G(**) and [6s5p](**) basis sets. Since the SCF results for [6s5p] system are the counterparts of that for 4-31G system, we discuss only the case of the latter basis set system from now on. The value $\nu_1=257$ cm^{-1} by 4-31G(**) CI calculation is only 3% greater than the experimental value. The value $\nu_3=686.2$ cm^{-1} is also in the same agreement with the average experimental ν_3 value 712 cm^{-1} (4% smaller). The same vibrational constants are predicted by the use of two dimensional analysis[43] of Lippinocott-Schröder potential.[11] By the use of vibrational SCF calculation for two dimensional potential surface, the results $\nu_3^H=652$ cm^{-1} and $\nu_3^D=459$ cm^{-1} ($\nu_3^H/\nu_3^D=1.42$) are obtained.[44] Whereas the prediction of ν_3 by one dimensional vibrational analysis results in $\nu_3^H=762$ cm^{-1} and $\nu_3^D=455$ cm^{-1} ($\nu_3^H/\nu_3^D=1.67$).[11] That is, the vibrational interaction between ν_1 and ν_3 makes the harmonic value of isotope frequency ratio. But these will be a fortuitious results. The results by larger basis sets including 3d polarization functions on Cl atoms predict the larger vibrational frequencies and shorter R_{Cl-Cl} distance The value $\nu_1=352$ cm^{-1} by 4-31G** CI(2) calculation is 41% greater than the experimental values except for $Na^+HCl_2^-$, but is only 17% over estimation for $Na^+HCl_2^-$. If the calculated ν_3 value 1050 cm^{-1} is overestimated, the predicted ν_3 value by the same correction (41% or 17%) comes to be 620 cm^{-1} or 872 cm^{-1}. It is possible to predict that ν_3 value in type II salt is about 700 cm^{-1}. In comparison with the experimental ν_3 value for $CsCl\cdot 1/3$ [$H_3O^+HCl_2^-$] is 1050—1200 cm^{-1}, calculated value 1050 cm^{-1} is in underestimation, which is the same in the case of 4-31G(**). It is also possible to predict that the shorter hydrogen bond ($R_{Cl-Cl}=3.14$ Å) may have the ν_3 value about 1050 cm^{-1} and have a single minimum potential. Since Schröder have not obtained the IR spectra for $CsCl\cdot 1/3$ [$H_3O^+DCl_2^-$], we can not clarify which of the ν_3 values are reasonable from the view point of isotope effect. At least we can predict that HCl_2^- anion in the shorter R_{Cl-Cl} distance ($R_{Cl-Cl}=3.14$ Å) has a single minimum potential and that the symmetric HCl_2^- anion causes the type II spectra which is perfectly different from type I in smaller ν_3 value.

We have not calculated the potential surface of ν_2 mode. From the group theory consideration in centrosymmetric HCl_2^- anion ($D_{\infty h}$ symmetry) ν_1, ν_2, and ν_3 modes have the symmetry species Σ_g^+, Π_u, and Σ_u^+ respectively.[18] This implies that the inter-mode interaction is negligible between ν_2 and ν_3 and between ν_1 and ν_3. Experimentally ν_1 and ν_2 values indicate no significant shifts between type I and type II salts in comparison with the great shift of ν_3. Thus we concern mainly with the one dimesional potential surface along the D_∞ axis for the ion.

^{35}Cl Nuclear Quadrupole Resonance (NQR) spectroscopy provides the information about the position of H atom in HCl_2^- ion, *i.e.* whether the ion is centrosymmetric or not. Type I salts indicate ^{35}Cl NQR value near 20 MHz, *i.e.* 20.22 MHz for $(CH_3)_4N^+HCl_2^-$ (at 77 K),[24,45,46] 21.27 MHz for $Cs^+HCl_2^-$ (at 166 K).[24] Whereas type II show the value about 12 MHz, *i.e.* 11.89 MHz[24] or 12.48 MHz[47] for $(C_2H_5)_4N^+HCl_2^-$ (at 77K), 11.94 MHz for $CsCl\cdot 1/3$ [$H_3O^+HCl_2^-$] (at 203 K).[24] Townes-Dailey theory relates the ^{35}Cl quadrupole coupling constant e^2qQ/h with the charge δ_{Cl} on Cl by the following formula,

$$(e^2qQ/h)_{ion}(e^2qQ/h)_{atom} = 1 - \delta_{Cl}, \quad (6)$$

where δ_{Cl} is corresponding to q'_{Cl} in Fig. 5. Using this relation and the experimental NQR data, Evans and Lo estimated the net-charge density distribution of symmetric HCl_2^- anion.[47] The results are Cl(0.86)··· H(0.57)–Cl(0.57) for asymmetric anion and Cl(0.74)–H(0.52)–Cl(0.74) for symmetric one. This suggests that the large ^{35}Cl NQR frequency is attributed to the small net-charge density of Cl atom on HCl side of asymmetric ion and the low frequency to the relatively high density of the symmetric one. This picture is supported by Cousseau *et al.* (1973) on the same estimation for $[(C_2H_5)_3NH]^+HCl_2^-$ salt.[48] A priori accurate theoretical prediction of ^{35}Cl NQR frequency on HCl_2^- ion is given by Thomson *et al.*[14] ^{35}Cl NQR value by the use of Townes-Dailey theory and MO calculation is 21.0 and 6.3 MHz for asymmetric ion ($R_{Cl-Cl}=3.22$ Å and $R_{HCl}=1.365$ Å), 13.11 MHz for symmetric ion ($R_{Cl-Cl}=3.14$ Å and $R_{HCl}=1.57$ Å). We have the net charge distribution on HCl_2^- ion for the variation of basis set and the method (SCF and CI). (See Figs. 5 and 6.) From Fig. 5 we can see that the charge distribution on Cl split into Cl^- and Cl in HCl molecule with the variation of H position. The q'_{Cl} value at the symmetric

position is estimated about 0.62—0.65 which is in somewhat underestimation with the result by Evans and Lo.[47] In the asymmetric position of proton our result by 4-31G(**) predicts q'_{Cl} values as 0.52 and 0.70 (at r_H= 0.228 Å), which are in well agreements with the results by Evans and Lo.[47] The tendencies are same in larger basis sets. There are some discussions on the reliability of Mulliken population analysis.[51] But we can explain qualitatively the shift of charge density according to the equilibrium position of proton. These gross population on atoms are not so unrealistic. Cousseau *et al.* (1973)[49] also discussed the proton NMR shift on HCl_2^- ion. The proton NMR chemical shift values are 9.6 ppm for asymmetric ion and 13.9 ppm for symmetric ion. Martin and Fujiwara (1971)[50] suggested that in these cylindrically symmetric system all the significant contributions to the ^1H shielding increasing 1s orbital population of H atom. Estimated δ_H values by Cousseau *et al.* are 0.50 for asymmetric and 0.42 for symmetric ion. Thus the large ^1H shift is the corresponding with the low density on H atom of symmetric HCl_2^- ion. Figure 6 shows that our results on δ_H at symmetric position are scattered in region from 0.77 to 0.69, where δ_H is corresponding to $1.0-q'_H$ in Fig. 6. The result by 4-31G** SCF is 0.69 (at symmetric position). This result is relatively great in comparison with the results by Evans and Lo[47] and Cousseau *et al.*[49] But we can see from Fig. 6 that the increacing tendency of δ_H from the symmetric to asymmetric position seems to explain the difference of ^1H chemical shift between the symmetric position and the asymmetric position of H atom. The relatively low net-charge density on H atom is also explained by the spacing of MO in the occupied valence and virtual regions. Figures 7 and 8 show the orbital correlation diagrams of HCl_2^- ion for 4-31G(**) and 4-31G** basis sets. Both in HCl and HCl_2^- 1s orbital of hydrogen forms the LUMO and the orbital energy of LUMO is increasing in HCl_2^- in comparison with isolated HCl molecule. Whereas HOMO consists of σ_u orbital which is accompanied by the degenerate orbitals π_g and π_u with the slightly small energy differences. This is due to the long Cl—Cl distance which decrease the in phase overlapping of orbitals and minimize the out of phase overlapping. Then the anti-bonding orbitals σ_u and π_g become stable. As a result 1s orbital of H comes to be LUMO to decrease δ_H and σ_u become HOMO to increase the absolute value of δ_{Cl}. Estimated net-charge density of HCl (literature value) is H(0.62)–Cl(0.38), which turned out to be an opposite net-charge distribution both in symmetric and asymmetric HCl_2^- ions.[47] It is the same in our case that H(0.85)–Cl(0.15) turns out to be Cl(0.63)–H(0.74)–Cl(0.63) for 4-31G(**) SCF. Martin and Fujiwara note that, "As the halide ion, X^-, approaches the positive (H) region of the HX molecule, electronic charge is repelled out of the hydrogen orbital." The situation is well established not only by the shift of q'_{Cl} and q'_H (Figs. 5 and 6) but also by the orbital correlation diagram of HCl_2^- (Figs. 7 and 8).

Figure 8 also explains the anomalous CI potential surface of proton by 4-31G** CI(1) (*i.e.* CI expansion terms are 4005). CI correction energy is abnormally minimized at the center of HCl_2^-. CSF of CI(1) is

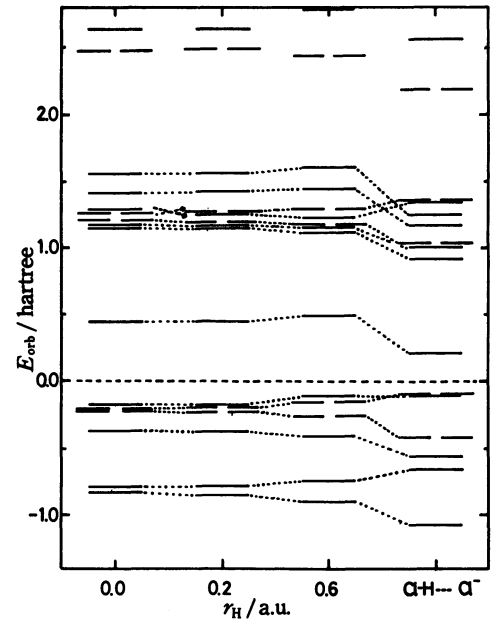

Fig. 7. Orbital correlation diagram of HCl_2^-(4-31G(**) basis set) on the proton displacement from the central position at R_{Cl-H}=3.228 Å. Cl–H···Cl⁻ denotes the position at r_{H-Cl}=1.257 Å and $r_{H\cdots Cl^-}$=211.7 Å, which corresponds to the dissociation limit. Only the orbitals numbered 10—18 (occupied) and 19—31 (unoccupied) are shown. Correlation among the polarization functions are not shown.

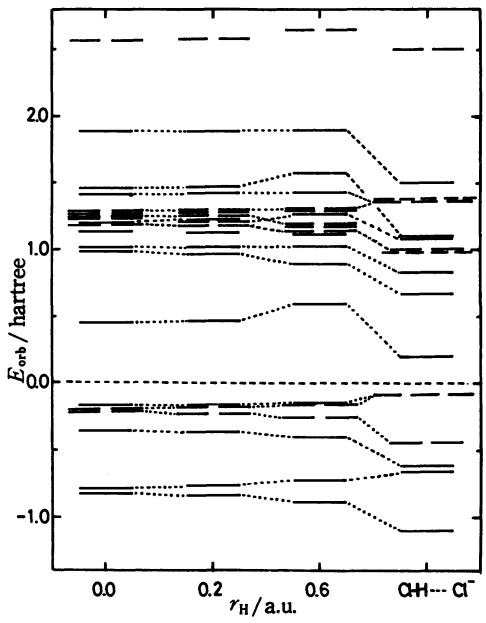

Fig. 8. Orbital correlation diagram of HCl_2^- (4-31G** basis set) on the proton displacement from the central position at R_{Cl-Cl}=3.140 Å. Cl–H···Cl⁻ denotes the position r_{H-Cl}=1.275 Å and $r_{H\cdots Cl^-}$=211.7 Å, which corresponds to the dissociation limit. Only the orbitals numbered 10—18 (occupied) and 19—38 (unoccupied) are shown. Correlation among the polarization functions are not shown.

constructed by the higher 8 occupied valence orbitals and lower 11 unoccupied orbitals. From Fig. 8 we can see eight doubly degenerate orbitals from 26th to 31st orbital, which correspond to 3d orbitals of Cl atoms. Since the crossing occurs between the lowest degenerate 3d orbitals (26th and 27th orbitals) and the 25th orbital in a region 0 a.u.$<r_H<$0.2 a.u., the contributions to the CI correction energy from these orbitals indicate significant change. Since CSF of CI(2) (CI expansion terms are 13041) consists of 8 occupied orbitals and 20 virtual orbitals, the anomalous potential surface is not formed. Though 4-31G(**) orbital correlation diagram (Fig. 7) indicates such crossings among the orbitals 24th, 25th (degenerate), and 26th, CSF consists of 8 occupied orbitals and 10 (CI expansion terms are 3321) or 13 (CI expansion terms are 5565) virtual orbitals. Thus the anomalous proton potential surface is not formed by any CI calculation for 4-31 G(**) basis set.

Now we have arrived at the conclusion summarized as follows:

(i) Symmetric HCl_2^- ions are formed in the salts which indicate ν_3 mode classified into type II IR spectra. But there is the possibility that the type II salts are classfied into the two types of molecules; *i. e.* one is the salts which indicate ν_3=700 cm^{-1} (*e.g.* $(C_2H_5)_4N^+HCl_2^-$ in aprotic solution or $Rb^+HCl_2^-$ in argon matrix), and another is the salts which possibly indicate ν_3=1050 cm^{-1} and has a single minimum potential of proton and the hydrogen bond length 3.14 Å (*e.g.* CsCl·1/3 [H_3O^+-HCl_2^-] in crystalline state).

(ii) At least we can predict by the largest CI calculation that the isolated linear symmetric HCl_2^- ion has the value R_{Cl-Cl}=3.14 Å and single minimum potential which causes the harmonic value of isotope frequency ratio. The SCF calculation by the largest basis set supports this prediction. (*i.e.* SCF barrier is very low and CI reduces the central barrier.) But we can hardly clarify which ν_3 values represents that of the linear symmetric HCl_2^- ion by the lack of accuracy of calculated potential curvature.

(iii) Calculated net-charge distribution also supports the conclusion (i)—(ii) in self consistent standpoint with the ^{35}Cl NQR spectra and ^1H NMR spectra which distinguish type II salts from type I salts. But the realistic structures of the former type II salts are not known. Thus we conclude with some reserve that type II HCl_2^- anion has symmetric structure of $D_{\infty h}$ symmetry.

The authors wish to express their thanks to Institute of Molecular Science (IMS) at Okazaki for the permission of the use of HITAC M-200H computer system for the MO calculation.

References

1) T. C. Waddington, *Trans. Faraday Soc.*, **54**, 25 (1958).
2) H. P. Dioxn, H. D. B. Jenkins, and T. C. Waddington, *J. Chem. Phys.*, **57**, 4338 (1978).
3) B. L. McGraw and J. A. Ibers, *J. Chem. Phys.*, **39**, 2667 (1963).
4) J. A. Ibers, *J. Chem. Phys.*, **40**, 402 (1964).
5) H. Boutin, G. Safford, and V. Brajovic, *J. Chem. Phys.*, **39**, 3135 (1963).
6) G. L. Cote and H. W. Thompson, *Proc. R. Soc. London. Ser. A*, **210**, 206 (1951).
7) J. A. A. Ketelaar, *Recl. Trav. Chim. Pays-Bas*, **60**,523 (1941)
8) J. J. Rush, L. W. Schröder, and A. J. Melveger, *J. Chem. Phys.*, **56**, 2793 (1972).
9) T. R. Singh and J. L. Wood, *J. Chem. Phys.*, **48**, 4567 (1968); **50**, 3572 (1969).
10) J. Almlöf, *Chem. Phys. Lett.*, **17**, 49 (1972).
11) G. J. Jiang and G. R. Anderson, *J. Phys. Chem.*, **77**, 1764 (1973).
12) S. A. Barton and W. R. Thorson, *J. Chem. Phys.*, **71**, 4263 (1979).
13) J. M. Williams and L. F. Schneemeyer, *J. Am. Chem. Soc.*, **95**, 5780 (1973).
14) C. Thomson, D. T. Clark, T. C. Waddington, and H. D. B. Jenkins, *J. Chem. Soc., Faraday Trans. 2*, **71**, 1942 (1975).
15) S. N. Vinogradov and R. H. Linnell, "Hydrogen Bonding," Van Nostrand Reinhold, New York (1971), p, 172,
16) T. C. Waddington, *J. Chem. Soc.*, **1958**, 1708.
17) J. C. Evans and G. Y-S. Lo, *J. Phys. Chem.*, **70**, 11, 20 (1966).
18) J. W. Nibler and G. C. Pimentel, *J. Chem. Phys.*, **47**, 710 (1967).
19) G. C. Stirling, G. C. Ludman, and T. C. Waddington, *J. Chem. Phys.*, **52**, 2730 (1970).
20) J. A. S. Smith, F. P. Temme, C. J. Ludman, and T. C., Waddington, *J. Chem. Soc., Faraday Trans. 2*, **69**, 1447 (1973).
21) J. Howard and T. C. Waddington, *Chem. Phys.*, **42**, 113 (1979).
22) L. W. Schröder and J. A. Ibers, *J. Am. Chem. Soc.*, **88**, 2601 (1966).
23) L. W. Schröder, *J. Chem. Phys.*, **52**, 1972 (1970).
24) C. J. Ludman and T. C. Waddigton, *J. Chem. Soc., Chem. Commun.*, **1970**, 405.
25) M. Dixon, R. E. Overill, and E. Platt, *J. Mol. Struct.*,**48**, 115 (1978).
26) B. S. Ault and L. Andrews, *J. Am. Chem. Soc.*, **97**, 3824 (1975); *J. Chem. Phys.*, **63**, 2466 (1975).
27) P. N. Noble and G. C. Pimentel, *J. Chem. Phys.*,**49**, 3156 (1968).
28) D. E. Milligan and M. E. Jacox, *J. Chem. Phys.*, **53**, 2034 (1970).
29) R. Ditchfield, W. J. Hehre, and J. A. Pople, *J. Chem. Phys.*, **54**, 724 (1971).
30) T. H. Dunning, Jr., *Chem. Phys. Lett.*, **7**, 423 (1970).
31) T. H. Dunning, Jr., *J. Chem. Phys.*, **53**, 2823 (1970).
32) C. M. Cook, GAUSSIAN 76, QCPE No. 391 (1980).
33) S. Rothenberg, R. H. Young, and H. F. Schaefer, III, *J. Am. Chem. Soc.*, **92**, 3243 (1970).
34) R. Ahlrichs and P. R. Taylor, *J. Chim. Phys.*, **78**, 315 (1981).
35) T. H. Dunning, Jr., and P. J. Hay, "Method of Electronic Structure Theory," in "Modern Theoretical Chemistry," ed by H.F. Schaefer, III, Plenum Press, New York and London (1977), Vol. 3, Chap. 1, pp. 1—49.
36) W. J. Hehre, W. A. Lathan, R. Ditchfield, M. D. Newton, and J. A. Pople, GAUSSIAN 70, QCPE No. 236, (1973).
37) B. J. Rothenberg, W. C. Ermler, and I. Shavitt, *J. Chem. Phys.*, **65**, 4072 (1976).
38) B. Roos *Chem. Phys. Lett.* **15**, 153 (1972).
39) S. R. Langhoff and E. R. Davidson, *Intern. J. Quantum Chem.*, **78**, 61 (1974).
40) R. Janoschek, E. G. Weidemann and G. Zundel, *J. Chem. Soc., Faraday Trans. 2*, **63**, 505 (1973).

41) K. P. Huber and G. Herzberg, "Constants of Diatomic Molecules," Van Nostrand Reinhold, New York (1979).
42) G. Alagona, E. Scrocco, and J. Tomasi, *Theoret. Chim. Acta*, **47**, 133 (1978).
43) T. Saitoh, K. Mori, and R. Itoh, *Chem. Phys.*, **60**, 161 (1981).
44) T. Saitoh, K. Mori, and R. Itoh, Annual Meetings of Molecular Electronic State and Molecular Structure of Japan, Kyoto, October 1981, Abstr., No, 4A16.
45) T. E. Haas and S. M. Welsh, *J. Phys. Chem.*, **71**, 3363 (1967).
46) J. C. Evans and G. Y-S. Lo, *J. Phys. Chem.*, **70**, 2702 (1966).
47) J. C. Evans and G. Y-S. Lo, *J. Phys. Chem.*, **71**, 3697 (1967).
48) C. H. Townes and B. P. Dailey, *J. Chem. Phys.*, **17**, 782 (1949).
49) J. Cousseau, L. Gouin, L. Jones, G. Jugie, and J. A. S. Smith, *J. Chem. Soc., Faraday Trans. 2*, **69**, 1821 (1973).
50) J. S. Martin and F. Y. Fujiwara, *Can. J. Chem.*, **49**, 3071 (1971).
51) S. Iwata, *Chem. Phys. Lett.*, **69**, 305 (1980).

 © 1983 The Chemical Society of Japan Bull. Chem. Soc. Jpn., 56, 2889—2893 (1983)

Microscopic Viscosity of the Interior Water Pool in Dodecylammonium Propionate Reversed Micelles

Kaoru Tsujii,† Junzo Sunamoto,*,†† and Janos H. Fendler*,†††

††*Department of Industrial Chemistry, Faculty of Engineering, Nagasaki University, Nagasaki 852*

†††*Department of Chemistry, Clarkson College of Technology, Potsdam, New York 13676, U.S.A.*

(Received February 5, 1983)

^{13}C-Chemical shifts and spin lattice relaxation times have been determined for dodecylammonium propionate/water/benzene or CCl_4 reversed micelles and for [^{13}C]glycine cosolubilized therein. Data obtained have been discussed in terms of the mobility of glycine molecules being effectively isolated from the surfactant headgroups by water molecules. The determined relaxation times of [^{13}C]glycine in glycerol-water mixtures correlated well with the macroscopic and microscopic viscosities of the reversed micellar solution. In a relatively small water pool, the apparent viscosity of water surrounding glycine in the micelle (microviscosity) was corresponding to that of 78% aqueous glycerol solution. Increasing the size of water pool resulted in decrased microviscosities.

Equilibria, rates, and pathways of inorganic and organic reactions are dramatically and specifically controlled by surfactant–water aggregates in apolar solvents, termed revesed micelles.[1] The reacting substrates are localized in a specific and restricted field provided by reversed micelles. In many respects, this water pool represents a unique and versatile reaction field. Depending on its water content, the microscopic polarity,[2,3] and viscosity[3-5] of the field and reactivity of water[6,7] can vary markedly, by which one can control chemical reactions as required. Therefore, detailed understanding of the nature of specific reaction field is not only inherently interesting, but is essential for the meaningful interpretation of the observed effects in controlling rate, equilibrium, and pathway.

As part of our overall program on the interactions and reactions in reversed micelles, we have investigated the microscopic viscosity of the water pool in the micelles using ^{13}C-NMR technique. The major advantage of this technique is that the use of probes which may perturb the system is avoided.[8] Additionally, ^{13}C-relaxation time measurements provide information on factors which determine molecular motions.[9] ^{13}C-NMR techniques have been applied to the investigations of aqueous micelles so far.[10] The present work reports data on ^{13}C-chemical shifts and spin lattice relaxation times for dodecylammonium propionate (DAP) aggregates in benzene or carbon tetrachloride and ^{13}C-labeled glycine cosolubilized therein. Glycine was chosen as the probe since it completely partitions into the water pool and the substantial rate enhancements have been observed in its ligand exchange reactions with vitamin B_{12}.[6a] The obtained data allows the elucidation of the apparent microscopic viscosity around glycine encapsulated in the restricted field provided by reversed micelles.

Experimental

DAP was prepared and purified by the established procedures.[11] Samples of [1-^{13}C]glycine and [2-^{13}C]glycine (90% enriched) were used as received from Merck, Sharp, and Dohm Co. Inc., N. J. Reagent grade benzene and carbon tetrachloride were distilled and stored over Linde 5A molecular sieve.

Special care was taken to eliminate paramagnetic impurities in sample preparations. The recommendations of Drs. Roberts[12a] and Smith[12b] were followed. Specifically, all glassware and NMR sample tubes were washed by caustic methanol (NaOH : MeOH : H_2O=1 : 4 : 1, w/w), soaked overnight in 0.35% EDTA (pH 8) and rinsed extensively by deionized and doubly distilled water. All NMR tubes were additionally steamed for 10—15 min prior to placing the sample solutions. Subsequent to introducing the sample into the NMR tubes, gaseous hydrogen sulfide was bubbled through them for approximately 10 min. Although any precipitate of metal sulfides was not discernible, the sample tubes were centrifuged just prior to commencing the measurements. Using these precautions, the observed spin lattice relaxation times for the carboxyl carbon of glycine agreed well with those reported.[12]

^{13}C-NMR chemical shifts and relaxation times (T_1) were determined at 25.0 MHz on a JEOL PFT-100 pulse-Fourier transform spectrometer connected to a Nicolet 1080 computer system. Wilmad coaxial NMR tubes were employed. First, a mixture of TMS and acetone-d_6 (1 : 1, by vol) in the coaxial tube was used to obtain the external standard and the NMR lock signal for 1.0 M (M=mol dm^{-1}) aqueous ammonium propionate as well as for the initial experiment in reversed micellar systems. Subsequently, solvent benzene was used as the second internal standard using external D_2O placed in a coaxial tube to obtain the lock signal. All the chemical shifts were given in ppm measured downfield form TMS. The inversion-recovery method was utilized for T_1-measurements under conditions of complete proton noise decoupling. FID signals for each spectrum were accumulated 8—32 times, depending on the glycine concentration. T_1-Values were computationally calculated employing either peak heights or areas. Differences between the two methods were less than the experimental error, ±10%. Viscosities of benzene solutions containing DAP–water aggregates, so-called macroscopic viscosities, were determined with use of an Ostwald viscometer at 27.0 °C (the temperature of the NMR probe). The viscometer was frequently calibrated with pure water.

Results and Discussion

Chemical shifts for the magnetically discrete carbon atoms of 1.0 M DAP in benzene with and without glycine ([1-^{13}C]glycine and [2-^{13}C]glycine) as a function

† On leave from Kao Corporation, Tochigi Research Laboratories, Ichikai-machi, Haga-gun, Tochigi 321-34

Table 1. ^{13}C-Chemical shifts of surfactant molecule and glycine in DAP/H_2O/benzene reversed micelles[a)]

$[H_2O]$ M	10^3[Glycine] M	δ DAP Carbons[b)] 1	2	3	4–5	6–9	10	11	12	1′	2′	3′	α-Carbon[c)] of glycine	Carboxyl carbon[d)] of glycine
<6 ppm	0.0	40.1	28.8	27.5	30.2	30.6	32.7	23.5	14.8	181.6	31.8	11.6		
1.3	0.0	40.5	28.8	27.8	30.3	30.6	32.8	23.6	14.8	182.3	31.9	11.7		
1.3	10.0	40.5	28.7	27.7	30.3	30.6	32.7	23.5	14.7	182.1	31.8	11.6	43.0	173.8
2.5	10.0	40.6	28.7	27.8	30.3	30.6	32.8	23.5	14.8	182.5	31.8	11.6	43.0	
2.5	50.0	40.5	28.7	27.8	30.4	30.7	32.9	23.6	14.8	182.6	31.9	11.7	43.1	
6.0	10.0	40.6	28.6	27.8	30.4	30.7	32.8	23.5	14.8	183.1	31.8	11.5	42.9	
9.0	10.0	40.6	28.6	27.8	30.4	30.7	32.8	23.6	14.8	183.4	31.8	11.6	42.9	

a) In ppm, relative to TMS, at 27.0 °C (probe temperature). b) DAP carbon are designated as $^{12}_{C}\text{-}^{11}_{C}\text{-}^{10}_{C}\text{-}^{9}_{C}\text{-}^{8}_{C}\text{-}^{7}_{C}\text{-}^{6}_{C}\text{-}^{5}_{C}\text{-}^{4}_{C}\text{-}^{3}_{C}\text{-}^{2}_{C}\text{-}^{1}_{C}\text{-}^{+}_{NH_3}\,^{-}_{O_2}\overset{1'}{C}\text{-}\overset{2'}{C}\text{-}\overset{3'}{C}$. c) In water, $\delta = 43.0$. d) In water, $\delta = 173.7$.

of water content are given in Table 1. Table 1 also contains values of the glycine carbon atoms cosolubilized in the micelles. The assignment for DAP carbon atoms was based on the known chemical shifts of alkyl amines and ammonium ions.[13,14)] The chemical shifts of C-1, C-2, and C-3 carbon atoms of DAP in benzene, 40.1, 28.8, and 27.5 ppm (Table 1), respectively, agree well with those of the corresponding carbon atoms of octylammonium trifluoroacetate in D_2O (40.2, 28.3, and 27.7 ppm). Although DAP is known to undergo polydispersion type association such as monomer$\rightleftharpoons$dimer $\rightleftharpoons$ trimer$\cdots\rightleftharpoons n$-mer,[15)] there were no observable distinct chemical shifts for monomers and aggregates. This implies, of course, that the equilibration between monomers and aggregates are rapid on the NMR time scale. Similar observations have been made for a variety of normal aqueous micelles.[10a)]

Addition of water alters the chemical shifts of only the carboxyl carbon (C-1′) and the carbon atom nearest to the cationic headgroup (C-1) of the surfactant. However, the magnitude of the change was modest (Table 1). This is not unexpected since the shielding of carbon nucleus is known to be less sensitive to medium change than that of hydrogen nucleus.[8b)] Even when propylammonium dodecanoate was employed instead of DAP, the effect of water content on the chemical shift of the C-1′ atom was larger than that of the C-1 atom. This may be explicable in terms of the difference in the type and strength of hydrogen bonding between the two headgroups and water: namely, $-\overset{\overset{O}{\|}}{C}-O^-\cdots H-OH$ and $-\overset{+}{N}H_2-H\cdots OH_2$.[16)] As expected, chemical shifts of the inner methylene carbon atoms (C-2 to C-12) of DAP are unaffected by solubilized water. These observations substantiate our proposal[1,3,16)] that water is solubilized upon interacting with the ionic headgroups of DAP and is isolated from the bulk apolar solvent by surfactant aggregates. Chemical shift of the C-1′ carbon atom of 1.0 M DAP shifts downfield from 181.6 ppm in the least amount (<6 ppm) of water to 183.4 ppm in the presence of 9.0 M water (Table 1). Chemical shifts of the methyl, methylene, and carboxyl carbon atoms of 1.0 M ammonium propionate in water at pH 7 were determined to be 11.7, 32.1, and 186.2 ppm, respectively. Chemical shifts of the methyl and methylene carbon atoms of propionate ion in the DAP/benzene reversed micellar system agreed well (Table 1) with those of ammonium propionate in water. Conversely, the chemical shift of the carboxyl carbon atom of 1.0 M ammonium propionate differs substantially from that of C-1′ of 1.0 M DAP in benzene. These results preclude the possibility of an experimental artifact in the observed chemical shift differences. Apparently, even at $R=9.0$ ($R=[H_2O]/[DAP]$), the environment of the surfactant headgroups is significantly different from that in bulk water. Chemical shifts of the surfactant carbon atoms are not altered by adding glycine. Magnetic resonances of the glycine carbon atoms in bulk water and reversed micellar core were found to be identical, implying that the amino acid, at least in the present series of experiments, is free enough from the direct interaction with headgroups of DAP.

^{13}C-Spin lattice relaxation times, T_1, of the carbon atoms of DAP are in Table 2. Since the exchange of DAP molecules between monomeric and aggregated environments is rapid with respect to $1/T_1$, the observed spin lattice relaxation times represent weighted averages of relaxation times in these environments:

$$1/T_1 = X_m/T_{1m} + X_d/T_{1d} + X_t/T_{1t} + \cdots X_i/T_{1i},$$

where suffixes, m, d, t, and i, stand for monomeric, dimeric, trimeric, and i-meric environments in the mole fraction, X, and relaxation time, T_1, respectively. Lack of information of the distribution of different sized aggregates in the 1.0 M DAP/benzene micelle precludes the dissection of T_1-values. Since ^{13}C-spin lattice relaxation times of micellar alkylammonium ions are considerably shorter than those of their monomers,[13)] the reported T_1-values are considered to represent upper limits in the environment of the aggregates. The relaxation times for the resolved carbon atoms of dodecylammonium ion in benzene (Tabel 2) are even longer than those reported for hexyl- and decylammonium ions in the same solvent,[13)] indicating further overall restriction in the motion of the ions.

T_1-Values for carbon atoms of the dodecylammonium ion increase along with the carbon chain on going from C-1 to C-12 (Table 2), indicating an increase in the segmental motion of methylene units.[13)] The segmental motion of a molecule can be expressed in terms of its ω/α-value, defined as the ratio of the spin lattice relaxa-

Table 2. ^{13}C-Spin-lattice relaxation times of dodecylammonium propionate in 1.0 M DAP/H_2O/glycine/benzene reversed micelles

$[H_2O]$/M	10^3[Glycine]/M	T_1/s[a]											ω/α[b]
		1	2	3	4–5	6–9	10	11	12	1′	2′	3′	
<6 ppm	0.0	0.15	0.36	0.54	0.82	0.79	1.8	2.5	3.0	4.1	0.83	2.7	20.0
1.3	0.0	0.15	0.35	0.34	0.78	0.64	1.7	2.6	3.4	5.5	0.83	2.8	22.7
1.3	10.0	0.15	0.31	0.25	0.79	0.61	1.6	2.0	2.8	5.5	0.80	3.1	18.7
2.5	10.0		0.28	0.30	0.59	0.51	1.3	2.1	2.8	7.2	0.70	2.9	
2.5	50.0	0.14	0.37	0.36	0.77	0.60	1.4	2.2		5.1	1.1	3.3	
6.0	10.0		0.33	0.33	0.56	0.48	1.3	1.8	2.3	10	1.3	2.6	
9.0	10.0	0.24	0.35	0.73	0.69	0.51	1.4	1.9	3.1	10	1.4	2.9	12.9

a) See footnote b in Table 1 for designation of the carbon atoms of DAP. b) Segmental motion, see text.

Table 3. ^{13}C-Spin lattice relaxation times of glycine in DAP reversed micelles[a]

Solvent	[DAP]/M	$[H_2O]$/M	10^3[Glycine]/M	T_1/s	
				α-Carbon of glycine	Carboxyl carbon of glycine
H_2O				3.7, 3.9	40 (44)[b]
C_6H_6	1.0	1.3	10	0.14	2.9
	1.0	2.5	10	0.29	
	1.0	2.5	50	0.35	
	1.0	6.0	10	0.96	
	1.0	9.0	10	1.3	
	0.20	1.3	10		13
	0.20	1.3	50		13
CCl_4	0.20	2.0	10		22
	0.20	2.0	20		21
	0.20	2.0	30		20
	0.20	2.0	40		19
	0.20	2.0	50	1.3	22

a) Using 90% enriched [1-^{13}C]glycine and [2-^{13}C]glycine. b) Ref. 12.

Table 4. Macroscopic and microscopic viscosities in DAP reversed micellar solutions

Solvent	[DAP]/M	$[H_2O]$/M	10^3[Glycine]/M	Viscosity/cP	
				Macroscopic[a]	Microscopic[b]
C_6H_6	1.0	1.3	10	2.70	32[c]
	1.0	2.5	10	3.89	13[c]
	1.0	2.5	50		11[c]
	1.0	6.0	10	6.90	3.5[c]
	1.0	9.0	10	8.48	2.6[c]
	0.2	1.3	10		3.1[d]
	0.2	1.3	50		3.1[d]
	1.0	0	0	1.64	
CCl_4	0.2	2.0	10		1.7[d]
	0.2	2.0	20		1.8[d]
	0.2	2.0	30		1.8[d]
	0.2	2.0	40		2.0[d]
	0.2	2.0	50		1.7[d]

a) Determined by the Ostwald viscosimeter at 27.0 °C in the absence of glycine. b) Estimated using Fig. 1. c) Using T_1-values of α-carbon atom. d) Using T_1-values of carbonyl carbon atom.

tion time of the terminal methyl carbon (ω) to that on or the nearest one to the ionic headgroup (α).[13] The higher the ω/α-value is, the more the segmental motion is pronounced. In the absence of glycine, ω/α for 1.0 M dodecylammonium ion in DAP/benzene micelle was 20.0. This value should be compared to 19.5 which was determined for 1.2 M decylammonium ion in benzene-d_6.[13] Solubilizing 0.01 M glycine in 1.3 and 9.0 M water/DAP/benzene micellar systems results in ω/α-values of 18.7 and 12.9 respectively. It should be pointed out that changes in ω/α-values is predominantly the consequence of changes in the relaxation times of the

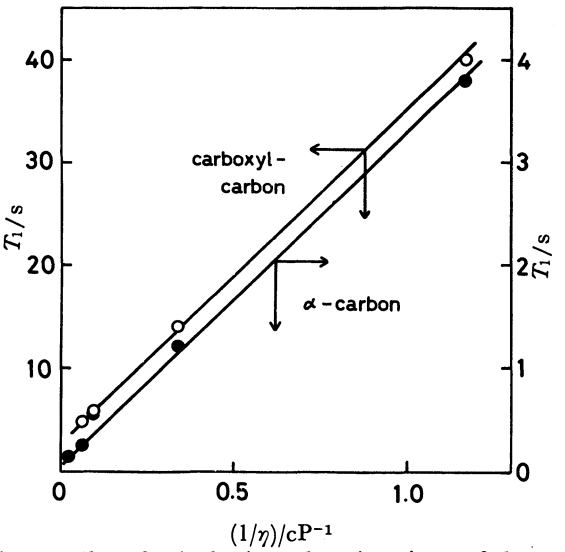

Fig. 1. Plot of spin lattice relaxation times of the carboxyl and α-carbon atoms of glycine in aqueous glycerol against the reciprocal viscosity of the solvent.

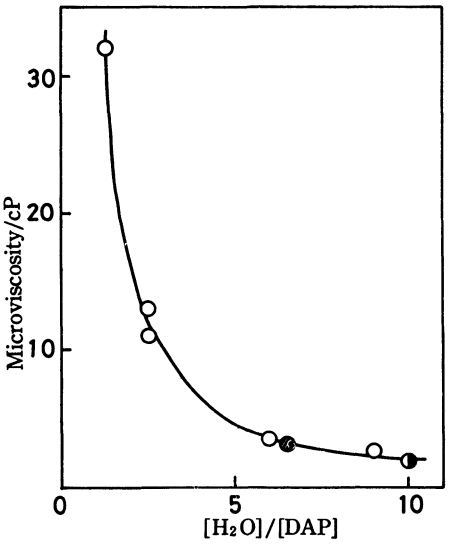

Fig. 2. Microscopic viscosity of the water pool estimated from T_1-values of glycine solubilized in DAP reversed micells as a function of R (=[H_2O]/[DAP])-value: ○, 1.0 M DAP/benzene micelle; ●, 0.2 M DAP/benzene micelle, and ◑, 0.2 M DAP/CCl_4 micelle, respectively.

C-1 carbon atoms (Table 2). A decrease in the segmental motion is brought about by an increase in the hydration at the site of the ionic headgroups. Increased hydration reduces the dipole-dipole interactions between surfactant headgroups and increases in the overall molecular motion.

Using ^{13}C-enriched glycine allowed the determination of spin lattice relaxation times of the carboxyl and α-carbon atoms of glycine (Table 3). Taking appropriate precautions, the determined T_1-values for the carboxyl carbon atom agree well with those cited.[12] The most significant fact emerged from Table 3 is the dramatic reduction in the relaxation times of both α and carboxyl carbon atoms in the water pool of DAP reversed micelles compared with those in bulk water. Evidently, the molecular motion of glycine is considerablly restricted in the micellar core. Macroscopic viscosities of the DAP/benzene reversed micellar system, the viscosity of the whole solution, were determined as a function of water content (Table 4). Increasing the water content results in an increase in the macroscopic viscosity of the whole system, which is ascribed to an increase in the size of water pool and the aggregation number. Consideration of the microenvironment of glycine in the DAP reversed micelle is more meaningful. Microscopic viscosities of the water pool of micelles have been assesed from the ruler obtained by the determined viscosities and ^{13}C-spin lattice relaxation times of glycine in aqueous glycerol solutions. A linear relationship has been obtained between the T_1-values of both the carboxyl and α-carbon atoms of glycine in glycerol–water mixtures and the reciprocal viscosities of the corresponding solution (Fig. 1). Using this correlation as a ruler, microviscosities of the water pool of DAP micelles have been read off (Table 4). Surprisingly, the apparent viscosity of the water pool of 1.0 M DAP/1.3 M water/benzene micelle containing 1.0×10^{-2} M glycine resembles that of approximately 78% aqueous glycerol solution. Conversely to the observed trend in the macroscopic viscosity, increasing the size of water pool resulted in a decreased microviscosity (Fig. 2). Figure 2 shows that the microscopic viscosity is determined predominantly by the R-value irrespective of the bulk organic solvent and the surfactant concentration, and that the microviscosity drastically decreases at the lower R-value region. Similar trends are seen in the relaxation time of water proton in ^{1}H-NMR[5b] and in the fluorescence polarization of pyranine[3] as a function of R-value. It is of interest to observe that changes of glycine concentration in a given DAP reversed micelle do not alter the microviscosity (Table 4). This is in accord with the above postulate that glycine may be appreciably isolated from the surfactant headgroup by water in the present systems. This means also that glycine must be localized in the "type II phase"[3] of water pool of reversed micelles.

This work had been carried out mostly in Texas A & M University when Janos H. Fendler was Professor of Chemistry in Department of Chemistry, Texas A & M University.

Supports by the Robert A. Welch Foundation, the National Science Foundation, U. S. Energy Research and Development Administration, and Grants-in-Aid for Scientific Research from the Ministry of Education, Science and Culture, Japan (447068 and 56550594) are gratefully acknowledged.

References

1) J. H. Fendler and E. J. Fendler, "Catalysis in Micellar and Macromolecular Systems," Academic Press, New York (1975); J. H. Fendler, *Acc. Chem. Res.*, **9**, 153 (1976); J. H. Fendler, "Membrane Mimetic Chemistry," John Wiley and Sons, New York (1982); J. Sunamoto and H. Kondo, *Yukagaku*, **26**, 389 (1977); J. Sunamoto, "Kagaku Sosetzu," ed by the Chemical Society of Japan, Japan Scientific Societies Press,

Tokyo (1983), No. 40, p. 105.

2) F. M. Menger and G. Saito, *J. Am. Chem. Soc.*, **100**, 4376 (1978).

3) H. Kondo, I. Miwa, and J. Sunamoto, *J. Phys. Chem.*, **86**, 4826 (1982).

4) J. Sunamoto, K. Iwamoto, M. Akutagawa, M. Nagase, and H. Kondo, *J. Am. Chem. Soc.*, **104**, 4904 (1982); J. Sunamoto, H. Kondo, J. Kikuchi, H. Yoshinaga, and S. Takei, *J. Org. Chem.*, **48**, 2423 (1983).

5) a) M. Wong, J. K. Thomas, and M. Grätzel, *J. Am. Chem. Soc.*, **98**, 2391 (1976); b) M. Wong, J. K. Thomas, and T. Nowak, *ibid.*, **99**, 4730 (1977); c) F. M. Menger, G. Saito, G. V. Sanzero, and J. R. Dodd, *ibid.*, **97**, 909 (1975).

6) a) C. J. O'Connor, E. J. Fendler, and J. H. Fendler, *J. Am. Chem. Soc.*, **95**, 600 (1973); b) C. J. O'Connor, E. J, Fendler, and J. H. Fendler, *J. Chem. Soc., Dalton Trans. 1*, **1974**, 625; c) J. H. Fendler, F. Nome, and H. C. vanWoert, *J. Am. Chem. Soc.*, **96**, 6745 (1974).

7) J. Sunamoto, H. Kondo, and K. Akimaru, *Chem.Lett.*, **1978**, 821 ; J. Sunamoto and T. Hamada, "Fundamental Research in Homogeneous Catalysis," ed by M. Tsutsui, Plenum Press, New York (1978), Vol. 3, p. 809.

8) a) G. C. Levy and G. L. Nelson, "Carbon-13 Nuclear Magnetic Resonance for Organic Chemists," Wiley Interscience, New York (1972); b) J. B. Stothers, "Carbon-13 NMR Spectroscopy," Academic Press, New York (1972).

9) G. C. Levy, *Acc. Chem. Res.*, **6**, 161 (1973); E. Breitmaier, K.-H. Spohn, and S. Berger, *Argew. Chem., Int. Ed. Engl.*, **14**, 144 (1975).

10) a) T. Nakagawa and F. Tokiwa, *Surface and Colloid Sci.*, **9**, 69 (1976); b) K. Kalyanasundaran, M. Grätzel, and J. K. Thomas, *J. Am. Chem. Soc.*, **97**, 3915 (1975).

11) A. Kitahara, *Bull. Chem. Soc. Jpn.*, **28**, 234 (1955); **30**, 586 (1957).

12) a) H. Pearson, D. Gust, I. M. Armitage, H. Huber, J. D. Roberts, R. E. Stark, R. R. Vold, and R. L. Vold, *Proc. Natl. Acad. Sci. U.S.A.*, **72**, 1599 (1975); b) I. C. P. Smith, private communication.

13) G. C. Levy, R. A. Kamoroski, and J. A. Halstead, *J. Am. Chem. Soc.*, **96**, 5456 (1974).

14) H. Eggert and C. Djerassi, *J. Am. Chem. Soc.*, **95**, 3710 (1973).

15) F. Y.-F. Lo, B. M. Escott, E. J. Fendler, E. T. Adams, Jr., R. D. Larsen, and P. W. Smith, *J. Phys. Chem.*, **79**, 2609, (1975); K. Tsujii, J. Sunamoto, F. Nome, and J. H. Fendler, *ibid.*, **82**, 423 (1978).

16) J. Sunamoto, T. Seto, and S. Yamamoto, *Bull. Chem. Soc. Jpn.*, **53**, 583 (1980).

The Crystal Structure of Tetramethyltetraselenafulvalenium Perrhenate, (TMTSF)(ReO_4)($C_2H_3Cl_3$)$_{0.25}$

Hayao KOBAYASHI,* Akiko KOBAYASHI,† Yukiyoshi SASAKI,† Gunzi SAITO,†† and Hiroo INOKUCHI††

Department of Chemistry, Faculty of Science, Toho University, Funabashi, Chiba 274

†*Department of Chemistry, Faculty of Science, The University of Tokyo, Hongo, Bunkyo-ku, Tokyo 113*

††*Institute for Molecular Science, Okazaki 444*

(Received February 7, 1983)

The crystal structure of (TMTSF)(ReO_4)($C_2H_3Cl_3$)$_{2.25}$ was determined. The crystals are monoclinic P2/c, $a=18.573(3)$, $b=7.418(2)$, $c=26.210(6)$Å, $\beta=107.85(2)°$, $Z=8$. TMTSF molecules are stacked to form diadic columns along the b axis. The mode of intermolecular overlapping between adjacent TMTSF molecules shows a new mode of overlapping. The strong alternation of the intermolecular Se–Se distances along the TMTSF columns indicates that this compound is a Peierls insulator, which is consistent with the semiconducting behavior. The Peierls instability is accompanied by a bending distortion of the planar TMTSF molecules. The room-temperature conductivity is 3×10^{-4} $(\Omega\,cm)^{-1}$, and the activation energy is 0.18 eV. There are some short Se–O contacts between ReO_4 anions and TMTSF stacks. The solvent molecnles ($C_2H_3Cl_3$) are located in the channel formed along the b axis.

Since the discovery of the organic superconductors, (TMTSF)$_2$X(X=ClO_4, PF_6···), a number of works have been undertaken to elucidate various aspects of the organic metal systems (TMTSF: tetramethyltetraselenafulvalene). The crystal structure analyses of (TMTSF)$_2$X compounds have revealed that these compounds have both one-dimensional (1-D) and two-dimensional (2-D) characters.[1] The TMTSF molecules are stacked face-to-face to form columns typically observed in 1-D organic metal systems. The interstack Se–Se contacts indicate the two-dimensionality of the crystals. Unlike the complex 2 : 1 salts of TMTSF, though no crystal-structure determination has been made on the simple 1 : 1 salts. In this paper, we report on the crystal structure of (TMTSF) (ReO_4) ($C_2H_3Cl_3$)$_{0.25}$.

Experimental

The black needle crystals were grown electrochemically from 1,1,2-trichloroethane by using twice-crystallized Bu_4NReO_4 as the electrolyte. The crystal data are: ($C_{10}H_{12}Se_4$) (ReO_4) ($C_2H_3Cl_3$)$_{0.25}$, $a=18.573(3)$, $b=7.418(2)$, $c=26.210(6)$ Å, $\beta=107.85(2)°$, $V=3489.7$ Å^3; monoclinic, space group P2/c, $Z=8$. The intensities were measured on a Rigaku automated four-circle diffractometer with Mo $K\alpha$ radiation ($\lambda=0.7107$ Å). The size of the crystal used was $0.04\times0.10\times0.30$ mm. The structure was solved by the direct method and has been refined to $R=0.089$, using 2742 independent reflections for which $|F|>3\sigma(|F|)$. The hydrogen atoms were not included in the calculations. The atomic coordinates are given in Table 1.[2]**

Table 1. Atomic coordinates of (TMTSF) (ReO_4)($C_2H_3Cl_3$)$_{0.25}$

Atom	x	y	z
Re(1)	0.2996 (1)	0.4890 (4)	0.0457 (1)
Re(2)	0.1916 (1)	0.0831 (4)	0.2630 (1)
Se(1)	0.0457 (2)	0.1889 (8)	0.0805 (2)
Se(2)	-0.1205 (2)	0.2189 (7)	0.0056 (2)
Se(3)	0.1084 (2)	0.3085 (7)	-0.0234 (2)
Se(4)	-0.0601 (2)	0.3351 (8)	-0.0953 (2)
Se(5)	0.4906 (2)	0.0543 (9)	0.3344 (2)
Se(6)	0.6291 (2)	0.0563 (8)	0.2907 (2)
Se(7)	0.3770 (2)	0.5263 (8)	0.1948 (2)
Se(8)	0.4463 (2)	0.5256 (9)	0.3173 (2)
Cl(1)	0.4212 (17)	0.3103 (71)	0.4484 (15)
Cl(2)	0.4260 (19)	0.7012 (73)	0.4519 (15)
C(1)	-0.0124 (25)	0.2315 (83)	0.0160 (19)
C(2)	0.0016 (23)	0.2789 (77)	-0.0305 (21)
C(3)	-0.0321 (32)	0.1368 (81)	0.1120 (15)
C(4)	-0.1080 (26)	0.1470 (80)	0.0695 (28)
C(5)	0.0921 (33)	0.3603 (79)	-0.0912 (22)
C(6)	0.0129 (26)	0.3678 (77)	-0.1313 (18)
C(7)	-0.0071 (29)	0.0820 (100)	0.1639 (20)
C(8)	-0.1741 (25)	0.0965 (82)	0.0916 (22)
C(9)	0.1564 (32)	0.3941 (102)	-0.1156 (25)
C(10)	-0.0069 (33)	0.4026 (77)	-0.1843 (18)
C(11)	0.5172 (23)	0.0501 (84)	0.2761 (19)
C(12)	0.5897 (30)	0.0155 (82)	0.3846 (25)
C(13)	0.6491 (22)	0.0217 (85)	0.3618 (21)
C(14)	0.5874 (30)	0.0097 (70)	0.4399 (23)
C(15)	0.7267 (26)	0.0015 (91)	0.3962 (26)
C(16)	0.4651 (22)	0.5202 (78)	0.2551 (16)
C(17)	0.3142 (29)	0.5505 (88)	0.2375 (18)
C(18)	0.3393 (26)	0.5620 (60)	0.2841 (19)
C(19)	0.2255 (27)	0.5796 (98)	0.2058 (21)
C(20)	0.2973 (36)	0.5839 (132)	0.3325 (29)
O(1)	0.2538 (20)	0.4967 (74)	0.0917 (13)
O(2)	0.3945 (16)	0.4921 (88)	0.0868 (16)
O(3)	0.2772 (19)	0.3254 (104)	0.0069 (16)
O(4)	0.2808 (22)	0.6591 (89)	0.0046 (17)
O(5)	0.1894 (23)	0.0915 (80)	0.2044 (19)
O(6)	0.1492 (24)	0.2706 (62)	0.2799 (18)
O(7)	0.2745 (36)	0.0774 (134)	0.3122 (21)
O(8)	0.1505 (27)	-0.1015 (72)	0.2784 (19)
C(21)	0.4821 (56)	0.5464 (155)	0.4785 (37)
C(22)	0.4684 (84)	0.4093 (233)	0.4773 (59)

Result and Discussion

The crystal structure is shown in Fig. 1. There are three crystallographically independent TMTSF molecules. One is on the general position, and the others, on the two-fold axis. They will hereafter be named molecules A, B, and B′ respectively (see Fig. 1). The crystal has channels along the b axis. The structure refinements have revealed the existence of solvent molecules in the channels. A similar inclusion of the $C_2H_3Cl_3$ solvent molecules has been observed in (BEDT–TTF)$_2$-ClO_4($C_2H_3Cl_3$)$_{0.5}$.[3] The volume of the channel indicates that two solvent molecules can be accommodated in the unit cell. However, the atoms of the solvent molecules are highly disordered and could not be located definitely. Fourier maps gave four large and four small peaks around (1/2, 1/2, 1/2), which were assumed to be the positions of the Cl and C atoms of $C_2H_3Cl_3$.

** A list of the observed and calculated structure amplitudes and a table of the thermal parameters are kept at the Chemical Society of Japan as Document No. 8339.

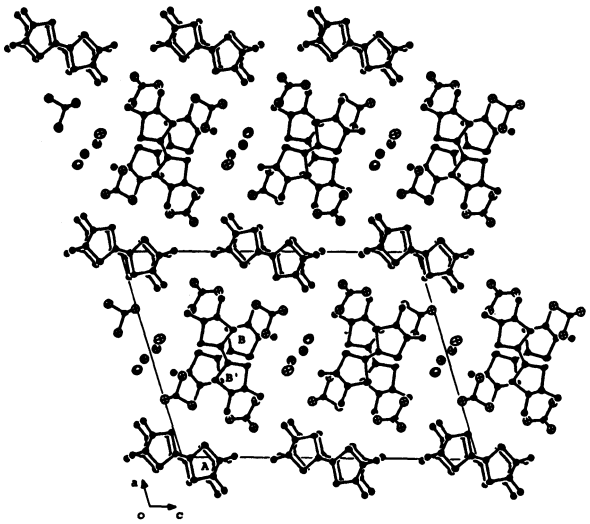

Fig. 1. The b axis projection of the structure of (TMTSF)(ReO_4) ($C_2H_3Cl_3$)$_{0.25}$.

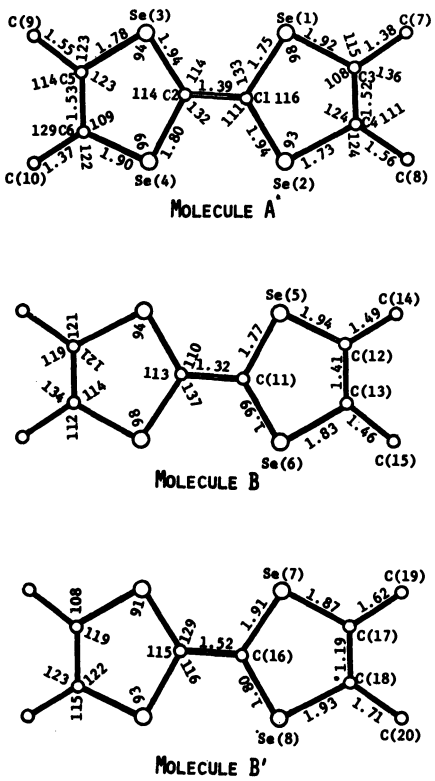

Fig. 2. Bond lengths (Å) and angles (°) of TMTSF. The standard deviations are: 0.06—0.07 Å (Se–C), 0.09—0.10 Å (C–C), 2—3° (C–Se–C), and 5—6° (C–C–Se and C–C–C).

In the least-squares refinements, the atomic populations of Cl and C atoms were taken to be 0.75 and 0.5 respectively.

Unlike (TMTSF)$_2ReO_4$,[4] (TMTSF)(ReO_4)($C_2H_3Cl_3$)$_{0.25}$ does not show the orientational disorder of ReO_4. However, the large temperature factors of some oxygen atoms of the ReO_4 anions indicate a large thermal motion. The isotropic thermal parameters (B/Å^2) are: O(1), 5.6; O(2), 6.1; O(3), 6.4; O(4), 6.7; O(5), 7.8; O(6), 6.5; O(7), 10.7; O(8), 7.7; Re(1), 4.6; Re(2), 5.1.[5] It is natural that the ReO_4 anion, with its relatively large thermal parameters (Re(2), O(5), O(6), O(7), and O(8)), shows a loose contact with

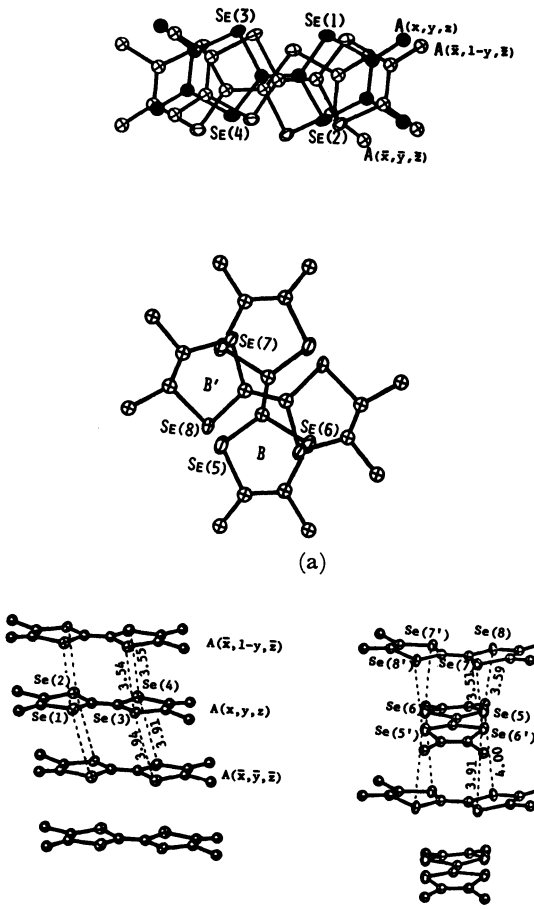

(a)

(b)

Fig. 3. (a) The modes of intermolecular overlapping. A(x, y, z), B(x, y, z), and B′(x, y, z) indicate three independent TMTSF molecules (see Fig. 1 and Table 1). A(u, v, w) indicates the molecule related to A(x, y, z) by the symmetry operation (u, v, w). (b) The intermolecular short Se–Se distances along the stacks.

Table 2. Bond lengths and angles of ReO_4. The standard deviations are: 0.05—0.10 Å (Re–O) and 2—4° (O–Re–O)

Bond length	l/Å	Bond angle	φ/°
Re(1)···O(1)	1.69	O(1)–Re(1)–O(2)	100
Re(1)···O(2)	1.79	O(1)–Re(1)–O(3)	114
Re(1)···O(3)	1.57	O(1)–Re(1)–O(4)	114
Re(1)···O(4)	1.64	O(2)–Re(1)–O(3)	116
		O(2)–Re(1)–O(4)	112
		O(3)–Re(1)–O(4)	101
Re(2)···O(5)	1.55	O(5)–Re(2)–O(6)	111
Re(2)···O(6)	1.72	O(5)–Re(2)–O(7)	121
Re(2)···O(7)	1.69	O(5)–Re(2)–O(8)	114
Re(2)···O(8)	1.68	O(6)–Re(2)–O(7)	101
		O(6)–Re(2)–O(8)	109
		O(7)–Re(2)–O(9)	100

TABLE 3. THE BEST PLANES OF THE TMTSF MOLECULES

Molecule A

(1) The best plane calculated from the atomic coordinates of the non-hydrogen atoms.
$-2.1187X + 7.1702Y + 6.7436Z = 1.770$ (Å)
(X, Y, and Z are coordinates referred to the direct lattice)
Deviations (Å): Se(1), 0.03; Se(2), 0.09; Se(3), 0.05; Se(4), 0.12; C(1), 0.02; C(2), 0.02; C(3), 0.04; C(5), 0.00; C(6), −0.05; C(7), −0.06; C(8), −0.09; C(9), −0.06; C(10), −0.11.

(2) The best plane calculated from the atomic coordinates of Se(1), Se(2), Se(3), Se(4), C(1), and C(2).
$-1.8954X + 7.1483Y + 7.0873Z = 1.817$
Deviations: Se(1), 0.02; C(1), 0.02; Se(3), 0.02; Se(4), 0.02; C(1), −0.02; C(2), −0.04.

(3) The best plane calculated from the atomic coordinates of Se(1), Se(2), C(3), C(4), C(7), and C(8).
$-2.6425X + 7.0702Y + 7.9249Z = 1.892$
Deviations: Se(1), −0.04; Se(2), 0.02; C(3), 0.05; C(4), −0.02; C(7), 0.01; C(8), −0.02.

(4) The best plane calculated from the atomic coordinates of Se(3), Se(4), C(5), C(6), C(9), and C(10).
$-1.5359X + 7.2652Y + 5.33982Z = 1.978$
Deviations: Se(3), −0.03; Se(4), 0.04; C(5), 0.01; C(6), −0.03; C(9), 0.03, C(10), −0.03.

Molecule B

(1) The plane calculated from the atomic coordinates of Se(5), Se(6), and C(11).
$7.418Y = 0.398$
Deviations: Se(5), 0.01; Se(6), 0.02; C(11), −0.03.

(2) The best plane calculated from the atomic coordinates of Se(5), Se(6), C(12), C(13), C(14), and C(15).
$0.9258X + 7.3500Y + 2.7742Z = 1.783$
Deviations: Se(5), 0.00; Se(6), 0.02; C(12), −0.06; C(13), −0.02; C(14), 0.05; C(15), 0.00.

Molecule B′

(1) The plane calculated from the atomic coordinates of Se(7), Se(8), and C(16).
$7.418Y = 3.888$
Deviations: Se(7), 0.02; Se(8), 0.01; C(16), −0.03.

(2) The best plane calculated from the atomic coordinates of Se(7), Se(8), C(18), C(19), and C(20).
$2.6087X + 7.3425Y - 1.7261Z = 4.490$
Deviations: Se(7), 0.02; Se(8), −0.01; C(17), −0.04; C(18), 0.03; C(19), 0.00; C(20), 0.00.

The bending angle α.

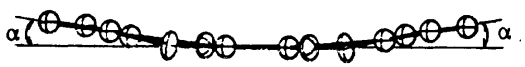

Molecule A 2.6, 3.9°
Molecule B 7.8
Molecule B′ 8.2

surrounding molecules: the (Se(6)···O(5)) contact is the only contact which is slightly shorter than the van der Waals distance (Table 4).

The bond lengths and angles are given in Fig. 2 and Table 2. As a result of the relatively small number of reflections, the standard deviations are fairly large. The least-squares planes of TMTSF molecules are listed in Table 3.

The TMTSF molecules are stacked face-to-face to form diadic columns. The modes of intermolecular overlapping are shown in Fig. 3. The A(x, y, z), A($\bar{x}, \bar{y}, \bar{z}$), and A($\bar{x}$, $1-y$, $\bar{z}$) molecules are stacked in a manner similar to that found in usual organic conductors, where A(u, v, w) indicates the molecule related to the A(=A(x, y, z)) molecule, by the symmetry operation (u, v, w). The mode of overlapping between A(x, y, z) and A($\bar{x}, \bar{y}, \bar{z}$) is similar to that observed in $(TMTSF)_2X$.[1] However, the mode between A(x, y, z) and A($\bar{x}$, $1-y$, $\bar{z}$) is that of a slightly modified direct overlap. The B and B′ molecules have C_2 symmetry, and the mode of intermolecular overlapping is of a new type. The longest axis of the B molecule is approximately perpendicular to that of the B′ molecule. This new overlapping mode appears to be natural, because this structure indicates a large intermolecular Se–Se interaction and a small intermolecular C–C repulsion. Since the symmetry of the highest occupied molecular orbital(HOMO) of TMTSF

TABLE 4. INTERMOLECULAR SHORT CONTACTS[a] (l/Å)

(x, y, z)···(x, y, z)		(x, y, z)···($\bar{x}, \bar{y}, \bar{z}$)	
Se(5)···Se(8)	3.59 Å	Se(1)···Se(4)	3.55
Se(3)···O(3)	2.99	Se(2)···Se(3)	3.94
Se(7)···O(1)	2.99		
Se(7)···O(2)	3.00	(x, y, z)···($1-x, y-1, 1/2-z$)	
		Se(6)···Se(7)	3.95
(x, y, z)···($\bar{x}$, $1-y$, $\bar{z}$)		Se(5)···Se(8)	4.00
Se(1)···Se(4)	3.55		
Se(2)···Se(3)	3.54	(x, y, z)···($1-x, y, 1/2-z$)	
Se(2)···O(4)	3.04	Se(6)···Se(7)	3.51
O(4)···C(8)	3.27	Se(6)···O(5)	3.34
(x, y, z)···(x, $1-y$, $z-1/2$)		(x, y, z)···($\bar{x}, y$, $1/2-z$)	
C(9)···C(20)	3.31	Se(6)···O(5)	3.34

a) The standard deviations are: 0.008 Å (Se···Se), 0.07 (Se···O), and 0.10 (C···O).

with ideal D_{2h} symmetry is b_{1u} (the coefficients of the atomic orbitals of the four Se atoms are identical), the magnitude of the intermolecular overlap integral of HOMO for this configulation will be almost equal to that for the direct overlapping. The short intermolecular Se–Se distances are given in Table 4 and Fig. 3. The average Se–Se distance between the A(x, y, z) and A($\bar{x}$, $1-y$, $\bar{z}$) molecules is 3.55 Å, but that between A(x, y, z) and A($\bar{x}$, $\bar{y}$, $\bar{z}$) is 3.93 Å. Similarly, the Se–Se separation between B(x, y, z) and B′(x, y, z) is 3.55 Å, and that between B(x, y, z) and B′(x, $y-1$, z) is 3.96 Å. Thus, the positions of the Se atoms are shifted alternately along the b axis from the positions of the regular arrangement, which makes the molecules nonplanar (see Fig. 3 and Table 3). The shortest Se–Se distance of 3.51 Å is much shorter than the van der Waals distance (4.0 Å). In (TMTSF)$_2$X, the Se–Se distance in the TMTSF stack is longer than 3.85 Å.[1,3] Unlike the case in (TMTSF)$_2$$ReO_4$, the TMTSF columns in (TMTSF)(ReO_4)($C_2H_3Cl_3$)$_{0.25}$ have no short Se–Se contact between adjacent columns (see Table 4). The only significantly short contact between TMTSF column can be seen between methyl carbons (C(9)–C(20), 3.31 Å). Thus, the TMTSF columns can be regarded as 1-D systems.

The temperature depence of the electrical conductivity shows that this compound is a semiconductor with the room-temperature conductivity of 3×10^{-4} $(\Omega\,cm)^{-1}$ and the activation energy of 0.18 eV (see Fig. 4).[6] Contrary to the semiconductive behavior of (TMTSF)(ReO_4)($C_2H_3Cl_3$)$_{0.25}$, (TMTSF)$_2$$ReO_4$ is metallic above 180 K(T_c), where a metal-insulator transition occurs.[7] The superconductivity appears above 9.5 kbar at 1.3 K.[8]

Since the stoichiometry of TMTSF to ReO_4 is 1 : 1, the diadic column of TMTSF indicates that the 1-D band formed along the TMTSF column is filled. Thus, the semiconductive nature of this salt is quite reasonable. The strong alternation of the intermolecular Se–Se distance is consistent with the Peierls instability of the 1-D metallic system. The intermolecular repulsion between the adjacent molecules in the same stack will tend to make the intermolecular spacings regular. On the other hand, the $2k_F$-(Peierls) instability of the 1-D chain tends to produce a diadic distortion in order to to gain the electronic stabilization energy. Since the 1-D band is considered to be made up of atomic orbitals of the Se atoms,[9] the periodical displacements of the other atoms do not contribute to the stabilization of the 1-D electronic system. Therefore, as a result of the Peierls instability, the intermolecular repulsion will make TMTSF molecules nonplanar. Besides the intra-stack interaction, the interaction between TMTSF molecules and ReO_4 anions may also be important. Since only a few short contacts can be seen between oxygen atoms and methyl carbons (Table 4), the steric repulsion between methyl carbons and ReO_4 is not important. However, significantly short contacts can be seen between the Se atoms of TMTSF and the O atoms of ReO_4. Consequently, some interaction must exist between these atoms. Similar short Se–O (or F) contacts have been observed in (TMTSF)$_2$X.[1]

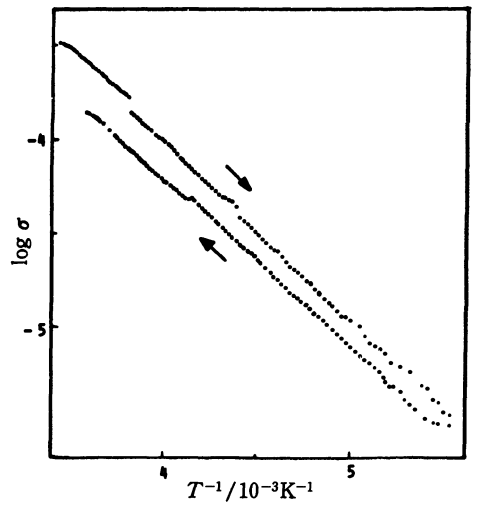

Fig. 4. The electrical conductivity of (TMTSF) (ReO_4) ($C_2H_3Cl_3$)$_{0.25}$.

A recent X-ray study by Moret, Pouget, Comes, and Bechgaard[10] has revealed that TMTSF columns in (TMTSF)$_2$$ReO_4$ are strongly modulated by the $2k_F$-wave below T_c(=180 K), where (TMTSF)$_2$$ReO_4$ is an insulator. They suggested that the correlation between the TMTSF molecules and the anion displacements can be analyzed as a cooperative phenomenon. The activation energy of about 0.20 eV in (TMTSF)$_2$$ReO_4$ is approximately equal to that of (TMTSF)(ReO_4)($C_2H_3Cl_3$)$_{0.25}$ (0.18 eV).

Since the elctron-phonon coupling in the commensurate system is considered to be strong, the large distortion must be related to that period of the $2k_F$-wave in (TMTSF)(ReO_4)($C_2H_3Cl_3$)$_{0.25}$, which is strongly commensurate with the lattice spacing.[11] The structure of this compound shows that the $2k_F$-wave is accompanied by molecular deformation. The bending deformation of the planar molecule has also been found in the partially oxidized platinum compound, $Rb_{1.67}[Pt(C_2O_4)_2]\cdot1.5H_2O$ (RbDOX), which has six-fold commensurate $2k_F$-structure.[14]

The average intermolecular Se–Se distance in the TMTSF stack is much smaller than that of (TMTSF)$_2$X ($\approx$3.9 Å). Therefore, if the TMTSF stack of (TMTSF)(ReO_4)($C_2H_3Cl_3$)$_{0.25}$ were regular, it would be a 1-D metal with a sufficiently large band width. However, the interstack interaction is not large enough to prevent the Peierls instability.

References

1) N. Thorup, G. Rindorf, H. Soling, and K. Bechgaard, *Acta Crystallogr., Sect. B*, **37**, 1236 (1981); F. Wudl, *J. Am. Chem. Soc.*, **103**, 7064 (1981); J. M. Williams, M. A. Beno, E. H. Appelman, and J. M. Capriott, *Mol. Cryst. Liq. Cryst.*, **79**, 319 (1982); H. Kobayashi, A. Kobayashi, G. Saito, and H. Inokuchi, *Chem. Lett.*, **1982**, 245; K. Bechgaard, K. Carneiro, F. B. Rasmussen, M. Olsen, G. Rindorf, C. S. Jacobsen, H. J. Pedersen, and J. C. Scott, *J. Am. Chem. Soc.*, **103**, 2440 (1981); J. M. Williams, M. A. Beno, J. C. Sullivan, L. M. Banovetz, J. M. Braam, G. S. Blackman, C. D. Carlson, D. L. Geer, and D. M. Loesing, *J. Am. Chem. Soc.*, to be published.

2) Adopting anisotropic temperature factors for the Se and Cl atoms and isotropic ones for C and O atoms, the block-

diagonal least-squares refinements gave the R value of 0.093. The subsequent anisotropic refinements of all the non-hydrogen atoms produced only a little improvement ($R=0.089$), but the temperature factor of C(3) became singular. Therefore, the isotropic temperature factors are adopted for C and O atoms (Table 1).

3) H. Kobayashi, A. Kobayashi, Y. Sasaki, G. Saito, and H. Inokuchi, *J. Am. Chem. Soc.* **105**, 297 (1983).

4) N. Thrup, G. Rindorf, and H. Soling, private communication; H. Kobayashi, unpublished paper.

5) Equivalent isotropic temperature factors as defined by W. C. Hamilton (*Acta Crystallogr.*, **12**, 609 (1959)).

6) The d.c. conductivity was measured along the b axis by using the four-probe method. Gold wires 0.025 mm in diameter were bonded to the specimen with silver paint.

7) C. S. Jacobsen, H. J. Pedersen, K. Mortensen, G. Rindorf, N. Thorup, J. B. Torrance, and K. Bechgaard, *J. Phys. C.*, **15**, 2651 (1982).

8) S. S. Parkin, D. Jerome, and K. Bechgaard, *Mol. Cryst. Liq. Cryst.*, **79**, 213 (1982).

9) T. Mori, A. Kobayashi, Y. Sasaki, and H. Kobayashi, *Chem. Lett.*, **1982**, 1923.

10) R. Moret, J. P. Pouget, R. Comes, and K. Bechgaard, *Phys. Rev. Lett.*, **49**, 1008 (1982).

11) The amplitude of the $2k_F$-wave is considered to be small. However, it has not been determined definitely in any organic conductors. In partially oxidized platinum complexes, the amplitudes of the $2k_F$-wave have been estimated as: 0.025 Å $K_2[Pt(CN)_4]\cdot Br_{0.3}\cdot 3H_2O$ (KCP), 0.025 Å;[12] $K_{1.81}[Pt(C_2O_4)_2]\cdot 1.5H_2O$ (γ-KDOX), 0.17 Å;[13] $Rb_{1.67}[Pt(C_2O_4)_2]\cdot 1.5H_2O$ (RbDOX), 0.17 Å[14]

12) J. M. Lynn, M. Iizumi, and G. Shirane, *Phys. Rev. B*, **12**, 1154 (1975).

13) H. Kobayashi, I. Shirotani, A. Kobayashi, and Y. Sasaki, *Solid State Commun.*, **23**, 409 (1977); A. Kobayashi, Y. Sasaki, I. Shirotani, and H. Kobayashi, *ibid.*, **26**, 653 (1978).

14) A. Kobayashi, Y. Sasaki, and H. Kobayashi, *Bull. Chem. Soc. Jpn.*, **52**, 3682 (1979).

 © 1983 The Chemical Society of Japan Bull. Chem. Soc. Jpn., 56, 2899—2904 (1983)

Demonstration of Electrostatic Field Effect Working on Dipolar Liquids with Correlation to Their Structures

Goro WADA,* Yasuko TERUTA, Takako KATO, and Naoko BITOH
Department of Chemistry, Faculty of Science, Nara Women's University, Nara 630
(Received February 7, 1983)

When an electrically charged body is allowed to come close to a fine water stream falling down from the tip of a capillary, the vertical stream is bent a little towards the charged body by an attractive force due to the electricity-water dipole interaction. We constructed a simple equipment for the purpose of quantitative determination of the attractive force by defining a quantity P to search the correlation between the permittivity ε and the dipole momemt μ of polar liquids. For various pure polar liquids and mixtures at various mole fractions x of the components, we found a proportional correlationship $P\bar{\varepsilon}=k\bar{\mu}$ with a common constant k, when the electric potential applied on an electrode, temperature, and flow velocity are fixed. In the cases of mixtures, $\bar{\varepsilon}=\sum x_i\varepsilon_i$ and $\bar{\mu}=\sum x_i\mu_i$ are used. Pure liquids, such as methanol, ethanol, 1-propanol, acetic acid, acetone, acetonitrile, tetrahydrofuran, 1,4-dioxane, nitromethane, dimethyl sulfoxide, and nitrobenzene and mixtures, such as benzene–ethanol and benzene–nitrobenzene obey the proportionality rule approximately. On the other hand, water and some mixtures such as benzene–acetic acid and benzene–tetrahydrofran fail the rule, suggesting the possibility that molecular association occurs due to their mutual interactions in the liquids. Thus, this method may be considered as a simple demonstration illustrating the states of molecular aggregation in polar liquids.

We often experience a phenomenon even in our daily life that when something electrically charged such as mechanically rubbed plastics is brought close to a fine and smooth water current falling down from an end of a tap, the vertical pillar of water is forced to bend considerably towards the electrically charged body. This is caused by the interaction between the electricity on the charged body and the electric dipoles of water molecules. An idea that this may be caused, instead, by the frictional electricity produced on water surface when it is made to flow down off the end of the tap is easily denied by the facts that the phenomenon is not observed at all if water is replaced by nonpolar liquids such as benzene or 1,4-dioxane and that the interaction force occurs always to be attractive but never repulsive indifferent to whether the sign of the electricity on the rubbed body is positive or negative.

Some effects of electric[1,2] or magnetic[3] fields have ever been found and investigated on the viscosities of water and other several liquids. But the attractive force itself working on polar liquids in electric fields have never been quantitatively measured yet. In the present investigation, we constructed an equipment suitable for quantitative determinations of the forces applied to a variety of dipolar liquids; pure water, some organic substances, their mixtures, and various aqueous solutions of electrolytes. It was necessary to set up a device for reproducing the desired electric fields of constant strength and maintaining the stationary flow of liquids for the purpose. Then, the correlations of the dipole moments of liquids with their permittivities (dielectric constants) will be discussed as a convenient clue for the molecular association in liquids.

Experimental

Equipment. In order to apply a stable and reproducible electric field, a Hamamatsu Regulated DC Power Supply Model HTV-C752 was used as a high voltage source. The electrode of high voltage was made of a copper plate of 2 cm width and 4 cm length. The apparatus for the observation was constructed by wholly connected glass for the use of organic substances, as is shown in Fig. 1. The notations in the figure indicate as follows; A: sample liquid reservoir, B: overflow branch for keeping constant liquid level, C: reservoir bottle for waste liquid, D: capillary tip, E: electrode, F: thermostat, S: high-voltage source, and T: telescope with micrometer. Among the numbered stopcocks 1—6, only cock 1 is of three-way. The electrode and the capillary are settled vertically, and the vertical center line on the electrode surface was arranged to face just in paralled to the liquid current which was steadily flowing down from the end of the capillary tip. The distance between the electrode and the

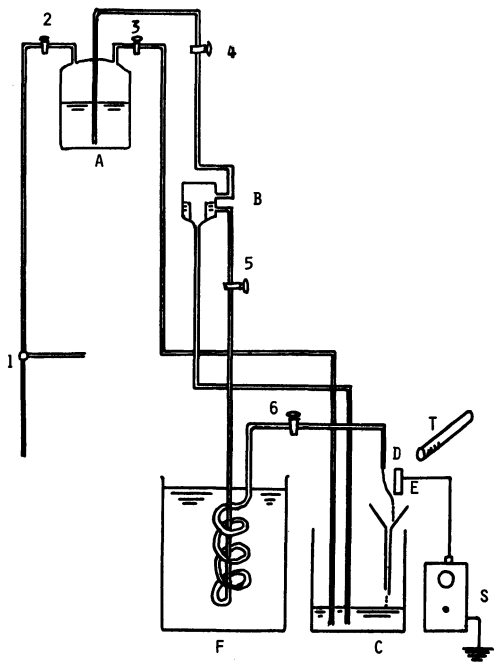

Fig. 1. Glass-connected apparatus for stationary liquid flux.
A: Sample liquid reservoir, B: overflow branch device, C: reservoir bottle for waste liquid, D: capillary tip, E: electrode, F: thermostat, S: high-voltage source, T: telescope with micrometer, cocks: 1—6.

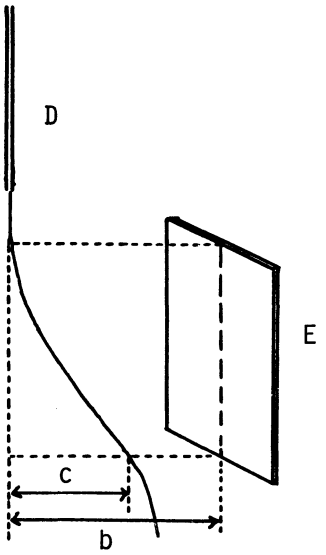

Fig. 2. Arrangement of capillary tip and electrode.

liquid stream was easily varied. The overflow branch B was deviced to make the pressure of the liquid at the capillary tip unchanged and reproducible in order to allow the liquid to flow down steadily during the cource of the observation. The telescope was used to measure the distance between the stream and the electrode to see how far the liquid stream was forced to displace horizontally towards the electrode.

Procedure. After an appropriate portion of the sample liquid in the reservoir C is pumped up to the reservoir A by use of an aspirator, slightly compressed air is applied on the liquid in A through the cock 1 to let the liquid flow down towards the overflow branch B *via* the cock 4. The main flow goes as far as to the capillary tip D through the thermostat F and the cocks 5 and 6 on the way as a steady current, while the overflowed liquid returns directly to the reservoir bottle C. The liquid in C can be used repeatedly. The regulation of the current was carried out at the cock 6. Cock 5 was used only for the interuption of the liquid current. The temperature of the liquid was 25 °C, except otherwise noted. The voltage on the electrode was variable 0—2.5 kV by the DC power supply and was generally kept at 2.5 kV.

In Fig. 2, the arrangement of the capillary tip and the electrode is shown. The distance b denotes the initial separation between the liquid and the electrode with no electric charge, while c is the distance of displacement caused by attraction when the electrode is charged. The distances b and c are measured horizontally at the bottom height of the electrode. Many conples of b and c were determined for the respective sample liquds.

Since the viscosities and the densities of the liquids differ from one another, it is necessary to regulate the flow velocity fixed for the purpose of comparison; the flow velocity was adjusted according to the amount of the liquid fallen during a definite time. The densities of the respective liquids were measured by use of a small pycnometer.

Materials. Water was purified by double distillation after being deionized through ion-exchange resin. Organic substances used were methanol, ethanol, 1-propanol, acetone, acetonitrile, nitromethane, 1,4-dioxane, tetrahydrofuran, acetic acid, dimethyl sulfoxide (DMSO), benzene, nitrobenzene, phenol, and pyridine, and electrolytes used were LiCl, NaCl, KCl, RbCl, $MgCl_2$, $(CH_3)_3NHCl$, and $(C_2H_5)_3$-NHCl, all of which were of the special reagent grade, being further purified by distillation or recrystallization for the use.

Results and Discussion

Evaluation of Magnitude of Attractive Force. The distances b and c have been defined above in Fig. 2. In general, the smaller the value of b, the larger becomes that of c; finally the liquid stream may touch the bottom edge of the electrode, where a length A is defined at the extreme distance, as $A \equiv b = c$. Figure 3 shows the relationships of c with b in the case of pure water, in which $\log(b/c)$ is found to be linear with respect to $\log b$ with an empirical formula,

$$\log \frac{b}{c} = m + n \log b.$$

Accordingly, the value of A is obtained by the linear extrapolation of $\log(b/c)$ to zero as equal to $A = 10^{-(m/n)}$. Thus, A is characteristic of the dipolar property of the liquid so far as the temperature and flow velocity are given in a definite electric field.

Since A is an integrated distance of horizontal displacement of liquid attracted towards the electrode with the lapse of time during which the falling liquid stream passes just the vertical length of the electrode. Therefore, the value of A multiplied by the liquid density d may be proportional to the attractive force f wrought on the dipolar liquid ($f \propto Ad$). If it is hypothesized for the sake of simplicity that the electricity on the electrode is a point charge (q) and that the dipolar liquid is fixed at the distance of $b-c$ apart from the point charge, the dipoles of the liquid are attracted by a force f as expressed below:

$$f = -\frac{2\mu q}{\varepsilon(b-c)^3},$$

where μ and ε are the dipole moment and the permittivity of the liquid, respectively. This correlation may hold approximately under the more complicated circum-

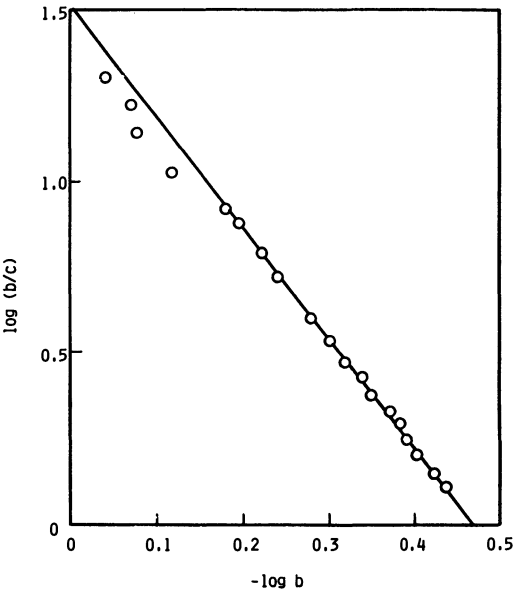

Fig. 3. Linear relationship of $\log(b/c)$ *vs.* $\log b$ in the case of pure water.

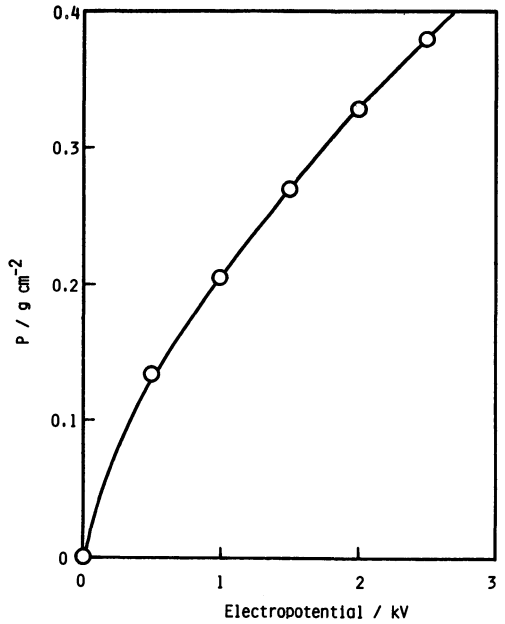

Fig. 4. Correlation of P with the electric potential of the electrode in the case of pure water at a flowing rate 0.810 cm^3 s^{-1} and 25 °C.

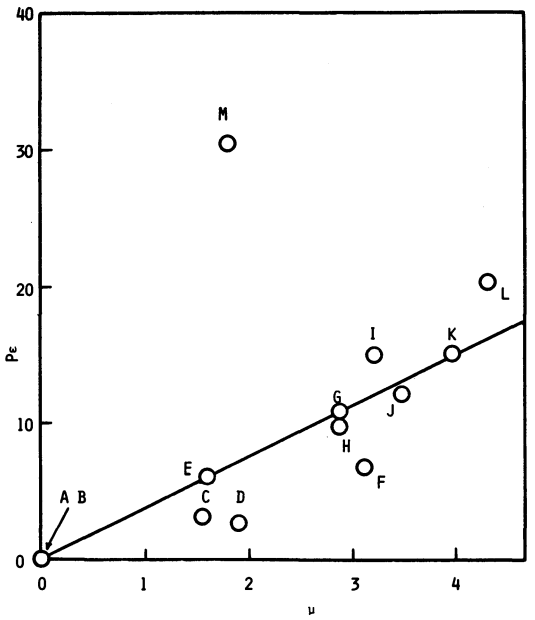

Fig. 5. Proportionality between $P\varepsilon$ and μ.
A: Benzene, B: 1,4-dioxane, C: tetrahydrofuran, D: acetic acid, E: 1-propanol, F: acetone, G: methanol, H: ethanol, I: nitromethane, J: acetonitrile, K: nitrobenzene, L: dimethyl sulfoxide, M: water.

stances like the present experimental conditions, as $f \propto \mu/\varepsilon$. Combining the former proportionality with this, the following equation can be derived, if Ad is denoted by P and k is put as a proportional constant.

$$P \equiv Ad = k\frac{\mu}{\varepsilon} \quad (1)$$

After all, the proportionality of $P\varepsilon$ to μ will be confirmed by measuring A and d for various polar substances, and the obedience to and violation against the proportionality rule may lead us to the discussion on the problems on their molecular structures in liquidous state, as in the followings.

Dependence of P upon Electric Potential of Electrode. Figure 4 shows the correlation of P with the electric potentials of the electrode in the case of water at the flow velocity 0.810 cm^3 s^{-1} and 25 °C. The value of P increases with the increasing potential. In the following observations, the potential will be always fixed at 2.5 kV.

Dependence of P upon Temperature. P exhibited no significant variation with temperature within the range of 10—40 °C, $P=0.39\pm0.03$ g cm^{-2} in the case of water. Nevertheless, the orientation of dipoles in an electric field may be more perturbed by thermal agitation, and therefore P is expected to be smaller at higher temperatures. In the following observations, the temperature will be fixed at 25 °C.

Dependence of A upon Flow Velocity of Liquids. The flow velocity of a liquid current falling down from the tip of the capillary is expressed by $\pi r^2 u$ in cm^3 s^{-1}, where r and u represent the internal radius of the capillary and the current velocity of liquid stream, respectively. On the other hand, since the current velocity u is approximately equal to l/t where l and t are vertical length of the front of the electrode and the time of passing as far as l for the liquid, respectively, the flow velocity is given by $\pi r^2 l/t$. Since A is affected by t, t as well as both r and l should be fixed constant by adjusting the current by use of cock 6, for the purpose of relative comparisons of A with one another among various polar liquids. The flow velocity used throughout the investigation was 0.735 cm^3 s^{-1}. In the cases of different velocities from this value, A was corrected to the standard velocity by virtue of a calibration curve.

Proportional Correlation of Pε vs. μ for Pure Liquids. Figure 5 represents the proportionality between $P\varepsilon$ and μ for 13 pure substances:[4-6] water ($\varepsilon=78.5$, $\mu=1.80$), methanol (32.63, 2.87), ethanol (24.30, 2.89), 1-propanol (20.1, 1.66), acetic acid (6.15, 1.92), acetone (20.7, 3.11), acetonitrile (37.5, 3.45), tetrahydrofuran (7.39, 1.63), 1,4-dioxane (2.21, 0), nitromethane (35.87, 3.23), dimethyl sulfoxide (48.9, 4.30), benzene (2.274, 0), and nitrobenzene (34.82, 3.97). The proportional relationship due to Eq. 1 is well recognized to be approximately established with only one exception of water. When ε, instead of $P\varepsilon$, is plotted against μ for many polar substances, no proportionality is seen but ε grows up more rapidly as μ increases.[7] The reason why only water deviates severely from the proportionality of Eq. 1 is supposed because the used value of dipole moment 1.85 D. U. for water is that in gas phase and the essential value in liquid phase is probably as high as 7, estimated from the proportionality rule, due to the molecular association between themselves forming so-called clusters or icebergs.

Aqueous Mixtures of Some Organic Liquids. The variations of P with the mole fraction x of organic liquids in water are plotted in Fig. 6, where no linearity holds between P and x. But when $P\bar{\varepsilon}$'s are plotted against the

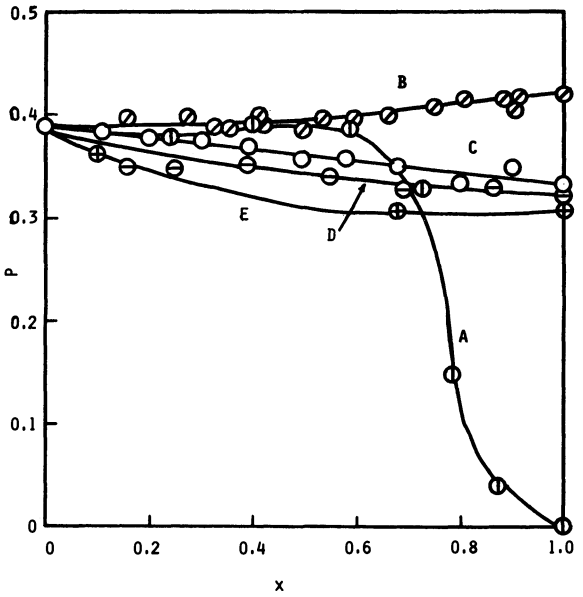

Fig. 6. Variations of P with mole fraction x of organic liquids in aqueous mixtures.
A: 1,4-Dioxane, B: dimethyl sulfoxide, C: methanol, D: acetone, E: 1-propanol.

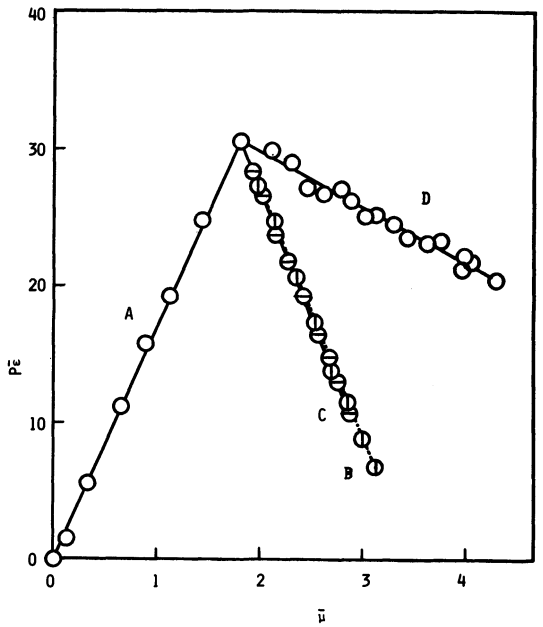

Fig. 7. Linear relationships between $P\bar{\varepsilon}$ and $\bar{\mu}$ for aqueous mixtures of organic substances.
A: 1,4-Dioxane, B: acetone, C: methanol, D: dimethyl sulfoxide.

individual apparent dipole moments of the mixed liquids, $\bar{\mu}$, as shown in Fig. 7, there appear straight lines connecting two limiting points for individual pure liquids respectively. The apparent permittivity $\bar{\varepsilon}$ and dipole moment $\bar{\mu}$ of mixture of two substances 1 and 2 are represented by

$$\bar{\varepsilon} = x_1\varepsilon_1 + x_2\varepsilon_2, \tag{2}$$

$$\bar{\mu} = x_1\mu_1 + x_2\mu_2, \tag{3}$$

at mole fraction x, respectively. The linearities appearing in Fig. 7 indicate that the mixtures behave like pure substances with $\bar{\varepsilon}$ and $\bar{\mu}$ exhibiting their dielectric and dipolar properties proportional to the concentrations of components, although the more delicate and fine properties have been noticed as stoichiometric and structured association of molecules at characteristic mole ratios in the mixtures of water with dimethyl sulfoxide,[8-10] 1,4-dioxane,[10,11] 1-propanol,[12,13] and tetrahydrofuran,[14,15] for instances.

As noticed above, Eq. 1 is valid to normal mixtures as well as pure substances, only if it is modified to be $P=k\bar{\mu}/\bar{\varepsilon}$. Therefore, the variation of P with x_1 may be expressed by the following equation:

$$\frac{dP}{dx_1} = k\frac{\mu_1\varepsilon_2-\mu_2\varepsilon_1}{(\varepsilon_1x_1+\varepsilon_2x_2)^2}. \tag{4}$$

Consequently, the increasing trend at $x_1\to 0$ can be presumed by

$$\left(\frac{dP}{dx_1}\right)_{x_1\to 0} = k\frac{\mu_1\varepsilon_2-\mu_2\varepsilon_1}{\varepsilon_2^2}, \tag{5}$$

where the suffixes 1 and 2 correspond to an organic substance and water, respectively. Then, the calculated values of $(dP/dx_1)_{x_1\to 0}$ are in a sequence: dimethyl sulfoxide>acetone>methanol>1, 4-dioxane, which coincides qualitatively with the observed one except for acetone: dimethyl sulfoxide>methanol>1,4-dioxane>acetone, this discrepancy being not interpreted at the present stage.

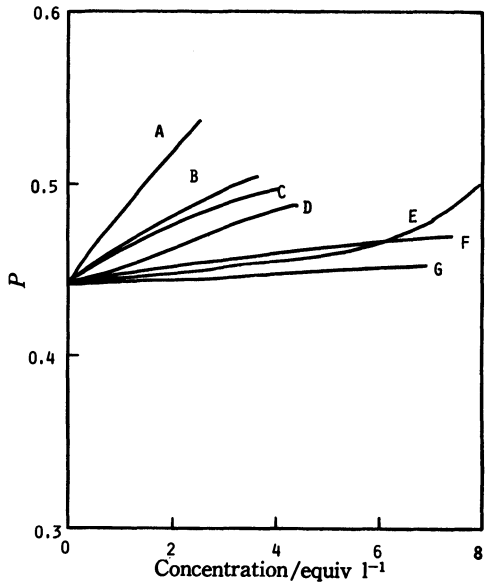

Fig. 8. Variations of P with concentrations of electrolytes in water.
A: RbCl, B: KCl, C: NaCl, D: $MgCl_2$, E: LiCl, F: $(C_2H_5)_3NHCl$, G: $(CH_3)_3NHCl$.
Observations were performed so many times that only smoothed curves are shown as general tendencies in order to avoid the complexity, in the figure.

Aqueous Solutions of Electrolytes. Figure 8 presents the variations of P with respect to the concentrations c/equiv dm^{-3} of electrolytes. The values of $(dP/dc)_{c\to 0}$ are all positive in a sequence: RbCl>KCl>NaCl>$MgCl_2$>LiCl>$(C_2H_5)_3NHCl\approx(CH_3)_3NHCl$. Concern-

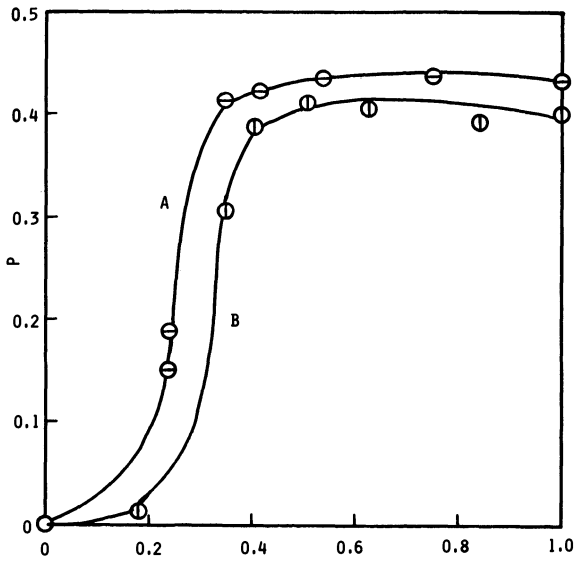

Fig. 9. Variations of P with mole fractions of polar substances in benzene.
A: Nitrobenzene, B: ethanol.

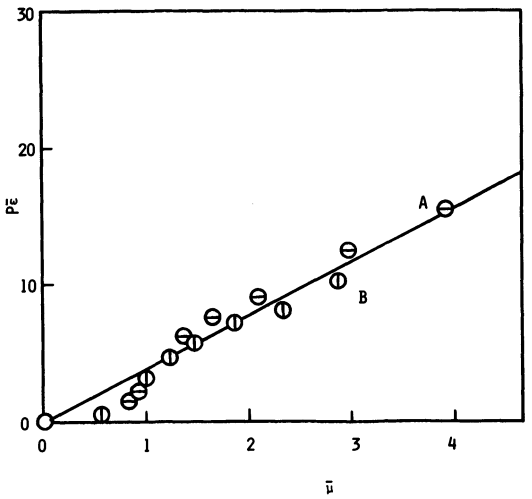

Fig. 10. Proportionality between $P\bar{\varepsilon}$ and $\bar{\mu}$ for benzene solutions of polar substances at various mole fractions.
A: Nitrobenzene, B: ethanol.

ing the cases of alkali chlorides, the observed order coincides with the nature of alkali ions changing from structure breakers to structure formers. Water molecules surrounding ions are classified into three categories, A, B, and C; water molecules in A layer are firmly attached to the central ions by the Coulombic interactions between ion and dipole, and water molecules in C range are bulk water having the ordinary nature as pure water, while water molecules in B layer are located intermediate between A and C and therefore are free from the restrictions due to both the Coulombic attraction as in A and the hydrogen bondings between themselves as in C. Accordingly, the electric dipoles of water molecules in B layer may be enabled to take proper orientations towards the outer electric field more easily than those in A or C area.[16] The structure-breaking

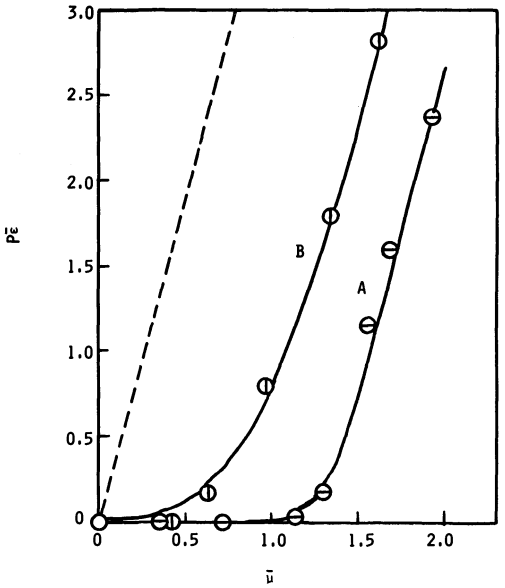

Fig. 11. Variations of $P\bar{\varepsilon}$ with $\bar{\mu}$ for benzene solutions.
A: Acetic acid, B: tetrahydrofuran.

ions have more water molecules in B layer and therefore aqueous solutions of structure breakers may exhibit larger P value than the structure making ions. The observed order of the values of $(dP/dc)_{c\to 0}$ is thus well understood.

Although $(C_2H_5)_3NH^+$ and $(CH_3)_3NH^+$ ions have large ionic radii, they are not structure breakers but structure makers, because the hydrophobicity of CH_3 and C_2H_5 groups promotes the icelike hydrogen-bonded structure around ions.[17] This is the reason why alkyl ammonium ions exhibit smaller value of $(dP/dc)_{c\to 0}$ than Li^+ ion.

Benzene Solutions with Polar Substances. In order to make the matter simpler, we used mixtures of polar substances with nonpolar liquid: benzene with $\mu_2=0$ and $\varepsilon_2=2.274$. In this case, Eq. 5 becomes $(dP/dx_1)_{x_1\to 0}=k\mu_1/\varepsilon_2$. Although Fig. 9 shows that the correlationship between P and x_1 do not explicitly exhibit the expected slopes at the limiting concentration $x_1\to 0$ in mixtures of nitrobenzene or ethanol in benzene, respectively, the proportionality of $P\bar{\varepsilon}$ *vs.* $\bar{\mu}$ is approximately established over the whole concentration range for both mixtures, as shown in Fig. 10. This fact may indicate that individual molecules of both nitrobenzene and ethanol exist independently and freely in benzene without occurrence of any molecular association, respectively.

On the other hand, Fig. 11 shows the cases of benzene solutions of acetic acid and tetrahydrofuran, in which no proportionality is recognized between $P\bar{\varepsilon}$ and $\bar{\mu}$. Therefore, it seems that they are not simple mixtures but there probably happen mutual interactions between polar molecules of themselves in benzene solutions. Acetic acid is known to dimerize by hydrogen bondings in benzene, giving

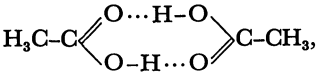

which has a nonpolar structure and therefore may dimi-

TABLE 1. EXAMINATION FOR ADDITIVITY OF $P\bar{\varepsilon}$ BETWEEN PHENOL AND PYRIDINE IN BENZENE SOLUTIONS

Solute	x	$\bar{\varepsilon}$	$\bar{\mu}$	$P\bar{\varepsilon}$
Phenol	0.4	5.276	0.588	0.280
Pyridine	0.4	6.284	0.972	0.798
Mixture of phenol and pyridine	0.4 0.4	9.287	1.560	3.752

nish the apparent dipole moment, making the solutions to disobey the proportionality correlation in the result. Tetrahydrofuran also fails to obey the proportionality rule to the similar direction to acetic acid. But the reason for the depression of its apparent dipole moment in benzene is not understood at the present stage of the investigation.

As has been indicated in Fig. 5, the observed point for water appears far above the straight line of the proportionality between $P\varepsilon$ and μ. The apparent increment of μ is supposed to be caused by the molecular association of the type head to tail $(+-)(+-)\cdots$, while the apparent depression of μ as experienced in the case of acetic acid and presumably that of tetrahydrofuran in benzene solutions may be attributed to the formation of dimers of the type head to head $(+-)(-+)$.

Ternary Mixtures of Phenol, Pyridine, and Benzene. If two solutes S_1 and S_2 are independently dissolved in benzene without mutual interaction between molecules of the same species as well as between the different ones, an additivity correlation with respect to $P\bar{\varepsilon}$ values should hold in solutions of the both solutes. Table 1 gives data proving whether the additivity holds in the cases of phenol ($\varepsilon=9.78$, $\mu=1.47$) and pyridine (12.3, 2.43) or not. According to the table, the observed $P\bar{\varepsilon}$ for the ternary mixture of phenol ($x=0.4$), pyridine ($x=0.4$), and benzene ($x=0.2$) is 3.752, which is much larger than the value of the sum of the respective solutions in benzene of the same mole fraction, $0.280+0.798=1.078$. This discrepancy may suggest that there occurs molecular association between phenol and pyridine, forming a molecular complex with apparently large dipole moment as compared with those for respective species. Although the detailed structure of the molecular complex is not clear, the bonding between the two species would be a hydrogen bond of the type O–H···N and the resultant electron density at benzene ring may be larger than that at pyridine ring. Thus, the point for the observed $P\bar{\varepsilon}$ should appear above the simply expected one from the additivity as a normal mixture, in a $P\bar{\varepsilon}$-$\bar{\mu}$ diagram.

Conclusion. The attractive force wrought on polar substances in an outer electric field has been found to be proportional to the observable quantity P as defined above. The value of P offers a simple means to detect the structures of pure liquids or mixtures in liquids. $P\varepsilon$ *vs.* μ for various pure liquids and $P\bar{\varepsilon}$ *vs.* $\bar{\mu}$ for mixtures of some components give a straight line with a common proportional constant k, if no molecular association occurs, although ε *vs.* μ for various polar substances is not linear.

When $P\bar{\varepsilon}$ value *vs.* $\bar{\mu}$ fails to come on the straight line with the slope k, there probably happens to take place molecular association. The association to cause an apparently larger dipole moment makes the point locate above the straight line, and *vice versa.* The former instances are seen in the cases of water and mixture of phenol–pyridine–benzene, and the latters in those of mixtures of acetic acid–benzene and of tetrahydrofuran–benzene.

References

1) O. Kimura, *Bull. Chem. Soc. Jpn.*, **12**, 147 (1937).
2) O. Kimura, *Bull. Chem. Soc. Jpn.*, **14**, 243 (1939).
3) J. Lielmezs, H. Aleman, and L. Fish, *Z. Phys. Chem. Neue Folge*, **99**, 117 (1976).
4) A. Weissberger, E. S. Proskauer, J. A. Riddick, and E. E. Toops, Jr., "Organic Solvents, Physical Properties and Methods of Purification," Interscience Publishers, Inc., New York (1955).
5) M. Senoh and T. Arai, "Solvent Effects in Organic Reactions," (in Japanese), ed by S. Asahara, Sangyo-Tosho, Tokyo (1970).
6) "Chemistry Handbook (Kagaku Binran)," Fundamental Part, ed by the Chem. Soc. Japan, Maruzen, Tokyo (1975).
7) L. Pauling, "General Chemistry," 3rd ed, W. H. Freeman and Company, San Francisco (1970), Chap. 12.
8) D. H. Rasmussen and A. P. McKenzie, *Nature*, **220**, 1315 (1968).
9) G. Wada, *Wakojunyaku-Jiho*, **45**, 3 (1976).
10) D. Oakenfull and D. E. Fenwick, *J. Chem. Soc., Faraday Trans. 1*, **1979**, 636.
11) N. M. Murthy and S. V. Subrahmanyam, *Can. J. Chem.*, **56**, 2412 (1979).
12) K. Hallenga, J. R. Grigera, and H. J. C. Berendesen, *J. Phys. Chem.*, **84**, 2381 (1980).
13) G. H. Grossmann and K. H. Ebert, *Ber. Bunsenges. Phys. Chem.*, **85**, 1026 (1981).
14) S. R. Gough, *J. Solution Chem.*, **8**, 371 (1979).
15) G. Atkinson, S. Rajagopalan, and B. L. Atkinson, *J. Phys. Chem.*, **85**, 733 (1981).
16) R. E. Verral, "Water," ed by F. Franks, Plenum Press, New York (1973), Vol. 3, Chap. 5.
17) G. Wada, E. Nagao, N. Kawamura, and K. Kinumoto, *Bull. Chem. Soc. Jpn.*, **51**, 1937 (1978).

Free Energy, Enthalpy, and Entropy Changes of Mixing of Aqueous Solutions of D-Glucose and Tetraalkylammonium Bromide at 25 °C

Koichiro MIYAJIMA,* Masahiro SAWADA, and Masayuki NAKAGAKI
Faculty of Pharmaceutical Sciences, Kyoto University, Yoshida Shimoadachi-cho, Sakyo-ku, Kyoto 606
(Received March 16, 1983)

Changes of free energy and enthalpy of mixing of aqueous solutions of D-glucose and tetraalkylammonium bromide were measured at 25 °C by isopiestic method and calorimetry, and excess thermodynamic quantities and transfer functions were calculated. All transfer functions were positive and mutual salting-out was observed. The positive value of free energy of transfer of tetrabutylammoniun bromide from water to aqueous D-glucose solution comes from the predominance of enthalpic term over entropic term. These results are interpreted in terms of the structural incompatibility of hydration cospheres around these two kinds of solutes.

The tetraalkylammonium salt (TAAB) is known to enhance the structure of water by formation of a cage-like structure around itself. Judging from the results of x-ray analysis of the tetrabutylammonium fluoride,[1] the hydrogen bond network of clathrate compound is different from that of tridymite structure of ice, though the hydrogen bond length and the bond angle are similar.

Various monosaccharides, such as D-glucose, also promote the water structure by directly forming hydrogen bonds with water molecules. Kabayama and Patterson[2] postulated that the spacing of the equatorial oxygen atoms of the hexopyranose of the chair conformation nearly fits the spacing of oxygen atoms in the tridymite-like structure of water. In a previous paper,[3] we reported the excess thermodynamic quantities of aqueous monosaccharide solutions, and concluded D-glucose to be a structure maker from the negative value of excess partial molar entropy of water. Therefore, the water structure around D-glucose and that around the tetraalkylammonium bromide must be different from each other.

On the other hand, various saccharides and polyalcohols are reported to be an anti-denaturating agents of proteins in aqueous solutions,[4] and the mechanism is considered to be related to the strengthening of hydrophobic interaction in protein molecule by the presence of these compounds. Therefore, the study on the structural interaction of these two kinds of solutes, one is hydrophobic solute and the other hydrophilic, in aqueous solutions seems to be important as a model system of such a protein denaturation in aqueous solutions.

From these points of view, we measured the activity coefficients and heat of dilution on the ternary system D-glucose–tetrabutylammonium bromide (TBAB)–water at 25 °C, and discussed the interaction of these solutes through the structural change of water on the basis of the thermodynamic excess quantities and the transfer functions.

Theory

Activity Coefficient. Activity coefficients of solutes 1 (D-glucose) and 2 (TAAB) are determined from the isopiestic data by the Ellerton-Dunlop method.[5] Assume that the activity coefficient of solute 1 (γ_1) is expressed by Eq. 1.

$$\ln \gamma_1 = \sum_{i=0}^{4}\sum_{j=0}^{4} g_{ij} m_1^i m_2^j \quad (A_{00}=0,\ i+j\leq 4), \tag{1}$$

where g_{ij}'s are the interaction parameters and m_1 and m_2 the molalities of solutes 1 and 2, respectively. In Eq. 1, the four terms $g_{10}m_1$, $g_{20}m_1^2$, $g_{30}m_1^3$, and $g_{40}m_1^4$ correspond to the contributions of activity coefficient of binary system (γ_1°). Therefore, Eq. 1 is rewritten as

$$\begin{aligned}\ln \gamma_1 = \ln \gamma_1^\circ &+ g_{01}m_2 + g_{11}m_1m_2 + g_{02}m_2^2 + g_{21}m_1^2m_2 \\ &+ g_{12}m_1m_2^2 + g_{03}m_2^3 + g_{31}m_1^3m_2 + g_{22}m_1^2m_2^2 \\ &+ g_{13}m_1m_2^3 + g_{04}m_2^4.\end{aligned} \tag{2}$$

Here the cross differential relation holds between two solutes.

$$\left(\frac{\partial \ln \gamma_1}{\partial m_2}\right)_{m_1} = \nu \left(\frac{\partial \ln \gamma_2}{\partial m_1}\right)_{m_2}, \tag{3}$$

where ν is the number of moles of ions formed from 1 mole of solute 2 (TAAB). Introducing Eq. 2 to Eq. 3, we obtain Eq. 4 as an expression of activity coefficient for solute 2.

$$\begin{aligned}\nu \ln \gamma_2 = \nu \ln \gamma_2^\circ &+ g_{01}m_1 + \frac{1}{2}g_{11}m_1^2 + 2g_{02}m_1m_2 \\ &+ \frac{1}{3}g_{21}m_1^3 + g_{12}m_1^2m_2 + 3g_{03}m_1m_2^2 + \frac{1}{4}g_{31}m_1^4 \\ &+ \frac{2}{3}g_{22}m_1^3m_2 + \frac{3}{2}g_{13}m_1^2m_2^2 + 4g_{04}m_1m_2^3.\end{aligned} \tag{4}$$

Combining Eqs. 2 and 4 with Gibbs-Duhem relation, experimental quantity defined by Eq. 5 is expressed by Eq. 6 using g_{ji}'s.

$$\Delta = \nu_R m_R \phi_R - m_1\phi_1^\circ - \nu m_2 \phi_2^\circ, \tag{5}$$

and

$$\begin{aligned}\Delta/m_1m_2 = g_{01} &+ g_{11}m_1 + 2g_{02}m_2 + g_{21}m_1^2 + \frac{3}{2}g_{12}m_1m_2 \\ &+ 3g_{03}m_2^2 + g_{31}m_1^3 + \frac{4}{3}g_{22}m_1^2m_2 + 2g_{13}m_1m_2^2 \\ &+ 4g_{04}m_2^3.\end{aligned} \tag{6}$$

In these equations, ν_R is the number of moles of ions produced by the dissociation of 1 mol of reference salt, and m_R and ϕ_R are the molality and the osmotic coefficient of reference salt, respectively. ϕ_1° and ϕ_2° are osmotic coefficients of solutes 1 and 2 in binary aqueous solutions, respectively. The activity coefficients of solutes 1 and 2 can be calculated from g_{ij}'s obtained by the application of the least squares method to Eq. 6.

Heat of Dilution. Assume that the excess enthalpy of ternary system is expressed by the polynomials involving terms up to quartic.

$$H^{ex} = (m_1\phi_{L,1}^{ex,0} + m_2\phi_{L,2}^{ex,0}) + h_{11}m_1m_2 + h_{21}m_1^2m_2 + h_{12}m_1m_2^2 + h_{31}m_1^3m_2 + h_{22}m_1^2m_2^2 + h_{13}m_1m_2^3, \quad (7)$$

where $\phi_{L,1}^{ex,0}$ and $\phi_{L,2}^{ex,0}$ are the apparent molar excess enthalpies in aqueous binary solutions, and h_{ij}'s are interaction parameters. M and x being the total molality and the mole fraction of solute 1, respectively, excess mean apparent molar enthalpy (ϕ_L^{ex}) is expressed by Eq. 8.

$$\phi_L^{ex} = H^{ex}/M = [x\phi_{L,1}^{ex,0} + (1-x)\phi_{L,2}^{ex,0}] + h_{11}x(1-x)M + h_{21}x^2(1-x)M^2 + h_{12}x(1-x)^2M^2 + h_{31}x^3(1-x)M^3 + h_{22}x^2(1-x)^2M^3 + h_{13}x(1-x)^3M^3. \quad (8)$$
$$(M=m_1+m_2,\ x=m_1/M)$$

Q_D is defined as mean molar heat evolved on dilution from M to M', then Q_D is expressed by

$$-Q_D(M \to M') = \phi_L^{ex}(x, M) - \phi_L^{ex}(x, M'). \quad (9)$$

Introducing Eq. 8 to Eq. 9, we obtain

$$\begin{aligned} Q_D(M \to M') &- x[\phi_{L,1}^{ex,0}(xM) - \phi_{L,1}^{ex,0}(xM')] \\ &- (1-x)\{\phi_{L,2}^{ex,0}[(1-x)M] - \phi_{L,2}^{ex,0}[(1-x)M']\} \\ &= h_{11}x(1-x)(M-M') + h_{21}x^2(1-x)(M^2-M'^2) \\ &+ h_{12}x(1-x)^2(M^2-M'^2) + h_{31}x^3(1-x)(M^3-M'^3) \\ &+ h_{22}x^2(1-x)^2(M^3-M'^3) + h_{13}x(1-x)^3(M^3-M'^3). \quad (10) \end{aligned}$$

The left hand terms of Eq. 10 can be experimentally measurable quantities, because the first term corresponds to the enthalpy of dilution of ternary system and the second and the third terms correspond to the enthalpy of dilution of each binary system. Therefore, Q_D was measured with variations of total molarities and degree of dilution, and the interaction parameters were determined by the least squares method. H^{ex} and ϕ_L^{ex} were calculated from these h_{ij}'s using Eqs. 7 and 8.

Excess Thermodynamic Quantities of Mixing. Excess free energy change of mixing of each component is expressed by the Eqs. 11, 12, and 13.[6,8]

$$\Delta_m G_1^{ex} = RTm_1 \ln(\gamma_1/\gamma_1^\circ), \quad (11)$$

$$\Delta_m G_2^{ex} = \nu RTm_2 \ln(\gamma_2/\gamma_2^\circ), \quad (12)$$

and

$$\Delta_m G_w^{ex} = -RT\Delta, \quad (13)$$

where subscripts 1, 2, and w denote D-glucose, TAAB, and water, respectively. Total excess free energy change of mixing is the sum of three components.

$$\Delta_m G^{ex} = \Delta_m G_1^{ex} + \Delta_m G_2^{ex} + \Delta_m G_w^{ex}. \quad (14)$$

Excess enthalpy change of mixing is expressed by Eq. 15.

$$\Delta_m H^{ex} = H^{ex} - m_1\phi_{L,1}^{ex} - m_2\phi_{L,2}^{ex}. \quad (15)$$

Therefore, excess entropy change of mixing is obtained from $\Delta_m G^{ex}$ and $\Delta_m H^{ex}$,

$$\Delta_m S^{ex} = (\Delta_m H^{ex} - \Delta_m G^{ex})/T. \quad (16)$$

Change of the Partial Molar Thermodynamic Quantities of Transfer of the Solute from Water to Aqueous Solution; Thermodynamic Transfer Functions. Free energy change on transferring 1 mol of solute 1 from water to aqueous solution ($\Delta\bar{G}_1^{tr}$) is expressed by Eq. 17.

$$\Delta\bar{G}_1^{tr} = RT\ln(\gamma_1/\gamma_1^\circ). \quad (17)$$

Similarly in the case of solute 2 $\Delta\bar{G}_2^{tr}$ is expressed by Eq. 18.

$$\Delta\bar{G}_2^{tr} = \nu RT\ln(\gamma_2/\gamma_2^\circ). \quad (18)$$

Partial molar enthalpy change on transferring 1 mol of solute 1 or solute 2 from water to aqueous solution is expressed by Eq. 19 or Eq. 20.

$$\begin{aligned} \Delta\bar{H}_1^{tr} &= \left(\frac{\partial\Delta_m H^{ex}}{\partial m_1}\right)_{m_2} \\ &= h_{11}m_2 + 2h_{21}m_1m_2 + h_{12}m_2^2 + 3h_{31}m_1^2m_2 \\ &\quad + 2h_{22}m_1m_2^2 + h_{13}m_2^3, \quad (19) \end{aligned}$$

or

$$\begin{aligned} \Delta\bar{H}_2^{tr} &= \left(\frac{\partial\Delta_m H^{ex}}{\partial m_2}\right)_{m_1} \\ &= h_{11}m_1 + h_{21}m_1^2 + 2h_{12}m_1m_2 + h_{31}m_1^3 \\ &\quad + 2h_{22}m_1^2m_2 + 3h_{13}m_1m_2^2. \quad (20) \end{aligned}$$

Therefore, partial molar entropy change on transferring 1 mol of solute 1 or solute 2 from water to aqueous solution is written by Eq. 21.

$$\Delta\bar{S}_k^{tr} = (\Delta\bar{H}_k^{tr} - \Delta\bar{G}_k^{tr})/T. \quad (k=1 \text{ or } 2) \quad (21)$$

Experimental

Materials. Reagent grade D-glucose obtained from Nakarai Chemical Co. Ltd., was dried *in vacuo* for several days at room temperature over P_2O_5 before use. TBAB and TMAB purchased from Nakarai Chemical Co. Ltd. were recrystallized twice from appropriate solvent described elsewhere,[7] and dried *in vacuo* for 2 d at 80 °C before use. Reagent grade sodium chloride was obtained from Matsunaga Chemical Co. Ltd., and dried *in vacuo* for a day at 100 °C. Solutions were prepared with water purified by distillations and deionization.

Methods. Osmotic coefficients were measured at 25±0.2 °C by isopiestic comparison method described elsewhere.[8] Sodium chloride and TBAB were used as reference solutes. Measurement of heat of dilution was carried out by using a flow microcalorimeter (LKB 10700-1) at 25±0.001 °C. Experimental procedure and accuracy were the same as those reported elsewhere.[9] The least squares fittings were carried out by using FACOM OSIV/F4 in Data Processing Center of Kyoto university.

Results

Activity Coefficient. Isopiestic molalities of solutes 1 (D-glucose) and 2 (TAAB) in the ternary systems and of the reference solutes are shown in Table 1 together with the experimental quantity Δ/m_1m_2 and percentage errors (Diff. %) defined by Kelly *et al.*[10] The osmotic coefficients of aqueous binary solutions were taken from the literatures given by Robinson and Stokes[11] for NaCl, Lindenbaum and Boyd[12] and Wen *et al.*[13] for TBAB, Levien[14] for TMAB, and authors[3] for D-glucose. Parameters in Eq. 6 calculated from the data in Table 1 by the least squares method were shown in Table 2. The activity coefficient *vs.* molality curves for D-glucose and TBAB in binary and ternary solutions are shown in Figs. 1 and 2, respectively. The activity coefficient of

TABLE 1. ISOPIESTIC DATA FOR THE TERNARY SYSTEMS AT 25 °C

m_R[a)]	m_1	m_2	Δ/m_1m_2	Diff.%
	D-Glucose–TBAB–Water			
5.58547[b)]	1.88173	2.43312	0.106_7	0.23
	2.45491	1.66757	0.143_9	0.28
	3.01205	1.09892	0.183_5	0.56
	3.51991	0.69762	0.211_7	0.83
4.83019[b)]	1.01674	3.07606	0.087_3	0.79
	1.63818	2.11820	0.130_4	−0.05
	2.16277	1.46913	0.174_0	0.02
	2.67844	0.97721	0.217_0	0.28
	3.14644	0.62360	0.247_6	0.54
	3.59751	0.34642	0.261_8	0.71
3.01293[b)]	0.63513	2.05193	0.152_1	0.45
	1.13429	1.44160	0.199_1	0.63
	1.45981	1.10247	0.244_0	0.39
	1.90703	0.73042	0.284_2	0.84
	2.35036	0.42425	0.324_6	0.81
	2.78284	0.18193	0.361_5	0.39
2.55046[b)]	0.54959	1.77558	0.173_3	0.54
	0.99392	1.26320	0.230_6	0.44
	1.29479	0.97784	0.262_9	0.70
	1.69558	0.64943	0.310_2	0.79
	2.09777	0.37865	0.350_0	0.75
	2.49051	0.16282	0.388_6	0.34
3.19897	4.11496	1.05103	0.170_0	0.92
	4.63770	0.66049	0.194_4	0.68
	5.23109	0.30484	0.219_3	0.29
3.04387	1.22289	4.79463	0.064_4	−0.63
	2.51047	2.53846	0.111_9	0.29
	2.98874	1.86965	0.139_0	−0.30
	3.48175	1.34172	0.163_6	0.00
	3.90509	0.96251	0.190_2	−0.05
	4.34530	0.63886	0.214_8	−0.08
	4.89791	0.31015	0.240_1	−0.12
3.02745	1.17178	4.91373	0.051_7	−0.15
	2.48856	2.56977	0.104_8	0.94
	2.97920	1.88543	0.130_2	0.42
	3.48210	1.32319	0.161_6	0.23
	3.85308	0.98530	0.186_7	0.07
	4.35193	0.62052	0.211_7	0.12
	4.92406	0.28729	0.229_3	0.17
3.00226	1.18078	4.79459	0.056_1	−0.05
	2.50085	2.47096	0.109_9	0.48
	2.98549	1.81767	0.134_5	0.24
	3.38927	1.36985	0.159_2	0.19
	3.82790	0.96826	0.188_5	0.06
	4.31823	0.60771	0.216_4	−0.00
	4.79664	0.32369	0.236_7	−0.02
2.95340	1.17417	4.60363	0.064_9	−0.23
	1.88423	3.32784	0.083_4	−1.42
	2.41522	2.44214	0.115_2	−0.22
	2.88180	1.80275	0.143_4	−0.57
	3.35513	1.29293	0.172_9	−0.41
	3.77127	0.92953	0.198_7	−0.29
	4.20068	0.61759	0.223_3	−0.23
	4.73634	0.29992	0.250_3	−0.23
2.86386	1.11887	4.38683	0.071_4	−0.34
	1.80350	3.18527	0.088_1	0.66
	3.22973	1.24460	0.183_5	−0.77
	3.63781	0.89664	0.209_1	−0.52
	4.05782	0.59659	0.233_0	−0.36
	4.56492	0.28907	0.276_0	−0.63
2.69620	1.02361	4.01334	0.078_5	−0.17
	1.66112	2.93380	0.094_6	0.12
	2.57995	1.61393	0.160_1	−0.76
	3.01173	1.16060	0.198_2	−0.82
	3.40422	0.83906	0.222_0	−0.43
	3.79793	0.55838	0.249_8	−0.39
	4.29541	0.27200	0.272_1	−0.20
2.67229	0.97211	4.07643	0.068_2	0.47
	1.65960	2.86335	0.097_7	−0.02
	2.10914	2.17797	0.124_8	−0.49
	2.55073	1.61427	0.156_0	−0.42
	3.00739	1.14280	0.192_7	−0.33
	3.34902	0.85640	0.216_4	−0.16
	3.80127	0.54200	0.238_2	0.14
	4.31330	0.25165	0.247_5	0.35
2.44087	0.85889	3.48754	0.080_6	0.66
	1.35217	2.66616	0.113_5	−0.50
	1.90085	1.87813	0.152_0	−0.76
	2.30898	1.40578	0.185_9	−0.58
	2.65214	1.07192	0.217_4	−0.50
	3.02725	0.76574	0.248_9	−0.37
	3.44249	0.48446	0.276_4	−0.19
	3.88367	0.25905	0.299_9	−0.16
2.37975	0.84140	3.29891	0.096_6	0.03
	1.38237	2.44149	0.127_2	−0.77
	1.81172	1.83192	0.163_9	−1.12
	2.20690	1.38056	0.198_4	−0.96
	2.60620	1.00432	0.234_8	−0.76
	2.95772	0.72901	0.262_5	−0.52
	3.32277	0.48852	0.282_1	−0.18
	3.76170	0.23820	0.314_6	−0.25
2.20377	0.73640	2.99016	0.103_7	0.33
	1.17137	2.30968	0.134_5	−0.32
	1.67033	1.65037	0.175_6	−0.37
	2.04440	1.24470	0.213_6	−0.36
	2.36286	0.95500	0.244_6	−0.25
	2.70716	0.68477	0.277_8	−0.21
	3.09209	0.43515	0.301_4	0.04
	3.44982	0.23281	0.333_9	−0.18
2.00818	0.66368	2.57654	0.126_0	0.18
	1.10181	1.98079	0.140_5	0.84
	1.46915	1.50836	0.188_5	0.25
	1.83187	1.13442	0.228_1	0.25
	2.13293	0.87272	0.257_2	0.39
	2.44249	0.63582	0.288_0	0.38
	2.79087	0.41377	0.305_7	0.63
	3.12781	0.22434	0.329_3	0.38
1.84657	0.62926	2.18474	0.178_6	−0.92
	1.01585	1.68954	0.197_8	−0.55
	1.34154	1.32358	0.232_8	−0.53
	1.67233	1.00653	0.269_9	−0.42
	1.97911	0.75860	0.297_0	−0.06
	2.23993	0.56952	0.323_4	0.01
	2.55794	0.37676	0.333_5	0.48
	2.92561	0.17304	0.387_5	−0.11

TABLE 1. (Continued)

m_R [a)]	m_1	m_2	Δ/m_1m_2	Diff.%
1.72165	0.53468	2.07574	0.159_4	0.19
	0.90015	1.61826	0.184_4	0.58
	1.22334	1.25599	0.228_3	0.34
	1.54421	0.95628	0.263_0	0.54
	1.80721	0.73945	0.292_7	0.59
	2.08163	0.54188	0.318_1	0.70
	2.38295	0.35329	0.340_3	0.71
	2.67364	0.19177	0.377_2	0.24
1.72014	0.53374	2.07208	0.160_8	0.16
	0.89719	1.61294	0.189_2	0.39
	1.22304	1.25568	0.226_6	0.42
	1.54343	0.95580	0.261_8	0.59
	1.80770	0.73965	0.289_3	0.73
	2.08179	0.54193	0.314_7	0.81
	2.38235	0.35320	0.337_2	0.79
	2.67368	0.19177	0.370_2	0.35
1.66148	0.54735	1.90036	0.199_0	−0.65
	0.89133	1.48245	0.227_7	−0.57
	1.18704	1.17111	0.262_2	−0.53
	1.48276	0.89247	0.308_5	−0.78
	1.75821	0.67393	0.340_8	−0.62
	1.99480	0.50719	0.369_8	−0.57
	2.29072	0.33740	0.369_0	0.23
	2.61563	0.15471	0.469_5	−0.78
1.65133	0.50384	1.95600	0.177_3	−0.06
	0.85360	1.53458	0.198_2	0.42
	1.15968	1.19063	0.251_7	−0.17
	1.46642	0.90810	0.288_3	−0.05
	1.71645	0.70231	0.323_0	−0.13
	1.98236	0.51604	0.346_3	0.12
	2.27509	0.33730	0.366_6	0.30
	2.55028	0.18292	0.427_6	−0.34
1.52498	0.49139	1.70606	0.213_2	−0.43
	0.80679	1.34184	0.245_0	−0.40
	1.08153	1.06701	0.276_1	−0.24
	1.35470	0.81539	0.324_8	−0.59
	1.60557	0.61542	0.365_3	−0.74
	1.82688	0.46450	0.389_6	−0.56
	2.09572	0.30871	0.398_8	−0.03
	2.40353	0.14216	0.486_1	−0.70
1.16782	0.58872	0.99294	0.330_0	−1.06
	0.79884	0.80461	0.347_5	−0.72
	0.99409	0.64322	0.372_5	−0.54
	1.21426	0.48665	0.379_2	0.19
	1.40921	0.35518	0.409_0	0.14
	1.62676	0.23288	0.404_0	0.65
	1.87534	0.10024	0.496_9	−0.23
1.08472	0.37254	1.09560	0.288_5	−0.29
	0.68320	0.81449	0.294_7	0.74
	0.89775	0.60861	0.401_8	−1.05
	1.11795	0.45023	0.417_3	−0.50
	1.38310	0.28338	0.437_1	−0.04
	1.62650	0.14437	0.531_8	−0.74
0.97360	0.33073	0.97264	0.305_8	−0.23
	0.60764	0.72441	0.324_0	0.37
	0.81048	0.54945	0.386_0	−0.23
	1.00721	0.40563	0.414_2	−0.10
	1.24238	0.25455	0.452_9	−0.11
	1.46512	0.13005	0.530_4	−0.56
0.85712	0.28895	0.84976	0.303_5	0.14
	0.53325	0.63573	0.329_7	0.57
	0.72015	0.48821	0.349_7	0.89
	0.89362	0.35989	0.389_8	0.65
	1.10740	0.22689	0.395_0	0.97
	1.29838	0.11525	0.498_0	−0.11
	D-Glucose–TMAB–Water			
1.91152	0.48715	1.96769	0.158_1	−1.00
	0.93162	1.68599	0.092_5	0.52
	1.33629	1.39716	0.094_4	0.00
	1.78118	1.09182	0.089_9	−0.20
	2.15133	0.83482	0.092_3	−0.42
	2.48582	0.61450	0.085_7	−0.08
	2.79602	0.40039	0.097_8	−0.25
	3.14369	0.18392	0.087_1	0.11
1.70685	0.44492	1.76339	0.102_4	0.55
	0.83753	1.47662	0.104_7	0.26
	1.17620	1.23765	0.103_1	0.07
	1.59513	0.94465	0.106_6	−0.09
	1.91060	0.74199	0.094_2	0.66
	2.22795	0.51261	0.122_7	0.05
	2.50445	0.33584	0.128_6	0.26
	2.76084	0.17256	0.167_6	−0.17
1.68047	0.52713	1.66379	0.111_7	0.28
	1.04867	1.28887	0.109_0	−0.08
	1.47862	0.98701	0.111_8	−0.28
	1.85253	0.73013	0.117_5	−0.17
	2.17128	0.51619	0.126_5	0.02
	2.55559	0.26705	0.153_7	−0.05
1.64520	0.43052	1.69558	0.098_2	0.63
	0.80845	1.41666	0.106_7	0.20
	1.11714	1.20543	0.097_2	0.40
	1.50432	0.93028	0.106_4	0.07
	1.81728	0.71551	0.111_7	0.19
	2.11276	0.51668	0.120_4	0.34
	2.37423	0.34799	0.128_4	0.47
	2.60853	0.19767	0.162_2	0.04
1.41469	0.43669	1.27833	0.136_3	−0.41
	0.86934	1.06847	0.127_9	−0.60
	1.22748	0.81937	0.131_1	−0.51
	1.53933	0.60669	0.142_4	−0.29
	1.80924	0.43012	0.154_3	0.02
	2.13236	0.22282	0.211_2	−0.39
1.18671	0.36223	1.14330	0.143_8	−0.58
	0.72168	0.88698	0.138_1	−0.72
	1.01798	0.67953	0.150_8	−0.77
	1.27600	0.50291	0.173_4	−0.77
	1.50770	0.35843	0.177_4	−0.17
	1.77647	0.18563	0.271_8	−0.96
1.03352	0.23036	1.05712	0.092_4	0.25
	0.48086	0.87825	0.104_1	0.17
	0.71980	0.71322	0.107_6	0.34
	0.93200	0.57014	0.112_4	0.62
	1.12111	0.44379	0.125_3	0.72
	1.33817	0.30535	0.138_3	0.87
	1.51967	0.19509	0.152_8	0.80
	1.63203	0.12882	0.176_6	0.49
0.82982	0.18159	0.83330	0.135_8	−0.21

TABLE 1. (Continued)

m_R[a)]	m_1	m_2	Δ/m_1m_2	Diff.%	m_R[a)]	m_1	m_2	Δ/m_1m_2	Diff.%
	0.37979	0.69364	0.135_5	−0.26	0.78509	0.19603	0.77297	0.088_0	0.30
	0.56942	0.56421	0.137_3	−0.11		0.52910	0.54012	0.129_6	0.10
	0.73869	0.45188	0.142_2	0.11		0.67487	0.43953	0.156_4	−0.15
	0.89047	0.35249	0.157_7	0.15		0.84104	0.33489	0.151_7	0.31
	1.06446	0.24289	0.182_4	0.11		1.00853	0.22766	0.192_5	−0.01
	1.21713	0.15625	0.170_0	0.52		1.12271	0.15532	0.265_2	−0.65
	1.30755	0.10321	0.209_1	0.16		1.22800	0.09720	0.301_2	−0.60

a) Reference solute is sodium chloride except for b). b) Reference solute is TBAB.

TABLE 2. THE VALUES OF g_{ij} IN Eq. 6

	D-Glucose–TBAB–Water	D-Glucose–TMAB–Water
g_{01}	0.47840	0.27828
g_{11}	0.09192	−0.06649
g_{02}	−0.12984	−0.19866
g_{21}	−0.05170	0.06080
g_{12}	−0.04619	0.05685
g_{03}	0.02332	0.10087
g_{31}	0.00500	−0.01642
g_{22}	0.01359	−0.01939
g_{13}	0.00393	−0.02080
g_{04}	−0.00175	−0.01707

TABLE 3. THE VALUES OF h_{ij} *in* Eq. 10 FOR THE SYSTEM D-GLUCOSE–TBAB–WATER

h_{11}	1266.4
h_{21}	−52.9
h_{12}	−86.2
h_{31}	−13.5
h_{22}	23.7
h_{13}	−100.1

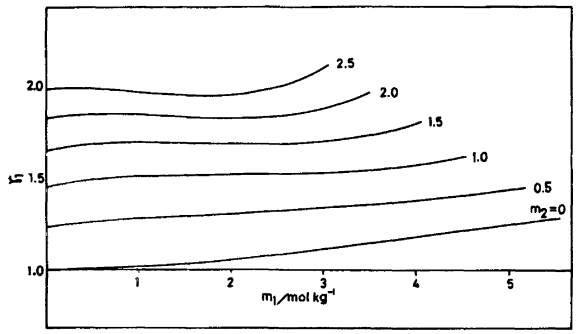

Fig. 1. Activity coefficients of D-glucose (γ_1) in aqueous TBAB solutions of various concentrations at 25 °C.
m_1; Molality of D-glucose, m_2; molality of TBAB.

each solute increases in the presence of the other solute. Similar tendency was observed in the ternary system D-glucose–TMAB–water.

Heat of Dilution. Figure 3 shows the mean molar heat of dilution as a function of total concentration difference before and after dilution ($M-M'$). The values of molar heat of dilution for the binary systems, D-glucose–water and TBAB–water, obtained from this work agree with those of literatures.[15-17] Using the least squares method, interaction parameters in Eq. 10 are calculated and are shown in Table 3.

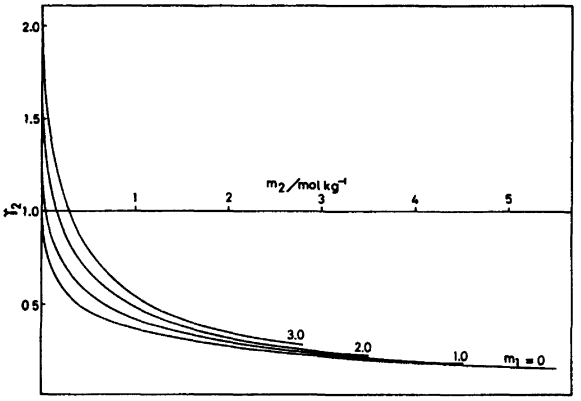

Fig. 2. Activity coefficients of TBAB (γ_2) in aqueous D-glucose solutions of various concentrations at 25 °C.
m_1; Molality of D-glucose, m_2; molality of TBAB.

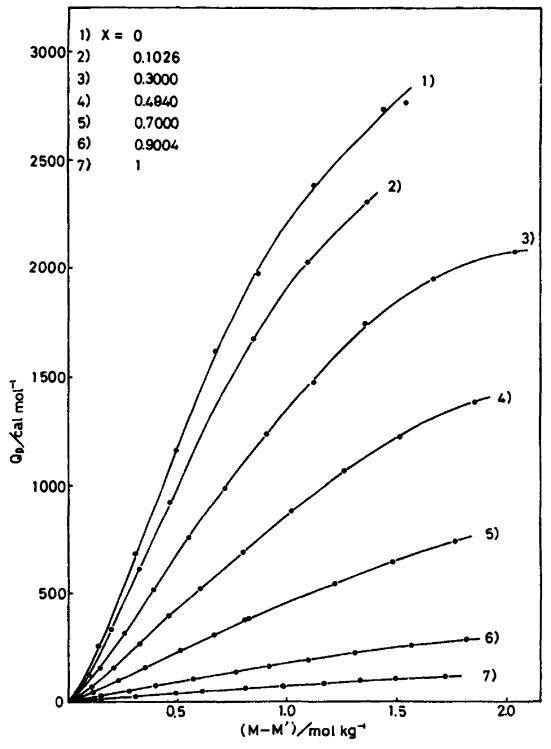

Fig. 3. Mean molar heat of dilution (Q_D) as a function of total concentration difference before and after dilution ($M-M'$) at 25 °C.
x; Mole fraction of D-glucose.

Discussion

As seen in Figs. 1 and 2, activity coefficient of each solute in ternary system increases in the presence of the other solute, showing mutual salting-out. Therefore, the repulsive force is working between these two solutes. Similar result, except for small in magnitude, was observed in the D-glucose–TMAB–water system. Taking into account the both solutes being strongly hydrated, the mutual salting-out observed in the D-glucose–TBAB–water system should be due to the structural salting-out arising from the structural difference of hydration cospheres around these two kinds of solutes.

Figures 4-(a) and -(b) show the relations between the changes of the excess thermodynamic quantities of mixing and the mole fraction of D-glucose at total molalities 1 and 2 mol kg^{-1}, repsectively. In these figures, the solid lines with star sign denote the excess free energy change of mixing for the D-glucose–TMAB–water system. The values of $\Delta_m G^{ex}$ for the both systems are positive, but the magnitude for the D-glucose–TBAB–water system is larger than that for the D-glucose–TMAB–water system. This result indicates that the hydrophobic hydration plays an important role on the magnitude of $\Delta_m G^{ex}$. The positive value of $\Delta_m G^{ex}$ implies that the system becomes unstable by mixing.

On the D-glucose–TBAB–water system, the positive value of $\Delta_m G^{ex}$ comes from the difference between large positive excess enthalpy change and entropy change, that is, the predominance of excess enthalpy term over excess entropy term makes $\Delta_m G^{ex}$ positive. Thus the unstableness of the system caused by mixing is due to the large positive excess enthalpy change.

Let us consider the mechanism of interaction between two kinds of solutes on the basis of the thermodynamic results obtained in this work. As stated in the introduction of this paper, both solutes are strongly hydrated but their structures of hydration cospheres are different each other. Accordingly the structural incompatibility causes the destruction of water structure around each solute, resulting in the increase of positive $\Delta_m S^{ex}$. The destruction of water structure accompanies the cleavage of hydrogen bonds among water molecules and makes the $\Delta_m H^{ex}$ value positive.

In order to compare the thermodynamic quantities of this system with those of the urea–TBAB–water system, thermodynamic transfer quantities were calculated by Eqs. 20, 21, and 22, and shown in Figs. 5 and 6 together with those for the urea–TBAB–water system reported by Wen *et al.*[18] As seen in Fig. 5, free energy ($\Delta\bar{G}_1^{tr}$), enthalpy ($\Delta\bar{H}_1^{tr}$), and entropy ($\Delta\bar{S}_1^{tr}$) of transfer of D-glucose from water to aqueous TBAB solution at infinite dilution are all positive, indicating the transfer process is disfavoured in enthalpic sence. The positive values of ΔH_1^{tr} and ΔS_1^{tr} mean the decrease of water structure around D-glucose in the transfer process. It is striking that the $T\Delta\bar{S}_1^{tr}$ *vs.* m_2 and $\Delta\bar{H}_1^{tr}$ *vs.* m_2 curves have maximum points around $m_2=1.5$, although the $\Delta\bar{G}_1^{tr}$ *vs.* m_2 curve gradually increases with m_2. The concentration of TBAB showing the maximum values of $\Delta\bar{H}_1^{tr}$ and $\Delta\bar{S}_1^{tr}$ nearly corresponds to the concentration at the minimum point observed in partial molar volume *vs.* concentration curve in aqueous TBAB solution.[19] At the concentration showing the minimum point, clusters around TBAB arrive at maximum cooperation in constructing a clathrate-like structure.[20] Therefore, this fact indicates that the water structure around D-glucose is destructed most strongly by TBAB at this concentration.

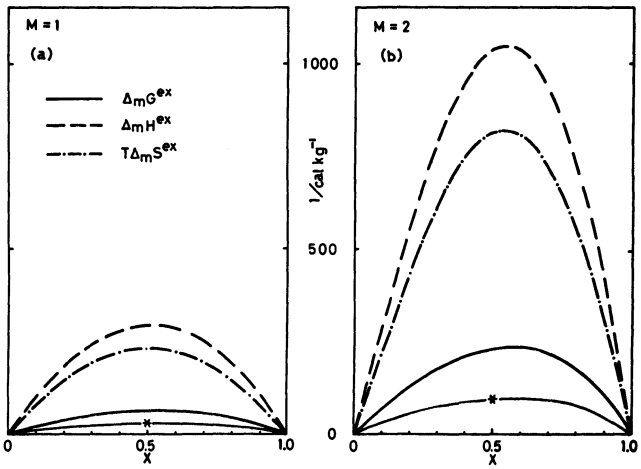

Fig. 4. Changes of excess thermodynamic quantities of mixing for the D-glucose–TBAB–water system at total molality (a) 1 or (b) 2 mol kg^{-1} at 25 °C. x; Mole fraction of D-glucose.
The solid lines with star sign denote change of excess free energy of mixing for the D-glucose–TMAB–water system.

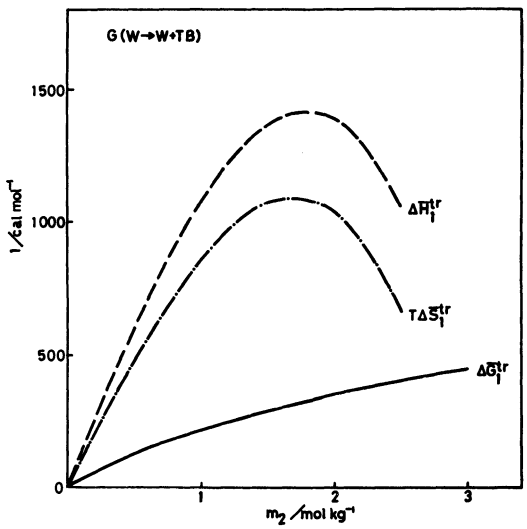

Fig. 5. Thermodynamic transfer functions of D-glucose from water to aqueous TBAB solution at infinite dilution at 25 °C.
m_2; Molality of TBAB.

Thermodynamic transfer functions of TBAB from water to aqueous D-glucose solution at infinite dilution are shown in Fig. 6-(a) as a function of the concentration of D-glucose. Similarly to Fig. 5, signs of all transfer functions are positive indicating that salting-out are caused by the large enthalpic contribution. Both positive $\Delta\bar{H}_2^{tr}$ and $\Delta\bar{S}_2^{tr}$ mean that the clathrate-like

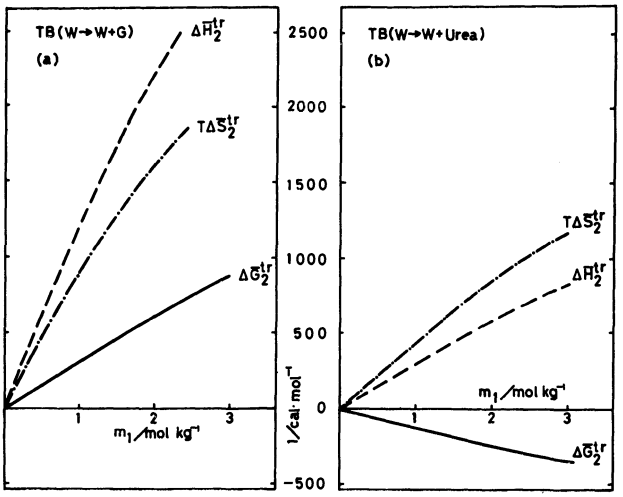

Fig. 6. Thermodynamic transfer functions of TBAB from water to (a) aqueous D-glucose solution or (b) aqueous urea solution[18] at infinite dilution at 25 °C.
m_1; Molality of D-glucose or urea.

structure of water around TBAB decreases in the presence of D-glucose. Figure 6-(b) shows the thermodynamic transfer functions of TBAB from water to various concentrations of aqueous urea solutions.[18] Comparing Fig. 6-(a) with Fig. 6-(b), one can find that both $\Delta\bar{H}_2^{tr}$ and $\Delta\bar{S}_2^{tr}$ are positive in each system but their relative magnitudes are different, that is, $\Delta\bar{H}_2^{tr} > T\Delta\bar{S}_2^{tr}$ for the D-glucose–TBAB–water system while $\Delta\bar{H}_2^{tr} < T\Delta\bar{S}_2^{tr}$ for the urea–TBAB–water system. Thus $\Delta\bar{G}_2^{tr}$ for the urea–TBAB–water system is negative, indicating salting-in. The positive value of $\Delta\bar{S}_2^{tr}$ in these two systems indicate that both D-glucose and urea decrease the clathrate-like structure of water around TBAB, but D-glucose needs more energy to break down the hydrogen bonds in clathrate-like structure than urea does. We can not explain the detail mechanism of destruction of clathrate-like structure by D-glucose at the present stage. However, it is plausible that the incompatibility of structure of hydration cosphere around D-glucose and that around TBAB enforces the mutual structure breaking action, because both solutes are known to be structure makers.

The conclusion drawn from the comparison of our results with Wen's results is that hydrophobic hydration is destabilized in the presence of both D-glucose (hydrophilic structure maker) and urea (hydrophilic structure breaker).

Saccharides and polyalcols are known to stabilize the native conformation of protein in aqueous solution, while urea destabilizes it. Hydrophobic interactions are considered to play an important role for the maintenance of the native conformation of protein.[21] The positive value of $\Delta\bar{G}_2^{tr}$ in aqueous D-glucose solution suggests that the hydrophobic moieties of protein may be more unstable in aqueous D-glucose solution than in water. Therefore, the salting-out effect of D-glucose for the hydrophobic TBAB may be related to the stabilization of native conformation of protein in aqueous D-glucose solution.

In conclusion, the excess enthalpy change ($\Delta_m H^{ex}$) and the excess entropy change ($\Delta_m S^{ex}$) of mixing for the ternary system D-glucose–TBAB–water are positive, showing that the degree of hydration of each solute in ternary solution decreases as compared with that in binary solution. The positive value of $\Delta_m G^{ex}$ which originates from the difference between $\Delta_m H^{ex}$ and $T\Delta_m S^{ex}$ indicates that each binary solution is more stable than the mixed ternary solution. Enthalpy and entropy changes of transfer of TBAB from water to D-glucose solution are positive similarly to those from water to urea solution. However, free energy of transfer of TBAB from water to D-glucose solution is positive in contrast to the case of urea–TBAB–water system. These differences seem to reflect the difference of structural effect between D-glucose and urea.

The authors express the sincere gratitude to Professor Sachio Murakami of Osaka City University for the permission and guidance of calorimetric measurements.

References

1) R. K. McMullan, M. Bonamico, and G. A. Jeffrey, *J. Chem. Phys.*, **39**, 3925 (1963).
2) M. A. Kabayama and D. Patterson, *Can. J. Chem.*, **36**, 563 (1958).
3) K. Miyajima, M. Sawada, and M. Nakagaki, *Bull. Chem. Soc. Jpn.* **56**, 1620 (1983).
4) S. Y. Gersma and E. R. Stuur, *Int. J. Pept. Protein Res.*, **4**, 377 (1972).
5) H. D. Ellerton and P. J. Dunlop, *J. Phys. Chem.*, **70**, 1831 (1966).
6) R. B. Cassel and R. H. Wood, *J. Phys. Chem.*, **78**, 2460 (1974).
7) B. E. Conway, R. E. Verrall, and J. E. Desnoyers, *Trans. Faraday Soc.*, **62**, 2738 (1966).
8) K. Miyajima, S. Nakanishi, and M. Nakagaki, *Bull. Chem. Soc. Jpn.*, **52**, 967 (1979).
9) I. Fujihara, M. Kobayashi, and S. Murakami, *J. Chem. Thermodyn.*, **15**, 1 (1983).
10) F. J. Kelly, R. A. Robinson, and R. H. Stokes, *J. Phys. Chem.*, **65**, 1958 (1961).
11) R. A. Robinson and R. H. Stokes, "Electrolyte Solutions," 2nd ed, Butterworths, London (1959).
12) S. Lindenbaum and G. E. Boyd, *J. Phys. Chem.*, **68**, 911 (1964).
13) W.-Y. Wen, K. Miyajima, and A. Otsuka, *J. Phys. Chem.*, **75**, 2148 (1971).
14) B. J. Levien, *Aust. J. Chem.*, **18**, 1161 (1965).
15) J. J. Savage and R. H. Wood, *J. Solution Chem.*, **5**, 773 (1976).
16) G. Barone, P. Cacace, G. Castronuovo, and V. Elia, *Carbohydr. Res.*, **91**, 101 (1981).
17) S. Lindenbaum, *J. Phys. Chem.*, **70**, 814 (1966).
18) R. B. Cassel and W.-Y. Wen, *J. Phys. Chem.*, **76**, 1370 (1972).
19) W.-Y. When and S. Saito, *J. Phys. Chem.*, **68**, 2639 (1964).
20) W.-Y. Wen, "Water and Aqueous Solutions," ed by R. A. Horne, John Wiley and Sons New York (1972), Chap. 15, p. 621.
21) C. Tanford, *J. Am. Chem. Soc.*, **84**, 4240 (1962).

Thermodynamics of the Electrocapillarity of Oil-Water Interfaces

Takashi KAKIUCHI and Mitsugi SENDA*
Department of Agricultural Chemistry, Faculty of Agriculture, Kyoto University, Sakyo-ku, Kyoto 606
(Received March 26, 1983)

General electrocapillary equations for the interfaces between two immiscible or partially miscible electrolyte solutions have been derived. The theory includes both nonpolarized and ideal polarized interfaces. The electrocapillary equation for the latter has been derived from the equation for the former as a special case where no common ionic species are distributed between the two phases. Implications of the general electrocapillary equation for oil–water interfaces are indicated.

Recent advances[1-3] in electrochemistry of the interfaces between two immiscible or partially miscible electrolyte solutions allow us to obtain various thermodynamic quantities characterizing the interface from the electrocapillary measurements. Koryta *et al.* have first interpreted the polarizability of the interfaces in terms of the transfer free energies of ions from one solvent to the other.[4] Kakiuchi and Senda have shown that the interface between a nitrobenzene solution of tetrabutylammonium tetraphenylborate and an aqueous solution of lithium chloride has a certain polarized potential region, where the ion transfer current across the interface is negligibly small, and gives an electrocapillary curve of parabolic shape.[5,6] The electrocapillary curves of nonpolarized nitrobenzene–water interfaces have been measured by Gros *et al.*[7] To analyze these electrocapillary data at full length, exact thermodynamic treatment of these interfaces is indispensable. Several thermodynamic treatments so far reported[7-10] suffer from limited applicability due to simplifications and various assumptions introduced.

The purpose of this study is to present a general thermodynamic theory of electrocapillarity for the planar interface between two immiscible or partially miscible electrolyte solutions, which we hereafter call the oil–water interface. In this paper, we first establish the basic electrocapillary equations for a nonpolarized oil–water interface at equilibrium, where some of the ions as well as some of the neutral components can pass through the interface and are distributed between the two phases in equilibrium. Then the electrocapillary equation for an ideal polarized oil–water interface, which is defined as the interface where no ionic species is common in both phases or where each charged species is present in appreciable amounts in only one of the two phases,[11] is derived from the equation for the nonpolarized interface by eliminating the terms involving the common ionic species.

Theoretical

Nonpolarized Oil–Water Interface. The System: We shall consider the following cell:

$$\mathrm{M}\,|\mathrm{R1}|\,\mathrm{O}\,|\,\mathrm{W}\,|\,\mathrm{R2}|\,\mathrm{M}', \qquad \text{(I)}$$

where M and M′ are two pieces of the same metal between which we measure the potential difference, and R1 and R2 are the appropriate reference electrodes, each of which is reversible to one of the ions in the adjoining solution phase. We assume a planar interface between the oil phase (O) and the water phase(W). The oil phase contains i cations, j anions, and k uncharged nondissociating components, which we hereafter simply call neutral components, while the water phase contains p cations, q anions, and h neutral components. These sets of the components are also designated by i, j, k, p, q, and h, respectively, so that these symbols are used to indicate both the set and the number of the components. Suppose that α cations, β anions and l neutral components are able to pass through the interface and are commonly distributed over the two phases; the interface is nonpolarizable with respect to these common ions. In other words, i-α cations, j-β anions, and k-l neutral components stay solely within the oil phase, while p-α cations, q-β anions, and h-l neutral components stay within the water phase. Let the sets of these common cations, anions, and neutral components also be denoted by α, β, and l, respectively.

The number of the intensive variables for this system is $i+j+k+p+q+h+2$ including temperature and pressure, but not all of them are independent. Since $\alpha+\beta+l$ components are common in both phases, there are $\alpha+\beta+l$ equations relating the chemical potentials of the common components in the two phases with each other. In addition, there are two Gibbs-Duhem equations: one for the oil phase and one for the water phase. Moreover, the potential difference between the two terminals of the cell (I) correlates the two electrochemical potentials of the two ions which are reversible to the reference electrodes R1 and R2. The number of the independent intensive variables which define the present system is, therefore, $i+j+k+p+q+h-(\alpha+\beta+l)-1$.

The Electrocapillary Equation: We adopt the concept of a surface phase[12,13] to describe the interface. An exact definition of the surface phase which the present treatment rests on has been given by Eriksson.[14] The analogue of the Gibbs-Duhem equation for the surface phase with a planar interface is[14]

$$-\mathrm{d}\gamma = \eta\,\mathrm{d}T - \tau\,\mathrm{d}P + \sum_x \Gamma_x \mathrm{d}\mu_x, \qquad (1)$$

where γ is the interfacial tension, η is the entropy of the surface phase per unit area of the interface, T is the temperature, τ is the thickness of the surface phase, P is the pressure, and Γ_x is the number of moles of the x component per unit area of the interface, which may be called the surface concentration of the x component.

The summation in the right hand side of Eq. 1 includes all the components in the system including ionic species. In Eq. 1 μ_x represents the electrochemical potential for a charged component and the chemical potential for a neutral component. For the present system Eq. 1 takes the form

$$-\mathrm{d}\gamma = \eta\,\mathrm{d}T - \tau dP + \sum_{i\neq\alpha}\Gamma_i\mathrm{d}\tilde{\mu}_i + \sum_{j\neq\beta}\Gamma_j\mathrm{d}\tilde{\mu}_j + \sum_{k\neq l}\Gamma_k\mathrm{d}\mu_k + \sum_{p\neq\alpha}\Gamma_p\mathrm{d}\tilde{\mu}_p + \sum_{q\neq\beta}\Gamma_q\mathrm{d}\tilde{\mu}_q + \sum_{h\neq l}\Gamma_h\mathrm{d}\mu_h + \sum_{\alpha}\Gamma_\alpha\mathrm{d}\tilde{\mu}_\alpha + \sum_{\beta}\Gamma_\beta\mathrm{d}\tilde{\mu}_\beta + \sum_{l}\Gamma_l d\mu_l. \quad (2)$$

In Eq. 2, we have made a distinction between the electrochemical potential, $\tilde{\mu}_x$, for a charged component $x(x=i, j, p, q, \alpha, \beta)$, and the chemical potential, μ_y, for a neutral component $y(y=h, k, l)$. The symbol $\sum_{f\neq g}$ means that the summation covers all the f components except g. There are $i+j+k+p+q+h-(\alpha+\beta+l)+2$ intensive variables and hence three of them are dependent variables as described above.

Suppose that the reference electrodes R1 and R2 are reversible to a cation i' among the cations $i\neq\alpha(i$ except $\alpha)$ and an anion q' among the anions $q\neq\beta(q$ except $\beta)$. Furthermore, we choose the anion j' out of $j\neq\beta$ anions as a counter anion of the cation i' to make up an indicator salt[15] $i'j'$ and the cation p' out of the $p\neq\alpha$ cations as a counter cation of the anion q' to make up an indicator salt $p'q'$. Then the electrochemical potentials of the ionic components can be related to the chemical potentials of the salt containing one of the ions: i', j', p', or q'.

In many practical cases, the ions constituting the indicator salts may also be commonly distributed in the two phases. To make the present treatment general enough to include these cases, we further suppose here that, in addition to the common ions, α and β, the ions consituting the indicator salts also are commonly distributed in the two phases. There are then $\alpha+2$ common cations and $\beta+2$ common anions in the system. Although these newly added four ions could be included in the sets α and β, we retain in the following treatment a distinction between these ions and the sets of ions α and β for later convenience when deriving the electrocapillary equation for an ideal polarized oil–water interface. Obviously, this extension does not change the number of independent variables. Then we have the following equations relating the electrochemical potentials of the ionic components with the chemical potential of their salt:

$$\mathrm{d}\mu_{i'j'} = \nu^+_{i'j'}\mathrm{d}\tilde{\mu}_{i'} + \nu^-_{i'j'}\mathrm{d}\tilde{\mu}_{j'} \quad (3\text{-}1)$$

$$\mathrm{d}\mu_{ij'} = \nu^+_{ij'}\mathrm{d}\tilde{\mu}_i + \nu^-_{ij'}\mathrm{d}\tilde{\mu}_{j'} \quad (i\neq i', \alpha) \quad (3\text{-}2)$$

$$\mathrm{d}\mu_{i'j} = \nu^+_{i'j}\mathrm{d}\tilde{\mu}_{i'} + \nu^-_{i'j}\mathrm{d}\tilde{\mu}_j \quad (j\neq j', \beta) \quad (3\text{-}3)$$

$$\mathrm{d}\mu_{\alpha j'} = \nu^+_{\alpha j'}\mathrm{d}\tilde{\mu}_\alpha + \nu^-_{\alpha j'}\mathrm{d}\tilde{\mu}_{j'} \quad (3\text{-}4)$$

$$\mathrm{d}\mu_{i'\beta} = \nu^+_{i'\beta}\mathrm{d}\tilde{\mu}_{i'} + \nu^-_{i'\beta}\mathrm{d}\tilde{\mu}_\beta \quad (3\text{-}5)$$

$$\mathrm{d}\mu_{p'q'} = \nu^+_{p'q'}\mathrm{d}\tilde{\mu}_{p'} + \nu^-_{p'q'}\mathrm{d}\tilde{\mu}_{q'} \quad (3\text{-}6)$$

$$\mathrm{d}\mu_{pq'} = \nu^+_{pq'}\mathrm{d}\tilde{\mu}_p + \nu^-_{pq'}\mathrm{d}\tilde{\mu}_{q'} \quad (p\neq p', \alpha) \quad (3\text{-}7)$$

$$\mathrm{d}\mu_{p'q} = \nu^+_{p'q}\mathrm{d}\tilde{\mu}_{p'} + \nu^-_{p'q}\mathrm{d}\tilde{\mu}_q \quad (q\neq q', \beta) \quad (3\text{-}8)$$

$$\mathrm{d}\mu_{\alpha q'} = \nu^+_{\alpha q'}\mathrm{d}\tilde{\mu}_\alpha + \nu^-_{\alpha q'}\mathrm{d}\tilde{\mu}_{q'} \quad (3\text{-}9)$$

$$\mathrm{d}\mu_{p'\beta} = \nu^+_{p'\beta}\mathrm{d}\tilde{\mu}_{p'} + \nu^-_{p'\beta}\mathrm{d}\tilde{\mu}_\beta \quad (3\text{-}10)$$

$$\mathrm{d}\mu_{i'q'} = \nu^+_{i'q'}\mathrm{d}\tilde{\mu}_{i'} + \nu^-_{i'q'}\mathrm{d}\tilde{\mu}_{q'} \quad (3\text{-}11)$$

$$\mathrm{d}\mu_{p'j'} = \nu^+_{p'j'}\mathrm{d}\tilde{\mu}_{p'} + \nu^-_{p'j'}\mathrm{d}\tilde{\mu}_{j'}, \quad (3\text{-}12)$$

where μ_{CA} is the chemical potential of a salt $(C)_{\nu^+_{CA}}(A)_{\nu^-_{CA}}$, and ν^+_{CA} and ν^-_{CA} are the stoichiometric numbers for the dissociation of the salt:

$$(C)_{\nu^+_{CA}}(A)_{\nu^-_{CA}} = \nu^+_{CA}C^{z_C} + \nu^-_{CA}A^{z_A}, \quad (4)$$

where C and A represent a cation and an anion and z_C and z_A are their ionic charges. By using the Gibbs-Duhem equations for the oil and water phases, we can eliminate any two of the intensive variables in Eq. 1. Usually, it is convenient to eliminate the chemical potentials of the two neutral components, which may be identified as the solvents in each phase, *e.g.*, water in the water phase and an oil in the oil phase. These two components are called the reference components. Since most organic solvents used in electrochemistry of oil–water interfaces have a certain solubility in water and *vice versa*, let l' and l'' out of l neutral components be chosen as the reference components.

The Gibbs-Duhem equations for the oil and water phases may then be written in the form

$$\bar{s}^{O}\mathrm{d}T - \bar{v}^{O}\mathrm{d}P + \sum_{i\neq i',\alpha}x^{O}_{ij'}\mathrm{d}\mu_{ij'} + \sum_{\alpha}x^{O}_{\alpha j'}\mathrm{d}\mu_{\alpha j'} + \sum_{j\neq j',\beta}x^{O}_{i'j}\mathrm{d}\mu_{i'j} + \sum_{\beta}x^{O}_{i'\beta}\mathrm{d}\mu_{i'\beta} + x^{O}_{i'j'}\mathrm{d}\mu_{i'j'} + x^{O}_{i'q'}\mathrm{d}\mu_{i'q'} + x^{O}_{p'j'}\mathrm{d}\mu_{p'j'} + \sum_{k\neq l}x^{O}_{k}\mathrm{d}\mu_k + \sum_{l\neq l',l''}x^{O}_{l}\mathrm{d}\mu_l + x^{O}_{l'}\mathrm{d}\mu_{l'} + x^{O}_{l''}\mathrm{d}\mu_{l''} = 0, \quad (5)$$

and

$$\bar{s}^{W}\mathrm{d}T - \bar{v}^{W}\mathrm{d}P + \sum_{p\neq p',\alpha}x^{W}_{pq'}\mathrm{d}\mu_{pq'} + \sum_{\alpha}x^{W}_{\alpha q'}\mathrm{d}\mu_{\alpha q'} + \sum_{q\neq q',\beta}x^{W}_{p'q}\mathrm{d}\mu_{p'q} + \sum_{\beta}x^{W}_{p'\beta}\mathrm{d}\mu_{p'\beta} + x^{W}_{p'q'}\mathrm{d}\mu_{p'q'} + x^{W}_{i'q'}\mathrm{d}\mu_{i'q'} + x^{W}_{p'j'}\mathrm{d}\mu_{p'j'} + \sum_{h\neq l}x^{W}_{h}\mathrm{d}\mu_h + \sum_{l\neq l',l''}x^{W}_{l}\mathrm{d}\mu_l + x^{W}_{l'}\mathrm{d}\mu_{l'} + x^{W}_{l''}\mathrm{d}\mu_{l''} = 0, \quad (6)$$

where $\bar{s}$ and $\bar{v}$ are the mean molar entropy and the mean molar volume of the bulk phase and x is the mole fraction. The superscript O and W denote the oil phase and the water phase, respectively. Substituting Eqs. 3, 5, and 6 into Eq. 2 to eliminate the chemical potential terms for l' and l'' and for all the ionic components except i' and q', we obtain

$$-\mathrm{d}\gamma = (\eta - J\bar{s}^{o} - K\bar{s}^{W})\mathrm{d}T - (\tau - J\bar{v}^{o} - K\bar{v}^{W})\,\mathrm{d}P + \sum_{k\neq l}(\Gamma_k - Jx^{O}_{k})\mathrm{d}\mu_k + \sum_{h\neq l}(\Gamma_h - Kx^{W}_{h})\,\mathrm{d}\mu_h + \sum_{l\neq l',l''}(\Gamma_l - Jx^{O}_{l} - Kx^{W}_{l})\,\mathrm{d}\mu_l + \sum_{i\neq i',\alpha}\left(\frac{\Gamma_i}{\nu^+_{ij'}} - Jx^{O}_{ij'}\right)\mathrm{d}\mu_{ij'} + \sum_{j\neq j',\beta}\left(\frac{\Gamma_j}{\nu^-_{i'j}} - Jx^{O}_{i'j}\right)\mathrm{d}\mu_{i'j} + \sum_{p\neq p',\alpha}\left(\frac{\Gamma_p}{\nu^+_{pq'}} - Kx^{W}_{pq'}\right)\mathrm{d}\mu_{pq'} + \sum_{q\neq q',\beta}\left(\frac{\Gamma_q}{\nu^-_{p'q}} - Kx^{W}_{p'q}\right)\mathrm{d}\mu_{p'q} + \sum_{\alpha}\left(\frac{\Gamma_\alpha}{\nu^+_{\alpha q'}} - Jx^{O}_{\alpha j'}\frac{\nu^+_{\alpha j'}}{\nu^+_{\alpha q'}} - Kx^{W}_{\alpha q'}\right)\mathrm{d}\mu_{\alpha q'} + \sum_{\beta}\left(\frac{\Gamma_\beta}{\nu^-_{p'\beta}} - Jx^{O}_{i'\beta}\frac{\nu^-_{i'\beta}}{\nu^-_{p'\beta}} - Kx^{W}_{p'\beta}\right)\mathrm{d}\mu_{p'\beta} + \frac{1}{\nu^-_{i'j'}}\Big(\Gamma_{j'} - \sum_{i\neq i',\alpha}\frac{z_i}{|z_{j'}|}\Gamma_i - J\sum_{\alpha}\nu^-_{\alpha j'}x^{O}_{\alpha j'} - J\nu^-_{p'j'}x^{O}_{p'j'} - K\nu^-_{p'j'}x^{W}_{p'j'} - J\nu^-_{i'j'}x^{O}_{i'j'}\Big)\mathrm{d}\mu_{i'j'}$$

$$+\frac{1}{\nu^{+}_{p'q'}}\Big(\Gamma_{p'}-\sum_{q\neq q'}\frac{|z_q|}{z_{p'}}\Gamma_q+J\sum_{\beta}\frac{|z_\beta|}{z_{p'}}\nu^{-}_{i'\beta}x^{0}_{i'\beta}$$
$$-J\nu^{+}_{p'j'}x^{0}_{p'j'}-K\nu^{+}_{p'j'}x^{W}_{p'j'}-K\nu^{+}_{p'q'}x^{W}_{p'q'}\Big)\mathrm{d}\mu_{p'q'}$$
$$-\frac{Q^{W}}{z_{i'}F}\mathrm{d}\tilde{\mu}_{i'}+\frac{Q^{0}}{|z_{q'}|F}\mathrm{d}\tilde{\mu}_{q'}, \tag{7}$$

where F is the Faraday and Q^{W}, Q^{0}, J, and K are given by

$$\frac{Q^{W}}{F}=\sum_{p}z_p\Gamma_p-\sum_{q}|z_q|\Gamma_q-J\sum_{\alpha}|z_{j'}|\nu^{-}_{\alpha j'}x^{0}_{\alpha j'}$$
$$+J\sum_{\beta}z_{i'}\nu^{+}_{i'\beta}x^{0}_{i'\beta}+J(z_{i'}\nu^{+}_{i'q'}x^{0}_{i'q'}-|z_{j'}|\nu^{-}_{p'j'}x^{0}_{p'j'})$$
$$+K(z_{i'}\nu^{+}_{i'q'}x^{W}_{i'q'}-|z_{j'}|\nu^{-}_{p'j'}x^{W}_{p'j'}), \tag{8}$$
$$\frac{Q^{0}}{F}=\sum_{i\neq\alpha}z_i\Gamma_i-\sum_{j\neq\beta}|z_j|\Gamma_j+J\sum_{\alpha}z_\alpha\nu^{+}_{\alpha j'}x^{0}_{\alpha j'}$$
$$-J\sum_{\beta}|z_\beta|\nu^{-}_{i'\beta}x^{0}_{i'\beta}-J(z_{j'}\nu^{+}_{i'q'}x^{0}_{i'q'}-|z_{j'}|\nu^{-}_{p'j'}x^{0}_{p'j'})$$
$$-K(z_{i'}\nu^{+}_{i'q'}x^{W}_{i'q'}-|z_{j'}|\nu^{-}_{p'j'}x^{W}_{p'j'}), \tag{9}$$
$$J=\frac{\Gamma_{l'}x^{W}_{l''}-\Gamma_{l''}x^{W}_{l'}}{x^{W}_{l'}x^{0}_{l''}-x^{0}_{l'}x^{W}_{l''}}, \tag{10}$$
$$K=\frac{\Gamma_{l'}x^{0}_{l''}-\Gamma_{l''}x^{0}_{l'}}{x^{W}_{l'}x^{0}_{l''}-x^{0}_{l'}x^{W}_{l''}}. \tag{11}$$

The electroneutrality condition of the interface can be written in the form

$$\sum_{i\neq\alpha}z_i\Gamma_i+\sum_{p\neq\alpha}z_p\Gamma_p+\sum_{\alpha}z_\alpha\Gamma_\alpha-\sum_{j\neq\beta}|z_j|\Gamma_j$$
$$-\sum_{q\neq\beta}|z_q|\Gamma_q-\sum_{\beta}|z_\beta|\Gamma_\beta=0, \tag{12}$$

from which it can be shown that $Q^{W}=-Q^{0}$. Then the last two terms in the right hand side of Eq. 7 become

$$\frac{Q^{0}}{F}\Big(\frac{1}{z_{i'}}\mathrm{d}\mu_{i'}+\frac{1}{|z_{q'}|}\mathrm{d}\mu_{q'}\Big)=$$
$$-\frac{Q^{W}}{F}\Big(\frac{1}{z_{i'}}\mathrm{d}\mu_{i'}+\frac{1}{|z_{q'}|}\mathrm{d}\mu_{q'}\Big). \tag{13}$$

Since the reference electrodes R1 and R2 in the cell (I) are reversible to i' and q' ions, respectively, we may write[15]

$$\mathrm{d}\tilde{\mu}_{i'}=-z_i\mathrm{d}\tilde{\mu}^{M}_{e}+\mathrm{d}\mu^{\cdot,R1}_{+}$$
$$=-z_i\mathrm{d}\tilde{\mu}^{M}_{e}+s^{\cdot}_{R1}\mathrm{d}T-v^{\cdot}_{R1}\mathrm{d}P, \tag{14}$$

and

$$\mathrm{d}\tilde{\mu}_{q'}=|z_{q'}|\mathrm{d}\tilde{\mu}^{M'}_{e}+\mathrm{d}\mu^{\cdot,R2}_{-}$$
$$=|z_{q'}|\mathrm{d}\tilde{\mu}^{M'}_{e}+s^{\cdot}_{R2}\mathrm{d}T-v^{\cdot}_{R2}\mathrm{d}P, \tag{15}$$

where $\tilde{\mu}^{M}_{e}$ and $\tilde{\mu}^{M'}_{e}$ are the electrochemical potentials of electron in M and M′, and $\mu^{\cdot}$, $s^{\cdot}$, and $v^{\cdot}$ are linear combinations of the chemical potentials, the molar entropies and the molar volumes of the neutral substances involved in the electrochemical reactions at the reference electrodes[15] and hence are dependent only on the nature of the reference electrodes. Substitution of Eqs. 13, 14, and 15 into Eq. 7 yields the basic electrocapillary equation for the cell (I),

$$-\mathrm{d}\gamma=\Big[\eta-J\bar{s}^{0}-K\bar{s}^{W}-\frac{Q^{W}}{F}\Big(\frac{s^{\cdot}_{R1}}{z_{i'}}+\frac{s^{\cdot}_{R2}}{|z_{q'}|}\Big)\Big]\mathrm{d}T$$
$$-\Big[\tau-J\bar{v}^{0}-K\bar{v}^{W}-\frac{Q^{W}}{F}\Big(\frac{v^{\cdot}_{R1}}{z_{i'}}+\frac{v^{\cdot}_{R2}}{|z_{q'}|}\Big)\Big]\mathrm{d}P$$
$$+\sum_{k\neq l}(\Gamma_k-Jx^{0}_{k}-Kx^{W}_{k})\mathrm{d}\mu_k+\sum_{h\neq l}(\Gamma_h-Kx^{W}_{h})\mathrm{d}\mu_h$$
$$+\sum_{l\neq l',l''}(\Gamma_l-Jx^{0}_{l}-Kx^{W}_{l})\mathrm{d}\mu_l$$
$$+\sum_{i\neq i',\alpha}\Big(\frac{\Gamma_i}{\nu^{+}_{ij'}}-Jx^{0}_{ij'}\Big)\mathrm{d}\mu_{ij'}+\sum_{j\neq j'\beta}\Big(\frac{\Gamma_j}{\nu^{-}_{i'j}}-Jx^{0}_{i'j}\Big)\mathrm{d}\mu_{i'j}$$
$$+\sum_{p\neq p',\alpha}\Big(\frac{\Gamma_p}{\nu^{+}_{pq'}}-Kx^{W}_{pq'}\Big)\mathrm{d}\mu_{pq'}+\sum_{q\neq q',\beta}\Big(\frac{\Gamma_q}{\nu^{-}_{p'q}}-Kx^{W}_{p'q}\Big)\mathrm{d}\mu_{p'q}$$
$$+\sum_{\alpha}\Big(\frac{\Gamma_\alpha}{\nu^{+}_{\alpha q'}}-J\frac{\nu^{+}_{\alpha j'}}{\nu^{+}_{\alpha q'}}x^{0}_{\alpha j'}-Kx^{W}_{\alpha q'}\Big)\mathrm{d}\mu_{\alpha q'}$$
$$+\sum_{\beta}\Big(\frac{\Gamma_\beta}{\nu^{-}_{p'\beta}}-J\frac{\nu^{-}_{i'\beta}}{\nu^{-}_{p'\beta}}x^{0}_{i'\beta}-Kx^{W}_{p'\beta}\Big)\mathrm{d}\mu_{p'\beta}$$
$$+\frac{1}{\nu^{-}_{i'j'}}\Big(\Gamma_{j'}-\sum_{i\neq i',\alpha}\frac{z_i}{|z_{j'}|}\Gamma_i-J\sum_{\alpha}\nu^{-}_{\alpha j'}x^{0}_{\alpha j'}-J\nu^{-}_{p'j'}x^{0}_{p'j'}$$
$$-K\nu^{-}_{p'j'}x^{W}_{p'j'}-J\nu^{-}_{i'j'}x^{0}_{i'j'}\Big)\mathrm{d}\mu_{i'j'}+\frac{1}{\nu^{+}_{p'q'}}\Big(\Gamma_{p'}-\sum_{q\neq q'}\frac{|z_q|}{z_{p'}}\Gamma_q$$
$$+J\sum_{\beta}\frac{|z_\beta|}{z_{p'}}\nu^{-}_{i'\beta}x^{0}_{i'\beta}-J\nu^{+}_{p'j'}x^{0}_{p'j'}-K\nu^{+}_{p'j'}x^{W}_{p'j'}-K\nu^{+}_{p'q'}x^{W}_{p'q'}\Big)\mathrm{d}\mu_{p'q'}$$
$$+Q^{W}\mathrm{d}E^{W-}_{O+}, \tag{16}$$

where $\mathrm{d}E^{W-}_{O+}=(\mathrm{d}\tilde{\mu}^{M}_{e}-\mathrm{d}\tilde{\mu}^{M'}_{e})/F$ is the change in the potential of the right hand side terminal, M′, in the cell (I) with respect to the left, M. The superscript W− and the subscript O+ indicate that the reference electrodes are reversible to the anion in the water phase and the cation in the oil phase, respectively. In Eq. 16 there are $k+h+i+p+q-(\alpha+\beta+l)-1$ intensive variables, and hence all of them are independent variables.

Generalization of the Electrocapillary Equation: In the derivations of Eq. 16 we have chosen the chemical potentials of the salts of $\alpha q'$ and $p'\beta$ types as the independent variables for all the salts containing the commonly distributed ions α and β. In principle, we can choose as the independent variables either one of $\mu_{\alpha q'}$, and $\mu_{\alpha j'}$ for each of α and either one of $\mu_{p'\beta}$ and $\mu_{i'\beta}$ for each of β. In the present treatment we consider only the simple cases where all the chemical potentials of the salts of the same type are either simultaneously dependent variables or simultaneously independent variables. There are then four possible cases to choose the sets of the independent variables involving the commonly distributed ions α and β: ($\alpha q'$ and $p'\beta$), ($\alpha q'$ and $i'\beta$), ($\alpha j'$ and $p'\beta$), and ($\alpha j'$ and $i'\beta$). The change of the independent variables among these variables results in the corresponding changes in the coefficients of $\mathrm{d}E^{W-}_{O+}$, $\mathrm{d}\mu_{i'j'}$, and $\mathrm{d}\mu_{p'q'}$ in Eq. 16 as well as those of the terms involving the chosen independent variables. Furthermore, the expressions of the coefficients of $\mathrm{d}\mu_{i'j'}$ and $\mathrm{d}\mu_{p'q'}$ depend upon the set of the ions reversible to the reference electrodes R1 and R2. There are four possible cases for the choice of the set of the ions among the ions i', j', p', and q': (i' and p'), (i' and q'), (j' and p'), and (j' and q'). The coefficients of the $\mathrm{d}T$ and $\mathrm{d}P$ terms also depend upon the choice of the set of these ions.

Taking account of these possible cases, we have a general formula for the basic electrocapillary equation for the non-polarized interface:

$$-\mathrm{d}\gamma=\Big\{\eta-J\bar{s}^{0}-K\bar{s}^{W}-\frac{Q^{W}}{F}(\mathrm{A}+\mathrm{A}')\Big\}\mathrm{d}T$$
$$-\Big\{\tau-J\bar{v}^{0}-K\bar{v}^{W}-\frac{Q^{W}}{F}(\mathrm{B}+\mathrm{B}')\Big\}\mathrm{d}P$$

$$+ Cd\mu_{i'j'} + Dd\mu_{p'q'} + Gd\mu_{\alpha x} + Hd\mu_{y\beta} + Q^{W}dE^{W\pm}_{0\pm}$$
$$+ \sum_{k\neq l}(\Gamma_k - Jx^{O}_k)d\mu_k + \sum_{h\neq l}(\Gamma_h - Kx^{W}_h)d\mu_h$$
$$+ \sum_{l\neq l',l''}(\Gamma_l - Jx^{O}_l - Kx^{W}_l)d\mu_l$$
$$+ \sum_{i\neq i',\alpha}\left(\frac{\Gamma_i}{\nu^{+}_{ij'}} - Jx^{O}_{ij'}\right)d\mu_{ij'} + \sum_{j\neq j',\beta}\left(\frac{\Gamma_i}{\nu^{-}_{i'j}} - Jx^{O}_{i'j}\right)d\mu_{i'j}$$
$$+ \sum_{p\neq q',\alpha}\left(\frac{\Gamma_p}{\nu^{+}_{\alpha q'}} - Kx^{W}_{pq'}\right)d\mu_{pq'} + \sum_{q\neq q',\beta}\left(\frac{\Gamma_q}{\nu^{-}_{p'q}} - Kx^{W}_{p'q}\right)d\mu_{p'q}, \quad (17)$$

where G, H, and Q^{W} are given in Tables 1 and 2, and A, A′, B, B′, C, and D are in Tables 3 and 4. In Eq. 17 $\mu_{\alpha x}(x=j' \text{ or } q')$ and $\mu_{y\beta}(y=i' \text{ or } p')$ are the chemical potentials of the salts containing α and β, respectively, and $E^{W\pm}_{0\pm}$ is the potential of M′ with respect to M in the cell (I), where the plus(minus) sign is taken when the reference electrode is reversible to a cation(anion).

Ideal Polarized Oil–Water Interfaces: When no common ionic species is present between the oil and the water phases the interface may be called an ideal polarized oil–water interface. In general, the ideal polarized oil–water interface permits the equilibrium distribution of neutral compounds between the two phases. In this case the terms involving the common ionic species α and β in Eqs. 8, 9, 16, and 17 vanish. The terms involving the mole fractions of $p'j'$ and $i'q'$ in the two phases also reduce to zero. We then obtain for the ideal polarized oil–water interface corresponding to Eq. 16:

$$-d\gamma = \left[\eta - J\bar{s}^{O} - K\bar{s}^{W} - \frac{Q^{W}}{F}\left(\frac{s^{*}_{R1}}{z_{i'}} + \frac{s^{*}_{R2}}{|z_{q'}|}\right)\right]dT$$
$$-\left[\tau - J\bar{v}^{O} - K\bar{v}^{W} - \frac{Q^{W}}{F}\left(\frac{v^{*}_{R1}}{z_{i'}} + \frac{v^{*}_{R2}}{|z_{q'}|}\right)\right]dP$$
$$+ \sum_{k\neq l}(\Gamma_k - Jx^{O}_k)d\mu_k + \sum_{h\neq l}(\Gamma_h - Kx_h)d\mu_h$$
$$+ \sum_{l\neq l',l''}(\Gamma_l - Jx^{O}_l - Kx^{W}_l)d\mu_l$$
$$+ \sum_{i\neq i'}\left(\frac{\Gamma_i}{\nu^{+}_{ij'}} - Jx^{O}_{ij'}\right)d\mu_{ij'} + \sum_{j\neq j'}\left(\frac{\Gamma_i}{\nu^{-}_{i'j}} - Jx^{O}_{i'j}\right)d\mu_{i'j}$$
$$+ \sum_{p\neq p'}\left(\frac{\Gamma_p}{\nu^{+}_{pq'}} - Kx^{W}_{pq'}\right)d\mu_{pq'} + \sum_{q\neq q'}\left(\frac{\Gamma_q}{\nu^{-}_{p'q}} - Kx^{W}_{p'q}\right)d\mu_{p'q}$$
$$+ \frac{1}{\nu^{-}_{i'j'}}\left(\Gamma_{j'} - \sum_{i\neq i'}\frac{z_i}{|z_{j'}|}\Gamma_i - J\nu^{-}_{i'j'}x^{O}_{i'j'}\right)d\mu_{i'j'}$$
$$+ \frac{1}{\nu^{+}_{p'q'}}\left(\Gamma_{p'} - \sum_{q\neq q'}\frac{|z_q|}{z_{p'}}\Gamma_q - K\nu^{+}_{p'q'}x^{W}_{p'q'}\right)d\mu_{p'q'}$$
$$+ q^{W}dE^{W-}_{0+}, \quad (18)$$

where $q^{W}(=-q^{O})$ is the surface charge density due to the components in the water phase (q^{O} is the surface charge density due to the components in the oil phase) and is defined by

$$q^{W} = F\left(\sum_{p} z_p\Gamma_p - \sum_{q}|z_q|\Gamma_q\right)$$
$$= F\left(\sum_{j}|z_j|\Gamma_j - \sum_{i} z_i\Gamma_i\right) = -q^{O}. \quad (19)$$

The degree of freedom of Eq. 18 is $k+h+i+j+p+q-l-1$ and, hence, all the intensive variables are independent. When the pair of the ions reversible to the reference electrodes R1 and R2 is not the $i'q'$ pair, one can easily find a corresponding electrocapillary equation using Eq. 17 and Tables 1, 3, and 4 if we omit the terms involving the common ionic species α and β and the mole fractions of $p'j'$ and $i'q'$.

Discussion

Ideal non-polarized interface is characterized by the lack of the degree of freedom concerning the electrical state of the interface; it is not possible to change the electrical potential difference between the interface or the surface charge density if we keep all other intensive variables constant. In the basic electrocapillary equation for the ideal nonpolarized interface represented by Eq. 16, or in more general terms in Eq. 17, there appears the potential difference between the two terminals of the cell (I) as an independent variable. This does not mean that one can apply a voltage to the interface without changing the equilibrium state of the interface. The potential difference between the two terminals can of course be measured, but the change of this potential can be achieved only through the change of the chemical potential of at least one of the salts containing α and β. In fact, the dE^{W-}_{0+} term in Eq. 16 can be rewitten in terms of the chemical potential of one of these salts which has been taken as a dependent variable in Eq. 16.

Let $\mu_{p'\beta'}$ instead of E^{W-}_{0+} be the independent variable, where β' is any one of β common anions. By using Eq. 3 the last two terms in the right hand side of Eq. 7 become

$$-\frac{Q^{W}}{z_{i'}F}d\mu_{i'} + \frac{Q^{O}}{|z_{q'}|F}d\mu_{q'} =$$
$$-\frac{Q^{W}}{F}\left(\frac{1}{z_i\nu^{+}_{i'\beta'}}d\mu_{i'\beta'} - \frac{1}{|z_\beta|\nu^{-}_{p'\beta'}}d\mu_{p'\beta'} + \frac{1}{z_{p'}\nu^{+}_{p'q'}}d\mu_{p'q'}\right).$$

Therefore, dE^{W-}_{0+} may be rewritten as

$$dE^{W-}_{0+} = \frac{1}{|z_{\beta'}|\nu^{-}_{p'\beta'}}d\mu_{p'\beta'} - \frac{1}{z_{i'}\nu^{+}_{i'\beta'}}d\mu_{i'\beta'} - \frac{1}{z_{p'}\nu^{+}_{p'q'}}d\mu_{p'q'}.$$

Necessary changes in Eq. 16 accompanied by the change of the independent variable from E^{W-}_{0+} to $\mu_{p'\beta'}$ are given in Table 5. Thus, in ideal nonpolarized oil–water interfaces one can always replace the electromotive force of the cell with the chemical potential of one of the salts containing a common ion. Namely, a change of the chemical potential is always accompanied by a change of the chemical potential and is achieved only through the change of the chemical potential of the salt, as described above. When the interface is ideally polarized, there is no salt whose constituent ion is commonly distributed in both phases. In this case, one can arbitrarily change E^{W-}_{0+} by applying a voltage between the two reference electrodes.

Equations 16 and 17 show that the partial derivative of the interfacial tension with respect to the potential drop across the terminals of the cell (I) gives the quantity Q^{W}. This Q^{W} is different from the surface charge density in the water phase q^{W} defined by Eq. 19 for an ideal polarized oil–water interface. First, Q^{W} defined by Eq. 8 contains the terms of the surface concentrations of the ions commonly distributed in the two phases, and, second, in comparison with q^{W}, Q^{W} has four additional terms involving the mole fractions of the salts containing the common ions. Unlike the ideal polarized interfaces, the potential of the electrocapillary maximum of the electrocapillary curve for a nonpolarized oil–water

TABLE 1. COEFFICIENTS G AND H IN Eq. 17

Independent variable		Coefficient G	Coefficient H
$\mu_{\alpha x}$	$\mu_{\alpha q'}$ [a]	$\sum_{\alpha}\frac{\Gamma_{\alpha}}{\nu^{+}_{\alpha q'}} - J\frac{\nu^{+}_{\alpha j'}}{\nu^{+}_{\alpha q'}}x^{0}_{\alpha j'} - Kx^{W}_{\alpha q'}$	—
	$\mu_{\alpha j'}$	$\sum_{\alpha}\frac{\Gamma_{\alpha}}{\nu^{+}_{\alpha j'}} - Jx^{0}_{\alpha j'} - K\frac{\nu^{+}_{\alpha q'}}{\nu^{+}_{\alpha j'}}x^{W}_{\alpha q'}$	—
$\mu_{y\beta}$	$\mu_{p'\beta}$ [a]	—	$\sum_{\beta}\frac{\Gamma_{\beta'}}{\nu^{-}_{p'\beta}} - J\frac{\nu^{-}_{i'\beta}}{\nu^{-}_{p'\beta}}x^{0}_{i'\beta} - Kx^{W}_{p'\beta}$
	$\mu_{i'\beta}$	—	$\sum_{\beta}\frac{\Gamma_{\beta}}{\nu^{-}_{i'\beta}} - Jx^{0}_{i'\beta} - K\frac{\nu^{-}_{p'\beta}}{\nu^{-}_{i'\beta}}x^{W}_{p'\beta}$

a) This choice of independent variables corresponds to Eq. 16.

TABLE 2. COEFFICIENTS Q^{W} IN Eq. 17 FOR VARIOUS SETS THE INDEPEDENT VARIABLES CONCERNING THE COMMON IONIC SPECIES

Set of independent variables	Q^{W}
$\alpha q'$ and $p'\beta$ [a]	$F\{\sum_{p}z_{p}\Gamma_{p} - \sum_{q}\lvert z_{q}\rvert\Gamma_{q} - J\sum_{\alpha}\nu^{+}_{\alpha j'}z_{\alpha}x^{0}_{\alpha j'} + J\sum_{\beta}\lvert z_{\beta}\rvert\nu^{-}_{i'\beta}x^{0}_{i'\beta}$ $+ J(z_{i'}\nu^{+}_{i'q'}x^{0}_{i'q'} - \lvert z_{j'}\rvert\nu^{-}_{p'j'}x^{0}_{p'j'}) + K(z_{i'}\nu^{+}_{i'q'}x^{W}_{i'q'} - \lvert z_{j'}\rvert\nu^{-}_{p'j'}x^{W}_{p'j'})\}$
$\alpha q'$ and $i'\beta$	$F\{\sum_{p}z_{p}\Gamma_{p} - \sum_{q\neq\beta}\lvert z_{q}\rvert\Gamma_{q} - J\sum_{\alpha}z_{\alpha}\nu^{+}_{\alpha j'} - K\sum_{\beta}\lvert z_{\beta}\rvert\nu^{-}_{p'\beta}x^{W}_{p'\beta}$ $+ J(z_{i'}\nu^{+}_{i'q'}x^{0}_{i'q'} - \lvert z_{j'}\rvert\nu^{-}_{p'j'}x^{0}_{p'j'}) + K(z_{i'}\nu^{+}_{i'q'}x^{W}_{i'q'} - \lvert z_{j'}\rvert\nu^{-}_{p'j'}x^{W}_{p'j'})\}$
$\alpha j'$ and $p'\beta$	$F\{\sum_{p\neq\alpha}z_{p}\Gamma_{p} - \sum_{q}\lvert z_{q}\rvert\Gamma_{q} + K\sum_{\alpha}z_{\alpha}\nu^{+}_{\alpha q'}x^{W}_{\alpha q'} + J\sum_{\beta}\lvert z_{\beta}\rvert\nu^{-}_{i'\beta}x^{0}_{i'\beta}$ $+ J(z_{i'}\nu^{+}_{i'q'}x^{0}_{i'q'} - \lvert z_{j'}\rvert\nu^{-}_{p'j'}x^{0}_{p'j'}) + K(z_{i'}\nu^{+}_{i'q'}x^{W}_{i'q'} - \lvert z_{j'}\rvert\nu^{-}_{p'j'}x^{W}_{p'j'})\}$
$\alpha j'$ and $i'\beta$	$F\{\sum_{p\neq\alpha}z_{p}\Gamma_{p} - \sum_{q\neq\beta}\lvert z_{q}\rvert\Gamma_{q} + K\sum_{\alpha}z_{\alpha}\nu^{+}_{\alpha q'}x^{W}_{\alpha q'} - K\sum_{\beta}\lvert z_{\beta}\rvert\nu^{-}_{p'\beta}x^{W}_{p'\beta}$ $+ J(z_{i'}\nu^{+}_{i'q'}x^{0}_{i'q'} - \lvert z_{j'}\rvert\nu^{-}_{p'j'}x^{0}_{p'j'}) + K(z_{i'}\nu^{+}_{i'q'}x^{W}_{i'q'} - \lvert z_{j'}\rvert\nu^{-}_{p'j'}x^{W}_{p'j'})\}$

a) This choice of independent variables corresponds to Eq. 16.

TABLE 3. EXPRESSSIONS OF A, B, AND C IN Eq. 17

Coefficient in Eq. 17	Choice of αx and $y\beta$	Ion reversible to R1 i'	Ion reversible to R1 j'
A	—	$s^{*}_{R1}/z_{i'}$ [a]	$-s^{*}_{R1}/\lvert z_{j'}\rvert$
B	—	$v^{*}_{R1}/z_{i'}$ [a]	$-v^{*}_{R1}/\lvert z_{j'}\rvert$
C	$(\alpha q', p'\beta)$ $(\alpha q', i'\beta)$	$\frac{1}{\nu^{-}_{i'j'}}(\Gamma_{j'} - \sum_{i\neq j',\alpha}\frac{z_{i}}{\lvert z_{j'}\rvert}\Gamma_{i} - J\sum_{\alpha}\nu^{-}_{\alpha j'}x^{0}_{\alpha j'}$ [a] $- J\nu^{-}_{i'j'}x^{0}_{i'j'} - J\nu^{-}_{p'j'}x^{0}_{p'j'} - K\nu^{-}_{p'j'}x^{W}_{p'j'})$	$\frac{1}{\nu^{+}_{i'j'}}(\Gamma_{i} - \sum_{i\neq j',\beta}\frac{\lvert z_{j}\rvert}{z_{i'}}\Gamma_{j} - J\sum_{\beta}\nu^{+}_{i'\beta}x^{0}_{i'\beta}$ $- J\nu^{+}_{i'j'}x^{0}_{i'j'} - J\nu^{+}_{i'q'}x^{0}_{i'q'} - K\nu^{+}_{i'q'}x^{W}_{i'q'})$
	$(\alpha j', i'\beta)$ $(\alpha j', p'\beta)$	$\frac{1}{\nu^{-}_{i'j'}}(\Gamma_{j'} - \sum_{i\neq i'}\frac{z_{i}}{\lvert z_{j'}\rvert}\Gamma_{i} + K\sum_{\alpha}\nu^{+}_{\alpha q'}x^{W}_{\alpha q'}$ $- J\nu^{-}_{i'j'}x^{0}_{i'j'} - J\nu^{-}_{p'j'}x^{0}_{p'j'} - K\nu^{-}_{p'j'}x^{W}_{p'j'})$	$\frac{1}{\nu^{+}_{i'j'}}(\Gamma_{i'} - \sum_{i\neq j'}\frac{\lvert z_{j}\rvert}{z_{i'}}\Gamma_{j} + K\sum_{\alpha}\frac{\lvert z_{\beta}\rvert}{z_{i'}}\nu^{-}_{p'\beta}x^{W}_{p'\beta}$ $- J\nu^{+}_{i'j'}x^{0}_{i'j'} - J\nu^{+}_{i'q'}x^{0}_{i'q'} - K\nu^{+}_{i'q'}x^{W}_{i'q'}$

a) This choice of independent variables corresponds to Eq. 16.

TABLE 4. EXPRESSIONS OF A', B', AND D IN Eq. 17

Coefficient in Eq. 17	Choice of αx and $y\beta$	Ion reversible to R2 p'	Ion reversible to R2 q'
A'	—	$-s^{*}_{R1}/z_{p'}$	$s^{*}_{R2}/\lvert z_{q'}\rvert$ [a]
B'	—	$-v^{*}_{R2}/z_{p'}$	$v^{*}_{R2}/\lvert z_{q'}\rvert$ [a]
D	$(\alpha q', p'\beta)$ $(\alpha j', p'\beta)$	$\frac{1}{\nu^{-}_{p'q'}}(\Gamma_{q'} - \sum_{p\neq p'}\frac{z_{p}}{\lvert z_{q'}\rvert}\Gamma_{p} + J\frac{z_{\alpha}}{\lvert z_{q'}\rvert}\nu^{-}_{\alpha j'}x^{0}_{\alpha j'}$ $- K\nu^{-}_{p'q'}x^{W}_{p'q'} - J\nu^{-}_{i'q'}x^{0}_{i'q'} - K\nu^{-}_{i'q'}x^{W}_{i'q'})$	$\frac{1}{\nu^{+}_{p'q'}}(\Gamma_{p'} - \sum_{q\neq q'}\frac{\lvert z_{q}\rvert}{z_{p'}}\Gamma_{q} + J\frac{\lvert z_{\beta}\rvert}{z_{p'}}\nu^{-}_{i'\beta}x^{0}_{i'\beta}$ $- K\nu^{+}_{p'q'}x^{W}_{p'q'} - J\nu^{+}_{p'j'}x^{0}_{p'j'} - K\nu^{+}_{p'j'}x^{W}_{p'j'})$ [a]
	$(\alpha q', i'\beta)$ $(\alpha j', i'\beta)$	$\frac{1}{\nu^{-}_{p'q'}}(\Gamma_{q'} - \sum_{p\neq p'}\frac{z_{p}}{\lvert z_{q'}\rvert}\Gamma_{p} - K\sum_{\alpha}\nu^{+}_{\alpha q'}x^{W}_{\alpha q'}$ $- K\nu^{-}_{p'q'}x^{W}_{p'q'} - J\nu^{-}_{i'q'}x^{0}_{i'q'} - K\nu^{-}_{i'q'}x^{W}_{i'q'})$	$\frac{1}{\nu^{+}_{p'q'}}(\Gamma_{p'} - \sum_{q\neq q',\beta}\frac{\lvert z_{q}\rvert}{z_{p'}}\Gamma_{q} - K\sum_{\beta}\nu^{+}_{p'\beta}x^{W}_{p'\beta}$ $- K\nu^{+}_{p'q'}x^{W}_{p'q'} - J\nu^{+}_{p'j'}x^{0}_{p'j'} - K\nu^{+}_{p'j'}x^{W}_{p'j'})$

a) This choice of independent variables corresponds to Eq. 16.

TABLE 5. CHANGE OF THE TERMS IN Eq. 16 ACCOMPANIED BY THE CHANGE OF AN INDEPENDENT VARIABLES FROM E^{W-}_{0+} to $\mu_{i'\beta'}$

E^{W-}_{0+}	$\mu_{i'\beta'}$
$\sum_{\beta}\frac{\Gamma_\beta}{\nu^-_{p'\beta}} - J\frac{\nu^-_{i'\beta}}{\nu^-_{p'\beta}}x^O_{i'\beta} - Kx^W_{p'\beta})\mathrm{d}\mu_{p'\beta}$	$\sum_{\beta\neq\beta'}\left(\frac{\Gamma_\beta}{\nu^-_{p'\beta}} - J\frac{\nu^-_{i'\beta}}{\nu^-_{p'\beta}}x^O_{i'\beta} - Kx^W_{p'\beta}\right)\mathrm{d}\mu_{p'\beta}$
	$+\left(\frac{\Gamma_{\beta'}}{\nu^-_{p'\beta'}} - J\frac{\nu^-_{i'\beta'}}{\nu^-_{p'\beta'}}x^O_{i'\beta'} - Kx^W_{p'\beta'} + \frac{1}{\lvert z_{\beta'}\rvert\nu^-_{p'\beta'}}\cdot\frac{Q^W}{F}\right)d\mu_{p'\beta'}$
$\frac{1}{\nu^+_{p'q'}}X\,\mathrm{d}\mu_{p'q'}$ [a]	$\frac{1}{\nu^+_{p'q'}}\left(X - \frac{Q^W}{z_{p'}F}\right)\mathrm{d}\mu_{p'q'}$ [a]
$\frac{Q^W}{F}\mathrm{d}E^{W-}_{0+}$	$-\frac{Q^W}{Fz_{i'}\nu^+_{i'\beta'}}\mathrm{d}\mu_{i'\beta'}$

a) $X = \Gamma_{p'} - \sum_{q\neq q'}\frac{\lvert z_q\rvert}{z_{p'}}\Gamma_q + J\sum_{\beta}\frac{\lvert z_\beta\rvert}{z_{p'}}\nu^-_{i'\beta'} - J\nu^+_{p'j'}x^O_{p'j'} - K\nu^+_{p'j'}x^W_{p'j'} - K\nu^+_{p'q'}x^W_{p'q'}$.

interface, therfore, does not generally correspond to the potential of zero charge, which, however, can be defined only through an assumption of a dividing surface in the case of nonpolarized interfaces. The difference between Q^W and q^W originates in the difference in thermodynamic polarizability of the interfaces and is free from any particular model which assumes a physical dividing surface.[16] The surface charge density due to the components in the water phase q^W defined by Eq. 19 is conventionally called the surface charge density in water phase and q^O the surface charge density in oil phase. Note that the surface charge density $q^W(=-q^O)$ is a thermodynamically defined quantity for an ideal polarized oil–water interface and may not correspond to the physical surface charge density.[11,16] For example, the ionic charge due to the hydrophilic group of an amphiphile which is present only in the oil phase and is adsorbed at an oil–water interface should be considered as a part of the "surface charge density in the oil phase" even when the hydrophilic ionic groups protrude into the water phase and are exposed to the aqueous medium, as is the case of the adsorption of phospholipids at the oil–water interface.[17]

In Eqs. 16, 17, and 18 the partial derivative of the interfacial tension with respect to the chemical potential of any one of the neutral components gives the relative surface concentration of the corresponding component, *i.e.*, the surface concentration relativised by the surface concentrations of the two reference components l' and l'', which enter into the measured quantity through J and K terms. Similarly, the partial derivative of the interfacial tension with respect to the chemical potential of any one of the salt components gives the relative surface concentration of the corresponding ionic component. When the mutual solubility between l' and l'' is considerably high, the denominators of Eqs. 10 and 11 become very small. This means that the relative surface concentrations can be significantly different from the actual surface concentrations. This is due to the fact that the relative surface concentrations in Eqs. 16–18 are relativised by the two reference components; hence, this is one of the features of the oil–water interfaces which distinguish them from the metal-solution interfaces.[15]

When there occurs an ion pair formation or an incomplete dissociation of a salt, which may be expected especially in the oil phase having lower dielectric constant, the surface concentration of an ion pair or an undissociated salt appears in the relevant terms in Eq. 17 (and also in Eqs. 16 and 18). Extension of the basic electrocapillary equation to meet these cases is feasible. For example, suppose that the cation $\bar{i}$ in the cations i (except i' and α) and the anion $\bar{j}$ in the anions j (except j' and β) form a neutral ion pair $\bar{i}\bar{j}$ in the oil phase. There then appears an additional term $\Gamma_{\bar{i}\bar{j}}\mathrm{d}\mu_{\bar{i}\bar{j}}$ in Eq. 2, where $\Gamma_{\bar{i}\bar{j}}$ and $\mu_{\bar{i}\bar{j}}$ are the surface concentration and the chemical potential of the ion pair $\bar{i}\bar{j}$. Since the differential of the chemical potential of $\bar{i}\bar{j}$, $\mathrm{d}\mu_{\bar{i}\bar{j}}$, can be written in terms of those of the electrochemical potentials of $\bar{i}$ and $\bar{j}$ ions, $\mathrm{d}\mu_{\bar{i}}$ and $\mathrm{d}\mu_{\bar{j}}$, as

$$\mathrm{d}\mu_{\bar{i}\bar{j}} = \nu^+_{\bar{i}\bar{j}}\mathrm{d}\mu_{\bar{i}} + \nu^-_{\bar{i}\bar{j}}\mathrm{d}\mu_{\bar{j}},$$

where $\nu^+_{\bar{i}\bar{j}}$ and $\nu^-_{\bar{i}\bar{j}}$ are the stoichiometric numbers of the ion pair formation reaction represented by the equation similar to Eq. 4, the term $\Gamma_{\bar{i}\bar{j}}\mathrm{d}\mu_{\bar{i}\bar{j}}$ can be rewritten in the form:

$$\Gamma_{\bar{i}\bar{j}}\mathrm{d}\mu_{\bar{i}\bar{j}} = \Gamma_{\bar{i}\bar{j}}(\nu^+_{\bar{i}\bar{j}}\mathrm{d}\mu_{\bar{i}} + \nu^-_{\bar{i}\bar{j}}\mathrm{d}\mu_{\bar{j}}).$$

Substituting Eqs. 3-1 to 3-3 into this equation, we obtain

$$\Gamma_{\bar{i}\bar{j}}\mathrm{d}\mu_{\bar{i}\bar{j}} = \Gamma_{\bar{i}\bar{j}}\left(\frac{\nu^+_{\bar{i}\bar{j}}}{\nu^+_{\bar{i}j'}}\mathrm{d}\mu_{\bar{i}j'} - \frac{\nu^-_{\bar{i}\bar{j}}}{\nu^-_{i'\bar{j}}}\mathrm{d}\mu_{i'\bar{j}} - \frac{z_{\bar{i}}}{\lvert z_{j'}\rvert}\cdot\frac{\nu^+_{\bar{i}\bar{j}}}{\nu^+_{i'j'}}\mathrm{d}\mu_{i'j'}\right).$$

Consequently, the ion pair formation between the ions $\bar{i}$ and $\bar{j}$ gives rise to additional terms involving the surface concentration of the ion pair, $(\nu^+_{\bar{i}\bar{j}}/\nu^+_{\bar{i}j})\Gamma_{\bar{i}\bar{j}}$, $(\nu^-_{\bar{i}\bar{j}}/\nu^-_{i'\bar{j}})\Gamma_{\bar{i}\bar{j}}$, and $(z_{\bar{i}}/\lvert z_{j'}\rvert)(\nu^+_{\bar{i}\bar{j}}/\nu^+_{i'j'})\Gamma_{\bar{i}\bar{j}}$, in the coefficients of $\mathrm{d}\mu_{\bar{i}j'}$, $\mathrm{d}\mu_{i'\bar{j}}$, and $\mathrm{d}\mu_{i'j'}$ terms, respectively, in Eq. 17 (and also in Eqs. 16 and 18). Thus the ion pair formation or incomplete dissociation of a salt is easily taken into account in the general electrocapillary equation. The case of the formation of a charged ion pair may be considered similarly.

If we introduce a new function defined by $\xi = Q^W E^{W\pm}_{0\pm} + \gamma$, which has been proposed by Parsons[18] for an ideal polarized metal-solution interface, we can replace the independent variable $E^{W\pm}_{0\pm}$ with Q^W in Eq. 17. Then several useful relationships can be obtained from the cross-differentiation relationship. For example, the Esin–Markov coefficient of a neutral component k, which is defined as the slope of a plot of $E^{W\pm}_{0\pm}$ *vs.* the chemical potential of component k at constant T, P, Q^W, and chemical potentials of all other components, is related to the rate of the change of the relative surface concentration of a component k with Q^W at constant T, P, and composition:

$$\left(\frac{\partial E^{w\pm}_{0\pm}}{\partial \mu_k}\right)_{T,P,Q^w,\mu\neq\mu_k} = -\left(\frac{\partial(\Gamma_k - Jx^{0}_{k})}{\partial Q^w}\right)_{T,P,\mu}$$

(for $k\neq l$).

Similar relations are easily obtained for the Esin–Markov coefficients of the neutral components $h(\neq l)$ and $l(\neq l', l'')$ and of the salts $i'j'$, $p'q'$, αx ($x=j'$ or q'), $y\beta$($y=i'$ or p'), ij'(for $i\neq i'$, α), $i'j$(for $j\neq j'$, β), pq'(for $p\neq p'$, α), and $p'q$(for $q\neq q'$, β). Such cross-differentiation relations have been employed to analyze the Esin-Markov coefficients at the interface between a nitrobenzene solution of tetrabutylammonium tetraphenylborate and an aqueous solution of lithium chloride to detect the specific adsorption of the ions.[6]

References

1) A. Watanabe and H. Tamai, *Hyomen*, **13**, 67 (1975).

2) J. Koryta, *Anal. Chim. Acta*, **61**, 329 (1972); **91**, 1 (1977); 111, 1 (1979); **139**, 1 (1982).

3) J. Koryta and P. Vaňysek, "Advances in Electrochemistry and Electrochemical Engineering," ed by H. Gerischer and C. W. Tobias, John Wiley and Sons, New York (1981), Vol. 12, p. 113.

4) J. Koryta, P. Vaňysek, and M. Březina, *J. Electroanal. Chem. Interfacial Electrochem.*, **75**, 211 (1977).

5) T. Kakiuchi and M. Senda, *Bull. Chem. Soc. Jpn.*, **56**, 1322 (1983).

6) T. Kakiuchi and M. Senda, *Bull. Chem. Soc. Jpn.*, **56**, 1753 (1983).

7) M. Gros, M. Grom, and C. Gavach, *J. Electroanal. Chem. Interfacial Electrochem.*, **89**, 29 (1978).

8) A. Watanabe, M. Matsumoto, H. Tamai, and R. Gotoh, *Kolloid Z. Z. Polym.*, **220**, 152 (1967).

9) M. Dupeyrat and E. Nakache, *J. Colloid Interface Sci.*, **73**, 332 (1980).

10) M. Senda and T. Kakiuchi, *Rev. Polarogr. (Kyoto)*, **27**, 49 (1981).

11) D. C. Grahame and R. B. Whitney, *J. Am. Chem. Soc.*, **64**, 1548 (1942).

12) G. Bakker, "Handbuch der Experimentalphysik," Hg. von W. Wien und F. Harms, Akademische Verlag., Leipzig (1928), Band 6, Kap. XV.

13) E. A. Guggenheim, "Thermodynamics," 6th ed, North-Holland, Amsterdam (1977), p. 45.

14) J. C. Eriksson, *Ark. Kemi*, **25**, 331 (1966).

15) D. M. Mohilner, "Electroanalytical Chemistry," ed by A. Bard, Marcel Dekker, New York (1966), Vol. 1, p. 241.

16) A. N. Frumikin, O. A. Petrii, and B. B. Damaskin, "Comprehensive Treatise of Electrochemistry," ed by J. O'M. Bockris, B. E. Conway, and E. Yeager, Plenum Press, New York (1980), Vol. 1, Chap. 5.

17) A. Watanabe, M. Matsumoto, H, Tamai, and R. Gotoh, *Kolloid Z. Z. Polym.*, **228**, 58 (1968).

18) R. Parsons, *Trans. Faraday Soc.*, **51**, 1518 (1955).

 © 1983 The Chemical Society of Japan Bull. Chem. Soc. Jpn., 56, 2919—2921 (1983)

Homoconjugation in Bicyclo[2.2.1]hept-2-en-7-yl and 1,4-Dihydro-1,4-methanonaphthalen-9-yl Radicals

Takashi KAWAMURA,* Yoshio SUGIYAMA, and Teijiro YONEZAWA
Department of Hydrocarbon Chemistry, Faculty of Engineering, Kyoto University, Sakyo-ku, Kyoto 606
(Received March 28, 1983)

2,3-Dimethylbicyclo[2.2.1]hept-2-en-7-yl and 6-methyl-1,4-dihydro-1,4-methanonaphthalen-9-yl radicals are examined wiht ESR. Comparisons of their hyperfine splitting constants with those of bicyclo[2.2.1]hept-2-en-7-yl (**1a**) and 1,4-dihydro-1,4-methanonaphthalen-9-yl (**2a**) radicals show that the odd electron on the tervalent carbon atom is delocalized to the extent of 10% into the π system of the vinylene bridge in **1a**, and 5% at maximum into the π system of the phenylene bridge in **2a**, respectively. This odd eletron delocalization is accompanied by an increase of carbanion character of the tervalent carbon atom. The nonplanarity of their tervalent carbon atoms is discussed in relation to the carbanion character.

Molecules with bicyclo[2.2.1]hept-2-en-7-yl, 1,4-dihydro-1,4-methanonaphthalen-9-yl and related frameworks are of interest because of possible involvement of homoconjugation. In a previous communication,[1] the tervalent carbon atom of the bicyclo[2.2.1]hepta-2,5-dien-7-yl radical was shown to have a deep pyramidal geometry, which was proposed to arise mainly from intramolecular charge transfer interactions from the vinylene bridges onto the tervalent carbon atom. To estimate the extent of this type of charge transfer interaction, 2,3-dimethylbicyclo[2.2.1]hept-2-en-7-yl (**1b**) and 6-methyl-1,4-dihydro-1,4-methanonaphthalen-9-yl (**2b**) radicals are examined with ESR and compared with results of bicyclo[2.2.1]hept-2-en-7-yl (**1a**) and 1,4-dihydro-1,4-methanonaphthalen-9-yl (**2a**) radicals.

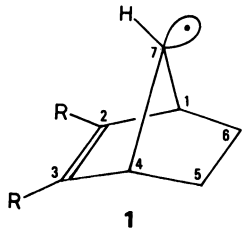

1
a : R = H
b : R = CH_3

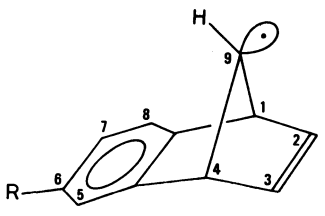

2
a : R = H
b : R = CH_3

Results

The ESR spectrum of **1b** (Fig. 1) was observed during photolysis of a cyclopropane solution of a mixture of 7-bromo-2,3-dimethylbicyclo[2.2.1]hept-2-ene, triethylsilane, and di-*t*-butyl peroxide at −127 °C. The hyperfine structure of the spectrum arises from a proton (0.992 mT), two pairs of equivalent protons (0.173 and 0.161 mT), and six equivalent protons (0.140 mT). The *g* factor is 2.00240. On the basis of the comparison of these hyperfine splitting constants (hfsc) with those of **1a**,[2,3] the formers are assigned as shown below:

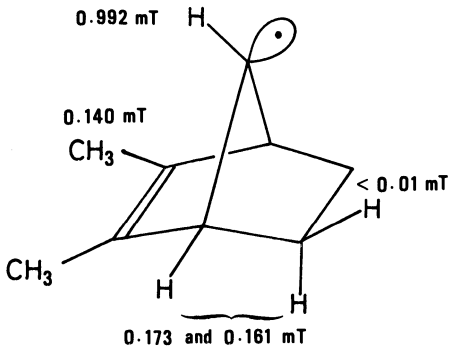

Figure 2 shows the ESR spectrum of **2b** generated similarly from 9-*anti*-bromo-6-methyl-1,4-dihydro-1,4-dihydro-1,4-methanonaphthalene. The spectrum consists of a doublet of 0.812 mT split into triplets of 0.166 mT further into quintets of 0.028 mT. By comparing these hfsc's with those of **2a**,[3] the formers can be most reasonably assigned as shown on the next page.

The hfsc's of phenylene protons and vinylene protons of **2a** could not be uniquely assigned in the previous communication[3] due to lack of sufficient data. The present assignment of phenylene proton hfsc of **2b** leads to following assignment of the observed hfsc's of **2a**:

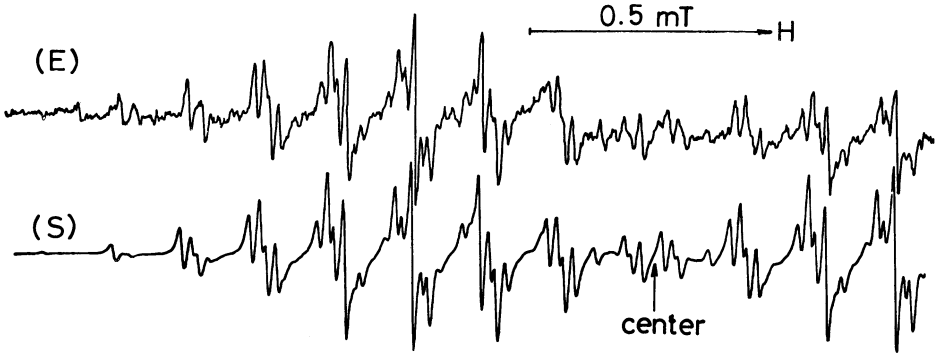

Fig. 1. Observed (E) and simulated (S) ESR spectra of **1b**.

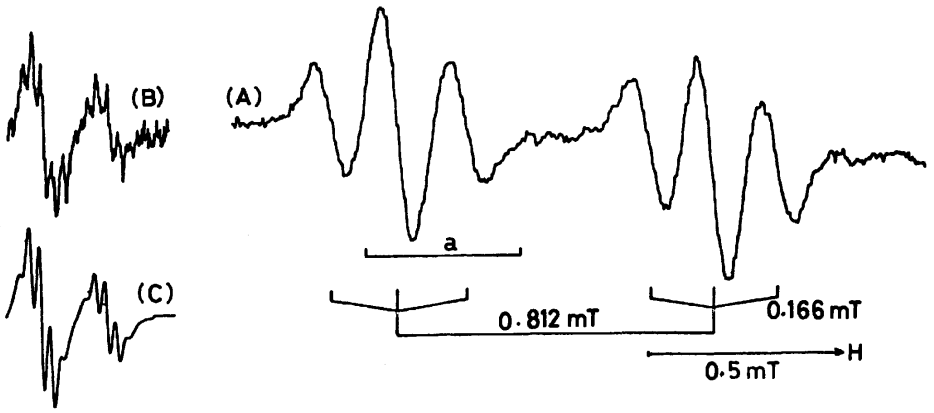

Fig. 2. (A) ESR spectrum of **2b**. (B) Underlined part a of (A) observed with higher resolution. (C) Simulated spectrum corresponding to (B).

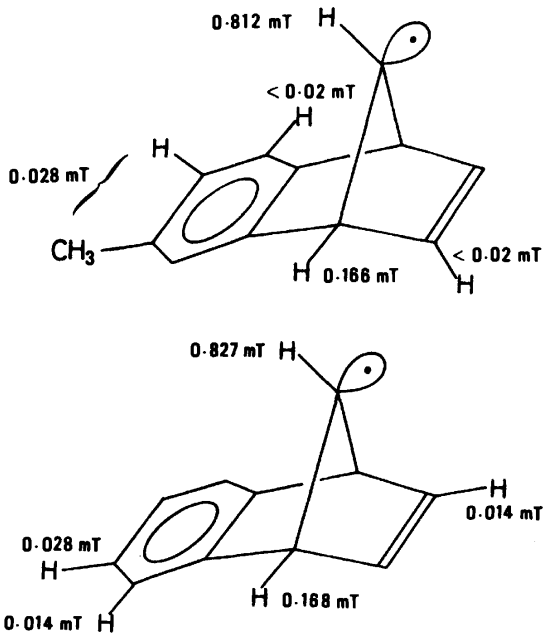

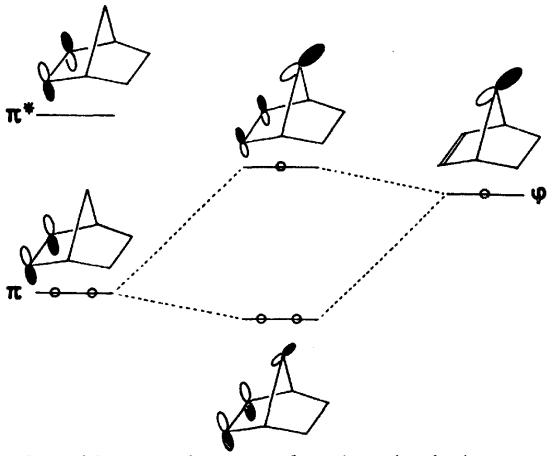

Fig. 3. Bishomocyclopropenyl conjugation in **1a** and **1b**. The mixing of π^* and φ is symmetry-forbidden.

Discussion

Homoconjugation in 1a and 1b. The bishomocyclopropenyl conjugation in **1a** and **1b** is the symmetry-allowed intramolecular charge transfer interaction from the vinylene π system to the tervalent carbon atom as shown in Fig. 3. This conjugation gives the tervalent carbon atom a carbanion character and delocalizes the odd electron onto a π atomic orbital of a vinylene carbon atom from the tervalent carbon atom. When the electron density of δ is transferred from the vinylene bridge onto the tervalent carbon atom, the odd electron density on a vinylene carbon atom is $\delta/2$ in the present simple model. If this mechanism is the major source of the hfsc of the vinylene proton of **1a** (0.12 mT),[2,3] this hfsc, $a(H_2)$, can be correlated with the odd electron density, $\delta/2$, as

$$a(H_2) = Q_\alpha\delta/2, \quad Q_\alpha = 2.3 \text{ mT},$$

and the methyl proton hfsc of **1b**, $a(CH_3)$, with $\delta/2$ as:

$$a(CH_3) = Q_\beta\delta/2, \quad Q_\beta = 2.7 \text{ mT}.$$

Both of the equations are satisfied when $\delta=0.10$, showing that both $a(H_2)$ of **1a** and $a(CH_3)$ of **1b** originate from the odd electron delocalization onto the vinylene π system from the tervalent carbon atom through the homoconjugation and that the extent of this delocalization is about 10%.

Homoconjugation in 2a and 2b. The bishomobenzocyclopropenyl conjugation in **2a** and **2b** is the symmetry-allowed mixing of the odd electron orbital on C_9 (φ) with phenylene orbitals of π_1, π_2, and π_3 shown in Fig. 4. Since the orbital energy difference between π_1 and φ is larger than those between φ and the other two π orbitals in Fig. 4, the mixing between π_1 and φ can be neglected for the present semiquantitative analysis of the homoconjugation.

Protons and/or those in the methyl moiety bonding to C_6 and C_7 of **2a** and **2b** have larger hfsc's than those of protons bonding to C_5 and C_8. This shows that the odd electron is delocalized onto π_2 rather than π_3. This mixing of the odd electron orbital on C_9, φ, with the doubly occupied π_2 orbital induces a carbanion character of the tervalent carbon atom. The extra electron density accumulated on the tervalent carbon atom by this bishomobenzocyclopropenyl conjugation is estimated from the phenylene proton hfsc's of **2a** and **2b** as 0.05 at maximum, which is smaller than that of the bishomocyclopropenyl conjugation in **1a** and **1b**.

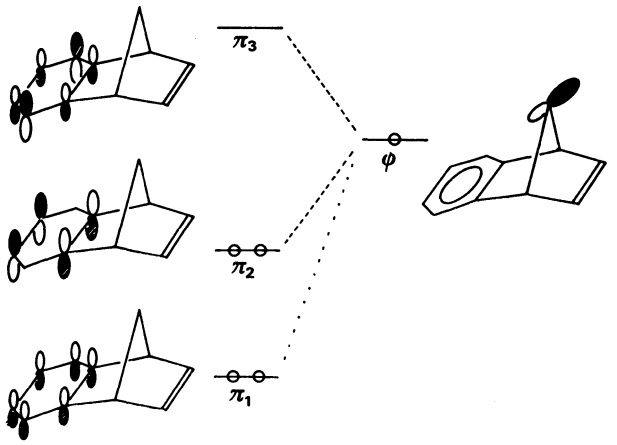

Fig. 4. Bishomobenzocyclopropenyl conjugation in **2a** and **2b**. The other three π molecular orbitals of the phenylene ring are symmetry-forbidden to interact with the odd electron orbital, φ.

The resolved small hyperfine splittings by H_5 and H_8 of **2a** indicate that there exists a minor mixing of π_3 into φ. This mode of interaction is stabilizing, but it transfers electron density from C_9 onto the phenylene π system. Therefore, even if the total electron density accumulated on the tervalent carbon atom by bishomobenzocyclopropenyl interaction is smaller than that by bishomocyclopropenyl interaction, the former can be more stabilizing than the latter.

Pyramidal Geometry of Tervalent Carbon Atom. The decrease of the α proton hfsc in the order of bicyclo[2.2.1]hept-7-yl radical (**3**) (1.678 mT),[2] 1,2,3,4-tetrahydro-1,4-methanonaphthalen-9-yl radical (**4**) (1.278 mT),[3] **1a** (1.087 mT),[2] **2a** (8.27 mT),[3] and bicyclo[2.2.1]hepta-2,5-dien-7-yl radical (**5**) (0.449 mT)[1] indicates the increase of the nonplanarity of the tervalent carbon atom, because these hfsc's have negative signs.[1,3] We suggested previously that the extent of the bending of the tervalent carbon atom of **3** and related radicals would correlate with the angle between C_1–C_7 and C_7–C_4 bonds.[3] However, the difference between C_1–C_7–C_4 angles of **3** and **5** is expected to be small, since the corresponding angle in bicyclo[2.2.1]heptane (93.2°) is only slightly larger than that of bicyclo[2.2.1]hepta-2,5-diene (92.0°).[4] It seems difficult to attribute the difference between the bendings of the tervalent carbon atoms of **3** and **4** entirely to the small difference between their C_1–C_7–C_4 bond angles.[1]

The introduction of methyl substituent(s) onto a bridging unsaturated moiety of **1a** or **2a** induces an increase of the nonplanarity of the tervalent carbon atom as shown by the decrease of their α proton hfsc's. Thus we propose that the increase of the nonplanarity of the tervalent carbon atom of **1a**, **1b**, **2a**, **2b**, **4**, and **5** from that of **3** would have been induced mainly by the increase of the carbanion character of their tervalent carbon atoms arising from homoconjugation(s). Indeed, the small bond angle of C_1–C_7–C_4 of **3** should be one of major factors inducing the pyramidal geometry of its tervalent carbon atom.

The geometry of the tervalent carbon atom of the radicals appearing in the present discussion suggests the following trends: (i) bishomocyclopropenyl interaction induces more carbanion character of the tervalent tarbon atom than bishomobenzocyclopropenyl interaction, but the latter is more stabilizing than the former; and (ii) a geometry in which the rear-lobe of the odd electron orbital on the tervalent carbon atom overlaps with the π orbital(s) of the bridging moiety is preferred than the geometry of the front-lobe overlap, but the extent of charge transfer by homoconjugation in the front-lobe overlap geometry is not negligibly small.

Experimental

The equipments and procedures for the photolysis-ESR experiments have been described earlier.[5]

7-anti-Bromo-2,3-dimethylbicyclo[2.2.1]hept-2-ene. 2,3-Dimethylbicyclo[2.2.1]hept-2-en-7-one (2.4 g, 0.18 mmol) was reduced to 7-hydroxybicyclo[2.2.1]hept-2-ene by $LiAlH_4$ in ether.[6] The alcohol, freed from ether, was dissolved into 20 ml of pentane without purification and shaken with 22 ml of 47% HBr aqueous solution for 10 min at room temperature. After evaporation of the pentane from the organic layer, *anti*-7-bromo-2,3-dimethylbicyclo[2.2.1]hept-2-ene (bp 95 °C/21 Torr)[7] was obtained in 42% yield based on the starting ketone. 60 MHz ^{1}H NMR (CCl_4): δ 1.10 (H_{5endo}, H_{6endo}). 1.63 (CH_3), 2.03 (H_{5exo}, H_{6exo}), 2.5 (H_1, H_4), 3.73 (H_{7syn}).

9-anti-Bromo-6-methyl-1,4-dihydro-1,4-methanonaphthalene. To a stirred solution of 6-methyl-1,4-dihydro-1,4-methanonaphthalene[8] (3.0 g, 19 mmol) in 11 ml of CCl_4 kept below 10 °C, bromine (3.4 g, 21 mmol) in 25 ml of CCl_4 was added dropwise in 10 min and stirred for 1 h at room temperature thenafter. After evaporation of the solvent and excess of the bromine, crude 2-*exo*,9-*anti*-dibromo-6-methyl-1,4-dihydro-1,4-methanonaphthalene was obtained as a viscous residue. The crude dibromide was reacted with potassium *t*-butoxide (2.2 g, 20 mmol) in dry dimethyl sulfoxide under nitrogen atmosphere at 70—80 °C for 1.5 h. The reaction mixture was poured into water and extracted with ether. After evaporation of the ether, the residue was recrystallized from ethanol to give 9-*anti*-bromo-6-methyl-1,4-dihydro-1,4-methanonaphthalene (1.1 g, 4.7 mmol) as white crystals. 220 MHz ^{1}H NMR (CCl_4) δ 2.25 (s, 3H), 3.95 (s, 2H), 4.28 (s, 1H), 6.58 (s, 2H), 6.67 (m, 1H), 6.95—7.00 (m, 2H). (s: singlet. m: multiplet.).

We are indebted to Drs H. Tanida and T. Tsushima (Shionogi Research Laboratory, Osaka) for the offer of 6-methyl-1,4-dihydro-1,4-methanonaphthalene.

References

1) Y. Sugiyama, T. Kawamura, and T. Yonezawa, *J. Chem. Soc., Chem. Commun.*, **1978**, 804.

2) P. Bakuzis, J. K. Kochi, and P. J. Krusic, *J. Am. Chem. Soc.*, **92**, 1434 (1970); J. K. Kochi, P. Bakuzis, and P. J. Krusic, *ibid.*, **95**, 1515 (1973).

3) T. Kawamura, Y. Sugiyama, M. Matsunaga, and T. Yonezawa, *J. Am. Chem. Soc.*, **97**, 1627 (1975).

4) Y. Morino, K. Kuchitsu, and A. Yokozeki, *Bull. Chem. Soc. Jpn.*, **40**, 1552 (1967).

5) T. Kawamura, M. Tsumura, Y. Yokomichi, and T. Yonezawa, *J. Am. Chem. Soc.*, **99**, 8251 (1977).

6) P. G. Gassman and D. S. Patton, *J. Am. Chem. Soc.*, **91**, 2160 (1969).

7) Torr=133 Pa.

8) H. Tanida, R. Muneyuki, and T. Tsuji, *Bull. Chem. Soc. Jpn.*, **37**, 40 (1964).

The Crystal Structure of 11-(*p*-Bromophenyl)-11-cyano-12-phenyl-6b-(1-pyrrolidinyl)-6b,6c,11,12a-tetrahydroindeno[1′2′ : 3,4]-cyclopenta[1,2-*a*]acenaphthylene Acetone Solvate

Tetsuo UECHI,* Otohiko TSUGE,† Shigeru OKITA,† and Shuji KANEMASA†

College of General Education, Kyushu University 01, Ropponmatsu, Fukuoka 810

†*Research Institute of Industrial Science, and Department of Molecular Science and Technology, Interdisciplinary Graduate School of Engineering Sciences, Kyushu University 86, Kasuga, Kasugashi, Fukuoka 816*

(Received April 4, 1983)

The title compound crystallizes in the triclinic space group $P\bar{1}$ with two fomrula units in a unit cell of dimensions; $a=11.621(3)$, $b=15.177(3)$, $c=10.229(2)$ Å, $\alpha=95.63(2)$, $\beta=105.46(2)$, and $\gamma=76.43(2)°$. The crystal structure was solved by a conventional heavy-atom method and refined by block-diagonal least-squares procedures to give a final R value of 0.050 for 3428 reflections, with $F_o>2\sigma(F_o)$, collected on a four-circle diffractometer. The bond distance shared between the acenaphthene and the cyclopentane rings is unusually long at 1.596(6) Å, which may result from the additional strain induced by the fusion of these rings. The solvent molecules are disordered in the channel composed of the main molecules.

As a part of our studies of the reaction of enamines with triafulvenes, we have recently reported that 1-(1-pyrrolidinyl)acenaphthylene reacts with 2-phenyl-2-(2,3-diphenyl-2-cyclopropenylidene)acetonitrile to give two isomeric 1 : 1 adducts.[1] This reaction was regared as the first example in which a phenyl group on the three-membered ring of methylenecyclopene had taken part in a cyclization. On the basis of chemical and spectroscopic techniques alone, the stereochemical structures of the adducts could not be elucidated unambiguously. In order to confirm the structure as well as to explore the essential features of this reaction, we have undertaken an X-ray structural study of the title main molecule (abbreviated as ICPA) which was the major product from the reaction of 1-(1-pyrrolidinyl)acenaphthylene with 2-(*p*-bromophenyl)-2-(2,3-diphenyl-2-cyclopropenylidene)acetonitrile under the same reaction conditions. The X-ray structural study was not applied to the minor product because the crystals obtained were unsuitable.

Experimental

The title compound was obtained by recrystallization from acetone as colorless prisms elongated along the c axis. The crystal used for the X-ray work was approximately triclinic in shape, with dimensions of 0.2 mm × 0.3 mm × 0.4 mm, and it was coated with nail enamel to prevent deterioration in air. The density was measured by flotation in an aqueous KI solution. Preliminary X-ray photographs showed the crystal to be triclinic. The unit-cell parameters and intensity data were measured on a Rigaku automated four-circle diffractometer with monochromated Mo $K\alpha$ radiation ($\lambda=0.71073$ Å). The unit-cell parameters were determined by a least-squares procedure using 25 reflections within the range of $23<2\theta<27°$. The crystal data are given in Table 1.

TABLE 1. CRYSTAL DATA[a]

Formula unit	$C_{39}H_{29}N_2Br\cdot C_3H_6O$
Formula weight	663.66
Space group	$P\bar{1}$
$a=11.621$ (3) Å	$\alpha=95.63$ (2)°
$b=15.177$ (3) Å	$\beta=105.46$ (2)°
$c=10.229$ (2) Å	$\gamma=76.43$ (2)°
$V=1689.1$ (6) Å^3	$Z=2$
$D_M=1.310$ g cm^{-3}	$D_X=1.305$ g cm^{-3}
$\mu=1.24$ mm^{-1} (for Mo $K\alpha$ radiation)	$F(000)=688$

a) The numbers in parentheses, here and elsewhere in this paper, are the e.s.d.'s in the last significant digits.

Intensity data of 4404 independent reflections within a range of $2\theta<45°$ were collected by an ω-2θ scanning technique. Of these, 3434 reflections with $F_o>2.0\sigma(F_o)$ were used for the structure analysis. The intensity data were corrected for Lorentz and polarization effects, but not for absorption or extinction. The statistical distribution of the normalized structure factors favoured the centrosymmetric space group, which was confirmed by the convergence of the structure at a later stage of the refinement.

Structure Determination and Refinement

The Br-atom position was easily deduced from a Patterson synthesis, and the remaining non-H atoms of ICPA molecule were located in a subsequent Fourier map. Refinement was carried out by the block-diagonal least-squares procedures, in which initially equal weights and later Cruickshank's weighting scheme were adopted.[2] After several cycles of refinements with isotropic and then anisotropic thermal parameters, the H atoms were located in difference Fourier maps, in which also eight peaks with three times the height of these H atoms were found between ICPA molecules. These peaks were interpreted as disordered acetone atoms with an occupancy factor of 0.5. After the removal of the five strong reflections affected by secondary extinction and of one reflection with a strong imbalance of the background intensities, refinement was terminated when all shift/e.s.d. for non-H atoms of ICPA became less than 0.3. The final difference Fourier synthesis showed two implausible peaks of *ca.* 0.6 eÅ^{-3} in the vicinity of the Br atom and eight peaks of 0.3—0.5 eÅ^{-3} distributed at random in the vicinities of the acetone atoms. This suggested that the model of the disordered acetone was yet ambiguous, but no attempt was made to clarify the disorder. Thus, the molecular dimensions of the acetone were omitted from the later table and discussion. The final conventional R index was 0.050 for 3428 measurable reflections. The

TABLE 2. FRACTIONAL ATOMIC COORDINATES AND THERMAL PARAMETERS

(a) Non-H atoms of ICPA molecule.
The coordinate values have been multiplied by 10^4. The B_{eq}'s are the equivalent values of the anisotropic thermal parameters, following the definition given by Hamilton.[8]

Atom	x	y	z	B_{eq}/Å^2
Br	5802.4(6)	6295.0(4)	6888.7(5)	5.36(1)
C(1)	4436(4)	8939(3)	-2034(5)	4.0(2)
C(2)	4095(5)	9078(4)	-3438(6)	4.7(2)
C(3)	4930(6)	9055(4)	-4172(5)	4.9(2)
C(3a)	6198(5)	8870(3)	-3549(5)	3.8(1)
C(4)	7183(5)	8834(3)	-4131(5)	4.4(2)
C(5)	8358(5)	8617(3)	-3384(5)	4.2(2)
C(6)	8665(4)	8415(3)	-1995(5)	3.7(1)
C(6a)	7735(4)	8458(3)	-1381(4)	3.0(1)
C(6b)	7739(4)	8235(3)	48(4)	2.8(1)
C(6c)	7903(4)	7184(3)	140(4)	2.6(1)
C(6d)	9014(4)	6550(3)	935(4)	2.9(1)
C(7)	10235(4)	6433(3)	947(5)	3.9(1)
C(8)	11078(5)	5739(4)	1673(6)	5.1(2)
C(9)	10709(5)	5159(4)	2348(6)	5.4(2)
C(10)	9504(5)	5262(3)	2354(6)	4.4(2)
C(10a)	8653(4)	5964(3)	1638(4)	3.0(1)
C(11)	7261(4)	6175(3)	1458(4)	2.7(1)
C(11a)	6899(4)	7082(3)	757(4)	2.5(1)
C(12)	6006(4)	7829(3)	698(4)	2.5(1)
C(12a)	6340(4)	8580(3)	83(4)	2.8(1)
C(12b)	5660(4)	8753(3)	-1386(4)	3.0(1)
C(12c)	6521(4)	8707(3)	-2146(4)	3.0(1)
N(1)	8640(3)	8606(2)	1094(4)	3.1(1)
C(13)	8616(5)	9572(3)	951(5)	4.1(2)
C(14)	9346(6)	9860(4)	2308(6)	5.4(2)
C(15)	9373(6)	9178(5)	3301(6)	6.1(2)
C(16)	8614(5)	8531(4)	2504(5)	4.0(2)
C(17)	6762(4)	5477(3)	488(4)	2.9(1)
N(2)	6390(4)	4945(3)	-265(4)	4.4(1)
C(18)	6871(4)	6191(3)	2783(4)	2.8(1)
C(19)	5922(4)	5814(3)	2870(4)	3.5(1)
C(20)	5589(5)	5861(4)	4081(5)	4.2(2)
C(21)	6216(4)	6261(3)	5209(4)	3.4(1)
C(22)	7166(4)	6640(3)	5150(4)	316(1)
C(23)	7487(4)	6610(3)	3945(5)	3.4(1)
C(24)	4831(4)	7962(3)	1060(4)	2.7(1)
C(25)	4151(4)	7299(3)	712(6)	4.2(2)
C(26)	3021(5)	7420(4)	965(7)	5.5(2)
C(27)	2541(5)	8215(4)	1585(6)	5.1(2)
C(28)	3193(5)	8884(3)	1948(6)	4.4(2)
C(29)	4330(4)	8764(3)	1687(5)	3.5(1)

(b) H atoms of ICPA molecule.
The H atoms are labelled in terms of the C atom to which they are are attached. The coordinate values have been multiplied by 10^3.

Atom	x	y	z	B/Å^2
H(1)	384(4)	895(3)	-152(4)	4(1)
H(2)	322(4)	918(3)	-387(5)	4(1)
H(3)	466(4)	921(3)	-504(5)	5(1)
H(4)	704(4)	897(3)	-500(5)	5(1)
H(5)	906(4)	860(3)	-380(4)	4(1)
H(6)	949(4)	825(3)	-153(4)	3(1)
H(6c)	774(3)	695(2)	-77(3)	2(1)
H(7)	1048(4)	683(3)	45(4)	4(1)
H(8)	1187(4)	571(3)	167(5)	5(1)
H(9)	1125(5)	475(4)	280(5)	6(1)
H(10)	924(5)	489(3)	280(5)	5(1)
H(12a)	622(3)	916(3)	66(4)	3(1)
H(13)1	772(4)	993(3)	76(5)	4(1)
H(13)2	898(4)	964(3)	21(4)	4(1)
H(14)1	1015(5)	986(3)	232(5)	5(1)
H(14)2	902(6)	1048(4)	261(6)	8(2)
H(15)1	1024(5)	884(4)	369(6)	7(1)
H(15)2	909(6)	939(4)	411(6)	8(2)
H(16)1	776(5)	878(3)	264(5)	6(1)
H(16)2	882(5)	790(4)	285(6)	7(1)
H(19)	554(5)	550(4)	213(5)	6(1)
H(20)	494(4)	563(3)	414(5)	5(1)
H(22)	754(4)	692(3)	587(4)	4(1)
H(23)	816(4)	693(3)	387(5)	5(1)
H(25)	445(4)	681(3)	20(5)	4(1)
H(26)	255(4)	691(3)	67(4)	4(1)
H(27)	171(5)	830(4)	173(5)	6(1)
H(28)	283(5)	953(4)	242(6)	8(1)
H(29)	479(4)	918(3)	199(5)	5(1)

(c) Disordered acetone atoms.
The occupancy factor was fixed at 0.5. The coordinate values have been multiplied by 10^3.

	x	y	z	B/Å^2
O	775(1)	313(1)	266(1)	12(1)
C(30)	841(2)	289(1)	411(2)	9(1)
C(31)	800(2)	350(2)	499(3)	14(1)
C(32)	958(2)	300(1)	448(2)	10(1)
O'	760(1)	293(1)	524(1)	11(1)
C(30)'	804(2)	258(2)	403(2)	12(1)
C(31)'	860(1)	191(1)	387(2)	8(1)
C(32)'	857(2)	333(2)	380(2)	13(1)

atomic scattering factors for Br, O, N, and C_{cov}, with correction factors for anomalous dispersion, were taken from International Tables for X-ray Crystallography.[3] Those for H were adopted from the table of Stewart *et al.*[4] All the calculations were carried out on a FACOM M-200 computer in the Computer Center of Kyushu University by the use of locally modified versions of the UNICS-III program system.[5,6] Figures. 1 and 3 were drawn by the use of the ORTEP program.[7] The final atomic parameters are listed in Table. 2, together with their e.s.d.'s. Lists of the structure factors and anisotropic thermal parameters have been deposited as Document No. 8341 at the Office of the Editor of the Bulletin of the Chemical Society of Japan.

Results and Discussion

The molecular structure of ICPA was confirmed by

Table 3. Bond angles

Bond angle	θ/°	Bond angle	θ/°	Bond angle	θ/°
C(12b)-C(1)-C(2)	118.3(5)	C(8)-C(9)-C(10)	121.6(5)	C(6b)-N(1)-C(13)	114.7(3)
C(1)-C(2)-C(3)	122.7(5)	C(9)-C(10)-C(10a)	118.2(6)	C(6b)-N(1)-C(16)	116.5(4)
C(2)-C(3)-C(3a)	121.0(5)	C(10)-C(10a)-C(6d)	120.8(5)	C(13)-N(1)-C(16)	105.7(4)
C(3)-C(3a)-C(12c)	115.3(5)	C(10)-C(10a)-C(11)	126.8(5)	N(1)-C(13)-C(14)	104.4(4)
C(3)-C(3a)-C(4)	129.0(5)	C(6d)-C(10a)-C(11)	112.4(4)	C(13)-C(14)-C(15)	106.3(5)
C(12c)-C(3a)-C(4)	115.7(4)	C(10a)-C(11)-C(11a)	100.2(4)	C(14)-C(15)-C(16)	106.0(5)
C(3a)-C(4)-C(5)	121.1(5)	C(10a)-C(11)-C(17)	107.7(4)	C(15)-C(16)-N(1)	104.3(6)
C(4)-C(5)-C(6)	122.4(6)	C(10a)-C(11)-C(18)	114.2(3)	C(11)-C(17)-N(2)	179.1(6)
C(5)-C(6)-C(6a)	118.6(4)	C(11a)-C(11)-C(17)	109.1(3)	C(11)-C(18)-C(19)	122.7(4)
C(6)-C(6a)-C(12c)	119.0(4)	C(11a)-C(11)-C(18)	115.5(4)	C(11)-C(18)-C(23)	119.0(5)
C(6)-C(6a)-C(6b)	132.1(4)	C(17)-C(11)-C(18)	109.6(4)	C(19)-C(18)-C(23)	118.4(4)
C(12c)-C(6a)-C(6b)	108.9(4)	C(11)-C(11a)-C(6c)	109.8(4)	C(18)-C(19)-C(20)	120.6(4)
C(6a)-C(6b)-C(6c)	109.9(3)	C(11)-C(11a)-C(12)	136.0(5)	C(19)-C(20)-C(21)	120.1(6)
C(6a)-C(6b)-(12a)	103.2(3)	C(6c)-C(11a)-C(12)	113.6(4)	C(20)-C(21)-C(22)	120.5(5)
C(6a)-C(6b)-N(1)	112.2(4)	C(11a)-C(12)-C(12a)	108.9(4)	C(21)-C(22)-C(23)	119.7(4)
C(12a)-C(6b)-C(6c)	100.8(4)	C(11a)-C(12)-C(24)	129.4(5)	C(22)-C(28)-C(18)	120.8(5)
C(12a)-C(6b)-N(1)	117.1(4)	C(12a)-C(12)-C(24)	121.6(4)	C(20)-C(21)-Br	120.5(4)
C(6c)-C(6b)-N(1)	112.7(3)	C(12)-C(12a)-C(6b)	106.5(3)	C(22)-C(21)-Br	119.0(3)
C(6b)-C(6c)-C(11a)	104.9(4)	C(12)-C(12a)-C(12b)	114.5(4)	C(12)-C(24)-C(25)	120.1(4)
C(6b)-C(6c)-C(6d)	126.1(4)	C(6b)-C(12a)-C(12b)	104.5(4)	C(12)-C(24)-C(29)	122.2(5)
C(11a)-C(6c)-C(6d)	103.2(4)	C(12a)-C(12b)-C(12c)	108.6(4)	C(25)-C(24)-C(29)	117.6(5)
C(6c)-C(6d)-C(10a)	109.7(4)	C(12a)-C(12b)-C(1)	132.4(5)	C(24)-C(25)-C(26)	121.7(5)
C(6c)-C(6d)-C(7)	130.1(5)	C(1)-C(12b)-C(12c)	119.0(5)	C(25)-C(26)-C(27)	119.9(6)
C(10a)-C(6d)-C(7)	120.0(4)	C(3a)-C(12c)-C(6a)	123.2(5)	C(26)-C(27)-C(28)	119.9(6)
C(6d)-C(7)-C(8)	119.0(5)	C(3a)-C(12c)-C(12b)	123.6(4)	C(27)-C(28)-C(29)	120.2(5)
C(7)-C(8)-C(9)	120.6(5)	C(6a)-C(12c)-C(12b)	113.2(4)	C(28)-C(29)-C(24)	120.6(5)

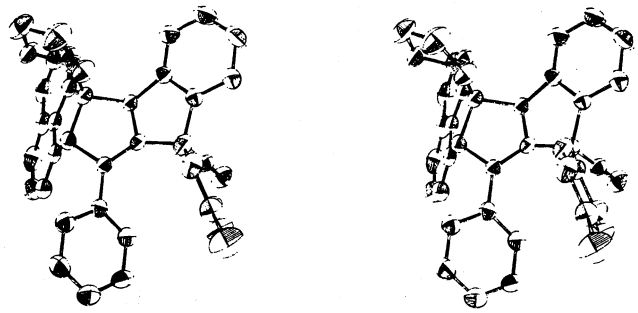

Fig. 1. Stereoscopic view of the molecular structure of ICPA. The thermal-motion ellipsoids are scaled to enclose 50% probability. The H atoms have been omitted for clarity, and likewise in the following figures.

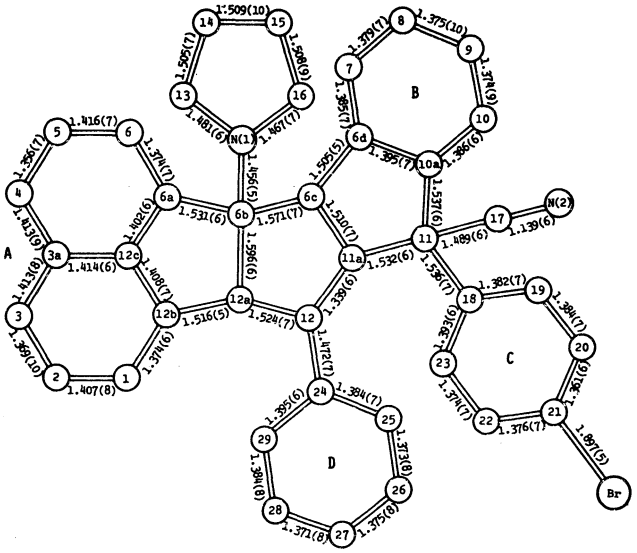

Fig. 2. Bond distances (l/Å) of the schematically drawn ICPA molecule with atomic-nomenclature scheme. The C atoms are shown by the position-numbers.

this X-ray structural study. A stereoscopic view of this molecular structure is shown in Fig. 1. The bond distances(l) are shown schematically in Fig. 2, together with the atomic-nomenclature scheme. The bond angles(θ) are listed in Table 3.

The naphthalene ring [A] deviates slightly from planarity, the maximum deviation being 0.04 Å, as shown in Table 4. C(6b) is shifted by 0.17 Å from this plane, whereas C(12a) is displaced 0.11 Å in the opposite direction, so that the acenaphthene ring has a somewhat twisted conformation. The distance of the C(6b)–C(12a) bond, which is shared between the acenaphthene and the central cyclopentane ring [C(6b), C(6c), C(11a), C(12), and C(12a)], is unusually long (1.596(6) Å). This may result from the additional strain induced on the bond by the fusion of these rings. A similar phenomenon has been observed in a series of fused acenaphthylenes, $C_{14}H_{10}$, $C_{18}H_{12}$, $C_{22}H_{14}$, and $C_{26}H_{14}N_2$.[9–12] The central cyclopentane ring is slightly puckered in an envelope-like conformation; the maximum torsion angle is 21.8(4)° about the C(6b)–C(6c) bond, and C(6b) is shifted by 0.38 Å from the plane through the other four atoms. The B ring [C(6d) through C(10a)] is planar within limits of the experimental error. C(6c) and C(11a) were found to lie almost equidistant from the plane on different sides, and so the indane ring has a

TABLE 4. LEAST-SQUARES PLANES AND TORSION ANGLES

(a) Deviations (l/Å) from least-squares planes.
Atoms with an asterisk are not included in the plane calculation.

ring A		ring B		ring C		ring D	
C(1)	0.017	C(6d)	−0.000	C(18)	−0.002	C(24)	−0.001
C(2)	−0.033	C(7)	−0.005	C(19)	−0.006	C(25)	0.002
C(3)	−0.028	C(8)	0.008	C(20)	0.009	C(26)	−0.001
C(3a)	0.002	C(9)	−0.006	C(21)	−0.005	C(27)	−0.001
C(4)	0.035	C(10)	0.001	C(22)	−0.003	C(28)	0.002
C(5)	0.020	C(10a)	0.002	C(23)	0.006	C(29)	−0.001
C(6)	−0.030	C(6c)*	−0.137	C(11)*	0.011	C(12)*	−0.079
C(6a)	0.039	C(11)*	−0.052	Br*	−0.042		
C(12b)	0.042	C(11a)*	0.174				
C(12c)	0.014						
C(6b)*	−0.166						
C(12a)*	0.109						

(b) Selected torsion angles (θ/°)

Central cyclopentane ring		Pyrrolidine ring	
C(6b)-C(6c)-C(11a)-C(12)	17.1(5)	N(1)-C(13)-C(14)-C(15)	−19.6(6)
C(6c)-C(11a)-C(12)-C(12a)	−3.4(5)	C(13)-C(14)-C(15)-C(16)	−2.2(7)
C(11a)-C(12)-C(12a)-C(6b)	−11.6(5)	C(14)-C(15)-C(16)-N(1)	23.4(6)
C(12)-C(12a)-C(6b)-C(6c)	20.5(4)	C(15)-C(16)-N(1)-C(13)	−36.3(5)
C(12a)-C(6b)-C(6c)-C(11a)	−21.8(4)	C(16)-N(1)-C(13)-C(14)	35.0(5)
Around the C(6b)-N(1) bond			
C(6a)-C(6b)-N(1)-C(13)	48.4(5)		
C(6c)-C(6b)-N(1)-C(13)	173.1(4)		
C(12a)-C(6b)-N(1)-C(13)	−70.6(5)		

somewhat twisted conformation. The plane of the B ring makes an angle of 42.0° with the naphthalene ring. Thus, the body of the molecule has an uncomfortable chair form.

The pyrrolidine ring is in the normal envelope conformation, with N(1) out of the plane of the other four atoms. The torsion angles about the C(6b)–N(1) bond are close to 50, 170, and 290°, so that the lone pair of electrons of N(1) is *cis* to C(12a). The D ring [C(24) through C(29)] is planar within the limits of experimental error, and this plane is tuned from the plane through the four atoms [C(11a), C(12), C(12a), and C(24)] by an angle of 42.1° away from the naphthalene moiety. The bromophenyl group faces the D ring at an angle of *ca.* 60°. The bromophenyl group is *cis* to the pyrrolidine, so that the close contact between the two groups is 2.26(9) Å of the H(16)2···H(23) distance.

The C–H bond distances are in the range from 0.84 to 1.09 Å, with an average of 0.96(6) Å, and the bond angles involving the H atoms are reasonable. These bond distances and angles have been omitted in Table 3, since the H atoms were unlikely to play a role except in crystal packing.

The crystal structure projected along the c axis is shown in Fig. 3. There is a channel parallel to the c axis extending throughout the entire crystal. Acetone molecule is contained in this channel, without close contact with the main molecule. This explains the easy loss of acetone from the crystal.

The structure of the minor product was presumed to be stereoisomer of the present compound, with a different configuration only at the C(11) atom.[1)]

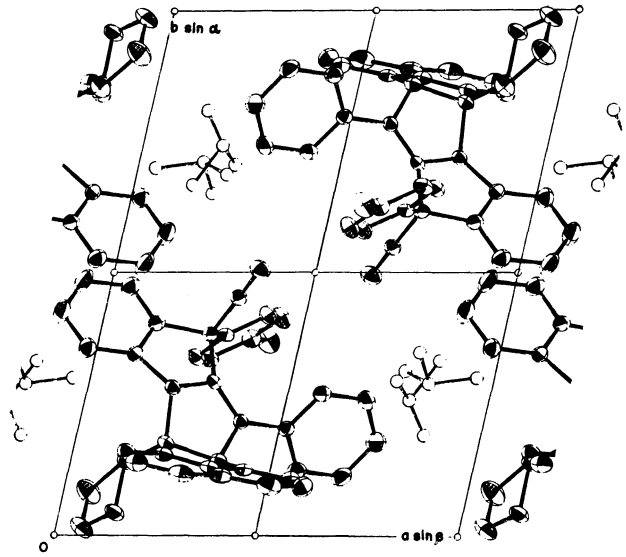

Fig. 3. The crystal structure projected along the c axis. The thermal-motion elliposids are scaled to enclose 30% probability, and acetone atoms are shown as open circles of arbitrary size.

The authors are grateful to Professor Shigeo Kida of the Faculty of Science, Kyushu University, for allowing us to use the automated diffractometer, and to Asst. Professor Shigeaki Kawano of the College of General Eduction of this University for his advice with regard to the computation process.

References

1) O. Tsuge, S. Okita, M. Noguchi, and S. Kanemasa, *Chem. Lett.*, **1982**, 993.
2) D. W. J. Cruickshank, "Computing Methods in Crystallography," ed by J. S. Rollett, Pergamon Press, Oxford (1965), p. 112.
3) "International Tables for X-ray Crystallography," Kynoch Press, Birmingham (1974), Vol. IV, p. 72.
4) R. F. Stewart, E. R. Davidson, and W. T. Simpson, *J. Chem. Phys.*, **42**, 3175 (1965).
5) T. Sakurai and K. Kobayashi, *Rikagaku Kenkyusho Hokoku* (in Japanese), **55**, 69 (1979).
6) S. Kawano, *Rep. Comp. Cent. Kyushu Univ.* (in Japanese), **16**, 113 (1983).
7) C. K. Johnson, ORTEP, Report ORNL-3794, Oak Ridge National Laboratory, Tennessee (1965).
8) W. C. Hamilton, *Acta Crystallogr.*, **12**, 609 (1959).
9) A. C. Hazell, *Acta Crystallogr., Sect. B*, **32**, 2010 (1976).
10) A. C. Hazell and R. G. Hazell, *Acta Crystallogr., Sect. B*, **33**, 360 (1977).
11) A. C. Hazell and Å. Weigelt, *Acta Crystallogr., Sect. B*, **32**, 306 (1976).
12) C. Courseille, B. Busetta, M. Hospital, and A. Castellan, *Cryst. Struct. Commun.*, **1**, 337 (1972).

 © 1983 The Chemical Society of Japan Bull. Chem. Soc. Jpn., 56, 2927—2931 (1983)

Acidic and Catalytic Properties of Niobium Pentaoxide

Tokio Iizuka,* Kazuharu Ogasawara, and Kozo Tanabe
Department of Chemistry, Faculty of Science, Hokkaido University, Sapporo 060
(Received April 30, 1983)

The surface acidic property of $Nb_2O_5 \cdot nH_2O$ and its catalytic activities for the isomerization of 1-butene, the polymerization of propylene and the dehydration of 2-butanol were examined. The activities were high on $Nb_2O_5 \cdot nH_2O$ evacuated at moderate temperatures (100—150 °C) in all of the reactions and decreased drastically on evacuation at higher temperatures (400—500 °C). The surface of $Nb_2O_5 \cdot nH_2O$ showed a strong acidic character ($H_0 \leqq -5.6$) even after heating in air at 100 °C, but the strong acid sites disappeared on heat treatment at higher temperatures. The active sites on the catalysts heat-treated at moderate temperatures were ascribed mainly to Brönsted acid sites on the basis of the IR study of adsorbed pyridine.

Although niobium oxides are reported in the patents to catalyze several reactions such as the oxidation of organic molecules,[1] oxidative dehydrogenation of olefins or paraffins,[2] and the decomposition of NO_x,[3] the details of surface property and catalytic activity are not known. On the other hand, catalysts containing molybdenum and vanadium, neighbors of niobium in the periodic table, are the most important industrial catalysts and their catalytic properties have been studied extensively by many workers. In this sense, it will be possible to use niobium oxides as a catalyst or an active component of catalysts for certain reaction. For this purpose, a fundamental knowledge about niobium oxides is required. Thus, we have studied the surface acid-base properties and the catalytic activities for the reactions of 1-butene, propylene, and 2-butanol as model reactions.

Experimental

Niobium oxide was prepared by heating $Nb_2O_5 \cdot nH_2O$ (CBMM AD-108) in a vacuum or in air at various temperatures. The $Nb_2O_5 \cdot nH_2O$ was used after washing with distilled water followed by drying at 100 °C. The content of Nb in $Nb_2O_5 \cdot nH_2O$ was 55.54% and no impurity of K or Na was detected.

The differential thermal analysis (DTA) and thermogravimetry (TG) were done by using a Rigaku TG-DTA apparatus with the heating program rate of 10 °C/min. The X-ray diffraction pattern was taken by a Shimadzu XRD spectrometer with Cu *Ka* source. The surface area of $Nb_2O_5 \cdot nH_2O$ was measured by using a conventional BET apparatus.

For the measurement of acidic and basic properties, Nb_2O_5 was suspended in a benzene solution, basic or acidic indicators were adsorbed and the color change of indicators was observed.[4] The indicators used were anthraquinone ($pK_a = -8.2$), benzylideneacetophenone (−5.6), dicinnamylideneacetone (−3.0), Crystal Violet (+0.8), 4-anilinoazobenzene (+1.5), 4-dimethylaminoazobenzene (+3.3), Methyl Red (+4.8), and Bromthymol Blue (+7.1).

Infrared spectra were recorded with a JASCO-701G spectrometer using an in situ cell. The sample was pressed into a thin wafer and placed in the cell. Pyridine was adsorbed on $Nb_2O_5 \cdot nH_2O$ which had been evacuated at various temperatures for 2 h and degassed at certain temperatures for 30 min. The IR spectra of adsorbed CO_2 was also measured by the same method as in pyridine adsorption.

For the reactions of 1-butene and 2-butanol, a closed recirculation reactor having a volume of 300 cm^3 was used. After the evacuation of $Nb_2O_5 \cdot nH_2O$ at various temperatures for 2 h, 6.7 kPa of 1-butene or 1.4 kPa of 2-butanol was introduced at the reaction temperature. The polymerization activity of propylene was measured by observing the pressure decrease in a static reactor. The activity was obtained by measuring the rate of decrease in reactant pressure (initial pressure = 13.3 kPa) at 5 min reaction time to avoid the pressure decrease due to the adsorption in the initial stage of the reaction.

Results

X-Ray and Thermal Analysis of $Nb_2O_5 \cdot nH_2O$. The results of DTA and TG of $Nb_2O_5 \cdot nH_2O$ are shown in Fig. 1(A). At around 90 and 180 °C, two endothermic peaks with the decrease of gravity were observed. These can be ascribed to the dehydration process of $Nb_2O_5 \cdot nH_2O$. The dehydration was completed by heating up to 300 °C and the gravity change of the sample was not observed at 300—700 °C. The exothermic peak at

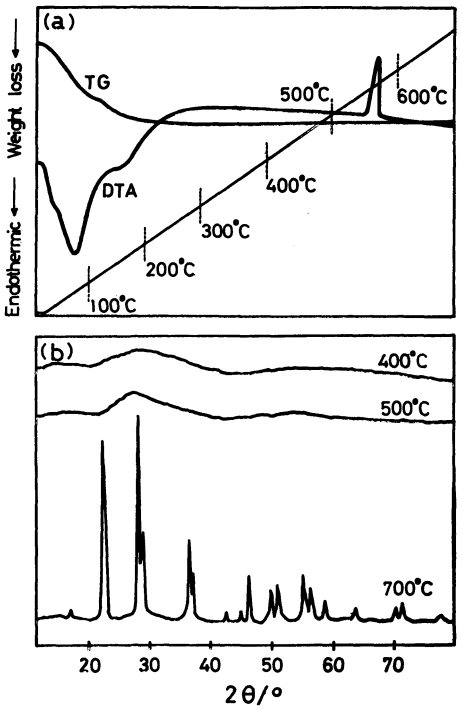

Fig. 1. (A) Thermogravimetry and differential thermal analysis of $Nb_2O_5 \cdot nH_2O$. (B) X-Ray diffraction patterns of $Nb_2O_5 \cdot nH_2O$ heat-treated at various temperatures in air.

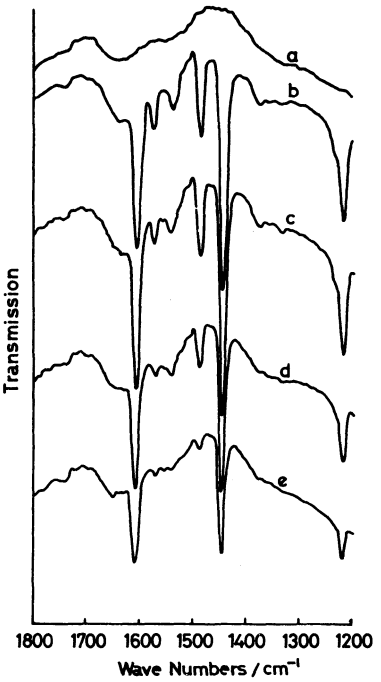

Fig. 2. IR spectra of pyridine adsorbed on $Nb_2O_5 \cdot nH_2O$. a: Background, b: degassed at room temperature after the adsorption, c: degassed at 100 °C, d: degassed at 200 °C, e: degassed at 300 °C.

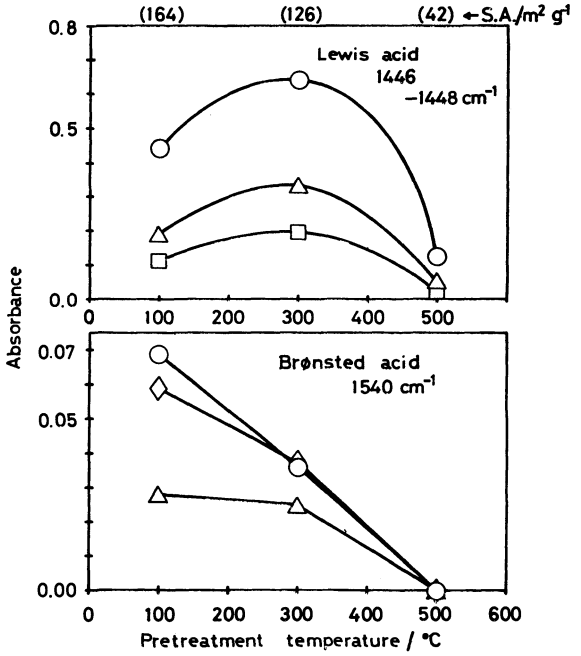

Fig. 3. Acidity change of $Nb_2O_5 \cdot nH_2O$ with pretreatment temperature.
◇: Evacuated at room temperature after adsorption of pyridine, ○: at 100 °C, △: at 200 °C, □: at 300 °C.

about 550—570 °C with no gravity change might be due to a phase transformation.

X-Ray diffraction patterns of the samples which were heat-treated at different temperatures are shown in Fig. 1(B). After heating $Nb_2O_5 \cdot nH_2O$ at 400 °C in air, very broad peaks at $2\theta \simeq 30°$ and around 55° were

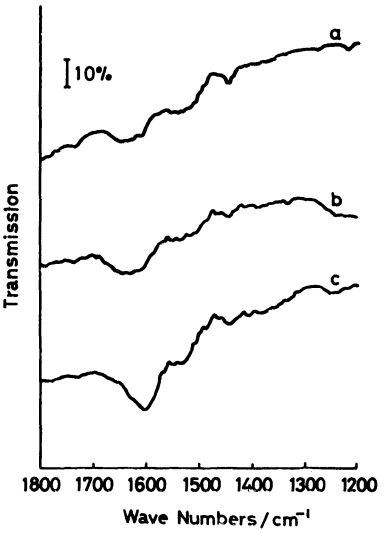

Fig. 4. IR spectra of CO_2 adsorbed on $Nb_2O_5 \cdot nH_2O$ evacuated at 300 °C, a: background, b: evacuated at room temperature after the adsorption for 15 min, c: adsorption for 15 h.

observed. Upon heating at 500 °C in air, those peaks sharpened slightly. A good crystallinity was observed by heating at 700 °C and the diffraction pattern corresponded well to the T–T phase Nb_2O_5.[5]

The surface areas of $Nb_2O_5 \cdot nH_2O$ were 164, 126, and 42 $m^2 g^{-1}$ after the evacuation at 100, 300, and 500 °C, respectively.

Acidic and Basic Character of $Nb_2O_5 \cdot nH_2O$. The acid strength of $Nb_2O_5 \cdot nH_2O$ examined by the indicator adsorption method is mentioned first. After drying at 100 °C, $Nb_2O_5 \cdot nH_2O$ changed the color of benzylideneacetophenone ($pK_a = -5.6$) indicator to its acidic color (yellow), but no color change of anthraquinone ($pK_a = -8.2$) was observed. After heat treatment at 300 °C, all the indicators of $pK_a \geqq -8.2$ also changed their colors to those of the acidic forms. Thus, $Nb_2O_5 \cdot nH_2O$ which was heated at 100—300 °C has an acid strength of $H_0 \leqq -5.6$. However, the strong acid sites disappeared and only an acid strength of $H_0 \leqq +3.3$ was observed by heating at 500 °C.

In order to obtain further information about the acidity of $Nb_2O_5 \cdot nH_2O$, the infrared spectroscopic study of the adsorbed pyridine was examined. The results are shown in Fig. 2. Upon the adsorption of pyridine over $Nb_2O_5 \cdot nH_2O$ which had been evacuated at various temperatures, the bands at 1610, 1540, 1480, and 1440 cm^{-1} were observed after degassing at 100—150 °C. The bands at 1610, 1480, and 1440 cm^{-1} are due to coordinated pyridine and the band at 1540 cm^{-1} is ascribed to pyridinium ion.[6] Thus, $Nb_2O_5 \cdot nH_2O$ has both Lewis and Brönsted acid sites on the surface. The pyridinium ion band almost disappeared after degassing at 300 °C, but the Lewis acid bands still remained. The band intensity changes with evacuation temperature on $Nb_2O_5 \cdot nH_2O$ which had been preheated in a vacuum at different temperatures are shown in Fig. 3. The Brönsted acid band intensity was strongest on the sample evacuated at 100 °C and decreased with the increase of

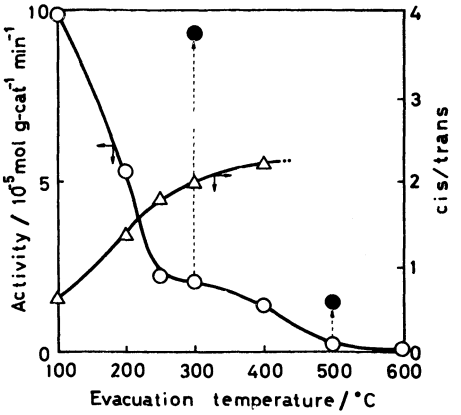

Fig. 5. Activity and selectivity of 1-butene isomerization.
●: H_2O added after pretreatment and evacuated at 100 °C.

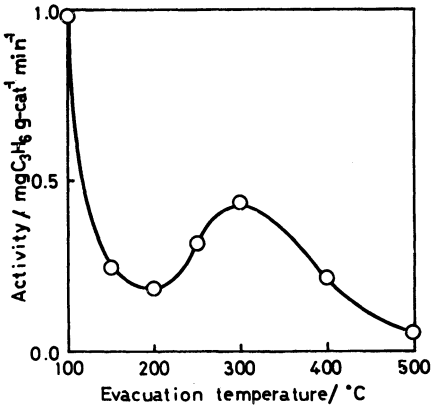

Fig. 6. Polymerization activity of propylene over $Nb_2O_5 \cdot nH_2O$.

pretreatment temperature. However, Lewis acid band intensity showed a maximum on the sample which had been evacuated at 300 °C. Upon preheating at 500 °C, both the acidic sites decreased remarkably.

The adsorption of CO_2 on $Nb_2O_5 \cdot nH_2O$ was examined to obtain an information about surface basic property. The spectra are shown in Fig. 4. After the introduction of CO_2 (2.7 kPa) on the sample which had been evacuated at 300 °C, no distinct change on the spectrum was observed. When the sample was contacted with CO_2 for 15 h, a slight increase of the bands at 1600 and 1390 cm^{-1} were noticed.

Isomerization of 1-Butene. The activity and selectivity changes of 1-butene isomerization with evacuation temperature are shown in Fig. 5. The $Nb_2O_5 \cdot nH_2O$ which was evacuated at 100 °C for 2 h showed a remarkable isomerization activity, the selectivity (the ratio of *cis*-2-butene to *trans*-2-butene) being less than unity. However, if the pretreatment temperature was increased to 200—250 °C, the activity decreased remarkably and the selectivity increased to about 2. In the range of evacuation temperature of 250—400 °C, the activity was not sensitive to the treatment temperature but diminished after the treatment at 500—600 °C. When $Nb_2O_5 \cdot nH_2O$ which had been evacuated at 300 °C was exposed to H_2O vapor at room temperature followed by

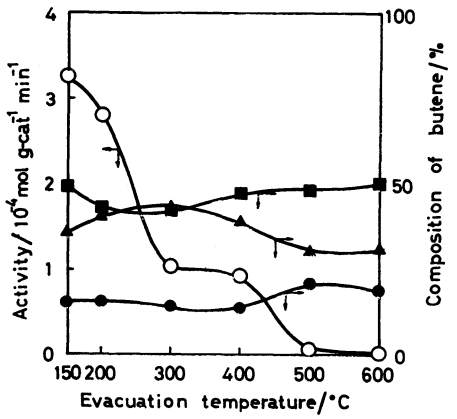

Fig. 7. Activity and selectivity changes of 2-butanol over $Nb_2O_5 \cdot nH_2O$ evacuated at various temperatures.
●: 1-Butene, ▲: *trans*-2-butene, ■: *cis*-2-butene

evacuation at 100 °C, almost the same activity as the catalyst originally evacuated at 100 °C was restored. On the other hand, after evacuation at 500 °C, the activity actually increased by the same treatment but the effect was far less compared to the case evacuated at 300 °C.

Polymerization of Propylene. The change of polymerization activity at 100 °C with evacuation temperature is shown in Fig. 6. The activity was highest on the sample evacuated at 100 °C and decreased remarkably after evacuation at 150—200 °C. However, upon evacuation at higher temperatures, the activity increased again and attained a maximum on treatment at 300 °C. After evacuation at the temperatures higher than 500 °C, the catalyst became almost inactive. The products of polymerization were not thoroughly analyzed due to the adsorption on the sample, but a considerable amount of butenes and pentenes along with the higher hydrocarbons desorbed at higher temperature (300 °C).

Dehydration of 2-Butanol. The changes of activity and selectivity of 2-butanol dehydration reaction with evacuation temperature are shown in Fig. 7. The activity gradually decreased with evacuation temperature. However, the activity was not changed by evacuation between 300—400 °C. The activity finally diminished on evacuation at 500—600 °C.

The formation of dehydrogenated product was not observed in the reaction at 150 °C over the whole catalysts. The ratio of formed *cis*- and *trans*-2-butenes was almost unity and the amount of 1-butene was less than 20% of the products over the catalysts evacuated at lower temperatures (150—300 °C), but the amount of 1-butene increased and that of *trans*-2-butene decreased after evacuation at 400—500 °C.

Discussion

The surface of $Nb_2O_5 \cdot nH_2O$ showed a considerable strong acidic character and rather weak basic property. After heat treatment at 100 °C, the strong acid sites of $H_0 \leqq -5.6$ were found to exist on the surface. Over the typical solid acid catalysts such as SiO_2–Al_2O_3 and SiO_2–TiO_2, the strong acid sites appear only after heat treatment at high temperature ($\simeq$500 °C)[7] along with the

removal of surface water. The acid sites on those catalyst surfaces are thought to be the isolated OH groups as Brönsted acid sites and the exposed metal ions as Lewis acid sites both of which appear after rigorous heat treatment.[7] However, $Nb_2O_5 \cdot nH_2O$ has acidic OH groups (Brönsted acid sites) as observed by IR experiment even after the mild heat treatment at 100 °C. Thus, the surface acidic property of $Nb_2O_5 \cdot nH_2O$ pretreated at mild temperatures is very peculiar and interesting because the residual water might cover almost the whole surface after the treatment. Upon pretreatment at 300 °C, H_2O was almost removed from $Nb_2O_5 \cdot nH_2O$ as observed in DTA experiment, and Lewis acidity increased along with the decrease of Brönsted acidity. However, after treatment at 500 °C, Nb_2O_5 became very inactive and the acidic property was very weak. This surface change is considered to be due to a phase transformation of amorphous $Nb_2O_5 \cdot nH_2O$ to T–T phase Nb_2O_5[5] at around 500—600 °C as observed by DTA and XRD. The catalytic activity of Nb_2O_5 was diminished by heat treatment at 500 °C or higher temperatures in the whole cases of 1-butene isomerization, propylene polymerization and 2-butanol dehydration reactions. In the case of 1-butene isomerization, $Nb_2O_5 \cdot nH_2O$ was very active on evacuation at 100 °C. The ratio of produced cis- and trans-isomers was around unity as observed in a typical case of acid-catalyzed reaction over SiO_2–Al_2O_3.[8] Though the activity decreased drastically after the sample was evacuated at 300 °C, almost the same activity as the sample evacuated at 100 °C was restored only by the introduction of H_2O vapor followed by evacuation at 100 °C. This fact indicates that the isomerization is catalyzed mainly by Brönsted acid sites whose amount decreases with the increase of evacuation temperature as shown in Fig. 3. However, after evacuation at 500 °C, only a slight increase of activity was observed by the introduction of H_2O vapor. The decrease of surface area due to the phase transformation at around 500 °C might prevent the regeneration of Brönsted acid sites on the surface.

In the reaction of 2-butanol dehydration, a high activity was achieved by evacuation at 150—200 °C. The activity on the catalyst evacuated at 150 °C was almost comparable to that on SiO_2–Al_2O_3 (3.7×10^{-4} mol min^{-1} g^{-1} at 200 °C).[9] Since the activity was reduced remarkably by evacuation at 300 °C, the activity would be also ascribed to Brönsted acidity, but Lewis acid sites might also act as active sites on evacuation at 300—400 °C. It is known that the selectivity of produced butenes from 2-butanol is very sensitive to the surface acidic and basic property.[10] The oxide catalysts which have both acidic and basic sites such as ThO_2 and ZrO_2 produce 1-butene dominantly.[11] However, over the strongly acidic catalysts such as SiO_2–Al_2O_3 produce less amount of 1-butene than 2-butene.[12] The $Nb_2O_5 \cdot nH_2O$ in this experiment is the latter case. It would be reasonable because the surface of $Nb_2O_5 \cdot nH_2O$ was mainly acidic and only very weak basic sites were observed in IR of CO_2 adsorption or indicator adsorption.

The polymerization of propylene is known as a model reaction catalyzed by Brönsted acid sites over SiO_2–Al_2O_3 or other acid catalysts.[13] In this work, $Nb_2O_5 \cdot nH_2O$ evacuated at 100 °C showed the highest activity for the polymerization, but the activity decreased remarkably when evacuated at 200—250 °C. In this case, it might be reasonable that the activity is ascribed to Brönsted acidity. However, the activity increased again on evacuation at 300—400 °C in contrast to the cases of 1-butene isomerization and dehydration of 2-butanol. This fact suggests the importance of Lewis acidity in the polymerization of propylene over Nb_2O_5 evacuated at higher temperatures. It is known that niobium compounds such as niobium trichloride distearate and niobium tetrachloride butanoate can polymerize ethylene, propylene, and 1,3-butadiene.[14] The promoting effect of niobium halide in the polymerization in Ziegler-Natta system is also known in the patent.[15] Since the importance of niobium ion as an active site for the polymerization is apparent in those cases, the Lewis acid site is thought to be an active site even on the oxide of niobium. Thus, we conclude that the polymerization of propylene proceeds on Brönsted acid sites on $Nb_2O_5 \cdot nH_2O$ pretreated at low temperatures ($\simeq$100 °C), but Lewis acid sites become main active sites after treatment at higher temperatures.

In conclusion, niobium oxide treated at 100 °C is characterized as a very strong Brönsted acid and can be used as a potential catalyst for Brönsted acid-catalyzed reactions at mild conditions. It should be emphasized that niobium oxide exhibits the highest acid strength among all of the metal oxides pretreated at 100 °C.

We are indebted to Dr. Hideshi Hattori for his valuable suggestion and kind cooperation and to CBMM LTDA for their kind supply of niobium samples and financial support.

References

1) R. Parthasarathy and J. G. Ciapetta, France Patent, No. 1555139 (1968); T. Shirasaki, K. Moriya, and I. Furuoya, Japan Patent, 76-143615 (1976); Y. Oda, K. Uchida, and T. Morimoto, Japan Patent, 73-49715 (1973); Y. Nanba, T. Suzuki, Y. Nakanishi, and Y. Okuda, Japan Patent, 75-39292 (1975).

2) J. F. McMahon, France Patent, No. 1500632 (1966); R. C. Hansford, U. S. Patent, No. 3480684 (1969); L. Bajars, U. S. Patent, No. 3291854 (1966); L. Bajars, U. S. Patent, No. 3308200 (1967); L. Bajars, U. S. Patent, No. 3308196 (1967); L. Bajars, U. S. Patent, No. 3308191 (1967).

3) K. Ohdan, H. Sasaya, K. Yoshida, and H. Ohtsuka, Japan Patent, No. 73-55870 (1973).

4) K. Tanabe, "Solid Acids and Bases," Kodansha, Tokyo, Academic Press, New York (1970).

5) M. L. Robinson, *J. Phys. Chem. Solids*, **29**, 2064 (1967).

6) E. P. Parry, *J. Catal.*, **2**, 371 (1963).

7) M. Itoh, H. Hattori, and K. Tanabe, *J. Catal.*, **35**, 225 (1974).

8) J. W. Hightower and W. K. Hall, *Chem. Eng. Prog., Symp. Ser.*, **63**, 122 (1967).

9) K. Tanabe, A. Kayo, and T. Yamaguchi, *J. Chem. Soc., Chem. Commun.*, **1981**, 602.

10) M. E. Winfield, *Catalysis*, **7**, 93 (1960).

11) A. J. Lundeen and R. V. Hoozer, *J. Org. Chem.*, **32**,

3386 (1967); T. Yamaguchi, H. Sasaki, and K. Tanabe, *Chem. Lett.*, **1973**, 1017.
12) A. J. Lundeen and R. V. Hoozer, *J. Am. Chem. Soc.*, **85**, 2180 (1963).
13) M. W. Tamele, *Discuss. Faraday Soc.*, **8**, 270 (1960).
14) J. E. Bwileigh and C. A. Uraneck, U. S. Patent, No. 3640986 (1972).
15) K. Tashiro, M. Yokoyama, and S. Kitazume, Japan Patent, 74-15631 (1974).

The Effect of Surfactant on Formation of Calcium Carbonate

Tsuneo SUHARA, Kunio ESUMI,* and Kenjiro MEGURO
Department of Applied Chemistry and Institute of Colloid and Interface Science, Science University of Tokyo, Kagurazaka, Shinjuku-ku, Tokyo 162

(Received May 23, 1983)

Calcium carbonate was precipitated by rapidly mixing calcium chloride solution, sodium carbonate solution, and aqueous surfactant solution at 25 °C in order to elucidate the effect of addition of surfactant on the formation. The samples obtained were examined by scanning electron microscopy, X-ray powder diffraction, and a specific surface area study. The sample without surfactant proved to be calcite crystals. When a cationic surfactant was added, the crystal structure was transferred from calcite and vaterite to calcite with an increase of the concentration of the cationic surfactant. On the other hand, the addition of a lower concentration of an anionic surfactant provided a mixture of calcite and vaterite, but in higher concentration, amorphous material was obtained. The samples with nonionic surfactant were vaterite crystals. It was found that the spherical particle ratio (N_{sp}) and the vaterite crystal ratio (F_v) in the sample depend on the concentration of the nonionic surfactant.

The preparation of the spherical particles of inorganic compounds has been the subject of many studies.[1-14] However, the spherical particles can be obtained only under limited synthesis conditions, depending on the concentration of solution, temperature, reaction rate, pH, and the ripening method.

Anhydrous calcium carbonate as an inorganic compound is known to exist in three crystalline modifications: calcite, aragonite, and vaterite. Calcite is a stable form at ordinary temperatures and pressures. Aragonite and vaterite are metastable modifications which transform to calcite on heating.[10-12]

Miyata and Nakahara[13] have reported that vaterite was prepared by an interfacial reaction method in which calcium carbonate was formed by the reaction of K_2CO_3 aqueous solution emulsified in benzene with $CaCl_2$ aqueous solution. Inoue and Kanaji[11] prepared vaterite by reacting the concentrated aqueous solution of $CaCl_2$ with Na_2CO_3 and the same process was also employed in the system of $Ca(NO_3)_2$ with Na_2CO_3. Enomoto *et al.*[14] obtained vaterite by mixing $CaCl_2$, $NaHCO_3$, and NH_3 at 45 °C to attain a final pH of 6.8.

In this work, calcium carbonate was precipitated by mixing $CaCl_2$–Na_2CO_3 solutions in the presence of aqueous surfactant solution at 25 °C. The effects of addition of aqueous surfactant solution on the morphology and polymorphism of calcium carbonate were examined.

Experimental

Preparation of Calcium Carbonate. Nonionic surfactants used in this experiment were supplied by Nikko Chemicals Co., Ltd.; other chemicals were of reagent grade.

Calcium carbonate was precipitated by rapidly mixing 2.5×10^{-2} mol dm^{-3} of $CaCl_2$ solution, 2.5×10^{-2} mol dm^{-3} of Na_2CO_3 solution, and aqueous surfactant solution at 25 °C. The concentrations of the surfactant added were 5.0×10^{-5}, 9.0×10^{-4}, and 5.0×10^{-3} mol dm^{-3} (cationic surfactant: hexadecyltrimethylammonium bromide, CTAB), 5.0×10^{-5}, 3.2×10^{-3}, and 8.0×10^{-3} mol dm^{-3} (anionic surfactant: sodium dodecyl sulfate, SDS), and 5.0×10^{-6}, 1.0×10^{-5}, 5.0×10^{-5}, 1.0×10^{-4}, 5.0×10^{-4}, and 1.0×10^{-3} mol dm^{-3} (nonionic surfactant: poly(oxyethylene) nonylphenyl ether, NP-n: n=10, 20). Each solution was mixed for 10 s and unstirred thereafter. Precipitation commenced less than 5 s after mixing, with a rapid onset of turbidity, and crystals gradually settled out of the solutions. In this experiment, the precipitate of calcium carbonate adhered tenaciously to the walls and bottom of the reaction cell after 3 h of aging. The precipitate obtained was washed with water to remove unreactive salts and by-products, washed again with methanol to remove the surfactant, then dried *in vacuo*. Each dried precipitate was used as a sample.

pH Measurement. The pH of the supernatant was measured by a Corning pH meter 130.

Scanning Electron Microsopy (SEM). The morphology and polymorphic composition of samples obtained were taken with a JEOL JSM-T20 SCANNING MICROSCOPE and a AKASHI ALPHA-10 after coating by the thick 30 nm of gold on each sample was carried out by a JEOL COAT ION SPUTTER JEC-1100. Further, the spherical particle ratio (N_{sp}) was determined by counting the number of spherical and unspherical particles on the microphotgraphs taken with different fields.

Specific Surface Area. The specific surface area of calcium carbonate was measured by a Shimadzu GAS CHROMATOGRAPH GC-7A connected with a Shimadzu SORPTOGRAPH ADS-1B. The area was determined by applying the BET method to the nitrogen adsorption at liquid nitrogen temperature.

X-Ray Powder Diffraction.[15] An X-ray powder diffraction was measured by a Rigaku Denki Geigerflex RAD-IIIA MJ 200 DX with nickel filtered copper $K\alpha$ radiation (35 kV and 10 mA). To evaluate the crystal transfer ratio in vaterite to calcite in the presence of surfactant, the following equations were employed:

$$F_c = \frac{I_{104(c)}}{I_{110(v)} + I_{104(c)} + I_{112(v)} + I_{114(v)}} \times 100, \quad (1)$$

$$F_c + F_v = 100. \quad (2)$$

Here diffraction intensities (I) of the (104) reflection of calcite and of the (110), (112), and (114) reflections of vaterite are obtained and the vaterite (F_v) and calcite (F_c) crystal ratios can be determined by the X-ray diffraction measurement using Eqs. 1 and 2.

Results and Discussion

The crystals obtained in the absence of surfactant had a characteristic calcite(rhombohedral) morphology, as shown in Fig. 1. Further, the X-ray powder diffraction

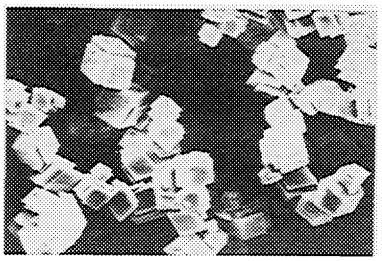

Fig. 1. SEM photomicrograph of calcium carbonate crystals precipitated in the absence of surfactant.

analysis showed the calcite (ASTM No. 5-586) diffraction peak. The pH values of each reacting solution, with and without the surfactant solutions, were 10.30, and 10.30—10.40, indicating that the effect of pH on the formation of calcium carbonate by the addition of surfactant will be negligibly small.

Figure 2 shows a scanning electron microphotograph of the powders prepared in the presence of CTAB, whose critical micelle concentration(cmc) is 9.0×10^{-4} mol dm^{-3}. The samples obtained in the presence of 5.0×10^{-5} mol dm^{-3} of CTAB were a mixture of characteristic calcite and vaterite(hexagonal) whose morphology is shown in Fig. 2(A). With an increase of the concentration of CTAB (9.0×10^{-4} and 5.0×10^{-3} mol dm^{-3}), the morphology became that characteristic of calcite, as shown in Figs. 2(B) and (C). The above results indicate that the vaterite fraction in the samples decreases with an increase of the concentration of CTAB added. Especially. in the concentration of 5.0×10^{-5} mol dm^{-3} of CTAB, the spherical particle ratio (N_{sp}), the vaterite crystal ratio (F_v), and the specific surface area were 82.5%, 47.0%, and 2.8 m^2/g, respectively. The decrease in the vaterite crystal ratio with an increase of the concentration of CTAB might be caused by the slow diffusion of water owing to the thick layer of CTAB adsorbed around the calcium carbonate particles.

Figure 3 gives the SEM pictures of the powders prepared in the presence of SDS, whose cmc is 8.0×10^{-3} mol dm^{-3}. The morphology of the samples obtained in the presence of 5.0×10^{-5} mol dm^{-3} of SDS exhibited a mixture of calcite and vaterite, as shown in Fig. 3(A). The addition of higher concentrations of SDS (3.2×10^{-3} and 8.0×10^{-3} mol dm^{-3}) provided amorphous precipitates, as shown in Figs. 3(B) and (C). Thus, vaterite and calcite crystals become amorphous with increasing the concentration of SDS added. In the concentration of 5.0×10^{-5} mol dm^{-3} of SDS, N_{sp}, F_v, and specific surface area were 70.0%, 32.0%, and 2.3 m^2/g, respectively.

The adsorption of SDS onto calcium carbonate powder has been studied by Chibowski.[16] According to his report, in the low concentration of SDS, the adsorption in the synthesis reaction step of calcium carbonate was appreciable, while in the highcon centration, this solution dissociated similarly to Eq. 3, and Ca^{2+} and $2DS^-$ in this solution produced $Ca(DS)_2$ after reacting like Eq. 4. Since this reaction affects significantly the reaction of calcium carbonate, it is considered that calcite and vaterite crystals become amorphous by the addition of SDS.

$$Na\text{–}Ds \longrightarrow Na^+ + DS^-, \quad (3)$$

$$Ca^{2+} + 2DS^- \longrightarrow Ca(DS)_2. \quad (4)$$

Thus, cationic and anionic species of the surfactant play important roles in the formation of calcium carbonate. As nonionic surfactants have no charge groups, the formation of calcium carbonate in the presence of nonionic surfactant proceeds without taking into consideration the charge effect.

Figure 4 gives the SEM pictures of the powders prepared in the presence of NP-10, whose cmc is $(7.5—9.0)\times10^{-5}$ mol dm^{-3}. The samples in the presence of NP-10 (5.0×10^{-6} and 1.0×10^{-4} mol dm^{-3}) had a characteristic calcite and vaterite morphology, as shown in Fig. 4(C). The vaterite crystal ratio (F_v) calculated

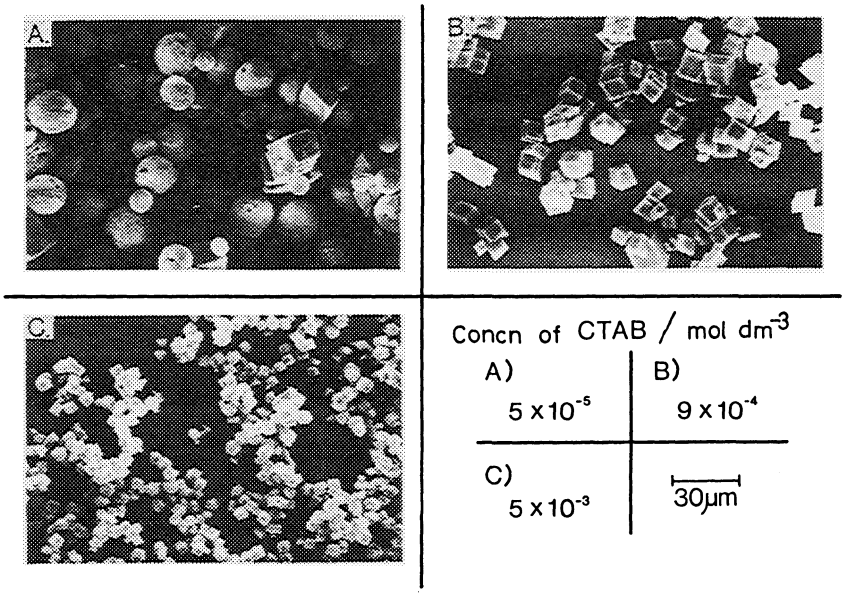

Fig. 2. SEM photomicrographs of calcium carbonate crystals precipitated in the presence of various concentrations of CTAB.

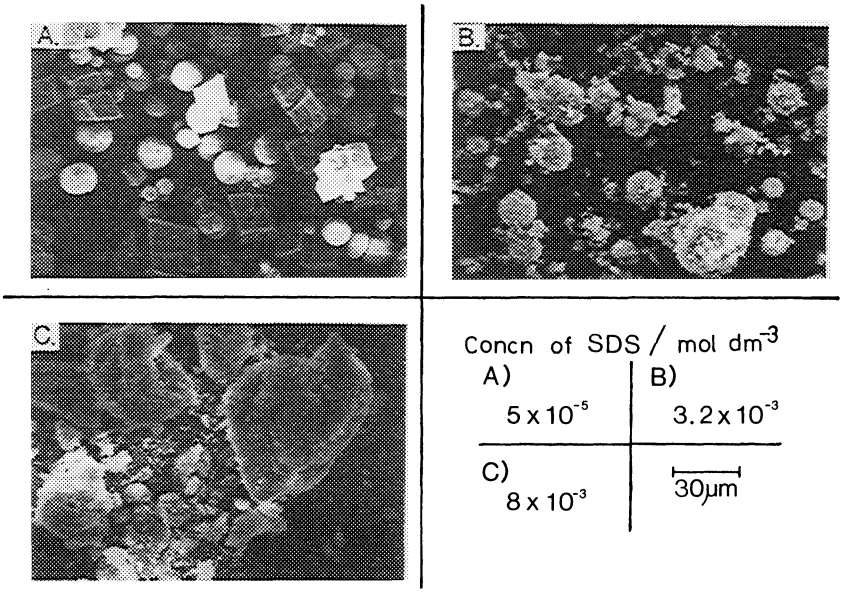

Fig. 3. SEM photomicrographs of calcium carbonate crystals precipitated in the presence of various concentrations of SDS.

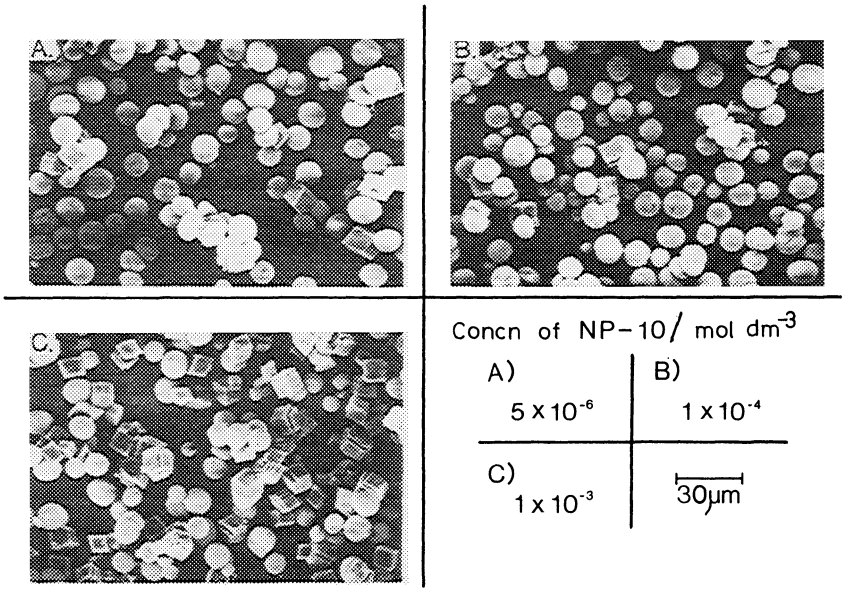

Fig. 4. SEM photomicrographs of calcium carbonate crystals precipitated in the presence of various concentrations of NP-10.

by Eqs. 1 and 2 is plotted against the concentration of surfactant shown in Fig. 5. In the case of NP-10, the F_v increased until the concentration of 5.0×10^{-5} mol dm^{-3}, then decreased slowly with an increase of the concentration until 1.0×10^{-4} mol dm^{-3}, and then decreased rapidly. In the case of NP-20, the F_v increased gradually with an increase of the concentration of surfactant. Thus, it is found that the vaterite crystal ratio depends on the concentration of the nonionic surfactant.

The spherical particle ratio (N_{sp}) is also plotted against the concentration of nonionic surfactant in Fig. 6. In the range of concentration of NP-10 from 5.0×10^{-6} to 5.0×10^{-4} mol dm^{-3}, the crystals were spheres, cubes, and amorphous. Further, at concentrations above 5.0×10^{-4} mol dm^{-3}, the N_{sp} decreased with an increase of the concentration of NP-10. Similarly, in the range of concentration of NP-20 from 5.0×10^{-6} to 1.0×10^{-3} mol dm^{-3}, the N_{sp} increased with an increase of the concentration of NP-20. The magnitude of N_{sp} obtained by using NP-10 is larger than that of NP-20.

The adsorption of nonionic surfactant onto inorganic powders has been studied by several investigators.[17-20] Akers and Riley[19] and Hsiao and Dunning[20] examined the adsorption of nonionic surfactants onto calcium carbonate or sands. They reported that the adsorption increases with decrease in the length of oxyethylene chain of the surfactant. According to their results, as the film thickness of the surfactant adsorbed on the powder particle increases with an increase of the concen-

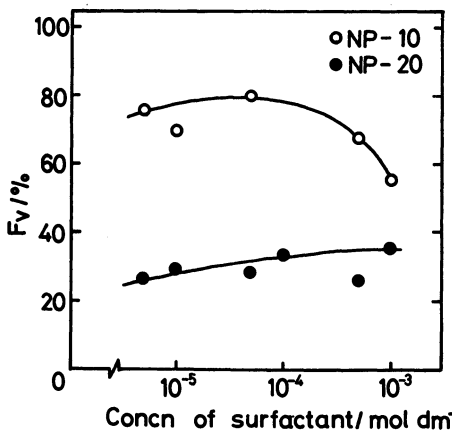

Fig. 5. Relation between vaterite ratio (F_v) in calcium carbonate and concentration of surfactant added.

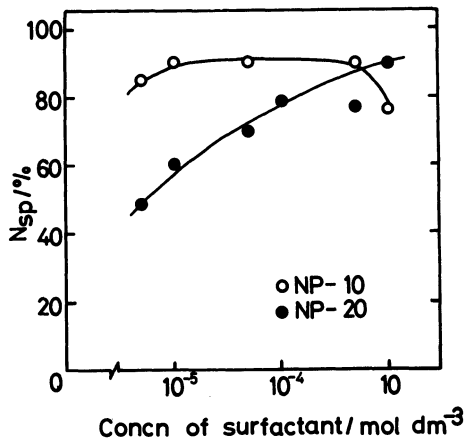

Fig. 6. Relation between spherical particle ratio (N_{sp}) in calcium carbonate and concentration of surfactant added.

tration of the surfactant, the film prevents the surface of the particle from contacting the water. Thus, the increase of the vaterite crystal ratio might be caused by preventing the vaterite particle from coming into contact with the water; this would result in stability of the vaterite crystal. On the other hand, at higher concentrations of the surfactant, the decrease in the vaterite crystal ratio is due to the slow diffusion of water through the thick film layer of the surfactant adsorbed around the particle. The above results show that the N_{sp} and F_v depend on the concentration of the surfactant and the length of their oxyethylene chain. Here, the N_{sp} in the case of NP-10 and NP-20 were 20—30% and 40—50% greater than those of their F_v, respectively. This difference might be interpreted if some of the sherical particles in the preparation of the above conditions are amorphous vaterite rather than vaterite crystals.

The mean particles size (arithmetic mean diameter, D) and specific surface area (S_N, S_D) of calcium carbonate are given in Table 1. The S_D value was determined by calculating from the mean particle size, employing Eq. 5:

$$S_D = 6/D \times \rho, \quad (5)$$

where D is an arithmetic mean diameter estimated from

Table 1. Mean particle size and surface area of calcium carbonate precipitated in the presence of surfactant

Surfactant mol dm^{-3}	Mean particle μm	S_N $m^2\,g^{-1}$	S_D $m^2\,g^{-1}$
None	10.50	1.48	0.22
NP-10			
1×10^{-5}	14.12	3.56	0.16
5×10^{-5}	12.32	3.02	0.18
1×10^{-4}	11.56	3.74	0.20
5×10^{-4}	10.56	4.81	0.21
NP-20			
5×10^{-6}	13.69	2.05	0.17
1×10^{-5}	12.57	2.80	0.18
5×10^{-4}	10.36	2.58	0.22
1×10^{-3}	12.44	4.59	0.18

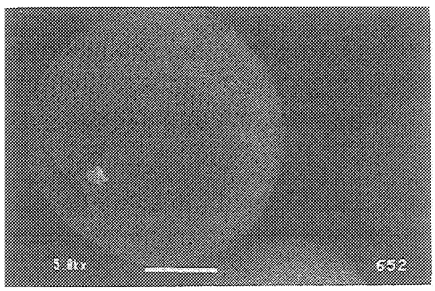

Fig. 7. SEM photomicrograph of a vaterite crystal enlarged.

the SEM pictures and ρ is the specific gravity, 2.65. The S_N value was also determined by the BET method from the nitrogen adsorption. From Table 1, it is seen that the S_N value is larger than that of the S_D, indicating that the calcium carbonate formed by the addition of nonionic surfactant is porous. Further, to elucidate the surface morphology of vaterite crystal, the SEM picture was taken and is shown in Fig. 7. It is found that, as predicted by the S_N/S_D value, the surface of vaterite seems to have many pores.

References

1) Y. Nakahara and K. Miyata, *Hyomen*, **15**, 319 (1977).
2) Y. Nakahara and K. Miyata, *Nippon Kagaku Kaishi*, **1976**, 1525.
3) K. Miyata and Y. Nakahara, *Nipppon Kagaku Kaishi*, **1976**, 727.
4) K. Miyata and Y. Nakahara, *J. Jpn. Colour Material*, **49**, 349 (1976).
5) K. Miyata and Y. Nakahara, *J. Jpn. Colour Material*, **49**, 643 (1976).
6) S. Hamada and E. Matijević, *J. Colloid Interface Sci.*, **84**, 274 (1981).
7) E. Matijević and P. Scheiner, *J. Colloid Interface Sci.*, **63**, 509 (1978).
8) E. Matijević, R. Sapieszko, and J. B. Melville, *J. Colloid Interface Sci.*, **50**. 567 (1975).
9) A. Tentorio, E. Matijević, and J. P. Kratohvil, *J. Colloid Interface Sci.*, **77**, 418 (1980).
10) Y. Kitano, *Kogyo Kagaku Zasshi*, **59**, 1343 (1959).
11) Y. Inoue and Y. Kanazi, *Hyomen*, **7**, 665 (1969).

12) P. E. Cloud, *Geochem. Cosmochem. Acta*, **26**, 867 (1962).
13) K. Miyata and Y. Nakahara, *J. Jpn. Colour Material*, **50**, 67 (1977).
14) T. Enomoto, T. Mizuno, M. Fujinaga, and R. Nakamura, Japan Kokai Tokkyo Koho 79 150 397 (1979).
15) M. S. Rao, *Bull. Chem. Soc. Jpn.*, **46**, 1414 (1973).
16) S. Chibowski, *J. Colloid Interface Sci.*, **76**, 371 (1980).
17) J. A. Shropshire, *J. Colloid Interface Sci.*, **25**, 389 (1967).
18) K. G. Mathai and R. H. Ottewill, *Trans. Faraday Soc.*, **62**, 750 (1966).

 © 1983 The Chemical Society of Japan Bull. Chem. Soc. Jpn., 56, 2937—2940 (1983)

The Preparation and Some Properties of Potassium Tris(1,1′-ferrocenedicarboxylato)ferrate(III)

Tomoko NOMURA

Department of Chemistry, Faculty of Science and Engineering, The Aoyama Gakuin University, Shibuya, Shibuya-ku, Tokyo 150

(Received October 5, 1982)

The K_3[Fe(1,1′-ferrocenedicarboxylato)$_3$] complex was synthesized. The infrared absorption bands of the ligand (parent) acid, its potassium and barium salts, and the complex were assigned in studying the nature of the oxygen-to-metal bond in the complex. The electronic absorption spectra of the ligand acid and the complex were also measured. The techniques of thermogravimetry (TG) and differential thermal analysis (DTA) were used to establish the thermal decomposition of the complex.

There are some complexes in which ferrocenyl groups are introduced into the ligand,[1,7,9] but no complexes with 1,1′-ferrocenedicarboxylic acid (H_2fdc) as ligands have yet been reported. The K_3[Fe(1,1′-ferrocenedicarboxylate)$_3$] (K_3[Fe(fdc)$_3$]) complex was synthesized by using iron(III) sulfate and barium 1,1′-ferrocenedicarboxylate. Its properties was investigated in the present study.

Experimental

Preparation of Ligand. H_2fdc was prepared according to Rausch and Ciappenelli.[2] The product recrystallized from glacial acetic acid was orange and melted, with decomposition, at *ca.* 246 °C (lit: decomposition over 240 °C). The product was identified by means of IR[3] and NMR measurments. Calcd for $C_{12}H_{10}O_4Fe$: Fe, 20.38%. Found: Fe, 20.1%.

Preparation of the Complex. The K_3[Fe(fdc)$_3$] complex could not be synthesized by the following procedure:

$$2Fe(OH)_3 + 3H_2fdc \longrightarrow Fe_2(fdc)_3 + 6H_2O,$$

$$Fe_2(fdc)_3 + 3K_2fdc \longrightarrow 2K_3[Fe(fdc)_3].$$

However, the procedure of Bailar and Jones[4] could be successfully applied:

$$Fe_2(SO_4)_3 \cdot nH_2O + 3Bafdc \longrightarrow Fe_2(fdc)_3 + 3BaSO_4,$$

$$Fe_2(fdc)_3 + 3K_2fdc \longrightarrow 2K_3[Fe(fdc)_3].$$

$Fe_2(SO_4)_3$ (0.55 g), Bafdc (2.2 g) (prepared from $Ba(OH)_2 \cdot 8H_2O$ (3.15 g) and H_2fdc (2.74 g)), and K_2fdc (1.6 g) (prepared from K_2CO_3 (1.38 g) and H_2fdc (2.74 g)) were placed in water (400 cm^3) and digested for 3 h on a water bath. A crystalline substance then began to precipitate. After centrifugation, the filtrate was evaporated to *ca.* 70 cm^3, at which point crystals precipitated. The product, which formed after standing for 1 h, was filtered with suction and washed with 50% ethanol several times. Yellowish brown, flat crystals of K_3[Fe(fdc)$_3$] were thus prepared in a nearly quantitative yield . The complex was stable in air, decomposed at 284 °C, and was insoluble in most organic solvents. It was dried *in vacuo* over silica gel at room temperature. Found: C, 44.86; H, 2.95; Fe, 22.1%. Calcd for K_3[Fe(fdc)$_3$]: C, 43.70; H, 2.42; Fe, 22.6%. Attempted recrystallizations with water and *N,N*-dimethylformamide were unsuccessful. In the case of a protogenic solvent such as acetic acid or an amphiprotic solvent such as water, the K_3[Fe(fdc)$_3$] was changed to H_2fdc. In an organic solvent such as *N,N*-dimethylformamide, a slight decomposition was observed after one week.

Measurements. The electronic spectra were measured with a Shimadzu UV-200 spectrophotometer in cells with a 1-cm light path. The infrared spectra were measured with a JASCO IRA-1 spectrophotometer in the range of 650—4000 cm^{-1} on KBr pellets. The TG and DTA measurements were made with a Shimadzu DTA-20B differential thermal microbalance under two conditions, in static N_2 and air at the heating rate of 10 °C/min. The sample amounts taken in the TG runs were *ca.* 5 mg, and in the DTA runs, *ca.* 2 mg.

Results and Discussion

Composition of the Chelate. The K_3[Fe(fdc)$_3$] complex crystals obtained in a solid state could not be recrystallized, and they were too fine for any powder X-ray study. The complex was, however, homogeneous and was found to be composed of single crystals under a polarizing microscope. Therefore it was considered that the complex was pure enough for the structural study. DTA and TG measurements showed that no water molecules existed in the complex. Considering that the majority of Fe(III) complexes are octahedral, like the tris(oxalato) complex, the molar ratio of Fe : H_2fdc (1 : 3) seems to be natural. The molecular weight and conductivity of the complex were not measured, since no suitable solvent could be found.

IR Spectra. A) Assignment of the Observed Frequencies of 1,1′-Ferrocenedicarboxylic Acid and Its Potassium and Barium Salts: The main bands are listed in Table 1. Characteristic bands for the carboxylic acid[3] were observed at 2625, 2545, and 914 cm^{-1} in the spectrum of the H_2fdc, which could be assigned to the OH stretching and out-of-plane OH deformation vibrations. A very strong band at about 1680—1720 cm^{-1} in the H_2fdc spectrum was assigned to the C=O stretching vibrations. Bands at 1492 and 1300 cm^{-1} in the H_2fdc spectrum were assigned to the C–O vibrations, coupled with the in-plane OH deformation vibration. Very strong bands at about 1600 cm^{-1} and other strong band at about 1400 cm^{-1} observed in the spectra of K_2fdc and Bafdc were assigned to the antisymmetric and symmetric OCO stretching vibration respectively. Strong bands at 1465 cm^{-1} in the K_2fdc spectrum and at 1475 cm^{-1} in the Bafdc spectrum were also assigned to the symmetric OCO stretching vibrations.

B) Assignment of the Observed Frequencies of the Potassium Tris(1,1′-ferrocenedicarboxylato)ferrate(III) Complex: On the basis of the reported data on the bands of similar complexes, such as the oxalato,[5] malonato,[6] and 1,1′-diacetylferrocenato complexes,[7] the absorption bands

TABLE 1. IR SPECTRA OF 1,1′-FERROCENEDICARBOXLIC ACID, POTASSIUM, AND BARIUM SALTS[a)]

$H_2fdc(\tilde{\nu}/cm^{-1})$	$K_2fdc\cdot xH_2O(\tilde{\nu}/cm^{-1})$	$Bafdc\cdot H_2O(\tilde{\nu}/cm^{-1})$	Assignment
	3380 m,b	3380 m,b	$\nu(H_2O)$[b)]
3120 ⌇ 2860	3070 w	3090 w	$\nu(CH)F_c$
			$\nu(OH)$
2625 vw			$\nu(OH)$
2545 vw			$\nu(OH)$
1720 s,sh 1680 vs,b			$\nu_a(C{=}O)$
	1575 vs,b	1555 vs,b 1525 vs,b	$\nu_a(OCO)$
1492 s			$\nu_s(CO)+\delta(OH)$
	1465 s	1475 s	$\nu_s(OCO)$
1405 m			$\nu(CC)F_c$
1374 w			
	1387 s 1362 s 1340 m,sh	1388 s 1358 m 1346 m	$\nu_s(OCO)$
1300 s			$\delta(OH)+\nu_s(CO)$
1166 m	1187 w 1176 w	1183 w	$\nu_a(CC)$
1025 m	1035 w 1010 w	1028 m	$\delta(CH)F_c$
914 m,b			$\pi(OH)$
823 m,b	808 m 784 m	808 m 780 w,sh	$\delta(OCO)+\pi(CH)F_c$
775 vw			
742 w			

a) The absorption bands: s=strong, w=weak, m=medium, v=very, sh=shoulder, b=broad, *a*=antisym., *s*=sym., F_c=ferrocenyl group, δ=in-plane def., π=out-of-plane def. b) The stretching vibration of H_2O.

TABLE 2. IR SPECTRA OF POTASSIUM TRIS(1,1′-FERROGENEDICARBOXYLATO)FERRATE(III)

$K_3[Fe(fdc)_3]$ ($\tilde{\nu}/cm^{-1}$)	Assignment
3100 vw, b	$\nu(CH)F_c$
1677 vs	$\nu_a(C{=}O)$
1586 m 1542 m	$\nu_a(OCO)$
1465 s,b	$\nu_s(OCO)$
1380 m 1353 w 1325 w	$\nu_s(OCO)$
1280 vs,b	$\nu_s(CO)+\delta(OCO)$
1160 m	
1025 w	$\delta(CH)F_c$
905 vw	
816 w 775 w	$\delta(OCO)$
724 w,b	

of $K_3[Fe(fdc)_3]$ were assigned; they are shown in Table 2 and Fig. 1 (——). The bands at 2860—3120, 2625, and 2545 cm^{-1} assignable to the OH stretching vibration were not observed. The very strong C=O stretching vibration at 1680—1720 cm^{-1} in the ligand was shifted to a lower frequency, 1677 cm^{-1}, in the complex. New bands were observed at 1586 and 1542 cm^{-1}; they were assigned to the antisymmetric OCO stretching vibrations corresponding to the bands at 1555 and 1525 cm^{-1} respectively present in the spectrum of Bafdc. The band at 1465 cm^{-1} corresponded to the bands of symmetric OCO stretching vibration in the K_2fdc and Bafdc spectra. The band at 1380 cm^{-1} and new weak bands at 1353 and 1325 cm^{-1} assigned to the symmetric OCO stretching vibrations corresponded to the bands at 1387, 1362, and 1340 cm^{-1} respectively in the K_2fdc spectrum and to the bands at 1388, 1358, and 1346 cm^{-1} in the Bafdc spectrum. The nature of the metal-to-ligand

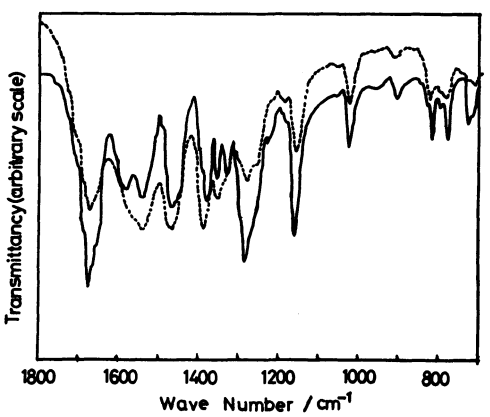

Fig. 1. IR spectra of $K_3[Fe(fdc)_3]$ (——) and the thermal decomposition product of $K_3[Fe(fdc)_3]$ after heating at 290 °C in N_2 in the DTA procedure (------).

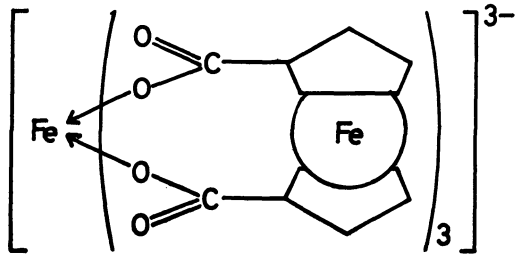

Fig. 2. The structure of $K_3[Fe(fdc)_3]$.

TABLE 3. ELECTRONIC SPECTRAL DATA FOR LIGAND AND COMPLEX

Compound	Solvent	$\tilde{\nu}/10^3$ cm^{-1} (logϵ)		
H_2fdc	95% EtOH	32.4(3.12),	28.6(2.58),	22.3(2.47)
	H_2O	32.3sh,		22.1
	DMSO	32.3sh(3.13),	28.6(2.60),	22.2(2.46)
$K_3[Fe(fdc)_3]$				
	95% EtOH	32.3sh,	28.6sh,	22.3
	H_2O	32.3sh,		22.0sh
	DMSO	32.3sh(3.63),	28.6sh(3.25),	22.0(2.95)

The ligand did not dissolve enough in H_2O, and the complex, in 95% EtOH and H_2O, to enable us determine the extinction coefficients. sh=shoulder.

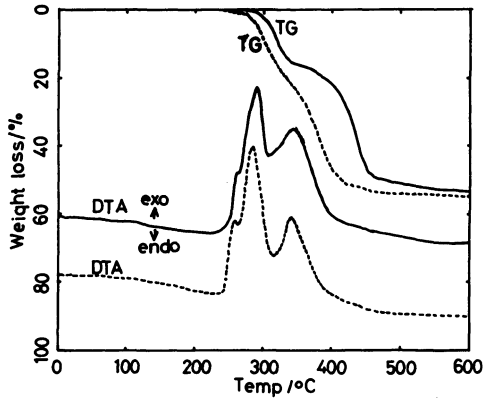

Fig. 3. TG and DTA curves of $K_3[Fe(fdc)_3]$ in N_2 (——) and in air (------).

bond (M–O) could thus be studied indirectly from the value of the CO stretching frequency, without determining the M–O stretching vibration, which appears at a much lower frequency. The structure deduced from these data is shown in Fig. 2.

Electronic Spectra. The electronic spectra of H_2fdc and its complex was measured in three solvents: 95% ethanol (EtOH), dimethyl sulfoxide (DMSO), and H_2O. The absorption bands in the $(12.5—33.5)\times10^3$ cm^{-1} region are given in Table 3. In these spectra, a broad low-intensity band around 440 nm, which is identified as a forbidden d-d transition localized on the iron atom, and another band at 325 nm, which is identified as a N–Q transition or as a symmetry-forbidden N–V transition, are characteristic. In comparison with the absorption bands of ferrocene (325 nm (ε, 49), 440(91)) and ferrocenemonocarboxylic acid (342^{sh}-(361), 445(223)) in 95% EtOH,[8] the spectrum of the H_2fdc showed a bathochromic shift. These bands shifted with substitution on the cyclopentadienyl ring, and the intensity increased in such derivatives where a ferrocene was conjugated with COOH. In the spectrum of the complex, the positions of the absorption bands were negligibly changed, while the intensities increased. Interestingly, the change in the electronic spectrum was not so pronounced as would be expected when COOH groups substituted on ferrocene are coordinated to Fe^{III}. The H_2fdc ligand has a strongly aromatic nature with π electrons. When such ligands are coordinated to a metal, the spectrum of the complex is almost the same as that of a free ligand. Therefore the electronic spectrum of the complex showed the absorption bands based on the ligand.

TG and DTA. The data for $K_3[Fe(fdc)_3]$ are shown in Fig. 3. They show that the thermal-decomposition process of $K_3[Fe(fdc)_3]$ proceeds in two stages, corresponding to the exothermic peaks at 284 and 339 °C in air and at 289 and 343 °C in N_2. The H_2fdc ligand is decomposed with an exothermic peak at 246 °C in air. In the investigation of the thermal decomposition of $K_3[Fe(fdc)_3]$ in N_2, the solid residue obtained at 290 °C (loss in weight 12%) was identified by means of its IR spectra. Figure 1 (------) shows that the strong absorption band at 1677 cm^{-1} assigned to the C=O stretching vibration and that at 1280 cm^{-1} assigned to the C=O stretching and the O–C=O deformation vibrations were both very much reduced. The weak absorption bands at 1586, 1325, and 730 cm^{-1} disappeared. These spectral changes show that the Fe–O bonds are partially dissociated by heating. After the extraction of this solid residue with *N,N*-dimethylformamide, ferrocene or its derivative was not found by studying IR spectra of the extract. It seems that such an organic compound is sublimed in the thermal decomposition process, as has been described in the literature.[9] The solid residue obtained at 360 °C (loss weight in 49.8%) was identified by means of its IR spectra; it was found to be potassium carbonate. A comparison of the thermal decomposition of the chelate of H_2fdc and that of the chelate of oxalic acid[10] shows that the thermal stability rises a little upon the introduction of the carboxyl groups into ferrocene, which is thermally stable.

The author wishes to express her deep gratitude to Professor Shoichiro Kawakubo of Aoyama Gakuin University.

References

1) C. R. Hauser and C. E. Cain, *J. Org. Chem.*, **23**, 1142 (1958); C. R. Hauser and J. K. Lindsay, *ibid.*, **22**, 482 (1957); H. Imai and T. Ota, *Bull. Chem. Soc. Jpn.*, **47**, 2497 (1974); D. M. Wiles and T. Suprunchuk, *Can. J. Chem.*, **46**, 1865 (1968); I. Pavlík, K. Handlíř, and V. Dvořák, *Collect. Czech. Chem. Commun.*, **30**, 3052 (1965); I. Pavlík, J. Klikorka, and K. Handlíř, *Z. Chem.*, **8**, 390 (1968); L. M. Dyagileva, O. S. Morozov, N. N. Vyshinskii, V. G. Tsvetkov, and Y. A. Aleksandrov, *Zh. Obshch. Khim.*, **50**, 1859 (1980); P. P. Singh and R. Chard, *J. Inorg. Nucl. Chem.*, **37**, 45 (1975); A. N. Nesmeyanov, Y. T. Struchkov, N. N. Sedova, V. G. Andrianov, Y. V. Volgin, and V. A. Sazonova, *J. Organomet. Chem.*, **137**, 217 (1977); D. J. Booth and B. W. Rockett,

Inorg. Nucl. Chem. Lett., **6**, 121 (1970); A. W. Rudie, D. W. Lichtenberg, M. L. Katcher, and A. Davison, *Inorg. Chem.*, **17**, 2859 (1978).

2) M. D. Rausch and D. J. Ciappenelli, *J. Organomet. Chem.*, **10**, 127 (1967).

3) M. D. Rausch, E. O. Fischer, and H. Grubert, *J. Am. Chem. Soc.*, **82**, 76 (1960).

4) J. C. Bailar, Jr., and E. M. Jones, *Inorg. Synth.* Vol. III, 35 (1939).

5) K. Nakamoto, "Infrared and Raman Spectra of Inorganic and Coordination Compounds," John Wiley & Sons, New York (1978), p. 233.

6) M. J. Schmelz, I. Nakgawa, S. Mizushima, and J. V. Quagliano, *J. Am. Chem. Soc.*, **81**, 287 (1959).

7) I. Pavlík and K. Handlíř, *Collect. Czech. Chem. Commun.*, **31**, 1958 (1966).

8) R. T. Lundquist and M. Cais, *J. Org. Chem.*, **27**, 1167 (1962).

9) Y. G. Orlik, P. N. Gaponik, A. I. Lesnikovich, and A. I. Vrublevskii, *Zh. Obshch. Khim.*, **48**, 1601 (1978).

10) W. W. Wendlant and T.D. George, *J. Inorg. Nucl. Chem.*, **21**, 69 (1961).

 © 1983 The Chemical Society of Japan Bull. Chem. Soc. Jpn., 56, 2941—2944 (1983)

Particle Size of Nickel in Nickel-Alumina Catalysts and Its Effects on Propene Hydrogenation

Yoriko TAKAI, Akifumi UENO,* and Yoshihide KOTERA
Department of Materials Science, Toyohashi University of Technology, Tempaku-cho, Toyohashi 440
(Received November 30, 1982)

The particle size of nickel in Ni/Al_2O_3 catalysts prepared by the alkoxide technique is well controlled by changing the metal concentration in the catalyst. The rate of propene hydrogenation over the catalyst increases with decrease in Ni particle size, and this phenomenon is explained on the assumption that nickel atoms located on edges and/or corners of crystallites may contribute predominantly to the hydrogenation of propene.

The relation between dispersion states and catalytic behavior of a metal has been of current interest in the field of catalysis, since it was reported that physical properties of a fine metal particle should be different from those of bulk metal when the particle size is smaller than 100 Å.[1] Boudart[2] proposed that there are two types of catalytic reactions, each called the structure sensitive reaction and the structure insensitive reaction. The hydrogenation of ethylene, cyclopropane, or benzene on Pt/Al_2O_3 is considered to be structure insensitive,[3] while the hydrocracking, isomerization, and dehydrocyclization of 2-methylpentane are likely to be structure sensitive.[4] For a structure sensitive reaction, Brunelle *et al.*[5] tried to explain the effect of metal particle size on reaction selectivity by assuming a simple geometrical arrangement of metal atoms exposed on the surface of crystallite. Otero-Schipper *et al.*[6] also applied the idea to the hydrogenation of propene or butadiene on Pt/Al_2O_3 catalyst. The idea of simple geometrical arrangement was first proposed by van Hardeveld and van Montfoort[7] and developed by Anderson.[8] On the contrary, Primet *et al.*[9] studied the influence of metal particle size on chemisorption properties of supported platinum by means of infrared spectroscopy. They discussed size effects on the basis of an idea that electronic properties of a metal would change with its particle size when it is less than 100 Å.

In the present work the hydrogenation of propene was studied on Ni/Al_2O_3 catalysts prepared by the alkoxide technique.[10] The nickel metal particle size was well controlled by adjusting the metal concentration in the catalyst. The rate of hydrogenation increased with decrease in the metal particle size and this was interpreted by an assumption that the reaction would take place preferentially on nickel atoms located on edges and/or corners of crystallites.

Experimental

Catalyst Preparation. The catalyst employed was Ni/Al_2O_3 prepared by hydrolysis of a mixed solution of aluminium isopropoxide dissolved in butyl alcohol and nickel nitrate dissolved in ethylene glycolate: The nickel nitrate was heated at 90 °C to remove water *via* $Ni(NO_3)_2 \cdot 6H_2O \longrightarrow Ni(NO_3)_2 \cdot H_2O$, and the butyl alcohol and ethylene glycolate were distilled before use; about 5.0 g of nickel nitrate was dissolved in ethylene glycolate at 80 °C. Depending upon the concentration of nickel in the designed catalyst, the corresponding amount of this solution was poured into the aluminium isopropoxide dissolved in butyl alcohol and stirred at 80 °C in an N_2 atmosphere. Water was then added to the mixed solution. The volume of water added was about 4 times the volume of aluminium isopropoxide employed. The solution was stirred at 80 °C for 4 h and then cooled to room temperature without stirring. A gel was obtained, filtered, and dried at 110 °C in an oven. The powder thus obtained was calcined at 500 °C for 4 h in air and then reduced with hydrogen at 500 °C for 4 h. The loading of Ni ions on the catalyst could be controlled by varying the concentration of nickel nitrate in the mixed solution employed. The Ni ions in the catalyst were extracted by heating the catalyst in an aqueous solution of nitric acid and the concentration of nickel ions was determined with a X-ray fluorescence spectrometer. In the present experiment the concentrations of nickel in the catalysts prepared were 0.39, 0.78, 3.96, and 13.9 wt%.

Measurement of Particle Size of Nickel Metal by Transmission Electron Micrography. The particle size of Ni in the catalyst was measured with a transmission electron microscope (TEM) operated at an accelerating voltage of 75 kV (Hitachi, H-300). The sample was first ground in an agate mortar and then suspended in water or ethyl alcohol by using supersonic waves. Some of the finest parts of the suspension was pipetted onto a microgrid covered with collodion film (400 mesh, Nisshin Film Co.). Micrographs were obtained with an instrumental magnification of $\times 50000$ and enlarged with $\times 2$ for print.

Measurement of Mean Particle Size by Hydrogen Chemisorption. After the reduction of catalyst samples at 500 °C, they were evacuated at the same temperature for 3 h and cooled to room temperature to be sebjected to hydrogen chemisorption measurement. The measurement was carried out by using an absolute pressure gauge (MKS Baratoron type 222B) in the hydrogen pressure range 5—50 mmHg (1 mmHg = 133.322 Pa) as registered at adsorption equilibrium. The volume adsorbed was determined by extrapolating the linear part of the isotherm to zero pressure as proposed by Hall and Wilson.[11] The specific surface area of Ni in the catalyst was estimated on the assumption that a nickel atom will occupy an area of 6.8 Å^2 [12] and the mean particle size was calculated by

$$d = 5/\rho S,$$

where ρ is the density of nickel metal and S is the specific surface area of nickel particle in the catalyst. In this calculation nickel particles were assumed to be in the f.c.c. packing.

Magnetic Measurement of Nickel Reduced to Metal. In order to obtain the specific surface area of nickel in a catalyst, the fraction of nickel reduced to metel should be estimated, because hydrogen adsorbs on metallic nickel but not on Ni cations in the catalyst. After the reduction of catalyst samples, they were loaded on a vibrating sample magnetometer (Toei Kogyo Co., Model VSM-2) at a vibration frequency of 80 kHz with a magnetic field strength up to 10 kOe†. The

† 1 Oe = $(1000/4\pi)$A m^{-1}.

Table 1. Measurement of saturation magnetization of catalysts and the fractions reduced to metal

Ni Concentration/wt%	Reduction temperature/°C	Time/h	Saturation magnetization[a)] of Ni in catalyst /emu cm^3 g^{-1}	Fraction of Ni metal/%
0.39	500	2	0.0671	23.6
0.78	500	2	0.1000	31.7
3.96	500	2	0.6850	31.9
3.96	500	4	0.7250	33.7
3.96	700	4	1.250	58.2
13.9	500	2	2.370	31.4

a) Saturation magnetization of Ni: 54.39 emu cm^3 g^{-1}.

magnetization was measured at room temperature. One problem in the measurement was the exposure of the reduced catalyst to air a few minutes while being packed into the sample holder.

Particle Size Effects on Reaction Rate. As a model reaction the hydrogenation of propene was selected since Ni catalysts are often employed for the hydrogenation of olefinic hydrocarbons. The reaction was carried out at 50 °C with a closed circulating reactor, made of glass, containing about 0.5 g of catalyst. Feed gases were usually composed of propene and hydrogen each of 20 cmHg pressure. Gas products were analyzed with a gas chromatograph equiped with columns packed with molecular sieves 13X and Polapak Q. The rate of propene hydrogenation was calculated from the amount of propane produced during the initial 5 min of reaction.

Results

Particle Size of Nickel Measured by TEM and H_2 Chemisorption. Typical photographs obtained by TEM are shown in Fig. 1 for the 0.78, 3.96, and 13.9 wt% Ni/Al_2O_3 catalysts. The particle size distributions were obtained by measuring 500—1000 particles in the photographs. Unfortunately, no qualified photographs were obtained for the 0.39 wt% Ni/Al_2O_3 catalyst so as to allow the determination of particle size distribution. It must be mentioned that small nickel particles often coagulated with each other when irradiated by an electron beam from the microscope.

The mean particle size obtained by hydrogen chemisorption measurements is given in Fig. 3. The mean particle size increases with increase in the concentration of nickel in the catalyst. To obtain the mean particle size, the specific surface area of Ni was calculated by

$$S/\text{Å} = 13.6\, VN_AR^{-1},$$

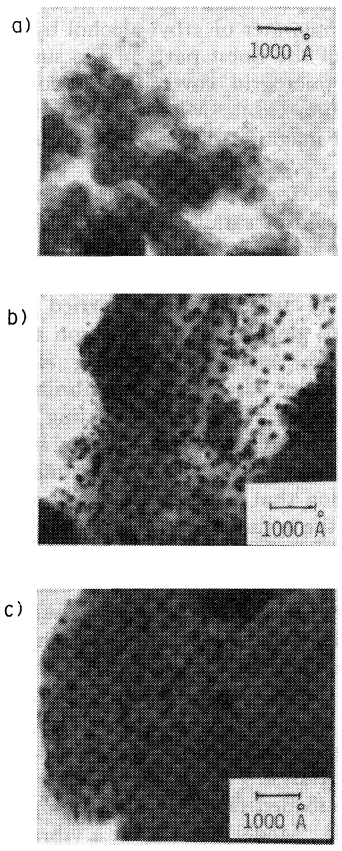

Fig. 1. Transmission electron micrographs ($\times 10^5$).
a): 0.78 wt% Ni/Al_2O_3, b) 3.96 wt% Ni/Al_2O_3, c): 13.9 wt% Ni/Al_2O_3.

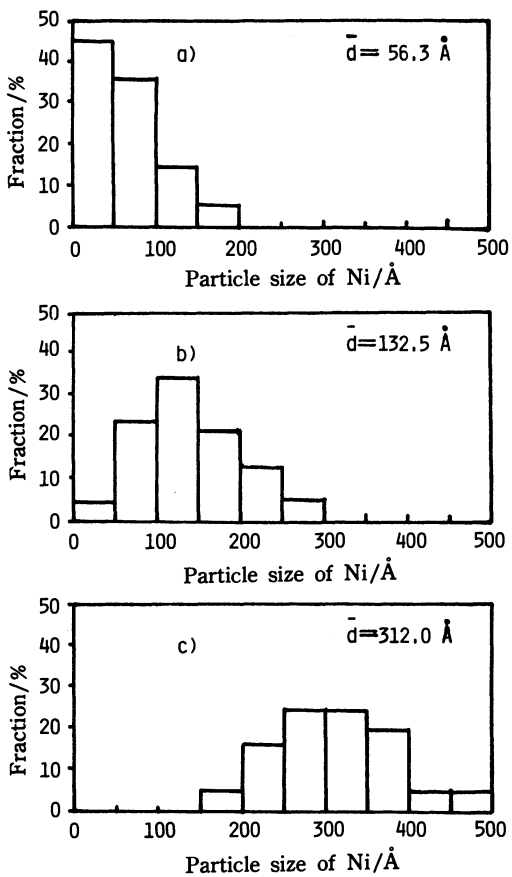

Fig. 2. Particle size distribution of Ni in Ni/Al_2O_3 catalyst.
a): 0.78% Ni/Al_2O_3, b): 3.96% Ni/Al_2O_3, c): 13.9% Ni/Al_2O_3.

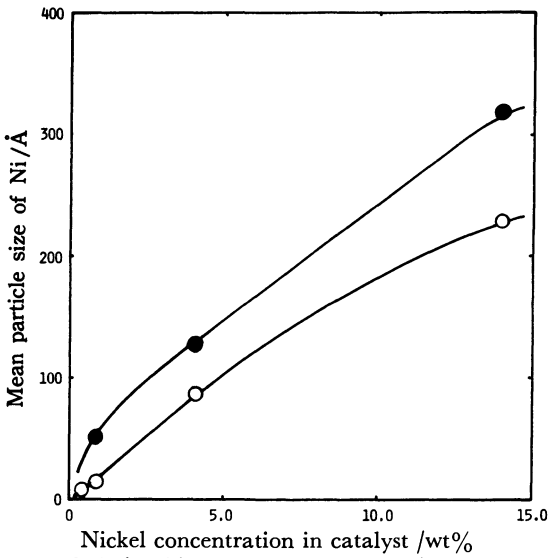

Fig. 3. Relationship between mean particle size of Ni and nickel concentration in Ni/Al_2O_3 catalyst.
—○—: Calculated from hydrogen chemisorption,
—●—: measured by transmission electron micrograph.

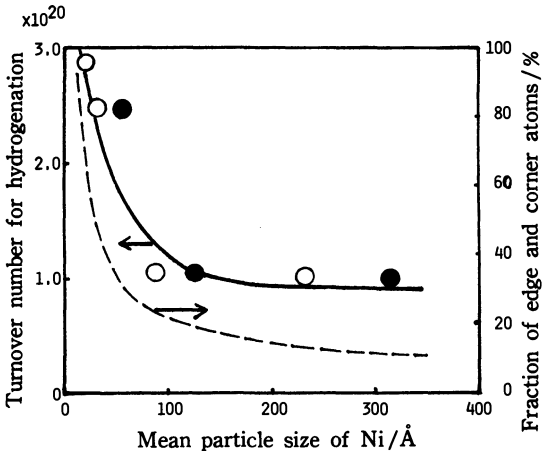

Fig. 4. Effects of particle size upon catalytic activity and fraction of atoms located on edges and corners of nickel crystallites assumed to be f.c.c.
—○—: Particle size calculated by H_2 chemisorption,
—●—: particle size measured by TEM.

where V is the mole of hydrogen adsorbed on the unit mass of Ni, N_A is Avogadro's number, and R is the fraction of nickel reduced to metal. For catalysts prepared by the usual impregnation method the fraction of metal reduced is almost 1.0, while for the present catalysts it was as low as 0.3 (Table 1).

Magnetic Measurements. Measurements were made for the saturated magnetization of Ni with catalysts reduced by hydrogen at 500 and/or 700 °C (Table 1). Since the saturated magnetization of Ni is 34.59 emu $cm^3\ g^{-1}$,[13] the fraction of nickel reduced to metal was calculated from the magnetization observed, the results being given in Table 1.

Effects of Ni Particle Size on the Rate of Propene Hydrogenation. The rate obtained for the initial 5 min of reaction was expressed in terms of (the number of the molecules of propane formed per min)/(the number of the nickel atoms exposed on the surface), which is the so-called turnover number. In Fig. 4, the turnover number increased with decrease in the particle size when the size was less than 50 Å, indicating that a size effect is involved in the propene hydrogenation on Ni/Al_2O_3 catalyst.

Discussion

The most important factor for studying effects of particle size on catalytic activity is that the catalyst should be free from any impurities which will affect the activity. In the present work, the catalyst was prepared by the alkoxide technique, because one of the best methods of obtaining a pure metal oxide is hydrolysis of its alkoxide in a proper solvent. It has been reported that most metals form their alkoxides by the reaction between metal chloride and sodium alkoxide in the presence of an excess of alcohol and a hydrocarbon solvent.[14] The elimination of the chlorine and sodium ions from alkoxides thus prepared is difficult. It was reported that a well dispersed Ni/Al_2O_3 catalyst was prepared by using a mixture of aluminium *s*-butylate and nickel acetate.[15]

A highly dispersed Ni/SiO_2 was prepared[10] by hydrolysis of a mixture of nickel nitrate dissolved in ethylene glycolate and ethyl silicate. In this work aluminium isopropoxide dissolved in butyl alcohol was employed in place of ethyl silicate in hope of formation of the Ni–O–Al structure in the catalyst since the Ni–O–Si structure was observed by infrared spectroscopy in Ni/SiO_2 catalyst as mentioned in the previous paper.[10] Although the Ni–O–Al structure was not identified here by infrared spectroscopy, we believe the formation of the structure in the catalyst thus prepared. This will be discussed later.

Homogeneous dispersion of metal particles is also important to investigate the relation between particle size and activity. The particle size of Ni in the catalyst thus prepared was measured by use of hydrogen chemisorption, leading to a conclusion that the mean particle size is well controllable by varying the concentration of Ni in the catalyst. At a glance over the photographs shown in Fig. 1, it is clear that the size of the Ni particles are almost the same with each other. The size distribution of nickel shown in Fig. 2 also indicates that the nickel particles are controlled so as to be in an even size level, although the mean particle sizes calculated from the results by TEM are larger than those obtained by hydrogen chemisorption. The particles of Ni in the 0.39 wt% Ni/Al_2O_3 catalyst may be too small to be observed by TEM.

The nickel ions in the catalyst prepared by the usual impregnation method are ready to be reduced by hydrogen at 500 °C, while the nickel ions in the present catalyst prepared by the alkoxide technique are hard to be reduced under the same conditions. The fraction of the nickel reduced to metal was determined by measuring the saturation magnetization of Ni in the catalyst. The magnetization would be affected by the nickel particle size,[16] but this effect was ignored here in

calculating the fraction of nickel reduced. The low fraction of nickel metal in the present catalyst suggests that the nickel cations in the catalyst are strongly bound to the Al_2O_3 support. This interaction is due to formation of the Ni–O–Al structure possibly *via* the reaction between cyclic glycolate of nickel and aluminium isopropoxide

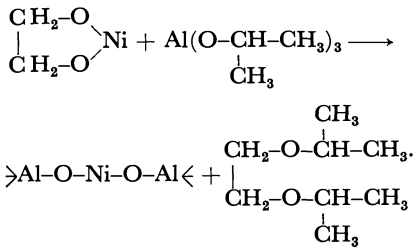

In this sense, Ni atoms may be atomically dispersed in the bulk of alumina and hence they are hardly reduced by hydrogen. The fraction of Ni reduced to metal increased gradually with increase in the reduction temperature (see Table 1).

Thus, it was confirmed that the particle size can be controlled by the concentration of Ni in the catalyst and that the particles are well dispersed in an even size level, when the catalyst is prepared by the alkoxide technique. Accordingly, a discussion on the relation between particle size and catalytic activity will be available. The hydrogenation of propene was employed as a model reaction since Ni catalysts are often used for hydrogenation processes. It is well known that catalytic hydrogenation of an olefin accompanies hydrocracking at higher temperatures, so the reaction was carried out at 50 °C where no hydrocracking takes place. The amount of propane formed is in a linear relation with reaction time during the initial 5 or 10 min of reaction. The rate of hydrogenation was estimated from the slope for the initial 5 min. The relation between the catalyst is shown in Fig. 4. It was found that the rate significantly increased when the particle size became smaller than 50 Å. Schwab[17] proposed that catalytic reactions might be divided into two groups; one consists of donor reactions in which the rate determining step involves an electron transfer from the reactant molecule to the catalyst and the other consists of acceptor reactions where the reactant must accept an electron from the catalyst. Hydrogenation belongs to the group of donor reactions so that an electron transfers to the catalyst from the reactant. Since it was reported that electrons in a metal particle will move to the carrier when the particle size is so small,[18] the observation is understandable that the rate of hydrogenation was enhanced when the size of nickel particle was less than 50 Å. Three kinds of nickel atoms may be considered to exist on the surface of particles; one is a nickel atom located on the surface plane of a crystallite and the other two are those on the edge and corner of a crystallite, respectively. The fraction of the atoms located on edges and corners of crystallites is a function of the dimension of the crystallite and the fraction is shown in Fig. 4 on an assumption that the Ni particles are f.c.c. crystallites.[7,8] The turnover number for nickel atom for the hydrogenation is also plotted against particle size in Fig. 4. Both the curves are similar to each other, suggesting that the hydrogenation might taken place over the nickel atoms located on edges and corners of crystallites. There will be a question why the atoms on edges and corners are more active for the hydrogenation. Mott and Davis[19] describe that atoms on edges and corners have two and three dangling bonds, respectively, whereas those located on surface planes have one such bond, and that the total energies (electron plus lattice) of a crystallite are lowered by the interaction of these dangling bonds: $2D^0 \rightarrow D^+ + D^-$, where D^0 is a dangling bond unperturbed, D^+ is a dangling bond from which an electron is released, and D^- is a dangling bond to which an electron has moved. In the present nickel particles, it might be possible that electrons in the dangling bonds of nickel atoms at the edges and corners will transfer to the dangling bonds of the nickel atoms located on surface planes. This will result in an enhancement of the positive character of nickel atoms located on edges and corners, hence the activity for olefin hydrogenation will also be enhanced.

The present authors would like to express their thanks to Drs. J. Tasaki, Y. Murase, and T. Mori at the Japanese Government Industrial Research Institute, Nagoya for the measurement of saturation magnetization and transmission electron micrograph.

References

1) R. Kubo, *J. Phys. Soc. Jpn.*, **17**, 975 (1962).
2) M. Boudart, *Adv. Catal.*, **20**, 153 (1960).
3) M. Boudart, *Proc. 6th Int. Congr. Catal.*, p. 1 (1976).
4) J. M. Dartigues, A. Chmbellan, and F. G. Gault, *J. Am. Chem. Soc.*, **98**, 856 (1976).
5) J. P. Brunelle, A. Sugier, and J. F. LePage, *J. Catal.*, **43**, 273 (1976).
6) P. H. Otero-Schipper, W. A. Wachter, J. B. Butt, R. L. Burwell, and J. B. Cohen, *J. Catal.*, **50**, 494 (1977).
7) R. van Hardeveld and A. van Montfoort, *Sur. Sci.*, **4**, 396 (1964).
8) J. R. Anderson, "Structure of Metallic Catalyst," Academic Press, New York (1975).
9) M. Primet, J. M. Basset, E. Garbowski, and M. V. Mathieu, *J. Am. Chem. Soc.*, **97**, 3655 (1975).
10) A. Ueno, H. Suzuki, and Y. Kotera, *J. Chem. Soc., Faraday Trans. 1*, **79**, 127 (1983); H. Suzuki, S. Takasaki, F. Koga, A. Ueno, and Y. Kotera, *Chem. Lett.*, **1982**, 127.
11) G. R. Wilson and W. K. Hall, *J. Catal.*, **17**, 190 (1970); E. Kikuchi, K. Ito, T. Ino, and Y. Morita, *J. Catal.*, **46**, 382 (1977).
12) D. G. Mustard, and C. H. Bartholomew, *J. Catal.*, **67**, 186 (1981).
13) "Kagaku Binran (Kiso-hen II)," ed by the Chemical Society of Japan, Maruzen, Tokyo (1975), p. 1233.
14) D. Bradley, R. Mehrotra, and D. Gauer, "Metal Alkoxides," Academic Press, New York (1978).
15) M. Astier, A. Bertrand, D. Bianchi, A. Chenard, G. E. E. Gardes, G. Pajonk, M. B. Taghavi, S. J. Teichner, and B. L. Villemin, "Preparation of Catalyst," ed by B. Delmon, P. A. Jacobs, and G. Poncelot, Elsevier, Brussels (1976), p. 315.
16) P. W. Selwood, *J. Phys. Chem.*, **70**, 3003 (1966).
17) G. M. Schwab, *Adv. Catal.*, **27**, 1 (1978).
18) K. Forger and J. R. Anderson, *J. Catal.*, **54**, 318 (1978).
19) N. F. Mott and E. A. Davis, "Electronic Process in Noncrystalline Materials," Clarendon Press, Oxford (1979), p. 465.

The Preparation and X-Ray Structures of Di-μ-sulfido- and μ-Oxo-μ-sulfido-bis[tris(isothiocyanato)oxomolybdate(V)] Ions

Takashi SHIBAHARA, Hisao KUROYA, Keiji MATSUMOTO,*,† and Shun'ichiro OOI†

Department of Chemistry, Okayama University of Science, Ridai-cho 1-1, Okayama 700

†*Department of Chemistry, Faculty of Science, Osaka City University, Sumiyoshi-ku, Osaka 558*

(Received March 3, 1983)

The crystal structures of $(pyH)_4[Mo_2O_2S_2(NCS)_6]$ (**1**) (pyH=pyridinium ion) and $(pyH)_4[Mo_2O_3S(NCS)_6]\cdot 2H_2O$ (**2**) have been determined from the diffractometer data. The **1** and **2** structures were refined by the least-squares method to R 0.041 and 0.064 for 2728 and 2349 non-zero reflections respectively. The two structures are isomorphous. Each Mo(V) ion has a distorted octahedral coordination, and two coordination octahedra share a common edge to form a binuclear complex. The binuclear complex contains a mirror plane through two bridging atoms. The two terminal oxo ligands on each Mo(V) are *cis* to each other and *cis* to the bridging oxo or sulfido. The Mo–N(NCS) bond length *trans* to the Mo–O_t (terminal oxo) is *ca.* 0.1 Å longer than the other Mo–N(NCS) bond lengths, showing the large *trans* effect of the O_t ligand.

Although the preparation and X-ray structure of the $(pyH)_4[Mo_2O_4(NCS)_6]\cdot H_2O$ complex with the di-μ-oxo bridge have been reported,[1] no similar complex containing the di-μ-sulfido or μ-oxo-μ-sulfido bridge has yet been prepared. In this paper, we wish to describe the preparation and structures of $(pyH)_4[Mo_2O_2S_2(NCS)_6]$ (**1**) and $(pyH)_4[Mo_2O_3S(NCS)_6]\cdot 2H_2O$ (**2**) and to compare the structures of the two complexes with that of $(pyH)_4[Mo_2O_4(NCS)_6]\cdot H_2O$[1] in connection with the *trans* bond-weekening effects of the terminal oxo, bridging oxo, and bridging sulfido.

Experimental

Preparation of 1 and 2. Complex **1** was prepared by the addition of sodium thiocyanate about six times the molar quantity of the aqua-ion $[Mo_2O_2S_2(H_2O)_6]^{2+}$ in 1 mol dm^{-3} of HCl,[2] followed by the drop-by-drop addition of pyridine (*ca.* one thirtieth of the volume of the aqua-ion solution). After the solution had stood in a refrigerator a couple of days, the red crystals which had deposited were filtered by suction and air-dried. Yield, 85%. Found: N, 14.67; C, 32.51; H, 2.53%. Calcd for $(pyH)_4[Mo_2O_2S_2(NCS)_6]$: N, 14.64; C, 32.64; H, 2.53%.

Complex **2** was prepared similarly by the use of the aqua ion $[Mo_2O_3S(H_2O)_6]^{2+}$ in 1 mol dm^{-3} HCl[3] instead of the $[Mo_2O_2S_2(H_2O)_6]^{2+}$ used for the preparation of **1**. Yield, 70%. Found: N, 14.87; C, 33.29; H, 2.50%. Calcd for $(pyH)_4[Mo_2O_3S(NCS)_6]\cdot 2H_2O$: N, 14.34; C, 31.97; H, 2.89%.

X-Ray-data Collection. Complex **1** crystallizes in the form of red square-prisms. The crystal of **2** is thin red plate. The **1** and **2** crystals were mounted in an arbitrary orientation on a Philips PW1100 automated diffractometer. The PW1100 programs obtained 17 centered reflections for **1** and 15 for **2**, and an orientation matrix for each crystal, and then identified the monoclinic cells for the two crystals. The $P2_1/m$ space group for **1** and **2** was assumed throughout the structure analyses and was confirmed by the successful refinement of the structures. The unit-cell dimensions were refined by the least-squares analyses of the θ values of 36 reflections for **1** and of 38 for **2**. The crystal data and experimental details for **1** and **2** are given in Table 1. The intensity data were collected by the use of Mo $K\alpha$ radiation. During the data collection, three standard reflections were monitored every 4 h to check the stability and orientation of each crystal. Both compounds remained quite stable. Each data set was corrected for Lorenz-polarization effects,[4] but not for absorption.

Structure Solution and Refinement. The structure of **1** was first solved by the Patterson-Fourier method. The structure solution of **2** was straightforward because the **1** and **2** structures are isomorphous. The refinement of the structures was carried out by the use of the block-diagonal least-squares method. The function minimized was $\sum w(F_o-|F_c|)^2$, where $w=1/\sigma^2(F_o)$ was used. The neutral atomic scattering factors for the Mo, S, O, N, and C atoms were taken from Ref. 5, with an anomalous dispersion corrections ($\Delta f'$) for the Mo and S atoms. The final R values were 0.041 for **1** and 0.064 for **2**. No attempt was made to locate hydrogen atoms. The N atom of the pyridinium ion could not be identified in either crystal. The positions of the N atoms were detemined on the basis of short contact distances (Table 4), because the N–H group of the pyridinium ion is expected to form a hydrogen bond. No chemically significant peaks were observed on the final difference Fourier maps for **1** and **2**. The maximum peaks were 0.6 e Å^{-3} for **1** and 0.6 e Å^{-3} for **2**. No water of crystallization was found in **1**. The F_o-F_c tables for **1** and **2** and the anisotropic temperature factors are preserved by the Chemical Society of Japan (Document No. 8340). The final atomic coordinates are given in Tables 2 and 3. The figures were drawn by the use of ORTEP.[6] The computations were performed by the use of a FACOM 230-60 computer at Osaka City University and an ACOS-900 computer at the Crystallographic Research Center, Institute for Protein Research, Osaka University, using Programs in the UNICS.[7]

Results and Discussion

Perspective views of the complex ions in **1** and **2** are given in Figs. 1 and 2. Each complex contains a crystallographic mirror plane through the two bridging atoms. Therefore, both complexes have the *cis*-dioxo structure. Each structure consists of two distorted octahedra sharing as SS or OS edge. The geometries and dimensions of $Mo_2O_2S_2$ and Mo_2O_3S cores do not significantly differ from those of the corresponding cores in the other binuclear Mo(V) complexes. The deviation of the Mo atom from the mean plane defined by the S_2N_2 plane to O1 is 0.28 Å in **1**, while that from the OSN_2 plane to O1 is 0.28 Å in **2**. The bond distances and angles are listed in Table 4, while important interatomic distances and dihedral angles are compared in Table 5. The Mo–Mo and O1–O1 distances are larger in **1** than in **2**, in

TABLE 1. SUMMARY OF CRYSTAL DATA AND EXPERIMENTAL DETAILS

Compound	**1** $(pyH)_4[Mo_2O_2S_2(NCS)_6]$	**2** $(pyH)_4[Mo_2O_3S(NCS)_6]\cdot 2H_2O$
Crystal system	Monoclinic	Monoclinic
Space group	$P2_1/m$	$P2_1/m$
a/Å	15.669 (5)	15.898 (9)
b/Å	13.107 (4)	13.207 (4)
c/Å	9.173 (3)	9.085 (4)
β/°	96.77 (3)	94.04 (4)
$F(000)$	996	980
F.W.	993.0	976.9
U/Å^3	1870.8 (10)	1902.7 (15)
Z	2	2
D_m/g cm^{-3}	1.74	1.68
D_c/g cm^{-3}	1.76	1.70
μ(Mo $K\alpha$)/cm^{-1}	11.4	10.7
Crystal size/mm^3	0.08×0.08×0.13	0.04×0.08×0.14
Scan type	ω	ω
Scan speed/° s^{-1}	0.033	0.033
Scan range/°	0.9	1.0
$2\theta_{max}$/°	50	50
Background measurement	Half of the scan time	Half of the scan time
Number of unique reflections with $F_o^2 \geqq 3\sigma(F_o^2)$	2728	2349
$R(R')$	0.041 (0.060)	0.064 (0.085)

TABLE 2. ATOMIC COORDINATES (×10^5 FOR Mo AND ×10^4 FOR OTHERS) AND TEMPERATURE FACTORS (×10^4 FOR Mo AND ×10^3 FOR OTHERS) FOR **1** $(pyH)_4[Mo_2O_2S_2(NCS)_6]$, WITH THEIR ESTIMATED STANDARD DEVIATIONS IN PARENTHESES

Atom	x	y	z	U_{eq}/Å^2 a)
Mo	18082 (3)	35785 (5)	3970 (5)	427
S1	3411 (2)	5890 (2)	3932 (3)	92
S2	848 (2)	5915 (3)	−3625 (3)	112
S3	4557 (2)	4035 (2)	−1945 (2)	70
S4	1319 (2)	2500	−1516 (2)	44
S5	2643 (2)	2500	1948 (2)	48
O1	929 (3)	3747 (4)	1260 (5)	58
N1	2457 (4)	4788 (5)	1724 (6)	63
N2	1400 (4)	4796 (5)	−1154 (6)	63
N3	3003 (4)	3851 (5)	−725 (6)	57
C1	2852 (4)	5229 (5)	2668 (7)	53
C2	1166 (4)	5247 (5)	−2192 (7)	55
C3	3636 (4)	3943 (5)	−1240 (6)	49
NA1	1108 (6)	2500	4380 (9)	96
CA2	1479 (6)	1603 (6)	4714 (8)	75
CA3	2299 (6)	1603 (6)	5479 (7)	81
CA4	2710 (7)	2500	5846 (10)	68
NB1	9335 (7)	2500	9750 (11)	146
CB2	9242 (7)	1614 (8)	9021 (13)	130
CB3	8959 (7)	1657 (9)	7402 (13)	129
CB4	8863 (9)	2500	6836 (15)	111
NC1	4732 (5)	2500	1428 (10)	72
CC2	4741 (4)	1609 (5)	2167 (8)	60
CC3	4756 (5)	1592 (6)	3617 (9)	68
CC4	4771 (6)	2500	4402 (11)	70
ND1	7000 (7)	2500	2766 (13)	103
CD2	6952 (6)	1593 (6)	2026 (11)	88
CD3	6860 (6)	1584 (8)	520 (9)	96
CD4	6774 (8)	2500	−236 (12)	114

a) $U_{eq} = (U_{11}+U_{22}+U_{33})/3$.

TABLE 3. ATOMIC COORDINATES (×10^5 FOR Mo AND ×10^4 FOR OTHERS) AND TEMPERATURE FACTORS (×10^4 FOR Mo AND ×10^3 FOR OTHERS) FOR **2** $(pyH)_4[Mo_2O_3S(NCS)_6]\cdot 2H_2O$, WITH THEIR ESTIMATED STANDARD DEVIATIONS IN PARENTHESES

Atom	x	y	z	U_{eq}/Å^2 a)
Mo	17567 (6)	35176 (7)	2266 (8)	480
S1	3264 (3)	5870 (4)	3701 (5)	120
S2	837 (4)	5843 (5)	−3682 (6)	157
S3	4492 (2)	4074 (3)	−2173 (5)	90
S4	1294 (3)	2500	−1732 (4)	51
O2	2391 (6)	2500	1397 (9)	54
O1	895 (5)	3687 (6)	1145 (7)	63
N1	2416 (6)	4630 (7)	1644 (10)	69
N2	1422 (6)	4766 (7)	−1246 (9)	66
N3	2984 (6)	3752 (7)	−863 (9)	63
C1	2771 (7)	5156 (9)	2487 (12)	67
C2	1196 (7)	5241 (9)	−2217 (11)	62
C3	3605 (7)	3890 (8)	−1373 (10)	57
NA1	1165 (10)	2500	4271 (14)	103
CA2	1562 (10)	1609 (10)	4586 (12)	93
CA3	2386 (10)	1625 (11)	5241 (12)	98
CA4	2794 (13)	2500	5558 (17)	90
NB1	9319 (10)	2500	9760 (15)	153
CB2	9238 (10)	1592 (13)	9007 (19)	133
CB3	9010 (10)	1594 (13)	7589 (18)	123
CB4	8826 (14)	2500	6943 (23)	126
NC1	3994 (11)	2500	2236 (17)	93
CC2	4301 (10)	1702 (12)	2634 (16)	117
CC3	4968 (10)	1599 (9)	3701 (17)	104
CC4	5313 (15)	2500	4220 (23)	113
ND1	5962 (11)	2500	−201 (18)	107
CD2	6275 (11)	1600 (12)	285 (22)	131
CD3	6933 (10)	1619 (13)	1384 (27)	150
CD4	7252 (15)	2500	1858 (34)	142
OW	9026 (8)	1291 (10)	3301 (13)	146

a) $U_{eq} = (U_{11}+U_{22}+U_{33})/3$.

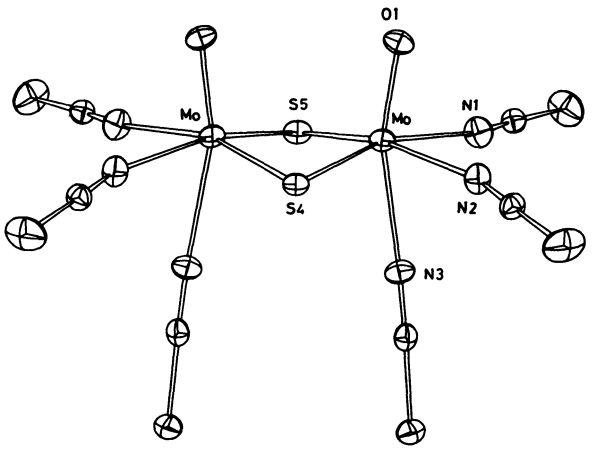

Fig. 1. A perspective view of $[Mo_2O_2S_2(NCS)_6]^{4-}$. The thermal ellipsoid was drawn at the 40% probability level.

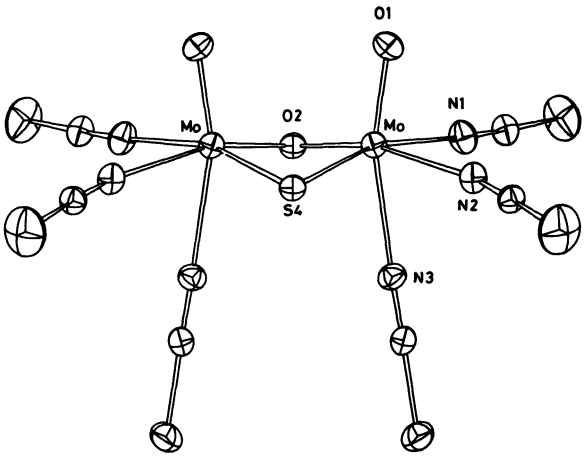

Fig. 2. A perspective view of $[Mo_2O_3S(NCS)_6]^{4-}$.

accordance with the larger size of the sulfur compared to that of the oxygen in the bridge. On the other hand, the S_b–Mo–O1 (S_b: bridging sulfido) and O_b–Mo–O1 (O_b : bridging oxo) angles in the cores in **1** and **2** have similar values. The angle between the two MoS_2 planes in **1** is very close to that between the two MoOS planes in **2**. The MoS_2–MoS_2 dihedral angle of 153.4° and the MoOS–MoOS dihedral angle of 153.8° are similar to those in $Ba[Mo_2O_4(ox)_2(H_2O)_2]\cdot 10H_2O$[8] and $Cs_2[Mo_2O_2S_2(ox)_2(H_2O)_2]\cdot 2H_2O$,[9] but smaller than those in $K_6[\{Mo_2O_3S(ox)_2\}_2(ox)]\cdot 10H_2O$[3] and $K_6[\{Mo_2O_4(mal)_2\}_2(mal)]\cdot 4H_2O$.[10] The Mo–O1 distance in **1** is 1.683 Å and that in **2**, 1.669 Å. These values are in agreement with those previously reported.[11] The Mo–S (bridging sulfido) distances in **1** and **2** range from 2.301 to 2.313 Å, and the Mo–O (bridging oxo) distance in **2** is 1.950 Å. The S–Mo–S, O–Mo–S, Mo–S–Mo, and Mo–O–Mo angles in the bridges agree well with those in $Na_2[Mo_2S_2O_2(R\text{-pdta})]\cdot 4H_2O$,[12] and $Na_2[Mo_2O_3S(R\text{-pdta})]\cdot 4H_2O$.[12] The bond lengths and angles for the $Mo_2S_2O_2$ core in **1** are similar to those in $Na_2[Mo_2O_2S_2(R\text{-pdta})]\cdot 4H_2O$, and the bond lengths and angles for the Mo_2O_3S core in **2** are similar to those in $Na_2[Mo_2O_3S(R\text{-pdta})]\cdot 4H_2O$. The large trans effect of terminal oxo (O_t=O1) was observed in these cases,

Table 4. Interatomic distances and angles, with their estimated standard deviations in parentheses

Bond length	l/Å		Bond angle	ϕ/°	
	1	2		1	2
Mo–O1	1.683(6)	1.669(6)	S4–Mo–S5	101.95(8)	
Mo–S4	2.313(2)	2.308(4)	S4–Mo–O2		98.3(3)
Mo–S5	2.301(2)		Mo–S4–Mo	75.36(7)	71.2(2)
Mo–O2		1.950(9)	Mo–S5–Mo	75.81(7)	
Mo–N1	2.176(6)	2.17(2)	Mo–O2–Mo		87.1(4)
Mo–N2	2.183(6)	2.17(3)	S5–Mo–O1	103.1(2)	
Mo–N3	2.269(6)	2.27(2)	S4–Mo–O1	102.8(2)	103.6(3)
N1–C1	1.16(1)	1.15(3)	O2–Mo–O1		103.4(4)
N2–C2	1.14(1)	1.12(4)	N1–Mo–O1	89.7(3)	89.5(5)
N3–C3	1.15(1)	1.13(2)	N2–Mo–O1	91.0(3)	91.8(7)
C1–S1	1.620(7)	1.61(3)	N3–Mo–O1	163.4(3)	163.9(5)
C2–S2	1.609(7)	1.62(4)	Mo–N1–C1	162.8(6)	174(2)
C3–S3	1.655(7)	1.65(3)	Mo–N2–C2	163.9(6)	164(3)
Mo–Mo	2.827(2)	2.688(2)	Mo–N3–C3	175.7(6)	178(1)
O1···O1	3.269(9)	3.14(2)	N1–C1–S1	177.2(7)	178(2)
N3···N3	3.54(2)	3.31(4)	N2–C2–S2	178.0(7)	175(3)
Short contact			N3–C3–S3	177.9(6)	178(2)
NA1···S2(I)[a]	3.699(9)				
NA1···O1(II)	3.28(1)	3.25(2)			
NB1···O1(III)	3.16(2)	3.14(2)			
NC1···S5(II)	3.363(9)				
NC1···O2(II)		2.61(2)			
ND1···S3(II)		3.52(2)			

a) Roman numerals refer to the following equivalent positions: (I) $-x$, $-1/2+y$, $-z$; (II) x, $1/2-y$, z; (III) $1+x$, $1/2-y$, $1+z$.

TABLE 5. COMPARISON OF THE INTERATOMIC DISTANCES[a] AND DIHEDRAL ANGLES

	l/Å								ϕ/° D[e]
	Mo–O_t	Mo–O_b	Mo–S_b	Mo–N[b]	Mo–N[c]	Mo–N[d]	Mo–Mo	$O_t\cdots O_t$	
1	1.683 (6)		2.301 (2)	2.269 (6)	2.176 (6)		2.827 (2)	3.269 (9)	153.4
			2.313 (2)		2.183 (6)				
2	1.669 (6)	1.950 (9)	2.308 (4)	2.27 (2)	2.17 (2)	2.17 (3)	2.688 (2)	3.14 (2)	153.8
3[f]	1.645 (5)	1.954 (3)		2.251 (7)		2.142 (4)	2.581 (1)		

a) O_t: Terminal oxo; O_b: bridging oxo; S_b: bridging sulfido, b) *trans* to O_t, c) *trans* to S_b, d) *trans* to O_b, e) Dihedral angle between the two MoS_2 or MoOS planes. f) Average values except for the Mo–Mo distance in $(pyH)_4[Mo_2O_4(NCS)_6]\cdot H_2O$; Ref. 1.

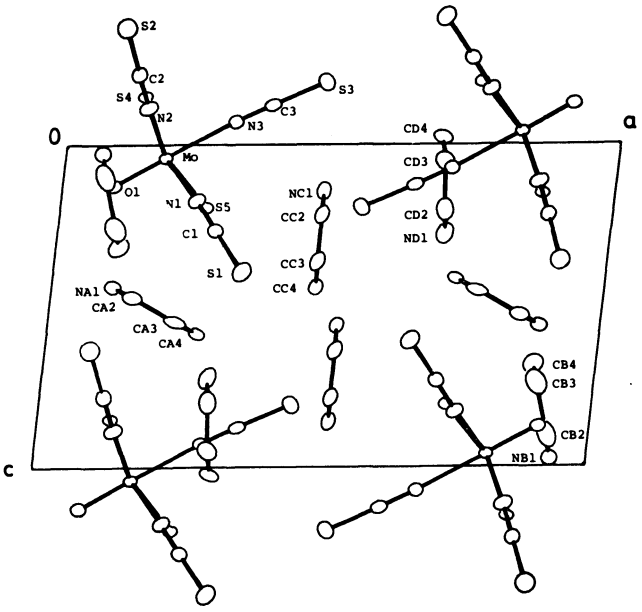

Fig. 3. Crystal structure of $(pyH)_4[Mo_2O_2S_2(NCS)_6]$ viewed down the b axis.

too. The Mo–N bonds trans to O_t(O1) are *ca.* 0.1 Å longer than the other Mo–N bonds, as in the case of $(pyH)_4[Mo_2O_4(NCS)_6]\cdot H_2O$.[1] We found no significant difference between the Mo–N bond lengths *trans* to the bridging oxo and those trans to the bridging sulfido.

The crystal structure of **1**, as viewed down the b axis, is shown in Fig. 3. The crystal consists of $[Mo_2O_2S_2(NCS)_6]^{4-}$ ions, and $(pyH)^+$ ions. The short contact distances are given in Table 4.

References

1) B. Jezowska-Trzebiatowska, T. Glowiak, M. F. Rudolf, M. Sabat, and J. Sabat, *Russ. J. Inorg. Chem.*, **22**, 1950 (1977).
2) F. A. Armstrong, T. Shibahara, and A. G. Sykes, *Inorg. Chem.*, **17**, 189 (1978).
3) T. Shibahara, S. Ooi, and H. Kuroya, *Bull. Chem. Soc. Jpn.*, **55**, 3742, (1982).
4) J. Hornstra and B. Stubbe, PW1100 Data Processing Programs, Philips Research Laboratories, Eindhoven, Holland.
5) "International Tables for X-Ray Crystallography," Kynoch Press, Birmingham (1974), Vol. IV, pp. 71, 148.
6) C. K. Johnson, "OREP," Report ORNL-3794, Oak Ridge National Laboratory, Oak Ridge, Tenn. (1965).
7) "The Universal Crystallographic Computation Program System," The Crystallographic Society of Japan, Tokyo (1969).
8) F. A. Cotton and S. M. Morehouse, *Inorg. Chem.*, **4**, 1377 (1965).
9) W. S. McDonald, *Acta Crystallogr., Sect. B*, **1978**, 2850.
10) T. Shibahara, H. Kuroya, K. Matsumoto, and S. Ooi, *Inorg. Chim. Acta*, **54**, L75 (1981).
11) B. Spivack and Z. Dori, *Coord. Chem. Rev.*, **17**, 99 (1975); E. I. Stiefel, *Prog. Inorg. Chem.*, **22**, 1 (1977), and the references cited therein.
12) A. Kojima, S. Ooi, Y. Sasaki, K. Z. Suzuki, K. Saito, and H. Kuroya, *Bull. Chem. Soc. Jpn.*, **54**, 2457 (1981).

 © 1983 The Chemical Society of Japan Bull. Chem. Soc. Jpn., 56, 2949—2951 (1983)

Retention Behavior of Iron(III) Chelates with Amine-*N*-carboxylic Acids on Silica-gel and Octadecyl-silica Columns

Akihiro YAMAGUCHI, Atsuko TODA, Kunio OHZEKI,* and Tomihito KAMBARA
Department of Chemistry, Faculty of Science, Hokkaido University, Sapporo 060
(Received March 31, 1983)

The separation of iron(III)–edta, –methyl-edta, –dtpa, and –cdta was investigated by high performance liquid chromatography on silica-gel (ZORBAX SIL) and octadecyl-silica (ZORBAX ODS) columns. The chelates were retained on both columns from phosphate buffer mobile phase of pH 3, while the baseline separation was not achieved on the ODS column. The degree of increase in retention caused by the addition of tetrabutylammonium bromide to the eluent was greater on the ODS column than on the silica-gel column, and well separated chelates were eluted in the order, iron(III)–edta, –methyl-edta, –dtpa, and –cdta on both columns.

The application of reversed-phase high performance liquid chromatography (RPHPLC) to analysis of metal chelates has become of interest in recent years.[1,2] The mobile phase containing hydrophobic counter ions has been used to enhance retention and resolution of charged metal complexes on alkyl-bonded silica gel[1] and silica-gel columns.[3]

We have recently shown[4] that iron(III) complexes with EDTA and the analogous compounds were retained from phosphate buffer mobile phase on a silica-gel column, and that the retention increased either with increasing buffer concentration or with increasing amount of sodium sulfate added to the eluent. The purpose of this paper is to show the effect of a tetra-alkylammonium ion on the retention behavior of the chelates on the silica-gel column, and to compare the results with those observed on the octadecyl-silica column.

Experimental

Apparatus. A Shimadzu Model LC-3A chromatograph equipped with a Model SIL-1A syringe injector and a Model SPD-2A variable wavelength UV-detector was used in combination with a Chromatopac C-R1A recorder. The pre-packed columns of ZORBAX SIL and ZORBAX ODS, (DuPont Co.) were used. Both columns were 25 cm × 4.6 mm i.d. A Horiba Model F-7C pH meter was used.

Reagents. The chelating agents were obtained from Dojin Laboratory. The compounds and their abbreviations are disodium salt of ethylenediamine-*N,N,N',N'*-tetraacetic acid (EDTA), 1,2-propanediamine-*N,N,N',N'*-tetraacetic acid (Methyl-EDTA), diethylenetriamine-*N,N,N',N'',N''*-pentaacetic acid (DTPA), and 1,2-cyclohexanediamine-*N,N,N',N'*,-tetraacetic acid (CDTA). Inorganic salts used were of analytical reagent grade. Iron(III) standard solution was prepared from ammonium iron(III) sulfate dodecahydrate. Tetrabutylammonium bromide (TBAB) and chromatographic grade acetonitrile were obtained from Wako Pure Chemicals Co. Deionized and redistilled water was used.

Procedure. Sample solutions were prepared by mixing standard iron(III) and chelating agent solutions in the stoichiometric ratio. The final concentration of each chelate was 20 μmol dm^{-3}. The 10-μl portions were injected. All experiments were carried out at room temperature. The capacity factors were calculated in the usual way.[5] The retention time of a nonretained component was evaluated from the first detectable peak on the chromatogram.

Results and Discussion

Effect of TBAB on Silica-gel Column. The retention of iron(III)–edta, –methyl-edta, –dtpa, and –cdta complexes on the silica-gel column was remarkably enhanced by the addition of TBAB to the phosphate buffer mobile phase. In the presence of 0.1 mmol dm^{-3} TBAB in 2.3 mmol dm^{-3} phosphate buffer eluent of pH 3, the retention time increased from 3.4 to 12.7 min for iron(III)–edta, and 12.6 to 107 min for iron(III)–cdta complexes, respectively, at a flow rate of 1 ml min^{-1}. The capacity factor of each chelate increased with increasing concentration of TBAB in the mobile phase, as generally occurs in reversed-phase chromatography. Among mechanisms which were reviewed[6] to describe the effect of lipophilic alkyl ions in RPHPLC the ion-exchange model[7] seems to be most familiar.

Effect of Electrolyte. The effect of electrolyte added to the phosphate buffer mobile phase was studied in the

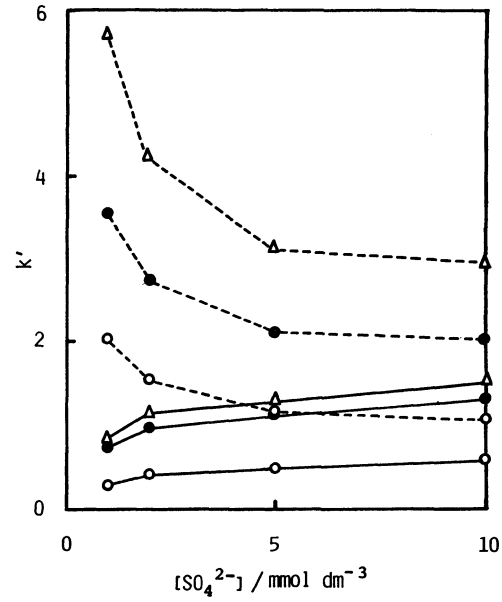

Fig. 1. Effect of sodium sulfate concentration in 2.3 mmol dm^{-3} phosphate buffer eluent (pH 3) on the capacity factor in the absence (solid line) and in the presence (dashed line) of 0.1 mmol dm^{-3} TBAB. Column: ZORBAX SIL, 25 cm × 4.6 mm i.d.; sample: (○) Fe^{III}–edta, (●) Fe^{III}–methyl-edta, (△) Fe^{III}–dtpa.

TABLE 1. THE CAPACITY FACTORS OF IRON(III) CHELATES ON ZORBAX SIL AND ODS

	ZORBAX SIL			ZORBAX ODS		
	k'_1	k'_2	k'_2/k'_1	k'_1	k'_2	k'_2/k'_1
Fe^{III}-edta	0.20	0.46	2.3	0.13	1.78	13.7
Fe^{III}-methyl-edta	0.35	0.68	1.9	0.29	2.57	8.9
Fe^{III}-dtpa	0.44	0.88	2.0	0.29	3.28	11.3
Fe^{III}-cdta	1.11	1.72	1.5	2.26	12.31	5.4

Eluent: 0.012 mol dm^{-3} phosphate buffer solution, 5% (V/V) acetonitrile, pH 3. k'_1: Capacity factor in the absence of TBAB. k'_2: Capacity factor in the presence of 0.1 mmol dm^{-3} TBAB.

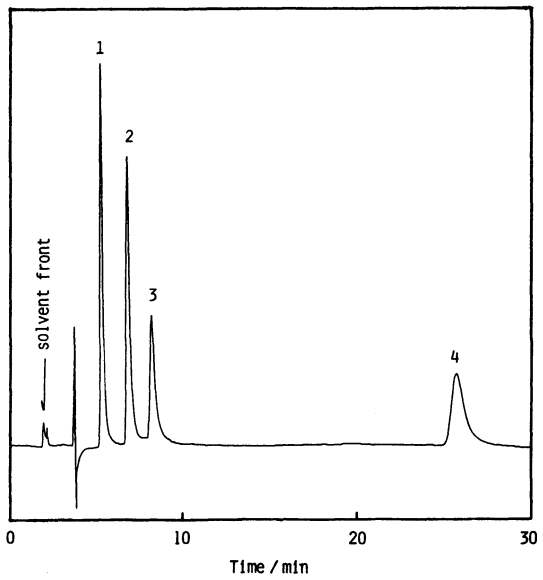

Fig. 2. Separation of iron(III) chelates on ZORBAX ODS in the presence of TBAB. Eluent: 12.0 mmol dm^{-3} phosphate buffer solution containing 0.1 mmol dm^{-3} TBAB and 5% (V/V) acetonitrile, pH 3; flow rate: 1 ml min^{-1}; detection at 260 nm, 0.01 a.u.f.s.; sample: 10 μl containing each chelate in 20 μmol dm^{-3}; peak 1, Fe^{III}-edta; peak 2, Fe^{III}-methyl-edta; peak 3, Fe^{III}-dtpa; peak 4, Fe^{III}-cdta.

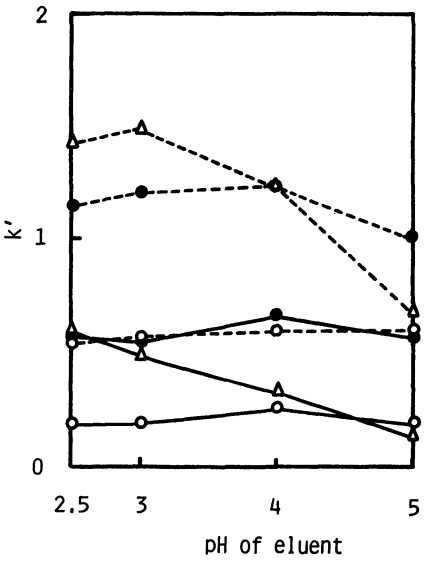

Fig. 3. Effect of pH on the capacity factor. Column: ZORBAX ODS (solid line), ZORBAX SIL (dashed line); eluent: phosphate buffer solution containing 10 mmol dm^{-3} sodium sulfate; sample: (○) Fe^{III}-edta, (●) Fe^{III}-methyl-edta, (△) Fe^{III}-dtpa.

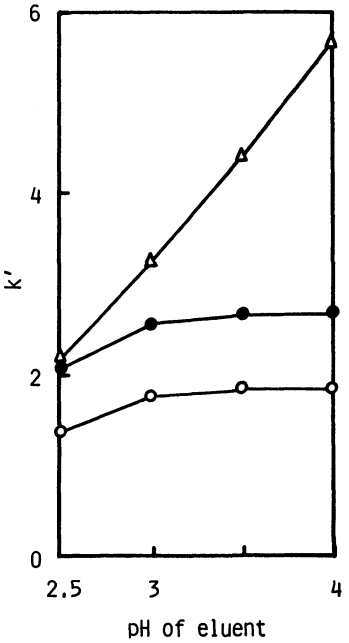

Fig. 4. Effect of pH on the capacity factor in the presence of TBAB. Column: ZORBAX ODS; eluent: phosphate buffer solution containing 0.1 mmol dm^{-3} TBAB and 5% acetonitrile; sample: (○) Fe^{III}-edta, (●) Fe^{III}-methyl-edta, (△) Fe^{III}-dtpa.

presence and absence of TBAB (Fig. 1). In the absence of TBAB, the retention of each complex increased gradually with increasing concentration of sodium sulfate in the mobile phase. The increase in retention is caused by the salting-out effect[8] of the electrolyte, the hydrophobic interaction[4] between the solute and stationary phase being facilitated. On the other hand, in the presence of TBAB, the retention decreased with increasing concentration of sodium sulfate, and reached almost constant value for each chelate in the concentration range of 5 to 10 mmol dm^{-3} of sodium sulfate. It is clearly concluded that the retention observed in the presence of TBAB is governed by at least two factors, namely, ion-exchange and salting-out effects. With increasing concentration of electrolyte in the eluent, the retention due to ion-exchange decreases and the retention caused by salting-out effect becomes predominant.

Separation of Chelates. The capacity factors of the chelates on silica-gel and ODS columns obtained by using mobile phase of the same composition were summarized in Table 1. The acetonitrile was used to reduce the retention time. The degree of increase in retention

caused by the addition of TBAB to the mobile phase was much greater on the ODS column than on the silica-gel column. The results suggested that the hydrophobic tetrabutylammonium ion is more feasibly adsorbed on the hydrocarbonaceous silica gel than on the original silica gel. The typical chromatogram was shown in Fig. 2. In the absence of TBAB, baseline separation of the iron(III) chelates were not achieved on the ODS column, even though the retention and resolution of the chelates were enhanced with increasing buffer concentration. The iron(III)–dtpa complex eluted between EDTA and Methyl–EDTA complexes on the ODS column, while the compound was eluted after the Methyl–EDTA complex on the silica-gel column. In the presence of TBAB, the chelates were well separated and eluted in the following order, iron(III)–edta, –methyl-edta, –dtpa, and –cdta on both columns. The elution sequence depends on the hydrophobicity of the chelates[4] and the pH of mobile phase as described below.

The Effect of Eluent pH. The effect of eluent pH was examined on the silica-gel and alkyl-modified silica-gel columns. On both columns, the retention of iron(III)–dtpa decreased with increasing pH of the mobile phase (Fig. 3). The DTPA complex has two carboxyl groups which do not participate in the complexation.[9] The dissociation of one or two uncoordinated carboxyl groups will reduce the hydrophobicity of the complex. The retention of DTPA complex begins to decrease at lower pH on the ODS column than on the silica-gel column. The silanol groups on the silica-gel surface will suppress the dissociation of carboxyl groups. The effect of pH on the ODS column was also studied in the presence of TBAB (Fig. 4). The retention of iron(III)–dtpa increased with increasing pH, which suggested also the dissociation of uncoordinated carboxyl groups.

References

1) H. Hoshino and T. Yotsuyanagi, *Kagaku*, **36**, 657 (1980).
2) A. R. Timerbaev, O. M. Petruchin, and Yu. A. Zolotov, *Zh. Anal. Chem.*, **36**, 1160 (1981).
3) S. Igarashi, M. Nakano, and T. Yotsuyanagi, *Bunseki Kagaku*, **32**, 67 (1983).
4) K. Ohzeki, A. Yamaguchi, A. Toda, and T. Kambara, *Bunseki Kagaku*, **32**, E133 (1983).
5) A. M. Krstulovic, and P. R. Brown, "Reversed-Phase High-Performance Liquid Chromatography," John Willey and Sons, New York (1982), p. 6.
6) B. A. Bidlingmeyer, *J. Chromatogr. Sci.*, **18**, 525 (1980).
7) J. L. M. van de Vanne and J. L. H. M. Hendrikx, *J. Chromatogr.*, **167**, 1 (1978).
8) C. Horvath, "High-Performance Liquid Chromatography," Academic Press, New York (1980), Vol. 1, p. 135.
9) S. Ooi, *Kagaku No Ryoiki*, **24**, 47 (1970).

Normal Pulse Polarographic Study of the Electrode Reaction of Copper(II) Complexes with Ethylenediaminetetraacetic Acid(EDTA) and *N*-(2-Hydroxyethyl)ethylenediamine-*N*,*N*′,*N*′-triacetic Acid(HEDTA)

Shuichiro YAMAGUCHI, Hiroaki MATSUDA, Takeo OHSAKA,† and Noboru OYAMA*,†

Department of Electronic Chemistry, Graduate School at Nagatsuta, Tokyo Institute of Technology, Nagatsuta, Midori-ku, Yokohama 227

†*Department of Applied Chemistry for Resources, Tokyo University of Agriculture and Technology, Koganei, Tokyo 184*

(Received April 21, 1983)

The normal pulse polarographic behavior of the Cu(II)–EDTA and –HEDTA complexes was examined in a wide range of pH values to elucidate the mechanisms of their electrode reactions and to evaluate the relevant electrochemical kinetic parameters. From analysis of the dependence of the half-wave potentials on the sampling time and the hydrogen ion concentration, it was shown that the reduction wave of the Cu(II)–EDTA complexes observed in the pH range of 2.0 to 9.5 at −0.1 to −0.5 V *vs.* SCE corresponds to the simultaneous reduction of four complex species, CuH_3L^+, CuH_2L^0, $CuHL^-$, and CuL^{2-}, where $CuH_pL^{(p-2)+}$ and L^{4-} denote the protonated complex species with p protons and the unprotonated EDTA ion, respectively. The reduction wave of the Cu(II)–HEDTA complexes in the pH range of 3.0 to 9.0 at −0.25 to −0.4 V *vs.* SCE corresponds to the simultaneous reduction of two complex species, $CuHL^0$ and CuL^-, where L^{3-} denotes the unprotonated HEDTA ion. The kinetic parameters of the corresponding complex species (*i.e.* the cathodic transfer coefficient and the standard rate constant of electrode reaction) were evaluated.

In a series of papers,[1-3] we have examined the electrode reaction mechanism of the Cd(II) and Pb(II) complexes with ethylenediamine-*N*,*N*,*N*′,*N*′-tetraacetic acid (EDTA) and *N*-(2-hydroxyethyl)ethylenediamine-*N*,*N*′,*N*′-triacetic acid (HEDTA) and it has been shown that many protonated complex species of the type MH_pL (p=1,2,3 for the EDTA complex and p=1,2 for the HEDTA complex) complex species, as well as the ordinary unprotonated complex species can participate directly in the charge transfer processes. The relevant electrochemical kinetic parameters have been evaluated therein.

Our careful analysis of the d.c. polarograms for the Cu(II) complexes with EDTA and HEDTA confirmed that the electrode reactions are the quasi-reversible[4] in the range of pH=1.0 to 11.0, although their electrode processes have been considered to be reversible in the polarographic time scale.[5-8] It has been recognized that in the case of the quasi-reversible processes less reliable data regarding the electrochemical kinetic parameters are obtained from the analysis of the d.c. polarograms.

Normal pulse polarography (NPP) among the numerous pulse techniques is most suitable for the examination of the kinetics of polarographically quasi-reversibel electrode processes, because the current measuring time in NPP can be widely varied from 10^{-4} to a few seconds and the shape of normal pulse polarograms is similar to that of d.c. polarograms, so that the analysis of the normal pulse polarograms can be easily carried out by using the procedure similar to that of the analysis of the d.c. polarograms.[9] However, NPP has been ever applied to the examination of the electrode kinetics in only a few examples.[10-13] In general many pulse techniques[14] have been used for the microanalysis so far, since they were proposed by Barker[15,16] in 1957.

In this paper, we demonstrate that NPP is the powerful method to elucidate in detail the mechanism of the electrode processes of Cu(II)–EDTA and –HEDTA complexes and determine the values of the kinetic parameters of many protonated complexes and the unprotonated complexes being participating in the electrode reactions. Previously,[4] we have performed the examination of complex equilibrium of the Cu(II) aqua ion with EDTA and HEDTA by potentiometric titration measurements and reported the values of the formation constants of many protonated complexes and hydroxo complexes, being newly found.

Experimental

Instrumentation. Current-potential curves were measured by home-made instruments with multifunctions (d.c. polarography, differential pulse polarography, and normal pulse polarography). The program controlling potentials was generated by CMOS logic IC and programmable timer counter IC (Intersil ICM 7250) with a quartz oscillator, which acted through a 12-bit D/A converter driving the potentiostat. The current response, which was converted to the voltage at the current follower of the potentiostat, was fed through a sample-hold circuits (Intersil IH 5110) into two integrator-type sample-hold circuits (using Analog Devies AD515k) with very small drift rate (<1 μV s^{-1}) at the hold-mode. Individual storing information was recorded with a two-pen X-Y-Y recorder. The sampling times of normal pulse polarography can be set at two arbitrary values from 0.1 ms to 9.9 s. The magnitude of the increase in the potential pulse height, ΔE, at each mercury drop can be changed from 1 to 99 mV. As an another current sampling method, we also used the following method: the current was integrated over a time interval, which is shorter than one-tenth of the pulse width, near the end of the pulse and the average value of the integrated current was taken as the current sampled. In order to increase the signal-to-noise ratio, especially when the faradic current is small,

A spike-like pulse which is generated between a dropping mercury electrode and a counter electrode at the moment of mercury drop fall is employed as a signal indicating the drop birth.[17] A chatter-free wetting mercury relay was employed to remove the counter electrode from potentiostatic control after measuring the current.

In the differential pulse polarographic mode operation, the dual slope integrating technique reported by Kalvoda and Trojanek[18,19] was employed.

Procedure. An electrolytic cell which was specially designed to be able to monitor continuously the concentration of hydrogen ion during the polarographic measurements, was a seven-neck vesel which was set with a dropping mercury electrode (DME), an 1.0 M (1 M=1 mol dm^{-3}) NaCl agar-agar bridge for connection with a saturated calomel electrode (SCE), a Pt wire counter electrode, a glass electrode, an Ag–AgCl reference electrode and two burets. A digital pH/mV meter (Orion Research, model 801) was used for pH measurements, in combination with a Beckman 40495 glass electrode and an Ag/AgCl electrode. The determination of the pH values was carried out in a similar manner as reported previously.[1,20] The flow rate of the mercury of the DME was $m=0.97$ mg s^{-1} and the drop time 6 s at the height of mercury head $h=60$ cm in 1 M $NaClO_4$ solution.

All measurements were performed in a parafine oil thermostat at (25.0±0.1) °C. The hydrogen ion concentration of the test solution was varied and measured before and after the recording of each polarogram. The difference in these pH values was within 0.01 pH unit as a rule. The composition of the test solution was 4.00×10^{-4} M of Cu(II) aqua ion, 8.00×10^{-3} M of EDTA or 2.00×10^{-2} M for HEDTA, and 1.0 M $NaClO_4$, unless otherwise noted. No buffer was added in the pH ranges 1.0—3.5 and 5.5—10.0 because the ligands are expected to have a large buffer capacity in these pH ranges. In the pH range 3.5—5.5, the acetate buffer was used at three different concentrations, 20, 40, and 80 mM CH_3COONa. The acetate ion did not show any influence on the shape and the position of the polarograms obtained. No maximum suppressor was added, since no polarographic maximum appeared in the pH range 1.0—11.5. The test solution was deaerated for 30 min with argon gas before each measurement of the polarograms.

Reagents. Ethylenediaminetetraacetic acid (disodium salt) (reagent grade, Dojindo Lab.) was recrystallized twice, dried and stored over silica gel in a desiccator. *N*-(2-Hydroxyethyl)-ethylenediamine-*N*,*N*′,*N*′-triacetic acid (Dojindo Lab.) was recrystallized from distilled water and dried under a reduced pressure. Copper(II) perchlorate was prepared by dissolving $CuCO_3$ in a $HClO_4$ solution and purified by recrystallizing three times from distilled water. The stock solution contained a small amount of $HClO_4$ to prevent hydrolysis of Cu(II) aqua ion. The concentration of Cu(II) aqua ion in the stock solution was determined by electrogravimetry.

Sodium perchlorate, sodium hydroxide and perchloric acid stock solutions were prepared by the methods described previously.[20]

Results

The Cu(II)–EDTA Complexes. Normal pulse polarograms for the reduction of the Cu(II) complexes were measured in the pH range from 1.0 to 11.0. Typical normal pulse polarograms are shown in Fig. 1. The half-wave potential of reduction waves shifted to cathodic direction with increasing the pH value and with decreasing sampling time, θ. Their limiting current was diffusion-controlled, as proved from the fact that the product of the limiting current and $\theta^{1/2}$ is always constant.

As has been described previously,[4] a number of protonated complex species of the MH_pL type (p= 1,2,3) for the EDTA complex are formed in the bulk of the solution and any possibility of the formation of polynuclear or polyligand complexes can be disregarded, when the solution contains an excess of EDTA ligand relative to the Cu(II) aqua ion. Since no Cu(II) aqua ion is present above pH=1.0[4] and no its kinetic behavior was observed in the normal pulse polarograms in the pH range 1.0 to 11.0, it seems reasonable to assume that the mechanism of the electrode processes under consideration can generally be expressed by

$$\begin{array}{l} CuH_NL + 2e \rightleftarrows Cu(Hg) + H_NL \\ \quad\updownarrow \qquad\quad \alpha_N, k_N^\circ \\ \cdots\cdots\cdots\cdots\cdots\cdots \\ \quad\updownarrow \\ CuH_pL + 2e \rightleftarrows Cu(Hg) + H_pL \\ \quad\updownarrow \qquad\quad \alpha_p, k_p^\circ \\ \cdots\cdots\cdots\cdots\cdots\cdots \\ \quad\updownarrow \\ CuL + 2e \rightleftarrows Cu(Hg) + L \\ \qquad\quad \alpha_0, k_0^\circ \end{array} \qquad (1)$$

We have previously reported the d.c. polarographic current-potential relationship for the similar mechanism of the electrode processes and its application to the analysis of the polarograms for the reduction of the Cd(II) and Pb(II) complexes with EDTA and HEDTA.[1-3] The current-potential relationship for normal pulse polarograms of the electrode process, assuming that the CuH_pL complex predominantly participates in the charge transfer process, is given by Eq. 2 which can be derived from the modification of the general current-potential relationship for normal pulse polarograms of the simple electrode process, $Ox+ne \rightleftarrows Red$.[9,13,21]

$$E = E^* - \frac{2.3RT}{2a_pF}\log\left[\frac{\sqrt{3x}}{4\sqrt{\theta}}\left\{\frac{1.75+x^2(1+\exp\zeta)^2}{1-x(1+\exp\zeta)}\right\}^{1/2}\right] \qquad (2)$$

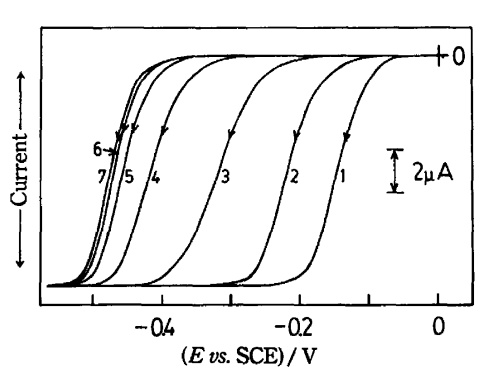

Fig. 1. Typical normal pulse polarograms for the reduction of the Cu(II)–EDTA complexes in 1.0 M $NaClO_4$ solution containing 0.4 mM Cu(II) aqua ion and 8 mM EDTA.
Sampling time θ=27 ms, drop time of DME τ=4.0 s and rate of the increase in potential pulse height ΔE=5 mV/drop.
$-\log[H^+]$: (1) 2.12, (2) 3.06, (3) 4.02, (4) 5.85, (5) 7.36, (6) 8.59, (7) 9.37.

with

$$E^* = E^r_{1/2.p} + \frac{2.3RT}{2a_pF} \log\left[\frac{k^\circ_p(\beta_{0p1})^{a_p}(\beta_{1p1})^{1-a_p}[H^+]^p\{F([H^+])+G([H^+])/C_L\}^{1+a_p}}{\{D_C^{1-a_p}D^{a_p}_{Cu(Hg)}\}^{1/2}\{G([H^+])/C_L\}^{a_p}F([H^+])^2}\right], \quad (3)$$

$$X = i/(i_d)_{Cott}, \quad (4)$$

$$\zeta = (2F/RT)(E-E^r_{1/2.p}), \quad (5)$$

$$E^r_{1/2.p} = E^\circ_p + \frac{2.3RT}{2F} \log\left[\left(1+\frac{F([H^+])}{G([H^+])/C_L}\right)\frac{\beta_{0p1}}{\beta_{1p1}}\right] + \frac{2.3RT}{2F}\log\frac{D_C}{D_{Cu(Hg)}}, \quad (6)$$

$$F([H^+]) = \sum_{p=0}^{N}\beta_{1p1}[H^+]^p, \quad (7)$$

$$G([H^+]) = \sum_{p=0}^{N}\beta_{0p1}[H^+]^p, \quad (8)$$

$$\beta_{qpr} = [Cu_qH_pL_r^{2q+p-nr}]/[Cu^{2+}]^q[H^+]^p[L^{n-}]^r, \quad (9)$$

$$C_c = \sum_{p=0}^{N}[CuH_pL^{2+p-n}], \quad (10)$$

$$D_c = \sum_{p=0}^{N}\beta_{1p1}[H^+]^pD_p/F([H^+]). \quad (11)$$

In these equation, E is the electrode potential; i is the normal pulse polarographic current; θ is the sampling time; E°_p, $E^r_{1/2.p}$, k°_p, and α_p are the standard potential, the reversible half-wave potential, the standard rate constant and the cathodic transfer coefficient, respectively, of the electrode reaction: $CuH_pL^{2+p-n}+2e \rightleftarrows Cu(Hg)+H_pL^{p-n}$; D_p and $D_{Cu(Hg)}$ are the diffusion coefficients of the complex species CuH_pL^{2+p-n} in the solution and of the copper atoms Cu(Hg) in the amalgam, respectively; β_{qpr} which is designated by Eq. 9 is the equilibrium constant for the reaction: $qCu^{2+}+pH^++rL^{n-} \rightleftarrows Cu_qH_pL_r^{2q+p-nr}$; C_L is the total concentration of the ligand; $[H^+]$ is the concentration of hydrogen ion; $[Cu^{2+}]$ and $[CuH_pL^{2+p-n}]$ are the concentrations of the Cu(II) aqua ion and the complex species CuH_pL^{2+p-n}, respectively; $[L^{n-}]$ is the concentration of the free ligand; $(i_d)_{Cott}$ denotes the diffusion current expressed by the Cottrell equation.[22]

D.c. polarograms of Cu(II)–EDTA complexes were measured in the same solutions as used in NPP. The reversible half-wave potentials, $E^r_{1/2.p}$, were evaluated from these d.c. polarograms by means of extrapolation method.[23] Thus, the values of the logarithmic term of r.h.s. of Eq. 2 and ζ can be calculated by using Eqs. 2 and 5, respectively, at any electrode potential. The modified log-plots of the normal pulse polarograms, in which the log-term on r.h.s. of Eq. 2 is plotted against E, gave straight lines for the reduction of the Cu(II)–EDTA complexes over the whole pH range examined (Fig. 2). These straight lines have constant slopes, the values of which are equal to $-2a_pF/2.3RT$, in the range of pH 1.0—2.5, 3.0—4.5, 5.5—7.5, and 8.0—10.0 within experimental errors. The cathodic transfer coefficients were evaluated from their reciprocal slopes. The values obtained are given in Table 1. The constant value of α_p obtained in each pH range seems to permit us to assume that only one species predominantly participates in the charge transfer process in limited pH ranges. Thus we can apply Eq. 3 to the determination of the composition of the discharging species.

After some rearrangements of Eq. 3, we obtain

$$Z_p \equiv \frac{2a_pF}{2.3RT}(E^*-E^r_{1/2.p}) + \log\left[\frac{\{G([H^+])/C_L\}^{a_p}F([H^+])^2}{\{F([H^+])+G([H^+])/C_L\}^{1+a_p}}\right], \quad (12)$$

$$= \log[k^\circ_p(\beta_{0p1})^{a_p}(\beta_{1p1})^{1-a_p}] - \frac{1}{2}\log[D_c^{1-a_p}D_{Cu(Hg)}{}^{a_p}] + p\log[H^+]. \quad (13)$$

The values of the function Z_p, defined by Eq. 12, were calculated as a function of $[H^+]$ for each pH range. Hence, the composition of the discharging complex species, *i.e.*, p can be determined from the dependence of the function, $-Z_p$, upon $-\log[H^+]$. In Fig. 3, the values of $-Z_p$ are plotted against $-\log[H^+]$. As can readily be seen from Fig. 3, a linear relationship is obtained with $p=3$ in the pH range 1.0—2.5, indicating that the discharging species is the species CuH_3L^+. Similarly, the discharging species is primarily CuH_2L^0 in the pH range 3.0—4.5, $CuHL^-$ in 5.5—7.5 and CuL^{2-} in pH 8.0—10.0, respectively. Thus, it can be concluded

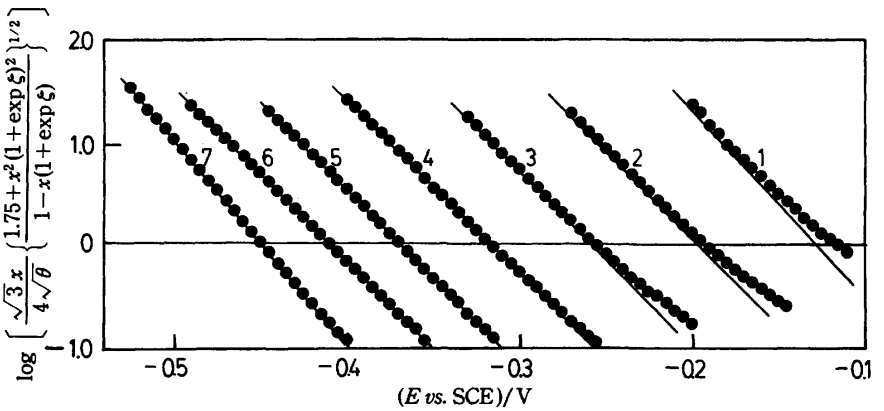

Fig. 2. Modified log-plots of normal pulse polarograms for the reduction of the Cu(II)–EDTA complexes.
$-\log[H^+]$: (1) 2.17, (2) 3.06, (3) 3.72, (4) 4.44, (5) 5.33, (6) 6.56, (7) 8.59.
Other experimental conditions are the same as in Fig. 1.

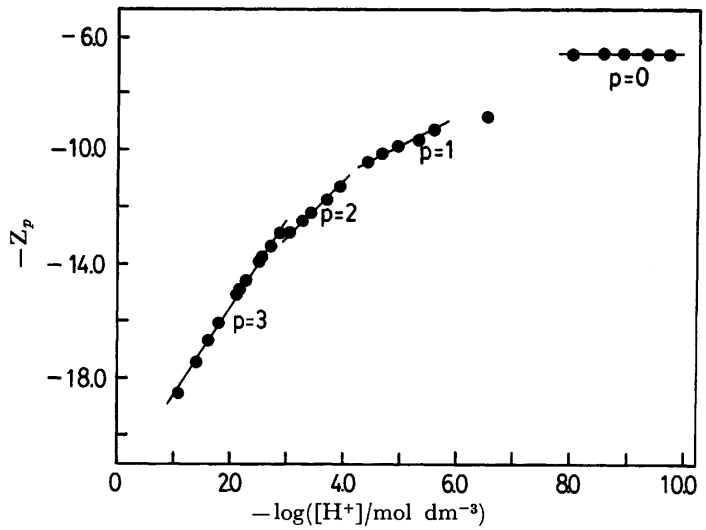

Fig. 3. Dependence of the function, $-Z_p$, upon $-\log[H^+]$ for the Cu(II)–EDTA complexes.
Experimental conditions are the same as in Fig. 1.

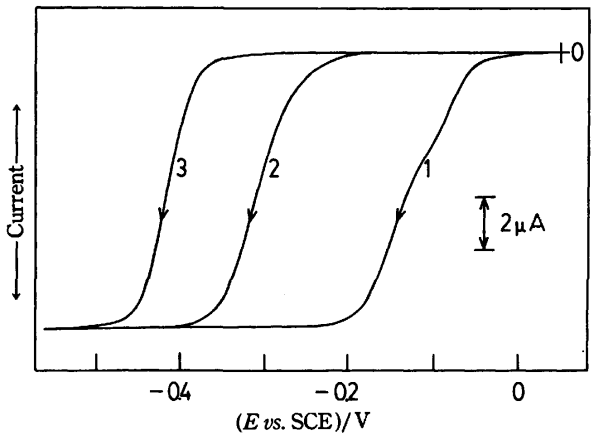

Fig. 4. Normal pulse polarograms for the reduction of the Cu(II)–HEDTA complexes.
Solution composition: 0.4 mM Cu(II) aqua ion, 20 mM HEDTA and 1.0 M $NaClO_4$. Sampling time $\theta=27$ ms, drop time of DME $\tau=4.0$ s and rate of the increase in potential pulse height $\Delta E=5$ mV/drop.
$-\log[H^+]$: (1) 1.91 (2) 4.63, (3) 9.21.

that the normal pulse polarographic wave for the reduction of the Cu(II)–EDTA complexes is composed of the four charge transfer processes, $CuH_pL^{p-2}+2e \rightleftarrows Cu(Hg)+H_pL^{p-4}$ ($p=3, 2, 1, 0$). The standard rate constant, k_p°, of each charge transfer process can be evaluated from the value of the intercept of the plots shown in Fig. 3 and by introducing the experimental data into Eq. 13, where the values of D_p and $D_{Cu(Hg)}$ were 5.4×10^{-6} cm^2 s^{-1} and 1.06×10^{-5} cm^2 s^{-1},[24] respectively. The above value of D_p was obtained from the cathodic limiting currents of d.c. polarograms by using the Ilkovic equation.[14] The kinetic parameters obtained are given in Table 1.

The Cu(II)–HEDTA Complexes. Figure 4 shows a set of normal pulse polarograms for the reduction of the system of the Cu(II)–HEDTA complexes in the solution of various pH. Figure 5 shows the modified log-plots of the normal pulse polarograms. These log-plots satisfied the straight lines and their slopes were constants in the range of pH 3.0—6.0 and 7.5—9.5, respectively. The cathodic transfer coefficients were evaluated from their reciprocal slopes. In Fig. 6, the values of $-Z_p$, calculated from Eq. 12, are plotted against $-\log[H^+]$. It is apparent from this figure that the discharging species is primarily $CuHL'^0$ and CuL'^- ($L'=hedta^{3-}$) in the pH range 3.0—6.0 and 7.5—9.5, respectively. The standard rate constants for these discharging species were evaluated by means of the same method as described in the previous section. The values obtained are summarized in Table 1.

In the acidic solution below pH 3.0, the modified log-plots of the normal pulse polarograms deviated from the straight line, as shown in Fig. 5, when the value of the logarithmic term of r.h.s. of Eq. 2 is below zero. The deviation seems to result from that the

Table 1. Electrochemical kinetic parameters of the Cu(II)–EDTA and –HEDTA complexes in 1.0 M $NaClO_4$ at 25 °C ($L=edta^{4-}$ and $L'=hedta^{3-}$)

Discharging species	Cu(II)–EDTA complex				Cu(II)–HEDTA complex	
	CuL^{2-}	$CuHL^-$	CuH_2L^0	CuH_3L^+	CuL'^-	$CuHL'^0$
k_p°/cm s^{-1}	9.3×10^{-4}	8.7×10^{-3}	1.6×10^{-2}	3.6×10^{-3}	2.7×10^{-2}	1.5×10^{-1}
α_p	0.59	0.50	0.48	0.52	0.58	0.47
(E_p° *vs.* SCE)/mV	−488	−321	−205	−171	−460	−266
$\Delta\phi_2$/mV	−6.0	13	25	29	−3.7	20
$(k_p^\circ)_{corr}$/cm s^{-1}	4.4×10^{-4}	2.4×10^{-2}	9.2×10^{-3}	1.7×10^{-2}	2.0×10^{-2}	3.0×10^{-1}

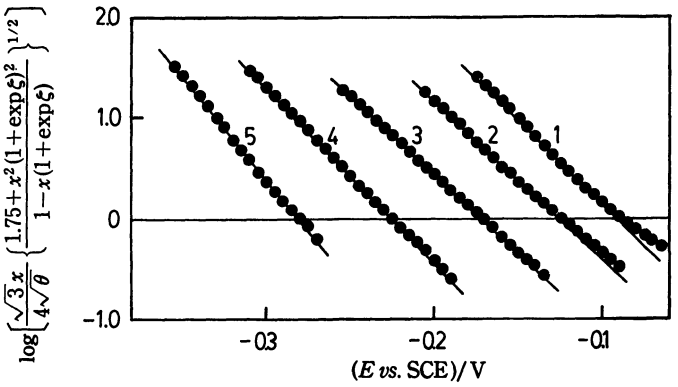

Fig. 5. Modified log-plots of normal pulse polarograms for the reduction of the Cu(II)–HEDTA complexes.
Total concentration of HEDTA=20 mM and concentration of Cu(II) aqua ion=0.4 mM. Sampling time θ=6 ms, drop time of DME τ=4.0 s and rate of the increase in potential pulse height ΔE=10 mV/drop.
$-\log[H^+]$: (1) 2.96, (2) 3.62, (3) 4.40, (4) 6.07, (5) 8.89.

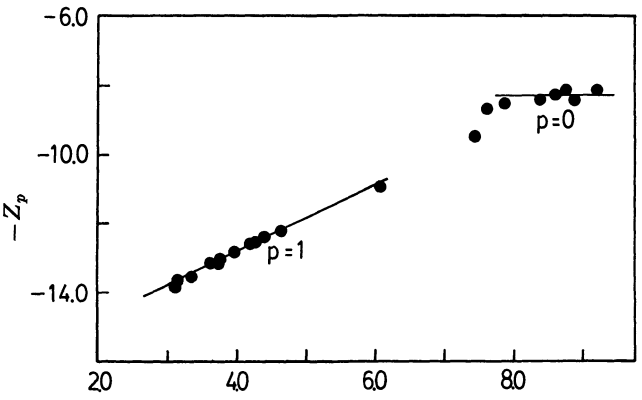

Fig. 6. Dependence of the function, $-Z_p$, upon $-\log[H^+]$ for the Cu(II)–HEDTA complexes.
Experimental conditions are the same as in Fig. 4.

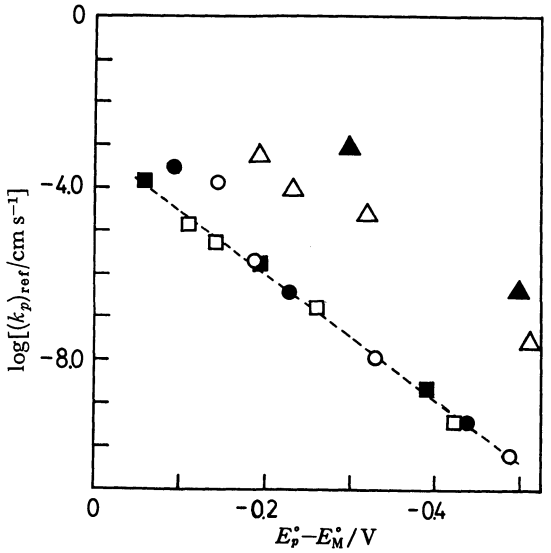

Fig. 7. Plots of $\log(k_p^\circ)_{ref}$ against $E_p^\circ - E_M^\circ$ ($= -(2.3\,RT/2F) \times \log(\beta_{1p1}/\beta_{0p1})$) for the M(II)–EDTA complexes and the M(II)–HEDTA complexes.
(▲): Cu(II)–HEDTA complexes, (△): Cu(II)–EDTA complexes, (●): Pb(II)–HEDTA complexes, (○): Pb-(II)–EDTA complexes, (■): Cd(II)–HEDTA complexes, (□): Cd(II)–EDTA complexes.

polarogram probably consists of the overlap of two waves for the reduction of Cu(II) aqua ion and the protonated Cu(II) complexes, as seen from polarogram 1 in Fig. 4. By the differential pulse polarography the two humps in polarogram were observed. However, since two waves closely overlapped, the waves could not be satisfctorily separated by using the non-linear least-squares method.[25]

Discussion

The results obtained above demonstrate that normal pulse polarography is one of the most useful pulse techniques for the examination of the electrode kinetics in d.c. polarographically quasi-reversible electrode processes. The kinetic parameters obtained are summarized in Table 1 together with the values of the standard rate constants, $(k_p^\circ)_{corr}$, corrected for the double layer effect by means of the Frumkin theory,[26] in which the values of ϕ_2 were taken from Russell's tables.[27] The values of the standard rate constants, $(k_p^\circ)_{corr}$ increase in the following order: $CuL^{2-} \ll CuH_2L^0 < CuHL^- < CuH_3L^+$ (L=edta^{4-}) for the Cu-(II)–EDTA complexes and $CuL'^- < CuHL'^0$ (L'=hedta^{3-}) for the Cu(II)–HEDTA complexes. In both systems, the values of k_p° ($p \geqq 1$) for the protonated complex species are larger than those for the ordinary unprotonated complex species. The corrected rate constant, $(k_p^\circ)_{corr}$, of the Cu(II)–EDTA and –HEDTA complexes except CuH(hedta)^0 and Cu(edta)$^{2-}$ were almost the same order of magnitude ($\approx 10^{-2}$ cm s^{-1}) as that of the Cu(II) aqua ion.[28] The values of the cathodic transfer coefficients for the species under consideration were in the range of 0.47 to 0.59, as summarized in Table 1.

Previously[1-3] we have found that the linear relation between the cathodic rate constants at some reference

potential and the corresponding standard potentials holds for the Cd(II) and Pb(II) complexes with EDTA and related compounds and further suggested that the protonation of acetate groups of these ligands, leading to the cleavage of the metal-oxygen bonds within the complex species, accelerates the rate of charge transfer process. We examined whether such a correlation prevails for the present series of the Cu(II) complexes. In Fig. 7 the logarithms of $(k_p^\circ)_{ref}$'s are plotted against $E_p^\circ - E_{Cu}^\circ (= -2.3(RT/2F)\log(\beta_{1p1}/\beta_{0p1}))$, where E_p° is the standard potential of the couple $CuH_pL/Cu(Hg)$ or $CuH_pL'/Cu(Hg)$ and E_{Cu}° is the standard potential of Cu(II) aqua ion. As can readily be seen from this figure, a linear relationship between the cathodic rate constants and the corresponding standard potentials could not be obtained. We have no idea to explain such a different behavior at present, but this may probably be associated with the difference between the ordinary octahedral structure of the Cd(II) and Pb(II) complexes and the pseudo octahedral structure of the Cu(II) complex.[29-31]

References

1) N. Oyama and H. Matsuda, *J. Electroanal. Chem.*, **78**, 89 (1977).
2) N. Oyama and H. Matsuda, *J. Electroanal. Chem.*, **78**, 103 (1977).
3) N. Oyama, T. Shirato, and H. Matsuda, *J. Electroanal. Chem.*, **81**, 67 (1977).
4) S. Yamaguchi, N. Oyama, K. Ikeda, and H. Matsuda, *Bull. Chem. Soc. Jpn.*, **54**, 3753 (1981).
5) R. L. Pescok, *Anal. Chem.*, **25**, 561 (1953).
6) G. Schwarzenbach, R. Gut, and G. Anderegg, *Helv. Chem. Acta*, **37**, 937 (1954).
7) M. C. Benett and N. O. Schmidt, *Trans. Faraday Soc.*, **51**, 1412 (1955).
8) N. Tanaka and K. Kato, *Bull. Chem. Soc. Jpn.*, **32**, 1376 (1959).
9) H. Matsuda, *Bull. Chem. Soc. Jpn.*, **53**, 3439 (1980).
10) A. W. Fonds, J. L. Molenaar, and J. M. Los, *J. Electroanal. Chem.*, **22**, 229 (1969).
11) J. M. Los, A. A. A. M. Brinkman, and B. J. C. Wetsema, *J. Electroanal. Chem.*, **56**, 187 (1974).
12) J. M. Los, L. F. Roeleveld, and B. J. C. Wetsema, *J. Electroanal. Chem.*, **75**, 819 (1977).
13) T. Ohsaka, N. Oyama, S. Yamaguchi, and H. Matsuda, *Bull. Chem. Soc. Jpn.*, **54**, 2475 (1981).
14) A. M. Bond, "Modern Polarographic Methods in Analytical Chemistry," Marcel Dekker, New York (1980), Chap. 6.
15) G. C. Barker, Proc. Congr. on Modern Anal. Chem. in Ind., St. Andrew, 1957, p. 199.
16) G. C. Barker and A. W. Gardner, *Z. Anal. Chem.*, **173**, 79 (1960).
17) T. Rohko, M. Kogoma, and S. Aoyagui, *J. Electroanal. Chem.*, **38**, 45 (1972).
18) R. Kalvoda and A. Trojanek, *J. Electroanal. Chem.*, **75**, 151 (1977).
19) Sam Ben-Yaakov and H. Gutermen, *J. Electroanal. Chem.*, **125**, 41 (1981).
20) N. Oyama, T. Shirato, H. Matsuda, and H. Ohtaki, *Bull. Chem. Soc. Jpn.*, **49**, 3047 (1976).
21) K. Sato, H. Matsuda, T. Ohsaka, and N. Oyama, *Bull. Chem. Soc. Jpn.*, **56**, 2004 (1983).
22) F. G. Cottrell, *Z. Phys. Chem.*, **42**, 385 (1903).
23) H. Matsuda, *Tokyo Kogyo Shikensho Hokoku*, **61**, 315 (1966).
24) N. H. Furman and W. C. Cooper, *J. Chem. Soc.*, **72**, 5667 (1950).
25) C. Nishihara and H. Matsuda, *J. Electroanal. Chem.*, **28**, 17 (1970).
26) A. N. Frumkin, *Z. Phys. Chem.*, **164**, 121 (1933).
27) C. D. Russell, *J. Electroanal. Chem.*, **6**, 486 (1963).
28) N. Tanaka and R. Tamamushi, *Electrochim, Acta*, **9**, 963 (1964).
29) L. E. Orgel, "An Introduction to Transition-Metal Chemistry: Ligand-Field Theory," Methuen and Co., Ltd., London (1966).
30) B. F. Figgis, "Introduction to Ligand Fields," Interscience Pub. New York-London-Sydney (1966).
31) R. H. Nuttall and D. M. Stalker, *Inorg. Nucl. Chem. Lett.*, **12**, 636 (1976).

Preparation, Racemization, and Deuteration of 2-(Methylthio)propionato-*S,O* and 2-Sulfinatopropionato-*S,O* Complexes of Cobalt(III)

Masaaki Kojima and Junnosuke Fujita*
Department of Chemistry, Faculty of Science, Nagoya University, Chikusa-ku, Nagoya 464
(Received April 28, 1983)

$(+)_{589}$-[Co{SCH(CH_3)COO}(tren)]$^+$, $(-)_{589}$-[Co{CH_3SCH(CH_3)COO}(tren)]$^{2+}$, and $(+)_{589}$-[Co{$S(O)_2$-CH(CH_3)COO}(tren)]$^+$ (tren=tris(2-aminoethyl)amine) were prepared and assigned to the trans (*tertiary amine nitrogen, S*) isomer with the *R* carbon atom on the basis of the absorption, CD, and ^{1}H NMR spectra. Racemization of the complexes was studied in aqueous solutions with ionic strength of 0.1, 0.2, or 1.0 ($NaClO_4$) in the pH and temperature ranges of 5.96—6.86 and 19.9—49.5 °C, respectively. The $CH_3SCH(CH_3)COO^-$ and $^-O_2SCH(CH_3)$-COO^- complexes follow the rate law, $R=k_r[OH^-][complex]$. The second-order rate constants (k_r) for the former and the latter complexes are 4.6×10^3 (35.3 °C) and 7.8×10^3 (35.2 °C) mol^{-1} dm^3 s^{-1}, respectively. The $^-SCH(CH_3)COO^-$ complex did not racemize under these conditions. Deuteration of the methine protons in the complexes was found to proceed simultaneously with the racemization. The differences in reactivity to racemization and proton exchange among three complexes were accounted for by the difference in electron-withdrawing effect of the $^-S-$, $S(CH_3)-$, and $^-S(O)_2-$ groups, and by the difference in net charge of the complex ions.

It is known that methine or methylene groups of α-amino acids become reactive on chelation to metals. The activation leads to such reactions as deuteration of the methine or methylene protons,[1-3] racemization at the α-carbon atom,[2] and condensation with aldehydes to afford α-substituted amino acids.[4] Activation of methylene groups of ethylenediaminetetraacetato[1] and malonato[5,6] metal chelates has also been demonstrated. All these reactions are base-catalyzed and occur at methine or methylene groups located between two electron-withdrawing groups. 2-(Methylthio)propionato-*S,O* and 2-sulfinatopropionato-*S,O* chelates both of which contain two electron-withdrawing groups are also expected to have similar reactivity. Recently Adzamli *et al.*[7] reported that the methylene protons of *S,O* chelates in [Co{$S(O)_nCH_2COO$}$(en)_2$]$^+$ (n=0, 1, 2; en: ethylenediamine) undergo deuterium exchange in basic D_2O solutions. However, no kinetic studies have been done. It is of interest to compare quantitatively the activity of methylene groups of such *S,O* chelates with that of amino acidato-*N,O* and dicarboxylato-*O,O* chelates.

This paper reports kinetic studies on racemization and deuteration of optically active $CH_3SCH(CH_3)$-COO^- and $^-O_2SCH(CH_3)COO^-$ chelates in tris(2-aminoethyl)amine(tren) cobalt(III) complexes as well as deuteration of $CH_3SCH_2COO^-$ and $^-O_2SCH_2COO^-$ chelates in some related complexes. Preparation, stereochemistry, and circular dichroism (CD) spectra of these tren complexes are also described in this paper.

Experimental

$(+)_{589}$-[Co{SCH(CH_3)COO}(tren)]ClO_4. To an aqueous solution (30 cm^3) of [$CoCl_2$(tren)]Cl[8] (1.24 g, 4 mmol) was added an aqueous solution (30 cm^3) of 2-mercaptopropionic acid (0.24 g, 4 mmol). The pH of the solution was adjusted to *ca.* 9 with Na_2CO_3, and the mixture was stirred for 1 h at 65 °C. The color of the solution changed from violet to dark brown. The solution was cooled and then mixed with $NaClO_4$ to yield brown crystals of the complex perchlorate, which were filtered and washed with ethanol. Yield: 1.1 g. No evidence indicative of the presence of the other isomer was obtained in both the ^{1}H NMR spectrum of the isolated complex and chromatography (SP-Sephadex C-25, 0.1 mol dm^{-3} NaBr) of the reaction mixture. The sparingly soluble perchlorate was converted into chloride by use of Dowex 1×8 (Cl^- form). Brown crystals were obtained by adding ethanol to the concentrate of the complex chloride. Yield: 85%. The complex was resolved as follows: To an aqueous solution (9 cm^3) of the complex chloride (2.68 g, 7.78 mmol) was added an aqueous solution (9 cm^3) of $(+)_{546}$-$Na[Co(C_2O_4)_2(en)]\cdot3.5H_2O$[9] (1.48 g, 3.89 mmol). The solution was mixed with 10 cm^3 of ethanol and allowed to stand overnight at room temperature. The dark purple crystals precipitated were collected by filtration and recrystallized six times from water–ethanol. Yield: 0.72 g. The crystals were dissolved in water, and the solution was passed through a column (ϕ1.5 cm×5 cm) of SP-Sephadex C-25 (Na^+ form). After washing the column with water the complex adsorbed was eluted with 0.5 mol dm^{-3} $NaClO_4$. The crystalline $(+)_{589}$-isomer was obtained by further addition of $NaClO_4$ to the effluent, filtered, and washed with ethanol. Yield: 0.37 g. Found: C, 26.30; H, 5.44; N, 13.73%. Calcd for $C_9H_{22}N_4ClCoO_6S$: C, 26.45; H, 5.42; N, 13.71%.

$(-)_{589}$-[Co{CH_3SCH(CH_3)COO}(tren)]$(ClO_4)_2\cdot H_2O$. To a stirred suspension of $(+)_{589}$-[Co{SCH(CH_3)COO}-(tren)]ClO_4 (0.80 g, 1.96 mmol) in dimethyl sulfoxide (20 cm^3) was added CH_3I (2.78 g, 19.6 mmol) in dimethyl sulfoxide (20 cm^3). An orange solution was obtained within a few minutes. After a day the solution was diluted with 0.01 mol dm^{-3} HCl (200 cm^3), excess CH_3I was extracted with $CHCl_3$ (300 cm^3), and the orange aqueous phase was passed through a column (ϕ1.5 cm×3 cm) of SP-Sephadex C-25. The Sephadex charged with the product was placed on the top of a column (ϕ6 cm×30 cm) of SP-Sephadex C-25, and the product was eluted with 0.2 mol dm^{-3} NaCl adjusted to pH 2 with HCl. The column showed only one band. The effluent was diluted twenty times with 0.01 mol dm^{-3} HCl and passed again through an SP-Sephadex C-25 column (ϕ1.5 cm×3 cm). After washing the column with 0.01 mol dm^{-3} $HClO_4$, the complex adsorbed was eluted with 0.7 mol dm^{-3} $NaClO_4$ adjusted to pH 2 with $HClO_4$. The effluent was evaporated to a small volume under reduced pressure to yield orange crystals of the $(-)_{589}$-isomer, which were filtered, washed with ethanol, and recrystallized from 0.01 mol dm^{-3} $HClO_4$. Yield: 0.65 g. Found: C, 22.24; H, 4.68; N, 10.59%. Calcd for $C_{10}H_{27}N_4Cl_2CoO_{11}S$: C, 22.19; H, 5.03; N, 10.35%.

$(+)_{589}$-[Co{$S(O)_2$CH(CH_3)COO}(tren)]$ClO_4\cdot H_2O$. To

a suspension of $(+)_{589}$-[Co{SCH(CH_3)COO}(tren)]ClO_4 (0.82 g, 2 mmol) in 0.1 mol dm^{-3} $HClO_4$ (20 cm^3) was added 35% aqueous H_2O_2 (1.94 g, 20 mmol) in 0.1 mol dm^{-3} $HClO_4$ (30 cm^3) with stirring. The color of the mixture changed from purple to orange, and the starting material dissolved completely in 10 min. After a day $NaClO_4$ was added to the resulting solution to yield yellow crystals, which were filtered and washed with ethanol. No other complex was formed. Yield: 0.53 g. Found: C, 23.57; H, 5.16; N, 12.44%. Calcd for $C_9H_{24}N_4ClCoO_9S$: C, 23.56; H, 5.27; N, 12.21%.

$(-)_{589}$-[Co{S(O)CH(CH_3)COO}(tren)]$^+$. This complex was less stable than the above sulfinato complex and could not be isolated as the pure solid. To a solution of $(+)_{589}$-[Co{SCH(CH_3)COO}(tren)]ClO_4 (8.2 mg, 0.02 mmol) in 0.01 mol dm^{-3} $HClO_4$ (10 cm^3) was added 35% aqueous H_2O_2 (2.1 mg, 0.022 mmol) in 0.01 mol dm^{-3} $HClO_4$ (25 cm^3). The color of the solution changed immediately from purple to orange. After 30 min the solution showed an absorption band at 365 nm characteristic of the S-bonded sulfenato moiety.[7] The solution was used for CD measurements without isolating the complex.

[Co(SCH_2COO)(tren)]ClO_4, [Co(CH_3SCH_2COO)(tren)]$(ClO_4)_2$, and [Co{S(O)$_2CH_2COO$}(tren)]ClO_4. These complexes were prepared by the same methods as those for the corresponding 2-mercaptopropionate, and its derivative complexes. Found: C, 24.32; H, 5.13; N, 14.22%. Calcd for $C_8H_{20}N_4ClCoO_6S$=[Co(SCH_2COO)(tren)]ClO_4: C,24.34; H, 5.11; N, 14.19%. Found: C, 21.17; H, 4.55; N, 10.95%. Calcd for $C_9H_{23}N_4Cl_2CoO_{10}S$=[Co($CH_3SCH_2COO$)(tren)]$(ClO_4)_2$: C, 21.23; H, 4.55; N, 11.00%. Found: C, 22.81; H, 4.85; N, 13.14%. Calcd for $C_8H_{20}N_4ClCoO_8S$=[Co{S(O)$_2$-CH_2COO}(tren)]ClO_4: C, 22.52; H, 4.72; N, 13.13%. Each complex was confirmed to yield only one isomer by column chromatography on SP-Sephadex and ^1H NMR spectra.

p- and t-[Co($CH_3SCH_2CH_2NH_2$)(tren)]$(ClO_4)_3\cdot H_2O$. These complexes were prepared from CH_3I and the corresponding isomers of [Co($SCH_2CH_2NH_2$)(tren)]$ZnCl_4$[10] by a method similar to that for $(-)_{589}$-[Co{CH_3SCH(CH_3)COO}(tren)]$(ClO_4)_2\cdot H_2O$. Found for the *p*-isomer: C, 17.56; H, 4.51; N, 11.39%. Found for the *t*-isomer: C, 17.58; H, 4.70; N, 11.57%. Calcd for $C_9H_{29}N_5Cl_3CoO_{13}S$: C, 17.64; H, 4.77; N, 11.43%.

[Co(SCH_2COO)$(en)_2$]ClO_4, [Co(CH_3SCH_2COO)$(en)_2$]$(ClO_4)_2$, and [Co{S(O)$_2CH_2COO$}$(en)_2$]$Cl\cdot H_2O$. These complexes were prepared by literature procedures.[7,11-13]

[Co{S(O)$_2$C(CH_2OH)$_2COO$}$(en)_2$]$ClO_4\cdot 0.5CH_3OH$. To a mixture of [Co{S(O)$_2CH_2COO$}$(en)_2$]$Cl\cdot H_2O$ (0.68 g, 2 mmol) and Na_2CO_3 (0.12 g, 1 mmol) in water (25 cm^3) was added an aqueous solution (25 cm^3) containing 8 mmol of formaldehyde. The mixture was stirred for a day at room temperature and filtered to remove a small amount of precipitate. The filtrate was chromatographed using a column (ϕ3 cm×40 cm) of SP-Sephadex C-25 and an eluent of 0.2 mol dm^{-3} $NaClO_4$. The effluent of the fast-moving main band was collected and evaporated to a small volume under reduced pressure. On addition of methanol the concentrate gave large orange crystals, which were filtered, washed with methanol, and recrystallized from water–methanol. Yield: 0.13 g. The presence of 0.5 mol of methanol in the complex salt was confirmed by the ^1H NMR spectrum. Found: C, 21.22; H, 5.06; N, 11.86%. Calcd for $C_{8.5}H_{24}N_4ClCoO_{10.5}S$: C, 21.41; H, 5.07; N, 11.75%.

Measurements. Absorption and CD spectra were recorded on a Hitachi 323 spectrophotometer and a JASCO J-40CS spectropolarimeter, respectively. Optical rotations at 589 nm were measured with a JASCO DIP-4 polarimeter. ^1H NMR spectra were obtained in D_2O or DCl–D_2O solutions with a JEOL PMX-60 spectrometer using sodium 3-(trimethylsilyl)propionate-d_4 or sodium 2,2-dimethyl-2-silapentane-5-sulfonate (DSS) as an internal reference.

Racemization Studies. Racemization rates were followed by monitoring CD strength changes at 465 nm ([Co{CH_3SCH(CH_3)COO}(tren)]$^{2+}$) or at 420 nm ([Co{S(O)$_2$CH(CH_3)COO}(tren)]$^+$) as a function of reaction time. All experiments were carried out in aqueous solutions with ionic strength of 0.1, 0.2, or 1.0 ($NaClO_4$) in the pH and temperature ranges of 5.96—6.86 ($NaCH_3COO$–HCl) and 19.9—49.5 °C, respectively. The complex concentrations were in the range of (2.5—9.6)×10^{-3} mol dm^{-3}. The absorption spectra were also measured to check the stability of the complexes toward decomposition.

Deuteration Studies. Deuteration rates were followed by monitoring signal changes in ^1H NMR spectra. The complex perchlorates were converted into chlorides with a Dowex 1×8 anion exchanger in the chloride form in order to increase the solubility. The complex concentrations were 0.21—0.25 mol dm^{-3}, and no attempt was made to keep ionic strength constant. The samples in NMR tubes were placed in a thermostat at 34.5 °C, and the spectra were recorded at timed intervals at 34.5 °C. The peak areas of signals were determined by weighing paper cutouts maching the peak areas. The pD=pH+0.4,[14] and $[OD^-]=2.89\times10^{-15}$ $[D^+]^{-1}$ [15] formulae were used to evaluate $[D^+]$ and $[OD^-]$, respectively.

Results and Discussion

Preparation and Characterization of the Complexes. The thiolato complexes, [Co{SCH(CH_3)COO}(tren)]$^+$ and [Co(SCH_2COO)(tren)]$^+$ were prepared from [$CoCl_2$(tren)]$^+$ and the thiolate ligands in fairly good yields (60—70%). A number of thiolatobis(ethylenediamine)cobalt(III) complexes have been prepared by oxidizing bis(ethylenediamine)cobalt(II) ions with the disulfide derivative of a thiol in the absence of air.[16] However, this method was not effective for the tren complex, no redox reaction taking place between tren-cobalt(II) ions and either disulfide, ($^-OOCCH_2S$–)$_2$ or (^-OOCCH-(CH_3)S–)$_2$. On the other hand, analogous ligands, ($^-OOCCH_2Se$–)$_2$ and ($NH_2CH_2CH_2S$–)$_2$ oxidize tren-cobalt(II) ions to yield [Co($SeCH_2COO$)(tren)]$^+$[19] and [Co($NH_2CH_2CH_2S$)(tren)]$^{2+}$,[10] respectively, although the reaction with the latter ligand is slow. Such differences in reactivity may be related with oxidizing strength of these ligands toward the tren-cobalt(II) ion.

Two geometrical (*p*- and *t*-) isomers[18] are possible for

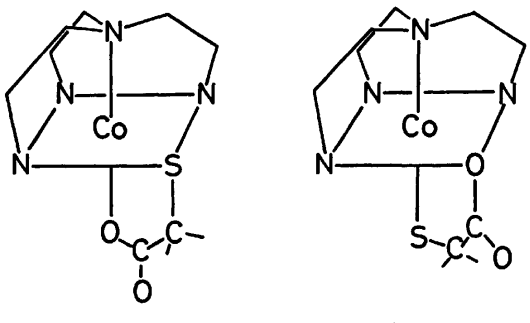

Fig. 1. Two geometrical isomers of [Co(*S,O* chelate)(tren)]$^{n+}$.

TABLE 1. ABSORPTION AND CD SPECTRAL DATA

Complex	Absorption $\tilde{\nu}_{max}/cm^{-1}(\log\varepsilon)$	CD $\tilde{\nu}_{ext}/cm^{-1}(\Delta\varepsilon)$
$[Co(SCH_2COO)(tren)]^+$	17000(1.81)[b]	
	20330(2.07)	
	22000(2.03)[b]	
	27500(2.42)[b]	
	34600(4.17)	
	44840(4.18)	
$(+)_{589}$-$[Co\{SCH(CH_3)COO\}(tren)]^+$	17000(1.82)[b]	17150(−0.59)
	20330(2.07)	19880(+3.10)
	22000(2.02)[b]	22990(−2.72)
	27500(2.40)[b]	
	34720(4.18)	34970(+4.63)
	44350(4.16)	41490(−3.05)
$[Co(CH_3SCH_2COO)(tren)]^{2+}$	20620(2.13)	
	28000(2.41)[b]	
	34660(3.99)	
	42830(4.13)	
$(-)_{589}$-$[Co\{CH_3SCH(CH_3)COO\}(tren)]^{2+}$[a]	20640(2 22)	21510(−0 93)
	28000(2.44)[b]	28170(+0 40)
	34970(4.03)	34360(+2 86)
	43290(4.13)	39220(−3.04)
$[Co\{S(O)_2CH_2COO\}(tren)]^+$	23040(2.52)	
	33170(4.09)	
	44740(4.15)	
$(+)_{589}$-$[Co\{S(O)_2CH(CH_3)COO\}(tren)]^+$[a]	22990(2.60)	20200(−0.17)
		23920(+0.79)
	33000(4.10)	33220(+4.11)
	44540(4.13)	42020(−1.95)
p-$[Co(CH_3SCH_2CH_2NH_2)(tren)]^{3+}$	20530(2.29)	
	34720(3.88)	
	43200(4.17)	
t-$[Co(CH_3SCH_2CH_2NH_2)(tren)]^{3+}$	20790(2.15)	
	34420(4.05)	
	44540(4.18)	
$[Co\{S(O)_2C(CH_2OH)_2COO\}(en)_2]^+$	22300(2.45)	
	33110(4.01)	
	44740(4.14)	
$[Co\{S(O)_2CH_2COO\}(en)_2]^+$	22300(2.37)	
	33840(3.96)	
	44740(4.15)	

a) Measured in 10^{-2} mol dm^{-3} $HClO_4$. b) Shoulder.

$[Co(SCHRCOO)(tren)]^+$ (R=H, CH_3; Fig. 1). These thiolatocarboxylato complexes form only one geometrical isomer as confirmed by column chromatography and ^1H NMR spectra. The absorption spectra of both complexes are quite similar and the complexes will have the same geometrical configuration. The spectra show a shoulder around 17000 cm^{-1} on the low energy side of the first absorption band, and an intense sulfur-to-cobalt(III) charge-transfer band around 34700 cm^{-1} (Table 1 and Fig. 2). The spectral pattern is characteristic of cobalt(III)-thiolato complexes.[19]

The $[Co(NH_2CH_2CH_2S)(tren)]^{2+}$ complex forms both *p*- and *t*-isomers. The isomers give the first absorption band at nearly the same position, but the patterns differ remarkably from each other. The spectral pattern of the $^-SCHRCOO^-$ complexes is very similar to that of the *t*-isomer of the $NH_2CH_2CH_2S^-$ complex, showing strong shoulder absorption on the low energy side of the first absorption band (Fig. 2). The *p*-isomer exhibits only weak shoulder in this region. Thus both thiolatocarboxylato complexes can be assigned to the *t*-isomer. This assignment agrees with that obtained from absorption spectra of methylthio complexes derived from the present $^-SCHRCOO^-$ complexes described below.

The sulfenato-, sulfinato-, and methylthio-carboxylato complexes were prepared from the $^-SCHRCOO^-$ complexes by stoichiometric oxidation with H_2O_2,[7,20] by oxidation with excess H_2O_2,[7,20] and by methylation with CH_3I in dimethyl sulfoxide,[10,11,21,22] respectively. These reactions do not involve Co–S cleavage, and geometrical structures of the complexes should be retained.[23,24] The $[Co(CH_3SCH_2COO)(tren)]^{2+}$ complex thus obtained gives the first absorption band (20620 cm^{-1}) between those of *p*-(20530 cm^{-1}) and *t*-(20790

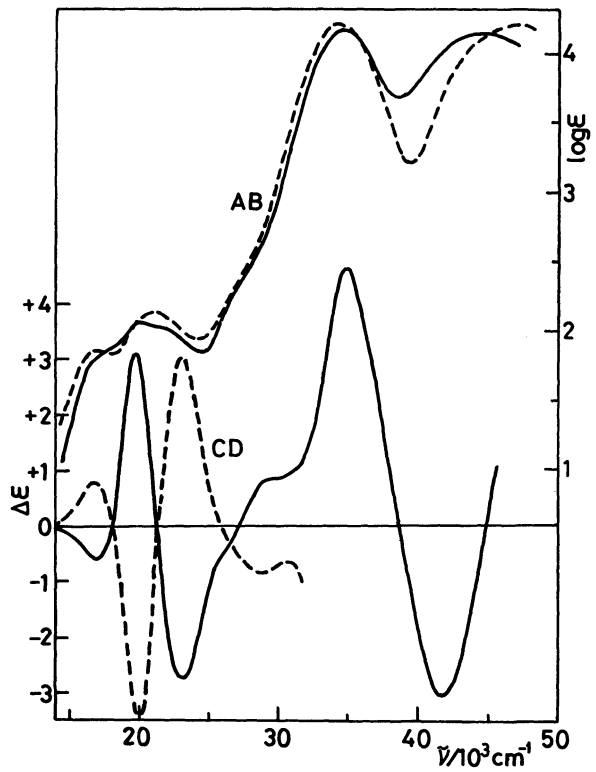

Fig. 2. Absorption and CD spectra of $(+)_{589}$-[Co{SCH(CH_3)COO}(tren)]$^+$ (——) and *t*-[Co{(*S*)-SCH(CH_3)-CH_2NH_2}(tren)]$^{2+}$ (------)[26] in water.

cm^{-1}) isomers of [Co($CH_3SCH_2CH_2NH_2$)(tren)]$^{3+}$ (Table 1). Since $CH_3SCH_2COO^-$ will exert a weaker ligand field than $CH_3SCH_2CH_2NH_2$, the CH_3SCH_2-COO^- complex will show the d-d absorption bands at lower energy than those of the $CH_3SCH_2CH_2NH_2$ complex with the same geometrical configuration. Thus [Co(CH_3SCH_2COO)(tren)]$^{2+}$ and all the *S,O* chelate complexes obtained in this study can be assigned to the *t*-isomer.

The difference in absorption maxima of the d-d bands between *t*- and *p*-[Co($CH_3SCH_2CH_2NH_2$)-(tren)]$^{3+}$ may partly be ascribed to the difference in strain involved in the isomers. Molecular models indicate that the *p*-isomer will be strained by steric hindrance between the methyl group and the tren ligand. On the other hand, the *t*-isomer has no such hindrance around the methyl group. Accordingly the strained *p*-isomer will show the first absorption band at lower energy than that of the *t*-isomer. When the methyl group in the *p*-isomer is replaced by a small hydrogen atom, the hindrance with the tren ligand will be diminished, and the energy difference between the first absorption bands of the *p*- and *t*-isomers will be decreased. In concd H_2SO_4, where the thiolato chelates will be completely protonated,[25] both isomers show the first absorption band at the same position (20640 cm^{-1}). Thus the position of the first absorption band of [Co-($RSCH_2CH_2NH_2$)(tren)]$^{3+}$ seems to depend strongly on the steric conditions.

The ^1H NMR spectrum of [Co(CH_3SCH_2COO)-(tren)]$^{2+}$ in DCl–D_2O (pD *ca.* 2) gives an AB quartet (3.53—4.22 ppm, J=18 Hz, $\Delta\nu$=14 Hz) attributable to the methylene protons of the (methylthio)acetate ligand. The result demonstrates that the inversion at the sulfur atom is slow on the NMR time scale. However, attempts to resolve the complex by column chromatography were unsuccessful, suggesting that the inversion is not so slow as to be resolved by conventional techniques. The ^1H NMR spectrum of [Co{CH_3SCH-(CH_3)COO}(tren)]$^{2+}$ shows only one kind of quartet (4.07 ppm) and doublet (1.65 ppm) assignable to the methine and methyl protons of the –$CH(CH_3)$– group, respectively. From a comparison with the above (methylthio)acetato complex, it is unlikely that the spectrum is brought about by rapid inversion at sulfur (coalesced spectrum) or accidental degeneracies. Thus it is concluded that the disposition of the S–CH_3 group is stereospecific in the (methylthio)propionato complex (*vide post*). In general, sulfur atoms in cobalt(III)-sulfide complexes are labile toward inversion, although the rate is slow on the NMR time scale.[10]

Figure 2 compares the absorption and CD spectra of $(+)_{589}$-[Co{SCH(CH_3)COO}(tren)]$^+$, which has been assigned to the *t*-isomer, with those of *t*-[Co{(*S*)-SCH-(CH_3)CH_2NH_2}(tren)]$^{2+}$.[26] The absorption spectra of both complexes are similar, but the CD spectra are almost enantiomeric to each other in the d-d absorption band region. Thus the carbon atom of $(+)_{589}$-[Co-{SCH(CH_3)COO}(tren)]$^+$ can be assigned to *R* configuration. The absolute configuration of the sulfur atom in $(-)_{589}$-[Co{S(O)CH(CH_3)COO}(tren)]$^+$ which was derived from $(+)_{589}$-[Co{SCH(CH_3)COO}-(tren)]$^+$ can be assigned by comparing the CD spectrum with that of *Λ*-[Co{*S*(S), *R*(C)-cysO}$(en)_2$]$^{+}$[23] whose absolute configuration has been determined by the X-ray method[27] (*S*(S), *R*(C)-cysO=(*S*(S), *R*(C))-2-amino-3-sulfenatopropionate-*N,S*). In the Co–S charge-transfer band region (25000—39000 cm^{-1}) the CD pattern of $(-)_{589}$-[Co{S(O)CH(CH_3)COO}(tren)]$^+$ is almost enantiomeric to that of the *Λ*[*S*(S), *R*(C)]-cysO complex, and very similar to that of the *Λ*[*R*(S), *R*(C)]-cysO complex.[23] Thus the sulfur atom in $(-)_{589}$-[Co{S(O)CH(CH_3)COO}(tren)]$^+$ can be assigned to *R* configuration. The oxidation of the sulfur atom in the $^-SCH(CH_3)COO^-$ complex will occur selectively at the *anti* position to the methyl group to afford the (*R*(S), *R*(*C*))- or (*S*(S), *S*(C))-$^-S(O)CH(CH_3)COO^-$ complex, since the incoming oxidant to this position has less steric interaction with the methyl group (Fig. 3). Thus the carbon atom in $(+)_{589}$-[Co{SCH(CH_3)COO}(tren)]$^+$ which gives the (*R*(S))-$^-S(O)CH(CH_3)COO^-$ complex should have *R* configuration. This conclusion for the carbon atom agrees with the previous one obtained on the basis of the CD spectrum of the (*S*)-SCH(CH_3)-CH_2NH_2 complex.

Very recently, the structure of $(-)_{589}$-[Co{CH_3SCH-(CH_3)COO}(tren)]$^{2+}$ which was derived from $(+)_{589}$-[Co{SCH(CH_3)COO}(tren)]$^+$ has been determined by X-ray analysis to have *S*(S), *R*(C) configuration.[28] The disposition of the methyl group on the sulfur atom in this complex is the same as that of the oxygen atom in the above *R*(S), *R*(C)-sulfenato complex, the notation, *R* and *S* for the chiral sulfur atom being reversed between the methylthio and sulfenato complexes.

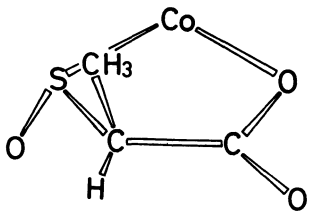

Fig. 3. Proposed structure of the $^{-}OSCH(CH_3)COO^{-}$ chelate.

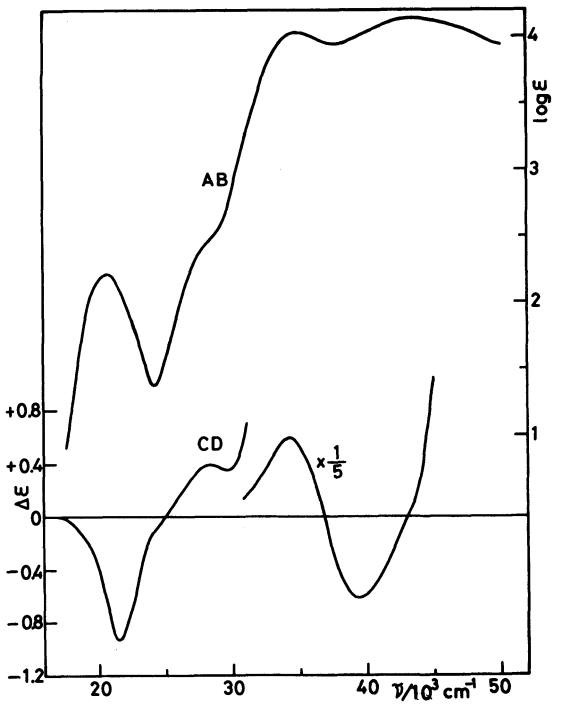

Fig. 4. Absorption and CD spectra of $(-)_{589}$-$[Co\{CH_3SCH(CH_3)COO\}(tren)]^{2+}$ in 10^{-2} mol dm^{-3} $HClO_4$.

Kinetics of Racemization and Deuteration Reactions. Absorption and CD spectra of $(-)_{589}$-$[Co\{CH_3SCH(CH_3)COO\}(tren)]^{2+}$ in acidic water are given in Fig. 4. The complex which was prepared from $(+)_{589}$-$[Co\{SCH(CH_3)COO\}(tren)]^{+}$ gives a CD extreme at 465 nm (21510 cm^{-1}), and this wavelength was used to follow the racemization rates. Measurements were carried out over the temperature range of 20.0 to 45.3 °C in the pH region of 5.96 to 6.86. In every kinetic run the plot of $\log(\Delta\varepsilon_{465})$ *vs.* time at a constant pH gave a straight line for at least two half-lives. Thus the racemization rate at a constant pH can be expressed as $-d[complex]/dt=k_{r(obsd)}[complex]$, where $k_{r(obsd)}$ is the pseudo-first-order rate constant for racemization at a constant pH. The $k_{r(obsd)}/[OH^-]$ $(=k_r)$ values are constant at a given temperature, indicating that the reaction is first-order in $[OH^-]$. The values of $k_{r(obsd)}$ and k_r are listed in Table 2, where the variation of ionic product of water, $k_w=[H^+][OH^-]$ with change in temperature[29] was taken into consideration. The average value of k_r is $(4.6\pm0.1)\times10^3$ mol^{-1} dm^3 s^{-1} at 35.3 °C (Table 3). No detectable change in the absorption spectrum was observed during the measurements. The rate was independent of ionic strength in the range of 0.1 to 1.0 ($NaClO_4$). Eyring treatments of $\log(k_r/T)$ *vs.* T^{-1} yielded an activation enthalpy of 46 ± 1 kJ mol^{-1} and an activation entropy of -26 ± 4 J mol^{-1} K^{-1}. The sulfur atom in the complex is also chiral, but racemizes more rapidly than does the carbon atom as stated previously. Thus the racemization observed should be for the carbon atom.

Table 2. Rate constants for the racemization of $(-)_{589}$-$[Co\{CH_3SCH(CH_3)COO\}(tren)]^{2+}$ and $(+)_{589}$-$[Co\{S(O)_2CH(CH_3)COO\}(tren)]^{+}$ $(I=0.2)$

pH	t/°C	$k_{r(obsd)}$/s^{-1}	k_r/mol^{-1} dm^3 s^{-1}
	$(-)_{589}$-$[Co\{CH_3SCH(CH_3)COO\}(tren)]^{2+}$		
5.96	24.9	$(2.20\pm0.03)\times10^{-5}$	$(2.41\pm0.05)\times10^3$
5.96	35.3	$(9.05\pm0.05)\times10^{-5}$	$(4.74\pm0.12)\times10^3$
6.29	35.3	$(1.86\pm0.02)\times10^{-4}$	$(4.57\pm0.10)\times10^3$
6.57	20.0	$(4.26\pm0.02)\times10^{-5}$	$(1.68\pm0.04)\times10^3$
6.57	25.0	$(9.00\pm0.03)\times10^{-5}$	$(2.42\pm0.05)\times10^3$
6.57	30.3	$(1.83\pm0.02)\times10^{-4}$	$(3.35\pm0.08)\times10^3$
6.57	35.3	$(3.52\pm0.02)\times10^{-4}$	$(4.53\pm0.11)\times10^3$
6.57	40.3	$(6.88\pm0.03)\times10^{-4}$	$(6.37\pm0.13)\times10^3$
6.57	45.3	$(1.21\pm0.03)\times10^{-3}$	$(8.12\pm0.17)\times10^3$
6.86	35.3	$(6.70\pm0.06)\times10^{-4}$	$(4.44\pm0.12)\times10^3$
6.32[a]	30.3	$(8.83\pm0.05)\times10^{-5}$	$(2.88\pm0.06)\times10^3$
6.66[b]	30.3	$(2.62\pm0.04)\times10^{-5}$	$(3.90\pm0.09)\times10^3$
	$(+)_{589}$-$[Co\{S(O)_2CH(CH_3)COO\}(tren)]^{+}$		
6.21	19.9	$(3.71\pm0.03)\times10^{-5}$	$(3.37\pm0.06)\times10^3$
6.21	25.1	$(8.62\pm0.10)\times10^{-5}$	$(5.32\pm0.16)\times10^3$
6.21	30.1	$(1.46\pm0.02)\times10^{-4}$	$(6.13\pm0.14)\times10^3$
6.21	35.2	$(2.65\pm0.02)\times10^{-4}$	$(7.82\pm0.18)\times10^3$
6.21	39.7	$(4.74\pm0.02)\times10^{-4}$	$(1.00\pm0.03)\times10^4$
6.21	40.2	$(5.09\pm0.03)\times10^{-4}$	$(1.08\pm0.03)\times10^4$
6.21	42.5	$(6.53\pm0.03)\times10^{-4}$	$(1.13\pm0.03)\times10^4$
6.21	45.5	$(8.92\pm0.03)\times10^{-4}$	$(1.37\pm0.03)\times10^4$
6.21	49.5	$(1.39\pm0.01)\times10^{-3}$	$(1.57\pm0.03)\times10^4$
6.67	25.2	$(2.46\pm0.02)\times10^{-4}$	$(5.26\pm0.08)\times10^3$
6.80	25.1	$(3.70\pm0.03)\times10^{-4}$	$(5.86\pm0.10)\times10^3$

a) Ionic strength 1.0. b) Ionic strength 0.1.

Table 3. Rate constants for racemization and deuteration

Complex	k/mol^{-1} dm^3 s^{-1} (t/°C)
Racemization	
$[Co\{CH_3SCH(CH_3)COO\}(tren)]^{2+}$	$(4.6\pm0.1)\times10^3$ (35.3)
$[Co\{S(O)_2CH(CH_3)COO\}(tren)]^{+}$	$(7.8\pm0.2)\times10^3$ (35.2)
Deuteration	
$[Co\{CH_3SCH(CH_3)COO\}(tren)]^{2+}$	$(1.5\pm0.3)\times10^4$ (34.5)
$[Co\{S(O)_2CH(CH_3)COO\}(tren)]^{+}$	$(4.5\pm0.9)\times10^4$ (34.5)
$[Co\{S(O)_2CH_2COO\}(tren)]^{+}$	$(3.0\pm0.6)\times10^5$ (34.5)
$[Co\{S(O)_2CH_2COO\}(en)_2]^{+}$	$(4.3\pm0.9)\times10^5$ (34.5)

The absorption and CD spectra of $(+)_{589}$-$[Co\{S(O)_2CH(CH_3)COO\}(tren)]^{+}$ in 0.01 mol dm^{-3} $HClO_4$ are given in Fig. 5. The complex was also prepared from $(+)_{589}$-$[Co\{SCH(CH_3)COO\}(tren)]^{+}$, and the racemization was studied by the same procedure as the above. The decrease in CD strength also obeyed second-order kinetics; first-order in each of the concentrations of complex and OH^- ions. The results are given in Table 2. The second-order rate constant (k_r) is $(7.8\pm$

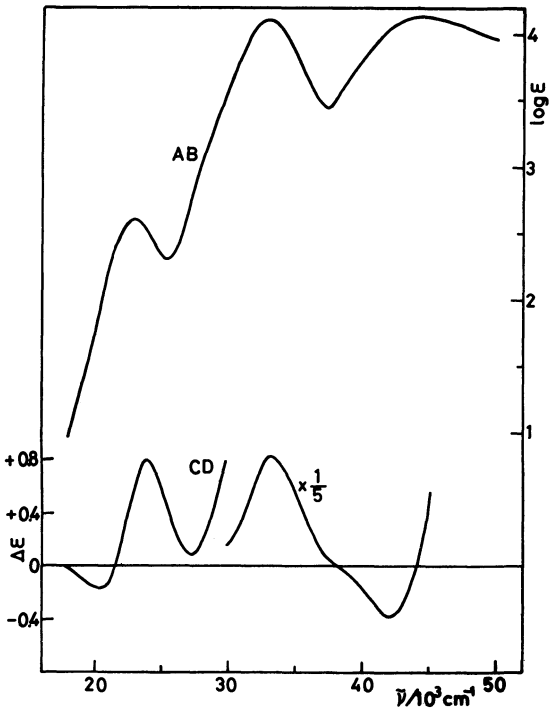

Fig. 5. Absorption and CD spectra of $(+)_{589}$-$[Co\{S(O)_2CH(CH_3)COO\}(tren)]^+$ in 10^{-2} mol dm^{-3} $HClO_4$.

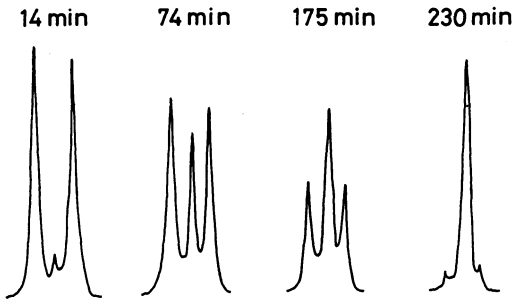

Fig. 6. Signal change of the C–CH_3 of $[Co\{S(O)_2CH(CH_3)COO\}(tren)]^+$ in D_2O (pD 5.75, 34.5 °C).

$0.2)\times10^3$ mol^{-1} dm^3 s^{-1} at 35.2 °C, and the values of activation enthalpy and entropy are 40 ± 1 kJ mol^{-1} and -40 ± 4 J mol^{-1} K^{-1}, respectively.

Deuteration rates of the methine protons of *S,O* chelates in $[Co\{CH_3SCH(CH_3)COO\}(tren)]Cl_2$ and $[Co\{S(O)_2CH(CH_3)COO\}(tren)]Cl$ were obtained by monitoring signal changes in the ^1H NMR spectra. The C–CH_3 doublet signals become a singlet by the proton-deuteron exchange (Fig. 6). For both complexes, the plot of log(peak area of the doublet) *vs.* time was linear, from which the pseudo-first-order rate constant for the deuteration $k_{D(obsd)}$ was obtained. The rates for the $CH_3SCH(CH_3)COO^-$ and $^-S(O)_2CH(CH_3)COO^-$ complexes were $(7.3\pm0.5)\times10^{-5}$ s^{-1} (pD 5.75, 34.5 °C) and $(6.4\pm0.4)\times10^{-5}$ s^{-1} (pD 6.16, 34.5 °C), respectively. The deuteration was completed in 1 h at pD 7.5 and 34.5 °C for both complexes. The rates are 10^5—10^6-fold greater than that for the methine proton in $[Co(alaninate)(en)_2]^{2+}$ (8.5×10^{-11} s^{-1} at pD 5.75 and 34.3 °C, and 2.2×10^{-10} s^{-1} at pD 6.16 and 34.3 °C).[30]

Table 4. ^1H NMR spectral data for S–CH and S–CH_2 protons in $[CoN_4OS]^{n+}$-type complexes in D_2O, δ[a]

Complex	S–CH	S–CH_2
$[Co\{SCH(CH_3)COO\}(tren)]^+$	3.5(q)[b]	
$[Co\{CH_3SCH(CH_3)COO\}(tren)]^{2+}$	4.07(q)	
$[Co\{S(O)_2CH(CH_3)COO\}(tren)]^+$	4.38(q)	
$[Co(SCH_2COO)(en)_2]^+$		3.21(s)
$[Co(CH_3SCH_2COO)(en)_2]^{2+}$		3.85(q_{AB})
$[Co\{S(O)_2CH_2COO\}(en)_2]^+$		4.45(q_{AB})

a) The complexes of which methine or methylene protons are susceptible to deuterium exchange were measured in DCl–D_2O. b) The signal overlapped with those of tren-CH_2, and the chemical shift was determined by the spin decoupling technique. s: singlet, q: quartet, q_{AB}: AB quartet.

As shown previously, the racemization rates of $CH_3SCH(CH_3)COO^-$ and $^-S(O)_2CH(CH_3)COO^-$ chelates in the tren complex are proportional to the concentration of OH^-. The results support that the reactions proceed with a mechanism analogous to that for racemization of α-amino acidato chelates,[2] where the rate-determining step is release of the methine proton by the nucleophilic attack of OH^-. If the proton exchange and the racemization take place simultaneously and there is no isotopic effect between H and D, the ratio of k_D to k_r (k_D/k_r) should be 2. The observed ratios are 3.2 and 5.7 for $[Co\{CH_3SCH(CH_3)COO\}(tren)]^+$ and $[Co\{S(O)_2CH(CH_3)COO\}(tren)]^+$, respectively, at 35 °C, the k_D values being obtained by the formula $k_D = k_{D(obsd)}[D^+]/2.89\times10^{-15}$.[15] Although the reliability of these values is uncertain because of difficulty in determining accurate $[D^+]$ values,[14] we assume that both reactions of the proton exchange and the racemization in these tren complexes proceed simultaneously, forming carbanions as intermediate.

Table 4 shows that the NMR signals of the methine or methylene protons adjacent to sulfur shift remarkably to a lower magnetic field in the order of the $^-SCHRCOO^-$, $CH_3SCHRCOO^-$, and $^-S(O)_2CHRCOO^-$ (R=H and CH_3) complexes. Such large lower shifts may be brought about by the increasing electron-withdrawing effect of $^-S-$, $S(CH_3)-$, and $^-S(O)_2-$ groups. When the electron-withdrawing effect is small, the methine or methylene group will require larger energy in forming a carbanion and will have less reactivity to proton exchange or racemization. In fact, $[Co\{SCH(CH_3)COO\}(tren)]^+$ which has two lone pairs of electrons on the sulfur atom and gives the methine proton signal at 3.5 ppm does not racemize over 6 days at pH 9.22 and 25 °C. The methylene protons of $^-SCH_2COO^-$ in $[Co(SCH_2COO)(tren)]^+$ do not either undergo deuterium exchange over at least a day at pD 10.4 and 30 °C, although Adzamli *et al.*[7] reported that the deuteration occured in basic D_2O solution. The complex decomposes at higher pH. The sulfinato complex is expected to be more labile than the methylthio complex in deuteration or racemization reactions, since the sulfinato group is more electronegative than the methylthio group. However, the rates of $[Co\{S(O)_2CH(CH_3)-$

COO}(tren)]$^+$ in these reactions are similar to those of [Co{$CH_3SCH(CH_3)COO$}(tren)]$^{2+}$. The result may be accounted for by a difference in net charge of the complex ions. It has been reported that reactivity of glycine chelates in cobalt(III) complexes toward base-catalyzed condensation with acetaldehyde decreases with a decreasing positive net charge of the complex ion.[2,31,32]

The [Co{$S(O)_2CH_2COO$}$(en)_2$]$^+$ complex easily reacts with formaldehyde under basic conditions to afford [Co{$S(O)_2C(CH_2OH)_2COO$}$(en)_2$]$^+$ (Experimental). A similar condensation reaction has been reported to occur between [Co(glycinate)$(en)_2$]$^{2+}$ and formaldehyde in aqueous solution saturated with Li_2CO_3.[33]

The free $CH_3SCHRCOO^-$ (R=H, CH_3) ligand is stable to proton exchange. For example, $CH_3SCH(CH_3)COO^-$ does not undergo deuterium exchange for 4 d at pD *ca.* 9 and 30 °C. Thus the cobalt(III) ion activates the methine or methylene protons of these *S,O* chelate ligands. The activity of the protons seems to be much higher than that of the corresponding protons of amino acidato chelates as indicated by the proton exchange or racemization reactions.

References

1) D. H. Williams and D. H. Busch, *J. Am. Chem. Soc.*, **87**, 4644 (1965).
2) D. A. Buckingham, L. G. Marzilli, and A. M. Sargeson, *J. Am. Chem. Soc.*, **89**, 5133 (1967).
3) T. Ama, H. Kawaguchi, M. Kanekiya, and T. Yasui, *Bull. Chem. Soc. Jpn.*, **53**, 956 (1980).
4) M. Sato, K. Okawa, and S. Akabori, *Bull. Chem. Soc. Jpn.*, **30**, 937 (1957).
5) H. Yoneda and Y. Morimoto, *Inorg. Chim. Acta*, **1**, 413 (1967).
6) U. Sakaguchi, K. Morito, and H. Yoneda, *Chem. Lett.*, **1979**, 19.
7) I. K. Adzamli, K. Libson, J. D. Lydon, R. C. Elder, and E. Deutsch, *Inorg. Chem.*, **18**, 303 (1979).
8) D. A. Buckingham, P. J. Cresswell, and A. M. Sargeson, *Inorg. Chem.*, **14**, 1485 (1975).
9) J. H. Worrell, *Inorg. Chem.*, **10**, 870 (1971).
10) W. G. Jackson and A. M. Sargeson, *Inorg. Chem.*, **17**, 2165 (1978).
11) R. H. Lane, F. A. Sedor, M. J. Gilroy, P. F. Eisenhardt, J. P. Bennett, Jr., R. X. Ewall, and L. E. Bennett, *Inorg. Chem.*, **16**, 93 (1977).
12) K. Yamanari, J. Hidaka, and Y. Shimura, *Bull. Chem. Soc. Jpn.*, **50**, 2299 (1977).
13) K. Hori, *Bull. Chem. Soc. Jpn.*, **48**, 2209 (1975).
14) P. K. Glasoe and F. A. Long, *J. Phys. Chem.*, **64**, 188 (1960).
15) The data of ionic product for D_2O were taken from A. K. Covington, R. A. Robinson, and R. G. Bates, *J. Phys. Chem.*, **70**, 3820 (1966).
16) D. L. Nosco and E. Deutsch, *Inorg. Synth.*, **21**, 19 (1982) and references cited therein.
17) K. Tozaki, K. Nakajima, M. Kojima, and J. Fujita, unpublished data.
18) The *p*- and *t*-isomers have the S atom at the trans position to the primary(*p*) and tertiary(*t*) amine nitrogens of tren, respectively.
19) M. H. Dickman, R. J. Doedens, and E. Deutsch, *Inorg. Chem.*, **19**, 945 (1980).
20) C. P. Sloan and J. H. Krueger, *Inorg. Chem.*, **14**, 1481 (1975).
21) K. Hori, *Nippon Kagaku Zasshi*, **90**, 561 (1969).
22) V. Kothari and D. H. Busch, *Inorg. Chem.*, **8**, 2276 (1969).
23) D. L. Harting, C. P. Sloan, A. W. Cabral, and J. H. Krueger, *Inorg. Chem.*, **17**, 1649 (1978).
24) G. J. Gainsford, W. G. Jackson, and A. M. Sargeson, *J. Chem. Soc., Chem. Commun.*, **1979**, 802.
25) I. K. Adzamli, D. L. Nosco, and E. Deutsch, *J. Inorg. Nucl. Chem.*, **42**, 1364 (1980).
26) K. Nakabayashi, M. Kojima, and J. Fujita, unpublished data.
27) W. G. Jackson, A. M. Sargeson, and P. O. Whimp, *J. Chem. Soc., Chem. Commun.*, **1976**, 934.
28) S. Ohba and Y. Saito, private communication.
29) H. S. Harned and R. A. Robinson, *Trans. Faraday Soc.*, **36**, 973 (1940).
30) The rates were calculated from the rate law, $R = k_D[OD^-][complex]$, $k_{D_2O} = 2.9 \times 10^{-15}$ mol^2 dm^{-6} and $k_D = 5.3 \times 10^{-2}$ mol^{-1} dm^3 s^{-1} at 34.3 °C.[2]
31) J. C. Dabrowiak and D. W. Cooke, *Inorg. Chem.*, **14**, 1305 (1975).
32) P. R. Norman and D. A. Phipps, *Inorg. Chim. Acta*, **28**, L161 (1978).
33) R. J. Geue, M. R. Snow, J. Springborg, A. J. Heart, A. M. Sargeson, and T. Taylor, *J. Chem. Soc., Chem. Commun.*, **1975**, 285.

 © 1983 The Chemical Society of Japan Bull. Chem. Soc. Jpn., 56, 2965—2968 (1983)

Immunoassay Using a Metal-complex Compound as a Chemiluminescent Catalyst. II. An Improvement of the Analytical Method for Practical Use

Tadashi HARA,* Motohiro TORIYAMA, and Kazuhiko TSUKAGOSHI
Dapartment of Chemical Engineering, Faculty of Engineering, Doshisha University, Karasuma Imadegawa, Kamigyo-ku, Kyoto 602
(Received April 30, 1983)

Immunoassay using a synthesized metal-complex compound as a labeling reagent has been investigated. Iron(III) 2,9,16,23-tetrakis(chlorocarbonyl)phthalocyanine, which showed a marked catalytic action in the chemiluminescence reaction between luminol and H_2O_2, was synthesized, and albumin was labeled with it. Albumin in the range from 50 ng/tube to 50 μg/tube could be determined by measuring the chemiluminescence intensity in a competitive immunoassay using glass beads immobilized with an antibody. The present method became about 40 time as sensitive as the previous method by optimizing the labeling procedure, the chemiluminescence reaction, and the immune reaction.

A chemiluminescence complex catalyst immunoassay (CLCCIA), in which a synthesized metal-complex compound acting as a catalyst for chemiluminescence reaction was used as a labeling reagent, was previously reported by the authors for the determination of human serum albumin(HSA) as a model compound for the protein.[1] Since the CLCCIA was carried out by measuring the catalyst effect of conjugated iron(III) 2,9,16,23-tetracarboxyphthalocyanine(TCP–Fe(III)) on the chemiluminescence reaction between 5-amino-2,3-dihydro-1,4-phthalazinedione(luminol) and hydrogen peroxide(H_2O_2), CLCCIA was expected to have the following advantages: 1) A sensitive and rapid analysis can be made by the use of a simple and inexpensive apparatus; 2) the TCP–Fe(III) used as a labeling reagent is more stable and cheaper than a radioactive isotope and enzyme; 3) no steric hindrance of the immune reaction is caused by TCP–Fe(III) because its molecular weight is very small as compared with that of enzyme, and 4) no counterplan is necessary for hazards of radioactivity. These advantages were almost all verified in the previous work, but its sensitivity was still unsatisfactory for practical use in immunoassay.

In order to make the CLCCIA a practical method of immunoassay, the following were examined: 1) The carboxyl group in TCP–Fe(III) used as a labeling reagent in the previous work was converted into acyl chloride, and the product, iron(III) 2,9,16,23-tetrakis-(chlorocarbonyl)phthalocyanine(TCCP–Fe(III)), was used as a labeling reagent in the present work. Labeled HSA was easily obtained by only adding TCCP–Fe(III) to a HSA solution; it was more homogeneous than that obtained by the tedious and complicated carbodiimide method. 2) Optimization for chemiluminescence reaction was made with regard to the experimental conditions, such as the luminol concentration, the H_2O_2 concentration, and the total volume of the mixed solution. 3) Optimization was also made for the amounts of labeled HSA and the sample which were used for the competitive immunoassay. As a result, an improved CLCCIA was found to be about 40 times as sensitive as the previous method. This sensitivity enabled an improved CLCCIA to determine HSA on a picomole level which corresponded to the practical sensitivity in a common immunoassay.

Experimental

Reagents. TCCP–Fe(III) was synthesized by the acyl chlorination of TCP–Fe(III).[2] The labeling of HSA with TCCP–Fe(III) was made by the following method: Thirty milligrams of HSA (Sigma, Fraction V) was dissolved in 10 cm^3 of a potassium dihydrogenphosphate-disodium hydrogenphosphate buffer solution (pH 7.2), a 5-mg portion of TCCP–Fe(III) was added to it, and the mixed solution was incubated for 48 h at 4 °C. After the reaction, the mixture was centrifuged at 10000 *g*, and the precipitate was removed. To the supernatant we then added 10 cm^3 of a saturated ammonium sulfate solution ,and the mixed solution was held at 4 °C overnight. The supernatant was removed by centrifugation at 10000 *g*, and the precipitate thus obtained was dissolved in 1 cm^3 of a phosphate buffer solution (pH 7.0), after which the solution was dialyzed to remove the ammonium sulfate. After dialysis, the precipitate was removed by centrifugation, and the supernatant was submitted to gel chromatography on a TOYOPEARL HW-50 (TOYO SODA) column (150 cm^3), using a phosphate buffer solution (pH 7.0) as an eluent. Twenty cubic centimeters of an albumin fraction containing HSA labeled with TCCP–Fe(III) were thus obtained.

The glass beads immobilized with the antibody (Ab-bead) were prepared by the previously reported method.[1] The other reagents used were of a commercially available analytical grade.

Apparatus. The same apparatus as in the previous paper was used for the measurement of the chemiluminescence intensity (CL intensity).[1]

Procedure. Seventy cubic millimeters of a phosphate buffer solution (pH 7.2), containing a definite amount of HSA as an analyte and 30 mm^3 of a labeled HSA solution (containing about 200 ng of conjugated TCCP–Fe(III)), were placed in a 50×6 mm diam. test tube, and one particle of the Ab-beads was soaked in its solution. Thus, the labeled HSA and the free HSA used as an analyte were made to react competitively overnight at 4 °C with the antibody immobilized on the Ab-beads. After the immune reaction, the Ab-beads were twice washed with a phosphate buffer solution (pH 7.2). On the other hand, 0.5 cm^3 of a 1.0×10^{-3} mol/dm^3 luminol solution (pH 10.2; a boric acid–potassium hydroxide buffer solution) and 0.5 cm^3 of a 7.5×10^{-3} mol/dm^3 H_2O_2 solution were mixed in a 90×10 mm diam. test tube; the mixture was then allowed to stand for 30 min before measurement to stabilize

the chemiluminescence background. The above Ab-beads were put into the mixed solution, and the CL intensity was immediately measured by means of the photon counter.

Results and Discussion

Labeling with TCCP-Fe(III). The labeling of HSA with TCP-Fe(III) in the previous paper was carried out by allowing the carboxyl group of TCP-Fe(III) to combine covalently with the amino group of HSA by the use of the water-soluble carbodiimide reagent. However, this labeling method resulted in lowering the homogeneity of labeled HSA because in HSA containing both carboxyl and amino groups the two groups easily combined with each other.

The labeling of HSA with TCCP-Fe(III) in the present work was easily carried out by adding TCCP-Fe(III) as an acyl chloride to a HSA solution, and no linkage was produced between one HSA molecule and others. The absorption spectra of HSA, TCP-Fe(III), TCCP-Fe(III), HSA labeled with TCP-Fe(III) by the carbodiimide method, and HSA labeled with TCCP-Fe(III) by the present method were measured by the use of their respective phosphate buffer solutions (pH 7.0); the results are shown in Fig. 1. Each albumin fraction prepared by gel chromatography was used for the respective HSA labeled with TCP-Fe(III) and TCCP-Fe(III) (*cf.* Fig. 1). The spectrum of TCCP-Fe(III) was obtained after TCCP-Fe(III) had been dissolved in a phosphate buffer solution (pH 7.0) and the solution kept at 4 °C for 48 h. As can be seen from Fig. 1, the spectrum of TCCP-Fe(III) agreed well with that of TCP-Fe(III). Each shoulder at 675 nm, which was not quite observed for TCP-Fe(III) and TCCP-Fe(III) alone, was newly found for HSA labeled with TCP-Fe(III) and TCCP-Fe(III) respectively. In addition, slight peak shifts at 325 and 639 nm were also observed for both labeled HSA's. It still remains to be determined if the above-mentioned phenomena are based on either the formation of a covalent bond between HSA and a labeling reagent or the formation of a coordination linkage between the functional group of HSA and the residual coordination sites of the iron(III) complex as a labeling reagent. The absorption spectrum of HSA labeled with TCCP-Fe(III) was rather more similar to that of TCP-Fe(III) than to that of HSA labeled with TCP-Fe(III). By assuming that the molar absorptivity of HSA at 280 nm and of TCCP-Fe(III) and TCP-Fe(III) at 639 nm do not change upon labeling, the approximate mole ratio of a labeling reagent to HSA was obtained by the use of the calibration curves for TCCP-Fe(III), TCP-Fe(III), and HSA, the results being TCCP-Fe(III) : HSA=1 : 1 and TCP-Fe(III) : HSA=1 : 5. It is concluded from the amount of the conjugated iron(III) complex that the present method using TCCP-Fe(III) as a labeling reagent is superior to the carbodiimide method using TCP-Fe(III) as a labeling reagent.

Optimum Conditions for the Measurement of the CL Intensity. To find out the optimum conditions for the measurement of the CL intensity, the effects of the concentrations of H_2O_2 and luminol and of the total volume of a H_2O_2–luminol mixed solution on the CL intensity were examined. The CL intensity was measured by the use of Ab-beads which had been submitted to an immune reaction overnight at 4 °C in 100 mm³ of a phosphate buffer solution (pH 7.2) containing 30

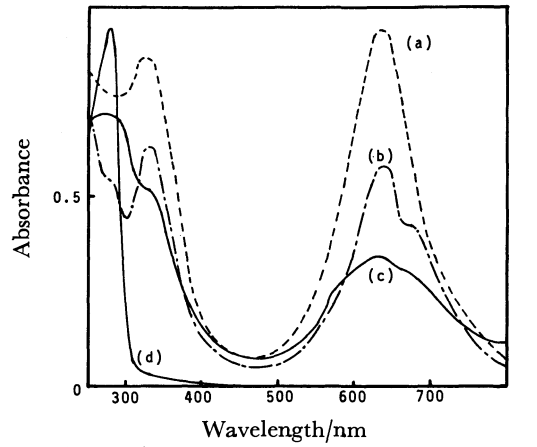

Fig. 1. Absorption spectra.
a: TCP-Fe(III) and TCCP-Fe(III), b: HSA labeled with TCCP-Fe(III), c: HSA labeled with TCP-Fe(III), and d: HSA.

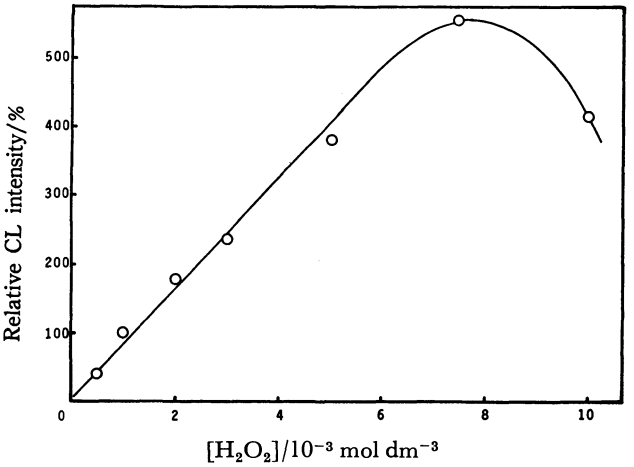

Fig. 2. Effect of H_2O_2 concentration on relative CL intensity at 1.0×10^{-3} mol/dm³ luminol.

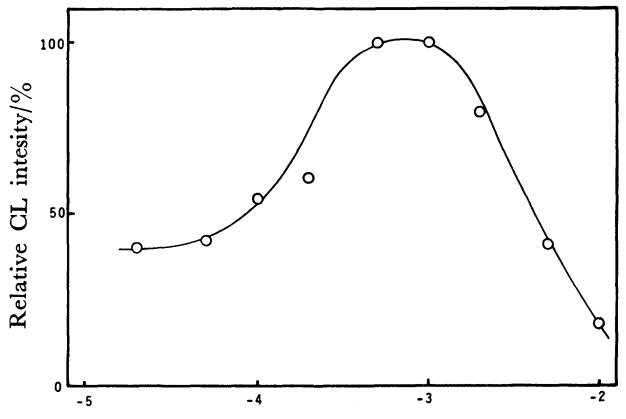

Fig. 3. Effect of luminol concentration on relative CL intensity at 7.5×10^{-3} mol/dm³ H_2O_2.

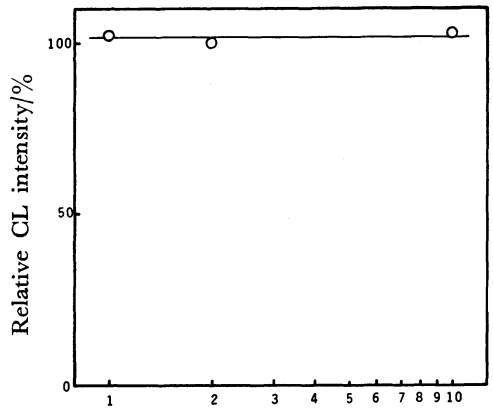

log(Volume of a mixed solution/cm^3)

Fig. 4. Relationship between volume of luminol–H_2O_2 mixed solution and relative CL intensity at 1.0×10^{-3} mol/dm^3 luminol and 7.5×10^{-3} mol/dm^3 H_2O_2.

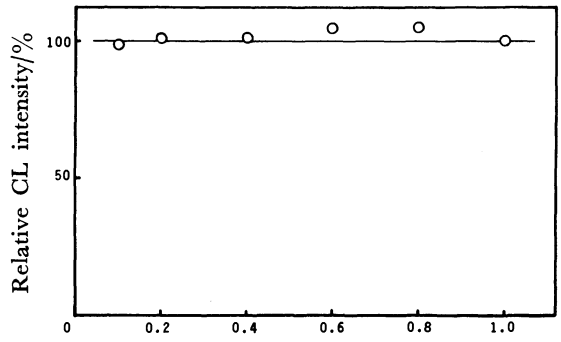

Volume of immune reaction solution/cm^3

Fig. 5. Relationship between total aqueous volume in immune reaction and relative CL intensity in a mixed solution of luminol (0.5 cm^3, 1.0×10^{-3} mol/dm^3) and H_2O_2 (0.5 cm^3, 7.5×10^{-3} mol/dm^3).

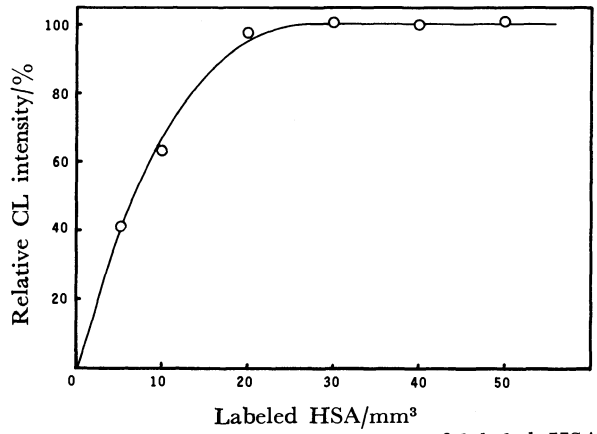

Labeled HSA/mm^3

Fig. 6. Relationship between volume of labeled HSA and relative CL intensity.

mm^3 of a labeled HSA solution. The results are shown in Figs. 2, 3, and 4. The CL intensity increased proportionally with an increase in the concentration of H_2O_2 and gave a maximum value at 7.5×10^{-3} mol/dm^3 H_2O_2, followed by its decrease. The maximum CL intensity was also obtained at 1.0×10^{-3} mol/dm^3 luminol. The total volume of a luminol–H_2O_2 mixed

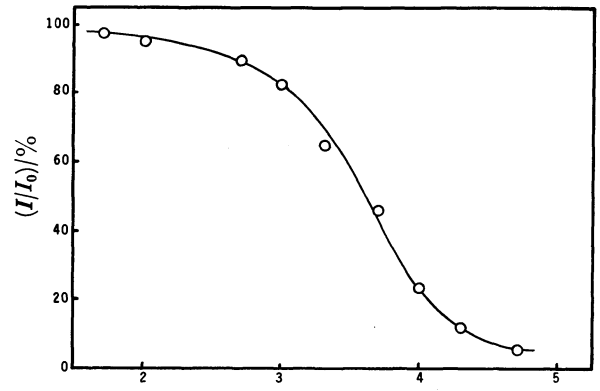

log(HSA/ng tube^{-1})

Fig. 7. Standard curve for HSA.
I, I_0: CL intensity of the sample in the presence or absence of HSA.

solution did not affect the CL intensity.

On the basis of these results, 0.5 cm^3 of a 7.5×10^{-3} mol/dm^3 H_2O_2 solution and 0.5 cm^3 of a 1.0×10^{-3} mol/dm^3 luminol solution were mixed to obtain an optimum result.

Optimum Conditions for a Competitive Immune Reaction. The relationship between the CL intensity and the total aqueous volume for an immune reaction is shown in Fig. 5. A definite concentration of labeled HSA was allowed to react with the antibody on Ab-beads at a total aqueous volume of from 0.1 to 1 cm^3. After the immune reaction, each Ab-bead showed approximately the same CL intensity. Since a minimum aqueous volume of 0.1 cm^3 was necessary to keep an Ab-bead in a solution, a total aqueous volume of 0.1 cm^3 was recommended for practical use.

The amount of labeled HSA required for a competitive immune reaction with HSA was examined by changing the amount of labeled HSA in a 0.1 cm^3 aqueous solution and by measuring the CL intensities, the results are shown in Fig. 6. As can be seen from Fig. 6, the active site of an antibody on an Ab-bead was completely saturated with more than 30 mm^3 of labeled HSA. To satisfy the requirements that 1) the total amount of antigen and labeled antigen has to surpass the corresponding amount of the immobilized antibody in a competitive immunoassay and 2) the sensitivity for a competitive immunoassay has to be enhanced as much as possible, 30 mm^3 of labeled HSA was chosen for the immunoassay.

Immunoassay. The immunoassay of HSA was carried out by the use of HSA labeled with TCCP–Fe(III), and a standard curve was obtained for HSA of from 50 ng/tube to 50 μg/tube (Fig. 7). For the preparation of the standard curve for HSA, the CL intensities of five equal amounts of HSA were separately measured, and their mean value(I) was obtained. The relative CL intensity(I/I_0) was represented as the ratio of I to the CL intensity(I_0) of a labeled HSA alone. The CL intensity of a HSA of more than 50 ng/tube was always smaller than the I_0 value, while the CL intensity of a HSA of less than 50 ng/tube was often larger than the I_0 value. Therefore, 50 ng/tube of HSA was defined

TABLE 1. IMMUNOASSAY USING A METAL COMPLEX COMPOUND AS A LABELING REAGENT

Immunoassay	Method		Chemical amplification[a)]	Detection limit	Sample	Analyte
	Component	Measurement				
CLCCIA	Catalytic activity	Chemiluminescence	+	50 ng/tube (7.6×10^{-9} mol/dm^3)	70 mm^3	HSA
VIA	In	Differential pulse anodic stripping voltammetry	−	5.0 μg/cm^3 (7.6×10^{-8} mol/dm^3)	5000 mm^3	HSA
MIA	Fe, Mn	Atomic-absorption spectrometry	−	0.1 μg/cm^3 (3.5×10^{-7} mol/dm^3)	30 mm^3	Oestrogen steroids (hapten)

a) +, −: Shows the presence or absence of chemical amplification.

as the detection limit. Judging from the detection limit for the previous and the present methods, the present method was about 40 times as sensitive as the previous method. This enhancement is attributed to 1) the optimization of the chemiluminescence reaction and the immune reaction, and 2) the use of HSA labeled sufficiently with TCCP–Fe(III). Voltammetric immunoassay (VIA)[3] and metalloimmunoassay (MIA)[4,5] have previously been reported as immunoassays using a metal-complex compound as a labeling reagent. In Table 1 they are compared with the present method. According to the present method, the picomole level of albumin can be determined; this sensitivity satisfies the sensitivity required for a practical immunoassay. Since the present method makes use of the catalytic action of a metal-complex compound as a labeling reagent, its sensitivity would be much more improved by using a sandwich method or some other such method. Further study is now in progress.

References

1) T. Hara, M. Toriyama, and K. Tsukagoshi, *Bull. Chem. Soc. Jpn.*, **56**, 2267 (1983).
2) H. Shirai, A. Maruyama, K. Kobayashi, and N. Hojo, *J. Polym. Sci., Polym. Lett. Ed.*, **17**, 661 (1979).
3) M.J. Doyle, H. B. Halsall, and W. R. Helneman, *Anal. Chem.*, **54**, 2318 (1982).
4) M. Cais, S. Dani, Y. Eden, O. Gandolfi, M. Horn, E. E. Isaacs, Y. Josephy, Y. Saay, E. Slovin, and L. Snarsky, *Nature*, **270**, 534 (1977).
5) M. Cais, E. Slovin, and L. Snarsky, *J. Organomet. Chem.*, **160**, 223 (1978).

Synthesis of Mesoionic Triazolopyridine. II. *N*-Acylation of 1,2,4-Triazolo[4,3-*a*]pyridin-3(2*H*)-one

Akio SAITO* and Bunji SHIMIZU
Chemical Research Laboratories, Sankyo Co., Ltd., Hiromachi, Shinagawa-ku, Tokyo 140
(Received December 25, 1982)

N-Acyl and *N*-alkoxycarbonyl mesoionic triazolopyridines were synthesized by selective *N*-acylation of 1,2,4-triazolo[4,3-*a*]pyridin-3(2*H*)-one. Some properties of these new-type azolides were also investigated.

In a previous work[1] in this series, we reported a novel approach for the synthesis of mesoionic triazolopyridines (**2**) by the selective alkylation of 1,2,4-triazolo[4,3-*a*]-pyridin-3(2*H*)-one (**1**). The interesting properties of *N*-alkyl mesoionic triazolopyridines (**2**) have called our attention to mesoionic *N*-acyl derivatives (**3**). These compounds (**3**) are characterized by combination of *N*-acyl azole(azolide) with mesoionic ring. Hence, a term "mesoionic azolide" will be used for these compounds. Only one example of this class of compounds has so far been reported.[2]

N-Acyl azoles, such as imidazolides (**4**) or triazolides (**5**) have been known as active amides, and widely used as acylating reagents.[3-8] The remarkable reactivity of these azolides has been attributed[7] to their resonance structures. Hence, it is thought that the reactivity of the acyl group of **3** reflects the particular resonance structure of the mesoionic ring. Possible use of the compounds (**3**) as acylating reagents would also be expected. Therefore, we have studied *N*-acylation of **1**. In this paper, we wish to report the selective *N*-acylation of **1** and some properties of the *N*-acyl mesoionic triazolopyridines.

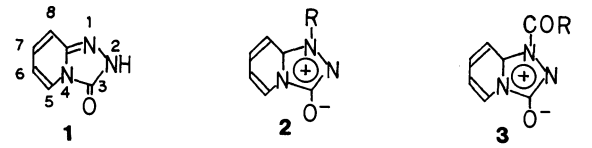

1 **2** **3**

4 **5**

Fig. 1.

Results and Discussion

The followings are typical known preparative methods of *N*-acyl azoles(azolides): 1) direct acylation of parent azoles with acid halides,[5,9,10] 2) acylation of *N*-(trimethylsilyl)azoles with acid halides,[11] 3) reaction of carbonyl(diazolide)s with carboxylic acids.[5,12] We attempted several methods for the preparation of the mesoionic azolides (Fig. 2).

Almost all attempts to obtained the *N*-acyl mesoionic triazolopyridinones (**3**) by the reaction of **1** with acid chloride failed. Thus, heating of **1** with acid chloride in boiling chloroform resulted in the exclusive formation of

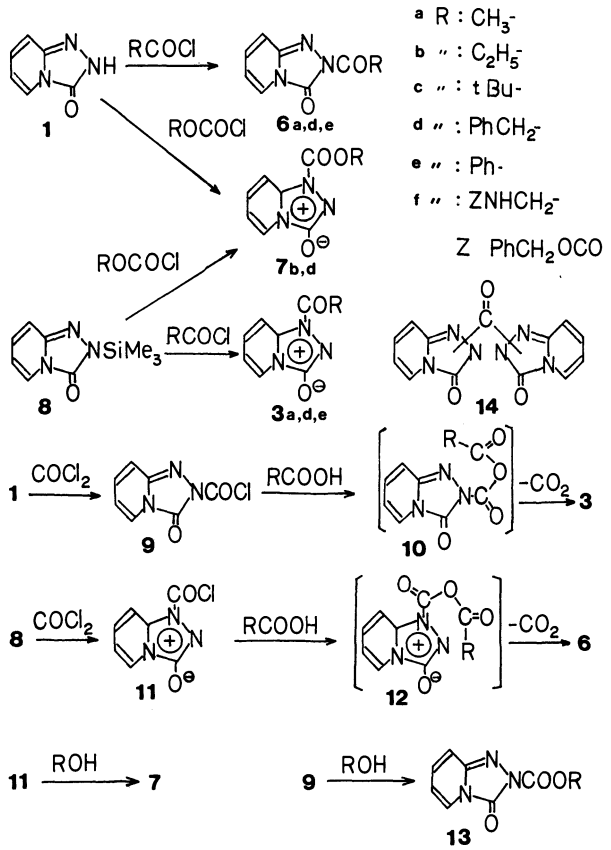

Fig. 2.

nonmesoionic compounds, which were assigned to N^2-acyltriazolopyridinones (**6**) based on their physical data. Details on the structural assignment are described in the following section. On the other hand, reaction of **1** with alkokycarbonyl chlorides gave mesoionic compounds (**7**) in moderate yields. For example, heating **1** with benzyl chloroformate gave a pale yellowish crystalline product which showed strong fluorescence when it was dissolved in an aprotic solvent. By comparing its IR, UV, and NMR spectra with those of *N*-alkyl mesoionic triazolopyridinones (**2**), this compound was found to have a mesoionic structure (**7d**) as shown in Table 1. *N*-acyl mesoionic triazolopyridinones (**3**) were obtained by using 2-(trimethylsilyl)triazolopyridine (**8**)[1] instead of **1**. Reaction of **8** with acid chlorides proceeded smoothly to give the desired mesoionic compounds (**3**) even at low temperature. When the reaction is carried out in a nonpolar solvent, such as benzene, the product is easily isolated by filtration, because it precipitates during reaction in most cases. Reaction of

Table 1. Comparison of physical data of mesoionic azolide with those of N^2-acyl and N-alkyl analogs

Compound	UV(H_2O) λ/mm	UV(THF) λ/mm	IR $\tilde{\nu}$/cm^{-1} (ring C=O)	NMR (δ) 5H	6H	CH_2 (benzyl)
3d	338	385 (ε 7550)	1700	8.14	7.25	4.42
7d	—	377 (ε 6100)	1705	8.55	7.55	5.48
2d	330	384 (ε 7550)	1660	8.19	7.02	5.41
6d	—	350 (ε 4000)	1740	7.75	6.50	4.45
13d	337	347 (ε 3600)	1730	7.88	6.64	5.47
15	338	350 (ε 4000)	1720	7.89	6.63	5.15

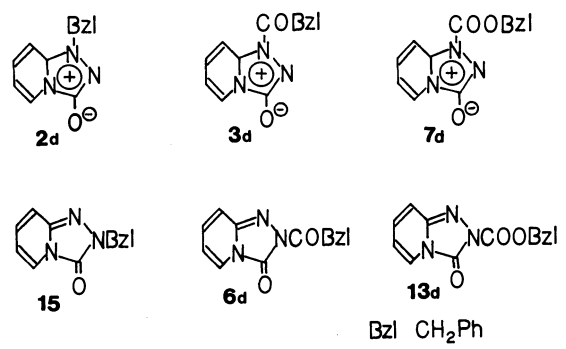

Fig. 3.

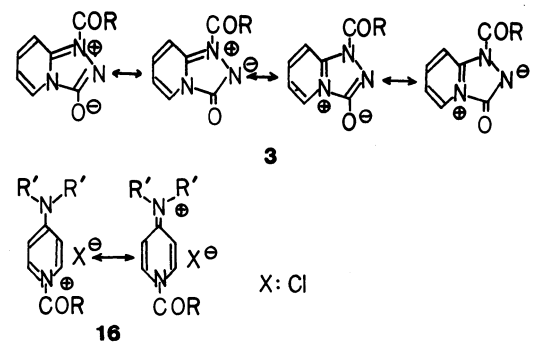

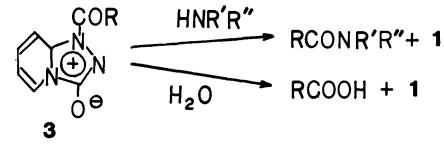

Fig. 4.

8 with alkoxycarbonyl chlorides gave the urethane-type mesoionic triazolopyridines (**7**) in the same manner.

When phosgene was used as the acylating reagent for the reaction of **1** or **8**, the N-chloroformyl derivative, **9** or **11** respectively, was obtained instead of the expected[4] carbonyldi(triazolopyridine) (**14**).

Structure of **9** and **11** were assigned on the basis of their UV spectra. It became clear that these compounds were useful reagents for the preparation of N-acyltriazolopyridines, similar to the carbonyldi(azole) for the preparation of N-acyl azoles[5,12] Thus, reaction of **9** with a variety of carboxylic acids proceeded in the presence of one equivalent-molar bases to give the mesoionic azolides (**3**) accompanying evolution of carbon dioxide. Since **3** was the sole product in this reaction, it was supposed that intramolecular transacylation of the intermediate mixed anhydride (**10**) occurred exclusively on the N^1-atom of the triazolopyridine ring. Similar transacylation was assumed in the reaction of **11** with a carboxylic acid, in this case **6** was the sole product. Reactions of these reagents, **9** and **11**, with alcohols in the presence of pyridine gave urethane-type mesoionic and nonmesoionic triazolopyridines, **7** and **13**, respectively. Thus, it became possible to obtain these mesoionic azolides (**3** and **7**) from appropriate carboxylic acids or alcohols by using these reagents (**9** or **11**). Both reagents are stable crystalline masses and may be stored in a desiccator at room temperature for a few months, but preferably in a refrigerator for longer storage.

Some Properties of the Mesoionic Azolides (3 and 7).
A comparison of physical data of the mesoionic azolides (**3d** and **7d**) with those of N-alkyl and N^2-acyl analogs (Fig. 3) is shown in Table 1. It can be seen that the spectra of the N-acyl mesoionic triazolopyridines (**3d** and **7d**) are closely related to those of N-benzyl mesoionic triazolopyridine (**2d**). In an aprotic solvent, mesoionic triazolopyridines (**2**, **3**, and **7**) showed characteristic UV absorption in the region from 360 to 400 nm with intensity (ε 5500—10000) and large hypsochromic shifts (35—40 nm) of the maxima were observed when the solvents were changed to a protic solvent. In the case of nonmesoionic triazolopyridines (**6**, **13**, and **15**), these maxima were found in the region from 350 to 360 nm in an aprotic solvent with relatively low intensity (ε 3500—4500), and small hypsochromic shifts (*ca.* 10 nm) were observed. In the IR spectra, absorption bands for ring carbonyl of these mesoionic compounds (**3**, **7**, and **2**) were found in a lower frequency region than those of the corresponding nonmesoionic N^2-analogs (**6**, **13**, and **15**). In the NMR spectra, the chemical shifts of the pyridine-ring protons of the mesoionic compounds (**3**, **7**, and **2**) were always found at a lower field than those of the nonmesoionic analogs (**6**, **13**, and **15**). Thus, UV absorption and chemical shift of the pyridine-ring protons are effective in discriminating mesoionic compounds from their nonmesoionic analogs.

The mesoionic azolides (**3**) were found to have a tendency to transform to the thermodynamically more stable N^2-acyl analogs (**6**) under the conditions described below.

On heating in boiling 1,2-dichloroethane, slow conversion of **3d** to **6d** was found. In a previous paper,[1]

it was found that benzyl bromide acted as an effective catalyst for the N^1—N^2 benzyl migration on the triazolopyridine ring. Conversion of **3d** to **6d** was accelerated by addition of phenylacetyl chloride. The exclusive formation of **6** in the reaction of **1** with acyl chloride may be explained by the finding described above. Tertiary amine was found to be a more efficient catalyst for the conversion. When triethylamine was used as a catalyst, conversion of **3d** to **6d** took place even at room temperature, and completed within 3 h. The resonance structure of the mesoionic ring is illustrated in Fig. 4, which is very close to that of 1-acyl-4-dialkylaminopyridinium chloride (**16**),[13,14] a very reactive acylating reagent (Fig. 4). This similarity indicates that these acyl azolides (**3** or **7**) should act as powerful acylating agents. In fact, a reaction of **3d** with aniline in dichloromethane at room temperature completed within 2 h, yielding phenylacetanilide in nearly quantitative yield.

Relative reactivity of the mesoionic azolide (**3**) was determined on the reaction of **3a** with diethylamine or water, according to the method of Staab.[3] The mesoionic azolide (**3a**) was found to be 4 times more reactive than *N*-acetylimidazole[3] toward diethylamine in THF. On the other hand, hydrolytic decomposition of **3a** was found to proceed fairly slowly in spite of the high reactivity to an amine. The half life of the mesoionic azolide (**3a**) in water was found to be 380 min as determined by the change of the UV absorption at 25 °C. In the literature, the half lives of *N*-acetylimidazole,[3] *N*-acetyltriazole,[3] and 1-acetyl-4-dimethylaminopyridinium chloride were reported as 33—45, 6.6, and 3.9 min respectively under the same conditions. From these facts it appears that *N*-acyl mesoionic triazolopyridines (**3**) should be quite stable against water but very reactive toward amines. Although the relationship between the mesoionic structure and the selective reactivity of the mesoionic azolide against different nucleophiles is still uncertain, the stability toward hydrolytic decomposition makes the reagent (**3**) easy to handle. These findings together with their easy preparation suggest the usefulness of these mesoionic azolides (**3** and **7**) as acylating reagent. Details of their applications as acylating reagents will be reported in a subsequent paper.

Experimental

Melting points were determined on a Yazawa hot-stage apparatus and are uncorrected. IR, UV, and NMR spectra were recorded on JASCO A-102, Hitachi 200-20 and Varian EM 360L spectrometers, respectively. Triazolopyridine (**1**) was prepared by the method of Potts and Burton.[16]

1-Ethoxycarbonyl-1,2,4-triazolo[4,3-a]pyridinium-3-olate (7b). *a)*: A mixture of 5.4 g (40 mmol) of 1,2,4-triazolo[4,3-*a*]-pyridin-3(2*H*)-one (**1**) and ethyl chloroformate (100 ml) was heated under reflux for 3 h, cooled, and evaporated *in vacuo*. The residue was crystallized from methanol to give yellow fine needles, mp 144—145 °C. Yield 5.87 g (71%). UV (THF) λ_{max}: 378 nm (ε 5500). IR (Nujol): 1735, 1720 cm^{-1} (C=O). NMR ($CDCl_3$–DMSO-d_6); δ=8.57 (m, 1, H-5), 8.40 (m, 1, H-8), 8.16 (m, 1, H-7), 7.54 (m, 1, H-6), 4.51 (q, J=7 Hz, 2, COOC$\underline{H}_2$), 1.47 (t, J=7 Hz, 3, COOCH$_2$C$\underline{H}_3$). Found: C, 51.96; H, 4.23; N, 20.16%. Calcd for $C_9H_9N_3O_3$: C, 52.17; H, 4.23; N, 20.27%.

b): To a solution of 2.07 g (10 mmol) of 2-trimethylsilyl-1,2,4-triazolo[4,3-*a*]pyridin-3(2*H*)-one (**8**)[11] in dry benzene(20 ml) was added ethyl chloroformate (1.19 g, 11 mmol) with stirring. After the mixture had been stirred for 1 h, the crystalline precipitate was collected by filtration, washed with dry benzene and recrystallized from methanol to give pure **7b** (1.81 g, 87%). This product was identical with the sample prepared by route *a)*.

1-Benzyloxycarbonyl-1,2,4-triazolo[4,3-a]pyridinium-3-olate (7d). *a)*: A mixture of **1** (3.95 g, 2.93 mmol) and benzyl chloroformate (50 ml) was stirred at 90 °c for 1 h, and evaporated *in vacuo*. The residue was crystallized from ethanol to give **7d** as fine needles, mp 140°C. Yield 4.10 g (52%). UV (THF) λ_{max}: 224 (ε 4800), 254 (4300), 314 (3300), 377 nm (6100). IR (Nujol): 1745, 1710 cm^{-1} (C=O). NMR ($CDCl_3$–DMSO-d_6); δ=8.55 (m, 1, H-5), 8.4—8.0 (m, 2, H-7 and H-8), 7.42 (m, 1, H-6), 7.41 (s, 5, C$_6\underline{H}_5$), 5.48 (s, 2, PhC$\underline{H}_2$). Found: C, 62.48; H, 4.09; N, 15.81%. Calcd for $C_{14}H_{11}N_3O_3$: C, 62.45; H, 4.12; N, 15.61%.

b): To a solution of **8** (2.07 g, 10 mmol) in dry benzene (20 ml) was added benzyl chloroformate (1.82 g, 10.7 mmol) with stirring. After the mixture had been stirred for 1 h at room temperature, the crystalline precipitate was collected, recrystallized from ethanol to give **7d** (2.48 g, 92%). This product was identical with the sample prepared by route *a)*.

1-Acetyl-1,2,4-triazolo[4,3-a]pyridinium-3-olate (3a). To a solution of **8** (2.07 g, 10.0 mmol) in dry THF (20 ml) was added 0.80 g (10.2 mmol) of acetyl chloride with stirring. The reaction was slightly exothermic, and yellow crystals precipitated off immediately from the solution. After the mixture had been stirred for 1 h at room temperature, the product was collected by filtration, washed with dry THF and dried *in vacuo*: 1.29 g (73%) of **3a** was obtained, mp 150—153°C. UV (THF) λ_{max}: 374 nm (ε 6220). IR (Nujol): 1720 cm^{-1} (C=O). Found: C, 53.97; H, 4.00; N, 23.76%. Calcd for $C_8H_7N_3O_2$: C, 54.24; H. 3.98; N, 23.72%.

Reactions of 1 with Acid Chlorides. *a) With Acetyl Chloride*: A mixture of **1** (1.35 g, 10 mmol) and acetyl chloride (1.57 g, 20 mmol) in chloroform (15 ml) was boiled under reflux for 4 h, then, cooled to room temperature. A small amount of solid was filtered off, and the filtrate was evaporated *in vacuo* to dryness. The residue was crystallized from chloroform–hexane to give 1.63 g (92%) of 2-acetyl-1,2,4-triazolo[4,3-*a*]pyridin-3-(2*H*)-one (**6a**), mp 176 °C. UV (THF) λ_{max}: 351 nm (ε 3750). IR (Nujol): 1720 cm^{-1} (C=O). NMR ($CDCl_3$); δ=7.79 (m, 1, H-5), 7.4—7.1 (m, 2, H-7 and H-8), 6.55 (m, 1, H-6), 2.72 (s, 3, C$\underline{H}_3$CO). Found: C, 54.34; H. 3.86; N, 23.83%. Calcd for $C_8H_7N_3O_2$: C, 54.24; H, 3.98; N, 23.72%.

b) With Phenylacetyl Chloride: A mixture of **1** (1.35 g, 10 mmol) and phenylacetyl chloride (1.57 g, 20 mmol) in chloroform (15 ml) was boiled under refiux, and the reaction mixture was worked up in the manner described above expt; 2.43 g (96%) of 2-phenylacetyl-1,2,4-triazolo[4,3-*a*]pyridin-3(2*H*)-one (**6d**) was obtained, mp 142—143 °C. UV (THF) λ_{max}: 257 (ε 4300), 266 (4100), 350 nm (4000). IR (Nujol): 1740 cm^{-1} (C=O). NMR ($CDCl_3$); δ=7.75 (m, 1, H-5), 7.40 (s, 5, C$_6\underline{H}_5$), 7.5—7.0 (m, 2, H-7 and H-8), 6.50 (m, 1, H-6), 4.45 (s, 2, PhCH_2). Found: C, 66.56; H, 4.22; N, 16.71%. Calcd for $C_{14}H_{11}N_3O_2$: C, 66.39; H, 4.38; N, 16.59%.

c) With Benzoyl Chloride: A mixture of **1** (1.35 g, 10 mmol) and benzoyl chloride (2.81 g, 20 mmol) in chloroform (15 ml) was boiled under reflux for 96 h and the reaction mixture was worked up in the manner described above to give 1.78 g (74%) of 2-benzoyl-1,2,4-triazolo[4,3-*a*]pyridin-3(2*H*)-

one (**6e**), mp 145 °C. UV (THF) λ_{max}: 358 nm (ε 4300). IR (Nujol): 1730, 1695 cm^{-1}. NMR (DMSO-d_6): δ=8.03 (m, 1, H-5), 8.0—7.0 (m, 7, H-7, H-8 and $C_6\underline{H}_5$), 6.66 (m, 1, H-6). Found: C, 65.28; H, 3.59; N, 17.70%. Calcd for $C_{13}H_9N_3O_2$: C, 65.27; H, 3.79; N, 17.57%.

*2-Chloroformyl-1,2,4-triazolo[4,3-a]pyridin-3(2H)-one (**9**).* To a suspension of **1** (27 g, 200 mmol) in dry THF (600 ml) was introduced phosgene (40 g) with stirring. The resulting mixture was boiled under reflux for 2 h to afford a clear soln and then cooled to room temperature. The resulting crystalline product was collected by filtration, washed with a small amount of dry THF, and dried *in vacuo* to give **9**. The filtrate was combined with the washing, concentrared *in vacuo*, giving a second crop of **9**. Mp 230 °C. Yield 36.78 g (93%). UV (CH_2Cl_2) λ_{max}: 262, 272, 283, 356 nm. Found: C, 42.30; H, 2.33; N, 21.26; Cl, 17.99%. Calcd for $C_7H_4N_3O_2Cl$: C, 42.55; H, 2.04; N, 21.27; Cl, 17.95%.

*1-Chloroformyl-1,2,4-triazolo[4,3-a]pyridinium-3-olate (**11**).* To a solution of **8** (20.7 g, 100 mmol) in dry benzene was slowly added a solution of phosgene (9.90 g, 100 mmol) in dry THF (50 ml) at a temperature between 4 °C and 10 °C with stirring. After the mixture had been stirred at room temperature for 1 h, the crystalline precipitate was collected by filtration, washed with dry benzene, and dried *in vacuo* to give **11**, mp 320 °C (decomp). UV (CH_2Cl_2) λ_{max}: 247, 375 nm. Found: C, 42.56; H, 2.14; N, 21.54; Cl, 17.72%. Calcd for $C_7H_4N_3O_2Cl$: C, 42.55; H, 2.04; N, 21.27; Cl, 17.95%.

*Reaction of **9** with Carboxylic Acids.* *a) With Acetic Acid*: To a solution of acetic acid (0.48 g, 10 mmol) in dichloromethane (40 ml) was added triethylamine (1.40 ml, 10 mmol). The mixture was cooled to 4 °C and 1.98 g (10 mmol) of **9** was added. With evolution of gas, the solution became yellow-green. After 1 h-stirring at 4 °C, the solution was washed twice with cold water, dried over anhydrous sodium sulfate, and concentrated *in vacuo* to *ca.* 10 ml. Ether was added to give a crystalline product of 1-acetyl-1,2,4-triazolo[4,3-*a*]-pyridinium-3-olate (**3a**), mp 167 °C. Yield 1.10 g (62%). The physical properties of this product agreed with those of the sample obtained in the above expt.

b) With Phenylacetic Acid: By treating phenylacetic acid (1.36 g, 10 mmol) with **9** (1.98 g, 10 mmol) as in the previous experiment, 2.26 g (89%) of 1-phenylacetyl-1,2,4-triazolo[4,3-*a*]pyridinium-3-olate (**3d**) was obtained, mp 155—157 °C. UV (THF) λ_{max}: 232 (ε 8150), 258 (3100), 384 nm (7550). IR (Nujol): 1720, 1700 cm^{-1} (C=O). NMR ($CDCl_3$); δ=8.16 (m, 1, H-5), 8.0—7.3 (m, 7, H-7, H-8, and $C_6\underline{H}_5$), 7.25 (m, 1, H-6), 4.42 (s, 2, $PhCH_2$). Found: C, 66.50; H, 4.28; N, 16.65%. Calcd for $C_{14}H_{11}N_3O_2$: C, 66.39; H, 4.38; N, 16.59%.

c) With Benzoic Acid: By treating benzoic acid (1.22 g, 10 mmol) with **9** (1.98 g, 10 mmol) in the manner described above, 1-benzoyl-1,2,4-triazolo[4,3-*a*]pyridinium-3-olate (**3e**) was obtained, mp 134—136 °C. Yield 2.06 g (86%). UV (THF) λ_{max}: 398 nm (ε 9950). IR (Nujol): 1730, 1695 cm^{-1} (C=O). NMR ($CDCl_3$); δ=8.8—7.3 (m, triazolopyridine ring and benzene ring protons). Found: C, 65.22; H, 3.63; N, 17.74%. Calcd for $C_{13}H_9N_3O_2$: C, 65.27; H, 3.79; N, 17.57%.

d) With N-(Benzyloxycarbonyl)glycine: By treating *N*-*Z*-glycine (2.09 g, 10 mmol) with **9** (1.98 g, 10 mmol) in the manner described above, 1-[*N*-(benzyloxycarbonyl)glycyl]-1,2,4-triazolo[4,3-*a*]pyridinium-3-olate (**3f**) was obtained, mp 173—176 °C. Yield 2.87 g (88%). UV (THF) λ_{max}: 375 nm. IR (Nujol): 1720, 1695 cm^{-1} (C=O). Found: C, 58.69; H, 4.23; N, 17.34%. Calcd for $C_{16}H_{14}N_4O_4$: C, 58.89; H, 4.32; N, 17.17%.

*Reaction of **11** with Phenylacetic Acid.* To a solution of phenylacetic acid (0.68 g, 5 mmol) in dichloromethane (20 ml) was added triethylamine (0.70 ml, 5 mmol), and the mixture was cooled to 4 °C, then, **11** (0.985 g, 5 mmol) was added. After stirring at room temperature for 1 h, the reaction mixture was washed twice with cold water, dried over anhydrous sodium sulfate, and evaporated *in vacuo* to dryness. The residue was crystallized from chloroform–hexane to give 1.18 g (93%) of **6d**. The physical properties of this product agreed with those of the sample obtained in the above expt.

*Reaction of **11** with Alcohols.* *a) With Benzyl Alcohol*: A suspension of **11** (1.98 g, 10 mmol) in ethanol–free chloroform (50 ml) prepared by passing through an alumina column before use was cooled to 4 °C, and 1.05 ml of pyridine was added. After the mixture had been stirred at 4 °C for 1 h, benzyl alcohol (1.19 g, 11 mmol) was added. The reaction mixture became a clear solution, and soon after yellow crystals separated out from the solution. After the mixture had been stirred at room temperature for 30 min, the product was collected by filtration, washed with chloroform, and dried *in vacuo* to give **7d**. The filtrate and washings were combined, washed twice with water, dried over anhydrous sodium sulfate, and concentrated *in vacuo*, giving a second crop of **7d**. The total yield of **7d** was 2.50 g (94%). The physical properties of this product were identical to those of the sample in the above expt.

b) With t-Butyl Alcohol: A suspension of **11** (1.98 g, 10 mmol) in ethanol–free chloroform was cooled to 4 °C, dry pyridine (1.05 ml) was added, and the mixture was stirred at 4 °C for 40 min then, anhydrous *t*-butyl alcohol (2 ml) was added. On stirring at room temperature, the reaction mixture became a clear solution within 20 min. After a further 1 h-stirring, the solution was washed twice with cold water, dried over anhydrous sodium sulfate, and evaporated *in vacuo*. The residue was crystallized from chloroform–ether to give 2.04 g (69%) of 1-(*t*-butoxycarbonyl)-1,2,4-triazolo-[4,3-*a*]pyridinium-3-olate (**7c**) as a chloroform adduct, mp 119—121 °C. UV (THF) λ_{max} 374 nm. IR (Nujol): 1757, 1722 cm^{-1} (C=O). Found: C, 46.95; H, 4.62; N, 14.47%. Calcd for $C_{11}H_{13}N_3O_3 \cdot 1/2CHCl_3$: C, 46.82; H, 4.61; N, 14.25 %.

*2-Benzyloxycarbonyl-1,2,4-triazolo[4,3-a]pyridin-3(2H)-one (**13d**).* To a suspension of **9** (1.0 g) in dichloromethane were added pyridine (0.40 g) and benzyl alcohol (0.65 g), and the mixture was stirred for 1 h at room temperature. The resulting solution was washed twice with water, dried over anhydrous sodium sulfate, and evastallized *in vacuo* to dryness. The residue was crystallized from ether to give **13d** (1.257 g, 93%), mp 138 °C. UV (THF)λ_{max}: 254 (ε 3500), 264 (3500), 276 (2200), 347 nm (3600). IR (Nujol): 1730 cm^{-1} (C=O). NMR (DMSO-d_6); δ=7.88 (m, 1, H-5), 7.7—7.0 (m, 2, H-7 and H-8), 7.51 (s, 5, C_6H_5), 6.64 (m, 1, H-6), 5.47 (s, 2, $PhC\underline{H}_2$). Found: C, 62.24; H, 4.00; N, 15.60%. Calcd for $C_{14}H_{11}N_3O_3$: C, 62.45; H, 4.12; N, 15.61%.

*Conversion of **3d** to **6d**.* *a) Thermal Conversion*: A solution of **3d** (100 mg) in 5 ml of 1,2-dichloroethane was heated under reflux for 20 h, then, the solvent was removed by evaporation *in vacuo*. The NMR spectrum of the residue in $CDCl_3$ showed that it consisted of **3d** and **6d** (43 : 57).

b) Conversion Catalyzed by Acid Chloride: A mixture of **3d** (253 mg, 1 mmol) and phenylacetyl chloride (155 mg, 1 mmol) in 1,2-dichloroethane (2.5 ml) was stirred at 80 °C for 45 min; TLC on silica gel in 40% ethyl acetate in benzene showed disappearance of the starting material (**3d**) within 40 min. The reaction mixture was evaporated *in vacuo*, and the residue was crystallized from chloroform–hexane to give 232 mg of **6d**.

c) Conversion Catalyzed by Triethylamine: To a solution of

3d (100 mg) in 1,2-dichloroethane (5 ml) was added triethylamine (0.04 ml), and the mixture was stirred at room temperature. TLC on silica gel showed that **3d** was almost completely converted to **6d** within 3 h.

Reaction of Mesoionic Azolide (3d) with Aniline. A mixture of **3d** (1.27 g, 5 mmol) and aniline (0.49 g, 5.25 mmol) in dichloromethane (10 ml) was stirred at room temperature for 2 h, filtered, and the filtrate was washed successively with 0.5 M citric acid, water, 4% sodium hydrogencarbonate, and water. The dichloromethane solution was dried over anhydrous sodium sulfate, and evaporated *in vacuo* to give crystalline phenylacetanilide (1.02 g, 97%), mp 117—118 °C. The physical properties of this product agreed with those of authentic phenylacetanilide.

Measurement of the Reactivities of 3a. The rates of aminolysis and hydrolysis were measured at 25 °C according to the direction of Staab.[3] The rate of the aminolysis of **3a** (1.830×10^{-4} mmol/ml) in THF containing 5% diethylamine was measured by observing the decrease in its UV absorption maximum at 389 nm. The rate of the hydrolysis of **3a** in water (2.25×10^{-4} mmol/ml) was also measured by means of the change of the maximum at 340 nm. Pseudo-first order rate constants of the amonolysis in 5% diethylamine–THF was 3.84×10^{-2} and that of hydrolytic decomposition was 1.8×10^{-3}.

The authors wish to thank Dr. Genshun Sunagawa, Dr. Keisuke Murayama, and Dr. Hideo Nakao for their continuing interest and encouragement and Dr. Masakatsu Kaneko for his helpful comments.

References

1) A. Saito and B. Shimizu, *Bull. Chem. Soc. Jpn.*, **50**, 1596 (1977).
2) A. Chinone and M. Ohta, *Chem. Lett.*, **1972**, 969.
3) H. A. Staab, *Chem. Ber.*, **89**, 1927 (1956).
4) H. A. Staab, *Chem. Ber.*, **90**, 1326 (1957).
5) H. A. Staab and K. Wendel, *Chem. Ber.*, **93**, 2910 (1960).
6) H. W. Anderson and R. Paul, *J. Am. Chem. Soc.*, **80**, 4423 (1958); R. Paul and G. W. Anderson, *ibid.*, **82**, 4596 (1960).
7) H. A. Staab, *Angew. Chem., Int. Ed. Engl.*, **1**, 351 (1962).
8) Y. Nomura, *Yuki Gosei Kagaku Kyokai Shi*, **21**, 585 (1963).
9) O. Gerngross, *Ber.*, **46**, 1912 (1913).
10) T. Wieland and G. Schneider, *Justus Liebigs Ann. Chem.*, **580**, 159 (1953).
11) L. Birkofer, P. Richter, and A. Ritter, *Chem. Ber.*, **93**, 2804 (1960).
12) H. A. Staab, M. Lüking, and F. H. Dürr, *Chem. Ber.*, **95**, 1275 (1962).
13) L. M. Litvinenko and A. I. Kirichenko, *Dokl. Akad. Nauk SSSR, Ser. Khim.*, **176**, 97 (1967); *Chem. Abstr.*, **68**, 68325u (1968).
14) W. Steglich and G. Höfle, *Angew. Chem.*, **81**, 1001 (1969); *Angew. Chem., Int. Ed. Engl.*, **8**, 981 (1969).
15) M. Wakselman and E. Guibé-Jampel, *Tetrahedron Lett.*, **1970**, 1521.
16) K. T. Potts and H. R. Burton, *J. Org. Chem.*, **31**, 251 (1966).

Synthesis of Mesoionic Triazolopyridine. III. Applications of *N*-Acyl Mesoionic Triazolopyridines as Acylating Reagents

Akio SAITO* and Bunji SHIMIZU
Chemical Research Laboratories, Sankyo Co., Ltd., Hiromachi, Shinagawa-ku, Tokyo 140
(Received September 11, 1982)

Utility of *N*-acyl mesoionic triazolopyridines as acylating reagents was investigated concerning with peptide synthesis. Several dipeptides and *N*-alkoxycarbonyl amino acids were prepared by use of these reagents.

N-Acylimidazoles(imidazolides, **1**) are widely used for organic synthesis[1] as acylating reagents because of their easy preparation and appropriate reactivity. Thus, imidazolides are readily prepared[2] from carboxylic acids under very mild conditions, and are utilized in a wide variety of synthetic processes, *e.g.*, amides[1,2] esters,[3] aldehydes,[4] ketones,[1] and C–C bond formations.[5] However, the instability of imidazolides on hydrolytic decomposition requires careful handling and delineates their appricatons. To remove this defect, other types of active amides are being developed.[6–8]

In the preceding paper[9] of this series, we described the synthesis and some properties of *N*-acyl and *N*-alkoxycarbonyl mesoionic triazolopyridines† (**2** and **3**). These compounds are readily synthesized from carboxylic acids or alcohols by using *N*-(chloroformyl)-triazolopyridines (**5** and **6**) under the very mild conditions. Preliminary study[9] revealed that the active amide of these types (**2** and **3**) was relatively stable toward hydrolytic decomposition but more active than corresponding imidazolide in the reaction with amines. These properties of the mesoionic azolide have indicated the potential of these compounds as acylating reagents. To examine the utility of the mesoionic azolides as acylating reagents, we have first applied them for a synthesis of amides. In this paper, we wish to describe the applications of these mesoionic azolides (**2** and **3**) for peptide synthesis including both of peptide-bond formation and introduction of urethane-type protecting groups to amine moieties of amino acids.

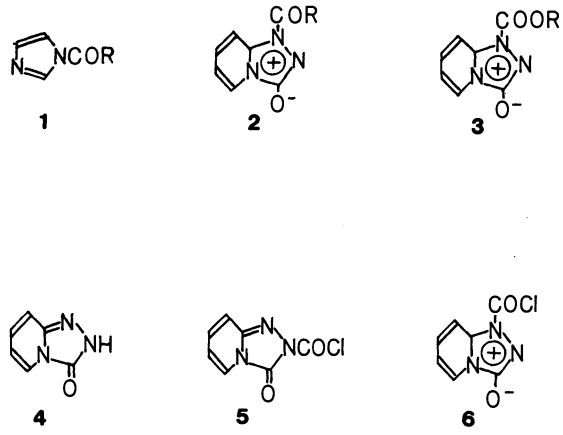

1 2 3 4 5 6

Fig. 1.

† Both classes of compounds are characterized by combination of *N*-acylazole(azolide)[1] with mosoionic ring. Hence, we wish to use a term "mesoionic azolide" for the compounds (**2** and **3**) in this paper.

Results and Discussion

The *N*-acyl mesoionic azolides (**2**) were applied for peptide-bond formation, and the urethane-type mesoionic azolides (**3**) were utilized for the introduction of amineprotecting groups.

Peptide-bond Formation. One of the major problem in peptide synthesis is racemization, which proceeds[10] *via* 5(4*H*)-oxazolone (**8**) formation at the activated carboxyl group of an *N*-acyl amino acid or acyl peptide (Scheme 1). To avoid this problem, the *N*-blocked amino acids (**9**) by urethane-type protecting groups, which suppress the oxazolone formation, are usually used for the coupling reactions of amino acids.

N^{α}-Benzyloxycarbonyl (Z) or N^{α}-(*t*-butoxycalbonyl) (Boc) amino acids reacted rapidly with **5** in the presence of one equimolor of tertiary amines in an aprotic solvent with evolution of gas. The reactions completed within 10 min at 4—25 °C, and the reaction mixture turned fluorescent yellow-green, indicating the formation of the mesoionic azolides (**2**). The products (**10**) were isolated easily by washing the reaction mixture with water, followed by removing the solvent *in vacuo*. However, in most cases, the reaction mixtures were used to the following coupling reactions without isolation of the mesoionic azolides. Reactions of the mesoionic azolides, such as **10**, with amino acid esters (**11**, R^3=alkyl) took place smoothly and generally completed within 1—3 h; in the case of sterically hindered amino acids, *e.g.*, isoleucine or valine, longer time (—15 h) was required to complete the reaction. According to the progress of the reaction, disappearance of the fluorescence of the reaction mixture and precipitation of the by-product (**4**) were found. These changes can be used to monitor the reaction. The by-product (**4**) is only slightly soluble in most of solvents. Therefore, it was almost separated by filtration, and the small amount of **4** remaining in the filtrate was completely removed by washing with 4% sodium hydrogencarbonate or 0.5 M copper(II) sulfate buffered with sodium citrate. Thus, desired dipeptide esters (**12**, R^3= alkyl) were isolated from the reaction mixture without any difficulties. The yields of the products were good.

When the mesoionic azolide (**10a**) was treated with sodium salts of amino acids (**11**, R^3=Na) in aqueous solution, dipeptides (**12**, R^3=H) were obtained in good yield. The yield of 93% for *N*-Z-glycylphenylalanine is obviously superior than those of other methods including imidazolide method; the yields of 55—66% were reported.[2,8,11] It seemed that this good yield could be ascribed to the stability of the mesoionic azolide toward hydrolytic decomposition. The conditions of the coupl-

TABLE 1. PREPARATION OF DIPEPTIDES. REACTION CONDITIONS AND YIELDS

Run	Synthesized dipeptide	Reaction conditions			Yield/%[a]
		Temp/°C	Time/h	Solvent	
1	Z-Ile-Gly-OEt[b]	r.t.[d]	3	$CHCl_3$	96
2	Z-Ile-Leu-OEt[b]	r.t.	15	$CHCl_3$	73
3	Z-Arg(NO_2)-Pro-OBzl[b]	r.t.	3	$CHCl_3$	82
4	Z-pyro-Glu-His-OBzl[c]	r.t.	2	$CHCl_3$	87
5	Boc-Pro-Gly-OEt[c]	r.t.	0.5	$CHCl_3$	99
6	Z-Gly-Ala-OH[b]	4	3	Me_2CO-H_2O	91
7	Z-Gly-Phe-OH[b]	r.t.	0.5	Me_2CO-H_2O	93

a) Isolated yield. b) Isolated mesoionic azolide was used. c) The coupling was carried out without isolation of the mesoionic azolide. d) Room temperature.

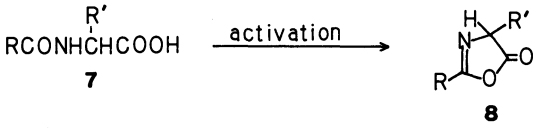

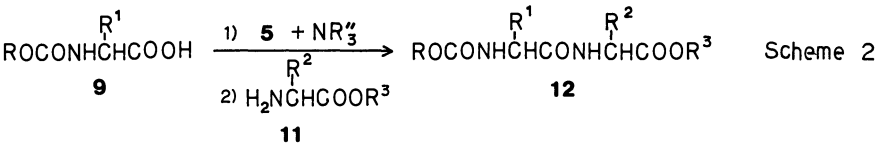

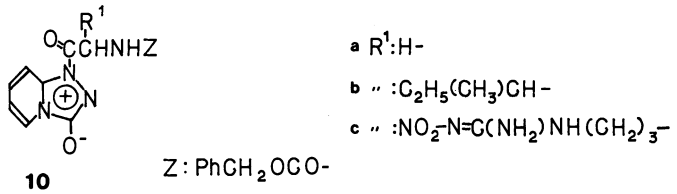

Fig. 2.

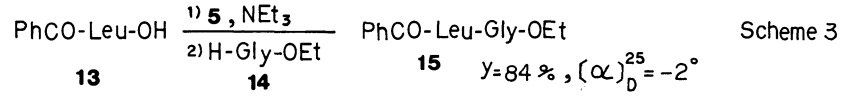

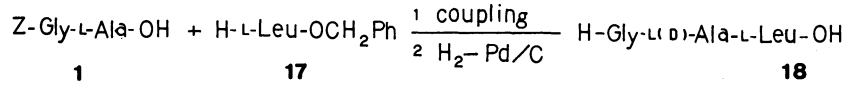

Fig. 3.

ing reaction and the yields of dipeptides are summarized in Table 1. The physical properties of the dipeptides are in agreement with those of the samples reported in literature.[2,24-26]

When *N*-benzoyl-L-leucine (**13**) was treated with **5**, instead of *N*-Boc or *N*-*Z* amino acid, relatively weak fluorescence of the reaction mixture and precipitation of **4** were found. These facts suggest the formation of oxazolone (**8**) instead of mesoionic azolide such as **10**. The following treatment of this reaction mixture with glycine ethyl ester (**14**) gave the dipeptide (**15**) with loss of optical activity. This peptide-bond formation seemed to proceed via oxazolone, which causes the racemization. To determine exact degree of the racemization in this method, Izumiya test[12] was achieved. The results are shown in Table 2. The racemization was minimized to 6.7% when the reaction was carried out in THF and in lower temperature (−20 °C). Further attempts to overcome the racemization were not achieved, since polypeptides are generally synthesized by stepwise condensation using an N^{α}-protected amino acid with a urethane-type protecting group, and practical methods[13,14] for fragment condensation now became available.

TABLE 2. IZUMIYA TEST

Run	Activation conditions			Tripeptide	
	Temp °C	Time min	Solvent	Yield %	Extent of racemization %
1	0	20	$CHCl_3$	90	16.3
2	−20	10	THF	97	6.7

Protection of Amino Function by Using the Mesoionic Azolide (3). Since benzyloxycarbonyl fragment was introduced as an amino-protecting group in peptide synthesis, a number of analogous groups with a variety of

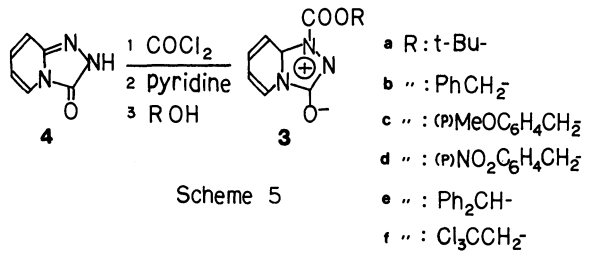

4 3

Scheme 5

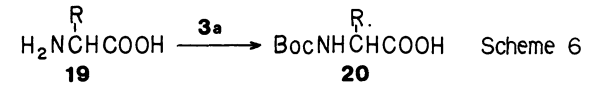

19 20 Scheme 6

21 22 Scheme 7

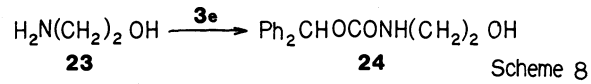

23 24 Scheme 8

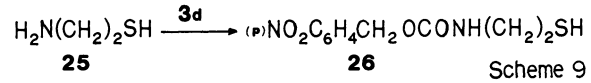

25 26 Scheme 9

Fig. 4.

the deblocking conditions have been utilized, *e.g.*, *t*-butoxycarbonyl (Boc),[15] *p*-methoxybenzyloxycarbonyl (PMZ),[15,16] *p*-nitrobenzyloxycarbonyl (PNZ),[17] benzhydryloxycarbonyl (Bhoc),[18] trichloroethoxycarbonyl (Troc),[19] and the others. Introduction of these blocking groups to amino acids has been done by using corresponding chloride or azide. However, the former procedure suffers from the instability of the reagents and the later cases have a fear of explosion in the synthesis of the reagent. To overcome these defects, some of reagents[20,21] have been developed in connection with the synthesis of *N*-Boc amino acid, which are most widely used for peptide synthesis.

Table 3. Urethane-type mesoionic azolides (3)

	R	Yield/%	Mp θ_m/°C
3a	*t*-Bu-	87	112—114
3b	$PhCH_2$-	90	140
3c	*p*-$MeOC_6H_4CH_2$-	82	127—130
3d	*p*-$NO_2C_6H_4CH_2$-	92	230
3e	Ph_2CH-	95	147—149
3f	Cl_3CCH_2-	88	140

The urethane-type mesoionic azolides (**3**) are obtained in good yield from a variety of alcohols by using **6**, or more conveniently by subsequent treatment of **4** with phosgene, pyridine and appropriate alcohols, (Fig. 4) and (Table 3). These mesoionic azolides were highly crystalline solids and could be stored in the air at room temperature for several months without any practical decomposition. It was found these reagents are applicable to the introduction of a variety of urethane-type *N*-protecting groups. Reactions of mesoionic *N*-Boc triazolopyridine (**3a**) with sodium salts of amino acids in aqueous acetone took place smoothly at room temperature, and generally completed in about 1—5 h, and the yields of the *N*-Boc amino acids were good (80—100%) (Table 4). The other urethane-type protecting groups were also easily introduced by using corresponding mesoionic azolide (**3**). For example mesoionic *N*-*Z*-triazolopyridine (**3b**) reacted with glycine sodium salt under the same conditions to give *N*-(benzyloxycarbonyl)glycine in 86% yield. In case of amino acid, like phenylglycine which has low solubility in aqueous solution, precipitation of the amino acid frequently occurred during the course of the eraction. This causes lowering the yields of the products. This problem was overcome by controlling the pH (10.2—10.5) of the reaction mixture or by exchanging the solvent from aqueous acetone to aqueous pyridine. Another problem in this procedure is the competitive conversion of the mesoionic azolide (**3**) into less reactive nonmesoionic N^2-acyl analogs.[9] However, this problem was overcome using excess of the reagent (1.2—2.0 molar equivalent). By using these conditions, several *N*-(alkoxycarbonyl)-

Table 4. Boc-amino acids. yields and reaction conditions

Boc-Amino acid[a]	Reagent mol	Solvent	Reaction time/h	Yield %	Mp θ_m/°C	Ref θ_m/°C
Boc-L-Trp-OH	1.4	A	6	90	137—139	137—138[21]
Boc-L-Glu-OH	1.4	A	3	82	113—114	110—112[23]
Boc-L-Ile-OH·DCHA	1.4	A	4	86	124—126	123—125[21]
Boc-L-Met-OH·DCHA	1.4	A	4	92	136—138	137—139[21]
Boc-L-Arg(NO_2)-OH	1.4	A	5	85	116(decomp)	115—116(decomp)[21]
Boc-L-Pro-OH	1.1	B	2	88	133—134	132—133[21]
Boc-L-Phe-OH	1.4	C	4	77	87—89	84—86[21]
Boc-L-Tyr-OH·DCHA	1.4	A	4	81	198(decomp)	202(decomp)[21]
Boc-L-Val-OH·DCHA	1.4	A	3	89	138—139	
Boc-L-Ser-OH·DCHA	1.4	A	4	71	136—138	140—142[23]
Boc-D-Phg-OH	2.0	A	4	77	85—88	87—89.5[21]
Boc-D-Phg-OH	2.0	A(pH 10.5)	2	84	86—88	

a) Each of amino acids (10 mmol) was dissolved in 10 ml of 1 M sodium hydroxide, then organic solvents were added. A: Acetone (10 ml)-pyridine (2 ml), B: no additive, C: dioxane (10 ml)-pyridine (2 ml).

phenylglycines (**22a**, **c**, **f**) were obtained in satisfactory yields. These results show that the mesoionic azolides (**3**) are useful reagents for the introduction of a variety of urethane-type protecting groups. These reactions of **3** with amino acids proceed in aqueous solution under mild conditions, and the yields of the *N*-protected amino acids are satisfactory. These good results are probably attributed to the feature of the mesoionic azolide. Thus, both of polar structure of the mesoionic ring and higher reactivity toward amines compared with water are favorable for reaction in aqueous solution. Alternative example of the highly selective reactivity of the mesoionic azolide were found in the following experiments. The reaction of **3e** with 2-aminoethanol (**23**) gave *N*-Boc-2-aminoethanol (**24**) in 96% yield (Scheme 8). More interesting result was obtained in the case of 2-aminoethanethiol (**25**). The reaction of **3d** with **25** gave *N*-protected product (**26**) in good yield (Scheme 9). It was reported[22] that **26** was hardly prepared by direct *N*-acylation of **25** since *N*- and *S*-acylations compete in the reaction.

As described above, *N*-Boc and *N*-*Z* amino acids were converted readily to the mesoionic azolide (**2**) under very mild conditions by using the reagent (**5**). Coupling reactions of these mesoionic azolides with amino acid esters or amino acid salts proceeded smoothly yielding dipeptides. The yields were satisfactory even in the reaction being conducted in aqueous solution. A variety of urethane-type mesoionic azolides were also utilized successfully for the specific introduction of urethane-type protecting groups to the amino moieties of several amines having another functional groups. Remarkable selective reactivity of these mesoionic azolides (**2** and **3**) toward amino moiety was found in the experiments described above. The results revealed the utility of these mesoionic azolides (**2** and **3**) as acylating reagents, and indicate possible use for the acylation of complicated molecules.

Experimental

Melting points were determined on a Yazawa hot-stage apparatus and were uncorrected. IR, UV, and NMR spectra were recorded on JASCO A102, Hitachi 200-20 and Varian EM 360L spectrometers respectively.

N-(Chloroformyl)triazolopyridines (**5** and **6**) were prepared in the manner previously reported.[9]

*1-[N-(Benzyloxycarbonyl)glycyl]-1,2,4-triazolo[4,3-a]pyridinium-3-olate (**10a**).* To a solution of *N*-(benzyloxycarbonyl)-glycine (6.27 g, 30 mmol) in chloroform (80 ml) were successively added triethylamine (4.20 ml, 30 mmol) and 5.91 g (30 mmol) of 2-chloroformyl-1,2,4-triazolo[4,3-*a*]pyridin-3(2*H*)-one (**5**). After the mixture had been stirred at room temperature for 1 h, the precipitate formed was collected by filtration to give 8.23 g (84%) of **10a**. The filtrate was washed twice with cold water, dried over anhydrous sodium sulfate, and evaporated *in vacuo*. The residue was crystallized from chloroform–ether to give second crop of **10a** (328 mg, 3.3%); mp 173—176 °C. UV (THF) λ_{max}: 375 nm. IR (Nujol): 1720, 1695 cm^{-1} (C=O). Found: C, 58.65; H, 4.13; N, 17.05%. Calcd for $C_{16}H_{14}N_4O_4$: C, 58.89; H, 4.32; N, 17.17%.

*1-(N-Benzyloxycarbonyl-L-isoleucyl)-1,2,4-triazolo[4,3-a]pyridinium-3-olate (**10b**).* To a solution of *N*-benzyloxycarbonyl-L-isoleucine (7.96 g, 30 mmol) in chloroform (100 ml) was added triethylamine (4.2 ml, 30 mmol), and the mixture was cooled to 4 °C, then 5.91 g (30 mmol) of **5** was added. After having been stirred for 1 h, at room temperature, the reaction mixture was washed twice with cold water, dried over anhydro us sodium sulfate, and evaporated *in vacuo*. The residue was crystallized from chloroform–ether giving pure **10b** (10.83 g, 95%); mp 165—170 °C. UV (THF) λ_{max}: 374 nm. Found: C, 62.92; H, 5.84; N, 14.65%. Calcd for $C_{20}H_{22}N_4O_4$: C, 62.81; H, 5.80; N, 14.65%.

*1-(N^a-Benzyloxycarbonyl-N^g-nitro-L-arginyl)-1,2,4-triazolo[4,3-a]pyridinium-3-olate (**10c**).* A solution of N^a-benzyloxycarbonyl-N^g-nitro-L-arginine (7.06 g, 20 mmol) and triethylamine (2.80 ml, 20 mmol) in dichloromethane (30 ml) was added dropwise into a suspension of **5** (4.00 g, 20 mmol) in dichloromethane (50 ml) at a temperature between 4 °C to 7 °C with stirring. The mixture was stirred for 1 h at 4 °C, then allowed to stand at room temperature for 2 h. The crystalline precipitate was collected by filtration, washed with chloroform, dried *in vacuo* to give **10c** (8.08 g, 85.5%). The filtrate and the washing were combined, washed twice with cold water, dried over anhydrous sodium sulfate, and evaporated *in vacuo*. The residue was crystallized from chloroform–ether to give second crop of **10c** (1.381 g, 14.5%); mp 120 °C. UV (CH_2Cl_2) λ_{max}: 378 nm. Found: C, 49.24; H, 4.96; N, 22.68%. Calcd for $C_{20}H_{22}N_8O_6 \cdot H_2O$: C, 49.16; H, 4.95; N, 22.95%.

*Reaction of **10b** with H–Gly–OEt.* To a solution of glycine ethyl ester (356 mg, 3.15 mmol) in chloroform (10 ml) was added **10b** (1.15 g, 3 mmol), and the mixture was stirred at room temperature for 3 h. The reaction mixture was filtered to remove the by-product (**4**), and the filtrate was washed successively with 2% hydrochloric acid, water, 4% sodium hydrogencarbonate, and water, then dried over anhydrous sodium sulfate, and evaporated *in vacuo*. The residue was crystallized from methanol to give *N*-benzyloxycarbonyl-L-isoleucylglycine ethyl ester (1.01 g, 96%); mp 155—156 °C; $[\alpha]_D^{25}$ −27° (c 0.9, CH_3OH). Lit[24] mp 155 °C; $[\alpha]_D$ −26° (*c* 1, CH_3OH). Found: C, 61.67; H, 7.63; N, 8.26%. Calcd for $C_{18}H_{26}N_2O_5$: C, 61.70; H, 7.48; N, 7.99%.

*Reaction of **10b** with H-L-Leu-OEt.* Triethylamine (0.70 ml, 5 mmol) was added to a solution of leucine ethyl ester hydrochloride (1.00 g, 5 mmol) in chloroform (10 ml), then **10b** (1.91 g, 5 mmol) was added. After having been stirred at room temperature for 15 h, the reaction mixture was worked up in the same manner as described in the preceding experiment. Crystallization from ether gave *N*-benzyloxycarbonyl-L-isoleucyl-L-leucine ethyl ester (1.433 g, 71%); mp 116—117 °C; $[\alpha]_D^{25}$ −43.5° (*c* 0.8, CH_3OH). Found: C, 64.69; H, 8.44; N, 6.72%. Calcd for $C_{22}H_{34}N_2O_5$: C, 64.99; H, 8.43; N, 6.89%.

*Reaction of **10c** with H-L-Pro-OBzl.* To a suspension of L-proline benzyl ester hydrochloride (2.64 g, 11 mmol) in chloroform (20 ml) was added triethylamine (1.54 ml, 11 mmol), and the mixture was stirred for 10 min, then **10c** (4.88 g, 10 mmol) was added. After having been stirred at room temperature for 2 h, the reaction mixture was worked up in the same manner as described in the preceding experiment. Crystallization from ethanol–ether gave N^a-benzyloxycarbonyl-N^g-nitro-L-arginyl-L-proline benzyl ester (4.33 g, 82%); mp 145—146 °C; $[\alpha]_D^{22}$ −59° (*c* 1, CH_3OH). Lit,[25] $[\alpha]_D$ −61° (*c* 1.1, CH_3OH). Found: C, 57.49; H, 6.09; N, 15.46%. Calcd for $C_{26}H_{32}N_6O_7$: C, 57.77; H, 5.97; N, 15.55%.

*Coupling of Z-L-pyro-Glu-OH with H-L-His-OBzl by Use of **5**.* To a solution of *N*-benzyloxycarbonyl-L-pyroglutamic acid (526 mg, 2 mmol) in chloroform (10 ml) were added triethylamine (0.28 ml, 2 mmol) and **5** (396 mg, 2 mmol), and the

mixture was stirred at room temperature for 30 min, then L-histidine benzyl ester (490 mg, 2 mmol) was added. After having been stirred at room temperature for 2 h, the reaction mixture was filtered to remove the by-product (**4**). The filtrate was washed successively with water, 2% hydrochloric acid, 4% sodium hydrogencarbonate and water, then dried over anhydrous sodium sulfate, and evaporated *in vacuo*. The residue was crystallized from ethyl acetate to give *N*-benzyloxycarbonyl-L-pyroglutamyl-L-histidine benzyl ester (852 mg, 87%); mp 125—126 °C; $[\alpha]_D^{22}$ −40° (*c* 1.2, CH_3OH). Found: C, 63.40; H, 5.33; N, 11.33%. Calcd for $C_{19}H_{22}N_4O_5$: C, 63.68; H, 5.34; N, 11.42%.

Coupling of Boc-L-Pro-OH with H-Gly-OEt by Use of ***5***. To a stirred solution of Boc-L-proline (5.37 g, 25 mmol) in chloroform (50 ml) were added successively *N*-methylmorpholine (2.74 ml, 25 mmol) and **5** (4.95 g, 25 mmol) at a temperature below 10 °C, and the mixture was stirred at room temperature for 40 min, then glycine ethyl ester (2.83 g, 27.5 mmol) was added. After having been stirred at room temperature for 30 min, the reaction mixture was filtered to remove the by-product (**4**). The filtrate was washed successively with water, 0.5 M citric acid, water, 4% sodium hydrogencarbonate and water, then dried over anhydrous sodium sulfate, and evaporated *in vacuo*. The oily residue was chromatographically pure *N*-Boc-L-prolylglycine ethyl ester (7.43 g, 99%). Found: C, 56.23; H, 8.22; N, 9.15%. Calcd for $C_{14}H_{24}N_2O_5$: C, 55.97; H, 8.05; N, 9.32%.

Reaction of ***10a*** *with H-Ala-OH.* To a solution of L-alanine (1.60 g, 18 mmol) in a mixture of 1 M sodium hydroxide (18 ml) and acetone (18 ml) was added **10a** (4.89 g, 15 mmol) at 4 °C. The mixture was stirred at 4 °C for 3 h, evaporated *in vacuo* to remove the acetone, and filtered to remove by-product. The filtrate was washed with ethyl acetate, acidified by adding 1 M hydrochloric acid, and extracted with ethyl acetate (×2). The ethyl acetate solution was washed successively with a 1 : 1 mixture of 0.5 M copper(II) sulfate and 1/6 M sodium citrate, and with water, dried over anhydrous sodium sulfate, and concentrated *in vacuo* giving a crystalline product. The product was collected by filtration, washed with small amount of ethyl acetate, and dried. *N*-(Benzyloxycarbonyl)glycyl-L-alanine (3.864 g, 91%) was obtained: mp 117 °C; $[\alpha]_D^{22}$ −9.7° (*c* 3, C_2H_5OH). Lit,[26]: mp 119.5 °C; $[\alpha]_D$ −9.8° (*c* 2.8, C_2H_5OH). found: C, 55.98; H, 5.60; N, 9.97%. Calcd for $C_{13}H_{16}N_2O_5$: C, 55.68; H, 5.75; N, 9.99%.

Reaction of ***10a*** *with H-L-Phe-OH.* To a solution of L-phenylalanine (2.48 g, 15 mmol) in a mixture of 1 M sodium hydroxide (15 ml) and acetone (15 ml) was added **10a** (4.89 g, 10 mmol). The mixture was stirred at room temperature for 30 min, then allowed to stand overnight in a refrigerator. The crystalline by-product (**4**) was removed by filtration. Sodium hydrogencarbonate (4%, 10 ml) was added to the filtrate. The mixture was washed with ethyl acetate, acidified by adding 1 M hydrochloric acid (17 ml), and then extracted with ethyl acetate. The ethyl acetate extract was washed with 1 : 1 mixture of 0.5 M copper(II) sulfate and 1/6 M sodium citrate, and with water, then dried over anhydrous sodium sulfate, and evaporated *in vacuo*. The residue was crystallized from ether to give *N*-(benzyloxycarbonyl)glycyl-L-phenylalanine (5.02 g, 93%): mp 124—125.5 °C; $[\alpha]_D^{22}$ +40° (*c* 1, C_2H_5OH). Lit,[2]: mp 126.5 °C; $[\alpha]_D$ +40° (C_2H_5OH). Found: C, 64.11; H, 5.55; N, 7.96%. Calcd for $C_{19}H_{20}N_2O_5$: C, 64.03; H, 5.66; N, 7.86%.

Coupling of Bz-Leu-OH with H-Gly-OEt by Use of ***5***. A solution of *N*-benzoyl-L-leucine (1.175 g, 5 mmol) and triethylamine (1.40 g, 5 mmol) in chloroform (5 ml) was added dropwise with stirring into a suspension of **5** (1.0 g, 5 mmol) in chloroform at −15 °C. Gas evolution, followed by precipitation of insoluble material was found. The mixture was stirred at −10 °C for 1 h, and glycine ethyl ester (515 mg, 5 mmol) was added. After having been stirred at −10 °C for 30 min, then at 4 °C for 3 h, the reaction mixture was filtered. The filtrate was washed with water, dried over anhydrous sodium sulfate, and evaporated *in vacuo*. The residue was crystallized from ether to give *N*-(benzoyl) leucylglycine ethyl ester (1.342 g, 84%); mp 144—147 °C; $[\alpha]_D^{22}$ −2° (*c* 1, C_2H_5OH): the value of $[\alpha]_D^{20}$ −34.0° (*c* 3.1, C_2H_5OH) was reported[10] for *N*-benzoyl-L-leucylglycine ethyl ester. Found: C, 63.88; H, 7.41; N, 9.03%. Calcd for $C_{17}H_{24}N_2O_4$: C, 63.73; H, 7.55; N, 8.75%.

Izumiya Test. Z-Gly-L-Ala-OH and authentic samples of H-Gly-L-Ala-L-Leu-OH and H-Gly-D-Ala-L-Leu-OH were prepared by the methods in the literature.[12] The dipeptide (Z-Gly-L-Ala-OH) was treated with **5** under the condotions summarized in Table 2, and then allowed to react with L-leucine benzyl ester at room temperature overnight to give tripeptide. After hydrogenation to remove the protecting group, the tripeptide (**18**) were analyzed according to the procedure in the literature.[12]

General Procedure for Synthesis of the Urethane-type Mesoionic Azolide (3). *Synthesis of* ***3a***: Finely powdered 1,2,4-triazolo[4,3-*a*]pyridin-3(2*H*)-one[23] (40.5 g, 0.3 mol) was suspended in ethanol-free chloroform (1.2 l) prepared by passing through an alumina column, and a solution of phosgene (33 g, 0.33 mol) in THF (150 ml) was added with stirring at a temperature below 10 °C. The mixture was stirred at 4 °C for 45 min, pyridine (53.5 ml, 0.66 mol) was added. After the mixture had been stirred for 30 min at 4 °C, *t*-butyl alcohol (50 ml) was added, and resultant mixture was stirred at room temperature for 40 min. The reaction mixture was washed with cold water (×3), dried over anhydrous sodium sulfate, and concentrated *in vacuo* giving crystalline product, and ether was added slowly to complete the crystallization. The product (**3a**) was collected by filtration, washed with ether, and dried *in vacuo*. Yield; 77.0 g (87% as a one-half molar chloroform adduct). UV (CH_2Cl_2) λ_{max}: 363 nm. IR (Nujol): 1757, 1722 cm^{-1} (C=O). Found: C, 46.75; H, 4.52; N, 14.52%. Calcd for $C_{11}H_{13}N_3O_3 \cdot 1/2\ CHCl_3$: C, 46.82; H, 4.61; N, 14.25%.

Other mesoionic azolides (**3**) were prepared in the same manner by using appropriate alcohols instead of *t*-butyl alcohol. In some cases, the products were crystallized off from the reaction mixture during the course of the reaction, hence they could be collected by filtration. Result was summarized in Table 3. The physical data of **3** were as follows:

a) **3b**; mp 140 °C, Physical properties of this compound were identical to those of authentic samples.[9]

b) **3c**; mp 127—130 °C. UV (CH_2Cl_2) λ_{max} 363 nm. NMR ($CDCl_3$–CD_3OD); δ=8.53 (m, 1, H-5), 8.5—7.9 (m, 2, H-7 and H-8), 7.45 (m, 1, H-6), 7.42 (d, J=9 Hz, 2, aromatic H), 6.88 (d, J=9 Hz, 2, aromatic H), 5.42 (s, 2, $PhC\underline{H}_2$), 3.81 (s, 3, OCH_3). Found: C, 59.93; H, 4.54; N, 14.31%. Calcd for $C_{15}H_{13}N_3O_4$: C, 60.20; H, 4.38; N, 14.04%.

c) **3d**; mp 230 °C (decomp). UV (CH_2Cl_2) λ_{max} 363 nm. Found: C, 56.65; H, 3.01; N, 16.38%. Calcd for $C_{16}H_{10}N_4O_5$: C, 56.80; H, 2.98; N, 16.56%.

d) **3e**; mp 147—149 °C. UV (CH_2Cl_2)λ_{max} 263, 363 nm. Found: C, 68.59; H, 4.56; N, 12.23%. Calcd for $C_{20}H_{15}N_3O_3$ 1/4 H_2O: C, 68.65; H, 4.46; N, 12.01%.

e) **3f**; mp 140 °C. UV (CH_2Cl_2) λ_{max} 364 nm. NMR ($CDCl_3$–CD_3OD); δ=8.67 (m, 1, H-5), 8.6—8.1 (m, 2, H-7 and H-8), 7.61 (m, 1, H-6), 5.18 (s, 2, $Cl_3CC\underline{H}_2$). Found: C, 35.03; H, 1.99; N, 13.66; Cl, 34.13%. Calcd for $C_9H_6N_3$-

O_3Cl_3: C, 34.82; H, 1.95; N, 13.53; Cl, 34.25%.

General Procedure of Synthesis of N-*Boc Amino Acids.* *a) A Typical Procedure*: To a solution of L-tryptophan (2.04 g, 10 mmol) in a mixture of 1 M sodium hydroxide (10 ml), acetone (10 ml) and pyridine (2 ml), **3a** (4.14 g, 14 mmol as 1/2 $CHCl_3$ adduct) was added, and the mixture was stirred at room temperature for 3 h then evaporated *in vacuo* to remove the acetone, and the residual aqueous solution was allowed to stand overnight in a refrigerator. Crystalline by-product (**4**) was removed by filtration, and the filtrate was acidified with 0.5 M citric acid to pH 3, then extracted with ethyl acetate. The ethyl acetate solution was washed with a 1 : 1 mixture of 0.5 M copper(II) sulfate and 1/6 M sodium citrate, and with water, then dried over anhydrous sodium sulfate, and evaporated *in vacuo*. The residue was crystallized from ethyl acetate–hexane to give *N*-Boc-L-tryptophan (2.74 g, 90%); mp 137—139 °C. Found: C, 62.97; H, 6.40; N, 9.35%. Calcd for $C_{16}H_{20}N_2O_4$: C, 63.14; H, 6.62; N, 9.20%. Other *N*-Boc amino acids were synthesized in the almost same manner, under the conditions summarized in Table 4; *N*-Boc-glutamic acid was extracted with 1-butanol instead of ethyl acetate.

b) By pH Control: To a solution of D-phenylglycine (3.03 g, 20 mmol) in a mixture of 1 M sodium hydroxide (20 ml) and acetone (20 ml) was added **3a** (11.80 g, 40 mmol as 1/2 $CHCl_3$ adduct), and the mixture was stirred at room temperature for 30 min. pH of the reaction mixture was kept around 10.5 by adding 2 M sodium hydroxide. The reaction mixture was stirred for additional 1.5 h without the pH control, and then evaporated *in vacuo* to remove the acetone. The resultant aqueous solution was allowed to stand for 1 h in a refrigerator, then filtered to remove the by-product (**4**). The filtrate was worked up in the same manner as described in preceding experiment. Crystallization from hexane gave *N*-Boc-D-phenylglycine (4.21 g, 84%); mp 86—88 °C; lit,[21] 87—89.5 °C. $[\alpha]_D^{22}$ −148° (*c* 1, C_2H_5OH); lit,[23] $[\alpha]_D$ +150° (*c* 1, C_2H_5OH) for *N*-Boc-L-phenylglycine.

N-*(p-Methoxybenzyloxycarbonyl)-D-phenylglycine.* D-Phenylglycine (3.03 g, 20 mmol) was treated with **3c** (8.95 g, 30 mmol) in the same manner as described before in the preparation of *N*-Boc-D-phenylglycine. Crystallization of the crude product from ethyl acetate–hexane gave desired product (5.16 g, 82%); mp 130—132 °C; $[\alpha]_D^{22}$ −102° (*c* 1, CH_3OH). NMR (DMSO-d_6–$CDCl_3$); δ=7.92 (d, J=8 Hz, 1, NH), 7.34 (s, 5, C_6H_5), 7.25 (d, J=9 Hz, 2, aromatic H), 6.84 (d, J=9 Hz, 2, aromatic H), 5.13 (d, J=8 Hz, 1, PhC<u>H</u>), 4.94 (s, 2, PhC<u>H</u>$_2$), 3.72 (s, 3, OCH_3). Found: C, 43.22; H, 8.91; N, 7.23%. Calcd for $C_{17}H_{17}NO_5$: C, 43.06; H, 8.78; N, 7.18%.

N-*(Benzyloxycarbonyl)glycine.* To a solution of glycine (375 mg, 5 mmol) in 1 M sodium hydroxide (5 ml) was added **3b** (1.48 g, 5.5 mmol), and the mixture was stirred at room temperature for 1 h and then allowed to stand for 3 h in a refrigerator. The reaction solution was filtered to remove the by-product (**4**). The filtrate was washed twice with ethyl acetate, acidified by adding 1 M hydrochloric acid (6 ml) and extracted with ethyl acetate. The ethyl acetate solution was washed twice water, dried over anhydrous sodium sulfate, and evaporated *in vacuo*. The residue was extracted with ether, and the extract was evaporated *in vacuo*. The residue was crystallized from ether–petroleum ether to give desired compound (898 mg, 86%); mp 120—121 °C. Found: C, 57.25; H, 5.34; N, 6.75%. Calcd for $C_{10}H_{11}NO_4$: C, 57.40; H, 5.30; N, 6.70%.

N-*Trichloroethoxycarbonyl-D-phenylglycine (22f).* To a solution of D-phenylglycine (1.51 g, 10 mmol) in a mixture of 1 M sodium hydroxide (10 ml), acetone (10 ml) and pyridine (2 ml) was added **3f** (3.5 g, 11 mmol), and the mixture was stirred at 4 °C for 2 h, then evaporated *in vacuo* to remove the acetone. The residual aqueous solution was allowed to stand overnight in a refrigerator, and then filtered to remove the by-product. The filtrate was washed with ethyl acetate, acidified with 1 M hydrochloric acid to pH 2.5, and extracted with ethyl acetate. The ethyl acetate solution was washed with a 1 : 1 mixture of 0.5 M copper(II) sulfate and 1/6 M sodium citrate, and with water, then dried over anhydrous sodium sulfate, and evaporated *in vacuo*. The residue was crystallized from ether–petroleum ether to give desired product (3.10 g, 93%); mp 140—141.5 °C; $[\alpha]_D^{22}$ −105° (*c* 1.2, CH_3OH). Lit[21]: mp 141—143 °C. Found: C, 40.43; H, 3.15; N, 4.36; Cl, 31.91%. Calcd for $C_{11}H_{10}NO_4Cl_3$: C, 40.45; H, 3.09; N, 4.29; Cl; 32.56%.

Reaction of 3e with 2-Aminoethanol. To a solution of 2-aminoethanol (1.22 g, 20 mmol) in dichloromethane (30 ml) was added **3e** (6.0 g, 17.4 mmol), and the mixture was stirred at room temperature for 20 min, then filtered to remove the by-product (**4**). The filtrate was washed successively with 0.5 M citric acid, water, 5% sodium hydrogencarbonate, and water, then dried over anhydrous sodium sulfate, and concentrated giving crystalline product which was collected by filtration. 4.50 g (95.6%) of 2-(benzhydryloxycarbonylamino)ethanol was collected; mp 66—67 °C. NMR ($CDCl_3$); δ=7.36 (s, 10, C_6H_5), 6.84 (s, 1, $Ph_2C\underline{H}$), 5.68 (t, J=5 Hz, 1, NH), 3.5—3.0 (m, 5, CH_2 and OH). Found: C, 71.25; H, 6.36; N, 5.25%. Calcd for $C_{16}H_{17}NO_3$: C, 70.83; H, 6.32; N, 5.16%.

Reaction of 3d with 2-Aminoethanethiol. To a suspension of 2-aminoethanethiol hydrochloride (1.25 g, 11 mmol) in dichloromethane was added triethylamine (1.4 ml, 10 mmol), and the mixture was stirred at room temperature for 30 min under nitrogen atmosphere, then **3d** (3.14 g, 10 mmol) was added. After having been stirred at room temperature for 30 min, the reaction mixture was filtered, and the filtrate was washed successively with water, 0.5 M citric acid, water, 4% sodium hydrogencarbonate and water. The chloroform solution was dried over anhydrous sodium sulfate, and evaporated *in vacuo* to give a solid, which was washed with diisopropyl ether to give 2-(*p*-nitrobenzyloxycarbonylamino)ethanethiol (1.950 g, 81%); mp 66—68 °C. NMR ($CDCl_3$); δ=8.14 (d, J=8.5 Hz, 2, aromatic H), 7.47 (d, J=8.5 Hz, 2, aromatic H), 5.61 (broad-s, 1, NH), 5.19 (s, 2, PhC<u>H</u>$_2$), 3.46 (t, J=7 Hz, 2, NC<u>H</u>$_2$), 2.68 (m, 2, SC<u>H</u>$_2$), 1.44 (t, J=8 Hz, 1, SH).

References

1) H. A. Staab, *Angew, Chem., Int. Ed. Engl.*, **1**, 351 (1962).

2) G. W. Anderson and R. Paul, *J. Am. Chem. Soc.*, **80**, 4423 (1958); R. Paul and G. W. Anderson, *ibid*, **82**, 4596 (1960).

3) H. A. Staab, W. Rohr, and A. Mannschreck, *Angew. Chem.*, **73**, 143 (1961); H. A. Staab and A. Mannschreck, *Chem. Ber.*, **95**, 1284 (1962).

4) H. A. Staab and H. Bräunling, *Justus Liebigs Ann. Chem.*, **654**, 119 (1962).

5) D. W. Brooks, L. D.-L. Lu, and S. Masamune, *Angew. Chem., Int. Ed. Engl.*, **18**, 72 (1979).

6) T. Kunieda, T. Higuchi, Y. Abe, and M. Hirobe, *Tetrahedron Lett.*, **21**, 3065 (1980).

7) Y. Nagao, K. Seno, K. Kawabata, T. Miyasaka, S. Takao, and E. Fujita, *Tetrahedron Lett.*, **21**, 841 (1980).

8) L. Chung-hsi, Y. Yuen-hwa, L. Yao, L. Yong-jun, C, Ai-hsueh, and H. Chi-yi, *Tetrahedron Lett.*, **22**, 3467 (1981).

9) A. Saito and B. Shimizu, *Bull. Chem. Soc. Jpn.*, **56**, 2969 (1983).

10) M. W. Williams and G. T. Young, *J. Chem. Soc.*, **1964**, 3701.

11) J. R. Vaughan, Jr., and R. L. Osato, *J. Am. Chem. Soc.*, **74**, 676 (1952).
12) N. Izumiya, M. Muraoka, and H. Aoyagi, *Bull. Chem. Soc. Jpn.*, **44**, 3391 (1971).
13) W. König and R. Geiger, *Chem. Ber.*, **103**, 788 (1970); **103**, 2024 (1970); **103**, 2034 (1970).
14) M. Fujino, S. Kobayashi, M. Obayashi, T. Fukuda, S. Shinagawa, and O. Nishimura, *Chem. Pharm. Bull.*, **22**, 1857 (1974).
15) F. C. Mckay and N. F. Albertson, *J. Am. Chem. Soc.*, **79**, 4686 (1957).
16) F. Weygand and K. Hunger, *Chem. Ber.*, **95**, 1 (1962).
17) F. H. Carpenter and D. T. Gish, *J. Am. Chem. Soc.*, **74**, 3818 (1952).
18) R. G. Hiskey and J. B. Adams, Jr., *J. Am. Chem. Soc.*, **87**, 3969 (1965).
19) R. B. Woodward, K. Hensler, J. Gosteli, P. Naegeli, W. Oppolzer, R. Ramage, S. Ranganthan, and H. Vorbrüggen, *J. Am. Chem. Soc.*, **88**, 852 (1966).
20) D. S. Tarbell, Y. Yamamoto, and M. B. Pope, *Proc. Natl. Acad. Sci. U. S. A.*, **69**, 730 (1972).
21) M. Itoh, D. Hagiwara, and T. Kamiya, *Tetrahedron Lett.*, **1974**, 4493.
22) I. Shinkai, T. Liu, R. Reamer, and M. Sletzinger, *Synthesis*, **1980**, 924.
23) E. Schnabel, *Justus Liebigs Ann. Chem.*, **702**, 188 (1967).
24) M. Miyoshi, *Bull. Chem. Soc. Jpn.*, **46**, 1489 (1973).
25) K. Okamoto and S. Shimaura, *Yakugaku Zasshi*, **96**, 315 (1976).
26) B. F. Erlanger and E. Brand, *J. Am. Chem. Soc.*, **73**, 3508 (1951).

 © 1983 The Chemical Society of Japan Bull. Chem. Soc. Jpn., 56, 2981—2984 (1983)

Revision of Structure of Anhydronellionol Triacetate

Takashi MATSUMOTO,* Sachihiko IMAI, Masanori MITSUKI, and Seiji MAETA
Department of Chemistry, Faculty of Science, Hiroshima University, Higashisenda-machi, Naka-ku, Hiroshima 730
(Received January 27, 1983)

The structure of anhydronellionol triacetate was revised to 11,12,16-triacetoxy-6-hydroxyabieta-5,8,11,13-tetraen-7-one (**18**) by the following syntheses. Acetylation of 16-acetoxyabieta-8,11,13-trien-12-ol, followed by oxidation with chromium trioxide, afforded 12,16-diacetoxyabieta-8,11,13-trien-7-one. This was converted into 6,12,16-triacetoxyabieta-5,8,11,13-tetraen-7-one (**17**) *via* 12,16-diacetoxyabieta-8,11,13-trien-6-one. Oxidation of 11,12,16-triacetoxyabieta-8,11,13-trien-6-one with Jones reagent gave **18**, whose ^{1}H NMR spectrum was in good agreement with that of natural anhydronellionol triacetate. 11,12,16-Triacetoxyabieta-5,8,11,13-tetraen-7-one (**28**) was also synthesized from 11,12,16-triacetoxyabieta-8,11,13-trien-7-one. The ^{1}H NMR spectra of **17** and **28** were different from that of natural anhydronellionol triacetate. Since the revised structure **18** corresponds to dehydronellionol triacetate, the name of anhydronellionol should now be dropped from the list of natural diterpenes.

Recently three tricyclic aromatic diterpenes, nellionol, dehydronellionol, and anhydronellionol, have been isolated from the root bark of *Premna latifolia* Roxb. by Rao *et al.*[1] On the basis of chemical and spectroscopic studies, they deduced the structures of nellionol, dehydronellionol, and anhydronellionol to be 6α,11,14,16-tetrahydroxyabieta-8,11,13-trien-7-one (**1**), 6,11,14,16-tetrahydroxyabieta-5,8,11,13-tetraen-7-one (**2**), and 11,14,16-trihydroxyabieta-5,8,11,13-tetraen-7-one (**3**), respectively. The isolation of several abietane type diterpenes possessing two oxygen functions in the C-ring have already been reported. In these natural products oxygen functions are usually present at the C-11 and C-12 positions such as cryptojaponol (**4**),[2] fuerstione (**5**),[3] taxodione (**6**),[4] and carnosolone (**7**).[5] However, the proposed structures (**1**, **2**, and **3**) are unique because they possess two oxygen functions at the C-11 and C-14 positions and no oxygen function at the C-12 position. In the previous paper[6] we have reported the revised structures of nellionol and dehydronellionol to be respectively 6α,11,12,16-tetrahydroxyabieta-8,11,13-trien-7-one (**8**) and 6,11,12,16-tetrahydroxyabieta-5,8,11,13-tetraen-7-one (**9**); these possess two oxygen functions in the C-ring at the C-11 and C-12 positions. As an extension of the previous work,[6] we have now examined the published spectral data[1] of natural anhydronellionol triacetate to confirm the validity of the proposed structure **3**. The ^{1}H NMR spectrum of anhydronellionol triacetate showed singlet signals at δ 7.11 and 8.16 which were assigned respectively to the C-6 olefinic proton and the C-12 aromatic proton in the proposed structure (**10**). However, the chemical shift (δ 8.16) of the aromatic proton is different from those (δ 7.04 and 7.09) of the C-12 aromatic protons in methyl 11,14-diacetoxy-7-oxoabieta-8,11,13-trien-18-oate (**11**)[6] and 11,14-diacetoxy-13-(acetoxymethyl) podocarpa-8,11,13-trien-7-one (**12**),[7] but very similar to those (δ 8.15, 8.13, and 8.23) of the C-14 aromatic protons in methyl 11,12-diacetoxy-7-oxoabieta-5,8,11,13-tetraen-20-oate (**13**),[8] 12-acetoxyabieta-5,8,11,13-tetraen-7-one (**14**),[9] and carnosolone diacetate (**15**).[5] These spectral data strongly suggested that the aromatic proton in anhydronellionol triacetate is located at the C-14 position ortho to a carbonyl group. Furthermore the assignment of the signal at δ 7.11 to the C-6 olefinic proton was also unusual, because the olefinic protons in the same moiety of **13** and **14** were observed as singlets at δ 6.57 and 6.50 respectively. On the other hand, the ^{1}H NMR spectrum of **14** showed a singlet signal at δ 7.20 due to the C-11 aromatic proton and that of 6-hydroxyabieta-5,8,11,13-tetraen-7-one (**16**)[10] showed a singlet signal due to an enolic hydroxyl group at δ 7.08. From these spectral analyses, together with consideration of the other spectral data, we deduced a preferable structure of anhydronellionol triacetate to be 6,12,16-triacetoxyabieta-5,8,11,13-tetraen-7-one (**17**) or 11,12,16-triacetoxy-6-hydroxyabieta-5,8,11,13-tetraen-7-one (**18**). To obtain final confirmation of the structure of anhydronellionol triacetate, syntheses of **17** and **18** have been attempted.

Acetylation of 16-acetoxyabieta-8,11,13-trien-12-ol (**19**)[6,11] with acetic anhydride in pyridine, followed by oxidation of the resulting acetate (**20**: 91%) with chromium trioxide in acetic acid at room temperature, afforded 12,16-diacetoxyabieta-8,11,13-trien-7-one (**21**:

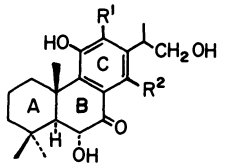

1 R¹=H, R²=OH
8 R¹=OH, R²=H

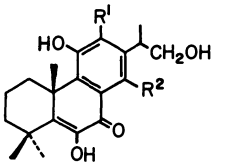

2 R¹=H, R²=OH
9 R¹=OH, R²=H

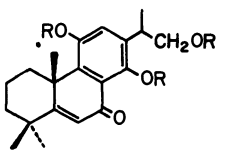

3 R=H
10 R=Ac

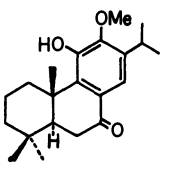

4

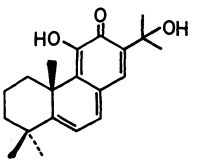

5

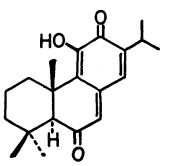

6

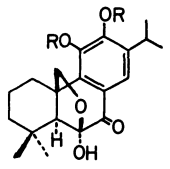
7 R=H
15 R=Ac

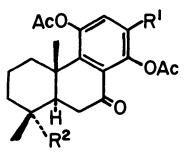
11 R^1=$CHMe_2$, R^2=CO_2Me
12 R^1=CH_2OAc, R^2=Me

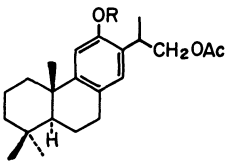
19 R=H
20 R=Ac

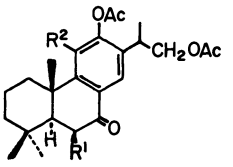
21 R^1=R^2=H
26 R^1=H, R^2=OAc
27 R^1=Br, R^2=OAc

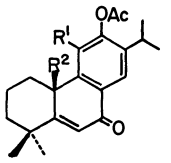
13 R^1=OAc, R^2=CO_2Me
14 R^1=H, R^2=Me

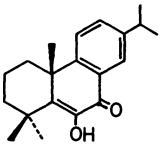
16

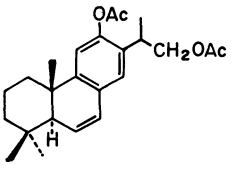
22

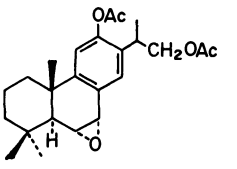
23

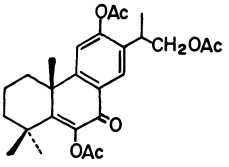
17

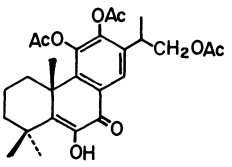
18

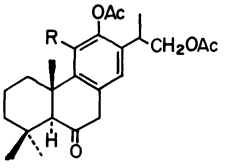
24 R=H
25 R=OAc

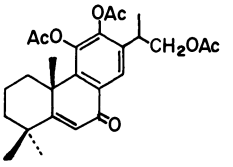
28

65%). The ketone **21** was reduced with sodium borohydride in methanol and the resulting mixture of epimeric 7-hydroxy compounds was immediately subjected to dehydration with dilute hydrochloric acid in refluxing methanol. Under these conditions, the acetoxyl groups were hydrolyzed. Therefore, the crude product was acetylated with acetic anhydride in pyridine to give 12,16-diacetoxyabieta-6,8,11,13-tetraene (**22**). This was treated with *m*-chloroperbenzoic acid in dichloromethane at room temperature. The resulting crude epoxide (**23**) was refluxed with dilute hydrochloric acid in methanol and then acetylated[12] with acetic anhydride in pyridine to afford 12,16-diacetoxyabieta-8,11,13-trien-6-one (**24**: 48% from **21**). The structure of **24** was supported by its ^{1}H NMR spectrum which showed singlet signals at δ 2.39 (1H) due to the $C_{5\alpha}$ proton and at δ 3.61 (2H) due to the C-7 methylene protons. Oxidation of **24** with Jones reagent at room temperature, followed by treatment with anhydrous sodium acetate in refluxing acetic anhydride, afforded the desired **17** (55%). The ^{1}H NMR spectrum of synthetic **17** showed singlet signals due to three acetoxyl groups at δ 2.01 (3H) and 2.36 (6H), and due to two aromatic protons at δ 7.21 (1H) and 8.08 (1H). However, the spectrum of **17** was different from that of natural anhydronellionol triacetate.

Subsequently, 11,12,16-triacetoxyabieta-8,11,13-trien-6-one (**25**)[6,11] was oxidized with Jones reagent and the resulting crude product purified by column chromatography on silica gel to give the desired **18** (49%). The ^{1}H NMR spectrum of synthetic **18** showed singlet signals due to three acetoxyl groups at δ 2.01 (3H), 2.32 (3H), and 2.35 (3H), due to an enolic hydroxyl group at δ 7.05 (1H), and due to an aromatic proton at δ 8.15 (1H). The spectrum of **18** was in good agreement with that of natural anhydronellionol triacetate.

For comparison, 11,12,16-triacetoxyabieta-5,8,11,13-tetraen-7-one (**28**) was also synthesized as follows. Bromination of 11,12,16-triacetoxyabieta-8,11,13-trien-7-one (**26**)[6,11] with pyridinium tribromide in a mixture of chloroform and ethanol (2 : 1) at room temperature produced 11,12,16-triacetoxy-6β-bromoabieta-8,11,13-trien-7-one (**27**). The β-configuration of the bromine atom in **27** was supported by its ^{1}H NMR spectrum, which showed a signal due to the C-10 methyl group in low field (δ 1.75), owing to the 1,3-diaxial interaction between the bromine atom and the C-10 methyl group. Dehydrobromination of the crude bromide **27** with 1,5 diazabicyclo[4.3.0]non-5-ene in refluxing benzene, followed by acetylation,[12] afforded **28** (37% from **26**). The ^{1}H NMR spectrum of **28** showed signals due to the C-6 olefinic proton at δ 6.53 (1H) and due to an aromatic proton at δ 8.13 (1H), which were different from those of natural anhydronellionol triacetate.

From the present study, the proposed structure[1] of natural anhydronellionol triacetate must be revised to **18**, which corresponds to dehydronellionol 11,12,16-triacetate.[6] Therefore, the name of anhydronellionol should now be dropped from the list of natural diterpenes.

Experimental

The IR spectra were measured in chloroform, and the ^{1}H NMR spectra in deuterochloroform at 60 MHz, with tetramethylsilane as an internal standard, unless otherwise stated. The chemical shifts are reported in terms of δ values; s: singlet, d: doublet, bd: broad doublet, m: multiplet. Column chromatography was performed using Merck silica gel.

*12,16-Diacetoxyabieta-8,11,13-triene (**20**).* A solution of

16-acetoxyabieta-8,11,13-trien-12-ol (**19**)[6,11] (678 mg) and acetic anhydride (1.5 ml) in pyridine (2.0 ml) was heated at 75—85 °C for 2 h. After the usual work-up, the crude product was chromatographed on silica gel (20 g), using ether–benzene (3 : 97) as the eluent, to give **20** (690 mg: 91%). IR: 1750, 1730 cm^{-1}; ^1H NMR (CCl_4): δ=0.95 (6H, s, $-C(CH_3)_2$), 1.18 (3H, d, J=7 Hz, C_{15}–CH_3), 1.19 (3H, s, C_{10}–CH_3), 1.95 (3H, s, C_{16}–$OCOCH_3$), 2.24 (3H, s, C_{12}–$OCOCH_3$), 3.97 (d, J=7 Hz) and 4.01 (d, J=7 Hz) (2H, $-CH_2OCOCH_3$), 6.78 (1H, s) and 6.85 (1H, s) (C_{11}–H and C_{14}–H).

*12,16-Diacetoxyabieta-8,11,13-trien-7-one (**21**).* Anhydrous chromium trioxide (416 mg) was added to a solution of **20** (913 mg) in acetic acid (10 ml) with cooling in an ice–water bath. The mixture was stirred at this temperature for 15 min and then at room temperature for 22 h. The mixture was diluted with water and extracted with ether. The ether extract was washed successively with aqueous sodium hydrogencarbonate and brine, dried over sodium sulfate, and evaporated *in vacuo*. The residue was chromatographed on silica gel (40 g), using ether–benzene (4 : 96) as the eluent, to give the starting **20** (103 mg: 11%). Further elution with ether–benzene (7 : 93) gave **21** (615 mg: 65%). IR: 1750, 1730, 1673, 1607 cm^{-1}; ^1H NMR: δ=0.95 (3H, s) and 1.02 (3H, s) ($-C(CH_3)_2$), 1.26 (3H, d, J=7 Hz, C_{15}–CH_3), 1.27 (3H, s, C_{10}–CH_3), 2.04 (3H, s, C_{16}–$OCOCH_3$), 2.38 (3H, s, C_{12}–$OCOCH_3$), 4.13 (2H, d, J=7 Hz, $-CH_2OCOCH_3$), 7.07 (1H, s, C_{11}–H), 8.03 (1H, s, C_{14}–H).

*12,16-Diacetoxyabieta-8,11,13-trien-6-one (**24**).* A mixture of **21** (767 mg) and sodium borohydride (150 mg) in methanol (10 ml) was stirred at 0—5 °C for 30 min and then at room temperature for 1 h. The mixture was acidified with dilute hydrochloric acid (10%: 2.0 ml), refluxed for 1 h, and evaporated *in vacuo*. The residue was extracted with ether. The ether extract was washed with brine, dried over sodium sulfate, and evaporated *in vacuo*. The residual oil was acetylated with acetic anhydride (2.0 ml) in pyridine (2.0 ml) at 75—85 °C for 2 h to give the crude 12,16-diacetoxyabieta-6,8,11,13-tetraene (**22**) (743 mg) which was used without purification in the next reaction.

A mixture of the crude tetraene **22** (743 mg) and *m*-chloroperbenzoic acid (590 mg) in dichloromethane (10 ml) was stirred at 0—5 °C for 1 h and then at room temperature for 14 h. The mixture was diluted with ether and washed successively with aqueous potassium iodide, aqueous sodium thiosulfate, aqueous sodium hydrogencarbonate, and brine. The ether solution was dried over sodium sulfate and evaporated *in vacuo* to give a crude epoxide (**23**) (871 mg) which was used without purification in the next reaction.

A mixture of the crude epoxide **23** (871 mg) and dilute hydrochloric acid (10%: 2.0 ml) in methanol (10 ml) was refluxed for 1 h. The mixture was evaporated *in vacuo*, diluted with water, and extracted with ether. The ether extract was washed with water, dried over sodium sulfate, and evaporated *in vacuo* to give an oil (784 mg). This was acetylated with acetic anhydride (2.0 ml) in pyridine (2.0 ml) at 75—85 °C for 2 h. After the usual work-up, the crude product was purified by column chromatography on silica gel (40 g), using ether–benzene (3 : 97) as the eluent, to give **24** (368 mg: 48% from **21**). IR: 1750sh, 1732, 1710 cm^{-1}; ^1H NMR: δ=1.09 (3H, s), 1.18 (3H, s), and 1.34 (3H, s) ($-C(CH_3)_2$ and C_{10}–CH_3), 1.23 (3H, d, J=7 Hz, C_{15}–CH_3), 2.05 (3H, s, C_{16}–$OCOCH_3$), 2.36 (3H, s, C_{12}–$OCOCH_3$), 2.39 (1H, s, $C_{5\alpha}$–H), 3.61 (2H, s, $-COCH_2-$), 4.12 (2H, d, J=7 Hz, $-CH_2OCOCH_3$), 7.01 (2H, s, C_{11}–H and C_{14}–H).

*6,12,16-Triacetoxyabieta-5,8,11,13-tetraen-7-one (**17**).* A solution of **24** (368 mg) in acetone (8.0 ml) was oxidized with Jones reagent [2.5 M (1 M=1 mol dm^{-3}): 1.2 ml] at 0—5 °C for 10 min and then at room temperature for 2.5 h. The mixture was diluted with water and extracted with ether. The ether extract was washed with brine, dried over sodium sulfate, and evaporated *in vacuo* to give a crude 6,7-dioxo compound. This was immediately refluxed with acetic anhydride (15 ml) in the presence of anhydrous sodium acetate (900 mg) for 2.5 h with stirring. The mixture was diluted with water and benzene, evaporated *in vacuo* to remove the excess acetic anhydride, and extracted with ether. The ether extract was washed successively with aqueous sodium hydrogencarbonate and brine, dried over sodium sulfate, and evaporated *in vacuo*. The residue was chromatographed on silica gel (20 g), using ether–benzene (5 : 95) as the eluent, to give **17** (229 mg: 55%). IR: 1760, 1735sh, 1660, 1615 cm^{-1}; ^1H NMR (90 MHz): δ=1.27 (d, J=7 Hz) and 1.30 (d, J=7 Hz) (3H, C_{15}–CH_3), 1.33 (3H, s) and 1.40 (3H, s) ($-C(CH_3)_2$), 1.59 (3H, s, C_{10}–CH_3), 2.01 (3H, s, C_{16}–$OCOCH_3$), 2.36 (6H, s, C_6 –$OCOCH_3$ and C_{12}–$OCOCH_3$), 4.04—4.18 (2H, m, $-CH_2-OCOCH_3$), 7.21 (1H, s, C_{11}–H), 8.08 (1H, s, C_{14}–H). The ^1H NMR spectrum of **17** was different from that of natural anhydronellionol triacetate. Found: C, 68.12; H, 7.17%. Calcd for $C_{26}H_{32}O_7$: C, 68.40; H, 7.07%.

*11,12,16-Triacetoxy-6-hydroxyabieta-5,8,11,13-tetraen-7-one (Dehydronellionol 11,12,16-Triacetate) (**18**).* A solution of 11,12,16-triacetoxyabieta-8,11,13-trien-6-one (**25**)[6,11] (71 mg) in acetone (2.0 ml) was oxidized with Jones reagent (2.5 M: 0.1 ml) at 0—5 °C for 10 min and then at room temperature for 2 h. The mixture was diluted with water and extracted with ether. The ether extract was washed with brine, dried over sodium sulfate, and evaporated *in vacuo*. The residue was chromatographed on silica gel (7.0 g), using ether–benzene (3 : 97) as the eluent, to give **18** (36 mg: 49%). IR: 3405, 1775, 1730, 1631, 1605 cm^{-1}; ^1H NMR (90 MHz): δ=1.30 (d, J=7 Hz) and 1.32 (d, J=7 Hz) (3H, C_{15}–CH_3), 1.46 (3H, s) and 1.48 (3H, s) ($-C(CH_3)_2$), 1.59 (3H, s, C_{10}–CH_3), 2.01 (3H, s, C_{16}–$OCOCH_3$), 2.32 (3H, s) and 2.35 (3H, s) (C_{11} –$OCOCH_3$ and C_{12}–$OCOCH_3$), 4.10 (d, J=7 Hz) and 4.13 (d, J=7 Hz) (2H, $-CH_2OCOCH_3$), 7.05 (1H, s, –OH), 8.15 (1H, s, C_{14}–H). The ^1H NMR spectrum of **18** was compatible with that of natural anhydronellionol triacetate, except for the signals due to the corresponding C-15 epimer.

*11,12,16-Triacetoxy-6β-bromoabieta-8,11,13-trien-7-one (**27**).* A mixture of 11,12,16-triacetoxyabieta-8,11,13-trien-7-one (**26**)[6,11] (68 mg) and 80% pyridinium tribromide (120 mg) in chloroform (1.0 ml) and ethanol (0.5 ml) was stirred at room temperature for 2 h. The mixture was diluted with water and extracted with ether. The ether extract was washed successively with water, aqueous sodium thiosulfate, and brine. The dried solution was evaporated *in vacuo* to give a crude bromide (**27**) (87 mg). ^1H NMR (CCl_4): δ=1.42 (6H, s, $-C(CH_3)_2$), 1.75 (3H, s, C_{10}–CH_3), 1.98 (3H, s, C_{16}–$OCOCH_3$), 2.39 (6H, s, C_{11}–$OCOCH_3$ and C_{12}–$OCOCH_3$), 4.80 (1H, bd, J=2.5 Hz, $W_{1/2}$=4 Hz, $C_{6\alpha}$–H), 8.05 (1H, s, C_{14}–H).

*11,12,16-Triacetoxyabieta-5,8,11,13-tetraen-7-one (**28**).* A mixture of the crude bromide **27** (87 mg) and 1,5-diazabicyclo-[4.3.0]non-5-ene (0.1 ml) in dry benzene (2.0 ml) was refluxed for 2 h in a stream of nitrogen. The mixture was cooled, acidified with dilute hydrochloric acid, and extracted with ether. The ether extract was washed with aqueous sodium thiosulfate and brine, dried over sodium sulfate, and evaporated *in vacuo*. The residue was immediately acetylated[12] with acetic anhydride (0.5 ml) in pyridine (0.5 ml) at room temperature for 20 h. After the usual work-up, the crude product was chromatographed on silica gel (7.0 g), using ether–benzene (3 : 97) as the eluent, to give **26** (18 mg: 26%). Further elution with ether–benzene (5 : 95) afforded **28** (25 mg: 37% from **26**). IR: 1772, 1727, 1650, 1605 cm^{-1}; ^1H

NMR (90 MHz): $\delta=1.30$ (3H, s) and 1.38 (3H, s) ($-\dot{C}(CH_3)_2$), 1.31 (3H, d, $J=7$ Hz, C_{15}–CH_3), 1.59 (3H, s, C_{10}–CH_3), 2.01 (s) and 2.02 (s) (3H, C_{16}–$OCOCH_3$), 2.33 (3H, s) and 2.34 (3H, s) (C_{11}–$OCOCH_3$ and C_{12}–$OCOCH_3$), 3.25 (1H, m, C_{15}–H), 4.09 (d, $J=7$ Hz) and 4.12 (d, $J=7$ Hz) (2H, $-C\underline{H}_2OCOCH_3$), 6.53 (1H, s, C_6–H), 8.13 (1H, s, C_{14}–H). The ^{1}H NMR spectrum of **28** was different from that of natural anhydronellionol triacetate.

The authors are grateful to Professor Ch. B. Rao for kindly supplying the spectral data of the natural product.

References

1) Ch. B. Rao, T. N. Rao, and E. K. S. Vijayakumar, *Curr. Sci.*, **47**, 455 (1978); *Indian J. Chem.*, **18B**, 513 (1979).
2) T. Kondo, M. Suda, and M. Teshima, *J. Pharm. Soc. Jpn.*, **82**, 1252 (1962).
3) D. Karanatsios, J. S. Scarpa, and C. H. Eugster, *Helv. Chim. Acta*, **49**, 1151 (1966).
4) S. M. Kupchan, A. Karim, and C. Marcks, *J. Am. Chem. Soc.*, **90**, 5923 (1968); *J. Org. Chem.*, **34**, 3912 (1969).
5) F. Yoshizaki, P. Rüedi, and C. H. Eugster, *Helv. Chim. Acta*, **62**, 2754 (1979).
6) T. Matsumoto, S. Imai, S. Takeda, and M. Mitsuki, *Bull. Chem. Soc. Jpn.*, **56**, 2013 (1983).
7) T. Matsumoto, S. Imai, and S. Yuki, *Bull. Chem. Soc. Jpn.*, **55**, 3836 (1982).
8) H. Linde, *Helv. Chim. Acta*, **47**, 1234 (1964).
9) R. C. Cambie, R. C. Hayward, J. L. Jurlina, P. S. Rutledge, and P. D. Woodgate, *J. Chem. Soc., Perkin Trans. 1*, **1978**, 126.
10) T. Matsumoto, S. Imai, H. Masuda, and K. Fukui, *Chem. Lett.*, **1974**, 1001.
11) The compound was a mixture of the corresponding C-15 epimers.
12) Under these conditions, the acetoxyl groups were hydrolyzed.

 © 1983 The Chemical Society of Japan Bull. Chem. Soc. Jpn., 56, 2985—2993 (1983)

Functionalization of (*R*)-3-(3-Acetoxypropyl)-2,3-dihydro-7-isopropyl-3,4-dimethylnaphtho[2,3-*b*]furan-2-one and Some Related Compounds

Takashi MATSUMOTO,* Sachihiko IMAI,* Kenji ONDO, Hideo KATAOKA, and Kyoko KATO
Department of Chemistry, Faculty of Science, Hiroshima University, Higashisenda-machi, Naka-ku, Hiroshima 730
(Received February 7, 1983)

Oxidation of (*R*)-3-(3-acetoxypropyl)-2,3-dihydro-6-hydroxy-7-isopropyl-3,4-dimethylnaphtho[2,3-*b*]furan-2-one with Fremy's radical afforded the corresponding *o*-quinone, which was converted into (*R*)-5,6,8-triacetoxy-3-(3-acetoxypropyl)-2,3-dihydro-7-isopropyl-3,4-dimethylnaphtho[2,3-*b*]furan-2-one and its 5,6,9-triacetoxy isomer. (*R*)-3-(3-Acetoxypropyl)-2,3-dihydro-7-isopropyl-3,4-dimethylnaphtho[2,3-*b*]furan-2-one was also converted into (*R*)-9-acetoxy- and (*R*)-5,8,9-triacetoxy-2,3-dihydro-7-isopropyl-3-(3-methoxypropyl)-3,4-dimethylnaphtho[2,3-*b*]-furan-2-one. Transformation of (*R*)-2,3-dihydro-6-hydroxy-3-(3-hydroxypropyl)-7-isopropyl-3,4-dimethylnaphtho-[2,3-*b*]furan-2-one into (*R*)-6-acetoxy-3-allyl-2,3-dihydro-7-isopropyl-3,4-dimethylnaphtho[2,3-*b*]furan-2-one was also achieved.

In previous papers,[1,2] we have reported the conversion of methyl abieta-6,8,11,13-tetraen-18-oate derivatives (**Ia**, **b**, **c**) into (*R*)-3-(3-acetoxypropyl)-2,3-dihydro-7-isopropyl-3,4-dimethylnaphtho[2,3-*b*]furan-2-one derivatives (**IIIa**, **b**, **c**) *via* the corresponding 6-hydroxy-5β*H*-abieta-6,8,11,13-tetraen-18-oic acid 18,6-lactones (**IIa**, **b**, **c**). These naphthalene derivatives (**III**) seem to be useful intermediates for the synthesis of coleon A (**1**),[3,4] a rare highly oxygenated 1,10-secoabietane derivative isolated from the leaves of *Coleus igniarius* Schweinf. (Labiatae) by Eugster *et al.*[5] In order to devise an efficient synthetic route for coleon A, we have now attempted, as a preliminary experiment, to introduce oxygen functions into the naphthalene skeleton of **III** and to transform an acetoxypropyl side chain into an allyl group. This paper describes the syntheses of (*R*)-5,6,8-triacetoxy-3-(3-acetoxypropyl)-2,3-dihydro-7-isopropyl-3,4-dimethylnaphtho[2,3-*b*]furan-2-one (**2**) and its 5,6,9-triacetoxy isomer (**3**), and some related compounds, starting from **IIIa**, **b**, **c**.

Oxidation of (*R*)-3-(3-acetoxypropyl)-2,3-dihydro-6-hydroxy-7-isopropyl-3,4-dimethylnaphtho[2,3-*b*]furan-2-one (**IIIa**)[2] in aqueous acetone with Fremy's radical[6] in the presence of potassium dihydrogenphosphate at room temperature afforded a hydroxy-*p*-quinone (IR: 3355, 1645 cm^{-1}), (*R*)-3-(3-acetoxypropyl)-2,3,5,8-tetrahydro-6-hydroxy-7-isopropyl-3,4-dimethylnaphtho[2,3-*b*]furan-2,5,8-trione (**4**: 5%), and an *o*-quinone (IR: 1678, 1661 cm^{-1}),[7] (*R*)-3-(3-acetoxypropyl)-2,3,5,6-tetrahydro-7-isopropyl-3,4-dimethylnaphtho[2,3-*b*]-furan-2,5,6-trione (**5**: 40%), together with the starting **IIIa** (22%). The *o*-quinone **5** was then submitted to Thiele-Winter acetoxylation[8] with acetic anhydride and concentrated sulfuric acid at room temperature to give an acetoxy-*p*-quinone (IR: 1775, 1735, 1667 cm^{-1}), (*R*)-6-acetoxy-3-(3-acetoxypropyl)-2,3,5,8-tetrahydro-7-isopropyl-3,4-dimethylnaphtho[2,3-*b*]furan-2,5,8-trione (**6**: 7%), and **2** (43%). The *p*-quinones **4** and **6** were each converted into **2** in quantitative yield by reductive acetylation with zinc and acetic anhydride in pyridine at room temperature. Similar treatment of **5** with zinc and acetic anhydride in pyridine afforded (*R*)-5,6-diacetoxy-3-(3-acetoxypropyl)-2,3-dihydro-7-isopropyl-3,4-dimethylnaphtho[2,3-*b*]furan-2-one (**7**: 89%). The structure of **2** was supported by its ^1H NMR spectrum, which showed a doublet signal due to isopropyl methyls at δ 1.25 (6H) and singlet signals due to two methyls at δ 1.53 and 2.62 (each 3H), four acetoxyls at δ 1.89 (3H), 2.26 (6H), and 2.33 (3H), and an aromatic proton at δ 7.08 (1H). (*R*)-2,3-dihydro-6-hydroxy-3-(3-hydroxypropyl)-7-isopropyl-3,4-dimethylnaphtho[2,3-*b*]furan-2-one (**8**), prepared from (*R*)-6-acetoxy-3-(3-acetoxypropyl)-2,3-dihydro-7-isopropyl-3,4-dimethylnaphtho[2,3-*b*]furan-2-one (**IIIb**)[2] by hydrolysis with dilute hydrochloric acid in refluxing methanol, was similarly oxidized with Fremy's radical to give the corresponding *o*-quinone (**9**) (IR: 1673, 1658 cm^{-1}), which was converted into **7** (63% from **IIIb**) by reductive acetylation with zinc and acetic anhydride in pyridine. Attempts to introduce an acetyl group at C-9 in **2** and at C-8 or C-9 in **7** by Friedel-Crafts acylation with acetyl chloride and anhydrous aluminium chloride in refluxing carbon disulfide were unsuccessful, giving the starting **2** and **7**. However, nitration of **2** with fuming nitric acid in acetic anhydride at 0 °C and then at room temperature afforded a nitro compound (IR: 1547, 1340 cm^{-1}), (*R*)-5,6,8-triacetoxy-3-(3-acetoxypropyl)-

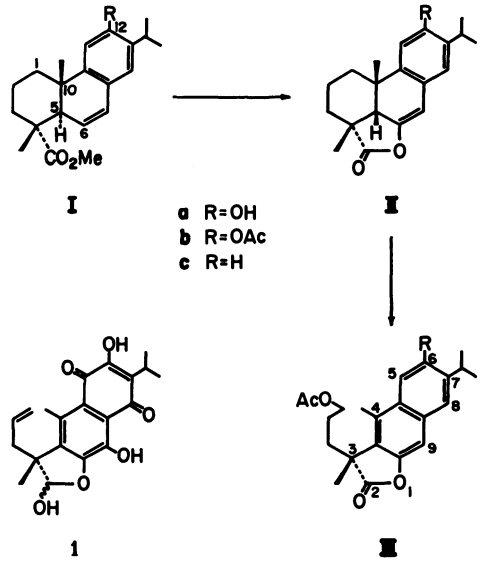

2,3-dihydro-7-isopropyl-3,4-dimethyl-9-nitronaphtho-[2,3-*b*]furan-2-one (**10**: 41%), together with **6** (18%) and an acetoxy-*o*-quinone (IR: 1778, 1735, 1672, 1659 cm^{-1}), (*R*)-8-acetoxy-3-(3-acetoxypropyl)-2,3,5,6-tetrahydro-7-isopropyl-3,4-dimethylnaphtho[2,3-*b*]furan-2,5,6-trione (**11**: 17%). Reductive acetylation of **11** with zinc and acetic anhydride in pyridine produced **2** in quantitative yield. For conversion of the nitro group into the hydroxyl group *via* the corresponding amine (**12**), the nitro compound **10** in ethanol was submitted to catalytic hydrogenation over PtO_2 at room temperature under an atmosphere of hydrogen. The IR spectrum of the product (**13**: 51%) showed absorption bands at 1809 (γ-lactone), 1774 and 1736 (acetoxyls), 1660 cm^{-1} (C=N), and no absorption band at 3500—3400 cm^{-1} (NH_2). The ^1H NMR spectrum of **13** showed a doublet signal at δ 1.30 (6H) due to isopropyl methyls and singlet signals at δ 1.56, 1.92, 2.23, 2.24, 2.26, and 2.50 (each 3H) due to three methyls and three acetoxyls. From these spectral data, the structure of **13** was tentatively assigned to be (*R*)-5,6-diacetoxy-8-(3-acetoxypropyl)-8,9-dihydro-4-isopropyl-2,7,8-trimethylfuro-[2′,3′ : 2,3]naphtho[1,8-*de*][1,3]oxazin-9-one. Since the desired amine **12** could not be obtained, the following approach was adopted. Nitration of **7** in acetic anhydride with fuming nitric acid at −10 °C and then at 0—5 °C afforded, in addition to **5** (10%), **6** (4%), and the starting **7** (11%), three nitro compounds **14** (21%) **15** (1%), and **16** (38%). The IR spectrum of **14** showed absorption bands at 1823 (γ-lactone), 1737 (acetoxyl), 1680 and 1658 (*o*-quinone), 1548 and 1309 cm^{-1} (NO_2), and its ^1H NMR spectrum showed a multiplet signal due to an isopropyl methine at very high field (δ 2.66), compared with that (δ 2.98) of **5**. From these spectral data, the structure of **14** was assigned to be (*R*)-3-(3-acetoxypropyl)-2,3,5,6-tetrahydro-7-isopropyl-3,4-dimethyl-8-nitronaphtho[2,3-*b*]furan-2,5,6-trione. The ^1H NMR spectrum of **16** showed signals at δ 1.29 (6H) and 3.02 (1H) due to an isopropyl, at δ 1.63 and 2.70 (each 3H) due to two methyls, at δ 1.91, 2.30, and 2.31 (each 3H) due to three acetoxyls, and at δ 7.74 (1H) due to an aromatic proton. Since the long-range coupling between the isopropyl methine at δ 3.02 and the aromatic proton at δ 7.74 was observed,[9] the structure of **16** was assigned to be (*R*)-5,6-diacetoxy-3-(3-acetoxypropyl)-2,3-dihydro-7-isopropyl-3,4-dimethyl-9-nitronaphtho[2,3-*b*]furan-2-one. The IR and ^1H NMR spectra of **15** were very similar to those of **16**, except for a singlet NMR signal at δ 7.02 (1H) due to an aromatic proton. Therefore, both compounds **15** and **16** should be position-isomers with regard to the nitro group. The compound **15** was also obtained by reductive acetylation of **14** with zinc and acetic anhydride in pyridine. Thus, the structure of **15** was assigned to be (*R*)-5,6-diacetoxy-3-(3-acetoxypropyl)-2,3-dihydro-7-isopropyl-3,4-dimethyl-8-nitronaphtho[2,3-*b*]furan-2-one. Catalytic hydrogenation of **16** with PtO_2 in acetic acid afforded the corresponding amine (**17**: 80%), which was converted into **3** (20%) and **7** (25%) by successive treatments with sodium nitrite and dilute hydrochloric acid in acetic acid at 0—5 °C, with dilute sulfuric acid at 80 °C, and then with zinc and acetic anhydride in pyridine. The structure of **3** was supported by its ^1H NMR spectrum, which showed signals at δ 1.31 (6H, doublet) and 3.02 (1H, multiplet) due to an isopropyl, at δ 1.64 and 2.66 (each 3H and singlet) due to two methyls, at δ 1.93 (3H), 2.29 (6H), and 2.44 (3H) (each singlet) due to four acetoxyls, and at δ 7.60 (1H, singlet) due to an aromatic proton. Friedel-Crafts acylation of **3** with acetyl chloride and anhydrous aluminium chloride in refluxing carbon disulfide afforded only the starting compound, as in the case of **2**. However nitration of **3** with fuming nitric acid or dilute nitric acid gave a complex mixture. Since functionalization of C-8 in **3** was also unsuccessful, the following experiments were carried out for the introduction of a functional group at C-9 of the naphthalene skeleton.

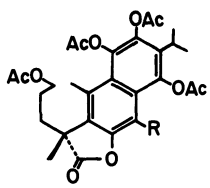

2 R=H
10 R=NO_2
12 R=NH_2

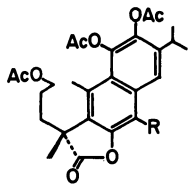

3 R=OAc
16 R=NO_2
17 R=NH_2

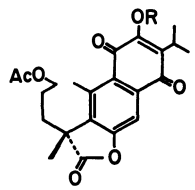

4 R=H
6 R=Ac

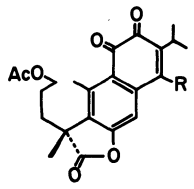

5 R=H
11 R=OAc
14 R=NO_2

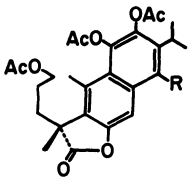

7 R=H
15 R=NO_2

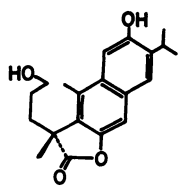

8

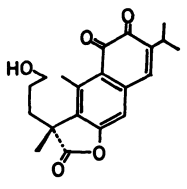

9

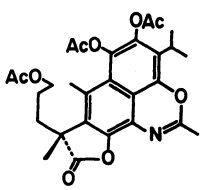

13

Reduction of (*R*)-2,3-dihydro-7-isopropyl-3,4-dimethyl-3-propylnaphtho[2,3-*b*]furan-2-one (**18**)[2] with lithium aluminium hydride in refluxing ether afforded (*R*)-2,3-dihydro-7-isopropyl-3,4-dimethyl-3-propylna-

phtho[2,3-*b*]furan (**19**: 29%) and an epimeric mixture at C-2 of 2,3-dihydro-2-hydroxy-7-isopropyl-3,4-dimethyl-3-propylnaphtho[2,3-*b*]furan (**20**: 60%) which gave the corresponding acetate (**21**: 90%) with acetic anhydride in pyridine. The compound **20** was also obtained in quantitative yield by reduction of **18** with sodium borohydride in methanol. Oxidation of **20** with Jones reagent at 0—5 °C gave **18** (93%). Treatment of **21** in acetic anhydride with boron trifluoride etherate at room temperature afforded the corresponding 9-acetyl (**22**: 58%) and 9-acetoacetyl (**23**: 29%) derivatives. Both compounds **22** and **23** were also obtained by the same treatment of **20** in 58% and 20% yields, respectively. The ^{1}H NMR spectrum of **22** showed an acetyl signal at δ 2.58 (3H, singlet) and three aromatic proton signals at δ 7.21 (1H, double doublet, J=2 and 9 Hz), 7.81 (1H, doublet, J=9 Hz), and 8.15 (1H, doublet, J=2 Hz). These chemical shifts and coupling pattern of the aromatic protons suggested the presence of the acetyl group at C-9. The ^{1}H NMR spectrum of **23** also showed similar signals due to three aromatic protons at δ 7.22 (1H, double doublet, J=2 and 9 Hz), 7.82 (1H, doublet, J=9 Hz), and 8.13 (1H, doublet, J=2 Hz), and signals due to an acetoacetyl at δ 2.13 (3H, singlet), 5.93 (1H, singlet), and 15.95 (1H, broad). These spectral data also suggested that the acetoacetyl group was present at C-9 as its enol form. Acetylation of **19** in acetic anhydride with boron trifluoride etherate also gave the corresponding 9-acetyl derivative (**24**: 77%). It is noteworthy that the compounds **19**, **20**, and **21** were each acetylated at C-9 with acetic anhydride and boron trifluoride etherate, because when the lactone **18** was treated in the same manner only the starting material was recovered. In contrast to the above results, acetylation of (*R*)-3-(3-acetoxypropyl)-2,3-dihydro-7-isopropyl-3,4-dimethylnaphtho[2,3-*b*]furan-2-one (**IIIc**)[2] with acetyl chloride and anhydrous aluminium chloride in refluxing carbon disulfide afforded the corresponding 8-acetyl derivative (**25**: 54%). The structure of **25** was supported by its ^{1}H NMR spectrum, which showed an acetyl signal at δ 2.54 (3H, singlet) and three aromatic proton signals at δ 7.01 (1H, broad singlet), 7.36 (1H, doublet, J=9 Hz), and 7.91 (1H, doublet, J=9 Hz). Hydrolysis of **IIIc** with concentrated hydrochloric acid in refluxing methanol quantitatively produced the corresponding alcohol (**26**), which was methylated with diazomethane in the presence of boron trifluoride etherate to give (*R*)-2,3-dihydro-7-isopropyl-3-(3-methoxypropyl)-3,4-dimethylnaphtho [2,3-*b*] furan-2-one (**27**: 85%). In order to introduce an acetyl group at C-9, the lactone **27** was reduced with sodium borohydride in ethanol and the resulting hemiacetal (**28**) was treated with acetic anhydride and boron trifluoride etherate to give an epimeric mixture at C-2 of 2-acetoxy-9-acetyl-2,3-dihydro-7-isopropyl-3-(3-methoxypropyl)-3,4-dimethylnaphtho[2,3-*b*]furan (**29**: 70% from **27**). Hydrolysis of **29** with dilute hydrochloric acid in refluxing methanol afforded the corresponding hemiacetal (**30**), which was oxidized with Jones reagent at 0—5 °C to give (*R*)-9-acetyl-2,3-dihydro-7-isopropyl-3-(3-methoxypropyl)-3,4-dimethylnaphtho[2,3-*b*]furan-2-one (**31**: 69% from **29**). Treatment of **31** in refluxing dichloromethane with *m*-chloroperbenzoic acid in the presence of *p*-toluenesulfonic acid monohydrate afforded, after column chromatography on silica gel, the corresponding 9-acetoxy derivative (**32**: 11%), together with an acetoxy-*p*-quinone (**33**: 4%) and a mixture of **32** and the starting **31**. The mixture of **31** and **32** was hydrolyzed with dilute hydrochloric acid in refluxing methanol and then purified by column chromatography on silica gel to give **31** (16%) and the 9-hydroxy derivative (**34**: 22% from **31**). Acetylation of **34** with acetic anhydride in pyridine afforded **32** (87%). The structure of **32** was supported by its ^{1}H NMR spectrum, which showed signals due to an acetoxyl at δ 2.45 (3H, singlet) and

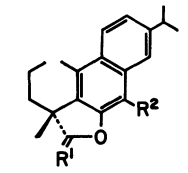

18 R^1=O, R^2=H
19 R^1=H$_2$, R^2=H
24 R^1=H$_2$, R^2=Ac

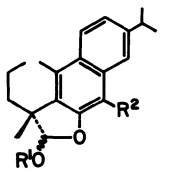

20 R^1=R^2=H
21 R^1=Ac, R^2=H
22 R^1=R^2=Ac
23 R^1=Ac, R^2=COCH=C(OH)Me

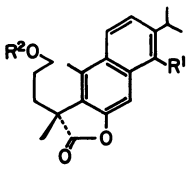

25 R^1=R^2=Ac
26 R^1=R^2=H
27 R^1=H, R^2=Me

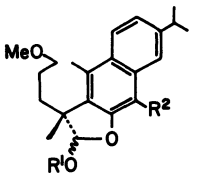

28 R^1=R^2=H
29 R^1=R^2=Ac
30 R^1=H, R^2=Ac

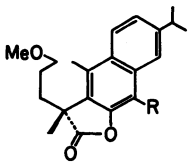

31 R=Ac
32 R=OAc
34 R=OH

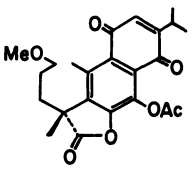

33

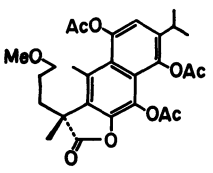

35

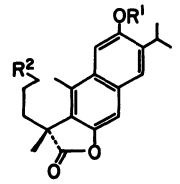

36 R^1=H, R^2=SeC$_6$H$_4$NO$_2$(o-)
37 R^1=Ac, R^2=SeC$_6$H$_4$NO$_2$(o-)

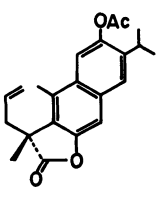

38

three aromatic protons at δ 7.37 (1H, double doublet, J=2 and 9 Hz), 7.62 (1H, broad singlet), and 7.94 (1H, doublet, J=9 Hz). The IR spectrum of **33** showed absorption bands at 1821 (γ-lactone), 1779 (acetoxyl), 1659 cm^{-1} (p-quinone), and its ^{1}H NMR spectrum showed signals due to an acetoxyl at δ 2.42 (3H, singlet), an olefinic proton at δ 6.55 (1H, doublet, J=1.5 Hz), and no aromatic proton. From these spectral data, the structure of **33** was assigned to be (*R*)-9-acetoxy-2,3,5,8-tetrahydro-7-isopropyl-3-(3-methoxypropyl)-3,4-dimethylnaphtho[2,3-*b*]furan-2,5,8-trione. Reductive acetylation of **33** with zinc and acetic anhydride in pyridine afforded the corresponding triacetate (**35**: 45%). It is of interest that the oxygen functions were introduced to C-5, C-8, and C-9 of **31** in one stage by oxidation with *m*-chloroperbenzoic acid, although the yield was low. Therefore if the yield is improved, the 9-acetyl derivatives seem to be useful intermediates for the synthesis of coleon A (**1**).

Finally, transformation of a hydroxypropyl side chain into an allyl group was also carried out as follows. Treatment[10] of **8** with *o*-nitrophenyl selenocyanate and tributylphosphine in pyridine at room temperature under a stream of nitrogen yielded a selenide (**36**), which was immediately acetylated with acetic anhydride in pyridine to give the corresponding 6-acetoxy selenide (**37**: 56% from **8**). Oxidation of **37** with 50% hydrogen peroxide in tetrahydrofuran at room temperature afforded the desired (*R*)-6-acetoxy-3-allyl-2,3-dihydro-7-isopropyl-3,4-dimethylnaphtho[2,3-*b*]furan-2-one (**38**: 89%). The structure of **38** was supported by its ^{1}H NMR spectrum, which showed signals due to an acetoxyl at δ 2.32 (3H, singlet), an allyl at δ 2.76 (2H, doublet, J=6.5 Hz) and 4.7—5.6 (3H, multiplet), and three aromatic protons at δ 7.20, 7.50, and 7.58 (each 1H and singlet). Application of the present results for the synthesis of coleon A (**1**) will describe in the succeeding paper.

Experimental

All melting points are uncorrected. The IR spectra and optical rotations were measured in chloroform, and the ^{1}H NMR spectra in carbon tetrachloride at 90 MHz, with tetramethylsilane as an internal standard, unless otherwise stated. The chemical shifts are presented in terms of δ values; s: singlet, bs: broad singlet, d: doublet, bd: broad doublet, dd: double doublet, t: triplet, m: multiplet. The column chromatography was performed using Merck silica gel.

Oxidation of (R)-3-(3-Acetoxypropyl)-2,3-dihydro-6-hydroxy-7-isopropyl-3,4-dimethylnaphtho[2,3-b]furan-2-one (IIIa) with Fremy's Reagent. A solution of freshly prepared Fremy's reagent [potassium nitrosodisulfonate (4.2 g) and aqueous potassium dihydrogenphosphate (0.17 M:† 150 ml) in water (300 ml)] was added to a stirred solution of **IIIa** (1522 mg) in acetone (260 ml) at room temperature. After being stirred for 3 h and then 2 h more, additional Fremy's reagent [potassium nitrosodisulfonate (2.8 g) and aqueous potassium dihydrogenphosphate (0.17 M: 100 ml) in water (200 ml)] was added twice. The mixture was further stirred for 24 h, diluted with brine, and extracted with ether. The ether extract was washed with brine, dried over sodium sulfate, and evaporated *in vacuo*. The residue was chromatographed on silica gel (150 g), using ether–benzene (5 : 95) as the eluent, to give (*R*)-3-(3-acetoxypropyl)-2,3,5,8-tetrahydro-6-hydroxy-7-isopropyl-3,4-dimethylnaphtho[2,3-*b*]furan-2,5,8-trione (**4**) (85 mg: 5.2 %). IR: 3355, 1817, 1732, 1645, 1598, 1585 cm^{-1}; ^{1}H NMR: δ=1.30 (6H, d, J=7 Hz, -CH(C$\underline{H}_3$)$_2$), 1.61 (3H, s, C_3-CH_3), 1.94 (3H, s, -OCOCH_3), 2.72 (3H, s, C_4-CH_3), 3.32 (1H, m, -C$\underline{H}$(CH$_3$)$_2$), 3.88 (2H, t, J=6.5 Hz, -C$\underline{H}_2$OAc), 7.70 (1H, s, C_6-OH, disappeared with D_2O), 7.75 (1H, s, C_9-H).

Subsequent elution gave (*R*)-3-(3-acetoxypropyl)-2,3,5,6-tetrahydro-7-isopropyl-3,4-dimethylnaphtho[2,3-*b*]furan-2,5,6-trione (**5**) (637 mg: 40.3%). $[\alpha]_D$ +125° (*c* 5.36); IR: 1815, 1735, 1678, 1661, 1598, 1580 cm^{-1}; ^{1}H NMR: δ=1.17 (6H, d, J=7 Hz, -CH(C$\underline{H}_3$)$_2$), 1.60 (3H, s, C_3-CH_3), 1.94 (3H, s, -OCOCH_3), 2.63 (3H, s, C_4-CH_3), 2.98 (1H, m, -C$\underline{H}$(CH$_3$)$_2$), 3.87 (2H, t, J=6 Hz, -C$\underline{H}_2$OAc), 6.89 (1H, s, C_9-H), 6.99 (1H, bs, C_8-H); UV: λ_{max}^{EtOH} 265 nm (log ε 4.38), 358 (3.63). Found: C, 68.56; H, 6.29%. Calcd for $C_{22}H_{24}O_6$: C, 68.73; H, 6.29%.

Further elution gave the recovered **IIIa** (332 mg: 21.8%).

Thiele-Winter Reaction of 5. Concentrated sulfuric acid (0.08 ml) was added to a stirred solution of **5** (802 mg) in acetic anhydride (8.0 ml) at 0—5 °C. The solution was stirred at room temperature for 4 h, poured into aqueous sodium hydrogencarbonate, and extracted with ether. The ether extract was washed with brine, dried over sodium sulfate, and evaporated *in vacuo*. The residue was chromatographed on silica gel (85 g), using ether–benzene (5 : 95) as the eluent, to give (*R*)-6-acetoxy-3-(3-acetoxypropyl)-2,3,5,8-tetrahydro-7-isopropyl-3,4-dimethylnaphtho[2,3-*b*]furan-2,5,8-trione (**6**) (63 mg: 6.8%). $[\alpha]_D$ +10° (*c* 0.77); IR: 1816, 1775, 1735, 1667, 1603, 1588 cm^{-1}; ^{1}H NMR: δ=1.27 (6H, d, J=7 Hz, -CH(C$\underline{H}_3$)$_2$), 1.61 (3H, s, C_3-CH_3), 1.93 (3H, s, -CH_2-OCOC$\underline{H}_3$), 2.36 (3H, s, C_6-OCOCH_3), 2.68 (3H, s, C_4-CH_3), 3.21 (1H, m, -C$\underline{H}$(CH$_3$)$_2$), 3.86 (2H, t, J=6.5 Hz, -C$\underline{H}_2$OAc), 7.71 (1H, s, C_9-H); UV: λ_{max}^{EtOH} 252 nm (log ε 4.31), 353 (3.45). Found: C, 64.91; H, 6.15%. Calcd for $C_{24}H_{26}O_8$: C, 65.15; H, 5.92%.

Further elution with ether–benzene (15 : 85) afforded (*R*)-5,6,8-triacetoxy-3-(3-acetoxypropyl)-2,3-dihydro-7-isopropyl-3,4-dimethylnaphtho[2,3-*b*]furan-2-one (**2**) (478 mg: 43.3%). $[\alpha]_D$ +13° (*c* 1.13); IR: 1807, 1778, 1733, 1641, 1617 cm^{-1}; ^{1}H NMR: δ=1.25 (6H, d, J=7 Hz, -CH(C$\underline{H}_3$)$_2$), 1.53 (3H, s, C_3-CH_3), 1.89 (3H, s, -CH_2OCOC$\underline{H}_3$), 2.26 (6H, s) and 2.33 (3H, s) (C_5-OCOCH_3, C_6-OCOCH_3, and C_8-OCOCH_3), 2.62 (3H, s, C_4-CH_3), 3.10 (1H, m, -C$\underline{H}$(CH$_3$)$_2$), 3.77 (2H, t, J=6 Hz, -C$\underline{H}_2$OAc), 7.08 (1H, s, C_9-H); UV: λ_{max}^{EtOH} 241.5 nm (log ε 5.00), 274 (3.81), 285.5 (3.86), 296.5 (3.77), 320.5 (3.17), 335 (3.25). Found: C, 63.91; H, 6.27%. Calcd for $C_{28}H_{32}O_{10}$: C, 63.62; H, 6.10%.

Reductive Acetylation of 5. Zinc powder (0.1 g) was added to a stirred solution of **5** (470 mg) and acetic anhydride (2.0 ml) in pyridine (2.0 ml) with cooling in an ice–water bath. The mixture was stirred at this temperature for 5 min and then at room temperature for 1 h, poured into aqueous sodium hydrogencarbonate, and extracted with ether. The ether extract was washed with brine, dried over sodium sulfate, and evaporated *in vacuo*. The residue was chromatographed on silica gel (60 g), using ether–benzene (1 : 9) as the eluent, to give (*R*)-5,6-diacetoxy-3-(3-acetoxypropyl)-2,3-dihydro-7-isopropyl-3,4-dimethylnaphtho[2,3-*b*]furan-2-one (**7**) (512 mg: 89.0%). $[\alpha]_D$ +23° (*c* 1.92); IR: 1798, 1769, 1729, 1638 cm^{-1}; ^{1}H NMR: δ=1.30 (6H, d, J=7 Hz, -CH(C$\underline{H}_3$)$_2$), 1.60 (3H, s, C_3-CH_3), 1.92 (3H, s, -CH_2OCOC$\underline{H}_3$), 2.28 (6H, s, C_5-OCOCH_3 and C_6-OCOCH_3), 2.66 (3H, s, C_4-CH_3), 2.99 (1H, m, -C$\underline{H}$(CH$_3$)$_2$), 3.84 (2H, t, J=6 Hz, -C$\underline{H}_2$OAc), 7.24 (1H, s, C_9-H), 7.50 (1H, s, C_8-H); UV: λ_{max}^{EtOH} 239 nm (log ε

† 1 M=1 mol dm^{-3}.

4.94), 272 (3.78), 283 (3.83), 294 (3.71), 318.5 (3.03), 332.5 (3.11). Found: C, 66.29; H, 6.58%. Calcd for $C_{26}H_{30}O_8$: C, 66.37; H, 6.43%.

Nitration of **2**. A solution of fuming nitric acid ($d=1.50$, 0.62 ml) in acetic anhydride (1.24 ml) was added dropwise over a period of 5 min to a stirred solution of **2** (410 mg) in acetic anhydride (4.1 ml) with cooling in an ice–water bath. The mixture was stirred at room temperature for 30 min, poured into brine, and extracted with ether. The ether extract was washed successively with brine, aqueous sodium hydrogencarbonate, and brine, dried over sodium sulfate, and evaporated *in vacuo*. The residue was chromatographed on silica gel (40 g), using ether–benzene (5 : 95) as the eluent, to give a diacetoxy-*p*-quinone (60 mg: 17.5%), whose IR and ^{1}H NMR spectra were identical with those of the authentic **6**.

Subsequent elution gave (*R*)-8-acetoxy-3-(3-acetoxypropyl)-2,3,5,6-tetrahydro-7-isopropyl-3,4-dimethylnaphtho[2,3-*b*]-furan-2,5,6-trione (**11**) (59 mg: 17.2%). $[\alpha]_D$ +45° (*c* 0.31); IR: 1818, 1778, 1735, 1690, 1672, 1659, 1622, 1600, 1583 cm^{-1}; ^{1}H NMR: $\delta=1.23$ (6H, d, $J=7$ Hz, $-CH(C\underline{H}_3)_2$), 1.59 (3H, s, C_3-CH_3), 1.94 (3H, s, $-CH_2OCOC\underline{H}_3$), 2.44 (3H, s, $C_8-OCOCH_3$), 2.64 (3H, s, C_4-CH_3), 2.80 (1H, m, $-C\underline{H}(CH_3)_2$), 3.86 (2H, t, $J=6$ Hz, $-C\underline{H}_2OAc$), 6.91 (1H, s, C_9-H); UV: λ_{max}^{EtOH} 241.5 nm (log ε 4.61), 290sh (3.74), 298sh (3.71), 302sh (3.71), 335.5 (3.53). Found: C, 65.45; H, 6.21%. Calcd for $C_{24}H_{26}O_8$: C, 65.15; H, 5.92%.

Further elution with ether–benzene (15 : 85) gave (*R*)-5,6,8-triacetoxy-3-(3-acetoxypropyl)-2,3-dihydro-7-isopropyl-3,4-dimethyl-9-nitronaphtho[2,3-*b*]furan-2-one (**10**) 181 mg: (40.7%). This was crystallized from ethanol, mp 171.5—172.5 °C, $[\alpha]_D$ +7° (*c* 1.04); IR: 1827, 1787, 1737, 1650, 1614, 1547, 1340 cm^{-1}; ^{1}H NMR: $\delta=1.23$ (6H, bd, $J=7$ Hz, $-CH(C\underline{H}_3)_2$), 1.59 (3H, s, C_3-CH_3), 1.92 (3H, s, $-CH_2OCOC\underline{H}_3$), 2.27 (9H, s, $C_5-OCOCH_3$, $C_6-OCOCH_3$, and $C_8-OCOCH_3$), 2.56 (3H, s, C_4-CH_3), 3.00 (1H, m, $-C\underline{H}(CH_3)_2$), 3.82 (2H, t, $J=6$ Hz, $-C\underline{H}_2OAc$). Found: C, 58.88; H, 5.74; N, 2.38%. Calcd for $C_{28}H_{31}O_{12}N$: C, 58.63; H, 5.45; N, 2.44%.

Reductive Acetylation of **4**, **6**, *and* **11**. *a)*: A solution of **4** (80 mg) and acetic anhydride (0.4 ml) in pyridine (0.4 ml) was treated with zinc powder (26 mg) in the same manner as described for the preparation of **7**. The crude product was purified by column chromatography on silica gel (10 g) to give **2** (104 mg: 98%), whose IR and ^{1}H NMR spectra were identical with those of an authentic sample.

b): A solution of **6** (113 mg) and acetic anhydride (0.6 ml) in pyridine (0.6 ml) was treated with zinc powder (33 mg) to give **2** (129 mg: 96%).

c): A solution of **11** (50 mg) and acetic anhydride (0.3 ml) in pyridine (0.3 ml) was treated with zinc powder (15 mg) to give **2** (58 mg: 97%).

*Conversion of (*R*)-6-Acetoxy-3-(3-acetoxypropyl)-2,3-dihydro-7-isopropyl-3,4-dimethylnaphtho[2,3-*b*]furan-2-one (**IIIb**) into* **7**. A solution of **IIIb**[2] (4120 mg) and dilute hydrochloric acid (6 M: 83 ml) in methanol (412 ml) was refluxed for 1 h, and then evaporated *in vacuo*. The residue was diluted with brine and extracted with ether. The ether extract was washed with brine, dried over sodium sulfate, and evaporated *in vacuo* to give the crude (*R*)-2,3-dihydro-6-hydroxy-3-(3-hydroxypropyl)-7-isopropyl-3,4-dimethylnaphtho[2,3-*b*]furan-2-one (**8**) which, without purification, was used in the next reaction. IR: 3575, 3325br, 1785, 1621 cm^{-1}; ^{1}H NMR (60 MHz, $CDCl_3$): $\delta=1.33$ (6H, d, $J=7$ Hz, $-CH(C\underline{H}_3)_2$), 1.59 (3H, s, C_3-CH_3), 2.50 (3H, s, C_4-CH_3), 3.35 (1H, m, $-C\underline{H}(CH_3)_2$), 3.46 (2H, t, $J=6$ Hz, $-C\underline{H}_2OH$), 6.70 (1H, br, C_6-OH), 7.20 (2H, s, C_5-H and C_9-H), 7.51 (1H, s, C_8-H).

A stirred solution of the above crude **8** in acetone (656 ml) was oxidized with Fremy's reagent [potassium nitrosodisulfonate (13.42 g) and aqueous potassium dihydrogenphosphate (0.17 M: 300 ml) in water (600 ml)] at room temperature. After being stirred for 5 h, additional Fremy's reagent [potassium nitrosodisulfonate (5.36 g) and aqueous potassium dihydrogenphosphate (0.17 M: 120 ml) in water (240 ml)] was added. The mixture was further stirred for 14 h, diluted with brine, and extracted with chloroform. The chloroform extract was washed with brine, dried over sodium sulfate, and evaporated *in vacuo* to give the crude (*R*)-2,3,5,6-tetrahydro-3-(3-hydroxypropyl)-7-isopropyl-3,4-dimethylnaphtho[2,3-*b*]-furan-2,5,6-trione (**9**) which, without purification, was used in the next reaction. IR: 3580sh, 3490, 3370sh, 1808, 1673, 1658, 1596, 1577 cm^{-1}; ^{1}H NMR (60 MHz, $CDCl_3$): $\delta=1.19$ (6H, d, $J=7$ Hz, $-CH(C\underline{H}_3)_2$), 1.63 (3H, s, C_3-CH_3), 2.68 (3H, s, C_4-CH_3), 3.55 (2H, t, $J=6$ Hz, $-C\underline{H}_2OH$), 6.99 (1H, s, C_9-H), 7.09 (1H, bs, C_8-H).

Zinc powder (650 mg) was added to a stirred solution of the above crude **9** and acetic anhydride (17 ml) in pyridine (17 ml) at 0—5 °C. After being stirred at 0—5 °C for 5 min and then at room temperature for 1 h, the mixture was filtered and the filtrate was extracted with chloroform. The chloroform extract was washed successively with aqueous sodium hydrogencarbonate and brine, dried over sodium sulfate, and evaporated *in vacuo*. The residue was chromatographed on silica gel (220 g), using ether–benzene (5 : 95) as the eluent, to give the starting **IIIb** (640 mg: 15.5%) and **7** (2940 mg: 62.6%). Further elution with ether–benzene (2 : 8) gave **2** (60 mg: 1.1%). The IR and ^{1}H NMR spectra of **2** and **7** were identical with those of authentic samples.

Catalytic Hydrogenation of **10**. A mixture of **10** (57 mg) and PtO_2 (12 mg) in ethanol (5.7 ml) was submitted to catalytic hydrogenation at room temperature for 34 h. After the usual work-up, the crude product was chromatographed on silica gel (5.0 g), using ether–benzene (1 : 3) as the eluent, to give an oxazine derivative (**13**) (27 mg: 51%). IR: 1809, 1774, 1736, 1660, 1623 cm^{-1}; ^{1}H NMR: $\delta=1.30$ (6H, d, $J=7$ Hz, $-CH(C\underline{H}_3)_2$), 1.56 (3H, s, C_3-CH_3), 1.92 (3H, s, $-CH_2-OCOC\underline{H}_3$), 2.23, 2.24, and 2.26 (each 3H and s, $C_5-OCOCH_3$, $C_6-OCOCH_3$, and $-N=CCH_3$), 2.50 (3H, s, C_4-CH_3), 3.04 (1H, m, $-C\underline{H}(CH_3)_2$), 3.84 (2H, t, $J=6$ Hz, $-C\underline{H}_2OAc$).

Nitration of **7**. A solution of fuming nitric acid ($d=1.50$, 0.94 ml) in acetic anhydride (4.7 ml) was added dropwise to a stirred solution of **7** (2350 mg) in acetic anhydride (35 ml) at −10 °C over a period of 30 min. After being stirred at −10—−5 °C for 1 h and then at 0—5 °C for 50 h, the mixture was poured into aqueous sodium hydrogencarbonate and extracted with chloroform. The extract was washed with brine, dried over sodium sulfate, and evaporated *in vacuo*. The residue was chromatographed on silica gel (260 g), using ether–benzene (5 : 95) as the eluent, to give **6** (85 mg: 3.8%) and (*R*)-3-(3-acetoxypropyl)-2,3,5,6-tetrahydro-7-isopropyl-3,4-dimethyl-8-nitronaphtho[2,3-*b*]furan-2,5,6-trione (**14**) (459 mg: 21.4%). IR: 1823, 1737, 1680, 1658, 1629, 1601, 1583, 1548, 1309 cm^{-1}; ^{1}H NMR: $\delta=1.29$ (6H, d, $J=7$ Hz, $-CH(C\underline{H}_3)_2$), 1.61 (3H, s, C_3-CH_3), 1.92 (3H, s, $-CH_2OCOC\underline{H}_3$), 2.66 (1H, m, $-C\underline{H}(CH_3)_2$), 2.67 (3H, s, C_4-CH_3), 3.86 (2H, t, $J=6$ Hz, $-C\underline{H}_2OAc$), 6.69 (1H, s, C_9-H).

Subsequent elution gave **5** (187 mg: 9.7%), the starting **7** (253 mg: 10.8%), and (*R*)-5,6-diacetoxy-3-(3-acetoxypropyl)-2,3-dihydro-7-isopropyl-3,4-dimethyl-8-nitronaphtho[2,3-*b*]-furan-2-one (**15**) (25 mg: 1.0%). This was recrystallized from ether, mp 153—154.5 °C, $[\alpha]_D$ +18° (*c* 0.55); IR: 1810, 1780, 1732, 1642, 1532, 1331 cm^{-1}; ^{1}H NMR (60 MHz): $\delta=$ 1.32 (6H, d, $J=7$ Hz, $-CH(C\underline{H}_3)_2$), 1.58 (3H, s, C_3-CH_3), 1.91 (3H, s, $-CH_2OCOC\underline{H}_3$), 2.33 (6H, s, $C_5-OCOCH_3$ and $C_6-OCOCH_3$), 2.70 (3H, s, C_4-CH_3), 3.06 (1H, m, $-C\underline{H}-(CH_3)_2$), 3.85 (2H, t, $J=6$ Hz, $-C\underline{H}_2OAc$), 7.02 (1H, s, C_9-H).

Found: C, 60.54; H, 5.69; N, 2.72%. Calcd for $C_{26}H_{29}O_{10}N$: C, 60.57; H, 5.67; N, 2.72%.

Further elution gave (*R*)-5,6-diacetoxy-3-(3-acetoxypropyl)-2,3-dihydro-7-isopropyl-3,4-dimethyl-9-nitronaphtho[2,3-*b*]-furan-2-one (**16**) (970 mg: 37.7%). This was recrystallized from chloroform-carbon tetrachloride, mp 181—182 °C, $[\alpha]_D$ +6° (*c* 0.71); IR: 1820, 1774, 1729, 1642, 1530, 1327 cm^{-1}; ^1H NMR: δ=1.29 (6H, d, J=7 Hz, $-CH(C\underline{H}_3)_2$), 1.63 (3H, s, C_3-CH_3), 1.91 (3H, s, $-CH_2OCOC\underline{H}_3$), 2.30 and 2.31 (each 3H and s, $C_5-OCOCH_3$ and $C_6-OCOCH_3$), 2.70 (3H, s, C_4-CH_3), 3.02 (1H, m, $-C\underline{H}(CH_3)_2$), 3.83 (2H, t, J=6 Hz, $-C\underline{H}_2OAc$), 7.74 (1H, s, C_8-H); UV: λ_{max}^{EtOH} 236 nm (log ε 4.86), 265sh (3.98), 322sh (3.47), 335 (3.52). Found: C, 60.86; H, 5.76; N, 2.55%. Calcd for $C_{26}H_{29}O_{10}N$: C, 60.57; H, 5.67; N, 2.72%. The IR and ^1H NMR spectra of **5**, **6**, and **7** were identical with those of authentic samples.

Reductive Acetylation of ***14***. Zinc powder (17 mg) was added to a stirred solution of **14** (108 mg) and acetic anhydride (0.5 ml) in pyridine (0.5 ml) at 0—5 °C. After being stirred at 0—5 °C for 5 min and then at room temperature for 1 h, the mixture was diluted with ether. The ether solution was washed successively with aqueous sodium hydrogencarbonate, dilute hydrochloric acid, and brine, dried over sodium sulfate, and evaporated *in vacuo*. The residue was chromatographed on silica gel (10 g), using ether–benzene (1 : 4) as the eluent, to give **15** (53 mg: 40.9%). The IR and ^1H NMR spectra of **15** were identical with those of an authentic sample.

*(R)-5,6-Diacetoxy-3-(3-acetoxypropyl)-9-amino-2,3-dihydro-7-isopropyl-3,4-dimethylnaphtho[2,3-b]furan-2-one (**17**).* A mixture of **16** (515 mg) and PtO_2 (103 mg) in acetic acid (10 ml) was submitted to catalytic hydrogenation with 1 atm hydrogen pressure at room temperature for 3.5 h. After the usual work-up, the crude product was recrystallized from ethanol to give **17** (388 mg: 80.0%), mp 192.5—193 °C, $[\alpha]_D$ +23° (*c* 0.52); IR: 3440, 3370, 1792, 1770, 1732, 1658, 1625 cm^{-1}; ^1H NMR ($CDCl_3$): δ=1.31 (6H, d, J=7 Hz, $-CH(C\underline{H}_3)_2$), 1.62 (3H, s, C_3-CH_3), 1.98 (3H, s, $-CH_2OCOC\underline{H}_3$), 2.36 (6H, s, $C_5-OCOCH_3$ and $C_6-OCOCH_3$), 2.60 (3H, s, C_4-CH_3), 3.07 (1H, m, $-C\underline{H}(CH_3)_2$), *ca.* 3.7—4.3 (2H, br, $-NH_2$), 3.91 (2H, t, J=6 Hz, $-C\underline{H}_2OAc$), 7.62(1H, s, C_8-H). Found: C, 64.01; H, 6.39; N, 2.84%. Calcd for $C_{26}H_{31}O_8N$: C, 64.31; H, 6.44; N, 2.89%.

*(R)-5,6,9-Triacetoxy-3-(3-acetoxypropyl)-2,3-dihydro-7-isopropyl-3,4-dimethylnaphtho[2,3-b]furan-2-one (**3**).* A solution of sodium nitrite (522 mg) in water (10.5 ml) was added dropwise at 0—5 °C to a stirred solution of **17** (1440 mg) and dilute hydrochloric acid (4 M: 18.6 ml) in acetic acid (30 ml). After being stirred at 0—5 °C for 20 min, urea (900 mg) was added. The mixture was stirred for 10 min more, diluted with dilute sulfuric acid (3 M: 500 ml), and then heated at 80 °C for 1 h. After standing overnight at room temperature, the mixture was extracted with chloroform. The extract was washed with brine, dried over sodium sulfate, and evaporated *in vacuo*.

The above residue was treated with zinc powder (390 mg) and acetic anhydride (6.5 ml) in pyridine (6.5 ml) at room temperature for 1 h. After the same work-up as described for the preparation of **7**, the crude product was chromatographed on silica gel (170 g), using ether–benzene (7 : 93) as the eluent, to give **7** (342 mg: 24.5%) and **3** (315 mg: 20.1%), $[\alpha]_D$ +15° (*c* 2.50); IR: 1802, 1770, 1729, 1653 cm^{-1}; ^1H NMR: δ=1.31 (6H, d, J=7 Hz, $-CH(C\underline{H}_3)_2$), 1.64 (3H, s, C_3-CH_3), 1.93 (3H, s, $-CH_2OCOC\underline{H}_3$), 2.29 (6H, s, $C_5-OCOCH_3$ and $C_6-OCOCH_3$), 2.44 (3H, s, $C_9-OCOCH_3$), 2.66 (3H, s, C_4-CH_3), 3.02 (1H, m, $-C\underline{H}(CH_3)_2$), 3.87 (2H, t, J=6 Hz, $-C\underline{H}_2OAc$), 7.60 (1H, s, C_8-H). Found: C, 63.90; H, 6.10%. Calcd for $C_{28}H_{32}O_{10}$: C, 63.62; H, 6.10%.

*Reduction of (R)-2,3-Dihydro-7-isopropyl-3,4-dimethyl-3-propylnaphtho[2,3-b]furan-2-one (**18**) with Lithium Aluminium Hydride.* A mixture of **18**[2] (300 mg) and lithium aluminium hydride (80 mg) in dry ether (12 ml) was refluxed for 4 h with stirring. The mixture was poured into ice-dilute hydrochloric acid and extracted with ether. The ether extract was washed with brine, dried over sodium sulfate, and evaporated *in vacuo*. The residue was chromatographed on silica gel (50 g), using hexane–benzene (9 : 1) as the eluent, to give (*R*)-2,3-dihydro-7-isopropyl-3,4-dimethyl-3-propylnaphtho[2,3-*b*]furan (**19**) (84 mg: 29%), $[\alpha]_D$ +28° (*c* 4.02); IR: 1635, 1583 cm^{-1}; ^1H NMR (60 MHz): δ=1.31 (6H, d, J=7 Hz, $-CH(C\underline{H}_3)_2$), 1.47 (3H, s, C_3-CH_3), 2.60 (3H, s, C_4-CH_3), 3.00 (1H, m, $-C\underline{H}(CH_3)_2$), 4.14 (2H, ABq, δ_{AB}=14.5 Hz, J_{AB}=8.5 Hz, C_2-H_2), 6.77 (1H, s, C_9-H), 7.05 (1H, dd, J=2 and 9 Hz, C_6-H), 7.31 (1H, d, J=2 Hz, C_8-H), 7.70 (1H, d, J=9 Hz, C_5-H). Found: C, 85.26; H, 9.39%. Calcd for $C_{20}H_{26}O$: C, 85.05; H, 9.28%.

Further elution with ether–benzene (2 : 98) gave an epimeric mixture at C-2 of 2,3-dihydro-2-hydroxy-7-isopropyl-3,4-dimethyl-3-propylnaphtho[2,3-*b*]furan (**20**) (*ca.* 4 : 1 mixture, 180 mg: 59.6%), IR: 3590, 3400br, 1633, 1591 cm^{-1}; ^1H NMR (60 MHz): δ=1.29 (6H, d, J=7 Hz, $-CH(C\underline{H}_3)_2$), 1.35 and 1.43 (3H, each s, *ca.* 1: 4, C_3-CH_3), 2.58 (3H, s, C_4-CH_3), 2.99 (1H, m, $-C\underline{H}(CH_3)_2$), 5.39 and 5.48 (1H, each bs, *ca.* 1 :4, C_2-H), 6.82 (1H, s, C_9-H), 7.09 (1H, dd, J=2 and 8.5 Hz, C_6-H), 7.33 (1H, d, J=2 Hz, C_8-H), 7.71 (1H, d, J=8.5 Hz, C_5-H). Found: C, 80.64; H, 8.81%. Calcd for $C_{20}H_{26}O_2$: C, 80.49; H, 8.78%.

Reduction of ***18*** *with Sodium Borohydride.* A mixture of **18** (444 mg) and sodium borohydride (114 mg) in methanol (22.2 ml) was stirred at 0—5 °C for 1 h and then allowed to stand overnight at room temperature. The mixture was evaporated *in vacuo*, acidified with dilute hydrochloric acid, and extracted with ether. The ether extract was washed with brine, dried over sodium sulfate, and evaporated *in vacuo* to give a product (*ca.* 4 : 1 mixture, 423 mg: 94.6%), whose IR and ^1H NMR spectra were identical with those of authentic **20**.

A stirred solution of **20** (31.4 mg) in acetone (2.0 ml) was oxidized with four drops of Jones reagent (2M) at 0—5 °C for 15 min. The mixture was diluted with water and extracted with ether. The ether extract was washed with brine, dried over sodium sulfate, and evaporated *in vacuo* to give a lactone (29.1 mg: 93.0%), whose IR and ^1H NMR spectra were identical with those of authentic **18**.

A mixture of **20** (182 mg) and acetic anhydride (1.0 ml) in pyridine (0.5 ml) was allowed to stand overnight at room temperature. After the usual work-up, the crude product was chromatographed on silica gel (20 g), using benzene as the eluent, to give an acetate (**21**) (187 mg: 90.1%). IR: 1735, 1633, 1587 cm^{-1}; ^1H NMR (60 MHz): δ=1.30 (6H, d, J=7 Hz, $-CH(C\underline{H}_3)_2$), 1.41 and 1.49 (3H, each s, *ca.* 1 : 4, C_3-CH_3), 2.01 (3H, s, $-OCOCH_3$), 2.62 (3H, s, C_4-CH_3), 3.00 (1H, m, $-C\underline{H}(CH_3)_2$), 6.34 and 6.44 (1H, each s, *ca.* 1 : 4, C_2-H), 6.92 (1H, s, C_9-H), 7.14 (1H, dd, J=2 and 8.5 Hz, C_6-H), 7.40 (1H, d, J=2 Hz, C_8-H), 7.78 (1H, d, J=8.5 Hz, C_5-H). Found: C, 77.73; H, 8.31%. Calcd for $C_{22}H_{28}O_3$: C, 77.61; H, 8.29%.

Acetylation of ***19***, ***20***, *and* ***21***. *a)*: Boron trifluoride etherate (0.09 ml) was added to a stirred solution of **19** (84 mg) in acetic anhydride (1.8 ml) with cooling in an ice-water bath. The mixture was stirred at room temperature for 3 min, poured into a mixture of ice and aqueous sodium hydrogencarbonate, and extracted with ether. The ether extract was washed with brine, dried over sodium sulfate, and evaporated *in vacuo*. The residue was chromatographed on silica gel (10 g), using benzene as the eluent, to give (*R*)-9-acetyl-2,3-dihydro-7-isopropyl-3,4-dimethyl-3-propylnaphtho[2,3-*b*]furan (**24**)

(74 mg: 77%), $[\alpha]_D$ +7.3° (*c* 3.01); IR: 1661, 1613, 1585 cm^{-1}; ^1H NMR: δ=1.30 (6H, d, J=7 Hz, $-CH(C\underline{H}_3)_2$), 1.45 (3H, s, C_3-CH_3), 2.57 (6H, s, C_4-CH_3 and C_9-COCH_3), 3.00 (1H, m, $-C\underline{H}(CH_3)_2$), 4.24 (2H, ABq, δ_{AB}=22.5 Hz, J_{AB}= 8.5 Hz, C_2-H_2), 7.16 (1H, dd, J=2 and 8.5 Hz, C_6-H), 7.75 (1H, d, J=8.5 Hz, C_5-H), 8.15 (1H, d, J=2 Hz, C_8-H). Found: C, 81.20; H, 8.78%. Calcd for $C_{22}H_{28}O_2$: C, 81.44; H, 8.70%.

b): A solution of **20** (99.8 mg) in acetic anhydride (2.0 ml) was treated with boron trifluoride etherate (0.1 ml) as described for the preparation of **24**. The crude product was chromatographed on silica gel (20 g), using ether–benzene (2 : 98) as the eluent, to give an epimeric mixture at C-2 of 2-acetoxy-9-acetyl-2,3-dihydro-7-isopropyl-3,4-dimethyl-3-propylnaphtho[2,3-*b*]furan (**22**) (74.0 mg: 57.9%); IR: 1740, 1665, 1613, 1587 cm^{-1}; ^1H NMR: δ=1.31 (6H, d, J=7 Hz, $-CH(C\underline{H}_3)_2$), 1.44 and 1.50 (3H, each s, C_3-CH_3), 2.04 and 2.06 (3H, each s, *ca.* 4 : 1, $C_2-OCOCH_3$), 2.58 (3H, s, C_9-COCH_3), 2.63 (3H, s, C_4-CH_3), 3.02 (1H, m, $-C\underline{H}(CH_3)_2$), 6.40 and 6.51 (1H, each s, *ca.* 1 : 4, C_2-H), 7.21 (1H, dd, J=2 and 9 Hz, C_6-H), 7.81 (1H, d, J=9 Hz, C_5-H), 8.15 (1H, d, J=2 Hz, C_8-H). Found: C, 75.22; H, 7.91%. Calcd for $C_{24}H_{30}O_4$: C, 75.36; H, 7.91%.

Further elution with ether–benzene (1 : 9) gave an epimeric mixture at C-2 of 9-acetoacetyl-2-acetoxy-2,3-dihydro-7-isopropyl-3,4-dimethyl-3-propylnaphtho[2,3-*b*]furan (**23**) (28.4 mg: 20.0%), whose acetoacetyl group existed only in the enol form. IR: 1737, 1640—1530br cm^{-1}; ^1H NMR: δ=1.30 (6H, d, J=7 Hz, $-CH(C\underline{H}_3)_2$), 1.49 (3H, s, C_3-CH_3), 2.05 (3H, s, $-OCOCH_3$), 2.13 (3H, s, $-COCH=C(OH)C\underline{H}_3$), 2.63 (3H, s, C_4-CH_3), 3.03 (1H, m, $-C\underline{H}(CH_3)_2$), 5.93 (1H, s, $-COC\underline{H}=C(OH)CH_3$), 6.52 (1H, s, C_2-H), 7.22 (1H, dd, J=2 and 9 Hz, C_6-H), 7.82 (1H, d, J=9 Hz, C_5-H), 8.13 (1H, d, J=2 Hz, C_8-H), 15.95 (1H, br, $-COCH=C(O\underline{H})CH_3$). Found: C, 73.54; H, 7.69%. Calcd for $C_{26}H_{32}O_5$: C, 73.56; H, 7.60%.

c): A solution of **21** (84.5 mg) in acetic anhydride (1.8 ml) was treated with boron trifluoride etherate (0.09 ml) as described for the preparation of **24**. The crude product was chromatographed on silica gel (10 g) to give **22** (55.0 mg, 57.9%) and **23** (31.0 mg: 29.4%).

(R)-3-(3-Acetoxypropyl)-8-acetyl-2,3-dihydro-7-isopropyl-3,4-dimethylnaphtho[2,3-b]furan-2-one (25). A solution of (*R*)-3-(3-acetoxypropyl)-2,3-dihydro-7-isopropyl-3,4-dimethylnaphtho[2,3-*b*]furan-2-one (**IIIc**)[2] (71.0 mg) and acetyl chloride (160 mg) in carbon disulfide (1.4 ml) was added dropwise to a stirred solution of anhydrous aluminium chloride (266 mg) in carbon disulfide (2.7 ml) over a period of 15 min. The mixture was refluxed for 4 h and evaporated *in vacuo*. The residue was decomposed with a mixture of ice and dilute hydrochloric acid, and extracted with ether. The ether extract was washed with brine, dried over sodium sulfate, and evaporated *in vacuo*. The crude product was purified by column chromatography on silica gel (7.0 g), using ether–benzene (3 : 97) as the eluent, to give **25** (43.0 mg: 54.1%). IR: 1802, 1735, 1697, 1642 cm^{-1}; ^1H NMR: δ=1.30 (6H, d, J=7 Hz, $-CH(C\underline{H}_3)_2$), 1.62 (3H, s, C_3-CH_3), 1.92 (3H, s, $-OCOCH_3$), 2.54 (3H, s, $-COCH_3$), 2.64 (3H, s, C_4-CH_3), 2.94 (1H, m, $-C\underline{H}(CH_3)_2$), 3.86 (2H, t, J=6.5 Hz, $-C\underline{H}_2OAc$), 7.01 (1H, bs, C_9-H), 7.36 (1H, d, J=9 Hz, C_6-H), 7.91 (1H, d, J=9 Hz, C_5-H). Found: C, 72.98; H, 7.16%. Calcd for $C_{24}H_{28}O_5$: C, 72.70; H, 7.12%.

(R)-2,3-Dihydro-7-isopropyl-3-(3-methoxypropyl)-3,4-dimethylnaphtho[2,3-b]furan-2-one (27). The diazomethane ether solution (600 ml) was prepared from *N*-methyl-*N*-nitrosourea (60 g) by the known procedure and it was then dried over potassium hydroxide. To a stirred solution of (*R*)-2,3-dihydro-3-(3-hydroxypropyl)-7-isopropyl-3,4-dimethylnaphtho[2,3-*b*]-furan-2-one (**26**)[2] (9.94 g) in ether (500 ml) was added successively boron trifluoride etherate (1.9 ml) and the above diazomethane ether solution (600 ml). The mixture was allowed to stand at room temperature for 30 min and then filtered to remove a resinous material. The filtrate was washed successively with aqueous sodium hydrogencarbonate and brine, dried over sodium sulfate, and evaporated *in vacuo*. The residue was chromatographed on silica gel (300 g), using benzene as the eluent, to give **27** (8.87 g: 85.4%). $[\alpha]_D$ +27° (*c* 1.71); IR: 1792, 1637, 1592 cm^{-1}; ^1H NMR: δ=1.32 (6H, d, J=7 Hz, $-CH(C\underline{H}_3)_2$), 1.59 (3H, s, C_3-CH_3), 2.62 (3H, s, C_4-CH_3), 3.01 (1H, m, $-C\underline{H}(CH_3)_2$), 3.12 (3H, s, $-OCH_3$), 3.13 (2H, t, J=6 Hz, $-C\underline{H}_2OMe$), 7.18 (1H, s, C_9-H), 7.24 (1H, dd, J=2 and 8.5 Hz, C_6-H), 7.48 (1H, d, J=2 Hz, C_8-H), 7.82 (1H, d, J=8.5 Hz, C_5-H). Found: C, 77.28; H, 7.97%. Calcd for $C_{21}H_{26}O_3$: C, 77.27; H, 8.03%.

(3R)-2ξ-Acetoxy-9-acetyl-2,3-dihydro-7-isopropyl-3-(3-methoxypropyl)-3,4-dimethylnaphtho[2,3-b]furan (29). A mixture of **27** (699 mg) and sodium borohydride (163 mg) in ethanol (35 ml) was stirred at room temperature for 20 h. The mixture was evaporated *in vacuo*, acidified with dilute hydrochloric acid, and extracted with ether. The ether extract was washed with brine, dried over sodium sulfate, and evaporated *in vacuo* to give an epimeric mixture at C-2 of the corresponding alcohol (**28**) (713 mg) which, without purification, was used in the next reaction. IR: 3600, 3350br, 1635, 1593 cm^{-1}; ^1H NMR (60 MHz): δ=1.31 (6H, d, J=7 Hz, $-CH(C\underline{H}_3)_2$), 1.37 and 1.44 (3H, each s, C_3-CH_3), 2.59 (3H, s, C_4-CH_3), 2.99 (1H, m, $-C\underline{H}(CH_3)_2$), 3.19 and 3.26 (3H, each s, $-OCH_3$), *ca.* 3.1—3.4 (2H, m, $-C\underline{H}_2OMe$), 4.1 (1H, br, -OH), 5.37 and 5.50 (1H, each bs, *ca.* 1 : 3, C_2-H), 6.84 (1H, s, C_9-H), 7.11 (1H, bd, J=9 Hz, C_6-H), 7.36 (1H, bs, C_8-H), 7.76 (1H, d, J=9 Hz, C_5-H).

Boron trifluoride etherate (0.71 ml) was added to a stirred solution of the above crude **28** (713 mg) in acetic anhydride (14.2 ml) at 0—5 °C. The mixture was stirred at this temperature for 4 min and then treated as described for the preparation of **24**. The crude product was chromatographed on silica gel (90 g), using ether–benzene (5 : 95) as the eluent, to give **29** (618 mg: 70.0% from **27**). IR: 1748, 1675, 1621, 1597 cm^{-1}; ^1H NMR (60 MHz): δ=1.30 (6H, d, J=7 Hz, $-CH(C\underline{H}_3)_2$), 1.45 and 1.52 (3H, each s, C_3-CH_3), 2.04 and 2.07 (3H, each s, $C_2-OCOCH_3$), 2.60 (3H, s, C_9-COCH_3), 2.64 (3H, s, C_4-CH_3), 3.02 (1H, m, $-C\underline{H}(CH_3)_2$), 3.17 and 3.24 (3H, each s, $-OCH_3$), *ca.* 3.1—3.4 (2H, m, $-C\underline{H}_2OMe$), 6.40 and 6.50 (1H, each s, *ca.* 1 : 3, C_2-H), 7.20 (1H, dd, J= 2.5 and 9 Hz, C_6-H), 7.77 (1H, d, J=9 Hz, C_5-H), 8.11 (1H, d, J=2.5 Hz, C_8-H). Found: C, 72.62; H, 7.83%. Calcd for $C_{25}H_{32}O_5$: C, 72.79; H, 7.82%.

(R)-9-Acetyl-2,3-dihydro-7-isopropyl-3-(3-methoxypropyl)-3,4-dimethylnaphtho[2,3-b]furan-2-one (31). A mixture of **29** (484 mg) and dilute hydrochloric acid (6M: 0.6 ml) in methanol (20 ml) was refluxed for 1 h. The mixture was evaporated *in vacuo* and extracted with ether. The ether extract was washed successively with aqueous sodium hydrogencarbonate and brine, dried over sodium sulfate, and evaporated *in vacuo* to give an epimeric mixture at C-2 of the corresponding alcohol (**30**) (436 mg) which, without purification, was used in the next reaction. IR: 3600, 3325br, 1667, 1619, 1591 cm^{-1}; ^1H NMR (60 MHz): δ=1.33 (6H, d, J=7 Hz, $-CH(C\underline{H}_3)_2$), 1.38 and 1.43 (3H, each s, C_3-CH_3), 2.60 (3H, s, C_4-CH_3), 2.63 (3H, s, C_9-COCH_3), 3.02 (1H, m, $-C\underline{H}(CH_3)_2$), 3.17 and 3.24 (3H, each s, $-OCH_3$), *ca.* 3.05—3.35 (2H, m, $-C\underline{H}_2OMe$), 5.49 (1H, bs, C_2-H), 7.16 (1H, dd, J=2 and 9 Hz, C_6-H), 7.78 (1H, d, J=9 Hz, C_5-H), 8.07 (1H, d, J=2 Hz, C_8-H).

A solution of the above crude **30** (436 mg) in acetone (20 ml) was oxidized with Jones' reagent (2 M: 0.8 ml) at 0—5 °C

for 45 min. After the usual work-up, the crude product was chromatographed on silica gel (45 g), using ether–benzene (3 : 97) as the eluent, to give **31** (300 mg: 69.4% from **29**). $[\alpha]_D$ +11° (*c* 4.76); IR: 1805, 1685, 1627, 1597 cm^{-1}; ^1H NMR (60 MHz): δ=1.33 (6H, d, J=7 Hz, $-CH(C\underline{H}_3)_2$), 1.63 (3H, s, C_3-CH_3), 2.65 (3H, s, C_4-CH_3), 2.71 (3H, s, C_9-COCH_3), 3.03 (1H, m, $-C\underline{H}(CH_3)_2$), 3.13 (3H, s, $-OCH_3$), 3.15 (2H, t, J=6 Hz, $-C\underline{H}_2OMe$), 7.32 (1H, dd, J=2 and 9 Hz, C_6–H), 7.84 (1H, d, J=9 Hz, C_5–H), 8.07 (1H, d, J=2 Hz, C_8–H). Found: C, 74.77; H, 7.90%. Calcd for $C_{23}H_{28}O_4$: C, 74.97; H, 7.66%.

*Oxidation of **31** with* m-*Chloroperbenzoic Acid.* A mixture of **31** (3490 mg), *m*-chloroperbenzoic acid (85%: 8170 mg), and *p*-toluenesulfonic acid monohydrate (175 mg) in dichloromethane (240 ml) was refluxed for 30 h and then diluted with ether. The ether solution was washed successively with aqueous potassium iodide, aqueous sodium thiosulfate, aqueous sodium hydrogencarbonate, and brine, dried over sodium sulfate, and evaporated *in vacuo*. The residue was chromatographed on silica gel (130 g), using ether–benzene (2 : 98) as the eluent, to give (*R*)-9-acetoxy-2,3-dihydro-7-isopropyl-3-(3-methoxypropyl)-3,4-dimethylnaphtho[2,3-*b*]-furan-2-one (**32**) (395 mg: 10.8%). $[\alpha]_D$ +16° (*c* 1.40); IR: 1807, 1773, 1655, 1623 cm^{-1}; ^1H NMR (60 MHz): δ=1.34 (6H, d, J=7 Hz, $-CH(C\underline{H}_3)_2$), 1.64 (3H, s, C_3-CH_3), 2.45 (3H, s, $-OCOCH_3$), 2.62 (3H, s, C_4-CH_3), 2.98 (1H, m, $-C\underline{H}(CH_3)_2$), 3.15 (3H, s, $-OCH_3$), 3.16 (2H, t, J=6 Hz, $-C\underline{H}_2OMe$), 7.37 (1H, dd, J=2 and 9 Hz, C_6–H), 7.62 (1H, bs, C_8–H), 7.94 (1H, d, J=9 Hz, C_5–H). Found: C, 72.12; H, 7.37%. Calcd for $C_{23}H_{28}O_5$: C, 71.85; H, 7.34%. Subsequent elution gave a mixture of **32** and the starting **31** (1320 mg), whose purification is described later. Further elution gave (*R*)-9-acetoxy-2,3,5,8-tetrahydro-7-isopropyl-3-(3-methoxypropyl)-3,4-dimethylnaphtho[2,3-*b*]furan-2,5,8-trione (**33**) (162 mg: 4.1%). $[\alpha]_D$ +25° (*c* 1.01); IR: 1821, 1779, 1659, 1633, 1607, 1562 cm^{-1}; ^1H NMR (60 MHz): δ=1.20 (6H, d, J=7 Hz, $-CH(C\underline{H}_3)_2$), 1.63 (3H, s, C_3-CH_3), 2.42 (3H, s, $-OCOCH_3$), 2.68 (3H, s, C_4-CH_3), 3.04 (1H, m, $-C\underline{H}(CH_3)_2$), 3.16 (3H, s, $-OCH_3$), 3.20 (2H, t, J=6 Hz, $-C\underline{H}_2OMe$), 6.55 (1H, d, J=1.5 Hz, C_6–H). Found: C, 66.83; H, 6.38%. Calcd for $C_{23}H_{26}O_7$: C, 66.65; H, 6.32%.

The above mixture (1320 mg) of **31** and **32** was treated with dilute hydrochloric acid (6 M: 8.0 ml) in refluxing methanol (50 ml) for 1 h. The mixture was concentrated *in vacuo*, diluted with brine, and extracted with ether. The ether extract was washed with brine, dried over sodium sulfate, and evaporated *in vacuo*. The residue was chromatographed on silica gel (120 g), using ether–benzene (5 : 95) as the eluent, to give the starting **31** (541 mg: 15.5%) and (*R*)-2,3-dihydro-9-hydroxy-7-isopropyl-3-(3-methoxypropyl)-3,4-dimethylnaphtho[2,3-*b*]furan-2-one (**34**) (706 mg: 21.8%); IR: 3570, 3340br, 1793, 1653, 1620, 1603 cm^{-1}; ^1H NMR (60 MHz): δ=1.33 (6H, d, J=7 Hz, $-CH(C\underline{H}_3)_2$), 1.59 (3H, s, C_3-CH_3), 2.48 (3H, s, C_4-CH_3), 3.18 (3H, s, $-OCH_3$), 7.21 (1H, bd, J=9 Hz, C_6–H), 7.30 (1H, br, –OH), 7.63 (1H, d, J=9 Hz, C_5–H), 7.98 (1H, bs, C_8–H).

A solution of **34** (2.01 g) and acetic anhydride (2.0 ml) in pyridine (2.0 ml) was allowed to stand at room temperature for 1 h. After the usual work-up, the crude product was chromatographed on silica gel (100 g) to give **32** (1.96 g: 86.9%).

*(R)-5,8,9-Triacetoxy-2,3-dihydro-7-isopropyl-3-(3-methoxypropyl)-3,4-dimethylnaphtho[2,3-b]furan-2-one (**35**).* Zinc powder (65 mg) was added to a stirred solution of **33** (85 mg) and acetic anhydride (0.4 ml) in pyridine (0.4 ml) at 0—5 °C. The mixture was stirred at room temperature for 1 h and then treated as described for the preparation of **7**. The crude product was chromatographed on silica gel (30 g), using ether–benzene (1 : 9) as the eluent, to give **35** (46 mg: 45%). $[\alpha]_D$ +18° (*c* 2.33); IR: 1818, 1767, 1654,1628 cm^{-1}; ^1H NMR: δ=1.22 (6H, d, J=7 Hz, $-CH(C\underline{H}_3)_2$), 1.59 (3H, s, C_3-CH_3), 2.29, 2.30, and 2.32 (each 3H and s, $C_5-OCOCH_3$, $C_8-OCOCH_3$, and $C_9-OCOCH_3$), 2.67 (3H, s, C_4-CH_3), 3.07 (2H, t, J=6 Hz, $-C\underline{H}_2OMe$), 3.07 (1H, m, $-C\underline{H}(CH_3)_2$), 3.09 (3H, s, $-OCH_3$), 6.96 (1H, s, C_6–H). Found: C, 65.02; H, 6.48%. Calcd for $C_{27}H_{32}O_9$: C, 64.79; H, 6.44%.

*(R)-6-Acetoxy-2,3-dihydro-7-isopropyl-3,4-dimethyl-3-[3-(o-nitrophenylseleno)propyl]naphtho[2,3-b]furan-2-one (**37**).* Tributylphosphine (0.75 ml) was added to a stirred mixture of **8** (242 mg) and *o*-nitrophenyl selenocyanate (665 mg) in pyridine (6.0 ml) at room temperature under a stream of nitrogen. The mixture was stirred at room temperature for 1 h, diluted with ether, and then filtered to remove yellow precipitates. The filtrate was evaporated *in vacuo* to give a crude selenide (**36**), which was immediately acetylated with acetic anhydride (1.0 ml) in pyridine (1.0 ml) at room temperature for 1 h. After the usual work-up, the product was purified by column chromatography on silica gel (150 g), using benzene as the eluent, to give **37** (229 mg: 56.0%). $[\alpha]_D$ +47° (*c* 2.83); IR: 1793, 1752, 1638, 1600, 1588, 1567, 1507, 1330 cm^{-1}; ^1H NMR ($CDCl_3$): δ=1.32 (6H, d, J=7 Hz, $-CH(C\underline{H}_3)_2$), 1.64 (3H, s, C_3-CH_3), 2.40 (3H, s, $-OCOCH_3$), 2.55 (3H, s, C_4-CH_3), *ca.* 2.5—3.0 (2H, m, $-C\underline{H}_2SeC_6H_4-$), 3.11 (1H, m, $-C\underline{H}(CH_3)_2$) *ca.* 7.0—7.2 (3H, m) and *ca.* 8.0—8.25 (1H, m) ($-SeC_6\underline{H}_4-$), 7.29 (1H, s, C_9–H), 7.56 (1H, s, C_5–H), 7.66 (1H, s, C_8–H).

*(R)-6-Acetoxy-3-allyl-2,3-dihydro-7-isopropyl-3,4-dimethylnaphtho[2,3-b]furan-2-one (**38**).* A mixture of **37** (229 mg) and 50% hydrogen peroxide (0.26 ml) in tetrahydrofuran (9.2 ml) was stirred at room temperature for 19 h. The mixture was diluted with brine and extracted with ether. The ether extract was washed successively with aqueous potassium iodide, aqueous sodium thiosulfate, aqueous sodium hydrogencarbonate, and brine, dried over sodium sulfate, and evaporated *in vacuo*. The residue was chromatographed on silica gel (15 g), using benzene as the eluent, to give **38** (129 mg: 88.6%). $[\alpha]_D$ +105° (*c* 2.82); IR: 1794, 1753, 1640, 1622 cm^{-1}; ^1H NMR: δ=1.30 (6H, d, J=7 Hz, $-CH(C\underline{H}_3)_2$), 1.61 (3H, s, C_3-CH_3), 2.32 (3H, s, $-OCOCH_3$), 2.62 (3H, s, C_4-CH_3), 2.76 (2H, d, J=6.5 Hz, $C_3-C\underline{H}_2CH=CH_2$), *ca.* 4.7—5.6 (3H, m, $C_3-CH_2C\underline{H}=C\underline{H}_2$), 7.20 (1H, s, C_9–H), 7.50 (1H, s, C_5–H), 7.58 (1H, s, C_8–H). Found: C, 75.27; H, 7.07%. Calcd for $C_{22}H_{24}O_4$: C, 74.97; H, 6.86%.

The authors are grateful to Messrs. Tatsuo Arioka, Shuji Takauchi, and Yutaka Fukuda for their technical assistance.

References

1) T. Matsumoto, S. Imai, K. Ondo, N. Takeyama, and K. Fukui, *Chem. Lett.*, **1980**, 425.

2) T. Matsumoto, S. Imai, K. Ondo, N. Takeyama, H. Kataoka, Y. Yamamoto, and K. Fukui, *Bull. Chem. Soc. Jpn.*, **55**, 891 (1982).

3) D. Karanatsios and C. H. Eugster, *Helv. Chim. Acta*, **48**, 471 (1965).

4) C. H. Eugster, *Ber. Deutsch. Bot. Ges.*, **88**, 141 (1975).

5) C. H. Eugster, H.-P. Küng, H. Kühnis, and P. Karrer, *Helv. Chim. Acta*, **46**, 530 (1963).

6) H. Zimmer, D. C. Lankin, and S. W. Horgan, *Chem. Rev.*, **71**, 229 (1971).

7) W. Otting and G. Staiger, *Chem. Ber.*, **88**, 828 (1955).

8) J. F. W. McOmie and J. M. Blatchly, *Org. React.*, **19**, 199 (1972).
9) By irradiation of a signal at δ 3.02, the half-height width of a signal at δ 7.74 was changed from 1.5 Hz to 1.0 Hz.
10) P. A. Grieco, S. Gilman, and M. Nishizawa, *J. Org. Chem.*, **41**, 1485 (1976).

An Improved Resolution of β-Hydroxy-DL-aspartic Acid on Optically Active Resin Containing L-Lysine or L-Ornithine[1,2]

Shigeharu Anpeiji, Yasunobu Toritani, Kazunori Kawada, Seiji Kondo, Shinji Murai, Hideo Okai,* Hisanobu Yoshida,† and Hideo Imai†

Department of Fermentation Technology, Faculty of Engineering, Hiroshima University, Shitami, Saijo-cho, Higashihiroshima 724

†*Institute of Pharmaceutial Science, Hiroshima University School of Medicine, Kasumi 1, Minami-ku, Hiroshima 734*

(Received March 9, 1983)

A series of experiments on column chromatography of the optically active resin containing L-lysine or L-ornithine were carried out with pyridinium acetate and ammonium acetate solvent systems as the eluents. *threo*-β-Hydroxy-DL-aspartic acid was found to be resolved on the optically active resin containing L-lysine with ammonium acetate solvent system; *erythro*-β-hydroxy-DL-aspartic acid could be resolved on that containing L-ornithine with pyridinium acetate solvent system. The *threo* or *erythro* racemate was resolved on a preparative scale, and the resolution including the complete characterization of enantiomers resolved was first accomplished.

Resolution of racemic compounds on the optically active resin has become familiar. In the initial stage, the resolution was carried out using naturally occurring adsorbent materials such as wool,[3] (+)-quartz,[4] and cellulose,[5-7] but the optical purity of the enantiomers obtained was low. The possibility of using synthetic optically active polymers as agents for the resolution was first studied by Bunnett and Marks in 1952.[8] The application of this principle to the resolution of racemic amino acids was first reported by Losse *et al.*[9] They attempted to resolve eight kinds of racemic amino acids on three types of copolymers composed by L-tyrosine and some suitable crosslinking agents. Roberts and Haigh also reported the synthesis of polymer of *S*-(*o*- and *p*-vinylbenzyl)-L-cysteine and its use in the partial resolution of DL-methionine.[10] Yamashita and Nakamura synthesized three types of optically active polymers by the homogeneous copolymerization of *N*-acryloylated α-amino acids with *N*,*N*′-dimethacryloyl-1,6-hexanediamine, and then partially resolved several kinds of DL-amino acid anilides by the use of these copolymers.[11] Snyder *et al.* resolved DL-valine, DL-isoleucine, DL-norvaline, DL-α-aminobutyric acid, DL-alanine, and DL-proline on styrene–divinylbenzene copolymers containing (*N*-carboxymethyl-L-valine)copper(II) at 40—70% optical purity.[12] These authors suggested that the degree of resolution increased with an increase in the bulkiness of the side chain on the α-carbon of the amino acid. Davankov *et al.* reported that DL-proline was resolved at 100% optical purity using an asymmetric resin containing optically active L-proline in the Cu^{2+} form.[13] In all cases mentioned above, however, there has been no work on the resolution involving the complete characterization of enantiomers resolved.

One of the present authors has previously reported the resolution of *threo*- or *erythro*-β-hydroxy-DL-aspartic acid by the fractional crystallization of diastereomeric salt.[14] Although the *threo* racemate has been most satisfactorily resolved with L-lysine, and the *erythro* racemate with L-ornitine, these resolutions have required a highly skilled experimental technique. The resolutions of β-hydroxyaspartic acid were expected to become technically easier by the application of these resolutions to column chromatography. So the authors have tried to resolve *threo*- or *erythro*-β-hydroxy-DL-aspartic acid on the optically active resin containing L-lysine or L-ornithine. In this paper, we deal with the preparations of the optically active resins and their use in the resolutions.

The optically active resins were prepared by the modification of the solid phase peptide synthesis by Merrifield.[15,16] N^{α}, N^{ϵ}-Bis(*t*-butoxycarbonyl)-L-lysine and chloromethylated styrene–divinylbenzene copolymer (PS–DVB) (DVB 2%, 200—400 Mesh, 1.32 mmol of Cl/g-resin) were coupled in *N*,*N*-dimethylformamide containing triethylamine for 72 h at 50 °C. The desired resin was afforded by the removal of the *t*-butoxycarbonyl group from the resin mentioned above by treatment with hydrogen chloride in dioxane for 90 min at room temperature. After the acidic hydrolysis

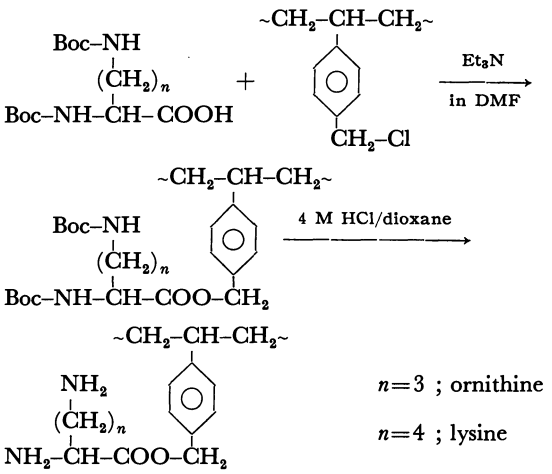

of the prepared resin, L-lysine content was determined by amino acid analysis and found to be 0.58 mmol/g-resin (correspond to 44% yield). L-Ornithylstyrene–divinylbenzene copolymer (Orn-PS–DVB) was prepared in the same manner as described for the preparation of L-lysylstyrene–divinylbenzene copolymer (Lys-PS–DVB) ;the L-ornithine content was 0.97 mmol/g-resin (yield 73%). The chromatography was carried out as follows: The aqueous solution of an aliquot of the racemate was applied to a column (1.2×10 cm) and eluted with various solvent systems at room temperature and

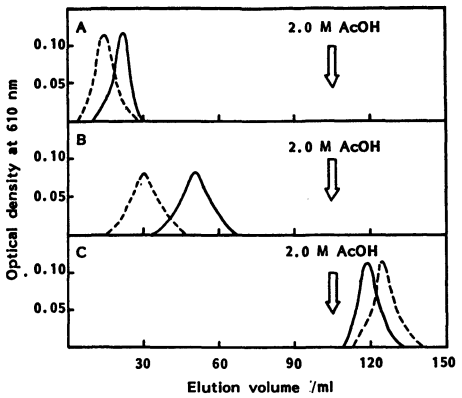

Fig. 1. Effect of pH in 0.1 M pyridinium acetate solvent system on resolution of *threo*-DL-Hyasp.
Column: Lys-PS–DVB (solid line), Orn-PS–DVB (dotted line). A: pH 4.0, B: pH 6.0, C: pH 8.0.

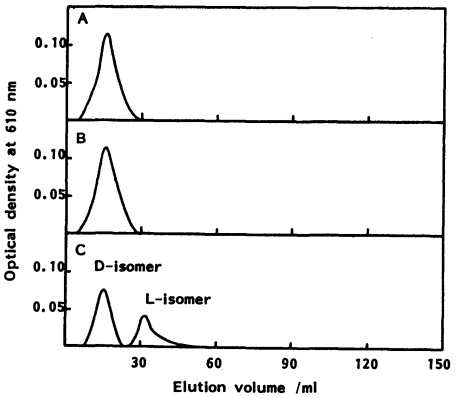

Fig. 2. Effect of pH in 0.1 M ammonium acetate solvent system on resolution of *threo*-DL-Hyasp.
Column: Lys-PS–DVB. A: pH 6.0, B: pH 7.0, C: pH 8.0.

a flow rate of *ca.* 5 ml h^{-1}.

The elution patterns of *threo*-β-hydroxy-DL-aspartic acid with 0.1 M (1 M=1 mol dm^{-3}) pyridinium acetate solvent system are shown in Fig. 1. The effect of variation of pH was examined on Lys-PS–DVB and Orn-PS–DVB; in no cases was any *threo* racemate resolved. A similar experiment was run by the use of 0.1 M ammonium acetate instead of 0.1 M pyridinium acetate as an eluent. The elution patterns of the *threo* racemate are shown in Fig. 2. The *threo* racemate was successfully resolved with the column of Lys-PS–DVB using 0.1 M ammonium acetate of pH 8.0. It was confirmed that D-isomer eluted faster than L-isomer by separately eluting each enantiomer under the conditions described above. The effect of variation in concentration of ammonium acetate in the solvent system was also examined on Lys-PS–DVB; 0.1 M concentration proved to be the optimal condition for the resolution of the *threo* racemate (Fig. 3).

The resolution of *erythro*-β-hydroxy-DL-aspartic acid was carried out with column of Lys-PS–DVB and Orn-PS–DVB using 0.1 M pyridinium acetate of pH 4.0, 6.0, and 8.0. The elution patterns of the *erythro* racemate are shown in Fig. 4. The *erythro* racemate was found

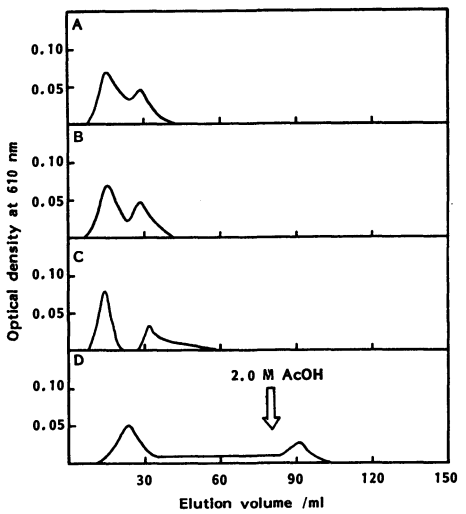

Fig. 3. Effect of concentration of ammonium acetate in solvent system (pH 8.0) on resolution of *threo*-DL-Hyasp.
Column: Lys-PS–DVB. A: 0.2 M, B: 0.15 M, C: 0.1 M, D: 0.05 M.

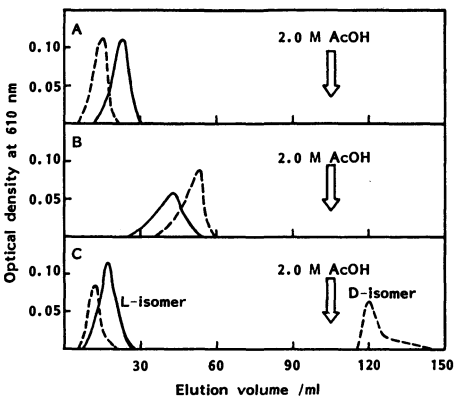

Fig. 4. Effect of pH in 0.1 M pyridinium acetate solvent system on resolution of *erythro*-DL-Hyasp.
Column: Lys-PS–DVB (solid line), Orn-PS–DVB (dotted line). A: pH 4.0, B: pH 6.0, C: pH 8.0.

to be successfully resolved with the column of Orn-PS–DVB using 0.1 M pyridinium acetate of pH 8.0. The faster peak was eluted easily, as shown in Fig. 4, whereas 2.0 M acetic acid was required for the elution of the slower peak. The faster peak proved to be L-isomer, and the slower peak was D-isomer.

As an experiment on a preparative scale, we attempted to resolve the *threo* racemate with the column (1.8×40 cm) of Lys-PS–DVB, and the *erythro* racemate with the column of Orn-PS–DVB, under the optimal conditions which had been found previously for the resolutions on a smaller scale. Two hundred milligrams of *threo*-β-hydroxy-DL-aspartic acid was resolved, and the eluate containing each enantiomer was collected. The resolution was repeated five times, and each faster (or slower) peak was combined. We observed the presence of a small amount of lysine in the collected eluates, which seemed to be attributable to the liberation of lysine from the resin. After the removal of lysine by ion-exchange chromatography with an appropriate eluent,

Table 1. Comparison of specific rotations and yields of the four optical isomers of β-hydroxyaspartic acid

Compound	Chemical procedure[14]		Present procedure	
	$[\alpha]_D^{a)}$/°	Yield/%	$[\alpha]_D^{a)}$/°	Yield/%
threo-L-Hyasp	− 8.5(H_2O) + 6.4(5 M HCl)	67	− 8.1(H_2O) + 6.2(5 M HCl)	80
threo-D-Hyasp	+ 8.6(H_2O) − 6.5(5 M HCl)	57	+ 8.3(H_2O) − 6.4(5 M HCl)	84
erythro-L-Hyasp	+ 47.0(H_2O) + 52.0(5 M HCl)	81	+ 47.4(H_2O) + 52.1(5 M HCl)	92
erythro-D-Hyasp	− 46.8(H_2O) − 51.8(5 M HCl)	72	− 47.0(H_2O) − 51.6(5 M HCl)	90

a) Temperature, 20 °C; *c* 1.0 in H_2O or 5 M HCl.

Table 2. Amino acid contents and spontaneous liberations relating to the prepared resins

Resin	Content (mmol/g-resin)	Yield[a]/%	Liberated amino acid[b]					
			pH 4.0 mmol/g-resin	%	pH 6.0 mmol/g-resin	%	pH 8.0 mmol/g-resin	%
Gly-PS-DVB	0.85	64	0.11	13	0.04	5	0.04	5
Ala-PS-DVB	0.66	50	0.15	23	0.12	18	0.10	15
Val-PS-DVB	0.80	61	0.01	1	<0.01	<1	<0 01	<1
Leu-PS-DVB	0.70	53	0.03	4	<0.01	<1	<0.01	<1
Ile-PS-DVB	0.65	49	<0.01	<1	<0.01	<1	<0.01	<1
Phe-PS-DVB	0.78	59	0.01	1	<0.01	<1	<0.01	<1
Tyr-PS-DVB	0.52	39	0.01	2	<0.01	<1	<0.01	<1
Pro-PS-DVB	0.91	69	0.51	56	0.12	13	0.13	14
Ser-PS-DVB	0.56	42	0.05	9	0.01	2	<0.01	<1
Thr-PS-DVB	0.69	52	0.02	3	<0.01	<1	<0.01	<1
Orn-PS-DVB	0.97	73	0.06	6	0.01	1	0.01	1
Lys-PS-DVB	0.58	44	0.07	12	0.11	19	0.04	7

a) The yields are based on Cl content (1.32 mmol/g-resin) of chloromethylated PS-DVB (DVB 2%, 200—400 Mesh).
b) The amounts of liberated amino acids below 0.01 mmol/g-resin are described as <0.01, and the percentages of liberation below 1% as <1.

the faster fraction (containing D-isomer) or the slower fraction (containing L-isomer) was concentrated *in vacuo*; optically pure *threo*-β-hydroxy-D-aspartic acid or *threo*-β-hydroxy-L-aspartic acid was obtained, in a good yield. *erythro*-β-Hydroxy-DL-aspartic acid was resolved by the elution of 500 mg of the racemate. Each enantiomer was obtained in the same manner as described for the resolution of the *threo* racemate. The specific rotations and yields of the four optical isomers so obtained are summarized in Table 1, together with those obtained by the fractional crystallization. As shown in Table 1, it was obvious that the *threo* or *erythro* racemate was completely resolved. This chromatographic procedure was far more useful than the resolution by the fractional crystallization: Such as could be obtained both a high yield and high optical purity, in a chemical procedure, were given by a facile operation.

In order to estimate the degree of the above-mentioned spontaneous degradation in PS-DVB substituted with amino acids, the authors prepared twelve kinds of resins, including Lys-PS-DVB and Orn-PS-DVB, and compared the liberations of amino acids from resins. They were prepared in the same manner as described for the preparations of Lys-PS-DVB and Orn-PS-DVB. Amino acid contents of resins are shown in Table 2. An aliquot of each resin so obtained was immersed in 0.1 M pyridinium acetate of pH 4.0, 6.0, and 8.0 for 7 d at room temperature, and the liberated amino acid in the supernatant was determined by amino acid analysis (Table 2). Table 2 revealed the liberations of amino acids from resins, whereas amino acid benzyl esters in liquid phase were not entirely hydrolyzed under such mild conditions. The percentage of the liberated amino acid based on each amino acid content varied with the kinds of bonded amino acid. Gly-, Ala-, Pro-, and Lys-PS-DVB were unstable, while the resins containing amino acids possessing hydrophobic side chains were relatively stable. The variation of pH in the solvent also affected the liberation. The degree of liberation was greater under the acidic conditions than under the neutral and basic conditions, but only Lys-PS-DVB was unstable under the neutral conditions. These phenomena were greatly different from the commonly known propensity of hydrolysis of amino acids benzyl ester in aqueous acidic or basic solution. It seemed that an amino acid benzyl ester fixed on the stationary phase behaved in different ways from that in the liquid phase.

There have been some reports on successful resolutions of racemic amino acid derivatives by gas chromatography on optically active stationary phases,[17,18] but they have been used only on the analytical scale for the determination of configurations and optical purity and have restricted the variation of the racemates. For the resolutions of various kinds of racemic amino acids on a preparative scale, liquid-chromatographic resolutions have been more effective than gas-chromatographic resolutions. This report is the first on the complete resolution of a racemic amino acid on the

optically active stationary phase. It will be possible to apply the principles of this procedure to the resolutions of other racemic amino acids.

Experimental

All the melting points were uncorrected. The optical rotations were measured on a Union PM-101 Polarimeter. The quantitative analyses of amino acids were run with the high-performance liquid chromatography (HPLC) apparatus composed of; Toyo soda HLC-805, Toyo soda solvent feeder, Toyo soda sequence controller, Toyo soda reactor, Shimadzu fluorescence spectromonitor RF-500LC (for phthalaldehyde as fluorogenic reagent), Toyo soda visible spectrophotometer (for ninhydrin as color-developing reagent), and TSK pen recorder. The amounts of color developed were determined by an Atago AG-4 densitometer (slit 1 × 18 mm, 610 nm).

Syntheses of N-*(t-Butoxycarbonyl) Amino Acid Derivatives.* All the *N*-(*t*-butoxycarbonyl) amino acid derivatives were synthesized by the ordinary manner. *N*-(*t*-Butoxycarbonyl) derivatives of lysine, ornithine, valine, isoleucine, phenylalanine, tyrosine, serine, and threonine were stored as a DCHA salt, and that of leucine as the hemihydrate. Boc–Lys(Boc)–OH·DCHA: mp 134—136 °C; $[\alpha]_D^{20}$ −4° (*c* 3, AcOH). Boc–Orn(Boc)–OH·DCHA: mp 164—166 °C; $[\alpha]_D^{20}$ +2° (*c* 4, AcOH). Boc–Gly–OH: mp 93—94 °C (lit,[19] 94—95 °C). Boc–Ala–OH: mp 81–83 °C (lit,[20] 83—84 °C); $[\alpha]_D^{20}$ −22° (*c* 1, AcOH) (lit,[20] −24° (*c* 1, AcOH)). Boc–Val–OH·DCHA: mp 138—140 °C; $[\alpha]_D^{20}$ −1° (*c* 4, AcOH). Boc–Leu–OH·1/2 H_2O: mp 80—82 °C (lit,[19] 78—81 °C); $[\alpha]_D^{20}$ −21° (*c* 2, AcOH). Boc–Ile–OH·DCHA: mp 125—127 °C (lit,[21] 127—128 °C); $[\alpha]_D^{20}$ +7° (*c* 1.5, DMF) (lit,[21] +6° (*c* 1.5, DMF)). Boc–Phe–OH·DCHA: mp 213—214 °C (lit,[22] 210—212 °C); $[\alpha]_D^{20}$ +30° (*c* 1, methanol) (lit,[22] +29.2° (*c* 1.025, methanol at 23 °C)). Boc–Tyr–OH·DCHA: mp 208—210 °C (lit,[20] 205—208 °C); $[\alpha]_D^{20}$ +4° (*c* 1, AcOH) (lit,[20] +3.8° (*c* 1, AcOH)). Boc–Pro–OH: mp 133—134 °C (lit,[23] 133—134 °C); $[\alpha]_D^{20}$ −59° (*c* 2, AcOH) (lit,[23] −60.8° (*c* 2.04, AcOH at 25 °C)). Boc–Ser–OH·DCHA: mp 140—142 °C (lit,[24] 142—144 °C); $[\alpha]_D^{20}$ +13° (*c* 3, methanol) (lit,[24] +13.3° (*c* 3.044, methanol at 25.5 °C)). Boc–Thr–OH·DCHA: mp 148—151 °C; $[\alpha]_D^{20}$ −2° (*c* 4, AcOH). Elemental analyses of these compounds also agreed with the theoretical values.

Preparations of Optically Active Resins. L-*Lysylstyrene–divinylbenzene Copolymer (Lys-PS–DVB)*: The chloromethylated PS–DVB (DVB 2%, 200—400 Mesh, 1.32 mmol of Cl/g-resin) (10.0 g) was suspended in DMF (80 ml). The suspension was degassed for 1 h *in vacuo*. The solvent was decanted and the residual resin was washed three times with DMF by decantation. Boc–Lys(Boc)–OH which was released from its DCHA salt (13.9 g, 26.4 mmol) with 1 M sulfuric acid in the usual manner was dissolved in DMF (80 ml). The solution and triethylamine (3.3 ml, 23.8 mmol) were added to the residual resin and the mixture was shaken for 72 h at 50 °C. Then the resin was filtered, washed throughly with DMF, acetic acid, methanol, DMF, and methanol by gradual changes of solvent composition and sucked dry. The resin was kept overnight in a vacuum desiccator: yield 12.8 g. The resulting resin was suspended in dioxane (80 ml) and the suspension was degassed for 1 h *in vacuo*. The solvent was decanted and the residual resin was washed three times with dioxane by decantation. To the residual resin, 4 M hydrogen chloride in dioxane (50 ml) was added. After shaking for 90 min at room temperature, the resin was filtered, washed with dioxane, 1 M acetic acid, water and finally methanol and sucked dry. The resin was kept overnight in a vacuum desiccator: yield 11.0 g. Lys-PS–DVB (41 mg) weighed out precisely was introduced into a tube and hydrolyzed with a mixture of 6 M HCl (0.5 ml) and propionic acid (0.5 ml) at 110 °C in a sealed tube for 24 h. Lys-PS–DVB was filtered and the filtrate was evaporated to dryness *in vacuo*. The residue was dissolved in water (1.0 ml) and the solution was diluted with water. Lysine content was determined by applying a part of the dilute solution on HPLC and found to be 0.58 mmol/g-resin. The PS–DVB substituted with ornithine, glycine, alanine, valine, leucine, isoleucine, phenylalanine, tyrosine, proline, serine, and threonine were prepared in the same manner as described for the preparation of Lys-PS–DVB. *N*-(*t*-Butoxycarbonyl) derivatives of glycine, alanine and proline were used for the coupling directly, and Boc–Leu–OH·1/2 H_2O was used after dehydration. The amino acid content of each resin is presented in Table 2.

Resolution of threo- *or* erythro-DL-*Hyasp on Optically Active Resin.* *Resolution of* threo-DL-*Hyasp*: Lys-PS–DVB or Orn-PS–DVB (7.5 g) was packed into a column (1.2 × 10 cm); each column was equilibrated by washing with an eluent. 0.1 M ammonium acetate was prepared in the following manner. Ammonium acetate (7.7 g) was dissolved in water (500 ml), and the pH of the solution was adjusted with acetic acid. The solution was made up to 1 L with water, and adjusted again to the desired pH by acetic acid or aqueous ammonia. 0.1 M Pyridinium acetate was also prepared in the same manner by using pyridine (8.1 ml) instead of ammonium acetate. The solution of *threo*-DL-Hyasp[14] (20 mg/1 ml water) was put on the column and eluted with the appropriate solvent system at room temperature and a flow rate of *ca.* 5 ml h^{-1}. The volume of each fraction was one milliliter. When the elution volume exceeded 90 ml, 2.0 M acetic acid was used as an eluent. The color development, the determination of the developed color, and the plotting on a graph were run according to the manner by H. Okai *et al.*[14] The elution patterns are shown in Fig. 1—3.

Resolution of erythro-DL-*Hyasp*: *erythro*-DL-Hyasp[14] (20 mg) was treated in the same manner as has been described for the resolution of *threo*-DL-Hyasp. For the elution of the slower peak, 2.0 M acetic acid was used as an eluent. The elution patterns are shown in Fig. 4.

Preparative Resolution of threo-DL-*Hyasp*: A solution of *threo*-DL-Hyasp[14] (0.2 g) in a suitable volume (*ca.* 10 ml) of 0.1 M ammonium acetate solvent of pH 8.0 was put on a column (1.8 × 40 cm) of Lys-PS–DVB (70 g, 0.63 mmol of Lys/g-resin), and eluted with the same solvent at a flow rate of *ca.* 10 ml h^{-1}. Each fraction (2 ml) was tested on a paper strip with ninhydrin, and then the ninhydrin-positive fractions were applied on paper chromatography (developing solvent, 1-butanol–acetic acid–pyridine–water (4 : 1 : 1 : 2, v/v)) to find the fractions containing hydroxyaspartic acid. The resolution of 0.2 g of the racemate was repeated five times in the above-mentioned manner. The faster eluting fractions were combined and then evaporated to dryness *in vacuo*. Most of the ammonium acetate was removed by sublimation *in vacuo* for *ca.* 1 h at 100 °C. To remove the contaminated lysine, the residue was treated with Dowex 1 (acetate form). A column (1.8 × 12 cm) of Dowex 1 was washed with 0.5 M acetic acid (30 ml) and then with 2.0 M acetic acid (70 ml) to elute hydroxyaspartic acid. The residue obtained by the evaporation of the eluate was crystallized from water–ethanol: yield of *threo*-D-Hyasp 0.42 g (84%).

Found: C, 31.99; H, 4.88; N, 9.32%. Calcd for $C_4H_7O_5N$: C, 32.22; H, 4.73; N, 9.40%. The slower eluting fractions were combined and then treated in the manner described above: yield of *threo*-L-Hyasp 0.40 g (80%).

Found: C, 31.96; H, 4.90; N, 9.28%. The specific rotations of each enantiomer are presented in Table 1.

Preparative Resolution of erythro-DL-*Hyasp*: A solution of *erythro*-DL-Hyasp[14] (0.5 g) in a suitable volume (*ca.* 20 ml) of 0.1 M pyridinium acetate of pH 8.0 was put on a column (1.8×40 cm) of Orn-PS–DVB (70 g, 0.91 mmol of Orn/g-resin), and eluted with the same solvent at a flow rate of *ca.* 10 ml h^{-1}. After the faster eluting fractions containing hydroxyaspartic acid were found in the above-mentioned manner, 2.0 M acetic acid was used as an eluent. The resolution was repeated twice, and *erythro*-L-Hyasp was obtained from the faster eluting fractions by the method described for the separation of *threo*-D-Hyasp: yield of *erythro*-L-Hyasp 0.46 g (92%).

Found: C, 32.02; H, 4.82; N, 9.35%. The slower eluting fractions were combined and then treated as in the separation of *threo*-D-Hyasp: yield of *erythro*-D-Hyasp 0.45 g (90%).

Found: C, 32.18; H, 4.77; N, 9.42%. The specific rotations of each enantiomer are presented in Table 1.

Spontaneous Degradation. Determination of Liberated Amino Acid: The prepared resin (*ca.* 300 mg) was weighed out precisely and introduced into three test tubes. To the tubes 6.0 ml of 0.1 M pyridinium acetate (pH 4.0, 6.0, and 8.0) were added; the tubes were then sealed and allowed to stand at room temperature. The time-course of the spontaneous degradation was followed by determining the amino acid in the supernatant at daily intervals. The supernatant (0.5 ml) was withdrawn and evaporated to dryness *in vacuo*, and an aliquot of the residue was applied on HPLC. The amounts of the amino acids in the supernatant at each time were derived by correcting the experimental values, and those at zero time were subtracted from those at each time. The amounts of the liberated amino acids after 7 d are presented in Table 2.

We wish to express our thanks to Professor Nobuo Izumiya of Kyushu University and Professor Sakuzo Fukui of Hiroshima University for their helpful discussions.

References

1) This article was in preliminary form communicated at the 13th Symposium on Peptide Chemistry, Nov. 1975, Tokyo.

2) The abbreviations recommended by the IUPAC-IUB commission of Biochemical Nomenclature (*J. Biol. Chem.*, **247**, 977 (1972)) have been used. Amino acid symbols except glycine denote the L-configuration unless otherwise noted. Additional abbreviations: AcOH, acetic acid: DCHA, dicyclohexylamine; DMF, *N,N*-dimethylformamide, Et_3N, triethylamine; Hyasp, β-hydroxyaspartic acid; PS–DVB, styrene–divinylbenzene copolymer.

3) W. Bradley and R. Brindley, *Chem. Ind.* (*London*), **1954**, 579.

4) R. Tsuchida, M. Kobayashi, and N. Nakamura, *Nippon Kagaku Zasshi*, **56**, 1339 (1935).

5) N. Nakamura, *Nippon Kagaku Zasshi*, **72**, 789 (1951).

6) K. Closs and C. Haug, *Chem. Ind.* (*London*), **1953**, 103.

7) C. Dalgliesh, *J. Chem. Soc.*, **1952**, 3940.

8) J. F. Bunnett and J. L. Marks, *J. Am. Chem. Soc.*, **74**, 5893 (1952).

9) G. Losse, H. Jeschkeit, G. Fickert, and H. Rabe, *Z. Naturforsch.*, **176**, 419 (1962).

10) C. W. Roberts and H. Haigh, *J. Org. Chem.*, **27**, 3375 (1962).

11) T. Yamashita and N. Nakamura, *Bull. Chem. Soc. Jpn.*, **43**, 1809 (1970).

12) R. V. Snyder, R. J. Angelici, and R. B. Meck, *J. Am. Chem. Soc.*, **94**, 2660 (1971).

13) V. A. Davankov and S. V. Rogozhin, *J. Chromatogr.*, **60**, 280 (1971); V. A. Davankov, S. V. Rogozhin, A. V. Semechkin and T. P. Sachkova, *ibid.*, **82**, 359 (1973); I. Peslekas, S. V. Rogozhin, and V. A. Davankov, *Izv. Akad. Nauk SSSR, Ser. Khim.*, **1974**, 1972.

14) H. Okai, N. Imamura, and N. Izumiya, *Bull. Chem. Soc. Jpn.*, **40**, 2154 (1967).

15) R. B. Merrifield, *J. Am. Chem. Soc.*, **85**, 2149 (1963).

16) J. M. Stewart and J. D. Young, "Solid Phase Peptide Synthesis," Freeman, San Francisco (1969).

17) S. Weinstein, F. Feibush, and E. Gil-Av, *J. Chromatogr.*, **126**, 97 (1976).

18) H. Frank, G. J. Nicholson, and E. Bayer, *J. Chromatogr.*, **146**, 197 (1978).

19) E. Schnabel, *Justus Liebigs Ann. Chem.*, **702**, 188 (1967).

20) T. Nagasawa, K. Kuroiwa, K. Narita, and Y. Isowa, *Bull. Chem. Soc. Jpn.*, **46**, 1269 (1973).

21) H. C. Beyerman, C. A. M. Boers-Boonekamp, and H. Maassen van den Brink-Zimmermannova, *Recl. Trav. Chim. Pays-Bas*, **87**, 257 (1968).

22) M. Fujino and C. Hatanaka, *Chem. Pharm. Bull.* (*Tokyo*), **15**, 2015 (1967).

23) E. Bayer, G. Jung, and H. Hagenmaier, *Tetrahedron*, **24**, 4853 (1968).

24) H. Otsuka, K. Inouye, F. Shinozaki, and M. Kanayama *Bull. Chem. Soc. Jpn.*, **39**, 1171 (1966).

Synthetic Studies on the Validamycins. IX. Synthesis of Some Racemic Isomers of Validoxylamine A[1]

Tatsushi Toyokuni, Seiichiro Ogawa, and Tetsuo Suami*
Department of Applied Chemistry, Faculty of Science and Technology, Keio University, Hiyoshi, Kohoku-ku, Yokohama 223
(Received March 23, 1983)

Two racemic isomers of validoxylamine A have been synthesized by use of coupling reactions of the protected DL-validamine and the allyl bromides, the precursors of the unsaturated branched-chain cyclitol moiety. The racemic diastereomers thus formed can be separated by chromatography on silica gel. It indicates that optically pure validoxylamine A analogs should be obtained if chiral validamine derivative is used in place of the racemate.

The validamycins,[2] isolated from the culture filtrate of *Streptomyces hygroscopicus* var. *limoneous*, is a complex mixture of novel aminocyclitol antibiotics[3] containing a single amino group linked to two separate branched-chain cyclitols. The antibiotics are widely used for the treatment of sheath blight disease of rice plants. Among them, validamycin A (**1**) is the major and most active component.[4]

Hydrolysis of **1** with 1 M (=1 mol dm^{-3}) sulfuric acid gave validoxylamine A (**2**)[5,6] and D-glucose. Compound **2** was assigned as *N*-[(1*S*)-(1,4,6/5)-3-hydroxymethyl-4,5,6-trihydroxycyclohex-2-enyl]-(1*S*)-(1,2,4/3,5)-2,3,4-trihydroxy-5-(hydroxymethyl)cyclohexylamine, and was also found in the validamycin producing culture.[4b] It is not only an aglycon part of **1** but also a common structural unit of other validamycins (C, D, E, and F),[7] except for validamycin B which has validoxylamine B,[8] the C-6 hydroxy analog of **2**, as an aglycon. Although **2** showed a low activity compared with validamycin A in the "dendroid-test method," it exhibits a considerable activity in the green house test.[4b]

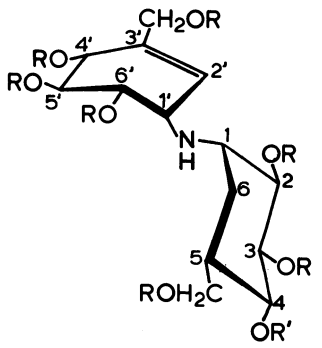

	R	R'
Validamycin A (1)	H	β-D-glucopyranosyl
Validoxylamine A (2)	H	H
Validoxylamine A octa-O-acetate (3)	Ac	Ac

As a part of the study directed toward the total synthesis of **1** and the related substances,[9] we now wish to describe the stereoselective synthesis of two racemic isomers of **2**, that is, "reversed" validoxylamine A (**18a** and **18b**) and 1′-epivalidoxylamine A (**23a** and **23b**), in order to elucidate the structure activity relationships of this type of pseudo-disaccharides. For the synthesis of the validoxylamine A analogs, we have undertaken a coupling reaction of the protected DL-validamine (**11**) and appropriate allyl bromides (**15** and **19**),[10] the precursors of the unsaturated branched-chain cyclitol moiety.

Results and Discussion

Preparation of Protected DL-*Validamine.* Di-*O*-isopropylidene derivative **11** of DL-validamine was prepared from readily available DL-1,2,3-tri-*O*-acetyl-(1,3/2,4,6)-4-bromo-6-acetoxymethyl-1,2,3-cyclohexanetriol (**4**).[11]

Hydrolysis of **4** with 2 M hydrochloric acid yielded the hydroxy compound **5**, which was then treated with 2,2-dimethoxypropane in *N*,*N*-dimethylformamide (DMF) in the presence of a small amount of *p*-toluenesulfonic acid at 60 °C to give the di-*O*-isopropylidene derivative **9** in 77% overall yield. When **9** was allowed to react with sodium azide in dimethyl sulfoxide at 110 °C, the azido compound **10** was produced in 78% yield. In agreement with the inversion of the configuration at C-4, the ^{1}H NMR spectrum of **10** showed a quartet (J= 3 Hz) at δ=4.26, assignable to the C-4 equatorial proton.

Alternatively, **10** was provided, in less satisfactory yield, from DL-1,2,3-tri-*O*-acetyl-(1,3,4/2,6)-6-acetoxymethyl-4-azido-1,2,3-cyclohexanetriol (**6**),[11] which was obtained by treatment of **4** with sodium azide. Thus, *O*-deacetylation of **6** with methanolic sodium methoxide gave the hydroxy compound **7** in 52% yield, together with elimination product, DL-(1,3/2,4)-4-hydroxymethyl-5-cyclohexene-1,2,3-triol (**8**) in 12% yield. Similar isopropylidenation of **7** afforded **10** in 83% yield.

The IR spectrum and the elemental analysis supported the assigned structure of **8**.[12] As far as we are aware, such an elimination of an azido function as hydrazoic acid under basic conditions have not hitherto been encountered in the literature except for the report by Uryu *et al.*[13]

Catalytic hydrogenation of **10** with Raney nickel T-4[14] in ethanol gave the protected validamine **11** in 76% yield, which was further characterized as the *N*-acetyl derivative **12**. As it is well known that introduction of the electron-withdrawing group into an amino group increases the nucleophilicity of the nitrogen atom,[15] the *N*-(*p*-tolysulfonyl) **13** and *N*-(trifluoroacetyl) derivatives

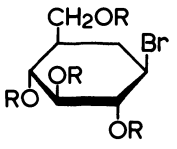

4 R=Ac
5 R=H

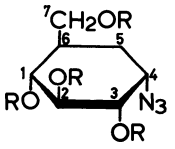

6 R=Ac
7 R=H

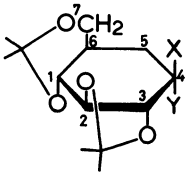

	X	Y
9	Br	H
10	H	N_3
11	H	NH_2
12	H	NHAc
13	H	NHTs
14	H	$NHCOCF_3$

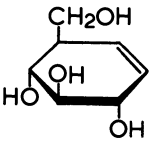

8

11 +

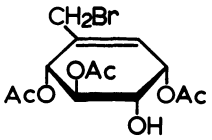

15

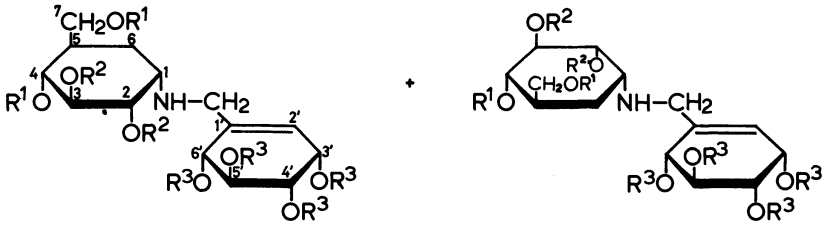

	R^1	R^2	R^3
16 a,b	$>C(CH_3)_2$	$>C(CH_3)_2$	Ac
17 a,b	Ac	Ac	Ac
18 a,b	H	H	H

14 were prepared as the nucleophiles for the allyl bromides.

Synthesis of Racemic Reversed Validoxylamine A. The allyl bromide, DL-1,3,4-tri-*O*-acetyl-(1,2,4/3)-5-bromomethyl-5-cyclohexene-1,2,3,4-tetrol (**15**), was prepared according to the procedure described previously.[10] The coupling reaction of **11** with **15** in chloroform in the presence of *N,N*-diisopropylethylamine under reflux for 3 d, followed by the conventional acetylation, gave the expected two racemic isomers **16a** and **16b** in 80% yield. Isolation of the diastereomeric mixture by use of a silica-gel column eluting with 1 : 3 2-butanone–toluene gave **16a** (19%) and **16b** (27%). In agreement with the postulated structures, the ^{1}H NMR spectra of **16a** and **16b** showed the presence of four acetoxyl and two isopropylidene groups. The splitting pattern of the signals due to the ring protons of the unsaturated cyclitol moiety appeared to be somewhat different each other. The elemental analyses were also consistent with their structures.

Removal of the isopropylidene groups of **16a** and **16b**, followed by acetylation, gave the corresponding octa-*O*-acetyl derivatives **17a** and **17b**, respectively. The ^{1}H NMR spectra of **17a** and **17b** were very similar and the C-2′ olefinic proton of **17b** resonated at higher field (0.07 ppm) than that of **17a**. It is noteworthy that acetylation, even under the forcing conditions, gave no *N*-acetylated compound.

O-Deacetylation of **17a** and **17b** was effected by treatment with methanolic sodium methoxide in methanol to give the racemic "reversed" validoxylamine A (**18a** and **18b**), respectively. They showed the similar chromatographic behaviors (R_f 0.11) on TLC [4 : 1 : 1 1-propanol–acetic acid–water, *cf.* validoxylamine A (**2**):[16] R_f 0.33]. In the present stage, it is not possible to determine which diastereomer is which, for instance, on

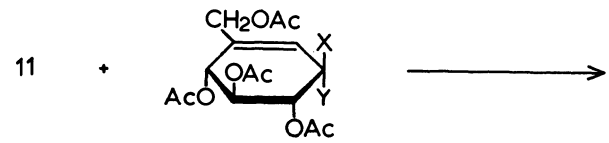

	X	Y
19	H	Br
20	Br	H

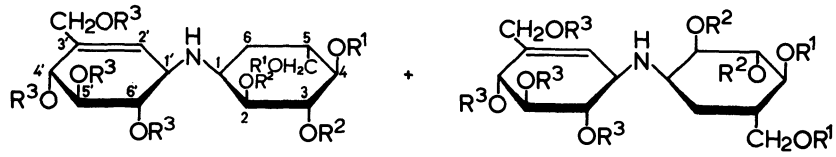

	R^1	R^2	R^3
21 a,b	$>C(CH_3)_2$	$>C(CH_3)_2$	Ac
22 a,b	Ac	Ac	Ac
23 a,b	H	H	H

the basis of ^{1}H NMR spectroscopy.

Synthesis of Racemic 1'-Epivalidoxylamine A. Next the synthesis of the racemic 1'-epivalidoxylamine A (**23a** and **23b**) was carried out by a coupling of **11** with DL-1,2,3-tri-*O*-acetyl-(1,3,6/2)-4-acetoxymethyl-6-bromo-4-cyclohexene-1,2,3-triol (**19**).[10]

When molar equivalent of **11** and **19** were allowed to react in DMF in the presence of *N,N*-diisopropylethylamine at room temperature for 20 d, the pseudo-disaccharide **21a** and **21b** were obtained mainly, after chromatography on silica gel, as a homogeneous mixture in 40% yield, together with a mixture of pentaacetate **24** and **25**[10] (7%), a mixture of tetraacetate **26** and **27**[10] (23%), the *N*-acetyl derivative **12** (18%) of **11**, and recovered **11** (17%). These compounds were identified with authentic samples by comparing the ^{1}H NMR spectra. In the ^{1}H NMR spectrum of the mixture of **21a** and **21b**, the signals for the isopropylidene and acetoxymethyl groups appeared at δ=1.36—1.56 and 1.92—2.20, respectively, and that of the olefinic proton at δ=5.83.

For the synthesis of validoxylamine A, the C-6 epimer **20** of **19** would be a desirable substrate, if the nucleophilic substitution reaction with **11** proceeds *via* an S_N2 mechanism. As **20** had not been available as a pure compound, a 3.5 : 1 mixture of **19** and **20** was used in the coupling reaction with **11**. However, the reaction gave no desired products at all but the same mixture of products as was obtained from **19**. This facts indicate that the reaction pathway might be independent of the configuration of the allylic bromine atom, and the reaction mechanism may be speculated as follows: Due to a low nucleophilicity of **11**, **20** is likely to be converted into the 1,6-cyclic acetoxonium ion, by neighboring group participation of the C-1 acetoxyl group, which is cleaved by moisture or a back-side attack of **11** at C-6. On the other hand, **19** may suffer an S_N2 attack by **11** and/or by a bromide ion generated from the initial reaction of **19** with **11**, giving rise to an equilibrium mixture of **19** and **20**.

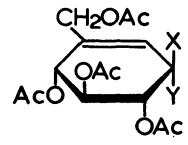

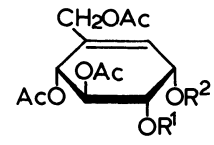

	X	Y
24	H	OAc
25	OAc	H

	R^1	R^2
26	H	Ac
27	Ac	H

The similar reaction was carried out by using **13** or **14** instead of **11**. However, desired secondary amines were not obtained at all, presumably due to the steric hindrance.

When the coupling reaction was conducted at elevated temperature (60 °C), the formation of the side-products became preferable.

Separation of the mixture of **21a** and **21b** was not possible because of their similar chromatographic behaviors. Removal of the isopropylidene groups, followed by the conventional acetylation, gave the diastereomeric mixture (**22a** and **22b**) of 1'-epivalidoxylamine A octaacetate, which were fractionated by a silica-gel column with 1 : 2 ethyl acetate–toluene to give **22a** and **22b** in 23 and 41% isolated yields, respectively. Their elemental analyses and ^{1}H NMR spectral data were consistent with the structures proposed. In both ^{1}H NMR spectra, the signals due to the acetoxymethyl protons of the saturated cyclitol moiety and those of the unsaturated cyclitol moiety could be assignable.

Compounds **22a** and **22b** showed R_f 0.40 and 0.35, respectively on TLC in 1 : 1 ethyl acetate–toluene, while validoxylamine A octaacetate (**3**)[17] R_f 0.32. The ^{1}H NMR spectrum of **3** revealed a doublet (J=5.3 Hz) at δ=5.95, ascribable to the C-2 olefinic proton, whereas those of **22a** and **22b** have a broad singlet at δ=5.70 and 5.65, respectively, indicative of the pseudoequatorial orientation of the imino group.

It is interesting to note that, in the ^{1}H NMR spectrum of **22b**, the chemical shifts and the splitting pattern of the signals due to the ring protons of the saturated cyclitol part as well as the acetoxylmethyl protons resemble those of **3**, suggesting that **22b** adopts more similar conformation to that of **3** in chloroform than does **22a**. Similar to the case of the reversed validoxylamine A, the *N*-acetyl derivatives of 1'-epivalidoxylamine A could not be prepared.

O-Deacetylation of **22a** and **22b** with sodium methoxide in methanol afforded the racemic 1'-epivalidoxylamine A (**23a**) and (**23b**), respectively, which showed almost similar mobilities (*Rf* 0.28) on TLC in 4 : 1 : 1 1-propanol–acetic acid–water [*cf.* validoxylamine A (**2**): R_f 0.31].

The present results indicate that resolution of the coupling products should be possible by using optically active validamine[18] instead of the racemate. Biological and biochemical studies on the isomers of validoxylamine A obtained here are on the way.

Experimental

Melting points were determined on a Büchi 510 capillary melting point apparatus and are uncorrected. ^{1}H NMR spectra were recorded on a Varian EM-390 (90 MHz) spectrometer in chloroform-*d*. Chemical shifts were reported as ppm relative to tetramethylsilane as an internal standard. TLC was performed on precoated silica gel 60 F-254 plates (Merck, Darmstadt; 0.25 mm thickness), and the spots were visualized by concd sulfuric acid spray (heating at 120 °C) or ninhydrin spray. Conventional chromatography was carried out with Wakogel C-300 (silica gel, Wako Pure Chemical Industries, Ltd.). Solutions were dried over anhydrous sodium sulfate and concentrated below 50 °C under reduced pressure. Catalytic hydrogenation was carried out in a Parr shaker type apparatus in the initial hydrogen pressure of 3.5 kg/cm^2 at room temperature.

DL-*(1,3/2,4,6)-4-Bromo-6-hydroxymethyl-1,2,3-cyclohexanetriol (5).* To a solution of DL-1,2,3-tri-*O*-acetyl-(1,3/2,4,6)-6-acetoxymethyl-4-bromo-1,2,3-cyclohexanetriol (**4**)[11] (2.84 g) in ethanol (18 ml) was added 2 M hydrochloric acid (17 ml), and the mixture was heated for 3 h at 80 °C. The mixture was evaporated and then coevaporated with ethanol several times to give a crystalline residue, which was recrystallized from ethanol giving **5** (1.5 g, 90%): mp 155.5—156 °C.

Found: C, 34.97; H, 5.26; Br, 33.28%. Calcd for $C_7H_{13}BrO_4$: C, 35.09; H, 5.43; Br, 33.15%.

DL-*1,7:2,3-Di-O-isopropylidene-(1,3/2,4,6)-4-bromo-6-hydroxymethyl-1,2,3-cyclohexanetriol (9).* A mixture of **5** (1.40 g), 2,2-dimethoxypropane (DMP) (21 ml), *p*-toluenesulfonic acid monohydrate (TsOH) (35 mg), and *N,N*-dimethylformamide (DMF) (30 ml) was heated for 3 h at 60 °C. The mixture was then neutralized with Amberlite IRA-400 (OH^-) and concentrated to dryness. Recrystallization of the crude product from ethanol gave **9** (1.56 g, 86%) as feathers: mp 148—149 °C; ^{1}H NMR (60 MHz)[19] δ=1.45 (6H, s) and 1.68 (6H, s) (isopropylidene), 1.71—2.31 (3H, m, H-5, H-5', and H-6), and 3.30—4.20 (6H, m, H-1, H-2, H-3, H-4, and C$\underline{H}_2$O).

Found: C, 48.59; H, 6.51; Br, 24.79%. Calcd for $C_{13}H_{21}BrO_4$: C, 48.61; H, 6.59; Br, 24.88%.

DL-*(1,3,4/2,6)-4-Azido-6-hydroxymethyl-1,2,3-cyclohexanetriol(7) and* DL-*(1,3/2,4)-4-Hydroxymethyl-5-cyclohexene-1,2,3-triol (8).* To a solution of DL-1,2,3-tri-*O*-acetyl-(1,3,4/2,6)-4-azido-6-acetoxymethyl-1,2,3-cyclohexanetriol (**6**)[11] (1.36 g) in methanol (80 ml) was added 1 M methanolic sodium methoxide (2.0 ml), and the mixture was allowed to stand at room temperature overnight. After treatment with Amberlite IR-120 (H^+) resin, the mixture was concentrated to a syrup, which was shown by TLC to contain two components (R_f 0.42 and 0.33, 3 : 1 chloroform–methanol). The products were fractionated on a silica-gel column (30 g) with 3 : 1 chloroform–methanol as an eluent. The first fraction gave **7** (378 mg, 52%) as feathers: mp 112.5—113 °C.

Found: C, 41.13; H, 6.33; N, 20.41%. Calcd for $C_7H_{13}N_3O_4$: C, 41.38; H, 6.45; N, 20.68%.

The second fraction gave **8** (70 mg, 12%): mp 136—138 °C; ^{1}H NMR (90 MHz)[20] δ=2.13—2.47 (1H, m, H-4), 3.39—4.15 (5H, H-1, H-2, H-3, and C$\underline{H}_2$OH), and 5.60 (2H, s, H-5 and H-6), identical with the compound obtained by the different route.[12]

DL-*1,7 : 2,3-Di-O-isopropylidene-(1,3,4/2,6)-4-azido-6-hydroxymethyl-1,2,3-cyclohexanetriol (10).* *a)*: A mixture of **7** (284 mg), DMP (5 ml), TsOH (8 mg), and DMF (9 ml) was heated for 3 h at 60 °C. After neutralization with Amberlite IRA-400 (OH^-) resin, the mixture was concentrated, and the residue was crystallized from ethanol giving **10** (329 mg, 83%) as needles: mp 109—110.5 °C; ^{1}H NMR (90 MHz) δ=1.45 (6H, s) and 1.50 (6H, s) (isopropylidene), 3.51 (1H, dd, J=3 and 9 Hz, H-3), 3.60—3.87 (3H, m, H-1 and C$\underline{H}_2$O), 3.98 (1H, t, J=9 Hz, H-2), and 4.26 (1H, q, J=3 Hz, H-4).

Found: C, 55.33; H, 7.46; N, 14.71%. Calcd for $C_{13}H_{21}N_3O_4$: C, 55.11; H, 7.47; N, 14.83%.

b): A mixture of **9** (1.40 g), sodium azide (1.47 g, 4 molar equivalent), and dimethyl sulfoxide (30 ml) was heated at 110 °C for 15 h. The mixture was then diluted with ethyl acetate and washed with water thoroughly. The organic layer was dried and concentrated, and the residue was recrystallized from ethanol giving **10** (960 mg, 78%), identical with the compound obtained from **9**.

DL-*1,7:2,3-Di-O-isopropylidene-(1,3,4/2,6)-4-amino-6-hydroxymethyl-1,2,3-cyclohexanetriol*[DL-*Di-O-(isopropylidene)validamine*] *(11).* A solution of **10** (946 mg) in ethanol (30 ml) was hydrogenated in the presence of Raney nickel T-4[14] (one spoonful) at room temperature overnight. The catalyst was removed by filtration and the filtrate was concentrated to give a crystalline residue, which was recrystallized from ethanol giving **11** (653 mg, 76%) as needles: mp 153—154 °C; ^{1}H NMR (90 MHz) δ=1.43 (9H, s) and 1.50 (3H, s) (isopropylidene), 3.42 (1H, dd, J=3 and 9 Hz, H-3), 3.53—3.81 (4H, m, H-1, H-4, and C$\underline{H}_2$O), and 3.97 (1H, t, J=9 Hz, H-2).

Found: C, 60.59; H, 8.72; N, 5.65%. Calcd for $C_{13}H_{23}NO_4$: C, 60.67; H, 9.00; N, 5.44%.

DL-*1,7: 2,3-Di-O-isopropylidene-(1,3,4/2,6)-4-acetamido-1,2,3-cyclohexanetriol (12).* Compound **11** (30 mg) was treated with acetic anhydride (1 ml) in pyridine (1 ml) at room temperature overnight. The mixture was concentrated to a syrup, which was purified by passage through a short column of alumina with chloroform. The eluate was concentrated and the residue was crystallized from ethanol giving **12** (29 mg, 84%) as prisms: mp 231—232 °C; ^{1}H NMR (90 MHz) δ=1.43 (3H, s), 1.47 (6H, s), and 1.51 (3H, s) (isopropylidene), 2.00 (3H, s, NAc), 3.37—3.83 (5H, m, H-1, H-2, H-3, and C$\underline{H}_2$O), 4.33—4.57 (1H, m, H-4), and 6.04 (1H, m, N$\underline{H}$).

Found: C, 60.30; H, 8.28; N, 4.68%. Calcd for $C_{15}H_{25}NO_5$: C, 60.17; H, 8.43; N, 4.68%.

DL-*1,7: 2,3-Di-O-isopropylidene-(1,3,4/2,6)-6-hydroxymethyl-4-(p-toluenesulfonamido)-1,2,3-cyclohexanetriol (13).* To a solution of **11** (100 mg) in pyridine (3 ml) was added *p*-toluenesulfonyl chloride (173 mg), and the mixture was

stirred at room temperature for 3 h. The reaction mixture was poured into ice–water (10 ml) and extracted with chloroform. The extracts were washed successively with saturated hydrogencarbonate solution and water, and concentrated. The residue was recrystallized from ethanol giving **13** (140 mg, 87%): mp 190—191 °C; ^{1}H NMR (90 MHz) δ=1.39 (6H, s), 1.41 (3H, s), and 1.46 (3H, s) (isopropylidene), 2.42 (3H, s, tosyl C$\underline{H}_3$), 3.30—3.83 (6H, m, H-1, H-2, H-3, H-4, and C$\underline{H}_2$O), and 7.27 (2H, d, J=12 Hz) and 7.54 (2H, d, J=12 Hz) (phenyl).

Found: C, 58.10; H, 6.99; N, 3.17; S, 7.62%. Calcd for $C_{20}H_{29}NO_6S$: C, 58.36; H, 7.12; N, 3.40; S, 7.79%.

DL-*1,7 : 2,3-Di-O-isopropylidene-(1,3,4/2,6)-6-hydroxymethyl-4-trifluoroacetamido-1,2,3-cyclohexanetriol (**14**).* To a stirred solution of **11** (100 mg) in pyridine (3 ml) was added dropwise trifluoroacetic anhydride (0.25 ml) under ice cooling, and the mixture was stirred at room temperature overnight. The mixture was diluted with chloroform (10 ml) and washed with water. The solution was dried and concentrated to a syrup, which was solidified upon standing in a desiccator giving **14** (129 mg, 94%): ^{1}H NMR (90 MHz) δ=1.47 (9H, s) and 1.53 (3H, s) (isopropylidene), 3.47—3.90 (6H, m, H-1, H-2, H-3, and C$\underline{H}_2$O), 4.30—4.51 (1H, m, H-4), and 6.17—6.40 (1H, m, N$\underline{H}$).

Found: C, 51.20; H, 6.39; N, 3.96%. Calcd for $C_{15}H_{22}F_3NO_5$: C, 50.98; H, 6.29; N, 3.96%.

DL-N-[*(3,4,6/5)-3,4,5,6-Tetraacetoxy-1-cyclohexenylmethyl*]-*2,3:4,7-di-O-isopropylidene-(1,2,4/3,5)-2,3,4-trihydroxy-5-(hydroxymethyl)cyclohexylamine (**16a** and **16b**).* A mixture of **11** (73 mg, 0.28 mmol), DL-1,3,4-tri-*O*-acetyl-(1,2,4/3)-5-bromomethyl-5-cyclohexene-1,2,3,4-tetrol (**15**)[10] (103 mg, 0.28 mmol)- and *N,N*-diisopropylethylamine (0.10 ml, 0.28 mmol) in chloroform (4 ml) was refluxed for 3 d. The mixture was evaporated and the residue was acetylated in the usual way. The product was shown to consist of two components (TLC: R_f 0.29 and 0.23, 1 : 3 2-butanone–toluene). It was fractionated on a silica-gel column (10 g) with 1 : 3 2-butanone–toluene as an eluent. The first fraction gave, after crystallization from ethanol, **16a** (32 mg, 19%): mp 176—177 °C; ^{1}H NMR (90 MHz) δ=1.43 (9H, s) and 1.50 (3H, s) (isopropylidene), 1.99 (3H, s), 2.02 (3H, s), 2.07 (3H, s), and 2.10 (3H, s) (OAc), 3.16—3.35 (3H, m, H-1 and C=CC$\underline{H}_2$), 3.47 (1H, dd, J=3.3 and 9 Hz, H-2), 3.55—3.83 (3H, m, H-4 and CC$\underline{H}_2$O), 3.99 (1H, t, J=9 Hz, H-3), 5.08 (1H, ddd, J=1.8, 3.8, and 9 Hz, H-4′), 5.36—5.71 (3H, m, H-3′, H-5′, and H-6′), and 5.96 (1H, br d, J=*ca.* 7 Hz, H-2′).

Found: C, 57.68; H, 7.00; N, 2.28%. Calcd for $C_{28}H_{41}NO_{12}$: C, 57.62; H, 7.08; N, 2.40%.

The second fraction gave **16b** (45 mg, 27%) as a syrup: ^{1}H NMR (90 MHz) δ=1.46 (9H, s) and 1.49 (3H, s) (isopropylidene), 2.00 (3H, s), 2.02 (3H, s), 2.07 (3H, s), and 2.10 (3H, s) (OAc), 3.12—3.32 (3H, m, H-1 and C=CC$\underline{H}_2$), 3.47 (1H, dd, J=3.3 and 9 Hz, H-2), 3.56—3.82 (3H, m, H-4 and CC$\underline{H}_2$O), 3.94 (1H, t, J=9 Hz, H-3), 5.09 (1H, dd, J=3.8 and 10 Hz, H-4′), 5.51 (1H, dd, J=6.8 and 10 Hz, H-5′), 5.47—5.65 (1H, m, H-3′), 5.74 (1H, br d, J=6.8 Hz, H-6′), and 5.85 (1H, br d, J=6 Hz, H-2′).

Found: C, 57.65; H, 6.95; N, 2.26%. Calcd for $C_{28}H_{41}NO_{12}$: C, 57.62; H, 7.08; N, 2.40%.

The fraction containing unresolved mixture of **16a** and **16b** weighed 58 mg (34%).

DL-N-[*(3,4,6/5)-3,4,5,6-Tetrahydroxy-1-cyclohexenylmethyl*]-*(1,2,4/3,5)-2,3,4-triacetoxy-5-(acetoxymethyl)cyclohexylamine (**17a** and **17b**).* Compound **16a** (21 mg) was treated with 70% aqueous acetic acid (2 ml) at room temperature overnight. The mixture was concentrated to a syrup, which was acetylated in the usual way. The product was purified by a silica-gel column with 1 : 3 2-butanone–toluene as an eluent, giving **17a** (16 mg, 65%) as a syrup: ^{1}H NMR (90 MHz) δ=1.93 (3H, s), 1.97 (6H, s), 1.98 (3H, s), 2.00 (3H, s), 2.05 (6H, s), and 2.07 (3H, s) (OAc), 2.08—3.18 (3H, m, H-1 and C=CC$\underline{H}_2$), 3.79 (1H, br dd, J=3.8 and 11 Hz) and 4.00 (1H, br dd, J=4 and 11 Hz) (CC$\underline{H}_2$OAc), 4.75—5.12 (3H, m, H-2, H-3, and H-4), 5.19—5.63 (4H, m, H-3′, H-4′, H-5′, and H-6′), and 5.81 (1H, br d, J=*ca.* 6 Hz, H-2′).

Found: C, 53.77; H, 6.03; N, 1.94%. Calcd for $C_{30}H_{41}NO_{16}$: C, 53.65; H, 6.15; N, 2.09%.

Similarly, *O*-deisopropylidenation of **16b** followed by acetylation gave **17b** (37 mg, 71%) as a syrup: ^{1}H NMR (90 MHz) δ=1.94 (3H, s), 1.97 (6H, s), 2.00 (6H, s), 2.04 (6H, s), and 2.06 (3H, s) (OAc), 2.85—3.32 (3H, m, H-1 and C=CC$\underline{H}_2$), 3.78 (1H, br dd, J=3.2 and 12 Hz) and 4.02 (1H, br dd, J=4.5 and 12 Hz) (CC$\underline{H}_2$OAc), 4.69—5.07 (3H, m, H-2, H-3, and H-4), 5.16—5.54 (4H, m, H-3′, H-4′, H-5, and H-6′), and 5.74 (1H, br d, J=5 Hz, H-2′).

Found: C, 53.64; H, 6.00; N, 1.97%. Calcd for $C_{30}H_{41}NO_{16}$: C, 53.65; H, 6.15; N, 2.09%.

DL-N-[*(3,4,6/5)-3,4,5,6-Tetrahydroxy-1-cyclohexenylmethyl*]-*(1,2,4/3,5)-2,3,4-trihydroxy-5-(hydroxymethyl)cyclohexylamine (Racemic Reversed Validoxylamine A) (**18a** and **18b**).* De-*O*-acetylation of **17a** and **17b** was carried out by treatment with 1 M methanolic sodium methoxide in methanol at room temperature overnight giving **18a** and **18b**, respectively, in quantitative yields. Both **18a** and **18b** showed the same R_f value (0.11) on TLC (4 : 1 : 1 1-propanol–acetic acid–water, *cf.* validoxylamine A,[16] R_f 0.33).

DL-N-[*(1,5/4,6)-4,5,6-Triacetoxy-3-acetoxymethyl-2-cyclohexenyl*]-*2,3: 4,7-di-O-isopropylidene-(1,2,4/3,5)-2,3,4-trihydroxy-5-(hydroxymethyl)cyclohexylamine (**21a** and **21b**).* A mixture of **11** (368 mg, 1.43 mmol), DL-1,2,3-tri-*O*-acetyl-(1,3,6/2)-4-acetoxymethyl-6-bromo-4-cyclohexene-1,2,3-triol (**19**)[10] (582 mg, 1.43 mmol), and *N,N*-diisopropylethylamine (0.80 ml, 4.58 mmol) in DMF (15 ml) was stirred at room temperature for 20 d. At this time, TLC indicated the formation of many components (R_f 0.50, 0.41, 0.30, 0.27, and 0.16, 1 : 8 ethanol–toluene). The mixture was concentrated to a syrup, which was fractionated on a silica-gel column (50 g) with 1 : 5 2-butanone–toluene as an eluent. The first fraction (R_f 0.50) gave a syrupy mixture (39 mg, 7%) of DL-1,2,3,4-tetra-*O*-acetyl-(1,2,4/3)- (**24**) and -(1,3/2,4)-5-acetoxymethyl-5-cyclohexene-1,2,3,4-tetrol (**25**), identical with authentic samples.[10]

The second fraction (R_f 0.41) gave a mixture (334 mg, 40%) of **21a** and **21b** as a glass: ^{1}H NMR (90 MHz) δ=1.36—1.56 (12H, m, isopropylidene), 1.92—2.20 (12H, m, OAc), and 5.83 (1H, br s, H-2′).

Found: C, 57.39; H, 6.92; N, 2.35%. Calcd for $C_{28}H_{41}NO_{12}$: C, 57.62; H, 7.08; N, 2.40%.

The third fraction (R_f 0.30) gave a mixture (113 mg, 23%) of DL-1,3,4-tri-*O*-acetyl-(1,2,4/3)-5-acetoxymethyl-5-cyclohexene-1,2,3,4-tetrol (**26**) and DL-2,3,4-tri-*O*-acetyl-(1,2,4/3)-5-acetoxymethyl-5-cyclohexene-1,2,3,4-tetrol (**27**), identical with authentic samples.[10]

The fourth fraction (R_f 0.27) gave **12** (77 mg, 18%): mp 229—230.5 °C, identical with the compound prepared above.

The fifth fraction gave recovered **11** (63 mg, 17%).

DL-N-[*(1,5/4,6)-4,5,6-Triacetoxy-3-acetoxymethyl-2-cyclohexenyl*]-*(1,2,4/3,5)-2,3,4-triacetoxy-5-(acetoxymethyl)cyclohexylamine (**22a** and **22b**).* The syrupy mixture of **21a** and **21b** (189 mg) was treated with a small amount of *p*-toluenesulfonic acid in ethanol (5 ml) at room temperature for 1 d, and then the mixture was neutralized with Amberlite IRA-400 (OH^-). The mixture was concentrated and the residue was acetylated in the usual way. The product was shown by TLC to consist of two components (R_f 0.40 and 0.35, 1 : 1 ethyl acetate–toluene).

The mixture was fractionated on a silica-gel column (10 g) with 1 : 2 acetone–toluene as eluent. The first fraction (R_f 0.40) gave **22a** (89 mg, 41%) as a syrup: ^{1}H NMR (90 MHz) δ=1.89—2.06 (24H, m, OAc), 3.30—3.52 (2H, m, H-1 and H-1′), 3.83 (1H, dd, J=4.2 and 12 Hz) and 4.03 (1H, dd, J=4.7 and 12 Hz) (CC$\underline{H}_2$OAc), 4.24 (1H, d, J=13 Hz) and 4.60 (1H, br d, J=13 Hz) (C=C$\underline{H}_2$OAc), 4.67—5.10 (3H, m, H-2, H-3, and H-4), 5.11—5.49 (2H, m, H-5′ and H-6′), 5.53—5.69 (1H, m, H-4′), and 5.70 (1H, br s, H-2′).

Found: C, 53.74; H, 6.09; N, 2.06%. Calcd for $C_{30}H_{41}NO_{16}$: C, 53.65; H, 6.15; N, 2.09%.

The fraction (R_f 0.35) gave **22b** (50 mg, 23%) as a syrup: ^{1}H NMR (90 MHz) δ=1.90—2.07 (24H, m, OAc), 3.18—3.41 (2H, m, H-1 and H-1′), 3.79 (1H, dd, J=3.2 and 12 Hz) and 4.01 (1H, dd, J=4.5 and 12 Hz) (CC$\underline{H}_2$OAc), 4.26 (1H, d, J=14 Hz) and 4.52 (1H, br d, J=14 Hz) (C=CC$\underline{H}_2$OAc), 4.70—5.15 (3H, m, H-2, H-3, and H-4), 5.15—5.39 (2H, m, H-5′ and H-6′), 5.58 (1H, m, H-4′), and 5.65 (1H, br s, H-2′).

Found: C, 53.78; H, 6.07; N, 2.17%. Calcd for $C_{30}H_{41}NO_{16}$: C, 53.65; H, 6.15; N, 2.09%.

The fraction containing unresolved mixture of **22a** and **22b** weighed 50 mg (23%).

DL-N-[*(1,5/4,6)-3-Hydroxymethyl-4,5,6-trihydroxy-2-cyclohexenyl*]-*(1,2,4/3,5)-2,3,4-trihydroxy-5-(hydroxymethyl)cyclohexylamine (Racemic 1′-Epivalidoxylamine A) (**23a** and **23b**).* O-Deacetylation of **22a** and **22b** in the usual way gave **23a** and **23b**, respectively, in quantitative yields. Both showed the same R_f value (0.28) on TLC (4 : 1 : 1 1-propanol–acetic acid–water, *cf.* validoxylamine A:[16] R_f 0.31).

This work was supported in part by a Grant-in-Aid for Scientific Research No. 56550617 from the Ministry of Education, Science and Culture. We wish to thank Mr. Saburo Nakada for elemental analyses and Dr. Satoshi Horii of Takeda Chemical Industries, Ltd. (Osaka) for a gift of validoxylamine A. We also thank Messrs. Yasuo Abe, Masayuki Oya, and Yoshikazu Iwasawa for their assistance in some preparative work.

References

1) A preliminary account of portions of this articles was previously presented: S. Ogawa, T. Toyokuni, and T. Suami, *Chem. Lett.*, **1981**, 947. The nomenclature used in this paper is based on the IUPAC-IUB Tentative Cyclitol Nomenclature Rule [*J. Biol. Chem.*, **243**, 5809 (1968)]. For convenience, all the formulas depict one of the respective enatiomers.

2) T. Iwasa, H. Yamamoto, and M. Shibata, *J. Antibiot.*, **23**, 595 (1970).

3) K. L. Rinehart, Jr., and L. S. Shield, "Aminocyclitol Antibiotics: An Introduction," ed by K. L. Rinehart, Jr., and T. Suami, American Chemical Society, Washington, D. C. (1980), pp. 1—11.

4) a) T. Iwasa, Y. Kameda, M. Asai, S. Horii, and K. Mizuno, *J. Antibiot.*, **24**, 119 (1971); b) S. Horii, Y. Kameda, and K. Kawahara, *ibid.*, **25**, 48 (1972).

5) A. Horii, T. Iwasa, and Y. Kameda, *J. Antibiot.*, **24**, 57 (1971).

6) S. Ogawa, T. Ogawa, N. Chida, T. Toyokuni, and T. Suami, *Chem. Lett.*, **1982**, 749 and the references cited therein.

7) O. Wakae and K. Matsuura, *Rev. Plant Protec. Res.*, **8**, 81 (1975).

8) S. Ogawa, T. Toyokuni, Y. Iwasawa, Y. Abe. and T. Suami, *Chem. Lett.*, **1982**, 279 and the references cited therein.

9) For paper VIII of this series, see S. Ogawa, H. Ito, and T. Suami, *Bull. Chem. Soc. Jpn.*, **56**, 2326 (1983).

10) T. Toyokuni, Y. Abe, S. Ogawa, and T. Suami, *Bull. Chem. Soc. Jpn.*, **56**, 505 (1983).

11) S. Ogawa, K. Nakamoto, M. Takahara, Y. Tanno, N. Chida, and T. Suami, *Bull. Chem. Soc. Jpn.*, **52**, 1174 (1979).

12) S. Ogawa, N. Chida, and T. Suami, *J. Org. Chem.*, **48**, 1203 (1983).

13) T. Uryu, K.Hatanaka, K. Matsuura, and H. Kuzuhara, 5th Carbohydrate (Toshitsu) Symposium, Nagoya, July 1982, Abstr. No. 35.

14) S. Nishimura, *Bull. Chem. Soc. Jpn.*, **32**, 61 (1959).

15) A. Guggisherg, P. van den Broek, M. Hesse, H. Schmid, F. Schneider, and K. Bernauer, *Helv. Chim. Acta*, **59**, 3013 (1976); J. E. Nordlander, D. B. Catalane, T. H. Eberlein, L. V. Farks, R. S. Howe, R. M. Stevens, and N. A. Tripopulas, *Tetrahedron Lett.*, **1978**, 4987.

16) Provided by Dr. Satoshi Horii of Takeda Chemical Industries Ltd. Osaka.

17) Prepared from **2**[16] by treatment with acetic anhydride in pyridine.

18) S. Ogawa, Y. Shibata, N. Chida, and T. Suami, The ACS/CSJ Chemical Congress: 1979, Honolulu, Hawaii, April 1979, Abstr. CARB 89: *Bull. Chem. Soc. Jpn.*, **56**, 494 (1983).

19) Taken on a Varian EM 360A (60 MHz).

20) Taken in deuterated methan-d_3-ol.

Studies on the β-Turn of Peptides. V.[1] Turn Preference of Peptide Sequences Analyzed by Conformational Energy Calculation on Dipeptide Models and by CD Spectra of Chromophoric Derivatives

Masao KAWAI,*,† Kazuki SATO, Rika SUGAWARA, and Ukon NAGAI
Mitsubishi-Kasei Institute of Life Sciences, Minamiooya 11, Machida, Tokyo 194
†*Department of Synthetic Chemistry, Nagoya Institute of Technology, Gokiso-cho, Showa-ku, Nagoya 466*
(Received April 8, 1983)

Empirical conformational energy calculations were performed on Ac–L-Pro–D-Ala–$NHCH_3$ and Ac–D-Ala–L-Pro–$NHCH_3$. In order to study the turn tendency of the dipeptide sequences turn probabilities and average interterminal distances were calculated. Much larger turn preference of D-Ala containing sequences was indicated compared with the corresponding L-Ala containing sequences. The turn tendency of the dipeptide sequences were shown to be in the order: L-Pro–D-Ala>D-Ala–L-Pro>L-Pro–L-Ala>L-Ala–L-Pro. This order coincides with the order of the magnitude of the Cotton effects in the CD spectra of the chromophoric derivatives having 2,4-dinitrophenylglycyl and glycine-*p*-nitroanilide at the *N*- and the *C*-termini, respectively, of the corresponding dipeptide sequences. This agreement supports the validity of the chiroptical method to study the turn tendency of the peptide sequences using chromophoric derivatives reported earlier.

CD spectra of *N*-(2,4-dinitrophenyl)tetrapeptide *p*-nitroanilides (Dnp–tetrapeptide–pNA)[2] exhibit characteristic Cotton effects when they take β-turn conformation. Exciton coupling of the electric transition moments of the two chromophores were assumed to explain the spectra and the mgnitude of the Cotton effects around 310 and 350 nm were shown to reflect the β-turn preference of the derivatives.[3] A question was raised, however, whether such chiroptical method using chromophoric derivatives as mentioned above reveals well the conformational characteristics of the original peptide sequences lacking those chromophoric groups. For the purpose of answering the question we have attempted empirical conformational energy calculations on model peptides having acetyl and *N*-methylamide groups at the *N*- and the *C*-termini, respectively. In this paper the conformational energy studies on model dipeptides are described and the results are compared with the CD spectral data of tetrapeptide derivatives having Dnp–Gly and Gly–pNA moieties at the *N*- and the *C*-termini, respectively.

Results and Discussion

The CD spectra of Dnp–Gly–X–Y–Gly–pNA are shown in Fig. 1 where X–Y represents a dipeptide sequence consisting of L- or D-Ala and L-Pro residues. Marked difference in the magnitude of the Cotton effects observed for this series of tetrapeptide derivatives can be attributed to the divergent β-turn tendency of the central dipeptide sequences X–Y. Theoretical study has been attempted to elucidate the turn preference of the X–Y sequences by means of empirical conformational energy calculation on the model dipeptides Ac–X–Y–$NHCH_3$. Computations were carried out using the program ECEPP[4] with the Powell's minimization subroutine.[5] The conformational properties of Ac–L-Pro–L-Ala–$NHCH_3$ and Ac–L-Ala–L-Pro–$NHCH_3$ had been already elucidated by Zimmerman and Scheraga[6] by use of ECEPP. Essentially same procedure as reported by them was followed for the calculation of Ac–L-Pro–D-Ala–$NHCH_3$ and Ac–D-Ala–L-Pro–$NHCH_3$ except that

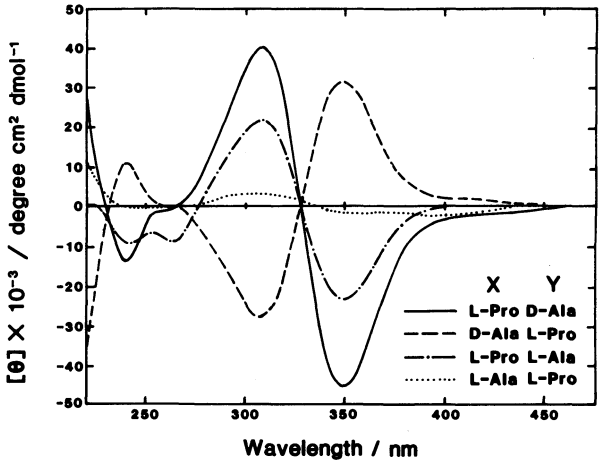

Fig. 1. CD spectra of Dnp–Gly–X–Y–Gly–pNA in methanol.

the contribution of librational entropy is not included in our calculation.

For the calculation of Ac–L-Pro–D-Ala–$NHCH_3$ all combination of low energy conformations of Ac–L-Pro–$NHCH_3$[7] (C −75°, −79°; F −75°, 159°; A −75°, 48°; A −75°, −23°)[8] and of Ac–D-Ala–$NHCH_3$[7] (C* 84°, −79°; E* 154°; −153°; D* 150°, −72°; F* 75°, −145°; A* 74°, 45°; G* 158°, 85°; A −54°, −57°)[8] were used as the starting conformations for energy minimization. All ω values were fixed to 180°. In Table 1 are listed 19 low-energy conformations obtained through energy minimization of Ac–L-Pro–D-Ala–$NHCH_3$. The interatomic distance *R*, defined as the distance between the methyl carbons of the acetyl and the *N*-methylamide groups, and the O(Ac)···N($NHCH_3$) distance *h* are given along with the relative conformational energy ΔE and the normalized statistical weight *v* of each conformation. For each conformation with the *R* value less than 7.0 Å the bend type is given according to the classification by Zimmerman and Scheraga.[6] In the case of energy minimization of Ac–D-Ala–L-Pro–$NHCH_3$ some starting conformations having *cis* peptide linkage which were taken from the minimum energy conforma-

TABLE 1. MINIMUM-ENERGY CONFORMATIONS[a] OF Ac-L-Pro-D-Ala-$NHCH_3$

Conformation letter code[b]	ΔE[c]/kcal mol^{-1}	v[b]	h[d]/Å	R[d]/Å	Bend[b] type	Dihedral angles[e]/°			
						ϕ_{pro}	$\phi_{D\text{-}Ala}$	$\psi_{D\text{-}Ala}$	$\chi_{D\text{-}Ala}$
C A*	0.00	0.278	3.59	4.81	II	82	78	42	59
C C*	0.14	0.219	4.87	5.93	V	78	85	−77	59
C D*	0.30	0.168	3.39	5.33	V	80	153	−47	59
C F*	0.79	0.074	5.72	7.19		77	73	−142	58
F C*	0.95	0.057	4.29	6.37	V	159	85	−76	59
C E*	1.10	0.044	5.11	7.13		80	154	−149	61
C G*	1.33	0.030	3.80	6.34	IV	76	155	58	66
A C*	1.43	0.025	6.32	8.83		−47	84	−80	59
A E*	1.51	0.022	7.23	8.65		−47	154	−155	60
F E*	1.55	0.021	6.47	9.60		161	155	−152	61
F D*	1.69	0.016	4.97	8.22		154	149	−68	61
A F*	1.97	0.010	6.75	9.21		−46	76	−138	58
A F*	2.02	0.009	6.71	9.00		−27	77	−139	58
A D*	2.10	0.008	6.80	8.15		−47	150	−68	61
C A	2.38	0.005	5.43	8.67		78	−54	−58	55
A A*	2.56	0.004	6.50	8.47		−45	75	44	59
A A*	2.56	0.004	6.24	7.94		−25	75	43	59
A G*	2.69	0.003	6.22	5.79	IV	−23	159	58	67
A G*	2.75	0.003	5.91	6.65	IV	−44	159	58	66

a) All minimum-energy conformations with $\Delta E < 3$ kcal mol^{-1} are listed. b) See Ref. 6. c) Relative energy taking the energy value ($E = -14.58$ kcal mol^{-1}) of the lowest-energy conformation as 0.0 kcal mol^{-1}. d) See text. e) Only variable dihedral angles are listed; all others are 180°, except $\phi_{Pro} = -75°$.

TABLE 2. MINIMUM-ENERGY CONFORMATIONS[a] of Ac-D-Ala-L-Pro-$NHCH_3$

Conformation letter code[b]	ΔE[c] kcal mol^{-1}	v[b]	h[d]/Å	R[d]/Å	Bend type[b]	Dihedral angles[e]/°				
						$\phi_{D\text{-}Ala}$	$\psi_{D\text{-}Ala}$	$\omega_{D\text{-}Ala}$	$\chi_{D\text{-}Ala}$	ψ_{Pro}
D*C	0.00	0.243	6.76	6.73	IV	151	−72	173	61	78
F*C	0.13	0.198	3.95	5.63	II′	70	−143	175	60	76
E*C	0.31	0.144	6.67	7.02		153	−146	179	64	79
D*F	0.41	0.122	7.78	7.83		152	−71	172	61	164
F*A	0.68	0.078	3.18	5.36	II′	71	−140	175	59	−18
A C	0.68	0.078	3.24	4.88	I	−53	−69	169	57	75
E*F	0.99	0.046	7.95	8.66		154	−147	180	65	161
D*A	1.22	0.032	5.95	5.59	III	150	−72	172	61	−46
E*A	1.48	0.020	6.33	7.32		153	−147	−179	64	−48
D*F	1.69	0.014	3.88	6.62	VI	147	−78	−4	62	160
D*F	1.69	0.014	5.79	7.61		80	−145	180	60	158
A F	2.36	0.005	4.69	6.17	I	−53	−69	169	56	151
A A	2.53	0.003	3.47	4.06	III	−52	−68	171	57	−39
D*A	2.70	0.003	5.46	7.88		153	−76	−7	62	−46

a) All minimum-energy conformations with $\Delta E < 3$ kcal mol^{-1} are listed. b) See Ref. 6. c) Relative energy taking the energy value (-13.12 kcal mol^{-1}) of the lowest-energy conformation as 0.0 kcal mol^{-1}. d) See text. e) Only valuable dihedral angles are listed; all others are 180°, except $\phi_{Pro} = -75°$.

tions with *cis* Ac-Pro bond of Ac-L-Pro-$NHCH_3$[7] (A −75°, −48°; F −75°, 162°)[8] were also included. The results of energy minimization are given in Table 2.

In order to evaluate the turn tendency of the dipeptide sequences the bend probability P_b and the averaged interterminal distance $\langle R \rangle$ were calculated for each model peptide. As defined by Zimmerman and Scheraga[6] the quantity P_b is the probability of occurrence (or mole fraction) of bend conformations ($R < 7$ Å) in a particular dipeptide and the quantity $\langle R \rangle$ is the statistical average of the interterminal distance R.[6] In Table 3 are shown the calculated P_b and $\langle R \rangle$ values for the D-Ala containing model peptides along with the reported values[6] for Ac-L-Pro-L-Ala-$NHCH_3$ and Ac-L-Ala-L-Pro-$NHCH_3$. The larger P_b values and the smaller $\langle R \rangle$ values for the D-Ala containing dipeptides compared with the corresponding L-Ala derivatives indicated the larger turn tendency of D-Ala containing sequences. Stability of turn conformation of LL and LD sequences and the role of proline in the formation of the LL and the LD bends were studied by Chandrasekaran *et al.*[9] Our results afforded semiquantitative evaluation of turn tendency of these sequences.

As can be seen from Table 3 theoretical conforma-

Table 3. Magnitude of cotton effects of Dnp–Gly–X–Y–Gly–pNA and bend probability P_b[a] and average interterminal distance $\langle R \rangle$[a] of Ac–X–Y–NHCH$_3$

X	Y	CD Spectral data $\lvert[\theta]^{max}_{\approx 350} - [\theta]^{max}_{\approx 310}\rvert$	Calculated value P_b	Calculated value $\langle R \rangle$/Å
L-Pro	D-Ala	84.7×10^3	0.76	6.06
D-Ala	L-Pro	58.8×10^3	0.65	6.51
L-Pro	L-Ala	44.8×10^3	0.26[b]	7.99[b]
L-Ala	L-Pro	3.3×10^3	0.02[b]	9.13[b]

a) See Ref. 6. b) Values taken from Ref. 6.

tional study clearly demonstrated the turn tendency of the dipeptide sequences to be in the order: L-Pro–D-Ala>D-Ala–L-Pro>L-Pro–L-Ala>L-Ala–L-Pro. This order coincides with the order of the magmitude of the Cotton effects in the CD spectra of Dnp–Gly–X–Y–Gly–pNA as summarized in Table 3. In other words turn preference of dipeptide sequences studied by the chiroptical approach has been shown to agree with the results of theoretical conformational analysis, indicating the usefulness of the chiroptical method. Though librational entropy was not calculated in our study, the sequence dependence of turn tendency obtained in this study is assumed to be valid since the deviation of the $\langle R \rangle$ and P_b values due to neglection of librational entropy is at most 0.36 Å and 0.14, respectively, among the 12 proline containing dipeptides.[6]

Conformational properties of the tetrapeptide derivatives studied by their CD spectra were discussed with relation to the intrinsic turn tendency of the central dipeptide units disclosed by theoretical study. Conformational energy calculations were performed on the dipeptide models which contain acetyl and *N*-methylamide groups in place of Dnp–Gly and Gly–pNA moieties, respectively, of the tetrapeptide derivatives. These achiral terminal moieties in the chromophoric tetrapeptide derivatives, however, make some contribution to the absolute turn tendency of these molecules. Acetyl and *N*-methylamide groups of the dipeptide models correspond to the CH_2CO group of the 1st Gly residue and the $NHCH_2$ group of the 4th Gly residue, respectively, but Dnp–NH and CO–pNA groups were not included in the calculation. It was shown that intramolecular interaction between the two chromophoric groups stabilizes turn conformers without changing relative turn prefernce of the peptide sequences of the same series of compounds.[10] Replacement of the 1st and the 4th Gly residues of Dnp–Gly–X–Y–Gly–pNA by chiral amino acids markedly changes the turn tendency,[11] which is not dealt with in this paper.

In summary intrinsic turn tendency of proline containing dipeptide sequences were estimated semiquantitatively by means of empirical conformational energy calculation on model peptides. Calculation on Ac–L-Pro–D-Ala–NHCH$_3$ and Ac–D-Ala–L-Pro–NHCH$_3$ demonstrated the larger turn tendency of these D-Ala containing dipeptides than the corresponding L-Ala analogs, which is consistent with the CD spectral data of the tetrapeptide derivatives having Dnp–Gly and Gly–pNA groups. We consider that the results described here proved the validity of the chiroptical method using Dnp,pNA derivatives.[3] NMR study of acetyltetrapeptide *N*-methylamide also supported the chiroptical analysis as described elsewhere.[10]

Experimental

Materials. Synthesis of Dnp–Gly–L-Pro–L-Ala–Gly–pNA,[12] Dnp–Gly–L-Pro–D-Ala–Gly–pNA,[12] and Dnp–Gly–D-Ala–L-Pro–Gly–pNA[13] were already described.

Synthesis of Dnp–Gly–L-Ala–L-Pro–Gly–pNA. All the melting points were measured on a Yanagimoto micromelting point apparatus and were uncorrected. TLC's were carried out on Merck silica gel 60 F_{254} plates with the following solvent systems: R_f^1, $CHCl_3$–MeOH (5 : 1, v/v); R_f^2, $CHCl_3$–MeOH–AcOH (95 : 5 : 1, v/v); R_f^3, *n*-BuOH–AcOH–pyridine–H_2O (4 : 1 : 1 : 2, v/v). Optical rotations were measured on an Union automatic polarimeter PM-201.

Boc-L-Pro–Gly–pNA. To a chilled solution of Boc-L-Pro–OH (1.075 g, 5 mmol) and H–Gly–pNA (0.975 g, 5 mmol) in DMF (20 ml) was added EDC·HCl (0.959 g, 5 mmol). The mixture was stirred at 0 °C for 1 h and at room temperature overnight and evaporated under reduced pressure. The residue was dissolved in EtOAc, and the solution was washed successively with 10% citric acid, 4% $NaHCO_3$, and water, dried (Na_2SO_4), and evaporated. The residue was solidified by addition of ether and petroleum ether, and the product was recrystallized from EtOAc–ether–petroleum ether; yield, 1.523 g (77%); mp 204—205 °C; $[\alpha]_D^{22}$ −18.8° (*c* 0.5, MeOH); R_f^1 0.70, R_f^2 0.41, R_f^3 0.83.

Found: C, 55.34; H, 6.23%; N, 14.20%. Calcd for $C_{18}H_{24}O_6N_4$: C, 55.09; H, 6.17%; N, 14.28%.

H–L-Pro–Gly–pNA·HCl. Boc-L-Pro–Gly–pNA (785 mg, 2 mmol) was dissolved in 0.1 M (1 M=1 mol dm^{-3}) hydrogen chloride in formic acid (24 ml). The solution was allowed to stand at room temperature for 30 min and evaporated under reduced pressure to leave crystals, which were collected by filtration with the aid of ether; yield, 651 mg (99%); mp 217—219 °C; $[\alpha]_D^{22}$ −25.6° (*c* 1, MeOH); R_f^1 0.13, R_f^3 0.53.

Found: C, 47.40; H, 5.15; N, 17.12%. Calcd for $C_{13}H_{17}O_4N_4Cl$: C, 47.49; H, 5.21; N, 17.05%.

Boc–L-Ala–L-Pro–Gly–pNA. To a chilled solution of H–L-Pro–Gly–pNA·HCl (625 mg, 1.9 mmol) were added TEA (0.27 ml, 1.9 mmol) and Boc–L-Ala–ONSu (653 mg, 2.3 mmol). The mixture was treated as described for the synthesis of Boc–L-Pro–Gly–pNA. The product was recrystallized from MeOH–ether; yield, 511 mg (59%); mp 220—222 °C; $[\alpha]_D^{22}$ −12.6° (*c* 1, MeOH); R_f^1 0.64, R_f^3 0.23, R_f^3 0.76.

Found: C, 54.31; H, 6.25; N, 15.11%. Calcd for $C_{21}H_{29}O_7N_5$: C, 54.42; H, 6.31; N, 15.11%.

H–L-Ala–L-Pro–Gly–pNA·HCl. Boc–L-Ala–L-Pro–Gly–pNA (278 mg, 0.6 mmol) was treated with 0.1 M hydrogen chloride in formic acid (7 ml) as described for H–L-Pro–Gly–pNA·HCl. The product was highly hygroscopic crystals; yield, 240 mg (100%); $[\alpha]_D^{22}$ −11.0° (*c* 1, MeOH); R_f^1 0.07, R_f^3 0.54.

Found: C, 45.84; H, 5.84; N, 16.56%. Calcd for $C_{16}H_{22}O_5N_5Cl \cdot H_2O$: C, 45.99; H, 5.79; N, 16.76%.

Boc–Gly–L-Ala–L-Pro–Gly–pNA. This compound was prepared from H–L-Ala–L-Pro–Gly–pNA·HCl (200 mg, 0.5 mmol) and Boc–Gly–ONSu (163 mg, 0.6 mmol) as described for Boc–L-Ala–L-Pro–Gly–pNA; yield, 151 mg (58%); mp 135—138 °C; $[\alpha]_D^{22}$ −34.2° (*c* 1, MeOH); R_f^1 0.52, R_f^2 0.09, R_f^3 0.77.

Found: C, 52.47; H, 6.04; N, 15.82%. Calcd for $C_{23}H_{32}O_8N_6 \cdot 1/2\ H_2O$: C, 52.17; H, 6.28; N, 15.87%.

H–Gly–L-Ala–L-Pro–Gly–pNA·HCl. Boc–Gly–L-Ala–L-Pro–Gly–pNA (78 mg, 0.15 mmol) was dissolved in 0.1 M hydrogen chloride in formic acid (1.8 ml). After 30 min, the solution was evaporated to leave an oil, which was used for the next reaction without further treatment; yield was quantitative; R_f^1 0.02, R_f^3 0.51.

Dnp–Gly–L-Ala–L-Pro–Gly–pNA. To a solution of H–Gly–L-Ala–L-Pro–Gly–pNA·HCl (69 mg, 0.15 mmol) in DMF (1 ml) were added TEA (0.063 ml, 0.45 mmol) and N_2ph–F (56 mg, 0.3 mmol). The reaction mixture was stirred at room temperature for 3 h and evaporated *in vacuo*. The residue dissolved in $CHCl_3$ (10 ml) was applied to a column (1.8×18 cm) of silica gel 60 (Merck) and the column was washed with $CHCl_3$. The desired product was eluted with a mixture of $CHCl_3$ and MeOH (5 : 1, v/v). The fractions containing the desired product were evaporated to leave an oil, which was crystallized by addition of ether and recrystallized from MeOH–ether; yield, 73 mg (83%); mp 162—163 °C; $[\alpha]_D^{22}$ −26.2° (*c* 1, DMF); R_f^1 0.54, R_f^2 0.09, R_f^3 0.74.

Found: C, 48.31; H, 4.59; N, 18.56%. Calcd for $C_{24}H_{26}O_{10}N_8 \cdot 1/2\ H_2O$: C, 48.40; H, 4.57; N, 18.82%.

Measurements. CD spectra were recorded in methanol solution on JASCO J-40 spectropolarimeter.

Computation. ECEPP program and minimization subroutine VA04A were obtained from Quantum Chemistry Program Exchange, Indiana University. Computations were performed with FACOM 260F computer. All bond lengths and bond angles were taken from the standard ECEPP data for residues and end groups. The proline ring was taken in the puckered down position ($\phi = -75°$).

The authors are grateful to Dr. Tadakazu Maeda in our Institute and the members of System Center, Mitsubishi-Kasei Industries, Ltd. for their assistance during computation and also to the members of System Engineering Laboratory, Mitsubishi-Kasei Industries, Ltd., for performing elemental analyses.

References

1) Part IV: K. Sato, N. Taki, U. Nagai, and T. Higashijima, *Bull. Chem. Soc. Jpn.*, **56**, 2476 (1983).

2) The abbreviations used in this paper are those recommended by IUPAC-IUB; *J. Biol. Chem.*, **247**, 977 (1972). Additional abbreviations: Boc, *t*-butoxycarbonyl; Dnp, 2,4-dinitrophenyl; pNA, p-nitroanilide; ONSu, *N*-hydroxysuccinimide ester; EDC·HCl, 1-ethyl-3-(3′-dimethylaminopropyl)-carbodiimide hydrochloride; N_2ph–F, 1-fluoro-2,4-dinitrobenzene; TEA, triethylamine; DMF, *N*,*N*-dimethylformamide; TLC, thin-layer chromatography.

3) K. Sato, M. Kawai, and U. Nagai, *Biopolymers*, **20**, 1921 (1981).

4) F. A. Momany, R. F. McGuire, A. W. Burgess, and H. A. Scheraga, *J. Phys. Chem.*, **79**, 2361 (1975).

5) M. J. D. Powell, *Computer J.*, **7**, 151 (1964).

6) S. S. Zimmerman and H. A. Scheraga, *Biopolymers*, **16**, 811 (1977).

7) S. S. Zimmerman, M. S. Pottle, G. Nemethy, and H. A. Scheraga, *Macromolecules*, **10**, 1 (1977).

8) Conformational letter code[7] and ϕ and ψ values are given for each conformation.

9) R. Chandrasekaran, A. V. Lakshminarayanan, U. V. Pandya, and G. N. Ramachandran, *Biochim. Biophys. Acta*, **303**, 14, (1973).

10) K. Sato, T. Higashijima, T. Miyazawa, R. Sugawara, and U. Nagai, "Peptide Chemistry 1982; Proceedings of the 20th Symposium on Peptide Chemistry," ed by S. Sakakibara, Protein Research Foundation, Osaka (1983), p. 299.

11) M. Kawai, K. Sato, and U. Nagai, "Peptide Chemistry 1982; Proceedings of the 20th Symposium on Peptide Chemistry," ed by S. Sakakibara, Protein Research Foundation, Osaka (1983), p. 317.

12) K. Sato, U. Nagai, and T. Higashijima, *Bull. Chem. Soc. Jpn.*, **56**, 1657 (1983).

13) K. Sato, M. Kawai, and U. Nagai, *Bull. Chem. Soc. Jpn.*, **56**, 1527 (1983).

 © 1983 The Chemical Society of Japan Bull. Chem. Soc. Jpn., 56, 3009—3014 (1983)

Conversion of Disilanes to Functional Monosilanes. XIII.[1] The Palladium Catalyzed Reductive Coupling of Benzylidene Dichlorides and Benzylidyne Trichlorides Using Disilanes as Reducing Agents

Hideyuki MATSUMOTO,* Takeshi ARAI, Masatoshi TAKAHASHI, Toshiyuki ASHIZAWA, Taichi NAKANO, and Yoichiro NAGAI*

Department of Chemistry, Gunma University, Kiryu, Gunma 376

(Received April 11, 1983)

The reaction of benzylidene dichlorides or benzylidyne trichlorides with 1,2-dichloro-1,1,2,2-tetramethyldisilane or hexamethyldisilane proceeded smoothly in the presence of a catalytic amount of $Pd(PPh_3)_4$ to give (*E*)-stilbenes or (*E*)- and (*Z*)-α,β-dichlorostilbenes in high yields, respectively. Also, in the presence of the palladium(0) catalyst, α,α-dichlorobenzyltrimethylsilanes reacted with hexamethyldisilane yielding (*E*)-α,β-bis(trimethylsilyl)stilbenes in quantitative yield.

The reductive coupling of benzylidene dichlorides and benzylidyne trichlorides has been studied extensively and previous work employed active metal agents in low-oxidation state such as zero-valent titanium, iron, cobalt, and nickel compounds or slurries[2] as well as copper(I), titanium(II), vanadium(II), chromium(II), iron(II), cobalt(I), and cobalt(II) species.[3]

In connection with our continuing interest in the Si–Si cleavage of disilanes by organic halides,[1,4] we examined the interaction of benzylidene dichloride with methylchlorodisilanes, *e.g.*, 1,2-dichloro-1,1,2,2-tetramethyldisilane, in the presence of $Pd(PPh_3)_4$.[5] The reaction afforded the coupling products of the *gem*-dichlorides, stilbenes, in good yields. The result in this preliminary investigation demonstrates that such methylchlorodisilanes, formally tetravalent silicon species, can be effectively used for the coupling reaction as reducing agents. We have now extended this approach to use of other active *gem*-polychloro compounds such as benzylidyne trichlorides and α,α-dichlorobenzyltrimethylsilanes. The present paper is intended to summarize our work on this palladium(0) complex-catalyzed reductive coupling reaction.

Results and Discussion

Results for the reaction of benzylidene dichloride and benzylidyne trichloride with methylchlorodisilanes, $Me_{6-n}Si_2Cl_n$ (n=0, 2, 4), are given in Tables 1 and 2.

As shown in the tables, both hexamethyldisilane and 1,2-dichloro-1,1,2,2-tetramethyldisilane can bring about the coupling reaction. However, there is somewhat a puzzling difference in the effectiveness of these disilanes and choice of disilane depends upon the nature of the polychloromethylbenzene. The dichlorotetramethyldisilane is much more effective for converting benzylidene dichloride to (*E*)-stilbene than hexamethyldisilane, and optimum yield is obtained at initial disilane/substrate molar ratio of 2. On the other hand, the coupling of benzylidyne trichloride can be achieved smoothly with the permethyldisilane rather than with the dichlorotetramethyldisilane. The observed trend seems to reflect a compromise of the controlling factors in the sequence of the steps involved in the present catalytic reaction.

These reactions were run at 130 °C in a refluxing system. However, we note that the coupling can be also achieved at lower temperatures. For example, benzylidyne trichloride reacted with the permethyldisilane at 100 °C to give α,β-dichlorostilbene in 97% yield after 10 h.

In contrast with the case of these disilanes, the reaction of 1,1,2,2-tetrachloro-1,2-dimethyldisilane with benzylidene dichloride and benzylidyne trichloride afforded a complex mixture of products involving polysilanes due to the competitive disproportionation of the disilane itself.

The fact that the product ratio [PhCClXCClXPh: PhCX=CXPh (X=H, Cl)] is markedly affected by the ratio of the reactants (Tables 1 and 2) suggests that the formation of PhCX=CXPh occurs by a two-step process, Eqs. 1 and 2. This is further confirmed by the time-concentration profiles for the coupling of $PhCCl_2X$, indicating the initial formation of the dichlorodiphenylethane (**2**) followed by conversion of **2** to the

Table 1. Reaction of benzylidene dichloride with methylchlorodisilanes in the presence of $Pd(PPh_3)_4$[a]

Disilane	$PhCHCl_2$: Disilane	Time / h	Yield[b]/% PhCHClCHClPh	Yield[b]/% PhCH=CHPh	(*E*)/(*Z*)[c]
Me_6Si_2	1 : 2	6	51	4	—
$Me_4Si_2Cl_2$[d]	1 : 2	3	0	78[e]	100/0
$Me_4Si_2Cl_2$	1 : 1	3	65	18	100/0
$Me_4Si_2Cl_2$	2 : 1	3	44	5	—
$Me_2Si_2Cl_4$[f,g]	1 : 2	2	4	35	100/0

a) Carried out at 130 °C in mesitylene. The catalyst concentration was 1 mol % based on $PhCHCl_2$ charged. b) Based on $PhCHCl_2$ charged and determined by GLC. c) Determined by GLC. d) 1,2-Dichloro-1,1,2,2-tetramethyldisilane. e) $PhCH(SiMe_2Cl)_2$ was also formed in 22 % yield. f) 1,1,2,2-Tetrachloro-1,2-dimethyldisilane. g) In this run the disilane was completely consumed.

Table 2. Reaction of benzylidyne trichloride with methylchlorodisilanes in the presence of $Pd(PPh_3)_4$[a)]

Disilane	$PhCCl_3$: Disilane	Time / h	Yield[b)]/%		$(E)/(Z)$[c)]
			$PhCCl_2CCl_2Ph$	$PhCCl{=}CClPh$	
Me_6Si_2	1 : 2	2	0	quant.	30/70
Me_6Si_2	1 : 1	6	4	81	30/70
Me_6Si_2	2 : 1	12	50	0	—
$Me_4Si_2Cl_2$[d)]	1 : 2	6	49	45	30/70
$Me_2Si_2Cl_4$[e),f)]	1 : 2	2	0	15	—

a—d) See the corresponding footnotes in Table 1. e) 1,1,2,2-Tetrachloro-1,2-dimethyldisilane. f) In this run the disilane was completely consumed.

Table 3. Reaction of $ArCCl_2X$ with methylchlorodisilanes in the presence of $Pd(PPh_3)_4$[a)]

Substrate Ar	X	Disilane	Time / h	Yield[b)] of $ArCX{=}CXAr$/%	$(E)/(Z)$[c)]
2-Cl_6H_4	H	$Me_4Si_2Cl_2$	0.5	94	100/0
4-ClC_6H_4	H	$Me_4Si_2Cl_2$	0.5	quant.	100/0
2,4-$Cl_2C_6H_3$	H	$Me_4Si_2Cl_2$	3	95	100/0
2-ClC_6H_4	Cl	Me_6Si_2	2	96	40/60
4-ClC_6H_4	Cl	Me_6Si_2	2	79	30/70
2,4-$Cl_2C_6H_3$	Cl	Me_6Si_2	2	86	48/52
C_6H_5	C_6H_5	Me_6Si_2	10	90[d)]	—

a) $[ArCCl_2X]/[disilane]/[Pd(0)] = 1/2/0.01$; at 130 °C in mesitylene. b) Based on $ArCCl_2X$ charged and determined by GLC unless otherwise stated. c) Determined by GLC. d) Isolated yield.

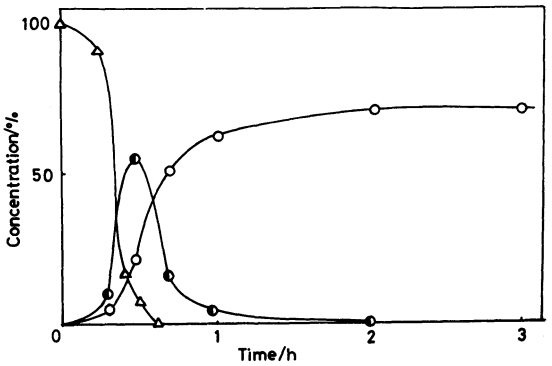

Fig. 1. Time-concentration profiles for the reaction of $PhCHCl_2$ with $ClMe_2SiSiMe_2Cl$ in the presence of $Pd(PPh_3)_4$ at 130 °C.
△: $PhCHCl_2$, ◐: PhCHClCHClPh, ○: (*E*)-PhCH=CHPh.

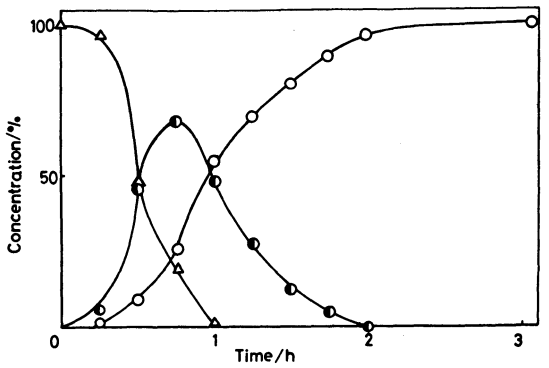

Fig. 2. Time-concentration profiles for the reaction of $PhCCl_3$ with $Me_3SiSiMe_3$ in the presence of $Pd(PPh_3)_4$ at 130 °C.
△: $PhCCl_3$, ◐: $PhCCl_2CCl_2Ph$, ○: (*E*)- and (*Z*)-PhCCl=CClPh.

$$2PhCCl_2X + YMe_2SiSiMe_2Y \xrightarrow{[Pd]} \underset{\mathbf{1}}{} \quad PhCClXCClXPh + 2Me_2SiClY \quad (1)$$
$$\underset{\mathbf{2}}{}$$

$$\mathbf{1} + \mathbf{2} \xrightarrow{[Pd]} PhCX{=}CXPh + 2Me_2SiClY \quad (2)$$
$$(X{=}H, Cl;\ Y{=}Cl, Me)$$

corresponding stilbenes (Figs. 1 and 2).

Under optimum conditions, the coupling of substituted benzylidene dichlorides and benzylidyne trichlorides was achieved in high yields by the reaction with the dichloroteramethyldisilane or with the permethyldisilane. As shown in Table 3, (*E*)-stilbenes are only coupled products obtained by the reaction with the dichlorides, whereas a mixture of (*E*)- and (*Z*)-isomers is obtained from the trichlorides.[6)] The geometrical isomerism for previously unreported stilbenes, *e.g.*, α,β,-2,2′-tetrachlorostilbene and α,β,2,2′,4,4′-hexachlorostilbene, was assigned based on differences in the physical properties of these isomers: (i) in ^1H NMR spectra, the phenyl proton signals in the (*E*)-isomers appear at lower fields compared to those on the (*Z*)-isomers. ii) In IR spectra, the C=C stretching frequences around 1600 cm^{-1} of the (*E*)-isomers are very weak and broad, due to their symmetrical structures, while those of the (*Z*)-isomers are relatively strong and sharp. (iii) The conjugation bands of the UV spectra for the (*E*)-isomers occur at shorter wave length than those of the (*Z*)-isomers. (iv) The melting points of the (*E*)-isomers are

Table 4. Effect of some other common group VIII metal complexes on the reaction of $PhCHCl_2$ with $ClMe_2SiSiMe_2Cl$[a]

Complex	Time / h	Yield[b]/% PhCHClCHClPh	Yield[b]/% PhCH=CHPh
$PdCl_2L_2$	2	0	59[c]
PtL_4	2	28	19
$PtCl_2L_2$	2	25	12
$RhClL_3$	2	16	15
$NiCl_2L_2$	5	1	1

a) $[PhCHCl_2]/[disilane]/[Pd(0)] = 1/2/0.01$; at 130 °C in mesitylene. b) Determined by GLC. c) $PhCH(SiMe_2Cl)_2$ was also produced in 40% yield.

higher than those of the (*Z*)-isomers. Similar observations have been made in such pairs of the geometrical isomers of α,β-dichlorostilbene and α,β,4,4′-tetrachlorostilbene.[2,3,7]

The data accumulated in Tables 1-3 clearly reveal that the present system provides a workable procedure for the selective coupling of these polychloromethylbenzenes to the stilbenes. This has advantages: (i) the methylchlorodisilanes employed are readily available in large quantities.[8] (ii) Removal of the counter products, Me_2SiCl_2 (bp 70 °C) and Me_3SiCl (bp 57 °C), can be easily achieved by evaporation. The formation of large amounts of nonvolatile and solid inorganic salts as oxidation products is the drawback of the conventional methods using stoichiometric amount of low-valent metals as reducing agents.[2,3] Further, the fact that only catalytic amounts of the palladium(0) complex are required in the present reaction also increases the potential synthetic utility of our method.

Catalytic efficiency was tested briefly for other common group VIII metal–phosphine complexes using the reaction of benzylidene dichloride with 1,2-dichloro-1,1,2,2-tetramethyldisilane as a standard. As shown in Table 4, $PdCl_2(PPh_3)_2$ showed the catalytic activity for the coupling. However, the reaction was less selective compared to that in the presence of the palladium(0) complex and gave a considerable amount of $PhCH(SiMe_2Cl)_2$ as well as (*E*)-stilbene. The complexes $Pt(PPh_3)_4$, $PtCl_2(PPh_3)_2$, and $RhCl(PPh_3)_3$ also induced the reaction, but their catalytic ability was much lower. $NiCl_2(PPh_3)_2$ failed to effect the expected reaction to any appreciable extent.

$$ArCHCl_2 + ClMe_2SiSiMe_2Cl$$
$$\xrightarrow{a:\ [Pd]}$$
$$ArCHClSiMe_2Cl\ (\mathbf{3}) + Me_2SiCl_2$$
$$\xrightarrow{b:\ ArCHCl_2/[Pd]}$$
$$ArCHClCHClAr + Me_2SiCl_2$$
$$\xrightarrow{c:\ ClMe_2SiSiMe_2Cl/[Pd]}$$
$$ArCHClCH(SiMe_2Cl)Ar\ (\mathbf{4}) + Me_2SiCl_2$$
$$\xrightarrow{d:\ \Delta}$$
$$(E)\text{-}ArCH{=}CHAr + Me_2SiCl_2$$

Scheme 1.

Mechanistically, the coupling reaction perhaps consists of several steps as shown in Scheme 1. This involves the palladium-catalyzed dechlorinative silylation of a benzylidene dichloride $ArCHCl_2$ with 1,2-dichloro-1,1,2,2-tetramethyldisilane to give the α-chlorobenzyldimethylchlorosilane (**3**) (path a), followed by the metathesis between **3** and $ArCHCl_2$ yielding a coupling product ArCHClCHClAr (path b). Support for the transient intermediate **3** was found in the reaction of $PhCHCl_2$ with excess of the dichlorotetramethyldisilane. The reaction afforded $PhCH(SiMe_2Cl)_2$, as a by-product, which should arise from **3** (Ar=Ph) by the reaction with the disilane (Table 1). Path b is the reminiscent of the palladium-catalyzed metathesis of allyltrimethylsilane with allyl bromide that gives 1,5-hexadiene together with trimethylbromosilane.[4c] The reaction of ArCHClCHClAr with the dichlorotetramethyldisilane to give the 1-chloro-2-(dimethylchlorosilyl)-1,2-diarylethane **4** (path c), which releases spontaneously dimethyldichlorosilane *via* β-elimination[9] resulting in the formation of (*E*)-ArCH=CHAr (path d), should be also involved. A similar mechanism may be given for the coupling of benzylidyne trichlorides.

Alternatively, a scheme might be proposed whereby the dichlorotetramethyldisilane as well as the permethyldisilane acts as reducing agents to regenerate the palladium(0) from the palladium(II) formed upon the coupling (Eqs. 3 and 4). This scheme, however, seems

$$ArCCl_2X + Pd(PPh_3)_4 \longrightarrow ArCClXCClXAr + PdCl_2(PPh_3)_2 + 2PPh_3 \quad (3)$$

$$PdCl_2(PPh_3)_2 + YMe_2SiSiMe_2Y \longrightarrow Pd(PPh_3)_2 + 2MeSiClY \quad (4)$$

to be unlikely, since vigorous conditions (*e.g.*, 160—200 °C) are generally required to bring about reduction of this type.[10] Moreover, the recent finding by Stille and Lau,[11] and Eaborn *et al.*[12] that trimethylchlorosilane reacts with $Pd(PPh_3)_4$ to give hexamethyldisilane and $PdCl_2(PPh_3)_2$ strongly indicates that reaction 4 is much less favorable.

In consideration of the catalytic cycles for paths a and b in Scheme 1, it is likely that the cycles are initiated by the reaction of $ArCHCl_2$ with $Pd(PPh_3)_4$, since we found that such a reaction occurs rapidly at a room temperature, although an attempt to isolate the expected oxidative adduct, *e.g.*, $PdCl(CHClPh)(PPh_3)_2$, failed due to the instability of this complex. On the other hand, 1,2-dichloro-1,1,2,2-tetramethyldisilane is much less reactive toward the palladium(0) complex under comparable conditions.[1] Thus, plausible catalytic cycles are shown in Scheme 2. Cycle A was inferred from the mechanism proposed for the palladium(0)-catalyzed metathesis between benzyl chlorides and the dichlorotetramethyldisilane to give benzyldimethylchlorosilanes.[1] Cycle B involves the transmetallation of the palladium(II) complex, $PdCl(CHClAr)(PPh_3)_2$, with the α-chlorobenzyldimethylchlorosilane (**3**). Analogous transmetallation process has been proposed for the cleavage of silicon-alkyl and silicon-aryl bonds by palladium(II) compounds which takes places at 60—120 °C[13] and also for the palladium-catalyzed coupling

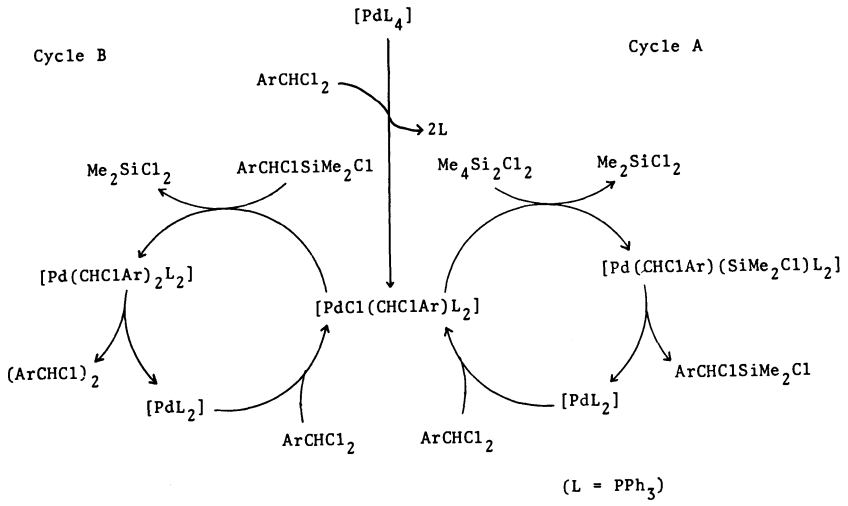

Scheme 2.

TABLE 5. REACTION OF $ArCCl_2SiMe_3$ WITH $Me_3SiSiMe_3$ IN THE PRESENCE OF $Pd(PPh_3)_4$[a]

Substrate Ar	Time / h	Yield[b]/% ArCCl=CArSiMe$_3$	Yield[b]/% Ar(Me$_3$Si)C=C(SiMe$_3$)Ar[c]
C_6H_5	2	42[d]	44[d]
C_6H_5	18	—	quant.
4-ClC_6H_4	24	—	quant.

a) [Substrate]/[disilane]/[Pd(0)] = 1/2/0.01; at 130 °C in mesitylene. b) Isolated yields unless otherwise stated. c) Only the (*E*)-isomers were formed. d) Determined by GLC.

of tetraorganotin compounds with aryl and benzyl halides.[14] Further, it has been found by Pitt *et al.*[15] that silicon-benzyl bond is cleaved by palladium under certain conditions.

In view of this proposed mechanism, it is expected that α,α-dichlorobenzyltrimethylsilanes could be readily enter into the coupling and this was found to be the case (Table 5). For example, $PhCCl_2SiMe_3$ reacted very smoothly with hexamethyldisilane in the presence of the palladium(0) catalyst to give (*E*)-α,β-bis(trimethylsilyl)stilbene together with α-chloro-β-(trimethylsilyl)-stilbene (presumably, (*E*)-isomer). Further, the bis-(trimethylsilyl)stilbene could be obtained in quatitative yield by continuing the reaction until virtual disappearance of the monosilylstilbene. The formation of the bis(silyl)stilbene can be rationalized in terms of the palladium-catalyzed metathesis between the monosilylstilbene and the permethyldisilane (Eq. 5).[16] The results in the table again emphasize the utility of our

$$PhCCl{=}C(SiMe_3)Ph + Me_3SiSiMe_3 \xrightarrow{[Pd]} Me_3Si(Ph)C{=}C(SiMe_3)Ph + Me_3SiCl \quad (5)$$

procedure as a selective route (*E*)-α,β-bis(trimethylsilyl)-stilbenes which would be of interest for the study of physico-chemical properties.[17]

Experimental

Melting points were uncorrected. IR spectra were taken on a JASCO A102 spectrophotometer. ^1H NMR spectra were obtained with a Varian EM-360 spectrometer using tetramethylsilane as an internal standard. UV spectra were taken on a Hitachi 200-10 spectrophotomter. Mass spectra were obtained with a JEOL JMS-07 spectrometer. GLC analyses were performed on an Ohkura GC-103 instrument with thermal conductivity detector using 0.4×100-200 cm Teflon and Pyrex glass columns packed with 10%SE-30, 10% DCQF-1, 10%KF-96, and 10%Carbowax 20M on Celite 545 (80—100 mesh). Corrections were made thermal conductivity of the various components.

Materials. Benzylidene dichloride was commercially available and used as received. Substituted benzylidene dichlorides were prepared by the benzoyl peroxide-catalyzed chlorination of the corresponding benzyl chlorides with sulfuryl chloride.[18] Benzylidyne trichlorides were commercially available and used as received. α,α-Dichlorobenzyltrimethylsilanes were prepared according to literature directions.[19] Hexamethyldisilane was commercially available and purified by distillation prior to use. 1,2-Dichloro-1,1,2,2-tetramethyldisilane[8f] and 1,1,2,2-tetrachloro-1,2-dimethyldisilane[8e] were prepared according to published procedures.

The complexes $Pd(PPh_3)_4$,[20] $PdCl_2(PPh_3)_2$,[21] $Pt(PPh_3)_4$,[22] $PtCl_2(PPh_3)_2$,[23] $RhCl(PPh_3)_3$,[24] and $NiCl_2(PPh_3)_2$[25] were prepared according to literature procedures.

Other organic reagents and solvents were commercially available and purified according to standard procedures.

Procedure for the Coupling of Benzylidene Dichlorides and Benzylidyne Trichlorides. All the reactions were carried out under nitrogen in a refluxing system and typical examples are described below.

(a) Reaction of 2-Chlorobenzylidene Dichloride with 1,2-Dichloro-1,1,2,2-tetramethyldisilane: A mixture of 1.98 g (10.2 mmol) of the dichloride, 3.75 g (20.0 mmol) of the disilane, 0.12 g (0.1 mmol) of $Pd(PPh_3)_4$, and 3 ml of mesitylene was heated at 130 °C for 0.5 h with stirring. GLC analysis showed that the dichloride had been completely consumed and that 2,2′-dichlorostilbene (4.7 mmol, 94% yield) had been produced. The reaction mixture was then diluted with 30 ml of pentanes to precipitate the catalyst which was removed by filtration. The filtrate was concentrated to yield 1.03 g (85% yield) of

stilbene as colorless crystals.

(b) Reaction of Benzylidyne Trichloride with Hexamethyldisilane: A mixture of 1.95 g (10.0 mmol) of the trichloride, 2.90 g (19.8 mmol) of the disilane, 0.12 g (0.1 mmol) of the palladium(0) complex, and 5 ml of mesitylene was heated at 130 °C for 2 h with stirring. GLC analysis showed that the reaction had given 5.0 mmol (100% yield) of α,β-dichlorostilbene as a 30 : 70 mixture of the (*E*)- and (*Z*)-isomers. Work-up as described above afforded 1.20 g (97% yield) of the product as colorless crystals.

The physical data of the products obtained are given below. PhCHClCHClPh: mp 176—190 °C (lit,[3a] *meso*, mp 191—193 °C; *dl*, 93—94 °C); NMR (CCl_4) δ=5.05 (s, 2H) and 7.31 (s, 10H). (*E*)-PhCH=CHPh: mp 123—124 °C (lit,[26] 124 °C); NMR (CCl_4) δ=7.10 (s, 2H) and 7.50 (m, 10H). $PhCH(SiMe_2Cl)_2$: IR (neat) 1255 (s) cm^{-1}; NMR (CCl_4) δ=0.46 (s, 12H); 1.88 (s, 1H) and 7.12 (s, 5H); MS (30 eV), *m/e*, 276 (M^+). This compound gave a poor analytical result due to high susceptibility to hydrolysis. (*E*)-2-ClC_6H_4CH=CHC_6H_4-2-Cl: mp 97—98 °C (lit,[26] 98—99 °C); NMR (CCl_4) δ=6.98 (s, 2H) and 7.53 (s, 8H). 4-ClC_6H_4CH=CHC_6H_4-4-Cl: mp 174—176 °C (lit,[26] 176—176.5 °C); NMR (CCl_4) δ=6.92 (s, 2H) and 7.30 (s, 8H). (*E*)-2,4-$Cl_2C_6H_3CH$=CHC_6H_3-2,4-Cl_2: mp 159—161 °C (lit,[26] 161—161.5 °C); NMR (CCl_4) δ=7.00 (s, 2H) and 7.31 (m, 6H). $PhCCl_2CCl_2Ph$: mp 166—167 °C (lit,[3b] 167 °C). (*E*)-PhCCl=CClPh: mp 139.5—140.5 °C (lit,[3c] 140 °C); IR (KBr disk) 1605 (vw) cm^{-1}; NMR (CCl_4) δ=7.53 (m). (*Z*)-PhCCl=CCl-Ph: mp 55—56 °C (lit,[3c] 62—64 °C); IR (KBr disk) 1615 (m) cm^{-1}; NMR (CCl_4) δ=7.17 (s). (*E*)-2-ClC_6H_4CCl=$CClC_6H_4$-2-Cl: mp 170—170.5 °C; UV_{max} (heptane) 251 nm (ε 5100); IR (KBr disk) 1598 (vw) cm^{-1}; NMR (CCl_4) δ=7.41 (m); MS (30 eV), *m/e*, 316 (M^+). Found: C, 52.96; H, 2.55%. Calcd for $C_{14}H_8Cl_4$: C, 52.87; H, 2.54%. (*Z*)-2-ClC_6H_4CCl=$CClC_6H_4$-2-Cl: mp 133—133.5 °C; UV_{max} (heptane) 265 nm (ε 5140); IR (KBr disk) 1595 (m) cm^{-1}; NMR (CCl_4) δ=7.16 (m); MS (30 eV), *m/e*, 316 (M^+). Found: C, 52.95; H, 2.65%. Calcd for $C_{14}H_8Cl_4$: C, 52.87; H, 2.54%. (*E*)-4-ClC_6H_4CCl=$CClC_6H_4$-4-Cl: mp 163—165 °C (lit,[7a] 164—165 °C); IR (KBr disk) 1590 (vw) cm^{-1}; NMR (CCl_4) δ=7.55 (m). (*Z*)-4-ClC_6H_4-CCl=$CClC_6H_4$-4-Cl: mp 90—91 °C (lit,[7a] 85—86 °C); IR (KBr disk) 1590 (m) cm^{-1}; NMR (CCl_4) δ=7.19 (s). (*E*)-2,4-$Cl_2C_6H_3CCl$=$CClC_6H_3$-2,4-Cl_2: mp 171—172 °C; UV_{max} (heptane) 236 nm (ε 19300); IR (KBr disk) 1585 (vw) cm^{-1}; NMR (CCl_4) δ=7.39 (m, 4H) and 7.55 (m, 2H), MS (30 eV), *m/e*, 384 (M^+). Found: C, 43.75; H, 1.71%. Calcd for $C_{14}H_6Cl_6$: C, 43.46; H, 1.71%. (*Z*)-2,4-$Cl_2C_6H_3CCl$=$CClC_6H_3$-2,4-Cl_2: mp 124—125 °C; UV_{max} (heptane) 266 nm (ε 6400); IR (KBr disk) 1580 (m) cm^{-1}; NMR (CCl_4) δ=7.21 (m, 4H) and 7.36 (m, 2H); MS (30 eV) *m/e* 384 (M^+). Found: C, 42.94; H, 1.62%. Calcd for $C_{14}H_6Cl_6$: C, 43.46; H, 1.56%.

Time-concentration Profiles for the Coupling of Benzylidene Dichloride and Benzylidyne Trichloride. Typically, a mixture of 1.61 g (10.0 mmol) of benzylidene dichloride, 3.75 g (20.0 mmol) of 1,2-dichloro-1,1,2,2-tetramethyldisilane, 0.12 g (0.1 mmol) of the palladium(0) complex, 3 ml of mesitylene, and 0.488 g (2.00 mmol) of triphenylmethane as an internal standard was heated at 130 °C under nitrogen with stirring. The course of the reaction was monitored by GLC.

Effect of Some Common Group VIII Metal Complex on the Reaction of Benzylidene Dichloride with 1,2-Dichloro-1,1,2,2-tetramethyldisilane. A mixture of 1.61 g (10.0 mmol) of the dichloride, 3.75 g (20.0 mmol) of the disilane, 0.1 mmol of a complex, and 3 ml of mesitylene was heated at 130 °C under nitrogen with stirring. After 2—5 h, the resulting mixture was subjected to GLC analysis.

Reaction of α,α-Dichlorobenzyltrimethylsilane with Hexamethyldisilane. Typical examples are described below. *i)* A mixture of 2.34 g (10.0 mmol) of $PhCCl_2SiMe_3$, 2.93 g (20.0 mmol) of hexamethyldisilane, 0.12 g (0.1 mmol) of the palladium(0) complex, and 5 ml of mesitylene was heated at 130 °C under nitrogen for 2 h. GLC analysis showed that the reaction had given α,β-bis(trimethylsilyl)stilbene in 44% yield together with a 42% yield of α-chloro-β-(trimethylsilyl)-stilbene.

ii) A mixture of 1.34 g (5.0 mmol) of α,α,4-trichlorobenzyltrimethylsilane, 1.50 g (10.3 mmol) of the permethyldisilane, 0.058 g (0.05 mmol) of the palladium(0) complex, and 3 ml of mesitylene was heated at 130 °C for 24 h under nitrogen. The resulting mixture was diluted with 50 ml of pentanes and the precipitated catalyst was removed by filtration. The filtrate was concentrated to dryness under reduced pressure to yield 1.05 g (100% yield) of (*E*)-α,β-bis(trimethylsilyl)-4,4′-dichlorostilbene.

The physical data of the products obtained are given below. (*E*)-$Ph(Me_3Si)C$=$C(SiMe_3)Ph$: mp 112 °C (lit,[17] 116 °C); IR (KBr disk) 1600 (vw) and 1248 (s) cm^{-1}; NMR (CCl_4) δ=7.22 (m, 10H) and −0.38 (s, 18H). $PhCCl$=$C(SiMe_3)Ph$: mp 52—53 °C; IR (KBr disk) 1600 (vw) and 1250 (s) cm^{-1}; NMR (CCl_4) δ=7.02 (m, 10H) and 0.18 (s, 9H); MS (30 eV), *m/e* 286 (M^+). Found: C, 71.67; H, 6.25%. Calcd for $C_{17}H_{19}ClSi$: C, 71.18; H, 6.68%. (*E*)-4-$ClC_6H_4(Me_3Si)C$=$C(SiMe_3)C_6H_4$-4-Cl: mp 178—181 °C; IR (KBr disk) 1600 (vw) and 1252 (s) cm^{-1}; NMR (CCl_4) δ=6.98 (d, 2H, J=7 Hz), 7.12 (d, 2H, J=7 Hz) and −0.08 (s, 18H); MS (30 eV), *m/e*, 392 (M^+). Found: C, 60.89; H, 6.15%. Calcd for $C_{20}H_{26}Cl_2Si_2$: C, 61.05; H, 6.61%.

Reaction of Benzylidene Dichloride with $Pd(PPh_3)_4$. To a solution of 0.23 g (0.20 mmol) of the palladium(0) complex in 5 ml of benzene was added 0.064 g (0.40 mmol) of the dichloride under nitrogen. The reaction mixture was stirred at a room temperature for 5 h and then diluted with 20 ml of pentanes. The yellow microcrystals that separated were filtered, washed with ether and dried *in vacuo*. IR spectrum of this product was in complete agreement with that of the complex $PdCl_2(PPh_3)_2$; 0.083 g (64% yield). Further, GLC analysis of the filtrate showed the formation of (*E*)-stilbene (0.07 mmol) and 1,2-dichloro-1,2-diphenylethane (0.02mmol).

References

1) Part XII: H. Matsumoto, M. Kasahara, I. Matsubara, M. Takahashi, T. Arai, M. Hasegawa, T. Nakano, and Y. Nagai, *J. Organomet. Chem.*, **250**, 99 (1983).

2) A. Merijanian, T. Mayer, J. S. Helling, and F. Klemick, *J. Org. Chem.*, **37**, 3945 (1972); Y. Ogata and H. Nakamura, *ibid.*, **21**, 1170 (1956); C. E. Coffey, *J. Am. Chem. Soc.*, **83**, 1623 (1961); T. A. Cooper and T. Takeshita, *J. Org. Chem.*, **36**, 3517 (1971); D. Seyferth and M. D. Millar, *J. Organomet. Chem.*, **38**, 373 (1972); S. Inaba, H. Matsumoto, and R. D. Rieke, *Tetrahedron Lett.*, **23**, 4215 (1982).

3) a) H. Nozaki, T. Shirafuji, and Y. Yamamoto, *Tetrahedron*, **25**, 3461 (1969); b) T. A. Cooper, *J. Am. Chem. Soc.*, **95**, 4158 (1973); c) G. Olah and G. K. Surya Parahashi, *Synthesis*, **1976**, 607; d) Y. Okude, T. Hiyama, and H. Nozaki, *Tetrahedron Lett.*, **1977**, 3829; e) T. Wellmann and E. Steckhan, *Synthesis*, **1978**, 901; f) K. Onuma, J. Yamashita, and H. Hashimoto, *Bull. Chem. Soc. Jpn.*, **43**, 836 (1970); **46**, 333 (1973); g) Y. Yamada and D. Momose, *Chem. Lett.*, **1981**, 1277; h) F. Stoneberger and A. L. Crumbliss, *J. Organomet. Chem.*, **215**, 229 (1981).

4) a) H. Matsumoto, S. Nagashima, K. Yoshiro, and Y. Nagai, *J. Organomet. Chem.*, **85**, Cl (1975); b) H. Matsumoto, K. Yoshiro, S. Nagashima, H. Watanabe, and Y. Nagai, *ibid.*,

128, 409 (1977); c) H. Matsumoto, T. Yako, S. Nagashima, and Y. Nagai, *ibid.*, **148**, 97 (1978); d) H. Matsumoto, S. Nagashima, T. Kato, and Y. Nagai, *Angew. Chem.*, **90**, 288 (1978); e) H. Matsumoto, K. Shono, and Y. Nagai, *Org. Proc. Prep. Intl.*, **13**, 118 (1981); f) H. Matsumoto, K. Shono, and Y. Nagai, *J. Organomet. Chem.*, **208**, 145 (1981); g) H. Matsumoto, K. Ohkawa, T. Nakano, and Y. Nagai, *Chem. Lett.*, **1980**, 721.

5) T. Nakano, M. Takahashi, T. Ashizawa, T. Arai, S. Seki, H. Matsumoto, and Y. Nagai, *Chem. Lett.*, **1982**, 613.

6) The formation of silylated products, *e.g.*, α-chloro-β-(trimethylsilyl)stilbenes, was virtually negligible in each run shown in Tables 2 and 3. It may be thus concluded that the reaction of the resulting α,β-dichlorostilbenes with hexamethyldisilane did not take place under the conditions employed. This is further confirmed by a control experiment in which α,β-dichlorostilbene [30%(*E*)- and 70%(*Z*)-isomers] was allowed to react with excess (10 equiv) of the permethyldisilane in the presence of 1 mol% of the palladium(0) complex at 130 °C for 5 h. The reaction resulted in the complete recovery of the starting dichlorostilbene.

7) a) C. D. Weis, *Helv. Chim. Acta*, **49**, 234 (1966); b) S. Uemura, H. Okazaki, A. Onoe, and M. Okanao, *J. Chem. Soc., Perkin Trans. 1*, **1977**, 676.

8) a) M. Kumada, Y. Yamaguchi, Y. Yamamoto, and K. Shiina, *J. Org. Chem.*, **21**, 1264 (1956); b) M. Kumada and M. Ishikawa, *J. Organomet. Chem.*, **1**, 153 (1963); c) M. Kumada, M. Ishikawa, and S. Maeda, *ibid.*, **2**, 278 (1963); d) H. Sakurai, T. Watanabe, and M. Kumada, *ibid.*, **7**, P15 (1967); e) H. Watanabe, M. Kobayashi, Y. Koiche, S. Nagashima, H. Matsumoto, and Y. Nagai, *ibid.*, **128**, 173 (1977); f) H. Matsumoto, T. Motegi, M. Hasegawa, and Y. Nagai, *ibid.*, **142**, 149 (1977).

9) C. Eaborn and R. W. Bott, "Organometallic Compounds of the Group IV Elements," ed by MacDiamid, Marcel Dekker, New York (1968), Vol. 1, Part 1, p. 378.

10) R. Calas, E. Frainnet, and Y. Dentone, *Compt. Rend.*, **259**, 3777 (1964): *Chem. Abstr.*, **62**, 9166 (1965); H. Urata, H. Suzuki, Y. Moro-oka, and T. Ikawa, *J. Organomet. Chem.*, **234**, 367 (1982).

11) J. K. Stille and K. S. Lau, *J. Am. Chem. Soc.*, **98**, 5841 (1976).

12) C. Eaborn, R. W. Griffiths, and A. Pidcock, *J. Organomet. Chem.*, **225**, 331 (1982).

13) I. S. Akhrem, N. M. Chistovalova, E. I. Mysov, M. E. Vol'pin, *J. Organomet. Chem.*, **72**, 171 (1974).

14) D. Milstein and J. K. Stille, *J. Am. Chem. Soc.*, **101**, 17 (1979).

15) C. G. Pitt, A. E. Friedman, D. H. Rector, and M. G. Wani, *J. Organomet. Chem.*, **121**, 37 (1976).

16) The results seem to demonstrate that the reactivity of the chlorine atom in α-chloro-β-(trimethylsilyl)stilbenes toward hexamethyldisilane is substantially increased by β-trimethylsilyl substituent, when compared with those of the α,β-dichlorostilbenes, coupling products from benzylidyne trichlorides (see Ref. 6). Such an anchimeric effect of β-silicon will be discussed in future.

17) Y. Kiso, K. Tamao, and M. Kumada, *J. Organomet. Chem.*, **76**, 105 (1974).

18) M. S. Kharasch and H. C. Brown, *J. Am. Chem. Soc.*, **61**, 2142 (1939).

19) J. Dunogues, E. Jousseaume, and R. Calas, *J. Organomet. Chem.*, **71**, 377 (1974).

20) D. R. Coulson, *Inorg. Synth.*, **13**, 121 (1972).

21) J. Chatt and F. G. Mann, *J. Chem. Soc.*, **1939**, 1631.

22) R. Ugo, F. Gariati, and G. La Monica, *Inorg. Synth.*, **11**, 105 (1968).

23) L. Malatesta and C. Cariello, *J. Chem. Soc.*, **1958**, 2323.

24) J. A. Osborn, F. A. Jardine, J. F. Young, and G. Wilkinson, *J. Chem. Soc., A*, **1966**, 1711.

25) F. A. Cotton, O. D. Faut, and D. M. L. Goodgame, *J. Am. Chem. Soc.*, **83**, 344 (1961).

26) D. F. Hoeg and D. I. Lusk, *J. Organomet. Chem.*, **5**, 1 (1965).

 © 1983 The Chemical Society of Japan Bull. Chem. Soc. Jpn., 56, 3015—3019 (1983)

A Novel Cyclization Reaction of Alkylthiodiphenylcyclopropenium Ions with Acyclic 1,3-Diketones to Give Cyclopentadienols

Hiroshi Yoshida,* Mikito Nakajima, Tsuyoshi Ogata, Kiyoshi Matsumoto,†
R. Morrin Acheson,†† and John D. Wallis†††
Department of Applied Chemistry, Faculty of Engineering, Shizuoka University, Hamamatsu 432
†*College of Liberal Arts and Sciences, Kyoto University, Kyoto 606*
††*Department of Biochemistry, University of Oxford, South Parks Road, Oxford OX1 3QU, U.K.*
†††*The Chemical Crystallography Laboratory, 9 Parks Road, Oxford OX1 3PD, U.K.*
(Received April 19, 1983)

Reaction of methylthio-, ethylthio-, and benzylthiodiphenylcyclopropenium salts with 2,4-pentanedione (**3a**) and ethyl acetoacetate (**3b**) yielded the cyclopentadienol derivatives (**4**) by ring expansion. One of the products **4a** was shown to be 4-acetyl-5-hydroxy-5-methyl-1-methylthio-2,3-diphenyl-1,3-cyclopentadiene by X-ray crystallography. Chemical transformation of the products yielded some cyclopentenones. Triphenylcyclopropenium perchlorate reacted with **3a** and **3b** affording the ketocyclopropene in good yields.

Cyclopropenium ions with phenyl, amino, and alkylthio groups as substituents condense with nitrogenous nucleophiles such as hydrazine, aliphatic amines, and azides to give 5- or 6-membered nitrogen heterocycles,[1-4] whereas 1,2-diphenyl-3-ethoxycyclopropenium tetrafluoroborate (**1**) reacts with 1,3-diketones yielding fulvenes.[5,6] In the course of our studies on the chemistry of some cyclopropenone derivatives[7,8] we found a novel cyclization reaction of 3-alkylthio-1,2-diphenylcyclopropenium salts (**2**) with 2,4-pentanedione (**3a**) or ethyl acetoacetate (**3b**).

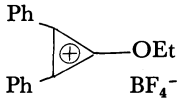

1

Diphenylcyclopropenethione reacted easily with alkyl halides, such as methyl bromide, ethyl iodide, or benzyl bromide, to give the corresponding cyclopropenium salts (**2a—c**) in good yields. A mixture of **2**, **3**, and triethylamine in approximately 1 : 1.2 : 2 molar ratio was stirred in benzene at room temperature for 20 min. Column chromatography of the products on silica gel afforded pale yellow crystals of the cyclopentadienols (**4**) (Table 1). The use of acetonitrile as reaction solvent or diisopropylamine as base lowered the yield of **4a**. Although many isomeric structures are mechanistically possible for the products, the ^{1}H- and ^{13}C-NMR, and mass spectra did not permit clear choice to be made.

Table 1. Reactions of cyclopropenium salts **2** or **11** with carbonyl compounds **3**.

Product	Reactant		R	R′	Yield/%[a]
4a	**2a**	**3a**	Me	Me	73, 59,[b] 61[c]
4b	**2a**	**3b**	Me	EtO	36
4c	**2b**	**3a**	Et	Me	71
4d	**2b**	**3b**	Et	EtO	45
4e	**2c**	**3a**	$PhCH_2$	Me	65
4f	**2c**	**3b**	$PhCH_2$	EtO	14
12a	**11**	**3a**	—	Me	73
12b	**11**	**3b**	—	EtO	61

Tertiary amine and solvent used: a) triethylamine in benzene, b) triethylamine in acetonitrile, c) diisopropylamine in acetonitrile.

The structure of 4-acetyl-5-hydroxy-5-methyl-1-methylthio-2,3-diphenylcyclopentadiene (**4a**) was ascertained by an X-ray crystal structure determination. There are two molecules of **4a** in the asymmetric unit and their relationship is shown in the stereo diagram, Fig. 1. Thermal ellipsoid plots of both molecules are shown in Fig. 2 and some of the more interesting bond lengths and angles are presented in Tables 2 and 3. There are no significant differences between the parameters for the two molecules. The two phenyl groups make angles of ≈58° (range 55.6—61°) in the same sense with the best plane through the respective cyclopentadiene ring. The bond length data suggests that there is electron delocalization from the sulfur atom through the butadiene system and into the acetyl group. In particular the S(1)–C(1) and C(2)–C(3) single bonds are shortened and the carbon-carbon and carbon-oxygen double bonds lengthened. The *S*-methyl carbons lie almost in the plane of their respective cyclopentadiene rings (deviation from plane: C(6)-0.307, C(6A)-0.211 Å)

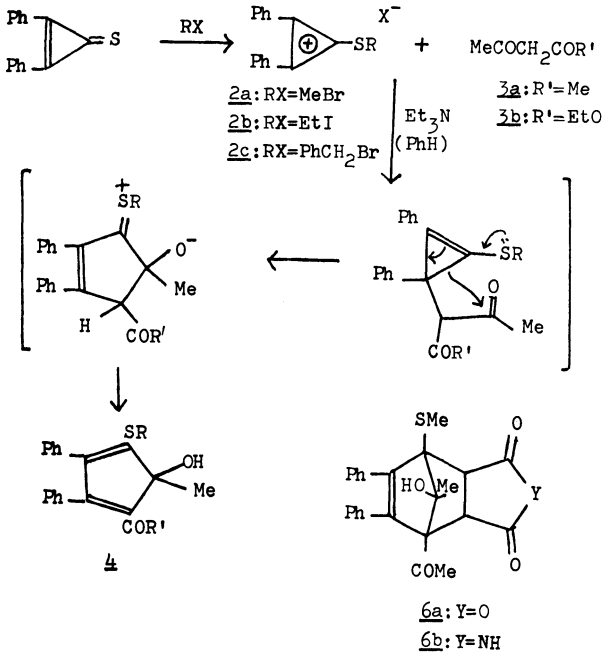

Scheme 1.

TABLE 2. BOND LENGTHS FOR **4a** WITH e.s.d.'s IN PARENTHESES

Bond length	l/Å	
	Molecule 1	Molecule 1A
S(1)–C(1)	1.744(6)	1.732(7)
S(1)–C(6)	1.769(8)	1.747(9)
O(1)–C(19)	1.235(7)	1.234(7)
O(2)–C(5)	1.440(7)	1.450(8)
C(1)–C(2)	1.359(8)	1.355(8)
C(1)–C(5)	1.504(8)	1.513(9)
C(2)–C(3)	1.389(8)	1.468(8)
C(2)–C(7)	1.481(8)	1.478(8)
C(3)–C(4)	1.351(8)	1.354(8)
C(3)–C(13)	1.484(8)	1.491(8)
C(4)–C(5)	1.523(8)	1.517(9)
C(4)–C(19)	1.456(8)	1.461(9)
C(5)–C(21)	1.525(9)	1.502(9)
C(19)–C(20)	1.502(9)	1.491(9)

Carbon-carbon bond lengths in the phenyl rings range between 1.361 and 1.397 Å with e.s.d.'s ranging from 0.008 to 0.011 Å.

TABLE 3. BOND ANGLES FOR **4a** WITH e.s.d.'s IN PARENTHESES

Bond angle	ϕ/°	
	Molecule 1	Molecule 1A
C(1)–S(1)–C(6)	107.4(4)	109.4(4)
S(1)–C(1)–C(2)	122.1(5)	124.0(5)
S(1)–C(1)–C(5)	126.4(5)	126.0(5)
C(2)–C(1)–C(5)	110.7(5)	109.6(6)
C(1)–C(2)–C(3)	107.3(5)	109.2(5)
C(1)–C(2)–C(7)	127.6(6)	126.0(6)
C(3)–C(2)–C(7)	125.2(5)	124.8(5)
C(2)–C(3)–C(4)	110.3(5)	109.3(5)
C(2)–C(3)–C(13)	119.7(5)	122.0(5)
C(4)–C(3)–C(13)	129.9(5)	128.8(6)
C(3)–C(4)–C(5)	108.6(5)	109.4(6)
C(3)–C(4)–C(19)	132.0(6)	132.1(6)
C(5)–C(4)–C(19)	119.3(6)	118.4(6)
O(2)–C(5)–C(1)	109.7(5)	109.5(6)
O(2)–C(5)–C(4)	111.7(5)	113.3(6)
O(2)–C(5)–C(21)	110.6(5)	110.5(5)
C(1)–C(5)–C(4)	102.6(5)	102.3(5)
C(1)–C(5)–C(21)	112.1(6)	111.3(6)
C(4)–C(5)–C(21)	110.0(5)	109.8(6)
O(1)–C(19)–C(4)	119.4(6)	118.4(7)
O(1)–C(19)–C(20)	117.9(6)	119.0(7)
C(4)–C(19)–C(20)	122.7(6)	122.4(6)

C–C–C bond angles at the phenyl ring carbons vary between 118.2 and 121.3° with e.s.d.'s ranging between 0.6 and 0.8°.

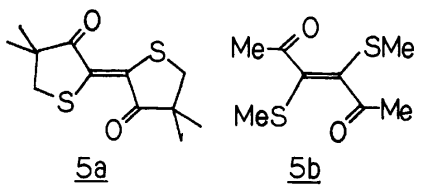

5a 5b

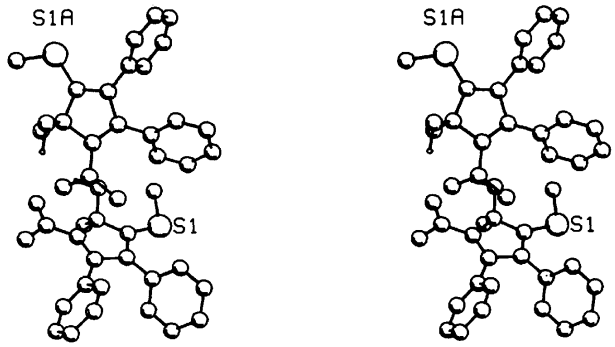

Fig. 1. A stereo view of the contents of the asymmetric unit of the crystal structure of **4a** drawn with SNOOPI.[10]

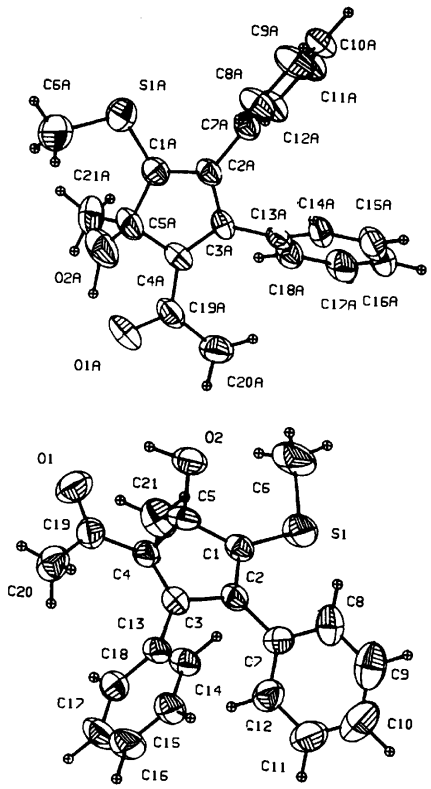

Fig. 2. Thermal ellipsoid plots, drawn at the 50% level of the two independent molecules of **4a** drawn with SNOOPI.[10]

suggesting that the conjugated sulfur lone pair is in an essentially p-type orbital. From a comparison with the accurately measured[9] bond length data for *trans*-$\Delta^{2,2'}$-bis(4,4-dimethylthiolan-3-one) (**5a**) and *trans*-3,4-bis-(methylthio)-3-hexene-2,5-dione (**5b**) it would appear that electron delocalization from sulfur into an acetys group through a butadiene system was more effectivel than through just one carbon-carbon double bond. Thus the average C(1)–S(1) bond and the average C(4)–C(19) bond in **4a** are both shorter (by 0.010 and 0.028 Å respectively) while all the double bonds are longer than the equivalent bonds in **5a** and **5b**. However this may be misleading since further shortening of the bonds

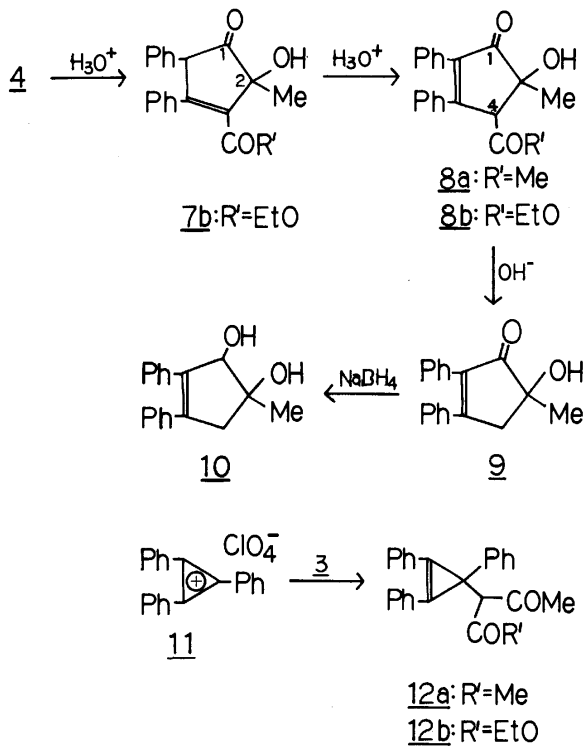

joining the sulfur and acetyl moieties to the double bond in **5a, b** would further reduce the distance between the sulfur and carbonyl oxygen which is already (2.8 Å) within the sum of the van der Waals radii for these two atoms (3.2 Å).

The other compounds listed in Table 1 and given similar structures have similar spectra. In agreement with the dienol structure, **4a** underwent Diels-Alder reactions with maleic anhydride and maleimide at room temperature in benzene to give the adducts **6a** and **6b** in 81 and 66% yields and both showed characteristic AB quartets due to the two methine protons in their ^{1}H-NMR spectra.

Chemical transformation of **4** yielded some new cyclopentene derivatives **7**—**10**, the structures of which are based on their spectra and the reagents employed. Raney nickel (W1 and W5) desulfurization of **4a** and **4b** gave only tarry mixtures.

On hydrolysis with a mixture of trifluoroacetic acid–mercury(II) chloride–water–chloroform, both **4a** and **4c** gave the cyclopentenone (**8a**) in 88 and 81% yield respectively. In the absence of the mercury(II) chloride the product was a tarry mixture. In contrast, **4b** and **4d** were hydrolyzed easily with hydrochloric acid in ethanol to give β,γ-unsaturated cyclic ketone **7b**, which isomerized to **8b** under further acid treatment.

On heating in aqueous sodium hydroxide **8a** and **8b** smoothly cleaved to yield the cyclopentenone (**9**) in good yields. This type of cleavage of vinylogous β-keto esters or diketones has been studied.[11]

Reduction of **9** with sodium borohydride gave the cyclic glycol **10** quantitatively. The structure of **7**—**10** are consistent with their ^{1}H- and ^{13}C-NMR, IR, and mass spectra. The mass spectra of **8**—**9** showed peaks at *m/e* 178, corresponding to PhC≡CPh, indicaing that the PhC=CPh grouping splits out intact; **7b** showed no such peak. Since ^{1}H- and ^{13}C-NMR spectra indicated that only one isomer was obtained for **8a**, **8b**, and **10**, their structures were not settled.

Eicher and his coworkers have reported reactions of **1**, with various carbon nucleophiles,[12] at position 1 or 3 of the cyclopropene ring depending on the conditions and reactant used.

Although the reactions of **2** with **3** were expected to give similar products to those obtained from **1**, several attempts (careful column chromatography or varieties of reaction conditions) to isolate products other than **4** were unsaccessful.

In contrast to the behavior of **2**, triphenylcyclopropenium perchlorate (**11**) with **3** in the presence of triethylamine in benzene produced the triphenylcyclopropenes (**12**) (Table 1). Their structures are clear from their ^{1}H-NMR (one proton exchanged by NaOD) and IR (2000—1700 cm^{-1} due to the cyclopropene ring) spectra. These cyclopropenes **12** were stable at 100 °C in the presence or absence of triethylamine.

The marked difference in reaction between **2** and **11** may be ascribed to electron-releasing properties of the alkylthio group.[13] The exact mechanism for the formation of **4** is not clear but most probably involves the formation of an intermediate corresponding to **12**, ring expansion, and proton movement as shown in Scheme 1.

Experimental

General. Melting points are uncorrected. The ^{13}C FT NMR spectra were recorded on a JEOL JNM FX-60 spectrometer (15.04 MHz), and ^{1}H-NMR spectra, on a Hitachi-Perkin Elmer R-24 (60 MHz). The IR spectra were recorded on a JASCO A-3 spectrometer.

Preparation of Alkylthiodiphenylcyclopropenium Salts (2a—c). The alkyl halide (25 mmol) was added in one portion to a solution of diphenylcyclopropenthione (4.3 g) in benzene (50 ml), and after 2 d at room temperature the precipitated salt **2** was collected, washed with dry benzene, and all solvent removed under reduced pressure. The following were prepared: *methylthiodiphenylcyclopropenium bromide (2a)*: yield 88%; mp 131—132 °C; ^{1}H-NMR ($CDCl_3$–10% CF_3CO_2H) δ=3.24 (3H, s, MeS) and 7.1—8.3 (10H, m, Ph). *Ethylthiocyclopropenium iodide (2b)*: yield 62%; mp 130—132 °C; ^{1}H-NMR ($CDCl_3$–10% CF_3CO_2H) δ=1.52 (3H, t, J=7.5 Hz, $\underline{Me}CH_2$), 3.66 (2H, q, CH_2), and 7.1—8.3 (10H, m, Ph). *Benzylthiodiphenylcyclopropenium bromide (2c)*: yield 79%; mp 131—134 °C; ^{1}H-NMR ($CDCl_3$–10% CF_3CO_2H) 5.09 (2H, s, $Ph\underline{C}H_2$) and 7.1—8.3 (15H, m, Ph).

The Reactions of Alkylthiodiphenylcyclopropenium Ions (2) with 2,4-Pentanedione (3a) or Ethyl Acetoacetate (3b). (a): Methylthiodiphenylcyclopropenium bromide with **3a**. A mixture of **2a** (10 mmol), **3a** (12 mmol), and triethylamine (20 mmol) in dry benzene (100 cm^3) was stirred for 20 min. After filtration from the precipitate, the benzene solution was concentrated and chromatographed over silica gel (petroleum ether : benzene : ethyl acetate, 10 : 2 : 1 v/v) to give *4-acetyl-5-hydroxy-5-methyl-1-methylthio-2,3-diphenyl-1,3-cyclopentadiene (4a)*, yellow crystals (73%): mp 105—106 °C; IR (KBr) 3300—3500 (OH) and 1615 cm^{-1} (CO); ^{1}H-NMR ($CDCl_3$) δ=1.79 (3H, s, MeCO), 1.82 (3H, s, $\underline{Me}COH$), 2.39 (3H, s, MeS), 4.36 (1H, s, OH), and 6.9—7.5 (10H, m, Ph); ^{13}C-NMR ($CDCl_3$) δ=15.0 (q, MeS), 27.1 (q, $\underline{Me}COH$), 29.7 (g, $\underline{Me}CO$) 87.2 (s, COH), 127.7 (d), 128.2 (d), 128.6 (d),

129.7 (d), 133.4 (s), 134.7 (s), 139.6 (s), 143.6 (s), 154.0 (s), 155.4 (s), and 196.0 (s, C=O); MS (*m/e*) 336 (M^+); Found: C, 74.73; H, 5.91%. Calcd for $C_{21}H_{20}O_2S$: C, 74.97; H, 5.99%.

Acetonitrile as reaction solvent gave 61% of **4a**, and replacing the triethylamine by diisorpylamine as well reduced the yield to 59%.

The subsequent reactions were carried out in benzene as described above. (*b*): Methylthiodiphenylcyclopropenium bromide (**2a**) with ethyl acetoacetate (**3b**) yielded *4-ethoxycarbonyl-5-hydroxy-5-methyl-1-methylthio-2,3-diphenyl-1,3-cyclopentadiene* (***4b***) (36%): mp 96—97 °C; IR (KBr) 3300—3500 (OH) and 1670 cm^{-1} (C=O); ^{1}H-NMR ($CDCl_3$) δ=0.99 (3H, t, J=7.5 Hz, MeCH$_2$), 1.78 (3H, s, MeCO), 2.31 (3H, s, MeS) 3.88 (1H, s, OH), 4.06 (2H, q, MeCH$_2$), and 7.0—7.6 (10H, m, Ph); ^{13}C-NMR ($CDCl_3$) δ=13.6 (q, MeS), 15.1 (q, MeCH$_2$O), 21.6 (q, MeCOH), 59.9 (t, CH$_2$O), 86.1 (s, COH), 127.1 (d), 127.5 (d), 128.1 (d), 129.7 (d), 133.5 (s), 134.2 (s), 134.7 (s), 139.9 (s), 154.2 (s), 155.1 (s), and 164.1 (s, CO$_2$); MS (*m/e*) 366 (M^+); Found: C, 71.74; H, 5.98%. Calcd for $C_{22}H_{22}O_3S$: C, 72.12; H, 6.05%. (*c*): Ethylthiodiphenylcyclopropenium iodide (**2b**) with 2,4-pentanedione (**3a**) yielded *4-acetyl-1-ethylthio-5-hydroxy-5-methyl-2,3-diphenyl-1,3-cyclopentadiene* (***4c***) (71%): mp 107—107.5 °C; IR (KBr) 3300—3500 (OH) and 1610 cm^{-1} (CO); ^{1}H-NMR ($CDCl_3$) δ=1.13 (3H, t, J=7.5 Hz, MeCH$_2$), 1.74 (3H, s, MeC=O), 1.78 (3H, s, MeCOH), 2.4—3.6 (2H, m, CH$_2$), 4.05 (1H, s, OH), and 6.8—7.4 (10H, m, Ph); ^{13}C-NMR ($CDCl_3$) δ=15.1 (q, MeCH$_2$), 25.8 (t, CH$_2$S), 27.5 (q, MeCOH), 29.4 (q, MeC=O), 87.2 (s, COH), 127.7 (d), 128.2 (d), 128.6(d), 129.6(d), 133.6 (s), 134.8 (s), 140.6 (s), 144.0 (s), 153.4 (s), 155.2 (s), and 195.9 (s, C=O); MS (*m/e*) 350 (M^+); Found: C, 75.50; H, 6.28%. Calcd for $C_{22}H_{22}O_2S$: C, 75.40; H, 6.23%. (*d*) Ethylthiodiphenylphenylcyclopropenium iodide (**2b**) with ethyl acetoacetate (**3b**) yielded *4-ethoxycarbonyl-1-ethylthio-5-hydroxy-5-methyl-2,3-diphenyl-1,3-cyclopentadiene* (***4d***) (45%): mp 62—63 °C; IR (KBr) 3300—3500 (OH) and 1660 cm^{-1} (CO): ^{1}H-NMR ($CDCl_3$) δ=0.98 (3H, t, J=7.5 Hz, MeCH$_2$O), 1.15 (3H, t, J=7.5 Hz, MeCH$_2$S), 1.77 (3H, s, MeCOH), 2.4—3.6 (2H, m, CH$_2$), 4.08 (2H, q, J=7.5 Hz, CH$_2$O), and 6.8—7.4 (10H, m, Ph); ^{13}C-NMR ($CDCl_3$) δ=13.7 (q, MeCH$_2$S), 15.2 (q, MeCH$_2$O), 25.8 (t, CH$_2$S), 26.4 (q, MeCOH), 59.9 (t, CH$_2$O), 86.1 (s, COH), 127.0 (d), 127.3 (d), 127.6 (d), 127.7 (d), 128.9 (d), 129.6 (d), 133.7 (s), 134.2 (s), 135.2 (s), 141.1 (s), 150.5 (s), 154.1 (s), and 164.2 (s, CO$_2$); MS (*m/e*) 380 (M^+); Found: C, 72.50; H, 6.48%. Calcd for $C_{23}H_{24}O_3S$: C, 72.60; H, 6.36%. (*e*): Benzylthiodiphenylcyclopropenium bromide (**2c**) with 2,4-pentanedione (**3a**) yielded *4-acetyl-1-benzylthio-5-hydroxy-5-methyl-2,3-diphenyl-1,3-cyclopentadiene* (***4e***) (65%): mp 116—117 °C; IR (KBr) 3300—3500 (OH) and 1620 cm^{-1} (CO); ^{1}H-NMR ($CDCl_3$) δ=1.76 (3H, s, MeCO), 1.99 (3H, s, MeCOH), 4.04 and 4.30 (2H, ABq, J=13 Hz, CH$_2$), 4.16 (1H, s, OH), and 6.7—7.4 (15H, m, Ph); MS (*m/e*) 412 (M^+); Found: C, 78.61; H, 5.97%. Calcd for $C_{27}H_{24}O_2S$: C, 78.61; H, 6.06%. (*f*): Benzylthiodiphenylcyclopropenium bromide (**2c**) with ethyl acetoacetate (**3b**) gave *1-benzylthio-4-ethoxycarbonyl-5-hydroxy-5-methyl-2,3-diphenyl-1,3-cyclopentadiene* (***4f***) (14%): mp 120—121 °C; IR (KBr) 3300—3500 (OH) and 1675 cm^{-1} (CO); ^{1}H-NMR ($CDCl_3$) δ=0.98 (3H, t, J=7.5 Hz, MeCH$_2$), 1.76 (3H, s, MeCOH), 4.08 (2H, q, CH$_2$O), 4.08 (1H, s, OH), 4.13 (2H, s, PhCH$_2$) and 6.6—7.7 (15H, m, Ph); MS (*m/e*) 442 (M^+); Found; C, 76.28; H, 6.09%. Calcd for $C_{28}H_{26}O_3S$: C, 75.99; H, 5.92%.

Diels-Alder Reaction of ***4a***. (*a*): A solution of **4a** (1 mmol) and maleic anhydride (2 mmol) in benzene (25 cm^3) was stirred at room temperature for 3 h. The precipitate of needles was collected, washed with small amount of benzene, and dried to give *the adduct* **6a** (81%): mp 151—165 °C; IR (KBr) 3450 (OH), 1855, 1770, and 1690 cm^{-1}; ^{1}H-NMR ($CDCl_3$–DMSO-d_6 1/1) δ=1.63 (3H, s, MeCOH), 2.03 (3H, s, MeCO), 2.22 (3H, s, MeS), 3.10 (1H, bs, OH), 4.33 (1H, d, J=9 Hz, CH), 4.83 (1H, d, CH), and 6.6—7.6 (10H, m, Ph) MS (*m/e*) 434 (M^+); Found: C, 68.54; H, 5.01%. Calcd for $C_{25}H_{20}O_5S$: C, 69.11; H, 5.10%. (b) A solution of **4a** (1 mmol) and maleimide (1 mmol) in ethanol (50 cm^3) was left at room temperature for 3 h. The solvent was removed *in vacuo* and the residual crystalline mass washed with benzene and hot ethanol to yield *the adduct* **6b** (66%): mp 234—238 °C; IR (KBr) 3475 (OH), 1860, 1780, and 1700 cm^{-1} (CO); ^{1}H-NMR ($CDCl_3$: DMSO-d_6, 1 : 1) δ=1.06 (3H, s, MeCOH), 2.14 (3H, s, MeCO), 2.16 (3H, s, MeS), 3.24 (1H, s, OH), 3.86 (1H, d, J=7.5 Hz, CH), 4.52 (1H, d, CH), 5.91 (1H, s, NH), and 6.6—7.3 (10H, m, Ph); MS (*m/e*) 443 (M^+); Found: C, 68.44; H, 5.12; N, 3.10%. Calcd for $C_{25}H_{21}NO_4S$: C, 69.26; H, 5.35; N, 3.23%.

Hydrolysis of ***4a***. A mixture of **4a** (160 mg, 0.48 mmol), mercury(II) chloride (260 mg, 0.96 mmol), trifluoroacetic acid (0.56 cm^3, 48 mmol), water (0.4 cm^3), and chloroform (15 cm^3) was vigorously stirred at room temperature for 3 d. Water (15 cm^3) was added and the organic layer separated. Removal of the solvent and chromatography of the residue over silica gel (chloroform: ethyl acetate, 3 : 1, v/v) yielded *4-acetyl-5-hydroxy-5-methyl-2,3-diphenyl-2-cyclopentenone* (**8a**) (88 %): mp 184—185 °C (2-propanol); IR (KBr) 3450 (OH), 1700, 1690 (sh) (CO), and 1620 cm^{-1}; ^{1}H-NMR ($CDCl_3$) δ=1.60 (3H, s, MeCOH), 2.20 (3H, s, MeCO), 2.92 (1H, OH, D_2O exchangeable), 4.28 (1H, s, CH), and 7.28—7.31 (10H, m, Ph); ^{13}C-NMR ($CDCl_3$) δ=27.3 (q, MeCOH), 30.5 (q, MeCO), 67.7 (d, C_4H), 78.4 (s, C_5), 128.3 (d), 128.6 (d), 128.8 (d), 129.2 (d), 129.5 (d), 130.5 (d), 131.2 (s), 134.2 (s), 138.0 (s), 163.2 (s), 204.9 (s, MeC=O), and 206.8 (s, C_1=O); MS (*m/e*) 304 (M^+); Found: C, 78.28; H, 5.83%. Calcd for $C_{20}H_{18}O_3$: C, 78.41; H, 5.92%.

Hydrolysis of ***4b*** *to* ***7b***. A solution of **4b** (270 mg, 0.55 mmol) and concentrated hydrochloric acid (0.4 cm^3) in ethanol (10 cm^3) was stirred at 10 °C for 2 d. The mixture was quenched with water and the product was extracted with chloroform. The extract was dried and evaporated under reduced pressure to give colorless crystals of *3-ethoxycarbonyl-2-hydroxy-2-methyl-4,5-diphenyl-3-cyclopentenone* (***7b***) (86% crude yield) which after recrystallization from 2-propanol (48%) has mp 150—151 °C: IR (KBr) 3450 (OH), 1730, 1710 (CO), and 1630 cm^{-1}; ^{1}H-NMR ($CDCl_3$) δ=1.16 (3H, t, J=7 Hz, MeCH$_2$), 1.60 (3H, s, MeC$_2$), 3.01 (1H, s, OH), 4.06 (1H, s, CH), 4.07 (2H, q, CH$_2$), and 7.0—7.4 (10H, m, Ph); ^{13}C-NMR ($CDCl_3$) δ=13.7 (q, MeCH$_2$), 26.4 (q, MeCOH), 61.0 (d, C_5H), 61.7 (t, CH$_2$), 78.1 (s, C_2), 128.3 (d), 128.5 (d), 129.2 (d), 130.0 (d), 130.3 (d), 131.3 (s), 134.1 (s), 137.9 (s), 161.0 (s), 169.6 (s, CO$_2$), and 206.2 (s, C_1=O); MS (*m/e*) 396 (M^+); Found: C, 75.08; H, 5.83%. Calcd for $C_{21}H_{20}O_4$: C, 74.98; H, 5.99%.

Similar treatment of **4d** yielded **7b** in 83% yield.

Isomerization of ***4b*** *to* ***8b***. A solution of **4b** (0.5 mmol) and concentrated HCl (1 cm^3) in ethanol (10 cm^3) was left at 25 °C for 2 d. The mixture was quenched with water, extracted with chloroform and the dried extracts evapolated *in vacuo* to yield a crystalline mass of *4-ethoxy-5-hydroxy-5-methyl-2,3-diphenylcyclopent-2-enone* (***8b***) (83%) mp: 158—159 °C (benzene–petroleum ether); IR (KBr) 3470 (OH), 1730, and 1710 cm^{-1} (CO); ^{1}H-NMR ($CDCl_3$) δ=1.06 (3H, t, J=7.5 Hz, MeCH$_2$), 1.46 (3H, s, MeC$_5$), 3.13 (1H, s, OH, D_2O exchangeable), 4.08 (2H, q, CH$_2$), 4.27 (1H, s, CH), and 7.0—7.5 (10H, m, Ph); ^{13}C-NMR ($CDCl_3$) δ=14.0 (q, MeCH$_2$), 21.7 (q, Me), 60.0 (t, CH$_2$), 61.2 (d, CH), 77.2 (s,

MeCOH), 128.4 (d), 128.4 (d), 129.5 (d), 130.1 (d), 130.9 (s), 134.3 (s), 137.3 (s), 163.5 (s), 169.8 (s, CO_2), and 206.3 (s, C=O); MS (*m/e*) 396 (M^+) and 178 (PhC≡CPh); Found: C, 74.75; H, 5.85%. Calcd for $C_{21}H_{20}O_4$: C, 74.98; H, 5.99%.

The compound **8b** was prepared in the same way from **7b** in 96% yield.

*Preparation of 2,3-Diphenyl-5-hydroxy-5-methylcyclopent-2-en-1-one (**9**).* A suspension of **8a** (272 mg, 0.89 mmol) in 20% aqueous hydroxide (15 cm^3) was refluxed for 20 min. The first formed red solution precipitated crystals. After cooling these were collected and purified by chromatography over silica gel (ethyl acetate : chloroform, 1 : 3, v/v) to give **9** (60%): mp 146—147 °C (benzene); IR (KBr) 3425 (OH) and 1690 cm^{-1} (CO); ^{1}H-NMR ($CDCl_3$) δ=1.53 (3H, s, Me), 2.68 (1H, s, OH), 2.94 and 3.31 (2H, d, J=18 Hz, CH_2), and 7.1—7.4 (10H, m, Ph); ^{13}C-NMR ($CDCl_3$) δ=24.1 (q, Me), 44.2 (t, CH_2), 73.2 (COH), 126.4 (d), 126.8 (d), 127.7 (d), 128.6 (d), 130.4 (s), 133.4 (s), 134.2 (s), 163.5 (s), and 207.2 (s, C=O); MS (*m/e*) 264 (M^+) and 178 (PhC≡CPh); Found: C, 81.55; H, 6.00%. Calcd for $C_{18}H_{16}O_2$: C, 81.79; H, 6.10%. similar treatment of **8b** with aqueous sodium hydroxide yielded **9** in a 74% yield.

*Reduction of **9** with Sodium Borohydride.* A solution of **9** (1 mmol) and sodium borohydride (1 mmol) in ethanol (25 cm^3) was stirred at room temperature for 1 d, quenched with water and extracted with chloroform. The extract was chromatographed over silica gel (chloroform : ethyl acetate, 3 : 1, v/v) to yield *3,4-diphenyl-1-methyl-3-cyclopentene-1,2-diol (**10**)* (75%): mp 110—111 °C; IR (KBr) 3100—3700 cm^{-1} (OH); ^{1}H-NMR ($CDCl_3$) δ=1.45 (3H, s, Me), 2.20 (2H, s, OH), 2.58 and 3.20 (2H, d, J=16 Hz, CH_2), 4.07 (1H, s, CH), and 7.1—7.3 (10H, m, Ph); MS (*m/e*) 266 (M^+) and 178 (PhC≡CPh); Found: C, 80.58; H, 6.84%. Calcd for $C_{18}H_{18}O_2$: C, 81.17; H, 6.81%.

*Reactions of Triphenylcyclopropenium Perchlorate (**11**). (a) With 2,5-Pentanedione (**3a**)*: A mixture of **11** (0.5 mmol), **3a** (0.6 mmol), and triethylamine (1.0 mmol) in benzene (10 cm^3) was stirred for 20 min. The solution was concentrated and chromatographed over silica gel (petroleum ether : ethyl acetate, 4 : 1, v/v). Evaporation of the elute gave a solid which recrystallized from 2-propanol to give *3-(1,2,3-triphenyl-2-cyclopropenyl)-2,4-pentanedione (**12a**)* (73%): mp 135—137 °C; IR (KBr) 1810, 1730, and 1700 cm^{-1}; ^{1}H-NMR ($CDCl_3$) δ=2.07 (6H, s, MeCO), 5.22 (1H, s, CH), and 7.0—8.1 (15H, m, Ph); ^{13}C-NMR ($CDCl_3$) δ=31.2 (q, Me), 33.0 (s, C_3), 72.1 (d, CH), 116.9 (s), 125.9 (d), 126.2 (d), 128.0 (d), 128.2 (s), 128.3 (d), 128.6 (d), 128.9 (d), 129.7 (d), 144.3 (s), and 204.2 (C=O); MS (*m/e*) 366 (M^+); Found: C, 85.28; H, 6.00%. Calcd for $C_{26}H_{22}O_2$: C, 85.22; H, 6.05%. *(b) With Ethyl Acetoacetate **3b***: A mixture of **11** (0.5 mmol), ethyl acetoacetate **3b** (0.6 mmol), and triethylamine (1 mmol) in benzene yielded *ethyl 2-(1,2,3-triphenyl-2-cyclopropenyl)-3-oxobutyrate (**12b**)* (61%): mp 133—134 °C; IR (KBr) 1950, 1890, 1730, and 1710 cm^{-1}; ^{1}H-NMR ($CDCl_3$) δ=0.94 (3H, t, J=7 Hz, MeCH$_2$) 2.12 (s, MeCO), 3.98 (2H, q, CH_2O), 4.96 (1H, CH), and 7.1—8.0 (15H, m, Ph); ^{13}C-NMR ($CDCl_3$) δ=13.6 (q, MeCH$_2$), 30.3 (q, MeCO), 32.5 (s, C_3), 61.1 (t, CH_2O), 64.6 (d, CH), 116.0 (s), 116.3 (s), 125.8 (d), 126.2 (s), 128.0 (s), 128.2 (d), 128.7 (d), 129.0 (d), 129.7 (d), 129.8 (d), 144.2 (s), 169.1 (s, CO_2), and 202.5 (s, COMe); MS (*m/e*) 396(M^+); Found: C, 81.99; H, 6.28%. Calcd for $C_{27}H_{24}O_3$: C, 81.79; H, 6.10%.

Crystal Structure Determination. Crystal Data: $C_{21}H_{20}O_2S$, M_r 336.5, monoclinic, $P2_1/n$, a=10.365(4), b=24.659(8), c=14.394(5) Å, β=101.63(3)°, U=3603.4 Å, Z=8, D_c=1.25 g cm^{-3}, μ=0.19 mm^{-1} (Mo $K\alpha$), R=0.053 for 2225 observed reflections.

A crystal of **4a** mounted on a glass fibre, was transferred to a CAD-4F four-circle diffractometer. Cell dimensions were determined from the positions of strong reflections located by the SEARCH routine and intensity data was collected by $\omega/2\theta$ scans out to 2θ=44° with periodic checking of the intensity and orientation of three standered reflections. After the application of Lorentz and polarization corrections, elimination of systematic absences and the merging of equivalent reflections, 3520 structure amplitudes were derived. The structure was solved using MULTAN 80[14] whic hlocated all but one of the non-hydrogen atoms. The structure was refined by blocked-matrix least squares with isotropic temperature factors and with Waser constrains[15] applied to the phenyl ring (bond lengths: 1.40 Å, e.s.d. 0.01 Å, bond angles: 120°, e.s.d. 0.5°). The missing atom was located by a difference Fourier synthesis and refinement continued with anisotropic temperature factors. The hydroxyl hydrogen atoms were placed from a difference Fourier synthesis but all the other hydrogens were placed geometrically and all were assigned an isotropic temperature factor of 0.075 and excluded from the refinement. The constrains on the phenyl ring were removed and weights for the final rounds of refinement were computed from Chebyshev series $w=[19.33t_0(x)+25.87t_1(x)+8.733t_2(x)]^{-1}$, where $(x)=F_o/F_{max}$.[16] The structure converged at an R-value of 0.053. All calculations were performed with the CRYSTALS[17] package on a VAX 11/750 computer.

References

1) E. A. Chandross and G. Smolinsky, *Tetrahedron Lett.*, **1960**, 19.

2) S. Yoneda, H. Hirai, and Z. Yoshida, *Chem. Lett.*, **1976**, 1051.

3) T. Eicher and D. Lerch, *Tetrahedron Lett.*, **21**, 3751 (1980).

4) S. Yoneda, H. Hirai, and Z. Yoshida, *Heterocycles*, **15**, 865 (1981).

5) T. Eicher and A. Loschner, *Z. Naturforsch., B*, **21**, 295 (1966).

6) T. Eicher and A. Loschner, *Z. Natursch., B*, **21**, 899 (1966).

7) H. Yoshida, M. Nakajima, and T. Ogata, *Synthesis*, **1981**, 36.

8) H. Yoshida, M. Nakajima, T. Ogata, and K. Matsumot, *Bull. Chem. Soc. Jpn.*, **55**, 1973 (1982).

9) H. L. Ammon and H. Hermann, *J. Org. Chem.*, **43**, 4581 (1978).

10) E. K. Davies, SNOOPI User Guide, Chemical Crystallography Laboratory, University of Oxford, Oxford, 1981.

11) H. O. House, "Modern Synthetic Reactions," 2nd ed, W. A. Benjamin Inc., Menlo Park, California (1972), p. 518.

12) T. Eicher and A. Hansen, *Chem. Ber.*, **102**, 319 (1969).

13) E. Block, "Reactions of Organosulfur Compounds," Academic Press, New York (1978).

14) P. Main, "MULTAN 80. A System of Computer Programs for the Automatic Solution of Crystal Structures from X-ray Diffraction Data," Department of Physics, University of York, York (1980).

15) J. S. Rollet, "Crystallographic Computing," ed by F. R. Ahmed, Munksgaard, Copenhagen (1970), p. 170.

16) J. R. Carruthers and D. J. Watkin, *Acta Crystallogr., Sect. A*, **35**, 698 (1979).

17) D. J. Watkin and J. R. Carruthers, CRYSTALS User Guide, Chemical Crystallography Laboratory, University of Oxford, Oxford.

Stereoselective Syntheses of 3-Acetyl-1,2-dimethyl-1-cyclopentanols. Syntheses of *dl*-Plinols A, B, and C

Takeshi IMAGAWA, Kazuyuki MATSUURA, Nobuyuki MURAI, Tetsuo AKIYAMA, and Mituyosi KAWANISI*

Department of Industrial Chemistry, Faculty of Engineering, Kyoto University, Sakyo-ku, Kyoto 606

(Received May 9, 1983)

c- and *t*-3-Acetyl-1,*c*-2-dimethyl-*r*-1-cyclopentanols and *c*-3-acetyl-1,*t*-2-dimethyl-*r*-1-cyclopentanol are synthesized stereoselectively and *dl*-plinols A, B, and C are prepared therefrom.

Isomeric 3-acetyl-1,2-dimethyl-1-cyclopentanols have been obtained by ozonolysis of four isomeric plinols separated gas-chromatographically from a mixture of A, B, C, and D, which was derived from linalool by ene reaction.[1] Meanwhile, the title cyclopentanols have been recognized[2] as the key substance for synthesis of a variety of terpenoids. For instance, cyclonerodiol, a biogenetically important fungal metabolite, has been synthesized from an isomer of the cyclopentanols.[3] However, procurement of the aforementioned plinols in stereochemically pure state is not necessarily easy task. Therefore, facile preparation of each cyclopentanol isomer seems highly desirable.

In this report we wish to describe a streoselective synthesis of *c*- and *t*-acetyl-1,*c*-2-dimethyl-*r*-1-cyclopentanols (**1** and **2**, respectively) and *c*-3-acetyl-1,*t*-2-dimethyl-*r*-1-cyclopentanol (**3**) by a methodology based on Wagner-Meerwein rearrangement of 7-oxabicyclo[2.2.1]hept-2-yl cation to 2-oxabicyclo[2.2.1]hept-3-yl cation employing anodic oxidative decarboxylation.[4]

Additionally the transformation of the cyclopentanols into *dl*-plinols A, B, and C is described.

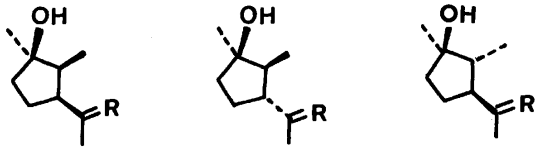

1 : R = O 2 ; R = O 3 : R = O

6 ; R = CH_2 4 : R = CH_2 5 : R = CH_2

Results and Discussion

The anhydride **8**,[5] obtained from the Diels-Alder adduct (**7**) of maleic anhydride and 2,5-dimethylfuran followed by hydrogenation, was reduced by sodium borohydride to give lactone **9**. Lactone **9** was treated with benzenethiolate anion to afford carboxylic acid **10**. Raney nickel desulfurization of **10** gave *exo*-methyl carboxylic acid **11** in 31% overall yield from **7**.

Acid **11** was electrolyzed in methanolic solution with addition of sodium methanolate using graphite electrodes to give cyclic acetal **12**.[4] Addition of aqueous acetic acid to this mixture gave ketone **1** in 84% yield. The configuration of this compound was obvious from consideration of the reaction course as well as from comparison with the reported data.[1] It was further established by transformation into *dl*-plinol C (**6**) as follows.

Methylenation of **1** with dibromomethane–zinc–titanium tetrachloride[6] gave exclusively *dl*-plinol C (**6**) in 50% yield. Its structure was confirmed by comparison with the reported spectral data.[1]

Alternatively the methyl ketone **1** was efficiently epimerized[1,3] to isomeric ketone **2** which was a synthetic intermediate for cyclonerodiol.[3] Methylenation of ketone **2** in the same manner yielded *dl*-plinol A (**4**) in 66% yield.

The *endo*-anhydride **17** obtained from the Diels-Alder adduct (**13**) of 2,5-dimethylfuran and dimethyl acetylenedicarboxylate gave lactone **18** by sodium borohydride reduction. Cleavage of lactone **18** by benzenethiolate anion, followed by desulfurization gave *endo*-methyl carboxylic acid **20** isomeric to **11** in 77% yield.

Similarly, electrolysis of **20** followed by hydrolysis gave stereoselectively *trans*-methyl ketone **3** in 63% yield. Methylenation of **3** gave *dl*-plinol B (**5**) in 51% yield.

In summary three isomeric 3-acetyl-1,2-dimethyl-1-cyclopentanols were prepared in stereochemically pure form and it was demonstrated that they are useful starting materials for synthesis of natural products.

Experimental

All mp's were uncorrected. Distillation was performed on a Buchi Kugelrohr apparatus. ^{1}H-NMR spectra were obtained with a Varian EM-360 or EM-390 spectrometer using tetramethylsilane as an internal standard. ^{13}C-NMR spectra were obtained with a Varian CFT-20 spectrometer in $CDCl_3$ solution unless otherwise noted, using tetramethylsilane as an internal standard. IR spectra were recorded with a Shimazu IR-27 spectrophotometer as Nujol mull.

Synthesis of c-*3-Acetyl-1,*c-*2-dimethyl-*r-*1-cyclopentanol (1).*

(a) Hydrogenation of 7: Hydrogenation of 5.23 g (26.9 mmol) of **7** in 30 ml of ethyl acetate using palladium black catalyst (0.5 g) gave 5.03 g (95%) of the product **8** after filtration, removal of the solvent and distillation; mp 126.2—126.7 °C (lit,[5] 121.5 °C); ^{1}H-NMR ($CDCl_3$): δ=3.16 (s, 2H), 1.81 (s, 4H), 1.64 (s, 6H).

(b) exo-*3-Hydroxymethyl-1,4-dimethyl-7-oxabicyclo[2.2.1]heptane-*exo-*2-carboxylic Lactone (9)*: To an ice-cooled and stirred solution of 2.8 g (73.7 mmol) of $NaBH_4$ in 100 ml of dry EtOH 9.03 g (46.0 mmol) of the anhydride **8** was added slowly. After the evolution of the reaction heat subsided, the reaction mixture was kept for 3 h at room temp and 35 ml of 5 M hydrochloric acid (1 M=1 mol dm^{-3}) was added with cooling in an ice bath. The solution was diluted with water and extracted with dichloromethane. The organic layer was dried over anhydrous Na_2SO_4 and concentrated *in vacuo*. Distillation gave 7.41 g (88%) of **9**; bp 116—117 °C/3 kPa; ^{1}H-NMR ($CDCl_3$): δ=4.5—4.1 (m, 2H), 2.2—2.9 (2H), 1.74 (m, 4H), 1.59 (s, 3H), 1.47 (s, 3H); ^{13}C-NMR: δ=176.6 (s), 85.8 (s),

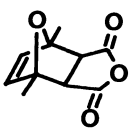

7

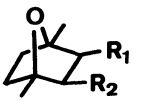

8 : R_1, R_2 = -COOCO-
9 : R_1, R_2 = $-CH_2OCO-$
10 : R_1 = CH_2SPh, R_2 = COOH
11 : R_1 = CH_3, R_2 = COOH

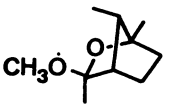

12

13

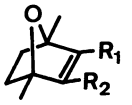

14 : R_1 = R_2 = COOMe
15 : R_1 = R_2 = COOH

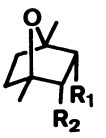

16 : R_1 = R_2 = COOH
17 : R_1 = R_2 = -COOCO-
18 : R_1 = R_2 = $-CH_2OCO-$
19 : R_1 = CH_2SPh, R_2 = COOH
20 : R_1 = CH_3, R_2 = COOH

85.0 (s), 68.7 (t), 52.7 (d), 48.0 (d), 38.7 (t), 37.5 (t), 18.0 (q), 17.4 (q); MS: *m/e* 182 (M^+, 1), 124, 98 (100), 97, 43. Found: C, 66.20; H, 7.83%. Calcd for $C_{10}H_{14}O_3$: C, 65.92; H, 7.74%.

*(c) 1,4-Dimethyl-*exo*-3-phenylthiomethyl-7-oxabicyclo[2.2.1]-heptane-*exo*-2-carboxylic Acid (**10**)*: Sodium benzenethiolate, freshly prepared from 0.74 g (32 mmol) of Na and 3.5 ml (34 mmol) of benzenethiol by stirring overnight at room temp. and evaporation of the solvent (THF), and 2.374 g (13.03 mmol) of **9** were dissolved in 25 ml of DMF. The solution was heated at 130 °C for 16 h. After having been cooled to room temp, the reaction mixture was acidified with 20 ml of 2 M hydrochloric acid and extracted with dichloromethane. The organic layer was extracted with 2% aq NaOH four times (30 ml×2, 20 ml×2). The combined aqueous layer was acidified and extracted with diethyl ether. The organic layer was dried over anhydrous Na_2SO_4 and concentrated *in vacuo*. Crude crystals thus obtained were recrystallized from benzene to give 2.468 g (65%) of pure **10**; mp 122.0—124.0 °C; ^{1}H-NMR ($CDCl_3$): δ=7.4 (m, 5H), 3.3—2.9 (3H), 2.42 (m, 1H), 1.70 (bs, 4H), 1.52 (s, 3H), 1.48 (s, 3H); ^{13}C-NMR: δ 177.4 (s), 135.7 (s), 129.9 (d), 128.9 (d), 126.3 (d), 85.2 (s), 84.9 (s), 56.1 (d), 49.8 (d), 39.3 (t), 38.7 (t), 33.0 (t), 18.3 (q), 17.8 (q) Found: C, 65.57; H, 6.98; S, 11.13%. Calcd for $C_{16}H_{20}O_3S$: C, 65.73; H, 6.89; S, 10.96%.

*(d) 1,*exo*-3,4-Trimethyl-7-oxabicyclo[2.2.1]heptane-*exo*-2-carboxylic Acid (**11**)*: To a solution of 6.04 g of NaOH and 612 mg (2.093 mmol) of **10** in 40 ml of water, 3.06 g of Ni–Al alloy was added slowly with cooling with running water. After addition of the alloy the suspension was stirred for 1 h and refluxed for 2.5 h. The Raney nickel was removed by filtration and the filtrate was acidified with hydrochloric acid. Extraction with diethyl ether, drying over Na_2SO_4, removal of the solvent, and distillation gave 364 mg (94%) of **11**; mp 67.5—68.5 °C; ^{1}H-NMR ($CDCl_3$): δ=9.1 (COOH), 2.95 (d, 1H), 2.3 (m, 1H), 1.70 (bs, 4H), 1.54 (s, 3H), 1.37 (s, 3H), 0.98 (d), 3H); ^{13}C-NMR: δ=174.6 (s), 85.8(s), 84.5 (s), 58.4 (d), 44.0 (d), 39.3 (t), 38.4 (t), 18.6 (q), 17.4 (q), 13.3 (q); MS: *m/e* 184 (M^+, 15), 169, 139, 123, 109, 97 (100). Found: C, 64.93; H, 8.79%. Calcd for $C_{10}H_{16}O_3$: C, 65.19; H, 8.75%.

*(e) Electrolysis of **11***: A solution of 351 mg (1.906 mmol) of **11** and 30 mg of NaOMe in 25 ml of dry MeOH was electrolyzed using graphite electrode in an undivided cell with ice cooling. After **11** had been consumed, 4 ml of water and 1 ml of AcOH were added to the reaction mixture. The solution was kept overnight at room temp. and concentrated *in vacuo*. The residue was diluted with water, neutralized with $NaHCO_3$ and extracted with dichloromethane. The organic layer was washed with sat. aq NaCl, dried over Na_2SO_4, concentrated, and distilled to give 250 mg (84%) of **1**; ^{13}C-NMR: δ=216.4 (s), 79.3 (s), 54.9 (d), 46.4 (d), 41.6 (t), 32.4 (q), 26.6 (t), 24.8 (q), 9.1 (q); other spectral data of **1** were in accord with those previously reported.[1]

Synthesis of dl-*Plinol C (**6**)*. To a suspension of 779 mg (11.9 mmol) of zinc powder in 10 ml of dry THF, 756 mg (4.35 mmol) of CH_2Br_2 was added under argon atmosphere. At 0 °C 3.0 ml of 1 M solution of $TiCl_4$ in CH_2Cl_2 was added and stirring was continued for 20 min. A solution of 44.4 mg of **1** in 2 ml of THF was added to this solution. After having been stirred overnight at r.t., the mixture was diluted with 10 ml of diethyl ether and 20 ml of 1 M hydrochloric acid and stirring was continued for an additional hour. Ether extract of the solution was washed with sat. aq NaCl, dried over Na_2SO_4, concentrated, and distilled to give 21.9 mg (50%) of *dl*-plinol C (**6**); ^{13}C-NMR: δ=148.2 (s), 110.6 (t), 80.3 (s), 48.9 (d), 45.7 (d), 39.5 (t), 29.4 (q), 25.5 (t), 23.3 (q), 9.3 (q); other spectra were identical with the reported full spectra.[1] (−)-Plinols C and B are reported to be crystals[1] but *dl*-plinols C and B were obtained as oils.

Preparation of t-*3-Acetyl-1,*c-*2-dimethyl-*r-*1-cyclopentanol (**2**)*. Isomerization of **1** (123 mg; 0.787 mmol) was performed by the published procedure[3] to give 107 mg (87%) of **2**; ^{13}C-NMR: δ=211.3 (s), 80.7 (s), 57.8 (d), 46.2 (d), 40.2 (t), 29.8 (q), 25.8 (q), 11.6 (q); other spectral data were consistent with those previously reported.[1]

Synthesis of dl-*Plinol A (**4**)*. *dl*-Plinol A (**4**) was prepared from **2** (31.6 mg; 0.203 mg) according to the method described above for plinol C as a liquid (20.7 mg; 66%); ^{13}C-NMR: δ=147.2 (s), 110.3 (t), 80.4 (s), 52.9 (d), 47.2 (d), 40.2 (t), 27.6 (t), 26.6 (q), 19.1 (q), 10.6 (q); other spectra were identical with the reported full spectra.[1]

Synthesis of c-*3-Acetyl-1,*t-*2-dimethyl-*r-*1-cyclopentanol (**3**)*.

*(a) 1,4-Dimethyl-7-oxabicyclo[2.2.1]heptane-*endo*-2,3-dicarboxylic Anhydride (**17**)*: A mixture of 3.34 g (34.8 mmol) of 2,5-dimethylfuran and 4.47 g (31.5 mmol) of dimethyl acetylenedicarboxylate was heated in a pressure bottle at 100 °C

for 21 h. The reaction mixture was dissolved in 30 ml of acetone and hydrogenated over 0.82 g of 10% Pd/C. Removal of the catalyst and of the solvent gave **14** in quantitative yield; mp 158—160 °C; ^{1}H-NMR ($CDCl_3$): δ=3.81 (s, 6H), 1.76 (bs, 4H), 1.68 (s, 6H).

To a solution of 3.461 g (14.4 mmol) of **14** in 2.5 ml of THF, 6 ml of 20 M KOH solution was added . After stirring for 2 h at r.t., the reaction mixture was acidified to pH 1 and concentrated. The residue was extracted with diethyl ether. Drying over Na_2SO_4 and removal of the solvent gave 3.003 g (98%) of **15**; mp 158—160 °C; ^{1}H-NMR (CD_3COCD_3): δ=1.72 (bs, 4H), 1.68 (s, 6H).

Hydrogenation of **15** (1.156 g; 5.45 mmol) (Pd black; EtOH) gave quantitiatively **16**; mp 155—158 °C; ^{1}H-NMR (CD_3COCD_3): δ=3.00 (s, 2H), ≈1.5 (4H), 1.47 (s, 6H).

A solution of 656 mg (3.06 mmol) of **16** in 8 ml of acetyl chloride was heated under reflux for 3 h. Removal of the volatile material by evaporation and washing the residue with ligroine gave 549 mg (92%) of **17**; mp 140—143 °C; ^{1}H-NMR (CD_3COCD_3): δ=3.62 (s, 2H), 1.82 (s, 4H), 1.59 (s, 6H). Found: C, 60.98; H, 5.87%. Calcd for $C_{10}H_{12}O_4$: C, 61.21; H, 6.17%.

endo-*3-Hydroxymethyl-1,4-dimethyl-7-oxabicyclo*[*2.2.1*]*heptane*-endo-**2**-*carboxylic Lactone* (**18**). According to the procedure for the reduction of **8**, 278 mg (1.42 mmol) of **17** was reduced to the lactone **18** (246 mg; 95%); mp 103.0—104.5 °C. ^{1}H-NMR (CD_3COCD_3): δ=4.21 (m, 2H), 2.97 (m, 2H), ≈1.7 (4H), 1.46 (s, 3H), 1.37 (s, 3H); ^{13}C-NMR (CD_3COCD_3): δ=177.1 (s), 87.3 (s), 86.6 (s), 67.6 (t), 56.3 (d), 52.4 (d), 35.2 (t), 31.4 (t), 21.4 (q), 21.0 (q); MS: *m/e* 182 (M^+, 9), 125. 124, 108 (100), 107; IR: 1760 cm^{-1}. Found: C, 65.74; H, 7.78%. Calcd for $C_{10}H_{14}O_3$: C, 65.92; H, 7.74%.

1,4-Dimethyl-endo-*3-phenylthiomethyl-7-oxabicyclo*[*2.2.1*]*heptane*-endo-*2-carboxylic Acid* (**19**). As described above, 545 mg (2.99 mmol) of **18** yielded 777 mg (89%) of **19**; ^{1}H-NMR ($CDCl_3$): δ=7.2 (5H), 2.7—3.5 (3H), 1.5—2.5 (5H), 1.42 (s, 3H), 1.32 (s, 3H); ^{13}C-NMR: δ=177.2 (s), 135.8 (s), 130.0 (d), 129.0 (d), 126.4 (d), 87.1 (s), 86.4 (s), 54.1 (d), 49.8 (d), 33.2 (t), 31.7 (t), 31.7 (t), 21.2 (q), 20.4 (q). IR: 3000, 1725, 1580, 1450 cm^{-1}. Found: C, 65.46; H, 6.61; S, 11.13%. Calcd for $C_{16}H_{20}O_3S$: C, 65.73; H, 6.89; S, 10.96%.

1,endo-*3,4-Trimethyl-7-oxabicyclo*[*2.2.1*]*heptane*-endo-*2-carboxylic Acid* (**20**). As described above, 145 mg (0.496 mmol) of **19** gave 82 mg (90%) of **20**; mp 102.9—104.2 °C; ^{1}H-NMR ($CDCl_3$): δ=9.6 (COOH), 2.93 (d, 1H), 2.6—1.8 (5H), 1.51 (s, 3H), 1.40 (s, 3H), 1.05 (d, 3H); ^{13}C-NMR: δ=177.2 (s), 87.8 (s), 85.7 (s), 55.4 (d), 44.2 (d), 32.7 (t), 31.2 (t), 21.4 (q), 20.1 (q), 12.5 (q); MS: *m/e* 184 (M^+), 166, 139, 97 (100); IR: 2900, 1740 cm^{-1}. Found: C, 65.38; H, 9.01%. Calcd for $C_{10}H_{16}O_3$; C, 65.19; H, 8.75%.

Electrolysis of **20** (114 mg; 0.619 mmol) gave 61 mg (63%) of **3** after hydrolysis; ^{13}C-NMR: δ=211.8 (s), 81.2 (s), 58.8 (d), 47.4 (d), 40.0 (t), 29.4 (q), 25.6 (t), 23.1 (q), 16.4 (q); other spectral characteristics were consistent with those previously reported.[1]

Synthesis of dl-*Plinol B* (**5**). Similar methylenation of 50.2 mg (0.321 mmol) of **3** gave 25.4 mg (51%) of *dl*-plinol B (**5**): ^{13}C-NMR: δ=135.4 (s), 110.2 (t), 80.4 (s), 53.3 (d), 48.0 (d), 40.6 (t), 27.0 (t), 23.5 (q), 19.0 (q), 12.8 (q); other spectra were in accord with the reported full spectra.[1]

References

1) H. Strickler, G. Ohloff, and E. sz. Kováts, *Helv. Chim. Acta*, **50**, 759 (1967).

2) A. F. Thomas, "The Total Synthesis of Natural Products," ed by J. ApSimon, Wiley-interscience, New York (1973), Vol. 2, p. 60, and references cited therein.

3) S. Nozoe, N. Morisaki, and M. Goi, *Tetrahedron Lett.*, **1971**, 3701.

4) T. Akiyama, T. Fujii, H. Ishiwari, T. Imagawa, and M. Kawanisi, *Tetrahedron Lett.*, **1978**, 2165; T. Imagawa, T. Nakagawa, K. Matsuura, T. Akiyama, and M. Kawanisi, *Chem. Lett.*, **1981**, 903; T. Imagawa, S. Sugita, T. Akiyama, and M. Kawanisi, *Tetrahedron Lett.*, **22**, 2564 (1981); T. Imagawa, N. Murai, T. Akiyama, and M. Kawanisi, *ibid.*, **1979**, 1961; T. Imagawa, T. Sonobe, H. Ishiwari, T. Akiyama, and M. Kawanisi, *J. Org. Chem.*, **45**, 2005 (1980).

5) O. Diels and S. Olsen, *J. Prakt. Chem.*, **156**, 285 (1940).

6) K. Takai, Y. Hotta, K. Oshima, and H. Nozaki, *Bull. Chem. Soc. Jpn.*, **53**, 1698 (1980).

 © 1983 The Chemical Society of Japan Bull. Chem. Soc. Jpn., 56, 3023—3027 (1983)

Restricted Rotation Involving the Tetrahedral Carbon. L. Rotamer Distributions and Rotational Barriers in Some 9-(1-Methoxyethyl)triptycene Derivatives[1]

Yoshiyuki TANAKA, Gaku YAMAMOTO, and Michinori ŌKI*
Department of Chemistry, Faculty of Science, The University of Tokyo, Bunkyo-ku, Tokyo 113
(Received April 22, 1983)

1,4-Dimethyl- and 1,2,3,4-tetrahalo-9-(1-methoxyethyl)triptycenes (halogen=F, Cl, and Br) were synthesized by reactions of 9-(1-methoxyethyl)anthracene with appropriate benzynes. Rotamer distributions and rotational barriers about the bridgehead-to-substituent bond were studied by NMR spectroscopy. Rotamer distributions are governed mainly by the steric effect; the major rotamer is assigned to *sc**(*S**), the minor one to *ap*, and the third one found only in the tetrafluoro derivative to *sc**(*R**). Rotational barriers are 21—23 kcal mol^{-1} which are slightly lower than those for the corresponding 9-isopropyltriptycenes.

We have reported on the energy barriers to rotation about the bridgehead-to-substituent bond in triptycene derivatives carrying several types of secondary alkyl groups at the bridgehead position and on the dependence of the barriers upon *peri*-substituents. Among the compounds investigated are 9-isopropyl-,[2] 9-(2-methoxy-1-methylethyl)-,[3] and 9-(1-methyl-2-propenyl)triptycenes.[4] These compounds have rather similar barrier heights irrespective of the type of 9-alkyl groups. These findings allured us to study the rotational barriers in 9-(1-methoxyethyl)triptycenes which carry an oxygen function in the α-position of the 9-substituent and to compare the behavior with that exhibited by the 9-*s*-alkyltriptycenes mentioned above. We also found that singly *peri*-substituted 9-(1-hydroxy or methoxy-1-methylethyl)triptycenes have strong preference for the $\pm sc$ rotamers over the *ap* because of the smaller bulkiness of an oxy group than a methyl.[5] Therefore, the rotamer distributions in 9-(1-methoxyethyl)triptycenes are of interest because they are determined by the differential steric interactions of the methoxyl and methyl groups with the *peri*-substituent. Furthermore, the populations of rotamers may be affected by other factors than the steric because of the polar nature of a methoxyl group.

In this paper we report the syntheses of 9-(1-methoxyethyl)triptycenes **1**—**4** and the studies of the rotational equilibria and the rotational barriers measured by means of NMR spectroscopy.

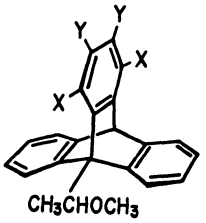

1: X = Y = F
2: X = Y = Cl
3: X = Y = Br
4: X = CH_3, Y = H

The compounds studied were prepared as follows. 9-(1-Hydroxyethyl)anthracene (**5**) obtained by reduction of 9-acetylanthracene was methylated to give 9-(1-methoxyethyl)anthracene (**6**). Reactions of **6** with appropriate benzynes afforded the desired triptycene derivatives **1**—**4**. Tetrafluorobenzyne was generated by lithiation of bromopentafluorobenzene followed by *in situ* elimination of lithium fluoride. The other benzynes were generated by aprotic diazotization of the corresponding anthranilic acids followed by *in situ* pyrolysis of the resulting 2-diazoniobenzoates.

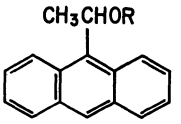

5: R = H
6: R = CH_3

Experimental

Melting points are not corrected. ^{1}H and ^{19}F NMR spectra at ambient temperature (*ca.* 35 °C) were obtained on a Varian EM 390 spectrometer at 90.0 and 84.67 MHz, respectively. ^{1}H NMR spectra were obtained also on a Hitachi R-20B spectrometer at 60.0 MHz. ^{1}H NMR data for **1**—**4** are compiled in Table 1. ^{19}F chemical shifts are shown in ppm downfield from internal hexafluorobenzene.

9-(1-Hydroxyethyl)anthracene (5). To a solution of 5.0 g (23 mmol) of 9-acetylanthracene[6] in 250 mL of diethyl ether was added 500 mg (13 mmol) of lithium tetrahydridoaluminate and the mixture was heated under reflux for 4 h with stirring. The reaction mixture was treated with 10 mL of ethyl acetate and then with 50 mL of water. The ether layer was washed with water and dried over magnesium sulfate. After the solvent was evaporated, the residue was recrystallized from dichloromethane-hexane to afford 4.3 g (85%) of the desired compound, mp 122—123 °C (lit,[7]: 125—126 °C). ^{1}H NMR ($CDCl_3$, δ): 1.85 (3H, d, J=6.3 Hz), 2.1 (1H, br s), 6.35 (1H, q, J=6.3 Hz), 7.3—7.6 (4H, m), 7.8—8.1 (2H, m), 8.30 (1H, s), 8.5—8.7 (2H, m).

9-(1-Methoxyethyl)anthracene (6). To a solution of 2.2 g (10 mmol) of **5** in 70 mL of tetrahydrofuran was added 10 mL of 1.5 mol L^{-1} solution of butyllithium in hexane and the mixture was stirred for 1 h at room temperature. To this solution was added dropwise 10 mL of methyl iodide and the mixture was stirred for 2 h. After evaporation of the volatile part of the reaction mixture, the residue was taken up in ether. The ether layer was washed with water and dried over magnesium sulfate. Evaporation of the solvent followed by recrystallization from dichloromethane–pentane gave 1.85 g (78%) of **6** as yellow crystals, mp 94—95 °C. Found: C, 86.41; H, 6.82%. Calcd for $C_{17}H_{16}O$: C, 86.48; H, 6.81%. ^{1}H NMR ($CDCl_3$, δ): 1.84 (3H, d, J=6.3 Hz), 3.19 (3H, s), 5.89 (1H, q, J=6.3 Hz), 7.3—7.6 (4H, m), 7.8—8.1 (2H, m), 8.37 (1H, s), 8.5—8.8 (2H, m).

1,2,3,4-Tetrafluoro-9-(1-methoxyethyl)triptycene (1). To a solution of 908 mg (3.8 mmol) of **6** and 1.1 g (4.5 mmol) of bromopentafluorobenzene in 100 mL of diethyl ether was

TABLE 1. ^{1}H NMR DATA AND POPULATION OF THE ROTAMERS IN $CDCl_3$ AT *ca.* 35°C[a]

Compd	Rotamer[b]	Population/%	9-Substituent			10-H	Other signals
			CH_3	OCH_3	CH		
1	*ap*	39	2.05 dd (5.9, *7.1*)	3.73	5.19 dq (5.9, *2.9*)	5.69 d (*1.5*)	6.9—7.6 m, 7.9—8.2 m
	sc(S*)*	55	2.00 dd (6.0, *1.0*)	3.69 d (*0.9*)	5.16 dq (6.0, *1.6*)	5.71 d (*1.5*)	
	sc(R*)*	6	1.99 dd (5.9, *7.4*)	3.71	5.01 dq (5.9, *2.7*)	5.71[c]	
2	*ap*	24	2.13 d (5.8)	3.71	5.77 q (5.8)	5.94	6.8—7.6 m, 7.9—8.2 m
	sc(S*)*	76	1.90 d (6.0)	3.65	5.75 q (6.0)	5.96	
3	*ap*	22	2.13 d (5.9)	3.71	6.00 q (5.9)	6.01	6.8—7.6 m, 7.9—8.2 m
	sc(S*)*	78	1.88 d (6.0)	3.67	5.97 q (6.0)	6.05	
4	*ap*	22	2.12 d (6.0)	3.71	5.44 q (6.0)	5.54	2.47[d]; 6.62 d, 6.70 d (7.8) (7.8) 6.8—7.4 m, 7.9—8.2 m
	sc(S*)*	78	1.92 d (6.0)	3.65	5.40 q (6.0)	5.54	2.40, 2.55; 6.59

a) Chemical shifts are given in δ. Signals are singlets unless otherwise noted; d: doublet, dd: double doublet, q: quartet, dq: double quartet, m: multiplet. In parentheses are coupling constants in Hz. Those in italics are couplings with 1-F. b) For the rotamer assignments, see text. c) Not definitely identified. d) Two methyl signals coincide.

TABLE 2. DYNAMIC NMR DATA

Compd	Obsd protons	T_c / °C	$\Delta\nu_c$ / Hz	k_c[a] / s^{-1}	$\Delta G_c^{\ddagger}$[a] / kcal mol^{-1}	K_c[b]	ΔH°[a] / kcal mol^{-1}	ΔS°[a] / eu	Solvent
2	CH_3	145.5[c]	15.4	8.0 (20.0)	23.1±0.1 (22.3±0.1)	0.40	1.6	1.9	C_6H_5Cl
3	OCH_3	109.5	1.8	0.53 (1.6)	23.2±0.1 (22.2±0.1)	0.33	2.1	3.4	1-$ClC_{10}H_7$
4	CH_3	114[c]	11.8	4.3 (13.0)	21.7±0.1 (20.9±0.1)	0.33	1.3	1.0	C_6H_5Cl
	OCH_3	106	4.7	2.7 (8.7)	21.6±0.1 (20.7±0.1)	0.31			

a) Refers to the *sc*(S*)*→*ap* process. In parentheses are the data for the *ap*→*sc*(S*)* process. b) $K=[ap]/[sc^*(S^*)]$. c) The temperature at which the rate constant was obtained by simulation.

added 3.0 mL of 1.5 mol L^{-1} solution of butyllithium in hexane at −78 °C.[8] The mixture was stirred at this temperature for 1 h, allowed to warm up to room temperature and then heated under reflux for 40 h. The reaction mixture was treated with dilute hydrochloric acid. The organic layer was washed with water and dried over magnesium sulfate. Column chromatography of the product on silica gel with hexane–dichloromethane as the eluent followed by recrystallization from dichloromethane–hexane gave 180 mg (12%) of **1** as colorless crystals, mp 193—195 °C. Found: C, 71.84; H, 4.19%. Calcd for $C_{23}H_{16}F_4O$: C, 71.87; H, 4.20%. ^{19}F NMR ($CDCl_3$): 2.0—4.0 (m, 2- and 3-F of the three rotamers), 12.0—14.0 (m, 4-F of the three rotamers), 19.6 (apparent quintet, 1-F of *sc*(S*)*), 25.3 (br, 1-F of *ap*) 33.5 (br, 1-F *sc*(R*)*).

1,2,3,4-Tetrachloro-9-(1-methoxyethyl)triptycene (2). To a boiling solution of 498 mg (2.1 mmol) of **6** and 1 mL of isopently nitrite in 40 mL of 1,2-dimethoxyethane (DME) was added a solution of 1.1 g (4.1 mmol) of tetrachloroanthranilic acid[9] in 50 mL of DMF during the course of 3 h. The mixture was heated under reflux for 1 h. Evaporation of the solvent followed by column chromatography of the residue on silica gel with hexane–dichloromethane as the eluent and recrystallization from dichloromethane–hexane gave 84 mg (9%) of **2**, mp 264.5—266 °C. Found: C, 61.22; H, 3.50; Cl, 31.63%. Calcd for $C_{23}H_{16}Cl_4O$: C, 61.36; H, 3.58; Cl, 31.50%.

1,2,3,4-Tetrabromo-9-(1-methoxyethyl)triptycene (3), mp 288—289 °C, was synthesized similarly as **2** from **6** and tetrabromoanthranilic acid[10] in 8% yield. Found: C, 44.13; H, 2.64; Br, 50.75%. Calcd for $C_{23}H_{16}Br_4O$: C, 43.99; H, 2.57; Br, 50.89%.

9-(1-Methoxyethyl)-1,4-dimethyltriptycene (4), mp 219—220 °C, was synthesized similarly as **2** from **6** and 3,6-dimethylanthranilic acid[11] in 25% yield. Found: C, 88.18; H, 7.00%. Calcd for $C_{25}H_{24}O$: C, 88.20; H, 7.10%.

Dynamic NMR Studies. Variable temperature NMR spectra were recorded on a Hitachi R-20B spectrometer at 60.0 MHz as solutions in chlorobenzene or 1-chloronaphthalene. Temperatures were calibrated using an ethylene glycol sample.[12] Chemical shift differences ($\Delta\nu_c$) at the coalescence temperatures (T_c) were obtained by linearly extrapolating the chemical shift differences at low tempera-

tures. Equilibrium constants (K_c) at T_c were calculated using the van't Hoff parameters shown in Table 2 which were obtained from the equilibrium constants at low temperatures. Rate constants (k_c) at T_c of the methoxyl signals were obtained by two methods: graphically following Jaeschke *et al.*[13] and by computer simulation of the spectra. Values obtained by the two methods agreed quite well. As for the coalescence of the methyl doublets, it was difficult to define T_c and the rate constants were obtained by simulating the spectra at a temperature which was estimated to be close to T_c.

Computer Simulation of the NMR Spectra. The calculations of the theoretical spectra were carried out on a Hitachi M280H computer at the Computer Center of the University of Tokyo, using a modified version of the DNMR 3 program by Binsch.[14] Spectra of **2**—**4** at or near T_c were simulated using the parameters obtained as described in the preceding section and modifying them if necessary to give the rate constants shown in Table 2. The methyl proton signal of **1** at ambient temperature was also simulated putting the exchange rates as zero. As our version of the program can not accommodate a three-site exchange problem of a five-spin system (AM_3X with a methine and methyl protons and a fluorine nucleus), we treated the system as a three-spin system regarding the methyl group as a single nucleus. The fluorine chemical shifts were assumed to be 9000 Hz upfield of the methyl protons, because the computation failed if the actual chemical shift differences between the proton and fluorine were used. Attempt at rigorous simulation of the variable temperature spectra of **1** was abandoned because of too many variable parameters: three independent rate constants, and temperature dependent chemical shifts and rotamer populations. Instead, the theoretical spectra were calculated using the parameters at ambient temperatures and assuming $k_{ap\rightarrow sc^*(S^*)} = 10\ k_{ap\rightarrow sc^*(R^*)} = 10\ k_{sc^*(S^*)\rightarrow sc^*(R^*)}$. Those with $k_{ap\rightarrow sc^*(S^*)}$ of 10—20 s^{-1} gave the best resemblance with the experimental spectrum at 122 °C, which gives a rough estimate of $\Delta G^{\ddagger}$ of 20.5—21.5 kcal mol^{-1} for the $ap\rightarrow sc^*(S^*)$ process.

Results and Discussion

Rotamer Assignments and Equilibria. The compounds examined have high rotational barriers on the NMR time scale and the rotamers about the bridgehead-to-substituent bond are separately observed at room temperature by NMR spectroscopy. Three racemic rotamers, *ap*, *sc**(*S**), and *sc**(*R**),[15] are possible and the Newman projections along the bond in question for those with *R*-configuration are shown in Scheme 1.

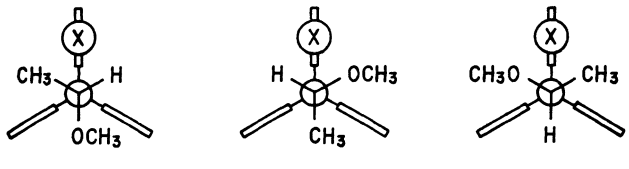

ap *sc*(S*)* *sc*(R*)*

Scheme 1.

It is shown that all the three rotamers are present in chloroform-*d* solution of the tetrafluoro derivative (**1**). In the ^{19}F NMR spectrum, three separate signals due to 1-F are observed at 19.6, 25.3, and 33.5 ppm downfield from internal hexafluorobenzene with an intensity ratio of 55 : 39 : 6, besides the signals due to 2-, 3-, and 4-F. The least abundant rotamer with the lowest-field 1-F signal can be assigned to *sc**(*R**) because the *sc**(*R**) rotamer should be least stable on the steric ground and the 1-F in this rotamer should be most deshielded: a downfield shift known as the van der Waals (steric compression) shift. Similarly from the standpoint of steric compression, the most abundant rotamer with the highest-field 1-F signal can be assigned to *sc**(*S**) and thus the remainder to *ap*.

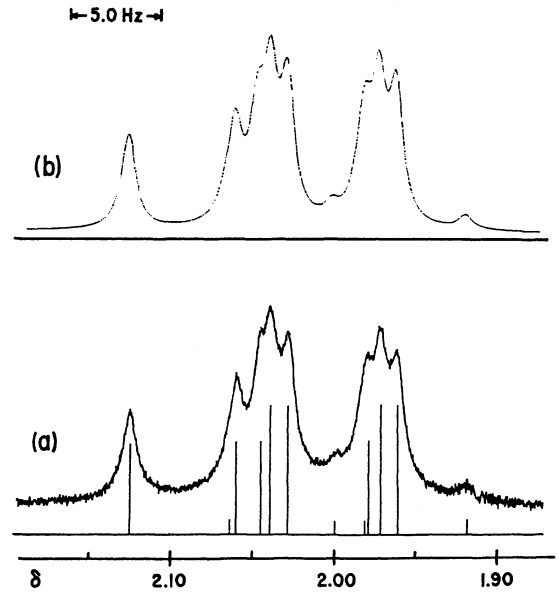

Fig. 1. (a) Observed 90 MHz ^1H NMR spectrum of the methyl region of compound **1** in chloroform-*d* at *ca.* 35 °C. (b) Calculated spectrum using the parameter values given in Table 1.

These assignments are supported by the analysis of the ^1H NMR spectrum of **1**. As found in our previous studies on 1-fluoro-9-(1,1-dimethyl-2-phenylethyl)triptycene atropisomers[16] and on 1-fluoro-9-isopropyltriptycene,[2] the methyl group in a $\pm sc$ site to the *peri*-fluoro substituent shows a large long-range spin-spin coupling with 1-F with a magnitude of 6—9 Hz, while the methyl in an *ap* site which is remote from the *peri*-fluoro group shows only a small coupling, if any, reflecting the through-space nature of the coupling.[17]

The methyl proton signal of **1** looks very complex consisting of three overlapping sets of double doublets due to the coupling with the methine proton and with the 1-F nucleus. The spectrum at 90.0 MHz is shown in Fig. 1. The analysis of the signals is almost unambiguously made by comparing the spectra obtained at 60 and 90 MHz. Furthere, the calculated spectrum (Fig. 1b) using the chemical shifts, the coupling constants and the rotamer populations, given in Table 1, properly reproduces the experimental spectrum.

The methyl signal due to the most abundant rotamer shows a small coupling with 1-F (1.0 Hz) indicating that the methyl group is in the *ap* site and therefore the rotamer is *sc**(*S**). The second abundant rotamer has a large ^1H–^{19}F coupling of 7.1 Hz which is consistent with the *ap* rotamer. The least abundant rotamer also gives a large coupling of 7.4 Hz.

The chemical shifts of the methyl protons in **1** fall in a

narrow range of δ 1.99—2.05 and are not helpful in rotamer assignments but those of the methine proton are shown to be clearly site dependent: the protons in the *ap* and *sc**(*S**) rotamers have nearly identical chemical shifts and the proton in the *sc**(*R**) rotamer appears at a higher field by more than 0.15 ppm than the others. A methine proton synclinal to the *peri*-fluorine is deshielded due probably to the steric compression and/or anisotropy effect exerted by the *peri*-substituent.[18]

The tetrachloro compound **2** shows the presence of only two rotamers in equilibrium in a ratio of 76 : 24. It is reasonable to deduce that the absent rotamer is *sc**(*R**), because the population of the *sc**(*R**) rotamer of **1** is only 6% and the *peri*-chloro substituent in **2** is bulkier than the *peri*-fluoro one in **1**. The methine proton signals of the two rotamers have nearly the same chemical shifts of δ 5.77 and 5.75 and this supports that the two rotamers have their methine protons in similar environments, *i.e.* $\pm sc$ sites to the *peri*-substituent and that they are the *ap* and *sc**(*S**) rotamers.

Differentiation between the *ap* and *sc**(*S**) rotamers is made by consideration of the chemical shifts of the methyl proton signals. As was shown in our previous studies on 9-*t*-alkyl-[16] and 9-*s*-alkyltriptycenes[2-4] carrying a single *peri*-substituent, a methyl group located synclinal to the *peri*-substituent gives its signal at a considerably lower field than the one antiperiplanar to the *peri*-group probably because of the steric compression effect of the flanking *peri*-substituent. *peri*-Fluoro compounds behave exceptionally as mentioned above. Assuming that this generalization applies to compound **2**, we can assign *sc**(*S**) to the major rotamer because the methyl doublet at a higher field is more intense than that at a lower field (Table 1).

The same arguments apply to compounds **3** and **4**, both of which reside as two rotamers in a ratio of 78 : 22 in chloroform-*d*. In either of the compounds the more intense doublet for the methyl group appears at a higher field, and thus the *sc**(*S**) conformation is assigned to the major rotamer.

It becomes clear from the discussion above that the rotamer distribution in **1**—**4** is principally governed by the steric factor, the electrostatic effect being insignificant. A methoxyl group is less bulky than a methyl and is more confortably accommodated in a $\pm sc$ site, resulting in the predominance of the *sc**(*S**) rotamers. Operation of other factors than the steric one, *i.e.* electrostatic and hydrogen bonding effects, was observed in several 1-oxy-substituted 9-(1-methoxyethyl)triptycenes, which will be discussed in the following paper.[19]

The absence of the *sc**(*R**) rotamer in **2**—**4** may be in accordance with the absence of the corresponding rotamers **7** in 9-*s*-alkyltriptycenes hitherto examined.[2-4] The

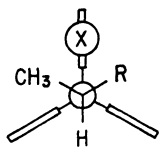

R = CH_3, CH_2OCH_3, $CH{=}CH_2$

7

presence of a small amount of the *sc**(*R**) rotamer in **1** corresponds to the existence of the *ap* rotamer (**7**: R=CH_3, X=F) in 1-fluoro-9-isopropyltriptycene.[2b]

Rotational Barriers. Dynamic NMR behavior of **2**—**4** were studied in solutions of chlorobenzene or 1-chloronaphthalene by observing the methyl and/or methoxyl proton signals. These compounds reside as two rotamers, *ap* and *sc**(*S**), in these solvents as well as in chloroform-*d*, although the rotamer ratios are slightly different from those shown in Table 1. Rate constants for the $ap \rightleftharpoons sc^*(S^*)$ interconversion at or near the coalescence temperatures were evaluated by a graphical method or by computer simulation. These data and the free energies of activation therefrom are given in Table 2. The barriers for **2**—**4** are lower than those for the corresponding 9-isopropyltriptycenes[2] by 0.2—0.8 kcal mol^{-1} (1 cal=4.184 J). This may be due to the smaller bulkiness of a methoxyl than a methyl group. The higher barriers for **2** and **3** than for **4** may be ascribed to the operation of the positive buttressing effect in **2** and **3**[2,20] and also to the effective raise of the ground state in **4** due to the bulkiness of the *peri*-substituent as found in 9-isopropyltriptycenes.[2] The barrier for **1** is roughly estimated to be 20.5—21.5 kcal mol^{-1} as described in the Experimental section and this is evidently lower than the barriers for **2** and **3**.

Conformation in Crystalline States. Many compounds reside as only one of the possible rotamers in the crystalline states and this fact constituted a basis for the assignment of rotational isomers in the pioneering spectroscopic studies.[21] There are however some examples in which a crystal contains more than one rotamer.[22] Therefore it is interesting to see whether the crystals obtained here contain one or more rotamers. Although the rotational barriers found in **2**—**4** are too low for the rotamers to be separately isolated at room temperature, they are high enough for the rotamer composition in the crystalline state to be retained on dissolution in a solvent at low temperatures.

Crystals of compound **4** were dissolved in chloroform-*d* at *ca.* −50 °C and the ^1H NMR spectrum of the solution was taken at −40 °C. The sample was shown to be rotamerically homogeneous under these conditions and the rotamer was the one to which we have assigned *sc**(*S**) in the discussion above. The ^1H NMR spectra of **2** and **3** taken at −10——40 °C after dissolving the crystalline compounds at *ca.* −50 °C showed the presence of a small amount of the *ap* rotamer in addition to the *sc**(*S**). This may have been caused by the elevation of the sample temperature in the dissolution process. The crystals of **2**—**4** are therefore inferred to consist solely of the *sc**(*S**) rotameric state which is the major rotamer in solution. X-ray crystallographic studies on these compounds will afford an unambiguous evidence for the rotamer assignments in solution and are now in progress.

References

1) Part IL: Ref. 2b.
2) a) F. Suzuki, M. Ōki, and H. Nakanishi, *Bull. Chem. Soc. Jpn.*, **47**, 3114 (1974); b) G. Yamamoto and M. Ōki, *ibid.*,

56, 2082 (1983).

3) M. Suzuki, G. Yamamoto, H. Kikuchi, and M. Ōki, *Bull. Chem. Soc. Jpn.*, **54**, 2383 (1981).

4) H. Kikuchi, S. Hatakeyama, G. Yamamoto, and M. Ōki, *Bull. Chem. Soc. Jpn.*, **54**, 3832 (1981).

5) M. Ōki, Y. Tanaka, G. Yamamoto, and N. Nakamura, *Bull. Chem. Soc. Jpn.*, **56**, 302 (1983).

6) C. Merrit, Jr. and C. E. Braun, *Org. Syn.*, Coll. Vol. IV, 8 (1963).

7) L. F. Fieser and J. L. Hartwell, *J. Am. Chem. Soc.*, **60**, 2555 (1938).

8) For generation of tetrafluorobenzyne by metallation of bromopentafluorobenzene, see for example: P. L. Coe, R. Stephens, and J. C. Tatlow, *J. Chem. Soc.*, **1962**, 3227.

9) V. Villiger and L. Blangey, *Ber.*, **42**, 3549 (1909).

10) H. Heaney, K. G. Mason, and J. M. Sketchley, *J. Chem. Soc., C*, **1971**, 567.

11) S. Gronowitz and G. Hansen, *Ark. Kemi*, **27**, 145 (1967).

12) A. L. Van Geet, *Anal. Chem.*, **40**, 2227 (1968).

13) A. Jaeschke, G. Munsch, H. G. Schmid, H. Friebolin, and A. Mannschreck, *J. Mol. Spectrosc.*, **31**, 14 (1969).

14) G. Binsch, *Top. Stereochem.*, **3**, 97 (1968).

15) Nomenclature of conformations involving a chiral center is discussed elsewhere: M. Ōki, *Top. Stereochem.*, **14**, 1 (1983). *R** means a racemic mixture of *R* and *S* configurations as is recommended by IUPAC: L. C. Closs and W. Klyne, *Pure Appl. Chem.*, **45**, 11 (1976). *sc**(*R**) denotes a racemic mixture of $+sc(R)$ and $-sc(S)$, whereas *sc**(*S**) denotes that of $-sc(R)$ and $+sc(S)$.

16) G. Yamamoto, M. Suzuki, and M. Ōki, *Bull. Chem. Soc. Jpn.*, **56**, 306 (1983).

17) Details of long-range ^{1}H–^{19}F spin-spin couplings in triptycene derivatives will be discussed elsewhere.

18) That an *α*-proton of a bridgenead substituent resonates at a lower field when it is in a $\pm sc$ site than when it is in an *ap* site is also observed in 1-substituted 9-(arylmethyl)triptycenes: F. Suzuki and M. Ōki, *Bull. Chem. Soc. Jpn.*, **48**, 596 (1975); G. Yamamoto and M. Ōki, *ibid.*, **54**, 481 (1981).

19) G. Yamamoto, Y. Tanaka, and M. Ōki, *Bull. Chem. Soc. Jpn.*, **56**, 3028 (1983).

20) For the "positive" and "negative" buttressing effects, see: G. Yamamoto, M. Suzuki, and M. Ōki, *Bull. Chem. Soc. Jpn.*, **56**, 809 (1983).

21) S. Mizushima, "Structure of Molecules and Internal Rotation," Academic Press, New York (1954).

22) For example, see: N. Nogami, M. Ōki, S. Sato, and Y. Saito, *Bull. Chem. Soc. Jpn.*, **55**, 3580 (1982).

Restricted Rotation Involving the Tetrahedral Carbon. LI. Electrostatic and Hydrogen Bonding Effects on the Rotamer Distribution in 1-Oxy-substituted 9-(1-Methoxyethyl)triptycenes[1)]

Gaku YAMAMOTO, Yoshiyuki TANAKA, and Michinori ŌKI*
Department of Chemistry, Faculty of Science, The University of Tokyo, Bunkyo-ku, Tokyo 113
(Received April 22, 1983)

1-Hydroxy-4-methoxy- (**5**) and 1,4-dimethoxy-9-(1-methoxyethyl)triptycenes (**6**) were obtained by the reaction of 9-(1-methoxyethyl)anthracene with *p*-benzoquinone followed by enolization and methylation. Rotamer equilibrium in **6** is principally governed by the electrostatic effects favoring the *ap* rotamer. In weakly proton-accepting chloroform-*d*, **5** exists as *sc**(*R**) and *sc**(*S**) rotamers with the former predominating, both of which contain a strong intramolecular hydrogen bonding between the 1-hydroxyl and the methoxyl group in the 9-substituent. In strongly proton-accepting dimethyl-d_6 sulfoxide, all the three rotamers exist with the *ap* rotamer predominating. It is noteworthy that the *sc**(*R**) rotamer, which is present in 20% ratio in dimethyl sulfoxide, still retains the intramolecular hydrogen bonding in this solvent.

In the preceding paper[1)] we reported that the rotamer equilibrium in 9-(1-methoxyethyl)triptycenes **1**—**4** carrying a halogen or a methyl substitutent in a *peri*-position is principally governed by steric effects, the less crowded *sc**(*S**) rotamer being favored. We report here on the dynamic behavior of 1-oxy-substituted 9-(1-methoxyethyl)triptycenes **5** and **6** in which electrostatic and hydrogen bonding effects are the crucial factors governing the rotamer distribution.

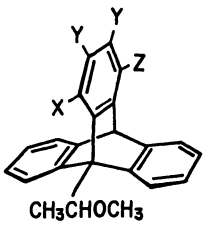

1 : X = Y = Z = F
2 : X = Y = Z = Cl
3 : X = Y = Z = Br
4 : X = Z = CH_3, Y = H
5 : X = OH, Y = H, Z = OCH_3
6 : X = Z = OCH_3, Y = H

Results and Discussion

Syntheses. Reaction of 9-(1-methoxyethyl)anthracene (**7**) with *p*-benzoquinone in acetonitrile gave a 9,10-adduct (**8**) which essentially consists of one diastereomer. In our previous studies on several 9-*s*-alkyl systems,[3)] enolization followed by methylation of a *p*-benzoquinone-anthracene adduct to give a 1,4-dimethoxytriptycene derivative was carried out in one pot under base-catalysis conditions. However, this method was unsatisfactory in the present case and thus the enolization of **8** was effected with acid and the 1,4-dihydroxy compound **9** was once isolated. Action of dimethyl sulfate on **9** in the presence of an aqueous base and a phase-transfer catalyst afforded a monomethylated compound **5**, which was then converted to the dimethylated derivative **6** by action of butyllithium and methyl iodide.

That the monomethylated compound is actually the 1-hydroxy-4-methoxy derivative **5** comes from the following observations. ^{1}H NMR spectrum of the hydroquinone **9** in chloroform-*d* exhibits two types of hydroxyl proton signals. One is a broad signal at δ 5.6 and the other consists of two sharp singlets at δ 9.12 and 9.27 with an intensity ratio of 3 : 1 which is identical with the rotamer ratio of **9** obtained by integration of the methyl and methoxyl signals. The former is assigned to the 4-hydroxyl proton because the chemical shift is in the normal region of phenolic hydroxyl protons.[4)] The latter is ascribed to the 1-hydroxyl group which forms a strong intramolecular hydrogen bonding with the methoxyl group in the bridgehead substituent, as is discussed in detail in the later section. The monomethylated compound **5** in chloroform-*d* shows only the latter type of hydroxyl proton signals, *i.e.* two sharp singlets at δ 9.06 and 9.16 in 3 : 1 ratio, consistent with the presence of the 1-hydroxyl group.

Rotamer Distributions. ^{1}H NMR spectrum of the

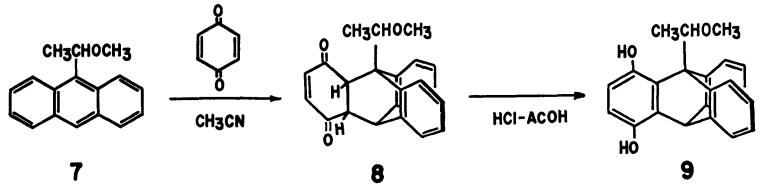

7 **8** **9**

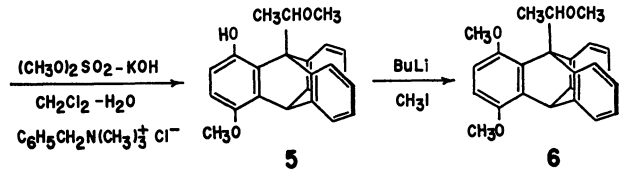

5 **6**

TABLE 1. ^{1}H NMR DATA AND POPULATIONS OF ROTAMERS[a)]

Compd	Solvent	Rotamer[b)]	Population/%	9-Substituent			10-H	2,3-H	Other Aromatic H	1-OR	4-OR
				CH_3	OCH_3	CH					
9	$CDCl_3$	*sc**(*R**)	75	2.09 d (6.0)	3.84	5.11 q (6.0)	5.80	6.48	6.7—7.5 m	9.12	5.6 br
		*sc**(*S**)	25	2.01 d (6.0)	3.79	5.40 q (6.0)	5.78	6.30 d, 6.38 d (8.4) (8.4)	6.7—7.5 m	9.27	
5	$CDCl_3$	*sc**(*R**)	75	2.08 d (5.9)	3.82[c)]	5.10 q (5.9)	5.85	6.61	6.8—7.5 m	9.06	3.81[c)]
		*sc**(*S**)	25	2.00 d (6.1)	3.79[c)]	5.40 q (6.1)	5.83	6.47	6.8—7.5 m 7.8 m	9.16	3.73[c)]
	DMSO-d_6	*sc**(*R**)	20	1.95 d (5.9)	3.82[c)]	5.22 q (5.9)	5.83	6.49 d, 6.71 d (8.9) (8.9)	6.7—7.5 m	9.18	3.77[c)]
		*sc**(*S**)	18	1.86 d (6.0)	3.63[c)]	5.42 q (6.0)	5.77	6.38 d, 6.48 d (8.9) (8.9)	6.7—7.5 m 7.85 m	8.97	3.69[c)]
		ap	62	1.99 d (5.8)	3.59[c)]	5.40 q (5.8)	5.74	6.42 d, 6.55 d (8.9) (8.9)	6.7—7.5 m 7.85 m	9.04	3.73[c)]
6	$CDCl_3$	*ap*	75	2.01 d (5.7)		5.42 q (5.7)	5.79	6.46 d, 6.53 d (8.9) (8.9)	6.7—7.5 m		3.68, 3.70, 3.78[d)]
		*sc**(*S**)	25	1.94 d (6.0)		5.46 q (6.0)	5.79	6.46	7.8—8.2 m		3.66, 3.72, 3.75[d)]
	DMSO-d_6	*ap*	78	1.91 d (5.7)		5.33 q (5.7)	5.79	6.62 d, 6.68 d (9.0) (9.0)	6.7—7.5 m		3.59, 3.67, 3.76[d)]
		*sc**(*S**)	22	1.82 d (6.0)		5.35 q (6.0)	5.79	6.59	7.8—8.2 m		3.55, 3.70, 3.72[d)]

a) Chemical shifts are given in δ. Signals are singlets unless otherwise noted. d: doublet, q: quartet, m: multiplet, br: broad signal. In parentheses are coupling constants in Hz. b) For the rotamer assignments, see text. c) Assignments are unambiguously made by comparing the spectrum of 1-hydroxy-4-trideuteriomethoxy-9-(1-methoxyethyl) triptycene. d) Assignments of the methoxyl signals are not made.

1,4-dimethoxy compound **6** in chloroform-*d* shows that it exists as two rotamers about the bridgehead-to-substituent bond in a ratio of 3 : 1. A criterion for making rotamer assignments is the chemical shifts of the methyl and methine protons in the bridgehead substituent as discussed in the preceding paper.[1)] We rely on the general tendency that either the methyl group or the methine proton gives its signal at a lower field when it is synclinal to the *peri*-substituent than when it is antiperiplanar due mainly to the steric compression effect exerted by the *peri*-substituent.[5)]

From the fact that the methine signals for the two rotamers have very similar chemical shifts (Table 1), it is inferred that the two rotamers are *ap* and *sc**(*S**) because the methine protons in these rotamers are in similar environments, *i.e.* are flanked by the *peri*-methoxyl group. The absence of the *sc**(*R**) rotamer is reasonable because this rotamer should be least stable of the three on both steric and electrostatic grounds.

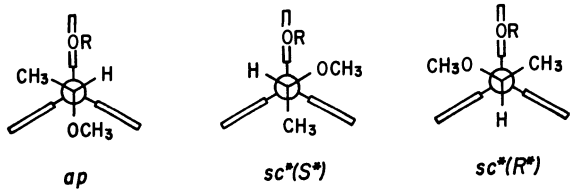

Differentiation between *ap* and *sc**(*S**) comes from the inspection of the methyl signals. The doublet at a low field is more intense than that at a high field, and thus the major rotamer should be *ap* from the criterion. Although similar assignments were made for the rotamers in **2**—**4**,[1)] the one in the present case may be less reliable because the chemical shift difference between the methyl doublets is far smaller in **6** (0.07 ppm) than in **2**—**4** (0.20—0.23 ppm).

In order to confirm the assignment, we studied the effect of solvent polarity on the rotamer ratio. Upon changing the solvent from chloroform-*d* to more polar dimethyl-d_6 sulfoxide (DMSO-d_6), the more abundant rotamer increased its population (75→78%), whereas the less abundant decreased. As is clearly shown by molecular model consideration, *ap*-**6** is more polar than *sc**(*S**)-**6**, and the major rotamer is reasonably assigned to *ap* because a more polar isomer is stabilized in a more polar solvent.

The predominance of the *ap* rotamer in **6** is in sharp contrast with the behavior exhibited by the *peri*-halo compounds **1**—**3** and the *peri*-methyl one **4** where the *sc**(*S**) rotamer is predominant. As shown in the preceding paper, steric effect is the major factor governing the rotamer distribution in **1**—**4**.[1)] The findings here indicate that the electrostatic effect overweighs the steric effect in **6**: the electrostatic repulsion between the oxygen lone pairs in the 1-methoxyl and the 9-(1-methoxyethyl) groups destabilizes the *sc**(*S**) rotamer. An alternative explanation may be possible which includes a hypothetical C–H···O hydrogen bonding.[3,9)] We prefer to attribute the phenomenon to the electrostatic effect until afirm basis of the C–H···O hydrogen bonding is laid.

Compounds **5** and **9**, carrying a hydroxyl group at a *peri*-position, behaved very similarly with each other in ^{1}H NMR spectra, and a detailed study was carried out mainly on **5** because of the low solubility of **9**. ^{1}H NMR spectrum of **5** in chloroform-*d* shows the presence of two rotamers in a ratio of 3 : 1 (Table 1). The most distinguished feature of the spectrum is the appearance of the *peri*-hydroxyl proton signal as two sharp singlets at δ 9.06 and 9.16 in an intensity ratio of 3 : 1. This clearly indicates that the hydroxyl group in each of the rotamers forms a strong intramolecular hydrogen bonding and thus the two are *sc**(*R**) and *sc*(*S**), in both of which the methoxyl group in the 9-substituent flanks the *peri*-hydroxyl. The hydroxyl group in the *ap* rotamer, if present, would appear at a far higher field.[4]

This situation is also evidenced by IR spectroscopy.[10] A dilute solution (*ca.* 2×10^{-3} mol L^{-1}) of **5** in chloroform shows an absorption at 3220 cm^{-1} ($\varepsilon\approx150$) with a half band width of *ca.* 200 cm^{-1} as the only one ascribable to O–H stretching. This frequency is lower by nearly 400 cm^{-1} than the normal one of 3610 cm^{-1} for a phenolic hydroxyl group, suggesting the occurence of an unusually strong intramolecular hydrogen bonding. Such a large shift as found here is unprecedented in an intramolecular hydrogen bonding between a hydroxyl and an alkoxyl group although several examples of large shifts have been reported on *o*-nitrophenol derivatives.[10b]

This spectral feature is retained in a more concentrated solution of **5** (*ca.* 8×10^{-2} mol L^{-1}) in chloroform-*d*, which is the same sample as is used in the ^{1}H NMR measurement.[11] Therefore IR spectroscopy also indicates that **5** in chloroform resides only as the rotamers capable of intramolecular hydrogen bonding: *sc**(*R**) and/or *sc**(*S**).

Conformational assignments of the two rotamers present in chloroform-*d* come again from the chemical shifts of the methyl and methine proton signals. As the lower-field methyl signal and the higher-field methine signal are more intense than their respective counterparts, the major rotamer is deduced to be *sc**(*R**), and thus the minor *sc**(*S**). This assignment looks quite unusual from the standpoint of steric effect because the *sc**(*R**) rotamer is apparently more crowded. The explanation for this still remains unknown.

Although **5** was shown to exist solely as intramolecularly hydrogen-bonded rotamers in chloroform which is very weak as a proton acceptor, the compound was expected to behave differently in a strongly proton-accepting solvent. Actually, ^{1}H NMR spectrum of **5** in DMSO-d_6 disclosed the presence of three rotamers in a ratio of 62 : 20 : 18. As the direct comparison of the spectrum with that in chloroform-*d* did not allow an unambiguous assignment of the rotamers, the change of the rotamer distribution was followed by gradually varying the solvent composition in a mixture of chloroform-*d* and DMSO-d_6. The results, as shown in Fig. 1, clearly reveal that the most abundant rotamer in DMSO is the one which is absent in chloroform, namely *ap*. The major rotamer in chloroform, *sc**(*R**), becomes less and less populous with the increasing content of DMSO, and the minor one in chloroform, *sc**(*S**), does not significantly change its population by the solvent composition.

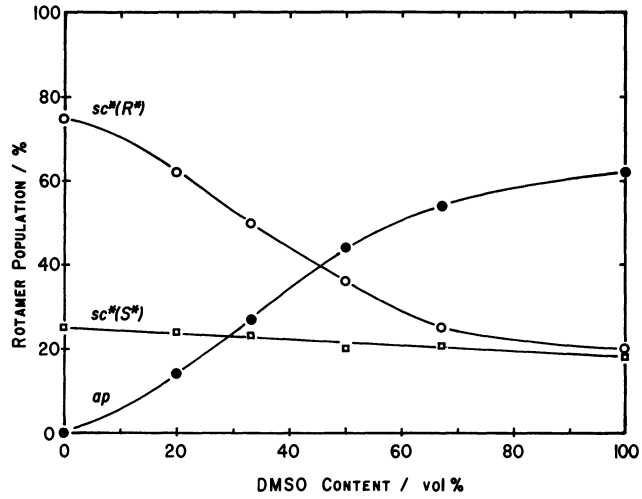

Fig. 1. Dependence of the rotamer populations in **5** upon the solvent composition in $CDCl_3$–DMSO-d_6. ●: *ap*, ○: *sc**(*R**), □: *sc**(*S**).

In a fraction of molecules of **5**, intramolecular hydrogen bonding in chloroform switches to intermolecular hydrogen bonding with a solvent molecule in DMSO. In intermolecularly hydrogen-bonded species the attractive interaction between the *peri*-hydroxyl group and the methoxyl in the side chain disappears, rendering the electrostatic repulsion between the lone pairs a ruling factor. This results in the destabilization of *sc**(*S**)-**5** and the predominance of *ap*-**5** (Scheme 1).

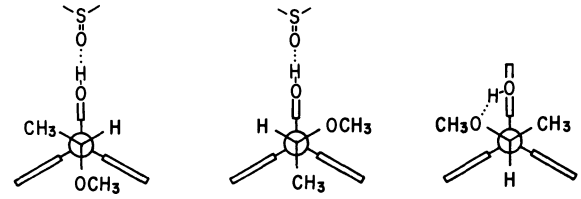

ap-**5** *sc**(*S**)-**5** *sc**(*R**)-**5**

Scheme 1.

It is noticed that the population ratio of the *ap* and *sc**(*S**) rotamers of **5** in DMSO is identical with that of **6** in DMSO within the experimental error (3.4 *vs.* 3.5). This suggests that the same factor dominates in controlling the distribution between the *ap* and *sc**(*S**) rotamers, *i.e.* the electrostatic repulsion between the lone pair electrons, and that the 1-hydroxyl group in the *sc**(*S**) rotamer forms an intermolecular hydrogen bonding with a DMSO molecule.

The fact that the *sc**(*R**) rotamer of **5** still exists in 20% population in DMSO, in contrast with the absence of the corresponding *sc**(*R**) rotamer of **6**, suggests that *sc**(*R**)-**5** is stabilized by a special factor which is absent in **6**, *i.e.* an intramolecular hydrogen bonding (Scheme 1).

Intra- and intermolecularity of the hydrogen bonding in **5** is also reflected in the chemical shifts, especially of the hydroxyl and methoxyl proton signals. The dependence of the chemical shifts of these signals upon the solvent composition is shown in Fig. 2. The hydroxyl

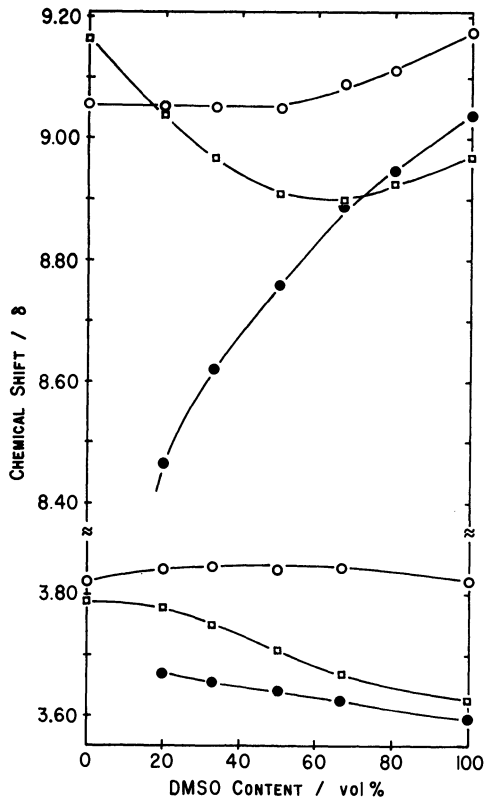

Fig. 2. Dependence of the chemical shifts of the 1-hydroxyl proton and the methoxyl protons in the 9-substituent in rotamers of **5** upon the solvent composition in $CDCl_3$–DMSO-d_6. ●: *ap*, ○: *sc**(*R**), □: *sc**(*S**).

proton signal of the *sc**(*R**) rotamer stays at the initial position of δ 9.06 and then gradually shifts downfield as the DMSO content increases. The signal retains its sharpness (a half-band width of less than 1.7 Hz) irrespective of the solvent composition reflecting the intramolecularity of the hydrogen bonding throughout the solvent range. The hydroxyl proton signal of the *sc**(*S**) rotamer, which appears at δ 9.16 in chloroform-*d*, rapidly shifts upfield and broadens as the DMSO content increases up to 50 vol%. It then moves downfield and resharpens. Appearance of the broad signal at the intermediate region of the DMSO content should be due to exchange between the intramolecular hydrogen-bonded species and the intermolecularly hydrogen-bonded ones. A small broad signal due to *ap*-**5** is observed at δ 8.45 when the DMSO content is *ca.* 20 vol%, which increases in its intensity, sharpens and shifts downfield as the DMSO content increases until it appears at δ 9.04 as a sharp singlet in DMSO.[12]

Dependence of the chemical shifts of the methoxyl protons of the 9-substituent upon the solvent composition also seems to reflect whether the methoxyl group participates in the hydrogen bonding. Although the chemical shifts of the methoxyl protons depend on several other factors, their contributions would be rather small in view of the fact that the chemical shift differences of the methoxyl protons between the rotamers in **1**—**4** is at most 0.06 ppm. The methoxyl group of *sc**(*R**)-**5** which forms the hydrogen bonding with the hydroxyl group gives its signal at a low field of δ 3.82—3.85, while that of *ap*-**5** which does not participate in hydrogen bonding appears at a high field of δ 3.59—3.67. The methoxyl proton signal due to *sc**(*S**)-**5** is located near that due to *sc**(*R**)-**5** in chloroform-*d* but it shifts upfield with the increasing content of DMSO and appears closely to that due to *ap*-**5** in DMSO, suggesting that the hydrogen bonding in *sc**(*S**)-**5** switches from intramolecular in chloroform to intermolecular in DMSO.

^{1}H NMR spectrum of **5** obtained in acetone-d_6 indicates the presence of three rotamers in a ratio of 66 : 22 : 12. The behavior of the chemical shifts and populations in mixtures of chloroform-*d* and acetone-d_6 reveals that the most abundant rotamer in acetone-d_6 is *sc**(*R**), the second abundant *sc**(*S**) and the least abundant *ap*. This ratio is almost identical with the rotamer ratio of **5** in chloroform-*d* containing 15 vol% of DMSO-d_6 (Fig. 1). Therefore the rotamer distribution in **5** may serve as a measure of the proton accepting ability of a solvent system. In benzene-d_6, **5** exists as two rotamers, *sc**(*R**) and *sc**(*S**), in a ratio of 3 : 1 just as in chloroform-*d*, indicating that benzene is as weak a proton acceptor as chloroform.

Rotational Barriers. Variable temperature ^{1}H NMR spectra of **5** and **6** were obtained in chlorobenzene. Both of them showed the presence of two rotamers in this solvent. As there is no reason to assume that the rotamer distributions significantly alter by changing the solvent from chloroform-*d* to chlorobenzene, the existing rotamers of **5** are assigned to *sc**(*R**) and *sc**(*S**) and those of **6** to *ap* and *sc**(*S**), the former predominating in each compound. Rate constants for the interconversion between the two rotamers at or near the coalescence temperatures (T_c) and the free energies of activation therefrom are given in Table 2. The barrier to the $ap \rightleftarrows sc^*(S^*)$ process in **6** is a little lower than that to the $+sc \rightleftarrows -sc$ process in 1,4-dimethoxy-9-isopropyltriptycene ($\Delta G_c^{\ddagger}$=23.0 kcal mol^{-1} at 140 °C),[7] both occurring through similar transition states in which the methine hydrogen in the 9-substituent eclipses the *peri*-

Table 2. Dynamic NMR data in chlorobenzene

Compound	Obsd signal	Process	T_c / °C	$\Delta\nu_c$ / Hz	k_c / s^{-1}	$\Delta G_c^{\ddagger}$ / kcal mol^{-1}	K_c
5	OCH_3	*sc**(*R**)→*sc**(*S**)	112	5.5	9.3	21.0±0.1	3.0
		*sc**(*S**)→*sc**(*R**)			3.1	21.9±0.1	
6	CH_3	*ap*→*sc**(*S**)	114	9.2	13.2	20.9±0.1	2.2
		*sc**(*S**)±*ap*			6.0	21.5±0.1	

methoxyl group. The barrier difference may be ascribed to the smaller bulkiness of a methoxyl than a methyl. The barriers in the *peri*-methoxy compound **6** are almost the same as those in the *peri*-methyl one **4**.[1] In the 9-isopropyl series, the *peri*-methoxy compound has a higher barrier than the *peri*-methyl one (ΔG_c^*: 23.0 *vs.* 22.0 kcal mol^{-1}), which was ascribed to the destabilization of the ground state in the latter due to molecular deformation. The destabilization of the ground state in **4** may be less significant because of the smaller congestion in the 9-(1-methoxyethyl) series.

Observation of the *sc**(*R**)⇌*sc**(*S**) process in **5** is unique in the point that the methoxyl group in the 9-substituent eclipses the *peri*-hydroxyl group in the transition state, because every barrier heigen hitherto examined in 9-*s*-alkyl- and 9-(1-methoxylethyl)-triptycenes has referred to the process in which the methine hydrogen eclipses the *peri*-substituent in the transition state.

Experimental

Melting points are not corrected. ^{1}H NMR spectra were obatined on a Hitachi R-20B (60 MHz) or a Varian EM-390 (90 MHz) spectrometer at *ca.* 35 °C. IR spectra were recorded on a Hitachi 260-30 or a Hitachi 260-50 spectrophotometer using a 0.1 mm KRS-5 cell for samples of *ca.* 0.1 mol L^{-1} and a 5.0 mm quartz cell for samples of *ca.* 10^{-3} mol L^{-1}.

1,4-Dihydroxy-9-(1-methoxyethyl)triptycene (9). A mixture of 944 mg (4.0 mmol) of 9-(1-methoxyethyl)anthracene (**7**)[1] and 2.1 g (20 mmol) of *p*-benzoquinone in 7 mL of acetonitrile was heated under reflux for 3 h with stirring. The mixture was cooled and the precipitate was collected by filtration. The solid was washed with diethyl ether to remove the unreacted *p*-benzoquinone. The 9,10-adduct (**8**) was obtained in 99% yield, mp 177—179 °C (decomp), which was shown by ^{1}H NMR to consist of a single diastereomer. ^{1}H NMR ($CDCl_3$, δ): 1.79 (3H, d, J=6.0 Hz), 2.97 (1H, dd, J=8.5 and 2.5 Hz), 3.45 (1H, d, J=8.5 Hz), 3.67 (3H, s), 4.43 (1H, q, J=6.0 Hz), 4.58 (1H, d, J=2.5 Hz), 5.99 (2H, s), 7.0—7.4 (7H, m), 7.95 (1H, m). A suspension of 500 mg of the adduct **8** in 50 mL of acetic acid containing 2 mL of concentrated hydrochloric acid was stirred overnight at room temperature. The solid was collected by filtration, washed with water and dried in air. Recrystallization from dichloromethane–hexane gave 475 mg (95%) of **9**, mp 166 °C (decomp). This compound was directly used for the next reaction.

1-Hydroxy-4-methoxy-9-(1-methoxyethyl)triptycene (5). A solution of 500 mg (1.45 mmol) of **9**, 3 mL (32 mmol) of dimethyl sulfate and 100 mg of benzyltrimethylammonium chloride in 50 mL of dichloromethane was stirred overnight at room temperature with 30 mL of a 1 mol L^{-1} aqueous solution of potassium hydroxide. The excess of dimethyl sulfate was decomposed by warming the organic layer with 10 mL of a 1 mol L^{-1} aqueous solution of potassium hydroxide. The organic layer was separated and concentrated by evaporation. The residue was taken up in ether. The ethereal solution was washed successively with dilute hydrochloric acid, aqueous sodium hydrogencarbonate and water, and dried over magnesium sulfate. Recrystallization of the product from chloroform–hexane gave 260 mg (50%) of **5**, mp 265—266 °C. Found: C, 80.16; H, 6.22%. Calcd for $C_{24}H_{22}O_3$: C, 80.42; H, 6.19%.

1,4-Dimethoxy-9-(1-methoxyethyl)triptycene (6). To a solution of 113 mg (0.32 mmol) of the monomethylated compound **5** in 30 mL of tetrahydrofuran was added dropwise 0.3 mL of 1.5 mol L^{-1} butyllithium in hexane and the mixture was stirred for 3 h at room temperature. To the solution was added dropwise 10 mL (160 mmol) of methyl iodide and the mixture was stirred for 24 h at room temperature. The mixture was taken up in ether and the ethereal solution was washed successively with dilute hydrochloric acid, aqueous sodium hydrogencarbonate and water. The ether layer was dried over magnesium sulfate and the solvent was evaporated. The residue was recrystallized from dichloromethane–hexane to give 62 mg (53%) of **6**, mp 204—205 °C. Found: C, 80.83; H, 6.23%. Calcd for $C_{25}H_{24}O_3$: C, 80.62; H, 6.49%.

DNMR Studies. Variable temperature ^{1}H NMR spectra were recorded on the Hitachi R-20B spectrometer. Temperatures were calibrated with the use of an ethylene glycol sample.[13] Rate constants at or near T_c were evaluated by simulating the spectra using a modified version of the DNMR 3 program by Binsch.[14] While T_c for the methoxyl proton signal in **6** was easily defined, that for the methyl signal in **5** was not definitely identified and a spectrum obtained at a temperature which was estimated to be close to T_c was simulated.

References

1) Part L: Y. Tanaka, G. Yamamoto, and M. Ōki, *Bull. Chem. Soc. Jpn.*, **56**, 3023 (1983).
2) For nomenclature of rotamers, see Ref. 1 and also: M. Ōki, *Top. Stereochem.*, **14**, 1 (1983).
3) M. Suzuki, G. Yamamoto, H. Kikuchi, and M. Ōki, *Bull. Chem. Soc. Jpn.*, **54**, 2383 (1981); H. Kikuchi, S. Hatakeyama, G. Yamamoto, and M. Ōki, *ibid.*, **54**, 3832 (1981).
4) A hydroxyl proton signal of phenols which do not form an intramolecular hydrogen bonding is said to appear at δ 4-7: R. M. Silverstein, G. C. Bassler, and T. C. Morrill, "Spectroscopic Identification of Organic Compounds," 4th ed, Wiley, New York (1981), p. 196.
5) This tendency has been observed in our previous studies for the methyl signals in 9-*t*-alkyl-[6] and 9-*s*-alkyl-triptycenes[3,7] and for the methylene protons in 9-(arylmethyl)-triptycene.[8]
6) G. Yamamoto, M. Suzuki, and M. Ōki, *Bull. Chem. Soc. Jpn.*, **56**, 306 (1983).
7) F. Suzuki, M. Ōki, and H. Nakanishi, *Bull. Chem. Soc. Jpn.*, **47**, 3114 (1974); G. Yamamoto and M. Ōki, *ibid.*, **56**, 2082 (1983).
8) F. Suzuki and M. Ōki, *Bull. Chem. Soc. Jpn.*, **48**, 596 (1975); G. Yamamoto and M. Ōki, *ibid.*, **54**, 481 (1981).
9) S. Zushi, Y. Kodama, K. Nishihata, K. Umemura, M. Nishio, J. Uzawa, and M. Hirota, *Bull. Chem. Soc. Jpn.*, **53**, 3631 (1980) and references cited therein.
10) a) L. J. Bellamy, "The Infrared Spectra of Complex Molecules," 3rd ed, Wiley, New York (1975), Chap. 6; b) M. Tichý, *Adv. Org. Chem.*, **5**, 115 (1965).
11) The corresponding 1-deuteroxy compound shows an absorption at 2365 cm^{-1} as a sole signal ascribable to O–D stretching.
12) The hydroxyl proton of phenol in DMSO appears at δ 9.25: O. L. Chapman and K. W. King, *J. Am. Chem. Soc.*, **86**, 1256 (1964).
13) A. L. Van Geet, *Anal. Chem.*, **40**, 2227 (1968).
14) G. Binsch, *Top. Stereochem.*, **3**, 97 (1968).

 © 1983 The Chemical Society of Japan Bull. Chem. Soc. Jpn., 56, 3033—3036 (1983)

Production of $C_2(d^3\Pi_g)$ by Controlled Electron Impact on Acetylene, Ethylene, and Ethane

Teiichiro OGAWA,* Yasuhiro UEDA,† and Morihide HIGO††
Department of Molecular Science and Technology, Kyushu University 39, Kasuga, Fukuoka 816
(Received January 20, 1983)

The emission spectra produced by controlled electron impact on C_2H_2, C_2H_4, and C_2H_6 have been analyzed to gain insight into the production mechanisms of $C_2(d^3\Pi_g)$ from the three molecules. There are four thresholds on the excitation function of $C_2(d^3\Pi_g)$ from C_2H_2. Its vibrational temperatures are 22000 K for C_2H_2, 30000 K for C_2H_4 and 56000 K for C_2H_6 at an electron energy of 100 eV. Doubly-excited states are involved in the dissociative excitation of C_2H_2.

The observation of the diatomic C_2 radicals can be traced back to the nineteenth century. The intense emission bands of C_2 are prominent in all kinds of flames and electrical discharges of carbon compounds. Laser photolysis combined with laser-induced fluorescence detection is an efficient method to produce and to monitor this radical, and has been applied for studying elementary processes of C_2.[1] The mechanism of C_2 production in the infrared multiphoton dissociation has been investigated under collisionless conditions.[2,3] This radical has been produced by excimer laser photolysis;[4,5] the vibrational and the rotational temperatures of $C_2(d^3\Pi_g)$ from acrylonitrile have been determined to be 7150 and 4960 K, respectively.[5]

The molecular excitation process by electrons is somewhat different from that by photons; excitation into a triplet state and into a doubly-excited state is more feasible for the former. The $C_2(d^3\Pi_g)$ radical has been observed by controlled electron impact on acetylene,[6,7] ethylene,[8] and benzene;[9] however, no detailed discussion on their production mechanism has been carried out.

In the present paper, the emission spectra of C_2H_2, C_2H_4, and C_2H_6 produced by controlled electron impact have been measured under higher resolution than those in the previous papers, and the vibrational distributions and excitation functions of $C_2(d^3\Pi_g)$ have been analyzed to elucidate its production mechanisms.

Experimental

The details of the apparatus have been described.[10,11] In brief, the sample gas jet (10^{-4} Torr, 1 Torr≈133.322 Pa) was made to collide with an electron beam and the photoemission was measured with a Spex 1269 monochromator. The photons were detected with an HTV R585 photomultiplier and were counted with an NF PC545A photoncounter. The wavelength response was corrected with an Ushio JC-24-150 halogen lamp.[12] All the spectra were measured in a region where the intensity was proportional to both the electron-beam current and to the gas pressure. The sample gases were used as supplied (C_2H_2, Fuji Gas Ind.; C_2H_4, Seitetsu Chemicals; C_2H_6, Takachiho Chemicals); bulb-to-bulb distillation did not induce any change on the spectrum.

† Present address: Atsugi Plant, Sony Corporation Atsugi, Kanagawa 243.

†† Present address: Faculty of Engineering, Kagoshima University, Korimoto, Kagoshima 890.

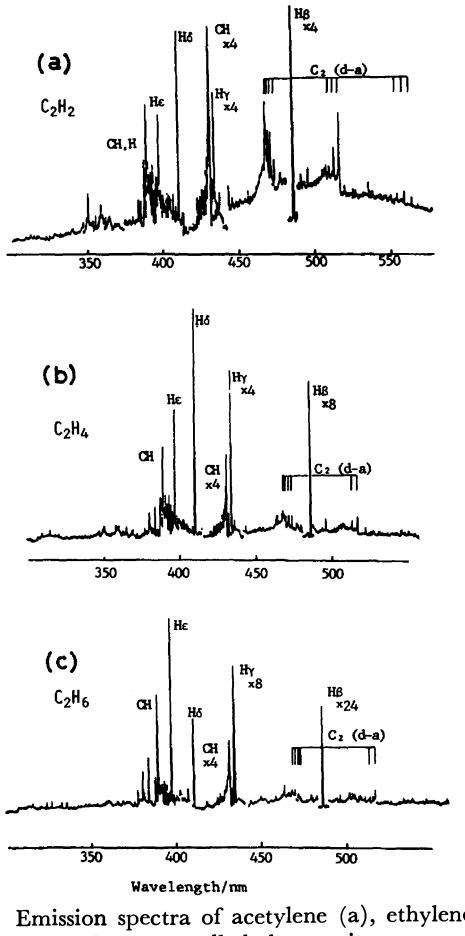

Fig. 1. Emission spectra of acetylene (a), ethylene (b), and ethane (c) by controlled electron impact.
Electron energy 100 eV; electron-beam current 100 μA (a, b), 1000 μA (c); gas pressure 3×10^{-4} Torr; optical resolution 3.2 Å.

Results and Discussion

Spectra. The emission spectra of acetylene, ethylene, and ethane by controlled electron impact show the Balmer lines of the excited hydrogen atom and bands of the CH radical (the A–X and B–X transition) and of the C_2 radical (the Swan system: the d–a transition),[13] as are shown in Fig. 1. The detailed spectra of the Swan system of C_2 from acetylene are shown in Fig. 2. The weak intensity of this system, especially for ethane, makes a quantitative analysis difficult. The band shape was independent of pressure

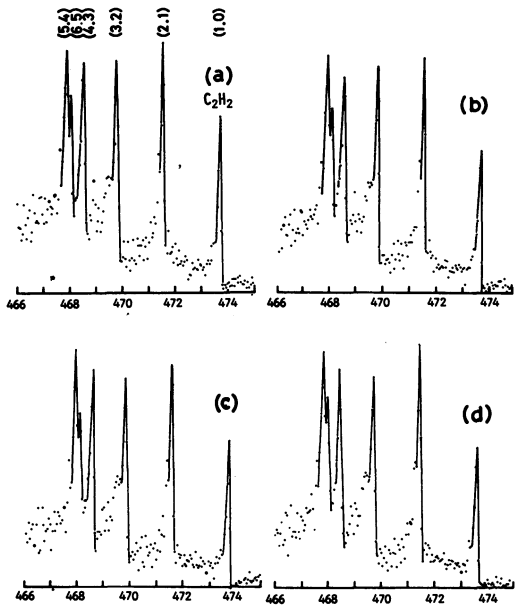

Fig. 2. The detailed spectra of the Swan system of acetylene at 100 eV (a), 50 eV (b), 30 eV (c), and 20 eV (d).
Electron-beam current 200—400 μA; optical resolution 0.8 Å.

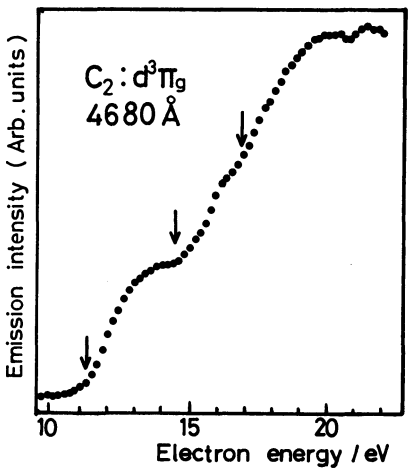

Fig. 3. The excitation function of $C_2(d^3\Pi_g)$ from acetylene at 4680 Å.
Electron-beam current 2 μA; electron energy resolution 0.6 eV; gas pressure 3×10^{-4} Torr.

$(6—50)\times10^{-5}$ Torr. The Swan bands are slightly polarized (1—2%) for electron energies from the threshold to 100 eV: this finding indicates that direct dissociation processes are involved in the dissociative excitation of the three molecules.

The excitation function of $C_2(d^3\Pi_g)$ from acetylene is shown in Fig. 2. There are four thresholds; their values are 11.2 ± 0.8, 14.5 ± 1.1, 16.9 ± 0.8, and 24.0 ± 1.0 eV. Those of ethylene and probably of ethane also have four thresholds.[14] These findings indicate that there are four major processes for the formation of C_2 from acetylene and ethylene, and probably also from ethane. The existence of two or more processes for dissociative excitation is usual for electron impact dissociations.[15]

Vibrational Population. The Vibrational distribution of the fragments produced in a collision process has much to do with the kinematics. The intensity of each vibrational band of the $\Delta v=+1$ transition of $C_2(d^3\Pi_g)$ has been obtained from its peak intensity, following the method of Danylewych and Nicholls.[16] The vibrational population thus obtained are shown in Fig. 3 for the three molecules excited by an electron beams of 100 eV. The values are relative to that $v'=0$, which is set to 1.0. The error bars shown are due to random experimental fluctuations. The observed distribution represents the nascent one, since the pressure is so low that the collisional deactivation can be ignored over the lifetime of the emitting level ($\approx$119 ns[4]).

The vibrational population of C_2 decreased as v' increased. If the excess energy of the primarily excited species are distributed randomly over various freedoms of motions, the vibrational population may be a Poisson distribution. This is not the case, as is shown in Fig. 4.

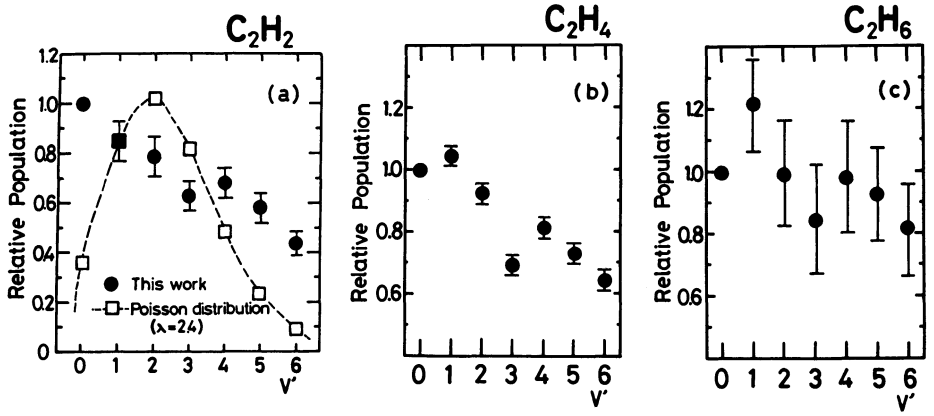

Fig. 4. Vibrational populations of $C_2(d^3\Pi_g)$ from C_2H_2 (a), C_2H_4 (b), and C_2H_6 (c) at an excitation energy of 100 eV.
The error bars represent random scatterings. A poisson distribution is shown for the case of C_2H_2, where λ is determined as a parameter for the least-square fitting with the observed values.

Table 1. Vibrational temperature ($T_{vib.}$) of C_2 at various electron energies (E_{el})

C_2H_2		C_2H_4		C_2H_6	
E_{el}/eV	T_{vib}/K	E_{el}/eV	$T_{vib.}$/K	E_{el}/eV	$T_{vib.}$/K
100	22000	100	30000	100	56000
50	26000	50	32000		
16	25000	30	46000		
13	30000	21	36000		

Estimated errors: C_2H_2 and C_2H_4 at 100—50 eV; ±10%, the others; ±20%.

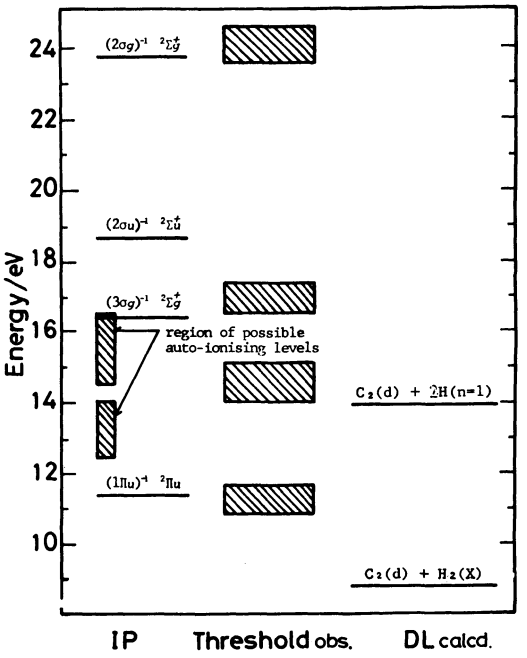

Fig. 5. Energy diagram of acetylene.
The ionization potentials, the observed threshold energies and the calculated dissociation limits are shown. The width of the threshold energy represents its uncertainty.

The vibrational distributions of C_2 are rather similar to a Boltzmann distribution. Semi-logarithmic plots of the vibrational populations give the vibrational temperatures of $C_2(d^3\Pi_g)$, as are shown in Table 1. The vibrational temperatures tend to increase for a larger parent molecule. This finding seems to be inconsistent with a statistical prediction,[17] which has been successfully applied to multiphoton dissociation of benzene.[18] This means either that the three molecules are too simple to be treated statistically or that there are some predominant processes.

Assignments for Acetylene. The core-ion model of molecular dissociation may be extended to the low-Rydberg fragments.[15] If this is also the case for the production of C_2, dissociative ionization to produce C_2^+ should be correlated with dissociative excitation. The electron configuration of acetylene is $KK(2\sigma_g)^2(2\sigma_u)^2(3\sigma_g)^2(1\pi_u)^4$. The energy diagram for dissociation is shown in Fig. 5.

The first component of C_2, which has the threshold at 11.2 eV, is assigned to be produced from dissociative excitation through Rydberg states converging to the $(1\pi_u)^{-1}$ ionized state, which lies in this region.[19] The final state should be $C_2(d^3\Pi_g)+H_2(X)$ from energy considerations. The excess energy of this process is about 2.6 eV and is almost equal to the vibrational energy of C_2 excited at 13 eV (30000 K=2.6 eV); thus, the excess energy mostly goes into the vibrational freedom of C_2 in this process.

There are auto-ionizing levels[20] near the second threshold (14.5 eV), Rydberg states converging to the $(2\sigma_u)^{-1}$ and $(3\sigma_g)^{-1}$ ionized states[19] near the third threshold (16.9 eV), and Rydberg states converging to the $(2\sigma_g)^{-1}$ ionized state[19] near the fourth threshold (24.0 eV). The $(3\sigma_g)^{-1}$ state dissociates into C_2H^+ and then into C_2^+ quickly.[21] The $(2\sigma_u)$ orbital is strongly bonding for the C–H bonds and the $(2\sigma_u)^{-1}$ state is expected to dissociate into C_2^+. Thus, these states are expected to be important for the formation of $C_2(d^3\Pi_g)$ in the respective energy regions.

Assignments of C_2 production mechanism may be carried out similarly for ethylene and ethane; however, insufficient information on their highly-excited states and larger experimental fluctuations made any detailed discussion difficult.

Concluding Remarks. An electron is a very efficient source for molecular excitation in the 10—1000 eV range, and an electron source is much easily operated than a synchrotron orbital radiation facility. Furthermore, the electron has a distinct advantage; it is able to excite optically forbidden processes, which are often important in the dissociation dynamics.[15] The vibrational distributions of $C_2(d^3\Pi_g)$ produced by IR multiphoton dissociation of C_2H_3CN concentrate in the lower vibrational level,[3] whereas those produced by UV multiphoton dissociation of C_2H_3CN have a vibrational temperature of 7150 K.[5] These results disclose differences in the excitation mechanisms. Recent demands for the dynamics and kinetics of C_2 from combustion engineering, atmospheric and environmental sciences warrant further investigation on this subject.

The authors thank Professor Nobuhiko Ishibashi for his encouragement. The present study was partially supported by a Grant-in-Aid from the Ministry of Education, Science and Culture.

References

1) H. Reisler, M. Mangir, and C. Witting, "Chemical and Biochemical Applications of Lasers," ed by C. B. Moore, Academic Press, New York (1980), Vol. 5, p. 139.

2) R. V. Anbartzumian, N. V. Chekalin, V. S. Letoknov, and E. A. Ryabov, *Chem. Phys. Lett.*, **36**, 301 (1975); N. V. Chekalin, V. S. Letoknov, V. N. Lokhman, and A. N. Shibanov, *Chem. Phys.*, **36**, 415 (1979).

3) J. D. Campbell, M. H. Yu, M. Mangir, and C. Wittig, *J. Chem. Phys.*, **69**, 3854 (1978); M. H. Yu, M. R. Levy, and C. Wittig, *ibid.*, **72**, 3789 (1980).

4) J. R. McDonald, A. P. Baronavski, and V. M. Donnelly, *Chem. Phys.*, **33**, 161 (1978).

5) N. Nishi, H. Shinohara, and I. Hanazaki, *J. Chem. Phys.*, **77**, 246 (1982).

6) C. I. M. Beenakker and F. J. de Heer, *Chem. Phys.*, **6**, 291 (1974).

7) M. Tsuji, T. Ogawa, Y. Nishimura, and N. Ishibashi, *Bull. Chem. Soc. Jpn.*, **49**, 2913 (1976).
8) D. E. Donobue, J. A. Schiavone, and R. S. Freund, *J. Chem. Phys.*, **67**, 769 (1977).
9) M. Tsuji, T. Ogawa, T. Imasaka, Y. Nishimura, and N. Ishibashi, *Bull. Chem. Soc. Jpn.*, **49**, 53 (1976).
10) T. Ogawa and M. Higo, *Chem. Phys.*, **52**, 55 (1980).
11) T. Ogawa, N. Yamami, M. Tsuji, and Y. Nishimura, *Bull. Chem. Soc. Jpn.*, **54**, 1203 (1981).
12) The authors are indebted to Dr. M. Suzuki of the Electrotechnical Laboratory for his determination of the spectral irradiance of this lamp.
13) R. W. B. Pearse and A. G. Gaydon, "The Identification of Molecular Spectra," 4th ed, Chapman and Hall, London (1976).
14) T. Ogawa, Y. Ueda, and M. Higo, *Eng. Sci. Repts. Kyushu Univ.*, **5**, 1 (1983).
15) T. Ogawa, J. Kurawaki, and M. Higo, *Chem. Phys.*, **61**, 181 (1981); M. Higo, S. Kamata, and T. Ogawa, *ibid.*, **66**, 243 (1982).
16) L. L. Danylewych and R. W. Nicholls, *Proc. R. Soc. London, Ser. A*, **339**, 197, 213 (1974).
17) J. Silberstein and R. D. Levine, *Chem. Phys. Lett.*, **74**, 6, (1980).
18) N. Ohmichi, J. Silberstein, and R. D. Levine, *Chem. Phys. Lett.*, **84**, 228 (1981).
19) K. Kimura, S. Katsumata, Y. Achiba, T. Yamazaki, and S. Iwata, "Handbook of HeI Photoelectron Spectra of Fundamental Organic Molecules," Japan Sci. Soc. Press, Tokyo (1981).
20) R. Botter, V. H. Dibeler, J. A. Walker, and H. M. Rosenstock, *J. Chem. Phys.*, **44**, 1271 (1966); T. Hayaishi, S. Iwata, M. Sasanuma, E. Ishiguro, Y. Morioka, Y. Iida, and M. Nakamura, *J. Phys. B*, **15**, 79 (1982).
21) R. S. Lehrle and R. S. Mason, *Int. J. Mass Spectrom. Phys.*, **21**, 165 (1976).

 © 1983 The Chemical Society of Japan Bull. Chem. Soc. Jpn., 56, 3037—3041 (1983)

The Crystal Structure of 2,11,20-Trithia[3.3.3](1,2,4)(1,3,5)cyclophane and Molecular Structures of Unsymmertically Tris-bridged [2.2.2](1,2,4)(1,3,5) and [2.2.2](1,2,4)(1,2,5)Cyclophanes, Estimated by Molecular Conformational Analysis†

Yasushi KAI, Takashi MIZUMA,†† Noritake YASUOKA,††† and Nobutami KASAI*
Department of Applied Chemistry, Faculty of Engineering, Osaka University, Yamadaoka, Suita, Osaka 565
(Received January 24, 1983)

The crystal structure of 2,11,20-trithia[3.3.3](1,2,4)(1,3,5)cyclophane has been determined by the X-ray diffraction method and compared with the molecular structures of unsymmetrically tris-bridged [2.2.2](1,2,4)(1,3,5) and [2.2.2](1,2,4)(1,2,5)cyclophanes, estimated by molecular conformational analysis.

In a series of recent synthetic studies of layered cyclophane compounds with more than two ethano bridges holding two benzene rings,[1-4] a new type of unsymmetrically tris-bridged [2.2.2]cyclophanes (**1** and **2**) has been reported by Nakazaki and his co-workers.[5]

The molecular structures of **1** and **2** are expected to have unusually deformed benzene rings with a new mode of overlapping structures among the various kinds of layered cyclophane compounds. In the synthetic paths to **1** and **2**, trithia[3.3.3]cyclophanes (**3** and **4**) are the intermediate products, followed by the preparation of trisulfones and their pyrolysis.

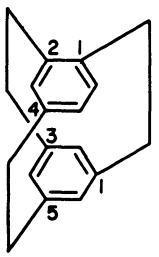

1

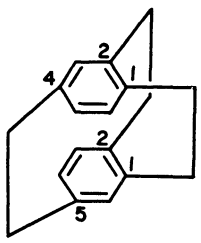

2

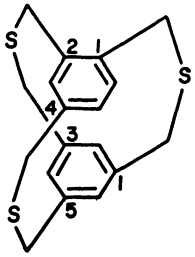

3

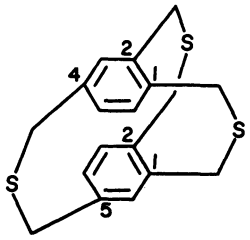

4

As a first step in structural studies of these unsymmetrically tris-bridged [2.2.2]cyclophanes, the crystal structure of **3** has been determined by the X-ray diffraction method. The crystals of **1** and **2** were of a poor quality for the X-ray experiment. The molecular structures of **1** and **2**, therefore, have been estimated by the intramolecular-strain-energy-minimization method with semi-empirical potential functions by Boyd,[6] and have been compared with the molecular structure of **3**.

Experimental

Crystal Data. $C_{18}H_{18}S_3$, *F.W.* 330.5, monoclinic, space group $P2_1/c$, $a=15.466(4)$, $b=13.068(5)$, $c=8.409(2)$ Å, $\beta=115.39(2)°$, $V=1535.4(8)$ Å^3, $D_m=1.43$ (by flotation), $D_c=1.430$ g cm^{-3}, $Z=4$.

The three-dimensional X-ray data were collected using a crystal with dimensions of $0.3\times0.3\times0.35$ mm by the use of Zr-filtered Mo $K\alpha$ radiation on a Rigaku automated four-circle diffractometer. The θ-2θ scan method was employed at a rate of 4° min^{-1}. The backgrounds were measured for 5 s before and after each scan. A total of 3384 (2513 non-zero) reflections was collected up to $2\theta=54°$. Usual *Lp* corrections were made but no absorption correction was employed [μ(Mo $K\alpha$) = 4.5 cm^{-1}].

The structure was solved by the direct method (*MULTAN* 74)[7] and refined anisotropically by the block-diagonal least-squares procedure (*HBLS*-V).[8] After the *R* value had converged to 0.113, all the H atoms located on the difference Fourier map were included in the refinement with the isotropic temperature factors. The weighting scheme used was $w=[\sigma^2(F_o)+a|F_o|+b|F_o|^2]^{-1}$ and $w=c$ for non-zero and zero reflections respectively. The final *R* value was 0.098 for non-zero reflections (0.149 for all), and $R_w=0.138$, with $a=0.0796$, $b=0.0017$, and $c=0.1320$. The atomic scattering factors for the S and C atoms were taken from the "International Tables for X-Ray Crystallography," Vol. IV,[9] and those for the H atom from Stewart *et al.*[10] The final atomic coordinates are listed in Table 1.††††

Results and Discussion

Molecular Structure of 2,11,20-Trithia[3.3.3](1,2,4)-(1,3,5)cyclophane (3). The perspective view of the molecule are shown in Fig. 1 by the *ORTEP* drawings,[12] together with the atomic numberings. The bond distances and angles are listed in Table 2.

In the crystal structure of **3**, no conformational disorder of the sulfide bridges is found, in contrast with the crystal structures of related compounds, 2,11,20-trithia[3.3.3](1,3,5)cyclophane (**5**),[13] and *syn*-2,11-dithia-9,18-dimethyl[3.3]cyclophane (**6**).[14] The conformational disorder observed in **5** and **6** was inter-

† Structural Chemistry of Layered Cyclophanes. IX.

†† Present address: Fuji-FACOM Coorporation, 23-5 Nishi Shimbashi, 3-Chome, Minato-ku, Tokyo 105.

††† Present address: Institute for Protein Research, Osaka University, Yamadaoka, Suita, Osaka 565.

†††† Tables of observed and calculated structure factors and anisotropic thermal parameters are deposited as Document No. 8342 at the Chemical Society of Japan.

TABLE 1. FRACTIONAL ATOMIC COORDINATES OF THE **3** MOLECULE WITH ESTIMATED STANDARD DEVIATIONS IN PARENTHESES

a) S and C atoms with equivalent temperature factors.[11]

Atom	x	y	z	B_{eq}/Å^2
S(2)	0.48268(12)	0.60850(15)	0.8016(3)	4.32
S(11)	0.14673(14)	0.37512(14)	0.0391(3)	4.32
S(20)	0.04427(11)	0.61177(14)	0.4316(3)	3.73
C(1)	0.3724(5)	0.5682(5)	0.8135(8)	3.8
C(3)	0.4414(5)	0.6905(6)	0.6085(10)	4.8
C(4)	0.3496(5)	0.6605(5)	0.4574(8)	3.6
C(5)	0.2654(5)	0.7056(5)	0.4427(8)	3.4
C(6)	0.1774(4)	0.6738(5)	0.3156(8)	3.0
C(7)	0.1739(5)	0.5972(5)	0.1994(8)	3.3
C(8)	0.2564(5)	0.5486(5)	0.2126(8)	3.3
C(9)	0.3449(5)	0.5810(5)	0.3420(8)	3.6
C(10)	0.2509(5)	0.4573(6)	0.0973(8)	4.1
C(12)	0.1811(5)	0.2914(6)	0.2326(8)	4.0
C(13)	0.2259(5)	0.3510(5)	0.4036(8)	3.2
C(14)	0.3223(5)	0.3400(5)	0.5145(9)	3.6
C(15)	0.3660(5)	0.4069(5)	0.6514(8)	3.6
C(16)	0.3167(4)	0.4868(5)	0.6819(7)	3.0
C(17)	0.2170(4)	0.4913(5)	0.5826(7)	2.8
C(18)	0.1736(5)	0.4233(5)	0.4465(8)	3.2
C(19)	0.1526(5)	0.5686(6)	0.6165(8)	3.7
C(21)	0.0878(5)	0.7086(5)	0.3261(9)	3.8

b) H atoms with isotropic temperature factors.

Atom	x	y	z	B/Å^2
H(1A)	0.334(6)	0.626(6)	0.803(11)	4(2)
H(1B)	0.395(7)	0.545(8)	0.919(12)	6(3)
H(3A)	0.493(7)	0.688(7)	0.566(12)	5(3)
H(3B)	0.440(6)	0.759(7)	0.629(12)	5(3)
H(5)	0.266(5)	0.765(6)	0.511(9)	3(2)
H(7)	0.107(6)	0.570(6)	0.106(10)	3(2)
H(9)	0.413(6)	0.549(7)	0.349(11)	4(2)
H(10A)	0.248(7)	0.482(8)	0.007(14)	6(3)
H(10B)	0.308(6)	0.410(7)	0.139(11)	4(2)
H(12A)	0.232(6)	0.242(7)	0.240(11)	4(2)
H(12B)	0.115(8)	0.259(9)	0.225(15)	8(3)
H(14)	0.352(7)	0.293(8)	0.497(13)	6(3)
H(15)	0.433(8)	0.408(8)	0.718(14)	7(3)
H(18)	0.093(7)	0.431(8)	0.369(13)	6(3)
H(19A)	0.123(7)	0.546(8)	0.709(13)	6(3)
H(19B)	0.197(7)	0.631(7)	0.696(11)	4(2)
H(21A)	0.099(7)	0.769(7)	0.397(12)	5(3)
H(21B)	0.033(6)	0.712(7)	0.222(12)	5(2)

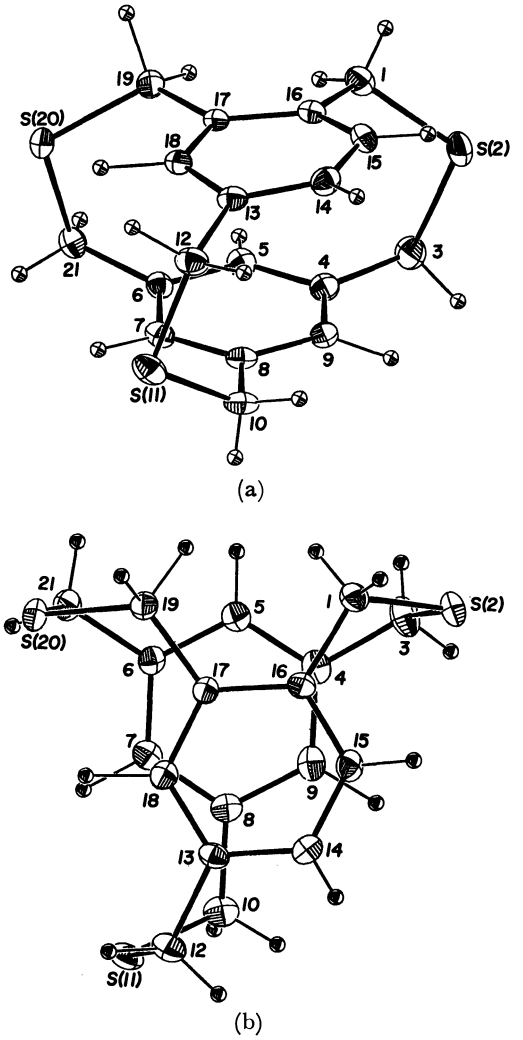

Fig. 1. Molecular structures of **3** with the numbering scheme of the atoms. Thermal ellipsoids for non-hydrogen atoms are drawn at the 30% probability level. H atoms are shown as spheres with arbitrary temperature factor of 1.0 Å^2. a) Side view of the molecule. b) Projection of the molecule onto the mean plane of (1, 3, 5) benzene.

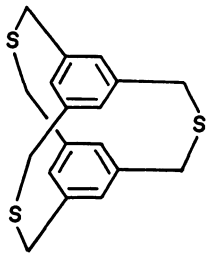

5

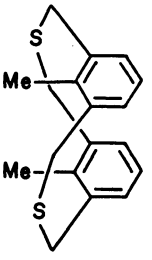

6

preted in terms of a temperature-modulated flipping of the sulfide bridges[13] between two positions related by the local 2-fold symmetry. The lack of local 2-fold symmetry in **3** may be an important factor in preventing the sulfide bridges from flipping in the crystal structure.

The structures of the two benzene rings in this molecule are different from each other. The benzene ring with three sulfide bridges symmetrically on its 1, 3, and 5 positions [abbreviated as (1,3,5)benzene hereafter] is planar within a maximum deviation of 0.015 Å. On the other hand, the other benzene ring, with three sulfide bridges unsymmetrically on its 1, 2, and 4 positions [(1,2,4)benzene], deviates from a plane to boat structure. The C(14), C(15), C(17), and C(18) atoms make a base plane within a 0.003 Å deviation, with the C(13) and C(16) atoms as the bow and/or stern atoms. The dihedral angles between the base plane and the bow and/or stern planes [C(14), C(13), and C(18)] and [C(15), C(16), and C(17)] are both 6.4°, a value of which is much smaller than the corresponding angles (12—14°) of the boat-form benzene rings in [2.2]paracyclophane[15] and its derivatives.[16,17] In the **5** molecule, the two benzene rings are both planar and are parallel to each other within a 1° deviation. In the **3** molecule, the mean plane of the (1,3,5)benzene ring makes an angle of 6.8° with the base plane of the (1,2,4)-benzene ring. The distances of the carbon atoms in (1,3,5)benzene from the base plane of (1,2,4)benzene lie between 2.902 and 3.238 Å, the average of which [3.077 Å] is shorter than the corresponding distance of **5**, 3.192 Å.

The C–S–C angles about the S(2), S(11), and S(20) atoms are 103.9(3), 103.1(3), and 103.5(3)° respectively. The C–S distances range from 1.817(8) to 1.840(8) Å [av. 1.827 Å]. The S–C–C angles, distributed in the

TABLE 2. SELECTED BOND LENGTHS AND BOND ANGLES IN THE **3** MOLECULE WITH THEIR ESTIMATED STANDARD DEVIATIONS IN PARENTHESES

Bond length	l/Å	Bond length	l/Å
S(2)–C(1)	1.829(7)	S(2)–C(3)	1.817(8)
S(11)–C(10)	1.820(8)	S(11)–C(12)	1.840(8)
S(20)–C(19)	1.820(7)	S(20)–C(21)	1.833(7)
C(1)–C(16)	1.510(9)	C(3)–C(4)	1.495(10)
C(4)–C(5)	1.386(9)	C(4)–C(9)	1.403(9)
C(5)–C(6)	1.385(9)	C(6)–C(7)	1.383(9)
C(6)–C(21)	1.496(9)	C(7)–C(8)	1.386(9)
C(8)–C(9)	1.400(9)	C(8)–C(10)	1.516(7)
C(12)–C(13)	1.517(10)	C(13)–C(14)	1.387(9)
C(13)–C(18)	1.388(9)	C(14)–C(15)	1.371(9)
C(15)–C(16)	1.379(9)	C(16)–C(17)	1.406(8)
C(17)–C(18)	1.375(9)	C(17)–C(19)	1.528(9)
C–H 0.81—1.14(8—12), av. 0.99(10)			
Bond angle	**ϕ/°**	**Bond angle**	**ϕ/°**
C(1)–S(2)–C(3)	103.9(3)	C(10)–S(11)–C(12)	103.1(4)
C(19)–S(20)–C(21)	103.5(3)	S(2)–C(1)–C(16)	114.5(5)
S(2)–C(3)–C(4)	116.5(5)	C(3)–C(4)–C(5)	118.6(6)
C(3)–C(4)–C(9)	122.1(6)	C(5)–C(4)–C(9)	119.0(6)
C(4)–C(5)–C(6)	121.1(6)	C(5)–C(6)–C(7)	119.3(6)
C(5)–C(6)–C(21)	119.5(6)	C(7)–C(6)–C(21)	120.3(6)
C(6)–C(7)–C(8)	121.3(6)	C(7)–C(8)–C(9)	118.9(6)
C(7)–C(8)–C(10)	120.8(6)	C(9)–C(8)–C(12)	120.0(6)
C(4)–C(9)–C(8)	120.3(6)	S(11)–C(10)–C(8)	115.9(5)
S(11)–C(12)–C(13)	112.0(5)	C(12)–C(13)–C(14)	120.4(6)
C(12)–C(13)–C(18)	121.1(6)	C(14)–C(13)–C(18)	118.3(6)
C(13)–C(14)–C(15)	119.9(6)	C(14)–C(15)–C(16)	121.8(6)
C(1)–C(16)–C(15)	118.8(6)	C(1)–C(16)–C(17)	122.8(6)
C(15)–C(16)–C(17)	118.3(6)	C(16)–C(17)–C(18)	119.1(6)
C(16)–C(17)–C(19)	123.6(5)	C(18)–C(17)–C(19)	117.3(5)
C(13)–C(18)–C(17)	121.7(6)	S(20)–C(19)–C(17)	118.7(5)
S(20)–C(21)–C(6)	111.1(5)		
S–C–H 96—116 (5—8), av. 106(6)			
C–C(sp^3)–H 104—118 (5—8), av. 110(6)			
C–C(sp^2)–H 116—122 (4—8), av. 119(6)			
H–C(sp^3)–H 90—117 (7—9), av. 107(8)			

range from 111.1(5) to 118.7(5)° [av. 114.8°], are greater than the tetrahedral angle of 109.5°.

The angular deviation of the C(3)–C(4) bond from the plane defined by the C(4), C(5), and C(9) atoms, that of the C(6)–C(21) bond from the plane defined by the C(5), C(6), and C(7) atoms, and that of the C(8)–C(10) bond from the plane defined by the C(7), C(8), and C(9) atoms are 5.9, 9.5, and 3.4° respectively. The corresponding angular deviations of the C(1)–C(16), C(17)–C(19), and C(12)–C(13) bonds are 2.7, 0.2, and 4.1° respectively. These angles are much smaller than the corresponding angles (11—15°) in [2.2]paracyclophane[15] and related compounds.[16,17]

The above results suggest that the intramolecular strain of the **3** molecule may be much smaller than the layered cyclophanes with ethano bridges and a little greater than those of the symmetrically tris-bridged analogue (**5**) and the di-bridged related compound (**6**).

Estimated Molecular Structures of Unsymmetrically Tris-bridged [2.2.2](1,2,4)(1,3,5) and [2.2.2](1,2,4)(1,2,5)-Cyclophanes. The molecular structures of [2.2.2](1,2,4)(1,3,5)cyclophane (**1**) and [2.2.2](1,2,4)(1,2,5)-cyclophane (**2**) were obtained by the conformational analysis of Boyd's *MOLBD*-3 program.[6] The starting molecular models were generated by Mansfield's *MOLGEN* program[18] using the standard structural parameters. The starting molecular models were refined through the energy-minimization procedure by means of the *MOLBD*-3 program to converged structures with strain energies of 39.1 (**1**) and 28.3 kcal mol^{-1} (**2**).†††† The calculated molecular structures of **1** and **2** are shown in Fig. 2. The molecular structures thus obtained give quite reasonable results, with a significantly greater strain energy in **1** than in **2**. The strain energy of [2.2]-paracyclophane was reported by Boyd to be 35.1 kcal mol^{-1}.[6]

The additional strain energy in **1** compared with that in **2** is based on the difference in bridging positions between the facing benzene rings. In the **2** molecule, the bridging from the 1, 2, and 4 positions of one benzene ring to the 1, 2, and 5 positions of the other benzene ring is done by sliding and rotating two benzene

†††† 1 cal=4.186 J.

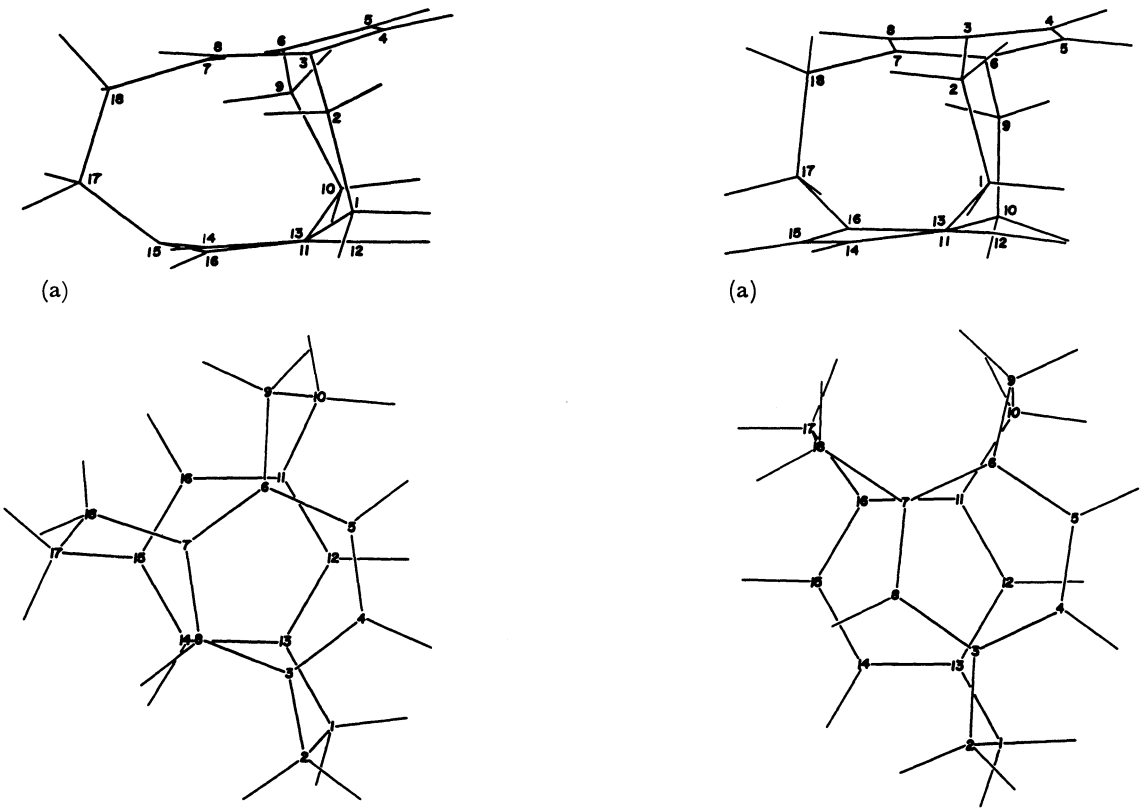

(a) (a)

(b) **1** (b) **2**

Fig. 2. Molecular structures of **1** and **2** estimated by the molecular conformational analysis by the use of *MOLBD*-3 program. a) Side views of the molecules projected along the C(13)–C(11) bond. b) Projections of the molecules onto the least-squares planes of (1, 3, 5)benzene for **1** and (1, 2, 5) benzene for **2**, respectively.

rings from the eclipsed position without adding an extra strain energy to its molecular structure. In the **1** molecule, however, the deviation of the two benzene rings from the eclipsed position is smaller than that of **2** because of the more constrained bridging positions of 1, 3, and 5 of the second benzene ring. This causes the rather large deformations of the structural parameters from the standard values. Almost all of the difference between the intramolecular strain energies of **1** and **2** [10.2 kcal mol^{-1}] is due to the difference in the strain energies of the angular deformations about C(benzene) connecting to the ethano bridges [2.7 kcal mol^{-1}] and out-of-plane deformations of C(benzene)–C(bridge) from the C(benzene) plane [6.5 kcal mol^{-1}] between **1** and **2**.

In the **1** molecule, the (1,2,4)benzene ring takes an approximately boat form, with the base plane including C(4), C(5), C(7), and C(8) atoms, while the (1,3,5)-benzene ring is roughly planar. The structures of these benzene rings in **1** are similar to those found in trithia-[3.3.3]cyclophane, which has the same bridging structure (**3**). In the **2** molecule, the (1,2,4)benzene ring also takes a boat form, with the base plane including C(4), C(5), C(7), and C(8), while the planality of the (1,2,5)-benzene ring is lower than that of the (1,3,5)benzene ring in **1**. The distances of the atoms in the (1,3,5)-benzene ring from the base plane of the (1,2,4)-benzene ring in **1** range from 2.57 to 3.02 Å [av. 2.82 Å], while

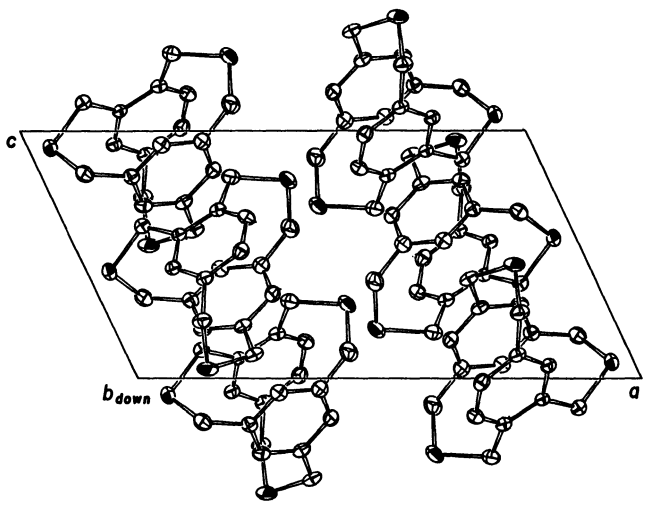

Fig. 3. Crystal structure of **3** projected along the b axis.

the corresponding values in **2** range from 2.52 to 3.01 Å [av. 2.81 Å]. It is noteworthy that the projection of **3** onto the mean plane of (1,3,5)benzene (Fig. 1), which shows an overlapping structure of two benzene rings, is essentially the same as the projection of **1** in Fig. 2.

Crystal Structure of 2,11,20-Trithia[3.3.3](1,3,5)cyclophane (3). The crystal structure of the **3** molecule is shown in Fig. 3. No unusually short contacts were found, the shortest ones being as follows: S(11)–C(13)

[x, 1/2−y, 1/2+z] 3.567 Å, S(11)–C(21) [x, 1/2−y, −1/2+z] 3.583 Å, and S(20)–S(20) [−x, 1−y, 1−z] 3.617 Å.

All the computations were carried out on an ACOS 800 computer at the Computation Center, Osaka University, and on an ACOS 700S computer at the Crystallographic Research Center, Institute for Protein Research, Osaka University.

The authors wish to express their deep thanks to Professor Masao Nakazaki and his co-workers of Osaka University for their kindness in supplying samples and their valuable discussions. We would also like to thank Professor Richard H. Boyd and Dr. Marc Mansfield for supplying their excellent computer programs. The present work was partially supported by a Grant-in-Aid for Co-operative Research (No. 434026) from the Ministry of Education, Science and Culture.

References

1) V. Boekelheide and R. A. Hollins, *J. Am. Chem. Soc.*, **93**, 3512 (1970); **95**, 3201 (1973).
2) D. J. Cram and E. A. Truesdale, *J. Am. Chem. Soc.*, **95**, 5825 (1973).
3) V. Boekelheide and R. Gray, *Angew. Chem., Int. Ed. Engl.*, **14**, 107 (1975).
4) W. Gilb, K. Menke, and H. Hopf, *Angew. Chem., Int. Ed. Engl.*, **16**, 191 (1977).
5) M. Nakazaki, K. Yamamoto, and Y. Miura, *J. Org. Chem.*, **43**, 1041 (1978).
6) R. H. Boyd, *J. Chem. Phys.*, **49**, 2574 (1968).
7) P. Main, M. M. Woolfson, L. Lessinger, G. Germain, and J. P. Declercq, *MULTAN* 74; "A System of Computer Programs for the Automatic Solution of Crystal Structures from X-Ray Diffraction Data," Univs. of York, England, and Louvain, Belgium (1974).
8) T. Ashida, *HBLS*-V, "The Universal Crystallographic Computing System-Osaka," The Computation Center, Osaka Univ. (1973), pp. 55—61.
9) "International Tables for X-Ray Crystallography," Kynoch Press, Birmingham (1974), Vol. IV, p. 71.
10) R. F. Stewart, E. R. Davidson, and W. T. Simpson, *J. Chem. Phys.*, **42**, 3175 (1965).
11) W. C. Hamilton, *Acta Crystallogr.*, **12**, 609 (1959).
12) C. K. Johnson, *ORTEP*-II, Report ORNL-5138, Oak Ridge National Laboratory, Tennessee (1974).
13) A. W. Hanson and E. W. Macaulay, *Acta Crystallogr., Sect. B*, **28**, 1255 (1972).
14) B. R. Davis and I. Bernal, *J. Chem. Soc., B*, **1971**, 2307.
15) H. Hope, J. Bernstein, and K. N. Trueblood, *Acta Crystallogr., Sect. B*, **28**, 1733 (1972).
16) H. Goto, Y. Kai, N. Yasuoka, and N. Kasai, 10th Symposium on Structural Organic Chemistry, Matsuyama, October 1977, Abstr., p. 219.
17) Y. Kai, H. Goto, N. Yasuoka, and N. Kasai, *Acta Crystallogr., Sect. A*, **34**, S292 (1978).
18) M. Mansfield, private communication.

The Crystal and Molecular Structure of Albocycline

Akio FURUSAKI,* Takeshi MATSUMOTO, Ken-ichi HARADA,† Makoto SUZUKI,†
Kenji KINOSHITA,†† Mitsuo HAYASHI,†† and Kazumi NAKATSU††
Department of Chemistry, Faculty of Science, Hokkaido University, Kita-ku, Sapporo 060
†*Faculty of Pharmacy, Meijo University, Tempaku-ku, Nagoya 468*
††*Faculty of Science, Kwansei Gakuin University, Nishinomiya 662*
(Received March 11, 1983)

The detailed molecular geometry of albocycline ($C_{18}H_{28}O_4$) has been examined by X-ray crystal analysis. The crystals are monoclinic, with four molecules in a unit cell with dimensions of $a=16.177(2)$, $b=9.562(1)$, $c=11.742(2)$ Å, and $\beta=90.43(1)°$; the space group is $P2_1$. 3062 unique intensity data were collected on a four-circle diffractometer with graphite-monochromated Mo $K\alpha$ radiation. The structure was elucidated by the Monte Carlo direct method, using the 30 reflections with the greatest $|E|$ values as the starting set; the 174th random phase set led to the correct solution. The R value reached 0.057 by block-diagonal least-squares refinements. The two crystallographically-independent molecules are connected by two O–H···O hydrogen bonds, forming a hydrogen-bonded dimer. The conformations of the fourteen-membered macrolide rings in these two molecules are considerably different from each other; *e.g.*, great differences of 165, 153, and 108° are found for the torsion angles around the C(4)–C(5), C(6)–C(7), and C(7)–C(8) single bonds respectively.

Albocycline is a macrolide antibiotic isolated from such strains of *Streptomyces* as *S. brunneogriseus*[1] and *S. maizeus*,[2] and is active mainly against staphylococci. On the basis of degradative and spectroscopic experiments,[3-5] the **1** structure was proposed for this antibiotic. A nuclear-Overhauser-effect study later suggested that the C(8)=C(9) double bond might be not *cis* but *trans*.[6] Therefore, in order to establish the molecular structure, we undertook an X-ray crystal structure analysis of albocycline itself. However, soon after this analysis has completed, the results of the X-ray study of (*p*-bromobenzoyl)albocycline (**2**) were published.[7] According to that report, albocycline has the **3** structure, which agrees with our conclusion. The present paper gives a detailed description of the two different molecular conformations found in the albocycline crystal.

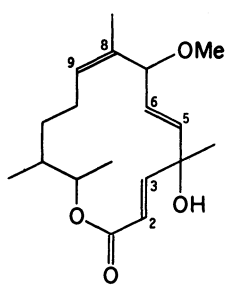

1

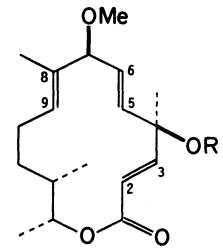

2 : R = p-BrC$_6$H$_4$CO
3 : R = H

Experimental

Colorless single crystals of albocycline were grown from a hexane–diethyl ether solution. The sample used for the X-ray experiment had dimensions of about $0.3\times0.4\times0.5$ mm^3. The crystal data are summarized in Table 1. The unit-cell dimensions and diffraction intensities were measured on a Rigaku four-circle diffractometer with graphite-monochromated Mo $K\alpha$ radiation ($\lambda=0.71069$ Å). The ω-2θ scan technique was applied at a 2θ scan rate of 4° min^{-1}; the scan width in ω was $(0.9+0.34\tan\theta)°$. The background was measured for 10 s at each end of the scan range. The intensities were corrected for the Lorentz and polarization factors, but not for the absorption or the extinction effect. In the range of 2θ value s up to 55°, 3062 independent structure factors above the $\sigma(F)$ level were selected for the structure determination.

TABLE 1. THE CRYSTAL DATA

$C_{18}H_{28}O_4$	Mol wt 308 42
Crystal system	Monoclinic
Space group	$P2_1$
Cell dimensions	a = 16.177(2) Å
	b = 9.562(1) Å
	c = 11.742(2) Å
	β = 90.43(1)°
V	1816.2 Å^3
Z	4
D_c	1.128 g cm^{-3}
μ(Mo $K\alpha$)	0.730 cm^{-1}

Structure Determination

In the early stage of the structure determination, various attempts were made to solve the structure with the MULTAN-78 program,[8] but all such attempts were unsuccessful. The structure was finally elucidated by the Monte Carlo direct method,[9] using the reflections with 2θ values less than 50°. The starting set was composed of the 30 reflections having the greatest $|E|$ values. In order to extend each of the tentative-phase sets derived from random numbers, 12 cycles of the tangent procedure were carried out by the use of 711 $|E|$ values above 1.30. Since the 174th random phase set showed a low R_K value of 0.316 ($R_K=\Sigma||E_o|-k|E_c||/\Sigma|E_o|$), 6 additional cycles of the tangent procedure were performed using 861 $|E|$ values above 1.20; consequently, the R_K value was reduced to 0.266. An E-map based on 828 phases revealed the locations of all the 44 non-hydrogen atoms.

The structure thus obtained was refined by the block-diagonal least-squares method with anisotropic temperature factors, using all the 3062 reflections. After all the 56 hydrogen atoms had been located in a difference Fourier map, further least-squares refine-

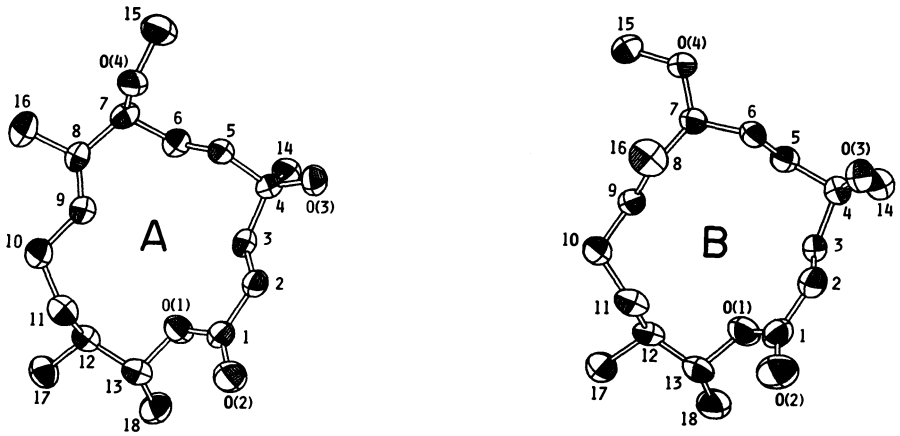

Fig. 1. The skeletons of the two crystallographically-independent albocycline molecules, A and B, viewed perpendicularly to their respective ring planes. Each non-hydrogen atom is represented as a thermal ellipsoid enclosing a 50% probability.

TABLE 2. THE FINAL ATOMIC PARAMETERS AND ESTIMATED STANDARD DEVIATIONS. The coordinates and B_{eq}[a)] values are multiplied by 10^4 and 10^2 respectively.

Atom	x	y	z	B_{eq}/Å^2	Atom	x	y	z	B_{eq}/Å^2
O(A1)	60(2)	4466(4)	5275(3)	436	O(B1)	5068(2)	4724(5)	9356(3)	524
O(A2)	856(2)	5718(6)	6451(3)	606	O(B2)	4361(3)	3584(6)	10685(4)	686
O(A3)	2528(2)	4936(4)	2861(3)	419	O(B3)	2341(2)	5092(5)	7696(3)	498
O(A4)	343(2)	6669(4)	328(3)	465	O(B4)	3650(2)	3078(5)	4163(3)	471
C(A1)	757(3)	5075(5)	5575(4)	367	C(B1)	4370(3)	4294(6)	9849(4)	455
C(A2)	1388(3)	4926(6)	4674(4)	362	C(B2)	3641(3)	4741(7)	9183(4)	444
C(A3)	1265(3)	4166(5)	3762(4)	326	C(B3)	3683(3)	5651(6)	8363(4)	380
C(A4)	1790(3)	4149(5)	2701(3)	339	C(B4)	3030(3)	5949(6)	7461(4)	403
C(A5)	1256(3)	4978(5)	1861(3)	338	C(B5)	3480(3)	5455(6)	6394(4)	381
C(A6)	554(3)	4533(5)	1413(4)	367	C(B6)	3412(2)	4238(5)	5937(4)	355
C(A7)	-37(3)	5433(6)	739(4)	404	C(B7)	4058(3)	3636(6)	5144(4)	382
C(A8)	-798(3)	5869(6)	1406(4)	398	C(B8)	4561(3)	2574(5)	5809(3)	342
C(A9)	-922(3)	5521(6)	2480(4)	402	C(B9)	5321(3)	2855(6)	6134(4)	373
C(A10)	-1633(3)	5945(6)	3216(4)	453	C(B10)	5858(3)	1981(6)	6911(5)	465
C(A11)	-1404(3)	6009(6)	4478(4)	418	C(B11)	5760(3)	2314(6)	8174(4)	450
C(A12)	-1375(3)	4607(5)	5082(4)	380	C(B12)	6243(3)	3578(6)	8612(4)	422
C(A13)	-676(3)	4590(6)	5979(4)	394	C(B13)	5867(3)	4134(7)	9708(4)	498
C(A14)	1976(3)	2678(6)	2315(4)	448	C(B14)	2794(4)	7467(8)	7416(5)	563
C(A15)	846(5)	6471(10)	-633(6)	698	C(B15)	4205(4)	2495(9)	3353(4)	582
C(A16)	-1387(4)	6770(11)	744(6)	776	C(B16)	4103(4)	1262(7)	6132(5)	538
C(A17)	-2217(3)	4220(6)	5591(5)	479	C(B17)	7150(3)	3181(8)	8795(5)	571
C(A18)	-676(4)	3388(8)	6809(5)	597	C(B18)	6333(5)	5304(9)	10294(6)	713

a) $B_{eq} = 8\pi^2(u_1^2+u_2^2+u_3^2)/3$, where u_i is the root-mean-square deviation in the i-th principal axis of the thermal ellipsoid.

ments were carried out including the hydrogen atoms with isotropic temperature factors. For these refinements, the following weighting scheme was used:

$$w=1/\{\sigma(F)^2 \exp(c_1X^2+c_2Y^2+c_3XY+c_4X+c_5Y)\},$$

where $X=|F_o|$ and $Y=\sin\theta/\lambda$. The c_1, c_2, c_3, c_4, and c_5 coefficients were evaluated from the $(\Delta F)^2$ distribution: $c_1=-0.377\times10^{-4}$, $c_2=24.1$, $c_3=0.0518$, $c_4=-0.265\times10^{-2}$, and $c_5=-27.3$. In this manner, the R value reached 0.057. The final atomic parameters are listed in Table 2.[10)]

The calculations were done on a HITAC M-200H computer at the Hokkaido University Computing Center, using our own programs. The atomic scattering factors were taken from the International Tables.[11)]

Results and Discussion

Molecular Structure. The frameworks of the two crystallographically-independent molecules, A and B, are illustrated in Fig. 1, while the bond distances and angles and the torsion angles are given in Tables 3 and 4 respectively. These results demonstrate that albocycline has the **3** structure in which the fourteen-membered macrolide ring contains a *trans,trans,trans*-triene system.

Notwithstanding the incorporation in the macrolide ring, the ester moiety in each of the A and B molecules keeps the geometry characteristic of secondary alcohol esters, *i.e.*, the synperiplanar configuration of the

Table 3. The bond distances and angles with their standard deviations

The e.s.d.'s given in parentheses refer to the last decimal position.

Bond distance	l/Å		Bond distance	l/Å	
	Mol. A	Mol. B		Mol. A	Mol. B
C(1)–C(2)	1.482(6)	1.472(7)	C(7)–O(4)	1.419(7)	1.427(6)
C(1)–O(1)	1.315(6)	1.338(7)	C(8)–C(9)	1.321(7)	1.312(6)
C(1)–O(2)	1.208(6)	1.194(7)	C(8)–C(16)	1.498(10)	1.508(8)
C(2)–C(3)	1.308(6)	1.300(7)	C(9)–C(10)	1.499(7)	1.508(7)
C(3)–C(4)	1.513(6)	1.518(6)	C(10)–C(11)	1.527(7)	1.525(7)
C(4)–C(5)	1.528(6)	1.530(7)	C(11)–C(12)	1.516(7)	1.526(8)
C(4)–C(14)	1.509(8)	1.501(9)	C(12)–C(13)	1.541(6)	1.522(7)
C(4)–O(3)	1.422(5)	1.411(6)	C(12)–C(17)	1.536(7)	1.529(7)
C(5)–C(6)	1.318(6)	1.286(7)	C(13)–C(18)	1.507(9)	1.512(10)
C(6)–C(7)	1.507(7)	1.517(6)	C(13)–O(1)	1.459(6)	1.467(7)
C(7)–C(8)	1.523(7)	1.515(7)	C(15)–O(4)	1.410(8)	1.426(7)

Bond angle	θ/°		Bond angle	θ/°	
	Mol. A	Mol. B		Mol. A	Mol. B
C(2)–C(1)–O(1)	111.1(4)	110.9(4)	C(8)–C(7)–O(4)	107.5(4)	114.1(4)
C(2)–C(1)–O(2)	124.7(4)	125.9(5)	C(7)–C(8)–C(9)	123.4(4)	120.8(5)
O(1)–C(1)–O(2)	124.1(4)	123.1(5)	C(7)–C(8)–C(16)	113.9(4)	115.1(4)
C(1)–C(2)–C(3)	122.4(4)	122.8(5)	C(9)–C(8)–C(16)	122.7(5)	124.0(5)
C(2)–C(3)–C(4)	126.6(4)	127.1(4)	C(8)–C(9)–C(10)	127.2(5)	126.6(5)
C(3)–C(4)–C(5)	102.0(3)	100.4(4)	C(9)–C(10)–C(11)	112.9(4)	114.1(5)
C(3)–C(4)–C(14)	111.8(4)	112.4(4)	C(10)–C(11)–C(12)	115.2(4)	115.9(4)
C(3)–C(4)–O(3)	111.2(3)	107.5(4)	C(11)–C(12)–C(13)	110.4(4)	110.8(4)
C(5)–C(4)–C(14)	113.8(4)	113.1(4)	C(11)–C(12)–C(17)	111.8(4)	109.8(5)
C(5)–C(4)–O(3)	106.3(4)	111.3(4)	C(13)–C(12)–C(17)	112.4(4)	110.9(4)
C(14)–C(4)–O(3)	111.3(4)	111.6(4)	C(12)–C(13)–C(18)	116.5(5)	116.3(5)
C(4)–C(5)–C(6)	124.8(4)	125.6(4)	C(12)–C(13)–O(1)	102.2(3)	104.7(4)
C(5)–C(6)–C(7)	124.5(5)	122.8(4)	C(18)–C(13)–O(1)	108.0(4)	106.1(5)
C(6)–C(7)–C(8)	113.5(4)	108.0(4)	C(1)–O(1)–C(13)	120.9(4)	120.3(4)
C(6)–C(7)–O(4)	112.3(4)	108.7(3)	C(7)–O(4)–C(15)	114.5(5)	113.3(4)

Table 4. The torsion angles[a)]

Torsion angle	ϕ/°		Torsion angle	ϕ/°	
	Mol. A	Mol. B		Mol. A	Mol. B
O(1)–C(1)–C(2)–C(3)	-5.9	-12.2	O(4)–C(7)–C(8)–C(9)	-123.4	132.4
O(2)–C(1)–C(2)–C(3)	176.9	171.4	O(4)–C(7)–C(8)–C(16)	54.8	-52.2
C(2)–C(1)–O(1)–C(13)	-174.1	-165.6	C(6)–C(7)–O(4)–C(15)	77.5	179.5
O(2)–C(1)–O(1)–C(13)	3.1	10.9	C(8)–C(7)–O(4)–C(15)	-156.9	-60.0
C(1)–C(2)–C(3)–C(4)	168.0	165.3	C(7)–C(8)–C(9)–C(10)	177.5	172.3
C(2)–C(3)–C(4)–C(5)	-104.6	-114.0	C(16)–C(8)–C(9)–C(10)	-0.6	-2.7
C(2)–C(3)–C(4)–C(14)	133.4	125.6	C(8)–C(9)–C(10)–C(11)	-151.4	-88.3
C(2)–C(3)–C(4)–O(3)	8.3	2.4	C(9)–C(10)–C(11)–C(12)	-79.2	-81.4
C(3)–C(4)–C(5)–C(6)	-70.0	95.3	C(10)–C(11)–C(12)–C(13)	144.1	158.7
C(14)–C(4)–C(5)–C(6)	50.6	-144.7	C(10)–C(11)–C(12)–C(17)	-90.1	-78.4
O(3)–C(4)–C(5)–C(6)	173.4	-18.3	C(11)–C(12)–C(13)–C(18)	168.1	174.6
C(4)–C(5)–C(6)–C(7)	169.6	-159.2	C(11)–C(12)–C(13)–O(1)	-74.5	-68.8
C(5)–C(6)–C(7)–C(8)	-103.6	103.1	C(17)–C(12)–C(13)–C(18)	42.6	52.3
C(5)–C(6)–C(7)–O(4)	18.6	-132.6	C(17)–C(12)–C(13)–O(1)	160.0	169.0
C(6)–C(7)–C(8)–C(9)	1.4	-106.6	C(12)–C(13)–O(1)–C(1)	145.9	124.6
C(6)–C(7)–C(8)–C(16)	179.7	68.8	C(18)–C(13)–O(1)–C(1)	-90.7	-112.0

a) The e.s.d.'s are 0.4—0.9°.

C(13)–O(1)–C(1)=O(2) segment and the eclipsed conformation of the H(13)–C(13)–O(1)–C(1) segment. This geometry brings the O(2) and H(13) atoms close to each other; their distances are 2.49(4) and 2.30(5) Å for the A and B molecules respectively. The C(2)=C(3) and C(1)=O(2) conjugated double bonds are transoid and nearly coplanar for both molecules. Consequently, the C(13)–O(1)–C(1)(O(2))–C(2)=C(3)–C(4) segment as a whole has a rigid and nearly-planar configuration. This coplanarity of the five consecutive bonds makes it

impossible for the ring to take a rectangular form.

As will be seen from Fig. 1, the ring conformations of the A and B molecules differ considerably from each other. The C(5) and C(6) atoms in the former molecule are situated above and below the mean plane of the ring respectively, while those in the latter are placed in the opposite way. This remarkable variation in the orientation of the C(5)=C(6) double bond is caused mainly by great changes (165, 153, and 108° respectively) of the C(3)–C(4)–C(5)=C(6), C(5)=C(6)–C(7)–C(8), and C(6)–C(7)–C(8)=C(9) torsion angles. These torsional changes further alter the orientations of the atomic groups at the C(4) and C(7) atoms in a regular manner; *i.e.*, the O(3)H, C(14)H_3, and O(4)–C(15)H_3 groups in the A molecule are pseudo-equatorial, pseudo-axial, and pseudo-axial respectively, whereas those in the B molecule are pseudo-axial, pseudo-equatorial, and pseudo-equatorial respectively. On the other hand, the C(17)H_3 and C(18)H_3 groups remote from the C(4)–C(5)=C(6)–C(7) segment are pseudo-equatorial for both molecules.

When the macrolide ring in the B molecule is viewed along the normal of its mean plane, it looks like a somewhat-deformed trapezoid having the nearly-planar C(13)–O(1)–C(1)(O(2))–C(2)=C(3)–C(4), C(4)–C(5)=C(6)–C(7), C(7)–C(8)(C(16))=C(9)–C(10), and C(10)–C(11)=C(12)–C(13) segments as the four sides (see Fig. 1). The mean planes for these segments make angles of 33, 12, 5, and 16° with the normal of the ring plane respectively. On the other hand, the macrolide ring in the A molecule is too greatly deformed to be regarded as having such a trapezoid form. That is to say, the mean planes for the C(13)–O(1)–C(1)(O(2))–C(2)=C(3)–C(4) and C(7)–C(8)(C(16))=C(9)–C(10) segments incline at large angles of 46 and 70° with the normal of the ring plane respectively, although those for the C(4)–C(5)=C(6)–C(7) and C(10)–C(11)–C(12)–C(13) segments are at small angles of 17 and 9° with this normal respectively. The marked inclination of the C(7)–C(8)(C(16))=C(9)–C(10) segment results mainly from the eclipsed conformation of the C(6)–C(7)–C(8)=C(9) segment. The (*p*-bromobenzoyl)albocycline molecule[7] has almost the same ring conformation as the A molecule of albocycline. A ring conformation such as the B molecule takes may be unfavorable for the derivative molecule because of the pseudo-axial orientation of the large *p*-bromobenzoyloxyl group.

The ring formation results in considerable deformation of the vinylene groups. The deviations of the C(1)–C(2)=C(3)–C(4), C(4)–C(5)=C(6)–C(7), and C(7)–C(8)=C(9)–C(10) torsion angles from the value (180°) for the ideal planar *trans* configuration are 12.0, 10.4, and 2.5° for the A molecule respectively, and are 14.7, 20.8, and 7.7° for the B molecule respectively. It is of interest to note that each vinylene group in the B molecule is more greatly deformed than the corresponding group in the A molecule. Apart from the O(1)–C(1)–C(2)=C(3) segment which has the synperiplanar conformation because of the strong conjugation between the C(2)=C(3) and C(1)=O(2) double bonds, there are three and four synperiplanar segments of the C=C–C–X type in the A and B molecules respectively (see Table 5). Of these seven segments, two are the C(2)=C(3)–C(4)–O(3) segments in the two molecules. It is known that, in the preferred conformations of *unsym*-butene (CH_2=CH–CH_2–CH_3) and allyl alcohol (CH_2=CH–CH_2–OH), the C=C double bond eclipses one of the hydrogen atoms at the allylic position.[12] The C(5)=C(6)–C(7)–H(7) and H(7)–C(7)–C(8)=C(9) segments in the B molecule have such eclipsed conformations. On the other hand, the eclipsed conformations of the C(5)=C(6)–C(7)–O(4) and C(6)–C(7)–C(8)=C(9) segments in the A molecule result in significant enlargement of the C(5)=C(6)–C(7), C(6)–C(7)–O(4), C(6)–C(7)–C(8), and C(7)–C(8)=C(9) bond angles, the observed values of which are greater than the corresponding values in the B molecule by 1.7, 3.6, 5.5, and 2.6° respectively. The O(3)–C(4)–C(5) bond angle in the B molecule is greater than that in the A molecule by 5.0°. This is also explained by the fact that, while the C(5)=C(6) double bond in the former molecule eclipses the C(4)–O(3) bond, that in the latter is gauche to the C(3)–C(4) and C(4)–C(14) bonds.

Crystal Structure. The molecular arrangement viewed along the b axis is shown in Fig. 2. There are two kinds of hydrogen bonds, O(A3)–H···O(B4) and

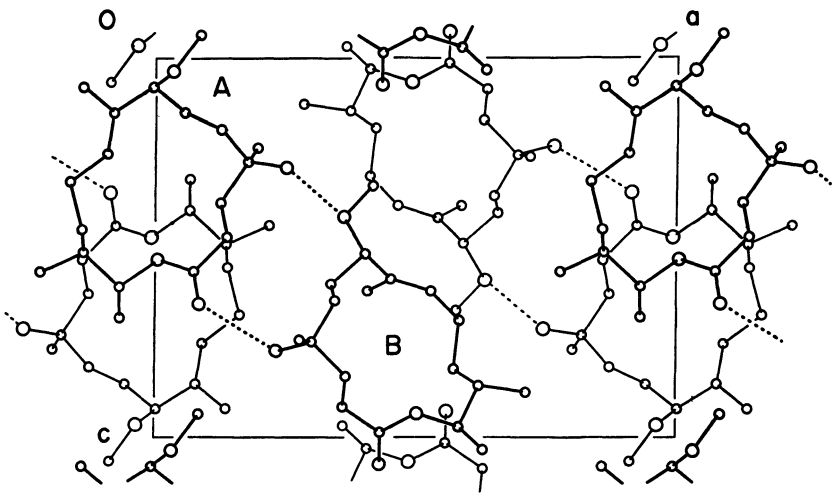

Fig. 2. The molecular arrangement viewed along the b axis.

Table 5. The synperiplanar segments of the C=C–C–X type and their torsion angles(ϕ/°)

(1) Molecule A	
C(2)=C(3)–C(4)–O(3)	8.3(7)
C(5)=C(6)–C(7)–O(4)	18.6(6)
C(6)–C(7)–C(8)=C(9)	1.4(7)
(2) Molecule B	
C(2)=C(3)–C(4)–O(3)	2.4(7)
O(3)–C(4)–C(5)=C(6)	−18.3(7)
C(5)=C(6)–C(7)–H(7)	−15(3)
H(7)–C(7)–C(8)=C(9)	9(3)

O(B3)–H···O(A2); their O···O distances are 2.957(5) and 2.867(5) Å respectively. Through these hydrogen bonds, the O(2)–C(1)–C(2)=C(3)–C(4)–O(3)–H(O3) segment in the A molecule and the H(O3)–O(3)–C(4)–C(5)=C(6)–C(7)–O(4) segment in the B molecule are connected to form a fourteen-membered ring; consequently, the two molecules form a hydrogen-bonded dimer oriented nearly in the [101] direction. The macrolide-ring planes of the A and B molecules in the same dimer make an angle of 30° with each other, and incline at angles of 15 and 37° to the (010) plane respectively. The hydrogen-bonded dimers are further held together mainly by the van der Waals interactions.

References

1) N. Nagahama, M. Suzuki, S. Awataguchi, and T. Okuda, *J. Antibiot., Ser. A*, **20**, 261 (1967).
2) F. Reusser, *J. Bacteriol.*, **100**, 11 (1969).
3) N. Nagahama, I. Takamori, K. Kotera, and M. Suzuki, *Chem. Pharm. Bull.*, **19**, 649 (1971).
4) N. Nagahama, I. Takamori, and M. Suzuki, *Chem. Pharm. Bull.*, **19**, 655 (1971).
5) N. Nagahama, I. Takamori, and M. Suzuki, *Chem. Pharm. Bull.*, **19**, 660 (1971).
6) K.-I. Harada, F. Nishida, H. Takagi, and M. Suzuki, unpublished.
7) R. C. Thomas and C. G. Chidester, *J. Antibiot.*, **35**, 1658 (1982).
8) P. Main, S. E. Hull, L. Lessinger, G. Germain, J. P. Declercq, and M. M. Woolfson, "MULTAN 78, A System of Computer Programs for the Automatic Solution of Crystal Structures from X-Ray Diffraction Data," Universities of York, England, and Louvain, Belgium (1978).
9) A. Furusaki, *Acta Crystallogr., Sect. A*, **35**, 220 (1979).
10) The tables of the anisotropic thermal parameters and hydrogen parameters and the F_o-F_c table are kept at the Chemical Society of Japan (Document No. 8336).
11) "International Tables for X-Ray Crystallography," The Kynoch Press, Birmingham (1974), Vol. IV.
12) D. R. Herschbach and L. C. Krischner, *J. Chem. Phys.*, **28**, 728 (1958).

 © 1983 The Chemical Society of Japan Bull. Chem. Soc. Jpn., 56, 3047—3051 (1983)

Kinetic Parameters of the Electrode Reaction of Carbonatocobalt(III) Complexes at Mercury Electrodes

Akifumi YAMADA,* Yutaka KADO, and Yu YOKOYAMA

Department of Materials Science and Technology, Technological University of Nagaoka, Kamitomioka, Nagaoka 949-54

(Received January 27, 1983)

The electroreduction of $[Co(CO_3)(NH_3)_5]^+$, $[Co(CO_3)(NH_3)_4]^+$, $[Co(CO_3)(tn)_2]^+$, $[Co(CO_3)(pn)_2]^+$, $[Co(CO_3)(en)_2]^+$, and $[Co(CO_3)_2(en)]^-$ (tn=trimethylenediamine, pn=propylenediamine, en=ethylenediamine) have been studied at mercury electrodes in weak acid solutions. All complexes exhibit two irreversible reduction waves; the first corresponds to $Co^{III} \longrightarrow Co^{II}$, and the second, to $Co^{II} \longrightarrow Co^0$. The kinetic parameters of the electrode reactions of the first step were determined by means of Tast and pulse polarography in solutions containing 0.005 M sodium acetate–acetic acid buffer (pH=6) and 0.995 M sodium nitrate at 25 °C. The differential pulse polarograph hic characteristics of these complexes are also given.

The polarography of carbonatocobalt(III) complexes has been briefly reported in the course of the survey of the half-wave potential for mixed ammine cobalt[1,2] and ethylenediamine cobalt[3] complexes. However, a systematic study of a series of carbonatocobalt(III) complexes under the same conditions has not yet been made. Data for electrochemical kinetic parameters are of importance in the discussion not only of the properties of electrode reactions but also the effect of the solvent, the supporting electrolytes and the electrical double layer on the reactions.

In this paper, the kinetic parameters of the electrode reactions of several carbonatocobalt(III) complexes were examined by means of Tast and pulse polarography.

Experimental

Materials. The complexes, $[Co(CO_3)(en)_2]ClO_4$,[4] $[Co(CO_3)(pn)_2]NO_3$,[5] $[Co(CO_3)(tn)_2]ClO_4$,[6] $[Co(CO_3)(NH_3)_4]NO_3 \cdot 0.5H_2O$,[7] $[Co(CO_3)(NH_3)_5]NO_3 \cdot 0.5H_2O$,[8] $K[Co(CO_3)_2(en)]$,[9] $[Co(NH_3)_6](NO_3)_3$,[10] and $Na[Co(edta)]$[11] were prepared by the literature methods. The concentration of 0.001% polyacrylamide (PAA) was used as the maximum suppressor. All the other chemicals used were of a guaranteed reagent-grade.

Electrochemical Measurements. A three-electrode cell[12] equipped with a saturated calomel electrode (Yanagimoto MR-P2-05-1) and a platinum wire electrode was employed. The dropping mercury electrode (flow rate, 1.25 mg s^{-1} and drop time, 2.99 s in 1 M (1 M=1 mol dm^{-3}) sodium nitrate solutions) served as a working electrode. The kinetic parameters of the electrode reactions were determined by means of Tast and pulse polarography. The polarograms were recorded on Yanagimoto Model P-1000 polarograph with a Riken Denshi Model F3EP x-y recorder. A Takeda Riken digital multimeter, Model TR-6355, was used; the current and the potential were thus measured precisely. Electrolytic solutions were deaerated by bubbling purified nitrogen gas through the solution. All measurements were made at 25±0.1 °C.

In a series of determination of the electrochemical kinetic parameters of various cobalt(III) complexes, the electrochemical procedure was as follows. After measurements of residual current of 10 ml of supporting electrolyte solution, a solid sample of the cobalt complex under test was added to the solution. The electrode potential which is premeditatedly selected was applied. The current was then measured. Measurements were made within ten minutes to avoid the decomposition of complexes in the solution.

Results and Discussion

Many mixed cobalt(III) complexes with various ligands have been prepared, but the kinetic parameters of the electrode reactions have been studied only for a few.[13] For the carbonatocobalt(III) complexes, the polarographic half-wave potentials in neutral solutions have been reported only for carbonatopentaamminecobalt(III),[1] carbonatotetraamminecobalt(III),[2] and carbonatobis(ethylenediamine)cobalt(III)[3] complexes. These cobalt(III) complexes are reduced in two steps: the first corresponds to $Co^{III} \rightarrow Co^{II}$ and the second, to $Co^{II} \rightarrow Co^0$. This work reports extensive kinetic studies of carbonatocobalt(III) complex ions, such as $[Co(CO_3)(en)_2]^+$, $[Co(CO_3)(pn)_2]^+$, $[Co(CO_3)(tn)_2]^+$, $[Co(CO_3)(NH_3)_4]^+$, $[Co(CO_3)(NH_3)_5]^+$, and $[Co(CO_3)_2(en)]^-$. They are made in acid solutions at mercury electrodes.

The carbonatocobalt(III) complexes gave two polarographic waves. The limiting currents of both the first and the second wave were diffusion-controlled and were proportional to the concentration of the complex. The limiting current of the second wave was twice that of the first one, which suggests that a one-electron reduction is followed by a two-electron reduction. From a polarographic log-plot analysis[14] and other polarographic experiments, both steps are considered to be totally irreversible. The present investigation is concerned only with the reduction of cobalt(III) to cobalt(II).

Figure 1 shows the Tast polarogram of the first wave of several carbonatocobalt(III) complexes obtained in solutions containing 0.005 M sodium acetate-acetic acid buffer (pH=6) and 0.995 M sodium nitrate. In the carbonatocobalt(III) complexes studied, the CO_3^{2-} acts as a bidentate ligand, except for $[Co(CO_3)(NH_3)_5]^+$, in which the carbonate ions are unidentate ligands. An examination of Fig. 1 shows the half-wave potentials for the first wave of the complex depend on the types of coordination. The order of the half-wave potential in the series of complexes is:

$$[Co(CO_3)(NH_3)_5]^+ > [Co(CO_3)(NH_3)_4]^+ > [Co(CO_3)_2(en)]^-$$

and

$$[Co(CO_3)(tn)_2]^+ > [Co(CO_3)(pn)_2]^+ > [Co(CO_3)(en)_2]^+.$$

In the first series, carbonatopentaamminecobalt(III)

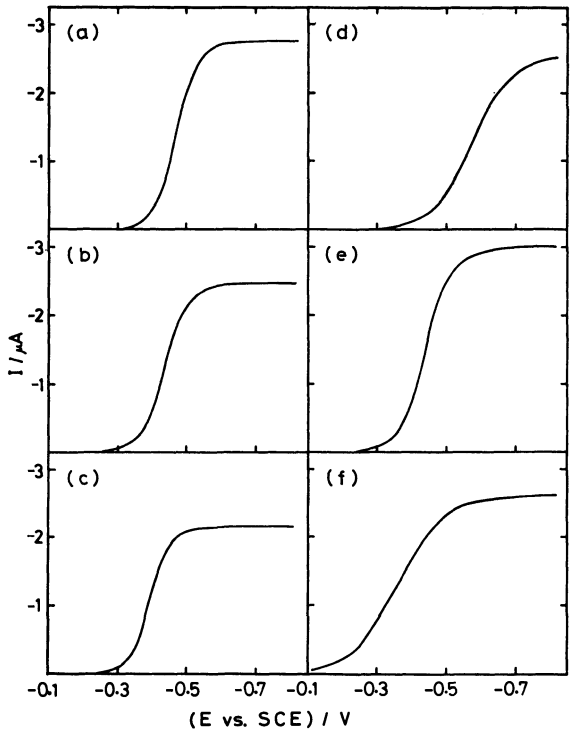

Fig. 1. Tast polarograms for the first wave of several carbonatocobalt(III) complex ions obtained in 0.005 M acetate buffer (pH=6), 0.995 M sodium nitrate and 0.001% PAA at 25 °C.
(a) $[Co(CO_3)(en)_2]^+$, (b) $[Co(CO_3)(pn)_2]^+$, (c) $[Co(CO_3)(tn)_2]^+$, (d) $[Co(CO_3)_2(en)]^-$, (e) $[Co(CO_3)(NH_3)_4]^+$, (f) $[Co(CO_3)(NH_3)_5]^+$.

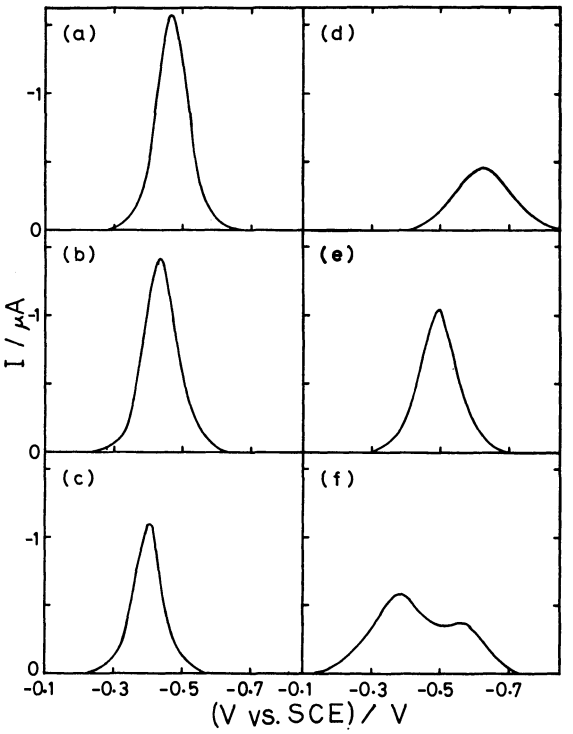

Fig. 2. Differential pulse polarograms for the first wave of several carbonatocobalt(III) complex ions obtained in 0.005 M acetate buffer (pH=6), 0.995 M sodium nitrate and 0.001% PAA at 25 °C.
(a) $[Co(CO_3)(en)_2]^+$, (b) $[Co(CO_3)(pn)_2]^+$, (c) $[Co(CO_3)(tn)_2]^+$, (d) $[Co(CO_3)_2(en)]^-$, (e) $[Co(CO_3)(NH_3)_4]^+$, (f) $[Co(CO_3)(NH_3)_5]^+$.

TABLE 1. DIFFERENTIAL-PULSE POLAROGRAPHIC CHARACTERISTICS OF THE ONE-ELECTRON REDUCTION OF 1 mM COBALT(III) COMPLEXES OBTAINED IN 0.005 M ACETATE BUFFER (pH=6), 0.995 M SODIUM NITRATE AND 0.001% PAA AT 25 °C.

Complex	E_p *vs.* SCE / V	I_p / μA	ΔW / mV
$[Co(CO_3)_2(en)]^-$	−0.630	−0.45	194
$[Co(CO_3)(en)_2]^+$	−0.470	−1.5	106
$[Co(CO_3)(pn)_2]^+$	−0.436	−1.4	111
$[Co(CO_3)(tn)_2]^+$	−0.410	−1.1	90
$[Co(CO_3)(NH_3)_4]^+$	−0.495	−1.0	123
$[Co(CO_3)(NH_3)_5]^+$	−0.382	−0.59	218
	(−0.57)[a]	(−0.38)[a]	—
$[Co(NH_3)_6]^{3+}$	−0.363	−1.3	113
$[Co(edta)]^-$	+0.145	−3.2	102

a) Corresponds to the second peak.

may be less stable than carbonatotetraamminecobalt(III) since the ligand CO_3^{2-} acts as unidentate in $[Co(CO_3)(NH_3)_5]^+$. Dicarbonatoethylenediaminecobaltate(III) may be more stable than carbonatotetraamminecobalt(III) because the CO_3^{2-} ligand occupies four coordination positions in the former, but only two in the latter. In the second series, the order of the half-wave potential is in accordance with that of the tris-type complexes ($[Co(tn)_3]^{3+}$>$[Co(pn)_3]^{3+}$>$[Co(en)_3]^{3+}$).[15] The trimethylenediamine chelate ring is more bulky than the ethylenediamine chelate ring, and carbonatobis(trimethylenediamine)cobalt(III) may be less stable than carbonatobis(ethylenediamine)cobalt(III).

Figure 2 shows the differential pulse polarograms of the first wave of several carbonatocobalt(III) complexes. The wave height of $[Co(CO_3)_2(en)]^-$ was about one-third of $[Co(CO_3)(en)_2]^+$. The differential pulse polarogram of $[Co(CO_3)(NH_3)_5]^+$ showed two peaks while the Tast polarogram gave a single wave as is seen in Fig. 1. Tast and pulse polarograms of this complex were observed over a wide potential range.

Various parameters which characterize a differential pulse polarogram were obtained; they are shown in Table 1 together with those of hexaamminecobalt(III) and ethylenediaminetetraacetatocobaltate(III) ions. The electrode reaction of $[Co(NH_3)_6]^{3+}$ at a mercury electrode is recognized as a typical key reaction for an irreversible electron-transfer process.[13] On the contrary, the electrode reaction of $[Co(edta)]^-$ is known to proceed reversibly at a mercury electrode.[16] For all the complexes studied, the peak currents of the first wave were found to be much smaller than that expected for a reversible electron-transfer process indicating that the electrode reaction is irreversible.

The reduction of carbonatocobalt(III) to cobalt(II) species in an acid solution was considered to be irrever-

sible from the facts described above. For a totally irreversible electrode reaction, the following relations of the Tast polarography are derived:[17,18]

$$(\boldsymbol{R}T/an\boldsymbol{F})\ln[2x(3-x)/5(1-x)] = E_{1/2} - E, \quad (1)$$

with:

$$x = I/I_d, \quad (2)$$

and:

$$E_{1/2} = (\boldsymbol{R}T/an\boldsymbol{F})\ln[1.35\, k_c^\circ (t_d/D)^{1/2}], \quad (3)$$

where I is the current at the potential E; I_d the diffusion-controlled current; D, the diffusion coefficient; t_d, the drop time; α, the transfer coefficient; k_c°, the cathodic rate constant at $E=0$; n, the number of electrons; $\boldsymbol{R}$, $\boldsymbol{F}$, and T have usual meanings. According to Eq. 1, a plot of $\ln[2x(3-x)/5(1-x)]$ *vs.* E should be a straight line. The transfer coefficient, α, can be obtained from $E_1/_2$ by applying Eq. 3. These relations are derived under the assumptions that a transfer coefficient is independent on electrode potentials and extrapolation to $E=0$ is possible for the rate constants. The analysis of electrode kinetics by these relations, therefore, may be limited to a first approximation. However, such kinetic parameters of electrode reactions play an important role in the interpretation of electrode kinetics, because the available data have been reported only few.[13]

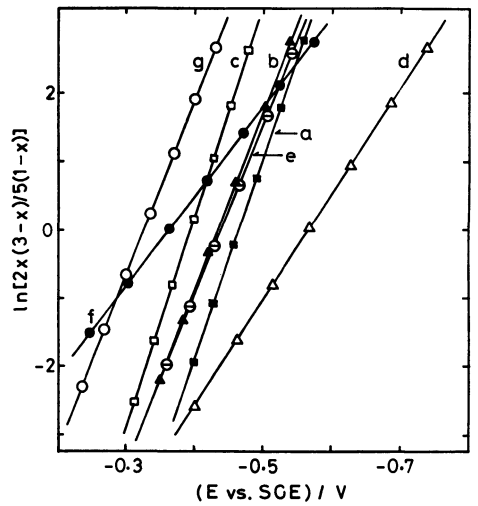

Fig. 3. Tast polarographic log plots for the first wave of several carbonatocobalt(III) complex ions obtained in 0.005 M acetate buffer (pH=6), 0.995 M sodium nitrate and 0.001% PAA at 25 °C.
(a) $[Co(CO_3)(en)_2]^+$, (b) $[Co(CO_3)(pn)_2]^+$, (c) $[Co(CO_3)(tn)_2]^+$, (d) $[Co(CO_3)_2(en)]^-$, (e) $[Co(CO_3)(NH_3)_4]^+$, (f) $[Co(CO_3)(NH_3)_5]^+$, (g) $[Co(NH_3)_6]^{3+}$.

An example of the plots for Eq. 1 is given in Fig. 3. Table 2 summarizes the kinetic parameters of the electrode reactions corresponding to the first wave for various carbonatocobalt(III) complexes. The diffusion coefficients required for the calculation of kinetic parameters were taken from the earlier work.[19] These kinetic parameters obtained were checked by calculating the current according to the relation:

$$2x(3-x)/5(1-x) = 1.35\, k_c^\circ (t_d/D)^{1/2} \exp(-an\boldsymbol{F}E/\boldsymbol{R}T). \quad (4)$$

The calculated currents were in agreement with the observed ones except for the case of $[Co(CO_3)(NH_3)_5]^+$. The order of a specific rate constant (k_c°) was found to be 10^{-6}—10^{-9} cm s^{-1}. The transfer coefficients were found to be above 0.5 except for the cases of $[Co(CO_3)(NH_3)_5]^+$ and $[Co(CO_3)_2(en)]^-$.

The kinetic parameters of electrode reactions for these carbonatocobalt(III) complexes are also determined by means of pulse polarography. To a pulse response of totally irreversible system, the following equations are applied:[17,18]

$$(\boldsymbol{R}T/2an\boldsymbol{F})\ln[x^2(1.75+x)/(1-x)] = E_{1/2} - E, \quad (5)$$

with:

$$E_{1/2} = (\boldsymbol{R}T/an\boldsymbol{F})\ln[2.31\, k_c^\circ (t_d/D)^{1/2}]. \quad (6)$$

where x is defined by Eq. 2. In this case a plot of $\ln[x^2(1.75+x)/(1-x)]$ *vs.* E should give a straight line. The transfer coefficient (α) and the specific rate constant (k_c°) can be claculated if a linear plot is obtained.

Examples of the plot of Eq. 5 obtained at various electrode potentials are given in Fig. 4. A linear plot was obtained except for $[Co(CO_3)(NH_3)_5]^+$. The log plot for $[Co(CO_3)(NH_3)_5]^+$ is somewhat sigmoid in shape. The kinetic parameters obtained from these plots are given in Table 3. The half-wave potentials obtained by means of pulse polarography were found to shift to more negative potentials. This is expected from the magnitude of the sampling time as is given by Eqs. 3 and 6. The measurements were made at sampling times of 2.99 and 0.04 s for the Tast and the pulse polarography, respectively.

The transfer coefficients obtained by means of those

Table 2. Kinetic parameters of electrode reactions of the one-electron reduction of cobalt(III) complexes obtained by Tast polarography in 0.005 M acetate buffer (pH=6), 0.995 M sodium nitrate and 0.001% PAA at 25 °C.

Complex	$E_{1/2}$ *vs.* SCE / V	α	$k_c^\circ/\sqrt{D}$ / $s^{-1/2}$	k_c° / cm s^{-1}	D[a] / 10^{-6} cm^2 s^{-1}
$[Co(CO_3)_2(en)]^-$	−0.567	0.40	5.9×10^{-5}	1.5×10^{-7}	6.74
$[Co(CO_3)(en)_2]^+$	−0.465	0.74	6.4×10^{-7}	1.8×10^{-9}	7.85
$[Co(CO_3)(pn)_2]^+$	−0.435	0.68	4.3×10^{-6}	1.1×10^{-8}	6.21
$[Co(CO_3)(tn)_2]^+$	−0.395	0.79	2.3×10^{-6}	5.0×10^{-9}	4.76
$[Co(CO_3)(NH_3)_4]^+$	−0.439	0.65	6.7×10^{-6}	2.0×10^{-8}	9.04
$[Co(CO_3)(NH_3)_5]^+$	−0.360	0.34	3.6×10^{-3}	9.6×10^{-6}	7.09
$[Co(NH_3)_6]^{3+}$	−0.327	0.65	1.1×10^{-4}	3.1×10^{-7}	8.06

a) Taken from the previous work.[19]

TABLE 3. KINETIC PARAMETERS OF ELECTRODE REACTIONS OF THE ONE-ELECTRON REDUCTION OF COBALT(III) COMPLEXES OBTAINED BY PULSE POLAROGRAPHY IN 0.005 M ACETATE BUFFER (pH=6), 0.995 M SODIUM NITRATE AND 0 001% PAA AT 25 °C.

Complex	$E_{1/2}$ *vs.* SCE / V	α	$k_c^\circ/\sqrt{D}$ / $s^{-1/2}$	k_c° / cm s^{-1}
$[Co(CO_3)_2(en)]^-$	−0.624	0.48	1.8×10^{-5}	4.7×10^{-8}
$[Co(CO_3)(en)_2]^+$	−0.490	0.82	3.4×10^{-7}	9.5×10^{-10}
$[Co(CO_3)(pn)_2]^+$	−0.456	0.75	3.8×10^{-6}	9.5×10^{-9}
$[Co(CO_3)(tn)_2]^+$	−0.437	0.80	2.6×10^{-6}	5.7×10^{-9}
$[Co(CO_3)(NH_3)_4]^+$	−0.508	0.67	4.0×10^{-6}	1.2×10^{-8}
$[Co(CO_3)(NH_3)_5]^+$	−0.430	0.35	7.9×10^{-3}	2.1×10^{-5}
$[Co(NH_3)_6]^{3+}$	−0.379	0.67	1.1×10^{-4}	3.1×10^{-7}

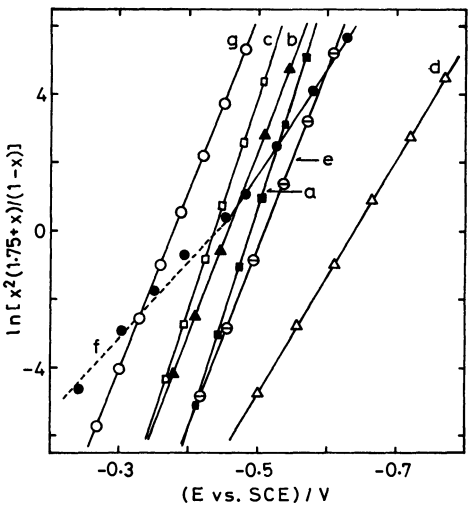

Fig. 4. Pulse polarographic log plots for the first wave of several carbonatocobalt(III) complex ions obtained in 0.005 M acetate buffer (pH=6), 0.995 M sodium nitrate and 0.001% PAA at 25 °C.
(a) $[Co(CO_3)(en)_2]^+$, (b) $[Co(CO_3)(pn)_2]^+$, (c) $[Co(CO_3)(tn)_2]^+$, (d) $[Co(CO_3)_2(en)]^-$, (e) $[Co(CO_3)(NH_3)_4]^+$, (f) $[Co(CO_3)(NH_3)_5]^+$, (g) $[Co(NH_3)_6]^{3+}$.

Tast polarography, however, were found to be smaller than those of the pulse polarography. In the Tast polarography, the electrolysis proceeds simultaneously during the drop life, while in the pulse polarography the faradaic current is negligibly small before the pulse is applied. Therefore, the differencies of the kinetic parameters obtained by the two electrochemical methods may be mainly attributed to the depletion effect as was pointed out by Hans *et al.*[20] Furthermore, the electrode reactions of the cobalt complex studied here are followed by chemical reactions as described below. This may enhance the depletion effect. The evaluated specific rate constant (k_c°) may be smaller when the transfer coefficient increases as is seen from Eqs. 3 and 6.

As for $[Co(CO_3)(NH_3)_5]^+$, the current-potential curves between −0.25 and −0.45 V *vs.* SCE were used in this calculation. The alternative value of $\alpha=0.44$, and $k_c^\circ/\sqrt{D}=7.8\times10^{-4}$ $s^{-1/2}$ were obtained for the use of the current between −0.45 and −0.60 V *vs.* SCE. If the whole data are used the following values can be determined: $\alpha=0.32$, and $k_c^\circ/\sqrt{D}=1.1\times10^{-2}$ $s^{-1/2}$. N. Maki *et al.*[1] have reported the half-wave potential of carbonato- and dicarbonatoethylenediaminecobalt(III) complex in solution of 0.5 M K_2SO_4: $E_{1/2}=-0.50_0$ V *vs.* SCE for $[Co(CO_3)(NH_3)_5]^+$ and $E_{1/2}=-0.50_2$ V *vs.* SCE for $[Co(HCO_3)(NH_3)_5]^{2+}$. The hydrogencarbonate complex may exist partly in the solution, but no further experiments were done.

Among the cobalt complexes used here, cobalt(III) is substitution-inert towards solvolysis, while cobalt(II) is substitution-labile. In general, dissociation of the inert cobalt(III) complexes can be neglected from the standpoint of polarography, whereas that of the labile cobalt(II) complexes occurs rapidly compared with the scanning rate of the applied potential. Therefore, the cobalt(II) complex results in the formation of an aquacobalt(II) mixture in an equilibrium state with water molecules in aqueous solutions.

The overall electrode reaction for the first wave was evaluated by a comparison of its electrode reaction with that of other cobalt(III) complexes.[13] Thus,

$$[Co(CO_3)(NH_3)_5]^+ + e \longrightarrow [Co(CO_3)(NH_3)_5], \quad (7a)$$

$$[Co(CO_3)(NH_3)_5] + pH_2O \longrightarrow [Co(H_2O)_p(NH_3)_{6-p}]^{2+} + CO_3^{2-} + (p-1)NH_3, \quad (7b)$$

for the pentaammine complex, and

$$[Co(CO_3)(NH_3)_4]^+ + e \longrightarrow [Co(CO_3)(NH_3)_4], \quad (8a)$$

$$[Co(CO_3)(NH_3)_4] + (p+2)H_2O \longrightarrow [Co(H_2O)_{p+2}(NH_3)_{4-p}]^{2+} + CO_3^{2-} + pNH_3, \quad (8b)$$

for the tetraammine complex. With the bis(diamine) complex:

$$[Co(CO_3)(N)_2]^+ + e \longrightarrow [Co(CO_3)(N)_2], \quad (9a)$$

$$[Co(CO_3)(N_2)] + (2p+2)H_2O \longrightarrow [Co(H_2O)_{2+2p}(N)_{2-p}]^{2+} + CO_3^{2-} + p(N). \quad (9b)$$

((N)=en, pn, tn)

The electrode reaction of dicarbonatoethylenediaminecobaltate(III) complex may be:

$$[Co(CO_3)_2(en)]^- + e \longrightarrow [Co(CO_3)_2(en)]^{2-}, \quad (10a)$$

$$[Co(CO_3)_2(en)]^{2-} + (2p+q)H_2O \longrightarrow [Co(H_2O)_{2p+2q}(en)_{1-p}]^{2-} + pCO_3^{2-} + q\text{en}. \quad (10b)$$

The kinetic parameters given in Table 2 and 3 correspond to the electrode reactions $Co^{III}\rightarrow Co^{II}$ (Eqs. 7a, 8a, 9a, and 10a). Furthermore, the experimental data obtained for complexes $[Co(CO_3)(en)_2]^+$, $[Co(CO_3)(pn)_2]^+$, $[Co(CO_3)(tn)_2]^+$, $[Co(CO_3)(NH_3)_4]^+$, and [Co-

$(NH_3)_6]^{3+}$ show transfer coefficients above 0.5, indicating that the electrode process follows outer-sphere pathways.[21]

The authors wish to thank the Ministry of Education, Science and Culture for the financial support granted for this research.

References

1) N. Maki, Y. Shimura, and R. Tsuchida, *Bull. Chem. Soc. Jpn.*, **32**, 23 (1959).
2) N. Maki, Y. Shimura, and R. Tsuchida, *Bull. Chem. Soc. Jpn.*, **32**, 833 (1959).
3) N. Maki, Y. Shimura, and R. Tsuchida, *Bull. Chem. Soc. Jpn.*, **32**, 150 (1959).
4) P. Pfeiffer, S. Golther, and O. Angern, *Ber.*, **60**, 308 (1927).
5) F. P. Dwyer and T. E. MacDermott, *Inorg. Chem.*, **2**, 871 (1963).
6) Y. Kojima, *Bull. Chem. Soc. Jpn.*, **48**, 2033 (1975).
7) S. M. Jørgensen, *Z. Anorg. Chem.*, **2**, 279 (1892).
8) F. Basolo and R. K. Murmann, "Inorganic Syntheses," ed by J. C. Bailar, Jr., McGraw-Hill, New York (1953), Vol. 4, p. 171.
9) M. Shibata, *Nippon Kagaku Zasshi*, **87**, 771 (1966).
10) J. Bierrum and J. P. McReynolds, "Inorganic Syntheses," ed by W. C. Fernelius, McGraw-Hill, New York (1946), Vol. 2, p. 216.
11) F. P. Dwyer, E. C. Gyafas, and D. P. Mellor, *J. Phys. Chem.*, **59**, 296 (1953).
12) A. Yamada, T. Yoshikuni, Y. Kato, and N. Tanaka, *Anal. Chim. Acta*, **133**, 421 (1981).
13) "Encyclopedia of Electrochemistry of the Elements," ed by A. J. Bard, Marcel Dekker, New York (1975), Vol. 3, Chap. III-2.
14) I. M. Kolthoff and J. J. Lingane, "Polarography," Interscience Publishers, New York (1964), Vol. 1, Chap. 11.
15) T. Yoshikuni, Doctoral Thesis, Thoku University, Sendai, Japan, 1979.
16) A. Yamada and N. Tanaka, *Sci, Repts. Tohoku Univ., Ser. I*, **52**, 73 (1969).
17) K. B. Oldham and E. P. Parry, *Anal. Chem.*, **40**, 65 (1968).
18) H. Matsuda, *Bull. Chem. Soc. Jpn.*, **53**, 3439 (1980).
19) A. Yamada, Y. Kato, T. Yoshikuni, Y. Tanaka, and N. Tanaka, *Anal. Chim. Acta*, **112**, 55 (1979).
20) W. Hans, W. Henne, and E. Meuner, *Z. Elektrochem.*, **58**, 836 (1954).
21) F. C. Anson, M. G. Finn, and A. Yamada, *Inorg. Chem.*, **16**, 2124 (1977).

 © 1983 The Chemical Society of Japan Bull. Chem. Soc. Jpn., 56, 3052—3056 (1983) [Vol. 56, No. 10

Ion-chromatographic Behavior of Silica Gels Modified by Poly- and Bis(crown ether)s of Benzo-18-crown-6

Masaki NAKAJIMA, Keiichi KIMURA,* and Toshiyuki SHONO*
Department of Applied Chemistry, Faculty of Engineering, Osaka University, Yamadaoka, Suita, Osaka 565
(Received February 25, 1983)

Chromatographic behavior of crown ether modified silicas, in which poly- and bis(benzo-18-crown-6)s were attached covalently to silica gel, was investigated on separation of alkali and alkaline earth metal salts, using water or water/methanol as the mobile phase. Poly- and bis(benzo-18-crown-6)-modified silicas have a large affinity for Cs^+, the retention time of alkali metal cations being in the order $Li^+ < Na^+ < Rb^+ < K^+ < Cs^+$. Various anions having a common cation are separable as well as the metal cations on the modified silicas. Also, alkaline earth metal cations were separated on the stationary phases. The temperature effect of retention of alkali metal chlorides was also examined on bis(benzo-18-crown-6)-modified silica.

In the previous papers,[1,2] we have already reported the syntheses of silica gels modified by poly- and bis-(benzo-15-crown-5) derivatives as stationary phases of liquid chromatography, and the chromatographic separation of alkali and alkaline earth metal salts on the modified silicas using water or water/methanol as the mobile phase. The following conclusions were attained on the crown ether modified silicas: 1) The stationary phases have a great affinity for K^+ among alkali metal cations, and the retention time increases in the order $Li^+ < Na^+ < Cs^+ < Rb^+ < K^+$; 2) pure solvents such as water or water/methanol can be utilized as the mobile phase without addition of acids, alkalies, and salts unlike the case of conventional ion chromatography; 3) the separation can be controlled by changing the fraction of methanol in the water mobile phase. Thus, poly- and bis(benzo-15-crown-5)-modified silicas have obviously many attractive properties as compared with conventional ion-exchange resins.

On the other hand, poly- and bis(crown ether)s containing benzo-18-crown-6 moiety have exhibited great cation-binding ability for Cs^+ among alkali and alkaline earth metal cations,[3] which has also been verified by the studies of solvent extraction[4] and ion-selective electrodes[5] using them. This specific cation-binding ability of poly- and bis(benzo-18-crown-6) derivatives is expected to be applied to the stationary phase of liquid chromatography.

This paper describes the liquid chromatography of alkali and alkaline earth metal salts on silica gels modified by poly- and bis(benzo-18-crown-6) derivatives. The temperature effect on the chromatographic behavior of the crown ether modified silicas is also discussed.

Experimental

Syntheses of Stationary Phases. Poly(benzo-18-crown-6)-modified silica (I) and bis(benzo-18-crown-6)-modified silica (II) were synthesized in similar ways to the poly- and bis(benzo-15-crown-5)-modified silicas, respectively, as reported in our previous work.[2] The silica gel employed was an irregular type and the average particle diameter was 10 μm. The crown ether contents of poly(benzo-18-crown-6)-modified silica, which were calculated from the weight increase and the carbon elemental analysis, are 0.28 mmol and 0.27 mmol per 1 g of dry modified silica, respectively. The bis(crown ether) contents of bis(benzo-18-crown-6)-modified silica are 0.31 mmol and 0.33 mmol per 1 g of dry modified silica, respectively. The expected structures of them are shown in Fig. 1.

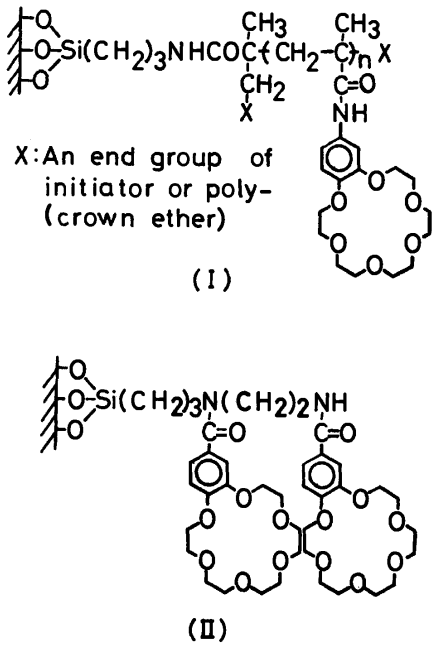

Fig. 1. Expected structures of poly(benzo-18-crown-6)-modified silica and bis(benzo-18-crown-6)-modified silica.

Materials. Alkali and alkaline earth metal salts employed here were of analytical grade. Water and methanol used as the LC mobile phase were purified by fractional distillation, followed by ultrafiltration, and then were degassed with an ultrasonic cleaner.

Instrumentation. Chromatographic experiments were performed with two chromatograph systems. One was the system assembled with commercially available modules, consisting of a pump (Milton Roy 0369-57), a sample injector (Kyowaseimitsu KHP-UI-130), and a refractometer detector (Waters Associates R-401). The other was also assembled with commercially available modules, consisting of a pump (Waters Associates 6000A), a sample injector (Waters Associates U6K), and a conductivity detector (LDC C-203). In this study, the former and the latter systems were referred to as chromatograph systems 1 and 2, respectively.

A stainless steel column (4 mm i.d., 300 mm length) was

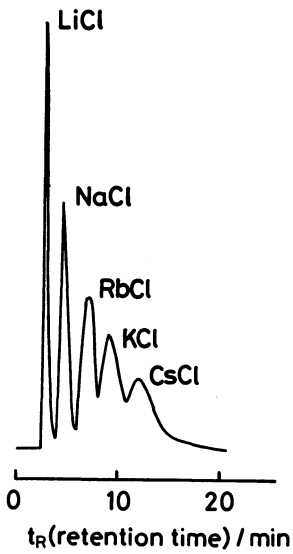

Fig. 2. Separation of alkali metal chlorides on poly-(benzo-18-crown-6)-modified silica.
LiCl, 0.08 mg; NaCl, 0.21 mg; KCl, 0.15 mg; RbCl, 0.24 mg; CsCl, 0.34 mg; mobile phase, water/methanol (90/10 vol/vol).

packed with the modified silica (I), by a balanced-density slurry technique, and incorporated to chromatograph system 1. The other stainless steel column (4 mm i.d., 150 mm length) was packed with the modified silica (II), and incorporated to chromatograph system 2.

After the columns were conditioned by elution with a large quantity of water or water/methanol, sample (50 μl (1 l= 1 dm^3)) containing 0.02—0.04 mol l^{-1} salts was injected into systems 1 and 2. Chromatography was performed at a flow rate of 1.0 ml min^{-1} and at room temperature unless otherwise stated. The pressure drops ranged from 40 to 90 kg cm^{-2} on the chromatograph systems. In spite of the longer column length, the pressure drop on system 1 was not so high as that on system 2, of which the double damper system induced extra pressure drop. In some cases, the column temperature on chromatograph system 2 was controlled using a glass column jacket connected to a circulating water bath.

Results and Discussion

Separation of Alkali Metal Salts. A typical chromatogram of alkali metal chlorides on poly(benzo-18-crown-6)-modified silica is depicted in Fig. 2. A mixture of alkali metal (Li^+, Na^+, K^+, Rb^+, and Cs^+) chlorides was separated successfully on the crown ether modified silica, their retention time increasing in the sequence $Li^+ < Na^+ < Rb^+ < K^+ < Cs^+$. The crown ether modified silica showed a large affinity for Cs^+, which is presumably attributed to the cation-binding ability of the crown ether. Since poly- and bis(crown ether)s possessing neighboring crown ether moieties are favorable for forming sandwich-type 2 : 1 crown ether ring to cation complexes with particular metal cations which are slightly larger than the crown ether cavity, they often exhibit excellent selectivities and great cation-binding abilities for Cs^+ compared to the corresponding monocyclic crown ethers.[3-5] This cooperative effect of poly(benzo-18-crown-6) on binding metal cations is reflected on the chromatographic behavior of the modified silica. As a result, Cs^+ was retained longer than other alkali metal cations. K^+, which can fit into the cavity of benzo-18-crown-6, forms stable 1 : 1 crown ether ring to cation complexes. Rb^+, which is between Cs^+ and K^+ in cation size, is thought to form both 1 : 1 and 2 : 1 crown ether ring to cation complexes, but they may not be very stable. Na^+, which has a smaller cation size than K^+, is not bound very strongly by the crown ether. Conceivably, there is no appreciable interaction between the crown ether and Li^+, which has the smallest size among alkali metal cations. Obviously, the complexing ability of poly-(benzo-18-crown-6) derivatives is reflected on the elution sequence of alkali metal salts.

Table 1. Retention time of alkali metal chlorides on poly(benzo-18-crown-6)-modified silica

	Retention time/min		
		H_2O/MeOH	
	H_2O	90/10	75/25
Li^+	2.8	2.7	2.9
Na^+	4.3	4.5	5.8
K^+	7.7	9.0	12.5
Rb^+	6.2	7.0	9.5
Cs^+	8.7	12.0	20.7

Table 2. Separation factor of alkali metal chlorides on poly(benzo-18-crown-6)-modified silica

	Separation factor[a]		
		H_2O/MeOH	
	H_2O	90/10	75/25
Na^+	3.8	5.2	5.8
K^+	1.2	1.5	1.8
Rb^+	1.7	2.2	2.6

a) Separation factor of Na^+, K^+, and Rb^+ over Cs^+.

The retention time of alkali metal chlorides and the separation factors of NaCl, KCl, and RbCl over CsCl on poly(benzo-18-crown-6)-modified silica with water and water/methanol elution systems are given in Tables 1 and 2, respectively. Although the difference of retention time between K^+ and Cs^+ was observed by elution of pure water, the Cs^+ peak was too broad to be separated completely from the neighboring K^+ one. When a mixture of metal chlorides was eluted by water, the chromatogram gave four apparent peaks, which can be assigned to Li^+, Na^+, Rb^+, and K^+/Cs^+. If a water/methanol mixture is utilized instead of pure water as the mobile phase, the retention time of alkali metal cations increases with the rise of methanol fraction in the mobile phase except for Li^+ which is scarcely complexed by the crown ether. Consequently, the differences of retention time among their cations also increased. This is mainly due to the increased complexing abilities of the crown ether in water/methanol compared with that in water. The separation factor

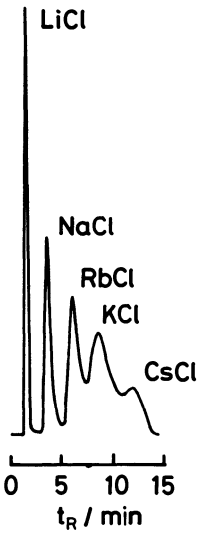

Fig. 3. Separation of alkali metal chlorides on bis-(benzo-18-crown-6)-modified silica.
LiCl, 0.08 mg; NaCl, 0.12 mg; KCl, 0.15 mg; RbCl, 0.25 mg; CsCl, 0.34 mg; mobile phase, water/methanol (75/25 vol/vol).

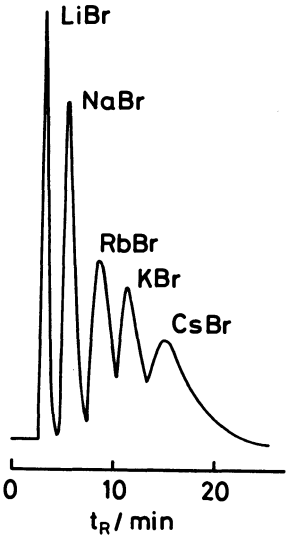

Fig. 4. Separation of alkali metal bromides on poly-(benzo-18-crown-6)-modified silica.
LiBr, 0.17 mg; NaBr, 0.24 mg; KBr, 0.24 mg; RbBr, 0.34 mg; CsBr, 0.53 mg; mobile phase, water/methanol (90/10 vol/vol).

of K^+ over Cs^+ changed from 1.2 with water to 1.8 with water/methanol (75/25 vol/vol). In practice, the elution with water/methanol led to the base-line separation of K^+ and Cs^+, while their peaks overlapped each other on elution with water. However, the chromatography of alkali metal halides by elution with water/methanol (75/25 vol/vol) is rather time-consuming, and the separation of Rb^+ and K^+ is slightly inferior to that with water/methanol (90/10 vol/vol). Thus, the best chromatographic separation of alkali metal chlorides on poly(benzo-18-crown-6)-modified silica was attained using water/methanol (90/10 vol/vol) as the mobile phase, as can be seen in Fig. 2. Chromatographic retention of alkali metal chlorides on bis(crown ether)-modified silica containing benzo-18-crown-6 moiety is similar to that on the poly(crown ether)-modified silica. The alkali metal cation affinity to the modified silica increased again in the sequence $Li^+ < Na^+ < Rb^+ < K^+ < Cs^+$, and thus the modified silica retained Cs^+ longer. In this case, some cooperative effect of bis(crown ether)s on binding alkali metal cations also seems to contribute to the Cs^+ selectivity. On this stationary phase, K^+ and Cs^+ were not separated at all when pure water was used as the mobile phase, but addition of methanol to the mobile phase allowed them to separate each other. A typical chromatogram of alkali metal chlorides on bis(benzo-18-crown-6)-modified silica is demonstrated in Fig. 3. Each peak of Rb^+, K^+, and Cs^+ was so broad that their separations were not base-line ones. The retention time of alkali metal chlorides is summarized in Table 3. Naturally, they were eluted faster on bis(benzo-18-crown-6)-modified silica because of the difference in the column length.

With the stationary phase consisting of poly(benzo-18-crown-6)-modified silica, alkali metal bromides and iodides were also separated (Fig. 4). The elution orders

Table 3. Retention time of alkali metal chlorides on bis(benzo-18-crown-6)-modified silica

	Retention time/min			
	H_2O	H_2O/MeOH		
		90/10	75/25	50/50
Li^+	1.4	1.4	1.4	1.5
Na^+	2.1	2.6	2.8	5.9
K^+	4.2	5.6	7.5	18.0
Rb^+	3.1	3.9	5.3	13.4
Cs^+	4.8	6.5	11.6	25.4

of alkali metal bromides and iodides were the same as that of alkali metal chlorides. Generally, the complexing abilities of crown ethers for metal cations are also governed by the kind of counter anions, and cations possessing a large anion tend to be complexed easily by crown ether. Capacity factors of alkali metal chlorides, bromides, and iodides in chromatographic separation on the modified silica by elution with water/methanol (90/10 vol/vol) are shown in Fig. 5. The capacity factor of anions having a common cation increased in the sequence $Cl^- < Br^- < I^-$. Salts containing a much larger anion such as thiocyanate had greater capacity factors than the metal halides. Chromatographic retention of alkali metal bromides and iodides also depended on the fraction of water and methanol. Similar anion-dependence was observed for bis(benzo-18-crown-6)-modified silica as well. There is a remarkable difference in capacity factors among alkali metal chlorides, bromides, and iodides, as shown in Fig. 5. This means that separation of anions possessing a common cation can be attained, as demonstrated in Fig. 6.

Separation of Alkaline Earth Metal Salts. Crown ethers have an ability to form complexes with alkaline

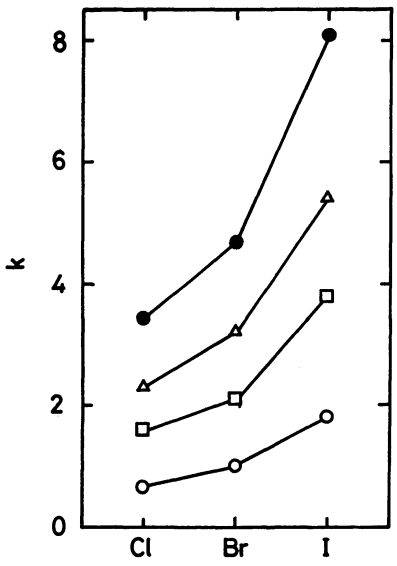

Fig. 5. Capacity factor on poly(benzo-18-crown-6)-modified silica.
Mobile phase, water/methanol (90/10 vol/vol); (○), NaCl; (△), KCl; (□), RbCl; (●), CsCl.

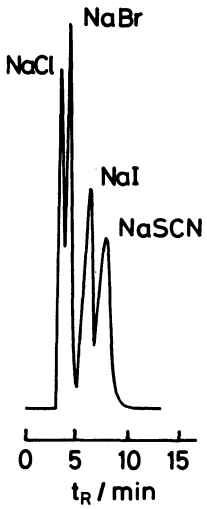

Fig. 6. Separation of a mixture of sodium salt on bis-(benzo-18-crown-6)-modified silica.
NaCl, 0.12 mg; NaBr, 0.24 mg; NaI, 0.30 mg; NaSCN, 0.16 mg; mobile phase, water/methanol (75/25 vol/vol).

Table 4. Retention time of alkaline earth metal chlorides on poly(benzo-18-crown-6) modified silica

	Retention time/min		
	H_2O	H_2O/MeOH	
		90/10	75/25
Mg^{2+}	2.9	2.8	3.0
Ca^{2+}	3.1	3.3	3.8
Sr^{2+}	5.1	6.3	7.9
Ba^{2+}	8.4	9.0	12.6

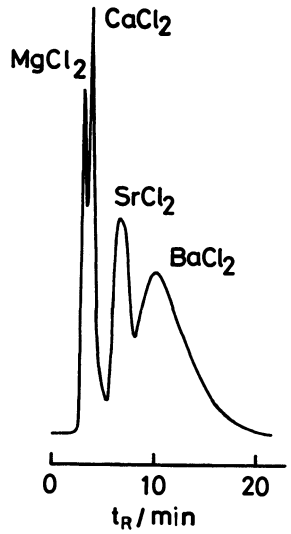

Fig. 7. Separation of alkaline earth metal chlorides on poly(benzo-18-crown-6)-modified silica.
$MgCl_2$, 0.10 mg; $CaCl_2$, 0.15 mg; $SrCl_2$, 0.27 mg; $BaCl_2$, 0.63 mg; mobile phase, water/methanol (90/10 vol/vol).

earth metal cations as well. However, not only the relative size of alkaline earth metal cation and crown ether ring, but also their strong hydration affects the complexing ability of the crown ethers. When alkaline earth metal chlorides were chromatographed on poly-(benzo-18-crown-6)-modified silica, the retention time increased in the sequence $Mg^{2+}<Ca^{2+}<Sr^{2+}<Ba^{2+}$. That is to say, this modified silica has a large affinity for Ba^{2+} among alkaline earth metal cations. Mg^{2+} and Ca^{2+} were slightly separated using pure water as the mobile phase, but their separation was improved with addition of methanol, successful separation being observed with water/methanol (75/25 vol/vol). However, since the peak of Ba^{2+} is broadened on this elution condition, the peaks of Sr^{2+} and Ba^{2+} overlapped with each other. A typical chromatogram of alkaline earth metal salts on poly(benzo-18-crown-6)-modified silica is given in Fig. 7, the retention time being listed in Table 4. Bis(benzo-18-crown-6)-modified silica exhibited chromatographic behavior analogous to poly(benzo-18-crown-6)-modified silica. Also, in the chromatographic separation of alkaline earth metal salts on the crown ether modified silica, the anion dependence was the same as that for alkali metal salts.

Temperature Effect of Retention of Alkali Metal Chlorides on Bis(benzo-18-crown-6)-modified Silica. Generally, the column temperature plays an important role in the sample solubility, the retention time, the viscosity of the mobile phase, and the column efficiency. Therefore, the temperature dependence of the retention time for alkali metal chlorides was examined using bis(benzo-18-crown-6)-modified silica. The retention time decreased with increasing column temperature except that of Li^+ which scarcely changed at any temperature. Plots of ln k (capacity factor) *vs.* $1/T$ for the alkali metal cations gave straight lines with positive slopes (Fig. 8). It is known that the complexation of crown ethers with cation is an exothermic reaction, which is reflected in

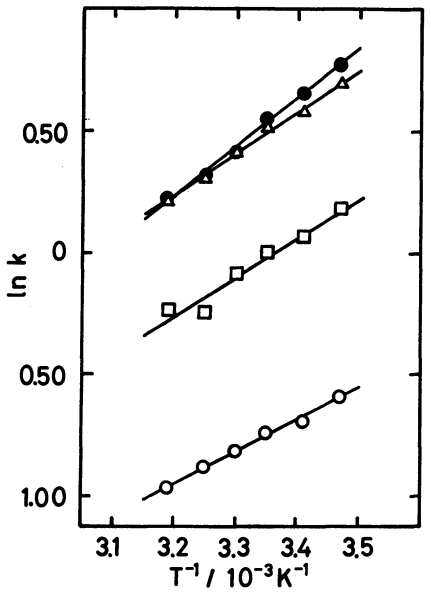

Fig. 8. Plots of ln k *vs.* $1/T$ on bis(benzo-18-crown-6)-modified silica.
(○), NaCl; (△), KCl; (□), RbCl; (●), CsCl.

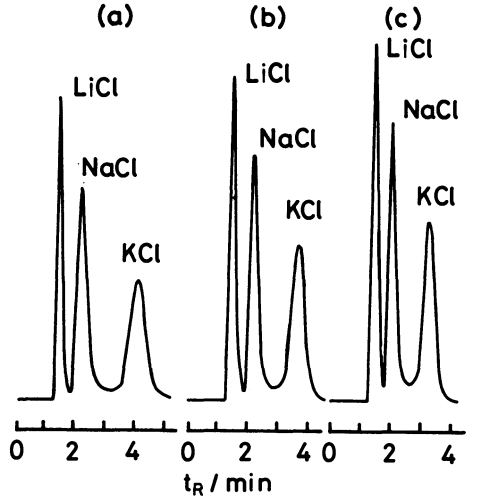

Fig. 9. Temperature dependence of chromatographic behavior of alkali metal chlorides on bis(benzo-18-crown-6)-modified silica.
LiCl, 0.09 mg; NaCl, 0.12 mg; KCl, 0.15 mg; mobile phase, water; (a), 20 °C; (b), 30 °C; (c), 40 °C.

the negative enthalpy changes (the positive slopes of the straight lines). Although the retention time approached to each other with the rise of temperature, separation of a mixture of Li^+, Na^+, and K^+ was rather excellent at elevated temperatures (Fig. 9). This is mainly due to the high column efficiency derived from a large diffusion coefficient of the mobile phase. Furthermore, the separation time was shorter at 40 °C (within 4 min) than at 15 °C (within 5.5 min). Thus the separation time can be easily adjusted to the best one by varying the column temperature.

The present work was partially supported by a Grant-in-Aid for Scientific Research No. 57750671 from the Ministry of Education, Science and Culture.

References

1) K. Kimura, M. Nakajima, and T. Shono, *Anal. Lett.*, **13** 741 (1980).
2) M. Nakajima, K. Kimura, and T. Shono, *Anal. Chem.*, **55**, 463 (1983).
3) S. Kopolow, T. E. Hogen Esch, and J. Smid, *Macromolecules*, **6**, 133 (1973).
4) K. Kimura, T. Maeda, and T. Shono, *Talanta*, **26**, 945 (1979).
5) K. Kimura, H. Tamura, and T. Shono, *J. Electroanal. Chem. Interfacial Electrochem.*, **105**, 335 (1979).

 © 1983 The Chemical Society of Japan Bull. Chem. Soc. Jpn., 56, 3057—3061 (1983)

Ion-pair Extraction of Pyrocatechol Violet into Chloroform with Quaternary Ammoniun Salts

Yoshio HIRANO,† Masahito ANDO,†† Kunishige NAITO,* and Shinsuke TAKEI

Department of Industrial Chemistry, Faculty of Engineering, Ibaraki University, Nakanarusawa-cho, Hitachi 316

(Received March 19, 1983)

An extraction method was first examined for establishing possible distributions of surface-active dodecyltrimethylammonium chloride (DTMAC) and non-surface active tetrabutylammonium chloride (TBAC) between aqueous and organic phases. Both quaternary ammonium salts seem to be present in the form of a free ion in the aqueous phase and in the forms of an ion pair(monomer) and a dimer in the organic phase. A possible distribution of DTMAC in the organic phase was confirmed spectrometrically by following the formation of a 1 : 1 DTMAC–iodine adduct in chloroform solution. On the basis of the possible distribution of quaternary ammonium salts, an ion pair forming extraction of Pyrocatechol Violet (PV) can be successfully interpreted in terms of the anion-exchange mechanism.

Spectrophotometric determinations of metal ions with various ligands in the presence of some cationic surfactants have provided some interesting advantages, such as improved sensitivity and/or selectivity, and a considerable reduction in analytical operation. Such analytical methods have been much advanced in practical applications but fundamental studies have been rare. We intended first to confirm possible distribution of water-soluble cationic surfactant species in aqueous and nonaqueous solutions for clarifying some questions, such as what the true roles of the surfactant species are in the formation of ternary metal–ligand–surfactant complexes.

A surfactant solution is a complicated system involving different chemical species equilibrated with each other through ion associations and molecular aggregations. To examine such a complex system, an extraction method has often been used under well-defined conditions because of its flexibilities. H. K. Biswas and B. M. Mandal[1] successfully analyzed their experimental data of extraction of hexadecyltrimethylammonium bromide with a dyestuff, on the condition that the quaternary ammonium salt was present in the form of free ion in an aqueous phase and an ion pair(monomer) in an organic phase at the low concentration (10^{-5} mol dm^{-3}). In the present study, extractions of two different types of quaternary ammonium salts from aqueous chloride solutions into chloroform were studied in order to establish possible distributions of their chemical species in both solutions. Surface-active dodecyltrimethylammonium chloride (DTMAC) was selected to provide a more complicated system than that of H. K. Biswas and B. M. Mandal because of its relatively higher cmc. A part of the extraction results was confirmed by following the reaction of DTMAC with free iodine in chloroform. And finally, the extraction of Pyrocatechol Violet (PV) with both quaternary ammonium salts was studied on the basis of the possible distributions of quaternary ammonium species.

Experimental

Reagent. A DTMAC solution was prepared by dissolving a weighed amount of DTMAC in distilled water or purified chloroform. The solution was diluted precisely to 100 cm^3 and was used without further dilution. A TBAC solution was prepared by dissolving about 7 g of TBAC in 250 cm^3 of distilled water and standardized by Mohr's argentimetric titration before use. Stock solution of PV (2.50×10^{-3} mol dm^{-3}) and Thymol Blue (TB) (5.00×10^{-4} mol dm^{-3}) were prepared with Dotite PV and TB for a pH indicator, respectively. They were dried to a constant weight under vacuum. An iodine solution (1.00 g dm^{-3}) in chloroform was prepared for each experimental run and was used without dilution. Chrlorform, of chemically pure reagent grade, was purified by the ordinary method and kept in an amber glass bottle; 0.5% (v/v) of ethanol was added as a stabilizer. The other chemicals, of guaranteed reagent grade or chemically pure reagent grade, were used without further purification.

Procedure. Determination of Distribution of DTMAC and TBAC: Ten cubic centimetres of an aqueous phase, containing a fixed amount of DTMAC or TBAC, sodium chloride and hydrochloric acid, was equilibrated with 10 cm^3 of purified chloroform in a 50 cm^3 glass-stoppered test tube by shaking for about 20 min (the first extraction). The quaternary ammonium salt extracted was spectrophotometrically determined as its 1 : 1 ion pair with TB extracted at pH 6.5 into chloroform. From this determination and the original amount of quaternary ammonium salt, distribution ratios of DTMAC and TBAC in the first extraction were calculated.

Reaction of DTMAC with Iodine in Chloroform: A desired amount of DTMAC solution and iodine solution in chloroform were mixed to be diluted precisely to 10 cm^3 with purified chloroform. Absorbance of the solution was measured in a quartz cell with 1 cm path length at 364 nm.

Extraction of PV with DTMAC and with TBAC: Fifteen cubic centimetres of an aqueous phase, containing PV (5.00×10^{-4} mol dm^{-3} except for the varying concentration), DTMAC or TBAC, sodium chloride and hydrochloric acid, was equilibrated with 15 cm^3 of purified chloroform in a 50 cm^3 glass-stoppered test tube by shaking for 10 min. Absorbances of the aqueous and chloroform layers were measured at 445 and 440 nm, respectively, after separating the clear liquid phases.

Results and Discussion

Partition of DTMAC and TBAC between Aqueous and Chloroform Phases. We first examined an extraction of surface-active DTMAC from an aqueous chloride solution into chloroform at a constant pH and at a fixed total concentration of chloride ion, but at various total concentrations of DTMAC. Figure 1 shows that

† Present address: Japan Capacitor Industrial Co., Ltd., Uenohara, Kitatsuru-gun, Yamanashi 409-01.

†† Present address: Yazaki Densen, Gotenba 412.

TABLE 1. INTERCEPT AND SLOPE OF LINEAR D *vs.* C_w GRAPHS

DTMAC			TBAC		
C°_{Cl} / mol dm^{-3}	Intercept	Slope / dm^3 mol^{-1}	C°_{Cl} / mol dm^{-3}	Intercept	Slope / dm^3 mol^{-1}
0.05	0.209	205	0.75	0.215	16.6
0.10	0.440	422	1.0	0.381	26.0
0.15	0.669	712	1.3	0.432	56.0
0.20	0.897	1070	1.5	0.554	86.7
0.30	1.353	1980	1.6	0.579	107
0.40	1.800	3180			
0.50	2.260	4660			

pH 1.5 (DTMAC), pH 1.0 (TBAC).

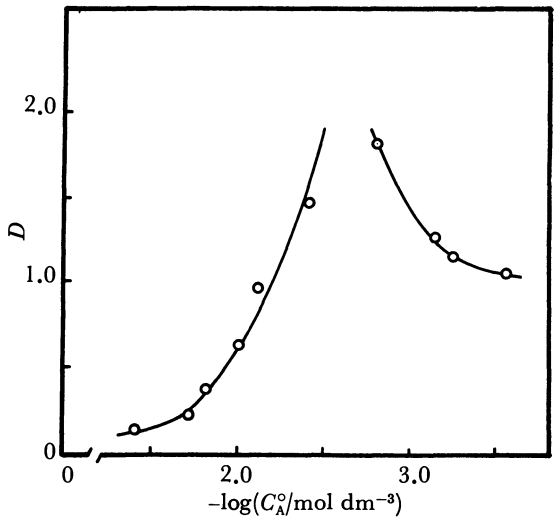

Fig. 1. Distribution ratio of DTMAC between aqueous and chloroform phases.
pH 1.8 and $C^\circ_{Cl}=0.20$ mol dm^{-3}.

the distribution ratio of DTMAC is influenced through the formation of higher aggregates in the organic phase than in the aqueous phase at a concentration lower than 2.5×10^{-3} mol dm^{-3}. These dependences reverse at higher concentrations. Because of a violent emulsification which occurred at concentrations above 2.5×10^{-3} mol dm^{-3}, our extraction method was exclusively applied to examinations at a lower concentration than this one.

The distribution ratios of DTMAC and TBAC were determined as a function of the total concentration of quaternary ammonium salt and chloride ion at a constant pH of an aqueous phase. The distribution ratio of both quaternary ammonium salts was increased with an increase of the total concentration of them and of chloride ions. This concentration dependence suggests that the extraction was enhanced with quaternary ammonium salt itself and with chloride ion. A higher aggregate of quaternary ammonium salt may be formed in a chloroform layer than in an aqueous phase. The present extraction system can be thus interpreted in terms of the following equilibria: formation of an ion pair of quaternary ammonium salt in the aqueous phase, partition of it into the chloroform layer, and formations of its aggregates such as a dimer and a trimer in chloroform. The distribution ratio of quaternary ammonium salt, D, can be written as,

$$D=\frac{[\mathrm{ACl}]_o+2[(\mathrm{ACl})_2]_o+3[(\mathrm{ACl})_3]_o+\cdots}{[\mathrm{A}^+]_w+[\mathrm{ACl}]_w}, \quad (1)$$

where A^+, ACl, $(ACl)_2$, and $(ACl)_3$ are a free quaternary ammonium ion, an ion pair of it with chloride ion (monomer) and its molecular aggregates, a dimer and trimer, respectively. Two subscripts, w and o, denote the aqueous phase and the organic layer. From the material balance of quaternary ammonium salt and the experimental conditions, Eq. 1 can be rewritten

$$D=\left(\frac{KPC^\circ_{Cl}}{1+KC^\circ_{Cl}}\right)+2K_2\left(\frac{KPC^\circ_{Cl}}{1+KC^\circ_{Cl}}\right)^2C_w + 3K_3\left(\frac{KPC^\circ_{Cl}}{1+KC^\circ_{Cl}}\right)^3C_w^2+\cdots, \quad (2)$$

where K, P, K_2, and K_3 are the formation constant of the ion pair in the aqueous phase, its partition coefficient, and the formation constants of the dimer and the trimer in the chloroform layer, respectively. C°_{Cl} represents the total concentration of chloride ion in the extraction system and C_w that of quaternary ammonium salt in the aqueous phase. This equation predicts a linear or a curved graph on D *vs.* C_w diagram at every constant C°_{Cl} value.

A practical plotting of D against C_w gave a series of straight lines with varying slopes and intercepts as a function of C°_{Cl} for both quaternary ammonium salts. Their results suggests that quaternary ammonium salt can be present in the monomeric and dimeric forms in chloroform under the conditions studied. K. Inoue *et al.*[2] and K. Inoue and Y. Baba[3] have reported a similar result in their paper of extraction equilibria of hydrochloric and acetic acids with a long-chain alkylamine. From Table 1, intercepts of these lines were directly proportional to C°_{Cl}, so that the first term of Eq. 2 can be regarded as KPC°_{Cl}, that is, $KC^\circ_{Cl}\ll1$. This is supported by the fact that a linear graph with a small intercept is obtained by plotting slopes of the serial straight lines against $C^{\circ 2}_{Cl}$. These suggest that a free quaternary ammonium ion is a predominant species in the aqueous phase. Under these conditions, the distribution ratio of quaternary ammonium salt can be expressed by

$$D=KPC^\circ_{Cl}+2K_2(KPC^\circ_{Cl})^2C_w. \quad (3)$$

From these linear relations, the extraction constant of

the ion pair of quaternary ammonium salt, *KP*, and its dimerization constant, K_2, can be estimated as 4.45 and 440 $dm^3\ mol^{-1}$ for DTMAC and as 0.35 and 140 $dm^3\ mol^{-1}$ for TBAC, respectively.

Reaction of DTMAC with Free Iodine in Chloroform. To confirm the above conclusion, the reaction of DTMAC with isolated iodine was followed spectrophotometrically in a chloroform solution. An iodine solution in chloroform showed an absorption maximum near 514 nm and one near 364 nm on the absorption spectra in the absence and presence of DTMAC, respectively. Since only one isosbestic point is found on the spectra, only one DTMAC–iodine adduct may be formed on adding DTMAC into an iodine solution. This adduct composition was found to be the 1 : 1 molar ratio by the continuous variation method.

In the presence of an excess of free iodine, absorbance of the solution at 364 nm increased linearly with the total concentration of DTMAC, C_A°. A slope of this linear graph increased with an increase of the total concentration of free iodine, $C_{I_2}^\circ$. In the presence of an excess of DTMAC, a similar linear graph was obtained on an absorbance-$C_{I_2}^\circ$ diagram. We considered for simplicity that quaternary ammonium salt was present in three different forms: a monomer, a dimer and a 1 : 1 adduct of monomeric DTMAC with free iodine, and that iodine was present as two species: free iodine and the 1 : 1 DTMAC–iodine adduct in the chloroform solution. Since $C_{I_2}^\circ = [I_2]_o$ in the presence of an excess of free iodine, the absorbance of the solution can be approximated as

$$A_s = \varepsilon_{I_2} \cdot C_{I_2}^\circ + \varepsilon \cdot [ACl \cdot I_2]_o, \quad (4)$$

where $[I_2]_o$ is the actual concentration of free iodine in the solution and ε_{I_2} and ε are molar absorptivities of free iodine and the 1 : 1 DTMAC–iodine adduct at 364 nm, respectively. On the other hand, in the presence of an excess of DTMAC, the absorbance of free iodine, $\varepsilon_{I_2} \cdot [I_2]_o$, was negligible as compared with that of the adduct because of small values of ε_{I_2} and $[I_2]_o$. Thus, absorbance of the solution can be approximated as $A_s = \varepsilon \cdot [ACl \cdot I_2]_o$. Taking account of the dimerization of DTMAC and the formation of the 1 : 1 DTMAC–iodine adduct, the following equations can be derived in the presence of an excess of free iodine and of DTMAC, respectively:

$$\frac{C_A^\circ}{A_s - \varepsilon_{I_2} \cdot C_{I_2}^\circ} = \frac{1 + K_f \cdot C_{I_2}^\circ}{\varepsilon \cdot K_f \cdot C_{I_2}^\circ} + \frac{2K_2}{\varepsilon^2 \cdot K_f^2 \cdot C_{I_2}^{\circ 2}} (A_s - \varepsilon_{I_2} \cdot C_{I_2}^\circ) \quad (5)$$

and

$$\frac{(C_A^\circ - A_s/\varepsilon) \cdot (C_{I_2}^\circ - A_s/\varepsilon)}{A_s/\varepsilon} = \frac{1}{K_f} + \frac{2K_2}{\varepsilon^2 \cdot K_f^2 \cdot C_{I_2}^{\circ 2}} \cdot \frac{A_s/\varepsilon}{C_{I_2}^\circ - A_s/\varepsilon}, \quad (6)$$

where K_f and K_2 are formation constants of the adduct and the dimeric DTMAC, respectively. A series of straight lines on the $C_A^\circ/(A_s - \varepsilon_{I_2} \cdot C_{I_2}^\circ)$ *vs.* $(A_s - \varepsilon_{I_2} \cdot C_{I_2}^\circ)$ diagram indicate the validity of Eq. 5. Table 2 summarizes the intercept and slope of these straight lines determined by the least-square regression method. A linear graph was then drawn by plotting the intercept against $1/C_{I_2}^\circ$. From the intercept and the slope of this graph, the molar absorptivity and the formation constant of the 1 : 1 DTMAC–iodine adduct were estimated as $\varepsilon = 7622\ dm^3\ mol^{-1}\ cm^{-1}$ and $K_f = 711\ dm^3\ mol^{-1}$, respectively. Logarithmic plot of the slope *vs.* $C_{I_2}^\circ$ also gave a straight line with a slope of -1.97. From the intercept of this graph, the formation constant of the dimeric DTMAC was found as $K_2 = 683\ dm^3\ mol^{-1}$, closed fairly to that of $K_2 = 440\ dm^3\ mol^{-1}$ estimated through the extraction experiment. On the other hand, a reversed L-shaped curve appeared on the $(C_A^\circ - A_s/\varepsilon) \cdot (C_{I_2}^\circ - A_s/\varepsilon)/(A_s/\varepsilon)$ *vs.* $(A_s/\varepsilon)/(C_{I_2}^\circ - A_s/\varepsilon)$ diagram (Fig. 2). This suggests that a monomeric DTMAC is the dominant species at DTMAC concentrations below about $9.0 \times 10^{-4}\ mol\ dm^{-3}$ and the dimeric one is dominant above this concentration. From the constant value of the graph, the formation constant of the adduct was also estimated as $K_f = 797\ dm^3\ mol^{-1}$, closed to that of $K_f = 711\ dm^3\ mol^{-1}$. And from the slope of the linearly increasing part of the curve, the formation constant of the dimeric DTMAC was found to be $K_2 = 626\ dm^3\ mol^{-1}$, comparable to that of $K_2 = 638\ dm^3\ mol^{-1}$. These results lead to the same conclusion as that of the extraction experiment of DTMAC.

Extraction of PV with DTMAC and with TBAC from Aqueous Phase into Chloroform. PV was extracted into chloroform with DTMAC or with TBAC but only

Table 2. Intercept and slope of linear plots of $C_A^\circ/(A_s - \varepsilon_{I_2}^\circ \cdot C_{I_2}^\circ)$ against $(A_s - \varepsilon_{I_2} \cdot C_{I_2}^\circ)$

$C_{I_2}^\circ$ / mol dm^{-3}	Intercept / mol dm^{-3}	Slope / mol dm^{-3}
3.28×10^{-4}	6.98×10^{-4}	1.16×10^{-3}
7.91×10^{-4}	3.42×10^{-4}	1.02×10^{-4}
1.16×10^{-3}	3.10×10^{-4}	3.50×10^{-5}
2.32×10^{-3}	2.52×10^{-4}	1.17×10^{-5}
8.58×10^{-3}	1.51×10^{-4}	8.28×10^{-6}

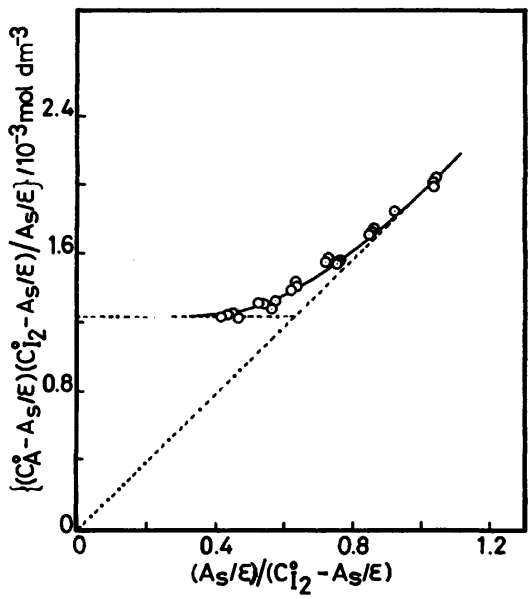

Fig. 2. $(C_A^\circ - A_s/\varepsilon) \cdot (C_{I_2}^\circ - A_s/\varepsilon)/(A_s/\varepsilon)$ *vs.* $(A_s/\varepsilon)/(C_{I_2}^\circ - A_s/\varepsilon)$ plot.

with difficulty without such quaternary ammonium salts. Depending upon the pH value of the aqueous phase, two different PV species could be extracted into chloroform. They were extractable at a pH lower than 6 and between pH 7 and 11, and showed absorption bands near 450 and 610 nm on the spectra. For the PV species extracted at a pH above 7, time-dependent absorptions spectra were observed, so that the extraction of PV with DTMAC and TBAC was examined more in detail at a low pH. The literature[4-6] reports a stable PV species in the low pH range to be a protonated form with three dissociative hydroxyl groups (H_3L^-). In the range lower than pH 2, another PV species with an absorption band near 560 nm newly appeared in the aqueous phase. This was regarded as a more protonated form of the H_3L^- species, such as H_4L or H_5L^+. Comparing the absorption spectra of chloroform and aqueous solutions containing PV, we considered that the H_3L^- species was the extractable species of PV with quaternary ammonium salt in this pH range. Since very similar absorption spectra were observed in the absence and presence of the quaternary ammonium salt, we conclude that no PV species interacting with it was present in the aqueous phase equilibrated once with chloroform. No aggregated form of the PV species may be present in either phase because the ratio of absorbances of the two related phases stayed constant at any concentration of PV(C_L°). Even in the presence of a large excess of quaternary ammonium salt, quantitative extraction of PV could occur only with difficulty in the present study. Thus, an absorbance ratio of both phases, $Y = A_{s_o}/A_{s_w}$, was used for analyzing experimental data, instead of a distribution ratio. Figure 3 shows a parabolic curve on the Y *vs.* C_A° diagram for the DTMAC–PV system. This suggests the formation of an aggregated DTMAC species involving only one PV molecule in a chloroform layer. A similar curve was observed for the TBAC–PV system. We considered that PV species were present in the form of H_3L^-, H_4L, and H_5L^+ in the aqueous phase and H_3LA and $H_3LA \cdot ACl$, regarded as anion-exchanged forms of ACl and $(ACl)_2$, in the chloroform layer. According to Beer's law and linear additivity of absorbances, the absorbance ratio, Y, can be expressed as

$$Y = \frac{\varepsilon_o \cdot [H_3LA]_o + \varepsilon_o' \cdot [H_3LA \cdot ACl]_o}{\varepsilon_{w(3)} \cdot [H_3L^-]_w + \varepsilon_{w(4)} \cdot [H_4L]_w + \varepsilon_{w(5)} \cdot [H_5L^+]_w}, \quad (7)$$

where ε_o, ε_o', $\varepsilon_{w(3)}$, $\varepsilon_{w(4)}$, and $\varepsilon_{w(5)}$ are molar absorptivities of the species, H_3LA, $H_3LA \cdot ACl$, H_3L^-, H_4L, and H_5L^+, respectively. Using equilibrium constants of extraction reaction and dimerization of ACl, extraction reactions of PV with ACl and with $(ACl)_2$ by anion exchange, and protonation of the H_3L^- species in an aqueous phase, the following equation was derived:

$$Y = \frac{\varepsilon_o K_{ex(1)} KP[A^+]_w + \varepsilon_o' K_2 K_{ex(2)} K^2 P^2 C_{Cl}^\circ [A^+]_w^2}{\varepsilon_{w(3)} + \varepsilon_{w(4)} K_{H(4)} [H^+]_w + \varepsilon_{w(5)} K_{H(4)} K_{H(5)} [H^+]_w^2}, \quad (8)$$

where $K_{ex(2)}$ and $K_{ex(2)}$ are extraction constants of PV with ACl and with $(ACl)_2$, and $K_{H(4)}$, and $K_{H(5)}$ are successive protonation constants of the H_3L^- species. Under the experimental conditions, $C_A^\circ \gg C_L^\circ$, so that the following relation is approximately valid:

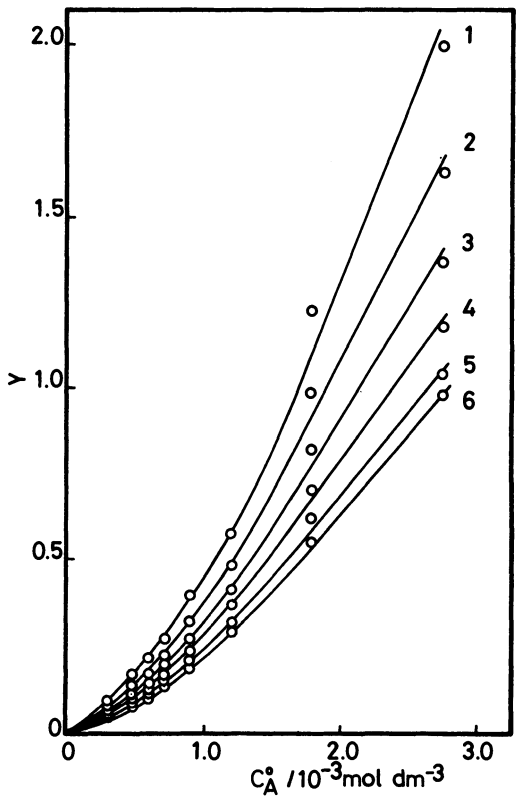

Fig. 3. Y *vs.* C_A° plot for DTMAC.
pH 2.3, $C_L^\circ = 4.03 \times 10^{-5}$ mol dm^{-3} and C_{Cl}°: 1; 0.10, 2; 0.20, 3; 0.30, 4; 0.40, 5; 0.50, 6; 0.60 mol dm^{-3}.

$$C_A^\circ = [A^+]_w + [ACl]_o + 2[(ACl)_2]_o,$$

that is,

$$C_A^\circ = (1 + KPC_{Cl}^\circ)[A^+]_w + 2K_2(KPC_{Cl}^\circ)^2[A^+]_w^2. \quad (9)$$

Since KP and K_2 are known, $[A^+]_w$ could be calculated at any C_{Cl}° from this equation. Equation 8 predicts that a series of straight lines with the same intercept but with the C_{Cl}°-dependent slopes may be obtained by plotting $Y/[A^+]_w$ *vs.* $[A^+]_w$ at a constant pH of the aqueous phase. This prediction was experimentally confirmed for the DTMAC–PV system. The intercept and slope of the regression line are listed in Table 3. The values of $(\varepsilon_o/\varepsilon_w)K_{ex(1)}$ and $(\varepsilon_o'/\varepsilon_w)K_{ex(2)}$ were estimated as 46 and 855 from these values. However, extraction constants, $K_{ex(1)}$ and $K_{ex(2)}$, were difficult to be determined because of our failure to find the molar absorptivities. For the TBAC–PV system, a

Table 3. Intercept and slope of linear graph of $Y/[A^+]_w$ against $[A^+]_w$ for DTMAC

C_{Cl}° / mol dm^{-3}	Intercept / dm^3 mol^{-1}	Slope / dm^6 mol^{-2}
0.1	209	0.724×10^6
0.2	218	1.38×10^6
0.3	193	2.13×10^6
0.4	199	2.95×10^6
0.5	208	3.66×10^6
0.6	191	4.76×10^6

$C_L^\circ = 4.03 \times 10^{-5}$ mol dm^{-3} and pH 2.3.

series of linear graphs was drawn at a fixed C°_{Cl} on the $Y/[A^+]_w$ *vs.* $[A^+]_w$ diagram. Their different intercepts and slopes, calculated by the least-square regression method, are shown in Table 4. The reciprocals of the intercept and the slope was well correlated linearly to the square of hydrogen ion concentration. This suggests a simultaneous protonation of the H_3L^- species with two hydrogen ions. I. S. Mustafin *et al.*[6] have reported the simultaneous uptake of two hydrogen ions due to a quinone and a sulfonate groups of the PV molecule. From the intercept and the slope of the linear reciprocal plots, $(\varepsilon_o/\varepsilon_{w(3)})K_{ex(1)}$, $(\varepsilon'_o/\varepsilon_{w(3)})K_{ex(2)}$, $(\varepsilon_o/\varepsilon_{w(5)})K_{ex(1)}/K_{H(4)}K_{H(5)}$, and $(\varepsilon'_o/\varepsilon_{w(5)})K_{ex(2)}/K_{H(4)}K_{H(5)}$ were determined to be 69, 550, 20 $dm^3\ mol^{-1}$ and 127 $dm^3\ mol^{-1}$, respectively, for the TBAC–PV system. In this case, the absorbance ratio can be written simply

$$Y = \frac{\varepsilon_o K_{ex(1)} KP[A^+]_w + \varepsilon_o' K_2 K_{ex(2)} K^2 P^2 C^\circ_{Cl}[A^+]^2_w}{\varepsilon_{w(3)} + \varepsilon_{w(5)} K_{H(4)} K_{H(5)} [H^+]^2_w}. \quad (10)$$

From these results and discussion, we concluded that both surface-active DTMAC and non-surface active TBAC were present in the form of free ions in an aqueous phase and in the monomeric and dimeric forms in a chloroform layer. The extraction of PV with quaternary ammonium salt could be successfully interpreted by an anion-exchange mechanism on the basis of the distributions of quaternary ammonium salt established. It should be noted that the same distributions could be established for quaternary ammonium salts with and without surface activity. We continue our interest in studying possible distributions of chemical species in the surfactant solution.

Table 4. Intercept and slope of linear graph of $Y/[A^+]_w$ against $[A^+]_w$ for TBAC

$[H^+]_w$ / mol dm^{-3}	Intercept / dm^3 mol^{-1}	Slope / dm^6 mol^{-2}
0.04	19.1	1.15×10^4
0.05	23.2	1.08×10^4
0.10	23.1	9.74×10^3
0.15	20.3	8.92×10^3
0.20	20.1	7.96×10^3
0.25	19.7	7.16×10^3
0.30	14.7	6.84×10^3
0.40	15.7	5.40×10^3
0.50	13.5	4.37×10^3
0.60	10.7	3.84×10^3
0.80	10.2	2.49×10^3
0.98	7.93	1.82×10^3

$C^\circ_L = 5.00 \times 10^{-5}$ mol dm^{-3} and $C^\circ_{Cl} = 1.0$ mol dm^{-3}.

References

1) H. K. Biswas and B. M. Mandal, *Anal. Chem.*, **44**, 1636 (1972).
2) K. Inoue, Y. Kawano, F. Nakashio, and W. Sakai, *Kagaku Kogaku*, **38**, 41 (1974).
3) K. Inoue and Y. Baba, *Kagaku Kogaku Ronbunshu*, **4**, 95 (1978).
4) E. Bishop, "Indicators," Pergamon Press, Oxford (1972), p. 355.
5) R. M. Saginashvili and V. I. Petrashen', *Zh. Anal. Khim.*, **22**, 984 (1967).
6) I. S. Mustafin, L. A. Molot, and A. S. Arkhangel'skaya, *Zh. Anal. Khim.*, **22**, 1808 (1967).

Response of a Copper(II) Ion-selective Electrode in Cupric Buffers Based on Macrocyclic Polyamines

Akinori Jyo,* Akiyoshi Nagamoto, Takashi Khono, and Akira Ohyoshi
Department of Industrial Chemistry, Faculty of Engineering, Kumamoto University, Kurokami, Kumamoto 860
(Received April 11, 1983)

The behavior of a copper(II) ion-selective electrode at extremely low activity levels of free copper(II) was examined in copper(II) buffers based on macrocyclic triamines ([9]aneN$_3$ and [10]aneN$_3$) and macrocyclic tetramines ([12]aneN$_4$, [14]aneN$_4$, and [16]aneN$_4$). Although the electrode showed the ideal behavior in the buffers based on [12]aneN$_4$ and [16]aneN$_4$, non-ideal behavior was observed for the macrocyclic triamines and [14]aneN$_4$. Thus, the macrocyclic polyamines did not always give the ideal copper(II) buffers for the electrode, in contrast to the case of acyclic polyamines. Stability constants, which were in good agreement with the reported values, could be determined only for [12]aneN$_4$ and [16]aneN$_4$. An application of the cyclic tetramines to complexiometry is also presented.

Recently, much attention is being paid to metal complexes of macrocyclic polyamines. Particular attention has been paid for copper(II) complexes of the amines, since some of them can be regarded as simplified models for naturally occurring structures in proteins.[1] The solution chemistry of the copper(II) complexes has produced a number of stability constants. Although several techniques have been used in determination of stability constants of copper(II)–macrocyclic polyamine complexes,[2,3] no use of a copper(II) ion-selective electrode in determination of their stability constants has been reported.

An ion-selective electrode provides a simple method for determination of a stability constant if the electrode behaves ideally in buffered solutions of the objective ion of the electrode. However, the copper(II) ion-selective electrode does not always respond to its objective ion at extremely low activity levels. In this connection, Nakagawa *et al.* and Heijne *et al.* have found the ideal behavior of the electrode down to 10^{-22}—10^{-23} M (M=mol dm^{-3}) of free copper(II) activity in copper(II) buffers based on acyclic polyamines.[4-6] This led us to investigate the behavior of the electrode in copper(II) buffers based on the macrocyclic polyamines, since the complexing behavior of copper(II) with the macrocyclic polyamines is considerably different from that with the acyclic polyamines.[2,3] This paper describes the behavior of the electrode in the copper(II) buffers based on the following macrocyclic polyamines (L^1—L^5).

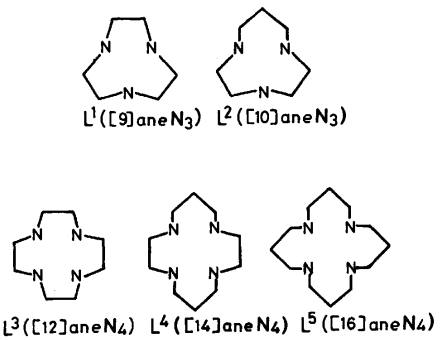

Scheme 1.

Experimental

Materials. The macrocyclic triamines, L^1 and L^2 (as 3HBr salts), were prepared by the method of Koyama *et al.*[7] The macrocyclic tetramines, L^3—L^5 (L^3 and L^5 as 4HCl salts, L^4 as $2H_2SO_4$ salt) were prepared by the method of Richman *et al.*[8] Their purities were checked by CHN analysis, ^{1}H NMR, melting point or potentiometric titration. A copper(II) standard was prepared from a reagent grade copper(II) sulfate and standardized against an EDTA solution by the use of a copper(II) ion-selective electrode as an indicator. Other reagents were of reagent grade and were used as received.

Apparatus. A Denki Kagaku Keiki (DKK) digital mV meter IOC 10 was used in potential and pH measurements. The following cell was arranged by using an Orion 94-29A copper(II) ion-selective electrode and a DKK reference electrode (silver/silver chloride electrode of a double junction type): Ag/AgCl/stand. KCl//10% KNO_3//test solution/copper(II) ion-selective electrode.

The ionic strength of the test solution was adjusted with potassium nitrate. During potential measurements, the test solution was stirred. At first, preliminary measurements were made under ambient conditions, and then almost the same measurements were repeated at 25±0.1 °C.

Testing of Electrode Response in the Copper(II) Buffers. The behavior of the electrode was examined in the presence of a given macrocyclic polyamine in excess. Here, the total concentration of copper(II) was varied, while that of the amine, pH, and ionic strength were maintained at appropriate values. In the case of the triamines, the electrode response was examined in the pH range 5.5—6.8, because of the relatively small stability constants of the copper(II)–triamine complexes.[2,3] For the tetramines, the electrode response was tested in the pH range of 10.4—11.1 since the tetramines form extremely stable copper(II) complexes.[2,3]

Determination of Stability Constants. Two kinds of solutions containing copper(II) and a given polyamine were prepared. Both had the same compositions except for pH. In each solution, the total concentration of the amine is greater than that of copper(II) by about ten times. One solution had a high pH and the other a low pH; the pH of each was adjusted with sodium hydroxide or nitric acid. The solution with a high pH was titrated with the solution with a low pH. Potentials of the electrode and pH were measured during the titration.

Results and Discussion

Electrode Response in the Copper(II) Buffers. In the case of the triamines, ideal behavior of the electrode was

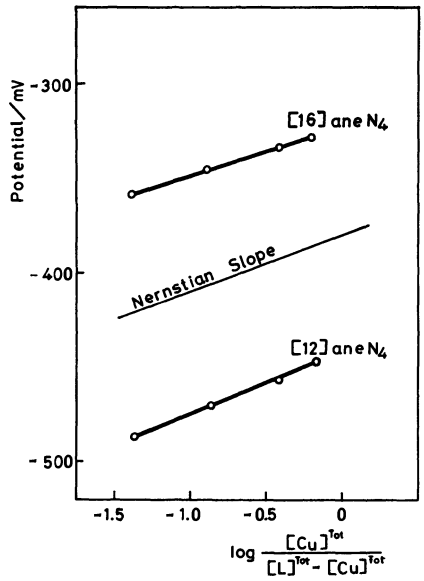

Fig. 1. Electrode response in cupric buffers at 25 °C. $[L]^{Tot}$: $8.9_2\times10^{-3}$ M, $[Cu^{2+}]^{Tot}$: $3.5_8\times10^{-4}$—$3.5_8\times10^{-3}$ M, pH: 10.85±0.05 for [12]aneN$_4$ and 10.55±0.15 for [16]aneN$_4$, ionic strength: 0.14.

not observed. Potentials were not so stable and prolonged response time longer than 10 min was frequently observed. In addition, electrode potentials themselves were not highly reproducible. In the case of the tetramines, on the other hand, the response was rapid and the potentials were stable. However, [14]aneN$_4$ gave rather strange results; the response was rapid and potentials were stable, but the potential values changed from run to run. Accordingly, only [12]aneN$_4$ and [16]aneN$_4$ gave satisfactory results.

As described later, [12]aneN$_4$ and [16]aneN$_4$ form the 1 : 1 complexes with copper(II) and their stability constants are extremely large. Thus, one can get the relation at a given pH:

$$[Cu^{2+}] \propto [Cu^{2+}]^{Tot}/([L]^{Tot}-[Cu^{2+}]^{Tot}), \quad (1)$$

where $[Cu^{2+}]^{Tot}$ and $[L]^{Tot}$ are respective total concentrations of copper(II) and the ligand, and $[Cu^{2+}]$ represents the concentration of free copper(II). Then, if the electrode shows a Nernstian response even in the copper(II) buffers, one can expect that the plot of the electrode potential against log $([Cu^{2+}]^{Tot}/([L]^{Tot}-[Cu^{2+}]^{Tot}))$ will give a straight line having a slope of $2.303RT/2F$. This expectation is satisfied for the copper(II) buffers based on [12]aneN$_4$ and [16]aneN$_4$, as is shown in Fig. 1.

Determination of Stability Constants. As mentioned in the previous section, one can expect that the stability constants of the copper(II) complexes with [12]aneN$_4$ and [16]aneN$_4$ can be determined by the copper(II) ion-selective electrode. The results for potentiometric titrations are shown in Fig. 2. From the definition, and from the mass balance, one can get the relations:

$$pCu = \log\beta_n - npL - \log[CuL_n], \quad (2)$$

$$[CuL_n] = [Cu^{2+}]^{Tot} - [Cu^{2+}], \quad (3)$$

$$[L] = ([L]^{Tot} - n[CuL_n])/\alpha_{L(H)}. \quad (4)$$

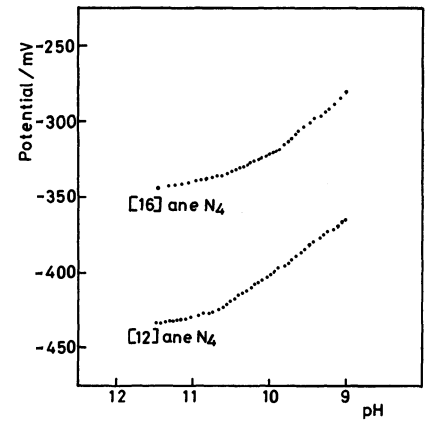

Fig. 2. Response potentials *vs.* pH at 25 °C. [12]aneN$_4$: $[L]^{Tot}=5.0_0\times10^{-3}$ M, $[Cu^{2+}]^{Tot}=5.0_0\times10^{-4}$ M, ionic strength=0.10. [16]aneN$_4$: $[L]^{Tot}=1.0_0\times10^{-2}$ M, $[Cu^{2+}]^{Tot}=1.0_0\times10^{-3}$ M, ionic strength =0.10.

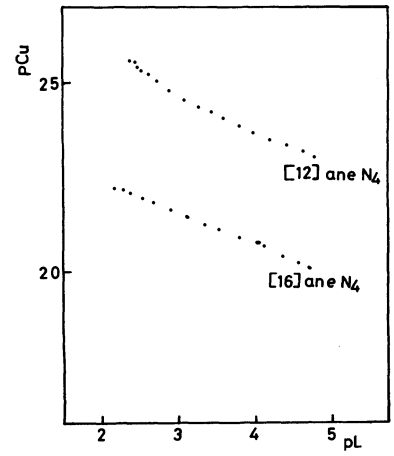

Fig. 3. Plots of pCu *vs.* pL. Conditions are given in Fig. 2.

Here, $\alpha_{L(H)}$ is a side reaction coefficient of the ligand and other symbols have their usual meanings. As pCu can be estimated from the electrode potential, β_n can be calculated from Eqs. 2, 3, and 4. The relations between pCu and pL are shown in Fig. 3. Figure 3 shows that the coordination number, n, is unity for both ligands. The stability constants determined are given in Table 1. Although our experimental conditions are somewhat different from the reported ones, the determined stability constants are in fair agreement with the reported values.

In conclusion, the macrocyclic polyamines do not always give the copper(II) buffers in which the electrode responds to free copper(II) ideally. This is in contrast to the case of acyclic polyamines; most of them give the ideal copper(II) buffers for the electrode.[4-6,9] In this work, we could show that the electrode responds to free copper(II) down to 10^{-25}—10^{-26} M in the copper(II) buffer based on [12]aneN$_4$.

Application of the Macrocyclic Tetramines to Complexiometry. Although fundamental works on macro-

Table 1. Stability constants of Cu(II) complexes at 25 °C

Ligand	$\log \beta_1$	
	Determined[a]	Reported
[12]aneN$_4$	24.4	24.8[b]
[16]aneN$_4$	21.6	20.9[c]

a) Ionic strength: 0.10 (KNO_3). b) Taken from Ref. 2a. Determined by polarography, ionic strength: 0.20 (KNO_3). c) Taken from Ref. 3g. Determined by potentiometric titration with a glass electrode, ionic strength: 0.50 (KNO_3).

cyclic polyamines have been reported, practical studies are rare. In this work, the solutions of the tetramines were standardized against a copper(II) sulfate solution by the use of the electrode as an indicator. Some examples of titration curves are shown in Fig. 4. The ligands, [12]aneN$_4$ and [16]aneN$_4$, give greater breaks than EDTA. This means that both amines are preferable to EDTA as the reagent for complexation titration of copper(II) as long as the end point is detected with the electrode. Although the stability constants predict that [14]aneN$_4$ will give a greater break than [12]aneN$_4$ does, the reversed results are observed. This may be ascribable to the anomalous response of the electrode in the presence of [14]aneN$_4$.

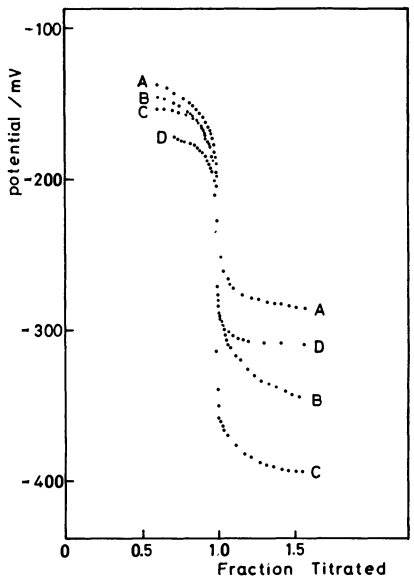

Fig. 4. Titration curves of copper(II) with macrocyclic tetramines and EDTA.
Sample: 10.0 ml of $1.01_0 \times 10^{-2}$ M $CuSO_4$ (pH 10.0, NH_3–NH_4Cl buffer). Titrant: *ca.* 10^{-2} M of each ligand, A: [16]aneN$_4$, B: [14]aneN$_4$, C: [12]aneN$_4$, D: EDTA.

The authors would like to express their gratitude to Denki Kagaku Keiki Co. Ltd., for gifts of reference and glass electrodes.

References

1) E. Kimura, *Kagaku No Ryoiki*, **35**, 865 (1981).
2) a) M. Kodama and E. Kimura, *J. Chem. Soc., Dalton Trans.*, **1976**, 116; b) **1976**, 2341; c) **1977**, 1473; d) **1978**, 104; e) **1978**, 1081; f) **1980**, 2536.
3) a) T. Arishima, K. Hamada, and S. Takamoto, *Nippon Kagaku Kaishi*, **1973**, 1119; b) N. Watanabe, T. Ohe, and S. Takamoto, *ibid.*, **1975**, 298; c) R. W. Renfrew, R. S. Jamison, and D. C. Weatherburn, *Inorg. Chem.*, **18**, 1854 (1979); d) R. Yang and L. J. Zompa, *ibid.*, **15**, 1499 (1976); e) L. Fabbrizzi, P. Paoletti, and A. B. P. Lever, *ibid.*, **15**, 1502 (1976); f) L. J. Zompa, *ibid.*, **17**, 2351 (1978); g) E. Gallori, E. Martini, M. Micheloni, and P. Paoletti, *J. Chem. Soc., Dalton Trans.*, **1980**, 1722; h) M. Micheloni, P. Paoletti, A. Poggi, and L. Fabbrizzi, *ibid.*, **1982**, 61; i) T. J. Riedo and T. A. Kaden, *Helv. Chim. Acta*, **62**, 1089 (1979).
4) G. Nakagawa, H. Wada, and T. Hayakawa, *Bull. Chem. Soc. Jpn.*, **48**, 424 (1975).
5) G. Nakagawa, H. Wada, and T. Sako, *Bull. Chem. Soc. Jpn.*, **53**, 1303 (1980).
6) G. J. M. Heijne and W. E. van der Linden, *Anal. Chim. Acta*, **96**, 13 (1978).
7) H. Koyama and T. Yoshino, *Bull. Chem. Soc. Jpn.*, **45**, 481 (1972).
8) J. E. Richman and T. J. Atkins, *J. Am. Chem. Soc.*, **96**, 2268 (1974).
9) A. Jyo and N. Ishibashi, unpublished work.

 © 1983 The Chemical Society of Japan Bull. Chem. Soc. Jpn., 56, 3065—3072 (1983)

Double Potential Step Chronoamperometry for Reversible Follow-up Chemical Reactions. Application to the Aquation Kinetics of Bis(ethylenediaminemonoacetato)cobalt(II)

Takeo OHSAKA, Tadashi SOTOMURA,†,†† Hiroaki MATSUDA,† and Noboru OYAMA*

Department of Applied Chemistry for Resources, Tokyo University of Agriculture and Technology, Koganei, Tokyo 184

†*Department of Electronic Chemistry, Graduate School at Nagatsuta, Tokyo Institute of Technology, Nagatsuta, Midori-ku, Yokohama 227*

(Received April 30, 1983)

A theory of double potential step chronoamperometry (DPSCA) is developed for the reversible follow-up reactions represented as $Ox+ne \rightleftarrows Red$, $Red \underset{kK}{\overset{k}{\rightleftarrows}} Z$, where k and K are the rate and the equilibrium constants of the follow-up chemical reaction, respectively. DPSCA is applied to investigate the kinetics of aquation reaction of $[Co(edma)_2]^0$ (edma: ethylenediamine-*N*-acetate), which is produced by electrolytic reduction of $[Co(edma)_2]^+$ in the range of pH 1.5 to 10.5. At pH$<$4.5, the aquation reaction of $[Co(edma)_2]^0$ is irreversible. The rate of aquation reaction is accelerated by hydrogen ions and approaches an upper limiting value (2.1×10^3 s^{-1}). At pH$>$4.5, on the other hand, the hydrogen ions do not substantially contribute to the aquation and thus the rate approaches a lower limiting value (4.7×10^2 s^{-1}), which is in good agreement with that obtained in neutral region (4.5$<$pH$<$7), where the reverse (complex formation) reaction must be taken into consideration. Above pH 7, the $[Co(edma)_2]^0$ species exists as main species in the solution and thus the kinetic behavior of the aquation is not observed. It is demonstrated that DPSCA is a useful method for kinetic studies of the dissociation-association reactions of labile complexes.

The double potential step (DPS) chronoamperometry (CA) and the DPS chronocoulometry (CC) are well-developed techniques for studying the kinetics of homogeneous chemical reactions of the species, which may be produced by charge transfer reactions. Schwarz and Shain[1] first presented the DPSCA to determine the rate constant of the benzidine rearrangement reaction and showed that this technique has a high potentiality for the determination of rate constants of follow-up chemical reactions. Christie[2] modified the technique originally devised by Schwarz and Shain by recording the charge *vs.* time variations instead of the current *vs.* time curves, and this modified technique is usually referred to as DPSCC. Since then, various authors have reported several modifications of these techniques[3-9] as well as their application to practical problems.[10-20] However, almost all treatments reported up to date are restricted to completely irreversible follow-up reactions. The recent paper of Hanafey *et al.*[9] is only one exceptional one, in which they reported the explicit finite difference simulation of DPS current, charge and absorbance responces for 22 two-parameter electrochemical mechanisms, including the second-order kinetics.

Recently, we have attempted an application of DPSCA to the kinetics of aquation reactions of labile complexes which may be produced by charge transfer reactions of the corresponding inert complexes. In this case, if it is desired to perform measurements in a wide range of free ligand concentrations or of pH, the effects of the reverse (complex formation) reactions should be taken into consideration. Then, the follow-up reactions must be regarded as reversible. In the present paper, we shall develope a theory of DPSCA for reversible follow-up reactions in an analytical way and apply it to determining the rate constant of aquation reaction of bis(ethylenediaminemonoacetato)cobalt(II), which is produced by electrolytic reduction of bis(ethylenediaminemonoacetato)cobalt(III) (corresponding inert complex species).

Theoretical

Consider the electrode reaction followed by a first-order chemical reaction, which is symbolically represented by

$$Ox + ne \rightleftarrows Red, \quad Red \underset{kK}{\overset{k}{\rightleftarrows}} Z,$$

where k and K are the rate and the equilibrium constants of the follow-up chemical reaction, respectively. The plane boundary value problem for the diffusion processes corresponding to the above mechanism can be solved by utilizing the method of Laplace transformation under the assumption that the diffusion coefficients of Red and Z have the common value.[21] Thus, the concentration of Ox and Red at the electrode surface, C_O^s and C_R^s, can be expressed as

$$C_O^s = C_O^\circ - \frac{1}{\sqrt{D_O\pi}}\int_0^t \frac{[i(u)/nFA]}{\sqrt{t-u}}du, \tag{1}$$

$$C_R^s = \frac{1}{(1+K)\sqrt{D\pi}}\int_0^t \frac{K+\exp[-\rho(t-u)]}{\sqrt{t-u}}[i(u)/nFA]du, \tag{2}$$

with

$$\rho = k(1+K), \tag{3}$$

where C_O° denotes the bulk concentration of Ox; the bulk concentrations of Red and Z are assumed to be equal to zero; D_O is the diffusion coefficient of Ox; D is the common diffusion coefficient of Red and Z; $i(t)$ denotes the current intensity; A is the surface area of the electrode; t is the lapse of the time after the beginning of the electrolysis.

The electrolysis condition of DPSCA is as follows:

†† Present address: Matsushita Electric Industrial Co., Ltd., 1006, Kadoma, Kadoma, Osaka 571.

the potential is stepped from some initial value, where no current flows, to a value which causes the electrode reaction product, Red, to be generated at a diffusion-controlled rate. After a given generation time, τ, the potential is returned to the initial value, where the electrode reaction is reversed, consuming Red at a diffusion-controlled rate. Thus, the electrolysis condition can be expressed by

$$0 < t < \tau : C_O^S = 0, \tag{4}$$

$$\tau < t : C_R^S = 0, \tag{5}$$

For $0<t<\tau$, inserting Eq. 1 into Eq. 4 and solving the resultant Abel integral equation yields immediately the cathodic limiting diffusion current, i_c:

$$i_c = nFA\, C_O^\circ \sqrt{D_O}/\sqrt{\pi t}. \tag{6}$$

For $t>\tau$, on the other hand, substituting Eq. 2 into Eq. 5 and noting that the current intensity during the first potential pulse ($0<t<\tau$) is given by Eq. 6, we obtain after some rearrangements

$$\int_\tau^t \frac{K+\exp[-\rho(t-u)]}{\sqrt{t-u}} \left\{ \frac{-i_a(u)}{nFA} + \frac{C_O^\circ \sqrt{D_O}}{\sqrt{\pi u}} \right\} du = \frac{C_O^\circ \sqrt{D_O}}{\sqrt{\pi}} \int_0^t \frac{K+\exp[-\rho(t-u)]}{\sqrt{u(t-u)}} du, \tag{7}$$

where i_a denotes the anodic current to be measured for $t>\tau$. Here, it is convenient to introduce the dimensionless variable:

$$\xi = (t-\tau)/\tau, \tag{8}$$

which denotes the portion of the lapse of time after the beginning of the second potential pulse to the switching time τ. Further, we introduce new integral variables: $u=\tau(1+v)$ and $u=\tau(1+\xi)(1-v)$ into the left- and right-hand sides of Eq. 7, respectively. Then we obtain after evaluating the definite integral on the right-hand side of the resulting equation[22]

$$\int_0^\xi \frac{K+\exp[-\rho\tau(\xi-v)]}{\sqrt{v(\xi-v)}} \Psi(v) dv = \pi \left\{ K+\exp[-(\rho\tau/2)(1+\xi)] I_0\left(\frac{\rho\tau}{2}[1+\xi]\right) \right\}, \tag{9}$$

with

$$\Psi(v) = (-i_a/i_c) + \sqrt{\xi/(1+\xi)}, \tag{10}$$

where I_0 is the zero-order modified Bessel function of the first kind. $(-i_a/i_c)$ denotes the ratio of the anodic current measured at a given time t during the second pulse to the cathodic current measured at $(t-\tau)$ during the first pulse, and will be used for constructing the working curves, following the suggestion of Schwarz and Shain.[1] Since Eq. 9 is the Volterra integral equation of the first kind with respect to $\Psi(\xi)$, its analytical solution may be obtained in a closed form by utilizing the method of Laplace transformation. However, when practically constructing the working curves by using the analytical solution, it is necessary to evaluate numerically the definite integral. Such a numerical method is described in Appendix. Numerical calculations were performed for various combinations of the values of K and $k\tau$ by means of a digital computer FACOM M-160, and the values of $\Psi(\xi)$ were obtained as functions of ξ. Then, for a given constant value of ξ, say $\xi=1$, the working curves, *i.e.*, $(-i_a/i_c)$ *vs.* $k\tau$ plots, were drawn for a series of values of K. As examples, such working curves constructed for $\xi=1$ are shown for a series of values of K in Fig. 1. Of course, the curve for $K=0$ is in agreement with that of Schwarz and Shain.[1] As can be seen from Fig. 1, when the parameter $k\tau$ is increased, the working curves are at first decreased and then, after passing through the corresponding minima, they are increased. This behavior is understandable in view of the fact that Red may be reproduced from Z by the reverse reaction during the second pulse. Thus, there arises a problem that one measured value of $(-i_a/i_c)$ corresponds to the two values of $k\tau$. This problem may simply be solved by examining whether $(-i_a/i_c)$ is decreased or increased when the switching time τ is slightly increased.

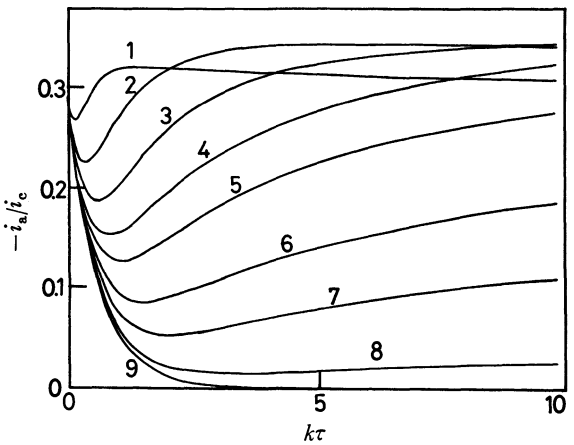

Fig. 1. Typical working curves for a series of values of K at $\xi=1$.
K: (1) 3; (2) 1; (3) 0.5; (4) 0.3; (5) 0.2; (6) 0.1; (7) 0.05; (8) 0.01; and (9) 0.

Experimental

Reagents. *Trans*-bis(ethylenediaminemonoacetato)cobalt(III) chloride dihydrate, *trans*-[Co(edma)$_2$]Cl·2H$_2$O, and ethylenediaminemonoacetic acid dihydrochloride dihydrate, Hedma·2HCl·2H$_2$O, were prepared and purified by the method of Fujii *et al.*,[23] where edma$^-$ is an abbreviation of $H_2NCH_2CH_2NHCH_2COO^-$. Sodium acetate and disodium hydrogen phosphate were purified by recrystallizing twice from water. All other chemicals used were prepared and purified by the methods described previously.[24]

Cell and Electrodes. The electrolytic cell used was all-glass six neck vessel of the same type as described previously,[25] which was equipped with various electrodes, argon gas inlet and outlet, and two burets. The electrode assembly consisted of a dropping mercury working electrode (DME), a saturated calomel reference electrode (SCE) and a mercury pool auxiliary electrode (AE), the latter being placed at the bottom of the cell. The characteristics of DME used were: drop time = 7.9 s and flow rate of mercury = 1.45 mg s^{-1} in 1.0 M (1 M = 1 mol dm^{-3}) $NaClO_4$ solution at 45 cm of the height of mercury head with no applied potential. The SCE was connected to the cell throught a junction salt bridge containing sodium chloride solution. A glass electrode (Beckman No. 40495) and a Ag–AgCl reference electrode were used for pH measurements of the test solutions.

Instrumentation. The pulse experiments were performed

on the solid state instrument constructed from readily available components, which consisted of a drop fall detector, timing control logic circuitry, a pulse generator and a potentiostat. A spike-like pulse, generated at the moment of drop detachment from the capillary tip, was employed as a trigger signal for the timing controlling pulse train.[26] When the spike was detected, the AE was disconnected from the potentiostat by means of a FET switch. The measuring device was a Nicolet 1090A Explorer digital oscilloscope. The current responces were monitored and stored on it and then the enlarged current-time curves were displayed on an X-Y recorder (Riken-Denshi Model F-42CP). No IR compensation was employed.

The polarograph used for preliminary experiments was the same as described previously.[24] The pH measurements were performed on an Orion Research Model 801 digital pH/mV meter.

Procedures. All measurements were performed in a paraffin oil thermostat at 25.0±0.1 °C. Two kinds of the solution composition were used: 1.0 mM *trans*-$[Co(edma)_2]^+$, 20 and 50 mM Hedma, and 1.0 M $NaClO_4$. No buffer was added in the pH ranges 1.0—3.5 and 6.5—10.0, because the ligand present in a large excess was expected to have a sufficiently large buffer capacity in these pH ranges. In the pH range 3.5—6.5, the acetate (for pH 3.5—5.5) and phosphate (for pH 5.5—6.5) buffers were used at the concentration of 50 mM. The pH values of the test solutions were changed and measured following the procedure described previously.[27] Deaeration of the solution was accomplished with pure argon gas by bubbling through the solution for 1 h before each run and with a steady flow maintained over the solution during measurements.

The potential applied to the working electrode was a single square pulse with an amplitude of 0.55 V and this pulse was applied at the moment when the mercury drop sufficiently grew, *i.e.*, 4—5 s after the beginning of the drop growth. The initial d.c. level E_1 was selected from the behavior of d.c. polarographic reduction waves of *trans*-$[Co(edma)_2]^+$ as follows: $E_1=-0.05$ *V vs.* SCE for pH 1—6, $E_1=-0.10$ *V vs.* SCE for pH 6—8 and $E_1=-0.20$ *V* vs. SCE for pH 8—10. In acidic solutions the applied potentials always fell in the diffusion-controlled limiting current region for each depolarizer species. However, in the alkaline region, the foot of the mercury desolution wave slightly overlapped with the reduction wave of $[Co(edma)_2]^+$ species. Thus, data obtained in alkaline solutions may be less reliable, although several trials for selection of E_1 were performed and a blank correction was made using current-time curves measured in solutions containing no $[Co(edma)_2]^+$ species.

Results and Discussion

The electrode reaction of Co(III)/Co(II)–edma system may be formally expressed by Scheme 1, where, $(k_1)_{app}$ and $(k_2)_{app}$ denote the apparent rate constants of the step-wise aquation processes, respectively.

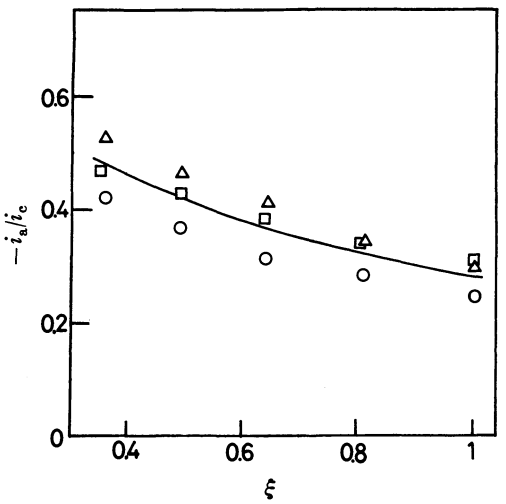

Fig. 2. Typical plots of the current ratio $(-i_a/i_c)$ *vs.* ξ under the diffusion-controlled conditions.
Concentration of *trans*-$[Co(edma)_2]^+=1.0$ mM. Total concentration of Hedma=20 mM. (□): pH 7.38, (○): pH 8.75, (△): pH 10.66. Solid line represents the theoretical curve calculated by Eq. 11.

β_{101} and β_{102} are the overall formation constants of $[Co(edma)]^+$ and $[Co(edma)_2]^0$ species, respectively, the values of which were determined previously[27] as follows: $\log \beta_{101}=7.51$ and $\log \beta_{102}=14.05$.

First, consider the reaction in the alkaline region higher than pH 7. In this pH region, $[Co(edma)_2]^0$ species is stable for the ligand concentrations of 20—50 mM and thus the aquation reaction does not occur. Therefore, the anodic-cathodic current ratio, $(-i_a/i_c)$, must satisfy the following equation for the diffusion-controlled conditions:[1]

$$(-i_a/i_c) = 1 - [\xi/(1+\xi)]^{1/2}, \qquad (11)$$

where ξ is defined by Eq. 8. Some typical results of $(-i_a/i_c)$ *vs.* ξ plot for several pH values are shown in Fig. 2, where the points are the experimental values, and the solid line represents the theoretical behavior calculated by Eq. 11. The results show that the anodic currents are essentially controlled by diffusion of $[Co(edma)_2]^0$ to the electrode surface. Slight deviations of $(-i_a/i_c)$ from theory could be attributed to the overlapping of the mercury desolution current with the anodic current of $[Co(edma)_2]^0$.

Next, the reaction in the acidic region lower than pH 4.5 will be examined. In this acidic region, the first step aquation process becomes irreversible, because the rate of the corresponding reverse process may be neglected, as can be proved from the concentrations of $[Co(edma)]^+$ and $edma^-$ calculated by the use of the

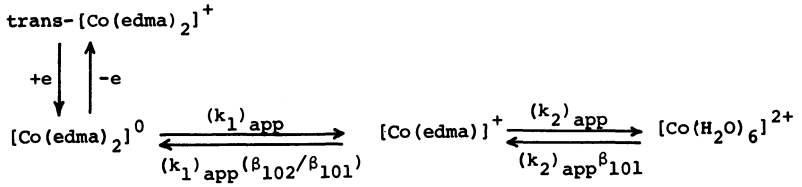

Scheme 1.

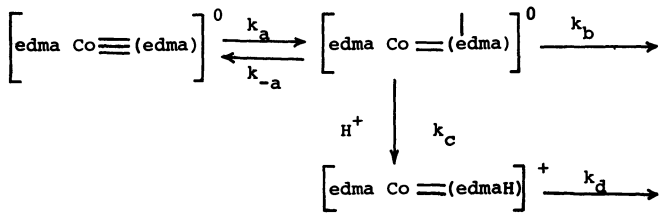

Scheme 2.

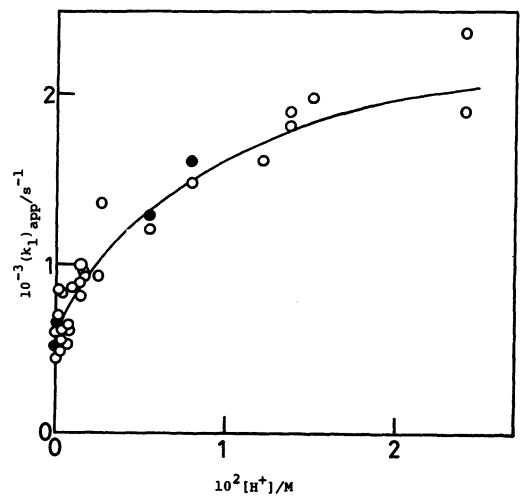

Fig. 3. Dependence of the apparent rate constant of the aquation reaction of $[Co(edma)_2]^0$ upon the concentration of hydrogen ion.
$[Co(edma)_2]^0$ was produced by the electrolytic reduction of 1.0 mM *trans*-$[Co(edma)_2]^+$ in 1.0 M $NaClO_4$ solutions containing 20 mM Hedma (open circle) or 50 mM Hedma (solid circle). The solid curve indicates the values of $(k_1)_{app}$ calculated by the use of Eq. 12 with the values of k_a, k_b/k_{-a}, and k_c/k_{-a} obtained.

formation constants of complex species and the protonation constants of edma$^-$, $\log \beta_{011}=9.97$, $\log \beta_{021}=16.71$, and $\log \beta_{031}=18.76$.[27] Therefore, analysis of the current-time curves was made by using the working curves with $K=0$ (*e.g.*, see curve 9 in Fig. 1.). The values of $(k_1)_{app}$ thus obtained for various pH values are shown in dependence of the hydrogen ion concentration, $[H^+]$, in Fig. 3. We see that the apparent rate constant greatly increases with an increase in $[H^+]$, indicating that the first aquation step is accelerated by the presence of hydrogen ion. A possible mechanism for such an acid-catalyzed dissociation of multidentate ligands may be expressed by Scheme 2, where it is assumed that the protonation of the intermediate containing bidentated edma$^-$ is irreversible, because of the fact that no evidence for the presence of protonated species was observed in potentiometric titrations.[27] Similar schemes were previously proposed for the dissociation of nickel(II),[28] iron(II),[29,30] and cobalt(II)[31-35] complexes with polyamines such as ethylenediamine (en), diethylenetriamine (dien), triethylenetetraamine (trien), 2,2′-bipyridine (bpy), 2,2′ : 6′,2″-terpyridine (terp) and 1,10-phenanthroline (phen), and the 2,4-pentanedionate complexes[36] of chromium(II), cobalt(II), and ruthenium(II). According to Sheme 2 and considering stationary-state kinetics for

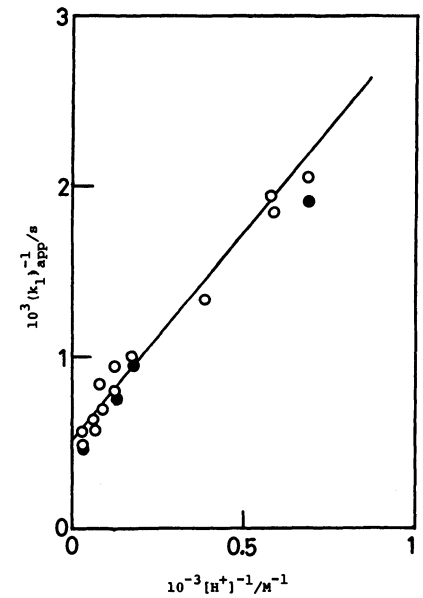

Fig. 4. Plot of $1/(k_1)_{app}$ *vs.* $1/[H^+]$.
The experimental conditions and the symbols used are the same as those in Fig. 3.

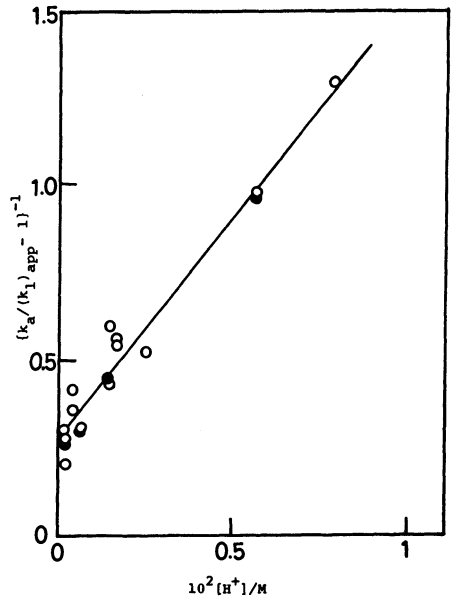

Fig. 5. Plot of $1/\{(k_a/(k_1)_{app})-1\}$ *vs.* $[H^+]$.
The experimental conditions and the symbols used are the same as those in Fig. 3.

unprotonated bidentated species, $(k_1)_{app}$ will be given by

$$(k_1)_{app}=\frac{k_a(k_b+k_c[H^+])}{k_{-a}+k_b+k_c[H^+]}. \quad (12)$$

Equation 12 can be rearranged to

$$\frac{1}{(k_1)_{app}}=\frac{1}{k_a}+\frac{k_{-a}}{k_a(k_b+k_c[H^+])}. \quad (13)$$

At sufficiently low pH where $k_b \ll k_c[H^+]$, a plot of $1/(k_1)_{app}$ *vs.* $1/[H^+]$ is linear, and k_a is derived by extrapolation to $1/[H^+]\rightarrow 0$. The graph for the first step dissociation of $[Co(edma)_2]^0$ is shown in Fig. 4. The corresponding values of the rate constants derived from the intercept and the slope are

$$k_a = 2.1 \times 10^3\ s^{-1}$$
$$(k_c/k_{-a}) = 1.9 \times 10^2.$$

Further rearrangement of Eq. 12 yields

$$1/[\{k_a/(k_1)_{app}\} - 1] = (k_b/k_{-a}) + (k_c/k_{-a})[H^+]. \quad (14)$$

Figure 5 shows the plots of $1/[\{k_a/(k_1)_{app}\} - 1]$ *vs.* $[H^+]$, which is linear as expected from Eq. 14. The intercept and the slope give the following values for the corresponding rate constants:

$$(k_b/k_{-a}) = 2.9 \times 10^{-1}$$
$$(k_c/k_{-a}) = 1.4 \times 10^2.$$

Two values of (k_c/k_{-a}) obtained from the two different plots are in good agreement with each other. To summarize briefly, the rate constant of the first step dissociation of $[Co(edma)_2]^0$ approaches to a limiting value ($2.1 \times 10^3\ s^{-1}$) for pH$<$1.3, in which the first bond rupture is the rate determining step for the dissociation and the hydrogen ion acts as an effective scavenger for the detached bond of bidentated edma. On the other hand, the rate constant is reduced to another limiting value ($4.7 \times 10^2\ s^{-1}$) for pH$<$4.3, in which the hydrogen ion does not participate directly in the dissociation process. We can calculate $(k_1)_{app}$ at various concentrations of hydrogen ion by the use of Eq. 12 with the values of k_a, k_b/k_{-a}, and k_c/k_{-a} obtained. The calculated values (solid curve in Fig. 3) are in agreement with the measured ones.

Two mechanisms are possible, depending on whether the first bond rupture occurs on the Co–N bond of a primary amino group or on the Co–O bond of carboxyl group, where the rupture of Co–N bond of secondary amino group is ruled out taking into account the steric factors. If the first bond rupture occurs on the Co–N bond of a primary amino group, the dissociation reaction proceeds through "glycinate intermediate".[37,38] On the other hand, if the Co–O bond of carboxyl group ruptures first, the subsequent dissociation reaction proceeds *via* "ethylenediamine intermediate."[37,38] The both possible reaction paths for the first step of the dissociation of $[Co(edma)_2]^0$ complex produced by the electrochemical reduction of the corresponding cobalt(III) complex can be expressed by Scheme 3, where edma$^-$ and N–N–O$^-$ stand for NH_2–CH_2–CH_2–NH–COO^- and Hedma denotes the protonated edma$^-$.

As being obtained above, the rate constant of the first bond rupture corresponding to $k_{a'}$ or $k_{a''}$ is $2.1 \times 10^3\ s^{-1}$. This value is almost equal to those of the corresponding first bond rupture of $[Co(en)_2]^{2+}$ and $[Co(trien)]^{2+}$ (1.4×10^3 and 2.1×10^3, respectively).[31] Each of these three cobalt(II) complexes has four nitrogen atoms as a donating atom. Further, the rate constants of the first bond rupture of cobalt(II) complexes with edma$^-$ or such aliphatic polyamines as en, dien and trien increase in the order:[31] $[Co(en)]^{2+} < [Co(dien)]^{2+} < [Co(en)_2]^{2+} \approx [Co(trien)]^{2+} \approx [Co(edma)_2]^0 < [Co(en)_3]^{2+} \approx [Co(dien)_2]^{2+}$. It is likely that in the dissociation of cobalt(II) complexes with aliphatic polyamines and polyamine-*N*-carboxylates the rate constant of the first bond rupture increases with an increase in the number of nitrogen donor atoms. From the fact that the rate constant of the first bond rupture for $[Co(edma)_2]^0$ is almost equal to those for $[Co(trien)]^{2+}$ and $[Co(en)_2]^{2+}$, it seems reasonable that the first bond rupture occurs on the Co–N bond of a primary amino group.

The ratio k_c/k_{-a} ($(1.7 \pm 0.3) \times 10^2$) for $[Co(edma)_2]^0$ is almost equal to those for $[Co(trien)]^{2+}$ and $[Co(en)_2]^{2+}$ (3.6×10^2 and 1.6×10^2, respectively).[31] This means that for these cobalt(II) complexes the hydrolysis involving protonation is much faster than the re-

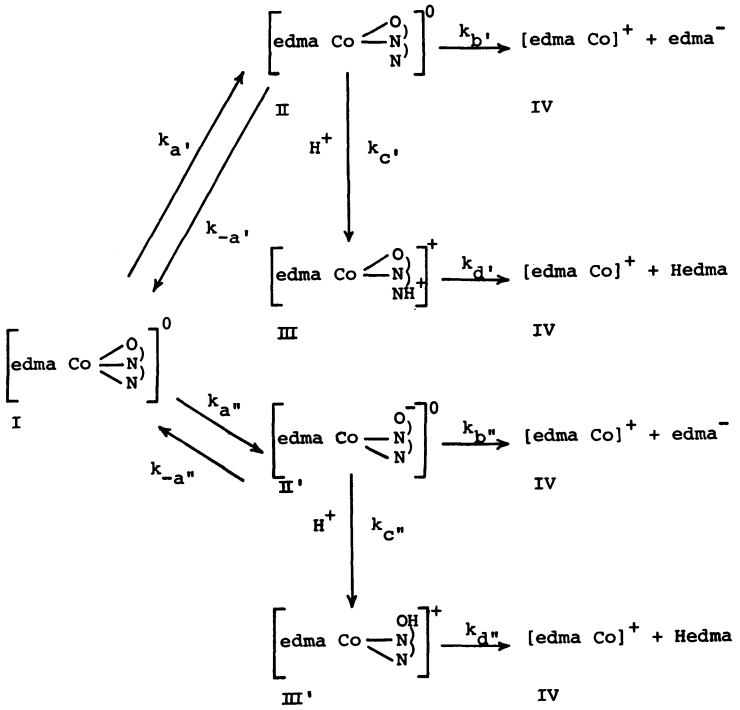

Scheme 3.

formation of the chelate ring and further for the $[Co(edma)_2]^0$ complex the protonation of an uncoordinated ligand can occur with the same easiness as those in the $[Co(en)_2]^{2+}$ and $[Co(trien)]^{2+}$ complexes.

The ratio k_b/k_{-a} is a measure of the probability for complete dissociation of a ligand once the first bond rupture occurred. The value (2.9×10^{-1}) of k_b/k_{-a} for $[Co(edma)_2]^0$ is about forty times larger than those (7.9×10^{-3})[31] for $[Co(en)_2]^{2+}$ and $[Co(trien)]^{2+}$. This may be due to the difference between the type of the bond of the still-bound ligand after the first bond rupture in the $[Co(edma)_2]^0$ dissociation and that for $[Co(en)_2]^{2+}$ and $[Co(trien)]^{2+}$. In the former the still-bound ligand has a possibility to make "glycinate intermediate" (II) and/or "ethylenediamine intermediate" (II'), while in the latter the formation of "ethylenediamine intermediate"[31] can be only expected. The processes II→IV and II'→IV shown in Scheme 3 may be considered to be similar to the first detachment processes of glycine (gly) and ethylenediamine (en) from the cobalt(II) complexes with gly and en, respectively. The rate constant of the first step of the dissociation of the $[Co(gly)_3]^-$ is by *ca.* 10 times larger than that of the $[Co(en)_3]^{2+}$.[36,39-41] Similarly, the dissociation of the nickel(II)–glycine complexes is faster than that of the corresponding ethylenediamine complexes.[42] Thus, the large difference between the value of k_b/k_{-a} for $[Co(edma)_2]^0$ and those for $[Co(en)_2]^{2+}$ and $[Co(trien)]^{2+}$ seems to eliminate the possibility of an ethylenediamine reaction mechanism in the $[Co(edma)_2]^0$ dissociation. This finding is contrary to the observation of Kodama *et al.*[37,38] obtained in their kinetic study of the substitution reactions of nickel(II)–edma$^-$ complex with diethylenetriamine-*N*,*N*,*N'*,*N''*,*N''*-pentaacetic acid (DTPA). The substitution reaction of nickel(II)–edma$^-$ complex with DTPA proceeds through "ethylenediamine intermediates."

Lastly, consider the reaction in the near neutral region of pH values from 4.5 to 7. In this pH region, the $[Co(edma)_2]^0$, $[Co(edma)]^+$, and $[Co(H_2O)_6]^{2+}$ species coexist in the solution, as can be seen from the concentration distributions calculated by the use of the formation constants of the $[Co(edma)_2]^0$ and $[Co(edma)]^+$ species and the protonation constants of edma$^-$.[27] Then the effects of the reverse (complex formation) reactions should be taken into consideration. It has been well known[41-46] that the rate constant of the first detachment step of the ligand (*i.e.*, dissociation reaction) of the labile complexes is larger than those of the subsequent steps. Thus, we assumed that the second step process $[Co(edma)]^+ \rightleftarrows [Co(H_2O)_6]^{2+}$ dose not proceed substantially compared with the first step process $[Co(edma)_2]^0 \rightleftarrows [Co(edma)]^+$ within the time scale of DPSCA. Further, the experiments were mainly conducted under the experimental conditions where $[Co(H_2O)_6]^{2+}$ ion is scarcely present in the solution. The second step process was thus ignored in examining the mechanism of overall aquation reaction of $[Co(edma)_2]^0$. Furthermore, the reaction path through the protonation of the amino group, which is the main path of the dissociation in an acidic solution, can be neglected, since the ratio of $k_c[H^+]$ to k_b which

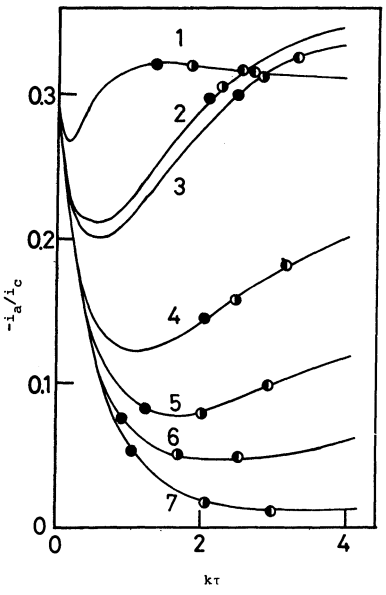

Fig. 6. Dependence of the measured values of the current ratio $(-i_a/i_c)$ on $k\tau$ for various values of K at $\xi=1$.
(●): $\tau=3.0$ ms, (◑): $\tau=4.7$ ms, (◐): $\tau=6.5$ ms.
(1): $K=3.00$, [Hedma]=20.0 mM, pH 6.22; (2): $K=0.592$, [Hedma]=20.0 mM, pH 5.84; (3): $K=0.541$, [Hedma]=15.7 mM, pH 5.90; (4): $K=0.173$, [Hedma]=60.9 mM, pH 5.32; (5): $K=0.110$, [Hedma]=40.5 mM, pH 5.30; (6): $K=0.048$, [Hedma]=20.0 mM, pH 5.20; (7): $K=0.05$, [Hedma]=14.0 mM, pH 5.00. In all cases, the concentration of *trans*-$[Co(edma)_2]^+$ is 1.0 mM. Solid lines represent the theoretical curves for various values of K which correspond to the solution compositions ((1)—(7)).

can be estimated by using the values of k_b/k_{-a} and k_c/k_{-a} obtained above is sufficiently small at pH>*ca.* 5. According to the reaction scheme (Scheme 1), the apparent rate constant, $(k)_{app}$, and the equilibrium constant, K, can be expressed by $(k_1)_{app}$ and $l(\beta_{102}/\beta_{101})$, respectively, in which l is the concentration of free edma$^-$. In Fig. 6 the experimental values of the ratio $(-i_a/i_c)$ are shown as a function of the product of the rate of the follow-up chemical reaction (k) and the switching time (τ) at various analytical concentrations of Hedma and pH's. The value of $(k_1)_{app}$ was independent of the analytical concentrations of Hedma and pH's within the experimental error, as can be expected from the above mentions. The value of $(k_1)_{app}$ was estimated to be $(4.1\pm0.6)\times10^2\,s^{-1}$, which is almost equal to the value $(4.7\times10^2\,s^{-1})$ obtained in the acidic region (pH<4.5).

The results may be summarized as follows: The mechanism of the aquation of the $[Co(edma)_2]^0$ can be described by Scheme 1 in the range of pH 1.5 to 10.6. At pH<4.5, the process of the detachment of the first edma$^-$ from the $[Co(edma)_2]^0$ is irreversible and the rate of this process is accelerated by hydrogen ions (Scheme 2). The first step of the dissociation of the $[Co(edma)_2]^0$ is the bond rupture of the Co–N bond of a primary amino group and the dissociation reaction proceeds through "glycinate intermediate" (see Scheme 3). In the region of further lower pH (pH<1), the

rate of the dissociation approaches an upper limiting value ($2.1\times10^3\ s^{-1}$). At pH>4.5, on the other hand, the hydrogen ions do not substantially contribute to the aquation and thus the rate approaches a lower limiting value ($4.7\times10^2\ s^{-1}$), which is in good agreement with that obtained in neutral region (4.5<pH<7), where the reverse (complex formation) reaction must be also taken into consideration. Above pH 7, the $[Co(edma)_2]^0$ species exists as main species in the solution and thus the kinetic behavior of the aquation is not observed.

Appendix

If we make the following substitution:

$$\eta = \sqrt{v}, \tag{A-1}$$

$$\sigma = \sqrt{\xi}. \tag{A-2}$$

Eq. 10 can be converted into the following equation;

$$2\int_0^{\sigma} \frac{K+\exp[-\rho\tau(\sigma^2-\eta^2)]}{\sqrt{\sigma^2-\eta^2}}\Psi(\eta)d\eta = C(\sigma^2,K,\rho\tau), \tag{A-3}$$

with

$$C(\sigma^2,K,\rho\tau) = \pi\left[K+\exp\left\{-\frac{\rho\tau(1+\sigma^2)}{2}\right\}\cdot I_0\left(\frac{\rho\tau[1+\sigma^2]}{2}\right)\right]. \tag{A-4}$$

Equation A-4 can be solved numerically in the following way:[22] First, divide the σ -axis into N equal intervals of $\Delta\sigma$, and transform Eq. A-3 into

$$2\sum_{p=1}^{N}\int_{(p-1)\Delta\sigma}^{p\Delta\sigma}\Psi(\eta)\frac{K+\exp[-\rho\tau\{(N\Delta\sigma)^2-\eta^2\}]}{\sqrt{(N\Delta\sigma)^2-\eta^2}}d\eta = C((N\Delta\sigma)^2,K,\rho\tau), \tag{A-5}$$

with

$$C((N\Delta\sigma)^2,K,\rho\tau) = \left[K+\exp\left\{-\frac{\rho\tau(1+(N\Delta\sigma)^2)}{2}\right\}\cdot I_0\left(\frac{\rho\tau(1+(N\Delta\sigma)^2)}{2}\right)\right]. \tag{A-6}$$

Next, approximate the function $\Psi(\eta)[K+\exp\{-\rho\tau((N\Delta\sigma)^2-\eta^2\}]$ in the interval $(p-1)\Delta\sigma\leqq\eta\leqq p\Delta\sigma$ by its arithmetic mean

$$\frac{1}{2}\{\Psi(p\Delta\sigma)[K+\exp\{-\rho\tau(N^2-p^2)(\Delta\sigma)^2] + \Psi([p-1]\Delta\sigma)[K+\exp\{-\rho\tau(N^2-[p-1]^2)(\Delta\sigma)^2]\}, \tag{A-7}$$

and perform the integration of the remaining part. Then, we obtain, after some rearrangements,

$$\Psi(\Delta\sigma) = \frac{C((N\Delta\sigma)^2,K,\rho\tau)-\Psi(0)[K+\exp\{-\rho\tau(\Delta\sigma)^2\}]H(1,1)}{(K+1)H(1,1)}, \tag{A-8}$$

$$\Psi(N\Delta\sigma) = \frac{1}{(K+1)H(N,N)}\Big[C((N\Delta\sigma)^2,K,\rho\tau)-\Psi(0)H(N,N)[K+\exp\{-\rho\tau(\Delta\sigma)^2N^2\}]-\sum_{p=1}^{N}\Psi(p\Delta\sigma)[K+\exp\{-\rho\tau(\Delta\sigma)^2(N^2-p^2)\}][H(N,p)+H(N,p-1)\Big], \tag{A-9}$$

with

$$H(N,p) = \sin^{-1}\left(\frac{p}{N}\right)-\sin^{-1}\left(\frac{p-1}{N}\right), \tag{A-10}$$

where

$$\Psi(0) = \frac{1}{K+1}\left[K+\exp\left(-\frac{\rho\tau}{2}\right)\cdot I_0\left(\frac{\rho\tau}{2}\right)\right]. \tag{A-11}$$

The condition A-11 is given by solving the Eq. 9 at $\xi\to0$. Thus, the numerical values of $\Psi(\sigma)$ can be obtained stepwise with $N=1,2,3,\cdots$ for the various choices of the parameters K and $\rho\tau$. Numerical calculations were carried out on a digital computer FACOM M-160 for a series of values of K and $\rho\tau$ ranging from 0 to 100 and 0 to 10, respectively, by setting $\Delta\sigma=0.001$.

References

1) W. M. Schwarz and I. Shain, *J. Phys. Chem.*, **69**, 30 (1965).
2) J. H. Christie, *J. Electroanal. Chem.*, **13**, 79 (1967).
3) J. H. Christie, R. A. Osteryoung, and F. C. Anson, *J. Electroanal. Chem.*, **13**, 236 (1967).
4) R. J. Lawson and J. T. Maley, *Anal. Chem.*, **46**, 559 (1974).
5) K. Holub, *J. Electroanal. Chem.*, **65**, 193 (1975).
6) K. Holub and J. Weber, *J. Electroanal. Chem.*, **73**, 126 (1976).
7) R. C. Bess, S. E. Cranston, and T. H. Ridgway, *Anal. Chem.*, **48**, 1619 (1976).
8) T. H. Ridgway, R. P. Van Duyne, and C. N. Reilly, *J. Electroanal. Chem.*, **67**, 1 (1976).
9) M. K. Hanafey, R. L. Scott, T. H. Ridgway, and C. N. Reilly, *Anal. Chem.*, **50**, 116 (1978) and references therein.
10) S. P. Perone and W. J. Krethow, *Anal. Chem.*, **38**, 1760 (1966).
11) F. C. Anson, *Anal. Chem.*, **38**, 54 (1966).
12) F. C. Anson, J. H. Christie, and R. A. Osteryoung, *J. Electroanal. Chem.*, **13**, 343 (1967).
13) A. Zweig, A. K. Hoffmann, D. L. Maricle, and A. H. Maurer, *J. Am. Chem. Soc.*, **90**, 261 (1968).
14) K. H. Houser, D. E. Bartak, and M. D. Hawley, *J. Am. Chem. Soc.*, **95**, 6033 (1973).
15) E. Temmerman, R. Abel, and R. A. Osteryoung, *J. Electroanal. Chem.*, **55**, 173 (1974).
16) D. L. Jeanmaire and R. P. Van Duyne, *J. Electroanal. Chem.*, **66**, 235 (1975).
17) C. M. Elson, *Inorg. Chem.*, **15**, 469 (1976).
18) J. Weber, K. Holub, D. Homolka and J. Pradac, *J. Electroanal. Chem.*, **73**, 151 (1976).
19) C. J. Myall and D. Pletcher, *J. Electroanal. Chem.*, **75**, 269 (1977).
20) O. G. De Alvarez and L. Gierst, *J. Electroanal. Chem.*, **100**, 819 (1979).
21) H. Matsuda and Y. Ayabe, *Z. Electrochem.*, **59**, 494 (1955).
22) C. Nishihara and H. Matsuda, *J. Electroanal. Chem.*, **51**, 287 (1974).
23) Y. Fujii, E. Kyuno, and R. Tsuchiya, *Bull. Chem. Soc. Jpn.*, **43**, 786 (1970).
24) T. Ohsaka, N. Oyama, S. Yamaguchi, and H. Matsuda, *Bull. Chem. Soc. Jpn.*, **54**, 2475 (1981).
25) N. Oyama and H. Matsuda, *J. Electroanal. Chem.*, **78**, 89 (1977).
26) T. Rohko, M. Kogoma, and S. Aoyagui, *J. Electroanal. Chem.*, **78**, 89 (1977).
27) T. Ohsaka, N. Oyama, and H. Matsuda, *Bull. Chem. Soc. Jpn.*, **53**, 3601 (1980).
28) J. P. Jones and D. W. Margerum, *J. Am. Chem. Soc.*, **92**, 470 (1970).
29) J. H. Baxendale and P. George, *Trans. Faraday Soc.*, **46**,

736 (1950).
30) J. Burgess and M. V. Twigg, *J. Chem. Soc., Dalton Trans.*, **1974**, 2032.
31) N. Shinohara, J. Lilie, and M. G. Simic, *Inorg. Chem.*, **16**, 2809 (1976).
32) J. Lilie, N. Shinohara, and M. G. Simic, *J. Am. Chem. Soc.*, **98**, 6516 (1976).
33) M. G. Simic, M. Z. Hoffman, R. P. Cheney, and Q. G. Mulazzani, *J. Phys. Chem.*, **83**, 439 (1979).
34) R. Farina, R. Hogg, and R. G. Wilkins, *Inorg. Chem.*, **7**, 170 (1968).
35) R. Davies, M. Green, and A. G. Sykes, *J. Chem. Soc. Dalton Trans.*, **1972**, 1171.
36) D. Meisel, K. H. Schmidt, and D. Meyerstein, *Inorg. Chem.*, **18**, 971 (1979).
37) M. Kodama, Y. Fujii, and T. Ueda, *Bull. Chem. Soc. Jpn.* **43**, 2085 (1970).
38) M. Kodama, M. Hashimoto, and T. Watanabe, *Bull. Chem. Soc. Jpn.*, **45**, 2761 (1972).
39) G. G. Hammes and J. I. Steinfeld, *J. Am. Chem. Soc.*, **84**, 4639 (1962).
40) K. Kustin, R. F. Pasternack, and E. M. Weinstock, *J. Am. Chem. Soc.*, **88**, 4610 (1966).
41) A. Kowalak, K. Kustin, R. F. Pasternack, and S. Petrucci, *J. Am. Chem. Soc.*, **89**, 3126 (1967).
42) A. K. S. Ahmed and R. G. Wilkins, *J. Chem. Soc.*, **1960**, 2901.
43) R. F. Pasternack, M. Angwin, L. Gippand, and R. Reingold, *J. Inorg. Nucl. Chem.*, **34**, 2329 (1972).
44) R. G. Wilkins, *J. Chem. Soc.*, **1957**, 4521.
45) R. Hogg and R. G. Wilkins, *J. Chem. Soc.*, **1962**, 341.
46) "Coordination Chemistry," ed by A. E. Martell, American Chemical Society, Washington, D. C. (1978), Vol. 2, p. 85.

 © 1983 The Chemical Society of Japan Bull. Chem. Soc. Jpn., 56, 3073—3077 (1983)

Synthesis of *N*-Unsubstituted Di- and Triaza Crown Ethers

Hirokazu MAEDA, Shigeo FURUYOSHI, Yohji NAKATSUJI, and Mitsuo OKAHARA*

Department of Applied Chemistry, Faculty of Engineering, Osaka University, Yamada-oka 2-1, Suita, Osaka 565

(Received March 1, 1983)

Facile syntheses of di- and triaza crown ethers by intramolecular cyclization of oligoethylene glycols containing two or three imino groups or by their intermolecular cyclization with oligoethylene glycol bis(*p*-toluenesulfonate)s are described.

N-Unsubstituted oligoaza crown ethers are important as intermediate in the synthesis of cryptands[1] or macrotricyclic compounds.[2-8] They can also be transformed into polymers having crown rings in the backbone.[9-13] Diaza crown ethers as *N*-unsubstituted oligoaza crown ethers have been synthesized by the reaction between diamine and bis(acyl chloride),[1,14] bis(tosylamide) or sodium tosylamine and ditosylate or dichloride,[15-17] and bis(trifluoroacetamide) and ditosylate.[18] However, in all these methods, the elimination of protecting groups is needed in the final step. The reaction of triethylene glycol dichloride with excess ammonia gives diaza-18-crown-6 in low yield with many by-products.[18] Although the preparation by *N*-alkylation of diamine with dichloride[19] or diiodide[20] has been reported, the synthesis of *N*-unsubstituted diaza crown ethers by *O*-alkylation has not been published except some preparations of special diaza crown ethers.[21,22]

We have previously reported that *N*-unsubstituted monoaza crown ethers can be obtained by the reaction of readily available dialkanolamines with oligoethylene glycol bis(*p*-toluenesulfonate)s without protection of the amino group, based on the higher reactivity of alkoxide anion.[23-25] We have also reported one-pot synthesis of substituted and unsubstituted crown ethers by treating various oligoethylene glycol derivatives with arenesulfonyl chlorides.[26] In this paper, the results of the syntheses of *N*-unsubstituted di- and triaza crown ethers by intramolecular cyclization of oligoethylene glycols including two or three imino groups or by intermolecular cyclization of them with oligoethylene glycol bis(*p*-toluenesulfonate)s are described.

Results and Discussion

The starting materials, oligoethylene glycols (**3**) containing two imino groups, were obtained from 2-amino-1-hydroxy compounds (**1**) and oligoethylene glycol dichlorides (**2**) (Scheme 1). When **2** ($m=1$) was used in this reaction, a morpholine derivative was obtained from the intramolecular substitution by the attack of the amino group of the intermediate compound.[18] On the other hand, as the use of 1,2-dichloroethane (**2**, $m=0$) may result in the formation of aziridine derivatives, it is necessary to use **2** having more than two oxyethylene units ($m\geq 2$) in order to get **3** in satisfactory yield. 2-[2-(2-Hydroxyethylamino)ethylamino]ethanol (**4**) and N^{α},N^{ω}-bis(2-hydroxycyclohexyl)-oligoazaalkane-α,ω-diamines (**6**) were obtained from the reaction of excess 2-(2-aminoethylamino)ethanol with 2-chloroethanol and the reaction of oligoazaalkane-α,ω-diamine (**5**) with cyclohexene oxide, respectively.

The preparation of diaza crown ethers by the intramolecular cyclization of **3** was achieved (Scheme 2). After **3** was treated with an equimolar amount of *p*-toluenesulfonyl chloride in dioxane suspension of powdered alkali metal hydroxide at 60 °C, the product

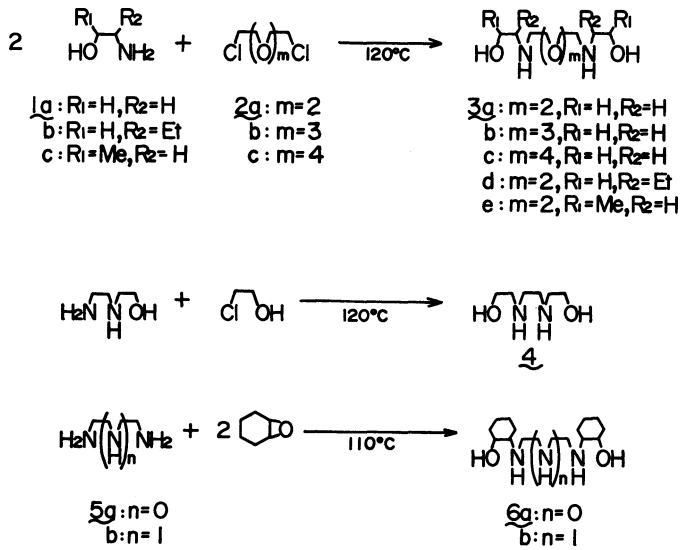

Scheme 1.

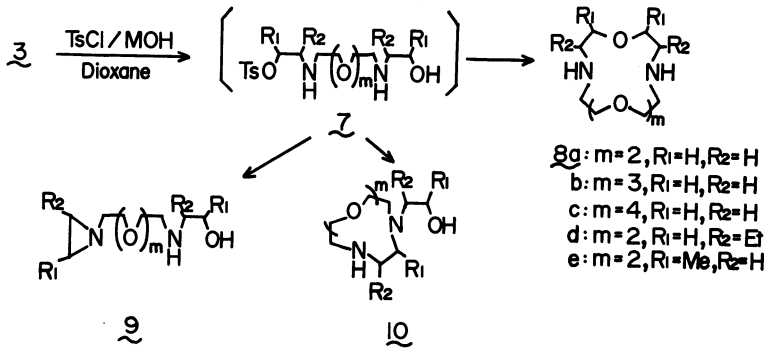

Scheme 2.

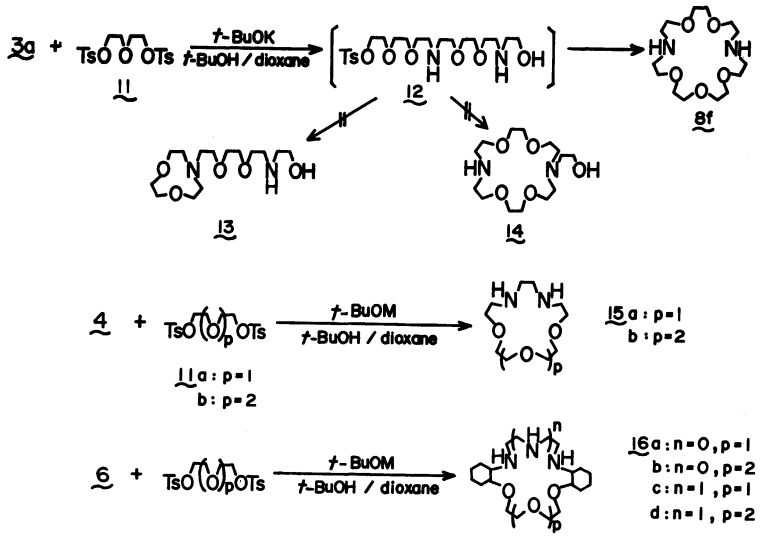

Scheme 3.

TABLE 1. SYNTHESIS OF DIAZA CROWN ETHERS BY THE REACTION OF **3** WITH *p*-TOLUENESULFONYL CHLORIDE

Diaza crown ether	Starting meterial	Base	Yield %	Mp θ_m/°C or Bp θ_b/°C (Torr)
7,13-Diaza-15-crown-5(**8a**)[a]	**3a**	NaOH	26[b]	91—93 80—85(0.015)
10,16-Diaza-18-crown-6(**8b**)	**3b**	NaOH	11[b]	101—103 100—105(0.002)
13,19-Diaza-21-crown-7(**8c**)	**3c**	KOH	11[b]	120—125(0.005)
8,12-Diethyl-7,13-diaza-15-crown-5(**8d**)	**3d**	NaOH	12[c]	100—105(0.04)
9,11-Dimethyl-7,13-diaza-15-crown-5(**8e**)	**3e**	NaOH	17[c]	90—95(0.02)

a) Total amine number(calcd): 505.6(514.0), tertiary amine number: 18.1. b) Purified by distillation. c) Purified by column chromatography.

was obtained by distillations in a Kugelrohr apparatus.

In this reaction, *p*-toluenesulfonyl chloride is first attacked by alkoxide anion to give mono(*p*-toluenesulfonate)s (**7**), and then an intramolecular attack by an alternative alkoxide anion can generate the diaza crown ethers (**8**). If *p*-toluenesulfonyl chloride reacts with imino groups, sulfonamide derivatives may be formed. But, the resonance of *p*-toluenesulfonamides is hardly observed in the ^{1}H NMR spectrum of the crude products of **8a**—**e** before distillation. While, intramolecular reactions of **7** with imino groups may result in *N*-substituted derivatives (**9** and **10**). In the ^{1}H NMR spectrum of the crude product, in fact, resonances are observed at δ 1.16, 1.72, and 2.41, which are ascribed to the protons of aziridine derivatives. However, it is found that the products (**8a**—**c**) obtained by distillations are almost pure *N*-unsubstituted diaza crown ethers (**8**), probably because of the thermal instability of aziridine derivatives. As the distillation product for **8d**, **e** is a mixture of aziridine compound, **8d**, **e** is further purified by alumina column chromatography. Although the product obtained is a mixture of stereoisomers, further purification was not performed. These results are shown in Table 1.

3a and potassium metal were dissolved in *t*-butyl alcohol, then diethylene glycol bis(*p*-toluenesulfonate) (**11a**) in dioxane was added dropwise to the solution at 40 °C. The crude product was distilled in a Kugelrohr apparatus to give diaza 21-crown-7 (**8f**) in 38% yield (Scheme 3).

This synthetic method is similar to that previously reported for the synthesis of monoaza crown ethers,[22,23] and **8f** generated from selective *O*-alkylation under these conditions. Although it is confirmed by the measure-

Table 2. Synthesis of oligoaza crown ethers by the reaction of dihydroxy amine and oligoethylene glycol bis(*p*-toluenesulfonate)s (**11**)

Crown ether	Dihydroxy amine	Disulfonate (11)	Base	Yield %	Mp θ_m/°C or Bp θ_b/°C (Torr)
10,19-Diaza-21-crown-7(**8f**)	**3a**	**11a**	*t*-BuOK	38	120—125 (0.005) 39—41
10,13-Diaza-15-crown-5(**15a**)	**4**	**11a**	*t*-BuONa	32	85—90 (0.02) 46—48
13,16-Diaza-18-crown-6(**15b**)	**4**	**11b**	*t*-BuONa	39	105—110 (0.02)
"Dicyclohexyl-10,13-diaza-15-crown-5"(**16a**)	**6a**	**11a**	*t*-BuONa	42	137—141 (0.015)
"Dicyclohexyl-13,16-diaza-18-crown-6"(**16b**)	**6a**	**11b**	*t*-BuONa	42	155—160 (0.005)
"Dicyclohexyl-10,13,16-triaza-18-crown-6"(**16c**)	**6b**	**11a**	*t*-BuONa	27	161—165 (0.02)
"Dicyclohexyl-13,16,19-triaza-21-crown-7"(**16d**)	**6b**	**11b**	*t*-BuOK	21	170—173 (0.03)

ment of tertiary amine content of product **8f** that the isomeric hydroxy compounds (**13** and **14**) to be formed by *N*-alkylation of **12** are scarcely generated, diethylene glycol di-*t*-butyl ether is formed by the attack of *t*-butoxide anion on **11a** as a by-product.[27]

In a similar manner to **8f**, di- and triaza crown ethers (**15** and **16**) have also been obtained (Table 2). The better yields of crown compounds (**16a**, **b**) with a cyclohexane ring than compounds (**15a**, **b**) without the ring may be explained by the higher solubility of their intermediate alkoxides in the solvent. In the case of crown ethers (**16c**, **d**) having three imino groups, the yields are lower and about half of the starting (**6b**) is recovered unreacted. This is due to the decrease of the template effect, because a softer *N*-doner than *O*-doner is not apt to complex with a hard alkali metal cation.[28]

Experimental

IR and ^{1}H NMR spectra were recorded on a Hitachi 260 spectrometer and a JEOL JNM-PS-100 spectrometer respectively. Mass spectral data were measured with a Hitachi RMU-6E mass spectrometer at an ionization potential of 70 eV. GLC analyses were performed on a Shimadzu gas chromatograph GC-3BF using two 1 m×3 mm columns packed with 10% Silicone SE-30 on Celite 545 and OV-1 on Uniport KS or on a Shimadzu gas chromatograph GC-3BT employing 0.7 m×3 mm column packed with 10% Carbowax on Celite 545. Amine contents were determined by titration.[29,30]

Most starting materials were obtained from commercial sources. Their purity was checked by GLC and when necessary they were purified by distillation. α-(2-Chloroethyl)-ω-chlorooligo(oxyethylenes)(**2b**, **c**) were prepared from the corresponding glycols and thionyl chloride. 6,9-Dioxa-3,12-diazateradecane-1,14-diol (**3a**)[18] and oligoethylene glycol bis(*p*-toluenesulfonate)s (**11a**, **b**)[31] were synthesized as described previously.

7,10-Dioxa-4,13-diazahexadecane-2,15-diol (3e). 1,8-Dichloro-3,6-dioxaoctane (18.7 g, 0.1 mol) was added to a suspension of 1-amino-2-propanol (75.1 g, 1.0 mol) and powdered sodium carbonate (15.9 g, 0.15 mol), and the mixture was heated at 120 °C with stirring. After 30 h, methanol (100 ml) was added. The mixture was filtered, and the excess amine and methanol were removed from the filtrate. The residue was distilled in a Kugelrohr apparatus at 175—180 °C (0.03 Torr) to give a crude product (15.5 g). It was purified by recrystallization from hexane–THF (50 : 50) to afford 11.9 g (45%) of **3e** as a white solid: mp 65—67.5 °C; ^{1}H NMR ($CDCl_3$) δ=1.16 (d, 6H), 2.30—2.92 (m, 8H), 3.29 (s, 4H), 3.47—3.68 (m, 8H), 3.69—3.99 (m, 2H); MS, *m/e* (relative intensity) 249(3), 219(100), 164(59), 132(25), 102(76) 88(68), 44(49); IR (KBr) 3300, 2920, 2880, 1460, 1355, 1120 cm^{-1}. Found: C, 54.25; H, 10.60; N, 10.33. Calcd for $C_{12}H_{28}N_2O_4$: C, 54.52; H, 10.68; N, 10.60. Using a similar procedure, **3b**, **3c**, and **3d** were also obtained.

6,9,12-Trioxa-3,15-diazaheptadecane-1,17-diol (3b). Bp 180—185 °C (0.01 Torr,** Kugelrohr distillation); yellowish viscous liquid; 20% yield; ^{1}H NMR ($CDCl_3$) δ=2.56—2.93 (m, 8H), 3.39—3.95 (m, 16H), 3.64 (s, 4H); *m/e* (relative intensity) 249(11), 194(20), 176(28), 165(15), 88(42), 74(100), 44(30); IR (neat) 3300, 2930, 2880, 1460, 1360, 1110 cm^{-1}. Found: C, 51.12; H, 9.89; N, 10.19. Calcd for $C_{12}H_{28}N_2O_5$: C, 51.41; H, 10.07; N, 9.99.

6,9,12,15-Tetraoxa-3,18-diazaeicosane-1,20-diol (3c). Bp 190—195 °C (0.005 Torr, Kugelrohr distillation); yellowish viscous liquid; 22% yield; ^{1}H NMR ($CDCl_3$) δ=2.56—2.96 (m, 8H), 3.28 (s, 4H), 3.44—3.85 (m, 20H); MS, *m/e* (relative intensity) 293(18), 238(43), 220(37), 132(24), 100(24), 88(41), 74(100); IR(neat) 3290, 2930, 1460, 1355, 1100 cm^{-1}. Found: C, 51.56; H, 10.02; N, 8.71. Calcd for $C_{14}H_{32}N_2O_6$: C, 51.83; H, 9.94; N, 8.64.

2,13-Diethyl-6,9-dioxa-3,12-diazatetradecane-1,14-diol (3d). Bp 170—175 °C (0.01 Torr, Kugelrohr distillation); white waxy solid at 30 °C; 49% yield; ^{1}H NMR ($CDCl_3$) δ=0.92 (t, 6H), 1.24—1.64 (m, 4H) 2.37—2.96 (m, 6H), 3.02 (s, 4H), 3.24—3.76 (m, 12H); MS, *m/e* (relative intensity) 292 (M^+, 1), 261(100), 243(6), 178(27), 116(61), 102(53), 44(71); IR (KBr) 3300, 2910, 2880, 1460, 1360, 1120 cm^{-1}. Found: C, 57.88; H, 10.76; N, 9.71. Calcd for $C_{14}H_{32}N_2O_4$: C, 57.50; H, 11.03; N, 9.58.

2-[2-(2-Hydroxyethylamino)ethylamino]ethanol (4). 2-Chloroethanol (8.5 g, 0.1 mol) was added to a suspension of 2-(2-aminoethylamino)ethanol (104 g, 1 mol) and powdered sodium carbonate (8.0 g, 0.08 mol); the reaction was continued with stirring at 120 °C for 29 h. After the reaction mixture cooled to room temperature, methanol (150 ml) was added, and the mixture was filtered. Evaporation of the filtrate gave a crude

** 1 Torr≈133.322 Pa.

product (15.5 g), which was recrystallized twice from THF to give 7.6 g (51%) of **4** as a white solid: mp 98—100 °C; ^{1}H NMR (CD_3OD) δ=2.40—2.92 (m, 8H), 3.63 (t, 4H); MS, *m/e* (relative intensity) 118(10), 74(100), 56(59), 44(62); IR (KBr) 3330, 2950, 2875, 1450, 1360, 1070 cm^{-1}. Found: C, 48.34; H, 10.63; N, 19.14. Calcd for $C_6H_{16}N_2O_2$: C, 48.63; H, 10.88; N, 18.90.

*N,N'-Bis(2-hydroxycyclohexyl)ethylenediamine (**6a**).* Cyclohexene oxide (19.6 g, 0.2 mol) was added dropwise to ethylenediamine (6.02 g, 0.1 mol) at 85 °C. After the addition, the mixture was heated at 110 °C for 3 h and gradually became a solid. The crude product was recrystallized from methanol–water (99 : 1) to give 8.32 g (32%) of **6a** as a white solid: mp 190—193 °C; ^{1}H NMR (CD_3COOD) δ=1.02—2.49 (m, 16H), 2.76—3.36 (m, 2H), 3.37—4.05 (m, 6H); MS, *m/e* (relative intensity) 220(8), 128(100), 100(27), 81(19), 44(17); IR (KBr) 3290, 2950, 2880, 1475, 1090 cm^{-1}. Found: C, 65.55; H, 11.01; N, 10.90. Calcd for $C_{14}H_{28}N_2O_2$: C, 65.59; H, 11.01; N, 10.93.

*Bis[2-(2-hydroxycyclohexylamino)ethyl]amine (**6b**).* The above procedure was followed, using cyclohexene oxide (19.6 g, 0.2 mol) and bis(2-aminoethyl)amine (10.3 g, 0.1 mol). The crude product was recrystallized from THF to give 7.6 g (25%) of **6b** as a white solid: mp 132—135 °C; ^{1}H NMR ($CDCl_3$) δ=0.69—2.13 (m, 16H), 2.14—3.03 (m, 10H), 2.86 (s, 5H), 3.04—3.47 (m, 2H); MS, *m/e* (relative intensity)

TABLE 3. CHARACTERIZATION OF DI- AND TRIAZA CROWN ETHERS

Crown ether	IR(neat) $\tilde{\nu}$/cm^{-1}	^{1}H NMR($CDCl_3$) δ	MS(70 eV), *m/e* (relative intensity)
8a	3330, 1110[a)]	2.47(s,2H), 2.75(t,8H), 3.48—3.76(m,12H)	217(M^+−1,1), 187(4), 173(6), 150(36), 132(100), 118(10)
8b	3320, 1110[a)]	2.21(s,2H), 2.76(t,8H), 3.32—3.85(m,16H)	261(M^+−1,1), 194(28), 176 (100), 100(31), 88(54)
8c	3320, 2930, 2880, 1460, 1350, 1120	2.45(s,2H), 2.78(t,8H), 3.49—3.92(m,20H)	305(M^+−1,2), 288(5), 275(9), 238(37), 220(100), 206(19)
8d	3320, 2970, 2890, 1465, 1355, 1130	0.93(t,6H), 1.22—1.61(m,4H), 2.34—2.97(m,6H), 2.81(s,2H), 3.46—3.80(m,12H)	274(M^+), 243(89), 160(76), 128 (17), 103(45), 84(100)
8e	3320, 2980, 2880, 1460, 1355, 1125	0.99—1.35(m,6H), 2.19—3.11 (m,8H), 2.41(s,2H), 3.43—3.39(m,10H)	246(M^+,3), 201(11), 146(76), 118(22), 100(74), 74(100)
8f	3360, 2920, 2880, 1460, 1355, 1110	2.57(s,2H), 2.70(t,8H), 3.48—3.80(m,20H)	305(M^+−1,2), 275(9), 238(25), 231(15), 187(13), 176(100)
15a	3310, 2910, 2875, 1460, 1355, 1130	2.33(s,2H), 2.62—2.91(m,8H), 3.41—3.90(m,12H)	218(M^+,2), 162(100), 118(21), 112(25), 100(36), 85(26)
15b	3310, 2920, 2880, 1460, 1360, 1120	2.57(s,2H), 2.68—2.95(m,8H), 3.44—3.84(m,16H)	262(M^+,1), 206(100), 162(9), 111(13), 100(23)
16a	3320, 2940, 2890, 1460, 1360, 1120	0.80—2.23(m,16H), 2.24—2.69 (m,2H), 2.47(s,2H), 2.75(s,4H), 2.86—3.28(m,2H), 3.32—4.04(m,8H)	325(M^+−1,3), 220(39), 216 (100), 198(5), 155(11), 111(63)
16b	3320, 2950, 2880, 1455, 1365, 1115	0.80—2.22(m,16H), 2.22—2.56 (m,2H), 2.71(s,4H), 2.73(s,2H), 2.90—3.31(m,2H), 3.32—3.99(m,12H)	369(M^+−1,5), 260(100), 220(38), 123(20), 111(35)
16c	3300, 2950, 2870, 1460, 1370, 1110	0.77—2.26(m,16H), 2.26—2.97 (m,10H), 2.75(s,3H), 2.97—3.31 (m,2H), 3.38—4.21(m,8H)	368(M^+−1,4), 325(100), 313(64), 247(86), 216(48), 110(58)
16d	3320, 2940, 2875 1460, 1360, 1120	0.73—2.16(m,16H), 2.22—3.00 (m,10H), 2.84(s,3H), 3.00—3.33 (m,2H), 3.34—3.95(m,12H)	412(M^+−1,4), 369(88), 357(61), 260(67), 171(92), 128(91), 110(91), 81(80), 44(100)

a) Nujol.

TABLE 4. ELEMENTAL ANALYSIS OF DI- AND TRIAZA CROWN ETHERS

Crown ether	Molecular formula	Found (Calcd) (%)		
		H	C	N
8a	$C_{10}H_{22}N_2O_3$	10.32(10.16)	54.65(55.02)	12.89(12.83)
8b	$C_{12}H_{26}N_2O_4$	10.26(9.99)	54.78(54.94)	10.76(10.68)
8c	$C_{14}H_{30}N_2O_5$	9.92(9.87)	54.78(54.88)	8.80(9.14)
8d	$C_{14}H_{30}N_2O_3$	11.13(11.02)	61.12(61.28)	10.32(10.21)
8e	$C_{12}H_{26}N_2O_3$	10.76(10.64)	58.70(58.51)	11.18(11.37)
8f	$C_{14}H_{30}N_2O_5$	9.65(9.87)	55.01(54.88)	8.97(9.14)
15a	$C_{10}H_{22}N_2O_3$	10.35(10.16)	55.14(55.02)	12.90(12.83)
15b	$C_{12}H_{26}N_2O_4$	10.15(9.99)	54.83(54.94)	10.45(10.68)
16a	$C_{18}H_{34}N_2O_3$	10.69(10.50)	65.84(66.22)	8.65(8.58)
16b	$C_{20}H_{38}N_2O_4$	10.53(10.34)	64.40(64.83)	7.62(7.56)
16c	$C_{20}H_{39}N_3O_3$	10.98(10.64)	64.65(65.00)	11.48(11.37)
16d	$C_{22}H_{43}N_3O_4$	10.78(10.48)	63.79(63.89)	9.88(10.16)

171(100), 159(31), 128(83), 98(21); IR (KBr) 3270, 2950, 2870, 1460, 1140 cm^{-1}. Found: C, 64.08; H, 11.08; N, 13.92. Calcd for $C_{16}H_{33}N_3O_2$: C, 64.18; H, 11.11; N, 14.03.

*1,4,10-Trioxa-7,13-diazacyclopentadecane (**8a**)* via *Intramolecular Cyclization.* *p*-Toluenesulfonyl chloride (3.81 g, 0.02 mol) dissolved in 20 ml of dioxane, was slowly added dropwise to a suspension of powdered sodium hydroxide (6.3 g, 0.15 mol) and 6,9-dioxa-3,12-diazatetradecane-1,14-diol (**3a**, 4.73 g, 0.02 mol) in 60 ml of dioxane over a period of 2 h at 60 °C. After the addition, the reaction was continued for 3 h and the reaction mixture filtered. The precipitate was washed with dichloromethane, and the solvent removed from the combined solution of filtrate and washings. Water (10 ml) was added to the residue and the solution extracted five time with dichloromethane. The solvent was removed from the dichloromethane extracts to give the crude product (3.51 g). In the ^1H NMR ($CDCl_3$) spectrum of it, resonances were observed at δ 1.16 and 1.72, which were ascribed to the aziridine ring protons. No resonances for *p*-toluenesulfonamides were observed. After the crude product was neutralized by hydrochloric acid, it was distilled in the presence of sodium carbonate (2.12 g, 0.02 mol) by Kugelrohr distillation at 75—90 °C (0.03 Torr) to give a white waxy solid (1.61 g, 37%). It was again distilled in a Kugelrohr apparatus at 80—85 °C (0.015 Torr) to afford 1.14 g (26%) of GLC-pure **8a** as a white solid: mp 91—93 °C (lit,[1] 89—90 °C). In the ^1H NMR of the product, resonances of aziridine ring protons were no longer observed, because aziridine derivatives were lost by further reaction during distillation. This procedure was typical for the preparation of diaza crown ethers (**8b—e**) by intramolecular cyclization, and **8d**, **e** were separated from the first distillation product by alumina column chromatography (acetone–hexane 50 : 50), and further purified by distillation. Characterization of **8** was accomplished by a standard method (Tables 1 and 3) and elemental analysis of **8** is shown in Table 4.

*1,4,7,13,16-Pentaoxa-10,19-diazacycloheneicosane (**8f**)* via *Intermolecular Cyclization.* 6,9-Dioxa-3,12-diazatetradecane-1,-14-diol (**3a**, 4.73 g, 0.02 mol) and potassium metal (1.72 g, 0.044 mol) were dissolved in *t*-butyl alcohol (160 ml), and diethylene glycol bis(*p*-toluenesulfonate) (**11a**, 8.29 g, 0.02 mol) in dioxane (60 ml) was added dropwise to the solution at 40 °C during 2 h. After the addition, the reaction was continued for 2 h, when the reaction mixture was filtered. The precipitate was washed with dichloromethane, and the solvent removed from the combined solution of filtrate and washings. Water (10 ml) was added to the residue and the solution was extracted twice with hexane to remove by-products. It was then extracted several times with dichloromethane. The hexane was removed from the extracts, and the main by-product was isolated from the residue by preparative GLC and identified as diethylene glycol di-*t*-butyl ether: ^1H NMR ($CDCl_3$) δ=1.19 (s, 18H), 3.47—3.71 (m, 8H). The dichloromethane extracts were combined, the solvent evaporated. The crude product (5.48 g) was purified two distillations in a Kugelrohr apparatus at 120—124 °C (0.005 Torr) to give GLC-pure **8f** (2.33 g, 38%) as a clear liquid. The tertiary amine number of the product was found to be almost negligible (11.5), but the total amine number (363.6) agreed well with the calculated number (366.2). Using a similar procedure, oligoaza crown ethers (**15** and **16**) were also obtained (Tables 2 and 3).

References

1) B. Dietrich, J. M. Lehn, and J. P. Sauvage, *Tetrahedron Lett.*, **1969**, 2885; *Tetrahedron*, **29**, 1629 (1973).
2) R. Wiest and R. Weiss, *J. Chem. Soc., Chem. Commun.*, **1973**, 678.
3) J. Fisher, M. Mellinger, and R. Weiss, *Inorg. Chim. Acta*, **21**, 256 (1977).
4) M. Johnson, I. O. Sutherland, and R. F. Newton, *J. Chem. Soc., Chem. Commun.*, **1979**, 309.
5) F.K.-Hibert, J. M. Lehn, and P. Vierling, *Tetrahedron Lett.*, **21**, 941 (1980).
6) J.-P. Kintzinger, F.K.-Hibert, J. M. Lehn, A. Pagelot, and K. Saigo, *J. Chem. Soc., Chem. Commun.*, **1981**, 833.
7) N. F. Jones, A. Kumar, and I. O. Sutherland, *J. Chem. Soc., Chem. Commun.*, **1981**, 990.
8) M. J. Calverley and J. Dale, *J. Chem. Soc., Chem. Commun.*, **1981**, 1084.
9) S. Bormann, J. Brossas, E. Franta, and P. Gramain, *Tetrahedron*, **31**, 2791 (1975).
10) E. Blasius and P.-G. Maurer, *Makromol. Chem.*, **178**, 649 (1977).
11) Ph. Gramain and Y. Frere, *Macromolecules*, **12**, 1038 (1979); *Ind. Eng. Chem., Prod. Res. Dev.*, **20**, 524 (1981).
12) I. Cho, S.-K. Chang, *Makromol. Chem., Rapid Commun.*, **2**, 155 (1981).
13) G. Manecke and P. Reuter, *Makromol. Chem.*, **182**, 1972 (1981).
14) D. J. Chadwick, I. A. Cliffe, and I. O. Sutherland, *J. Chem. Soc., Chem. Commun.*, **1981**, 992.
15) J. E. Richman, T. J. Atkins, *J. Am. Chem. Soc.*, **96**, 2268 (1974).
16) E. Buhleier, W. Rasshofer, W. Wehner, F. Luppertz, and F. Vögtle, *Justus Liebigs Ann. Chem.*, **1977**, 1344.
17) W. Rasshofer and F. Vögtle, *Justus Liebigs Ann. Chem.*, **1978**, 552.
18) A. P. King and C. G. Krespan, *J. Org. Chem.*, **39**, 1315 (1974).
19) J. C. Lockhart, A. C. Robson, and M. E. Thompson, *J. Chem. Soc., Perkin Trans. 1*, **1973**, 577.
20) S. Kulstad and L. A. Malmsten, *Acta Chem. Scand., Ser. B*, **33**, 469 (1979); *Tetrahedron*, **36**, 521 (1980).
21) C. G. Krespan, *J. Org. Chem.*, **40**, 1205 (1975).
22) M. Tomoi, O. Abe, M. Ikeda, K. Kihara, and H. Kakiuchi, *Tetrahedron Lett.*, **1978**, 3031.
23) H. Maeda, Y. Nakatsuji, and M. Okahara, *J. Chem. Soc., Chem. Commun.*, **1981**, 471.
24) H. Maeda, S. Furuyoshi, Y. Nakatsuji, and M. Okahara *Bull. Chem. Soc. Jpn.*, **56**, 212 (1983).
25) H. Maeda, T. Kikui, Y. Nakatsuji, and M. Okahara, *J. Org. Chem.*, **47**, 5167 (1982).
26) I. Ikeda, S. Yamamura, Y. Nakatsuji, and M. Okahara, *J. Org. Chem.*, **45**, 5355 (1980); P.-L. Kuo, N. Kawamura, M. Miki, and M. Okahara, *Bull. Chem. Soc. Jpn.*, **53**, 1689 (1980).
27) P. Veeravagu, R. T. Arnold, and E. W. Eigenman, *J. Am. Chem. Soc.*, **86**, 3072 (1964).
28) H. K. Frensdorff, *J. Am. Chem. Soc.*, **93**, 600 (1971).
29) D. E. Terry, K. R. Eilar, and O. A. Moe, *Anal. Chem.*, **24**, 313 (1952).
30) C. D. Wagner, R. H. Brown, and E. D. Peters, *Anal. Chem.*, **19**, 2609 (1947).
31) J. Dale and P. O. Kristiansen, *Acta Chem. Scand.*, **26**, 1471 (1972).

Regiocontrolled Formation of 4,5-Dihydro-3(2*H*)-furanones from 2-Butyne-1,4-diol Derivatives. Synthesis of Bullatenone and Geiparvarin

Hiroyuki Saimoto, Tamejiro Hiyama,*† and Hitosi Nozaki
Department of Industrial Chemistry, Kyoto University, Yoshida, Sakyo-ku, Kyoto 606
(Received March 23, 1983)

Two new methods for selective hydration of 1,1,4-trisubstituted 2-butyne-1,4-diols (**1**) to give 4,5-dihydro-3(2*H*)-furanone derivatives are reported. The first involves selective monoacetylation of the less hindered hydroxyl group of **1** followed by Ag(I)-catalyzed rearrangement and cyclization to give 3-acetoxy-2,2,5-trisubstituted 2,5-dihydrofurans (**2**). Final hydrolysis yielded 2,2,5-trisubstituted 4,5-dihydro-3(2*H*)-furanones. Oxidation of the enol acetates **2** with 2,3-dichloro-5,6-dicyano-1,4-benzoquinone gave 3(2*H*)-furanones. The new method was applied to the synthesis of naturally occurring 3(2*H*)-furanones such as bullatenone and geiparvarin from the corresponding 2-butyne-1,4-diol derivatives. The second approach is concerned with the synthesis of the opposite regioisomer, 2,5,5-trisubstituted 4,5-dihydro-3(2*H*)-furanones, from diols **1** with a polymer reagent Hg/Nafion-H.

In extension of our efforts in regio- and stereoselective cyclopentannulation starting with 2-butyne-1,4-diol derivatives,[1] we have found that the acetylenic diols provide excellent means of regiocontrolled construction of 3(2*H*)-furanone skeleton.[2] Compounds of this type are important in view of their distribution in nature,[3] cytotoxic and antitumor actions,[4] and versatility as synthetic intermediates[5,6] in the synthesis of muscarine alkaloids,[7] for example. The furanones are valued by perfumers,[8] pharmacologists,[7] and the food and beverage industries.[9] The 3-hydroxyfurans have been investigated with theoretical interest[10] in keto-enol tautomerism. Among the methods for the construction of the 3(2*H*)-furanone ring, the transformation of 2-butyne-1,4-diol derivatives into 4,5-dihydro-3(2*H*)-furanones is most promising in a practical sense because of the simple synthetic pathway.[11] Though well-established for symmetrical 2-butyne-1,4-diols, this process has not been used for the synthesis of furanone derivatives in general, due mainly to the lack of the regiocontrol in the hydration of the carbon-carbon triple bond.[12,13] Many naturally occurring 3-furanones possess the 2,2,5-trisubstituted 3(2*H*)-furanone ring-system,[3] which is not readily accessible by previous methods.[11,12] Selective hydration at the position *a* (or *b*) in the formula **1** is, therefore, important in respect of regiocontrolled construction of the 3(2*H*)-furanone skeleton.

We have found that introduction of an oxygen function at the position *a* of the triple bond of **1** to give **3** is achieved by method A (Scheme 1) with complete regioselectivity. This involves selective monoacetylation of unsymmetrical 2-butyne-1,4-diols **1** followed by Ag(I)-catalyzed cyclization with acetoxyl migration to give enol acetates **2**, whose hydrolysis yields 2,2,5-trisubstituted 4,5-dihydro-3(2*H*)-furanones (**3**). In contrast, the opposite regioisomer **4** of the dihydrofuranones was prepared directly from the diol **1** by treatment with a polymer reagent Hg/Nafion-H[14] (method B). Details are reported herein.[15]

*Transformation of Diols **1** into 4,5-Dihydro-3(2H)-furanones of Type **3** (Method A).* Unsymmetrically substituted 2-butyne-1,4-diols (**1**) were prepared from corresponding carbonyl compounds and propargyl alcohol derivatives. Treatment of **1** with acetic anhydride and pyridine at 25 °C resulted in acetylation of the less hindered hydroxyl group. The intermediates **1** were not necessarily isolated and were subjected directly to the monoacetylation; especially effective for **6f** and **6g**.

The monoacetates **6** were then treated with 5 mol% of silver perchlorate (or silver tetrafluoroborate) in refluxing benzene in the dark to give the enol acetates **2**[16] in good yields. Results are summarized in Table 1. The transformation can be explained by assuming Ag(I)-catalyzed isomerization[17] of the monoacetates **6** to allenyl acetates **7** followed by Ag(I)-assisted cyclization[18] (Scheme 2). The selective introduction of an

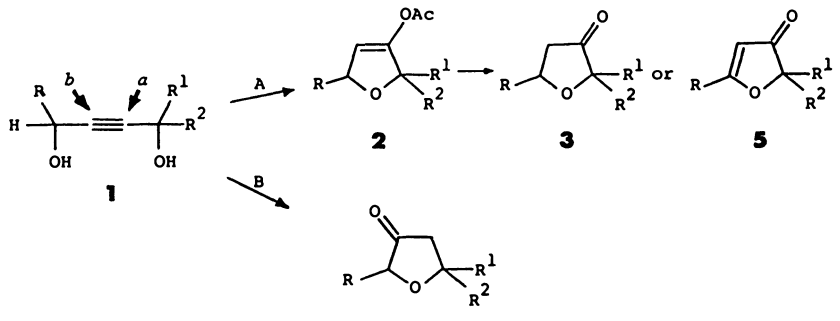

Scheme 1.

† Present address: Sagami Chemical Research Center, 4-4-1, Nishiohnuma, Sagamihara, Kanagawa 229.

Table 1. Ag(I)-Catalyzed synthesis of dihydro-3(2*H*)-furanone enol acetates 2[a)]

2-Butyne-1,4-diol derivative **1**	Yield[b)]/% of monoacetate **6**	Yield[b)]/% of dihydro-3(2*H*)-furanone enol acetate **2**
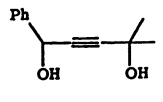 **1a**	99	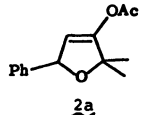 **2a** 83
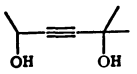 **1b**	>99	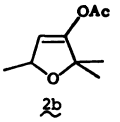 **2b** 99
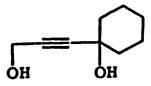 **1c**	>99	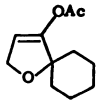 **2c** 63[c)]
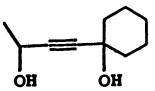 **1d**	>99	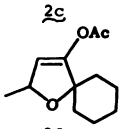 **2d** 80
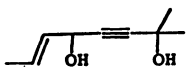 **1e**	90	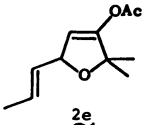 **2e** 74
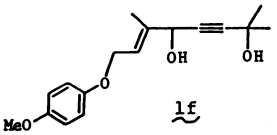 **1f**	81[d)]	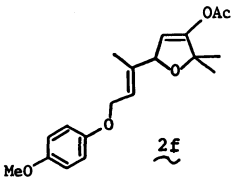 **2f** 63
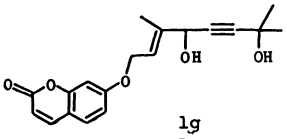 **1g**	86[d)]	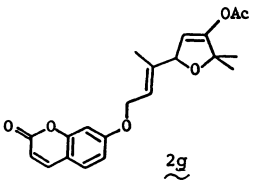 **2g** 61[d)]

a) The monoacetates **6** were treated with 5 mol% of silver perchlorate. b) Isolated yields. c) Silver tetrafluoroborate (10 mol%) was used. d) Overall yields from the corresponding aldehyde and 2-methyl-3-butyn-2-ol. e) Silver perchlorate (15 mol%) was employed.

oxygen function at the position *a* is now achieved by this Ag(I)-mediated intramolecular rearrangement. Although this reaction was monitored very carefully, the allenyl acetates **7** were never isolated. It is worthy to note that the carbon-carbon double bond in the substrate **1** was not affected (Table 1, compounds **2e**, **2f**, and **2g**) and the olefinic configuration was completely retained through the reaction.

Finally, the enol acetate **2** was converted into the 4,5-dihydro-3(2*H*)-furanone **3** by treatment with sodium methoxide in methanol at r.t. (Scheme 3).

Oxidation of the Enol Acetates 2 to 3(2H)-Furanones 5. Application to a Practical Synthesis of Bullatenone (5a) and Geiparvarin (5g). The attempted transformation of **2** into the corresponding 3(2*H*)-furanones **5** involves the bromination dehydrobromination process (Scheme 3). Molecular bromine was allowed to react with the enol acetates **2** and the resulting bromodihydrofuranones **8** were treated with Li_2CO_3 (and LiCl) in *N*,*N*-dimethylformamide (DMF) or hexamethylphosphoric triamide (HMPA) to give **5**. Although this transformation was effective for **5a** and **5e**, the yield of **5f** was disappointedly low.

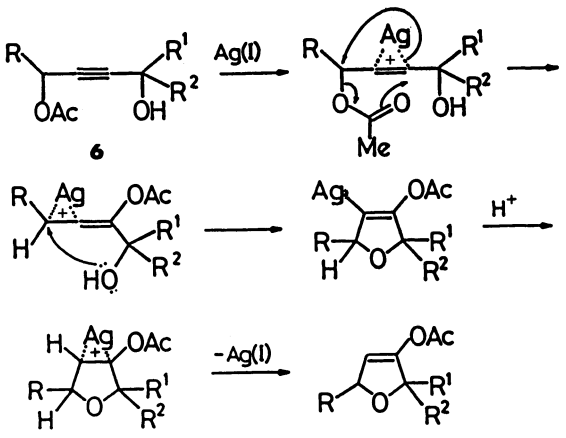

Scheme 2.

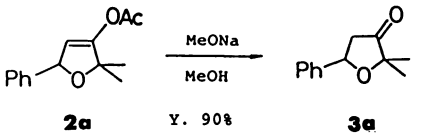

Scheme 3.

The use of 2,3-dichloro-5,6-dicyano-1,4-benzoquinone (DDQ) very much improved the oxidation step. Treatment of **2** with DDQ in benzene at 25 °C for several hours afforded **5** quantitatively (Table 2). The present transformation of the diols **1** into 3-furanones of type **3** and **5** should hold considerable promise as a general synthetic method.

Thus, the combined process allowed us to synthesize bullatenone (**5a**),[19)] a naturally occurring 3(2*H*)-

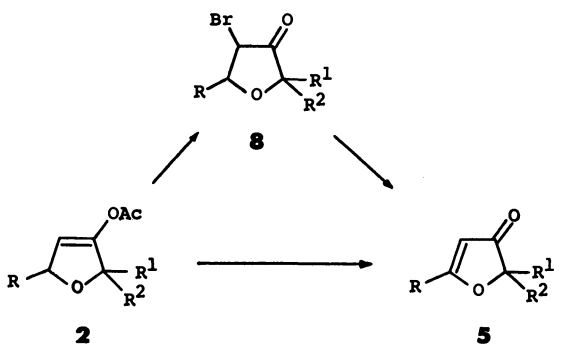

Scheme 4.

Table 2. Isolated yields (%) of 3(2*H*)-furanones **5**

Enol acetate **2**	3(2*H*)-Furanone **5**	Oxidation with DDQ[a]	Bromination and dehydromination[b]
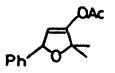 **2a**	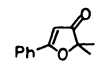 bullatenone **5a**	99	85
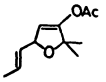 **2e**	**5e**	>99	66
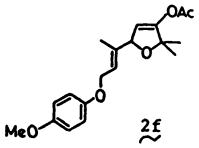 **2f**	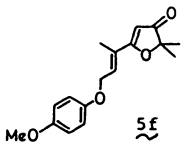 **5f**	>99	46
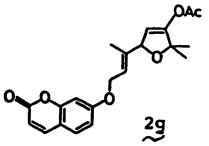 **2g**	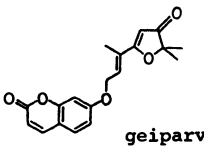 geiparvarin **5g**	>99	

a) The enol acetates were treated with DDQ (1.2—1.9 equiv). b) See the experimental part for each transformation.

furanone isolated from blistered leaf myrtle (*Myrtus bllata*),[3b] a shrub endemic to New Zealand, in 81% overall yield from benzaldehyde. The dilithium salt of 2-methyl-3-butyn-2-ol was allowed to react with benzaldehyde in THF to give 4-methyl-1-phenyl-2-pentyne-1,4-diol (**1a**) (98% yield). The adduct **1a** was converted into the monoacetate **6a** (99% yield) which was then subjected to Ag(I)-catalyzed rearrangement and cyclization to yield the enol acetate **2a** (84% yield); finally oxidation of **2a** with DDQ afforded bullatenone **5a** in a quantitative yield.

Similarly, an antitumor 3(2*H*)-furanone, geiparvarin (**5g**)[3e-h] isolated from *Geijera parviflora*, was stereospecifically synthesized from (*E*)-4-(2-oxo-2*H*-chromen-7-yloxy)-2-methyl-2-butenal (**9**)[20] in 52% overall yield. Treatment of **9** with 2-methyl-3-butyn-2-ol dianion followed by acetylation gave the corresponding monoacetate **6g** (86% overall yield). The monoacetate **6g** was then treated with 15 mol% of silver perchlorate in refluxing benzene, giving rise to **2g** (61% yield), whose oxidation with DDQ yielded geiparvarin (**5g**) quantitatively. The spectral data (IR, ^{1}H-NMR) and mp were identical with those of the natural product.[3d-f] The absence of the (*Z*) isomer[9a,b] in the reaction product was ascertained by the ^{1}H-NMR spectra.

Hg/Nafion-H Catalyzed Transformation of Acetylenic Diols ***1*** *into 4,5-Dihydro-3(2*H*)-furanones of Type* ***4*** *(Method B).* In order to introduce an oxygen function at the position *b* in the formula **1** to obtain **4**, diols **1** were treated with the polymer reagent Hg/Nafion-H in the presence of 5 equiv of water in ethanol at 25 °C for several hours; results are summarized in Table 3. Apparently, introduction of the oxygen function into **1** takes place at the acetylenic carbon of less steric hindrance.[21] Although the selectivity in **1a**, **1b**, and **1d** (secondary *vs.* tertiary hydroxyl) was moderate (4 : 1 to 1 : 1), the preference of the primary hydroxyl group over the tertiary one was excellent. This is exemplified in the reaction of **1c** and **1i—n**.

In order to gain an insight into the reaction mechanism, the propargyl alcohol adducts of 2-methylcyclohexanone were prepared. Cyclization of the 3 : 2 mixture of the diastereomers[1] **1j** and **1j'** gave the dihydro-3(2*H*)-furanones **4j** and **4j'** as a 40 : 60 diastereomeric mixture. The separately isolated **1j** or **1j'** also produced a 48 : 52 or 45 : 55 mixture of **4j** and **4j'**; the ratio being very similar irrespective of the stereochemistry of the diol (**1j** or **1j'**). The hypothetical mechanism of Scheme 5 explains the results. The Hg(II)-catalyzed hydration and elimination of the hydroxyl group lead to **10** and/or **11** and final cyclization produces the desired dihydro-3(2*H*)-furanones **4**.

Although the Hg/Nafion-H catalyzed formation of **4** is extremely efficient, a side reaction sometimes competes with the transformation of **1m**[22] into **4m** particularly.

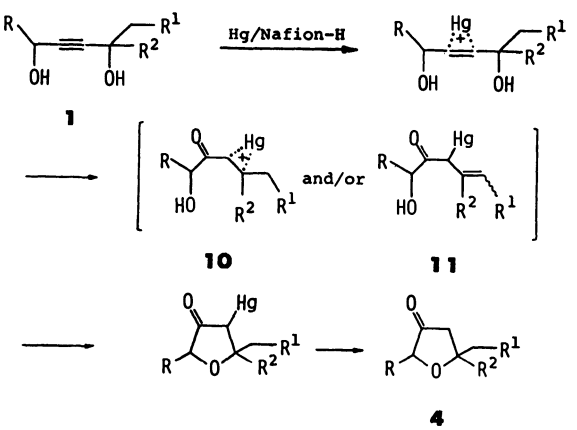

Scheme 5.

TABLE 3. Hg/NAFION-H CATALYZED DIHYDRO-3(2*H*)-FURANONE SYNTHESIS

Entry	Diol	Yield/% of dihydro-3(2*H*)-furanone[a]		3 : 4	Entry	Diol	Yield/% of dih-ydro-3(2*H*)-furanone[a]	
1	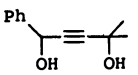 **1a**	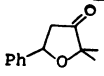 **3a**	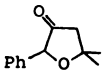 **4a**	70[b]	1 : 4	10	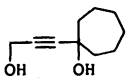 **1k**	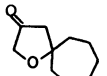 **4k**	62[d]
2	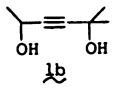 **1b**	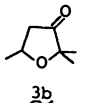 **3b**	**4b**	80	1 : 2	11	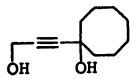 **1l**	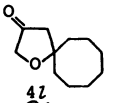 **4l**	50[e]
3	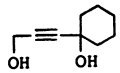 **1c**		**4c**	62		12	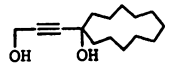 **1m**	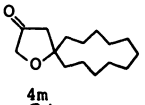 **4m**	68[f]
4	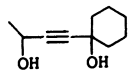 **1d**	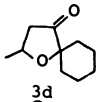 **3d**	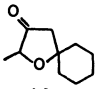 **4d**	70	1 : 1–2	13	**1m**	**4m**	66[g]
						14	**1m**	**4m**	58[h]
5	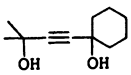 **1h**	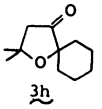 **3h**	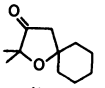 **4h**	95	1 : 2	15	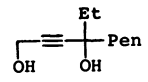 **1n**	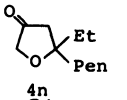 **4n**	59[i]
6	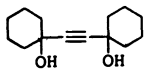 **1i**		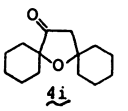 **4i**	90		16	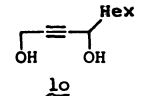 **1o**	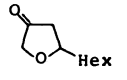 **4o**	43[j]
7	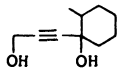 **1j** + **1j'**	**4j** + **4j'**		78	40 : 60[c]	17	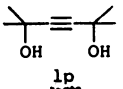 **1p**	**4p**	90[k]
8	**1j**	**4j** + **4j'**		63	48 : 52[c]				
9	**1j'**	**4j** + **4j'**		82	45 : 55[c]				

a) Isolated yields refer to fully characterized compounds produced from the diols **1** on treatment with Hg/Nafion-H. b) (*E*)-4-Hydroxy-4-methyl-1-phenyl-1-penten-3-one (**12a**) was produced (11% yield) as a by-product. c) The diastereomeric ratio of **4j** to **4j'**. d) The transformation was carried out at 60 °C in a 1 : 1 mixture of hexane–ethanol. 3-Cycloheptylidene-1-hydroxy-2-propanone (**12k**) was produced (13% yield) along with **4k**. e) A by-product, 3-cyclooctylidene-1-hydroxy-2-propanone (**12l**) was formed in 23% yield. f) 3-Cyclododecylidene 1-hydroxy-2-propanone (**12m**) was produced (10% yield) along with **4m**. g) The reaction was carried out at 50 °C, **12m** being produced in 3% yield. h) The transformation was carried out at 0—10 °C. The yield of **12m** was 22% i) 4-Ethyl-1-hydroxy-3-nonen-2-one (**12n**) was formed(30% yield) as a by-product. *j*) 1-Ethoxy-4-hydroxy-3-decanone (**12o**) was produced (15% yield) along with **4o**. k) Using the recoverd polymer regent, **1p** was converted into **4p** in 82% yield.

A by-product, 3-cyclododecylidene-1-hydroxy-2-propanone (**12m**), was produced in 10% yield which was slowly converted into **4m** under the reaction conditions. Formation of **12m** was temperature-dependent; at 50 °C only 3%; at 0—10 °C as much as 22% yield, whereas the yield of **4m** remained almost constant. In any event, the procedure is applicable to the synthesis of dihydrofuranones of type **4**.

As is usual with polymer reagent, the experimental procedure for Hg/Nafion-H mediated transformation is very simple. Workup involves only removal of the catalyst by filtration and concentration of the filtrates. The polymer reagent could be recovered easily by washing with dichloromethane and drying, and reused: For example, the diol **1p** was converted into **4p** repeatedly (first run, 90% yield, and second run with the recovered reagent, 82% yield). The present Hg/Nafion-H catalyzed transformation proceeded under milder conditions (25 °C) with higher selectivity than the previous methods.[11,12] Whereas the diol **1b** gives a 1 : 1 mixture of 3-furanones **3b** and **4b** with a conventional catalyst, HgO,[12d] in ether-aqueous sulfuric acid, the transformation with Hg/Nafion-H preferred **4b** formation (**3b** : **4b** 1 : 2).

Experimental

Distillation was carried out by use of Kugelrohr (Büchi) and boiling points were determined by measuring the bath temperature. All mp and bp are not corrected. ^{1}H-NMR spectra (tetramethylsilane as an internal standard) were obtained on a Varian EM 390 spectrometer, chemical shifts being given in ppm units, IR spectra of neat liquid film samples (unless otherwise noted) on a Shimadzu IR-27G spectrometer, MS on a Hitachi RMU-6L spectrometer, and exact mass on a Hitachi M 80 spectrometer. Gas-liquid phase chromatography (GLC) analyses were performed with a Yanagimoto

GCG-550F chromatograph, and preparative GLC with a JEOL-JGC-20K chromatograph. Preparative TLC plates (20 cm×20 cm) were prepared with Merck Kiesel-gel PF_{254}. Column chromatography was carried out with silica gel (Wakogel C-100) at atmospheric pressure. Propargyl alcohol and 2-methyl-3-butyn-2-ol were distilled before use. 3-Butyn-2-ol (Tokyo Kasei-Kogyo Co. or Nakarai Chemicals Ltd., 55% aqueous solution) was used.

*Preparation of 4-Methyl-1-phenyl-2-pentyne-1,4-diol (**1a**) (A Typical Procedure).* A hexane solution of butyllithium (1.53 M,† 19.6 ml, 30.0 mmol) was added at −78 °C under an argon atmosphere to a THF (150 ml) solution of 2-methyl-3-butyn-2-ol (1.26 g, 15.0 mmol). The reaction mixture was stirred for 2 h at −78 °C. To this solution a THF (4 ml) solution of benzaldehyde (1.06 g, 10.0 mmol) was added at −65 °C. The whole was stirred for 6 h and allowed to warm to 25 °C. The resulting solution was then poured into water (50 ml) and extracted with ethyl acetate. The extracts were dried with anhydrous sodium sulfate and concentrated to yield a crude product. Purification of the residue by column chromatography (hexane–ethyl acetate 1 : 1) gave the diol **1a**[19a] (1.87 g, 98% yield) having ^{1}H-NMR (CCl_4): δ=1.43 (s, 6H), 4.13 (br s, 1H), 5.34 (s, 1H), 7.1—7.6 (m, 5H); IR (CCl_4): 3330, 1162, 942 cm^{-1}; MS: *m/e* 190 (M^+).

In general, experiments of no less than 10 mmol scale are preferable in order to secure high yields of the adducts **1**. This procedure applies to the synthesis of **1b**, **1c**, **1e**, **1h**, **1i**, **1k**, **1l**, **1n**, and **1o**. The yields and spectral properties are summarized below.

*2-Methyl-3-hexyne-2,5-diol (**1b**).*[23] Yield 95%. Bp 132—140 °C (bath temp)/3.0 Torr;** ^{1}H-NMR (CCl_4): δ=1.41 (d, J=6.8 Hz, 3H), 1.49 (s, 6H), 4.4—4.7 (m, 3H); IR: 3320, 1165 cm^{-1}; MS: *m/e* 113 (M^+-CH_3).

*1-(3-Hydroxy-1-propynyl)cyclohexanol (**1c**).*[24] Yield 88%. ^{1}H-NMR (CCl_4): δ=1.0—2.2 (m, 10H), 4.33 (s, 2H), 4.56 (br s, 2H); IR: 3330, 1073 cm^{-1}; MS: *m/e* 154 (M^+).

*2-Methyl-6-octen-3-yne-2,5-diol (**1e**).*[25] Yield 90%. ^{1}H-NMR (CCl_4): δ=1.49 (s, 6H), 1.74 (d, J=6.0 Hz, 3H), 4.28 br s, 2H), 4.79 (d, J=5.3 Hz, 1H), 5.57 (dd, J=15.2, 5.3 Hz, 1H), 5.78 (dq, J=15.2, 6.0 Hz, 1H); IR: 3340, 1164, 963, 944 cm^{-1}; MS: *m/e* 139 (M^+-CH_3).

*1-(3-Hydroxy-3-methyl-1-butynyl)cyclohexanol (**1h**).*[5a,26] Yield 84%. Mp 95.0—96.0 °C (methanol); ^{1}H-NMR (CCl_4): δ=1.0—2.1 (m+s (δ=1.53), 16H), 4.10 (br s, 2H); IR (Nujol): 3250, 1460, 1080, 950 cm^{-1}; MS: *m/e* 182 (M^+).

*Bis(1-hydroxycyclohexyl)acetylene (**1i**).*[27] This product was prepared from cyclohexanone and 1-ethynylcyclohexanol (51% yield, 99% yield based on consumed 1-ethynylcyclohexanol). ^{1}H-NMR ($CDCl_3$): δ=0.9—2.2 (m, 20H), 2.27 (br s, 2H); IR (Nujol): 3350, 1070 cm^{-1}; MS: *m/e* 222 (M^+).

*1-(3-Hydroxy-1-propynyl)cycloheptanol (**1k**).* Yield 79%. Bp 131—132 °C (bath temp)/0.15 Torr; ^{1}H-NMR (CCl_4): δ=1.2—2.2 (m, 12H), 4.27 (br s, 2H), 4.37 (s, 2H); IR: 3340, 1461, 1445, 1026 cm^{-1}; MS: *m/e* (rel intensity) 168 (M^+, 4), 150(11), 111(71), 65(75), 55(100), 40(93). Found: C, 71.15; H, 9.80%. Calcd for $C_{10}H_{16}O_2$: C, 71.39; H, 9.59%.

*1-(3-Hydroxy-1-propynyl)cyclooctanol (**1l**).* Yield 54%. Bp 153—154 °C (bath temp)/0.10 Torr; ^{1}H-NMR ($CDCl_4$): δ=1.1—2.1 (m, 14H), 4.26 (s, 2H), 4.46 (br s, 2H); IR: 3340, 1447, 1040, 1014 cm^{-1}; MS: *m/e* (rel intensity) 182 (M^+, trace), 164(7), 111(46), 93(48), 79(50), 65(57), 55(100), 41(99). Found: *m/e* 164.1226. Calcd for $C_{11}H_{16}O$: M^+-H_2O, 164.1201

*4-Ethyl-2-nonyne-1,4-diol (**1n**).* Yield 81%. Bp 109—110 °C (bath temp)/0.13 Torr; ^{1}H-NMR (CCl_4): δ=0.9—2.0 (m+t (δ=0.97, J=6.6 Hz)+t (δ=1.01, J=7.5 Hz), 16H), 3.30 (br s, 1H), 3.55 (br s, 1H), 4.26 (s, 2H); IR: 3350, 1465, 1011 cm^{-1}; MS: *m/e* (rel intensity) 155 ($M^+-C_2H_5$, 37), 113 (100), 67 (89), 43 (82). Found: C, 71.67; H, 11.13%. Calcd for $C_{11}H_{20}O_2$: C, 71.70; H, 10.94%.

*2-Decyne-1,4-diol (**1o**).*[28] Yield 77%. ^{1}H-NMR (CCl_4): δ=0.7—1.9 (m, 13H), 4.1—4.8 (m, 5H); IR: 3310, 1017 cm^{-1}; MS: *m/e* 170 (M^+).

*1-(3-Hydroxy-1-butynyl)cyclohexanol (**1d**).* Potassium hydroxide (3.36 g, 60.0 mmol) was dissolved in a 55% aqueous solution of 3-butyn-2-ol (2.86 g, 22.5 mmol) and the resulting mixture was stirred at 40 °C for 10 min. To this solution cyclohexanone (1.47 g, 15.0 mmol) dissolved in THF (3 ml) was added drop by drop during 2 h at 25 °C. The whole was stirred for 26 h at 40 °C, then diluted with ether (20 ml) and cold water (10 ml). Extractive workup with ether gave an oil (3.05 g). Purification of the crude adduct by column chromatography (hexane-ethyl acetate 2 : 1 to 1 : 1) afforded the diol **1d**[23] (2.27 g, 90% yield). ^{1}H-NMR (CCl_4): δ=1.0—2.1 (m+d (δ=1.43, J=6.9 Hz), 13H), 4.01 (br s, 2H), 4.53 (q, J=6.9 Hz, 1H); IR: 3330, 1072 cm^{-1}; MS: *m/e* 168 (M^+).

*Transformation of the Diols **1** into the Enol Acetates **2**.*

*Preparation of 3-Acetoxy-2,2-dimethyl-5-phenyl-2,5-dihydrofuran (**2a**) (A Typical Procedure):* A dichloromethane (0.25 ml) solution of **1a** (0.21 g, 1.1 mmol) was treated with acetic anhydride (0.5 ml) and pyridine (0.05 ml) at 25 °C. As soon as the starting diol was consumed (1.5 h), all the volatile materials were evaporated. Purification of the residue by column chromatography (hexane–ethyl acetate 10 : 1 to 2 : 1) gave 5-acetoxy-2-methyl-5-phenyl-3-pentyn-2-ol (**6a**) (0.25 g, 99% yield) having ^{1}H-NMR (CCl_4): δ=1.51 (s, 6H), 2.03 (s, 3H), 2.96 (br s, 1H), 6.41 (s, 1H), 7.2—7.6 (m, 5H); IR: 3400, 1740, 1220 cm^{-1}; MS: *m/e* (rel intensity) 232 (M^+, trace), 190 (4), 189(4), 172(33), 129(31), 43(100).

A benzene (1 ml) solution of **6a** (77 mg, 0.33 mmol) was heated at 80 °C in the presence of silver perchlorate (4 mg, *ca.* 5 mol%) for 10 h in the dark under an argon atmosphere. The reaction mixture was then diluted with dichloromethane (10 ml) at 25 °C and washed with 10% aqueous ammonia (3 ml) and sat. aqueous sodium chloride solution (3 ml). Concentration of the organic phase gave the crude product which was purified by column chromatography (hexane–ethyl acetate 10 : 1) to afford **2a** (65 mg, 84% yield). Bp 122—124 °C (bath temp)/ 0.04 Torr; ^{1}H-NMR (CCl_4): δ=1.36 (s, 3H), 1.38 (s, 3H), 2.17 (s, 3H), 5.70 (d, J=1.5 Hz, 1H), 5.81 (d, J=1.5 Hz, 1H), 7.26 (br s, 5H); IR: 1781, 1698, 1658, 1207, 1193, 1050 cm^{-1}; MS: *m/e* (rel intensity) 232 (M^+, 2), 217(2), 190(34), 189(19), 105(41), 102(27), 77(32), 43(100). Found: C, 72.48; H, 6.84%. Calcd for $C_{14}H_{16}O_3$: C, 72.39; H, 6.94%.

This procedure applies to the synthesis of **6b—e**, **2b**, and **2d—g**, whose physical properties are summarized below.

*5-Acetoxy-2-methyl-3-hexyn-2-ol (**6b**) and 3-Acetoxy-2,2,5-trimethyl-2,5-dihydrofuran (**2b**):* The monoacetate **6b** showed ^{1}H-NMR (CCl_4): δ=1.43 (d, J=6.8 Hz, 3H), 1.44 (s, 6H), 2.01 (s, 3H), 2.66 (br s, 1H), 5.33 (q, J=6.8 Hz, 1H); IR: 3425, 1740, 1230 cm^{-1}; MS: *m/e* (rel intensity) 196 (M^+, trace), 144(3), 118(7), 99(20), 84(39), 56 (28), 43(100). The Bp of **2b**: 101—102 °C (bath temp)/18 Torr; ^{1}H-NMR (CCl_4): δ=1.22 (s, 3H), 1.23 (d, J=6.0 Hz, 3H), 1.27 (s, 3H), 2.14 (s, 3H), 4.83 (dq, J=1.7, 6.0 Hz, 1H), 5.66 (d, J=1.7 Hz, 1H); IR: 1782, 1760, 1660, 1204, 1033 cm^{-1}; MS: *m/e* (rel intensity) 170 (M^+, trace), 155(6), 128(9), 126(13), 113(30), 68(23), 43(1000). Found: C, 63.62; H, 8.46%. Calcd for $C_9H_{14}O_3$: C, 63.51; H, 8.29%.

*1-(3-Acetoxy-1-propynyl)cyclohexanol (**6c**) and 4-Acetoxy-1-oxaspiro[4.5]dec-3-ene (**2c**):* ^{1}H-NMR (CCl_4) of **6c**: δ=1.0—2.0 (m, 10H), 2.06 (s, 3H), 2.30 (br s, 1H), 4.64 (s, 2H); IR:

† 1 M=1 mol dm^{-3}.

** 1 Torr=133.322 Pa.

3420, 1747, 1229 cm^{-1}; MS: *m/e* (rel intensity) 196 (M^+, 1), 154(19), 153(22), 139(48), 111(52), 43(100). Silver tetrafluoroborate (10 mol%) was used instead of silver perchlorate for the transformation of **6c** into **2c** having bp 122—125 °C (bath temp)/0.04 Torr; ^{1}H-NMR (CCl_4): δ=1.4—1.9 (m, 10H), 2.13 (s, 3H), 4.54 (d, J=1.7 Hz, 5.73 (t, J=1.7 Hz, 1H); IR: 1780, 1757 (sh), 1658, 1194 cm^{-1}; MS: *m/e* (rel intensity) 196 (M^+, 3), 168(8), 153(12), 111(28). 97(17), 81(12), 69(13), 55(27), 43(100). Found: C, 67.60; H, 8.33%. Calcd for $C_{11}H_{16}O_3$: C, 67.32; H, 8.22%.

*1-(3-Acetoxy-1-butynyl)cyclohexanol (**6d**) and 4-Acetoxy-2-methyl-1-oxaspiro[4.5]dec-3-ene (**2d**)*: The monoacetate **6d** showed ^{1}H-NMR (CCl_4): δ=1.1—2.0 (m+d (δ=1.45, J=6.9 Hz), 14H), 2.03 (s, 3H), 5.41 (q, J=6.9 Hz, 1H); IR: 3425, 1740, 1235 cm^{-1}; MS: *m/e* (rel intensity) 168 ($M^+-C_2H_2O$, 15), 107(30), 80(58), 43(100). The bp of **2d**: 92 °C (bath temp)/0.05 Torr; ^{1}H-NMR (CCl_4): δ=1.22 (d, J=6.3 Hz, 3H), 1.2—1.9 (m, 10H), 2.10 (s, 3H), 4.73 (dq, J=1.5, 6.3 Hz, 1H), 5.60 (d, J=1.5 Hz, 1H); IR: 1784, 1758, 1659, 1198 cm^{-1}; MS: *m/e* (rel intensity) 210 (M^+, 4), 168(16), 153(24), 125(42), 111(51), 69(22), 55(25), 43(100). Found: C, 68.37;H, 8.87%. Calcd for $C_{12}H_{18}O_3$: C, 68.54; H, 8.63%.

*5-Acetoxy-2-methyl-6-octen-3-yn-2-ol (**6e**) and 3-Acetoxy-2,2-dimethyl-5-[(E)-1-propenyl]-2,5-dihydrofuran (**2e**)*: ^{1}H-NMR (CCl_4) of **6e**: δ=1.48 (s, 6H), 1.77 (d, J=6.8 Hz, 3H), 2.04 (s, 3H), 2.17 (br s, 1H), 5.66 (dd, J=15.3, 6.5 Hz, 1H), 5.84 (d, J=6.5 Hz, 1H), 6.03 (dq, J=15.3, 6.8 Hz, 1H); IR: 3430, 1738, 1224 cm^{-1}; MS: *m/e* (rel intensity) 196 (M^+, trace), 136(39), 121(47), 77(45), 43(100). The enol acetate **2e** showed bp 117—118 °C (bath temp)/0.04 Torr; ^{1}H-NMR (CCl_4): δ=1.25 (s, 3H), 1.28 (s, 3H), 1.69 (d, J=5.3 Hz, 3H), 2.14 (s, 3H), 5.02 (dd, J=1.5, 5.9 Hz, 1H), 5.52 (dd, J=5.9, 15.0 Hz, 1H), 5.61 (d, J=1.5 Hz, 1H), 5.62 (dq, J=15.0, 5.3 Hz, 1H); IR: 1781, 1761 (sh), 1656, 1200, 1041, 963 cm^{-1}; MS: *m/e* (rel intensity) 154 (M^+, 30), 139(42), 113(12), 111(18) 69(26), 43(100). Found: C, 67.40; H, 8.42%. Calcd for $C_{11}H_{16}O_3$: C, 67.32; H, 8.22%.

*Preparation of (E)-5-Acetoxy-2,6-dimethyl-8-(4-methoxyphenoxy)-6-octen-3-yn-2-ol (**6f**)*: Under an argon atmosphere a THF (8 ml) solution of 4-methoxyphenol (**13**) (1.30 g, 10.5 mmol) was added to sodium hydride (50% in oil, 0.50 g, 10.5 mmol) in THF (15 ml) at 25 °C in 10 min. After stirring for 30 min ethyl 4-bromotiglate (2.07 g, 10.0 mmol) dissolved in THF (3 ml) was added to the reaction mixture . The whole was stirred for 4.5 h at reflux temperature. Workup followed by column chromatography (hexane–ethyl acetate 5 : 1 to 2 : 1) gave ethyl (*E*)-4-(4-methoxyphenoxy)-2-methyl-2-butenoate (**14**) (1.61 g, 51% yield; 97% yield based on the consumed phenol **13**). ^{1}H-NMR (CCl_4): δ=1.30 (t, J=7.2 Hz, 3H), 1.88 (s, 3H), 3.74 (s, 3H), 4.20 (q, J=7.2 Hz, 2H), 4.62 (d, J=6.2 Hz, 2H), 6.7—7.0 (m, 5H); IR: 1712, 1658, 1593, 1510, 1233, 1134, 1039, 826 cm^{-1}; MS: *m/e* (rel intensity) 250 (M^+, 18), 177(9), 133(9), 124(100), 123(71), 109(26), 99(18), 95(13), 43(24). Found: *m/e* 250.1219. Calcd for $C_{14}H_{18}O_4$: M^+, 250.1205.

An ether (10 ml) solution of **14** (1.28 g, 5.1 mmol) was added at 0 °C to an ether (20 ml) suspension of lithium aluminum hydride (0.18 g, 4.6 mmol). After stirring for 5 min at 0 °C, extractive workup gave (*E*)-4-(4-methoxyphenoxy)-2-methyl-2-buten-1-ol (**15**) (0.90 g, 85% yield) having ^{1}H-NMR ($CDCl_3$): δ=1.73 (s, 3H), 3.67 (br s, 1H), 3.75 (s, 3H), 4.05 (s, 2H), 4.50 (d, J=7.2 Hz, 2H), 5.75 (t, J=7.2 Hz, 1H), 6.80 (s, 4H).

A dichloromethane (10 ml) solution of the crude alcohol **15** (0.86 g, 4.1 mmol) was added to pyridinium chlorochoromate (1.34 g, 6.2 mmol) and sodium acetate (0.10 g, 1.2 mmol) in dichloromethane (10 ml) at 0 °C. The reaction mixture was stirred for 2 h at 0—25 °C, and then diluted with ether (50 ml). The resulting solution was filtered through silica gel and celite. Concentration of the filtrate gave (*E*)-4-(4-methoxyphenoxy)-2-methyl-2-butenal (**16**) (0.58 g, 70% yield), ^{1}H-NMR (CCl_4): δ=1.82 (s, 3H), 3.77 (s, 3H), 4.81 (d, J=3.6 Hz, 2H), 6.65 (t, J=3.6 Hz, 1H), 6.82 (s, 4H), 9.54 (s, 1H). The crude aldehyde **16** was subjected to the next transformation without further purification.

A hexane solution of butyllithium (1.57 M, 5.3 ml, 8.3 mmol) was added at −78 °C to 2-methyl-3-butyn-2-ol (0.35 g, 4.2 mmol) in THF (55 ml). The mixture was stirred for 2 h. To this solution was added a THF (5 ml) solution of **16** (0.57 g, 2.8 mmol) at −50 °C. The resulting solution was stirred for 4 h and allowed to warm to 25 °C. Water (30 ml) and ethyl acetate (30 ml) were then added. Extraction with ethyl acetate and concentration of the extracts gave (*E*)-2,6-dimethyl-8-(4-methoxyphenoxy)-6-octen-3-yne-2,5-diol (**1f**) (0.82 g) having ^{1}H-NMR (CCl_4): δ=1.50 (s, 6H), 1.78 (s, 3H), 3.50 (br s, 2H), 3.70 (s, 3H), 4.46 (d, J=6.0 Hz, 2H), 4.70 (s, 1H), 5.84 (t, J=6.0 Hz, 1H), 6.71 (s, 4H).

The crude adduct **1f** (0.81 g, 2.8 mmol) in dichloromethane (0.5 ml) was treated with acetic anhydride (1.5 ml) and pyridine (0.15 ml) for 1.6 h at 25 °C. Purification of the concentrated residue (0.89 g) by column chromatography (hexane–ethyl acetate 5 : 1 to 2 : 1) gave **6f** (0.74 g, 81% yield from **16**). Bp 168—170 °C (bath temp)/0.05 Torr; ^{1}H-NMR (CCl_4): δ=1.48 (s, 6H), 1.79 (s, 3H), 2.06 (s, 3H), 2.66 (br s, 1H), 3.73 (s, 3H), 4.50 (d, J=6.0 Hz, 2H), 5.78 (s, 1H), 5.93 (t, J=6.0 Hz, 1H), 6.75 (s, 4H); IR: 3450, 1739, 1510, 1224, 1037, 1015 cm^{-1}; MS: *m/e* (rel intensity) 332 (M^+, 1), 314(1), 272(1), 191(6), 149(19), 124(57), 109(26), 43(100). Found: C, 68.93; H, 7.21%. Calcd for $C_{19}H_{24}O_5$: C, 68.65; H, 7.28%.

*3-Acetoxy-2,2-dimethyl-5-[(E)-3-(4-methoxyphenoxy)-1-methyl-1-propenyl]-2,5-dihydrofuran (**2f**)*: Bp 160—162 °C (bath temp)/0.05 Torr; ^{1}H-NMR (CCl_4): δ=1.27 (s, 3H), 1.30 (s, 3H), 1.67 (s, 3H), 2.15 (s, 3H), 3.71 (s, 3H), 4.49 (d, J=6.0 Hz, 2H), 5.11 (br s, 1H), 5.63 (d, J=1.5 Hz, 1H), 5.70 (t, J=6.0 Hz), 6.73 (s, 4H); IR: 1778, 1657, 1592, 1509, 1230, 1205, 1040, 1013 cm^{-1}; MS: *m/e* (rel intensity) 332 (M^+, 1), 209(6), 167(91), 124(100), 113(45), 78(97), 52(25), 43(72). Found: C, 68.80; H, 7.25%. Calcd for $C_{19}H_{24}O_5$: C, 68.65; H, 7.28%. The double bond in the appendage was supposed to have the (*E*) configuration on analogy of the results of **2e**, **2g**, and **5g**.

*(E)-5-Acetoxy-2,6-dimethyl-8-(2-oxo-2H-chromen-7-yloxy)-6-octen-3-yn-2-ol (**6g**)*: A hexane solution of butyllithium (1.67 M, 18.0 ml, 30.0 mmol) was added at −78 °C to 2-methyl-3-butyn-2-ol (1.3 g, 15.0 mmol) in THF (120 ml). After stirring for 3 h (*E*)-4-(2-oxo-2*H*-chromen-7-yloxy)-2-methyl-2-butenal (**9**)[20] (2.4 g, 10.0 mmol) dissolved in THF (5 ml) was added at −78 °C. The reaction mixture was stirred for 3 h, being warmed to −20 °C and treated with methanol (30 ml) and water (20 ml). Extractive workup gave the crude adduct **1g** (3.06 g), whose dichloromethane (3 ml) solution was stirred with acetic anhydride (1.9 ml) and pyridine (4.0 ml) for 3 h at 20 °C and then concentrated. Purification of the residue by column chromatography (hexane–ethyl acetate 1 : 1) gave **6g** (3.2 g, 86% yield from **9**). Bp 205—210 °C (bath temp)/0.02 Torr; ^{1}H-NMR ($CDCl_3$): δ=1.50 (s, 6H), 1.84 (s, 3H), 2.09 (s, 3H), 4.63 (d, J=6.0 Hz, 2H), 5.84 (s, 1H), 5.93 (t, J=6.0 Hz, 1H), 6.25 (d, J=9.3 Hz, 1H), 6.7—6.9 (m, 2H), 7.34 (d, J=5.8 Hz, 1H), 7.61 (d, J=9.3 Hz, 1H); IR: 3435, 1734, 1613, 1225, 1123 cm^{-1}. Found: C, 68.13; H, 6.03%. Calcd for $C_{21}H_{22}O_6$: C, 68.09; H, 5.99%.

*3-Acetoxy-5-[(E)-3-(2-oxo-2H-chromen-7-yloxy)-1-methyl-1-propenyl]-2,2-dimethyl-2,5-dihydrofuran (**2g**)*: Bp 180—183 °C

(bath temp)/0.05 Torr; ^{1}H-NMR ($CDCl_3$): δ=1.35 (s, 3H), 1.38 (s, 3H), 1.74 (s, 3H), 2.21 (s, 3H), 4.66 (d, J=6.0 Hz, 2H) 5.23 (br s, 1H), 5.69 (d, J=1.5 Hz, 1H), 5.83 (t, J=6.0 Hz, 1H), 6.25 (d, J=9.6 Hz, 1H), 6.8—7.0 (m, 2H), 7.3—7.5 (m, 1H), 7.68 (d, J=9.6 Hz, 1H); IR (CCl_4): 1780, 1745, 1615, 1196, 1121 cm^{-1}; MS: *m/e* (rel intensity) 370 (M^+, trace), 343 (1), 326(1), 167(15), 162(8), 59(23), 55(18), 43(100). Found: C, 68.29; H, 5.75%. Calcd for $C_{21}H_{22}O_6$: C, 68.09; H, 5.99%.

Transformation of **2a** *into 2,2-Dimethyl-5-phenyl-4,5-dihydro-3(2H)-furanone (***3a***).* The enol acetate **2a** (33 mg, 0.14 mmol) was treated with a methanol solution of sodium methoxide (0.01 M, 1 ml, 0.01 mmol) at 25 °C for 40 min. Workup followed by column chromatography (hexane–ethyl acetate 10 : 1) gave **3a**[13q,29] (25 mg, 90% yield). ^{1}H-NMR (CCl_4): δ=1.27 (s, 3H), 1.34 (s, 3H), 2.39 (dd, J=10.4, 18.0 Hz, 1H), 2.79 (dd, J=6.3, 18.0 Hz, 1H), 5.15 (dd, J=6.3, 10.4 Hz, 1H), 7.2—7.5 (m, 5H); IR: 1752, 1171, 1010, 693 cm^{-1}; MS: *m/e* 190 (M^+).

Oxidation of the Enol Acetates **2** *to 3(2H)-Furanones* **5**.

(1) Bromination-dehydrobromination of **2a** *(A Typical Procedure)*: A chloroform solution of bromine (0.5 M, 1.4 ml, 0.69 mmol) was added at −20 °C in 10 min to **2a** (0.16 g, 0.69 mmol) dissolved in chloroform (0.5 ml). The reaction mixture was stirred for 30 min and allowed to warm up to 25 °C. Concentration of the resulting solution afforded crude 4-bromo-2,2-dimethyl-5-phenyl-4,5-dihydro-3(2*H*)-furanone (**8a**) (*ca.* 0.19 g) having ^{1}H-NMR (CCl_4): δ=1.35 (s, 3H), 1.64 (s, 3H), 4.38 (d, J=3.6 Hz, 1H), 5.25 (d, J=3.6 Hz, 1H), 7.43 (s, 5H); IR: 1725, 1172, 1110 cm^{-1}.

The bromide **8a** (*ca.* 0.19 g) dissolved in DMF (1 ml) was treated with lithium carbonate (0.23 g, 3.5 mmol) at 120 °C for 40 min. Workup followed by column chromatography (hexane–ethyl acetate 10 : 1) gave bullatenone (**5a**) (0.11 g, 85% yield from **2a**). Mp 67.5—68.0 °C (hexane); ^{1}H-NMR (CCl_4): δ=1.43 (s, 6H), 5.89 (s, 1H), 7.3—7.6 (m, 3H), 7.7—7.9 (m, 2H); IR (CCl_4): 1702, 1608, 1594, 1568, 1162 cm^{-1}; MS: *m/e* (rel intensity) 188 (M^+, 22), 102 (100). The spectral data (IR, ^{1}H-NMR) and mp were identical with the recorded ones.[10f,10g,19]

*2,2-Dimethyl-5-[(E)-1-propenyl]-3(2H)-furanone (***5e***).* According to the method described above **2e** (0.31 g, 1.6 mmol) was transformed into the corresponding bromide which was treated with lithium chloride (0.20 g, 4.8 mmol) and lithium carbonate (0.35 g, 4.8 mmol) in HMPA (2 ml) at 80 °C for 11 h. Workup and purification by column chromatography (hexane–ethyl acetate 5 : 1) gave **5e** (0.16 g, 66% overall yield). Bp 120—122 °C (bath temp)/0.04 Torr; ^{1}H-NMR (CCl_4): δ=1.33 (s, 6H), 1.96 (d, J=6.8 Hz, 3H), 5.29 (s, 1H), 6.23 (d, J=15.8 Hz, 1H), 6.74 (dq, J=15.8, 6.8 Hz, 1H); IR: 1700, 1651, 1565, 1382, 1177, 984, 964 cm^{-1}; MS: *m/e* (rel intensity) 152 (M^+, 23), 137(8), 94(11), 66(100). Found: C, 71.32; H, 8.09%. Calcd for $C_9H_{12}O_2$: C, 71.02; H, 7.95%.

*2,2-Dimethyl-5-[(E)-3-(4-methoxyphenoxy)-1-methyl-1-propenyl]-3(2H)-furanone (***5f***).* According to the method for the transformation of **2e** into **5e**, the enol acetate **2f** was converted into **5f** (46% overall yield) having mp 77.5—78.0 °C (methanol); bp 165—168 °C (bath temp)/0.05 Torr; ^{1}H-NMR (CCl_4): δ 1.35 (s, 6H), 1.96 (s, 3H), 3.70 (s, 3H), 4.62 (d, J=6.0 Hz, 2H), 5.43 (s, 1H), 6.66 (t, J=6.0 Hz, 1H), 6.70 (s, 4H); IR (CCl_4): 1702, 1564, 1509, 1226, 1181, 1041 cm^{-1}; MS: *m/e* (rel intensity) 288 (M^+, 5), 200(9), 151(11), 124(18), 109(18), 79(45), 40(100). Found: C, 70.70; H, 7.09%. Calcd for $C_{17}H_{20}O_4$: C, 70.81; H, 6.99%. The double bond in the appendage was supposed to have the (*E*) configuration by comparison with the results of **5e** and **5g**.

(2) Oxidation of the Enol Acetate **2a** *with DDQ (A Typical Procedure)*: The enol acetate **2a** (0.11 g, 0.49 mmol) was treated with DDQ (0.16 g, 0.71 mmol) in benzene (1 ml) at 25 °C for 1.8 h. The reaction mixture was washed with sat. aqueous sodium sulfite solution. The aqueous layer was extracted with dichloromethane. Concentration of the combined organic layer followed by column chromatography of the residue (dichloromethane–ethyl acetate 20 : 1) gave **5a** (92 mg, 99% yield). This procedure applies to the synthesis of **2e—g**.

*5-[(E)-3-(2-oxo-2H-chromen-7-yloxy)-1-methyl-1-propenyl]-2,2-dimethyl-3(2H)-furanone, Geiparvarin (***5g***).* Mp 159.5—160.5 °C (colorless prisms from methanol); ^{1}H-NMR ($CDCl_3$): δ=1.39 (s, 6H), 2.01 (s, 3H), 4.82 (d, J=6.0 Hz, 2H), 5.57 (s, 1H), 6.22 (d, J=9.3 Hz, 1H), 6.6—7.0 (m+t (δ 6.73, J=6.0 Hz), 3H), 7.37 (d, J=8.7 Hz, 1H), 7.61 (d, J=9.3 Hz, 1H); IR ($CHCl_3$): 1727, 1696, 1615, 1561, 1278, 1171, 1158, 1123, 1017, 838 cm^{-1}; MS: *m/e* (rel intensity) 326 (M^+, trace), 249(11), 247(11), 149(19), 99(48), 83(63), 55(85), 43(100). The synthetic material showed more than 97% purity of the (*E*) isomer as evidenced by the ^{1}H-NMR spectrum consistent with the literature values.[3e-g,9b]

Hg/Nafion-H Catalyzed Transformation of Acetylenic Diols **1** *into 4,5-Dihydro-3(2H)-furanones of Type* **4** *(Method B, a Typical Procedure).* The polymer reagent Hg/Nafion-H[14] was prepared as follows. Nafion® 511 (20.4 g) was treated with 12% hydrochloric acid (25 ml) for 6 h and the resin was filtered and superficially washed with water. This procedure was repeated 5 times. Finally the resin was washed more thoroughly with water and dried at 85 °C for 10 h under *ca.* 1 Torr to give Nafion®-H, perfluorinated resin-sulfonic acid, which contained 0.94 mmol of $-SO_3H$ group per 1 g. The resin-sulfonic acid (20.4 g) was stirred in sat. aqueous mercury(II) acetate solution (25 ml) at 25 °C for 7 h. The resin was collected by filtration, washed with water, and dried at 25°C under 1 Torr for 1 d. Hg/Nafion-H thus prepared contained 0.38 mmol of Hg(II) per 1 g.

The diols **1** (1 mmol) in ethanol (1 ml) were treated with Hg/Nafion-H (*ca.* 0.5 g) in the presence of water (5 mmol) at 25 °C for several hours. The reaction mixture was filtered, and the catalyst was washed with dichloromethane. Concentration of the combined filtrates followed by purification gave the desired products.

*5,5-Dimethyl-2-phenyl-4,5-dihydro-3(2H)-furanone (***4a***).* The reaction of **1a** with Hg/Nafion-H afforded a 1 : 4 mixture of **3a** and **4a** (14% and 56% isolated yield respectively) along with a by-product, (*E*)-4-hydroxy-4-methyl-1-phenyl-1-penten-3-one (**12a**) (11% yield). Physical properties of **4a** are given. Bp 108—109 °C (bath temp)/0.05 Torr; ^{1}H-NMR (CCl_4): δ=1.40 (s, 3H), 1.55 (s, 3H), 2.35 (s, 2H), 4.82 (s, 1H), 7.2—7.5 (m, 5H); IR: 1758, 1182, 1056, 699 cm^{-1}; MS: *m/e* (rel intensity) 190 (M^+, 4), 162(11), 107(100), 105(35), 56(98). Found: C, 75.90; H, 7.59%. Calcd for $C_{12}H_{14}O_2$: C, 75.76; H, 7.42%. The enone **12a** showed bp 131—132 °C (bath temp)/0.14 Torr; ^{1}H-NMR (CCl_4): δ=1.40 (s, 6H), 3.64 (br s, 1H), 7.04 (d, J=15.6 Hz, 1H), 7.3—7.7 (m, 5H), 7.81 (d, J=15.6 Hz, 1H); IR: 3450, 1681, 1610, 1600, 1071, 973, 764 cm^{-1}; MS: *m/e* (rel intensity) 172 (M^+-H_2O, 2), 147(25), 132(32), 131(47), 104(34), 59(100). Found: C, 75.50; H, 7.51%. Calcd for $C_{12}H_{14}O_2$: C, 75.76; H, 7.42%.

*2,2,5-Trimethyl-4,5-dihydro-3(2H)-furanone (***3b***) and 2,5,5-Trimethyl-4,5-dihydro-3(2H)-furanone (***4b***).* A mixture of **3b**[12b] and **4b**[12b] (**3b** : **4b** being 1 : 2 based on ^{1}H-NMR) were produced in 80% yield. The mixture showed bp 135—140 °C (bath temp)/20 Torr; IR: 1759, 1371, 1195, 1098 cm^{-1}; MS: *m/e* 128 (M^+); ^{1}H-NMR (CCl_4) of **3b**: δ 1.13 (s, $C\underline{H}_3$–C–CH_3), 1.18 (s, CH_3–C–$C\underline{H}_3$), 1.29 (d, J=5.2 Hz, CH–$C\underline{H}_3$), 2.03 (dd, J=9.9, 17.4 Hz, $\underline{H}$–C–H), 2.49 (dd, J=6.0, 17.4 Hz,

H-C-H), 4.0—4.4 (m, CH-CH_3, 0.33H); ^{1}H-NMR (CCl_4) of **4b**: δ=1.25 (d, J=6.9 Hz, CH-CH_3), 1.31 (s, CH_3-C-CH_3), 1.40 (s, CH_3-C-CH_3), 2.25 (s, H-C-H), 3.91 (q, J=6.9 Hz, CH-CH_3, 0.67H).

*1-Oxaspiro[4.5]decan-3-one (**4c**).*[12a] ^{1}H-NMR (CCl_4): δ=1.1—2.0 (m, 10H), 2.24 (s, 2H), 3.94 (s, 2H), IR: 1760, 1184, 1064 cm^{-1}; MS: *m/e* 154 (M^+).

*2-Methyl-1-oxaspiro[4.5]decan-4-one (**3d**) and 2-Methyl-1-oxaspiro[4.5]decan-3-one (**4d**).* The ratio of **3d**[12g] to **4d**[12d] (1 : 1 to 1 : 2) was estimated by the examination of the ^{1}H-NMR spectrum of the mixture having IR: 1755, 1450, 1190, 1105, 1065 cm^{-1}; MS: *m/e* 168 (M^+); ^{1}H-NMR (CCl_4, *refers to **4d**): δ=1.0—2.0 (m+d (δ=1.22*, J=6.8 Hz)+d (δ=1.38, J=6.3 Hz), 13H), 2.05 (dd, J=10.2, 17.9 Hz), 2.20* (d, J=17.6 Hz), 2.32* (d, J=17.6 Hz), 2.50 (dd, J=6.0, 17.9 Hz), 3.88* (q, J=6.8 Hz, CH-CH_3, 0.69—0.50H), 4.23 (ddq, J=6.0, 10.2, 6.8 Hz, CH-CH_3, 0.31—0.50H).

*2,2-Dimethyl-1-oxaspiro[4.5]decan-4-one (**3h**) and 2,2-Dimethyl-1-oxaspiro[4.5]decan-3-one (**4h**).* The ratio of **3h**[5e] to **4h**[5e] was estimated by GLC (PEG 20 M, 10% on Celit 545, 2 m, 123 °C, N_2 carrier gas 0.5 kg/cm^2, FID detector) to be *ca.* 1 : 2, R_t being 5.7 min and 6.4 min respectively; each isomer could be isolated by preparative GLC (PEG 20 M, 30% on Celite 545, 3 m, 150 °C, He carrier gas 0.8 kg/cm^2, TCD detector; **3h** R_t 7.0 min; **4h**, R_t 8.5 min). The structure of regioisomers was established by the examination of the ^{1}H-NMR spectra in the presence of Eu(fod)$_3$. ^{1}H-NMR (CCl_4) of **3h**: δ=1.1—1.8 (m+s (δ=1.36), 16H), 2.39 (s, 2H); **4h**: δ=1.22 (s, 6H), 1.2—1.9 (m, 10H), 2.36 (s, 2H). The mixture showed IR: 1754, 1159, 990 cm^{-1}; MS: *m/e* 182 (M^+).

*7-Oxadispiro[5.1.5.2]pentadecan-14-one (**4i**).*[30] Bp 150—151 °C (bath temp)/8 Torr; ^{1}H-NMR (CCl_4): δ=1.0—2.2 (m, 20H), 2.38 (s, 2H); IR: 1750, 1451, 1064, 990 cm^{-1}; MS: *m/e* 222 (M^+).

*6-Methyl-1-oxaspiro[4.5]decan-3-one (**4j**) and (**4j'**).* A 3 : 2 diastereomeric mixture of **1j** and **1j'** (TLC, hexane–ethyl acetate 1 : 2, R_f 0.14 and 0.22 respectively)[1] was transformed into **4j** and **4j'**, which were separated by preparative TLC (hexane–ethyl acetate 5 : 1, double development) to give **4j** (R_f 0.35—0.45) and **4j'** (R_f 0.45—0.55). Physical properties of **4j** are given. Bp 111—112 °C (bath temp)/0.12 Torr; ^{1}H-NMR (CCl_4): δ=0.94 (d, J=6.9 Hz, 3H), 1.0—2.0 (m, 9H), 2.06 d, J=18.3 Hz, 1H), 2.35 (d, J=18.3 Hz, 1H), 3.92 (s, 2H); IR: 1761, 1184, 1067 cm^{-1}; MS: *m/e* (rel intensity) 168 (M^+, 41), 125(43), 111(100), 98(45), 67(42). Found: C, 71.41; H, 9.84%. Calcd for $C_{10}H_{16}O_2$: C, 71.39; H, 9.59%. The isomer **4j'** showed bp 92—93 °C (bath temp)/0.05 Torr; ^{1}H-NMR (CCl_4): δ=0.97 (d, J=5.9 Hz, 3H), 1.0—2.0 (m, 9H), 2.06 (d, J=18.0 Hz, 1H), 2.51 (d, J=18.0 Hz, 1H), 3.90 (s, 2H); IR: 1760, 1188, 1066 cm^{-1}; MS: *m/e* (rel intensity) 168 (M^+, 38), 125(48), 111(100), 98(46), 67(46). Found: C, 71.25; H, 9.86%. Calcd for $C_{10}H_{16}O_2$: C, 71.39, H, 9.59%.

*1-Oxaspiro[4.6]undecan-3-one (**4k**).* Isolated by preparative TLC (hexane–ethyl acetate 2 : 1, R_f 0.60—0.75) along with 3-cycloheptylidene-1-hydroxy-2-propanone (**12k**) (R_f 0.40—0.50). The furanone **4k** showed bp 109 °C (bath temp)/0.15 Torr; ^{1}H-NMR (CCl_4): δ=1.2—2.1 (m, 12H), 2.24 (s, 2H), 3.88 (s, 2H); IR: 1760, 1462, 1447, 1066 cm^{-1}; MS: *m/e* (rel intensity) 168 (M^+, 16), 111(100), 98(44), 83(44), 67(47). Found: C, 71.26; H, 9.76%. Calcd for $C_{10}H_{16}O_2$: C, 71.39; H, 9.59%. Bp of **12k**: 120—125 °C (bath temp)/0.20 Torr; ^{1}H-NMR (CCl_4): δ=1.3—2.0 (m, 8H), 2.42 (t, J=5.0 Hz, 2H), 2.95 (t, J=5.0 Hz, 2H), 3.05 (br s, 1H), 4.13 (s, 2H), 5.99 (s, 1H); IR: 3455, 1704, 1678, 1605, 1444, 1066 cm^{-1}; MS: *m/e* (rel intensity) 168 (M^+, 4), 137(76), 113(100), 95(67), 67(65), 55(80). Found *m/e* 168.1145. Calcd for $C_{10}H_{16}O_2$: M^+, 168.1149.

*1-Oxaspiro[4.7]dodecan-3-one (**4l**).* Isolated by preparative TLC (hexane–ethyl acetate 3 : 1, R_f 0.61—0.72) together with 3-cyclooctylidene-1-hydroxy-2-propanone (**12l**) (R_f 0.50—0.60). Physical properties of **4l** are given. Bp 110—112 °C (bath temp)/0.15 Torr; ^{1}H-NMR (CCl_4): δ=1.0—2.4 (m+s (δ=2.22), 16H), 3.89 s, 2H); IR: 1760, 1180, 1064 cm^{-1}; MS: *m/e* (rel intensity) 182 (M^+, 12), 111 (100), 98(63), 83(35), 55(40). Found: C, 72.42; H, 10.20%. Calcd for $C_{11}H_{18}O_2$: C, 72.49; H, 9.95%. The enone **12l** showed bp 102—103 °C (bath temp)/0.18 Torr; ^{1}H-NMR (CCl_4): δ=1.1—2.1 (m, 10H), 2.34 (t, J=6.0 Hz, 2H), 2.79 (t, J=6.0 Hz, 2H), 2.99 (br s, 1H), 4.10 (s, 2H), 6.02 (s, 1H); IR: 3450, 1682, 1607, 1449, 1050 cm^{-1}; MS: *m/e* (rel intensity) 182 (M^+, 4), 151(69), 81(100), 67(71), 55(83). Found: C, 72.26; H, 10.20%. Calcd for $C_{11}H_{18}O_2$: C, 72.49; H, 9.95%.

*1-Oxaspiro[4.11]hexadecan-3-one (**4m**).* Mp 81.5—82.0 °C (colorless needles from hexane); ^{1}H-NMR (CCl_4): δ=1.2—2.0 (m, 22H), 2.19 (s, 2H), 3.87 (s, 2H), IR ($CHCl_3$): 1763, 1471, 1448, 1180, 1062 cm^{-1}; MS: *m/e* (rel intensity) 238 (M^+, 8), 111 (100), 98(56), 55(48). Found: C, 75.64; H, 10.98%. Calcd for $C_{15}H_{26}O_2$: C, 75.58; H, 11.00%. The by-product was proved to be 3-cyclododecylidene-1-hydroxy-2-propanone (**12m**) having mp 43.0—44.0 °C (hexane); bp 136—138 °C (bath temp)/0.04 Torr; ^{1}H-NMR (CCl_4): δ=1.1—1.9 (m, 18H), 2.27 (t, J=6.8 Hz, 2H), 2.80 (t, J=6.8 Hz, 2H), 3.09 (br s, 1H), 4.61 (s, 2H), 6.07 (s, 1H); IR (CCl_4): 3455, 1687, 1614, 1063 cm^{-1}; MS: *m/e* (rel intensity) 238 (M^+, 3), 207(33), 83(56), 55(100). Found: C, 75.41; 11.13%. Calcd for $C_{15}H_{26}O_2$: C, 75.58; H, 11.00%.

*5-Ethyl-5-pentyl-4,5-dihydro-3(2H)-furanone (**4n**).* Bp 89 °C (bath temp)/0.13 Torr; ^{1}H-NMR (CCl_4): δ=0.6—1.9 (m, 16H), 2.24 (s, 2H), 3.89 (s, 2H); IR: 1761, 1465, 1185, 1067 cm^{-1}; MS: *m/e* (rel intensity) 155 ($M^+-C_2H_5$, 38), 113(100), 85(55), 57(72), 55(84). Found: *m/e* 155.1057. Calcd for $C_9H_{15}O_2$: $M^+-C_2H_5$, 155.1071. The by-product, (*E*)- and (*Z*)-4-ethyl-1-hydroxy-3-nonen-2-one (**12n**) showed bp 110 °C (bath temp)/0.08 Torr; ^{1}H-NMR (CCl_4): δ=0.7—2.0 (m, 12H), 2.22 (m, 2H), 2.63 (m, 2H), 3.07 (br s, 1H), 4.12 (s, 2H), 5.87 (s, 0.5H), 5.97 (s, 0.5H); IR: 3450, 1688, 1618, 1462, 1071, 1053 cm^{-1}; MS: *m/e* (rel intensity) 184 (M^+, trace), 153(73), 83(59), 69(59), 57(64), 55(50), 41(100). Found: C, 71.45; H, 11.19%. Calcd for $C_{11}H_{20}O_2$: C, 71.70; H, 10.94%.

*5-Hexyl-4,5-dihydro-3(2H)-furanone (**4o**).* Bp 120 °C (bath temp)/0.15 Torr; ^{1}H-NMR (CCl_4): δ=0.7—1.9 (m, 13H), 2.04 (dd, J=9.5, 17.7 Hz, 1H), 2.46 (dd, J=6.3, 17.7 Hz, 1H), 3.70 (d, J=17.3 Hz, 1H), 3.99 (d, J=17.3 Hz, 1H), 4.18 (m, 1H); IR: 1765, 1170, 1064 cm^{-1}; MS: *m/e* (rel intensity) 170 (M^+, 6), 140(34), 85(97), 57(100), 55(83), 43(77) Found: C, 70.30; H, 10.75%. Calcd for $C_{10}H_{18}O_2$: C, 70.55; H, 10.66%. The by-product was proved to be 1-ethoxy-4-hydroxy-3-decanone (**12o**) having bp 113—114 °C (bath temp)/0.09 Torr; ^{1}H-NMR (CCl_4): δ=0.7—2.0 (m+t (δ=1.15, J=7.1 Hz), 16H), 2.63 (t, J=6.3 Hz, 2H), 3.30 (br s, 1H), 3.45 (q, J=7.1 Hz, 2H), 3.65 (t, J=6.3 Hz, 2H), 4.04 (m, 1H); IR: 3480, 1712, 1115 cm^{-1}. Found: C, 66.88; H, 11.42%. Calcd for $C_{12}H_{24}O_3$: C, 66.63; H, 11.18%.

*2,2,5,5-Tetramethyl-4,5-dihydro-3(2H)-furanone (**4p**).* Using the recovered polymer reagent Hg/Nafion-H (200 mg), **1p** (91 mg, 0.64 mmol) was converted into **4p**[11] (74 mg, 82% yield) having ^{1}H-NMR (CCl_4): δ=1.20 (s, 6H), 1.33 (s, 6H), 2.37 (s, 2H); IR: 1757, 1369, 1153, 990 cm^{-1}; MS: *m/e* 142 (M^+).

This work was financially supported by the Ministry of Education, Science and Culture (Grant-in-Aid No. 57118006).

References

1) T. Hiyama, M. Shinoda, H. Saimoto, and H. Nozaki, *Bull. Chem. Soc. Jpn.*, **54**, 2747 (1981).

2) For a preliminary communication on this work, see H. Saimoto, T. Hiyama, and H. Nozaki, *J. Am. Chem. Soc.*, **103**, 4975 (1981).

3) For example, a) Budlein-A and B: A. Romo de Vivar, C. Guerrero, E. Diag, E. A. Bratoeff, and L. Jimenetz, *Phytochemistry*, **15**, 525 (1976); b) Bullatenone: C. W. Brandt, W. I. Taylor, and B. R. Thomas, *J. Chem. Soc.*, **1954**, 3245; c) Eremantholides: R. F. Raffauf, R.-K. C. Huang, P. W. Le Queane, S. B. Levery, and T. E. Brennan, *J. Am. Chem. Soc.*, **97**, 6884, (1975); d) P. W. Le Quesne, S. B. Levery, M. D. Menachery, T. F. Brennan, and R. F. Raffauf, *J. Chem. Soc., Perkin Trans. 1*, **1978**, 1572; e) Geiparvarin: F. N. Lahey and J. K. MacLeod, *Aust. J. Chem.*, **20**, 1943 (1967); f) R. M. Carman, F. N. Lahey, and J. K. MacLeod, *ibid.*, **20**, 1957 (1967); g) D. L. Dreyer and A. Lee, *Phytochemistry*, **11**, 763 (1972); h) K. Padmawinata, *Acta Pharm.*, **4**, 1 (1973); *Chem. Abstr.*, **79**, 75897n (1973); i) Goyazensolide: W. Vichnewski, S. J. Sarti, B. Gilbert, and W. Herz, *Phytochemistry*, **15**, 191 (1976); j) Jatrophone: S. M. Kupchan, C. W. Sigel, M. J. Matz, J. A. Saenz Renauld, R. C. Haltiwanger, and H. F. Bryan, *J. Am. Chem. Soc.*, **92**, 4476 (1970); k) S. M. Kupchan, C. W. Sigel, M. J. Matz, C. J. Gilmore, and R. F. Bryan, *ibid.*, **98**, 2295 (1976); l) Sirodesmins: P. J. Curtis, D. Greatbanks, B. Hesp, A. F. Cameron, and A. A. Freer, *J. Chem. Soc., Perkin Trans. 1*, **1977**, 180; m) J. P. Férézou, C. Riche, A. Quesneau-Thierry, C. Pascard-Billy, M. Barbier, J. F. Bousquet, and G. Boudart, *Nouv. J. Chem.*, **1**, 327 (1977); *Chem. Abstr.*, **87**, 179449z (1977); n) A flavor component of pineapple and strawberry: J. O. Rodin, C. M. Himel, R. M. Silverstein, R. W. Leeper, and W. A. Gortner, *J. Food Sci.*, **30**, 280 (1965); o) B. Willharm, M. Stoll, and A. F. Thomas, *Chem. Ind. (London)*, **1965**, 1629.

4) Biological activity[3d,h,j-l] was discussed in connection with the addition reaction of model biological nucleophiles to many antitumor agents: S. M. Kupchan, D. C. Fessler, M. A. Eakin, and T. J. Giacobbe, *Science*, **168**, 376 (1970); E. Fujita and Y. Nagao, *Bioorg. Chem.*, **6**, 287 (1977) and Ref. 13q.

5) For example, preparation of tetrahydrofuran-3,4-diones and their monooximes connected with the synthesis of 4-hydroxy-3-furanones: a) G. B. Bennett, W. J. Houlian, R. B. Mason, and R. G. Engstrom, *J. Med. Chem.*, **19**, 709 (1976); b) I. K. Korobitsyna, Yu. K. Yur'ev, Yu. A. Cheburkov, and E. M. Lukia, *Zh. Obshch. Khim.*, **25**, 734 (1955); *Chem. Abstr.*, **50**, 2536f (1956); c) I. K. Korobitsyna, Yu. K. Yur'ev, and K. V. Kuznetsova, *ibid.*, **27**, 1792 (1957); *Chem. Abstr.*, **52**, 4659i (1958); d) I. K. Korobitsyna, I. G. Zhukova, and Yu. K. Yur'ev, *ibid.*, **29**, 2190 (1959); *Chem. Abstr.*, **54**, 10989a (1960); e) I. K. Korobitsyna, K. K. Pivnitskii, and Yu. K. Yur'ev, *ibid.*, **29**, 3880 (1959); *Chem. Abstr.*, **54**, 21032i (1960); f) I. K. Korobitsyna, I. G. Zhukova, V. V. Voronkova, and Yu. K. Yur'ev, *Dokl. Akad. Nauk SSSR*, **117**, 237 (1957); *Chem. Abstr.*, **52**, 9062i (1958). Photochemical ring expansion: g) P. Yates, A. K. Verma, and J. C. L. Tam, *J. Chem. Soc., Chem. Commun.*, **1976**, 933; h) P. Yates and R. O. Loutfy, *Acc. Chem. Res.*, **8**, 209 (1975). Preparation of tetronic acid derivatives: i) S. Gelin and D. Hartmann, *J. Heterocycl. Chem.*, **13**, 521 (1976); j) T. Reffstrup and P. M. Boll, *Acta Chem. Scand., Ser. B*, **31**, 727 (1977). Synthesis of 2-, 4-, and 5-oxopyrrol derivatives: k) S. Gelin and R. Gelin, *J. Org. Chem.*, **44**, 808 (1979); l) S. Gelin, *Synthesis*, **1978**, 291; m) B. Chantegrel and S. Gelin, *J. Heterocycl. Chem.*, **15**, 1215 (1978).

6) a) A. B. Smith, III and P. J. Jerris, *Tetrahedron Lett.*, **21**, 711 (1980); b) P. J. Jerris and A. B. Smith, III, *J. Org. Chem.*, **46**, 577 (1981); c) A. B. Smith, III, M. A. Guaciaro, S. R. Schow, P. M. Wovkulich, B. H. Toder, and T. W. Hall, *J. Am. Chem. Soc.*, **103**, 219 (1981); d) W. H. Rastetter and J. Adams, *Tetrahedron Lett.*, **23**, 1319 (1982); J. D. White, T. Nishiguchi, and R. W. Skeean, *J. Am. Chem. Soc.*, **104**, 3923 (1982).

7) Reviews: C. H. Eugster, *Adv. Org. Chem.*, **2**, 427 (1960); S. Wilkinson, *Q. Rev. Chem. Soc.*, **15**, 153 (1961). Recent methods for the synthesis of muscarine alkaloids, see: Z. Lysenko, F. Ricciardi, J. E. Semple, P. C. Wang, and M. M. Joullié, *Tetrahedron Lett.*, **1978**, 2679; A. M. Mubarak and D. M. Bromn, *ibid.*, **21**, 2453 (1980); R. Amouroux, B. Gerin, and M. Chastrette, *ibid.*, **23**, 4341 (1982); H. Meister, *Justus Liebigs Ann. Chem.*, **701**, 174 (1967); **752**, 163 (1971); W. C. Still and J. A. Schneider, *J. Org. Chem.*, **45**, 3375 (1980); Y. Hayakawa, H. Takaya, S. Makino, N. Hayakawa, and R. Noyori, *Bull. Chem. Soc. Jpn.*, **50**, 1990 (1977) and references cited therein.

8) R. Teranishi, "Gustation and Olfaction," ed by G. Ohloff and A. F. Thomas, Academic Press, New York (1971), p. 165.

9) M. A. Gianturco, P. Friedel, and A. S. Gimmarino, *Tetrahedron*, **20**, 1763 (1964); G. Büchi, E. Demole, and A. F. Thomas, *J. Org. Chem.*, **38**, 123 (1973); L. Re and G. Ohloff, Swiss Patent 540 650 (1974); *Chem. Abstr.*, **80**, 69406f (1974); L. Re, B. Maurer, and G. Ohloff, *Helv. Chim. Acta*, **56**, 1882 (1973).

10) a) Elguero, C. Marzin, A. R. Katritzky, and P. Linda, "Advances in Heterocyclic Chemistry, Supplement 1, The Tautomerism of Heterocycles," ed by A. R. Katritzky and A. J. Boulton, Academic Press, New York (1976), pp. 222—228; b) A. R. Katritzky and J. M. Lagowski, "Advances in Heterocyclic Chemistry," ed by A. R. Katritzky, Academic Press, New York (1963), Vol. 2, pp. 5—8; c) P. Bosshard and C. H. Eugster, "Advances in Heterocyclic Chemistry," ed by A. R. Katritzky and A. J. Boulton, Academic Press, New York (1966), Vol. 7, pp. 462—468; d) M. Anteunis and M. Vandewalle, *Spectrochim. Acta, Part A*, **27**, 2119 (1971); e) I. K. Korobitsyna, I. G. Zhukova, and Yu. K. Yur'ev, *Zh. Obshch. Khim.*, **29**, 2196 (1959); *Chem. Abstr.*, **54**, 10989f (1960); f) R. E. Rosenkranz, K. Allner, R. Good, W. V. Philipsborn, and C. H. Eugster, *Helv. Chim. Acta*, **46**, 1259 (1963); g) A. Hofmann, W. V. Philipsborn, and C. H. Eugster, *ibid.*, **48**, 1322 (1965); h) A. Hofmann and C. H. Eugster, *ibid.*, **49**, 53 (1966); i) P. M. Burke, W. F. Reynold, J. C. L. Tam, and P. Yates, *Can. J. Chem.*, **54**, 1449 (1976); j) D. W. Henry and R. M. Silverstein *J. Org. Chem.*, **31**, 2391 (1966); k) E. C. Kendall and Z. Hajos, *J. Am. Chem. Soc.*, **82**, 3219, 3220 (1960). Conformational equilibrium constants for a number of 1-oxaspiro[*n*. 5]-alkanes, see: l) P. Picard and J. Moulines, *Tetrahedron*, **34**, 671 (1978).

11) H. Richet, *Ann. Chim.*, **3**, 317 (1948); F. Leonard, A. Wajngurt, and H. Horn, *J. Org. Chem.*, **21**, 1402 (1956); M. S. Newman and W. R. Reichle, *Org. Synth.*, Coll. Vol. V, 1024 (1973).

12) a) J. Colonge, R. Falcotet, and R. Gaumont, *Bull. Soc. Chim. Fr.*, **1958**, 211; b) S. A. Vartanyan, G. A. Chukhadzhyan R. A. Melikyan, and Sh. A. Babanya, *Izv. Akad. Nauk Arm. SSR, Khim. Nauki*, **15**, 45 (1962); *Chem. Abstr.*, **58**, 6756b (1963); c) A. S. Medvedeva, M. F. Shostakoviskii, G. G. Chichkareva, T. A. Favorskaya, and V. K. Voronov, *Zh. Org. Khim.*, **7**, 641 (1971); *J. Org. Chem. USSR*, **7**, 649 (1971); d) A. S. Medvedeva, L. P. Safronova, I. D. Kalikhuman, and V. M. Vlasov, *Izv. Akad. Nauk SSSR, Ser. Khim.*, **1975**, 1175; *Bull. Acad. Sci. USSR, Chem. Sci.*, **1975**, 1082; Ref. 5b, 5c, and 5e.

13) Other methods for the synthesis of 3-furanones, see: a) J. E. Semple and M. M. Joullié, *Heterocycles*, **14**, 1825 (1980);

b) I. N. Nazarov and S. G. Matsoyan, *Zh. Obshch. Khim.*, **27**, 2951 (1957); *Chem. Abstr.*, **52**, 8080f (1958); c) G. Casnati and A. Ricca, *Tetrahedron Lett.*, **1967**, 327, d) M.-A. Barrow, A. C. Richards, R. H. Simithers, and H. M. R. Hoffmann, *ibid.*, **1972**, 3101; e) M. Bertrand, J. P. Dulcere, G. Gil, J. Grimaldi, and P. Sylvestre-Panthet, *ibid.*, **1976**, 1507; f) D. Caine and W. D. Samuels, *ibid.*, **21**, 4057 (1980); g) J. E. Semple, A. E. Guthrie, and M. M. Joullie, *ibid.*, **21**, 4561 (1980); h) T. H. Chan and B. S. Ong, *Tetrahedron*, **36**, 2269 (1980); i) P. Picard and J. Moulines, *Bull. Soc. Chim. Fr.*, **1974**, 2889; j) R. Gerin, A. Galliand, B. Chantegrel, and S. Gelin, *ibid.*, **1974**, 1043; k) M. Yamamoto, *J. Chem. Soc., Perkin Trans. I*, **1976**, 1688; l) J. Yoshimura, S. Kondo, M. Ihara, and H. Hashimoto, *Chem. Lett.*, **1979**, 819; m) Ch. Meister and H.-D. Scharf, *Synthesis*, **1981**, 733, 737; n) M. Matsui, T. Ogawa, T. Kitahara, and K. Takagi, Japan Kokai Patent 79, 115, 369 (1978); *Chem. Abstr.*, **92**, 110828h (1980); o) D. Gange and P. Magnus, *J. Am. Chem. Soc.*, **100**, 7746 (1978); p) K. C. Nicolaou, R. L. Magolda, W. J. Sipio, W. E. Barnette, Z. Lysenko, and M. M. Joullié, *ibid.*, **102**, 3784 (1980); q) A. B. Smith, III, P. A. Levenberg, P. J. Jerris, R. M. Scarborough, Jr., and P. M. Wovkulich, *ibid.*, **103**, 1501 (1981) and references cited therein.

14) Nafion® is a perfluorinated resin-sulfonic acid commercially available from E. I. du Pont de Nemours and Co. The author is indebted to E. I. du Pont de Nemours and Co. and Mitsui Fluorochemical Co. for a generous gift of the potassium salt of Nafion® 511. *Cf.* G. A. Olah and D. Meider, *Synthesis*, **1978**, 671; G. A. Olah, J. Kaspi, and J. Bukala, *J. Org. Chem.*, **26**, 4187 (1977).

15) Other approaches to 3(2*H*)-furanone derivatives, see: T. Hiyama, M. Shinoda, H. Saimoto, and H. Nozaki, *Heterocycles*, **15**, 263 (1981) and references cited therein. Preparation of 3-furanones from acetylene derivatives, see: F. Bohlmann, *Chem. Ber.*, **94**, 1104 (1961); c) H. Meister, German Patent 1147593 (1963); *Chem. Abstr.*, **59**, 11427b (1963); d) German Patent 1150658 (1964); *Chem. Abstr.*, **60**, 2895e (1964); e) S. A. Vartanyan, L. V. Oganova, and Sh. O. Badanyan, *Izu. Akad. Nauk Arm. SSR, Khim. Nauki*, **17**, 709 (1964); *Chem. Abstr.*, **63**, 4232e (1965); f) B. P. Gusev, I. I. Nazarova, and V. F. Kucherov, *Izv. Akad. Nauk SSSR, Ser. Khim.*, **1965**, 688; g) I. I. Nazarova, B. P. Gusev, and V. F. Kucherov, *ibid.*, **1967**, 1580; h) V. M. Al'bitskaya and E. D. Venus-Danilova, *Zh. Obshch. Khim.*, **30**, 349 (1960); *Chem. Abstr.*, **54**, 22558g (1960); i) A. N. Volkov, A. V. Bogdanova, and G. P. Kugatova-Shemyakina, *Zh. Org. Khim.*, **3**, 316 (1967); *Chem. Abstr.*, **66**, 115346x (1967); j) L. I. Vereshchagin, S. R. Gainulina, L. P. Kirillova, and T. V. Lipovich, *ibid.*, **5**, 1557 (1969); *Chem. Abstr.*, **72**, 12456c (1970); k) B. P. Gusev, I. I. Nazarova, and V. F. Kucherov, *Khim. Atsetilena*, **1968**, 88; *Chem. Abstr.*, **71**, 61082r (1969); l) D. R. Williams, A. Abbaspour, and R. M. Jacobson, *Tetrahedron Lett.*, **22**, 3564 (1981). For preparation of 4-hydroxy-3-furanones, see: m) M. Baumann and W. H. Hoffmann, *Synthesis*, **1981**, 709; Ref. 9, 10j, and 10k. For preparation of 2-alkylidene-3(2*H*)-furanones, see: n) I. da Rocha Pitta, M. do Socorro Lacerda, and C. Luu Duc, *J. Heterocycl. Chem.*, **16**, 821 (1979); o) B. Chantegrel and S. Gelin, *Synthesis*, **1981**, 45.

16) Similar enol acetates were prepared from the corresponding dihydro-3(2*H*)-furanones and transformed into 4-chloro-4,5-dihydro-3(2*H*)-furanones, see: I. K. Korobitsyna, I. G. Zhukova, V. A. Kuvshinova, N. N. Gaidamovich, and Yu. K. Yur'ev, *Dokl. Akad. Nauk SSSR*, **114**, 327 (1957); *Chem. Abstr.*, **52**, 349f (1958). See also Ref. 10l.

17) D. G. Oelberg and M. D. Schiavelli, *J. Org. Chem.*, **42**, 1804 (1977); W. R. Been, *ibid.*, **33**, 3113 (1968); P. D. Landor and S. R. Landor, *J. Chem. Soc.*, **1956**, 1015; G. Saucy, R. Marbet, H. Lindlar, and O. Isler, *Helv. Chim. Acta*, **42**, 1945 (1959); H. Schlossarczyk, W. Sieber, M. Hesse, H.-J. Hansen, and H. Schmid, *ibid.*, **56**, 875 (1973); F. Hoffmann-La-Roche and Co., A.-G. Belgian Patent 617174 (1962); *Chem. Abstr.*, **59**, 1540f (1963); A. C. Day and M. C. Whiting ,*J. Chem. Soc., C*, **1966**, 464.

18) G. Leandri, H. Monti, and M. Bertrand, *Tetrahedron*, **30**, 289 (1974); L.-I. Olsson and A. Claesson, *Synthesis*, **1979**, 743; P. Audin, A. Doutheau, and J. Gore, *Tetrahedron Lett.*, **23**, 4337, (1982); J.-J. Chilot, A. Doutheau, and J. Gore, *ibid.*, **23**, 4693 (1982).

19) a) W. Parker, R. A. Raphael, and D. I. Wilkinson, *J. Chem. Soc.*, **1958**, 3871; b) A. Takeda, S. Tsuboi, and T. Sakai, *Chem. Lett.*, **1973**, 425; c) L. D. Gavrilov, M. I. Klopotova, and L. I. Vereshchagin, *Zh. Org. Khim.*, **10**, 2064 (1974); d) J. E. Baldwin, R. C. Thomas, L. I. Kruse, and L. Silberman, *J. Org. Chem.*, **42**, 3846 (1977); e) A. B. Smith, III and P. J. Jerris, *Synth. Commun.*, **8**, 421 (1978); f) M. Ito, M. Ohno, E. Takeo, Y. Oda, and K. Tsukida, *Heterocycles*, **12**, 505 (1979); g) Y. Takahashi, H. Hagiwara, H. Uda, and H. Kosugi, *ibid.*, **15**, 225 (1981).

20) The aldehyde **9** was prepared by selenium dioxide oxidation of 7-(3-methyl-2-butenyloxy)coumarin, see: E. V. Lassak and I. A. Southwell, *Aust. J. Chem.*, **25**, 2451 (1972).

21) *Cf.* Ref. 12d.

22) M. Karpf and A. S. Dreiding, *Helv. Chim. Acta*, **59**, 1226 (1976).

23) M. F. Shostakovskii, V. M. Vlasov, and A. A. Vasileva, *Izv. Akad. Nauk SSSR, Ser. Khim.*, **1964**, 696.

24) K. Zeil and H. Meyer, *Ber. Deuch. Chem. Ges.*, **75**, 356 (1942).

25) A. I. Nogaideli, K. Ya. Dzagnidze, and R. PaPava, *Zh. Obshch. Khim.*, **28**, 116 (1958); *Chem. Abstr.*, **52**, 12758a (1958).

26) S. A. Vartanyan, G. A. Chukhadzhyan, and V. N. Zhamagortsyan, *Izv. Akad. Nauk Arm. SSR, Khim. Nauki*, **12**, 107 (1959); *Chem. Abstr.*, **55**, 5370c (1961).

27) A. Babayan, B. Akopyan, and R. G. Kevhyan, *J. Gen. Chem.*, **9**, 1631 (1939); *Chem. Abstr.*, **34**, 2788 (1940).

28) M. Gouge, *Ann. Chim.*, **6**, 648 (1951).

29) I. N. Nazarov and A. N. Elizarova, *Bull. Akad. Sci. U. R. S. S., Classe Sci. Chim.*, **1948**, 107; *Chem. Abstr.*, **42**, 7738a (1948).

30) I. K. Korobitsyna, L. A. Kazitsyna, and Yu. K. Yur'ev, *Zh. Obshch. Khim.*, **25**, 1349 (1955); *Chem. Abstr.*, **49**, 15481h (1955).

31) For Nafion®-H catalyzed ether formation, see: G. A. Olah, A. P. Fung, and P. Malhotra, *Synthesis*, **1981**, 474.

New Methods for the Synthesis of 3(2*H*)-Furanones and 2(5*H*)-Furanones

Hiroyuki Saimoto, Masaki Shinoda, Seijiro Matsubara, Koichiro Oshima, Tamejiro Hiyama,*,† and Hitosi Nozaki

Department of Industrial Chemistry, Kyoto University, Yoshida, Sakyo-ku, Kyoto 606

(Received March 23, 1983)

New procedures for the synthesis of 3(2*H*)-furanones and 4-alkoxy-2(5*H*)-furanones are reported. Reaction of ketones with the lithium salt of propynal diethyl acetal, followed by treatment of the resulting 4-hydroxy-2-alkynal diethyl acetals with sulfuric acid–methanol, gave 2,2-disubstituted 3(2*H*)-furanones. The action of a polymer reagent Hg/Nafion-H upon 4-hydroxy-2-alkynones produced 2,2,5-trisubstituted 3(2*H*)-furanones. Reaction of 1,1,1-triethoxy-2-alkyn-4-ols (**4**) with trifluoroacetic acid and mercury(II) acetate provided 5-ethoxy-2,2-disubstituted 3(2*H*)-furanones. In contrast, the adducts **4** were converted into 4-alkoxy-5,5-disubstituted 2(5*H*)-furanones upon reaction with Hg/Nafion-H.

In the preceding paper we have reported new methods for regiocontrolled synthesis of 4,5-dihydro-3(2*H*)-furanones from 2-butyne-1,4-diol derivatives.[1] As the final step of the procedure was the oxidation to 3(2*H*)-furanones, it was anticipated that employing the derivatives of 2-butyne-1,4-diols with higher oxidation stage as the starting materials would lead to 3(2*H*)-furanones[2] directly. This was indeed the case as demonstrated by the reactions summarized in Scheme 1.

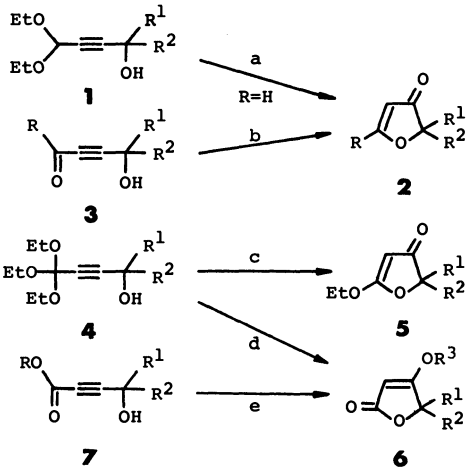

a) H_2SO_4–MeOH; b,d,e) Hg/Nafion-H; c) CF_3COOH, $Hg(OAc)_2$.

Scheme 1.

Transformation of 4-Hydroxy-2-alkynal Diethyl Acetals **1** *into 3(2H)-Furanones* **2**. The carbonyl addition of the lithiated propynal diethyl acetals to ketones produced the acetylenic alcohols **1**.[3] Treatment of the adducts **1** with a 1 : 1 mixture of sulfuric acid and methanol at 0 °C gave 3(2*H*)-furanones **2**.[4] Results are summarized in Table 1. The new transformation is understood in terms of the sequence in Scheme 2. Initial elimination of an ethoxyl group and hydration of the triple bond are followed by intramolecular nucleophilic attack of the tertiary hydroxyl group. The Baldwin's rule[5] says that the 5-*exo-trig.* reaction is allowed. It is worthy to note

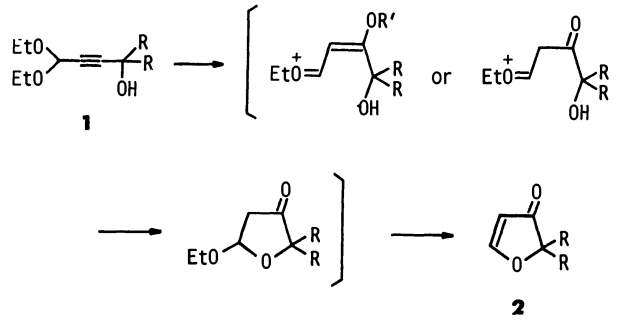

Scheme 2.

that the propargylic tertiary hydroxyl group in **1** remains intact under the acidic conditions.[6]

Synthesis of 3(2H)-Furanones **2** *from 4-Hydroxy-2-alkynones* **3**. The hydroxy ketones **3** were previously prepared by MnO_2 oxidation of the corresponding 2-butyne-1,4-diols in poor yields.[7,8] We found that treatment of the 2-butyne-1,4-diol derivatives with *t*-butyl hydroperoxide and Nafion-H[9] at 25 °C provided ketones **3** effectively. They were converted by step b in Scheme 1 into 3(2*H*)-furanones **2** in excellent yields with Hg/Nafion-H reagent[1] in the presence of 5 equivalents of water in ethanol at 40 °C[10] (Table 2). The conjugate addition of water to the triple bond took place efficiently with complete regioselectivity.

The combined process was applied to the synthesis of a naturally occurring 3(2*H*)-furanone, bullatenone (**2f**)[11] of Table 2. Oxidation of 4-methyl-1-phenyl-2-pentyne-1,4-diol with *t*-butyl hydroperoxide and Nafion-H followed by treatment with Hg/Nafion-H gave the furanone **2f** in a quantitative yield.

Transformation of 1,1,1-Triethoxy-2-alkyn-4-ols **4** *into 5-Ethoxy-3(2H)-furanones* **5** *and 4-Alkoxy-2(5H)-furanones* **6**. The starting alkynols **4** were prepared by the reaction of ketones with the lithium salt of 3,3,3-triethoxypropyne in THF. Treatment of the adduct **4** with trifluoroacetic acid and mercury(II) acetate at reflux temperature (step c in Scheme 1) afforded the 3-furanones **5** in moderate yields (Table 3).

On the other hand, the reaction of the ortho ester **4a** with the Hg/Nafion-H reagent and 5 equivalents of water in ethanol gave 2(5*H*)-furanone[12] **6a** in 81% yield (step d in Scheme 1). This transformation could

† Present address: Sagami Chemical Research Center, 4-4-1, Nishiohnuma, Sagamihara, Kanagawa 229.

Table 1. 3(2*H*)-Furanones **2** from 4-hydroxy-2-alkynal diethyl acetals **1**

Ketone	Yield/% of the adduct[a,b]		Yield/% of 3(2*H*)-furanone[a,c]	
Acetone	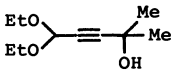 **1a**	64	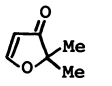 **2a**	98
Cyclohexanone	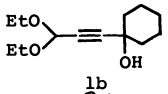 **1b**	99	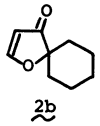 **2b**	67
Cyclododecanone	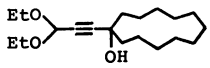 **1c**	79	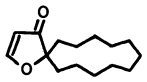 **2c**	70

a) Isolated yields. b) Ketones were allowed to react with the lithium salt of propynal diethyl acetal. c) The adducts **1** were treated with H_2SO_4–MeOH.

Table 2. Transformation of 4-hydroxy-2-alkynones **3** into 3(2*H*)-furanones **2**

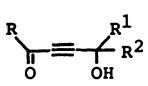
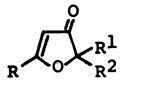
Yield/%[a,b]

	R	R^1	R^2		
3a	Me	Me	Me	**2d**	92
3b	Me		$-(CH_2)_5-$	**2e**	87
3c	Ph	Me	Me	**2f**	100
3d		$-(CH_2)_8-$	H	**2g**	90[c]

a) Isolated yields. b) Alkynols **3** were treated with Hg/Nafion-H. c) 4-Acetoxy-2-cyclododecyn-1-one was employed as a starting material.

Table 3. Synthesis of 5-ethoxy-3(2*H*)-furanones **5** from 1,1,1-triethoxy-2-alkyn-4-ols **4**

Ketone	Yield/% of the adduct[a,b]		Yield/% of 3(2*H*)-furanone[b,c]	
Acetone	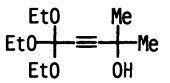 **4a**	67	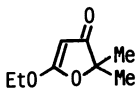 **5a**	63
Cyclohexanone	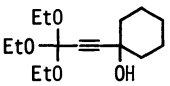 **4b**	66	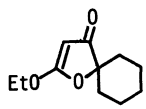 **5b**	49

a) Ketones were allowed to react with lithium salt of triethyl orthopropiolate. b) Isolated yields. c) The adducts **4** were treated with CF_3CO_2H–$Hg(OAc)_2$.

be effected by a mixture of sulfuric acid–methanol less efficiently[13] (Table 4). Monitoring experiments revealed the intermediacy of ethyl 4-hydroxy-2-alkynoates. Thus the methyl ester **7b** generated independently gave the 2(5*H*)-furanone **6c** on treatment with Hg/Nafion-H (step e in Scheme 1).

Table 4. Synthesis of 4-alkoxy-2(5*H*)-furanones **6**

Starting alkynol	Yield/% of **6**[a]	
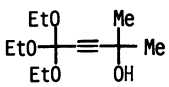 **4a**	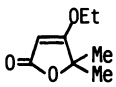 **6a**	81[b]
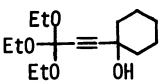 **4b**	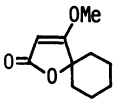 **6b**	30[c]
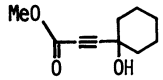 **7b**	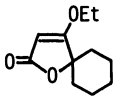 **6c**	85[b]

a) Isolated yields. b) Hg/Nafion-H was used for the cyclization. c) The alkynol **4b** was treated with H_2SO_4–MeOH.

Experimental

Distillation was carried out by use of Kugelrohr (Büchi) and boiling points were determined by measuring the bath temperature. All mp and bp are not corrected. ^{1}H-NMR spectra (tetramethylsilane as an internal standard) were obtained on a Varian EM 390 spectrometer, chemical shifts being given in ppm units, IR spectra of neat liquid film samples (unless otherwise noted) on a Shimadzu IR-27G spectrometer, MS on a Hitachi RMU-6L spectrometer, and exact mass on a Hitachi M 80 spectrometer. Gas-liquid phase chromatography (GLC) analyses were performed with a Yanagimoto GCG-550F chromatograph, and preparative GLC with a JEOL JGC-20K chromatograph. Preparative TLC plates were prepared with Merck Kiesel-gel PF_{254}. Column chromatography was carried out with silica gel (Wakogel C-100) at atmospheric pressure. Commercial sulfuric acid (97%) and *t*-butyl hydroperoxide (Nakarai Chemicals Ltd., 70% aqueous solution) were used.

Synthesis of 1-Oxaspiro[4.11]hexadec-2-en-4-one (2c) from Cyclo-

dodecanone (A Typical Procedure). To a THF (10 ml) solution of propynal diethyl acetal[14] (0.96 g, 7.5 mmol) was added a hexane solution of butyllithium (1.85 M,** 4.1 ml, 7.5 mmol) at −78 °C. After 10 min cyclododecanone (0.91 g, 5.0 mmol) dissolved in THF (7 ml) was added in 15 min. The reaction mixture was stirred at −78 °C for 1 h and at 25 °C for 30 min. Workup followed by column chromatography (hexane–ether 5 : 1) gave 1-(3,3-diethoxypropynyl)cyclododecanol **1c** (1.22 g, 79% yield). Mp 45.0—45.5 °C (hexane); bp 192—193 °C (bath temp)/0.15 Torr;†† ^{1}H-NMR (CCl_4): δ=1.19 (t, J=7.5 Hz, 6H), 1.2—2.2 (m, 23H), 3.3—3.8 (m, 4H), 5.11 (s, 1H); IR: 3430, 2270, 1121, 1055, 1008 cm^{-1}; MS: *m/e* (rel intensity) 310 (M^+, 5), 265(20), 149(8), 119(98), 117(100), 103(60). Found: C, 73.25; H, 11.02%. Calcd for $C_{19}H_{34}O_3$: C, 73.50; H, 11.04%.

The adduct **1c** (0.22 g, 0.71 mmol) was dissolved in methanol (1.0 ml) and cooled at 0 °C. To this solution was added sulfuric acid (1.0 ml) dropwise over 10 min. After stirring for 30 min, the reaction mixture was diluted with ether and neutralized with aqueous sodium hydrogencarbonate solution. Extractive workup followed by preparative TLC purification (hexane–ether 1 : 1, R_f 0.33—0.47) gave **2c** (0.12 g, 70% yield). Mp 81.0—81.5 °C (hexane); IR (Nujol): 1709, 1684, 1569 cm^{-1}; ^{1}H-NMR (CCl_4): δ=1.2—1.8 (m, 22H), 5.43 (d, J=2.7 Hz, 1H), 8.04 (d, J=2.7 Hz, 1H); MS: *m/e* (rel intensity) 236 (M^+, 32), 123(32), 110(31), 97(100). Found: C, 75.92; H, 10.23%. Calcd for $C_{15}H_{24}O_2$: C, 76.22; H, 10.24%.

This procedure applies to the synthesis of **1a**, **1b**, **2a**, and **2b**, whose physical properties are summarized below.

*5,5-Diethoxy-2-methyl-3-pentyn-2-ol (**1a**).*[38] ^{1}H-NMR (CCl_4): δ=1.19 (t, J=7.5 Hz, 6H), 1.48 (s, 6H), 2.96 (br s, 1H), 3.3—3.8 (m, 4H), 5.12 (s, 1H); IR: 3400, 2270, 1104, 1045, 1009 cm^{-1}; (Found: *m/e* 185.1198, M^+-1).

*5,5-Dimethyl-3(2H)-furanone (**2a**).*[15] ^{1}H-NMR (CCl_4): δ=1.33 (s, 6H), 5.48 (d, J=2.7 Hz), 8.06 (d, J=2.7 Hz, 1H); IR: 1702, 1555, 794 cm^{-1}; MS: *m/e* 112 (M^+).

*1-(3,3-Diethoxypropynyl)cyclohexanol (**1b**).* Bp 103—110 °C (bath temp)/0.05 Torr; ^{1}H-NMR (CCl_4): δ=1.20 (t, J=7.5 Hz, 6H), 1.2—2.0 (m, 10H), 2.6—3.0 (m, 1H), 3.3—3.9 (m, 4H), 5.15 (s, 1H); IR: 3405, 2260, 1112, 1048, 1005 cm^{-1}; MS: *m/e* (rel intensity) 226 (M^+, 5), 197(3), 181(100), 153(29), 107(25), 79(35), 55(57). Found: C, 68.81; H, 9.74%. Calcd for $C_{13}H_{22}O_3$: C, 68.99; H, 9.80%.

*1-Oxaspiro[4.5]dec-2-en-4-one (**2b**).*[16] ^{1}H-NMR (CCl_4): δ=1.1—2.0 (m, 10H), 5.48 (d, J=2.6 Hz, 1H), 8.09 (d, J=2.6 Hz, 1H); IR: 1700, 1562, 1173 cm^{-1}; MS: *m/e* 152 (M^+).

*Transformation of 4-Hydroxy-4-methyl-1-phenyl-2-pentyn-1-one (**3c**) into Bullatenone (**2f**) (A Typical Procedure).* 4-Methyl-1-phenyl-2-pentyne-1,4-diol[1] (28 mg, 0.15 mmol) was treated with Nafion®-H[1,9] (24 mg) in 70% aqueous *t*-butyl hydroperoxide (1 ml) at 25 °C for 42 h. The reaction mixture was filtered, and the catalyst was washed with dichloromethane. Concentration of the combined filtrates *in vacuo* afforded **3c**[10a] (28 mg) quantitatively. An ethanol (1 ml) solution of **3c** (37 mg, 0.20 mmol) was stirred with Hg/Nafion-H[1] (52 mg) in the presence of water (18 mg, 1.0 mmol) at 40 °C for 14 h. Removal of the polymer reagent by filtration and concentration of the filtrate gave bullatenone (**2f**)[11] (37 mg, 100%) whose spectral data were identical with the recorded ones.

Spectral properties of **2d** and **3e** are listed below.

*2,2,5-Trimethyl-3(2H)-furanone (**2d**)*[17] *from **3a**.*[18] ^{1}H-NMR (CCl_4): δ=1.29 (s, 6H), 2.17 (s, 3H), 5.20 (s, 1H); IR: 1700, 1601, 1390, 1179 cm^{-1}; MS: *m/e* 126 (M^+).

*2-Methyl-1-oxaspiro[4.5]dec-2-en-4-one (**2e**)*[19] *from **3b**.*[20] ^{1}H-NMR (CCl_4): δ=1.0—2.1 (m, 10H), 2.21 (s, 3H), 5.26 (s, 1H); IR: 1697, 1601, 1386, 1348, 1062 cm^{-1}; MS: *m/e* 166 (M^+).

*13-Oxabicyclo[8.2.1]tridec-1(12)-en-11-one-1(**2g**).* 2-Cyclododecyne-1,4-diol[21] (284 mg, 1.5 mmol) was treated with acetic anhydride (148 mg, 1.5 mmol) and pyridine (1 ml) at 25 °C for 5 h, and the reaction mixture was concentrated. Purification of the residue by column chromatography (hexane–ethyl acetate 5 : 1) gave 4-acetoxy-2-cyclodecynol (159 mg, 46% yield) together with the diol (76 mg) and the diacetate (92 mg). ^{1}H-NMR (CCl_4) of the monoacetate: δ= δ=1.1—2.1 (m+s (δ=2.00), 20H), 4.2—4.4 (m, 1H), 5.1—5.4 (m, 1H); IR: 3430, 1741, 1229, 1020 cm^{-1}; MS: *m/e* 238 (M^+).

A dichloromethane (3 ml) solution of the monoacetate (64 mg, 0.27 mmol) was added to pyridinium chlorochromate (87 mg, 0.40 mmol) and sodium acetate (7 mg, 0.08 mmol) in dichloromethane (0.5 ml) at 0 °C. After stirring for 6 h at 25 °C, workup followed by column chromatography (ether) gave 4-acetoxy-2-cyclododecyn-1-one (55 mg, 90%yield). Bp 140—142 °C (bath temp)/0.09 Torr; ^{1}H-NMR (CCl_4): δ= 1.1—2.1 (m+s (δ=2.04), 17H), 2.3—2.6 (m, 2H), 5.46 (t, J=6.0 Hz, 1H); IR: 2250, 1742, 1672, 1218, 1020 cm^{-1}; MS: *m/e* (rel intensity) 236 (M^+, trace), 194(3), 123(11), 97(17), 79(17), 55(21), 43(100). Found: C, 70.91; H, 8.51%. Calcd for $C_{14}H_{20}O_3$: C, 71.16; H, 8.53%.

An ethanol (0.5 ml) solution of the acetylenic ketone (30 mg 0.13 mmol) was stirred with Hg/Nafion-H (31 mg) in the presence of water (11 mg, 0.64 mmol) at 40 °C for 7 h. Filtration of the reaction mixture and concentration of the filtrate gave **2g** (22 mg, 90% yield). Mp 60.5—61.5 °C (hexane); ^{1}H-NMR (CCl_4): δ=0.8—2.9 (m, 16H), 4.34 (t, J=7.8 Hz, 1H), 5.34 (s, 1H), IR (CCl_4): 1700, 1590, 1376, 1158 cm^{-1}; MS: *m/e* (rel intensity) 194 (M^+, 5), 148(41), 122(44), 81(55), 69(68), 67(62), 55(74), 40(100). Found: *m/e* 195.1295. Calcd for $C_{12}H_{19}O_2$: M^++1, 195.1383.

*Synthesis of 2-Ethoxy-1-oxaspiro[4.5]dec-2-en-4-one (**5b**) (A Typical Procedure).* A hexane solution of butyllithium (1.60 M, 4.4 ml, 7.0 mmol) was added at −78 °C to 3,3,3-triethoxypropyne[22] (1.20 g, 7.0 mmol) in THF (10 ml). After stirring for 40 min, cyclohexanone (0.97 g, 9.9 mmol) dissolved in THF (6 ml) was added in 20 min. Stirring at −78 °C for 50 min, at 25 °C for 20 min, followed by workup and column chromatography (hexane–ethyl acetate 5 : 1) gave the adduct **4b** (1.24 g, 66% yield). Bp 148—150 °C (bath temp)/0.12 Torr; ^{1}H-NMR (CCl_4): δ=1.0—2.4 (m+t (δ=1.20, J=6.6 Hz), 20H), 3.57 (q, J=6.6 Hz, 6H); IR: 3400, 2230, 1240, 1084, 1041 cm^{-1}; MS: *m/e* (rel intensity) 225 (M^+ $-C_2H_5O$, 100), 179(40), 141(26), 105(35), 95(30), 81(30). Found: *m/e* 255.1557. Calcd for $C_{14}H_{23}O_4$: M^+-CH_3, 255.1594.

Trifluoroacetic acid (3 ml) was added at 25 °C to the adduct **4b** (122 mg, 0.45 mmol) and mercury(II) acetate (144 mg, 0.45 mmol). After stirring for 15 min at reflux temperature, workup and preparative TLC purification (hexane–ethyl acetate 2 : 1, double development) gave **5b** (R_f 0.30—0.40, 43 mg, 49% yield). Mp 54.1 °C (hexane); ^{1}H-NMR (CCl_4): δ=1.0—2.0 (m+t (δ=1.48, J=7.5 Hz), 13H), 4.21 (q, J= 7.5 Hz, 2H), 4.57 (s, 1H); IR: 1696, 1573, 1427, 1360, 881 cm^{-1}; MS: *m/e* (rel intensity) 197 (M^++1, 4), 196 (M^+, 24), 141(21), 115(21), 83(36), 81(36), 69(77), 40(100). Found: C, 67.44; H, 8.36%. Calcd for $C_{11}H_{16}O_3$: C, 67.32; H, 8.22%.

This procedure was applied to the synthesis of **4a** and **5a**.

*4,4,4-Triethoxy-2-methyl-3-pentyn-2-ol (**4a**) and 2,2-Dimethyl-5-ethoxy-3(2H)-furanone (**5a**).* The ortho ester **4a** showed bp 135—136 °C (bath temp)/0.12 Torr; ^{1}H-NMR (CCl_4):

** 1 M=1 mol dm^{-3}; †† 1 Torr=133.322 Pa.

δ=0.80 (t, J=7.2 Hz, 9H), 1.12 (s, 6H), 1.4—1.8 (m, 1H), 3.17 (q, J=7.2 Hz, 6H); IR: 3450, 2250, 1240, 1170, 1085, 1034 cm^{-1}; MS: *m/e* (rel intensity) 185 ($M^+-C_2H_5O$, 84), 111(44), 95(100), 71(36), 67(37), 59(42), 43(80). Found: *m/e* 231.1578. Calcd for $C_{12}H_{23}O_4$: M^++1, 231.1594.

Physical properties of the 3-furanone **5a** are given. Bp 98—100 °C (bath temp)/0.13 Torr; ^{1}H-NMR (CCl_4): δ=1.39 (s, 6H), 1.47 (t, J=7.2 Hz, 3H), 4.28 (q, J=7.2 Hz, 2H), 4.55 (s, 1H); IR: 1675, 1567, 1175, 1057 cm^{-1}; MS: *m/e* (rel intensity) 157 (M^++1, 4), 156 (M^+, 23), 111(2), 97(12), 87(12), 69(100), 59(55), 43(30). Found: *m/e* 156.0885. Calcd for $C_8H_{12}O_3$: M^+, 156.0786.

*5,5-Dimethyl-4-ethoxy-2(5H)-furanone (**6a**).* An ethanol (1 ml) solution of **4a** (40 mg, 0.17 mmol) was stirred with Hg/Nafion-H (46 mg) in the presence of water (13 mg, 0.74 mmol) at 40 °C for 40 h. Filtration of the reaction mixture followed by concentration of the filtrate gave **6a**[13a] (22 mg, 81% yield). Bp 114—115 °C (bath temp)/0.12 Torr; ^{1}H-NMR (CCl_4): δ=1.41 (t, J=6.9 Hz, 3H), 1.42 (s, 6H), 4.05 (q, J=6.9 Hz, 2H), 4.81 (s, 1H); IR: 1754, 1634, 1342, 1266, 1260 cm^{-1}; MS: *m/e* 156 (M^+).

When the reaction was carried out at 25 °C for 1.5 h, ethyl 4-hydroxy-4-methyl-2-pentynoate (**7a**)[23] was produced in a quantitative yield. Bp 100—101 °C (bath temp)/0.5 Torr; ^{1}H-NMR (CCl_4): δ=1.29 (t, J=7.2 Hz, 3H), 1.52 (s, 6H), 3.26 (s, 1H), 4.14 (q, J=7.2 Hz, 2H); IR: 3410, 2230, 1712, 1253, 1030 cm^{-1}; MS: *m/e* 141 (M^+).

*4-Methoxy-1-oxaspiro[4.5]dec-3-en-one (**6b**).* A mixture of sulfuric acid (0.15 ml) and methanol (0.15 ml) was added to **4b** (62 mg, 0.23 mmol) dissolved in methanol (0.15 ml) at 25 °C in 10 min. After stirring for 2 h, workup followed by preparative TLC separation (hexane–ether 1 : 1) gave **6b**[13a] (R_f 0.08—0.12, 13 mg, 30% yield) having ^{1}H-NMR (CCl_4): δ=1.0—2.5 (m, 10H), 3.77 (s, 3H), 5.03 (s, 1H); IR: 1711, 1614, 1228, 1030 cm^{-1}; MS: *m/e* 182 (M^+).

*4-Ethoxy-1-oxaspiro[4.5]dec-3-en-2-one (**6c**).* Methyl 4-(1-hydroxycyclohexyl)-2-butynoate (**7b**)[13a] (50 mg, 0.28 mmol) dissolved in ethanol (1 ml) was treated with Hg/Nafion-H (103 mg) in the presence of water (25 mg, 1.4 mmol) at 40 °C for 50 h. Removal of the polymer reagent by filtration and concentration of the filtrate gave **6c** (46 mg, 85% yield). Mp 70—71 °C (hexane); bp 95—97 °C (bath temp)/0.07 Torr; ^{1}H-NMR (CCl_4): δ=0.9—2.1 (m+t(δ=1.40, J=6.8 Hz), 13H), 4.00 (q, J=6.8 Hz, 2H), 4.74 (s, 1H); IR: 1751, 1627, 1336, 1195, 976 cm^{-1}; MS: *m/e* (rel intensity) 196 (M^+, 25), 168(22), 153(28), 140(56), 125(34), 112(41), 69(100), 55(56), 43(31). Found: C, 67.37; H, 8.48%. Calcd for $C_{11}H_{16}O_3$: C, 67.32; H, 8.22%.

Financial support by the Nissan Kagaku Kogyo Ltd. and the Ministry of Education, Science and Culture (Grant-in-Aid for Special Project Research No. 57118006) is acknowledged.

References

1) H. Saimoto, T. Hiyama, and H. Nozaki, *Bull. Chem. Soc. Jpn.*, **56**, 3078 (1983); *J. Am. Chem. Soc.*, **103**, 4975 (1981).

2) Reports of new naturally occurring 3-furanones are abundant in the literature, for example: F. Bohlmann, U. Fritz, R. M. King, and H. Robinson, *Phytochemistry*, **20**, 743 (1981); F. Bohlmann, C. Zdero, J. Pickard, H. Robinson, and R. M. King, *ibid.*, **20**, 1323 (1981); P. Bloch and C. Tamm, *Helv. Chim. Acta*, **64**, 304 (1981); W. Breitenstein, K. K. Chexal, P. Mohl, and C. Tamm, *ibid.*, **64**, 379 (1981).

3) *Cf.* a) E. P. Serebryakov, L. M. Kostochka, and V. F. Kucherov, *Zh. Org. Chem.*, **9**, 1617 (1973); *J. Org. Chem. USSR*, **9**, 1640 (1973); b) D. R. Williams, A. Abbaspour, and R. M. Jacobson, *Tetrahedron Lett.*, **22**, 3565 (1981).

4) For a preliminary communication on this work, see: T. Hiyama, M. Shinoda, H. Saimoto, and H. Nozaki, *Heterocycles*, **15**, 263 (1981).

5) J. E. Baldwin, *J. Chem. Soc., Chem. Commun.*, **1976**, 734, 738, J. E. Baldwin, J. Cutting, W. Dupont, L. Kruse, L. Silberman, and R. C. Thomas, *ibid.*, **1976**, 736; J. E. Baldwin in "Further Perspectives in Organic Chemistry," Ciba Foundation Symposium 53, Elsevier, Amsterdam (1978), pp. 85—99.

6) Under the reaction conditions, elimination of the acetylenic hydroxyl groups of 2-butyne-1,4-diol derivatives took place to yield cyclopentenones: T. Hiyama, M. Shinoda, H. Saimoto, and H. Nozaki, *Bull. Chem. Soc. Jpn.*, **54**, 2747 (1981). Elimination of the propargylic hydroxyl group of **1** led to cyclopentenone formation, see Ref. 3b.

7) a) L. I. Vereshchagin, S. R. Gainulina, and L. P. Kirilova, *Biol. Activ. Soedin.*, **1968**, 154; *Chem. Abstr.*, **71**, 123446y (1969); b) M. F. Shostakovskii, T. A. Favorskaya, A. S. Medvedeva, L. P. Safronova, and V. K. Voronov, *Zh. Org. Khim.*, **6**, 2377 (1970); *J. Org. Chem. USSR*, **6**, 2390 (1970).

8) For preparation of **3** from ketones and 1-alkyn-3-ones, see: D. I. Mikhailovskii, V. N. Rozhkova, and T. A. Favorskaya, *Zh. Org. Khim.*, **6**, 397 (1970); *J. Org. Chem. USSR*, **6**, 386 (1970); D.I. Mikhailovskii, V.N. Mikhailovskaya and T. A. Favorskaya, *ibid.*, **9**, 1804 (1973); *J. Org. Chem. USSR*, **9**, 1829 (1973); **10**, 188, 190 (1974). For the reaction of ketones with the anion of 3,3-ethylenedioxy-1-butyne, see: C. Feugeas and G. Giusti, *C. R. Akad. Sci., Paris, Ser. C*, **264**, 1772 (1967) and Ref. 3b also.

9) We are indebted to E. I. du Pont de Nemours and Co. and Mitsui Fluorochemical Co. for generous gift of Nafion.®

10) Previously the transformation of the alkynones **3** into 3(2*H*)-furanones **2** proceeded less efficiently: a) W. Parker, R. A. Raphael, and D. I. Wilkinson, *J. Chem. Soc.*, **1958**, 3871; b) S. A. Vartanyan, L. V. Oganova, and Sh. O. Badanyan, *Izv. Akad. Nauk Arm. SSR, Khim. Nauki*, **17**, 709 (1964); *Chem. Abstr.*, **63**, 4232e (1965); c) L. I. Vereshchagin, S. R. Gainulina L. P. Kirillova, and T. V. Lipovich, *Zh. Org. Khim.*, **5**, 1557 (1969); *Chem. Abstr.*, **72**, 12456c (1970); d) L. I. Vereshchagin, L. D. Gavrilov, E. I. Titova, L. G. Tikhonova, S. R. Buzilova, *Khim. Geterotsikl. Soedin.*, **1976**, 1471; *Chem. Abstr.*, **86**, 139749v (1977) and Ref. 7b. For preparation of 3(2*H*)-furanones **2** from acetals of **3**, see Ref. 3b. For transformation of methyl ethers of **3** into **2**, see: e) W. Reid and A. Marhold, *Chem. Ber.*, **107**, 1714 (1974).

11) C. R. Brandt, W. I. Taylor, and B. R. Thomas, *J. Chem. Soc.*, **1954**, 3245; R. E. Rosenkranz, K. Allner, R. Good, W. v. Philipsborn, C. H. Eugster, *Helv. Chim. Acta*, **46**, 1259 (1963) and Refs. 1, 10a.

12) Reviews: Y. S. Rao, *Chem. Rev.*, **76**, 625 (1976); A. A. Avetisyan and M. T. Dangyan, *Russ. Chem. Rev.*, **46**, 643 (1977). Recent methods for the synthesis of 2(5*H*)furanones, see: K. Iwai, H. Kosugi, H. Uda, and M. Kawai, *Bull. Chem. Soc. Jpn.*, **50**, 242 (1977); R. R. Schmidt and J. Talbiersky, *Angew. Chem., Int. Ed. Engl.*, **17**, 204 (1978); A. S. Berg and P. Kolsaker, *Acta Chem. Scand., Ser. B*, **32**, 665 (1978); D. Caine and S. Frobese, *Tetrahedron Lett.*, **1978**, 5167; D. Goldsmith, D. Liotta, C. Lee, and G. Zima, *ibid.*, **1979**, 4801; A. Pelter, R. Al-Bayati, R. Hansel, H. Dinter, and B. Burke, *ibid.*, **22**, 1545 (1981); M. Larcheveque, Ch. Legueut, A. Debal, and J. Y. Lallemand, *ibid.*, **22**, 1595 (1981); P. Barbier and C. Benezra, *ibid.*, **23**, 3511 (1982); M. Ito and K. Tsukida, *Heterocycles*, **19**, 1385 (1982); J. J. Bourguignon and C. G. Wermuth, *J. Org. Chem.*, **46**, 4889 (1981); P. Camps, J. Cardellach, J. Font, R. M. Ortuno, and O. Ponsati, *Tetrahedron*, **38**, 2395 (1982); J. Cardellach, C. Estopa, J. Font, M. Moreno-Manas, R. M.

Ortuno, F. Sanchez-Ferrando, S. Valle, and L. Vilamajo, *ibid.*, **38**, 2377 (1982) and references cited therein.

13) a) E. R. H. Jones and M. C. Whiting, *J. Chem. Soc.*, **1949**, 1423. For the synthesis of δ-lactones, see: b) R. M. Carlson and A. R. Oyler, *Tetrahedron Lett.*, **1974**, 2615; c) R. M. Oylar and J. R. Peterson, *J. Org. Chem.*, **40**, 1960 (1975) and Ref. 10d.

14) M. Grard, *Ann. Chim.* (*Paris*), **13**, 336 (1930); L. Brandsma, "Preparative Acetylenic Chemistry," Elsevier, Amsterdam (1971), p. 118.

15) P. Margaretha, *Tetrahedron Lett.*, **1971**, 4891; B. K. Carpenter, K. E. Clemens, E. A. Schmidt, and H. M. R. Hoffmann, *J. Am. Chem. Soc.*, **94**, 6213 (1972); Ch. Meister and H.-D. Scharf, *Synthesis*, **1981**, 737.

16) F. Sehr, J. L. Isidor, H. R. Taneja, R. M. Carlson, *Tetrahedron Lett.*, **1973**, 557 and Ref. 3b.

17) a) I. N. Nazarov and S. G. Matsoyan, *Zh. Obshch. Khim.*, **27**, 2951 (1957); *Chem. Abstr.*, **52**, 8080f (1958); b) B. P. Gusev, I. I. Nazarova, and V. F. Kucherov, *Izv. Akad. Nauk SSSR, Ser. Khim.*, **1965**, 688.

18) N. A. Milas and J. T. Nolan, Jr., *J. Am. Chem. Soc.*, **80** 5826 (1958) and Ref. 7b.

19) H. Meister, German Patent, 1147593 (1963); *Chem. Abstr.*, **59**, 11427b (1963); D. Caine and W. D. Samuels, *Tetrahedron Lett.*, **21**, 4057 (1980) and Refs. 10d, 17b.

20) M. S. Newman, I. Waltcher, and H. F. Ginsberg, *J. Org. Chem.*, **17**, 962 (1952) and Ref. 7b.

21) B. Chabaud and K. B. Sharpless, *J. Org. Chem.*, **44**, 4202 (1979).

22) H. Stetter and W. Uerdingen, *Synthesis*, **1973**, 207.

23) L. J. Haynes and E. R. H. Jones, *J. Chem. Soc.*, **1946**, 503.

 © 1983 The Chemical Society of Japan Bull. Chem. Soc. Jpn., 56, 3093—3098 (1983)

A Novel Synthesis of α-Methylene-γ-butyrolactones

Hiroyuki Saimoto, Koji Nishio, Hajime Yamamoto, Masaki Shinoda, Tamejiro Hiyama,*,† and Hitosi Nozaki

Department of Industrial Chemistry, Kyoto University, Yoshida, Sakyo-ku, Kyoto 606

(Received March 23, 1983)

A new method is reported for constructing α-methylene-γ-butyrolactone moiety under neutral, anhydrous conditions. Olefin–dibromocarbene adducts were transformed into methyl 1-(dimethylaminomethyl)cyclopropanecarboxylates (**3**). Treatment of **3** with trimethylsilyl iodide followed by thermolytic distillation of the crude products gave α-methylene-γ-butyrolactones with high regio- and stereoselectivity.

Many compounds of natural or synthetic origin having α-methylene-γ-butyrolactone moiety possess a variety of biological activity.[1] Efforts for synthesizing the structural unit have been made extensively,[2,3] but a highly selective method seems still awaited. We found a novel method for constructing the structure under neutral, anhydrous conditions. The process involves ring reorganization of methyl 1-(dimethylaminomethyl)cyclopropanecarboxylates (**3**) with concomitant elimination of the amino group,[4] and is characterized by its high stereo- and regioselectivity. The transformation is accomplished by treatment of **3** with trimethylsilyl iodide[5] followed by thermolytic distillation.[6]

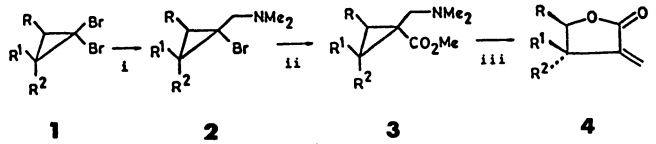

1 **2** **3** **4**

	R	R^1	R^2
a	Ph	H	H
b	n-C_6H_{13}	H	H
c	$-(CH_2)_4-$		H
d	n-C_6H_{13}	n-C_6H_{13}	H
e	n-C_6H_{13}	H	n-C_6H_{13}

i) BuLi, $CH_2{=}N^+Me_2I^-$; ii) BuLi (or *t*-BuLi), $(MeO)_2C{=}O$; iii) Me_3SiI, distillation.

Scheme 1.

The amino esters **3** were prepared as shown in Scheme 1. *gem*-Dibromocyclopropanes **1** underwent bromine–lithium exchange reaction on treatment with butyllithium at −95 °C.[7] The resulting carbenoids then reacted with *N,N*-dimethylmethaniminium iodide[8] to give amino bromides **2**. The configuration of the dimethylaminomethyl group was inferred to be *cis* or *endo* relative to the substituents R and R^1 of **2a—d** on the analogy of our previous observation.[9] Successively, **2** were converted into cyclopropyllithium by the action of butyllithium (for **2a**) or *t*-butyllithium (for **2b—e**) at −78 °C. The bromine–lithium exchange was particularly facilitated by the dimethylamino group which coordinates lithium cation.[10] The cyclopropyllithium reacted with dimethyl carbonate to give **3**.

The amino esters **3** were treated with 3 mol of trimethylsilyl iodide in benzene (for **3a**, **3b**) or 1,2-dichloroethane (for **3c—e**) at 50—95 °C for several hours. After the starting esters were consumed (TLC), all the volatile materials were evaporated *in vacuo*. At first, we dissolved the residue in high boiling solvents and heated as high as 200 °C, but no trace of the desired product was formed.[11] The transformation into the lactones **4** was effectively executed by the thermolytic distillation of the residue under reduced pressure with bath temperature of 170 °C or above by use of Kugelrohl, thermally unstable product being immediately removed from the hot reaction pot. The results are summarized in Table 1.

The transformation of **3a** afforded a plant growth inhibitory α-methylene-γ-lactone (**4a**)[11] as the sole product. Thus, the bond between the substituted carbons of cyclopropane ring is preferentially cleaved. The same preference was observed in the reaction of **3b** which gave **4b** as the major product (71%) accompanied by the regioisomer (29%).[12] The carbon-carbon bond cleavage and carbon-oxygen bond formation proceeded with retention of configuration as observed in the reaction of **3c—e**. Only the *cis* product **4c** was produced from **3c**, and **4d** (*cis-trans* 94 : 6) from **3d** which was derived from **1d** (*cis-trans* 84 : 16). The reaction of *trans* isomer **3e** gave only the *trans* lactone **4e**.

Of special interest in the transformation is the intermediary species leading to **4**. Treatment of **3c** with trimethylsilyl iodide followed by evaporation as above gave an oil which exhibited a singlet peak at δ 3.69 (^{1}H-NMR in $CDCl_3$) without reasonably intense

Table 1. Synthesis of α-methylene-γ-butyrolactones[a]

	Starting dibromide **1** R	R^1	R^2	Yield[b] of **2**/%	Yield[b] of **3**/%	Yield[b] of **4**/%
a	Ph	H	H	59	73	62
b	n-C_6H_{13}	H	H	71[c]	60[c]	58[d]
c	$-(CH_2)_4-$		H	61	61	64
d[e]	n-C_6H_{13}	n-C_6H_{13}	H	49[e]	51[e]	67[f]
e	n-C_6H_{13}	H	n-C_6H_{13}	51	48	73

a) See the Experimental part for each transformations. b) Isolated yields. c) Contained 12% of the stereoisomer. d) Contained 29% of the regioisomer. e) Derived from 7-tetradecene (*cis*: *trans* 84 : 16). f) Contaminated by **4e** (6%).

† Present address: Sagami Chemical Research Center, 4-4-1, Nishiohnuma, Sagamihara, Kanagawa 229.

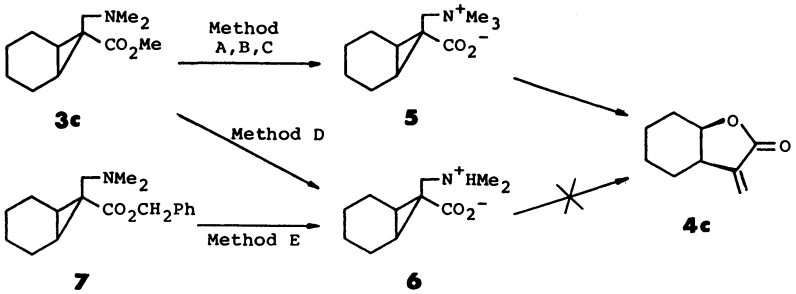

Scheme 2.

TABLE 2. SYNTHESIS OF THE LACTONE **4c** BY MEANS OF VARIOUS METHODS[a]

Starting amino ester	Method		Yield[b] of **4c**/%
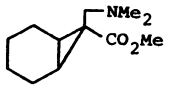 **3c**	A	1) MeI 2) Me_3SiI (2 equiv) 3) dist.	49
	B	1) MeI 2) aq KOH 3) dist.	43
	C	1) aq KOH 2) MeI 3) dist.	34
	D	1) KOH (1.2 equiv) 2) HCl (1.2 equiv) 3) dist.	—
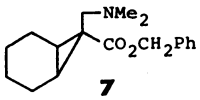 **7**	E	1) Pd/C, H_2 2) dist.	—
	F	1) Me_3SiI 2) dist.	61
	G	1) Pd/C, H_2 2) MeI 3) dist.	51

a) For the detail procedures, see the Experimental parts. b) Isolated yields.

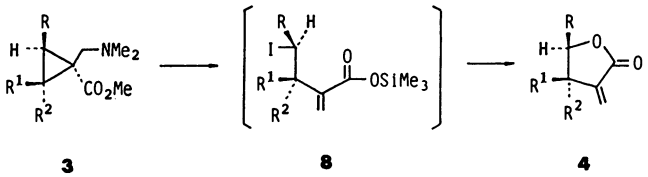

Scheme 3.

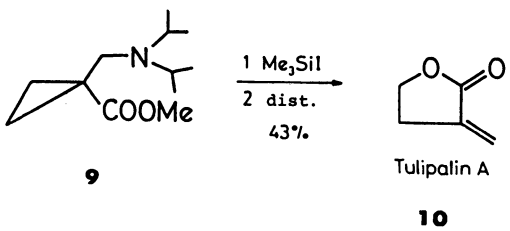

Scheme 4.

peaks due to trimethylsilyl groups. The IR spectrum (neat) revealed the presence of carboxylate (1620, 1400 cm^{-1}) and/or carboxylic acid (3650—2200, 1710 cm^{-1}) functional group(s). Thus, the most likely intermediate seems to be **5** which is derived from trimethylsilyl iodide mediated ester hydrolysis and quaternization. The initial phase of the reaction would be *N*-trimethylsilyl ammonium formation followed by trimethylsilyl-methyl exchange.[13] Indeed, when **5** was produced alternatively by quaternization with methyl iodide and hydrolysis with a base, subsequent thermolysis gave **4c** albeit in somewhat lower yields (Table 2, method A—C). Another possible intermediate **6** could clearly be eliminated as following two procedures failed to give **4c** (Scheme 2): D, (1) hydrolysis of **3c** with aq KOH, (2) neutralization with HCl, (3) distillation; E, (1) hydrogenolysis of benzyl ester **7**, (2) distillation. Of course, the benzyl ester **7** was transformed into **4c** by the standard procedure or by hydrogenolysis followed by quaternization and distillation (Table 2, method F, G). According to recent studies on the trimethylsilyl iodide mediated ring opening of cyclopropanecarboxylates,[14] the stereoselectivity can be explained by the intermediacy of **8** (Scheme 3).

Thus the α-methylene-γ-butyrolactone synthesis described herein has a remarkable feature involving anhydrous, neutral conditions in sharp contrast to the related system which employs aqueous strong acidic conditions.[15] Furthermore, the method has wide applicability as the starting *gem*-dibromocyclopropanes are readily available from olefins and dibromocarbene.

Finally, the sequence was successfully applied to the synthesis of tulipalin A (**10**), a cytotoxic lactone isolated from tulip bulbs[16] and also from Adder's Tongue (*Erythronium americanum*),[17] starting from amino ester **9** (Scheme 4). In this reaction diisopropylamino group is especially pertinent as the dimethylamino derivatives gave only trace amount of **10**. The bulky amino leaving group seems essential for the isolation of the remarkably unstable product.[17]

Experimental

Bulb-to-bulb distillation was carried out by use of Kugelrohr (Büchi) and boiling points were determined by measuring the bath temperature. All mp and bp are not corrected. ^1H-NMR spectra (tetramethylsilane as an internal standard) were obtained on a Varian EM-390 spectrometer, chemical shift being given in ppm units, IR spectra of neat liquid film samples (unless otherwise noted) on a Shimadzu IR-27G spectrometer, MS on a Hitachi RMU-6L spectrometer, and exact mass on a Hitachi M 80 spectrometer. Preparative TLC plates were prepared with Merck Kiesel-gel PF_{254}. Column chromatography was carried out with silica gel

(Wakogel C-100) at atmospheric pressure.

*Transformation of 7,7-Dibromonorcarane (**1c**) into the Lactone **4c** (A Typical Procedure).* *7-exo-Bromo-7-endo-(dimethylaminomethyl)norcarane (**2c**)*: At −95 °C a hexane solution of butyllithium (1.7 M†, 3.4 ml, 5.8 mmol) was added under an argon atmosphere to **1c**[18] (1.32 g, 5.2 mmol) dissolved in THF (30 ml). After 10 min stirring *N,N*-dimethylmethaniminium iodide (1.40 g, 7.5 mmol) was added portionwise at −95 °C. The heterogeneous reaction mixture was stirred for 15 h and warmed gradually to r.t. Workup followed by column chromatography (hexane–ether 10 : 1 to 1 : 100) gave **2c** (0.73 g, 61% yield). Bp 70—80 °C (bath temp)/0.3 Torr;†† ^{1}H-NMR (CCl_4): δ=0.9—2.0 (m, 10H), 2.27 (s, 6H), 2.63 (s, 2H); IR: 2950, 2870, 2835, 2780, 1450, 1025 cm^{-1}; MS: *m/e* (rel intensity) 233 (M^++2, 1), 232 (M^++1, 0.7), 231 (M^+, 1), 152(21), 91(19), 79(31), 68(21), 59(81), 58(43), 46(100), 44(86). Found: *m/e* 231.0641. Calcd for $C_{10}H_{18}BrN$: M^+, 231.0622.

*7-exo-Methoxycarbonyl-7-endo-(dimethylaminomethyl)norcarane (**3c**)*: A pentane solution of *t*-butyllithium (2.3 M, 1.5 ml, 3.4 mmol) was added to a THF (25 ml) solution of **2c** (0.71 g, 3.1 mmol) at −78 °C under an argon atmosphere. After stirring for 1 h, dimethyl carbonate (0.54 g, 6.0 mmol) was added at −78 °C. The whole was stirred for 15 h and warmed to r.t. Workup and column chromatography (hexane–ether 5 : 1 to 1 : 100) gave **3c** (0.39 g, 61% yield). Bp 85—100 °C (bath temp)/0.5 Torr; ^{1}H-NMR (CCl_4): δ=1.1—2.0 (m, 10H) 2.17 (s, 6H), 2.67 (s, 2H), 3.57 (s, 3H); IR: 2950, 2870, 2830, 2780, 1720, 1238, 1186, 1164, 1145 cm^{-1}; MS: *m/e* (rel intensity) 211 (M^+, 1), 168(3), 107(5), 99(4), 90(4), 79(9), 67(4), 59(87), 45(100). Found: C, 68.13; H, 10.25; N, 6.39%. Calcd for $C_{12}H_{21}NO_2$: C, 68.21; H, 10.02; N, 6.63%.

*cis-Hexahydro-3-methylene-2(3H)-benzofuranone (**4c**)*: Trimethylsilyl iodide (0.52 g, 2.6 mmol) was added to **3c** (170 mg, 0.81 mmol) in 1,2-dichloroethane (7 ml) under an argon atmosphere, and the reaction mixture was stirred at reflux temperature for 14 h. Concentration and distillation of the residue (Kugelrohr) gave the crude product collected at 160—210 °C (bath temp) at 0.05 Torr. Purification by preparative TLC (hexane–ether 1 : 1) gave **4c** (R_f 0.4, 78 mg, 64% yield) identical in all respects with the reported data.[19] Bp 105—110 °C (bath temp)/0.5 Torr; ^{1}H-NMR (CCl_4): δ=1.1—2.2 (m, 8H), 2.8—3.2 (m, 1H), 4.46 (dq, *J*=5.1, 6.2 Hz, 1H), 5.43 (d, *J*=2.6 Hz, 1H), 6.08 (d, *J*=2.6 Hz, 1H); IR: 2950, 2860, 1765, 1665, 1255, 1123, 1100, 1010, 889 cm^{-1}; MS: *m/e* 152 (M^+).

This procedure applies to the transformation of **1a**, **1b**, **1d**, and **1e** into **4a**, **4b**, **4d**, and **4e** respectively. Physical properties are summarized below.

*r-1-Bromo-1-(dimethylaminomethyl)-t-2-phenylcyclopropane (**2a**) from **1a**:*[18] Bp 105—115 °C (bath temp)/0.2 Torr; ^{1}H-NMR (CCl_4): δ=1.4—1.7 (m, 2H), 1.88 (d, *J*=13.8 Hz, 1H), 2.12 (s, 6H), 2.56 (d, *J*=13.8 Hz, 1H), 2.75 (t, *J*=8.5 Hz, 1H), 7.20 (s, 5H); IR: 2950, 2830, 2780, 1602, 1500, 1452, 1036, 774, 701 cm^{-1}; MS: *m/e* (rel intensity) 255 (M^++2, 3), 254 (M^++1, 1), 253 (M^+, 3), 175(10), 135(12), 134(100), 129(27), 128(18), 115(15), 91(13), 77(10), 70(15), 59(13), 58(100). Found: *m/e* 253.0472. Calcd for $C_{12}H_{16}BrN$: M^+, 253.0466.

*1-(Dimethylaminomethyl)-r-1-methoxycarbonyl-t-2-phenylcyclopropane (**3a**)*: Bp 105—115 °C (bath temp)/2 Torr; ^{1}H-NMR (CCl_4): δ=1.42 (dd, *J*=3.0, 4.7 Hz, 1H), 1.44 (d, *J*=8.4 Hz, 1H), 1.86 (dd, *J*=3.0, 5.8 Hz, 1H), 1.92 (s, 6H), 2.46 (dd, *J*=4.7, 5.8 Hz, 1H), 2.66 (d, *J*=8.4 Hz, 1H), 3.44 (s, 3H), 6.6—6.9 (m, 5H); IR: 2970, 2840, 2780, 1718, 1605, 1502, 1460, 1437, 1243, 1176, 765, 700 cm^{-1}; MS: *m/e* (rel intensity) 234 (M^++1, 2), 233 (M^+, 4), 219(2), 142(72), 134(19), 129(26), 115(8), 91(9), 58(100). Found: C, 71.84; H, 8.25; N, 6.06%. Calcd for $C_{14}H_{19}NO_2$: C, 72.07; H, 8.21; N, 6.00%.

*5-Phenyl-4,5-dihydro-3-methylene-2(3H)-furanone (**4a**)*:[2x,20] Mp 48—49.5 °C; ^{1}H-NMR (CCl_4): δ=2.88 (ddt, *J*=6.6, 17.0, 2.9 Hz, 1H), 3.40 (ddt, *J*=8.0, 17.0, 2.5 Hz, 1H), 5.50 (dd, *J*=6.6, 8.0 Hz, 1H), 5.66 (dd, *J*=2.5, 2.9 Hz, 1H), 6.28 (dd, *J*=2.5, 2.9 Hz, 1H), 7.34 (s, 5H); IR: 1760, 1665, 1500, 1265, 1120, 1015 cm^{-1}; MS: *m/e* 174 (M^+).

*r-1-Bromo-1-(dimethylaminomethyl)-t-2-hexylcyclopropane (**2b**)*: The dibromocyclopropane **1b**[18] was converted into a stereoisomeric mixture of **2b** and **2b′**, *r*-1-bromo-1-(dimethylaminomethyl)-*c*-2-hexylcyclopropane. The ratio of **2b** to **2b′** (88 : 12) was estimated by the examination of the ^{1}H-NMR spectrum of a mixture of **3b** and **3b′**. The mixture of **2b** and **2b′** showed bp 72—80 °C (bath temp)/0.5 Torr; ^{1}H-NMR (CCl_4): δ=0.5—1.6 (m, 15H), 2.04 (m, 1H), 2.26 (s, 6H), 2.32 (d, *J*=13.5 Hz, 1H), 2.79 (d, *J*=13.5 Hz, 1H); IR: 2950, 2870, 2825, 2780, 1460, 1250, 1190, 1128, 1038 cm^{-1}; MS: *m/e* (rel intensity) 263 (M^++2, 2), 262 (M^++1, 1), 261 (M^+, 2), 182(18), 142(5), 96(6), 85(9), 70(8), 67(11), 58(100), 55(20), 46(55), 45(46), 44(46), 43(44). Found: *m/e* 261.1068. Calcd for $C_{12}H_{24}BrN$: M^+, 261.1092.

*1-(Dimethylaminomethyl)-r-1-methoxycarbonyl-t-2-hexylcyclopropane (**3b**)*: The mixture of **2b** and **2b′** was transformed into an 88 : 12 mixture of **3b** and the stereoisomer **3b′**, 1-(dimethylaminomethyl)-*r*-1-methoxycarbonyl-*c*-2-hexylcyclopropane, having ^{1}H-NMR (CCl_4): δ=0.5—1.6 (m, 16H), 2.08 (d, *J*=13.1 Hz, 1H), 2.13 (s, 6H), 2.98 (d, *J*=13.1 Hz, 1H), 3.57 (s, CO_2Me, 2.64H), 3.61 (s, CO_2Me, 0.36H); IR: 2935, 2860, 2820, 2770, 1725, 1245, 1185, 1152, 1133, 1025 cm^{-1}; MS: *m/e* (rel intensity) 241 (M^+, 3), 198(2), 170(2), 157(2), 142(13), 98(4), 58(100), 46(34), 45(78), 44(21). Found: C, 69.45; H, 11.52; N, 5.55%. Calcd for $C_{14}H_{27}NO_2$: C, 69.66; H, 11.28; N, 5.80%. Bp 72—80 °C (bath temp)/0.5 Torr.

*5-Hexyl-4,5-dihydro-3-methylene-2(3H)-furanone (**4b**)*:[2g,20] The 88 : 12 mixture of **3b** and **3b′** gave the lactones **4b** and **4b′**, 4-hexyl-4,5-dihydro-3-methylene-2(3*H*)-furanone, as a 71 : 29 regioisomeric mixture,[12] ^{1}H-NMR (CCl_4): δ=0.7—1.9 (m, 13H), 1.1—1.8 (m, 10H), 2.41 (ddt, *J*=6.0, 17.0, 3.0 Hz, HCH of **4b**, 0.71H), 2.9—3.1 (m+ddt (δ=3.00, *J*=7.5, 17.0, 2.6 Hz, HCH of **4b**), 1H), 3.93 (dd, *J*=5.7, 9.0 Hz, HCH of **4b′**, 0.29H), 4.35—4.55 (m+dd(δ=4.42, *J*=8.3, 9.0 Hz, HCH of **4b′**), 1H), 5.55 (d, *J*=2.8 Hz, 0.29H), 5.58 (dd, *J*=2.6, 3.0 Hz, 0.71H), 6.18 (dd, *J*=2.6, 3.0 Hz, 0.71H), 6.23 (d, *J*=2.8 Hz, 0.29H); IR: 1760, 1662 cm^{-1}; MS: *m/e* (rel intensity) 182 (M^+, 1), 140(10), 97(100), 41(42); bp 102—108 °C (bath temp)/0.5 Torr. Found: *m/e* 181.1274. Calcd for $C_{11}H_{17}O_2$: M^+−1, 181.1226.

When stereochemically pure **3b** was subjected to the reaction conditions, the product ratio was improved a little (**4b**: **4b′** 82 : 18).

*r-1-Bromo-c-2,c-3-dihexyl-1-(dimethylaminomethyl)cyclopropane (**2d**)*: The reported procedure[21] was applied to the transformation of 7-tetradecene (*cis* : *trans* 84 : 16)[22] into the dibromocyclopropane **1d** together with the *trans* isomer **1e** (85% tield), bp 120—125 °C/0.11 Torr; ^{1}H-NMR (CCl_4): δ=0.7—1.6 (m, 28H); IR: 1464, 1455, 715 cm^{-1}. Found: *m/e* 366.0516. Calcd for $C_{15}H_{28}Br_2$: M^+, 366.0558.

The stereoisomer **2d** showed ^{1}H-NMR (CCl_4): δ=0.7—1.7 (m, 28H), 2.26 (s, 6H), 2.48 (s, 2H); IR: 1466, 1034 cm^{-1}; MS: *m/e* (rel intensity) 347 (M^++2, trace), 345 (M^+, trace), 267(8), 266(10), 69(16), 58(100), 55(26), 46(22), 45(66), 43(29), 41(29); bp 165—167 °C (bath temp)/0.12 Torr. Found: C, 62.68; H, 10.70; N, 3.96%. Calcd for $C_{18}H_{36}BrN$: C, 62.41; H, 10.48; N, 4.04%.

† 1 M=1 mol dm^{-3}; †† 1 Torr=133.322 Pa.

t-*2*,t-*3-Dihexyl-1-(dimethylaminomethyl)*-r-*1-(methoxycarbonyl)-cyclopropane (3d)*: Bp 142 °C (bath temp)/0.07 Torr; ^{1}H-NMR (CCl_4): δ=0.7—1.7 (m, 28H), 2.23 (s, 6H), 2.64 (s, 2H), 3.58 (s, 3H); IR: 1721, 1476, 1259, 1197 cm^{-1}; MS: *m/e* (rel intensity) 325 (M^+, trace), 310 (trace), 240(14), 58(93), 46(76), 45(100), 44(23), 43(17), 41(19). Found: C, 73.58; H, 12.23; N, 4.07%. Calcd for $C_{20}H_{39}NO_2$: C, 73.79; H, 12.08; N, 4.03%.

cis-*4,5-Dihexyl-4,5-dihydro-3-methylene-2(3H)-furanone (4d)*: A 94 : 6 stereoisomeric mixture of **4d** and its *trans* isomer **4e** was synthesized from the amino esters (**3d** and **3e**) which were derived from 7-tetradecene (*cis* : *trans* 84 : 16). The mixture of **4d** and **4e** showed bp 141—142 °C (bath temp)/0.18 Torr; ^{1}H-NMR (CCl_4): δ=0.7—1.6 (m, 26H), 2.80 (m, 1H), 4.30 (dt, J=5.1, 6.3 Hz, 1H), 5.30 (d, J=2.3 Hz, 1H), IR: 1764, 1660, 1464, 1264, 1111 cm^{-1}; MS: *m/e* (rel intensity) 266 (M^+, 2), 152(56), 96(72), 95(72), 82(100), 55(64), 54(92). Found: C, 76.46; H, 11.49%. Calcd for $C_{17}H_{30}O_2$: C, 76.64; H, 11.35%.

r-*1-Bromo*-c-*2*,t-*3-dihexyl-1-(dimethylaminomethyl)cyclopropane (2e)*: *trans*-1,1-Dibromo-2,3-dihexylcyclopropane (**1e**) was prepared from *trans*-7-tetradecene[22] according to the reported procedure[21] (75% yield, 97% yield based on the consumed olefin). ^{1}H-NMR (CCl_4) of **1e**: δ=0.7—1.7 (m, 28H); IR: 1466, 733, 722 cm^{-1}; bp 105—115 °C/0.08 Torr. Found: C, 49.02; H, 7.70%. Calcd for $C_{15}H_{28}Br_2$: C, 48.93; H, 7.67%.

The amino bromide **2e** showed bp 162—163 °C (bath temp)/0.11 Torr; ^{1}H-NMR (CCl_4): δ=0.7—1.8 (m, 28H), 2.23 (s, 6H), 2.28 (d, J=12.8 Hz, 1H), 2.85 (d, J=12.8 Hz, 1H); IR: 1464, 1454, 1033 cm^{-1}; MS: *m/e* (rel intensity) 266 (M^+—Br, 5), 81(5), 79(4), 69(5), 67(5), 58(100), 46(13), 45(43). Found: *m/e* 266.2854. Calcd for $C_{18}H_{36}N$: M^+—Br, 266.2846.

c-*2*,t-*3-Dihexyl-1-(dimethylaminomethyl)*-r-*1-(methoxycarboxyl)-cyclopropane (3e)*: Bp 165 °C (bath temp)/0.11 Torr; ^{1}H-NMR (CCl_4): δ=0.7—1.7 (m, 28H), 2.16 (s, 6H), 2.30 (d, J=13.2 Hz, 1H), 2.75 (d, J=13.2 Hz, 1H), 3.65 (s, 3H); IR: 1724, 1461, 1190, 1158 cm^{-1}; MS: *m/e* (rel intensity) 325 (M^+, trace), 310(1), 382(1), 240(12), 226(4), 58(100), 46(45), 45(55). Found: C, 73.56; H, 12.28; N, 4.17%. Calcd for $C_{20}H_{39}NO_2$: C, 73.79; H, 12.08; N, 4.30%.

trans-*4,5-Dihexyl-4,5-dihydro-3-methylene-2(3H)-furanone (4e)*: Bp 140—142 °C (bath temp)/0.18 Torr; ^{1}H-NMR (CCl_4): δ=0.7—1.8 (m, 26H), 2.53 (m, 1H), 4.04 (dt, J=3.6, 5.3 Hz, 1H), 5.45 (d, J=2.6 Hz, 1H), 6.13 (d, J=2.6 Hz, 1H); IR: 1763, 1658, 1465, 1265, 1116 cm^{-1}; MS: *m/e* (rel intensity) 266 (M^+, 1), 181(16), 152(39), 95(45), 82(52), 67(41), 55(57), 43(91), 41(100). Found: C, 76.83; H, 11.23%. Calcd for $C_{17}H_{30}O_2$: C, 76.64; H, 11.35%.

Preparation of the Lactone 4c from the Amino Ester 3c or 7.

Method A: Treatment of **3c** (98 mg, 0.47 mmol) with methyl iodide (1 ml) at reflux temperature for 14 h was followed by concentration. The resulting residue was allowed to react with trimethylsilyl iodide (186 mg, 0.93 mmol) in 1,2-dichloroethane at 50 °C for 15 h. Evaporation of all the volatile materials and the subsequent thermolysis gave **4c** (35 mg, 45% yield).

Method B: The ester **3c** (105 mg, 0.50 mmol) in methyl iodide (2 ml) was stirred for 2 h at reflux temperature, and the excess reagent was then removed. The residue was treated with a methanol–water (1 : 1) solution of potassium hydroxide (0.24 M, 0.59 mmol) at 80 °C (bath temp) for 15 h. Concentration of the reaction mixture *in vacuo* followed by distillation gave **4c** (33 mg, 43% yield).

Method C: Treatment of **3c** (90 mg, 0.43 mmol) with a methanol–water (1 : 1) solution of potassium hydroxide (0.23 M, 0.51 mmol) followed by concentration gave a solid. Methyl iodide (2 ml) was added to the residue and the whole was stirred at reflux temperature for 2.5 h. Removal of excess methyl iodide and the thermolytic distillation gave **4c** (22 mg, 34% yield).

Method D: Hydrolysis of **3c** (90 mg, 0.43 mmol) with a methanol–water (1 : 1) solution of potassium hydroxide (0.24 M, 0.51 mmol) was followed by neutralization with hydrochloric acid (1.0 M, 0.51 mmol). Concentration of the reaction mixture *in vacuo* and the subsequent distillation failed to give the desired lactone **4c**.

Method E: Benzyl alcohol (0.23 g, 2.1 mmol) was treated with sodium hydride (1.8 mmol) in benzene (4 ml) at 80 °C for 30 min, and **3c** (192 mg, 0.91 mmol) in benzene (1 ml) was then added at r.t. After stirring for 3 h at 80 °C, workup and distillation gave 7-*exo*-benzyloxycarbonyl-7-*endo*-(dimethylaminomethyl)norcarane (**7**) (108 mg, 42% yield); bp 162—163 °C (bath temp)/0.11 Torr; ^{1}H-NMR (CCl_4): δ=1.0—2.1 (m, 10H), 2.16 (s, 6H), 2.71 (s, 2H), 4.98 (s, 2H), 7.26 (br s, 5H); IR: 1710, 1244, 1172, 695 cm^{-1}; MS: *m/e* (rel intensity) 287 (M^+, trace), 196(15), 91(95), 65(29), 58(100), 46(74), 45(94), 44(42). Found: C, 74.97; H, 8.80; N, 4.78%. Calcd for $C_{18}H_{25}NO_2$: C, 75.22; H, 8.77; N, 4.87%.

An ethanol (1 ml) solution of **7** (115 mg, 0.42 mmol) was treated with Pd on carbon (5%, 12 mg) under a hydrogen atmosphere for 20 h. Filtration followed by concentration and the thermolysis failed to give **4c**.

Method F: Treatment of **7** (72 mg, 0.25 mmol) with trimethylsilyl iodide (51 mg, 0.51 mmol) in refluxing 1,2-dichloroethane (2 ml) for 15 h was followed by concentration. Thermolysis of the residue gave **4c** (23 mg, 60% yield).

Method G: An ethanol (1 ml) solution of **7** (94 mg, 0.33 mmol) was stirred with Pd on carbon (5%, 10 mg) under a hydrogen atmosphere for 15 h. Filtration and concentration gave a solid, which was treated with methyl iodide (3 ml) at reflux temperature for 1.5 h. Removal of the excess reagent followed by the thermolysis gave **4c** (25 mg, 51% yield).

Synthesis of Tulipalin A (10). Methyl 2-(bromomethyl)acrylate was prepared from dimethyl bis(hydroxymethyl)-malonate according to reported methods[23] (32% overall yield). ^{1}H-NMR (CCl_4): δ=3.78 (s, 3H), 4.12 (s, 2H), 5.91 (s, 1H), 6.27 (s, 1H); IR: 1716, 1628, 1440, 1321, 1300, 1210, 1187, 1162, 1110 cm^{-1}; MS: *m/e* (rel intensity) 180 (M^++2, 17), 178 (M^+, 18), 149(21), 147(21), 121(21), 119(21), 99(100), 69(21), 59(50), 45(16), 41(24). Found: C, 33.65; H, 4.07%. Calcd for $C_5H_7BrO_2$: C, 33.56; H, 3.91%. Bp 85—90 °C/32 Torr.

A reported procedure[23b] was applied to the transformation of methyl 2-(bromomethyl)acrylate into methyl 2-(diisopropylaminomethyl)acrylate (91% yield). Bp 70—78 °C/1 Torr; ^{1}H-NMR (CCl_4): δ=0.98 (d, J=6.6 Hz, 12H), 2.99 (septet, J=6.6 Hz, 2H), 3.21 (t, J=1.8 Hz, 2H), 5.8—5.9 (m, 1H), 6.0—6.1 (m, 1H); IR: 2980, 1717, 1630, 1436, 1366, 1287, 1250, 1172, 1125 cm^{-1}; MS: *m/e* (rel intensity) 199 (M^+, 11), 185(100), 142(43), 110(100), 69(54), 41(47). Found: C, 66.37; H, 10.90; N, 6.95%. Calcd for $C_{11}H_{21}NO_2$: C, 66.29; H, 10.62; N, 7.03%.

Thus prepared amino ester (1.1 g, 5.58 mmol) was treated with an ether (10 ml) solution of diazomethane (large excess) for 15 h at 25 °C and the reaction mixture was concentrated. A benzene (50 ml) solution of the residue was placed in a Pyrex tube and irradiated with a 200 W high-pressure mercury lamp externally for 7 h at 25 °C under a nitrogen atmosphere. Purification of the concentrated residue by column chromatography (hexane–ether 5 : 1) gave methyl 1-(diisopropylaminomethyl)cyclopropanecarboxylate (**9**) (0.42 g, 35% yield). Bp 118 °C (bath temp)/1 Torr; ^{1}H-NMR (CCl_4): δ=0.5—0.8 (m, 2H), 0.8—1.1 (m+d (δ=0.95, J=6.3 Hz), 14H), 2.78 (s, 2H), 2.96 (septet, J=6.3 Hz, 2H), 3.57 (s, 3H); IR: 2990, 1720,

1436, 1348, 1241, 1180, 1134 cm^{-1}; MS: *m/e* (rel intensity) 213 (M^+, 9), 198(100), 124(46), 114(42), 113(26), 86(20), 83(27), 81(35), 44(36), 43(25), 41(27). Found: C, 67.78; H, 10.79; N, 6.61%. Calcd for $C_{12}H_{23}NO_2$: C, 67.56; H, 10.87; N, 6.57%.

A 1,2-dichloroethane (6 ml) solution of **9** (107 mg, 0.51 mmol) was treated with trimethylsilyl iodide (402 mg, 2.01 mmol) at reflux temperature for 15 h under an argon atmosphere. Thermolysis of the concentrated residue yielded the crude product. Purification by preparative TLC (hexane–ether 1 : 1) gave **10** (21 mg, 43% yield, R_f 0.3) identical in all respects with the reported data.[24] Bp 92—95 °C (bath temp)/11 Torr; ^{1}H-NMR (CCl_4): δ=2.97 (tt, J=2.9, 7.4 Hz, 2H), 4.63 (t, J=7.4 Hz, 2H), 5.64 (t, J=2.9 Hz, 1H), 6.24 (t, J=2.9 Hz, 1H); IR ($CHCl_3$): 1759, 1667, 1107, 1021, 940 cm^{-1}; MS: *m/e* 98 (M^+).

This work was financially supported by the Ministry of Education, Science and Culture (Grant-in-Aid Nos. 303023 and 56430027).

References

1) a) H. Shibaoka, *Plant Cell Physiol.*, **2**, 175 (1961); b) M. Mitsuhashi and H. Shibaoka, *ibid.*, **6**, 87 (1965); c) L. Sequeire, R. J. Hemingway, and S. M. Kupchan, *Science*, **161**, 789 (1968); d) S. M. Kupchan, D. C. Fessler, M. A. Eakin, and T. J. Giacobbe, *ibid.*, **168**, (1970); e) R. L. Hanson, H. A. Lardy, and S. M. Kupchan, *ibid.*, **168**, 378 (1970); f) J. L. Hartwell and B. J. Abbott, *Adv. Pharmacol. Chemother.*, **7**, 117 (1969); g) S. M. Kupchan, J. E. Kelsey, M. Maruyama, J. M. Cassady, J. C. Hemingway, and J. R. Knox, *J. Org. Chem.*, **34**, 3876 (1969); h) S. M. Kupchan, *Trans. N. Y. Acad. Sci.*, **32**, 85 (1970); i) Y. Iino, A. Tanaka, and K. Yamashita, *Agric. Biol. Chem.*, **36**, 2505 (1972); j) C. H. Smith, J. Larner, A. M. Thomas, and S. M. Kupchan, *Biochem. Biophys. Acta*, **276**, 94 (1972); k) P. A. Grieco, J. A. Noguez, Y. Masaki, K. Hiroi, N. Nishizawa, A. Rosowsky, S. Oppenheim, and H. Lazarus, *J. Med. Chem.*, **20**, 71 (1977); l) G. Schlewer, J. L. Stampf, and C. Benezra, *ibid.*, **23**, 1031 (1980); m) K. Yamashita, *Kagaku No Ryoiki*, **27**, 899 (1973).

2) Reviews: a) R. B. Gammill, C. A. Wilson, and T. A. Bryson, *Synth. Commun.*, **5**, 245 (1975); b) P. A. Grieco, *Synthesis*, **1975**, 67; c) S. S. Newaz, *Aldrichimica Acta*, **10**, 64, (1977); d) H. Takei, *Kagaku, No Ryoiki*, **33**, 680 (1979); T. Shono and Y. Matsumoto, *Yuki Gosei Kagaku Kyokai Shi*, **39**, 358 (1981). Recent methods for the synthesis of α-methylene-γ-butyrolactones, see: e) A. W. McCulloch and A. G. McInnes, *Tetrahedron Lett.*, **1979**, 1963; f) K. Yamamoto, Y. Tomo, and S. Suzuki, *ibid.*, **21**, 2861 (1980); g) H. Nishiyama, H. Yokoyama, S. Narimatsu, and K. Itoh, *ibid.*, **23**, 1267 (1982); h) K. Tanaka, N. Yamagishi, H. Uneme, R. Tanikaga, and A. Kaji, *Chem. Lett.*, **1978**, 197; i) K. Tanaka, H. Uneme, N. Yamagishi, N. Ono, and A. Kaji, *ibid.*, **1978**, 653; j) I. Matsuda *ibid.*, **1978**, 773; k) M. F. Semmelhack and E. S. C. Wu, *J. Am. Chem. Soc.*, **98**, 3384 (1976); l) N. L. Holy and Y. F. Wang, *ibid.*, **99**, 944 (1977); m) M. F. Semmelhack and S. J. Brickner, *ibid.*, **103**, 3945 (1981); n) T. F. Murray, E. G. Samsel, V. Varma, and J. R. Norton, *ibid.*, **103**, 7520 (1981); o) R. M. Carlson and A. R. Oyler, *J. Org. Chem.*, **41**, 4065 (1976); p) A. Hassner, H. W. Pinnick, and J. M. Ansell, *ibid.*, **43**, 1774 (1978); q) P. F. Hudrlik, J. M. Takacs, D. T. W. Chou, and L. R. Rudnick, *ibid.*, **44**, 786 (1979); r) L. G. Mueller and R. G. Lawton, *ibid.*, **44**, 4741 (1979); s) V. Nair and A. K. Sinhababu, *ibid.*, **45**, 1893 (1980); t) J.-P. Corbet and C. Benezra, *ibid.*, **46**, 1141 (1981); u) M. F. Semmelhack and S. J. Brickner, *ibid.*, **46**, 1723 (1981); v) N. S. Pantaleo, K. D. Berlin, and D. van der Helm, *ibid.*, **46**, 4284 (1981); w) T. C. T. Chang and M. Rosenblum, *ibid.*, **46**, 4626 (1981); x) M. Okabe M. Abe, and M. Tada, *ibid.*, **47**, 1775 (1982); y) L.-C. Yu and P. Helquist, *ibid.*, **46**, 4536 (1981) and references cited therein.

3) Recent reports for the synthesis of natural products: T. Sakai, M. Yoshida, S. Kohmoto, M. Utaka, and A. Takeda, *Tetrahedron Lett.*, **23**, 5185 (1982), H. Ohrui and S. Emoto, *ibid.*, **1975**, 3653; R. E. Damon and R. H. Schlessinger, *ibid.*, **1975**, 4551; R. C. Anderson and B. Fraser-Reid, *ibid.*, **1977**, 2865; I. Paterson and I. Fleming, *ibid.*, **1979**, 993, R. H. Wollenberg, *ibid.*, **21**, 3139 (1980); P. Barbier and C. Benezra, *ibid.*, **23**, 3513 (1982); J. L. Herrmann, M. H. Berger, and R. H. Schlessinger, *J. Am. Chem. Soc.*, **101**, 1544 (1979); R. C. Anderson and B. Fraser-Reid; *ibid.*, **97**, 3870 (1975); S. W. Rollinson, R. A. Amos, and J. A. Katzenellenbogen, *ibid.*, **103**, 4114 (1981); W. L. Parker and F. Johnson, *J. Org. Chem.*, **38**, 2489 (1973); J. Martin, P. C. Watts, and F. Johnson, *ibid.*, **39**, 1676 (1974); T. Sakai, H. Horokawa, and A. Takeda, *ibid.*, **45**, 2039 (1980); A. S. Kende and B. H. Toder, *ibid.*, **47**, 163 (1982); K. Yamada, M. Kato, M. Iyoda, and Y. Hirata, *J. Chem. Soc., Chem. Commun.*, **1973**, 499; A. Murai, K. Takahashi, H. Takatsuru, and T. Masamune, *ibid.*, **1981**, 221; H. Takei, Y. Fukuda, and T. Taguchi, *Chem. Lett.*, **1980**, 1311; A. Tanaka and K. Yamashita, *ibid.*, **1981**, 319.

4) The dimethylamino group is often utilized for protection of the α-methylene moiety of α-methylene-γ-butyrolactones. See, S. Danishefsky, T. Kitahara, R. McKee, and P. F. Schuda, *J. Am. Chem. Soc.*, **98**, 6715 (1976); S. Danishefsky, P. F. Schuda, T. Kitahara, and S. J. Etheredge, *ibid.*, **99**, 6066 (1977).

5) M. E. Jung and M. A. Lyster, *J. Am. Chem. Soc.*, **99**, 968 (1977); *J. Org. Chem.*, **42**, 3761 (1977); T.-L. Ho and G. A. Olah, *Angew. Chem.*, **88**, 847 (1976); A. Hosomi, *Yuki Gosei Kagaku Kyokai Shi*, **40**, 545 (1982); A. H. Schmidt, *Aldrichimica Acta*, **14**, 31 (1981).

6) Preliminary communication on this work, see T. Hiyama, H. Saimoto, K. Nishio, M. Shinoda, H. Yamamoto, and H. Nozaki, *Tetrahedron Lett.*, **1979**, 2043.

7) K. Kitatani, T. Hiyama, and H. Nozaki, *Bull. Chem. Soc. Jpn.*, **50**, 3288 (1977).

8) J. Schreiber, H. Maag, N. Hashimoto, and A. Eschenmoser, *Angew. Chem., Int. Ed. Engl.*, **10**, 330, (1971).

9) The observed stereoselectivity is consistent with the results obtained in thermodynamically controlled generation of the lithium carbenoid. See Ref. 7.

10) Bromine–lithium exchange of 7-substituted 7-bromonorcarane system proceeds often sluggishly by means of butyllithium or *t*-butyllithium. See, H. Yamamoto, K. Kitatani, T. Hiyama, and H. Nozaki, *J. Am. Chem. Soc.*, **99**, 5816 (1977).

11) On treatment of **3c** with trimethylsilyl iodide, **4c** was produced to some extent (less than 40% yield estimated by ^{1}H-NMR) without thermolysis.

12) The ratio of **2b** to **2b'**, 4-hexyl-4,5-dihydro-3-methylene-2(3*H*)-furanone, was originally reported[6] as 88 : 12. However, upon detailed reexamination of the ^{1}H-NMR spectra of the mixture, the ratio was determined to be 71 : 29.

13) The similar phenomenon is observed, see: J. Minamikawa and A. Brossi, *Tetrahedron Lett.*, **1978**, 3085.

14) S. P. Brown, B. S. Bal, and H. W. Pinnick, *Tetrahedron Lett.*, **22**, 4891 (1981); R. D. Miller and D. R. McKeen, *J. Org. Chem.*, **26**, 2412 (1981).

15) P. F. Hudrlik, L. R. Rudnick, and S. H. Korzeneniowski *J. Am. Chem. Soc.*, **95**, 6848 (1973).

16) U. N. Brongersma-Oosterhoff, *Recl. Trav. Chim. Pays-Bas*, **86**, 705 (1967); B. H. H. Pergaman, J. C. M. Beijersbergen J. C. Overeem, and A. K. Sijpesteijn, *ibid.*, **86**, 709 (1967).

17) C. J. Cavallito and T. H. Haskell, *J. Am. Chem. Soc.*, **68**, 2332 (1946). *Cf.* R. Tschesche, F.-J. Kammerer, and G. Wulff, *Chem. Ber.*, **102**, 2057 (1969).

18) W. von E. Doering and A. K. Hoffmann, *J. Am. Chem. Soc.*, **76**, 6162 (1954) and Ref 7.

19) J. A. Marshall and N. Cohen, *J. Org. Chem.*, **30**, 3475 (1965) and Refs. 2x, 2y.

20) L. S. Hegedus, S. D. Wagner, E. L. Waterman, and K. Siirala-Hansen, *J. Org. Chem.*, **40**, 593 (1975).

21) H. Nozaki, S. Kato, and R. Noyori, *Can. J. Chem.*, **44**, 1021 (1966) and Ref. 18.

22) H. J. Bestmann, W. Stranaky, and O. Vostrowsky, *Chem. Ber.*, **109**, 1694 (1976). According to the reported procedures *cis*- and *trans*-7-tetradecene were prepared: E. C. Ashby and S. A. Noding, *J. Org. Chem.*, **45**, 1035 (1980); E. F. Magoon and L. H. Slangh, *Tetrahedron*, **23**, 4509 (1967).

23) a) A. F. Ferris, *J. Org. Chem.*, **20**, 780 (1955); b) J. Dickstein, M. Bodnar, and R. M. Hoegerle, U. S. Patent 3094554 (1963); *Chem. Abstr.*, **59**, 12647h (1963).

24) C. R. Hutchinson, *J. Org. Chem.*, **39**, 1854 (1974) and Refs. 16, 17.

 © 1983 The Chemical Society of Japan Bull. Chem. Soc. Jpn., 56, 3099—3105 (1983)

A Facile Synthesis of Colchiceine Analogues [4-(1-Acetamido-3-arylpropyl)tropolones][1,2]

Tetsuo NOZOE,*,† Kahei TAKASE,* Norio KAWABE†† Toyonobu ASAO,††† and Hiroshi YAMAMOTO*,††††

Department of Chemistry, Faculty of Science, Tohoku University, Aramaki, Aoba, Sendai 980

††††*Department of Chemistry, Faculty of Science, Okayama University, Tsushima, Okayama 700*

(Received March 28, 1983)

The condensation of 4-acetyltropolone with various arenecarbaldehydes gave a wide variety of 4-cinnamoyltropolone derivatives in good yield. The same reaction with 2-furaldehyde and cinnamaldehyde also afforded the corresponding 4-substituted tropolones. These products were converted to their oximes (with hydroxylamine hydrochloride), which in turn were hydrogenated over 5% Pd/C in acetic acid and then acetylated with acetic anhydride, to yield 4-(1-acetamido-3-aryl-2-propenyl)tropolones. The catalytic hydrogenation of these olefinic products over 10—30% Pd/C in aqueous KOH gave various 4-(1-acetamido-3-arylpropyl)tropolones, which possess a B-ring-open structure of colchiceine. The structures of these products are discussed on the basis of UV, IR, and ^{1}H-NMR spectra.

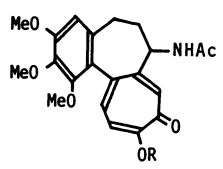

1 R = Me
2 R = H

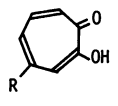

3 R = $CHMe_2$
4 R = $C(=CH_2)Me$
5 R = Ac

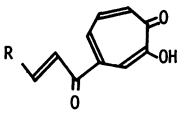

10 R =
11 R = CH=CHPh

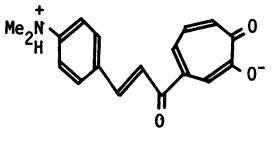

12

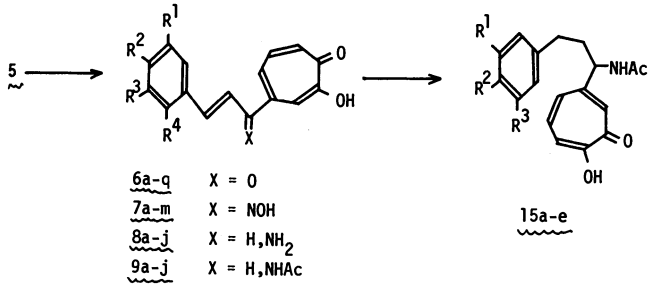

6a-q X = O
7a-m X = NOH
8a-j X = H,NH_2
9a-j X = H,NHAc

15a-e

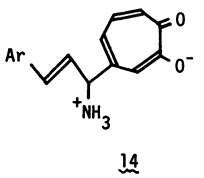

14

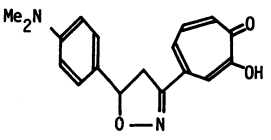

13

6 - 9, 15	R^1	R^2	R^3	R^4
a	OMe	OMe	OMe	H
b	OMe	OMe	H	H
c	O—CH_2—O		H	H
d	H	H	H	H
e	H	Me	H	H
f	OMe	OCH_2Ph	H	H
g	OCH_2Ph	OMe	H	H
h	H	Cl	H	H
i	H	Cl	H	Cl
j	H	OMe	H	H
k	H	Br	H	H
l	NO_2	OMe	H	H
m	NO_2	H	H	H
n	H	NO_2	H	H
o	OH	OMe	H	H
p	H	H	H	OH
q	H	NMe_2	H	H

Colchicine (**1**), one of the major alkaloid constituents of the autumn crocus (*Colchicum automnale L.*), is well known to block cell division during mitosis, and has been valued for its use in the treatment of gout.[3] This compound has also drawn the attention of synthetic organic chemists for almost three decades, and the total synthesis has been accomplished by several groups.[4] These synthetic routes, however, are apparently unsuitable not only for the practical synthesis of colchicine but also for the preparation of various kinds of colchicine analogues having potential utility of their biological activity.

A considerable interest in the physiological activity of colchicine, particularly concerning the binding sites of the microtubrins in the muscle and nerve cells,[3] led us to complete our longstanding, convenient synthetic scheme involving variously substituted 4-cinnamoyltropolones as intermediates.[1,2] As the intial part of our reinvestigation, we have recently reported[5] a convenient synthesis of 4-acetyltropolone (**5**) from hinokitiol (**3**), because of the limited supply of naturally occurring β-dolabrin[6] (**4**) which had previously been used[1,2] as the starting material for the preparation of **5**. We now wish to describe a convenient synthesis of analogues of colchiceine (**2**) starting from 4-acetyltropolone (**5**).

The condensation of compound **5** with various

† Present address: 811, 2-5-1, Kamiyoga, Setagaya-ku, Tokyo 158.

†† Present address: Torey Co. Ltd., Otsu 520.

††† Present address: Department of Chemistry, College of General Education, Tohoku University, Kawauchi, Sendai 980.

Table 1. Analysis and spectra of thf 4-substituted tropolones

Compd	Formula	Calcd Found (%) C	H	N	IR Spectra[a] (KBr) $\tilde{\nu}$/cm^{-1}	UV Spectra[b] λ_{max}/nm	log ε	S[c]
4-Cinnamoyltropolones and related compounds								
6a	$C_{19}H_{18}O_6$	66.66	5.30	—	3226, 1664,	255, 342	4.41, 4.31	0
		67.06	5.09	—	1597	260, 347, 441	4.20, 4.41, 3.73	—
6b	$C_{18}H_{16}O_5$	69.22	5.16	—	3268, 1653,	252, 368	4.45, 4.30	0
		69.21	5.21	—	1610	263, 350, 430	4.34, 4.47, 3.86	—
6c	$C_{17}H_{12}O_5$	68.91	4.08	—	3279, 1642,	255, 335	4.33, 4.30	0
		69.31	3.91	—	1610	270, 350, 430	4.27, 4.39, 3.79	—
6d	$C_{16}H_{12}O_3$	76.18	4.80	—	3155, 1664,	252, 318, 380	4.43, 4.37, 3.82	0
		76.25	5.01	—	1623, 1602	265, 318, 444	4.23, 4.36, 3.80	—
6e	$C_{17}H_{14}O_3$	76.67	5.30	—	3185, 1661,	253, 328, 384	4.33, 4.27, 3.87	0
		76.46	5.37	—	1592	266, 326, 440	4.14, 4.27, 3.57	—
6f	$C_{24}H_{20}O_5$	74.21	5.19	—	3205, 1626,	254, 332, 375	4.44, 4.19, 4.32	0
		73.95	5.01	—	1613, 1600	262, 353, 440	4.31, 4.44, 3.80	—
6g	$C_{24}H_{20}O_5$	74.21	5.19	—	3155, 1656,	253, 332, 376	4.48, 4.15, 4.44	0
		74.40	5.30	—	1608	263, 351, 440	4.33, 4.44, 3.80	—
6h	$C_{16}H_{11}O_3Cl$	66.95	3.86	—	3135, 1667,	254, 322, 380	4.42, 4.39, 3.86	0
		66.99	3.89	—	1623, 1600	284, 316, 440	4.28, 4.31, 3.66	—
6i	$C_{16}H_{10}O_3Cl_2$	59.86	3.16	—	3205, 1669,	254, 320, 380	4.43, 4.34, 3.82	0
		59.54	3.13	—	1621, 1597	240, 283, 445	4.25, 4.29, 3.63	—
6j	$C_{17}H_{14}O_4$	72.33	5.00	—	3185, 1634,	250, 348	4.45, 4.38	0
		72.16	5.34	—	1616, 1605	267, 347, 440	4.23, 4.52, 3.79	—
6k	$C_{16}H_{11}O_3Br$	58.05	3.35	—	3226, 1664,	252, 322, 385	4.39, 4.39, 3.77	0
		58.33	3.59	—	1621, 1600	324, 440	4.35, 3.73	—
6l	$C_{17}H_{13}O_6N$	62.38	4.00	4.28	3125, 1658,	252, 326, 390	4.26, 4.30, 3.70	0
		62.64	4.06	4.10	1592	278, 330, 440	4.28, 4.44, 3.74	—
6m	$C_{16}H_{11}O_5N$	64.64	3.73	4.71	3226, 1664,	259, 300, 386	4.40, 4.25, 3.68	0
		64.48	3.98	4.37	1605	270, 345, 444	4.26, 3.90, 3.49	—
6n	$C_{16}H_{11}O_5N$	64.64	3.73	4.71	3240, 1672,	255, 318, 400	4.35, 4.51, 3.73	0
		64.61	3.93	4.89	1610	271, 319, 448	4.27, 4.43, 4.68	—
6o	$C_{17}H_{14}O_5$	68.45	4.73	—	3236, 1653,	258, 350	4.35, 4.41	0
		68.15	4.94	—	1592	268, 345, 426	4.39, 4.43, 4.28	— —
6p	$C_{16}H_{12}O_4$	71.63	4.51	—	3145, 1637,	250, 320, 370	4.40, 4.16, 4.20	0
		71.67	4.25	—	1613	259, 335, 444	4.34, 4.21, 4.17	—
6q	$C_{18}H_{17}O_3N$	73.20	5.80	4.74	3236, 1642,	252, 312, 393	4.48, 4.37, 3.94	+
		72.94	5.54	5.07	1613	255, 325, 432	4.39, 4.13, 4.47	±
						273, 345, 430	4.35, 4.18, 4.57	—
10	$C_{14}H_{10}O_4$	69.42	4.16	—	3326, 1664,	250, 347	4.41, 4.33,	0
		69.41	4.02	—	1605	264, 345, 445	4.19, 4.50, 3.77	—
11	$C_{18}H_{14}O_3$	77.68	5.07	—	3226, 1653,	258, 345	4.28, 4.57,	0
		77.43	5.30	—	1603	280, 342, 450	4.25, 4.63, 3.78	—
4-Cinnamoyltropolone oximes								
7a	$C_{19}H_{19}O_6N$	63.86	5.36	3.92	3333, 1608	238, 315, 375	4.58, 4.48, 3.82	0
		63.72	5.55	3.95		395	3.68	
7b	$C_{18}H_{17}O_5N$	66.05	5.24	4.28	3367, 3145,			
		65.76	5.03	4.63[d]	1605[d]	243, 328, 390	4.49, 4.46, 3.84[d]	0
		66.41	4.97	4.57[e]		245, 328, 395	4.51, 4.48, 3.90[e]	0
7c	$C_{17}H_{13}O_5N$	65.59	4.21	4.50	3311, 1608[d]			
		65.59	3.99	4.54[d]		245, 333, 402	4.53, 4.50, 3.96[d]	0
		65.50	4.43	4.61[e]		243, 330, 402	4.53, 4.47, 3.90[e]	0
7d	$C_{16}H_{13}O_3N$	71.96	4.90	5.24	3205, 3096			
		71.68	4.85	5.35[d]	1603[d]	246, 290, 372	4.43, 4.44, 3.79[d]	0
		71.77	4.95	5.37[e]		245, 288, 372	4.45, 4.51, 3.78[e]	0
7e	$C_{17}H_{15}O_3N$	72.58	5.37	4.98	3333, 1608	231, 302, 370	4.43, 4.45, 3.70	0
		72.75	5.40	5.27		230, 301, 402	4.21, 4.28, 3.51	—
7f	$C_{24}H_{21}O_5N$	71.45	5.25	3.47	3378, 1613	240, 325, 375	4.51, 4.47, 3.92	0
		71.20	5.23	3.42		239, 326, 402	4.39, 4.33, 3.69	—

Table 1. (Continued)

Compd	Formula	Calcd Found (%) C	H	N	IR Spectra[a] (KBr) $\tilde{\nu}$/cm^{-1}	UV Spectra[b] λ_{max}/nm	log ε	S[c]
7g	$C_{24}H_{21}O_5N$	71.45	5.25	3.47	3195, 1603	241, 325, 380	4.50, 4.42, 3.77	0
		71.27	5.32	3.49		240, 325, 402	4.38. 4.31, 3.69	—
7h	$C_{16}H_{12}O_3NCl$	63.63	4.01	4.64	3205, 1608	245, 293, 380	4.38, 4.48, 3.74	0
		63.90	4.35	4.46				
7i	$C_{16}H_{11}O_3NCl_2$	55.70	3.21	4.06	3333, 3125,	238, 293, 363	4.49, 4.47, 3.83	0
		55.98	3.35	4.04	1613	248, 331, 406	4.48, 4.45, 4.13	—
7j	$C_{17}H_{15}O_4N$	68.67	5.08	4.77	3226, 3155,	233, 317, 378	4.44, 4.50, 3.83	0
		68.53	5.12	4.83	1600			
7k	$C_{16}H_{12}O_3NBr$	55.54	3.50	4.05				
		55.93	3.74	3.85				
7l	$C_{17}H_{14}O_6N_2$	59.65	4.12	8.18				
		58.97	4.36	7.93				
7m	$C_{16}H_{12}O_5N_2$	61.54	3.87	8.97	3268, 3096,	249, 272, 377	4.52, 4.55, 3.79	0
		60.94	3.78	8.42	1610	227, 273, 403	4.13, 4.26, 3.55	—
13	$C_{18}H_{18}O_3N_2$	69.66	5.85	9.03	3257, 1613	266, 380, 400	4.49, 3.83, 3.78	0
		69.93	5.88	8.85				
4-(1-Amino-3-aryl-2-propenyl)tropolones								
8a	$C_{19}H_{21}O_5N$	66.46	6.16	4.08	3534, 3414,	245, 335, 395	4.44, 3.96, 3.52	±
		64.78[f]	6.15	4.26	1590			
8b	$C_{18}H_{19}O_4N$	68.99	6.11	4.47		228, 317, 350	4.52, 4.20, 3.85	+
		68.21[f]	6.07	4.49	1587	245, 307, 393	4.47, 4.13, 3.70	±
8c	$C_{17}H_{15}O_4N$	68.67	5.08	4.71		237, 317, 355	4.46, 4.17, 3.82	+
		68.04[f]	5.02	4.55	1590	245, 317, 395	4.41, 4.12, 3.72	±
8d	$C_{16}H_{15}O_2N$	76.96	5.70	5.28		245, 335, 395	4.49, 3.96, 3.57	±
		[f]			1590			
8e	$C_{17}H_{17}O_2N$	76.38	6.41	5.24		247, 335, 394	4.45, 3.99, 3.77	±
		75.29[f]	6.31	4.92	1590			
8f	$C_{24}H_{23}O_4N$	74.02	5.95	3.60	3425, 1590	246, 309, 393	4.47, 4.16, 3.72	±
		73.27[f]	5.73	3.46				
8g	$C_{24}O_{23}O_4N$	74.02	5.95	3.60				
		[f]			1587			
8h	$C_{16}H_{14}O_2NCl$	66.79	4.90	4.86		248, 335, 373,	4.44, 3.90, 3.83,	±
		64.45[f]	4.98	4.28	1587	400	3.50	
8i	$C_{16}H_{13}O_2NCl_2$	59.68	4.07	4.35		260, 335, 373,	4.45, 3.99, 3.74,	±
		59.14	4.10	4.52	1590	394	3.77	
8j	$C_{17}O_{17}O_3N$	72.06	6.05	4.49		247, 334, 372,	4.44, 4.02, 3.74,	±
		69.61[f]	6.10	4.83	1608, 1592	394	3.76	
4-(1-Acetamido-3-aryl-2-propenyl)tropolones								
9a	$C_{21}H_{23}O_6N$	65.44	6.02	3.63	3268, 3165,	242, 335, 370	4.52, 3.96, 3.79	0
		65.17	6.31	3.96	1639, 1610			
9b	$C_{20}H_{21}O_5N$	67.59	5.96	3.94	3311, 3125,	243, 313, 350	4.52, 4.17, 3.81	+
		67.19	5.81	3.86	1637, 1608	245, 307, 370	4.53, 4.15, 3.97	0
						248, 337, 395	4.52, 4.12, 4.14	—
9c	$C_{19}H_{17}O_5N$	67.25	5.05	4.13	3322, 3195,	246, 315, 372	4.49, 4.19, 3.75	0
		67.22	4.97	4.08	1637, 1613			
9d	$C_{18}H_{17}O_3N$	73.20	5.80	4.74	3311, 3125,	243, 328, 370	4.56, 3.96, 3.76	0
		72.15[f]	5.85	4.57	1639, 1610			
9e	$C_{19}H_{19}O_3N$	73.76	6.19	4.53	3322, 3125,	245, 333, 370	4.56, 3.96, 3.75	0
		73.46	6.18	4.35	1642, 1610			
9f	$C_{26}H_{25}O_5N$	72.37	5.84	3.25	3250, 3210,	247, 309, 371	4.49, 4.17, 3.73	0
		72.58	5.77	3.14	1644, 1611	251, 339, 402	4.48, 4.11, 4.09	—
9g	$C_{26}H_{25}O_5N$	72.37	5.84	3.25	3247, 1642,	250, 305, 370	4.40, 4.10, 3.60	0
		72.09	6.07	3.14	1610	265, 340, 401	4.26, 3.93, 3.75	—
9h	$C_{18}H_{16}O_3NCl$	65.51	4.89	4.24	3322, 3135,	246, 335, 370,	4.56, 3.96, 3.75,	0
		65.41	4.66	4.19	1645, 1613	394	3.65	
9i	$C_{18}H_{15}O_3NCl_2$	59.39	4.15	3.85	3322, 3175,	248, 309, 335,	4.51, 3.85, 3.97,	0
		59.70	4.07	3.83	1645, 1613	371, 397	3.77, 3.67	

TABLE 1. (Continued)

Compd	Formula	Calcd Found (%) C	H	N	IR Spectra[a] (KBr) $\tilde{\nu}$/cm^{-1}	UV Spectra[b] λ_{max}/nm	log ε	S[c]
9j	$C_{19}H_{19}O_4N$	70.14	5.89	4.31	3310, 1643,	244, 305, 352,	4.45, 3.99, 3.78,	0
		69.85	5.78	4.17	1608	368	3.74	
4-(1-Acetamido-3-arylpropyl)tropolones								
15a	$C_{21}H_{25}O_6N$	65.10	6.50	3.62	3333, 3226,	238, 325, 370,	4.49, 4.09, 3.87,	0
		65.01	6.57	3.54	1647, 1610	386	3.84	
15b	$C_{20}H_{23}O_5N$	67.21	6.49	3.92	3333, 3155,	233, 325, 370	4.45, 3.80, 3.67	0
		67.49	6.50	3.76	1642, 1610	235, 338, 399	4.32, 3.90, 3.85	—
15c	$C_{19}H_{19}O_5N$	66.85	5.61	4.10	3300, 3226,	240, 330, 369	4.46, 3.89, 3.71	0
		67.18	5.51	3.99	1642, 1608,			
15d	$C_{18}H_{19}O_3N$	72.70	6.44	4.71	3300, 1640,	244, 327, 359	4.45, 3.91, 3.76	0
		72.49	6.16	4.96	1611			
15e	$C_{19}H_{21}O_3N$	73.29	6.80	4.50	3333, 3155,	245, 327, 368	4.43, 3.87, 3.70	0
		73.12	6.67	4.41	1642, 1610	251, 337, 400	4.43, 4.05, 4.09	—

a) Characteristic absorptions due to NH, OH, and C=O groups. b) Inflections in underlines. c) Species: Monocation (+) in 0.1 M (1 M=1 mol dm^{-3}) HCl/MeOH; neutral species (0) and Zwitterion (±) in MeOH; monoanion (−) and dianion (− −) in 0.1 M NaOH/MeOH. d) For oximes of the lower melting point. e) For oximes of the higher melting point. f) No satisfactory analytical figures available even by repeating the analysis.

substituted benzaldehydes in methanolic potassium hydroxide at 0 °C readily afforded 17 4-cinnamoyltropolones (**6a**—**q**) in most cases in excellent yields. Similarly, the reaction of **5** with 2-furaldehyde and cinnamaldehyde gave 4-[3-(2-furyl)propenoyl]- (**10**) and 4-(5-phenyl-2,4-pentadienoyl)tropolone (**11**), respectively. However, the condensation with isovanilline and salicylaldehyde afforded the products (**6o** and **6p**, respectively) in moderate or poor yields, whereas that with vanilline failed to give any condensation products. These results, together with the elemental analysis and spectral data, are summarized in Table 1.

The presence of a conjugated carbonyl group was supported by the IR (≃1660 cm^{-1}) and ^{1}H-NMR spectra: The *E*-configuration of the olefinic group of these products was established from the large magnitude (14—16 Hz) of the coupling constants of the olefinic proton signals in the NMR spectra. The neutral species of these compounds exhibited the longest wavelength absorption maxima at 340—390 nm in the UV spectra, whereas the anionic species (troponate anions) showed a significant bathochromic shift (50—100 nm) in these absorption maxima; the acidic pK_a values of these compounds are considered to be *ca.* 6, as exemplified by the value (6.08)[5] of **6a**. The red-colored *p*-dimethylamino derivative (**6q**) apparently exists mostly as the Zwitterion form (**12**) on the evidence of the UV spectrum in methanol; the spectra of the neutral and anionic species of **6q** closely resembled those of anionic species of other cinnamoyltropolones, whereas the spectrum of the monocation of **6q** corresponded to those of the neutral species of the other derivatives (**6**) (see Table 1).

The treatment of compounds **6** with hydroxylamine hydrochloride in refluxing ethanol gave the corresponding oximes (**7a**—**m**); in some cases two isomers (*syn* and *anti*) were separated by fractional recrystallization. The structures of these oximes were supported by the elemental analysis and the IR spectra (namely, the disappearance of the strong absorptions at ≃1660 cm^{-1} due to the conjugated carbonyl group; see Table 1).

The isoxazoline structure (**13**) was assigned for the product derived from the *p*-dimethylamino compound (**6q**) on the basis of the ^{1}H-NMR spectrum, which showed three aliphatic proton signals of an ABX type at δ 3.32, 3.67, and 5.71 in addition to the signals due to the dimethylamino group (δ 2.94) and the aromatic ring-protons [δ 6.68 (2H), 7.1—7.4 (5H), and 7.77 (1H)]. Moreover, the UV spectrum of **13** closely resembled that of the 4-acetyltropolone oxide,[6] supporting the isoxazoline structure for this product. The exclusive formation of **13** (instead of an oxime derivative **7q**) from **6q** could be explained by the presence of the strongly electron-donating *p*-dimethylamino group, which should facilitate protonation at the intermediately formed oxime nitrogen even under the weakly acidic conditions compared to other oximes **7a**—**m**; the resonance-stabilized monocation (**15**) thus formed would in turn easily result in the isoxazoline ring closure to give **13** (Scheme 1).

The catalytic hydrogenation of the oximes (**7**) in the presence of 5% Pd/C in acetic acid containing a small amount of hydrochloric acid smoothly afforded the corresponding 4-(1-amino-3-aryl-2-propenyl)tropolones (**8a**—**j**) in good yields (see Table 1 for the summarized results). These yellow-colored amino compounds were considered to exist mostly as the Zwitterion form (**14**)

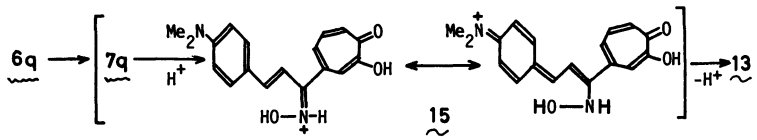

Scheme 1. A reaction pathway for the formation of **13** from **6q**.

on the evidence of the UV spectra; in this case, the longest wavelength absorptions of the neutral species of **8** resembled those of the troponate anions and, on acidification, an appreciable hypsochromic shift (≃40 nm) was observed in these absorptions (see Table 1). This ionic form **14** would be in conformity with the generally observed pK_a values of usual primary amines (9—10)[7] and tropolones (6.7—7.1).[5,8]

These amino compounds were acetylated with acetic anhydride to afford the stable acetamido derivatives (**9a**—**j**) (see Table 1). The presence of an acetamido group and two olefinic protons of *E*-configuration in **9** were confirmed by the IR and ^{1}H-NMR spectra. Because of the disappearance of the basic amino group, compounds **9** exist in the normal tropolone form, as shown by the UV spectra of their neutral species, which became similar to those of the cationic species of the amino compounds **8**.

After intensive studies, we found that the reduction of the olefinic group in compounds **9** was best accomplished by catalytic hydrogenation over 10—30% Pd/C in aqueous potassium hydroxide at room temperature (*ca.* 50 h). The 4-(1-acetamido-3-arylpropyl)tropolones (**15a**—**e**) were thus obtained in good yields. The structures of these reduced products were readily established by elemental analysis and spectroscopy (NMR, IR, and UV, see Table 1 and Experimental part).[9]

Among these products, compound **15a**, which was readily available from **5** in four steps in an overall yield of *ca.* 40—45% as shown above, possesses a structure analogous to that of colchiceine (**2**), in which the C_{1a}–C_{12a} bond is disconnected, having the B-ring-open form.

These findings so far described are believed to be of considerable value not only for the exploration of a convenient and efficient route to prepare various kinds of colchicine analogues but also for the development of the fundamental chemistry of troponoid compounds,[10] which are currently under investigation.

Experimental

All melting points are uncorrected. The microanalyses were carried out at Tohoku University and the results are summarized in Table 1. The ^{1}H-NMR spectra were recorded in $CDCl_3$ with a Hitachi R-22 (90 MHz). Chemical shifts are reported as δ values in parts per million relative to tetramethylsilane (δ 0.0) as an internal standard. Spin decoupling was performed for each proton signal to confirm the coupling constants. IR and UV spectra were obtained on Hitachi 215 and 340 spectrometers, respectively, and the characteristic absorption maxima are recorded in Table 1. All reactions were monitored by paper chromatography (on phosphoric acid-treated Toyo paper developed in benzene) or TLC [conducted on plates precoated with silica gel (0.25 mm, Merck)]. The yields referred to in this section are in most cases those of crude, but chromatographically pure, products; specimens for analysis can be purified by recrystallization from the appropriate solvents.

General Procedure for the Reaction of 4-Acetyltropolone (5) with Arenecarbaldehydes. A 50% aqueous potassium hydroxide solution (5 ml) was added dropwise, at 0 °C, to a stirred suspension of **5** (4.0 g) and 1.2 mol equiv of an arenecarbaldehyde in methanol (60 ml) over a period of 20 min. The mixture was stirred for 4—10 h, allowed to stand overnight at 0 °C, and then diluted with cold water (100 ml). On acidification with 6 M HCl, the corresponding 4-cinnamoyltropolone (**6**) [or compounds **10** and **11**] precipitated. The product was filtered off and recrystallized.

4-(3,4,5-Trimethoxycinnamoyl)tropolone (6a): Yellow needles (≃100% yield), mp 185—186 °C (from MeOH–$CHCl_3$); ^{1}H-NMR 3.92 (9H, s, 3MeO), 6.87 (2H, s, H-2′,6′), 7,21 (1H, d, J=14 Hz, H-9), 7.5 (3H, m, H-5,6,7), 7.6 (1H, m, HO-2, exchangeable with D_2O), 7.67 (1H, d, J=14 Hz, H-10), and 7.80 (1H, s, H-3).

4-(3,4-Dimethoxycinnamoyl)tropolone (6b): Yellow crystals (≃100% yield), mp 154—155 °C (from MeOH–$CHCl_3$).

4-(3,4-Methylenedioxycinnamoyl)tropolone (6c): Orange-yellow scales (≃100% yield), 162—163 °C (from AcOH).

4-Cinnamoyltropolone (6d): Yellow crystals (≃100% yield), mp 132—133 °C (from AcOH).

4-(4-Methylcinnamoyl)tropolone (6e): Yellow plates (≃100% yield), mp 175—176 °C (from EtOAc).

4-(4-Benzyloxy-3-methoxycinnamoyl)tropolone (6f): Yellow plates (≃100% yield), mp 146—147 °C (from MeOH).

4-(3-Benzyloxy-4-methoxycinnamoyl)tropolone (6g): Yellow crystals (95% yield), mp 143—144 °C (from EtOH).

4-(4-Chlorocinnamoyl)tropolone (6h): Yellow prisms (≃100%) mp 208—209 °C (from $CHCl_3$).

4-(2,4-Dichlorocinnamoyl)tropolone (6i): Yellow scales (≃100 % yield), mp 162—163 °C (from EtOAc).

4-(4-Methoxycinnamoyl)tropolone (6j): Yellow needles (≃100 % yield), mp 163—164 °C (from $CHCl_3$).

4-(4-Bromocinnamoyl)tropolone (6k): Yellow crystals (94% yield), mp 213—214 °C (from $CHCl_3$).

4-(4-Methoxy-3-nitrocinnamoyl)tropolone (6l): Yellow crystals (≃100% yield), mp 272—273 °C (from dioxane).

4-(3-Nitrocinnamoyl)tropolone (6m): Yellow crystals (≃100% yield), mp 185—186 °C (from EtOH–dioxane).

4-(4-Nitrocinnamoyl)tropolone (6n): Orange needles (77% yield), mp 216—217 °C (from AcOH).

4-(3-Hydroxy-4-methoxycinnamoyl)tropolone (6o): Yellow crystals (49% yield), mp 174—175 °C (from AcOH).

4-(2-Hydroxycinnamoyl)tropolone (6p): Pale yellow crystals (22% yield), mp 172—173 °C (from EtOAc).

4-[4-Dimethylamino)cinnamoyl]tropolone (6q): Red needles (79% yield), mp 160—161 °C (from AcOH).

4-[3-(2-Furyl)propenoyl]tropolone (10): Yellow needles (91% yield), mp 160—161 °C (from EtOAc).

4-(5-Phenyl-2,4-pentadienoyl)tropolone (11): Yellow crystals (83% yield), mp 134—135 °C (from AcOH).

General Procedure for the Preparation of Oximes (7a—m) and Isoxazoline (13). A solution of 4-cinnamoyltropolone **6** (1 g) and 6.6 mol equiv of hydroxylamine hydrochloride in ethanol (10 ml) was refluxed for 4—13 h, and then, after cooling, diluted with water (30 ml), affording **7** (or **13**) as precipitates.

4-(3,4,5-Trimethoxycinnamoyl)tropolone Oxime (7a): Pale yellow crystals (75% yield), mp 230 °C (decomp) (from AcOH).

4-(3,4-Dimethoxycinnamoyl)tropolone Oximes (7b): Two isomers both as pale yellow crystals (75% combined yield), mp 216—217 and 219—220 °C after fractional recrystallization from dioxane.

4-(3,4-Methylenedioxycinnamoyl)tropolone Oximes (7c): Two isomers both as pale yellow crystals (76% combined yield), mp 176—178 and 208—209 °C (decomp) after fractional recrystallization from dioxane.

4-Cinnamoyltropolone Oximes (7d): Two isomers of colorless needles, mp 171—172 °C, and colorless prisms, mp 190—191 °C (43% combined yield) after fractional recrystallization

from EtOH.

4-(4-Methylcinnamoyl)tropolone Oxime (7e): Pale amber crystals (85% yield), mp 177—178 °C (from benzene).

4-(4-Benzyloxy-3-methoxycinnamoyl)tropolone Oxime (7f): Pale yellow crystals (92% yield), mp 180—181 °C (from benzene).

4-(3-Benzyloxy-4-methoxycinnamoyl)tropolone Oxime (7g): Pale yellow crystals (59% yield), mp 174—175 °C (from benzene).

4-(4-Chlorocinnamoyl)tropolone Oxime (7h): Pale yellow crystals (90% yield), mp 153—154 °C (from benzene).

4-(2,4-Dichlorocinnamoyl)tropolone Oxime (7i): Colorless crystals (59% yield), mp 219—220 °C (from EtOAc–dioxane).

4-(4-Methoxycinnamoyl)tropolone Oxime (7j): Pale amber crystals (45% yield), mp 178—179 °C (from dioxane).

4-(4-Bromocinnamoyl)tropolone Oxime (7k): Colorless crystals (81% yield), mp 163—164 °C (from benzene).

4-(4-Methoxy-3-nitrocinnamoyl)tropolone Oxime (7l): Yellow crystals (73% yield), mp 167—168 °C (decomp) (from benzene–EtOAc).

4-(3-Nitrocinnamoyl)tropolone Oxime (7m): Pale amber crystals (86% yield), mp 196—197 °C (from acetone).

4-[5-[4-(Dimethylamino)phenyl]-4, 5-dihydro-3-isoxazolyl]tropolone (13): Yellow crystals (91% yield), mp 172—173 °C (from benzene–$CHCl_3$); ^{1}H-NMR 2.94 (6H, s, Me_2N), 3.32, 3.67 (1H each, dd, J=16, 10 Hz, 2H-9), 5.71 (1H, t, J=10 Hz, H-10), 6.68 (2H, d, J=8.8 Hz, H′-3,5), 7.1—7.4 (5H, m, H-4,5,6 and H′-2,6), and 7.77 (1H, s, H-3).

General Procedure for the Hydrogenation of Oximes (7). A solution of the oxime (3.8 g) in acetic acid (47 ml) containing conc hydrochloric acid (5 ml) was hydrogenated in the presence 5% Pd/C at room temperature, until 2 mol equiv of hydrogen was absorbed. The catalyst was removed by filtration, the filtrate diluted with water (150 ml) and then washed with chloroform. The aq layer was neutralized with 59% aq KOH, depositing the corresponding amino compounds (**8**).

4-[1-Amino-3-(3,4,5-trimethoxyphenyl)-2-propenyl]tropolone (8a): Yellow crystals (82% yield), mp 153—154 °C (decomp) (from aq MeOH).

4-[1-Amino-3-(3,4-dimethoxyphenyl)-2-propenyl]tropolone (8b): Yellow crystals (85% yield), mp 154—155 °C (decomp) (from EtOH).

4-[1-Amino-3-(3, 4-methylenedioxyphenyl)-2-propenyl]tropolone (8c): Yellow crystals (77% yield), mp 187—188 °C (decomp) (from EtOH).

4-(1-Amino-3-phenyl-2-propenyl)tropolone (8d): Yellow crystals (98% yield), mp 191—192 °C (decomp) (from dioxane).

*4-(1-Amino-3-*p*-tolyl-2-propenyl)tropolone (8e)*: Yellow crystals (97% yield), mp 185—186 °C (decomp) (from dioxane).

4-[1-Amino-3-(4-benzyloxy-3-methoxyphenyl)-2-propenyl]tropolone (8f): Yellow crystals (80% yield), mp 146—147 °C (decomp) (from EtOH).

4-[1-Amino-3-(3-benzyloxy-4-methoxyphenyl)-2-propenyl]tropolone (8g): Yellow crystals (88% yield), mp 155—156 °C (decomp) (from EtOH).

4-[1-Amino-3-(4-chlorophenyl)-2-propenyl]tropolone (8h): Yellow crystals (93% yield), mp 198—199 °C (decomp) (from MeOH).

4-[1-Amino-3-(2,4-dichlorophenyl)-2-propenyl]tropolone (8i): Yellow crystals (93% yield), mp 185—186 °C (decomp) (from MeOH).

4-[1-Amino-3-(4-methoxyphenyl)-2-propenyl]tropolone (8j): Yellow crystals (90% yield), mp 182—183 °C (decomp) (from EtOH).

General Procedure for the Acetylation of the Amino Compounds (8). A mixture of **8** (2 g) and acetic anhydride (8 ml) was heated until it became a solution and then, after cooling, diluted with water (50 ml), depositing the acetamido compounds (**9**).

4-[1-Acetamido-3-(3,4,5-trimethoxyphenyl)-2-propenyl]tropolone (9a): Colorless leaflets (85% yield), mp 192—193 °C (from EtOH); ^{1}H-NMR 2.06 (3H, s, AcN), 3.84 (9H, s, 3MeO),5.2 (2H, m, OH. NH, exchangeable with D_2O), 5.60 (1H, m, H-8), 6.48 (1H, dd, J=14, 5 Hz, H-9) 6.55 (2H, s, H-2′,6′), 7.05—7.35 (4H, m, H-5,6,7,10), 7.25 (1H, d, J=14 Hz, H-10), and 7.40 (1H, s, H-3).

4-[1-Acetamido-3-(3, 4-dimethoxyphenyl)-2-propenyl]tropolone (9b): Colorless needles (93% yield), mp 183—184 °C (from MeOH).

4-[1-Acetamido-3-(3,4-methylenedioxyphenyl)-2-propenyl]tropolone (9c): Colorless needles (86% yield), mp 177—178 °C (from MeOH).

4-(1-Acetamido-3-phenyl-2-propenyl)tropolone (9d): Colorless needles (79% yield), mp 162—163 °C (from MeOH).

*4-(1-Acetamido-3-*p*-tolyl-2-propenyl)tropolone (9e)*: Colorless needles (92% yield), mp 182—183 °C (from EtOAc).

4-[1-Acetamido-3-(4-benzyloxy-3-methoxyphenyl)-2-propenyl]tropolone (9f): Colorless crystals (62% yield), mp 148—149 °C (from EtOAc).

4-[1-Acetamido-3-(3-benzyloxy-4-methoxyphenyl)-2-propenyl]tropolone (9g): Colorless crystals (89% yield), mp 154—155 °C (from EtOAc).

4-[1-Acetamido-3-(4-chlorophenyl)-2-propenyl]tropolone (9h): Colorless crystals (95% yield), mp 154—155 °C (from EtOAc).

4-[1-Acetamido-3-(2,4-dichlorophenyl)-2-propenyl]tropolone (9i): Colorless needles (54% yield), mp 121—122 °C (from EtOAc).

4-[1-Acetamido-3-(4-methoxyphenyl)-2-propenyl]tropolone (9j): Colorless crystals (90% yield), mp 122—123 °C (from EtOH).

General Procedure for the Preparation of Compounds **15**. A solution of the olefin **9** (3 g) in 0.25—1.0 M aq KOH (30 ml) was reduced with hydrogen in the presence of 10—30% Pd/C at room temperature until the starting material disappeared (*ca.* 50 h). After filtration of the catalyst, the filtrate was acidified with 6 M HCl, depositing the product **15**; when necessary, the product was extracted with chloroform.

4-[1-Acetamido-3-(3,4,5-trimethoxyphenyl)propyl]tropolone (15a): Colorless needles (98% yield), mp 129—130 °C (from EtOAc); ^{1}H-NMR 1.97 (3H, s, AcN), 2.0 (2H, m, 2H-9), 2.55 (2H, m, 2H-10), 3.92 (9H, s, 3MeO), 4.3 (1H, m, NH), 4.90 (1H, q, J=7 Hz), 6.36 (2H, s, H-2′,6′), and 7.1—7.4 (4H, m, H-3,4,6,-7).

4-[1-Acetamido-3-(3,4-dimethoxyphenyl)propyl]tropolone (15b): Colorless crystals (93% yield), mp 143—144 °C (from EtOAc–MeOH).

4-[1-Acetamido-3-(3, 4-methylenedioxyphenyl)propyl]tropolone (15c): Colorless crystals (67% yield), mp 168—169 °C (from EtOAc).

4-(1-Acetamido-3-phenylpropyl)tropolone (15d): Colorless needles (88% yield), mp 148—149 °C (EtOH).

*4-(1-Acetamido-3-*p*-tolypropyl)tropolone (15e)*: Colorless needles (90% yield), mp 149—150 °C ($CHCl_3$).

We are grateful to Mr. H. Akiyama for carrying out a part of the experiments. The present work was partially supported by a Grant-in-Aid for Scientific Research from the Ministry of Education, Science and Culture and also a Research Grant from Sankyo Co. Ltd., Tokyo, to which we wish to express our thanks.

References

1) An initial part of the results have been presented: a) T. Nozoe, 16th IUPAC Congress, Paris, July, 1957, *Experientia, Suppl. VII*, 306 (1957); b) T. Nozoe, K. Takase, Y. Kitahara, and K. Doi, 132nd National Meeting of the American Chemical Society, New York, Sept. 1957; c) T. Nozoe, K. Takase, and

H. Matsumura, "Comprehesive Organic Chemistry (Dai Yuki Kagaku)," ed by M. Kotake, Asakura, Tokyo (1960), Vol. 13, pp. 340—374; T. Nozoe, *Prog. Org. Chem.*, **5**, 132 (1961).

2) A part of the results in the Experimental section have been taken from M. Sc. Thesis of N. Kawabe, Tohoku Univ. (1965); publication of the present work has been delayed for a long period for various reasons.

3) M. H. Zweig and C. F. Chignell, *Biochem. Pharmacol.*, **22**, 2141 (1973); J. B. Olmstead and G. G. Borisy, *Annu. Rev. Biochem.*, **42**, 507 (1973).

4) J. Schreiber, W. Leimgruber, M. Pesaro, P. Schudel, T. Threefall, and A. Eschenmoser, *Helv. Chim. Acta*, **44**, 540 (1961); E. E. van Tamelen, T. R. Spencer, Jr., D. B. Allen, and R. L. Orvis, *Tetrahedron*, **14**, 8 (1961); T. Nakamura, Y. Murase, R. Hayashi, and Y. Endo, *Chem. Pharm. Bull.*, **10**, 281 (1962), G. Sunagawa, T. Nakamura, and J. Nakazawa, *ibid.*, **10**, 291 (1962), T. Nakamura, *ibid.*, **10**, 299 (1962); A. I. Scott, F. McCapra, R. L. Buchanan, A. C. Day, and D. W. Young, *Tetrahedron*, **21**, 3605 (1965); R. B. Woodward, "The Harvey Lecture," Ser. 59, 31, Academic Press, New York, N. Y. (1965); J. Martel, E. Toromonoff, and C. Huyuh, *J. Org. Chem.*, **30**, 1752 (1965); S. Kaneko and M. Matsui, *Agric. Biol. Chem.*, **32**, 995 (1968); K. Kato, F. Kido, M. D. Wu, and A. Yoshikoshi, *Bull. Chem. Soc. Jpn.*, **47**, 1516 (1974); E. Kotani, F. Miyazaki, and S. Tobinaga, *J. Chem. Soc., Chem. Commun.*, **1974**, 300; D. A. Evans, S. P. Tanis, and D. J. Hart, *J. Am. Chem. Soc.*, **103**, 5813 (1981).

5) H. Yamamoto, A. Hara, A. Noguchi, H. Kawamoto, S. Inokawa, and T. Nozoe, *Bull. Chem. Soc. Jpn.*, **55**, 1594 (1982).

6) T. Nozoe, *Fortschr. Chem. Org. Naturst.*, **13**, 232 (1956); T. Nozoe, K. Takase, and M. Ogata, *Chem. Ind.*, **1957**, 1070.

7) See, *e.g.* A. Albert and E. P. Sergent, "The Determination of Ionization Constants of Acids and Bases," Chapman and Hall, London (1972); D. D. Perrin, B. Dempsey, and E. P. Sergent, "pK_a Prediction for Organic Acids and Bases," Chapman and Hall, London (1981).

8) J. W. Cook, A. R. Gibb, R. A. Raphael, and A. R. Sommerville, *Chem. Ind.*, **1950**, 427, *J. Chem. Soc.*, **1951**, 503; W. von E. Doering and L. H. Knox, *J. Am. Chem. Soc.*, **72**, 2305 (1950); **73**, 828 (1951).

9) Employing our method,[1,2] M. Oda and H. Ogawa have prepared a dichloro compound (**15**; $R^1=R^2=Cl$, $R^3=H$) from **5**: Japan Kokai Koho 61156-61158 (1979); *Chem. Abstr.*, 193025 (1980).

10) Ref. 1c, pp. 1—691; D. Lloyd, "Carbocyclic Nonbenzenoid Aromatic Compounds," Elsevier, Amsterdam (1966), pp. 134—144; F. Pietra, *Chem. Rev.*, **73**, 293 (1973).

Synthesis and the Spectral Analysis of 4- and 6-[1-Acetamido-3-(3,4,5-trimethoxyphenyl)propyl]-2-methoxytropones (B-Ring-open Analogues of Colchicine)[1]

Hiroshi YAMAMOTO,* Atsushi HARA, Saburo INOKAWA, and Tetsuo NOZOE†
Department of Chemistry, Faculty of Science, Okayama University, Tsushima, Okayama 700
(Received April 16, 1983)

The treatment of 4-[1-acetamido-3-(3,4,5-trimethoxyphenyl)propyl]tropolone with ethereal diazomethane gave the 6- and 4-substituted title compounds in 51 and 38% yields, respectively. The 270-MHz ^{1}H-NMR spectral analysis performed on these compounds, colchicine, and two methyl ethers of hinokitiol permits unequivocal assignment of the position of the *C*-substituent on these 2-methoxytropone rings. Attempts were made to effect the direct B-ring closure of these intermediates and 4-[1-acetamido-3-(3,4,5-trimethoxyphenyl)propyl]-5-aminotropolone using various oxidizing reagents.

In our effort to explore a convenient and efficient route for the preparation of colchicine (**1**) and its analogues, and also as a part of our study of troponoid chemistry, we have previously reported[2,3] a facile synthesis of 4-(1-acetamido-3-arypropyl)tropolones (*e.g.* **4**) from 4-acetyltropolone (**3**). We wish to describe herein the preparation of B-ring-open colchicine analogues and an effective use of ^{1}H-NMR spectroscopy in the structural assignment of the related 2-methoxytropone derivatives.

As a representative example of the derivatization to colchicine analogues, 4-[1-acetamido-3-(3,4,5-trimethoxyphenyl)propyl]tropolone (**4**) prepared[3] from **3** in five steps with an overall yield of *ca.* 35—40% was treated with ethereal diazomethane at 0 °C to furnish colorless needles of **5** (mp 119—121 °C) and **6** (180—182 °C) after chromatographic separation. The high-resolution EI mass spectra of both compounds clearly gave the molecular ions at *m/e* 401 ($C_{22}H_{27}O_6N$) corresponding to the methyl ethers of **4**. The structural assignments of these two isomers were effectively made by the analysis of the 270 MHz ^{1}H-NMR spectral signals at δ 6.7—7.3 due to their tropolone ring moiety (see Fig. 1). Namely, the doublet at δ 6.70 in the spectrum of **5** was readily assigned to H-3 on the evidence of a long-range spin coupling (J=0.3 Hz) with the methoxyl group on C-2, as had been observed for methyl ether derivatives of salicylaldehyde[4] and 5-aminotropolones.[5] The other ring-proton signals were then automatically assignable by decoupling experiments, leading to structure **5**, 6-[1-acetamido-3-(3,4,5-trimethoxyphenyl)propyl]-2-methoxytropone (the colchicine molecule being cleaved at the C_{1a}–C_{12a} bond), for the product available from the faster-eluting fraction; see Table 1 for parameters of the NMR spectrum of **5**.

Similarly, the spectrum of the other product can be rationalized in terms of the isomeric structure, 4-substituted 2-methoxytropone (**6**) (an analogue of isocolchicine); the parameters of the spectrum and the assignments of the signals are also summarized in Table 1.

The remarkable difference in the splitting patterns of the H-3 signals between these two isomers **5** (doublet) and **6** (slightly broadened singlet) readily permits the assignment of the position of the *C*-substituent on the 2-methoxytropone nucleus. This evidence is of value for distinguishing between the 4- and 6-positional isomers of the methyl ethers derived from many kinds of naturally occurring 4-substituted troponoids,[6,7] such as colchiceine (**2**), hinokitiol (**7**), and β-dolabrin (**8**). The two methyl ethers **9** and **10**, which had been reported as an inseparable mixture upon treatment of **7** with diazomethane,[8,9] have now been separated into pure components by silica-gel column chromatography. Their structures can easily be established by their ^{1}H-NMR spectral analysis even at 60 MHz; see the assignments for each compound recorded in Table 1.[10] The distinction between these two isomers **9** and **10** had

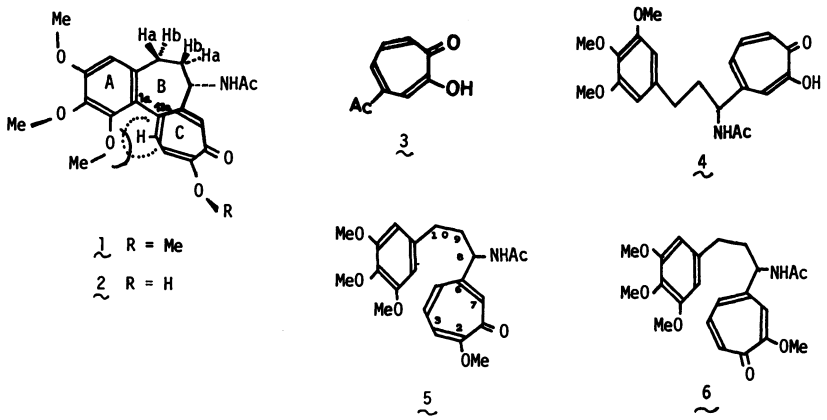

† 811, 2-5-1, Kamiyoga, Setagaya-ku, Tokyo 158.

Table 1. ^{1}H-NMR (270 MHz) Parameters for colchicine and its analogues in $CDCl_3$

Compound	Chemical shifts, δ									
	MeO-2	H-3	H-4	H-5	H-6	H-7	H-8 NH-8 AcN-8	H_a-9 H_b-9	H_a-10 H_b-10	MeO-4′ MeO-3′,5′ H-2′,6′
1[a]	4.02	6.92	7.38	—	—	7.65	4.62 8.38 1.97	2.00[b] 2.36[b]	2.40[b] 2.53[b]	3.91 3.67, 3.95 6.55
2[c]	6.7[d]	7.30	7.69	—	—	7.58	4.72 4.7 1.99	2.0 2.2	2.40 2.48	3.93 3.65, 3.93 6.57
4[c]	6.4[d]	7.3	7.3	7.1	—	7.3	4.90 4.3 1.97	2.0 2.0	2.5 2.5	3.82 3.83, 3.83 6.36
5	3.92	6.70	7.07	6.88	—	7.27	4.80 6.79 1.99	2.02 2.02	2.61 2.68	3.82 3.83, 3.83 6.37
6	3.89	6.73	—	6.88	7.19	7.12	4.86 6.49 2.03	2.07 2.11	2.60 2.65	3.82 3.83, 3.83 6.36
9[c]	3.93	6.65	7.0[e]	6.9[e]	—	7.20	2.80	1.21[f]		
10[c]	3.98	6.70	—	6.82	7.2[e]	7.1[e]	2.86	1.27[f]		
11[c]	7.1	7.33	8.10	2.45[g] 7.35[h] 7.72[h]	—	7.51	6.15 6.60	2.1 2.1	2.5 2.6	3.80 3.75, 3.75 6.30
12	7.15	7.1	7.35	5.2[i]	—	7.43	5.1 5.2 2.02	2.1	2.6	3.83 3.83, 3.83 6.40

Coupling constants/Hz[j]

	$J_{3,4}$	$J_{3,5}$	$J_{3,OMe}$	$J_{4,5}$	$J_{5,6}$	$J_{5,7}$	$J_{6,7}$	$J_{8,9a}$	$J_{8,9b}$	$J_{8,NH}$	$J_{9,9}$	$J_{9,10}$	$J_{10,10}$
1	10.8	—	0.3	—	—	—	—	11.2	5.2	6.2	15	[b]	15
2	11.0	—	—	—	—	—	—						
4			—		—		—	7.0	7.0	7.0			
5	10.0	0.5	0.3	10.7	—	1.3	—	7.0	7.0	7.0	—	7.5[k]	14
6	—	0.5	0.3	—	8.2	1.2	12.2	7.0	6.5	8.5	14	7.5[k]	14
9	8.0	1.5	0.5[e]	10[e]	—	1.3	—	7.0[l]					
10	—	0.5[e]	0.5[e]	—	8[e]	1[e]	12[e]	7.0[l]					
11	12.0	—	—	—	—	—	—	7.0	7.0	7.0			

a) The numbering of compounds **1**, **2**, **4**, **11**, and **12** corresponds to that of **5** for the purpose of comparison. b) The AMNX spin system was used for the calculation of the approximate J values (*cf.* Ref. 10): $J_{9a,10a}$ 11, $J_{9a,10b}$ 0, $J_{9b,10a}$ 4, and $J_{9b,10b}$ 6 2 Hz. c) Measured at 60 MHz. d) HO-2. e) Approximate value. f) $2H_3$-9. g) *p*-$C\underline{H}_3C_6H_4N_2$-5. h) $MeC_6\underline{H}_4N_2$-5 (both 2H, d, J=7.5 Hz). i) NH_2-5. j) J Values confirmed by double resonance. k) All $J_{9,10}$ values are almost identical. l) $J_{8,9}$

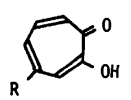

7 R = $CHMe_2$

8 R = $C(=CH_2)Me$

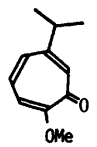

9

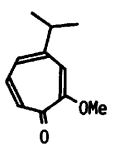

10

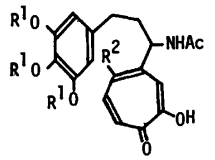

11 R^1 = Me R^2 = $N_2C_6H_4Me(p)$

12 R^1 = Me R^2 = NH_2

13 R^1 = Me R^2 = N_2^+

14 R^1 = H R^2 = H

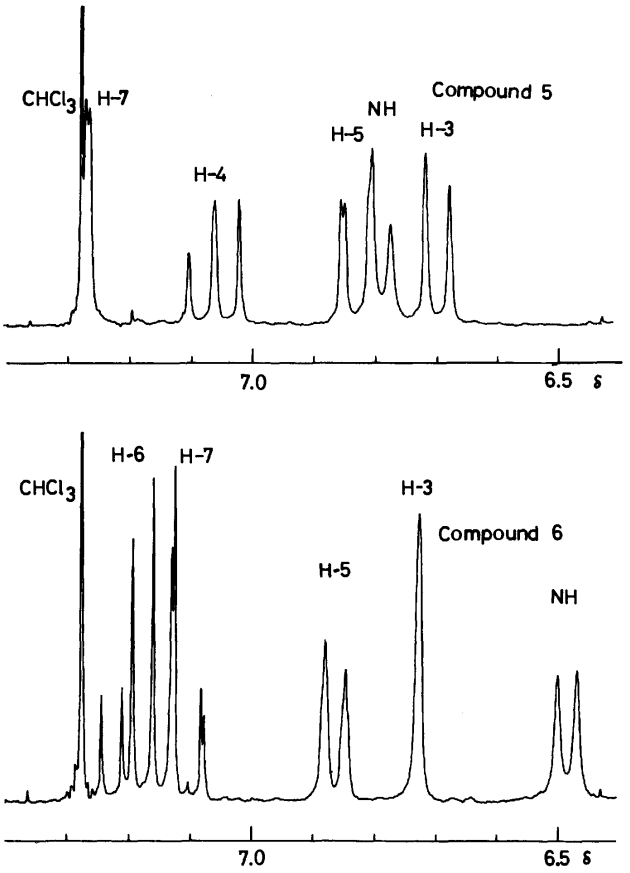

Fig. 1. Aromatic regions of the ^{1}H-NMR (270 MHz) spectra of **5** and **6**.

previously been made either by chemical conversion to the known tropolone derivatives[11] or by examining the out-of-plane bending bands in their IR spectra.[12] Although the latter method is useful for relatively simple tropolone derivatives, the distinction by the NMR spectroscopy is obviously more reliable and has a wider applicability.

The ^{1}H-NMR spectrum of colchicine (**1**) taken at 270 MHz is in accord with the characteristic features discussed above. The assignment of all signals, which can reasonably be made by considering (with the aid of the CPK and Dreiding models) the dihedral angles between the A and C rings, are recorded in Table 1. It is noted that, when **1** is hydrolyzed to colchiceine (**2**) either with hot, dilute hydrochloric acid[13] or with cold alkali, an appreciable downfield shift (0.3—0.4 ppm) of the H-3 and H-4 signals occurs. A similar shift can be seen, when the H-3 and -4 signals of the analogue **5** are compared with those of **4** (see Table 1).[14]

Various attempts were made to effect the B-ring-closure of compounds **4** and **5** to provide **2** and **1**, respectively, using the following oxidizing reagents which have been effective for the oxidative coupling of phenols:[15] i) diphenyl selenoxide,[16] ii) thallium(III) tris(trifluoroacetate),[17] and iii) manganese(III) acetylacetonate.[18] However, these procedures were found to be unsuccessful and the starting materials remained unchanged in most cases. Alternatively, in order to utilize the Pschorr reaction for the ring-closure,[19] the amino compound **12**, obtained from **4** *via* 5-*p*-tolylazo compound (**11**),[20] was first diazotized to the 5-diazonium salt (**13**) and subjected to various conditions of the Pschorr reaction,[21] but no appreciable amount of anticipated colchiceine (**2**) was detected among the reaction products. Attempts at partial or total demethylation of the methoxyl groups on the phenyl ring in **4** (to lead to *e.g.* compound **14**) using trimethylsilyl iodide[22] or conc hydrobromic acid resulted in extensive decomposition.

These findings are believed to be of value, not only from the viewpoint of modifications of the ring-closure for an efficient synthesis of various kinds of colchicine analogues having a potential biological activity, but also from that of the development of the fundamental chemistry of troponoids.[23]

Experimental

Melting points were measured with a Yanagimoto MP-3 instrument and are uncorrected. The ^{1}H-NMR spectra were recorded in $CDCl_3$ with a Hitachi R-20A (60 MHz) [or Brucker WH-270 cryospectrometer (270 MHz) for compounds **1**, **5**, and **6**]. Chemical shifts are reported as δ values in parts per million relative to tetramethylsilane (δ 0.0) as an internal standard. Spin decoupling was performed for all proton signals to confirm the coupling constants. Mass spectra were measured with a Hitachi M-80 high-resolution instrument and are given in terms of *m/e* (relative intensity) compared with the base peak and possible assignments. IR And UV spectra were obtained on Hitachi 215 and 340 spectrometers, respectively. All reactions were monitored by TLC [conducted on plates precoated with silica gel (0.25 mm, Merck)]. Column chromatography was performed using Merck Lobar silica gel.

6-[1-Acetamido-3-(3,4,5-trimethoxyphenyl)propyl]-2-methoxytropone (5) and Its 4-Propyl Isomer (6). A solution of 257 mg of the tropolone[3] **4** in 20 ml of dry dichloromethane was treated with an excess amount of *ca.* 0.5 M (1 M=1 mol dm^{-3}) ethereal diazomethane at 0 °C for 1 h. The solvent was evaporated *in vacuo*, and the residue chromatographed on a column of silica gel with CCl_4 (which was gradually changed to $CHCl_3$) as eluent, giving **5** (136 mg, 51%) and **6** (100 mg, 38%).

5: Colorless needles, mp 119—121 °C (from CH_2Cl_2–EtOAc); R_f 0.60 (10% MeOH/$CHCl_3$, v/v); ^{1}H-NMR, see Table 1; IR (KBr) 3280, 2910, 1660, 1590, 1450, 1220, 1120, 1000, 790, and 780 cm^{-1}; EI MS *m/e* (rel intensity) 401 (29; M$^+$), 342 (35; M−$AcNH_2$), 220 (28; M−Ar*CH_2), 207 (100; M−Ar*CH=CH_2), 195 (48; Ar*CH=CH_2), 182 (43; Ar*CH_2), 181 (25), and 164 (44; M−Ar*CH=CH_2−Ac); exact mass, calcd for $C_{22}H_{27}O_6N$ 401.1837, found 401.1855.

6: Colorless needles, mp 180—182 °C (from EtOAc–hexane); R_f 0.55 (10% MeOH/$CHCl_3$); ^{1}H-NMR, see Table 1; IR (KBr) 3250, 2900, 1655, 1590—1500, 1440, 1270, 1250, 1225, 1200, 1120, 1020, 960, 820, 790, and 770 cm^{-1}; EI MS *m/e* (rel intensity) 401 (76; M$^+$), 342(18), 220(85), 207(58), 195(89), 182(51), 181(100), and 164(45); exact mass, Calcd for $C_{22}H_{27}O_6N$ 401.1837, Found 401.1841.

6- and 4-Isopropyl-2-methoxytropone (9 and 10). Hinokitiol (**7**; 200 mg) was similarly treated with cold ethereal diazomethane, and the crude products chromatographed on a column of silica gel, using benzene–ethyl acetate as eluent, thus giving **9** (47% yield) and **10** (31% yield).

Ar*: 3,4,5-Trimethoxyphenyl.

9 and **10**: Both colorless oil (*cf.* Ref. 11, oil): R_f 0.45 and 0.50, respectively, (3% EtOH–EtOAc, v/v); ^{1}H-NMR, see Table 1.

Colchiceine (2). A mixture of 49 mg of **1**, 0.5 ml of ethanol, and 0.5 ml of 1 M KOH was stirred at 20 °C for 17 h. The ethanol was removed *in vacuo*, and the residue brought to pH 4, extracted with CH_2Cl_2, dried (Na_2SO_4), and evaporated, thus giving, after recrystallization from ethyl acetate, 37 mg (78%) of **2**, mp 177—178 °C (Ref. 13, 178—179 °C).

4-[1-Acetamido-3-(3,4,5-trimethoxyphenyl)propyl]-5-(p-tolylazo)-tropolone (11). A cold solution of *p*-toluenediazonium chloride prepared from 12 mg of *p*-toluidine and 8 mg of sodium nitrite by the usual method was added to a solution of 40 mg of **4** in 0.15 ml of dry pyridine at 0 °C. After having been stirred for 3 h, the mixture was diluted with cold water (1 ml), and the precipitates were filtered off and washed with benzene, thus affording 40 mg (88% yield) of **11** as reddish orange crystals: mp 127—128 °C; ^{1}H-NMR, see Table 1; λ_{max} (MeOH) 230, 285, 430 nm (log ε 4.48, 4.06, 4.43); Found: C, 63.85; H, 6.36; N, 7.80%. Calcd for $C_{28}H_{31}O_6N_3 \cdot H_2O$: C, 64.23; H, 6.35; N, 8.03%.

4-[1-Acetamido-3-(3, 4, 5-trimethoxyphenyl)propyl]-5-aminotropolone (12). A suspension of 37 mg of **11** in 1 ml of methanol was hydrogenated over 1 mg of 10% Pd/C at 27 °C under atmospheric pressure until two equivalents of hydrogen was absorbed (20 min). The catalyst was filtered off and the filtrate was concentrated *in vacuo* to give 28 mg (95% yield) of **12** as yellow needles: mp 122—123 °C (from EtOAc); ^{1}H-NMR, see Table 1; λ_{max} (MeOH) 232, 360, 400 nm (log ε 4.42, 4.06, 3.96); Found: C, 62.67; H, 6.76; N, 7.21%. Calcd for $C_{21}H_{26}O_6N_2$: C, 62.67; H, 6.51; N, 6.96%.

We wish to thank Mr. K. Suzuki for carrying out a part of experiments and Dr. T. Takita of Institute of Bioorganic Chemistry, Kawasaki, for the kind measurements of the 270 MHz ^{1}H-NMR and the high-resolution mass spectra. The present work was partially supported by a Research Grant (to H.Y.) from the Suntory Institute of Bioorganic Research, Osaka, to which we wish to express our thanks.

References

1) A part of the results have been presented: A. Hara, A. Noguchi, H. Yamamoto, S. Inokawa, and T. Nozoe, the 45th National Meeting of the Chemical Society of Japan, Tokyo, April 1982, Abstr., No. 1096; A. Noguchi, A. Hara, H. Yamamoto, S. Inokawa, T. Nozoe, the Regional Meeting of the Chemical Society of Japan, Takamatsu, November 1982, Abstr., No. 196.

2) H. Yamamoto, A. Hara, A. Noguchi, H. Kawamoto, S. Inokawa, and T. Nozoe, *Bull. Chem. Soc. Jpn.*, **55**, 1594 (1982).

3) T. Nozoe, K. Takase, N. Kawabe, T. Asao, and H. Yamamoto, *Bull. Chem. Soc. Jpn.*, **56**, 3099 (1983).

4) S. Forsen, *J. Phys. Chem.*, **67**, 1749 (1963); S. Forsen, B. Akermark, and T. Alm, *Acta Chem. Scand.*, **18**, 2313 (1964).

5) S. Seto, K. Ogura, H. Toda, Y. Ikegami, and T. Ikenoue, *Bull. Chem. Soc. Jpn.*, **41**, 2696 (1968).

6) T. Nozoe, K. Takase, and H. Matsumura, "Dai Yuki Kagaku (Comprehensive Organic Chemistry)," ed by M. Kotake, Asakura, Tokyo (1960), Vol. 13, pp. 21—45.

7) T. Nozoe, *Fortschr. Chem. Org. Naturst.*, **13**, 232 (1956); T. Nozoe, K. Takase, and M. Ogata, *Chem. Ind.*, **1957**, 1070.

8) Ref. 6, pp. 178—213.

9) R. D. Haworth and J. D. Hobson, *J. Chem. Soc.*, **1951**, 561.

10) For the analysis of the NMR spectra, see *e.g.*, P. L. Corio, *Chem. Rev.*, **60**, 363 (1960).

11) T. Nozoe, S. Seto, H. Takeda, S. Morosawa, and K. Matsumoto, *Proc. Jpn. Acad.*, **28**, 192 (1952).

12) M. Yasunami, K. Takase, and T. Nozoe, to be published.

13) F. Santavy and V. Macak, *Coll. Czech. Chem. Commun.*, **19**, 805 (1954); F. Santavy, "Alkaloidy Ocunovitych Rostlin Ajejich Derivaty," Statni Zdravotinicke, Nakladatelstivi (1958).

14) Physiological activities of compounds **4**, **5**, and **6** are being tested, and the results will be reported elsewhere.

15) *E.g.*, W. I. Taylor and A. R. Battersby, "Oxidative Coupling of Phenols," Marcel Dekker, New York (1967).

16) J. P. Marino and A. Schwarz, *Tetrahedron Lett.*, **1975**, 3252.

17) M. A. Schwarz and I. S. Mami, *J. Am. Chem. Soc.*, **97**, 1239 (1975).

18) M. J. S. Dewar and T. Nakaya, *J. Am. Chem. Soc.*, **90**, 7134 (1968).

19) A preliminary account of the attempted ring-closure by this method has been presented: T. Nozoe, 16th IUPAC Congress, Paris, July, 1957; *Experientia, Suppl. VII*, 306 (1957).

20) A part of the results in the Experimental section have been taken from M.Sc. Thesis of K. Suzuki, Tohoku Univ. (1960).

21) D. F. De Tar, *Org. React.*, **9**, 409 (1957); T. Kametani and K. Fukumoto, *J. Heterocycl. Chem.*, **8**, 341 (1971).

22) M. E. Jung and M. A. Lyster, *J. Org. Chem.*, **42**, 3761 (1977).

23) Ref. 6, pp. 1—437; D. Lloyd, "Carbocyclic Non-benzenoid Aromatic Compounds," Elsevier, Amsterdam (1966), pp. 134—144; F. Pietra, *Chem. Rev.*, **73**, 293 (1973).

 © 1983 The Chemical Society of Japan Bull. Chem. Soc. Jpn., 56, 3110—3117 (1983) [Vol. 56, No. 10

The Conformational Analysis of 1-*p*-Tolyl-2-phenyl-1-propanols, 1-*p*-Tolyl-2-phenylethanol, and 1-*p*-Tolyl-2-phenyl-1-propanone by Means of NMR Spectroscopy

Norio KUNIEDA,*,† Hiroko ENDO,†† Minoru HIROTA,††
Yoshio KODAMA, and Motohiro NISHIO*

Central Research Laboratories, Meiji Seika Kaisha Ltd., Morooka, Kohoku-ku, Yokohama 222
†*Department of Applied Chemistry, Faculty of Engineering, Osaka City University, Sumiyoshi-ku, Osaka 558*
††*Department of Applied Chemistry, Faculty of Engineering, Yokohama National University, Tokiwadai, Hodogaya-ku, Yokohama 240*

(Received April 18, 1983)

The conformations of the diastereomers of 1-*p*-tolyl-2-phenyl-1-propanols[(*RS*/*SR*)-**3** and (*RR*/*SS*)-**3**], 1-*p*-tolyl-2-phenylethanol (**4**), and 1-*p*-tolyl-2-phenyl-1-propanone (**5**) were studied by means of NMR spectroscopy, mostly with the aid of the computer-simulation of the lanthanoid-induced shifts. It has been suggested that the rotamers in which the tolyl group lies close to the phenyl group are preferred in the conformational equilibria of (*RS*/*SR*)-**3**, **4**, and **5**. For (*RR*/*SS*)-**3**, the most stable rotamer (in $CDCl_3$) has been suggested to have the tolyl group *anti* to the phenyl group and *gauche* to the methyl group. The results have been discussed in view of the general occurrence of the folded conformation.

Our recent nuclear magnetic resonance studies of several diastereomeric 1-phenylalkyl aryl sulfoxides, (*RS*/*SR*)- or (*RR*/*SS*)-$C_6H_5CH(R)$–SO–Ar (**1**),[1] have demonstrated that the conformational equilibria of these compounds are like those illustrated in Scheme 1. That is to say, it has been found that the rotamers in which the aromatic group(Ar) is positioned *gauche* to the phenyl group (Ph) (**a** and **b** rotamers) are most populated in the conformational equilibria of these compounds.

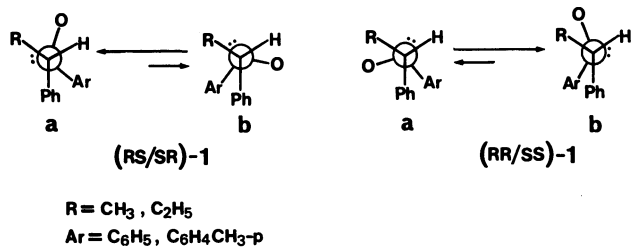

Scheme 1.

This phenomenon (favored *gauche* interactions) is interesting in relation to a similar one hitherto observed for the compounds of the following type: $C_6H_5CH(CH_3)$–X–R (**2**) [X=S,[14] SO,[1,10] CH_2,[13] CHOH,[4,7] CO;[9] R=CH_3, C_2H_5, *i*-C_3H_7, *t*-C_4H_9]. These findings have now prompted us to investigate the conformational analysis of a few alcohols, the diastereomeric pairs of 1-*p*-tolyl-2-phenyl-1-propanol [(*RS*/*SR*)-**3** and (*RR*/*SS*)-**3**], 1-*p*-tolyl-2-phenylethanol (**4**), and a ketone, 1-*p*-tolyl-2-phenyl-1-propanone (**5**), which have the structural resemblance to **1**. It is quite important to explore the generality of the phenomenon (favored *gauche* interactions) in order to know the nature of the interactions, which provide the molecular shapes of these compounds. In this paper we wish to report the results for the conformational assignments of the compounds (**3**—**5**) accomplished with the aid of NMR spectroscopy and comments concerning the interactions involved in the conformational equilibria.

Experimental

(RS/SR)- *and* (RR/SS)-*1*-p-*Tolyl-2-phenyl-1-propanols (3).* 2-Phenylpropionaldehyde (50 g, 0.37 mol) was treated with a Grignard reagent derived from 70 g (0.41 mol) of *p*-bromotoluene and 10 g (0.41 mol) of magnesium in dry ether. After the usual work-up, the crude product was purified by fractional distillation to yield a diastereoisomeric mixture of **3** (73 g, 87% yield); bp 138—139 °C/1—2 Torr (1 Torr≈133.322 Pa). The diastereomeric ratio, (*RS*/*SR*)-**3** : (*RR*/*SS*)-**3**, of the products evaluated by NMR was about 6 : 1. The separation of the diastereoisomers was carried out using a procedure similar to that described for 1,2-diphenylpropanols by Cram and Erhafez.[2] Thus the above mixture (15.2 g, 67 mmol) was treated with *p*-nitrobenzoyl chloride (12.5 g, 67 mmol) in 25 cm^3 of dry pyridine at 90—95 °C for 2 h. Five recrystallizations of the resulting mixture of esters from ethyl acetate yielded the *p*-nitrobenzoyl ester of (*RS*/*SR*)-**3** (9.3 g, 37%); mp 98 °C. The hydrolysis of the above ester (5.3 g, 14 mmol) was carried out in a mixture of 10 cm^3 of water and 10 cm^3 of methanol, with 0.8 g of potassium hydroxide and 0.6 g of sodium hydroxide, to yield 2.9 g of (*RS*/*SR*)-**3**. This was purified by column chromatography on silica gel using ether–hexane (1 : 3) as the eluent. Yield 2.4 g (76%); bp 138 °C/1—2 Torr. Found: C, 84.55; H, 7.98%. Calcd for $C_{16}H_{18}O$: C, 84.92; H, 8.02%.

1-*p*-Tolyl-2-phenyl-1-propanone (**5**) (9.9 g, 44 mmol) was treated with 1.5 g of lithium alminium hydride to yield a mixture of the diastereoisomeric alcohols (9.1 g, 91%); bp 135 °C/1 Torr. The diastereomeric ratio, (*RS*/*SR*)-**3** : (*RR*/*SS*)-**3**, was evaluated to be *ca.* 1 : 4 by NMR. The above mixture (2.5 g, 11 mmol) was treated with 1.7 g (11 mmol) of phthalic anhydride in 2 cm^3 of dry pyridine at 100 °C for 2 h to produce the phthalic acid monoesters of **3**. Four recrystallizations of the ester from ethyl acetate–hexane yielded the ester of (*RR*/*SS*)-**3** (1.9 g, 46%); mp 131—132 °C. The free alcohol (1.0 g) was obtained by hydrolyzing the ester (1.75 g, 4.7 mmol) in 6 cm^3 of methanol–water (1 : 1) using a mixture of potassium hydroxide (0.5 g) and sodium hydroxide (0.5 g). The subsequent column chromatography on silica gel, eluting with ether–hexane (1 : 3), afforded analytically pure (*RR*/*SS*)-**3** (0.95 g, 90%). Found: C, 84.91; H, 8.05%. Calcd for $C_{16}H_{18}O$: C, 84.92; H, 8.02%.

1-p-*Tolyl-2-phenylethanol (4).* This compound was

prepared by the reaction of phenylacetaldehyde (18 g) with *p*-tolylmagnesium bromide (derived from 27 g of *p*-bromotoluene and 3.9 g of magnesium) in dry ether. After the usual work-up, column chromatography of the crude product on silica gel (ether : hexane=1 : 3), followed by the recrystallization from hexane, yielded analytically pure **4** (23.5 g, 74%); mp 68—69 °C (lit,[3] 68—69 °C).

1-p-Tolyl-2-phenyl-1-propanone (5). The diastereomeric mixture of 1-*p*-tolyl-2-phenyl-1-propanols(**3**) (10.4 g, 46 mmol) was oxidized with 50 mmol of Jones reagent in 200 cm^3 of acetone. The usual work-up, followed by the fractional distillation of the crude product gave analytically pure **5** (7.6 g, 74%); bp 125 °C/1 Torr. Found C, 85.13; H, 7.14%. Calcd for $C_{16}H_{16}O$: C, 85.68; H, 7.19%.

NMR Measurements. The ^1H and ^{13}C NMR spectra were measured for solutions in $CDCl_3$ and/or C_6D_6 (*ca.* 0.3 mol/dm^3) on a JEOL FX-90Q spectrometer. The chemical shifts are given in ppm downfield from internal tetramethylsilane (TMS). The assignments for the carbon resonances were aided by the comparisons of the lanthanoid-induced shifts (LIS).

Lanthanoid-induced Shifts (LIS) Measurements. The LIS were determined, for $CDCl_3$ and C_6D_6 solutions, as described in the preceding paper[1] using $Yb(fod)_3$ or $Eu(fod)_3$ as the lanthanoid shift-reagents (LSR). Table 1 lists the relative LIS's for protons and carbons in (*RS/SR*)-**3**, (*RR/SS*)-**3**, **4**, and **5**. The vicinal coupling constants, $^3J_{H_aH_x}$, have been found to be insensitive to the addition of the LSR. Perturbation to the conformational equilibria by coordination is therefore unimportant for **3** and **4**.

Computer-simulation of LIS. The computer simulation of the LIS was carried out according to the procedure described in the previous papers.[4,10] Thus, the distribution of the LSR and the conformation of the molecule (with regard to the central C–C bond) were varied, step by step, in the search for an acceptable fit of the computed LIS's [assuming the McConnell–Robertson's relationship: $LIS_i^{calcd}=K(3\cos^2\chi_i-1)r_i^{-3}$] with the observed values. For the methyl and aromatic protons, and for C(2) and C(3), the contribution of the individual nuclei was calculated and then averaged. The Hamilton reliability factor, $AF=[\sum_i(LIS_i^{obsd}-LIS_i^{calcd})^2/\sum_i(LIS_i^{obsd})^2]^{1/2}$, was used in order to assess the agreement between the computed LIS's and the experimental ones. The calculated shifts were normalized to the average experimental LIS in the computational process.

Results

Figure 1 plots the agreement factor (*AF*) against the O–C(8)–C(7)–C_6H_5 dihedral angle (ϕ) for (*RS/SR*)-**3**. The values of *R* (LSR–O distance), θ (LSR–O–C angle), and *A* (index for the LSR-distribution)[4] are fixed at 0.32 nm, 130°, and 0.8, respectively (see Scheme 2).

An interesting feature of these profiles is the appearance

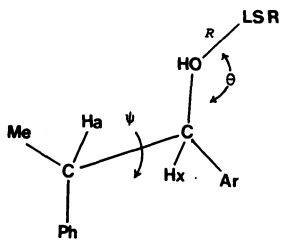

Scheme 2. A typical model for the (*RS/SR*)-3-LSR complex (Ph: C_6H_5, Ar: $C_6H_4CH_3$-*p*, Me: CH_3).

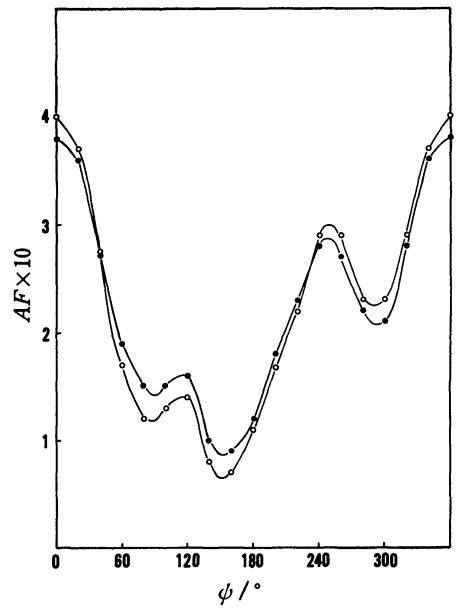

Fig. 1. Plots of *AF vs.* the OH/Ph dihedral angle (ϕ) for (*RS/SR*)-**3**. ●—●: H_a, Me_1, H_x, H_{o1}, H_{o2}, C_1, and C_{16} were used as the monitor nuclei. ○—○: Computed with five proton LIS's.

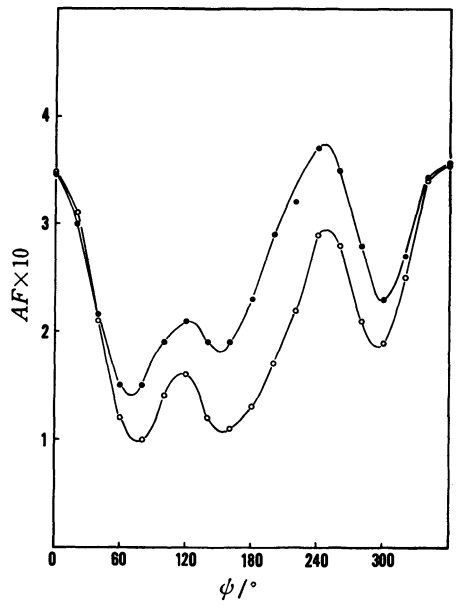

Fig. 2. Plots of *AF vs.* the OH/Ph dihedral angle (ϕ) for (*RR/SS*)-**3**. ●—●: H_a, Me_1, H_x, H_{o1}, H_{o2}, C_1, C_{12}, and C_{16} were used as the monitor nuclei. ○—○: Computed with five proton LIS's.

of three minima at around the staggered geometries (ϕ 80—100°, 140—160°, and 280—300°) of the molecule. Meantime, these results do not differ significantly from those obtained for the sulfoxide analogue, (*RS/SR*)-**1**.[1] For reasons described in previous papers,[1,4,10] we believe that the values of ϕ and *AF* at the minima reflect, although in an indirect manner, the approximate geometries and the contribution of the possible rotamers.[5] Thus, it is suggested that a rotamer in which the tolyl group (Ar) lies about *anti* to the methyl group (Me) and *gauche* to the phenyl group (Ph) (**a** rotamer;

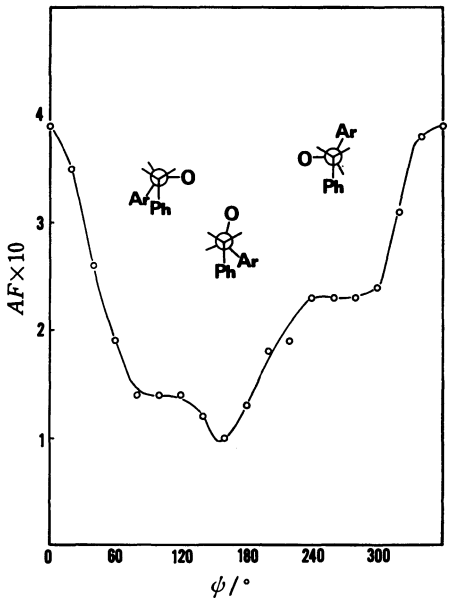

Fig. 3. A plot of *AF vs.* the OH/Ph dihedral angle (ψ) for **4**. The monitor nuclei are H_a, H_x, H_{o1}, H_{o2}, C_1, C_4, C_9, and C_{12}.

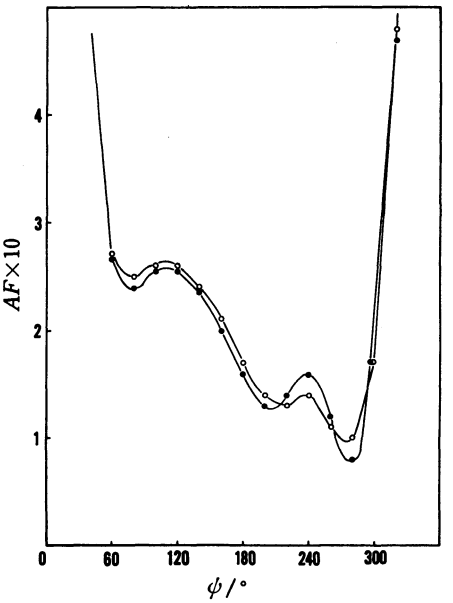

Fig. 4. Plots of *AF vs.* the C=O/Ph dihedral angle(ψ) for **5**. The monitor nuclei are H_a, Me_1, H_{o1}, H_{o2}, C_1, C_4, C_9, C_{12}, and C_{16}. ●—●: R=0.34 nm; ○—○: R= 0.32 nm.

see Fig. 5) is most preferred in the conformational equilibrium of this compound. The second most stable one is suggested to be the **b** rotamer in which Ar is flanked by Me and Ph.

Figure 2 represents the AF/ψ profiles[6] for (*RR*/*SS*)-**3**. The smallest *AF* is recorded at ψ 60—80° and the second minimum is found at 140—160°; here the most stable rotamer seems to have Ar *anti* to Ph but close to Me (**c** rotamer; see Fig. 5).

In Fig. 3 is given an AF/ψ profile[6] recorded for the benzylic alcohol (**4**). The result is rather similar to those obtained previously for its analogues, in which

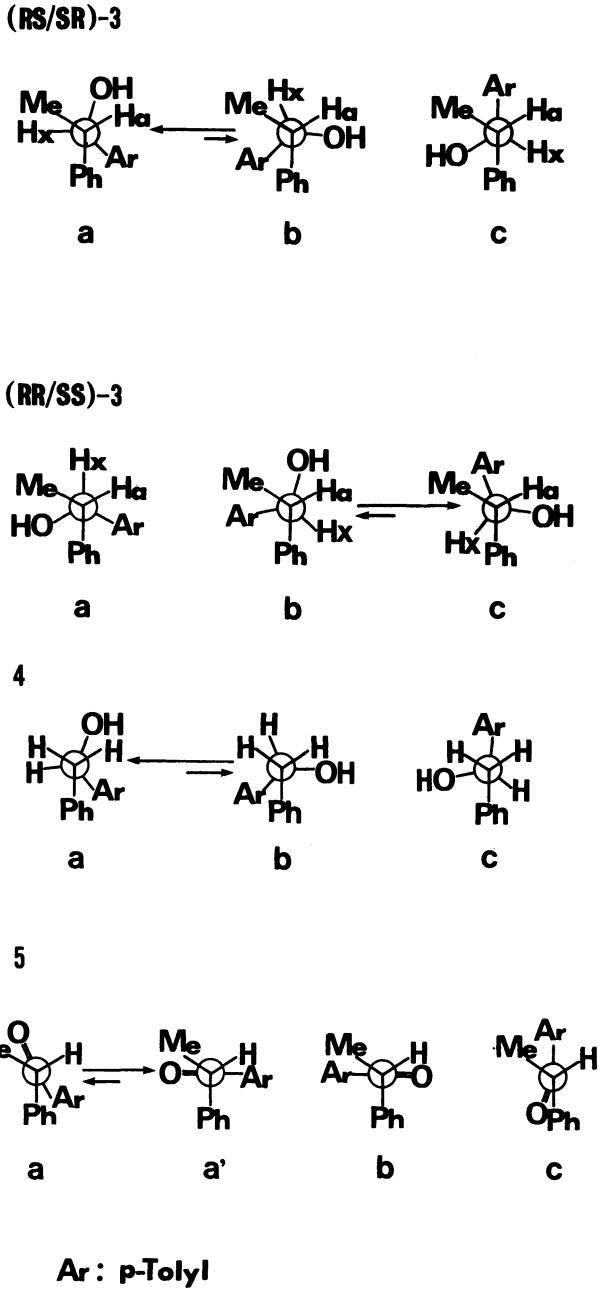

Fig. 5. Plausible conformations and the rotameric equilibria suggested by the LIS-simulation for (*RS*/*SR*)-**3**, (*RR*/*SS*)-**3**, **4**, and **5**.

the tolyl group of **4** is replaced by an alkyl group.[7] Thus, the rotamer having the OH group *anti* to Ph (ψ *ca.* 160°) is suggested to be most preferred.

The profiles obtained for the 1-*p*-tolyl-2-phenyl-1-propanone (**5**) are shown in Fig. 4[8] (R=0.34 nm, θ= 140°, p=0.4). The smallest *AF* values are recorded at ψ [O(=C)/Ph dihedral angle] *ca.* 280° and then 200—220°; the results are analogues to its alkyl derivative, in which the tolyl group in **5** is replaced by an isopropyl group.[9]

Discussion

Figure 5 summarizes the results obtained by the LIS

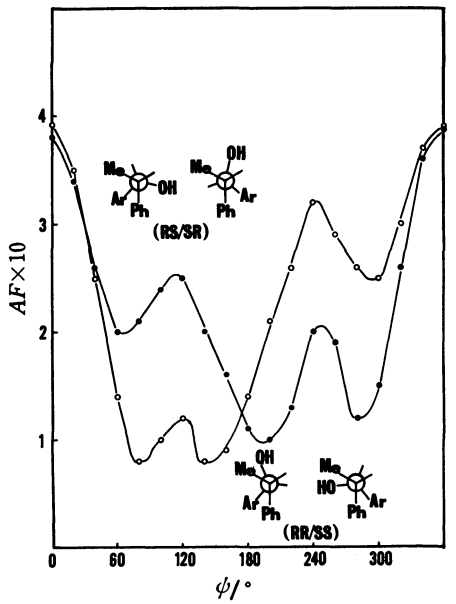

Fig. 6. Plots of *AF vs.* the OH/Ph dihedral angle (ϕ) for (*RS/SR*)-**3** (○—○) and (*RR/SS*)-**3** (●—●). The LIS's were obtained with the use of Eu(fod)$_3$ in C_6D_6 for five protons (H_a, Me_1, H_x, H_{o1}, and H_{o2}).

method for the four compounds, (*RS/SR*)-**3**, (*RR/SS*)-**3**, **4**, and **5**.

We do not wish to mean that the molecular geometries illustrated in Fig. 5 correspond exactly to the shapes of the stable rotameres, since the model (on which the computation is based) is rather primitive and a number of approximations were introduced in the simulation process. The values of *AF*, either, do not necessarily reflect the correct order of the stability (above all, if the difference is small) of the possible rotamers. We may conclude from above results, however, that the folded rotamers are generally preponderant in the conformational equilibria of these compounds. Thus, in the cases of (*RS/SR*)-**3**, the benzylic alcohol (**4**), and the ketone (**5**), the most populated rotamers are suggested to have their tolyl group *gauche* to Ph [rotamers **a** and **b** for (*RS/SR*)-**3** and **4**; rotamers **a** and **a'** for **5**]. The results are consistent with those obtained for the sulfoxide analogues,[1,10] (*RS/SR*)-**1**[11] and the alkyl analogues (**2**).[4,7,9] Meanwhile, in the conformational equilibrium of **5**, the conformer in which the tolyl group is *anti* to Ph (rotamer **c**; C=O is eclipsed to Ph) is least favorable (Fig. 4). The absence of this rotamer has been reported also for other carbonyl compounds.[9] In this respect, it is noteworthy that, in all of the conformations suggested to be preferred (see Figs. 1—4, Figs. 8 and 9 in Ref. 4, Fig. 4 in Ref. 9, and Fig. 3 in Ref. 7), the C=O and OH groups have never been found to lie eclipsed with the phenyl group; *AF*'s are always largest at ϕ *ca.* 0°.

The compound (*RR/SS*)-**3** represents a somewhat different case; here the most stable rotamer seems to have the tolyl group *anti* to the phenyl group but close to the methyl group (**c** rotamer). The second most populated one seems to be the **b** rotamer whereby the tolyl group is flanked by the methyl group and the phenyl group. The result differs from those obtained for the sulfoxide analogue,[1] (*RR/SS*)-**1**.[11] In order to confirm the above suggestions the NMR parameters listed in Tables 2 and 3 were examined in detail.

Chemical Shifts. In harmony with the suggested predominance of the *gauche* Tolyl/Ph conformations, appreciable upfield shifts are observed for the aromatic protons of (*RS/SR*)-**3**. The *ortho* protons (H_{o1} and H_{o2}) give rise to peaks at considerably higher magnetic field (δ 7.07—7.09) as compared to those in reference compounds (δ 7.18—7.23 for alkyl homologues: **2**, X= CHOH).[4] The high-field shifts are not significant in

Table 1. The lanthanoid-induced shifts[a] of 1-*p*-tolyl-2-phenyl-1-propanols(**3**), 1-*p*-tolyl-2-phenylethanol(**4**), and 1-*p*-tolyl-2-phenyl-1-propanone(**5**)

	Me_1	Me_2	H_a	H_x	H_{o1}	H_{o2}	C_1	C_2	C_3	C_4	C_7	C_8	C_9	C_{10}	C_{11}	C_{12}	C_{15}	C_{16}
(*RS/SR*)-**3**	22.6	2.6	42.5	64.5	20.5	27.2	28.7	21.4	11.9	10.7	48.9	100	45.3	28.7	13.5	10.7	3.7	30.9
	(37.6)	(5.5)	(73.6)	(100)	(37.3)	(54.5)[b]												
(*RR/SS*)-**3**	23.3	2.9	40.1	65.0	24.1	30.0	37.1	27.6	15.6	13.3	49.1	100	50.1	28.6	11.7	8.5	3.4	29.7
	(42.0)	(3.9)	(54.5)	(100)	(35.4)	(54.0)												
4	—	2.8	36.9	61.5	16.7	26.7	26.7	20.3	10.8	9.5	48.2	100	45.1	28.2	12.8	9.2	4.1	—
5	24.6	1.7	26.6	—	20.2	22.1	24.6	16.2	8.7	6.2	44.8	100	40.6	23.0	9.8	8.4	1.7	30.8

a) Relative values. b) The data in parentheses are obtained in C_6D_6 with the use of Eu(fod)$_3$.

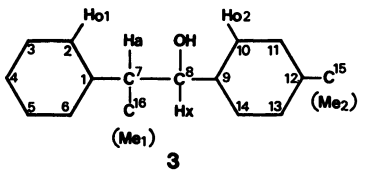

3

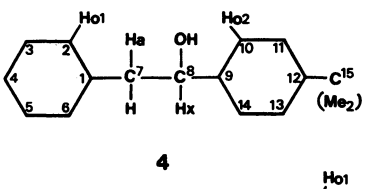

4

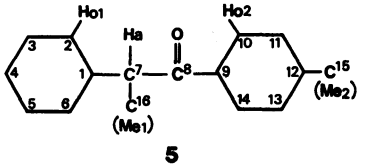

5

TABLE 2. PROTON NMR PARAMETERS[a] OF 1-*p*-TOLYL-2-PHENYL-1-PROPANOLS(**3**), 1-*p*-TOLYL-2-PHENYLETHANOL(**4**), AND 1-*p*-TOLYL-2-PHENYL-1-PROPANONE(**5**)

Compound	Solvent	Me_1	Me_2	H_a	H_x	H_{o1}[b]	H_{o2}	OH[c]	$^3J_{H_aH_x}$
(*RS/SR*)-**3**	$CDCl_3$	1.29	2.29	3.07	4.75	7.09	7.07	1.79	5.8[d]
	C_6D_6	1.32	2.07	2.97	4.52	7.16	7.20		6.1
	ASIS[e]	−0.03	+0.22	+0.10	+0.23	−0.07	−0.13		
(*RR/SS*)-**3**	$CDCl_3$	1.05	2.34	2.98	4.60	7.22	7.24	1.79	8.8
	C_6D_6	1.03	2.13	2.92	4.46	7.14	7.19		7.8
	ASIS	+0.02	+0.21	+0.06	+0.14	+0.04	+0.06		
4	$CDCl_3$	—	2.33	2.97[f]	4.83	7.10	7.13	1.89	
	C_6D_6	—	2.14	2.89	4.62				
	ASIS		+0.19	+0.08	+0.21				
5	$CDCl_3$	1.52	2.32	4.66	—	7.24	7.24	—	

a) The chemical shifts are reported in ppm downfield from internal TMS. b) The chemical shifts of aromatic protons were determined by extraporating the linear LIS plots to the intercept at zero of the $Ln(fod)_3$ concentration. c) Extraporated to infinite dilution. d) Reported in Hz; insensitive to the addition of the LSR. e) ASIS = $\delta(CDCl_3) - \delta(C_6D_6)$. f) Equivalent for the diastereotopic protons.

TABLE 3. ^{13}C CHEMICAL SHIFTS[a] OF 1-*p*-TOTLY-2-PHENYL-1-PROPANOLS(**3**), 1-*p*-TOLYL-2-PHENYLETHANOL(**4**), AND 1-*p*-TOLYL-2-PHENYL-1-PROPANONE(**5**)

	C_1	C_2	C_3	C_4	C_7	C_8	C_9	C_{10}	C_{11}	C_{12}	C_{15}	C_{16}
(*RS/SR*)-**3**	143.7	128.1	128.1	126.4	47.2	78.5	139.9	126.2	128.9	136.8	21.1	15.1
(*RR/SS*)-**3**	143.6	128.0	128.0	127.0	48.1	79.5	139.6	126.9	129.0	137.4	21.2	18.4
4	138.2	129.5	128.5	126.6	46.0	75.2	140.9	125.9	129.1	137.2	21.2	
5	141.6	127.6	128.8	126.8	47.7	199.8	133.9	129.0	128.8	143.5	21.5	19.4

a) Reported in ppm downfield from internal TMS in $CDCl_3$.

the case of (*RR/SS*)-alcohol. This is not unexpected since the aromatic groups are remote from each other in the most preferred rotamer of this compound. Noteworthy in this regard, is the chemical shift of the methyl protons. The signal attributed to Me (δ 1.05) is remarkably shifted upward in the (*RR/SS*)-isomer as compared with that in (*RS/SR*)-**3** (δ 1.29). This is consistent with the suggestion that in (*RR/SS*)-**3** Me is close to the tolyl group in both of the preferred rotamers (**c** and **b**).

Vicinal Coupling Constants. The spin-coupling constant regarding the vicinal protons ($^3J_{H_aH_x}$) is smaller in (*RS/SR*)-**3** than in (*RR/SS*)-**3**. This may be an indication that the H_a/H_x torsional angle (see Fig. 5) in the most important contributor [rotamer **a** for (*RS/SR*), rotamer **c** for (*RR/SS*)] is closer to 180° in (*RR/SS*)-alcohol than in (*RS/SR*)-isomer, or the proportion of the most stable rotamer is larger in (*RR/SS*)-alcohol than in (*RS/SR*)-alcohol.

Conformational Change in C_6D_6. It is noted that $^3J_{H_aH_x}$ of (*RS/SR*)-**3** does not differ significantly in $CDCl_3$ and in C_6D_6 (Table 2), however, for (*RR/SS*)-**3** it becomes appreciably smaller by replacing the solvent from $CDCl_3$ (8.8 Hz) to C_6D_6 (7.8 Hz). We therefore determined the LIS in C_6D_6 for the diastereoisomeric alcohols and carried out the simulation with the use of these data (Table 1). For (*RS/SR*)-isomer, the profiles are similar to each other in these two solvents. A remarkable difference is found, on the other hand, in the case of (*RR/SS*)-alcohol (Figs. 2 and 6). In C_6D_6 solution, the **b** and **a** rotamers seem to become the most important contributors. The results are compatible with the coupling data. We, however, reserve further discussion on this matter, until more exact knowledge about the conformational equilibria becomes available.

Aromatic Solvent-induced Shifts (ASIS).[46] The ASIS data are listed in Table 2. The results are consistent with the suggested equilibria of these alcohols, but here we only cite an interesting observation that ASIS's for the methyl and aromatic protons are negative in (*RS/SR*)-**3**; at present we have no clear explanation for this phenomenon.

^{13}C NMR Data. The peak attributed to the methyl carbon [C(16)] appears at considerably higher magnetic field (δ 15.1) in (*RS/SR*)-**3** than in the (*RR/SS*)-alcohol (δ 18.4) (Table 3). This is well understood in terms of the *γ-gauche* effect.[1,12] In the most stable rotamer of (*RS/SR*)-**3** (**a** rotamer) OH is *gauche* to Me, but in (*RR/SS*)-**3** this is remote from Me in the most preferred rotamer (**c** rotamer).

In summary, inspection of these conformational analyses reveals that the molecules, (*RS/SR*)-**3**, **4**, and **5**, tend to adopt the folded conformations in solution. In addition, we felt it probable that the phenomenon is general to other kind of molecules, in view of the common preference of the *gauche* rotamers, at least in these simplest systems studied thus far [$C_6H_5CH(R^1)$-X-R^2 : R^1=H, CH_3, or C_2H_5; R^2=alkyl or aryl group; X=CH_2,[13] CHOH,[4,7] CO,[9] S,[14] SO,[1,10] or SO_2,[14]]. The generality of the favored *gauche* alkyl/phenyl conformation (CH/π interaction)[15] was argued previously.[9,16] The scope was therefore examined for the phenomenon in systems, where aromatic groups are incorporated in each end of the molecules.

Table 4 is a summary of a literature survey on compounds relevant to this problem. X-ray studies of 1,2-

TABLE 4. TYPICAL COMPOUNDS WHICH EXHIBIT THE PREFERENTIAL FOLDED CONFORMATION

Compound	Method	Favored conformation	Ref.
$PhCH_2CH_2Ph$(**6**)	X-ray	anti	17
	EFF, CNDO/2	folded	22
	EFF	folded	23
	EFF/EHMO	anti	25
$ArCH_2CH_2Ar$(**6′**)	dipole moment	anti	26
	IR/Raman, Kerr Const.	anti	27
$XC_6H_4CH_2SO_2C_6H_4Y$(**7**)			
(X = MeO, Y=Cl)	EFF	folded	18
	X-ray	anti	18
(X = Me_2N, Y = NO_2)	EFF	folded	18
	X-ray	folded	18
$ArCH_2SO_2Ar$(**7′**)	UV, NMR-2	folded	21
$ArCH_2SOAr$	NMR-2	folded	21b
PhCH(Me)SOPh(**1**)	X-ray	anti	19
PhCH(Me)SOAr(**1**)	NMR-2,4,5	folded	1, 20
PhCH(Me)SAr	indirect evidence	folded	14
PhCH(R)SO_2Ph, R = Me, Et	NMR-4	folded	20
PhCH(Me)CH_2Ph(**8**)	EFF	folded	23
	NMR-1	anti	23, 24
	EFF/EHMO	anti	25
ArCH(Me)CH(Me)Ar(**9**)	IR/Raman, Kerr const.	anti	27
$ArCH_2CH_2OSO_2C_6H_4CH_3$(**10**)	NMR-2	folded	28
$ArCH_2NHPh$(**11**)	UV	folded	29
$Ar(CH_2)_nOCOC_6H_2(NO_2)_3$(**12**)	UV	folded	30
$[ArSO_2CH(Ph)NH]_2CO$(**13**)	NMR-2	folded	31a
	X-ray	folded	31b
$ArSO_2CH_2N(Me)CO_2Ar$(**14**)	NMR-2, UV	folded	32a
	X-ray, EFF	folded	32b
$Fl(CH_2)_3COR$(**15**)			
R = aromatic amino acid residues (Phe, Tyr, Trp)	FL	folded	33
Fl = 3- or 10-flavinyl			
NAD(**16**)	NMR-2	folded	34
	NMR-2	folded	35
	NMR-3	folded	36
$Ade(CH_2)_3Nic$(**17**)			
Ade = 9-adenyl	UV	folded	37
Nic = 1-(3-carbamoyl-1-pyridyl)			
$Ade(CH_2)_3Nic^+$	X-ray	anti	38
$AdeH^+(CH_2)_3Nic^+$	X-ray	folded	39
$Ade(CH_2)_3$iPAde(**18**)			
iPAde = 6-(3-methyl-2-butenyl)adenin-9-yl	UV, FL	folded	40
M(ATP)(Trp)(**19**)			
M = Mn, Cu, Zn	UV, NMR-2	folded	41a
M(ATP)(phen)(**19′**)			
M = Mg, Ca, Zn	NMR-2	folded	41b
phen=1,10-phenanthroline			
NH_2–Ala–Gly–Cys–Lys–Asn–Phe–Phe–Trp–Lys–Thr–Phe–Thr–Ser–Cys–COOH(**20**)			
	CD	folded	42
PhCH(Me)CH(OH)$C_6H_4CH_3$(**3**)	NMR-2,4,5	folded	this work
$PhCH_2$CH(OH)$C_6H_4CH_3$(**4**)	NMR-5	folded	this work
PhCH(Me)$COC_6H_4CH_3$(**5**)	NMR-5	folded	this work

Methods: NMR-1 = vicinal coupling constant: NMR-2 = ^1H chemical shift; NMR-3 = T_1 measurement (^{13}C); NMR-4 = *γ-gauche* effect; NMR-5 = LIS-simulation; UV = observation of charge-transfer band; CD = circular dichroism; FL = fluorometry; EFF = empirical force-field calculation; EFF/EHMO = EFF/extended Hückel MO hybrid method.

diphenylethane (**6**),[17] *p*-methoxybenzyl *p*-chlorophenyl sulfone (**7**),[18] and (*RS*/*SR*)-**1**[19] demonstrated that these molecules adopt the extended conformations (*anti* aromatic groups) in the crystal fields. In solution, however, **7**,[18] **1**,[1,20] and their analogues[14,20,21] have been shown to be present in folded (*gauche* aromatic groups) conformations. For solution (or gas phase) conformation of **6** and its homologue, 1,2-diphenylpropane(**8**), the results obtained earlier are rather contradictory. Thus, force-field and semi-empirical MO calculations showed that **6**[22] and **8**[23] are more stable in *gauche* Ph/Ph conformations. On the other hand, NMR spin-coupling data of **8**[23,24] (as well as the EFF/EHMO results on **6** and **8**[25] were reported to be incompatible with this conclution. We do not know the reason for the above disagreement, but it may be pointed out that an argument based only on coupling constants often leads to an ambiguous conclusion. Huang *et al.* studied the conformations of substituted 1,2-diphenylethanes(**6'**)[26] and 2,3-diphenylbutane derivatives (**9**),[27] and reported that these molecules prefer the *anti* Ar/Ar conformations (an appreciable proton resides in the *gauche* conformation, however). The conformations of 2-arylethyl *p*-toluenesulfonate (**10**),[28] (*N*-substituted benzyl)anilines (**11**),[29] arylalkyl 2,4,6-trinitrobenzoates (**12**),[30] *N*,*N'*-bis(α-tosylbenzyl)-urea(**13**),[31] *p*-dimethylaminophenyl *N*-methyl-*N*-(*p*-nitrophenylsulfonylmethyl)carbamate(**14**),[32] certain flavinyl peptides (**15**),[33] nicotinamide-adenine dinucleotides (**16**),[34–36] and its analogues (**17**),[37–39] 9-[3-(adenin-9-yl) propyl]-6-(3-methyl-2-butenylamino)-purine (**18**),[40] several mixed-ligand metal complexes (**19**),[41] and somatostatin (**20**)[42] (a cyclic tetradecapeptide) were also studied and they have been shown to exist preferentially in folded forms, whereby two aromatic groups in the molecules are approached to each other.

The reason of the discrepancy cited as above for the conformations of **6** (or **6'**) and **8** remains to be clarified. We believe, however, that the folding tendency of groups (Ar/Ar, Alkyl/Ar,[9,16] and Alkyl/Alkyl[43]) is general to a wide variety of compounds. It may be a rule rather than an exception. In other words, one must seek an explanation if one finds an extended conformation.

As to the origin of the folded conformations, it may be the dispersion force,[13,28,43b,43d] CH/π interaction,[15,44] CH/n interaction,[9,44] and/or other interactions which are not yet disclosed. A folded conformation may, of course, be brought about by other type (such as the hydrogen bonding,[45] dipole/quadrupole,[46] quadrupole/quadrupole, *gauche*-vicinal H/H[47]) of interactions. In any event, the geometry of a molecule is determined as a result of a compromise of various (attractive as well as repulsive) effects. In view of this, it is surprising that the important contribution of weak, attractive interactions has hitherto been underestimated in organic chemistry.[48]

We wish to thank Prof. Masayoshi Kinoshita of Osaka City University for his encouragement.

References

1) K. Kobayashi, Y. Kodama, M. Nishio, T. Sugawara, and H. Iwamura, *Bull. Chem. Soc. Jpn.*, **55**, 3560 (1982).
2) D. J. Cram and F. A. Abd Erhafez, *J. Am. Chem. Soc.*, **74**, 5828 (1952).
3) B. M. Benjamin and C. J. Collins, *J. Am. Chem. Soc.*, **78**, 4952 (1956).
4) J. Uzawa, S. Zushi, Y. Kodama, K. Nishihata, Y. Fukuda, K. Umemura, M. Nishio, and M. Hirota, *Bull. Chem. Soc. Jpn.*, **53**, 3623 (1980).
5) The position and the goodness of fit at the respective *AF*-minimum reflect, although in an indirect manner, the plausible geometry and the relative importance of a substrate-LSR complex.[4]
6) The parameters are fixed as in Fig. 1.
7) S. Zushi, Y. Kodama, Y. Fukuda, K. Nishihata, M. Nishio, M. Hirota, and J. Uzawa, *Bull. Chem. Soc. Jpn.*, **54**, 2113 (1981).
8) *R*, θ, and *p* [index for the LSR-distribution; see Ref. 9 and P. Finocchiaro, A. Recca, P. Maravigna, and G. Montaudo, *Tetrahedron*, **30**, 4159 (1974)] are fixed at 0.32 (or 0.34) nm, 140°, and 0.4, respectively.
9) S. Zushi, Y. Kodama, K. Nishihata, K. Umemura, M. Nishio, J. Uzawa, and M. Hirota, *Bull. Chem. Soc. Jpn.*, **53**, 3631 (1980).
10) Y. Kodama, K. Nishihata, M. Nishio, and Y. Iitaka, *J. Chem. Soc., Perkin Trans. 2*, **1976**, 1490; **1980**, 1306; M. Hirota, Y. Takahashi, M. Nishio, and K. Nishihata, *Bull. Chem. Soc. Jpn.*, **51**, 2358 (1978).
11) The reason for the difference observed between the sulfoxides and alcohols with the (*RR*/*SS*)-configuration remains to be explained.
12) D. M. Grant and E. G. Paul, *J. Am. Chem. Soc.*, **86**, 2984 (1964); J. D. Roberts, F. J. Weigert, J. I. Kroschwitz, and H. J. Reich, *ibid.*, **92**, 1338 (1972).
13) M. Hirota, K. Abe, T. Sekiya, H. Tashiro, M. Nishio, and E. Osawa, *Chem. Lett.*, **1981**, 685.
14) K. Nishihata and M. Nishio, *J. Chem. Soc., Perkin Trans. 2*, **1973**, 758; *Tetrahedron Lett.*, **1977**, 1041.
15) Y. Kodama, K. Nishihata, M. Nishio, and N. Nakagawa, *Tetrahedron Lett.*, **1977**, 2105; M. Nishio, *Kagaku No Ryoiki*, **31**, 998 (1977). [*cf.* M. Cherest and N. Prudent, *Tetrahedron*, **36**, 1599 (1980); H. Okawa, Y. Numata, A. Mio, and S. Kida, *Bull. Chem. Soc. Jpn.*, **53**, 2248 (1980); *Chem. Lett.*, **1981**, 547; B. E. Fischer and H. Sigel, *J. Am. Chem. Soc.*, **102**, 2998 (1980); Y. Yokoo, T. Sakurai, M. Saburi, and S. Yoshikawa, *Nippon Kagaku Kaishi*, **1981**, 1904; H. Okawa, K. Ueda, and S. Kida, *Inorg. Chem.*, **21**, 1594 (1982).]
16) Y. Kodama, K. Nishihata, S. Zushi, M. Nishio, J. Uzawa, K. Sakamoto, and H. Iwamura, *Bull. Chem. Soc. Jpn.*, **52**, 2661 (1979).
17) D. W. J. Cruickshank, *Acta Crystallogr.*, **2**, 65 (1949); C. J. Brown, *ibid.*, **7**, 97 (1954).
18) I. Tickle, J. Hess, A. Vos, and J. B. F. N. Engberts, *J. Chem. Soc., Perkin Trans. 2*, **1978**, 460.
19) N. Sakabe, K. Sakabe, N. Sasaki, Y. Kodama, and M. Nishio, unpublished X-ray results.
20) K. Kobayashi, T. Sugawara, and H. Iwamura, *J. Chem. Soc., Chem. Commun.*, **1981**, 479.
21) R. van Est-Stammer and J. B. F. N. Engberts, *Tetrahedron Lett.*, **1971**, 3215; *Can. J. Chem.*, **51**, 1187 (1973); R. van Est-Stammer, Ph. D. Thesis, University of Groningen, 1973.
22) P. Ivanov, I. Pojarlieff, and N. Tyutyulkov, *Tetrahedron Lett.*, **1976**, 775.

23) J. Jacobus, *Tetrahedron Lett.*, **1976**, 2927.
24) S. L. Spassov, A. S. Orahovats, and S. M. Mishev, *Tetrahedron*, **30**, 365 (1974).
25) D. A. Dougherty and K. Mislow, *J. Am. Chem. Soc.*, **101**, 1401 (1979).
26) K. K. Chiu, H. H. Huang, and P. K. K. Lin, *J. Chem. Soc., B*, **1970**, 304. [*cf.* A. M. North, R. A. Pethrick, and A. D. Wilson, *Spectrochim. Acta, Part A*, **30**, 1317 (1974).]
27) K. K. Chiu, H. H. Huang, and L. H. L. Chia, *J. Chem. Soc., Perkin Trans. 2*, **1972**, 286.
28) M. D. Bentley and M. J. S. Dewar, *Tetrahedron Lett.*, **1967**, 5043.
29) M. Ōki and K. Mutai, *Tetrahedron Lett.*, **1968**, 2019; *Tetrahedron*, **26**, 1181 (1970). [*cf*, K. Mutai, *Tetrahedron Lett.*, **1971**, 1125.]
30) H. A. H. Craenen, J. W. Verhoeven, and Th. J. de Boer, *Tetrahedron*, **27**, 2561 (1971).
31) R. M. Tel and J. B. F. N. Engberts, *Recl. Trav. Chim. Pays-Bas*, **93**, 37 (1974); *J. Chem. Soc., Perkin Trans. 2*, **1976**, 483; R. M. Tel, Ph. D. Thesis, University of Groningen, 1977.
32) R. van Est-Stammer and J. B. F. N. Engberts, *Recl. Trav. Chim. Pays-Bas*, **91**, 1289 (1972); R. J. J. Visser, A. Vos, and J. B. F. N. Engberts, *J. Chem. Soc., Perkin Trans. 2*, **1978**, 634.
33) R. E. McKenzie, W. Föry, and D. B. McCormick, *Biochemistry*, **8**, 1839 (1969).
34) O. Jardetzky and N. G. Wade-Jardetzky, *J. Biol. Chem.* **241**, 85 (1966).
35) R. H. Sarma and N. O. Kaplan, *Biochemistry*, **9**, 539 (1970).
36) W. D. Hamill, Jr., R. J. Pugmire, and D. M. Grant, *J. Am. Chem. Soc.*, **96**, 2885 (1974).
37) N. J. Leonard, T. G. Scott, and P. C. Huang, *J. Am. Chem. Soc.*, **89**, 7137 (1967).
38) P. L. Johnson, C. A. Maier, and I. C. Paul, *J. Am. Chem. Soc.*, **95**, 5370 (1973).
39) P. L. Johnson, J. K. Frank, and I. C. Paul, *J. Am. Chem. Soc.*, **95**, 5377 (1973).
40) N. J. Leonard, H. Iwamura, and J. Eisinger, *Proc. Natl. Acad. Sci. U. S. A.*, **64**, 352 (1969).
41) H. Sigel and C. F. Naumann, *J. Am. Chem. Soc.*, **98**, 730 (1976); P. R. Mitchell and H. Sigel, *ibid.*, **100**, 1564 (1978); P. R. Mitchell, B. Prijs, and H. Sigel, *Helv. Chim. Acta*, **62**, 1723 (1979).
42) L. A. Holladay and D. Puett, *Proc. Natl. Acad. Sci. U. S. A.*, **73**, 1199 (1976); L. A. Holladay, J. Rivier, and D. Puett, *Biochemistry*, **16**, 4895 (1977).
43) a) D. C. Best, G. Underwood, and C. A. Kingsbury, *J. Chem. Soc., Chem. Commun.*, **1969**, 627; S. Aime, R. K. Harris, and E. M. McVicker, *ibid.*, **1974**, 426; **1975**, 886; H, C. E. McFarlane and W. McFarlane, *ibid.*, **1975**, 582; b) R. E. Carter and P. Stilbs, *J. Am. Chem. Soc.*, **98**, 7515 (1976); B. Aurivillius and R. E. Carter, *J. Chem. Soc., Perkin Trans. 2*, **1978**, 1033; c) S. Brownstein, J. Dunogues, D. Lindsay, and K. U. Ingold, *J. Am. Chem. Soc.*, **99**, 2073 (1977); S. G. Baxter, D. A. Dougherty, J. P. Hummel, J. F. Blount, and K. Mislow, *ibid.*, **100**, 7795 (1978) and references cited therein; d) M. H. Lyttle, A .Streitwieser, Jr., and R. Q. Kluttz, *ibid.*, **103**, 3232 (1981).
44) M. Nishio, *Kagaku No Ryoiki*, **33**, 422 (1979).
45) G. C. Pimentel and A. L. McClellan, "The Hydrogen Bond," W. H. Freeman, San Francisco (1960).
46) K. Nikki and N. Nakagawa, *Bull. Chem. Soc. Jpn.*, **51**, 3267 (1978); **48**, 2902 (1975); *Chem. Lett.*, **1972**, 1239; **1974**, 699. [unstable with the O/Ph approached orientation.]
47) D. H. Wertz and N. L. Allinger, *Tetrahedron*, **30**, 1579 (1974).
48) J. D. Watson, "The Importance of Weak Chemical Interactions," in "Molecular Biology of the Gene," W. A. Benjamin, Menlo Park, Calif. (1965), Chap. 4; M. Nishio, *Kagaku No Ryoiki*, **37**, 243 (1983).

Photoinduced Intramolecular Cyclization of 9-(ω-Anilinoalkyl)phenanthrenes

Akira Sugimoto,* Katsumi Sumi, Keiji Urakawa, Mamoru Ikemura, Satoshi Sakamoto, Shigeo Yoneda, and Yoshio Otsuji*

Department of Applied Chemistry, University of Osaka Prefecture, Mozu-Umemachi, Sakai, Osaka 591

(Received April 23, 1983)

Photoreactions of a series of compounds of the type 9-phenanthryl–A–$CH_2NHC_6H_5$ [–A–=*o*-phenylene (**1b**), $-(CH_2)_2-$ (**1c**), $-(CH_2)_3-$ (**1d**), $-(CH_2)_4-$ (**1e**), $-CH_2-$ (**1f**)] in benzene were studied. From **1b—d**, the spiro compounds are obtained by an intramolecular *cis*-addition of the N–H function to the C_9, C_{10}-double bond of the phenanthrene ring. These photoproducts can be converted to the starting materials by treating with trifluoroacetic acid or heating above their melting temperatures. The mechanistic features of these reactions are described.

Photoreactions between excited aromatic hydrocarbons and amines in their ground states have been extensively studied in recent years.[1] For example, primary and secondary amines undergo the photoaddition to aromatic hydrocarbons such as benzene,[2] naphthalene,[3] and anthracene[4] *via* an exciplex or an electron-transfer from the amines to the excited aromatics.[5]

In a previous paper, we reported that irradiation of 9-(2-anilinomethyl-1-naphthyl)phenanthrene (**1a**) in benzene affords pyrroline derivative **2a** in high yield by an intramolecular addition of the anilino function to the phenanthrene ring (Scheme 1).[6] The high efficiency of this photoreaction was attributed to a structural feature that the anilino function lies close to the phenanthrene ring in **1a** by a steric reason. We now report the photoinduced intramolecular cyclization of 9-(ω-anilinoalkyl)phenanthrenes **1b—f** which have a much greater flexibility in conformation compared with **1a**.

Results and Discussion

The phenanthrene derivatives, **1b—f**, were prepared by the routes shown in Scheme 2 and characterized from their ^1H NMR and IR spectral data and elemental analyses.

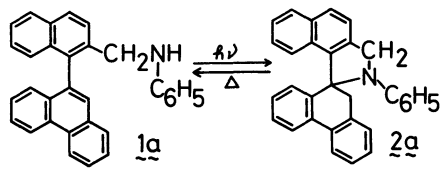

Scheme 1.

Photoproducts. Irradiation of a degassed benzene solution of **1b** (1.6×10^{-2} mol/dm^3) through a Pyrex filter with a 300 W Hg lamp for 90 min gave spiro compound **2b** in 73% yield. The irradiation for 3 h gave **2b** in quantitative yield. Similar irradiation of **1c** and **1d** afforded the corresponding spiro compounds **2c** and **2d**, respectively. The yields are shown in Table 1, together with the UV and fluorescence spectral data of the starting materials.

The spiro compounds produced by the photoreaction could be converted to the starting materials in quantitative yields by treating with trifluoroacetic acid or by heating above their melting temperatures. Structures of the photoproducts were established from their spectral data and chemical behaviors. The pertinent ^1H NMR and IR spectral data are listed in Table 2, together with those of the starting materials.

The IR spectrum of **2b** showed no NH stretching band. The ^1H NMR spectrum of **1b** changed markedly upon UV irradiation. A characteristic multiplet around δ 8.5 (2H, the H-4 and H-5 protons on the phenanthrene ring) shifted to up-field and became overlapped with signals due to other aromatic protons. A broad singlet at δ 3.54 (1H, NH) disappeared. A singlet at δ 3.91 (2H, $-CH_2-N=$) shifted to δ 4.81. A new AB quartet (J=16 Hz) centered at δ 2.60 (1H) and δ 4.30 (1H) appeared, and these signals were assigned to the H_A

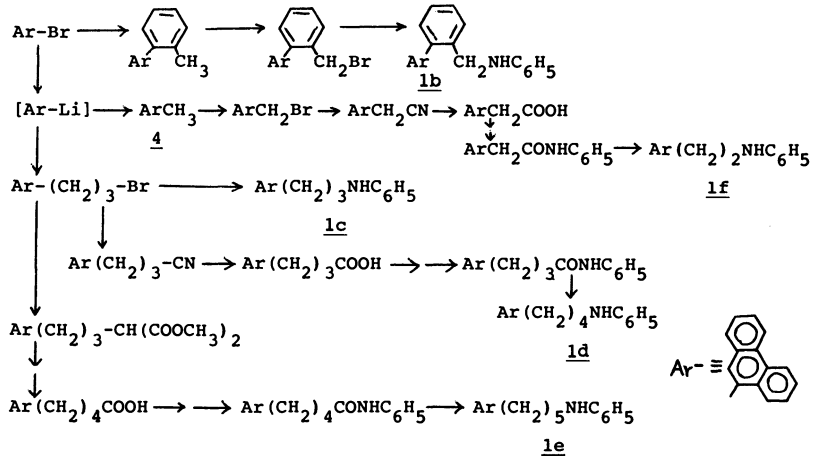

Scheme 2.

Table 1. Photoreaction and spectral data of phenanthrene derivatives[a)]

Compd	UV absorption maximum λ/nm (log ε)	Relative intensity of fluorescence at 366 nm[b)]	Product	Yield (Recovery)[c)]/% In C_6H_6		In CH_3CN	
1b	299 (4.11)	1	**2b**	73[d)]	(27)[d)]	69[d)]	(31)[d)]
1c	298 (4.11)	11	**2c**	76	(12)	68	(16)
1d	298 (4.11)	20	**2d**	31	(61)	40	(52)
1e	298 (4.11)	61	—		(83)		(82)
1f	298 (4.00)	69	**3**	56	(26)	38	(41)
4	297 (4.06)	780	—		(100)		—

a) All the photoreactions were carried out by irradiating 1.6×10^{-2} mol/dm³ solutions with a 300 W Hg lamp for 90 min under the same conditions. b) Excited by a 300 nm light in hexane. c) Isolated yields. d) Estimated from the intensity of ^{1}H NMR signals.

Table 2. ^{1}H NMR and IR data of starting materials and photoproducts

Compd	δ –A–**CH₂**–N–	H_A	H_B	J_{AB}/Hz	ν_{NH}/cm^{-1}
1b	3.91	—	—	—	3430
1c	2.8—3.2	—	—	—	3420
1d	2.8—3.7	—	—	—	3380
1e	2.8—3.2	—	—	—	3400
1f	3.1—3.8	—	—	—	3400
2b	4.81	2.60	4.30	16	—
2c	3.5—3.75	2.30	4.03	16	—
2d	3.5—4.0	2.94	3.84	16	—
1a[6)]	4.10	—	—	—	3400
2a[6)]	5.00	3.45	3.97	19	—

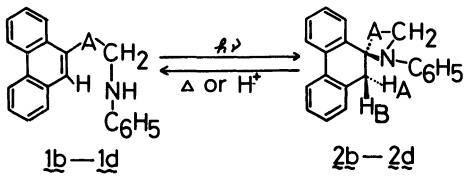

1b—1d 2b—2d

b : A = , **c** : A = $-CH_2CH_2-$, **d** : A = $-CH_2CH_2CH_2-$

Scheme 3.

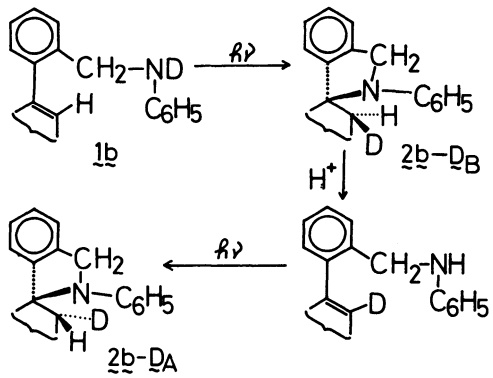

1b

Scheme 4.

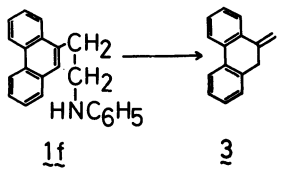

1f 3

Scheme 5.

and H_B protons on the pyrroline ring of **2b** (Scheme 3), respectively. A down-field shift of the H_B proton compared with the H_A proton may be due to a deshielding effect of lone-pair electrons on the nitrogen atom of the pyrroline ring. A similar spectral pattern was also observed in **2a**.[6)] A further support for the structure of **2b** was obtained from the following observations.

Irradiation of **1b** in a D_2O-saturated benzene gave a monodeuterated compound of **2b** (**2b**-$\mathbf{D_B}$) which showed a singlet at δ 2.60 (1H) but no signal at δ 4.30 in its ^{1}H NMR spectrum. Other ^{1}H NMR pattern of this compound was identical to that of **2b**. Treatment of **2b**-$\mathbf{D_B}$ with trifluoroacetic acid, followed by irradiation in benzene, afforded as a major product the other monodeuterated compound of **2b** (**2b**-$\mathbf{D_A}$), whose ^{1}H NMR spectrum showed a singlet at δ 4.30 but no signal at δ 2.60, along with a small amount of **1b**. These results can be explained in terms of the reaction pathway shown in Scheme 4 and support the assigned structure for **2b**. A remarkable feature of the photocyclization of **1b** to the spiro compound **2b** is that the N–H function adds stereospecifically to the C_9, C_{10} double bond of the phenanthrene ring in a *cis*-mode. The acid-catalyzed conversion of **2b** to **1b** occurs preferentially *via* the *trans*-elimination of the N–H function.

Compounds **1c** and **1d** behaved similarly when the compounds were irradiated in a D_2O-saturated benzene, supporting the assigned structures for **2c** and **2d**. In the case of **1e**, no photoreaction occurred. However, irradiation of **1f** in benzene gave 9-methylene-9,10-dihydrophenanthrene (**3**) (Scheme 5) which was characterized by ^{1}H NMR and IR spectra (see Experimental) and chemical evidence.[7)]

Mechanistic Features. UV spectra of **1b**—**f** in hexane were similar to each other in shape and resemble that of 9-methylphenanthrene (**4**) (Table 1). All these compounds also displayed fluorescence spectra similar to the fluorescence spectrum of **4** in the region of 340—450 nm in hexane (Fig. 1). Their intensities of the emission at 370 nm decreased in the order; **4**>**1f**>**1e**>**1d**>**1c**>**1b** (Table 1). The fluorescence of **4** was quenched by *N*-methylaniline. The low intensities of

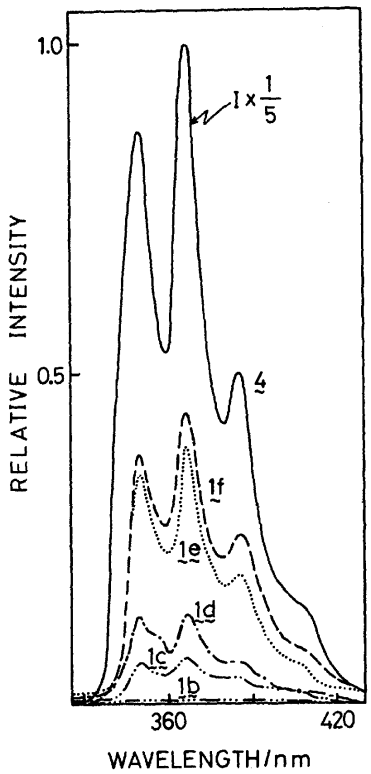

Fig. 1. Fluorescence spectra of the phenanthrene derivatives in hexane: concentration 1.00×10^{-4} mol/dm^3, excited at 300 nm.

1b—**f** compared with **4** suggest that an intramolecular quenching of fluorescence by the anilino group occurs in these compounds. The quenching of fluorescence of an aromatic hydrocarbon by a primary or secondary amine has been attributed to the formation of an exciplex between the excited aromatic hydrocarbon and the amine.[5] Accordingly, the above results strongly suggest that intramolecular exciplexes are formed between the excited phenanthrene moiety and the anilino group in **1b**—**d**, and that the Hirayama rule[8] in intramolecular exciplex formation can also be applicable to these systems.

In the photoreactions of **1b**—**e**, the less emissive compounds afford the photoproducts in the higher yields as shown in Table 1. No appreciable solvent effect on the yields of the photoproducts was observed in these photoreactions (Table 1).

On the basis of all the results presented above, we propose the mechanistic pathways of the photoreactions as shown in Scheme 6. In benzene, the photoreactions probably occur from exciplexes formed by interaction between the excited phenanthrene moiety and the anilino group. In acetonitrile, the exciplexes may dissociate to ion-radical pairs **5**. However, no appreciable solvent effect on these photoreactions suggests that the photoreactions occur in a solvent cage even if the ion-radical pairs are formed. This assumption was supported by the fact that no quenching was observed when the photoreactions were carried out in triethylamine: irradiations of **1b** and **1c** in triethylamine for 90 min gave **2b** in 80% yield and **2c** in 82% yield (compare these yields with those cited in Table 1). The mechanism of the formation of **3** from **1f** remains equivocal.

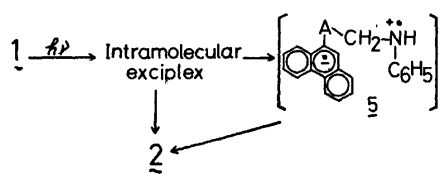

Scheme 6.

Experimental

All melting points are uncorrected. IR spectra were obtained on a Hitachi 215 infrared spectrophotometer. ^{1}H NMR spectra were recorded on a Hitachi R-24A spectrometer (60 MHz) with tetramethylsilane as an internal standard. UV and visible absorption spectra were obtained on a Hitachi EPS-3T spectrometer. Fluorescence spectra were obtained for degassed samples with a Nippon Bunko FP-500S Fluorophotometer by exciting with 300 nm light.

Materials. *9-(o-Anilinomethylphenyl)phenanthrene (**1b**)*: A Grignard reagent, prepared from *o*-bromotoluene (17.5 g, 0.102 mol) and magnesium (2.5 g, 0.103 mol) in ether (40 cm^3) was added to a solution of 9-bromophenanthrene (15.5 g, 0.06 mol) and dichlorobis(triphenylphosphine)nickel(II) (0.20 g) in benzene–ether (1 : 1, v/v) (100 cm^3) over 1.5 h under gentle refluxing.[9] The mixture was refluxed further for 30 min and acidified with dil hydrochloric acid. The organic layer was separated, dried (Na_2SO_4), and evaporated. The residue solidified upon trituration with petroleum ether to give 11.7 g (69% based on 9-bromophenanthrene) of 9-(*o*-tolyl)phenanthrene. Recrystallization from hexane gave an analytical sample; mp 132—133 °C: ^{1}H NMR (CCl_4) δ 7.0—8.7 (13H, m, aromatic), 2.00 (3H, s, CH_3). Found: C, 93.98; H, 5.83%. Calcd for $C_{21}H_{16}$: C, 93.99; H, 6.01%.

A mixture of 9-(*o*-tolyl)phenanthrene (2.7 g, 7.8 mmol), *N*-bromosuccinimide (1.9 g, 10.7 mmol) and a small amount of benzoyl peroxide in CCl_4 (50 cm^3) was refluxed for 16 h. After cooling, the mixture was filtered and the filtrate was concentrated to give 9-(*o*-bromomethylphenyl)phenanthrene as a viscous oil which was purified by chromatography on silica gel with hexane.

A mixture of 9-(*o*-bromomethylphenyl)phenanthrene (2.9 g, 8 mmol) and aniline (3 g, 32 mmol) in 1,2-dimethoxyethane (10 cm^3) was stirred for 20 h at room temperature and filtered. The filtrate was concentrated under reduced pressure. The viscous oily residue was washed with dil hydrochloric acid to give a solid which was suspended in benzene and washed with dil aqueous sodium hydroxide. The benzene layer was dried and evaporated. The residue was recrystallized from hexane to give **1b** as a colorless needles in 57% yield; mp 141—141.5 °C: ^{1}H NMR (CCl_4) δ 6.0—8.7 (18H, m, aromatic), 3.91 (2H, s, CH_2), 3.55 (1H, s, NH); IR (KBr) 3430 cm^{-1} (NH). Found: C, 90.50; H, 5.61; N, 3.86%. Calcd for $C_{27}H_{21}N$: C, 90.21; H, 5.89; N, 3.90%.

*9-(3-Anilinopropyl)phenanthrene (**1c**).* To a stirred solution of 7.8 g (30 mmol) of 9-bromophenanthrene in 40 cm^3 of anhydrous ether was added butyllithium (60 mmol) in hexane and then 13 g (64 mmol) of 1,3-dibromopropane. After refluxing for 4 h, the mixture was poured into water and extracted with ether. The extract was dried (Na_2SO_4) and evaporated. The oily residue was chromatographed on silica gel with hexane to give 1.96 g (22%) of 1-bromo-3-(9-phenanthryl)propane as colorless solid; mp 55—57 °C: ^{1}H NMR

($CDCl_3$) δ 7.3—8.7 (9H, m, aromatic), 3.0—3.5 (4H, m, $-CH_2-C-CH_2$), and 2.1—2.5 (2H, m, $C-CH_2-C$).

A mixture of 1-bromo-3-(9-phenanthryl)propane (670 mg, 2.2 mmol), aniline (5 cm³, 54 mmol), and Na_2CO_3 (5 g) in DMF (30 cm³) was stirred for 42 h at room temperature. The deposited solid was filtered off and washed with a small amount of benzene. The filtrate and the benzene washing were combined and evaporated. The residue was washed with 100 cm³ of hydrochloric acid to give a solid which was dissolved in benzene and washed with an aqueous Na_2CO_3 solution. The benzene layer was dried (Na_2SO_4) and evaporated. TLC of the residue gave 450 mg (65%) of **1c**; mp 77—79 °C: ^1H NMR ($CDCl_3$) δ 6.3—8.7 (14H, m, aromatic), 3.4 (1H, br s, NH), 2.8—3.2 (4H, m, CH_2-C-CH_2), and 1.6—2.2 (2H, m, $C-CH_2-C$). IR (KBr) 3420 cm^{-1} (NH). Found: C, 88.98; H, 6.69; N, 4.57%. Calcd for $C_{23}H_{21}N$: C, 88.71; H, 6.80; N, 4.50%.

*9-(4-Anilinobutyl)phenanthrene (**1d**).* A mixture of 1-bromo-3-(9-phenanthryl)propane (1.49 g, 5 mmol) and KCN (0.4 g, 6.1 mmol) in ethanol (40 cm³) was refluxed for 42 h. The solvent was evaporated under reduced pressure and the residue was washed with water and extracted with ether. The extract was dried (Na_2SO_4) and evaporated to give 1.17 g (96%) of 4-(9-phenanthryl)butanenitrile as colorless needles which was recrystallized from hexane–benzene (9 : 1); mp 90—91 °C: IR (KBr) 2250 cm^{-1} (CN); ^1H NMR ($CDCl_3$) δ 7.4—8.8 (9H, m, aromatic), 3.22 (2H, t, $J=7$ Hz, $Ar-CH_2-$), 1.9—2.5 (4H, m, $-CH_2CH_2CN$). Found: C, 87.99; H, 5.78; N, 5.48%. Calcd for $C_{18}H_{15}N$: C, 88.13; H, 6.16; N, 5.71%.

The hydrolysis of 4-(9-phenanthryl)butanenitrile with KOH in ethanol by refluxing for 20 h gave 4-(9-phenanthryl)-butanoic acid in 90% yield; mp 169—170 °C (lit,[10] 172.8—174 °C); IR (KBr) 1710 cm^{-1} (CO).

4-(9-Phenanthryl)butanoic acid (1.1 g, 4.1 mmol) was added in small portions to thionyl chloride (13 cm³) and the mixture was refluxed for 10 min. Excess thionyl chloride was removed by evaporation under reduced pressure. The residue was dissolved in ether (140 cm³) and added to a solution of aniline (3 cm³, 32 mmol) in ether (15 cm³). The mixture was stirred for 4.5 h at room temperature, washed with 3 M hydrochloric acid, and the ether layer was separated. The aqueous layer was extracted with dichloromethane. Both the organic solutions were combined and evaporated to give 1.35 g (98%) of *N*-phenyl-4-(9-phenanthryl)butanamide; mp 152.5—155.5 °C: IR (KBr) 3300 (NH) and 1660 cm^{-1} (CO).

To a stirred solution of *N*-phenyl-4-(9-phenanthryl)butanamide (1.27 g, 3.7 mmol) in THF–ether (40 cm³) was added $LiAlH_4$ (1.0 g) in small portions over 10 min. After refluxing for 3.5 h, the mixture was washed with a saturated aqueous solution of ammonium chloride and extracted with ether. Evaporation of the solvent from the ether extract under reduced pressure gave the amine **1d** (1.1 g, 90%) which was chromatographed on silica gel with benzene and then recrystallized from hexane; mp 101—102 °C: IR (KBr) 3380 cm^{-1} (NH); ^1H NMR ($CDCl_3$) δ 9.0—6.5 (14H, m, aromatic), 2.8—3.7 (5H, m, NH and CH_2), and 1.5—2.2 (4H, m, CH_2). Found: C, 88.53; H, 7.08; N, 4.25%. Calcd for $C_{24}H_{23}N$: C, 88.57; H, 7.12; N, 4.30%.

*9-(5-Anilinopentyl)phenanthrene (**1e**).* A solution of 1-bromo-3-(9-phenanthryl)propane (0.86 g, 2.85 mmol) in benzene (10 cm³) was added at 50 °C to a stirred mixture of sodium methoxide (prepared from 0.1 g of sodium) and dimethyl malonate (0.7 cm³, 6.1 mmol) in methanol (10 cm³). The mixture was refluxed for 3 d and diluted with a large amount of water, and then extracted with ether. The extract was dried (Na_2SO_4) and the solvent was evaporated completely. The residue was added to a solution of KOH (3 g) in methanol (20 cm³) and water (3 cm³), and the mixture was refluxed for 40 h. After removal of the solvent, the residue was shaken with a mixture of water and ether. The aqueous layer was separated, acidified with hydrochloric acid and extracted with ether. The extract was dried (Na_2SO_4) and evaporated. The colorless solid obtained (0.69 g) was heated up to its melting temperature under argon atmosphere to give 5-(9-phenanthryl)pentanoic acid (0.45 g); mp 145—150 °C: IR (KBr) 1710 cm^{-1} (CO).

5-(9-Phenanthryl)pentanoic acid was converted to the amine **1e** in 60% yield by the method similar to that used for the preparation of **1d**. Colorless solid; mp 101.5—103 °C: IR (KBr) 3400 cm^{-1} (NH); ^1H NMR ($CDCl_3$) δ 6.3—8.7 (14H, m, aromatic), 3.4 (1H, br s, NH), 2.8—3.2 (4H, m, CH_2), and 1.3—2.1 (6H, m, CH_2). Found: C, 88.38; H, 7.53; N, 4.11%. Calcd for $C_{25}H_{25}N$: C, 88.45; H, 7.42; N, 4.13%.

*9-(2-Anilinoethyl)phenanthrene (**1f**).* 9-Phenanthreneacetic acid[11] (2.4 g, 10.2 mmol) was converted to the corresponding anilide by a standard method *via* the acid chloride, mp 225—226 °C; IR (KBr) 3300 (NH), 1670 cm^{-1} (CO). Found: C, 84.85; H, 5.33; N, 4.63%. Calcd for $C_{22}H_{17}NO$: C, 84.86; H, 5.50; N, 4.50%. To a solution of this anilide (1.56 g) in THF–ether (2 : 1, v/v, 140 cm³) was added $LiAlH_4$ (1.0 g) in small portions at room temperature. The mixture was refluxed for 5 h and washed with an aqueous ammonium chloride solution, and then extracted with ether. The extract was dried (Na_2SO_4) and evaporated. The residue was recrystallized from hexane to give **1f** as colorless needles (840 mg, 56%); mp 108—108.5 °C: IR (KBr) 3400 cm^{-1} (NH); ^1H NMR ($CDCl_3$) δ 6.3—8.7 (14H, m, aromatic), 3.1—3.8 (5H, m, CH_2 and NH). Found: C, 89.01; H, 6.50; N, 4.34%. Calcd for $C_{22}H_{19}N$: C, 88.85; H, 6.44; N, 4.71%.

Photoreactions. A general procedure is shown with the photoreaction of **1b**. A solution of **1b** in benzene (1.6×10^{-2} mol/dm³) in a Pyrex tube was degassed by three freeze-pump-thaw cycles under argon, and the tube was sealded under reduced pressure. The solution was irradiated externally with a 300 W high-pressure mercury lamp using a merry-go-round apparatus (Eikosha PIH-300): The distance between the light source and the sample solutions was 5 cm. After irradiation for 90 min, the solvent was removed under reduced pressure and the residue was chromatographed on silica gel. Elution with benzene–hexane (1 : 1) gave **2b**, mp 96—135 °C: ^1H NMR ($CDCl_3$) δ 6.3—8.0 (17H, m, aromatic), 4.81 (2H, s, CH_2), and AB quartet signals centered at 4.30 and 2.60 (2H, $J=16$ Hz, CH_2). Found: C, 90.25; H, 5.74; N, 3.62%. Calcd for $C_{27}H_{21}N$: C, 90.22; H, 5.89; N, 3.90%. **2c**: mp 100—102 °C; ^1H NMR ($CDCl_3$) δ 6.3—7.8 (13H, m, aromatic), AB quartet signals centered at 4.03 and 2.30 (2H, $J=$ 16 Hz, CH_2), 3.5—3.75 (2H, m, $=N-CH_2$), and 1.7—2.2 (4H, m, $-CH_2CH_2-$). Found: C, 88.56; H, 6.57; N, 4.67%. Calcd for $C_{23}H_{21}N$: C, 88.70; H, 6.80; N, 4.50%. **2d**: mp 117—120 °C; ^1H NMR ($CDCl_3$) δ 6.5—8.0 (13H, m, aromatic), AB quartet signals centered at 3.84 and 2.94 (2H, $J=$ 16 Hz, CH_2), 3.5—4.0 (2H, m, $N-CH_2-C$), 2.2—1.3 (6H, m, $CH_2CH_2CH_2$). Found: C, 88.64; H, 7.05; N, 4.46%. Calcd for $C_{24}H_{23}N$: C, 88.57; H, 7.12; N, 4.30%. **3**[7]: IR (liquid film) 3060, 3030, 2945, 1635, 1605, 1490, 1455, 895, 770, and 745 cm^{-1}; ^1H NMR ($CDCl_3$) δ 7.0—7.8 (8H, m, aromatic), 5.26 (1H, d, $J=1.5$ Hz, $=CH_2$), 5.06 (1H, d, $J=1.5$ Hz, $=CH_2$), and 3.65 (2H, s, CH_2). Found: C, 93.71; H, 6.02%. Calcd for $C_{15}H_{12}$: C, 93.71; H, 6.29%.

References

1) S. G. Cohen, A. Parola, and G. H. Parson, Jr., *Chem.*

Rev., **73**, 141 (1973); N. Mataga, "Kagaku Sousetsu," ed by the Chemical Society of Japan, Japan Scientific Societies Press, Tokyo (1982), No. 33, p. 19; M. Ohashi, *Kagaku No Ryoiki*, **32**, 830 (1978).

2) M. Bellas, D. Bryce-Smith, and A. Gilbert, *Chem. Commun.*, **1967**, 263, 862; M. Bellas, D. Bryce-Smith, M. T. Clarke, A. Gilbert, G. Klunkin, S. Krestonosich, C. Manning, and S. Wilson, *J. Chem. Soc., Perkin Trans. 1*, **1977**, 2571 and references cited therein.

3) J. A. Barltrop and R. J. Owers, *Chem. Commun.*, **1970**, 1492.

4) N. C. Yang and J. Libman. *J. Am. Chem. Soc.*, **95**, 5783 (1973); N. C. Yang, D. M. Shold, and B. Kim, *ibid.*, **98**, 6587 (1976).

5) T. Okada, I. Karaki, and N. Mataga, *J. Am. Chem. Soc.*, **104**, 7191 (1982) and references cited therein.

6) A. Sugimoto, R. Sumida, N. Tamai, H. Inoue, and Y. Otsuji, *Bull. Chem. Soc. Jpn.*, **54**. 3500 (1981).

7) A. Sugimoto and S. Yoneda, *J. Chem. Soc., Chem. Commun.*, **1982**, 376.

8) F. Hirayama, *J. Chem. Phys.*, **42**, 3163 (1965).

9) K. Tamao, K. Sumitani, Y. Kiso, M. Zembayashi, A. Fujioka, S. Kodama, I. Nakajima, A. Minato, and M. Kumada *Bull. Chem. Soc. Jpn.*, **49**, 1958 (1976).

10) L. F. Fieser and L. M. Joshel, *J. Am. Chem. Soc.*, **61**, 2958 (1939).

11) E. Mosettig and J. van de Kamp, *J. Am. Chem. Soc.*, **55**, 2995 (1933).

 © 1983 The Chemical Society of Japan Bull. Chem. Soc. Jpn., 56, 3123—3128 (1983)

The Sulfuranyl Radical Structure and Reactions of *o*-(Thio)benzoyloxyl Radicals Formed by the Decomposition of *t*-Butyl *o*-(Thio)-perbenzoates Studied by ^{1}H and ^{13}C CIDNP and ^{17}O NMR

Warō Nakanishi,* Yoshiaki Kusuyama, Yoshitsugu Ikeda, and Hiizu Iwamura*,†
Department of Chemistry, Faculty of Education, Wakayama University, Masagocho, Wakayama 640
†*Division of Applied Molecular Science, Institute for Molecular Science, Myodaiji, Okazaki 444*
(Received May 4, 1983)

^{1}H and ^{13}C CIDNP signals were observed in the methyl group of *o*-(methylthio)benzoic acid and the methylene group of 3,1-benzoxathian-4-one (**6**) during the thermal decomposition of *t*-butyl *o*-(methylthio)perbenzoate. The results show that the free "*o*-(methylthio)benzoyloxyl radical" itself is better represented as the bridged sulfuranyl radical in which most of the spin density is localized at the sulfur atom rather than in the carboxyl. Thermolysis of *t*-butyl *o*-(methylthio)- and *o*-(phenylthio)perbenzoates-*carbonyl*-^{17}O was carried out and the oxygen labels were detected by ^{17}O NMR spectroscopy preferentially at the carbonyl oxygen of **6** and diphenyl 2,2′-dithiodibenzoate ruling out the zwitterionic radical structure. The migration of phenyl group and the peroxomonosulfate oxidation of *o*-(phenylthio)benzoic acid are also discussed.

The rate of thermolysis of *t*-butyl perbenzoate is enhanced by the substitution at the *ortho* positions with iodo,[1] vinyl,[2] and thio[1,3] groups. In the case of *t*-butyl *o*-(methylthio)- and *o*-(phenylthio)perbenzoates (**1a** and **1b**, respectively), for example, the rate acceleration reaches upwards of 10^4 times relative to the unsubstituted system (**1e**) at 60 °C in chlorobenzene. The decomposition proceeds with the significant lower $\Delta H^{\ddagger}$ and negative $\Delta S^{\ddagger}$ values.[1] The transition state is also considered to accompany a considerable polar character[4] as shown in the susceptibility of the rate of the thermal decomposition of **1b** to the substituents, solvent ionizing powers, and added salts. Martin *et al.*

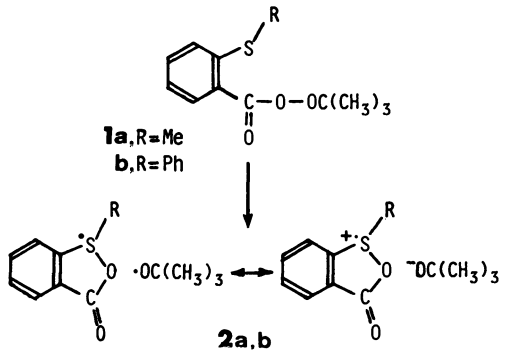

2a,b

proposed a mechanism of the homolytic O–O bond cleavage anchimerically assisted by the neighboring sulfur atom with structure **2** contributing to the transition state.[1] The heavy atom effect as seen in *o*-iodo derivative[5] was excluded here and the steric acceleration was not important because *o*-(*t*-butyl) derivative showed little rate enhancement.[1]

The question we want to raise is if the sulfuranyl radical structure (**3** and/or **4**) should only be the contributing structure in the transition state for the thermolysis reaction or could also be an important representation of the resulting "*o*-(thio)benzoyloxyl radicals." Our strategy was two-fold: The CIDNP method and ^{17}O labeling technique. The CIDNP method has been employed to the elucidation of a number of free radical reaction mechanisms.[6] When applied to the structural study of 2-chloroethyl,[7] 2-bromoethyl,[8] phenethyl,[7] and neophyl[9] radicals, only the classical structures were concluded. In the present case, the cyclic sulfuranyl radical *vs.* "*o*-(thio)benzoyloxyl radical" will be answered by the CIDNP effect in the S-methyl protons and carbon.[10] Secondly, in contrast to the ^{18}O tracer technique[11] widely used to elucidating structures and reaction mechanisms in organic chemistry, the ^{17}O labeling coupled with ^{17}O NMR determination[12] has not been very much publicized and yet has the strong advantage as a nondestructive method; by employing chemical shifts and integration of the signal intensities, the site and distribution of the isotopes in the product molecules can be determined directly.

^{17}O NMR spectroscopy has now been applied to thermal decomposition of ^{17}O labeled *t*-butyl *o*-(methylthio)- and *o*-(phenylthio)perbenzoates (**1a*** and **1b***, respectively).[12]

Quite independently from ours, Martin *et al.* treated the problem by using ESR spectroscopy.[13]

Results and Discussion

The CIDNP Results. Thermolysis of *t*-butyl *o*-(methylthio)perbenzoate (**1a**) produces *o*-(methylthio)-benzoic acid (**5a**: 30%), 3,1-benzoxathian-4-one (**6**: 12%), *t*-butyl alcohol (62%), and acetone (21%) in chlorobenzene at 70 °C.[1]

When a solution of 5 mg of **1a** in 0.5 ml of *o*-dichlorobenzene was heated at 80 °C in a ^{1}H NMR probe, strong emission (E) and enhanced absorption (A) signals were observed at δ 2.38 and 5.21, respectively (Fig. 1).[14] By adding a small amount of the authentic samples to the completed reaction mixture and observing increase in the corresponding signal intensities, it was found that the methyl protons of **5a** were in E and methylene protons[15] of **6** were in A. The signals due to acetone and *t*-butyl alcohol were not spin-polarized. CIDNP was not clear in the aromatic protons for the reaction run in tetrachloroethylene or decalin. The ^{13}C experiments of **1a** were carried out on a solution of 150 mg of **1a** in 1 ml of *o*-dichlorobenzene at 75 °C.

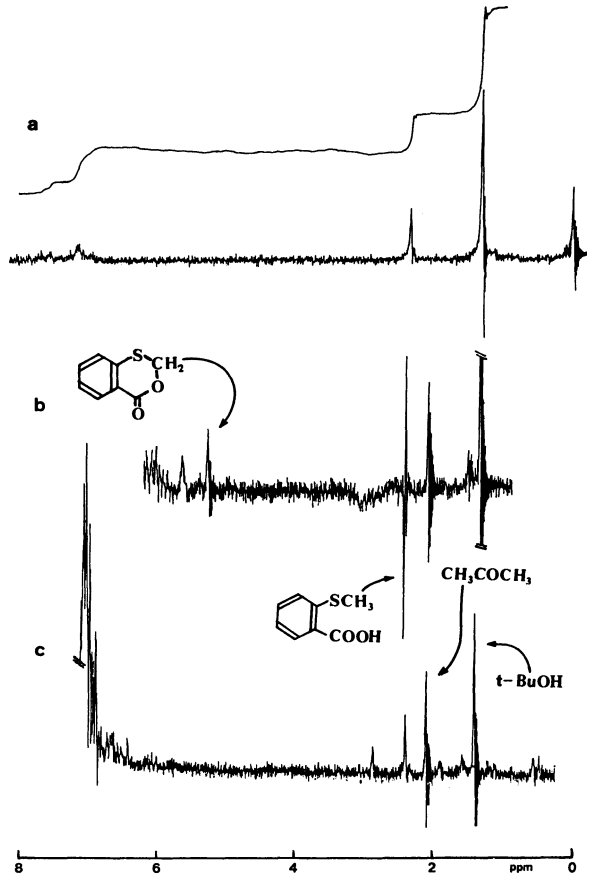

Fig. 1. ^{1}H NMR spectra of **1a**. a: In carbon tetrachloride at 27 °C, b: during the decomposition in *o*-dichlorobenzene at 80 °C, c: after the reaction at 80 °C.

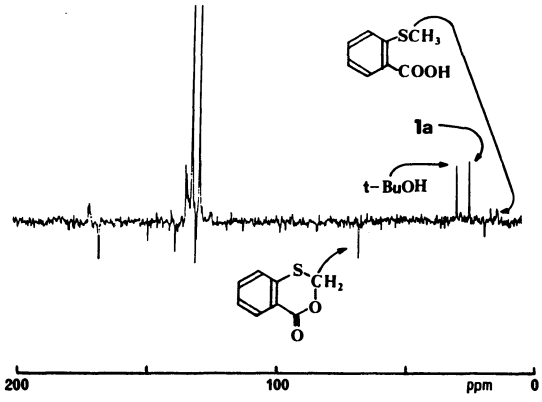

Fig. 2. ^{13}C CIDNP spectrum obtained during the decomposition of **1a** in *o*-dichlorobenzene at 75 °C. See also Ref. 16.

As shown in Fig. 2, the methylene carbon of **6** was in strong E at δ 68.7. The *S*-methyl carbon of **5a** at 15.5 was in A. There were some polarization signals yet to be assigned in the aromatic carbons. There were no polarization signals in the C=O carbon region of **5a** and **6**.[16]

All the results, especially strong polarization in the *S*-methyl group and no polarization in the carbonyl carbons in **5a** and **6** indicate that hyperfine interactions of the methyl protons and carbons are quite large and that the considerable spin density must be localized at the sulfur atom and not in the carboxyl group in the "*o*-(methylthio)benzoyloxyl radical" (**3a**). This is in accordance with the ESR measurement of **3a** and a close analog of **3a** performed by Martin *et al.*[13] The *g*-value of **3a** is 2.0080 and the proton hyperfine splitting of *S*-methyl group is 9.0 G and that of aromatic proton *ortho* to carbonyl group is 1.5 G. The ESR results are best interpreted in terms of a bridged radical with an S–O bond, in which the odd electron is in a σ-type orbital with a large spin density on sulfur. The sign for hyperfine coupling are expected to be plus for the β-H and minus for the α-C in the methyl group of *S*-centered radical **3a**.

The CIDNP spectra are reasonably explained only when the radical has structure of **3a** (or **4a**). In reference to the Kaptein rule,[6b] Scheme 1 is proposed for the observed CIDNP.

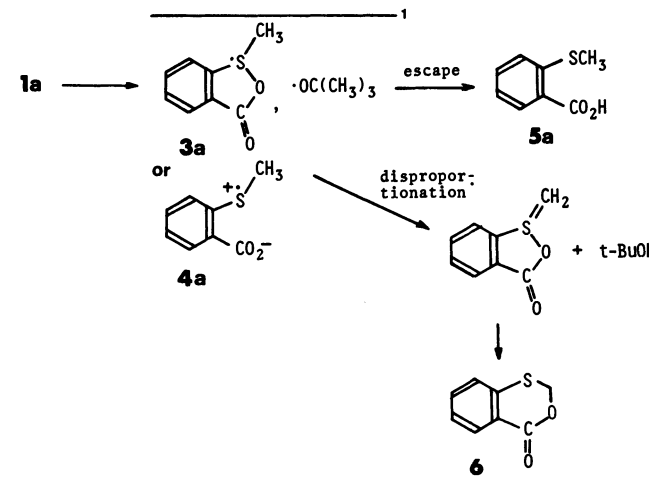

Scheme 1.

$$\Gamma_{ne}(i) = \mu\varepsilon\Delta g A_i,$$

where the sign of polarization of nucleous i due to the net effect (Γ_{ne}(i)) is given by the product of signs of the spin multiplicity of the precursor, the mode of the reaction, the difference in the *g* factors in the radical pair, and the hyperfine coupling constant of nucleus i. The Δg term is negative for **3a** because *g*-value of **3a** is 2.0080 while that of *t*-butoxyl radical is 2.009.[14] The opposite signs of polarization found in the *S*-methyl group of **5a** and the methylene group of **6** are reasonably ascribed to the different mode of formation of these products:[6] **5a** is an escape product ($\varepsilon<0$) while ε for **6** is positive which may be formed by cage-disproportionation followed by rearrangement.

Similar CIDNP experiments on *t*-butyl *p*-(methylthio)perbenzoate and the *o*-methoxyl derivative (**1c**) gave negative results. The ^{1}H signals due to acetone, *t*-butyl alcohol, and methyl protons of *p*-(methylthio)-benzoic acid of the products increased monotonically during the decomposition of *t*-butyl *p*-(methylthio)-perbenzoate in hexachlorobutadiene at 155 °C. No CIDNP was observed in the methoxyl groups of anisole and *o*-methoxybenzoic acid in thermolysis of **1c** in *o*-dichlorobenzene at 147 °C.

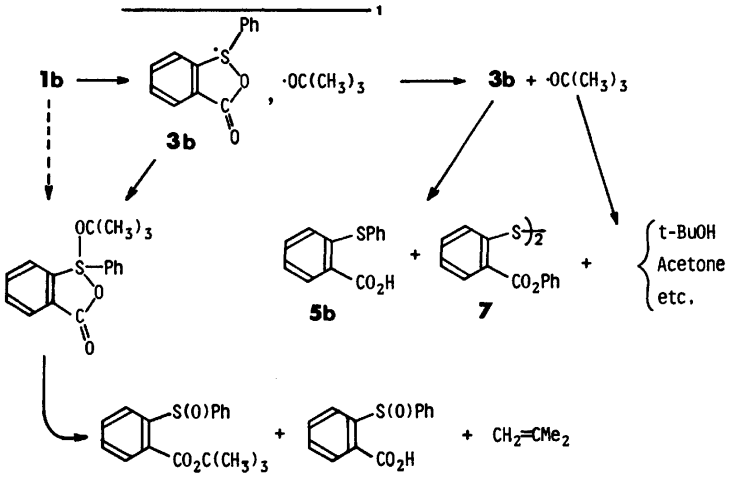

Scheme 2.

CIDNP experiments were also carried out on the thermolysis of *t*-butyl *o*-(phenylthio)perbenzoate (**1b**). Some polarized signals were observed in the phenyl carbon region, but none of them could be assigned to *o*-(phenylthio)benzoic acid (**5b**), diphenyl 2,2′-dithiodibenzoate (**7**), or *o*-(phenylsulfinyl)benzoic acid. Strong polarization was ascribed only to the solvent reacted products. The decomposition mechanism of **1b** proposed by Martin *et al.* is shown in Scheme 2.[3c]

Thus the CIDNP experiments clearly exhibit that most of the spin density should be localized at the sulfur atom. This is possible only when the radical has either the cyclic sulfuranyl radical (**3a**) or a zwitterion radical (**4a**) structure. The "*o*-(thio)benzoyloxyl radical" structure is very unlikely.

Decomposition of ^{17}O-labeled Peroxy Esters. As an operational test to differentiate between the two possibilities, we had recourse to the ^{17}O labeling technique in which the carbonyl oxygen of the starting peroxy esters was specifically enriched with ^{17}O and distribution of the isotope in the cyclic product was examined. Unfortunately scrambling of the two oxygen sites in the carboxyl group did not allow us to study the ^{17}O distribution in the major product **5a**.

Thermal decomposition of *t*-butyl *o*-(methylthio)-perbenzoate enriched with ^{17}O selectively at the carbonyl group (**1a***) was carried out in chlorobenzene at 76 °C. Carbonyl oxygen in **1a*** is estimated to be enriched by *ca.* 4.6 atom%. The contribution from the natural abundance isotope to ^{17}O NMR spectra is less than 1%, since natural abundance of ^{17}O is only 0.037 atom%.

^{17}O-labeled 3,1-benzoxathian-4-one (**6***) was isolated as a decomposition product. As shown in Fig. 3, the ^{17}O NMR spectrum of the lactone contains two signals: The downfield signal (365 ppm from external D_2O) due to the carbonyl oxygen and the higher one (159 ppm) due to the ether oxygen.[17] They were found to be in the integration ratio of 66 : 34. The ratio was 50 : 50 when the ^{17}O NMR spectrum of **6** in natural abundance was measured. Thus the oxathianone-*carbonyl*-^{17}O (**6***[**C=O***]) and the oxathianone-3-^{17}O (**6***[**–O***–]) were found in the ratio of 66 : 34 when **1a*** was decomposed under the conditions described above.[18] As shown in Table 1, the formation of **6***[**C=O***] in preference to **6***[**–O***–] was more favored as the temperature of decomposition was lowered.

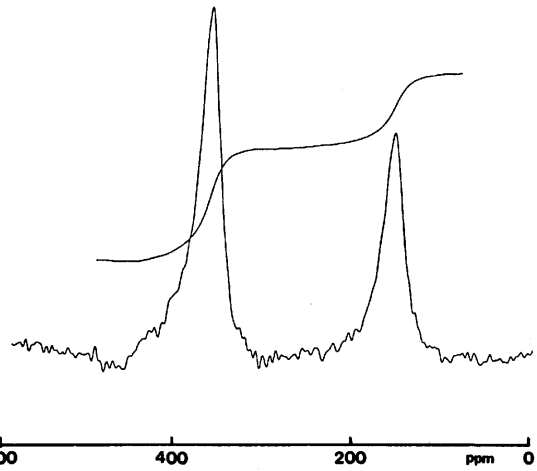

Fig. 3. ^{17}O NMR spectrum of **6*** derived from the thermal decomposition of **1a*** at 76 °C.

Table 1. Population of the ^{17}O label in **6** and the temperature of decomposition of **1a***

Temperature/°C	**6***[**C-O***]	**6***[**–O***–]
76	66	34
62	69	31
40	74	26

A similar study has been carried out on the decomposition of *t*-butyl *o*-(phenylthio)perbenzoate-*carbonyl*-^{17}O (**1b***). Thermolysis of **1b** gives diphenyl 2,2′-dithiodibenzoate (**7**) among many other products as shown in Scheme 2.[1,3c] ^{17}O-labeled **7** (**7***) was isolated as a decomposition product of **1b*** in chlorobenzene at 52 °C. Here we encountered a typical example showing the limitation of the ^{17}O NMR method. Since the line width of ^{17}O NMR signals is governed by quadrupolar relaxation, line broadening of the signal becomes serious as the size (represented by a^3 of a spherical molecule of the radius *a*) of molecules increases.

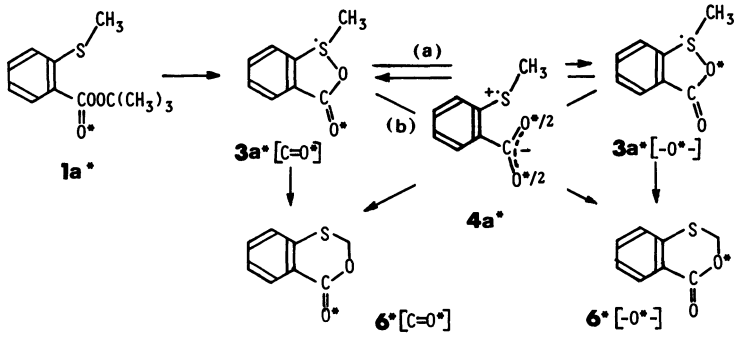

Scheme 3.

Whereas the signal due to the ^{17}O enriched carbonyl oxygen was easily determined, it was difficult to get a reasonable S/N for ^{17}O poor ether oxygen of **7***. Therefore a strategy of carrying out the measurement on a smaller molecule was adopted. Population of the ^{17}O label was thus determined on phenyl *o*-mercaptobenzoate obtained by cleavage of the S–S bond of **7*** into two halves by the method of Overman *et al.*[19] Integration of the peaks at δ 363 and 191 for the carbonyl and ether oxygens, respectively, gave a ratio of 71 : 29.

Martin and Koenig[2b] investigated the distribution of ^{18}O in 3-benzhydrylphthalide obtained from the decomposition of *t*-butyl *o*-(2,2-diphenylvinyl)perbenzoate labeled with ^{18}O in the carbonyl position. By comparing the content of the ^{18}O isotope before and after the saponification/relactonization procedure, it was found that the identity of the carbonyl oxygen of the phthalide was in 88% retention.

As shown in Scheme 1, thermal decomposition of **1a** produces **5a** and **6** as escape and disproportionation products, respectively, of the primary radical pair formed by the O–O bond cleavage of **1a**.[1] If the anchimerically assisted O–O bond cleavage takes place by intramolecular electron transfer from the sulfur to the antibonding O–O orbital and the structure of "*o*-(methylthio)benzoyloxyl radical" formed is **3a**, **6*[C=O*]** should be exclusively formed from **1a***. Structure **4a** should operationally lead to scrambling of the label between the two oxygen atoms, although there may be some lifetime before the requisite rotation of the Ar–CO_2^- bond takes place. The results in Table 1 indicate that the identity of the carbonyl oxygen can be kept through the reaction path to lactone **6*** and that there is a competitive channel available for the scrambling of the oxygen label which has the higher activation energy of the reaction than that retentive path by 2.3 kcal/mol. The scrambling of the label between the carbonyl and endocyclic oxygens may take place either before or during the course of the Pummerer type rearrangement (a or b in Scheme 3). Zwitterionic radical is supposedly an intermediate or a transient species in these scrambling processes. Therefore it is concluded that the "*o*-(methylthio)benzoyloxyl radical" should be described as cyclic structure **3a**. However the contribution of the induced decomposition[1] which could be another mechanism for the retention of oxygen label may take place in the decomposition of **1a**.* In

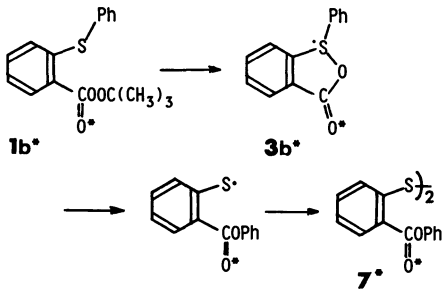

Scheme 4.

the case of **1b***, the contribution of the induced decomposition such as **1a*** is negligible.[1] The 71% of ^{17}O retention in the carbonyl oxygen of **7*** well establishes the sulfuranyl radical structure **3b** for the "*o*-(phenylthio)benzoyloxyl radical" (Scheme 4).

Thus the sulfuranyl radical structure has been well established by a combination of CIDNP and ^{17}O NMR spectroscopy.

Phenyl Migration in o-*Phenoxy- and* o-*(Phenylthio)-benzoyloxyl Radicals.* DeTar and Hlynsky[20] reported predominant phenyl migration in *o*-phenoxybenzoyloxyl radical produced by the decomposition of bis(2-phenoxybenzoyl) peroxide. In this study, the decomposition of *t*-butyl *o*-phenoxyperbenzoate (**1d**) was examined. As shown in Table 2, the decomposition rate constant for **1d** in chlorobenzene at 132 °C is 4.13×10^{-4} s^{-1} which is almost as fast as that calculated from the kinetic parameters (ΔH^*=33.5 kcal/mol and ΔS^*= 7.8 e.u.)[21] of *t*-butyl perbenzoate (**1e**) at the temperature. Phenyl salicylate was produced in 7—10% in this reaction.[22] The rate constant for the decomposition of *t*-butyl *o*-methoxyperbenzoate (**1c**) was also determined as 5.23×10^{-4} s^{-1} in chlorobenzene at 118 °C. The rate constant is 6.7 times larger than that estimated for nonsubstituted one. *o*-Methoxybenzoic acid was produced in *ca.* 40% yield at 118 °C. However it was

Table 2. Rate constant for decomposition of *t*-butyl *o*-(oxy)perbenzoates

Compound	k/s^{-1}	(Temp/°C)	k_{rel}
1c	5.23×10^{-4}	(118)	6.7
1d	4.13×10^{-4}	(132)	1.1
1e[a]			1.0

a) Ref. 21.

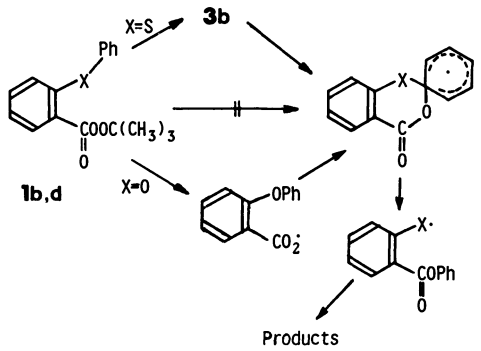

Scheme 5.

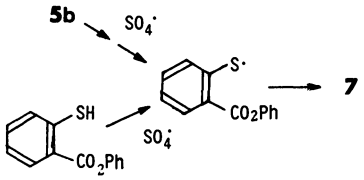

Scheme 6.

ca. 10% at 132 °C in chlorobenzene with the formation of anisole in *ca.* 10%.

As also suggested by Martin,[1] the oxygen atom *ortho* to the peroxy ester moiety does not play an important role in the O–O bond homolysis, that is, anchimeric assistance is absent in *o*-(oxy)perbenzoates. By comparing the rate constant for **1d** with those of **1c** and nonsubstituted one, participation of phenyl ring can be excluded (Scheme 5). Therefore, the phenyl migration in **1b** and **1d** is explained by a two step mechanism. The phenyl migration in **3b** occurs *via* 1,2-shift of the phenyl group in sulfuranyl radical.[1] In the case of **3d**, the ipso attack by the carboxyl radical to the phenoxyl group may occur. The direct attack of the phenyl group to O–O bond is negligible.

The rearranged thiyl radical was directly formed by potassium peroxomonosulfate oxidation[23] of phenyl *o*-mercaptobenzoate. Treatment of phenyl *o*-mercaptobenzoate with equimolar peroxomonosulfate in boiling water gave **7** in 90—95% yield. Oxidation of *o*-(phenylthio)benzoic acid (**5b**) with peroxomonosulfate resulted in the formation of 30% of **7** and *ca.* 10% of by-products with *ca.* 60% of recovery of the starting material. In the presence of catalytic amount of silver ion and 3 molar excess peroxomonosulfate, the yield of **7** was very much improved. The formation of **7** from H-abstraction of **5b** shows that the phenyl migration also occurs in this case (Scheme 6).

Experimental

^{1}H spectra were obtained on a JEOL C 60HL spectrometer operating at 60 MHz. ^{13}C spectra were obtained on a Varian PFT 80 CFT 20 Pulse Fourier Transform spectrometer operating at 20.1 MHz or on a JEOL FX-60Q spectrometer operating at 15 MHz.

CIDNP Measurement. For a typical run, a solution of 5 mg of **1a** in 0.5 ml of chlorobenzene was sealed in a 5 mm ϕ NMR sample tube. ^{1}H NMR spectra were measured at room temperature. Then the sample was put into an NMR probe preheated at 80 °C. The CW ^{1}H NMR spectra were obtained at 20 s, 60 s, and so on after the sample tube was brought into the probe. Time-dependent spectra containing polarized signals were obtained. After the reactions were over, a small amount of authentically prepared compounds was added to assign the CIDNP signals. The chemical shifts were determined from acetone, one of the products, as δ 2.18.

^{13}C CIDNP spectra were obtained in a similar manner on a solution of 150 mg of **1a** in 1 ml of *o*-dichlorobenzene at 75 °C using a Varian CFT-20 spectrometer. A 8 μs pulse was applied with an acquisition time of 0.909 s over the spectral width of 4.5 kHz. The number of data points was 8 K and the number of transients accumulated was *ca.* 300.

As solvents, chlorobenzene, *o*-dichlorobenzene, tetrachloroethylene, 1,1,2,2-tetrachloroethane, hexachlorobutadiene, and decalin were employed after distillation and checked by ^{1}H NMR.

^{17}O NMR Measurement. ^{17}O NMR spectra were measured on a Varian FT-80A spectrometer at 10.782 MHz, using a 90° pulse of 0.02 s. A spectral width was 8000 Hz with 323 data points, the Fourier number being kept at 16384. The labeled sample (*ca.* 300 mg) was dissolved in chloroform-*d* and the temperature of the probe was set at 60 °C in order to obtain a better S/N of the signals due to narrower half-band widths. A reasonable S/N of *ca.* 8 of the spectra was obtained by 1 h's accumulation (the number of transients accumulated was 10^{5}) for enriched samples of this size of molecules. Three to four such data were averaged; the reporoducibility of the relative peak areas was ±2%.

Materials. *t*-Butyl *o*-(methylthio)- and *o*-(phenylthio)-perbenzoates (**1a** and **1b**, respectively) and 3,1-benzoxathian-4-one (**6**) were prepared in analogy with Martin's method.[1] Physical properties agreed well with those in the literature.

t-Butyl o-Methoxyperbenzoate (1c) and t-Butyl o-Phenoxyperbenzoate (1d). These compounds were prepared in a similar manner to that for **1a** and **1b**.

1c: Recrystallization from pentane-ether after low temperature chromatography on basic alumina. Mp 52.0—52.5 °C. Found: C, 64.43; H, 7.31%. Calcd for $C_{12}H_{16}O_4$: C, 64.27; H, 7.19%.

1d: Purified by chromatography on basic alumina with ether as an eluent at low temperature. Colorless oil. Found: C, 71.19; H, 6.28%. Calcd for $C_{17}H_{18}O_4$: C, 71.31; H, 6.34%.

^{17}O Enriched o-(Methylthio)benzoic Acid (5a).* Sodium hydroxide 2.2 g (55.6 mmol) and 1 g of water enriched with ^{17}O in 20 atom% (Prochem, 55.6 mmol) were dissolved in 80 ml of dioxane in the presence of a small amount of 18-crown-6. Then 10.36 g (55.6 mmol) of *o*-(methylthio)benzoyl chloride in 20 ml of dioxane was added at 70 °C, and refluxed for 10 h. After evaporation of the solvent, the mixture was acidified with cold diluted hydrochloric acid (*ca.* 0.005 mol dm^{-3}). The precipitate was washed with cold water and recrystallized from hot water yielded 7.77 g (83%). Mp 169—170 °C (lit,[24] 169 °C). From Mass spectra, the *o*-(methylthio)benzoic acid prepared above was enriched with ^{17}O by 9.1%. So each oxygen in **5a*** is enriched with ^{17}O by 4.6%.

t-Butyl o-(Methylthio)perbenzoate-carbonyl-^{17}O (1a).* To a solution of 5.0 g (31 mmol) of 1,1′-carbonyldiimidazole in 100 ml of THF was added a solution of 5.0 g (30 mmol) of **5a*** in 50 ml of THF, then stirred at 40 °C for 2 h.[25] After evolution of carbon dioxide, 5.4 g (60 mmol) of *t*-butyl hydroperoxide in THF (50 ml) was dropped at −10 °C, and stirred for 2 h. After one night at −20 °C, the solvent was evaporated *in vacuo* below 0 °C. Then cold ether was added and washed with cold water as soon as possible. After drying

over calcium chloride at low temperature, the solvent was evaporated below 0 °C. The residue was purified by chromatography on basic alumina with ether as an eluent at −15 °C. Five and three tenth grams (74%) of **1a*** was obtained. Physical properties and ^{1}H and ^{13}C NMR spectra of **1a*** were the same as those of **1a**.

t-Butyl o-(Phenylthio)perbenzoate-carbonyl-^{17}O (1b).* This compound was prepared in the same manner as that for **1a***.

*Decomposition of 1a**. A solution of 5.3 g of **1a*** in 69 ml of chlorobenzene was stirred at 76 °C for 30 min under nitrogen atmosphere. The solvent was removed *in vacuo*. The residue was chromatographed on silica gel with chloroform as an eluent. Pure **6*** (327 mg) was obtained with 300 mg of a mixture of **6*** and **5a***.

*S–S Bond Cleavage of 7**. Decomposition of **1b*** was carried out similarly at 52 °C and **7*** was isolated. Then **7*** (95 mg) and 52 mg of triphenylphosphine were dissolved in 2 ml of dioxane. The solution was acidified with 0.5 ml of 0.02 mol dm^{-3} hydrochloric acid and kept under nitrogen at 40 °C for 1 h. After removing most of the solvent under reduced pressure, the risidue was extracted with ether, dried over anhydrous magnesium sulfate and chromatographed on silica gel to give 73 mg of phenyl *o*-mercaptobenzoate[19] enriched with ^{17}O.

Oxidation of 5b with Potassium Peroxomonosulfate. To a suspention of 1.0 g of **5b** in boiling water (30 ml) was added a solution of 1.17 g of potassium peroxomonosulfate in 20 ml of water and refluxed for 3 h.[23] After cooling and acidified with diluted hydrochloric acid, crude products were obtained. The crude products contained **7** (30%), **5b** (*ca.* 60%), and by-products. When the mixture was chromatographed on basic alumina, **7** and one of by-products were isolated. In the presence of silver ion and 3 molar excess peroxomonosulfate, the yield of **7** was very much increased but that of the by-product was not improved and occasionally it was not found in the mixture.

Oxidation of phenyl *o*-mercaptobenzoate with peroxomonosulfate yielded 90—95% of **7** without silver ion.

References

1) W. G. Bentrude and J. C. Martin, *J. Am. Chem. Soc.*, **84**,1561 (1962).

2) a) T. W. Koenig and J. C. Martin, *J. Org. Chem.*, **29**, 1520 (1964); b) J. C. Martin and T. W. Koenig, *J. Am. Chem. Soc.*, **86**, 1771 (1964).

3) a) T. H. Fisher and J. C. Martin, *J. Am. Chem. Soc.*, **88**, 3382 (1966); b) J. C. Martin and M. M. Chau, *ibid.*, **96**, 3319 (1974); c) P. Livant and J. C. Martin, *ibid.*, **98**, 7851 (1976).

4) D. L. Tuleen, W. G. Bentrude, and J. C. Martin, *J. Am. Chem. Soc.*, **85**, 1938 (1963).

5) M. Kasha, *J. Chem. Phys.*, **20**, 71 (1952); J. E. Leffler, R. D. Faulkner, and C. C. Petropoulos, *J. Am. Chem. Soc.*, **80**, 5435 (1958).

6) a) "Chemically Induced Magnetic Polarization," ed by A. R. Lepley and G. L. Closs, Wiley, New York (1973); b) R. Kaptein, *J. Am. Chem. Soc.*, **94**, 6251 (1972), and references cited therein.

7) W. Nakanishi, M. Ohara, K. Suyama, Y. Kusuyama, and Y. Ikeda, *Bull. Fac. Educ. Wakayama Univ. Nat. Sci.*, **32**, 1 (1983).

8) J. H. Hargis and P. B. Shevlin, *J. Chem. Soc., Chem. Commun.*, **1973**, 179.

9) P. B. Shevlin and H. J. Hansen, *J. Org. Chem.*, **42**, 3011 (1977).

10) A preliminary report has been published: W. Nakanishi, S. Koike, M. Inoue, Y. Ikeda, H. Iwamura, Y. Imahashi, H. Kihara, and M. Iwai, *Tetrahedron Lett.*, **1977**, 81.

11) For example, see Ref. 2b and references cited therein.

12) For a preliminary publication, see: W. Nakanishi, T. Jo, K. Miura, Y. Ikeda, T. Sugawara, Y. Kawada, and H. Iwamura, *Chem. Lett.*, **1981**, 387.

13) C. W. Perkins, J. C. Martin, A. J. Arduengo, W. Lau, A. Alegria, and J. K. Kochi, *J. Am. Chem. Soc.*, **102**, 7753 (1980).

14) There is an argument that the *t*-butoxyl radical has probably a very short electron relaxation time due to large *g*-tensor anisotropy and therefore ESR observation of this radical in solution is difficult. The radical may not be able to be a component of a radical pair responsible for CIDNP effect (J. den Hollander, Ph. D. Thesis, University of Leiden, Leiden, The Netherlands, 1976.). However, there are some reports in which the pair containing the *t*-butoxyl radical does produce CIDNP (P. D. Bartlett and N. Shimizu, *J. Am. Chem. Soc.*, **97**, 6253 (1975).).

15) As shown in Ref. 1, the chemical shift of the methylene protons of **6** shows rather large solvent dependence.

16) A strong emission was observed at δ 165.4 and enhanced absorptions at 168.8 and 169.2. However they are not assigned to carbonyl carbons of **5a** and/or **6**, because the chemical shifts of the carbons of **5a** and **6** are 171.2 and 163.2, respectively, under the same conditions.

17) T. Sugawara, Y. Kawada, M. Katoh, and H. Iwamura, *Bull. Chem. Soc. Jpn.*, **52**, 3391 (1979); T. Sugawara, Y. Kawada, and H. Iwamura, *Kagaku No Ryoiki*, **34**, 207 (1980).

18) The results are consistent with that the sulfur atom in **1a** attacks the oxygen next to the carbonyl group in the anchimeric assistance. See also Ref. 3a and 3b.

19) L. E. Overman, J. Smoot, and J. D. Overman, *Synthesis*, **1974**, 59.

20) D. F. DeTar and A. Hlynsky, *J. Am. Chem. Soc.*, **77**, 4411 (1955).

21) The values for activation parameters were obtained in *p*-chlorotoluene. A. T. Blomquist and A. F. Ferris, *J. Am. Chem. Sco.*, **73**, 3408 (1951).

22) When the decomposition of **1d** was carried out in decalin, phenyl salicylate was produced over 80% yield.

23) G. Sosnovsky and D. J. Rawlinson, "Organic Peroxide," ed by D. Swern, Wiley, New York (1971), Vol. 2, p. 317; Peroxomonosulfate oxidation of *o*-phenoxybenzoic acid gives a dimer of *o*-(phenoxycarbonyl)phenoxyl radical, see R. H. Thomson and A. G. Wylie, *J. Chem. Soc., C*, **1966**, 321.

24) The mp is for **5a**; T. Zincke and G. Siebert, *Ber.*, **48**, 1242 (1915).

25) R. Hecht and C. Rüchardt, *Chem. Ber.*, **96**, 1281 (1963).

 © 1983 The Chemical Society of Japan Bull. Chem. Soc. Jpn., 56, 3129—3133 (1983)

The Formation and Thermal Decomposition of Hydrous Lead(II) Oxide Prepared by the Alkoxide Method

Eiichi NARITA,* Makito KOBAYASHI, Hirobumi SHINJO, Hisashi TSUCHIDA,** and Hiroyuki NAITO**

Department of Applied Chemistry, Faculty of Engineering, Tohoku University, Aramaki, Sendai 980

***Mizusawa Factory, Mizusawa Industrial Chemicals, Ltd., Nishime, Tsuruoka 999-75*

(Received December 7, 1982)

Lead(II) isopropoxide was hydrolyzed by addition to water in order to investigate the effects of temperature, rate of hydrolysis, seeds and anions added in aqueous phase on the formation of hydrous lead(II) oxide. Thermal decomposition of the resulting hydrous lead(II) oxide was also investigated using TG and DTA techniques. It was found that the metastable phase of lead(II) oxide, $3PbO \cdot H_2O$ (tetragonal), was formed only under certain strict conditions, *i.e.*, at higher rate of hydrolysis and at temperatures below 40 °C, whereas the anhydrous lead(II) oxides such as massicot (orthorhombic), litharge (tetragonal), or a mixture of the two were formed under conditions other than those described above. In the presence of massicot seed in aqueous phase, massicot was predominantly formed under the formation conditions of $3PbO \cdot H_2O$. It was also found that the presence of anions such as citrate and EDTA ions, which have higher complexing ability with Pb^{II} ion, facilitated the formation of $3PbO \cdot H_2O$ even under the formation conditions of massicot. In the heating process, $3PbO \cdot H_2O$ was changed to litharge at 168 °C with the release of its water of crystallization and then transformed to massicot at 650 °C. The reaction order and activation energy for the dehydration were 0.9 and 112.6 kJ mol^{-1}, respectively.

Although many hydrous lead(II) oxides such as $5PbO \cdot 2H_2O$,[1,2] $8PbO \cdot 3H_2O$,[2] $3PbO \cdot H_2O$,[3-5] and $2PbO \cdot H_2O$[3,4] have been prepared by the hydrolysis of $Pb(NO_3)_2$ and $Pb(CH_3COO)_2$ solutions, these contents of the water of crystallization have been thought to be ambiguous. This is because of this small amounts compared with the total weights of these hydrous lead(II) oxides and of the strong affinities for carbon dioxide in air.[5] Therefore, an investigation to clarify the relationship between the formation conditions and the chemical composition and other properties of the hydrous lead(II) oxides is desirable.

The authors have previously proposed a new industrial method for the production of lead(II) oxide ("Oxygen Pressurized Wet Milling Method"[6,7]), in which many spherical granules of metallic lead (3—5 mm in diameter) are oxidized with pressurized oxygen in the presence of water at temperatures below about 60 °C in a rotating mill. In the course of this developments further information about the formation of the hydrous lead(II) oxides was also necessary, since the hydrous lead(II) oxide ($3PbO \cdot H_2O$) was formed together with massicot and litharge according to the conditions. $3PbO \cdot H_2O$ is characterized by its very small particle size and higher activity for chemical reactions; which properties seem to be advantageous for a variety of industrial uses.

On the other hand, it is well known that the products obtained by the hydrolysis of lead(II) salts tend to be affected by the presence of anions such as CH_3COO^-, NO_3^-, and Cl^-, and anhydrous lead(II) oxides or basic lead(II) compounds are often formed instead of the hydrous lead(II) oxides.[8,9] As a starting material for the hydrolysis of $lead^{II}$ ion without the effect of anions, lead(II) isopropoxide can be used conveniently.[10]

This study will deal with the formation of hydrous lead(II) oxide by the hydrolysis of lead(II) isopropoxide, especially with the effects of changes in temperature, rate of hydrolysis, and additions of seeds and anions. The thermal decomposition of the resulting hydrous lead(II) oxide was also studied by TG and DTA techniques.

Experimental

Reagents. All the reagents used were of extra pure grade. The isopropyl alcohol was purified by fractional distillation. Anhydrous lead(II) acetate was used after drying overnight at 110 °C. The water used was obtained by double distillation of dilute potassium manganate(VII) aqueous solution.

Procedure. An alcoholic solution containing 3.0 wt% lead(II) isopropoxide was prepared according to the method reported by Yamaguchi *et al.*[10] Sodium isopropoxide was first prepared by the reaction of 0.68 g metallic sodium with a 200 cm^3 of isopropyl alcohol (Eq. 1). Then, 4.8 g of anhydrous lead(II) acetate was

$$Na + C_3H_7OH \longrightarrow Na(OC_3H_7) + 1/2H_2, \quad (1)$$

added to the alcoholic solution and the mixture refluxed for 6 h (Eq. 2). After centrifuging to remove sodium acetate, 3.0 wt% lead(II) isopropoxide solution was obtained.

$$Pb(CH_3COO)_2 + 2NaOC_3H_7 \xrightarrow[C_3H_7OH]{83\,^\circ C,\ 6\ h} Pb(OC_3H_7)_2 + 2CH_3COONa\downarrow \quad (2)$$

The hydrolysis of the alkoxide was carried out as follows: A 400 cm^3 of the distilled water was transferred to a 1 dm^3 three-necked glass flask equipped with a reflux condenser, a dropping funnel, a thermometer, and a magnetic stirrer, and heated to the desired temperature under nitrogen atmosphere. Subsequently, a 200 cm^3 portion of alcoholic solution of the alkoxide in the dropping funnel was added to the distilled water with vigorous stirring (Eq. 3). The resulting suspension was stirred for further 30 min.

$$Pb(OC_3H_7)_2 + H_2O \longrightarrow PbO\downarrow + 2C_3H_7OH \quad (3)$$

After measuring the pH of the suspension, the product was filtered off, washed with acetone and diethyl ether, and dried over P_2O_5 under reduced pressure.

Analysis. The X-ray diffraction patterns were obtained using a Rigaku Denki Geigerflex D-2F with Ni filtered Cu *Ka* radiation, with 30 kV and 15 mA. The observation of the product was carried out with a Hitachi-Akashi Scanning

Electron Microscope MSM 4C-102. The IR absorption spectra were obtained on a Nippon Bunko IR-E spectrometer with the KBr pellet technique. DTA and TG were performed using a Rigaku Denki Thermoflex over the range from room temperature to 700 °C. α-Al_2O_3 was used as a standard substance and the rate of temperature rise was 10 °C/min.

Results and Discussion

Effects of Temperature and Hydrolysis Rate. The effects of temperature and hydrolysis rate on the crystal form of the product are given in Table 1. In these experiments, the hydrolysis rate was changed by controlling the rate of addition of the alkoxide solution to the aqueous phase. Figure 1 also shows the X-ray diffraction patterns of these typical products shown in Table 1. According to the conditions, three kinds of lead(II) oxides, *i.e.*, $3PbO \cdot H_2O$,[11] massicot,[12] and litharge[13] were formed as single phases or as binary mixtures. A product consisting of only $3PbO \cdot H_2O$ was obtained under the conditions of low temperatures (<40 °C) and high hydrolysis rate. With decreasing hydrolysis rate, the amount of massicot in addition $3PbO \cdot H_2O$ was gradually increased. One other noticeable result was that the formation of $3PbO \cdot H_2O$ was independent of the pH of the resulting suspension in the range of 9—12. On the other hand, a product consisting of only litharge was obtained under the conditions of high temperatures and hydrolysis rate. Similarly the amount of massicot in addition to litharge increased with decreasing hydrolysis rate, and a product consisting of only massicot was obtained at low hydrolysis rate. Thus formation of massicot and litharge is identical

Table 1. Effects of temperature and hydrolysis rate on the crystal form of the lead(II) oxide prepared by the alkoxide method

No.	Temp °C	Addition speed of alkoxide s/200 cm³	Product[a]
1	25	2	H
2	40	2	H
3	50	2	L
4	60	2	L
5	80	2	L
6	25	5	H
7	25	3×10^2	M+H
8	25	1.2×10^3	M+H
9	25	6×10^3	M
10	60	5	L+M
11	80	5	L+M

a) H: $3PbO \cdot H_2O$, L: litharge, M: massicot.

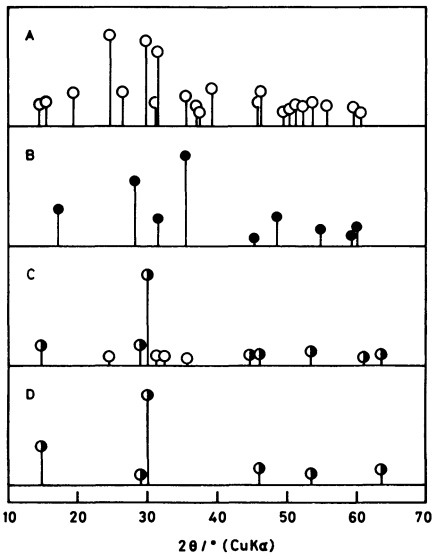

Fig. 1. X-Ray diffraction patterns of the lead(II) oxides prepared by the alkoxide method.
○: $3PbO \cdot H_2O$, ◑: massicot, ●: litharge, (A): sample No. 1, (B): sample No. 4, (C): sample No. 7, (D): sample No. 9 in Table 1.

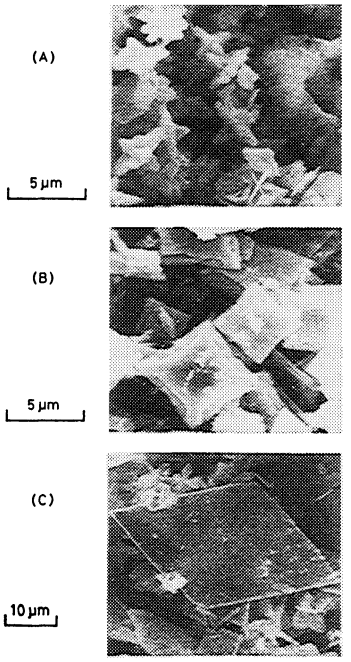

Fig. 2. Scanning electron micrographs of the lead(II) oxides prepared by the alkoxide method.
(A): $3PbO \cdot H_2O$, (B): litharge, (C): massicot.

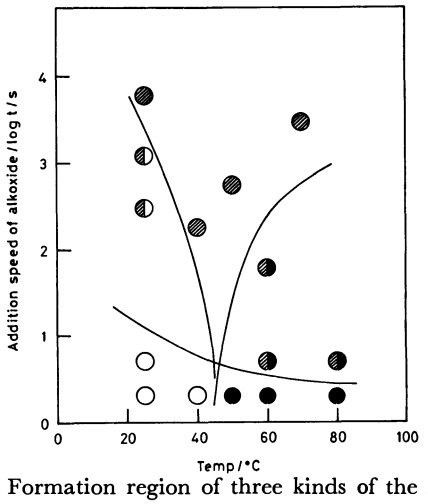

Fig. 3. Formation region of three kinds of the lead(II) oxides prepared by the alkoxide method.
○: $3PbO \cdot H_2O$, ◍: massicot, ●: litharge, ◍●: mixture.

Table 2. Free energies of formation of lead(II) oxide

Lead(II) oxide	ΔG_f° / kJ mol^{-1}	
	Latimer[14]	Spencer *et al.*[15]
$3PbO \cdot H_2O$	—	−187.7
Massicot	−188.5	−188.1
Litharge	−189.4	−188.7

with that reported by Yamaguchi *et al.*[10] As shown in Fig. 2, the precipitated $3PbO \cdot H_2O$ was a petal shaped crystal of 2—5 μm in size, which were smaller than those of massicot and litharge. Figure 3 demonstrates the formation regions of these three lead(II) oxides. It was found that the formation of pure $3PbO \cdot H_2O$ was limited to a sharply defined region of low temperature and high hydrolysis rate.

In general, a crystal nuclei generated from a homogeneous phase during a reaction (Eq. 3) does not always correspond with that of the thermodynamically stable phase. A crystal nuclei of a metastable phase is often formed under nonequilibrium states of supersaturation. The standard free energies of formation of these three lead(II) oxides are given in Table 2.[14,15] The thermodynamical stability is found to be litharge>massicot> $3PbO \cdot H_2O$ in that order. Thus, $3PbO \cdot H_2O$ is a metastable phase.

Effect of Seed. A series of experiments was carried out in which three kinds of lead(II) oxides prepared by the alkoxide method were previously added in an aqueous phase and the results of the effect of various seeds on the crystal form of the product are given in Table 3. When 0.2 g (corresponding 20 wt% amount for the product yield) of massicot seed was added, the product, consisting only of massicot, was obtained even under the formation conditions of $3PbO \cdot H_2O$, whereas the addition of 0.1 g of massicot seed had no affect because its amount was not enough against the supersaturation. The same results in the presence of massicot seed was also observed under the formation conditions of litharge. This result means that massicot is apparently more stable than litharge in this experiment, contrary to the thermodynamical stability order. It is generally known that the crystal form of lead(II) oxide is affected by a small amount of impurities (especially Si^{IV} ion) and massicot is predominantly formed.[16] Following the addition of $3PbO \cdot H_2O$ and litharge seeds under the formation conditions of massicot, the crystal form of the product was always massicot, as expected from the apparent stability order.

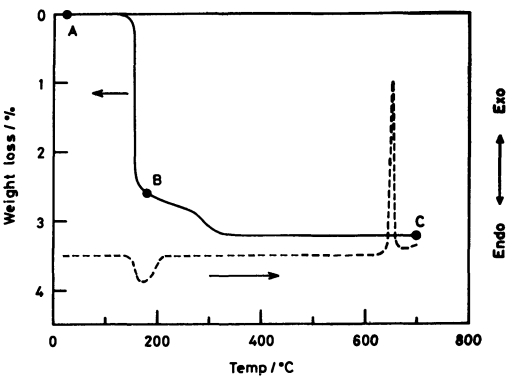

Fig. 4. TG and DTA curves of the hydrous lead(II) oxide ($3PbO \cdot H_2O$) under an air atmosphere.
Heating rate of furnace: 10 deg/min, amount of sample: 37.4 mg.

Effect of Anions. A series of experiments was carried out under the formation conditions of massicot in which several anions were previously dissolved in aqueous phase in a concentration range of 1×10^{-4}—1×10^{-3} mol dm^{-3}. The results of the effect of these anions on the formation of $3PbO \cdot H_2O$ are given in Table 4. A product consisting only of $3PbO \cdot H_2O$ was obtained instead of massicot following the addition of citrate ion or EDTA ion. A minor amount of $3PbO \cdot H_2O$ was also obtained, together with massicot, following the addition of sulfate ion. However, the coexisting acetate and chloride ions did not affected the crystal form of the product. The complexing ability of these anions with lead^{II} ion is decreased in the order: EDTA>citrate> sulfate>acetate>chloride.[17] Therefore, it was concluded that the presence of the anions having higher formation ability of the lead^{II} complex facilitated the selective formation of $3PbO \cdot H_2O$.

Lead^{II} ion forms an octahedron configuration coordinating H_2O molecule or OH^- ion in aqueous solution. If certain anions having high complexing ability with lead^{II} ion are presented in the solution, H_2O molecule or OH^- ion is rapidly substituted for these anions according to these complexing abilities and concentrations. It is generally known that the crystal form of the nuclei is affected by the coordinating anions when metal ions such as iron and titanium are precipitated by the hydrolysis.[18,19] In these studies, the polymorphism has been interpreted by a mechanism in which the order of the formation energy of the critical nuclei is

Table 3. Effect of seed on the crystal form of the lead(II) oxide prepared by the alkoxide method

No.	Seed (Amount / g)[a]	Temp / °C	Addition speed of alkoxide / s/200 cm^3	Product[a]	
				Without seed	With seed
1	M (0.1)	25	2	H	H+M
2	M (0.2)	25	2	H	M
3	M (0.2)	60	2	L	M
4	L (0.2)	25	2	H	M+H
5	L (0.2)	60	6×10^3	M	M
6	H (0.2)	25	3×10^2	M	M

a) H: $3PbO \cdot H_2O$, L: litharge, M: massicot.

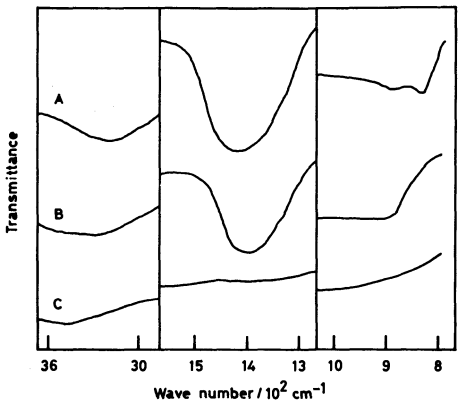

Fig. 5. Infrared spectra of the heating products of the hydrous lead(II) oxide ($3PbO \cdot H_2O$).
(A): Room temperature, (B): 180 °C, (C): 720 °C.

TABLE 4. EFFECT OF ADDITIVES ON THE CRYSTAL FORM OF THE LEAD(II) OXIDE PREPARED BY THE ALKOXIDE METHOD[a)]

No.	Additive	Concentration of additive / mol dm^{-3}	Product[b)]
1	None	—	M
2	Citric acid	1×10^{-4}	H
3	Citric acid	1×10^{-3}	H
4	Acetic acid	1×10^{-4}	M
5	Sulfuric acid	1×10^{-4}	M(+H)
6	Hydrochloric acid	1×10^{-4}	M+BS(+H)
7	EDTA	1×10^{-4}	M
8	EDTA	1×10^{-3}	H

a) All experiments were conducted under the conditions as follows: temperature, 25 °C; adding speed of alkoxide, 50 min/200 cm; pH of suspension, 9.5—9.8. b) H: $3PbO \cdot H_2O$, L: litharge, M: massicot, BS: basic salt.

reversed by the adsorption of the coordinating anions. The results obtained here are also consistant with the mechanism reported by earlier investigators.

Thermal Decomposition of $3PbO \cdot H_2O$. TG and DTA curves, in air, for $3PbO \cdot H_2O$ obtained by the alkoxide method are shown in Fig. 4. The weight loss on heating was indicated on the TG curve at 160—170 °C. This was due to the release of the water of crystallization, corresponded with the sharp endothermic peak of the DTA curve at 168 °C. A second weight loss was also indicated on the TG curve in the temperature range of 180—350 °C. The X-ray diffraction patterns of three samples obtained at A (before heating), B (180 C°), and C (720 °C) in Fig. 4 indicated that they were $3PbO \cdot H_2O$, litharge and massicot, respectively. That is, $3PbO \cdot H_2O$ was first changed to litharge with the release of the water of crystallization and then transferred to massicot in the heating process. Although

$$3PbO \cdot H_2O \xrightarrow{160\,^\circ C} PbO(\text{litharge}) \xrightarrow{650\,^\circ C} PbO(\text{massicot})$$

the weight loss calculated from the formula of $3PbO \cdot H_2O$ should be 2.5 wt%, the total weight loss obtained from the TG curve in Fig. 4 was 3.2 wt%. Therefore, it would seem that only the first weight loss (2.5 wt%) is due to the release of the water of crystallization and the second to the release of other impurities. Figure 5 shows the IR spectra for the three samples A, B, and C. The spectrum of sample A ($3PbO \cdot H_2O$) displays four distinct bands at 860, 1420, 1630, and 3200 cm^{-1}. The bands at 1630 and 3200 cm^{-1} are the OH stretching band and the OH bending band, respectively. The bands of 860 and 1420 cm^{-1} can be assigned to CO_3^{2-}. As described previously, $3PbO \cdot H_2O$ has strong affinity for CO_2 gas in air, which being responsible for the ambiguous amount of the water of crystallization of hydrous lead(II) oxides. Doi *et al.*[20] proposed the following thermal decomposition scheme for lead(II) carbonate:

$$3PbCO_3 \longrightarrow 2PbCO_3 \cdot PbO + CO_2\uparrow(316\,^\circ C), \quad (4)$$

$$2(2PbCO_3 \cdot PbO) \longrightarrow 3(PbCO_3 \cdot PbO) + CO_2\uparrow(339\,^\circ C), \quad (5)$$

$$3(PbCO_3 \cdot PbO) \longrightarrow 2(PbCO_3 \cdot 2PbO) + CO_2\uparrow(373\,^\circ C), \quad (6)$$

$$PbCO_3 \cdot 2PbO \longrightarrow 3PbO + CO_2\uparrow(\text{about } 435^\circ C). \quad (7)$$

From this result, it was concluded that the second weight loss at 180—350 °C in Fig. 4 was due to this decomposition of $PbCO_3$ in the precipitate.

The methods of Freeman-Carroll[21] and Coats-Redfern[22] were used to study the kinetics of the dehydration. These methods can only be used for a single elementary reaction. The formura of the Freeman-Carroll method is written as

$$\Delta \log(dW/dt)/\Delta \log W_r = n - \Delta(1/T)/2.303\,RT(\Delta \log W_r), \quad (8)$$

where dW/dt is the weight change in mg per minute, n the order of the reaction, T the absolute temperature, and $W_r = W - W_c$, where W is the weight (mg) at time t, and W_c the weight (mg) of the sample at the end of the reaction. E is the energy of activation. If the plot of the ratio $\Delta\log(dW/dt)/\Delta\log W_r$ values *vs.* $\Delta(1/T)/\Delta\log W_r$ is linear, the activation energy and the reaction order will be given by its slope and intercept, respectively. This is illustrated in Fig. 6, where the linear relationship is observed. The results are given in Table 5.

When the reaction order is other than unity, the formula of the Coats-Redfern method is written as

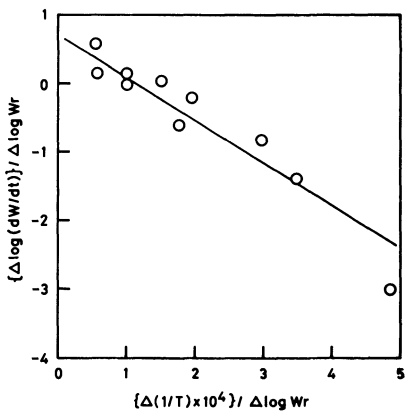

Fig. 6. Freeman-Carroll straight line for the dehydration step of the hydrous lead(II) oxide ($3PbO \cdot H_2O$).

Table 5. Reaction order and activation energy of the thermal dehydration of the hydrous lead(II) oxide

Method	Activation energy / kJ mol^{-1}	Reaction order
Freeman-Carroll	112.8	0.7
Coats-Redfern	112.4	1.0
Average	112.6	0.9

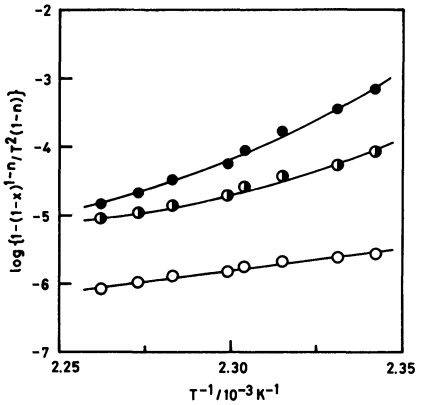

Fig. 7. Coats–Redfern straight line for the dehydration step of the hydrous lead(III) oxide ($3PbO \cdot H_2O$). order n —●: 1.0, ◑: 2.0, ○: 3.0.

$$\log\{1-(1-x)^{1-n}/(1-n)T^2\} = \log(AR/\phi E)(1-2RT/E) - E/2.303RT, \quad (9)$$

where x is the fraction of reaction, ϕ the heating rate of furnace and A the frequency factor. Graphic representation of the $\log\{1-(1-x)^{1-n}/(1-n)T^2\}$ values as a function of $1/T$ gives a straight line of slope $-E/2.303R$ for the correct value of n. This is illustrated in Fig. 7 and the results are given in Table 5. No difference between the results obtained by either method was observed and the average apparent activation energy and reaction order were 112.6 kJ mol^{-1} and 0.9, respectively.

The authors wish to thank Prof. Taijiro Okabe of the Department of Applied Chemistry, Tohoku University for his helpful discussion.

References

1) L. Clark and W. P. Tyler, *J. Am. Chem. Soc.*, **61**, 58 (1939).
2) S. Glasstone, *J. Chem. Soc.*, **121**, 58 (1922).
3) V. Köhlshütter and H. Rösti, *Ber. Deutsch. Chem. Ges.*, **56**, 275 (1923).
4) G. F. Hüttig and B. Steiner, *Z. Anorg. Allg. Chem.*, **197**, 257 (1931).
5) H. R. Oswald, J. R. Günter, and W. Shählin, *Helv. Chim. Acta*, **51**, 6 (1968).
6) H. Naito, H. Tsuchida, A. Takahashi, and Y. Noshi, *Nippon Kagaku Kaishi*, **1983**, 626.
7) H. Tsuchida, H. Noshi, H. Naito, H. Okayasu, and E. Narita, *Nippon Kagaku Kaishi*, **1983**, 633.
8) M. Kiyama, K. Murakami, T. Takada, I. Sugano, and T. Tsuji, *Chem. Lett.*, **1976**, 23.
9) H. Torii, M. Kiyama, T. Takada, *Bull. Inst. Chem. Res., Kyoto Univ.*, **56**, 247 (1978).
10) O. Yamaguchi, M. Yamadera, and K. Shimizu, *Bull. Chem. Soc. Jpn.*, **50**, 2805 (1977).
11) X-Ray powder data file (ASTM card 21-1134).
12) X-Ray powder data file (ASTM card 5-570).
13) X-Ray powder data file (ASTM card 5-561).
14) W. M. Latimer, "Oxidation Potentials," 2nd ed, Prentice-Hall, N. J. (1952), p. 152.
15) H. M. Spencer and J. H. Mote, *J. Am. Chem. Soc.*, **54**, 4618 (1932).
16) W. Kwestroo, J. D. Jonge, and P. H. G. M. Vromans, *J. Inorg. Nucl. Chem.*, **29**, 39 (1957).
17) L. G. Sillen and A. E. Martell, "Stability Constants of Metal-Ion Complexes," The Chem. Soc., London (1971).
18) K. Inoue, *Kagaku To Kogyo*, **27**, 571 (1974).
19) F. Izumi, *Bull. Chem. Soc. Jpn.*, **51**, 1771 (1978).
20) A. Doi and C. Kato, *Kogyo Kagaku Zasshi*, **73**, 488 (1970).
21) E. S. Freeman and B. Carroll, *J. Phys. Chem.*, **62**, 394 (1958).
22) A. W. Coats and J. P. Redfern, *Nature*, **201**, 68 (1964).

Semiexperimental Magnetic Study of Some Methyl Derivatives of Benzoic Acid

Mohamed Mahmoud Abdel-Kader
Physics Department, Faculty of Science, University of Cairo, Giza, Egypt
(Received October 6, 1982)

The mean molar susceptibilities of some methyl derivatives of benzoic acid have been measured. From these measurements and the calculated value of the in-plane susceptibilities (K_1, K_2) of each molecule, the semiexperimental magnetic anisotropy of the acid molecule has been determined. The obtained magnetic data are explained on the basis of the hydrogen bonding systems of these molecules.

The peculiar magnetic properties of aromatic compounds (besides exaltation, there are large magnetic anisotropies and anomalous nmr chemical shifts) are widely held to be results of the relatively large magnetic moment induced in the fully delocalized π-electrons characteristic of these molecules.[1-3] This has come to be called the "ring current." The contribution of the ring current to the magnetic susceptibility is amenable to theoretical calculation. The literature in this field is extensive.[4-9]

Although the contribution of the ring current to the magnetic susceptibility is comparatively large and is the main cause of the anisotropy of the diamagnetic susceptibility of a molecule,[6] yet other contribution of σ-electrons and localized π-electrons are also important.[10] Hoarau[11] suggested that the ring current probably accounts for not more than half of the observed anisotropy of benzene. He discussed the anisotropy of benzene and other aromatic hydrocarbons according to the scheme:

$$\Delta K_{\text{obsd}} = \Delta K_{\text{London}} + \Delta K_{\sigma} + n\Sigma\Delta K_{\pi}. \quad (1)$$

The first term is the anisotropy according to London theory, *i.e.* the component due to the ring currents in the delocalized π-electrons; the second term represents the anisotropy due to σ-electrons, and the third term is the sum of anisotropies due to localized π-electrons. The effect of the last term is to increase the anisotropy, not through the usual enhancement of the out-of-plane susceptibility (K_3), but by a decrease in the in-plane susceptibilities K_1 and K_2. Davies[10] calculated the π-electron susceptibility ΔK^{π} of benzene and other system and gave the empirical equation:[12]

$$\Delta K^{\pi} = K_3 - \Sigma\chi_{\text{atomic}}, \quad (2)$$

where K_3 is the experimental out-of-plane susceptibility. A more recent calculation of ΔK^{π} was given by Edwards and McWeeny.[6] A complete discussion of the use of ring current concept in the magnetic susceptibility, magnetic anisotropy and nmr chemical shift was given recently by Gomes.[13]

In general, the principal susceptibilities (K_1, K_2, and K_3) and therefore the anisotropy of the diamagnetic susceptibility for a molecule can be found from the measured values of the crystal susceptibilities (χ_1, χ_2, and χ_3) along the principal axes of the crystals, combined with the orientation of the molecule in it. The set of equations that commonly used is:

$$\left.\begin{aligned}\chi_1 &= K_1\cos^2\alpha_1 + K_2\cos^2\alpha_2 + K_3\cos^2\alpha_3,\\ \chi_2 &= K_1\cos^2\beta_1 + K_2\cos^2\beta_2 + K_3\cos^2\beta_3,\\ \chi_3 &= K_1\cos^2\gamma_1 + K_2\cos^2\gamma_2 + K_3\cos^2\gamma_3,\end{aligned}\right\} \quad (3)$$

where ($\cos\alpha_1$, $\cos\beta_1$, and $\cos\gamma_1$) are the direction consines of K_1 relative to the axes of the triaxial ellipsoide. These direction consines are determined from the atomic coordinates as given by X-ray structure analysis, but after performing the transformation needed for systems other than the orthogonal one. Several investigators have been made in this way.[14-21] According to Akamatu,[3] such a method is the orthodox one. Recently both the magnetic susceptibility and the anisotropy are calculated semiemperically or theoretically.[6-8,22-24]

In this paper, the method suggested by Hoarau[11] is used. Accordingly, the value of $(1/2)(K_1+K_2)_{\text{calcd}}$ is given by:

$$(1/2)(K_1+K_2)_{\text{calcd}} = \Sigma\chi_{\text{atomic}} + n\alpha, \quad (4)$$

where n is the number of trigonally hybridized carbon atoms and α is a constitutive correction ($\simeq +3.8\times 10^{-6}$ emu mol^{-1}) expressing quantitatively the effect of ΔK_{π} of Eq. 2 on the in-plane susceptibilities.

Since the magnetic anisotropy of a molecule is given by

$$\Delta K = K_3 - (1/2)(K_1+K_2),$$

and

$$\chi_{\text{M}}^{\text{obsd}} = (1/3)(K_1+K_2+K_3),$$

therefore

$$\Delta K_{\text{semi}} = 3[\chi_{\text{M}}^{\text{obsd}} - (1/2)(K_1+K_2)].$$

Experimental

The compounds studied in this paper are:
a) *o*-Methylbenzoic acid (*o*-Toluic acid).[25]
b) *m*-Methylbenzoic acid (*m*-Toluic acid).[26]
c) *p*-Methylbenzoic acid (*p*-Toluic acid).[27]

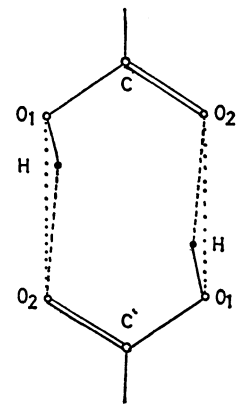

Fig. 1. The 8-membered ring.

d) 2,6-Dimethylbenzoic acid.[28]
e) 3,5-Dimethylbenzoic acid.[29]
f) 2,3,4-Trimethylbenzoic acid.[26]
g) 2,4,6-Trimethylbenzoic acid.[30]
h) 3,4,5-Trimethylbenzoic acid.[31]

The unit cell parameters of these compounds were previously obtained by different authors.[25-31] The purity of these compounds was tested by measuring their melting points. Purification by vacuum distillation and/or recrystallization from suitable solvents were carried out when the melting point of the compound is slightly different from those given in the literatures.

The Gouy method was employed for the measurements of the mean magnetic susceptibility of each compound. The apparatus consists essentially of an electromagnet and a sensitive Mettler balance. The magnetizing current is taken from a stabilized unit supplied with the electromagnet. The degree of stability of current amounts to 10^{-4}. The electromagnet is kept in a glass cabinet on top of which a sensitive Mettler balance is placed.

The purified material was finely powdered and was uniformally packed in the specimen tube. The later was made of Monax glass fitted with a glass stopper. The specimen in its container was suspended from one arm of the Mettler balance whose accuracy is 10^{-5} g. Suspension was done such that the tube is symmetrical with the pole pieces; its bottom being in the strong part of the field and the top well outside the field gap. The effect of the container and the correction of porosity of the packed powder were taken into account. Among a series of measurements, the calibration was checked with naphthalene and with benzoic acid.

In the Gouy method random orientation might be assumed since good powdering and packing were followed. The results obtained from adopting such a procedure gave consistent diamagnetic susceptibilities values with accuracy better than 1%.

Results and Discussion

The specific susceptibility χ_s, the observed molar susceptibility χ_M^{obsd} and the calculated molar susceptibility χ_M^{calcd} according to Pascal-Pacult method are given in Table 1. The atomic susceptibilities and the constitutive corrections (in 10^{-6} emu mol^{-1}) used in these calculations are:

$$\chi_C = -7.4,\ \chi_H = -2.0,\ \chi_{C\begin{smallmatrix}/O\\ \backslash O\end{smallmatrix}} = -15.15,$$

$$\chi_O = -5.30,\ \lambda_{benzene} = -1.40,\ \lambda_{CH_3} = -0.85$$

These values were given by Hoarau. For the CH_3 group, its magnetic susceptibility is taken as -13.24×10^{-6} emu mol^{-1}.[32]

It can be seen from Table 1 that the observed values of the molar susceptibilities of the *o*-, *m*-, and *p*-methylbenzoic acid are not equal. The slight difference (about one unit) in the χ_M^{obsd} of the *o*- and *m*-compound can be explained in terms of positional isomerism. According to Sriraman,[33] the CH_3 group is *o-p* directing and when substituted in the benzene ring gives higher value for ortho than for meta or isomers. The order of susceptibility should therefore be *o*->*p*->*m*-. French[34] pointed out that such an order should normally be expected. Since the CH_3 group is not strong *o-p* directing and no evidence exists for resonance in these compounds,[24,27] therefore the difference in χ_M^{obsd} is expected to be small. The results shown in Table 1 support these rules.

In Table 2, the values of $(1/2)(K_1+K_2)$, the out-of-plane susceptibility (K_3) and the semiexperimental magnetic anisotropy (ΔK_{semi}) of each compound are listed. For the benzoic acid, $\chi_M^{obsd} = -71.00\times 10^{-6}$ emu mol^{-1}, $(1/2)(K_1+K_2)_{calcd} = -47.80\times 10^{-6}$ emu mol^{-1}

Table 1. Observed and calculated magnetic susceptibilities[a]

Compound	Mol wt	χ_s	χ_M^{obsd}	χ_M^{calcd}	$\Delta\chi_M$
o-Methylbenzoic acid	136	−0.6117±0.001	−83.20	−85.04	−1.84
m-Methylbenzoic acid	136	−0.6036±0.001	−82.10	−85.04	−2.94
p-Methylbenzoic acid	136	−0.6073±0.002	−82.60	−85.04	−2.44
2,6-Dimethylbenzoic acid	150	−0.6300±0.002	−94.50	−97.13	−2.63
3,5-Dimethylbenzoic acid	150	−0.6240±0.001	−93.60	−97.13	−3.53
2,3,4-Trimethylbenzoic acid	164	−0.6420±0.001	−105.30	−109.22	−3.90
2,4,6-Trimethylbenzoic acid	164	−0.6451±0.002	−105.80	−109.22	−3.42
3,4,5-Trimethylbenzoic acid	164	−0.6402±0.001	−105.00	109.22	−4.22

a) Throughout this paper all values of χ's, K's, $\Delta\chi$'s and ΔK's are to be multiplied by 10^{-6} emu mol^{-1}.

Table 2. Semiexperimental magnetic anisotropies

Compound	$\Sigma\chi_{atomic}$	$(1/2)(K_1+K_2)_{calcd}$	K_3	ΔK_{semi}
o-Methylbenzoic acid	−85.8	−59.20	−131.20	−72.00
m-Methylbenzoic acid	−85.8	−59.20	−127.90	−68.70
p-Methylbenzoic acid	−85.8	−59.20	−129.40	−70.20
2,6-Dimethylbenzoic acid	−97.20	−70.60	−142.30	−71.70
3,5-Dimethylbenzoic acid	−97.20	−70.60	−139.60	−69.00
2,3,4-Trimethylbenzoic acid	−108.60	−82.00	−151.90	−69.90
2,4,6-Trimethylbenzoic acid	−108.60	−82.00	−153.40	−71.40
3,4,5-Trimethylbenzoic acid	−108.60	−82.00	−151.00	−69.00

TABLE 3. CONTRIBUTION OF THE HYDROGEN BONDING

Compound	ΔK_{mol}	$\Delta K_{benzene}$	Δ	ΔK_{semi}	ΔK_{calcd}	Δ
o-Methylbenzoic acid	−45.40	−38.20	−7.20	−72.00	−65.00	−7.00
m-Methylbenzoic acid	−42.10	−38.20	−3.90	−68.70	−65.00	−3.70
p-Methylbenzoic acid	−43.60	−38.20	−5.40	−70.20	−65.00	−5.20
2,6-Dimethylbenzoic acid	−45.10	−38.20	−6.90	−71.70	−65.00	−6.70
3,5-Dimethylbenzoic acid	−42.40	−38.20	−4.20	−69.00	−65.00	−4.00
2,3,4-Trimethylbenzoic acid	−43.30	−38.20	−5.10	−69.90	−65.00	−4.90
2,4,6-Trimethylbenzoic acid	−44.80	−38.20	−6.6	−71.40	−65.00	−6.40
3,4,5-Trimethylbenzoic acid	−42.60	−38.20	−4.4	−69.00	−65.00	−4.00

$\Delta = \Delta K'_{mol} - \Delta K'_{benzene}$ and $\Delta = \Delta K_{semi} - \Delta K_{calcd}$.

and $\Delta K_{semi} = -69.60 \times 10^{-6}$ emu mol^{-1}. The observed magnetic data of this compound (in 10^{-6} emu mol^{-1}) as previously obtained by the author[16-18] are:

$K_1 = -48.09$, $K_2 = -46.09$, $K_3 = -117.32$,

$(1/2)(K_1+K_2)_{obsd} = -47.53$ and $\Delta K = -69.79$

It is clear that the values of $(1/2)(K_1+K_2)_{obsd}$ and that calculated according to Eq. 2 are identical. This can be regarded as a check on the accuracy of this method. It is of interest to correlate the magnetic data of these molecules with their hydrogen-bonding systems.

In the crystalline state, these compounds are strongly hydrogen-bonded. The main feature of the crystal structure of the acid molecules is that, each two molecules are associated by intermolecular hydrogen bonding to form dimer. The carboxyl groups of the two molecules and the hydrogen bonds form an 8-membered ring. In recent years much attention has been paid to study the effect of hydrogen bonding on the magnetic properties of aromatic compounds.

Preliminary results on a general investigation of diamagnetism and hydrogen bonding were discussed by Rumpf and Seguin.[35] They used Pascal-Pacault method for the calculation of the mean susceptibility χ_M^{calcd} of some aromatic molecules associated with hydrogen bonds. Upon comparing the calculated value of χ_M^{calcd} of a given molecule with its observed one, a lowering was observed. They attributed this small difference between the calculated and the observed values of χ_M to the effect of the hydrogen bonding. The application of this method on the compounds under investigation is shown in Table 1. The small difference $\Delta\chi_M$ between χ_M^{calcd} and χ_M^{obsd} may be due to the contribution of the intermolecular hydrogen bonding of these molecules. This conclusion was confirmed recently by Haberditzl[36] on a similar work, who observed that a change in diamagnetism of 1—5% is obtained on the formation of the hydrogen bonds.

According to Lonsdale,[37] any satisfactory study of the effect of the hydrogen bonds on diamagnetism must take into account the three principal susceptibilities (K_1, K_2, and K_3) of the molecule. Furthermore, Mason[38] showed that the hydrogen bond can give rise to electron delocalization resulting in magnetic anisotropy. The effective delocalization term $\Delta K'$ as given by Mason, Davies,[12] and by Craig[39] is

$$\Delta K' = K_3 - \Sigma\chi_{atomic}.$$

Constitutive corrections are not used.[10] For benzene ring, $K_3 = -94.60 \times 10^{-6}$ emu mol^{-1} [40] and $\Sigma\chi_{atomic} = -56.40 \times 10^{-6}$ emu mol^{-1}, thus the value of $\Delta K'$ is -38.20×10^{-6} emu mol^{-1}. This value of $\Delta K'$ for benzene ring is in agreement with a value of -37.80×10^{-6} emu mol^{-1} as calculated recently by Edwards and McWeeny.[9] The values of the effective delocalization term of each compound are shown in Table 3. As can be seen from Table 3, the value of $\Delta K'$ of each molecule of the eight compounds is numerically higher than that of the benzene ring. This may be due to the additional delocalization resulting from the intermolecular hydrogen bonding of these molecules as suggested by Mason.

The contribution of the hydrogen bonding on the magnetic anisotropy of the molecule may also be investigated by comparing the semiexperimental magnetic anisotropy with the calculated one. The most recent calculated values of the magnetic anisotropy (in 10^{-6} emu mol^{-1}) of the benzene ring are: −60.90,[6] −58.61,[8] −60.24,[22] and 60.00.[23] Its observed that magnetic anisotropy is −59.70.[40] The magnetic anisotropy of the benzene ring is taken as −60.00 through this paper. The magnetic anisotropy of the COOH group is -5×10^{-6} emu mol^{-1}.[20] The CH_3 group or (groups) is or (are) assumed to be magnetically isotropic. Thus the magnetic anisotropy of any acid molecule is -65×10^{-6} emu mol^{-1}. The difference between the semiexperimental anisotropy and the calculated one is taken as the effect of the hydrogen bonding.

From Table 3, it is clear that the numerical increase in the semiexperimental magnetic anisotropy over the calculated one for one molecule is about -5×10^{-6} emu mol^{-1}. Thus for one dimer (two molecules), this contribution is about -10×10^{-6} emu mol^{-1}. Referring to the crystal structures, this value is ascribed to the magnetic anisotropy of an 8-membered ring formed by the two hydrogen bonds linking the two molecules of the dimer.

References

1) L. Pauling, *J. Chem. Phys.*, **4**, 673 (1936).
2) F. London, *J. Phys. Rad.*, **8**, 397 (1937).
3) H. Akamatu and Y. Matsunaga, *Bull. Chem. Soc. Jpn.*, **26**, 364 (1953).
4) R. McWeeny, *Mol. Phys.*, **1**, 311 (1958).
5) H. Haberditzl, *Angew. Chem., Int. Ed. Engl.*, **5**, 288

(1966).
6) A. T. Amos and Ff. Roberts, *J. Chem. Phys.*, **50**, 2375 (1969).
7) E. R. Long and J. D. Memory, *J. Chem. Phys.*, **65**, 2918 (1976).
8) P. Lazzeretti and F. Taddei, *J. Chem. Soc., Faraday Trans.* 2, **68**, 1825 (1972).
9) T. G. Edwards and R. McWeeny, *Chem. Phys. Lett.*, **10**, 283 (1971).
10) J. A. Pople, *J. Chem. Phys.*, **41**, 2559 (1964).
11) J. Hoarau, *Ann. Chim.*, **13**, 544 (1956).
12) D. W. Davies, *Nature*, **190**, 1102 (1961).
13) J. A. N. Gomes, *Mol. Phys.*, **40**, 765 (1980).
14) K. Lonsdale and K. S. Krishnan, *Proc. R. Soc. London, Ser. A*, **156**, 597 (1936).
15) S. Banerjee, *Z. Krist*, **100**, 316 (1938).
16) M. M. Abdel-Kader, M. Sc. Thesis, Cairo University (1974).
17) M. M. Abdel-Kader, *Acta Phys. Pol. A*, **63**, 539 (1983); *Chem. Phys. Lett.*, **93**, 297 (1982); *Mol. Phys.*, **48**, 1145 (1983).
18) S. Salem, S. A. Abdel-Hadi, and M. M. Abdel-Kader, *Z. Phys. Chem.* (Leipzig), **257**, 641 (1976) 4, S.
19) M. A. Lasheen, *Phil. Trans. R. Soc. London, Ser. A*, **256**, 357 (1964).
20) A. Mookherji, S. N. Mookherji, and D. Neogy, *Bull. Chem. Soc. Jpn.*, **34**, 233 (1961).
21) J. Japmakowicz and J. W. Rohleder, *Acta Phys. Pol.*, **35**, 897 (1969).
22) R. Benassi, P. Lazzeretti, and F. Taddei, *J. Phys. Chem.*, **79**, 848 (1975).
23) P. H. Blustin, *Mol. Phys.*, **36**, 1441 (1978).
24) J. I. Musher, *J. Chem. Phys.*, **43**, 4081 (1965).
25) C. Katayama, A. Furusaki, and I. Nitta, *Bull. Chem. Soc. Jpn.*, **40**, 1293 (1967).
26) J. L. Elias and S. Garcia-Blanco, *Acta Crystallogr.*, **16**, 434 (1963).
27) M. G. Takwale and M. Pant, *Acta Crystallogr., Sect B*, **27**, 1152 (1971).
28) R. Anca, S. Martinez-Carrera, and S. Garcia-Blanco, *Acta Crystallogr.*, **23**, 1010 (1967).
29) S. Marting-Carrera and S. Garcia-Balanco, *Ann. Real. Soc. Espan, Fis Quim. Ser. A*, **63**, 313 (1967).
30) F. Florencio and P. Smith, *Acta Crystallogr., Sect. B*, **26**, 659 (1970).
31) F. H. Cano, S. Martinez-Carrera, and S. Garcia-Blanco, *Acta Crystallogr., Sect B*, **26**, 972 (1970).
32) V. C. G. Trew, *Trans. Faraday Soc.*, **49**, 604 (1953).
33) S. Sriraman and R. Sabesan, *Trans. Faraday Soc.*, **58**, 1080 (1962).
34) C. M. French, *Trans. Faraday Soc.*, **41**, 676 (1945).
35) P. Rumpf and M. Séguin, *Bull. Soc. Chim. Fr.*, **1949**, 366.
36) W. Haberditzl, "Uber ein neues Diamagnetismus-Inkrement system," Akademic-Verlag, Berlin (1964).
37) K. Lonsdale, *Trans. Faraday Soc.*, **36**, 937 (1940).
38) R. Mason, *Mol. Phys.*, **4**, 191 (1961), *Acta Crystallogr.*, **14**, 720 (1961).
39) D. P. Craig, M. L. Heffernan, R. Mason, and N. L. Paddock, *J. Chem. Soc.*, **1961**, 1376.
40) J. Hoarau, N. Lumbroso, and A. Pacault, *C. R. Acad. Sci.*, **242**, 1702 (1956).

Polarographic Studies on Mixed Ligand Complexes of Cadmium with DL-3-(3,4-Dihydroxyphenyl)alanine and Some Dicarboxylic Acids

Nishi GUPTA, Chandra Pal Singh CHANDEL, Prakash Chandra GUPTA, and Chand Mal GUPTA*

Chemical Laboratories, Rajasthan University, Jaipur 302004, India

(Received November 18, 1982)

The reductiou of Cd(II) has been carried out polarographically in the aqueous solution of DL-3-(3,4-dihydroxyphenyl)alanine(DOPA). The stability constants were determined for the simple Cd-DOPA system first, and then mixed-ligand complexes of cadmium with DOPA and dicarboxylic acids (oxalic and malic) have been studied. The stability constants of mixed-ligand complexes have been evaluated by the method of Schaap and McMasters. With these data the statistical and electrostatic effects have also been considered.

The importance of amines and their derivatives has been widely recognised in the biochemical, analytical, and pharmaceutical fields. These compounds are therefore attracting wide attention in different areas of research. Potentiometric investigations of the complexation behaviour of some metal ions with DOPA has been carried out by Rajan and coworkers.[1-4] However, there is not a single reference about the polarographic studies of cadmium with DOPA. Hence the present work has been undertaken. This communication deals with the study of simple and mixed ligand complexes of cadmium with DOPA and some dicarboxylic acids.

Theory

Since Cd forms hexacoordinated complexes with DOPA–oxalate and malate ions, there can be, at maximum a possibility of the existence of three mixed complex species of the type Cd(XY), $Cd(XY_2)$, and $Cd(X_2Y)$, the total number of ligands being limited to three due to the bidentate nature of the ligands under investigation.

Hence for a complexation reaction,

$$M + iX + jY \rightleftharpoons MX_iY_j. \quad (1)$$

Where i, j are stoichiometry numbers, X and Y are two different ligands and charges have been ignored for simplicity.

The overall stability constant β_{ij} for the above reaction is given by

$$\beta_{ij} = \frac{MX_iY_j}{M[X]^i[Y]^j}.$$

The DeFord and Hume function $F_o(X)$ may be extended to a new function $F_{oo}(X,Y)$ given by,

$$F_{oo}(X,Y) = \sum MX_iY_j[X]^i[Y]^j = \text{antilog}\frac{0.4343\,nF}{RT}\Delta E_{1/2} + \log\frac{I_m}{I_c}. \quad (2)$$

Where activity coefficients have been ignored and n is the number of electrons involved in the reversible reduction, F the Faraday number, R the gas constant, T the absolute temperature and I_m and I_c are the diffusion current constants for the metal and mixed complex respectively.

The factorization of $F_o(X,Y)$ using Leden's approach[14] leads to,

$$F_{oo}(X,Y) = \{\beta_{oo} + \beta_{01}[Y] + \beta_{02}[Y]^2 + \beta_{03}[Y]^3\}[X]^\circ + \{\beta_{10}+\beta_{11}[Y]+\beta_{12}[Y]^2\}[X] + \{\beta_{20}+\beta_{21}[Y]\}[X]^2 + \{\beta_{30}\}[X]^3 \quad (3)$$

or

$$F_{oo}(X,Y) = A + B[X] + C[X]^2 + D[X]^3 \quad (4)$$

Where A, B, C, and D have values as defined by Eq. 3.

The graphical method may be extended to the $F_{oo}(X,Y)$ data if the activity of one of the ligands is kept constant while that of the other, (Y) is varied. The intercept on the F_{oo} axis in the plot of F_{oo} *versus* [X] gives A. Therefore,

$$F_{10}(X,Y) = \frac{F_{oo}(X,Y)-A}{[X]} = B + C[X] + D[X]^2 \quad (5)$$

By a similar plotting of $F_{10}(X,Y)$ *versus* [X] and taking the intercept on $F_{10}(X,Y)$ axis as B, we have,

$$F_{20}(X,Y) = \frac{F_{10}(X,Y)-B}{[X]} = C + D[X] \quad (6)$$

and so on.

From the knowledge of C, the mixed stability constant β_{21} may be calculated. The values of β_{11} and β_{12} may be computed by the values of B at two [Y] concentrations.

Experimental

DOPA, oxalic acid, and malic acid used were of AnalaR grade and were used as complexing agents. Potassium nitrate as supporting electrolyte was used to maintain ionic strength at 1.0 M and 0.004% gelatin in the final solution sufficed to suppress the maxima observed. The temperature was maintained constant at 303±1 K.

The experimental technique was the same as described earlier.[5]

Results

Simple Systems. Before the study of the mixed ligand complexes, the formation constants of the complexes of Cd^{2+} with DOPA, oxalic acid, and malic acid were determined by the method of DeFord and Hume.[6] The results which are in good agreement with the previous studies[7-10] are tabulated in Table 1.

The Mixed Systems. The cadmium–DOPA–oxalate and cadmium–DOPA–malate systems were studied by keeping the concentration of the weaker ligand (oxalic and malic acid) constant at two values, while varying the concentration of the second ligand.

At each fixed concentration of oxalate and malate ions with varying concentration of DOPA, the slope

of the straight line for the plot of $E_{d.e.}$ *versus* $\log \frac{i}{id-i}$ was 31±1 mV. The direct proportionality of the diffusion current to the square root of effective height of mercury column indicated that the reduction is entirely diffusion controlled.

A shift in half-wave potential to more negative side with increase in DOPA concentration was observed. This shift in half-wave potential is greater in presence of the weaker ligands (oxalic and malic acid) than in their absence. This indicates mixed ligand complex formation by the DOPA and oxalate and malate ions.

The Schaap and McMasters[11] treatment was applied for calculating the $F_{1o}(X,Y)$ functions and Leden's graphical extrapolation method to calculate *A*, *B*, *C*, and *D* at two concentrations of [Ox] and [Mal]. The details of the calculations are presented in Tables 2 and 3.

The formation constant β_{11} and β_{12} were evaluated

Table 1. Dissociation constants of DOPA, oxalate, and malate and stability constants of their simple complexes with Cd(II)
μ=1.0 M, T=30 °C.

	pK_1^H	pK_2^H	$\log \beta_1$	$\log \beta_2$	$\log \beta_3$
DOPA	9.50	—	5.39	8.30	11.79
Oxalate	1.30	4.28	2.82	4.22	5.16
Malate	3.40	5.05	1.90	2.80	3.40

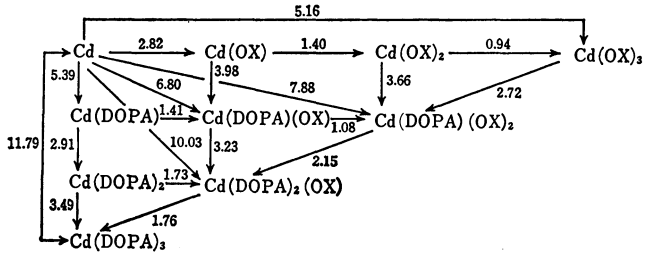

Scheme 1. Cd-DOPA-oxalate system.

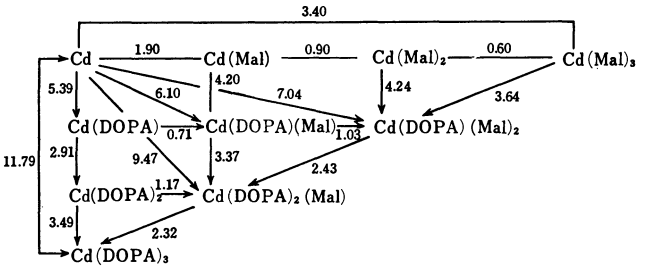

Scheme 2. Cd-DOPA-malate system.

Table 2(a). Data and results for cadmium-DOPA-oxalate system
Oxalate=0.02 M, $E_{1/2}$(M)=0.580 V *vs.* SCE.

[X] ×10³	$\Delta E_{1/2}$ V	$\log \frac{I_m}{I_c}$	F_{oo} ×10⁻³	F_{10} ×10⁻⁶	F_{20} ×10⁻⁸	F_{30} ×10⁻¹¹	F_{oo}(Cal) ×10⁻³	ΔF/%*
0.25	0.066	0.0100	0.16	0.55	6.00	8.00	0.16	±0.00
0.50	0.077	0.0250	0.39	0.74	6.80	5.60	0.40	+0.63
1.50	0.106	0.0400	3.69	2.45	13.67	6.45	3.63	−0.93
2.00	0.115	0.0500	7.52	3.75	16.75	6.38	7.43	−1.19
3.00	0.128	0.0580	20.07	6.68	20.93	5.64	20.17	+0.49
4.00	0.138	0.0690	45.74	11.43	27.58	5.90	48.15	+5.18
5.00	0.146	0.0840	87.38	17.47	34.14	6.03	90.39	+3.45
7.50	0.161	0.0970	284.10	37.80	49.97	6.13	290.03	+2.11
10.00	0.172	0.1100	679.89	67.90	67.59	6.36	671.02	−1.17
12.50	0.180	0.1200	1284.10	102.73	81.86	6.23	1239.63	−3.46

A=22.00 (Cal), B=4×10⁵, C=4×10⁸, D=(6.27±1.73)×10¹¹.

Table 2(b). Data and results for cadmium-DOPA-oxalate system
Oxalate=0.2 M, $E_{1/2}$(M)=0.580 V *vs.* SCE.

[X] ×10³	$\Delta E_{1/2}$ V	$\log \frac{I_m}{I_c}$	F_{oo} ×10⁻³	F_{10} ×10⁻⁶	F_{20} ×10⁻⁹	F_{30} ×10⁻¹¹	F_{oo}(Cal) ×10⁻³	ΔF/%*
0.25	0.106	0.0014	3.37	5.64	4.54	—	3.28	−2.67
0.50	0.111	0.0071	5.01	6.10	3.20	—	4.99	−0.39
1.50	0.126	0.0106	15.94	9.32	3.21	4.73**	16.41	+2.88
2.00	0.132	0.0186	25.72	11.88	3.69	5.95	25.88	+0.62
3.00	0.142	0.0230	55.89	17.98	4.49	6.63	54.60	−2.46
4.00	0.149	0.0275	96.55	23.65	4.79	5.93	99.32	+2.86
5.00	0.156	0.0327	167.04	33.02	5.70	6.40	163.83	−1.90
7.00	0.166	0.0365	362.51	51.51	6.72	6.03	366.90	+1.21
10.00	0.178	0.0403	916.98	91.50	8.70	6.20	911.96	−0.54
12.50	0.185	0.0600	1640.40	131.08	10.13	6.10	1650.00	+0.57

A=1.96×10³, B=4.5×10⁶, C=2.5×10⁹, D=(6.15±0.48)×10¹¹.

TABLE 3(a). DATA AND RESULTS FOR CADMIUM-DOPA-MALATE SYSTEM
Malate=0.04 M, $E_{1/2}$(M)=0.588 V *vs.* SCE.

[X] $\times 10^4$	$\Delta E_{1/2}$ V	$\log \frac{I_m}{I_c}$	F_{oo} $\times 10^{-2}$	F_{10} $\times 10^{-5}$	F_{20} $\times 10^{-8}$	F_{30} $\times 10^{-11}$	F_{oo}(Cal) $\times 10^{-2}$	ΔF/%*
0.50	0.038	0.060	0.21	3.12	0.40	—	0.22	+4.76
1.50	0.052	0.073	0.64	3.91	5.40	14.7**	0.61	−4.68
2.50	0.059	0.100	1.16	4.42	5.28	8.32**	1.13	−2.58
3.50	0.064	0.118	1.77	4.90	5.14	5.54	1.79	+1.12
4.50	0.069	0.139	2.72	5.92	6.27	6.82	2.66	−2.20
5.00	0.071	0.149	3.24	6.37	6.54	6.68	3.18	−1.85
10.00	0.088	0.156	12.13	12.08	8.98	5.78	12.50	+3.05
15.00	0.100	0.176	31.84	21.19	12.06	5.91	32.66	+2.57

A=5.4 (Cal), $B=3.10\times10^5$, $C=3.20\times10^8$, $D=(6.15\pm0.67)\times10^{11}$.

TABLE 3(b). DATA AND RESULTS FOR CADMIUM-DOPA-MALATE SYSTEM
Malate=0.2 M, $E_{1/2}$(M)=0.588 V *vs.* SCE.

[X] $\times 10^4$	$\Delta E_{1/2}$ V	$\log \frac{I_m}{I_c}$	F_{oo} $\times 10^{-2}$	F_{10} $\times 10^{-5}$	F_{20} $\times 10^{-8}$	F_{30} $\times 10^{-11}$	F_{oo}(Cal) $\times 10^{-2}$	ΔF/%*
0.50	0.059	0.032	0.99	7.36	5.20	—	1.00	+1.0
1.50	0.067	0.045	1.88	8.39	8.60	4.67**	1.89	+0.53
2.50	0.073	0.049	3.00	9.51	9.64	6.96	3.00	±0.00
3.50	0.078	0.057	4.49	11.05	11.29	9.69**	4.38	−2.44
4.50	0.082	0.063	6.18	12.35	11.67	8.38	6.06	−1.94
10.00	0.098	0.094	22.62	22.00	14.90	7.00	22.72	+0.44
15.00	0.108	0.101	49.45	32.55	16.97	6.05	53.00	+8.08

A=62.20 (Cal), $B=7.10\times10^5$, $C=7.90\times10^8$, $D=(7.10\pm1.28)\times10^{11}$.

TABLE 4. STABILITY CONSTANTS OF MIXED-LIGAND COMPLEXES OF Cd(II) WITH DOPA AND OXALATE, MALATE (μ=1.0, T=30 °C)

System	$\log \beta_{11}$	$\log \beta_{12}$	$\log \beta_{21}$
Cd-DOPA-oxalate	6.80	7.88	10.03
Cd-DOPA-malate	6.10	7.04	9.47

from the two values of B, the two values of C gave two values of β_{21} in good agreement with each other and have been presented in Table 4.

The experimental values of D should also coincide with β_{30} as at the final concentration of DOPA, all the dicarboxylate ions have been replaced and only $Cd(DOPA)_3$ complex exists in solution. This indeed is found to be so.

$$\log \beta_{30} = 11.790$$

$$\log D = \begin{cases} 11.797,\ 11.789 \text{ (for oxalate)} \\ 11.789,\ 11.851 \text{ (for malate)} \end{cases}$$

The results are summarised in the form of Schemes 1 and 2 where the numerical values indicate the logarithms of the equilibrium constant.

Discussion

The mixed ligand complex formation may also be explained by considering Schemes 1 and 2. The tendency to add X (X=DOPA) to CdX and CdY (Y= oxalate and malate) can be compared. The logarithm of stability constants of the above complexes are (2.91 and 3.98) and (2.91 and 4.20) for cadmium-DOPA-oxalate and cadmium-DOPA-malate respectively. The largest part of the difference in $\log K$ must be attributed to entropy and electrostatic effects which would favour the formation of a charged complex. The logarithm of stability constants of addition of oxalate to Cd(Ox) and Cd(DOPA) and malate to Cd(mal) and Cd(DOPA) are 1.40 and 1.41 and 0.90 and 0.71 respectively, indicating that the mixed ligand complexation is favoured.

The $\log K$ values for addition of X to $Cd(X)_2$, Cd(XY), and $Cd(Y)_2$ are (3.49, 3.23, and 3.66) and (3.49, 3.37, and 4.24) for Cd-DOPA-oxalate and Cd-DOPA-malate respectively and show that the addition of amino acids is preferred to a weaker ligand.

The $\log K$ values for the addition of Y to $Cd(Y)_2$, Cd(XY), and $Cd(X)_2$ are (0.94, 1.08, and 1.73) and (0.60, 1.03, and 1.17) for oxalate and malate systems respectively, indicating that the addition of dicarboxylate ion is preferred to [Cd(dicarboxylate)(DOPA)] as compared to Cd(dicarboxylate)$_2$ and $Cd(DOPA)_2$.

The case of mixed ligand complex formation by the addition of dicarboxylate ions to $Cd(DOPA)_2$ and [Cd(DOPA)(dicarboxylate)] may easily be confirmed on the basis of statistical considerations[12] using Eqs. 7—9 as proposed by Watter's and Dewitt.[13]

$$\beta_{11} = 2 \times 3 \times \beta_{20}^{1/3} \times \beta_{03}^{1/3} \quad (7)$$

$$\beta_{12} = 3 \times \beta_{30}^{1/3} \times \beta_{03}^{2/3} \quad (8)$$

$$\beta_{21} = 3 \times \beta_{30}^{2/3} \times \beta_{03}^{1/3} \quad (9)$$

The values of stability constants so obtained from

Table 5. Values of stability constants of mixed-ligand complexes of Cd(II) with DOPA and oxalate and malate as calculated by Watters and Dewitteqs

System	$\log \beta_{11}$	$\log \beta_{12}$	$\log \beta_{21}$
Cd-DOPA-oxalate	6.42	7.84	10.05
Cd-DOPA-malate	5.84	6.67	9.46

above equations are given in Table 5 and when compared with the observed values, it indicates that MXY, MXY_2, and MX_2Y complexes have been formed purely on the statistical factors.

The tendency of formation of simple and mixed complexes can be easily expressed by calculating the disproportionation constant K^D for the equilibria

$$2Cd(XY) \rightleftharpoons Cd(X)_2 + Cd(Y)_2$$

The value of $\log K^D$ is -0.6 statistically but the observed values are found to be -1.08 and -1.10 for the Cd(DOPA)(Ox) and Cd(DOPA)(Mal) systems respectively. More negative values of $\log K^D$ for each equilibria account for the stability of the mixed ligand complexes.

One of the authors (Nishi Gupta) is thankful to U.G.C. for providing junior research fellowship and C.P.S. Chandel is thankful to C.S.I.R., New Delhi for financial support. They are also thankful to the Head, Chemistry Department for providing the laboratory facilities.

References

1) K. S. Rajan, S. Mainer, and J. M. Danis, *Bio. Inorg. Chem.*, **9**, 187 (1978).
2) Gergely. Arthur Kiss, *Tamas. Magy. Kem. Foly.*, **81**, 264 (1975).
3) J. E. Gorton and R. F. Jameson, *J. Chem. Soc., Dalton. Trans*, **1972**, 310.
4) K. S. Rajan, S. Mainer, and J. M. Danis, *J. Inorg. Nucl. Chem.*, **40**, 2089 (1978).
5) S. C. Khurana and C. M. Gupta, *Aust. J. Chem.*, **26**, 971 (1973).
6) D. D. DeFord and D. N. Hume, *J. Am. Chem. Soc.*, **73**, 5321 (1951).
7) D. J. Perkins, *Biochem. J.*, **53**, 649 (1953).
8) S. K. Shah Ph. D. Thesis, University of Rajasthan, Jaipur (India) (1980).
9) N. P. Sachan, C. P. S. Chandel, and C. M. Gupta, *Chemica Scripta*, **20**, 111 (1982).
10) S. C. Khurana, J. K. Gupta, and C. M. Gupta, *Electrochim. Acta*, **18**, 59 (1973).
11) W. B. Schaap and D. L. McMasters, *J. Am. Chem. Soc.*, **83**, 4699 (1961).
12) D. D. Perrin and V. S. Sharma, *J. Chem. Soc.*, **17**, 2060 (1969).
13) J. I. Watters and R. Dewitt, *J. Am. Chem. Soc.*, **82**, 1333 (1960).
14) I. Leden, *Z. Phys. Chem.*, **188**, 160 (1941).

Capillary Ripple Response of Cholesterol and Lecithin Monolayers

Jamil Ahmad
Chemistry Department, University College, Bahrain
(Received November 27, 1982)

Capillary ripple characteristics of monolayers of cholesterol and dipalmitoyllecithin and a 1:1 mixture of the two over air-water interface were studied. The ripple damping coefficient and the wavelength were determined as a function of the surface concentration. A stronger chain-chain interaction exists between the molcules in the pure cholesterol monolayer compared to pure lecithin as indicated by the sharp maximum in the damping coefficient curve for the former case. In the monolayer of the mixture, there is evidence of an interaction between the chains of the two substances.

The focus of this paper is the exploration of the capillary ripple response of the monolayers from lecithin, cholesterol and a 1:1 cholesterol–lecithin mixture on air-water interface. In particular, the dependence of the ripple damping coefficient and the wavelength on the surface concentration was studied. It is expected that this work would generalize into a new technique for the study of biomembrane surface properties.

The capillary ripple method allows study of the dynamic response of monolayers over the frequency range of 10 Hz to 2 kHz. In this method, ripples are generated on the air-water interface on which the appropriate monolayer is spread and the damping coefficient and the wave number are measured. The value of these parameters reflect the elastic and viscous response of the monolayer. The review article by Hansen and Ahmad[1] summarizes several studies using the method.[2–5] The dependence of the values of the ripple parameters on the surface tension and the surface tension gradient was shown by van den Tempel and coworkers.[6] Hansen and Mann[7] included additional elastic and viscosity terms in their treatment.

Experimental

The experimental set up was similar to the one used by other workers.[1] It involved generation of ripples at the air/water interface on which a monomolecular film of interest was spread. The ripples were generated by a probe made from a stainless steel razor blade. A steel wire was soldered to the end of the blade and connected to the coil of an electromechanical transducer, essentially a modified speaker. The speaker was excited by the output from the reference channel of a precision lock-in amplifier. The frequency and the level of the input signal were monitored. For the results reported here, the input signal of 200 Hz was used. The ripple sensing probe was similar in design to the generating probe. The waves generated are reflected by the sensing probe and a stationary wave pattern is set up with the probes acting as boundaries. The sensing probe is fitted to a phonographic cartridge in the place of the usual needle. The motion of the receiving probe was converted into an electrical signal which was fed into the lock-in amplifier, where only that part of the signal was amplified which had the same frequency as the reference signal used to drive the generating probe.

The precise determination of the ripple parameters by the method described by Mann and Ahmad[8] is a tedius procedure and is impractical when several measurements have to be made. Instead, a variation of the method was followed in the present set of experiments. The probe output voltage, a quantity assumed proportional to the wave amplitude, is given by Eq. 2 of Mann and Ahmad.[8] This quantity is an oscillatory function of the distance between the probes. The maxima in the voltage-distance curve $\overline{V}(L)$, are given by

$$\overline{V}(L) = \frac{V_o\{1-\exp(\beta)\}}{1-\exp\{-(2\alpha L+\beta)\}}\exp(-\alpha L), \quad (1)$$

where V_0 is the output voltage, when the probe separation, L, is zero. α is the ripple damping coefficient and β is the reflection coefficient at the boundaries. If α is of the order of 0.4 cm^{-1}, L is kept around 4 cm or more and the reflection coefficient, β, is of the order of 1, then

$$1 - \exp\{-(2\alpha L+\beta)\} \approx 1.$$

The upper limit to the error introduced by this approximation is 2%. Thus Eq. 1 can be rewritten as

$$\overline{V}(L) = C\exp(-\alpha L). \quad (2)$$

If for pure water, the distance between the probes is fixed such that they are perfectly in phase at a desired frequency, the output voltage is given by Eq. 2. If the monolayer is now spread on the surface, the wave number will be different from the case of the pure water and the two probes may not be in phase. If the probe separation is adjusted slightly to bring back the probes in phase, Eq. 2 can be applied. The maximum adjustment needed will not be more than one half of a wavelength. The maximum error introduced by this change of the probe separation is about 2%. If for the monolayer covered surface, output voltage is $\overline{V}'(L)$, then

$$\overline{V}'(L) = C\exp(-\alpha' L). \quad (3)$$

From Eq. 2 and 3 $\ln\frac{V'(L)}{\overline{V}(L)} = L(\alpha - \alpha')$.

Thus knowing L and the damping coefficient for pure water, α', the damping coefficient for the monolayer can be calculated. The procedure is repeated at various film pressures. The other important parameter of the capillary ripple experiment, the wavelength, can be measured in a separate experiment by observing the voltage change as the probe separation is increased in small steps, and measuring the distance between the probe positions corresponding to successive maxima and minima. The wave number, k, can then be calculated by the relation

$$k = \frac{2\pi}{\lambda};\ \lambda \text{ being the wavelength.}$$

Along with the ripple measurements, simultaneous measurements of the film pressure were made with a balance similar to the one described by Mann and Hansen.[9] The film balance system involved a Teflon trough milled out of a single Teflon slab, and a movable surface piston or "barrier". Near one and of the trough was a torsion balance.

A Teflon float was coupled to the torsion wire by the help of a vertical bar. A horizontal bar was fixed to the torsion wire, and was coupled to the core of a 0.084 cm travel linear variable differential transformer (LVDT). The LVDT output as monitored on a strip chart recorder was calibrated in terms of the force acting on one cm of the float.

The reproducibility of the values of the damping coefficient and the wave number is 4% or better. The film balance could detect a change in surface pressure of 5×10^{-5} N m^{-1}.

Solutions of known concentration of synthetic β,γ-dipalmitoyl-DL-α-lecithin, cholesterol and an equimolar mixture of the two were made in chloroform. The lecithin used was supplied by Nutritional Biochemical Corporation, Cleveland, Ohio, U.S.A. and cholesterol by General Biochem. Lab., Chagrin Falls, Ohio, U.S.A. The concentration of the solute was such that approximately 200 microliters of the solution spread on the trough gave a sub-monomolecular layer suitable for compression to full coverage. Line distilled water distilled from the alkaline $KMnO_4$ solution and redistilled from a quartz still was used as the substrate. The monolayer was spread from a microsyringe drop by drop. The surface piston was then moved in steps to decrease the area available to the monolayer. After each change of the barrier position, the surface was allowed to come to equilibrium, indicated by a constant film pressure. The ripple measurements were then made. A series of measurements was made until the monolayer collapsed as indicated by leveling off of the surface pressure.

From the measured values of α and k, dimensionless parameters $Y_1\left(=\frac{\rho\omega^2}{\gamma k^3}\right)$ and $Y_2\left(=\frac{\alpha}{k}\right)$ were obtained. Here ρ is the density of water, γ the surface tension calculated from the film pressure, and ω is the angular frequency given by $\omega=2\pi\nu$; ν being the frequency of the probe vibration.

Results and Discussion

Figure 1 shows the damping coefficient curves. The curve for the mixture is intermediate in character between the curves for the pure compounds. All the damping coefficient curves show a maximum which is sharp in the case of cholesterol and a plateau rather than a distinct maximum for lecithin.

The mixed film also shows a relatively sharp maximum.

The damping coefficient and the sharpness of its maximum can be related to the chain-chain interaction in the molecules forming the monolayer. The effect of the surface diffusion on the wave damping has been calculated from the hydrodynamic theory.[1] This theory predicts a maximum in the damping coefficient as the surface elastic modulus increases. This has been verified experimentally for various soluble and insoluble film-forming substances.

Physically we can interpret the results as follows. As the wave passes, the surface is alternately compressed and expanded. Because of the surface elasticity in the presence of the surfactant molecules, the waves are damped. The damping is caused by the surface tension gradients set up by the stretching and contraction of the surface as the wave passes. If there is appreciable surface to bulk or surface to surface diffusion of the surfactant molecules in one wave period, these surface tension gradients are reduced and the damping is reduced. For insoluble monolayer like cholesterol and lecithin, the bulk to surface diffusion is irrelevant, only the surface to surface diffusion is important. If the chain-chain interaction in the monolayer is strong, this diffusion is low, resulting in a high damping coefficient.

From the results it is obvious that the chain-chain interaction in cholesterol monolayer is stronger than in the lecithin film. The relatively sharp maximum in the curve for the mixture indicates that there is appreciable interaction between the molecules of the mixture. This evidence favors the suggestion by Demel and Joos[10] that at low surface pressures, there is an interaction between the chains of the two substances in a monolayer.

The capillary ripple theory[1] makes it obvious that the ripple damping coefficient is sensitive to the elastic modulus only at intermediate values of the elastic modulus *i.e.* near the damping coefficient maximum. At low or high surface elasticity values the damping coefficient is virtually independent of the surface elastic modulus. This method is therefore sensitive to the value of the surface elastic modulus and hence to any property affecting this modulus only at such intermediate values. Thus, though this study suggests that there is an appreciable molecular interaction at intermediate surface elasticity which corresponds to quite dense films for these systems, it does not rule out such interaction at lower surface pressures.

A consideration of the dimensionless group Y_1 and

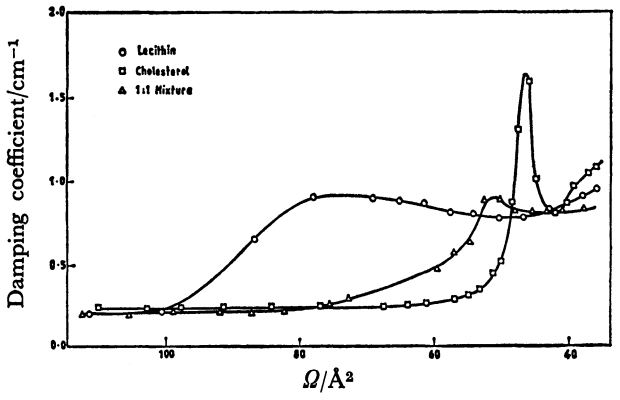

Fig. 1. Capillary ripple damping coefficient for the monolayers at various surface concentrations, frequency=200 Hz, temperature=25 °C.

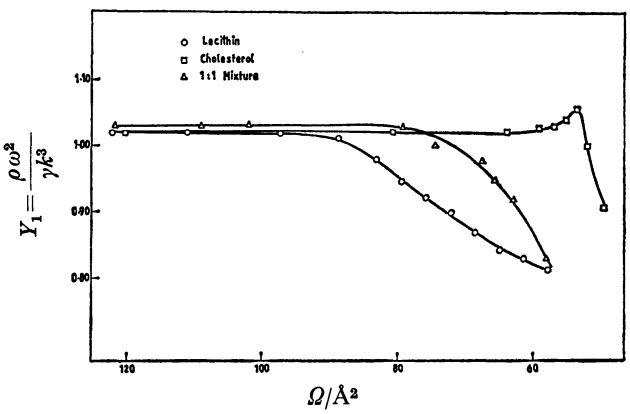

Fig. 2. Dimensionless parameter Y_1 for the monolayers.

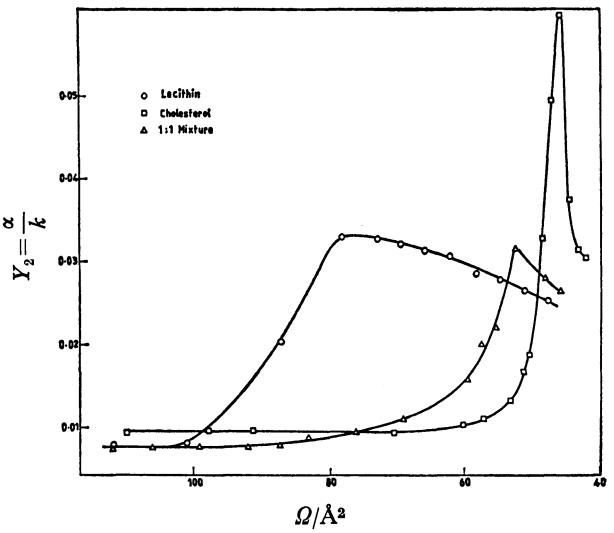

Fig. 3. Parameter Y_2 as a function of area per molecule, Ω, for the various monolayers.

Y_2 is useful when comparing monolayers formed by different substances. $Y_1=1$ is the Kelvin equation and is followed by pure water and by the monolayers in the limits of zero surface elasticity and surface viscosity. The curves in Fig. 2 follow this pattern. At high film densities the deviation from ideality sets in, this being due to compressional elastic modulus as well as surface viscosity. The different surface elastic moduli in the pure and the mixed film cause the curves to separate out at higher densities.

The amplitude of the waves in this study was small enough that the monolayer did not collapse by the passage of the waves, even for the near rigid films. This was confirmed by the stability of the values of the film pressures during the course of the ripple experiment.

References

1) R. S. Hansen and J. Ahmad, "Progress in Surface and Membrane Science," ed by Danielli *et al.*, Academic Press (1971).

2) J. A. Mann. Jr., and R. S. Hansen, *J. Colloid Sci.*, **18**, 757, 805 (1963).

3) J. Lucassen and R. S. Hansen, *J. Colloid Interface Sci.*, **23**, 319 (1967).

4) R. S. Hansen and J. Lucassen, *J. Colloid Interface Sci.*, **22**, 32 (1966).

5) R. S. Hansen, J. Lucassen, R. L. Bendure, and G. P. Bierwagen, *J. Colloid Interface Sci.*, **26**, 198 (1968).

6) M. van den Tempel and R. P. van de Riet, *J. Chem. Phys.*, **42**, 2769 (1965).

7) R. S. Hansen and J. A. Mann., Jr., *J. Appl. Phys.*, **32**, 158 (1964).

8) J. A. Mann, Jr., and J. Ahmad, *J. Colloid Interface Sci.*, **29**, 158 (1969).

9) J. A. Mann Jr., and R. S. Hansen, *Rev. Sci. Instr.*, **34**, 702 (1963).

10) R. A. Demel and P. Joos, *Chem. Phys. Lipids*, **2**, 35 (1968).

 © 1983 The Chemical Society of Japan Bull. Chem. Soc. Jpn., 56, 3145—3151 (1983)

Thermal Investigation of Nickel(II) Diamine Complexes in Solid State

Goutam De, Prasanta Kumar Biswas, and Nirmalendu Ray Chaudhuri*

Department of Inorganic Chemistry, Indian Association for the Cultivation of Science, Calcutta 700032, India

(Received August 24, 1982)

Three tris(ethylenediamine)nickel(II) chloride dihydrate having identical composition, apparently similar in color, magnetic moment and spectral properties showed differences in thermal profile. Thermal investigations of $[Ni(en)_3]Br_2\cdot 2H_2O$, $[Ni(tn)_3]Cl_2\cdot 2H_2O$, and $[Ni(tn)_3]Br_2\cdot H_2O$ where en=ethylenediamine and tn=1,3-propanediamine were carried out. Several bis and mono(diamine) complexes were synthesized in solid state from the corresponding tris complexes. All the bis and mono(diamine) complexes were found to be O_h and T_d symmetry respectively. All tris(diamine) complexes generate *cis* bis(diamine) species upon heating. But only one tris(ethylenediamine)nickel(II) chloride dihydrate generates *cis* bis species by the isomerization from the *trans* species temporarily formed. Monodiamine complexes decomposed through $[Ni_2(diamine)Cl_4]$ species which showed unusually high magnetic moment. The probable mechanistic path for each step of decomposition was also reported.

Thermal investigations of transition metal diamine complexes have been carried out by several workers.[1-4] Solid state kinetics of Cr^{III} complexes of ethylenediamine are well known in literature.[5] Thermal investigations of metal complexes of 1,2-propanediamine are known.[1] But the studies on the complexes of 1,3-propanediamine (tn) are scanty.[4] It is reasonable to expect that the thermal decomposition of $[Ni^{II}(tn)_3]X_2$ (X=Cl or Br) would be a matter of great interest as the complexes may lead to the formation of some new stoichiometric 1,3-propanediamine complexes of nickel(II) in solid state which could not be synthesized even in solution. Previously some work[2] on the thermal decomposition of $[Ni^{II}(en)_3]X_2$ (X=Cl or Br) has been done. Since thermal decomposition pattern is sometimes governed by the instrumental techniques used as also on the experimental conditions, studies on $[Ni^{II}(en)_3]X_2$ are also relevant. The present paper reports the thermal studies of $[Ni^{II}L_3]X_2$, where L=en or tn and X=Cl or Br. It deals with the synthesis and characterization of some new compounds derived in solid state. It also reports the probable mechanistic path for each step of decomposition.

Experimental

Preparation. *$[Ni(en)_3]Cl_2\cdot 2H_2O$ (**1**), $[NiCl_2(en)_2]$ (**4**)*: These were prepared following the method described in literature.[6]

*$[Ni(en)_3]Cl_2\cdot 2H_2O$ (**2**)*: Methylhydrazine or *N,N*-dimethylhydrazine or *N,N*-diethylethylenediamine (3 mmol) was added slowly to $[NiCl_2(en)_2]$ (**4**) (1 mmol) dissolved in water–ethanol (1:9) mixture. Shining pinkish crystals separated out. These crystals were collected and purified by washing with ethanol.

*$[Ni(en)_3]Cl_2\cdot 2H_2O$ (**3**)*: Addition of pyridine (3 mmol) to $[NiCl_2(en)_2]$ (**4**) (1 mmol) dissolved in water–ethanol (1:9) mixture, yielded shining pinkish crystals. These crystals were collected and purified by washing with ethanol.

*$[NiCl_2en]$ (**5**)*: This was synthesized by pyrolysis of the complexes **2** or **3** or **4** at 325 °C for 5 min in nitrogen atmosphere.

*$[Ni(en)_3]Br_2\cdot 2H_2O$ (**6**), $[Ni(tn)_3]Cl_2\cdot 2H_2O$ (**3**), and $[Ni(tn)_3]Br_2\cdot H_2O$ (**12**)*: These were prepared by mixing ethanolic solution of diamine (3 mmol) drop by drop to the ethanolic solution of nickel salt (1 mmol). While stirring the mixture, shining crystals separated out slowly. These crystals were collected and purified by washing with ethanol.

*$[NiBr_2(en)_2]$ (**7**)*: This was synthesized by pyrolysis of $[Ni(en)_3]Br_2\cdot 2H_2O$ (**6**) at 275 °C in nitrogen atmosphere.

*$[NiCl_2(tn)_2]$ (**9**)*: This was prepared by pyrolysis of $[Ni(tn)_3]Cl_2\cdot 2H_2O$ at 180 °C for 5 min in nitrogen atmosphere.

*$[NiCl_2tn]$ (**10**)*: This was prepared by pyrolysis of $[Ni(tn)_3]Cl_2\cdot 2H_2O$ (**8**) or $[NiCl_2(tn)_2]\cdot 1.5H_2O$ (**11**) at ≈278 °C in nitrogen atmosphere.

*$[NiCl_2(tn)_2]\cdot 1.5H_2O$ (**11**)*: This was synthesized by the same method adopted for the preparation of $[NiCl_2(en)_2]$ (**4**). This was also synthesized by keeping $[NiCl_2(tn)_2]$ (**9**) in an open air.

*$[NiBr_2(tn)_2]$ (**13**)*: This was synthesized by pyrolysis of $[Ni(tn)_3]Br_2\cdot H_2O$ (**12**) at 230 °C in nitrogen atmosphere.

Thermal Measurements. The thermal analysis was carried out using a Shimadzu DT-30 thermal analyzer. A constant flow of nitrogen (30 $cm^3\ min^{-1}$) was maintained. Platinum crucibles were used. Heating rate (10 °C min^{-1}) was maintained. The particle size of the samples was within 150—200 mesh. Aluminum oxide was used as reference. Zinc metal was used as calibrant for evaluation of enthalpy change.

Other Measurements. Infrared spectra in KBr (4000—250 cm^{-1}) and electronic spectra in mull (28570—11111 cm^{-1}) were recorded using a Beckman IR-20A and Pye Unicam SP8-150 spectrophotometers respectively. Cary 17D was also used for mull spectra in some cases. Magnetic moments of the compounds were evaluated at room temperature from the magnetic susceptibilities of the samples, corrected by applying Pascal's constants of the elements involved, using the Gouy technique where $Hg[Co(SCN)_4]$ was taken as standard. EG and G PAR 155 vibrating sample magnetometer was also used for measuring magnetic moment in some cases.

Results

$[Ni(en)_3]Cl_2\cdot 2H_2O$ (**1**) becomes anhydrous at 140 °C (Fig. 1, Table 1). The anhydrous species is thermally stable upto 190 °C. On further heating, it starts to lose en and transforms to metal chloride through bis, mono and hemi(diamine) species. None of the intermediate species and even the metal chloride are isolable. TG curve (Fig. 1) hints the elimination of water taking place in two steps. But the corresponding DTA curve predicts the water elimination occurring

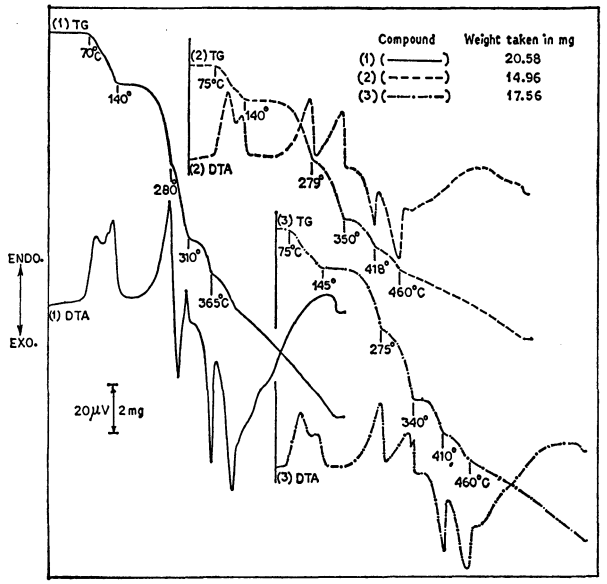

Fig. 1. Thermal curves of $[Ni(en)_3]Cl_2 \cdot 2H_2O$ (**1**) (——), $[Ni(en)_3]Cl_2 \cdot 2H_2O$ (**2**) (— — — —), and $[Ni(en)_3]Cl_2 \cdot 2H_2O$ (**3**) (—·—·—·—).

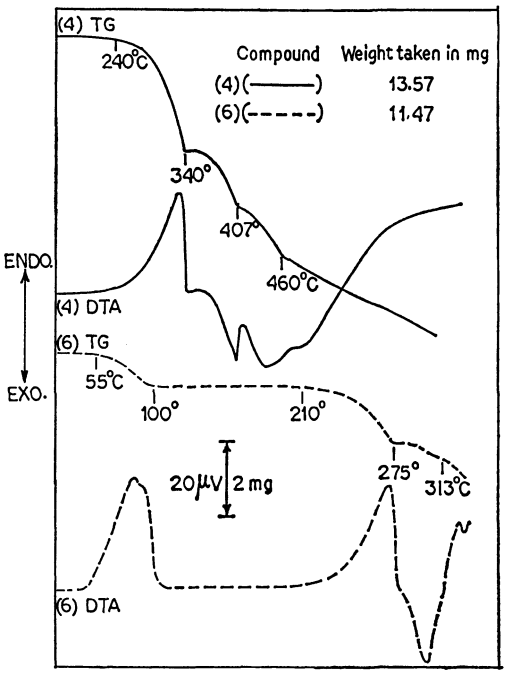

Fig. 2. Thermal curves of $[NiCl_2(en)_2]$ (**4**) (——) and $(Ni(en)_3]Br_2 \cdot 2H_2O$ (**6**) (— — — —).

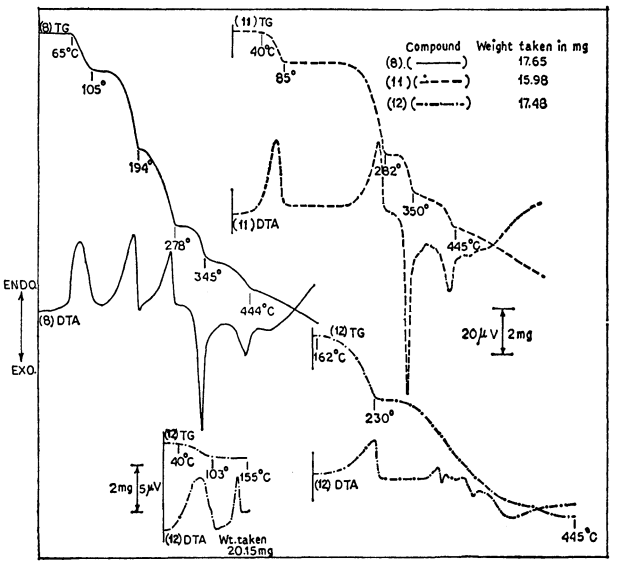

Fig. 3. Thermal curves of $[Ni(tn)_3]Cl_2 \cdot 2H_2O$ (**8**) (——), $[NiCl_2(tn)_2] \cdot 1.5H_2O$ (**11**) (— — — —), and $[Ni(tn)_3]Br_2 \cdot H_2O$ (**12**) (—·—·—·—).

actually in three steps. DTA profile for the elimination of two molecules of en shows first an endotherm followed by an exotherm followed by an another endotherm. It shows two prominent exotherms for the elimination of last molecule of en. On the other hand, $[Ni(en)_3]Cl_2 \cdot 2H_2O$ (**2**) loses two molecules of water in two steps as evident from its TG as well as DTA curves (Fig. 1). TG curve of the anhydrous species is almost similar to that of the complex **1**. But the DTA curve shows two prominent endotherms for the elimination of first two molecules of en and two exotherms for the elimination of last molecule of en. Thermal profile (Fig. 1) of complex **3** is almost similar to that of complex **2**. The only difference observed in the DTA curve is that endotherm responsible for the elimination of second molecule of en splits here. Thermal behavior of $[NiCl_2(en)_2]$ (**4**) is practically similar to that of the complex **2** in the decomposition from the stage of $[NiCl_2(en)_2]$. The isolation of mono(diamine) species is feasible by temperature arrest technique in nitrogen atmosphere from the complexes **2**, **3**, and **4**.

$[Ni(en)_3]Br_2 \cdot 2H_2O$ (**6**) becomes anhydrous at 100 °C in single step as observed from TG curve (Fig. 2, Table 1). But DTA curve shows elimination of water taking place in two steps. The anhydrous species starts to decompose at 210 °C and generates $[NiBr_2(en)_2]$ (**7**) at 275 °C showing a prominent endotherm in the DTA curve. An exotherm is displayed at the quite early stage of decomposition of the bis species which melts on further heating.

$[Ni(tn)_3]Cl_2 \cdot 2H_2O$ (**8**) becomes anhydrous at 105 °C (Fig. 3, Table 1). The anhydrous species starts to lose tn at 135 °C and transforms to metal chloride through bis (**9**), mono (**10**) and hemi(diamine) species. Bis and mono complexes are isolated in solid state by temperature arrest technique in nitrogen atmosphere. But we could not isolate the hemi species in pure form. The DTA curve shows two distinctly separated endotherms for the elimination of first two molecules of tn and two exotherms for the elimination of rest tn molecule.

$[Ni(tn)_3]Br_2 \cdot H_2O$ (**12**) starts to lose its water molecule at 40 °C and becomes anhydrous at 103 °C (Fig. 3, Table 1). This anhydrous species shows an endothermic peak in the temperature range 135—155 °C without showing any mass loss. After this change it starts to lose one molecule of tn at 162 °C and becomes $[NiBr_2(tn)_2]$ (**13**) at 230 °C which is isolable in the solid state. On further heating it transforms to metal bromide at 415 °C. But this transformation is found to be very complicated as evident from its TG and

Table 1. Thermal parameters of nickel(II) diamine complexes

Decomposition reactions	Temperature range/°C	DTA peak temperature/°C		ΔH/kJ mol^{-1}
		Endo	Exo	
$[Ni(en)_3]Cl_2\cdot 2H_2O$ (**1**) → $[Ni(en)_3]Cl_2$	70—140	98, 115, 135		153
$[Ni(en)_3]Cl_2$ → $[NiCl_2(en)_2]$	190—280	277		b)
$[NiCl_2(en)_2]$ → $[NiCl_2en]$	280—310	308	290	b)
$[NiCl_2en]$ → $[Ni_2Cl_4en]$	310—365		360	b)
$[Ni_2Cl_4en]$ → $NiCl_2$	365—416		398	b)
$[Ni(en)_3]Cl_2\cdot 2H_2O$ (**2**) → $[Ni(en)_3]Cl_2$	75—140	100, 135		141
$[Ni(en)_3]Cl_2$ → $[NiCl_2(en)_2]$	195—279	275		104
$[NiCl_2(en)_2]$ → $[NiCl_2en]$	279—350	347		100
$[NiCl_2en]$ → $[Ni_2Cl_4en]$	362—418		417	36
$[Ni_2Cl_4en]$ → $NiCl_2$	418—460		460	79
$[Ni(en)_3]Cl_2\cdot 2H_2O$ (**3**) → $[Ni(en)_3]Cl_2$	75—145	100, 136		144
$[Ni(en)_3]Cl_2$ → $[NiCl_2(en)_2]$	200—275	270		105
$[NiCl_2(en)_2]$ → $[NiCl_2en]$	275—340	330, 340		70
$[NiCl_2en]$ → $[Ni_2Cl_4en]$	350—410		406	52
$[Ni_2Cl_4en]$ → $NiCl_2$	410—460		450	69
$[NiCl_2(en)_2]$ (**4**) → $[NiCl_2en]$ (**5**)	240—340	335		116
$[NiCl_2en]$ → $[Ni_2Cl_4en]$	345—407		399	b)
$[Ni_2Cl_4en]$ → $NiCl_2$	407—460		440	b)
$[Ni(en)_3]Br_2\cdot 2H_2O$ (**6**) → $[Ni(en)_3]Br_2$	55—100	80, 90		130
$[Ni(en)_3]Br_2$ → $[NiBr_2(en)_2]$ (**7**)	210—275	271		124
$[NiBr_2(en)_2]$ → $[NiBr_2(en)_2]$[d]	280—313		300	b)
$[Ni(tn)_3]Cl_2\cdot 2H_2O$ (**8**) → $[Ni(tn)_3]Cl_2$	65—105	88		135
$[Ni(tn)_3]Cl_2$ → $[NiCl_2(tn)_2]$ (**9**)	135—195	190		129
$[NiCl_2(tn)_2]$ → $[NiCl_2tn]$ (**10**)	200—278	274		83
$[NiCl_2tn]$ → $[Ni_2Cl_4tn]$	305—345		343	104
$[Ni_2Cl_4tn]$ → $NiCl_2$	345—444		440	41
$[NiCl_2(tn)_2]\cdot 1.5H_2O$ (**11**) → $[NiCl_2(tn)_2]$ (**9**)	40— 85	72		92
$[NiCl_2(tn)_2]$ → $[NiCl_2tn]$ (**10**)	205—282	278		102
$[NiCl_2tn]$ → $[Ni_2Cl_4tn]$	310—350		348	134
$[Ni_2Cl_4tn]$ → $NiCl_2$	350—445		442	51
$[Ni(tn)_3]Br_2\cdot H_2O$ (**12**) → $[Ni(tn)_3]Br_2$	40—103	75, 98		37
$[Ni(tn)_3]Br_2$ → $[Ni(tn)_3]Br_2$	135—155	153		8
$[Ni(tn)_3]Br_2$ → $[NiBr_2tn_2]$ (**13**)	161—230	228		121
$[NiBr_2(tn)_2]$ → $NiBr_2$	250—400	c)	c)	b)

a) $en=NH_2CH_2CH_2NH_2$; $tn=NH_2CH_2CH_2CH_2NH_2$. b) Value of enthalpy change could not be evaluated. c) Very weakly resolved peaks. d) Thermal decomposition of $[NiBr_2(en)_2]$ (**7**) could not be done.

Table 2. Analytical and magnetic data of nickel(II) diamine complexes

Compound		Color	Found (Calcd) (%)			$\frac{\mu_{eff}}{BM}$
			Metal	Nitrogen	Halogen	
$[Ni(en)_3]Cl_2\cdot 2H_2O$	(**1**)	Pink	16.82 (16.98)	24.25 (24.29)	20.51 (20.53)	3.06
$[Ni(en)_3]Cl_2\cdot 2H_2O$	(**2**)	Pink	16.90 (16.98)	24.24 (24.29)	20.50 (20.53)	3.07
$[Ni(en)_3]Cl_2\cdot 2H_2O$	(**3**)	Pink	16.92 (16.98)	24.26 (24.29)	20.50 (20.53)	3.07
$[NiCl_2(en)_2]$	(**4**)	Blue	23.47 (23.51)	22.39 (22.42)	28.40 (28.43)	3.18
$[NiCl_2en]$	(**5**)	Green	30.98 (30.94)	14.72 (14.76)	37.45 (37.42)	3.55
$[Ni(en)_3]Br_2\cdot 2H_2O$	(**6**)	Pink	13.52 (13.51)	19.30 (19.32)	36.80 (36.77)	3.09
$[NiBr_2(en)_2]$	(**7**)	Blue	17.38 (17.34)	16.50 (16.54)	47.22 (47.20)	3.28
$[Ni(tn)_3]Cl_2\cdot 2H_2O$	(**8**)	Bluish pink	15.09 (15.14)	21.61 (21.66)	18.29 (18.31)	3.01
$[NiCl_2(tn)_2]$	(**9**)	Blue	21.10 (21.14)	20.14 (20.16)	25.54 (25.56)	3.17
$[NiCl_2tn]$	(**10**)	Green	28.79 (28.82)	13.76 (13.74)	34.86 (34.85)	3.54
$[NiCl_2(tn)_2]\cdot 1.5H_2O$	(**11**)	Blue	19.20 (19.27)	18.34 (18.37)	23.26 (23.30)	3.15
$[Ni(tn)_3]Br_2\cdot H_2O$	(**12**)	Bluish pink	12.78 (12.80)	18.35 (18.31)	34.87 (34.85)	3.10
$[Ni(tn)_2Br_2]$	(**13**)	Blue	16.03 (16.01)	15.26 (15.27)	43.62 (43.60)	3.20

DTA curves (Fig. 3).

Discussion

Ethylenediamine Complexes of Nickel(II) Chloride. It is interesting to note that complexes **1**, **2**, and **3** seem apparently identical (Table 2) but they are basically different in structures as evident from their DTA profiles. These structural differences may be due to the changes in conformation of the individual chelate ring as may be expected for these complexes. But the possession of similar IR bands by these three tris complexes rules out the possibility of conformational changes. Structural changes observed against these three complexes are not due to the changes in microsymmetry (D_3) as evident from their identical electronic spectra (Table 3). It is expected that the differences as observed during the decomposition appear to be due to the existence of different crystal symmetries belonged to them or due to some other factors (*vide supra*). It is difficult to understand what mechanism plays while synthesizing complexes **2** and **3** by adding pyridine, methylhydrazine *etc.* to the bis complex **4**. However, it is expected that non-bridging of halide ion in $[NiCl_2(en)_2]$ resulting in bond stretching phenomenon as reported by Benson and Haim[7] is responsible for the transformation of $[NiCl_2(en)_2]$ to $[Ni(en)_3]Cl_2$. It is observed that dehydration pattern of complex **1** is different (Fig. 1) from the complexes **2** and **3**. One interesting observation is that these three anhydrous tris complexes take two molecules of water while keeping them in air. The difference exhibited in the dehydration process does not exist in the dehydration of the rehydrated complexes in solid state. This is probably due to different attachment of H_2O molecules between **1** and the rehydrated compounds of anhydrous **1**. DTA profile for the transformation of bis→mono species in complex **1** is an exotherm followed by an endotherm (Fig. 1) which suggests that the decomposition takes place after geometrical isomerization. In complex **1** three chelated en are arranged in such a manner that during tris→bis transformation, a square pyramidal intermediate[8] is expected to be formed by chelate opening followed by the instantaneous axial coordination by chloride ion to the unstable intermediate (Scheme 1). The further heating develops unstable *trans*-$[NiCl_2(en)_2]$ which transforms to *cis* variety as Cl^- acts as reasonably good *cis* directing product.[5] As a consequence, the exotherm at the beginning of the decomposition of bis species is responsible for the *trans*→*cis* isomerization as evident from literature[9] that such isomerization would generally cause exotherm in the system. Moreover, a weakly resolved plateau in TG curve for tris→bis formation in **1**, unlike the cases of **2** and **3** (Fig. 1) is probably due to the formation of unstable *trans* intermediate (Scheme 1). On the other hand, during the isomerization process complexes **2** and **3** exhibit simply endotherms for bis→mono transformation. Occurrence of splitting in endotherm in complex **3** suggests that complexes **2** and **3** are possibly structurally different, which would indicate that bis→mono transformation occurs in two steps though the corresponding TG curve shows no inflexion due to the extreme instability of the intermediate complex species. The above observation indicates that the complex **2** possesses more simple structure in comparison to that of complex **3**. $[NiCl_2(en)_2]$ (**4**) is undoubtedly *cis* as evident from IR assignments[10–13] and X-ray crystallographic studies.[14] TG curves (Fig. 1) of the decomposition of **1**, **2**, and **3** do not permit the isolation of bis$[NiCl_2(en)_2]$ in very pure state. However, we have isolated the bis species from complexes **2** and **3**. The IR spectral data of these two bis species support the configuration as that (Table 4) of complex *cis*-$[NiCl_2(en)_2]$ (**4**). This shows that basic *cis* form of complex **4** is not disturbed at all while synthesizing the complexes **2** and **3**.

It is a matter of great interest that mono species, $[NiCl_2en]$ (**5**), green in color, has been isolated in pure form in solid state, whilst attempt for the preparation of this compound in solution has been unsuccessful. The IR spectrum (Table 4) of this compound suggests that en is chelated. Moreover, the medium broad band at $\approx 330\ cm^{-1}$ in IR spectrum is well

Table 3. Electronic spectra of nickel(II) diamine complexes in mull

Compound		Absorbance[a] maxima λ/nm
$[Ni(en)_3]Cl_2\cdot 2H_2O$	(**1**)	(625sh, 575sh, 540, 500sh, 465sh, 345)[b]
$[Ni(en)_3]Cl_2\cdot 2H_2O$	(**2**)	(625sh, 575sh, 540, 500sh, 465sh, 345)[b]
$[Ni(en)_3]Cl_2\cdot 2H_2O$	(**3**)	(625sh, 575sh, 540, 500sh, 465sh, 345)[b]
$[NiBr_2(en)_2]$[c]	(**7**)	580, 366
$[NiCl_2en]$	(**5**)	672, 398
$[NiCl_2(tn)_2]$[c]	(**9**)	570, 352
$[NiCl_2tn]$[c]	(**10**)	664, 408
$[NiBr_2(tn)_2]$[c]	(**13**)	564, 364

a) Arbitrary absorbance. b) Spectral data of the crystals of the corresponding complexes. c) Compound synthesized in solid state.

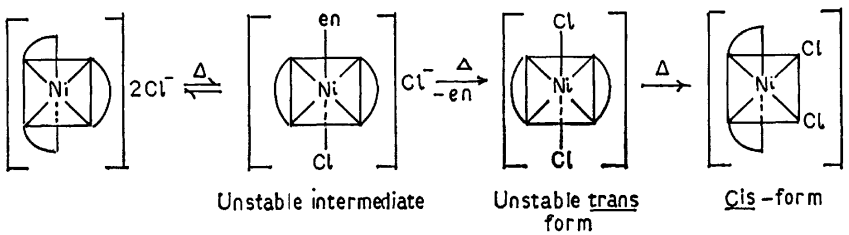

Scheme 1.

Table 4. IR spectral data of nickel(II) diamine complexes in KBr

Compound		Assignments									
		$\nu_{(NH_2)}$	$\nu_{(CH_2)}$	$\delta_{(NH2)}$	$\delta_{(CH_2)}$	$\rho_{w\,(CH_2)}$	$\tau_{(NH_2)}+\rho_{w\,(NH_2)}+\tau_{(CH_2)}$		Stretching vibrations of skeleton $\nu_{C-N}+\nu_{C-C}$		$\rho_{r\,(CH_2)}+\nu_{(MN)}$	
$[NiCl_2(en)_2]$[a]	(**4**)	3330 w, 3280 s, 3235 m, 2195 m, 3145 m, 3120 m	2960 m, 2940 m, 2880 m	1580 sh, 1570 s	1445 m, 1435 m	1385 w, 1360 vw	1330 m, 1280 w, 1135 m,	1320 w, 1265 m, 1100 sh	1090 s, 1010 sh, 960 sh	1020 vs, 970 w,	870 vw, 665 m, 500 m,	855 w, 650 sh,
$[NiBr_2(en)_2]$[b]	(**7**)	3335 w, 3290 s, 3250 m, 3200 m, 3160 m, 3127 m	2962 w, 2950 m, 2886 m	1590 sh, 1580 s	1455 m, 1445 m	1392 w, 1370 vw	1330 m, 1290 w, 1142 m,	1320 w, 1275 m, 1105 sh	1100 s, 1020 sh,	1030 vs, 980 w	860 vw, 660 m,	675 m, 515 m
$[NiCl_2(tn)_2]$[b]	(**9**)	3340 w, 3300 s, 3230 m	2970 m, 2930 m, 2880 m	1628 m, 1580 s, 1560 m, 1555 w	1468 w, 1452 w, 1440 w	1404 w, 1390 w, 1352 vw	1325 w, 1315 w, 1280 m, 1165 s		1090 vw, 1070 m, 1020 s		908 s, 730 sh, 630 m,	879 vw, 690 br, 585 m
$[NiBr_2(tn)_2]$[b]	(**13**)	3358 m, 3303 s, 3235 m	2970 m, 2928 m, 2880 m	1622 m, 1576 s, 1550 m, 1555 m	1460 w, 1450 vw, 1442 w	1400 w, 1385 m, 1350 vw	1320 w, 1310 w, 1275 m, 1152 s		1085 w, 1060 m, 1012 s		900 s, 720 sh, 621 m,	870 w, 680 br, 585 m
$[NiCl_2en]$[b]	(**5**)	3260 sbr	2960 w, 2940 w, 2880 w	1640 m, 1600 m, 1570 s, 1565 sh	1462 w, 1455 w	1400 vw, 1375 vw	1330 m, 1285 m, 1145 w, 1105 sh	1335 sh, 1155 w, 1112 m,	1050 sh, 1035 vs, 1015 sh, 1000 sh, 970 m		875 vw, 685 s, 665 sh, 620 sh, 515 m	
$[NiCl_2tn]$[b]	(**10**)	3340 m, 3315 m, 3260 m, 3040 m	2970 sh, 2900 m, 2800 w	1590 sh, 1580 s	1470 s, 1460 s, 1450 sh	1405 m	1315 vw, 1245 vw, 1185 w, 1120 m	1265 m, 1212 m, 1140 s,	1100 m, 1052 w, 1000 s	1070 sh, 1010 sh,	942 s, 870 vw, 595 vw,	918 m, 642 br, 550 sh

s=strong, vs=very strong, m=medium, w=weak, br=broad, sh=shoulder, vw=very weak, sbr=strong broad. a) IR spectral data of two bis species from complexes **2** and **3** are similar to that of complex **4**. b) Synthesized in solid state.

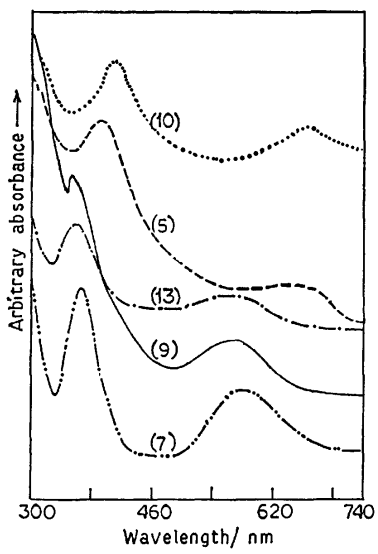

Fig. 4. Electronic spectra of $[NiBr_2(en)_2]$ (**7**) (—··—··—··—), $[NiCl_2(tn)_2]$ (**9**) (——), $[NiBr_2(tn)_2]$ (**13**) (—·—·—·—), $[NiCl_2en]$ (**5**) (— — — —), and $[NiCl_2tn]$ (**10**) (·····) in mull).

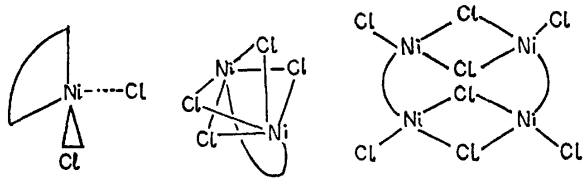

significant for Ni–Cl terminal coordination in T_d symmetry.[15] Magnetic moment (Table 2) is higher than those of the complexes **2**, **3**, and **4** which suggests that the symmetry is lowered in $[NiCl_2en]$ causing greater orbital contribution. The electronic spectra in mull (Fig. 4) display the characteristic band of the T_d Ni^{II} system (Structure 1) at ≈650 nm which is tentatively assignable to the $^3T_1 \rightarrow {}^3T_1(P)$ transition (ν_3).[16,17]

We could not isolate $[Ni_2Cl_4en]$ in pure form as TG curve (Fig. 1) does not indicate stable step. But we have measured magnetic moment of this species isolated by temperature arrest technique at the temperature (410 °C) where the desired composition corresponds to the TG curve. The compound possesses unusually high magnetic moment (μ_{eff}=10.0 BM using the formula, $[Ni_2Cl_4en]$). This may be due to the ferromagnetic behavior which is possibly developed from the Cl^- bridging[18–20] and metal-metal interaction.[21] These phenomena and the stoichiometry of the compound would require either pentacoordinated species (Structure 2) developed from monomeric $[Ni_2Cl_4en]$ or tetracoordinated tetrahedral species (Structure 3) formed from dimeric $[Ni_2Cl_4en]$ *i.e.*, $[Ni_4Cl_8(en)_2]$. In this type of geometry two Ni^{II} ions probably come closer with each other to satisfy the proposed interaction. Since the compound is hygroscopic (in nature) its IR spectrum is not well resolved. However, comparing the complicated IR spectrum of $[NiCl_2en]$ (**5**) with the simpler IR of $[Ni_2Cl_4en]$ it is expected that en is possibly bridged and *trans*. Electronic spectrum in mull of $[Ni_2Cl_4en]$ is not also well resolved. As a result it would not be prudent to support the structures from electronic spectrum.

Ethylenediamine Complexes of Nickel(II) Bromide. Dehydration of $[Ni(en)_3]Br_2\cdot 2H_2O$ (**6**) occurs in two steps like complexes **2** and **3**. Isolation of $[NiBr_2(en)_2]$ (**7**) in pure state from complex **6** is possible unlike the corresponding chloro complexes. This bis complex (**7**) is expected to possess *cis* configuration as the IR spectrum of it closely resembles that of *cis* variety of $[NiCl_2(en)_2]$ (**4**). Though the method or preparation of complexes **4** and **7** are different the complexes are having *cis* configuration. As the intermediate bis species obtained from the complexes **2** and **3** are exhibiting almost similar IR spectra with those of **4** and **7** the possession of similar *cis* configuration like that of complexes **4** and **7** is also supported here for the bis species isolated from **2** and **3**. It is interesting to note that an exotherm appears in DTA profile (Fig. 2) at the threshold of decomposition of *cis*-$[NiBr_2(en)_2]$. This exotherm is probably due to the isomerization process. However, it is difficult to say which configuration is being formed here. On the contrary, it is expected that melting process generally happens to more symmetric species. As *trans* species is more symmetric than *cis*, *trans* configuration is possibly formed before melting. As a consequence, it seems that the initial configurations of the bis products obtained from the decomposition of **1** and **6** are not similar. Such differences are possibly due to the different polarizability of halide ions. It is reasonable to expect that, Br^- has stronger bridging character owing to its higher polarizability and larger size than Cl^- which prefers *cis* configuration as evident from the isolable *cis* complex **7**. On the other hand, the less polarizability and smaller size of Cl^- possibly hinders bridging character, and so the *cis* form (Scheme 1) generated is less stable (Fig. 1, Table 1).

Attempt to prepare $[Ni(en)_3]Br_2$ by the treatment of complex $[NiBr_2(en)_2]$ with pyridine, methylhydrazine *etc.* has been unsuccessful unlike the cases of complexes **2** and **3**. It is not unlikely to expect that bond stretching phenomenon of Ni–Br in $[NiBr_2(en)_2]$ is not pronounced here since the Br^- has greater tendency to form bridge.

1,3-Propanediamine Complexes of Nickel(II) Chloride. $[Ni(tn)_3]Cl_2\cdot 2H_2O$ (**8**) shows almost similar thermal behavior as observed by the complex **2**. We have synthesized $[NiCl_2(tn)_2]\cdot 1.5H_2O$ in two ways. We thought initially that two types of $[NiCl_2(tn)_2]\cdot 1.5H_2O$ would be generated due to the difference in synthetic procedure. But we find no difference in structure between the two bis species owing to their similar spectral and thermal behavior. This bis species is also suggested to possess *cis* configuration like $[NiCl_2(en)_2]$ (**4**) as evident from a number of bands in the region 1550—1650 cm^{-1} (Table 4) which are mainly contributed due to $\delta_{(NH_2)}$ vibration. Here also, this bis species did not yield tris species at all by the reaction with pyridine, methylhydrazine *etc.* unlike the complex **4**. The reason is probably due to the longer chain of chelate ring in the complex than en, whose effect is

pronounced for Br^- rather than Cl^- ion. Another intermediate complex, $[NiCl_2tn]$ (**10**) synthesized in solid state from complex **8** is much hygroscopic in nature, and green in color like **5**. IR, electronic spectra (in mull) as well as magnetic moment of $[NiCl_2tn]$ suggests its T_d symmetry similar to the corresponding en complex. Here also, we could not isolate $[Ni_2Cl_4tn]$ in pure form. It is interesting to note that $[Ni_2Cl_4tn]$ is also ferromagnetic like $[Ni_2Cl_4en]$.

1,3-Propanediamine Complexes of Nickel(II) Bromide. $[Ni(tn)_3]Br_2 \cdot H_2O$ (**11**) after dehydration, exhibits an endotherm with no weight loss. The detail studies of the observed phase change is to be reported separately[22] along with the other phase transition phenomena occurring in diamine complexes. Decomposition of this dehydrated complex species (**12**) to bis complex follows the path similar to that of complex **2** (Fig. 3). The $[NiBr_2(tn)_2]$ (**13**) is O_h suggested by its magnetic moment (Table 2) and electronic spectra in mull (Table 3). IR spectrum of $[NiBr_2(tn)_2]$ also shows more bands than *trans* chelated $[Ni(NCS)_2(tn)_2]$[23] which indicate that two tn molecules are chelated (Table 4). The decomposition of $[NiBr_2(tn)_2]$ to $NiBr_2$ follows in multiple steps, unlike $[NiCl_2(tn)_2]$.

It is clear from the decomposition patterns of the complexes that change of halide ion in the system causes remarkably different decomposition, whilst the increase in chain length in the diamines does not affect it much.

Water elimination in tris(diamine) complexes of nickel(II) bromide takes place at lower temperature (Table 1) in comparison to those of the corresponding chloride. This is probably due to anion variation in the complexes. The value of enthalpy change for water elimination appears very low in $[Ni(tn)_3]Br_2 \cdot H_2O$ (**12**) which indicates that attraction of water molecule towards nickel(II) is less here in comparison of enthalpy changes among **1**, **2**, **3**, **6**, and **8** complexes (Table 1). It is reasonable to expect that the water molecule in **12** is attached by van der Waals force only. On the other hand, water molecules in the **1**, **2**, **3**, **6**, and **8** complexes are probably attached by hydrogen bonding as well as van der Waals force causing more attraction of the water molecules in the species.

It is interesting to note that the ΔH value for the decomposition of $[NiCl_2tn]$ to $[Ni_2Cl_4tn]$ is considerably high (Table 1) in comparison to that for $[NiCl_2en]$ to $[Ni_2Cl_4en]$ transformation. Here the ΔH values involve the metal ligand bond energies, polarization energies of the ligands and other contributions. However, it is rather difficult to say which factor is predominant to cause such difference in the ΔH values of the two transformations.

References

1) T. D. George and W. W. Wendlandt, *Tex. J. Sci.*, **14**, 47 (1962).
2) T. D. George and W. W. Wendlandt, *J. Inorg. Nucl. Chem.*, **25**, 395 (1963).
3) W. W. Wendlandt, *Anal. Chim. Acta*, **27**, 309 (1962).
4) F. Ya. Kul'ba, Yu. A. Makashev, D. M. Maskhaevn, and A. V. Barsukov, *Russ. J. Inorg. Chem.*, **16**, 511 (1971).
5) J. E. House, Jr., and John C. Bailar, Jr., *J. Am. Chem. Soc.*, **91**, 67 (1969), and the references therein.
6) "Inorganic Synthesis," ed by E. G. Rochow, McGrow-Hill Book Company, Inc., New York (1960), Vol. VI, pp. 198, 200.
7) P. Benson and A. Haim, *J. Am. Chem. Soc.*, **87**, 3826 (1965).
8) F. A. Cotton and G. Wilkinson, "Advanced Inorganic Chemistry," 3rd ed, John Wiley and Sons, Inc., New York (1972), p. 670.
9) S. Mitra, T. Yoshikuni, A. Uehara, and R. Tsuchiya, *Bull. Chem. Soc. Jpn.*, **52**, 2569 (1979).
10) M. E. Baldwin, *J. Chem. Soc.*, **1960**, 4369.
11) J. M. Rigg and E. Sherwin, *J. Inorg. Nucl. Chem.*, **27**, 653 (1965).
12) J. A. McLean, A. F. Schreiner, and A. F. Laethem, *J. Inorg. Nucl. Chem.*, **26**, 1245 (1964).
13) M. L. Morris and D. H. Busch, *J. Am. Chem. Soc.*, **82**, 1521 (1960).
14) A. S. Antsyshkina and M. A. Porai Koshits, *Dokl. Akad. Nauk SSSR*, **143**, 105 (1962).
15) K. Shobatake and K. Nakamoto, *J. Am. Chem. Soc.*, **92**, 3332 (1970).
16) M. Goodgame, D. M. L. Goodgame, and F. A. Cotton, *J. Am. Chem. Soc.*, **83**, 4161 (1961).
17) J. T. Donoghue and R. S. Drago, *Inorg. Chem.*, **1**, 866 (1962).
18) O. Kahn, P. Tola, J. Galy, and H. Coudanne, *J. Am. Chem. Soc.*, **100**, 3931 (1978).
19) S. Foner, R. B. Frankel, H. Wong, W. M. Reiff, and G. J. Long, *J. Chem. Phys.*, **68**, 478 (1978).
20) S. O'Brien, R. M. Gaura, C. P. Landee, and R. D. Willett, *Solid State Commun.*, **39**, 1333 (1981).
21) S. Yamada and A. Takeuchi, *Coord. Chem. Rev.*, **43**, 187 (1982).
22) G. De, P. K. Biawas, and N. Ray Chaudhuri, unpublished work.
23) N. F. Curtis and Y. M. Curtis, *Aust. J. Chem.*, **19**, 1423 (1966).

 © 1983 The Chemical Society of Japan Bull. Chem. Soc. Jpn., 56, 3152—3158 (1983) [Vol. 56, No. 10

Graphical Enumeration of the Sextet Polynomials. Novel Identities of Resonant Sextet Numbers of Cata-condensed Benzenoid Hydrocarbons†

Sherif EL-BASIL
Faculty of Pharmacy, Kasr El-Aini Street, Cairo, Egypt
(Received November 20, 1982)

Novel graph-theoretical identities of resonant sextet numbers of certain nonbranched and branched cata-condensed benzenoid hydrocarbons are given, which are based on transforming Kekulé valence-bond structures into the subspace of their double bonds. Analytic expressions are given which allow construction of sextet polynomials of certain types of benzenoid hydrocarbons of very large sizes in a few seconds without drawing any graphs.

A little more than a decade ago Hosoya introduced his concept of nonadjacent numbers[1] as the sum of a set of numbers $p(G,k)$'s defined as the number of ways in which k bonds in graph G are so chosen that no two of them are connected. Thus $p(G,2)$ *e.g.* would be the number of disconnected K_2 graphs in G. Hosoya correlated such numbers with boiling points of alkanes.[1] The concept is related to the so called bond eigenfunctions of many-electron molecules adopted in old resonance theory.[2] The reference polynomial[3] of benzenoid hydrocarbons, BH's is expressed as simple functions of such disconnected K_2 graphs.[4]

Some years later Hosoya and Yamaguchi[5] extended the "nonadjacent" concept to Clar's sextet theory[6] by defining a resonant sextet number, $r(G,k)$ for a BH graph G as the number of ways in which k disconnected but mutually resonant sextets are chosen from G. Such resonant sextet numbers are used to construct sextet polynomials, $B_G(X)$'s, as given by

$$B_G(X) = \sum_{k=0}^{m} r(G,k)X^k,$$

where $r(G,0)$ is defined as unity and m is the maximal number of disconnected sextets in G. Two years later, Gutman[7] correlated sextet polynomials with characteristic polynomials of certain trees, $P_T(X)$, corresponding to nonbranched cata-condensed BH's, where

$$P_T(X) = \sum_{k=0}^{(N/2)} (-1)^k p(T,k)X^{N-2k},$$

N is the number of vertices in the tree, and $p(T,k)$ is the number of ways in which k nonincident edges are selected from T. Gutman demonstrated and proved the equality of the two variables, *viz.*,

$$r(G,k) = p(T,k).$$

In quite a recent development, Gutman[8] constructed his so called C graphs associated with a BH composed of y hexagons, $h_1, h_2, \ldots, h_y$. The vertices of the C graph $v_1, v_2, \ldots, v_y$ correspond to the h's such that v_r and v_s are adjacent if and only if h_r and h_s in BH are mutually nonresonant. Gutman[8] discovered the interesting relation that such C graphs are actually the line graphs[9] corresponding to tree graphs associated with nonbranched cata-condensed BH's so that we may write:

$$L^{-1}(C) = T.$$

In a related development Aihara[10] defined a new polynomial based on the $r(G,k)$ numbers from which an expression was deduced for resonance energies of BH's. The above history of the sextet polynomial stimulated many people of deriving algorithms for its construction[11] due to its importance to both theorists and organic chemists.

In this work we analyze the sextet polynomial from a novel vent, namely from the permutation[12] of double bonds in Kekulé structures of BH's. First we cite some terms and their meanings.

Definitions

Types of Benzenoid Hydrocarbons. We shall adopt the following terminology in this paper: A molecular network which is entirely composed of hexagons is called benzenoid. If all benzene rings in one of the Kekulé structures have an aromatic sextet the hydrocarbon is called all-benzenoid (in the opposite sense, a nonall benzenoid). If no three hexagons have a common atom, the system is called cata-condensed. If every hexagon of a cata-condensed system has at most two neighbouring hexagons, it is said to be nonbranched. If there is at least one hexagon in a cata-condensed hydrocarbon that is surrounded by three other hexagons, it is said to be branched.

Modes of Ring Annellation, the L,A-Sequence.[7] The nonterminal hexagons in a nonbranched cata-condensed system can be annellated in just two ways,[7] *viz.*,

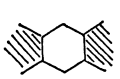

L-mode

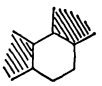

A-mode

Furthermore we shall adopt an additional convention that a hexagon which is fused simultaneously to three other hexagons (*i.e.* a branched hexagon) will be assigned the symbol A, *viz.*,

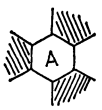

Therefore an ordered R-tuple of symbols L,A, the so called L,A-sequence,[7] might be associated with a cata-condensed BH containing R hexagons, thus: $S_1, S_2, \ldots, S_R$ where, by definition[7] $S_1 = S_R = L$ while S_n, $1 < n < R$, is assigned the symbol L or A depending on its mode of annellation. As an illustration we consider G(I)

† This paper is dedicated to Professor Nenad Trinajstić.

and G(II) representing molecular graphs of a non-branched and a branched cata-condensed BH and their L,A sequences

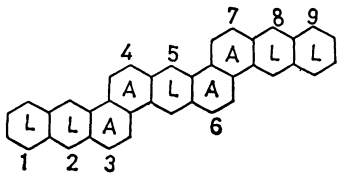

G(I)

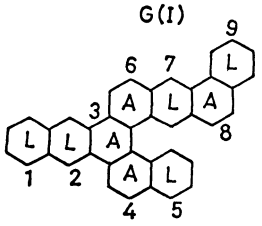

G(II)

We distinguish three types of induced subgraphs[9] which might be partitioned out of the molecular graph of the BH, *viz*,

$$\langle g_1 \rangle = \mathrm{L}^{s_1}\mathrm{A}, \tag{1}$$

$$\langle g_2 \rangle = \mathrm{AL}^{s_2}\mathrm{A}, \tag{2}$$

$$\langle g_3 \rangle = \mathrm{AL}^{s_3}. \tag{3}$$

where L^s means L repeated s times (thus L^3 means L L L and so on). The values of s_1 and $s_3 \neq 0$ while s_2 may or may not be zero depending on the structure of G. As an illustration we consider all the induced subgraphs in G(I) and G(II). For G(I) we have:

$$\langle g_1 \rangle \supset \langle S_1, S_2, S_3 \rangle$$

$$\langle g_2 \rangle \supset \langle S_3, S_4 \rangle \; ; \; \langle S_4, S_5, S_6 \rangle \; ; \; \langle S_6, S_7 \rangle$$

$$\langle g_3 \rangle \supset \langle S_7, S_8, S_9 \rangle.$$

While G(II) is partitioned into:

$$\langle g_1 \rangle \supset \langle S_1, S_2, S_3 \rangle$$

$$\langle g_2 \rangle \supset \langle S_3, S_6 \rangle \; ; \; \langle S_3, S_4 \rangle \; ; \; \langle S_6, S_7, S_8 \rangle$$

$$\langle g_3 \rangle \supset \langle S_8, S_9 \rangle \; ; \; \langle S_4, S_5 \rangle.$$

The number of induced subgraphs will be denoted as L. Thus $L(\mathrm{G(I)})=5$; $L(\mathrm{G(II)})=6$; L(linear acene)$=1$.

Clar Representation of Kekulé Structures, Dualist and Factor Graphs. In a recent graph-theoretical analysis of Clar sextet theory,[6] Hosoya *et al.*[13] distinguished two types of sextets proper and improper, *viz.*,

proper sextet

improper sextet

If, in a Kekulé structure circles are placed into hexagons containing proper sextets and then double bonds are replaced by single bonds a Clar formula, $\mathcal{C}$, results. When a Kekulé structure is transformed into the subspace of its double bonds, a factor graph,[14] $F(K)$ results. If the benzene rings of the benzenoid hydrocarbon are replaced by vertices and then connecting adjacent ones, a dualist,[15] D, results. As an illustration we consider a Kekulé structure for G(I), its Clar formula, factor graph and dualist:

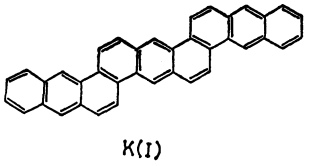

K(I)

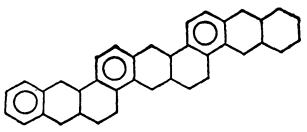

$\mathcal{C}$(I)

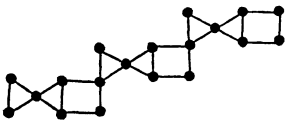

F(K,I)

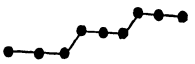

D(I)

Partition Sequence, $S(P)$ of the Factor Graphs

The factor graphs corresponding to the Kekulé structures of a BH might be partitioned according to the degrees of vertices composing them. Our treatment is restricted to BH's and the vertices of their factor graphs might have only degrees of 2, 3, and/or 4.[16] Figure 1 shows all $F(K)$'s of picene where the numbers in braces are populations of bivalent, tervalent and quadrivalent vertices respectively. We might, therefore, construct the following partition sequence for picene

$$S(P) = \{7,0,4\} + 5\{6,2,3\} + 6\{5,4,2\} + \{4,6,1\}.$$

One observes that the sextet polynomial of picene is given by $B_{\mathrm{G}}(X)=1+5X+6X^2+X^3$. The identity between the coefficients of our sequence and those of the polynomial is obvious.[17] In general one might define as ith partition, P_i as:

$$P_i = \{v_{2,i} \; ; \; v_{3,i} \; ; \; v_{4,i}\},$$

where $v_{2,i}$ is the number of bivalent vertices in ith partition and similarly for $v_{3,i}$ and $v_{4,i}$. Since, however, v_2, v_3, and v_4 for a BH are linearly related,[16] we might record only one variable, say v_2's. Thus our partition sequence takes the following general form for a set of $F(K)$'s with n partitions:

$$S(P) = a_{\bar{m}}[\bar{m}] + a_{\bar{m}-1}[\bar{m}-1] + \cdots + a_{\bar{m}-n+1}[\bar{m}-n+1], \tag{4}$$

where $[\bar{m}]$ is a partition for which v_2 is maximum and $a_{\bar{m}}$ is its population. The value $\bar{m}-n+1$ is minimum $v_2=\underline{m}$, and n is the number of partitions. Equation 4 might be written as:

$$S(P) = \sum_{j=0}^{n-1} a_{\bar{m}-j}[\bar{m}-j]$$

where

$$\sum_{j=0}^{n-1} a_{\bar{m}-j} = K,$$

being the Kekulé count. For picene we have

$$n = 4 \; ; \; a_{\bar{m}} = 1 \; ; \; a_{\bar{m}-1} = 5 \; ; \; a_{\bar{m}-2} = 6 \; ; \; a_{\bar{m}-3} = 1$$

whence K(picene)$=1+5+6+1=13$. One observes that the corresponding $r(\mathrm{G},k)$'s are:

$$r(G,0) = 1 \; ; \; r(\mathrm{G},1) = 5 \; ; \; r(\mathrm{G},2) = 6 \; ; \; r(\mathrm{G},3) = 1.$$

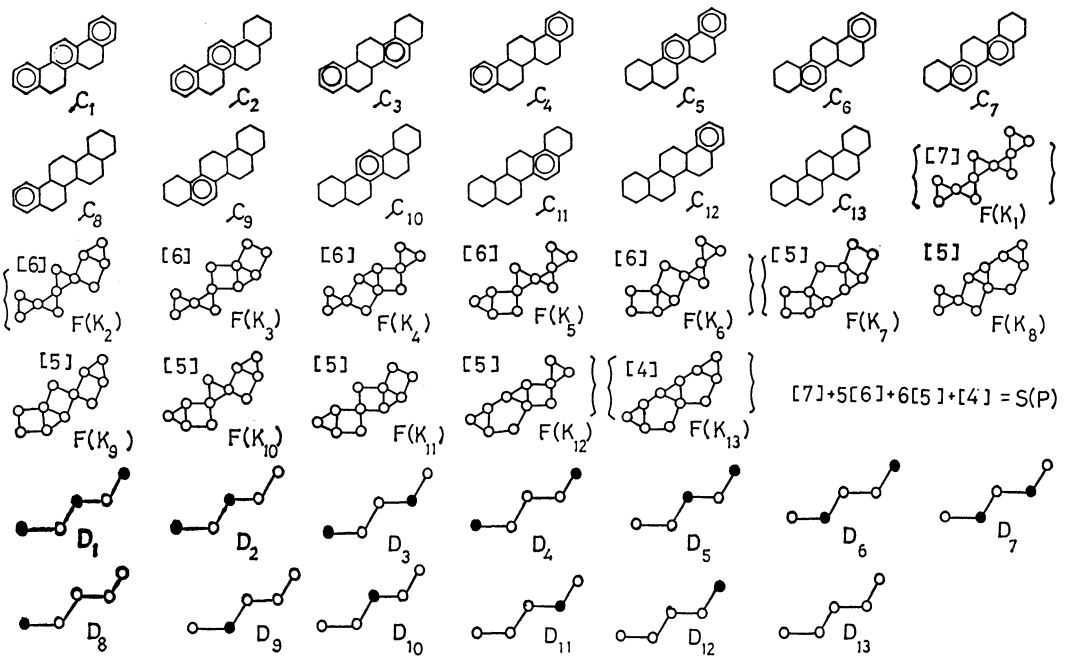

Fig. 1. Graphical illustration of Sextet Polynomial of pentaphene (a NBCCABH). The ⟋C's are Clar formulas, $F(K)$'s are the corresponding factor graphs while the D's being the corresponding dualists colored such that solid vertices correspond to hexagons containing circles. Thus dualists containing one solid vertex correspond to $r(G,1)$ or $N(1)$, those containing two solid vertices correspond to $r(G,2)$ or $N(2)$ and so on. Numbers in square brackets are v_2's in each $F(K)$.

Results

The Linear Acenes. $S(P)$'s and $B_G(X)$'s of the lower numbers of the linear acenes are listed below

Benzene	:	$0[4] + 2[3]\ ;\ 1 + X$,
Naphthalene	:	$[4] + 2[3]\ ;\ 1 + 2X$,
Anthracene	:	$2[4] + 2[3]\ ;\ 1 + 3X$,
Naphthacene:	:	$3[4] + 2[3]\ ;\ 1 + 4X$,
Pentacene	:	$4[4] + 2[3]\ ;\ 1 + 5X$.

The following relations hold for a linear acene

$$a_4 = a_{\bar{m}} = R - 1 = r(G,1) - 1, \tag{5}$$

$$a_{\underline{m}} = a_3 = 2, \tag{6}$$

$$n = 2. \tag{7}$$

Theorem: The vertices of a set of $F(K)$'s of a linear acene partition themselves in only two distinct ways; such that two of these $F(K)$'s have only three bivalent vertices while the remaining factor graphs contain four bivalent vertices each. *i.e.*

$$S(P)_{\text{Linear acene}} = (R-1)[4] + 2[3]. \tag{8}$$

R being the number of benzene rings.

Proof: We consider the most general case first, of a linear acene containing R rings, $R \geqslant 4$. One can easily show that there are three types of factor graphs belonging to such a linear acene, A, B, and C, *viz.*,

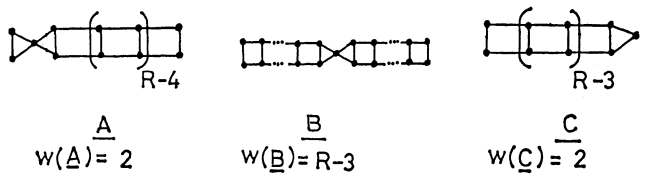

Where w is the multiplicity of factor graph type. *E.g.* there are two forms of A *i.e.* A and its mirror image and similarly for C, while the B type generates $(R-3)$ $F(K)$'s. The number of cycles in B is, of course, R. We observe that the sum of w's is $2+R-3+2=R+1=K$. Furthermore types A and B lead to partition with maximum number of bivalent vertices, thus $a_{\bar{m}}=w(A)+w(B)=2+R-3=R-1$. Type C leads to $[\underline{m}]$, and since $w(C)=2$, $\bar{m}=4$ and $\underline{m}=3$ Eq. 8 is proved for $R \geq 4$.

The proof can easily be demonstrated for $R<4$. *E.g.* when $R=2$, A=B= and w (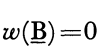) $=1$;

C= $w(C)=2$. When $R=3$, $w(B)=0$ while

A= 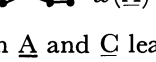 $w(A)=2$, and C= 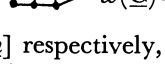 $w(C)=2$.

Again A and C lead to $[\bar{m}]$ and $[\underline{m}]$ respectively, where $\bar{m}=4$, $\underline{m}=3$. When the values of w's are used, Eq. 8 results.

Nonbranched Cata-condensed All-benzenoid Hydrocarbons NBCCABH's. An all-benzenoid cata-condensed hydrocarbon is defined above. In terms of Eqs. 1—3, only three types of induced subgraphs[9] might be factored out of the molecular graph of a NBCCABH, *viz.*,

$$\langle g_1 \rangle = \text{LA},$$

$$\langle g_2 \rangle = \text{A}^2,$$

$$\langle g_3 \rangle = \text{AL}.$$

Thus for a NBCCABH containing R rings the L,A sequence would be LA^{R-2}L. Consequently for this

TABLE 1. PARTITION SEQUENCES $S(P)$'s, (ABOVE), AND SEXTET POLYNOMIALS, $B_G(X)$'s, (BELOW), OF SOME NONBRANCHED ALLBENZENOID SYSTEMS

R	Example	$S(P)$; $B_G(X)$
3		$[5]+3[4]+[3]$ $1+3X+X^2$
4		$[6]+4[5]+3[4]$ $1+4X+3X^2$
5		$[7]+5[6]+6[5]+[4]$ $1+5X+6X^2+X^3$
6		$[8]+6[7]+10[6]+4[5]$ $1+6X+10X^2+4X^3$
7		$[9]+7[8]+15[7]+10[6]+[5]$ $1+7X+15X^2+10X^3+X^4$
10		$[12]+10[11]+36[10]+56[9]+35[8]+6[7]$ $1+10X+36X^2+56X^3+35X^4+6X^5$

class of BH's we may write:

$$R = L + 1. \tag{9}$$

Table 1 outlines $S(P)$'s and $B_G(X)$'s for some representative members of this topology. The following identity holds for NBCCABH's:

$$a_{\bar{m}-j} = r(G,j). \tag{10}$$

Equation 10 might easily be induced from observation of the results. The following relations hold for population coefficients:

$$a_{\bar{m}} = 1 = a_{R+2}\ ;\ (\bar{m}=R+2), \tag{11}$$
$$a_{\bar{m}-1} = R, \tag{12}$$
$$a_{\bar{m}-2} = 2^{-1}(R-2)(R-1), \tag{13}$$
$$a_{\bar{m}-3} = 6^{-1}(R-4)(R-3)(R-2), \tag{14}$$
$$a_{\bar{m}-4} = 24^{-1}(R-6)(R-5)(R-4)(R-3), \tag{15}$$
$$a_{\bar{m}-5} = 120^{-1}(R-8)(R-7)(R-6)(R-5)(R-4), \tag{16}$$
$$a_{\bar{m}-6} = 720^{-1}(R-10)(R-9)(R-8)(R-7)(R-6)(R-5). \tag{17}$$

Thus, a general expression is given by:

$$a_{m-j} = r(G,j) = (j!)^{-1}(R+1-j)\prod_{m=0}^{j-2}(R-j-m) \tag{18}$$
$$= \binom{R+1-j}{j}.$$

The algebraic properties of the above factorials make the derivation of higher populations possible. Naturally the sum of these coefficients will lead to K. The number of different partitions, n, is related to R in the following way:

R	n
3, 4	3
5, 6	4
7, 8	5
9, 10	6 ··· *etc.*

Thus

$$n = \frac{(R+1)}{2} + 1 \qquad (R \text{ odd})$$
$$= \frac{R}{2} + 1 \qquad (R \text{ even})$$

or by using the Gaussian brackets

$$n = \left[\frac{(R+1)}{2}\right] + 1.$$

The value of $a_{\underline{m}} = a_{\bar{m}-n+1}$ is given by:

$$a_{\underline{m}} = 1 \qquad (R \text{ odd}) \tag{19}$$
$$a_{\underline{m}} = \frac{R}{2} + 1 \qquad (R \text{ even}) \tag{20}$$

Non-branched Cata-condensed Nonall-benzenoid Hydrocarbons for Which $L=2$, (NBCCNABH's)$_{L=2}$. Dualists of this class of BH's are characterised by having just one bend (kink),[18] *i.e.* $L=2$ (See Table 2 for some representative members). It is convenient to express their partition sequence as:

TABLE 2. PARTITION SEQUENCES, $S(P)$, (ABOVE), AND SEXTET POLYNOMIALS, $B_G(X)$, (BELOW), OF NONBRANCHED NONALL-BENZENOIDS CONTAINING TWO LINEAR SUBGRAPHS

R	Dualist	$S(P)$; $S_G(X)$
4		$[3]+4[4]+2[5]$; $1+4X+2X^2$
5		$[3]+5[4]+4[5]$; $1+5X+4X^2$
5	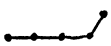	$[3]+5[4]+3[5]$ $1+5X+3X^2$
6	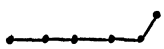	$[3]+6[4]+4[5]$ $1+6X+4X^2$
6	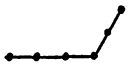	$[3]+6[4]+6[5]$; $1+6X+6X^2$
7	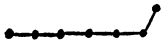	$[3]+7[4]+5[5]$; $1+7X+5X^2$
7		$[3]+7[4]+9[5]$; $1+7X+9X^2$
7	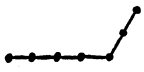	$[3]+7[4]+8[5]$; $1+7X+8X^2$

$$S(P)_{(\text{NBCCNABH})_{L=2}} = a_3[3] + a_4[4] + a_5[5], \quad (21)$$

i.e. $\underline{m}=3$; $\bar{m}=5$; $n=3$ for this class of BH's. Furthermore, their resonant numbers are identified with their population coefficients as given by:

$$a_{\underline{m}+i} = r(\mathrm{G},i). \quad (22)$$

Equation 22 can easily be induced from observation of the results (Table 2). Equation 22 leads to three explicit expressions of the individual resonant numbers, .,*viz*

$$a_3 = r(\mathrm{G},0) = 1, \quad (23)$$

$$a_4 = r(G,1) = R, \quad (24)$$

$$a_5 = r(\mathrm{G},2) = e\langle g_1\rangle\, e\langle g_3\rangle, \quad (25)$$

where $e\langle g_1\rangle$ is size of $\langle g_1\rangle$ *i.e.* number of its edges and similarly for $e\langle g_3\rangle$. (*c.f.* Eqs. 1, 3). Thus for pentaphene, *e.g.* $e\langle g_1\rangle = e\langle g_3\rangle = 2$; whence $a_5=4$. An expression for K for this class of BH's is:

$$K_{(\text{NBCCNABH})_{L=2}} = \sum_{i=0}^{2} a_{\underline{m}+i} = 1 + R + e\langle g_1\rangle \cdot e\langle g_3\rangle. \quad (26)$$

Conjecture: The set of $F(K)$'s of a NBCCNABH for which $L=2$ (*i.e.* whose graph has only one hexagon with an A annellation mode) may partition themselves into three subsets only, in which the number of bivalent vertices may take on values of three, four, or five.

Non-branched Cata-condensed Nonall-benzenoid Hydrocarbons for which $L=3$; $(NBCCNABH's)_{L=3}$. We report results for only two types of this class as illustrations, *viz.*,

Class i for which the size of the middle subgraph is unity, *i.e.* $e\langle g_2\rangle = 1$ (Table 3).

Class ii for which $e\langle g_2\rangle = 2$ (Table 4).

We conjecture that for both types, the partition sequence is described by Eq. 27, *viz.*

$$S(P)_{(\text{NBCCNABH})_{L=3}} = a_4[4] + a_5[5] + a_6[6]. \quad (27)$$

Table 3. Partition sequences, $S(P)$, (above), and sextet polynomials, $B_G(X)$, (below), of nonbranched nonall-benzenoids containing three G_L's such that the middle G_L has only one edge *i.e.*, $e(G_{L_2})=1$

R	Dualist	$S(P)$; $B_G(X)$
5	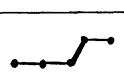	3[4]+6[5]+2[6]; $1+5X+5X^2$
6	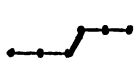	3[4]+8[5]+4[6]; $1+6X+8X^2$
6	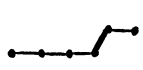	3[4]+8[5]+3[6]; $1+6X+7X^2$
7	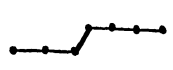	3[4]+10[5]+6[6]; $1+7X+11X^2$
8	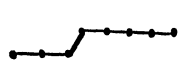	3[4]+12[5]+8[6]; $1+8X+14X^2$
8	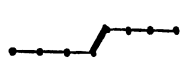	3[4]+12[5]+9[6]; $1+8X+15X^2$

Table 4. Partition sequences, $S(P)$, (above), and sextet polynomials, $B_G(X)$, (below), of nonbranched nonallbenzenoid systems containing three linear subgraphs, in which the middle one contains two edges *i.e.* $e(G_{L_2})=2$

R	Dualist	$S(P)$; $B_G(X)$
5		4[4]+6[5]+2[6]; $1+5X+5X^2+X^3$
6	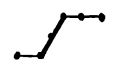	4[4]+9[5]+4[6]; $1+6X+8X^2+2X^3$
7		4[4]+12[5]+8[6]; $1+7X+12X^2+4X^3$
8	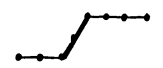	4[4]+14[5]+12[6]; $1+8X+16X^2+6X^3$

Table 5. Topological properties of $(\text{NBCCNABH's})_{L=3}$

Property	Class i	Class ii
$e\langle g_2\rangle$	1	2
a_4	3	4
a_5	$2(R-2)$	$3(R-3)$
a_6	$e\langle g_1\rangle \cdot e\langle g_3\rangle$	$2e\langle g_1\rangle \cdot e\langle g_3\rangle$
$a_5(R+1)-a_5(R)$[a]	2	3
$r(\mathrm{G},2)$	$a_6+(R-2)$	$\frac{1}{2}a_6+2(R-3)$
$r(\mathrm{G},3)$	0.00	$e\langle g_1\rangle \cdot e\langle g_3\rangle$
K	$2R+e\langle g_1\rangle \cdot e\langle g_3\rangle - 1$	$3R+2e\langle g_1\rangle \cdot e\langle g_3\rangle - 5$

a) $a_5(R)$ is population coefficient of partition whose $v_2=5$ of a BH containing R rings and similary for $a_5(R+1)$.

We outline the following useful topological properties for these two classes of graphs:

Branched Cata-condensed Benzenoid Hydrocarbons. The structure of the sextet polynomials of branched cata-condensed systems depends on the mode of growth of the hexagons on the triphenylene unit. We consider the two modes of ring annellation *viz.* linear and angular ways as illustrated below on dualists of some triphenylene derivatives:

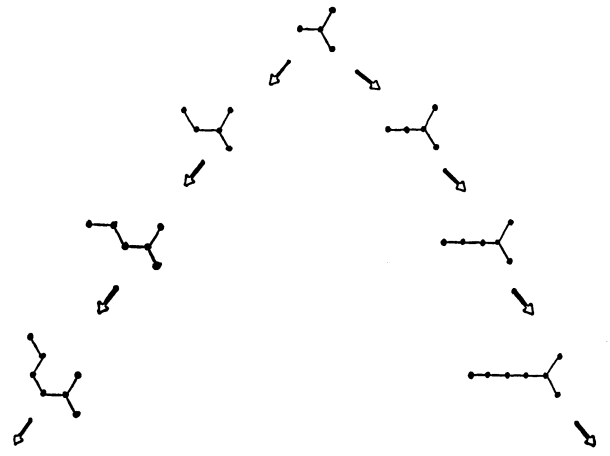

TABLE 6. PARTITION SEQUENCES, $S(P)$'s (ABOVE), AND SEXTET POLYNOMIALS, $B_G(X)$'s, (BELOW), OF SOME BRANCHED CATACONDENSED BENZENOID HYDROCARBONS

R	Dualist	$S(P)$; $B_G(X)$
4		$2[6]+3[5]+3[4]+[3]$ $1+4X+3X^2+X^3$
5		$3[6]+5[5]+4[4]+[3]$ $1+5X+5X^2+2X^3$
6	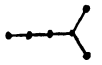	$4[6]+7[5]+5[4]+[3]$ $1+6X+7X^2+3X^3$
5		$2[7]+5[6]+5[5]+2[4]$ $1+5X+6X^2+2X^3$
6		$2[8]+7[7]+8[6]+5[5]+[4]$ $1+6X+10X^2+5X^3+X^4$
7	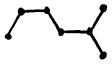	$2[9]+9[8]+13[7]+10[6]+3[5]$ $1+7X+15X^2+11X^3+3X^4$

The group of dualists to the right are derived from triphenylene by linear annellation of hexagons while those to the left by angular annellation. Table 6 lists $S(P)$'s and $B_G(X)$'s of these dualists. We now list some of the mathematical properties of these branched systems.

i) Systems Derived by Linear Ring Annellation: Throughout the following equations, by definition of a branched cata-condensed system, $R \geqslant 4$:

$$a_{\bar{m}} = R-2 = a_6, \tag{28}$$

$$a_{\bar{m}-1} = 2R-5 = a_5 = r(\mathrm{G},2), \tag{29}$$

$$a_{\bar{m}-2} = R-1 = a_4, \tag{30}$$

$$a_{\bar{m}-3} = a_{\underline{m}-3} = a_3 = 1, \tag{31}$$

$$r(\mathrm{G},3) = R-3. \tag{32}$$

One can easily deduce an expression for the Kekulé count of branched cata-condensed benzenoid hydrocarbons whose dualists have the general formula:

, $m=0, 1, 2, \cdots$

as:

$$K = a_6 + a_5 + a_4 + a_3 = 4R-7. \tag{33}$$

ii) Systems Derived by Angular Ring Annellation:

$$a_{\bar{m}} = 2 = a_{R+2}, \tag{34}$$

$$a_{\bar{m}-1} = 2R-5, \tag{35}$$

$$a_{\bar{m}-2}(\mathrm{R}) + a_{\bar{m}-2}(R+1) = a_{\bar{m}-2}(R+2), \tag{36}$$

where $a_{\bar{m}-2}(R)$ is population of the partition $[\bar{m}-2]$ for an allbenzenoid benzenoid hydrocarbon containing R rings and one branched ring (*i.e.* a ring which is fused simultaneously to three other rings) and similarly for $a_{\bar{m}-2}(R+1)$ and $a_{\bar{m}-2}(R+2)$. *I.e.* the coefficients of $[\bar{m}-2]$ in a homologous series of this class of branched systems define a Fibonacci sequence.[19]

The relation among the coefficients of the partition sequences of this class of hydrocarbons is best shown in the following diagram (see Table 6) where the first row corresponds to triphenylene:

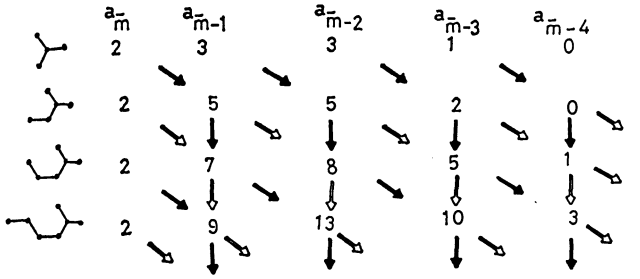

The above relation might be expressed as:

$$a_{\bar{m}}(R) + a_{\bar{m}-1}(R+1) = a_{\bar{m}-1}(R+2). \tag{37}$$

A similar relation holds for the resonant numbers as diagramed below: (the first row correspond to triphenylene).

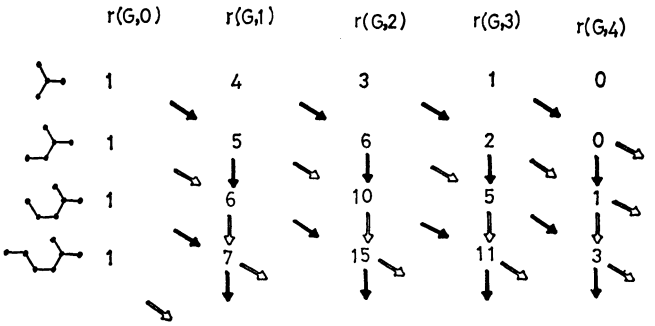

So that we may write

$$r(\mathrm{G},j)_R + r(\mathrm{G},j+1)_{R+1} = r(\mathrm{G},j+1)_{R+2}, \tag{38}$$

where $r(\mathrm{G},j)_R$ is $r(\mathrm{G},j)$ for a member of this set of branched hydrocarbons containing R rings and similarly for other notations. Diagrams like the ones shown above allow the systematic synthesis of sextet polynomials of very large graphs. Furthermore we have:

$$r(\mathrm{G},2) = \sum_{j=2}^{R-1} (R-j)\ ;\ R \geqslant 4. \tag{39}$$

Restricted Disjoint Interactions, RDI's

A pair of RDI is defined between two dualist vertices v_r and v_s such that:

i) v_r and v_s are not part of the same induced subgraph defined by Eqs. 1—3.

ii) v_r and v_s are never adjacent.

i) and ii) are equivalent to saying that v_r and v_s form a pair of RDI if and only if the corresponding hexagons, h_r and h_s, in BH are resonant. We now recall that the so called C(Clar) graph recently introduced by Gutman[8] has its v_r and v_s adjacent only if the corresponding h_r and h_s are nonresonant. We might, there-

fore, call the elements of our RDI's "non-Clar graphs". Examples of such pairs of RDI's are shown as solid circles in dualists of pentaphene (Fig. 1). The number of such pairs of RDI's will be denoted as $N(2)$.

Analogously we define $N(3)$ as triplet of RDI's *e.g.* $N(3)$ for pentaphene=1 (Fig. 1).

Quartets, Quintets *etc.* might similarly be defined. It can be shown that for any type of cata-condensed BH. The following identity holds:

$$N(j) = r(G,j). \tag{40}$$

The validity of the above identity is a result of the definition of RDI's and the fact that in a cata-condensed BH every induced subgraph (Eqs. 1—3) might have only one resonant sextet. This topology makes $N(j)$ identical with the number of ways in which j mutually resonant but disconnected sextets are selected from BH graph. For NBCCABH's the sextet numbers are related to population coefficients by:

$$r(G,j) = a_{\bar{m}-j}. \tag{41}$$

Whence

$$a_{\bar{m}-j} = r(G,j) = N(j). \tag{42}$$

Therefore finding expressions for $N(j)$'s allows construction of sextet polynomials and generation of partition sequences of nonbranched allbenzenoid hydrocarbons without actually writing any Kekulé structures.

For the purpose of illustration we consider a NBCCABH containing ten rings. One such dualist is shown below:

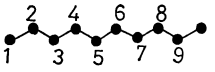

We would like to compute, *e.g.* $r(G,5)$ *i.e.* coefficient of X^5 in sextet polynomial or $a_{\bar{m}-5}$ and since $\bar{m}=R+2$ (for NBCCABH) we are looking for $a_{12-5}=a_7$ *i.e.* population of [7] (that is the number of factor graphs for which $v_2=7$). We simply list the following quintets of RDI's (1,3,5,7,9); (1,3,5,8,10); (1,3,5,7,10); (1,3,6,8,10); (1,4,6,8,10); and (2,4,6,8,10). Therefore there are six Kekulé structures containing each, five disconnected but mutually resonant sextets. Alternatively, we say, there are six $F(K)$'s containing, each, seven bivalent vertices. Actually we do not have to "synthesize" these RDI's we may use Eq. 16, *viz.*,

$$a_{m-5} = 120^{-1}(R-8)(R-7)(R-6)(R-5)(R-4)$$
$$= 120^{-1}(2)(3)(4)(5)(6) = 6.$$

Obviously to use the approach originally suggested by Hosoya and Yamaguchi[5] would be rather a formidable task, especially for higher tuplets. Also, Gutman's method[7,8] requires the construction of the C graph and its $L^{-1}C$ as well as knowledge on characteristic polynomials of trees. To our knowledge our method is simple enough to be carried out by an "average" chemistry student !.

I wish to thank Professor Nenad Trinajstić for correcting some of my mathematical terms, namely dualist instead of dual graph and K_2 subgraphs for non-adjacent numbers. I am also indebted to Professor Ivan Gutman for sending me his recent work on the subject (Ref. 8).

References

1) H. Hosoya, *Bull. Chem. Soc. Jpn.*, **44**, 2332 (1971).
2) See, *e.g.*, H. Eyring, J. Walter, and G. Kimball, "Quantum Chemistry," John Wiley & Sons, New York (1944), pp. 238, 239.
3) The reference polynomial is sometimes referred to as acyclic polynomial (*c.f.* N. Trinajstic, *Croat. Chem. Acta*, **49**, 593 (1977)). Gutman refers to the reference polynomial as the matching polynomial (*c.f.* I. Gutman, *Publ. Inst. Math.*, **27**, 61 (1980)).
4) J. Aihara, *J. Am. Chem. Soc.*, **98**, 2750 (1976).
5) H. Hosoya and T. Yamaguchi, *Tetrahedron Lett.*, **52**, 4659 (1975).
6) E. Clar, "The Aromatic Sextet," John Wiley & Sons, London (1972).
7) I. Gutman, *Theoret. Chim. Acta (Berlin)*, **45**, 309 (1977).
8) I. Gutman, *Z. Naturforsch., A*, **37**, 69 (1982).
9) F. Harary, "Graph Theory," Addison-Wesley, Reading (1969), Chap. 8.
10) J. Aihara, *Bull. Chem. Soc. Jpn.*, **50**, 2010 (1977).
11) I. Gutman, H. Hosoya, T. Yamaguchi, A. Motoyama, and N. Kuboi, *Bull. Soc. Chim. Beograd*, **42**, 503 (1977); S. El-Basil, *Croat. Chem. Acta*, **56** (1983), in press, I. Gutman and S. El-Basil, work in progress.
12) Although Kekulé structures are mathematical states that represent permutation of double bonds, this fact was explicitely stated only recently; D. Cvetkovic, I. Gutman, and N. Trinajstic, *J. Chem. Phys.*, **61**, 2700 (1974).
13) N. Ohkami, A. Motoyama, T. Yamaguchi, H. Hosoya, and I. Gutman, *Tetrahedron*, **37**, 1113 (1981).
14) The concept of transforming a Kekulé structure into the subspace of its double bonds was first introduced by: H. Joela, *Theoret. Chim. Acta (Berlin)*, **39**, 241 (1975) and was adopted to study MO-VB characters of Kekulé structures: S. El-Basil, *Int. J. Quantum Chem.*, **21**, 771, 779, 793 (1982). Such graphs were called submolecule graphs. However, this name has been changed now to factor graphs, (M. Randić, private communication, 1982).
15) *C.f.*, A. T. Balaban, *Rev. Roum Chim.*, **22**, 45 (1977); S. El-Basil, *Math. Chem. (Mülheim)*, **11**, 97 (1981).
16) A recent account of some of the mathematical properties of factor graphs of benzenoid hydrocarbons is available: S. El-Basil, *Math. Chem.*, **13**, 209 (1982).
17) This observation has been reported recently: S. El-Basil, *Chem. Phys. Lett.*, **89**, 145 (1982); S. El-Basil and I. Gutman, *ibid.*, **94**, 188 (1983).
18) *C.f.*, A. T. Balaban, *Tetrahedron*, **25**, 2949 (1969).
19) N. N. Vorobev, "Fibonacci Numbers," Pergamon, New York (1966); See also, H. Hosoya, *Fibonacci Quart.*, **14**, 173 (1976).

Partial Reduction of Dinitroarenes to Nitroanilines with Hydrazine Hydrate†

Nagaraj R. Ayyangar,* Uttam R. Kalkote, Ananda G. Lugade,
Pandurang V. Nikrad, and Vasant K. Sharma
National Chemical Laboratory, Poona 411008, India

(Received December 7, 1982)

Dinitroarenes containing substituents such as hydroxyl and amine groups could be conveniently reduced with 3 molar equivalents of hydrazine hydrate in presence of Raney nickel catalyst in ethanol/1,2-dichloroethane solvent mixture to give a product wherein one of the two nitro groups was reduced to the amino group. The yields of the partial reduction products are good. Under similar conditions alkoxyl substituents in the *o,p*-position to the nitro groups were displaced by the hydrazino group to give 2,4-dinitrophenylhydrazine as the main product. The details of the reduction reaction are described.

We reported the high reduction ability of hydrazine hydrate in presence of Raney nickel in ethanol/1,2-dichloroethane solvent mixture to reduce nitroarenes under mild conditions.[1] The reaction conditions and solvent system are ideal for the reduction of nitro compounds having limited solvent solubility. The scope of the method has been extended for the reduction of one of the two nitro groups of dinitroarenes. The results of the partial reductions are discussed here.

Usually partial reduction is carried out in aqueous medium by using sodium sulfide under alkaline conditions (Zinin reduction) or tin(II) chloride under acidic conditions. The latter has a tendency to reduce the less hindered nitro group. The dinitro compounds such as 2,4-dinitrophenol, its ethers and 2,4-dinitroaniline derivatives undergo reduction with sulfide reagents at the nitro group ortho to the phenolic or ether oxygen or amino substituent.[2] Ruthenium-on-carbon catalyst, which can be used for the partial reduction of 2,4-dinitroaniline to 4-nitro-*o*-phenylenediamine with hydrazine, was shown to be useful for the synthesis of 1-*N*-substituted 4-nitro-*o*-phenylenediamines.[3] Use of Raney nickel catalyst under identical conditions yielded a complex mixture. Catalytic hydrogenation of 2,4-dinitroaniline at 2.72 atm in presence of 5% rhodium on alumina catalyst and ammonia in DMF yielded 4-nitro-*o*-phenylenediamine in 87% yield.[4] 4-Nitro-*o*-phenylenediamine has commercial utility as an analytical reagent, as an ingredient of hair dyes and as a drug and dye intermediate.

Results and Discussion

We found that 1,3-dinitrobenzene (**1a**) could be conveniently reduced to *m*-nitroaniline (**2a**) by using 3 mol of hydrazine hydrate per mol of **1a** in presence of Raney nickel catalyst in ethanol/1,2-dichloroethane solvent mixture at 50—60 °C.[1] The yield of **2a** exceeded 90%. The procedure is advantageously used for the partial reduction of dinitroarene derivatives containing various substituents. Ethanol/1,2-dichloroethane (1:1) mixture was used as the solvent. In general, the ortho nitro group in 2,4-dinitroarylamine derivatives was preferentially reduced, giving 2-amino-4-nitroarylamine derivatives as the main products. The less hindered para-nitro groups was reduced to a small extent. The results are summarised in Table 1. It can be seen that the yield of the partial reduction products by our method are excellent.

Reduction of 2,4-dinitrophenol (**1b**) with 3 molar equivalent of hydrazine hydrate in presence of Raney nickel in ethanol/1,2-dichloroethane (1:1) at 50—60 °C for 4 h gave 2-amino-4-nitrophenol (**2b**) and 4-amino-2-nitrophenol (**2c**) in 92% and 7% isolable yields respectively. Similarly, 2,4-dinitroaniline (**1c**), under identical conditions for 6 h gave 4-nitro-*o*-phenylenediamine (**2d**) and 2-nitro-*p*-phenylenediamine (**2e**) in 95% and 3% isolable yields. Quantitative yield of 2-amino-*N*-ethyl-4-nitro-aniline (**2f**) was obtained from *N*-ethyl-2,4-dinitroaniline (**1d**). With *N*-isopropyl-2,4-dinitroaniline (**1e**), however, the reduction was effected only upto the hydroxylamine stage. The hitherto unknown 2-hydroxy-*N*-isopropyl-4-nitroaniline (**2g**) was isolated in quantitative yield. With *N*-phenyl-substituted amino compounds such as 2,4-dinitrodiphenylamine (**1f**), the yield of the ortho-amino product, 2-amino-4-nitrodiphenylamine (**2h**) fell down to 70% and that of the isomeric para-amino product, 4-amino-2-nitrodiphenylamine (**2i**) increased to 29%. Thus, in the cases described so far, nitro group in the ortho position to amino or hydroxyl substituent was preferentially reduced giving ortho-amino derivatives as major or sole products. Apparently the hydrogen bonding between the amino or the hydroxyl substituent and the ortho-nitro group plays a decisive role in these cases. If such a hydrogen bonding is not possible, as in the case of 2,4-dinitrotoluene (**1j**), the reduction of the para-nitro group was predominant resulting in 88% of 2-nitro-*p*-toluidine (**2n**) and only 10% of 4-nitro-*o*-toluidine (**2o**). Sodium sulfide also selectively reduces the para-nitro group of 2,4-dinitrotoluene.[5,6] The reduction of 2,6-dinitro-*p*-creasol (**1g**) yielded 2-amino-6-nitro-*p*-cresol (**2j**) in 98% yield. During the partial reduction of 3,5-dinitrobenzoic acid, hydrazine salt of 3,5-dinitrobenzoic acid (mp 170 °C, lit,[7] 168 °C) was found to be an intermediate product, which could be isolated and characterized. Ultimately, 3-amino-5-nitrobenzoic acid (**2k**) was isolated in 85% yield. As a representative example of naphthalene series, the partial reduction of 1,5-dinitronaphthalene (**1i**), using 3 molar equivalents of hydrazine hydrate was studied. The reduction product consisted of 20.33% 5-nitro-1-naphthylamine (**2l**), 47.26% 1,5-naphthalenediamine (**2m**) and 32.41% of the starting 1,5-dinitronaphthalene (**1i**). The product analysis was carried out by using IATROSCAN TH

† NCL Communication No. 3130.

Table 1. Partial reduction[a] of dinitroarenes **1** with hydrazine hydrate/raney nickel

Substrate **1** No.		Time h	Product **2**		Yield[b] %	Mp θ_m/°C Found	Ref.
1a,	$1,3\text{-}(NO_2)_2C_6H_4$	3	**2a**,	$3\text{-}NO_2C_6H_4NH_2$	94	113—114	(113—114)[1]
1b,	$2,4\text{-}(NO_2)_2C_6H_3OH$	4	**2b**,	$2\text{-}NH_2\text{-}4\text{-}NO_2C_6H_3OH$	92	141	(142—143)[15]
			2c,	$2\text{-}NO_2\text{-}4\text{-}NH_2C_6H_3OH$	7	130	(131)[16]
1c,	$2,4\text{-}(NO_2)_2C_6H_3NH_2$	6	**2d**,	$2\text{-}NH_2\text{-}4\text{-}NO_2C_6H_3NH_2$	95	200	(200)[17]
			2e,	$2\text{-}NO_2\text{-}4\text{-}NH_2C_6H_3NH_2$	3	140	(140—141)[18]
1d,	$2,4\text{-}(NO_2)_2C_6H_3NHC_2H_5$	6	**2f**,	$2\text{-}NH_2\text{-}4\text{-}NO_2C_6H_3NHC_2H_5$	98	139	(140)[19]
1e,	$2,4\text{-}(NO_2)_2C_6H_3NHCH(CH_3)_2$	4	**2g**,	$2\text{-}NHOH\text{-}4\text{-}NO_2C_6H_3NHCH(CH_3)_2$	100	165	c)
1f,	$2,4\text{-}(NO_2)_2C_6H_3NHPh$	4	**2h**,	$2\text{-}NH_2\text{-}4\text{-}NO_2C_6H_3NHPh$	70	134	(134)[20]
			2i,	$2\text{-}NO_2\text{-}4\text{-}NH_2C_6H_3NHPh$	29	80	(80—81)[21]
1g,	$2,6\text{-}(NO_2)_2\text{-}4\text{-}CH_3C_6H_2OH$	6	**2j**,	$2\text{-}NH_2\text{-}4\text{-}CH_3\text{-}6\text{-}NO_2C_6H_2OH$	98	118	(119)[22]
1h,	$3,5\text{-}(NO_2)_2C_6H_3COOH$	8	**2k**,	$3\text{-}NH_2\text{-}5\text{-}NO_2C_6H_3COOH$	85	210	(210—212)[23]
1i,	$1,5\text{-}(NO_2)_2C_{10}H_6$	8	**2l**,	$5\text{-}NO_2\text{-}C_{10}H_6NH_2$	20.33	118	(118—119)[24]
			2m,	$1,5\text{-}(NH_2)_2C_{10}H_6$	47.26	188	(188)[25]
1j,	$2,4\text{-}(NO_2)_2C_6H_3CH_3$	4	**2n**,	$2\text{-}NO_2\text{-}4\text{-}NH_2C_6H_3CH_3$	88	78	(78)[26]
			2o,	$2\text{-}NH_2\text{-}4\text{-}NO_2C_6H_3CH_3$	10	107	(107)[27]

a) Dinitroarene **1**: hydrazine hydrate ratio 1:3, 0.3 g of catalyst; 10 ml of solvent $C_2H_5OH/ClCH_2CH_2Cl$ (1:1 v/v) per g of **1**. Temperature 50—60 °C. b) Yield of isolated products. c) Characterized by spectral and elemental analysis.

Table 2. Partial reduction[a] of dinitrophenol ethers **3** with hydrazine hydrate/Raney nickel

Substrate **3** No.		Time h	Product[b]		Yield[c] %	Mp θ_m/°C Found	Ref.
3a,	$2,4\text{-}(NO_2)_2C_6H_3OCH_3$	4	**4a**,	$2\text{-}NH_2\text{-}4\text{-}NO_2C_6H_3OCH_3$	8	118	(118)[28]
3b,	$2,4\text{-}(NO_2)_2C_6H_3OC_2H_5$	4	**4b**,	$2\text{-}NH_2\text{-}4\text{-}NO_2C_6H_3OC_2H_5$	6	96	(96)[13]
3c,	$2,4\text{-}(NO_2)_2C_6H_3O(CH_2)_2OH$	4	**4c**,	$2\text{-}NH_2\text{-}4\text{-}NO_2C_6H_3O(CH_2)_2OH$	1	105	(105)[8]
3d,	$2,4\text{-}(NO_2)_2C_6H_3O(CH_2)_2OCH_3$	4	**4d**,	$2\text{-}NH_2\text{-}4\text{-}NO_2C_6H_3O(CH_2)_2OCH_3$	1	94	(95)[29]
3e,	$2,4\text{-}(NO_2)_2C_6H_3OCH(CH_3)_2$	4	**4e**,	$2\text{-}NH_2\text{-}4\text{-}NO_2C_6H_3OCH(CH_3)_2$	1	63	(62.5—63.5)[13]
3f,	$2,4\text{-}(NO_2)_2C_6H_3O(CH_2)_2CH_3$	4	**4f**,	$2\text{-}NH_2\text{-}4\text{-}NO_2C_6H_3O(CH_2)_2CH_3$	0.8	48	(47.5—48.5)[13]
3g,	$2,4\text{-}(NO_2)_2C_6H_3OC_6H_3(Cl)_2\text{-}2,4$	3	**4g**,	$2\text{-}NH_2\text{-}4\text{-}NO_2C_6H_3OC_6H_3Cl_2\text{-}2,4$	0.5	125	d)
3h,	$2,4\text{-}(NO_2)_2C_6H_3OC_6H_5$	3	**4h**,	$2\text{-}NH_2\text{-}4\text{-}NO_2C_6H_3OC_6H_5$	0.5	105	(107)[30]
3i,	$2,4\text{-}(NO_2)_2C_6H_3OCH_2\text{-}CH(OH)CH_2OH$	3	**4i**,	$2\text{-}NH_2\text{-}4\text{-}NO_2C_6H_3\text{-}OCH_2CH(OH)CH_2OH$	1	117	(117)[8]
3j	$2,4\text{-}(NO_2)_2C_6H_3OCH_2C_6H_5$	3	**4l**,	$2\text{-}NH_2\text{-}4\text{-}NO_2C_6H_3OCH_2C_6H_5$	1	105	(105)[13]

a) Dinitrophenol ether **3**: hydrazine hydrate ratio 1:3; 0.3 g of catalyst; 10 ml of solvent $C_2H_5OH/ClCH_2CH_2Cl$ (1:1 v/v) per g of **3**. Temperature 50—60 °C. b) The rest of the product amounting 91—99% is 2,4-dinitrophenylhydrazine (**5**) isolated in every case; mp 200 °C (Ref. 31, 200 °C). c) Yield isolated product. d) Characterized by spectral and elemental analysis.

10 TLC/FID analyzer (Iatron Laboratories, Inc., Japan). Apparently, the initially formed partially reduced product undergoes parallel reduction reaction to give **2m** in organic solvent medium.

Using the same conditions as mentioned above, alkyl and aryl ethers of 2,4-dinitrophenol were allowed to react with 3 molar equivalents of hydrazine hydrate in presence of Raney nickel catalyst. The reactions resulted in rapid replacement of the alkoxyl or the aryloxyl groups with the formation of 2,4-dinitrophenylhydrazine (**5**) as the predominant product. The results are summerised in Table 2. Partial reduction products having amino groups in ortho positions to the alkoxyl or the aryloxyl substituents were isolated in yields ranging from 0.5 to 8%. In general, the bulkier groups (such as 2-hydroxyethoxy, 2-methoxyethoxy, propoxy, isopropoxy 2,4-dichlorophenoxy, phenoxy, 2,3-dihydroxypropoxy, and benzyloxy groups of **3c**—**3j** are replaced with ease with the formation of 2,4-dinitrophenylhydrazine (**5**). The yields of the corresponding partial reduction products **4c**—**4i** and **4l** ranged from 0.5 to 1%. The compound **4f**, known as P4000, is the sweetest material known and is 4000 times sweeter than sucrose.[8] In the case of **3a** and **3b** with less bulkier methoxyl and ethoxyl substituents, the yields of 4-nitro-*o*-anisidine (**4a**) and 4-nitro-*o*-phenetidine (**4b**) were 8% and 6% respectively. The formation of **5** involves nucleophilic substitution reaction similar to the reaction of amines with 2,4-dinitrophenyl ethers, resulting in the formation of 2,4-dinitroanilines.[8–10] The 2,4-dinitrophenylhydrazine (**5**), which is formed in high yields within 4 h, has a tend-

ency to undergo subsequent reaction, if prolonged further, resulting in the formation of side products as indicated by TLC. Under basic reaction conditions, triazoles and other products arising from partial and complete reduction of **5** are produced.[11] Apparently, the catalyst played no role, when 2,4-dinitrophenyl ethers were allowed to react with hydrazine under our conditions. When 2,4-dinitrophenyl ethers **3a**, **3b**, **3c**, **3e**, and **3g** were allowed to react with 3 molar equivalents of hydrazine hydrate in the absence of catalyst in ethanol/1,2-dichloroethane solvent at 60 °C for 4 to 6 h the expected 2,4-dinitriphenylhydrazine (**5**) was obtained as the sole product. There was no trace of any side product.

In order to study the role of solvent, 1,3-dinitrobenzene (**1a**) was allowed to react with 3 molar equivalents of 20, 40, 60, and 80% hydrazine hydrate in aqueous medium at 90 °C for 16—18 h. The yields (based on TLC/FID analysis using IATROSCAN TH 10) of *m*-nitroaniline (**2a**) were 74, 86, 100, and 100% respectively. Since 60% hydrazine hydrate gave quantitative yield of **2a**, it was used for the noncatalytic reduction of other dinitroarenes. The results are summerised in Table 3. The partially reduced products, 2-amino-4-nitrophenol (**2b**) and 2-nitro-*p*-toluidine (**2n**) were obtained in 98% and 92% yields from 2,4-dinitrophenol (**1b**) and 2,4-dinitrotoluene (**1j**) respectively. The reductions were, however, slow and took 16 to 18 h for completion. In the case of *N*-ethyl-2,4-dinitroaniline (**1d**), the yield of **2f** was 70%. The success of this method is noteworthy in the case of 1,5-dinitronaphthalene (**1i**). The yield of the partially reduced product, 5-nitro-1-naphthylamine (**2l**) was 80%. The rest of the product consisted of the starting material **1i**. Apparently in this case, the partially reduced product **2l** falls out of the reaction medium and is inaccesible for further reduction to **2m**. Such a partial reduction of 1,5-dinitronaphthalene by noncatalytic hydrazine hydrate in the absence of solvents has been reported in a patent.[12] Mononitro compounds such as *p*-nitrotoluene (**6**) or difficultly soluble dinitro compounds such as bis(3-nitrodiphenyl) sulfone (**7**) were not reduced under similar conditions even after 36 h. Their complete insolubility in aqueous 60% hydrazine hydrate is responsible for the nonreducibility. The dinitrophenol ethers **3a**, **3b**, **3e**, **3f**, **3g**, and **3i**, as expected yielded 2,4-dinitrophenylhydrazine (**5**) quantitatively within 0.5 h even at 65 °C. Lower concentrations of hydrazine hydrate (*e.g.* 20%) also yielded **5** quantitatively at 90 °C for 2 h. Alkaline sulfide reductions of 2,4-dinitriphenol ethers are known to give the corresponding partial reduction products.[13]

Recently it was shown that if nitro compounds containing *N*- or *O*-benzyl groups were added to a refluxing mixture of excess of hydrazine hydrate, Raney nickel and methanol, nitro groups got reduced to the amino groups; but the benzylamino or the benzyloxy groups were unaffected. Thus 2,4-dinitrophenyl benzyl ether (**3j**) gave 2,4-diaminophenyl benzyl ether with 10 molar equivalents of hydrazine hydrate.[14] We carried out the same reaction under identical conditions by using 3 molar equivalents of hydrazine hydrate and obtained 2,4-diaminophenyl benzyl ether in 43% yield (isolated as dihydrochloride, mp 134 °C), the rest of the product consisted of unreacted starting material. Apparently the mode of addition of the nitro compounds and other reaction conditions play an important role in the selective reduction of dinitroarenes. Thus, when 2,4-dinitroanisole, **3a** (**3a**: hydrazine hydrate ratio 1:3, 0.3 g Raney nickel, 0.01 mol **3a** and methanol 40 ml per g of **3a**, 4 h reaction time) was added to hydrazine hydrate, methanol and Raney nickel mixture at 0 °C, about 95% of unreacted **3a** and 5% 2-amino-4-nitroanisole (**4a**) were isolated. At 28—30 °C, there was 94% formation of **5** and the rest a complex mixture giving a series of spots on silica gel TLC plate. At 40—50 °C, the formation of **5** was 86% and that of **4a** was 8.8% (isolated yield). There was also evidence for the formation of other complex reduction products as noticed by TLC analysis. When **3a** was added to a refluxing mixture of methanol, hydrazine hydrate and Raney nickel, formation of **5** was not noticed. Only 2,4-diaminoanisole was isolated as dihydrochloride, mp 248 °C (mixed mp with an authentic sample was not depressed) in 46% yield. Under identical conditions, **3j** was reduced with 3 molar equivalents of hydrazine hydrate to give a product consisting of 44% of unreacted **3j**, and 43% of 2,4-diaminophenyl benzyl ether isolated as dihydrochloride. Finally, a mixture of methanol, hydrazine hydrate and Raney nickel was refluxed for 10—12

Table 3. Reduction[a] of nitroarene (**6**), dinitroarenes (**7** and **1**) and dinitrophenol ethers (**3**) with 60% aq. hydrazine hydrate alone

Substrate No.	Time / h	Temperature / °C	Product	Yield[b] / %	Mp θ_m/°C Found	Mp θ_m/°C Ref.
6, 4-$NO_2C_6H_4CH_3$	36	90	No reduction	—	—	—
7, $(3\text{-}NO_2C_6H_4)_2SO_2$	36	90	No reduction	—	—	—
1b	18	90	**2b**	98	141	(142—143)[15]
1d	18	90	**2f**	70[c]	139	(140)[19]
1i	16	90	**2l**	80[d]	118	(118—119)[24]
1j	16	90	**2n**	92	78	(78)[26]
3a, **3b**, **3e**, **3f**, **3g**, **3i**	0.5	65	**5**	100	200	(200)[31]
3a[e]	2	90	**5**	100	200	(200)[31]

a) Substrate: hydrazine hydrate ratio, 1:3. b) Yield of isolated product. c) 30% unreacted **1d** is isolated. d) 20% unreacted **1i** is isolated. e) 20% aq. hydrazine hydrate is used.

min, dinitroarenes **3a**, **3d**, **3f**, **3g**, and **3j** (1 mol per 3 mol of hydrazine) were added to the cooled mixture at 5 °C, and stirred for 45 min at that temperature. Hydrazine hydrate in this case probably has decomposed to hydrogen and nitrogen (along with ammonia) in the beginning, leaving most of the alkoxyl of aryloxyl group unaffected. Here, thus, we could isolate partially reduced products without the replacement of *O*-

Table 4. Partial reduction[a] of dinitrophenol ethers (**3**) with hydrazine hydrate/Raney nickel

Substrate No.	Product		Yield[b] %	Mp θ_m/°C Found	Ref.
3a	**4a**,		33	118	(118)[28]
	9a,	$(2\text{-}CH_3O\text{-}5\text{-}NO_2C_6H_3)_2N_2O$	22.9	210	c)
3d	**4j**,	$2\text{-}NHOH\text{-}4\text{-}NO_2C_6H_3OCH_2CH_2OCH_3$	30	116	c)
	9b,	$[2\text{-}(CH_3OCH_2CH_2O)\text{-}5\text{-}NO_2C_6H_3]_2N_2O$	36	178	c)
3f	**4f**		10	48	(47.5—48.5)[13]
	9c,	$[2\text{-}(CH_3CH_2CH_2O)\text{-}5\text{-}NO_2C_6H_3]_2N_2O$	24	106	c)
3g	**4g**		22.5	125	c)
	4k,	$2\text{-}NO_2\text{-}4\text{-}NH_2C_6H_3OC_6H_3Cl_2\text{-}2,4$	20	86	c)
3j	**4l**,	$2\text{-}NH_2\text{-}4\text{-}NO_2C_6H_3OCH_2C_6H_5$	6	105	(105)[13]
	9d,	$[2\text{-}(C_6H_5CH_2O)\text{-}5\text{-}NO_2C_6H_3]_2N_2O$	31	205	c)

a) Substrate: Hydrazine hydrate ratio 1:3; 0.3 g of catalyst; 40 ml of methanol per g of **3**. Temperature 4—5 °C, time 45 min. b) Yield of isolated products. c) Compounds characterized by spectral and elemental analysis.

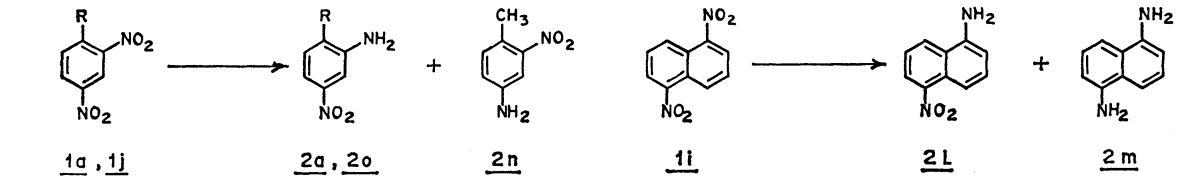

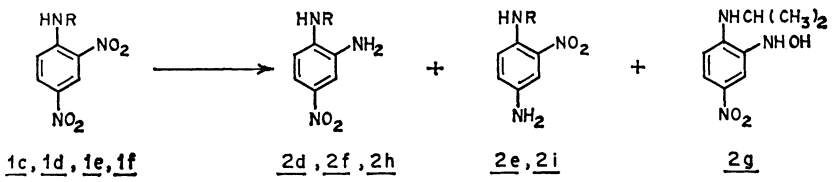

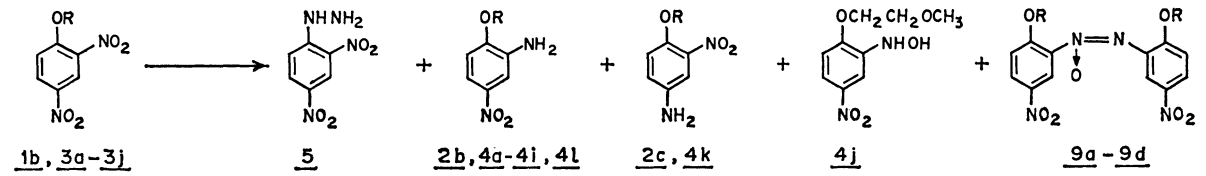

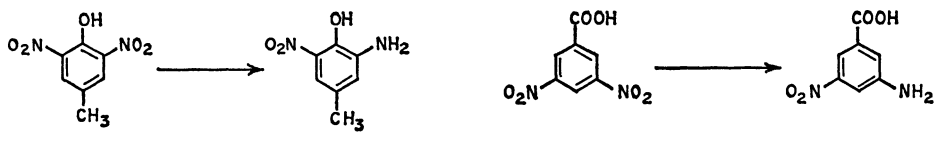

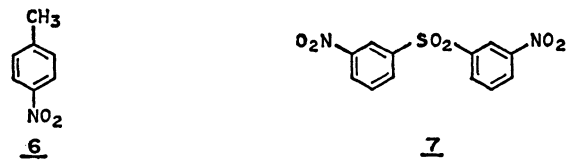

alkyl or *O*-aryl groups (Table 4). The reduction of **3a** gave 2-amino-4-nitroanisole (**4a**) in 33% yield. Under similar conditions, the yields of 2-amino-4-nitro-1-propoxybenzene (**4f**), 2-amino-4-nitro-2′,4′-dichlorodiphenyl ether (**4g**) and 2-amino-4-nitrophenyl benzyl ether (**4l**) were 10, 22.5, and 6% respectively. The 2,4-dinitrophenyl 2-methoxyethyl ether (**3d**), however, gave only 2-hydroxyamino-4-nitrophenyl 2-methoxyethyl ether (**4j**) in 30% yield. In the case of **3a**, **3d**, **3f**, and **3j**, we could additionally isolate the hitherto unknown pale yellow azoxy compounds, 2,2′-disubstituted 5,5′-dinitroazoxybenzenes, **9a**—**9d** as major products in 22.9, 36, 24, and 31% yields respectively. Such azoxy compounds were not isolated during the reduction of dinitroarenes **1**. The compound **3g** yielded the para-nitro reduction product, 4-amino-2-nitro-2′,4′-dichlorodiphenyl ether (**4k**) in 20% yield. About 49% of **3g** and 53% of **3j** were recovered unreacted. All the unknown compounds were characterized by their spectral and analytical data.

Features of the present method are: (1) the preferential formation of 2-amino-4-nitroanilines from the corresponding dinitroanilines, (2) the formation of 2,4-dinitrophenylhydrazine (**5**) by the replacement of *O*-alkyl or *O*-aryl groups in 2,4-dinitrophenyl ethers by hydrazino group; and (3) the simplicity of the work-up procedures.

Experimental

Melting points were uncorrected. IR spectra were recorded on a Perkin-Elmer infrared spectrometer-model 137B, ^{1}H NMR spectra on a Varian T-60 spectrometer using TMS as internal standard. Mass spectra were determined on CEC-2L-11OB spectrometer.

*Reduction of Dinitroarenes **1** and **3**. General Procedure*: A mixture of dinitroarene (0.1 mol), 1:1 (v/v) ethanol/1,2-dichloroethane (10 ml per g of **1** and **3**), and hydrazine hydrate (0.3 mol) is stirred for 10 min at 28—30 °C. Raney nickel (0.3 g) is added with stirring in three portions over a period of 40 min. The reaction is vigorous and the temperature increases to 50—60 °C. (Temperature is not allowed to rise above 60 °C). After 30 min, when the reaction has subsided, stirring is continued for 3 to 8 h at 50—60 °C (Tables 1 and 2). Complete conversion of the dinitroarene can be confirmed by TLC analysis on silica gel using benzene/ethanol (19:1) as eluent and colour development with iodine vapours. The catalyst is removed by filtration. The solvent is evaporated and the residue is crystallized from ethanol (**1a**—**1e**; **1g**—**1i**) and from pet.ether/benzene (**1f**). The filtrates were chromatographed to give minor aminonitroarenes, **2c**, **2e**, and **2i**. In case of **1i**, the product mixture is analyzed by IATROSCAN TH 10 TLC/FID analyzer using benzene:ethanol (99:1, v/v) as solvent to give 1,5-dinitronaphthalene (**1i**) 32.41%, 5-nitro-1-naphthylamine (**2l**), 20.33%, and 1,5-naphthalenediamine (**2m**), 47.26%. The reduction product from **1j** is chromatographed on silica gel (eluent, benzene) to give **2n** and **2o** respectively. The aminonitroarenes **2a**—**2f** and **2h**—**2o** are characterized by mp, mixed mp and elemental micro analysis. The orange product, 2-hydroxyamino-*N*-isopropyl-4-nitroaniline (**2g**) is isolated from the reduction of *N*-isopropyl-2,4-dinitroaniline (**1e**); mp 165 °C. IR (nujol) 3345, 3200, 1585, 1535, 1445, 1370, 1300, 1280 1240, 1220, 1155, 1120, 1100 cm^{-1}; ^{1}H NMR (pyridine) δ 1.26 (s, 3H), 1.40 (s, 3H), 4.1 (q, 1H); (DMSO), 4.63 (d, 1H, exchangeable with D_2O), 4.93 (s, 1H exchangeable with D_2O), 5.6 (s, 1H, exchangeable with D_2O), 6.33 (d, 1H), 7.10—7.4 (m, 2H); MS *m/e* 211. Found: C, 50.62; H, 6.52; N, 19.82%. Calcd for $C_9H_{13}N_3O_3$: C, 51.17; H, 6.20; N, 19.89%.

Dinitrophenylhydrazine (**5**), a major product from dinitrophenol ethers (**3a**—**j**) (Table 2) is isolated by crystallisation from ethanol, mp 200 °C (Lit,[34] mp 200 °C). The filtrate is evaporated and the residue is chromatographed on silica gel (eluent, benzene) to obtain minor partial reduction products (**4**). They are characterized (**4a**—**4f**; **4h**, **4i**, **4l**) by mp (mixed mp with authentic sample is not depressed). The unknown 2-amino-4-nitro-2′,4′-dichlorodiphenylether (**4g**) is characterized by spectral and microanalytical data. IR (Nujol) 3425, 3300, 3200, 1625, 1570, 1510, 1460, 1380, 1340, 1270, 1250, 1230, 1140, 1100, 1050, 865 cm^{-1}. ^{1}H NMR (CH_3CN) δ 4.57 (br s, 2H), 6.66—7.53 (m, 6H); MS *m/e* 299. Found: C, 47.81; H, 2.96; N, 9.33%. Calcd for $C_{12}H_8Cl_2N_2O_3$: C, 48.18; H, 2.69; N, 9.36%.

*Reduction of Nitroarene (**6**), Dinitroarenes (**1b**, **1d**, **1i**, **1j**, and **7**) and Dinitrophenol Ethers (**3a**, **3b**, **3e**, **3f**, **3g**, **3i**) with 60% Hydrazine Hydrate Alone.* A mixture of 2,4-dinitrophenol (**1b**) (0.05 mol), and 60% hydrazine hydrate (0.15 mol) is stirred for 10 min at 28—30 °C. Temperature is then raised to 90 °C in 45 min and stirring is continued for 18 h at 90 °C on water bath. Complete conversion of the nitroarene (**1b**) can be confirmed by TLC analysis on silica gel using benzene/ethanol (19:1) as eluent and colour development with iodine vapours. The dark red coloured reaction mixture is neutralized with dilute hydrochloric acid, when 2-amino-4-nitrophenol (**2b**) gets precipitated out. The solid filtered and crystallized from ethanol. Yield 7.53 g (98%), mp 141 °C (Lit,[16] mp 142—143 °C); mixed mp not depressed. Similar reactions of **1d**, **1i**, and **1j** give **2f**, **2l**, and **2n** in 70, 80, and 92% yields respectively (Table 3). In the case of **6** and **7**, there is no reduction and starting material can be recovered even after 36 h heating at 90 °C. The dinitrophenol ethers under similar treatment give 2,4-dinitrophenylhydrazine exclusively at 65 °C in 0.5 h.

*Reduction of Dinitrophenol Ethers (**3a**, **3d**, **3f**, **3g**, **3j**) in Methanol at 5 °C.* A mixture of methanol (40 ml), 80% hydrazine hydrate (1.9 ml) and Raney nickel (0.3 g) is refluxed for 10—12 min and cooled to 5 °C. To this cold solution is added 2,4-dinitroanisole (**3a**) (1.98 g, 10 mmol) in methanol (40 ml) under stirring. The reaction is continued for additional 45 min. Complete conversion of **3a** can be confirmed by TLC analysis on silica gel using benzene/ethanol (19:1) as eluent and colour development with iodine vapours. The catalyst is removed by filtration. The solvent is evaporated and the residue is chromatographed on silica gel (eluent, benzene). The aminonitrophenolic ethers (**4a**, **4f**, **4g**, **4l**) are characterized by mp, mixed mp and microanalysis. The unknown partial reduction product, 2-hydroxyamino-4-nitrophenyl 2-methoxyethyl ether (**4j**) mp 116 °C, from **3d** is characterized by spectral and microanalytical data. IR (Nujol) 3280, 3180, 1510, 1460, 1333, 1290, 1270, 1200, 1140, 1120, 1080, 1030, 973 cm^{-1}; ^{1}H NMR ($CDCl_3$) δ 3.44 (s, 3H), 3.8 (t, 2H), 4.16—4.54 (m, 3H, 1H exchangeable with D_2O), 4.72 (br s, 1H, exchangeable with D_2O), 7.08—7.40 (m, 1H), 7.92—8.72 (m, 2H). MS *m/e* 228. Found: C, 47.68; H, 5.58; N, 12.01%. Calcd for $C_9H_{12}N_2O_5$: C, 47.37; H, 5.20; N, 12.27%. The hitherto unknown compound 4-amino-2-nitro-2′,4′-dichlorodiphenyl ether (**4k**), mp 86 °C, isolated from **3g** is characterized by spectral and microanalytical data. IR (Nujol) 3480, 3365, 3300, 1625, 1580, 1510, 1460, 1380, 1340, 1270, 1250, 1230,

1140, 1100, 1050, 865 cm^{-1}; ^1H NMR (CH_3CN) δ 3.77 (brs, 2H), 6.43—7.23 (m, 6H); MS *m/e* 299. Found: C, 48.20; H, 3.07; N, 9.73%. Calcd for: $C_{12}H_8N_2Cl_2O_3$: C, 48.18; H, 2.69; N, 9.36%.

The major products, 2',2'-disubstituted 5,5'-dinitroazoxybenzenes (**9a**, **9b**, **9c**, **9d**) were isolated from **3a**, **3d**, **3f**, and **3j** respectively by column chromatography on silica gel column using benzene as eluent. They were characterized as follows:

2,2'-Dimethoxy-5,5'-dinitroazoxybenzene (**9a**), mp, 210 °C. IR (Nujol) 3090, 1600, 1525, 1450, 1340, 1290, 1145, 1090, 1020, 895, 815 cm^{-1}; ^1H NMR ($CDCl_3$) δ 4.26 (d, 6H), 7.16—7.56 (m, 3H), 8.36—9.23 (m, 3H). MS *m/e* 348. Found: C, 48.08; H, 4.00; N, 16.16%. Calcd for $C_{14}H_{12}N_4O_7$: C, 48.28; H, 3.47; N, 16.08%.

2,2'-Bis(2-methoxyethoxy)-5,5'-dinitroazoxybenzene (**9b**), mp 178 °C. IR (Nujol) 3100, 2850, 1600, 1590, 1450, 1340, 1290, 1280, 1200, 1140, 1125, 1080, 1040, 940, 860, 810 cm^{-1}; ^1H NMR ($CDCl_3$) δ 3.66 (s, 6H), 4.0 (m, 4H), 4.56 (m, 4H), 7.20—7.66 (m, 3H), 8.33—8.93 (m, 3H); MS *m/e* 436. Found: C, 50.10; H, 4.89; N, 12.31%. Calcd for $C_{18}H_{20}N_4O_9$: C, 49.54; H, 4.62; N, 12.84%.

2,2'-Dipropoxy-5,5'-dinitroazoxybenzene (**9c**), mp 106 °C. IR (Nujol) 3080, 1605, 1515, 1455, 1375, 1350, 1280, 1150, 1070, 1000, 900, 820, 800 cm^{-1}; ^1H NMR ($CDCl_3$) δ 1.20 (t, 6H) 1.72—2.30 (m, 4H), 4.40 (t, 4H), 7.2—7.66 (m, 3H), 8.56—9.33 (m, 3H); MS *m/e* 404. Found: C, 52.95; H, 5.25; N, 13.24%. Calcd for $C_{18}H_{20}N_4O_7$: C, 53.46; H, 4.29; N, 13.85%.

2,2'-Bis(benzyloxy)-5,5'-dinitroazoxybenzene (**9d**), mp 205 °C. IR (Nujol) 3080, 1600, 1530, 1415, 1345, 1275, 1142, 1085, 905, 815 cm^{-1}; ^1H NMR ($CDCl_3$) δ 5.43 (d, 4H), 7.16—7.76 (m, 13H), 8.26—8.80 (m, 3H); MS *m/e* 500. Found: C, 62.25; H, 4.57; N, 11.41%. Calcd for $C_{26}H_{20}N_4O_7$: C, 62.40; H, 4.00; N, 11.20%.

References

1) N. R. Ayyangar, A. G. Lugade, P. V. Nikrad, and V. K. Sharma, *Synthesis*, **1981**, 640.

2) H. K. Porter, *Org. React.*, **20**, 455 (1973).

3) J. L. Miesel, G. O. P. O'Doherty, and J. M. Owen, "Catalysis in Organic Synthesis," ed by P. N. Rylander and H. Greenfield, Academic Press, New York, (1976), p. 273.

4) R. J. Alaimo and R. J. Storrin, "Catalysis of Organic Reactions," ed by W. R. Moser, Marcel Dekker Inc., New York, (1981), p. 473.

5) H. Limprict, *Ber.*, **18**, 1400 (1885).

6) A. S. Wingrove and R. L. Caret, "Organic Chemistry," Harper and Row Publishers, New York (1981), p. 1122.

7) *Beilstein*, **9**, 414 (1942).

8) J. J. Blanksma and P. G. Fohr, *Recl. Trav. Chim.*, **65**, 711 (1946).

9) L. Bartolotti and A. Cerniani, *Bull. Sci. Fac. Chim. Ind. Bologna*, **14**, 33 (1956); *Chem. Abstr.*, **50**, 15182 (1956).

10) Y. Ogata and M. Okano, *J. Am. Chem. Soc.*, **71**, 3211 (1949).

11) C. C. Clark, "Hydrazine," Mathieson Chemical Corporation, Maryland, (1953), p. 32.

12) H. E. Oelinek and I. Zugravescu, Romanian Patent 49844 (1972); *Chem. Abstr.*, **79**, 146173 (1973).

13) P. E. Verkade, C. P. Van Dijk, and W. Meerburg, *Recl. Trav. Chim.*, **65**, 346 (1946).

14) F. Yuste, M. Saldana, and F. Walls, *Tetrahedron Lett.*, **23**, 147 (1982).

15) W. W. Hartman and H. L. Silloway, *Org. Synth.*, Coll. Vol. 3, 82 (1965).

16) P. Friedländer and M. Zeitlin, *Ber.*, **27**, 196 (1894).

17) K. P. Griffin and W. D. Peterson, *Org. Synth.*, **21**, 20 (1941).

18) B. M. Webster and P. E. Verkade, *Recl. Trav. Chim.*, **68**, 77, 83 (1949).

19) R. Foster, *J. Chem. Soc.*, **1957**, 4687.

20) W. Ozegowski, D. Krebs, and M. Wunderwald, *J. Prakt. Chem.*, **20**, 166 (1963).

21) A. T. Peters, *J. Appl. Chem. Biotechnol.*, **26**, 131 (1976).

22) H. Lindemann and S. Romanoff, *J. Prakt. Chem.*, **122**, 214 (1929); *Chem. Abstr.*, **24**, 91 (1930).

23) D. Pitre and E. Lorenzotti, *Chimica (Aarau)*, **19**, 462 (1965); *Chem. Abstr.*, **63**, 13128 (1965).

24) G. Schröeter, *Ber.*, **63**, 1308, 1317 (1930).

25) N. J. Leonard and A. M. Hyson, *J. Am. Chem. Soc.*, **71**, 1961 (1949).

26) E. Nölting and A. Collin, *Ber.*, **17**, 261 (1884).

27) A. G. Green and T. A. Lawson, *J. Chem. Soc.*, **59**, 1013 (1891).

28) C. Niemann, J. F. Mead, and A. A. Benson, *J. Am. Chem. Soc.*, **63**, 609 (1941).

29) J. F. Manning and J. P. Mason, *J. Am. Chem. Soc.*, **62**, 3136 (1940).

30) C. I. Brodrick, J. S. Nicholson, W. F. Short, and D. G. Wibberely, *J. Chem. Soc.*, **1953**, 1080.

31) A. I. Vogel, "A Text Book of Practical Organic Chemistry," 3rd ed., Longmans, London, (1956), p. 610.

The Resonance Raman Spectra of (*meso*-Tetraphenylporphinato)-cobalt(II)-d_0 [Co (TPP)-d_0], -d_8, and -d_{20}

Muneteru KOZUKA* and Masamoto IWAIZUMI
Chemical Research Institute of Non-Aqueous Solutions, Tohoku University, Katahira, Sendai 980
(Received January 6, 1983)

Synopsis. The resonance Raman spectra of the title complexes were measured, and a normal coordinate analysis was carried out. The 1604 and 1243 cm^{-1} polarized bands of Co(TPP)-d_0 were assigned to resonance-enhanced phenyl modes. This suggests the presence of appreciable porphine-phenyl resonance interaction in this complex.

Many vibrational studies have been devoted to the TPP ligand. Since there is no physiological porphine with aromatic groups at its *meso* positions, it is important to check the TPP's characteritic features which are caused by the peripheral phenyl group. Recently, Burke *et al.* tentatively assigned the 1240 cm^{-1} band of Fe(TPP) and the corresponding bands of the analogues to a mode mainly associated with the C_m–Ph (mesocarbon-phenyl) stretching vibration and stated that the porphine-phenyl resonance interaction in the ground state was no required to interpret any of the RR data.[1,2] On the other hand, Fuchsman *et al.* assigned the halogen-sensitive resonance Raman (RR) bands (1100 — 1050 cm^{-1}) of tetra(*p*-halophenyl)porphine derivatives[3] and the 1234 cm^{-1} band of Cu(TPP)[4] to phenyl modes and pointed out that this was direct evidence of the resonance interaction. Adequate vibrational data to shed light on this controversial point were not found in the literature. Fortunately, however, our understanding of the fundamental vibration of the porphine core has been extensively advanced by Kitagawa *et al.*'s detailed experimental[5] and theoretical[6] studies of (octaethylporphinato)nickel(II) [Ni(OEP)]. Although the pattern of peripheral substitution in TPP is quite different from that in OEP, X-ray crystallographic studies suggest that the bonding within the porphine core is essentially the same in both porphines.[7,8] Hence, we tried to explain our RR data with reference to the results of normal coordinate analyses.

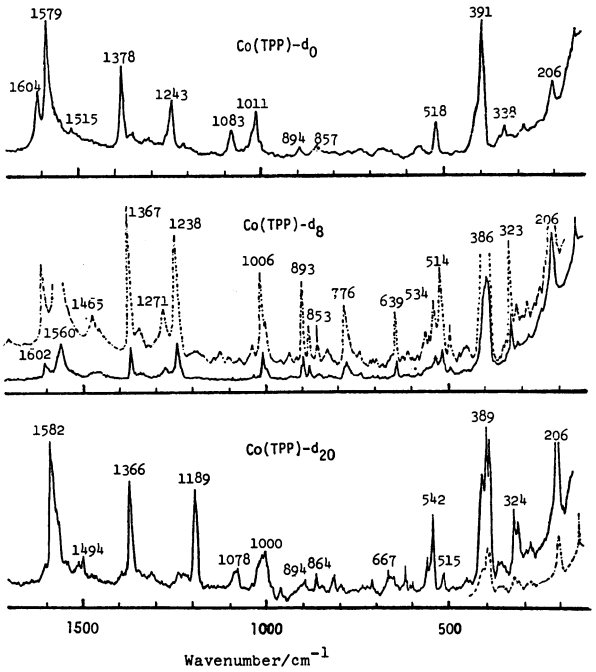

Fig. 1. RR spectra of Co(TPP)-d_0, -d_8, and -d_{20}. The samples were deposited on a cold tip at 10 K as films and excited by the 457.9 nm line of an Ar-ion laser.

Figure 1 shows the RR spectra of the well-purified samples, which were vaporized from a "miniature oven" and deposited onto a cold Cu tip to make films. The films at 10 K were excited by the 457.9 nm line of an Ar-ion laser. The details and the spectrometer have been described previously.[9] The spectra closely resemble those in Ar matrices.[9] All the strong bands were found to be polarized, as was expected from the fact that the RR spectra of metalloporphines were dominated by the totally symmetric modes (A_{1g} species

TABLE 1. CALCULATED AND OBSERVED A_{1g} FUNDAMENTAL FREQUENCIES (cm^{-1}) OF Co(TPP)-d_0, -d_8, -d_{20}, AND M(T_{piv}PP).

Modes	Co(TPP)-d_0		Co(TPP)-d_8		Co(TPP)-d_{20}		Fe(T_{piv}PP)[a]	Co(T_{piv}PP)
	Obsd	Calcd	Obsd	Calcd	Obsd	Clacd	Obsd	Calcd
ν_1	—	3057	—	2264	—	3057	—	3057
ν_2	1579(vs)	1578	1560(vs)	1569	1582(vs)	1578	1566(vs)	1578
ν_3	1497(w)[b]	1493	1465(mw)	1471	1494(mw)	1493	1480(vw)	1493
ν_4	1378(s)	1378	1367(ms)	1356	1366(s)	1378	1370(s)	1377
ν_5	1083(m)	1092	776(m)	769	1078(m)	1092	1080(mw)	1092
ν_6	1011(ms)	1000	1006(ms)	1017	1000(ms)	1000	996(m)	994
ν_7	894(w)	886	893(mw)	883	894(w)	885	—	881
ν_8	391(vs)	385	386(vs)	379	389(s)	384	372(s)	375
ν_9	206(m)	208	206(s)	208	206(s)	203	—	143

a) The data were cited from Ref. 6. b) This band was distinctly detected in Ar matrices, but was smeared out in films (Ref. 9).

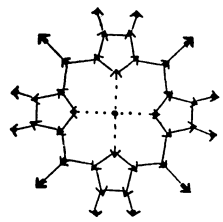

Fig. 2. The eigenvector of the Co(TPP)-d_0's ν_9 mode (A_{1g}, 206 cm^{-1}).

under D_{4h} symmetry) when the exciting frequency approaches that of the Soret band.[10] An experimental assignment is shown in Table 1, along with the calculated frequencies.

To carry out the normal coordinate calculation, the following assumptions were adopted: the symmetry of the porphine core is D_{4h}, and the phenyl group is regarded as a single dynamic unit with a mass of 77 ($-d_0$ and $-d_8$) and 82 ($-d_{20}$). The structural parameters were taken from the result of X-ray crystallographic analysis of Co(TPP),[8] but slightly modified to keep the D_{4h} symmetry. The potential energy was expressed with the same type of modified Urey-Bradley force field as that used for (NiOEP) by Abe *et al.*[6] The calculations were carried out by means of a NEAC-ACOS 1000 computer system at Tohoku University with AXSMZ and LSMX programs.[11]

The A_{1g}-calculated frequencies are in good agreement with the observed frequencies. The determined stretching and repulsive force constants were slightly different from those of Ni(OEP) in a manner roughly corresponding to their structural change. The experimental Teller-Redlich A_{1g} product ratios of Co(TPP)-d_8 and $-d_{20}$ to $-d_0$ were 0.499 and 0.970, which were close to the theoretical values of 0.500 and 0.969 respectively.[12] The 1604 and 1243 cm^{-1} bands ($-d_0$) were not included in the A_{1g} mode. Some other weakly observed bands were explained with B_{1g}, A_{2g}, and B_{2g} frequencies calculated at the same time.

Although Fuchsman *et al.* supposed that some porphine-core modes of Cu(TPP) shifted to a frequency range lower by about 35 cm^{-1} upon the phenyl deuteration,[4] the calculated frequencies of Co(TPP)-d_0 and $-d_{20}$ show that the maximum frequency shift is only 5 cm^{-1} in the ν_9 mode (Fig. 2). In this mode, the phenyl groups vibrate in-phase with each other and with the largest amplitude, while those in the other core modes are negligibly small. The mesocarbons vibrate in the same phase as do the phenyl groups, but with a slightly smaller amplitude. From the calculation, it is now evident that the 1243 cm^{-1} band ($-d_0$) shifted to 1189 cm^{-1} ($-d_{20}$). This large frequency shift and the disappearance of the 1604 cm^{-1} band upon the phenyl deuteration suggest that they are phenyl modes.

To confirm this assignment, a normal coordinate treatment for [*a,a,a,a-meso*-(*o*-pivaloylamidophenyl)porphinato]cobalt(II), [Co(T_{piv}PP)], was also carried out, where the same structural parameters and force constants as those used for Co(TPP) were employed. The calculated frequencies well explained the observed frequencies of Fe(T_{piv}PP)[2] in Table 1. A comparison between the calculated frequencies of Co(TPP)-d_0 and Co(T_{piv}PP) shows that the drastic changes in the mass (from 77×4 to 176×4 amu) and structure in the periphery do not substantially affect the A_{1g} normal frequencies, except for the ν_9 mode. This means that the second assumption, or the separation of the phenyl modes from the porphine-core modes, is appropriate. If the 1240 cm^{-1} band of Fe(TPP) is one of the core modes, as assigned by Burke *et al.*,[2] its counterpart in Fe(T_{piv}PP) should be found in a slightly lower frequency region. However, this is not the case.

The present work thus supports Fuchsman *et al.*'s results.

The authors wish to thank Professor Ichiro Nakagawa and Dr. Yoshiyuki Morioka of Tohoku University for their critical reading of the manuscript and their helpful discussions. We are also indebted to Professor Kazuo Nakamoto of Marquette University for his kindness in allowing us to use the RR data recorded at his laboratory, and to Dr. James Kincaid of Kentucky University for the gift of the deuterated samples.

References

1) J. M. Burke, J. R. Kincaid, and T. G. Spiro, *J. Am. Chem. Soc.*, **100**, 6077 (1978).
2) J. M. Burke, J. R. Kincaid, S. Peters, R. R. Gagne, J. R. Collman, and T. G. Spiro, *J. Am. Chem. Soc.*, **100**, 6083 (1978).
3) W. H. Fuchsman, Q. R. Smith, and M. M. Stein, *J. Am. Chem. Soc.*, **99**, 4177 (1977).
4) W. H. Fuchsman, J. M. Goldberg, D. D. Levy, and Q. R. Smith, *Bioinorg. Chem.*, **9**, 461 (1978).
5) T. Kitagawa, M. Abe, and H. Ogoshi, *J. Chem. Phys.*, **69**, 4516 (1978).
6) M. Abe, T. Kitagawa, and Y. Kyogoku, *J. Chem. Phys.*, **69**, 4526 (1978).
7) D. C. Cullen and E. F. Meyer, Jr., *J. Am. Chem. Soc.*, **96**, 2095 (1974).
8) P. Madura and W. R. Scheidt, *Inorg. Chem.*, **15**, 3182 (1976).
9) M. Kozuka and K. Nakamoto, *J. Am. Chem. Soc.*, **103**, 2162 (1981).
10) R. H. Felton and Nai-Teng Yu, "The Porphyrins," ed by D. Dolphin, Academic Press, New York (1978), Vol. III, p. 371.
11) T. Shimanouchi, "Computer Program of Polyatomic Molecules," The University of Tokyo (1968).
12) E. B. Wilson, Jr., J. C. Decius, and P. C. Cross, "Molecular Vibrations," McGraw-Hill, New York (1955), p. 125.

Carbon-13 Relaxation Times of Poly(vinylnaphthalene)s in Solution

Kazuhiko SEKI* and Yoshio IMAMURA

Department of Chemistry, Faculty of Science, Science University of Tokyo, Kagurazaka, Shinjuku-ku, Tokyo 162

(Received January 31, 1983)

Synopsis. Carbon-13 spin-lattice relaxation times and nuclear Overhauser enhancement factors were measured at 25.03 MHz and 40 °C for a solution of poly(1-vinylnaphthalene)(P1VN) and poly(2-vinylnaphthalene)(P2VN). The backbone motions in P1VN and P2VN were characterized by a distribution of correlation times. The relative mobilities of P1VN, P2VN, and polystyrene were as follows: $\bar{\tau}_{\text{polystyrene}} < \bar{\tau}_{\text{P2VN}} < \bar{\tau}_{\text{P1VN}}$ for the average correlation times. These results were explained on the basis of the energy contour maps for polystyrene, P2VN, and P1VN.

In our previous papers,[1-3] we explained the conformational characteristics of poly(1-vinylnaphthalene) (P1VN) and poly(2-vinylnaphthalene) (P2VN), by estimating the steric compression energies of the rotational isomeric states (RIS) of the naphthyl side groups and the conformational energies of the skeletal bonds.

The revealed differences of the characteristics between P1VN and P2VN corresponded well with the difference of the solution properties of P1VN and P2VN, such as in transition[1] phenomenon, NMR spectra patterns[2] and in fluorescence spectra of the solution.[3]

Futhermore, some information about the molecular dynamics of P1VN and P2VN can be also drawn from the previous calculations. The segmental motion of P1VN chain may undergo the steric restriction of the neighboring 1-naphthyl groups. Since the P2VN chain is not so spatially crowded by neighboring 2-naphthyl groups as the chain in P1VN is, the motion of the main chain in the former would not be so influenced by the restriction of neighboring groups. Consequently, the relative mobilities of P1VN, P2VN, and polystyrene chains can be predicted as follows: $\tau_{\text{polystyrene}} < \tau_{\text{P2VN}} < \tau_{\text{P1VN}}$ for the correlation time τ. These correlation times can be estimated by the measurement o carbon-13 spin relaxation time and nuclear Overhauser enhancement. The purpose of this paper is to discuss the segmental motion in P1VN and P2VN chain as characterized by a distribution of the correlation times.

Experimental

Samples of P1VN and P2VN were prepared by radical polymerization, using α,α'-azobisisobutyronitrile as an initiator. The number-average molecular weights of these polymers were determined using a "KUNAUAR's Membrance Osmometer" in chloroform solution at 37 °C. The average molecular weights of P1VN and P2VN were 4.0×10^4 and 7.5×10^4, respectively. In the vinyl aromatic polymers with this range of the degree of polymerization, the T_1 values are almost independent of the chain lengths.[4,5]

Natural abundance ^{13}C NMR spectra were obtained at 25.03 MHz by Fourier transform techniques using a JEOL JNM PS-100 spectrometer; details described before.[2] Spin-lattice relaxation times T_1 were measured from PRFT spectra obtained from 180°-t-90° sequences. The spectra of the polymer solutions of *ca.* 30% concentrations in dioxane-d_8 were observed at 40 °C. Nuclear Overhauser enhancements (NOE) were measured by comparison of coupled and decoupled spectra. The maximum errors in T_1 and NOE were within ±10%.

Calculation

Assuming only the dipolar interactions between a methine carbon and the proton bonded to it, the ^{13}C T_1 and NOEF (NOE-1) are given by[6,7]

$$1/T_1 = 2.190\times10^9(f(\omega_1)+3f(\omega_2)+6f(\omega_3))\ \text{s}^{-1}, \quad (1)$$

$$\text{NOEF} = \frac{(-f(\omega_1)+6f(\omega_2))}{(f(\omega_1)+3f(\omega_2)+6f(\omega_3))}\times 3.976, \quad (2)$$

$$\omega_1 = \omega_H - \omega_C, \quad (3)$$

$$\omega_2 = \omega_C, \quad (4)$$

and

$$\omega_3 = \omega_H + \omega_C, \quad (5)$$

where ω_C and ω_H are the Larmor frequencies for ^{13}C and ^{1}H, respectively and for ^{13}C measurement at 25.03 MHz, $\omega_1=4.682\times10^8$ rad s^{-1}, $\omega_2=1.573\times10^8$ rad s^{-1}, $\omega_3=7.828\times10^8$ rad s^{-1}. As the backbone motion in a polymer is characterized by a distribution of correlation times, the spectral density function $f(\omega_i)$ is written by considering a log $-\chi^2$ distribution,[8,9] as follows:

$$f(\omega_i) = \frac{\bar{\tau}\Gamma^{(p)}(s)(b^s-1)\mathrm{d}s}{(b-1)(1+\omega_i^2\bar{\tau}^2((b^s-1)/(b-1))^2)} \quad (6)$$

$$\Gamma^{(p)}(s) = \frac{1}{\Gamma(p)}(ps)^{p-1}\exp(-ps)p\mathrm{d}s, \quad (7)$$

and

$$s = \log_b(1+(b-1)\tau/\bar{\tau}) \quad (8)$$

where Γ function, $\Gamma(p)$, normalizes $\Gamma^{(p)}(s)$ to unity, and the width of the distribution is characterized by p. The value of log base $b=1000$ is used. The $\bar{\tau}$ represents an average correlation time. Using Eqs. 1—8, T_1 and NOEF were computed by varying the width parameter p from 1 to 100 in 1-unit steps, and by varying the average correlation time $\bar{\tau}$ from 1.0×10^{-7} to 1.0×10^{-12} s^{-1}.

Results and Discussion

The proton-decoupled ^{13}C NMR spectra of P1VN and P2VN at 40 °C are shown in Figs. 1a and b, respectively. The signal peaks of naphthyl carbons are denoted by the symbols A, B, C, D, E, and F from the order of the low magnetic field. Table 1 shows the ^{13}C T_1 values for the aromatic peaks in P1VN and P2VN, together with those for polystyrene reported in the literature.[5,10,11] The T_1 for the aromatic carbons suggests that A–C peaks correspond to the nonprotonated carbons, and that D–F for P1VN and D, E for P2VN correspond to the protonated carbons. The line widths of A peaks in P1VN and P2VN are somewhat broader than that of B or C peak. Since this feature is attributed

Table 1. ^{13}C Spin-lattice relaxation times of aromatic carbon in P1VN, P2VN, and polystyrene

Polymer	Solvent	Temp/°C	Aromatic carbons T_1/ms					
			A	B	C	D	E	F
P1VN	Dioxane-d_8	40	968	1320	1520	78	85	86
P2VN	Dioxane-d_8	40	928	1380	1440	91	84	—
			Meta, ortho carbon			Para carbon		Ref.
Atactic polystyrene	Toluene-d_8	30	140			120		10
Atactic polystyrene	Tetrachloroethylene	44	98			89		5
Atactic polystyrene	Tetramethylene oxide	30	126			110		11

Table 2. ^{13}C Spin-lattice relaxation times and NOE of methine carbon in P1VN, P2VN, and polystyrene in solution

Polymer	Solvent	Temp/°C	T_1/ms	NOE	$\bar{\tau}$/s^{-1}	p	Ref.
P1VN	Dioxane-d_8	40	66	1.40	1.6×10^{-8}	20	—
P2VN	Dioxane-d_8	40	64	1.70	5.3×10^{-9}	12	—
Isotactic polystyrene	*o*-Dichlorobenzene	35	65	1.80	1.0×10^{-9}	18	9
Atactic polystyrene	Pentachloroethane	30			4.5×10^{-9}	20	12

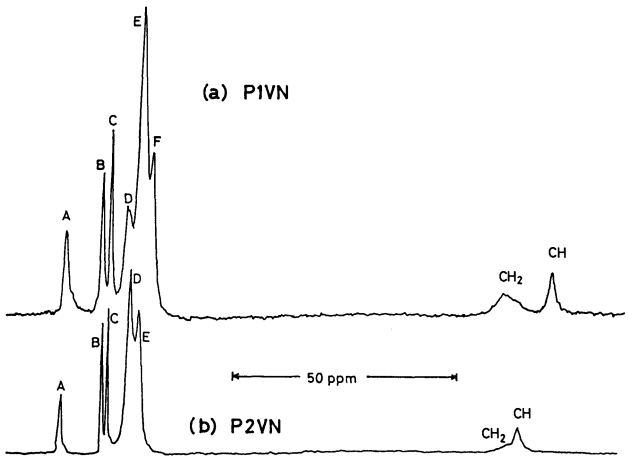

Fig. 1. Proton-decoupled, natural abundance ^{13}C FT NMR spectra of (a) P1VN and (b) P2VN in dioxane-d_8 at 25.03 MHz and 40 °C.

to the tacticity number in the polymer samples used, the A peak can be assigned to the naphthyl carbons, which bond to α-carbon. A similar phenomenon was observed in polystyrene. The other peaks of the aromatic carbons can not be assigned to each carbon in the naphthyl group at the present stage. T_1 values of the protonated carbon in P1VN and P2VN are smaller than that of polystyrene. This observation suggests that the naphthyl ring rotation is perturbed by the neighboring naphthyl rings, CH and CH_2 groups.

The average correlation times $\bar{\tau}$ and width parameter p satisfying the observed values (T_1 and NOE) are given in Table 2. T_1 value of methine carbon in P1VN was approximately equal to that of P2VN or polystyrene. It is apparent that the correlation time can not be adequately approximated by the T_1 value, and the $\bar{\tau}$ values for the segmental motion of these polymer are mainly influenced by the NOEF.

The segmental motion of P1VN was estimated to be slower than that for P2VN and polystyrene, as was expected. The order of the relative mobilities of the polymer chains agreed with that described above. These experimental results are explained as follows. The mobility of the main chain would be correlated to the values of the contour lines of the energy maps, which surround all the minima (tt, gt, tg, and gg) positions, since the energy value of each contour has a influence upon the magnitude of the change in RIS (t and g) of the molecular chain. In a previous paper,[3] all minima in the conformational energy maps of P1VN chain were shown to be surrounded by the contour lines of 9 kcal mol^{-1},† in the P2VN chain, the lines were 7—8 kcal mol^{-1}, while in polystyrene, it was sufficient to surround the all minima by contours of 5—6 kcal mol^{-1}. The order of the energy of these contours was found to be that of the chain mobilities described above.

References

1) K. Seki, Y. Ichimura, and Y. Imamura, *Macromolecules*, **14**, 1831 (1981).
2) K. Seki, S. Mori, and Y. Imamura, *Bull. Chem. Soc. Jpn.*, **55**, 2739 (1982).
3) K. Seki and Y. Imamura, *Bull. Chem. Soc. Jpn.*, **55**, 3711 (1982).
4) F. Heatley and B. Wood, *Polymer*, **19**, 1405 (1978).
5) A. Allerhand and R. K. Hailstone, *J. Chem. Phys.*, **56**, 3718 (1972).
6) J. Schaefer and D. F. S. Natusch, *Macromolecules*, **5**, 416 (1972).
7) A. Allerhand, D. Doddrell, and R. Komoroski, *J. Chem. Phys.*, **55**, 189 (1971).
8) J. R. Lyerla, T. T. Horikawa, and D. E. Johnson, *J. Am. Chem. Soc.*, **99**, 2463 (1977).
9) J. Schaefer, *Macromolecules*, **6**, 882 (1973).
10) Y. Inoue and T. Konno, *Polym. J.*, **8**, 457 (1976).
11) W. Gronski and N. Murayama, *Makromol. Chem.*, **179**, 1509 (1978).
12) F. Heatley and A. Begum, *Polymer*, **17**, 399 (1976).

†: In SI units: 1 kcal mol^{-1}=4.184 kJ mol^{-1}.

Wetting of Coal by Nonionic Surfactant and Mixtures of Nonionic and Anionic Surfactants

Kunio Esumi,* Kenjiro Meguro, and Hidemasa Honda
Department of Applied Chemistry and Institute of Colloid and Interface Science, Science University of Tokyo, Kagurazaka, Shinjuku-ku, Tokyo 162
(Received May 16, 1983)

Synopsis. The rates of wetting of coals with various carbon contents by aqueous nonionic surfactants and mixtures of nonionic and anionic surfactants were examined. It was found that the wetting rate of each coal decreased with an increase of the length of oxyethylene chain in the nonionic surfactant. Further, the wetting rate of coal by anionic surfactant was enhanced by the addition of nonionic surfactant. This enhancement was most effective for coals with relatively low carbon content.

Wettability of coal allows us to understand mechanisms of coal flotation, coal dust suppression, and coal–water mixing. A number of techniques[1-3] have been used to measure the wettability of coal. Glanville and Wightman[4] have employed a wetting time method. They have reported that rates of wetting of coal by aqueous surfactant solution are accelerated by addition of dipositive metal ions. Esumi *et al.*[5] have studied the effect of dipositive metal ions on wetting of coals with various carbon contents by anionic surfactant solutions. They have demonstrated that the rates of wetting of coals are enhanced more effectively by anionic surfactants with long-chain hydrophobic groups than those with short-chain ones, in the presence of dipositive metal ions.

In this work, effects of nonionic surfactants and mixtures of nonionic and anionic surfactant solutions on the wetting of coals were investigated by measuring the wetting rates and the zeta potential of wetted coal particles.

Experimental

Materials. The coals used in this work were Yallourn, Taiheiyo, Miike, and Hon-gay coals, whose carbon contents were 61.6, 74.8, 85.2, and 93.0 wt%, respectively. They were sieved between 60 and 100 mesh. The other physical properties for them have been described elsewhere.[6]

Sodium 1,2-bis(2-ethylhexyloxycarbonyl)ethanesulfonate (Aerosol OT), sodium 1,2-bis(2-methylpentyloxycarbonyl)-ethanesulfonate(Aerosol MA), and sodium 1,2-bis[diamyl-(mixture of 2-methylbutyl and 3-methylbutyl)oxycarbonyl]-ethanesulfonate (Aerosol AY) were obtained from the American Cyanamid Co. Poly(oxyethylene)nonylphenyl ethers (NP-*n*, where *n* indicates the average mole number of oxyethylene units) were supplied by Nikko Chemicals Co., Ltd. These surfactants were used without further purification.

The water used was purified by passing through Milli-Q Reagent-Grade Water Systems until its specific conductivity fell below $10^{-7}\ \Omega^{-1}\ cm^{-1}$.

Measurements. To estimate rates of wetting of coal, sink times were measured for 0.30 g of coal gently deposited on the surface of the aqueous surfactant solution in a 100 ml beaker at 25 °C. The time taken for the last trace of unwetted coal particles to break through the surface of the aqueous surfactant solution was measured with a stopwatch. The average value of four or five run was taken as the final sink time. Here, the rate of wetting of coal was expressed as the surface area of coal wetted per second to compare the wettability of coals with different surface area.

The zeta potential of coal particles after exposure to the aqueous surfactant solution was measured using a Pen Kem Laser Zee^{tm} Model 500. The surface tension of the aqueous surfactant solution was measured using a Wilhelmy-type tensiometer at 25 °C.

Results and Discussion

Figure 1 shows the wetting rates of coals with various carbon contents as a function of the concentration of nonionic surfactants. It can be seen that the wetting rate of each coal is enhanced with an increase of the concentration of nonionic surfactant. Further, the wetting rates of coals are influenced by the length of the oxyethylene chain in the nonionic surfactant; the wetting rate of each coal decreases with an increase of the length of oxyethylene chain from 7.5 to 50. In this study, the optimum oxyethylene chain at which a maximum wetting rate of all the coals except Hon-gay coal is attained is located at 7.5—15 mol. Glanville and Haley[7] have also studied the wetting rates of coal obtained from the Pocahontas No. 3 Seam of McDowell County, West Virginia by using a series of polyethoxylated alkylphenol and have reported that there is an optimum degree of ethoxylation for a maximum wetting rate of coal dust. Thus, the above results can be interpreted by considering the surface tension of the nonionic surfactant and the diffusion rate to the coal surfaces: as the surface tension of nonionic surfactant

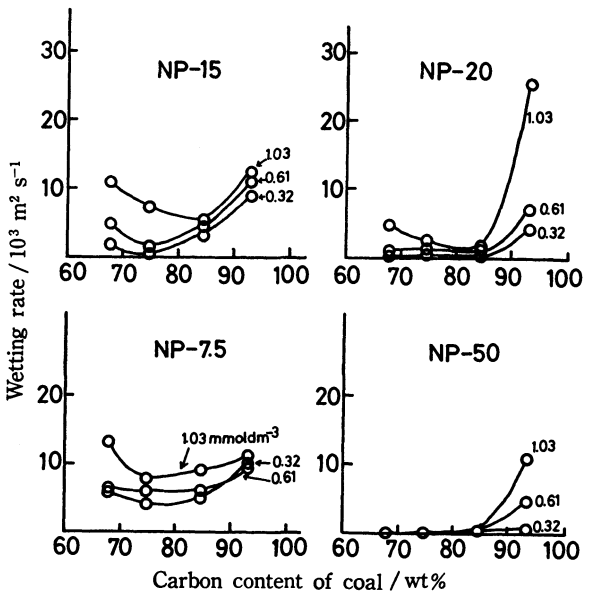

Fig. 1. The rates of wetting of coals with various carbon content by nonionic surfactant solutions.

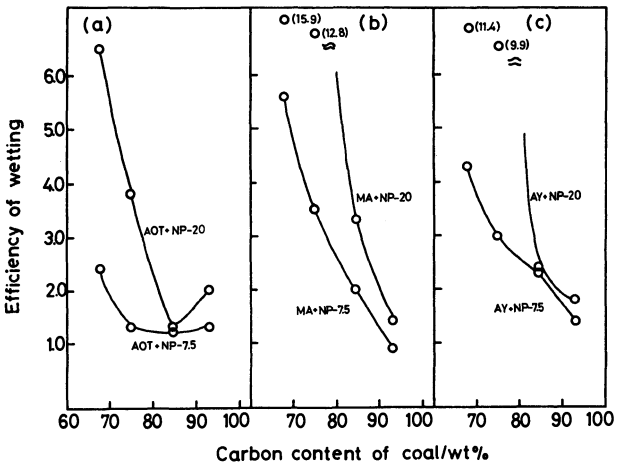

Fig. 2. The efficiency of wetting of coals with various carbon content by addition of nonionic surfactant in the presence of anionic surfactant.
(a): Aerosol OT, 1.38 mmol dm^{-3}, NP-*n*, 0.61 mmol dm^{-3}, (b): Aerosol MA, 7.5 mmol dm^{-3}, NP-*n*, 0.61 mmol dm^{-3}, (c): Aerosol AY, 14 mmol dm^{-3}, NP-*n*, 0.61 mmol dm^{-3}.

at a same concentration increases from NP-7.5 to NP-50, the wetting rate of coal by the nonionic surfactant is accelerated from NP-50 to NP-7.5 and the nonionic surfactants with longer oxyethylene chains are believed to diffuse more slowly than those with shorter ones. Compared with anionic surfactants[5] such as Aerosol OT, MA, and AY, the addition of the nonionic surfactants is less effective on the wetting rate of coal.

As the addition of nonionic surfactant has been shown to increase the wetting power for textile[8] by some anionic surfactants, a similar effect will be expected for the wettability of coal. So, the effect of nonionic surfactants on the wetting rate of coal by anionic surfactant solution was examined. Here, the efficiency of wetting rate of coal by the addition of nonionic surfactant can be evaluated by the ratio of the wetting rate of coal by the addition of nonionic surfactant in the presence of anionic surfactant to the sum of wetting rates of coal in each surfactant. The results are given in Fig. 2. In Aerosol OT–NP-*n* system, the efficiency of wetting decreases with an increase of carbon content and shows a minimum at 85.2 wt%, then increases for both NP-7.5 and NP-20. On the other hand, the efficiency of wetting decreases gradually with an increase of carbon content until 74.8 wt%, then rapidly for Aerosol MA–NP-*n* and Aerosol AY–NP-*n* systems. Particularly, the wetting rates of Yallourn and Taiheiyo

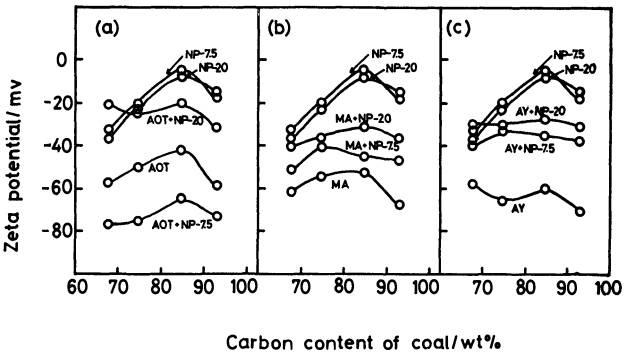

Fig. 3. The zeta potentials of coals shown in Fig. 2.

coals are enhanced most effectively by the addition of NP-20 in the presence of Aerosol MA and AY, respectively. Since the surface tensions of these systems are not so different, this enhancement might be attributed to an increase caused by the nonionic surfactant in the mobility of the anionic surfactant, resulting in more rapid diffusion to the surface of coal particles.

To elucidate the interaction of coal surfaces and the anionic surfactant by the addition of the nonionic surfactant, the zeta potentials of coal particles after their exposure to the aqueous surfactant solution were measured. The results are depicted in Fig. 3. The magnitudes of zeta potentials of coal particles after the exposure to the anionic surfactant–NP-*n* systems are located between that of anionic and of nonionic surfactants alone, except for the Aerosol OT–NP-7.5 system. The above results imply that co-adsorption of anionic and nonionic surfactants occurs on the coal surface and weakens the repulsion forces between anionic surfactant molecules, resulting in the promotion of the wetting rates of coal.

References

1) T. Murata, *Nippon Kogyo Kaishi*, **94**, 547 (1980).
2) D. T. Hornsby and J. Leja, *Colloids and Surfaces*, **1**, 425 (1980).
3) E. L. Fuller, Jr., *J. Colloid Interface Sci.*, **75**, 577 (1980).
4) J. O. Glanville and J. P. Wightman, *Fuel*. **58**, 819 (1979).
5) K. Esumi, K. Meguro, and H. Honda, *Bull. Chem. Soc. Jpn.*, **56**, 933 (1983).
6) K. Esumi, K. Meguro, and H. Honda, *Bull. Chem. Soc. Jpn.*, **55**, 3021 (1982).
7) J. O. Glanville and L. H. Haley, *Colloids and Surfaces*, **4**, 213 (1982).
8) A. K. Biswas and B. K. Mukherji, *J. Appl. Chem.*, **10**, 73 (1960).

Enthalpies of Combustion of Organic Compouds. V. 3- and 4-Nitroanilines†

Keiichi NISHIYAMA, Minoru SAKIYAMA,* and Syûzô SEKI††
Chemical Thermodynamics Laboratory and Department of Chemistry, Faculty of Science, Osaka University, Toyonaka 560
(Received June 13, 1983)

Synopsis. Precision oxygen bomb combustion calorimetry was carried out for the title compounds in the crystalline states. Standard enthalpies of formation at 298.15 K for the crystalline and gaseous states were derived.

Although standard enthalpies of combustion has been reported for 3- and 4-nitroanilines by several authors,[1-4] the agreement between these values is poor. In order to obtain more reliable values, oxygen bomb combustion calorimetry accompanying carbon dioxide analysis has been conducted for these compounds.

Experimental

Materials. Microanalytical standard 4-nitroaniline (Kishida, SMA-SP-18) was used after applying the pellet drying procedure.[5] Commercial 3-nitroaniline (Wako, special Grade) was purified by recrystallization from aqueous solution and then from ethanol solutions (three times). After preliminary drying, the purified material was subjected to the pellet drying.

Combustion Calorimetry. An isoperibol rotating bomb calorimeter, described elsewhere,[6,7] was used without rotating the bomb. The calorimeter was calibrated by burning thermochemical standard benzoic acid (N. B. S. SRM 39i) under certificate conditions. Mean and standard deviation of the mean for the energy equivalent of the empty calorimeter, ε° (calor), was obtained to be (15 163.52±0.51) J K^{-1} from eight calibration experiments. The substances were found to produce a small amount of soot, when a pellet weighing about 1.2 g was ignited alone in an ordinary open crucible at 3 MPa of oxygen pressure. The use of a deep crucible with a small lid[8] or the use of a higher pressure (4 MPa) was not efficient in preventing the soot formation. Consequently, a pellet of the thermochemical standard benzoic acid, weighing 0.3 g, was placed on a pellet of either substance in the ordinary crucible, and they were ignited at 3 MPa of oxygen pressure. In this way, the soot formation was effectively suppressed. In order to examine the completeness of combustion and/or the purity of tha sample, carbon dioxide recovery was determined by the method described previously.[7] Carbon monoxide was barely detected. Nitric acid was determined by titration with aqueous sodium hydroxide solution.

Table 1. Auxiliary data for the calculation of standard energy of combustion

Material	Formula	ρ / g cm^{-3}	c_p / J K^{-1} g^{-1}	$-(\partial U/\partial p)_T$ / J MPa^{-1} g^{-1}
3-Nitroaniline	$C_6H_6O_2N_2$	1.430	1.15	(0.048)
4-Nitroaniline	$C_6H_6O_2N_2$	1.424	1.116	(0.048)
Benzoic acid	$C_7H_6O_2$	1.320	1.21	0.0527
Cotton fuse	$CH_{1.86}O_{0.93}$	1.5	1.7	0.0290

Auxiliary Quantities. Relative atomic masses were taken from the recommendation of IUPAC Commission on Atomic Weights (1977). Densities, specific heat capacities, and $(\partial U/\partial p)_T$ values are collected in Table 1. Other auxiliary quantities are as follows: T_h=298.15 K, V(bomb)=0.3469 cm^3, ΔU_c°(fuse)=−16507 J g^{-1}, and $\Delta U_c^\circ/M$(benzoic acid)=−(26414±1) J g^{-1}, where uncertainty is the estimated standard deviation of the mean.

Results

Molar srandard energies and enthalpies of combustion, given in this paper, refer to the following idealized combustion reaction at 298.15 K: $C_6H_6O_2N_2(c)+(13/2)O_2(g)=6CO_2(g)+N_2(g)+3H_2O(l)$. Details of the combustion calorimetry are presented in Table 2. Most of the symbols in the table are essentially similar to those used by Hubbard *et al.*[9] Mean and standard deviation of the mean for molar standard energy of combustion, $\Delta U_c^\circ(c)$, and those for relative total carbon dioxide recovery, $[m(CO_2,\text{obsd})/m(CO_2,\text{calcd})]$, are

Table 2. Summary of combustion calorimetric results on 3- and 4-nitroanilines

Experiment	3-Nitoaniline				4-Nitroaniline				
	1	2	3	4	1	2	3	4	5
m'(compd)/g	0.85161	0.84414	0.84702	0.84879	0.84963	0.84914	0.84788	0.85055	0.85704
m''(B-acid)/g	0.30065	0.29354	0.30007	0.29804	0.30266	0.29427	0.29286	0.30742	0.30647
m'''(fuse)/g	0.00234	0.00257	0.00270	0.00220	0.00191	0.00230	0.00236	0.00205	0.00273
$m^i(H_2O)$/g	3.14	3.17	3.05	3.15	3.07	3.17	3.13	3.07	3.00
$(T_i/K)-273.15$	23.14719	23.14226	23.14067	23.14000	23.13275	23.13830	23.14895	23.12804	23.12626
$(T_f/K)-273.15$	24.99401	24.97222	24.98451	24.98326	24.97713	24.97061	24.97411	24.97976	24.98690
ΔT_{corr}/K	0.02699	0.02882	0.02700	0.02743	0.02357	0.02719	0.02434	0.02167	0.02135
$n^f(HNO_3)$/mmol	1.152	1.160	1.167	1.167	1.142	1.129	1.192	1.154	1.154
ΔU_{ign}/J	7.7	7.7	7.8	7.8	7.8	7.8	2.5	7.5	7.6
ΔU_Σ/J	22.1	21.8	21.8	22.0	22.0	21.9	21.7	22.0	22.0
$\Delta U_d(HNO_3)$/J	67.8	68.3	68.7	68.7	67.2	66.5	70.2	68.0	68.0
ε^i(cont)/J K^{-1}	26.3	26.4	25.9	26.3	26.0	26.4	26.2	24.0	23.7
ε^f(cont)/J K^{-1}	27.3	27.4	26.9	27.3	27.0	27.4	27.2	25.0	24.7
$-\Delta U_{IBP}$/J	27717.0	27351.6	27590.9	27575.8	27649.4	27411.5	27351.1	27784.3	27923.7
$-\{\Delta U_c^\circ/M(\text{compd})\}$/kJ g^{-1}	23.0706	23.0597	23.0571	23.0640	22.9916	22.9791	22.9805	22.9739	22.9787
$-\Delta U_c^\circ$(compd)/kJ mol^{-1}	3186.63	3185.13	3184.77	3185.72	3175.72	3173.98	3174.19	3173.26	3173.93
$[m(CO_2,\text{obsd})/m(CO_2,\text{calcd})]$	1.0000	1.0001	—	1.0005	1.0002	1.0001	1.0005	0.9995	0.9997

† Contribution No. 59 from Chemical Thermodynamics Laboratory, Faculty of Science, Osaka University.
†† Present address: School of Science, Kwansei Gakuin University, Nishinomiya 662.

Table 3. Standard thermodynamic quantities at 298.15 K of 3- and 4-nitroanilines

	3-Nitroaniline	4-Nitroaniline
$-\Delta U_c^\circ$(c)/kJ mol^{-1}	3185.56 ± 0.88	3174.22 ± 0.90
$-\Delta H_c^\circ$(c)/kJ mol^{-1}	3184.32 ± 0.88	3172.98 ± 0.90
$-\Delta H_f^\circ$(c)/kJ mol^{-1}	34.2 ± 1.2	45.6 ± 1.2
ΔH_{sub}°/kJ mol^{-1}	96.7 ± 1.3[a]	100.8 ± 1.3
ΔH_f°(g)/kJ mol^{-1}	62.5 ± 1.8	55.2 ± 1.8

a) Ref. 11.

Table 4. Comparison of the present results with literature values

	$-\Delta H_c^\circ$(c)/kJ mol^{-1}
3-Nitroaniline	
Médard and Thomas(1957)[a]	3190.3 ± 6.3
Lebedeva *et al.* (1971)[b]	3180.3 ± 0.4
Present study	3184.32 ± 0.88
4-Nitroaniline	
Cole and Gilbert (1951)[c]	3177.08 ± 0.63
Médard and Thomas(1954)[d]	3180.1 ± 3.2
Lebedeva *et al.* (1971)[b]	3175.7 ± 0.8
Present study	3172.98 ± 0.98

a) Ref. 2. b) Ref. 3. c) Ref. 1. d) Ref. 4.

$-(3185.56\pm0.41)$ kJ mol^{-1} and (1.0002 ± 0.0001), respectively, for 3-nitroaniline, and $-(3174.22\pm0.41)$ kJ mol^{-1} and (1.0002 ± 0.0001), respectively, for 4-nitroaniline.

Derived standard thermodynamic quantities are presented in Table 3. CODATA key values of thermodynamics[10] and the calorimetric values of standard enthalpy of sublimation, reported by Malaspina *et al.*,[11] were used to calculate ΔH_f°(c) and ΔH_f°(g), respectively. Uncertainties for ΔU_c°(c) and ΔH_c°(c) are the uncertainty intervals defined by Rossini.[12] Those for ΔH_f°(c) and ΔH_f°(g) were calculated by combining the relevant uncertainties by use of the equation of error propagation.

Discussion

The present values are compared with literature values in Tabel 4. The present value for 3-nitroaniline is intermediate between the literature values. The one for 4-nitroaniline is less negative than the rest. Although the present value is closer to that of Levedeva *et al.*,[3] they do not agree with each other within the sum of the uncertainties. The present results for both substances, seem to be more reliable, since the chemical aspect of the combustion calorimetry is evidenced to be quite normal by the results of carbon dioxide analysis.

References

1) L. G. Cole and E. C. Gilbert, *J. Am. Chem. Soc.*, **73**, 5423 (1951).
2) L. Médard and M. Thomas, *Mém. Poudres*, **39**, 195 (1957).
3) N. D. Lebedeva, N. M. Gutner, and V. L. Ryadnenko, *Zh. Fiz. Khim.*, **45**, 999 (1971); *VINITI*, No. 2502-71.
4) L. Médard and M. Thomas, *Mém. Poudres*, **36**, 97 (1954).
5) C. E. Vanderzee and M. Månsson, *J. Chem. Thermodyn.*, **4**, 533 (1972), and references cited therein.
6) M. Sakiyama, T. Nakano, and S. Seki, *Bull. Chem. Soc. Jpn.*, **48**, 705 (1975).
7) K. Nishiyama, M. Sakiyama, S. Seki, H. Horita, T. Otsubo, and S. Misumi, *Bull Chem.. Soc. Jpn.*, **53**, 869 (1980).
8) A. Kamaguchi, T. Sato, M. Sakiyama, and S. Seki, *Bull. Chem. Soc. Jpn.*, **48**, 2203 (1975).
9) W. N. Hubbard, D. W. Scott, G. Waddington, "Experimental Thermochemistry," Vol. 1, ed by F. D. Rossini, Interscience, New York (1956), Chap. 5.
10) CODATA Task Group on Key Values of Thermodynamics, 1977, *CODATA Bull.* **28** (1978); *J. Chem. Thermodyn.*, **10**, 903 (1978).
11) L. Malaspina, R. Gigli, G. Bardi, and G. de Maria, *J. Chem. Thermodyn.*, **5**, 699 (1973).
12) F. D. Rossini, "Experimental Thermochemistry," ed by F. D. Rossini, Interscience, New York (1956), Vol. 1, Chap. 12.

Distribution of Calcium Ion in the Crystal of $MgTiO_3$–$CaTiO_3$ System

Eiji NAGATA,† Junzo TANAKA,* Masayuki TSUTSUMI, and Eisuke BANNAI
National Institute for Research in Inorganic Materials, Namiki 1-1, Sakura-Mura, Niihari-Gun, Ibaragi 305
†*Taki Chemical Co., Midorimachi 2, Befu-Cho, Kakogawa, Hyogo 675-01*

(Received February 17, 1983)

Synopsis. The crystal of 0.96 $MgTiO_3$–0.04 $CaTiO_3$ was grown by a TSFZ method. The distribution of $CaTiO_3$ in the crystal was analyzed by SEM and EPMA. The results obtained suggest that the change of dielectric properties of $MgTiO_3$ by adding $CaTiO_3$ results from the independent distribution of $CaTiO_3$ in $MgTiO_3$.

Some dielectric materials have been studied up to date to develope high-quality filters of microwave resonator. From the characteristics of practical filters, the following three dielectric properties are required for materials: (i) high dielectric constant, (ii) high dielectric Q value, and (iii) low temperature coefficient ($=\eta_f$) of resonant frequency.[1] There exsist, for example, systems of BaO–TiO_2, $MgTiO_3$–$CaTiO_3$, $Ba(Zn_{1/3}Nb_{2/3})O_3$–$Ba(Zn_{1/3}Ta_{2/3})O_3$ *etc.*[2-4] which satisfy such requirements.

In the system of $MgTiO_3$–$CaTiO_3$, to add a slight amount of $CaTiO_3$ into $MgTiO_3$ betters the temperature coefficient η_f of $MgTiO_3$.[2] The purposes of the present report are to study the crystal growth of $(Mg_{0.96}Ca_{0.04})TiO_3$ by a travelling solvent floating zone method and to study the detailed phase diagram of the system of $MgTiO_3$–$CaTiO_3$ just near both end-members in order to make clear an effect of adding $CaTiO_3$ on the dielectric properties, especially on the coefficient η_f, of $MgTiO_3$–$CaTiO_3$ system.

Starting materials were MgO, $CaCO_3$ (99% purity), and TiO_2 (99.5% purity). They were weighed at the molar ratio of Mg : Ca : Ti=0.96 : 0.04 : 1, sufficiently mixed in acetone for 2 h, and fired at 1200 °C for 12 h. After the compound obtained was remixed in acetone for 2 h, it was pressed into a cylindrical rod of 10 mm in diameter and 100 mm in length under the hydrostatic pressure of 1 t/cm². The rod was sintered at 1400 °C in oxygen gas for 2 h; this rod was used as a feed of the crystal growth. An apparatus used for the crystal growth was the ellipsoidal image furnace (Nippon Electric Co.) whose heater source was a halogen lamp of 1.5 kW located at one focus position. The sintered rod was set up at the other focus position of the furnace where the light emitted from the halogen lamp focuses. The crystal was grown under the following conditions: the seed and feed were counter-rotated at the rate of 35 cm^{-1}, the growth rate was 2 mm/h, and the flow rate of air was 5 l/min. The dimension of the crystal obtained was 10 mm in diameter and 50 mm in length. The chemical analysis of the middle part of the crystal indicates Mg=19.1, Ca=1.20, and Ti=39.7 in wt%, which agrees with the composition of the starting material, that is, Mg=19.3, Ca=1.33, and Ti=39.6 in wt%.

The microscopic analysis in the middle part of the crystal was performed by the scanning electron microscope (SEM) and by the electron probe microanalyzer (EPMA). Figure 1 shows the result of qualitative analysis by SEM, together with the variation of intensities of the characteristic X-rays of both Mg and Ca ions along a straight line a. As seen from the figure, there exsist two domains; one is a light enclosed domain and the other is a dark dominant domain. The content of Mg is large outside of the light domain, while inside of the light domain, its content is very small. The behaviors of Ca is quite opposite to that of Mg: the content is extremely small outside of the light domain but large inside. On contrary to Mg and Ca, the content of Ti changes little over both the domains.

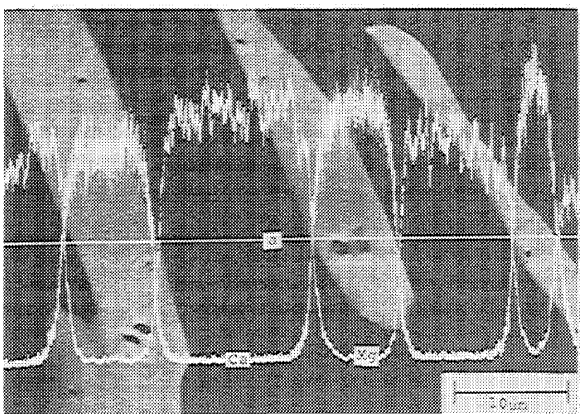

Fig. 1. Composition image of SEM for the middle part of the crystal $(Mg_{0.96}Ca_{0.04})TiO_3$. Lines denoted by Mg and Ca respectively show the results of the line analysis of Mg and Ca contents along a line a.

TABLE 1. EPMA ANALYSIS OF THE CRYSTAL

	Mg(wt %)	Ca(wt %)	Ti(wt %)	O(wt %)
Dark domain	20.15	0.06	40.85	40.53
Light domain	0.29	29.77	34.81	32.81

In order to determine the compositions of both the domains, the distribution of Mg, Ca, Ti, and O was quantitatively analyzed by EPMA; the results are summarized in Table 1. Two kinds of product could be observed as predicted from the phase diagram reported by Rouf *et al.*,[5] the products being roughly expressed by $MgTiO_3$ and $CaTiO_3$, respectively. $MgTiO_3$ occupies dominant part of the crystal corresponding to the dark domain in Fig. 1, while $CaTiO_3$ is a little interpersed as inclusions along the growth direction, corresponding to the light domain in Fig. 1. Table 1 shows that $CaTiO_3$ is solved into $MgTiO_3$ by 0.2 wt% ($=C_1$), while $MgTiO_3$ also into $CaTiO_3$ by 1.4 wt% ($=C_2$). This suggests that there exsist solid solutions just near both the end-members of the system $MgTiO_3$–$CaTiO_3$, which are not shown in the diagram reported by Rouf *et al.*[5] The result that $C_2 \gg C_1$ is reasonable since Mg ions more easily substitute Ca ions than Ca ions do Mg ions because of $r_{Ca} > r_{Mg}$, where r

indicates a radius. The result of powdered X-ray diffraction shows that both solid solutions have same crystal structures and lattice constants as $MgTiO_3$ (ilmenite type) and $CaTiO_3$ (perovskite type), respectively. The physical properties of the solid solution are, therefore, almost same as the original materials, $MgTiO_3$ and $CaTiO_3$.

As mentioned above, the temperature coefficient η_f changes by adding $CaTiO_3$ by about 4—6 mol% into $MgTiO_3$. In practice, the η_f of the crystal is −38 ppm/deg although it contains oxygen defects, the absolute value of the η_f being smaller than that (η_f= −60 ppm/deg) of $MgTiO_3$ reported by Courtney.[3] Thus, the experimental results lead us the conclusion that the change of the coefficient η_f does not result from forming solid solution such as $(Mg,Ca)TiO_3$ whose temperature coefficient η_f is nearly equal to zero, but from the independent distribution of $CaTiO_3$ and $MgTiO_3$ whose coefficients η_f have mutually opposite sign.[2]

The authors thank Prof. Shioichiro Nomura, Dr. Isamu Shindo and Dr. Masayuki Tsukioka for their valuable suggestions concerning the crystal growth and the dielectric properties of $MgTiO_3$. The authors also thank Mr. Satoshi Takenouchi and Mrs. Michiko Kobayashi to perform the chemical analysis.

References

1) H. M. O' Bryan, J. Thomson, and J. K. Plourde, *J. Am. Ceram. Soc.*, **57**, 450 (1974).
2) H. Tamura and M. Katsube, Japan Patent, 138008 (1979); *Chem. Abstr.*, **92**, 120665s (1980).
3) W. E. Courtney, *IEEE Trans,. MTT*-**18**, 476 (1970).
4) T. Makino and A. Hashima, *IEEE Trans.*, *MTT*-**27**, 633 (1979).
5) M. A. Rouf, A. H. Cooper, and H. B. Bell, *Trans. Brit. Ceram. Soc.*, **68**, 265 (1969).

cyclo-Octasulfur in Swine Manure

Akio YASUHARA,* Sumio NAGAI,† Keiichiro FUWA, and Masayuki JIMBU††
Division of Chemistry and Physics, National Institute for Environmental Studies, Yatabe, Tsukuba-gun, Ibaraki 305
††*Department of Animal Genetics, National Institute of Animal Industry, Kukizaki, Inashiki-gun, Ibaraki 305*
(Received February 22, 1983)

Synopsis. Pale-yellowish white needles were isolated from a rotten mixture of swine urine and feces by vacuum distillation and identified to be *cyclo*-octasulfur by means of mass spectrometry and other methods. This is the first time that this compound has been detected in swine manure.

cyclo-Octasulfur is the most stable form having a crown structure[1] and a main component in monoclinic and rhombic sulfurs.[2] Khare and Sagan[3] detected large amounts of *cyclo*-octasulfur in photoreaction products of hydrogen sulfide and other gaseous compounds. This compound was also isolated from a culture filtrate when a marine fungus was cultivated in a sulfite-pulp waste-liquor medium and was characterized by mass spectrometry.[4] White and Lee[5] found *cyclo*-octasulfur in a coal extract by gas chromatography-mass spectrometry using a capillary column and flame photometric detection. *cyclo*-Octasulfur has hardly been detected in other environmental samples. This article describes an identification of *cyclo*-octasulfur in swine manure.

Experimental

Isolation of cyclo-*Octasulfur.* A rotten mixture of swine urine (700 mL) and feces (400 g) was frozen at *ca.* −80 °C and vacuum-distilled in a frozen state at a pressure of *ca.* 10^{-4} Torr (1 Torr=133.322 Pa): The trap for volatile substances was cooled at −80 to −100 °C. The sample flask was kept at room temperature for 1 d, heated at 40 °C for 2 d, and finally heated at 100 °C for 4 d. The distillation residue (35 g) was mixed with diethyl ether (1 L) for 1 d. The filtrate was concentrated to *ca.* 50 mL and then vacuum-distilled in order to separate volatile from nonvolatile matters. The volatile matters were combined with the volatile in the trap as described below.

The ice (960 mL) containing the volatile compounds in the trap was melted and the volatile substances were extracted with diethyl ether (200 mL) by a liquid-liquid continuous extractor for 2 d. The extracted solution was combined with the volatile matters from the residue and then concentrated at atmospheric pressure with a Kuderna–Danish concentrator. When most of the diethyl ether was removed, white needle crystals were precipitated from the solution. The isolated crystals (3.35 mg), mp 112—119 °C, were characterized by mass spectrometry and other methods.

Gas Chromatography–Mass Spectrometry. The gas chromatographic conditions used were as follows: apparatus, HEWLETT PACKARD HP5710A gas chromatograph; column, glass column (3 m×3 mm i.d.) packed with 5% Thermon-3000 on 80—100 mesh Chromosorb W (AM-DMCS); column temperature, 50 °C initially for 2 min, increased to 250 °C at a rate of 4 °C/min; injection temperature, 250 °C; helium flow rate, 20 mL/min. The mass spectrometric conditions used were as follows: apparatus, JEOL JMS-DX 300 mass spectrometer and JEOL JMA 3500 mass data analysis system; ionizing current, 300 μA; electron energy, 70 eV; accelerating voltage, 3 kV; scan range, *m/e* 10—400; scan speed, 1.6 s/scan; repetition time, 2.5 s; ionization chamber pressure, 1—2×10^{-6} Torr; ionization chamber temperature, 180—210 °C.

† Present address: Hokkaido Research Institute for Environmental Pollution, West 12, North 19, Kita-ku, Sapporo Hokkaido 060.

Results and Discussion

The needle crystals isolated from rotten swine manure were pale-yellowish white and smelled of sulfur, which we usually experience near volcanos. They were easily soluble in benzene and chloroform, slightly soluble in diethyl ether and tetrahydrofuran, and insoluble in acetone. Their mass spectra were measured both by the direct inlet method and by the GC/MS method. The mass spectra, shown in Fig. 1, were identical with each other and only one peak was observed in a total ion monitoring by GC/MS, as shown in Fig. 2. Therefore, these crystals are not a mixture but a single compound. The mass spectrum measured in this study is the same as that of *cyclo*-octasulfur, though the relative intensities of the peaks at *m/e* 128, 160, 192, and 256 are somewhat different from those already reported.[4,6,7] With the direct inlet method, all mass spectra are essentially identical irrespective of sample temperature. No signals were observed in a measurement of ^{1}H NMR spectra, indicating that there is no hydrogen atom in the molecule. The electronic spectrum of this compound in

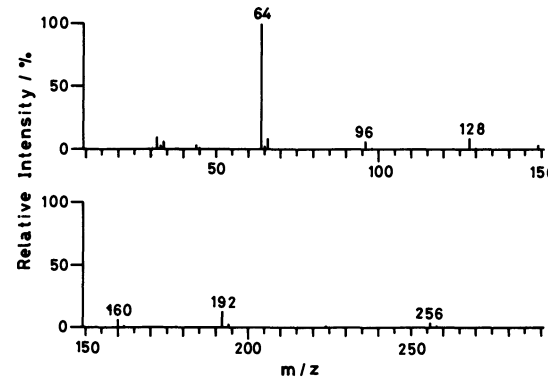

Fig. 1. Mass spectrum of *cyclo*-octasulfur.

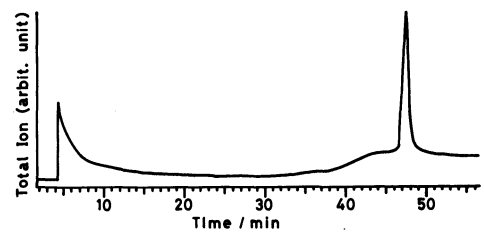

Fig. 2. Total ion monitoring of *cyclo*-octasulfur in GC/MS.

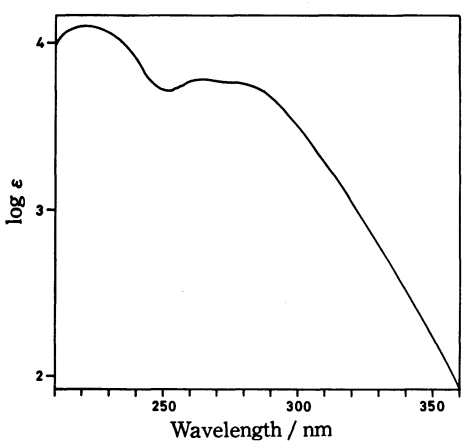

Fig. 3. Electronic spectrum of *cyclo*-octasulfur. Solvent, THF.

tetrahydrofuran solution, shown in Fig. 3, is slightly different from the one in the literature.[8] The IR spectrum of *cyclo*-octasulfur has already been reported by a few investigators,[3,9] although it is not clear-cut because of too small a sample amount. From these results, this compound has been decided to be *cyclo*-octasulfur.

cyclo-Octasulfur was detected only in rotten mixtures of swine urine and feces (two samples) and not in rotten swine urine (two samples). A semiquantitative result gave an amount of 3.35 mg of *cyclo*-octasulfur with a rotten mixture of 700 mL urine and 400 g feces. This compound has not always been detected in swine manure, since the formation of *cyclo*-octasulfur as a single substance of elemental sulfur might require some specific conditions which can seldom been realized in natural environment. According to Yurovskii's theory,[10] *cyclo*-octasulfur might be produced *via*

$$2FeSO_4+5H_2S \longrightarrow 2FeS_2+2S+H_2SO_4+4H_2O,$$

where the hydrogen sulfide is anaerobically formed from sulfate by bacteria. It has been known that a large amount of hydrogen sulfide is produced from liquid swine manure by anaerobic digestion.[11] Furthermore, dimethyl disulfide is found in swine manure.[12] It is reasonable to consider that *cyclo*-octasulfur results from the hydrogen sulfide evolved in swine manure. Since the offensive hydrogen sulfide raises environmental odor problems, the conversion of hydrogen sulfide to *cyclo*-octasulfur is very desirable. Also, it is interesting to examine whether or not *cyclo*-octasulfur is to be detected in other environments where hydrogen sulfide is evolved.

cyclo-Octasulfur can be detected by means of GC/MS or GC with a flame photometric detector, since GC with a flame ionization detector cannot have any responses. The ionization efficiency of *cyclo*-octasulfur in mass spectrometry was roughly investigated. Dimethylsulfone was used as a reference material, because it is often contained in swine manure and it gives a weak peak at mass number 64 (SO_2^+) in its mass spectrum. In the mass spectrum of *cyclo*-octasulfur, a base peak (S_2^+) locates at mass number 64. The molar ratio in peak intensity of *cyclo*-octasulfur to dimethylsulfone at *m/e* 64 is 0.200. As the relative intensity of the peak at *m/e* 64 to the base peak at *m/e* 79 ($CH_3SO_2^+$) in dimethylsulfone is 0.021, the molar ratio in base peak intensity of *cyclo*-octasulfur to dimethylsulfone is 0.0041. Namely, the ionization efficiency of *cyclo*-octasulfur is very low compared with dimethylsulfone which is detectable at usual sensitivities. The detection limit is around 100 ng. Therefore, the determination of a trace amount of *cyclo*-octasulfur by mass spectrometry is very difficult.

References

1) J. Chao, *Hydrocarbon Process.*, **59**, 217 (1980).
2) L. K. Templeton, D. H. Templeton, and A. Zalkin, *Inorg. Chem.*, **15**, 1999 (1976).
3) B. N. Khare and C. Sagan, *Science*, **189**, 722 (1975).
4) T. Fukuzumi, Y. Miyauchi, K. Tubaki, and K. Minami, *Mokuzai Gakkai Shi*, **21**, 558 (1975).
5) C. M. White and M. L. Lee, *Geochim. Cosmochim. Acta*, **44**, 1825 (1980).
6) S. R. Heller and G. W. A. Milne, "EPA/NIH Mass Spectral Data Base," U. S. Government Printing Office, Washington (1978), p. 1823.
7) E. Stenhagen, S. Abrahamsson, and F. W. McLafferty, "Registery of mass Spectral Data," Wiley-Interscience, New York (1974), p. 1573.
8) B. Meyer, M. Gouterman, D. Jensen, T. V. Oommen, K. Spitzer, and T. Stroyer-Hansen, *Adv. Chem. Ser.*, **110**, 53 (1972); *Chem. Abstr.*, **76**, 160464b (1972).
9) A. Anderson and P. G. Boczar, *Chem. Phys. Lett.*, **43**, 506 (1976).
10) A. Z. Yurovskii, "Sera Kamennykh Uglei," Izdatel. Akad. Nauk S. S. S. R., Moscow (1960); English translation available from the U. S. Department of Commerce, National Technical Information Service, Springfield, VA 22161, U. S. A. (Ref. No. TT 70—57216); cited from Ref. 5.
11) A. Yasuhara and K. Fuwa, *Chemosphere*, **7**, 833 (1978).
12) A. Yasuhara and K. Fuwa, *Agric. Biol. Chem.*, **44**, 2379 (1980).

A Reinforced Oleophilic Anion-exchange Resin Membrane as a Sensitive Membrane of Anion-selective Electrodes

Akinori Jyo,*,† Toshihiko Imato, Hirofumi Kohno, and Nobuhiko Ishibashi
Department of Applied Analytical Chemistry, Faculty of Engineering, 36, Kyushu University, Fukuoka 812
(Received April 8, 1983)

Synopsis. Based on an impregnation technique for the preparation of ion-exchange resin membranes, a simple way was proposed for the preparation of a reinforced oleophilic anion-exchange resin membrane as an anion-selective electrode membrane with a chemically fixed site. The resulting exchange resin membrane is thin (*ca.* 25 μm) and flexible. It gives anion-selective electrodes with high performances.

We have developed anion-selective electrodes based on an oleophilic anion-exchange resin membrane, which is a homogeneous crosslinked polystyrene membrane with a chemically fixed benzyltrioctylammonium ion as the anion-exchange site.[1] The resin membrane performs almost the same as the sensitive membrane of a liquid membrane anion-selective electrode when it is impregnated with a water-immiscible organic solvent.[1] Since the membrane is based on a homogeneous crosslinked polystyrene matrix, it is hard and weak to bending. In addition, much experience and skill are generally required for the preparation of homogeneous ion-exchange resin membranes.[2,3] Thus from a practical point of view, it is desirable to develope a simple method of preparing a flexible membrane.

Based on an impregnation technique widely used in the preparation of usual hydrophilic ion-exchange resin membranes,[2] we have developed a simpler way to prepare an oleophilic anion-exchange resin membrane. The newly developed membrane is thinner and more flexible than the previously reported membrane. This note will describe the preparation of the membrane. The performances of anion-selective electrodes based on the membrane will also be presented.

Experimental

Preparation of the Oleophilic Anion-exchange Resin Membrane. A sheet of Duragard (macroporous film of polypropylene, thickness, 25 μm; Polyplastic Co.) was cut into appropriate squares (3 cm × 3 cm or 4 cm × 4 cm). They were immersed in a styrene–divinylbenzene mixture (20 ml : 0.5 ml) containing benzoyl peroxide (0.2 g) for 24 h. The sheets impregnated with the monomers were then inserted between piled glass plates. After the glass plates had been fastened, they were immersed in a hot solution of saturated sodium sulfate (70 °C) for 8—10 h in order to polymerize the monomers.[3] Although the original Duragard itself was opaque, a translucent membrane was thus obtained. After the membrane had been soaked in hot water for 1 h, it was washed with ethanol for 2 h and then with acetone for 30 min in a Soxhlet extractor. After drying in a vacuum desiccator, it was weighed. The increase in weight was 48% of the initial weight of the sheet. The membrane was then chloromethylated by the conventional method.[4] After the chloromethylated membrane had been soaked in a mixture of hydrochloric acid and ethanol (1 : 10) overnight, it was washed with acetone in a Soxhlet extractor for 20 h and then dried. After it had swollen in a trioctylamine–ethanol mixture (2 : 1) overnight at room temperature, the mixture was maintained at 80 °C for 30 h in order to effect the quaternization of the membrane with the amine. In this stage, the membrane expanded in every direction by 1.2 times, while no marked change in the size was observed before the quaternization process. The resulting anion-exchange resin membrane was washed with ethanol in a Soxhlet extractor for 30 h. The conditioning of the membrane and determination of the exchange capacity were performed by the previously reported procedures.[1]

Ion-selective Electrode Assemblies. The membrane was converted into the nitrate or perchlorate form according to the previously reported procedures.[1] As a solvent to be impregnated in the membrane, nitrobenzene was used. The fabrication of the electrode and the evaluation of the electrode performances have been reported in detail elsewhere.[1]

Results and Discussion

The exchange capacity of the membrane is 0.68 mequiv./g of resin, which is smaller than those of the previously reported homogeneous membranes (1.0—1.1 mequiv./g of resin).[1] This may be due to the fact that the present membrane contains polypropylene as a reinforcing material. The membrane is thin (*ca.* 25 μm) and flexible. It is strong for bending. In the case of the homogeneous membrane, it took more than a week to change its ionic form by means of ion exchange since it is relatively thick (0.2—0.5 mm). The thickness of the present membrane is reduced to about one-tenth of the previous one. Accordingly, the ion exchange could be easily finished within a week. The present membrane also showed the oleophilic property; it is easily wetted with organic solvents, but is hardly to wet with water.[5]

Nitrate and perchlorate ion-selective electrodes were fabricated by using the membranes in nitrate and perchlorate forms respectively. The results for electrode

Table 1. Performances of anion-selective electrodes based on oleophilic anion-exchange resin membranes

Membrane	Sensing ion of electrode	Slope[a] (mV/log *a*)	Lower limit of linear response/M
Present membrane	NO_3^-	−57	$10^{-4.3}$
(Reinforced membrane)	ClO_4^-	−59	$10^{-4.3}$
Previous membrane	NO_3^-	−57	$10^{-4.3}$
(Homogeneous membrane)	ClO_4^-	−58	$10^{-4.3}$

a) The solvent impregnated in the membrane is nitrobenzene. The electrodes were calibrated at an ionic strength of 0.3 (0.10 M Na_2SO_4).

† Present address: Department of Industrial Chemistry, Faculty of Engineering, Kumamoto University, Kumamoto 860.

Table 2. Selectivity coefficients of nitrate ion-selective electrodes based on oleophilic anion-exchange resin membrane

Membrane	Selectivity coefficient ($\log K^{pot}_{NO_3,j}$)[a]			
(j)	Cl^-	NO_2^-	CH_3COO^-	
Concn of j-ion/M	0.0050	0.0010	0.10	
Present membrane	−2.1	−1.1	−3.6	
Previous membrane	−2.0	−1.4	−3.4	

a) The solvent impregnated in the membrane is nitrobenzene.

calibrations are summarized in Table 1. The performances are almost the same as those of the previously reported electrodes based on the homogeneous membranes.[1] Although the response of the present electrodes was also rapid within the concentration range of the linear response, a small oscillation of potentials was sometimes observed. This presents no serious problem, however, since the oscillation is less than ± 0.3 mV.

Table 2 gives the selectivity coefficients of the nitrate ion-selective electrode. They were determined by the mixed-solution method under fixed activity of an interferent ion.[6] No marked difference in selectivity is seen between the present and previous electrodes when a common solvent, nitrobenzene, is impregnated in the membranes. That is, no marked influence of polymer matrices on the electrode selectivity can be seen. This observation is in accordance with the view that the selectivity of anion-selective electrodes of the liquid membrane type is essentially governed by the solvent of the membrane.[7]

References

1) T. Imato, A. Jyo, and N. Ishibashi, *Anal. Chem.*, **52**, 1893 (1980).

2) F. Hellferich, "Ion Exchange," McGraw-Hill, New York (1962), pp. 61—65.

3) "Kireto Jyushi, Ion Kokan Jyushi," ed by N. Hojyo, Kodansya, Tokyo (1976), p. 229.

4) T. Ohtsu and M. Kinoshita, "Kobunshi Gosei No Jikkenho," Kagaku Dojin, Kyoto (1972), p. 375.

5) H. P. Gregor, G. K. Hoeschele, J. Potenza, A. G. Tsuk, R. Feinland, M. Shida, and Ph. Teyssie, *J. Am. Chem. Soc.*, **87**, 5525 (1965).

6) P. L. Bailey, "Analysis with Ion-selective Electrodes," Heiden, London (1976), pp. 45—50.

7) N. Yoshida and N. Ishibashi, *Chem. Lett.*, **1974**, 493; A. Jyo, M. Torikai, and N. Ishibashi, *Bull. Chem. Soc. Jpn.*, **47**, 2862 (1974); N. Yoshida and N. Ishibashi, *ibid.*, **50**, 3189 (19.7).

Extractive Spectrophotometric Determinaton of Molybdenum(VI) with 8-Hydroxy-5-quinolinesulfonic Acid and Methyltrioctylammonium Chloride

Masao SUGAWARA,* Masayuki UTO, and Tomihito KAMBARA
Department of Chemistry, Faculty of Science, Hokkaido University, Kita-ku, Sapporo 060

(Received April 19, 1983)

Synopsis. Molybdenum(VI) complex with 8-hydroxy-5-quinolinesulfonic acid (H_2qs) is reduced to the quinquevalent state by hydrazinium sulfate and extracted into chloroform as the ion-association complex with methyltrioctylammonium chloride(Q^+Cl^-). Molybdenum(VI) in the ppm range is determined spectrophotometrically. The composition of the extracted species was estimated to be $[(MoO_2qs)_2(Hqs)_3(Q)_5]$.

When molybdenum(VI) in a weakly acidic solution in the presence of 8-hydroxy-5-quinolinesulfonic acid (H_2qs) is reduced by hydrazine, a yellow molybdenum(V)–H_2qs complex is formed, which changes to a red-purple complex on heating.[1,2] The formation of the red-purple complex is the basis of spectrophotometric determination of molybdenum in water.[3] The composition of yellow complex has been ascribed[4] to two monomers, *i.e.*, $[MoO_2qs(OH)]^{2-}$ and $[MoO_2qs]^-$, and the red-purple complex to the dimer $[(MoO_2qs)_2(Hqs)_3]^{5-}$.

In the present work, spectrophotometric determination of molybdenum after extraction of the red-purple complex as an ion-association complex with a quaternary ammonium salt is described. Determination of molybdenum in the organic phase is more sensitive than in water, owing to the concentration effect, and selectivity of the method has also been improved.

Experimental

Apparatus. Spectrophotometric measurements were carried out with a Shimadzu spectrophotometer UV-240 and a 10-mm cell. A Hitachi-Horiba glass electrode pH meter F-7LC was used for pH measurements. A Yamato Shaker FA-31 was used.

Reagents. A 0.01 M (1 M=1 mol dm^{-3}) of stock solution of molybdenum(VI) was prepared from hexaammonium heptamolybdate tetrahydrate $(NH_4)_6Mo_7O_{24}\cdot 4H_2O$ and standardized chelatometrically. Commercially available 8-hydroxy-5-quinolinesulfonic acid (H_2qs) was recrystallized from water. A 0.1 M stock solution of NaHqs was prepared by dissolving the weighed amount of H_2qs into the equivalent amount of sodium hydroxide solution and diluting to the volume with water. A 1.9 M hydrazine solution was prepared by dissolving 123.9 g of hydrazinium sulfate into water, neutralizing to about pH 7 with sodium hydroxide solution and diluting to 500 cm^3 with water. A 0.01 M methyltrioctylammonium chloride (Q^+Cl^-) solution was prepared by diluting 25 g of Capriquat (Dojindo Laboratories) to 500 cm^3 with chloroform. Acetate buffer solutions were prepared in the usual way. Deionized water was used. Other reagents used were of G. R. grade.

Procedure. To a sample up to 5 cm^3 containing 38—288 μg molybdenum(VI) in a 100-cm^3 Erlenmeyer flask are added 5 cm^3 of 0.1 M NaHqs solution, 5 cm^3 of 1 M acetate buffer solution (pH 4.6) and 5 cm^3 of 1.9 M hydrazine solution. The mixture is diluted to 20 cm^3 with water and heated for 20 min over a boiling water-bath. The solution at room temperature is transferred into a 100-cm^3 separatory funnel and diluted to 50 cm^3 with water. After addition of 10 cm^3 of 0.01 M QCl–chloroform solution, two phases are shaken for 5 min and allowed to stand for 5 min. The organic phase, dehydrated with anhydrous sodium sulfate, is subjected to optical measurements at 570 nm against the reagent blank obtained in the same manner.

Results and Discussion

Reduction of Mo^{VI}–H_2qs Complex. To a solution containing 96 μg molybdenum(VI) are added 5 cm^3 of 0.1 M NaHqs solution, 5 cm^3 of 1 M acetate buffer solution (pH 4.6) and different amount of 1.9 M hydrazine solution. After diluting the mixture to 20 cm^3 with water, the solution was heated for 40 min over a boiling water-bath. The solution at room temperature was transferred into a 50-cm^3 volumetric flask and diluted to the volume with water. Absorbance of the solution at 538 nm was measured against the reagent blank. It was found that the addition of more than 5 cm^3 of 1.9 M hydrazine solution is required for quantitative color development of the red molybdenum(V) complex. With 5 cm^3 of 1.9 M hydrazine solution, a maximum and constant absorbance of the molybdenum(V) complex was obtained for the heating time above 25 min. Effect of pH on the absorbance of the molyb-

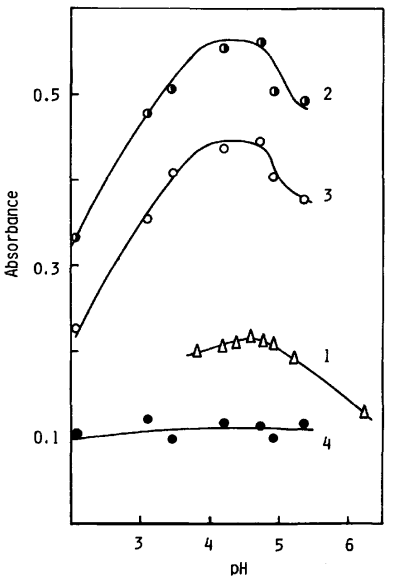

Fig. 1. Effect of pH on the absorbance of Mo^V–H_2qs complex in aqueous solution and chloroform extracts. 1: 96 μg Mo in 25-cm^3 aqueous solution, 538 nm *vs.* reagent blank, 2: 96 μg Mo in 10-cm^3 $CHCl_3$-extracts, 570 nm *vs.* $CHCl_3$, 3: 2 *vs.* reagent blank, 4: reagent blank *vs.* $CHCl_3$.

Table 1. Effect of diverse ions

Foreign ion	Added as	Added (μg)	Mo found (μg)	Error %
Ca^{II}	Sulfate	10000	94.9	−1.1
Mg^{II}	Sulfate	9700	96.4	+0.4
Zn^{II}	Chloride	1000	99.6	+3.7
Al^{III}	Chloride	200	98.9	+3.0
W^{VI}	Sodium salt	200	98.9	+3.0
V^{IV}	Sulfate	50	99.6	+3.7
Ni^{II}	Sulfate	20	99.5	+3.6
Cr^{III}	Chloride	20	96.7	+0.7
Cu^{II}	Sulfate	20	90.7	−5.5
Mn^{II}	Sulfate	20	94.1	−2.0
Co^{II}	Chloride	12	97.8	+1.9
Fe^{III}	Mohr's salt	10	159.1	+65.7
Fe^{III}	Mohr's salt	10[a)]	102.4	+6.4

Mo^{VI} taken: 96.0 μg. a) Backwashed with 0.2 M sodium oxalate solution (pH 4).

denum(V) complex is shown in Fig. 1. The absorbance of the complex is constant in the pH range from 4.5 to 4.8.

Extraction of Mo^{V}–H_2qs Complex. The molybdenum(V) complex extracted according to the above procedure shows absorption maxima at 372 and 570 nm. The complex is quantitatively extracted in the pH range from 4.0 to 4.7, as shown in Fig. 1. A maximum and stable absorbance of the extracts at 570 nm was obtained for the addition of more than 4 cm^3 of 0.1 M NaHqs solution and for QCl concentration above 40 mM. The molybdenum(V) complex is quantitatively extracted for shaking time of 1—10 min at an aqueous-to-organic volume ratio of 5 : 1. Absorbance of the extracts remains constant at least for 30 min.

Calibration Curve. The calibration curve does not pass through the origin, but it is linear in the concentration range of molybdenum(V) from 38 to 288 μg in 10-cm^3 extracts. The results of regression analysis for the linear calibration range gave $Y=-(61\pm6.7)\times10^{-3}+(51\pm0.47)\times10^{-3}\ X$ at a significance level of $\alpha=0.05$, where Y is absorbance of the extracts at 570 nm and X is the concentration of molybdenum(V) in μg/cm^3-extracts.

Effect of Diverse Ions. Effect of foreign metal ions on the determination of molybdenum is given in Table 1. Interference by vanadium(IV) and iron(III) was significantly diminished as compared with the method of Busev and Fan.[3)]

Composition of the Extracted Species. When the molybdenum(V)–H_2qs complex having the absorption maximum at 570 nm is predominantly extracted, the equilibrium is given by

$$M^{m-} + m\,QCl_o \rightleftharpoons MQ_{m,o} + m\,Cl^- \quad (1)$$

where M^{m-} indicates the anionic Mo^{V}–H_2qs complex and subscript o the organic phase. The distribution ratio D of molybdenum(V) complex is given by

$$D = \frac{A}{A_{max}-A} \quad (2)$$

where A is the absorbance of the extracts at 570 nm and A_{max} that of the extracts where molybdenum(V) is quantitatively extracted. Thus, a plot of log D *vs.* log $[QCl]_o$ should give a straight line with a slope of m. As shown in Fig. 2, the plot has a slope of $m=4.7$, suggesting the composition of $[(MoO_2qs)_2(Hqs)_3(Q)_5]_o$.

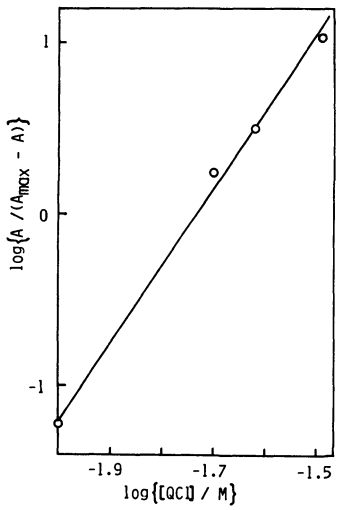

Fig. 2. A plot of log D *vs.* log[QCl] at pH 4.6.
Aqueous layer: [Mo]=96 μg, [NaHqs]=0.01 M, [Hydrazine]=0.19 M, [NaCl]=0.1 M.
The plot has a slope of 4.7 as evaluated by the method of least squares.

References

1) A. I. Busev and C. Fan, *Zh. Anal. Khim.*, **15**, 455 (1960).
2) A. I. Busev, "Analytical Chemistry of Molybdenum," translated by I. Schmork, Ann Arbor-Humphery Science, Ann Arbor (1969).
3) A. I. Busev and C. Fan, *Talanta*, **9**, 107 (1962).
4) M. Cadiot and M. Blasse, *Bull. Soc. Chim. Fr.*, **1975**, 1555.

Fluorescence as a Means for Kinetic Studies. III. Bimolecular Reaction of Fluorescent Reagent as Quenching Probes

Hideharu Ushiki,* Akio Okamoto,† Kazuyuki Horie,† and Itaru Mita,†
Laboratory of Chemistry, Faculty of General Education, Tokyo University of Agriculture and Technology, 3-5-8, Saiwai-cho, Fuchu, Tokyo 183
†*Institute of Interdisciplinary Research, Faculty of Enginnering, The University of Tokyo, 4-6-1, Komaba, Meguro-ku, Tokyo 153*
(Received April 28, 1983)

Synopsis. In order to study the rate of bimolecula reaction between 9-(3-aminopropyl)carbazole and dansyl chloride, the change of fluorescent intensity of dansyl group has been measured. It has been found that the rate of increase in fluorescent intensity of the dansyl group is equal to the rate of decrease in fluorescent intensity of the carbazolyl group during progress of this bimolecular reaction. Another *quenching probe* was also examined briefly.

Fluorescent probes are defined as fluorescent molecules whose spectral response (quantum yield, excitation, and emission) varies as a function of the physical and chemical environment with which the probe is associated.[1] In recent years the studies of bimolecular reaction rates in nonaqueous solution by using the fluorescent probe have been reported by many authors.[2-7] Especially, the fluorescent probe method is effective for the study on reaction rate of macromolecules because the rates of bimolecular reaction between polymers must be measured in a very dilute solution.[8]

Instrumental sensitivity for the detection of fluorescence emission is usually several orders of magnitude greater than that for absorption measurements. Thus the fluorescent probe method is the most effective for the study on rates of organic reaction in dilute solution. But there is a difficult problem on fluorescent probe method because the probes are restricted to special organic compounds. The most remarkable characteristics of fluorescent probe is the fact that these probes must have a fluorescence emission only after this reaction.

The reaction product between the one having energy donor group and the other having energy acceptor group shows the intramolecular energy transfer such as 9-[3-(5-dimethylamino-1-naphthylsulfonylamino)propyl]carbazole (DNSPC) shows the intramolecular singlet-singlet energy transfer between carbazolyl group (energy donor) and dansyl group (energy acceptor). So, it is contemplated that the decrease in fluorescent intensity based upon singlet-singlet energy transfer will be observed during progress of the bimolecular reaction between the compound having energy donor group and the other having energy acceptor group.

In this paper, the rates of bimolecular reaction between amino group and chlorosulfonyl or carbonyl chloride groups in nonaqueous solution have been measured by *quenching probe method.*

Experimental

Materials. 9-(2-Cyanoethyl)carbazole (CEC) was prepared in a similar way to that reported by other authors.[9]

9-(3-Aminopropyl)carbazole (APC) was prepared by the reduction of CEC by using lithium aluminium hydride r($LiAlH_4$).[10]

Anthraquinone-2-sulfonyl chloride (ASCl) was prepared in a similar way to that reported by other author.[11] The each product was identified by infrared and NMR spectra.

Measurements. Sample solution in a rectangular quartz cell with cap was set in a thermostat (60 °C), and the fluorescence spectra were measured by using JASCO FP-550 spectrofluorometer. Dotite-Luminasol-grade ethyl acetate was used as a solvent for fluorescent measurements.

Results and Discussion

The fluorescence spectra in the bimolecular reaction between 9-(3-aminopropyl)carbazole (APC) and 5-dimethylamino-1-naphthalenesulfonyl chloride (dansyl chloride, DNSCl) in ethyl acetate at 60 °C are shown in Fig. 1. The kinetic scheme of this bimolecular reaction is shown below.

$$\mathrm{CazCH_2CH_2CH_2NH_2} + \mathrm{DNSCl} \longrightarrow \mathrm{CazCH_2CH_2CH_2NHSO_2DN} + \mathrm{HCl} \quad (1)$$

In organic solvents, hydrogen chloride formed reacts immediately with amine.[12]

$$\mathrm{CazCH_2CH_2CH_2NH_2} + \mathrm{HCl} \longrightarrow \mathrm{CazCH_2CH_2CH_2NH_3^+Cl^-} \quad (2)$$

The rate of this bimolecular reaction can be measured by the increase in fluorescent intensity of the dansyl group (499 nm) because the dansyl group shows a fluorescence emission only after this reaction. The rate constants for pseudo-first-order reaction under the concentrations of $[APC]=3.9\times10^{-5}$ M, 1.0×10^{-3} M, and 2.0×10^{-3} M, $[DNACl]=3.9\times10^{-5}$ M were measured in ethyl acetate at 60 °C by the increase in fluorescent intensity of the dansyl group. The plots of pseudo-first-order reaction show a straight line. The values of k_2 for second-order reaction are 0.059 s^{-1} M^{-1} ($[APC]=3.9\times10^{-5}$ M), 0.038 s^{-1} M^{-1} ($[APC]=1.0\times10^{-3}$ M), and 0.032 s^{-1} M^{-1} ($[APC]=2.0\times10^{-3}$ M). On the other hand, it has been supposed that the rate of increase in fluorescent intensity for the dansyl group is equal to the rate of increase in fluorescent intensity for the carbazolyl group during progress of bimolecular reaction in Fig. 1. DNSPC must show the intramolecular singlet-singlet energy transfer between carbazolyl group (energy donor : 81 kcal) and dansyl group (energy acceptor : 57 kcal). Consequently, the rate for this bimolecular reaction can be determined by the decrease in fluorescent intensity of the carbazolyl group, and the values of k_2 obtained by *quenching probe method* agree well with that by fluorescent probe method.

The value of k_2 for the bimolecular reaction between buthylamine and dansyl chloride was measured in ethyl acetate at 60 °C by the fluorescent probe method, and

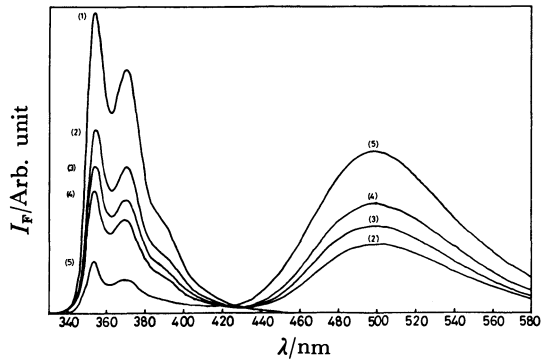

Fig. 1. Fluorescence spectra in the bimolecular reaction between 9-(3-aminopropyl)carbazole (APC) and dansyl chloride (DNSCl) in ethyl acetate. [APC]=[DNSCl]=3.9×10^{-5} M. Excitation wavelength: 350 nm. (1); 0 h (in the absence of DNSCl), (2); 51 h, (3); 94 h, (4); 143 h, (5); 598 h (at end point).

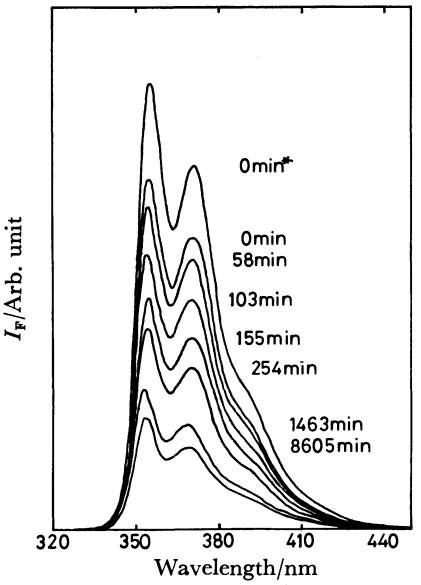

Fig. 2. Fluorescence spectra in the bimolecular reaction between 9-(3-aminopropyl)carbazole (APC) and antraquinone-2-sulfonyl chloride (ASCl) in ethyl acetate. [APC]=[ASCl]=3.9×10^{-5} M. Excitation wavelength: 350 nm. 0 min* is the condition in the absence of ASCl.

was 0.20 s^{-1} M^{-1}.[6] But the value of k_2 for the bimolecular reaction between APC and dansyl chloride under the above conditions was about 0.2—0.3 times as large as that for bimolecular reaction between butylamine and dansyl chloride. The bimolecular reaction between amino group and chlorosulfonyl group is well-known as the bimolecular nucleophilic substitution reaction (S_N2). The S_N2 displacement is less affected by electrometric effect (resonance, inductive, *etc.*) since there is relatively little charge on sulfur in the transition state.[13] Consequently, it seems reasonable to assume that the bimolecular reaction between APC and dansyl chloride is reduced by nonpolar effect of its own carbazolyl group.

The rates of bimolecular reactions between APC and ASCl or anthraquinone-2-carbonyl chloride (ACCl) in ethyl acetate at 60 °C can be measured by *quenching probe method* but not by fluorescent probe method. The kinetic schemes of those bimolecular reactions are below.

$$CazCH_2CH_2CH_2NH_2 + AQSO_2Cl \longrightarrow CazCH_2CH_2CH_2NHSO_2AQ \quad (3)$$

$$CazCH_2CH_2CH_2NH_2 + AQCOCl \longrightarrow CazCH_2CH_2CH_2NHCOAQ \quad (4)$$

The products formed by this bimolecular reaction shows the intramolecular singlet-singlet energy transfer between carbazolyl group (energy donor : 81 kcal) and anthraquinon-2-yl group (energy acceptor : 67 kcal). Moreover, anthraquinon-2-yl group does not fluoresce. The fluorescence spectra in the bimolecular reaction between APC and ASCl under the conditions of [APC]=[ASCl]=3.9×10^{-5} M in ethyl acetate at 60 °C are shown in Fig. 2. These values of k_2 obtained by plots for second-order reaction are 3.2 s^{-1} M^{-1}(between APC and ASCl) and 7.6 s^{-1} M^{-1} (between APC and ACCl). The values of k_2 for bimolecular reactions between APC and ASCl or ACCl in ethyl acetate at 60 °C are about 54 or 129 times as large as that for the bimolecular reaction between APC and dansyl chloride. The accelerating effect in the reaction with ASCl should be predictable from the distinction of electromeric effect on the sulfur atom in sulfonyl group between anthraquinon-2-yl group and dansyl group. These results are compatible with ones in other reaction between amino group and chlorosulfonyl or carbonyl chloried groups.

In conclusion, DNSPC formed by bimolecular reaction between APC and dansyl chloride shows the intramolecular singlet-singlet energy transfer between carbazolyl group and dansyl group. So, the decrease in fluorescent intensity based upon singlet-singlet energy transfer was observed during progress of the bimolecular reaction between the compound having energy donor group and the other having energy acceptor group. The rates of bimolecular reaction between APC and ASCl or ACCl could be measured by *quenching probe method.*

References

1) L. Stryer, *Science*, **162**, 526 (1968).
2) Y. Eckstein and P. Dreyfuss, *Anal. Chem.*, **52**, 537 (1980).
3) T. Sekine, K. Ando, M. Machida, and Y. Kanaoka, *Anal. Biochem.*, **48**, 557 (1972).
4) Y. Kanaoka, M. Machida, K. Ando, and T. Sekine, *Biochem. Biophys. Acta*, **207**,269 (1970).
5) L. K. Tan and R. A. Patsiga, *Anal. Lett.*, **10**, 437 (1977).
6) A. Okamoto, K. Uchiyama, and I. Mita, *Bull. Chem. Soc. Jpn.*, **55**, 3068 (1982).
7) A. Okamoto, K. Toyoshima, and I. Mita, *Bull. Chem. Soc. Jpn.*, **56**, 333 (1983).
8) A. Okamoto, K. Toyoshima, and I. Mita *Eur. Polym. J.*, **19**, 341 (1983).
9) F. C. Whitmore, H. S. Mosher, R. R. Adams, R. B. Taylor, E. C. Chapin, C. Weisel, and W. Yanko, *J. Am. Chem. Soc.*, **66**, 725 (1944).
10) L. H. Amundersen and L. S. Nelson, *J. Am. Chem. Soc.*, **73**, 242 (1951).
11) H. H. Bosshard, *Helv. Chim. Acta*, **17**, 1653 (1953).
12) L. M. Litbinenko and A. F. Popov, *Dokl. Acad. Nauk SSSR*, **160**, 1124 (1965).
13) A. J. Parker, *Chem. Rev.*, **69**, 1 (1969).

Single-step Lithium-ion Exchange on α-Hafnium Phosphate

Isao TOMITA,* Kazuo MAGAMI,† Hiroshi WATANABE,†
Koji SUZUKI,† and Toshihiro NAKAMURA†
Tokyo University of Fisheries, Konan, Minato-ku, Tokyo 108
Department of Industrial Chemistry, Faculty of Engineering, Meiji University, Higashi-Mita, Tama-ku, Kawasaki 214
(Received May 7, 1983)

Synopsis. Forward and backward pH titration curves were measured for lithium-ion exchange on crystalline α-hafnium phosphate. The forward reaction proceeded in a single step, in contrast to the corresponding process in α-zirconium phosphate. In the backward process, no intermediate crystalline phases were observed during the exchange, and the exchanger was gradually converted into gel.

The ion-exchange properties of crystalline α-hafnium bis(hydrogenphosphate) monohydrate, $Hf(HPO_4)_2 \cdot H_2O$ (referred to as α-HP), had been expected to be similar to those of α-zirconium phosphate, $Zr(HPO_4)_2 \cdot H_2O$ (α-ZP), but had scarcely been investigated[1] because of its difficulty in practical use and because of the rather easy inference of the properties due to the nearly identical chemistries of zirconium and hafnium. The authors have found that many properties are similar to those of α-ZP, as was expected. Attention has, however, been attracted to Li^+ ion exchange because the behavior of this ion is quite different between α-titanium phosphate (α-TP)[2,3] and α-ZP,[4] which have almost the same structure and interlayer distance. Information on Li^+ ion exchange behavior on α-HP is thus worth mentioning in the interpretation of ion exchange on this type of exchanger.

Experimental

Crystalline α-HP was prepared by refluxing newly formed amorphous hafnium phosphate in from 11 to 12 $mol \cdot dm^{-3}$ of H_3PO_4 at the boiling point for more than 210 h. The resulting crystallite was identified by means of X-ray diffractometry and thermal analysis (TG–DTA). The fully exchanged Li^+ form of the exchanger, $Hf(LiPO_4)_2 \cdot 4H_2O$ (Li–HP) was prepared from α-HP in two ways. One was prepared by the gradual addition of 0.1 $mol \cdot dm^{-3}$ LiOH to a suspension of α-HP in distilled water, keeping the pH of the mixed solution as high as about 9. Another Li–HP was produced by the batch technique in the same way as in the forward exchange.

The ion exchange experiment was carried out by the batch method. Forward and backward pH titration curves were measured at 25 °C. In the forward process, where H^+ ions of α-HP were replaced by Li^+ ions, mixed solutions of 0.1 $mol \cdot dm^{-3}$ LiCl and 0.1 $mol \cdot dm^{-3}$ LiOH were prepared at variable mixing ratios to give solutions of differing LiOH concentrations, keeping the lithium concentration constant. Then, α-HP (200 mg) was placed in contact with a 20-cm^3 portion of each of the above-mentioned mixed solutions, and the mixture was shaken for 4 d. The solution was centrifuged, and the supernatant liquid was subjected to pH measurement, as well as to the determination of lithium and phosphate by means of flame photometry and absorptiometry respectively. The analytical data for lithium were used for the calculation of the lithium ionic fractions ($\overline{XLi}$) of the exchanger, while those for phosphate were used for examining the degradation of the exchanger. The solid phase was analyzed by means of X-ray powder diffractometry and thermogravimetry. In the backward titration, the solutions to be placed in contact with Li–HP consisted of 0.1 $mol \cdot dm^{-3}$ LiCl and 0.1 $mol \cdot dm^{-3}$ HCl at variable mixing ratios. Twenty-cm^3 portions of each of the solutions were used, and the amount of Li–HP taken was such that it was equivalent to 200 mg of α-HP. Thus, the solution-to-solid ratio was kept constant (100 cm^3/g) in both the forward and backward titrations.

Results and Discussion

The forward titration curve is shown in Fig. 1. It gives a single plateau at a pH value around 5.3. An initial slope up to about 20% of conversion corresponds to the solid-solution formation of Li^+ ions in the α-HP lattice. There is no indication of a pH jump at a half-exchange. The lowest-angle region of the X-ray powder diffraction patterns of the exchanger are presented in Fig. 2. Up to $\overline{XLi}$ of 0.3, only the reflection peak due to the interlayer distance (d_{002}) of α-HP was found; *i.e.*, the Li^+ ions are incorporated with α-HP without any essential change in the crystal structure. This region corresponds to the initial slope of the titration curve. In the subsequent plateau region, a new phase with the interlayer distance of 10 Å appeared. As the exchange proceeded, the intensity of the reflection of this phase increased with a decrease in that of α-HP. Beyond a half-exchange, however, the α-HP was not completely converted into the new phase, but coexisted with that phase. Another phase with the interlayer distance of 7.9 Å appeared at a relatively higher conversion, and sometimes three reflection lines (at 7.6, 7.9, and 10.1 Å) coexisted. If the sample for the X-ray measurement was dried under an infrared lamp for 10, 40, and 70 m, the peak at 10.1 Å gradually diminished and peak at 7.9 Å increased in intensity.

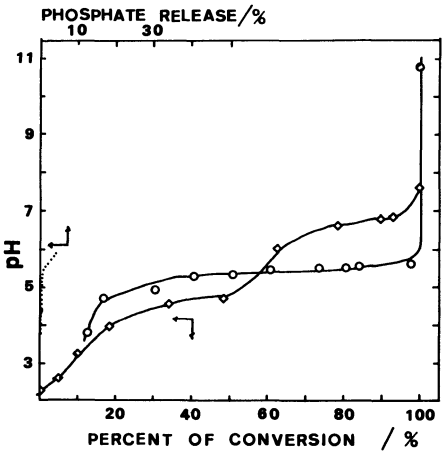

Fig. 1. The forward and backward pH titration curves for Li^+ ion exchange and the phosphate release curve in the forward titration.
○: Forward, ◇: Backward. The point at 13% conversion in the forward run was obtained when contacting the exchanger with 0.1 $mol \cdot dm^{-3}$ LiCl only.

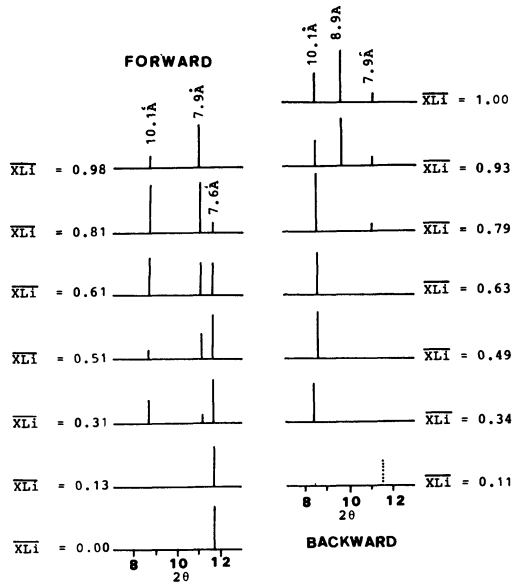

Fig. 2. The lowest angle regions of the X-ray powder diffraction patterns of the exchanger at several stages of exchange. $\overline{XLi}$ denotes the lithium ionic fraction.

From these results as well as the data for α-ZP, the 7.9- and 10.1 Å peaks were ascribed to Li–HP monohydrate and tetrahydrate respectively. Whether or not the exchanged phases with different hydration numbers exist *in situ* during exchange is difficult to confirm, though at equilibrium the phase-rule requirement rules out the coexistence of three solid phases including α-HP. From the shape of the curve and the X-ray evidence the Li^+ ion exchange on α-HP is considered to proceed essentially in a single step, without the formation of any intermediate Li^+ ion-exchanged phases.

The backward titration curve is given in Fig. 1. The curve has some slopes, and an inflection point is seen around a half-exchange. No evidence, however, of a two-step exchange has been obtained from the X-ray data shown in Fig. 2. Further, as the backward exchange progressed, the conversion of the crystalline exchanger into gel became extensive. This phenomenon is what has been observed in the backward titration of Li^+ form of α-ZP.[5] If the resulting gels were stored for a few months, a partial recrystallization into α-HP was found, the phenomenon being shown as dotted reflection lines at $\overline{XLi}$=0.11 in Fig. 2.

It should be noted that the X-ray powder patterns of the Li–HP forms prepared by the different methods are not the same. The exchanged form prepared by the gradual addition of LiOH had an additional reflection peak at 8.9 Å besides the 10- and 7.9 Å peaks. The intensity of the 8.9 Å reflection depended on the drying conditions of the sample for the X-ray measurement. Thus, the peak is to be ascribed to the di- or trihydrate of Li–HP. The results of thermogravimetry also depended upon the drying condition of the sample, but a typical air-dried product had 3.7 mol of water per formula weight. This is a mixture of Li–HP forms with varing numbers of hydration, the majority of them being tetrahydrate. The curve given in Fig. 1 is the one obtained for Li–HP prepared by the slow addition of LiOH, but the curve for Li–HP prepared by the batch method has almost the same shape. It is of interest that even the latter product gave the 8.9 Å peak at the initial stage of the backward titration.

The phosphate release into the solution was measured at every stage of exchange. The result of the forward titration are given in Fig. 1; they were usually less than 0.1 mmol P/g α-HP. In the backward titration, the release was between 0.1 and 0.15 mmol P/g α-HP. Since the theoretical capacity of α-HP is 5.15 mequiv./g, the phosphate release affects the capacity by only 3% or less as long as the exchanger is used in acidic media.

The interlayer distances of α-ZP and α-TP are almost the same, 7.6 Å.[6] It is, therefore, quite likely that the ion-exchange behavior of these exchangers also has a strong resemblance in many respects—for example, the ion-sieve effect, the selectivity sequence, and the exchange mechanism. The Li^+ ion-exchange behavior on α-TP does differ from that of α-ZP in that the former exhibits a single-step exchange, in contrast to three-step exchange in the latter. This process in α-ZP may be expressed as follows:[6]

$$\underset{(7.6\text{ Å})}{\overline{HH}\cdot H_2O} \longrightarrow \underset{(10.1\text{ Å})}{\overline{HLi}\cdot 4H_2O} \longrightarrow \underset{(10.1\text{ Å})}{\overline{H_{0.5}Li_{1.5}}\cdot 4H_2O} \longrightarrow \underset{(10.0\text{ Å})}{\overline{LiLi}\cdot 4H_2O} \quad (\alpha\text{-ZP})$$

Here, $\overline{HH}$, $\overline{HLi}$, $\overline{H_{0.5}Li_{1.5}}$, and $\overline{LiLi}$ denote α-ZP, monolithium form, the 1.5 Li^+-exchanged form, and the dilithium form respectively. The hydration numbers are given as H_2O and $4H_2O$. The interlayer distances are given in the parentheses. The lithium-ion exchange on α-TP may be shown in the same fashion:

$$\underset{(7.6\text{ Å})}{\overline{HH}\cdot H_2O} \longrightarrow \underset{(7.6\text{ Å})}{\overline{LiLi}\cdot H_2O} \quad (\alpha\text{-TP})$$

In α-HP, the Li^+ ion exchange in the forward directions is between those of α-TP and α-ZP:

$$\underset{(7.6\text{ Å})}{\overline{HH}\cdot H_2O} \longrightarrow \underset{(10.1\text{ Å})}{\overline{LiLi}\cdot 4H_2O} \quad (\alpha\text{-HP})$$

This is also nearly the case for zirconium titanium phosphate mixed crystals (ZTP):[7]

$$\underset{(7.6\text{ Å})}{\overline{HH}\cdot H_2O} \longrightarrow \underset{(9.9\text{—}10.1\text{ Å})}{\overline{LiLi}\cdot 4H_2O} \quad (\text{ZTP})$$

As the presence of any intermediate exchanged phase corresponds to a step-by-step ion exchange, α-HP does not seem to form as many exchanged phases as α-ZP.

References

1) G. Alberti, "Inorganic Ion Exchange Materials," ed by A. Clearfield, CRC Press, Florida (1982), Chap. 2.
2) G. Alberti, P. Gardini-Galli, U. Costantino, and E. Torracca, *J. Inorg. Nucl. Chem.*, **29**, 571 (1967).
3) K. Takaguchi and I. Tomita, *J. Chromatogr.*, **118**, 263 (1976).
4) A. Clearfield, "Inorganic Ion Exchange Materials," CRC Press, Florida (1982), Chap. 1.
5) A. Clearfield and J. Troup, *J. Phys. Chem.*, **74**, 314 (1970).
6) G. Alberti, *Acc. Chem. Res.*, **11**, 163 (1978).
7) I. Tomita, K. Iwase, K. Saito, and Y. Sugiyama, *Bull. Chem. Soc. Jpn.*, **54**, 749 (1981).

Synthesis and Properties of Crown Compounds Containing Anthraquinone Nuclei[1)]

Shin'ichi NAKATSUJI, Yuko OHMORI, Masahiko IYODA,†
Kenichiro NAKASHIMA, and Shuzo AKIYAMA*
Faculty of Pharmaceutical Sciences, Nagasaki University, 1-14 Bunkyomachi, Nagasaki 852
†*Department of Chemistry, Faculty of Science, Osaka University, Toyonaka, Osaka 560*
(Received January 24, 1983)

Synopsis. 2,5,8,20,23,26-Hexaoxa[7.7]- and 2,5,8,11,23,26,29,32-Octaoxa[10.10](1,8)anthraquinonophanes (**2** and **3**) were synthesized, examined for complexation behavior with alkali and alkaline earth metal cations, and observed to show significant selectivity among the cations studied. The electroreduction of **2** by cyclic voltammetry was studied with the related compounds.

Crown compounds including a quinone-hydroquinone redox system in the molecule demonstrate complexation behavior. Recently, Vögtle *et al.* synthesized 4,7,10-trioxa-1,13-dithia[13](9,10)anthraquinonophane[2a)] and 1,4,7,10,13-pentaoxa[13]- and 1,4,7,10,13,16-hexaoxa-[16](1,2)anthraquinonophanes.[2b)] Misumi *et al.* have reported the synthesis of "crowned" quinone-hydroquinone redox systems, for which the 2,4-dinitrophenylhydrazone derivatives exist only as tautometric "crowned" dinitrophenylazophenols. They showed cation selectivity for Li(I).[3a,b)] These compounds were applied to the spectrophotometric determination of Li(I).[3c)]

Here, we report the synthesis of a new series of "crowned" anthraquinone (**1**, **2**, **3**, and **6**) according to Chart 1.

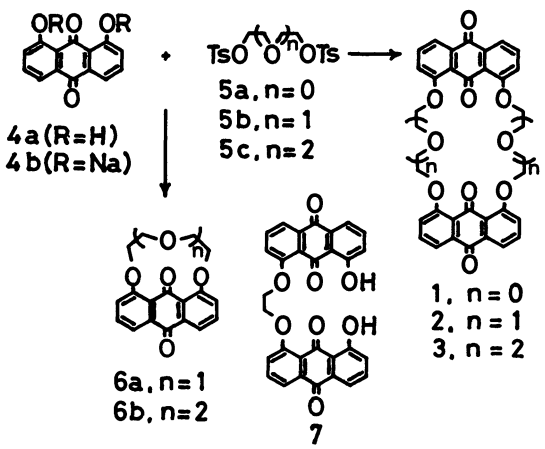

Chart 1.

TABLE 1. RESULTS OF SOLVENT EXTRACTION AT 20 °C

Ion	**2**(%)	**3**(%)	**7**(%)	Ionic radius/Å
Li^+	5.8	12.8	0.7	0.60
Na^+	9.9	22.6	2.1	0.95
K^+	12.8	56.6	2.8	1.33
Rb^+	28.6	49.9	3.1	1.48
Cs^+	25.5	35.7	2.7	1.69
Mg^{2+}	2.4	3.2	1.4	0.65
Ca^{2+}	3.8	7.1	2.6	0.99
Sr^{2+}	3.4	4.0	2.4	1.13
Ba^{2+}	5.4	30.4	2.3	1.35

Treatment of the sodium salt (**4b**) of 1,8-dihydroxyanthraquinone with ethylene glycol ditosylate (**5a**) in the presence of NaOH in xylene under reflux for 10—15 h did not gave the cyclic ether **1** but the acyclic ether **7** in 2.5% yield. On the other hand the reactions of **4b** with **5b** and **5c** afforded **2** (8.9%) and **3** (0.6%). Neither the expected **6a** and **6b** were obtained. An attempt to synthesize **6** ($n=1$ or 2) by the reaction of **4b** with the corresponding **5b** or **5c** was unsuccessful. The structures of **2**, **3**, and **7** obtained here, were identified by elemental analyses, IR, mass spectra, and ^1H NMR. The complex formation between a macrocyclic polyether (**2** or **3**) and a variety of alkali and alkaline earth metal salts could be readily established by Pedersen's solvent extraction method.[4)] Results obtained by the solvent extraction of the complexed crowns from a mixture of picric acid, alkali, or alkaline earth metal salt (Li^+, Na^+, K^+, Rb^+, Cs^+, Mg^{2+}, Ca^{2+}, Sr^{2+}, or Ba^{2+}) and the crown (**2** or **3**) in CH_2Cl_2–H_2O are shown in Table 1.

Appreciable selectivity was shown by **2** for Rb^+ and Cs^+, and by **3** for K^+, Rb^+, and Cs^+ among alkali cations and also by **3** for Ba^{2+} among alkaline earth metal cations. It was also clear that the acyclic diol **7** did not participate significantly in the extraction. These facts seem to be related to the relative size of the cations and the cavity of **2** or **3**.[5)]

Electrochemical properties of **2** were studied by cyclic voltammetry together with related quinones.[6)] The reduction potentials of these quinones are summarized in Table 2. The acyclic compound **7** has two redox couples (−0.66 and −1.35 V), whose difference ($E_{p1}-E_{p2}$) corresponds well to that of 9,10-anthraquinone. In contrast the cyclic voltammogram of **2** gave a well-defined three wave pattern contrary to that expected for two or four redox couples. The differences between the redox potentials ($E_{p1}-E_{p2}$ and $E_{p2}-E_{p3}$) of **2** were characteristically very small, *i.e.*, 0.22 and 0.33 V, respectively. This behavior of **2** is not completely explained but seems to be related to the easy delocalization of the electron(s) in the corresponding dianion species (dianion or dianion diradical) arising from the reduction of **2**. Thus, the dianion species appear to be more stabilized by delocalization than the corresponding mono-, tri-, or tetraanion species

TABLE 2. ELECTROCHEMICAL REDUCTION POTENTIALS (V *vs.* SCE)

Compound	E_{p1}	E_{p2}	E_{p3}	$E_{p1}-E_{p2}$	$E_{p2}-E_{p3}$
9,10-Anthraquinone	−0.96	−1.67	—	0.71	—
7	−0.66	−1.35	—	0.69	—
2	−0.85	−1.07	−1.40	0.22	0.33

derived from **2**.

Experimental

Ultraviolet absorption (UV) spectra and IR spectra were measured on Shimadzu UV-300 and JASCO IRA-2 spectrometers, respectively. ^{1}H NMR spectra were obtained on a JEOL FX 90Q spectrometer. The chemical shifts are in ppm using TMS as an internal standard. Mass spectra were obtained with a JEOL JMS-01SG mass spectrometer.

General Procedure. *Polyethylene glycol ditosylate* (**5a**, **5b**, or **5c**, 80 mmol) was added to a solution of disodium 9,10-dioxo-1,8-anthracenediolate prepared by azeotropic distillation of a mixture of aqueous NaOH solution (160 mmol), 1,8-dihydroxyanthraquinone (19.20 g, 80 mmol), and xylene (500 ml). The above mixture was refluxed for 10—15 h. The reaction mixture was filtered and the residue washed thoroughly with xylene (100 ml). The combined xylene solution was evaporated *in vacuo* and the solid residues were washed with acetone to give **2**, **3**, and **7**, respectively. The unreacted tosylate was recovered from the filtrate. The compounds (**2**, **3**, and **7**) were recrystallized from toluene.

2,5,8,20,23,26-Hexaoxa[7.7](1,8)anthraquinonophane (2): Yellow crystals; mp 190 °C; IR (KBr): 1670, 1630, and 1585 cm^{-1}; ^{1}H NMR ($CDCl_3$): δ=4.04—4.36 (m, 16H, $-CH_2-$) and 7.15—7.98 (m, 12H, aromatic H); UV (CH_2Cl_2): 396 nm (ε 9750); Found: C, 69.70; H, 5.00%; M$^+$, 620. Calcd for $C_{36}H_{28}O_{10}$: C, 69.67; H, 4.55%; M, 620.

2,5,8,11,23,26,29,32-Octaoxa[10.10](1,8)anthraquinonophane (3): Pale yellow crystals; mp 278—280 °C; IR (KBr): 1670, 1625, and 1590 cm^{-1}; ^{1}H NMR ($CDCl_3$): δ=3.60—4.22 (m, 24H, $-CH_2-$) and 7.12—7.83 (m, 12H, aromatic H); UV (CH_2Cl_2): 380 nm (ε 8490); Found: C, 66.10; H, 4.99%: M$^+$, 708. Calcd for $C_{40}H_{36}O_{12}\cdot H_2O$: C, 66.11; H, 5.27%; M, 708.

1,1'-Bis(8-hydroxy-9,10-dioxo-1-anthryloxy)ethylene (7): Yellow crystals; mp 280 °C decomp; IR (KBr): 3400, 1675, 1635, and 1585 cm^{-1}; ^{1}H NMR ($CDCl_3$): δ=4.74 (s, 4H, $-CH_2-$), 12.72 (s, 2H, OH), and 7.25—7.96 (m, 12H, aromatic H); UV (CH_2Cl_2): 411 nm (ε 11000); Found: C, 73.48; H, 4.54%; M$^+$, 506. Calcd for $C_{30}H_{18}O_8\cdot 1/2C_7H_8$: C, 73.69; H, 4.18%; M 506.

Solvent Extraction Experiments of Metal Ions by 2, 3, and 7:[4] After a mixture of picric acid (7×10^{-5} M, 5 ml of aqueous solution; 1 M=1 mol dm^{-3}), metal chloride (0.1 equiv., 5 ml of aqueous solution) was shaked vigorously with **2**, **3**, or **7** (7×10^{-4} M, 5 ml of CH_2Cl_2 solution), the absorbance of the aqueous layer was measured. The extraction ratios obtained by the reduced absorbance to that of the original aqueous layer are shown in Table 1.

Electrochemical Measurements of the Quinones: According to Ref. 6 all measurements were carried out in *N,N*-dimethylformamide containing 0.1 M tetrabutylammonium perchlorate at 20±0.2 °C using a three electrode cell.

The authors wish to express their thanks to Professor Soichi Misumi and Dr. Takahiro Kaneda of Osaka University for valuable discussions.

References

1) Development and Application of Organic Analytical Reagents, Part III. Part II: S. Akiyama, K. Nakashima, S. Nakatsuji, M. Hamada, and Y. Izaki, *Bull. Chem. Soc. Jpn.*, **56**, 361 (1983).

2) a) E. Buhleier and F. Vögtle, *Chem. Ber.*, **111**, 2729 (1978); b) J. P. Dix and F. Vögtle, *ibid.*, **114**, 638 (1981).

3) a) K. Sugihara, H. Kamiya, M. Yamaguchi, T. Kaneda and S. Misumi, *Tetrahedron Lett.*, **22**, 1691 (1981); b) T. Kaneda, K. Sugihara, H. Kamiya, and S. Misumi, *ibid.*, **22**, 4407 (1981); c) K. Nakashima, S. Nakatsuji, S. Akiyama, T. Kaneda, and S. Misumi, *Chem. Lett.*, **1982**, 1781.

4) C. J. Pedersen, *Fed. Proc., Fed. Am. Soc. Exp. Biol.*, **27**, 1305 (1968).

5) The cavity sizes of **2** and **3** were estimated by using the CPK model: **2**, 2.6×3.6 Å; **3**, 4.2×5.4 Å.

6) M. Iyoda, Y. Onishi, and M. Nakagawa, *Tetrahedron Lett.*, **22**, 3645 (1981).

Studies of Tritylated Pentoses and 6-Deoxyhexoses. III. The *O*-Tritylation of Methyl α- and β-D-Xylopyranoside[1)]

Toshiki OTAKE* and Toru SONOBE†

Department of Food and Nutrition, Yamanashi Gakuin Junior College, 502, Sakaori-machi, Kofu 400

†*Tobishi Pharmaceutical Co., Ltd., Omori-Nishi, Ota-ku, Tokyo 143*

(Received March 14, 1983)

Synopsis. The tritylation of methyl α- and β-D-xylopyranoside afforded three isomeric trityl ethers in both cases. All the ethers were separated by column chromatography in almost pure forms on TLC. Among them, methyl 2-*O*-trityl-α- and methyl 3-*O*-trityl-β-D-xylopyranoside were crystallized from aqueous ethanol. The position of the trityl group in each ether was mainly established by the use of ^{1}H NMR with its diacetyl derivative.

In previous papers of this series, it was shown that methyl α-D-fucopyranoside[2)] and methyl α- and β-L-rhamnopyranoside[3)] readily formed trityl ethers, although they had no primary hydroxyl group in their molecules. In these glycosides, the equatorial hydroxyl groups, each of which is in a *cis*-form with an axial hydroxyl group, seem reactive toward tritylation.

Jackson, Hockett, and Hudson[4-5)] have reported that methyl β-D-xylopyranoside (**2**) reacted with trityl chloride in dry pyridine to give ethers. This glycoside also has no primary hydroxyl group in its molecule. They isolated two crystalline ditrityl ethers and two monotrityl ethers as crystalline di-*O*-acetates. However, they did not describe their structures. Robertson and Speedie[6)] prepared methyl 2,4-di-*O*-methyl-3-*O*-tosyl-β-D-xylopyranoside from a syrupy tritylation product of **2** through crystalline methyl di-*O*-acetyl-β-D-xylopyranoside mononitrate. From the position of the tosyl group in the resulting compound, they assumed that the starting tritylation product consisted mainly of methyl 3-*O*-trityl-β-D-xylopyranoside. They did not describe any physical data of the trityl ether or the presence of other tritylation products of **2**. Also, there has been no report about the tritylation of methyl α-D-xylopyranoside (**1**). This paper will deal with the chromatographic isolation of the three possible trityl ethers from each tritylation product of **1** and **2** and with their structures.

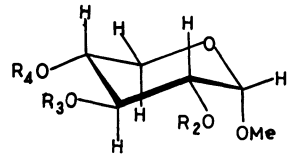

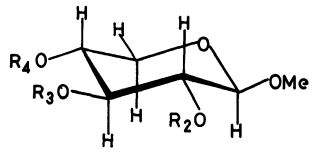

1	R_2=R_3=R_4=H	**2**	R_2=R_3=R_4=H
3a	R_2=Tr, R_3=R_4=H	**6a**	R_2=Tr, R_3=R_4=H
3b	R_2=Tr, R_3=R_4=Ac	**6b**	R_2=Tr, R_3=R_4=Ac
4a	R_3=Tr, R_2=R_4=H	**7a**	R_3=Tr, R_2=R_4=H
4b	R_3=Tr, R_2=R_4=Ac	**7b**	R_3=Tr, R_2=R_4=Ac
5a	R_4=Tr, R_2=R_3=H	**8a**	R_4=Tr, R_2=R_3=H
5b	R_4=Tr, R_2=R_3=Ac	**8b**	R_4=Tr, R_2=R_3=Ac

Tr : -C(C_6H_5)$_3$

Results and Discussion

The reaction of **1** with 1.5 molar equivalents of trityl chloride in pyridine afforded three monotrityl ethers: the 2-*O*- (**3a**), 3-*O*- (**4a**), and 4-*O*-trityl derivatives (**5a**), in a ratio of 45 : 34 : 21 and in a combined yield of 58%. Among them, **3a** was crystallized from aqueous ethanol. A dark green spot, the R_f value of which was higher than that of triphenylmethanol, was observed on a TLC of the reaction mixture; it was assumed to correspond to the ditrityl ether of **1**. The analogous tritylation of **2** gave a 39 : 34 : 27 mixture of three monotrityl ethers: the 2-*O*- (**6a**), 3-*O*- (**7a**), and 4-*O*-trityl derivatives (**8a**), in a combined yield of 67%. Among them, **7a** was crystallized from aqueous ethanol. Two dark green spots with high R_f values on a TLC of the reaction mixture were assumed to be the di-*O*-trityl derivatives of **2**. All the mono-*O*-trityl-di-*O*-acetyl derivatives (**3b**, **4b**, **5b**, **6b**, **7b**, and **8b**) derived from each monotrityl ether were crystallized from aqueous ethanol. Two acetates, **6b** and **8b**, have almost the same mp's as the compounds reported by Jackson *et al.*;[5)] however the $[\alpha]_D$'s of **6b** and **8b** do not agree with those of the compounds in their report. The ^{1}H NMR spectra of the trityl acetyl derivatives were analyzed with a favorable Cl conformation, aided by the nuclear magnetic double resonance (NMDR) technique, thus confirming the structures. *O*-Trityl-methine proton signals are distinguished by their high-field shifts from signals of acetylmethine protons. The ^{1}H NMR data in the first-order analysis of the trityl acetyl derivatives are summarized in Table 1.

In the reactions of both **1** and **2**, the sequence of the reactivity of the hydroxyl groups toward tritylation was OH-2, OH-3, and OH-4. No considerable difference was recognized in the ratios of the three monotrityl ethers between the tritylation products of **1** and **2**.

Table 1. ^{1}H NMR parameters of methine protons in the trityl acetyl derivatives

	Chemical shifts, δ					
	H-1	H-2	H-3	H-4	H-5ax	H-5eq
3b	3.85(d)	3.38(dd)	5.61(dd)	4.62(ddd)	3.45(dd)	3.57(dd)
4b	4.71(d)	4.93(dd)	3.17(dd)	4.93(ddd)	3.60—3.75(multi)	
irr 4.7	—	d	dd	ddd	multi	
5b	4.64(d)	4.52(dd)	5.60(dd)	2.78(ddd)	3.50(dd)	3.45(dd)
6b	3.90(d)	3.43(dd)	5.24(dd)	4.66(ddd)	3.92(dd)	3.45(dd)
irr 4.7	d	dd	d	—	d	d
7b	4.14(d)	4.89(dd)	3.53(dd)	4.66(ddd)	3.05(dd)	4.09(dd)
irr 3.1	d	dd	dd	dd	—	d
irr 3.5	—	d	—	dd	—	—
8b	4.29(d)	4.65(dd)	5.30(dd)	3.60(ddd)	3.0—3.3(multi)	

	Coupling constants/Hz					
	$J_{1,2}$	$J_{2,3}$	$J_{3,4}$	$J_{4,5ax}$	$J_{4,5eq}$	$J_{5ax,5eq}$
3b	3.9	10.0	10.0	11.0	6.5	11.0
4b	4.0	9.2	*ca.* 10	*ca.* 10	6.0	—
5b	4.0	10.0	8.7	*ca.* 10	*ca.* 6	*ca.* 10
6b	4.4	6.5	6.6	6.0	4.5	12.5
7b	5.1	7.0	7.0	6.5	4.2	12.5
8b	6.7	9.0	9.0	9 0	5 2	—

d: doublet, dd: d of d's, ddd: d of dd's, irr: irradiated at.

Experimental

General Methods. The solutions were evaporated under reduced pressure below 40 °C. The optical rotations were measured with a Japan Spectroscopic DIP-SL polarimeter. The TLC was performed using a DC-Alufolien Kieselgel 60 F_{254} plate, 0.2 mm in thickness (Merck), developed two times with a solvent system of methanol–acetone–pyridine–water–chloroform (1.5 : 1.5 : 0.5 : 0.5 : 96). Preparative column chromatography was achieved using Wakogel C-200 (Wako Junyaku Co., Ltd.), eluted with the same solvent system as that used in the TLC described above. The ^{1}H NMR spectra were recorded with a Varian EM 390 (90 MHz), a Varian XL-100 (100 MHz) or a JEOL XF-200 (200 MHz) spectrometer, chloroform-*d* being used as the solvent and tetramethylsilane as the internal standard.

Tritylation of Methyl α- (1) and β-D-Xylopyranoside (2). Xyloside **1** and **2** were prepared from commercial D-xylose. A mixture of **1** or **2** and trityl chloride in a molar ratio of 1 : 1.5, dissolved in dry pyridine (×5), was allowed to stand for five days at room temperature. Thus, a small amount of water was added to the solution. After concentration, the residue was dissolved in toluene (×5). Triphenylmethanol (TPM) was then filtered from the toluene solution, and the TPM-free concentrate was subjected to recycling column chromatography eight times on silica gel (30 g). In the reaction of **1** (3.28 g), the evaporation of the eluting solvent in the fraction with R_f values of 0.29, 0.57, and 0.39 gave 2.128 g of **3a**, 1.599 g of **4a**, and 1.022 g of **5a** respectively. Compound **3a** was crystallized from 80% ethanol as white prisms: mp 135—136 °C. $[\alpha]_D^{20}$ (*c* 2.0 chloroform): **3a**, +41.3°; **4a**, +5.9°; **5a**, +53.3°. Found: **3a**, C, 73.67; H, 6.49%; **4a**, C, 74.02; H, 6.60%; **5a**, C, 73.86; H, 6.56%. Calcd for $C_{25}H_{26}O_5$: C, 73.86; H, 6.45%.

The TPM-free concentrate of the tritylation product of **2** (3.28 g) was chromatographed on silica gel (30 g) in a recycling manner eight times. The concentration of the fractions with R_f values of 0.71, 0.60, and 0.52 on a TLC gave 2.101 g of **6a**, 1.875 g of **7a**, and 1.500 g of **8a** respectively. Compound **7a** was crystallized from 80% ethanol as white needles: mp 80—81 °C. $[\alpha]_D^{20}$ (*c* 2.0 chloroform): **6a**, +10.4°; **7a**, −48.0°; **8a**, −73.5°. Found: **6a**, C, 73.57; H, 6.48%; **7a**, C, 73.63; H, 6.45%; **8a**, C, 73.58; H, 6.57%. Calcd for $C_{25}H_{25}O_5$: C, 73.86; H, 6.45%.

Acetylation of Methyl O-Tritylxylopyranosides. Each sample was acetylated under standard conditions for 2 d. After chromatographic purification, all the acetates were recrystallized from 80% ethanol in yields of 70—80%. Mp: **3b**:176—177 °C; **4b**, 154 °C; **5b**, 107—108 °C; **6b**, 169—171 °C; **7b**, 162—163 °C; **8b**, 125—126 °C. $[\alpha]_D^{20}$ (*c* 2.0 chloroform): **3b**, +61.8°; **4b**, +65.5°; **5b**, +55.6°; **6b**, −6.4°; **7b**, −27.6°; **8b**, −54.2°. Chemical shifts of methyl protons in ^{1}H NMR δ=**3b**, 1.84, 1.98, 3.24; **4b**, 1.52, 1.59, 3.17; **5b**, 1.87, 2.03, 3.31; **6b**, 1.79, 2.11, 2.99; **7b**, 1.57, 1.73, 3.39; **8b**, 1.70, 2.05, 3.39. Found: **3b**, C, 71.14; H, 6.29%; **4b**, C, 70.83; H, 6.30%; **5b**, C, 70.89; H, 6.30%; **6b**, C, 71.11; H, 6.28%; **7b**, C, 70.86; H, 6.35%; **8b**, C, 70.76; H, 6.37%. Calcd for $C_{29}H_{30}O_7$: C, 71.00; H, 6.16%.

References

1) Presented in part at the 32nd National Meeting of the Chemical Society of Japan, Tokyo, April 1975, Abstr. Vol. 3, p. 1725.

2) T. Otake and T. Sonobe, *Bull. Chem. Soc. Jpn.*, **49**, 1050 (1976).

3) T. Otake, T. Sonobe, and T. Suami, *Bull. Chem. Soc. Jpn.*, **52**, 3109 (1979).

4) R. C. Hockett and C. S. Hudson, *J. Am. Chem. Soc.*, **53**, 4456 (1931).

5) E. L. Jackson, R. C. Hockett, and C. S. Hudson, *J. Am. Chem. Soc.*, **56**, 947 (1934).

6) G. J. Robertson and T. H. Speedie, *J. Chem. Soc.*, **1934**, 824.

Synthesis of Cyclic Guanidines Fused with Aromatic Ring through Metal Ion Promoted Cyclization

Hiroyuki OBASE,* Nobuhiro NAKAMIZO, Haruki TAKAI, and Masayuki TERANISHI
Tokyo Research Laboratory, Kyowa Hakko Co., Ltd., Asahimachi 3-6-6, Machida, Tokyo 194

(Received March 29, 1983)

Synopsis. A convenient synthetic method of five- and six- membered cyclic guanidines fused with aromatic ring was presented. 2-Aminoaniline or 2-(aminomethyl)aniline was treated with dimethyl carbonimidodithioates to give isothiourea which was cyclized to cyclic guanidine by using soft metal cations (Ag^+, Hg^{2+}).

As part of a program directed towards the preparation of potential antiphypertensive agents, it was necessary to synthesize cyclic guanidines fused with aromatic ring under mild conditions. We describe herein a new and mild synthesis of cyclic guanidines with formula **5** which is the key intermediate for the preparation of hypotensive agents, utilizing metal ion promoted reaction.

There are methods available for the synthesis of cyclic guanidines from 2-amino- or 2-(aminomethyl)aniline derivatives.[1-3] However, their syntheses need drastic conditions because of the poor reactivity of an anilino nitrogen. 2-(Cyanoimino)tetrahydroquinazoline **2** has been prepared in 54% yield by heating 2-(benzylaminomethyl)aniline (**1**) with dimethyl cyanocarbonimidodithioate (**6**) at 180—200 °C.[1] Rodricks *et al.* reported

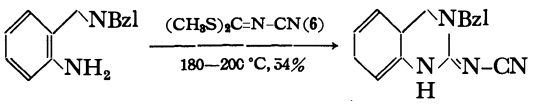

1 **2**

that 2-(tosylamino)benzimidazole could be obtained from the reaction of dimethyl tosylcarbonimidodithioate with *o*-phenylenediamine in DMF at 150—160 °C for 12—16 h.[2] The reactivity of anilino nitrogen in **3** is reduced considerably due to the hindered nature of these molecules. Therefore, the reaction conditions to obtain cyclic guanidine **5** would be more drastic than that reported earlier. Our two-step method is depicted below.

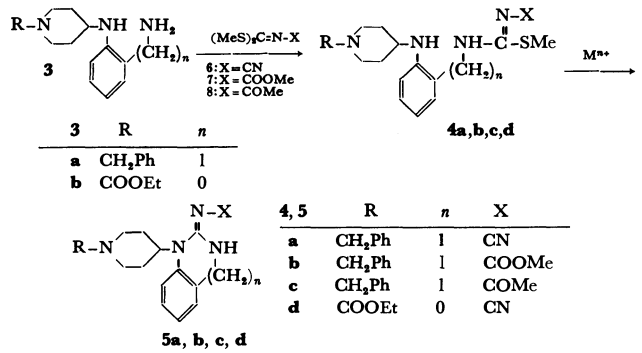

3	R	n
a	CH_2Ph	1
b	COOEt	0

4, 5	R	n	X
a	CH_2Ph	1	CN
b	CH_2Ph	1	COOMe
c	CH_2Ph	1	COMe
d	COOEt	0	CN

The synthesis of cyclization precursor **4** was attained as follows. Wittenbrook and coworker reported the preparation of 2-(cyanoimino)-1*H*-benzimidazole *via* base catalyzed reaction of *o*-phenylenediamine with **6**.[3] However, when 1-ethoxycarbonyl-4-(2-aminoanilino)-piperidine (**3b**) was reacted with **6** under the reaction conditions described by them (using triethylamine as a base, in refluxing ethanol), neither **4d** or **5d** could be detected and unchanged starting materials were recovered. The reaction carried out in dioxane in the presence of 1,8-diazabicyclo[5.4.0]undec-7-ene (DBU) at 80 °C gave an isothiourea **4d** in a moderate yield. In this case, side product such as 2-(methylthio)benzimidazole derivative reported by D' Amico[4] was not detected. The other cyclization precursors **4a**—**c** required for the synthesis of 1,2,3,4-tetrahydroquinazoline **5a**—**c** were obtained in high yields under milder conditions (at room temperature, in ethanol). The yield and physical properties of **4** are summarized in Table 1.

The cyclization of **4** to cyclic guanidine **5** was achieved by using soft metal cations. The result are shown in Table 2.

The kinds of soft metal ion available in this reaction were Hg^{2+} [$HgCl_2$, $Hg(OAc)_2$] and Ag^+ (CH_3COOAg, CF_3COOAg, CH_3SO_3Ag, and CF_3SO_3Ag). The table clearly indicates that the reaction becomes faster as increase with the softness of the metal cations. Cu(I) and Cu(II) did not promote this reaction because of preferential δ or π complexation of amino group to copper.[5-6]

Table 1. Yield and physical properties of compound **4** and **5**

Compd	Yield[a] %	Mp θ_m/°C	IR $\tilde{\nu}$/cm^{-1}		NMR ($CDCl_3$, δ)
4a	92	165—165.5	KBr	2300, 1560—1550	2.51 (s, 3H, SCH_3), 3.55 (s, 2H, CH_2Ph), 4.50 (s, 2H, $ArCH_2NHC$-N)
4b	85	Oil	$CHCl_3$	1640, 1565(br), 1555(br)	2.47 (s, 3H, SCH_3), 3.49 (s, 2H, CH_2Ph), 3.67 (s, 3H, $COOCH_3$), 4.37 (s, 2H, $ArCH_2NHC$-N)
4c	75	Oil	$CHCl_3$	1620, 1583, 1573(sh)	2.11 (s, 3H, $COCH_3$), 2.48 (s, SCH_3), 3.52 (s, 2H, CH_2Ph), 4.29, 4.34 (s, 2H, $ArCH_2NHC$-N)
4d	45	160—161	KBr	2350, 1690—1685 1570	1.27 (t, 3H, CH_3CH_2), 2.35 (s, 3H, SCH_3), 4.17 (q, 2H, CH_2CH_3)
5a	b)	204—205	KBr	2300, 1600, 1585	3.58 (s, 2H, CH_2Ph), 4.28, 4.30 (s, 2H, quinazoline ring H)
5b	b)	120—121	KBr	1633, 1610, 1595, 1582	3.58 (s, 2H, CH_2Ph), 3.73 (s, 3H, $COOCH_3$), 4.27, 4.29 (s, 2H, quinazoline ring H)
5c	b)	104—104.5	KBr	1600, 1575, 1570	2.16 (s, 3H, $COCH_3$), 3.59 (s, 2H, CH_2Ph), 4.26 (s, 2H, quinazoline ring H)
5d	b)	235—235.5	KBr	2330, 1695—1680, 1629, 1609	1.31 (t, 3H, CH_3CH_2), 4.20 (q, 2H, CH_2CH_3), 12.25 (NH)

a) Isolated yield. b) See Table 2.

Table 2. Cyclization of **4** to **5** by metal cations

Starting material	M^{n+}	Conditions[a] Temp/°C	Time/h	Product	Yield[b] %
4a	CF_3COOAg	50	1	**5a**	95
4a	CH_3SO_3Ag	50	2	**5a**	88
4a	CH_3COOAg	50	5	**5a**	90
4a	$Hg(OAc)_2$	20	0.2	**5a**	96
4a	$HgCl_2$	20	2	**5a**	95
4b	CH_3COOAg	50	3	**5b**	87
4c	CH_3COOAg	50	3	**5c**	79
4d	$Hg(OAc)_2$	20	0.1	**5d**	93

a) Starting material (0.25 mmol) in 2 ml of methanol.
b) Isolated yield.

A thiol ester is known to react with an alcohol in the presence of soft metal cations to afford the corresponding ester or lactone,[7] and also a selenol ester was demonstrated to serve as active acyl-transfer agent in the presence of copper(I) or mercury(II).[5-6] However, no example of intramolecular C–N bound formation with soft metal cations has been reported. Thus, it is noteworthy that this novel metal ion promoted reaction can afford cyclic guanidines in good yield under very simple and mild conditions and will be useful for constructing a variety of nitrogen heterocycles.

Experimental

The melting points for the samples were determined with a Mitamura hot-stage apparatus and are uncorrected. IR spectra were recorded on a Shimadzu, IR-27G grating IR spectrometer. ^{1}H NMR spectra were determined on a JNM-FX-100 spectrometer. Chemical shifts are reported in δ values relative to Me_4Si as a standard. The physical properties for samples in the experimental section are presented in Table 1.

N-[3-(1-Benzyl-4-piperidinylamino) phenylmethyl]-N′-cyano-S-methylisothiourea (4a). A solution of 1-benzyl-4-[2-(aminomethyl)anilino]piperidine[8] (**3a**, 1.0 g, 3.4 mmol), dimethyl dithiocarboimidate[9] (**6**, 0.59 g, 4 mmol), and triethylamine (0.5 g, 4.9 mmol) in 15 ml of EtOH was stirred for 2 h and concentrated under reduced pressure. The residue was triturated with 2-propanol. The crystals were collected by filtration and recrystallized from EtOH to give 1.4 g (92%) of **4a**. Found: C, 67.37; H, 6.98; N, 17.92%. Calcd for $C_{22}H_{27}N_5S$: C, 67.14; H, 6.91; N, 17.92%.

N-[2-(1-Benzyl-4-piperidinylamino) phenylmethyl]-N′-methoxycarbonyl-S-methylisothiourea (4b). Similarly **3a** (1.0 g, 3.4 mmol) was reacted with **7**[10] (0.68 g, 3.8 mmol) in the presence of triethylamine (0.5 g, 4.9 mmol) in 10 ml of EtOH. The reaction mixture was concentrated under reduced pressure and the residue was purified by chromatography on silica gel with $CHCl_3$–MeOH, 30 : 1. Pure **4b** was obtained in 85% yield as an oil. Found: C, 64.72; H, 7.12; N, 12.94%. Calcd for $C_{23}H_{30}N_4O_2S$: C, 64.76; H, 7.09; N, 13.13%.

N-[2-(1-Ethoxycarbonyl-4-piperidinylamino)phenyl]-N′-cyano-S-methylisothiourea (4d). A solution of 1-ethoxycarbonyl-4-(2-aminoanilino)piperidine[11] (**3b**, 1.5 g, 5.7 mmol), **6** (1.5 g, 5.8 mmol), and DBU (1.5 g, 12.1 mmol) in 20 ml of dioxane was heated at 80 °C for 12 h and concentrated. The residue was extracted with ethyl actate and the extract was washed successively with 0.3 mol dm^{-3} acetic acid, 0.57 mol dm^{-3} hydrochloric acid and water. After being dried over Na_2SO_4, the solvent was removed under reduced pressure and the residue was purified by silica-gel chromatography using $CHCl_3$–MeOH, 50 : 1 as eluent to afford 0.93 g (45%) of **4d**. An analytical sample was recrystallized from 2-propanol. Found: C, 56.36; H, 6.44; N, 19.19%. Calcd for $C_{17}H_{23}N_5O_2S$: C, 56.49; H, 6.41; N, 19.38%.

1-(1-Benzyl-4-piperidinyl)-2-cyanoimino-1,2,3,4-tetrahydroquinazoline (5a). A mixture of **4a** (973 mg, 2.5 mmol) and silver acetate (450 mg, 2.7 mmol) in 10 ml of MeOH was heated at 50 °C for 5 h and filtered through Celite. The filtrate was concentrated. The residue was dissolved in water, basified with 1 mol dm^{-3} NaOH, and extracted with $CHCl_3$. The extract was washed with aqueous NaCl and water, and dried over Na_2SO_4. Removal of the solvent gave essentially pure **5a** (777 mg, 90%). An analytical sample was recrystallized from 2-propanol. Found: C, 73.09; H, 6.77; N, 20.24%. Calcd for $C_{21}H_{23}N_5$: C, 73.01; H, 6.71; N, 20.28%.

1-(1-Benzyl-4-piperidinyl)-2-methoxycarbonylimino-1,2,3,4-tetrahydroquinazoline (5b). Similar reaction as described for **5a** was repeated by using **4b** (1.29 g, 3 mmol) and silver acetate (0.6 g, 3.6 mmol) in 20 ml of MeOH afforded 990 mg (87%) of **5b**. An analytical sample was recrystallized from AcOEt–hexane. Found: C, 69.76; H, 6.92; N, 14.77%. Calcd for $C_{22}H_{26}N_4O_2$: C, 69.81; H, 6.92; N, 14.81%.

2-Cyanoimino-3-(1-ethoxycarbonyl-4-piperidinyl)-2,3-dihydro-1H-benzimidazole (5d). A solution of **4d** (600 mg, 1.66 mmol) and mercury(II) acetate (535 mg, 1.68 mmol) in 10 ml of MeOH was stirred at room temperature for 1 h and concentrated. The residue was dissolved in $CHCl_3$ and the solution was washed with aqueous NaCl and water. The organic layer was separated and filtered through Celite. The filtrate was dried over Na_2SO_4 and concentrated. The residue almost pure **5d** (485 mg, 93%). An analytical sample was recrystallized from 2-propanol. Found: C, 61.54; H, 6.11; N, 22.18%. Calcd for $C_{16}H_{19}N_5O_2$: C, 61.32; H, 6.11; N, 22.35%.

References

1) F. Ishikawa, Y. Watanabe, and J. Saegusa, *Chem. Pharm. Bull.*, **28**, 1357 (1980).
2) J. V. Rodricks and H. Rapoport, *J. Org. Chem.*, **36**, 46 (1971).
3) L. S. Wittenbrook, *J. Heterocycl. Chem.*, **12**, 37 (1975).
4) J. J. D'Amico, K. Boustany, A. B. Sullivan, and R. H. Campbell, *Int. J. Sulfur Chem., Part A*, **2**, 37 (1972).
5) A. P. Kozikowski and A. Ames, *J. Am. Chem. Soc.*, **102**, 860 (1980).
6) A. P. Kozikowski and A. Ames, *J. Org. Chem.*, **43**, 2735 (1978).
7) S. Masamune, S. Kamata, and W. Schilling, *J. Am. Chem. Soc.*, **97**, 3515 (1975).
8) H. Takai, M. Teranishi, N. Nakamizo, K. Kubo, and Y. Kasuya, Japan Kokai, 56—92884 (1981).
9) R. J. Timmons and L. S. Wittenbrook, *J. Org. Chem.*, **32**, 1566 (1967).
10) M. M. Fawzi and W. Del., U. S. Patent 3562290 (1971).
11) P. A. J. Janseen, A. H. M. T. Tan Heertum, J. Vandenberk, and M. J. M. C. van Aa, Ger. Offen. 2527261 (1976).

A Kinetic Study on Denitration of 9,9′-Dinitro-9,9′-bifluorenyl by Tin(II) Chloride in *N,N*-Dimethylformamide

Kimitoshi FUKUNAGA* and Makoto KIMURA
Faculty of Engineering, Yamaguchi University, Tokiwadai, Ube, Yamaguchi 755
(Received April 25, 1983)

Synopsis. The kinetics of the reductive elimination of nitro groups from 9,9′-dinitro-9,9′-bifluorenyl by tin(II) chloride in *N,N*-dimethylformamide (DMF) at 20 °C was investigated. It was found that the present elimination is a second-order reaction.

The potential usefulness of a radical anion-radical chain elimination reaction ($E_{RC}l$) has been widely recognized.[1] Although numerous works have been published on the $E_{RC}l$ of vicinal dinitro compounds,[2,3] α-cyano-β-nitro esters,[4] α-acetyl-β-nitro ketones,[5] and β-nitro sulfones,[6] little was known of their kinetics. The kinetic approach to the $E_{RC}l$, in general, suffers from the drawbacks that the reaction system is heterogeneous, and that the reaction is carried out under the photoirradiation or at elevated temperatures. However, in the previous work[3] it was found that the denitration of α,β-diaryl vicinal dinitro compounds with tin(II) chloride in DMF proceeded readily at room temperature. Moreover, the $E_{RC}l$ product from 9,9′-dinitro-9,9′-bifluorenyl (**1**) is 9,9′-bifluorenylidene (**2**), which has absorptions in the visible region probably attributable to a π-π^* electronic transition. The large molar absorptivity of product **2** permits low concentrations of the reactants to be used, thus eliminating problems arising from the limted solubility of tin(II) chloride. Based on these preliminary findings, a kinetic study on $E_{RC}l$ of **1** with tin(II) chloride in DMF has been made.

Experimental

Chemicals. Commercial anhydrous tin(II) chloride and DMF of the purest grade were used without further purification. Compound 1 was prepared according to the literature method.[3]

Procedure and Apparatus. The reaction of **1** with tin(II) chloride in DMF was initiated by the addition of the latter solution into a stirred solution of **1**, which was placed in the spectrophotometric cell (width 1 cm, quartz) immersed in a water bath thermostated at 20±0.1 °C. Red compound **2** has an extremely large absorptivity in DMF, $\varepsilon = 2.30 \times 10^4$ $dm^3\ mol^{-1}\ cm^{-1}$ at 458 nm, while the other species in the reaction solution are transparent under the given concentrations. Consequently the absorbance of **2** formed was measured at an appropriate reaction time using a Hitachi Model 330 spectrophotometer.

Results and Discussion

A typical spectral change of the reaction mixture is shown in Fig. 1. Figure 2 shows a typical reaction profile. The concentrations used were 4.54×10^{-4}—9.5×10^{-3} mol dm^{-3} for **1** and 1.96×10^{-3}—2.78×10^{-2} mol dm^{-3} for tin(II) chloride. The runs were carried out to about 0.07—0.7% completion. For the reaction under consideration, we may write as follows:

$$r = d[\mathbf{2}]/dt = k[\mathbf{1}]^a[SnCl_2]^b, \quad (1)$$

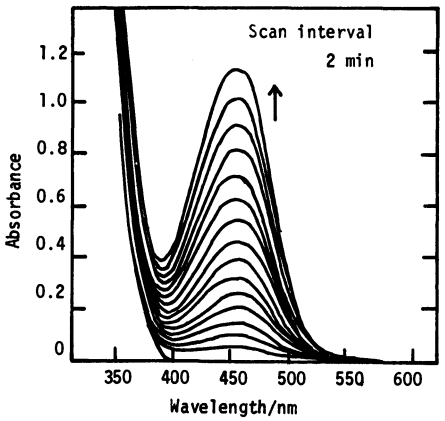

Fig. 1. Absorption spectral change due to the increase of 9,9′-bifluorenylidene (**2**) in the reaction of 9,9′-dinitro-9,9′-bifluorenyl (**1**) (2.73×10^{-3} mol dm^{-3}) with tin(II) chloride (1.86×10^{-2} mol dm^{-3}) in DMF at 20 °C.

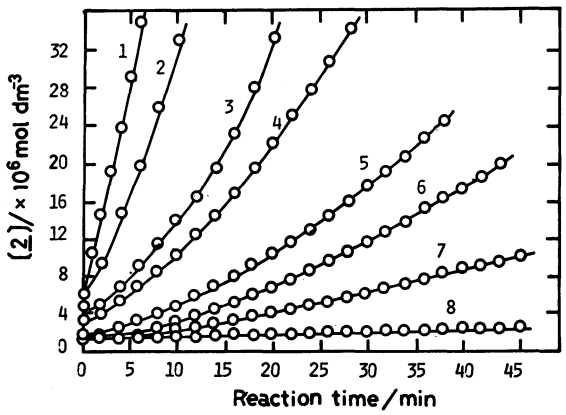

Fig. 2. Formation of **2** from **1** in a DMF solution at 20 °C.
The concentrations were as follows: 1, $[\mathbf{1}] = 9.50 \times 10^{-3}$ M and $[SnCl_2] = 2.78 \times 10^{-2}$ M; 2, $[\mathbf{1}] = 5.68 \times 10^{-3}$ M and $[SnCl_2] = 2.78 \times 10^{-2}$ M; 3, $[\mathbf{1}] = 2.73 \times 10^{-4}$ M and $[SnCl_2] = 2.78 \times 10^{-2}$ M; 4, $[\mathbf{1}] = 2.73 \times 10^{-4}$ M and $[SnCl_2] = 1.86 \times 10^{-2}$ M; 5, $[\mathbf{1}] = 2.73 \times 10^{-4}$ M and $[SnCl_2] = 1.43 \times 10^{-2}$ M; 6, $[\mathbf{1}] = 2.73 \times 10^{-4}$ M and $[SnCl_2] = 1.07 \times 10^{-2}$ M; 7, $[\mathbf{1}] = 2.73 \times 10^{-4}$ M and $[SnCl_2] = 5.27 \times 10^{-3}$ M; 8, $[\mathbf{1}] = 2.73 \times 10^{-4}$ M and $[SnCl_2] = 1.96 \times 10^{-3}$ M.

where r, [ ], t, k, a, and b denote the reaction rate, the concentration, the time, the rate constant, kinetic order with respect to **1**, and that with respect to tin(II) chloride, respectively. From Eq. 1, we get

$$\log r = \log(d[\mathbf{2}]/dt) = \log k + a \log[\mathbf{1}] + b \log[SnCl_2]. \quad (2)$$

Thus from measurements of the initial rate of the reaction in separate experiments, in which either of the reactants

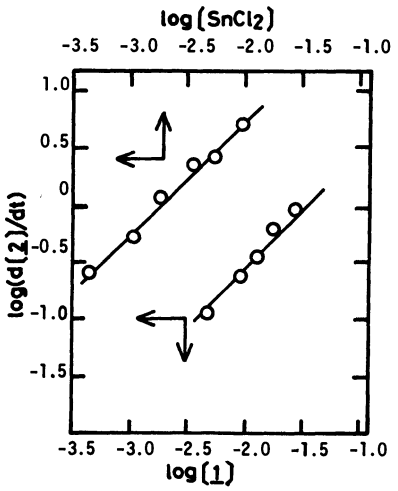

Fig. 3. log-log plots of the initial rate of the reaction of **1** with tin(II) chloride in DMF at 20 °C against the concentrations of **1** and tin(II) chloride.

is kept constant, we may find orders a and b. Plots of both log [**1**] and log [$SnCl_2$] *vs.* og $r_{t\to 0}$ will give a straight line with each slope of a and b. Each linear plot with a slope of $a=1.00$ and $b=1.04$ in Fig. 3 suggests that the reaction rate is expressed by an equation

$$r = d[\mathbf{2}]/dt = k[\mathbf{1}]^{1.00}[SnCl_2]^{1.04} \quad (3)$$

with a second-order constant $k=1.49\times10^4$ M^{-1} min^{-1} (1 M=1 mol dm^{-3}) at 20 °C. The net reaction is thus given by the following equation:

$$\mathbf{1} + Sn(II) \longrightarrow \mathbf{2} + Sn(IV) + 2\,NO_2^- . \quad (4)$$

The mechanism of the present elimination appears to be one of the $E_{RC}1$[1] whose mechanism has been confirmed in the reaction of vicinal dinitro compounds or β-nitro sulfones with tributyltin hydride,[6] and the elimination seems to proceed according to the following reactions. By combining Eqs. 5—8 we obtain Eq. 4.

The k value is *ca.* 7×10^5 times greater than the second-order rate constant for a similar reductive elimination of *meso*-stilbene dibromide with tin(II) chloride in DMF at 59.4 °C reported by Kwok and

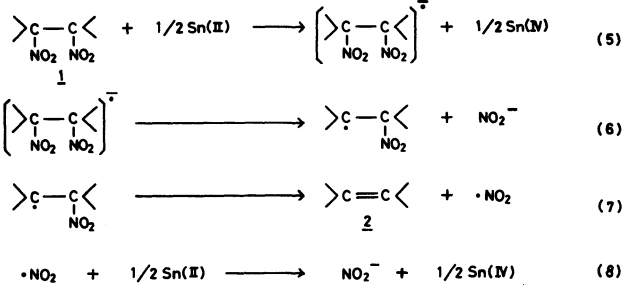

Miller.[7] It is also important to note that the k value is comparable to those for second-order electron transfer reactions among metal ions in liquid phase such as $Fe^{2+}+Co^{3+}\to Fe^{3+}+Co^{2+}$ at 0—25 °C.[8] The observed rate constant appears to be accounted for by the fact that the nitro group accepts most readily one electron among all the common functional groups.[6]

References

1) N. Kornblum, *Angew. Chem., Int. Ed. Engl.*, **14**, 734 (1975); N. Ono and A. Kaji, *Yuki Gosei Kagaku Kyokai Shi*, **35**, 165 (1977); D. J. Girdler and R. K. Norris, *Tetrahedron Lett.*, **1975**, 2375; D. J. Freeman and R. K. Norris, *Aust. J. Chem.*, **29**, 2631 (1976).

2) N. Kornblum, S. D. Boyd, H. W. Pinnick, and R. G. Smith, *J. Am. Chem. Soc.*, **93**, 4316 (1971); N. Kornblum and L. Cheng, *J. Org. Chem.*, **42**, 2944 (1977).

3) K. Fukunaga, *Synthesis*, **1975**, 442; K. Fukunaga and M. Kimura, *Bull. Chem. Soc. Jpn.*, **52**, 1107 (1979).

4) N. Ono, R. Tamura, J. Hayami, and A. Kaji, *Chem. Lett.*, **1977**, 189.

5) R. Tamura, T. Nakatsuka, N. Ono, and A. Kaji, *Chem. Lett.*, **1980**, 281.

6) N. Ono, R. Tamura, T. Nakatsuka, J. Hayami, and A. Kaji, *Bull. Chem. Soc. Jpn.*, **53**, 3295 (1980); N. Ono, H. Miyake, R. Tamura, I. Hamamoto, and A. Kaji, *Chem. Lett.*, **1981**, 1139.

7) W. K. Kwok and S. I. Miller, *J. Am. Chem. Soc.*, **92**, 4599 (1970).

8) L. E. Bennett and J. C. Sheppard, *J. Phys. Chem.*, **66**, 1275 (1962).

Condensations of 3,4-Bis(diphenylmethylene)-1,2-cyclobutanedione with *o*-Phenylenediamine under Ionic and Radical Reaction Conditions

Zaiko Ro,† Koichi Tanaka, and Fumio Toda*
Department of Industrial Chemistry, Faculty of Engineering, Ehime University, Matsuyama 790
(Received May 9, 1983)

Synopsis The title condensations under ionic and radical reaction conditions gave 1,2-bis(diphenylmethylene)-1,2-dihydrocyclobuta[*b*]quinoxaline and 7,8-bis(diphenylmethylene)-7,8-dihydrobenzo[*b*][1,4]diazocine-6,9(5*H*,10*H*)-dione respectively.

Recently, McOmie and his co-workers have found that the kind of the condensation product of substituted benzocyclobutene-1,2-dione (**1**) with *o*-phenylenediamine (**2**) is very sensitively affected by the substituents of the former. For example, the condensation of **1a**—**c** with **2** in MeOH containing AcOH gave the corresponding 5,10-diazabenzo[*b*]biphenylenes (**3a**—**c**), whereas the similar condensation of **1d**—**f** gave the corresponding dibenzo[*b*,*f*][1,4]diazocine-6,11(5*H*,12*H*)-diones (**4d**—**f**).[1] However, the reason for the difference has not been clear.

We have now found that the condensations of 3,4-bis(diphenylmethylene)-1,2-cyclobutanedione (**5**) with **2** under ionic and radical reaction conditions gave 1,2-bis(diphenylmethylene)-1,2-dihydrocyclobuta[*b*]quinoxaline (**7**) and 7,8-bis(diphenylmethylene)-7,8-dihydrobenzo[*b*][1,4]diazocine-6,9(5*H*,10*H*)-dione (**8**) respectively. When a solution of **5**[2] and an equimolar amount of **2** in CCl_4 was kept at room temperature for 120 min, **7** and **8** were obtained in 46 and 53% yields respectively (Table 1). When the reaction was carried out in the dark, the yield of **7** increased slightly. The condensation reaction was accelerated by the addition of AcOH. The reaction in CCl_4 containing 3% AcOH ceased within 15 min and gave **7** and **8** in 56 and 43% yields respectively. When the concentration of AcOH was increased to 20 or 50%, the reaction was much more accelerated and gave only **7** in a 98% yield in both cases. The termination of the reaction can easily be followed by observing the disappearance of the deep green color of **5**. The above results clearly show that the acide catalyzed condensation of **5** and **2** gives **7**.

On the contrary, the reaction in the presence of the radical initiator $CBrCl_3$ gave **8** in an 85% yield in addition to a small amount of **7**. When the same reaction was carried out in the dark, however, the yield of **8** decreased to 50% and the yield of **7** increased to 44%. The homolysis of $CBrCl_3$ to trihalomethyl and halogeno radicals is accelerated by light.[3] The formation of **8** by the reaction in CCl_4 in the dark may be due to radical species produced by a dark reaction of **2** and CCl_4, for no reaction occurred in MeOH in the dark.

The plausible reaction pathways are shown in Scheme 1. The reaction of **5** and **2** gives the diol intermediate (**6**), which, upon acid-catalyzed dehydration and radical-induced dehydrogenation, affords **7** and **8** respectively. When the halogeno radical abstracts hydrogen from **6**, **8**, and hydrogen halide are formed. The hydrogen halide thus formed catalyzes the dehydration of **6**. This would be the reason that the formation of **8** always accompanies that of **7**.

Nonetheless, it is not clear whether McOmie's case is similar to ours or not.[4]

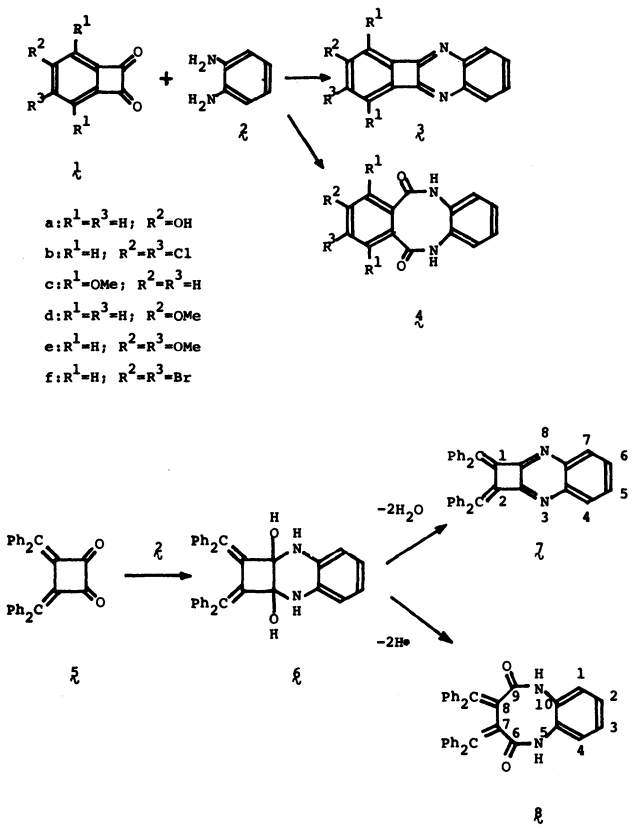

Scheme 1.

Table 1. Reaction of **5** with **2** in CCl_4

Additive (v/v%)		Reaction time/min	Yield/%	
			7	**8**
—		120	46	53
—	(dark)	240	51	48
AcOH	3	15	56	43
AcOH	20	10	98	—
AcOH	50	5	98	—
$CBrCl_3$	10	20	14	85
$CBrCl_3$	10 (dark)	40	44	50

† Present address: Institute of Chemistry, Ryannei Teachers College, Dalian, Peoples Republic of China.

Experimental

*Condensation Reaction of **5** with **2** in the Absence of AcOH.* When a solution of **5**[2] (0.24 g, 0.58 mmol) and **2** (0.063 g, 0.58 mmol) in CCl_4 (20 ml) was kept at room temperature for 120 min, the deep green color of **5** disappeared completely, resulting in an orange-colored CCl_4 solution. This solution was poured into a column filled with silica gel; it was subsequently eluted by $CHCl_3$ and THF to give **7** as yellow prisms (0.128 g; 46%; mp 240—241 °C (lit,[2] mp 240—241 °C)) and **8** as colorless prisms (0.16 g; 53% mp 287—288 °C) respectively. IR (Nujol) 3170 (NH) and 1660 cm^{-1} (CO). UV ($CHCl_3$) 298 (ε 8300) and 356 nm (3400). MS (75 eV) *m/e* (rel intensity) 518 (M^+; 100), 340(90), and 322(20), ^1H NMR ($CDCl_3$) δ=4.38 (s, NH, 2H) and 6.5—7.6 (m, Ar, 24H).

Found: C, 83.11; H, 5.07; N, 5.29%. Calcd for $C_{36}H_{26}O_2N_2$: C, 83.37; H, 5.05; N, 5.40%.

The reaction mixture obtained by carrying out the reaction in the dark and in the presence of $CBrCl_3$ was treated by the same method as above (Table 1).

*Condensation Reaction of **5** with **2** in the Presence of AcOH.* The reaction was carried out by a method similar to that used for the reaction in the absence of AcOH. The reaction mixture was washed with aq $NaHCO_3$ and water, and dried over Na_2SO_4. The dried CCl_4 solution was then column-chromatographed on silica gel in the same manner as that described above (Table 1).

References

1) O. Abou-Teim, N. P. Hacker, R. B. Jansen, J. F. W. McOmie, and D. H. Perry, *J. Chem. Soc., Perkin Trans. 1*, **1981**, 988.

2) F. Toda and K. Akagi, *Tetrahedron*, **27**, 2801 (1971).

3) E. S. Huyser, *J. Am. Chem. Soc.*, **82**, 391 (1960).

4) According to our request, McOmie and his co-workers tried their condensation reactions under our reaction conditions, but they could not get clear results; private communication.

Stereoselective Cross-Aldol Reactions of Silyl Enol Ethers with Acetals Catalyzed by Iodotrimethylsilane[1)]

Hideki SAKURAI,* Koshi SASAKI, and Akira HOSOMI
Department of Chemistry, Tohoku University, Sendai 980

(Received May 20, 1983)

Synopsis. Iodotrimethylsilane catalyzes effectively erythroselective aldol type condensation of silyl enol ethers with acetals.

Recently, much attention has been focused on the stereoselective aldol condensations[2)] in relation to syntheses of acyclic β-hydroxy ketones as a structural unit of natural macrolide antibiotics.[3)] We have found previously that iodotrimethylsilane is an efficient catalyst for the regiospecific allylation of acetals with allylsilanes.[4)] As an extension of the work, we report here that highly nucleophilic silyl enol ethers (**2**), like allylsilanes, undergo the reaction with acetals (**3**) in the presence of a catalytic amount of iodotrimethylsilane (**1**), prepared from hexamethyldisilane and iodine at ambient temperature,[5)] to afford erythro-selective β-alkoxy ketones (**4**) in excellent yield. (Eq. 1).

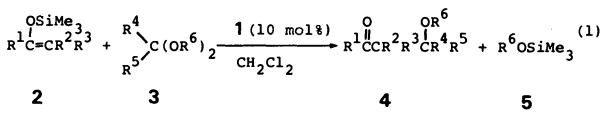

(1)

2 **3** **4** **5**

Results and Discussion

The essential feature of the reaction is rather similar to the trimethylsilyl triflate-catalyzed reaction,[6)] and the results are listed in Table 1.

In all cases, the reaction of **2** with a variety of **3** proceeds very smoothly and completes within 30 min at −78 °C.[7)] It is important to note that the reaction mixture should be hydrolyzed by a saturated hydrogen sodium carbonate solution at −78 °C. One of the important features of the present reaction is the erythro selective aldol condensation. For example, reactions of benzaldehyde dimethyl acetal (**3a**) with silyl enol ethers, **2a** and **2b**, derived from cyclopentanone and cyclohexanone, gave mixtures of erythro and threo derivatives in a ratio of 99 : 1 and 95 : 5, respectively. (Eq. 2).

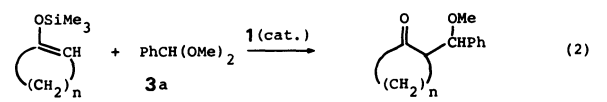

(2)

2a, n = 3 — **4a**, 87%; Erythro:Threo = 99:1

b, n = 4 — b, 89%; Erythro:Threo = 95:5

On the other hand, 3-trimethylsiloxy-2-pentene (**2c**, *E* : *Z*=21 : 79), prepared by Et_3N/Me_3SiCl in DMF,[8)] gave a 57 : 43 mixture of erythro and threo derivatives. (Eq. 3).

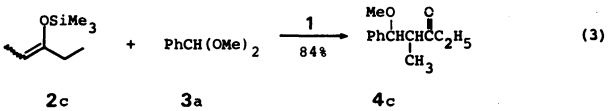

(3)

2c **3a** **4c**

E:Z = 21:79 — Erythro:Threo = 57:43

Table 1. Reactions of silyl enol ethers (**2**) with acetals (**3**) and orthoformates (**6**) catalyzed by iodotrimethylsilane (**1**) in dichloromethane at −78 °C

Silyl enol ether	Acetal or orthoformate	Reaction time/min	Product	Yield[a)]/% erythro[b)] /threo
(**2a**)	$PhCHC(OMe)_2$ (**3a**)	20[c]	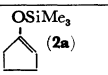 (**4a**)	87 (99/ 1)
2a	$Ph(CH_2)_3CH(OEt)_2$ (**3b**)	30		90 (83/17)
2a	$CH_3(CH_2)_3CH(OMe)_2$ (**3c**)	30		70 (70/30)
2a	$PhCH{=}CHCH(OMe)_2$ (**3d**)	50		82 (80/20)
2a	$CH_3CH_2CH(OCH_2Ph)_2$	90		65
2a	$(CH_3)_2C(OMe)_2$ (**3e**)	50		90
2a	$CH(OMe)_3$ (**6a**)	60		81
$OSiMe_3$ (**2b**)	**3a**	60	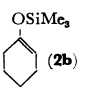 (**4b**)	89 (95/ 5)
2b	$(CH_3)_2CHCH_2(OMe)_2$	25	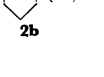	70 (79/21)
2b	**3b**	30		87 (86/14)
2b	**3d**	60		92 (89/11)
2b	**3e**	60		82
2b	**6a**	60		80
$OSiMe_3$ (**2c**)	**3a**	55	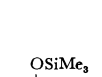	84 (57/43)
2c	**3e**	60	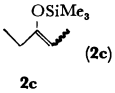	86
$OSiMe_3$ Ph (**2d**)	**3a**	40	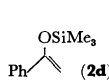	90
2d	**3c**	50	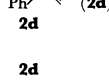	90
2d	**3e**	50	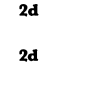	84
2d	**6a**	60	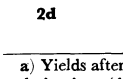	88
2d	$CH(OEt)_3$	60	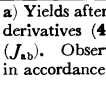	87

a) Yields after isolation by TLC. b) Determined by NMR. Erythro and threo derivatives (**4**) were characterized by comparing the vicinal coupling constants (J_{ab}). Observations that J_{threo} of *e.g.* **4b** (13 Hz) is greater than $J_{erythro}$ (4 Hz) is in accordance with other erythro–threo systems.[6,10)] c) At −35 °C.

It is notable that orthoformate (**6**) reacts with **2** by catalysis of **1** to give β-keto acetal (**7**). No further reaction with the resulting β-keto acetal occurred. Apparently, the reaction of **7** with **2** is slower than the reaction of **6**.

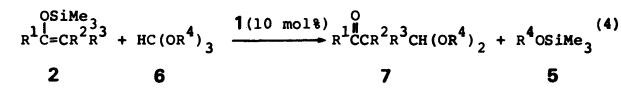

2 **6** **7** **5**

From the mechanistic point of view, it is interesting that reactions with α,β-unsaturated acetals catalyzed by **1** proceed very selectively on the acetal carbon (see Table 1). This fact suggests strongly that a silyloxonium ion A, not a carbenium ion like B, is the most important intermediate in the reaction.

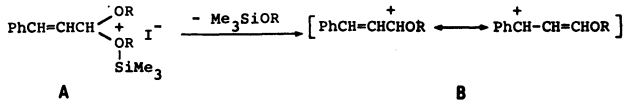

A **B**

Experimental

Reactions Summarized in Table 1. The following procedure is typical. To a mixture of **2** (1.2 mmol) and **3** (or **6**) (1.0 mmol) in dry dichloromethane (2 ml) was added iodotrimethylsilane (0.02 g, 0.1 mmol) by a syringe under nitrogen at −78 °C. The reaction mixture was stirred for given conditions in Table 1 and hydrolyzed with a saturated solution of hydrogen sodium carbonate at −78 ° C.After usual work-up, the crude product was purified by preparative thin-layer chromatography on silica gel.[9]

References

1) Chemistry of Organosilicon Compounds. 179.

2) C. H. Heathcock, C. T. Buse, W. A. Kleschick, M. C. Pirrung, J. E. Shon, and J. Lampe, *J. Org. Chem.*, **45**, 1066 (1980); M. Hiramura, D. S. Garvey, L. D. Lu, and S. Masamune, *Tetrahedron Lett.*, **1979**, 3937; D. A. Evans, J. V. Nelson, E. V. gel and T. R. Taber, *J. Am. Chem. Soc.*, **103**, 3099 (1981); K. Maruoka, S. Hashimoto, and H. Nozaki, *ibid.*, **99**, 7705 (1977); T. Mukaiyama, K. Banno, K. Narasaka, *ibid.*, **96**, 7503 (1974); Y. Yamamoto, H. Yatagai, Y. Naruta, and K. Maruyama, *ibid.*, **102**, 7107 (1980), and references cited therein.

3) For review articles, see S. Masamune, *Aldrichimica Acta*, **11**, 23 (1978); P. A. Bartlett, *Tetrahedron*, **36**, 3 (1980).

4) H. Sakurai, K. Sasaki, and A. Hosomi, *Tetrahedron Lett.*, **23**, 745 (1981).

5) H. Sakurai, A. Shirahata, K. Sasaki, and A. Hosomi, *Synthesis*, **740**, (1979).

6) S. Murata, M. Suzuki, and R. Noyori, *J. Am. Chem. Soc.*, **102**, 3248 (1980).

7) Reactions can be catalyzed by a smaller amount of iodotrimethylsilane but in a slower rate.

8) E. Nakamura, K. Hashimoto, and I. Kuwajima, *Tetrahedron Lett.*, **1978**, 2079.

9) All compounds gave satisfactory spectral data and correct elemental analyses.

10) *E. g.*; T. Mukaiyama, K. Narasaka, and K. Banno, *J. Am. Chem. Soc.*, **96**, 7503 (1974); H. O. House, D. C. Crumrine, A. Y. Teranishi, and M. D. Olmstead, *ibid.*, **95**, 3310; Y. Yamamoto, H. Yatagai, and K. Maruyama, *ibid.*, **103**, 3229 (1981).

Reactivity of Aromatic *o*-Hydroxy Oximes. II. The Use of Esters of Aromatic *o*-Hydroxy Oximes in Peptide Synthesis

Ikuo HAYASHI* and Kiyoshi SHIMIZU

Research and Development Laboratory of Nitto Boseki Co., Ltd., Fukuyama-cho, Koriyama 963

(Received March 1, 1983)

Synopsis. Esters of *N*-protected amino acids with *o*-hydroxybenzaldehyde oxime, *o*-hydroxyacetophenone oxime, *o*-hydroxybenzophenone oxime, and their 5-Cl and 5-NO_2 derivatives were prepared by several methods. Various dipeptide derivatives with high purity were obtained in good yield by use of these active ester reagents.

There are numerous reports on the use of oxime compounds and their derivatives for peptide synthesis.[1,2] The reactivity of oxime esters with an amine component is generally low.[2] Therefore, weak acid catalysts are often used to enhance the reactivity of oxime esters. We reported in the previous paper[3] that esters with *N*-(benzyloxycarbonyl)glycine (Z–Gly) of aromatic *o*-hydroxy oximes, *e.g.*, *o*-hydroxybenzaldehyde oxime (HOHBA), *o*-hydroxyacetophenone oxime (HOHAP), *o*-hydroxybenzophenone oxime (HOHBP), and their 5-Cl and 5-NO_2 derivatives of (*E*)-configuration, react rapidly with benzylamine without use of any acids in THF at 30 °C. In the present study, we report that some new esters of the above-mentioned oximes with various acylamino acids have been prepared and that these oxime esters are very effective for peptide synthesis.

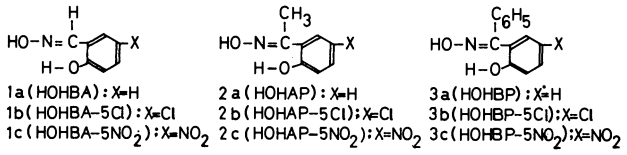

Results and Discussion

The active esters of *N*-protected amino acids were prepared from the amino acids and the oxime **1**, **2**, or **3** (A) by a direct condensation using dicyclohexylcarbodiimide (DCC), (B) with carbonic carboxylic anhydride, or (C) with acid chloride. Method (A) appears to be more useful than the others because of its mild reaction conditions.

Table 1. Oxime esters of amino acids

Ester[a]	Method	Yield %	Mp θ_m/°C	$[\alpha]_D^{24}$/° (*c* 1, DMF)
Boc–Gly–OHBA	(B)	68.0	123—126	—
Boc–Gly–OHAP	(A)	73.5	135—138	—
Z–Ala–OHBA	(A)	86.9	94—96	−19.7
Z–Ala–OHAP	(A)	66.2	99.5—100	−42.4
Boc–Ala–OHBA	(A)	82.0	100—102	−26.4[b]
Boc–Ala–OHAP	(A)	44.3	104—106	−67.1
Boc–Phe–OHBA	(A)	47.9	113—115.5	−2.9
Boc–Phe–OHAP	(A)	39.2	114.5—116.5	−21.0
Z–Phe–OHAP	(A)	68.6	116.5—118.5	−21.1
Nps–Phe–OHAP	(A)	87.7	132—134	−129.1
Nps–Phe–OHAP–5NO_2	(A)	57.0	145.5—148.5	−90.7
Z–Leu–OHAP	(A)	78.7	112—113.5	−36.5
Boc–Lys(Z)–OHAP	(A)	72.8	105—107	−32.9
Nps–Pro–OHAP	(A)	85.5	152.5—154	−193.5

a) Abbreviations were used in the same mode as in the previous paper[3] and all oxime esters were characterized by elemental analysis. b) In $CHCl_3$.

The active esters of the oximes are shown in Table 1 except those[3] of Z–Gly previously reported. Although the oximes themselves have a bifunctional nature, only the hydroxyimino group in the molecule is esterified with *N*-protected amino acids.[3] Therefore, it is not necessary to protect the phenolic hydroxyl group for the preparation of these esters. When **4** is prepared by these methods, alkaline washing of the reaction mixture cannot be applied in the case of the reaction with **1c**, **2c**, or **3c** because of the existence of *o*-hydroxyl group which is considerably acidic, and therefore the procedure for the isolation of **4** requires some considerations.

The results are summarized in Table 2. The yield of reaction products was always good and their purity was also quite satisfactory. The most significant advantage of our oxime ester method is that no addition of acid

Table 2. Synthesis of dipeptide derivatives[a] by using active esters **4**

Active ester[b]	Amine component	Yield[c] %	Mp θ_m/°C Observed	Mp θ_m/°C Lit	$[\alpha]_D^{24}$/° Observed (Lit, °C)	*c*/%	Solvent
Z–Gly–OHBA[3]	Gly–OEt	88.9	76—78	80—81[5]	—		
Z–Gly–OHAP[3]	Gly–OEt	77.5	76—78		—		
Z–Ala–OHBA	Gly–OEt	65.2	96—97	98—99[6]	−22.4(−21.3, 22)[6]	1	EtOH
Z–Ala–OHAP	Gly–OEt	72.0	95—96	97.5—98[7]	−24.3(−24.4, 20)[7]	1	EtOH
Z–Ala–OHBP[d]	Gly–OEt	48.8	97—98		−21.5	1	EtOH
Boc–Leu–OHBA[e]	Gly–OMe	35.0	129—130	128—131[8]	−21.2(−20.7, 24)[8]	1	EtOH
Boc–Leu–OHAP[e]	Gly–OMe	42.3	131—131.5		−21.0	1	EtOH
Z–Leu–OHBA	Gly–OEt	66.9	100—100.5	102—104[10]	−26.6(−27.5, 20)[10]	5	EtOH
Z–Leu–OHAP	Gly–OEt	50.8	101.5—102		−28.0	5	EtOH
Boc–Phe–OHBA	Gly–OEt	48.2	87—88	89.5—90[9]	−4.9 (−4.3, 25)[9]	2	EtOH
Boc–Phe–OHAP	Gly–OEt	56.4	88—90		−4.7	2	EtOH
Z–Phe–OHBA	Gly–OEt	36.2	109—109.5	111[6]	−15.7(−16.8, 22)[6]	2	EtOH
Z–Phe–OHAP	Gly–OEt	65.2	108.5—111		−14.4	2	EtOH
Z–Phe–OHAP–5Cl[d]	Gly–OEt	72.4	106—108		−15.5	2	EtOH
Boc–Lys(Z)–OHAP	Gly–OEt	83.3	61—63	68[11]	−12.1(−13.1, 25)[11]	1	MeOH

a) All dipeptide derivatives were characterized by elementary analysis. b) Abbreviations were used in the same mode as in the previous paper.[3] c) **4** coupled with an amine component. d) A viscous oil. e) A colorless oil.

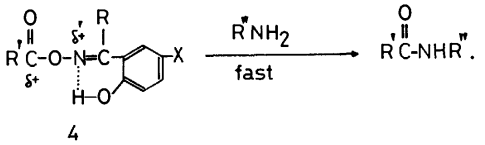

4

catalyst is required for enhancing the reactivity of **4**, since the aminolysis accelerates by the favorable mechanism of intramolecular acid-catalysis.[3]

With this new coupling method, the reaction of **4** with the amine component can progress successfully without any addition of weak acid catalyst. To check the reactivity of **4**, the reaction of Z–Gly–OHAP (**4**; $R=CH_3$, $X=H$)[3] and Z–Gly–OAP (**5**; $R=CH_3$, $X=H$)[2] with ethyl glycinate (Gly–OEt) in THF at room temperature was carried out with a reaction time of 60 min. The yields of Z–Gly–Gly–OEt obtained were 75 and 35%, respectively. From the above instances, a period of one night may be regarded as a sufficient reaction time for the completion of the condensation. The dipeptide derivative from a reaction mixture is easily isolated by alkaline washing in the usual fashion, since the free oxime has an acidic *o*-hydroxyl group, especially with the 5-NO_2 derivatives. Because of high reactivity of **4** and easy availability of the peptide derivatives, these esters appear to be quite useful for peptide synthesis.

Experimental

The purity of products was tested by TLC.[3] The IR spectra of all compounds were determined by a JASCO A-102 spectrophotometer. The specific rotations were measured with a JASCO automatic polarimeter DIP-140. All the amino acids except Gly were of L-configuration. All the oximes and active esters **4** were prepared as described in the previous paper.[3] *N*-Benzyloxycarbonyl amino acids and *N*-(*t*-butoxycarbonyl) (Boc) amino acids were prepared in the usual way. *N*-(*o*-Nitrophenylsulphenyl) (Nps) amino acids were prepared as described by Zervas *et al.*[4]

Preparation of Dipeptides. Twenty mmol of *N*-protected amino acid oxime ester **4**, 20 mmol of hydrohalide of amino acid alkyl ester, and 20 mmol of triethylamine were dissolved in THF or DMF (about 150 ml). The mixture was stirred overnight at room temperature and then the solvent was removed. The crude products was dissolved in ethyl acetate. The solution was washed successively with 5% citric acid, 1 mol dm^{-3} $NaHCO_3$, and water, and dried over magnesium sulfate. The ethyl acetate was removed *in vacuo*. The resulting residue was triturated with petroleum ether to give a solid. The purified product was recrystallized from an appropriate solvent.

Comparison of Reactivity between Z–Gly–OHAP and Z–Gly–OAP. Triethylamine (1.4 ml, 10 mmol) was added to a suspension of Gly–OEt·HCl (1.40 g, 10 mmol) in THF (50 ml) with stirring. After 15 min, Z–Gly–OHAP (3.42 g, 10 mmol) was added to the solution at room temperature. After 60 min, a cold 2 mol dm^{-3} HCl was added to the mixture in order to terminate the coupling, and the mixture was worked up similarly to the above procedure. A recrystallization of crude product from ethyl acetate-petroleum ether gave Z–Gly–Gly–OEt: 2.21 g; mp 79.5—80.5 °C. The reaction of Z–Gly–OAP with Gly–OEt was carried out simultaneously under the same conditions with the result: 1.04 g, mp 76—78.5 °C.

References

1) *E.g.*, Houben-Weyl, "Methoden der Organischen Chemie," Georg-Thieme Verlag, Stuttgart (1974), Band XV, Teil 2.

2) G. Losse, A. Barth, and K. Schatz, *Justus Liebigs Ann. Chem.*, **677**, 185 (1964).

3) I. Hayashi, K. Ogihara, and K. Shimizu, *Bull. Chem. Soc. Jpn.*, **56**, 2432 (1983). Abbreviations were used in the same mode as in this paper.

4) L. Zervas, D. Borovas, and E. Gazis, *J. Am. Chem. Soc.*, **85**, 3660 (1963).

5) H. Kinoshita, I. Inomata, O. Miyano, and H. Kotake, *Bull. Chem. Soc. Jpn.*, **52**, 2119 (1979).

6) M. Fujino and C. Hatanaka, *Chem. Pharm. Bull.*, **16**, 929 (1968).

7) M. Bergmann, L. Zervas, J. S. Fruton, F. Schneider, and H. Schleich, *J. Biol. Chem.*, **109**, 325 (1935).

8) A. S. Dutta and J. S. Morley, *J. Chem. Soc., C*, **1971**, 2896.

9) G. Anderson and A. C. McGregor, *J. Am. Chem. Soc.*, **79**, 6180, (1957).

10) M. Itoh, *Chem. Pharm. Bull.*, **18**, 784 (1970).

11) K. Khodadadeh, K. Heppenheimer, and E. A. Heidemann, *Makromol. Chem.*, **78**, 1897 (1977).

Synthesis of Cyclic Imines Having Conjugated Exocyclic Double Bond

Yujiro NOMURA,* Takashi BANDO, Yoshito TAKEUCHI, and Shuji TOMODA
Department of Chemistry, College of Arts and Sciences, The University of Tokyo, Komaba, Meguro-ku, Tokyo 113

(Received April 15, 1983)

Synopsis. Cyclic imines with conjugated exocyclic double bond have been synthesized by the reaction of 1-pyrroline trimer or 2,3,4,5-tetrahydropyridine trimer with various aldehydes in methanol in moderate to decent yields.

Cyclic amines possessing the general structure **1** and their quaternary ammonium salts have attracted attention because of their intriguing pharmacological activities. In particular, the five-membered analogs **1a**, in which both R^1 and R^2 are phenyl, have been known to exhibit potent antihistamine and anticholine activities and indeed some of them have been subjected to clinical applications.[1)]

The synthesis of these compounds (**1**) heavily depends on the availability of the unsaturated imines (**2**) for which a number of synthetic methods have been reported to date.[2)] Herein we wish to describe a novel method for the synthesis of **2**.

The new method rests on ready availability of 1-pyrroline trimer (**3a**), the synthesis of which we reported some time ago,[3)] and 2,3,4,5-tetrahydropyridine trimer (**3b**).[4)] We have now found that these imines react with a variety of aldehydes to give **2** in the yields shown in Table 1.

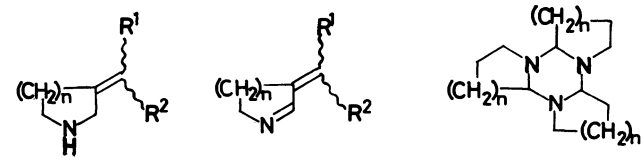

1 a ($n=1$) b ($n=2$) **2** a ($n=1$) b ($n=2$) **3** a ($n=1$) b ($n=2$)

Table 1. Reaction of **3** with aldehydes in methanol

Entry	3	Aldehyde (RCHO) R=	Temp	Time / h	Method[a)]	Yield / %	Mp θ_m/°C
1	a	Ph	r.t.	64	A	28	71.0—71.5[b)]
2	b	Ph	reflux	3	A	40	36.0—38.0[c)]
3	b	Ph	reflux	3	B	38	—
4	b	Ph	r.t.	43	A	39	—
5	b	Ph	r.t.	91	B	50	—
6	b	*p*-MeC_6H_4	r.t.	111	B	42	47.0—48.0[c)]
7	b	*p*-$MeOC_6H_4$	r.t.	108	B	27	73.0—73.5[b)]
8	b	*p*-$Me_2NC_6H_4$	r.t.	114	B	10	108.5—109.5[d)]
9	b	*p*-ClC_6H_4	r.t.	87	B	55	oil
10	b	*p*-NCC_6H_4	r.t.	86	B	56	66.5—67.0[d)]
11	b	*p*-$O_2NC_6H_4$	r.t.	86	B	74	66.5—67.0[d)]
12	b	*i*-Pr	r.t.	74	A	37	oil
13	b	2-furyl	r.t.	87	A	77	oil

a) Method A: In the absence of molecular sieves. Method B: In the presence of molecular sieves. b) Recrystallized from hexane. c) Purified by sublimation. d) Recrystallized from cyclohexane.

Table 2. Spectroscopic and analytical data for **2**

Compd (R²=H)	R¹	M⁺(*m/e*)	Found (Calcd)(%) C	H	N	ν(C=N)/cm⁻¹	δ_C(C=N)[a)]	δ_H[a)]
2a	Ph	157	83.90 (84.04)	6.92 (7.05)	8.85 (8.91)	1630	168.21	2.77 (m, 2H), 4.13 (m, 2H), 6.73 (t, J=2.5 Hz, 1H), 7.37 (m, 5H), 7.80 (t, J=2.5 Hz, 1H)
2b	Ph	171	84.04 (84.21)	7.73 (7.60)	8.29 (8.19)	1613	163.64	1.71(qui, J=7 Hz, 2H), 2.70 (dt, J=7, 2.7 Hz, 2H), 3.72 (dt, J=7, 2.7 Hz, 2H), 6.64 (t, J=2.7 Hz, 1H), 7.36 (m, 5H), 7.96 (t, J=2.7 Hz, 1H)
2b	*p*-MeC_6H_4	185	84.16 (84.28)	7.89 (8.16)	7.83 (7.56)	1597	163.66	1.67 (qui, J=6 Hz, 2H), 2.35 (s, 3H), 2.68 (d, t, J=6, 2.5 Hz, 2H), 3.65 (d, t, J=6, 2.5 Hz, 2H), 6.53 (br s, 1H), 7.16 (m, 4H), 7.93 (t, J=2.5 Hz, 1H)
2b	*p*-$MeOC_6H_4$	201	77.64 (77.58)	7.42 (7.51)	6.87 (6.96)	1595	163.64	1.70 (qui, J=6 Hz, 2H), 2.63 (dt, J=6, 2.5 Hz, 2H), 3.63 (dt, J=6, 2.5 Hz, 2H), 3.80 (s, 3H), 6.46 (br s, 1H), 6.83 (d, J=9 Hz, 2H), 7.28 (d, J=9 Hz, 2H), 7.90 (br t, J=2.5 Hz, 1H)
2b	*p*-NMe_2-C_6H_4	214	—	—	—	1592	164.31	1.70 (qui, J=6 Hz, 2H), 2.70 (dt, J=6, 2.5 Hz, 2H), 3.00 (s, 6H), 3.63 (dt, J=6, 2.5 Hz, 2H), 6.47 (br s, 1H), 6.67 (d, J=9 Hz, 2H), 7.28 (d, J=9 Hz, 2H), 7.90 (br s, 1H)
2b	*p*-ClC_6H_4	205	69.84 (70.07)	6.03 (5.88)	6.64 (6.81) Cl 17.23 (17·24)	1610	163.28	1.70 (qui, J=6 Hz, 2H), 2.65 (dt, J=6, 2.5 Hz, 2H), 3.67 (br t, 2H), 6.57 (br t, 1H), 7.30 (m, 4H), 7.97 (br s, 1H)
2b	*p*-CNC_6H_4	196	79.50 (79.56)	6.04 (6.16)	14.23 (14.27)	1605	162.74	1.72 (qui, J=6 Hz, 2H), 2.70 (dt, J=6, 2.7 Hz, 2H), 3.72 (dt, J=6, 2.7 Hz, 2H), 6.62 (br t, J=2.7 Hz, 1H), 7.45 (d, J=9 Hz, 2H), 7.67 (d, J=9 Hz, 2H), 8.01 (t, J=2.7 Hz, 1H)
2b	*p*-NO_2-C_6H_4	216	66.52 (66.65)	5.65 (5.59)	13.22 (12.95)	1605	162.57	1.75 (qui, J=6 Hz, 2H), 2.72 (dt, J=6, 2.7 Hz, 2H), 3.73 (dt, J=6, 2.7 Hz, 2H), 6.67 (br s, 1H), 7.50 (d, J=9 Hz, 2H), 8.02 (t, J=2.7 Hz, 1H), 8.20 (d, J=9 Hz, 2H)
2b	*i*-Pr	—	—	—	—	1640	163.50	1.00 (d, J=6 Hz, 6H), 1.67 (qui, J=6 Hz, 2H), 2.36 (dt, J=6, 2.5 Hz, 2H), 2.60 (m, 1H), 3.53 (dt, J=6, 2.5 Hz, 2H), 5.53 (br d, J=9 Hz, 1H), 7.77 (t, J=2.5 Hz, 1H)
2b	2-Furyl	167	74.23 (74.51)	6.95 (6.88)	8.49 (8.69)	1605	162.74	1.70 (qui, J=6 Hz, 2H), 2.73 (dt, J=6, 2.5 Hz, 2H), 3.73 (dt, J=6, 2.5 Hz, 2H), 6.37 (t, J=2.5 Hz, 1H), 6.47 (m, 2H), 7.40 (br s, 1H), 7.90 (t, J=2.5 Hz, 1H)

a) In $CDCl_3$ relative to TMS.

The yields of the reactions involving benzaldehyde (entries 2—5) were about 40% at reflux or room temperature, but the presence of molecular sieves did improve the yield of room temperature reaction (entry 5). It is clear that among para-substituted benzaldehydes (entries 6—11), the yield was significantly increased with electron-withdrawing substituents. As seen in entry 12, the reaction is equally effective for aliphatic aldehydes. The best yield was obtained with 2-furaldehyde (entry 13).

The structures of these conjugated imines (**2**) were elucidated by spectral data (MS, IR, ^{1}H- and ^{13}C-NMR) as well as by combustion analysis. The presence of conjugated imine moiety was inferred from the following spectral evidence; a strong to medium IR band between 1592 and 1640 cm^{-1}, a low-field doublet near δ 165 in ^{13}C NMR[5] and a characteristic triplet ($\delta\approx8$, $J=$ 2.5—2.7 Hz) in ^{1}H NMR spectra. A small coupling between allylic methylene protons ($\delta\approx2.7$, m, 2H) and the exocyclic olefin proton ($\delta\approx6.5$, t, $^4J=2.5$—2.7 Hz) suggested the trans-relationship of these protons.[6] The spectroscopic data together with analytical results are summerized in Table 2.

Experimental

Methanol was purified by distillation over sodium under dry nitrogen atmosphere. All reactions were performed under dry nitrogen. Spectral data were obtained by the following spectrometers; Hitachi-Perkin Elmer RMU-6D mass spectrometer, JASCO DS-403G IR spectrometer, JEOL FX-90Q spectrometer, JEOL MH-100 spectrometer. All chemical shifts are reported in δ relative to internal TMS in $CDCl_3$.

General Procedure for the Preparation of **2**. A mixture of **3a** or **3b** (2 mmol) and an aldehyde (6 mmol) in methanol (20 ml) was stirred magnetically in the presence or absence of 3A molecular sieves under the conditions indicated in Table 1. After having been stirred for appropriate period (see Table 1), it was concentrated *in vacuo* and the residue purified by silica gel column chromatography. The product was further purified by distillation, sublimation or recrystallization if necessary.

References

1) S. Ohki, N. Ozawa, Y. Yabe, and H. Matsuda, *Chem. Pharm. Bull.*, **24**, 1362 (1976) and references cited therein.

2) Representative methods; Bischler-Napieraliski reaction, S. Sugasawa and S. Ushioda, *Tetrahedron*, **5**, 48 (1959); Ritter reaction; A. I. Meyers and J. J. Ritter, *J. Org. Chem.*, **23**, 1918 (1958).

3) Y. Nomura, K. Ogawa, Y. Takeuchi, and S. Tomoda, *Chem. Lett.*, **1977**, 693; K. Ogawa, Y. Nomura, Y. Takeuchi, and S. Tomoda, *J. Chem. Soc., Perkin Trans. 1*, **1982**, 3031.

4) α-isomer; The stereoisomer possessing C_3 Symmetry; the three methine hydrogens adjacent to the two nitrogen atoms are all cis.

5) J. M. Ruxer, A. Solladia-Cavallo, G. Solladie, and D. Olliero, *Org. Magn. Reson.*, **10**, 105 (1977).

6) For similar cases previously reported see; A. K. Bose, J. L. Fahey, and M. S. Manhas, *Tetrahedron*, **30**, 3 (1974).

Studies on Bile Salt Solutions. Part 2. Acid Catalyzed Hydrolysis of Trimethyl Orthobenzoate in Solutions of Glycine and Taurine Conjugated Bile Salts

Charmian J. O'Connor* and Beng Tatt Ch'ng
Chemistry Department, University of Auckland, Private Bag, Auckland, New Zealand

(Received November 1, 1982)

Synopsis. The reactivity of trimethyl orthobenzoate has been studied, at 310.5 K, in solutions of the glycine and taurine conjugates of the cholanic acids. The rate-concentration profiles are characterized by peaks and troughs which coincide with discontinuities in the slopes of the surface tension-concentration profiles.

Trimethyl orthobenzoate **1** is one of the few substrates whose acid catalyzed hydrolysis is subject to catalysis by anionic surfactants.[1-6] The kinetic effects are accentuated when the hydrophobic interactions between **1** and surfactants are accentuated. Increasing the hydrocarbon chain length of sodium alkyl sulfates causes a more dramatic increase in rate.[1]

Bile salts **2** are important surfactants in the biological system and they offer an attractive opportunity for

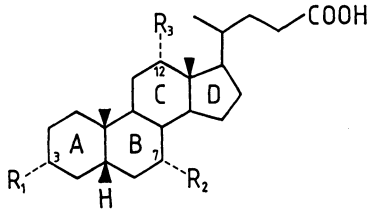

correlating chemical composition with micellar properties in a series of molecules differing only slightly in their chemical structure. It is therefore surprising that only five publications can be identified[7-11] which report kinetic investigations by these amphiphiles in aqueous solution in the absence of enzymes.

We now report on the reactivity of **1** in solutions of the taurine and glycine conjugates of trihydroxy- and dihydroxy cholates; taurocholate, TC, and glycocholate, GC, ($R_1=R_2=R_3=OH$); taurochenodeoxycholate, TCDC, and glycochenodeoxycholate, GCDC, ($R_1=R_2=OH$, $R_3=H$); and taurodeoxycholate, TDC, and glycodeoxycholate, GDC, ($R_1=R_3=OH$, $R_2=H$). In contrast to the literature studies[7-11] on reactivity in bile salt solutions which have concentrated, for the most part, on concentrations greater than CMC and in solutions of alkaline pH where all the bile salts are converted to the anionic form, we have used solutions of pH<7. Inevitably this has placed a relatively low limit on the maximum concentration able to be solubilized so that many of our data refer to concentrations well below CMC.

Experimental

Materials. The bile salts and bile acids were Sigma products. Their purity was monitored by TLC analysis using the solvent system of acetone: dibutyl ether in the ratio 3:7 and development in an iodine chamber. Acetic acid used for preparation of buffer solutions was freshly distilled. All water was triply distilled and the pH of each solution was measured, using as a standard BDH buffer for blood pH determination with pH 6.840 at 311 K, with a Radiometer PHM 4d pH meter and a dual walled sample holder held at 310.5 K by means of a Grant thermocirculator. Trimethyl orthobenzoate was prepared according to the method of McElvain and Venerable[14] (Bp 387—388 K at 25 mmHg).

Measurement of Rate Constants of Hydrolysis. The hydrolysis of **1** was followed by measuring the appearance of methyl benzoate at 228 nm. (Under acidic conditions methyl benzoate is converted slowly to benzoic acid but the extinction coefficients of the intermediate and final products of hydrolysis are identical at 228 nm.) The reaction was initiated by injecting 8—20 μl of a 5.8×10^{-4} mol dm^{-3} solution of **1** in absolute ethanol into the contents of the reaction cell which had previously been brought to equilibrium temperature (310.5 K) in the cell compartment of a Cary 219 recording Spectrophotometer. Pseudo first order rate constants were calculated from the absorbance data on a Burroughs B6700 or Commodore 3032 minicomputer. Rate data were duplicated and showed a reproducibility of $<+2\%$.

Results and Discussion

The pseudo first order rate constant, k_ψ, for hydrolysis of **1** in acid solution is linearly dependent on the hydronium ion concentration. At 310.5 K in 0.03 mol dm^{-3} sodium acetate buffer the values of k_ψ are 2.07×10^{-2} and 0.070×10^{-2} s^{-1} at pH values of 4.07 and 5.47 respectively. All rate measurements described in this investigation were made within this pH range and using this buffer medium and temperature.

Figures 1—3 show the values of k_ψ for hydrolysis of **1** in the bile salt solutions. Superimposed on all the rate concentration profiles are plots of the surface tension values of these same bile salt solutions measured under identical conditions of pH and temperature. Determination of these surface tension values has been reported separately.[12]

In contrast to the relatively simple multiphasic rate-concentration profile reported for hydrolysis of **1** in sodium alkyl sulfate solutions[1] the profiles presented here are quite complicated, being characterized by plateaux, peaks and troughs. Each change in slope in the rate-profile is matched by a discontinuity in the slope of the corresponding surface tension-profile.

We were able to explain the surface tension data by use of a multi-equilibrium model involving the step-wise aggregation of monomers or small oligomers. We believe that micelle formation of bile salts passes through several successive distinct stages, each one being characterized by constant properties of the solute. Our rate data support this postulate, for it seems that, at the pH values we have used, the association process in bile salts is one of multiple association rather than a monomer$\rightleftharpoons$*n-mer* equilibrium and that each of the small aggregates has its own characteristic binding constant leading to an individual kinetic identity, as well as an unique ability to modify the surface tension properties of the solvent.

However, the changes we have observed are small. The maximum percentage change observed was

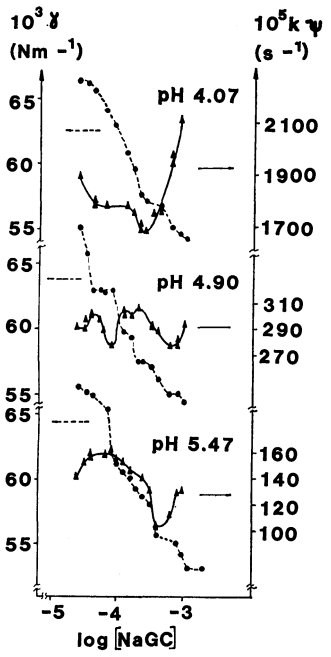

Fig. 1.

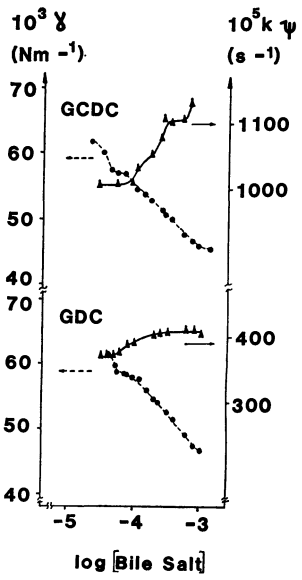

Fig. 2.

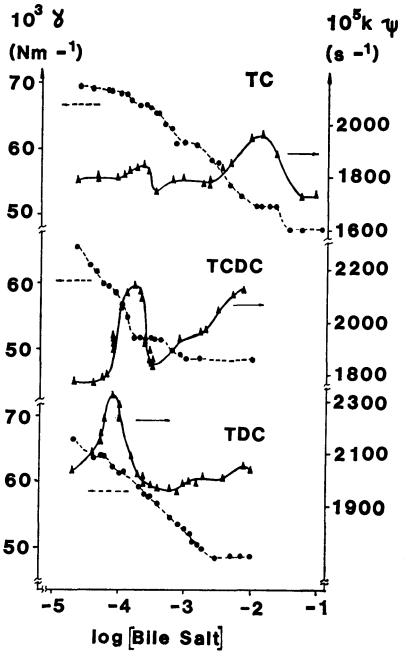

Fig. 3.

Fig. 1—3. The pseudo first order rate constant of hydrolysis, k_ψ, of trimethyl orthobenzoate (▲ and solid line) and the equilibrium surface tension values, γ, (● and broken line) in solutions of bile salts in 0.03 mol dm^{-3} acetate buffer at 310.5 K. Fig. 1, sodium glycochoate at pH values of 4.07, 4.90, and 5.47 (43%, 10%, and 3% protonation respectively); Fig. 2, sodium glycochenodeoxycholate at pH 4.34 and sodium glycodeoxycholate at pH 4.77 (both 43% protonated); Fig. 3, sodium taurocholate, sodium taurochenodeoxycholate and sodium taurodeoxycholate at pH 4.09.

+100% for GC at pH 5.47 and TDC was the only other salt to show a significant increase in rate (+22%) at its maximum value. At the minimum values of k_ψ all the salts except TDC were slightly inhibitory (the maximum inhibition of −16% was observed for GC at pH 4.07).

The pK_a values for GC, GDC and GCDC range from 3.8—4.1, 4.7—4.8, and 4.2—4.3 respectively[13] while those for the taurine conjugates have pK_a values less than 2. This means that a substantial portion of the glycine conjugates is present in the undissociated form at the pH values we have used (43%, 10%, and 3% protonation at pH values of 4.07, 4.90, and 5.47 respectively) while the taurine conjugates will be 100% deprotonated. Increasing the pH from 4.07 to 4.47 increases the value of k_2 (min) for GC (where $k_2=k_\psi/[H_3O^+]$ is the second order rate constant) from 198 to 301 dm^3 mol^{-1} s^{-1} and the value of k_2 (max) from 248 to 472 dm^3 mol^{-1} s^{-1}. Thus the presence of the acid form of the bile salt inhibits the rate of hydrolysis. The bile acids are sparingly soluble in water and cannot themselves form micelles, but they are solubilized as "mixed" micelles of anion and acid. Solubilization of free acid in the mixed micelles will lessen the hydrophobic environment and thereby inhibit the catalytic efficiency for hydrolysis of **1**.

The hydrophobicity of the bile salts increases in order TC<TCDC<TDC and this is also the order of increasing values of k_2 (max), *i.e.* the more hydrophobic the surfactant, the more of **1** is in the micellar phase and the greater is the catalysis. However in these micellar systems the aggregation number, the pK_a value and the binding constant of substrate to micelle will depend very delicately upon the reaction conditions and these will also affect the rate of hydrolysis. In the light of these factors further discussion of the small rate enhancements does not seem warranted.

Equipment grants from the New Zealand Universities' Grants Committee and the University of Auckland are gratefully acknowledged.

References

1) R. B. Dunlap and E. H. Cordes, *J. Am. Chem. Soc.*, **90**, 4395 (1968).
2) R. B. Dunlap and E. H. Cordes, *J. Phys. Chem.*, **73**, 361 (1969).
3) M. T. A. Behme, J. G. Fullington, R. Noel, and E. H. Cordes, *J. Am. Chem. Soc.*, **87**, 266 (1965).
4) R. B. Dunlap, G. A. Ghanim, and E. H. Cordes, *J. Phys. Chem.*, **73**, 1898 (1969).
5) L. R. Romsted and E. H. Cordes, *J. Am. Chem. Soc.*, **90**, 4404 (1968).
6) E. H. Cordes and C. Gitler, *Progr. Bioorganic Chem.*, **2**, 1 (1973).
7) F. Alhaique, C. Botré, G. Lionetti, M. Marchetti, and F. M. Riccieri *J. Pharm. Sci.*, **56**, 1555 (1967).
8) S. Shinkai and T. Kunitake, *Bull. Chem. Soc. Jpn.*, **44**, 3086 (1971).
9) F. M. Menger and M. J. McCreery, *J. Am. Chem. Soc.*, **96**, 121 (1974).
10) A. G. Cairns-Smith and S. Rasool, *J. Chem. Soc., Perkin Trans.* 2, **1978**, 1007.
11) S. Miyagishi and M. Mishida, *Yakugaku*, **28**, 923 (1979).
12) C. J. O'Connor, B. T. Ch'ng, and R. G. Wallace, *J. Colloid Interface Sci.*, in press.
13) D. M. Small, "The Bile Acids, Chemistry, Physiology and Metabolism," ed by P. P. Nair and D. Kritchevsky, Plenum Press, New York (1971), Vol. 1, p. 303.
14) S. M. McElvain and J. T. Venerable, *J. Am. Chem. Soc.*, **72**, 1661 (1950).

 © 1983 The Chemical Society of Japan Bull. Chem. Soc. Jpn., 56, 3203—3207 (1983)

Light-induced Redox Characteristics of [Tetrakis(4-methylpyridyl)-porphyrinato]manganese(III)

Koushin TAKAHASHI,* Teruhisa KOMURA, and Hiroto IMANAGA
Faculty of Technology, Kanazawa University, Kanazawa 920

(Received March 10, 1983)

[Tetrakis(4-methylpyridyl)porphyrinato]manganese(III) (Mn^{III}(tmpp)) undergoes reversible one-electron transfer reactions in aqueous solutions. The half-wave potential of $Mn^{III/II}$(tmpp) redox couple is −0.21 V (*vs.* 3.33 M KCl, AgCl/Ag) between pH 4 and 12. On the other hand, the half-wave potential of $Mn^{IV/III}$-(tmpp) redox couple becomes less positive with increasing pH in alkaline solution. A small amount of methylviologen cation radical ($MV^{+\cdot}$) is built up by irradiating with visible light an alkaline solution containing Mn^{III}(tmpp), methylviologen (MV^{2+}), and sacrificial electron donors. The formation of $MV^{+\cdot}$ is attributed to either the reduction of photoexcited Mn^{III}(tmpp) ($^*Mn^{III}$(tmpp)) with an electron donor or the oxidation of $^*Mn^{III}$(tmpp) with MV^{2+}.

Much attention has been drawn to light-induced electron transfer reactions sensitized by tris(2,2′-bipyridyl)ruthenium(II) complex and metalloporphyrins from the standpoint of conversion of solar to chemical energy.[1–5] For example, MV^{2+} is reduced to $MV^{+\cdot}$ under irradiation with light in the presence of tris(2,2′-bipyridyl)ruthenium(II) complex and ethylenediaminetetraacetic acid (EDTA),[1] and colloidal platinum catalyzes the hydrogen generation from water in this system.[6,7] Ruthenium dioxide catalyzes the oxygen generation when it substitutes for EDTA. On the other hand, a Mn-protein possibly catalyzes the oxygen generation in the photosynthesis, but the mechanism has hardly been known. Calvin[8] has proposed a general scheme for the photochemical generation of oxygen sensitized by manganese porphyrin. Harriman *et al.*[9–11] reported on the photoredox characteristics of water-soluble Mn(III) porphyrin. The electron transfer reactions sensitized by these compounds are probably very complex since Mn can take several oxidation number.

We previously reported on the redox and photoreductive properties of Mn^{III}(tmpp).[13] This paper presents the light-induced redox characteristics of Mn^{III}(tmpp) in the presence of MV^{2+} and electron donors.

Experimental

The preparation of Mn^{III}(tmpp) was described in the previous paper.[13] [Tetrakis(4-methylpyridyl)porphyrinato]-zinc(II) (Zn(tmpp))[14] and tris(2,2′-bipyridyl)ruthenium(II) chloride ($[Ru(bpy)_3]Cl_2$)[15] were prepared according to literature methods. Sodium acetate, sodium borate, and potassium phosphate (special grade) were recrystallized from water, and sodium sulfate (special grade) was recrystallized three times from water. Methylviologen dichloride (special grade) was recrystallized from ethanol and dried for 7 h at 60 °C *in vacuo*. Other chemicals (reagent grade) were used without further purification. All solutions were prepared with doubly distilled water.

Cyclic voltammetric experiments were performed in a purified nitrogen atmosphere by using a potentiostat (Nikko Keisoku NPGS-301), a potential sweeper (Nikko Keisoku NPG-2), and a three-electrode configuration. A Pt-wire was used as the warking electrode, a Pt-coil as the counter-electrode, and a commercially available 3.33 M KCl, AgCl/Ag electrode as the reference electrode (1 M = 1 mol dm^{-3}). An X-Y plotter (Riken Denshi Co., Ltd. Model F-3B) was used to record current-voltage curves. Half-wave potentials were measured as the average of cathodic and anodic peak potentials.

The pH of solutions was adjusted to a desired pH with 0.01 M acetate, phosphate, or borate buffer solution. The N_2-purged sample solution was transferred to an optical glass cell with a 1 cm-photopath length and a stopper in a nitrogen atmosphere. A 500 W Xenon arc lamp (Ushio Electric, Co., Ltd. UXL-500D-O) was used for steady-state irradiation experiments. The light was passed through a cut-off filter (Toshiba L-39) and water (1 cm), and focused onto a sample cell thermostated at 25 °C. The sample solution was continuously stirred with a magnetic stirrer throughout the irradiation period. Absorption spectra were measured with a Hitachi Model 124 spectrophotometer.

Results and Discussion

Cyclic Voltammetry of Mn^{III}(tmpp). [Tetrakis(4-methylpyridyl)porphyrinato]manganese(III) was reduced to Mn^{II}(tmpp) with sodium dithionite in a deoxygenated aqueous solution between pH 4 and 12, and was oxidized to Mn^{IV}(tmpp) with potassium peroxodisulfate, sodium hypochlorite, or pentaamminechlorocobalt(III) chloride between pH 9 and 12.[9,13] Table 1 shows the molar extinction coefficients for the absorption peaks of Mn^{II}(tmpp), Mn^{III}(tmpp), and Mn^{IV}(tmpp) in aqueous solution.[13]

Figure 1 shows a typical cyclic voltammogram of Mn^{III}(tmpp) in 0.2 M Na_2SO_4 aqueous solution at pH 12.0. The current-voltage curve shows two reversible waves. The following electrode reactions probably occur:

$$Mn^{III}(tmpp) + e^- \rightleftharpoons Mn^{II}(tmpp), \quad (1)$$

$$Mn^{IV}(tmpp) + e^- \rightleftharpoons Mn^{III}(tmpp). \quad (2)$$

TABLE 1. THE MOLAR EXTINCTION COEFFICIENTS AT ABSORPTION PEAK (λ_{max}/nm) OF Mn(tmpp) IN AQUEOUS SOLUTION[a]

	pH	λ_{max}/nm	ε/M^{-1} cm^{-1}
Mn^{II}(tmpp)	6.0	449	1.92×10^{5} [b]
Mn^{III}(tmpp)	6.0	463	1.59×10^{5}
Mn^{IV}(tmpp)	10.0	429	9.80×10^{4} [c]

a) From Ref. 13. b) Mn^{II}(tmpp) was formed by the reduction of Mn^{III}(tmpp) with $Na_2S_2O_4$. c) Mn^{IV}-(tmpp) was formed by the oxidation of Mn^{III}(tmpp) with $[CoCl(NH_3)_5]Cl_2$.

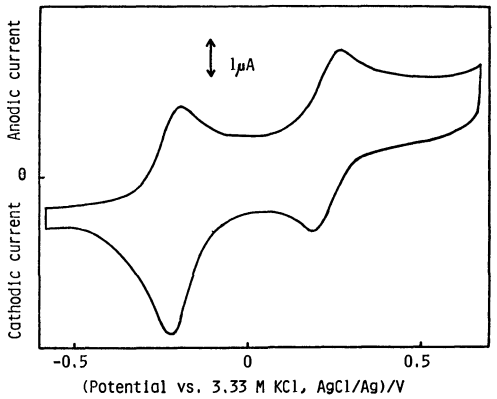

Fig. 1. A typical cyclic voltammogram of 1.0×10^{-3} M Mn^{III}(tmpp) in 0.2 M Na_2SO_4 aqueous solution at pH 12.0 (scan rate 20 mV/s).

TABLE 2. HALF-WAVE POTENTIALS/V (*vs.* 3.33 M KCl AgCl/Ag) OF $Mn^{III/II}$(tmpp) AND $Mn^{IV/III}$(tmpp) REDOX COUPLES IN 0.2 M Na_2SO_4 AQUEOUS SOLUTION AT ROOM TEMPERATURE

pH	$E_{1/2}$(III/III)	$E_{1/2}$(IV/III)
4.1	−0.20	—
5.6	−0.22	—
10.2	−0.21	0.45
10.7	−0.20	0.38
12.0	−0.22	0.23

The half-wave potentials of the two redox couples are given in Table 2. The half-wave potential of Reaction 1, $E_{1/2}$(III/II), is −0.21 V (*vs.* AgCl/Ag) between pH 4 and 12, but that of Reaction 2, $E_{1/2}$(IV/III), becomes less positive with increasing pH in alkaline solution. No anodic peak of Mn^{III}(tmpp) was observed below pH 8 because of the oxidation of water.

Photoreduction of Mn^{III}(tmpp). When a solution of Mn^{III}(tmpp) was irradiated with visible light in the presence of an electron donor (D) such as EDTA, triethanolamine (TEOA), triethylamine (TEA), or nicotine (NT), Mn^{III}(tmpp) was reduced to Mn^{II}(tmpp). Figure 2 shows the pH dependence of the concentration of Mn^{II}(tmpp) produced by irradiating an aqueous solution containing Mn^{III}(tmpp) (9.0×10^{-6} M) and EDTA (1×10^{-4} M) or TEOA (0.01 M).[13] The concentration of Mn^{II}(tmpp) ($C_{Mn^{II}}$) was estimated from the following equation:

$$C_{Mn^{II}} = (A_{449}-A_{449}^{\circ})/(\varepsilon_{449}^{II}-\varepsilon_{449}^{III}), \quad (3)$$

where A_{449}° and A_{449} are the absorbances at 449 nm before and after irradiation, and ε_{449}^{II} and ε_{449}^{III} are the molar extinction coefficients at 449 nm of Mn^{II}-(tmpp) and Mn^{III}(tmpp), respectively. As shown in Fig. 2, Mn^{III}(tmpp) was almost completely reduced to Mn^{II}(tmpp) with EDTA between pH 6 and 10, but only at pH 10 with TEOA. Figure 3 shows the concentration of Mn^{II}(tmpp) produced by irradiation for 30 min at different concentrations of electron donor at pH 10.0. In a high concentration (0.01 M) of EDTA, the chromophore was partly bleached. The reducing power of electron donors can be regarded as being in the order EDTA>TEOA>TEA>NT.

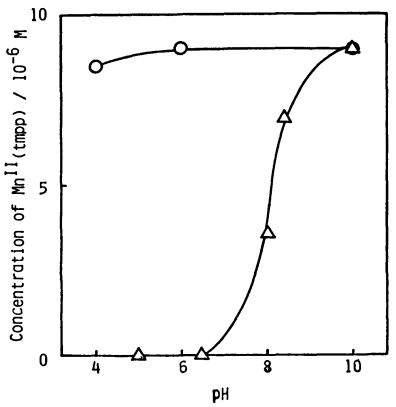

Fig. 2. The pH dependence of the concentration of Mn^{II}(tmpp) produced by irradiation for 30 min.
Total concentration of Mn(tmpp): 9.0×10^{-6} M.
○, 1×10^{-4} M EDTA; △, 0.01 M TEOA.

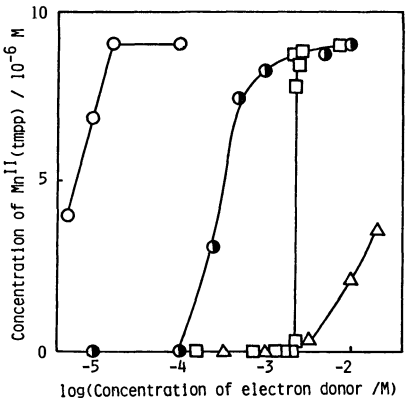

Fig. 3. The concentration of Mn^{II}(tmpp) produced by irradiation for 30 min at different concentrations of electron donors at pH 10.0.
Total concentration of Mn(tmpp): 9.0×10^{-6} M.
○, EDTA; ◑, TEOA; △, NT; □, TEA.

The following reactions can be proposed as the mechanism of the photoreduction of Mn^{III}(tmpp):

$$Mn^{III}(tmpp) \xrightarrow{h\nu} {}^{*}Mn^{III}(tmpp), \quad (4)$$

$$^{*}Mn^{II}(tmpp) + D \longrightarrow Mn^{II}(tmpp) + D_{ox}, \quad (5)$$

or

$$^{*}Mn^{III}(tmpp) + Mn^{III}(tmpp) \longrightarrow Mn^{II}(tmpp) + Mn^{IV}(tmpp), \quad (6)$$

$$Mn^{IV}(tmpp) + D \longrightarrow Mn^{III}(tmpp) + D_{ox}, \quad (7)$$

where D_{ox} is an oxidative decomposition product of D. Reaction 5 means that an excited Mn^{III}(tmpp) ($^{*}Mn^{III}$(tmpp)) is reduced to Mn^{II}(tmpp) with D. Reaction 6 means that $^{*}Mn^{III}$(tmpp) is reduced or oxidized with a ground-state Mn^{III}(tmpp), and Reaction 7 means that Mn^{IV}(tmpp) is scavenged with D.

Porphyrinatomanganese(III)-sensitized Reduction of MV^{2+} with Strong Electron Donors. In an aqueous solution containing Mn^{III}(tmpp) (2.0×10^{-5} M), MV^{2+} (2.0×10^{-3} M), and EDTA (0.01 M) between pH 5 and 11, the color of the solution did not change in the dark, but under irradiation it rapidly changed from orange to yellow green and finally into green. Figure 4 shows

the change in the absorption spectra of the solution as a function of irradiation time at pH 10.9. The absorption peaks at 463 and 570 nm of Mn^{III}(tmpp) rapidly disappeared under irradiation, and the new peaks at 395, 451, 579, and 606 nm appeared. The peaks at 395 and 606 nm originate from MV^{+},[16] and those at 451 and 579 nm from Mn^{II}(tmpp).[13] As shown in Fig. 4, Mn^{III}(tmpp) was almost completely reduced to Mn^{II}(tmpp) under irradiation. Because MV^{2+} was not photoreduced to MV^{+} in the absence of Mn^{III}(tmpp) or EDTA, Mn^{III}(tmpp) acts as a sensitizer and EDTA as an electron donor. Figure 5 shows the concentration of MV^{+} produced by irradiation for 30 min an aqueous solution containing Mn^{III}(tmpp) (2.0×10^{-5} M), MV^{2+} (2.0×10^{-3} M), and EDTA or TEOA (0.01 M). The concentration of MV^{+} ($C_{MV^{+}}$) was estimated on the following equation from the measurements of absorbance at 606 nm (A_{606}):

$$C_{MV^{+}} = (A_{606} - C_t\varepsilon_{606}^{II})/\varepsilon_{606}, \quad (8)$$

where C_t is the total concentration of Mn(tmpp), ε_{606}^{II} (7.9×10^{3} M^{-1} cm^{-1}) and ε_{606} (1.37×10^{4} M^{-1} cm^{-1})[18] are the molar extinction coefficients at 606 nm of Mn^{II}(tmpp) and MV^{+}, respectively. As shown in Fig. 5, a small amount of MV^{+} was built up between pH 5 and 8 in the presence of EDTA, but not in the presence of TEOA. On the other hand, above pH 9 MV^{+} was formed in considerable quantity in the presence of both the electron donors. This can be attributed to the pH dependence of the reducing powers of EDTA and TEOA. Their reducing powers increase with an increase in pH because the oxidative decompositions of EDTA and TEOA are attended by the formation of proton.[17,18] It is inferred from a comparison of Fig. 5 with Fig. 2 that a certain amount of MV^{+} is built up only when Mn^{III}(tmpp) is photoreduced to Mn^{II}(tmpp) with an electron donor. Figure 6 shows the concentration of MV^{+} produced by irradiation for 30 min and the turnover number of Mn^{III}(tmpp) at different concentrations of Mn^{III}(tmpp) at pH 10.1. The turnover number (N) was calculated by the following equation:

$$N = C_{MV^{+}}/C_t. \quad (9)$$

The concentration of MV^{+} rapidly increased with an increase in the concentration of Mn^{III}(tmpp) below 2×10^{-6} M, and the maximum turnover number of Mn^{III}(tmpp) was 37 at 5×10^{-7} M Mn^{III}(tmpp). Above 1×10^{-6} M Mn^{III}(tmpp), a photoexcited Mn(tmpp) is possibly self-quenched at high concentrations of Mn(tmpp).

The reaction scheme in Fig. 7 can be proposed as the mechanism for the Mn^{III}(tmpp)-sensitized reduction of MV^{2+} with strong electron donors. An excited Mn^{III}(tmpp) can first be reduced to Mn^{II}(tmpp) with an electron donor (Reaction 5). Furthermore, an excited Mn^{II}(tmpp) ($*Mn^{II}$(tmpp)) can be oxidized to

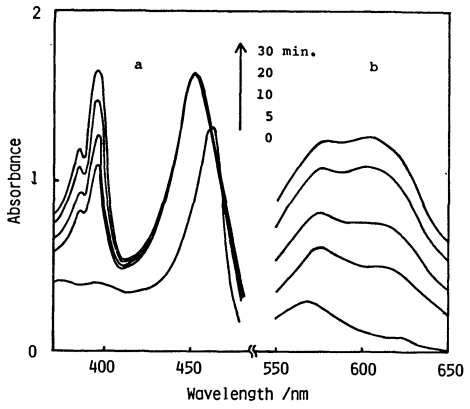

Fig. 4. Absorption spectral profiles showing the appearance of MV^{+} and Mn^{II}(tmpp) as a function of irradiation time at pH 10.9.
a, The concentrations of Mn^{III}(tmpp), MV^{2+}, and EDTA are 9.0×10^{-6}, 5.3×10^{-4}, and 0.01 M, respectively. b, The concentrations of Mn^{III}(tmpp), MV^{2+}, and EDTA are 2.0×10^{-5}, 2.1×10^{-3}, and 0.01 M, respectively.

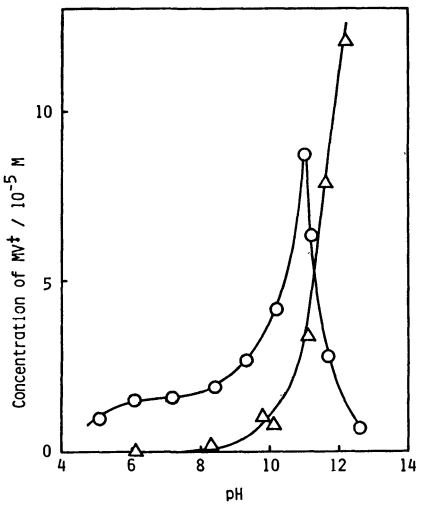

Fig. 5. The pH dependence of the concentration of MV^{+} produced by irradiation for 30 min.
Concentration of Mn^{III}(tmpp): 2.0×10^{-5} M. Concentration of MV^{2+}: 2.0×10^{-3} M. ○, 0.01 M EDTA; △, 0.01 M TEOA.

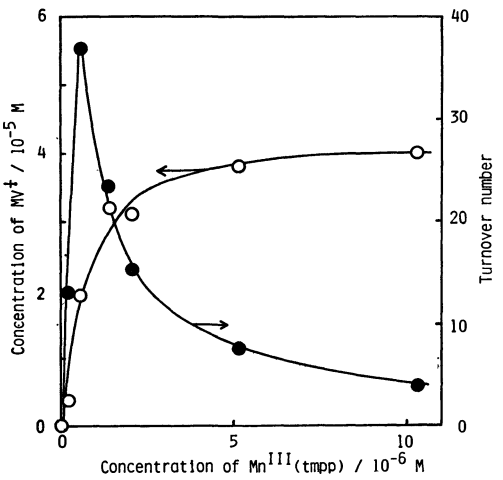

Fig. 6. The concentration of MV^{+} produced and the turnover number of Mn^{III}(tmpp) at different concentrations Mn^{III}(tmpp) at pH 10.1.
Concentration of MV^{2+}: 1.8×10^{-3} M. Concentration of EDTA: 0.01 M. Irradiation time: 30 min.

$Mn^{III}(tmpp)$ with MV^{2+}, and MV^{+} can be produced:

$$Mn^{II}(tmpp) \xrightarrow{h\nu} {}^{*}Mn^{II}(tmpp), \quad (10)$$

$$^{*}Mn^{II}(tmpp) + MV^{2+} \longrightarrow Mn^{III}(tmpp) + MV^{+}. \quad (11)$$

MV^{2+} is not reduced with the ground-state $Mn^{II}(tmpp)$ because the values of $E°(MV^{2+}/MV^{+})$ and $E_{1/2}(III/II)$ are -0.67 and -0.21 V (*vs.* AgCl/Ag), respectively. The energy level of $^{*}Mn^{II}(tmpp)$ is probably over 0.46 eV higher than that of $Mn^{II}(tmpp)$. $Mn^{III}(tmpp)$ is also reduced to $Mn^{II}(tmpp)$ with MV^{+} because of the back electron transfer:

$$Mn^{III}(tmpp) + MV^{+} \longrightarrow Mn^{II}(tmpp) + MV^{2+}. \quad (12)$$

The rate of Reaction 11 is probably higher than that of Reaction 12 because an appreciable amount of MV^{+} is built up.

Porphyrinatomanganese(III)-sensitized Reduction of MV^{2+} with Weak Electron Donors. Figure 8 shows the concentration of MV^{+} produced by irradiation for 30 min at different concentrations of electron donors in an aqueous solution containing $Mn^{III}(tmpp)$ (2.1×10^{-5} M) and MV^{2+} (2.0×10^{-3} M) at pH 10.1. The concentration of MV^{+} monotonously increased with an increase in the concentration of EDTA or TEA,

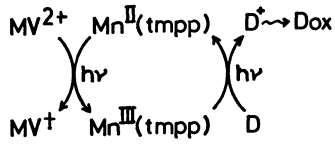

Fig. 7. A schematic representation of photosensitized reaction in the presence of EDTA.

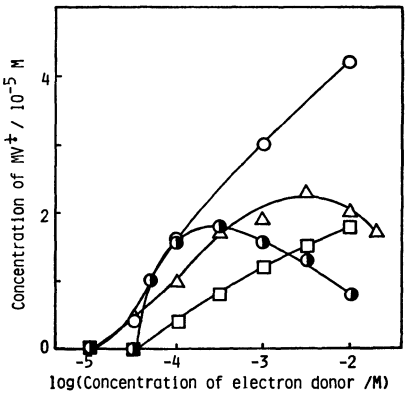

Fig. 8. The concentration of MV^{+} produced by irradiation for 30 min at different concentrations of electron donors at pH 10.1.
Concentration of $Mn^{III}(tmpp)$: 2.1×10^{-5} M. Concentration of MV^{2+}: 2.0×10^{-3} M. ○, EDTA; ◑, TEOA; △, NT; □, TEA.

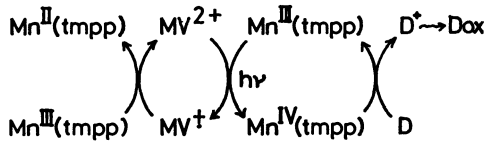

Fig. 9. A schematic representation of photosensitized reaction in the presence of weak electron donors (TEA, NT) below 2×10^{-3} M.

but exhibited a maximum in the case of TEOA or NT. A comparison of Fig. 8 with Fig. 3 shows that a certain amount of MV^{+} was built up even at the low concentration of NT, TEA, or TEOA, at which $Mn^{III}(tmpp)$ was not photoreduced in the absence of MV^{2+}. The formation of $Mn^{II}(tmpp)$ was also observed at such a low concentration (1×10^{-4} M) of NT, TEA, or TEOA.

The reaction scheme in Fig. 9 can be proposed as the mechanism for the $Mn^{III}(tmpp)$-sensitized reduction of MV^{2+} with weak electron donors at low concentrations. An excited $Mn^{III}(tmpp)$ can first be oxidized to $Mn^{IV}(tmpp)$ with MV^{2+}, and MV^{+} can be produced:

$$^{*}Mn^{III}(tmpp) + MV^{2+} \longrightarrow Mn^{IV}(tmpp) + MV^{+}. \quad (13)$$

The energy level of $^{*}Mn^{III}(tmpp)$ is probably over 1.12 eV higher than that of $Mn^{III}(tmpp)$ at pH 10 because the values of $E°(MV^{2+}/MV^{+})$ and $E_{1/2}(IV/III)$ are -0.67 and 0.45 V (*vs.* AgCl/Ag), respectively. The back electron transfer reaction (14) can be suppressed if $Mn^{IV}(tmpp)$ can rapidly be scavenged with an electron donor (Reaction 7):

$$Mn^{IV}(tmpp) + MV^{+} \longrightarrow Mn^{III}(tmpp) + MV^{2+}. \quad (14)$$

Furthermore, Reactions 12 and 11 can occur although Reaction 5 does not proceed with weak electron donors.

Figure 10 shows the dependence of the concentration of $Mn^{II}(tmpp)$ photoproduced at pH 6.0 on the concentration of MV^{2+} in an aqueous solution containing $Mn^{III}(tmpp)$ (5.3×10^{-6} M) and TEOA (0.01 M). Porphyrinatomanganese(III) was reduced to Mn^{II}-(tmpp) above 5×10^{-3} M MV^{2+}, but the formation of MV^{+} was not observed. At pH 6 the rate of Reaction 13 is slow since $E_{1/2}(IV/III)$ becomes more positive with decreasing pH. When $Ru(bpy)_3^{2+}$ or Zn(tmpp) was used as a sensitizer, 6.1×10^{-5} or 1.6×10^{-4} M MV^{+}, respectively, was built up by irradiating for 10 min a solution (pH 6.0) containing the sensitizer (2.0×10^{-5} M), MV^{2+} (2.0×10^{-3} M), and TEOA (0.01 M). [Tetrakis(4-methylpyridyl)porphyrinato]manga-

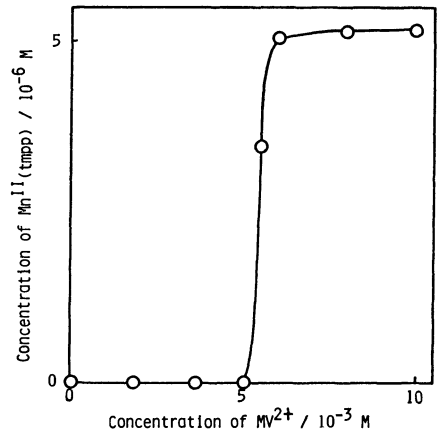

Fig. 10. The concentration of $Mn^{II}(tmpp)$ photoproduced at pH 6.0 at different concentrations of MV^{2+}.
Total concentration of Mn(tmpp): 5.3×10^{-6} M. Concentration of TEOA: 0.01 M. Irradiation time: 30 min.

nese(III) emitted a very weak luminescence around 540 nm in aqueous solutions. The excited triplet state lifetime of [tetrakis(4-pyridyl)porphyrinato]manganese(III) in ethanol glass at 77 K is below 0.1 ms,[10] but that of [tetrakisphenylporphyrinato]zinc(II) in methylcyclohexane at 77 K is 26 ms.[19] The oxidative electron transfer quenching of the excited Mn(III) porphyrin with MV^{2+} is less effective than that of the excited Zn(II) porphyrin.

References

1) K. Takuma, M. Kajiwara, and T. Matsuo, *Chem. Lett.*, **1977**, 1199.
2) N. Sutin, *J. Photochem.*, **10**, 19 (1979).
3) K. Kano, K. Takuma, T. Ikeda, D. Nakajima, Y. Tsutsui, and T. Matsuo, *Photochem. Photobiol.*, **27**, 695 (1978).
4) K. Kalyanasundaram and M. Grätzel, *Helv. Chem. Acta*, **63**, 478 (1980).
5) A. Harriman, G. Porter, and M. C. Richoux, *J. Chem. Soc., Faraday Trans. 2*, **77**, 833 (1981).
6) K. Kalyanasundaram and M. Grätzel, *Angew. Chem., Int. Ed. Engl.*, **18**, 701 (1979).
7) M. Grätzel, *Ber. Bunsenges. Phys. Chem.*, **84**, 981 (1980).
8) M. Calvin, *Faraday Discuss. Chem. Soc.*, **70**, 383 (1980).
9) A. Harriman and G. Porter, *J. Chem. Soc., Faraday Trans. 2*, **75**, 1532 (1979).
10) A. Harriman and G. Porter, *J. Chem. Soc., Faraday Trans. 2*, **75**, 1543 (1979).
11) I. A. Duncan, A. Harriman, and G. Porter, *J. Chem. Soc., Faraday Trans. 2*, **76**, 1415 (1980).
12) A. Harriman and G. Porter, *J. Chem. Soc., Faraday Trans. 2*, **76**, 1429 (1980).
13) K. Takahashi, T. Komura, and H. Imanaga, *Memoirs of the Faculty of Technology, Kanazwa University*, **16**, 103 (1983).
14) R. F. Pasternack, L. Francesconi, D. Raff, and E. Spiro, *Inorg. Chem.*, **12**, 2606 (1973).
15) "Shinjikken Kagaku Kohza 8, Mukikagohbutsu No Gohsei [III]," ed by the Chemical Society of Japan, Maruzen, Tokyo (1977), p. 1475.
16) T. Watanabe and K. Honda, *J. Phys. Chem.*, **86**, 2617 (1982).
17) W. E. Ford, J. W. Otvos, and M. Calvin, *Nature*, **274**, 507 (1978).
18) S. F. Chan, M. Chou, C. Creutz, T. Matsubara, and N. Sutin, *J. Am. Chem. Soc.*, **103**, 369 (1981).
19) A. Harriman, *J. Chem. Soc., Faraday Trans. 1*, **76**, 1978 (1980).

Decomposition of 2-Butanol Catalyzed by Iron Oxide and Mixed Oxides Containing Iron

Tuo JIN, Hideshi HATTORI, and Kozo TANABE*

Department of Chemistry, Faculty of Science, Hokkaido University, Sapporo 060

(Received March 29, 1983)

Three types of binary oxides, Fe_2O-TiO_2, Fe_2O_3-ZrO_2, and Fe_2O_3-ZnO, were prepared by a coprecipitation method, and their catalytic behaviors in the decomposition of 2-butanol were examined. The activities and selectivities of the catalysts varied with the type of the oxide with which Fe_2O_3 was combined, with the content of Fe_2O_3 in the binary oxides, and with the reduction temperature of the catalysts. Over the Fe_2O_3-TiO_2 catalysts, 2-butanol underwent primarily dehydration and the activity decreased with an increase in Fe_2O_3 content. Over the Fe_2O_3-ZnO catalysts, dehydrogenation preferentially occurred, the maximum activity being observed for the catalyst containing 67% Fe_2O_3. The Fe_2O_3-ZrO_2 catalysts exhibited an intermediate nature between the Fe_2O_3-TiO_2 catalysts and Fe_2O_3-ZnO catalysts. Reduction of catalysts tended to increase the dehydrogenation selectivity. Reduction also brought about the formation of butane. The maximum formation of butane was observed when the catalysts were reduced with hydrogen at about 350—400 °C. The reaction mechanisms of the formation of butane were elucidated by tracer experiments, and it was concluded that butane was formed by the mechanism involving the first order nucleophilic substitution (S_N1) of OH^- by H^- which was liberated in the dehydrogenation of butanols.

The catalysts containing iron have been used in various reactions such as ammonia synthesis, Fischer-Tropsch synthesis, water gas shift reaction, dehydrogenation of hydrocarbons, and oxidation reactions.[1] Meanwhile, combination of two types of oxides has been known to result in generation of acidic properties in many cases.[2] The acid-base properties of the catalysts containing iron, however, have not extensively been studied. Decomposition of 2-butanol generally yields butenes by dehydration over acidic catalyst and yields ethyl methyl ketone by dehydrogenation over basic catalyst.[3] Therefore, decomposition of 2-butanol seems to be an appropriate diagnostic reaction to see the acidic and basic properties of the catalysts. In the present work, variations in the catalytic activities and selectivities of the catalysts containing iron were examined as functions of catalyst composition, of reduction temperature and of types of oxides with which Fe_2O_3 was combined.

As previously reported, the formation of butane was observed during decomposition of 2-butanol over Fe_2O_3 catalyst.[4] In order to elucidate the reaction mechanism of the formation of butane, tracer experiments were also undertaken.

Table 1. Compositions and surface areas of catalysts

Nomenclature	Composition Fe/(Fe+X)/%[a]	Surface area $m^2\ g^{-1}$
TiO_2	0	42
Fe_2O_3-TiO_2(1/9)	10	62
Fe_2O_3-TiO_2(1/3)	25	42
Fe_2O_3-TiO_2(1/1)	50	38
Fe_2O_3-TiO_2(7/3)	70	40
Fe_2O_3-TiO_2(9/1)	90	21
ZrO_2	0	64
Fe_2O_3-ZrO_2(1/9)	10	77
Fe_2O_3-ZrO_2(3/7)	30	112
Fe_2O_3-ZrO_2(1/1)	50	96
Fe_2O_3-ZrO_2(7/3)	70	53
Fe_2O_3-ZrO_2(9/1)	90	36
ZnO	0	5
Fe_2O_3-ZnO(2/9)	18	10
Fe_2O_3-ZnO(2/1)	67	27
Fe_2O_3-ZnO(18/1)	95	14
Fe_2O_3	100	16

a) X represents Ti, Zr, or Zn.

Experimental

Catalyst Preparation. The Fe_2O_3-TiO_2 catalysts with different compositions were prepared by hydrolysis of mixed solutions of ferric nitrate and titanium tetrachloride in different molar ratios with aqueous ammonia, the final pH being 8—9. The Fe_2O_3-ZrO_2 catalysts and the Fe_2O_3-ZnO catalysts with different compositions were similarly prepared from mixed solutions of iron(III) nitrate and zirconium nitrate or zinc nitrate. The precipitates obtained by the hydrolysis were washed with deionized water, dried at 100 °C for 20—30 h, and finally calcined at 500 °C in air for 2—3 h. The compositions, surface areas and nomenclatures of the resulting catalysts are given in Table 1.

X-Ray Diffraction. X-Ray diffraction patterns were measured with powdered samples on a Toshiba GD-3 diffractometer, the radiation source being Ni-filtered Cu $K\alpha$. For the samples reduced with hydrogen, the sample was cooled to room temperature under a helium stream, and slowly exposed to air to prevent the sample from rapid oxidation.[5,6]

Hydrogen Consumption during Reduction. The amounts of hydrogen consumed during reduction at different temperatures were measured for the Fe_2O_3 catalyst, the Fe_2O_3-ZrO_2 (7:3) catalyst, the Fe_2O_3-ZnO (2:1) catalyst, and the Fe_2O_3-TiO_2 (7:3) catalyst by use of a recirculation system of a small volume, 40 ml. The sample (0.1 g) was placed in a U tube and outgassed at 500 °C for 2 h. After cooling the sample to room temperature, hydrogen (200 Torr, 1 Torr = 133.3 Pa) was introduced in the system and circulated in the loop which was attached by a liquid nitrogen trap. The temperature of the sample was raised to 250 °C and kept at the temperature for 30 min. The amount of hydrogen consumed for reduction of the sample was measured by decrease in the pressure. Then the sample was heated stepwise by 50 °C increment to 500 °C. At each increment, the temperature was kept for 30 min.

Reaction Procedures. For the kinenic measurement of

decomposition of 2-butanol, a microcatalytic pulse reactor was employed. A catalyst (0.1 g) was placed in a U-tube reactor and pretreated in a helium stream at 500 °C for 2 h. The catalyst was then cooled to the reaction temperature of 250 °C in a helium stream. In experiments with reduced catalysts, the catalysts were pretreated in a hydrogen stream for 30 min before cooling to the reaction temperature. The flow rate of helium was adjusted to 75 ml/min. 2-Butanol (10 μl) was injected by a syringe into a helium stream ahead of the catalyst. The reaction products were once trapped in a liquid nitrogen and flash-evaporated into gas chromatographic columns. The columns, PEG-20 M and VZ-7, were arranged in series for total analysis. By the former column operated at 80 °C, butenes plus butane, ethyl methyl ketone, and 2-butanol were separated. By the latter column operated at 0 °C, each isomer of butenes and butane were separated. The data of Figs. 2—5 and Table 4 were taken from No. 5 pulses which gave steady rates.

For carrying out some reactions, a closed recirculation reactor having a volume of 1280 ml was also employed. A catalyst (0.2 g) was outgassed at 500 °C for 2 h and reduced at 350 °C for 30 min by circulating hydrogen (150 Torr) in a loop of the reactor which was equipped with a trap of liquid nitrogen temperature. The catalyst was then outgassed at 240 °C for 30 min. A mixture of 1-butene (16 Torr) and hydrogen (18 Torr) or a mixture of 1-butene (3 Torr) and 2-propanol (27 Torr) was allowed to react at 242 °C over the Fe_2O_3 catalyst.

Two tracer experiments were also carried out in a closed recirculation reactor. One tracer experiment was the reaction of a mixture of 2-butanol (16 Torr) and deuterium (40 Torr). The other was the reaction of a mixture of monodeuterio 2-butanol ($CH_3CH_2CH(OD)CH_3$, 16 Torr) and heavy water (D_2O, 14 Torr). The isotopic distribution of butane was determined by mass spectrometry.

Results

X-Ray Diffraction. Crystalline structures detected by X-ray diffraction for the samples calcined at 500 °C in air are summarized in Table 2. For binary oxides of Fe_2O_3–ZrO_2 and Fe_2O_3–TiO_2, the crystalline structures detected were those of the mixture or one of the component oxides. New crystalline structures were not detected. For the Fe_2O_3–ZnO (2/9) and the Fe_2O_3–ZnO (2/1), a spinel structure of $ZnFe_2O_4$ was detected. All peaks detected for binary oxides calcined at 500 °C were weak in intensity and broad as compared with those for single component oxides.

Crystalline structures detected for the samples, Fe_2O_3, Fe_2O_3–ZrO_2 (7/3), Fe_2O_3–ZnO (2/1), and Fe_2O_3–TiO_2 (7/3), reduced with hydrogen at different temperatures

Table 2. Crystalline structure of the catalysis detected by XRD

Catalyst[a)]	Observed spectra
TiO_2	TiO_2(sharp)
Fe_2O_3-TiO_2(1/9)	TiO_2(sharp)
Fe_2O_3-TiO_2(1/3)	TiO_2(broad), Fe_2O_3(very broad)
Fe_2O_3-TiO_2(1/1)	Fe_2O_3(very broad), TiO_2(very broad)
Fe_2O_3-TiO_2(7/3)	Fe_2O_3(broad)
Fe_2O_3-TiO_2(9/1)	Fe_2O_3
ZrO_2	ZrO_2(sharp)
Fe_2O_3-ZrO_2(1/9)	ZrO_2(sharp)
Fe_2O_3-ZrO_2(3/7)	ZrO_2(broad), Fe_2O_3(broad)
Fe_2O_3-ZrO_2(1/1)	Fe_2O_3(broad), ZrO_2(broad)
Fe_2O_3-ZrO_2(7/3)	Fe_2O_3(broad), ZrO_2(broad)
Fe_2O_3-ZrO_2(9/1)	Fe_2O_3(sharp)
ZnO	ZnO, (sharp)
Fe_2O_3-ZnO(2/9)	ZnO, $ZnFe_2O_4$(broad)
Fe_2O_3-ZnO(2/1)	$ZnFe_2O_4$(broad)
Fe_2O_3-ZnO(18/1)	Fe_2O_3(sharp)
Fe_2O_3	Fe_2O_3(sharp)

a) All the catalysts were calcined in air at 500 °C for 2 h.

Table 3. Crystalline structure of pretreated catalysts detected by XRD

Catalyst	Temp of H_2 treatment	Observed spectra
Fe_2O_3	Untreated	Fe_2O_3(sharp)
Fe_2O_3	250 °C	Fe_3O_4, Fe(trace)
Fe_2O_3	350 °C	Fe(trace), Fe_3O_4(trace)
Fe_2O_3	500 °C	Fe(sharp)
Fe_2O_3-ZnO(2/1)	Untreated	$ZnFe_2O_4$(broad)
Fe_2O_3-ZnO(2/1)	250 °C	ZnO(broad), Fe_3O_4(trace), Fe(trace)
Fe_2O_3-ZnO(2/1)	350 °C	ZnO, Fe(trace), FeO(trace)
Fe_2O_3-ZnO(2/1)	500 °C	Fe(sharp), ZnO(sharp)
Fe_2O_3-ZrO_2(7/3)	Untreated	Fe_2O_3(broad), ZrO_2(broad)
Fe_2O_3-ZrO_2(7/3)	250 °C	ZrO_2(broad), Fe_3O_4(tract)
Fe_2O_3-ZrO_2(7/3)	350 °C	ZrO_2(broad), Fe_3O_4(trace), FeO(trace)
Fe_2O_3-ZrO_2(7/3)	500 °C	Fe(sharp), ZrO_2(sharp)
Fe_2O_3-TiO_2(7/3)	Untreated	Fe_2O_3(broad)
Fe_2O_3-TiO_2(7/3)	250 °C	Fe_3O_4(trace)
Fe_2O_3-TiO_2(7/3)	350 °C	Almost nothing
Fe_2O_3-TiO_2(7/3)	500 °C	Fe(sharp)

are summarized in Table 3. By reduction at 250 °C, the pattern of Fe_2O_3 disappeared and the pattern of Fe_3O_4 appeared for all samples, though all peaks for the binary oxides were broad and weak. By raising the reduction temperature to 500 °C, the patterns of oxide forms of Fe such as Fe_2O_3, Fe_3O_4, and FeO diminished and the sharp patterns of metallic Fe appeared. The spinel structure, $ZnFe_2O_4$, in the Fe_2O_3–ZnO (2/1) sample disappeared on reduction at 250 °C.

Hydrogen Consumption during Reduction. The amounts of hydrogen consumed in reduction of the Fe_2O_3, Fe_2O_3–ZrO_2 (7/3), Fe_2O_3–ZnO (2/1), and Fe_2O_3–TiO_2 (7/3) are plotted against the reduction temperature in Fig. 1. The easiness of reduction of these samples is in the following order:

$Fe_2O_3 > Fe_2O_3$–ZrO_2 (7/3) $> Fe_2O_3$–ZnO (2/1) $> Fe_2O_3$–TiO_2 (7/3).

Assuming that a part of Fe^{3+} ions were reduced only to Fe^{2+} ions at 350 °C for all samples, the percentages of Fe^{3+} ions reduced to Fe^{2+} ions were calculated to be 50, 43, 32, and 22% for the Fe_2O_3, Fe_2O_3–ZrO_2 (7/3), Fe_2O_3–ZnO (2/1), and Fe_2O_3–TiO_2 (7/3), respectively. Since reduction of Ti^{4+} ions might occur to some extent for the Fe_2O_3–TiO_2 (7/3), the value, 22% is the maximum percentage of Fe^{3+} ions converted to Fe^{2+} ions.

Effects of Reduction of Catalysts on Activity and Selectivity for Reaction of 2-Butanol. Reaction of 2-butanol gave ethyl methyl ketone, butenes, and butane. The rate of conversion of 2-butanol and the product distribution varied with type of binary oxide and with pretreatment condition of catalysts. The percentage conversions of 2-butanol and the molar percentages of each product are plotted against the reduction temperature of catalysts in Figs. 2—5 for the Fe_2O_3 catalyst, the Fe_2O_3–ZrO_2 (7/3) catalyst, the Fe_2O_3–ZnO (2/1) catalyst, and the Fe_2O_3–TiO_2 (7/3) catalyst, respectively.

With the Fe_2O_3 catalyst, the main product was ethyl methyl ketone over the whole range of the reduction temperature. The conversion of 2-butanol exhibited a maximum at the reduction temperature of 300 °C, and the ketone yield exhibited a maximum at the reduction temperature of 250 °C. It should be noted that considerable amounts of butane were produced when the catalyst was reduced in the temperature range of 300—400 °C. The formation of butane became maximum at the reduction temperature

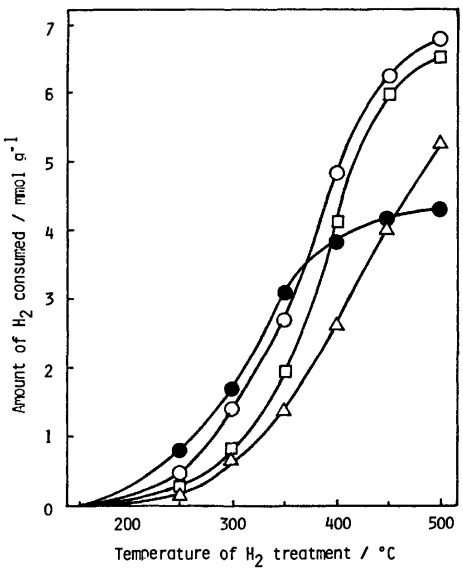

Fig. 1. Temperature programmed hydrogen treatment of iron oxide and binary oxides.
For binary oxides, the values of ordinate are based on 1 g of Fe_2O_3 contained in the catalysts. ●: Fe_2O_3, ○: Fe_2O_3-ZrO_2 (7/3), □: Fe_2O_3-ZnO (2/1), △: Fe_2O_3-TiO_2 (7/3).

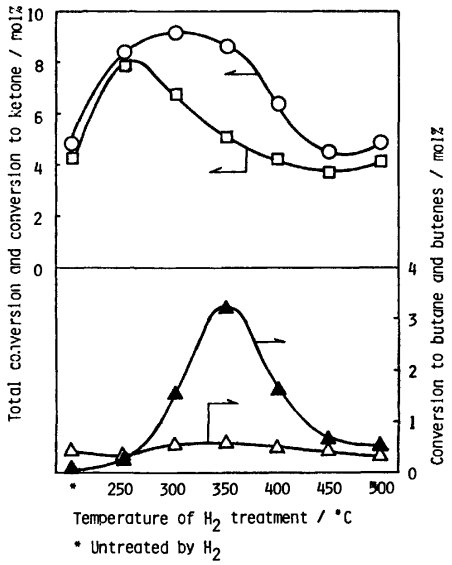

Fig. 2. Decomposition of 2-butanol over Fe_2O_3 at various temperatures of H_2 treatment.
Reaction at 250 °C with 0.1 g catalyst. ○: Total conversion, □: ketone, ▲: butane, △: butenes.

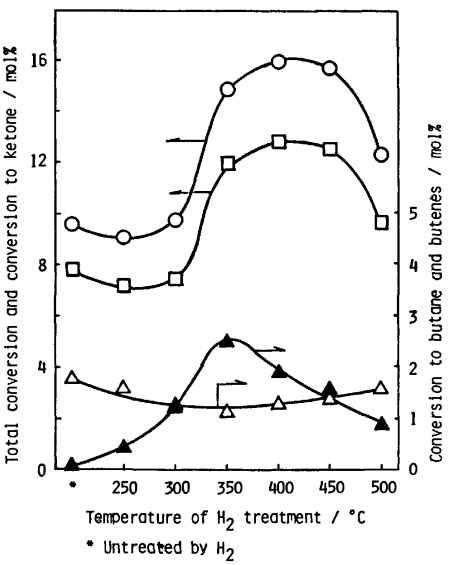

Fig. 3. Decomposition of 2-butanol over Fe_2O_3–ZrO_2 (7/3) at various temperatures of H_2 treatment.
Reaction at 250 °C with 0.1 g catalyst. ○: Total conversion, □: ketone, ▲: butane, △: butenes.

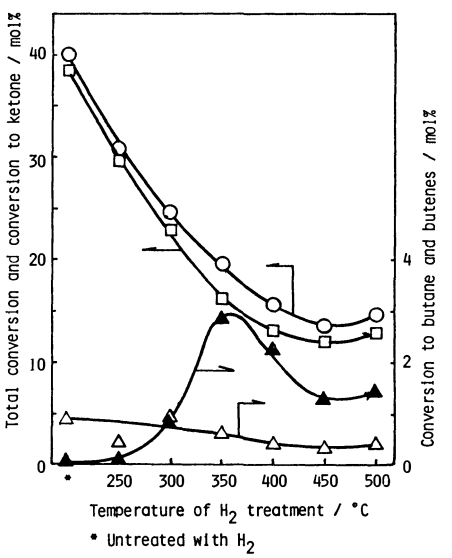

Fig. 4. Decomposition of 2-butanol over Fe_2O_3–ZnO (2/1) at various temperatures of H_2 treatment. Reaction at 250 °C with 0.1 g catalyst. ○: total conversion, □: ketone, ▲: butane, △: butenes.

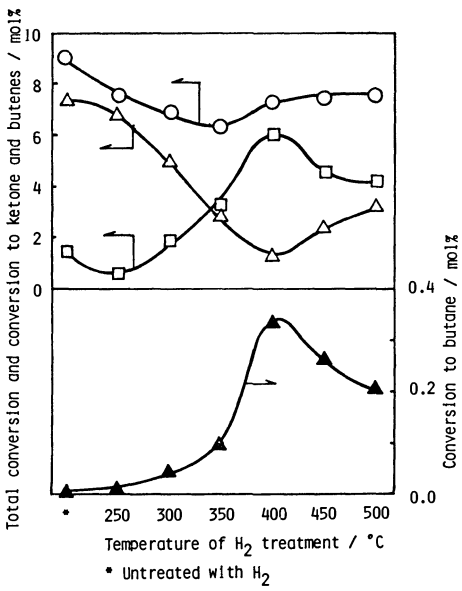

Fig. 5. Decomposition of 2-butanol over Fe_2O_3–TiO_2 (7/3) at various temperatures of H_2 treatment. Reaction at 250 °C with 0.1 g catalyst. ○: Conversion, □: ketone, ▲: butane, △: butenes.

of 350 °C.

With the Fe_2O_3–ZrO_2 catalyst, the main product was ethyl methyl ketone. The conversion of 2-butanol showed a maximum at the reduction temperature of 400 °C. The formation of butane was also observed over the wide range of the reduction temperature, 250—500 °C. The maximum formation was observed when the catalyst was reduced at 350 °C.

With the Fe_2O_3–ZnO (2/1) catalyst, the main product was also ethyl methyl ketone. The conversion of 2-butanol decreased steadily with an increase in the reduction temperature. The formation of butane reached maximum when the catalyst was reduced between 300—500 °C.

With the Fe_2O_3–TiO_2 (7/3) catalyst, the conversion of 2-butanol was almost independent of the reduction temperature. However, the ratios of ethyl methyl ketone/butenes changed much with the reduction temperature. When the reduction temperature was below 300 °C, butenes were produced much more than ethyl methyl ketone. On the contrary, ethyl methyl ketone was produced much more than butenes as the reduction temperature exceeded 350 °C. The amount of butane formed was less than 5% of total products, which was small as compared with the other catalysts. The maximum formation of butane was observed at the reduction temperature of 400 °C.

Activity and Selectivity of Catalysts with Different Compositions for Reaction of 2-Butanol. Product distributions in the reaction of 2-butanol over the binary oxides with different compositions and the component oxides are given in Table 4, in which the results both for the catalysts unreduced and for one reduced at 350 °C are included.

With unreduced Fe_2O_3–ZrO_2 catalysts, the dehydrogenation activities markedly increased as Fe_2O_3 was added to ZrO_2. The dehydration activities decreased with an increase in Fe_2O_3 content. The formation of butane was not observed. With the Fe_2O_3–ZrO_2 catalysts reduced at 350 °C, the maximum conversion of 2-butanol and activity for dehydrogenation were observed for the Fe_2O_3–ZrO_2 (1/1) catalyst. The formation of butane became maximum for the Fe_2O_3–ZrO_2 (7/3) catalyst.

With the unreduced Fe_2O_3–ZnO catalysts, the conversion of 2-butanol and the dehydrogenation activity became maximum for the Fe_2O_3–ZnO (2/1) catalyst. The dehydration activities were low, and the formation of butane was not appreciable for any compositions of the catalysts. With the reduced Fe_2O_3–ZnO catalysts, the conversion of 2-butanol and the dehydrogenation activity became maxima for the Fe_2O_3–ZnO (2/1) catalyst. The dehydration activity decreased as the content of Fe_2O_3 increased. The formation of butane was considerable and increased with an increase in the Fe_2O_3 content.

With the unreduced Fe_2O_3–TiO_2 catalysts, the dehydration activity decreased with an increase in the Fe_2O_3 content. The dehydrogenation activity became maximum for the Fe_2O_3–TiO_2 (1/1) catalyst. The formation of butane was not observed. With the reduced Fe_2O_3–TiO_2 catalysts, the dehydration activities decreased with an increase in Fe_2O_3 content. The dehydrogenation activity showed a maximum for the Fe_2O_3–TiO_2 (1/1) catalyst. The activities of the reduced Fe_2O_3–TiO_2 catalysts for the formation of butane were generally low as compared with those of the reduced Fe_2O_3–ZrO_2 catalysts and of Fe_2O_3–ZnO_2 catalysts.

Reaction of 1-Butene with Hydrogen. The compositions of the products in the reaction of 1-butene with H_2 over the Fe_2O_3 catalyst reduced at 350 °C are given in Table 5. The hydrogenation of butenes to butane was slow, the rate being 2.9×10^{-6} mol min^{-1} g^{-1}.

Reaction of 1-Butene in the Presence of 2-Propanol. The result for the reaction of a mixture of 1-butene and 2-propanol over the Fe_2O_3 catalyst reduced at

TABLE 4. PRODUCT DISTRIBUTION IN REACTION OF 2-BUTANOL

Catalyst	Conversion/%[a]	Butane/%[a]	Butenes/%[a]	Ketone/%[a]
TiO_2	32.5(18.0)	0.1(0.1)	31.9(17.8)	0.1(0.1)
Fe_2O_3-TiO_2(1/9)	22.5(18.6)	0.1(0.2)	22.0(16.6)	0.4(1.7)
Fe_2O_3-TiO_2(1/3)	14.6(14.3)	0.0(0.1)	11.3(12.4)	3.3(1.8)
Fe_2O_3-TiO_2(1/1)	16.2(17.4)	0.0(0.2)	11.2(12.8)	5.0(4.4)
Fe_2O_3-TiO_2(7/3)	8.6(7.1)	0.0(0.1)	7.2(3.8)	1.4(3.2)
Fe_2O_3-TiO_2(9/1)	2.6(3.7)	0.0(0.1)	1.8(1.0)	0.8(2.6)
ZrO_2	5.6(7.9)	0.0(0.0)	5.4(7.8)	0.2(0.1)
Fe_2O_3-ZrO_2(1/9)	11.9(9.6)	0.0(0.1)	6.5(4.3)	5.4(5.2)
Fe_2O_3-ZrO_2(3/7)	11.4(12.4)	0.0(0.7)	2.8(2.9)	8.4(8.8)
Fe_2O_3-ZrO_2(1/1)	10.5(13.6)	0.0(0.8)	2.4(1.7)	8.0(11.1)
Fe_2O_3-ZrO_2(7/3)	8.8(10.7)	0.0(2.4)	2.0(1.2)	6.8(7.1)
Fe_2O_3-ZrO_2(9/1)	4.8(7.0)	0.0(1.2)	0.8(0.8)	4.0(5.0)
ZnO	10.4(7.0)	0.0(0.0)	0.2(0.0)	10.2(9.0)
Fe_2O_3-ZnO(2/9)	13.9(17.9)	0.0(1.0)	1.3(1.7)	12.6(15.2)
Fe_2O_3-ZnO(2/1)	35.1(20.8)	0.0(3.2)	1.4(0.8)	33.7(16.8)
Fe_2O_3Z-ZnO(18/1)	5.1(11.4)	0.0(3.6)	0.5(0.3)	4.6(7.5)
Fe_2O_3	4.7(9.4)	0.0(3.8)	0.6(0.7)	4.1(4.9)

a) The data without parentheses represent the values over 0.1 g of unreduced catalysts, and thoses in parentheses are the values over 0.1 g of reduced catalysts.

TABLE 5. REACTION OF 1-BUTENE(6 Torr) IN H_2(18 Torr) OVER Fe_2O_3

Reaction temp	Reaction time	Conversion	Product yield/%		
°C	min	%	Butane	*t*-2-Butene	*c*-2-Butene
242	20	84.3	2.8	50.5	31.0

350 °C is shown in Table 6. The products consisted of propane, propene, and acetone. Butane was not formed, though propane was produced.

Reaction of 2-Butanol in the Presence of Deuterium. In the reaction of a mixture of 2-butanol and deuterium at 240 °C over the Fe_2O_3 catalyst reduced at 350 °C, monodeuteriobutane (butane-d_1) and dideuteriobutane (butane-d_2) were formed in addition to nondeuteriated butane. The percentages of butane-d_1 and butane-d_2 in total isotopic butanes are plotted against the conversion to butane in Fig. 6. Extrapolation to zero conversion gives nearly zero percentage for both the butane-d_1 and butane-d_2. The rate of the formation of butane was 4.0×10^{-6} mol min^{-1} g^{-1}, which was higher than the hydrogenation of 1-butene, 2.9×10^{-6} mol min^{-1} g^{-1}.

*Reaction of Deuterio 2-Butanol-*d *in the Presence of Heavy Water.* When a mixture of $CH_3CH_2CH(OD)CH_3$ and D_2O was allowed to react at 240 °C over the Fe_2O_3 catalyst reduced at 350 °C, formation of butane-d_1 was observed in addition to that of nondeuteriated butane. In Fig. 7, the percentage of butane-d_1 in total butane products is plotted against conversion of

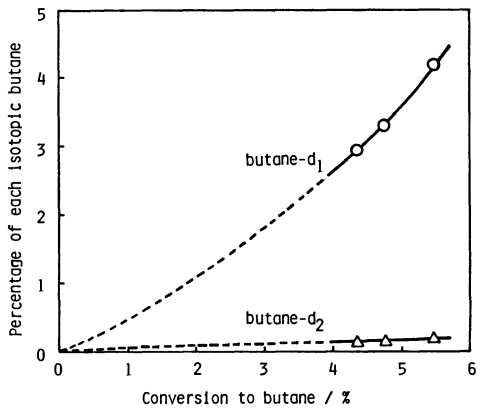

Fig. 6. Distribution of deuterated butane formed by reaction of 2-butanol with D_2. ○: butane-d_1, △: butane-d_2.

2-butanol. Extrapolation to the zero conversion gives less than 50% for butane-d_1 and approached to nearly zero percentage at the zero conversion.

Discussion

X-Ray diffraction patterns of the binary oxides were generally weak and broad. The binary oxides consisted mostly of amorphous parts. By treatment with hydrogen, one component oxide, Fe_2O_3, was reduced and converted mainly to amorphous species. Metallic iron was considerably yielded by raising the temperature to 500 °C. The reduction became difficult when Fe_2O_3 was mixed with the other oxides; ZrO_2,

Table 6. Reaction of mixture 1-butene and 2-propanol over Fe_2O_3[a)]

Reaction time	Composition of products/%					
min	1-Butene	2-Propanol	Propane	Propene	Acetone	Butane
0	10.00	90.00	0	0	0	0
40	10.06	64.87	1.53	0.56	22.98	0
70	10.07	50.18	2.17	0.99	36.59	0

a) The initial pressures of 1-butene and 2-propanol are 3 and 27 Torr, respectively.

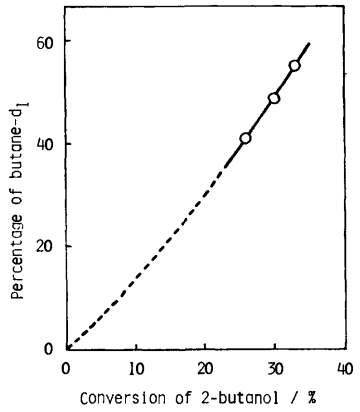

Fig. 7. Distribution of deuterated butane formed by reaction of 2-butanol with D_2O.

ZnO, and TiO_2. The difficulty of reduction of Fe_2O_3 in the binary oxides depended on the kinds of the other component oxides. There should be some chemical interactions between Fe_2O_3 and the other component oxides.

As for the activity and selectivity of the unreduced binary oxides, the catalytic properties of each component oxide seem to reflect on the activity and selectivity of the corresponding binary oxide catalysts. The catalytic properties of TiO_2 and ZrO_2 favored the dehydration, while those of ZnO and Fe_2O_3 favored the dehydrogenation. The binary oxides, Fe_2O_3–TiO_2 of any compositions and Fe_2O_3–ZrO_2 (1/9) mainly formed butenes, while Fe_2O_3–ZnO of any compositions and Fe_2O_3–ZrO_2 (3/7—9/1) gave ketone preferentially. It should be noted that a marked increase in the ketone yield was observed for the Fe_2O_3–ZnO (2/1) catalyst as compared with each component oxide.

Reduction of the catalysts brought about obvious changes in both the selectivity and activity. Direction of the changes depended upon types of the binary oxides. One of the factors to control the selectivity in decomposition of alcohols is an acid-base properties of catalyst.[3)] With acidic catalysts, the dehydration predominantly takes place, while, with basic catalysts, the dehydrogenation proceeds. Changes in the dehydration and dehydrogenation selectivity of the binary oxides suggest that the acidic and basic properties of the catalysts change with the reduction state of Fe_2O_3 in the binary oxides. The change was especially marked for the Fe_2O_3–TiO_2 (7/3) catalyst. It appears that the basic property of the Fe_2O_3–TiO_2 (7/3) catalyst was strengthened by reduction above 350 °C.

The most prominent change in the selectivity occurred on reduction was the appearance of the formation of butane. For the catalysts, Fe_2O_3, Fe_2O_3–ZnO (2/1), Fe_2O_3–ZrO_2 (7/3), and Fe_2O_3–TiO_2 (7/3), the reduction temperatures which gave maximum formation of butane were 350, 350, 350, and 400 °C, respectively. These temperatures are close to the temperatures which were required to reduce Fe_2O_3 in those catalysts to Fe_2O_{3-x} (x=0.5) as seen in Fig. 1. Besides, these temperatures are also the temperature at which most of Fe_2O_3 in the catalysts converted to an amorphous species. Although the amounts of butane formed on unit amount of Fe_2O_3 in the binary oxides were not the same for different binary oxides, the amorphous iron oxide formed by the reduction seems to be the active species for the formation of butane.

The formation of butane from 2-butanols was observed over TiO_2 for the first time by Vinek *et al.*[7)] However, the activity of the reduced Fe_2O_3 for the formation of butane is much higher than that of TiO_2 as shown in Table 4.

Several possibilities are considered as to the reaction mechanism of the formation of butane. Hydrogenation of butenes which were produced by dehydration of 2-butanol with hydrogen which resulted from dehydration would be one of them. However, the rate of hydrogenation of 1-butene was lower than that of the formation of butane from 2-butanol. In addition, the presence of hydrogen had no marked effect on the rate of butane formation from 2-butanol.[4)] Therefore, hydrogenation of butene should be ruled out. Another possibility that butenes are hydrogenated by use of adsorbed hydrogen atoms or ions which are formed by the dehydrogenation of 2-butanol might be taken into account. If the formation of butane from 2-butanol occurred *via* butene, the formation of propane from 2-propanol would also occur *via* propene. If this is the case, the reaction of a mixture of 1-butene and 2-propanol would yield both butane and propane, since propene undergoes hydrogenation only 1.5 times faster than 1-butene does.[8)] The observed results showed that propane was produced, while butane was not produced (Table 5). This rules out the possibility that butane was formed through butenes by use of adsorbed hydrogen.

Vinek *et al.*[7)] proposed on the basis of higher reactivity of 1-butanol as compared with 2-butanol that butane was formed *via* the second order nucleophilic substitution (S_N2) of OH^- by H^-. They concluded that the source of the H^- nucleophile is water which results from the dehydration of butanols, as they did not take into account the adsorbed H^- which results

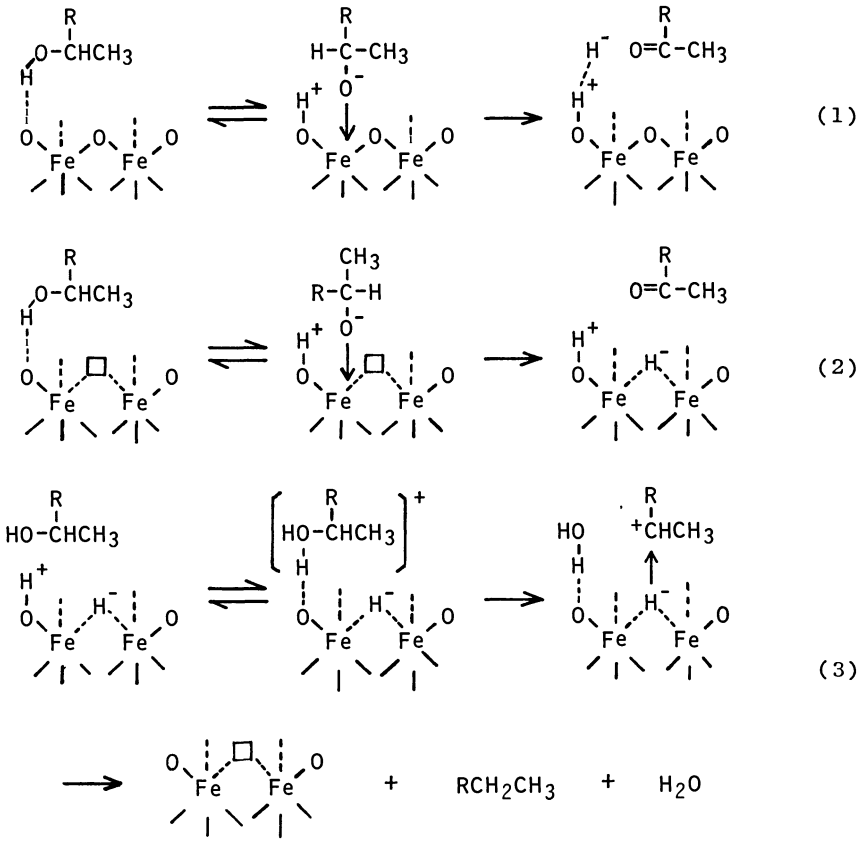

Scheme. Reaction scheme over Fe_2O_3 and reduced Fe_2O_3.

from the dehydrogenation.

In the present work, we propose that butane is formed *via* the first order nucleophilic substitution (S_N1) and that the H^- nucleophile is provided by the dehydrogenation of butanols. If the nucleophilic substitution proceeded by the S_N2 mechanism, 1-butanol would be easier to form butane than 2-butanol. If the substitution proceeded by the S_N1 mechanism, 2-butanol would undergo reaction much faster than 1-butanol. Our previous data[4] have shown that 2-butanol was easier to form butane than 1-butanol over the Fe_2O_3–ZrO_2 (7/3) catalyst. This suggests that the operating mechanism over the catalyst containing Fe_2O_3 is the first order nucleophilic substitution (S_N1) mechanism rather than the S_N2 mechanism.

The source of hydrogen would be either water[7] which results from dehydration or hydrogen which results from dehydrogenation. The amount of ethyl methyl ketone exceeded those of butane for all catalysts, whereas the amounts of butenes were lower than those of butane in the cases of some catalysts, Fe_2O_3, Fe_2O_3–ZnO (2/1—18/1), and Fe_2O_3–ZrO_2 (7/3—9/1) as seen in Table 4. It is, therefore, likely that the H^- nucleophile is supplied by the dehydrogenation of 2-butanol, but not from water. This is also supported by the percentage less than 50 of deuteriobutanes in total butane produced by the reaction of a mixture of the 2-butanol-*d* ($CH_3CH_2CH(OD)CH_3$) and heavy water, because if the hydride ion came from water formed from $CH_3CH_2CH(OD)CH_3$, the extrapolation to zero conversion should give 50% butane-d_1.

No incorporation of deuterium atoms into the butane molecules in the initial stage of the reaction of a mixture of 2-butanol and deuterium (Fig. 6) suggests that the hydrogen acting as the hydrogen source does not originate from molecular hydrogen, but from the adsorbed hydrogen which results from dehydrogenation of 2-butanol.

The reaction mechanism of the formation of butane could be drawn as follows. When dehydrogenation of alcohol occurs over the iron oxide catalyst, the alcohol dissociates into proton and alkoxide ion to adsorb on the catalyst surface at first, followed by losing of α hydrogen as hydride ion to form ketone (Scheme 1 or 2). The α hydrogen can be abstracted either by a proton or by an oxygen vacancy on the surface.[9] With the unreduced catalyst, the α hydrogen can be abstracted by H^+ (Scheme 1), since the metal ions are covered by oxygen atoms. In the case of the reduced catalyst, however, the α hydrogen tends to be abstracted as a hydride ion by an oxygen vacancy formed by reduction (Scheme 2). An alcohol molecule comes to the surface on which H^+ and H^- coexist and an alkoxonium ion is formed by the addition of H^+ to the alcohol. Since the present reaction was ascertained to proceed by the S_N1 mechanism, the alkoxonium ion must dissociate to form an alkyl cation. An alkane is produced by the nucleophilic attack of H^- to the alkyl cation (Scheme 3).

References

1) N. Todo, "Catalytic Engineering," Chijinshokan, (1967), Vol. X, p. 421.

2) K. Tanabe, T. Sumiyoshi, K. Shibata, T. Kiyoura, and J. Kitagawa, *Bull. Chem. Soc. Jpn.*, **47**, 1064 (1974).
3) O. V. Krylov, "Catalysis by Non-metals," Academic Press, New York (1970).
4) T. Jin, H. Hattori, and K. Tanabe, *Chem. Lett.*, **1981**, 1532.
5) J. P. Reymond, P. Meriauden, and J. S. Teichner, *J. Catal.*, **75**, 39, (1982).
6) J. A. Amelse, J. B. Butt, and L. H. Schwartz, *J. Phys. Chem.*, **82**, 558 (1978).
7) H. Vinek, J. Lercher, and H. Noller, Proc. 7th Inter. Congr. Catalysis, 1980, Tokyo, Part B, p. 1456, Elsevier (1981).
8) T. Jin and H. Hattori, unpublished data.
9) L. Nondek and J. Sedlacek, *J. Catal.*, **40**, 34 (1975).

A Further ESR Study of Irradiated D_2O Ice. On the Nature of the Species Appeared at $g=2.08$

Hirotomo HASE* and Takenobu HIGASHIMURA

Research Reactor Institute, Kyoto University, Kumatori-cho, Sennan-gun, Osaka 590-04

(Received April 6, 1983)

For D_2O ice warmed at *ca.* 120 K after the irradiation at 77 K, "$g=2.08$ line" was isolatedly detected at 4 K. The intensity of the line increased for the sample containing an electron scavenger. Photobleaching of solvated electrons caused no change in the intensity of the line. In D_2O single crystal, angular dependency of the line was not observed. The overall results were not accomodated to the hypothesis that "$g=2.08$ line" was due to O^- radical, but rather indicated the possibility that the species is a sort of positive ion or trapped hole.

Among numerous electron spin resonance (ESR) studies on irradiated ices, a few reports[1,2] described an asymmetric singlet line at $g=2.08$. However, the line was neither studied in detail nor identified until its thermal reversibility was firstly reported by Johnson and Moulton in 1978.[3] They found that in polycrystalline H_2O or D_2O ice irradiated at 4 or 77 K, "$g=2.08$ line" was observed only when ESR measurements were made at temperatures lower than 24 K. They proposed that "$g=2.08$ line" was probably due to H_2O^+ radical in irradiated H_2O ice, and D_2O^+ radical in irradiated D_2O ice.

Recently, however, Symons[4,5] has claimed that O^- radical is possibly responsible for "$g=2.08$ line". The experimental evidences on which the O^- hypothesis stands were: (i) the interconversion between OH radical and the species amounted to 50% for H_2O and 80% for D_2O ice[4] and (ii) when $D_2{}^{17}O$ ice was irradiated, a new line was observed in the $g=2.16$ region which was tentatively assigned to one of $g_{//}$ components of $^{17}O^-$ radical, although 6 $g_\perp$ components of $^{17}O^-$ radical could not be visible.[5] By analogy with NH_2^+ radical, Symons speculated that the H_2O^+ hypothesis must be rejected on the following reasons: (i) proton coupling of an order of 25 G† should be expected for H_2O^+; (ii) g-value should be close to 2.00 for H_2O^+. It was also stressed by Symons that ESR spectrum of the species was similar in profile to that for O^- in alkaline ice.

The argument by Symons for identification of the species is not completely convincing for us, since (i) the argument partly stands on the analogy with other radicals; (ii) there are scarecely any positive evidences which support the O^- hypothesis; (iii) direct observation of 6 hyperfine lines due to $^{17}O^-$ radical failed except for a new line at $g=2.16$ which might be attributed to $g_{//}$ component of $^{17}O^-$ radical.

Under these circumstances, it is worthwhile to study the nature of the species corresponding to "$g=2.08$ line" in order to further shed light on its identification.

In the present work, we have studied the effects of thermal annealing, addition of solute which is known as electron scavenger and photobleaching of solvated electrons(e^-_{sol}) on the "$g=2.08$ line" in polycrystalline D_2O ice containing NaOD. We have also studied the angular dependency of "$g=2.08$ line" in D_2O single crystal. Based on the results, we will discuss on the entity of "$g=2.08$ line".

† $1\,G=10^{-4}\,T$.

Experimental

D_2O(99.75%) and NaOD(40% in D_2O) were obtained from MSD (Japan) and used without further purification. Reagent grade $AgNO_3$ were used. Polycrystalline samples were made in suprasil quartz ESR tubes by immersing the liquid samples into liquid nitrogen. Single crystals of D_2O were made as described previously.[6] Samples were irradiated by ^{60}Co gamma rays at 77 and 4 K at a dose of 2.2 Mrad/h. ESR measurements were carried out with a Varian E-9 spectrometer at 77 and 4 K.

Results and Discussion

Figure 1 shows ESR spectra of polycrystalline D_2O ice irradiated at 77 K. Figure 1(A) presents the spectrum recorded at 4 K and shows an asymmetric singlet line at $g=2.08$ in addition to the lines due to OD radical in the $g=2.00$ region. Yields of species corresponding to "$g=2.08$ line" and OD radical increased linearly with gamma dose upto at least 20 Mrads. When ESR spectrum was recorded at 77 K, "$g=2.08$ line" was no longer visible. This spectral change is the same as reported firstly by Johnson and Moulton.[3] After the sample was warmed at *ca.* 120 K, ESR spectrum was recorded at 4 K. The spectrum is shown in Fig. 1(B). It is noted in Fig. 1(B) that "$g=2.08$ line" is still visible, although its intensity is reduced. The weak signal remaining in the $g=2.00$ region is

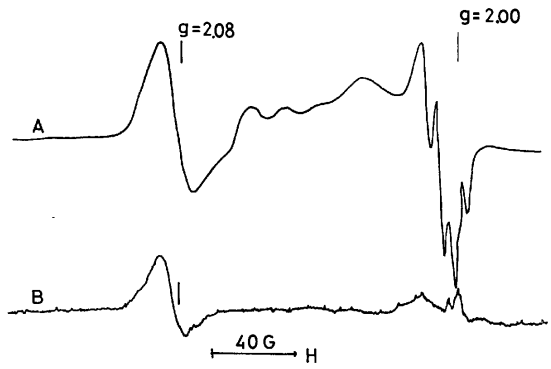

Fig. 1. ESR spectra of polycrystalline D_2O ice irradiated at 77 K. ESR spectrum at 4 K, (B) ESR spectrum at 4 K after warming to *ca.* 120 K. The ESR sensitivity for spectrum (B) was 5 times as large as that for spectrum (A).

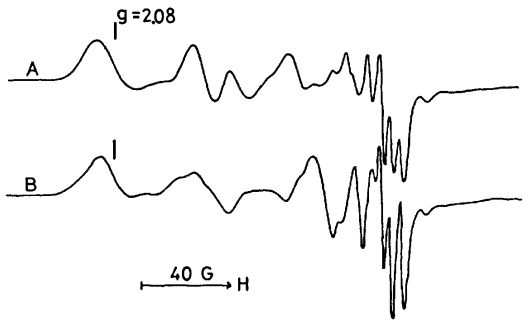

Fig. 2. ESR spectra of D_2O single crystal irradiated at 77 K. (A) ESR spectrum at 4 K, (B) ESR spectrum at 4 K after the cylindrical sample was rotated about 50°. The intensity of "g=2.08 line" remained nearly unchanged with any rotation angles.

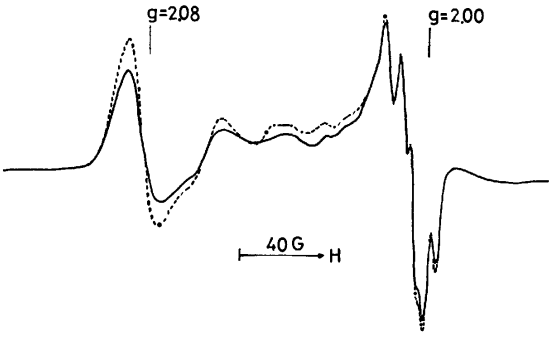

Fig. 3. ESR spectra of polycrystalline D_2O ice containing 0.1 M (solid line) and 0.5 M (dotted line) $AgNO_3$ which was irradiated at 77 K. ESR spectra were recorded at 4 K.

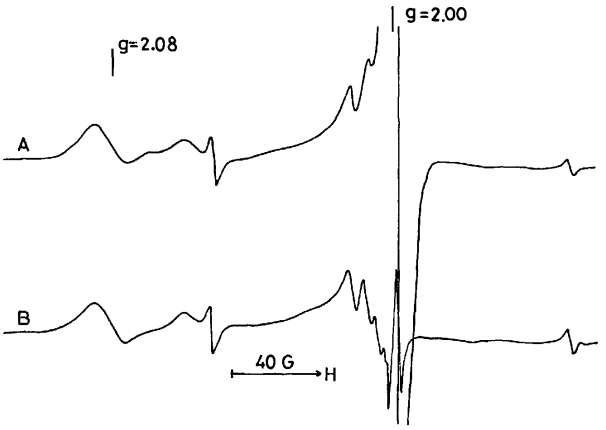

Fig. 4. ESR spectra of polycrystalline D_2O ice containing 1 M NaOD which was irradiated at 4 K. (A) ESR spectrum at 4 K, (B) ESR spectrum at 4 K after photobleaching the sample with the visible light at 4 K.

different from the signal due to either OD radical or $g_{//}$ component of O^- radical.

O^- radical is often reported for irradiated alkaline ices.[7,8] It is known that the $g_{//}$ component of O^- radical in the g=2.00 region provides a featureless broad line with ESR intensity comparable to that of the $g_\perp$ component in the g=2.07 region. Thus the signal remaining in the g=2.00 region in Fig. 1(B) is unlikely O^- radical.

The "g=2.08 line" was also observed in D_2O single crystal irradiated at 77 K. The relative intensities of the ESR lines due to OD radical changed remarkably with rotation of the cylindrical samples, while the intensity of "g=2.08 line" remained almost unchanged. This is illustrated in Fig. 2. The luck of the angular dependency for the "g=2.08 line" suggests that the line may be broadened partly by an unresolved hyperfine interactions with surrounding nuclei similar to those for trapped electrons in alkaline ices. This may also contrast to the result that ESR spectrum of bromine atom having an unpaired electron orbital like O^- radical showed a prominent angular dependency due to a large proton superhyperfine coupling in *N*-bromosuccinimide single crystal.[9]

When polycrystalline D_2O ice was irradiated at 4 K and ESR measurements were made at 4 K, the spectrum obtained was the same as that reported by Johnson and Moulton and showed "g=2.08 line" together with lines due to OD radical, trapped D atom and H atom.

Polycrystalline D_2O ices containing 0.1 or 0.5 M†† $AgNO_3$ were irradiated at 77 K. The "g=2.08 line" was observed in the ESR spectra recorded at 4 K. The intensity of "g=2.08 line" increased with concentration of $AgNO_3$, being 1.4 and 2.1 times for 0.1 and 0.5 M $AgNO_3$ solutions, respectively, as large as that for the solute-free D_2O ice. This is illustrated in Fig. 3. Since $AgNO_3$ is an electron scavenger, the observed effect of $AgNO_3$ in D_2O ice is consistent with the hypothesis that "g=2.08 line" is ascribed to a positive ion or hole, *e.g.* D_2O^+. O^- radical is also a cation-like species, but may not be a candidate for "g=2.08 line" in consideration of the previous result[7] that O^- yield was not affected by electron scavengers in alkaline ices at 77 K.

In polycrystalline D_2O ice containing 0.1 or 1.0 M NaOD, "g=2.08 line" was observed at 4 K. The intensity of the line was not affected by concentration of NaOD and remained nearly the same in both matrices. This result is in a remarkable contrast to the previous report[7] that O^- yield increased with concentration of NaOH. An intense singlet line due to e^-_{sol} was observed in the g=2.00 region in 1.0 M NaOD solution. Photobleaching of e^-_{sol} at 4 K caused little changes in the intensity of "g=2.08 line". That this is the case is shown in Fig. 4. It is previously reported[7] that complete photobleaching of e^-_{sol} in alkaline ices resulted in a decrease of about 70% of concentration of O^- radicals and that the decrease was attributed to the reaction of photodetached electrons with O^- radicals. Thus if "g=2.08 line" was attributed to O^- radicals, complete photobleaching of e^-_{sol} would reduce the intensity of "g=2.08 line". We infer that O^- radical must be produced in 1.0 M NaOD solution and that a broad ESR signal due to O^- radicals is probably masked in the apparent ESR spectrum. We also suppose that photodetached electrons in 1.0 M NaOD solution undergo a reaction

†† 1 M=1 mol dm^{-3}.

with O^- radicals more dominantly than another reaction with positive ion or hole. Thus the observed effects of NaOD in D_2O ice would be another evidence that "$g=2.08$ line" is not attributed to O^- radical.

In conclusion, we could not obtain any positive evidences for the hypothesis that "$g=2.08$ line" is ascribed to O^- radical.

This work was partially supported by a Grant-in-Aid for Scientific Research from Ministry of Education, Science and Culture. The authors are deeply indebted to Dr. Keisuke Kawabata at Radiation Center of Osaka Prefecture for his kind preparation of single crystal D_2O ice and fruitfull discussion throughout this study.

References

1) L. H. Piette, R. C. Rempel, and H. E. Weaver, *J. Chem. Phys.*, **30**, 1623 (1959).
2) S. Siegel, J. M. Flournoy, and L. H. Baum, *J. Chem. Phys.*, **34**, 1784 (1961).
3) J. E. Johnson and G. C. Moulton, *J. Chem. Phys.*, **69**, 3108 (1978).
4) M. C. R. Symons, *J. Chem. Soc., Chem. Commum.*, **1980**, 675.
5) M. C. R. Symons, *J. Chem. Soc., Faraday Trans. 1*, **78**, 1953 (1982).
6) K. Kawabata, *J. Chem. Phys.*, **55**, 3672 (1971).
7) L. Kevan, "Radiation Chemistry of Frozen Aqueous Systems," ed by G. Stein, Wiley-Interscience, New York (1968).
8) J. Kroh, B. C. Green, and J. W. T. Spinks, *J. Am. Chem. Soc.*, **83**, 2201 (1961).
9) H. Muto and L. D. Kispert, *J. Chem. Phys.*, **72**, 2300 (1980).

Adsorption of Dodecyltrimethylammonium Chloride–Decylammonium Chloride Mixtures at Water/Air Interface

Shozo URYU,† Makoto ARATONO, Michio YAMANAKA, Kinsi MOTOMURA,* and Ryohei MATUURA

Department of Chemistry, Faculty of Science, Kyushu University 33, Higashi-ku, Fukuoka 812

† *Chikushigaoka Highschool, 2-13-1 Noma, Minami-ku, Fukuoka 815*

(Received April 11, 1983)

The surface tension of the aqueous solution of dodecyltrimethylammonium chloride and decylammonium chloride mixture has been measured as a function of the total concentration and composition of the surfactants at 298.15 K under atmospheric pressure. It has been observed that the surface tension decreases with an increase in the composition of dodecyltrimethylammonium chloride at a fixed total concentration. A break point has been observed on the surface tension *vs.* total concentration curve. By applying the thermodynamic relations, the surface densities of surfactants have been evaluated numerically. It has been proved that the phase transition of the mixed adsorbed film takes place from a gaseous to an expanded state at the break point. By comparing the composition in the adsorbed film with that in the bulk phase, the difference between the compositions has been found to diminish as the surface tension decreases. It has been shown that the mutual relation between the compositions of the gaseous and expanded films at the transition point is described by the two-dimensional phase diagram.

The surface tension of the aqueous solution of surfactant mixture has been measured extensively and analyzed by applying the Gibbs adsorption equation.[1–14] However, most studies have been conducted in connection with the formation of mixed micelle at relatively high concentrations. In a recent paper,[15] we have investigated the adsorption of dodecylammonium chloride (DAC)–decylammonium chloride (DeAC) mixture at water/air interface in a relatively dilute concentration region; it has been shown that the phase transition of the mixed adsorbed film takes place from a gaseous state to an expanded one and its behavior can be treated thermodynamically by extending our method.[16] Further it has been shown that the two-dimensional phase diagram is useful to clarify the relation between the two coexisting phases.

In order to make sure that the occurence of the phase transition in mixed adsorbed films is a general phenomenon and our thermodynamic treatment is useful, we will investigate the mixed system of dodecyltrimethylammonium chloride (DTAC), of which the adsorbed film is accompanied by the phase transition,[17] with DeAC. The surface tension of the aqueous solution will be measured as a function of the total concentration and composition of the surfactants at constant temperature and pressure and analyzed by the thermodynamic equations advanced.

Experimental

Decylammonium chloride and dodecyltrimethylammonium chloride were synthesized and purified by the methods described previously.[15,17] Their purities were checked by the elementary analysis and guaranteed by the absence of minimum near the critical micelle concentration on the surface tension *vs.* concentration curves at 298.15 K. Water was distilled triply from alkaline permanganate.

The surface tension of solutions was measured by the drop volume technique described previously.[16] The temperature was kept constant at 298.15±0.01 K by immersing the measuring cell in a thermostat. The error estimated for the surface tension value was less than 0.05 mN m^{-1}.

Results and Discussion

The system under consideration is composed of two bulk phases and four components. Let us choose the total molality of surfactants m_t^w in the aqueous solution defined by

$$m_t^w = m_1^w + m_2^w, \tag{1}$$

and the composition of the second surfactant X_2^w defined by

$$X_2^w = m_2^w/(m_1^w + m_2^w), \tag{2}$$

as the thermodynamic independent variables at constant temperature T and pressure p. The subscripts 1 and 2 refer to DTAC and DeAC, respectively. The surface tension γ of the aqueous solution of surfactant mixture was measured as a function of m_t^w at fixed X_2^w and at 298.15 K under atmospheric pressure.

The values of γ are plotted against m_t^w at various X_2^w values in Fig. 1(a). It is seen that the curve has a break point and the m_t^w value of the break point increases, while the γ value decreases, as X_2^w increases. This can be seen more clearly from Fig. 1(b) which is the magnification of the γ *vs.* m_t^w curve in the neighborhood of the break point in Fig. 1(a). We confirmed the presence of the break by the fact that any extrapolation of the γ *vs.* m_t^w curve from concentrations above the break to zero concentration never gives, even if the experimental error is taken into account, the value for the pure water/air interface.[15] It has been proved thermodynamically that the presence of a break point on the surface tension *vs.* concentration curve means the phase transformation between two states in the adsorbed film.[15–17] Here also we may say that the phase transition takes place in the mixed adsorbed film of DTAC and DeAC.

In Fig. 2, the γ *vs.* X_2^w curves at fixed m_t^w values are illustrated, which are obtained from Fig. 1. It is found that γ increases with X_2^w and some curves have break points which are linked by the dotted line. It will be proved later that the region above and below the dotted line correspond to the gaseous and expanded states, respectively.

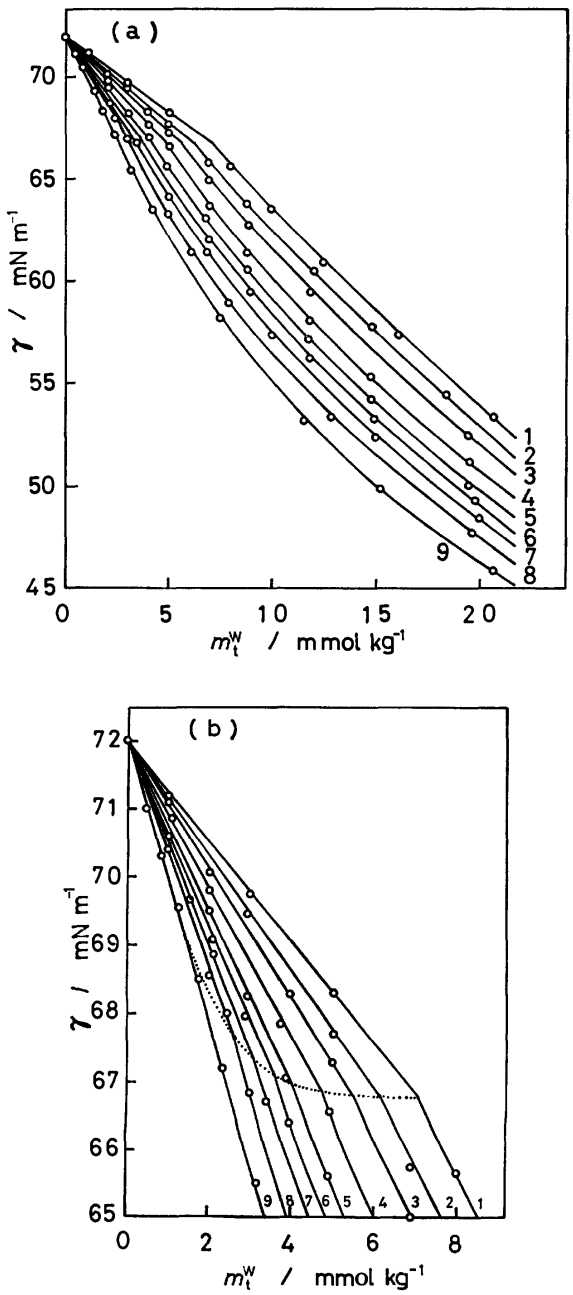

Fig. 1. Surface tension *vs.* total molality curves at constant bulk composition. (1) $X_2^w=1$, (2) 0.950, (3) 0.894, (4) 0.800, (5) 0.697, (6) 0.601, (7) 0.498, (8) 0.300, (9) 0.

Now let us consider the evaluation of the surface excess number of moles per unit area, Γ_i^H, of surfactant i defined with respect to the two dividing planes which are positioned so as to make the surface excess numbers of moles of water and air be zero.[18] Both surfactants in the present study are uni-uni valent strong electrolytes, which have the common anion and dissociate completely into ions. Then the surface tension can be expressed as a function of the total molality m_t^w and the composition X_2^w at constant temperature and pressure as[15]

$$d\gamma = -2RT[(\Gamma_1^H+\Gamma_2^H)/m_t^w]dm_t^w - RT[(X_1^w\Gamma_2^H-X_2^w\Gamma_1^H)/X_1^wX_2^w]dX_2^w. \quad (3)$$

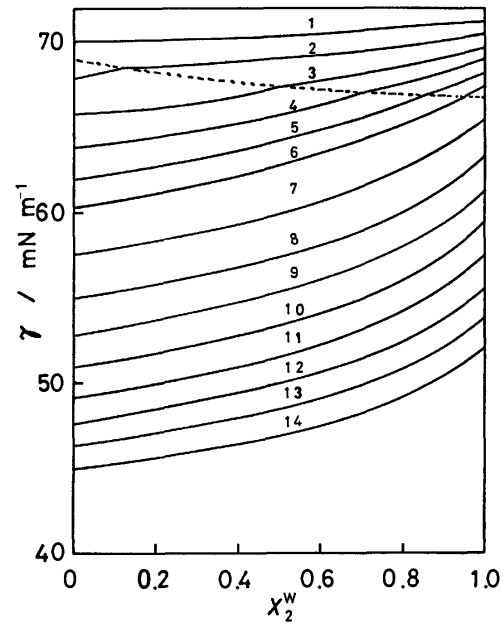

Fig. 2. Surface tension *vs.* bulk composition curves at constant total molality. (1) $m_t^w=1$ mmol kg^{-1}, (2) 2, (3) 3, (4) 4, (5) 5, (6) 6, (7) 8, (8) 10, (9) 12, (10) 14, (11) 16, (12) 18, (13) 20, (14) 22.

Introducing the total surface density Γ_t^H defined by

$$\Gamma_t^H = \Gamma_1^H + \Gamma_2^H, \quad (4)$$

Γ_t^H is found to be related to the change in γ with m_t^w at fixed X_2^w by the expression

$$\Gamma_t^H = -(m_t^w/2RT)(\partial\gamma/\partial m_t^w)_{T,p,X_2^w}, \quad (5)$$

which is derived from Eq. 3. On the other hand, the derivative of γ with respect to X_2^w at constant m_t^w is related to X_2^H in the form

$$X_2^H = X_2^w - (X_1^wX_2^w/RT\Gamma_t^H)(\partial\gamma/\partial X_2^w)_{T,p,m_t^w}, \quad (6)$$

where X_2^H is the composition of DeAC in the adsorbed film defined by

$$X_2^H = \Gamma_2^H/\Gamma_t^H. \quad (7)$$

Combination of Eqs. 5 and 6 gives the values of Γ_1^H and Γ_2^H. Further, Eq. 6 provides information regarding the difference between the compositions of surfactants in the adsorbed film and aqueous solution under the condition that T, p, and m_t^w are kept constant. It is noteworthy that the relation between X_2^H and X_2^w, when T, p, and γ are specified, is given by

$$X_2^H = X_2^w - (2X_1^wX_2^w/m_t^w)(\partial m_t^w/\partial X_2^w)_{T,p,\gamma}. \quad (8)$$

By applying Eq. 5 to the experimental data shown in Fig. 1, the value of Γ_t^H can be evaluated numerically. The Γ_t^H *vs.* m_t^w curves at various X_2^w values are drawn in Fig. 3. It should be noted that the values of Γ_t^H increase monotonously with increase in X_2^w although they change discontinuously at the m_t^w value of the break point in Fig. 1. Taking into account that the values of Γ_t^H at the discontinuous point are similar in magnitude to those of the DAC–DeAC system,[15] we can conclude that the phase transition occurs between a gaseous and an expanded state. It deserves further attention that the difference in the Γ_t^H value

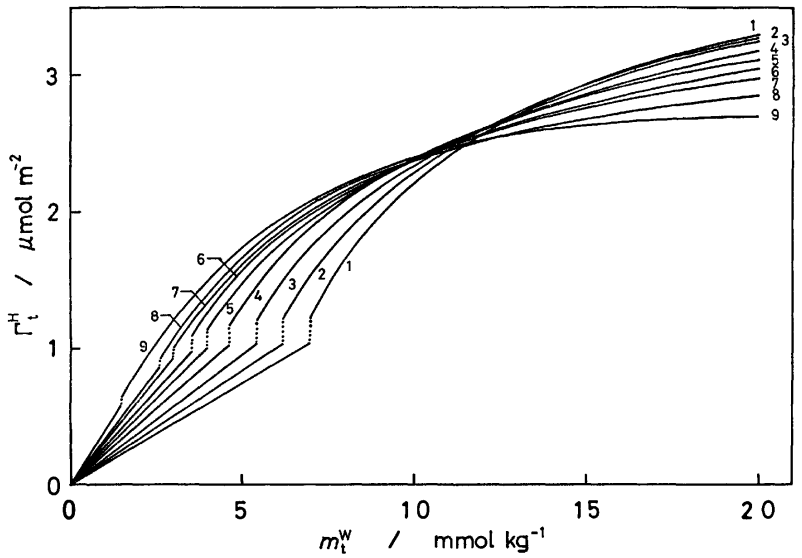

Fig. 3. Total surface density *vs.* total molality curves at constant bulk composition. (1) $X_2^W=1$, (2) 0.950, (3) 0.894, (4) 0.800, (5) 0.697, (6) 0.601, (7) 0.498, (8) 0.300, (9) 0.

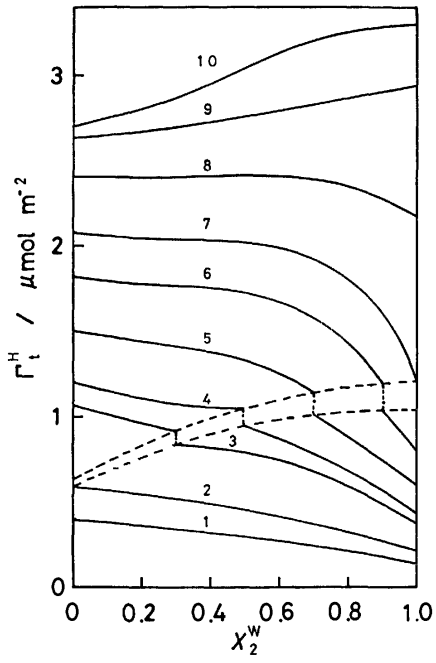

Fig. 4. Total surface density *vs.* bulk composition curves at constant total molality. (1) $m_t^W=1$ mmol kg^{-1}, (2) 1.5, (3) 2.6, (4) 3, (5) 4, (6) 5.45, (7) 7, (8) 10, (9) 15, (10) 20.

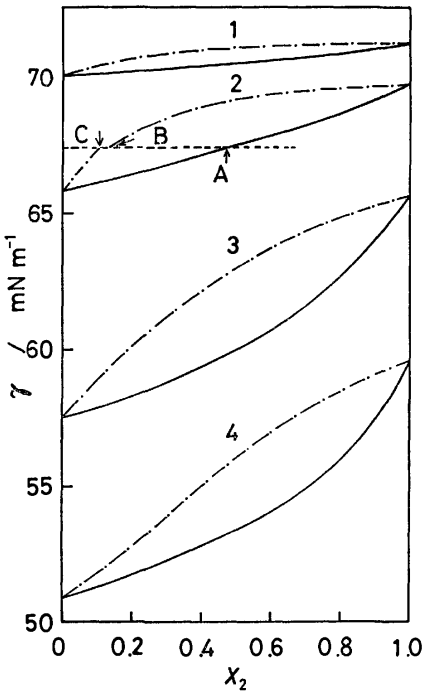

Fig. 5. Surface tension *vs.* composition curves at constant total molality. (1) $m_t^W=1$ mmol kg^{-1}, (2) 3, (3) 8, (4) 14, (——) γ *vs.* X_2^W, (----) γ *vs.* X_2^H.

between the two states becomes large as X_2^W increases.

In Fig. 4, the variation of Γ_t^H with X_2^W is drawn at constant m_t^W. It is seen that the value of Γ_t^H decreases with increasing X_2^W at a smaller value of m_t^W. However, the dependence of Γ_t^H on X_2^W reverses at about 11 mmol kg^{-1} in the expanded film. This observation seems to indicate that the hydrocarbon chain length of the surfactant has a great influence on the adsorption at water/air interface when the value of Γ_t^H is relatively small, but the effect of the size of ionic head group of DTAC becomes predominant as the value of Γ_t^H increases.

Next let us evaluate the composition of surfactants in the adsorbed film at given T, p, and m_t^W. Applying Eq. 6 to the γ *vs.* X_2^W curve shown in Fig. 2, the value of X_2^H can be calculated as a function of X_2^W. In Fig. 5, the results are illustrated in the form of the γ *vs.* X_2^H as well as the corresponding γ *vs.* X_2^W curve at various m_t^W values. We can read the relation between X_2^H and X_2^W at a given value of γ from the diagram indicated by 1 in the gaseous film and from the diagrams 3 and 4 in the expanded film. They are similar

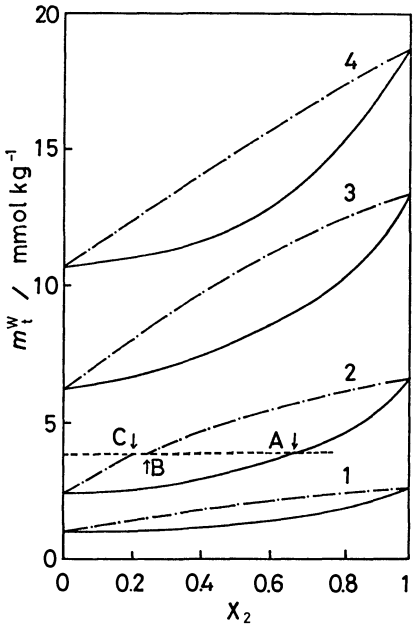

Fig. 6. Total molality *vs.* composition curves at constant surface tension. (1) $\gamma=70$ mN m^{-1}, (2) 67, (3) 60, (4) 55, (——) m_t^W *vs.* X_2^W, (– – –) m_t^W *vs.* X_2^H.

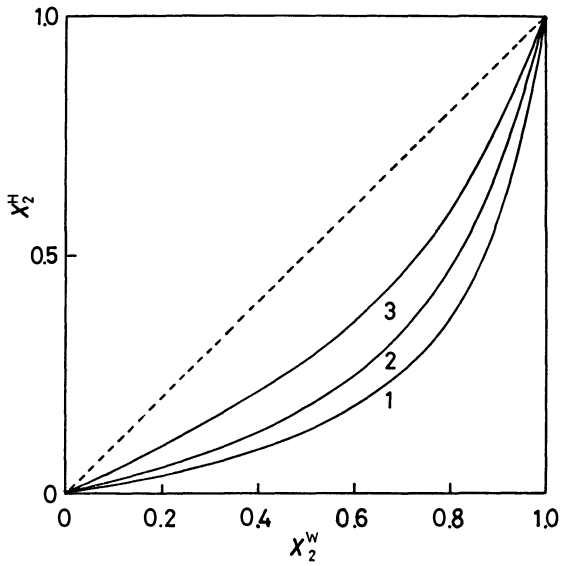

Fig. 7. Surface composition *vs.* bulk composition curves at constant surface tension. (1) $\gamma=70$ mN m^{-1}, (2) 60, (3) 50.

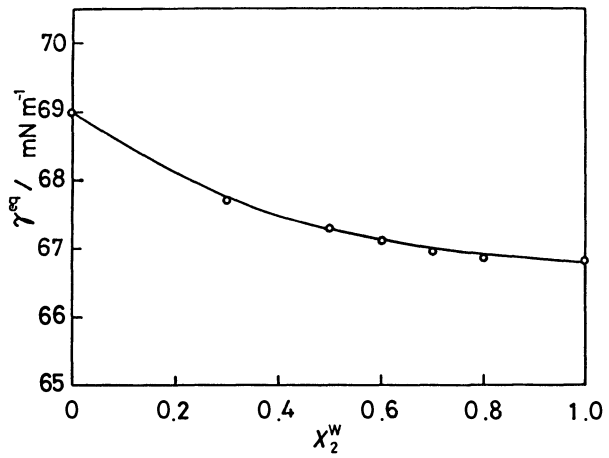

Fig. 8. Equilibrium surface tension *vs.* bulk composition curve.

in form to each other although the former takes the shape of a deflated cigar and the latters of a swollen cigar. However the diagram is slightly complex when the phase transition takes place in the adsorbed film. At $m_t^W=3$ mmol kg^{-1} (the diagram 2), the γ *vs.* X_2^W curve breaks at the point A and the γ *vs.* X_2^H curve changes discontinuously from the point B of the gaseous film to the point C of the expanded film. It should be noted that the alteration in the slope at A is related closely to the difference between the X_2^H values of B and C.

Further the value of X_2^H at constant T, p, and γ can be calculated by use of Eq. 8. The m_t^W *vs.* X_2^H and m_t^W *vs.* X_2^W are shown in Fig. 6. It is seen that the essential form of the diagram is quite similar to that in Fig. 5. It is important to note that the diagram 2, like the diagram 2 in Fig. 5, has a break point on the m_t^W *vs.* X_2^W curve and a discontinuous change on the m_t^W *vs.* X_2^H curve.

An interesting feature is manifested by plotting the value of X_2^H against X_2^W. The results at constant γ is illustrated in Fig. 7. We can see that the curve recedes from the diagonal line as the surface tension increases, *i.e.*, the difference between the compositions in the bulk phase and in the adsorbed film becomes large as the surface tension increases. This observation coincides with our previous result of the mixed system of DAC and DeAC.[15] Taking into account that DTAC and DAC are more surface active than DeAC, these facts indicate that the fraction of the more surface active molecule in the adsorbed film is enhanced remarkably at a larger value of γ.

Next, we shall elucidate the mutual relation between the compositions of the gaseous and expanded films at the phase transition point in connection with the two-dimensional phase diagram. When the two phases coexist in equilibrium, $X_2^{H,g}$ and $X_2^{H,e}$ are related to the equilibrium surface tension γ^{eq} by the expression

$$X_2^{H,g}-X_2^{H,e}=[X_1^W X_2^W(1/\Gamma_t^{H,e}-1/\Gamma_t^{H,g})/RT] \times(\partial\gamma^{eq}/\partial X_2^W)_{T,p}. \quad (9)$$

It is important to recognize that the variation in γ^{eq} with X_2^W, which is illustrated in Fig. 8, is determined by the difference $X_2^{H,g}-X_2^{H,e}$. By virtue of the diagram 2 in Fig. 5 and analogues, attended by the phase transition, we can obtain the γ^{eq} *vs.* $X_2^{H,g}$ and γ^{eq} *vs.* $X_2^{H,e}$ curves which are drawn in Fig. 9. It was found that the numerical value of $X_2^{H,g}-X_2^{H,e}$ calculated by applying Eq. 9 to the curve in Fig. 8 is approximately equal to the corresponding one in Fig. 9. This fact thermodynamically proves that the phase transition does take place at the break point on the γ *vs.* m_t^W curves.

It is seen in Fig. 9 that the value of $X_2^{H,e}$ is smaller than that of $X_2^{H,g}$. This means that the fraction of the more surface active component in the expanded film is larger than that in the gaseous film. A similar

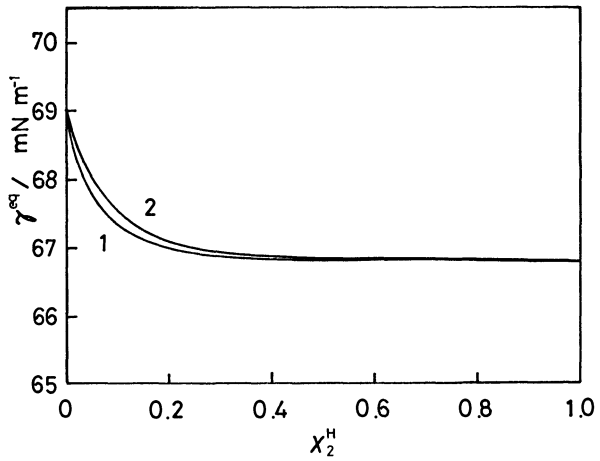

Fig. 9. Equilibrium surface tension *vs.* surface composition curves. (1) γ^{eq} *vs.* $X_2^{H,e}$, (2) γ^{eq} *vs.* $X_2^{H,g}$.

result has been obtained for the mixed adsorbed film of DAC and DeAC.[15] It is important to note that such a behavior has been observed in the case of mixed insoluble films on water if their equilibrium surface pressure *vs.* composition curves have no extremum.[19] Therefore, Fig. 9 is the two-dimensional phase diagram of the transition between the gaseous and expanded states of DTAC–DeAC mixed adsorbed film at 298.15 K under atmospheric pressure. It may be concluded that the phase transition in the mixed adsorbed film is described by the phase diagram like that in the mixed insoluble monolayer.

References

1) E. Huchinson, *J. Colloid Sci.*, **3**, 413 (1948).
2) K. Tajima, *Bull. Chem. Soc. Jpn.*, **44**, 1767 (1971).
3) E. H. Lucassen-Reynders, *J. Colloid Interface Sci.*, **41**, 156 (1972).
4) S. Ikeda, *Bull. Chem. Soc. Jpn.*, **50**, 1403 (1977).
5) A. Nakamura and M. Muramatsu, *J. Colloid Interface Sci.*, **62**, 165 (1977).
6) K. Tajima, A. Nakamura, and T. Tsutsui, *Bull. Chem. Soc. Jpn.*, **52**, 2060 (1979)
7) D. Góralczyk, *J. Colloid Interface Sci.*, **77**, 68 (1980).
8) E. H. Lucassen-Reynders, J. Lucassen, and D. Giles, *J. Colloid Interface Sci.*, **81**, 150 (1981).
9) E. H. Lucassen-Reynders, *J. Colloid Interface Sci.*, **85**, 178 (1982).
10) H. J. Schwuger, *Kolloid Z. Z. Polym.* **243**, 129 (1971).
11) H. Lange and K.-H. Beck, *Kolloid Z. Z. Polym.*, **251**, 424 (1973).
12) J. H. Clint, *J. Chem. Soc., Faraday Trans. 1*, **71**, 1327 (1975).
13) N. Funasaki and S. Hada, *Bull. Chem. Soc. Jpn.*, **49**, 2899 (1976).
14) B. T. Ingram and A. H. W. Luckhurst, *Surf. Act. Agents, SCI Symp. (Nottingham)*, **1979**, 89.
15) M. Aratono, S. Uryu, Y. Hayami, K. Motomura, and R. Matuura, *J. Colloid Interface Sci.*, **93**, 162 (1983).
16) K. Motomura, S. Iwanaga, Y. Hayami, S. Uryu, and R. Matuura, *J. Colloid Interface Sci.*, **80**, 32 (1981).
17) M. Aratono, S. Uryu, Y. Hayami, K. Motomura, and R. Matuura, *J. Colloid Interface Sci.*, in press.
18) K. Motomura, *J. Colloid Interface Sci.*, **64**, 348 (1978).
19) K. Motomura, *Adv. Colloid Interface Sci.*, **12**, 1 (1980).

Conformational Analysis of Terphenyls by Photoelectron Spectroscopy

Tsunetoshi KOBAYASHI

The Institute of Physical and Chemical Research, Wako, Saitama 351

The Institute for Solid State Physics, The University of Tokyo, Roppongi, Minato-ku, Tokyo 106

(Received April 21, 1983)

Vapor phase HeI photoelectron spectra of *o*- and *m*-terphenyl were measured, and conformational analysis of biphenyl, *o*-, *m*-, and *p*-terphenyl was made by comparing the observed photoelectron spectral patterns with the calculated ones by the CNDO/S method, the inter-ring twist angles in these compounds being estimated to be around 40°, 60°, 40°, and 40°, respectively. The result that the inter-ring twist angles in *o*-terphenyl are far smaller than 90° is completely in contrast to the long believed perpendicular model of *o*-terphenyl suggested by the gas electron diffraction study.

Concerning experimental studies of molecular conformations of terphenyls in the vapor phases, there has been only one research about *o*-terphenyl by Karle and Brockway[1] so far as we know. They studied the molecular structure of *o*-terphenyl by the gas electron diffraction (ED) method, concluding that the inter-ring twist angles θ about the apparently single CC bonds are 90°, and this result has long been believed. However, if their result be correct, it will be unusually interesting because in the case of (*Z*)-stilbene, which is structurally close to *o*-terphenyl, the two phenyl rings are twisted by only 43.2° from the central olefinic group plane according to the recent gas ED study.[2]

In this paper we study the conformation of *o*-terphenyl in the vapor phase from the standpoint of photoelectron (PE) spectroscopy to see if Karle and Brockway's result is reasonable. At the same time *m*- and *p*-terphenyl, the conformations of which have not been studied in the vapor phase as yet, are also treated here. This study forms a part of our program to investigate molecular conformations by PE spectroscopy,[3] and may present a typical example of the conformational analysis of rather large free molecules by PE spectroscopy.

Concerning the PE spectra of terphenyls, Dewar and Goodman[4] reported formerly the ionization energy (IE) values of *o*-, *m*-, and *p*-terphenyl with a low resolution instrument, and Hino *et al.*,[5] the PE spectrum of *p*-terphenyl by a high resolutior. instrument.

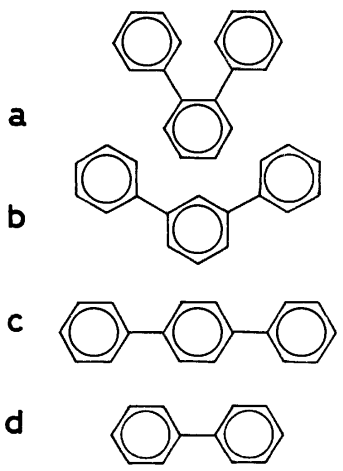

Fig. 1. Structural formulae of (a) *o*-, (b) *m*-, (c) *p*-terphenyl, and (d) biphenyl.

Experimental

Materials. Commercially available *o*- and *m*-terphenyl were recrystallized from methanol and ethanol, respectively, just before use.

Spectroscopic Measurements. Vapor phase HeI PE spectra of *o*- and *m*-terphenyl were measured with the PE spectrometer described formerly.[6] The sample inlet and target chamber systems were heated and kept at 104° for *o*-terphenyl and 105° for *m*-terphenyl by circulating hot silicone oil. Xe gas was used as the internal reference for the calibrations of the energy scale.

Computational

CNDO/S[7] calculations of biphenyl, *o*-, *m*-, and *p*-terphenyl were carried out on a FACOM 230-75 computer at the Institute of Physical and Chemical Research. All the atomic integral and parameter values necessary for the CNDO/S calculations were taken from or estimated according to Ref. 7.

In the calculations, all the benzene rings of the compounds treated here were assumed to be regular hexagons. In the case of biphenyl, the inter-ring CC single bond length was taken to be 1.489 Å and the CC bond lengths of the benzene rings, 1.396 Å according to the gas ED study.[8] All the CH bond lengths of biphenyl were assumed to be 1.0845 Å based on the gas ED data of benzene.[9]

Concerning *o*-terphenyl, Aikawa *et al.*[10] reported the molecular structural data in the crystalline state by X-ray diffraction (XD) and Brown and Levy,[11] by neutron diffraction (ND). In the present calculations, we used the averaged CC and CH bond lengths based on the data by ND, that is, the inter-ring CC bond lengths were assumed to be 1.487 Å, the benzene ring CC bond lengths, 1.390 Å, and the CH bond lengths, 1.090 Å.

In the calculations of *m*- and *p*-terphenyl, the CC and CH bond length values were assumed to be the same as those used in the calculations of biphenyl.

The CNDO/S calculations were carried out for various conformations of biphenyl and the terphenyls, the θ values being changed at intervals of 15° mostly. In the calculations the two phenyl rings in each terphenyl were twisted by the same angle.

Results and Discussion

Photoelectron Spectra. The PE spectra of *o*- and *m*-terphenyl are shown in Fig. 2 and the vertical IEs of these compounds obtained from these spectra are summarized in Table 1 with those of the related compounds.[5,12–15] The high resolution PE spectrum of

Table 1. Vertical ionization energies (E_{iv}) of terphenyls and related compounds

Compound	E_{iv}/eV					
o-Terphenyl	8.20	8.7	9.1[a]	9.5[a]	10.9	
m-Terphenyl	8.14	8.5	9.10	9.6	9.8	11.0
p-Terphenyl[b]	8.20	9.17	10.10	11.2		
Biphenyl[c]	8.32	9.05	9.15	9.80	11.20	
Toluene[d]	8.85	9.34	11.43			
o-Xylene[e]	8.57	9.10	11.18			
m-Xylene[f]	8.55	9.03				
p-Xylene[f]	8.43	9.14				

a) An apparent band maximum. b) Ref. 5. c) Ref. 12. d) Ref. 13. e) Ref. 14. f) Ref. 15.

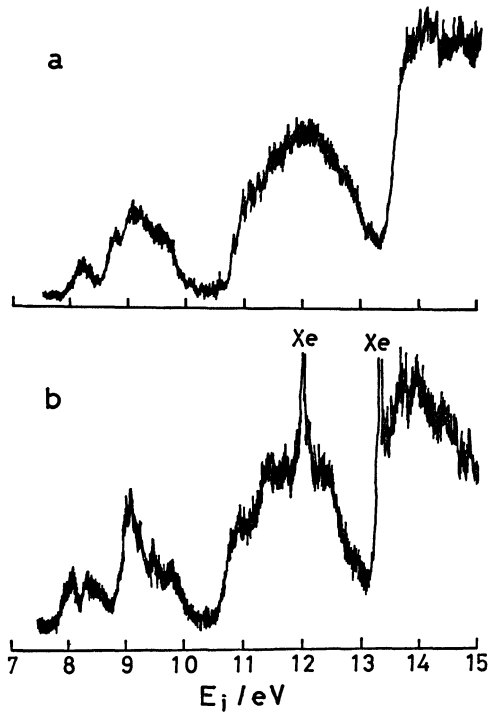

Fig. 2. Vapor phase HeI photoelectron spectra of (a) *o*-terphenyl and (b) *m*-terphenyl.

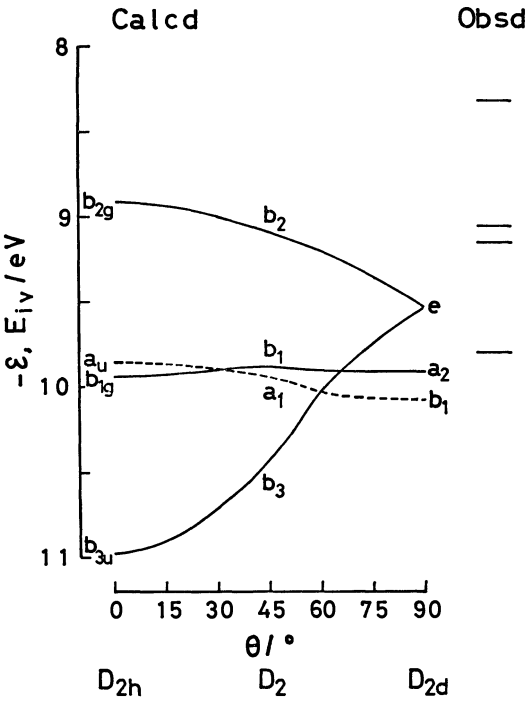

Fig. 3. Calculated orbital energy (ε) diagram with observed vertical ionization energies (E_{iv}) of biphenyl. The *z*-axis was taken along the long molecular axis.

p-terphenyl was formerly reported by Hino and coworkers.[5] In contrast to the simple pattern of the lower IE part of the PE spectrum of *p*-terphenyl, the lower energy part of the PE spectrum of *o*-terphenyl is highly complicated and the spectrum of *m*-terphenyl is regarded to be the intermediate case. Now we use these PE spectral patterns for the conformational analysis of the terphenyls by comparing the spectral patterns calculated by the CNDO/S method.

Conformational Analysis. Biphenyl: At first we examine the validity of the PE spectroscopic method for conformational analysis, which we are now going to use, in the case of biphenyl, as this compound is structurally very close to the terphenyls. The θ value of biphenyl in the vapor phase is $(41.6\pm2)°$ according to the gas ED study,[8] while this compound is essentially planar in the solid state.[16]

The PE spectrum of biphenyl shows four bands in the IE region from 7.5 eV to 10.5 eV, the second and third bands overlapping highly with each other, and these four bands correspond to the ionizations from the four HO-π-MOs formed by the interactions between the totally four e_{1g}-like π orbitals of the two benzene rings mainly.[12]

In Fig. 3 is shown the orbital energy diagram calculated by the CNDO/S method with the observed vertical IEs of biphenyl. If we compare the vertical IE difference between the first and fourth PE spectral bands with the calculated energy difference between the first and fourth HO-π-MOs, we get 39.3° as the estimated θ value for biphenyl in the vapor. This estimated θ value coincides almost perfectly with the observed one in the vapor by the ED method,[8] that is, in the case of biphenyl the calculated energy difference between the first and fourth HO-π-MOs can directly be compared with the observed splitting between the corresponding PE bands without any corrections in order to estimate the θ value. The similar situation was experienced also in the case of stilbenes[3d] closely related to terphenyls.

Concerning the absolute values of the first four IEs of biphenyl, the CNDO/S calculation for $\theta=39.3°$

predicts the IE values slightly higher (by *ca.* 0.8 eV) than the observed ones commonly, if we assume the validity of the Koopmans theorem,[17] though the intervals between the four bands are well predicted by the calculation.

The vertical IEs of the perpendicular type conformer of biphenyl with $\theta=90°$ are estimated to be 9.534 eV for the first e band, 9.906 eV for the second a_2 band, and 10.082 eV for the third b_1 band by using the CNDO/S orbital energies on the basis of the Koopmans theorem. The predicted splitting of the second and third bands of this conformer is due to a spiroconjugation.[18] By using the first two vertical IEs of toluene,[13] the e band IE of the perpendicular conformer is estimated to be 8.85 eV and the a_2 and b_1 band IEs, 9.34 eV, the spiroconjugation being neglected. That is, in the case of the perpendicular conformer also, the calculation seems to predict slightly higher (by 0.7 eV) IEs, but the difference between the first IE and the averaged IE of the second and third bands predicted by the CNDO/S calculation is 0.46 eV and this value is very close to the estimated one by using the experimental IEs of toluene, 0.49 eV. So far as the IE difference or orbital energy differences are concerned, the calculated orbital energy diagram seems to be realistic over a wide range of θ in the case of biphenyl.

As terphenyls are structurally close to biphenyl and stilbenes, now we may safely apply the same method as used for biphenyl to evaluate the θ values in the terphenyls.

p-*Terphenyl*: At first let us treat the simplest case, *p*-terphenyl. The PE spectrum of *p*-terphenyl shows three bands in the IE region from 7.5 eV to 10.5 eV with the intensity ratio 1:4:1.[5] Similarly to the case of biphenyl, in this energy region totally six bands are expected to appear, corresponding to the six HO-π-MOs formed by the interactions between the six e_{1g}-like π orbitals of the three benzene rings mainly. Therefore, the first and third bands are regarded to correspond to the ionizations from the first and sixth HO-π-MOs, respectively, judging from the above intensity ratio.[5]

In Fig. 4 is shown the orbital energy diagram for the D_{2h} and C_{2h} conformers calculated by the CNDO/S method with the observed vertical IEs[5] for *p*-terphenyl. The energy diagram for the D_{2h} and D_2 conformers is also similar to Fig. 4. By comparing the observed splitting between the first and apparently third PE spectral bands with the energy difference between the first and sixth HO-π-MOs just as in the case of biphenyl, we get 43° as the θ values of *p*-terphenyl if we assume the C_{2h} conformer and 42°, the D_2 conformer. That is, *p*-terphenyl is twisted in the vapor as biphenyl in the vapor, though the θ values of *p*-terphenyl were observed to be 0.4° in the room-temperature stable monoclinic crystal (space group, $P2_1/a$) by the XD and ND methods,[19a] and 15.2°, 18.2°, 23.4°, and 26.8° in the low-temperature stable crystal (space group, $P\bar{1}$) by XD.[19b]

Suzuki[20] estimated the θ values of *p*-terphenyl in solution by the HMO level consideration using the

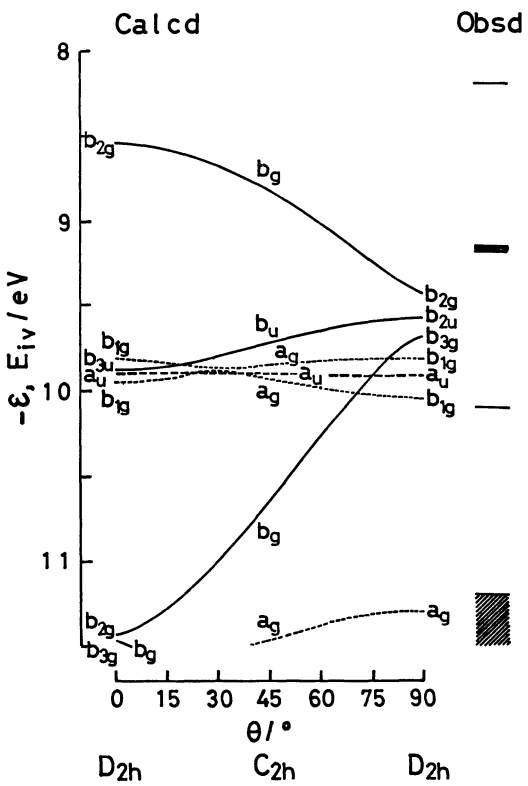

Fig. 4. Calculated orbital energy (ε) diagram with observed vertical ionization energies (E_{iv}) of *p*-terphenyl. The calculated results shown are for the D_{2h} and C_{2h} conformers. The *z*-axis was taken along the long molecular axis.

electronic absorption spectra and got 9.5—12.5°. These values do not seem to contradict ours, if we note the point that in the case of biphenyl the θ value was estimated to be 40—43° for the vapor phase and 19—26° for the solution phase by his method.[21] If we estimate the θ value ranges of biphenyl and *p*-terphenyl by using the van der Waals radii,[22] we get the result, $\theta\geq43°$. The value 43° is very close to the observed θ value of biphenyl in the vapor and those of *p*-terphenyl estimated just now. The reasonable result obtained here for *p*-terphenyl strongly supports the validity of the extended application of the method of conformational analysis tested in the case of biphenyl to the case of terphenyls.

The first and third PE spectral bands of *p*-terphenyl with the twist angles around 43° are ascribed to the ionizations from the two π orbitals delocalized completely over the entire carbon framework. In the case of *p*-terphenyl also the CNDO/S calculations predict the first six IE values slightly higher (by 0.6—0.8 eV) than the observed ones, though the intervals between the calculated ones are reasonable.

m-*Terphenyl*: Now we move to the slightly more complicated case, *m*-terphenyl. In this case, the PE spectrum shows apparently five bands in the energy region from 7.5 eV to 10.5 eV, the third band being stronger than the others. As in this energy region totally six PE spectral bands are expected to appear in the case of *m*-terphenyl also as in the case of *p*-terphenyl, the third band is regarded to be composed

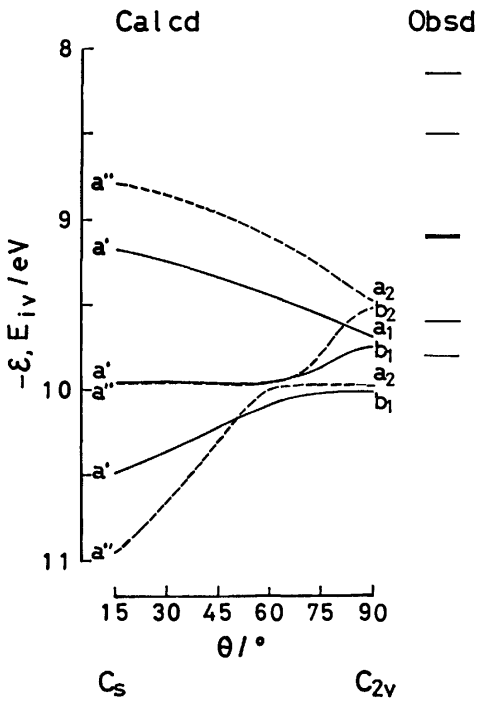

Fig. 5. Calculated orbital energy (ε) diagram with observed vertical ionization energies (E_{iv}) of *m*-terphenyl. The calculated results shown are for the C_{2v} and C_s conformers.

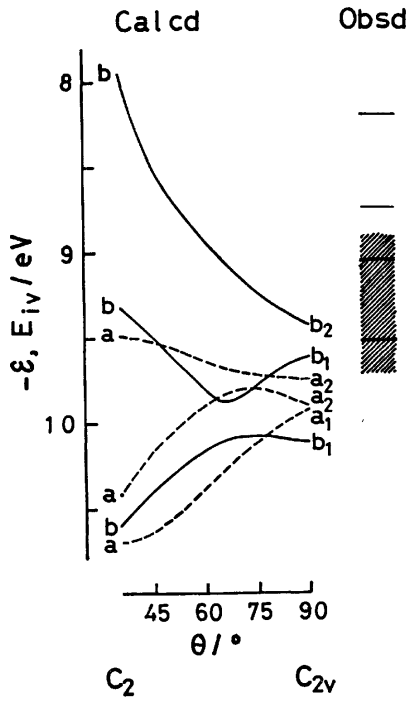

Fig. 6. Calculated orbital energy (ε) diagram with observed vertical ionization energies (E_{iv}) of *o*-terphenyl. The calculated results shown are for the C_{2v} and C_2 conformers.

of two bands overlapping highly with one another.

In Fig. 5 is shown the orbital energy diagram for the C_{2v} and C_s conformers calculated by the CNDO/S method with the observed vertical IEs for *m*-terphenyl. Just as in the case of *p*-terphenyl, by comparing the observed energy splitting between the first and apparently fifth PE spectral bands with the energy difference between the first and sixth HO-π-MOs calculated by the CNDO/S method, we get 35° as the θ values of *m*-terphenyl on the assumption of the C_s conformer and 38°, the C_2 conformer.

The θ value ranges for *m*-terphenyl are estimated to be $\theta \geq 43°$ by using the van der Waals radii,[22] and this value 43° is rather close to those estimated from the PE spectrum here. There have been no gas phase structural data about *m*-terphenyl, but the θ values of 1,3,5-triphenylbenzene closely related to *m*-terphenyl are (46±5)° according to the gas ED study by Bastiansen.[23] According to the XD study by Farag[24] the θ values of 1,3,5-triphenylbenzene are (34±2)°, (−27±2)°, and (24±2)° in the solid state. Recently Busing[25] estimated the θ values in an isolated 1,3,5-triphenylbenzene molecule to be 43.6° using the intramolecular potential function empirically determined from the crystalline data. These literature values for 1,3,5-triphenylbenzene are all consistent with our result for *m*-terphenyl by the PE spectroscopic method.

The calculated orbital sequence of the six HO-π-MOs of *m*-terphenyl is the same as that predicted by the simple HMO model around the twist angles estimated here. The first, second, fifth, and sixth HO-π-MOs are delocalized over the three benzene rings, the third and fourth ones being localized on the two *m*-phenyl groups. The CNDO/S calculations predict IEs slightly higher (by 0.7—0.9 eV) than the observed vertical ones for the first six IEs in the case of *m*-terphenyl also, but the calculated intervals between these six IEs are reasonable. Now the first apparently five bands of *m*-terphenyl are assigned to the a″ (a), a′ (b), overlapping a′ (b) and a″ (a), a′ (b), and a″ (a) bands from the top, respectively, for the C_s (C_2) conformer, the apparently third band being ascribed to the two highly overlapping bands.

o-Terphenyl: Now we may safely be able to treat our primary object, *o*-terphenyl, the most complicated one of the three terphenyls. The PE spectrum of *o*-terphenyl shows apparently four band maxima in the energy region from 7.5 eV to 10.5 eV. The first band is isolated from the following band group, their intensity ratio being approximately 1:5. As in this energy region totally six π bands are expected to appear in the case of *o*-terphenyl also just as in the case of *m*- and *p*-terphenyl, the first band is reasonably ascribed to the ionization from only the first HO-π-MO. As the 8.7 eV peak is also weak relative to the 9.1 and 9.5 eV apparent band maxima, the 8.7 eV peak may correspond to one ionization band, and each of the following two apparent strong band maxima may correspond to two overlapping bands. Keeping these points in mind let us carry out the conformational analysis of *o*-terphenyl.

In Fig. 6 is shown the orbital energy diagram calculated by the CNDO/S method for the C_{2v} and C_2 conformers of *o*-terphenyl with the observed vertical IEs. By comparing the observed energy difference between the first and the apparently fourth PE spectral bands with the calculated energy difference between

the first and sixth HO-π-MOs, we get 63° as the θ values of *o*-terphenyl on the assumption of the C_2 conformer and 66°, the C_s conformer. The θ value ranges estimated from the van der Waals radii are $\theta \geq 63°$ for the C_2 conformer and $\theta \geq 80°$ for the C_s conformer of *o*-terphenyl, and, therefore, we regard 63° for the C_2 conformer as the most probable θ values of *o*-terphenyl. These values are far from 90° determined by the gas ED method formerly,[1] and rather very close to those observed by the XD[10] and ND[11] methods for the solid states.

Suzuki estimated the θ values of *o*-terphenyl in solution as 42.5—43° by the electronic absorption spectroscopic method,[20] and these values do not contradict ours, if we remember the results for biphenyl mentioned just before in the discussion of *p*-terphenyl. Busing estimated the θ values in an isolated *o*-terphenyl molecule as 54.3° by the intramolecular potential function method.[25] These values are close to ours.

From the discussion given above, the θ values in *o*-terphenyl are around 60° in the vapor phase and at least far from 90°.

The calculated spectral pattern of *o*-terphenyl for the C_2 conformer around $\theta=63°$ based on the Koopmans theorem[17] reproduces well the overall feature of the observed one though the former is slightly shifted (by 0.6—0.9 eV) to the higher IE side relative to the latter. The orbital sequence of the fifth and sixth HOMOs predicted by the CNDO/S method is reversed to that predicted by the simple HMO model. In the case of *o*-terphenyl as in the case of (*Z*)-stilbene[26] the overlap integrals between the two twisted *o*-phenyl ring group π orbitals are not negligible and through-space orbital interactions between these orbitals, which are taken into account in the CNDO calculations automatically, may influence the orbital orderings. However, further detailed discussions about the orbital orderings of *o*-terphenyl are hindered by the highly overlapping nature of the PE spectral bands. Now the first apparently three bands of *o*-terphenyl are ascribed from the top, respectively, to the b, a, and overlapping b and a bands followed by the overlapping b and a bands corresponding to the fourth apparent band maximum for the C_2 conformer.

Summary of θ Values by Various Methods. Finally the θ values in the terphenyls and related compounds given by various methods for various phases are summarized in Table 2 for the sake of comparison. Le Fèvre *et al.*[27] estimated the θ values of the terphenyls and 1,3,5-triphenylbenzene in solution phases based on the molecular polarizability data or molar Kerr constants as given in Table 2. Their results are qualitatively consistent with ours. Recently Wakayama[28] estimated the θ values of *p*-terphenyl in solution at 77 K to be larger than 16° from its $S_1 \leftarrow S_0$ absorption in solution compared with that of crystalline state at 77 K on the basis of the XD data by Baudour *et al.*[19b] Theoretically Gamba *et al.*[29,30] calculated the θ values of biphenyl and the terphenyls by the molecules-in-molecule method by taking into account the non-bonded interactions, and their theoretical values are consistent with our present results.

TABLE 2. INTER-RING TWIST ANGLES(θ) IN TERPHENYLS AND RELATED COMPOUNDS

Compound	θ/°									
	PES[a]	EAS[b]		ED[c]	XD[d]	ND[e]	MP[f]	IMP[g]	MIM[h]	VDWR[i]
	(gas)	(gas)	(solution)	(gas)	(solid)	(solid)	(solution)	(free molecule)		
o-Terphenyl	63(C_2) 66(C_s)		42.5—43[k]	90[l]	42.5[o] 62.1	42.1[t] 62.1	55(C_2)	54.3	55[u]	≥63(C_2) ≥80(C_s)
m-Terphenyl	38(C_2) 35(C_s)						20		37[u]	≥43
p-Terphenyl	42(D_2) 43(C_{2h})		9.5—12.5[k]		15.2[q] 18.2 23.4 26.8	0.4[p]	20		37[u]	≥43
Biphenyl	39.3	40—43[j]	19—26[j]	41.6±2[m]	0[r]				40[v]	≥43
1,3,5-Triphenyl-benzene				46±5[n]	34±2[s] −27±2 24±2		38	43.6		≥43

a) This work by gas phase Hel photoelectron spectroscopy combined with CNDO/S calculations. Assumed molecular symmetries are given in parentheses after θ values. The error ranges for θ values are estimated to be several degrees from the result for biphenyl. b) Electronic absorption spectra treated on the HMO level. c) Gas electron diffraction. d) X-ray diffraction. e) Neutron diffraction. f) Molecular polarizability approach based on molar Kerr constants, Ref. 27. g) Empirical intramolecular potential function approach, Ref. 25. h) Molecules-in-molecule approach taking into account non-bonded interactions. i) This work using the van der Waals radii. j) Ref. 21. k) Ref. 20. l) Ref. 1. m) Ref. 8. n) Ref. 23. o) Ref. 10. p) At room temperature, Ref. 19a. q) At 113 K, Ref. 19b. r) Ref. 16. s) Ref. 24. t) Ref. 11. u) Ref. 29. v) Ref. 30.

Conclusion

Summing up the discussion given above it is concluded that *o*-terphenyl is more twisted than biphenyl, *m*- and *p*-terphenyl, but the inter-ring twist angles in *o*-terphenyl are around 60° and far from 90° in the vapor phase in contrast to the former gas ED result. It has been demonstrated that PE spectroscopy is very useful for the conformational analysis of rather large molecules in the vapor phase to which the other methods such as the gas ED method and the microwave spectroscopic method are not so easy to be applied.

The author thanks Professor Y. Maruyama of Ochanomizu University for his interest in this work.

References

1) I. L. Karle and L. O. Brockway, *J. Am. Chem. Soc.*, **66**, 1974 (1944).
2) M. Trætteberg and E. B. Frantsen, *J. Mol. Struct.*, **26**, 69 (1975).
3) a) R. Nakagaki, T. Kobayashi, and S. Nagakura, *Bull. Chem. Soc. Jpn.*, **53**, 901 (1980). b) R. Akaba, K. Tokumaru, T. Kobayashi, and C. Utsunomiya, *ibid.*, **53**, 2002 (1980); see also: R. Akaba, K. Tokumaru, and T. Kobayashi, *ibid.*, **53**, 1993 (1980). c) T. Kobayashi, T. Arai, H. Sakuragi, K. Tokumaru, and C. Utsunomiya, *ibid.*, **54**, 1658 (1981). d) T. Kobayashi, H. Suzuki, and K. Ogawa, *ibid.*, **55**, 1734 (1982).
4) M. J. S. Dewar and D. W. Goodman, *J. Chem. Soc., Faraday Trans. 2*, **68**, 1784 (1972).
5) S. Hino, K. Seki, and H. Inokuchi, *Chem. Phys. Lett.*, **36**, 335 (1975).
6) T. Kobayashi, K. Yokota, and S. Nagakura, *J. Electron Spectrosc. Relat. Phenom.*, **2**, 449 (1973).
7) R. L. Ellis, G. Kuehnlenz, and H. H. Jaffé, *Theor. Chim. Acta*, **26**, 131 (1972).
8) A. Almenningen and O. Bastiansen, *Det Kgl. Norsk. Vidensk. Selsk. Skrift.*, No. 4, 1 (1958).
9) "Handbook of Pure Chemistry," Revised 2nd ed, ed by the Chemical Society of Japan, Maruzen, Tokyo (1975), Part 2, p. 1399.
10) S. Aikawa, Y. Maruyama, Y. Ohashi, and Y. Sasada, *Acta Crystallogr., Sect. B*, **34**, 2901 (1978).
11) G. M. Brown and H. A. Levy, *Acta Crystallogr., Sect. B*, **35**, 785 (1979).
12) J. P. Mayer and D. W. Turner, *Faraday Discuss. Chem. Soc.*, No. 54, 149 (1972).
13) T. Kobayashi and S. Nagakura, *Bull. Chem. Soc. Jpn.*, **47**, 2563 (1974).
14) F. Brogli, E. Giovannini, E. Heilbronner, and R. Schurter, *Chem. Ber.*, **106**, 961 (1973).
15) T. Koenig, M. Tuttle, and R. A. Wielesek, *Tetrahedron Lett.*, **1974**, 2537.
16) a) J. Trotter, *Acta Crystallogr.*, **14**, 1135 (1961). b) A. Hargreaves and S. H. Rizvi, *ibid.*, **15**, 365 (1962).
17) T. Koopmans, *Physica*, **1**, 104 (1934).
18) A. Imamura and R. Hoffmann, *J. Am. Chem. Soc.*, **90**, 5379 (1968).
19) a) H. M. Rietveld, E. N. Maslen, and C. J. B. Clews, *Acta Crystallogr., Sect. B*, **26**, 693 (1970). b) J. L. Baudour, Y. Delugeard, and H. Cailleau, *ibid.*, **32**, 150 (1976).
20) H. Suzuki, *Bull. Chem. Soc. Jpn.*, **33**, 109 (1960).
21) H. Suzuki, *Bull. Chem. Soc. Jpn.*, **32**, 1340 (1959).
22) L. Pauling, "The Nature of the Chemical Bond," 3rd ed, Cornell University Press, Ithaca, NY (1960), p. 260.
23) O. Bastiansen, *Acta Chem. Scand.*, **6**, 205 (1952).
24) M. S. Farag, *Acta Crystallogr.*, **7**, 117 (1954).
25) W. R. Busing, *J. Am. Chem. Soc.*, **104**, 4829 (1982).
26) T. Kobayashi, K. Yokota, and S. Nagakura, *Bull. Chem. Soc. Jpn.*, **48**, 412 (1975).
27) R. J. W. Le Fèvre, A. Sundaram, and K. M. S. Sundaram, *J. Chem. Soc.*, **1963**, 3180.
28) N. I. Wakayama, *Chem. Phys. Lett.*, **70**, 397 (1980).
29) A. Gamba, G. F. Tantardini, and M. Simonetta, *Theor. Chim. Acta*, **29**, 335 (1973).
30) A. Gamba, G. F. Tantardini, and M. Simonetta, *Spectrochim. Acta, Part A*, **28**, 1877 (1972).

Liquid Crystal Formation in Binary Systems. VIII.[1] Induction of Smectic Phases by the Addition of 4-Alkoxynitrobenzene or 4-Alkoxybenzonitrile to *N*-(4-Propoxybenzylidene)-4-hexylaniline

Eiji CHINO and Yoshio MATSUNAGA*

Department of Chemistry, Faculty of Science, Hokkaido University, Sapporo 060

(Received April 25, 1983)

When 4-alkoxynitrobenzenes are mixed with *N*-(4-propoxybenzylidene)-4-hexylaniline, smectic A phases which are not found with the component compounds, are produced. The liquid crystals are stable if the number of carbon atoms in the alkoxyl group is eight or more, the maximum temperature being 49 °C with dodecyloxyl group, but they are entirely metastable if the number of carbon atoms is six or less. The extrapolation of the partly-observed smectic A-isotropic transition point curve indicates that 4-(dodecyloxy)-nitrobenzene has a latent transition point at about −25 °C and that all the examined *p*-disubstituted benzenes are potentially smectogenic. Smectic A phases are also induced by the addition of 4-alkoxybenzonitriles to the above Schiff base. The transition to the induced mesophase is enantiotropic when the alkoxyl group is decyloxyl or dodecyloxyl. The replacement of the propoxyl group in the Schiff base with an ethoxyl group makes the induced smectic A phases thermally less stable. The change is drastic when the alkoxyl group in the *p*-disubstituted benzene is hexyloxyl or shorter.

We reported in earlier papers,[2-5] that nematic and smectic liquid crystals can be induced by mixing a nonmesogenic electron donor and a nonmesogenic electron acceptor of the type 4-*X*-C_6H_4-*Z*-C_6H_4-*Y*-4. The appearance of mesophases in these binary systems was attributed to the thermal stabilization of the potential mesophases of the component compounds by the charge-transfer interaction introduced by mixing. It is generally believed that monomeric *p*-disubstituted benzenes are not mesogenic. However, the possibility that they are potentially mesogenic cannot be excluded. The observation of a smectic phase in the 4,4′-bis-(hexyloxy)azoxybenzene–4-(hexyloxy)nitrobenzene system covering the range as wide as 70 mol% reported by Schroeder and Schroeder[6] may be indicative of the potentially smectogenic behavior of 4-alkoxynitrobenzenes. We report here that the potential liquid crystal behavior of 4-alkoxynitrobenzenes and 4-alkoxybenzonitriles are readily demonstrable by the induction of new mesophases in the binary systems. For this purpose, we employed *N*-(4-propoxybenzylidene)-4-hexylaniline, which gives a nematic phase stable between 42 and 63 °C and a metastable smectic B phase below 21 °C, and its related compounds as the other components.[7]

Experimental

Materials. *N*-(4-Propoxybenzylidene)-4-hexylaniline, hereafter abbreviated as (3O, 6) designating the alkoxyl and alkyl carbon numbers for the substituents, was prepared by a condensation reaction between 4-propoxybenzaldehyde and 4-hexylaniline. The Schiff bases (2O, 6), (3O, 4), and (9O, 3) were similarly prepared. A homologous series of 4-alkoxynitrobenzenes was obtained by the alkylation of 4-nitrophenol following the procedure reported by Gray and Jones.[8] The compounds will be referred to as *n*O, NO_2 on the basis of the substituents where *n* is the number of carbon atoms in the alkoxyl group. By replacing 4-nitrophenol with 4-hydroxybenzonitrile, the 4-alkoxybenzonitriles, *n*O, CN, could be obtained.

Measurements. The calorimetric curves were recorded on a Rigaku Thermoflex differential scanning calorimeter equipped with a low-temperature unit. The heating and cooling rates in this work were 3 °C min^{-1}. The mesophases were identified by examining the texture with the aid of a polarizing microscope and by studying the continuous miscibility with the reference mesophases given by (9O, 3).

Results and Discussion

4-Alkoxynitrobenzenes, nO, NO_2. The even carbon number homologs up to $n=12$ were examined. Induced smectic A phases were observed in all the mixtures with (3O, 6). The phase diagrams of the binary systems containing each of 2O, NO_2, 6O, NO_2, and 10O, NO_2 are shown in Fig. 1. The open and shaded circles indicate the transitions recorded during the processes of heating and cooling respectively.

In Fig. 1a, the smectic phase found in the composition range from 61 to 87 mol% of (3O, 6) shows a texture different from the smectic B phase of (3O, 6); therefore, the induction of a smectic A phase by mixing is highly probable. This conclusion is confirmed by a study of the phase diagram of the pseudo-binary system consisting of the 81 mol% mixture (shown by an arrow in Fig. 1a) and (9O, 3). The latter compound gives a smectic A phase stable between 71.5 and 84 °C and also a smectic B phase stable between 48 and 71.5 °C.[9] The results presented in Fig. 1b firmly establish that the monotropic transition observed at 24 °C in the 81 mol% mixture is from a supercooled nematic phase to a smectic A phase. The smectic B phase exhibited by (3O, 6) appears to be drastically destabilized by the addition of 2O, NO_2.

The smectic A phase induced in the 4O, NO_2-(3O, 6) system covers the composition range from 50 to 82 mol% of (3O, 6), the maximum being located at 29 °C and near 80 mol%. This temperature is higher by 12 °C than that of the eutectic point. The transition temperature of (3O, 6) from the nematic phase to the smectic B phase is not much lowered by the addition of 4O, NO_2. At 89 mol% of (3O, 6) the supercooled nematic phase is transformed into the smectic B phase at 16 °C.

The compound 6O, NO_2 melts at 26 °C, the lowest among the melting points of *n*O, NO_2 examined. The

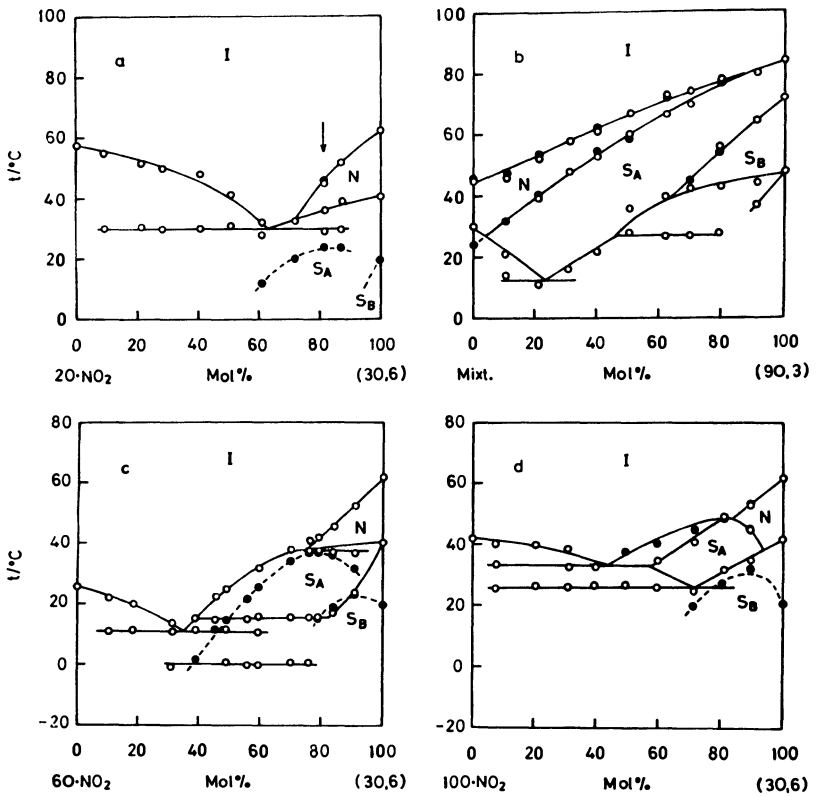

Fig. Phase diagrams of (a) 2O, NO_2-(3O, 6), (b) its 81 mol% mixture-(9O, 3), (c) 6O, NO_2-(3O, 6), and (d) 10O, NO_2-(3O, 6) systems. The open and shaded circles are transitions observed in the processes of heating and cooling respectively.

system with (3O, 6) exhibits a smectic A phase in the range from 39 to 91 mol% of (3O, 6). Around 78 mol%, the transition point curve reaches its maximum of 38 °C. The stabilization of the smectic B phase by 6O, NO_2 is also noted in this binary system. The monotropic transition at 91 mol% is found at 24 °C (see Fig. 1c).

The smectic A liquid crystals in the systems with each of 8O, NO_2, 10O, NO_2, and 12O, NO_2 can exist as stable phases. As the three phase diagrams are of the same type, they are exemplified by that of the 10O, NO_2-(3O, 6) system (see Fig. 1d). The transition between the isotropic liquid and the smectic A phase does not occur at a fixed temperature, that is, there is a range over which the isotropic liquid and the smectic A phase coexist. The smectic A-smectic B transition point curve is markedly convex upwards. As summarized in Fig. 2, the maximum smectic A-isotropic transition temperature against chain-length plot (see Curve a) shows a continued rise up to $n=10$ and then levels out. This change is of a common type for relationships known for homologous series of mesogenic compounds.[10]

The nematic-isotropic transition point curve is convex upwards in Fig. 1a, while the corresponding ones in the other systems are essentially straight (see Figs. 1c and 1d). Nevertheless, the latent transition point estimated for nO, NO_2 by the extrapolation to 0 mol% of (3O, 6) cannot be accurate since the observed fragment is not long enough. To a rough approximation, it is about −50 °C when $n=4$ and about −20 °C when

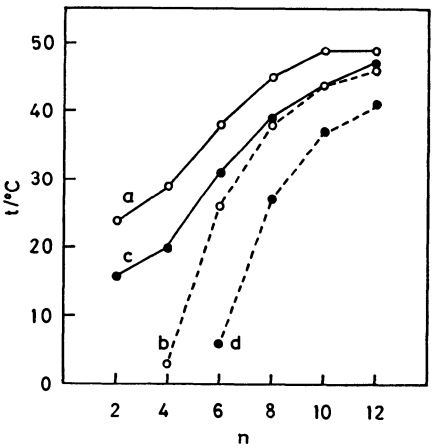

Fig. 2. Plots of the maximum temperatures of the induced smectic A phases against the length of the alkyl chain, n, for (a) nO, NO_2-(3O, 6) (b) nO, NO_2-(2O, 6), (c) nO, CN-(3O, 6), and (d) nO, CN-(2O, 6) systems.

$n=12$. If one similarly extrapolates plot of the smectic A-isotropic transition points against the composition, the latent smectic A-isotropic or -nematic transition point of nO, NO_2 may be estimated. Unfortunately, the plot is far from linear and the available points are limited to a high mol% range. By guess, one might infer about −60 °C for 6O, NO_2 and between −30 to −20 °C for 10O, NO_2 and 12O, NO_2: therefore, these temperatures are for transitions from smectic A phase to nematic phase.

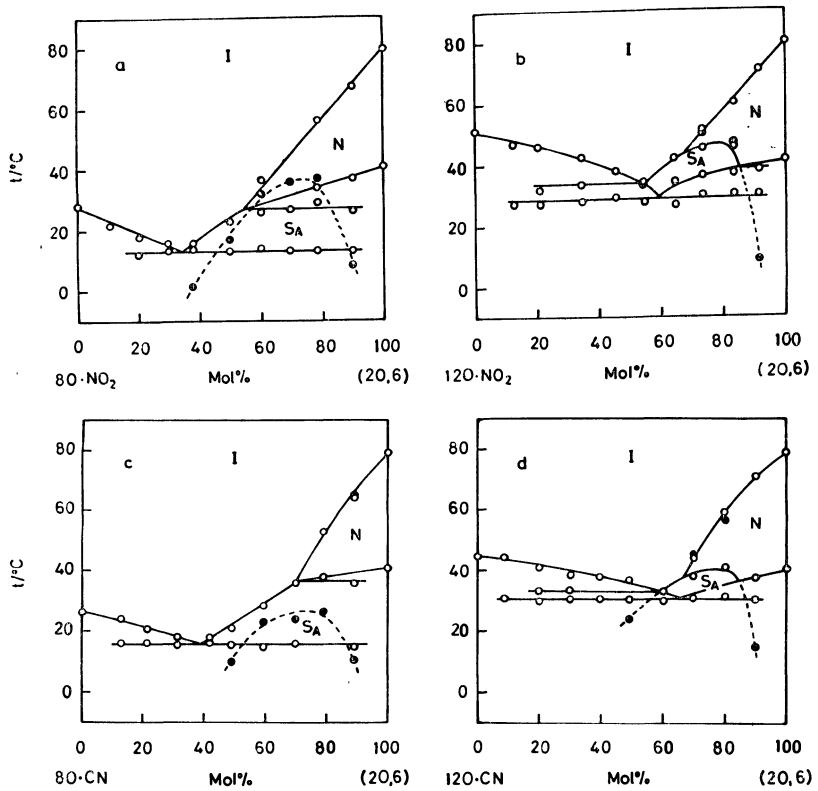

Fig. 3. Phase diagrams of (a) 8O, NO_2-(2O, 6), (b) 12O, NO_2-(2O, 6), (c) 8O, CN-(2O, 6), and (d) 12O, CN-(2O, 6) systems. As to the open and shaded circles, see the caption of Fig. 1.

The potential liquid crystal behavior of nO, NO_2 is supported also by the work on the systems with (2O, 6). The compound (2O, 6) is known to be nematogenic.[7] The mesophase is stable between 40.5 and 79.5 °C. Except for 2O, NO_2, smectic A phases are induced in all the combinations. The maximum smectic A-isotropic transition temperatures are given in Fig. 2 (see Curve b). Because of the steep rise between $n=4$ and 6 and that between $n=6$ and 8, Curve b lies far below Curve a at $n=2$ but the two approach to each other at $n=12$. Only when $n=10$ and 12, does the induced mesophase have a region of stable existence. The phase diagrams of the systems with each of 8O, NO_2 and 12O, NO_2 are presented in Fig. 3. The latent smectic A-nematic transition point of 8O, NO_2 may be estimated to be about −50 °C. As the smectic A phase induced in the 4O, NO_2-(2O, 6) system covers only the range from 70 to 80 mol% of (2O, 6), we studied further the system with (3O, 4). This mesogen exhibits a nematic phase stable between 41 and 58 °C and also a smectic B phase appearing from the supercooled nematic phase at 23.5 °C.[7] In the mixture with 4O, NO_2, the smectic A phase can be seen in the range from 50 to 90 mol% of (3O, 4), the maximum lying at 20 °C and about 75 mol%. Although the maximum temperature is lowered by 9 °C compared with that found in the corresponding system with (3O,6), there is no significant difference between the extent of the observable composition range. The latent smectic A phase of 4O, NO_2 may be located at a temperature as low as −70 °C. When 2O, NO_2 is mixed with (3O, 4), a smectic A phase is induced in the range from 70 to 88 mol%. In general, the stabilization of the smectic A phase by mixing with *N*-(4-alkoxybenzylidene)-4-alkylaniline appears to decrease in this order: (3O, 6)>(3O, 4)>(2O, 6).

4-Alkoxybenzonitriles, nO, CN. As exemplified by the binary systems consisting of (3O, 6) and each of 2O, CN, 6O, CN, and 10O, CN, these *p*-disubstituted benzenes are also potentially smectogenic. In Fig. 4a, the appearance of a new mesophase is indicated by the two monotropic transitions at 91 mol% of (3O, 6). The phase diagram of the pseudo-binary system, the 81 mol% mixture-(9O, 3), establishes that the newly-appeared phase is of the smectic A type (see Fig. 4b). The temperature range where this mesophase is observable is lower by 8 to 10 °C than that found in the 2O, NO_2-(3O, 6) system.

By mixing with (3O, 6), the compound 4O, CN produces a metastable smectic A phase covering the range from 40 to 90 mol%. The maximum temperature lies at 20 °C near 80 mol%. The transition to the smectic B phase located at 11 °C and 77 mol% may imply that the latent smectic B phase is thermally more stable than the smectic A phase when extrapolated to pure 4O, CN. It may be added that 4O, CN has the lowest melting point, 18.5 °C, among the 4-alkoxybenzonitriles employed in this work.

The phase diagram for the 6O, CN-(3O, 6) system is shown in Fig. 4c. In this system, the smectic A-smectic B transition point curve exhibits a maximum at about 90 mol% and 27 °C but the observation of the smectic B phase is limited to the range above 80 mol%.

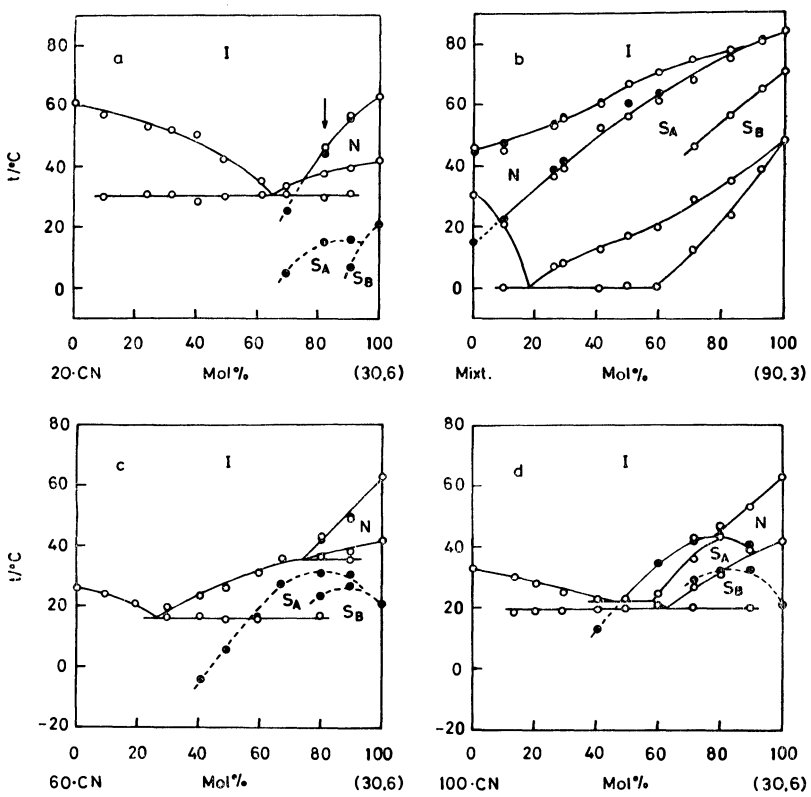

Fig. 4. Phase diagrams of (a) 2O, CN-(3O, 6), (b) its 81 mol% mixture-(9O, 3), (c) 6O, CN-(3O, 6), and (d) 10O, CN-(3O, 6) systems. As to the open and shaded circles, see the caption of Fig. 1.

With 8O, CN the stabilization of the smectic phases is appreciable. The maximum of the monotropic isotropic-smectic A transition point curve is at 39 °C and almost coincides with the horizontal line extending from the intersection between the isotropic-nematic transition point curve and the freezing point curve of (3O, 6). The smectic B phase is observable above 70 mol% with the maximum at 29 °C and about 85 mol%.

As is shown in Fig. 4d, a stable smectic A phase is found in the 10O, CN-(3O, 6) system. The compound 12O, CN also produces a diagram of the same type when it is mixed with (3O, 6). Although the diagram given in Fig. 4d bears a close similarity to that in Fig. 1d, it must be noted that the stabilization of smectic B phase with benzonitrile is more pronounced than that with nitrobenzene.

In Fig. 2, Curve c gives the plot of the maximum temperature of the smectic A-isotropic transition point curve against n. The temperature is 16 °C at $n=2$ and steadily increases to 47 °C at $n=12$.

Smectic A phases could be observed by mixing (2O, 6) with 6O, CN, 8O, CN, 10O, CN, and 12O, CN; however, only with the last benzonitrile the liquid crystal can be stable in a small region (see Figs. 3c and 3d). The maximum transition temperature in the nO, CN-(2O, 6) system is shown by Curve d in Fig. 2. The value is 6 °C at $n=6$ and 41 °C at $n=12$. Contrary to the 2O, NO_2-(3O, 4) system, the compound 2O, CN gives no smectic A phase when mixed with (3O, 4); however, the thermal stabilization of the smectic B phase is extensive and is observed to 78 mol% of (3O, 4), the temperature at this composition being 0 °C. When 4O, CN is employed with (3O, 4), a metastable smectic A phase appears in the range from 55 to 80 mol% of (3O, 4). The transition occurs at 16 °C at the upper limit and no maximum is located for this composition.

In conclusion, 4-alkoxynitrobenzenes and 4-alkoxybenzonitriles are potentially smectogenic. This potential liquid crystal behavior is possibly common to a wide range of *p*-disubstituted benzenes. The induction observed in the present systems may be partly attributed to the electron-donor-acceptor interaction as indicated by the pale yellow color developed on mixing and also may be partly due to a dipole-dipole interaction. As described above, the smectic A phases induced are observable mostly above 50 mol% of the Schiff base. This limitation may be ascribed to the relatively low latent transition temperatures of the *p*-disubstituted benzenes. In order to estimate the latent transition temperatures, it seems highly desirable to obtain essentially straight transition point curves in the binary systems with reference mesogens. With such systems, the effects of terminal substituents on liquid crystal behavior may be firmly established because of the simplicity of molecular structure. Attempts along this line are now in progress.

The present work was partly supported by a Grant-in-Aid for Scientific Research No. 543001 from the Ministry of Education, Science and Culture.

References

1) Part VII, M. Fukui and Y. Matsunaga, *Bull. Chem. Soc. Jpn.*, **55**, 3707 (1982).
2) K. Araya and Y. Matsunaga, *Bull. Chem. Soc. Jpn.*, **53**, 3079 (1980).
3) K. Araya and Y. Matsunaga, *Bull. Chem. Soc. Jpn.*, **54**, 2430 (1981).
4) K. Araya and Y. Matsunaga, *Bull. Chem. Soc. Jpn.*, **55**, 1710 (1982).
5) K. Araya, N. Homura, and Y. Matsunaga, *Bull. Chem. Soc. Jpn.*, **55**, 1953 (1982).
6) J. P. Schroeder and D. C. Schroeder, *J. Org. Chem.*, **33**, 591 (1968).
7) G. W. Smith, Z. G. Gardlund, and R. J. Curtis, *Mol. Cryst. Liq. Cryst.*, **19**, 327 (1973).
8) G. W. Gray and B. Jones, *J. Chem. Soc.*, **1954**, 1467.
9) C. Weygand and R. Gabler, *Naturwissenschaften*, **27**, 28 (1939). These authors have noted the appearance of two smectic phases. Our identification was made on the basis of the texture by thermal microscopy.
10) G. W. Gray and P. A. Winsor, "Liquid Crystals and Plastic Crystals," Ellis Horwood, Chichester (1974), Vol. 1, pp. 116—125.

 © 1983 The Chemical Society of Japan Bull. Chem. Soc. Jpn., 56, 3235—3242 (1983)

Excimer Formation and Phase Separation of Hydrocarbon and Fluorocarbon Bilayer Membranes[1)]

Toyoki KUNITAKE,* Shin-ichiro TAWAKI, and Naotoshi NAKASHIMA
Department of Organic Synthesis, Faculty of Engineering, Kyushu University, Higashi-ku, Fukuoka, 812
(Received June 3, 1983)

The benzene chromophore contained in double-chain(hydrocarbon) ammonium amphiphiles gives both of monomer and excimer fluorescence in the fluid(liquid crystalline) bilayer organization. The excimer emission disappears by phase transition to the rigid(crystalline) bilayer. In contrast, the corresponding fluorocarbon bilayer, in the absence of phase transition phenomena, shows excimer emission at all temperatures(15—50 °C). The excimer emission decreases when these probe amphiphiles are diluted in matrix bilayers. These results are applied to study the phase separation behavior of hydrocarbon and fluorocarbon bilayer membranes. The fluorocarbon bilayer is not extensively miscible with the hydrocarbon bilayer, and *vice versa*. The miscibility is influenced additionally by the chemical structure of amphiphiles. The rate of mixing is determined by the component miscibility as well as by the aggregate morphology. The DSC study supports these conclusions and further indicates that an unsymmetrical, double-chain(one hydrocarbon and one fluorocarbon chains) amphiphile can promote mixing of typical hydrocarbon and fluorocarbon bilayers.

It was recently reported from these laboratories that bilayer membranes are spontaneously formed from single-chain and double-chain ammonium amphiphiles with perfluoroalkyl groups.[2)] These fluorocarbon membranes combine organized assemblage similar to that of the hydrocarbon bilayer membrane and peculiar physicochemical properties of fluorocarbon compounds. For example, the fluorocarbon bilayer vesicle was more stable and less permeable to some organic probes than the hydrocarbon counterpart.

One of the interesting characteristics of fluorocarbon micelles is their limited miscibility with the hydrocarbon micelle.[3-7)] It is therefore expected that phase separation is readily induced in mixed membranes of hydrocarbon and fluorocarbon amphiphiles. Phase separation plays important roles in regulation of the biomembrane function. In the case of the synthetic bilayer membrane, phase separation was used to detect the interaction of the surface receptor with added ions,[8)] and the rates of hydroxide- and imidazole-catalyzed cleavage of phenyl esters were affected by phase separation of reacting species in the bilayer matrix.[9,10)]

The excimer formation has been used to probe the distribution and orientation of component amphiphiles in bilayers. For example, phosphatidylcholine lipids which contain covalently-bound pyrene chromophore were prepared by Sunamoto and coworkers and the excimer formation in the liposomal matrix was discussed in terms of membrane organization.[11,12)] Nagamura *et al.* reported that dialkylammonium salts which contain the phenoxy moiety in the alkyl chain portion gave weak excimer emission in the bilayer state.[13)] We reported recently that anthracene-containing, single-chain amphiphiles form bilayer membranes and that strong excimer emission is observed when the amphiphile is buried in the dialkylammonium bilayer matrix.[14)]

In the present paper, we describe our recent finding that double-chain ammonium amphiphiles which contain the benzene chromophore in the spacer portion

Fluorocarbon Bilayer Probe

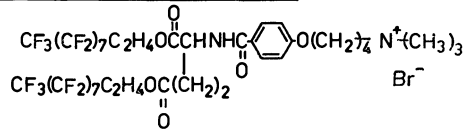

1, $2C_{10}^{F}$-L-Glu-ph-C_4-N^+

Fluorocarbon Bilayer Matrix

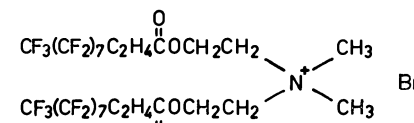

2, $2C_{11}^{F}$-de-N^+

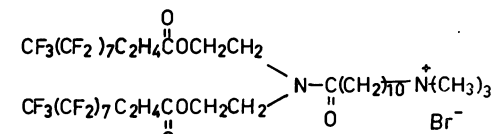

3, $2C_{11}^{F}$-de-C_{11}-N^+

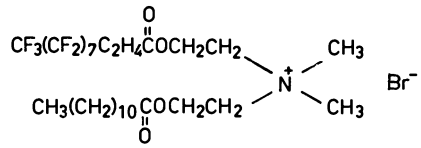

4, C_{11}^{F}, C_{12}-de-N^+

Hydrocarbon Bilayer Probe

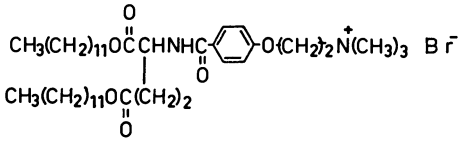

5, $2C_{12}$-L-Glu-ph-C_2-N^+

Hydrocarbon Bilayer Matrix

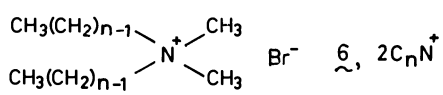

6, $2C_nN^+$

n=12, 14, 16

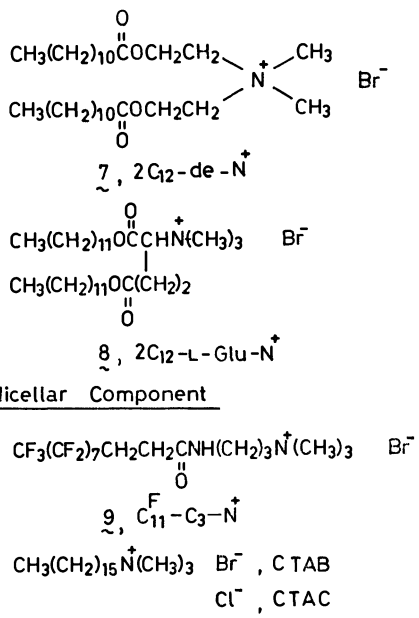

give strong excimer emission in the bilayer organization. Since the double-chain can be either hydrocarbon or fluorocarbon and since the excimer emission is highly dependent on the membrane physical state, these amphiphiles become very convenient probes for studying phase separation of hydrocarbon and fluorocarbon bilayers. The amphiphiles used are shown above together with their abbreviations.

Experimental

Fluorocarbon Amphiphile. 2*H*,2*H*,3*H*,3*H*-Perfluorundecanoic acid(24.6 g, 0.05 mol, Ugine Kuhlmann) was suspended in 18 g(0.15 mol) of thionyl chloride and the mixture was refluxed for 2 h and distilled *in vacuo*: colorless oil, yield 22.4 g(88%), bp 102—104 °C/13—14 mmHg(1 mmHg ≈133.3 Pa). The acid chloride(12 g, 0.024 mol) in 50 cm³ of $CHCl_3$ was added dropwise with stirring to an ice-cooled mixture of 1 g(8.4×10^{-3} mol) of commercial bis(2-hydroxyethyl)methylamine and 2 g(0.02 mol) of triethylamine in 100 cm³ of $CHCl_3$. The mixture was stirred further at room temperature for 1 h and at 40—50 °C for 24 h, and washed with water and aqueous Na_2CO_3 and dried over Na_2SO_4. The solvent was removed and the residue was distilled: colorless wax, yield 6.4 g(71%), bp 140—190 °C/0.03 mmHg. The formation of the diester was confirmed by IR and NMR spectroscopies. A large excess of CH_3Br was introduced to the diester(1 g, 9.4×10^{-4} mol) in 100 cm³ of tetrahydrofuran (THF). The mixture was stirred for 120 h at room temperature, and the precipitates formed were recrystallized from methanol and benzene: colorless flakes, yield 0.7 g(64%), mp 165—169.5 °C. The spectroscopic data(NMR and IR) were consistent with **2**. Found: C, 28.88; H, 1.87; N, 1.25%. Calcd for $C_{28}H_{22}NO_4F_{34}$: C, 28.93; H, 1.91; N, 1.20%.

A mixture of 4.5 g(0.042 mol) of commercial bis(2-hydroxyethyl)methylamine and 1.0 g(0.01 mol) of triethylamine in 100 cm³ of $CHCl_3$ was added dropwise to 5.0 g(0.01 mol) of the acid chloride in 50 cm³ of $CHCl_3$ with ice cooling. The mixture was then stirred at room temperature for 72 h, washed with water and aqueous Na_2CO_3, and dried. The solvent was removed, and toluene was added to the residual yellow oil, which was then kept in a refregerator. The colorless precipitates were recovered by quick separation, but they turned to colorless oil at room temperature: yield 3.0 g(51%). IR and NMR spectra showed the product to be the monoester. Undecanoyl chloride(1.3 g, 6.1×10^{-3} mol) in 40 cm³ of $CHCl_3$ was added dropwise to a solution of 3.0 g(5.1×10^{-3} mol) of the monoester and 0.6 g(6×10^{-3} mol) of triethylamine in 60 cm³ of $CHCl_3$ with ice cooling. The mixture was further stirred at 40 °C for 12 h, washed with water and aqueous $NaHCO_3$, and dried. The solvent was removed and colorless oil(TLC-FID, single peak) was recovered. A large excess of CH_3Br was introduced to 3.6 g(4.6×10^{-3} mol) of the product dissolved in 100 cm³ of dry THF, and the mixture stirred at room temperature for 24 h. The colorless precipitates were recrystallized from benzene, separated from the $CHCl_3$-insoluble by-product, and recrystallized again from benzene: colorless wax, yield 0.9 g (22%), mp 100→193 °C(the arrow indicates the liquid crystalline range). The structure (**4**) was confirmed by NMR spectroscopy. Found: C, 39.58; H, 4.74; N, 1.65%. Calcd for $C_{29}H_{41}F_{17}O_4NBr\cdot0.5H_2O$: C, 39.60; H, 4.81; N, 1.59%.

Amphiphiles **1**, **3**, and **9** were provided by S. Yasunami[2,15]

Hydrocarbon Amphiphile. *N*,*N*-bis[2-dodecanoyloxy)-ethyl]methylamine hydrochloride[15] (colorless powder, mp 105→120 °C)(2.5 g, 4.4×10^{-3} mol) in benzene was treated with aqueous Na_2CO_3 and dried. A large excess of CH_3Br gas was introduced to the solution and the mixture stirred at room temperature for 70 h. The colorless precipitates formed were recrystallized from ethyl acetate to give colorless powder of **7**: yield 1.4 g(55%), mp 173—175 °C. Found: C, 62.06; H, 10.38; N, 2.24%. Calcd for $C_{30}H_{60}O_4NBr$: C, 62.26; H, 10.45; N, 2.42%. Amphiphile **5** was provided by H. Fukushima.[16] Amphiphile **8** was described elsewhere.[19] The preparations of a series of dialkylammonium salts **6** were described briefly.[17,18] CTAB and CTAC are recrystallized from ethanol.

Miscellaneous. Electron micrographs were obtained with a Hitachi H-600 instrument, and fluorescence spectra were measured with a Hitachi 650-10S spectrofluorimeter. The degree of fluorescence polarization, P was obtained by Eq. 1.

$$P = \frac{I_{//\,//} - I_{//\perp}(I_{\perp//}/I_{\perp\perp})}{I_{//\,//} + I_{//\perp}(I_{\perp//}/I_{\perp\perp})}, \quad (1)$$

where $I_{//\,//}$ and $I_{\perp\perp}$ are emission measured with parallel polarizers(vertical and horizontal) and $I_{//\perp}$ and $I_{\perp//}$ are those measured with crossed polarizers.[20] UV-visible spectra were obtained with Hitachi spectrophotometers 200 and 220 A. Differential scanning calorimetry (DSC) was conducted for 20-mM samples with a Daini-Seikosha SSC/560 instrument. The temperature was raised from 0 °C at a rate of 2 °C/min.[21]

Results and Discussion

Aggregation Behavior. Figure 1 shows electron micrographs of $2C_{11}^F$-de-N^+, C_{11}^F,C_{12}-de-N^+, and $2C_{12}$-de-N^+. The sample preparation has been described before.[22] However, satisfactory staining was not attained by the previous method in the case of fluorocarbon membranes. In an improved procedure, crystalline membrane compounds and uranyl acetate were suspended in water and sonicated together. The bilayer structure(vesicle and lamella) is clearly observed for $2C_{11}^F$-de-N^+. C_{11}^F,C_{12}-de-N^+ gives very

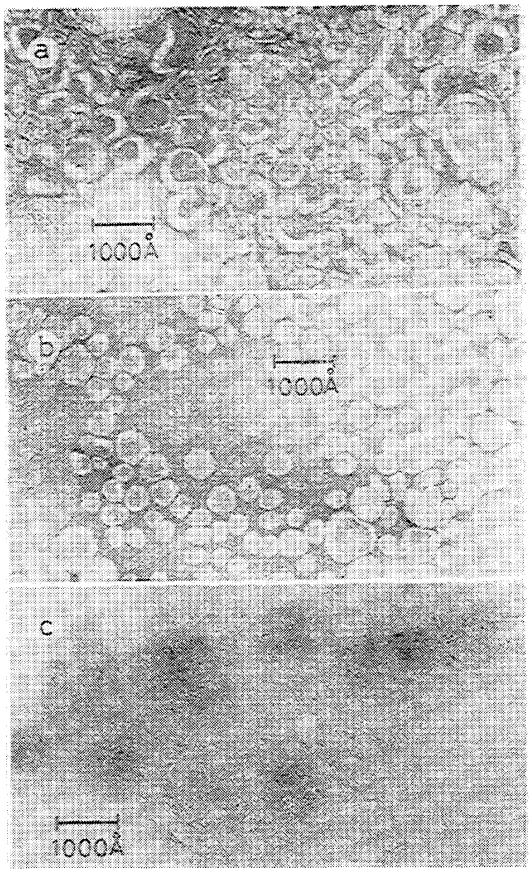

Fig. 1. Electron micrographs.
Sample 10 mM; initial magnification, ×30,000; stained by uranyl acetate, (a) $2C_{11}^{F}$-de-N^+ (b) C_{11}^{F}, C_{12}-de-N^+, (c) $2C_{12}$-de-N^+.

well dispersed, single-walled vesicles. The hydrocarbon counterpart, $2C_{12}$-de-N^+ gives multi-walled vesicles. These three compounds differ only in the long-chain portion(hydrocarbon or fluorocarbon). The bilayer organization is maintained when the hydrocarbon tail is replaced by the fluorocarbon tail of similar length, as mentioned previously.[2] However, it is interesting that the combination of hydrocarbon and fluorocarbon tails in an amphiphile gives single-walled vesicles that are much better dispersed than those of the bilayer aggregate of amphiphiles with two hydrocarbon(or fluorocarbon) tails.

All the other double-chain amphiphiles have been shown to form stable bilayer membranes.[2,15,16]

Excimer Emission of Hydrocarbon and Fluorocarbon Bilayers. Figure 2 describes fluorescence spectra of the aqueous bilayer of $2C_{12}$-L-Glu-ph-C_2N^+.[21] The excitation wavelength is set at 260 nm where the benzene ring absorbs. At 20 °C, the emission maximum appears at 320 nm, which is located close to that observed in methanol (312 nm). This peak is, therefore, attributed to the monomer emission. With rising temperature, this peak is lessened and a new, broader peak appears at 360 nm. The separation of the two peaks corresponds to *ca.* 4000 cm^{-1}, and this extent of energy difference is typical of the excimer formation.[24] The 360-nm peak shifts completely to 320 nm by addition of the CTAB micelle (2 mM), in consistence with excimer emission.

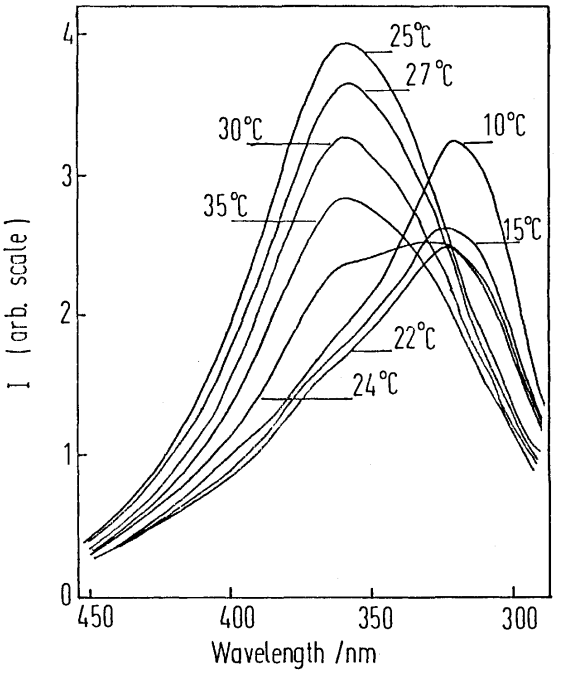

Fig. 2. Temperature dependence of fluorescence spectra of the aqueous $2C_{12}$-L-Glu-ph-C_2N^+ bilayer.
$2C_{12}$-L-Glu-ph-C_2N^+, 1.0×10^{-4} M, excitation at 260 nm.

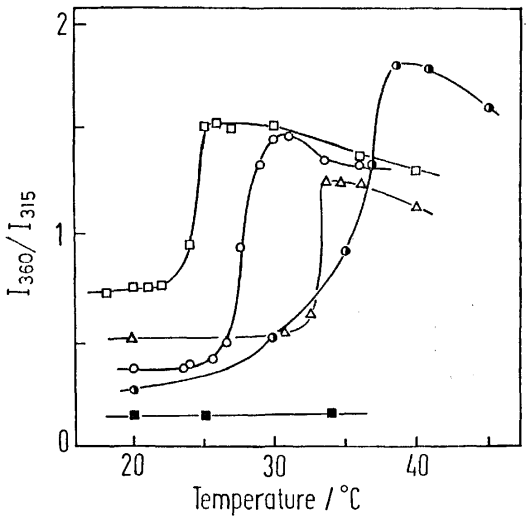

Fig. 3. Temperature dependence of I_{360}/I_{315} of hydrocarbon probes in water and in methanol.
[Amphiphiles] = 1.0×10^{-4} M.
—□—: $2C_{12}$-L-Glu-phC_2N^+ bilayer in water, —○—: $2C_{12}$-L-Glu-ph-C_4N^+ bilayer, in water, —◑—: $2C_{12}$-L-Glu-ph-C_6N^+ bilayer in water, —△—: $2C_{12}$-L-Asp-ph-C_4N^+ bilayer in water, —■—: $2C_{12}$-L-Glu-phC_2N^+ in methanol.

Figure 3 illustrates the temperature dependence of the ratio of fluorescence intensity at 360 and 315 nm. In the case of $2C_{12}$-L-Glu-ph-C_2N^+, this value increases rather abruptly in a narrow temperature range of 23 to 25 °C, and then gradually decreases with temperature. The maximum is located in the phase transition region: T_c (peak top temperature in the DSC thermogram)=27 °C. The I_{360}/I_{315} value in

methanol is smaller(0.15) and temperature-independent, as expected. Similar situations(excimer formation and temperature dependence) are found for other probe membranes in which the spacer length is different or the glutamate connector is replaced by the aspartate connector. The maxima exist more clearly in the case of the latter probes. It is interesting that the excimer emission is most enhanced with partially fluid membranes. Apparently the spatial arrangement of the neighboring benzene ring in the rigid bilayer is not suited for excimer formation.

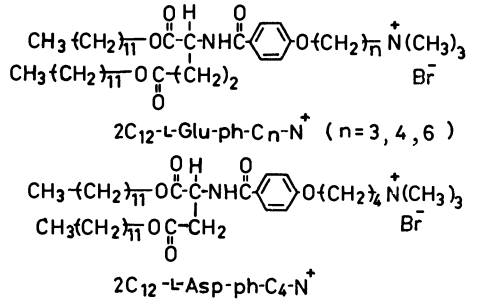

Figure 4 shows examples of the variation of fluorescence polarization(P) with temperature. In the case of a methanol solution in which $2C_{12}$–L-Glu–ph-C_4–N^+ is molecularly dispersed, P is 0.31 and temperature-independent. In the corresponding bilayer system, the emission at 310 nm gives a constant P value(0.43) in all temperature range, whereas P of the 360-nm emission changes in the phase transition region from 0.42 (low temperature) to 0.20(high temperature). The two P values (0.42 and 0.20) are mainly associated with the monomer and excimer emissions, respectively. The high P value observed for the monomer emission implies that this emission is derived from the benzene chromophore of fixed orientation. The lowered P value of the excimer emission is indicative of lessened orientation characteristic of the excimer. Similar results are found for $2C_{12}$–L-Glu–ph-C_2–N^+.

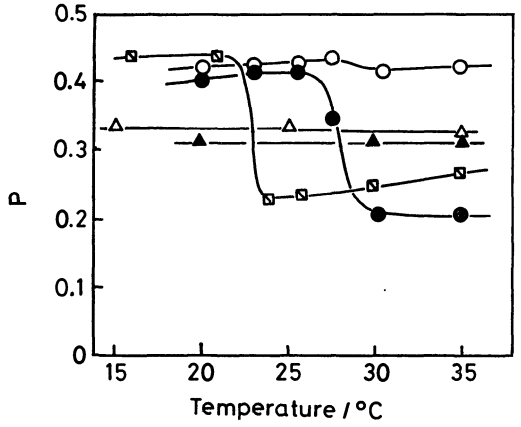

Fig. 4. Temperature dependence of the fluorescence polarization (P).
Sample, 1.0×10^{-4} M.
—▨—: $2C_{12}$-L-Glu-ph-C_2-N bilayer (Ex 265 nm, Em 360 nm), —○—: $2C_{12}$-L-Glu-ph-C_4N^+ bilayer (Ex 265 nm, Em 310 nm) —●—: $2C_{12}$-L-Glu-ph-C_4N^+ bilayer (Ex 265 nm, Em 360 nm), —△—: $2C_{12}$-L-Glu-ph-C_2N^+ in methanol (Ex 265 nm, Em 310 nm), —▲—: $2C_{12}$-L-Glu-phC_4N^+ in methanol (Ex 265 nm, Em 310 nm).

The fluorescence behavior of the corresponding fluorocarbon bilayer is not the same. The spectrum of the $2C^F_{10}$–L-Glu–ph-C_4–N^+ bilayer possesses a maximum at 365 nm with a shoulder at *ca.* 320 nm. This spectrum does not change in the temperature range examined (15—50 °C), in consistence with the lack of major changes in the physical state(no DSC peak observed). The I_{365}/I_{320} value decreases linearly with temperature: 1.8 at 15 °C and 1.3 at 45 °C. Apparently the excimer emission is predominant at all temperatures. The excimer emission is suppressed when the fluorocarbon probe is diluted by a large excess of a fluorocarbon membrane matrix. The pure monomer peak (320 nm) is observed when $2C^F_{10}$–L-Glu–ph-C_4N^+ is imbedded in 50 times excess of $2C^F_{11}$–de-N^+. The degree of polarization of the excimer peak (365 nm) was 0.11—0.13 at 14 to 47 °C, and that of the monomer peak (320 nm) was 0.3 in the same range.

Comparison of Excimer Formation of Hydrocarbon and Fluorocarbon Bilayers. A comparison of the fluorescence behavior(excimer formation) between the hydrocarbon and fluorocarbon probes is interesting. The excimer formation is determined by the distance and orientation of the two chromophore. The X-ray diffraction data indicate that the interplanar distance is 3.2 Å for typical excimer-forming pairs of the chromophore.[24] The bilayer membrane of the hydrocarbon probe gives strong circular dichroism (CD) enhancement due to the exciton coupling, if in the crystalline state.[25] This implies that there exist a long-range interaction among the aromatic chromophores due to their fixed orientation. However, the excimer formation is not observed for these rigid membranes. Apparently, the spatial arrangement of the fixed chromophore is not suitable in this case for excimer formation. Instead, the excimer is formed much more readily for partially or fully liquid-crystalline bilayers. The CD enhancement is not observed in the same temperature ranges.

The excimer-formation behavior of the fluorocarbon probe resembles that of the partially fluid hydrocarbon probe at all temperatures. This result, together with the lack of phase transition, suggests that the fluorocarbon probe maintains fluidity required for excimer formation in the whole temperature range. This is consistent with the absence of the CD enhancement for this probe.[26] The excimer naturally disappears upon dilution with a nonfluorescent fluorocarbon bilayer. It is well known that the intermolecular interaction of fluorocarbons is much smaller than that of the corresponding hydrocarbon. This difference can explain the fluorescence behavior of the two kinds of the membrane.

Phase Separation as Estimated by Fluorescent Probe. It is clear from the above results that the excimer emission is related to the formation of the probe cluster. Phase separation of hydrocarbon and fluorocarbon membranes was subsequently examined by using fluo-

Table 1. Phase separation of fluorocarbon probe

	Hydrocarbon matrix			Fluorocarbon matrix		
	$2C_{16}N^+$	$2C_{12}$-L-Glu-N^+	$2C_{12}$-de-N^+	$2C^F_{11}$-de-N^+	C^F_{11},C_{12}-de-N^+	$2C^F_{11}$-de-C_{11}-N^+
I_{365}/I_{320}	1.09	0.98	0.90	0.46	0.64	0.71
Cluster(%)	86	73	63	∞	30	39

$(I_{365}/I_{320})_{monomer}$=0.40. $(I_{365}/I_{320})_{cluster}$=1.20, [matrix]=1.0 mM, [probe]=0.1 mM, 33 °C.

Table 2. Phase separation of hydrocarbon probe

	Hydrocarbon matrix	Fluorocarbon matrix				
	$2C_{12}$-de-N^+ 1 mM	$2C^F_{11}$-de-N^+ 1 mM	C^F_{11},C_{12}-de-N^+			
			0.1 mM	1 mM	5 mM	10 mM
I_{355}/I_{320}	0.52	0.84	1.20	0.71	0.66	0.61
Cluster(%)	2	36	74	22	17	12

[Probe]=0.1 mM, 33 °C. $(I_{355}/I_{320})_{monomer}$=0.50, $(I_{355}/I_{320})_{cluster}$=1.45.

rocarbon probe $2C^F_{10}$-L-Glu-ph-C_4-N^+. Matrix (1 mM) and probe (0.1 mM) were cosonicated for 1 min to give clear solutions. The I_{365}/I_{320} values of the mixed membrane thus obtained did not virtually change with time.

The amount of the probe cluster(*i.e.*, extent of phase separation) is estimated by

$$\text{cluster}(\%) = \frac{(I_{365}/I_{320})_{obsd} - (I_{365}/I_{320})_{monomer}}{(I_{365}/I_{320})_{cluster} - (I_{365}/I_{320})_{monomer}} \times 100, \quad (2)$$

where I_{365}/I_{320} for cluster and monomer are obtainable from Fig. 5.

Table 1 summarizes the phase separation data of the fluorocarbon probe. In the case of the hydrocarbon matrices, most of the probe molecule are in the cluster, $2C_{16}N^+$ being least miscible. The fluorocarbon matrix is more miscible with the fluorocarbon probe, as expected. $2C^F_{11}$-de-N^+ is best miscible, as also shown in Fig. 5. The I_{365}/I_{320} value decreases linearly with decreasing molar ratios of the probe and matrix, and reaches a constant value (cluster disappears) when more than 10 times matrix molecules are present. Unsymmetrical double-chain matrix C^F_{11},C_{12}-de-N^+ solubilizes the probe less efficiently. It is interesting that a considerable amount of the probe cluster remains in the double fluoroalkyl matrix of $2C^F_{11}$-de-C_{11}-N^+. Apparently, the presence of the hydrocarbon spacer, $(CH_2)_{10}$, is responsible for this result.

The influence of the micellar matrix is similar to that of the membrane matrix. Thus, the probe (0.1 mM) exists predominantly as monomer (90%) in the fluorocarbon micelle of C^F_{11}-C_3-N^+ (10 mM). The amount of the cluster increases in CTAB (56%).

Subsequently, phase separation was examined by using hydrocarbon probe, $2C_{12}$-L-Glu-ph-C_2-N^+. This probe was selected because of its low T_c. The experimental procedures were the same as in the case of the fluorocarbon probe. The temperature used (33 °C) is higher than T_c of the probe membrane, so

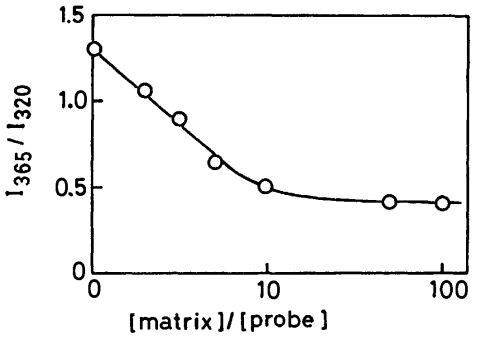

Fig. 5. Influence of the molar ratio ([matrix]/[probe]) on the relative excimer emission, I_{365}/I_{320}. 33 °C; $2C^F_{10}$-L-Glu-ph-C_4N^+ probe, 1.0×10^{-4} M; $2C^F_{11}$-de-N^+ matrix, 1×10^{-4}—1×10^{-2} M.

that the excimer formation is assured if the cluster is formed. The fluorescence intensities at 355 and 320 nm were compared, and the results are given in Table 2. The probe molecule exists almost completely as monomer in the hydrocarbon matrix (10 times excess) of $2C_{12}$-de-N^+. The cluster is formed more readily in the fluorocarbon matrix of $2C^F_{11}$-de-N^+ than in C^F_{11},C_{12}-de-N^+, and in the latter matrix, the cluster decreases with increasing matrix concentrations.

Membrane Mixing as Examined by Fluorescent Probe. Fusion and/or mixing processes of the bilayer aggregate can be followed by using the excimer emission. Sonicated solutions (0.9 cm^3) of the matrix membrane were aged in quartz cells for 30 min at 33 °C, and then sonicated solutions (0.1 cm^3) of the probe membrane were added. Figure 6 illustrates the decrease of I_{365}/I_{320} of the fluorocarbon probe with time in the fluorocarbon matrix. Mixing of the probe membrane with the C^F_{11},C_{12}-de-N^+ membrane proceeds more smoothly than with $2C^F_{11}$-de-N^+. This result is strange at first glance, since the extent of phase separation of the probe after sonication is larger with C^F_{11},C_{12}-de-N^+ than with $2C^F_{11}$-de-N^+ (Table 1). The mixing rate

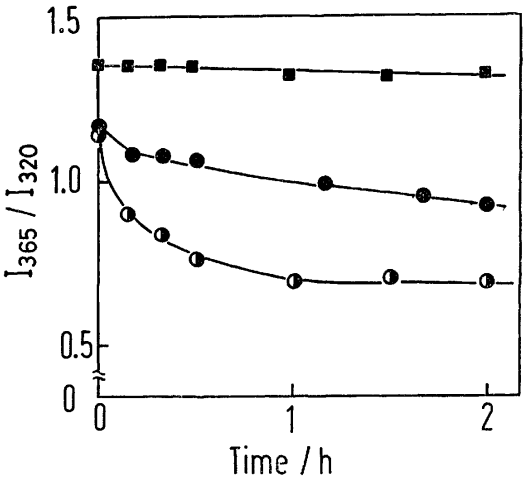

Fig. 6. Time course of I_{365}/I_{320} of the fluorocarbon bilayer probe upon mixing with fluorocarbon bilayer matrices.
33 °C; probe, 1.0×10^{-4} M; matrix, 1.0×10^{-3} M.
—■—: $2C_{11}^{F}$-de-$C_{11}N^{+}$ matrix, —●—: $2C_{11}^{F}$-de-N^{+} matrix, —◑—: C_{11}^{F},C_{12}-de-N^{+} matrix.

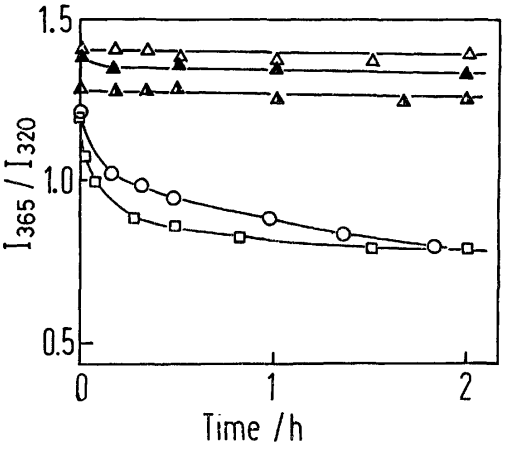

Fig. 7. Time course of I_{365}/I_{320} of the fluorocarbon bilayer probe upon mixing with hydrocarbon bilayer matrices.
33 °C; probe, 1.0×10^{-4} M; matrix, 1.0×10^{-3} M.
—△—, $2C_{12}N^{+}$; —▲—, $2C_{14}N^{+}$; —⏃—, $2C_{16}N^{+}$; —○—, $2C_{12}$-L-Glu-N^{+}; —□—, $2C_{12}$-de-N^{+}.

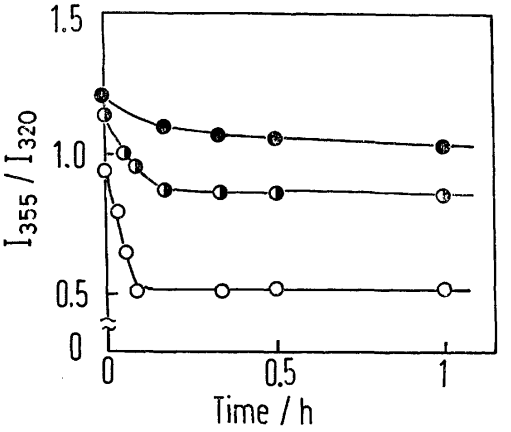

Fig. 8. Time course of I_{355}/I_{320} of the hydrocarbon bilayer probe upon mixing with hydrocarbon bilayer matrices.
33 °C; probe, 1.0×10^{-4} M; matrix, 1.0×10^{-4} M.
—●—: $2C_{11}^{F}$-de-N^{+} matrix. —◐—: C_{11}^{F},C_{12}-de-N^{+} matrix. —○—: $2C_{12}$-de-N^{+} matrix.

is determined by the kinetic and thermodynamic factors. Since the thermodynamic factor can be inferred from the extent of phase separation after sonication, the discrepancy may be associated with the kinetic factor. Electron microscopy indicates that the aqueous aggregate of C_{11}^{F},C_{12}-de-N^{+} is much better dispersed (single-walled vesicle) than that of $2C_{11}^{F}$-de-N^{+} (lamella and vesicle). Therefore, the initial mixing with the probe membrane would be more efficient in the case of C_{11}^{F},C_{12}-de-N^{+}.

Mixing of the fluorocarbon probe with $2C_{11}^{F}$-de-C_{11}-N^{+} is very slow in s ite of the fact that the two compounds possess the same fluoroalkyl chain in common. This result reflects the fact that $2C_{11}^{F}$-de-C_{11}-N^{+} does not mix well with the fluorocarbon probe probably because of the hydrocarbon spacer (Table 1). The morphological characteristics of $2C_{11}^{F}$-de-C_{11}-N^{+} (lamella)[15] may make the mixing even more sluggish.

Figure 7 displays the mixing process of the fluorocarbon probe and hydrocarbon matrices. The mixing with the dialkylammonium membranes is very slow, as anticipated from their extensive phase separation (Table 1). The mixing with the hydrocarbon membranes of $2C_{12}$-L-Glu-N^{+} and $2C_{12}$-de-N^{+} is unexpectedly facile, and comes close to the equilibrated phase separation of Table 1 within 1—2 h. The contact of probe and matrix must be efficient because of the morphologies of the latters.

Similar mixing experiments were carried out for the hydrocarbon probe (Fig. 8). As expected, this probe is readily mixed with the hydrocarbon matrix of $2C_{12}$-de-N^{+}. The miscibility is lessened with increasing fluoroalkyl contents. The I_{355}/I_{320} values become virtually constant in 15 min. The final values in the fluorocarbon matrix are larger than those obtained upon sonication. Therefore, complete mixing of the hydrocarbon probe and the fluorocarbon matrices cannot be attained without sonication.

DSC Study of Membrane Mixing. Synthetic bilayer membranes of dialkyl amphiphiles usually give DSC peaks due to the crystal-to-liquid crystal phase transition.[18] Therefore, the DSC technique can be conveniently applied to the study of the phase separation behavior of multi-component membranes when the spectroscopic probe is absent.

Three double-chain amphiphiles of closely related structures were selected for this purpose. Multi-component samples were prepared by sonication or simple mixing. Clear aqueous solutions were obtained by sonication of multi-component suspensions (20 mM each) in the sonication procedure, and the separately-prepared(by sonication) solutions were mixed without sonication in the simple-mixing procedure. The former procedure gives information on the final state of mixing, and the latter data are related to the mixing process.

Figure 9 illustrates the variation of the DSC peak of $2C_{12}$-de-N^{+}. The single-component sample gives a

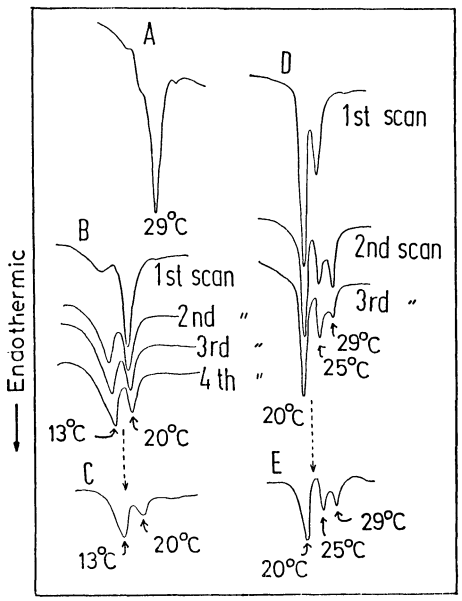

Fig. 9. DSC thermograms of the $2C_{12}$-de-N^+ bilayer alone and in combinations with related bilayers.
A, $2C_{12}$-de-N^+ alone (20 mM). B, an equimolar mixture with C_{11}^F,C_{12}-de-N^+. The sample was prepared by mixing of the two solutions without sonication. C, the same sample as B after sonication. D, an equimolar mixture with $2C_{11}^F$-de-N^+. The sample was prepared by mixing of the two solution without sonication. E, the same sample as D after sonication.

sharp peak at 29 °C with ΔH=38.5 kJ/mol, but those of $2C_{11}^F$-de-N^+ and C_{11}^F,C_{12}-de-N^+ do not give any DSC peak at 0 to 70 °C. An equimolar mixture of solutions of $2C_{12}$-de-N^+ and $2C_{11}^F$-de-N^+ (prepared without sonication) gives endothermic peaks at 20 °C (major peak) and 25 °C, in the first scan. In the second and third scans, three peaks appear at 20 (major peak), 25 and 29 °C. The DSC behavior observed upon repeated scans agrees with that of the sonicated sample. The ΔH value of the triplet peak is 15.9 kJ/mol, which is much smaller than 38.5 kJ/mol of $2C_{12}$-de-N^+ alone. An equimolar mixture (without sonication) of $2C_{12}$-de-N^+ with C_{11}^F,C_{12}-de-N^+ give peaks at 13 and 20 °C, and the latter peak becomes smaller upon repeated scans. In fact, a sonicated sample of the mixture gives peaks at 13(major) and 20 °C with reduced intensity(ΔH=10.0 kJ/mol).

It is suggested from these data that the fluorocarbon bilayer of $2C_{11}^F$-de-N^+ and the hydrocarbon bilayer of $2C_{12}$-de-N^+ are partially miscible. The decreased ΔH value implies the presence of rather small domains of $2C_{12}$-de-N^+. The miscibility is apparently improved in the mixture of $2C_{12}$-de-N^+ and $2C_{11}^F$-de-N^+, because the peaks appear at lower temperatures with smaller intensity.

Sturtevant and co-workers[27] prepared phospholipids labeled by fluorine at several positions of the acyl chain, and examined their mixing behavior with unlabeled phospholipids. The DSC data showed that the fluorine-labeled phosphocholines are not ideally distributed. These results are consistent with our data on a mixed membrane of $2C_{12}$-de-N^+ and $2C_{11}^F$-de-N^+ in that T_c shifts to lower temperatures and that ΔH decreases considerably.

The miscibility of the two-component membranes is improved in an equimolar, three-component mixture of $2C_{12}$-de-N^+, $2C_{11}^F$-de-N^+, and C_{11}^F,C_{12}-de-N^+. Very small DSC peaks appear at 16.5 and 22.5 °C in the first scan of this mixture(without sonication), but they disappear completely in the second scan. The peaks are totally absent in a sonicated mixture. This indicates that, although $2C_{12}$-de-N^+ is only partially miscible with either of $2C_{11}^F$-de-N^+ and C_{11}^F,C_{12}-de-N^+ it is completely miscible in a mixed membrane of $2C_{11}^F$-de-N^+ and C_{11}^F,C_{12}-de-N^+.

Conclusion

It is established that the excimer formation of the benzene unit is unusually facilitated due to the bilayer assemblage. This novel phenomenon is very useful for examining the phase separation behavior of hydrocarbon and fluorocarbon bilayers. We showed elsewhere that the anthracene chromophore included in the bilayer assemblage give strong excimer emission when it is partially buried in a bilayer matrix.[14] The intensity of the excimer emission depended on the mole ratio of the anthracene amphiphile and the dialkylammonium matrix. Thus, the excimer formation may be used widely as a means for elucidation of the phase separation.

The limited miscibility of hydrocarbon and fluorocarbon bilayers may also be used for developing novel catalytic functions. We already showed in the micellar system that high catalytic efficiency and selectivity are attainable by combinations of hydrocarbon and fluorocarbon reagents.[28]

References

1) Contribution No. 688 from Department of Organic Synthesis.
2) T. Kunitake, Y. Okahata, and S. Yasunami, *J. Am. Chem. Soc.*, **104**, 5547 (1982).
3) P. Mukerjee and A. Y. S. Yang., *J. Phys. Chem.*, **80**, 1388 (1976).
4) K. J. Mysels, *J. Colloid Interface Sci.*, **66**, 33 (1978).
5) P. Mukerjee and K. J. Mysels, *ACS Symp. Ser.*, No. 9, 239 (1975).
6) N. Funasaki and S. Hada, *Chem. Lett.*, **1979**, 717; *J. Phys. Chem.*, **84**, 763 (1980).
7) K. Shinoda and T. Nomura, *J. Phys. Chem.*, **84**, 365 (1980).
8) M. Shimomura and T. Kunitake, *J. Am. Chem. Soc.*, **104**, 1757 (1982).
9) Y. Okahata, H. Ihara, and T. Kunitake, *J. Am. Chem. Soc.*, in press (1983).
10) H. Ihara, Ph. D. Thesis, Faculty of Engineering, Kyushu Univ., 1982.
11) J. Sunamoto, T. Nomura, H. Okamoto, and H. Kondo, *J. Am. Chem. Soc.*, **102**, 1146 (1980).
12) J. Sunamoto, T. Nomura, and H. Okamoto, *Bull. Chem. Soc. Jpn.*, **53**, 2768 (1980).
13) T. Nagamura, T. Takayanagi, and T. Matsuo, *Int. J. Quantum Chem.*, **18**, 509 (1980).

14) M. Shimomura, H. Hashimoto, and T. Kunitake, *Chem. Lett.*, **1982**, 1285.
15) S. Yasunami, Master Thesis, Faculty of Engineering, Kyushu University, 1981.
16) Ref. 5 of N. Nakashima, H. Fukushima, and T. Kunitake, *Chem. Lett.*, **1981**, 1555.
17) T. Kunitake, Y. Okahata, K. Tamaki, F. Kumamuru, and M. Takayanagi, *Chem. Lett.*, **1977**, 387.
18) Y. Okahata, R. Ando, and T. Kunitake, *Bull. Chem. Soc. Jpn.*, **52**, 3647 (1979).
19) T. Kunitake, N. Nakashima, S. Hayashida, and K. Yonemori, *Chem. Lett.*, **1979**, 1413.
20) K. Kano, J. H. Fendler, *Chem. Phys. Lipids*, **23**, 189 (1979).
21) Y. Okahata, R. Ando, and T. Kunitake, *Ber. Bunsenges. Phys. Chem.*, **85**, 789 (1981).
22) T. Kunitake and Y. Okahata, *J. Am. Chem. Soc.*, **102**, 549 (1980).
23) The fluorescence spectrum of $2C_{12}$-L-Glu-ph-C_2-N^+ is affected by the extent of sonication. The temperature-dependent spectrum of Fig. 2 is obtained when the sonication time is less than 2 min(Branson cell disruptor 185, sonic power 60 W. When the aqueous sample was sonicated for more than 3 min, the spectrum consisted of a single peak at 363 nm at all temperatures. It seems that the delicate molecular arrangement is destroyed by extensive sonication and that an alternate (probably less ordered) bilayer structure is formed. This strange effect is not observed for the other membranes of $2C_{12}$-L-Glu-ph-C_n-N^+ ($n=3$, 4, 6, and 10).
24) W. Klöpffer, "Organic Molecular Photophysics," ed by J. B. Birks, Wiley-Interscience, New York (1973), Vol. 1, Chap. 7.
25) T. Kunitake, N. Nakashima, M. Shimomura, Y. Okahata, K. Kano, T. Ogawa, *J. Am. Chem. Soc.*, **102**, 6642 (1980).
26) Unpublished results in these laboratories.
27) J. M. Sturtevant, C. Ho, and A. Reimann, *Biochemistry*, **76**, 2239 (1979).
28) T. Kunitake, H. Ihara, and Y. Hashiguchi, submitted for publication.

Salt Effect on the Solubility of Copper and Beryllium Chelates of 4,4,4-Trifluoro-1-phenyl-1,3-butanedione

Yasuki YOSHIMURA,* Nobuyoshi SATO, and Makoto KIKUCHI

Laboratory of Chemistry, College of Humanities and Social Sciences, Iwate University, Ueda, Morioka 020

(Received February 18, 1983)

In order to examine whether the substitution of a trifluoromethyl group for a methyl group in metal chelates of 1-phenyl-1,3-butanedione (BA) affects the salt effect on the solubility of these chelates, the solubility of copper and beryllium chelates of 4,4,4-trifluoro-1-phenyl-1,3-butanedione (BFA) in water and in some aqueous salt solutions was measured at 25 °C. The solubility in water (S_0) was $9.07\pm0.22\times10^{-7}$ mol dm^{-3} for the copper chelate and $4.85\pm0.08\times10^{-6}$ mol dm^{-3} for the beryllium chelate. These solubility values are compared with those of the corresponding BA chelates and an influence of fluorination on the solubility of these BA chelates is discussed. It was found that the solubility of the above BFA chelates in the aqueous salt solutions (S) could be expressed satisfactorily by the equation, $\log(S_0/S)=a\sqrt{C_s}+bC_s$, where C_s is the concentration of salt. This result suggests that introduction of CF_3 group brings about a specific interaction between the fluorinated chelates and their surroundings.

In a series of our investigations, the salt effect on the solubility of bis(1-phenyl-1,3-butanedionato)copper-(II) ($Cu(bzac)_2$) and bis(1-phenyl-1,3-butanedionato)-beryllium(II) ($Be(bzac)_2$) has been studied and a generalized interpretation for the salt effect in the solvent extraction of metal chelates was presented[1,2]. The substitution of a trifluoromethyl group for a methyl group in the metal chelates of β-diketones affects their properties such as volatility.[3] The polarity of the metal chelates of the above fluorinated β-diketones is expected to be higher than that of parent chelates because of the high electronegativity of fluorine atoms.

On the other hand, in our studies on the salt effect on the solubility of BA and BFA, it was suggested that species of the latter was less polar than that of the former in aqueous solutions.[4,5] It is very interesting to see whether fluorination of β-diketone chelates affects the salt effect or not. Thus, in the present study, the solubility of bis(4,4,4-trifluoro-1-phenyl-1,3-butanedionato)copper(II) ($Cu(bfac)_2$) and bis(4,4,4-trifluoro-1-phenyl-1,3-butanedionato)beryllium(II) ($Be(bfac)_2$) in water and in aqueous salt solutions is measured and the salt effect on the solubility of these chelates is compared with that for $Cu(bzac)_2$ and $Be(bzac)_2$.

Experimental

Materials. The copper and beryllium chelates of BFA were prepared and purified by the same procedures as used for $Cu(bzac)_2$ and $Be(bzac)_2$.[1,2] The melting points of these chelates were 239 °C (Ref. 6, 241 °C) and 143 °C (Ref. 6, 143 °C), respectively. Aqueous solutions of LiCl, $NaClO_4$, NaCl, $NaNO_3$, and Na_2SO_4 were also prepared as previously reported.[1,2] Redistilled water was used and heptane was purified by an ordinary method.

Solubility Measurement. The apparatus and procedure used for the solubility measurement were similar to those previously reported,[1] except for the procedure modified to extract completely BFA into heptane. Filtered aliquots of the solution saturated with $Cu(bfac)_2$ or $Be(bfac)_2$ were acidified with one drop of 5 M (1 M = 1 mol dm^{-3}) HCl solution and then exact volume of these acidified solutions (30 cm^3 for $Cu(bfac)_2$ and 10—20 cm^3 for $Be(bfac)_2$) was transferred to 50 cm^3 centrifuge tubes in which Na_2SO_4 was previously placed. As the partition coefficient of BFA between water and heptane is lower than that of BA,[7] Na_2SO_4 was added to the above acidified solutions as a salting-out reagent to extract completely BFA. BFA was completely extracted at the concentrations of Na_2SO_4 over 1.5 M, and so in most cases Na_2SO_4 was added to give the concentration of 2 M. In the cases in which the addition of 2 M Na_2SO_4 results in the precipitation of salts while being extracted, for example, in the solubility measurement for $Be(bfac)_2$ in 3 M salt solutions, Na_2SO_4 concentration was reduced to 1 M. Even in these cases, the complete extraction of BFA was confirmed by stirring again aliquots of the aqueous phases, from which BFA was once extracted, with freshly added heptane. The mixtures of the aqueous solutions prepared as described above and 5 cm^3 of heptane were warmed at 30 °C to dissolve completely added Na_2SO_4 and stirred for 2 h with a magnetic stirrer.

The calibration curve to determine the concentration of BFA extracted into heptane phase was obtained as follows. Three independent series of standard solutions of BFA in heptane were prepared over the concentration range of 6.47×10^{-6}—3.24×10^{-5} M, and 5 cm^3 portions of these standard solutions were stirred for 2 h with 10—30 cm^3 of 2 M Na_2SO_4 acidified with one drop of 5 M HCl. After the heptane phases were separated by centrifugation, the absorbance at 323 nm in the heptane phases was measured, and the least-squares method was applied to these data. The calibration curve is expressed as

$$C=(A+0.0077)/(1.48\times10^4), \quad (1)$$

where C and A are the concentration(M) of BFA, and the absorbance at 323 nm in heptane phases, respectively.

The pH of sample solutions (250 cm^3) to be saturated with $Cu(bfac)_2$ or $Be(bfac)_2$ was adjusted within the ranges described in the following section by adding 0.1—0.4 cm^3 of 0.08 M sodium tetraborate-5 M HCl mixed solution of pH 7.4.

Results and Discussion

Solubility of $Cu(bfac)_2$ and $Be(bfac)_2$ in Water. The results of solubility measurement of $Cu(bfac)_2$ and $Be(bfac)_2$ in water are presented in Tables 1 and 2, respectively, in order to demonstrate influences of pH and equilibration time. The solubility values calculated from the concentration of BFA in heptane phases were practically constant over the pH ranges of 6.9—7.2 for $Cu(bfac)_2$ and 6.2—6.5 for $Be(bfac)_2$. For $Be(bfac)_2$, fairly long equilibration time was required to attain complete saturation.

Table 1. Solubility measurement for $Cu(bfac)_2$ in water at 25 °C

Equilibration time/h	pH[a]	pH[b]	Solubility 10^{-7} mol dm^{-3}	Equilibration time/h	pH[a]	pH[b]	Solubility 10^{-7} mol dm^{-3}
Run 1				Run 3			
32	7.21	6.99	9.27	42	7.20	7.16	9.59
48	7.01	6.99	9.15	66	7.09	7.01	9.18
54	6.99	7.01	8.93	90	7.06	7.11	9.03
72	7.16	7.09	8.82	114	7.02	6.99	9.01
Run 2							
72	7.19	7.10	9.20	Mean of all data 9.07±0.22			
95	7.01	7.03	8.85				
115	7.02	6.93	8.99				
142	7.00	7.01	8.85				

a,b) The pH of saturated solutions measured before and after being filtered to be equilibrated with heptane, respectively.

Table 2. Solubility measurement for $Be(bfac)_2$ in water at 25 °C

Equilibration time/h	pH[a]	pH[b]	Solubility 10^{-6} mol dm^{-3}	Equilibration time/h	pH[a]	pH[b]	Solubility 10^{-6} mol dm^{-3}
Run 1				Run 2			
90	6.40	6.40	4.70	235	6.26	6.24	4.86
114	6.49	6.44	4.89	264	6.29	6.23	4.88
138	6.42	6.42	4.84	283	6.24	6.24	4.78
168	6.40	6.38	4.96	314	6.21	6.17	4.81
186	6.48	6.41	4.90	332	6.24	6.22	4.85
210	6.39	6.43	4.84	356	6.30	6.24	4.73
234	6.39	6.43	4.96	380	6.49	6.48	4.96
				Mean of all data 4.85±0.08			

a,b) The pH of saturated solutions measured before and after being filtered to be equilibrated with heptane, respectively.

Table 3. Melting points and solubilities in water (S_0) at 25 °C for Cu and Be chelates with BA and BFA

Chelate	Mp θ_m/°C	S_0/mol dm^{-3}
$Cu(bzac)_2$[a]	195	1.38×10^{-6}
$Cu(bfac)_2$	239	9.07×10^{-7}
$Be(bzac)_2$[b]	211	9.98×10^{-7}
$Be(bfac)_2$	143	4.85×10^{-6}

a) Ref. 1. b) Ref. 2.

A comparison of the solubility of $Cu(bfac)_2$ and $Be(bfac)_2$ in water with that of $Cu(bzac)_2$ and $Be(bzac)_2$ is very interesting. As shown in Table 3, the higher the melting points of these chelates are, the smaller their solubilities are. This is a general phenomenon for the solubility of similar solids in their natures.[8] The extremely low melting point of $Be(bfac)_2$ may be ascribed to a mutual repulsion between molecules in its solid state caused by the introduction of CF_3 group.[6]

Salt Effect on the Solubility of $Cu(bfac)_2$ and $Be(bfac)_2$. For the solubility measurement in aqueous LiCl, $NaNO_3$, $NaClO_4$, NaCl, and Na_2SO_4 solutions, the pH ranges which gave constant values for BFA concentration in heptane phases were 6.4—6.9 for $Cu(bfac)_2$ and 6.0—6.5 for $Be(bfac)_2$. For each sample solution, the solubility measurement was made independently 4 times for $Cu(bfac)_2$ and 4—7 times for $Be(bfac)_2$ at adequate time intervals (*cf.* Tables 1 and 2). The number of solubility measurement for $Be(bfac)_2$ depends on the volume taken out of the saturated solutions. The standard deviations of these measurements were within 3% in all cases.

In the previous studies, it was confirmed that the solubility of $Cu(bzac)_2$ and $Be(bzac)_2$ in aqueous salt solutions (S) could be expressed by

$$\log S = \log S_0 - k_s C_s, \quad (2)$$

where S_0, k_s, and C_s were the solubility of these chelates in water, salting coefficient, and the concentration of salts, respectively.[1,2] For $Cu(bfac)_2$ and $Be(bfac)_2$, as the plot of log (S) *vs.* C_s did not give straight lines, Eq. 2 was not valid.

As shown in Figs. 1 and 2, where log (S_0/S) is plotted against $\sqrt{C_s}$ for $Cu(bfac)_2$ and $Be(bfac)_2$, it was found that the solubility data for these chelates might be expressed by

$$\log (S_0/S) = a\sqrt{C_s} + bC_s \quad (3)$$

The values for a and b in Eq. 3 obtained by applying the least-squares method to the solubility data are listed in Table 4, where the square root of the dispersions of residues of log (S_0/S), *i.e.*,

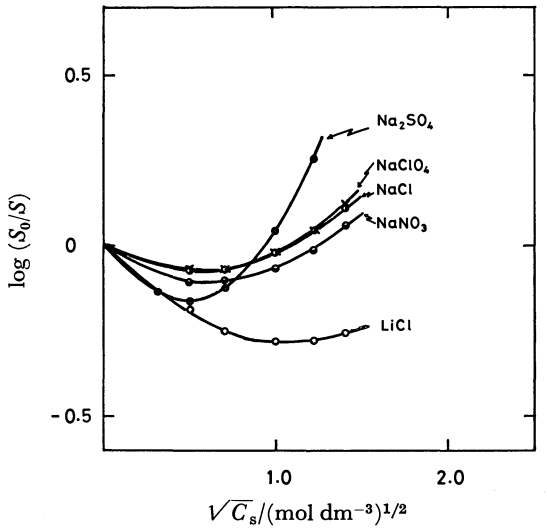

Fig. Plot of log (S_0/S) *vs.* $\sqrt{C_s}$ for $Cu(bfac)_2$. Solid lines are values calculated from log (S_0/S) = $a\sqrt{C_s}+bC_s$ by using the least-squares method.

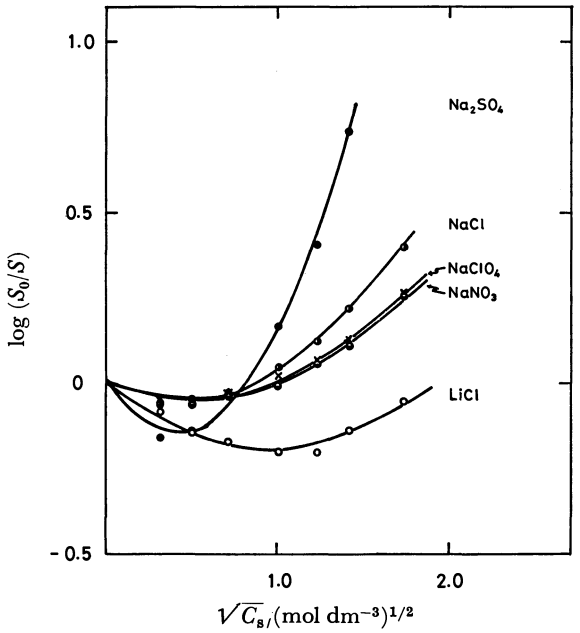

Fig. 2. Plot of log (S_0/S) *vs.* $\sqrt{C_s}$ for $Be(bfac)_2$. Solid lines are values calculated from log (S_0/S) = $a\sqrt{C_s}+bC_s$ by using the least-squares method.

$$\sigma = [\sum_{i=1}^{n} \{\log (S_0/S_i) - (a\sqrt{C_{si}} + bC_{si})\}^2/(n-1)]^{1/2}$$

is also tabulated. The S_0/S term in Eq. 3 represents the ratio of the activity coefficient of chelates in aqueous salt solutions to that of chelates in water.[9]

For all the salts studied in this work, the values for *a*-coefficient were negative and those for *b*-coefficient were positive (see Table 4). In a low region of C_s, the $a\sqrt{C_s}$ term is larger than the bC_s term and the solubility of $Cu(bfac)_2$ and $Be(bfac)_2$ in aqueous salt solutions is higher than the solubility in water. On the other hand, in a high region of C_s, the bC_s term is predominant and the solubility of these chelates decreases with increasing C_s. From a comparison of the salt effect on the solubility of $Cu(bfac)_2$ with that for $Be(bfac)_2$, it seems that the influence of the introduction of CF_3 group on the salt effect scarcely varies with the configuration of the chelates.

When the value for *a*-coefficient in Eq. 3 is negligible, Eq. 3 agrees with Eq. 2. Thus, a difference between the salt effect on the solubility of $Cu(bfac)_2$ or $Be(bfac)_2$ and that for $Cu(bzac)_2$ or $Be(bzac)_2$ is attributed to the $a\sqrt{C_s}$ term. Although the $a\sqrt{C_s}$ term must reflect a specific interaction between fluorinated chelates and water molecules or ions, more detailed study is required for clarifying the interaction.

Table 4. *a*- and *b*-coefficients in $\log(S_0/S)=a\sqrt{C_s}+bC_s$ for $Cu(bfac)_2$ and $Be(bfac)_2$

Salt	a/(mol dm^{-3})$^{1/2}$	b/mol dm^{-3}	σ[a]
	$Cu(bfac)_2$		
LiCl	−0.512	0.232	0.0060
$NaNO_3$	−0.336	0.267	0.0038
$NaClO_4$	−0.259	0.245	0.0040
NaCl	−0.270	0.247	0.0040
Na_2SO_4	−0.685	0.729	0.0046
	$Be(bfac)_2$		
LiCl	−0.411	0.216	0.0177
$NaNO_3$	−0.206	0.201	0.0097
$NaClO_4$	−0.204	0.206	0.0114
NaCl	−0.236	0.272	0.0099
Na_2SO_4	−0.707	0.868	0.0262

a) $\sigma^2 = \sum_{i=1}^{n} \{\log (S_0/S_i) - (a\sqrt{C_{si}} + bC_{si})\}^2/(n-1)$.

References

1) Y. Yoshimura, *J. Inorg. Nucl. Chem.*, **42**, 1749 (1980).
2) Y. Yoshimura, *J. Inorg. Nucl. Chem.*, **43**, 1615 (1981).
3) For example, a) W. D. Ross, *Anal. Chem.*, **35**, 1596 (1963); b) R. E. Sievers, B. W. Ponder, M. L. Morris, and R. W. Moshier, *Inorg. Chem.*, **2**, 693 (1963); c) W. D. Ross and G. Wheeler, Jr., *Anal. Chem.*, **36**, 266 (1964); d) W. R. Wolf, R. E. Sievers, and G. H. Brown, *Inorg. Chem.*, **11**, 1995 (1972).
4) Y. Yoshimura and N. Suzuki, *Anal. Chim. Acta*, **91**, 315 (1977).
5) Y. Yoshimura and N. Suzuki, *Talanta*, **25**, 489 (1978).
6) E. W. Berg and J. T. Truemper, *J. Phys. Chem.*, **64**, 487 (1960).
7) T. Sekine, Y. Hasegawa, and N. Ihara, *J. Inorg. Nucl. Chem.*, **35**, 3968 (1973).
8) K. Shinoda, "Yôeki To Yôkaido," Maruzen, Tokyo (1974), p. 247.
9) F. A. Long and W. F. McDevit, *Chem. Rev.*, **51**, 119 (1952).

Bis(2-aminoethanol)cadmium(II) Tetracyanonickelate(II)–Pyrrole (1/1) and 2-Aminoethanolcadmium(II) Tetracyanonickelate(II)–Benzene (1/2). Variation of Metal Complex Host Structure with the Size of Aromatic Guest Molecule

Shin-ichi Nishikiori and Toschitake Iwamoto*

Department of Chemistry, College of Arts and Sciences, The University of Tokyo, Komaba, Meguro-ku, Tokyo 153

(Received April 22, 1983)

Two modifications of the host structures analogous to that of Hofmann-type $Cd(NH_3)_2Ni(CN)_4$ have been found in the crystal structures of $Cd(mea)_2Ni(CN)_4\cdot C_4H_5N$ and $Cd(mea)Ni(CN)_4\cdot 2C_6H_6$ which were prepared using mea (2-aminoethanol=monoethanolamine) in place of the NH_3 as the ligands in the host metal complexes. In the former pyrrole clathrate, Hofmann-mea-type(1), the mea behaves as a unidentate ligand like the NH_3 in Hofmann-type, but in the latter benzene one, Hofmann-mea-type(2), it behaves ambidently like the en in Hofmann-en-type host $Cd(en)Ni(CN)_4$. In Hofmann-mea-type(1) host, the layered metal cyanide network is puckered, whereas that in Hofmann-ema-type(2) host is coplanar. The size of the guest molecule appears to control the behavior of mea and the structure of the metal cyanide network.

In the course of our studies involving the design and synthesis of clathrate compounds analogous to Hofmann-type $M(NH_3)_2M'(CN)_4\cdot 2G$, novel three-dimensional host structures have been developed using such ambident ligands as ethylenediamine (en), trimethylenediamine, propylenediamine (pn), in place of the NH_3 ligands in Hofmann-type host. Another strategy we have applied is to use tetrahedral tetracyanometallate(II) moieties such as $Cd(CN)_4$, $Hg(CN)_4$, in place of the square-planar $M'(CN)_4$ (M'=Ni, Pd, or Pt) in order to develop three-dimensional host structures.[1-5] The ambident ligands used are symmetric with respect to their coordination sites, although the skeletal structure of pn is asymmetric.[6]

In the present investigation, mea (monoethanolamine=2-aminoethanol: $NH_2CH_2CH_2OH$) was chosen as the ligand replacing the NH_3 in Hofmann-type to develop novel host structures; mea was expected to behave either as a unidentate ligand like the NH_3 in Hofmann-type or as an ambident one like the en in Hofmann-en-type $Cd(en)Ni(CN)_4\cdot 2G$.[7-11] In the former case, mea with a bulky $-CH_2CH_2OH$ group does not have any proper rotational axes like the threefold one of NH_3; in the latter case, it is also asymmetric with respect to the coordination sites $-NH_2$ and $-OH$. Both cases have been demonstrated in the host structures of novel clathrates, $Cd(mea)_2Ni(CN)_4\cdot C_4H_5N$ (**1**), and $Cd(mea)Ni(CN)_4\cdot 2C_6H_6$ (**2**), as has been reported briefly in the previous communication.[12] This paper describes their crystal structures in detail and discusses their structural features from the viewpoint of molecular inclusion phenomena occurring in the series of Hofmann-type and the analogous metal complex hosts.

Experimental

Preparation. Into 100 ml of 0.1 M $CdCl_2$ (M=mol dm^{-3}), 11.6 ml of 2-aminoethanol and 100 ml of 0.1 M $K_2[Ni(CN)_4]$ were added successively. The pH of the mixed solution was adjusted to *ca.* 9.5 by adding a few drops of 6 M HCl. The aqueous phase in a conical flask was covered with the organic phase of pyrrole-toluene (1:15) mixture, thiophene-*o*-xylene (1:1) mixture, or neat benzene to prepare the pyrrole, thiophene, or benzene clathrate, respectively. By leaving the flasks in a refrigerator at 5 °C for a few days, yellow crystals of the clathrates grew up at the interface between the aqueous and the organic phases. The freshly prepared crystals were subjected to the analyses of metal contents by chelatometry in this laboratory. The C, H, and N microanalyses were carried out for the specimens sealed in glass vials at the laboratory of elemental analysis in Department of Chemistry, Facultry of Science of this University a few days after the preparation. The pyrrole clathrate was stable enough to give the satisfiable analytical results, but the thiophene and the benzene ones were unstable even when reserved in sealed

Table 1. The analytical results and the compositions determined

Composition†	Found/Calcd(%)				
	C	H	N	Cd	Ni
$Cd(NH_2CH_2CH_2OH)_2Ni(CN)_4\cdot C_4H_5N$	31.2 / 31.03	4.17 / 4.12	21.2 / 21.11	23.8 / 24.20	12.7 / 12.63
$Cd(NH_2CH_2CH_2OH)_2Ni(CN)_4\cdot C_4H_4S$	29.1 / 29.93	3.28 / 3.77	17.6 / 17.45	23.2 / 23.34	12.4 / 12.19
$Cd(NH_2CH_2CH_2OH)Ni(CN)_4\cdot 2C_6H_6$	38.4 / 43.89	3.24 / 3.89	15.7 / 14.22	23.1 / 23.82	12.7 / 11.91

vials. The benzene clathrate was extremely unstable: it decomposed immediately at room temperature, even in contact with neat benzene. The analytical results listed in Table 1 appear to reflect the instability of the thiophene and the benzene clathrates, especially with respect to the values of C, H, and N.

Structure Determination

Data Collection. In order to avoid the spontaneous decomposition of the specimens under ambient conditions, each crystal was coated with epoxy resin before the X-ray experiments. Preliminary Weissenberg photographs were taken to check the crystal symmetries and lattice parameters for the pyrrole, the thiophene, and the benzene clathrates, respectively. The refinement of lattice parameters and the collection of Lp-corrected intensity data were carried out for the pyrrole clathrate (**1**), on a Rigaku automated four-circle diffractometer,[13] and for the benzene clathrate (**2**), on a Phillips one[14] using Mo $K\alpha$ radiation at ambient temperature. The lattice parameters were refined for **1** using 30 reflections with $45°<2\theta<50°$, and for **2** using 24 reflections with $20°<2\theta<64°$. The intensities of three standard reflections, recorded every fifty measurements, showed no significant variations. The experimental conditions and the crystallographic data are listed in Table 2.

Solution and Refinement of the Structures. The structures of **1** and **2** were solved by the heavy-atom method. The refinements were carried out by the successive Fourier and difference Fourier syntheses and by the block-diagonal least-squares method; for **2**, the full-matrix least-squares method was applied at the later stages. All the calculations were carried out on a HITAC M-200H computer at the Computer Center of this University using the programs in UNICS[15] and their local versions. The atomic scattering factors used were those in the *International Tables*.[16]

The Pyrrole Clathrate (1): The absorption correction for a cube was applied for the intensities of all the reflections used. From the observed systematic absences of reflections in the orthorhombic system, the space group was limited to either non-centrosymmetric $Pna2_1$ or centrosymmetric Pnam. On the Patterson map, the positions of Cd and Ni atoms were first found. Then those of C, N, and O atoms were revealed on the successive Fourier and difference Fourier maps.

Table 2. Crystallographic parameters and experimental data[a]

Compound	Host	$Cd(mea)_2Ni(CN)_4$		$Cd(mea)Ni(CN)_4$
	Guest	C_4H_5N	C_4H_4S	$2C_6H_6$
Chemical formula		$C_{12}H_{19}N_7O_2CdNi$	$C_{12}H_{18}N_6O_2SCdNi$	$C_{18}H_{19}N_5OCdNi$
Formula weight		470.44	481.48	492.49
Crystal system		orthorhombic	orthorhombic	tetragonal
Space group		$Pna2_1$	$P2_12_12_1$	P4/mmm
a/Å		14.691(1)	14.58	7.529(1)
b/Å		15.881(1)	16.34	7.529(1)
c/Å		7.575(1)	7.59	8.094(1)
Z		4	4	1
D_x/g cm^{-3}		1.76	1.74	1.75
D_o/g cm^{-3} [b]		1.74(1)	1.74(1)	1.75(1)
Crystal size/mm		0.35×0.35×0.35		0.25×0.25×0.30
Radiation		Mo $K\bar{\alpha}$[c]	Cu $K\bar{\alpha}$	Mo $K\bar{\alpha}$[c]
Monochromator		graphite		graphite
Scan mode		2θ-ω		ω
Scan range		$3.0°<2\theta<65°$		$7.5°<2\theta<70°$
No. of reflections				
in the range		3403		659
observed		3135		606
used[d]		3070		575
Systematic absences		($0kl$) $k+l=2n+1$	($h00$) $h=2n+1$	no
		($h0l$) $h=2n+1$	($0k0$) $k=2n+1$	
			($00l$) $l=2n+1$	
μ(Mo $K\bar{\alpha}$)/cm^{-1}		22.4		21.7
Correction		Lp and cubic absorption		Lp
No. of parameters determined		243		63
No. of variables refined		163		29
R[e]		0.041		0.047
R_w		0.047[f]		0.062[g]

a) Only the photographic data are listed for the thiophene clathrate. b) The values measured by the flotation method in bromoform-xylene mixture. c) $\lambda=0.710730$ Å. d) The reflections with $|F_o|>3\sigma(|F_o|)$. e) $R=\Sigma(|F_o|-|F_c|)/\Sigma|F_o|$. f) $R_w=(\Sigma w(|F_o|-|F_c|)^2/\Sigma|F_o|^2)^{1/2}$ with $w=(400/|F_o|)^2$ for $|F_o|\geq400$, $w=1.0$ for $400>|F_o|>40$, and $w=0.5$ for $|F_o|\leq40$. g) $R_w=(\Sigma w(|F_o|-|F_c|)^2/\Sigma w|F_o|^2)^{1/2}$ with $w=\{(\sigma(|F_o|)^2+(0.01|F_o|)^2\}^{-1/2}$.

At the stage of refinement with the anisotropic thermal parameters for the atoms of the host moieties except H's, and the isotropic ones fixed at 5.0 Å^2 for the skeletal atoms of pyrrole molecule, the possible space groups $Pna2_1$ and Pnam were compared. The $Pna2_1$ was chosen for the following reasons: (i) the R value of 0.043 was lower than 0.048, (ii) the preference in the Hamilton test with the significance level of 0.005, (iii) the acceptable bond lengths and angles, and (iv) the Patterson syntheses was fully supported by this space group.

In the final stage of refinement applying the $Pna2_1$ space group, the H atoms belonging to the host moieties, *i.e.*, those of the mea ligands, were located on the positions found on the difference Fourier map, except for those H's bonded to the O atoms. All the skeletal atoms of the pyrrole molecule were regarded as C because no significant discrimination of N was possible in the revealed structure. In the final block-diagonal least-squares calculations, the atomic coordinates of the host H atoms were fixed at the positions found on the difference Fourier map, and the thermal parameters of the host H atoms and the guest skeletal C atoms were fixed at 4.0 Å^2 and 5.0 Å^2, respectively, but these parameters were included in the evaluation of R values. After a few cycles of the calculations, the parameters to be determined converged into the range less than 0.5 times their

TABLE 3. THE FINAL POSITIONAL AND THERMAL PARAMETERS WITH THEIR ESTIMATED STANDARD DEVIATIONS IN THE PARENTHESES FOR $Cd(mea)_2Ni(CN)_4 \cdot C_4H_5N$[a]

Atom	x	y	z	U_{11}	U_{22}	U_{33}	U_{12}	U_{13}	U_{23}
Cd	4319(0)	7242(0)	0(2)	17(0)	32(0)	18(0)	1(0)	(0)	0(0)
Ni	3191(0)	2117(0)	47(0)	16(0)	33(0)	14(0)	−3(0)	−1(1)	−1(1)
C(1)	2262(4)	1964(4)	1678(8)	29(3)	28(3)	16(2)	−1(2)	0(2)	1(2)
C(2)	4005(4)	2321(5)	1855(9)	21(2)	38(4)	27(3)	−1(3)	5(2)	−1(3)
C(3)	881(4)	7267(4)	3360(8)	17(2)	34(3)	19(2)	2(2)	−2(2)	1(2)
C(4)	2659(4)	6995(5)	3225(9)	15(2)	53(4)	24(3)	1(3)	3(2)	7(3)
C(5)	4134(5)	5230(5)	9001(23)	36(3)	33(3)	50(8)	−3(2)	−1(4)	−1(4)
C(6)	4338(7)	4340(5)	422(12)	75(6)	35(4)	48(6)	−3(4)	4(5)	2(3)
C(7)	7807(5)	6226(5)	9727(28)	34(3)	40(4)	96(14)	−11(3)	1(6)	4(6)
C(8)	7569(6)	5310(6)	9505(14)	39(4)	53(5)	72(8)	−14(4)	6(4)	−7(5)
N(1)	1676(4)	1873(4)	2649(9)	27(3)	51(4)	31(3)	−7(3)	9(3)	−9(3)
N(2)	4542(4)	2447(4)	2967(8)	29(3)	53(4)	24(3)	−5(3)	−7(2)	−4(3)
N(3)	339(4)	7368(4)	2358(9)	31(3)	54(4)	27(3)	1(3)	−5(2)	4(3)
N(4)	3173(4)	6975(5)	2123(9)	34(3)	55(4)	25(3)	6(3)	6(3)	5(3)
N(5)	4749(4)	5879(4)	562(8)	32(3)	33(3)	34(3)	3(2)	0(2)	−1(2)
N(6)	8776(4)	6393(4)	9788(26)	29(2)	43(3)	88(10)	−4(2)	−8(5)	−20(8)
O(1)	5199(4)	4089(4)	9873(29)	60(3)	44(3)	108(9)	7(3)	−15(8)	−13(7)
O(2)	6642(5)	5242(5)	9721(38)	47(3)	56(4)	215(18)	−7(3)	−7(11)	1(11)
				B_{iso}/Å^2					
H(15)	530	580	0	4.0					
H(25)	470	590	160	4.0					
H(16)	410	880	880	4.0					
H(26)	390	890	100	4.0					
H(51)	370	540	20	4.0					
H(52)	430	520	820	4.0					
H(61)	450	440	180	4.0					
H(62)	390	390	0	4.0					
H(71)	750	660	100	4.0					
H(72)	750	660	900	4.0					
H(81)	770	540	780	4.0					
H(82)	810	500	50	4.0					
C(9)	590	80	0	5.0					
C(10)	650	960	0	5.0					
C(11)	530	40	100	5.0					
C(21)	570	960	120	5.0					
C(31)	670	40	940	5.0					
C(12)	530	40	900	5.0					
C(22)	570	960	880	5.0					
C(32)	670	40	60	5.0					

a) The U_{ij}'s are defined by $\exp[-2\pi^2(U_{11}h^2a^{*2}+U_{22}k^2b^{*2}+U_{33}l^2c^{*2}+2U_{12}hla^*b^*+2U_{13}hla^*c^*+2U_{23}klb^*c^*)]$. The positional and thermal parameters are multiplied by 10^4 and 10^3, respectively, for the atoms from Cd to O(2); those positional parameters for the atoms from H(15) to C(32) are multiplied by 10^3. The parameters lacking the estimated standard deviations were not refined, but were included in the evaluation of the R values (see text).

estimated standard deviations, except those for O(1) and O(2) atoms, and the R and R_w went down to 0.041 and 0.053, respectively.[17]

The Benzene Clathrate (2): On the Patterson map, the atomic coordinates of Cd and Ni atoms were fixed uniquely. Since the possible space groups predicted from the photographs and the collected intensity data are P4/mmm, P4mm, P422, P$\bar{4}$2m, and P$\bar{4}$m2, there should be statistical distributions at least in the orientation of mea molecule in the crystal structure. In the successive Fourier and difference Fourier syntheses and the block-diagonal least-squares calculations, the positions of the C and N atoms of cyanide group and the C atoms of benzene molecule were found out. By applying the anisotropic thermal parameters for the Ni and Cd, and the isotropic ones for the C and N atoms, the full-matrix least-squares calculations were done for the check of the most proper space group.

Table 4. The final atomic coordinates and thermal parameters with their estimated standard deviations in the parentheses for $Cd(mea)Ni(CN)_4 \cdot 2C_6H_6$[a]

Atom	x	y	z	U_{11}	U_{22}	U_{33}	U_{12}	U_{13}	U_{23}
Cd	0	0	0	22(0)	$=U_{11}$	34(0)	0	0	0
Ni	5000	5000	0	22(0)	$=U_{11}$	36(1)	0	0	0
C(1)	3263(5)	$=x$	0	29(1)	29(0)	41(2)	0(2)	0	0
N(1)	2185(5)	$=x$	0	33(1)	33(0)	65(3)	−3(2)	0	0
C(2)	5000	0	3275(13)	61(5)	84(6)	47(4)	*0*	0	0
C(3)	5000	1526(9)	4143(9)	123(7)	57(4)	77(4)	*0*	0	8(3)
				B_{iso}/Å^2					
N(2)	668(15)	0	2779(14)	3.1(2)					
C(4)	503(18)	0	4177(14)	3.1(3)					

a) The positional and thermal parameters U's are multiplied by 10^4 and 10^3, respectivealy. The U_{ij}'s are defined by: $\exp[-2\pi(U_{11}h^2a^{*2}+U_{22}k^2b^{*2}+U_{33}l^2c^{*2}+2U_{12}hka^*b^*+2U_{13}hla^*c^*+2U_{23}klb^*c^*)]$.

Table 5. Selected bond lengths and angles for $Cd(mea)_2Ni(CN)_4 \cdot C_4H_5N$ and their estimated standard deviations (in parentheses)

Bond length	l/Å	Bond length	l/Å	Bond length	l/Å
Ni-C(1)	1.856(6)	C(1)-N(1)	1.142(9)	N(1)-Cd	2.378(7)
Ni-C(2)	1.847(7)	C(2)-N(2)	1.172(9)	N(2)-Cd	2.326(6)
Ni-C(3)	1.885(6)	C(3)-N(3)	1.111(9)	N(3)-Cd	2.412(7)
Ni-C(4)	1.871(7)	C(4)-N(4)	1.126(9)	N(4)-Cd	2.367(7)
Cd-N(5)	2.295(6)	Cd-N(6)	2.320(7)		
N(5)-C(5)	1.49(1)	C(5)-C(6)	1.52(1)	C(6)-O(1)	1.391(1)
N(6)-C(7)	1.44(1)	C(7)-C(8)	1.51(1)	C(8)-O(2)	1.381(1)
C(5)-H(51)	0.76(1)	C(5)-H(52)	1.24(2)	C(6)-H(61)	1.075(9)
C(6)-C(62)	1.003(9)	C(7)-H(71)	1.22(2)	C(7)-H(72)	0.93(1)
C(8)-H(81)	1.31(1)	C(8)-H(82)	1.19(1)	N(5)-H(15)	0.93(1)
N(5)-H(25)	0.790(6)	N(6)-H(16)	0.95(2)	N(6)-H(26)	1.05(2)
C(9)-C(11 or 12)	1.33	C(11 or 12)-C(12 or 22)	1.41		
C(12 or 22)-C(10)	1.49	C(10)-C(31 or 32)	1.38		
C(31 or 32)-C(9)	1.41				
Bond angle	**ϕ/°**	**Bond angle**	**ϕ/°**		
C(1)-Ni-C(2)	90.3(3)	C(2)-Ni-C(3)	90.7(3)		
C(3)-Ni-C(4)	89.7(3)	C(4)-Ni-C(1)	89.3(3)		
Ni-C(1)-N(1)	178.3(6)	Ni-C(2)-N(2)	178.0(6)		
Ni-C(3)-N(3)	178.9(6)	NI-C(4)-N(4)	175.7(6)		
C(1)-N(1)-Cd	156.2(6)	C(2)-N(2)-Cd	175.2(6)		
C(3)-N(3)-Cd	170.9(6)	C(4)-N(4)-Cd	167.4(6)		
N(4)-Cd-N(5)	84.3(2)	N(5)-Cd-N(6)	172.0(2)		
N(1)-Cd-N(2)	89.4(2)	N(2)-Cd-N(3)	89.4(2)		
N(3)-Cd-N(4)	89.1(2)	N(4)-Cd-N(1)	91.6(2)		
Cd-N(5)-C(5)	114.5(5)	N(5)-C(5)-C(6)	113.8(9)		
C(5)-C(6)-O(1)	110.8(8)	H(15)-N(5)-H(25)	123.1(7)		
H(51)-C(5)-H(52)	125(2)	H(61)-C(6)-H(62)	120.9(9)		
Cd-N(6)-C(7)	121.3(5)	N(6)-C(7)-C(8)	114.2(7)		
C(7)-C(8)-O(2)	107.0(8)	H(16)-N(6)-H(26)	120.9(9)		
H(71)-C(7)-H(72)	88.8(8)	H(81)-C(8)-H(82)	124.8(8)		

Dihedral angle between the statistically distributed pyrrole molecular planes: 71.8°

Since the space groups P$\bar{4}$2m and P$\bar{4}$m2 require the mea and the benzene molecules to take extremely unusual arrangements and orientations, these two were discarded. Although no significant differences were observed in R values among the three possible space groups, those other than P4/mmm required the mea and the benzene molecules to be arranged with higher disorder. Because there are no positive reasons to take such unusual disorder, the space group P4/mmm was adopted. In this space group, however, the mea molecule should be distributed statistically about the fourfold axis and three sets of mirror planes of crystal. Therefore, the N and O atoms of mea were not distinguishable but the O atom was regarded as N, and each of the C and N(=O) of mea was distributed with the occupancy factor of 0.25 about the fourfold axis and the mirror planes in the refinement. By applying the anisotropic thermal parameters to the Cd, Ni, C, and N atoms of cyanide, and C atoms of benzene, and the isotropic ones to the C and N(=O) atoms of mea, the final full-matrix calculations converged to the R and R_w values of 0.047 and 0.063, respectively.[17]

Description of Structures and Discussion

As is shown in Table 1, the pyrrole and the thiophene clathrates have the composition $Cd(mea)_2Ni(CN)_4 \cdot G$ ($G = C_4H_5N$ or C_4H_4S) different from that of the benzene clathrate $Cd(mea)Ni(CN)_4 \cdot 2C_6H_6$ in the numbers of the mea ligands and of the guest molecules in the formula unit. The thiophene clathrate can be thought of as having a structure similar to the pyrrole one, as the crystallographic data in Table 2 show.

The atomic parameters determined for **1** and **2** are listed in Tables 3 and 4, and the illustrations of the structures are shown in Figs. 1 and 2 with the atomic notations; the selected bond lengths and angles are summarized in Tables 5 and 6.

The Structure of Pyrrole Clathrate (1). The pyrrole clathrate has the structure which is considerably distorted from those of the Hofmann-type and those of the analogous clathrates with the hosts containing square-planar $Ni(CN)_4$ moiety so far known, although some similarity to Hofmann-type host $Cd(NH_3)_2Ni(CN)_4$ is seen with regard to the layered two-dimensional network of metal cyanide and the projections of mea ligands from the six-coordinate Cd atoms in the network. The $Ni(CN)_4$ moiety, being almost coplanar by itself, is distorted from the D_{4h} symmetry with the bond angles slightly deviated from 90° about the central Ni atom and with the alignment of Ni–C–N linkages slightly bent from 180°. Furthermore, the joint between the $Ni(CN)_4$ moiety and the Cd atom is bent by 23.8° at the N(1) and by 12.6° at the N(4)

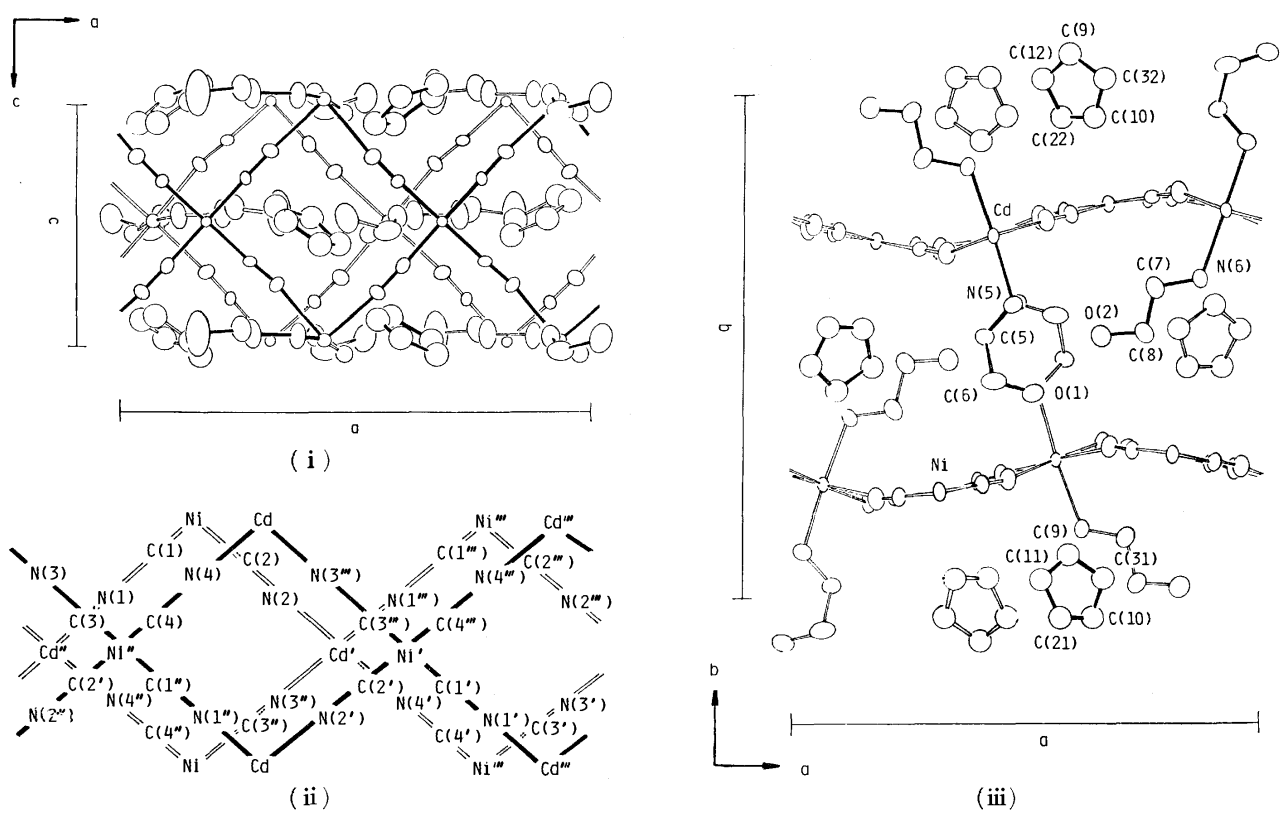

Fig. 1. The structure of $Cd(mea)_2Ni(CN)_4 \cdot C_4H_5N$. (i) Projection along the b axis: the bonds of the moieties belonging to the upper layer are shown with solid lines. (ii) Numbering of the atoms in the metal cyanide networks. Key: normal, x, y, z; with ′, $\bar{x}$, $\bar{y}$, $\frac{1}{2}+z$; with ″, $\frac{1}{2}-x$, $\frac{1}{2}+y$, $\frac{1}{2}+z$; and with ‴, $\frac{1}{2}+x$, $\frac{1}{2}-y$, z. (iii) Projection along the c axis with numbering of the atoms: the bonds of the moieties viewed on this side are shown with solid lines. In (i) and (ii), the hydrogen atoms of the pyrrole molecule and those of the mea, H(n5) at N(5), H(n6) at N(6) (n=1 or 2), H(mn) at C(m) (m=5—8, n=1 or 2), and those at O(1) and O(2), are not shown.

TABLE 6. SELECTED BOND LENGTHS AND ANGLES FOR $Cd(mea)Ni(CN)_4 \cdot 2C_6H_6$ AND THEIR ESTIMATED STANDARD DEVIATIONS (IN PARENTHESES)

Bond length	l/Å	Bond length	l/Å	Bond length	l/Å
Ni-C(1)	1.865(4)	C(1)-N(1)	1.158(5)	N(1)-Cd	2.346(4)
Cd-N(2)	2.31(1)	N(2)-C(4)	1.44(2)	C(4)-C(4′)	1.54(2)
Bond angle	ϕ/°	Bond angle	ϕ/°		
Ni-C(1)-N(1)	180.0(4)	C(1)-N(1)-Cd	180.0(4)		
N(1)-Cd-N(2)	81.1(3)	Cd-N(2)-C(4)	129.2(8)		
N(2)-C(4)-N(4′)	112(1)	C(2)-C(3)-N(3′)	121.2(7)		
C(3)-C(2)-C(3′)	117.6(9)				

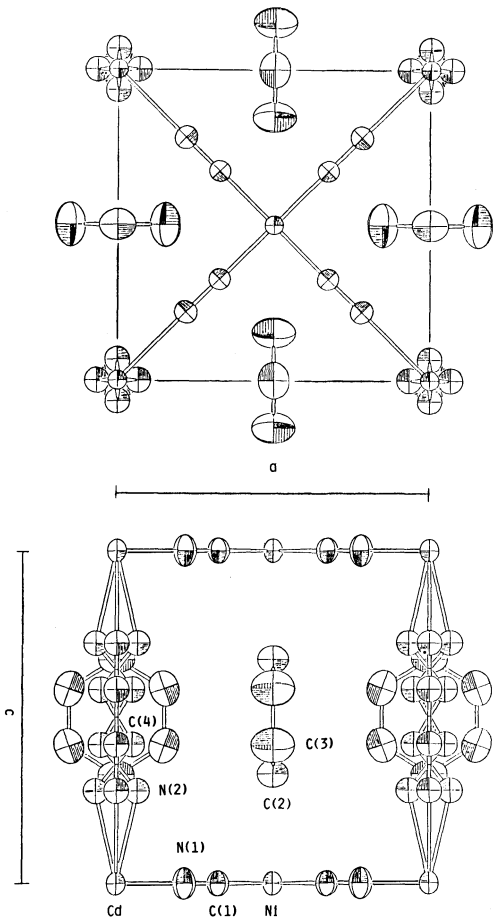

Fig. 2. The structure of $Cd(mea)Ni(CN)_4 \cdot 2C_6H_6$. Top: projection along the c axis, bottom: projection along the b axis.

atom, the distortion leading the layered network to a puckered structure along the crystal a-axis. However, the related bond distances are not unusual. The puckered metal cyanide networks are stacked along the crystal b-axis with an alternate shift approximately by $a/4$ and $c/2$, so that the six-coordinate Cd atom is approximately placed over or beneath the square-planar Ni atom along the crystal b-axis; in Hofmann-type host, the metal cyanide layers are arranged completely parallel to each other. There can be seen two kinds of cavities: one is a real cavity occupied by a guest pyrrole molecule; the other appears to be a pseudo-cavity occupied by the tail parts of two crystallographically-independent mea ligands. One mea plays a role of the column dividing the two kinds of cavities but its OH-end intrudes into the pseudo-cavity occupied mainly by another mea. The latter mea behaves as a pseudo-guest to insert its $-CH_2CH_2OH$ skeleton into the pseudo-cavity. The column mea has approximately a cis form of the N–C–C–O skeleton, and the pseudo-guest mea has a trans form. The O(2) of the latter appears to form hydrogen bonds with the O(1) and the N(5) of the former; the distances are 2.80(1) Å for O(2)–O(1), 3.30(1) Å for O(2)–N(5), and *ca.* 2.2 Å for O(2)–H(51). On the Fourier and difference Fourier maps, it was difficult to find out the positions of protons assigned to the OH groups of O(1) and O(2). As relatively large thermal parameters and their estimated standard deviations have been observed for the O(1) and O(2) atoms, the supposed hydrogen bonds are thought to be not so strong.

Although there should be only one crystallographically-independent pyrrole molecule in an asymmetric unit, three skeletal atoms (not C(9) and C(10)) are statistically distributed about a pseudo-mirror plane (001). If the space group Pnam had been applied, the symmetry operations would have required the statistical distributions not only for the pyrrole molecule but also for the mea ligands. The fact that the estimated standard deviations of the positional parameters are relatively large for the skeletal atoms of the mea ligands suggests the possibility of the Pnam space group. However, this space group was exclude from the consideration of structure because of the unacceptable molecular forms of the mea, as has been described in the Structure Determination section. Both the possible orientations of pyrrole molecule in a cavity appear to be almost equivalent to each other with respect to the host-guest contacts. Therefore, the respective atomic coordinates have been listed in Table 3, and both the orientations have been illustrated in Fig. 1.

The Structure of the Benzene Clathrate (2). The structure of $Cd(mea)Ni(CN)_4 \cdot 2C_6H_6$ is similar to that of Hofmann-en-type $Cd(en)Ni(CN)_4 \cdot 2C_6H_6$ (**2′**),[9] as expected from the similarity in the formula. The metal cyanide network keeps a D_{4h} symmetry and the unit cell contains a formula unit. Trivial differences between **2** and **2′** are found in that the aromatic plane of the guest benzene molecule is vertical to the (100) or (010) plane of the crystal in **2** (space group P4/mmm), whereas the inclination angle is 85° in **2′** (space group P4/m). Additionally, the N- and O-

ends of the mea ligand are indistinguishable from each other in the P4/mmm space group of **2**. The axial disorder of mea which bridges adjacent metal cyanide networks in **2** is also similar to that observed for en in **2'**. Although a rotating model about the fourfold axis of crystal has been applied for en in **2'**, the N(=O) and C atoms of mea in **2** are located on the (100) and (010) planes with an equal probability of 0.25. The deviation from the fourfold axis, *i.e.*, the radius in a rotating model, is 0.507 Å for the N(=O) and 0.382 Å for the C, whereas that of the N in **2'** is 0.63 Å.

Discussion. Each series of Hofmann-type and the analogous clathrates so far known, *e.g.*, Hofmann-type $M(NH_3)_2M'(CN)_4\cdot 2G$, en-Td-type $Cd(en)M'(CN)_4\cdot 2G$ (M'=Cd or Hg), Hofmann-pn-type $Cd(pn)Ni(CN)_4\cdot 1.5G$, *etc.*, has a general composition common to each member of the series for the various guests G, and the hosts are almost isostructural to each other. However, in the case of mea-containing hosts, two kinds of structures have been obtained under similar preparation conditions. In Hofmann-mea-type(1) $Cd(mea)_2Ni(CN)_4\cdot G$ ($G=C_4H_5N$ or C_4H_4S), the mea ligand behaves as a unidentate ligand, whereas in Hofmann-mea-type(2) $Cd(mea)Ni(CN)_4\cdot 2C_6H_6$, it behaves ambidently. The behavior of mea either as a unidentate in type(1) or as an ambident in type(2) probably depends on the size of the guest molecule, the diameter of which, approximated to a ring, is smaller by 0.75 Å for the pyrrole and thiophene than for the benzene in the gaseous state.

As the instability of the benzene clathrate shows, the mea-bridged structure appears to be essentially unfavorable owing to the lower affinity of the O atom of mea as the ligating site to the Cd(II) atom in the metal cyanide network. Except for the present type-(2) structure, few cases have been known where mea behaves as an ambident ligand between different metal atoms. Therefore the unidentate behavior in type(1) appears preferable to the ambident one in type(2) from the viewpoint of the coordination chemistry about the central Cd atom and the ligating atoms. However, the distortion of the metal complex network demonstrated in type(1) structure is unfavorable in terms of the conjugation of π-electrons of cyanide groups throughout the network. This unfavorable outcome may be recovered in a some extent by the interactions between the host mea ligands and the guest pyrrole molecule occupying the larger cavity, and by the interactions of the mea ligands through hydrogen bonds in the smaller pseudo-cavity. A benzene molecule may be too large as a guest to be enclathrated in type(1) host, because the distortion of the metal cyanide network should become too much to cancel the imbalance of the volumes between the benzene molecule in the larger cavity and the mea ligands in the smaller pseudo-cavity.

These observations suggested that we develop another way of design and synthesis of the clathrate compounds analogous to Hofmann-type, using the amine ligands with bulky substituents which bring about distortion of the cyanide network but provide cavities with the guest molecules in various size and shape. The first attempt has been reported briefly.[18,19]

The present work was partially supported by Grants-in-Aid for Scientific Research Nos. 56540357 and 57430011 from the Ministry of Education, Science and Culture.

References

1) T. Iwamoto, T. Miyoshi, T. Miyamoto, Y. Sasaki, and S. Fujiwara, *Bull. Chem. Soc. Jpn.*, **40**, 1174 (1967).
2) T. Iwamoto, T. Nakano, M. Morita, T. Miyoshi, T. Miyamoto, and Y. Sasaki, *Inorg. Chim. Acta*, **2**, 313 (1968).
3) T. Iwamoto, M. Kiyoki, Y. Ohtsu, and Y. Takeshige-Kato, *Bull. Chem. Soc. Jpn.*, **51**, 488 (1978).
4) T. Iwamoto, *Isr. J. Chem.*, **18**, 240 (1979).
5) T. Iwamoto, *J. Mol. Struct.*, **75**, 51 (1981).
6) S. Nishikiori, T. Iwamoto, and Y. Yoshino, *Bull. Chem. Soc. Jpn.*, **53**, 2236 (1980).
7) T. Iwamoto, *Inorg. Chim. Acta.*, **2**, 269 (1968).
8) T. Miyoshi, T. Iwamoto, and Y. Sasaki, *Inorg. Nucl. Chem. Lett.*, **6**, 21 (1970).
9) T. Miyoshi, T. Iwamoto, and Y. Sasaki, *Inorg. Chim. Acta*, **6**, 59 (1972).
10) T. Iwamoto and Y. Ohtsu, *Chem. Lett.*, **1972**, 463.
11) T. Iwamoto and M. Kiyoki, *Bull. Chem. Soc. Jpn.*, **48**, 2414 (1975).
12) S. Nishikiori and T. Iwamoto, *Chem. Lett.*, **1981**, 1775.
13) The diffractometer was used by the courtesy of Professor Yoshihiko Saito at the Institute for Solid State Physics of this University.
14) The diffractometer was used by the courtesy of Professor Yoichi Iitaka at the Faculty of Pharmaceutical Sciences of this University.
15) "The Universal Crystallographic Computation Program System (UNICS)," ed by T. Sakurai, Crystallographic Society of Japan, Tokyo (1967).
16) "International Tables for X-Ray Crystallography," Kynoch Press, Birmingham (1974), Vol. IV.
17) The tables of the structure factors are kept as Document No. 8345 at the Chemical Society of Japan.
18) S. Nishikiori and T. Iwamoto, *Chem. Lett.*, **1982**, 1035.
19) S. Nishikiori and T. Iwamoto, *Chem. Lett.*, **1983**, 1129.

Bis(crown ether) Dyes Incorporating Azophenol Structure

Sadaya KITAZAWA, Keiichi KIMURA,* and Toshiyuki SHONO*

Department of Applied Chemistry, Faculty of Engineering, Osaka University, Yamada-oka, Suita 565

(Received April 25, 1983)

Three types of bis(crown ether) dyes bearing one or two azophenol units were synthesized, which may be expected to show different cation-complexing properties from the corresponding monocyclic crown ether dyes. The extraction of alkali and alkaline-earth metal salts with the crown ether dyes suggested that some cooperative action of the two adjacent crown ether moieties of the bis(crown ether)s occurs on complexing metal cations, although the bis(crown ether) effect is not very remarkable.

Considerable attention has been focussed on crown ether dyes(or chromogenic crown ethers), where a chromophore such as picrylamine,[1,2] azo dye,[3-5] and other dye stuff,[6,7] is incorporated into a crown ether moiety. Some of the crown ether dyes possess a potential anionic site attached to their chromophore either inside or outside the crown ether cavity, which results in formation of intramolecular ion-pair complexes with alkali and alkaline-earth metal cations under basic conditions. The complex formation leads to marked color changes of dye solutions. In the other crown ether dyes which do not contain any dissociable group in the vicinity of the chromophore, crown ether amines are incorporated into dye molecules in such a manner that the chromophore directly affects the complexation with metal cations, thus showing characteristic coloration in the presence of various metal cations. The coloration of both types of crown ether dyes is influenced considerably by the relative size of crown ether cavity and complexed metal cations, and the charge density of cations, so they are often called ion-selective dyes. Thus, the crown ether derivatives bearing chromophore are promising analytical reagents for colorimetry and metal-ion indicators.

Bis(crown ether) derivatives, macrobicyclic polyethers containing two crown ether moieties at the end of a short aliphatic chain, are known to have attractive cation-complexing properties different from the corresponding monocyclic crown ethers.[8-10] They can form intramolecular sandwich-type metal complexes easily by cooperative action of two adjacent crown ether rings. The complexing behavior of the bis(crown ether)s is typical of certain alkali metal cations which are slightly larger in size than the cavity of the crown ether ring. It seems likely that this type of complex formation provides the bis(crown ether) derivatives with excellent cation-complexing abilities and/or selectivities.

These observations induced us to incorporate chromophore into bis(crown ether)s and to see what the difference in the ion-selectivity is between the bis(crown ether) dyes and the corresponding monocyclic ones. This paper concerns with the syntheses of various bis(crown ether) dyes containing azophenol skeleton and their coloration behavior on extraction of alkali and alkaline-earth metal salts.

Results and Discussion

Syntheses of Bis(crown ether) Dyes. Azophenol structure was selected as a chromophore of bis(crown ether) dyes. Three types of bis(crown ether) dyes **1** through **3** were synthesized as shown in scheme 1. The general procedure consists of a conventional diazotization-coupling reaction of aromatic amines with phenols containing crown ether moieties.

The first type of bis(crown ether) dyes **1** (n=1,2) are made up of two monocyclic crown ether bearing an intra-annular phenolic group in the azophenol structure. Diazotization of triethylene glycol bis(p-amino-

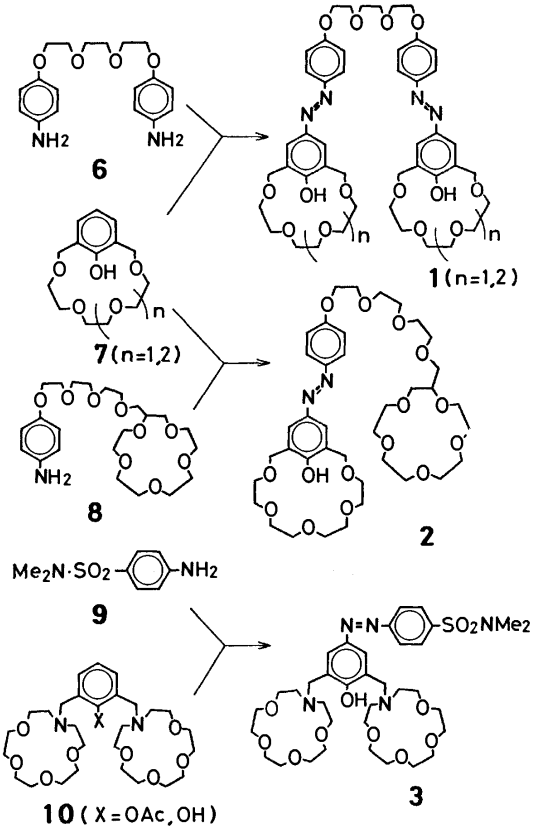

Scheme 1.

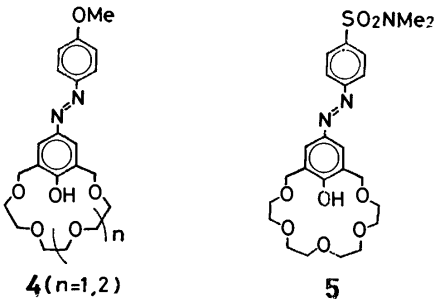

phenyl) ether (**6**), followed by coupling reaction with crown ether phenol **7** (n=1,2)[11] affords yellow-powdery bis(crown ether) dyes **1** (n=1,2).

In the second type of bis(crown ether) dye **2**, monocyclic crown ether dye **4** (n=2) is connected to 15-crown-5 using an oligo(oxyethylene) chain. The yellow oil of the unsymmetrical bis(crown ether) dye was obtained by the diazotization-coupling reaction of crown ether phenol **7** (n=2) with 15-crown-5 derivative carrying aminophenyl group, which can be prepared by the condensation of hydroxymethyl-15-crown-5 and triethylene glycol mono(p-nitrophenyl) ether, followed by hydrogenation over palladium-carbon.

In the third type of bis(crown ether) dye **3**, an azophenol dye is set up on the bridge containing two azacrown ether rings, the phenolic group being outside the crown ether cavity unlike the preceding ones. Bis(crown ether) **10** (X=$OCOCH_3$) was synthesized at first by condensation reaction of 2,6-bis(bromomethyl)phenyl acetate with two equivalents of monoaza-15-crown-5, and then hydrolyzed to bis(crown ether) phenol **10** (X=OH). The diazotization-coupling reaction of *N*,*N*-dimethyl-*p*-aminobenzenesulfonamide with the bis(crown ether) phenol gave orange oil of bis(crown ether) dye **3**.

Monocyclic crown ether dyes **4** (n=1,2) and **5** were also synthesized by the conventional diazotization-coupling reaction for comparison.

Complexation with Alkali and Alkaline-earth Metal Salts. For rapid screening of the complexing abilities of the bis(crown ether) dyes, **1** through **3**, extractions were carried out from aqueous solutions of alkali and alkaline-earth metal(Li^+, Na^+, K^+, Sr^{2+}, and Ba^{2+}) hydroxide with crown ether dye chloroform solutions. The corresponding monocyclic crown ether dyes, **4** and **5**, were also employed for comparison. Figures 1 and 2 depict the absorption spectra of the chloroform layer containing bis(crown ether) dyes **1** (n=1,2), which were obtained immediately after the extraction. The color of the chloroform layer changed from yellow to orange after the extraction of metal hydroxides, that

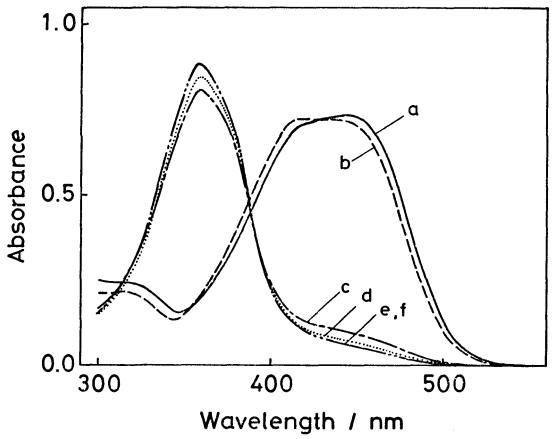

Fig. 1. Absorption spectra of 2×10^{-5} M **1**(n=1) in chloroform equilibrated with 0.04 M aqueous metal hydroxide solution. (1 M=1 mol dm^{-3})
a, $Ba(OH)_2$; b, $Sr(OH)_2$; c, LiOH; d, NaOH; e, KOH; f, without salt.

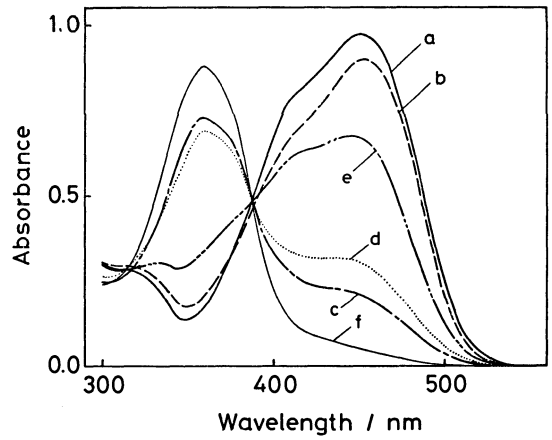

Fig. 2. Absorption spectra of 2×10^{-5} M **1**(n=2) in chloroform equilibrated with 0.04 M aqueous metal hydroxide solution.
The symbols are the same as those in Fig. 1.

is, a new peak appears at the higher wavelength, as the peak based on the uncomplexed crown ether dye diminishes at the lower wavelength. This indicates that when the crown ether dye complexes metal cations, the phenolic group interacts with the complexed cation appreciably. Since the molar absorptivity for the metal complexes does not change very much from one metal cation to the other, the complexing abilities of the crown ether dyes for metal cations can be discussed qualitatively from the absorbance of the new peaks. The complexing ability of bis(crown ether) dye **1**(n=1) decreases in the order $Ba^{2+}>Sr^{2+}\gg Li^+>Na^+>K^+$, while that of bis(crown ether) dye **1**(n=2) follows the order $Ba^{2+}>Sr^{2+}>K^+>Na^+>Li^+$. The corresponding monocyclic crown ether dyes **4** and **5** were essentially the same in the complexing tendency. However, it is worth noting that there is some difference in the absorption spectra between bis(crown ether) dye **1**(n=1) and monocyclic one **4**(n=1), as illustrated in Fig. 3. The complexing abilities of **4**(n=1) for Ba^{2+}, Sr^{2+}, Na^+, and K^+ were improved by the introduction of bis(crown ether) structure.

In the unsymmetrical bis(crown ether) dye **2**, the aliphatic crown ether moiety is expected to take an extra part in the complexation of the crown ether phenol moiety with metal cations. Unfortunately, the absorption spectra obtained in the **2**–metal hydroxide extraction system(Fig. 4) do not offer any distinct evidence about the cooperative complexation of two different crown ether moieties. Another possibility is that the aliphatic crown ether moiety complexes a metal cation by itself, then the crown ether phenol approaches the complex intramolecularly as the counter anion, but no further investigation was performed about this point.

In the third type of bis(crown ether) dye **3**, an azophenol unit exists on the bridge connecting two azacrown ethers, the phenolic group being outside the crown ether moieties unlike the preceding types of bis(crown ether) dyes, **1** and **2**. The absorption spectra obtained in the metal hydroxide extraction systems (Fig. 5) show that the complexing ability of bis(crown

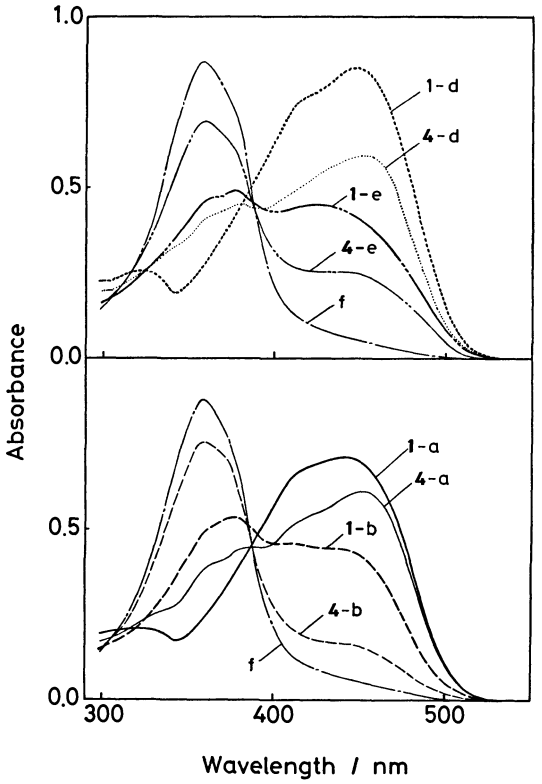

Fig. 3. Absorption spectra of **1**($n=1$) and **4**($n=1$) in chloroform equilibrated with aqueous metal hydroxide solution.
The symbols are the same as those in Fig. 1.
Crown ether unit concentration: 4×10^{-5} M, alkali metal concentration: 0.4 M, alkaline-earth metal concentration: 0.004 M.

ether) dye **3** for alkaline-earth metal cations is rather low compared to that of **1** and **2**. Crown ether dye **11**, the complexing ability of which has been studied by Nakamura *et al.*,[12] can be chosen as the corresponding monocyclic one of **3**, although the dye component is not azophenol but *p*-nitrophenol unit. Therefore,

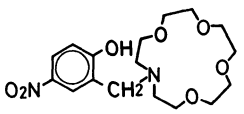

11

in order to compare the complexing ability of **3** with that of **11**, extractions were also made under the identical conditions in the **11** system, that is, from a metal chloride aqueous solution with a crown ether dye chloroform solution containing triethylamine. The extraction equilibrium constant(K_e) and the acid-dissociation constant(K_a) are listed in Table 1, together with the values for **11**. In the monocyclic crown ether dye **11**, the extractability(the complexing ability) decreases in the order $Li^+>Na^+>K^+$. This moderate lithium selectivity of **11** was explained in terms of the coordination interaction of the phenolate anion with the crown-complexed cation.[12] On the other hand, the extractability of bis(crown ether) dye **3** follows the order $Na^+>Li^+>K^+$, where the extractability for Na^+ is

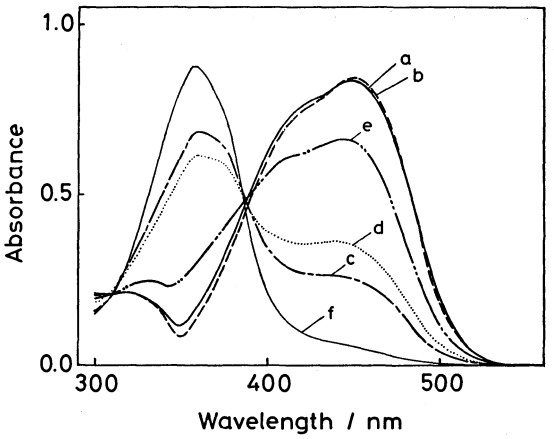

Fig. 4. Absorption spectra of 4×10^{-5} M **2** in chloroform equilibrated with 0.04 M aqueous metal hydroxide solution.
The symbols are the same as those in Fig. 1.

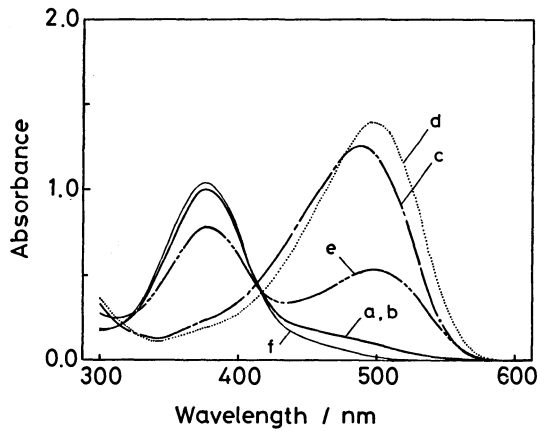

Fig. 5. Absorption spectra of 4×10^{-5} M **3** in chloroform equilibrated with 0.04 M aqueous metal hydroxide solution.
The symbols are the same as those in Fig. 1.

Table 1. Extraction equilibrium constant(K_e) and acid-dissociation constant(K_a) in the extraction of alkali metal salts

Crown ether dye	$-\log K_e$			$-\log K_a$
	Li^+	Na^+	K^+	
3	11.0	10.6	11.7	3.55[b]
11[a]	9.15	9.76	9.86	5.79

a) Taken from Ref. 12. b) Measured in H_2O containing about 0.1 M tetramethylammonium chloride.

slightly higher than that for Li^+. It has been discussed in detail by Nakamura *et al.*,[5] how the basicity(or acidity) of an anionic site can contribute to ion-selectivity of various crown ethers carrying a phenolic group in the periphery. It is likely that the anionic site possessing a localized charge(high basicity) coordinates to the crown-complexed metal cation, thus resulting in the preference for the smaller alkali metal cations. In contrast with the above site, the anionic site with a delocalized charge(low basicity) favors an

ion-pair interaction with the complexed metal cations. As the acid-dissociation constant of bis(crown ether) dye **3** is larger than monocyclic one **11** by about two orders of magnitude, the azophenol unit itself tends to enhance the Li^+-extractability of the crown ether dye compared with the *p*-nitrophenol unit. Nevertheless, bis(crown ether) dye **3** prefers Na^+ to Li^+ in the extraction of alkali metal salts. This finding indicates the possibility of such specific complex formation of the bis(crown ether) dye as often observed in the conventional bis(crown ether) derivatives.

Experimental

Syntheses of Crown Ether Dyes. General Procedure of Diazotization-coupling Reaction: An aniline derivative (10 mmol) in 1 M† HCl (30 cm^3) was diazotized by treating with $NaNO_2$ (12 mmol) at 0°C. The resulting diazonium salt solution was added dropwise to a phenol derivative dissolved in 0.25 M NaOH (50 cm^3) with vigorous stirring at room temperature. In the meantime the color of the solution changed to orange and then to yellow. To this mixture was added 1 M NaOH until the color turned again to orange, and then the mixture was allowed to stand overnight. Acidification of this solution by 1 M HCl gave yellow or orange precipitates, which were recovered by filtration and washed with water. The purification steps depended on the nature of the product, and most of the solid product were purified by recrystallization from ethanol–water(2:1).

Bis(crown ether) Dyes ***1****(n=1,2)*: The aniline component, 1,8-bis(*p*-aminophenoxy)-3,6-dioxaoctane, was obtained by the reaction of *p*-nitrophenol with 1,8-dibromo-3,6-dioxaoctane in acetone in the presence of K_2CO_3, followed by hydrogenation on palladium-carbon in dioxane. **1**(*n*=1): yellow crystals; mp 150 °C(decomp); UV($CHCl_3$) 358 nm (ε 5.3×10^4); IR(KBr) 3300(O–H), 1600(aromatic nuclei), 1590(N=N), and 1120 cm^{-1}(C–O–C); ^{1}H-NMR($CDCl_3$) δ= 3.55—3.98(36H, m, OCH_2CH_2O), 4.10(4H, t, CH_2OPh), 4.71(8H, s, CH_2Ph), 6.98(4H, d, aromatic H), 7.68—7.96 (8H, m, aromatic H), and 8.12(2H, s, OH); Found: C, 61.72; H, 6.64; N, 6.17%. Calcd for $C_{46}H_{58}N_4O_{14}$: C, 62.01; H, 6.56; N, 6.29%. **1**(*n*=2): yellow crystals; mp 123 °C(decomp); UV($CHCl_3$) 358 nm(ε 5.4×10^4); IR(KBr) 3250(O–H), 1590(aromatic nuclei), 1575(N=N), and 1100 cm^{-1}(C–O–C); ^{1}H-NMR($CDCl_3$) δ=3.60—3.98(44H, m, OCH_2CH_2O), 4.11(4H, t, CH_2OPh), 4.76(8H, s, CH_2PH), 7.02(4H, d, aromatic H), 7.75—7.99(8H, m, aromatic H), and 8.57(2H, s, OH). Found: C, 60.88; H, 6.75; N, 5.68%. Calcd for $C_{50}H_{66}N_4O_{16}$; C, 61.34; H, 6.79; N, 5.72%.

Bis(crown ether) Dye ***2***: The aniline component, [10-(*p*-nitrophenoxy)-2,5,8-trioxadecyl]-15-crown-5 (**8**) was prepared by the reaction of hydroxymethyl-15-crown-5 with 8-(*p*-nitrophenoxy)-3,6-dioxaoctyl tosylate in THF in the presence of NaH, followed by hydrogenation on palladium-carbon. After the coupling reaction and the acidification the product was extracted with chloroform(30 $cm^3\times5$). The combined extract was washed successively with 5% NaOH, water, 1 M HCl, and water and then dried. Bis(crown ether) dye **2** was purified by silica-gel column chromatography using chloroform–ethanol(5:2). **2**: orange oil: UV ($CHCl_3$) 358 nm(ε 2.2×10^4); IR(KBr) 3340(O–H), 1600 (aromatic nuclei), and 1110 cm^{-1}(C–O–C); ^{1}H-NMR($CDCl_3$) δ=3.50—3.90(47H, m, OCH_2CH_2O), 4.15(2H, m, CH_2OPh), 4.73(4H, s, CH_2Ph), 7.02(2H, d, aromatic H), 7.68—7.86 (4H, m, aromatic H), and 8.48(1H, s, OH).

Bis(crown ether) Dye ***3***: The precursor of the phenol component containing a bis(crown ether) moiety, **10**(X=$OCOCH_3$), was made up as follows. To an acetonitrile solution(50 cm^3) of monoaza-15-crown-5[13] (20 mmol) was added 2,6-bis(bromomethyl)phenyl acetate[14] (10 mmol) dissolved in acetonitrile(50 cm^3) under a nitrogen atmosphere at the refluxing temperature. After refluxing for 6 h, K_2CO_3 (20 mmol) was added to the reaction mixture, which was then continued to reflux with vigorous stirring for three more hours. The insoluble materials were filtered off and then washed with acetonitrile. Solvent evaporation of the filtrate gave a pale yellow oil of **10**(X=$OCOCH_3$); IR (neat) 1705(ester C=O), 1600(aromatic nucleus), and 1125 cm^{-1}(C–O–C); ^{1}H-NMR($CDCl_3$) δ=2.11(3H, s, CH_3CO), 2.70—3.00(8H, m, NCH_2), 3.50—3.90(32H, m, OCH_2), 3.83(4H, s, CH_2Ph), and 6.64—7.16(3H, m, aromatic H); MS(70 eV) *m/e*(rel intensity) 598(M^+, 4), 555(7), 379(32), 337(47), and 43(100). Bis(crown ether) phenol **10**(X=OH), which is accessible from **10**(X=$OCOCH_3$) by treating with 1 M NaOH, is labile to air oxidation, and subjected coupling reaction immediately after the hydrolysis. On the coupling reaction a small quantity of ethanol(10%) was required for solubilizing the aniline component **9**. After the reaction the crude product was extracted by chloroform (20 $cm^3\times5$) without the acidification process, and then back-extracted to 1 M HCl. The solution was adjusted to pH *ca.* 9 with concentrated aqueous ammonia and thereafter the product was again extracted with chloroform(20 $cm^3\times5$). The extract was washed with water, dried over Na_2SO_4, and concentrated to yield brown oil. Column chromatography[neutral alumina, ethanol–benzene(1:10)] affords pure bis(crown ether) dye **3**: reddish orange oil; UV($CHCl_3$) 378 nm(ε 2.6×10^4); IR(neat) 1600(aromatic nuclei), 1350 and 1165(SO_2), and 1125 cm^{-1}(C–O–C); ^{1}H-NMR($CDCl_3$) δ=2.74(6H, s, NCH_3), 2.86(8H, t, CH_2N), 3.50—3.90(32H, m, CH_2O), 3.86(4H, s, CH_2Ph), and 7.75—8.00(6H, m, aromatic H).

Monocyclic Crown Ether Dyes ***4*** *and* ***5***: They can be synthesized according to the general procedure. **4**(*n*=1): yellow crystals; mp 136—137 °C; UV($CHCl_3$) 358 nm(ε 2.2×10^4); IR(KBr) 3260(O–H), 1600(aromatic nuclei), 1580(N=N), and 1130 cm^{-1}(C–O–C); ^{1}H-NMR($CDCl_3$) δ=3.60—3.80 (12H, m, OCH_2CH_2O), 3.87(3H, s, OCH_3), 4.71(4H, s, CH_2Ph), 6.98(2H, d, aromatic H), 7.69—7.89(4H, m, aromatic H), and 8.12(1H, s, OH). **4**(*n*=2): yellow crystals; mp 95.5—96.5 °C; UV($CHCl_3$) 358 nm(ε 2.2×10^4); IR (KBr) 3260(O–H), 1590(aromatic nuclei), and 1100 cm^{-1} (C–O–C); ^{1}H-NMR($CDCl_3$) δ=3.60—3.80(16H, m, OCH_2-CH_2O), 3.87(3H, s, OCH_3), 4.75(4H, s, CH_2Ph), 6.98(2H, d, aromatic H), 7.73—7.79(4H, m, aromatic H), and 8.50 (1H, s, OH).

On the synthesis of **5**, the addition of ethanol was necessary because of the poor water-solubility, in a similar way to bis(crown ether) dye **3**. **5**: orange crystalline plates; mp 143.5—144.5 °C; UV($CHCl_3$) 364 nm(ε 2.9×10^4); IR (KBr) 3270(O–H), 1600(aromatic nuclei), 1350 and 1175 (SO_2), and 1120 cm^{-1}(C–O–C); ^{1}H-NMR($CDCl_3$) δ=2.74 (6H, s, NCH_3), 3.60—3.90(16H, m, OCH_2CH_2O), 4.77(4H, s, CH_2Ph), 7.79—8.04(6H, m, aromatic H), and 8.77(1H, s, OH).

Solvent Extraction. Extraction of Metal Hydroxide: In a stoppered 1-cm cell with about 10 cm^3 of volume was placed 4 cm^3 of a 0.04 M alkali or alkaline-earth metal hydroxide aqueous solution and 4 cm^3 of 4×10^{-5} M(for azophenol unit) crown ether dye chloroform solution, and

† 1 M=1 mol dm^{-3}.

then shaken vigorously at ambient temperature. After the complete phase separation the absorption spectrum of the chloroform layer was taken using a Hitachi 340 recording spectrometer.

Extraction of Metal Chloride in the Presence of Triethylamine: The experiments were done in a similar way to that in the literature.[2] Equal volumes(10 cm^3) of 0.5 or 0.1 M alkali metal chloride solution and$(0.5—2.5)\times10^{-5}$ M crown ether dye chloroform solution containing 0.2 M triethylamine were introduced into a stoppered flask and then shaken at 25.0 $\pm$0.1 °C for 30 min. Then, the absorbance of the chloroform layer was measured at 378 nm(uncomplexed, ε 2.61×10^4), and at 487 nm(Li^+ complex, ε 3.29×10^4), 493 nm(Na^+ complex, ε 3.49×10^4), or 500 nm(K^+ complex, ε 3.50×10^4) using 1-cm standard cell. Thus, each of the species in the chloroform layer can be calculated using the ε values, which were determined in separate experiments. The values of K_e and K_a were determined according to the published method.[2]

References

1) H. Nakamura, M. Takagi, and K. Ueno, *Talanta*, **26**, 921 (1979).

2) H. Nakamura, M. Takagi, and K. Ueno, *Anal. Chem.*, **52**, 1668 (1980).

3) K. Sugihara, T. Kaneda, and S. Misumi, *Heterocycles*, **18**, 57 (1982).

4) K. Nakashima, S. Nakatsuji, S. Akiyama, T. Kaneda, and S. Misumi, *Chem. Lett.*, **1982**, 1781.

5) H. Nakamura, H. Nishida, M. Takagi, and K. Ueno, *Anal. Chim. Acta*, **139**, 219 (1982).

6) J. P. Dix and F. Vögtle, *Chem. Ber.*, **113**, 457 (1980).

7) J. P. Dix and F. Vögtle, *Chem. Ber.*, **114**, 638 (1981).

8) M. Bourgoin, K. H. Wong, J. Y. Hui, and J. Smid, *J. Am. Chem. Soc.*, **97**, 3462 (1975).

9) K. Kimura, T. Maeda, and T. Shono, *Talanta*, **26**, 945 (1979).

10) K. Kimura, T. Maeda, H. Tamura, and T. Shono, *J. Electroanal. Chem. Interfacial Electrochem.*, **95**, 91 (1979).

11) M. A. McKervey and D. L. Mulholland, *J. Chem. Soc., Chem. Commun.*, **1977**, 438.

12) H. Nakamura, H. Sakka, M. Takagi, and K. Ueno, *Chem. Lett.*, **1981**, 1305.

13) M. J. Calverley and J. Dale, *Acta Chem. Scand., Ser. B*, **36**, 241 (1982).

14) F. Vögtle and P. Neumann, *Tetrahedron*, **26**, 5299 (1970).

Copper(II)–Sulfur Interactions in Pyridine- and Imidazole-containing Disulfide Complexes. Syntheses, Spectra, and Solution Equilibria

Osamu YAMAUCHI,* Hiroko SEKI, and Toshiya SHODA

Faculty of Pharmaceutical Sciences, Kanazawa University, Takaramachi, Kanazawa 920

(Received April 25, 1983)

Synthetic, spectroscopic, and potentiometric studies on the copper(II) complexes of pyridine-, quinoline-, and imidazole-ring-containing disulfides and related compounds have been made with emphasis on copper(II)–sulfur interactions. In the presence of copper(II), disulfide ligands, $(RCH_2NHCH_2CH_2S-)_2$, where R=4-imidazolyl (IMAD), 2-pyridyl (PMAD), 6-methyl-2-pyridyl (MPAD), and 2-quinolyl (QMAD), are more stable in acid solution than in neutral–alkaline solution. A stable 1:1 copper(II) complex, $Cu(IMAD)(ClO_4)_2 \cdot H_2O$, was isolated as crystals from aqueous solution, whereas a binuclear complex, $Cu_2(PMAD)Cl_4$, was obtained as crystals in ethanol. The Cu(II)–IMAD systems exhibit a single d-d peak at 585 nm indicative of a CuN_4 chromophore but no charge transfer (CT) band in the region 300—900 nm. The other Cu(II)–disulfide systems exhibit d-d bands at 650 and $\approx$850 nm. A shoulder at 310—330 nm observed for the Cu(II)–PMAD and –MPAD systems at pH $\approx$4 and $>$6, respectively, is assigned to the S$\rightarrow$Cu(II) CT transition. Thioether ligands, *N*-(2-pyridylmethyl)-L-methionine and *N*-(4-imidazolylmethyl)-DL-methionine, show the S$\rightarrow$Cu(II) CT peak at $\approx$310 nm at pH 9 in the 1:1 Cu(II)–ligand systems. Equilibrium constants of the proton-ligand and Cu(II)–ligand systems were determined by pH titrations at 25 °C and I=0.1(KNO_3). The Cu(II)–disulfide systems were analyzed by considering monomeric species CuL, CuLH, and $CuLH_2$ (L=ligand; H=proton) and a binuclear species Cu_2L; the $\log \beta_{110}$ values for CuL are 13.38, 13.32, and 9.46 for L=IMAD, PMAD, and MPAD, respectively. Conductivity measurements showed that the Cu(II)–IMAD complex isolated as crystals is monomeric in aqueous solution. Comparison of the electronic absorption and electron spin resonance spectral data and stability constants for various systems suggests that Cu(II)–PMAD has a square-pyramidal CuN_4S chromophore with a sulfur atom in an equatorial position, whereas Cu(II)–IMAD has a planar CuN_4 chromophore. The stability of disulfide bonds in copper(II) complexes in aqueous solution is briefly discussed on the basis of the modes of coordination.

Sulfur as a soft Lewis base is an important ligand atom in various metal complexes and is now established as a constituent of the biological copper site in plastocyanin[1] and azurin,[2] where copper is bound to a thiolate and a thioether sulfur and two imidazole nitrogens. For the copper(I)/copper(II) redox systems, the binding site should have a proper affinity for both oxidation states, and combination of sulfurs and aromatic nitrogens around copper in the proteins may be a necessary consequence.

Disulfide sulfurs, on the other hand, have been postulated to be involved in the copper binding in stellacyanin.[3–5] Because of the coordinating ability of sulfur and the redox activities of copper and disulfide groups,[6–8] copper–disulfide systems may play a unique role in biological systems. Disulfide and thioether groups usually exhibit weak ligation toward copper (II)[9] unless effective neighboring donor groups force them to be in the vicinity of copper(II). The interactions of copper(I) and copper(II) with multidentate disulfide ligands are particularly intriguing because (i) the disulfide group involved in a multidentate ligand with aromatic nitrogens and other donor groups may coordinate to copper to form a binuclear or a dimeric complex of potential biological significance and (ii) it may participate in redox reactions with copper(I) and/or copper(II) upon complex formation. Lewis acids such as silver(I) and mercury(I) are known to cleave disulfide bonds.[10] Seff and his collaborators found that the reaction of copper(II) with di-2-pyridyl disulfide gives the corresponding copper(I)–disulfide complex as the main product and a small amount of the copper(II) complex of 2-pyridinesulfinate.[11] We have recently observed that a pyridine-containing disulfide, bis[2-(2-pyridylmethylamino)-ethyl] disulfide (PMAD), reacts with copper(II) under aerobic conditions to give the copper(II) complex of 2-(2-pyridylmethylamino)ethanesulfinate[12] and that the oxygen atoms from molecular oxygen are partly incorporated into the sulfinate moiety.[13] Since

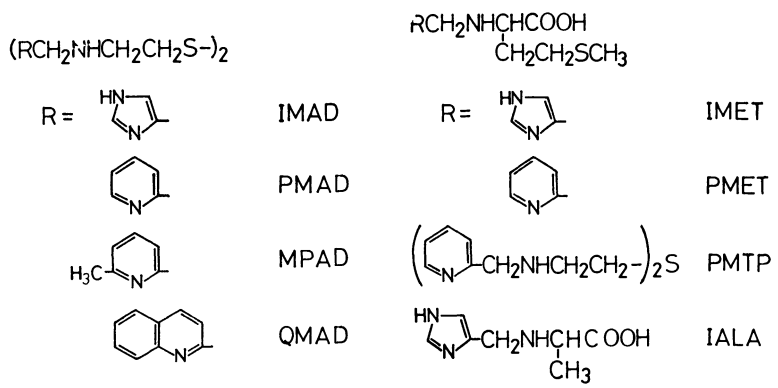

such reactions of disulfide ligands depend much on their structures, the modes of copper(II)–disulfide interactions would have a crucial effect on the stability of the disulfide bond in aqueous solution.

In view of the potential importance of the structural and functional properties expected for copper–disulfide systems and the paucity of relevant information, we now investigated the properties of the copper(II) complexes of disulfide and related ligands involving pyridine, quinoline, and imidazole rings in order to acquire basic information of the modes of copper(II)–sulfur interactions and their effects on the complex and disulfide bond stabilities in solution. We initiated this study on the presumption that only the complexes with weak or no disulfide sulfur–copper(II) interactions are stable in aqueous solution, whereas those with strong interactions suffer disulfide bond cleavage.

Experimental

Materials. 2-Pyridinecarbaldehyde was obtained from Tokyo Kasei Kogyo, and cystamine (bis(2-aminoethyl) disulfide) dihydrochloride and methyl L-alaninate hydrochloride from Nakarai Chemicals. Methyl L-methioninate was purchased from Sigma. 4-Imidazolecarbaldehyde was prepared from 4-(hydroxymethyl)imidazole hydrochloride by oxidation with nitric acid.[14] 1.9-Di-2-pyridyl-2,5,8-triazanonane (PDIEN) trihydrochloride[15] was prepared by reducing the Schiff base obtained from 2-pyridinecarbaldehyde and diethylenetriamine. All the materials used were of reagent grade, and distilled and deionized water was used throughout.

Syntheses.[16] *Bis[2-(4-imidazolylmethylamino)ethyl] Disulfide (IMAD)*: To a solution of cystamine dihydrochloride (11.26 g, 0.050 mol) in ethanol was added potassium hydroxide (5.61 g, 0.10 mol) dissolved in methanol, and the resulting inorganic salt (KCl) was removed by filtration. 4-Imidazolecarbaldehyde (9.60 g, 0.10 mol) in methanol was added to the filtrate, which was stirred for 30 min at 40—50 °C. A solution of $NaBH_4$ (3.8 g, 0.1 mol) in methanol was then added dropwise to the solution under cooling. The reaction mixture was neutralized with 1 M HCl (M= mol dm^{-3}), concentrated *in vacuo*, and extracted with methanol. Dry HCl gas was bubbled through the extract in methanol, when colorless crystals separated. These were filtered, washed with ethanol, and recrystallized from methanol to give IMAD·3HCl·H_2O in 80% yield. Found: C, 32.89; H, 5.73; N, 19.11; Cl, 24.18; S, 14.58%. Calcd for $C_{12}H_{23}N_6Cl_3S_2 \cdot H_2O$: C, 32.89; H, 5.76; N, 18.94; Cl, 24.15; S, 14.56%.

Bis[2-(2-pyridylmethylamino)ethyl] Disulfide (PMAD):[17] This disulfide was obtained as tetrahydrochloride in the same manner from cystamine dihydrochloride (11.26 g, 0.050 mol) and 2-pyridinecarbaldehyde (10.8 g, 0.10 mol) in 70% yield. Mp 167 °C (decomp). Found: C, 38.28; H, 5.40; N, 11.39; Cl, 28.49; S, 12.84%. Calcd for $C_{16}H_{26}N_4Cl_4S_2 \cdot H_2O$: C, 38.56; H, 5.66; N, 11.24; Cl, 28.46; S, 12.87%.

Bis[2-(6-methyl-2-pyridylmethylamino)ethyl] Disulfide (MPAD): This was prepared in methanol in the manner described for IMAD from cystamine dihydrochloride (4.68 g, 0.021 mol) and 6-methyl-2-pyridinecarbaldehyde (5.05 g, 0.042 mol) and recrystallized from methanol–ethanol. Yield, 25%; mp 191—193 °C. Found: C, 40.03; H, 6.30; N, 10.06%. Calcd for $C_{18}H_{30}N_4Cl_4S_2 \cdot 2H_2O$: C, 39.71; H, 6.29; N, 10.29%.

Bis[2-(2-quinolylmethylamino)ethyl] Disulfide (QMAD): This was prepared in tetrahydrofuran–methanol in an analogous manner from cystamine dihydrochloride (5.54 g, 0.024 mol) and 2-quinolinecarbaldehyde (7.60 g, 0.048 mol) and recrystallized from ethanol. Yield, 10%; mp 199—200 °C. Found: C, 56.53; H, 5.56; N, 10.79%. Calcd for $C_{24}H_{23}N_4Cl_2S_2$: C, 56.79; H, 5.56; N, 11.04%.

Bis[2-(2-pyridylmethylamino)ethyl] Sulfide (PMTP):[18,19] To a solution of bis(2-aminoethyl) sulfide dihydrochloride (9.65 g, 0.050 mol) in anhydrous ethanol was added potassium hydroxide (5.6 g, 0.1 mol) in ethanol under N_2. After the inorganic salt was quickly removed by filtration, 2-pyridinecarbaldehyde (10.8 g, 0.1 mol) was added to the filtrate and the mixture was stirred for 10 min at room temperature. Reduction with $NaBH_4$ (3.8 g, 0.1 mol) and isolation as a hydrochloride were performed in the manner described for IMAD. Repeated recrystallization from ethanol gave PMTP·2HCl·H_2O as a pale yellow powder, mp 148 °C, in 60% yield. Found: C, 48.89; H, 6.20; N, 14.14; Cl, 18.95; S, 7.91%. Calcd for $C_{16}H_{24}N_4Cl_2S \cdot H_2O$: C, 48.85; H, 6.66; N, 14.24; Cl, 18.10; S, 8.15%.

N-(4-Imidazolylmethyl)-DL-methionine (IMET): A solution of methyl L-methioninate in methanol, prepared from the hydrochloride (11.75 g, 0.050 mol) and potassium hydroxide (2.81 g, 0.050 mol) in methanol, was added dropwise to a solution of 4-imidazolecarbaldehyde (4.80 g, 0.050 mol) in methanol. The mixture was stirred for 1—2 h at 30—40 °C, cooled, and treated with $NaBH_4$ (1.90 g, 0.050 mol) in methanol and then with 1 M HCl as described for IMAD. Sodium hydroxide (2.0 g, 0.05 mol) dissolved in water was added to the mixture, which was stirred for 30 min at room temperature, acidified with hydrochloric acid, and concentrated *in vacuo*. The residue was extracted several times with methanol and concentrated *in vacuo*. Recrystallization from methanol containing hydrochloric acid gave IMET·HCl as a colorless powder, mp 240—242 °C (decomp), in 80% yield. Found: C, 40.71; H, 6.12; N, 16.21; Cl, 12.61; S, 11.62%. Calcd for $C_9H_{16}N_3O_2ClS$: C, 40.68; H, 6.07; N, 15.81; Cl, 13.34; S, 12.06%. The Cu(II)–IMET systems did not give the expected circular dichroism (CD) spectral peaks in the d-d region, and accordingly IMET·HCl is described as a racemic mixture.

N-(2-Pyridylmethyl)-L-methionine (PMET): This was prepared in 80% yield in the manner described for IMET from methyl L-methioninate hydrochloride (11.75 g, 0.050 mol) and 2-pyridinecarbaldehyde (5.36 g, 0.050 mol). Recrystallization from ethanol gave PMET as a colorless powder, mp 219—220 °C (decomp). Found: C, 54.98; H, 6.72; N, 11.33; S, 13.34%. Calcd for $C_{11}H_{16}N_2O_2S$: C, 54.98; H, 6.71; N, 11.66; S, 13.83%.

N-(4-Imidazolylmethyl)-L-alanine (IALA): This was prepared similarly from methyl L-alaninate hydrochloride (4.00 g, 0.025 mol) and 4-imidazolecarbaldehyde (2.4 g, 0.025 mol) in 50% yield. Recrystallization from methanol gave IALA·HCl·H_2O as a colorless powder, mp 215 °C (decomp). Found: C, 37.59; H, 6.31; N, 18.79%. Calcd for $C_7H_{12}N_3O_2Cl \cdot H_2O$: C, 37.05; H, 6.06; N, 18.32%.

[Cu(IMAD)](ClO$_4$)$_2$·H$_2$O: A concd solution of Cu-$(ClO_4)_2 \cdot 6H_2O$ (3.7 g, 0.01 mol) in water was added to a solution of IMAD·3HCl·H_2O (4.4 g, 0.01 mol) in water, and the pH of the resulting solution was adjusted at $\approx$6.0 with 2 M NaOH. The deep blue solution was passed through a column packed with Amberlite IRA-410 ion exchange resin in the ClO_4^- form and stored at 10—15 °C, when dark violet crystals separated. Recrystallization from water gave pure crystals of [Cu(IMAD)]$(ClO_4)_2 \cdot H_2O$. Found: C, 24.41; H, 3.89; N, 14.26%. Calcd for $C_{12}H_{20}N_6O_8Cl_2CuS_2 \cdot H_2O$: C, 24.31; H, 3.74; N, 14.18%.

Attempts to isolate pure complexes from solutions containing Cu(II) and IMAD in the molar ratio of 2:1 were unsuccessful.

[Cu_2(PMAD)]Cl_4: To a solution of PMAD·4HCl·H_2O (5.0 g, 0.01 mol) in ethanol (50 ml) was added with stirring a solution of $CuCl_2 \cdot 2H_2O$ (3.4 g, 0.02 mol) in ethanol (20 ml). The pale blue precipitate which separated from the solution was filtered and washed with ethanol. Found: C, 31.56; H, 3.69; N, 9.31; Cl, 23.43; S, 10.57%. Calcd for $C_{16}H_{22}N_4Cl_4Cu_2S_2$: C, 31.85; H, 3.67; N, 9.29; Cl, 23.50; S, 10.67%.

[Cu(PMET)]$ClO_4 \cdot H_2O$: To a solution of PMET (2.4 g, 0.01 mol) in aqueous methanol was added a solution of $Cu(ClO_4)_2 \cdot 6H_2O$ (3.7 g, 0.01 mol) in methanol. The resulting solution was neutralized with 1 M NaOH and kept in a refrigerator, when greenish blue crystals separated. These were recrystallized from methanol. Found: C, 31.25; H, 4.19; N, 6.32%. Calcd for $C_{11}H_{15}N_2O_6ClCuS \cdot H_2O$: C, 31.43; H, 4.08; N, 6.66%.

[Cu(PDIEN)]$(ClO_4)_2$: PDIEN·3HCl (3.9 g, 0.01 mol) and $Cu(ClO_4)_2 \cdot 6H_2O$ (3.7 g, 0.01 mol) were dissolved in water, and the pH of the resulting solution was adjusted at $\approx$7.0. The blue violet solution was passed through a column packed with Amberlite IRA-410 ion exchange resin in the ClO_4^- form and kept at room temperature, when blue violet needles separated. Found: C, 34.93; H, 4.10; N, 12.72%. Calcd for $C_{16}H_{23}N_5O_8Cl_2Cu$: C, 35.07; H, 4.24; N, 12.79%.

Spectroscopic Measurements. Absorption spectra were measured in water with a Hitachi 323 and a Union Giken SM-401 high-sensitivity recording spectrophotometer and CD spectra with a JASCO MOE-1 spectropolarimeter, the concentrations of samples being 1—4 mM for visible and 0.1—0.8 mM for ultraviolet spectral measurements. Electron spin resonance (ESR) spectra were measured for 4—5 mM solutions with JEOL FE-3X and FE-1X ESR spectrometers.

Conductivity Measurements. Conductivities of various copper(II) complexes were measured in water at 25 °C under N_2 with a Kyoto Denshi CM-07 conductivity meter calibrated with 0.01 M potassium chloride.

pH Titrations. *Reagents*: Carbonate-free 0.1 M KOH was prepared according to the method of Armstrong[20] and standardized against standard potassium hydrogen phthalate (Merck DIN 19226). Copper(II) nitrate (0.01 M) was prepared from $Cu(NO_3)_2 \cdot 3H_2O$ and standardized by chelatometry using metallic zinc (JIS primary standard) as standard.

Apparatus and Procedure: Measurements of pH were made with an Orion Research 901 ion meter equipped with an Orion 90-01-00 glass electrode and a 91-02-00 double junction reference electrode. The meter was calibrated with NBS standard buffer solutions (4.008, 7.413, and 9.180 at 25 °C). Conversion of pH meter reading (pH_M) to $-\log$ [H], where [H] refers to hydrogen ion concentration, was made by correcting the difference (0.060) between pH_M and $-\log$ [H] obtained by titrating 0.01 M HNO_3 with 0.1 M KOH at the ionic strength (I) of 0.1 M (KNO_3). The hydroxide ion concentration [OH] was calculated from the apparent ion product of water $pK_w' = 13.91$ ($= pH_M - \log$ [OH]) determined by titrating 0.1 M KNO_3 with 0.1 M KOH. Titrations were performed at 25±0.05 °C under N_2 for solutions containing a ligand only and those containing a ligand and Cu(II) in the molar ratio of 1:1, 1:2, and 2:1. Reproducibility was checked by multiplicate titrations.

Calculation of Equilibrium Constants. The equilibria in the present systems and the relevant equilibrium constants, β_{pqr}, are defined by Eqs. 1 and 2, respectively (charges are omitted for simplicity):

$$p\mathrm{Cu} + q\mathrm{L} + r\mathrm{H} \overset{\beta_{pqr}}{\rightleftharpoons} \mathrm{Cu}_p\mathrm{L}_q\mathrm{H}_r, \quad (1)$$

$$\beta_{pqr} = \frac{[\mathrm{Cu}_p\mathrm{L}_q\mathrm{H}_r]}{[\mathrm{Cu}]^p[\mathrm{L}]^q[\mathrm{H}]^r}, \quad (2)$$

where p, q, and r are the numbers of moles of Cu(II), ligand (L), and proton (H) in the complex $Cu_pL_qH_r$, respectively, and a negative value of r denotes the deprotonation from the complex. Calculation of β_{pqr} was made by the method of nonlinear least-squares with the use of the computer program MINIQUAD[21] where the function minimized is the sums of squares of the residuals in the mass balance equations for total hydrogen ion, total metal, and total ligand. A graphical method[22] was used for calculation of the stability constants for Cu(II)–PMET and –PMTP for which the least-squares treatment was not effective because of the small pH changes with the addition of alkali.

The β_{110} value for Cu(II)–PMTP was calculated by Eq. 3 derived from the material balance equations and the electroneutrality of solution:

$$\beta_{110} = \frac{(A\alpha - C_L\beta)(3\alpha - \beta)}{[(3C_M - A)\alpha + (C_L - C_M)\beta](3C_L - A)}, \quad (3)$$

where

$$A = 3[\mathrm{CuL}] + 3[\mathrm{L}] + 2[\mathrm{HL}] + [\mathrm{H_2L}],$$

$$\alpha = 1 + [\mathrm{H}]/K_{a_3} + [\mathrm{H}]^2/K_{a_3} \cdot K_{a_2} + [\mathrm{H}]^3/K_{a_3} \cdot K_{a_2} \cdot K_{a_1},$$

and

$$\beta = 2[\mathrm{H}]/K_{a_3} + [\mathrm{H}]^2/K_{a_3} \cdot K_{a_2}.$$

The K_a values are acid dissociation constants. The equation for Cu(II)–PMET (Eq. 4) was derived in a similar way:

$$\beta_{110} = \frac{(2\alpha - \beta)(A\alpha - C_L\beta)[\mathrm{H}]^2}{[(2C_M - A)\alpha + (C_L - C_M)\beta](2C_L - A)}, \quad (4)$$

where

$$A = 2[\mathrm{CuL}] + 2[\mathrm{L}] + [\mathrm{HL}],$$

$$\alpha = 1 + [\mathrm{H}]/K_{a_2} + [\mathrm{H}]^2/K_{a_2} \cdot K_{a_1},$$

and

$$\beta = 2 + [\mathrm{H}]/K_{a_2}.$$

Results

Synthesis of Complexes. At pH>6 PMAD is decomposed by Cu(II) in the presence of dioxygen to give the Cu(II) complex of the sulfinate derived from PMAD.[12,13] Probably because of the cleavage and subsequent redox reactions, preparation of the Cu(II)–PMAD complex was not feasible in aqueous solution (pH$\approx$7); in ethanol, however, PMAD·4HCl gave a binuclear complex of the composition, Cu_2(PMAD)Cl_4, as crystals. The imidazole-containing disulfide IMAD was less susceptible to the cleavage at pH 6—7, giving a 1:1 complex Cu(IMAD)$(ClO_4)_2 \cdot H_2O$ which is stable in water. At higher pH it also affords the Cu(II)–sulfinate complex.[23] The methionine derivative PMET and the pyridine-containing diethylenetriamine derivative PDIEN gave the corresponding 1:1 complexes with Cu(II), but attempted isolation of the Cu(II)–PMTP and –IALA complexes was not successful under the conditions used.

Spectra. The Cu(II)–disulfide systems are relatively stable in acid solution. Figure 1 illustrates the absorption spectra of some 1:1 Cu(II)–ligand systems, and Tables 1 and 2 show the spectral data for various binary and ternary systems, respectively, in acid–neutral solution. The 1:1 and 2:1 Cu(II)–PMAD systems have an absorption peak at 650 nm and a shoulder at ≈330 nm at pH≈4, whereas the 1:1 and 1:2 Cu(II)–2-(aminomethyl)pyridine (ampy) systems have a peak at 650 and 585 nm, respectively. An additional band is observed at 850 nm as a shoulder for the 1:1 Cu(II)–PMAD system and the 2:1 system at pH<4.0. Interestingly, the peak at 650 nm of Cu(II)–PMAD remained unchanged on going from the 1:1 binary system to the 1:1:1 Cu(II)–PMAD–ampy ternary system. The isolated complex $Cu_2(PMAD)Cl_4$ exhibited a peak at 760 nm in dimethyl sulfoxide and at 660 nm in water (pH 4.2). The Cu(II)–MPAD and –QMAD systems show spectral behavior partly similar to those of Cu(II)–PMAD; the d-d peaks are observed at ≈650 nm, but the band in the region 300—350 nm appears only at pH>6 for the Cu(II)–MPAD system, while it is undetectable for the Cu(II)–QMAD

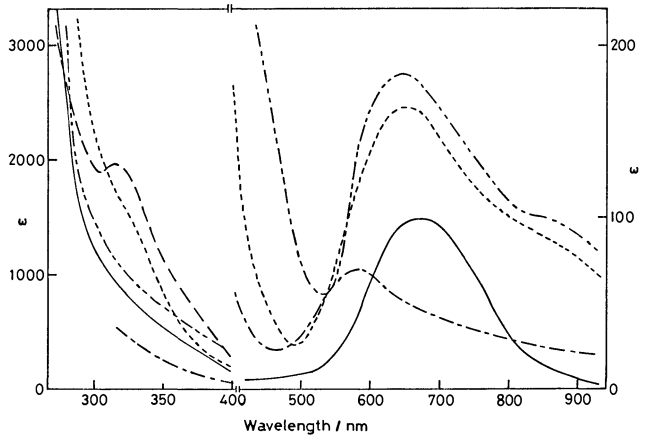

Fig. 1. Absorption spectra of 1:1 Cu(II)–ligand systems in water.
–––––: Cu(II)–IMAD (pH 5.0), ----: Cu(II)–PMAD (pH 4.5), ——: Cu(II)–MPAD (pH 4.7), ——: Cu(II)–PMET (pH 7.0), — — —: Cu(II)–PMET (pH 8.9).

Table 1. Absorption spectral data for binary systems in water[a)]

Ligand	Cu(II):Ligand	pH	λ_{max}/nm	ε / M^{-1} Cu^{-1} cm^{-1}	Ligand	Cu(II):Ligand	pH	λ_{max}/nm	ε / M^{-1} Cu^{-1} cm^{-1}
IMAD	1:1	3.4	720	21	MPAD			850sh	90
		3.7	630	32		2:1	4.0	680	39
		4.4	592	63			5.1—5.3	300sh	1840
		5.0	585	70				650	127
	2:1	4.0	600	40					
					QMAD[c)]	1:1	3.3	790	20
PMAD	1:1	3.5	330sh	1370			4.0	670	72
			650	137			5.0	650	184
			850sh	74				850sh	95
		4.5	330sh	1400		2:1	4.0	690	33
			650	164			5.2	650	107
			850sh	89					
	2:1	3.4	330sh	580	PMTP	1:1	7.0	320	3500
			650	73				600	190
			850sh	45				850	81
		4.1	330sh	770					
			650	82	PMET[d)]	1:1	7.0	680	100
		4.5	330	1100			8.8	307	1750
			650	101				680	100
			750sh	85	IMET	1:1	7.2	670	108
	2:1[b)]	(DMSO)	760	99			9.0	308	1600
		4.2	660	85				670	110
MPAD	1:1	4.0	660	56	IALA[d)]	1:1	7.4	660	83
			850sh	36					
		4.7	650	184	ampy[e)]	1:1	6.8	650	47
			850sh	100		1:2	6.3	585	76
		6.2—7.0	310	3700					
			650	177	bimen[f)]	1:1	6.5	585	110

a) sh=Shoulder. b) $Cu_2(PMAD)Cl_4$ in dimethyl sulfoxide (DMSO) and in water. c) The CT peak at 300—350 nm is undetectable because of the quinoline band. d) The CD spectral data, λ_{max}/nm ($\Delta\varepsilon$), for these systems are as follows: Cu(II)-PMET, 635 (−0.11) at pH 7.0 and 325 (-0.62) and 615 (−0.22) at pH 8.8; Cu(II)-IALA, 580 (-0.11) and 720 (0.11) at pH 7.4. e) ampy=2-(Aminomethyl)pyridine. f) bimen=*N*,*N*′-Bis(4-imidazolylmethyl)ethylenediamine.

TABLE 2. ABSORPTION SPECTRAL DATA FOR TERNARY SYSTEMS IN WATER[a)]

System	pH	λ_{max}/nm	ε/M^{-1} Cu^{-1} cm^{-1}
1:1:1 Cu(II)-IMAD-bpy	7.1	700br	75
		870sh	51
2:1:2 Cu(II)-IMAD-bpy	7.1	700	70
		870sh	48
1:1:1 Cu(II)-PMAD-ampy	4.1—4.3	330sh	1400
		650	139
		850sh	65
2:1:2 Cu(II)-PMAD-ampy	3.9—4.3	330sh	900
		650	100
		850sh	46
1:1:1 Cu(II)-PMAD-bpy	4.1	680	107
		850sh	64
2:1:2 Cu(II)-PMAD-bpy	4.1	680	96
		850sh	65

a) sh=Shoulder; br=broad.

system because of the strong quinoline peaks.

In the region 300—900 nm the 1:1 Cu(II)–IMAD system at pH 5 has a single peak at 585 nm with a normal intensity. The wavelength and molar absorption coefficient of the peak are not affected by concentrations of the solution covering the range 10^{-4}—10^{-2} M, suggesting that the 1:1 Cu(II)–IMAD complex has a monomeric structure with an N_4 donor set analogous to that of 1:2 Cu(II)–ampy and of 1:2 Cu(II)–4-(aminomethyl)imidazole (amim). The ESR spectrum shows at least seven resolved superhyperfine structures due to nitrogen donors, the g values, $g_{//}$= 2.23 and $g_{\perp}$=2.06, being typical of a tetragonal structure with axial symmetry (Table 3).

The 1:1 Cu(II)–PMTP system, where a thioether sulfur replaces the disulfide sulfurs of PMAD, exhibits a strong peak at 320 nm (ε=3500) and well-resolved d-d bands at 600 and 850 nm. The 320-nm peak has been assigned to the S→Cu(II) charge transfer (CT) transition,[18)] which is compatible with the equatorial S–Cu(II) bonding. Because no CT band is observed for the five-coordinate complex of PDIEN which is the nitrogen analog of PMTP, the chromophore of Cu(II)–PMTP is described as CuN_4S with an axial nitrogen coordination. Complexes of analogous pyridine-containing thioethers with CuN_2S_2 chromophores have been reported to show the S→Cu(II) CT band at 340—380 nm.[24)] The 1:1 systems with PMET and IMET give a d-d band at 670—680 nm corresponding with a CuN_2O_2 chromophore, but an additional band appears at ≈310 nm with pH increase. The negative CD peak at 325 nm and its absence in 1:1 Cu(II)–IALA reveal that the 310-nm peak is due to the S→Cu(II) CT transition. The Cu(II)–methionine system in ethanol has been reported to give two S→Cu(II) CT peaks at 380 and 450 nm.[25)]

Solution Equilibria. Figure 2 shows the titration curves for some ligands in the absence and the presence of Cu(II). The overall proton-ligand stability constants, log β_{01r}, calculated from these data are listed in Table 4 and the stepwise dissociation constants (pK_a) in Table 5. The two lower acid dissociation steps of IMAD are assigned to the imidazole nitrogens, because the imidazole moiety of amim has the pK_a value of 4.73.[26)] As observed for PDIEN,[15)] the protonation of the least basic pyridine rings of PMAD and PMTP occurs only at pH<2.5.

Since the disulfide bonds are susceptible to cleavage in the presence of Cu(II) at neutral and alkaline pH, the stability constants were calculated from the data covering the pH ranges 2—3.5 for PMAD, 2.6—5.0 for MPAD, and 2.8—5.9 for IMAD. Considering

TABLE 3. ESR SPECTRAL PARAMETERS FOR 1:1 Cu(II)-LIGAND SYSTEMS AT 77 K

Ligand	pH	$g_{//}$	$g_{\perp}$	$\lvert A_{//}\rvert$/10^{-4} cm^{-1}
IMAD	7.0	2.23	2.06	202
PMAD[a)]	4.0	2.25	2.07	182
PMTP	7.0	2.20	2.07	175
PMET	7.0	2.28	2.05	185
	8.8	2.27	2.06	179
IMET	7.2	2.28	2.07	188
IALA	7.4	2.27	2.06	187
bimen[b)]	7.0	2.21	2.06	206

a) Parameters for the predominant species. b) bimen= *N,N'*-Bis(4-imidazolylmethyl)ethylenediamine.

Table 4. Stability constants, $\log \beta_{01r}$, of proton-ligand complexes, LH_r, at 25 °C and I=0.1(KNO_3)[a]

Ligand	$\log \beta_{011}$	$\log \beta_{012}$	$\log \beta_{013}$	$\log \beta_{014}$
IMAD	8.74(0.007)	16.59(0.006)	21.21(0.006)	25.10(0.005)
PMAD	7.88(0.006)	14.90(0.007)	16.77(0.006)	
MPAD	7.80(0.001)	14.81(0.001)	17.60(0.004)	19.76(0.006)
PMTP	8.01(0.001)	15.01(0.001)	16.79(0.002)	
PMET	7.60(0.003)	9.70(0.004)		

a) Values in parentheses are estimated standard deviations.

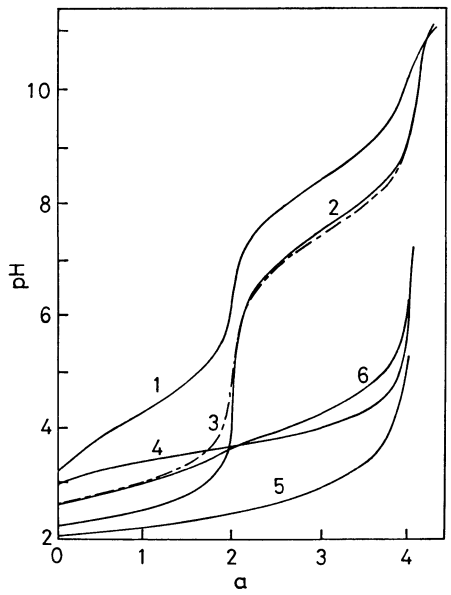

Fig. 2. Titration curves for proton- and Cu(II)-ligand systems at 25 °C.
a: Moles of KOH added per mole of ligand. 1: IMAD (0.004014 M), 2: PMAD (0.004000 M), 3: MPAD (0.002000 M), 4: Cu(II) (0.004027 M) and IMAD (0.004003 M), 5: Cu(II) (0.004027 M) and PMAD (0.004001 M), 6: Cu(II) (0.002029 M) and MPAD (0.002009 M).

that the absorption spectra of 1:1 and 2:1 Cu(II)–PMAD and –MPAD systems have a peak at 650 nm indicative of a monomeric species and that a complex with the composition Cu_2L (L=PMAD) was isolated, we attained convergence in the computer simulations by including the species $CuLH_2$ (for L=IMAD and MPAD), CuLH, CuL, and a binuclear species Cu_2L. The analysis of the 1:1 Cu(II)–IMAD system was possible either by the set of species $CuLH_2$, CuLH, and CuL, or by the set $CuLH_2$, CuLH, and Cu_2L_2, the sums of the squares of residuals being approximately the same. However, Cu_2L_2 was rejected in the simulation including both CuL and Cu_2L_2. From this fact and the absorption spectral behavior of the Cu(II)–IMAD systems, we preferred the set with monomeric species. This conclusion is further supported by the conductivity measurements of Cu(II) complexes (Fig. 3); $Cu(IMAD)(ClO_4)_2$ has the same molar conductivity as shown by $Cu(PDIEN)(ClO_4)_2$ and other

Table 5. Acid dissociation constants of ligands at 25 °C and I=0.1(KNO_3)

Ligand	pK_{a_1}	pK_{a_2}	pK_{a_3}	pK_{a_4}
IMAD	3.89	4.62	7.85	8.74
PMAD	a)	1.87	7.02	7.88
MPAD	2.16	2.79	7.01	7.80
PMTP	a)	1.78	7.00	8.01
	0.9[b]	1.9[b]	6.96[b]	7.98[b]
PMET	a)	2.10	7.60	

a) Not obtained. b) Ref. 19.

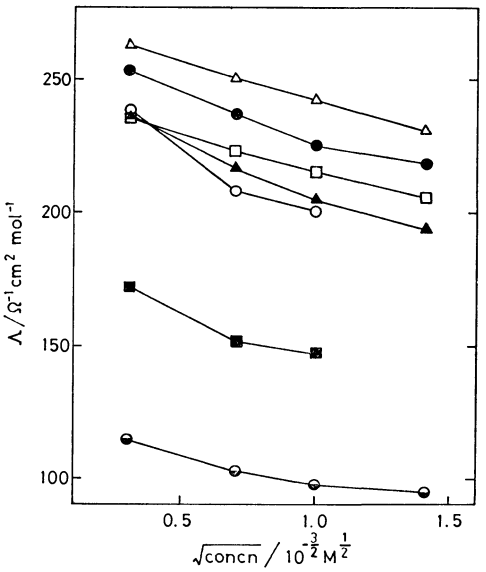

Fig. 3. Molar conductivities of copper(II) complexes in water at 25 °C.
△: $CuCl_2$, ●: $Cu(ClO_4)_2$, □: $Cu(bpy)(NO_3)_2$, ▲: $Cu(PDIEN)(ClO_4)_2$, ○: $Cu(IMAD)(ClO_4)_2$, ■: $Cu(PMET)ClO_4$, ◒: Cu(PMS)Cl (PMS=2-(2-Pyridylmethylamino)ethanesulfinate).

dipositive Cu(II) complex ions. The stability constants for Cu_2L were calculated from the data for the 2:1 Cu(II)–disulfide systems. Table 6 shows the overall stability constants for various complexes studied. The $\log \beta_{110}$ values for Cu(II)–PMAD and Cu(II)–IMAD are 13.32 and 13.38, respectively, which are much greater than those for 1:1 Cu(II)–ampy (=9.5)[27] and Cu(II)–amim (=9.22).[26] There is a drastic sta-

TABLE 6. STABILITY CONSTANTS, log β_{pqr}, OF COPPER(II) COMPLEXES, $Cu_pL_qH_r$, AT 25 °C AND I=0.1(KNO_3)[a]

Ligand	Species pqr	log β_{pqr}[b]
IMAD	112	20.51(0.02)
	111	17.22(0.007)
	110	13.38(0.006)
	210	16.30(0.04)[c]
PMAD	111	16.26(0.005)
	110	13.32(0.003)
	210	16.62(0.009)[c]
MPAD	112	16.75(0.018)
	111	13.54(0.005)
	110	9.46(0.003)
PMTP	110	16.3(0.1)[d]
		18.1(0.1)[e]
PMET	110	9.3(0.1)[d]
	11-1	0.5(0.06)
PDIEN	110	20.85(0.11)[f]
ampy[g]	110	9.5(0.2)[h]
	120	17.2(0.3)[h]
amim[i]	110	9.22(0.03)[j]
	120	17.17[j]

a) Values in parentheses are estimated standard deviations. b) Calculated for 1:1 Cu(II)-ligand systems. c) Calculated for 2:1 Cu(II)-ligand systems. d) Obtained by graphical methods. e) Ref. 19. f) Ref. 15. g) ampy=2-(Aminomethyl)pyridine. h) Ref. 27. i) amim=4-(Aminomethyl)imidazole. j) Ref. 26.

bility decrease in Cu(II)–MPAD due to the 6-methyl group, the log β_{110} value of 9.46 being as low as that of Cu(II)–ampy. The results imply that PMAD and IMAD behave as multidentate ligands coordinating through most of the available donor atoms, whereas MPAD coordinates to Cu(II) in the same way as ampy. We may compare the log β_{110} values for PMAD and IMAD with the log β_{120} values for ampy and amim: the log β_{110} values for the disulfides are smaller than these log β_{120} values, which could result from the difference in the ligand basicity and/or in the donor sets in the coordination plane.

The stability constants for Cu(II)–PMTP and Cu(II)–PMET were calculated by a graphical method. Both systems were analyzed by considering CuL only, and protonated species $CuLH_2$ and CuLH were negligible. The pyridine-containing thioether PMTP forms a 1:1 complex with log β_{110}=16,3,[28] whereas PDIEN forms a complex with log β_{110}=20.85.[15] The stability difference of 4.5 log unit is attributed to the difference in the coordinating ability of an amine nitrogen and a thioether sulfur, and further supports the conclusion derived from the spectra that Cu(II)–PMTP has an N_3S donor set in the coordination plane.

The amino acid derivative PMET forms a 1:1 complex with log β_{110}=9.30, which is smaller than the value of 11.8 reported for *N*-(2-pyridylmethyl)glycine with higher pK_a values.[29] At pH>7 the complex liberates an additional proton probably from the coordinated water molecule, whose dissociation constant was calculated by assuming the following step:

$$CuL \rightleftharpoons CuL(OH) + H. \quad (5)$$

Discussion

Structures of Complexes in Solution. The intensity and location of the S→Cu(II) CT band are affected by the mode of S–Cu(II) interactions.[30–32] The CT band due to equatorial thioether–Cu(II) bonding is strong, while the band due to apical bonding is sometimes too weak to be detected: the Cu(II) complex of an imidazole-containing thioether ligand, bis(4-phenyl-2-imidazolylmethyl) sulfide, has an apical S–Cu(II) bonding (2.824 Å) but shows no CT band.[32] The spectral properties of disulfide–Cu(II) bonding may be considered analogously, and the CT band arising from the apical disulfide–Cu(II) interaction may not be detected because of the poor overlap of the Cu(II) $d_{x^2-y^2}$ and S orbitals and the long axial S–Cu(II) bond as seen in the Cu(II) complexes of oxidized D-penicillamine (3.057 and 3.138 Å)[33] and glutathione (3.16 and 3.28 Å),[34] both of which apparently lack obvious S→Cu(II) CT bands. The Cu(II)···S separations in these complexes are much longer than the Cu(I)–S bonds (2.3—2.4 Å) in some Cu(I)–disulfide complexes.[35–38] Therefore, the 330-nm shoulder shown by Cu(II)–PMAD is assigned to the equatorial S→Cu(II) CT transition by analogy with the spectrum of the related system Cu(II)–PMTP.[18] The observed intensity (ε=1100) indicates that the S–Cu(II) interaction is weaker than that in Cu(II)–PMTP. For the system Cu(II)–tetramethylcystamine (=bis[2-(dimethylamino)ethyl] disulfide) Downes *et al.* observed three bands and suggested that both of the disulfide sulfur atoms are involved in the interactions with Cu(II).[39] Although a somewhat reduced $|A_{//}|$ value observed for Cu(II)–PMAD suggests sulfur coordination,[40] the ESR parameters do not explicitly point to the Cu(II)–S bonding. The splitting of the d-d band is ascribed to a square-pyramidal structure[41] with a donor group of PMAD occupying an apical position; in the 2:1 system the 850-nm band disappears at pH>4.1, indicating that the apical donor is used for forming a binuclear complex Cu_2L. The d-d band at 650 nm is remote from the band exhibited by 1:2 Cu(II)–ampy (585 nm) with a CuN_4 chromophore. Sterically PMAD may be coordinated to Cu(II) in the same way as ampy in 1:2 Cu(II)–ampy, but actually the maximum wavelength of 1:1 Cu(II)–PMAD is the same as that of 1:1 Cu(II)–ampy. Addition of ampy has no apparent effect on the spectrum of 1:1 Cu(II)–PMAD (Table 2), which may indicate either that the bonding by added ampy is similar to that by one of the two 2-pyridylmethylamino moieties of PMAD or that ampy does not coordinate to Cu(II) at all. With 2,2′-bipyridine (bpy), which probably

occupies two equatorial positions, the maximum at 650 nm shifts to 680 nm with concomitant loss of the 330-nm CT peak. An additional band is observed in both ternary systems at 850 nm as a shoulder. The 680-nm peak is close to the peak at 690 nm exhibited by 1:1:1 Cu(II)–ampy–bpy. This indicates that Cu(II)–PMAD–bpy and Cu(II)–ampy–bpy have a similar chromophore. Incidentally 1:2 Cu(II)–bpy complexes with various geometries often exhibit an electronic reflectance spectral peak at $\approx$650 nm.[42,43] From these considerations, the chromophore of 1:1 Cu(II)–PMAD in acid solution is best described as CuN_4S with apical coordination by a nitrogen donor, and we propose structure **1**, which is reminiscent of the probable structure of Cu(II)–PMTP.[18] Octahedral Ni(II)–PMAD complexes in the solid state have been reported to involve PMAD as a pentadentate ligand.[7,44]

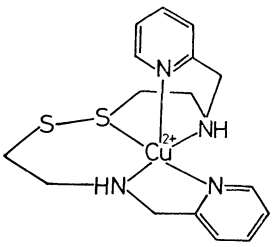

1

Another line of evidence is provided by the stability and the spectrum of the Cu(II)–MPAD system. In sharp contrast with the Cu(II)–PMAD system, it has the same stability constant as that of Cu(II)–ampy, which confirms an analogous mode of coordination in the square plane. The stability difference of 3.9 between Cu(II)–PMAD and Cu(II)–MPAD (Table 6) corresponds to the difference of one nitrogen donor in the plane, again indicating that at least three nitrogens are involved in the equatorial bonding in Cu(II)–PMAD. Space-filling molecular models show that, when MPAD is coordinated through the pyridine and amine nitrogens and the disulfide sulfur (structure **2**),

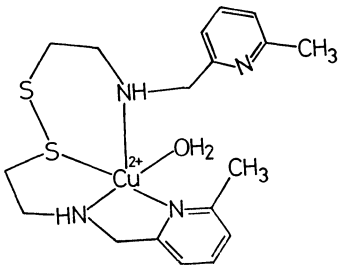

2

the methyl group severely interferes with the equatorial bonding by the rest of the donors. This is in accord with the lower stability and the lack of the S→Cu(II) CT band at pH<6.

On the other hand, the optical and ESR spectra (Tables 1 and 3) indicate that 1:1 Cu(II)–IMAD has a planar CuN_4 coordination structure with no strong Cu(II)–S bonding. Molecular models suggest that

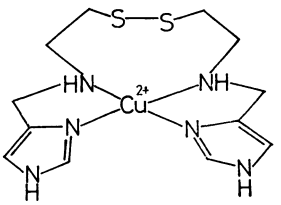

3

both *cis* and *trans* structures are possible with respect to the imidazole nitrogens and that the dithio group apically approaches Cu(II) in the *trans* structure. Although the apical S–Cu(II) interaction is not incompatible with lack of S→Cu(II) CT bands, we prefer the *cis* structure (**3**) with negligible S–Cu(II) interactions on the basis of the stability of the 1:1 complex toward the disulfide bond cleavage as has been observed for PMAD.[12,13] It should be noted in addition that the 1:1 Cu(II) complex of *N,N'*-bis(4-imidazolylmethyl)ethylenediamine with an N_4 donor set shows the same absorption and ESR spectral parameters as those of the 1:1 Cu(II)–IMAD system (Tables 1 and 3). The ternary Cu(II)–IMAD–bpy systems show a broad peak at 700 nm and a shoulder at 870 nm, indicating a change from the square-planar to the square-pyramidal structure. Structures **1** and **3** are related to each other and may be determined by steric requirements for pyridine and imidazole rings in the *cis* coordination positions.

Effects of Sulfur Coordination on Stability Constants of Copper(II) Complexes. The difference of $\approx$4.5 between the $\log \beta_{110}$ values for PMTP and PDIEN is attributed to the difference in the complexing ability of a thioether sulfur and an amine nitrogen. An analogous stability difference exists between the Cu(II) complexes of diethylenetriamine ($\log \beta_{110}=15.9$) and bis(2-aminoethyl) sulfide ($\log \beta_{110}=9.07$).[27] The complex of PMAD is less stable than that of PMTP in spite of similar coordination structures of CuN_4S as inferred from absorption spectra. An explanation for this is the orbital overlap in the S–Cu(II) interaction, which is considered from the CT band intensities to be small in Cu(II)–PMAD and large in Cu(II)–PMTP. Steric effects due to the presence of two sulfur atoms in one of the chelate rings should also affect the stability. The $\log \beta_{110}$ value for PMAD is expectedly smaller than $\log \beta_{120}$ for 1:2 Cu(II)–ampy with an N_4 donor set by 3.9 log units. The low stability of Cu(II)–MPAD is ascribed to the bidentate nature of MPAD due to the steric hindrance arising from the 6-methyl group.

Although 1:1 Cu(II)–IMAD and 1:2 Cu(II)–amim probably have the same donor groups in the coordination plane, the difference between $\log \beta_{110}$ of Cu(II)–IMAD and $\log \beta_{120}$ of Cu(II)–amim is rather large ($\approx$3.8) and may be caused by lower basicity of IMAD and steric strains due to the disulfide bond.

The terdentate thioether ligand PMET forms a 1:1 complex ($\log \beta_{110}=9.3$), which is more stable than the Cu(II)–L-methioninate complex ($\log \beta_{110}=7.849$).[45] The stability enhancement is due primarily to the pyridine nitrogen, and contribution by the

thioether moiety may be negligible, because Cu(II)–ampy has approximately the same stability. In this connection, L-methionylglycine and *S*-methyl-L-cysteinylglycine form Cu(II) complexes CuL with significantly higher stability than expected from the basicity of the terminal amino group of various dipeptides; the thioether sulfur of glycyl-L-methionine has no effect on the stability of CuL owing to the inaccessibility of the side chain to Cu(II).[46]

Dependence of the Disulfide Bond Stability on the Coordination Structure. Disulfides are susceptible to heterolytic cleavage by Ag(I), Hg(I), and other soft Lewis acids, forming sulfinic acids and thiols by the reaction with water and subsequent disproportionation.[10] Formation of 2-pyridylsulfinate from di-2-pyridyl disulfide in the presence of Cu(II) has been interpreted as due to the same heterolytic cleavage reaction.[11] PMAD is readily converted to 2-(2-pyridylmethylamino)ethanesulfinate in the presence of Cu(II) and dioxygen at pH $\approx$7.[12,13] Although this reaction has been found to require dioxygen,[13] it must involve the heterolytic cleavage and the reaction with water, because the oxygens incorporated from dioxygen account for only 25—30% of the total sulfinate oxygens. The 2:1 Cu(II)–PMAD system at pH$\approx$7 exhibits a transient but resolved peak at 330 nm,[13] indicating that the Cu(II)–S interaction is stronger than in acid solution where the 330-nm peak appears as a shoulder. The Cu(II)–tetramethylcystamine system in acetonitrile, whose disulfide bond is more stable than that in the Cu(II)–cystamine system, gives strong S$\rightarrow$Cu(II) CT peaks and is rapidly decomposed by addition of a second equivalent of sodium methoxide.[39] On the other hand, the Cu(II)–penicillamine disulfide[33] and –glutathione disulfide[34] complexes, which were isolated from aqueous solution, have long Cu(II)$\cdots$S distances (3.0—3.3 Å) and show no CT bands. Also, the Cu(II)–IMAD system is more stable in aqueous solution and gives a 1:1 complex as crystals; in line with this, the system shows no band ascribable to the S$\rightarrow$Cu(II) CT transition. Since the stability constants of Cu(II)–disulfide and –thioether complexes are usually low,[47–50] neighboring effective Cu(II)-binding sites which bring the disulfide group close to Cu(II) would promote the cleavage reaction. These observations probably indicate that only those complexes which involve weak Cu(II)–S bonds are stable in aqueous solution.

The disulfide bond has been proposed as a copper binding site in stellacyanin[3–5] which lacks the methionyl residue established as a binding site in plastocyanin and azurin. While the proposal is attractive in view of the coordinating ability of the disulfide sulfurs, it becomes necessary to cope with the dichotomy between coordination and disulfide bond cleavage. We may infer from the present observations that the copper site should meet one of the following requirements for the stability of the bond in the vicinity of Cu(II): (i) the S$\cdots$Cu(II) separation is as large as 3.0 Å; (ii) water and other nucleophiles are excluded from the copper binding site. Just as the Cu(II)$\cdots$S(methionine) distance found in plastocyanin is unusually long (2.90 Å),[1] a disulfide group would be able to contribute to the copper binding in stellacyanin through weak interaction with a large Cu(II)$\cdots$S separation.

We thank Mr. Kiyoshi Takami for assistance with the experiments. Thanks are also due to Dr. Yukio Sugiura of Kyoto University and Drs. Shinnichiro Suzuki and Takeshi Sakurai of Osaka University for ESR spectral measurements. We are indebted to Dr. P. Gans of the University of Leeds for suggestions on the use of the computer program MINIQUAD. This work was supported by a Grant-in-Aid for Special Project Research (No. 57102001) from the Ministry of Education, Science and Culture.

References

1) P. M. Colman, H. C. Freeman, J. M. Guss, M. Murata, V. A. Norris, J. A. M. Ramshaw, and M. P. Venkatappa, *Nature*, **272**, 319 (1978); H. C. Freeman, "Coordination Chemistry-21," ed by J. P. Laurent, Pergamon Press, Oxford(1981), p. 29.
2) E. T. Adman, R. E. Stenkamp, L. C. Sieker, and L. H. Jensen, *J. Mol. Biol.*, **123**, 35 (1978).
3) N. S. Ferris, W. H. Woodruff, D. B. Rorabacher, T. E. Jones, and L. A. Ochrymowycz, *J. Am. Chem. Soc.*, **100**, 5939 (1978).
4) M. Lundeen, *Inorg. Chim. Acta*, **56**, 149 (1981).
5) A. G. Lappin, "Metal Ions in Biological Systems," ed by H. Sigel, Marcel Dekker, New York (1981), Vol. 13, p. 15.
6) P. Hemmerich, "The Biochemistry of Copper," ed by J. Peisach, P. Aisen, and W. E. Blumberg, Academic Press, New York (1966), p. 15.
7) P. Kroneck, *J. Am. Chem. Soc.*, **97**, 3839 (1975).
8) P. J. M. W. L. Birker and H. C. Freeman, *J. Am. Chem. Soc.*, **99**, 6890 (1977).
9) R. B. Martin, "Metal Ions in Biological Systems," ed by H. Sigel, Marcel Dekker, New York (1979), Vol. 9, p. 1.
10) P. C. Jocelyn, "Biochemistry of the SH Group," Academic Press, London and New York (1972).
11) L. S. Higashi, M. Lundeen, E. Hilti, and K. Seff, *Inorg. Chem.*, **16**, 310 (1977).
12) A. Odani, T. Maruyama, O. Yamauchi, T. Fujiwara, and K. Tomita, *J. Chem. Soc., Chem. Commun.*, **1982**, 646.
13) O. Yamauchi and H. Seki, *Chem. Lett.*, **1982**, 1241.
14) F. L. Pyman, *J. Chem. Soc.*, **109**, 186 (1916).
15) W. R. Harris, I. Murase, J. H. Timmons, and A. E. Martell, *Inorg. Chem.*, **17**, 889 (1978).
16) All melting points are uncorrected.
17) This compound has been obtained earlier as a crude oil of low analytical purity (L. G. Warren, M. M. Kadooka, and K. Seff, *Inorg. Chem.*, **14**, 1773 (1975)).
18) T. Sakurai, S. Suzuki, and A. Nakahara, *Bull. Chem. Soc. Jpn.*, **54**, 2313 (1981).
19) S. A. Bedell, J. H. Timmons, A. E. Martell, and I. Murase, *Inorg. Chem.*, **21**, 874 (1982).
20) D. M. G. Armstrong, *Chem. Ind. (London)*, **1955**, 1405.
21) A. Sabatini, A. Vacca, and P. Gans, *Talanta*, **21**, 53 (1974).
22) M. Kodama and E. Kimura, *J. Chem. Soc., Dalton Trans.*, **1979**, 325.
23) Unpublished results.
24) D. E. Nikles, M. J. Powers, and F. L. Urback, *Inorg. Chim. Acta*, **37**, L499 (1979).

25) H. Kozlowski and T. Kowalík, *Inorg. Chim. Acta*, **34**, L231 (1979).
26) P. R. Huber, R. Griesser, and H. Sigel, *Inorg. Chem.*, **10**, 945 (1971).
27) R. M. Smith and A. E. Martell, "Critical Stability Constants," Plenum Press, New York and London (1975), Vol. 2.
28) The difference of 1.8 log units between this value and that reported by Bedell *et al.* (Ref. 19) may be due to the different methods of determination.
29) R. G. Lacoste, G. V. Christoffers, and A. E. Martell, *J. Am. Chem. Soc.*, **87**, 2385 (1965).
30) V. M. Miskowski, J. A. Thich, R. Solomon, and H. J. Schugar, *J. Am. Chem. Soc.*, **98**, 8344 (1976).
31) A. R. Amundsen, J. Whelan, and B. Bosnich, *J. Am. Chem. Soc.*, **99**, 6730 (1977).
32) H. J. Prochaska, W. F. Schwindinger, M. Schwartz, M. J. Burk, E. Bernarducci, R. A. Lalancette, J. A. Potenza, and H. J. Schugar, *J. Am. Chem. Soc.*, **103**, 3446 (1981).
33) J. A. Thich, D. Mastropaolo, J. Potenza, and H. J. Schugar, *J. Am. Chem. Soc.*, **96**, 726 (1974).
34) K. Miyoshi, Y. Sugiura, K. Ishizu, Y. Iitaka, and H. Nakamura, *J. Am. Chem. Soc.*, **102**, 6130 (1980).
35) C.-I. Branden, *Acta Chem. Scand.*, **21**, 1000 (1967).
36) T. Ottersen, L. G. Warner, and K. Seff, *J. Chem. Soc., Chem. Commun.*, **1973**, 876.
37) L. G. Warner, T. Ottersen, and K. Seff, *Inorg. Chem.*, **13**, 2819 (1974).
38) M. M. Kadooka, L. G. Warner, and K. Seff, *J. Am. Chem. Soc.*, **98**, 7569 (1976).
39) J. M. Downes, J. Whelan, and B. Bosnich, *Inorg. Chem.*, **20**, 1081 (1981).
40) U. Sakaguchi and A. W. Addison, *J. Am. Chem. Soc.*, **99**, 5189 (1977).
41) B. J. Hathaway and D. E. Billing, *Coord. Chem. Rev.*, **5**, 143 (1970).
42) B. J. Hathaway, I. M. Procter, R. C. Slade, and A. A. G. Tomlinson, *J. Chem. Soc., A*, **1969**, 2219.
43) R. J. Fereday, P. Hodgson, S. Tyagi, and B. J. Hathaway, *J. Chem. Soc., Dalton Trans.*, **1981**, 2070.
44) P. E. Rieley and K. Seff, *Inorg. Chem.*, **11**, 2993 (1972).
45) G. Brookes and L. D. Pettit, *J. Chem. Soc., Dalton Trans.*, **1977**, 1918.
46) H. Sigel, C. F. Naumann, B. Prijs, D. B. McCormick, and M. C. Falk, *Inorg. Chem.*, **16**, 790 (1977).
47) H. Sigel, V. M. Rheinberger, and B. E. Fischer, *Inorg. Chem.*, **18**, 3334 (1979).
48) H. Sigel, K. H. Scheller, V. M. Rheinberger, and B. E. Fischer, *J. Chem. Soc., Dalton Trans.*, **1980**, 1022.
49) H. Sigel, *Angew. Chem., Int. Ed. Engl.*, **21**, 389 (1982).
50) H. Sigel and K. H. Scheller, *J. Inorg. Biochem.*, **16**, 297 (1982).

Synthesis and Characterization of a New Quinquedentate Ligand Consisting of Salen Skeleton and Phenolic Tail Capable of Axial Coordination and Its Metal Complexes

Wakako KANDA, Hisashi ŌKAWA,* and Sigeo KIDA

Department of Chemistry, Faculty of Science, Kyushu University 33, Hakozaki, Higashi-ku, Fukuoka 812

(Received May 2, 1983)

A New quinquedentate ligand *N,N'*-disalicylidene-2-methyl-4-(2-hydroxy-5-methylphenyl)-1,2-butanediamine (H_2(sal-Hpen)) has been prepared, which is a salen derivative containing a phenolic tail capable of axial coordination. It formed the complexes of a general formula [M(sal-Hpen)] with copper(II), nickel(II), and cobalt(II) ions. Based on infrared, electronic and ESR spectra, the complexes were revealed to assume a planar coordination, free from axial coordination of the phenolic tail. On the other hand, distorted octahedral cobalt(III) and tetragonal pyramidal iron(III) complexes, [Co(sal-pen)py] and [Fe(sal-pen)], were obtained, where sal-pen^{3-} acts as a quinquedentate ligand.

Metal complexes of *N,N'*-disalicylideneethylenediamine (H_2salen) and its derivatives are known to assume planar coordination and show some characteristics relevant to biological systems, such as reversible oxygen adducts[1-11] and alkyl-cobalt(III) complexes[12,13] formations and catalytic function in substrate oxidation.[14-17] In these complexes, the fifth and sixth coordination at the axial positions plays a key role in the biomimetic functions. Therefore, it is interesting to synthesize salen derivatives possessing a tail group capable of axial coordination. However, synthesis of quinquedentate salen derivatives are limited to those with a thioether[18] or a pyridyl group[19] as an axial coordinating group.

In this study, a quinquedentate salen derivative, *N,N'*-disalicylidene-2-methyl-4-(2-hydroxy-5-methylphenyl)-1,2-butanediamine (abbreviated as H_2(sal-Hpen)), has been prepared. The complexes of this ligand may serve for elucidating the effects of the axial coordination of a phenolic oxygen on the electronic property and the reactivity of complexes and as a model for an intermediate in oxygenase reaction.[20]

In order to examine the net effect of axial phenolato donation, *N,N'*-disalicylidene-2-methyl-4-(2-methoxy-5-methylphenyl)-1,2-butanediamine (H_2(sal-mpen)) and its metal complexes were also prepared, where methyl group was substituted for phenolic hydrogen of H_2(sal-Hpen) so that practically no axial coordination is feasible. The synthetic methods for H_2(sal-Hpen) and H_2(sal-mpen) are schematically shown in Fig. 1.

Experimental

Syntheses. Methyl 2-(2-Methoxy-5-methylphenyl)ethyl Ketone: Ethyl acetoacetate (52 g) was added with stirring to a sodium ethoxide solution prepared by dissolving sodium (9.2 g) in absolute ethanol (350 cm^3). To this solution was added 2-methoxy-5-methylbenzyl chloride (68 g) with gentle boiling, and the mixture was refluxed for 3 h. When the reaction was completed, the mixture was cooled and sodium chloride separated was removed by filtration. The salt was washed with a small amount of ether and washings were combined with the main solution. The solution was evaporated to dryness to give a pale yellow substance. It

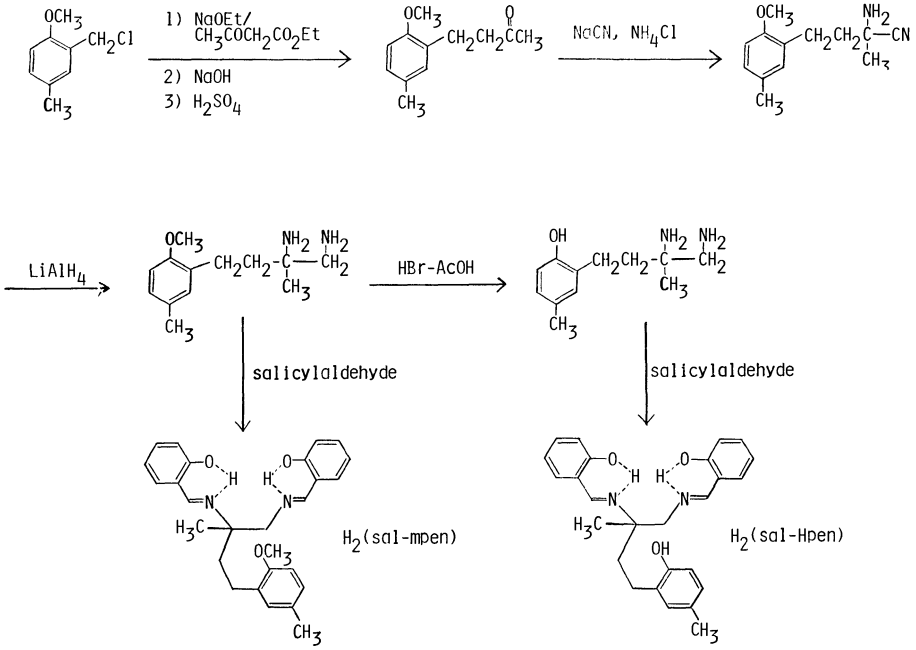

Fig. 1. Synthetic method for H_2(sal-Hpen) and H_2(sal-mpen).

was suspended in a 5% aqueous sodium hydroxide solution (640 cm^3) and the solution was stirred at room temperature overnight. The insoluble oily substance was removed and the aqueous solution was acidified by adding 50% sulfuric acid (160 cm^3). The mixture was refluxed for 2 h and the resulting yellow oily substance was separated with a separatory funnel. The aqueous layer was shaken with benzene and the extracts were combined and dried over anhydrous sodium sulfate. After the solvent was evaporated, the residue was distilled at 149—151 °C/13 mmHg (1 mmHg ≈133.322 Pa) to give a colorless liquid (30 g).

Found: C, 76.64; H, 8.42%. Calcd for $C_{12}H_{16}O_2$: C, 74.79; H, 8.39%.

2-Amino-2-methyl-4-(2-methoxy-5-methylphenyl)butanenitrile: A solution of ammonium chloride (5 g) in water (20 cm^3), sodium cyanide (4 g), and aqueous ammonia (28%, 11 cm^3) were mixed in a 500 cm^3 round-bottomed flask. To this was added methyl 2-(2-methoxy-5-methylphenyl)ethyl ketone (15 g), and the flask was sealed with a glass stopper and heated at 60 °C on a water bath for 5 h. The reaction mixture was shaken with five 60 cm^3 portions of ether, and the etherial extracts were combined and dried over sodium sulfate. On evaporating the solvent, the amino nitrile was obtained as an orange paste. It was used for the following reaction without purification.

2-Methyl-4-(2-methoxy-5-methylphenyl)-1,2-butanediamine Dihydrochloride (mpen·2HCl): To a stirred suspension of $LiAlH_4$ (25 g) in absolute ether (400 cm^3) was added a solution of the aminonitrile (10 g) in ether (50 cm^3). The reaction mixture was refluxed for 13 h and decomposed by adding water under ice cooling. The ethereal layer was separated and the residue was extracted with three 100 cm^3 portions of ether. The ethereal solutions were combined and dried over sodium sulfate. When dry hydrogen chloride was bubbled into the solution, crude mpen·2HCl was separated as a milky white precipitate. It was used for the following reaction without further purification because of its high hygroscopicity.

2-Methyl-4-(2-hydroxy-5-methylphenyl)-1,2-butanediamine Dihydrobromide (Hpen·2HBr): A mixture of crude mpen·2HCl (3.2 g), acetic acid (35 cm^3), hydrobromic acid (40%, 35 cm^3), and hydroiodic acid (55%, 3.5 cm^3) was refluxed for 20 h. The reaction mixture was evaporated to dryness to give dark brown mass. It was dissolved in methanol and decolorated with activated charcoal. When the solvent was evaporated, Hpen·2HBr was obtained as yellow mass. Since it was very hygroscopic, it was used for the preparation of H_2(sal-Hpen) without purification.

N,N′-Disalicylidene-2-methyl-4-(2-hydroxy-5-methylphenyl)-1,2-butanediamine (H_2(sal-Hpen)): This was obtained as yellow needles by the reaction Hpen·2HBr (0.3 g) and salicylaldehyde (0.2 g) in methanol (20 cm^3) in the presence of triethylamine (0.17 g).

Found: C, 74.74; H, 6.83; N, 6.74%. Calcd for $C_{26}H_{28}N_2O_3$: C, 74.79; H, 7.00; N, 6.89%.

N,N′-Disalicylidene-2-methyl-4-(2-methoxy-5-methylphenyl)-1,2-butanediamine (H_2(sal-mpen)): This was obtained as yellow needles in nearly the same way as that of H_2(sal-Hpen) except for using mpen·2HCl (0.2 g) instead of Hpen·2HBr.

Found: C, 75.15; H, 7.11; N, 6.52%. Calcd for $C_{27}H_{30}N_2O_3$: C, 75.32; H, 7.02; N, 6.51%.

[Cu(sal-Hpen)]: To a methanolic solution (30 cm^3) of H_2(sal-Hpen) (0.2 g) was added a methanolic solution of copper(II) acetate monohydrate (0.1 g). The mixture was heated at 60 °C for 5 h and allowed to stand overnight. Pu ple crystals separated were filtered and recrystallized from methanol.

Found: C, 64.58; H, 5.72; N, 5.79%. Calcd for $C_{26}H_{26}N_2O_3Cu\cdot\frac{1}{2}H_2O$: C, 64.12; H, 5.59; N, 5.75%.

[Ni(sal-Hpen)]: This complex was obtained as red crystals by the reaction of H_2(sal-Hpen) (0.2 g) and nickel (II) acetate tetrahydrate (0.12 g) in methanol. It was recrystallized from methanol.

Found: C, 65.69; H, 5.62; N, 6.00%. Calcd for $C_{26}H_{26}N_2O_3Ni$: C, 65.99; H, 5.53; N, 5.92%.

[Co(sal-Hpen)]: This complex was obtained as orange powder by the reaction of H_2(sal-Hpen) (0.2 g) and cobalt (II) acetate tetrahydrate (0.12 g) in absolute ethanol in an atmosphere of nitrogen.

Found: C, 65.60; H, 5.61; N, 5.94%. Calcd for $C_{26}H_{26}N_2O_3Co$: C, 65.96; H, 5.54; N, 5.92%.

[Fe(sal-pen)]: This complex was obtained as brownish purple crystalline powder by the reaction of H_2(sal-Hpen) (0.2 g) and iron(III) acetate (0.08 g) in absolute ethanol.

Found: C, 65.58; H, 5.44; N, 5.78%. Calcd for $C_{26}H_{25}N_2O_3Fe\cdot\frac{1}{2}H_2O$: C, 65.28; H, 5.47; N, 5.86%.

[Co(sal-pen)py]: [Co(sal-Hpen)] (0.1 g) was dissolved in dichloromethane (30 cm^3) containing pyridine (0.02 g), and to this was bubbled air for 3 h. On concentrating the solution, reddish brown crystalline powder was separated.

Found: C, 65.16; H, 5.39; N, 7.35%. Calcd for $C_{31}H_{30}N_3O_3Co\cdot H_2O$: C, 65.38; H, 5.66; N, 7.37%.

[Cu(sal-mpen)]: This complex was obtained as purple needles in the same way as that of [Cu(sal-Hpen)] except for using H_2(sal-mpen) (0.2 g) instead of H_2(sal-Hpen).

Found: C, 65.65; H, 5.74; N, 5.68%. Calcd for $C_{27}H_{28}N_2O_3Cu$: C, 65.77; H, 5.92; N, 5.68%.

[Ni(sal-mpen)]: This complex was obtained as red needles in the same way as that of [Ni(sal-Hpen)] except for using H_2(sal-mpen) (0.2 g) instead of H_2(sal-Hpen).

Found: C, 65.97; H, 5.86; N, 5.73%. Calcd for $C_{27}H_{28}N_2O_3Ni$: C, 66.42; H, 5.98; N, 5.73%.

[Co(sal-mpen)]: This complex was obtained as orange microcrystalline powder in the same way as that of [Co(sal-Hpen)] except for using H_2(sal-mpen) (0.2 g) instead of H_2(sal-Hpen).

Found: C, 66.34; H, 5.75; N, 5.79%. Calcd for $C_{27}H_{28}N_2O_3Co$: C, 66.39; H, 5.98; N, 5.73%.

Measurements. Infrared spectra were recorded on a Hitachi Infrared Spectrometer Model 215 on KBr disks or hexachlorobutadiene mulls. Electronic spectra were recorded on a Shimadzu Multipurpose Spectrophotometer Model MPS-5000 and a Shimadzu UV-VISIBLE Recording Spectrometer Model UV-240 in dichloromethane. Magnetic susceptibilities were measured by the Faraday method. The apparatus was calibrated by the use of $[Ni(en)_3]S_2O_3$.[21] Diamagnetic corrections were carried out using Pascal's constants and effective magnetic moments were calculated by the equation $\mu_{eff}=2.828(\chi_A\times T)^{1/2}$.

Results and Discussion

Infrared spectra of [M(sal-Hpen)](M=Cu^{II}, Ni^{II}, and Co^{II}) are quite similar to those of [M(sal-mpen)], except for a band at 3300—3200 cm^{-1} which is absent in the spectra of [M(sal-mpen)]. This band should be due to the stretching vibration of the phenolic hydroxy group in the tail.

Electronic spectra of [M(sal-Hpen)] and [M(sal-mpen)] were measured in dichloromethane and are shown in Fig. 2. The spectra of [Cu(sal-Hpen)] and [Cu(sal-mpen)] resemble each other in the region (15—35)$\times 10^3$ cm^{-1}, exhibiting a d-d band centered around

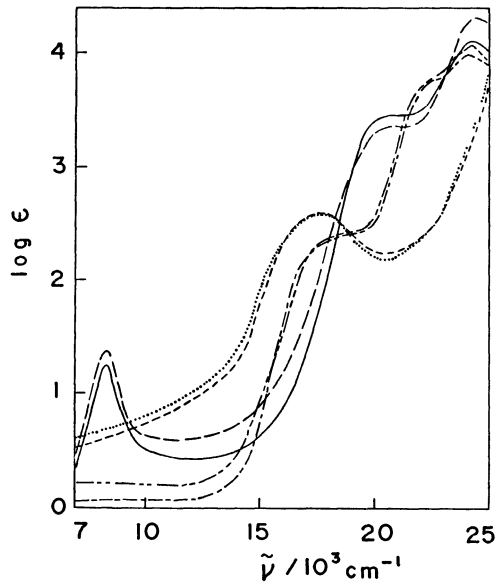

Fig. 2. Electronic spectra of (— — —)[Cu(sal-Hpen)], (·····) [Cu(sal-mpen)], (—·—·—) [Ni(sal-Hpen)], (—··—) [Ni(sal-mpen)], (——)[Co(sal-Hpen)], and (— — —) [Co(sal-mpen)].

18×10^3 cm^{-1}. Furthermore, these spectra are nearly the same as that of [Cu(salen)].[22-24] These facts clearly indicate that the geometry around the metal in the present complexes is essentialy planar without coordination of the hydroxyl or methoxyl group of the tail. Planar configuration for [Cu(sal-Hpen)] and [Cu(sal-mpen)] was also supported by their ESR spectra showing a tetragonal pattern, whose ESR parameters ([Cu(sal-Hpen)]: $g_{\parallel}=2.18$ and $A_{\parallel}=203$ G(1 G$=10^{-4}$T); [Cu(sal-mpen)]: $g_{\parallel}=2.18$ and $A_{\parallel}=201$ G) are practically the same as those of [Cu(salen)] ($g_{\parallel}=2.20$ and $A_{\parallel}$195 G).[25]

Electronic spectra of [Ni(sal-Hpen)] and [Ni(sal-mpen)] resemble each other in the region $(15—35) \times 10^3$ cm^{-1}. Both showed a d-d band at 18.5×10^3 cm^{-1}, which is nearly the same in frequency as that of [Ni(salen)].[24,26,27] Planar configuration around the metal in [Ni(sal-Hpen)] and [Ni(sal-mpen)] appeared to be reasonable, considered from the facts that [Ni(salen)] and its congeners are known to retain the planar configuration even in polar solvents such as pyridine.[26]

Effective magnetic moments of [Co(sal-Hpen)] and [Co(sal-mpen)] are *ca.* 2.4 BM at room temperature. Electronic spectra of these complexes show a weak band at 8.3×10^3 cm^{-1}, which is characteristic of low-spin, planar cobalt(II) complexes with salen-like Schiff bases.[28-30] Powder ESR spectra of [Co(sal-Hpen)] and [Co(sal-mpen)] both showed a typical ESR pattern of a low-spin, planar cobalt(II) with the $(d_{yz})^1$ ground state[31,32] (Fig. 3). The ESR parameters of the signal at the lower magnetic field are as follows: $g_{\parallel}=3.50$ and $A_{\parallel}=127$ G for [Co(sal-Hpen)]; $g_{\parallel}=3.50$ and $A_{\parallel}=121$ G for [Co(sal-mpen)]. From these facts we may conclude that the present cobalt(II) complexes are of square planar coordination.

Despite marked resemblance in electronic and ESR spectra, [Co(sal-Hpen)] distinctly differ from [Co(sal-mpen)] in reactivity to atmospheric oxygen; the former is very sensitive to molecular oxygen while the latter is practically insensitive in dichloromethane. This suggests that the hydroxy group in the tail exerts some effect on the oxygenation or oxidation at the metal though this group is free from coordination in the cobalt(II) complex.

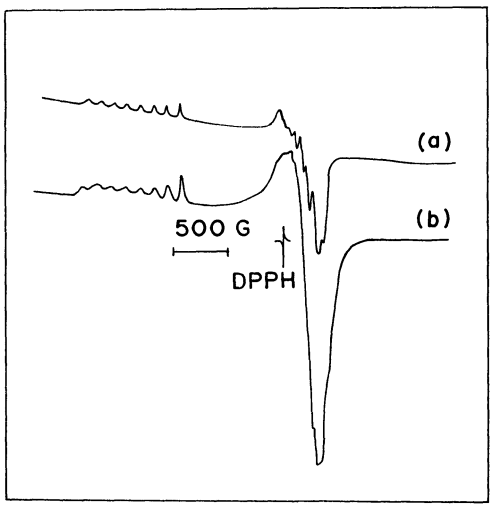

Fig. 3. ESR spectra of (a) [Co(sal-mpen)] and (b) [Co(sal-Hpen)].

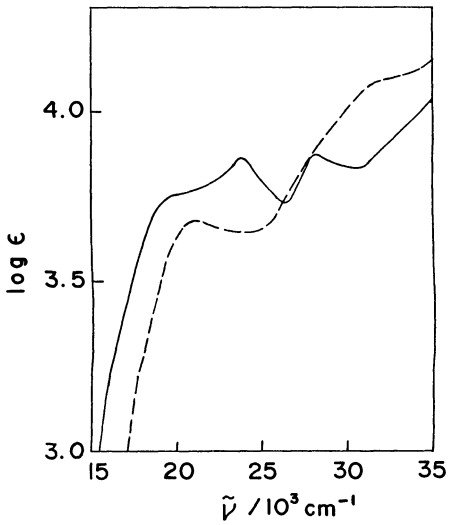

Fig. 4. Electronic spectra of (——) [Co(sal-pen)py] and (— — —) [Fe(sal-pen)].

Reddish brown [Co(sal-pen)py] prepared by air-oxidation of [Co(sal-Hpen)] in dichloromethane-pyridine is diamagnetic. Electronic spectrum of this complex shows an absorption at 20×10^3 cm^{-1} with a shoulder near 16.5×10^3 cm^{-1} (Fig. 4). Coordination of pyridine to the cobalt(III) ion was deduced by an IR band at 690 cm^{-1}. The absence of band due to O-H stretching mode in the region 3300—3200 cm^{-1} implies deprotonation of the phenolic OH group in the tail. All these facts suggest that H_2(sal-Hpen) acts as a quinquedentate ligand to form a six-coordinate cobalt(III) complex with the phenolic oxygen of the tail at the fifth donating site and a pyridine molecule

at the sixth site.

Magnetic susceptibility of [Fe(sal-pen)] is 5.8 BM at room temperature, which falls in the range for high-spin iron(III) complex. This complex exhibits no IR band in the region 3300—3200 cm^{-1}, implying the formation of a five-coordinate iron(III) complex with the deprotonated phenolic oxygen in the tail at the apex. It exhibits a visible spectrum with an absorption at 21×10^3 cm^{-1} ($\varepsilon \approx 4800$ M^{-1} cm^{-1}), which can be attributed to the charge transfer from the phenolic oxygen in the tail to the iron(III) ion (Fig. 4). Notably, this spectrum differs from those of [Fe(salen)-X] with phenolate or unidentate catecholate group as X; the latter complexes show the CT band in the region $(24.0—24.5) \times 10^3$ cm^{-1} ($\varepsilon \approx 7000$ M^{-1} cm^{-1}).[20] The reason for the absorption spectral difference between [Fe(sal-pen)] and [Fe(salen)X] is unclear at present. It is likely that the phenolic tail incorporated into the salen moiety affects the electronic property of iron(III) ion in a manner different from a monodentate phenolic donor. It is notable that the spectrum of [Fe(sal-pen)] resembles those of catechol 1,2-dioxygenase[33] and protocatechuate 3,5-dioxygenase,[34] which show the CT band from tyrosinate to iron at $(22.0—21.7) \times 10^3$ cm^{-1} ($\varepsilon \approx 3000—4000$ M^{-1} cm^{-1}).

References

1) T. Tsumaki, *Bull. Chem. Soc. Jpn.*, **13**, 252 (1938).
2) M. J. Carter, D. P. Rillema, and F. Basolo, *J. Am. Chem. Soc.*, **96**, 392 (1974).
3) D. Diemente, B. M. Hoffman, and F. Basolo, *J. Chem. Soc., Chem. Commun.*, **1970**, 467; B. M. Hoffman, D. L. Diemente, and F. Basolo, *J. Am. Chem. Soc.*, **92**, 61 (1970).
4) G. Amiconi, M. Brunori, E. Antonini, G. Tauzher, and G. Costa, *Nature (London)*, **228**, 549 (1970).
5) C. Floriani and F. Calderazzo, *J. Chem. Soc., A*, **1969**, 946.
6) A. Misono and S. Koda, *Bull. Chem. Soc. Jpn.*, **47**, 3048 (1969).
7) E. I. Ochiai, *J. Inorg. Nucl. Chem.*, **35**, 1727 (1973).
8) C. Busetto, C. Neri, N. Palladino, and E. Perrotti, *Inorg. Chim. Acta*, **5**, 129 (1971).
9) R. S. Gall and W. P. Schaefer, *Inorg. Chem.*, **15**, 2758 (1976).
10) A. Avdeef and W. P. Schaefer, *J. Am. Chem. Soc.*, **98**, 5153 (1976).
11) E. Cesarotti, M. Gullotti, A. Pasini, and R. Ugo, *J. Chem. Soc., Dalton. Trans.*, **1977**, 757.
12) G. Costa, G. Mestroni, and L. Stefani, *J. Organomet. Chem.*, **7**, 493 (1967).
13) G. Costa, G. Mestroni, and G. Pellizer, *J. Organomet. Chem.*, **11**, 333 (1968).
14) L. H. Vogt, Jr., J. G. Wirth, and H. L. Finkbeiner, *J. Org. Chem.*, **34**, 273 (1969).
15) T. J. Fullerton and S. P. Ahern, *Tetrahedron Lett.*, **1976**, 139.
16) A. Nishinaga, K. Watanabe, and T. Matsuura, *Tetrahedron Lett.*, **1974**, 1291.
17) A. Nishinaga, *Chem. Lett.*, **1975**, 273.
18) A. R. Amundsen, J. Whelan, and B. Bosnich, *Inorg. Chem.*, **18**, 206 (1979).
19) S. Nakagawa, H. Imai, Y. Uenori, A. Nakatsubo, and E. Kyuno, presented at the 32nd Symposium of Coordination Chemistry, Nagasaki, October 14, 1982.
20) R. H. Heistand II, R. B. Lauffer, E. Fikrig, and L. Que, Jr., *J. Am. Chem. Soc.*, **104**, 2789 (1982).
21) N. F. Curtis, *J. Chem. Soc.*, **1961**, 3147.
22) S. M. Crawford, *Spectrochim. Acta*, **19**, 255 (1963).
23) R. S. Downing and F. L. Urbach, *J. Am. Chem. Soc.*, **91**, 5977 (1969).
24) R. H. Holm, *J. Am. Chem. Soc.*, **82**, 5632 (1960).
25) A. H. Maki and B. R. McGarvey, *J. Chem. Phys.*, **29**, 31 (1958).
26) H. C. Clark and A. L. Odell, *J. Chem. Soc.*, **1955**, 3431.
27) B. Bosnich, *J. Am. Chem. Soc.*, **90**, 627 (1968).
28) H. Nishikawa and S. Yamada, *Bull. Chem. Soc. Jpn.*, **37**, 8 (1964).
29) C. J. Hipp and W. A. Baker, Jr., *J. Am. Chem. Soc.*, **92**, 792 (1970).
30) Y. Nishida and S. Kida, *Coord. Chem. Rev.*, **27**, 275 (1979).
31) M. A. Hitchman, *Inorg. Chem.*, **16**, 1985 (1977).
32) Y. Nishida and S. Kida, *Bull. Chem. Soc. Jpn.*, **51**, 143 (1978).
33) L. Que, Jr., R. H. Heistand II, R. Mayer, and A. L. Roe, *Biochemistry*, **19**, 2588 (1980).
34) L. Que, Jr., R. M. Epstein, *Biochemistry*, **20**, 2545 (1981).

Synthesis and Optical Resolution of $[Rh^{III}(S)_3(N)_3]$ Type Complexes Containing a Thiolato, Sulfenato, or Sulfinato Donor Group

Masakazu KITA,* Kazuaki YAMANARI, and Yoichi SHIMURA

Department of Chemistry, Faculty of Science, Osaka University, Toyonaka, Osaka 560

(Received May 4, 1983)

Rhodium(III) complexes, $[Rh(SCH_2CH_2NH_2)_3]$ and $[Rh\{S(O)CH_2CH_2NH_2\}_n\{S(O)_2CH_2CH_2NH_2\}_{3-n}]$ ($n=3$, 2, 1, and 0), were prepared and optically resolved by means of column chromatography or preferential crystallization of diastereomeric molecular compound with (*R,R*)-tartaric acid, d-$C_4H_6O_6\cdot(-)_{300}^{CD}$-$[Rh\{S(O)CH_2CH_2NH_2\}_3]\cdot H_2O$ or d-$C_4H_6O_6\cdot(+)_{300}^{CD}$-$[Rh\{S(O)CH_2CH_2NH_2\}_2\{S(O)_2CH_2CH_2NH_2\}]$. All the present complexes have only the *fac*(*S*) geometry. The (*R*) configuration of sulfenato group is more stable than the (*S*) one in the *Λ*-isomer.

In a previous paper[1] we have reported the synthesis, optical resolution, and stereoselectivity of neutral cobalt(III) complexes, $[Co(aet)_3]$ and $[Co(aese)_n(aesi)_{3-n}]$ ($n=3$, 2, 1, and 0).[2] These S-bonded sulfenato and sulfinato cobalt(III) complexes showed several unique chemical and spectrochemical behaviors. In particular, one of the isomers of $[Co(aese)_3]$ was resolved *via* diastereomeric molecular compound with (*R,R*)-tartaric acid. It is interesting to compare the properties of cobalt(III) complexes with those of the corresponding rhodium(III) complexes, because there is a general tendency for the metals of the second transition series to exhibit a greater affinity toward sulfur donors than do the metals of the first transition series.[3] No optically active sulfenato or sulfinato complexes has so far been reported for rhodium(III). This paper is concerned with the preparation, optical resolution, and stereochemistry of $[Rh(aet)_3]$ and $[Rh(aese)_n(aesi)_{3-n}]$ ($n=3$, 2, 1, and 0).

Experimental

Preparation, Separation, and Optical Resolution of Complexes. *(1)* $[Rh(aet)_3]$: To a solution of 3.0 g (39 mmol) of 2-aminoethanethiol and 1.5 g (38 mmol) of sodium hydroxide in 20 cm^3 of water was added 2.0 g (9.6 mmol) of $RhCl_3$ and the mixture was stirred at 95 °C for 4 h. The white curdy precipitate with a yellow tint (1.5 g, 47%) was filtered and washed with water. Found: C, 21.52; H, 5.41; N, 12.59%. Calcd for $[Rh(aet)_3]=C_6H_{18}N_3S_3Rh$: C, 21.75; H, 5.48; N, 12.68%.

(2) $[Rh(aese)_n(aesi)_{3-n}]$ *(n=3, 2, 1, and 0)*: These complexes were prepared *via* H_2O_2 oxidation of $[Rh(aet)_3]$ and isolated by the column chromatographic technique used for $[Co(aese)_n(aesi)_{3-n}]$ ($n=3$, 2, 1, and 0).[1]

To a suspension of 1.0 g (3.0 mmol) of $[Rh(aet)_3]$ in 20 cm^3 of water was added 20 cm^3 (9.0 mmol) of 1.5% aqueous H_2O_2 with stirring below 5 °C, leading to a faint yellow solution. On addition of acetone (100 cm^3) and diethyl ether (200 cm^3), a faint yellow precipitate (1.2 g) appeared. This was dissolved in a small amount of water, adsorbed on a column of anion-exchange resin {QAE Sephadex A-25, (*R,R*)-tartrate form} and eluted with water. The eluates were collected with five cm^3 portions. Four complexes, I, II, III, and IV, were eluted in this order. At this stage all complexes were partially resolved: The earlier eluted fractions of each complex showed positive CD at the longest wavelength regon of the first d-d absorption band.

Combined eluate of each the complex was concentrated in a vacuum rotary evaporator at *ca.* 8 °C to give the precipitate. The precipitate was collected by filtration and washed with ethanol–ether (1:1). The complex I partially isomerized into the complex II during the crystallization. The isomerization was confirmed by column chromatography and the ^{13}C NMR spectra. The sparingly soluble white complex V was obtained *via* oxidation of $[Rh(aet)_3]$ by an excess of 30% H_2O_2. Further oxidation of each complex I, II, III, or IV by dilute H_2O_2 showed that the oxidation process is stepwise in a series of I (or II)→III→IV→V and the complex V was the final oxidation product. On the basis of the absorption measurements and elemental analyses, the complexes I (and II), III, IV, and V were assigned to $n=3$, 2, 1, and 0 in $[Rh(aese)_n(aesi)_{3-n}]$ series, respectively. Found for I: C, 15.76; H, 5.60; N, 9.20%. Calcd for $[Rh(aese)_3]\cdot 4H_2O=C_6H_{26}N_3O_7S_3Rh$: C, 15.97; H, 5.80; N, 9.31%. Found for II: C, 16.75; H, 5.45; N, 9.76%. Calcd for $[Rh(aese)_3]\cdot 3H_2O=C_6H_{24}N_3O_6S_3Rh$: C, 16.63; H, 5.58; N, 9.70%. Found for III: C, 16.77; H, 5.14; N, 9.85%. Calcd for $[Rh(aese)_2(aesi)]\cdot 2H_2O=C_6H_{22}N_3O_6S_3Rh$: C, 16.71; H, 5.14; N, 9.74%. Found for IV: C, 16.52; H, 4.66; N, 9.52%. Calcd for $[Rh(aese)(aesi)_2]\cdot 1.5H_2O=C_6H_{21}N_3O_{6.5}S_3Rh$: C, 16.44; H, 4.83; N, 9.59%. Found for V: C, 16.77; H, 4.32; N, 9.58%. Calcd for $[Rh(aesi)_3]\cdot 0.5H_2O=C_6H_{19}N_3O_{6.5}S_3Rh$: C, 16.51; H, 4.39; N, 9.63%.

(3) Optical Resolution: The racemate II, $[Rh(aese)_3]\cdot 3H_2O$ (1.0 g, 2.3 mmol), or the racemate III, $[Rh(aese)_2(aesi)]\cdot 2H_2O$ (1.0 g, 2.3 mmol), was dissolved in an ethanol–water (2:1) mixture and then (*R,R*)-tartaric acid (0.35 g, 2.3 mmol) was added to the solution, and after a few minutes, a slightly yellow diastereomeric molecular compound, d-$C_4H_6O_6\cdot(-)_{300}^{CD}$-$[Rh(aese)_3]\cdot H_2O$ (II*) or a white diastereomeric molecular compound, d-$C_4H_6O_6\cdot(+)_{300}^{CD}$-$[Rh(aese)_2(aesi)]$ (III*) began to deposit, respectively. The crystals were filtered and washed with ethanol. Found for II*: C, 21.64; H, 4.71; N, 7.55%. Calcd for d-$C_4H_6O_6\cdot(-)_{300}^{CD}$-$[Rh(aese)_3]\cdot H_2O=C_{10}H_{26}N_3O_{10}S_3Rh$: C, 21.95; H, 4.79; N, 7.67%. Found for III*: C, 21.79; H, 4.44; N, 7.72%. Calcd for d-$C_4H_6O_6\cdot(+)_{300}^{CD}$-$[Rh(aese)_2(aesi)]=C_{10}H_{24}N_3O_{10}S_3Rh$: C, 22.02; H, 4.44; N, 7.70%.

The diastereomeric molecular compound, II* or III*, was converted into $(-)_{300}^{CD}$-II or $(+)_{300}^{CD}$-III by treating with an equimolar amount of $Ca(OH)_2$. The CD spectrum was measured for the filtrate whose concentration was calculated from the measured absorbance using the extinction coefficient of the corresponding racemate.

Optically pure complexes IV and V could be prepared by the oxidation of the optically active complex II or III, $(-)_{300}^{CD}$-$[Rh(aese)_3]$ or $(+)_{300}^{CD}$-$[Rh(aese)_2(aesi)]$. The oxidation product of $(-)_{300}^{CD}$-I, which was obtained by the column chromatography described above, was the same as that of $(-)_{300}^{CD}$-II.

(4) $[Co(aese)_3]$: The *rac*{*Λ*-(*S,S,S*)/*Λ*-(*R,R,R*)}-$[Co(aese)_3]$ was obtained by the previously reported procedure.[1]

Measurements. The visible and ultraviolet absorption spectra were measured on a Hitachi 330 spectrophotometer. The CD spectra were recorded on a JASCO MOE-1 spectropolarimeter and the MCD spectra were measured on the same instrument in 1.5 T magnetic field. The absorption, CD and MCD measurements of the complexes were made in aqueous solutions at room temperature. The ^{13}C NMR spectra were obtained with a Varian XL-100-15 NMR spectrometer in D_2O containing dioxane as an internal standard.

Results and Discussion

Geometry of [Rh(aet)$_3$]. The absorption spectra and data of [Rh(aet)$_3$] are shown in Fig. 1 and Table 1, respectively. The corresponding cobalt(III) complex [Co(aet)$_3$] takes the *fac(S)* geometry and its absorption peaks appear at 17200, 22700, and 36400 cm^{-1}, which were assigned to the first and second spin-allowed d-d transitions[1,4] ($^1T_1 \leftarrow {}^1A_1$), ($^1T_2 \leftarrow {}^1A_1$), and Co(σ^*)←S(σ) LMCT transition, respectively.[1,5] Analogously the absorption bands of [Rh(aet)$_3$] at 25000, 29500, and 44200 cm^{-1} are assigned to $^1T_1 \leftarrow {}^1A_1$, $^1T_2 \leftarrow {}^1A_1$, and Rh(σ^*)←S(σ) LMCT transitions, respectively.[4,5] The complex II, which was the oxidation product of [Rh(aet)$_3$], showed two ^{13}C NMR resonances, and therefore has C_3 symmetry (Table 2).

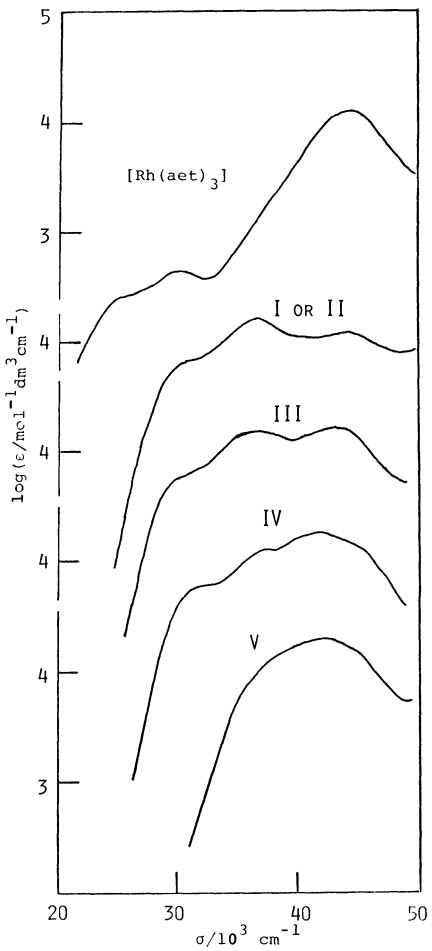

Fig. 1. Absorption spectra of [Rh(aet)$_3$] and [Rh(aese)$_n$(aesi)$_{3-n}$]: I or II (n=3), III (n=2), IV (n=1), and V (n=0).

As will be shown later both the complexes I and II have the *fac(S)* geometry. Therefore, it is concluded that the starting thiolato complex [Rh(aet)$_3$] exists in the *fac(S)* form.

Characterization of [Rh(aese)$_n$(aesi)$_{3-n}$] (n=3, 2, 1, and 0). The absorption spectra of the complexes for the series are shown in Fig. 1. All complexes showed an intense band in 42000—44000 cm^{-1} region, which is assigned to the Rh(σ^*)←S(σ) LMCT transition. The complexes I—IV show another intense band at *ca.* 36000 cm^{-1} whose molar absorption coefficient decreases successively with the decrease of the number of sulfenato groups. Therefore, the bands at *ca.* 36000 cm^{-1} can be assigned to LMCT Rh(σ^*)←sulfenato group. The d-d absorption bands of these oxidation products are somewhat obscured by the intense LMCT

Table 1. Absorption and CD spectral data

Complex	σ_{max}(log ε)[a]	σ_{ext}($\Delta\varepsilon$)[b]
[Rh(aet)$_3$]	25.0(2.5)^{sh}	
	29.5(2.7)	
	44.2(4.2)	
$(-)^{CD}_{300}$-[Rh(aese)$_3$] (I)	30.9(3.86)^{sh}	30.3(−7.69)^{sh}
	36.1(4.21)	35.3(−30.6)
		38.5(−16.1)
	43.6(4.06)	42.2(+15.5)
$(-)^{CD}_{300}$-[Rh(aese)$_3$] (II)	30.9(3.86)^{sh}	30.3(−15.5)^{sh}
	36.1(4.21)	35.5(−57.6)
	43.6(4.06)	43.9(+61.8)
$(-)^{CD}_{300}$-[Rh(aese)$_2$(aesi)] (III)	31.3(3.83)^{sh}	30.7(−15.5)^{sh}
	36.1(4.11)	35.1(−40.0)
		37.3(−27.7)
	43.1(4.23)	43.1(+38.5)
		49.5(+35.0)
$(-)^{CD}_{300}$-[Rh(aese)(aesi)$_2$] (IV)	32.0(3.75)^{sh}	32.3(−16.7)^{sh}
	37.0(4.07)	35.1(−25.2)
		38.5(−9.23)^{sh}
	42.4(4.25)	41.0(+5.65)^{sh}
		44.4(+11.1)
$(-)^{CD}_{300}$-[Rh(aesi)$_3$] (V)		35.7(−11.4)^{sh}
		39.1(−18.6)
	41.7(4.29)	44.1(+15.5)
[Co(aese)$_3$]	13.2(0.6)^{sh,c}	
	21.5(2.92)	
	27.9(4.21)	
	37.0(3.76)	

a, b) Wave numbers are given in 10^3 cm^{-1} unit, log ε or $\Delta\varepsilon$ (in parentheses) in mol^{-1} dm^3 cm^{-1}, and sh means a shoulder. c) This is assigned to the spin-forbidden ligand field transition, $^3T_1 \leftarrow {}^1A_1$.[4]

Table 2. Chemical shifts of ^{13}C NMR spectra[a]

Complex	δ
[Rh(aese)$_3$] (I)	40.53, 40.69, (41.07),[b] 41.88, 50.93, (51.31),[b] 51.91, 52.98
[Rh(aese)$_3$] (II)	41.07, 51.31

a) In D_2O containing dioxane (δ=67.40) as an internal standard. b) The signals are resulted from the partial isomerization of the complex I into II.

TABLE 3. MCD SPECTRAL DATA

Complex	*rac*{*Δ*-(*S,S,S*)/*Λ*-(*R,R,R*)}-[Co(aese)$_3$]	*rac*-[Rh(aese)$_3$] (II)
$\sigma_{ext}(\Delta\varepsilon_M)$[a]	12.7(+0.00052)	
	14.4(−0.00022)	
	17.7(−0.0013)	
	21.1(+0.123)	29.9(+0.180)
	25.3(−0.689)	34.3(−1.08)
	27.4(+0.434)	37.7(+0.507)
	30.0(−0.244)	42.6(−0.360)
	35.1(−0.488)	
	40.0(−0.651)	

a) Wave numbers are given in 10^3 cm^{-1} unit, $\Delta\varepsilon_M$ (in parentheses) in mol^{-1} dm^3 cm^{-1} T^{-1}.

bands. The MCD pattern of the racemic complex II is similar to that of *rac*{*Δ*-(*S,S,S*)/*Λ*-(*R,R,R*)}-[Co(aese)$_3$] in the spin-allowed d-d and LMCT region (Table 3 and Fig. 2). The *Λ*-(*R,R,R*)-[Co(aese)$_3$] showed the CD extrema at 20000 cm^{-1} ($\Delta\varepsilon$=+6.96) and 22400 cm^{-1} ($\Delta\varepsilon$=−4.12) in the ligand field transition region[1] and the corresponding MCD extremum at 21100 cm^{-1} ($\Delta\varepsilon_M$=+0.12). The MCD extremum of the rhodium(III) complex *rac*-II at 29900 cm^{-1} ($\Delta\varepsilon_M$=+0.18) is assigned to the ligand field transition on the analogy of the MCD pattern. The shoulder at *ca.* 30000 cm^{-1} of the complex III or IV in Fig. 3 is assigned to the ligand field transition band. A similar band of [Rh(aesi)$_3$] (V) was quite obscured in the absorption spectrum but the CD shoulder exists at 35700 cm^{-1}.

The complexes containing the sulfenato groups should have two CD contributions, one from the configurational chirality based on the skew pair of chelate rings (*Δ* or *Λ*) and the other from the chirality based on the asymmetric sulfur donor atom of sulfenato group (*S* or *R*). Since the complex $(-)^{CD}_{300}$-II has C_3 symmetry as determined from the ^{13}C NMR spectrum, the structure is one of the following four with *fac*(*S*) geometry, *Δ*-(*R,R,R*), *Δ*-(*S,S,S*), *Λ*-(*R,R.R*), or *Λ*-(*S,*-

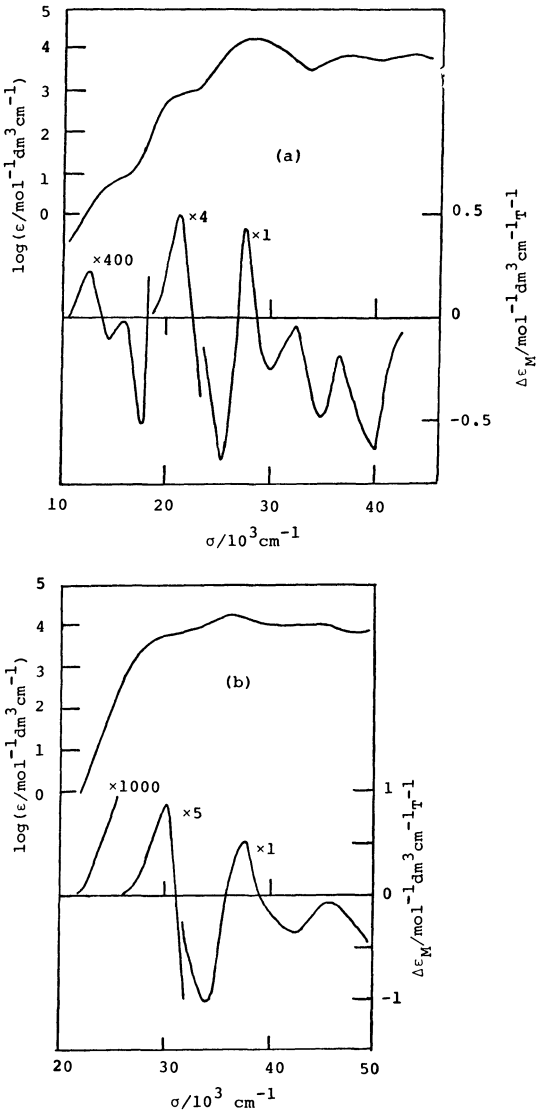

Fig. 2. Absorption and MCD spectra of (a): *rac*{*Δ*-(*S,S,S*)/*Λ*-(*R,R,R*)}-[Co(aese)$_3$] and (b): the complex II.

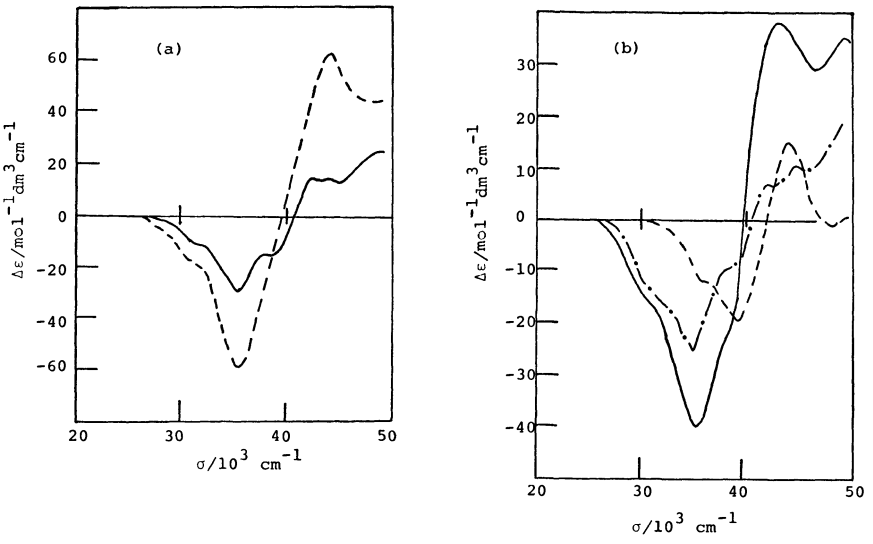

Fig. 3. CD spectra of the complexes (a): $(-)^{CD}_{300}$-I (——), and $(-)^{CD}_{300}$-II (—·—), and (b): $(-)^{CD}_{300}$-III (——), $(-)^{CD}_{300}$-IV (—·—), and $(-)^{CD}_{300}$-V (—·—).

S,S). The absolute configurations of sulfenato groups can be deduced from the cobalt(III) complexes by the CD sign and intensity ($\Delta\varepsilon$) in the sulfenato LMCT region.[1,6] For example, a positive CD band ($\Delta\varepsilon$= +11.71) was observed in the sulfenato LMCT reigon (*ca.* 27000 cm^{-1}) for *Λ-(S)*-[Co(aese)$(en)_2]^{2+}$, and a negative one for the *Λ-(R)* complex.[1] Assuming the same criterion for the sulfenato rhodium(III) complexes, it can be concluded that all the complexes $(-)^{CD}_{300}$-I, $(-)^{CD}_{300}$-II, $(-)^{CD}_{300}$-III, and $(-)^{CD}_{300}$-IV have mainly (*R*) sulfenato groups, because the $\Delta\varepsilon_{ext}$ values were −30.6, −57.6, −40.0, and −21.2 for $(-)^{CD}_{300}$-I, $(-)^{CD}_{300}$-II, $(-)^{CD}_{300}$-III, and $(-)^{CD}_{300}$-IV, respectively. The oxidation of the complexes $(-)^{CD}_{300}$-I and $(-)^{CD}_{300}$-II gave the same product $(-)^{CD}_{300}$-III, which in succession gave the $(-)^{CD}_{300}$-IV. These observations lead to the assignments *(R,R,S)*, *(R,R,R)*, *(R,R)*, and *(R)* for $(-)^{CD}_{300}$-I, $(-)^{CD}_{300}$-II, $(-)^{CD}_{300}$-III, and $(-)^{CD}_{300}$-IV, respectively. As in the case of *fac(S)*-[Co$(aese)_3$],[1] three sulfenato oxygen atoms of the *Λ-(R,R,R)* isomer should take the crowded axial positions on the *fac(S)* plane, whereas the oxygen atoms of the *Λ-(R,R,R)* isomer occupy the less-crowded equatorial ones. Therefore, the *Λ-(R,R,R)* configuration is desirable as the structure of the complex $(-)^{CD}_{300}$-II rather than the *Δ-(R,R,R)* one. The latter isomer was apparently undetectable in the preparation of *fac-(S)*-[Rh$(aese)_3$]. In conclusion the complex $(-)^{CD}_{300}$-I, $(-)^{CD}_{300}$-II, $(-)^{CD}_{300}$-III, $(-)^{CD}_{300}$-IV, or $(-)^{CD}_{300}$-V has *Λ-(R,R,S)*, *Λ-(R,R,R)*, *Λ-(R,R)*, *Λ-(R)*, or *Λ* configuration, respectively. These assignments rationalize the isomerization of $(-)^{CD}_{300}$-I into $(-)^{CD}_{300}$-II in the aqueous solutions, because the latter having less-crowded configuration than the former. The configurational chirality of [Co$(aese)_n(aesi)_{3-n}$] (n=3, 2, 1, or 0) was assigned on the basis of the sign of the longest wavelength CD band: the *Λ*-configuration show a positive CD.[1] It is noteworthy that this relation is reversed in the present complexes [Rh$(aese)_n(aesi)_{3-n}$] (n=3, 2, 1, and 0). This is probably due to the close overlapping of the d-d and LMCT bands (both in absorption and CD spectra) in the rhodium(III) complexes.

The column chromatographic behaviors also support the above chirality assignment. It the separation using QAE-Sephadex A-25 {(*R,R*)-tratrate form} with water as eluent, the *Λ* isomers were eluted more rapidly than the corresponding *Δ* ones in both the cobalt(III) and rhodium(III) complexes.

The optical resolution *via* diastereomeric molecular compound with *d*-tartaric acid was successful for the two kinds of rhodium(III) complexes, *fac(S)*-[Rh$(aese)_3$] and *fac(S)*-[Rh$(aese)_2(aesi)$]. The less soluble diastereomeric molecular compound *d*-$C_4H_6O_6\cdot(-)^{CD}_{300}$-[Rh$(aese)_3]\cdot H_2O$ has the same composition as the corresponding cobalt(III) compound *d*-$C_4H_6O_6\cdot(+)^{CD}_{500}$-[Co$(aese)_3]\cdot H_2O$. Since the X-ray diffraction study of the latter compound showed that the contains the *fac(S)-Λ-(R,R,R)* isomer,[7] it seems that the configuration of $(-)^{CD}_{300}$-[Rh$(aese)_3$] (III) is *fac(S)-Λ-(R,R,R)*. This is in accord with the above assignment from CD. The another molecular compound containing *fac(S)*-[M$(aese)_2(aesi)$] was found only in the rhodium(III) series and not in the cobalt(III) series. It remains puzzling that the isomer which forms the less soluble diastereomeric molecular compound with *d*-tartaric acid has the *Δ-(S,S)* configuration for the [Rh$(aese)_2(aesi)$] complex in contrast to the case of [Rh$(aese)_3$], for which the less soluble molecular compound contains the *Λ-(R,R,R)* isomer.

References

1) M. Kita, K. Yamanari, and Y. Shimura, *Bull. Chem. Soc. Jpn.*, **55**, 2873 (1982).

2) Abbreviations used for ligands are as follows: Haet, 2-aminoethanethiol $HSCH_2CH_2NH_2$; Haese, 2-aminoethanesulfenic acid $HS(O)CH_2CH_2NH_2$; Haesi, 2-aminoethanesulfinic acid $HS(O)_2CH_2CH_2NH_2$.

3) R. G. Pearson, *J. Am. Chem. Soc.*, **85**, 3533 (1963); Y. Zhang, *Inorg. Chem.*, **21**, 3889 (1982).

4) The assignments of d-d bands are in an approximation of O_h symmetry.

5) LMCT means ligand-to-metal charge transfer.

6) D. L. Herting, G. P. Sloan, A. W. Carbral, and J. H. Kruger, *Inorg. Chem.*, **17**, 1649 (1978).

7) M. Kita, K. Yamanari, K. Kitahama, and Y. Shimura, *Bull. Chem. Soc. Jpn.*, **54**, 2995 (1981).

An X-Ray Diffraction Study on the Structures of Bis- and Tris(ethylenediamine)copper(II) Complexes in Solution

Tadao FUJITA and Hitoshi OHTAKI*

Department of Electronic Chemistry, Tokyo Institute of Technology at Nagatsuta, Nagatsuta-cho, Midori-ku, Yokohama 227

(Received May 19, 1983)

The structure of copper(II) complexes with ethylenediamine (en) in solution has been determined by means of X-ray diffraction. The measurements were performed at 25 °C for aqueous ethylenediamine solutions of copper(II) nitrate, the mole ratio (en/Cu) in the solutions being 2.09 and 5.14. In the former solution the bis(ethylenediamine)copper(II) complex was contained as the main species, while the tris(ethylenediamine)copper(II) complex was predominantly formed in the latter solution. The analysis of the X-ray scattering data of the solutions showed that in the bis-complex four nitrogen atoms of the two ethylenediamine molecules coordinated to the central metal ion at the distance of 1.93 Å in a planar form and oxygen atoms of two water molecules were located at 2.92 Å above and below the plane. Since the axial Cu–OH_2 bond distance is very long, the structure of the bis-complex can be regarded as square-planar. In the tris-complex the equatorial Cu–N bond length was 1.92 Å, which was practically the same as that within the bis-complex. The axial Cu–N distance was 2.22 Å.

There exist nine electrons in the d-orbital of a copper(II) ion, and thus, a hexacoordinated copper(II) complex tends to have a distorted octahedral structure. Structures of copper(II) complexes have been extensively studied by the spectroscopic analysis of solutions, as well as by the crystallographic method. The distortion of the structure of the $[Cu(OH_2)_6]^{2+}$ complex was first investigated by the X-ray crystal analysis, and it was found that the equatorial Cu–O bond distance within the complex comparatively shortened to be 2.16 Å, while the axial Cu–O bond length was 2.2—2.5 Å.[1-5] The distorted octahedral structure of the $[Cu(OH_2)_6]^{2+}$ complex was also found in solution by the X-ray diffraction method.[6-8] Ohtaki and his coworkers[7,8] reported that the equatorial and axial Cu–O bond lengths within the $[Cu(OH_2)_6]^{2+}$ complex were 1.94 and 2.43 Å, respectively, in a copper(II) perchlorate solution.

Yamaguchi and Ohtaki[9] reported the structures of the $[Cu(NH_3)_4(OH_2)_2]^{2+}$ and $[Cu(NH_3)_5X]^{2+}$ (X= NH_3 or H_2O) complexes by means of X-ray diffraction in solution. The Cu–N_{eq} and Cu–O_{ax} distance within the former were 2.03 and 2.33 Å, respectively, whereas the Cu–N_{eq}, Cu–N_{ax}, and Cu–X_{ax} were 1.93, 2.30, and 2.30 Å, respectively, in the latter.

The structures of the copper(II)–ethylenediamine complexes have been investigated by the ESR spectroscopy[10] and the X-ray diffraction method in crystal. In the tris(ethylenediamine)copper(II) sulfate, the CuN_6 moiety of the complex has an octahedral structure in which all the Cu–N bond distances are 2.15 Å.[11] The indifferent bond length within the complex was explained in terms of the dynamic Jahn-Teller effect. Since the angle of the N–Cu–N bond within the complex was not 90 °, the symmetry of the complex was not O_h but D_3.[11]

A regular octahedral structure was also found for $K_2Pb[Cu(NO_2)_6]$ in which all the Cu–N distances were 2.11 Å.[12] However, most of the hexacoordinated copper(II) complexes have distorted octahedral structures with two elongated bonds along the axis of the octahedron. The tris-complexes of copper(II) ion containing 2,2′-bipyridine and 1,10-phenanthroline were distorted octahedral.[13,14] In the tris(2,2′-bipyridine)copper(II) complex, the equatorial Cu(II)–N bond distance was 2.031 Å, but the axial Cu–N bond lengths were 2.450 and 2.226 Å.[13] On the other hand, in the tris(1,10-phenanthroline)copper(II) complex the two axial Cu–N bond lengths were the same to be 2.33 Å, the equatorial Cu–N distance being 2.05 Å.[14]

Bertini *et al.*[15] investigated the effect of counter anions on the distortion of the octahedral structure of the tris(ethylenediamine)copper(II) complex in crystal containing various counter anions by using the ESR spectroscopy. They showed that the degree of the distortion varied with the counter anions.[15] The shape of the ESR spectra of the sulfate and nitrate salts was different and they suggested that the structure of the $[Cu(en)_3]^{2+}$ ion of the nitrate may be octahedrally distorted. On the contrary, the distortion of the structure of the $[Cu(en)_3]^{2+}$ ion in the sulfate was suggested to be small, which had also been studied crystallographically by Cullen and Lingafelter.[11]

The structure of the bis(ethylenediamine)copper(II) complex has been extensively investigated by the spectroscopic and crystallographic methods and it has been found that the complex ion has a distorted octahedral structure with counter anions or water molecules at the axial positions. The equatorial bond length within the bis-complex was about 2.05 Å, which was almost the same as that within the tris-complex.[14,16] When water molecules bound to the central copper(II) ion at the axial position, the Cu–OH_2 bond length remarkably changed from 2.22 Å to 2.89 Å depending on counter anions. The bond distance between the central copper ion and a thiocyante ion within the $[Cu(ClO_4)(NCS)(en)_2]$ complex was determined to be 2.73 Å by means of X-ray diffraction in the crystal.[17] Thus, the structure can be practically regarded as square-planar.

Although the structure of the $[Cu(en)_3](NO_3)_2$ compound has been assumed to be a distorted octahedron by a spectroscopic measurement,[15] the structure has not been determined by the X-ray diffraction method in crystal or in solution. In the present study, we have attempted to determine the structures of the bis-

and tris(ethylenediamine)copper(II) complexes in aqueous solutions and to compare them with the structures of copper-ammine complexes,[9] as well as those of ethylenediamine complexes of zinc(II),[18] cadmium-(II),[19] and nickel(II)[20] in solution.

Experimental

Preparation and Analysis of Sample Solutions. Ethylenediamine was purified by the method previously reported.[18] Copper(II) nitrate of reagent grade was purchased from Wako Pure Chemicals Co., Osaka, and recrystallized twice from water. The sample solutions were prepared by dissolving copper(II) nitrate into aqueous ethylenediamine solutions by the similar way to that described in previous papers.[18-20]

Concentrations of copper(II) ions in the test solutions were determined by electrogravimetry. The concentration of nitrate ions was calculated from the stoichiometry of copper-(II) nitrate. The density of the test solutions was measured pycnometrically. The composition of the test solutions is given in Table 1.

Method of Measurements and Treatment of X-Ray Scattering Data. The method of measurements and the apparatus used were essentially the same as those employed in the previous works.[7,8,18-20] Mo $K\alpha$ radiation ($\lambda=0.7107$ Å) was used for the measuremets over the range $1°<\theta<70°$ (2θ is the scattering angle). The data were recorded twice over the whole angle range. Corrections and analysis of the scattering data were performed in the same ways as those previously reported. Coherent and reduced intensities of the solutions are given in Figs. 1 and 2, respectively. The

Table 1. Composition of solutions A and B (mol dm^{-3})

	A	B
Cu	1.460	1.230
N	9.011	15.10
C	6.091	12.64
O	49.73	37.82
H	106.3	111.5
ρ/g cm^{-3}	1.195	1.159
V/Å	1267	1350
en/Cu	2.09	5.14

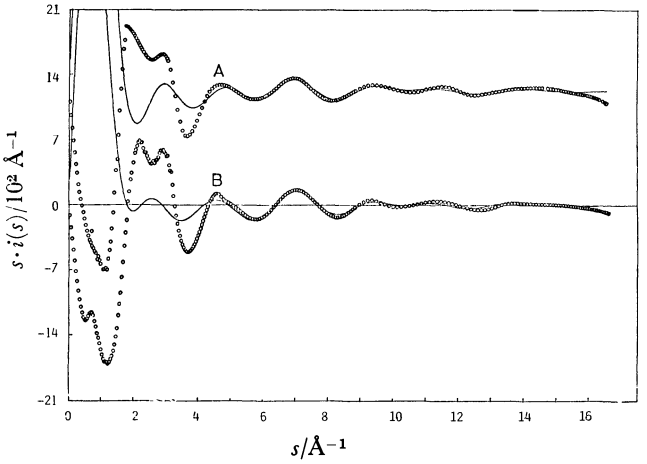

Fig. 2. The reduced intensities multiplied by s for solutions A and B. The observed $s\cdot i(s)$ curves are shown by circles and calculated ones by solid lines.

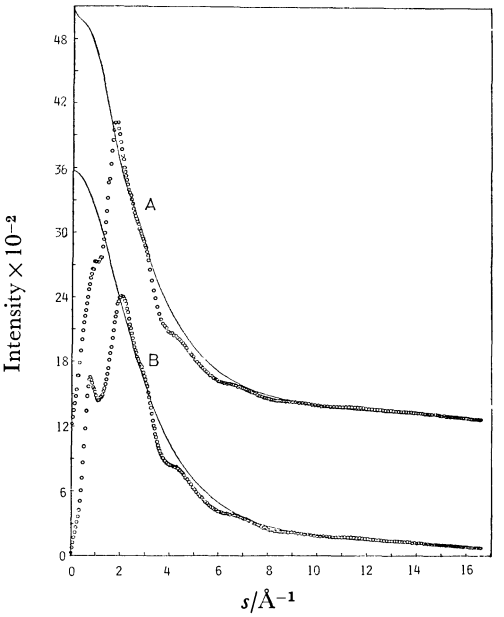

Fig. 1. Coherent scattering intensities of the sample solutions A and B. Experimentally obtained intensities I^{coh} are shown by circles and calculated independent scattering intensities by solid lines.

radial distribution function $D(r)$ was calculated by the following equation:

$$D(r) = 4\pi r^2\rho_0 + \frac{2r}{\pi}\int_0^{s_{max}} s\cdot i(s)\cdot M(s)\cdot\sin(rs)ds, \quad (1)$$

where ρ_0 is the average scattering density in the stiochiometric volume V of the solution per Cu atom and s_{max} denotes the maximum s-value attained in the measurements ($s_{max}=16.7$ Å^{-1}). $M(s)$ represents the modification function[21] and the reduced intensities $i(s)$ are given by

$$i(s) = I^{coh}(s) - \Sigma n_i\{(f_i(s)+\Delta f_i')^2+(\Delta f_i'')^2\}, \quad (2)$$

where n_i is the number of atom i and $f_i(s)$ denotes the scattering factor of atom i at s. $\Delta f_i'$ and $\Delta f_i''$ represent the real and imaginary parts of the anomalous dispersion, respectively.

The theoretical scattering intensities due to atom-pairs of all possible combinations were obtained as follows:

$$i_{calcd}(s) = \sum_{i}\sum_{\substack{j \\ i\neq j}} n_{ij}\{(f_i(s)+\Delta f_i')(f_j(s)+\Delta f_j') + (\Delta f_i'')(\Delta f_j'')\}\frac{\sin(r_{ij}s)}{(r_{ij}s)}\cdot\exp(-b_{ij}s^2), \quad (3)$$

where r_{ij}, b_{ij}, and n_{ij} denote the distance, the temperature factor and the frequency factor of the atom-pair i-j, respectively.

Calculations were mainly carried out with the computer M 160 and M 180 using NLPLSQ[21] and KURVLR[22] programs at the Tokyo Institute of Technology and partly with the computer M 200H at the Instituse for Molecular Science in Okazaki.

Results

According to the stability constants so far reported,[23] the bis(ethylenediamine)copper(II) complex is contained as the main species in solution A.

The stability constant of the tris(ethylenediamine)-copper(II) complex is comparatively small ($\log K_3 \simeq 1$[23]), and thus, the tris-complex can only exist in a solution containing a large excess of ethylenediamine. In solution B in which the mole ratio of ethylenediamine to copper(II) ion is 5.14, the tris(ethylenediamine)-copper(II) complex is expected to be formed as the predominant species. The coexistence of the bis-complex with the tris-complex in solution B must also be taken into account in the course of the analysis of the scattering data.

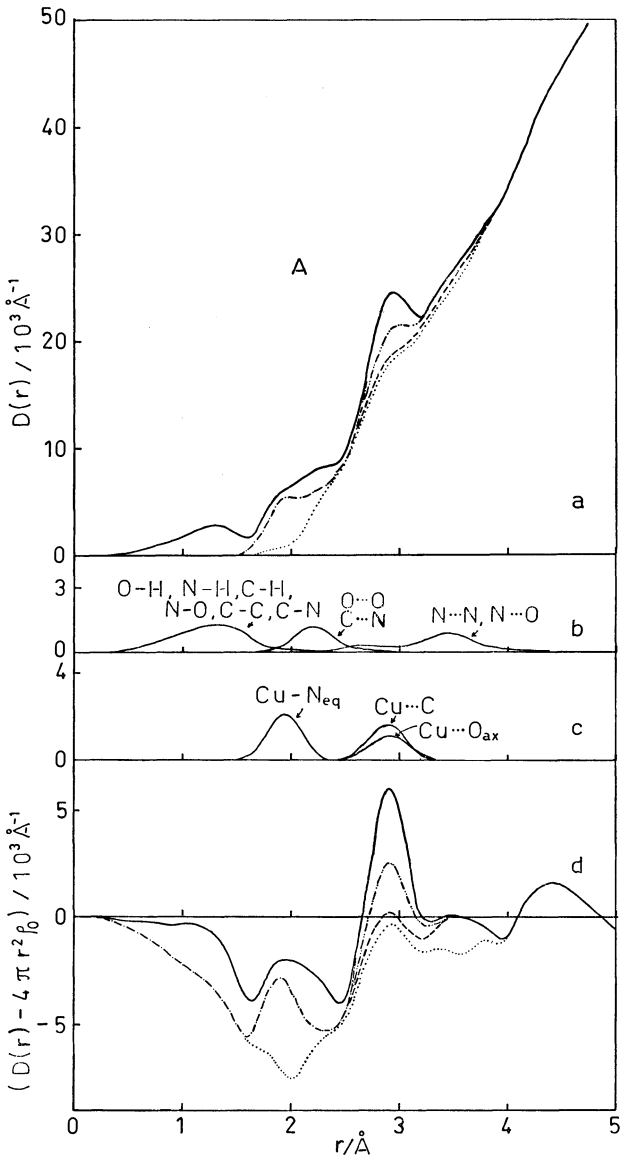

Fig. 3. (a); The $D(r)$ curve for solution A. The chain line (·—·—) shows the residual curve after subtraction of the theoretical peaks shown in b except for N···N and N···O interactions. The chain line (—··—··) shows the residual curve after subtraction of the theoretical peak shape due to the Cu···C interaction. Furthermore, after subtraction of the theoretical curve of the Cu–O_{ax} interaction, the dashed line is obtained. After subtraction of the theoretical peaks due to the Cu–N_{eq}, N···N, and N···O interactions the dotted line is obtained. (b) and (c); The theoretical peak shapes of each atom pair. (d); The corresponding $D(r)-4\pi r^2\rho_0$ curve to (a).

Solution A. From the corrected diffraction intensities (Fig. 1A) the $s \cdot i(s)$ curve was obtained (Fig. 2A), and thus, the radial distribution and differential radial distribution curves (Fig. 3, a and d, respectively) were calculated. In the radial distribution curve of solution A, five peaks were observed in the region 1—5 Å (see Fig. 3, a and d).

A broad and small peak at about 1.2 Å is composed of peaks due to the O–H bond within water molecules, the N–H, C–H, C–C, and C–N bonds within ethylenediamine molecules and the N–O bond within nitrate ions in the solution (see Fig. 3, b). The second peak appearing at about 2.0 Å may be attributed to the Cu–N bond within the metal complex, the O···O pair within nitrate ions and the C···N interaction within ethylenediamine molecules. The third peak around 2.9 Å may be ascribed to the nonbonding Cu···C interactions within the complex and the O···O interactions in the bulk water. The O···O pairs within nitrate ions may also contribute to this peak. The Cu–OH_2 bond, if it exists, can be expected to be included in this peak. A broad peak around 4 Å must include some longer intramolecular interactions, as well as intermolecular interactions between ions in the solution. The fifth peak at about 5 Å might consist of much longer intermolecular interactions, which will not be taken into consideration in the present analysis.

At the first step of analysis of the radial distribution curve, the theoretical peaks of the intramolecular interactions within ethylenediamine molecules and nitrate ions were subtracted from the original $D(r)$ curve, and then the curve expressed by the chain line (·—·—·) was obtained. The analysis of the residual curve revealed that the Cu–N_{eq} bond distance and its temperature factor were 1.93 Å and 0.002 Å^2, respectively. The frequency factor (n) of the Cu–N_{eq} bond was evaluated to be four from the area under the peak at 1.93 Å. The nonbonding Cu···C distance was estimated to be about 2.85 Å by using a suitable structure model of ethylendiamine and the Cu–N_{eq} distance estimated. After subtraction of the theoretical peak due to the Cu···C interactions, a double-dotted chain line (··—··—··) was obtained. A peak still remaining at about 2.9 Å was larger and sharper than that expected from the contribution of the only bulk water. Therefore, we assumed that the interaction between the central copper(II) ion and water molecules at the axial position may be included in the peak besides the H_2O···H_2O and NO_3···H_2O interactions. After subtraction of the Cu–O_{ax} interactions, the distance of which was assumed to be 2.95 Å, the dotted line (·····) with no appreciable peak was obtained in the region of 1.5—2.5 Å (Fig. 3, a and d). The N···N and N···O distances were estimated from the Cu–N_{eq} and Cu–O_{ax} lengths within the bis-complex on the basis of the structural model employed in the calculation mentioned above. Subtraction of the theoretical curve for the Cu–O_{ax} interaction, as well as the N···N and N···O interactions led to a smooth back-ground curve shown by the dotted line. A broad peak still left at about 2.9 Å could be ascribed to the adjacent O···O interac-

tions in the bulk water and hydrated nitrate ion, which were not taken into account in the calculation examined here. The parameter values were finally refined by the least-squares method by using the $s \cdot i(s)$ data of the high-angle region.

Solution B. An analytical procedure similar to that employed in the previous section was performed on the scattering data obtained from solution B. Subtraction of the theoretical peaks due to the O–H bond within H_2O, the N–H, C–H, C–C, C–N and C···N interactions within ethylenediamine molecules, and the N–O and O···O interactions within NO_3^- from the radial distribution curve of solution B led to a residual curve shown by a chain line (·—·—·) (Fig. 4, a and d). Two peaks observed at 1.9 and 2.2 Å in the residual curve may be identified to be due to the Cu–N_{eq} and Cu–N_{ax} bonds within the tris-complex. The area under the former and latter peaks corresponded to four and two Cu–N interactions, respectively. The former peak at 1.9 Å was, therefore, ascribed to the equatorial Cu–N bond. The temperature factors were estimated to be 0.002—0.0025 Å^2 to the former interaction and 0.003—0.0035 Å^2 to the latter. The peak obtained at 2.85 Å may partly be attributed to the nonbonding Cu···C interaction, and therefore, the double-dotted chain line (··—··—··) was obtained by subtracting the peak due to the nonbonding Cu···C interaction. A further subtraction of the peak due to the intramolecular N···N pairs within the tris-complex gave a dotted-line (·····) (Fig. 4, a and d). The parameter values were refined by using the least-squares procedure.

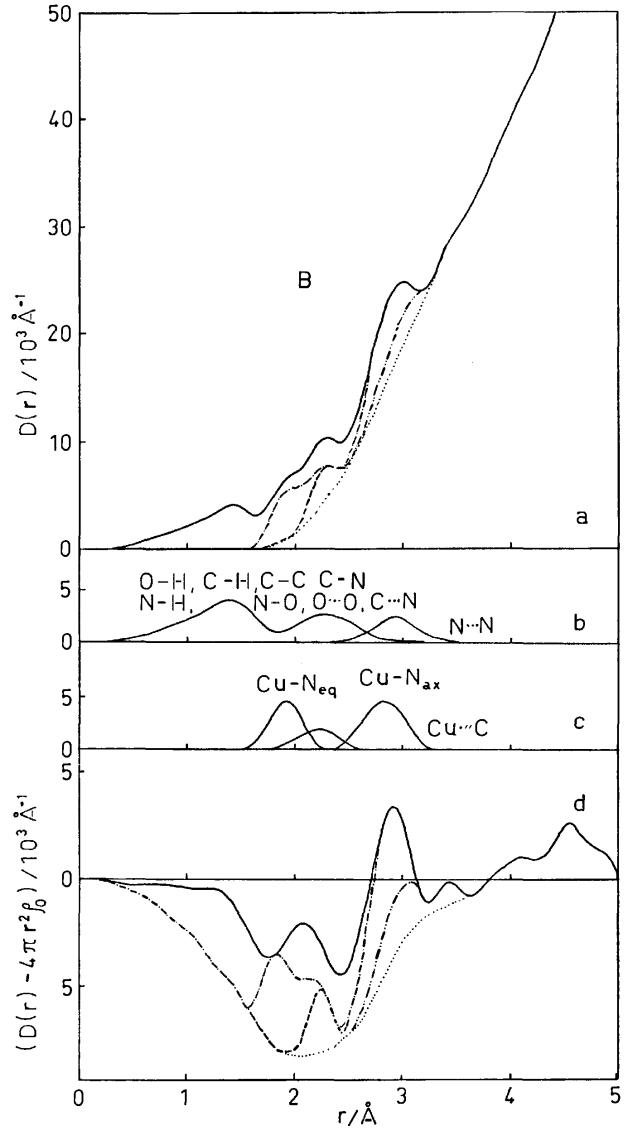

Fig. 4. (a); The $D(r)$ curve for solution B. The chain line (·—·—) shows the residual curve after subtraction of the theoretical peak shapes in (b) except for the N···N interaction from the original curve (solid line). After subtraction of the theoretical peak shape due to the Cu–N_{eq} bond from the chain line (·—·—·), the dashed line is obtained. The chain line (··—··—) shows the residual curve of the theoretical peak shape of the Cu···C interaction. After subtraction of the theoretical peak shapes of the Cu–N_{ax} and N···N interactions, the dotted line is obtained as the residual curve. (b) and (c); The theoretical peak shapes of atom-pairs indicated in the figure. (d); The corresponding $D(r)-4\pi r^2\rho_0$ curve to (a).

Least-squares Refinements. The $s \cdot i(s)$ data obtained in a high-angle region where $s>5$ Å^{-1} for solutions A and B were used for the least-squares refinement of the structure parameters of the bis- and tris-complexes in the solutions. In order to avoid introduction of errors by neglecting long-range intermolecular interactions in the solutions in the course of the refinements, the lower limit of the s-value was changed from 4.5 Å^{-1} to 7 Å^{-1}. In the least-squares calculations for solution A, in which the bis(ethylenediamine)copper(II) complex was predominantly formed, two types of calculations, I and II, were carried out. In type I, frequency factors n of all atom-pairs within the bis-complex were floated as well as the bond distances r and temperature factors b. In type II, on the other hand, the frequency factors were fixed and the only distances and temperature factors were refined. Throughout these refinements, the structure of the bis(ethylenediamine)copper(II) complex was assumed to be octahedral (Table 2).

The contribution from the O–H bond within water molecules was taken into account by using the structural parameters reported in the literature.[7,8,16,24] Structural parameters of the atom-pairs within ethylenediamine molecules were quoted from the work by Yokozeki and Kuchitsu[25] determined in the gas phase, as have been done in the previous studies.[18–20] The parameter values of the N–O pairs within NO_3^- were taken from the work by Caminiti *et al.*[26] and Maeda *et al.*[27] Contributions of all the atom-pairs were comparatively small in the s-region where we refined the structural parameters of the intramolecular interactions within the bis(ethylenediamine)copper(II) complex in the solution.

The parameter values for the O···O (NO_3^-), C···N (en), Cu···O_{ax}, Cu···C, and N···N ($Cu(en)_2(H_2O)_2$) atom-pairs were refined as independent variables. The change in the s-region in the course of the refinements did not practically affect the parameter values. The refined parameter values obtained by both I and II

Table 2. Least-squares refinements for solution A obtained over various s ranges
The parameter values, r=distance (Å), b=temperature factor (Å^2), and n=frequency factor, were refined. The values in parentheses are their standard deviations.

Interaction	Parameter	4.5 Å^{-1}<s<16.7 Å^{-1} I	4.5 Å^{-1}<s<16.7 Å^{-1} II	5.0 Å^{-1}<s<16.7 Å^{-1} I	5.0 Å^{-1}<s<16.7 Å^{-1} II*	6.0 Å^{-1}<s<16.7 Å^{-1} I	6.0 Å^{-1}<s<16.7 Å^{-1} II	7.0 Å^{-1}<s<16.7 Å^{-1} I	7.0 Å^{-1}<s<16.7 Å^{-1} II
O···O (NO_3^-)	r	2.21(3)	2.22(3)	2.22(3)	2.22(3)	2.20(4)	2.20(4)	2.20(3)	2.20(3)
C···N (en)	r	2.26(8)	2.25(8)	2.17(6)	2.18(6)	2.3(1)	2.3(1)	2.32(7)	2.18(6)
$Cu(en)_2^{2+}$									
Cu-N_{eq}	r	1.943(7)	1.948(7)	1.934(7)	1.934(6)	1.93(1)	1.94(1)	1.922(7)	1.924(7)
	b	0.0028(5)	0.0033(5)	0.0025(4)	0.0027(4)	0.0025(6)	0.0028(5)	0.0023(3)	0.0025(3
	n	3.8(1)	4[a]	3.81(9)	4[a]	3.6(2)	4[a]	3.9(1)	4[a]
Cu···O_{ax}[b]	r	2.92(4)	2.92(4)	2.92(3)	2.92(3)	2.91(5)	2.91(5)	2.90(3)	2.90(4)
	n	1.8(1)	2[a]	1.9(1)	2[a]	2.3(3)	2[a]	2.6(2)	2[a]
Cu···C[c]	r	2.89(2)	2.88(2)	2.89(2)	2.89(2)	2.89(3)	2.90(3)	2.88(2)	2.89(2)
	n	3.9(2)	4[a]	4.0(2)	4[a]	4.5(4)	4[a]	4.7(3)	4[a]
N···N[d]	r	2.7	2.7	2.7	2.7	2.7	2.7	2.7	2.7
	b	0.006	0.006	0.006	0.006	0.006	0.006	0.006	0.006
	n	4[a]	4[a]	4[a]	4[a]	4[a]	4[a]	4[a]	4[a]
N···O[d]	r	3.5	3.5	3.5	3.5	3.5	3.5	3.5	3.5
	b	0.006	0.006	0.006	0.006	0.006	0.006	0.006	0.006
	n	8[a]	8[a]	8[a]	8[a]	8[a]	8[a]	8[a]	8[a]

a) Fixed. b) The temperature factor of the interaction was fixed at 0.006 Å^2. c) The temperature factor of the interaction was fixed at 0.006 Å^2. d) The bond length, temperature factor, and frequency factor were fixed. *The calculated $s\cdot i(s)$ curve in Fig. 2 was obtained by using the parameter values given here.

types of calculations were almost consistent. The frequency factors of the Cu-N_{eq} and Cu-O_{ax} interactions obtained by the I-type calculation were close to four and two, respectively, and the frequency factor of the nonbonding Cu···C interaction was approximately four. Therefore, the distorted octahedral structure of the bis(ethylenediamine)copper(II) complex was thus confirmed from the least-squares calculations.

The Cu-N_{eq}, Cu-O_{ax}, and Cu···C distances were 1.93, 2.92, and 2.89 Å, respectively. Since the temperature factors of intramolecular interactions within the bis-complex except for the temperature factor of the Cu-N_{eq} bond were estimated to be about 0.006 Å^2 from the analysis of the radial distribution curve, they were assumed to be constant at 0.006 Å^2 in the course of the least-squares calculations.

The least-squares refinements of the parameter values of the tris(ethylenediamine)copper(II) complex were carried out by the similar way to that employed in the case of the bis-complex (Table 3). In the I-type calculation frequency factors n of all atom-pairs within the tris-complex were allowed to vary. In the II-type calculation frequancy factors of the atom-paris within the tris-complex were fixed by assuming the structure of the tris-complex to be distorted octahedral. In the III-type calculation the intramolecular N..N distance was also fixed. Throughout these calculations the temperature factors were kept constant at 0.003, 0.006, and 0.007 Å^2 for Cu-N_{ax}, Cu···C, and N···N interactions, respectively.

The frequency factors of the Cu-N_{eq}, Cu-N_{ax}, and Cu···C interactions found were practically four, two and six, respectively, in the I-type calculation. The Cu-N_{eq} distance within the tris-complex was almost the same as that of the bis-complex. In the analysis of the $s\cdot i(s)$ curve of solution B, the coexistence of the bis-complex together with the predominant tris-complex was taken into account. However, the experimental $s\cdot i(s)$ values were well reproduced by the structure model of the only tris-complex, and the contribution of the minor species of the bis-complex did not practically improve the result. Therefore, the values shown in Table 4 obtained by the least-squares method were those calculated on the assumption of the existence of the only bis-complex in solution A and the only tris-complex in solution B.

The final values for the distances of the Cu-N_{eq}, Cu-N_{ax}, Cu-O_{ax}, and Cu···C pairs of the bis- and tris-complexes are summarized in Table 4.

Discussion

In crystals the length of the axial Cu-OH_2 bond is affected by ligand molecules coordinated at the equatorial positions, counter ions and crystal structures (see Table 5). In copper(II) complexes in which nitrogen atoms are coordinated to the central copper(II) ion in the equatorial plane while two water molecules are located at the axial position, the shorter the equatorial Cu-N bond distance becomes, the longer the axial Cu-OH_2 bond length is[14] (Fig. 5, see also Tables 5 and 6). The Cu-N_{eq} distance (1.92 Å) within the tris(ethylenediamine)copper(II) complex in solution is shorter than that in other tris-complexes observed in

TABLE 3. LEAST-SQUARES REFINEMENTS FOR SOLUTION B OVER VARIOUS s RANGES
The parameter values, r=distance (Å), b=temperature factors (Å^2), and n=frequency factor, were refined. The values in parentheses are their standard deviations.

Interaction	Parameter	4.5 Å^{-1}<s<15.5 Å^{-1} I	4.5 Å^{-1}<s<15.5 Å^{-1} II	5.0 Å^{-1}<s<15.5 Å^{-1} I	5.0 Å^{-1}<s<15.5 Å^{-1} II	5.0 Å^{-1}<s<15.5 Å^{-1} III*
O···O (NO_3)	r	2.21(4)	2.23(4)	2.20(2)	2.20(2)	2.22(2)
C···N (en)	r	2.27(4)	2.24(4)	2.33(2)	2.31(2)	2.28(2)
$Cu(en)_3^{2+}$						
Cu-N_{eq}	r	1.909(7)	1.924(8)	1.911(4)	1.916(5)	1.919(5)
	b	0.0017(4)	0.0023(5)	0.0023(3)	0.0025(3)	0.0027(3)
	n	4.1(1)	4[a]	4.04(6)	4[a]	4[a]
Cu-N_{ax}[b]	r	2.21(2)	2.23(3)	2.20(8)	2.21(2)	2.22(2)
	n	2.8(1)	2[a]	2.52(8)	2[a]	2[a]
Cu···C[c]	r	2.81(2)	2.80(2)	2.83(1)	2.83(1)	2.829(9)
	n	5.3(2)	6[a]	5.7(1)	6[a]	6[a]
N···N	r	2,85(5)	2.97(5)	2.90(2)	2.944(6)	2.93[a]

Interaction	Parameter	5.5 Å^{-1}<s<15.5 Å^{-1} I	5.5 Å^{-1}<s<15.5 Å^{-1} II	6.0 Å^{-1}<s<15.5 Å^{-1} I	6.0 Å^{-1}<s<15.5 Å^{-1} II	6.0 Å^{-1}<s<15.5 Å^{-1} III
O···O (NO_3)	r	2.20(2)	2.20(2)	2.20(2)	2.20(2)	2.20(2)
C···N (en)	r	2.36(2)	2.33(2)	2.36(2)	2.33(2)	2.32(2)
$Cu(en)_3^{2+}$						
Cu-N_{eq}	r	1.904(4)	1.908(4)	1.903(5)	1.906(4)	1.905(5)
	b	0.0026(3)	0.0029(2)	0.0026(3)	0.0029(3)	0.0029(3)
	n	3.92(6)	4[a]	3.89(9)	4[a]	4[a]
Cu-N_{ax}[b]	r	2.205(9)	2.21(1)	2.20(1)	2.21(1)	2.20(1)
	n	2.47(9)	2[a]	2.47(9)	2[a]	2[a]
Cu···C[c]	r	2.842(9)	2.844(9)	2.84(1)	2.84(1)	2.83(9)
	n	6.3(1)	6[a]	6.4(2)	6[a]	6[a]
N···N[d]	r	2,87(2)	2.87(2)	2.87(3)	2.87(3)	2.93[a]

Interaction	Parameter	7.0 Å^{-1}<s<15.5 Å^{-1} I	7.0 Å^{-1}<s<15.5 Å^{-1} II	7.0 Å^{-1}<s<15.5 Å^{-1} III
O···O (NO_3)	r	2.20(2)	2.20(2)	2.20(2)
C···N (en)	r	2.38(3)	2.31(2)	2.29(2)
$Cu(en)_3^{2}$				
Cu-N_{eq}	r	1.899(6)	1.903(6)	1.904(6)
	b	0.0025(3)	0.0030(3)	0.0030(3)
	n	3.8(1)	4[a]	4[a]
Cu-N_{eqb}	r	2.21(9)	2.20(2)	2.20(2)
	n	2.8(1)	2[a]	2[a]
Cu···C[c]	r	2.84(1)	2.85(1)	2.83(1)
	n	6.6(2)	6[a]	6[a]
N···N[d]	r	2,86(4)	2.87(3)	2.93[a]

a) Fixed; b) Fixed (b=0.003 Å^2), c) Fixed (b=0.006 Å^2); d) Fixed (b=0.007 Å^2). *The calculated $s\cdot i(s)$ curve shown in Fig. 2 was obtained by using the parameter values of this type.

crystals (Table 7), but it is compared with the Cu–O_{eq} distance within the $[Cu(OH_2)_6]^{2+}$ complex.[7,8] On the contrary, the Cu–N_{ax} distance within the tris(ethylenediamine)copper(II) complex (2.22 Å) is shorter than the Cu–O_{ax} distance within the $[Cu(OH_2)_6]^{2+}$ complex, which has been reported to be 2.43 Å.[7,8]

In the $[Cu(NH_3)_4(OH_2)_2]^{2+}$ complex in solution, the Cu–N_{eq} and Cu–O_{ax} distances are 2.03 and 2.33 Å, respectively.[9] In the bis(ethylenediamine)copper(II) complex, the equatorial Cu–N bond is shorter than that within the tetraamminecopper(II) complex, which indicates a stronger Cu–N(en) interaction than

TABLE 4. FINAL PARAMETER VALUES FOR THE BIS- AND TRIS-(ETHYLENEDIAMINE)COPPER(II) COMPLEXES[a] (Å)

	Bis-complex	Tris-complex
$Cu-N_{eq}$	1.934(6)	1.919(5)
$Cu-N_{ax}$	—	2.22(2)
$Cu-O_{ax}$	2.92(3)	—
Cu···C	2.89(2)	2.829(9)
Structure	Distorted octahedral	

a) The values in parentheses are their standard deviations.

TABLE 5. CRYSTAL DATA FOR AXIAL $Cu-OH_2$ DISTANCE (Å)

Compound	$Cu-OH_2$	Author
$[Cu(NH_3)_4]SO_4\cdot H_2O$	2.59, 3.37	a)
$[Cu(C_5H_8N)_2]\cdot 2H_2O$	2.52	b)
$[Cu(en)_2(OH_2)Cl]Cl$	2.68	c)
	2.62	d)
$[Cu(en)_2(OH_2)Br]Br$	2.78	e)
$[Cu(C_6H_9O_2N_3)_2](NO_3)_2\cdot(H_2O)_2$	2.461, 2.778	f)
$[Cu(CH_2COO)_2NH]\cdot 2H_2O$	2.410	g)
$4[Cu(en)_2]\cdot Si_8O_{20}\cdot 38H_2O$	2.64, 2.74	h)
	2.60, 3.04	
$[Cu(en)_2(OH_2)]\cdot[Cu_2(CN)_2(SeCN)_2]$	2.483	i)
$[Cu(C_6H_6N_4)(OH_2)_4]\cdot(SO_4)(H_2O)$	2.384	j)
$[Cu(en)_2(OH_2)_2]^{2+}$	2.92	This work (in solution)

a) F. Mazzi, *Acta Crystallogr.*, **8**, 137 (1955). b) A. McL. Mathieson and H. K. Welsh, *Acta Crystallogr.*, **5**, 599 (1952). c) F. Mazzi, *R. C. Soc. Miner. Ital.*, **9**, 148 (1953). d) R. D. Ball, D. Hall, C. E. F. Richard, and T. N. Waters, *Inorg. Phys. Theor.*, **1967**, 1435. e) F. Mazzi, *R. C. Soc. Miner. Ital.*, **9**, 148 (1953). f) B. Evertson, *Acta Crystallogr., Sect. B*, **25**, 30 (1969). g) A. Podder, J. K. Dattagupta, N. N. Sana and W. Saenger, *Acta Crystallogr., Sect. B*, **35**, 53 (1979). h) Yu. I. Smolin, Yu. F. Shepelov, and I. K. Butikova, *Sov. Phys.-Crystallogr.*, **17**, 10 (1972). i) V. Vrabel and J. Garaj, *Acta Crystallogr., Sect. B*, **35**, 357 (1979). j) E. Sletten and E. Voland, *Acta Crystallogr., Sect. B*, **35**, 840 (1979)

the $Cu-N(NH_3)$ one. On the other hand, the $Cu-O_{ax}$ distance within the former complex becomes longer than that within the latter. Therefore, the bis(ethylenediamine)copper(II) complex is more distorted than the tetraamminecopper(II) complex owing, probably, to a higher electron density at the copper(II) atom of the bis(ethylenediamine)copper(II) complex by a stronger electron donation from the coordinated ethylenediamine molecules, and thus, a more weakened $Cu-OH_2$ interaction along the axis results.

In the bis(ethylenediamine)copper(II) complex, the axial $Cu-OH_2$ distance is so long (2.92 Å) that the complex can be regarded as square-planar.

In the CuN_4O_2-type complexes in solution the ratio of the axial bond length to the equatorial one is smaller than that in crystal (see Fig. 5). The enhanced lengthening in the $Cu-O_{ax}$ bond in crystal may be caused by interactions of the coordinated oxygen atom with another copper(II) ion (*e.g.*, in the case of $[Cu(NH_3)_4]SO_4\cdot H_2O$) or anions.

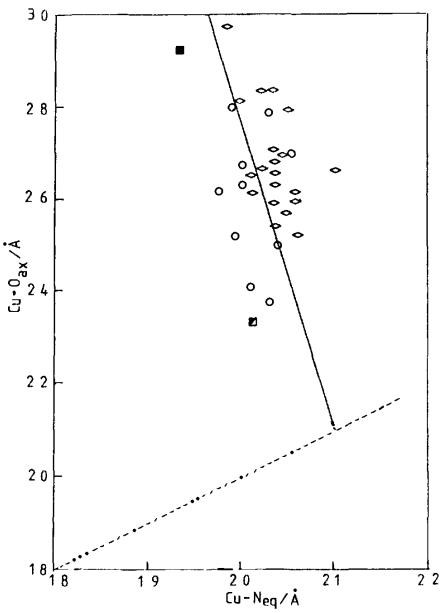

Fig. 5. A relationship between the equatorial Cu-N and axial Cu-O bond lengths of the CuN_4O_2 type complexes. ○: Complex containing only neutral ligands in crystal,[14] ◇: Complex containing neutral and anionic ligands in crystal,[14] ■: $[Cu(en)_2(OH_2)_2]^{2+}$ in solution, ◩: $[Cu(NH_3)_4(OH_2)_2]^{2+}$ in solution.[23]

TABLE 6. CRYSTAL DATA FOR Cu-N DISTANCE (Å) IN BIS(ETHYLENEDIAMINE)COPPER(II) COMPLEXES

Compound	Cu-N	Author
$[Cu(en)_2](BF_4)_2$	2.02	a)
$[Cu(en)_2(SCN)(ClO_4)]$	2.02	b)
$4[Cu(en)_2]\cdot Si_8O_{20}\cdot 38H_2O$	1.96—2.06	c)
$[Cu(en)_2(SCN)_2]$	1.99—2.01	d)
$[Cu(en)_2(OH_2)Cl]Cl$	1.98—2.02	e)
$[Cu(en)_2(OH_2)]\cdot[Cu_2(CN)_2(SeCN)_2]$	2.02—2.08	f)
$[Cu(en)_2](NO_3)_2$	2.01—2.04	g)
$[Cu(en)_2][Si(C_6H_4O_2)_3]$	1.990—2.018	h)
$[Cu(en)_2](ClO_4)_2$	2.03—2.05	i)
$[Cu(en)_2][Hg(SCN)_4]$	2.08—2.17	j)
$[Cu(en)_2(OH_2)Br]Br$	1.97—1.98	k)
$[Cu(en)_2(OH_2)_2]^{2+}$	1.93	This work (in solution)

a) D. S. Brown, J. D. Lee, and B. G. Melson, *Acta Crystallogr., Sect. B*, **24**, 730 (1968). b) M. Cammas, G. Carta, and G. Marongiu, *J. Chem. Soc., D*, **1971**, 1462; *J. Chem. Soc., Dalton Trans.*, **1973**, 251. c) Yu. I. Smolin, Yu. F. Shepelev, and I. K. Butikova, *Sov. Phys.-Crystallogr.*, **17**, 10 (1972). d) D. W. Brown and E. C. Lingafelter, *Acta Crystallogr.*, **17**, 254 (1964). e) R. D. Ball, D. Hall, C. E. F. Richard, and T. N. Waters, *Inorg. Phys. Theor.*, **1967**, 1435. f) V. Vrabel and J. Garaj, *Acta Crystallogr., Sect. B*, **35**, 357 (1979). g) K. Komiyama and E. C. Lingafelter, *Acta Crystallogr.*, **17**, 1145 (1964). h) V. D. Sackerer and G. Nagorsen, *Z. Anorg. Allg. Chem.*, **437**, 188 (1977). i) A. Pajunen, *Suomen Kem.*, **40**, 32 (1967). j) H. Scomloudi, *Acta Crystallogr.*, **6**, 148 (1953). k) F. Mazzi, *Rand. Soc. Miner. Ital.*, **9**, 148 (1953).

Table 7. Crystal data for $Cu-N_{eq}$ and $Cu-N_{ax}$ distances (Å) in the tris-complex containing bidentate ligands

Compound	$Cu-N_{eq}$	$Cu-N_{ax}$	Ref
$[Cu(en)_3]SO_4$	2.15	2.15	a)
$[Cu(bipy)_3](ClO_4)_2$	2.031	2.450, 2.226	b)
$[Cu(phen)_3](ClO_4)_2$	2.05	2.33	c)
$[Cu(en)_3]^{2+}$	1.92	2.22	This work[d]

a) D. L. Cullen and E. C. Lingafelter, *Inorg. Chem.*, **9**, 1858 (1970). b) Q. P. Anderson, *J. Chem. Soc.*, **1972**, 2597. c) Q. P. Anderson, *J. Chem. Soc., Dalton Trans.*, **1973**, 1237. d) In solution.

Only a few crystal structures of the CuN_6-type complexes have been reported so far (Table 7). In the X-ray analysis of the $[Cu(en)_3]SO_4$ in crystal, the structure was regularly octahedral. On the contrary, the tris(ethylenediamine)copper(II) ion in solution was concluded to have a distorted octahedral structure. The symmetrical structure of the $[Cu(en)_3]^{2+}$ ion in the $[Cu(en)_3]SO_4 \cdot H_2O$ crystal has been explained in terms of the dynamic Jahn-Teller effect.[11] In the solution, on the other hand, the distorted octahedral structure of the $[Cu(en)_3]^{2+}$ ion is clearly seen by the X-ray diffraction method, because such a dynamic distortion in the structure of a species is not observable but it is recognized as a random distribution of a distorted species in the analysis of scattering data in solution.

The $[Zn(en)_2]^{2+}$ ion has a regular tetrahedral structure with the Zn–N bond length of 2.131 Å.[18] A similar tetrahedral structure is kept in the $[Cd(en)_2]^{2+}$ complex, in which the Cd–N distance is found to be 2.339 Å.[19] The structure of the $[Ni(en)_2]^{2+}$ ion has an almost regular octahedral structure by combining with additional two water molecules in the coordination sphere.[20] The Ni–N distance, as well as the Ni–O distance, within the complex is 2.10 Å.[20] The bis(ethylenediamine)copper(II) complex is square-planar.

The $[Zn(en)_3]^{2+}$ complex is regular octahedral, and the Zn–N bond length is 2.276 Å,[18] which is larger than the Ni–N distance within the $[Ni(en)_3]^{2+}$ complex (2.202 Å[20]). In the $[Cu(en)_3]^{2+}$ complex the $Cu-N_{eq}$ bond is much smaller than the Zn–N and Ni–N distances of the relevant tris-complexes. The $Cu-N_{ax}$ bond, on the contrary, is longer than the Ni–N bond within the $[Ni(en)_3]^{2+}$ ion, although the Cu–N distance is slightly shorter than the Zn–N bond length within the $[Zn(en)_3]^{2+}$ complex. Obviously the Cu–N bond length within the $[Cu(en)_3]^{2+}$ complex is shorter than the Cd–N distance within the $[Cd(en)_3]^{2+}$ ion, because Cd^{2+} ion has a much larger ionic size than Cu^{2+} ion.

The work has been financially supported, in part, by the Grant-in-Aid for Scientific Research No. 57470054 from the Ministry of Education, Science and Culture. A part of the computer calculations carried out in the present work has been performed at the Institute for Molecular Science in Okazaki.

References

1) H. Montgomery and E. C. Lingafelter, *Acta Crystallogr.*, **20**, 659 (1966).
2) N. V. Mani and S. Ramaseshan, *Z. Kristallogr.*, **115**, 97 (1961).
3) J. Fischer and R. Weiss, *Acta Crystallogr., Sect. B*, **29**, 1958 (1973).
4) J. Fischer, R. Elchinger, and R. Weiss, *Acta Crystallogr., Sect. B*, 1967 (1973).
5) S. Ray, A. Zalkin, and D. H. Templeton, *Acta Crystallogr., Sect. B*, **29**, 2748 (1978).
6) L. M. Shapovalov and I. V. Radchenko, *Russ. J. Struct. Chem.*, **12**, 705 (1972).
7) H. Ohtaki and M. Maeda, *Bull. Chem. Soc. Jpn.*, **47**, 2197 (1974).
8) H. Ohtaki, T. Yamaguchi, and M. Maeda, *Bull. Chem. Soc. Jpn.*, **49**, 701 (1976).
9) T. Yamaguchi and H. Ohtaki, *Bull. Chem. Soc. Jpn.*, **52**, 415 (1979).
10) B. J. Hathaway and D. E. Billing, *Coord. Chem. Rev.*, **5**, 143 (1970).
11) D. L. Cullen and E. C. Lingafelter, *Inorg. Chem.*, **9**, 1858 (1970).
12) N. W. Isaacs and C. H. L. Kennard, *J. Chem. Soc., A*, **1969**, 386.
13) R. A. Palmer and T. S. Piper, *Inorg. Chem.*, **5**, 864 (1966); G. F. Kokoszka, G. W. Reimann, H. C. Allen, Jun., and G. Gordon, *ibid.*, **6**, 1657 (1967).
14) J. Gazo, I. B. Bersuker, J. Garaj, M. Kabešová, J. Hohout, H. Langferderová, M. Melník, M. Serátor, and F. Valach, *Coord. Chem. Rev.*, **19**, 253 (1976).
15) I. Bertini, D. Gatteschi, and A. Scozzafava, *Inorg. Chem.*, **16**, 1973 (1977).
16) I. M. Pecter, B. J. Hathaway, and P. Nichillis, *J. Chem. Soc., A*, **1968**, 1678.
17) M. Cammas, G. Carta, and G. Marongui, *J. Chem. Soc., D*, **1971**, 1462, *J. Chem. Soc., Dalton Trans.*, **1973**, 251.
18) T. Fujita, T. Yamaguchi, and H. Ohtaki, *Bull. Chem. Soc. Jpn.*, **52**, 3539 (1970).
19) T. Fujita and H. Ohtaki, *Bull. Chem. Soc. Jpn.*, **53**, 930 (1980).
20) T. Fujita and H. Ohtaki, *Bull. Chem. Soc. Jpn.*, **55**, 455 (1982).
21) T. Yamaguchi and H. Ohtaki, *Bull. Chem. Soc. Jpn.*, **51**, 3227 (1978).
22) G. Johansson and M. Sandström, *Chem. Scripta*, **4**, 195 (1973).
23) L. G. Sillén and A. E. Martell, "Stability Constants," Special Publication No. 17 (1964), Supplement No. 1 (Special Publication No. 25) (1971), The Chemical Society, London; D. D. Perrin, "Stability Constants, Part B, Organic Ligands," IUPAC Chemical Data Series No. 22, Pergamon Press, London (1979).
24) A. H. Narten, "X-Ray Diffraction Data on Liquid Water in the Temperature Range 4—200 °C," *ORNL*-4578 (1970).
25) A. Yokozeki and K. Kuchitsu, *Bull. Chem. Soc. Jpn.*, **44**, 2926 (1971).
26) R. Caminiti, G. Licheri, G. Piccaluga, and G. Pinna, *J. Chem. Phys.*, **68**, 1967 (1978).
27) M. Maeda, Y. Maegawa, T. Yamaguchi, and H. Ohtaki, *Bull. Chem. Soc. Jpn.*, **52**, 2545 (1979).

A Calorimetric Study on the Relative Thermal Stabilities of Some Cobalt(III)-Ammine Complexes in Solid Phase

Ryokichi TSUCHIYA,* Akira UEHARA, and Takashi NAKAYAMA
Department of Chemistry, Faculty of Science, Kanazawa University, Kanazawa 920
(Received May 20, 1983)

The enthalpy changes (ΔH) in the reaction of $[CoX_n(NH_3)_{6-n}]X_{3-n}$ type complexes with an alkaline sodium sulfide solution were calorimetrically measured at 25 °C, where X is Cl^-, Br^-, I^-, NO_3^-, or ClO_4^-. The thermal stabilities were found to decrease in the following orders: in the hexaammine series, chloride > bromide > nitrate > iodide > perchlorate; in the pentaammine series, chloride > bromide > nitrate; and in the *trans*-tetraammine series, chloride > bromide and chloro > bromo complexes. In addition, in the tetraammine series, the possibility of trans-to-cis isomerization, which has actually been observed, was reasonably explained on the basis of the difference in lattice energies between *trans*- and *cis*-$[CoCl_2(NH_3)_4]Cl$.

In the previous paper, we measured calorimetrically the enthalpy changes in the reaction of solid $Ni(AA)_2X_2 \cdot nH_2O$ (AA: *N,N*- or *N,N'*-diethylethylenediamine; X: Cl^-, Br^-, I^-, or NO_3^-; *n*: 0 or 2) with an aqueous potassium cyanide, and found that the thermal stabilities of the complexes decrease in the order, chloride > bromide > nitrate > iodide.[1] In addition, the enthalpy changes in the reaction of solid $[CoX_2(AA)_2]X$ type complexes (AA: diamine such as 1,2-ethanediamine; X: Cl^-, Br^-, or ClO_4^-) with an alkaline sodium sulfide solution were measured, and the differences in lattice energy among the above complexes were evaluated therefrom. Comparison of their lattice energies revealed that the thermal stabilities decrease in the order, chloride > bromide > perchlorate.[2] As a continuation of these calorimetric studies, the present study was undertaken to decide the order of the thermal stabilities among chloride, bromide, iodide, nitrate, and perchlorate in each series of the hexaammine-, pentaammine-, and tetraamminecobalt(III) complexes, and among the complexes of these three series when the anions involved are chloride, bromide and nitrate ions, respectively.

In $[CoX_2(en)_2]X$ type complexes (X=Cl^- or Br^-), the cis-to-trans isomerization was predicted to occur on the basis of the enthalpy measurement for trans- and cis-complexes, and the prediction was actually verified.[3] As for the corresponding ammine complexes, $[CoX_2(NH_3)_4]X$ (X:Cl^- or Br^-), however, no such calorimetric prediction has been made on the direction of isomerization (trans-to-cis or cis-to-trans). To solve this problem by the enthalpy measurement is the second purpose of this study.

Experimental

Preparation of Complexes. The following complexes were prepared by the literature methods: $[Co(NH_3)_6]Cl_3$, $[Co(NH_3)_6]Br_3$, $[Co(NH_3)_6](NO_3)_3$, $[Co(NH_3)_6]I_3$, $[Co(NH_3)_6](ClO_4)_3$,[4] $[CoCl(NH_3)_5]Cl_2$, $[CoCl(NH_3)_5]Br_2$,[5] $[CoBr(NH_3)_5]Br_2$, $[CoBr(NH_3)_5]Cl_2$,[6] $[Co(NO_3)(NH_3)_5](NO_3)_2$,[7] $[CoI(NH_3)_5]Cl_2$,[8] *trans*-$[CoCl_2(NH_3)_4]Cl$,[9] *cis*-$[CoCl_2(NH_3)_4]Cl$,[10] and *trans*-$[CoBr_2(NH_3)_4]Br$.[11]

Calorimetric Measurements. The enthalpy changes in the reaction of the complexes in the powder state with an alkaline sodium sulfide solution were measured with a Tokyo-Riko twin isoperibol calorimeter TIC-2S at 25 °C. In each run, the complex was accurately weighed and let react with 100 cm^3 of a mixture containing 2×10^{-2} mol dm^{-3} Na_2S and 1 mol dm^{-3} NaOH.

Results and Discussion

Thermal Stability of $[Co(NH_3)_6]X_3$ Complexes. The enthalpy changes (ΔH_{exp}) measured for the reaction of hexaammine cobalt(III) complexes with an alkaline sodium sulfide solution, *i.e.*, $[Co(NH_3)_6]X_3(s) + 3/2\ S^{2-}(aq) = 1/2\ Co_2S_3(s) + 6NH_3(aq) + 3X^-(aq)$ are summarized in Table 1. Combining these data with the values in the following changes,[12]

$$\left.\begin{array}{ll} Cl^-(aq) = Cl^-(g) & \Delta H = -76.5\ kJ\ mol^{-1} \\ Br^-(aq) = Br^-(g) & \Delta H = -110.5\ kJ\ mol^{-1} \\ NO_3^-(aq) = NO_3^-(g) & \Delta H = -128.9\ kJ\ mol^{-1} \\ I^-(aq) = I^-(g) & \Delta H = -154.0\ kJ\ mol^{-1} \\ ClO_4^-(aq) = ClO_4^-(g) & \Delta H = -217.6\ kJ\ mol^{-1} \end{array}\right\}, \quad (1)$$

the enthalpy changes (ΔH_{rel}) for the following reactions, $[Co(NH_3)_6]Cl_3(s) + 3X^-(g) = [Co(NH_3)_6]X_3(s) + 3Cl^-(g)$, were calculated as below:

for $X^- = Br^-$ $\Delta H_{rel} = 82.6\ kJ\ mol^{-1}$,
for $X^- = NO_3^-$ $\Delta H_{rel} = 125.2\ kJ\ mol^{-1}$,
for $X^- = I^-$ $\Delta H_{rel} = 210.0\ kJ\ mol^{-1}$,
for $X^- = ClO_4^-$ $\Delta H_{rel} = 377.5\ kJ\ mol^{-1}$.

These values correspond to the decreases of lattice energies of the solid complexes which give the magnitudes of instabilities of the bromide, nitrate, iodide, and perchlorate relative to that of the chloride as a standard. The enthalpy levels for the hexaammine complexes are diagrammatically shown in Fig. 1. The numeral attached to each level is the value obtained above. Inspection of the figure reveals that, in this series of complexes, the thermal stability decreases in

Table 1. Enthalpy changes, ΔH_{exp}, for the reaction of cobalt(III)-ammine complexes $[CoX_n(NH_3)_{6-n}]X_{3-n}$ with sodium sulfide solution (kJ mol^{-1})

X	$[Co(NH_3)_6]X_3$	$[CoX(NH_3)_5]X_2$	$[CoX_2(NH_3)_4]X$	
			trans	*cis*
Cl^-	29.5	12.2	−70.8	−56.2
Br^-	48.9	23.7	−215	
NO_3^-	61.5	29.6		
I^-	52.0			
ClO_4^-	75.3			

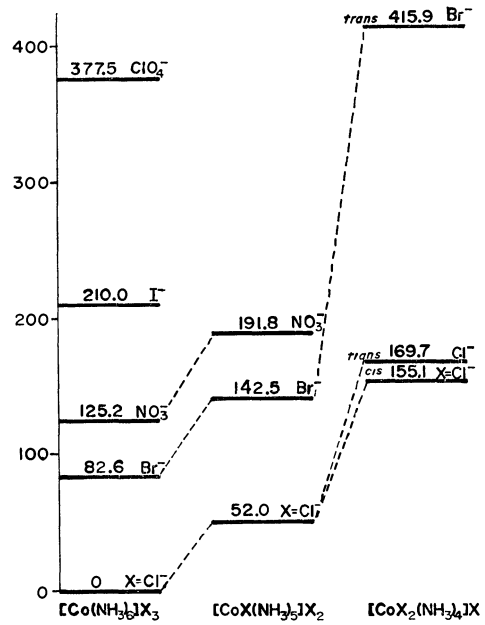

Fig. 1. Enthalpy level diagram for $[Co(NH_3)_6]X_3$, $[CoX(NH_3)_5]X_2$, and $[CoX_2(NH_3)_4]X$, where X is Cl^-, Br^-, NO_3^-, I^-, or ClO_4^-. The numerals are in kJ mol^{-1}.

the order, chloride>bromide>nitrate>iodide>perchlorate.

Thermal Stability of $[CoX(NH_3)_5]X_2$ *Complexes.* Combining the values of the enthalpy changes measured for the reaction of the pentaammine series of complexes (Table 1) with the values (1) concerned, the enthalpy changes (ΔH_{rel}) for substituting bromide and nitrate ions for chloride ions in chloropentaamminecobalt(III) chloride were calculated as below:

$$[CoCl(NH_3)_5]Cl_2(s) + 3X^-(g) = [CoX(NH_3)_5]X_2(s) + 3Cl^-(g),$$

for $X^- = Br^-$ $\quad \Delta H_{rel} = 90.5$ kJ mol^{-1},

for $X^- = NO_3^-$ $\quad \Delta H_{rel} = 139.8$ kJ mol^{-1}.

In the series of pentaammine complexes in which both the ion coordinated and the counter anions are the same, it is evident that the thermal stability decreases in the order, chloride>bromide>nitrate. The situation is parallel to the case of the hexaammine series (Fig. 1).

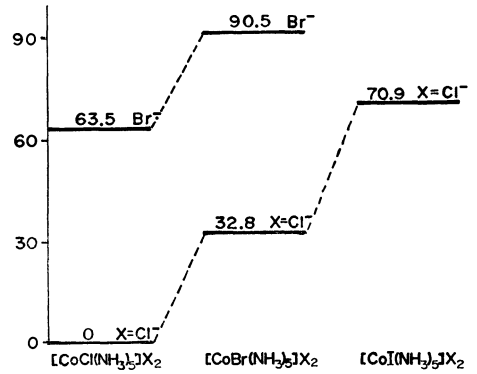

Fig. 2. Enthalpy level diagram for $[CoCl(NH_3)_5]X_2$, $[CoBr(NH_3)_5]X_2$ (X=Cl^- or Br^-) and $[CoI(NH_3)_5]Cl_2$. The numerals are in kJ mol^{-1}.

On the other hand, in the complexes where the counter halide ion is varied from Cl^- to Br^- without changing the coordinated ion, and where the coordinated ion is varied from Cl^- to Br^- and then to I^- without changing the counter ion, the enthalpy changes (ΔH_{exp}) measured and those (ΔH_{rel}) evaluated from them for successive substitution of halide anions inside and outside the coordination sphere are summarized in Table 2. The enthalpy levels of these pentaammine complexes are illustrated in Fig. 2. As seen in Table 2 and Fig. 2, if the counter ion is varied, the thermal stability of the bromides is less stable than that of the corresponding chlorides in both chloro- and bromo-complexes. The enthalpy changes (ΔH_{rel}) for substituting Br^- and I^- for Cl^- coordinated in the series of complex chlorides suggest that the thermal stabilities decrease in the order, chloro->bromo->iodo-complexes. And the enthalpy change for substituting Br^- for Cl^- coordinated in the bromide indicates the stability of the bromo complex to be lower than that of the chloro complex. This order coincides with that of the decrease of ligand field strength of halide ions.

It should be, in addition, noted from Fig. 2 that the enthalpy change for substituting Br^- for Cl^- per one mole of halide ion is about 30 kJ regardless of whether the halide ion is inside or outside the coor-

Table 2. Enthalpy changes, ΔH_{exp}, for the reaction with sodium sulfide solution and enthalpy changes, ΔH_{rel}, for substitution reaction of halide ion inside or outside the coordination sphere in series of pentaamminecobalt(III) complexes (kJ mol^{-1})

	Chloro series		Bromo series		
Chloride series	$[CoCl(NH_3)_5]Cl_2$		$[CoBr(NH_3)_5]Cl_2$		$[CoI(NH_3)_5]Cl_2$
ΔH_{exp}	12.2		13.4		18.8
ΔH_{rel}	0	⟶	32.8	⟶	70.9
	0		0		
ΔH_{rel}	↓		↓		
	63.5		57.7		
Bromide series	$[CoCl(NH_3)_5]Br_2$		$[CoBr(NH_3)_5]Br_2$		
ΔH_{exp}	16.7		23.7		
ΔH_{rel}	0	⟶	27.0		

dination sphere.

Comparison of Thermal Stability among Hexaammine, Pentaammine, and Tetraammine Complexes. By combining the enthalpy changes in Table 1 with the following value,[12]

$$NH_3(aq) = NH_3(g) \qquad \Delta H = 34.7\ kJ\ mol^{-1},$$

the enthalpy changes (ΔH_{rel}) for substituting chloride ion for ammonia in hexaamminecobalt(III) chloride to form chloropentaammine and dichlorotetraammine chlorides were obtained as follows:

$$[Co(NH_3)_6]Cl_3(s) = [CoCl(NH_3)_5]Cl_2(s) + NH_3(g)$$
$$\Delta H_{rel} = 52.0\ kJ\ mol^{-1},$$
$$[Co(NH_3)_6]Cl_3(s) = trans\text{-}[CoCl_2(NH_3)_4]Cl(s) + 2NH_3(g)$$
$$\Delta H_{rel} = 169.7\ kJ\ mol^{-1},$$
$$[Co(NH_3)_6]Cl_3(s) = cis\text{-}[CoCl_2(NH_3)_4]Cl(s) + 2NH_3(g)$$
$$\Delta H_{rel} = 155.1\ kJ\ mol^{-1}.$$

The enthalpy changes (ΔH_{rel}) for substituting bromide ion for ammonia in hexaamminecobalt(III) bromide and those for substituting nitrate ion in the corresponding nitrate were also obtained similarly as below,

$$[Co(NH_3)_6]Br_3(s) = [CoBr(NH_3)_5]Br_2(s) + NH_3(g)$$
$$\Delta H_{rel} = 59.9\ kJ\ mol^{-1},$$
$$[Co(NH_3)_6](NO_3)_3(s) = [Co(NO_3)(NH_3)_5](NO_3)_2(s) + NH_3(g)$$
$$\Delta H_{rel} = 66.6\ kJ\ mol^{-1}.$$

In order to illustrate the thermal stabilities of all the cobalt(III) ammine complexes, the enthalpy levels for pentaammine and tetraammine complexes are also shown in Fig. 1. The numeral designated at each enthalpy level reflects the difference of their lattice energies. Thus, the figure shows that the thermal stabilities decrease in the order,

$$[Co(NH_3)_6]X_3 > [CoX(NH_3)_5]X_2 > trans\text{- or } cis\text{-}[CoX_2(NH_3)_4]X,$$

where $X = Cl^-$ or Br^-.

Difference of Thermal Stability between trans- *and* cis-*$[CoCl_2(NH_3)_4]Cl$ complexes and Thermodynamic Possibility of Isomerization.* The occurrence of the partial trans-to-cis isomerization of $[CoCl_2(NH_3)_4]Cl$ has already been reported.[13] However, there have been no thermodynamical data to support this observation. Therefore, the enthalpy change of the trans-to-cis isomerization was estimated as below as shown in Table 1 and Fig. 1.

$$trans\text{-}[CoCl_2(NH_3)_4]Cl(s) = cis\text{-}[CoCl_2(NH_3)_4]Cl(s)$$
$$\Delta H = -14.6\ kJ\ mol^{-1}$$

Statistically, the entropy change of the isomerization is evaluated as[3]

$$\Delta S = 11.5\ J\ mol^{-1}\ K^{-1}.$$

The free energy change is, therefore, calculated as

$$\Delta G^\circ = -28.0\ kJ\ mol^{-1}$$

These data are consistent with the fact that the trans-to-cis isomerization takes place in $[CoCl_2(NH_3)_4]Cl$.

References

1) R. Tsuchiya, A. Uehara, and Y. Ohtsuka, *Bull. Chem. Soc. Jpn.*, **55**, 1858 (1982).
2) R. Tsuchiya, A. Uehara, T. Wazumi, and Y. Muramatsu, *Bull. Chem. Soc. Jpn.*, **56**, 2250 (1983).
3) R. Tsuchiya, A. Uehara, and Y. Muramatsu, *Bull. Chem. Soc. Jpn.*, **55**, 3770 (1982).
4) W. C. Fernelius, *Inorg. Synth.*, Vol. II, 216 (1946).
5) S. Y. Tyree, Jr., *Inorg. Synth.*, Vol. IX, 160 (1967).
6) H. S. Booth, *Inorg. Synth.*, Vol. I, 186 (1939).
7) A. Benrath and A. Miens, *Z Anorg. Allg. Chem.*, **177**, 289 (1929).
8) R. G. Yalmann, *J. Am. Chem. Soc.*, **77**, 3219 (1955).
9) S. M. Jörgensen, *Z. Anorg. Allg. Chem.*, **14**, 415 (1897).
10) C. Duval, *Compt. Rend.*, **182**, 636 (1926).
11) A. Werner and A. Wolberg, *Ber.*, **38**, 933 (1905).
12) F. D. Rossini, D. D. Wagman, W. H. Evans, S. Levine, and I. Jaffe, "Selected values of Chemical Thermodynamic Properties," U. S. Government Printing Office, Washington, D. C. (1952).
13) G. W. Watt and D. A. Butler, *Inorg. Chem.*, **5**, 1106 (1966).

 © 1983 The Chemical Society of Japan Bull. Chem. Soc. Jpn., 56, 3287—3290 (1983)

Extended X-Ray Absorption Fine Structure Studies in Some Aqueous Copper(II) Solutions

Mitsuru SANO,* Tetsuya MARUO,† and Hideo YAMATERA†

Laboratory of Inorganic Chemistry, College of General Education, Nagoya University, Chikusa-ku, Nagoya 464

† *Department of Chemistry, Faculty of Science, Nagoya University, Chikusa-ku, Nagoya 464*

(Received May 23, 1983)

With a laboratory EXAFS apparatus consisting of a usual X-ray generater, an LiF crystal, and a position sensitive X-ray detector with a self-scanning photodiode array, EXAFS spectra were obtained for aqueous $[Cu(NH_3)_4]SO_4$, $[Cu(en)_2]Cl_2$ (en = ethylenediamine), and $CuSO_4$ solutions. By reference to similar spectra of the corresponding crystals, the solution spectra were analyzed by the curve-fitting method. The values obtained for the distances between the metal and its first-shell atoms in the ammine and sulfate solutions are 2.03 (±0.02) and 1.98 (±0.03) Å, in accordance with those derived from the X-ray diffraction experiments. The Cu–N distance of $[Cu(en)_2]^{2+}$ in solution is 2.02 or 2.04 (±0.02) Å. These values obtained for the solutions are very close to those of corresponding solid complexes.

The chemistry of electrolyte solutions has made a great progress with the development of new methods such as nmr and laser-Raman spectroscopies and X-ray and neutron diffractions. Extended X-ray absorption fine structure (EXAFS) has also given significant information about the species dissolved in solution and become one of the most powerful techniques to study the local environment of the concerned atom.[1-3] However, there are some experimental difficulties in an EXAFS measurement, in which the total absorption coefficient, $\mu(E)$, must be measured with high accuracy. We have developed a laboratory apparatus utilizing a position sensitive detector to measure all the absorption coefficient at one time to improve the data collection efficiency.[4-5] In our previous EXAFS study[4] of the hydrated Cu^{2+} ion using a laboratory system equipped with a position sensitive photodiode array, the spectra was of low signal-to-noise ratio and their Fourier functions were not sufficiently reliable.[6] Thus we improved the apparatus by changing the electronic circuit of the preamplifier, adjusting the timing of the AD converter, cooling the SSPA, and so on, and used it in an EXAFS study of the aqueous cyanocuprate(I) solutions.[7] This paper is concerned with the EXAFS study of some aqueous copper(II) solutions on the laboratory EXAFS apparatus with position sensitive photodiode array. The purpose of the present study is to check the accuracy of obtained structual parameters as well as to compare the bond lengths of the species in solution with the solid complexes.

X-ray diffraction studies of aqueous solutions containing a copper(II) compound have been made by Ohtaki *et al.* (perchlolate,[8] the ammine complex,[9] and the ethylenediamine complex[10]), Wertz[11] (some chloride solutions), and Magini[12] (perchlolate, sulfate, and chloride). The EXAFS study for aqueous copper(II) perchlorate solution reported by Sham *et al.*[3] gave results in agreement with those from the X-ray diffraction studies. Lagarde *et al.*[1] studied $CuBr_2$ solutions of various concentrations reported that the local order of Cu^{2+} and Br^- ions at high concentration and is close to that found in the solid.

Experimental

The laboratory EXAFS system consists of three parts: a usual X-ray generater, an LiF crystal, and a position sensitive detector with a self-scanning photodiode array (SSPA). This is schematically shown in Fig. 1. We used a tungsten sealed X-ray tube (Philips fine focus tube, 1.5 kW) as the X-ray source, which was operated with a conventional X-ray power supply (Rigaku Co. Ltd., 1.5 kW) mostly with 25 mA at 17 kV. The generated continuous X-ray beam (uncollimated) is dispersed according to the Bragg condition by the LiF(200) crystal mounted on a goniometer. The SSPA (512 K MEL Matsushita Co. Ltd.) for one-dimensional X-ray detection consists of 512 photodiodes and MOS switches without pyrex window and has the total effective length of 14.4 mm (28 μm/channel); X-rays of different wavelengths can be detected by different channels of SSPA. The analog signal from SSPA is amplified, digitalized by an AD converter (Osaka Dempa Co. Ltd.), and transferred to the memory of a micro-computer (Sord M-100 ACE IV). The same type of the laboratory EXAFS system was used in our previous study.[7] A performance test has been carried out with Cu foil; Figure 2 shows the Cu *K* absorption spectrum for one-hour measurement at the condition of 17 kV and 25 mA. Except that

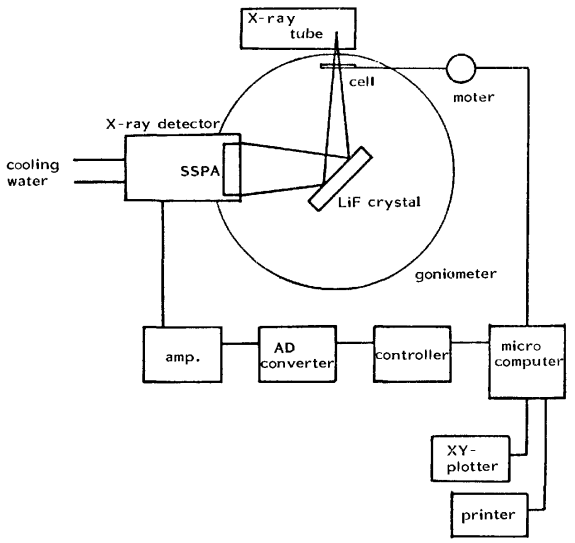

Fig. 1. The block diagram of the laboratory EXAFS system with a position sensitive photodiode array.

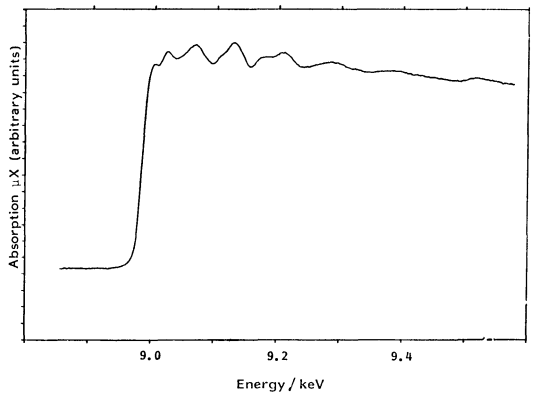

Fig. 2. X-Ray absorption spectrum of Cu-foil.

the spectrum shows a "glitch" at 9.52 keV from characteristic X-rays of W $L\beta_4$, it is comparable to that from other experiments.

The spectrum ($\mu X = \ln[(I_0 - I_d)/(I_s - I_d)]$) of each solution was obtained by measuring, in sequence and repeatedly, the beams transmitted by the sample (I_s) and by water (I_0) and the dark current without X-ray (I_d). Each step of the measurement was controlled by a micro-computer, which drives the cells at appropriate time intervals. A plastic cell contained a small volume of the sample solution between mylar windows spaced 0.6—1.0 mm apart. The solid sample was well grounded and deposited to scotch-tape.

Copper(II) sulfate and bis(ethylenediamine)copper(II) solutions were prepared by dissolving the corresponding copper salts in distilled water. The ammine solution was prepared by dissolving $[Cu(NH_3)_4]SO_4 \cdot H_2O$ in aqueous ammonia (0.14 M).† The known stability constants show that the main species contained in these solutions are $[Cu(H_2O)_6]^{2+}$ for the sulfate, $[Cu(en)_2]^{2+}$ for the ethylenediamine, and $[Cu(NH_3)_4]^{2+}$ for the ammonia solutions. The concentrations of copper ion were determined by titration with EDTA; 0.297 and 1.181 M for the sulfate, 0.321 M for the ammine, and 0.380 M for the ethylenediamine solutions.

Results and Discussion

The EXAFS spectrum $k^2\chi(k)$, in the k space, of crystalline bis(ethylenediamine)copper(II) salt ($[Cu(en)_2]Cl_2 \cdot 2H_2O$) is shown in Fig. 3 which was derived from the absorption spectrum. Fig. 4 shows the results of Fourier transformation from the k space to the r space; the transformation is applied to the $k^2\chi(k)$ values in the k range of 3.4—9.0 ($Å^{-1}$). The radial distribution curve shows two peaks, of which the larger one should corresponds to the N atoms of the coordinated ethylenediamine ligands and the smaller one may be due to the C atoms of the ligands.

The curve-fitting analysis was performed according to the method of Cramer *et al.*[13] using the following the formula for $k^2\chi(k)$:

$$k^2\chi(k) = c_0 N r^{-2} \exp(-c_1 k^2) k^{c_2} \sin[a_0 + (a_1 + 2r)k + a_2 k^2], \quad (1)$$

where N and r represent the coordination number and the interatomic distance, respectively, and c_0, c_1, and c_2 are the parameters for amplitude functions and

† 1 M = 1 mol dm^{-3}.

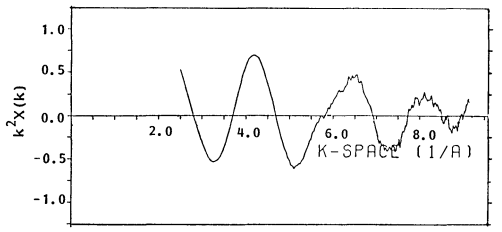

Fig. 3. EXAFS spectrum of $[Cu(en)_2]Cl_2 \cdot 2H_2O$.

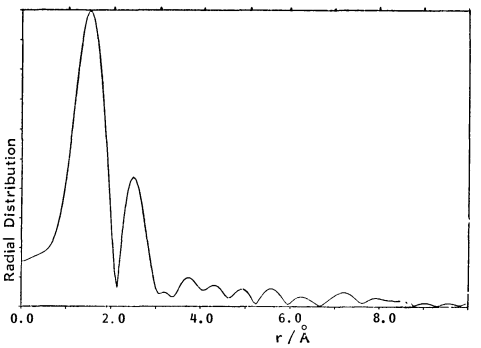

Fig. 4. Fourier transformation of the EXAFS spectrum (Fig. 3).

TABLE 1. CROSS-CHECK OF THE RESULTS OF LEAST-SQUARES FIT TO EXAFS DATA FOR CRYSTALLINE $[Cu(NH_3)_4]SO_4 \cdot H_2O$ AND $[Cu(en)_2]Cl_2 \cdot 2H_2O$

	Coordination number	Cu-N distance / Å
$[Cu(NH_3)_4]SO_4 \cdot H_2O$	4.01±0.73 (4.0)	2.03±0.02 (2.05) a)
$[Cu(en)_2]Cl_2 \cdot 2H_2O$	3.91±0.70 (4.0)	2.04±0.02 (2.03) b)

a) Obtained with parameters derived from EXAFS of the en complex. (The values in parentheses are the results of an X-ray diffraction study.[15]) b) Obtained with parameters derived from EXAFS of the ammine complex. (The values in parentheses are the results of an X-ray diffraction study.[14])

a_0, a_1, and a_2, the phase shift parameters. To determine the parameter values, we first examined the spectra of crystalline $[Cu(NH_3)_4]SO_4 \cdot H_2O$ and $[Cu(en)_2]Cl_2 \cdot 2H_2O$ of which the structures are known ($r_{Cu-N} = 2.05$ Å[14] for ammine-N and $r_{Cu-N} = 2.03$ Å[15] for ethylenediamine-N and $N = 4$ for both complexes). With fixed N and r, we obtained two sets of six parameters by curve-fitting the Fourier-filtered spectra for the isolated Cu–N interaction. For checking the accuracy of the analysis, the least-squares fit to the EXAFS spectrum of $[Cu(en)_2]Cl_2 \cdot 2H_2O$ was carried out in the range of $k = 3.8$—8.6 ($Å^{-1}$) with the set of parameters obtained above from the EXAFS spectrum of $[Cu(NH_3)_4]SO_4 \cdot H_2O$; the determined coordination number (N) and atomic distances (r_{Cu-N}) are shown in Table 1. On the other hand, the N and r_{Cu-N} values of the latter complex were obtained from the analysis of its EXAFS spectrum with the set of parameter values derived from the spectrum of the former (Table 1). The obtained values are within

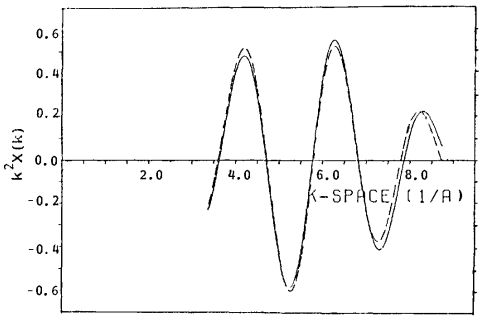

Fig. 5. First-shell fit for structure determination of an aqueous $[Cu(en)_2]^{2+}$ solution by use of a set of parameters obtained from the spectrum of solid $[Cu(NH_3)_4]SO_4 \cdot H_2O$. The solid line is the filtered EXAFS spectrum and dashed line is the least-squares fit.

Table 2. Results of curve-fitting analyses of aqueous $[Cu(NH_3)_4]^{2+}$ (0.32 M) and $[Cu(en)_2]^{2+}$ (0.38 M) solutions

	Set of parameters	Coordination number	Cu-N distance Å
$[Cu(NH_3)_4]^{2+}$	A	4.19±0.70	2.03±0.02
	B	4.24±0.71	2.02±0.02
$[Cu(en)_2]^{2+}$	A	4.59±0.72	2.04±0.02
	B	4.73±0.73	2.02±0.02

A: Parameters obtained from the spectrum of solid $[Cu(NH_3)_4]SO_4 \cdot H_2O$. B: Parameters obtained from the spectrum of solid $[Cu(en)_2]Cl_2 \cdot 2H_2O$.

the experimental error of those of X-ray diffraction analyses. This demonstrates that the analysis adopted here gives a reliable structural information.

Then we determined the structure parameters of the ammine and ethylenediamine complexes of copper(II) in aqueous solutions with both sets of parameters. The Fourier-filtered and least-squares fit curves are shown in Fig. 5 for a solution of ethylenediamine copper(II) chloride; a set of parameters obtained from the spectrum of solid $[Cu(NH_3)_4]SO_4 \cdot H_2O$ was used in the analysis. The numerical results are summarized in Table 2. Analyses with two different sets of parameters gave results in good agreement with each other. Obtained coordination numbers are about four and Cu–N distances are about 2.03 Å for both solutions;[16] these values are close to those for solid complexes. The values of ammine solution are also in good agreement with the results of Ohtaki *et al.*[9] for the concentrated aqueous solutions of ammine copper(II) salt by X-ray diffraction technique (coordination numbers of 4 and the Cu–N distances of 2.03 Å for the $[Cu(NH_3)_4]^{2+}$ solution). However, our r_{Cu-N} value (2.03 Å) for $[Cu(en)_2]^{2+}$ solutions is significantly larger than Ohtaki's (1.93 Å).[10] This inconsistency need to be further investigated by measurements of higher accuracy and precision. Generally speaking, however, the EXAFS method as applied to solutions has the advantage that it detects only the interatomic interactions in which the copper atom (or any other atom concerned) is involved, whereas the X-ray diffraction method gives a diffraction pattern which is the superposion of various diffractions by different pairs of atoms at different distances. One of the disadvantage of the EXAFS method is that the determination of interatomic distances include the estimation of the phase-shift parameter which cannot be predicted by the theory with satisfactory precision and was obtained here by an empirical method.

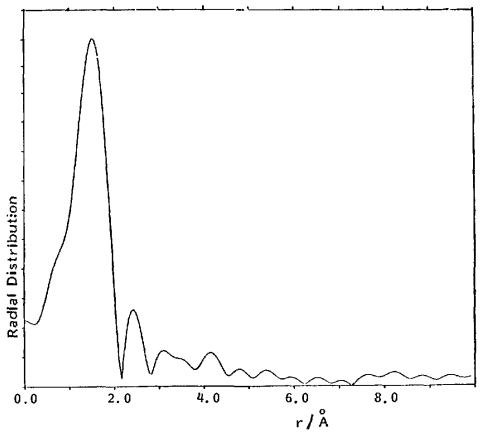

Fig. 6. Fourier transformation of the EXAFS spectrum of solid $CuSO_4 \cdot 5H_2O$.

Table 3. Results of curve-fitting analysis of aqueous $CuSO_4$ solutions

	Coordination number	Cu-O distance Å
0.30 M $CuSO_4$	4.25±0.57	1.98±0.03
1.18 M $CuSO_4$	4.13±0.57	1.98±0.03

Figure 6 shows the radial distribution from Fourier transformation of EXAFS for solid $CuSO_4 \cdot 5H_2O$, giving only one peak which corresponds to the Cu–O_{eq} interaction. Satelite at a distant position (2.3 Å) is doubtful to be a peak corresponding to Cu–O_{ax} because Fourier transformation may ripple beside the peak. Absence of the evidence for the second-nearest neighbour (O_{eq} at 2.4 Å) in the EXAFS spectrum has also been reported by Joyner.[17] To determine the Cu–O distances in solution, curve-fitting analysis was carried out using a set of parameters from solid $CuSO_4 \cdot 5H_2O$ (Cu–O=1.97 Å).[18] Table 3 shows the results for the structure parameters of two aqueous $CuSO_4$ solutions. The distance obtained is about 1.98 Å for both solutions, which generally agrees with the value from X-ray diffraction studies[8,12] within experimental error.

Concluding Remarks

An EXAFS study was carried out for aqueous solutions of some copper compounds with a position sensitive photodiode array, with which good spectra were easily obtained. The bond distance and coordination number obtained by curve-fitting method are 2.03 Å

and 4—5 for aqueous $[Cu(NH_3)_4]^{2+}$ and $[Cu(en)_2]^{2+}$ solutions. For $CuSO_4$ solutions, $Cu-O_{eq}$ is 1.98 Å and the first coordination sphere contains 4 O atoms. These results are very close to those of corresponding solid complexes.

This work was supported in part by a Grant-in-Aid from the Mitsubishi Fundation.

References

1) P. Lararde, A. Fontaine, D. Raoux, A. Sadoc, and P. Migliardo, *J. Chem. Phys.*, **72**, 3061 (1980); A. Fontaine, P. Lagarde, D. Raoux, M. P. Fontana, G. Maisano, P. Migliardo, and F. Wanderlingh, *Phys. Rev. Lett.*, **41**, 504 (1978).

2) T. K. Sham, J. B. Hastings, and M. L. Perlman, *J. Am. Chem. Soc.*, **102**, 5904 (1980).

3) J. Goulon, C. Goulon-Ginet, and M. Chabanel, *J. Solution Chem.*, **10**, 647 (1981).

4) M. Sano, K. Taniguchi, and H. Yamatera, *Chem. Lett.*, **1980**, 1285.

5) The same type of apparatus has been reported by following papers; H. Maeda, H. Terauchi, K. Tanabe, N. Kamijo, M. Hida, and H. Kawamura, *Jpn. J. Appl. Phys.*, **21**, 1342 (1982); M. Nomura, K. Asada, U. Kaminaga, T. Matsushita, K. Kohra, and H. Kuroda, *Bull. Chem. Soc. Jpn.*, **55**, 3911 (1982); K. Taniguchi, N. Yamaki, and S. Ikeda, to be published.

6) The first peak of the radial function can undoubtedly be attributed to the first H_2O shell, but the second peak was not sufficiently strong and cannot definitely be distinguished from the noise.

7) M. Sano, T. Maruo, and H. Yamatera, *Chem. Phys. Lett.*, in press.

8) H. Ohtaki, M. Maeda, and S. Ito, *Bull. Chem. Soc. Jpn.*, **47**, 2217 (1974); H. Ohtaki, T. Yamaguchi, and M. Maeda, *Bull. Chem. Soc. Jpn.*, **49**, 701 (1976).

9) T. Yamaguchi and H. Ohtaki, *Bull. Chem. Soc. Jpn.*, **52**, 415 (1979).

10) H. Ohtaki, *Rev. Inorg. Chem.*, **4**, 103 (1982).

11) J. R. Bell, J. L. Tyvoll, and D. L. Wertz, *J. Am. Chem. Soc.*, **95**, 1456 (1973); D. L. Wertz and J. L. Tyvoll, *J. Inorg. Nucl. Chem.*, **36**, 3713 (1974).

12) M. Magini, *J. Chem. Phys.*, **74**, 2523 (1981); *Inorg. Chem.*, **21**, 1535 (1982); A. Musinu, G. Paschina, G. Piccaluga, and M. Magini, *ibid.*, **22**, 1184 (1983).

13) S. P. Cramer, K. O. Hodgson, E. I. Stiefel, and N. E. Newton, *J. Am. Chem. Soc.*, **100**, 2748 (1978).

14) F. Mazzi, *Acta Crystallogr.*, **8**, 137 (1955).

15) Y. Komiyama and E. C. Lingafelter, *Acta Crystallogr.*, **17**, 1145 (1964).

16) The obtained values of coordination number, especially for the ethylenediamine case, indicate the possibility of partial five coordination of Cu^{2+} with an additional SO_4^{2-} or H_2O ligand. Further investigations are needed for the confirmation.

17) R. W. Joyner, *Chem. Phys. Lett.*, **72**, 162 (1980).

18) G. E. Bacon and N. A. Curry, *Proc. R. Soc. London*, **266**, 95 (1962).

 © 1983 The Chemical Society of Japan Bull. Chem. Soc. Jpn., 56, 3291—3293 (1983)

Mössbauer Studies of Mercury(II) Salt Adducts of [2]Ferrocenophane Derivatives

Masanobu WATANABE, Hajime ICHIKAWA, Izumi MOTOYAMA, and Hirotoshi SANO*

Department of Chemistry, Faculty of Science, Tokyo Metropolitan University, Fukasawa, Setagaya-ku, Tokyo 158

(Received May 23, 1983)

Various adducts of mercuric salts with [2]ferrocenophane and 1,1,2,2-tetramethyl[2]ferrocenophane, were prepared by treating HgX_2 ($X=Cl^-$, I^-, CN^-) with the [2]ferrocenophane derivatives in ether. The adducts were studied by Mössbauer spectroscopy and other physicochemical measurements. Anomalously large quadrupole splitting values of the adducts (about 3.10—3.30 mm s^{-1} at 78 K) suggest the presence of a strong direct interaction between the Fe and Hg atoms.

Since the discovery of ferrocene, the bonding states of this compound and its oxidized compounds, ferrocenium salts, have been investigated by various physicochemical measurements. Mössbauer spectroscopy has been applied to the investigation as one of the most useful tools to study the chemical state of iron atoms and it was found that Mössbauer parameters of ferrocene and ferrocenium salts are 2.41 mm s^{-1} and $\leq$0.5 mm s^{-1} in quadrupole splitting (Q.S.) value and 0.52 mm s^{-1} in isomer shift (I.S.) value both at 78 K. For most of the ferrocene and ferrocenium derivatives, the variation in isomer shift is slight, while the quadrupole splitting ranges from about 2.5 to 2.0 mm s^{-1} and 0 to 0.5 mm s^{-1}, respectively, depending upon the chemical state, such as the kind of substituent attached to the cyclopentadienyl rings.

Roger M. G. Roberts *et al.* recently reported Mössbauer spectroscopic studies of the $HgCl_2$ adduct of ferrocene synthesized from $HgCl_2$ and ferrocene in ether.[1] The Q.S. values of the adduct (3.09 mm s^{-1} at 78 K and 2.94 mm s^{-1} at 298 K) are one of the largest among values reported for most ferrocene derivatives suggesting an iron–mercury bonding interaction, although the adduct is not stable; *i.e.*, the orange-red color of the adduct changes into blue on standing at room temperature. Magnetic susceptibility measurements at room temperature have shown that the orange-red $Fe(Cp)_2\cdot 7HgCl_2$ compound is diamagnetic and the blue $Fe(Cp)_2\cdot 7HgCl_2$ compound paramagnetic with a magnetic moment of 2.36 BM, (1 BM$=9.274078\times10^{-24}$ J T^{-1}). This corresponds to that of a ferrocenium salt.[2]

Based on these results, it was concluded that there should be some kind of bonding interaction between Fe and Hg atoms in the orange compound, while on standing at room temperature the compound would suffer from a slow oxidation accompanying the Fe–Hg bond rupture.

Another interesting observation on the large quadrupole splitting value (2.72 mm s^{-1} at 80 K) was reported by R. M. G. Roberts *et al.* for the $Fe(Cp)_2$–$HAlCl_4$ adduct, suggesting an interaction between iron and hydrogen atoms.[3]

On the other hand, [2]ferrocenophane, one of the bridged ferrocenophane derivatives, was synthesized by H. L. Lentzner and W. E. Watts in 1971.[4] The structure was investigated by X-ray structural analysis and it was found that the cyclopentadienyl rings are inclined at *ca.* 23° to each other.[5] Various other studies of NMR,[4] electronic spectroscopy[4] and electric dipole moment measurements[6] on the [2]ferrocenophane are consistent with the "naked" structure of the iron atom in this compound. The present work was planned to study the possibility of producing an adduct of [2]ferrocenophane–HgX_2 ($X^-=Cl^-$, ClO_4^-, BF_4^-), which can be expected to be more stable than the ferrocene–$HgCl_2$ adduct because of the "naked" structure of iron atoms in the tilted-ring molecular structure.

Experimental

Materials. [2]Ferrocenophane·$3HgCl_2$ was prepared by mixing [2]ferrocenophane (1.0 g) dissolved in 50 ml diethyl ether with a large excess of $HgCl_2$ dissolved in diethyl ether. The red-orange precipitates were filtered, washed with ether and dried under vacuum. Calcd for $C_{12}H_{12}Fe\cdot 3HgCl_2$: C, 14.03, H, 1.16. Found: C, 13.18; H, 1.21.

1,1,2,2-Tetramethyl[2]ferrocenophane·$3HgCl_2$ was synthesized by the same method as that used for [2]ferrocenophane·$3HgCl_2$. Calcd for $C_{16}H_{20}Fe\cdot 3HgCl_2$: C, 17.97; H, 2.18%. Found: C, 18.00; H, 2.00%.

[2]Ferrocenophane·$0.5Hg(ClO_4)_2$ was prepared by mixing [2]ferrocenophane (0.21 g) dissolved in 150 ml absolute ethanol with about 10 drops of perchloric acid. Yellow-orange crystals started to precipitate. The precipitates were filtered, washed with absolute ethanol and dried under vacuum. Calcd for $C_{12}H_{12}Fe\cdot 0.5Hg(ClO_4)_2$: C, 34.97; H, 2.91%. Found: C, 32.88; H, 2.90%.

[2]Ferrocenophane·$0.5Hg(BF_4)_2$ was prepared by mixing [2]ferrocenophane (113 mg) with $Hg(CN)_2$ (0.32 mmol) each in 100 ml of absolute ethanol. To the solution, approximately 8 drops of 50% aqueous tetrafluoroboric acid was added. Yellow-orange crystals started to precipitate and the precipitates were filtered, washed with absolute ethanol and dried under vacuum. Calcd for $C_{12}H_{12}Fe\cdot 0.5Hg(BF_4)_2$: C, 36.08; H, 3.00%. Found: C, 35.92; H, 2.91%.

Measurements. ^{57}Fe-Mössbauer measurements were carried out using a ^{57}Co(Pt) source moving in a constant acceleration mode. The isomer shifts were determined relative to metallic iron foil. The experimental errors of the isomer shift and quadrupole splitting values are 0.02 mm s^{-1}. Electronic absorption spectra were measured in an acetonitrile solution with a Hitachi spectrophotometer model-220.

Results and Discussion

It has been reported that ferrocene reacts with $HgCl_2$ in ethanol or ether giving red-orange precipi-

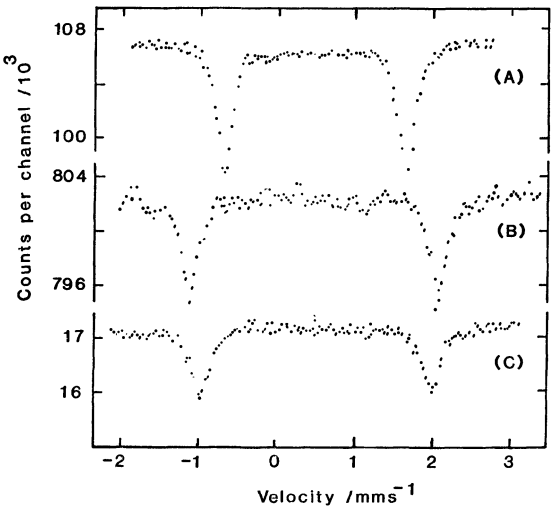

Fig. 1. Mössbauer spectra of (A) [2]ferrocenophane, (B) [2]ferrocenophane-$3HgCl_2$ adduct, and (C) [2]-ferrocenophane-$0.5Hg(BF_4)_2$ adduct all at 78 K.

tates. On standing at room temperature, this complex is also known to change color to blue. On the other hand, the present studies revealed that [2]ferrocenophane reacts with $HgCl_2$ in ether or ethanol giving red-orange precipitates, which are stable on standing, without change of color. Mössbauer spectra of [2]ferrocenophane and its mercury(II) chloride adduct are shown in Fig. 1. The quadrupole splitting of [2]ferrocenophane is found to be 2.41 mm s^{-1}, and that of 1,1,2,2-tetramethyl[2]ferrocenophane, 2.36 mm s^{-1}, both at 78 K. These values are almost the same as that of ferrocene (2.41 mm s^{-1}), indicating that the electric field gradient at the Fe nucleus in [2]ferrocenophane remains almost the same as that of ferrocene, although the cyclopentadienyl rings are largely inclined by *ca.* 23° each other.

A similar observation was reported by R. A. Abramovitch *et al.* in 1975 for 1-thia-2-aza[2]ferrocenophane 1,1-dioxide, in which cyclopentadienyl rings were bridged by sulfur and nitrogen atoms instead of carbon atoms.[7] The quadrupole splitting value of this compound is almost the same as that of ferrocene, as in the case of [2]ferrocenophane.

On the contrary, a remarkable difference was observed in the Mössbauer spectra of mercury(II) halide adducts of [2]ferrocenophane derivatives from that of ferrocene. The quadrupole splitting value of [2]ferrocenophane·$3HgCl_2$ is 3.29 mm s^{-1} at 78 K, which is the largest of all the reported ferrocene derivatives, while the Q.S. value of ferrocene·$7HgCl_2$ has been reported to be 3.09 mm s^{-1} at 78 K.

The large Q.S. value of [2]ferrocenophane·$3HgCl_2$ compound compared with that of ferrocene·$7HgCl_2$ suggests a stronger bonding formed between iron and mercury atoms in the adduct. The suggestion may also be supported by the fact that the [2]ferrocenophane·$3HgCl_2$ adduct remains more stable on standing, even after 180 d, than the ferrocene·$7HgCl_2$ adduct which changes to the ferrocenium salt. The results imply that the bonding formed by the "naked" electrons of Fe atom coordinating with an orbital of a Hg atom is so stable that the red-orange color of the mercury(II) chloride adduct of [2]ferrocenophane does not change on standing. The quadrupole splitting value of the mercury(II) iodide adduct, 1,1,2,2-tetramethyl[2]ferrocenophane·$2HgI_2$, is a little smaller than that of the mercury(II) chloride adduct of [2]-ferrocenophane.

D. N. Hendrickson *et al.* reported the structure and bonding state of ruthenocene compounds such as $[(Cp)_2Ru]_2HgX_2$ ($X=PF_6^-$, BF_4^-, ClO_4^-) by means of various physicochemical techniques.[8] It was found that a strong line component remained unchanged in the Raman spectra of $[(Cp)_2Ru]_2HgX_2$ except for the absorptions attributable to the different kinds of anion and that the strong Raman band observed at 110 cm^{-1} both in solid and in a solution containing the cation was assigned to a symmetrical Ru–Hg–Ru stretching mode. In their study of the electronic absorption spectrum of $[(Cp)_2Ru]_2Hg(PF_6)_2$ at room temperature, a strong new absorption band was observed at 320 nm and assigned to a transition associated with the Ru–Hg–Ru unit, based on studies of $M_2(CO)_{10}$ ($M=Mn$, Re) complexes.[9] From their results, they proposed that the structure of $[Ru(Cp)_2]_2HgX_2$ should be expressed as $[(Cp)_2Ru(II)–Hg(II)–Ru(II)(Cp)_2]X_2$.

Although ferrocene does not react with mercury(II) cyanide and does not form $[(Cp)_2Fe–Hg–Fe(Cp)_2]^{2+}$ but produces the ferrocenium salt, [2]ferrocenophane derivatives react with mercury(II) cyanide and produce mercury(II) salt adducts, $[(C_5H_4CH_2)_2Fe]_2HgX_2$, ($X^-=ClO_4^-$, BF_4^-), under similar conditions. Mössbauer parameters of the compounds are listed in Table 1 and typical Mössbauer spectra of the mercury(II) salt adducts are also shown in Fig. 1. The quadrupole splitting values of [2]ferrocenophane·$0.5Hg(BF_4)_2$ are 3.11 mm s^{-1} at 78 K and 3.10 mm s^{-1} at 300 K, and those of 1,1,2,2-tetramethylferrocenophane·$0.5Hg(BF_4)_2$ are 3.12 mm s^{-1} at 78 K and 3.08 mm s^{-1} at 300 K. Both values are larger than those of [2]ferrocenophane and 1,1,2,2-tetramethyl[2]ferrocenophane and are similar to that of mercury(II) chloride adducts, [2]ferrocenophane·$3HgCl_2$. This fact shows

Table 1. Mössbauer parameters of [2]ferrocenophane, $(C_5H_4CH_2)_2Fe$, and tetramethyl[2]ferrocenophane, $(C_5H_4C(CH_3)_2)_2Fe$, and their adducts with mercury(II) salts

Compound	Temp K	Q.S. mm s^{-1}	I.S. mm s^{-1}
$(C_5H_4CH_2)_2Fe$	78	2.41	0.49
$[(C_5H_4CH_2)_2Fe]·(HgCl_2)_3$	78	3.29	0.49
$[(C_5H_4CH_2)_2Fe]·$ 1/2 $Hg(ClO_4)_2$	78	3.14	0.53
$[(C_5H_4CH_2)_2Fe]·$ 1/2 $Hg(BF_4)_2$	78	3.11	0.53
	300	3.10	0.46
$(C_5H_4C(CH_3)_2)_2Fe$	78	2.36	0.53
$[(C_5H_4C(CH_3)_2)_2Fe]·$ 1/2 $Hg(BF_4)_2$	78	3.12	0.53
	300	3.08	0.44
$[(C_5H_4C(CH_3)_2)_2Fe]·$ $(HgI_2)_2$	78	3.09	0.51

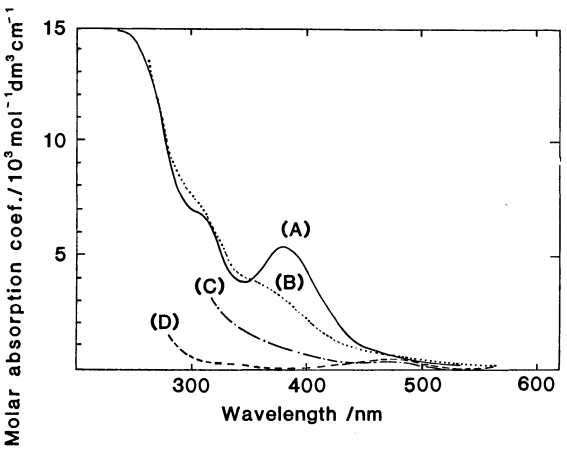

Fig. 2. Absorption spectra of an acetonitrile solution of bis([2]ferrocenophane)mercury(II) perchlorate, $[(C_5H_4CH_2)_2Fe]_2$-$Hg(ClO_4)_2$ (A) 4 min, (B) 20 min, (C) 50 min after preparation, and (D) an acetonitrile solution of [2]ferrocenophane, $(C_5H_4CH_2)_2Fe$.

that there is also a strong interaction between Fe–Hg atoms in these adducts described as $[(C_5H_4CH_2)_2Fe$–Hg–$Fe(C_5H_4CH_2)_2]^{2+}X^-_2$ in a similar way to the structure of $[Ru(Cp)_2]_2HgX_2$.

Figure 2 shows the electronic absorption spectra of $[(C_5H_4CH_2)_2Fe]_2Hg(ClO_4)_2$ dissolved in acetonitrile. A new absorption band, which is similar to that of the $[(Cp)_2Ru]_2HgX_2$ solution in spectral shape, appears at 380 nm, although the intensity of the band decreases gradually as the solution is allowed to stand, probably because of dissociation of the adduct in solution, as found in the solutions of $[(Cp)_2Ru]_2HgX_2$. The results suggest that the absorption band is assigned to an electronic transition associated with the Fe–Hg–Fe unit corresponding to that of the Ru–Hg–Ru unit.

All the results obtained in the present studies lead us to the conclusion that [2]ferrocenophane and 1,1,2,2-tetramethyl[2]ferrocenophane give stable adducts in which a direct bond is formed between iron and mercury atoms and that the bonding is stabilized by coordinating the "naked" electrons of iron atoms to one of the vacant orbitals of mercury atoms in the tilting structure of cyclopentadienyl rings in [2]ferrocenophanes, as in the case of [2]ferrocenophane–tin(IV) chloride adduct.[10]

References

1) R. M. G. Roberts, J. Silver, and I. G. Harrison, *J. Organomet. Chem.*, **209**, 385 (1981).
2) W. H. Morrison, Jr., and D. N. Hendrickson, *Inorg. Chem.*, **11**, 2912 (1972).
3) R. M. G. Roberts, J. Silver, R. J. Ranson, and I. E. G. Morrison, *J. Organomet. Chem.*, **219**, 233 (1981).
4) H. L. Lentzner and W. E. Watts, *Tetrahedron*, **27**, 4343 (1971).
5) M. B. Laing and K. N. Trueblood, *Acta Crystallogr.*, **19**, 373 (1965).
6) H. Lumbroso, C. Pigenet, H. L. Lentzner, and W. E. Watts, *Tetrahedron*, **28**, 111 (1972).
7) R. A. Abramovitch, J. L. Atwood, M. L. Good, and B. A. Lampert, *Inorg. Chem.*, **14**, 3085 (1975).
8) D. N. Hendrickson, Y. S. Sohn, W. H. Morrison, Jr., and H. B. Gray, *Inorg. Chem.*, **11**, 808 (1972).
9) R. Levenson and H. B. Gray, unpublished work; R. Leverson, Ph. D. Thesis, Columbia University, New York, N. Y., 1970.
10) M. Watanabe, H. Ichikawa, I. Motoyama, and H. Sano, *Chem. Lett.*, **1983**, 1009.

Kinetics of the Thermal Decomposition of Nickel Sulfate

Kaoru Onuki,* Saburo Shimizu, Hayato Nakajima, Yasumasa Ikezoe, and Shoichi Sato

Japan Atomic Energy Research Institute, Tokai-mura, Ibaraki, 319-11

(Received May 26, 1983)

The rate of thermal decomposition of nickel sulfate was measured in the temperature range from 1003 K to 1078 K. When a powder sample was used, this reaction was characterized as a contracting volume reaction, with apparent activation energy of 296 kJ mol^{-1}. The gaseous products were sulfur trioxide, sulfur dioxide, and oxygen. The composition of the gaseous products was near equilibrium in regard to the reaction, $SO_3 = SO_2 + 1/2\,O_2$, because the nickel oxide formed had high catalytic activity for this reaction.

We have proposed a thermochemical hydrogen production cycle composed of the following chemical reactions (NIS process).[1)]

$$SO_2 + I_2 + 2H_2O = 2HI + H_2SO_4 \quad (1\text{-}1)$$

$$2HI + H_2SO_4 + 2Ni = NiI_2 + NiSO_4 + 2H_2 \quad (1\text{-}2)$$

$$NiI_2 = Ni + I_2 \quad (2)$$

$$NiSO_4 = NiO + SO_3 \quad (3\text{-}1)$$

$$SO_3 = SO_2 + 1/2\,O_2 \quad (3\text{-}2)$$

$$NiO + H_2 = Ni + H_2O \quad (4)$$

Studies on the nickel salt separation[2)] and dehydration equilibrium of nickel iodide[3)] have been made about the process. In this paper, we report the study of reaction (3-1), the thermal decomposition of nickel sulfate.

The kinetics of the decomposition of nickel sulfate have been studied by a few investigators. Ingraham and Marier[4)] measured the rates of formation and decomposition of nickel sulfate by thermogravimetry. They reported that nickel oxide was formed at a well-defined interface between sulfate and oxide, and the interface migrated into the sulfate phase at a constant rate. Also, they found that a small amount of sulfur trioxide in the decomposition atmosphere caused a substantial decrease in the rate of decomposition. The same equation was reported by other investigators,[5–7)] but the apparent activation energies reported were widely different from each other as shown in Table 1. Dollimore and Pearce[8)] have measured the density and the surface area of a half- hour ignition sample at various temperatures, and observed the occurrence of cracking and adhesion of particles during decomposition.

In the present work, we studied the decomposition rate, the composition of the gaseous products and the characteristics of the solid product.

Experimental

Nickel sulfate hexahydrate ($NiSO_4 \cdot 6H_2O$) of analytical grade was dehydrated for 5 h at 723 K to the anhydrous form and then ground into powder.

Decomposition experiments were made with the apparatus shown in Fig. 1. The flow system was composed of a carrier gas flow controller, a vertical reactor, a sulfuric acid demister, a sulfur oxides (SO_x) trap, and oxygen meter. The reactor was made of a cylindrical quartz tube (o.d.=15 mm) and a sintered quartz disc. The powder sample was placed on the disc and covered with quartz wool. Temperature of the reaction zone was kept constant throughout the decomposition experiment, and was measured by two alumel–chromel thermocouples. One thermocouple was put in a quartz tube inside the reactor, and the other was set at the outer wall of the reactor. Gaseous decomposition products were carried away from the reactor by argon carrier gas and the sulfur oxides were absorbed in 0.1 mol dm^{-3} iodine solution added with potassium iodide. The acid mist in the product gas stream was caught efficiently by two sintered glass filters which was moistened with the iodine solution as shown in Fig. 1.

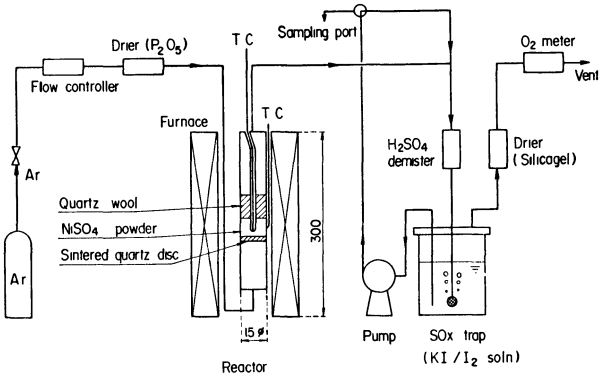

Fig. 1. Experimental apparatus (schematic).

The amounts of sulfur oxides produced were measured by acidimetry and iodometry. The oxygen concentration in the tail gas was continuously measured by an oxygen meter with zirconia solid electrolyte (Toray, Model LC 700-H).

Decomposition experiments were made with 1 g of the sample (in anhydrous form), in the temperature range from 1003 to 1078 K at 1.06×10^5 Pa pressure and 0.1 to 0.6 dm^3-NTP min^{-1} argon flow rate.

The scanning electron microscope (SEM) observation, the flowing BET surface area measurement,[9)] and X-ray diffraction measurement of the sample powder were done before and after decomposition.

Results and Discussion

First, all gaseous products from decomposition were measured at all stages of the reaction. The composition of the gaseous products was found to be almost constant throughout the decomposition. Then, the fraction decomposed, α was followed by measuring the oxygen concentration. The time dependent curves of α are shown in Fig. 2 at three temperatures and an argon flow rate of 0.5 dm^3 min^{-1}. The decomposition rates decrease continuously with time. The effect of argon flow rate on the reaction rate at a constant α of 0.3, $V_{0.3}$ is shown in Fig. 3. The decomposition

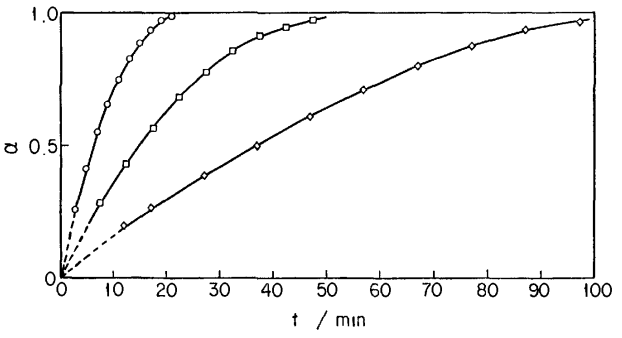

Fig. 2. Fraction decomposed (α) *vs.* time at various temperatures.
Argon flow rate: 0.5 $dm^3\ min^{-1}$. (◇); 1023 K, (□); 1043 K, (○); 1078 K.

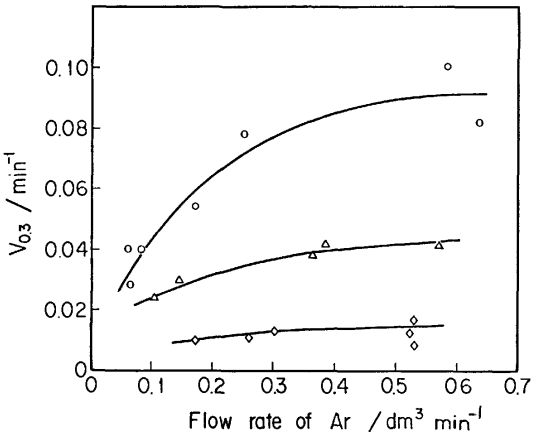

Fig. 3. Effect of argon flow rate on the decomposition rate of $NiSO_4$ when 30% of $NiSO_4$ is decomposed.
(◇); 1023 K, (△); 1063 K, (○); 1078 K.

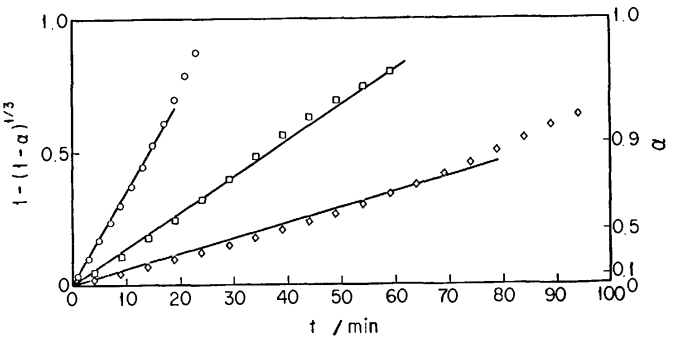

Fig. 4. $1-(1-\alpha)^{1/3}$ *vs.* time for the decomposition of $NiSO_4$.
(◇); 1023 K, (□); 1043 K, (○); 1078 K.

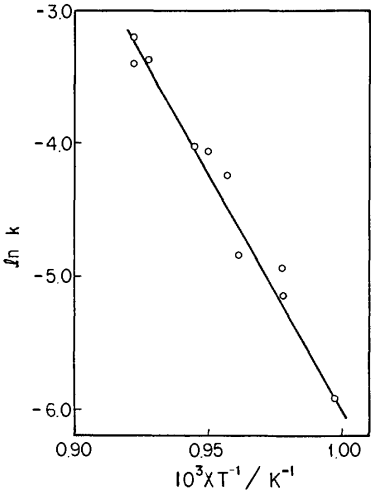

Fig. 5. Arrhenius' relationship for the decomposition of $NiSO_4$.

rates increase with increasing the flow rates to *ca.* 0.5 $dm^3\ min^{-1}$ and are constant above that flow rate. So, the data at a flow rate of 0.5 $dm^3\ min^{-1}$ are considered hereafter.

The rate equation of the reaction was obtained by Sharp-Brindley-Achar method.[10] By replotting α against the time normalized at $\alpha=0.5$, $t/t_{0.5}$, all data were expressed by a single curve. Then, the rate equation for the nickel sulfate decomposition could be expressed as follows:

$$1-(1-\alpha)^{1/3}=kt. \tag{5}$$

Here, k is the reaction rate constant and t is the reaction time. The plot of the experimental data according to Eq. 5 is shown in Fig. 4. A good linearity is found in the range of α to *ca.* 0.8. Equation 5 is considered for the contracting volume reaction.[11] The rate equation obtained is consistent with that previously reported.[4-7]

The Arrhenius' plot of the rate constants, k is shown in Fig. 5. From the plot, we can obtain the apparent rate parameters as follows:

$$k=1.18\times10^{11}\exp\left\{-\frac{296(\text{kJ mol}^{-1})}{RT}\right\}(\text{s}^{-1}). \tag{6}$$

Here, R is the gas constant. The apparent activation energies reported for the thermal decomposition of nickel sulfate are listed in Table 1 together with that obtained in the present study. Our result is close to those of Ingraham *et al.*[4] and Karwan *et al.*[6]

Table 1. Apparent activation energy for thermal decomposition of nickel sulfate

Decomposition atmosphere	Temperature range / K	Activation energy / kJ mol^{-1}	Reference
N_2	1031—1124	255±12	4)
Air	975—1064	115	5)
Air	1075—1250	305±32	6)
N_2 or Ar	1075—1220	162	7)
Ar	1003—1078	296	This work

The X-ray diffraction pattern showed the solid product was nickel oxide, NiO. The SEM picture of the sample powder before and after decomposition are shown in Figs. 6-a and 6-b, respectively. The granular product is very porous and fluffy, and the size of product particle is much larger than that of reactant. The specific surface areas of the sample powder before and after decomposition are 8.4 $m^2\ g^{-1}$ and 15.5 $m^2\ g^{-1}$, respectively. These observations are qualitatively explained assuming the following decomposition sequence.[8] As the decomposition proceeds, the particle is broken up into smaller particles due to the strain

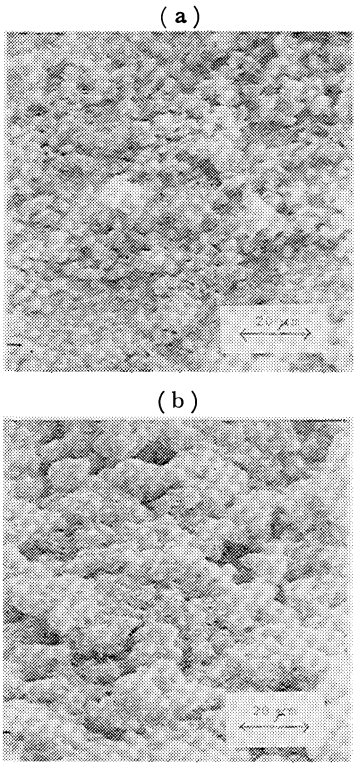

Fig. 6. (a) Scanning electron microscope picture of nickel sulfate powder used in the experiment. (b) Scanning electron microscope picture of the nickel oxide powder produced by the decomposition of sulfate at 1043 K.

imposed by the decomposition. Simultaneously, the adhesion of particles takes place and the porous and fluffy layer is formed.

The molar ratios of sulfur dioxide produced to the reactant, $NiSO_4$ at various decomposition temperatures and carrier gas flow rates are shown in Fig. 7. As seen in the figure, the ratio is almost independent of the reaction temperature and the carrier gas flow rate, and is very close to the equilibrium value which ranges from 0.88 to 0.96. The equilibrium value was calculated from the thermodynamic data[12] for the reaction:

$$SO_3 = SO_2 + 1/2\,O_2. \quad (3\text{-}2)$$

The sulfur trioxide concentration was estimated from the amount of the reactant, $NiSO_4$ and the time difference between the time of $\alpha=0.1$ and the time of $\alpha=0.9$.

The effect of oxygen on the product gas composition was also examined using air as the carrier gas as shown in Fig. 7. At 1043 K and 0.5 $dm^3\,min^{-1}$, the ratio is 0.66. This value is equal to the equilibrium one calculated for the oxygen fraction in the carrier gas, 0.21.

These results suggest that the decomposition product, NiO acts as an active catalyst for reaction (3-2) under the experimental conditions. The catalytic activity of the nickel oxide produced was tested as follows. After the nickel sulfate was completely decomposed by heating at 1073 K for 2.5 h in an argon stream, a gas mixture of argon and 3.8 vol% sulfur trioxide was introduced to the reactor and the oxygen

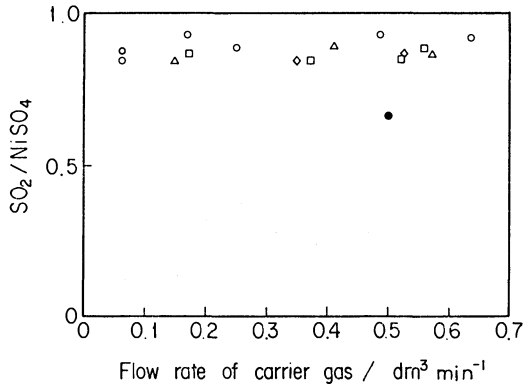

Fig. 7. Effect of the decomposition conditions on the molar ratio of SO_2 produced to $NiSO_4$.
Argon atmosphere: (◇); 1023 K, (□); 1043 K, (△); 1063 K, (○); 1078 K, air atmosphere: (●); 1043 K.

concentration of the tail gas was measured at 1073 K. At a contact time of 0.48 s, the fraction of sulfur trioxide decomposed was 0.77 ± 0.07. This concentration of SO_3 and the contact time were chosen so as to simulate the thermal decomposition condition in the present study. The equilibrium fraction of sulfur trioxide decomposed under the condition is calculated to be 0.90. Thus, it was proved that nickel oxide had an enough catalytic activity for reaction (3-2) under the experimental conditions. It should be noted that the reactor wall and the sintered quartz disc had no catalytic activity for reaction (3-2). These results suggest simplification of the NIS process, because reaction (3-1) and (3-2) may be operated in one step.

The authors are indebted to Dr. Norio Masaki for the X-ray diffractometry, to Mr. Hitoshi Otsu for the scanning electron microscope observation.

References

1) S. Shimizu, S. Sato, Y. Ikezoe, and H. Nakajima, *Denki Kagaku*, **49**, 699 (1981).
2) S. Shimizu, S. Sato, H. Nakajima, and K. Onuki, *Denki Kagaku*, **50**, 898 (1982).
3) S. Shimizu, K. Onuki, H. Nakajima, Y. Ikezoe, and S. Sato, *Denki Kagaku*, **50**, 904 (1982).
4) T. R. Ingraham and P. Marier, *Trans. Met. Soc. AIME*, **236**, 1067 (1966).
5) G. A. Kolta and M. H. Askar, *Thermochim. Acta*, **11**, 65 (1975).
6) T. Karwan, C. Malinowski, W. Ptak, and M. Sukiennik, *Thermochim. Acta*, **23**, 269 (1978).
7) M. Ducarroir, H. Romero-Paredes, D. Steinmetz, F. Sibieude, and M. Tmar, "Proc. 4th World Hydrogen Energy Conf.," Pergamon Press, Oxford (1982), Vol. 2, p. 451.
8) D. Dollimore and J. Pearce, *J. Therm. Anal.*, **6**, 321 (1974).
9) F. M. Nelson and F. T. Eggertson, *Anal. Chem.*, **30**, 1387 (1958).
10) J. H. Sharp, G. W. Brindley, and B. N. Achar, *J. Am. Ceram. Soc.*, **49**, 379 (1966).
11) W. E. Brown, D. Dollimore, and A. K. Galway, "Comprehensive Chemical Kinetics," ed by C. H. Bamford and C. F. H. Tipper, Elsevier, Amsterdam (1980), Vol. 22.
12) I. Barin and O. Knacke, "Thermochemical Properties of Inorganic Substances," Springer-Verlag, Dusseldorf (1973).

The Crystal and Molecular Structure of [Pd(tfac)(tfac-*O*){P(*o*-tolyl)$_3$}] Containing an *O*-Unidentate 1,1,1-Trifluoro-2,4-pentanedionate Anion as a Ligand

Shun'ichiro Ooi,* Toshio Matsushita, Kichisuke Nishimoto, Seichi Okeya,†
Yukio Nakamura, and Shinichi Kawaguchi*

Faculty of Science, Osaka City University, Sumiyoshi-ku, Osaka 558
† *Faculty of Education, Wakayama University, Masago-cho, Wakayama 640*

(Received May 30, 1983)

The title complex crystallizes in the monoclinic space group C2/c with $a=24.900(6)$ Å, $b=8.272(2)$ Å, $c=30.437(9)$ Å, and $\beta=97.23(2)°$. The structure analysis, which converged at $R=0.061$ and $R_w=0.083$ with 3017 reflections for which $F_o^2>3\sigma(F_o^2)$, showed that the palladium has a complete square-planar coordination geometry. While one of the tfac ligands is chelating, the other is bound to the metal only through the carbonyl oxygen adjacent to CH_3. The *O*-unidentate tfac ligand lies trans to the CF_3CO moiety of chelating tfac and has a planar structure in which the dangling CF_3CO group is situated trans to the bonding oxygen atom with respect to the C=C bond. The *ab initio* MO calculation for the *Z,Z*-form of the tfac anion indicated that the coordination ability of the acetyl oxygen is higher than that of the trifluoroacetyl oxygen in consistence with the observed structure.

In recent years the reactions of binary and mixed-ligand bis(β-diketonato)palladium(II) and -platinum(II) chelates[1] with various nitrogen bases[2-4] and tertiary phosphines[5] have been studied very extensively. Many types of products were obtained depending on the natures of the central metals, β-diketonate ligands, attacking Lewis bases, and solvents employed. For example, the [Pd(acac)(acac-C^3)L] complexes containing both the *O,O'*-chelated and the central-carbon-bonded 2,4-pentanedionate ligands (acac and acac-C^3, respectively) were afforded by the reactions of [Pd(acac)$_2$] with Lewis bases (L) such as diethylamine, pyridine, and triphenylphosphine as neat liquids and in benzene, respectively.[6]

The kinetic and equilibrium studies on the reaction of [Pd(acac)$_2$] with various alkylamines in solutions revealed that the carbon-bonded acac complexes are not derived directly from the starting bis-chelate, but resulted *via* the salt-like complexes [Pd(acac)L$_2$](acac).[7]

$$[Pd(acac)_2] + 2L \rightleftharpoons [Pd(acac)L_2](acac) \quad (1)$$

$$[Pd(acac)L_2](acac) \rightleftharpoons [Pd(acac)(acac\text{-}C^3)L] + L \quad (2)$$

In the first stage (Eq. 1) of the overall reaction, one of the chelating acac ligands seems to be displaced *via* the *O*-unidentate state although the intermediate complex [Pd(acac)(acac-*O*)L] was not detected spectrophotometrically in these particular reactions.[7]

In fact several [M(β-dik)(tfac-*O*)(PR$_3$)]-type complexes (M=Pd^{II} and Pt^{II}; β-dik=acac and tfac; R=ethyl, phenyl, *o*-tolyl, and cyclohexyl) containing the *O*-unidentate 1,1,1-trifluoro-2,4-pentanedionate anion (tfac-*O*) were prepared by the reactions of [M(β-dik)(tfac)] with tertiary phosphines.[5] According to the kinetic and equilibrium studies,[8] the reaction of [Pd(tfac)$_2$] with tri-*o*-tolylphosphine proceeds reversibly to afford the *O*-unidentate tfac complex exclusively, the equilibrium constant being 1.38×10^3, 4.35×10^3, and more than 10^9 dm^3 mol^{-1} in benzene, dichloromethane, and methanol, respectively, at 25 °C. The steric requirement of P(*o*-tolyl)$_3$ may prevent the formation of [Pd(tfac){P(*o*-tolyl)$_3$}$_2$](tfac) and [Pd(tfac)(tfac-C^3)-{P(*o*-tolyl)$_3$}].

The *O*-unidentate bonding of the β-diketonate anion was observed first for Me$_2$Si(acac-*O*)$_2$ and Me$_3$Si(acac-*O*)[9] followed by [Hg(β-dik-*O*)$_2$] (β-dik=acac, 2,6-dimethyl-3,5-heptanedionate, and 2,2,6,6-tetramethyl-3,5-heptanedionate anions),[10] [Pt(acac-*O*)$_2$L$_2$](L=PEt$_3$[11] and piperidine[12]), [Cu(acac)(hfac-*O*)(phen)] (hfac=1,1,1,5,5,5-hexafluoro-2,4-pentanedionate anion),[13] and [M(CO)$_3${PPh(acac-*O*)$_2$}] (M=Cr and W)[14] as well as the above-mentioned [M(β-dik)(tfac-*O*)(PR$_3$)] complexes.[5] This paper reports the crystal and molecular structure of [Pd(tfac)(tfac-*O*){P(*o*-tolyl)$_3$}] which was determined by the X-ray diffraction method in order to disclose for the first time the *O*-unidentate structure of tfac in a crystal.[15]

Experimental

The compound was prepared by the reaction of [Pd(tfac)$_2$] with P(*o*-tolyl)$_3$ in hot benzene and an orange plate ($0.09\times0.25\times0.25$ mm^3) for X-ray analysis was obtained on addition of hexane to the solution and spontaneous cooling to room temperature.[5] Crystal Data: Monoclinic, $a=24.900(6)$ Å, $b=8.272(2)$ Å, $c=30.437(9)$ Å, $\beta=97.23(2)°$, Space group C2/c, $D_m=1.52$ g cm^{-3}, $D_c=1.532$ g cm^{-3}, $Z=8$, μ(Mo $K\alpha$)$=7.14$ cm^{-1}. The Laue symmetry and the space group were determined from Weissenberg and precession photographs. The unit cell dimension was obtained from the least-squares treatment of 14 θ values of higher angle reflections ($\theta=7-15°$) measured on an automated diffractometer by use of Mo $K\alpha$ radiation.

The intensities were measured on the diffractometer by using the graphite-monochromated Mo $K\alpha$ radiation. The background was counted at each side of the scan range ($\omega=1.0+0.4\tan\theta$), the speed of ω scan being 0.033° s^{-1}. The intensities of three standard reflections monitored every 4 h showed no appreciable variation during the data collection.

Of 3839 independent reflections collected in the $2\theta\leq44°$ range, 3017 with $F_o^2>3\sigma(F_o^2)$ were used for the structure determination. The crystal structure was solved by the heavy atom technique. The positional and thermal parameters were refined by block-diagonal-matrix least-squares to R 0.061, R' ($=[\sum w\Delta^2/\sum wF_o^2]^{1/2}$) being 0.083. The minimized function was $\sum w(F_o-|F_c|)^2$, where $w=1/\sigma^2(F_o)$. No attempt was made to locate hydrogen atoms. In the course

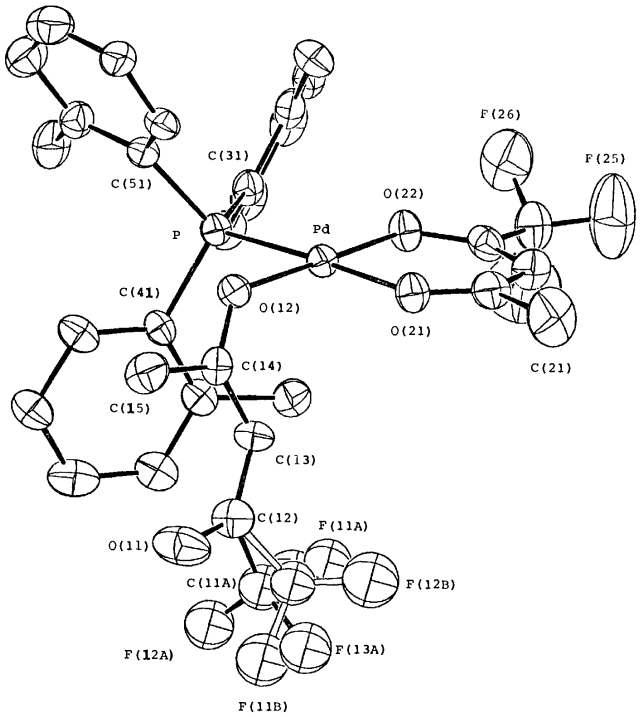

Fig. 1. ORTEP drawing of [Pd(tfac)(tfac-*O*){P(*o*-tolyl)$_3$}]. Thermal ellipsoids are drawn at 30% probability level. The CF_3 group composed of C 11), F(11), F(12), and F(13) is twofold disordered

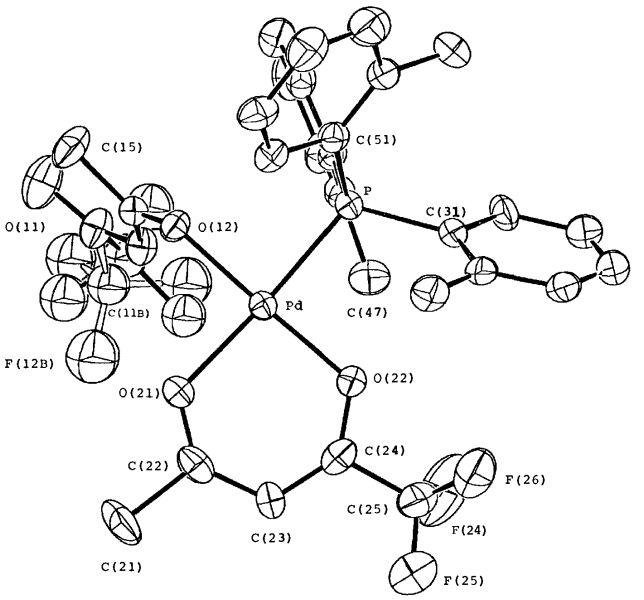

Fig. 2. Projection of the complex along the normal of coordination plane. Thermal ellipsoids are drawn at 30% probability level.

of the structure analysis, one of the CF_3 groups was found to be in disorder. The electron density distribution for this group was best interpreted by the model (twofold disorder) shown in Figs. 1 and 2. Occupancies for the disordered CF_3 groups were assumed to be equal. All parameter shifts in the final cycle of the refinement were less than 0.5σ except for the atomic parameters of the disordered CF_3 group, for which the shifts were in the $0.15\sigma-1.5\sigma$ range.

The atomic scattering factors with correction for anomalous dispersion of the metal atom were taken from Ref. 16. The

Table 1. Fractional coordinates and temperature factors for [Pd(tfac)(tfac-*O*){P(*o*-tolyl)$_3$}]. Standard deviations of the least significant figures are given in parentheses

Atom	x	y	z	B_{eq}/Å^2
Pd	0.10819(3)	0.1369(1)	0.15603(2)	3.60(2)
P	0.1351(1)	0.0126(3)	0.0967(1)	3.5(1)
C(31)	0.2020(4)	-0.080(1)	0.1062(3)	3.9(3)
C(32)	0.2481(4)	0.023(1)	0.1163(3)	4.8(3)
C(33)	0.2991(4)	-0.054(2)	0.1208(3)	5.5(4)
C(34)	0.3034(5)	-0.221(2)	0.1160(3)	6.2(4)
C(35)	0.2585(5)	-0.318(1)	0.1066(3)	6.0(4)
C(36)	0.2075(4)	-0.245(1)	0.1009(3)	4.7(3)
C(37)	0.2450(4)	0.205(1)	0.1220(4)	5.5(3)
C(41)	0.0850(3)	-0.148(1)	0.0824(3)	3.7(3)
C(42)	0.0752(4)	-0.269(1)	0.1120(3)	4.3(3)
C(43)	0.0344(4)	-0.377(1)	0.1006(4)	5.3(3)
C(44)	0.0008(5)	-0.364(1)	0.0599(4)	6.4(4)
C(45)	0.0081(4)	-0.239(1)	0.0297(4)	5.6(4)
C(46)	0.0519(4)	-0.132(1)	0.0424(4)	4.9(3)
C(47)	0.1075(5)	-0.290(1)	0.1586(3)	5.5(3)
C(51)	0.1368(3)	0.149(1)	0.0495(3)	3.8(3)
C(52)	0.1558(4)	0.101(1)	0.0108(3)	4.7(3)
C(53)	0.1585(5)	0.218(2)	-0.0235(4)	6.9(4)
C(54)	0.1451(5)	0.385(2)	-0.0150(4)	7.0(4)
C(55)	0.1262(4)	0.430(1)	0.0244(3)	5.5(3)
C(56)	0.1215(4)	0.311(1)	0.0558(3)	4.2(3)
C(57)	0.1742(5)	-0.066(2)	0.0008(4)	6.4(4)
O(21)	0.0790(3)	0.2534(8)	0.2072(2)	4.6(2)
O(22)	0.1753(2)	0.0676(8)	0.1930(2)	4.6(2)
C(21)	0.0745(6)	0.353(2)	0.2816(5)	9.3(6)
C(22)	0.1037(4)	0.254(1)	0.2465(3)	5.2(3)
C(23)	0.1526(4)	0.178(1)	0.2630(3)	5.1(3)
C(24)	0.1823(4)	0.093(1)	0.2358(3)	4.8(3)
C(25)	0.2329(5)	0.007(2)	0.2567(4)	6.8(4)
F(24)	0.2234(5)	-0.148(1)	0.2598(4)	16.4(5)
F(25)	0.2507(4)	0.056(2)	0.2953(3)	15.3(5)
F(26)	0.2741(3)	0.016(1)	0.2333(3)	10.9(3)
O(11)	-0.1094(3)	-0.032(1)	0.1267(3)	8.3(3)
O(12)	0.0409(2)	0.2037(8)	0.1167(2)	4.0(2)
C(15)	-0.0501(4)	0.209(2)	0.0849(4)	6.5(4)
C(14)	-0.0051(4)	0.138(1)	0.1186(3)	4.1(3)
C(13)	-0.0154(4)	0.016(1)	0.1469(3)	4.4(3)
C(12)	-0.0658(4)	-0.058(1)	0.1483(4)	5.3(3)
C(11A)	-0.068(1)	-0.219(4)	0.1721(9)	7.5(7)
F(11A)	-0.0201(6)	-0.250(2)	0.2013(5)	7.7(4)
F(12A)	-0.0796(6)	-0.341(2)	0.1503(5)	8.6(4)
F(13A)	-0.1058(6)	-0.205(2)	0.2034(5)	9.2(4)
C(11B)	-0.068(1)	-0.172(3)	0.1874(9)	7.0(7)
F(11B)	-0.1153(7)	-0.252(2)	0.1830(5)	9.7(4)
F(12B)	-0.0580(7)	-0.115(2)	0.2265(6)	11.2(5)
F(13B)	-0.0311(7)	-0.292(2)	0.1851(5)	10.3(4)

atomic coordinates are given in Table 1. The F_o—F_c table and the anisotropic thermal parameters are preserved at the Chemical Society of Japan (Document No. 8347). The computation was performed by a FACOM 230-60 computer at Osaka City University and an ACOS-700 computer at the Crystallographic Research Center of Osaka University by use of the programs in the UNICS[17] and ORTEP.[18]

Results and Discussion

Figures 1 and 2 show the perspective view of the molecule and its projection along the normal of the coordination plane, respectively. Figure 3 gives the view of the P(*o*-tolyl)$_3$ ligand along the M–P vector. Bond lengths and angles are summarized in Table 2. Average values are given for the parameters of CF_3 groups, since these groups have large thermal parameters indicative of a disorder (Table 1) and hence individual structural parameter is of less importance.

The Pd atom lies on a complete plane comprised of 3O and P atoms (Table 3). While one of the two tfac ligands is *O,O'*-chelated in the usual fashion, the other is linked to the metal atom only through the acetyl oxygen atom. Of the two Pd–O bonds constructing the chelate ring, the Pd–O(21) bond is more

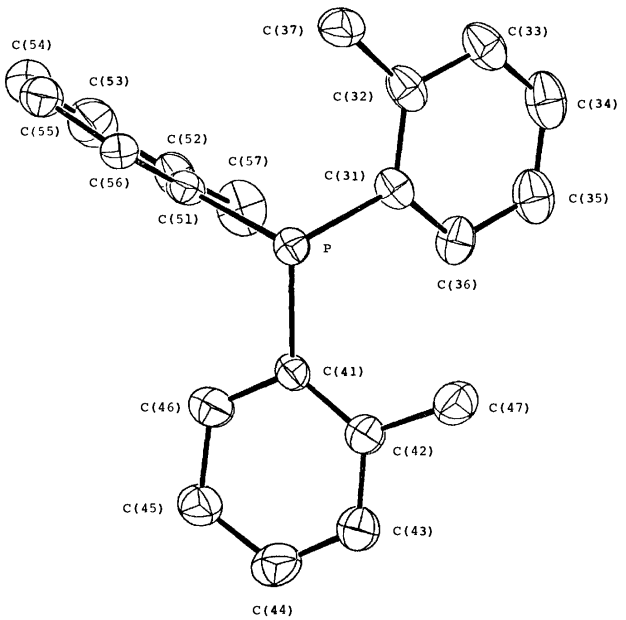

Fig. 3. The structure (30% ellipsoids) of the P(*o*-tolyl)$_3$ ligand viewed along the Pd–P vector.

Table 2. Bond lengths and angles

Bond length	*l*/Å	Bond length	*l*/Å
Pd-P	2.251(3)	P-C(31)	1.822(9)
-O(12)	2.011(6)	-C(41)	1.836(9)
-O(21)	2.041(7)	-C(51)	1.834(10)
-O(22)	1.979(6)		
C(11)-C(12)	A 1.52(3) B 1.53(3)	C(21)-C(22)	1.593(19)
C(12)-O(11)	1.217(12)	C(22)-O(21)	1.276(12)
C(12)-C(13)	1.403(14)	C(22)-C(23)	1.406(14)
C(13)-C(14)	1.372(14)	C(23)-C(24)	1.371(15)
C(14)-O(12)	1.274(11)	C(24)-O(22)	1.308(12)
C(14)-C(15)	1.538(14)	C(24)-C(25)	1.512(15)
C(11)-F	1.35[a]	C(25)-F	1.32[c]

Bond angle	ϕ/°	Bond angle	ϕ/°
O(21)-Pd-O(22)	93.4(3)	Pd-P-C(31)	115.0(3)
P-Pd-O(12)	87.6(2)	Pd-P-C(41)	105.0(3)
P-Pd-O(22)	90.5(2)	Pd-P-C(51)	112.6(3)
Pd-O(12)-C(14)	122.8(6)	C(31)-P-C(41)	108.3(4)
Pd-O(21)-C(22)	122.8(7)	C(31)-P-C(51)	105.8(4)
Pd-O(22)-C(24)	121.1(6)	C(41)-P-C(51)	110.0(4)
C(11)-C(12)-C(13)	A 119(1) B 115(1)	C(21)-C(22)-C(23)	116.1(9)
C(11)-C(12)-O(11)	A 110(1) B 115(1)	C(21)-C(22)-O(21)	115.0(9)
C(13)-C(12)-O(11)	130.1(11)	C(23)-C(22)-O(21)	128.8(10)
C(12)-C(13)-C(14)	125.5(9)	C(22)-C(23)-C(24)	121.5(9)
C(13)-C(14)-O(12)	125.6(8)	C(23)-C(24)-O(22)	132.0(9)
C(15)-C(14)-O(12)	112.9(8)	C(25)-C(24)-O(22)	110.1(9)
C(15)-C(14)-C(13)	121.5(9)	C(25)-C(24)-C(23)	117.9(9)
C(12)-C(11)-F	113[b]	C(24)-C(25)-F	113[d]
F-C(11)-F	106[b]	F-C(25)-F	106[d]

a) Mean value of six C(11)-F distances. b) Mean value of six C-C-F or F-C-F angles. c) Mean value of three C(25)-F distances. d) Mean value of three C-C-F or F-C-F angles.

Table 3. Atom deviation from mean plane and interplanar angle

Atom deviation	*d*/Å
Plane 1	[O(12), O(21), O(22), P] Pd, 0.002(3); O(12), 0.003(7); O(21), −0.003(7); O(22), 0.003(7); P, −0.003(4)
Plane 2	[O(11), O(12), C(12), C(13), C(14), C(15)] O(11), −0.003(12); O(12), −0.009(8); C(12), −0.005(14); C(13), 0.009(13); C(14), 0.005(13); C(15), 0.003(14); C(11A), −0.37(3); C(11B), 0.22(3)
Plane 3	[O(21), O(22), C(21), C(22), C(23), C(24), C(25)] O(21), −0.058(9); O(22), 0.055(9); C(21), 0.032(17); C(22), −0.006(15); C(23), 0.006(15); C(24), 0.016(14); C(25), −0.045(15)

Interplanar angle	φ/°
Plane 1-Plane 2	74.8(4)
[Pd, O(21), O(22)] plane-Plane 3	175.3(4)

than 0.06 Å longer than the other Pd–O(22) bond probably owing to the trans influence of the tertiary phosphine ligand. The unidentate tfac enolate ligand has a planar structure in which the dangling CF_3CO group lies trans to the bonding oxygen around the C=C bond, the torsion angle between the C(14)–C(15) and C(12)–O(11) bonds being 1.1°. The electron density due to the disordered CF_3 group is best interpreted by the model shown in Fig. 1. The C(12)–C(11A) and C(12)–C(11B) bonds make angles 13.1° and 9.4°, respectively, with the [O(11), C(12), C(13)] plane.

Since the chelating tfac ligand is unsymmetric, two geometrical arrangements around the metal atom are conceivable for this complex even if the unidentate tfac ligand is bound to the metal exclusively through the acetyl oxygen. In fact the two isomers exist in equilibrium in $CDCl_3$ and the present isomer (*trans*-[P,O(21)]) is overwhelmingly abundant (>80%) at ambient temperature.[5] As may be imagined from Fig. 2, there exists no severe atom overcrowding in the *cis*-[P,O(21)] isomer either and hence the higher stability of the *trans*-[P,O(21)] isomer seems to stem from some electronic origin. The σ-donating ability of the CH_3CO moiety of the chelating tfac is higher than that of the CF_3CO moiety (*vide infra*) and may strengthen the Pd-phosphine π-bonding.[5]

The planar *O*-unidentate β-diketonate ligand may have either the trans or cis configuration with respect to the C=C bond. By the ^{1}H NMR studies Pinnavaia and his collaborators found that the R_3Si(acac-*O*) complexes are composed of cis and trans isomers in

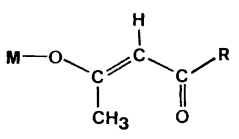

trans

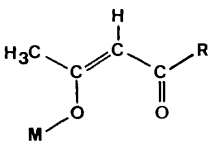

cis

equilibrium and the former is fluxional undergoing the head-to-tail coordinating atom exchange in solution.[19] On the other hand, the acac anions involved in $[Pt(acac\text{-}O)_2(PEt_3)_2]$[11] and $[Pt(acac\text{-}O)_2(piperidine)_2]$[4] have the cis configuration exclusively, exhibiting no fluxional motion. The cis configurations of acac in $[Cr(CO)_5\{PPh(acac\text{-}O)_2\}]$[14] and of hfac in [Cu(acac)(hfac-*O*)(phen)][13] were confirmed by X-ray analysis. The ^1H NMR spectrum of the present complex in $CDCl_3$ also indicated that the *O*-unidentate tfac ligand has the cis configuration[5] in contradiction with the present X-ray structure. The discrepancy between the structures in solution and a crystal can not be reasonably rationalized.

The *O*-unidentate tfac ligand should have a greater contribution from the structure $^-O\text{–}C(CH_3)\text{=}CH\text{–}C(CF_3)\text{=}O$, but no evidence for the π electron localization can be detected. Thus, although the C(12)–O(11) distance is shorter than the C(14)–O(12) distance (Table 2), it can not be the conclusive evidence for the π electron localization since (i) the thermal parameter is larger for O(11) than for O(12) and (ii) no significant difference exists between the C(12)–C(13) and C(13)–C(14) distances. On the contrary, the coplanar disposition of the O(12), C(14), C(15), C(13), C(12), and O(11) atoms is suggestive of some extent of π electron delocalization (Table 3). The nonbonded O(11)···C(15) distance (2.87(2) Å) is noteworthy, since it is considerably shorter than the value expected from the van der Waals radii of the components. Although the unidentate and bidentate tfac ligands differ in configuration, there is no remarkable difference between the corresponding structural parameters.

The enol tautomers of acacH[20] and hfacH[21] in gas phase were found by the electron diffraction method to have the planar symmetric hydrogen-chelate structure.[22] On the other hand, neutron diffraction data confirmed that the enol molecule of 1,3-diphenyl-1,3-propanedione has an asymmetric intramolecular hydrogen bond, the difference in the two O–H bond lengths being 0.199(17) Å.[25] The enol molecule of tfacH should certainly have an asymmetric hydrogen-chelate structure (A) or (B).

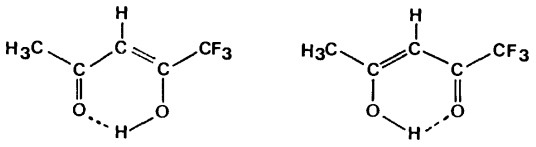

(A) (B)

Takeuchi and his collaborators compared the ^{13}C chemical shifts of the carbonyl carbons in tfacH in several solvents.[26] The intramolecular hydrogen bond retained in nonpolar solvents was supposed to be cleaved in dimethyl sulfoxide (DMSO-d_6) to form an intermolecular hydrogen bond. The signal from the carbonyl carbon adjacent to CH_3 showed a marked upfield shift (5.2 ppm) in DMSO-d_6 as compared with that in $CDCl_3$, while the chemical shift of the carbonyl carbon adjacent to CF_3 showed a minor difference (1.0 ppm) in these solvents. Based on this observation, Takeuchi *et al.* concluded that tfacH has structure (A) rather than (B) in nonpolar solvents.[26] If this structure assignment is correct, the proton affinity of the trifluoroacetyl oxygen (O(11)) must be higher than that of the acetyl oxygen (O(12)), and the tfac anion may be expected to be bound to a metal atom through O(11) when it serves as a unidentate ligand. The coordination mode found for the present complex is contrary to this expectation, the tfac anion being bound to palladium through O(12).

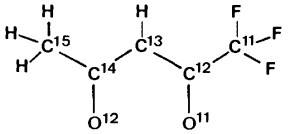

Coordination ability of the oxygen atom in a substituted 2,4-pentanedionate anion is enhanced with increase of the negative net charge on the donor atom, and also with increase of the square of AO coefficient at the oxygen in the σ-type HOMO. These values were calculated by the *ab initio* MO method with the STO-3G minimal base set and the results obtained are shown in Table 4. The negative net charge on either of oxygen atoms in the tfac anion is smaller than that in acac in accordance with higher acidity of tfacH than acacH.[28] In the tfac anion, both the negative charge and AO coefficient in the σ-type HOMO are larger on O(12) than on O(11), indicating that the coordination ability of the acetyl oxygen is higher than that of the trifluoroacetyl oxygen. These results are consistent with the unidentate structure of tfac in Pd^{II} and Pt^{II} complexes observed in crystals and solution.

Table 4. The net charge and AO coefficient in the σ-type HOMO at the oxygen atoms in the 2,4-pentanedionate and 1,1,1-trifluoro-2,4-pentanedionate anions of the *Z,Z*-form[a]

	Net charge on		AO coefficient in the σ-type HOMO at	
	O(11)	O(12)	O(11)	O(12)
acac	−0.374	−0.374	0.6577	0.6577
tfac	−0.346	−0.357	0.6179	0.6847

a) The following geometrical parameters[27] were used in the *ab initio* calculation for the tfac anion; bond lengths (Å): r(C(11)-C(12))=r(C(14)-C(15))=1.51, r(C(12)-C(13))=r(C(13)-C(14))=1.40, r(C(12)-O(11))=r(C(14)-O(12))=1.28, r(C(13)-H)=1.08, r(C(15)-H)=1.09, r(C(11)-F)=1.38; bond angles: CCC=CCO=HC(13)C=120°, HCH=FCF=109.47°

References

1) a) S. Okeya and S. Kawaguchi, *Inorg. Synth.*, **20**, 65 (1980); b) S. Okeya, S. Ooi, K. Matsumoto, Y. Nakamura, and S. Kawaguchi, *Bull. Chem. Soc. Jpn.*, **54**, 1085 (1981).

2) S. Okeya, H. Sazaki, M. Ogita, T. Takemoto, Y. Onuki, Y. Nakamura, B. K. Mohapatra, and S. Kawaguchi, *Bull. Chem. Soc. Jpn.*, **54**, 1978 (1981).

3) S. Okeya, H. Yoshimatsu, Y. Nakamura, and S. Kawaguchi, *Bull. Chem. Soc. Jpn.*, **55**, 483 (1982).
4) S. Okeya, Y. Nakamura, and S. Kawaguchi, *Bull. Chem. Soc. Jpn.*, **55**, 1460 (1982).
5) S. Okeya, Y. Nakamura, and S. Kawaguchi, *Bull. Chem. Soc. Jpn.*, **54**, 3396 (1981).
6) S. Baba, T. Ogura, and S. Kawaguchi, *Bull. Chem. Soc. Jpn.*, **47**, 665 (1974).
7) S. Matsumoto and S. Kawaguchi, *Bull. Chem. Soc. Jpn.*, **53**, 1577 (1980).
8) S. Matsumoto and S. Kawaguchi, *Bull. Chem. Soc. Jpn.*, **54**, 1704 (1981).
9) R. West, *J. Am. Chem. Soc.*, **80**, 3246 (1958).
10) G. S. Hammond, D. C. Nonhebel, and C.-H. S. Wu, *Inorg. Chem.*, **2**, 73 (1963); D. C. Nonhebel, *J. Chem. Soc.*, **1963**, 738.
11) T. Ito, T. Kiriyama, and A. Yamamoto, *Chem. Lett.*, **1976**, 835.
12) S. Okeya, F. Egawa, Y. Nakamura, and S. Kawaguchi, *Inorg. Chim. Acta*, **30**, L319 (1978).
13) N. A. Bailey, D. E. Fenton, M. V. Franklin, and M. Hall, *J. Chem. Soc., Dalton Trans.*, **1980**, 984.
14) J. von Seyerl, D. Neugebauer, G. Huttner, C. Kruger, and Y.-H. Tsay, *Chem. Ber.*, **112**, 3637 (1979).
15) A short communication appeared in S. Ooi, T. Matsushita, K. Nishimoto, Y. Nakamura, S. Kawaguchi, and S. Okeya, *Inorg. Chim. Acta*, **76**, L55 (1983).
16) "International Tables for X-Ray Crystallography," Kynoch Press, Birmingham (1974), Vol. IV.
17) "UNICS," The Crystallographic Society of Japan, Tokyo (1969).
18) C. K. Johnson, ORTEP II, Report ORNL-5138, Oak Ridge National Laboratory, Oak Ridge, TN (1976).
19) J. J. Howe and T. J. Pinnavaia, *J. Am. Chem. Soc.*, **91**, 5378 (1969); T. J. Pinnavaia, W. T. Collins, and J. J. Howe, *ibid.*, **92**, 4544 (1970).
20) A. H. Lowrey, C. George, P. D'Antonio, and J. Karle, *J. Am. Chem. Soc.*, **93**, 6399 (1971).
21) A. L. Andreassen, D. Zebelman, and S. H. Bauer, *J. Am. Chem. Soc.*, **93**, 1148 (1971).
22) Egan *et al.* determined the selected ^{13}C and ^{2}H spin-lattice relaxation times for the enol form of acacH and its perdeuterated analogue and concluded that the intramolecular hydrogen bond in the enolic acacH is of the double minimum type.[23] Brown reported on the basis of the X-ray photoelectron spectroscopic data that the two oxygen atoms in hfacH are inequivalent by virtue of an asymmetric hydrogen bond.[24]
23) W. Egan, G. Gunnarsson, T. E. Bull, and S. Forsén, *J. Am. Chem. Soc.*, **99**, 4568 (1977).
24) R. S. Brown, *J. Am. Chem. Soc.*, **99**, 5497 (1977); R. S. Brown, A. Tse, T. Nakashima, and R. C. Haddon, *ibid.*, **101**, 3157 (1979).
25) R. D. G. Jones, *Acta Cryst., Sect. B*, **32**, 1807 (1976).
26) J. Niwa, M. Yamazaki, and T. Takeuchi, *Chem. Lett.*, **1975**, 707; C. Shibata, T. Takeuchi, M. Yamazaki, and J. Niwa, *Nippon Kagaku Kaishi*, **1978**, 836.
27) L. E. Sutton, "Tables of Interatomic Distances and Configuration in Molecules and Ions," Supplement. The Chemical Society, London (1965).
28) T. Sekine, Y. Hasegawa, and N. Ihara, *J. Inorg. Nucl. Chem.*, **35**, 3968 (1973).

Solvent Effects on Dimerization of Copper(II) Decanoate in Alcohol Solvents

Hiromichi YAMADA,* Ryoji KITAZAKI, and Ikuo KAKIMI
Faculty of Engineering, Gifu University, 1-1, Yanagido, Gifu 501-11
(Received June 6, 1983)

The extraction of copper(II) with decanoic acid in some alcohol solvents was carried out at 25 °C and at 0.1 mol/dm³ ($NaClO_4$) aqueous ionic strength. Alcohols used are cyclohexanol, 1-pentanol, 1-hexanol, and 1-heptanol. In these solvents, monomeric and dimeric copper(II) decanoates are responsible for the extraction. Species involved in each organic phase are CuA_2, Cu_2A_4, and $Cu_2A_4(HA)_2$ (HA: decanoic acid). The dimerization and adduct formation of copper(II) decanoates in each organic phase are written as:

$$2CuA_2 \overset{K_{dim-1}}{\rightleftharpoons} Cu_2A_4$$

$$Cu_2A_4 + 2HA \overset{\beta_{ad,dim}}{\rightleftharpoons} Cu_2A_4(HA)_2$$

The following dimerization and adduct formation constants were obtained: $\log K_{dim-1} = 2.23$ and $\log \beta_{ad,dim} = 0.26$ for cyclohexanol, 2.26 and −0.03 for 1-pentanol, 2.77 and −0.04 for 1-hexanol, and 3.04 and −0.24 for 1-heptanol, respectively.

It is well-known that the dimeric copper(II) carboxylate involving free carboxylic acids, $Cu_2A_4(HA)_2$ is responsible for the extraction of copper(II) with aliphatic carboxylic acids in various inert solvents.[1-6] In the previous paper,[7] it has been shown that copper(II) is extracted with decanoic acid in several inert solvents as dimeric copper(II) decanoate, $Cu_2A_4(HA)_2$, and that the solvent effect on the extraction constants is interpreted in terms of the regular solution theory. In the subsequent paper,[8] the extracted species of copper(II) with decanoic acid in 1-octanol have been established to be not only the dimeric copper(II) decanoates(Cu_2A_4 and $Cu_2A_4(HA)_2$) but also the monomeric ones(CuA_2 and CuA_2HA). Also, the adduct formation and dimerization of copper(II) decanoates in 1-octanol have been mentioned.

The following solvent series, in which the formation of dimeric copper(II) carboxylates becomes more prominent, is reported: water, pyridine<methanol<ethanol, acetone, chloroform, benzene<carbon tetrachloride, dioxane<diethyl ether, and it is remarked that this solvent series can be discussed in terms of the dielectric constant of the solvents and the coordination power of the solvents to the metal or complex ion.[9]

The present paper describes the results of the extraction of copper(II) decanoates in several alcohol solvents. The solvent effect on the dimerization constant of copper(II) decanoate is interpreted in terms of the regular solution theory.

Experimental

Reagents. *Solvents*: 1-Pentanol, 1-hexanol, and 1-heptanol of reagent grade were washed successively first with dilute sodium hydroxide solution, secondly with dilute perchloric acid solution and thirdly with distilled water. Furthermore, they were purified by distillation and saturated with distilled water at 25 °C. Cyclohexanol of reagent grade was purified by distillation and saturated with distilled water at 25 °C.

Copper(II) perchlorate, sodium perchlorate, and decanoic acid were the same as presented previously.[8]

All other reagents were reagent grade and used without further purification.

Procedure. Experiments were carried out in the same manner as was stated in the previous report.[8]

Apparatus. The apparatus were similar to those previously used,[8] except for the use of Orion research microprocessor Ionalyzer 901(Orion Research Inc., U.S.A.) for the determination of hydrogen ion concentration in the aqueous phase.

Results and Discussion

Extraction Equilibrium. As previously described, if a j-merized copper(II) decanoate, $Cu_jA_{2j}(HA)_a$ is extracted into the organic phase, the extraction equilibrium can be expressed as follows:

$$jCu^{2+} + (2j+a)(HA)_o \rightleftharpoons (Cu_jA_{2j}(HA)_a)_o + 2jH^+$$

with the extraction constant:

$$K_{ex(ja)} = \frac{[Cu_jA_{2j}(HA)_a]_o[H^+]^{2j}}{[Cu^{2+}]^j[HA]_o^{(2j+a)}}, \quad (1)$$

where the subscript o refers to the organic phase.

Total concentration of copper in the organic phase, $C_{Cu,o}$ is represented as:

$$C_{Cu,o} = \sum_j \sum_a j[Cu_jA_{2j}(HA)_a]_o$$
$$= \sum_j \sum_a jK_{ex(ja)}[Cu^{2+}]^j[HA]_o^{(2j+a)}[H^+]^{-2j}. \quad (2)$$

It is expected from the results of the extraction of copper(II) with decanoic acid in 1-octanol that the monomer $CuA_2(HA)_a$ and the dimer $Cu_2A_4(HA)_p$ are both responsible for the present extraction systems. Then, the following equation can be derived from Eq. 2:

$$\log C_{Cu,o} - (\log C_{Cu,w} - 2\log[H^+]) = \log K_{ex(1a)} + (2+a)\log[HA]_o + \log\left(1 + \frac{2K_{ex(2p)}}{K_{ex(1a)}}[HA]_o^{(2+p-a)}C_{Cu,w}[H^+]^{-2}\right), \quad (3)$$

where the subscript w refers to the aqueous phase, and $K_{ex(1a)}$ and $K_{ex(2p)}$ represent the extraction constants of the monomer $CuA_2(HA)_a$ and the dimer $Cu_2A_4(HA)_p$, respectively. Then, by comparing the plot of the values of the left-hand side of Eq. 3 against ($\log C_{Cu,w}$—$2\log[H^+]$) at constant $[HA]_o$ with the

normalized curve, $\log(1+X)$ *vs.* $\log X$, we can check the degree of polymerization of the extracted species. The result obtained for 1-hexanol is shown in Fig. 1. As expected, it was proved that the monomeric and dimeric copper(II) decanoates were responsible for the extraction in which 1-hexanol was used as a diluent. For the other alcohols used the same results were obtained.

In the region where the monomer prevails, Eq. 2 is simplified to:

$$\log C_{Cu,o} - (\log C_{Cu,w} - 2\log[H^+]) = \log \sum_a (K_{ex(1a)}[HA]_o^{(2+a)}). \quad (4)$$

According to Eq. 4, we can find the number of decanoic acid molecules involved in the monomer from the slope of the plots of $\{\log C_{Cu,o} - (\log C_{Cu,w} - 2\log[H^+])\}$ against $\log[HA]_o$. The result for 1-hexanol is illustrated in Fig. 2. As evident from Fig. 2, the plot fits well a straight line with a slope of two, that is, $2+a=2$ or $a=0$. The same results were obtained for the other solvents. Consequently, the composition of the monomeric copper(II) decanoate is CuA_2 irrespective of the solvent. The monomeric species CuA_2HA for 1-octanol[8] is not extracted to any appreciable extent in these extraction systems. The extraction constant $K_{ex(10)}$ of the monomer can be determined from Eq. 4($a=0$). The values obtained for the respective solvent are summarized in Table 1 together with the other constants. The previous results for 1-octanol are also included in Table 1 for comparison.

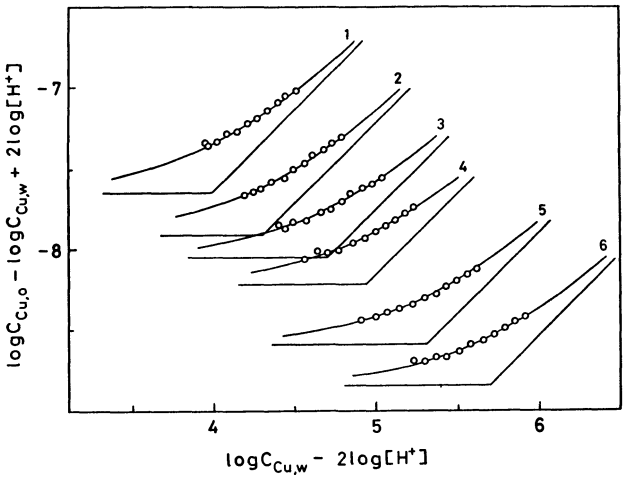

Fig. 1. The identification of the degree of polymerization of Cu(II) decanoates.
Solid curves are the normalized curves, $\log(1+X)$ *vs.* $\log X$. Solid lines are the asymptotes of the normalized curves. C_{HA}; No. 1: 2.0, No. 2: 1.5, No. 3: 1.25, No. 4: 1.0, No. 5: 0.7, No. 6: 0.5 mol/dm^3. Solvent: 1-hexanol.

On the other hand, in the region where the predominant extracted species are the dimer, that is, the plots shown in Fig. 1 fit with the straight line asymptotes with a slope of unity, the following expression is derived from Eq. 2:

$$\log C_{Cu,o} - 2(\log C_{Cu,w} - 2\log[H^+]) = \log 2\sum_p (K_{ex(2p)}[HA]_o^{(4+p)}). \quad (5)$$

According to Eq. 5, the slope of the plot of the left-hand side of Eq. 5 against $\log[HA]_o$ gives the number of decanoic acid molecules involved in the dimeric species. The results for 1-hexanol are shown in Fig. 3. As evident from Fig. 3, at least two dimeric copper(II) decanoates with the different number of decanoic acid molecules are responsible for the extraction. At lower concentration of decanoic acid in the organic phase, the plot is close to a straight line with a slope of 4.0. Therefore, one of the dimers is certainly Cu_2A_4 ($p=0$ in Eq. 5). In addition, the slope of the plot described above gets steeper with the concentration of decanoic acid in the organic phase. It is suggested that another dimer $Cu_2A_4(HA)_p$ ($p \geqq 1$) is responsible for the extraction at higher $[HA]_o$. Then, in the region where the dimer predominates, the fol-

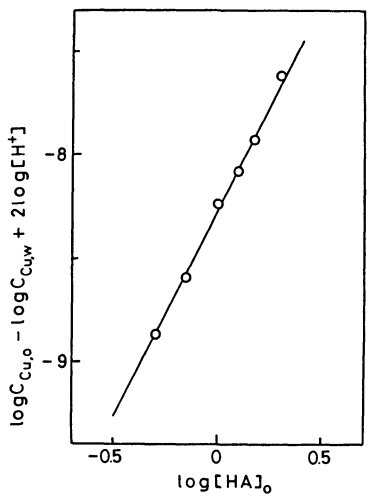

Fig. 2. Determination of the number of decanoic acid molecules involved in the monomeric Cu(II) decanoate.
Solid line is the straight line with a slope of 2.0. Solid line is the straight line with a slope of 2.0. Solvent: 1-hexanol.

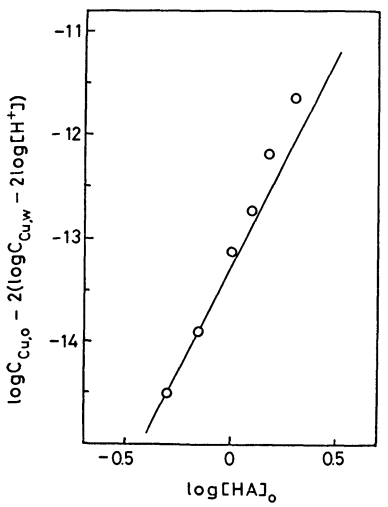

Fig. 3. Determination of the number of decanoic acid molecules involved in the dimeric Cu(II) decanoates.
Solid line is the straight line with a slope of 4.0. Solvent: 1-hexanol.

lowing expression can be written from Eq. 2:

$$C_{Cu,o} = 2([Cu_2A_4]_o + [Cu_2A_4(HA)_p]_o)$$
$$= 2K_{ex(20)}[Cu^{2+}]^2[HA]_o^4[H^+]^{-4} \times\left(1+\frac{K_{ex(2p)}}{K_{ex(20)}}[HA]_o^p\right), \quad (6)$$

which is rewritten as a logarithmic form:

$$\log C_{Cu,o} - 2(\log C_{Cu,w} - 2\log[H^+]) - 4\log[HA]_o$$
$$= \log\left(1+\frac{K_{ex(2p)}}{K_{ex(20)}}[HA]_o^p\right) + \log K_{ex(20)} + \log 2, \quad (7)$$

where $K_{ex(20)}$ and $K_{ex(2p)}$ represent the extraction constants of Cu_2A_4 and $Cu_2A_4(HA)_p$, respectively. Compared the plot of $\{\log C_{Cu,o} - 2(\log C_{Cu,w} - 2\log[H^+]) - 4\log[HA]_o\}$ *vs.* $\log[HA]_o$ with the normalized curves, $\log(1+X^n)$ *vs.* $\log X$, we find the composition of another dimeric copper(II) decanoate. The result for 1-hexanol is shown in Fig. 4. Figure 4 shows that the plot fits well the normalized curve, $\log(1+X^2)$ *vs.* $\log X$, that is, $p=n=2$. Thus, we have $Cu_2A_4(HA)_2$ together with Cu_2A_4 in the organic phase. From Fig. 4 we can also obtain the respective extraction constants, $K_{ex(20)}$ and $K_{ex(22)}$ by fitting the normalized curve to the observed values. In a similar manner as above, it was found that the same dimeric copper(II) decanoates as just described were responsible for the other extraction systems in which 1-heptanol, 1-pentanol, and cyclohexanol were used as solvents.

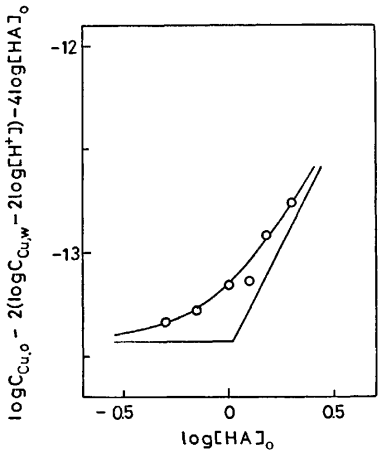

Fig. 4. Determination of the number of decanoic acid molecules involved in the dimeric Cu(II) decanoates by the curve fitting method.
Solid curve is the normalized curve, $\log(1+X^2)$ *vs.* $\log X$. Solid lines are the asymptotes of the normalized curve. Solvent: 1-hexanol.

Consequently, we conclude that the extraction equilibria for the present extraction systems are described as follows:

$$Cu^{2+} + 2(HA)_o \overset{K_{ex(10)}}{\rightleftharpoons} (CuA_2)_o + 2H^+,$$
$$2Cu^{2+} + 4(HA)_o \overset{K_{ex(20)}}{\rightleftharpoons} (Cu_2A_4)_o + 4H^+,$$
$$2Cu^{2+} + 6(HA)_o \overset{K_{ex(22)}}{\rightleftharpoons} (Cu_2A_4(HA)_2)_o + 4H^+.$$

The corresponding extraction constants are summarized in Table 1.

Then, the adduct formation and dimerization of copper(II) decanoates in these alcohol solutions can be described as follows:

$$Cu_2A_4 + 2HA \overset{\beta_{ad,dim}}{\rightleftharpoons} Cu_2A_4(HA)_2,$$
$$2CuA_2 \overset{K_{dim-1}}{\rightleftharpoons} Cu_2A_4.$$

The corresponding adduct formation and dimerization constants can be calculated from the respective extraction constants for each solvent. The results obtained are summarized in Table 1 together with the extraction constants.

Solvent Effects on the Dimerization of Copper(II) Decanoate in the Alcohol Solutions. According to the regular solution theory,[10] the activity of a solute A in a solvent S can be approximated in a dilute solution by the following equation:

$$\ln a_A = \ln \phi_A + \ln(V_s/V_A) + V_A(\delta_s-\delta_A)^2/RT, \quad (8)$$

where ϕ, V, and δ refer to the volume fraction, the molar volume and the solubility parameter, respectively. The molar concentration of a solute A is written as:

$$[A] = 1000\phi_A/V_A. \quad (9)$$

From Eqs. 8 and 9, the following expression can be derived:

$$\log a_A = \log[A] + \log V_s + 0.43V_A(\delta_s-\delta_A)^2/RT - 3. \quad (10)$$

The dimerization constant of copper(II) decanoate,

Table 1. Extraction, dimerization, and adduct formation constants of copper(II) decanoates

	Cyclohexanol	1-Pentanol	1-Hexanol	1-Heptanol	1-Octanol[8]
ε[a]	15.0	13.9	13.3	11.5	10.3
δ[b]/J$^{1/2}$ cm$^{-3/2}$	23.3	22.7	22.0	21.5	21.1
V[c]/cm^3	103	108	125	142	158
$\log K_{ex(10)}$	−8.34	−8.13	−8.25	−8.26	−8.41
$\log K_{ex(11)}$					−8.65
$\log K_{ex(20)}$	−14.45	−14.00	−13.73	−13.48	−13.36
$\log K_{ex(22)}$	−14.19	−14.03	−13.77	−13.72	−13.77
$\log K_{dim-1}$	2.23	2.26	2.77	3.04	3.46
$\log \beta_{ad,dim}$	0.26	−0.03	−0.04	−0.24	−0.41

a) Dielectric constant. b) Solubility parameter. c) Molar volume.

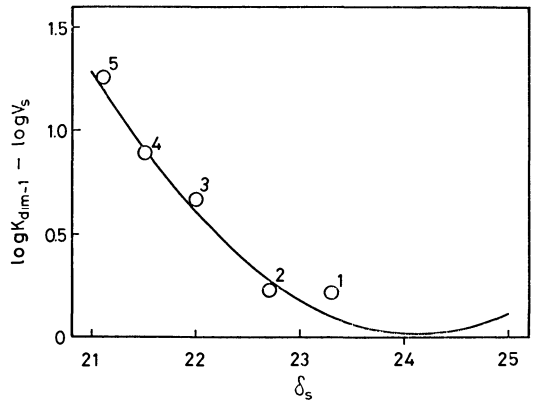

Fig. 5. Estimation of the solubility parameter of Cu(II) decanoate.
Solid line is the calculated curve of the second order with respect to δ_s on the basis of Eq. 12. No. 1: Cyclohexanol, No. 2: 1-pentanol, No. 3: 1-hexanol, No. 4: 1-heptanol, No. 5: 1-octanol.

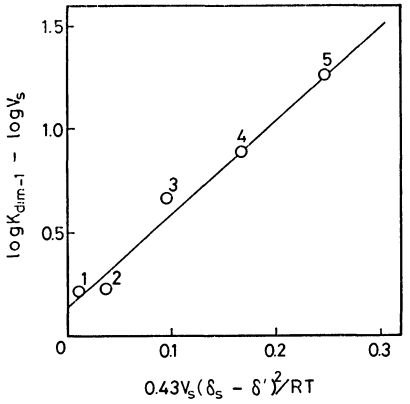

Fig. 6. Correlation of the dimerization constant of Cu(II) decanoate with the solubility parameter of solvents.
Solid line is the straight line with a slope of 4.5. $\delta'=24.1$ ($J^{1/2}/cm^{3/2}$). Numbers are the same as in Fig. 5.

K_{dim-1} is given as follows:

$$\log K_{dim-1} = \log K_{dim-1}^{\circ} + \log \frac{(f_{CuA_2})^2}{f_{Cu_2A_4}}, \qquad (11)$$

where K_{dim-1}° denotes the dimerization constant of copper(II) decanoate in an ideal solution and f's are the activity coefficients of the monomeric and dimeric copper(II) decanoates. If the monomeric and dimeric copper(II) decanoates have the same solubility parameter, we can obtain the following expression from Eq. 10:

$$\log K_{dim-1} - \log V_s = 0.43nV_s(\delta_s-\delta')^2/RT + \log K_{dim-1}^{\circ} - 3, \qquad (12)$$

where n denotes the number of solvent molecules set free in the dimerization of copper(II) decanoate, that is, $nV_s=2V_{CuA_2}-V_{Cu_2A_4}$, and $\delta'=\delta_{CuA_2}=\delta_{Cu_2A_4}$. Although the value of V_s in Eq. 12 varies from solvent to solvent, that of ($\log K_{dim-1}-\log V_s$) can be approximately related to the second order with respect to δ_s. Then it is expected that the value of ($\log K_{dim-1}-\log V_s$) is minimized at $\delta_s=\delta'$. This relationship between ($\log K_{dim-1}-\log V_s$) and δ_s is illustrated in Fig. 5. In Fig. 5, the plot was extrapolated as smooth as possible to find the value of δ', and resulted in $\delta'=24.1$ ($J^{1/2}/cm^{3/2}$). Further, according to Eq. 12, the plot of ($\log K_{dim-1}-\log V_s$) *vs.* $0.43V_s(\delta_s-\delta')^2/RT$ should yield a straight line with a slope of n. As expected, the validity of Eq. 12 is demonstrated in Fig. 6. The values of n and $\log K_{dim-1}^{\circ}$ were calculated to be 4.5 and 3.14, respectively, by the least squares method. Therefore, it is suggested that 4 to 5 molecules of solvent are liberated in the dimerization of copper(II) decanoate.

The authors wish to thank Professor Motoharu Tanaka of Nagoya University for his valuable discussion, and Professor Masateru Mizuta and Dr. Yukio Fujii of Gifu University for their interests in this work.

References

1) D. P. Graddon, *Nature*, **186**, 715 (1960).
2) A. W. Fletcher and D. S. Flett, *J. Appl. Chem.*, **14**, 250 (1964).
3) M. Tanaka and T. Niinomi, *J. Inorg. Nucl. Chem.*, **27**, 431 (1965).
4) W. J. Haffenden and G. J. Lawson, *J. Inorg. Nucl. Chem.*, **29**, 1133 (1967).
5) I. Kojima, M. Uchida, and M. Tanaka, *J. Inorg. Nucl. Chem.*, **32**, 1333 (1970).
6) M. J. Jaycock, A. D. Jones, and C. Robinson, *J. Inorg. Nucl. Chem.*, **36**, 887 (1974).
7) H. Yamada and M. Tanaka, *J. Inorg. Nucl. Chem.*, **38**, 1501 (1976).
8) H. Yamada, S. Suzuki, and M. Tanaka, *J. Inorg. Nucl. Chem.*, **43**, 1873 (1981).
9) M. Kato, H. B. Jonassen, and J. C. Fanning, *Chem. Rev.*, **64**, 99 (1964).
10) J. H. Hildebrand, J. M. Prausnitz, and R. L. Scott, "Regular and Related Solutions," Van Nostrand Reinhold, New York (1970).
11) M. Tanaka, *Z. Phys. Chem. N. F.*, **96**, 239 (1975).

Selective α-Monoalkylation of Phenylacetonitrile Using Alkali Metal Hydroxide Impregnated on Alumina

Kazuaki SUKATA

Nihon Tokushu Kagaku Kogyo Co., Ltd., 3-36, Tohda-cho, Moriguchi, Osaka 570

(Received January 26, 1983)

In the alkylation of phenylacetonitrile with alkyl halides, alkali metal hydroxides impregnated on alumina act as efficient bases for selective α-monoalkylation in benzene. It is proposed that the reaction may take place exclusively in the pore. The selectivity for α-monoalkylation is explained in terms of steric hindrance.

In recent years, processes using inorganic solids have been rapidly developed for organic syntheses.[1] The unique effectiveness of inorganic solids may be due to their large effective surface area, the presence of pores, and the adsorption of reactants.

This paper describes results of the following selective α-monoalkylation of phenylacetonitrile (PAN) with alkyl halides on a chromatographic-grade alumina impregnated with sodium or potassium hydroxide (NaOH/Al_2O_3 or KOH/Al_2O_3):

$$PhCH_2CN + RX \xrightarrow{\text{base}} PhCHRCN + PhCR_2CN. \quad (1)$$

Results and Discussion

In order to elucidate the effect of supports, the alkylation of PAN with ethyl bromide in the presence of different supports impregnated with KOH was carried out in benzene. Table 1 shows the results. The reactivity of KOH/Al_2O_3 was extremely high in comparison with the other solid suppotrs examined and its selectivity for α-monoalkylation was also high. The pore size of Al_2O_3[2] is much larger than those of Mc-lecular Sieves.[3] The surface area of Celite is very small in comparison with those of the other supports. These facts and the present findings suggest that the reaction of $[PhC\bar{H}CN]^-$ or $[PhC\bar{R}CN]^-$ with alkyl halide may take place predominantly in the pore, so that the reactivity of the impregnated KOH may be ascribed to the pore size of the support. The present findings can be interpreted as follows: The pore size of Al_2O_3 is suitable for the reaction,[4] whereas those of Molecular Sieves are too small. In the case of Celite, the reaction is very slow probably because of its small surface area.[5]

Table 1. Alkylation of PAN with ethyl bromide using KOH impregnated on several supports[a]

Support		Yield[b]/% Mono	Di
Molecular Sieve 5A	(60—80 mesh)	<1	—
	(powder)	<1	—
13X	(60—80 mesh)	<1	—
	(powder)	<1	—
Celite[c]	(powder)	3.5	—
Al_2O_3	(70—230 mesh)	91	4

a) Unless otherwise noted, reactions were carried out with KOH (75 mmol)/support (20 g), PAN (10 mmol), ethyl bromide (12 mmol), and benzene (30 mmol) as a solvent at 40 °C for 4 h. b) Determined by GLC with dodecane as an internal standard. c) Fifteen grams of Celite and 40 ml of benzene were used.

Table 2. Alkylation of PAN with ethyl bromide using KOH/Al_2O_3 in several solvents[a]

Solvent	Reaction time/h	Yield[b]/% Mono	Di
Acetonitrile	0.5	69	23
THF	2.0	81	12
Dioxane	2.0	83	4
	4.0	84	6
Benzene	4.0	91	4

a) All reactions were carried out with KOH (75 mmol)/Al_2O_3 (15 g), PAN (10 mmol), ethyl bromide (12 mmol), and a solvent (15 ml) at 40 °C. b) Determined by GLC with dodecane as an internal standard.

In order to reveal the effect of solvents, the alkylation of PAN with ethyl bromide was carried out using KOH/Al_2O_3 in several solvents. Table 2 shows the results. The order of rates of the reaction was acetonitrile > tetrahydrofuran > dioxane ≈ benzene. On the contrary, the order of the selectivities for α-monoalkylation was benzene>dioxane>tetrahydrofuran> acetonitrile. In a nonpolar solvent such as benzene, $[PhC\bar{R}CN]^-$ formed would be strongly adsorbed onto the wall of the pore as the carbanion is directed toward K^+:

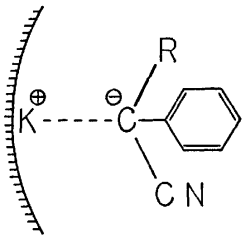

Consequently, the reaction of $[PhC\bar{R}CN]^-$ with the second alkyl halide will be strongly sterically hindered On the other hand, polar solvents would weaken the degree of the interaction, decreasing the degree of the steric hindrance. Also, the reaction in the bulk organic phase should not be ignored when polar solvents are employed.

The influence of the molecular size of alkylating agent was examined by use of the alkylation of PAN with various alkyl halides using KOH/Al_2O_3 or NaOH/Al_2O_3 in benzene. Table 3 summarizes the results. In a phase-transfer alkylation[6] using aqueous alkali

Table 3. Alkylation of PAN using KOH/Al_2O_3 or $NaOH/Al_2O_3$[a]

	Alkyl halide	Reaction Time h	Reaction Temp °C	Yield[b]/% Mono	Yield[b]/% Di
KOH/Al_2O_3	C_2H_5Br	4	40	91	4
	C_2H_5I	2	40	89	6
	C_2H_5I	2	30	92	3
	n-C_3H_7Br	6	40	91	2
	n-C_3H_7I	2	40	92.5	1.5
	n-C_4H_9Br	6	40	94	1.5
	n-C_4H_9I	2	40	94	1
	i-C_3H_7Br	7	40	70	≈0
	i-C_4H_9Br	7	40	68	≈0
	s-C_4H_9Br	7	40	69	≈0
$NaOH/Al_2O_3$	C_2H_5Br	4	40	90	1
	C_2H_5Br[c]	4	40	55	≈0
	C_2H_5I	4	40	64	≈0
	n-C_3H_7Br	6	40	82	≈0
	n-C_3H_7Br[c]	6	40	47	≈0
	n-C_3H_7I	6	40	68	≈0
	n-C_4H_9Br	6	40	79	≈0
	n-C_4H_9Br[c]	6	40	48	≈0
	n-C_4H_9I	6	40	55	≈0

a) All reactions were carried out with KOH or NaOH (75 mmol) / Al_2O_3 (15 g), PAN (10 mmol), alkyl halide (12 mmol), and benzene (15 ml) as a solvent. b) Determined by GLC with dodecane as an internal standard. c) Water was added to NaOH in 15% by weight.

metal hydroxide as a base, formation of *ca.* 10% of α,α-dialkylated products has been unavoidable under a similar molar ratio of alkyl halide to PAN. The alkylation using KOH/Al_2O_3 or $NaOH/Al_2O_3$ gave rapidly and exclusively α-monoalkylated products. In the case of $NaOH/Al_2O_3$, the addition of *ca.* 15% by weight of water to NaOH resulted only in slowing down the reaction. In regard to the selectivity for α-monoalkylation, however, $NaOH/Al_2O_3$ was better than KOH/Al_2O_3. When KOH/Al_2O_3 was employed, the reaction with alkyl iodides was faster than that with alkyl bromides. In contrast to KOH/Al_2O_3, the reaction with alkyl iodides was slower than that with alkyl bromides when $NaOH/Al_2O_3$ was employed. Since the ionic radius of Na^+ is smaller than that of K^+, Na^+ may attract the carbanion formed more closely to the wall of the pore than K^+, increasing to a greater extent the degree of the steric hindrance against the reaction of the carbanion with alkyl halide. It can also be explained in terms of the steric hindrance that the increase in the bulkiness of alkyl groups raises the selectivity for α-monoalkylation. In general, alkyl iodide is slightly better than alkyl bromide with respect to the selectivity for α-monoalkylation. Since alkyl iodide is bulkier than the corresponding alkyl bromide, alkyl iodide would be more sterically hindered than alkyl bromide for the reaction with $[PhC\bar{R}CN]^-$, giving a small amount of α,α-dialkylated product.

Experimental

Materials. Unless otherwise stated, all reagents were obtained commercially and dried with Molecular Sieve 4A. Alumina (Merck Ltd. Type 90 for column chromatography, activity I, 70—230 mesh), Molecular Sieves (for gas chromatography), Celite (for column chromatography), 85% KOH, and NaOH were also obtained commercially and used as obtained.

Impregnation of Alkali Metal Hydroxide on Inorganic Supports. An inorganic support was added to an aqueous alkali metal hydroxide, and the water was removed under reduced pressure at 50 °C. The impregnated reagent was further dried under vacuum (0.1 mmHg)(1 mmHg=133.322 Pa) at 90 °C for 1 h. By this procedure, the NaOH impregnated became nearly anhydrous. However, the KOH impregnated contained *ca.* 15% by weight of water. After the drying of the impregnated reagent for further 7 h, almost no decrease in its weight could be observed.

Typical Procedure for Alkylation of PAN. All the products were known compounds and identified by comparing GLC retention times with those of authentic samples prepared by the literature procedures.[6] A typical procedure is as follows: A mixture of KOH/Al_2O_3 (20.0 g) obtained from 85% KOH (5.0 g, 75 mmol) and Al_2O_3 (15.0 g), PAN (10 mmol), ethyl bromide (12 mmol), and benzene (15 ml) as a solvent was heated at 40 °C for 4 h with vigorous stirring. The yields of α-mono- and α,α-dialkylated products were determined by GLC with dodecane as an internal standard.

The author thanks Nihon Tokushu Kagaku Kogyo Co., Ltd. for permission to publish this article, and also Dr. Nobuaki Wada for useful suggestions during this work.

References

1) G. H. Posner, *Angew. Chem.*, **90**, 527(1978); A. McKillop and D. W. Young, *Synthesis*, **1979**, 401, 481; S. L. Regen, S. Quici, and S-J. Liaw, *J. Org. Chem.*, **44**, 2029 (1979); J. R. Dalton and S. L. Regen, *ibid.*, **44**, 4443 (1979); S. Quici and S. L. Regen, *ibid*, **44**, 3436 (1979); M. O. Brimeyer, A. Mehrota, S. Quici, A. Nigam, and S. L. Regen, *ibid.*, **45**, 4254 (1980); T. Ando, J. Yamawaki, T. Kawate, and T. Hanafusa, *Bull. Chem. Soc. Jpn.*, **55**, 2504 (1982); S. Tamagaki, K. Hotta, and W. Tagaki, *Chem. Lett.*, **1982**, 651; S. Tamagaki, K. Suzuki, and W. Tagaki, *ibid.*, **1982**, 1237.

2) According to Regen *et al.*, the average pore diameter of neutral alumina is 40 Å (80% being<120 Å): S. L. Regen, S. Quici, and M. D. Ryan, *J. Am. Chem. Soc.*, **101**, 7629 (1979).

3) The pore diameters of Molecular Sieves 5A and 13X are 5 and 10 Å, respectively.

4) The impregnated reagent was washed with water until almost all the alkali was recovered and then the amount of the eluted aluminium ion was determined to be *ca.* 4 mol% to the alkali used by the chelatometry using EDTA. This result indicates that the destruction of the pore structure of Al_2O_3 by concentrated aqueous alkali and the action of alkali metal aluminate as the base can be practically ignored under the present experimental conditions.

5) An alternative explanation is as follows. The KOH impregnated on Celite which is an acidic solid support might be neutralized and consequently the reactivity of KOH/Celite might be weakened.

6) E. Chiellini, R. Solaro, and S. D'Anton, *Makromol. Chem.*, **178**, 3165 (1977); E. Chiellini and R. Solar, *J. Org. Chem.*, **43**, 2550 (1978); K. Sukata, *Yuki Gosei Kagaku Kyokai Shi*, **39**, 1132 (1981).

 © 1983 The Chemical Society of Japan Bull. Chem. Soc. Jpn., 56, 3308—3313 (1983) [Vol. 56, No. 11

Pressure Dependence of Carboxypeptidase A Action

Mitsuhiro FUKUDA, Shigeru KUNUGI,* and Norio ISE

Department of Polymer Chemistry, Kyoto University, Sakyo-ku, Kyoto 606

(Received February 21, 1983)

The effect of pressure on the peptide hydrolysis by carboxypeptidase A and its inhibition by several substrate-analogs were investigated. The activation volumes for k_{cat} were -4 and -8 ml mol^{-1} for the hydrolysis of 3-(2-furyl)acryloyl–Gly–L-Phe and 3-(2-furyl)acryloyl–L-Phe–L-Phe, respectively. The reaction volumes for the binding process (ΔV_{ass}) for these dipeptide substrates and for the competitive inhibitors of the peptide hydrolysis (peptide-like inhibitors), such as Gly–L-Tyr and L-Phe, were about 30 ml mol^{-1}. In contrast, ΔV_{ass} values for 3-phenyllactate and L-mandelate, both of which are classified as the noncompetitive inhibitors for the peptide hydrolysis (ester-like inhibitors), were comparably small, 5 and 6 ml mol^{-1}, respectively. Furthermore the pressure dependence of the inhibition by D-Phe or D-mandelate was largely different from that of the corresponding L-form; namely ΔV_{ass} for D-Phe was 4 ml mol^{-1} and that for D-mandelate was 21 ml mol^{-1}. The pH dependence of the inhibition constant was classified into two groups; Gly–L-Tyr and L-Phe inhibited more strongly at higher pH while 3-phenyllactate and others did more effectively at lower pH. Taking into account the previously published result of the X-ray crystallographic studies (*e. g.*, J. A. Hartsuck and W. N. Lipscomb, "The Enzymes," 3rd ed, ed by P. D. Boyer, Academic Press, New York (1971), Vol. 3, p. 1), the present results were accounted for in terms of two different (electrostatic) interactions between the substrate or inhibitor and the active site of the enzyme.

The activation volumes or reaction volumes evaluated from the pressure dependence of chemical reactions often reflect the differences in the reaction mechanisms.[1] These parameters also provide important information on enzyme reaction,[2] as shown by the recent examinations of trypsin[3] or α-chymotrypsin catalysis.[4] By measuring the pressure dependence of enzyme reaction under appropriate experimental conditions, we can obtain the information on volumetric changes occurring in the reaction process, such as those due to changes in charge and bond states at the active site, higher-order structure of protein molecule and the hydration of the enzyme and the substrate. In the present study, we examined pressure dependence of peptide hydrolysis and the binding of several kinds of substrate analogs in bovine carboxypeptidase A (CPA). CPA is a representative zinc-containing metallo-protease, and various kinds of studies, such as primary and three dimensional structures,[5,6] metal substitution,[7,8] chemical modification,[9,10] and cryoenzymolozy,[11] have been carried out to reveal the role of the zinc together with that of other functional amino acid residues in the active site. However, due to the apparent complexities in its catalytic behavior toward peptides and esters or their analogs,[12] the detailed functional roles of these groups and the mode of catalytic functions are still ambiguous. Above all, the multiple binding of the substrate or inhibitor and a difference in the peptidase and esterase actions have prevented the straightforward interpretation of the kinetic data of this enzyme. In order to know much more details of the mechanism, especially to differentiate the mechanisms of the two kinds of enzyme activities, we measured the pressure dependence of kinetic parameters and inhibitory actions for several substrates and inhibitors.

Experimental

Materials. Bovine carboxypeptidase A (Cox) was purchased as an aqueous suspension with toluene preservative from Sigma Chemical Co., (St. Louis, Missouri, USA) (lot 119c8030). It was washed three times with cold deionized water followed by centrifugation and finally dissolved in 0.05 M Hepes buffer containing 1 M NaCl (1 M=1mol dm^{-3}). The enzyme concentration was determined spectrophotometrically at 25 °C, using ε=64200 at 280 nm.[13] 3-(2-Furyl)acryloylglycyl-L-phenylalanine (FuaGlyPhe), FuaGlyLeu and FuaPhePhe were synthesized according to the method in the literature.[14] FuaGlyPhe; mp 184—185 °C, Found; C, 62.93; H, 5.30; N, 8.12%. Calcd for $C_{18}H_{18}N_2O_5$: C, 63.15; H, 5.26; N, 8.18%. FuaGlyLeu; mp 202—204 °C, Found; C, 58.58; H, 6.56; N, 9.04%. Calcd for $C_{15}H_{20}N_2O_5$: C, 58.44; H, 6.49; N, 9.09%. FuaPhePhe; mp 203—205 °C, Found; C, 66.88; H, 5.87; N, 6.22%. Calcd for $C_{25}H_{24}O_5N_2\cdot H_2O$: C, 66.65; H, 5.82; N, 6.22%. Thinlayer chromatography on Kieselgel 60E (E. Merck, Darmstadt, West Germany) using chloroform–methanol–acetic acid (20:1:1) and/or 1-butanol–acetic acid–water–pyridine (15:10:12:3) showed a single UV quenching spot for each substrate. Inhibitors used were as follows ; Gly-L-Tyr, L-Phe, ZPhe (Protein Research Foundation, Osaka), L-2-hydroxy-3-phenylpropionic acid (3-phenyllactate), L-mandelate, D-mandelate (Aldrich, Milwaukee, Wisconsin, USA), 3-phenylpropionate, D-Phe (Wako Pure Chemicals, Osaka), L-Phe–L-Phe (Vega, Tucson, Arizona, USA). Good's buffers ; Mes, Hepes, and Taps were from Dojin Chem. Lab. (Kumamoto).

Methods. The rate of substrate hydrolysis was measured by following the absorbance change at around 340 nm due to the scission of the *C*-terminal peptide bond of Fua substituted amino acid, analogous to the case of thermolysin.[15,16] The difference extinction coefficient at 340 nm was determined as 870 (M^{-1} cm^{-1}) for FuaPhePhe and 830 (M^{-1} cm^{-1}) for FuaGlyPhe. An ultraviolet-visible spectrophotometer with a Drickamer type high pressure optical cell was used as previously described.[3] When the kinetics seem to follow a simple Michaelis-Menten scheme including only a competitive product inhibition, the steady-state rate expression is given by

$$v = -\mathrm{d}[S]/\mathrm{d}t = k_{cat}[E][S]/(K_m(1+([S]_0-[S])/K_p)+[S]), \quad (1)$$

where t is time, $[S]_0$ is the initial substrate concentration, [S] is the substrate concentration at time t, K_p is the product inhibitory constant and k_{cat} and K_m have their usual meanings.

In order to measure the second order rate constant (k_{cat}/

K_m), the substrate concentration is set sufficiently low with respect to both K_m and K_p, and Eq.1 is reduced to

$$v = -d[S]/dt = k_{cat}[E][S]/K_m. \quad (2)$$

In our experimental conditions, 0.03—0.05 mM FuaGlyPhe, Eq.2 is always satisfied (see results). The observed k_{cat}/K_m from the pseudo-first-order conditions (Eq. 2) is about 98% (pH 5—8), 95% (pH8—9), and 93% (pH above 9) confidence level. K_i values were measured under the condition of $[S]_0 \ll K_m$, K_p, where we cannot distinguish competitive and noncompetitive modes and therefore the inhibition constant was obtained from Eq. 3.

$$1 + [I]/K_I = (k_{cat}/K_m)_{[I]=0}/(k_{cat}/K_m)_{app}. \quad (3)$$

In the study of pH dependence, 0.05 M Hepes, 0.05 M Taps or 0.02 M Mes containing 0.33 M NaCl was used. At such a concentration the buffer dependence of the reaction was not significant.

The pressure dependence of pH of these buffers was examined according to the method of Neuman *et al.*[17] Hepes, Taps and Mes were rather pressure independent as was the case with Tris–HCl. The pH value given in this paper is the corrected one for the pressure dependence. Pressure dependence of K_i was measured in Hepes buffer at 270, 500, 750, and 1000 atm against the hydrolysis of FuaGlyPhe. In the case of L-Phe, FuaGlyLeu was also used as the substrate to avoid the influence of the product inhibition by L-Phe produced from FuaGlyPhe, since the K_p of L-Phe becomes markedly low at pH above 8, as shown in the results section. The change in the concentration of the solute in the solution under high pressure was corrected as previously reported.[3] The nonlinear regressions were carried out following the principle given in the literature.[18]

Results

Kinetic Parameters. First we examined the effect of pressure on the acid-base equilibria of the enzyme active site (Fig. 1) by using pseudo-first-order rate measurement with a substrate of poor K_m values (FuaGlyPhe). The pH dependence of k_{cat}/K_m at 25 °C, 1 atm showed a bell-shaped profile, as was previously reported for the hydrolysis of tripeptide substrate.[19] Under 1000 atm, though the activity was lower by a factor of three than that at 1 atm, a similar simple bell-shaped pH profile was obtained. By increasing pressure, the pK_{a1} shifted toward lower pH (from 6.04 to 5.72) and pK_{a2} changed in the same direction to a less extent (from 9.10 to 8.98). Though, in general, there can be a number of factors which may complicate the pH dependence of the enzyme and several mechanisms which can fit the result obtained, the simplest mechanism to explain these pH dependences is as follows:

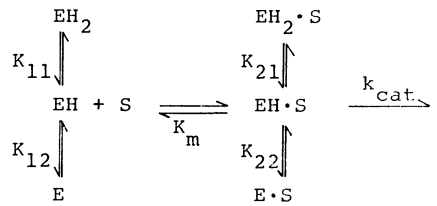

Scheme 1. K_{ij} means the proton dissociation constant for each species.

Then the observed two pK_a's are corresponding to the acid-base equilibria of the free enzyme (K_{11}, K_{12}), which shifted to the deprotonated state with an increase in pressure. We can estimate ΔV values for these deprotonation processes from the pK_a shifts; 18±5 ml mol^{-1} for pK_{a1} and 6±3 ml mol^{-1} for pK_{a2}. The following measurement under high pressure, therefore, was carried out at pH around 7 to minimize the influence from these pK_a shifts. FuaGlyPhe showed a substrate activation at high substrate concentration as shown in Fig. 2-a, similar to some other dipeptide

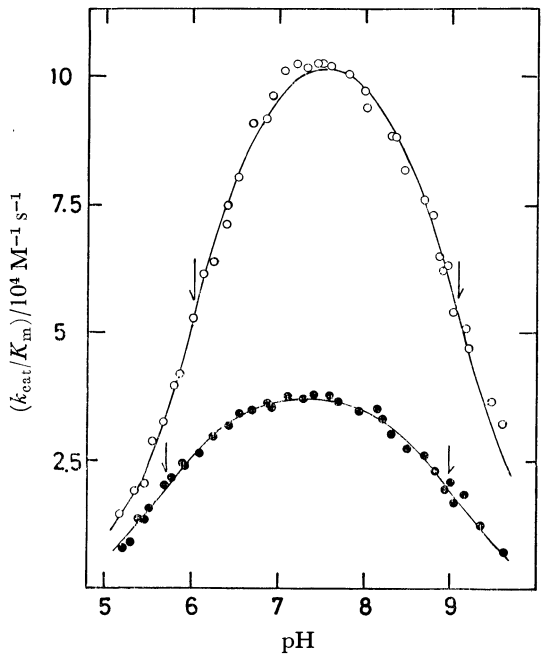

Fig. 1. The pH dependence of k_{cat}/K_m for FuaGlyPhe hydrolysis, (○) 1 atm, (●) 1000 atm. [FuaGlyPhe]=0.03—0.05 mM, [E]=(1—3)×10^{-7} M, 25 °C. 0.02 M Mes (pH 5.2—7.2), 0.05 M Hepes (pH 6.5—8.2), 0.05 M Taps (pH 7.5—9.5), NaCl 0.5 M. Arrows indicate the position of pK_a.

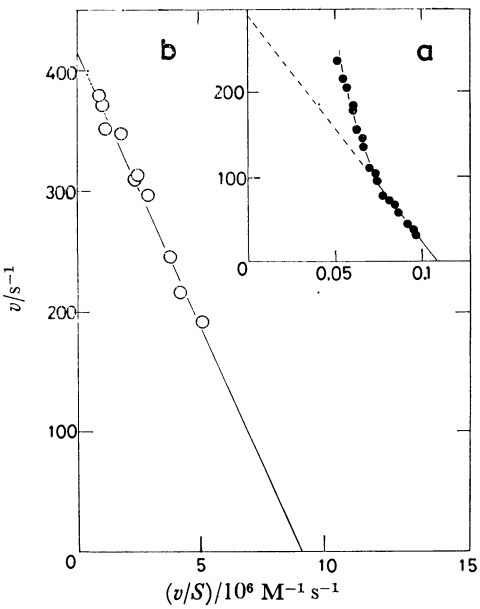

Fig. 2. Eadie plots for hydrolysis of FuaGlyPhe (a), and FuaPhePhe (b). 0.05 M Hepes, 0.33 M NaCl, pH 7.35, 25 °C.

substrates reported in the literature.[20] On the contrary, FuaPhePhe did exhibit neither substrate activation nor substrate inhibition within the concentration range studied here and its reactivity was considerably high (Fig. 2-b).

The hydrolytic rate of Fua–Phe was found to be very slow and its contribution was safely neglected in the interpretation of the observed rate process for FuaPhePhe. Table 1 shows k_{cat}, K_m, and k_{cat}/K_m at different pressures. The logarithms of these parameters were in linear relations with pressure and the activation and reaction volumes given in this paper were calculated at 1 atm.

The temperature dependence of k_{cat} and K_m was also studied for FuaPhePhe between 10 to 35 °C (in 0.05 M Hepes, 0.33 M NaCl pH 7.3). The thermodynamic parameters calculated are; $\Delta H^* = 8.0$ kcal mol^{-1} (1 cal=4.184 J) and $\Delta S^* = -20$ cal deg^{-1} mol^{-1} for k_{cat} and $\Delta H = 1.7$ kcal mol^{-1} and $\Delta S = 25$ cal deg^{-1} mol^{-1} for K_m^{-1}. The ΔH_{a1} value for pK_{a1} obtained from the temperature dependence of the pH profile of k_{cat}/K_m was about 4 kcal mol^{-1} for FuaGlyPhe hydrolysis.

Inhibition Constants. Figure 3 shows the pH dependence of the inhibition constants for various inhibitors. In order to prevent the complex multiple binding of these inhibitors on CPA,[21] the concentration of inhibitors were set below 1.5 fold of K_i over the whole range of pH examined. Under this condition, the [I] *vs.* [I]/K_i plot gave straight lines. As shown in Figs. 3-a and 3-b, K_i of GlyTyr, L-Phe and D-Phe increased as the pH became lower, and for GlyTyr, K_i showed a minimum at pH 8.5. On the contrary, the K_i values of 3-phenyllactate, L-madelate (Fig. 3-c), D-mandelate, 3-phenylpropionate and ZPhe (3-d) increased with pH increase. The profile of the last three were quite similar but the first two showed

TABLE 1. KINETIC PARAMETERS FOR PEPTIDE HYDROLYSIS BY CPA

Pressure atm	For FuaGlyPhe[a]			For FuaPhePhe[b]		
	k_{cat} / s^{-1}	K_m / 10^{-5} M	k_{cat}/K_m / 10^4 M^{-1} s^{-1}	k_{cat} / s^{-1}	K_m / 10^{-5} M	k_{cat}/K_m / 10_4 M^{-1} s^{-1}
1	85±2	52±3	16±1.3	410±10	4.6±0.2	980±60
500	91±4	98±8	9.3±0.8	480±20	8.3±0.5	580±40
1000	100±10	180±20	5.5±0.4	570±35	15±2	390±30
ΔV or $\Delta V^{\ddagger}$	−4±2	31±2		−8±2	30±3	

a) In 0.1 M Hepes, 0.1 M NaCl, pH 7.35, 25 °C. b) In 0.05 M Hepes, 0.33 M NaCl, pH 7.35, 25 °C.

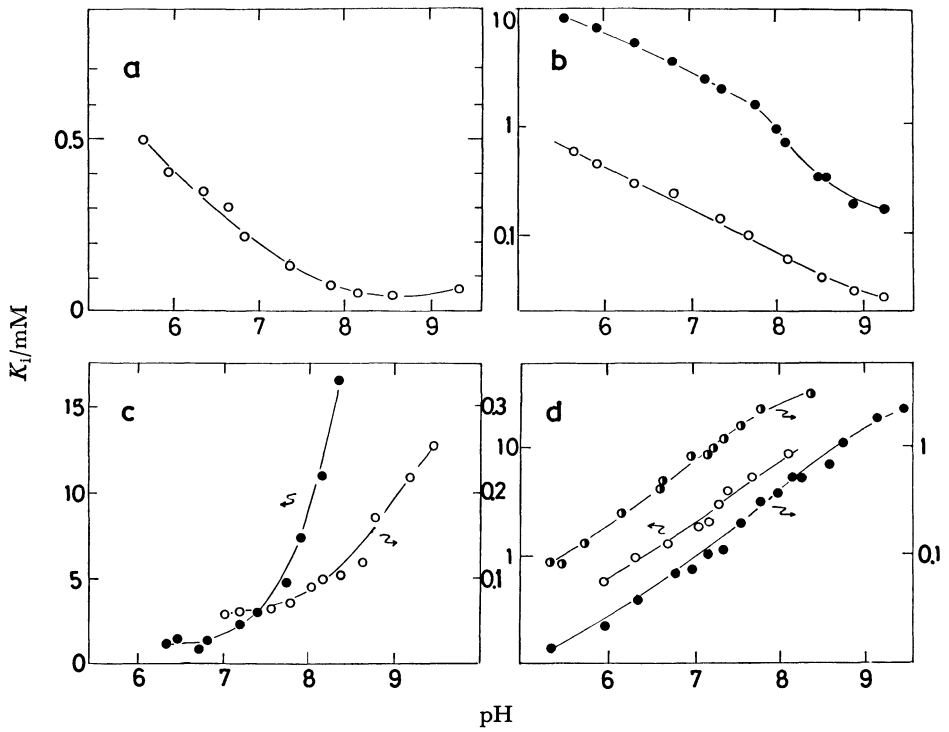

Fig. 3. pH dependence of K_i at 25 °C.
(a) GlyTyr (b) L-Phe (●), D-Phe (○) (c) 3-phenyllactate (○), L-mandelate (●) (d) ZPhe (◑), 3-phenylpropionate (●), D-mandelate (○), 0.02 M Mes, 0.05 M Hepes, or 0.05 M Taps, 0.33 M NaCl.

some characteristic features.

We note that the inhibitors of zwitter-ion type showed K_i decreasing with increasing pH while those having only carboxylate as the ionic residue showed K_i increasing with increasing pH. This classification is similar to that observed in the inhibitor interaction with thermolysin.[16] The fundamental feature of the pH dependence of the K_i of these zinc proteases, therefore, seems to be determined by the relation of the net charges of the inhibitor and the active site of the enzyme in both instances.

The pressure dependence of K_i was measured at pH around 7 (Table 2). Though, for some inhibitors which do not show maxima or minima around this pH, the measured pressure dependences involve influences

Table 2. Reaction volumes and inhibition constants of several substrate analogs[a]

Inhibitor	ΔV_{ass}/ml mol^{-1} [b]	$K_i/10^{-4}$ M
GlyTyr	33±2	1.3±0.1
PhePhe	34±5[c]	6.3±0.8
ZPhe	27±1[d]	11±1
L-Phe	23±1	23±2
D-Phe	4.0±0.5	1.4±0.1
3-Phenyllactate	5.1±1.0	0.64±0.03
3-Phenylpropionate	12±2	1.3±0.2
L-Mandelate	5.8±1.5[e]	33±2
D-Mandelate	21±3	13±2

a) Pressure dependence measured at pH 7.3, 0.05 M Hepes, 0.33 M NaCl, 25 °C unless otherwise mentioned. K_i's at pH 7.35, 0.05 M Hepes, 0.33 M NaCl, 25 °C, 1 atm. FuaGlyPhe was used as the substrate except for the case with L-Phe (see experimental). b) Volume change according to the complex formation. c) At pH 7.80. d) At pH 6.60. e) At pH 6.70.

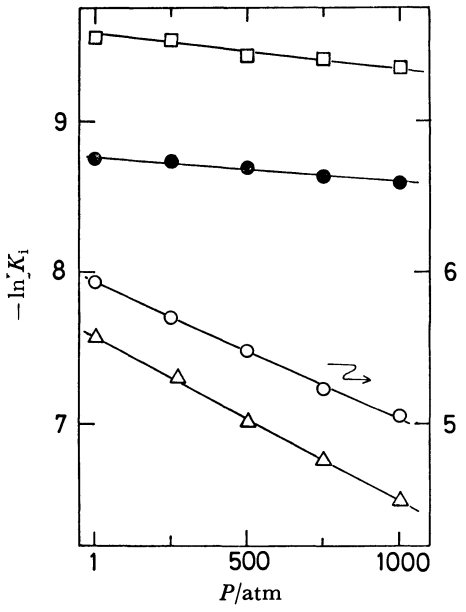

Fig. 4. Pressure dependence of K_i. Hepes 0.05 M, NaCl 0.33 M, pH 7.35 except for ZPhe (pH 6.60), 25 °C. (□) 3-phenyllactate, (●) D-Phe, (○) L-Phe, (△) ZPhe.

from the pK_a shifts of the residues which control the binding process of these inhibitors, the logarithm of the observed K_i values were in good linear relations to pressure as shown in Fig. 4. Inhibitors of CPA have been grouped into two; one such as GlyTyr acts competitive towards peptidase activity[20] and the other such as 3-phenylpropionate acts noncompetitive towards peptidase but competitive towards esterase.[7,20] By considering the structure of the inhibitors presently used and the inhibition studies on the related substances,[21,22] we understand that PhePhe, ZPhe and L-Phe fall in the former category (peptide-like inhibitors) while 3-phenyllactate and L-mandelate do in the latter (ester-like inhibitors). For the apparent reaction volumes of the formation process of the complex (ΔV_{ass}) we notice that the former group gave considerably large values, similar to that for the binding of the peptide substrates, FuaGlyPhe and FuaPhePhe, while the latter gave smaller values. We also notice that D-isomers of Phe and mandelate gave ΔV_{ass} values quite in contrast to the corresponding L-isomers.

Discussion

Assignment of Catalytic Group. From the pH dependences of the kinetic parameters of CPA, there have been arguments on the ionic state of the active site amino acid residues.[22-25] Based on the X-ray crystallographic studies of this enzyme which binds GlyTyr, three interpretations were given so far for the origin of the pK_{a1}: The ionization of the water molecules coordinated on Zn; the dissociation of a Zn–His bond followed by pH effects associated with His 69 or His 196; the interactions of the charged residue(s) (probably Glu 270) in the active site.[6] The measured ΔH_{a1} for the pK_{a1} process (4 kcal mol^{-1}) is comparable to the corresponding values (≈3 kcal mol^{-1}) reported for the hydrolysis of ZGlyGlyVal and ZGlyGlyLeu.[25] These values are intermediate between those reported for a free carboxyl (±1 kcal mol^{-1}) and a free imidazole or a water coordinated on zinc (6—7 kcal mol^{-1})[26-28] The presently obtained ΔV_{a1} value is apparently comparable to the ΔV value reported for a free carboxyl group (≈15 ml mol^{-1}).[27] Thus the ΔH_{a1} and ΔV_{a1} might give different interpretations. In general, ΔV has strong correlation with ΔS for various reactions in solution[2] and hence the problem is equivalent to telling which of the enthalpic and entropic factors plays a dominant part to determine the unusual (perturbed) pK_a values in the active site of the enzyme. The accumulated data on the thermodynamic measurement of the pK_a's of various acids in mixed solvents[28] tell us that, by changing the solvent composition, the entropic term varies significantly and the enthalpic one does partly compensate this change. This allows us to say that, at least in the case of pK_a, the enthalpic parameter is less influenced by the perturbation of the environments and it is better to assume the nature of the dissociative residues on the basis of this term. Then the value of ΔH_{a1} (3—4 kcal mol^{-1}) is considered to reflect the contributions from both carboxyl group and the H_2O on the zinc. In the hydrolysis by ther-

molysin, which is a microbial zinc protease similar to CPA with respect to the amino acid components of the active site and showed ΔH_{a1} of $\simeq$8 kcal,[16] there were two possible functional groups which dominated the pK_{a1}; the imidazol of His231 and the proton-sharing combination of the carboxylate of Glu and the zinc-coordinated water. Taking the absence of histidine residue in the active site of CPA into consideration, we can consider the latter is the case for the group controlling the pK_{a1} in the present enzyme.

Two Binding Modes of Inhibitors and Substrates. The X-ray crystallographic studies suggested that Arg-145, Glu270, Tyr248, and zinc ion at the active site are important in the CPA catalysis.[12] There have been many studies concerning the roles of these residues in the peptidase and esterase activities. A mechanistic difference between these two types of catalyses was inferred in most of the studies; *e.g.* different influence of metal substitution or metal extraction on the binding and/or catalytic processes of two types of the substrates[30] and a different influence of the chemical modification of the Arg residue.[9] One interpretation of these results was that the carboxyl group of the ester substrates interacts with zinc ion in the binding process while the carbonyl group of the peptide substrate does so during the hydrolytic process.[8] That is, in the binding process of peptide substrate, the Arg145 residue is considered to interact electrostatically with the terminal carboxylate. Such a purely electrostatic interaction is similar to the one observed in the substrate binding process of trypsin and its homologous proteases. Judging from the result on the pressure dependence of trypsin catalysis[3] and of other low molecular weight ionic associations[29] a fairly large and positive volume change is expected for such an association. In fact the pressure dependence of K_m^{-1} gave a large and positive ΔV_{ass} ($+30$ ml mol^{-1}) and the ΔV_{ass}'s for the peptide-like inhibitors such as GlyTyr, PhePhe, L-Phe, and ZPhe were also positive and large. In contrast, fairly small ΔV_{ass} values were observed for the binding of ester-like inhibitors such as 3-phenyllactate and L-mandelate. These smaller ΔV_{ass} values, then, would be related to the interaction of terminal carboxylate directly with the zinc ion instead of the guanidinium cation of Arg145. (Though these ester-like inhibitors behave noncompetitive to the peptidase activity, their competitive actions on ester one[22,23] and other physicochemical studies[6,30,31] comfirmed direct interaction of these inhibitors with the active site of enzyme.) The interaction of divalent metal ion with various carboxylic acids in aqueous solution has shown relatively small ΔV values (<10 ml mol^{-1}) as known in the literature.[29] Thus the present result gives strong support for the interpretation of Auld and Holmquist.[7] However it cannot exclude the possibility that such a direct coordination of terminal carboxylate to the zinc ion is limited to the case of ester-like *inhibitor* interacting with the active site where the peptide *substrate* is already located on the Arg residue and that the ester *substrate* might be bound in a similar manner to the peptide substrate.[32,33]

D-Phe showed a considerably different ΔV_{ass} value from L-form and this can be interpreted by the scheme

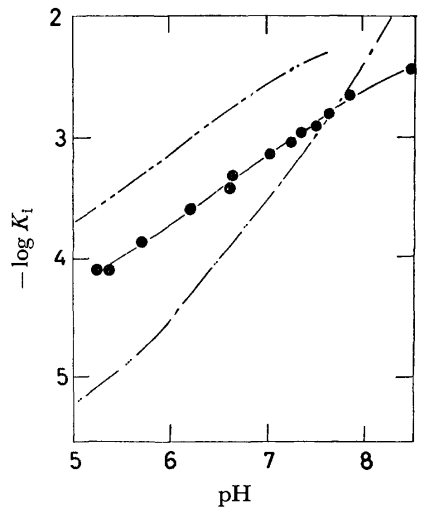

Fig. 5. Comparison of pH dependences of inhibitions by ZPhe for thermolysin and CPA.
●: Inhibition of CPA by ZPhe (taken from Fig. 3-d), ——: inhibition of thermolysin by ZPhe (taken from Ref. 16), – – – –: inhibition of thermolysin by ZLeuGly (taken from Ref. 16).

given by Lipscomb[34] that the terminal carboxylate of D-Phe does not interact with Arg but directly to zinc ion, just like the ester-type inhibitor. In fact D-Phe gave a ΔV_{ass} value which can be classfied into the latter. On the contrary D-form of mandelate showed a larger ΔV_{ass} value than L-form and in this case the D-isomer would interact with Arg residue just like peptide-like inhibitors.

pH-Dependent Alternation of Binding Modes. In the inhibition of thermolysin, ZPhe showed a very strong pH dependence and it was related to the direct interaction of terminal carboxylate of this inhibitor with zinc ion at a relatively low pH.[16,35] The inhibition of CPA by this inhibitor is less pH dependent as compared in Fig. 5 but it resembles the binding of the dipeptidyl inhibitor (ZLeuGly)[16] or tripeptidyl substrate (Fua-GlyLeuAla) (Fukuda *et al.*, unpublished result) on thermolysin. In the latter instances the pH profile can be interpreted as that the inhibitor or substrate interacts with the active site in a productive (normal) manner at neutral pH, while at lower pH it interacts in a nonproductive (reversed) manner just like ZPhe interaction with carboxylate coordinating on zinc. The situation seems analogous in the case of ZPhe interaction with CPA. At pH 7, where the pressure dependence was measured, the interaction of this inhibitor is normal and similar to the peptide substrate but at lower pH it would undergo a direct interaction with zinc ion and would have a character of ester-like inhibitor. D-Mandelate and 3-phenylpropionate showed fundamentally similar pH dependences to ZPhe and therefore a similar explanation can be valid for these inhibitors. Especially in the case of 3-phenylpropionate, we notice a ΔV_{ass} value of an intermediate between two extremes. Though this inhibitor behaved as a noncompetitive one for the peptidase,[7] a stopped-flow study revealed that an analogous inhibitor, phenylacetate, interacted with CPA in a mixed manner.[36]

Thus we can expect that the present intermediate ΔV_{ass} value of 3-phenylpropionate comes from two types of interactions. When the alternation of two binding modes occurs at relatively higher pH, as in these two instances, intermediate values of the parameters are observed even in ordinary measuring conditions. To substantiate this explanation further, we are measuring the pH dependence of ΔV_{ass} for these inhibitors.

References

1) T. Asano, Abstracts of the 23rd High Pressure Conference of Japan, p. 358 (1982).
2) K. J. Laidler and P. S. Bunting, "The Chemical Kinetics of Enzyme Reaction," 2nd ed, Clarendon Press, Oxford (1973), Chap.7.
3) S. Kunugi, M. Fukuda, and N. Ise, *Biochim. Biophys. Acta*, **704**, 107 (1982).
4) a) Y. Taniguchi and K. Suzuki, *Bull. Chem. Soc. Jpn.*, **53**, 1709 (1980); b) S. Makimoto, Y. Taniguchi, and K. Suzuki, Abstract of the 23rd High Pressure Conference of Japan, p. 328 (1982).
5) P. H. Petra and H. Neurath, *Biochemistry*, **10**, 3171 (1971).
6) W. N. Lipscomb, J. A. Hurtsuck, G-N. Reeke, F. A. Quiocho, P. H Bethge, M. L. Ludwig, T. A. Steitz, H. Muirhead, and J. C. Coppola, *Brookhaven Symp. Biol.*, **21**, 24 (1968).
7) D. S. Auld and B. Holmquist, *Biochemistry*, **13**, 4355 (1974).
8) H. E. Van Wart and B. L. Valle, *Biochemistry*, **17**, 3385 (1978).
9) J. F. Riordan, *Biochemistry*, **12**, 3915 (1973).
10) J. Suh and E. T. Kaiser, *J. Am. Chem. Soc.*, **98**, 1940 (1976).
11) M. W. Makinen, K. Yamamura, and E. T. Kaiser, *Proc. Natl. Acad. Sci. U.S.A.*, **73**, 3882 (1976).
12) F. A. Quiocho and W. N. Lipscomb, *Adv. Protein Chem.*, **25**, 1 (1971).
13) R. T. Simpson, J. F. Riordan, and B. L. Vallee, *Biochemistry*, **2**, 616 (1963).
14) S. Blumberg and B. L. Vallee, *Biochemistry*, **14**, 2410 (1975).
15) J. Feder, L. R. Bougham, and B. S. Wildi, *Biochemistry*, **13**, 1186 (1974).
16) S. Kunugi, H. Hirohara, and N. Ise, *Eur. J. Biochem.*, **124**, 157 (1982).
17) R. C. Neuman, Jr., W. Kauzman, and A, Zipp, *J. Phys. Chem.*, **77**, 2687 (1973).
18) D. W. Marquardt, *J. Sos. Ind. Appl. Math.*, **11**, 431 (1963).
19) D. S. Auld and B. L. Vallee, *Biochemistry*, **9**, 4352 (1970).
20) a) R. C. Davies, J. F. Riordan, D. S. Auld, and B. L. Vallee, *Biochemistry*, **7**, 1090 (1968); b) D. S. Auld and B. L. Vallee, *Biochemistry*, **9**, 602 (1970).
21) B. L. Vallee, J. F. Riordan, J. L. Coombs, D. S. Auld, and M. Sokolvsky, *Biochemistry*, **7**, 3574 (1968).
22) P. L. Hall, B. L. Kaiser, and E. T. Kaiser, *J. Am. Chem. Soc.*, **91**, 485 (1969).
23) F. W. Carson and E. T. Kaiser, *J. Am. Chem. Soc.*, **88**, 1212, (1966).
24) E. T. Kaiser and B. L. Kaiser, *Acc. Chem. Res.*, **5**, 219 (1972).
25) D. S. Auld and B. L. Vallee, *Biochemistry*, **10**, 2892 (1971).
26) J. T. Edsall and J. C. Wyman, "Biophysical Chemistry," Academic Press, New York (1958), Vol. 5, p. 456.
27) P. Woolley, *Nature (London)*, **258**, 677 (1975).
28) R. M. Izatt and J. J. Christensen, "Handbook of Biochemistry and Molecular Biology," 3rd ed, ed by G. D. Fasman, CRC Press, Cleaveland (1976), Phys. Chem. Data, Vol.1, p.151.
29) T. Asano and W. J. le Nobel, *Chem. Rev.*, **78**, 407 (1978).
30) J. E. Coleman and B. L. Vallee, *Biochemistry*, **3**, 1874 (1964).
31) G. Navon, R. G. Shulman, B. J. Wyluda, and T. Yamane, *J. Mol. Biol.*, **51**, 15 (1970).
32) W. W. Cleland, *Adv. Enzymol. Relat, Areas Mol. Biol.*, **45**, 273 (1977).
33) D. C. Ress and W. N. Lipscomb, *Proc. Natl. Acad. Sci. U.S.A.*, **78**, 5455 (1981).
34) W. N. Lipscomb, *Tetrahedron*, **30**, 1725 (1974).
35) W. R. Kester and B. W. Matthews, *Biochemistry*, **16**, 1506 (1977).
36) D. S. Auld, A. S. Latt, and B. L. Vallee, *Biochemistry*, **11**, 4994 (1972).

A Rubrene Problem. Reaction of 3,3,4,4-Tetrabromo-1,2-bis(diphenylmethylene)cyclobutane and Dichloroacetic Acid

Fumio Toda,* Michio Sasaoka, Yozo Todo, Kunio Iida, Toru Hino, Yasuaki Nishiyama, Hideo Ueda,† and Tokio Ōshima†

Department of Industrial Chemistry, Faculty of Engineering, Ehime University, Matsuyama 790

† *Central Research Laboratory, Ube Industries, Ltd., Ube 755*

(Received March 10, 1983)

Heating of 3,3,4,4-tetrabromo-1,2-bis(diphenylmethylene)cyclobutane in dichloroacetic acid afforded bridge-head olefin, 7-bromo-1,4,8-triphenyl-2,3-benzobicyclo[3.3.0]octa-2,4,7-trien-6-one, and spiroketone, 2-bromo-2′,3-diphenylspiro[1*H*-indene-1,1′(4′*H*)-naphthalen]-4′-one (**13**). Mechanism of the reaction was discussed. X-Ray structural study of the spiroketone **13** was also reported.

Formation of the bisallyl diradical intermediate (**2a**) in dimerization of chlorotriphenylallene (**1a**) or in thermal ring-cleavage of 3,4-dichloro-3,4-diphenyl-1,2-bis(diphenylmethylene)cyclobutane (**3a**) is the key-step of the *rubrene reaction* which finally gives so-called *rubrene*, 5,6,11,12-tetraphenylnaphthacene (**4a**).[1] We studied thermal reaction of 3,3,4,4-tetrabromo-1,2-bis-(diphenylmethylene)cyclobutane (**3b**)[2] in expectation of the formation of 5,11-dibromo-6,12-diphenylnaphthacene (**4b**) via the bisallyl diradical intermediate (**2b**), and we found that **3b** is thermally stable but heating of **3b** in dichloroacetic acid affords bridge-head olefin, 7-bromo-1,4,8-triphenyl-2,3-benzobicyclo-[3.3.0]octa-2,4,7-trien-6-one (**8a**) and spiroketone, 2-bromo-2′,3-diphenylspiro[1*H*-indene-1,1′(4′*H*)-naphthalen]-4′-one (**13**).

Heating of **3b** in dichloroacetic acid at 120 °C for 1 h gave **8a** and **13** in 30 and 36% yields, respectively. Plausible reaction pathways are shown in Scheme 1. Intermediacy of **5** and **6** was proven by preparing these by separate method. Heating of **3b** in benzene containing a small amount of conc H_2SO_4 under reflux for 7 h gave 7,8,8-tribromo-2,5,5-triphenyl-3,4-benzobicyclo[4.2.0]octa-1,3,6-triene (**5**) in 44% yield. Treatment of **5** with $AgClO_4$ in THF–MeOH gave 7,8-dibromo-5-methoxy-2,5,6-triphenyl-3,4-benzobicyclo[4.2.0]octa-1,3,7-triene (**6b**) in 81% yield. Heating of **5** in dichloroacetic acid for 30 min at 120 °C gave **8a** and **13** in 32 and 35% yields, respectively. Similar heating of **6b** gave **8a** in 88% yield. In the reaction of **5**, rearrangement of phenyl group which leads to **6** is probably competing with that of bromine atom which does to **9**. This was clarified by the reaction of the chloro-analog of **3a** (**3c**) in dichloroacetic acid which gives only the chloro-analog of **8a** (**8b**) in 90% yield. Much easier rearrangement of Br than Cl on four-membered ring has been reported.[3] Formation of cyclopropenyl-substituted indene intermediate such as **11** seems to be necessary for the conversion of **3** into **13**.

Due to distorted bridge-head olefinic linkage, **8** is reactive and shows interesting reactions. $KMnO_4$ oxidation of **8a** occurred vigorously at room temperature and 2-bromo-1,3,4-triphenylnaphthalene (**17**)[4] was obtained in 60% yield. A plausible reaction pathway is shown in Scheme 2. Ring-reconstruction of the carbonium ion intermediate (**14**) which was initially formed by an attack of hydroxyl cation on the distorted double bond of **8a** gives cyclic diketone (**16**) *via* **15**, which on decarbonylation finally affords **17**. Michael-type additions of MeOH by a base-catalyzed reaction and of benzene by an $AlCl_3$-catalyzed one to **8a** easily gave 7-bromo-4-methoxy-1,4,8-triphenyl-2,3-benzobicyclo[3.3.0]octa-2,7-dien-6-one (**18a**) and 7-bromo-1,4,4,8-tetraphenyl-2,3-benzobicyclo[3.3.0]octa-2,7-dien-6-one (**18b**), respectively.

From the viewpoint of structural resemblance of **13** to one bioactive component of *Cannabis sativa L*, cannabispirenone-B (**19**),[5] studies of crystal structure of **13** are interesting subjects. X-Ray crystallographic

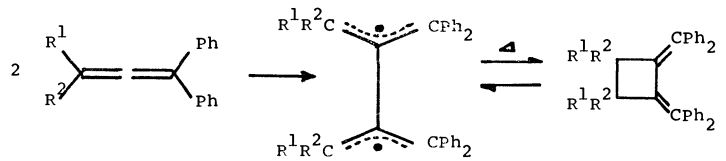

1 **2** **3**

a : R^1=Ph, R^2=Cl

b : R^1=R^2=Br

c : R^1=R^2=Cl

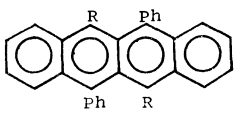

4

a : R=Ph

b : R=Br

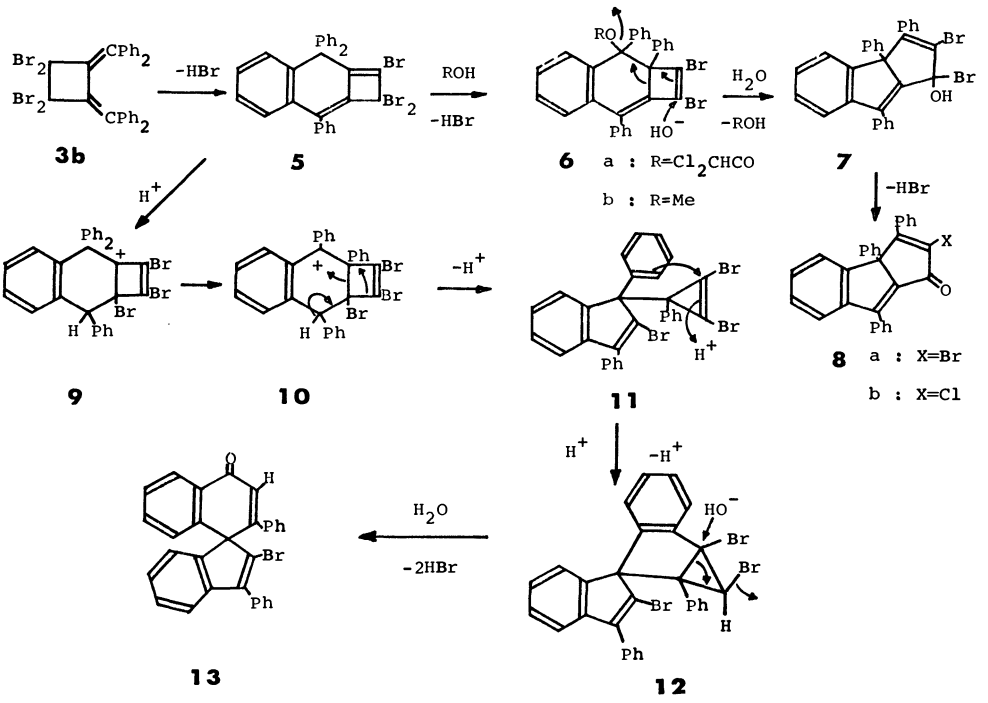

Scheme 1.

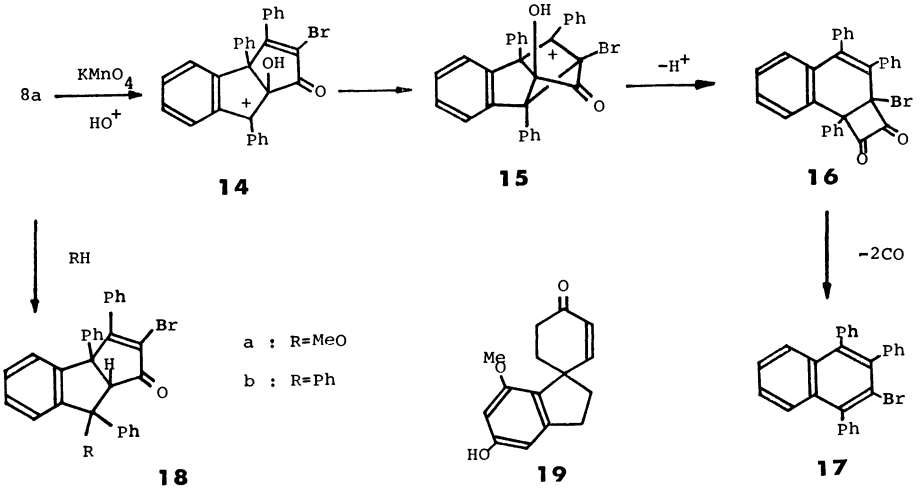

Scheme 2.

data are shown in Tables 1—5, and perspective view of **13** is shown in Fig. 1. Angles between the following two ring planes are shown in parentheses, A–C (55.3), B–C (3.6), C–E (89.6), D–F (50.4), and E–F (6.0°). These data show that two spiro rings are almost perpendicular each other. Distances between Br and the following atoms are shown in parentheses, C6 (3.42), C10 (3.37), C15 (3.79), and C25 (3.62 Å). However, absolute configuration of **13** was not determined.

Experimental

All the melting points are uncorrected. The IR, UV, and NMR spectra were measured in Nujol mull, $CHCl_3$, and $CDCl_3$, respectively. The mass spectra were obtained with an ionization energy of 75 eV.

*Thermal Reaction of 3,3,4,4-Tetrabromo- (**3b**) and 3,3,4,4-Tetrachloro-1,2-bis(diphenylmethylene)cyclobutane (**3c**) in Dichloroacetic Acid.* A solution of **3b** (5.6 g) in dichloroacetic acid (100 ml) was heated at 120 °C for 1 h. The crude solid obtained by addition of water to the reaction mixture was filtered and dried. Recrystallization of the solid from ethyl acetate gave yellow and colorless crystals, which were separated mechanically. Recrystallization of the former from ethyl acetate gave **8a** (1.14 g, 30%) as yellow prisms, mp 185—186 °C; IR 1690 cm^{-1} (C=O); UV 244 (23,400), 289 (14,100), and 364 nm (ε, 8900); ^{13}C NMR δ 70.5 (CPh); MS (*m/e*) 476 and 474 (M^+). Found: C, 75.73; H, 3.85%. Calcd for $C_{30}H_{19}OBr$: C, 75.80; H, 4.03%. Recrystallization of the latter from ethyl acetate gave **13** (1.37 g, 36%) as colorless needles, mp 197—198 °C; IR 1645 cm^{-1} (C=O); UV 243 (23,400), 270sh (15,600), and 283 nm (ε, 16,200); ^{13}C NMR δ 65.0 (spiro C); S (*m/e*) 476 and 474 (M^+). Found: C, 75.59; H, 4.11%. Calcd for $C_{30}H_{19}OBr$: C,

Table 1. Atomic coordinates and e.s.d.'s ($\times 10^4$) of non hydrogen atoms

Atom	x	y	z
Br	5646(1)	2502(1)	338(1)
O	7797(5)	449(3)	6571(7)
C(1)	4092(5)	2378(4)	1447(6)
C(2)	2729(5)	2744(3)	987(6)
C(3)	1880(5)	2439(5)	2208(6)
C(4)	2795(5)	1884(3)	3431(7)
C(5)	4360(5)	1832(3)	3111(7)
C(6)	5560(5)	2240(3)	4640(7)
C(7)	6736(6)	1788(4)	5795(8)
C(8)	6856(7)	875(4)	5530(8)
C(9)	5841(7)	520(4)	3913(8)
C(10)	4752(6)	935(3)	2735(8)
C(11)	371(5)	2576(6)	2203(7)
C(12)	9830(6)	2152(4)	3482(9)
C(13)	776(6)	1603(4)	4713(8)
C(14)	2263(6)	1476(4)	4696(9)
C(15)	5470(7)	3092(4)	4953(9)
C(16)	6542(7)	3496(4)	6292(9)
C(17)	7736(7)	3047(5)	7391(3)
C(18)	7802(6)	2191(4)	7166(8)
C(19)	2127(6)	3363(3)	−441(7)
C(20)	1575(7)	4116(4)	−20(9)
C(21)	1013(7)	4702(4)	−1360(11)
C(22)	990(7)	4522(5)	−3099(10)
C(23)	1529(8)	3784(5)	−3506(8)
C(24)	2107(7)	3204(4)	−2169(8)
C)25)	3931(6)	540(3)	1013(8)
C(26)	2380(7)	548(4)	327(9)
C(27)	1691(8)	141(5)	−1266(10)
C(28)	2555(8)	−260(4)	−2177(9)
C(29)	4095(9)	−264(5)	−1552(10)
C(30)	4793(11)	133(5)	78(14)

Table 2. Atomic parameters ($\times 10^3$) and isotropic temperature factors of hydrogen atoms

Atom	x	y	z	β/Å
H(9)	602(8)	0(5)	359(10)	4.2(19)
H(11)	−74	263	213	3.7
H(12)	1092	216	348	3.7
H(13)	−30	161	479	3.7
H(14)	296(6)	118(4)	540(8)	1.3(13)
H(15)	460(8)	336(5)	432(10)	3.8(18)
H(16)	639(7)	406(4)	661(9)	3.1(16)
H(17)	852(8)	335(4)	822(10)	4.0(18)
H(18)	876(7)	184(4)	796(9)	3.0(16)
H(20)	158(7)	417(4)	135(9)	2.1(14)
H(21)	44(9)	525(5)	−105(10)	5.0(20)
H(22)	56(7)	495(4)	−412(8)	2.5(16)
H(23)	151(7)	369(4)	−487(9)	2.8(15)
H(24)	253(6)	278(4)	−253(8)	2.5(15)
H(26)	172(7)	82(4)	87(9)	3.2(17)
H(27)	51(7)	15(4)	−174(9)	2.9(17)
H(28)	205(7)	−53(5)	−322(10)	3.9(18)
H(29)	488(8)	−59(5)	−199(10)	5.1(20)
H(30)	585(7)	11(4)	44(9)	3.5(17)

Table 3. Bond lengths and e.s.d.'s of non-hydrogen atoms

Bond length	l/Å	Bond length	l/Å
Br -C(1)	1.871(6)	O -C(8)	1.216(8)
C(1) -C(2)	1.332(8)	C(1) -C(5)	1.532(8)
C(2) -C(3)	1.473(9)	C(2) -C(19)	1.481(7)
C(3) -C(4)	1.400(9)	C(3) -C(11)	1.396(12)
C(4) -C)5)	1.521(8)	C(4) -C(14)	1.385(8)
C(5) -C)6)	1.527(8)	C(5) -C(10)	1.530(8)
C(6) -C(7)	1.399(8)	C)6) -C(15)	1.393(9)
C(7) -C(8)	1.486(9)	C(7) -C(18)	1.391(9)
C(8) -C(9)	1.460(9)	C(9) -C(10)	1.330(9)
C(10)-C(25)	1.490(9)	C(11)-C(12)	1.410(11)
C(12)-C(13)	1.409(9)	C(15)-C(16)	1.380(10)
C(16)-C(17)	1.388(10)	C(17)-C(18)	1.385(10)
C(19)-C(20)	1.383(9)	C(19)-C(24)	1.372(9)
C(20)-C(21)	1.395(11)	C(21)-C(22)	1.388(11)
C(22)-C(23)	1.352(11)	C(23)-C(24)	1.390(10)
C(25)-C(26)	1.369(9)	C(25)-C(30)	1.380(13)
C(26)-C(27)	1.393(10)	C(27)-C(28)	1.363(11)
C(28)-C(29)	1.355(11)	C(29)-C(30)	1.410(14)

Table 4. Bond angles and e.s.d.'s of non-hydrogen atoms

Bond angle	ϕ/°	Bond angle	ϕ/°
Br -C(1) -C(2)	127.0(5)	Br -C(1) -C(5)	119.6(4)
C(2) -C(1) -C(5)	113.3(5)	C(1) -C(2) -C(3)	107.5(5)
C(1) -C(2) -C(19)	128.4(5)	C(3) -C(2) -C(19)	124.2(5)
C(2) -C(3) -C(4)	109.5(6)	C(2) -C(3) -C(11)	130.1(7)
C(4) -C(3) -C(11)	120.2(67)	C(3) -C(4) -C(5)	109.3(5)
C(3) -C(4) -C(14)	121.9(6)	C(5) -C(4) -C(14)	128.8(5)
C(1) -C(5) -C(4)	100.1(5)	C(1) -C(5) -C(6)	109.4(5)
C(1) -C(5) -C(10)	111.3(5)	C(4) -C(5) -C(6)	110.5(6)
C(4) -C(5) -C(10)	111.3(5)	C(6) -C(5) -C(10)	113.4(5)
C(5) -C(6) -C(7)	122.7(5)	C(5) -C(6) -C(15)	119.5(5)
C(7) -C(6) -C(15)	117.8(5)	C(6) -C(7) -C(8)	119.5(5)
C(6) -C(7) -C(18)	120.3(6)	C(8) -C(7) -C(18)	120.2(6)
O -C(8) -C(7)	121.6(6)	O -C(8) -C(9)	121.6(6)
C(7) -C(8) -C(9)	116.8(6)	C(8) -C(9) -C(10)	125.4(6)
C(5) -C(10)-C(9)	120.4(6)	C(5) -C(10)-C(25)	119.2(5)
C(9) -C(10)-C(25)	120.4(6)	C(3) -C(11)-C(12)	117.8(8)
C(11)-C(12)-C(13)	121.2(7)	C(12)-C(13)-C(14)	120.3(6)
C(4) -C(14)-C(13)	118.8(5)	C(6) -C(15)-C(16)	122.0(6)
C(15)-C(16)-C(17)	119.7(7)	C(16)-C(17)-C(18)	119.3(7)
C(7) -C(18)-C(17)	120.8(6)	C(2) -C(19)-C(20)	119.2(5)
C(2) -C(19)-C(24)	121.5(5)	C(20)-C(19)-C(24)	119.4(6)
C(19)-C(20)-C(21)	119.3(6)	C(20)-C(21)-C(22)	120.0(7)
C(21)-C(22)-C(23)	120.5(8)	C(22)-C(23)-C(24)	119.5(7)
C(19)-C(24)-C(23)	121.3(6)	C(10)-C(25)-C(26)	123.8(6)
C(10)-C(25)-C(30)	117.7(7)	C(26)-C(25)-C(30)	118.6(7)
C(25)-C(26)-C(27)	120.4(7)	C(26)-C(27)-C(28)	120.5(7)
C(27)-C(28)-C(29)	120.6(7)	C(28)-C(29)-C(30)	119.1(8)
C(25)-C(30)-C(29)	120.9(9)		

75.80; H, 4.03%.

When a solution of **3c** (5.22 g) in dichloroacetic acid (100 ml) was heated at 120 °C for 1 h and the reaction mixture was worked up as above, **8b** (3.87 g, 90%) was obtained as yellow prisms, mp 189—191 °C; IR 1695 cm^{-1} (C=O); UV 240 (20,500), 295 (13,200), and 360 nm (ε, 9100). Found C, 83.38; H, 4.33%. Calcd for $C_{30}H_{19}OCl$: C,

Table 5. Deviations of the atoms from the least-squares planes

Plane A[a]		Plane B[b]		Plane C[c]		Plane D[d]	
C(2)	−0.002 Å	C(10)	0.015 Å	C(6)	−0.020 Å	C(3)	0.007 Å
C(19)	0.001	C(25)	−0.009	C(7)	0.004	C(4)	−0.009
C(20)	−0.003	C(26)	−0.016	C(15)	0.016	C(11)	−0.002
C(21)	0.005	C(27)	0.064	C(16)	0.004	C(12)	−0.000
C(22)	−0.004	C(28)	0.014	C(17)	−0.021	C(13)	−0.002
C(23)	−0.001	C(29)	−0.008	C(18)	0.017	C(14)	0.007
C(24)	0.004	C(30)	−0.003	C(8)[e]	−0.006	H(14)[e]	0.040
H(20)[e]	−0.061	H(26)[e]	−0.033	O[e]	0.103	C(2)[e]	−0.078
H(21)[e]	−0.140	H(27)[e]	0.014	C(9)[e]	−0.224	C(1)[e]	−0.158
H(22)[e]	−0.012	H(28)[e]	0.047	C(10)[e]	−0.313	C(5)[e]	−0.037
H(23)[e]	0.025	H(29)[e]	0.113	C(25)[e]	−0.723	Br[e]	−0.330
H(24)[e]	0.113	H(30)[e]	−0.011	C(5)[e]	−0.037	C(19)[e]	−0.042
				H(15)[e]	0.155		
				H(16)[e]	0.160		
				H(17)[e]	−0.126		
				H(18)[e]	−0.059		

The equation of plane is: $0.9017X+0.3990Y-0.0920Z-3.930=0$. b) The equation of plane is: $-0.2029X-0.8477Y+0.5273Z+1.035=0$. c) The equation of plane is: $-0.7690X-0.1649Y+0.8078Z+1.541=0$. d) The equation of plane is: $0.1259X+0.7591Y+0.5781Z-4.176=0$. e) Omitted from the least-squares plane calculation.

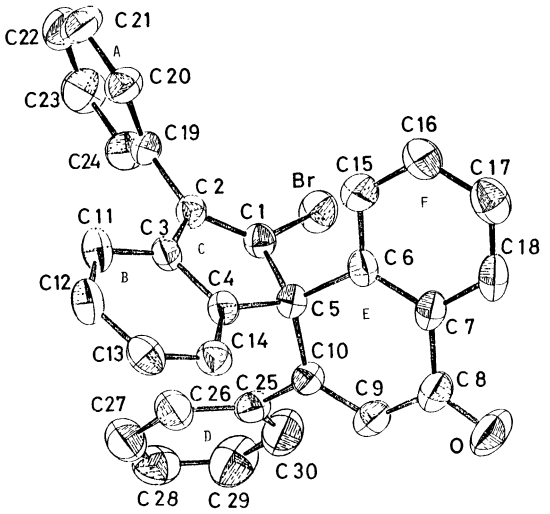

Fig. 1. Perspective view of **13** and the crystallographic numbering of carbon atoms.

83.62; H, 4.41%.

Synthesis of 7,8,8-Tribromo-2,5,5-triphenyl-3,4-benzobicyclo[4.2.0]octa-1,3,6-triene (5). A solution of **3b** (1.36 g) in benzene (35 ml) containing a small amount of conc H_2SO_4 was heated under reflux for 7 h. The crude product remained after evaporation of the solvent was recrystallized from acetone to give **5** (0.53 g, 44%) as colorless prisms, mp 159—160 °C; UV 326 (12,600) and 252 nm (ε, 21,400); MS (*m/e*) 622, 620, 618, and 616 (M^+). Found: C, 58.47; H, 2.86%. Calcd for $C_{30}H_{19}Br_3$: C, 58.19; H, 3.07%.

Synthesis of 7,8-Dibromo-5-methoxy-2,5,6-triphenyl-3,4-benzobicyclo[4.2.0]octa-1,3,7-triene (6b). A solution of **5** (0.4 g) in THF–MeOH (3:1, 20 ml) was treated with $AgClO_4$ (0.4 g) at room temperature. Excess $AgClO_4$ was decomposed with NaCl and filtered. The crude product remained after evaporation of the solvent of the organic layer was extracted with ether. The ether solution was washed with water and dried over Na_2SO_4. Crystals obtained from the ether solution were recrystallized from acetone–$CHCl_3$ (1:1) to give **6b** (0.3 g, 81%) as colorless prisms, mp 215—216.5 °C; IR 1075 cm^{-1} (ether); ^1H NMR δ 2.79 (s, MeO) and 6.3—7.8 (m, Ph). Found: C, 65.21; H, 3.81%. Calcd for $C_{31}H_{22}OBr$: C, 65.26; H, 3.86%.

Thermal Reaction of 5 and 6b in Dichloroacetic Acid. A solution of **5** (3.1 g) in dichloroacetic acid (50 ml) was heated at 120 °C for 1 h. The reaction mixture was worked up as done for the thermal reaction mixture of **3b** in dichloroacetic acid, and **8a** (0.76 g, 32%) and **13** (0.83 g, 35%) were obtained. When **6b** (0.1 g) was heated in dichloroacetic acid (10 ml) at 120 °C for 30 min and then worked up as above, **8a** (0.075 g, 88%) was obtained.

Potassium Permanganate Oxidation of 8a. When $KMnO_4$ (0.5 g) was added to a solution of **8a** (0.1 g) in acetone (10 ml), exothermic reaction occurred. After 3 h, excess $KMnO_4$ was decomposed with MeOH, and MnO_2 was filtered. Crude product remained after the evaporation of the solvent of acetone solution was recrystallized from acetone to give **17** (0.55 g, 60%) as colorless prisms, mp 244—245 °C (lit,[4] 245 °C). IR spectrum was identical to that of the authentic sample.[4]

Base-catalyzed Addition of MeOH to 8a. A solution of **2** (1.0 g) in THF (10 ml) was added to 5% KOH–MeOH (30 ml) and then heated under reflux for 1 h. Crude product remained after the evaporation of the solvent was washed with water, dried, and recrystallized from ethyl acetate to afford **18a** (0.95 g, 84%) as pale yellow prisms, mp 215—217 °C; IR 1710 cm^{-1} (C=O); UV 288 (18,600) and 358 nm (ε, 900); ^1H NMR δ 2.98 (s, MeO), 3.57 (s, CH), and 6.5—7.5 (m, Ph); MS (*m/e*) 508 and 506 (M^+). Found: C, 73.10; H, 4.35%. Calcd for $C_{31}H_{23}O_2Br$: C, 73.38; H, 4.54%.

$AlCl_3$-catalyzed Addition of Benzene to 8a. A mixture of **8a** (1.0 g), benzene (20 ml), and $AlCl_3$ (1.0 g) was stirred at room temperature for 3 h. The reaction mixture was decomposed with water and extracted with benzene. The benzene solution was washed with dil HCl and water, and dried over Na_2SO_4. Crude crystals obtained by the evaporation of the solvent were recrystallized from ethyl acetate to give **18b** (1.05 g, 90%) as colorless prisms, mp 255 °C; IR 1710 cm^{-1} (C=O); UV 215 (43,300) and 285 nm (ε,

8500); ^{1}H NMR δ 4.2 (s, CH) and 6.6—7.6 (m Ph); MS (*m/e*) 554 and 552 (M^+). Found: C, 77.82; H, 4.39%. Calcd for $C_{36}H_{25}OBr$: C, 77.93; H, 4.52%.

X-Ray Analysis of ***13***. A crystal used for the intensity measurement was $0.3\times0.2\times0.2$ mm^3. Intensity data were obtained on a Rigaku four-circle automatic diffractometer, equipped with graphite-monochromated Cu $K\alpha$ radiation, and using the $2\theta/\omega$ scan technique ($2\theta\leqq130°$). Two thousands sixty one independent reflections of $F_o\geqq3\sigma(F_o)$ were corrected for Lorentz and polarization factors but not for absorption.

Crystal data: $C_{30}H_{19}OBr$, monoclinic, $P2_1$, $Z=2$, $a=9.139(2)$, $b=16.020(3)$, $c=7.838(4)$ Å, $\beta=106.2(1)°$, $D_c=1.433$ g cm^{-3}, $\mu=3.2$ mm^{-1} (for Cu $K\alpha$)

The structure was solved by the heavy atom method. The positions of hydrogen atoms were located from the difference Fourier map. The positional and thermal parameters were refined by the block-diagonal least-squares method. The R factor was converged to 0.034 with an equal weight for each reflection.

We thank Professor H. H. R. Hoffmann of Technischen Universität at Hannover for sending IR spectrum of **17** (Ref. 4) which had been recorded by Professor G. Köbrich at the same University.

References

1) J. R. Rigaudy and P. Cadevielle, *Tetrahedron*, **33**, 767 (1977).
2) F. Toda and K. Akagi, *Tetrahedron Lett.*, **1970**, 5289.
3) F. Toda, F. Monden, and M. Ohi, *Bull. Chem. Soc. Jpn.*, **47**, 316 (1974).
4) G. Köbrich and H. Fröhlich, *Chem. Ber.*, **98**, 3637 (1965).
5) J. Novak and C. A. Salemink, *J. Chem. Soc., Perkin Trans. 1*, **1982**, 2403.

 © 1983 The Chemical Society of Japan Bull. Chem. Soc. Jpn., 56, 3319—3322 (1983)

The Reaction of Cyanoguanidine with Formaldehyde. I. Hydroxymethylation and Methoxymethylation of Cyanoguanidine

Michiaki Takimoto,* Toichi Ebisuno, and Ryuichi Shiba†

Department of Chemistry, Faculty of Science, Toho University, Miyama 2-2-1, Funabashi, Chiba 274

† *Department of Applied Science, Faculty of Technology, Tokyo Denki University, Kanda, Chiyoda-ku, Tokyo 101*

(Received April 7, 1983)

In order to examine the reactivity of cyanoguanidine (CG) with formaldehyde, CG was first hydroxymethylated, then methoxylated, and finally exhaustively hydroxymethylated with a large excess of formaldehyde. 4-Cyanoimino-3-methoxymethylperhydro-1,3,5-oxadiazine was isolated as a major reaction product of 1,3-bis(methoxymethyl)-2-cyanoguanidine with formaldehyde. This product is an adduct of 3 mol of formaldehyde per mole of CG and a six-membered cyclic ether. Minor products were further methoxylated and 3,5-bis(methoxymethyl)-4-methoxymethyl(carbamoylimino)perhydro-1,3,5-oxadiazine was isolated. This is an adduct of 2 mol of formaldehyde to the amidinated product derived from the major product by the hydration of the cyano group. The ring structure of perhydro-1,3,5-oxadiazine was so stable that it could not be decomposed under acidic conditions if the methoxymethyl groups were fully acid-hydrolyzed.

The resinous products of cyanoguanidine (CG) with formaldehyde are useful as sticking agents for dyes,[1] modifiers for urea- and melamine–formaldehyde resins[2] and commercial flocculants.[3] CG is first hydroxymethylated with formaldehyde; this procedure is followed by the condensation and polymerization into CG–formaldehyde resin. The reaction mechanism and properties of CG have seldom been reported, in contrast to the abundant reports on urea- and melamine–formaldehyde resins.[4–7]

Hamada,[8] Yamada,[9] and Miyaoka and Matsui[10] observed that the pH value of the reaction solution of CG with formaldehyde approached 8.5—9.0 from the initial value under acidic or alkaline conditions as the reaction proceeded. Under acidic conditions, a partial conversion of CG to amidinourea (AU), a basic compound, was confirmed by IR spectrometry. Under alkaline conditions, possible conversions of CG to cyanourea or urea and of formaldehyde to MeOH and formic acid have been speculated about, but the details of the reaction remained to be elucidated. Only two hydroxymethylated products, mono- and 1,3-bis-(hydroxymethyl)-2-cyanoguanidine (CG-1F and CG-2F), were isolated[8] and other hydroxymethylated products were not obtained in the reaction of CG with formaldehyde. Therefore, the reactivity of CG with formaldehyde (the maximal number of the introduced hydroxymethyl groups to CG) has been estimated to be 2 or 3 at the most. However, it can be anticipated to be 4 by analogy with urea which has the analogous structure to CG and reacts with formaldehyde into tetrakis(hydroxymethyl)urea derivatives.

Furthermore, the maximal wavelength of the strong absorption band in the UV region (λ_{max}) of hydroxymethylated products depends on the number of the introduced hydroxymethyl groups; their band positions shift to the longer wavelength side against the number of the hydroxymethyl groups in the reaction of melamine, melam, melem, ammelide or ammeline with formaldehyde.[11–12] If a similar relationship occurs for hydroxymethylated CG, our observation on λ_{max} of CG, CG-1F, CF-2F, and products of CG with a large excess of formaldehyde suggests that the reactivity of CG is about 4. In order to examine this suggestion, CG was exhaustively hydroxymethylated.

Results and Discussion

1,3-Bis(methoxymethyl)-2-cyanoguanidine (CG-2M) was used as a starting material for the exhaustive hydroxymethylation of CG with formaldehyde, because the usual hydroxymethylation is always attended by the reverse reactions and fails to prepare tris- and tetrakis(hydroxymethyl)-2-cyanoguanidine and because hydroxymethylated CG polymerizes and CG converts to AU together with other unknown compounds under severe reaction conditions. CG-2M could be prepared from CG-2F and MeOH in good yield by the addition of a large excess of an acid catalyst at low temperatures while, at the boiling point of MeOH in the presence of a small amount of an acid, intermolecular condensates were largely produced and CG-2M was poorly prepared. CG-2M was assigned by the elemental analysis and the appearance of ^{1}H-NMR signal of the methyl proton (δ=3.20) and the disappearance of the signal of the hydroxyl proton (δ=5.72 in CG-2F).

1-Methoxymethyl-2-cyanoguanidine (CG-1M) was obtained from CG-1F and MeOH and assigned in a similar way.

CG-2M was further hydroxymethylated in the presence of excess formaldehyde. The major product was assigned as 4-cyanoimino-3-methoxymethylperhydro-1,3,5-oxadiazine (CG-1Mcyc2F), a six-membered cyclic ether, by the elemental analysis, FD-MS and ^{1}H-NMR spectrometry. The X-ray diffraction data which will be reported elsewhere also confirmed this assignment. The λ_{max} of this product was plotted on the extrapolation of the linear λ_{max} *versus* the number of hydroxymethyl and/or methoxymethyl groups of CG, CG-1F, CG-1M, CG-2F, and CG-2M. Figure 1 shows that this contains three hydroxymethyl and/or methoxymethyl groups. This was probably derived by the intramolecular elimination of MeOH between the hydroxymethyl group which was introduced to one of two imino groups in CG-2M and the methoxymethyl group in the other imino group because the newly introduced hydroxymethyl group was labile and stabilized by the cyclization. This was an adduct of 3 mol of formaldehyde per mole of CG and showed that the reactivity of CG is 3 at least.

Then, in order to prepare 1,3-bis(hydroxymethyl)-1,3-bis(methoxymethyl)-2-cyanoguanidine (CG-2F2M) or 4-cyanoimino-3,5-bis(methoxymethyl)perhydro-1,3,5-oxadiazine (CG-2Mcyc2F), CG-2M was treated with formaldehyde under various conditions. Under mild conditions, no hydroxymethyl group was introduced into CG-2M. Under severe conditions, condensated polymers were mainly produced. The value of λ_{max} (232 nm) of the solution containing these products as shown in Fig. 1 suggested the possible production of CG-2F2M and/or CG-2Mcyc2F but none of them could be isolated.

CG-1Mcyc2F was also prepared from CG-1M and formaldehyde in a comparable yield with that from CG-2M and formaldehyde (scheme 1). In this preparation, two molecules of formaldehyde were added, one by one, to the free amino group and then to the imino group which had a methoxymethyl group. The dehydration from two of the hydroxymethyl groups selectively occurred and the MeOH elimination from one hydroxymethyl and one methoxymethyl group did not, because 4-cyanoimino-3-hydroxymethylperhydro-1,3,5-oxadiazine (CG-1Fcyc2F) could not be obtained.

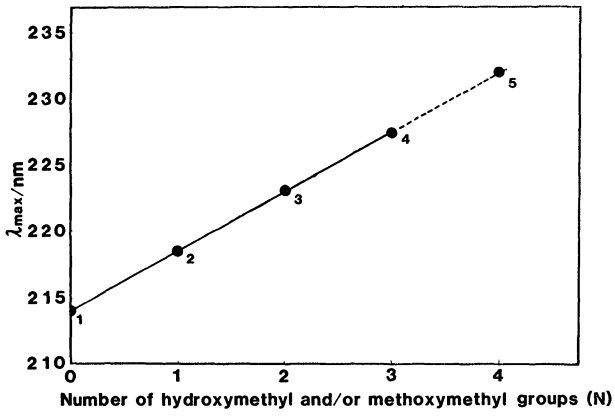

Fig. 1. Relationship of the maximal wavelength of absorption bands in UV region (λ_{max}) of CG, hydroxymethylated CG and methoxymethylated CG with the number (N) of hydroxymethyl and/or methoxymethyl groups.
1; CG, 2; CG-1F or CG-1M, 3; CG-2F or CG-2M, 4; CG-1Mcyc2F, 5; pasty products of CG-2M with a large excess of formaldehyde at 85—90 °C for 20 min.

4-Cyanoimino-3-ethoxymethylperhydro-1,3,5-oxadiazine (CG-1Ecyc2F) was prepared from 1-ethoxymethyl-2-cyanoguanidine (CG-1E) and formaldehyde in a 76% yield and condensated polymers and by-products were minimized. In the reaction of 1-alkoxymethyl-2-cyanoguanidine (CG-1M or CG-1E) with formaldehyde, the ring formation by the dehydration was a major reaction and preceded the intermolecular condensation, while in the reaction of hydroxymethylated CG which was not alkoxylated, this condensation preceded the ring formation.

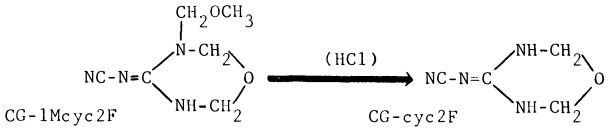

As 4-(cyanoimino)perhydro-1,3,5-oxadiazine (CG-cyc2F) could be obtained from CG-1Mcyc2F by acid-hydrolysis, the six-membered cyclic structure was so stable that it remained undecomposed but the methoxymethyl group was fully acid-hydrolyzed into formaldehyde, whose quantity was determined colorimetrically to be in agreement with the calculated amount.

After removal of the major reaction product of CG-2M with formaldehyde, the minor products were further treated with MeOH under acidic conditions. The isolated product lost the absorption band at 2140—2180 cm^{-1} in IR spectrum which is characteristic of

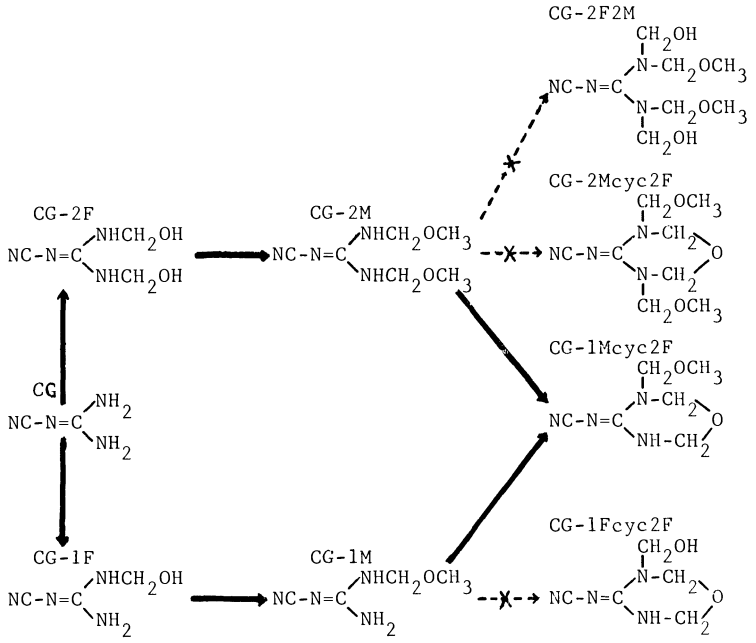

Scheme 1.

Table 1. ^{13}C-NMR spectra of CG and related compounds

	-CN	=N-CO-N=	-N=C(N=)(N=)
CG	118.3	—	163.1
Urea	—	159.7	—
AU	—	160.3	164.7
CG-1Mcyc2F	116.7	—	156.5
Hydrated product	—	155.3	163.6

the stretching vibration of -CN. The results in the ^{13}C-NMR spectrum shown in Table 1 suggest that this product has the structure of =N-CO-N= derived by the hydration of the cyano group of CG-1Mcyc2F and that the hydrated CG-1Mcyc2F is one of the minor products of CG-2M with formaldehyde. The λ_{max} of this product was 238 nm, which deviated to the wavelengths longer than the extrapolated value in Fig. 1 probably because of the structural conversion of CG itself to AU. This product had three easily acid-hydrolyzed methoxymethyl groups, whose presence was ascertained by the colorimetric determination of formaldehyde released. The following two structures were considered for this hydrated product. The structure of **1**, 3,5-bis(methoxymethyl)-4-methoxymethyl(carbamoylimino)perhydro-1,3,5-oxadiazine (AU-3Mcyc2F) is thought more feasible than **2** from the ^{13}C-NMR and ^{1}H-NMR spectra using a shift reagent.

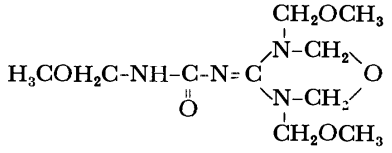

1

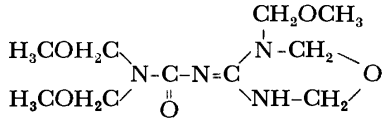

2

Two molecules of formaldehyde were added to the newly formed amino group and to the imino group in the ring, one by one, to form AU-3Mcyc2F. However, it remained obscure how the hydrogen of the imino group in the ring could be substituted for by the hydroxymethyl group in the presence of the cyano group which had not been hydrated.

The reaction mechanisms and characteristics of CG-1Mcyc2F and AU-3Mcyc2F are under investigation and will be reported elsewhere.

Experimental

NMR spectra of reaction products in DMSO-d_6 were obtained at 90 MHz on a JOEL FX-90Q instrument using TMS as an internal standard.

1,3-Bis(methoxymethyl)-2-cyanoguanidine (CG-2M). Keeping the temperature of the solution at 14—15 °C by using an ice bath, 5 ml of concentrated HCl was added dropwise with stirring to 2 g of CG-2F which was prepared according to the procedure of Hamada[8] in 50 ml of MeOH. After 15 min, the reaction solution was neutralized with 20% NaOH solution to the endpoint of phenolphthalein and evaporated to dryness under reduced pressure at low temperatures. A product, CG-2M, was recrystallized from EtOH as columnar crystals. (yield in crude; *ca.* 70%): mp 121.5—122.2 °C: Found: C, 41.75; H, 7.05; N, 32.15%: Calcd for $C_6H_{12}N_4O_2$, C, 41.86; H, 6.98; N, 32.56%: ^{1}H-NMR(DMSO-d_6): δ=3.20 (6H, s, -CH$_3$), 4.53 (4H, d, J=6 Hz, -CH$_2$OCH$_3$), 8.04 (2H, t, J=6 Hz, -NH-).

CG-1M was prepared from CG-1F and MeOH in a similar way as CG-2M (yield in crude; *ca.* 70%): mp 121.5—122.2 °C: Found: C, 37.38; H, 6.41; N, 43.54%: Calcd for $C_4H_8N_4O$, C, 37.49; H, 6.29; N, 43.73%: ^{1}H-NMR (DMSO-d_6): δ=3.09 (3H, s, -CH$_3$), 4.47 (2H, d, J=6 Hz, -CH$_2$OCH$_3$), 6.99 (2H, s, -NH$_2$), 7.62 (1H, t, J=7 Hz, -NH-).

4-Cyanoimino-3-methoxymethylperhydro-1,3,5-oxadiazine (CG-1Mcyc2F). Twenty-five ml of 37% formalin solution was added to 5 g of CG-2M (mole ratio of formaldehyde/CG-2M=10) and the pH of the solution was adjusted with 0.1 M NaOH solution to 8.8. After stirring for 10 min at 80 °C, the reaction mixture was cooled in an ice bath to stop the reaction and evaporated to dryness under reduced pressure at low temperatures. A large excess of acetone was added to the desiccated products. After the acetone-insoluble products were filtrated off, the acetone solution was concentrated to a viscous solution under reduced pressure; then a small amount of EtOH was added. On cooling, white powder was deposited (yield in crude; 51%). This was separated by filtration and recrystallized from 2-propanol to give plate crystals. Mp 113.8—114.0 °C: Found: C, 42.35; H, 5.88; N, 32.71%: Calcd for $C_6H_{10}N_4O_2$, C, 42.35; H, 5.88; N, 32.94%: ^{1}H-NMR(DMSO-d_6): δ=3.23 (3H, s, -CH$_3$), 4.73, 4.81 (4H, s, -CH$_2$OCH$_2$-), 4.90 (2H, s, -CH$_2$OCH$_3$), 8.47 (1H, t, J=4 Hz, -NH-): MS(FD): *m/e* 170 (M^+).

After removal of the major product, CG-1Mcyc2F, by filtration, the filtrate was concentrated to a viscous solution. A thin layer chromatogram of this viscous solution on silica gel (Merck F254) developed in 2-propanol showed three major spots under UV light. The isolation of these products by various solvents was, however, unsuccessful.

CG-1Mcyc2F was also prepared (yield in crude; 40%) from 5 g of CG-1M and 33 ml of 37% formalin solution (mole ratio of formaldehyde/CG-1M=10) in a way similar to the above.

The preparation conditions of 4-cyanoimino-3-ethoxymethylperhydro-1,3,5-oxadiazine (CG-1Ecyc2F) was virtually identical to that of CG-1Mcyc2F, but CG-1M was replaced with CG-1E. The yield of CG-1Ecyc2F was 76% in crude.

4-(Cyanoimino)perhydro-1,3,5-oxadiazine (CG-cyc2F). One g of CG-1Mcyc2F was dissolved in 50 ml of 0.1 M HCl and hydrolyzed at 80 °C for 20 min. The reaction mixture was neutralized and concentrated under reduced pressure. The resulting viscous solution was treated with EtOH and the deposited white crystals were recrystallized from dioxane. (yield in crude; 72%) mp 137.0—137.3 °C: Found: C, 38.12; H, 4.79; N, 44.31%: Calcd for $C_4H_6N_4O$, C, 38.09; H, 4.80; N, 44.42%: ^{1}H-NMR (DMSO-d_6): δ=4.73 (4H, s, -CH$_2$OCH$_2$-), 8.21 (2H, t, J=4 Hz, -NH-): MS (70 eV): *m/e*(rel intensity) 126 (M^+, 67), 96 (100), 68 (88).

3,5-Bis(methoxymethyl)-4-methoxymethyl(carbamoylimino)perhydro-1,3,5-oxadiazine (AU-3Mcyc2F). To 5 g of the viscous solution described in the preparation of CG-1Mcyc2F, 100 ml of MeOH was added. The solution was chilled to

below −10 °C by the use of Dry Ice and MeOH, then 5 ml of concentrated HCl was added and gradually allowed to warm to 10—12 °C. The reaction was carried out at 10—12 °C for 15 min. Keeping the temperature of the solution below −10 °C, the solution was neutralized with 20% NaOH solution. The solution was concentrated under reduced pressure at low temperatures. The resulting viscous solution was extracted with dioxane. Then, the dioxane soluble fraction was extracted with hexane three times. White crystals were obtained from hexane extracts (yield in crude; 12%). mp 58.0—58.6 °C: Found: C, 43.40; H, 7.27; N, 20.21%: Calcd for $C_{10}H_{20}N_4O_5$, C, 43.48; H, 7.25; N, 20.29%: ^{1}H-NMR(DMSO-d_6): δ=3.18 (6H, s, $-CH_3$), 3.24 (3H, s, $-CH_3$), 4.87 (4H, s, $-CH_2OCH_2-$), 4.93 (2H, s, $-CH_2OCH_3$), 9.86 (1H, t, J=4 Hz, $-NH-$): MS(FD): m/e 277 (MH^+).

References

1) L. Sellet and W. O. Dawson, U. S. Patent 2690434 (1954); *Chem. Abstr.*, **49**, 1370a (1955).
2) K. Ripper, U. S. Patent 2286228 (1942); *Chem. Abstr.*, **36**, 7189^5 (1942).
3) S. Sakai, *Kobunshi*, **8**, 612 (1959).
4) M. Nakajima, *Kobunshikako*, **1982**, 127, 162, 220, 268 (1982).
5) J. Merz and F. Raschdorf, *Textilveredlung*, **7**, 540 (1972).
6) S. M. Kambanis and R. C. Vasishth, *J. Appl. Polym. Sci.*, **15**, 1911 (1971).
7) B. Tomita and Y. Hirose, *J. Polym. Sci., Polym. Chem. Ed.*, **14**, 387 (1976).
8) M. Hamada, *Rep. Lab. Toyo Reiyon*, **1**, 28 (1954); **2**, 25 (1955).
9) E. Yamada, *Kogyo Kagaku Zasshi*, **62**, 1161 (1959).
10) U. Miyaoka and T. Matsui, *Kogyo Kagaku Zasshi*, **58**, 567 (1955).
11) M. Tajima, R. Shiba, T. Yatsuo and M. Takimoto, *Nippon Kagaku Kaishi*, **1982**, 125.
12) M. Takimoto, T. Funakawa, R. Shiba and M. Tajima, *Nippon Kagaku Kaishi*, **1982**, 662.

Studies on the β-Turn of Peptides. VI.[1] Nuclear Magnetic Resonance Study on the Conformations of *N*-(2,4-Dinitrophenyl)tetrapeptide *p*-Nitroanilides Related to the β-Turn Part of Gramicidin S

Tsutomu HIGASHIJIMA,† Kazuki SATO,* and Ukon NAGAI

Mitsubishi-Kasei Institute of Life Sciences, 11 Minamiooya, Machida, Tokyo 194

† *Department of Biophysics and Biochemistry, Faculty of Science, The University of Tokyo, Bunkyo-ku, Tokyo 113*

(Received April 21, 1983)

The conformations of *N*-(2,4-dinitrophenyl)-L-Leu-X-L-Pro-L-Val *p*-nitroanilides (**I**, X=D-Ala; **II**, X=Gly; **III**, X=L-Ala) were studied by nuclear magnetic resonance and circular dichroism spectroscopies. The L-Val-NH group of compound **I** takes part in an intramolecular hydrogen bonding, and the folded conformation is considered to be type II′ β-turn structure as in the case of [D-Ala$^{4,4'}$]-gramicidin S. The populations of β-turn conformer were considered to be in the order of **I**>**II**>**III**≈0 in methanol and *N*,*N*-dimethylformamide solutions, and decreased in dimethyl sulfoxide solution. Compound **II** in dimethyl sulfoxide and **III** in all the three solvents do not take a β-turn conformation. The data obtained from NMR and CD experiments showed a good correlation between the magnitudes of the Cotton effects (250—400 nm) and the populations of the β-turn conformation of these peptides. The proximity of the two chromophores was ascertained directly for compound **I** in *N*,*N*-dimethylformamide solution by nuclear Overhauser effects experiment. In addition, the β-turn preference of these peptides were in good accordance with the antibiotic activities of the gramicidin S analogs having the same tetrapeptide sequences at their β-turn parts.

Gramicidin S (GS) is a cyclic decapeptide antibiotic with the primary structure *cyclo*(-L-Val^1-L-Orn^2-L-Leu^3-D-Phe^4-L-Pro^5-L-Val$^{1'}$-L-Orn$^{2'}$-L-Leu$^{3'}$-D-Phe$^{4'}$-L-Pro$^{5'}$-).[2] Conformation of GS consists of the intramolecular antiparallel β-sheet with four hydrogen bonds between L-Val and L-Leu residues and two β-turns (type II′) around the D-Phe-L-Pro sequences (Fig. 1).[3] The characteristic feature of the conformation is the orientation of side chains in which the charged L-Orn side chains are on one side and the hydrophobic L-Val and L-Leu side chains on the other side of the molecule. The conformation of GS is considered to be stabilized not only by the four intramolecular hydrogen bonds but also by the stable β-turns formed by two D-Phe-L-Pro sequences. Izumiya *et al.* summarized the antibacterial activities of many GS analogs.[4] The activities of GS analogs were correlated to their conformations.[5] For example, the activities and the populations of GS-type β-sheet conformer were in the order of GS≈[D-Ala$^{4,4'}$]-GS>[Gly$^{4,4'}$]-GS≫[L-Ala$^{4,4'}$]-GS≈0.[6] It is of interest to study the β-turn preference of the amino acid sequences at the corner positions of GS analogs.

In the previous paper, we gave an outline of a new method to study the β-turn conformation of linear tetrapeptides.[7] *N*-(2,4-Dinitrophenyl)tetrapeptide *p*-nitroanilides (Dnp-tetrapeptide-pNA's) exhibited characteristic CD spectra above 250 nm, and the Cotton effects were considered to be due to the exciton coupling of the transition moments in the two terminal chromophores. The magnitudes of the Cotton effects near 310 and 350 nm were expected to reflect well the β-turn preference of the peptides.

This paper describes ^{1}H and ^{13}C nuclear magnetic resonance (NMR) studies on the conformations of tetrapeptide derivatives related to the β-turn part of GS, Dnp-L-Leu-X-L-Pro-L-Val-pNA (**I**, X=D-Ala; **II**, X=Gly; **III**, X=L-Ala), to study a correlation between the Cotton effects and the conformations of these peptides (Fig. 2). ^{1}H NMR measurements were systematically carried out including (a) temperature dependence of NH proton chemical shifts in various solutions, (b) nuclear Overhauser effects on amide, CH, and aromatic proton resonances, and (c) solvent dependences of NH and CH proton chemical shifts and spin-coupling constants ($^3J_{NH-C^{\alpha}H}$).

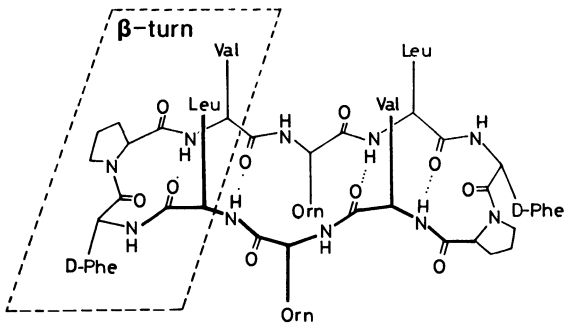

Fig. 1. β-Sheet conformation of gramicidin S.

Experimental

Syntheses of **I**—**III** were reported previously.[8] The solvent DMSO-d_6 (99.8%) was obtained from Commissariat a l'Energy Atomique and CD_3OH (99.5%) and DMF-d_7 (99.5%) from E. Merck.

^{1}H NMR spectra were recorded on a Bruker WH-270 spectrometer (270 MHz for ^{1}H), equipped with a Bruker B-ST-100/700 temperature control unit. ^{13}C NMR spectra were recorded on a JEOL FX-90Q (22.5 MHz for ^{13}C),

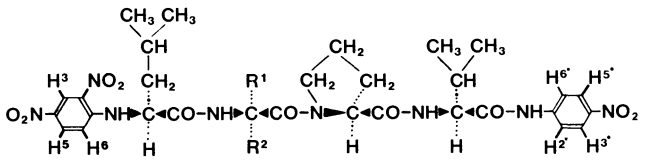

I (X = D-Ala) : R^1 = H, R^2 = CH_3
II (X = Gly) : R^1 = H, R^2 = H
III (X = L-Ala) : R^1 = CH_3, R^2 = H

Fig. 2. Primary structures of Dnp-tetrapeptide-pNA's (**I**—**III**).

with a variable-temperature unit. Internal references for chemical shift were DSS for ^1H and TMS for ^{13}C. Nuclear Overhauser effect (NOE) data were also recorded on a Bruker WH-270 instrument at the concentration of 5 mM (1 M=1 mol dm^{-3}) at 23 °C. The FID's were collected after applying a 5-s low power saturation pulse in alternating blocks of 16 on-resonance and 16 off-resonance spectra using a SW of 3000 Hz with 16K data points for 512 spectral acquisitions each, Fourier transformed and subtracted to obtain the difference spectra.

CD spectra were measured on a JASCO J-40A spectropolarimeter at the concentration of 0.1 mM at room temperature (23±2 °C).

Results

CD Measurements. CD spectra of **I**—**III** were measured in DMF and DMSO solutions, and the results are summarized in Fig. 3 together with those measured in MeOH solutions.[7] Compound **I** having D-Ala at the second position showed the largest Cotton effects in DMF and DMSO solutions as well as in MeOH solution of the three compounds. In DMSO solution, however, the Cotton effects decreased to about 40% of those in DMF and MeOH solutions. Compound **III** showed no significant CD band near 310 nm and 350 nm in any solutions, and **II** showed intermediate CD spectra between **I** and **III**. The strong CD bands of **I** are not due to intermolecular interaction, since CD spectra of **I** showed no concentration dependences at the range from 5 mM to 0.1 mM. Accordingly, the strong CD bands are attributed to the intramolecular interaction between the two terminal chromophores in **I**.

Assignments of ^1H Resonances. The ^1H NMR spectra of **I**—**III** were assigned with the aid of spin-decoupling, H–D exchange of NH protons, and saturation transfer (between the two conformers) in CD_3OH, DMSO-d_6, and DMF-d_7 solutions as shown in Table 1. All the spectra showed two sets of resonances for most of the protons due to *cis-trans* isomerism for the X–L-Pro bonds. Chemical shifts of aromatic protons are shown in Fig. 4, and those of the other protons are listed in Table 1 together with spin-coupling constants ($^3J_{NH-C^\alpha H}$). In all the solutions, aromatic protons of major conformer were shifted to higher field in the order of **I**>**II**>**III**, while those of minor conformers did not show such significant sequence dependences (Fig. 4). In DMSO-d_6 solution, the L-Pro–C$^\alpha$H proton of the major conformer of **I** showed higher field shift (4.41 ppm) than that of the minor conformer (4.87 ppm) suggesting that major conformer had *trans* D-Ala–L-Pro bond. This assignment was ascertained by ^{13}C NMR study as described in the next section. In the other solutions and also in the other compounds (**II** and **III**), the L-Pro–C$^\alpha$H protons of the major conformers showed the similar chemical shifts to that of the major conformer of **I** in DMSO-d_6 solution. The D-Ala residue in major conformer of **I** showed small spin-coupling constants ($^3J_{NH-C^\alpha H}$) of 3.9 and 4.0 Hz in CD_3OH and in DMF-d_7 solutions, respectively, suggesting that the ϕ angle of D-Ala residue is certainly fixed in these solutions, whereas the L-Ala residue of **III** showed spin-coupling constants

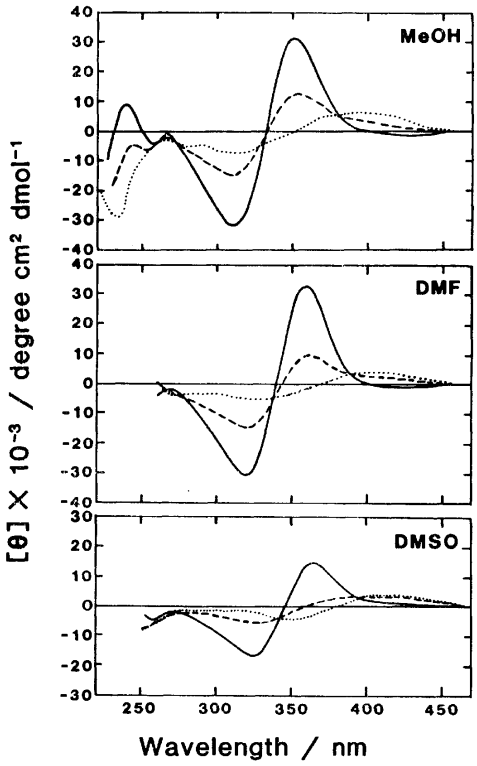

Fig. 3. CD spectra of Dnp-L-Leu-X-L-Pro-L-Val-pNA (**I**—**III**).
——: **I** (X=D-Ala), - - -: **II** (X=Gly), ……: **III** (X=L-Ala). Curves in MeOH solution were reproduced from Ref. 7 by kind permission of John Wiley & Sons, Inc.

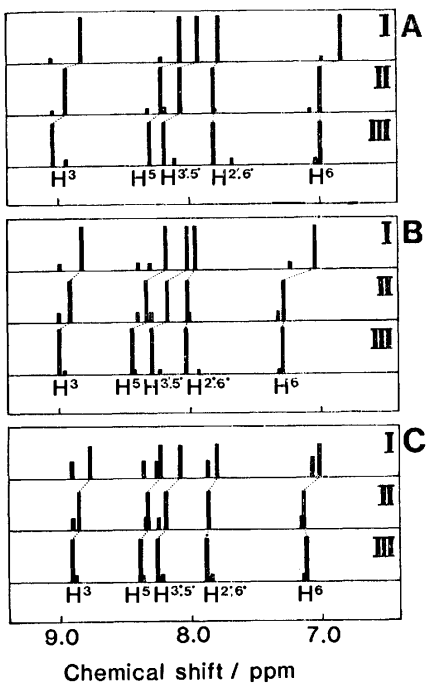

Fig. 4. Chemical shifts of aromatic protons of **I**—**III** in (A) CD_3OH in (B) DMF-d_7 and in (C) DMSO-d_6 solutions. The large bars and the small bars show the major and the minor resonances, respectively (for notation, see Fig. 2).

Table 1. ^{1}H NMR data of Dnp-L-Leu-X-L-Pro-L-Val-pNA (I—III) at 23 °C

Compound	Solvent	Conformer[a] %	Chemical shift from DSS ppm								$^3J_{NH-C^\alpha H}$ Hz		
			L-Leu		X		L-Pro	L-Val		pNA			
			NH	$C^\alpha H$	NH	$C^\alpha H$	$C^\alpha H$	NH	$C^\alpha H$	NH	L-Leu	X	L-Val
I	CD_3OH	*t*. 90	8.68	4.35	8.87	4.57	4.44	7.52	4.17	9.22	7.0	3.9	8.6
		c. 10											
	DMF-d_7	*t*. 83	8.83	4.66	9.19	4.69	4.45	7.45	4.30	9.57		4.0	8.8
		c. 17											
	DMSO-d_6	*t*. 65	8.72	4.55	8.90	4.59	4.41	7.59	4.20	10.00	7.8	6.1	8.3
		c. 35	8.79	4.55	8.79		4.87	8.54		10.79	8.0	7.5	8.5
II	CD_3OH	*t*. 88	8.70	4.63	8.69	4.08	4.47	7.96	4.24	9.95	7.3	13.6[b]	7.8
		c. 12	8.68		8.58			8.44					
	DMF-d_7	*t*. 78	8.92	4.76	8.83	4.21	4.54	7.92	4.83	10.27		9.2[b]	8.1
		c. 22			8.62								
	DMSO-d_6	*t*. 73	8.76	4.60	8.65	4.03	4.48	8.04	4.28	10.49	7.3	9.8	8.3
		c. 27	8.75		8.59			8.48				10.3[b]	
III	CD_3OH	*t*. 86	8.67	4.50	8.56	4.64	4.39	8.19	4.27	10.40	7.3	6.4	7.3
		c. 14	8.63		8.59			8.51		10.26			
	DMF-d_7	*t*. 88	8.94	4.73	8.76	4.77	4.59	8.07	4.44	10.73		7.0	
		c. 12											
	DMSO-d_6	*t*. 85	8.74	4.56	8.67	4.61	4.48	8.06	4.30	10.68	7.8	7.4	7.8
		c. 15											

a) *t*, *trans* X-L-Pro bond; *c*, *cis* X-L-Pro bond. b) Sum of *J* for two methylene protons.

typical to free rotation.

Assignments of ^{13}C Resonances. ^{13}C NMR is useful for the study of *cis-trans* isomerism of the X–L-Pro peptide bond.[9] Chemical shifts of the L-Pro–C^β and C^γ carbons of **I**—**III** in DMSO-d_6 solutions were determined in order to assign the two sets of resonances to the conformers with *trans* or *cis* X–L-Pro bond. Though the resonances of the L-Pro–C^γ carbons were overlapped with those of L-Leu–C^γ and C^δ carbons, those of the L-Pro–C^β carbons were clearly observed; the major and the minor resonances were 28.99 and 31.85 ppm for **I**, 29.10 and 31.97 ppm for **II**, and 28.75 and 31.56 ppm for **III**, respectively. The results indicate that major resonances can be attributed to the conformers with *trans* X–L-Pro bond.

Temperature Dependences of Proton Chemical Shifts. The temperature dependences of chemical shifts of amide proton resonances are useful for distinguishing between "exposed" and "intramolecularly hydrogen-bonded" amide proton;[10] exposed protons exhibit larger temperature coefficients than hydrogen-bonded amide protons. The temperature dependences of amide proton chemical shifts are shown in Fig. 5 for major conformers of **I**—**III**. The L-Val–NH proton of **I** showed much smaller temperature dependences (-2.72×10^{-3} and -2.13×10^{-3} ppm °C^{-1}) than the D-Ala–NH proton (-7.06×10^{-3} and -5.93×10^{-3} ppm °C^{-1}) in CD_3OH and in DMF-d_7 solutions, respectively, indicating that the L-Val–NH proton of **I** was involved in stable hydrogen bonding. In DMSO-d_6 solution, the L-Val–NH proton of **I** also showed smaller temperature dependence (-3.44×10^{-3} ppm °C^{-1}) than the D-Ala–NH proton (-4.59×10^{-3} ppm °C^{-1}), though the difference between the two NH protons was not so clear as that in CD_3OH or DMF-d_7 solution. The L-Val–NH proton of **II** showed a little smaller temperature dependence than the Gly–NH proton in CD_3OH and in DMF-d_7 solutions, though the values (-6.85×10^{-3} and -5.00×10^{-3} ppm °C^{-1}, respectively) were too large for strongly hydrogen-bonded species. The values for the L-Val–NH and Gly–NH protons of **II** were reversed in DMSO-d_6 solution. The L-Val–NH proton of **III** always showed larger temperature dependences than the L-Ala–NH proton. The temperature dependences of L-Val–NH protons were in the order of **I**<**II**<**III** in any solvents. Most of the protons other than amide ones showed little temperature dependences, suggesting that the conformations of **I**—**III** did not change significantly in the temperature range of these experiments.

Nuclear Overhauser Effects. Nuclear Overhauser effects (NOE's) are useful for the conformational analysis of peptides, since the effects are inversely proportional to the sixth power of the distance between the irradiated and observed protons. NOE's were observed for **I**—**III** in DMF-d_7 solutions at 23 °C as shown in Table 2. It is noteworthy that NOE's were observed for Dnp–H^3 resonance and D-Ala–$C^\alpha H$ proton resonance by the irradiation of pNA aromatic protons (Fig. 6A) and L-Pro–$C^\alpha H$ proton (Fig. 6B) resonances, respectively. On the other hand, the NOE enhancement was not observed for **III** between Dnp and pNA aromatic protons.

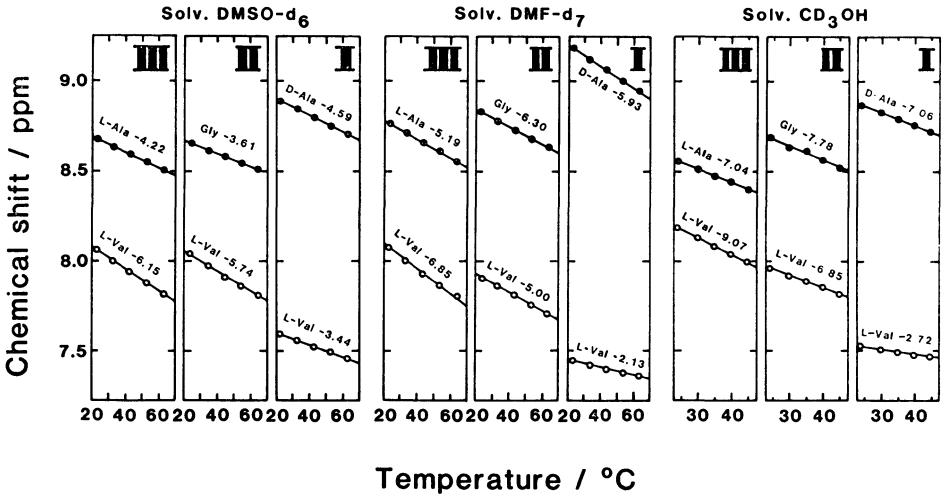

Fig. 5 Temperature dependences of amide proton chemical shifts of major resonances of **I**—**III**. Numbers on the lines refer to $10^3 \times$temperature coefficient in ppm $°C^{-1}$. ○: L-Val[4]-NH, ●: X^2-NH.

TABLE 2. NOE OBSERVATIONS FOR Dnp-L-Leu-X-L-Pro-L-Val-pNA (**I**—**III**) IN DMF-d_7 AT 23 °C[a)]

Compound	Signal irradiated	Signal observed (%)
I	L-Leu-C^αH(+D-Ala-C^αH)	Dnp-H^6 (19.4), pNA-$H^{2',6'}$ (<1), L-Leu-$C^{\beta,\gamma}$H (2), L-Leu-C^δH (<1)
	D-Ala-C^αH	Dnp-H^6 (14.5), L-Pro-C^δH (2.7), L-Pro-C^δH′ (1.7), L-Leu-$C^{\beta,\gamma}$H (2)
	L-Pro-C^αH	L-Pro-C^βH (5.7), L-Val-NH (2.3)
	L-Val-C^αH	L-Val-C^βH (6.1), L-Val-C^γH (<1)
	L-Pro-C^δH[b)]	D-Ala-C^αH (>3.7), L-Pro-C^δH′ (7.5), L-Pro-C^βH (2.2)
	L-Pro-C^δH′ [b)]	D-Ala-C^αH (>3.2), L-Pro-$C^{\beta,\gamma}$H (1.8)
	D-Ala-NH(+pNA-NH)	L-Leu-C^αH (6.3), D-Ala-C^αH (3.4), pNA-$H^{2',6'}$ (2.8), L-Val-C^αH (2)
	Dnp-H^6	Dnp-H^5 (18.9), L-Leu-C^αH (10.3)
	pNA-$H^{2',3',5',6'}$	Dnp-H^3 (2.1)
II	L-Leu-C^αH	Dnp-H^6 (18.7), L-Leu-C^αH (2.1)
	Gly-C^αH	L-Pro-C^δH (2.8), L-Pro-C^δH′ (4.7)
	L-Pro-C^αH	L-Val-NH (4.6)
	L-Val-C^αH	pNA-$H^{2',6'}$ (<1), L-Val-NH (3), L-Val-C^βH (4.7)
	L-Pro-C^δH	Gly-C^αH (small)
	L-Pro-C^δH′	Gly-C^αH (2.5)
	L-Leu-NH+pNA-NH+Dnp-H^3	pNA-H^2 (3.8), L-Leu-C^αH (3.3), L-Val-C^αH (4.5)
	Dnp-H^6	Dnp-H^5 (25), Dnp-H^3 (<1), L-Leu-C^αH (9.5)
	Dnp-H^5	Dnp-H^6 (6.8)
	pNA-$H^{2',6'}$	Dnp-H^3 (1.9)
	pNA-$H^{3',5'}$	Dnp-H^3 (3.8)
III	L-Leu-C^αH(+L-Ala-C^αH)	Dnp-H^6 (16.9), L-Ala-NH (4.3), L-Pro-C^δH (2.2), L-Leu-C^βH (2)
	L-Ala-C^αH(+L-Leu-C^αH)	L-Pro-C^δH (3.3), L-Leu-C^βH (3.8), Dnp-H^6 (14.7), L-Ala-NH (3.4)
	L-Pro-C^αH	L-Val-NH (>4.3), L-Pro-$C^{\beta,\gamma}$H (small)
	L-Val-C^αH	L-Val-C^βH (4.2)
	L-Ala-C^βH	L-Ala-C^αH (>5.5)
	L-Pro-C^δH	L-Ala-C^αH (>11.6), L-Pro-$C^{\alpha,\gamma}$H (small)
	L-Val-NH	L-Pro-C^αH (5.9), L-Val-C^αH (3)
	Dnp-H^6	Dnp-H^5 (16.2), Dnp-H^3 (1), L-Leu-C^αH (>6.7)
	Dnp-H^5	Dnp-H^3 (2), Dnp-H^6 (6.7)

a) Signals of minor conformer with *cis* X-L-Pro bond are omitted. b) C^δH and C^δH′ are a lower and a higher field signals, respectively.

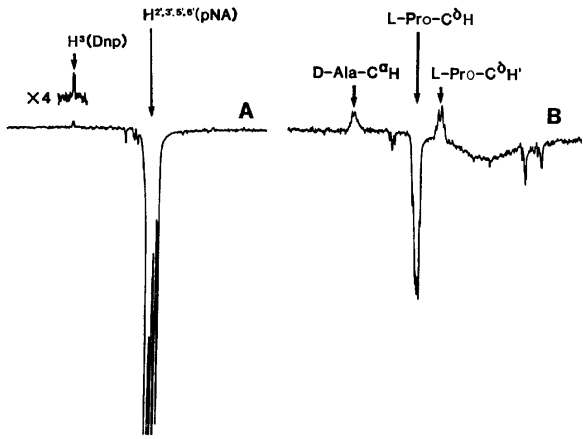

Fig. 6. NOE observations of **I** in DMF-d_7 solution. Signals irradiated were (A) pNA-$H^{2',3',5',6'}$ protons and (B) L-Pro-$C^{\beta}H$ proton.

Discussion

Cis-trans *Isomerism for X-L-Pro Bonds.* Major resonances of **I**—**III** in DMSO-d_6 solutions were attributed to the conformers with *trans* X–L-Pro bonds by ^{13}C NMR resonances. In CD_3OH and DMF-d_7 solutions, also, major resonances of **I**—**III** are considered to be due to the *trans* isomer, since all the major L-Pro–$C^{\alpha}H$ proton resonances showed similar chemical shifts to those in DMSO-d_6 solution. Populations of *trans* conformers of **I** and **II** increased in the order of in DMSO-d_6<DMF-d_7<CD_3OH solutions (Table 1). On the other hand, those of **III** did not show such large solvent dependences. It seems that the *cis* conformers of **I**—**III** are not in the fixed conformations in all solvents examined, since they showed similar chemical shifts of aromatic and some other protons for the three compounds (Fig. 4 and Table 1). These are ascertained by the large temperature dependences of the L-Val and X (X=D-Ala, Gly, or L-Ala) NH proton chemical shifts for the *cis* conformers. In contrast, the *trans* conformers of **I**—**III** showed large sequence and solvent dependences of chemical shifts for most of the NH and $C^{\alpha}H$ protons, indicating that their *trans* conformations depend on sequence and solvent. Detailed discussions are described hereafter for the conformations of *trans* (major) isomer of **I**—**III**.

Intramolecular Hydrogen Bonding. The L-Val–NH proton of **I** is concerned in a strong hydrogen bonding in CD_3OH or DMF-d_7 solution as shown in Fig. 5. In DMSO-d_6 solution, also, the L-Val–NH group is hydrogen-bonded. The hydrogen bonding is intramolecular, since **I** showed no concentration dependence of CD spectra. On the other hand, the L-Val–NH proton chemical shifts of **III** showed such large temperature dependences as that of *N*-methylacetamide in all the three solvents, indicating that the L-Val–NH group is not involved in an intramolecular hydrogen bonding. The temperature coefficients of L-Val–NH chemical shifts of **II** are intermediate of **I** and **III** for the three solutions. Accordingly, it seems that the magnitudes of the hydrogen bonding of the L-Val–NH protons of **I**—**III** are in the order of **I**>**II**>**III**≈0 in CD_3OH and DMF-d_7 solutions and **I**>**II**≥**III**≈0 in DMSO-d_6 solution.

The two CO groups of L-Leu (β-turn) and D-Ala (γ-turn) are the candidate for the acceptor of the intramolecular hydrogen bonding of L-Val–NH proton for compound **I**. It is noteworthy that the coupling constant ($^3J_{NH-C^{\alpha}H}$) of D-Ala residue for compound **I** is as small as 3.9 Hz and 4.0 Hz in CD_3OH and DMF-d_7 solution, respectively. The coupling constant ($^3J_{NH-C^{\alpha}H}$) of L-Ala residue is 8.5 Hz for Ac–L-Ala–$NHCH_3$, and 7.1 Hz for Ac–L-Ala–(*trans*)-L-Pro–OH,[11] which do not have specific conformations. These indicate that the ϕ angle of D-Ala residue of compound **I** is fairly fixed. This holds for the β-turn conformation (L-Leu^1–CO···HN–L-Val^4) of compound **I**: The ϕ angle of the second [$(i+1)$th] residue of β-turn conformation is known to be −60° for L-amino acid or +60° for D-amino acid, which indicates that the coupling constant ($^3J_{NH-C^{\alpha}H}$) for the residue is *ca.* 3.5 Hz.

In this series of compounds, the weaker is the hydrogen bonding of L-Val residue, the larger is the coupling constant ($^3J_{NH-C^{\alpha}H}$) of X-residue (X=L-Ala or D-Ala). On the other hand, the ϕ angle will not be fixed in the case of γ-turn conformation (D-Ala^2–CO···HN–L-Val^4).

*Type of the β-Turn of **I** and **II**.* [D-$Ala^{4,4'}$]-GS, which has similar conformation to that of GS,[6] is a good measure to estimate the type of the β-turn of **I**, though it is difficult usually to discriminate exactly the type of the β-turn of such a linear peptide as **I**. The NH protons of **I** in CD_3OH and DMF-d_7 solutions showed similar chemical shifts, coupling constants and temperature dependences to those of [D-$Ala^{4,4'}$]-GS in DMSO-d_6 solution (chemical shifts: D-Ala, 8.92 ppm; L-Val, 7.40 ppm; $^3J_{NH-C^{\alpha}H}$: D-Ala 3.7 Hz; L-Val, 8.8 Hz; temperature dependences: D-Ala, -7.50×10^{-3} ppm $°C^{-1}$; L-Val, -2.52×10^{-3} ppm $°C^{-1}$). Furthermore, NOE observation between D-Ala–$C^{\alpha}H$ and L-Pro–$C^{\beta}H$ protons of **I** indicates the proximity of these two protons (Fig. 6B). These results suggest that **I** takes the same type II′ β-turn as that of [D-$Ala^{4,4'}$]-GS. Since the corresponding residue of **II** to the D-Ala of **I** for the β-turn conformation is Gly, the type of the β-turn of **II** is expected to be similar to that of **I** (type II′).

Interaction between Dnp and pNA Chromophores. As the results of β-turn formation of peptide backbone, N- and C-terminal chromophores approach to each other. Certainly, higher-field shifts of aromatic proton chemical shifts of Dnp and pNA groups in *trans* isomer of **I** are due to ring-current effects, indicating the proximity of the two terminal chromophores (Fig. 4). On the other hand, aromatic protons of both isomers of **III** did not show large higher-field shifts but show the similar chemical shifts as those in *cis* isomer of **I**. Aromatic protons in the *trans* isomer of **II** showed intermediate higher-field shifts between those of the *trans* isomer of **I** and **III**. NOE observation between the aromatic protons of Dnp and pNA chromophores in the *trans* isomer of **I** is a direct evidence of the approach of these two chromophores (Fig. 6A).

Correlation between CD Spectra and β-Turn Conformations. The characteristic CD spectra of Dnp–tetrapeptide–pNA's are considered to be due to the exciton coupling of the transition moments in the two terminal chromophores. The order of Cotton effects of **I**—**III** shown in Fig. 3 is in a good accordance with the order of populations of β-turn conformers in **I**—**III** estimated from NMR measurements: In CD_3OH and in DMF-d_7 solutions, **I** has higher population of β-turn conformers than **II**, and **III** does not take a β-turn conformation. In DMSO-d_6 solution, **I** has some populations of β-turn conformer, though at a lower level than those in CD_3OH and in DMF-d_7 solutions, while **II** has little population of β-turn conformer as well as **III**. These good agreements suggest that the CD spectra of Dnp–pNA derivatives of tetrapeptides are good reflections of β-turn preference of the peptides.

Structure-activity Relationship of Gramicidin S Analogs. The β-turn preferences of **I**—**III** showed good correlation with the activities of the GS analogs having the same tetrapeptide sequences as **I**—**III** at their β-turn parts. This means that conformational preference of partial sequences of GS analogs seem to play a significant role for determining their biological activities as the results of stabilization of their active conformations.

We thank Professor Tatsuo Miyazawa of The University of Tokyo for helpful discussion.

References

1) Part V of this series: M. Kawai, K. Sato, R. Sugawara, and U. Nagai, *Bull. Chem. Soc. Jpn.*, **56**, 3005 (1983).

2) The abbreviations used in this paper are those recommended by IUPAC-IUB: *J. Biol. Chem.*, **247**, 977 (1972). Additional abbreviations: Dnp, 2,4-dinitrophenyl; pNA, *p*-nitroanilide; DSS, sodium 2,2-dimethyl-2-silapentane-5-sulfonate; TMS, tetramethylsilane; DMF, *N*,*N*-dimethylformamide; DMSO, dimethyl sulfoxide; FID, free induction decay.

3) A. Stern, W. A. Gibbons and L. C. Craig, *Proc. Natl. Acad. Sci. U.S.A.*, **61**, 734 (1968); R. Schwyzer and U. Ludescher, *Biochemistry*, **7**, 2591 (1968).

4) N. Izumiya, T. Kato, H. Aoyagi, M. Waki, and M. Kondo, "Synthetic Aspects of Biologically Active Cyclic Peptides–Gramicidin S and Tyrocidines, "Kodansha, Tokyo, and Halsted Press, New York (1979), pp. 49—70.

5) Ref. 4, pp. 71—97.

6) M. Kawai and U. Nagai, *Biopolymers*, **17**, 1549 (1978); T. Higashijima, M. Tasumi,T. Miyazawa, M. Kawai, and U. Nagai, "Peptide Chemistry 1977; Proceedings of the 15th Symposium on Peptide Chemistry," ed by T. Shiba, Protein Research Foundation, Osaka (1978), pp. 97—102.

7) K. Sato, M. Kawai, and U. Nagai, *Biopolymers*, **20**, 1921 (1981).

8) K. Sato, M. Kawai, and U. Nagai, *Bull. Chem. Soc. Jpn.*, **56**, 1527 (1983).

9) C. Deber, V. Madison, and E. R. Blout, *Acc. Chem. Res.*, **9**, 106 (1976) and references therein.

10) M. Ohnishi and D. W. Urry, *Biochem. Biophy. Res. Commun.*, **36**, 194 (1969); K. D. Kopple, M. Ohnishi, and A. Go, *Biochemistry*, **8**, 4087 (1969).

11) V. F. Bystrov, "Progress in Nuclear Magnetic Resonance Spectroscopy, 10" ed by J. W. Emsley, J. Feeney, and L. H. Sutcliffe, Pergamon Press, Oxford (1976), pp.41—81.

Studies on the β-Turn of Peptides. VII.[1] Syntheses and Antibiotic Activities of Gramicidin S Analogs with L-Pro-L-Asn or L-Pro-D-Ala Sequence at the β-Turn Part

Kazuki SATO* and Ukon NAGAI

Mitsubishi-Kasei Institute of Life Sciences, 11 Minamiooya, Machida, Tokyo 194

(Received April 30, 1983)

Two analogs of gramicidin S (GS), [L-Pro$^{4,4'}$, L-Asn$^{5,5'}$]-GS (**10a**) and [L-Pro$^{4,4'}$, D-Ala$^{5,5'}$]-GS were synthesized to investigate the possibility of replacing the β-turn part of GS by a different type of β-turn keeping the biological activity. For the synthesis of **10a**, three procedures were examined and satisfactory results were obtained by the active ester method applied to cyclization of linear decapeptide with L-Pro at the C-terminus. Neither analog showed antibiotic activity indicating that the β-turn part of GS could not be replaced with L-Pro-L-Asn or L-Pro-D-Ala sequences without affecting on its activity. The CD and ORD spectra of the analogs and their 2,4-dinitrophenyl derivatives showed weaker Cotton effects than those of GS and its derivative, respectively. So, the analogs were considered not to take GS-like β-sheet conformation. The reason why the analogs did not take such conformations was investigated by the model tetrapeptides with chromophoric substituents.

Gramicidin S (GS) is a cyclic decapeptide antibiotic with the primary structure shown in Fig. 1.[2] Several models have been proposed for the conformation of GS in solid state and solution.[3] The most favorable model is the intramolecular antiparallel β-sheet with four hydrogen bonds between Val and Leu residues, and two β-turns (type II') around the D-Phe–Pro sequences (Fig. 2).[4] The characteristic feature of this conformation is the orientation of side chains in which the charged Orn side chains are on one side and the hydrophobic Val and Leu side chains on the other side of the molecule.[5] Kato and Izumiya introduced the word "sidedness hypothesis" which means that the sidedness is important for the antibiotic activity of GS.[6,7] The hypothesis is supported by the results of many investigations of synthetic amino acid-substituted analogs.[8] The characteristic conformation of GS is considered to be stabilized not only by the four intramolecular hydrogen bonds but also by the stable β-turns formed by the two D-Phe–Pro sequences. The antibacterial activities of the GS analogs substituted both or either of 4,4' and 5,5' positions are summarized as follows:[8] The analogs in which D-Phe residues at the 4,4' positions are replaced with other D-amino acids show antibacterial activity, while replacement with L-amino acids leads to loss of activity, and the analog replaced with Gly shows weaker activity than the D-amino acid analogs. The Pro residues at the 5,5' positions can be replaced by a variety of amino acids (Gly, Sar, Leu, *etc.*) without loss of activity. One of the exceptions is [Aib$^{5,5'}$]-GS which shows no antibacterial activity. The activity of these analogs closely correlate to their conformations.[9] For example, the population of GS-type β-sheet conformer was in the order of GS≈[D-Ala$^{4,4'}$]-GS>[Gly$^{4,4'}$]-GS≫[L-Ala$^{4,4'}$]-GS≈0.[10]

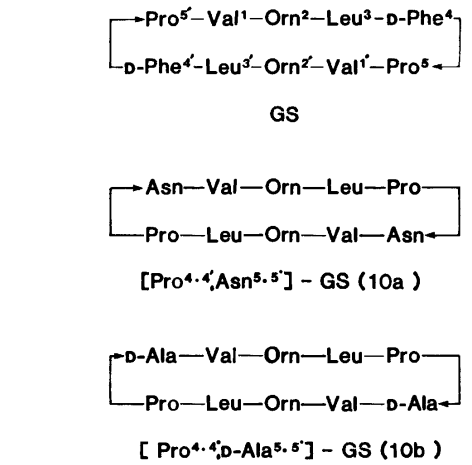

Fig. 1. Primary structures of GS and its analogs (**10a** and **10b**).

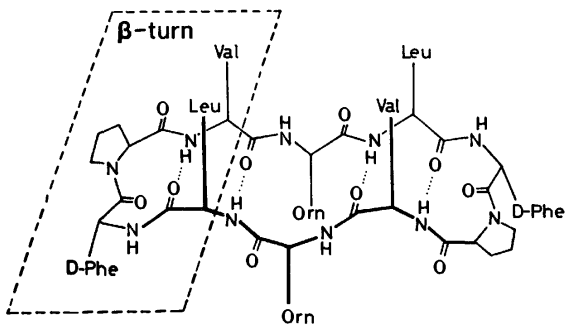

Fig. 2. β-Sheet conformation of GS.

In the course of studies on the β-turn of peptides, we proposed a new method to study the β-turn conformation of linear tetrapeptides.[1,11–15] *N*-(2,4-Dinitrophenyl)tetrapeptide *p*-nitroanilides (Dnp–tetrapeptide–pNA's) exhibit characteristic CD spectra above 250 nm when they take β-turn conformations. The Cotton effects are considered to be due to the exciton coupling of the transition moments in the two terminal chromophores. The magnitude of the Cotton effects near 350 and 310 nm were shown to reflect well the β-turn preference of the tetrapeptides.[11] In the case of model peptides related to the β-turn part of GS, β-turn preferences of the tetrapeptide derivatives had strong correlation with antibiotic activities of the GS analogs containing similar tetrapeptide sequences at their β-turn part.[12] Another series of compounds with a general structure Dnp–Gly–Pro–Y–Gly–pNA (Y=Asn, Gly, Ala, Gln, D-Ala) showed strong CD bands with opposite sign to those of GS-model peptides.[13] The

results indicated that the type of β-turn of the latter compounds were different from that of GS-model peptides (type II'). When Y was D-Ala, the strongest CD bands were observed and next ones were observed when Y was Asn (*cf.* Fig. 9).

It is of interest whether the β-turn part of GS can be replaced by a different type of β-turn keeping the biological activity. This paper describes the syntheses, antibiotic activities, and CD and ORD measurements of [Pro$^{4,4'}$, Asn$^{5,5'}$]-GS (**10a**) and [Pro$^{4,4'}$, D-Ala$^{5,5'}$]-GS (**10b**), in which the D-Phe–Pro sequences in GS were replaced by Pro–Asn and Pro–D-Ala sequences, respectively (Fig. 1). If Pro–Asn or Pro–D-Ala sequence could take stable β-turn conformation when incorporated in a cyclic decapeptide structure, the analogs would take GS-like β-sheet conformation, which would fulfil the "sidedness hypothesis," and would exhibit antibiotic activity.

Results and Discussion

Syntheses of Peptides. First, we chose the route A shown in Fig. 3 for the synthesis of **10a**, because GS and its analogs had been synthesized in satisfactory results by cyclization of linear decapeptides with Leu at the C-terminus.[16,17] Stepwise chain elongation from C-terminal tripeptide H–Val–Orn(Z)–Leu–OEt[17] gave Boc–pentapeptide ester (**3**), which was converted into pentapeptide ester (**4**) and Boc–pentapeptide hydrazide (**5**) with the aid of hydrogen chloride in formic acid and hydrazine hydrate, respectively. Fragment condensation of **4** and **5** by azide method afforded Boc–decapeptide ester (**6**), which was converted into the hydrazide derivative (**7**) by treatment with hydrazine hydrate. Deblocking of Boc-group of **7** gave N-terminal-free decapeptide hydrazide (**8**). Cyclization of **8** by azide method was examined, but the results were not satisfactory because of low yields ($\leq$11%) of the crude cyclized peptide and many by-products contaminated. These results forced us to change the synthetic strategy.

Next, we examined two different routes (routes B and C) concurrently, in which the Pro residue was placed at the C-terminus and azide method and active ester method were employed for cyclization as shown in Figs. 4 and 5, respectively. In route B, Boc–pentapeptide ester (**17**) was prepared by stepwise elongation from C-terminal H–Pro–OBzl. Pentapeptide ester (**18**) and Boc–pentapeptide hydrazide (**19**) both derived from **17** were coupled by azide method to afford Boc–decapeptide ester (**20**), which was converted into the

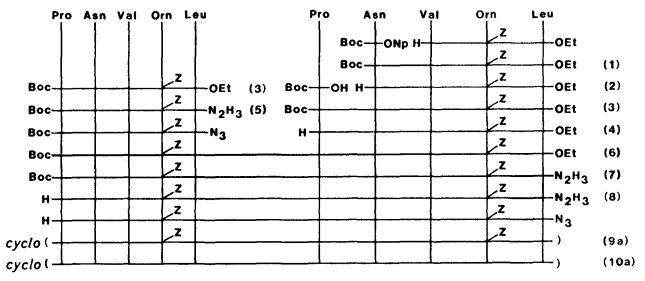

Fig. 3. Route A for the synthesis of **10a**.

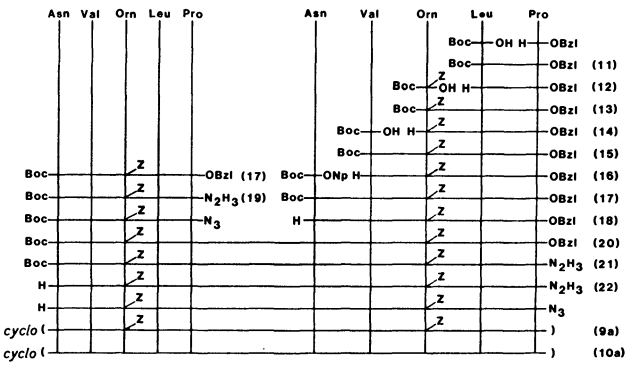

Fig. 4. Route B for the synthesis of **10a**.

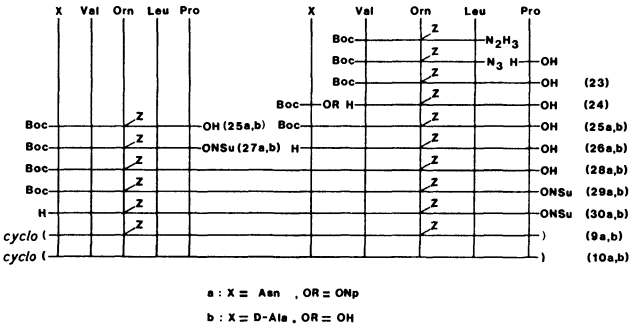

Fig. 5. Route C for the synthesis of **10a** and **10b**.

hydrazide derivative (**21**). Cyclization of **22** derived from **21** gave higher yield (38%) of crude cyclized peptide than that in route A. The crude product was purified by Sephadex LH-20 column chromatography and repeated recrystallization, however, small amount of by-product could not be removed. In route C, Boc-tetrapeptide with free carboxy terminus (**23**) was prepared by azide coupling of Boc–Val–Orn(Z)–Leu–N_2H_3[10] with H–Pro–OH. Compound **23** was treated with hydrogen chloride in formic acid, and subsequent active ester coupling of **24** with Boc–Asn–ONp afforded Boc–pentapeptide (**25a**). Pentapeptide (**26a**) and Boc–pentapeptide–ONSu (**27a**) both derived from **25a** were coupled to afford Boc–decapeptide (**28a**), which was converted into Boc–decapeptide–ONSu (**29a**). Boc-group of **29a** was removed with TFA to afford decapeptide–ONSu (**30a**). Cyclization of **30a** by active ester method gave satisfactory results: Yield of the crude cyclized peptide was 84%, and analytically pure **9a** was obtained after gel filtration with Sephadex LH-20 in 81% yield from **30a**. Compound **9a** prepared by route C was hydrogenated to afford [Pro$^{4,4'}$, Asn$^{5,5'}$]-GS (**10a**).

Another analog, [Pro$^{4,4'}$, D-Ala$^{5,5'}$]-GS (**10b**), was synthesized by the similar manner to that described for **10a** according to route C as shown in Fig. 5. The homogeneity of **10a** and **10b** was confirmed by thin-layer chromatography, paper electrophoresis, elemental analysis, and amino acid analysis.

It is interesting that the results of the cyclization largely depend on the sequence of the linear decapeptide precursor and on the activation method. Minematsu *et al.* reported high sequence dependence in the cyclization of linear pentapeptide precursor of GS.[18] They considered that steric character of terminal amino acids

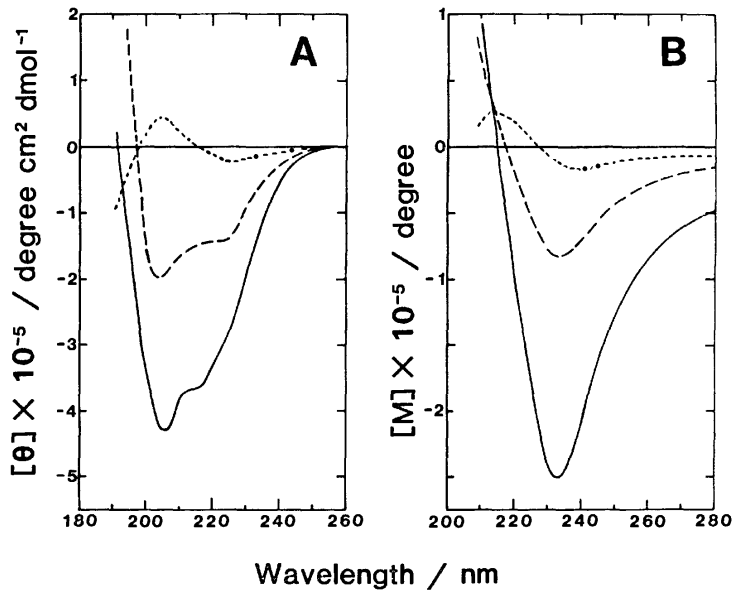

Fig. 6. CD (A) and ORD (B) spectra of GS and its analogs (**10a** and **10b**) in MeOH. ——: GS, – – –: **10a**, ·····: **10b**.

and conformation of peptide in the precursor might be important factors governing the marked differences in the mode of cyclization. Lee and Izumiya explained the sequence dependence in the cyclization of linear hexapeptide precursor of protodestruxin through the assumed conformation of the linear hexapeptide.[19] However, as far as we are aware, such a high sequence dependence as that shown in this work has not been reported in the case of cyclization of linear decapeptide precursor of GS and its analogs. Although the reason why such a high sequence dependence was observed is not clear, steric character of terminal amino acids is considered to play an important role for determining the mode of cyclization. Nucleophilic attack of amino group of Asn residue to carbonyl group of Pro residue (routes B and C) may be less hindered than that of imino group of Pro residue to carbonyl group of Leu residue (route A). As to activation method, active ester method seems to be more useful than azide method because of higher yield and experimental simplicity, when racemization-free amino acid such as Pro or Gly is used at the C-terminus of the linear precursor peptide.

CD and ORD Studies. Figure 6 shows the CD and ORD spectra of GS and its analogs (**10a** and **10b**). The analog **10a** shows similar curves to those of GS in shape, but the Cotton effects were much weaker than those of GS. In the case of **10b**, the shapes of the curves were also much different from those of GS. Usually, active analogs of GS having GS-like β-sheet conformation are considered to show similar ORD curves to that of GS.[9] It is possible for the analogs, **10a** and **10b**, to show the different CD and ORD spectra from those of GS even when they have β-sheet conformations, because the type of the β-turn of these analogs is considered to differ from that of GS. However, weak Cotton effects shown by the analogs suggest that they have some unordered conformations. The CD spectrum of the bis(Dnp) derivative of GS, [Orn(Dnp)[2,2']]-GS (**31c**), shows strong Cotton effects

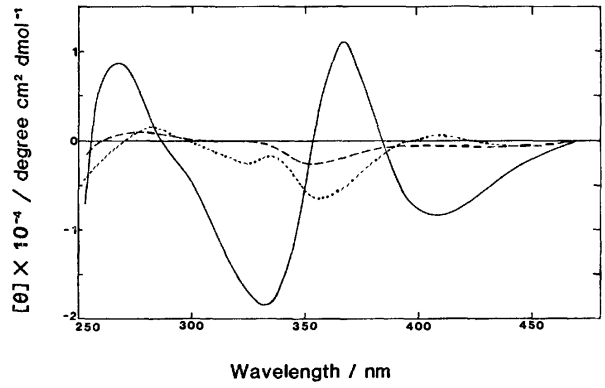

Fig. 7. CD spectra of bis(Dnp) derivatives of GS (**31c**), **10a** (**31a**), and **10b** (**31b**) in MeOH. ——: **31c**, – – –: **31a**, ·····: **31b**.

above 250 nm due to the interaction of the two Dnp chromophores, because the side chains of the two Orn residues in GS are close to each other owing to the β-sheet conformation of GS (Fig. 2).[10] Both of the bis(Dnp) derivatives of **10a** and **10b** (**31a** and **31b**, respectively) showed much weaker Cotton effects than that of GS, suggesting that neither **10a** nor **10b** took GS-like β-sheet conformation (Fig. 7).

Biological Activities. Neither **10a** nor **10b** showed antibiotic activities even at the concentration of 100 μg/ml. At such higher concentrations as 400 μg/ml and 200 μg/ml, respectively, **10a** and **10b** showed antibiotic activities on some Gram-positive bacteria, but practically they were inactive. The results indicate that the β-turn part of GS cannot be replaced with Pro–Asn or Pro–D-Ala sequences without affecting on its activity. Certainly, both analogs were hard to be absorbed on the cells of GS-sensitive strains (*B. subtilis* and *S. aureus*).[20]

Conformations and β-Turn Preferences. The inactivities of the analogs (**10a** and **10b**) seemed to result

from the fact that they did not take GS-like β-sheet conformation on the basis of the CD and ORD studies. So, the reason why they did not take such conformations was investigated. Heretofore, the high β-turn preferences of Pro–Asn and Pro–D-Ala sequences have been discussed by the model peptides with Gly residues at the first and the fourth positions of tetrapeptides,[13] however in the GS analogs these positions are occupied by Leu and Val residues, respectively. So, we synthesized Dnp–Leu–Pro–Asn–Val–pNA (**37a**) and Dnp–Leu–Pro–D-Ala–Val–pNA (**37b**), in which the terminal positions of Dnp–Gly–Pro–Y–Gly–pNA (Y=Asn or D-Ala) were replaced with Leu and Val residues, respectively (Fig. 8). Both of **37a** and **37b** showed weak Cotton effects similar to those of Dnp–Leu–Ala–Pro–Val–pNA which is considered to take random conformation (Figs. 9A and 9B).[11] The results indicated the importance of the terminal amino acid residues for the tetrapeptide sequences to take β-turn conformation. So, reluctance of the tetrapeptide sequences to take β-turn is considered to be the reason why **10a** and **10b** do not take GS-like β-sheet conformation. It is interesting to note that in the case of GS-model peptides, similar replacement of the terminal residues do not affect the β-turn preference (Fig. 9C).[12]

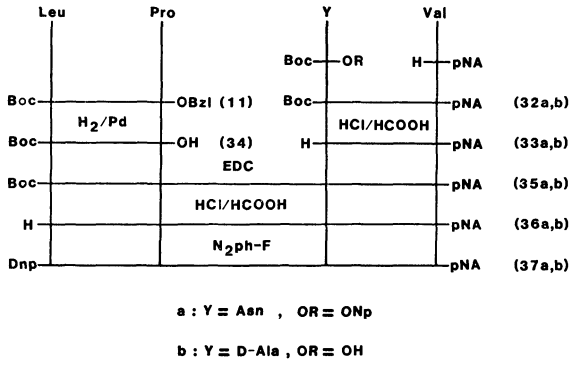

Fig. 8. Synthetic route of Dnp-Leu-Pro-Y-Val-pNA (**37a**: Y=Asn, **37b**: Y=D-Ala).

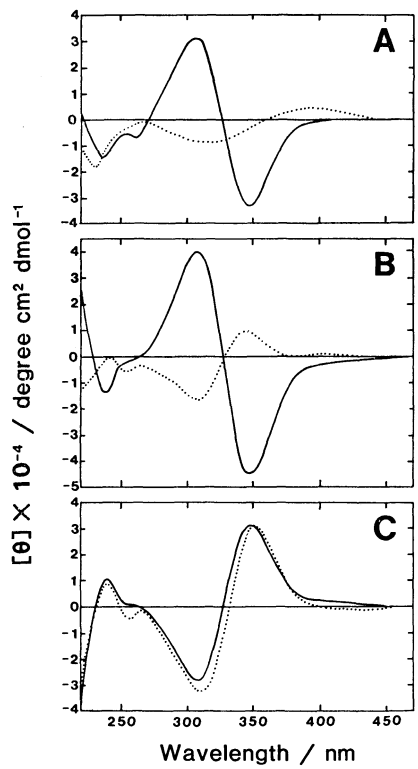

Fig. 9. CD spectra of Dnp-X′-Pro-Asn-Y′-pNA (A), Dnp-X′-Pro-D-Ala-Y′-pNA (B), and Dnp-X′-D-Ala-Pro-Y′-pNA (C)[12] in MeOH. ——: X′=Y′=Gly, ·····: X′=Leu, Y′=Val.

Experimental

Syntheses of Peptides. All the melting points were measured on a Yanagimoto micro melting point apparatus and were uncorrected. TLC's were carried out on Merck silica gel 60 F_{254} plates with the following solvent systems: R_f^1, $CHCl_3$–MeOH (5:1, v/v); R_f^2, $CHCl_3$–MeOH–AcOH (95:5:1, v/v); R_f^3, *n*-BuOH–AcOH–pyridine–H_2O (4:1:1:2, v/v). Optical rotations were measured on an Union automatic polarimeter PM-201. Amino acid analyses of peptides were performed by Durrum D-500 Amino Acid Analyzer after hydrolyses in 6 M (1 M=1 mol dm^{-3}) HCl at 105 °C for 20 h.

*Boc–Asn–Val–Orn(Z)–Leu–OEt (**1**).* To a solution of H–Val–Orn(Z)–Leu–OEt·HCl[17] (2.72 g, 5 mmol) and TEA (0.7 ml, 5 mmol) in DMF (20 ml) was added Boc–Asn–ONp (1.77 g, 5 mmol). The reaction mixture was stirred at room temperature overnight and evaporated to leave a solid which was collected by filtration with the aid of water and washed successively with 10% citric acid, 4% $NaHCO_3$, and water, and dried *in vacuo* over P_2O_5. The crude product was recrystallized from MeOH; yield, 2.67 g (74%); mp 214 °C; $[\alpha]_D^{22}$ −57.2° (*c* 1, MeOH); R_f^1 0.69, R_f^2 0.24, R_f^3 0.97.

Found: C, 58.58; H, 7.48; N, 11.47%. Calcd for $C_{35}H_{56}O_{10}N_6$: C, 58.32; H, 7.83; N, 11.66%.

*H–Asn–Val–Orn(Z)–Leu–OEt·HCl (**2**·HCl).* Compound **1** (2.16 g, 3 mmol) was dissolved in 0.1 M hydrogen chloride in formic acid (36 ml). The solution was allowed to stand at room temperature for 30 min and evaporated. The residue was solidified by the addition of ether; yield, 1.97 g (100%); mp 210—212 °C; $[\alpha]_D^{22}$ −33.0° (*c* 1, MeOH); R_f^1 0.25, R_f^3 0.71.

Found: C, 54.62; H, 7.51; N, 12.77%. Calcd for $C_{30}H_{49}O_8N_6Cl$: C, 54.83; H, 7.52; N, 12.79%.

*Boc–Pro–Asn–Val–Orn(Z)–Leu–OEt (**3**).* To a chilled solution of Boc–Pro–OH (344 mg, 1.6 mmol) and TEA (0.22 ml, 1.6 mmol) in THF (5 ml) was added isobutyl chloroformate (0.21 ml, 1.6 mmol) at −15 °C. After 10 min, a chilled solution of **2**·HCl (1.05 g, 1.6 mmol) and TEA (0.22 ml, 1.6 mmol) in DMF (5 ml) was added. The mixture was stirred at 0 °C for 1 h and at room temperature overnight and evaporated *in vacuo*. After the addition of water, the solid formed was collected by filtration and washed as described for **1**. The crude product was recrystallized from EtOH; yield, 1.11 g (85%); mp 193 °C; $[\alpha]_D^{22}$ −75.8° (*c* 1, MeOH); R_f^1 0.67, R_f^2 0.13, R_f^3 0.93.

Found: C, 58.54; H, 7.66; N, 11.71%. Calcd for $C_{40}H_{63}O_{11}N_7$: C, 58.73; H, 7.76; N, 11.99%.

*H–Pro–Asn–Val–Orn(Z)–Leu–OEt·HCl(**4**·HCl).* Compound **3** (409 mg, 0.5 mmol) was treated with 0.1 M hydrogen chloride in formic acid (6 ml) as described for **2**·HCl; yield, 362 mg (96%); mp 220—222 °C; $[\alpha]_D^{22}$ −62.8° (*c* 0.5, MeOH); R_f^1 0.12, R_f^3 0.69.

Found: C, 55.58; H, 7.17; N, 13.00%. Calcd for $C_{35}H_{56}O_9N_7Cl$: C, 55.73; H, 7.48; N, 13.00%.

*Boc–Pro–Asn–Val–Orn(Z)–Leu–N_2H_3 (**5**).* A solution of **3** (491 mg, 0.6 mmol) and hydrazine hydrate (0.58 ml,

12 mmol) in DMF (3 ml) was allowed to stand at room temperature for 2 d. The solution was poured dropwise into chilled water (100 ml), and the precipitate formed was collected by filtration, washed with water, and dried. The crude product was recrystallized from EtOAc; yield, 357 mg (74%); mp 235—236 °C; $[\alpha]_D^{22}$ −63.0° (*c* 0.2, MeOH); R_f^1 0.47, R_f^3 0.83.

Found: C, 56.33; H, 7.59; N, 15.65%. Calcd for $C_{38}H_{61}O_{10}N_9 \cdot 1/2\ H_2O$: C, 56.13; H, 7.69; N, 15.51%.

Boc–(Pro–Asn–Val–Orn(Z)–Leu)$_2$–OEt (**6**). To a solution of **5** (322 mg, 0.4 mmol) in DMF (2 ml) were added 2 M hydrogen chloride in EtOAc (0.8 ml) and isopentyl nitrite (0.056 ml, 0.4 mmol) at −60 °C. After being stirred at −20 °C for 10 min, the solution was cooled again to −60 °C and neutralized with TEA (0.22 ml, 1.6 mmol). To the solution was added a chilled solution of **4**·HCl (302 mg, 0.4 mmol) and TEA (0.056 ml, 0.4 mmol) in DMF (1 ml). The reaction mixture was stirred at 0 °C for 2 d and then evaporated. Addition of water to the residue gave a white precipitate, which was filtered, washed successively with 10 % citric acid, 4% $NaHCO_3$, and water, and dried over P_2O_5. The crude product dissolved in MeOH (5 ml) was applied to a column (3×170 cm) of Sephadex LH-20 and eluted with MeOH. The fractions with the desired product detected by UV absorption and TLC were collected and evaporated to leave a solid which was recrystallized from EtOH; yield, 439 mg (74%); mp 227—228 °C; $[\alpha]_D^{22}$ −96.0° (*c* 0.2, MeOH); R_f^1 0.64, R_f^3 0.86.

Found: C, 58.05; H, 7.33; N, 12.96%. Calcd for $C_{73}H_{112}O_{19}N_{14} \cdot H_2O$: C, 58.15; H, 7.62; N, 13.01%.

Boc–(Pro–Asn–Val–Orn(Z)–Leu)$_2$–N_2H_3 (**7**). A solution of **6** (402 mg, 0.27 mmol) and hydrazine hydrate (0.65 ml, 13.5 mmol) in DMF (5 ml) was treated as described for **5**. The crude product was recyrstallized from DMF–ether; yield, 325 mg (82%); mp 238—240 °C; $[\alpha]_D^{22}$ −76.0° (*c* 0.2, MeOH); R_f^1 0.31, R_f^3 0.83.

Found: C, 57.14; H, 7.41; N, 15.11%. Calcd for $C_{71}H_{110}O_{18}N_{16} \cdot H_2O$: C, 57.08; H, 7.56; N, 15.01%.

H–(Pro–Asn–Val–Orn(Z)–Leu)$_2$–N_2H_3·2HCl (**8**·2HCl). Compound **7** (295 mg, 0.2 mmol) was treated with 0.1 M hydrogen chloride in formic acid (5 ml) as described for **2**·HCl; yield, 284 mg (98%); mp 215—217 °C; $[\alpha]_D^{22}$ −89.0° (*c* 0.2, MeOH); R_f^1 0.02, R_f^3 0.66.

Found: C, 54.41; H, 7.11; N, 15.21%. Calcd for $C_{66}H_{104}O_{16}N_{16}Cl_2$: C, 54.72; H, 7.24; N, 15.47%.

cyclo(–(*Pro–Asn–Val–Orn(Z)–Leu)$_2$*–) (**9a**). To a solution of **8**·2HCl (174 mg, 0.12 mmol) in DMF (2 ml) were added 2 M hydrogen chloride in EtOAc (0.24 ml) and isopentyl nitrite (0.017 ml, 0.12 mmol) at −60 °C. After 20 min, the reaction mixture was added to pyridine (60 ml) at 0 °C. After being stirred at 0 °C for 3 d, the solution was evaporated and the residue was dissolved in a mixture (120 ml) of MeOH–H_2O (5:1, v/v). The solution was applied to columns (1.6×10 cm each) of Dowex 50 (H^+ form) and Dowex 1 (OH^- form). The columns were washed with the same solvent (200 ml) and the effluent was evaporated to leave a white solid, which was collected by filtration with the aid of water. Because of the low yield, 17 mg (11%), and the contaminated by-products (R_f^1, 0.40 and 0.35) estimated to 50% of the crude product, further treatment of the crude product was not carried out. Cyclizations examined further two times gave similar results.

Boc–Leu–Pro–OBzl (**11**). Boc–Leu–OH (4.63 g, 20 mmol) and H–Pro–OBzl·HCl (4.83 g, 20 mmol) were coupled by mixed anhydride method as described for **3**. The reaction mixture was evaporated and the residue was dissolved in EtOAc. The solution was washed successively with 10% citric acid, 4% $NaHCO_3$, and water, dried over Na_2SO_4, and evaporated to leave an oil; yield, 7.61 g (91%); R_f^1 0.89, R_f^2 0.76.

H–Leu–Pro–OBzl·HCl (**12**·HCl). Compound **11** (7.61 g, 18 mmol) was treated with 0.1 M hydrogen chloride in formic acid as described for **2**·HCl; yield, 6.36 g (90%); mp 150—151 °C; $[\alpha]_D^{22}$ −67.8° (*c* 1, MeOH); R_f^1 0.48, R_f^2 0.04, R_f^3 0.70.

Found: C, 60.52; H, 7.05; N, 8.01%. Calcd for $C_{18}H_{27}O_3N_2Cl$: C, 60.92; H, 7.67; N, 7.89%.

Boc–Orn(Z)–Leu–Pro–OBzl (**13**). This compound was prepared from Boc–Orn(Z)–OH (1.72 g, 4.7 mmol) and **12**·HCl (1.67 g, 4.7 mmol) as described for **11**; yield of an oil, 2.44 g (78%); R_f^1 0.88, R_f^2 0.58, R_f^3 0.92.

H–Orn(Z)–Leu–Pro–OBzl·HCl (**14**·HCl). A solution of **13** (2.44 g, 3.7 mmol) in 0.1 M hydrogen chloride in formic acid was allowed to stand at room temperature for 30 min and evaporated to leave an oil, which was kept over KOH pellets under reduced pressure overnight and used for the next reaction without further treatment; yield, 2.21 g (100%); R_f^1 0.71, R_f^2 0.09, R_f^3 0.75.

Boc–Val–Orn(Z)–Leu–Pro–OBzl (**15**). This compound was prepared from Boc–Val–OH (0.08 g, 3.7 mmol) and **14**·HCl (2.21 g, 3.7 mmol) as described for **11**; yield of an oil, 2.35 g (84%); R_f^1 0.89, R_f^2 0.54, R_f^3, 0.98.

H–Val–Orn(Z)–Leu–Pro–OBzl·HCl (**16**·HCl). Compound **15** (2.35 g, 3.1 mmol) was dissolved in 0.1 M hydrogen chloride in formic acid, and the solution was allowed to stand at room temperature for 30 min and evaporated. The residue dissolved in a mixture (5 ml) of $CHCl_3$–MeOH–AcOH (95:5:1, v/v) was applied to a column (3.3×35 cm) of silica gel 60 (Merck) and the column was washed with the same solvent. The desired product was eluted with a mixture of $CHCl_3$–MeOH (9:1, v/v); yield of an oil, 1.98 g (92%); R_f^1 0.36, R_f^2 0.07.

Boc–Asn–Val–Orn(Z)–Leu–Pro–OBzl (**17**). Boc–Asn–ONp (0.99 g, 2.8 mmol) and **16**·HCl (1.98 g, 2.8 mmol) were treated as described for **1**. The crude product dissolved in MeOH (5 ml) was applied to a column (3×170 cm) of Sephadex LH-20 and eluted with MeOH. The fractions with the desired product were collected and evaporated. Addition of ether to the residue gave a solid which was recrystallized from MeOH–ether; yield, 1.91 g (77%); mp 186—188 °C; $[\alpha]_D^{22}$ −90.0° (*c* 1, MeOH); R_f^1 0.75, R_f^2 0.25, R_f^3 0.95.

Found: C, 61.29; H, 7.52; N, 11.08%. Calcd for $C_{45}H_{65}O_{11}N_7$: C, 61.41; H, 7.45; N, 11.14%.

H–Asn–Val–Orn(Z)–Leu–Pro–OBzl·HCl (**18**·HCl). Compound **17** (409 mg, 0.46 mmol) was treated with 0.1 M hydrogen chloride in formic acid (5.5 ml) as described for **2**·HCl; yield, 376 mg (100%); mp 185—188 °C; $[\alpha]_D^{22}$ −72.2° (*c* 1, MeOH); R_f^1 0.31, R_f^3 0.72.

Found: C, 56.68; H, 7.02; N, 11.73%. Calcd for $C_{40}H_{58}O_9N_7Cl \cdot 3/2\ H_2O$: C, 56.96; H, 7.29; N, 11.62%.

Boc–Asn–Val–Orn(Z)–Leu–Pro–N_2H_3 (**19**). Compound **17** (491 mg, 0.6 mmol) was treated with hydrazine hydrate (1.16 ml, 24 mmol) as described for **5**; yield, 302 mg (68%); mp 176—178 °C; $[\alpha]_D^{22}$ −96.8° (*c* 0.5, MeOH); R_f^1 0.43, R_f^2 0.02, R_f^3 0.85.

Found: C, 56.58; H, 7.74; N, 15.35%. Calcd for $C_{38}H_{61}O_{10}N_9$: C, 56.77; H, 7.65; N, 15.68%.

Boc–(Asn–Val–Orn(Z)–Leu–Pro)$_2$–OBzl (**20**). This compound was prepared from **19** (260 mg, 0.35 mmol) and **18**·HCl (264 mg, 0.35 mmol) as described for **6**; yield, 410 mg (76%); mp 218—220 °C; $[\alpha]_D^{22}$ −90.4° (*c* 0.5, MeOH); R_f^1 0.58, R_f^3 0.89.

Found: C, 60.12; H, 7.37; N, 12.58%. Calcd for

$C_{78}H_{114}O_{19}N_{14}$: C, 60.37; H, 7.41; N, 12.64%.

*Boc-(Asn-Val-Orn(Z)-Leu-Pro)$_2$-N_2H_3 (**21**).* Compound **20** (372 mg, 0.24 mmol) was treated with hydrazine hydrate (0.58 ml, 12 mmol) as described for **4**. The crude product was recrystallized from EtOH; yield, 307 mg (87%); mp 201—203 °C; $[\alpha]_D^{22}$ −104° (*c* 0.2, MeOH); R_f^1 0.21, R_f^3 0.82.

Found: C, 57.07; H, 7.51; N, 15.06%. Calcd for $C_{71}H_{110}O_{18}N_{16}\cdot H_2O$: C, 57.09; H, 7.56; N, 15.00%.

*H-(Asn-Val-Orn(Z)-Leu-Pro)$_2$-N_2H_3·2HCl (**22**·2HCl).* Compound **21** (138 mg, 0.094 mmol) was treated with 0.1 M hydrogen chloride in formic acid (2.3 ml) as described for **2**·HCl; yield, 133 mg (98%); mp 168—169 °C; $[\alpha]_D^{22}$ −68.0° (*c* 0.2, MeOH); R_f^1 0.03, R_f^3 0.69.

Found: C, 52.67; H, 6.91; N, 14.73%. Calcd for $C_{66}H_{104}O_{16}N_{16}Cl_2\cdot 3H_2O$: C, 52.76; H, 7.37; N, 14.91%.

cyclo(-(Asn-Val-Orn(Z)-Leu-Pro)$_2$-) (**9a**). Cyclization of **22**·2HCl (123 mg, 0.085 mmol) was examined by the similar manner to that of **8**·2HCl. The crude product (43 mg, 38%) eluted from columns of Dowex 50 and Dowex 1 showed one major spot (R_f^1 0.66) and two minor spots (R_f^1 0.40 and 0.55) on TLC. All the crude product was dissolved in MeOH (5 ml) and applied to a column (3×170 cm) of Sephadex LH-20, and eluted with MeOH. The fractions containing the desired product were collected and evaporated to leave a white solid, which was collected by filtration with the aid of MeOH–ether; yield of semi-purified product, 34 mg (30%). By-product with R_f^1 0.40 was removed by this treatment but that with R_f^1 0.55 was not. Repeated recrystallization did not give satisfactory results.

*Boc-Val-Orn(Z)-Leu-Pro-OH (**23**).* To a solution of Boc-Val-Orn(Z)-Leu-N_2H_3[10] (2.37 g, 4 mmol) in DMF (10 ml) were added 2 M hydrogen chloride in EtOAc (6 ml) and isopentyl nitrite (0.56 ml, 4 mmol) at −60 °C. After being stirred at −20 °C for 10 min, the solution was cooled again to −60 °C and neutralized with TEA (1.68 ml, 12 mmol). To the solution was added a chilled solution of H-Pro-OH (0.59 g, 6 mmol) and TEA (0.84 ml, 6 mmol) in H_2O (4 ml). The reaction mixture was stirred at 0 °C for 3 days and evaporated. To the residue were added 3% NH_4OH and EtOAc. The aqueous layer was washed with EtOAc and acidified with 10% citric acid, and the oily product separated was extracted with EtOAc. The organic layer was washed with water, dried (Na_2SO_4), and evaporated. The residue was solidified by successive addition of ether and petroleum ether, and the crude product was dissolved in a mixture of $CHCl_3$–MeOH (5:1, v/v), applied to a column (3.3×35 cm) of silica gel 60 (Merck), and eluted with the same solvent. The fractions containing the desired product were collected and evaporated. Addition of a small amount of EtOAc to the residue gave colorless crystals; yield, 2.03 g (73%); mp 158—160 °C; $[\alpha]_D^{22}$ −62.2° (*c* 1, MeOH); R_f^1 0.44, R_f^2 0.24, R_f^3 0.83.

Found: C, 58.27; H, 7.51; N, 10.00%. Calcd for $C_{34}H_{53}O_9N_5\cdot 3/2\ H_2O$: C, 58.10; H, 8.03; N, 9.96%.

*H-Val-Orn(Z)-Leu-Pro-OH·HCl (**24**·HCl).* Compound **23** (946 mg, 1.4 mmol) was treated with 0.1 M hydrogen chloride in formic acid (15.4 ml) as described for **2**·HCl. The product was used for the next reaction without further treatment; yield, 857 mg (100%); R_f^3 0.71.

*Boc-Asn-Val-Orn(Z)-Leu-Pro-OH (**25a**).* To a chilled solution of **24**·HCl (857 mg, 1.4 mmol) and TEA (0.39 ml, 2.8 mmol) in DMF (10 ml) was added Boc-Asn-ONp (742 mg, 2.1 mmol). The mixture was stirred at 0 °C for 1 h and at room temperature overnight and evaporated. To the residue were added 10% citric acid and EtOAc. When the organic layer was being washed with water, crystallization of the product occurred. So, the crystals were filtered and dried *in vacuo* over P_2O_5. The crude product dissolved in MeOH (5 ml) was applied to a column (3×170 cm) of Sephadex LH-20 and eluted with MeOH. The fractions containing the desired product were collected and evaporated. The residue was crystallized by successive addition of MeOH and ether; yield, 867 mg (78%); mp 172—173 °C; $[\alpha]_D^{22}$ −78.0° (*c* 1, MeOH); R_f^1 0.61, R_f^2 0.03, R_f^3 0.80.

Found: C, 56.65; H, 7.47; N, 12.16%. Calcd for $C_{38}H_{59}O_{11}N_7\cdot H_2O$: C, 56.49; H, 7.61; N, 12.14%.

*H-Asn-Val-Orn(Z)-Leu-Pro-OH·HCl (**26a**·HCl).* Compound **25a** (158 mg, 0.2 mmol) was treated with 0.1 M hydrogen chloride in formic acid (3 ml) as described for **2**·HCl. The product was used for the next reaction without further treatment; yield, 145 mg (100%); R_f^3 0.61.

*Boc-Asn-Val-Orn(Z)-Leu-Pro-ONSu (**27a**).* To a chilled solution of **25a** (237 mg, 0.3 mmol) and HONSu (59 mg, 0.6 mmol) in a mixture of DMF (2 ml) and CH_2Cl_2 (2 ml) was added EDC·HCl (115 mg, 0.6 mmol), and the reaction mixture was stirred at 0 °C overnight and evaporated. The residue was triturated with the aid of chilled water, filtered, and dried *in vacuo* over P_2O_5. The product was used for the next reaction without further treatment; yield, 263 mg (99%); R_f^1 0.58, R_f^2 0.11, R_f^3 0.81.

*Boc-(Asn-Val-Orn(Z)-Leu-Pro)$_2$-OH (**28a**).* To a chilled solution of **26a**·HCl (145 mg, 0.2 mmol) and TEA (0.056 ml, 0.4 mmol) in DMF (2 ml) was added **27a** (222 mg, 0.25 mmol), and the mixture was stirred at 0 °C for 2 days and evaporated. The residue was solidified by addition of 10% citric acid, filtered, washed with water, and dried. The crude product was purified by column chromatography with Sephadex LH-20 as described for **6**; yield, 276 mg (94%); mp 210—211 °C; $[\alpha]_D^{22}$ −94.0° (*c* 0.5, MeOH); R_f^1 0.14, R_f^3 0.83.

Found: C, 57.25; H, 7.46; N, 13.15%. Calcd for $C_{71}H_{108}O_{19}N_{14}\cdot 3/2\ H_2O$: C, 57.28; H, 7.51; N, 13.17%.

*Boc-(Asn-Val-Orn(Z)-Leu-Pro)$_2$-ONSu (**29a**).* Compound **28a** (248 mg, 0.17 mmol) and HONSu (39 mg, 0.34 mmol) was treated as described for **27a**; yield, 265 mg (100 %); R_f^1 0.45, R_f^3 0.80.

*H-(Asn-Val-Orn(Z)-Leu-Pro)$_2$-ONSu·TFA (**30a**·TFA).* Compound **29a** (265 mg, 0.34 mmol) was dissolved in TFA (5 ml), and the solution was allowed to stand at 0 °C for 1 h and evaporated. The residue was solidified by addition of ether, filtered, dried *in vacuo* over KOH. The product was used for the next reaction without further treatment; yield, 243 mg (91%); R_f^1 0.35, R_f^3 0.74.

cyclo(-(Asn-Val-Orn(Z)-Leu-Pro)$_2$-) (**9a**). A solution of **30a**·TFA (243 mg, 0.16 mmol) in DMF (8 ml) was added dropwise to pyridine (80 ml) at room temperature, and the mixture was stirred overnight and evaporated. The residue was dissolved in a mixture (60 ml) of MeOH–H_2O (5:1, v/v), and the solution was applied to columns (1.6×10 cm each) of Dowex 50 (H^+ form) and Dowex 1 (OH^- form). The columns was washed with the same solvent (150 ml.) and the combined effluent was evaporated to leave a white solid, which was collected with the aid of water. The crude product was purified by column chromatography with Sephadex LH-20 as described for **6**. The product was recrystallized from MeOH–ether; yield, 168 mg (81%); mp 241—243 °C; $[\alpha]_D^{22}$ −102° (*c* 0.5, MeOH); R_f^1 0.66, R_f^2 0.08, R_f^3 0.83. Amino acid ratios in acid hydrolyzate: Asp (1.00), Val (0.95), Orn (1.00), Leu (1.00), Pro (1.06).

Found: C, 58.27; H, 7.44; N, 14.28%. Calcd for $C_{66}H_{98}O_{16}N_{14}\cdot H_2O$: C, 58.22; H, 7.40; N, 14.40%.

cyclo(-(Asn-Val-Orn-Leu-Pro)$_2$-)·2HCl (**10a**·2HCl). Compound **9a** (67 mg, 0.05 mmol) dissolved in 0.05 M hy-

drogen chloride in MeOH (4 ml) was hydrogenated with paradium black as a catalyst. After removal of the catalyst by filtration, the filtrate was evaporated to leave a solid, which was recrystallized from MeOH–ether; yield, 49 mg (86%); mp 228—230 °C; $[\alpha]_D^{22}$ −98° (*c* 0.5, MeOH); R_f^3 0.38. Amino acid ratios in acid hydrolyzate: Asp (0.98), Val (0.94), Orn (1.00), Leu (1.00), Pro (1.05).

Found: C, 49.48; H, 7.56; N, 15.84%. Calcd for $C_{50}H_{88}O_{12}N_{14}Cl_2 \cdot 4H_2O$: C, 49.21; H, 7.93; N, 16.07%.

*Boc-D-Ala-Val-Orn(Z)-Leu-Pro-OH (**25b**).* This compound was prepared from Boc-D-Ala-ONSu (401 mg, 1.4 mmol) and **24**·HCl (857 mg, 1.4 mmol) as described for **25a**; yield, 544 mg (52%); mp 174—175 °C; $[\alpha]_D^{22}$ −52.0° (*c* 0.5, MeOH); R_f^1 0.31, R_f^2 0.09, R_f^3 0.83.

Found: C, 58.84; H, 7.73; N, 11.09%. Calcd for $C_{37}H_{58}O_{10}N_6 \cdot 1/2\ H_2O$: C, 58.78; H, 7.87; N, 11.12%.

*H-D-Ala-Val-Orn(Z)-Leu-Pro-OH·HCl (**26b**·HCl).* Compound **25b** (0.185 mg, 0.25 mmol) was treated with 0.1 M hydrogen chloride in formic acid (4 ml) as described for **2**·HCl. The product was used for the next reaction without further treatment; yield, 177 mg (100%); R_f^3 0.68.

*Boc-D-Ala-Val-Orn(Z)-Leu-Pro-ONSu (**27b**).* This was prepared from **25b** (299 mg, 0.4 mmol) and HONSu (69 mg, 0.6 mmol) as described for **27a**. The product was used for the next reaction without further treatment; yield, 214 mg (63%); R_f^1 0.78, R_f^2 0.30.

*Boc-(D-Ala-Val-Orn(Z)-Leu-Pro)$_2$-OH (**28b**).* This was prepared from **26b**·HCl (150 mg, 0.22 mmol) and **27b** (186 mg, 0.22 mmol) as described for **28a**; yield, 162 mg (54%); mp 143—145 °C; $[\alpha]_D^{22}$ −52.0° (*c* 1, MeOH); R_f^1 0.48, R_f^2 0.07, R_f^3 0.83.

Found: C, 59.77; H, 7.74; N, 12.31%. Calcd for $C_{69}H_{106}O_{17}N_{12} \cdot 1/2\ H_2O$: C, 59.85; H, 7.79; N, 12.14%.

*Boc-(D-Ala-Val-Orn(Z)-Leu-Pro)$_2$-ONSu (**29b**).* This was prepared from **28b** (138 mg, 0.1 mmol) and HONSu (23 mg, 0.2 mmol) as described for **27a**. The product was used for the next reaction without further treatment; yield, 134 mg (91%); R_f^1 0.76, R_f^2 0.29.

*H-(D-Ala-Val-Orn(Z)-Leu-Pro)$_2$-ONSu·TFA (**30b**·TFA).* Compound **29b** (134 mg, 0.091 mmol) was treated with TFA (3 ml) as described for **30a**. The product was used for the next reaction without further treatment; yield, 136 mg (100%); R_f^1 0.54, R_f^2 0.13.

cyclo(-(D-Ala-Val-Orn(Z)-Leu-Pro)$_2$-) (**9b**). This was prepared from **30b**·TFA (136 mg, 0.091 mmol) as described for **9a**; yield; 74 mg (65%); mp >300 °C; $[\alpha]_D^{22}$ −44.9° (*c* 0.5, MeOH); R_f^1 0.66, R_f^2 0.13, R_f^3 0.85. Amino acid ratios in acid hydrolyzate: Ala (1.07), Val (1.04), Orn (1.06), Leu (1.00), Pro (1.11).

Found: C, 60.55; H, 7.68; N, 13.13%. Calcd for $C_{64}H_{96}O_{14}N_{12} \cdot H_2O$: C, 60.26; H, 7.74; N, 13.18%.

cyclo(-(D-Ala-Val-Orn-Leu-Pro)$_2$-)·2HCl (**10b**·2HCl). Compound **9b** (50 mg, 0.04 mmol) was hydrogenated as described for **10a**·2HCl; yield, 33 mg (78%); mp 261—263 °C; $[\alpha]_D^{22}$ −36.1° (*c* 0.5, MeOH); R_f^3 0.44. Amino acid ratios in acid hydrolyzate: Ala (1.00), Val (0.95), Orn (1.00), Leu (1.00), Pro (1.05).

Found: C, 52.11; H, 8.04; N, 15.04%. Calcd for $C_{48}H_{86}O_{10}N_{12}Cl_2 \cdot 2H_2O$: C, 52.49; H, 8.26; N, 15.30%.

*Bis(Dnp) Derivatives of **10a** and **10b** (**31a** and **31b**).* A small amount of **10a** and **10b** were treated with N_2ph–F as usual way[10] and purified by silica-gel (Merck) column chromatography; **31a**: R_f^1 0.63, R_f^2 0.08, R_f^3 0.78; **31b**: R_f^1 0.68, R_f^2 0.22, R_f^3 0.82.

*Boc-Asn-Val-pNA (**32a**).* Boc-Asn-ONp (706 mg, 2 mmol) and H-Val-pNA (476 mg, 2 mmol) were treated as described for **1**. The crude product was recrystallized from EtOH; yield, 666 mg (74%); mp 225—227 °C; $[\alpha]_D^{22}$ −121.0° (*c* 0.2, MeOH); R_f^1 0.63, R_f^2 0.16, R_f^3 0.92.

Found: C, 52.89; H, 6.36; N, 15.32%. Calcd for $C_{20}H_{29}O_7N_5$: C, 53.20; H, 6.47; N, 15.51%.

*H-Asn-Val-pNA·HCl (**33a**·HCl).* Compound **32a** (451 mg, 1 mmol) was treated with 0.1 M hydrogen chloride in formic acid (12 ml) as described for **2**·HCl; yield, 413 mg (100%); mp 160—162 °C; $[\alpha]_D^{22}$ −18.4° (*c* 1, MeOH); R_f^1 0.16, R_f^3 0.73.

Found: C, 45.26; H, 5.58; N, 17.56%. Calcd for $C_{15}H_{22}O_5N_5Cl \cdot 1/2\ H_2O$: C, 45.39; H, 5.84; N, 17.65%.

*Boc-Leu-Pro-OH (**34**).* Compound **11** (1.38 g, 3.3 mmol) dissolved in MeOH (10 ml) was hydrogenated with paradium black as a catalyst. After removal of the catalyst by filtration, the filtrate was evaporated to a foam, which was used for the next reaction without further treatment; yield, 1.08 g (100%); R_f^1 0.69, R_f^2 0.47, R_f^3 0.67.

*Boc-Leu-Pro-Asn-Val-pNA (**35a**).* To a chilled solution of **33a**·HCl (116 mg, 0.3 mmol) in $CHCl_3$ (3 ml) were added TEA (0.042 ml, 0.3 mmol), **34** (99 mg, 0.3 mmol), and EDC·HCl (58 mg, 0.3 mmol). The reaction mixture was treated as described for **11**, and the crude product obtained as a solid was purified by LH-20 column chromatography as described for **17**; yield, 75 mg (38%); mp 128—130 °C; $[\alpha]_D^{22}$ −130.0° (*c* 0.5, MeOH); R_f^1 0.67, R_f^2 0.15, R_f^3 0.81.

Found: C, 55.70; H, 7.13; N, 14.77%. Calcd for $C_{31}H_{47}O_9N_7 \cdot 1/2\ H_2O$: C, 55.51; H, 7.21; N, 14.62%.

*H-Leu-Pro-Asn-Val-pNA·HCl (**36a**·HCl).* Compound **35a** (47 mg, 0.07 mmol) was treated with 0.1 M hydrogen chloride in formic acid (0.8 ml) as described for **2**·HCl, and the residue was used for the next reaction without further treatment; yield was quantitative; R_f^1 0.18, R_f^3 0.74.

*Dnp-Leu-Pro-Asn-Val-pNA (**37a**).* To a solution of **36a**·HCl (42 mg, 0.07 mmol) and TEA (0.029 ml, 0.21 mmol) in DMF (2 ml) was added N_2ph–F (26 mg, 0.14 mmol), and the reaction mixture was stirred at room temperature for 3 h and evaporated. The residue dissolved in $CHCl_3$ (5 ml) was applied to a column (1.8×20 cm) of silica gel 60 (Merck), and the column was washed with $CHCl_3$. The fractions containing the desired product eluted with a mixture of $CHCl_3$–MeOH (19:1, v/v) were evaporated to leave a solid, which was recrystallized from EtOAc–ether; yield, 42 mg (83%); mp 145—148 °C; $[\alpha]_D^{22}$ −90.2° (*c* 1, MeOH); R_f^1 0.67, R_f^2 0.13, R_f^3 0.79.

Found: C, 52.44; H, 5.72; N, 17.11%. Calcd for $C_{32}H_{41}O_{11}N_9$: C, 52.82; H, 5.68; N, 17.32%.

*Boc-D-Ala-Val-pNA (**32b**).* This compound was prepared from Boc-D-Ala-OH (189 mg, 1 mmol) and H-Val-pNA (238 mg, 1 mmol) as described for **35a**. The crude product was recrystallized from EtOH–ether; yield, 306 mg (76%); mp 160 °C; $[\alpha]_D^{22}$ −47.0° (*c* 1, MeOH); R_f^1 0.82, R_f^2 0.45, R_f^3 0.91.

Found: C, 55.77; H, 6.98; N, 13.68%. Calcd for $C_{19}H_{28}O_6N_4$: C, 55.87; H, 6.91; N, 13.72%.

*H-D-Ala-Val-pNA·HCl (**33b**·HCl).* Compound **32b** (245 mg, 0.6 mmol) was treated with 0.1 M hydrogen chloride in formic acid (7 ml) as described for **2**·HCl; yield, 209 mg (100%); mp 170—173 °C; $[\alpha]_D^{22}$ −42.2° (*c* 1, MeOH); R_f^1 0.33, R_f^2 0.02, R_f^3 0.75.

Found: C, 48.01; H, 6.03; N, 16.19%. Calcd for $C_{14}H_{21}O_4N_4Cl \cdot 1/4\ H_2O$: C, 48.14; H, 6.20; N, 16.04%.

*Boc-Leu-Pro-D-Ala-Val-pNA (**35b**).* This compound was prepared from **33b**·HCl (209 mg, 0.6 mmol) and **34** (197 mg, 0.6 mmol) as described for **35a**; yield, 209 mg (56%); mp 140—142 °C; $[\alpha]_D^{22}$ −20.6° (*c* 1, MeOH); R_f^1 0.79, R_f^2 0.38, R_f^3 0.86.

Found: C, 57.36; H, 7.37; N, 13.09%. Calcd for $C_{30}H_{48}O_8N_6 \cdot 1/2\ H_2O$: C, 57.40; H, 7.55; N, 13.39%.

*H–Leu–Pro–D-Ala–Val–pNA·HCl (**36b**·HCl).* Compound **35b** (62 mg, 0.1 mmol) was treated with 0.1 M hydrogen chloride in formic acid (1.5 ml) as described for **2**·HCl, and the residue was used for the next reaction without further treatment; yield was quantitative; R_f^1 0.27, R_f^3 0.69.

*Dnp–Leu–Pro–D-Ala–Val–pNA (**37b**).* This compound was prepared from **36b**·HCl (56 mg. 0.1 mmol) as described for **37a**; yield, 59 mg (86%); mp 231 °C; $[\alpha]_D^{23}$ −38.4° (*c* 1, MeOH); R_f^1 0.77, R_f^2 0.36, R_f^3 0.82.

Found: C, 54.26; H, 5.78; N, 16.18%. Calcd for $C_{31}H_{40}O_{10}N_8$: C, 54.37; H, 5.89; N, 16.39%.

Paper Electrophoresis. Electrophoresis was carried out with Whatman No. 1 paper and a solvent system of HCOOH–AcOH–MeOH–H_2O (1:3:6:10, v/v, pH 1.8) for 2 h at 500 V/30 cm. Each of the analogs (**10a** and **10b**) showed single spot and their mobilities were as follows: **10a**, 7.3 cm; **10b**, 7.5 cm; GS, 7.1 cm.

CD and ORD Measurements. These spectra were recorded on a JASCO J-20 spectropolarimeter in MeOH solution at room temperature (23±2 °C).

Microbiological Assays. The minimum concentration of the compounds necessary for the complete inhibition of growth of several microorganisms was determined by a dilution method using a nutrient agar. Natural GS used as a reference showed complete inhibition at 3.13 and 6.25 μg/ml on *B. Subtilis* and *S. Aureus*, respectively, and was inactive on *E. Coli* at 100 μg/ml.

We thank Professor Tatsuo Miyazawa and Dr. Tsutomu Higashijima of The University of Tokyo for helpful discussions. We are indebted to Dr. Haruyasu Kinashi and Miss Kinumi Someno of this institute for the microbiological assays. We are also grateful to the members of Analytical Department of System Engineering Laboratory, Mitsubishi-Kasei Industries Ltd. for elemental analyses.

References

1) Part VI of this series: T. Higashijima, K. Sato, and U. Nagai, *Bull. Chem. Soc. Jpn.*, **56**, 3328 (1983).

2) The abbreviations used in this paper are those recommended by IUPAC-IUB: *J. Biol. Chem.*, **247**, 977 (1972). Additional abbreviations: Boc, *t*-butoxycarbonyl; Z, benzyloxycarbonyl; Dnp, 2,4-dinitrophenyl; pNA, *p*-nitroanilide; OBzl, benzyl ester; ONp, *p*-nitrophenyl ester; HONSu, *N*-hydroxysuccinimide; EDC, 1-ethyl-3-(3-dimethylaminopropyl)carbodiimide; N_2ph-F, 1-fluoro-2,4-dinitrobenzene;TEA, triethylamine; DMF, *N,N*-dimethylformamide; THF, tetrahydrofuran, MA, mixed anhydride; TLC, thin-layer chromatography; GS, gramicidin S. Symbols of optically active amino acids denote the L-configuration unless otherwise stated.

3) N. Izumiya, T. Kato, H. Aoyagi, M. Waki, and M. Kondo, "Synthetic Aspects of Biologically Active Cyclic Peptides—Gramicidin S and Tyrocidines," Kondansha, Tokyo, and Halsted Press, New York (1979), pp. 71—97.

4) D. C. Hodgkin and B. M. Oughton, *Biochem. J.*, **65**, 752 (1957), and the references cited in Ref. 3.

5) R. Schwyzer, "Amino Acids and Peptides with Antimetabolic Activity," Churchill, New York (1958) pp. 171—191.

6) T. Kato and N. Izumiya, *Biochim. Biophys. Acta*, **493**, 235 (1977).

7) In 1958, Schwyzer proposed the concept that GS shows the antibiotic activity because of a specific conformation of the molecule in which the charged side chains are on one side and the hydrophobic side chains on the other side.[5] For this concept, Kato and Izumiya introduced a term of "sidedness hypothesis" in 1977.[6] A term of sidedness itself appeared at first in 1975; N. G. Kumar, N. Izumiya, M. Miyoshi, H. Sugano, and D. W. Urry, *Biochemistry*, **14**, 2197 (1975).

8) Ref. 3, pp. 49—76.

9) T. Kato, M. Waki, S. Matsuura, and N. Izumiya, *J. Biochem.*, **68**, 751 (1970).

10) M. Kawai and U. Nagai, *Biopolymers*, **17**, 1549 (1978); T. Higashijima, M. Tasumi, T. Miyazawa, M. Kawai, and U. Nagai, "Peptide Chemistry 1977; Proceedings of the 15th Symposium on Peptide Chemistry," ed. by T. Shiba, Protein Research Foundation, Osaka (1978), p. 97.

11) K. Sato, M. Kawai, and U. Nagai, *Biopolymers*, **20**, 1921 (1981).

12) K. Sato, M. Kawai, and U. Nagai, *Bull. Chem. Soc. Jpn.*, **56**, 1527 (1983).

13) K. Sato, U. Nagai, and T. Higashijima, *Bull. Chem. Soc. Jpn.*, **56**, 1657 (1983).

14) K. Sato, N. Taki, U. Nagai, and T. Higashijima, *Bull. Chem. Soc. Jpn.*, **56**, 2476 (1983).

15) M. Kawai, K. Sato, R. Sugawara, and U. Nagai, *Bull. Chem. Soc. Jpn.*, **56**, 3305 (1983).

16) M. Ohno, K. Kuromizu, H. Ogawa, and N. Izumiya, *J. Am. Chem. Soc.*, **93**, 5251 (1971); K. Sato, H. Abe, T. Kato, and N. Izumiya, *Bull. Chem. Soc. Jpn.*, **50**, 1999 (1977); K. Sato, K. Ueda, M. Kondo, H. Aoyagi, and N. Izumiya, *ibid.*, **51**, 1830 (1978); K. Nonaka, K. Sato, S. Terada, T. Kato, and N. Izumiya, *ibid.*, **51**, 2127 (1978).

17) H. Abe, K. Sato, T. Kato, and N. Izumiya, *Bull. Chem. Soc. Jpn.*, **49**, 3113 (1976).

18) Y. Minematsu, M. Waki, K. Suwa, T. Kato, and N. Izumiya, *Tetrahedron Lett.*, **21**, 2179 (1980).

19) S. Lee and N. Izumiya, *Int. J. Peptide Protein Res.*, **10**, 206 (1977).

20) H. Yonezawa, K. Okamoto, M. Kaneda, N. Tominaga, and N. Izumiya, "Peptide Chemistry 1982; Proceedings of the 20th Symposium on Peptide Chemistry," ed by S. Sakakibara, Protein Research Foundation, Osaka (1983), pp. 283—288.

 © 1983 The Chemical Society of Japan Bull. Chem. Soc. Jpn., 56, 3337—3342 (1983)

The Substituent Effects in Thiophene Compounds. II.[1] ^{1}H NMR and IR Studies in Methyl (Substituted 3-Thiophenecarboxylate)s

Hajime SATONAKA

Industrial Research Institute of Kanagawa Prefecture, 3173, Showa-machi, Kanazawa-ku, Yokohama 236

(Received April 22, 1983)

The ^{1}H NMR spectra and the IR carbonyl stretching frequencies of methyl (2-, 4-, and 5-substituted 3-thiophenecarboxylate)s are reported. Good linear correlation between the chemical shifts of the ring protons in methyl (5-substituted 3-thiophenecarboxylate)s and those of the corresponding protons in substituted thiophenes was observed. It was found that in methyl (2- and 4-substituted 3-thiophenecarboxylate)s, which have the carbonyl or nitro group in an *ortho* position, the chemical shifts for the ring protons were considerable affected by the conformation of carbonyl group, the steric hindrance, and the intramolecular hydrogen bonding. Some of methyl (*ortho*-substituted 3-thiophenecarboxylate)s showed the two C=O stretching bands. They were assigned to *anti-s-trans* and *syn-s-trans* forms. The substitutent effects in the C=O frequencies are also discussed. The coupling constants between ring protons of methyl (substituted 3-thiophenecarboxylate)s were correlated very closely with the corresponding ones in substituted thiophenes. The coupling constants in methyl 3-thiophenecarboxylate series were found to vary linearly with the sum of the electronegativities of the substituent on the ring.

In an earlier paper,[1] the ^{1}H NMR spectra have been reported for 2-substituted thiophenes (**1**), 3-substituted thiophenes (**2**), methyl (3-substituted 2-thiophenecarboxylate)s (**3**), methyl (4-substituted 2-thiophenecarboxylate)s (**4**), and methyl (5-substituted 2-thiophenecarboxylate)s (**5**). The effects of the substituents were discussed.

The present study was undertaken to examine the substituent effects in methyl (2-, 4-, and 5-substituted 3-thiophenecarboxylate)s (**6**—**8**). The correlations of

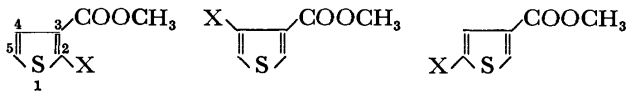

6 **7** **8**

the chemical shifts and of the coupling constants between methyl (substituted 3-thiophenecarboxylate)s and substituted thiophenes have been discussed in this paper. Attempts have also been made to compare the IR C=O stretching frequencies in methyl (substituted 3-thiophenecarboxylate)s with the chemical shifts in substituted thiophenes, and the coupling constants in methyl (substituted 3-thiophenecarboxylate)s with the electronegativities of the substituents. The influences of the conformation, steric hindrance, and intramolecular hydrogen bonding upon the chemical shifts of ring protons and C=O stretching frequencies in methyl (2- and 4-substituted 3-thiophenecarboxylate)s have been discussed.

Results and Discussion

The ^{1}H NMR spectra of methyl (2-, 4-, and 5-substituted 3-thiophenecarboxylate)s (**6**—**8**) were measured in deuteriochloroform at 25 °C. The assignments of the spectra were made on the basis of the chemical shifts and the characteristic ring coupling constants. The refined chemical shifts and coupling constants were obtained iteratively using LAOCN 3.[2] The results are given in Tables 1—3. For convenience, the notation H_r(**N**) for the rth(position)-proton on thiophene ring of the series of compounds **N**, δ_r(**N**) for its chemical shift, and *cc*, *p*, *i*, and *s* for the correlation coefficient, slope, intercept, and standard deviation in the least-squares analysis. For comparison of the effect of substituents on methyl (substituted 3-thiophenecarboxylate)s and substituted thiophenes, the chemical shifts of corresponding protons from the two series of compounds were plotted against each other. The plots of δ_4 (**8**) against δ_3(**1**)[1] (A, *cc* 0.999, *p* 0.958, *i* 0.069, *s* 0.019) and δ_2(**8**) against δ_5(**1**)(B, *cc* 0.999, *p* 0.847, *i* 1.857, *s* 0.011) gave excellent correlations as shown in Fig. 1. Line A runs almost parallel with B. The

Table 1. ^{1}H NMR chemical shifts and coupling constants of methyl (2-substituted 3-thiophenecarboxylate)s(series **6**)

No.	X	δ_{H_4}	δ_{H_5}	δ_{COOCH_3}	Others	J_{45}/Hz	Others	
1	H	7.53	7.30	3.87	8.10(H_2)	5.05	1.15(J_{24})	3.05(J_{25})
2	OCH_3	7.18	6.48	3.83	4.06(OCH_3)	6.00		
3	CH_3	7.37	6.97	3.84	2.74(CH_3)	5.40	0.35(J_{CH_3-4})	
4	Cl	7.35	7.05	3.88		5.85		
5	Br	7.36	7.21	3.88		5.75		
6	I	7.32	7.40	3.88		5.60		
7	CHO	7.58	7.64	3.96	10.62(CHO)	5.10	1.15(J_{CHO-5})	
8	$COCH_3$	7.35	7.46	3.91	2.61($COCH_3$)	5.10		
9	$COOCH_3$	7.45	7.28	3.89	3.91($COOCH_3$)	5.15		
10	NO_2	7.18	7.50	3.96		5.45		

Table 2. ^{1}H NMR chemical shifts and coupling constants of methyl (4-substituted 3-thiophenecarboxylate)s (series **7**)

No.	X	δ_{H_2}	δ_{H_5}	δ_{COOCH_3}	Others	J_{25}/Hz	Others	
1	H	8.10	7.30	3.87	7.53(H_4)	3.05	1.15(J_{24})	5.05(J_{45})
2	OCH_3	8.01	6.28	3.85	3.89(OCH_3)	3.60		
3	CH_3	8.06	6.91	3.84	2.46(CH_3)	3.40	0.35(J_{CH_3-2})	1.10(J_{CH_3-5})
4	Cl	8.12	7.18	3.88		3.70		
5	Br	8.11	7.31	3.88		3.60		
6	I	8.07	7.50	3.88		3.45		
7	CHO	8.16	8.18	3.94	10.50(CHO)	3.40	0.35(J_{CHO-2})	
8	$COCH_3$	7.89	7.68	3.88	2.53($COCH_3$)	3.20		
9	$COOCH_3$	7.85	7.85	3.88	3.88($COOCH_3$)	—		

Table 3. ^{1}H NMR chemical shifts and coupling constants of methyl (5-substituted 3-thiophenecarboxylate)s (series **8**)

No.	X	δ_{H_2}	δ_{H_4}	δ_{COOCH_3}	Others	J_{24}/Hz	Others	
1	H	8.10	7.53	3.87	7.30(H_5)	1.15	3.05(J_{25})	5.05(J_{45})
2	OCH_3	7.37	6.59	3.83	3.88(OCH_3)	1.65		
3	CH_3	7.85	7.17	3.83	2.47(CH_3)	1.35	1.15(J_{CH_3-4})	
4	Cl	7.86	7.33	3.85		1.60		
5	Br	7.98	7.47	3.85		1.55		
6	I	8.08	7.65	3.85		1.40		
7	CHO	8.44	8.16	3.91	9.94(CHO)	1.35	1.40(J_{CHO-2})	0.20(J_{CHO-4})
8	$COCH_3$	8.32	8.06	3.89	2.58($COCH_3$)	1.30		
9	$COOCH_3$	8.25	8.16	3.88	3.90($COOCH_3$)	1.40		
10	NO_2	8.24	8.28	3.92		1.80		

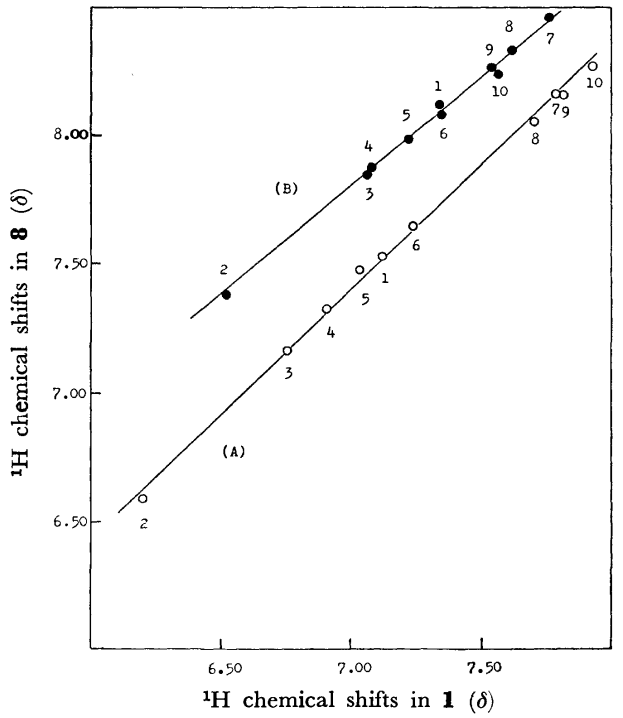

Fig. 1. Correlation between ^{1}H chemical shift in **8** and **1**; numbering as in Table 3. A, δ_4(**8**) *vs.* δ_3(**1**). B, δ_2(**8**) *vs.* δ_5(**1**).

correlation between δ_4(**8**) and δ_2(**8**) is in good accord with that between δ_3(**1**) and δ_5(**1**). These data seem to show that the introduction of methoxycarbonyl group into position 4 of 2-substituted thiophene is confined to the parallel transfer of the substituent effects on H_3 and H_5. The author further compared the chemical shifts of the ring protons in **8** with those in methyl (4-substituted 2-thiophenecarboxylate)s (**4**). The correlation between δ_4(**8**) and δ_3(**4**) was in agreement with that between δ_3(**1**) and δ_4(**2**). The correlation between δ_2(**8**) and δ_5(**4**) was also in agreement with that between δ_5(**1**) and δ_2(**2**). These correlations also demonstrate that the substituent effects in the series of compounds **8** and **4** follow the same trend.

Figure 2 shows the rough linearities between the effects of the substituents on δ_5(**6**) and those on δ_5(**1**) (A, *cc* 0.934, *p* 0.821, *i* 1.20, *s* 0.108) and between those on δ_4(**6**) and those on δ_4(**1**)(B, *cc* 0.868, *p* 0.590, *i* 3.28, *s* 0.055). The correlation between δ_5(**6**) and δ_4(**6**) is worse than that between δ_5(**1**) and δ_4(**1**). The author has compared the chemical shifts of the ring protons in **6** with those in methyl (3-substituted 2-thiophenecarboxylate)s (**3**), both of which belong to *ortho*-disubstituted thiophenes. The correlation between δ_4(**6**) and δ_4(**3**) was considerably worse than that between δ_4(**1**) and δ_4(**2**). Furthermore, the correlation between δ_5(**6**) and δ_5(**3**) was remarkably worse than that between δ_5(**1**) and δ_5(**2**). These results show that the additivity rule on the substituent effect in substituted thiophenes is not applicable to compounds **6**.

Figure 3 shows the good linearity between the effects of the substituents on δ_5(**7**) and those on δ_2(**2**)(A, *cc* 0.970, *p* 0.853, *i* 1.06, *s* 0.128), and no correlation between those on δ_2(**7**) and those on δ_5(**2**)(B, *cc* 0.085,

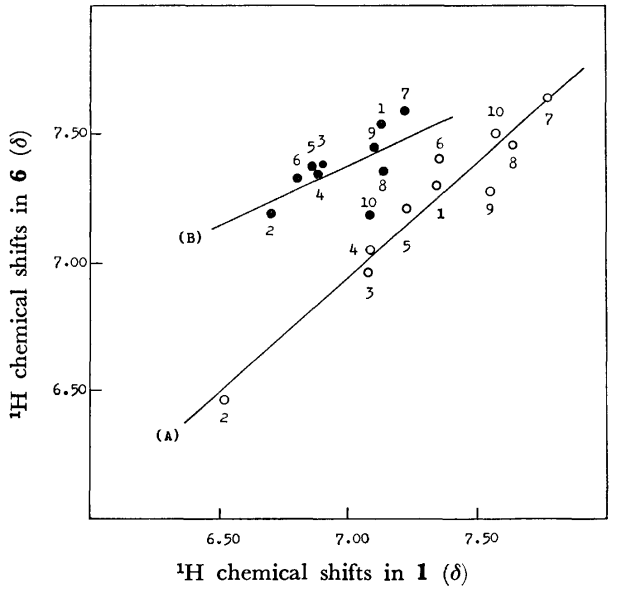

Fig. 2. Correlation between ^{1}H chemical shifts in **6** and **1**; numbering as in Table 1. A, δ_5(**6**) *vs.* δ_5(**1**). B, δ_4(**6**) *vs.* δ_4(**1**).

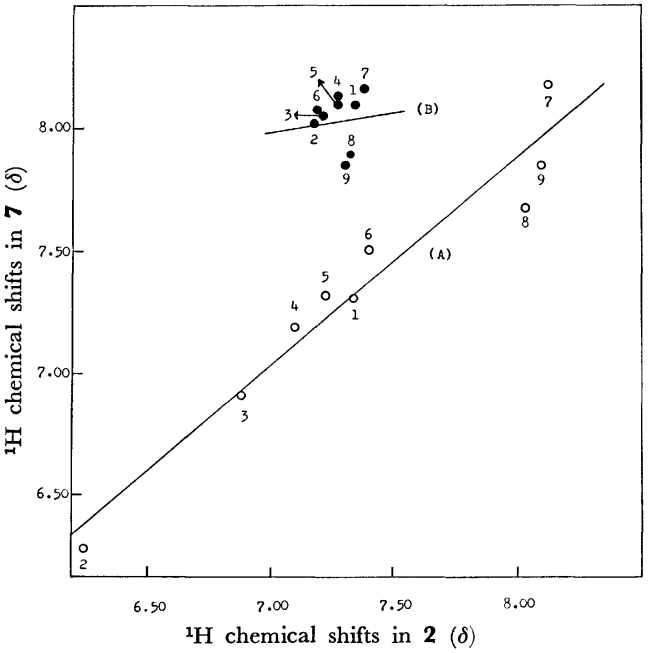

Fig. 3. Correlation between ^{1}H chemical shifts in **7** and **2**; numbering as in Table 2. A, δ_5(**7**) *vs.* δ_2(**2**). B, δ_2(**7**) *vs.* δ_5(**2**).

p 0.126, *i* 7.09, *s* 0.104). As given in Table 2, the chemical shifts of H_2 in the series of compounds **7** appear at significantly lower fields than those in the series of compounds **8**. It is noticeable that the H_2 signals of acetyl and methoxycarbonyl derivatives appear at higher fields than those in methoxy and methyl derivatives. These facts seem to account for the very poor correlation between δ_2(**7**) and δ_5(**2**).

Methyl proton chemical shifts of methyl (substituted 3-thiophenecarboxylate)s, which show the narrow range of variation, were found to be correlated with the chemical shifts of the corresponding protons of similarly substituted thiophenes. The result implies that the substituent effect is transmitted to the methyl group in a "through-bond" manner through the –CO–O–π system. The effect is attenuated by a factor of about 10.

The chemical shifts of the ring protons in methyl (2-, 4-, and 5-substituted 3-thiophenecarboxylate)s were calculated by making use of those of 2- and 3-substituted thiophenes. The observed chemical shifts are in good agreement with the calculated ones, within δ 0.1 in the series of compounds **8**. For example, the calculated ring proton chemical shifts were δ 7.83 and 7.16 for methyl 5-methyl-3-thiophenecarboxylate and δ 8.11 and 7.65 for methyl 5-iodo-3-thiophenecarboxylate. These calculated values were in good accord with the observed ones. This agreement suggests that the additivity rule, which is based on substituted thiophenes, is applicable to the chemical shifts of the ring protons in **8**, as well as in **4**.[1] In the series of compounds **6**, large deviations of the observed values from the calculated are seen in the carbonyl derivatives. As mentioned in the preceding paper,[1] methyl 2-formyl-3-thiophenecarboxylate and dimethyl 2,3-thiophenedicarboxylate are considered to take preferably the conformations **a** and **b**, respectively. The calculated chemical shifts of H_4 and H_5

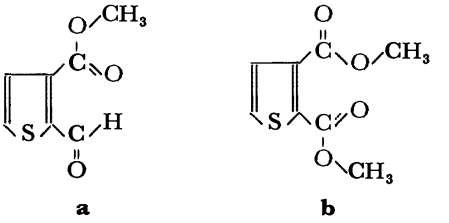

in methyl 2-acetyl-3-thiophenecarboxylate are δ 7.54 and 7.59 respectively, but the doublets occur at δ 7.35 and 7.46 and produce significant shifts to higher fields than the calculated values. The acetyl ester has a single ester carbonyl stretching band assignable to *anti-s-trans* form at 1731 cm^{-1}, quite analogous to methyl 2-formyl-3-thiophenecarboxylate (1729 cm^{-1}). It is confirmed that 2-acetylthiophene exists in *syn-s-trans* form **c**.[3] However, the C=O stretching band of acetyl group of this acetyl ester appears at 1671 cm^{-1} with a shoulder at 1686 cm^{-1}. Consequently, it is considered that another conformation **e** will exist in addition to the predominant conformation **d** in this compound. It is expected that the difference between the chemical shifts of H_4 and H_5 is enlarged by the presence of the conformation **e**. The signals at δ 7.35 and 7.46 may thus be assignable to those of H_4 and H_5, respectively. The discrepancy between the

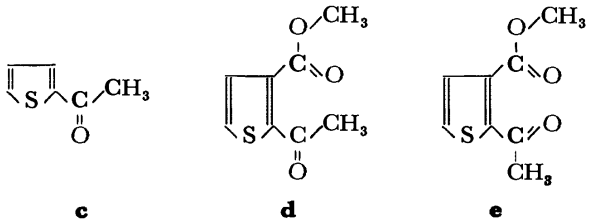

observed chemical shifts of H_4 and H_5 and those estimated seems to suggest that the coplanarity of carbonyl functions to the thiophene ring is lost by the steric hindrance. The H_4-chemical shift of methyl 2-nitro-3-thiophenecarboxylate is δ 7.18. This is a considerably higher field than the calculated value. The UV spectrum of nitro ester [λ_{max}: 284 nm(ε 6620)] is more similar to one of 2-nitrothiophene[λ_{max}: 300 nm(ε 6730), 282 nm(ε 5970)] than one of methyl 3-thiophenecarboxylate[λ_{max}: 239 nm(ε 7550)]. Consequently, it is considered that the methoxycarbonyl group at position 3 will exist with the considerable loss of the coplanarity to thiophene ring by the steric hindrance.

The discrepancy is largest in the series of compounds **7**, which is the *ortho*(3,4)-disubstituted derivative. It is considered that the contribution of the rotational isomer **f** involving a weak intramolecular hydrogen bond affects the chemical shifts of the ring and formyl protons in methyl 4-formyl-3-thiophenecarboxylate, as in methyl 3-formyl-2-thiophenecarboxylate[1] and methyl 2-formyl-3-thiophenecarboxylate. The H_2- and H_5-signals of this compound shift to significantly lower fields than the corresponding signals of acetyl derivative and dimethyl 3,4-thiophenedicarboxylate. The formyl proton chemical shift of methyl 4-formyl-3-thiophenecarboxylate is δ 10.50, and absorbs at δ *ca.* 0.6 lower field than that of methyl 4-formyl-2-thiophenecarboxylate(δ 9.91). The strong carbonyl band in IR spectrum appears at 1729 cm^{-1}, and is assignable to *syn-s-trans* form. Methyl 4-acetyl-3-thiophenecarboxylate has a single ester carbonyl band at 1730 cm^{-1} and a single acetyl carbonyl band at 1695 cm^{-1}. The observed chemical shifts of the ring protons in this ester are to significantly higher fields than the calculated values. This discrepancy suggests the loss of the coplanarity of carbonyl functions to thiophene ring by the steric hindrance, although this compound seems to exist in the preferred conformation **g**. The chemical shifts of H_2 and H_5 in dimethyl

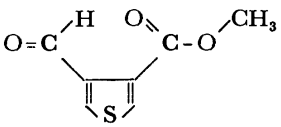

f

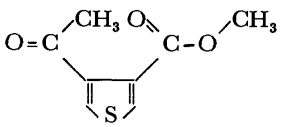

g

3,4-thiophenedicarboxylate are equivalent and δ 8.07 in the calculations, but appear at δ 7.85 in the experiment. This discrepancy suggests the participation of the repulsion by the lone pair electrons and the steric hindrance. The IR carbonyl band, which appears as a broad peak centered at 1735 cm^{-1}, also suggests coexistence of several conformations. The additional feature in this series is the discrepancy between the observed and the calculated values in halogen derivatives. Two carbonyl stretching vibrations, which are assignable to *syn-s-trans* and *anti-s-trans* forms, are observed in these compounds. The chemical shifts, which are calculated on the basis of the *syn-s-trans* form in methyl 3-thiophenecarboxylate, are considered to change largely due to the presence of the *anti-s-trans* form.

In summary, the discrepancy between the observed and estimated values in methyl (2-substituted 3-thiophenecarboxylate)s (**6**) and methyl (4-substituted 3-thiophenecarboxylate)s (**7**), which belong to *ortho*-substituted thiophenes, may be caused by (i) the change of the conformation in methoxycarbonyl, formyl, and acetyl groups, (ii) the loss of coplanarity of carbonyl functions to the thiophene ring by the steric hindrance and the repulsion of the lone pair electrons, and (iii) the electric field effect and the conformational effect by the weak intramolecular hydrogen bond.

The ester carbonyl stretching frequencies of methyl (substituted 3-thiophenecarboxylate)s, which were measured in CCl_4, are listed in Table 4. The correlations between the wavenumber of the C=O band (*syn-s-trans* form) and the proton chemical shift of the corresponding substituted thiophene were examined. A good correlation is obtained between $\nu_{C=O}$(**8**)[4] and δ_4(**1**). However, the C=O frequency data in other two series gave no correlation with ^1H chemical shifts of the corresponding substituted thiophenes. The correlation between the C=O frequencies of methyl (substituted 3-thiophenecarboxylate)s and methyl (substituted 2-thiophenecarboxylate)s was also examined. Reasonably good correlations were obtained between $\nu_{C=O}$(**6**) and $\nu_{C=O}$(**3**), and between $\nu_{C=O}$(**8**) and $\nu_{C=O}$(**4**), as well as $\nu_{C=O}$(**8**) and $\nu_{C=O}$(**5**). The correlation between $\nu_{C=O}$(**7**) and $\nu_{C=O}$(**3**) was excellent, and better than that between $\nu_{C=O}$(**6**) and $\nu_{C=O}$(**3**). It is interesting that these correlations are in good agreement with those between the chemical shifts of the ring protons in the three series of compounds **7**, **6**, and **3**, as mentioned above.

The plots of the proton-proton coupling constants in methyl (substituted 3-thiophenecarboxylate)s against those of the corresponding thiophenes gave good correlations, as shown in Fig. 4. The correlation of J_{45}(**3**)[5] against J_{45}(**1**) was found to be excellent, in contrast to that of the chemical shifts between both series. Furthermore, the correlations between the coupling constants of methyl (substituted 3-thiophenecarboxylate)s and those of methyl (substituted 2-thiophenecarboxylate)s were examined. Fair correlations were obtained between J_{45}(**6**) and J_{45}(**3**), and be-

Table 4. Frequencies of C=O stretching vibration for methyl (substituted 3-thiophenecarboxylate)s

No.	X	$\nu_{C=O}$/cm^{-1}					
		Series **6**		Series **7**		Series **8**	
		anti[a]	*syn*[b]	*anti*	*syn*	*anti*	*syn*
1	H		1726		1726		1726
2	OCH_3	1712	1725	1713	1734		1722
3	CH_3	1718	1731*	1720*	1725		1723
4	Cl	1718	1735	1720	1740		1729
5	Br	1716	1735	1718	1739		1727
6	I	1718*	1731	1724*	1735		1728
7	CHO	1729			1729		1731
8	$COCH_3$	1731			1730		1729
9	NO_2		1746				1735

a) *anti-s-trans* Form. b) *syn-s-trans* Form. * Shoulder.

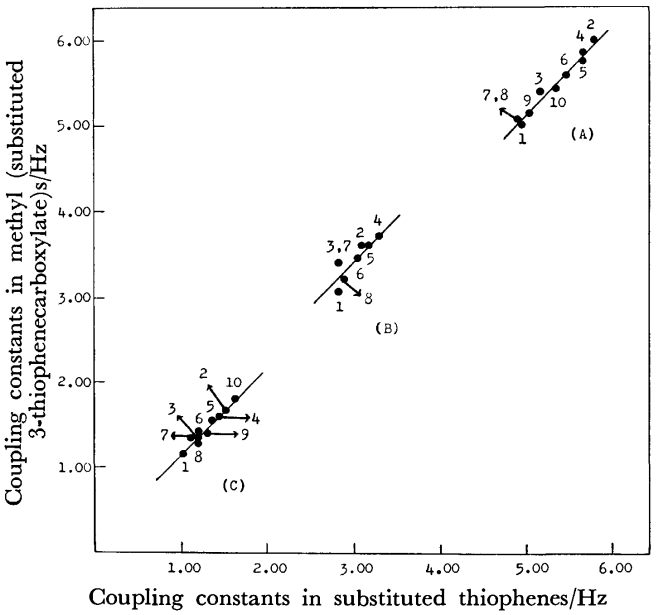

Fig. 4. Correlation between coupling constants in methyl (substituted 3-thiophenecarboxylate)s and substituted thiophenes, numbering as in Table 1. A, J_{45}(**6**) *vs.* J_{45}(**1**). B, J_{25}(**7**) *vs.* J_{25}(**2**). C, J_{24}(**8**) *vs.* J_{35}(**1**).

tween J_{24}(**8**) and J_{35}(**4**). For methyl (substituted 3-thiophenecarboxylate)s as well as for methyl (substituted 2-thiophenecarboxylate)s, the relationship of the coupling constants against the sum of the electronegativities of substituents including methoxycarbonyl group were examined. The individual coupling constants in the series of compounds **6**, **7**, and **8** gave good correlations with the electronegativities. The slope of the correlation for the series of compounds **6** is twice as large as those in the series of compounds **3**, **4**, **5**, **7**, and **8**. This fact shows that the electronegativity effect of the substituent on position 2 is more sensitive to J_{45} than those in all other cases, and is transmitted by a factor of about 2.

Experimental

The ^{1}H NMR spectra of the compounds were obtained at 100 MHz on a JEOL PS-100 spectrometer. The chemical shifts were determined with an accuracy of δ $\pm$0.005 relative to TMS as an internal standard and the coupling constants were determined with an accuracy of $\pm$0.02 Hz. The concentrations of solutions were adjusted approximately at 0.3 mol dm^{-3} with respect to substrates. The IR spectra were recorded on a Perkin-Elmer 257 spectrometer. The UV spectra were recorded on a Shimadzu MPS 5000 spectrometer in hexane.

Methyl 3-thiophenecarboxylate, methyl 2-bromo-3-thiophenecarboxylate, methyl 2-formyl-3-thiophenecarboxylate, methyl 4-methoxy-3-thiophenecarboxylate, methyl 4-bromo-3-thiophenecarboxylate, methyl 4-formyl-3-thiophenecarboxylate, dimethyl 3,4-thiophenedicarboxylate, methyl 5-chloro-3-thiophenecarboxylate, methyl 5-formyl-3-thiophenecarboxylate, and methyl 5-nitro-3-thiophenecarboxylate were prepared according to the reported procedures.[6-12]

Methyl 5-Methoxy-3-thiophenecarboxylate. This material was prepared by the oxidation of 5-methoxy-3-thiophenecarbaldehyde[13] followed by the esterification, bp 101.5—103 °C/4 mmHg (1 mmHg$\approx$133.322 Pa). Found: C, 48.68; H, 4.37; S, 18.88%. Calcd for $C_7H_8O_3S$: C, 48.82; H, 4.68; S, 18.62%. IR (neat, cm^{-1}): 3120(=C–H), 1720(C=O), 1552, 1438, 727(thiophene ring).

The following esters were prepared by the esterification of the corresponding carboxylic acids.[14-23]

Methyl 2-Methoxy-3-thiophenecarboxylate. Bp 146—147 °C/21 mmHg. Found: C, 48.96; H, 4.60; S, 18.53%. Calcd for $C_7H_8O_3S$: C, 48.82; H, 4.68; S, 18.62%. IR (neat, cm^{-1}): 3120(=C–H); 1716(C=O); 1542, 1438, 754 (thiophene ring).

Methyl 2-Methyl-3-thiophenecarboxylate. Bp 99—101 °C/16 mmHg. Found: C, 53.92; H, 5.04; S, 20.75%. Calcd for $C_7H_8O_2S$: C, 53.83; H, 5.16; S, 20.53%. IR (neat, cm^{-1}): 3110, 3090 (=C–H); 1712 (C=O); 1537, 1438, 708 (thiophene ring).

Methyl 2-Chloro-3-thiophenecarboxylate. Bp 124—125 °C/30 mmHg. Found: C, 40.68; H, 2.82; Cl, 20.33; S, 17.98%. Calcd for $C_6H_5ClO_2S$: C, 40.80; H, 2.85; Cl, 20.07; S, 18.15%. IR(neat, cm^{-1}); 3120, 3090(=C–H); 1712(C=O); 1529, 1440, 702(thiophene ring).

Methyl 2-Iodo-3-thiophenecarboxylate. Bp 127.5—128 °C/5 mmHg. Found: C, 26.90; H, 1.70; I, 47.50; S, 12.02%. Calcd for $C_6H_5IO_2S$: C, 26.88; I, 1.88; I, 47.34; S, 12.06%. IR(neat, cm^{-1}): 3100, 3090(=C–H); 1710(C=O); 1515, 1436, 707(thiophene ring).

Methyl 2-Acetyl-3-thiophenecarboxylate. Bp 118—119 °C/4.5 mmHg. Found: C, 52.08; H, 4.52; S, 17.35%. Calcd for $C_8H_8O_3S$: C, 52.16; H, 4.38; S, 17.41%. IR(neat, cm^{-1}): 3100(=C–H); 1728, 1672(C=O); 1527, 1438, 737 (thiophene ring).

Methyl 2-Nitro-3-thiophenecarboxylate. Bp 132—133.5 °C/3 mmHg. Found: C, 38.37; H, 2.58; N, 7.30; S, 17.25%. Calcd for $C_6H_5NO_4S$: C, 38.50; H, 2.69; N, 7.48; S, 17.13%. IR(neat, cm^{-1}): 3100(=C–H); 1737(C=O); 1515, 1345(NO_2); 1548, 1437, 742(thiophene ring).

Methyl 4-Methyl-3-thiophenecarboxylate. Bp 110—111 °C/21 mmHg. Found: C, 53.97; H, 5.29; S, 20.38%. Calcd for $C_7H_8O_2S$: C, 53.92; H, 5.16; S, 20.53%. IR (neat, cm^{-1}): 3120(=C–H); 1718(C=O); 1538, 1450, 777 (thiophene ring).

Methyl 4-Chloro-3-thiophenecarboxylate. Mp 51.5 °C. Found: C, 40.98; H, 2.92; Cl, 20.00; S, 18.01%. Calcd for $C_6H_5ClO_2S$: C, 40.80; H, 2.85; Cl, 20.07; S, 18.15%. IR(KBr, cm^{-1}): 3120(=C–H); 1715(C=O); 1507, 1440, 781 (thiophene ring).

Methyl 4-Iodo-3-thiophenecarboxylate. Mp 32 °C. Found: C, 26.92; H, 1.70; I, 47.15; S, 11.82%. Calcd for $C_6H_5IO_2S$: C, 26.88; H, 1.88; I, 47.34; S, 11.96%. IR (KBr, cm^{-1}): 3110(–C–H); 1710(C–O); 1488, 1438, 777 (thiophene ring).

Methyl 4-Acetyl-3-thiophenecarboxylate. Bp 108.5—110 °C/2.5 mmHg. Found: C, 52.08; H, 4.52; S, 17.30%. Calcd for $C_8H_8O_3S$: C, 52.16; H, 4.38; S, 17.41%. IR (neat, cm^{-1}): 3110(=C–H); 1712, 1683(C=O); 1512, 1453, 798(thiophene ring).

Methyl 5-Methyl-3-thiophenecarboxylate. Bp 118—120 °C/26 mmHg. Found: C, 53.97; H, 5.31; S, 20.38%. Calcd for $C_7H_8O_2S$: C, 53.83; H, 5.16; S, 20.53%. IR (neat, cm^{-1}): 3110(=C–H); 1718(C=O); 1550, 1468, 738 (thiophene ring).

Methyl 5-Bromo-3-thiophenecarboxylate. Mp 43 °C. Found: C, 32.47; H, 2.09; Br, 36.03; S, 14.63%. Calcd for $C_6H_5BrO_2S$: C, 32.60; H, 2.28; Br, 36.14; S, 14.50%. IR(KBr, cm^{-1}): 3100(=C–H); 1718(C=O); 1527, 1442, 738 (thiophene ring).

Methyl 5-Iodo-3-thiophenecarboxylate. Mp 72 °C. Found:

C, 26.98; H, 1.70; I, 47.23; S, 11.82%. Calcd for $C_6H_5IO_2S$: C, 26.88; H, 1.88; I, 47.34; S, 11.96%. IR (KBr, cm^{-1}): 3090(=C–H); 1700(C=O); 1520, 1439, 736 (thiophene ring).

Methyl 5-Acetyl-3-thiophenecarboxylate. Mp 114 °C. Found: C, 52.31; H, 4.53; S, 14.28%. Calcd for $C_8H_8O_3S$: C, 52.16; H, 4.38; S, 17.41%. IR(KBr, cm^{-1}): 3120, 3100 (=C–H); 1712, 1663 (C=O); 1534, 1428, 759 (thiophene ring).

The author wishes to thank to Professor Minoru Hirota of Yokohama National University for his kind suggestions and encouragement, to Dr. Hiroshi Ozawa of the University of Tokyo for his permission to use the Computation Program LAOCN 3, and to Mr. Takayoshi Ozawa for the elemental analyses.

References

1) Part I: H. Satonaka, *Bull. Chem. Soc. Jpn.*, **56**, 2463 (1983).
2) S. M. Castellano and A. A. Bothner-By, *J. Chem. Phys.*, **41**, 3863 (1964).
3) C. L. Cheng, I. G. John, and G. L. D. Ritchie, *J. Chem. Soc., Perkin Trans. 2*, **1975**, 744.
4) The notation $\nu_{C=O}$(**N**) in hereafter used for the carbonyl stretching frequency of the series of compounds **N**.
5) The notation J_{rs}(**N**) is hereafter used for the spin-spin coupling constant between r- and s-protons on thiophen ring of the series of compounds **N**.
6) R. H. Hoffman and S. Gronowitz, *Ark. Kemi*, **16**, 515 (1960).
7) L. S. Owen and F. F. Nord, *J. Org. Chem.*, **16**, 1864 (1951).
8) S. Gronowitz, A. Biezais, and B. Mathiasson, *Ark. Kemi*, **21**, 265 (1963).
9) J. B. Press, C. M. Hofmann, and S. R. Safir, *J. Org. Chem.*, **44**, 3292 (1979).
10) S. Gronowitz, P. Moes, A. Hornfeldt, and R. Hakansson, *Ark. Kemi*, **17**, 165 (1961).
11) C. Sone, Y. Abe, and T. Oikawa, *Nippon Kagaku Zasshi*, **92**, 1193 (1971).
12) I. J. Rinkes, *Recl. Trav. Chim. Pays-Bas*, **53**, 643 (1934).
13) Ya. L. Gol'dfarb, M. A. Kalik, and V. K. Zav'yalova, *Khim. Geterotsikl. Soedin.*, **1981**, 182.
14) A. Hallberg and S. Gronowitz, *Chem. Scr.*, **16**, 38 (1980).
15) G. Cousiglio, S. Gronowitz, A. B. Hornfeldt, R. Noto, K. Pettersson, and D. Spinell, *Chem. Scr.*, **13**, 20 (1979).
16) E. Campaigne and W. M. LeSuer, *J. Am. Chem. Soc.*, **71**, 333 (1949).
17) R. Guilard, P. Fournari, and M. Person, *Bull. Soc. Chim. Fr.*, **1967**, 4121.
18) M. Griffe, F. Durant, and A. F. Pieret, *Bull. Soc. Chim. Belg.*, **81**, 319 (1972).
19) W. Steinkopf and W. Hanske, *Ann.*, **532**, 236 (1937).
20) O. Hromatka, D. Binder, R. Pfister, and P. Zeller, Ger. Patent 2537070 (1975); *Chem. Abstr.*, **85**, 63077f (1976).
21) W. Steinkopf and W. Hanske, *Ann.*, **527**, 264 (1937).
22) E. Campaigne and R. C. Bourgeois, *J. Am. Chem. Soc.*, **76**, 2445 (1954).
23) I. B. Karmanova, Yu. B. Vol'ensktein, and L. I. Bolen'kii, *Khim. Geterotsikl. Soedin.*, **1973**, 490.

The Platinum Complex Catalyzed Reductive *N*-Carbonylation of Nitroarenes to the Carbamates

Yoshihisa WATANABE,* Yasushi TSUJI, Ryo TAKEUCHI, and Naoki SUZUKI

Department of Hydrocarbon Chemistry, Faculty of Engineering, Kyoto University, Sakyo-ku, Kyoto 606

(Received April 25, 1983)

The platium catalyst combined with triphenylphosphine, tin(IV) chloride, and triethylamine showed high activity for the reductive *N*-carbonylation of nitroarene in ethanol at 180 °C under carbon monoxide of 60 kg cm^{-2}. From nitrobenzene, ethyl phenylcarbamate was obtained in 83% yield. Iron(III) chloride, aluminum chloride and titanium(IV) chloride could be used as Lewis acids in place of tin(IV) chloride. Various nitroarenes were transformed into corresponding carbamate in moderate to excellent yields with the platinum catalyst.

Organic syntheses with carbon monoxide and synthesis gas are of current interest.[1,2] Many fundamental chemical feedstocks are derived by reaction with the gases. Among those chemicals, isocyanates are often employed for the production of urethane rubber, fiber, and synthetic leather. The conventional commercial methods for production of isocyanates consist of the catalytic hydrogenation of nitroarenes to aminoarenes and phosgenation of amines (Eq. 1).[3] However, this

$$ArNO_2 + 3H_2 \xrightarrow[-2H_2O]{} ArNH_2 \xrightarrow[-2HCl]{COCl_2} ArNCO \quad (1)$$

conventional process has several disadvantages: use of poisonous phosgen, formation of a lot of hydrogen chloride as a by-product, and consumption of a lot of electricity for production of phosgen. In place of this method, increasing attention has been paid to the reductive *N*-carbonylation of nitroarenes(Eq. 2). Intensive stud-

$$ArNO_2 + 3CO \longrightarrow ArNCO + 2CO_2 \quad (2)$$

ies have been focused on the catalyst for this reaction: several catalysts including palladium,[4] rhodium,[5] and selenium[6] compounds show high activities. When the reaction carried out in an alcohol medium, the carbonylation proceeds under milder conditions(Eq. 3).

$$ArNO_2 + 3CO + ROH \longrightarrow ArNHCOOEt + 2CO_2 \quad (3)$$

The products are arylcarbamates, which can be easily converted to the corresponding isocyanates by pyrolysis.[7]

Only a few studies have been reported on platinum complex catalyzed carbonylation with carbon monoxide. Ogata *et al.*[8] and Knifton[9] have reported that a platinum–tin(II) chloride catalyst system is effective for hydroformylation and hydroesterification of 1-alkene.

We recently reported the preliminary results of platinum complex catalyzed reductive *N*-carbonylation of nitrobenzene to ethyl phenylcarbamate.[10] To our knowledge, this is the first example of a platinum catalyst having a high activity for the reductive *N*-carbonylation nitrobenzene to the carbamate. In this paper, we describe the full details of our results(Eq. 4)

$$ArNO_2 + 3CO + EtOH \xrightarrow[Et_3N]{PtCl_2(PPh_3)_2\text{-}SnCl_4} ArNHCOOEt + 2CO_2 \quad (4)$$

Results and Discussion

The catalytic activity of dichlorobis(benzonitrile)-platinum ($Pt(PhCN)_2Cl_2$)–tin(II or IV) chloride system for reductive *N*-carbonylation of nitrobenzene was examined in the presence of different phosphorus(III) ligands. The results are listed in Table 1. Ethyl phenylcarbamate and aniline were obtained as the reaction products. In all cases, yields of the carbamate

Table 1. The reductive *N*-carbonylation of nitrobenzene in the absence of amine[a]

Run	Phosphorus(III) ligand	Tin halide	Conversion[b] %	Yield of products/%[b]	
				Carbamate[c]	Aniline
1	PPh_3	$SnCl_4$	97	22	34
2	$P(OPh)_3$	$SnCl_4$	52	13	26
3	$P(n\text{-}Bu)_3$	$SnCl_4$	20	0	15
4	—	$SnCl_4$	93	13	14
5	$Ph_2P(CH_2)_2PPh_2$	$SnCl_4$	27	10	11
6	$Ph_2P(CH_2)_3PPh_2$	$SnCl_4$	64	3	48
7	$Ph_2P(CH_2)_4PPh_2$	$SnCl_4$	78	1	61
8	PPh_3	$SnCl_2$	43	8	14
9	$P(OPh)_3$	$SnCl_2$	29	2	21
10	$P(n\text{-}Bu)_3$	$SnCl_2$	42	0	14

a) A mixture of nitrobenzene(40 mmol), $PtCl_2(PhCN)_2$(0.4 mmol; 1.0 mol% based on nitrobenzene), $SnCl_4$(2.0 mmol), phosphorus(III) ligand(1.6 mmol; 0.8 mmol for the bidentate ligands), and EtOH(20 ml) was reacted at 180 °C for 4 h under the initial pressure of 60 kg cm^{-2} carbon monoxide. b) Determined by GLC based on the amount of nitrobenzene charged. c) Ethyl phenylcarbamate.

TABLE 2. THE REDUCTIVE *N*-CARBONYLATION OF NITROBENZENE IN THE PRESENCE OF AMINE[a]

Run	Platinum complex	Phosphorus(III) ligand	Tin halide	Amine	Conversion[b] %	Yields of products/%[b] Carbamate[c]	Aniline
11	$PtCl_2(PPh_3)_2$	—	$SnCl_4$	Et_3N	97	83	8
12	$PtCl_2(PhCN)_2$	PPh_3[d]	$SnCl_4$	Et_3N	98	78	12
13	—	PPh_3[d]	$SnCl_4$	Et_3N	54	0	17
14	$PtCl_2(PhCN)_2$	—	$SnCl_4$	Et_3N	90	8	32
15	$PtCl_2(PPh_3)_2$	—	—	Et_3N	29	0	17
16	$PtCl_2(PPh_3)_2$	—	$SnCl_4$	—	96	19	42
17	$PtCl_2(PPh_3)_2$	—	$SnCl_2$	Et_3N	97	5	60

a) Nitrobenzene(40 mmol), platinum complex(0.2 mmol), $SnCl_4$(2.0 mmol), triethylamine(1.0 ml), EtOH(20 ml) at 180 °C for 4 h under the initial pressure of 60 kg cm^{-2} carbon monoxide. b) Determined by GLC based on the amount of nitrobenzene charged. c) Ethyl phenylcarbamate. d) 0.4 mmol.

were low. Among the phosphorus (III) ligands, triphenylphosphine, which is an effective ligand for the platinum catalyzed hydroformylation,[9a] gave the best yield(22%) of the carbamate, when combined with tin(IV) chloride(Run 1). However, tributylphosphine, a more basic ligand, gave no *N*-carbonylated product. Ogata and co-workers reported that diphosphorus(III) ligands ($Ph_2P(CH_2)_nPPh_2$), especially $n=4$, are highly effective for platinum catalyzed hydroformylation.[8] The diphosphorus(III) ligands such as 1,2-ethanediylbisdiphenylphosphine, 1,3-propanediylbisdiphenylphosphine, 1,4-butanediylbisdiphenylphosphine in this *N*-carbonylation, gave only low yields of the carbamate. But aniline was formed in large amounts with an increase in the methylene length of the ligands indicating that these ligands were not effective for *N*-carbonylation (Runs 5—7). These bidentate ligands were effective for transformation of nitrobenzene to aniline.

The catalytic activity of platinum–tin(IV) chloride for *N*-carbonylation was dramatically improved by the addition of a tertiary amine, such as triethylamine. The results are listed in Table 2. Some references indicated that in the transformation of nitroarenes to the corresponding isocyanates, activities of the palladium and rhodium catalysts are highly enhanced by adding a Lewis acid and an amine.[4-6] The platinum–tin(IV) chloride combined with triethylamine drastically enhanced the yield and selectivity of the carbamate(Runs 11 and 12). The triphenylphosphine-$PtCl_2(PhCN)_2$ pair showed a comparable catalytic activity with dichlorobis(triphenylphosphine)platinum ($PtCl_2(PPh_3)_2$).

The platinum catalyst showed the highest activity only when combined with triphenylphosphine, tin(IV) chloride, and triethylamine. If one of these components was removed from the reaction system, yield of the carbamate was reduced drastically(Runs 13—16). The carbamate was not obtained in the absence of the platinum complex or tin halide(Runs 13—15). It is well known that tin(II) chloride is effective as co-catalyst for platinum catalyzed hydroformylation[8,9a] and hydroesterification.[9b] When tin(II) chloride was used in place of tin(IV) chloride for this reaction, the yield of the carbamate was only 5%(Run 17), indicating that tin(IV) chloride is much more favorable for this reaction. Thus, the present platinum catalyst system was distinct from the previously reported platinum catalyst system.

TABLE 3. THE EFFECT OF AMINE ADDITIVES ON THE REDUCTIVE *N*-CARBONYLATION OF NITROBENZENE[a]

Run	Amine	Conversion %	Yield of products/%[b] Carbamate[c]	Aniline
18	*N*-Methyl piperidine	100	76	10
19	DBU[d]	98	62	16
20	Piperidine	96	46	26
21	Pyridine	97	23	35
22	Butylamine	90	13	31
23	Aniline	71	1	5

a) Nitrobenzene(40 mmol), $PtCl_2(PPh_3)_2$(0.2 mmol), $SnCl_4$(2.0 mmol), amine(1.0 ml), EtOH(20 ml) at 180 °C for 4 h under the initial pressure of 60 kg cm^{-2} carbon monoxide. b) Determined by GLC based on the amount of nitrobenzene charged. c) Ethyl phenylcarbamate. d) 1,8-Diazabicyclo[5.4.0.]undec-7-ene.

The carbamate was also produced in the presence of other tertiary amines(Table 3). There was no linear relationship between the pk_a value of the conjugated acid of amine and the yield of the carbamate. However, generally tertiary amines with high basicity were effective for the *N*-carbonylation. Secondary and primary amines were less favorable.

In Table 4, effects of different Lewis acids on the reaction were examined fixing a molar ratio of Lewis acid to Pt was 20. Tin(IV) chloride was the most effective among the Lewis acid examined. With tin(IV) halide, the yield of the carbamate was reduced in the following order; $SnCl_4 > SnBr_4 \gg SnI_4$. This is the order in which Lewis acidity decreased. In the precedent platinum catalyzed reactions(hydroformylation and hydroesterification),[8,9] only the combination of platinum complex with tin(II) chloride exhibits the high catalytic activity. It is noticeable that iron(III) chloride, aluminum chloride, and titanium(IV) chloride had comparable effectiveness to tin(IV) chloride as co-catalysts(Runs 28—30).

The reaction was remarkably affected by the nature of the diphosphorus(III) ligands. The results are listed

in Table 5. Triphenylphosphine was most effective. Chelating diphosphorus(III) ligands reduced the catalytic activity. Those bidentate ligands would form thermodynamically stable complexes and these rigid complexes would be unfavorable as catalysts. Tributylphosphine and triphenyl phosphite were less effective as ligands.

The optimum reaction temperature was 180 °C under the initial pressure of 60 kg cm^{-1} carbon monoxide. The results are listed in Table 6. Under the initial pressure of 40 kg cm^{-2} carbon monoxide, the yield of the carbamate decreased(Run 38, *cf.* Run 11). The carbamate was not obtained under lower pressure of carbon monoxide. The reaction at 200 °C reduced the selectivity of the carbamate and the reaction at 160 °C reduced both the conversion of nitrobenzene and the selectivity.

Various nitroarenes were also *N*-carbonylated by this procedure(Table 7). From nitroarenes with a methyl substituents, the corresponding carbamates were obtained in good to excellent isolated yields(Runs 42, 45, and 46). On the other hand, nitroarenes with a methoxyl substituent gave the corresponding

Table 4. The effect of Lewis acid on the reductive *N*-carbonylation of nitrobenzene[a]

Run	Lewis acid	Conversion[b] %	Yield of products/%[b]	
			Carbamate[c]	Aniline
24	$SnCl_4$	97	70	6
25	$SnCl_2$	98	40	25
26	$SnBr_4$	96	30	11
27	SnI_4	86	Trace	18
28	$FeCl_3$	98	64	15
29	$AlCl_3$	97	63	14
30	$TiCl_4$	95	61	12
31	$ZnCl_2$	28	0	14

a) Nitrobenzene (40 mmol), $PtCl_2(PPh_3)_2$ (0.2 mmol), Lewis acid(4.0 mmol), triethylamine(1.0 ml), EtOH(20 ml) at 180 °C for under the initial pressure of 60 kg cm^{-2} carbon monoxide. b) Determined by GLC based on the amount of nitrobenzene charged. c) Ethyl phenylcarbamate.

Table 5. The effect of phosphorus(III) ligand on the reductive *N*-carbonylation of nitrobenzene[a]

Run	Phosphorus(III) ligand	Conversion[b] %	Yield of products/%[b]	
			Carbamate[c]	Aniline
32	PPh_3	98	56	10
33	$Ph_2P(CH_2)_2PPh_2$	11	0	6
34	$Ph_2P(CH_2)_3PPh_2$	23	4	9
35	$Ph_2P(CH_2)_4PPh_2$	33	6	15
36	$P(n\text{-}Bu)_3$	97	29	31
37	$P(OPh)_3$	87	25	31

a) Nitrobenzene(40 mmol), $PtCl_2(PhCN)_2$(0.2 mmol), $SnCl_4$(2.0 mmol), phosphorus(III) ligand(0.8 mmol; 0.4 mmol for the bidentate ligands), triethylamine(1.0 ml), EtOH(20 ml) at 180 °C for 4 h under the initial pressure of 60 kg cm^{-2} carbon monoxide. b) Determined by GLC based on the amount of nitrobenzene charged. c) Ethyl phenylcarbamate.

Table 6. The effect of reaction temperature and carbon monoxide pressure on the reductive *N*-carbonylation of nitrobenzene[a]

Run	Initial carbon monoxide Pressure/kg cm^{-2}	Temp °C	Conversion[b] %	Yield of products/%[b]	
				Carbamate[c]	Aniline
11	60	180	97	83	8
38	40	180	97	68	7
39	20	180	87	0	14
40	60	200	93	69	5
41	60	160	62	30	5

a) Nitrobenzene(40 mmol), $PtCl_2(PPh_3)_2$(0.2 mmol), $SnCl_4$(2.0 mmol), triethylamine(1.0 ml), EtOH(20 ml) for 4 h. b) Determined by GLC based on the amount of nitrobenzene charged. c) Ethyl phenylcarbamate.

Table 7. The reductive *N*-carbonylation of various nitroarenes[a]

Run	Substrate	Product	Yield[b] %
42	*p*-Methylnitrobenzene	Ethyl 4-methylphenylcarbamate	87
43	*p*-Methoxynitrobenzene	Ethyl 4-methoxyphenylcarbamate	46
44	*p*-Chloronitrobenzene	Ethyl 4-chlorophenylcarbamate	59
45	*m*-Methylnitrobenzene	Ethyl 3-methylphenylcarbamate	64
46	*o*-Methylnitrobenzene	Ethyl 2-methylphenylcarbamte	74
47	*o*-Methoxynitrobenzene	Ethyl 2-methoxyphenylcarbamate	38
48	*o*-Chloronitrobenzene	Ethyl 2-chlorophenylcarbamate	42
49	1,4-Dimethyl-2-nitrobenzene	Ethyl 2,5-dimethylphenylcarbamate	71

a) Nitroarene(40 mmol), $PtCl_2(PPh_3)_2$(0.2 mmol), $SnCl_4$(4.0 mmol), triethylamine(1.0 ml), EtOH(20 ml) at 180 °C for 4 h under the initial pressure of 60 kg cm^{-2} carbon monoxide. b) Isolated yields.

carbamate in only moderate isolated yields and the reaction was accompanied by a considerable amount of tarry material (Runs 43 and 47). Under the same reaction conditions, *p*- or *o*- chloronitrobenzene gave moderate yields of the corresponding carbamates(Runs 44 and 48). 1-Nitronaphthalene gave only 1-naphthylamine as the product in 26% yield. From *p*-nitroaniline and *N*,*N*-dimethyl-3-nitroaniline, the corresponding *N*-carbonylated products were not obtained.

Two routes are possible for the reaction. One is the path in which aminoarene is carbonylated with carbon monoxide (Path A). Small amounts of aminoarenes were always detected as by-products. These would be formed by hydrogen transfer from ethanol to nitroarene or hydrogen abstraction by nitrene intermediate from ethanol. It is well known that the carbamates are obtained by transition metal catalyzed *N*-carbonylation of aminoarenes in the presence of an oxidant, such as nitroarenes or molecular oxygen.[11]

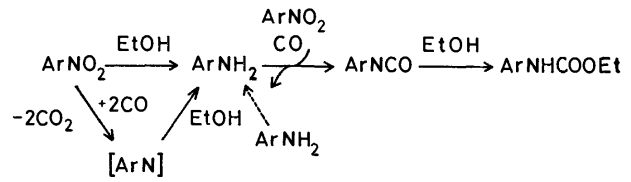

Path A.

In the present reaction, nitroarene may function as the oxidant for the carbonylation of aminoarene to the carbamate(Path A). However, an equimolar mixture of nitrobenzene and aniline under the same conditions as Run 11 gave low conversion of aniline, the yield of the carbamate was reduced to 38%, based on the total amount of nitrobenzene and aniline. This result indicated that Path A is unfavorable.

The other path is the route involving the carbonylation of a nitrene intermediate(Path B). Bennett *et al.* have reported formation of phenyl isocyanates from phenyl azide under carbon monoxide pressure.[12]

$$ArNO_2 \xrightarrow[-CO_2]{2CO} (ArN)[Pt] \xrightarrow{CO} (ArNCO)[Pt] \xrightarrow{EtOH} ArNHCOOEt + [Pt]$$

Path B.

They have proposed that phenylnitrene is the reaction intermediate. Collman *et al.* have also reported similar phenyl isocyanate formation from phenyl azide in the presence of a transition metal.[13] In our reaction, a nitrene intermediate would be generated by deoxygenation of nitroarene with carbon monoxide and the carbonylation of the nitrene intermediate would be followed, as shown in Path B. Iqbal also proposed the nitrene intermediate in the reaction of nitrobenzene with carbon monoxide.[14]

In this reaction, characterization of the active species could not be done. Several studies have indicated that a Lewis acid promotes migratory insertion of coordinated carbon monoxide to a carbon-metal bond.[15] In our reaction, a Lewis acid would be operative in promoted the insertion of carbon monoxide into a nitrogen-metal bond, which consequently generates an aryl isocyanate complex(Path B). Several transition metal nitrene complex[16] and isocyanate organometallic complex were isolated.[17] Schwetlick *et al.* isolated an isocyanate complex in the course of rhodium-catalyzed reductive *N*-carbonylation of nitromesitylene.[18] In the absence of amine, the yield of the carbamate was quite low and a considerable amount of tarry material was obtained. In the presence of amine, the reaction proceeded smoothly. The amine may function to weaken the Lewis acidity and to suppress side reaction promoted by Lewis acid.

Experimental

Material. The reagents employed in this study were purified before use. Carbon monoxide (>99.9%) was used without further purification. Ethanol(99.5%) was dried by reflux over freshly ignited and crushed CaO for 9 h and distilled carefully under Ar atmosphere. Platinum complexes were prepared by the literature methods.[19]

General Procedure. A 100 ml stainless steel autoclave (Nitto Koatsu) equipped with a magnetically driven stirrer was used. A glass liner was set in the autoclave and the inside of it was heated by a heat gun (400 W) for 2 min. After cooling in Ar steam, the reagents were charged in the following order: ethanol(20 ml), nitroarene(40 mmol), triethylamine(1.0 ml, 7.2 mmol), $PtCl_2(PPh_3)_2$ (158 mg, 0.2 mmol; 0.5 mol% based on nitroarene), and $SnCl_4$(0.47 ml, 4.0 mmol). After sealing and flushing with carbon monoxide, the reactor was pressured with carbon monoxide to 60 kg cm^{-2}. The autoclave was heated to 180 °C(20 min required) and then held at this temperature for 4 h. The reaction was terminated by rapid cooling and the autoclave was discharged. The resulting brown solution was analyzed with GLC. The products were isolated by vacuum distillation. The identification of the products was confirmed by elemental analysis, IR, ^{1}H-NMR, ^{13}C-NMR, and mass spectra. The boiling points and melting points are uncorrected. The GLC analysis was made with a column (3 mm $\phi \times 3$ m) packed with Silicone OV-17(2%) on Uniport HP 60—80 mesh. The oven temperature was programmed from 100 °C to 200 °C at a rate of 5 °C min^{-1}. The IR spectra were measured on a Hitachi model 215 grating spectrophotometer. The ^{13}C-NMR and ^{1}H-NMR spectra were recorded at 25.05 and 100 MHz respectively with a JEOL JNM FX 100 spectrometer. Samples were dissolved in $CDCl_3$, and the chemical shift values were expressed in relative to Me_4Si as an internal standard. Elemental analyses were performed at Microanalytical Center of Kyoto University. The mass spectra were recorded on a JMS OISG mass spectrometer.

The analytical data of the products are described below. The phenyl carbon resonances in the ^{13}C-NMR spectra were tentatively assigned by calculating their chemical shifts with additive parameters.[20]

Ethyl Phenylcarbamate. Yellow oil 117—119 °C/4 mmHg (1 mmHg≈133.322 Pa). All the spectral data (^{1}H-NMR, ^{13}C-NMR, and IR spectra) were consistent with those of an authentic sample.

Ethyl 4-Methylphenylcarbamate. Yellow oil, Kugelrohr distillation(65 °C/0.12 mmHg) ^{1}H-NMR (100 MHz)($CDCl_3$); δ 1.20 (t, 3H, $-OCH_2\underline{CH_3}$), 2.21 (s, 3H, $-\underline{CH_3}$), 4.41 (q, 2H, $-OC\underline{H_2}CH_3$), 6.98 (d, 2H, phenyl) 7.34 (d, 2H, phenyl). ^{13}C-NMR (25.05 MHz)($CDCl_3$); 14.6(q, $-OCH_2\underline{CH_3}$), 20.7 (q, $-\underline{CH_3}$), 60.9(t, $-O\underline{CH_2}CH_3$), 119.1 (d, phenyl 2, 6), 129.3 (d, phenyl 3, 5), 132.5(s, phenyl 4), 135.7(s, phenyl 1), 154.2

(s, C=O). IR(KBr): 3300 cm^{-1} (ν_{N-H}), 1710 cm^{-1} ($\nu_{C=O}$). MS(*m/e*): 179(M^+), 106(M^+—COOEt). Calcd for $C_{10}H_{13}NO_2$: C, 67.02; H, 7.31; N, 7.82%. Found: C, 67.06; H, 7.42; N, 7.91%.

Ethyl 4-Chlorophenylcarbamate. Yellow crystals, bp 114—120 °C/0.18 mmHg. ^{1}H-NMR (100 MHz)($CDCl_3$); δ 1.28(t, 3H, $-OCH_2C\underline{H}_3$), 4.21(q, 2H, $-OC\underline{H}_2CH_3$), 7.20 (d, 2H, phenyl), 7.35(d, 2H, phenyl). ^{13}C-NMR (25.05 MHz)($CDCl_3$); 14.5(q, $-OCH_2\underline{C}H_3$), 61.4(t, $-O\underline{C}H_2CH_3$), 120.0(d, phenyl 2, 6), 128.2(s, phenyl 4), 128.9(d, phenyl 3, 5), 136.7(s, phenyl 1), 153.7(s, C=O). IR(KBr): 3300 cm^{-1} (ν_{N-H}), 1690 cm^{-1} ($\nu_{C=O}$). MS(*m/e*): 199(M^+), 126 (M^+—COOEt). Calcd for $C_9H_{10}NO_2Cl$: C, 54.15; H, 5.05; N, 7.02; Cl, 17.76%. Found: C, 54.17; H, 5.09; N, 7.02; Cl, 17.91%.

Ethyl 3-Methylphenylcarbamate. Yellow oil, bp 93 °C/0.08 mmHg. ^{1}H-NMR (100 MHz)($CDCl_3$); δ 1.25(t, 3H, $-OCH_2C\underline{H}_3$), 2.25(s, 3H, $-C\underline{H}_3$), 4.18(q, 2H, $-OC\underline{H}_2CH_3$), 6.79—7.17(m, 5H, phenyl and NH). ^{13}C-NMR(25.05 MHz) ($CDCl_3$); 14.5 (q, $-OCH_2\underline{C}H_3$), 21.4 (s, $-\underline{C}H_3$), 61.0 (t, $-O\underline{C}H_2CH_3$), 115.9(d, phenyl 6), 119.4(d, phenyl 2), 124.0 (d, phenyl 4), 128.7(d, phenyl 5), 138.1(s, phenyl 3), 138.7 (s, phenyl 1), 153.9(s, C=O). IR(neat): 3320 cm^{-1} (ν_{N-H}), 1705 cm^{-1} ($\nu_{C=O}$). MS(*m/e*): 179(M^+), 106(M^+—COOEt). Calcd for $C_{10}H_{13}NO_2$: C, 67.02; H, 7.31; N, 7.82%. Found: C, 67.20; H, 7.22; N, 7.81%.

Ethyl 4-Methoxyphenylcarbamate. Yellow crystals, bp 126 °C/0.08 mmHg. ^{1}H-NMR (100 MHz) ($CDCl_3$); δ 1.27 (t, 3H, $-OCH_2C\underline{H}_3$), 3.74 (s, 3H, $-OC\underline{H}_3$), 4.19(q, 2H, $-OC\underline{H}_2CH_3$), 6.81(d, 2H, phenyl), 6.94(br, 1H, N$\underline{H}$), 7.29 (d, 2H, phenyl). ^{13}C-NMR (25.05 MHz)($CDCl_3$); 14.6(q, $-OCH_2\underline{C}H_3$), 55.5(q, $-O\underline{C}H_3$), 61.6(t, $-O\underline{C}H_2CH_3$), 114.1 (d, phenyl 3,5), 120.9(d, phenyl 2,6), 131.1(s, phenyl 1), 154.2(s, phenyl 4), 155.8(s, C=O). IR(KBr): 3310 cm^{-1} (ν_{N-H}), 1690 cm^{-1} ($\nu_{C=O}$). MS(*m/e*): 195(M^+), 122(M^+—COOEt). Calcd for $C_{10}H_{13}NO_3$: C, 61.53; H, 6.71; N, 7.18%. Found: C, 61.62; H, 6.63; N, 7.02%.

1-Naphthylamine. Red oil, bp 126 °C/0.12 mmHg. Spectra data of the isolated product were consistent with those of the authentic sample.

Ethyl 2-Methylphenylcarbamate. Colorless oil, bp 78—80 °C/0.06 mmHg. ^{1}H-NMR (100 MHz) ($CDCl_3$); δ 1.25 (t, 3H, $-OCH_2C\underline{H}_3$), 2.16 (s, 3H, $-C\underline{H}_3$), 4.16 (q, 2H, $-OC\underline{H}_2CH_3$), 6.65(br, 1H, N$\underline{H}$), 6.95—7.71(m, 4H, phenyl). ^{13}C-NMR(25.05 MHz)($CDCl_3$): 14.6(t, $-OCH_2\underline{C}H_3$), 17.6 (t, $-CH_3$), 61.6(t, $-O\underline{C}H_2CH_3$), 121.5(d, phenyl 6), 124.1 (d, phenyl 4), 126.6(d, phenyl 5), 128.0(s, phenyl 2), 130.3 (d, phenyl 3), 135.9(s, phenyl 1), 154.0(s, C=O). IR(neat): 3300 cm^{-1} (ν_{N-H}), 1730 cm^{-1} ($\nu_{C=O}$). MS(*m/e*): 179(M^+), 106(M^+—COOEt). Calcd for $C_{10}H_{13}NO_2$: C, 67.02; H, 7.31; N, 7.82%. Found: C, 67.45; H, 7.27; N, 7.84%.

Ethyl 2-Methoxyphenylcarbamate. Colorless oil, bp 95—97 °C/0.13 mmHg. ^{1}H-NMR (100 MHz) ($CDCl_3$): δ 1.28 (t, 3H, $-OCH_2C\underline{H}_3$), 3.78 (s, 3H, $-OC\underline{H}_3$), 4.20 (q, 2H, $-OC\underline{H}_2CH_3$), 7.23(br, 1H, N$\underline{H}$), 6.70—7.23(m, 3H, phenyl), 7.97—8.12(m, 1H, phenyl). ^{13}C-NMR(25.05 MHz)($CDCl_3$): 14.6(q, $-OCH_2\underline{C}H_3$), 55.8(q, $-O\underline{C}H_3$), 61.6(t, $-O\underline{C}H_2CH_3$), 110.0(d, phenyl 3), 118.2(d, phenyl 6), 121.0 (d, phenyl 5), 122.7(d, phenyl 4), 127.7(s, phenyl 1), 147.6 (s, phenyl 2), 153.5(s, C=O). IR (neat): 3420 cm^{-1} (ν_{N-H}), 1730 cm^{-1} ($\nu_{C=O}$). MS (*m/e*): 195 (M^+). Calcd for $C_{10}H_{13}NO_3$: C, 61.53; H, 6.71; N, 7.18. Found: C, 60.42; H, 6.51; N, 6.94.

Ethyl 2,5-Dimethylphenylcarbamate. Ethanol was removed from the reaction mixture *in vacuo* at 50 °C. Then, petroleum ether was added to the residue. A soluble part was separated by filtration, and then the solvent was removed *in vacuo*. The product was afforded as crystals: brown crystals, mp 94—95 °C. ^{1}H-NMR (100 MHz) ($CDCl_3$): δ 1.31(t, 3H, $-OCH_2C\underline{H}_3$), 2.19(s, 3H, $-C\underline{H}_3$), 2.31(s, 3H, $-C\underline{H}_3$), 4.22(q, 2H, $-OC\underline{H}_2CH_3$), 6.36(br, 1H, $-N\underline{H}$), 6.83 (d, 1H, phenyl), 7.02(d, 1H, phenyl), 7.61(s, 1H, phenyl). ^{13}C-NMR(25.05 MHz)($CDCl_3$): δ 14.6(q, $-OCH_2\underline{C}H_3$), 17.2 (q, $-\underline{C}H_3$), 21.1(q, $-\underline{C}H_3$), 61.2(t, $-O\underline{C}H_2CH_3$), 121.8(d, phenyl 6), 124.5(s, phenyl 2), 124.8(d, phenyl 4), 130.1(d, phenyl 3), 135.6(s, phenyl 5), 136.5(s, phenyl 1), 153.9(s, C=O). IR(KBr): 3290 cm^{-1} (ν_{N-H}), 1685 cm^{-1} ($\nu_{C=O}$). MS (*m/e*): 193(M^+), 120(M^+—COOEt). Calcd for $C_{11}H_{15}NO_2$: C, 68.37; H, 7.82; N, 7.25%. Found: C, 68.53; H, 7.92; N, 7.18%.

Ethyl 2-Chlorophenylcarbamate. Colorless oil, bp 70—72 °C/0.07 mmHg. ^{1}H-NMR(100 MHz)($CDCl_3$): δ 1.30(t, 3H, $-OCH_2C\underline{H}_3$), 4.22(q, 2H, $-OC\underline{H}_2CH_3$), 6.93(t of d, 1H, phenyl), 7.22 (t of d, 1H, phenyl), 7.29 (d of d, 1H, phenyl), 8.15(d of d, 1H, phenyl). ^{13}C-NMR(25.05 MHz) ($CDCl_3$): δ 14.5(t, $-OCH_2\underline{C}H_3$), 61.5(t, $-O\underline{C}H_2CH_3$), 119.9 (d, phenyl 6), 122.0 (s, phenyl 2), 123.6 (d, phenyl 4), 127.7 (d, phenyl 5), 129.0(d, phenyl 3), 134.8(s, phenyl 1), 153.2 (s, C=O). IR(neat): 3410 cm^{-1} (ν_{N-H}), 1730 cm^{-1} ($\nu_{C=O}$). MS(*m/e*): 199(M^+), 126(M^+—COOEt). Calcd for $C_9H_{10}NO_2Cl$: C, 54.15; H, 5.05; N, 7.02; Cl, 17.76%. Found: C, 54.97; H, 5.07; N, 7.36; Cl, 17.89%.

References

1) "New Synthesis with Carbon Monoxide," ed by J. Falbe Springer-Verlag, Berlin (1980).

2) V. I. M. Yuvenskii and B. K. Nefedov, *Russ. Chem. Rev.*, **50**, 470, (1980).

3) S. Ozaki, *Chem. Rev.*, **72**, 457 (1972).

4) P. Braunstein, R. Bender, and J. Kervennal, *Organometallics*, **1**, 1236 (1982); H. Tiez, K. Univerferth, and K. Schwetlick, *Z. Chem.*, **18**, 141 (1978); **20**, 296, 411 (1980); B. K. Nefedov and V. I. M. Yuvenskii, *Bull. Acad. Sci. USSR, Div. Chem. Sci.*, **1978**, 2066; A. N. Miyazov, B. K. Nefedov, Kh. O. Khoshdurdyev, and V. I. M. Yuvenskii, *Dokl. Chem. Acad. Soc. USSR. Chem. Sect.*, **1981**, 242; A. L. Lapidus, A. F. Lunin, S. D. Pirozhkov, N. B. Leonchick, P. Neitsel, and K. Schwetlick, *Bull. Acad. Sci. USSR, Div. Chem. Sci.*, **1982**, 1068.

5) K. Univerferth, R. Hontsch, and K. Schwetlick, *J. Prakt. Chem.*, **321**, 86 (1979); K. Univerferth and K. Schwetlick, *React. Kinet. Catal. Lett.*, **6**, 231 (1977); V. I. M. Yuvenskii, A. V. Smetanin, and B. K. Nefedov, *Bull. Acad. Sci. USSR, Div. Chem. Sci.*, **1980**, 1813, 1817; W. B. Hardy and R. P. Bennett, *Tetrahedron. Lett.*, **1967**, 961.

6) J. H. Bateman, *Chem. Tech.* **8**, 382 (1978); K. Kondo, N. Sonoda, and S. Tsutsumi, *Chem. Lett.*, **1972**, 373.

7) Japan Kokai 75-19721, 75-30832, 79-88201.

8) T. Hayashi, Y. Kawabata, T. Isoyama, and I. Ogata, *Bull. Chem. Soc. Jpn.*, **54**, 3483 (1981).

9) a) I. Schwanger and J. Knifton *J. Catal*, **45**, 256 (1976); b) J. F. Knifton, *J. Org. Chem.*, **41**, 793 (1976).

10) Y. Watanabe, Y. Tsuji, and N. Suzuki, *Chem. Lett.*, **1982**, 105.

11) Japan Kokai 80-120551, 80-120552, 80-124750.

12) R. B. Bennett and W. B. Hardy, *J. Am. Chem. Soc.*, **90**, 3295 (1968).

13) J. P. Collman, M. Kubota, D. F. Vastine, T. Y. Sun, and W. J. Kang, *J. Am. Chem. Soc.*, **90**, 5430 (1968).

14) A. F. M. Igbal, *J. Org. Chem.*, **37**, 2791 (1972); *Helv. Chim. Acta*, **55**, 26, 798, 2637 (1972).

15) S. B. Butts, S. H. Straus, E. M. Holt, R. E. Stimsom, N. W. Alcock, and D. F. Shriver, *J. Am. Chem. Soc.*, **102**,

5093 (1980); F. Correa, R. Nakamura, R. E. Stimson, R. L. Burwell, Jr., and D. F. Shriver, *ibid*, **102**, 5114 (1980); S. B. Butts, T. G. Richmond, and D. F. Shriver, *Inorg. Chem.*, **20**, 278 (1981); S. J. LaCroce and A. R. Culter, *J. Am. Chem. Soc.*, **104**, 2312 (1982).

16) M. Dekker and G. R. Knox, *J. Chem. Soc., Chem. Commun.*, **1967**, 1243; L. A. P. Kane-Murie, H. D. Gafeny, F. Basolo, and R. G. Pearson, *J. Am. Chem. Soc.*, **91**, 4610 (1969); A. T. Mcphail, G. R. Knox, C. G. Robertson, and G. A. Sim, *J. Chem. Soc.*, A, **1971**, 205.; R. A. Abramovitch, R. G. Sutherland, and A. K. V. Unni, *Tetrahedron Lett.*, **1972**, 1065; J. L. Reed, H. D. Gafeny, and F. Basolo, *J. Am. Chem. Soc.*, **96**, 1363 (1974); E. D. Johnson and F. Basolo, *Inorg. Chem.*, **16**, 554 (1977); M. Katz and H. D. Gafeny, *ibid.*, **16**, 554 (1978); S. Aime, G. Gervasio, L. Milone, R. Rossetti, and P. L. Stanghellini, *J. Chem. Soc., Dalton Trans.*, **1978**, 534; W. A. Neugent and R. L. Harlow, *J. Chem. Soc., Chem. Commun.*, **1978**, 579; **1979**, 342; B. L. Haymore, E. A. Maatta, and R. A. Wentworth, *J. Am. Chem. Soc.*, **101**, 2063 (1979); *Inorg. Chem.*, **19**, 1055 (1980).

17) M. F. Lapport and B. Porkai, *Adv. Organomet. Chem.*, **5**, 225 (1967); S. Cenini and G. La. Monica, *Inorg. Chim. Acta*, **18**, 279 (1976); H. L. M. Gaal and J. P. J. Verlaan, *J. Organomet. Chem.*, **133**, 93 (1977); D. H. M. W. Theweissen, *ibid.*, **192**, 115 (1980).

18) K. Univerferth, R. Hontsch, and K. Schwetlick, *J. Prakt. Chem.*, **321**, 928 (1978).

19) J. C. Bailar and H. Itatani, *Inorg. Chem.*, **4**, 1618 (1965); F. R. Hartley, "The Chemistry of Platinum and Palladium," Applied Science, London (1973), p. 462.

20) J. B. Stothers, "Carbon-13 NMR Spectroscopy," Academic Press, New York (1972), p. 197.

Photorearrangements of Some Methyl-substituted Cholest-5-en-3β-ol Nitrites[1)]

Hiroshi SUGINOME,* Norio MAEDA,† Makoto KAJI, and Kyohei TAKAKUWA

Organic Synthesis Division, Department of Chemical Process Engineering, Faculty of Engineering, Hokkaido University, Sapporo 060

† *Department of Chemistry, Faculty of Science, Hokkaido University, Sapporo 060*

(Received May 14, 1983)

Photolysis of 6-methylcholest-5-en-3β-ol nitrite and 4,4,6-trimethylcholest-5-en-3β-ol nitrite in benzene with monochromatic light respectively gave a seven-membered cyclic hydroxamic acid arising from rearrangement albeit in low yields. Photolysis of 3α-methylcholest-5-en-3β-ol nitrite and 3α,4,4-trimethylcholest-5-en-3β-ol nitrite respectively gave a nitroso dimer arising from β-scission.

In a series of previous papers,[2)] we have reported the results of the photorearrangements of several steroidal and nonsteroidal cyclic homoallyl alcohol nitrites.[2)]

These studies have shown that the products in the photorearrangement of cyclic homoallyl alcohol nitrites are always those arising from the combination of nitrogen monooxide and the less substituted carbon terminus of the allyl radical intermediates. These are generated by the β-scission of the corresponding oxyl radicals, with the formation of more highly substituted olefins.

We have found, however, an exception to this rule in the photorearrangement of 4,4-dimethylcholesteryl nitrite[2)] in which the nitrogen monooxide shifts regioselectively to the more substituted terminus of the intermediary allyl radical. This reverse regioselectivity observed in the radical combination between the allyl radical and nitrogen monooxide was explained as due to the shielding of the C-6 by the 10β-methyl group and the *quasi*-axial 7α-H.[3)]

In order to gain more insight into the effects of alkyl substitution around the reacting radical center, we investigated the photoreactions of two 6-methylcholest-5-en-3β-ol nitrites (**2**) and (**4**) and two 3α-methylcholest-5-en-3β-ol nitrites (**6**) and (**8**) with monochromatic light as well as with Pyrex-filtered light. The photolysis of these nitrites with monochromatic light was especially desirable in order to avoid the secondary photo-decomposition of the photo-products.

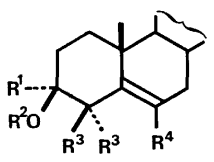

(1) $R^1=R^2=R^3=H$, $R^4=CH_3$
(2) $R^1=R^3=H$, $R^2=NO$, $R^4=CH_3$
(3) $R^1=R^2=H$, $R^3=R^4=CH_3$
(4) $R^1=H$, $R^2=NO$, $R^3=R^4=CH_3$
(5) $R^1=CH_3$, $R^2=R^3=R^4=H$
(6) $R^1=CH_3$, $R^2=NO$, $R^3=R^4=H$
(7) $R^1=R^3=CH_3$, $R^2=R^4=H$
(8) $R^1=R^3=CH_3$, $R^2=NO$, $R^4=H$

6-Methylcholest-5-en-3β-ol nitrite (**2**), 4,4,6-trimethylcholest-5-en-3β-ol nitrite (**4**) and 3α-methylcholest-5-en-3β-ol nitrite (**6**) were prepared from the corresponding 3β-ols (**1**),[4,5)] (**3**),[5)] and (**5**),[6)] by the standard method. Nitrosation of 3α,4,4-trimethylcholest-5-en-3β-ol (**7**)[7)] with nitrosyl chloride–pyridine by the standard method, was found to be difficult and to give a 1:2.4 mixture of the starting alcohol and nitrite **8** as determined by the signal ratio of 6-H in the ^1H NMR spectrum.

Irradiation of nitrite **2** in dry benzene with 370 nm monochromatic light gave mainly the parent alcohol (**1**) (57%) arising from a hydrogen abstraction of the corresponding oxy radical together with a 7% yield of a crystalline product (**9**). This was proved to be 4-hydroxy-6-methyl-4-aza-*A*-homocholest-5-en-3-one, a hydroxamic acid, from its spectroscopic data (Scheme 1).

Photolysis of nitrite **2** with a Pyrex-filtered light gave **9** in a much higher yield (37%) and the parent alcohol **1** (26%).

Photolysis of nitrite **4** with a 373 nm light also gave a mixture of products from which the parent alcohol **3** (18%), 4,6-dimethyl-4-methylene-3,4-secocholest-5-en-3-al (**10**) (25%) and 4-hydroxy-4a,4a,6-trimethyl-4-aza-*A*-homocholest-5-en-3-one (**11**) (13%) were obtained by preparative TLC (Scheme 2).

Photolysis of **4** with a Pyrex-filtered light was also found to give the parent alcohol **3** (18%) and a secoaldehyde **10** (6%) together with 4,4,6-trimethylcholest-5-en-3-one (**12**)[8)] (4%). No hydroxamic acid **11**, however, was found in the product mixture.

Although the observed differences between the results of the photolysis with monochromatic light and those with a Pyrex-filtered light are not clear at present, it has thus again been shown that seven-membered cyclic hydroxamic acid can be prepared from the photoreaction of 3-hydroxy-Δ^5-steroid nitrites.[2)] It should be noted that the product of the photorearrangement of (**2**) is a hydroxamic acid **9** and not the corresponding seven-membered cyclic nitrone.[9)] This

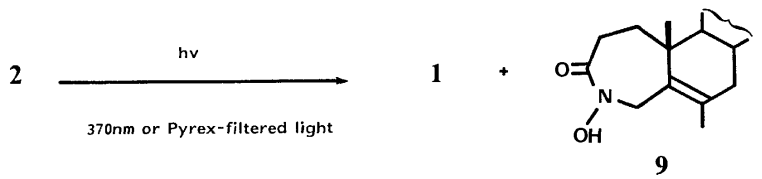

9

Scheme 1.

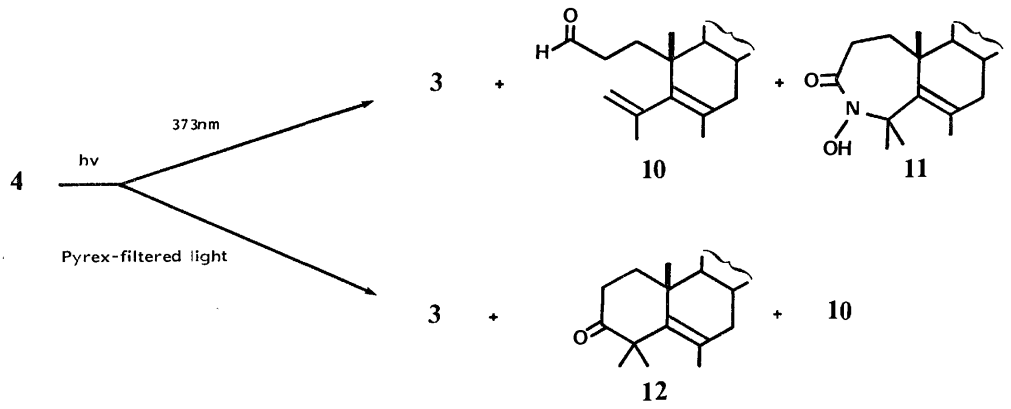

Scheme 2.

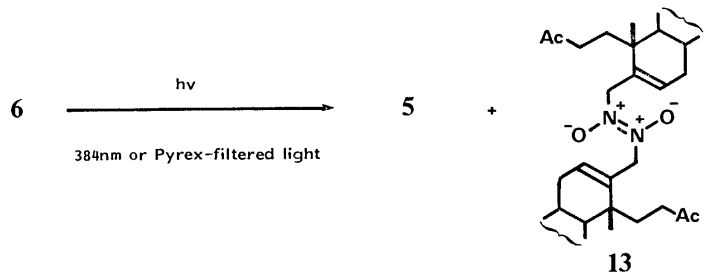

Scheme 3.

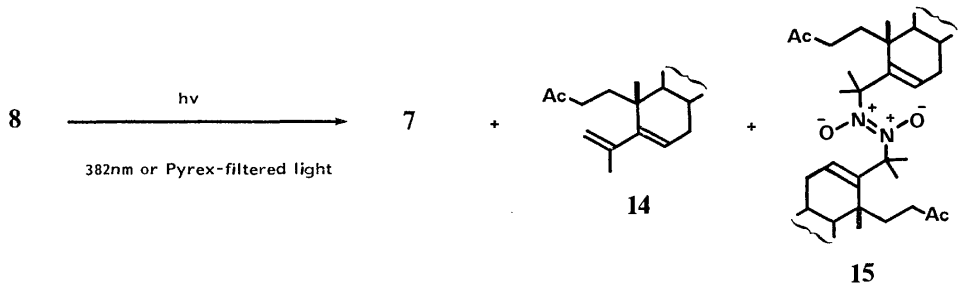

Scheme 4.

result is entirely parallel with that obtained in the photorearrangement of cholesterol nitrite.[2] The reason why the nitrone is not formed in this photorearrangement of cyclic homoallyl alcohol nitrite has already been discussed in the previous paper.[2]

We then studied the photolysis of two 3α-methylcholest-5-en-3β-ol nitrites (**6**) and (**8**) from which hydroxamic acids can not be formed even after β-scission.

The photolysis of 3α-methylcholest-5-en-3β-ol nitrite (**6**) with a 384 nm light resulted in the formation of a mixture of the products. Preparative TLC of the product gave the parent alcohol **5** (14%) and a crystalline nitroso dimer (**13**) (12%) together with several ill-defined products. The structure of the nitroso dimer **13** as (*E*)-4,4'-azobis(3,4-seco-3-methylcholest-5-en-3-one) *N*,*N*'-dioxide was confirmed by means of spectroscopy (see Experimental section). The photolysis of **6** with a Pyrex-filtered light gave a similar result with a better yield of the nitroso dimer (21%) (Scheme 3).

On the other hand, irradiation of a mixture of the alcohol **7** and the nitrite **8** with 382 nm monochromatic light gave three products; an amorphous seco-ketone (**14**)(13%), the parent alcohol **7** (23%) and an unstable amorphous nitroso dimer(**15**) (11%). The structures of **14** and **15** were shown to be 3,4-dimethyl-4-methylene-3,4-secocholest-5-en-3-one and (*E*)-4,4'-azobis (3,4-seco-3,4,4-trimethylcholest-5-en-3-one) *N*,*N*'-dioxide on the basis of their ^{1}H NMR, UV, IR, and Mass spectra (Scheme 4).

The photolysis of **8** with a Pyrex-filtered light also gave the seco-ketone **14** and the nitroso dimer **15** in better yields together with a lower yield of the parent 3β-ol **7**.

It has thus again been shown that the nitrogen monooxide migrates to the more substituted carbon terminus of the intermediary allyl radical in the photolysis of 4,4-dimethyl-3β-hydroxy-Δ^5-steroid nitrite. As has been discussed in the previous paper,[2] this anomaly in the site of the combination of radicals may be steric in its origin and may be due to the fact that the C-6 terminus of the intermediary allyl radical is more shielded for the approach of nitrogen monooxide.

Experimental

Mp's were determined with a Yanagimoto micro mp apparatus. IR spectra were determined for Nujol mulls, unless stated otherwise, with a JASCO IR-E spectrophotometer. UV spectra were determined with a Hitachi 124 double-beam spectrophotometer, unless stated otherwise. ^{1}H NMR spectra were determined with a JEOL PS 100 high-resolution spectrometer (100 MHz) (solvent $CDCl_3$, $SiMe_4$ as internal reference). ^{1}H NMR spectra of **8**, **11** and **15** were determined with a JEOL PS 200 high-resolution FT NMR spectrometer (200 MHz). ^{13}C NMR spectra were determined with a JNM-FX-100 (25 MHz) high-resolution spectrometer ($CDCl_3$, $SiMe_4$ as an internal reference). TLC was carried out on Wako silica gel B-5. Low resolution mass spectra of **9**, **10**, **13**, and **14** were recorded with JEOL JMS-D-300 spectrometer (70 eV) (The Faculty of Agriculture of this University.) Low resolution mass spectra of **11** and **15** were recorded with a JEOL JMS-D-300 spectrometer (70 eV) (The Faculty of Pharmaceutical Sciences of this University). The high resolution mass spectrum of **9** was determined with a JEOL JMS-D-300 spectrometer (70 eV). High resolution mass spectra of **13** and **14** were determined with a JEOL JMS-D 300 spectrometer (70 eV) (The Faculty of Agriculture) and that of **11** was determined with JEOL JMS-D-300 spectrometer (the Faculty of Pharmaceutical Sciences).

The Procedure of the Photolysis. (a) With a Pyrex-filtered Light: A benzene solution of each nitrite in a Pyrex tube was flushed with oxygen-free nitrogen and irradiated with a 100-W high pressure Hg arc (EIKOSHA PIH-100) until all the nitrite was decomposed. The progress of the photolysis was monitored by TLC at appropriate time intervals.

(b) With Monochromatic Light: A solution of each nitrite (2—300 mg) in dry benzene (2—3 cm^3) in a quartz cell (10×10×45 mm^3) was placed in a chamber of a JASCO CRM-FA grating spectro-irradiator equipped with 2KW Xe arc lamp and irradiated with appropriate monochromatic light until all the nitrite was decomposed. The progress of the photolysis was monitored by TLC.

Preparation of 6-Methylcholest-5-en-3β-ol Nitrite (2). To 6-methylcholesterol (800 mg) in pyridine (15 cm^3) cooled with Dry Ice–ethanol was added nitrosyl chloride in pyridine dropwise. The solution was stirred for 1 h and poured into water. The crystals (684 mg) of **2** were collected, washed with water and dried. Mp 88.5—90 °C; $[\alpha]_D^{25}$ −26.5° (*c* 1.0, $CHCl_3$); IR, 1645 and 1598 (*trans* and *cis* N–O), 782 (O–N), and 680 cm^{-1} (O–N=O); ^{1}H NMR, δ=0.69 (3H, s, 18-H), 1.03 (3H, s, 19-H), 1.64 (3H, s, 6-methyl), and 5.19 (1H, broad s, 3α-H); UV (benzene) 398 (ε 45), 374 (94), 362 (75), 348 (60), and 337 (45).

Photolysis of 2 with Pyrex-filtered Light. The nitrite (**2**) (620 mg) in benzene (40 cm^3) was irradiated for 3 h 20 min. The solvent was evaporated and the product (669 mg) was subjected to preparative TLC with hexane–ethyl acetate (5:1) to give eight fractions (A—H) in the order of decreasing mobilities. The fractions A (25 mg), B (33 mg), C (63 mg), E (30 mg), F (29 mg), and H (45 mg) could not be identified. The fraction D (150 mg, 26%) was the parent 3β-ol. The fraction G (231 mg, 37%) was 4-hydroxy-6-methyl-4-aza-*A*-homo-5-cholesten-3-one (**9**). This hydroxamic acid was recrystallized once from methanol and then from acetone to yield a specimen (179 mg) for analysis. Mp 180—184 °C; $[\alpha]_D^{20}$ −8.2° (*c* 1.6 $CHCl_3$); (Found: *m/z* 429.3632. Calcd for $C_{28}H_{47}NO_2$; M 429.3604. Found: C, 78.08; H, 11.06; N, 3.47%. Calcd for $C_{28}H_{47}NO_2$: C, 78.27; H, 11.03; N, 3.26%) IR, 3100 (OH), 1621 (amide C=O), 1230, and 768 cm^{-1}; ^{1}H NMR ($CDCl_3$), δ=0.69 (3H, s, 18-H), 0.98 (3H, s, 19-H), 1.74 (3H, s, 6-methyl), and 4.27 and 4.32 (2H, AB q, J=15 Hz, 4a-H_2); ^{13}C NMR, ($CDCl_3$), δ=167.9 (NCO), 136.1 (C-5) and 129.9 (C-6); MS *m/e* (rel intensity) 429 (M^+, 100), 413 (M^+—O, 16.8), 412 (M^+—OH, 52,3), 384 (57.7), 137 (67.4), 133 (45.7), 95 (28.0), 57 (32.0), 55 (36.9), and 43 (45.5).

Photolysis of 2 with 370 nm Monochromatic Light. A solution of 6-methylcholest-5-en-3β-ol nitrite (**2**) (260 mg) in dry benzene (2.5 cm^3) in a quartz cell was placed in a chamber of a JASCO CRM FA grating spectro-irradiator and was irradiated with 370 nm light for 9 h; complete decomposition of the nitrite had occurred after this period. The solvent was removed by distillation under vacuum and the photolysate was subjected to preparative TLC with hexane–ethyl acetate (5:1) as developer to give three fraction A—C in the order of increasing mobility. The least mobile fraction A (18 mg, 7%) was the hydroxamic acid **9**. Fraction B (138 mg, 57%) was the parent alcohol **1**. The most mobile fraction C (6 mg) was an intractable mixture.

Preparation of 4,4,6-Trimethylcholest-5-en-3β-ol Nitrite (4). To the 3β-ol **3** (428 mg) in pyridine (15 ml) cooled by Dry Ice–ethanol, was added nitrosyl chloride (1 cm^3). The solution was stirred for 30 min and poured into water and ice. The nitrite was collected by filtration and washed with water. The amount of the nitrite obtained was 440 mg (96%). It melted at 117.0—119.5 °C. This nitrite was recrystallized from acetone to yield an analytical specimen, mp 118.5—120 °C; $[\alpha]_D^{19}$ −26.8° (*c* 0.5, $CHCl_3$); IR, 1648 and 1613 (ONO), 801 and 776 cm^{-1} (ONO); ^{1}H NMR, δ=0.67 (3H, s, 18-H), 1.05 (3H, s, 19-H), 1.14 and 1.27 (each 3H, each s, 4,4-dimethyl), 1.76 (3H, s, 6-methyl), and 5.12 (1H, dd, J=5 and 11 Hz, 3α-H); UV (benzene) 386 (ε50), 373 (90), 357 (89), 345 (65), and 334 (48).

Photolysis of 4,4,6-Trimethylcholest-5-en-3β-ol Nitrite (4) with 373 nm Monochromatic Light. A solution of the nitrite (260 mg) in dry benzene (3 cm^3) in a quartz cell was placed in a chamber of a JASCO CRM-FA grating spectroirradiator and irradiated with 373 nm light for 12 h; complete decomposition of the nitrite had occurred after this period. The solvent was removed under vacuum and the photolysate (271 mg) was subjected to preparative TLC with benzene as developer to give six fractions, A—F in the order of increasing mobility. The least mobile fraction A (24 mg, 13%) was the hydroxamic acid **11**. It crystallized from acetone. Mp 178—181 °C. (Found: *m/z* 457.3907. Calcd for $C_{30}H_{51}NO_2$, M, 457.3919) MS, *m/z* (rel intensity) 457 (M^+, 21.9), 442 (M^+—CH_3, 18.3), 441 (M^+—0.69), 440 (M^+—OH, 9.5), 427 (M^+—$2CH_3$, 11.1), 426 (M^+—CH_3—O, 339), 369 (100), and 327 (52.6); IR 3400 (br, OH), and 1626 cm^{-1} (amide CO); ^{1}H NMR δ=0.68 (3H, s, 18-H), 1.22 (3H, s, 19-H), 1.67 and 1.73 (each 3H, each s, 4a-*gem* dimethyl), and 1.85 (3H, s, 6-methyl).

Fraction B (44 mg, 18%) was identical with the parent 3β-ol **3**. The fractions C (21 mg), D (15 mg), and E (8 mg) were intractable mixtures. Fraction F (60 mg, 25%) was the seco-aldehyde **10**. It could not be induced to crystallize but its spectroscopic data were identical with those of 4,6-dimethyl-4-methylene-3,4-secocholest-5-en-3-al obtained from the irradiation of 3β-ol **3** in benzene containing mercury (II) oxide and iodine.[5] [In the mass spectrometric data on compound **10** in the reference 5, 411 (M^+—CH_2CH_2CHO, 100) should read 411 (M^+—CH_3, 8.5), 369 (M^+—CH_2-CH_2CHO, 100)].

Photolysis of 4,4,6-Trimethycholest-5-en-3β-ol Nitrite with a Pyrex-filtered Light. The nitrite **4** (280 mg) in dry benzene (38 cm³) in a Pyrex vessel was irradiated for 10 h in a nitrogen atmosphere. The solvent was removed by rotary evaporation and the product was subjected to preparative TLC with benzene to yield 3β-ol (47 mg, 18%), 4,4,6-trimethylcholest-5-en-3-one (10 mg, 4%) and seco-aldehyde **10** (16 mg, 6%). No hydroxamic acid **11** was found in the product.

Preparation of 3α-Methylcholest-5-en-3β-ol Nitrite (6). The 3β-ol **5** (200 mg) in pyridine (6 cm³) was treated with nitrosyl chloride in pyridine in a usual manner to afford a crystalline nitrite, mp 115—117 °C (185 mg, 86%); $[\alpha]_D^{18}$ +6.9° (*c* 0.9, $CHCl_3$); IR 1628 (ONO), 810 (ONO), and 768 cm^{-1} (ONO); ^1H NMR, δ=0.68 (3H, s, 18-H), 1.07 (3H, s, 19-H), 1.54 (3H, s, 3α-methyl) and 5.45 (1H, br s, 6-H); UV (THF) 400 (ε49), 384 (75), 367 (67), 355 (46), and 342 (27).

Photolysis of 3α-Methylcholest-5-en-3β-ol Nitrite (6) with 384 nm Monochromatic Light. The nitrite (180 mg) in dry benzene (3 cm³) in a quartz vessel was placed in a chamber of JASCO CRM-FA grating spectroirradiator and was irradiated with 384 nm light for 10.5 h. The solvent was removed under vacuum and the brownish photolysate (155 mg) was subjected to preparative TLC with benzene–diethyl ether (10:1) to give four fractions A—D in the order of increasing mobility. The least mobile fraction A (21 mg, 12%) was the nitroso dimer **13**. This was recrystallized from methanol. Mp 111—113 °C; (Found: M^+ 429.3601. Calcd for $C_{28}H_{47}NO_2$: 429.3606); IR 1718 (acetyl) and 1196 cm^{-1}; ^1H NMR, δ=0.66 (3H, s, 18-H), 1.06 (3H, s, 19-H), 2.15 (3H, s, acetyl), 4.65 and 4.86 (each 1H, each d, *J*=13.5 Hz, 4-methylene), and 5.58 (1H, br, s, 6-H) MS, *m/z* (rel intensity), 429 (1.0), 341 (100, $M^+-CH_3COCH_2-CH_2$), 71 (91.2), 57 (89.2), and 43 (86.2). UV (dioxan) 294 (ε8300). Fraction B (20 mg) was an unidentified gum.

Fraction C (23 mg, 14%) was the parent 3β-ol. The most mobile fraction D (13 mg) was an unidentified gum.

Photolysis of 3α-Methylcholest-5-en-3β-ol Nitrite (6) with Pyrex-filtered Light. The nitrite (160 mg) in dry benzene (15 cm³) in a Pyrex-vessel was irradiated for 1.5 h. The crude product (173 mg) was subjected to preparative TLC with hexane–diethyl ether (5:1). The TLC plates were developed with the solvent twice to give five fractions A—E in the order of increasing mobility. The least mobile fraction A (110 mg) was again subjected to preparative TLC to afford three fractions E_1—E_3. Fractions E_1 (29 mg) and E_3 (112 mg) were not identified. Fraction E_2 (34 mg, 21%) was the nitrosodimer **13** which, after recrystallization, was identical with the specimen obtained by monochromatic light photolysis. The fractions B (7 mg), D (6 mg), and E (7 mg) were unidentified gums. Fraction C (27 mg, 18%) was the parent 3β-ol.

Preparation of 3α,4,4-Trimethylcholest-5-en-3β-ol Nitrite (8). The 3β-ol (330 mg) in pyridine (3 cm³) was treated with nitrosyl chloride–pyridine in a usual manner while the flask was cooled by ice. The solution was poured into water and the solid obtained was collected by filtration to give a gummy nitrite. This was dissolved in diethyl ether and the ethereal solution was dried over anhydrous sodium sulfate. The removal of the solvent gave a crystalline mixture of 3β-ol **7** and the nitrite 8, IR 1622 (ONO), 795 and 760 cm^{-1} (ONO); ^1H NMR δ=0.68 (s, 18-H of **7** and **8**), 1.05 (s, 19-H of **8**), 1.14 and 1.15 (each s, *gem*-dimethyl group at the C-4 of **8**), 1.52 (s, 3α-methyl of **8**), 5.49 (br s, 6-H of **7**), and 5.56 (br s, 6-H of **8**). The ratio of **7** to **8** estimated by the signal areas of 6-H of **7** and that of **8** was 1:2.4. UV (THF) 398, 382, 366, 353, and 340.

Photolysis of 3α,4,4-Trimethylcholest-5-en-3β-ol Nitrite (8) with 382 nm Monochromatic Light. The above nitrite (285 mg) in benzene (3 cm³) in a quartz cell was placed in a chamber of CRM-FA grating spectroirradiator and photolyzed with 382 nm light for 5.5 h. The solvent was evaporated and the product was subjected to preparative TLC to give six fractions (A—F) in the order of their mobility on the TLC plate. The most mobile fraction A (24 mg, 13%) was an oily methyl ketone **14** and this was again purified by TLC. (Found: *m/z* 426.3851. Calcd for $C_{30}H_{50}O$; M, 426.3858); MS, *m/z* (rel intensity) 426 (M^+, 34.6), 383 (18.1), 355 ($M^+-CH_3COCH_2CH_2$, 100), 313 (16.8), 147 (63.4), 133 (31.1) 121 (34.6), 105 (43.6), 95 (48.5), 84 (36.4), 69 (35.8), 57 (44.4), 55 (42.6), and 43 (71.3); IR (neat), 1724 (CH_3CO), 1164, and 898 cm^{-1}; ^1H NMR, δ=0.68 (3H, s, CH_3CO), 4.47 and 4.84 (each 1H, each br s, 4-methylene), and 5.61 (1H, br d, *J*=4.5 Hz, 6-H) UV (EtOH) 274 (ε 4000), and 203 (57600).

Fractions B (25 mg), D (8 mg), and F (11 mg) were intractable mixtures. Fraction C (126 mg, 23%) was identical with the parent alcohol **7**. Fraction E (23 mg, 11%) was, after purification by TLC, identified as an amorphous nitroso dimer **15**. MS, *m/z* (rel intensity) 427 (8.3) 426 (14.4), 355 (*m/z* 426 $-CH_3COCH_2CH_2$, 41.2) and 43 (100); IR (neat), 1717 (CH_3CO), 1541, and 1165 cm^{-1}; ^1H NMR, δ=0.67 (6H, s, 18- and 18′-H), 1.21 (6H, s, 19- and 19′-H), 1.40 (12H, s, *gem*-dimethyl groups at C-4 and C-4′), 2.15 (6H, s, 3- and 3′-methyl), and 5.67 (2H, 6H and 6′-H).

Photolysis of 3α,4,4-Trimethylcholest-5-en-3β-ol Nitrite with a Pyrex-filtered Light. The 3β-ol nitrite (485 mg) in benzene (32 cm³) was irradiated for 2.5 h under a nitrogen atmosphere. The product (482 mg) was subjected to preparative TLC with benzene to give 6 fractions A to F in the order of decreasing mobilities. The fraction A (112 mg, 35%) was an oily methyl ketone **14**.

Fraction D (161 mg, 6%) was, after further purification, identical with the parent 3β-ol **7**. Fraction F (54 mg, 16%) was the nitroso dimer **15**.

References

1) Photo-induced Transformations. Part 68. Part 67: H. Suginome, S. Yamada, and N. Miyaura, *Chem. Lett.*, **1983**, 55.

2) H. Suginome, N. Maeda, and M. Kaji, *J. Chem. Soc., Perkin Trans. 1*, **1982**, 111, and papers cited therein.

3) H. Suginome and A. Osada, *J. Chem. Soc., Perkin Trans. 1*, **1982**, 1963.

4) L. F. Fieser and J. Rigaudy, *J. Am. Chem. Soc.*, **73**, 4660 (1951).

5) H. Suginome, N. Maeda, Y. Seki, and K. Orito, *Bull. Chem. Soc. Jpn.*, **55**, 1653 (1982).

6) M. S. Patel and W. J. Peal, *Tetrahedron*, **20**, 2511 (1964); H. Suginome and N. Maeda, *Bull. Chem. Soc. Jpn.*, **53**, 2621 (1980).

7) H. Suginome, A. Furusaki, K. Kato, N. Maeda, and F. Yonebayashi, *J. Chem. Soc., Perkin Trans. 1*, **1981**, 236.

8) H. Suginome, N. Maeda, Y. Takahashi, and N. Miyata, *Bull. Chem. Soc. Jpn.*, **54**, 846 (1981).

9) H. Suginome, T. Mizuguchi, S. Honda, and T. Masamune, *J. Chem. Soc., Perkin Trans. 1*, **1977**, 927.

An X-Ray Crystallographic Study on the Absolute Configuration of Dihydroyashabushiketol and the Solvent-dependence of Its Optical Rotation

Takayuki SUGA,* Shinji OHTA, Tadashi AOKI, and Toshifumi HIRATA

Department of Chemistry, Faculty of Science, Hiroshima University, Higashisenda-machi, Naka-ku, Hiroshima 730

(Received May 16, 1983)

The absolute configuration of dihydroyashabushiketol was established to be *S* on the basis of the X-ray crystallographic analysis of the 4′,4″-dibromo derivative. In addition, it was found that the sense of the optical rotations of dihydroyashabushiketol and its dibromo derivative is determined by the interaction of their C-5 hydroxyl group with the solvent used for the measurements.

The absolute configurations of both dihydroyashabushiketol (**1**) and yashabushiketol (**2**) isolated from the male flowers of *Alnus sieboldiana* are reported to be *S*[1] on the basis of the benzoate rule[2] and Horeau's asymmetric synthesis.[3] However, the benzoate rule is not adapted to such a type of compounds in which the carbinyl carbon is flanked by two methylenes.[4] In the case of **1**, in addition, the optical yield of α-phenylbutyric acid was too low (only 1.5 %[1]) to determine the absolute configuration. These suspicious points necessitated the establishment of the absolute configuration of **1**† by use of an unambiguous method. Then, the absolute configuration was reexamined by the X-ray crystallographic analysis of the 4′,4″-dibromo derivative (**3**) prepared from **1**, and the absolute configuration proposed previously for **1** was validated. During the course of this reexamination, it was found that the sense of the optical rotation of **1** and **3** is determined by the interaction of their C-5 hydroxyl group with the solvent used for measurements of the optical rotation. We now wish to report these results.

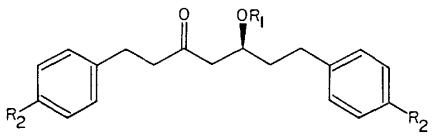

1 $R_1=R_2=H$
3 $R_1=H$, $R_2=Br$
4 $R_1=Ac$, $R_2=H$
5 $R_1=Ac$, $R_2=Br$

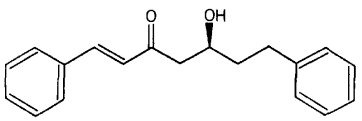

2

Experimental

General. The ^1H NMR spectra were taken on a Hitachi R-22 spectrometer using TMS as an internal standard. The ^{13}C NMR spectra were obtained on a Hitachi R-42 FT NMR (22.6 MHz) spectrometer ($\delta_{TMS}=0$). The Mass spectra were recorded by direct inlet at 70 eV ionization. The optical rotation was measured on a Yanaco Automatic Digital Polarimeter OR-50D spectrometer. The ORD curves were taken on a JASCO ORD/UV-5 spectropolarimeter at 25 °C by use of a 10 mm cell in path-length. The UV spectra were obtained on a Shimadzu UV-240 spectrometer. Analytical TLC and preparative TLC were carried out on 0.25 and 0.75 mm thick silica gel plates (Merck 60, GF_{254}), respectively.

The physical and spectral data of compounds **1** and **3**—**5** are summarized in Tables 1—4.

Isolation and Identification of Dihydroyashabushiketol (1). The benzene extract of the male flowers (13 kg) of *Alnus sieboldiana* MATSUM., which were collected on the mountain in the suburbs of Hiroshima City in February, was worked up in a similar manner as described in the literature[1] to give compound (**1**) (1.35 g). This compound (**1**) was

TABLE 1. PHYSICAL DATA OF **1**, **3**, **4**, AND **5**

Compd	Mp θ_m/°C	$[\alpha]_D^{25}$/°(Solvent)	Molecular formula	Found(Calcd)(%) C	H	Br
1	72.5—73.0	−2.7±0.6(*c* 0.67, MeOH)	$C_{19}H_{22}O_2$	80.64	7.94	
		+14.0±0.6(*c* 0.67, $CHCl_3$)		(80.81)	(7.85)	
3	96.0—96.5	−3.6±0.7(*c* 0.30, MeOH)	$C_{19}H_{20}O_2Br_2$	51.88	4.51	36.18
		+10.2±0.7(*c* 0.30, $CHCl_3$)		(51.84)	(4.58)	(36.31)
4	Viscous oil	+4.1±0.3(*c* 1.22, MeOH)				
		+3.6±0.3(*c* 1.22, $CHCl_3$)				
5	Viscous oil	+3.1±0.9(*c* 2.25, MeOH)				
		+2.7±0.9(*c* 2.25, $CHCl_3$)				

† Although the preparative TLC of the benzene extract of the male flowers was meticulously carried out in the same manner as previously described,[1] even a trace of yashabushiketol (**2**) was not found in the benzene extract.

Table 2. UV, IR, and Mass spectral data of **1**, **3**, **4**, and **5**

Compd	UV(EtOH) λ_{max}/nm (log ε)	IR ν_{max}/cm^{-1} a) OH	IR C=O	IR ν_{max}/cm^{-1}(CCl_4) intramolecular hydrogen bonded OH	Mass m/z(fragment ion and/or rel int.)
1	261(2.85), 264(2.80) 268(2.80), 287(2.64)	3410 and 3360	1708	3556(0.0006 M) b)	282(M^+, 0.8), 264(M−H_2O, 18), 159(18), 148(23), 133(22), 105(61), 91(100), 77(18), 43(25)
3	255(2.78), 262(2.87) 269(2.94), 277(2.85)	3355 and 3275	1711	3566(0.001 M) b)	442, 440, 438(M^+, 2, 4, 2), 424, 422, 420(M^+−H_2O, 24, 50, 24), 213(58), 211(56), 197(10), 195(13), 171(100), 169(100); 212.9770 and 210.9741 (C_9H_8OBr), 196.9749 and 194.9773 (C_9H_8Br)
4	260(2.95), 264(2.89) 268(2.88), 284(2.69)		1740 and 1719		324(M^+, 0.2), 264(M−AcOH, 21), 159(24), 133(18), 117(10), 105(40), 91(100), 77(15), 43(43)
5	255(2.84), 262(2.88) 269(2.93), 277(2.82)		1738 and 1718		424, 422, 420(M−AcOH, 11, 22, 11), 213(15), 211(19), 171(64), 169(61), 43(100)

a) IR spectra of **1** and **3** were taken in Nujol and those of **4** and **5** in the neat film. b) 1 M=1 mol dm^{-3}.

Table 3. ^{1}H NMR spectral data of **1**, **3**, **4**, and **5**(δ_H, CCl_4)a)

Compd	C_6-H_2	C_1-, C_2-, C_4-, C_7-H_2	C_5-H	Arom. H	OH	OAc
1	1.41—1.81 m	2.35—2.88 m	3.94 quin	7.11 m	2.95 brs	
3	1.43—1.71 m	2.35—2.87 m	3.87 quin	6.90—7.36AA′BB′	3.02 brs	
4	1.68—1.92 m	2.26—2.90 m	5.12 quin	7.12 m		1.88 s
5	1.66—2.05 m	2.28—2.87 m	5.08 quin	6.94—7.40AA′BB′		1.91 s

a) s: singlet, brs: broad singlet, m: multiplet, quin: quintet (J=6 Hz), AA′BB′: J=8 and/or 2 Hz.

Table 4. ^{13}C NMR spectral data of **1**, **3**, **4**, and **5**(δ_C, $CDCl_3$)

i) 5-Hydroxy(or acetoxy)-3-heptanone moiety

Compd	C-1	C-2	C-3	C-4	C-5	C-6	C-7	-OCOCH$_3$	-OCOCH$_3$
1	29.4	44.9	210.7	49.4	66.8	38.1	31.7		
3	28.6	44.5	209.8	49.2	66.4	37.8	30.9		
4	29.5	44.7	206.4	47.2	70.0	35.7	31.6	20.9	170.2
5	28.8	44.5	206.0	47.2	69.7	35.5	31.0	21.0	170.3

ii) Diphenyl moiety

Compd	C-1′	C-1″	C-2′	C-2″	C-3′	C-3″	C-4′	C-4″	C-5′	C-5″	C-6′	C-6″
1	140.7	141.8	128.4	128.4	128.4	128.4	126.1	125.8	128.4	128.4	128.4	128.4
3	139.5	140.6	130.1	130.1	131.4	131.4	119.8	119.4	131.4	131.4	130.1	130.1
4	140.9	141.2	128.4	128.4	128.4	128.4	126.1	126.1	128.4	128.4	128.4	128.4
5	139.8	140.0	130.1	130.1	131.5	131.5	119.9	119.9	131.5	131.5	130.1	130.1

confirmed to be identical with dihydroyashabushiketol[1] by direct comparison of the ^{1}H NMR spectra taken in $CDCl_3$ and the Mass spectra,[5] and then characterized as 1,7-diphenyl-5-hydroxy-3-heptanone on the basis of the elemental analysis and the UV, IR, ^{1}H and ^{13}C NMR, and Mass spectral data. Acetylation of **1** (96 mg) with a mixture of acetic anhydride (2 cm^3) and dry pyridine (2 cm^3) gave its acetate (**4**) (108 mg).

Bromination of 1. Following the method for the iodination of veratrole described in the literature,[6] the bromination of **1** (129 mg) was carried out by use of bromine (183 mg) in place of iodine under the conditions similar to those described. The resulting mixture was subjected to preparative TLC with EtOAc–hexane (3:7 v/v) to give a dibromo derivative (**3**) (48 mg), which was characterized as 1,7-bis(4-bromophenyl)-5-hydroxy-3-heptanone on the basis of the elemental analysis and the spectral data. Acetylation of **3** (48 mg) in the same way as in the case of **1** gave its acetate (**5**) (50 mg).

X-Ray Crystallographic Analysis. The single-crystals of **3** for the X-ray analysis were obtained by crystallization from MeOH–H_2O. The single-crystal used was about 0.2 mm×0.5 mm×0.7 mm in size. Cell dimensions were determined by least-squares calculations from 2θ values of 16 reflections measured on a Syntex R-3 automated four-circle diffractometer with graphite-monochromated Mo $K\alpha$ radiation. Crystal data: orthorhombic, space group $P2_12_12_1$, four molecules per unit cell with dimensions a=5.012(3), b=

Table 5. Bijvoet inequalities of **3**

h	k	l	$\langle\|F_c\|\rangle$	$\langle\|F_o\|\rangle$	$\Delta\|F_o\|$ [a]	$\Delta\|F_c\|$ [b]	$\|S\|$ [c]
1	1	4	133.1	132.6	3.82	8.12	6
1	1	3	169.3	169.8	4.38	6.69	5
1	3	9	47.2	45.8	7.54	6.61	5
1	1	5	113.9	114.2	−6.54	−6.54	5
2	1	1	71.6	67.0	−4.15	−6.05	4
1	2	11	54.2	52.5	−7.49	−5.57	4
1	6	4	36.4	37.5	−4.78	−5.56	4
1	1	1	118.2	124.2	−6.50	−5.47	4
1	1	6	134.3	134.3	4.30	5.22	4
2	3	4	75.4	75.9	4.35	4.67	3
1	1	16	34.2	31.8	6.03	4.58	3
1	2	1	54.6	59.2	3.55	4.53	3
2	5	8	12.9	16.4	4.72	4.50	3
1	4	6	25.5	22.6	−7.14	−4.46	3
1	5	15	20.7	25.0	3.39	4.45	3
2	3	11	40.0	40.1	3.67	4.42	3
1	2	10	42.1	41.7	−6.06	−4.27	3
1	6	12	17.6	17.5	−6.62	−4.27	3
1	3	6	84.7	91.2	−5.59	−4.24	3
2	5	2	27.3	28.0	−4.31	−4.18	3
1	3	8	40.1	37.5	4.89	4.13	3

a) $\Delta|F_o| = |F_o(hkl)| - |F_o(\bar{h}\bar{k}\bar{l})|$. b) $\Delta|F_c| = |F_c(hkl)| - |F_c(\bar{h}\bar{k}\bar{l})|$. c) $|S| = ||F_c(hkl)| - |F_c(\bar{h}\bar{k}\bar{l})||/\sigma(F_o)$.

12.315(6), c=30.480(15) Å; U=1881(2) Å; D_c=1.55 g cm^{-3}; D_m=1.54 g cm^{-3}; μ(Mo $K\alpha$)=45.7 cm^{-1}. A total of 2130 reflections with the Friedel pair of (h,k,l) and $(\bar{h},\bar{k},\bar{l})$ were collected by use of the ω-scan technique in the range $2\theta \leq 50.0°$. 1286 reflections having $F_o > 2\sigma(F_o)$ were used for the structure determination. The structure was solved by the conventional heavy-atom method. The bromine atom positions were obtained from a Patterson function, and then the positions of oxygen and carbon atoms were determined by difference-Fourier syntheses. A least-squares refinement was carried out by use of anisotropic temperature factors for bromine, carbon, and oxygen atoms and isotropic temperature factors for hydrogen atoms. In the least-squares calculation, the quantity minimized was $\sum w(|F_o| - |F_c|)^2$ with w=1.0 for all the reflections. Final refinements were done by use of the anomalous dispersion effect[7] of bromine and oxygen atoms and the index $R = [\sum(|F_o| - |F_c|)^2 / \sum|F_o|^2]^{1/2}$ was 0.094 for the S configuration and 0.105 for the R configuration, respectively. Bijvoet pairs[8] of 1286 reflections were considered for the S configuration and 20 pairs having the largest $||F_c(hkl)| - |F_c(\bar{h}\bar{k}\bar{l})||/\sigma(F_o)$ values are given in Table 5.

The complete $F_o - F_c$ data and the tables of anisotropic thermal parameters for **3** are deposited as Document No. 8346, at the Chemical Society of Japan.

Results and Discussion

The absolute configuration of dihydroyashabushiketol (**1**) was examined by the X-ray crystallographic analysis of the dibromo derivative (**3**). The absolute configuration of **3** was established by the X-ray anomalous-scattering technique.[7] Comparison of the R factors[9] for two enantiomeric configurations indicated that the absolute configuration of **3** is S. Final atomic

Table 6. Final atomic coordinates of **3**, with standard deviations in parentheses

Atom	10^4x	10^4y	10^4z	B_{eq}/Å^2 [a]
Br(1)	4247(7)	-1237(3)	2957(1)	9.1
Br(2)	11614(9)	8902(3)	-1247(1)	11.1
O(1)	14998(28)	2001(12)	1048(6)	6.0
O(2)	12933(29)	2653(10)	165(5)	4.7
C(1)	12506(38)	908(18)	1726(8)	6.2
C(2)	11040(37)	1812(20)	1448(8)	5.5
C(3)	12814(24)	2326(14)	1143(7)	4.7
C(4)	11990(32)	3314(17)	868(7)	4.3
C(5)	13323(29)	3549(13)	486(5)	3.4
C(6)	12475(37)	4537(14)	195(7)	3.2
C(7)	13898(67)	4774(20)	-150(9)	8.8
C(1')	10439(44)	354(21)	2008(8)	6.3
C(2')	9864(51)	751(20)	2344(9)	6.2
C(3')	7892(65)	493(19)	2716(9)	7.4
C(4')	6868(59)	-457(21)	2610(8)	7.0
C(5')	7201(46)	-1036(18)	2265(8)	6.5
C(6')	9054(56)	-690(17)	1903(10)	7.9
C(1'')	13323(46)	5765(22)	-436(8)	6.3
C(2'')	11475(71)	5747(20)	-711(10)	9.2
C(3'')	10765(63)	6717(22)	-944(10)	9.0
C(4'')	12353(75)	7650(19)	-860(8)	7.0
C(5'')	14174(67)	7589(24)	-578(12)	8.6
C(6'')	14783(53)	6685(22)	-356(12)	8.1

a) $B_{eq} = 8\pi^2(U_1 + U_2 + U_3)/3$, where U_1, U_2, and U_3 are the principal components by U matrix.

Table 7. Interatomic distances of **3**, with standard deviations in parentheses

Interatomic distance	l/Å	Interatomic distance	l/Å
C(1)-C(2)	1.58(3)	C(2')-C(3')	1.54(4)
C(1)-C(1')	1.51(3)	C(3')-C(4')	1.32(4)
C(2)-C(3)	1.43(3)	C(4')-C(5')	1.28(3)
C(3)-O(1)	1.20(2)	C(4')-Br(1)	1.94(3)
C(3)-C(4)	1.54(3)	C(5')-C(6')	1.51(4)
C(4)-C(5)	1.38(3)	C(1'')-C(2'')	1.25(4)
C(5)-O(2)	1.49(2)	C(1'')-C(6'')	1.37(4)
C(5)-C(6)	1.56(2)	C(2'')-C(3'')	1.43(4)
C(6)-C(7)	1.31(4)	C(3'')-C(4'')	1.42(4)
C(7)-C(1'')	1.53(4)	C(4'')-C(5'')	1.25(5)
C(1')-C(2')	1.17(4)	C(4'')-Br(2)	1.98(3)
C(1')-C(6')	1.50(3)	C(5'')-C(6'')	1.34(4)

Table 8. Bond angles of **3**, with standard deviations in parentheses

Bond angle	ϕ/°	Bond angle	ϕ/°
C(1')-C(1)-C(2)	108(2)	C(3')-C(4')-Br(1)	125(2)
C(1)-C(2)-C(3)	112(2)	Br(1)-C(4)-C(5')	105(2)
C(2)-C(3)-O(1)	125(2)	C(3')-C(4')-C(5')	130(3)
C(2)-C(3)-C(4)	122(2)	C(4')-C(5')-C(6')	122(2)
O(1)-C(3)-C(4)	112(2)	C(5')-C(6')-C(1')	112(2)
C(3)-C(4)-C(5)	120(2)	C(7)-C(1'')-C(2'')	121(3)
C(4)-C(5)-O(2)	110(1)	C(7)-C(1'')-C(6'')	117(2)
C(4)-C(5)-C(6)	121(2)	C(2'')-C(1'')-C(6'')	122(3)
O(2)-C(5)-C(6)	100(1)	C(1'')-C(2'')-C(3'')	120(3)
C(5)-C(6)-C(7)	119(2)	C(2'')-C(3'')-C(4'')	117(3)
C(6)-C(7)-C(1'')	122(2)	C(3'')-C(4'')-Br(2)	115(2)
C(1)-C(1')-C(2')	119(2)	Br(2)-C(4'')-C(5'')	126(2)
C(1)-C(1')-C(6'')	126(2)	C(3'')-C(4'')-C(5'')	119(3)
C(2')-C(1')-C(6')	116(2)	C(4'')-C(5'')-C(6'')	124(3)
C(1')-C(2')-C(3')	136(3)	C(1'')-C(6'')-C(5'')	118(3)
C(2')-C(3')-C(4')	105(2)		

coordinates, bond lengths, and bond angles are given in Tables 6—8. The observed and calculated Bijvoet inequalities[8] for the *S* configuration were in good agreement with each other, as shown in Table 5. Thus, the absolute configuration of **3** was determined to be *S*, as shown in the ORTEP drawing of Fig. 1, and that of dihydroyashabushiketol (**1**) was necessarily

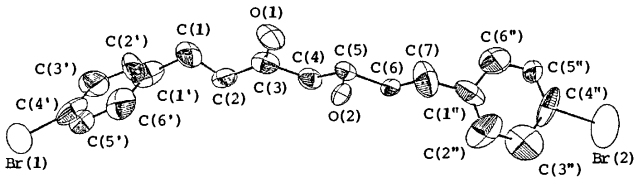

Fig. 1. ORTEP drawing[10] of the molecular structure of the 4′,4″-dibromo derivative (**3**).

Table 9. Torsion angles of **3**

Torsion angle	ϕ/°
C(2′)-C(1′)-C(1)-C(2)	+84.0
C(1′)-C(1)-C(2)-C(3)	−175.4
C(1)-C(2)-C(3)-C(4)	−173.2
C(1)-C(2)-C(3)-O(1)	+12.6
C(2)-C(3)-C(4)-C(5)	−157.7
O(1)-C(3)-C(4)-C(5)	+17.1
C(3)-C(4)-C(5)-C(6)	+178.6
C(3)-C(4)-C(5)-O(2)	+63.5
C(4)-C(5)-C(6)-C(7)	+175.6
O(2)-C(5)-C(6)-C(7)	−64.3
C(5)-C(6)-C(7)-C(1″)	−176.1
C(6)-C(7)-C(1″)-C(2″)	−78.7

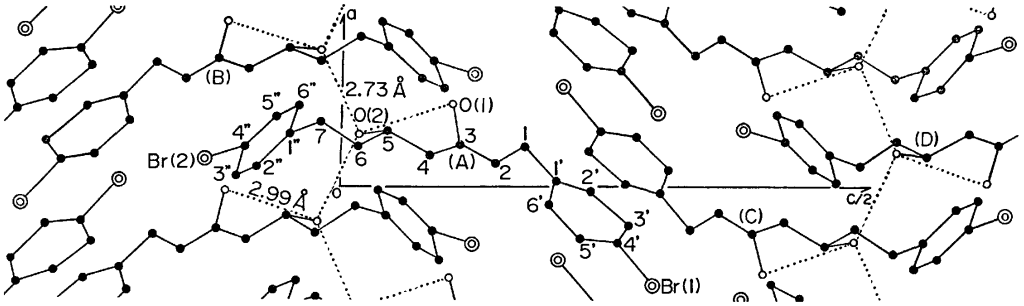

Fig. 2. Projection of the 4′,4″-dibromo derivative (**3**) along the b axis. The atoms indicated with ●, O, and ◎ denote carbon, oxygen, and bromine atoms respectively. The hydrogen bondings are shown by a broken line. The transformations of the atomic coordinates are (A) x, y, z; (B) $1/2+x$, $1/2-y$, $-z$; (C) $-x$, $1/2+y$, $1/2-z$; (D) $1/2-x$, $-y$, $1/2+z$.

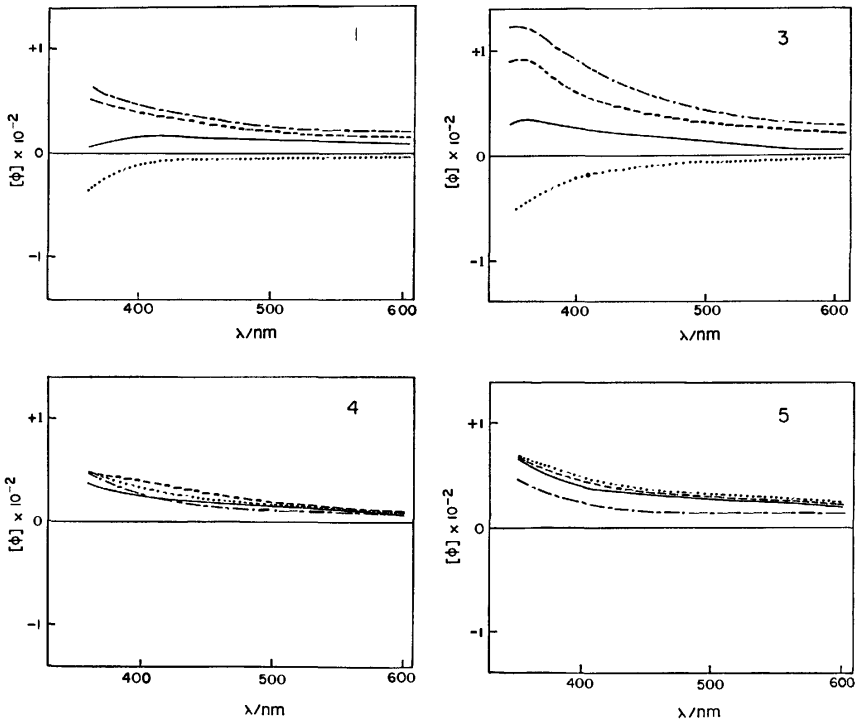

Fig. 3. ORD curves of **1**, **3**, **4**, and **5** in selected solvents at 25 °C; — — — in CCl_4; ---- in $CHCl_3$; —— in dioxane; ····· in MeOH. The measurements were carried out under the following concentrations in each solvent: **1**, *c* 0.85; **3**, *c* 2.20; **4**, *c* 0.97; **5**, *c* 2.60.

concluded to be *S*.

As shown in Table 2, the IR spectrum of **3** taken in a Nujol mull exhibited the bands at 3355 and 3275 cm^{-1} due to the inter- and intramolecular hydrogen bondings, respectively.[11] The presence of these bondings was confirmed by the diagnosis of the crystal structure as described below. The molecular arrangement and the hydrogen bond networks of **3** are given in Fig. 2. As shown in Table 9, the heptane chain was almost on the same plane, with the exception of the torsion angle of −157.7° at C2–C3–C4–C5. This torsion angle may result from the intramolecular hydrogen bonding between the carbonyl group at the 3-position and the hydroxyl group at C-5. This hydroxyl group is furthermore linked with the hydroxyl groups at C-5 of the adjacent molecules by intermolecular hydrogen bonds, and the molecules build up an infinite chain along the a axis by intermolecular hydrogen bondings. The chain is coupled with the next chain by the van der Waals force among the hydrophobic groups.

During the course of the study on the absolute configuration, it was observed that when the solvent used for measuring the optical rotation was changed from $CHCl_3$ to MeOH, the optical rotations of **1** and **3** changed from the dextrorotatory sense to the levorotatory one, but this was not the case for the corresponding acetates (**4** and **5**); these acetates were dextrorotatory in both of the solvents. These phenomena were also observed for ORD curves in the wavelength range of 350 to 600 nm, as shown in Fig. 3. The compounds **1** and **3** showed positive ORD curves in CCl_4, $CHCl_3$, and dioxane, while negative ORD curves in MeOH. On the other hand, their corresponding acetates (**4** and **5**) showed positive plain curves in all the solvents used. This indicates that the intermolecular hydrogen bonding between the hydroxyl group at C-5 of **1** and **3** and the functional or polar group of the solvent molecule participates in the inversion in the sense of their optical rotation. A similar solvent-dependence of the optical rotation is also observed for *cis*-verbenol,[12] (*S*)-marmesin,[13] and (*R*)-1-methylindan.[14] However, any causes for the inversion in the sense of the optical rotation have not been solved yet. Detailed investigations on causes involved for the inversion in the sense of the optical rotation of the diarylheptanoids are now in progress, and the results will be reported elsewhere.

The elemental analysis for bromine atom was performed in the Elemental Analytical Center of Kyoto University.

References

1) Y. Asakawa, *Bull. Chem. Soc. Jpn.*, **43**, 2223 (1970); **45**, 1794 (1972).
2) J. H. Brewster, *Tetrahedron*, **13**, 106 (1961).
3) A. Horeau and H. B. Kagan, *Tetrahedron*, **20**, 2431 (1964).
4) N. Harada, M. Ohashi, and K. Nakanishi, *J. Am. Chem. Soc.*, **90**, 7349 (1968).
5) Only the ^1H NMR spectrum taken in $CDCl_3$ and the MS spectrum were reliable for determining the identity of our diarylheptanoid (**1**) with dihydroyashabushiketol described in Ref. 1, because there were many ambiguous points about the reported physical and spectral data as follows: i) The values of elemental analysis are not in agreement with the calculated ones for dihydroyashabushiketol, ii) the mp (36.0—37.0 °C) and the absorbance in the UV spectrum are too low and small, respectively, in comparison with the data of our sample given in Tables 1 and 2, iii) the IR spectrum is taken in a liquid film, although dihydroyashabushiketol isolated by the author was crystalline in a pure state, and iv) the solvent used for the measurement of optical rotation is not shown in Ref. 1.
6) D. E. Jansen and C. V. Wilson, *Org. Synth.*, Coll. Vol. **IV**, 547 (1963).
7) "International Tables for X-Ray Crystallography," International Union of Crystallography, Kynoch Press, Birmingham (1974), Vol. 4, p. 149.
8) A. F. Peerdeman and J. M. Bijvoet, *Acta Crystallogr.*, **9**, 1012 (1956).
9) W. C. Hamilton, *Acta Crystallogr.*, **18**, 502 (1965).
10) C. K. Johnson, ORTEP. Oak Ridge National Laboratory Report ORNL-3794 (1965).
11) S. Ueji, K. Nakatsu, H. Yoshioka, and K. Kinoshita, *Tetrahedron Lett.*, **23**, 1173 (1982).
12) K. Mori, N. Mizumachi, and M. Matsui, *Agric. Biol. Chem.*, **40**, 1611 (1976).
13) H. Ishii, F. Sekiguchi, and T. Ishikawa, *Tetrahedron*, **37**, 285 (1981).
14) H.-J. Hansen, H.-R. Sliwka, and W. Hug, *Helv. Chim. Acta.*, **65**, 325 (1982).

Reactions of 3-Acetyltropolone and Its Methyl Ethers with 1,2-Ethanediamines

Yasunori SUDOH,† Katsunobu ONITSUKA,†† Kimiaki IMAFUKU,* and Hisashi MATSUMURA†††

Department of Chemistry, Faculty of Science, Kumamoto University, Kurokami, Kumamoto 860

(Received June 6, 1983)

3-Acetyltropolone reacted with 1,2-ethanediamine to give *N,N'*-bis(3-acetyl-2-oxo-3,5,7-cycloheptatrienyl)-1,2-ethanediamine (**3**) and 5-acetyl-3,4-dihydro-2*H*-cyclohepta[*b*]pyrazine (**4**), along with a small amount of by-products, which were 8-acetyl-1,2,3,4-tetrahydro-5-quinoxalinecarbaldehyde (**5**), 5-acetyl-1,2,3,4-tetrahydroquinoxaline (**6**), and 2-methyl-5,6-dihydro-4*H*-pyrrolo[1,2,3-*de*]quinoxaline (**7**). The minor products (**5**—**7**) resulted from the contraction of the seven-membered ring of the compound **4**. 2-Acetyl-7-methoxytropone (**2a**) also reacted with 1,2-ethanediamine to give the same products (**3**—**7**) in higher yields. On the other hand, the same reaction of 3-acetyl-2-methoxytropone (**2b**) readily gave **4**—**7**. The reaction of **2a** with *N*-methyl-1,2-ethanediamine gave *N*-(3-acetyl-2-oxo-3,5,7-cycloheptatrienyl)-*N'*-methyl-1,2-ethanediamine (**14**), 5-acetyl-1-methyl-2,3-dihydro-1*H*-cyclohepta[*b*]pyrazine (**15**), 8-acetyl-4-methyl-1,2,3,4-tetrahydro-5-quinoxalinecarbaldehyde (**16**), 5-acetyl-1-methyl-1,2,3,4-tetrahydroquinoxaline (**17**), and 2,6-dimethyl-5,6-dihydro-4*H*-pyrrolo[1,2,3-*de*]quinoxaline (**18**). The same reaction of **2b** also gave the products (**15**—**18**). The several reactions of these products are also described.

Recently, we found that 3-acetyltropolone and its methyl ethers reacted with a variety of nucleophilic reagents having two functional groups, such as amino and hydroxyl groups, to give heterocycle-fused troponoid compounds.[1] Amines[2] and *o*-aminophenol[3] reacted at the tropone carbonyl carbon atom and the adjacent carbon atom having the methoxyl group, while hydrazines[4-6] and hydroxylamine[7] reacted at the acetyl group and the adjacent carbonyl carbon atom or carbon atom having the methoxyl group. Furthermore, guanidine,[8] amidines,[8] and *o*-phenylenediamine[9] reacted in the former and in the latter forms to give two types of heterocycle-fused compounds. On the other hand, it was reported that the reactions of 5-nitroso- and 5-phenylazotropolones with 1,2-ethanediamine gave respectively oxime and phenylhydrazone of 7*H*-cyclohepta[*b*]pyrazin-7-one by dehydrogenation in the dihydropyrazine ring.[10] It was also found that 4,5-benzotropolone reacted with 1,2-ethanediamine to give benzo[4,5]cyclohepta[1,2-*b*]pyrazine.[11]

We now describe the reactions of 3-acetyltropolone (**1**) and its two isomeric methyl ethers——2-acetyl-7-methoxytropone (**2a**) and 3-acetyl-2-methoxytropone (**2b**)——with 1,2-ethanediamine and *N*-methyl-1,2-ethanediamine.

Results and Discussion

Reactions with 1,2-Ethanediamine. When 3-acetyltropolone (**1**) and 1,2-ethanediamine were refluxed for 2 h in methanol, *N,N'*-bis(3-acetyl-2-oxo-3,5,7-cycloheptatrienyl)-1,2-ethanediamine (**3**) and 5-acetyl-3,4-dihydro-2*H*-cyclohepta[*b*]pyrazine (**4**) were isolated in 1 and 3% yields, respectively. Their structures were determined by the elemental analyses and spectral data. The IR, UV, and ^{1}H NMR spectra of the compound **3** are very similar to those of 2-acetyl-7-ethylaminotropone.[2] The ^{13}C NMR spectrum of the compound **4** shows a signal at $\delta=202.13$, which is assigned to the acetyl carbonyl carbon atom. On the other hand, the acetyl carbonyl absorption in the IR spectrum is remarkably shifted to lower frequency region (1600 cm^{-1}) because of hydrogen-bonding with the 4-NH proton. The dehydrogenation reaction of **4** with 2,3-dichloro-5,6-dicyano-*p*-benzoquinone (DDQ) failed.

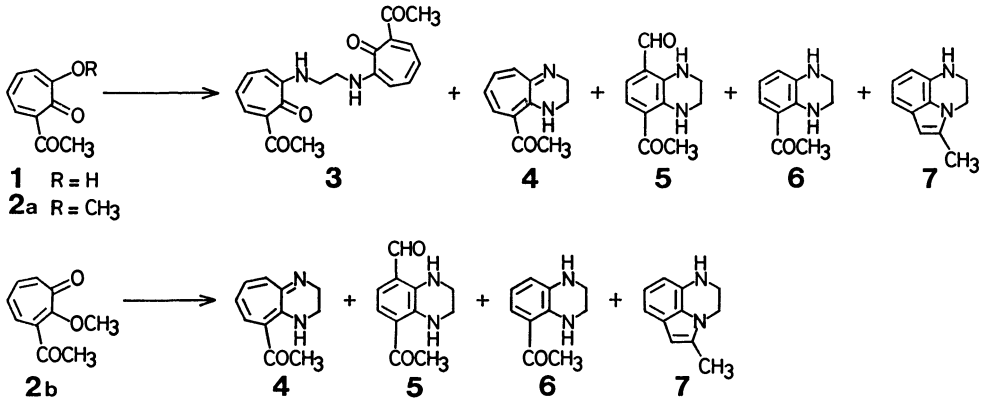

Scheme 1.

† Present address: Taiho Pharmaceutical Co., Ltd., Kawauchi-machi, Tokushima 771-01.

†† Present address: Kumamoto Municipal Institute of Public Health, Tamukae-machi, Kumamoto 862.

††† Present address: Kumamoto Institute of Technology, Ikeda, Kumamoto 860.

Prolonged reaction (24 h) of **1** with 1,2-ethanediamine afforded **3** and **4** in 4 and 6% yields, respectively, together with traces of 8-acetyl-1,2,3,4-tetrahydro-5-quinoxalinecarbaldehyde (**5**) (1%), 5-acetyl-1,2,3,4-tetrahydroquinoxaline (**6**) (trace), and 2-methyl-5,6-dihydro-4*H*-pyrrolo[1,2,3-*de*]quinoxaline (**7**) (1%). The products (**5**—**7**) were assigned on the basis of their elemental analyses and spectral data. Bromination of **4** with *N*-bromosuccinimide (NBS) gave 5-acetyl-9-bromo- (**9**) and 5-acetyl-7,9-dibromo-3,4-dihydro-2*H*-cyclohepta[*b*]pyrazine (**10**). The IR spectrum of the compound **5** shows the characteristic absorptions at 2840 and 2740 cm^{-1} for the formyl group and a broad absorption at 1670—1640 cm^{-1} for the acetyl and formyl groups which exhibited hydrogen-bonding with the NH protons at 1- and 4-positions, respectively. The ^1H NMR spectrum shows two doublets at δ=6.70 and 6.96 (J=9 Hz) for the two protons in the benzene ring. The ^{13}C NMR spectrum shows two peaks at δ=193.86 and 201.03, which are assigned to the formyl and acetyl carbonyl carbon atoms, respectively. The compound **5** reacted with NBS to afford 8-acetyl-6-bromo-1,2,3,4-tetrahydro-5-quinoxalinecarbaldehyde (**11**) and was dehydrogenated with DDQ to afford 8-acetyl-5-quinoxalinecarbaldehyde (**12**). For the compound **6**, the IR spectrum shows an absorption at 1635 cm^{-1} for the hydrogen-bonded acetyl group. In the ^1H NMR spectrum, the ABX pattern is observed at δ=6.35, 6.51, and 7.08 (J= 7, 7, and 3 Hz) for the three protons in the benzene ring. This compound **6** was also dehydrogenated with DDQ to afford 5-acetylquinoxaline (**13**). The compound **7** was very unstable on exposure to air. Difference in the UV spectra in methanol and in 6 M sulfuric acid (1 M=1 mol dm^{-3}) is very similar to behavior in spectra of indoles.[12] The ^1H NMR spectrum shows an ABX pattern for the three protons in the benzene ring at δ=6.23, 6.77, and 6.90 (J= 8, 6.5, and 2 Hz) and 1-H proton at δ=6.08 which exhibited a long-range coupling with the methyl protons (J=1 Hz). These compounds (**5**—**7**) were revealed to be secondary products from **4** by time dependence of the yields and conversion of **4** with base—1,2-ethanediamine. In addition, the compound **4** was treated with hydrogen peroxide to afford **5** and **6**, together with 8-acetyl-1,2,3,4-tetrahydro-6-quinoxalinecarbaldehyde (**8**). Although the compound **8** was very unstable, the assignment of the structure is based on the spectral evidences.

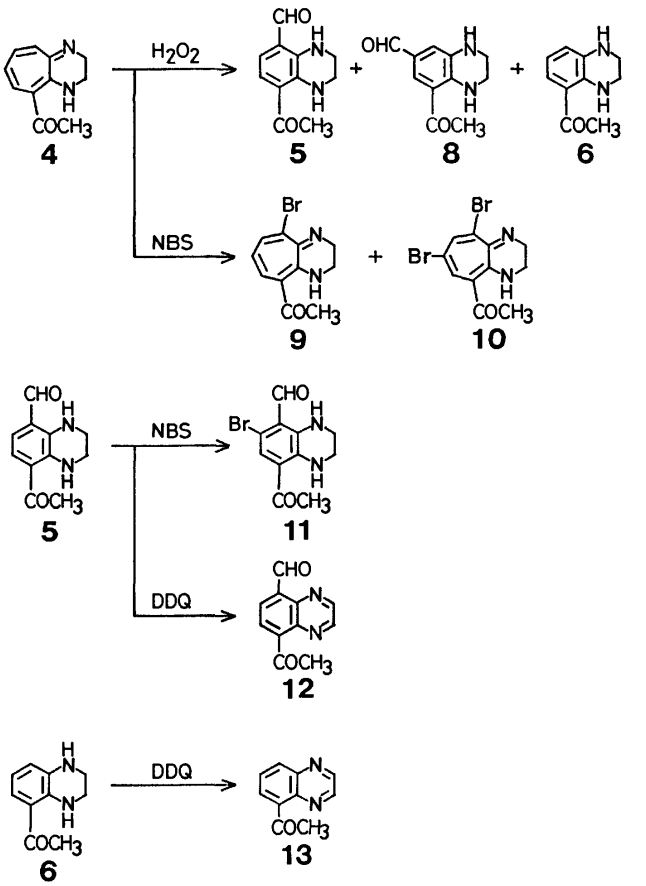

Scheme 2.

The reaction of 2-acetyl-7-methoxytropone (**2a**) with 1,2-ethanediamine also gave the five same products (**3**—**7**), as shown in Table 1. On the other hand, 3-acetyl-2-methoxytropone (**2b**) reacted with 1,2-ethanediamine to give the four products (**4**—**7**). The yield of the product (**4**) decreased, while the yields of the products (**5**—**7**) increased with reaction time.

Reactions with N-*Methyl-1,2-ethanediamine.* As shown in Table 2, 2-acetyl-7-methoxytropone (**2a**) reacted with *N*-methyl-1,2-ethanediamine to afford *N*-(3-acetyl-2-oxo-3,5,7-cycloheptatrienyl)-*N'*-methyl-1,2-ethanediamine (**14**), 5-acetyl-1-methyl-2,3-dihydro-1*H*-cyclohepta[*b*]pyrazine (**15**), 8-acetyl-4-methyl-1,2,3,4-

Table 1. Reactions with 1,2-ethanediamine

Substrate	Temperature	Reaction time / h	Yield/% 3	4	5	6	7
2a	Reflux	2	2	37	Trace	Trace	Trace
	Reflux	8	4	26	4	2	3
	Reflux	24	2	7	7	3	8
2b	R.t.	2		61	—	—	—
	R.t.	4.5		65	—	—	—
	Reflux	0.5		82	2	Trace	2
	Reflux	2		48	4	3	5
	Reflux	8		2	11	7	12

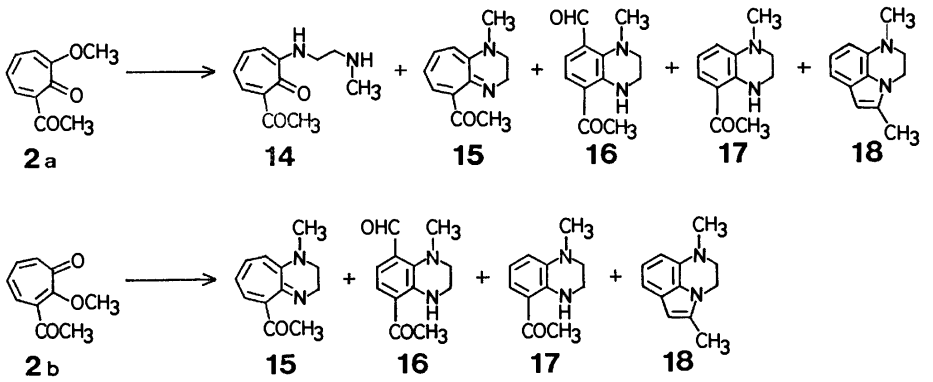

Scheme 3.

TABLE 2. REACTIONS WITH *N*-METHYL-1,2-ETHANEDIAMINE

Substrate	Temperature	Reaction time h	Yield/% 14	15	16	17	18
2a	R.t.	2	74	—	—	—	—
	Reflux	2	38	13	—	Trace	Trace
	Reflux	24	4	27	2	2	9
2b	R.t.	2		58	—	—	—
	Reflux	2		26	Trace	8	10
	Reflux	24		—	Trace	11	19

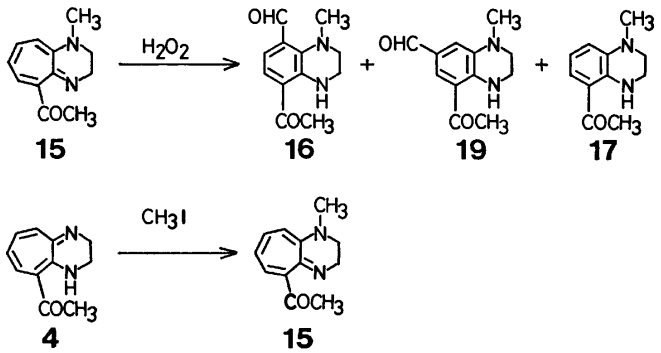

Scheme 4.

tetrahydro-5-quinoxalinecarbaldehyde (**16**), 5-acetyl-1-methyl-1,2,3,4-tetrahydroquinoxaline (**17**), and 2,6-dimethyl-5,6-dihydro-4*H*-pyrrolo[1,2,3-*de*]quinoxaline (**18**).

Their structures were assigned in comparison of the spectral data with those of the corresponding products from the reactions with 1,2-ethanediamine. The compound **15** was also obtained by methylation of **4** with methyl iodide and converted to the compounds (**16**—**18**) by heating in the presence of *N*-methyl-1,2-ethanediamine. Furthermore, the oxidation with hydrogen peroxide gave 8-acetyl-4-methyl-1,2,3,4-tetrahydro-6-quinoxalinecarbaldehyde (**19**), together with **16** and **17**. On the other hand, the reaction of 3-acetyl-2-methoxytropone (**2b**) with *N*-methyl-1,2-ethanediamine similarly gave the products (**15**—**18**).

Experimental

Measurements. The melting points were determined with a Yanagimoto MP-S2 apparatus and are uncorrected. The IR spectra were taken on a JASCO IRA-1 spectrophotometer, and the UV spectra on a Hitachi EPS-3T spectrophotometer. The ^1H and ^{13}C NMR spectra were recorded with a Hitachi R-24 (60 MHz) and a JEOL JNM-FX-100 spectrometer (100 MHz), respectively. The mass spectra were obtained with a JEOL JMS-01SG-2 and JMS-DX-300 spectrometers.

*Reactions of 3-Acetyltropolone (**1**) with 1,2-Ethanediamine. (a)*: A mixture of 3-acetyltropolone (**1**) (164 mg, 1.0 mmol) and 1,2-ethanediamine (0.1 ml, 1.5 mmol) in methanol (10 ml) was refluxed for 2 h on a water bath. After removal of the solvent, the residue was twice chromatographed on a Wakogel B-10 plate (30×30 cm^2) with ethyl acetate. The upper fraction was recrystallized from ethanol to give 4 mg (1%) of *N,N'*-bis(3-acetyl-2-oxo-3,5,7-cycloheptatrienyl)-1,2-ethanediamine (**3**) as yellowish brown needles; mp 214—215 °C (decomp); IR ($CHCl_3$) 3240 (NH), 1700 ($COCH_3$), and 1600 cm^{-1} (C=O); UV (CH_3OH) 248 (log ε 4.44), 354 (4.03), and 430 nm (4.22); ^1H NMR [$(CD_3)_2SO$] δ=2.41 (s, 6H, $CH_3\times2$), 3.6—3.9 (m, 4H, $CH_2\times2$), 6.4—6.9 (m, 4H, arom-H), 7.1—7.6 (m, 4H, arom-H), and 8.5 (br, 2H, NH×2). Found: C, 67.93; H, 5.59; N, 7.97%. Calcd for $C_{20}H_{20}N_2O_4$: C, 68.17; H, 5.72; N, 7.95%. The lower fraction was recrystallized from diethyl ether to give 6 mg (3%) of 5-acetyl-3,4-dihydro-2*H*-cyclohepta[*b*]pyrazine (**4**) as light brown prisms; mp 73—74 °C; IR ($CHCl_3$) 3180 (NH) and 1600 cm^{-1} ($COCH_3$); UV (CH_3OH) 254 (log ε 4.25), 303 (3.61), 386 (3.77), and 458 nm (3.97); ^1H NMR ($CDCl_3$) δ=2.48 (s, 3H, CH_3), 3.2—3.5 (m, 2H, CH_2), 3.7—3.9 (m, 2H, CH_2), 5.91 (ddd, 1H, J=12, 7, and 2 Hz, H-7), 6.41 (dd, 1H, J=12 and 2 Hz, H-6), 12.2 (br, 1H, NH); ^{13}C NMR ($CDCl_3$) δ=29.88 (CH_3), 38.69 (C-3), 49.90 (C-2), 108.26 (C-5), 116.77, 128.63, 131.16, 132.62, 149.71 (C-4a), 159.69 (C-9a), and 202.13 (C=O). Picrate: mp 216—218 °C. Found: C, 48.85; H, 3.67; N, 16.50%. Calcd for $C_{17}H_{15}N_5O_8$: C, 48.92; H, 3.62; N, 16.78%.

(b): A mixture of **1** (164 mg, 1.0 mmol) and 1,2-ethanediamine (0.1 ml, 1.5 mmol) in methanol (10 ml) was refluxed

for 8 h. After removal of the solvent, the residue was thrice chromatographed on a Wakogel B-10 plate (30×30 cm²) with chloroform. The first fraction was recrystallized from methanol–water to give 0.5 mg of 8-acetyl-1,2,3,4-tetrahydro-5-quinoxalinecarbaldehyde (**5**) as red needles; mp 132—133 °C; IR ($CHCl_3$) 3300 (NH), 2840 (CHO), 2740 (CHO), and 1670—1640 cm^{-1} (br, CHO and $COCH_3$); UV (CH_3OH) 214 (log ε 4.21), 240 (4.26), 277 (4.00), 328 (4.07), and 490 nm (3.74); ^1H NMR ($CDCl_3$) δ= 2.54 (s, 3H, CH_3), 3.50 (m, 4H, $CH_2\times2$), 6.70 (d, 1H, J=9 Hz, H-6), 6.96 (d, 1H, J=9 Hz, H-7), 8.57 (br, 1H, 4-NH), 9.05 (br, 1H, 1-NH), and 9.75 (s, 1H, CHO); ^{13}C NMR ($CDCl_3$) δ=28.47 (CH_3), 38.28 (C-2 or -3), 38.57 (C-2 or -3), 116.36 (C-4a or -8a), 116.48 (C-4a or -8a), 116.83 (C-6), 118.95 (C-7), 139.03 (C-5 or -8), 139.55 (C-5 or -8), 193.86 (CHO), and 201.03 (acetyl C=O). Found: C, 64.42; H, 6.07; N, 13.72 %. Calcd for $C_{11}H_{12}N_2O_2$: C, 64.69; H, 5.92; N, 13.72%. The second fraction was recrystallized from hexane to give 1 mg of 2-methyl-5,6-dihydro-4*H*-pyrrolo[1,2,3-*de*]quinoxaline (**7**) as colorless needles; mp 64—65 °C; IR ($CHCl_3$) 3380 cm^{-1} (NH); UV (CH_3OH) 226 (log ε 4.44) and 282 nm (3.89); ^1H NMR ($CDCl_3$) δ=2.29 (d, 3H, J=1 Hz, CH_3), 3.3—3.5 (m, 2H, CH_2), 3.58 (br, 1H, NH), 3.9—4.1 (m, 2H, CH_2), 6.08 (q, 1H, J=1 Hz, H-1), 6.23 (dd, 1H, J= 6.5 and 2 Hz, H-7), 6.81 (dd, 1H, J=8 and 6.5 Hz, H-8), and 6.90 (dd, 1H, J=8 and 2 Hz, H-9); ^{13}C NMR ($CDCl_3$) δ=11.57 (CH_3), 41.45 (C-4 or 5-), 41.98 (C-4 or -5), 99.16 (C-1), 102.27 (C-7), 110.02 (C-9), 119.94 (C-8), 125.87 (C-6a or -9a), 126.40 (C-6a or -9a), 132.16 (C-2 or -9b), and 134.33 (C-2 or -9b); MS *m/e* 172 (M^+). Found: C, 76.68; H, 7.11; N, 16.31%. Calcd for $C_{11}H_{12}N_2$: C, 76.71; H, 7.02; N, 16.27%. The third fraction was recrystallized from hexane to give 0.5 mg of 5-acetyl-1,2,3,4-tetrahydroquinoxaline (**6**) as yellow needles; mp 78—79 °C; IR ($CHCl_3$) 3310 (NH) and 1635 cm^{-1} ($COCH_3$); UV (CH_3OH) 215 (log ε 4.34), 262 (4.06), and 419 nm (3.72); ^1H NMR ($CDCl_3$) δ=2.49 (s, 3H, CH_3), 3.2—3.7 (m, 4H, $CH_2\times2$), 3.7 (br, 1H, 1-NH), 6.33 (dd, 1H, J=7 and 7 Hz, H-7), 6.49 (dd, 1H, J=7 and 3 Hz, H-8), 7.08 (dd, 1H, J=7 and 3 Hz, H-6), and 8.7 (br, 1H, 4-NH); MS *m/e* 176 (M^+). Found: C, 68.19; H, 6.93; N, 15.96%. Calcd for $C_{10}H_{12}N_2O$: C, 68.16; H, 6.86; N, 15.96%. The fourth fraction was rechromatographed on a Wakogel B-10 plate (30×30 cm²) with ethyl acetate to afford **3** (3 mg, 1%) and **4** (10 mg, 5%).

(c): A mixture of **1** (164 mg, 1.0 mmol) and 1,2-ethanediamine (0.1 ml, 1.5 mmol) in methanol (10 ml) was refluxed for 24 h and worked up, as mentioned above, to give **3** (17 mg, 5%), **4** (12 mg, 6%), **5** (2 mg, 1%), **6** (0.2 mg, trace), and **7** (2 mg, 1%).

*Reaction of 2-Acetyl-7-methoxytropone (**2a**) with 1,2-Ethanediamine.* A mixture of 2-acetyl-7-methoxytropone (**2a**) (178 mg, 1.0 mmol) and 1,2-ethanediamine (0.1 ml, 1.5 mmol) in methanol (10 ml) was refluxed and worked up, as mentioned above, to give the following results: (i) Reaction time, 2 h: **3** (8 mg, 2%), **4** (67 mg, 37%), **5** (0.2 mg), **6** (0.6 mg), and **7** (0.6 mg); (ii) Reaction time, 8 h: **3** (14 mg, 4%), **4** (48 mg, 26%), **5** (9 mg, 4%), **6** (3 mg, 2%), and **7** (4 mg, 3%); (iii) Reaction time, 24 h: **3** (8 mg, 2%), **4** (14 mg, 7%), **5** (14 mg, 7%), **6** (5 mg, 3%), and **7** (14 mg, 8%).

*Reaction of 3-Acetyl-2-methoxytropone (**2b**) with 1,2-Ethanediamine. (a)*: A solution of 3-acetyl-2-methoxytropone (**2b**) (357 mg, 2.0 mmol) and 1,2-ethanediamine (0.2 ml, 3.0 mmol) in methanol (10 ml) was allowed to stand for 2 h at room temperature. The reaction mixture was diluted with water and extracted with diethyl ether. After removal of the solvent, the residue was column-chromatographed on a Wakogel C-100 column (30 g) and recrystallized from diethyl ether to afford **4** (229 mg, 61%). Reaction time, 4.5 h: **4** (246 mg, 65%).

(b): A mixture of **2b** (178 mg, 1.0 mmol) and 1,2-ethanediamine (0.1 ml, 1.5 mmol) in methanol (10 ml) was refluxed and worked up, as mentioned above, to give the following results: (i) Reaction time, 30 min: **4** (152 mg, 82%), **5** (4 mg, 2%), **6** (1 mg), and **7** (3 mg, 2%); (ii) Reaction time, 2 h: **4** (91 mg, 48%), **5** (7 mg, 4%), **6** (5 mg, 3%), and **7** (8 mg, 5%); (iii) Reaction time, 8 h, **4** (3 mg, 2%), **5** (22 mg, 11%), **6** (12 mg, 7%), and **7** (20 mg, 11%).

*Treatment of the Compound (**4**) with 1,2-Ethanediamine.* A solution of the compound (**4**) (177 mg, 0.9 mmol) and 1,2-ethanediamine (0.1 ml, 1.5 mmol) in methanol (10 ml) was refluxed for 4 h. After evaporation of the solvent, the residue was thrice chromatographed on a Wakogel B-10 plate (30×30 cm²) with chloroform. The first fraction gave **5**. The second fraction was collected and rechromatographed on a Wakogel B-10 plate (30×30 cm²) with chloroform to give **5** and **7**. The third fraction gave **6**. Yields: **5** (23 mg, 12%), **6** (10 mg, 6%), and **7** (20 mg, 12%).

*Oxidation of the Compound (**4**) with Hydrogen Peroxide.* To a solution of **4** (98 mg, 0.5 mmol) in methanol (10 ml) was added 30% hydrogen peroxide aqueous solution (2 ml). The mixture was allowed to stand for 8 h at room temperature, diluted with water, and extracted with chloroform. After removal of the solvent, the residue was chromatographed on a Wakogel B-10 plate (30×30 cm²) with ethyl acetate to give **5** (3 mg, 3%), **6** (3 mg, 3%), and 8-acetyl-1,2,3,4-tetrahydro-6-quinoxalinecarbaldehyde (**8**) as semisolid (2 mg, 2%); IR ($CHCl_3$) 3390 (NH), 3270 (NH), 1690 (CHO), and 1630 cm^{-1} ($COCH_3$); ^1H NMR ($CDCl_3$) δ=2.57 (s, 3H, CH_3), 3.2—3.8 (m, 4H, $CH_2\times2$), 4.1 (br, 1H, 4-NH), 6.96 (d, 1H, J=1.5 Hz, H-5), 7.55 (d, 1H, J=1.5 Hz, H-7), 9.5 (br, 1H, 1-NH), and 9.52 (s, 1H, CHO).

*Bromination of the Compound (**4**) with NBS.* A mixture of **4** (95 mg, 0.5 mmol) and NBS (90 mg, 0.5 mmol) in benzene (10 ml) was refluxed for 30 min in the presence of benzoyl peroxide (catalytic amount). After removal of the solvent, the residue was twice chromatographed on a Wakogel B-10 plate (30×30 cm²) with ethyl acetate. The lower fraction was collected and recrystallized from benzene–hexane to afford 10 mg (7%) of 5-acetyl-9-bromo-3,4-dihydro-2*H*-cyclohepta[*b*]pyrazine (**9**) as brown plates; mp 102.5—103.5 °C; IR ($CHCl_3$) 1600 cm^{-1} (C=O); UV (CH_3OH) 245 (log ε 4.06), 252 (4.06), 270 (sh, 4.04), 380 (3.64), and 449 nm (3.82); ^1H NMR ($CDCl_3$) δ=2.45 (s, 3H, CH_3), 3.3—3.6 (m, 2H, CH_2), 3.8—4.1 (m, 2H, CH_2), 5.72 (dd, 1H, J= 10 and 8 Hz, H-7), 6.98 (d, 1H, J=10 Hz, H-8), 7.33 (d, 1H, J=8 Hz, H-6), and 10.8 (br, 1H, NH). Picrate: mp 206.5—207.5 °C (decomp). Found: C, 41.10; H, 2.90; N, 14.17%. Calcd for $C_{17}H_{14}N_5O_8Br$: C, 41.15; H, 2.84; N, 14.11%. The upper fraction was worked up, as mentioned above, to afford 11 mg (6%) of 5-acetyl-7,9-dibromo-3,4-dihydro-2*H*-cyclohepta[*b*]pyrazine (**10**) as brown prisms; mp 128 °C (decomp); IR ($CHCl_3$) 1620 cm^{-1} (C=O); UV (CH_3OH) 233 (log ε 4.13), 270 (4.07), 386 (3.75), and 461 nm (3.80); ^1H NMR ($CDCl_3$) δ=2.44 (s, 3H, CH_3), 3.2—3.5 (m, 2H, CH_2), 3.8—4.1 (m, 2H, CH_2), 7.31 (d, 1H, J= 1.5 Hz, H-8), 7.51 (d, 1H, J=1.5 Hz, H-6), and 12.1 (br, 1H, NH). Picrate: mp 154—155 °C (decomp). Found: C, 35.78; H, 2.34; N, 12.21%. Calcd for $C_{17}H_{13}N_5O_8Br_2$: C, 35.50; H, 2.28; N, 12.18%.

*Bromination of the Compound (**5**) with NBS.* A mixture of **5** (103 mg, 0.5 mmol) and NBS (89 mg, 0.5 mmol) in benzene (10 ml) was refluxed for 3 h in the presence of ben-

zoyl peroxide (catalytic amount), worked up, and twice chromatographed, as mentioned above. The upper fraction was collected and recrystallized from methanol to afford 16 mg (11%) of 8-acetyl-6-bromo-1,2,3,4-tetrahydro-5-quinoxalinecarbaldehdye (**11**) as red needles; mp 162—163 °C; IR ($CHCl_3$) 3270 (NH), 2870 (CHO), 2770 (CHO), 1645 cm^{-1} (CHO and $COCH_3$); UV (CH_3OH) 232 (log ε 4.24), 280 (3.81), 331 (3.98), 493 (3.74), and 515 nm (sh, 3.70); ^1H NMR ($CDCl_3$) δ=2.50 (s, 3H, CH_3), 3.5—3.7 (m, 4H, $CH_2\times2$), 7.11 (s, 1H, H-7), 9.2 (br, 1H, 4-NH), 9.6 (br, 1H, 1-NH), and 10.15 (s, 1H, CHO). Found: C, 46.88; H, 3.99; N, 9.86%. Calcd for $C_{11}H_{11}N_2O_2Br$: C, 46.67; H, 3.92; N, 9.90%. The starting material (**5**) (13 mg, 17%) was recovered from the lower fraction.

*Dehydrogenation of the Compound (**5**) with DDQ.* A mixture of **5** (76 mg, 0.4 mmol) and DDQ (85 mg, 0.4 mmol) in dry benzene (15 ml) was refluxed for 8 h. After removal of the solvent, the residue was twice chromatographed on a Wakogel B-10 plate (30×30 cm^2) with chloroform. The lower fraction was recrystallized from benzene to give 13 mg (17%) of 8-acetyl-5-quinoxalinecarbaldehyde (**12**) as pale yellow needles; mp 177 °C (decomp); IR ($CHCl_3$) 1710 cm^{-1} (CHO and $COCH_3$); UV (CH_3OH) 218 (log ε 4.28), 239 (4.05), 313 (3.72), and 322 nm (sh, 3.70); ^1H NMR ($CDCl_3$) δ=2.87 (s, 3H, CH_3), 8.08 (d, 1H, J=7 Hz, H-6), 8.36 (d, 1H, J=7 Hz, H-7), 8.97 (s, 2H, H-2,3), and 11.25 (s, 1H, CHO). Found: C, 66.12; H, 4.09; N, 13.99%. Calcd for $C_{11}H_8N_2O_2$: C, 65.99; H, 4.03; N, 13.99%. The compound **5** (22 mg, 29%) was recovered from the upper fraction.

*Dehydrogenation of the Compound (**6**) with DDQ.* A mixture of **6** (94 mg, 0.5 mmol) and DDQ (228 mg, 1.0 mmol) in dry benzene (10 ml) was refluxed for 1 h and chromatographed, as mentioned above, to give 14 mg (15%) of 5-acetylquinoxaline (**13**) as pale yellow plates; mp 75—76 °C; IR ($CHCl_3$) 1700 cm^{-1} (C=O); UV (CH_3OH) 214 (log ε 4.11), 238 (3.83), 315 (sh, 3.45), and 322 nm (3.46); ^1H NMR ($CDCl_3$) δ=2.91 (s, 3H, CH_3), 7.88 (dd, 1H, J=7 and 2 Hz, H-7), 8.06 (dd, 1H, J=7 and 2 Hz, H-8), 8.22 (dd, 1H, J=7 and 2 Hz, H-6), and 8.87 (s, 2H, H-2,3). Found: C, 69.68; H, 4.73; N, 16.30%. Calcd for $C_{10}H_8N_2O$: C, 69.75; H, 4.68; N, 16.27%.

*Reaction of 2-Acetyl-7-methoxytropone (**2a**) with* N-*Methyl-1,2-ethanediamine.* *(a)*: A solution of **2a** (178 mg, 1.0 mmol) and *N*-methyl-1,2-ethanediamine (0.1 ml, 1.4 mmol) in methanol (10 ml) was allowed to stand for 2 h at room temperature. The mixture was diluted with water and extracted with chloroform. After removal of the solvent, the residue was four-times chromatographed on two Kieselguhr G plates (30×30 cm^2) with hexane to give 163 mg (74%) of *N*-(3-acetyl-2-oxo-3,5,7-cycloheptatrienyl)-*N'*-methyl-1,2-ethanediamine (**14**) as a yellow oil; IR ($CHCl_3$) 3280 (NH), 1690 ($COCH_3$), and 1600 cm^{-1} (C=O); UV (CH_3OH) 247 (log ε 4.17), 349 (3.80), and 421 nm (3.96); ^1H NMR ($CDCl_3$) δ=1.7 (br, 1H, NH), 2.44 (br.s, 3H, *N*-CH_3), 2.55 (s, 3H, $COCH_3$), 2.7—3.1 (m, 2H, CH_2), 3.2—3.6 (m, 2H, CH_2), 6.4—6.8 (m, 2H, arom-H), 7.1—7.7 (m, 2H, arom-H), and 8.0 (br, 1H, NH). Picrate: mp 176 °C (decomp). Found: C, 47.89; H, 4.11; N, 15.27%. Calcd for $C_{18}H_{19}N_5O_9$: C, 48.11; H, 4.11; N, 15.58%.

(b): A mixture of **2a** (178 mg, 1.0 mmol) and *N*-methyl-1,2-ethanediamine (0.1 ml, 1.4 mmol) in methanol (10 ml) was refluxed for 2 h. After removal of the solvent, the residue was four-times chromatographed on two Kieselguhr G plates (30×30 cm^2) with hexane. The lower fraction gave **14** (84 mg, 38%). The upper fraction was collected and twice rechromatographed on a Wakogel B-10 plate (30×30 cm^2) with chloroform. The first fraction gave 1 mg of 2,6-dimethyl-5,6-dihydro-4*H*-pyrrolo[1,2,3-*de*]quinoxaline (**18**) as a colorless oil; UV (CH_3OH) 223 (log ε 4.32) and 284 nm (3.84); ^1H NMR ($CDCl_3$) δ=2.19 (s, 3H, CH_3), 2.73 (s, 3H, *N*-CH_3), 2.9—3.2 (m, 2H, CH_2), 3.7—4.0 (m, 2H, CH_2), 5.89 (s, 1H, H-1), 6.03 (dd, 1H, J=4.5 and 3 Hz, H-7), 6.64 (dd, 1H, J=7 and 4.5 Hz, H-8), 6.72 (dd, 1H, J=7 and 3 Hz, H-9). Found: MS *m/e* 186.1181 (M^+). Calcd for $C_{12}H_{14}N_2$: M^+ 186.1156. The second fraction was recrystallized from hexane to give 0.6 mg of 5-acetyl-1-methyl-1,2,3,4-tetrahydroquinoxaline (**17**) as yellow needles; mp 77—78 °C; IR ($CHCl_3$) 3300 (NH) and 1630 cm^{-1} (C=O); UV (CH_3OH) 212 (log ε 4.31), 268 (3.93), and 418 nm (3.67); ^1H NMR ($CDCl_3$) δ=2.49 (s, 3H, $COCH_3$), 2.78 (s, 3H, *N*-CH_3), 3.0—3.2 (m, 2H, CH_2), 3.4—3.7 (m, 2H, CH_2), 6.47 (dd, 1H, J=7 and 6 Hz, H-7), 6.56 (dd, 1H, J=7 and 3 Hz, H-8), 7.08 (dd, 1H, J=6 and 3 Hz, H-6), and 9.1 (br, 1H, NH). Found: C, 69.45; H, 7.39; N, 14.44%. Calcd for $C_{11}H_{14}N_2O$: C, 69.45; H, 7.42; N, 14.72%. The third fraction was recrystallized from benzene–hexane to afford 25 mg (13%) of 5-acetyl-1-methyl-2,3-dihydro-1*H*-cyclohepta[*b*]pyrazine (**15**) as orange prisms; mp 134—134.5 °C; IR ($CHCl_3$) 1680 cm^{-1} (C=O); UV (CH_3OH) 259 (log ε 4.18), 379 (3.75), and 466 nm (3.93); ^1H NMR ($CDCl_3$) δ=2.35 (s, 3H, $COCH_3$), 3.12 (s, 3H, *N*-CH_3), 3.3—3.5 (m, 2H, CH_2), 3.7—4.0 (m, 2H, CH_2), 5.79 (d, 1H, J=9.5 Hz, H-9), 6.06 (dd, 1H, J=10.5 and 8.5 Hz, H-7), 6.66 (ddd, 1H, J=10.5, 9.5, and 1.5 Hz, H-8), and 7.24 (dd, 1H, J=9.5 and 1.5 Hz, H-6); ^{13}C NMR ($CDCl_3$) δ=28.53 (*CO*-CH_3), 39.81 (*N*-CH_3), 50.37 (C-2), 51.96 (C-3), 101.86, 116.80, 132.86, 134.33, 134.97 (C-5), 147.83 (C-4a), and 202.49 (C=O). Picrate: mp 151—153 °C (decomp). Found: C, 50.31; H, 3.82; N, 15.92%. Calcd for $C_{18}H_{17}N_5O_7$: C, 50.12; H, 3.97; N, 16.24%.

(c): A mixture of **2a** (178 mg, 1.0 mmol) and *N*-methyl-1,2-ethanediamine (0.1 ml, 1.4 mmol) in methanol (10 ml) was refluxed for 24 h. The reaction mixture was worked up, as mentioned above, to give **14** (9 mg, 4%), **15** (54 mg, 27%), **17** (12 mg, 6%), **18** (17 mg, 9%), and 8-acetyl-4-methyl-1,2,3,4-tetrahydro-5-quinoxalinecarbaldehyde (**16**) (4 mg, 2%) as a red oil; IR ($CHCl_3$) 3300 (NH), 1695 (CHO), and 1640 cm^{-1} ($COCH_3$); UV (CH_3OH) 245 (log ε 4.30), 322 (3.62), and 467 nm (3.66); ^1H NMR ($CDCl_3$) δ=2.52 (s, 3H, $COCH_3$), 2.90 (s, 3H, *N*-CH_3), 3.3—3.7 (m, 4H, $CH_2\times2$), 6.94 (d, 1H, J=9 Hz, H-6), 7.40 (d, 1H, J=9 Hz, H-7), 9.1 (br, 1H, NH), and 10.25 (s, 1H, CHO). Found: MS *m/e* 218.0953 (M^+). Calcd for $C_{12}H_{14}N_2O_2$: M^+ 218.1055.

*Reaction of 3-Acetyl-2-methoxytropone (**2b**) with* N-*Methyl-1,2-ethanediamine.* *(a)*: A solution of 3-acetyl-2-methoxytropone (**2b**) (178 mg, 1.0 mmol) and *N*-methyl-1,2-ethanediamine (0.1 ml, 1.4 mmol) in methanol (10 ml) was allowed to stand for 2 h at room temperature. The mixture was diluted with water and extracted with chloroform. After removal of the solvent, the residue was twice chromatographed on two Wakogel B-10 plates (30×30 cm^2) with ethyl acetate to afford **15** (117 mg, 58%).

(b): A mixture of **2b** (178 mg, 1.0 mmol) and *N*-methyl-1,2-ethanediamine (0.1 ml, 1.4 mmol) in methanol (10 ml) was refluxed for 2 h. After removal of the solvent, the residue was twice chromatographed on two Wakogel B-10 plates (30×30 cm^2) with chloroform. The first, second, third, and fourth fractions gave **18** (20 mg, 10%), **17** (14 mg, 8%), **16** (2 mg), and **15** (52 mg, 26%), respectively.

(c): A mixture of **2b** (178 mg, 1.0 mmol) and *N*-methyl-1,2-ethanediamine (0.1 ml, 1.4 mmol) in methanol (10 ml)

was refluxed for 24 h. The mixture was worked up, as mentioned above, to give **16** (2 mg), **17** (20 mg, 11%), and **18** (35 mg, 19%).

*Treatment of the Compound (**15**) with* N-*Methyl-1,2-ethanediamine.* A solution of **15** (181 mg, 0.9 mmol) and *N*-methyl-1,2-ethanediamine (0.1 ml, 1.4 mmol) in methanol (10 ml) was refluxed for 7 h. After removal of the solvent, the residue was twice chromatographed on a Wakogel B-10 plate (30×30 cm^2) with chloroform to give **16** (19 mg, 10%), **17** (32 mg, 19%), and **18** (10 mg, 6%).

*Oxidation of the Compound (**15**) with Hydrogen Peroxide.* A mixture of **15** (66 mg, 0.3 mmol) and 30% hydrogen peroxide aqueous solution (1 ml) in methanol (5 ml) was allowed to stand for 6 h at room temperature, diluted with water, and extracted with chloroform. After removal of the solvent, the residue was chromatographed on a Wakogel B-10 plate (30×30 cm^2) with ethyl acetate to give **16** (9 mg, 12%), **17** (3 mg, 5%), and 8-acetyl-4-methyl-1,2,3,4-tetrahydro-6-quinoxalinecarbaldehyde (**19**) (6 mg, 9%) as a semisolid; IR ($CHCl_3$) 3240 (NH), 1680 (CHO), and 1625 cm^{-1} ($COCH_3$); ^{1}H NMR ($CDCl_3$) $\delta=2.60$ (s, 3H, $COCH_3$), 2.95 (s, 3H, *N*-CH_3), 3.0—3.4 (m, 2H, CH_2), 3.5—3.9 (m, 2H, CH_2), 7.02 (m, 1H, H-5), 7.65 (d, 1H, $J=1.5$ Hz, H-7), and 9.65 (s, 1H, CHO).

*Methylation of the Compound (**4**) with Methyl Iodide.* A solution of **4** (188 mg, 1.0 mmol) and methyl iodide (0.2 ml, 3.0 mmol) in dry acetone (20 ml) was allowed to stand for 6 h in the presence of silver oxide (695 mg, 3.0 mmol). The mixture was filtered, concentrated, and thrice chromatographed on a Wakogel B-10 plate (30×30 cm^2) with ethyl acetate to give **15** (26 mg, 13%). The starting material (**4**) was recovered in 35% yield.

We wish to thank Dr. Tetsuo Nozoe, Professor Emeritus of Tohoku University, for his continuous encouragement. We are also grateful to Professor Hitoshi Takeshita of Kyushu University and Mr. Masanori Tsumura of Ichikawa Chemical Laboratories, Higashi-Osaka, for their kind measurements of the ^{13}C NMR and the high-resolution mass spectra, respectively.

References

1) K. Imafuku and Z.-T. Jin, *Yanbian Daxue Xuebao*, **1983**, 35.
2) K. Imafuku and A. Shimazu, *Synthesis*, **1982**, 1043.
3) K. Imafuku, A. Shigenobu, and M. Ogura, *Bull. Chem. Soc. Jpn.*, **55**, 3337 (1982).
4) A. Yamane, M. Nagayoshi, K. Imafuku, and H. Matsumura, *Bull. Chem. Soc. Jpn.*, **52**, 1972 (1979).
5) A. Yamane, K. Imafuku, and H. Matsumura, *Bull. Chem. Soc. Jpn.*, **53**, 1461 (1980).
6) K. Imafuku, A. Yamane, and H. Matsumura, *J. Heterocycl. Chem.*, **17**, 1293 (1980).
7) Y. Sudoh, Z.-T. Jin, K. Imafuku, and H. Matsumura, *J. Heterocycl. Chem.*, **19**, 525 (1982).
8) Z.-T. Jin, K. Imafuku, and H. Matsumura, *J. Chem. Soc., Perkin Trans. 1*, **1982**, 1037.
9) K. Imafuku, A. Yamane, and H. Matsumura, *J. Heterocycl. Chem.*, **18**, 335 (1981).
10) S. Ito, *Sci. Repts. Tohoku Univ., I*, **42**, 247 (1958).
11) M. K. Eberle and G. G. Khale, *J. Heterocycl. Chem.*, **18**, 525 (1981).
12) R. L. Hinma and J. Lang, *J. Am. Chem. Soc.*, **86**, 3796 (1964).

Studies of Collectors. V.[1] The Preparation of Amidoxime-type Surfactants and the Flotation of a Trace Amount of Uranium

Yoshifumi KOIDE,* Hiroaki TAKAMOTO, Katsunori MATSUKAWA, and Kimiho YAMADA

Department of Synthetic Chemistry, Faculty of Engineering, Kumamoto University, Kurokami, Kumamoto 860

(Received February 3, 1983)

This study investigates the flotation of uranium with four amidoxime-type surfactants ($R_{12}Ax$, $R_{16}Ax$, Ls8.6Ax, and Ls7.2Ax6.0Hx). Ls7.2Ax6.0Hx was prepared by the telomerization of acrylonitrile and acrylamide using 1-dodecanethiol as a solvent, followed by treatment with hydroxylamine. Uranium could be floated effectively at pH 5.0 with $R_{12}Ax$, $R_{16}Ax$, or a combination of Ls8.6Ax and a nonionic surfactant. The floatability for uranium present in sea water was 43% after the addition of 1 mg $R_{16}Ax$ and 90% after the addition of 30 mg $R_{12}Ax$. Ls7.2Ax6.0Hx formed a soluble complex, and 72% of the uranium present in sea water could be collected at pH 8.0 by foam fractionation using Ls7.2Ax6.0Hx. Little surfactant remained in the residual solution, and it was regenerated from an acidic solution dissolving the scum or froth.

Ion flotation has been examined as a method of collecting specific metal ions.[2] The collectors used in such flotation are generally a combination of complexing agents, precipitants, or adsorbents, and oppositely charged surfactants.[3,4] However, floatability is apt to vary with the collector-adding method or with the pH, and a small amount of the collector remains in the residual solution.[5] In a previous paper[1] we prepared surfactants with a complex radical and applied them to collectors. The collectors formed floatable complexes with heavy metal ions, and little remained in the residual solution when the HLB (hydrophilic–lipophilic balance) value of the complexes was 4—14.[1] However, the flotation for trace amounts of metal ions dissolved in an aqueous solution was not investigated.

Fetscher,[6] Tani *et al.*,[7] and Egawa *et al.*[8] have reported that amidoxime-type resins adsorb uranium selectively from an aqueous solution or sea water, so that amidoxime-type surfactants may be expected to act as uranium-floating collectors. To get further information on collectors, in this paper we study the recovery of uranium in a 10-ppb uranium solution and in sea water by means of ion flotation and foam fractionation, using four amidoxime-type surfactants: $R_{12}Ax$, $R_{16}Ax$, Ls8.6Ax, and Ls7.2Ax6.0Hx.

Experimental

Synthesis of Amidoxime-type Surfactants. $R_{12}Ax$(3-dodecyloxy)propionamide oxime), $R_{16}Ax$(3-(hexadecyloxy)propionamide oxime), and Ls8.6Ax(telomer containing 8.6 unit moles of the amidoxime group[9]) were obtained as has been described in a previous paper.[1] Ls7.2Ax6.0Hx(cotelomer containing 7.2 unit moles of the amidoxime group, 6.0 unit moles of the hydroxamic acid group, and an amide group[9]) was synthesized as follows:

1-Dodecanethiol(10.1—40.4 g), acrylonitrile(9.5—16.0 g,bp 76.0—77.0 °C), and acrylamide(12.5—21.4 g, bp_{25} 123.0—125.0 °C) were added to 80 cm^3 of ethanol in a three-necked flask equipped with a stirrer, a reflux condenser, and a thermometer. After the air had been purged with nitrogen for 30 min, 1 wt% of α,α'-azobisisobutyronitrile per weight of monomers was added to the reaction mixture and the mixture was stirred at 70 °C. The cotelomer containing a nitrile group and an amide group[9] (Ls–AN–Am) precipitated gradually within 3—4 h; the remaining mixture was stirred for an additional 5 h at 70 °C. After cooling to room temperature, Ls–AN–Am was filtered by suction, washed first with 100 cm^3 of ethanol and second with 50 cm^3 of ether, and then dried. Then Ls7.7AN21.3Am (cotelomer containing 7.7 unit moles of the nitrile group and 21.3 unit moles of the amide group, 2 g) and hydroxylamine hydrochloride (2.1—8.4 g, Wako GR) were dissolved in 30 cm^3 of *N,N*-dimethylformamide in the above-mentioned flask, and the mixture was stirred at 80 °C. Sodium carbonate, in an amount equivalent to the hydroxylamine hydrochloride, was added to the mixture for over 30 min, after which the mixture was stirred for an additional 3 h at 80 °C. The sodium chloride thus precipitated was filtered out by suction, and the filtrate was cooled to room temperature. The white cotelomer, Ls–Ax–Hx, precipitated by the addition of the filtrate to 100 cm^3 of 2-propanol was filtered, rinsed with 200 cm^3 of methanol, and dried.

Collectors. The behavior of the amidoxime-type surfactants used as collectors was compared with that of the hydroxamic acid-type surfactants,[10] an EDTA-type surfactant(*N*-(1-carboxyundecyl)ethylenediamine-*N,N',N'*-triacetic acid, R-edta),[11] and sodium dodecyl sulfate (SDS). The chemical formulas and abbreviations of the amidoxime-type surfactants and hydroxamic acid-type surfactants are presented in Fig. 1.

Sample of Uranium. An aqueous solution containing 10 ppb of uranium ions was prepared by dissolving uranyl nitrate(Wako GR) in deionized water. Sea water was taken at the sea-coast of Akase, Uto-gun, Kumamoto, in Jan., 1979, and was filtered to remove any impure particles.

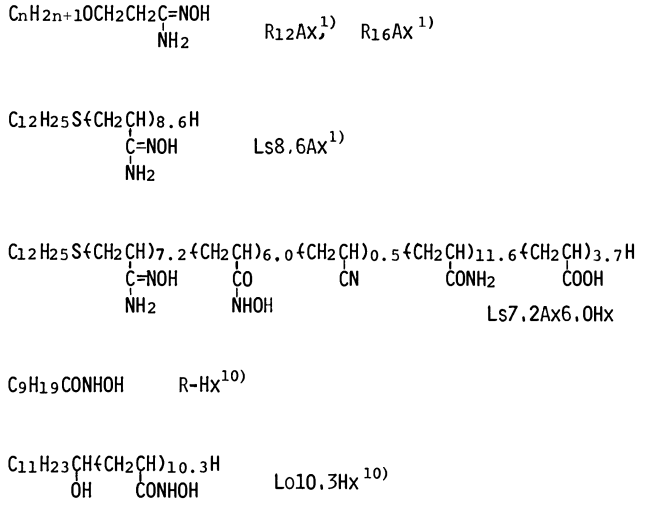

Fig. 1. Formulas and abbreviations.

Apparatus and Procedures. The flotation apparatus was the same as that previously reported.[1] A collector was added to 500 cm^3 of the sample of uranium in a flotation cell, and air, from which CO_2 had been removed with a NaOH solution, was passed into the sample through the glass filter at a rate of 30—40 cm^3/min for 20 min. The amount of uranium in the solution or in the scum was determined from the absorbance of the uranium–arsenazo III complex(660 nm).[12] The floatability(%) of uranium was calculated by the use of:

$$F = \frac{a_0 - a_1}{a_0} \times 100\%,$$

where a_0 and a_1 denote the initial and final concentrations of uranium in the solutions.

Results and Discussion

Synthesis of Ls7.2Ax6.0Hx. Ls–Ax–Hx was derived from Ls–AN–Am. Acrylonitrile was more difficult than acrylamide to introduce into the cotelomer, Ls–AN–Am. The IR spectrum of the compound prepared at 60 °C showed the absence of nitrile, even though the amount of acrylonitrile added was four times that of acrylamide. However, both acrylonitrile and acrylamide could be introduced into the cotelomer by raising the reaction temperature to 70 °C or 77 °C(bp of acrylonitrile), even in the monomer ratio of 1:1. The yield of cotelomer at 70 °C was more than that at 77 °C, and the elongation of the reaction time up to 3 h led to an increase in the yield. Therefore, the rest of the reactions were carried out for 5 h at 70 °C. The conditions for preparing Ls–AN–Am were listed in Table 1. The yields of cotelomer per monomer(acrylonitrile plus acrylamide) were all above 50%, and the plots of the fraction of 1-dodecanethiol(β) *vs.* the reciprocal of the polymerization degree(1/Pn) gave a straight line, as is seen in a usual chaintransfer reaction.[13]

The composition of the cotelomer was determined by means of its molecular weight (Corona 114 vapor pressure osmometer) and IR spectrum (Shimadzu IR-408). The IR spectrum of the cotelomer showed the characteristic absorptions of nitrile(ν_{CN} 2240 cm^{-1}), amide(ν_{CO} 1660, δ_{NH} 1610 cm^{-1}), and hydrocarbon(ν_{CH} 2920, 2850 cm^{-1}). The fraction of the cyano group and the carbamoyl group in the cotelomer was calculated from the absorption ratio for carbonitrile to carboxamide, based on the calibration curve made with the mixture of the nitrile-type telomer[1] and the amide-type telomer.[14] Moreover, the same structure was suggested by the ^1H NMR spectra integration(JEOL JMN-MH-100), as measured in a trifluoroacetic acid solvent with tetramethylsilane as the internal standard, *i.e.*, methyl(δ=0.89, 3H, t), methylene protons(δ=1.35, 20H) due to the dodecyl group, a broad peak of ethylene protons(δ=1.8—3.2), and carbamoyl protons(δ=7.5—7.7). The chemical formulas and results of the elementary analysis of four Ls–AN–Am are shown in Table 2. The calculated values of C, H, N, and S based on the chemical formulas agreed with the analytical data.

The carbamoyl group was introduced into the cotelomer to make the compound soluble even in a metallic solution. The four Ls–AN–Am in Table 2 were soluble in water, and stable foam was generated by bubbling air through the solution. The resulting

Table 1. Preparation of Ls-AN-Am

Conditions of reaction[a]			Products		
LSH (g)	AN+Am (g)	β / mol mol^{-1}	Abbreviation	Yield / g	Pn[b]
40.4	24.8	0.50	Ls0.7AN1.6Am	15.4	2.3
20.2	24.8	0.25	Ls3.5AN7.5Am	14.7	11.0
20.2	31.1	0.20	Ls3.7AN7.9Am	21.7	11.6
20.2	37.4	0.17	Ls4.2AN8.1Am	35.6	12.3
10.1	22.0	0.14	Ls5.0AN12.5Am	13.9	17.5
12.7	31.1	0.12	Ls7.7AN21.3Am	15.5	29.0

a) LSH=1-Dodecanethiol, AN=acrylonitrile, Am=acrylamide, β=LSH/(AN+Am), AN/Am=1 mol/mol. Temp: 70 °C, time: 5 h, AIBN: 1 wt% of (AN+Am). b) Polymerization degree.

Table 2. Elementary analysis of Ls-AN-Am

Ls-AN-Am	Formula	Calcd (Found) (%)			
		C	H	N	S
Ls3.5AN7.5Am	$C_{45.0}H_{74.0}N_{11.0}O_{7.5}S$	58.75	8.11	16.74	3.49
		(59.64)	(8.01)	(16.45)	(3.52)
Ls4.2AN8.1Am	$C_{48.9}H_{79.1}N_{12.3}O_{8.1}S$	58.68	7.96	17.21	3.20
		(59.34)	(7.91)	(16.30)	(3.40)
Ls5.0AN12.5Am	$C_{64.5}H_{103.5}N_{17.5}O_{12.5}S$	57.12	7.69	18.07	2.36
		(57.92)	(7.63)	(17.85)	(2.37)
Ls7.7AN21.3Am	$C_{99.0}H_{155.6}N_{29.0}O_{21.3}S$	55.94	7.37	19.10	1.50
		(55.23)	(7.45)	(18.75)	(1.20)

TABLE 3. REACTION OF Ls7.7AN21.3Am WITH HYDROXYLAMINE

Conditions of reaction[a]			Products		
$NH_2OH \cdot HCl$ (g)	*A*	*B*	Abbreviation	Yield	-CN[b]
	mol mol^{-1}			g	mol
2.1	4.2	1.2	Ls5.1Ax3.9Hx	1.7	2.6
4.2	8.3	2.4	Ls5.8Ax7.4Hx	2.0	1.9
8.4	16.7	4.8	Ls7.2Ax6.0Hx	1.9	0.5

a) Ls7.7AN21.3Am: 2g, *A*: NH_2OH/-CN, *B*: NH_2OH/(-CN+-$CONH_2$), Na_2CO_3: equiv wt to $NH_2OH \cdot HCl$, DMF: 30 cm^3, temp: 80 °C, time: 3 h. b) Numbers of cyano groups in Ls-Ax-Hx.

TABLE 4. ELEMENTARY ANALYSIS OF Ls-Ax-Hx

Ls-Ax-Hx	Calcd[a] (Found) (%)						
	C	H	N	S	Cl	Na	O
Ls5.1Ax3.9Hx	48.88	7.10	19.11	1.31	2.78	0.28	20.52
1	(48.78)	(7.60)	(19.08)	(1.30)	(2.43)	(0.30)	(20.51[b])
Ls5.8Ax7.4Hx	46.55	6.88	18.42	1.26	4.17	0.36	22.36
2	(46.12)	(7.36)	(18.28)	(1.48)	(4.23)	(0.32)	(22.21[b])
Ls7.2Ax6.0Hx	45.90	6.87	17.57	1.24	4.52	0.27	23.59
3	(45.64)	(6.75)	(17.48)	(1.86)	(4.50)	(0.30)	(23.47[b])

Formula[c]

1 $Ls\{Ax\}_{5.1}\{Hx\}_{3.9}\{CN\}_{2.6}\{Am\}_{16.5}\{Ac\}_{0.9}H \cdot 1.3HCl \cdot 0.3NaCl$

2 $Ls\{Ax\}_{5.8}\{Hx\}_{7.4}\{CN\}_{1.9}\{Am\}_{12.7}\{Ac\}_{1.2}H \cdot 2.6HCl \cdot 0.4NaCl$

3 $Ls\{Ax\}_{7.2}\{Hx\}_{6.0}\{CN\}_{0.5}\{Am\}_{11.6}\{Ac\}_{3.7}H \cdot 3.0HCl \cdot 0.3NaCl$

a) Calculated values based on the **1**, **2**, and **3** formulas. b) 100−(C+H+N+S+Cl+Na). c) Ls: $C_{12}H_{25}S$-, Ax: $-CH_2CH(C{=}NOH)NH_2$, Hx: $-CH_2CH(C{=}O)NHOH$, CN: $-CH_2CH(CN)-$, Am: $-CH_2CH(CONH_2)-$, Ac: $-CH_2CH(COOH)-$.

foam from the Ls7.7AN21.3Am solution was the richest, so that Ls7.7AN21.3Am was used for the next reaction. The amidoxime group resulted from the reaction of the cyano group with hydroxylamine. However, the carbamoyl group also reacted with hydroxylamine to give the hydroxamic acid group.[15] The conditions and yields of the reaction are shown in Table 3. All the yields were above 85%. The hydroxylamine used was 4.2—16.7 times the cyano group in molality, but a few unit moles of cyano group still remained in Ls-Ax-Hx. The amidoxime and hydroxamic-acid groups were identified by absorption at 265 nm and at 280 nm in an aqueous solution(pH 14).[1] The chemical formulas were determined by the use of the found C, H, N, S, Cl, and Na values of elementary analysis. The chemical formulas and elementary analysis are listed in Table 4.

Determination of Uranium. The amount of uranium in the aqueous solution, sea water, scum, or froth was determined from the absorbance of the arsenazo III- uranium complex(660 nm). Five cm^3 of 60 % HNO_3 was added to 500 cm^3 of the sample solution. The solution was shaken with 20 cm^3 of chloroform to remove any dissolved organic compounds and then concentrated to about 200 cm^3. To scum and froth, 2 cm^3 of 97% H_2SO_4 and 3 cm^3 of 60% HNO_3 were added. The mixture was heated till it became colorless, and then it was dissolved in 200 cm^3 of a 1% HNO_3 solution. After these pretreatments, the uranium was determined according to the procedure of Motojima *et al.*[12] To improve the lower limit of uranium detection, the volume of arsenazo III–31% perchloric acid solution was reduced from 10 cm^3 [12] to 4 cm^3 of the measurable minimum volume in a 1-cm cell. The 8-quinolinol was precipitated when extracted with that solution. Then the precipitate was filtered off. This reduction made the absorbance highly sensitive. The absorbance per 1 μg of uranium varied from 0.028[12] to 0.069; it was proportional to the amount of uranium within the range from 0 to 6 μg. The amount of uranium in 500 cm^3 of sea water was proved to be 1.50 μg (3.0 ppb) by the standard addition method. The addition of surfactants interfered little with the determination of uranium, because the amount of uranium in 500 cm^3 of sea water was proved to be 1.48 μg even when 0.5 g of $R_{12}Ax$ was added. It was presumed that the dissociation of the uranium–$R_{12}Ax$ complex and the formation of the uranium–arsenazo III complex proceeded quantitatively in a 31% perchloric acid solution.

Ion Flotation for 10 ppb Uranium Solution. It is well known that the resins containing the hydroxamic acid group[16] or the amidoxime group[6-8] adsorb uranium effectively. For comparison, the flotation for a 10 ppb uranium solution was examined with the above-mentioned collectors containing such groups.

The floatable pH range was 4—8, and the optimum pH was 5.0, with the amidoxime-type surfactants. The effects of amidoxime-type surfactants on the floatability of uranium at pH 5.0 are indicated in Fig. 2. The

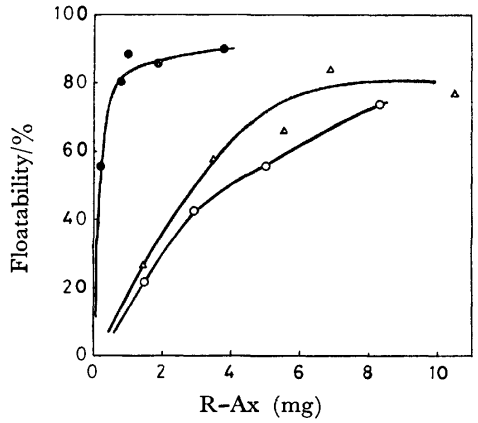

Fig. 2. Effects of R-Ax on the floatability of uranium. Uranium solution: 500 cm³; Concentration: 10 ppb; pH: 5.0. ○: $R_{12}Ax$, △: $R_{16}Ax$, ●: Ls8.6Ax+10 mg of nonionic surfactant.

highest floatability upon the addition of hydroxamic acid-type surfactants, R-edta, or SDS was as follows: 35%(pH 7.0) with 4.0 mg of R-Hx, 64%(pH 7.0) with both 2.1 mg of Lo10.3Hx and 10 mg of nonionic surfactant(Nissan nonion O-6), 51%(pH 7—8) with both 9.1 mg of R-edta and 10 mg of nonionic surfactant, and 21%(pH 7—8) with 20 mg of SDS.

It appears from these results and Fig. 2 that amidoxime-type surfactants were more effective than hydroxamic acid-type surfactants, R-edta, or SDS. The effect on flotation was $R_{12}Ax<R_{16}Ax<Ls8.6Ax$, as may be seen in Fig. 2, reversed to the solubility in water ($Ls8.6Ax<R_{16}Ax<R_{12}Ax$). Since $R_{12}Ax$ and $R_{16}Ax$ are floatable without any surfactant(Ls8.6Ax float with nonionic surfactant), it is considered that the amidoxime-uranium complexes are adsorbed or adhere to the excess of amidoxime-type surfactants and float with them. The HLB values of $R_{12}Ax$ and $R_{16}Ax$ calculated according to the Oda equation[17] were 5 and 4 respectively.

Ion Flotation for Uranium in Sea Water. The collectors used in uranium flotation are generally a combination of selective adsorbent and surfactant, or one of a selective complexing agent and the oppositely charged surfactant, *e.g.*, titanium dioxide and SDS, or arsenazo III and benzyldimethyltetradecylammonium chloride.[3,4] There has been no report on uranium flotation from sea water with a surfactant alone. Therefore, uranium flotation was investigated with amidoxime-type surfactants.

Flotation was carried out at the optimum pH of 5.0. The results are shown in Table 5. The floatability of uranium increased with the quantity of $R_{12}Ax$. In the case of $R_{16}Ax$ and Ls8.6Ax, known amounts of uranium(1, 2, and 3 μg) were further added to 500 cm³ of sea water. Although the amounts of the floatable uranium complexes increased, the floatability stayed approximately constant. The means of floatability were 44% with $R_{16}Ax$ and 47% with Ls8.6Ax, including the nonionic surfactant. Since the uranium complexes float, presumably because of the excess of the amidoxime-type surfactants, the floatability should increase with the increase in $R_{12}Ax$ and should not vary with the addition of uranium. The floatability coincided with the expectation, but the amount of uranium floated per gram of $R_{12}Ax$ decreased with the increase in $R_{12}Ax$, as may be seen in Table 5.

Flotation was carried out at the same pH as sea water(pH 8.0). The results are shown in Table 6. Amidoxime-type surfactants were also the most effective at pH 8.0, though the floatability at pH 8.0 was lower than at pH 5.0. Radioactive cobalt(^{60}Co) was also effectively floated at pH 5.0, as has been mentioned in a previous paper.[1] Because the isoelectric points

Table 5. Uranium flotation from sea water at pH 5.0

Conditions of flotation[a]			Uranium-floated	
Collector	(mg)	U added[b] (μg)	Floatability %	Amounts mg/g-collector
$R_{12}Ax$	0.3	—	32	1.60
$R_{12}Ax$	1.0	—	43	0.65
$R_{12}Ax$	2.5	—	41	0.25
$R_{12}Ax$	5.0	—	53	0.16
$R_{12}Ax$	10.0	—	69	0.10
$R_{12}Ax$	20.0	—	78	0.06
$R_{12}Ax$	30.0	—	90	0.05
$R_{16}Ax$	1.0	—	43	0.65
$R_{16}Ax$	1.0	1.0	46	1.15
$R_{16}Ax$	1.0	2.0	42	1.47
$R_{16}Ax$	1.0	3.0	45	2.03
Ls8.6Ax	0.3+N[c]	—	45	0.07
Ls8.6Ax	0.3+N[c]	1.0	50	0.12
Ls8.6Ax	0.3+N[c]	2.0	48	0.16
Ls8.6Ax	0.3+N[c]	3.0	45	0.20

a) 500 cm³ of sea water, pH adjusted to 5.0 with HNO_3. b) Uranium amount added to 500 cm³ of sea water. c) 10 mg of a nonionic surfactant. Note: Because of the trace amounts, the total amounts of uranium in sea water and scum were confirmed to be 1.50 μg after the flotation.

of amidoxime-type surfactants were presumed to be at pH 5.0, the differences between the floatability at pH 5.0 and that at pH 8.0 were considered to be due to the solubilities of amidoxime-type surfactants.

The residual amount of $R_{12}Ax$ and $R_{16}Ax$ in the sea water was then determined colorimetrically.[18] $R_{12}Ax$ and $R_{16}Ax$ were extracted with Orange II into chloroform at pH 1.0, and the absorbance of R–Ax–Orange II complexes in chloroform was measured at 485 nm. The residual amounts in sea water were 0.05 mg dm^{-3}(pH 5.0) and 0.06 mg dm^{-3}(pH 8.0) in $R_{12}Ax$, and less than 0.05 mg dm^{-3}(pH 5.0) and 0.05 mg dm^{-3} (pH 8.0) in $R_{16}Ax$.

Foam Fractionation of Uranium. Little of the used R-Ax remained in the sea water or the aqueous solution.[1] However, since the pH adjustment to 5.0 is unfavorable, the soluble amidoxime-type surfactant Ls–Ax–Hx was prepared and submitted to foam fractionation. The flotation effect for the 10-ppb uranium solution was observable in the range of pH 3.0—9.0. These floatability values were 52—56% with 40 mg of Ls7.2Ax6.0Hx. The floatability by Ls7.2Ax6.0Hx at pH 8.0 was 23% with 10 mg, 40% with 20 mg, and 56% with 40 mg.

The foam fractionation for uranium in sea water was also carried out(Fig. 3). Stable froth was formed by the addition of more than 30 mg of Ls7.2Ax6.0Hx, and the floatability of uranium was 67—70%. Even though sea water contains highly concentrated salts, the floatability was a little higher than that for the 10-ppb uranium solution. However, the effect varied with the content of the amidoxime group, and the floatability was about 30% with Ls5.1Ax3.9Hx. The floatability in foam fractionation is thought to be highly affected by the complexation and the bubbling ability. The largest amounts of uranium per gram of Ls7.2-Ax6.0Hx floated by foam fractionation were 106 μg/g for the 10-ppb uranium solution and 27 μg/g for sea water, lower than that by the ion flotation using R–Ax.

It is known that little collector for foam fractionation remains in an aqueous solution, since the foamy collector is adsorbed into the interface of the gas and the liquid and is almost completely removed as a froth.[19] The residual amount of Ls7.2Ax6.0Hx in sea water was determined at pH 8.0 by means of the less sensitive UV spectrum(235 nm), because Ls7.2Ax6.0-Hx could not be extracted with Orange II into chloroform. The sensitivity of this method was 0.5 mg/500 cm^3. The residual amount was below 0.5 mg/500 cm^3.

Foam fractionation can be expected to become more effective upon a modification of the apparatus or by a variation in the passing rate of air.[2]

Regeneration of Amidoxime-type Surfactants. The resulting scum or froth was dissociated to an amidoxime-type surfactant and a uranium solution by the addition of the acidic solution. Therefore, regeneration from the scum or froth was investigated after flotation. The hydrochloric acid solution(100 cm^3) prepared for pH prescription was added to the scum or froth and mixed for 5 min. $R_{12}Ax$ and $R_{16}Ax$ were extracted from the acidic solution with 15 cm^3 of chloroform, after which the chloroform was evaporated. Ls7.2Ax6.0Hx was floated as froth by foam fractionation from the acidic solution. The hydrophilic $R_{12}Ax$ in an acidic solution could be regenerated by both extraction and foam fractionation. However, the more hydrophilic Ls7.2-

TABLE 6. URANIUM FLOTATION FROM SEA WATER AT pH 8.0

Conditions of flotation[a]		Uranium-floated	
		Floatability	Amounts
Collector	(mg)	%	mg/g-collector
$R_{12}Ax$	1.0	13	0.20
$R_{12}Ax$	5.0	12	0.04
$R_{16}Ax$	1.0	27	0.41
Ls8.6Ax	0.3+N[b]	33	0.05
R-Hx	3.0+N[b]	5	0.01
Lo10.3Hx	3.2+N[b]	9	0.01
R-edta	1.3+N[b]	0	0
SDS	20.4	6	0.01

a) 500 cm^3 of sea water. b) 10 mg of a nonionic surfactant.

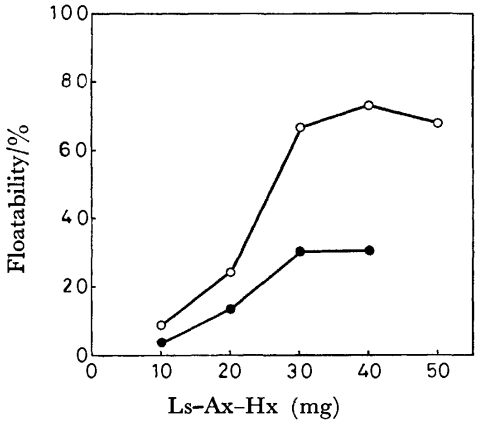

Fig. 3. Foam fractionation for uranium in 500 cm^3 of pH 8.0 sea water.
○: Ls7.2Ax6.0Hx, ●: Ls5.1Ax3.9Hx.

TABLE 7. REGENERATION OF AMIDOXIME-TYPE SURFACTANTS

Collector[a]	Regeneration[b]		Flotation[c]	
	Method	pH of aq soln	Method	Floatability %
$R_{12}Ax$	E	1.0	I	39(46)
$R_{12}Ax$	E	1.5	I	45(46)
$R_{12}Ax$	E	2.0	I	50(46)
$R_{16}Ax$	E	1.0	I	46(47)
$R_{12}Ax$	F	1.0	I	50(46)
Ls7.2Ax6.0Hx	F	1.0	F	68(70)
Ls7.2Ax6.0Hx	F	1.5	F	45(70)
Ls7.2Ax6.0Hx	F	2.0	F	44(70)

a) $R_{12}Ax$: 2 mg, $R_{16}Ax$: 2 mg, Ls7.2Ax6.0Hx: 40 mg. b) Regeneration of collector from resulting scum or froth. E: Extraction, F: foam fractionation. c) Ion flotation or foam fractionation for uranium in sea water by regenerated collectors. I: Ion flotation at pH 5.0, F: foam fractionation at pH 8.0. ( ): Floatability by original collectors.

Ax6.0Hx could not be extracted with chloroform. Furthermore, further flotation was carried out for other sea-water specimens using these regenerated amidoxime-type surfactants (Table 7). Uranium flotation with these surfactants was effective, even though a part of the surfactants might be lost because of adhering to the glass surface.

It is concluded from the above results that $R_{12}Ax$, $R_{16}Ax$, and Ls7.2Ax6.0Hx are excellent collectors for uranium flotation.

References

1) K. Yamada, Y. Koide, and A. Kagota, *Nippon Kagaku Kaishi*, **1981**, 1773.

2) R. Lemlich, "Adsorptive Bubble Separation Techniques," Academic Press, New York and London (1972); T. Sasaki, "Bunri To Seisei," in "Jikken Kagaku Koza," ed by the Chemical Society of Japan, Maruzen, Tokyo (1966), Ser. 2, Vol. 2, Sec. 15, pp. 565—603.

3) W. J. Williams and A. H. Gillam, *Analyst (London)*, **103**, 1239 (1978).

4) K. Sekine, *Mikrochim. Acta*, **1975**, 313.

5) A. Mizuike and M. Hiraide, *Hyomen*, **19**, 32 (1981).

6) C. A. Fetscher, U. S. Patents 3088798 (1963), 3088799 (1963); *Chem. Abstr.*, **59**, 4826d (1963), **59**, 3642e (1963).

7) H. Tani, H. Nakayama, and F. Sakamoto, Japan Kokai 134911 (1975); *Chem. Abstr.*, **84**, 93286v (1976).

8) H. Egawa, H. Harada, and T. Shuto, *Nippon Kagaku Kaishi*, **1980**, 1773.

9) "Amidoxime group," "hydroxamic acid group," "amide group," and "nitrile group" represent the structures of the N^2-hydroxyamidinoethylene group, the hydroxyaminocarbonylethylene group, the carbamoylethylene group, and the cyanoethylene group respectively. See Fig. 1 and Table 4 c).

10) K. Yamada, T. Kihara, H. Yamaguchi, and T. D. Chie, *Yukagaku*, **25**, 347 (1976).

11) Y. Koide, K. Izumi, K. Okuzono, and K. Yamada, *Nippon Kagaku Kaishi*, **1980**, 742.

12) K. Motojima, T. Yamamoto, and Y. Kato, *Bunseki Kagaku*, **18**, 208 (1969).

13) T. Tsuruta, "Kobunshi Gosei-kagaku," Nikkankogyo Shinbunsha, Tokyo (1976), p, 31.

14) K. Yamada, S. Ikeda, and H. Shosenji, *Yukagaku*, **28**, 605 (1979).

15) S. Soloway and A. Lipschitz, *Anal. Chem.*, **24**, 898 (1952).

16) W. Kern and R. C. Schulz, *Angew. Chem.*, **69**, 153 (1957).

17) R. Oda and K. Teramura, "Kaimen-kasseizai No Gosei To Sono-oyo," Makishoten, Tokyo (1962), p. 501.

18) K. Takahashi, Y. Nanba, M. Koike, and M. Kobayashi, "Kaimen-kasseizai," Kogakutosho, Tokyo (1978), p. 369.

19) T. Yoshida and T. Takeuchi, *Hyomen*, **8**, 65 (1970).

Studies on Thermodynamics for the Hydrolysis. II. The Temperature Effect on the Stereoselective Deacylation of Amino Acid Esters in Bilayer and Micellar Systems

Yōko Matsumoto and Ryuichi Ueoka*

Department of Industrial Chemistry, Kumamoto Institute of Technology, Ikeda, Kumamoto 860

(Received March 7, 1983)

Stereoselective deacylations of *p*-nitrophenyl *N*-acyl-D(or L)-phenylalaninates(D(or L)-S_n; n=2, 12, and 16) and *N*-benzyloxycarbonyl-D(L)-phenylalaninates(D(L)-ZS) by the bilayer and micellar catalytic systems of L-histidine derivatives (LauHis, MyrHis, PalHis, LauHisLeu, and MyrHisLeu) and surfactants ($2C_mN2C_1Br$ with m=12, 14, and 16, CTAB, OTAC, and (*R*)-(+)-SUR_{16}) were performed. It is noteworthy that the temperature dependence of enantioselectivity for the deacylation of S_{12} having a long acyl chain is bell-shaped with maxima at 25 °C and 15—25 °C in the bilayer systems of MyrHis+$2C_{12}N2C_1Br$ and MyrHisLeu+$2C_{12}N2C_1Br$, respectively. On the other hand, the enantioselectivity for the S_{12} deacylation catalyzed by LauHisLeu in the presence of the CTAB micelles increases as temperature is lowered (the highest enantiomer rate ratio ($k^L_{a,obsd}/k^D_{a,obsd}$=12) is attained at 20 °C). The enantioselectivity for the deacylation of S_2 having a short acyl chain, however, is almost constant and considerably lowered in comparison with that for the deacylation of S_{12} in both the bilayer and micellar systems. According to the isokinetic temperature (β), the deacylation of S_n (n=2 and 12) and ZS in the bilayer systems might be entropy-driven, whereas that in the micellar systems might be enthalpy-driven. The stronger hydrophobic microenvironment of the bilayer systems in the ester-deacylation would probably be connected with the entropy-driven nature.

The stereoselective deacylation of *N*-protected amino acid *p*-nitrophenyl esters has recently received considerable attention,[1] and a relatively high stereoselectivity was attaind in the deacylation of diastereomeric dipeptide[2] and of *N*-acylamino acid esters with the dipeptide-type L-histidine derivative in the presence of cationic surfactants[3] or in bilayer systems.[4] However, there has been no report on thermodynamic specificity for the enantioselectivity in the deacylation of amino acid esters.

This study deals with the temperature dependence of catalytic efficiency and enantioselectivity for the stereoselective deacylation of *p*-nitrophenyl *N*-acyl-D(or L)-phenylalaninates (D(or L)-S_n; n=2, 12, and 16) and *N*-benzyloxycarbonyl-D(L)-phenylalaninates (D(L)-ZS) by the bilayer and micellar catalytic systems of L-histidine derivatives (LauHis, MyrHis, PalHis, LauHisLeu, and MyrHisLeu) and surfactants ($2C_mN2C_1Br$ with m=12, 14, and 16, CTAB, OTAC, and (*R*)-(+)-SUR_{16}) and has been performed in an attempt to discuss on the hydrophobic microenvironment of aggregates on the basis of isokinetic temperature (β).[5]

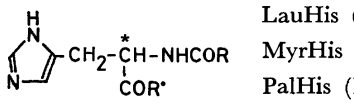

LauHis (R=$C_{11}H_{23}$, R′=OH)
MyrHis (R=$C_{13}H_{27}$, R′=OH)
PalHis (R=$C_{15}H_{31}$, R′=OH)

LauHisLeu (R=$C_{11}H_{23}$, R′=NH*CH(COOH)$CH_2CH(CH_3)_2$)
MyrHisLeu (R=$C_{13}H_{27}$, R′=NH*CH(COOH)$CH_2CH(CH_3)_2$)

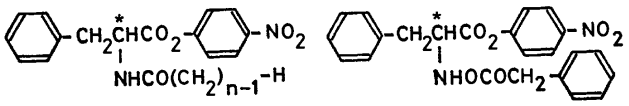

D(L)-S_n (n=2, 12, 16) D(L)-ZS

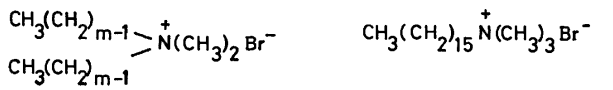

$2C_mN2C_1Br$ (m=12, 14, 16) CTAB

OTAC (*R*)-(+)-SUR_{16}

Experimental

Materials. *p*-Nitrophenyl *N*-acyl-D(L)-phenylalaninates (D(L)-S_n; n=2, 12, and 16) were prepared by the previous method.[6,7]

p-Nitrophenyl *N*-Cbz-D(L)-phenylalaninates (D(L)-ZS) were prepared from *N*-benzyloxycarbonyl-D(L)-phenylalanine by the esterification of the CO_2H group with *p*-nitrophenol and dicyclohexylcarbodiimide in a way similar to the previous method.[8] Satisfactory results of elemental analysis were obtained for D(L)-ZS. D-ZS: mp 121.5—123.5 °C (lit,[8] mp 126—126.5 °C). Found: C, 65.88; H, 4.70; N, 6.67%. Calcd for $C_{23}H_{20}N_2O_6$: C, 65.70; H, 4.78; N, 6.66%. L-ZS: mp 119—120 °C (lit,[8] mp 126—126.5 °C). Found: C, 65.65; H, 4.73; N, 6.59%. Calcd for $C_{23}H_{20}N_2O_6$: C, 65.70; H, 4.78; N, 6.66%.

N-Dodecanoyl-L-histidine (LauHis), *N*-tetradecanoyl-L-histidine (MyrHis), and *N*-hexadecanoyl-L-histidine (PalHis) were prepared by reaction of L-histidine and the corresponding acid chlorides.[9] Satisfactory results of elemental analysis were obtained for LauHis,[7] MyrHis, and PalHis.[7] MyrHis: dp 196 °C (lit,[9] dp 192 °C). Found: C, 65.87; H, 9.61; N, 11.30%. Calcd for $C_{20}H_{35}N_3O_3$: C, 65.75; H, 9.59; N, 11.51%.

N-Dodecanoyl-L-histidyl-L-leucine (LauHisLeu) and *N*-tetradecanoyl-L-histidyl-L-leucine (MyrHisLeu) were prepared by reaction of L-histidyl-L-leucine with anhydrous dodecanoic acid and tetradecanoyl chloride, respectively. Satisfactory results of elemental analysis were obtained for LauHisLeu and MyrHisLeu. LauHisLeu: mp 194—196 °C. Found: C, 63.81; H, 9.17; N, 12.33%. Calcd for $C_{24}H_{42}N_4O_4$: C, 63.97; H, 9.39; N, 12.43%. MyrHisLeu: mp 212—214 °C. Found: C, 65.03; H, 9.63; N, 11.19%. Calcd for $C_{26}H_{46}N_4O_4$: C, 65.24; H, 9.69; N, 11.71%.

Didodecyldimethylammonium bromide ($2C_{12}N2C_1Br$), ditetradecyldimethylammonium bromide ($2C_{14}N2C_1Br$), and

dihexadecyldimethylammonium bromide ($2C_{16}N2C_1Br$) were prepared by reaction of *N,N*-dimethylalkylamine and the corresponding alkyl bromides in refluxing ethanol in the presence of sodium carbonate, and purified by repeated recrystallizations from ethyl acetate according to the previous method.[10] Satisfactory results of elemental analysis were obtained for $2C_{12}N2C_1Br$, $2C_{14}N2C_1Br$, and $2C_{16}N2C_1Br$. $2C_{12}N2C_1Br$: Found: C, 67.77; H, 12.20; N, 2.98%. Calcd for $C_{26}H_{56}NBr$: C, 67.50; H, 12.20; N, 3.03%. $2C_{14}N2C_1Br$: Found: C, 69.18; H, 12.52; N, 2.68%. Calcd for $C_{30}H_{64}NBr$: C, 69.44; H, 12.46; N, 2.70%. $2C_{16}N2C_1Br$: Found: C, 70.46; H, 12.49; N, 2.52%. Calcd for $C_{34}H_{72}NBr$: C, 71.02; H, 12.65; N, 2.44%.

Commercially available hexadecyltrimethylammonium bromide (CTAB) and octadecyltrimethylammonium chloride (OTAC) were recrystallized from an anhydrous ethanol–ether mixture.

(+) - Hexadecyldimethyl[(*R*) - α - methylbenzyl]ammonium bromide ((*R*)-(+)-SUR_{16}) was prepared by reaction of (*R*)-(+)-*N,N,*α-trimethylbenzylamine and hexadecyl bromide in accordance with the previous method.[11] Satisfactory results of elemental analysis were obtained.[7]

Determination of Rate Constants. Rates of *p*-nitrophenol liberation from *p*-nitrophenyl esters were measured at 400 nm with a Shimadzu UV-200 spectrophotometer. Each run was usually initiated by adding an acetonitrile solution (0.1 ml) of a substrate ester to a reaction medium of tris(hydroxymethyl)methanamine (Tris) buffer (3.4 ml) containing both nucleophile and surfactant. The reaction obeyed the usual pseudo-first-order rate law, and the apparent second-order rate constant ($k_{a,obsd}$) for the deacylation of ester substrate was evaluated by the following equation on the basis of triplicate runs:

$$k_{a,obsd} = (k_t - k_s)/[\text{nucleophile}]_0, \quad (1)$$

where k_t and k_s refer to the observed first-order rate constant for the deacylation of S_n with and without a nucleophile, respectively, and $[\text{nucleophile}]_0$ denotes the initial nucleophile concentration.

In the case of the bilayer catalytic systems, clear stock solutions were prepared by dissolving the nucleophile and the surfactant in Tris–KCl buffer by sonication (Bransonic 12, Yamato Scientific Co.) at 50 °C for 1 h, and used for kinetic measurements.

Results and Discussion

Since the reaction rate of D(L)-S_n (1×10^{-5} M; 1 M=1 mol dm^{-3}) deacylation with PalHis (5×10^{-5} M) attains a maximum in the presence of *ca.* 1×10^{-3} M (critical micelle concentration (cmc) $=5\times10^{-5}$ M)[12] $2C_{12}N2C_1Br$,[4b] the relative activity of nucleophiles will be discussed with the stereoselective deacylation of D-(L)-S_n (n=2 and 12) and D(L)-ZS with the above concentration of the nucleophiles (PalHis, MyrHis, and MyrHisLeu) and the bilayer surfactants ($2C_mN2C_1Br$; m=12, 14, and 16). On the other hand, the concentrations of the micellar surfactants (CTAB, OTAC, and (*R*)-(+)-SUR_{16}) were set above their cmc's.

Catalytic Efficiency. It is obvious that the hydrophobicity of nucleophiles and substrates play an important role in enhancing the catalytic efficiency and stereoselectivity for the deacylation of amino acid esters in micellar[1d] and bilayer[4d] systems. Thus, in this study, we have employed the reactants having a hydrophobic segment.

Rate constants ($k_{a,obsd}$) as a function of temperature for the deacylation of D(L)-S_n (n=2 and 12) and D(L)-ZS catalyzed by the bilayer catalytic systems of MyrHis+$2C_{12}N2C_1Br$ and MyrHisLeu+$2C_{12}N2C_1Br$

Table 1. Temperature dependence of rate constant ($k_{a,obsd}$/M^{-1} s^{-1}) for the deacylation of S_n catalyzed by MyrHis and MyrHisLeu in the presence of $2C_{12}N2C_1Br$[a,b]

Substrate	10 °C	15 °C	20 °C	25 °C	30 °C	35 °C
L-S_2	100 (39)	140 (61)	150 (82)	340 (—)	—(140)	380 (200)
D-S_2	41 (31)	48 (43)	60 (59)	130 (—)	— (72)	140 (100)
L-S_{12}	390(270)	570(420)	810(590)	1500(670)	1900 (—)	2500(1200)
D-S_{12}	88 (71)	160 (80)	250(110)	380(130)	620 (—)	800 (430)
L-ZS	330(120)	490(180)	650(250)	970(300)	1300(470)	1400 (700)
D-ZS	87 (46)	140 (70)	220(100)	370(130)	500(200)	620 (310)

a) pH 7.6, 3%(v/v) CH_3CN-H_2O, 0.083 M Tris buffer (0.083 M KCl), [MyrHis]$=5\times10^{-5}$ M, [MyrHisLeu]$=3\times10^{-5}$ M, [Sub]$=1\times10^{-5}$ M, and [$2C_{12}N2C_1Br$]$=1\times10^{-3}$ M. b) Values in the parentheses are those for the deacylation of S_n catalyzed by MyrHisLeu in the presence of $2C_{12}N2C_1Br$.

Table 2. Temperature dependence of rate constant ($k_{a,obsd}$/M^{-1} s^{-1}) and enantioselectivity ($k^L_{a,obsd}/k^D_{a,obsd}$) for the deacylation of S_n catalyzed by LauHis and LauHisLeu in the presence of CTAB[a,b]

	20 °C	25 °C	30 °C	35 °C	40 °C
L-S_2	100 (15)	130 (26)	220 (52)	340(120)	500(150)
D-S_2	56 (15)	78 (26)	120 (47)	200(110)	300(120)
L-S_2/D-S_2[c]	1.8(1.0)	1.7(1.0)	1.8(1.1)	1.7(1.1)	1.7(1.3)
L-S_{12}	470(140)	530(210)	770(300)	1000(400)	1200(580)
D-S_{12}	120 (12)	150 (21)	180 (36)	280 (71)	300(150)
L-S_{12}/D-S_{12}[c]	3.9 (12)	3.5 (10)	4.3(8.3)	3.6(5.6)	4.0(3.9)

a) pH 7.6, 3%(v/v) CH_3CN-H_2O, 0.083 M Tris buffer (0.083 M KCl), [LauHis]=[LauHisLeu]$=5\times10^{-5}$ M, [Sub]$=1\times10^{-5}$ M, and [CTAB]$=3\times10^{-3}$ M. b) Values in the parentheses are those for the deacylation of S_n catalyzed by LauHisLeu in the presence of CTAB. c) These values include the experimental error within ±6%.

are summarized in Table 1. The magnitude of rate enhancement increases in the orders L-S_{12}>L-ZS≫L-S_2 and D-S_{12}≳D-ZS≫D-S_2 in the deacylation of L- and D-enantiomers, respectively, over the temperature range of 10—35 °C in both the bilayer systems. These orders agree fairly well with the hydrophobicity of substrates. The catalytic efficiency of MyrHis is superior to that of MyrHisLeu. The difference in catalytic efficiency between MyrHis and MyrHisLeu would be attributable to the framework of both nucleophiles. Namely, it is deduced that the bulky leucine part in MyrHisLeu might reduce the catalytic efficiency due to the steric hindrance against the substrate-incorporation by the mixed bilayer membrane.

Table 2 shows the temperature dependence of $k_{a,obsd}$ for the deacylation of D(L)-S_n (n=2 and 12) catalyzed by LauHis and LauHisLeu in the CTAB micellar systems. The $k_{a,obsd}$ values increase linearly as temperature is raised for the deacylation of all the substrates and were used for calculating activation parameters. Nucleophile LauHis is superior in catalytic efficiency to the dipeptide-type nucleophile (LauHisLeu). The difference in catalytic efficiency between LauHis and LauHisLeu in the micellar system is similar to that between MyrHis and MyrHisLeu in the bilayer system. It is suggested that the steric hindrance of the leucine part in the nucleophile cannot be neglected with respect to the substrate-incorporation into the micellar matrix. The hydrophobicity of the substrate is almost reflected in the order of its reactivity. Especially, substrate L-S_{12} having a long acyl chain is fairly superior to L-S_2 having a short acyl chain as shown in Table 2. These results for both the bilayer and micellar systems imply that the hydrophobic interaction between substrate and nucleophile and the easiness of substrate-incorporation into the aggregates are of great importance to the enhancement of catalytic efficiency.

It is known that the extent of incorporation of a substrate into a micellar phase agrees reasonably well with its binding properties.[13] The binding constants of the long-chain substrates are fairly larger than those of the short-chain substrates in both the bilayer and micellar systems.[4b] This result suggests that the hydrophobic interaction between the former and the aggregates might be stronger than that between the latter and the aggregates and is reflected in the larger rate enhancement for the deacylation of the long-chain substrates (L-S_{12} and D-S_{12}) than that of the short-chain ones (L-S_2 and D-S_2) in almost all the catalytic systems in the present study as shown in Tables 1 and 2.

Stereoselectivity. Enantioselective parameters ($k^L_{a,obsd}/k^D_{a,obsd}$) as a function of temperature for the deacylations of S_n (n=2 and 12) and ZS in the bilayer systems of MyrHis+$2C_{12}N2C_1Br$ and MyrHisLeu+$2C_{12}N2C_1Br$ are shown in Figs. 1 and 2, respectively.

As Fig. 1 indicates, the temperature dependence of enantioselectivity for the deacylation of S_n (n=2 and 12) and ZS with MyrHis and $2C_{12}N2C_1Br$ is divided into the following three trends over the temperature range of 10—35 °C: (a) the enantioselectivity in the deacylation of S_{12} having a long acyl chain tends to decrease as temperature is raised with a maximum

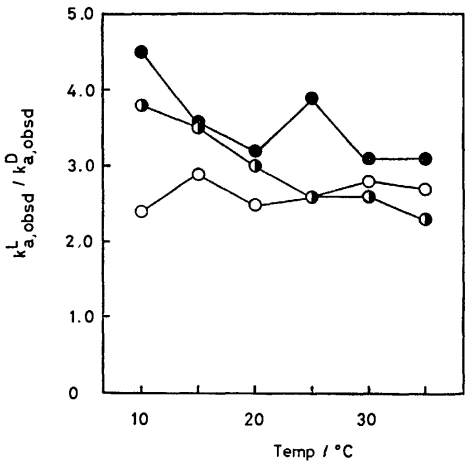

Fig. 1. Temperature dependence of enantioselectivity in the deacylation of S_n catalyzed by MyrHis with $2C_{12}N2C_1Br$.
pH 7.6, 3%(v/v) CH_3CN-H_2O, 0.083 M Tris-KCl buffer, [MyrHis]=5×10^{-5} M, [Sub]=1×10^{-5} M, [$2C_{12}N2C_1Br$]=1×10^{-3} M. ○: S_2, ●: S_{12}, ◑: ZS. The $k^L_{a,obsd}/k^D_{a,obsd}$ values include the experimental error within ±4%.

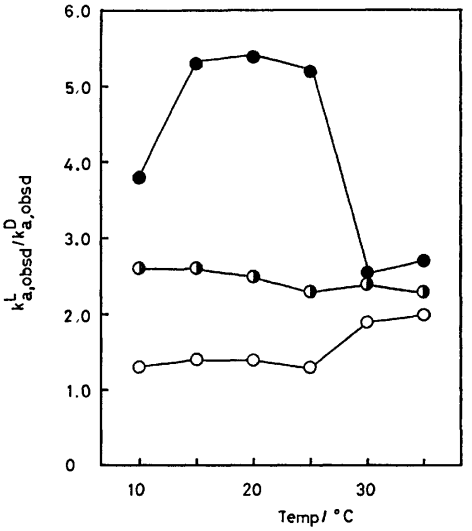

Fig. 2. Temperature dependence of enantioselectivity in the deacylation of S_n catalyzed by MyrHisLeu with $2C_{12}N2C_1Br$.
pH 7.6, 3%(v/v) CH_3CN-H_2O, 0.083 M Tris-KCl buffer, [MyrHisLeu]=3×10^{-5} M, [Sub]=1×10^{-5} M, [$2C_{12}N2C_1Br$]=1×10^{-3} M. ○: S_2, ●: S_{12}, ◑: ZS. The $k^L_{a,obsd}/k^D_{a,obsd}$ values include the experimental error within ±6%.

($k^L_{a,obsd}/k^D_{a,obsd}$=3.9) at 25 °C; (b) the $k^L_{a,obsd}/k^D_{a,obsd}$ value in the deacylation of ZS having a bulky side part decreases with rise in temperature; (c) the enantioselectivity in the deacylation of S_2 having a short acyl chain is almost constant ($k^L_{a,obsd}/k^D_{a,obsd}$=2.3—2.9) over the experimental temperature range. The difference in the temperature dependence of enantioselectivity among the deacylation of the three substrates (S_{12}, ZS, and S_2) would be attributed to the difference in the substrate-framework.

On the other hand, the temperature dependence for

the deacylation of S_n and ZS in the system of MyrHis-Leu+$2C_{12}N2C_1Br$ is different from that in the system of MyrHis+$2C_{12}N2C_1Br$ as shown in Fig. 2. It is especially worthy to note that the temperature dependence of enantioselectivity for the S_{12} deacylation is bell-shaped with a maximum ($k^L_{a,obsd}/k^D_{a,obsd}$=5.2—5.4) at 15—25 °C. The $k^L_{a,obsd}/k^D_{a,obsd}$ value for the deacylation of ZS is almost constant (2.3—2.6) over the whole temperature range examined, whereas that for the deacylation of S_2 is constant (1.3—1.4) in the temperature range of 10—25 °C and increases (1.9—2.0) at temperatures above 30 °C. Interestingly, the enantioselectivity for the deacylation of all the substrates (S_2, S_{12}, and ZS) employed converges at 30—35 °C.

These results for the bilayer and micellar systems suggest that the hydrophobic microenvironment would be changed delicately with temperature in the range of 10—35 °C and that the long-chain substrate (S_{12}) might be influenced by the change in microenvironment. At any rate, it is unique that the bilayer membrane system including the dipeptide-type nucleophile (MyrHisLeu+$2C_{12}N2C_1Br$) has displayed the high enantioselectivity in an adequate temperature range (15—25 °C) probably through a favorable hydrophobic interaction between the nucleophile (MyrHisLeu) and the substrate (D(L)-S_{12}). And, it is obvious that the leucine part of MyrHisLeu plays an important role in producing the high stereoselectivity.

Figure 3 and Table 2 show the temperature dependence of enantioselectivity for the deacylation of S_n (n=2, 12, and 16) in the micellar systems of PalHis+OTAC, LauHis+CTAB, and LauHisLeu+CTAB. Two interesting results were obtained: firstly, the temperature dependence of enantioselectivity for the S_{16} deacylation catalyzed by PalHis+OTAC is clearly bell-shaped with a maximum ($k^L_{a,obsd}/k^D_{a,obsd}$=3.6) at 30 °C and, secondly, the enantioselectivity for the S_{12} deacylation catalyzed by LauHisLeu+CTAB increases sharply as temperature is lowered. It is notable that the highest enantiomer rate ratio ($k^L_{a,obsd}/k^D_{a,obsd}$=12) is attained at 20 °C for the S_{12} deacylation in the micellar system of LauHisLeu+CTAB. This implies that the peculiar environments of the hydrophobic dipeptide (LauHisLeu) and the CTAB micelles, which are effective for the highly enantioselective deacylation of the hydrophobic substrate (S_{12}) at the lower temperature (20 °C), would be varied delicately as temperature is raised. The leucine part of LauHisLeu in the micellar system (CTAB) might play an important role in enhancing the enantioselectivity in common with that in the bilayer system (MyrHis-Leu+$2C_{12}N2C_1Br$). On the other hand, in the micellar systems of PalHis+OTAC and LauHis+CTAB, the stereoselectivity for the deacylation of S_n (n=2 and 12) remains almost constant over the temperature range of 20—35 (40) °C, though the magnitude of enantioselectivity for the long-chain substrate (S_{12}) is fairly larger than that for the short-chain substrate (S_2).

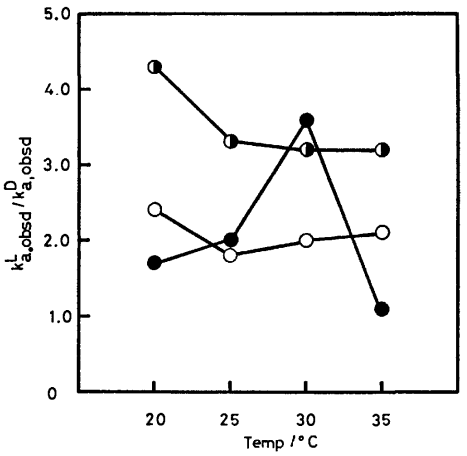

Fig. 3. Temperature dependence of enantioselectivity in the deacylation of S_n catalyzed by PalHis with OTAC.
pH 7.6, 3%(v/v) CH_3CN-H_2O, 0.083 M Tris-KCl buffer, [PalHis]=4×10^{-5} M, [S_n]=1×10^{-5} M, [OTAC]=8×10^{-4} M. ○: S_2, ◑: S_{12}, ●: S_{16}.
The $k^L_{a,obsd}/k^D_{a,obsd}$ values include the experimental error within ±3%.

Isokinetic Relationship. The isokinetic relationship appears to hold for the deacylation of D(L)-S_n (n=2 and 12) and D(L)-ZS in the bilayer and micellar systems from the relation between the entropy and enthalpy of activation on the basis of rate constant ($k_{a,obsd}$). The activation parameters (ΔG^*, ΔH^*, and ΔS^*) were evaluated by

$$\Delta G^* = 2.303RT \log (kT/hk_{a,obsd}) = \Delta H^* - T\Delta S^*, \quad (2)$$

where k and h stand for the Boltzmann and Planck constants, respectively. The linear relationship between the free energy of activation (ΔG^*) and the absolute temperature (T) is shown in Figs. 4 and 5. The ΔH^* and ΔS^* values obtained for the bilayer and micellar systems are summarized in Tables 3 and 4, respectively. Furthermore, the isokinetic temperatures (β) have been determined by plotting ΔH^* against ΔS^* according to Eq. (3)[5] and are summarized in Tables 3 and 4.

$$\Delta H^* = \Delta H^*_0 + \beta\Delta S^*, \quad (3)$$

where ΔH^*_0 is simply the intercept of ΔH^* correspond-

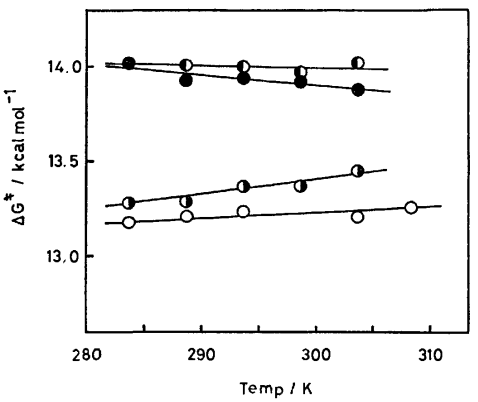

Fig. 4. Linear correlations between ΔG^* and absolute temperature (T) in the deacylation of S_n catalyzed by MyrHis with $2C_{12}N2C_1Br$.
pH 7.6, 3%(v/v) CH_3CN-H_2O, 0.083 M Tris-KCl buffer, [MyrHis]=5×10^{-5} M, [Sub]=1×10^{-5} M, [$2C_{12}N2C_1Br$]=1×10^{-3} M. ○: L-S_{12}, ●: D-S_{12}, ◑: L-ZS, ◐: D-ZS.

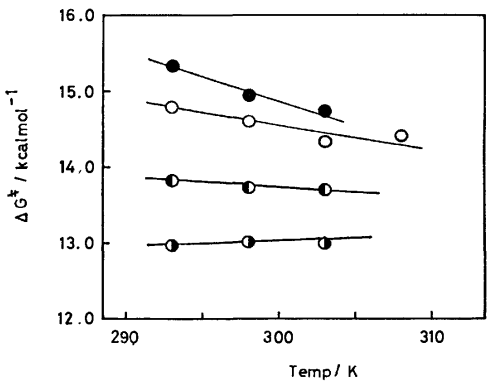

Fig. 5. Linear correlations between ΔG^* and absolute temperature (T) in the deacylation of S_n catalyzed by PalHis with OTAC.
pH 7.6, 3%(v/v) CH_3CN-H_2O, 0.083 M Tris-KCl buffer, [PalHis]$=4\times10^{-5}$ M, [S_n]$=1\times10^{-5}$ M, [OTAC]$=8\times10^{-4}$ M. ○: L-S_2, ●: D-S_2, ◑: L-S_{12}, ◐: D-S_{12}.

ing to ΔS^*.

It is known that hydrophobic interactions are mainly entropy driven, whereas lyophobic ones are mainly enthalpy driven.[14,15] On the other hand, it has been found that the β value based on apparent second-order rate constants ($k_{a,obsd}$) agrees fairly well with that based on k_m values for the simplified reaction ($M+S_n \overset{K_b}{\rightleftharpoons} MS_n \xrightarrow{k_m} P$; M, MS_n, and P stand for an aggregate composed of nucleophile and surfactant, an aggregate-substrate complex, and *p*-nitrophenol, respectively) in the deacylation of S_n (n=2, 12, and 16) with PalHis incorporated into OTAC micelles.[16] Then, we intend to discuss on the hydrophobic microenvironment for the stereoselective deacylation in the bilayer and micellar systems in terms of the β value obtained from the $k_{a,obsd}$ values in harmony with the k_m ones.

On the basis of the β value in connection with $\overline{T}$ (the average experimental temperature), the deacylation reaction in the bilayer systems may be governed by the entropy of activation in the temperature range of 10—40 °C, that is, $\overline{T}$ (296—306 K) exceeds β (245—269 K) in the bilayer systems of PalHis+$2C_{12}N2C_1Br$, MyrHis+$2C_{12}N2C_1Br$, MyrHisLeu+$2C_{12}N2C_1Br$, and PalHis+$2C_{14}N2C_1Br$, though β (302 K) is nearly equal to $\overline{T}$ (306 K) in the system of PalHis+$2C_{16}N2C_1Br$. This difference in β value between the systems of $2C_mN2C_1Br$ (m=12 and 14) and the $2C_{16}N2C_1Br$ system would be attributed to the difference in the state of bilayer phase. Namely, the bilayer systems of $2C_{12}N2C_1Br$ and $2C_{14}N2C_1Br$ and the system of $2C_{16}N2C_1Br$ are considered to be liquid crystals and a mixed state of liquid crystal and crystal over the experimental temperature range (see Table 3), respectively, in view of the phase transition temperature ($2C_{12}N2C_1Br$, 8 °C; $2C_{14}N2C_1Br$, 18 °C; $2C_{16}N2C_1Br$, 27 °C).[17] On the other hand, interestingly, the deacylation in the micellar systems may be governed by the enthalpy of activation in the temperature range of 20—40 (35) °C, that is, β (313—330 K) exceeds $\overline{T}$ (301—303 K) in the micellar systems of LauHis+

Table 3. Activation parameters (ΔH^* and ΔS^*) and isokinetic temperature (β) for the deacylation of S_n in the bilayer systems at pH 7.6[a,b]

Nucleophilic system	Substrate	ΔH^* / kcal mol^{-1} [d]	ΔS^* / cal K^{-1} mol^{-1}	β / K	$\overline{T}$[c] / K
PalHis+$2C_{12}N2C_1Br$	L-S_2	10.9	−10.6	267	306 (25—40 °C)
	D-S_2	9.2	−17.0		
	L-S_{12}	8.5	−15.6		
	D-S_{12}	9.6	−13.9		
MyrHis+$2C_{12}N2C_1Br$	L-S_2	10.4	−12.4	269	296 (10—35 °C)
	D-S_2	9.8	−16.8		
	L-S_{12}	12.6	−2.2		
	D-S_{12}	16.1	7.4		
	L-ZS	10.9	−8.4		
	D-ZS	14.4	1.4		
MyrHisLeu+$2C_{12}N2C_1Br$	L-S_2	10.3	−14.7	252	296 (10—35 °C)
	D-S_2	10.1	−16.0		
	L-S_{12}	11.8	−5.4		
	D-S_{12}	6.7	−26.2		
	L-ZS	10.9	−10.5		
	D-ZS	11.6	−9.7		
PalHis+$2C_{14}N2C_1Br$	L-S_2	7.4	−21.7	245	301 (20—35 °C)
	D-S_2	6.7	−25.0		
	L-S_{12}	8.3	−15.0		
	D-S_{12}	9.1	15.1		
PalHis+$2C_{16}N2C_1Br$	L-S_2	25.4	36.9	302	306 (25—40 °C)
	D-S_2	7.4	−22.9		
	L-S_{12}	19.3	21.0		
	D-S_{12}	14.6	3.0		

a) 3% (v/v) CH_3CN-H_2O, 0.083 M Tris buffer (0.083 M KCl), [PalHis]=[MyrHis]$=5\times10^{-5}$ M, [MyrHisLeu]$=3\times10^{-5}$ M, [Sub]$=1\times10^{-5}$ M, and [$2C_mN2C_1Br$]$=1\times10^{-3}$ M. b) Values in the parentheses are the temperature range. c) Average value of experimental temperatures. d) 1 cal=4.184 J.

Table 4. Activation parameters ($\Delta H^{\ddagger}$ and $\Delta S^{\ddagger}$) and isokinetic temperature (β) for the deacylation of S_n in the micellar systems at pH 7.6[a,b]

Nucleophilic system	Substrate	$\Delta H^{\ddagger}$ / kcal mol^{-1}	$\Delta S^{\ddagger}$ / cal K^{-1} mol^{-1}	β / K	$\overline{T}$[c] / K
LauHis+CTAB	L-S_2	14.4	−0.4	319	303 (20—40 °C)
	D-S_2	11.3	−11.7		
	L-S_{12}	7.2	−21.8		
	D-S_{12}	7.6	−23.2		
PalHis+(*R*)-(+)-SUR_{16}	L-S_2	9.9	−13.5	313	303 (20—40 °C)
	D-S_2	10.1	−13.8		
	L-S_{12}	8.2	−16.1		
	D-S_{12}	12.1	−5.1		
PalHis[d]+OTAC	L-S_2	23.3	29.0	330	301 (20—35 °C)
	D-S_2	32.6	59.0		
	L-S_{12}	9.9	−10.1		
	D-S_{12}	17.3	12.0		

a) 3%(v/v) CH_3CN-H_2O, 0.083 M Tris buffer (0.083 M KCl), [LauHis]=[PalHis]=5×10^{-5} M, [CTAB]=3×10^{-3} M, [(*R*)-(+)-SUR_{16}]=1×10^{-3} M, and [S_n]=1×10^{-5} M. b) Values in the parentheses are the temperature range. c) Average value of experimental temperature. d) [PalHis]=4×10^{-5} M, [OTAC]=8×10^{-4} M.

CTAB, PalHis+(*R*)-(+)-SUR_{16}, and PalHis+OTAC.

The difference in the driving parameter of activation ($\Delta S^{\ddagger}$ or $\Delta H^{\ddagger}$) for the deacylation reaction between the liquid-crystalline bilayer systems and the micellar ones would be attributable to the difference in the hydrophobic microenvironment of the aggregates. After all, it is concluded that the stereoselective deacylation in the liquid-crystalline bilayer systems would proceed through a stronger hydrophobic interaction between the reactants. So far, however, we have not found the relation between the β value and the catalytic efficiency and enantioselectivity.

We wish to thank Messrs. Akihiro Nakamura, Keizo Okada, and Toshihiro Kikuno for their technical assistance.

References

1) a) J. M. Brown and C. A. Bunton, *J. Chem. Soc., Chem. Commun.*, **1974**, 969; b) Y. Ihara, *ibid.*, **1978**, 984; c) K. Yamada, H. Shosenji, and H. Ihara, *Chem. Lett.*, **1979**, 491; d) R. Ueoka, T. Terao, and K. Ohkubo, *Nippon Kagaku Kaishi*, **1980**, 462.

2) a) R. A. Moss, Y.-S. Lee, and T. J. Lukas, *J. Am. Chem. Soc.*, **101**, 2499 (1979); b) R. A. Moss, Y.-S. Lee, and K. W. Alwis, *ibid.*, **102**, 6646 (1980).

3) a) K. Ohkubo, K. Sugahara, K. Yoshinaga, and R. Ueoka, *J. Chem. Soc., Chem. Commun.*, **1980**, 637; b) Y. Ihara, N. Kunikiyo, T. Kunimasa, M. Nango, and N. Kuroki, *Chem. Lett.*, **1981**, 667.

4) a) Y. Murakami, A. Nakano, A. Yoshimatsu, and K. Fukuya, *J. Am. Chem. Soc.*, **103**, 728 (1981); b) R. Ueoka, Y. Matsumoto, Y. Ninomiya, Y. Nakagawa, K. Inoue, and K. Ohkubo, *Chem. Lett.*, **1981**, 785; c) K. Ohkubo, N. Matsumoto, and H. Ohta, *J. Chem. Soc., Chem. Commun.*, **1982**, 738.

5) J. E. Leffler, *J. Org. Chem.*, **20**, 1202 (1955).

6) D. W. Ingles and J. R. Knowles, *Biochem. J.*, **104**, 369 (1976).

7) K. Ohkubo, K. Sugahara, H. Ohta, K. Tokuda, and R. Ueoka, *Bull. Chem. Soc. Jpn.*, **54**, 576 (1981).

8) M. Bodanszky and V. du Vigneaud, *J. Am. Chem. Soc.*, **81**, 6072 (1959).

9) C. Gitler and A. Ochoa-Solano, *J. Am. Chem. Soc.*, **90**, 5004 (1968).

10) Y. Okahata, R. Ando, and T. Kunitake, *Bull. Chem. Soc. Jpn.*, **52**, 3647 (1979).

11) R. A. Moss and W. L. Sunshine, *J. Org. Chem.*, **39**, 1083 (1974).

12) A. W. Ralston, D. N. Eggenberger, and P. L. DuBrow, *J. Am. Chem. Soc.*, **70**, 977 (1948).

13) C. A. Bunton and L. Robinson, *J. Am. Chem. Soc.*, **90**, 5972 (1968); *J. Org. Chem.*, **34**, 773 (1969).

14) G. Nemethy, *Angew. Chem., Int. Ed. Engl.*, **6**, 195 (1967); *Ann. N. Y. Acad. Sci.*, **155**, 492 (1969).

15) C. G. Overberger, R. C. Glowaky, and P.-H. Vandewyer, *J. Am. Chem. Soc.*, **95**, 6008 (1973).

16) R. Ueoka and Y. Murakami, *J. Chem. Soc., Perkin Trans. 2*, **1983**, 219.

17) The phase transition temperature values were estimated by the conductivity method and are in good agreement with those obtained with a differential scanning calorimeter described in Y. Okahata, S. Tanamachi, and T. Kunitake, *Nippon Kagaku Kaishi*, **1980**, 442.

Band-structure Parameters of Organic Conductors, $TSeT_2Cl$, TTT_2I_3, and $TSeT_2SCN$

Takehiko Mori,* Akiko Kobayashi, Yukiyoshi Sasaki, and Hayao Kobayashi†

Department of Chemistry, Faculty of Science, The University of Tokyo, Hongo, Bunkyo-ku, Tokyo 113

†*Department of Chemistry, Faculty of Science, Toho University, Funabashi, Chiba 274*

(Received March 24, 1983)

The band-structure parameters of organic conductors, $TSeT_2Cl$, TTT_2I_3, and $TSeT_2SCN$ (TSeT; 5,6:11,12-bis(diseleno)naphthacene; common name: tetraselenotetracene, and TTT; 5,6:11,12-bis(dithio)naphthacene; common name: tetrathiotetracene) were calculated using semiempirical molecular-orbital calculations. The longitudinal bandwidth W and the anisotropy parameter α of $TSeT_2Cl$ were obtained as 0.6 eV and 0.188 respectively. The shape of the Fermi surface, as calculated from the tight-binding theory and the large anisotropy parameter, agrees with its semimetallic nature at low temperatures. In TTT_2I_3, $W=0.56$ eV, and $\alpha=0.018$. This compound was regarded as a one-dimensional metal. The semiconductive conduction of $TSeT_2SCN$ was interpreted in terms of the small bandwidth, $W=0.26$ eV.

A number of highly-conducting complexes containing tetrathiotetracene (TTT) or tetraselenotetracene (TSeT) have been known, and their solid-state properties have been studied in some detail.[1,2] Among these compounds, $TSeT_2Cl$, $TSeT_2Br$, and $TSeT_2I$ show a high conductivity *ca.* $10^3\,\Omega^{-1}\,cm^{-1}$ at room temperature and retain their metallic conductivity down to 26 K.[3,4] Below this temperature the magnitude of the resistivity increases, but there is a tendency for $T\rightarrow 0$ to a finite value on the order of the room-temperature value. TTT_2I_3 also shows a high conductivity *ca.* $10^3\,\Omega^{-1}\,cm^{-1}$ at room temperature, but it has a conductivity maximum and its conductivity follows an activation process at low temperatures.[5] However, there is a considerable range of nonstoichiometry on iodine, and its physical properties suffer a serious influence from the disorder of the iodine sublattice.[5-8]

It is widely believed that an organic metal has a quasi-one-dimensional conduction band resulting from the π-π interaction of the planar organic molecules. However, the density-wave instabilities inherent in one-dimensional metals tend to destroy the metallic states of these compounds. The present authors have previously calculated the band-structure parameters of $TMTSF_2X$ and $(BEDT\text{-}TTF)_2ClO_4(C_2H_3Cl_3)_{0.5}$.[9-11] In the former, the authors concluded that the transverse transfer integrals, which are of the order of 0.1 of the longitudinal integrals, play an important role in the stabilization of the metallic states. On the other hand, $(BEDT\text{-}TTF)_2ClO_4(C_2H_3Cl_3)_{0.5}$ was regarded as a two-dimensional semimetal.

In the present investigation, the band-structure parameters of $TSeT_2Cl$ and TTT_2I_3 were calculated. To make a comparison, the calculation was also performed on an organic semiconductor, $TSeT_2SCN$. All these complexes have regular TSeT (or TTT) chains, and their conduction bands are three-quarters filled. In view of the calculated longitudinal bandwidths and the transverse interactions, their physical properties were also discussed.

Computation

The method of calculation was the same as has already been reported.[9-11] At first the molecular orbitals of a single molecule were calculated by the extended Hückel method using the parameters shown in Table 1.[12] Since the HOMO, which makes the conduction band in the crystal, is energetically separated enough from the other energy levels, as is shown in Fig. 1, only the overlaps of the HOMO's between the nearest-neighbor molecules were calculated. The transfer integrals t_i of the tight-binding theory are given from these overlaps S_i by the relation: $t_i=ES_i$, where E is a constant of the order of the ionization potential of the HOMO. From the energy level of the molecular orbital calculation (Fig. 1), in the present

Table 1. The exponents ζ and the ionization potentials ε (eV) for atomic orbitals

		ζ	ε			ζ	ε
S	3 s	2.122	−21.6	C	2 s	1.625	−21.4
	3 p	1.827	−15.5		2 p	1.625	−11.4
Se	4 s	2.44	−20.5	H	1 s	1.0	−13.6
	4 p	2.07	−14.4				

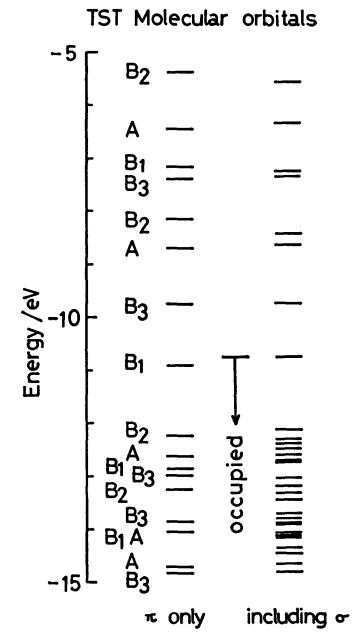

Fig. 1. Molecular orbital energy levels of TSeT. The left is the calculation including π-orbitals only, and the orbital symmetry of D_2 point group is shown.

paper E was assumed to be -10 eV. This value was also used in the calculations for the radical cation salts of TTF and BEDT–TTF when sulfur 3d orbitals were not included; it gave realistic magnitudes of transfer integrals which agrees well with the experimental results.[11] As will be discussed in the present paper, it also agrees consistently with various experiments on the salts of TTT and TSeT. The structural data were taken from the literature.[16–18]

Results and Discussion

$TSeT_2Cl$. The crystal structure of $TSeT_2Cl$ is shown in Fig. 2.[16] Because of the tetragonal symmetry, there are only two kinds of intermolecular interactions: the longitudinal interaction along the c axis, and the transverse interaction along the a axis. The calculated overlaps S, the bandwidth, and the anisotropy parameter α $(=t_\perp/t_{//})$ of the HOMO are shown in Table 2. The longitudinal bandwidth has been experimentally obtained as 0.6 eV from the magnetism.[3] This estimation agrees well with the results of the present calculation.

From the anisotropy of the conductivity, the anisotropy parameter can be roughly estimated using the following relation:[19]

$$\alpha = \left(\frac{t_\perp}{t_{//}}\right) \gtrsim \left(\frac{\sigma_\perp}{\sigma_{//}}\right)^{1/2}. \tag{1}$$

From the observed anisotropy of $TSeT_2Br$, $(\sigma_{//}/\sigma_\perp)=60$,[20] one obtains $\alpha=0.129$ ($t_a=0.077$ eV). The magnitude of the calculated $|\alpha|$ is slightly larger than this value.

From a standard tight-binding theory,[21] we obtained the following seqular equation for the conduction band.

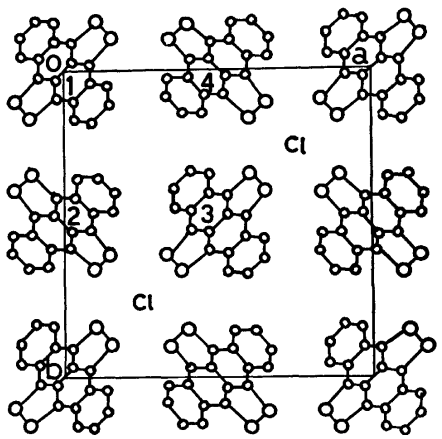

Fig. 2. Crystal structure of $TSeT_2Cl$, projection along c. The numbering of the molecules was used to derived Eq. 2.

Table 2. Band-structure parameters of $TSeT_2Cl$

Direction	Overlap	$4t_i$/eV	$\lvert\alpha_i\rvert$
c	-15.0×10^{-3}	0.60	
a	2.8×10^{-3}	-0.11	0.188

$$\begin{vmatrix} \lambda & \cos\frac{kb}{2}\cos\frac{kc}{2} & 0 & \cos\frac{ka}{2}\cos\frac{kc}{2} \\ \cos\frac{kb}{2}\cos\frac{kc}{2} & \lambda & \cos\frac{ka}{2}\cos\frac{kc}{2} & 0 \\ 0 & \cos\frac{ka}{2}\cos\frac{kc}{2} & \lambda & \cos\frac{kb}{2}\cos\frac{kc}{2} \\ \cos\frac{ka}{2}\cos\frac{kc}{2} & 0 & \cos\frac{kb}{2}\cos\frac{kc}{2} & \lambda \end{vmatrix} = 0, \tag{2}$$

$$\lambda = \frac{2t_c\cos kc-\varepsilon}{4t_a}.$$

This equation yields the dispersion relation:

$$\varepsilon(k) = 2t_c\left[\cos kc \pm 2\alpha\left(\cos\frac{ka}{2}\cos\frac{kc}{2} \pm \cos\frac{kb}{2}\cos\frac{kc}{2}\right)\right], \tag{3}$$

$$\alpha = t_a/t_c.$$

Since the conduction level is three-quarters filled, when $\alpha=0$ the Fermi surface consists of two pieces of fourfold degenerated planes at $k_F=\pm\pi/4c$. The shape of the Fermi surface depends only on the anisotropy parameter α. We numerically calculated their shapes for several values of α, as is shown in Fig. 3. When

$$\alpha = t_a/t_c = \frac{2}{8}\left(1-\cos\frac{\pi}{4c}c\right) = 0.07322,$$

one of the Fermi surfaces touches the $k_c=0$ plane, and if α is larger, a closed Fermi surface appears. At the calculated value of $\alpha=0.188$, two of the Fermi surfaces are closed, and though the other two remain open, they are seriously distorted. On the other hand, at the value of $\alpha=0.129$ obtained from the anisotropy of the conductivity of $TSeT_2Br$, one is closed, while the other three remain open. It is worth noting that, though the anisotropy parameter α of $TSeT_2Cl$ is only slightly larger than that of $TMTSF_2X$ (*ca.* 0.1),[9] the three-dimensional alignment and the larger number (8) of the neighbor molecules than that (4) of $TMTSF_2X$ effectively distort the Fermi surface.

From the anomaly of the magnetic susceptibility and the specific heat,[3,22] many authors have treated the transition at 26 K as of a Peierls type. Shchegolev and Yagubskii proposed a model where two of the four pairs of Fermi surfaces are nested, but the other two are unnested.[1] However, not only ideally planar Fermi surfaces, but also slightly distorted Fermi surfaces, can be effectively nested by a proper transfer vector.[23] Delhaes and his co-workers interpreted the properties below 26 K as a semimetallic state resulting from an imperfectly nested quasi-one-dimensional Fermi surface.[4] The observation of the anisotropic magnetoresistance also supports this interpretation.[20] The highly distorted Fermi surfaces in Fig. 3(d) agree with such semimetallic states. However, we are not certain whether a simple Peierls-type phase transition may occur on such a highly distorted Fermi surface as is shown in Fig. 3(d). A quantitative relation between the anisotropy and the Peierls transition in such a multi-band conductor remains unsolved.

In conclusion, we consider $TSeT_2Cl$ to be placed

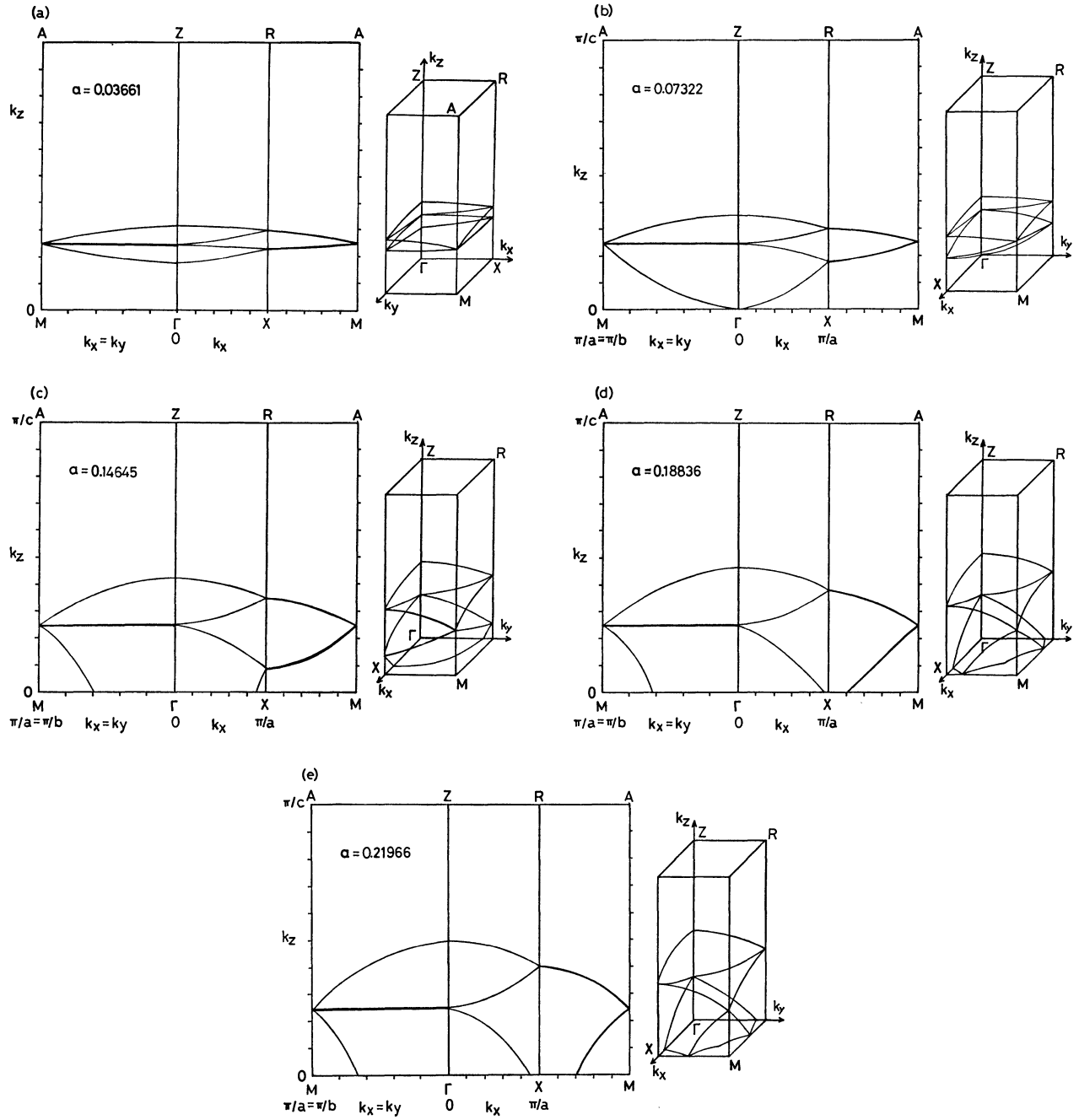

Fig. 3. Shape of the Fermi surfaces for various anisotropy parameters α, based on the dispersion of Eq. 3.

on the boundary between a one-dimensional metal and a three-dimensional metal.

TTT$_2$*I*$_3$. The crystal structure of TTT_2I_3 is shown in Fig. 4.[17] There are three kinds of intermolecular interactions. The calculated band-structure parameters are shown in Table 3. Since the magnetic susceptibility of TTT_2I_3 shows some temperature dependence, we cannot estimate the bandwidth directly from the magnetic data. However this fact qualitatively suggests that $U/4t$ in TTT_2I_3 is larger than that in $TSeT_2Cl$, and if the on-site Coulomb repulsion U is assumed to be unchanged, in TTT_2I_3 a slightly smaller bandwidth than that of $TSeT_2Cl$ is to be expected. There are some discrepancies as to the thermoelectric power because of the influence of disorder, but the bandwidth is estimated as 0.64 eV by Isett,[7] as 0.67 eV by Chaikin *et al.*,[24] as 0.7 eV by Khanna *et al.*,[8] and as 1.0 eV by Mihaly *et al.*[6] Since the magnitude of the thermoelectric power decreases with an increase in disorder,[8,24] we consider that the smallest W is the value free from the influence of disorder. Therefore, our calculated value agrees with the experimental results and can be regarded as the 'intrinsic' bandwidth free from disorder.

Though the shortest transverse S–S distance, 3.373 Å, along c is considerably smaller than the shortest longitudinal distance, 3.73 Å,[17] the calculated transverse overlap is much smaller than the longitudinal

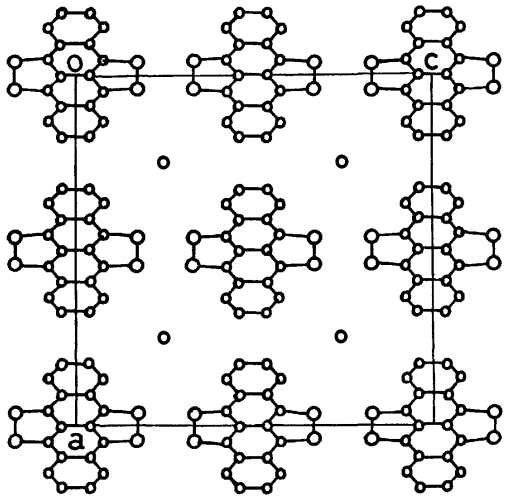

Fig. 4. Crystal structure of TTT_2I_3, projection along b.

Table 3. Band-structure parameters of TTT_2I_3

Direction	Overlap	$4t_i$/eV	$\|\alpha_i\|$
b	13.9×10^{-3}	−0.56	
c	-0.25×10^{-3}	0.010	0.018
a	0.064×10^{-3}	−0.0026	0.005

overlap and the anisotropy parameter, $\alpha=0.018$, is very small. It has been observed in the transverse interaction of TTF that the magnitude of the orbital overlap crosses zero between the σ-like and π-like overlap of the sulfur p-orbitals.[11] Because of the two similar sulfur atoms on the side of the molecule and the π-character of the HOMO, the change in the overlap between the two TTT molecules with side-by-side orientation is not very different from the case of TTF. Since the orientation between the two TTT molecules along c in TTT_2I_3 satisfies the crossover condition ($\phi=10°$ by the notation in Ref. 11, where ϕ is the angle between the molecular plane and the intermolecular transfer vector), t_c similarly happens to be small. Therefore, despite the relatively short transverse S–S distance, TTT_2I_3 has a highly-anisotropic band structure. This large anisotropy, $\alpha=0.018$, corresponds to that of the well-known organic metal, TTF–TCNQ ($\alpha=0.015$, for the largest transverse overlap).[19,25]

There are many pieces of evidence which suggest that the phase transition of TTT_2I_3 at 50 K is of a Peierls type. The magnetic susceptibility follows an exponential law with a gap 190 K below 50 K,[5,7] and the specific heat shows an anomaly of magnitude consistent with a mean-field model for a Peierls phase transition with correction for fluctuations.[26] The lack of the observation of distortion by X-ray scattering can be interpreted by the large scattering factor of iodine.[27] Though the influence of disorder seriously modifies the properties, especially those such as electrical conductivity and thermoelectric power, we regard TTT_2I_3 as essentially a quasi-one-dimensional metal, in which the bandwidth and the anisotropy parameter α are of about the same order as, or slightly larger than, those of TTF–TCNQ.

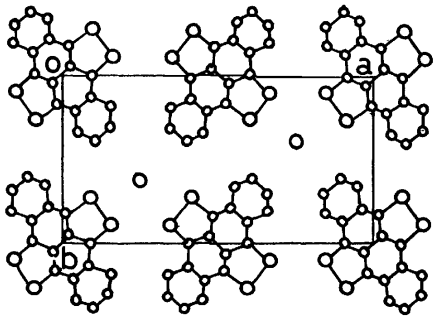

Fig. 5. Crystal sturcture of $TSeT_2SCN$, projection along c.

Table 4. Band-structure parameters of $TSeT_2SCN$

Direction	Overlap	$4t_i$/eV	$\|\alpha_i\|$
c	-6.6×10^{-3}	0.26	
a	-0.22×10^{-3}	0.0087	0.033
b	0.18×10^{-3}	−0.007	0.027

$TSeT_2SCN$. The crystal structure of $TSeT_2SCN$ is shown in Fig. 5.[18] Here again there are three kinds of intermolecular interactions. The calculated overlap and the bandwidths are shown in Table 4.

Though the degree of the occupancy of the TSeT chain is the same as that in $TSeT_2Cl$, its longitudinal conductivity is 20 Ω^{-1} cm^{-1} at room temperature and decreases with a lowering of the temperature.[18] This difference has been attributed to the larger interplanar separation (3.53 Å in $TSeT_2SCN$, and 3.37 Å in $TSeT_2Cl$), and to the pronounced anisotropy in the packing of the TSeT molecules which comes from the difference in the angle between the molecular plane and the chain direction.[18] The calculated small bandwidth and the small α reflect these structural differences. Though this anisotropy is large enough to produce a Peierls gap, it is more likely that the diffusive conduction occurs due to the larger electronic correlation in a narrowband conductor.

General Discussion. In the present paper, we neglected the interaction through anions. Since the Se–Cl distance, 3.024 Å, in $TSeT_2Cl$[16] and the Se–S distance, 3.160 Å, in $TSeT_2SCN$[18] are much shorter than the sum of the van der Waals radii, a considerable overlap of their orbitals is to be expected. These overlaps may contribute to the transport of electrons. Shchegolev and Yaguskii considered it as the dominant mechanism of the transverse interaction in $TSeT_2Cl$.[1] The contribution of such a transport to the transfer integral can be represented by a second-order perturbation theory as follows:

$$H_{ij}=\frac{H_{ia}H_{aj}}{E_a-E_o}, \tag{5}$$

where i and j represent the different organic molecules; E_a, the energy of the highest occupied level of the anion, and E_o, the energy of the HOMO. E_a-E_o is estimated to be usually of the order of several electron volts. In $TSeT_2Cl$, even if H_{ia} is assumed to be 10 times larger than the direct interaction, $W_a=0.01$ eV, H_{ij} is less than 0.05 eV. It is possible that this

second-order effect makes a considerable contribution to the transverse transport. However, it is unlikely that the calculated, not-small direct interaction is negligible compared with the indirect transport.

In summary, using semiempirical molecular orbital calculations, the present authors calculated the band-structure parameters of $TSeT_2Cl$, TTT_2I_3, and $TSeT_2SCN$. The bandwidth and the anisotropy parameter of $TSeT_2Cl$ are obtained as 0.6 eV and 0.188 respectively; this compound is considered to be on the boundary between a one-dimensional metal and a three-dimensional metal. In TTT_2I_3, the bandwidth is 0.56 eV and $\alpha=0.018$, and this compound is regarded essentially as a one-dimensional metal. On the contrary, the small bandwidth 0.26 eV of $TSeT_2SCN$ is considered to be responsible for the diffusive conduction.

References

1) I. F. Shchegolev and E. B. Yagubskii, "Extended Linear Chain Compounds," ed by J. S. Miller, Plenum, New York (1981), Vol. 2, p. 385.

2) R. P. Shibaeva, Ref. 1, p. 435.

3) S. P. Zolotukhin, V. F. Kaminskii, A. I. Kotov, R. B. Lyubovskii, M. L. Khidekel, R. P. Shibaeva, I. F. Shchegolev, and E. B. Yagubskii, *Pis'ma Zh. Eksp. Teor. Fiz.*, **25**, 480 (1977).

4) P. Delhaes, C. Coulon, S. Flandrois, B. Hilti, C. W. Mayer, G. Rihs, and J. Rivory, *J. Chem. Phys.*, **73**, 1452 (1980).

5) V. F. Kaminskii, M. L. Khidekel, R. B. Lyubovskii, I. F. Shchegolev, R. P. Shibaeva, E. B. Yagubskii, A. V. Zvarykina, and G. L. Zvereva, *Phys. Status Solidi A*, **44**, 77 (1977).

6) G. Mihaly, A. Janossy, and G. Grüner, *Solid State Commun.*, **22**, 771 (1977).

7) L. C. Isett, *Phys. Rev. B*, **18**, 439 (1978).

8) S. K. Khanna, S. P. S. Yen, R. B. Somoano, R. M. Chaikin, C. Lowe Ma, R. Williams, and S. Samson, *Phys. Rev. B*, **19**, 655 (1979).

9) T. Mori, A. Kobayashi, Y. Sasaki, and H. Kobayashi, *Chem. Lett.*, **1982**, 1923.

10) T. Mori, A. Kobayashi, Y. Sasaki, H. Kobayashi, G. Saito, and H. Inokuchi, *Chem. Lett.*, **1982**, 1963.

11) T. Mori, A. Kobayashi, Y. Sasaki, G. Saito, and H. Inokuchi, *Bull. Chem. Soc. Jpn.*, to be published.

12) The parameters were taken from Ref. 13 and Ref. 14, with the help of Ref. 15.

13) M.-H. Whangbo, W. M. Walsh, Jr., R. C. Haddon, and F. Wudl, *Solid State Commun.*, **43**, 637 (1982).

14) A. J. Berlinsky, J. F. Carolan, and L. Weiler, *Solid State Commun.*, **15**, 795 (1974).

15) C. F. Fischer, "The Hartree-Fock Method for Atoms," Wiley, New York (1977).

16) R. P. Shibaeva and V. F. Kaminskii, *Krystallografiya*, **23**, 1183 (1978).

17) D. L. Smith and H. R. Luss, *Acta Crystallogr., Sect. B*, **33**, 1744 (1977).

18) R. P. Shibaeva, V. F. Kaminskii, A. I. Kotov, E. B. Yagubskii, and M. L. Khidekel, *Kristallografiya*, **24**, 271 (1979).

19) G. Soda, D. Jerome, M. Weger, J. Alizon, J. Gallice, H. Robert, J. M. Fabre, and L. Giral, *J. Phys. Paris*, **38**, 931 (1977).

20) S. P. Zolotukin, Yu. S. Karimov, and T. F. Shchegolev, *Zh. Ekep. Teor. Fiz.*, **76**, 377 (1979).

21) For a review of the tight-binding calculation, see J.-M. Andre, *Adv. Quant. Chem.*, **12**, 65 (1980). For the construction of the energy matrix, see for example, S. Shitzkovsky, M. Weger, and H. Gutfreund, *J. Phys. Paris*, **39**, 711 (1978).

22) V. A. Merzhanov, S. I. Pesotskii, and V. N. Topnikov, *Pis'ma Zh. Eksp. Teor. Fiz.*, **30**, 197 (1979).

23) B. Horovitz, H. Gutfreund, and M. Weger, *Phys. Rev. B*, **12**, 3174 (1975).

24) P. M. Chaikin, G. Grümer, I. F. Shchegolev, and E. B. Yagubskii, *Solid State Commun.*, **32**, 1211 (1979).

25) A. John Berlinsky, J. F. Carolan, and L. Weiler, *Solid State Commun.*, **15**, 795 (1974).

26) B. Cort and D. G. Naugle, *Phys. Rev. B*, **24**, 3884 (1981).

27) C. Lowe-Ma, R. Williams, and S. Samson, *J. Chem. Phys.*, **74** 1966 (1981).

 © 1983 The Chemical Society of Japan Bull. Chem. Soc. Jpn., 56, 3381—3389 (1983)

Phosphorescence Studies of $^3\pi\pi^*$ Benzaldehyde, Acetophenone, and 1-Indanone in Benzoic Acid Host

Shin-ichi NAGAOKA and Noboru HIROTA*,†

Department of Chemistry, Faculty of Science, Kyoto University, Sakyo-ku, Kyoto 606

(Received March 26, 1983)

We have made a vibrational analysis of the phosphorescence spectra of benzaldehyde, deuterated benzaldehydes, acetophenone, and 1-Indanone in benzoic acid host. The emissions coming from different sites of benzaldehyde were separated with the help of microwave induced delayed phosphorescence (MIDP) spectroscopy. From the phosphorescence excitation spectra the locations of the $^3n\pi^*$ states were estimated to be about 2000 cm^{-1} above the $^3\pi\pi^*$ states. Contrary to the previous assignment, it was found that the aldehyde H wag is active in the spectra of benzaldehyde as in the cases of other host. The spectra of acetophenone and 1-indanone are similar to those obtained in other hosts, although the 0-0 bands are relatively stronger. The C=O stretching mode is, however, not clearly observable in all the systems studied here, suggesting that this mode is not active in the spectra of nearly pure $^3\pi\pi^*$ aromatic carbonyls. The main radiative mechanisms are discussed based on the present results and are compared with those of other aromatic carbonyls. Possible effects of hydrogen bonding on these properties are discussed.

The lowest excited triplet (T_1) states of aromatic carbonyls of the benzaldehyde type have mixed characters of $^3n\pi^*$ and $^3\pi\pi^*$ states. Their spectroscopic properties are interesting with regard to problems concerning the mixing of two nearby electronic states.[1,2] In recent years there have been considerable efforts to understand the details of the phosphorescence spectra of these molecules.[3–18] In order to fully understand the spectra of carbonyls with mixed characters, it seems desirable to understand first the spectra of pure $^3\pi\pi^*$ carbonyls.

Benzladehyde (abbreviated hereafter as BA) in benzoic acid (abbreviated as BAC), first studied by Koyanagi, Zwarich, and Goodman (KZG),[19] is nearly pure $^3\pi\pi^*$ in character because of the effect of hydrogen bonding. From a vibrational analysis of the phosphorescence spectrum KZG concluded that the aldehyde H wag mode is not active and that the couplings within the singlet manifold are more important than those in the triplet manifold, contrary to the cases of $^3\pi\pi^*$ benzladehydes in other hosts. It has also been a question whether or not the C=O stretching mode is present in the spectra of pure $^3\pi\pi^*$ aromatic carbonyls. Unfortunately the overlapping of the spectra coming from two sites and the presence of a broad background emission prevented KZG from making an unambiguous vibrational analysis. Here we have attempted to separate the emissions of the two sites using microwave induced delayed phosphorescence (MIDP) spectroscopy[20] and reexamined the spectrum of BA in BAC. We have also investigated the phosphorescence spectra of acetophenone (abbreviated as AP) and 1-indanone (abbreviated as 1ID) in BAC in order to see the general characteristics of the phosphorescence spectra of aromatic carbonyls of nearly pure $^3\pi\pi^*$ character.

It has been suggested that the properties of the $^3\pi\pi^*$ aromatic carbonyls of the benzaldehyde type are primarily determined by the energy separations between the $^3n\pi^*$ and $^3\pi\pi^*$ states.[21,22] However, an additional effect due to hydrogen bonding formation might be significant in the present systems. We also examine the magnetic and decay properties of the present systems in connection with those of the related $^3\pi\pi^*$ aromatic carbonyls.

Experimental

Sample Preparation. Commercially obtained BA and AP were purified by repeated distillations under reduced pressure. BA-d_1 (formyl hydrogen deuterated) and BA-d_6 obtained from Merck, Sharp, and Dohme of Canada were used without further purifications. 1ID was purified by recrystallization followed by zone refining. BAC used as host was purified by extensive zone refining. BAC crystals containing small amounts of BA, AP, and 1ID were grown by the Bridgman method. The initial concentrations of the guests in the melts were 2—3 wt%, but the actual concentrations in the crystals are considered to be very low. BAC crystals containing small amounts of anisole were used to obtain the BAC X-trap phosphorescence.

Phosphorescence and MIDP Spectra. The phosphorescence and MIDP spectra were taken at 4.2 K or 1.5 K with a zero field ODMR spectrometer similar to that described in a previous paper.[23] The light from a Xenon arc (XBO 900) or a mercury arc (Osram 500W) was filtered through a water solution saturated with $NiSO_4$ and a Toshiba UV transmitting filter (UVD33S). The phosphorescence emission was dispersed with a Spex 1704 spectrometer (blazed at 300 nm with linear dispersion of 0.83 nm/mm at 428.2 nm) and detected with an EMI 9502 photomultiplier. The phosphorescence intensities given in the tables were corrected for the wavelength dependence of the sensitivity of the detection system by the method given in Ref. 24 with quinine and 2-naphthol. In order to avoid the effect of polarization samples composed of small pieces were used to take the phosphorescence spectra. The polarization behavior of the emission was examined by observing the intensity variation of the phosphorescence with rotation of a polarizing sheet placed parallel to the ab plane of BAC crystal.

In the MIDP experiments microwaves generated by a HP 8900 series tunable microwave oscillator and amplified with a Hughes 1177H microwave amplifier were fed to the sample contained in a helix. In order to separate the spectra coming from the different sites microwave power corresponding to the transition frequency between the sublevels of one site was applied to produce MIDP signal. The

† Also at the Department of Chemistry, State University of New York at Stony Brook, N.Y. 11794.

MIDP signals generated at the rate of 0.5 Hz were lock-in detected with a PAR 128A lock-in amplifier, while the Spex spectrometer was scanned at the rate of 0.01 nm/s.

In order to take the phosphorescence excitation spectra the light from a 900 W Xenon arc was monochromatized by the Spex spectrometer and focused on the sample of the size of about $10\times5\times4$ mm which was immersed in liquid helium. The entire phosphorescence emission was monitored without using a monochromator.

Results and Discussion

Phosphorescence Excitation Spectra and the Locations of the $^1n\pi^*$ and $^3n\pi^*$ States. The phosphorescence excitation spectra of BA-d_1 in BAC and BAC X-trap obtained at 4.2 K are shown in Fig. 1. The triplet states of BA and AP in BAC host are generated by the direct absorption of the guests and the absorption of the host followed by the energy transfer to the guests.[25] Comparing the spectra of BAC containing BA or AP with that of BAC X-trap, we can assign the origins of the $S_1\leftarrow S_0$ and $S_2\leftarrow S_0$ transitions. The S_1 and S_2 states are considered to be $^1n\pi^*$ and $^1\pi\pi^*$ (^1L_b) states, respectively. The $T_2\leftarrow S_0$ ($^3n\pi^*$) transitions of the guests were not detected, presumably because the concentrations of the guests were very low. From the peak positions of the a_1 and b bands in Fig. 1 the origins of the $^1n\pi^*$ and $^1\pi\pi^*$ (^1L_b) states of BA-d_1 in BAC were located at 29500 and 32900 cm^{-1}, respectively. The $^1n\pi^*$ state is about 2700 cm^{-1} blue shifted compared with that in methylcyclohexane,[26] whereas the $^1\pi\pi^*$ (^1L_b) state is red shifted by 1500 cm^{-1}. The band a_2 is separated from the band a_1 by 1314 cm^{-1} and is assigned to the vibronic band associated with the C=O stretching vibration in the $^1n\pi^*$ state as in vapor and other hosts.[26] In taking the excitation spectrum of BA, emissions from the different sites were not distinguished. Therefore, the estimated energy separation has an ambiguity of about 200 cm^{-1}. Similarly, the energies of the $^1n\pi^*$ and $^1\pi\pi^*$ (^1L_b) states of AP in BAC were determined to be 29500 and 34000 cm^{-1}, respectively. The energy separations (ΔE_{TT}) between the $^3n\pi^*$ and $^3\pi\pi^*$ of the guests could not be determined directly from the present experiments, but approximate values may be obtained by noting that in the aromatic carbonyls of the benzaldehyde type the energy separations between the $^1n\pi^*$ and $^3n\pi^*$ states are about 1750 cm^{-1}.[21,27] ΔE_{TT} are then estimated using the $^3\pi\pi^*$ energies from the phosphorescence to be 2300 cm^{-1} for BA and 1750 cm^{-1} for AP. These values are much larger than those found for BA and AP in other systems.[26,28,29] This is presumably because hydrogen bonding increases the $^3n\pi^*$ and $^1n\pi^*$ energies. A smaller value of ΔE_{TT} and ΔE_{ST} (energy difference between $^1n\pi^*$ and $^3\pi\pi^*$ states) for AP than for BA probably indicates a weaker hydrogen bonding in AP.

Phosphorescence and ODMR Studies. The phosphorescence spectra of BA in the BAC host obtained at 4.2 K are shown in Fig. 2. In these spectra o and o′ peaks are the origins of the emissions coming from two sites as first suggested by Koyanagi *et al.* (KZG).[19] We designate the main vibronic bands using the notations adopted by KZG as much as possible. The phosphorescence spectrum of BA-d_6 in BAC reported by KZG has a broad background emission, but this emission could be eliminated easily by growing the crystals slowly from the melts.[30] It was found that the AP and 1ID spectra consist of the emissions from only one site (Fig. 3).

The o peak gives the ODMR signals at 4.35 and 0.48 GHz; the o′ peak at 4.23, 3.87, and 0.36 GHz in the case of BA-d_1. Deuteration effects on the ODMR frequencies are less than 0.06 GHz. In Table 1 we summarize the results of the ODMR study obtained at 1.5 K. The order of the sublevels is taken to be z, y, and x from the top.[22] It is notable that the energy separations between the z and y sublevels are very small. This situation is similar to that found

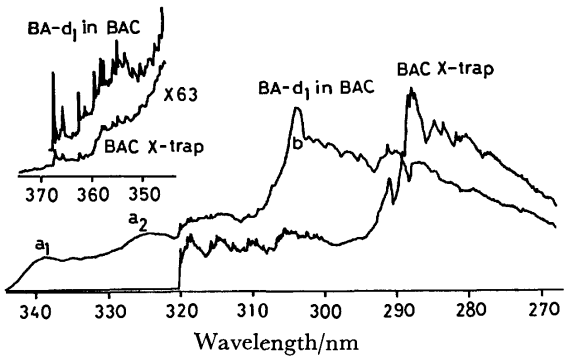

Fig. 1. Phosphorescence excitation spectra of BA-d_1 in BAC and BAC X-trap. The spectra shown in the upper left hand corner show the $T_1\leftarrow S_0$ absorption of BAC host.

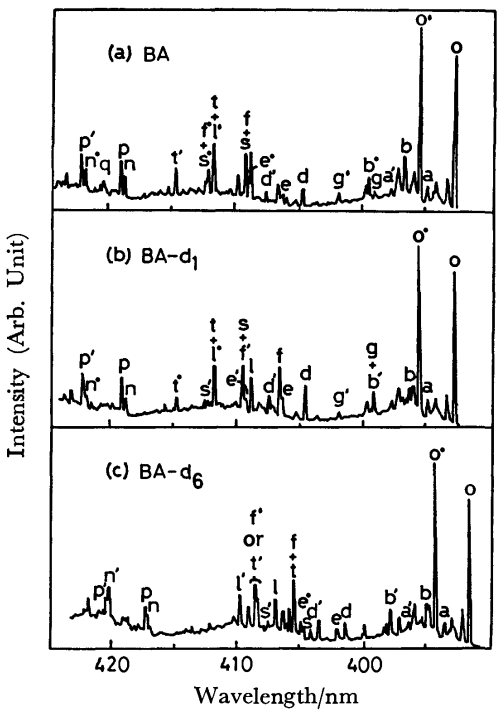

Fig. 2. Phosphorescence spectra of (a) BA, (b) BA-d_1, and (c) BA-d_6 in BAC. The spectra were taken with the slit width of 0.1 mm. No corrections for the peak intensities are made.

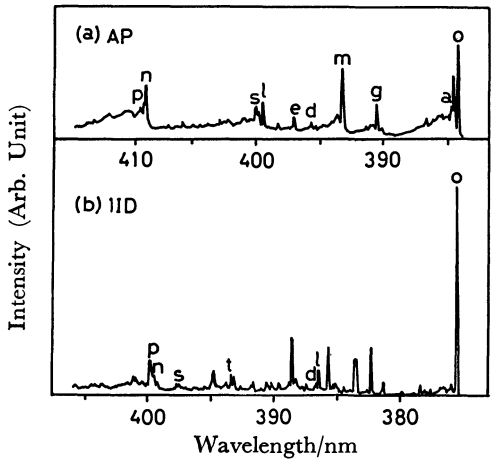

Fig. 3. Phosphorescence spectra of AP and 1ID in BAC. The spectra were taken with the slit width of 0.1 mm. No corrections for the peak intensities are made.

TABLE 1. ZFS AND DECAY RATES OF BA-d_1, AP, AND 1ID IN BAC

	BA-d_1		AP	1ID
	site 1	site 2		
$(Z-X)$/GHz	4.35	4.23	4.66	3.88
$(Z-Y)$/GHz	0.48	0.36	0.72	0.67
$(Y-X)$/GHz	—	3.87	—	—
D/cm^{-1}	−0.0805	−0.0765	−0.0897	−0.0758
E/cm^{-1}	0.0645	0.0645	0.0657	0.0535
k_z/s^{-1}	7.7	6.3	12	14
k_y/s^{-1}	0.33	4.9	1.1	0.53
k_x/s^{-1}	0.32	0.49	0.28	0.27
k_z^r/s^{-1}	1	1	1	—
k_y^r/s^{-1}	0.06	0.71	0.05	—
k_x^r/s^{-1}	0.03	0.06	≈0.02	—
T_1/cm^{-1}	25451	25276	26029	26615
S_1/cm^{-1}	29500		29500	—
S_2/cm^{-1}	32900		34000	—
ΔE_{ST}/cm^{-1}	4050		3500	—
ΔE_{TT}/cm^{-1}	2300		1750	—

for AP in ethylene glycol water studied by Lamola.[31] In spite of the poor molecular symmetry the radiative and total decays of the site 1 BA, AP, and 1ID take place almost exclusively from the z sublevels. The EPR study showed that the z axis is along the C=O direction in the site 1 BA.[32] The x axis is perpendicular to the molecular plane. This is also considered to be true in the cases of AP and 1ID. On the other hand, the EPR study showed that as expected from the decay characteristics the z axis deviates from the C=O direction by 45° in the case of site 2 BA.[32]

We obtained the MIDP spectrum of the z sublevel for the site 1 and those of the z and y sublevels for the site 2 at 1.5 K. The representative spectra are shown in Fig. 4. It was not possible to separate the two emissions completely, but the contribution of the undesired emission was less than 20% of the desired one. We could easily identify the main vibrational

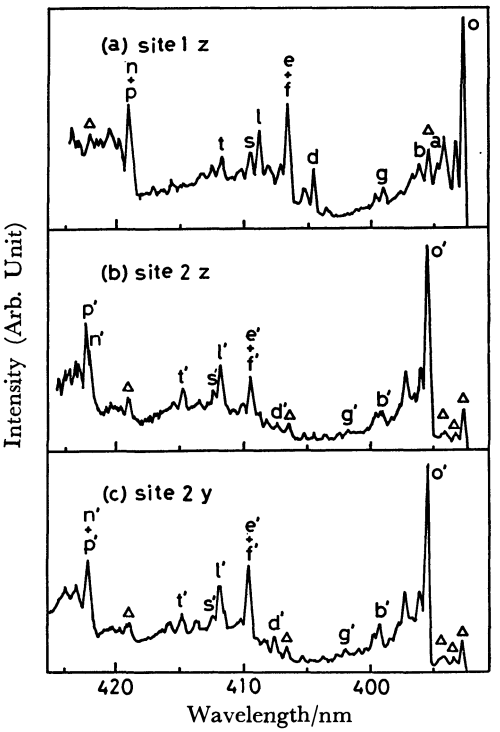

Fig. 4. MIDP specra of BA-d_1 in BAC. All spectra were taken with the slit width of 0.4 mm. The relative intensities of the peaks may not be accurate because of the use of long time constant. The peaks indicated with △ are due to the other site. (a) z sublevel spectrum of the site 1. (b) z subleved spectrum of the site 2. (c) y sublevel spectrum of the site 2.

bands of the emissions coming from the different sites. In Table 2 we give the results of our vibrational analysis. The analysis was made by comparison with the ground state vibrational frequencies given by Goodman *et al.*[33] The phosphorescence spectra of the site 1 and site 2 are slightly different from each other, but the difference is not large. Our assignments are mostly in agreement with those by KZG, but there are some important difference which are explained in the following.

The main difference is concerned with the assignments of the aldyhyde H wag (f) and ν_{19a} (s). KZG considered that the 0-1024 band (f) in the BA spectrum is due to the ν_{19a} vibration and the aldehyde H wag is not active. We think that this band is mainly due to the aldehyde H wag with a minor contribution from the ν_{19a} vibration, because we observe strong bands at 0-865 (f) and 0-870 (f+t) in the BA-d_1 and BA-d_6 spectra, which can be assigned to the aldehyde D wag. These vibrations are also very active in the site 2 spectra. In the MIDP spectra of BA-d_1 the band due to the ν_{19a} vibration is observable, but the intensity of this band is much weaker than that of the aldehyde D wag. This assignment is further supported by the observation that the polarization behavior of the 0-1024 band is similar to those of the other a″ bands such as CHO wag (b) and is different from those of the 0-0 and other a′ bands.[34] Among the a″ bands ν_{16b} and ν_4 vibrations seems to be less active than indicated by KZG.

TABLE 2. VIBRATIONAL ANALYSIS

Band number	Wave number[a]/cm^{-1}	Relative intensity[b]	$\Delta\tilde{\nu}$/cm^{-1}	Assignment	Designation
		BA site 1[c]			
0	25456	100	0	0-0 of $^3\pi\pi^*$-$^1A_1$	o
1	25417	20	39	0-39; lattice mode	
2	25359	15	97	0-97; lattice mode	
3	25348	7	108	0-108; lattice mode	
4	25316	13	140	0-140; a″ CHO torsion?	a
7	25202	25	254	0-254; a″ CHO wag	b
11	25096	3	360		
12	25049	5	407	0-407; a″ ν_{16a}	g
15	25009	7	447		
18	24705	13	751	0-751; a″ ν_{11}	d
19	24669	5	787		
21	24607	7	849	0-849; a″ ν_{10a}	e
22	24585	15	871		
24	24458	24	998	0-998; a′ ν_1	l
26	24435	32	1021	0-1021; a″ H wag and a′ ν_{19a}	f+s
28	24284	39	1172	0-1172; a′ ν_{9b}	t
30	24246	11	1210	0-1172-39?	
33	23872	20	1584	0-1584; a′ ν_{8b}	n
34	23857	28	1599	0-1599; a′ ν_{8a}	p
35	23776	8	1680		q
38	23607	13	1849		
		BA site 2[c]			
5	25281	118	0	0-0 of $^3\pi\pi$-$^1A_1$	o′
6	25247	15	34	0-34; lattice mode	
8	25187	5	94	0-94; lattice mode	
9	25168	16	113	0-113; lattice mode	
10	25131	7	150	0-150; a″ CHO torsion	a′
14	25024	12	257	0-257; a″ CHO wag	b′
17	24874	5	407	0-407; a″ ν_{16a}	g′
23	24527	8	754	0-754; a″ ν_{11}	d′
25	24451	10	830	0-830; a″ ν_{10a}?	e′
27	24395	17	886		
28	24284	39	997	0-997; a′ ν_1	l′
29	24256	17	1025	0-1025; a″ H wag and a′ ν_{19a}	f′+s′
31	24106	23	1175	0-1175; a′ ν_{9b}	t′
32	24066	8	1215	0-1175-34?	
36	23697	15	1584	0-1584; a′ ν_{8b}	n′
37	23683	27	1598	0-1598; a′ ν_{8a}	p′
40	23565	4	1716		
		BA-d_1 site 1[d]			
0	25451	100	0	0-0 of $^3\pi\pi^*$-$^1A_1$	o
1	25410	20	41	0-41; lattice mode	
2	25354	13	97	0-97; lattice mode	
3	25344	5	107	0-107; lattice mode	
4	25314	12	137	0-137; a″ CDO torsion	a
7	25221	11	230	0-230; a″ CDO wag	b
9	25186	5	265	0-230-41?	
12	25043	14	408	0-408; a″ ν_{16a}	g
14	25008	10	443	0-408-41?	
16	24762	4	689		
17	24709	25	742	0-742; a″ ν_{11}	d
18	24660	6	791		
19	24598	13	853	0-853; a″ ν_{10a}	e
20	24586	37	865	0-865; a″ D wag	f
21	24550	5	901		

TABLE 2. (Continued)

Band number	Wave number[a]/cm^{-1}	Relative intensity[b]	$\Delta\tilde{\nu}$/cm^{-1}	Assignment	Designation
24	24450	27	1001	0-1001; a′ ν_1	l
26	24409	33	1042	0-1042; a′ ν_{19a}	s
27	24277	30	1174	0-1174; a′ ν_{9b}	t
34	23954	4	1497		
35	23867	14	1584	0-1584; a′ ν_{8b}	n
36	23850	32	1601	0-1601; a′ ν_{8a}	p
37	23857	4	1645		
39	23767	4	1684		
40	23752	4	1699		
		BA-d_1 site 2[d]			
5	25276	114	0	0-0 of $^3\pi\pi^*$-$^1A_1$	o′
6	25243	15	33	0-33; lattice mode	
8	25203	5	73	0-73; lattice mode	
10	25116	15	110	0-110; lattice mode	
12	25043	14	233	0-233; a″ CDO wag	b′
14	25008	10	268	0-233-33?	
15	24869	5	407	0-407; a″ ν_{16a}	g′
22	24532	13	744	0-744; a″ ν_{11}	d′
25	24423	10	853	0-853; a″ ν_{10a}	e′
26	24409	33	867	0-867; a″ D wag	f′
27	24277	30	999	0-999; a′ ν_1	l′
29	24236	6	1040	0-1040; a′ ν_{19a}	s′
31	24098	12	1178	0-1178; a′ ν_{9b}	t′
42	23688	11	1588	0-1588; a′ ν_{8b}	n′
43	23674	27	1602	0-1602; a′ ν_{8a}	p′
44	23623	13	1653		
		BA-d_6 site 1[e]			
0	25523	100	0	0-0 of $^3\pi\pi^*$-$^1A_1$	o
1	25485	20	38	0-38; lattice mode	
2	25425	12	98	0-98; lattice mode	
3	25412	3	111	0-111; lattice mode	
4	25392	10	131	0-131; a″ CDO torsion	a
7	25306	18	217	0-217; a″ CDO wag	b
8	25277	7	246	0-217-38?	
11	25164	12	359		
17	24901	13	622	0-622; a″ ν_{11}	d
18	24859	9	664	0-664; a″ ν_{10a}	e
20	24772	18	751	0-751; a″ ν_{17b}	
23	24698	10	825	0-825; a′ ν_{19a}	s
25	24651	42	872	0-872; a′ ν_{9b} and/or a″ D wag	t+f
26	24633	17	890		
27	24613	8	910		
29	24563	23	960	0-960; a′ ν_1	l
33	24437	18	1086	0-1050-38?	
39	23964	12	1559	0-1559; a′ ν_{8b}	n
40	23955	21	1568	0-1568; a′ ν_{8a}	p
43	23874	6	1649		
44	23862	6	1661		
45	23851	6	1672		
		BA-d_6 site 2[e]			
5	25349	120	0	0-0 of $^3\pi\pi^*$-$^1A_1$	o′
6	25316	16	33	0-33; lattice mode	
9	25240	17	109	0-109; lattice mode	
10	25208	7	141	0-141; a″ CDO torsion	a′
12	25122	16	227	0-227; a″ CDO wag	b′
13	25101	7	248	0-227-33?	

TABLE 2. (Continued)

Band number	Wave number[a]/cm^{-1}	Relative intensity[b]	$\Delta\tilde{\nu}$/cm^{-1}	Assignment	Designation
14	25088	6	261		
15	24993	11	356		
22	24724	10	622	0-622; a″ ν_{11}	d′
24	24684	12	665	0-665; a″ ν_{10a}	e′
28	24596	16	753	0-753; a″ ν_{17b}?	
30	24522	8	827	0-827; a′ ν_{19a}	s′
31	24479	23	870	0-870; a′ ν_{9b} and/or a″ D wag	t′ or f′
32	24473	34	876	0-876; a′ ν_{9b} and/or a″ D wag	t′ or f′
33	24437	18	912		
34	24396	24	953	0-953; a′ ν_1	l′
35	24364	7	985	0-953-33?	
46	23792	26	1557	0-1557; a′ ν_{8b}	n′
47	23785	13	1564	0-1564; a′ ν_{8a}	p′
48	23699	17	1650		
		AP			
0	26029	100	0	0-0 of $^3\pi\pi^*$-$^1A_1$	o
1	26007	58	22	0-22; lattice mode	
2	25990	14	39	0-39; a″ $COCH_3$ torsion	a
3	25972	7	57		
4	25959	3	70		
5	25937	6	92		
6	25890	6	139	0-139; a″ CH_3 torsion	
7	25855	8	174		
8	25627	7	402		
9	25608	33	421	0-421; a″ ν_{16a}	
10	25584	4	445	0-421-22?	
11	25575	4	454		
12	25549	3	480	0-480; a″ ν_{16b}	
13	25430	70	599	0-599; a′ CCO bend	m
14	25399	10	630	0-599-22?	
15	25286	4	743		
16	25267	8	762	0-762; a″ ν_{11}	d
17	25182	14	847	0-847; a″ ν_{10a}	e
18	25097	7	932	0-932; a″ ν_{17a}	
19	25029	28	1000	0-1000; a′ ν_1	l
20	25005	18	1024	0-1000-22?	
21	24993	21	1036	0-1036; a′ ν_{19a}	s
22	24928	5	1101	0-1101; a′ ν(C–CH_3)	
23	24856	5	1173	0-1173; a′ ν_{9b}	
24	24812	6	1217		
25	24748	5	1281		
26	24727	3	1302		
27	24684	5	1345		
28	24638	5	1391		
29	24603	8	1426		
30	24575	5	1454		
31	24532	5	1497	0-1497; a′ ν_{18a}	
32	24503	3	1526		
33	24431	55	1598	0-1598; a′ ν_{8b}	n
34	24425	13	1604	0-1604; a′ ν_{8a}	p
35	24402	13	1627	0-1598-22?	
36	24336	10	1693		
37	24251	6	1778		
		1ID			
1	26615	100	0	0-0 of $^3\pi\pi^*$-$^1A_1$	o
2	26577	4	38	0-38; lattice mode	

TABLE 2. (Continued)

Band number	Wave number[a]/cm^{-1}	Relative intensity[b]	$\Delta\tilde{\nu}$/cm^{-1}	Assignment	Designation
3	26532	2	83	0-83; lattice mode	
4	26464	2	151		
5	26445	2	170		
6	26431	2	184		
7	26413	5	202		
8	26314	2	301		
9	26215	7	400	0-400; a″ ν_{16b}?	
10	26151	23	464	0-464; a″ γ(C=O)	
11	26125	2	490	0-464-38?	
12	26070	17	545	0-545; a′ ν_{6b}	
13	26065	17	550	0-550; a′ ν_{6a}	
14	26002	2	613	0-613; a′ δ(CCC$_p$)	
15	25956	4	659		
16	25942	3	673		
17	25920	22	695	0-695; a″ ν(CCC$_b$)	
18	25871	10	744	0-744; a′ ν_1	l
19	25854	3	761	0-761; a″ ν_{11}	d
20	25798	3	817	0-817; a″ γ(CH$_2$)	
21	25777	2	838	0-838; a′ ν_{12}	
22	25745	4	870		
23	25731	24	884	0-884; a″ ν_{10b}	
24	25713	3	902	0-884-38?	
25	25663	3	952	0-952; a′ ν(CC$_p$)	
26	25620	3	995	0-995; a″ ν_5	
27	25592	3	1023	0-1023; a′ w(CH$_2$)	
28	25528	5	1087	0-1087; a″ tw(CH$_2$)	
29	25514	2	1101	0-1101; a′ ν_{18b}	
30	25458	2	1157	0-1157; a′ ν_{15}	
31	25425	7	1190		
32	25410	7	1205	0-1205; a′ ν_{9b}	t
33	25384	4	1231	0-1231; a′ ν_{7b}	
34	25325	9	1290		
35	25148	3	1467	0-1467; a′ ν_{19a}	s
36	25136	3	1479	0-1479; a′ ν_{19b}	
37	25036	4	1579		
38	25018	5	1597	0-1597; a′ ν_{8b}	n
39	25005	12	1610	0-1610; a′ ν_{8a}	p
40	24933	4	1682		
41	24918	4	1697		

a) The wave numbers in this table refer to vacuum. b) The relative intensities in this table are peak ones and their ambiguities are about 5%. c) The following peaks could be assigned to neither site 1 nor site 2. (numbers in the parenthesis are the relative intensities) 25034(2), 25000(4), 24624(6), and 23589(4). d) 25130(7), 25029(3), 24482(7), 24256(4), 24218(7), 24081(4), 24042(8), 23781(4), 23710(6), and 23589(6). e) 24082(4), 24809(4), 24763(4), 24253(6), 24169(5), 23976(7), 23923(6), and 23900(4).

Another important difference exists concerning the estimate of the intensity of the C=O stretching bands. According to the KZG assignment the C=O stretching bands have moderate intensities in the spectra of BA, BA-d_1, and BA-d_6. Although there is a 0-1680 (q) band of moderate intensity in the BA, there is no corresponding band in the BA-d_1 spectrum. Therefore, the C=O stretching band is likely to be very weak in the present systems. The C=O stretching band is also not clearly observable in the AP and 1ID spectra. The vibrations appearing in the AP spectrum are similar to those appearing in the spectra of AP X-trap[35] and AP in AP-d_8[19] except that the C=O stretching band is not clearly observable in AP in BAC. The common features of the spectra of BA and AP in BAC may be summarized as follows.

1) The 0-0 band is very strong.

2) The C=O stretching band is not clearly observable.

3) The main a′ modes associated with the ring vibrations are ν_1 (l), ν_{19a} (s), ν_{9b} (t), ν_{8b} (n), and ν_{8a} (p).

4) In addition to the a″ vibrations associated with the CHO and CH$_3$CO groups ν_{16a} (g), ν_{11} (d), and ν_{10a} (e) a″ ring modes have moderate intensities.

In connection with the observations recently made

about the spectra of benzaldehyde, two points should be noted. One is about the intensity of the C=O stretching band. The C=O stretching vibration has been found widely in the phosphorescence spectra of the $^3\pi\pi^*$ aromatic carbonyls and it was suspected that it may have an intramolecular origin.[9] We have previously suggested that the appearance of this mode in the spectra of the $^3\pi\pi^*$ aromatic carbonyls is primarily due to the direct configurational mixing of the nearby $^3n\pi^*$ and $^3\pi\pi^*$ states caused by distortion and that it should not be active in the spectra of the nearly pure $^3\pi\pi^*$ aromatic carbonyls with large ΔE_{TT}.[5] The present result supports this suggestion further. Another point of interest is the relative intensities of the H wag and CHO torsion mode.[9] It was found that the intensity of the H wag is much stronger than that of the CHO torsion band as in the cases of many other $^3\pi\pi^*$ benzaldehydes.[12,25]

The phosphorescence spectrum of 1ID in BAC is also characterized by a very strong 0-0 band and a number of a″ vibronic bands with moderate to weak intensities. The vibrations appearing in the spectrum of 1ID in BAC are similar to those appearing in the 1ID X-trap spectrum,[33] but the relative intensity of the 0-0 band is much stronger in the BAC host. We made a vibrational analysis using infrared and Raman data.[36]

In the cases of BA, AP, and 1ID in BAC the phosphorescence takes place predominantly from the z sublevel. It was previously suggested that the z sublevel emissions of the $^3\pi\pi^*$ aromatic carbonyls are mainly due to the following three mechanisms.[5] (I) $^3n\pi^*$-$^3\pi\pi^*$ configurational mixing, (II) $^1n\pi^*$-$^3\pi\pi^*$ spin orbit coupling, (III) Herzberg-Teller vibronic spin orbit mechanism. However, the $^3n\pi^*$-$^3\pi\pi^*$ configurational mixing is not important in the present systems possibly because of large ΔE_{TT} and the planar structure of the T_1 states. Then the mechanism to produce the z sublevel emission at the 0-0 and the a′ band is,

$$\text{(II)}\ {}^3\pi\pi^*(z) \xleftrightarrow{\text{S.O.}} {}^1n\pi^* \xleftrightarrow{\vec{e}\,\vec{r}} S_0.$$

The Hertzberg-Teller vibronic spin orbit mechanism in both triplet and singlet manifolds gives rise to the a″ bands,

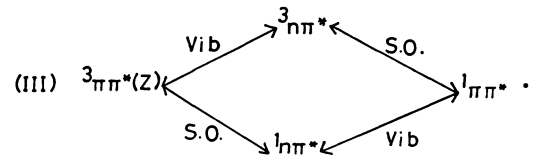

However, in view of the fact that ΔE_{TT} is smaller than the energy separations between the $^1n\pi^*$ and $^1\pi\pi^*$ states vibronic coupling within the triplet manifold is considered to be more important as in the other $^3\pi\pi^*$ benzladehydes.[5] The relative importance of the mechanism (III) with respect to that of (II) is reduced as ΔE_{TT} increases. This is the reason why the a″ vibronic bands are relatively weak compared with the 0-0 bands in the present systems. The phosphorescence spectra of the present systems are thus explained by the same radiative mechanisms as used previously to explain the other $^3\pi\pi^*$ aromatic carbonyls. It should be noted that the present mechanisms are essentially the same as those discussed for AP in ethylene glycol water by Lamola.[31]

The phosphorescence of the site 2 BA comes from both z and y sublevels with $k_z^r/k_y^r=0.71$ at the 0-0 band. Our EPR study showed that the z axis of the zero field tensor is 45° away from the C=O direction and this is the cause of the two sublevel activities in the site 2.[32] In fact, the y sublevel spectrum is quite similar to the z sublevel one. If the spin orbit mixing with the $^1n\pi^*$ state is responsible for the emissions from both y and z sublevels, the deviation of the z axis from the C=O direction is given by arctan $\sqrt{0.71}=40°$,[21] which is in reasonable agreement with the value determined by the EPR study.[33]

The EPR study showed that the spin distribution in the benzene ring of the T_1 state of BA in BAC is very similar to that of the T_1 state of benzonitrile. The T_1 states of BA in BAC and benzonitrile have similar quinonoid structures.[32,37] Then it may be expected that the modes associated with the benzene ring vibrations appearing in the phosphorescence spectra are similar in both systems. The phosphorescence spectrum of benzonitrile is simple consisting of the bands at 0-765, 0-1000, 0-1185, and 0-1610.[38] Indeed these bands have moderate intensities in the spectrum of BA in BAC.

Comparison with the Other $^3\pi\pi^*$ Carbonyls. The spectroscopic properties of BA, AP, and 1ID in BAC are mostly well explained by taking account of the fact that ΔE_{TT} are much larger than those of BA, AP, and 1ID in other hosts. However, there seem to be a few characteristics which are specific to the present systems.

It was shown previously that there is a good empirical correlation between the decay rate constant of the z sublevel of a $^3\pi\pi^*$ aromatic carbonyl and ΔE_{TT} or ΔE_{ST}.[21,22] This correlation with $\Delta E_{ST}=4050\ cm^{-1}$ predicts k_z of BA in BAC to be $17.6\ s^{-1}$, which is in good agreement with the observed $18\ s^{-1}$.[22] For a series of $^3\pi\pi^*$ aromatic carbonyls of the benzaldehyde type it was previously suggested that $k_y^r(0\text{-}0)/k_z^r(0\text{-}0)$ increases as ΔE_{TT} (ΔE_{ST}) increases.[5] There are a few carbonyls with large ΔE_{TT} in which $k_y^r(0\text{-}0)$ are even larger than $k_z^r(0\text{-}0)$.[39,40] Here, however, $k_y^r(0\text{-}0)/k_z^r(0\text{-}0)$ is very small in spite of rather large ΔE_{TT}. This is probably due to two causes. Firstly, $k_y^r(0\text{-}0)$ is very small. The fact that k_y of the site 1 BA and 1ID are much smaller than those of the other $^3\pi\pi^*$ aromatic carbonyls of the benzaldehyde type seems to indicate this. This shows that the radiative decay involving the spin-orbit mixing with the $^1\sigma\pi^*(^1\pi\sigma^*)$ state is not very effective in the present systems. Secondly, $k_z^r(0\text{-}0)$ is relatively large in the present systems probably because of the increased intensity of the $S_0\rightarrow S_1(^1n\pi^*)$ transition. Although we do not know the exact reason of the very small $k_y^r(0\text{-}0)/k_z^r(0\text{-}0)$ here, hydrogen bonding formation may be responsible.

The ZFS were determined by using the spin Hamiltonian, $H=-XS_x^2-YS_y^2-ZS_z^2$, with $D=-\frac{3}{2}Z$

and $E=\frac{1}{2}(Y-X)$. X, Y, and Z are the energies of the x, y, and z sublevels, respectively, with $X+Y+Z=0$. $|D|=0.0805$ cm^{-1} for BA-d_1, 0.0897 cm^{-1} for AP, and 0.0758 cm^{-1} for 1ID in BAC are rather small compared with those of the other $^3\pi\pi^*$ aromatic carbonyls. D is given as a sum of D_{SO} due to the second order effect of the spin orbit interaction and D_{SS} due to spin-spin interaction. D_{SO} is given approximately as[41,42]

$$D_{SO} = -G^2(1/\Delta E_{TT} - 1/\Delta E_{ST}).$$

Here G is the matrix element for the spin-orbit mixing between $^3n\pi^*$ and $^3\pi\pi^*$ states. G^2 was estimated to be $\approx$90, $\approx$60, and $\approx$20 cm^{-2} for a series of benzaldehydes, acetophenones, and 1-indanones.[21,22,43] With the values of ΔE_{TT} and ΔE_{ST} estimated in this work, these values give D_{SO} for BA, AP, and 1ID to be -0.017, -0.017, and -0.006 cm^{-1}, respectively. On the other hand, D_{SS} estimated for a series of benzaldehydes and 1-indanones are -0.11 cm^{-1} and -0.08 cm^{-1} from plots of D_{obs} *vs.* $1/\Delta E_{TT}-1/\Delta E_{ST}$.[21,22,43] These values predict D to be -0.127 and -0.086 cm^{-1}, respectively. The observed D are somewhat larger than these estimates. Our previous MO calculation showed that hydrogen bonding caused significant changes in the spin distribution on the carbonyl group.[31] D_{SS} and D_{SO} may be affected significantly through the changes in spin distribution.

We express our sincere thanks to Dr. Motohiko Koyanagi of Kyushu University for his helpful and critical discussions. Our thanks are also due to Dr. Seigo Yamauchi for valuable discussions, Mr. Yoshihiro Hirata for his help in the early stage of this work and Miss Yasuko Yamada for the correction of the wavelength dependence of the spectrometer and the polarization data. This work was partly supported by a Grant from the Ministry of Education, Science and Culture.

References

1) A. J. Duben, L. Goodman, and M. Koyanagi, "Interstate Interaction in Aromatic Aldehydes and Ketons," in "Excited States," ed by E. C. Lim, Academic Press, New York (1974), Vol. 1, pp. 295—329.
2) E. C. Lim, "Vibronic Interactions and Luminescence in Aromatic Molecules with Nonbonding Electrons," in "Excited States," ed by E. C. Lim, Academic Press, New York (1977), Vol. 3, pp. 305—337.
3) W. Moehle and M. Vala, *Chem. Phys. Lett.*, **41**, 149 (1976).
4) A. Despres and E. Migirdicyan, *Chem. Phys.*, **14**, 229 (1976).
5) E. T. Harrigan and N. Hirota, *Mol. Phys.*, **31**, 681 (1976).
6) M. Koyanagi, K. Higashi, and Y. Kanda, *Chem. Phys. Lett.*, **52**, 184 (1977).
7) O. S. Khalil, S. W. Hankin, and L. Goodman, *Chem. Phys. Lett.*, **52**, 187 (1977).
8) I-Fu Hung, D. F. Williams, and R. Yip, *J. Lumin.*, **15**, 231 (1977).
9) I. Özkan and L. Goodman, *Chem. Phys. Lett.*, **64**, 32 (1979).
10) M. Koyanagi and L. Goodman, *Chem. Phys.*, **39**, 237 (1979).
11) I. Özkan and L. Goodman, *Chem. Rev.*, **79**, 275 (1979).
12) A. Despres, V. Legeune, E. Migirdicyan, and W. Siebrand, *Chem. Phys.*, **36**, 41 (1979).
13) L. Goodman, M. Lamotte, and M. Koyanagi, *Chem. Phys.*, **47**, 329 (1980).
14) Y. Hirata and E. C. Lim, *J. Chem. Phys.*, **72**, 5505 (1980).
15) A. Despres and E. Migirdicyan, *Chem. Phys.*, **50**, 381 (1980).
16) J. S. Patel and D. M. Hanson, *Chem. Phys.*, **69**, 249 (1982).
17) I. C. Winkler and D. M. Hanson, *J. Chem. Phys.*, **76**, 5739 (1982).
18) A. Despres, V. Lejeune, and E. Migirdicyan, *Chem. Phys.*, **66**, 57 (1982).
19) M. Koyanagi, R. J. Zwarich, and L. Goodman, *J. Chem. Phys.*, **56**, 3044 (1972).
20) J. Schmidt, W. S. Veeman, and J. H. van der Waals, *Chem. Phys. Lett.*, **4**, 341 (1969); D. A. Antheunis, J. Schmidt, and J. H. van der Waals, *ibid.*, **6**, 255 (1970); *Mol. Phys.*, **22**, 1 (1971).
21) E. T. Harrigan and N. Hirota, *Mol. Phys.*, **31**, 663 (1976).
22) Y. Hirata and N. Hirota, *Mol. Phys.*, **39**, 129 (1980).
23) T. H. Cheng and N. Hirota, *J. Chem. Phys.*, **56**, 5019 (1972).
24) H. Kokubun, "Keiko," in "Shin Zikken Kagaku Koza" ed by the Chemical Society of Japan, Maruzen, Tokyo (1976), Vol. 4, Kiso Gizyutsu 3, Hikari (II), Chap. 8, pp. 505—549.
25) The bands starting at 320 and 292 nm of the excitation spectrum of the BAC trap are due to $T_2(^3n\pi^*)\leftarrow S_0$ and $S_1(^1\pi\pi^*)\leftarrow S_0$ absorptions of BAC, respectively.
26) L. Goodman and M. Koyanagi, *Mol. Photochem.*, **4**, 369 (1972).
27) H. Hayashi and S. Nagakura, *Mol. Phys.*, **27**, 969 (1974).
28) T. H. Cheng and N. Hirota, *Mol. Phys.*, **27**, 281 (1974).
29) W. A. Case and D. R. Kearns, *J. Chem. Phys.*, **52**, 2175 (1970).
30) Dr. M. Koyanagi also made the same observation. Private communication.
31) A. A. Lamola, *J. Chem. Phys.*, **47**, 4810 (1967).
32) S. Nagaoka and N. Hirota, *J. Chem. Phys.*, **74**, 1637 (1981).
33) R. Zwarich, J. Smolarek, and L. Goodman, *J. Mol. Spectrosc.*, **38**, 336 (1971).
34) The following values (numbers given in parenthesis) were obtained for I_b/I_c of the a′ and a″ bands of BA at site 1, respectively. a′ bands; 0-0(2.74), 0-998(1.88) 0-1584 (2.04), 0-1599(2.18), a″ bands; 0-254 (0.68), 0-751 (0.40), 0-1021 (0.81). Private communication from Y. Yamada.
35) S. Niizuma and N. Hirota, *J. Phys., Chem.*, **82**, 453 (1978).
36) L. Bardet, G. Fleury, R. Granger, and C. Sablayrolles, *J. Mol. Struct.*, **3**, 141 (1969).
37) N. Hirota, T. C. Wong, E. T. Harrigan, and K. Nishimoto, *Mol. Phys.*, **29**, 903 (1975).
38) L. Lebel and J. P. Laposa, *J. Mol. Spectrosc.*, **41**, 249 (1972).
39) E. T. Harrigan, A. Chakrabarti, and N. Hirota, *J. Am. Chem. Soc.*, **98**, 3460 (1976).
40) M. Baba, N. Hirota, and E. M. Kosower, *J. Phys. Chem.*, **85**, 1469 (1981).
41) H. Hayashi and S. Nagakura, *Mol. Phys.*, **24**, 801 (1972).
42) C. R. Jones, D. R. Kearns, and A. H. Maki, *J. Chem. Phys.*, **59**, 873 (1973).
43) S. Niizuma and N. Hirota, *J. Phys. Chem.*, **83**, 706 (1979).

Decomposition of Methylamine over Ruthenium Black

Hideo ORITA, Shuichi NAITO,* Takaharu ONISHI,† and Kenzi TAMARU

Department of Chemistry, Faculty of Science, The University of Tokyo, Hongo, Bunkyo-ku, Tokyo 113

(Received April 26, 1983)

The decomposition of methylamine over Ru black was investigated in the presence and absence of hydrogen, and the dependence of reaction rate on the pressures of reactants was also examined. Methylamine decomposes rapidly to gaseous ammonia and deposited carbon species (CH_x(a)) over clean Ru black in the absence of hydrogen. The hydrogenation of CH_x(a) after the decomposition of amines produced hydrocarbons in the range C_1—C_4 whose distribution was dependent on the way CH_x(a) was accumulated.

The reactions of aliphatic amines over some evaporated metal films (Ni, Fe, Pd, Pt, W, Co, V) were studied previously by Kemball and Moss,[1-3] and by Anderson and Clark.[4] Two most important reactions of methylamine have been considered to be (i) simple hydrocracking and (ii) disproportionation involving two amine molecules, which leave considerable amount of carbon on the catalysts.[1,4] On the other hand in the presence of hydrogen thermodynamics indicates that methylamine should be decomposed readily to methane and ammonia.

In the present work, ruthenium was chosen as a catalyst because of its high activity for ammonia synthesis and Fischer-Tropsch reaction, and the decomposition of methylamine over a ruthenium black was investigated in the presence and absence of hydrogen. The reaction mechanism has been discussed on the basis of the reaction kinetics and the nature of the carbon species deposited from amines.

Experimental

The catalytic reaction of amines was carried out in a conventional closed-circulation system, whose dead volume was 336 cm^3. The analysis of gas mixture was carried out by gas chromatography using Chromosorb 103 (3 m, 110—120 °C) for ammonia and amines, Molecular Sieve 5 A column (1.5 m, room temperature) for hydrogen and methane, and active alumina column (2 m, room temperature) for C_2—C_4 hydrocarbons.

The ruthenium black was purchased from Nippon Engelhard and was used as a catalyst after hydrogen reduction at 300 °C. After this treatment, no impurity was observed on the surface of ruthenium black by X-ray photoelectron spectroscopy. Methylamine was obtained from its hydrochloride solution and potassium hydroxide, followed by drying, purifying by vacuum distillation and out-gassing by freezing and pumping. Dried ethylamine (>99%) was purchased from Tokyo Kasei and was out-gassed before use. Hydrogen was purified by passing through a Deoxo catalyst (room temperature) and a liquid nitrogen cold trap.

Prior to each run of the reaction, the catalyst was reduced by hydrogen for 2 h and was evacuated for 1.5 h at 300 °C. The reaction temperature was fixed at 120±2 °C in order to prevent a secondary reaction. The exchange reaction with deuterium was investigated by IR, mass spectrometry, and gas chromatography (alumina+2% $MnCl_2$ column).

† Present address: Research Laboratory of Resources Utilization, Tokyo Institute of Technology, Midori-ku, Yokohama 227.

Results and Discussion

Decomposition of Methylamine. The decomposition of methylamine over ruthenium black was investigated in the presence and absence of hydrogen, which are shown in Figs. 1 and 2, respectively. In the presence of hydrogen (Fig. 1a) ammonia and methane were produced simultaneously, but the amount of ammonia was more than that of methane. This indicates that carbon is deposited on the catalyst during the reaction. (The deposited carbon may be partially hydrogenated in the presence of hydrogen, which will hereafter be designated as CH_x(a).) The rate of reaction became slower as the reaction proceeded, and small amounts of hydrocarbons in the range of C_2—C_4 were also produced in the later stage if the reaction was prolonged. (The ratio of ethane to methane was ≈0.07.) After evacuation for about 5 min, the gas mixture of methylamine and hydrogen was introduced again to the catalyst on which CH_x(a) had been accumulated (Fig. 1b). Rapid production of ammonia was not observed this time, but ammonia and methane were produced proportionally and almost stoichiometrically. The formation of higher amines over ruthenium black was not observed although the production of larger amounts of higher amines have been reported over Pd, Pt, and W films.[1,4]

The decomposition of methylamine occurred readily even in the absence of hydrogen (Fig. 2a), producing ammonia and hydrogen, whereas the production of methane was not detected under this reaction condi-

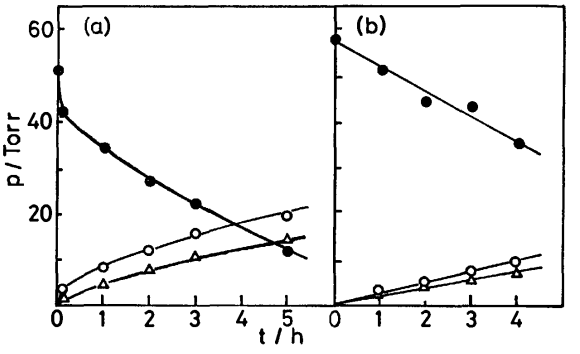

Fig. 1. (a) Reaction of CH_3NH_2 (51 Torr, 1 Torr= 133.3 Pa) and H_2 (241 Torr) over a Ru black at 120±2 °C; (b) reaction of CH_3NH_2 (58 Torr) and H_2 (241 Torr) over CH_x deposited Ru black at 120±2 °C; ●: CH_3NH_2, ○: NH_3, △: CH_4.

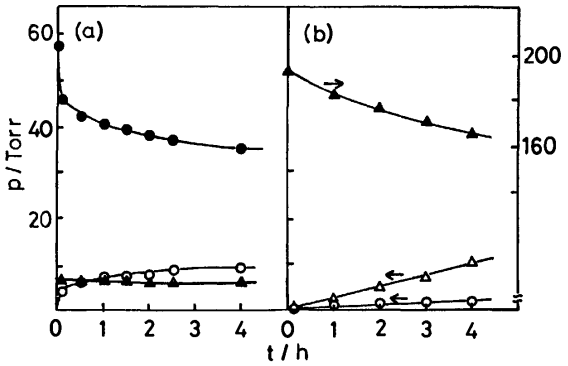

Fig. 2. (a) Decomposition of CH_3NH_2 (57 Torr) over clean Ru black at 120±2 °C; (b) hydrogenation (H_2, 200 Torr, 120 °C) of surface species after decomposition of CH_3NH_2; ●: CH_3NH_2, ○: NH_3, △: CH_4, ▲: H_2.

tion, and the reaction was almost stopped after 1 h. After evacuation for 5 min, only hydrogen was introduced onto the catalyst (Fig. 2b). A large amount of methane was produced, whose rate of formation was almost equal to that of steady-state conditions.

The exchange reaction of ammonia or hydrogen with deuterium and the hydrogenation of olefins during hydrogenolysis of methylamine were very fast and finished within 10 min, which indicates that chemisorption of hydrogen is not inhibited even in the presence of methylamine.

The dependences of the formation of methane and ammonia on the pressures of methylamine and hydrogen were examined. The formation of methane and ammonia was independent of the pressure of methylamine, but increased with increasing the pressure of hydrogen. The dependence of the formation of methane on hydrogen pressure was determined to be 0.9± 0.1, but that of ammonia could not be estimated because of the scatter of data. The independency of amine pressure suggests that the surface must be substantially covered by adsorbed amine under the experimental conditions. The increase of the reaction rate with increasing hydrogen pressure suggests that the removal of CH_x(a) from the surface with hydrogen may be an important process.

On the basis of the above mentioned experimental results, the reaction mechanism is considered as shown in Fig. 3. The decomposition of methylamine occurs

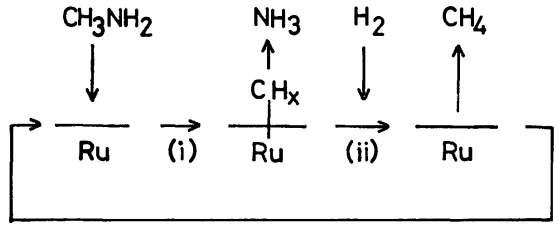

Fig. 3. Mechanism of hydrogenolysis of CH_3NH_2.

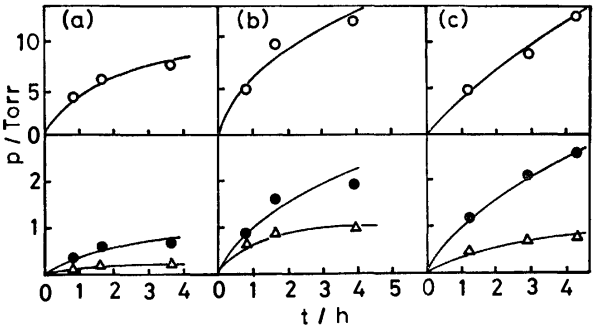

Fig. 4. Hydrogenation of surface hydrocarbon species after various of amines over 3 g Ru black at 120 °C; (a) $CH_3NH_2+H_2$ (20 h), (b) CH_3NH_2 decomposition (4.5 h), and (c) $C_2H_5NH_2$ decomposition (4.5 h); ○: CH_4, ●: C_2H_6, △: C_3H_8.

rapidly over freshly reduced ruthenium black even in the absence of hydrogen (step (i)), and then CH_x(a) is hydrogenated to methane slowly (step (ii)).

Hydrogenation of CH_x(a) after Various Reactions of Amines over Ruthenium Black. In order to investigate the nature of CH_x(a) produced from amines, the hydrogenation of CH_x(a) was carried out after various reactions of amines. The results are shown in Fig. 4 and Table 1. Main hydrogenation product was methane in all the cases, but the ratios of higher hydrocarbons to methane and the production rates were dependent on the way CH_x(a) was formed. The ratios of higher hydrocarbons to methane were larger in the hydrogenation of CH_x(a) produced from methylamine decomposition than that produced from the reaction of methylamine and hydrogen. This fact suggests that the CH_x(a) species produced from the reaction of methylamine and hydrogen is more easily hydrogenated to form methane than that from methylamine decomposition.

In the decomposition of methylamine and ethyl-

Table 1. Hydrogenation of surface species after various reactions of amines over Ru black (120 °C, 3 g-catalyst)

Reactions	Products of the hydrogenation of surface species						
	C_1	C_2	C_3	C_4	C_2/C_1	C_3/C_1	C_4/C_1
	Torr						
$CH_3NH_2 + H_2$ (20 h)[a)]	4.2	0.3	0.1	0.07	0.07	0.03	0.02
CH_3NH_2 decomp (4.5 h)[b),c)]	5.0	0.9	0.7	0.2	0.18	0.14	0.04
$C_2H_5NH_2$ decomp (4.5 h)[b),d)]	4.8	1.2	0.5	0.3	0.25	0.1	0.06

a) The time of hydrogenation is 50 min. b) Production of ammonia is almost stopped after 4.5 h. c) Amount of evolved ammonia is 28.7 Torr, and the time of hydrogenation is 50 min. d) Amount of evolved ammonia is 28.3 Torr, and the time of hydrogenation is 70 min.

amine, the same amount of ammonia was evolved, but when these CH_x(a) species were hydrogenated, smaller amount of methane and larger amount of ethane were produced in the case of ethylamine. Consequently, it is considered that CH_x(a) produced from the decomposition of ethylamine preserves the C–C bond to some extent. In the reaction of ethylene and hydrogen over clean ruthenium black at 120 °C, the hydrogenation of ethylene occurred rapidly and only a small amount of methane was produced. Therefore, the C–C bond is much more stable than the C–N bond over ruthenium black. Since CH_x(a) produced from amines has reactivity to produce C–C bonds, it may be similar to CH_x(a) species accumulated during CO–H_2 reaction over ruthenium metal.

References

1) C. Kemball and R. L. Moss, *Proc. R. Soc. London, Ser. A*, **238**, 107, (1956).
2) C. Kemball and R. L. Moss, *Proc. R. Soc. London, Ser. A*, **244**, 398, (1958).
3) R. L. Moss and C. Kemball, *Trans. Faraday Soc.*, **56**, 154, (1960).
4) J. R. Anderson and N. J. Clark, *J. Catal.*, **5**, 250, (1966).

 © 1983 The Chemical Society of Japan Bull. Chem. Soc. Jpn., 56, 3393—3399 (1983)

Amorphous Ni–Ti and Ni–Zr Alloys for Water Electrolysis Cathode Materials

Ken-ichi MACHIDA, Michio ENYO,* Isamu TOYOSHIMA, Koshiro MIYAHARA, Kenzo KAI,† and Kenji SUZUKI†

Research Institute for Catalysis, Hokkaido University, Sapporo 060

†*The Research Institute for Iron, Steel, and Other Metals, Tohoku University, Sendai 980*

(Received May 13, 1983)

Amorphous Ni–Ti and Ni–Zr alloys for their possible use in water electrolysis cathode materials were investigated. The hydrogen electrode reaction in 1 M NaOH (1 M=1 mol dm^{-3}) proceeds *via* the Volmer-Tafel reaction route with mixed rate-determining characteristics. The electrocatalytic activity is augmented significantly with a treatment of the alloy electrodes with aq HF. Thus, the exchange current density reaches 10^{-3} A cm^{-2} (apparent) at 303 K. The activation energy values are 9.4, 5.5, and 6.1 kcal mol^{-1} (1 cal=4.184 J) for the Volmer and Tafel step and the overall reaction, respectively. Surface analyses of the electrodes have indicated that such a high activity is caused by a stable porous Ni layer which is formed on the surface by the acid treatment. Such a porous Ni layer was not effectively formed if the alloys were in crystalline states.

Hydrogen is noted as a possible candidate for an energy carrier in the future as it is clean and fully recycleable substance of practically unlimited supply.[1] The energy system with hydrogen would consist mainly of three processes, the generation, transport or storage, and utilization. For its generation, the electrolysis of water is a simple and well established technique but, to make the technique economically practicable, improvements in electrode materials towards a minimized energy consumption are required.

Most of amorphous alloys prepared by a rapid quench from their melts, in general, possess high mechanical and corrosion resistant properties, and hence some of them have already been investigated for catalyst or electrode materials uses.[2,3] Also, a number of amorphous alloys, such as Ni alloys, containing, Ti, Zr, or Th, have been investigated towards hydrogen storage materials since they are not pulverized upon absorption and liberation of hydrogen and, in addition, have an improved amount and rate of absorption of hydrogen as compared with the corresponding crystalline alloys.[4] This indicates that there might be a possibility of using the amorphous alloys not only for a hydrogen evolving cathode but also for a hydrogen storage electrode.

One of the present authors investigated ealier the kinetics and mechanism of the hydrogen electrode reaction on Pd, a typical hydrogen absorbing metal.[5] It has been shown that the component overpotentials for each of the constituent steps are individually observable owing to the existence of a large amount of hydrogen stored in the electrode metal. Analysis of the overpotential rise and decay transient curves has shown that the hydrogen electrode reaction on Pd is comprised of two elementary steps, namely, Volmer and Tafel processes. The reaction rates of the elementary steps have thence been evaluated.

In this paper, we report the hydrogen electrode reaction characteristics of amorphous Ni–Ti and Ni–Zr alloys. In particular, the relationship between the electrodic property and the surface state of these electrodes will be discussed.

Experimental

Preparation of Electrodes. The amorphous alloys were prepared from the melts by a rapid quenching using a single roller type apparatus.[6] The specimens are of the following compositions, $Ni_{0.27}Ti_{0.73}$, $Ni_{0.33}Ti_{0.67}$, $Ni_{0.40}Ti_{0.60}$, $Ni_{0.25}Zr_{0.75}$, $Ni_{0.33}Zr_{0.67}$, $Ni_{0.50}Zr_{0.50}$, and $Ni_{0.65}Zr_{0.35}$. The crystalline Ni–Ti and Ni–Zr alloys were obtained by annealing the amorphous alloys at 873—1073 K for 30 min under a He atomosphere (20—30 kPa). The phase transition from the amorphous to the crystalline phase was monitored by observing changes of the electric conductivity and detected later by an X-ray diffraction analysis.

The specimens were in the shape of a ribbon, 0.6—1.4 mm in width, *ca.* 20 μm in thickness, and 1—2 cm in length, with the apparent surface area of 0.05—0.15 cm^2. Their ends were spot-welded to nickel wire which was in turn sealed into 8 mmϕ Pyrex glass tubings with epoxy resin ("Torr Seal" Varian Associates). These electrodes were treated with hot concentrated H_2SO_4, aqua regia, or 1 M HF solution in order to remove the oxide film on the surface (see below).

Electrochemical Measurements. The electrochemical measurements were carried out in a three compartment Pyrex glass electrolysis cell under a stream of H_2. A platinized Pt electrode was also used for comparison. The electrolytic solution, 1 M NaOH, was prepared from special grade NaOH (Merck Japan, Ltd.) with water from a Millipore pure water system. The temperature was controlled by a thermostat at 303 K except for the temperature dependence experiments. Details of the method and apparatus of the electrochemical measurements were described in a previous paper.[7]

X-Ray Photoelectron Spectroscopy. The surface analysis was performed by employing an ESCA apparatus (VG-III). Ar^+ bombardments were carried out at a condition of 800 eV and 3 μA cm^{-2} for 20 min in order to remove adsorbed carbon or hydroxyl groups from the surface of the alloys and to enhance the sensitivity of the detection. The spectra obtained were calibrated with the $4f_{7/2}$ peak from an Au plate which was employed as an internal standard. In order to avoid the overlap of the main spectra of Ti or Zr and Ni with their Auger signals, Al $K\alpha$ and Mg $K\alpha$ radiations were used for the Ni–Ti and Ni–Zr alloys, respectively.

Results and Discussion

Electrochemical Properties. The electrocatalytic activity of the amorphous Ni–Ti and Ni–Zr alloy electrodes in as-obtained form or after treatments with hot concentrated H_2SO_4 or aqua regia were very low and the reversible hydrogen electrode potential was not observed. However, when the samples, both the amorphous and crystalline alloys, were etched with a HF solution (1 M) for several minutes, the activity was strongly enhanced and the reversible potential was established. Alloys with relatively high Ni contents tended to require longer periods of time of the HF-treatment for the activation.

The galvanostatic overpotential rise transients give the rapidly growing overpotential component, η_1, which has the characteristics attributable to the Volmer process.[5,8] In Fig. 1 are shown the cathodic and anodic polarization behaviors with respect to η_1 on a series of the amorphous Ni–Ti alloys. The cathodic and anodic polarization curves appear to be essentially symmetrical with each other about the abscissa. This is expressed in terms of the symmetry factor β, which can be evaluated if we calculate the cathodic unidirectional current i_{-v}, by the relation,[5,8] $i_{-v}=i_{ov}\exp[-\beta F\eta/RT]=i/[1-\exp(F\eta/RT)]$. This is also shown in Fig. 1, a dashed line ($Ni_{0.27}Ti_{0.73}$), which gives almost a straight line with the slope of ≈ 95 mV or $\beta\simeq 0.63$. It is, therefore, concluded that η_1 represents the overpotential component responsible for an one electron transfer reaction, namely the Volmer (discharge) step.

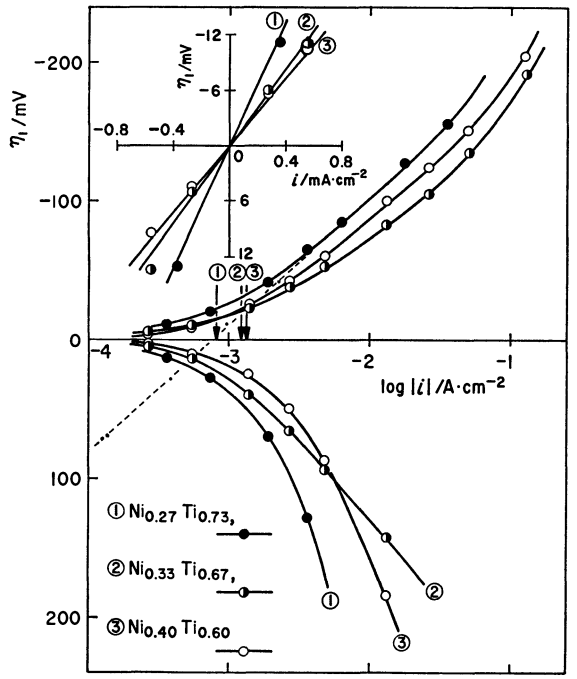

Fig. 1. Cathodic and anodic polarization behaviors of the rapidly rising overpotential component η_1 on a series of amorphous Ni-Ti alloys. The arrows on the abscissa indicate i_{ov} as evaluated from the linear plots (the inset figure) of η_1 *vs.* i near the reversible hydrogen electrode potential. 1 M NaOH, 303 K.

The exchange current density i_{ov} of the Volmer step has been evaluated[8] from the slope of a linear plot

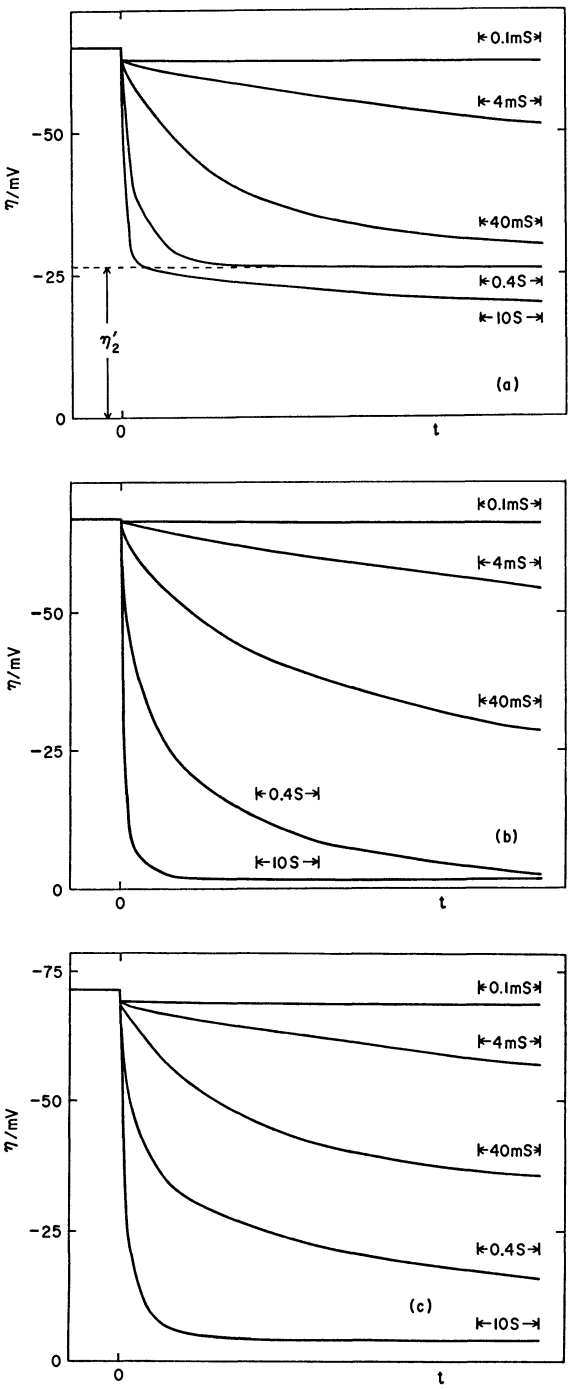

Fig. 2. Overpotential decay transients with various time scales. 1 M NaOH, 303 K.
(a) Amorphous $Ni_{0.33}Ti_{0.67}$ alloy electrode after a treatment with 1 M HF solution. $i=2.40$ mA cm^{-2} (apparent). (b) Crystalline $Ni_{0.33}Ti_{0.67}$ alloy electrode after a treatment with 1 M HF solution. $i=0.27$ mA cm^{-2} (apparent). (c) Amorphous $Ni_{0.33}Zr_{0.67}$ alloy electrode after a treatment with 1 M HF solution. $i=1.91$ mA cm^{-2} (apparent).

†† The current density and the exchange current densities are given, unless otherwise stated, on the apparent unit area basis.

of η_1 *vs.* current density at low overpotentials (the polarization resistance, r_1) with $i_{oV}=(RT/F)/r_1$. On the amorphous Ni–Ti alloy electrodes, i_{oV} was found to be of the order†† of 10^{-3} A cm^{-2} and did not depend appreciably on the alloy composition. The values are indicated by the arrows on the abscissa in Fig. 1.

The overpotential decay transients at various time scales on the amorphous and crystalline $Ni_{0.33}Ti_{0.67}$ alloy electrodes are shown in Figs. 2(a) and 2(b), respectively. The overpotential on the amorphous electrode decayed rapidly up to about 1 sec but, after that, the decay rate was greatly diminished so as to require several minutes for its complete decay (Fig. 2(a)). On the crystalline alloy electrodes, on the other hand, the overpotential decayed much more rapidly and no plateau was observed on the transient curves (Fig. 2(b)). These observations suggest that the rate of hydrogen absorption into or liberation from the amorphous Ni–Ti alloys is very rapid as compared with the surface reaction, but that may not be the case with the crystalline alloys.

The slowly decaying overpotential component η_2' is defined at the moment of completion of the initial rapid overpotential decay upon the termination of the polarization current. This was readily evaluated on the amorphous Ni–Ti electrodes by extrapolating the plateau on the overpotential decay curves, such as that in Fig. 2(a), to $t=0$. Results are shown in Fig. 3, together with the total overpotential η on the amorphous or cyrstalline Ni–Ti alloys, and also η on a platinized Pt electrode. The slope of the Tafel lines for η_2' was around 30 mV and the exchange current density value, evaluated by $i_{oT}=(RT/2F)/r_2'$ where r_2' is the polarization resistance with respect to η_2', was around 0.4×10^{-3} A cm^{-2}. The fact that the latter value is not much different from i_{oV} reported above indicates that the hydrogen electrode reaction is of mixed rate-determining type.

The Tafel slope and the exchange current density values associated with η_2' suggest, along with the Tafel (H(a) recombination) step, a significant contribution to η_2' of the H_2 diffusion process in the solution phase. To see this, the diffusion overpotential in the present experimental system was evaluated separately using a Au electrode of a similar dimension. As the overpotential on Au decays very rapidly (time constant $\approx10^{-3}$ s) except for a component attributed to the concentration overpotential due to H_2 diffusion, the overpotential decay transients could reveal only the latter component (the time constant $\approx10^{0}$ s). Results indicated that the concentration overpotential is of comparable magnitude with η_2'. This means that i_{oT} as determined from η_2' is in fact for the Tafel-plus-diffusion processes and hence the intrinsic value for the Tafel step should be considerably greater than the value quoted above or given below in Table 1.

The linear portion of the Tafel line with respect to the total overpotential η in the cathodic region has the slope of about 120 mV and its extrapolation to $\eta=0$ gives the exchange current density $i_{o,ext}$ of the order of 10^{-3} A cm^{-2}. It has been shown earlier from a general analysis of the mixed rate-determining Volmer-Tafel reaction[8] that the kinetics at high cathodic overpotentials should practically be determined by the Volmer step. This means that the electrocatalytic activity of the electrode under (deep) cathodic polarization is approximately represented by i_{oV} and not i_o or i_{oT}. Indeed, comparison of Fig. 3 with Fig. 1 reveals that $i_{o,ext}$ is in fair agreement with i_{oV} reported above.

In Table 1 are summarized the exchange current densities and the double layer capacitance obtained on the amorphous or crystalline Ni–Ti alloys, a Ni wire (0.25 mmϕ), and a platinized Pt electrode.

The exchange current density i_o of the overall reaction on the amorphous Ni–Ti electrodes is calculated from i_{oV} and i_{oT} by the relation,

$$\frac{1}{i_o}=\frac{1}{i_{oV}}+\frac{1}{i_{oT}}.$$

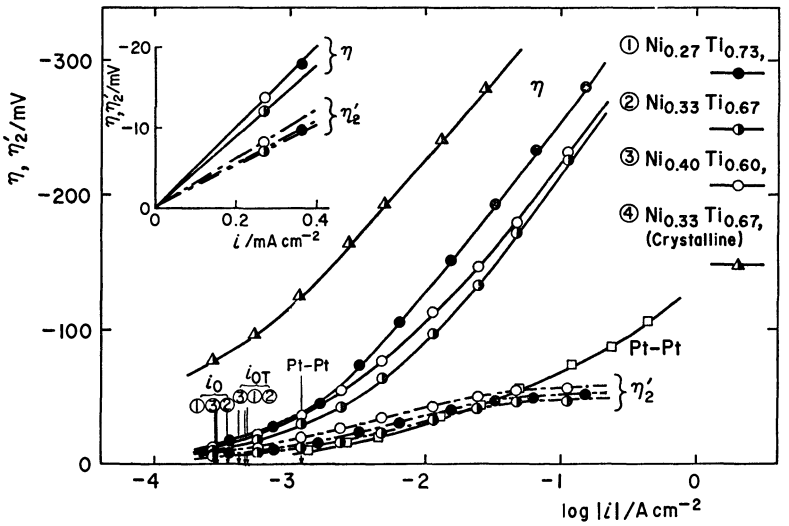

Fig. 3. Cathodic polarization behaviors of the total overpotential η and slowly decaying overpotential component η_2' on a series of amorphous and crystalline Ni–Ti alloy electrodes and on platinized Pt electrode. The arrows on the abscissa indicate i_o and i_{oT} obtained at low overpotentials (the inset figure). 1 M NaOH, 303 K.

Table 1. Exchange current densities[a] of the elementary steps and the overall reaction and the double layer capacitance on the cathodes of a series of Ni–Ti alloys in 1 M NaOH at 303 K

Composition	State	i_{oV} / mA cm^{-2}	i_{oT} / mA cm^{-2}	i_o / mA cm^{-2}	$i_{o,ext}$ / mA cm^{-2}	C / mF cm^{-2}
$Ni_{0.27}Ti_{0.73}$	Amorphous	0.82	0.47	0.28	0.83	2.3
$Ni_{0.33}Ti_{0.67}$	Amorphous	1.22	0.49	0.35	1.80	4.7
$Ni_{0.40}Ti_{0.60}$	Amorphous	1.32	0.37	0.29	1.60	2.1
$Ni_{0.33}Ti_{0.67}$	Crystalline				0.10	0.4
Ni	Crystalline				0.006	0.1
Pt–Pt	Crystalline			1.22		40.2

a) Per apparent unit area.

As mentioned above, i_o should not be identified with $i_{o,ext}$ in mixed rate-determining reactions such as in the present case ($i_o < i_{o,ext} \simeq i_{oV}$).

The evaluation of the step rates from the component overpotentials was not possible on the crystalline Ni–Ti electrode or on the Ni wire electrode. Accordingly, only $i_{o,ext}$ values are given, which may be compared with i_{oV}, at least approximately, as discussed above.

It is seen in Table 1 that the amorphous Ni–Ti alloy electrodes have electrocatalytic activities higher than the crystalline alloy electrode and far greater than that of the pure Ni electrode. The rate can further be increased if the H_2 diffusion rate were raised by improved stirring, *etc.* Even in the present stage, the activity is almost comparable with that of a smooth Pt electrode, particularly at low current densities.

It was seen that such a high electrocatalytic activity on the amorphous alloy electrodes were caused by a very large roughness factor value that was realized. The factor is evaluated from the capacitance values in Table 1 to be several hundreds, if one assumes a value of 18 μF cm^{-2} usually observed on Hg electrode to be the value per true unit area. Such an increase of the surface roughness factor must be a result of dissolution of the component metal Ti in the alloys by the treatment with hydrofluoric acid. If one counts $i_{o,ext}$ per true unit area on the amorphous and crystalline alloys, they are always in the range of 10^{-6}—10^{-5} A cm^{-2} (true) and are very close to that generally observed on smooth Ni electrodes. This is an indication that the electrocatalytic activity is caused by the layer of Ni and not by Ti.

The heat of activation determined from the Arrhenius plots of the exchange current densities (Fig. 4) on the amorphous $Ni_{0.33}Ti_{0.67}$ electrode was about 9.4, 5.5, and 6.1 kcal mol^{-1} for the Volmer and Tafel/diffusion step and the overall reaction, respectively. The value for the Volmer process was well comparable with the corresponding value of 8 kcal mol^{-1} observed on Pd.[8] The value for the Tafel/diffusion process is larger than *ca.* 3 kcal mol^{-1} anticipated for the diffusion process itself and thus indicates a significant contribution from the Tafel step which is likely[8] to be associated with some 6 kcal mol^{-1}.

The overpotential decay transients on the amorphous Ni–Zr alloy ($Ni_{0.33}Zr_{0.67}$) are shown in Fig. 2(c). The overpotential on both the amorphous and

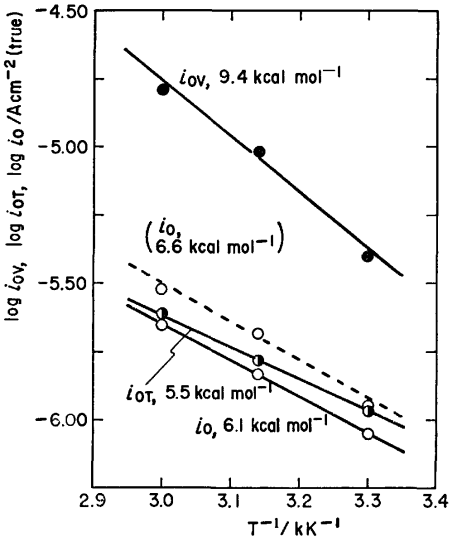

Fig. 4. Arrhenius plots of the exchange current densities and corresponding activation heats of the Volmer and Tafel step and the overall reaction on the amorphous $Ni_{0.33}Ti_{0.67}$ alloy electrode. The dashed-line and the value in the parenthesis represent those of i_o on the amorphous $Ni_{0.33}Zr_{0.67}$ alloy electrode. 1 M NaOH.

crystalline Ni–Zr alloys decayed rapidly with no plateau, and hence the kinetics of the component elementary reactions were not obtainable. Likewise, the evaluation of η_1 from the galvanostatic overpotential rise transients were not practicable.

The overall polarization characteristics on the amorphous or crystalline Ni–Zr alloys are shown in Fig. 5. It is seen that the electrodic characteristics are very similar with those of the Ni–Ti alloys. Thus, the slope of the Tafel line is around 120 mV and $i_{o,ext}$ is around 10^{-3} A cm^{-2}. One may hence conclude that the hydrogen electrode reaction on these alloys also proceeds *via* the Volmer-Tafel route with practically the same electrocatalytic activities, respectively, with the amorphous or crystalline Ni–Ti alloys reported above.

The polarization resistance around the reversible potential gives the values of i_o which are roughly in one order of magnitude smaller than $i_{o,ext}$. Along the line of arguments presented above, this fact may indicate that i_{oT} is at least several times smaller than

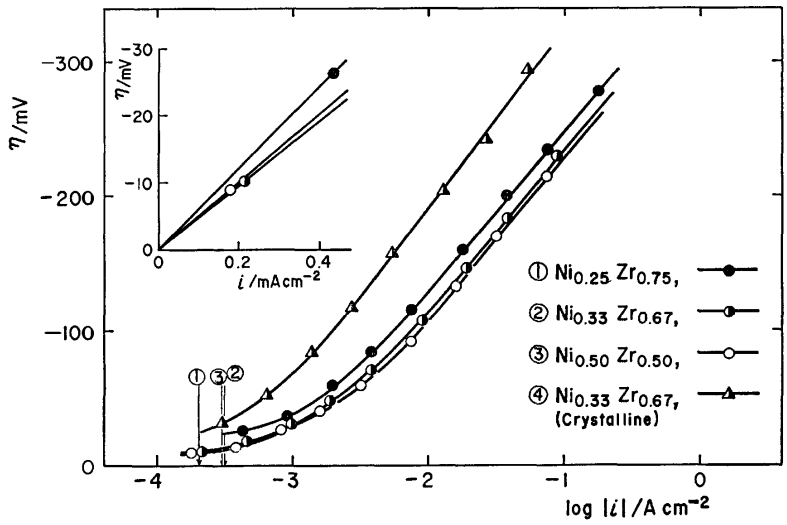

Fig. 5. Cathodic polarization behaviors of the total overpotential η on a series of the amorphous and crystalline Ni-Zr alloy electrodes. The arrows on the abscissa indicate i_0 obtained at low overpotentials (the inset figure). 1 M NaOH, 303 K.

Table 2. Exchange current densities[a] and double layer capacitance on the cathodes of a series of Ni–Zr alloys in 1 M NaOH at 303 K

Composition	State	i_0	$i_{0,ext}$	C
		mA cm^{-2}	mA cm^{-2}	mF cm^{-2}
$Ni_{0.25}Zr_{0.75}$	Amorphous	≈0.2	0.81	5.0
$Ni_{0.33}Zr_{0.67}$	Amorphous	≈0.3	1.10	4.1
$Ni_{0.50}Zr_{0.50}$	Amorphous	≈0.3	1.30	2.8
$Ni_{0.33}Zr_{0.67}$	Crystalline		0.34	0.9

a) Per apparent unit area.

i_{oV} and hence $i_o \simeq i_{oT}$. Values of i_o are hence evaluated by $i_o=(RT/2F)/r$ with $r=(d\eta/di)_{\eta\to 0}$ in a similar manner as i_{oT}. These are indicated by arrows in Fig. 5.

The exchange current density and the double layer capacitance obtained on a series of the amorphous Ni–Zr alloys and the crystalline $Ni_{0.33}Zr_{0.67}$ alloy are given in Table 2. Electrocatalytic activity measurements on $Ni_{0.65}Zr_{0.35}$ were unsuccessful because of its very low activity. The values of i_o on the amorphous Ni–Zr alloys was 0.2—0.3 mA cm^{-2}. As seen from Fig. 5, the electrocatalytic activity of the amorphous Ni–Zr alloys is considerably higher than that of the crystalline ones as in the case of the Ni–Ti systems. Also, it can be seen from Table 2 that the amorphous Ni–Zr alloys give nearly the same values of the double layer capacitance as on the amorphous Ni–Ti alloys and hence their true surface area is also very large.

The heat of activation was determined only for the overall reaction. It was 6.6 kcal mol^{-1} on the $Ni_{0.33}Zr_{0.67}$ alloy, as already shown in Fig. 4.

Surface Characterization. Surface analysis of the Ni–Ti or Ni–Zr alloy electrodes before and after the treatment with hydrofluoric acid were performed using the X-ray photoelectron spectroscopy (XPS) method. In Fig. 6 are recorded typical XPS spectrum patterns on the amorphous $Ni_{0.33}Ti_{0.67}$ and $Ni_{0.33}Zr_{0.67}$ alloys over a wide range of the binding energy. The non-treated (as-obtained) alloys, spectra a) ($Ni_{0.33}Ti_{0.67}$) and c) ($Ni_{0.33}Zr_{0.67}$), gave the signals with strong intensity of Ti or Zr and O, whereas the peaks to be assigned to Ni were very weak and almost undetectable. On the other hand, on the HF-treated samples, the

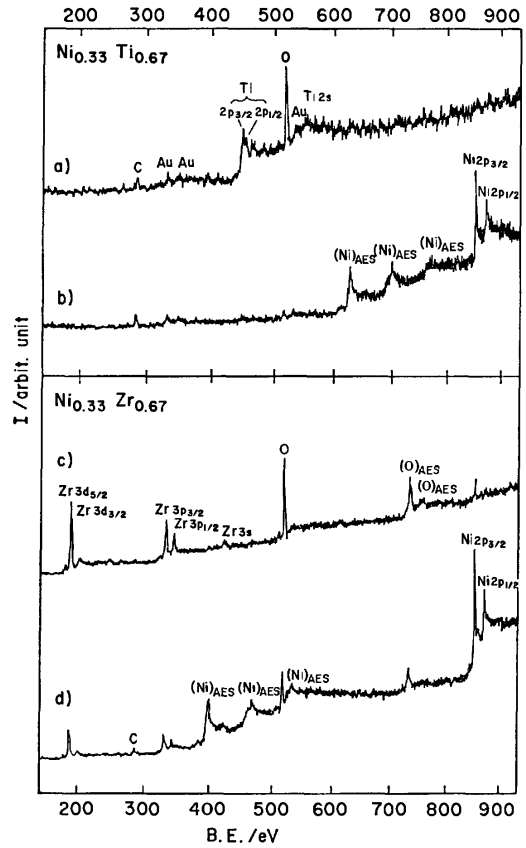

Fig. 6. XPS spectrum patters of the amorphous $Ni_{0.33}Ti_{0.67}$ and $Ni_{0.33}Zr_{0.67}$ alloys obtained with a wide range scan of the binding energy (*B.E.*=0—1000 eV). The X-ray source employed was Al $K\alpha$ for $Ni_{0.33}Ti_{0.67}$ and Mg $K\alpha$ for $Ni_{0.33}Zr_{0.67}$, respectively. a) and c), nontreated specimens; b) and d), HF-treated specimens.

XPS and Auger electron spectra from Ni increased remarkably while the signals of Ti or Zr were diminished (spectra b) and d)).

Figure 7 shows the XPS spectra ascribed to the Ti_{2p} or Zr_{3d} and the O_{1s} electrons from the nontreated amorphous $Ni_{0.33}Ti_{0.67}$ and $Ni_{0.33}Zr_{0.67}$ alloys. The signals of $Ti_{2p3/2}$ (or $Ti_{2p1/2}$) consists of three bands, as deconvoluted in Fig. 7, with the peak values around 455, 457, and 459 eV (or 461, 463, and 464.5 eV). These are attributable to metallic Ti or two oxides, Ti_2O_3 and TiO_2, on the basis of the data given in a handbook.[9] The Ti_2O_3 was probably formed from TiO_2 by the Ar^+ bombardments.[10] The $Ti_{2p3/2}$ and $Ti_{2p1/2}$ signals gave energy differences of 6.1 eV for metallic Ti or Ti_2O_3 and 5.6 eV for TiO_2. These values are in good agreement with the values in the literatures[9,11] for titanium in such valence states.

For the $Zr_{3d5/2}$ and $Zr_{3d3/2}$ electrons, there are each two bands respectively assigned to the Zr metal and its oxide (ZrO_2), with the peak positions about 179 or 182 eV for the former zirconium and about 183 or 185 eV for the latter one. The energy gaps of $Zr_{3d5/2}$ and $Zr_{3d3/2}$ were 2.3—2.4 eV as expected.[9] The O_{1s} signals are attributable to the lattice oxygens of Ti_2O_3, TiO_2, or ZrO_2. The XPS profiles similar to the Ti_{2p}, Zr_{3d}, or O_{1s} spectra in Fig. 7 were observed on the other amorphous or crystalline alloys.

The findings indicate that most of Ti or Zr on the surface of the alloys exists as dioxide, *viz.* TiO_2 or ZrO_2. On the other hand, the peak positions of $Ni_{2p3/2}$ and $Ni_{2p1/2}$ (≈853 and 870 eV) and the energy differences between these signals (≈17 eV) indicate that the nickel on the surface is metallic.

The surface atomic ratios, $C^S_{Ni/Ti}$ and $C^S_{Ni/Zr}$, were calculated from the integral peak intensity (I) of Ni_{2p} and $Ti_{2p3/2}$ or $Zr_{3d5/2}$, after taking into account their atomic sensitivity factors (S)[9] for X-ray in the following equation:

$$C^S_{Ni/M} = (I_{Ni}/S_{Ni})/(I_M/S_M), \quad M = Ti, Zr,$$

where the values employed were $S_{Ni}=5.4$, $S_{Ti}=1.1$, and $S_{Zr}=0.87$. The relationship between the surface and bulk Ni/Ti and Ni/Zr atomic ratios is shown in Fig. 8. It is seen that $C^S_{Ni/Ti}$ or $C^S_{Ni/Zr}$ values on the nontreated (amorphous and crystalline) samples are very low and entirely different from their bulk compositions. Thus, electrode surface is almost completely covered with a film of TiO_2 or ZrO_2. This explains why their electrocatalytic activity in the original form was so low that the reversible hydrogen electrode potential was hardly realized.

On the HF-treated alloys, the ratios $C^S_{Ni/Ti}$ and $C^S_{Ni/Zr}$ were found to be much higher than the values of $C^B_{Ni/Ti}$ and $C^B_{Ni/Zr}$ and this was particularly true on the amorphous alloys. It is conceivable that the concentration of Ni on the alloys would be increased by this treatment, above the level of its bulk composition, as hydrofluoric acid readily attacks the metal or oxides of Ti or Zr but not Ni. Further, the sufrace of the HF-treated alloys is very porous with the roughness factor as high as 300, as evaluated above from the

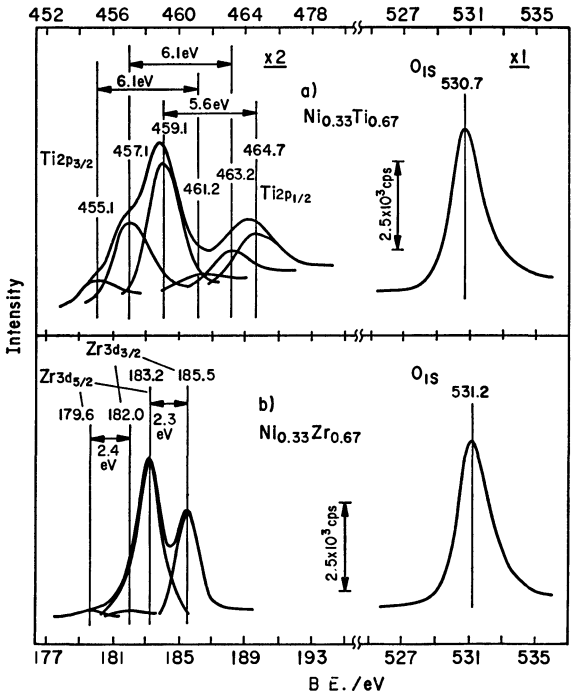

Fig. 7. XPS spectra of the Ti_{2p} or Zr_{3d} and the O_{1s} electrons from the amorphous $Ni_{0.33}Ti_{0.67}$ and $Ni_{0.33}Zr_{0.67}$ alloys (nontreated specimens). The X-ray source employed was Al $K\alpha$ for $Ni_{0.33}Ti_{0.67}$ and Mg $K\alpha$ for $Ni_{0.33}Zr_{0.67}$, respectively. The spectra of Ti_{2p} and Zr_{3d} were deconvoluted using Gaussian curves with reasonable half-band widths.

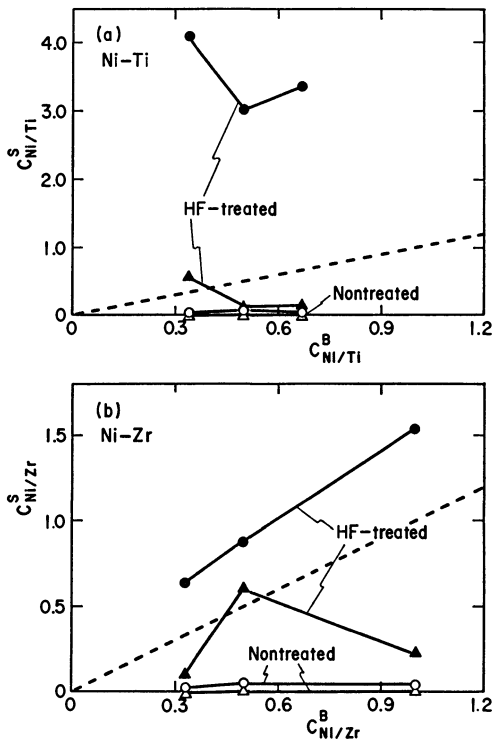

Fig. 8. Relationship between the surface and bulk atomic ratios ($C^S_{Ni/M}$ and $C^B_{Ni/M}$, M=Ti, Zr) of (a) Ni-Ti and (b) Ni-Zr alloys before and after the acid treatments. The dashed line represents a linear relationship of $C^S_{Ni/M}$ and $C^B_{Ni/M}$ when the surface concentration of the alloys is equal to the bulk one. Amorphous, ○ and ●; Crystalline, △ and ▲.

double layer capacitance (see Tables 1 and 2).††† The high electrocatalytic activity observed above is probably caused by the Ni-rich surface layer which is in the form of a Raney-type nickel. Indeed, the electrocatalytic activities per true unit area of the amorphous or cyrstalline Ni–Ti and Ni–Zr alloy electrodes are of the same order of magnitude with those on pure nickel electrodes.

It may be stressed that the amorphous, but not the crystalline, alloys could be readily brought to the state of very high roughness factor and hence of very high electrocatalytic activity by a simple acid treatment.

Conclusion

The amorphous Ni–Ti and Ni–Zr alloys after the treatment with aqueous HF have high electrocatalytic activity for the hydrogen electrode reaction in alkaline solutions. This is caused firstly by the removal of an inert film of TiO_2 of ZrO_2 from the surface, and secondly by producing a porous layer of Ni, which is stable on the amorphous alloys. Since the amorphous alloys in general show a high mechanical strength and high corrosion resistance, they can possibly be employed as water electrolysis cathode materials for hydrogen generation by water electrolysis.

††† The fact that the amorphous $Ni_{0.65}Zr_{0.35}$ alloy do not give an active electrode is likely to be due to a difficulty of removing Zr from the matrix by the acid treatments because of the high Ni content.

The present work is supported in part by Grants-in-Aid for Scientific Research No. 56119004 from the Ministry of Education, Science and Culture. Supports from the Mitsubishi Foundation, 1979, and from Ohtsuka Chemicals Co. Ltd. are also gratefully acknowledged.

References

1) G. G. Libowitz, "Hydrides for Energy Storage," ed by A. F. Andresen and A. J. Maeland, Pergamon Press, New York (1978), pp. 1—17.
2) A. Yokoyama, H. Komiyama, H. Inoue, T. Masumoto, and H. Kimura, *Shokubai*, **24**, 61 (1982).
3) a) M. Hara, K. Asami, K. Hashimoto, and T. Masumoto, *Electrochim. Acta*, **25**, 1091 (1980); b) K. Hashimoto and M. Hara, *Denki Kagaku*, **49**, 446 (1981).
4) a) A. J. Maeland, L. E. Tanner, and G. G. Libowitz, *J. Less-Common Met.*, **74**, 279 (1980); b) K. Aoki, A. Horata, and T. Masumoto, *Sci. Rep. Res. Inst. Tohoku Univ.*, **A29**, 218 (1981).
5) M. Enyo and T. Maoka, *J. Electroanal. Chem.*, **108**, 277 (1980).
6) M. Matsuura, M. Kikuchi, M. Yagi, and K. Suzuki, *Jpn. J. Appl. Phys.*, **19**, 1781 (1980).
7) T. Maoka and M. Enyo, *Surf. Technol.*, **8**, 441 (1979).
8) M. Enyo, *J. Electroanal. Chem.*, **134**, 75 (1982).
9) C. D. Wagner, W. M. Riggs, L. E. Davis, J. F. Moulder, and G. E. Muilenberg, "Handbook of X-Ray Phoelectron Spectroscopy," Perkin-Elmer Co., Physical Electronics Div. (1979).
10) B. A. Sexton, A. E. Hughes, and K. Foger, *J. Catal.*, **77**, 85 (1982).
11) T. L. Barr, *J. Phys. Chem.*, **82**, 1801 (1978).

Mechanism of Quenching of SO_2 $\tilde{C}(^1B_2)$ by He, Ar, and N_2

Takefumi Oka
Nagaoka Technical College, Nagaoka, Niigata 940

(Received May 23, 1983)

Sulfur dioxide gas was excited to $\tilde{C}(^1B_2)$ state by steady illumination and the total intensity and the spectrum of the fluorescence were measured in the SO_2 pressure range of 0.1—1 Torr (1 Torr≈133.322 Pa) both in the absence and in the presence of He, Ar, and N_2 up to 600 Torr. The observed fluorescence spectrum was broad but the wavelength of the maximum intensity was found to be dependent upon excitation wavelength in the range of 240—220 nm. Addition of foreign gases caused the blue shift of the fluorescence spectrum. The Stern-Volmer plots were nonlinear for quenching by the foreign gases but linear for self-quenching. It was suggested that the foreign gas molecules cause not only vibrational deactivation but also collision induced transition between $^1B_2$ state and a nonemitting state and that the rate constants of the transition to the nonemitting state are larger from higher vibrational levels than from lower ones.

Sulfur dioxide has three absorption systems in the ultra-violet region. The first weak absorption system ($400>\lambda>340$ nm) is due to $\tilde{a}(^3B_1)$ state and plays an important role in photochemistry in the lower atmosphere. The second system ($340>\lambda>250$ nm) consists of a banded structure due to $\tilde{A}(^1A_2)$ state and an underlying continuum due to $\tilde{B}(^1B_1)$ state. The fluorescence from this system shows nonexponential decay, indicating a strong coupling of $\tilde{A}(^1A_2)$ with $\tilde{B}(^1B_1)$. These two systems have been extensively studied.[1-4,13,18] On the other hand, only a few studies have been reported about the third system ($250>\lambda>175$ nm). A group of absorption bands in this system was once classified into two electronic states, α_1 and α_2 by Duchesne and Rosen[5] ($\tilde{C}$ and $\tilde{D}$ in Herzberg's summary[6]). Recently Brand and his co-workers have assigned these bands to one electronic state $^1B_2$ on the basis of the rotational analysis.[7-9]

Okabe examined absorption and fluorescence excitation spectra of this system and suggested the occurrence of predissociation below 220 nm.[10] He estimated quenching rate constant of one of the bands (at 220.6 nm in Fig. 2) by Ar to be 5×10^{-11} cm^3 molecule^{-1} s^{-1} by the intensity reduction on addition of Ar of 400 Torr assuming Stern-Volmer mechanism.

Hui and Rice studied the decay of the ten vibronic bands between 230 and 210 nm and observed simple exponential decay.[11] They measured the lifetimes and quantum yields of the fluorescence. The quantum yield was nearly unity at longer wavelengths, but decreased as wavelength approached to 220 nm and dropped abruptly below 220 nm. This abrupt change supports the occurrence of the predissociation below 220 nm. Observed radiative lifetimes were 30—50 ns while a lifetime calculated from the oscillator strength was 9 ns.

Very recently, quantum beat in the decay of $^1B_2$ due to the coupling with the ground electronic state was observed in a supersonic free jet.[12] As for fluorescence emission spectrum, only a broad spectrum centered at 320 nm was reported.[13,14]

In the present paper, the experimental results of self-quenching and foreign gas quenching will be presented and collision induced coupling of $^1B_2$ state with another state will be suggested.

Experimental

The sample gases were handled in a conventional vacuum line with a mercury diffusion pump. Pressure was measured with a mercury manometer and an oil manometer.

The excitation light beam was obtained with a combination of Ushio 500W Xenon lamp and Ritsu MC-20L monochromator, and passed through a T-shaped fluorescence cell along the principal axis. The geometric size of the cell with three quartz windows is shown in Fig. 1. The outside wall of the cell excluding the windows was painted black. The intensity of the transmitted light was monitored with a photomultiplier (1p28) behind the cell.

The emission was observed through a side window of the cell with an uncooled photomultiplier(HTV R585). The total intensity observed without any optical filters was used for quenching study. The excitation bandpass($\Delta\lambda_{ex}$) was 0.2 nm. The length of the view zone along the principal axis of the cell was about 3 cm (Fig. 1). For the measurements of fluorescence spectra, the second monochromator (JASCO CT-25N) was placed in front of the side window of the cell. The bandpasses used were $\Delta\lambda_{ex}=4$ nm for the excitation monochromator and $\Delta\lambda_{em}=9$ nm for the emission monochromator. The quantum efficiency of R585 was not constant over the range of 250—400 nm.[15] However, the correction for this effect did not affect the foreign gas quenching data.

A photon counter (HTV-C767) was used to count the number of photons emitted. The output of the counter and the 1p28 photomultiplier was fed into a two pen strip chart recorder. The nominal emission intensities were corrected for variation of the intensity of the excitation beam by using the intensity monitored with 1p28.

Sulfur dioxide synthesized from Na_2SO_3 and H_2SO_4 was bubbled through H_2SO_4, dryed over P_2O_5 and distilled *in vacuo* at −80 °C.

Helium, argon, and nitrogen used here were of purity

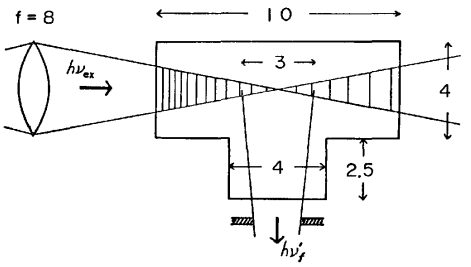

Fig. 1. Fluorescence cell. The unit of length is cm.

higher than 99.99% and passed through a liquid nitrogen trap before use. In the foreign gas quenching study, the cell was first filled with a certain pressure of SO_2 (mostly 0.8 Torr) and then a foreign gas of higher pressure (than 10 Torr) was added. The homogeneity of the mixture was confirmed by comparing the results obtained by this method with those of premixed sample. All the experiments were done at room temperature.

Results

Figure 2 shows the excitation spectrum of 0.9 Torr of SO_2 in the optical range of 240—216 nm. The vibrational assignment indicated in the figure is according to Brand.[6,8]

The bands located at wavelengths shorter than 225 nm could not be expressed by a combination of three normal modes because of the coupling of ν_1' and ν_3'. Quenching experiments were done with the resolved bands shown in Fig. 2. The emission spectra of 0.8 Torr SO_2 excited at various wavelengths are shown in Fig. 3. The emission spectra seemed to have structure[16] but the optical resolution in the present work ($\Delta\lambda_{ex}$=4 nm, $\Delta\lambda_{em}$=9 nm) was not high enough to resolve them. When the exciting light was changed to the longer wavelengths, the spectrum shifted to the blue.

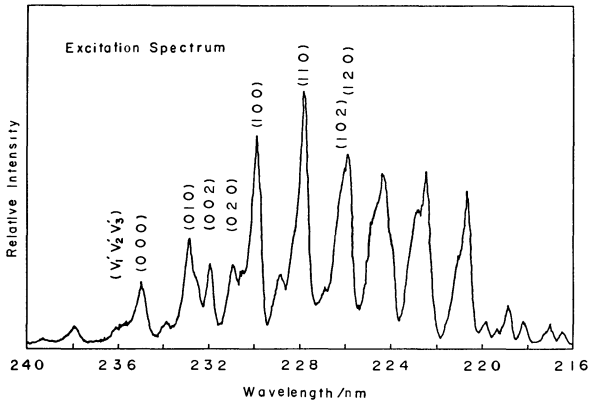

Fig. 2. Fluorescence excitation spectrum of $\tilde{C}^1B_2$ state. $p(SO_2)$=0.9 Torr and $\Delta\lambda_{ex}$=0.2 nm. The three figures in a parenthesis are a set of the vibrational quantum number of $^1B_2$ state, (v_1', v_2', v_3').

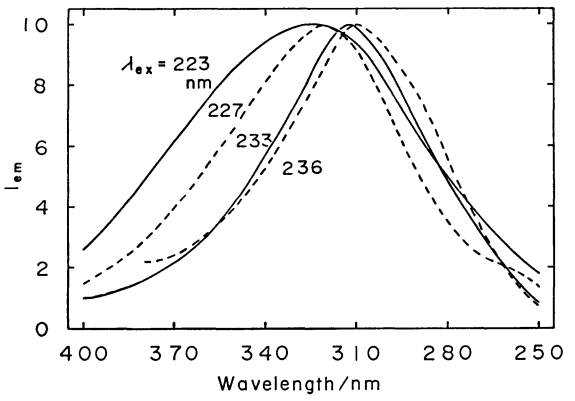

Fig. 3. Emission spectra excited at various wavelengths (λ_{ex}). $p(SO_2)$=0.8 Torr, $\Delta\lambda_{ex}$=4 nm, and $\Delta\lambda_{em}$= 9 nm. Spectra were not corrected for wavelength dependent sensitivity of the detection system.

The change of the emission spectrum due to the variation of SO_2 pressure from 0.1 to 1 Torr was negligibly small compared to that due to the high pressure foreign gas (*vide infra*). Foreign gas quenching of fluorescence excited at each vibronic band is shown in Fig. 4 for He, Fig. 5 for Ar, and Fig. 6 for N_2. The

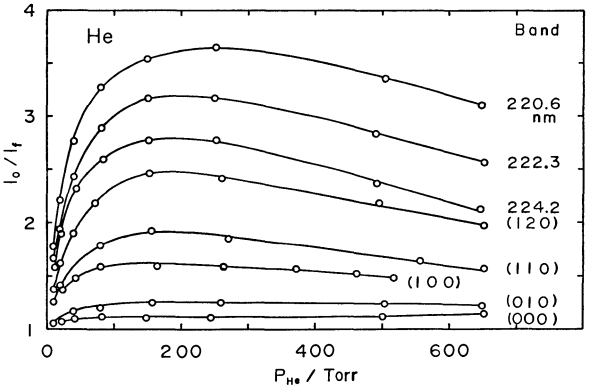

Fig. 4. Fluorescence quenching by He. $\Delta\lambda_{ex}$=0.2 nm and $p(SO_2)$=0.8 Torr. For the upper three curves, the bands are indicated by the wavelengths. I_f and I_0 are the fluorescence intensities with and without He, respectively.

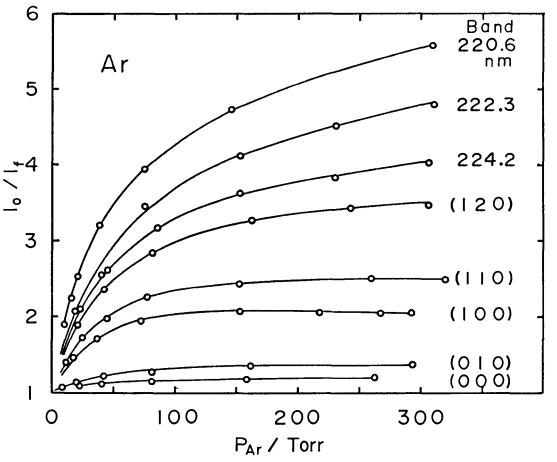

Fig. 5. Fluorescence quenching by Ar. See the legand of Fig. 4.

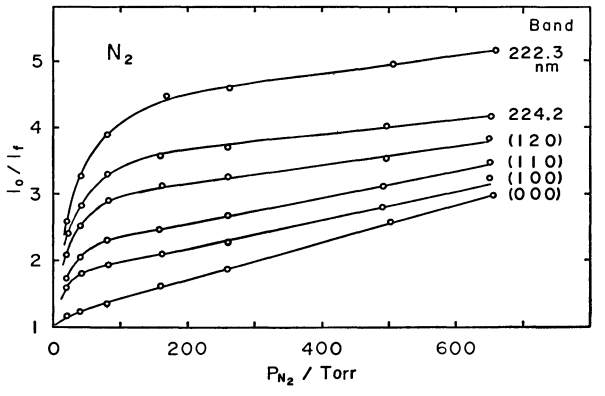

Fig. 6. Fluorescence quenching by N_2. See the legand of Fig. 4.

plots of I_0/I_F vs P_M are nonlinear, indicating that the quenching mechanism is not Stern-Volmer type.

As the foreign gas pressure increased from zero to about 200 Torr, intensity of emission decreased rapidly for all three gases. Above 200 Torr, the emission intensity showed different pressure dependence for the three gases, the intensity gradually increased for He, leveled off for Ar, and gradually decreased for N_2.[17]

The effects of addition of N_2 on the emission spectrum were the blue shift of the wavelength of emission maximum and the narrowing of the emission band width (Figs. 7-a,b).

The wavelength of maximum seems to converge to about 305 nm at the high pressure limit. The extent of the blue shift was large upon the excitation at shorter wavelengths.

The effects of addition of He and Ar on emission spectrum were similar to that of N_2. No difference among the three gases was observed upon the excitation at 233 nm. On the excitation at 223 nm, the efficiency of the effect decreased in the order of N_2, He, and Ar.

The self-quenching results of (110) band are compared in Fig. 8 for the cases in the absence and in the presence of high pressure argon. With Stern-Volmer mechanism, the straight lines with the same intercepts and with different slopes (larger in Ar) are expected. The plots in Fig. 8 show straight lines. However, the slope and the intercept in the presence of Ar are larger than those in the absence of Ar, though the difference in the intercepts is small. When He and N_2 were used in place of Ar, similar results were obtained. Table 1 summarizes the ratios of both the slope and the intercept in the presence of a foreign gas of about 200 Torr to those in the absence of the foreign gas.

Self-quenching was examined for each vibronic band of pure SO_2 in the SO_2 pressure range of 0.1—4 Torr. Self-quenching constants were determined as the ratio of intercept to slope in a plot of the type of Fig. 8 and are listed in the 2nd column of Table 3.

Discussion

Since the emission spectra were different for the excitation at different wavelengths as shown in Fig. 3, it can be said that the emitting species in pure SO_2 of 0.1—1 Torr is not vibrationally thermalized before the emission of fluorescence.

The blue shift of the emission spectra on the addition of the foreign gases can be interpreted as vibrational relaxation because the change of excitation level from higher to lower also caused the blue shift of the emission spectrum (Figs. 3 and 7). Since in the foreign gas quenching (Figs. 4—6) the rapid decrease followed by leveling off of the emission intensity as the foreign gas pressure increases from 0 to about 200 Torr is common to all the three gases, we may assume that

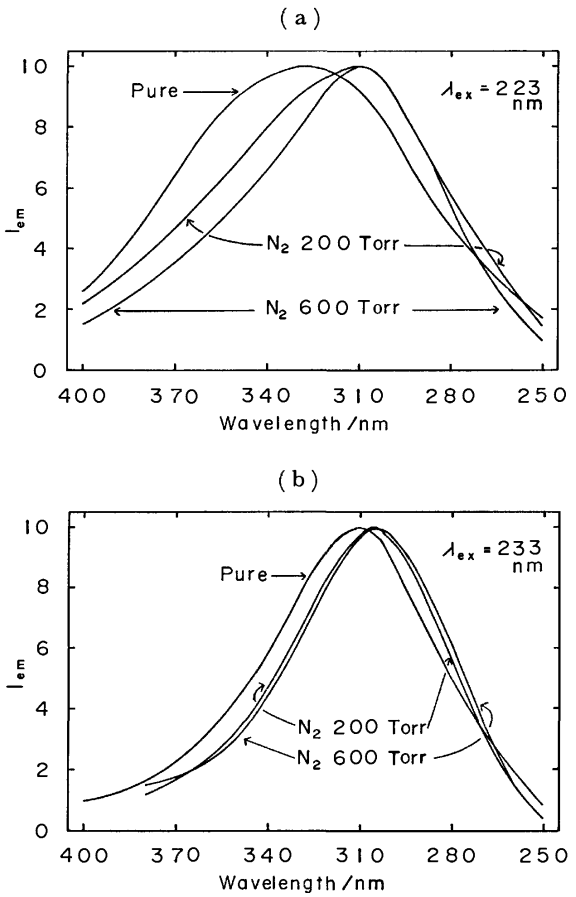

Fig. 7. Effect of addition of N_2 on the emission spectrum. $p(SO_2)$=0.8 Torr, $\Delta\lambda_{ex}$=4 nm, and $\Delta\lambda_{em}$ =9 nm. a) λ_{ex}=223 nm, b) λ_{ex}=233 nm.

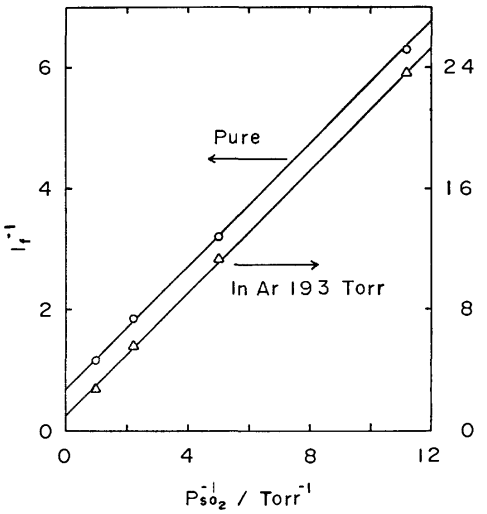

Fig. 8. Effect of Ar on self-quenching of (110) band. $\Delta\lambda_{ex}$=0.2 nm. I_f is corrected for the nonlinarity with respect to $p(SO_2)$.

TABLE 1. EFFECTS OF FOREIGN GASES ON SELF-QUENCHING OF (110) BAND

Foreign gas, M[a]	Intercept ratio[b]	Slope ratio[b]
He	1.1±0.1	2.9±0.1
Ar	1.3±0.1	4.2±0.1
N_2	1.4±0.1	4.1±0.1

a) p(M)=200 Torr and $p(SO_2)$=0.1—1.0 Torr. b) The intercept and the slope are those in the plot of $1/I_f$ *vs.* $1/p(SO_2)$.

this pressure dependence reflects the main structure of the foreign gas quenching mechanism.

Therefore, the mechanism we look for must be able to explain the following three features.

1) Foreign gases cause vibrational relaxation.

2) Fluorescence intensity decreases as foreign gas pressure increases and levels off above 200 Torr.

3) In the self-quenching, the plot of $1/I_f$ against reciprocal of SO_2 pressure is linear, and its slope is much larger in the presence of the foreign gas than in the absence of it while its intercept is only slightly larger in the presence of foreign gas.

First of all, we examine the equations for self- and foreign gas quenching expected with Stern-Volmer mechanism.

$$S + h\nu \xrightarrow{I_a} S^* \ (^1B_2, v'),$$
$$S^* \xrightarrow{k_r} S + h\nu'$$
$$S^* + S \xrightarrow{k_q} \text{self-quenching},$$
$$S^* + M \xrightarrow{k_m} \text{foreign gas quenching},$$

where S and M denote SO_2 and foreign gas molecules, respectively. I_a is the light intensity absorbed by SO_2 molecules at the view zone in the cell and is proportional to both the concentration of SO_2 and the incident light intensity I_l.

$I_a=\alpha I_l[S]$, where α is a proportional constant. Then the fluorescence intensity I_F is

$$I_F = k_r[S^*].$$

This mechanism leads to the equations;

$$I_0/I_f = 1 + \{k_m[M]/(k_r+k_q[S])\}, \quad (1)$$
$$1/I_f = [k_q+\{(k_r+k_m[M])/[S]\}]/(\alpha k_r), \quad (2)$$

where $I_f=I_F/I_l$, the fluorescence intensity relative to the incident light intensity, and I_0 is the value of I_f at $[M]=0$. Equation 2, when plotted I_f^{-1} *vs.* $[S]^{-1}$, gives a straight line with a slope $(k_r+k_m[M])/(\alpha k_r)$ and an intercept of $k_q/(\alpha k_r)$, and can explain the experimental results except for the slight dependence of the observed intercept on [M]. Equation 1 represents a straight line with a slope of $k_m/(k_r+k_q[S])$ in the plot of I_0/I_f *vs.* [M], while the experimental curves in Figs. 4—6 have slopes of decreasing functions of [M]. The vibrational relaxation is neither expected in this mechanism.

In the above mechanism, k_m is supposed to be a constant. However, if we would expect this mechanism to describe the experimental results, the slope, $k_m/(k_r+k_q[S])$, expected from Eq. 1 must be a decreasing function of [M] which approaches to zero at high pressure limit. We may attribute this [M] dependence to k_m. Secondly tested is the mechanism where vibrational relaxation takes place along with quenching processes. Higher vibrational levels are assumed to have larger quenching rate constants (k_m) than lower levels do. If Eq. 1 is applied to this system, the apparent k_m obtained would decrease as [M] increases because of vibrational relaxation. The following processes represent such a model where for simplicity only two levels are assumed.

$$S + h\nu \xrightarrow{I_a} S^*(1),$$
$$S^*(1) \xrightarrow{k_r} S + h\nu',$$
$$S^*(1) + S \xrightarrow{k_q} \text{self-quenching},$$
$$S^*(1) + M \xrightarrow{k_{m1}} \text{quenching}$$
$$\xrightarrow{k_v} S^*(0) + M,$$
$$S^*(0) \xrightarrow{k_r} h\nu' + S,$$
$$S^*(0) + S \xrightarrow{k_q} \text{self-quenching},$$
$$S^*(0) + M \xrightarrow{k_{m0}=0}$$
$$(k_{m1}>k_{m0}=0),$$

where $S^*(1)$ and $S^*(0)$ represent $v'=1$ and $v'=0$ levels of $^1B_2$ state respectively. The value of k_{m0} must be taken as zero otherwise emission intensity would not level off at high pressure of M. This mechanism leads to the Eqs. 1′ and 2′ below.

$$I_0/I_f = 1+\{k_m'[M]/(k_r+k_q[S])\}, \quad (1)'$$
$$k_m' = k_{m1}(k_r+k_q[S])/(k_r+k_q[S]+k_v[M]),$$

and when $k_q[S] \ll k_r+k_v[M]$,

$$1/I_f = [k_q\{1+k_{m1}k_v[M]^2/(k_r+k_v[M])^2\} +$$
$$k_r\{1+k_{m1}[M]/(k_r+k_v[M])\}/[S]]/(\alpha k_r). \quad (2)'.$$

This mechanism explains the first and second features but cannot explain the third feature because Eq. 2′ requires the slope and intercept in self-quenching increase by the same factor of $1+(k_{m1}/k_v)$ on addition of sufficiently high pressure of M. The origin of the failure of this mechanism is zero value of k_m at the lowest level. For the mechanism to be able to explain the third feature, k_m must be nonzero and et be a decreasing function of [M].

Then we hope to realize this situation by adding a back reaction of quenching process to the Stern-Volmer mechanism as follows;

$$S + h\nu \xrightarrow{I_a} S^*(^1B_2),$$
$$S^* \xrightarrow{k_r} S + h\nu',$$
$$S^* + S \xrightarrow{k_q} \text{self-quenching},$$
$$S^* + M \underset{k_m'}{\overset{k_m}{\rightleftarrows}} S^{**} + M,$$
$$S^{**} \xrightarrow{k_n'} \text{nonradiative decay},$$
$$S^{**} + S \xrightarrow{k_q'} \text{self-quenching},$$

where S^{**} denotes another electronic state. Again this mechanism does not contain electronic quenching processes of S^* and S^{**} to explain the leveling off of emission intensity at high pressures of M. This mechanism leads to the following equations 3 and 4.

$$I_0/I_f = 1 + [M]/(A+B[M]), \quad (3)$$

where

$$A = (k_r+k_q[S])/k_m \quad \text{and}$$
$$B = k_m'(k_r+k_q[S])/\{k_m(k_n'+k_q'[S])\},$$
$$1/I_f = \{k_q+(k_r+C[M])/[S]\}/(\alpha k_r), \quad (4)$$

where

$$C = k_m(k_n' + k_q'[S])/(k_n' + k_q'[S] + k_m'[M]).$$

Equation 4 can be approximated by Eq. 4', when

$$k_q'[S] \ll k_n' + k_m'[M], \quad (5)$$

$$1/I_f = [\{k_q + k_q'k_mk_m'[M]^2/(k_n' + k_m'[M])^2\} + \{k_r + k_mk_n'[M]/(k_n' + k_m'[M])\}/[S]]/(\alpha k_r). \quad (4)'$$

Equations 3 and 4' can explain the experimental results well. Fitting these equations to the experimental results, the quantities on the left-hand sides of the following equations can be experimentally determined.

$$k_m = (k_r + k_q[S])/A, \quad (6)$$

$$(k_n' + k_q'[S])/k_m' = A/B, \quad (7)$$

$$k_n'/k_m' = [M][k_m[M]/\{k_r(IR-1)\} - 1]^{-1}, \quad (8)$$

$$k_q'/k_m' = k_mk_q[M]^2(SR-1)/\{k_m[M] - k_r(IR-1)\}^2, \quad (9)$$

where IR and SR are respectively the ratios of the intercept and the slope of the self-quenching in the presence of foreign gas of [M] to those in the absence of it. It should be noted that the quantity of $(k_n' + k_q'[S])/k_m'$ can be obtained by the two independent ways, one with Eq. 7 and the other with a combination of Eqs. 8 and 9. The results of application of these equations to the data of (110) band are compared for the three gases in Table 2. It can be seen that the condition (5) is met and that Eqs. 7—9 are self-consistent. The results of application of Eqs. 6 and 7 to other levels are summarized in Table 3. It seems that k_m is smaller than k_q by an order and is an increasing function of vibrational energy.

Finally, by adding vibrational relaxation to the above mechanism, we have a mechanism that can explain all the three features. In this case, the quantities k_m and $(k_n' + k_q'[S])/k_m'$ in Table 3 must be interpreted as some sort of weighted averages over several levels.

In quenching by N_2, additional weak electronic quenching of S* and/or S** must be operating because continuous decrease of I_f was observed above 200 Torr as seen in Fig. 6. The recovery of I_f at high pressures observed in quenching by He (Fig. 4) cannot be explained by the proposed mechanism. The comparison of the quenching rate constant by Ar reported by Okabe with the k_m value of the present work is meaningless because Okabe's value was calculated with I_0/I_f at 400 Torr of Ar assuming Stern-Volmer mechanism. However, I_0/I_f values themselves in the two works coincide with each other within an experimental error.

Since the quantum beat in the fluorescence decay of $\tilde{C}(^1B_2)$ state due to the weak vibronic coupling of the state to the ground electronic state $\tilde{X}(^1A_1)$ has been observed,[12] the nonemitting state S** invoked in the proposed mechanism might be the ground state. To identify S** state, kinetic studies of $SO_2(^1B_2)$ in the presence of foreign gas are needed.

Table 2. The results of application of the proposed mechanism to (110) band

Gas M	k_m	$(k_n' + k_q'[S])/k_m'$	k_n'/k_m'	$k_q'[S]/k_m'$
	10^{-10} cm^3 molecule^{-1} s^{-1}	10^{18} molecule cm^{-3}		
He	0.67	1.0	1.0	0.06
Ar	0.91	1.4	1.3	0.16
N_2	1.3	0.91	0.86	0.14

$k_r = 3.1 \times 10^7$ s^{-1} from Ref. 11. $k_q = 1.25 \times 10^{-9}$ cm^3 molecule^{-1} s^{-1} calcd from Q in Table 3.

The author wishes to thank Professors Shin Sato and Shigeru Tsunashima of Tokyo Institute of Technology and Dr. Shigeyoshi Arai of the Institute of Physical and Chemical Research for helpful discussions and encouragements.

References

1) Y. Hamada and A. J. Merer, *Can. J. Phys.*, **52**, 1443 (1974).
2) R. J. Shaw, J. E. Kent, and M. F. O'Dwyer, *J. Mol. Spectrosc.*, **82**, 1 (1980).
3) E. K. C. Lee, B. G. MacDonald, D. L. Holtermann, and R. Nanes, *J. Photochem.* **17**, 495 (1981).
4) H. Watanabe, Y. Hyodo, S. Tsuchiya, and S. Koda, *Chem. Phys. Lett.*, **81**, 439 (1981).
5) J. Duchesne and B. Rosen, *J. Chem. Phys.*, **15**, 631 (1947).
6) G. Herzberg, "Electronic Spectra of Polyatomic Molecules," Van Nostrand, Princeton (1966), p. 605.

Table 3. Self-quenching constants and the results of application of the proposed mechanism

Band	Self-quenching const Q[a]	k_m[b]			$(k_n' + k_q'[S])/k_m'$[c]		
		He	Ar	N_2	He	Ar	N_2
220.6 nm	—	—	—	—	1.1	1.4	—
222.3 nm	3.2	2.4	2.0	3.8	0.90	1.9	0.93
224.2 nm	2.3	1.5	2.7	2.7	1.1	1.5	0.85
(120)	1.5	0.88	1.3	1.9	1.5	1.6	0.91
(102)	1.9	—	—	—	—	—	—
(110)	1.3	0.67	0.91	1.3	1.0	1.4	0.91
(100)	1.1	0.53	0.77	1.2	0.86	1.1	0.62
(010)	1.1	—	—	—	0.90	1.8	—
(000)	1.0	—	—	—	0.60	0.90	—

a) Q/Torr$^{-1} = 3.22 \times 10^{16}\ k_q/k_r$. Error $\pm 10\%$. b) Calculated with Eq. 6. In 10^{-10} cm^3 molecule^{-1} s^{-1}. k_r's are taken from Ref. 11. c) Calculated with Eq. 7. In 10^{18} molecule cm^{-3}. [S] $\approx 2.6 \times 10^{16}$ molecule cm^{-3}.

7) J. C. D. Brand, P. H. Chiu, and A. R. Hoy, *J. Mol. Spectrosc.*, **60**, 43 (1976).
8) J. C. D. Brand, D. R. Humphrey, A. E. Douglas, and I. Zanon, *Can. J. Phys.*, **51**, 530 (1973).
9) J. C. D. Brand and K. Srikameswaran, *Chem. Phys. Lett.*, **15**, 130 (1972).
10) H. Okabe, *J. Am. Chem. Soc.*, **93**, 7095 (1971).
11) Man-Him Hui and S. A. Rice, *Chem. Phys. Lett.*, **17**, 474 (1972).
12) W. Sharfin, M. Ivanco, and S. C. Wallace, *J. Chem. Phys.*, **76**, 2095 (1982).
13) H. Okabe, "Photochemistry of Small Molecules," Wiley-Interscience (1978).
14) H. Okabe, P. L. Splitstone, and J. J. Ball, *J. Air Pollution Control Assoc.*, **23**, 514 (1973).
15) The relative efficiencies (including the transmittance of the cell window) determined by compaison with thermopile data were 1:1:0.9:0.4 at 400, 350, 300, and 250 nm, respectively.
16) Weak bands buried were observed around 260 and 380 nm.
17) For the comparison, the quenching of $B(^1B_1)$ state excited at 285 nm measured for argon. The plot similar to Figs. 4—6 showed a straight line with argon pressure up to 80 Torr. The quenching rate constant obtained was 0.6×10^{-10} cm^3 molecule^{-1} s^{-1} which is compared to the value 0.5×10^{-10} reported by Mettee.[18]
18) H. D. Mettee, *J. Phys. Chem.*, **73**, 1071 (1969).

Structure of Liquid *N,N*-Dimethylformamide Studied by Means of X-Ray Diffraction

Hitoshi Ohtaki,* Sumiko Itoh, Toshio Yamaguchi, Shin-ichi Ishiguro and B. M. Rode†

Department of Electronic Chemistry, Tokyo Institute of Technology at Nagatsuta, 4259 Nagatsuta-cho, Midori-ku, Yokohama 227

†*Institute of Inorganic and Analytical Chemistry, University of Innsbruck, Innrain 52a, A-6020 Innsbruck, Austria*

(Received July 16, 1983)

The structure of *N,N*-dimethylformamide (DMF) was determined at 25 °C by means of X-ray diffraction using a θ-θ type X-ray diffractometer. The least-squares analysis of the reduced intensities results that a DMF molecule has a practically planar skeletal structure in the liquid state. Intramolecular structural parameters within a DMF molecule were determined as follows: C=O; 1.24 Å, N-C(CHO); 1.35 Å, and N-C(CH_3); 1.45 Å. The bond lengths are not appreciably different from those found in the gas phase, except for the C=O length, which is slightly longer by 0.04 Å in the liquid state than in the gaseous one. The radial distribution curve of DMF shows that the intermolecular arrangement of DMF molecules is practically fully disordered and no evidence has been found for the cluster formation of DMF molecules in the liquid state. The experimental result for the weak intermolecular interactions between DMF molecules is supported by *ab initio* MO-SCF calculations.

Structural studies of liquid amides have drawn considerable attentions of physical chemists and biochemists in connection with the conformation of amide moieties in polypeptides.[1-3] The structure of formamide has been extensively investigated in the liquid state,[4-9] as well as in the gaseous[10] and solid[11,12] phases. Theoretical considerations have also been carried out for the structure of formamide.[13,14] The molecular structure of *N,N*-dimethylformamide (DMF) has been determined in the gas phase by electron diffraction[15] and microwave[16] methods and they concluded that all atoms except hydrogen atoms at the methyl groups lay on one plane. The structure of DMF in the solid state has been studied for crystalline solvates,[17-19] but no crystal structure has been determined for pure DMF. Theoretical treatments for the molecular structure of DMF have also been done by some authors[2,20] for the electron distribution on the atoms within the DMF molecule. However, intermolecular interactions between DMF molecules have not been taken into the theoretical consideration.

Raman and infrared spectra of liquid DMF have been recorded by Fini and Mirone,[21] from which they concluded that DMF molecules formed clusters oriented in a partially ordered way. However, the cluster formation has not been conclusive from NMR measurements.[22-26] No X-ray study has been carried out so far for the structure of liquid DMF.

Since X-ray diffraction measurements can provide direct information for ordered structures of liquids, we aimed at investigating the liquid structure of DMF and comparing it with the structure of formamide examined in a previous work.[9]

Experimental

Reagents. Commercially available *N,N*-dimethylformamide of analytical grade was dried with Molecular Sieves (4A) and then distilled under a reduced pressure.

Method of Measurements and Analysis of Scattering Data. A sample solution was placed in a flat glass tray of 38 mm depth. X-Ray scattering measurements were carried out at (25±2) °C in a thermostatted room by using a JEOL θ-θ diffractometer with a bent LiF monochromator. Mo $K\alpha$ radiation (λ=0.7107 Å) was used. The scattered intensities were collected at discrete points over the s-range from 0.6 $Å^{-1}$ to 16.4 $Å^{-1}$ ($s=4\pi\lambda^{-1}\sin\theta$, where 2θ is the scattering angle). Details of the method of measurements have been described elsewhere.[27]

Experimental intensity data were corrected for background, absorption, double scattering, polarization and incoherent scatterings by the usual methods and then normalized to the absolute scale with respect to a stoichiometric unit volume V containing one DMF molecule.

The radial distribution curve was calculated by using a Fourier transform

$$D(r) = 4\pi r^2\rho_0 + 2r\pi^{-1}\int_{s_{min}}^{s_{max}} s\cdot i(s)\cdot M(s)\cdot\sin(sr)\mathrm{d}s, \quad (1)$$

were ρ_0 denotes the average scattering density, $M(s)$ a modification function of the form $[\sum n_i\{(f_i(0)+\Delta f_i')^2+(\Delta f_i'')^2\}/\sum n_i\{(f_i(s)+\Delta f_i')^2+(\Delta f_i'')^2\}]\cdot\exp(-0.01s^2)$. The s_{min} and s_{max} values are 0.6 $Å^{-1}$ and 16.4 $Å^{-1}$, respectively. The reduced intensities $i(s)$ were given as follows:

$$i(s) = I(s)_{obsd} - \sum n_i\{(f_i(s)+\Delta f_i')^2+(\Delta f_i'')^2\}, \quad (2)$$

and n_i is the number of atom i in the stoichiometric volume and $f_i(s)$ denotes the scattering factor of atom i at s. $\Delta f_i'$ and $\Delta f_i''$ are the real and imaginary parts of anomalous dispersion of atom i, respectively.

Theoretical reduced intensities were calculated by Eq. 3:

$$\begin{aligned} i(s) = \sum n_j[\sum n_{pq}\{(f_p(s)+\Delta f_p')(f_q(s)+\Delta f_q') \\ +\Delta f_p''\Delta f_q''\}\cdot\frac{\sin(sr_{pq})}{(sr_{pq})}\cdot\exp(-b_{pq}s^2)] \\ -\frac{4\pi R_j^3}{3V}\cdot\frac{3\{\sin(sR_j)-sR_j\cos(sR_j)\}}{(sR_j)^3} \\ \cdot\exp(-B_js^2)\cdot\{\sum n_i(f_i(s)+\Delta f_i')\sum n_j\cdot \\ (f_j(s)+\Delta f_j')+\sum n_i\Delta f_i''\sum n_j\Delta f_j''\}, \end{aligned} \quad (3)$$

where r_{pq}, b_{pq}, and n_{pq} stand for the distance, the temperature factor, and the frequency factor of the p-q atom-pair, respectively. R_j denotes the distance from an atom j beyond which a continuous electron distribution is assumed. A parameter B_j is introduced since the emergence of such a

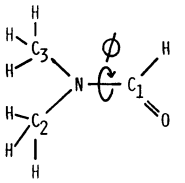

Fig. 1. The structure of DMF molecule.

continuous electron distribution around atom j is not sharp. Intramolecular interactions of all possible atom-pairs of DMF were calculated by using the first term of Eq. 3, while interactions between different molecules were approximated by using the second term of Eq. 3 on the assumption of the continuous electron distribution beyond the R_j values of each atom in one molecule. The R_j values were selected in order to obtain the best fit $s \cdot i(s)$ curve to the experimental one and assumed to be 2.50 Å for H and N atoms and 3.30 Å for O and C atoms by taking into consideration the interatomic distances found in the present work as will be shown later. The B_j values were set to be 0.05 Å^2 for all the atoms. The C–H bond length within a DMF molecule was fixed at 1.09 Å. The calculations were performed by using the KURVLR program.[28]

Distances of atom-pairs in the system were first assumed to be the same as those with the literature values reported from the electron diffraction measurement in the gas phase,[15] and then the structural parameters of the atom-pairs were refined by the least-squares method applied to the reduced intensities so as to minimize the error-square sum $U=\sum w\{i(s)-i(s)_{calcd}\}^2$, where the weighting function $w=I(s)_{obsd}^{-2}\cdot\cos\theta$. The NLPLSQ program was used for the calculations.[29]

For the sake of convenience of the discussion in the following section, we numbered the carbon atoms within a DMF molecule (Fig. 1).

Results and Discussion

The $s \cdot i(s)$ and radial distribution $(D(r)-4\pi r^2\rho_0)$ curves are shown in Figs. 2 and 3, respectively. The radial distribution curve of formamide is also shown in Fig. 3 for comparison.

Two distinct peaks are observed at 1.3 and 2.3 Å in the radial distribution curve of DMF (Fig. 3a). The former peak contains peaks due to the N–C_1, N–C_2, N–C_3, and C_1=O bonds within each DMF molecule, and the latter can be ascribed to the $C_1\cdots C_2$, $C_1\cdots C_3$, $C_2\cdots C_3$, and N···O nonbonding interactions. No significant peak is found in the range $r>3$ Å in the radial distribution curve of DMF, in contrast to that of formamide (see Fig. 3b).

NMR studies showed that a DMF molecule can rotate along the N–C_1 axis, although the free energy of activation of the rotation of the molecule is rather large (88 kJ mol^{-1}).[30] Therefore, we first attempted to postulate two possibilities of configuration of a DMF molecule; *i.e.*, a planar ($\phi=0°$) and a perpendicular ($\phi=90°$) structures (see Fig. 1). For the both model-structures we employed the least-squares calculation for the reduced intensities over the s-range from 3.5 Å^{-1} to 16 Å^{-1} in order to find structural parameters which can best reproduce the experimental $s \cdot i(s)$ values. In the course of the calculations we assumed a tetrahedral structure of the methyl groups within a DMF molecule and the C–H bond length to be 1.09 Å. The results obtained from the two models are compared with the experimental values in Fig. 2, and it is obvious that the planar model gives a much better fit to the experimental curve than the perpendicular one does. Moreover, when we introduced interatomic distances calculated from models at $\phi=30°$ and 60° as the initial values and allowed them to be optimized without fixing the rotation angle, the distances converged to the values resulted from the least-squares analysis at $\phi=0°$. Therefore, we concluded that the structure of a DMF molecule is practically planar. The final values of the bond distances thus obtained are listed in Table 1, together with the values found in the gaseous and solid states. The bond angles were estimated as follows: $\angle$N–C_1–O; (121±3)°, $\angle C_1$–N–$C_2=\angle C_1$–N–C_3; (116±4)°, and $\angle C_2$–N–C_3; (124±5)°.

The intramolecular bond distances of each atom-pair in DMF found in the liquid state are well consistent with those in the gas phase[15] except for the

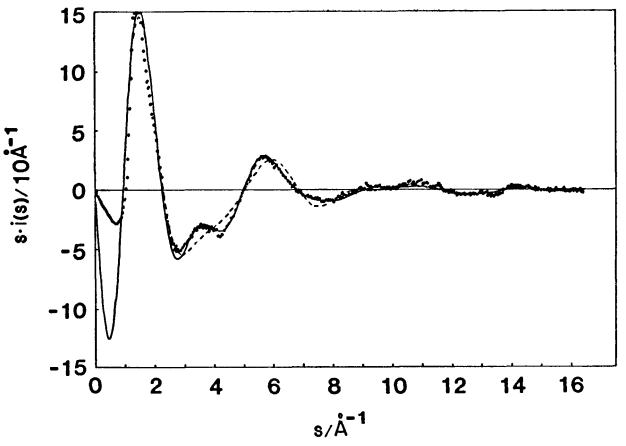

Fig. 2. The $s \cdot i(s)$ values of liquid DMF. Circles represent the $s \cdot i(s)$ values experimentally obtained. The solid line shows the theoretical $s \cdot i(s)$ values at $\phi=0°$ including those for interactions between atoms and electrons continuously distributed in the region of $r>R_j$. The dashed line shows the theoretical values at $\phi=90°$.

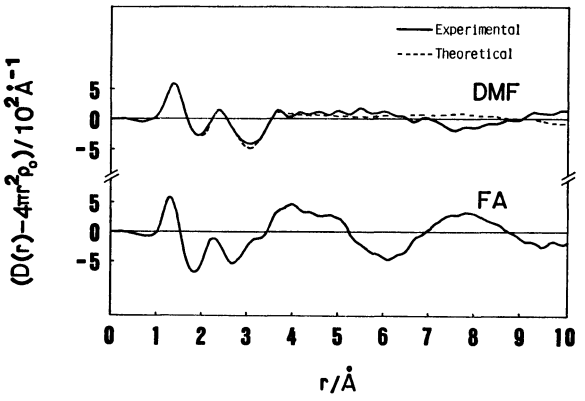

Fig. 3. Radial distribution curves $D(r)-4\pi r^2\rho_0$. (a) DMF. The solid and dashed lines represent experimental and theoretical curves, respectively. (b) Formamide.

TABLE 1. THE INTRAMOLECULAR DISTANCES (r) AND THE TEMPERATURE FACTORS (b) OF ATOM-PAIRS IN LIQUID DMF. THE VALUES IN PARENTHESES ARE THEIR STANDARD DEVIATIONS ESTIMATED (3σ). THE BOND LENGTHS WITHIN A DMF MOLECULE DETERMINED IN THE GAS PHASE AND IN A CRYSTALLINE SOLVATE ARE ALSO SHOWN

Atom-pair	Gas[15]	Liquid		Crystalline solvate[18]
	r/Å	r/Å	b/Å^2	r/Å
C_1=O	1.20	1.24(1)	0.003(1)	1.30
N-C_1	1.34	1.35(2)	0.002(1)	1.28
N-C_2	1.45	1.45(1)	0.004(1)	1.51
N-C_3	1.45	1.45(1)	0.004(1)	1.50

C=O bond length, which is slightly longer by 0.04 Å in the liquid state than in the gaseous one. The result may indicate a weak hydrogen-bonded interaction between DMF molecules. However, there are some discrepancies in the bond distances between in the liquid state and in a crystalline solvate,[18] probably because of strong ion-DMF interactions in the crystalline solvate compared with intermolecular interactions of DMF themselves in the liquid state.

In the radial distribution curve of DMF we do not find appreciable peaks in the range $r>3$ Å, in which we see still peaks due to intermolecular interactions of formamide molecules (Fig. 3). If we assumed a continuous electron distribution beyond R_j from each atom j within a DMF molecule, the reduced intensities calculated from Eq. 3 gave values which fitted satisfactorily with the experimental ones over the wide s-range of 1 Å^{-1} to 16 Å^{-1} (see solid line in Fig. 2). The radial distribution curve showed no distinct peak beyond $r=3$ Å, which indicated a practically random distribution of molecules in the system. Therefore, the result indicated that no significant interactions existed between molecules through, for instance, hydrogen bonds and thus the cluster formation of DMF molecules was not observed from the present X-ray diffraction work.

However, it is obvious that DMF molecules interact with each other to form a condensed phase at a room temperature. Therefore, we estimated the interaction energy between DMF molecules with the aid of the *ab initio* MO-SCF method by using some suitable structure models and minimal basis sets. The geometry of the DMF molecules was fixed at the experimental one obtained by the present work, and the distance between DMF molecules and the configuration of DMF associates were varied. The calculations were performed in a similar way as described previously.[9]

The dimer model used for the calculation is shown in Fig 4. At $\Theta=\Theta'=180°$, the dimer at $\Psi=0°$ was more stable by *ca.* 8.4 kJ mol^{-1} than that at $\Psi=180°$ when the intermolecular C-H···O distance was 3.2 Å. In the latter configuration the lowest energy of interaction was found at $\Theta=180°$ and $\Theta'=90°$ at $r_{C-H\cdots O}=$ 3.2 Å. At $\Theta'=120°$ a slightly higher energy of stabilization was estimated for the dimer, but the difference was too small (*ca.* 1 kJ mol^{-1}) to be significant.

The rotation barrier of the DMF dimer around the

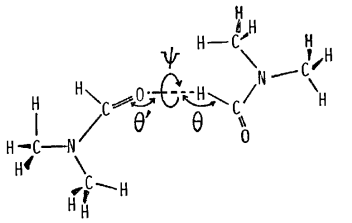

Fig. 4. The dimer model of DMF.

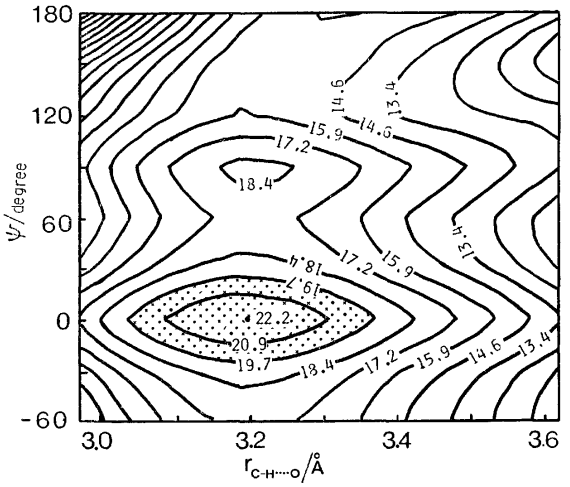

Fig. 5. The energy surface for the linear-dimer of DMF plotted against the C-H···O distance ($r_{C-H\cdots O}$) between molecules and the rotation angle Ψ around the C-H···O axis. The numbers indicated in the diagram show the stabilization energy of the dimer ($-\Delta E$) in kJ mol^{-1} units.

C-H···O axis at $\Theta=\Theta'=180°$ was calculated at various C-H···O distances. The energy surface diagram is plotted for varying bond distance $r_{C-H\cdots O}$ and rotation angle Ψ in Fig. 5. The numbers indicated in the diagram show stabilization energies of dimerization of DMF molecules ($-\Delta E$) in kJ mol^{-1} units. It is seen from the diagram that the configuration is most stable at $r_{C-H\cdots O}=3.2$ Å and $\Psi=0°$, but the curvature is so small that the bond distance and the rotation angle can change over the range ±0.15 Å and $\pm30°$, respectively, by the thermal energy (kT) at $T=300$ K. The crosshatched area in Fig. 5 indicates the region where the variation of the energy is smaller than the kT value at room temperature. The maximum stabilization energy of dimerization was estimated to be -22.2 kJ mol^{-1} (see Fig. 5), which is much smaller than the energies of hydrogen bonds of water molecules (-30 to -40 kJ mol^{-1}) and of formamide (-68 kJ mol^{-1}[19]). The ring-dimer structure of DMF was much less stable than the linear dimer examined above.

A chain-trimer connected by the C-H···O hydrogen bonds of DMF molecules had a similar stabilization energy (-23 kJ mol^{-1}) per bond as the linear dimer, and thus, no special stabilization is to be expected by the formation of oligomers. The vibrational amplitude of the C-H···O bond at room temperature was estimated to be about 0.23 Å from the surface of the stabilization energy of the trimer and the kT value. The amplitude of the trimer is practically the

same as that of the dimer (0.15 Å). Since the vibrational amplitude of DMF associates is fairly large, we may not expect to detect the associated species as discrete units in the liquid DMF. This conclusion is consistent with that obtained by the X-ray diffraction measurement demonstrated in the present study.

The present work has been financially supported by the Grant-in-Aid for Scientific Research (No. 57470054) from the Ministry of Education, Science and Culture. The Asahi Glass Foundation for Industrial Technology also financially supports the present work. The financial support by the Austrian Federal Ministry for Science and Research (Erl. Zl. 18.854/6—10/81) is also gratefully acknowledged.

References

1) E. B. Nielsen and J. A. Schellman, *J. Phys. Chem.*, **71**, 2297 (1967).
2) J. F. Yan, F. A. Momany, R. Hoffmann, and H. A. Scheraga, *J. Phys. Chem.*, **74**, 420 (1970).
3) J. Applequist, *J. Chem. Phys.*, **71**, 4324 (1979).
4) J. F. Hinton and K. H. Ladner, *J. Magn. Reson*, **6**, 586 (1972).
5) H. Siegbahn, L. Asplund, P. Kelfve, K. Harmin, L. Karlsson, and K. Siegbahn, *J. Electrosc. Relat. Phenom.*, **5**, 1059 (1974).
6) D. J. Gardiner, A. J. Lees, and B. P. Straughan, *J. Mol. Struct.*, **53**, 15 (1979).
7) R. J. DeSando and G. H. Brown, *J. Phys. Chem.*, **72**, 1088 (1968).
8) E. Kálmán, I. Serke, G. Pálinkás, M. D. Zeidler, F. J. Wiesmann, H. Bertagnolli, and P. Chieux, *Z. Naturforsch., A*, **38**, 231 (1983).
9) H. Ohtaki, A. Funaki, B. M. Rode, and G. J. Reibnegger, *Bull. Chem. Soc. Jpn.*, **56**, 2116 (1983).
10) M. Kitano and K. Kuchitsu, *Bull. Chem. Soc. Jpn.*, **47**, 67 (1974).
11) J. Ladell and B. Post, *Acta Crystallogr.*, **7**, 559 (1954).
12) E. D. Stevens, *Acta Crystallogr., Sect. B*, **34**, 544 (1978).
13) A. Pullman, H. Berthod, C. Giessner-Prettre, J. F. Hinton, and D. Harpool, *J. Am. Chem. Soc.*, **100**, 3991 (1978).
14) N. R. Carlsen, L. Random, N. V. Riggs, and W. R. Rodwell, *J. Am. Chem. Soc.*, **101**, 2233 (1979).
15) L. V. Vilkov, P. A. Akishin, and V. M. Presnyakova, *Zh. Strukt. Khim.*, **3**, 5 (1962); *J. Struct. Chem. USSR*, **3**, 3 (1962).
16) R. A. Elzaro, Ph. D. Thesis, Michigan State Univ., East Lansing, Mich., 1973, *Diss. Abstr., Int. B*, **34** (3), 1052 (1973).
17) Y. Gobillon, P. Piret, and M. V. Meerssche, *Bull. Soc. Chim. Fr.*, **1962**, 551.
18) L. Brun and C.-I. Brändén, *Acta Crystallogr.*, **20**, 749 (1966).
19) P. A. Koz'min, A. S. Kotel'nikova, M. D. Surazhskaya, T. B. Larina, Sh. A. Bagirov, and T. V. Misailova, *Kood. Khim.*, **4**, 1557 (1978); *Sov. J. Cood. Chem.*, **4**, 1183 (1978).
20) B. M. Rode and T. Pontani, *Mh. Chemie*, **109**, 871 (1978); B. M. Rode and R. Fussenegger, *J. Chem. Soc., Faraday Trans. 2*, **71**, 1958 (1975).
21) G. Fini and P. Mirone, *J. Chem. Soc., Faraday Trans., 2*, **70**, 1776 (1974).
22) A. G. Whittaker and S. Siegel, *J. Chem. Phys.*, **42**, 3320 (1965).
23) R. C. Neuman, Jr., W. Snider, and V. Jonas, *J. Phys. Chem.*, **72**, 2469 (1968).
24) W. T. Raynes and M. A. Raza, *Mol. Phys.*, **20**, 339 (1971).
25) H.-J. Bittrich and D. Kirsch, *Z. Phys. Chem. (Leipzig)*, **257**, 403 (1976).
26) M. Rabinovitz and A. Pines, *J. Chem. Soc., B*, **1968**, 1110.
27) H. Ohtaki, M. Maeda, and S. Ito, *Bull. Chem. Soc. Jpn.*, **47**, 2217 (1974).
28) G. Johansson and M. Sandström, *Chem. Scr.*, **4**, 195 (1973).
29) H. Ohtaki, T. Yamaguchi, and M. Maeda, *Bull. Chem. Soc. Jpn.*, **49**, 701 (1976).
30) W. E. Stewart and T. H. Siddall, III, *Chem. Rev.*, **70**, 517 (1970) and references therein.

Microwave Spectroscopy of Boron Chloride (BCl). The Chlorine Nuclear Quadrupole Coupling Constant

Yasuki Endo, Shuji Saito, and Eizi Hirota*
Institute for Molecular Science, Okazaki 444
(Received July 28, 1983)

The pure rotational spectrum of an unstable diatomic molecule, boron chloride (BCl), has been observed in the millimeter wave region. The BCl molecule was directly generated in a 3.7-m long free space absorption cell by a d.c. glow discharge in BCl_3. Rotational transitions of $^{11}B^{35}Cl$ and $^{11}B^{37}Cl$ in the ground vibrational state, which are split into a few components by the nuclear electric quadrupole interactions, have been observed and analyzed to yield molecular constants including the chlorine nuclear quadrupole coupling constant with high accuracy. The eQq constant thus determined is discussed along with those of other diatomic chlorides, to obtain information on the electronic structure of the molecules.

The chlorine nuclear quadrupole coupling constant [eQq(Cl)] has been determined in a number of molecules in the gas phase by means of microwave spectroscopy, and its significance for the electronic structure of the molecules has been explored in detail.[1] Thanks to recent developments in microwave spectroscopic techniques, several unstable molecules containing a chlorine nucleus have also been investigated; OCl,[2,3] CCl,[4] ClBO,[5] and NCl[6] are such examples. A diatomic molecule consisting of a second row element and a chlorine atom has the electron configuration in the ground state expressed as $KKL(5\sigma)^2(6\sigma)^2(2\pi)^4(7\sigma)^2(3\pi)^n$, where $n=1,2,3$, and 4 apply to CCl, NCl, OCl, and FCl.[7] As has been shown previously,[6] the eQq(Cl) constants of the molecules with $n=1$—4 fall on a smooth curve when they are plotted against n, the number of electrons in the 3π (HOMO) orbital, provided that the observed values of eQq for CCl, NCl, and OCl were corrected for π-electron back donation, as estimated from the magnetic hyperfine coupling constants. It is interesting to see whether the eQq(Cl) constant of BCl conforms with the prediction from those of other molecules; BCl is the first member with $n=0$ of this series.

The ground-state rotational and vibrational constants of BCl were first obtained by Herzberg and Hushley[8] from the analysis of the observed ultraviolet spectrum. Maki *et al.*[9] have recently observed vibration-rotation spectra of BCl by infrared diode laser spectroscopy in the 12-μm region. They generated BCl in the optical path by means of either a dc glow discharge or a 2450 MHz microwave discharge in BCl_3. They improved the accuracy of the ground-state constants over that of the previous study, but were unable to resolve the hyperfine structure. They have attempted to observe the pure rotational spectrum at around 80 GHz with a Stark-modulated microwave spectrometer without success.[9]

The present paper reports the observation of the rotational transitions of BCl and precise ground-state constants including eQq(Cl) obtained therefrom.

Experimental

The microwave spectrometer employed in the present study is a source modulation spectrometer with a free space absorption cell of 3.7-m length sealed with Teflon lenses at both ends.[10] The BCl molecule was generated directly in the cell by a dc glow discharge in BCl_3; BCl_3 was pumped continuously through the cell by a mechanical booster pump of 67 l s^{-1}. The optimum pressure for BCl_3 in the cell was about 20 mTorr (2.7 Pa) as measured by an uncalibrated Pirani gauge. The dc discharge current of 100 mA was required to obtain the S/N ratio sufficient for the measurement. We have also attempted to observe BCl lines using a 1-m long cell, where BCl was generated by a microwave discharge in BCl_3 in a side arm used as the inlet; the discharge products were rapidly pumped through the cell. Although the sample pressure (5 to 30 mTorr or 0.7 to 4.0 Pa) and the discharge current were carefully adjusted, we were unable to observe the BCl spectrum by this arrangement. This result indicates that BCl is short-lived and exists only in and near the discharged region.

Using the molecular constants of Maki *et al.*,[9] the frequency of the $J=4\leftarrow3$ transition of $^{11}B^{35}Cl$ was calculated to be about 163.3 GHz, and searching for this species was initiated in this region. A fairly strong absorption line with resolved hyperfine structure was observed at 13 MHz higher than that predicted for $J=4\leftarrow3$; its trace is shown in Fig. 1. It vanished immediately when the discharge was turned off, and was thus ascribed to a species of short life. Both the observed hyperfine structure and the short lifetime of the species indicated that the observed line is due to BCl. This assignment was confirmed by observing the corresponding transition of $^{11}B^{37}Cl$ and also the next lowest transition, $J=3\leftarrow2$. The $J=2\leftarrow1$ transition was found to be complicated because of additional splittings due to the ^{11}B nuclear quadrupole interaction, as exemplified by the trace shown in Fig. 2 (see also Table 1). The lowest $J=1\leftarrow0$ transition was also observed, but was too weak to measure the hyperfine components accurately.

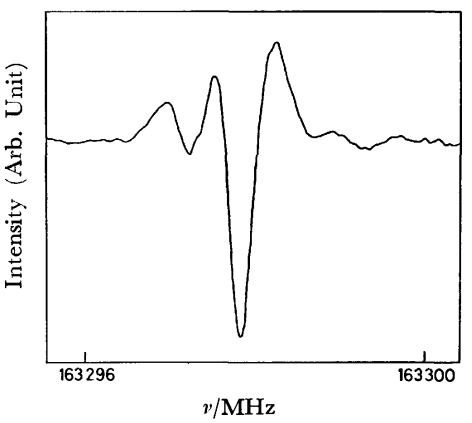

Fig. 1. The $J=4\leftarrow3$ transition of $^{11}B^{35}Cl$.

Table 1. Observed rotational transition frequencies of $^{11}B^{35}Cl$

$J \leftarrow J'$	$F_1' \leftarrow F_1$	$F' \leftarrow F$	ν_{obsd} / MHz	$\nu_{obsd} - \nu_{calcd}$ / MHz	Weight[a]
4←3	5.5←4.5	7←6	163 297.841	−0.002	0.035
		6←5		0.039	0.024
		5←4		0.075	0.016
		4←3		0.046	0.011
	4.5←3.5	6←5		−0.043	0.022
		5←4		0.082	0.014
		4←3		0.081	0.008
		3←2		−0.010	0.005
	3.5←2.5	4←3	163 297.234	0.012	0.113
		3←2		−0.022	0.057
	2.5←1.5	3←2		−0.003	0.054
		2←1		0.161	0.017
		1←0		−0.016	0.004
	4.5←4.5	6←6	163 293.573	0.000	1.000
	3.5←3.5	4←4	163 299.318	0.035	0.173
		5←5		−0.048	0.341
3←2	4.5←3.5	6←5	122 478.069	0.015	0.042
		5←4		0.093	0.026
		4←3		0.168	0.016
		3←2		0.094	0.010
	3.5←2.5	5←4		−0.063	0.022
		4←3		0.231	0.012
		3←2		0.127	0.006
		2←1		−0.084	0.003
	2.5←1.5	4←3	122 477.157	−0.001	0.123
		2←2		0.147	0.005
		2←1		0.147	0.015
		1←1		−0.174	0.003
		1←0		−0.174	0.003
	1.5←0.5	3←2		0.041	0.065
		1←1		0.073	0.008
	2.5←2.5	4←4	122 479.998	−0.089	0.261
		3←3		0.099	0.094
		2←2		−0.131	0.033
	1.5←1.5	3←3	122 481.348	0.019	1.000
2←1	3.5←2.5	5←4	81 654.517	0.041	0.082
		4←3		0.219	0.044
		3←3		−0.098	0.001
		3←2		0.105	0.022
		2←1		0.061	0.011
	2.5←1.5	4←3		−0.136	0.027
		2←1		0.010	0.003
	2.5←2.5	3←3	81 650.245	−0.067	0.391
		2←2		0.009	0.140
	2.5←2.5	1←1	81 649.812	−0.006	0.009
	1.5←0.5	3←2		0.085	0.191
		2←2		0.085	0.024
		2←1		−0.001	0.024
		1←1		−0.001	0.024
	3.5←2.5	4←4	81 653.804	0.048	0.006
	2.5←1.5	3←2		0.063	0.101
		2←2		−0.065	0.010
	0.5←0.5	2←2		−0.136	0.028
		2←1		−0.222	0.028
		1←2		−0.194	0.028
	1.5←1.5	3←3	81 657.597	0.014	0.424
		2←3		0.014	0.026
		2←1		−0.029	0.035
	1.5←1.5	3←2	81 656.947	−0.041	0.078
		2←2		−0.041	0.160
		1←2		−0.041	0.102

a) The weight for unresolved components is taken to be proportional to the square of the calculated relative intensity.

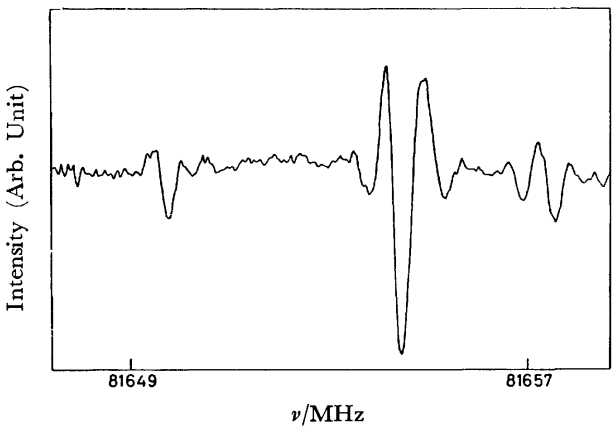

Fig. 2. The $J=2\leftarrow1$ transition of $^{11}B^{35}Cl$. The spectrum was synthesized from a few consecutive scans, each covering a region of 4 MHz.

The observed frequencies are listed in Table 1 with the assignment; each frequency was determined by taking the average of three up-sweep and three down-sweep measurements. A smaller number of lines were observed for $^{11}B^{37}Cl$ than for $^{11}B^{35}Cl$, because of poorer S/N ratio. The frequencies observed for $^{11}B^{37}Cl$ are given in Table 2. The standard deviation of the frequency measurement is less than 20 kHz except for a few weak lines.

Analysis of the Observed Spectrum

Because both nuclei in the BCl molecule show the quadrupole coupling interaction, a coupling scheme of the angular momenta, $\mathbf{F}_1=\mathbf{J}+\mathbf{I}(\mathrm{Cl})$ and $\mathbf{F}=\mathbf{F}_1+\mathbf{I}(^{11}\mathrm{B})$, was employed to analyze the hyperfine structure, where $\mathbf{J}$, $\mathbf{I}(\mathrm{Cl})$, and $\mathbf{I}(^{11}\mathrm{B})$ denote the rotational, Cl nuclear spin, and ^{11}B nuclear spin angular momenta, respectively; both $I(^{35,37}\mathrm{Cl})$ and $I(^{11}\mathrm{B})$ are 3/2. The $\Delta J=0$ matrix elements for the quadrupole coupling Hamiltonians, $\mathbf{H}_Q(\mathrm{Cl})$ and $\mathbf{H}_Q(\mathrm{B})$, are given by

$$\begin{aligned}&\langle I(\mathrm{Cl})JF_1'I(\mathrm{B})F'M_{F'}|\mathbf{H}_Q(\mathrm{Cl})|I(\mathrm{Cl})JF_1I(\mathrm{B})FM_F\rangle\\&=-\frac{1}{8}\delta_{F_1'F_1}\delta_{F'F}\delta_{M_{F'}M_F}\\&\times\frac{3C(C-1)-4J(J+1)I(\mathrm{Cl})[I(\mathrm{Cl})+1]}{(2J-1)(2J+3)I(\mathrm{Cl})[2I(\mathrm{Cl})-1]}eQq(\mathrm{Cl}),\end{aligned}\tag{1}$$

and

$$\begin{aligned}&\langle I(\mathrm{Cl})JF_1'I(\mathrm{B})F'M_{F'}|\mathbf{H}_Q(\mathrm{B})|I(\mathrm{Cl})JF_1I(\mathrm{B})FM_F\rangle\\&=-\delta_{F'F}\delta_{M_{F'}M_F}(-1)^{J+I(\mathrm{Cl})+F_1}[(2F_1+1)(2F_1'+1)]^{1/2}\\&\times\begin{Bmatrix}J & F_1 & I(\mathrm{Cl})\\ F_1' & J & 2\end{Bmatrix}(-1)^{I(\mathrm{B})+F_1+F}\\&\times\begin{Bmatrix}I(\mathrm{B}) & F_1 & F\\ F_1' & I(\mathrm{B}) & 2\end{Bmatrix}\left[\frac{J(J+1)(2J+1)}{(2J-1)(2J+3)}\right]^{1/2}\\&\times\left[\frac{[I(\mathrm{B})+1][2I(\mathrm{B})+1][2I(\mathrm{B})+3]}{I(\mathrm{B})[2I(\mathrm{B})-1]}\right]^{1/2}eQq(\mathrm{B})/4,\end{aligned}\tag{2}$$

where $C=J(J+1)+I(\mathrm{Cl})[I(\mathrm{Cl})+1]-F_1(F_1+1)$ and δ_{ij} and $\{\cdots\}$ denote Kronecker's delta and the Wigner 6j symbol, respectively. The matrix elements off-diagonal in J were ignored, since their contributions

Table 2. Observed rotational transition frequencies of $^{11}B^{37}Cl$

$J'\leftarrow J$	$F_1'\leftarrow F_1$	$F'\leftarrow F$	ν_{obsd} / MHz	$\nu_{obsd}-\nu_{calcd}$ / MHz	Weight[a]
4←3	5.5←4.5	7←6	161 191.074	−0.016	0.035
		6←5		0.027	0.024
		5←4		0.062	0.016
		4←3		0.035	0.011
	4.5←3.5	6←5		−0.059	0.022
		5←4		0.065	0.014
		4←3		0.062	0.008
		3←2		−0.011	0.005
3←2	4.5←3.5	6←5	120 879.834	−0.030	0.042
		5←4		0.052	0.026
		4←3		0.134	0.016
		3←2		0.058	0.010
	3.5←2.5	5←4		−0.111	0.022
		4←3		0.183	0.012
		3←2		0.074	0.006
		2←1		−0.115	0.003
	2.5←1.5	4←3	120 897.135	−0.059	0.123
		2←2		0.067	0.005
		2←1		0.067	0.015
		1←1		−0.212	0.003
		1←0		−0.212	0.003
	1.5←0.5	3←2		−0.009	0.065
		1←1		0.032	0.008
2←1	3.5←2.5	5←4	80 600.921	0.003	0.082
		4←3		0.183	0.044
		3←3		−0.136	0.001
		3←2		0.036	0.022
		2←1		0.018	0.011
	2.5←1.5	4←3		−0.178	0.027
		2←1		−0.029	0.003

a) See note a) of Table 1.

Table 3. Molecular constants of BCl[a)]

	$^{11}B^{35}Cl$		$^{11}B^{37}Cl$	
	Present	Ref. 9[b)]	Present	Ref. 9
B_0/MHz	20 413.942 2(91)	20 412.40(93)	20 150.562 0(182)	20 148.99
D_0/MHz	0.054 10(35)	0.055 10(157)	0.052 87(79)	0.053 68
eQq(Cl)/MHz	−16.737(11)		−13.191[d)]	
eQq(B)/MHz	−3.70[c)]		−3.70[d)]	

a) Values in parentheses denote 2.5 times the standard deviations of the fit. b) Converted from the Dunham coefficients of Ref. 9. c) Determined from a lineshape simulation. d) Assumed. Calculated from $eQq(^{35}Cl)$.

were found to be small. All other $\Delta J=0$ matrix elements off-diagonal in F_1 were taken into consideration. The Hamiltonian matrix was then factorized into blocks of 4×4 dimension or smaller, and was numerically diagonalized in carrying out the least-squares analysis.

The observed frequencies of $^{11}B^{35}Cl$ were thus analyzed taking B_0, D_0, and $eQq(^{35}Cl)$ as adjustable parameters, while $eQq(^{11}B)$ was determined separately by simulation; the calculated spectrum was obtained by assuming a Lorentzian line shape with the line width and modulation width of 0.25 and 0.2 MHz, respectively. For $^{11}B^{37}Cl$ only B_0 and D_0 were determined since the number of the observed lines was small, while $eQq(^{37}Cl)$ was fixed to $eQq(^{35}Cl)$ multiplied by the ratio of the nuclear quadrupole moments for ^{37}Cl and ^{35}Cl (1/1.26878). The frequencies of unresolved hyperfine components were calculated by weighting each component in proportion to the square of the normalized relative intensity. The molecular constants thus determined are listed in Table 3, where B_0 and D_0 calculated from the Dunham coefficients reported by Maki *et al.*[9] are also included for comparison.

Discussion

The eQq(Cl) constants obtained for the XCl type molecules are given in Table 4, where X=B, C, N, O, and F. The same Table also includes the values for CCl, NCl, and OCl that are obtained by correcting for the effect of π-electron delocalization estimated using the observed magnetic hyperfine coupling constants. Figure 3 plots the observed and corrected eQq values, indicated by open circles and solid circles, respectively, against the electronegativity difference. As is seen, the corrected values fall on a curve which is slightly shifted from that calculated by a formula proposed by Gordy and Cook.[1] The observed eQq(Cl) value of BCl also fits well with the curve; in order to obtain a better fit, only 0.12 π-electrons are necessary to be transferred from Cl to B, in other words, the 2π molecular orbital is required to involve the B $2p_\pi$ orbital by 3%. The fairly small eQq constant of BCl is thus primarily ascribed to the large ionic character of the B-Cl bond; the ionic character is estimated to be 79—85% using the relation $i_C=1+eQq/eQq_{310}$,[1] where eQq_{310} denotes the value for an atomic p electron in the 3p orbital.

Table 4. Chlorine nuclear quadrupole coupling constants of XCl

X	n[a)]	eQq/MHz	$eQq^{corr.b)}$/MHz	
B	0	−16.74(11)	(−23)[c)]	Present
C	1	−34.26(16)	−60.10	Ref. 4
N	2	−63.13(18)	−87.16	Ref. 6
O	3	−87.95(23)	−105.73	Ref. 3
F	4	−145.871		

a) The number of electrons in the 3π orbital. b) Corrected for π-electron delocalization. See Ref 6. c) 0.12 π-electrons were assumed to be transferred from Cl to B.

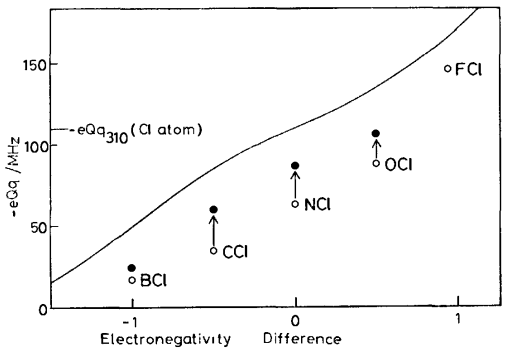

Fig. 3. The nuclear quadrupole coupling constants observed for second-row element chlorides *versus* the electronegativity difference. The observed values are shown by open circles, whereas the solid circles correspond to the corrected values. The arrows for OCl, NCl, and CCl designate the corrections for π-electron delocalization. For BCl the solid circle corresponds to 0.12 π-electron delocalization from Cl to B. The solid curve was calculated from a formula proposed by Gordy and Cook (see Ref. 1).

The B_0 constants of both $^{11}B^{35}Cl$ and $^{11}B^{37}Cl$ which Maki *et al.*[9] have reported differ from the present, more accurate values by four times their standard errors. The discrepancy may be ascribed to the fact that almost all transitions they observed belong to the R branch and the B_0 values are likely to be subjected to systematic errors.

We have also observed a few vibrational satellites. The relative intensity of these lines indicates the effective vibrational temperature of BCl in the discharge plasma to be much higher than the room temperature, namely 1000—2000 K.

Calculations in the present study were carried out at the Computer Center of the Institute for Molecular Science.

References

1) W. Gordy and R. L. Cook, "Microwave Molecular Spectra," Interscience, New York, N. Y. (1970).
2) T. Amano, S. Saito, E. Hirota, Y. Morino, D. R. Johnson, and F. X. Powell, *J. Mol. Spectrosc.*, **30**, 275 (1969).
3) R. K. Kakar, E. A. Cohen, and M. Geller, *J. Mol. Spectrosc.*, **70**, 243 (1978).
4) Y. Endo, S. Saito, and E. Hirota, *J. Mol. Spectrosc.*, **94**, 199 (1982).
5) K. Kawaguchi, Y. Endo, and E. Hirota, *J. Mol. Spectrosc.*, **93**, 381 (1982).
6) C. Yamada, Y. Endo, and E. Hirota, *J. Chem. Phys.*, in press.
7) B. Fabricant and J. S. Muenter, *J. Chem. Phys.*, **66**, 5274 (1977).
8) G. Herzberg and W. Hushley, *Can. J. Res., Sec. A*, **19**, 127 (1941).
9) A. G. Maki, F. J. Lovas, and R. D. Suenram, *J. Mol. Spectrosc.*, **91**, 424 (1982).
10) Y. Endo, S. Saito, and E. Hirota, *J. Chem. Phys.*, **75**, 4379 (1981).

 © 1983 The Chemical Society of Japan Bull. Chem. Soc. Jpn., 56, 3415—3420 (1983)

Phase Equilibria in the Ln_2O_3–V_2O_3–V_2O_5 (Ln=Eu and Yb) Systems at 1200 °C

Kenzo KITAYAMA,* Hidehiko SOU,† and Takashi KATSURA

Department of Chemistry, Faculty of Science, Tokyo Institute of Technology, Ookayama, Meguro-ku, Tokyo 152

(Received February 18, 1983)

Phase equilibria in the systems, Eu_2O_3–V_2O_3–V_2O_5 and Yb_2O_3–V_2O_3–V_2O_5, were established at 1200 °C by changing the oxygen partial pressure from −0.68 (air) to −13.00 atm in terms of $\log P_{O_2}$. In the Eu_2O_3–V_2O_3–V_2O_5 system, $0.81Eu_2O_3 \cdot 0.19V_2O_5$ ($Eu_{1.62}V_{0.38}O_{3.38}$) was stable; in the Yb_2O_3–V_2O_3–V_2O_5 system, a new compound $Yb_7V_3O_{16}$ was stable; and in both systems Ln_2O_3, $LnVO_4$, $LnVO_3$, V_nO_{2n-1} (n=2—7), and VO_2 were stable under the present experimental conditions. On the basis of the established phase diagrams, Gibbs energies of these reactions, $31/50\ Eu_2O_3 + 19/50\ EuVO_3 + 19/100\ O_2 = Eu_{1.62}V_{0.38}O_{3.38}$, $EuVO_3 + 1/2\ O_2 = EuVO_4$, $2\ Yb_2O_3 + 3\ YbVO_3 + 1/2\ O_2 = Yb_7V_3O_{16}$, $Yb_7V_3O_{16} + O_2 = 2\ Yb_2O_3 + 3\ YbVO_4$, and $YbVO_3 + 1/2\ O_2 = YbVO_4$, were determined to be −58.9, −126.0, −134.0, −210.0, and −117.7 kJ respectively. $EuVO_4$, $Eu_{1.62}V_{0.38}O_{3.38}$, $YbVO_4$, $Yb_7V_3O_{16}$, V_2O_3, and VO_2 have nonstoichiometric compositions.

Phase equilibria in the Ln_2O_3–V_2O_3–V_2O_5 systems (Ln=Sm, Lu, Er, Gd, La, Nd, and Tm) at 1200 °C have been established[1-7] by changing the oxygen partial pressure from −0.68 (air) to −12.50 or −13.00 atm†† in terms of $\log P_{O_2}$. These studies established phase diagrams whose different patterns are a result of the fact that different compounds coexist under the experimental conditions. We also succeeded in obtaining the Gibbs energies of reactions presented in the diagrams, the crystallographic data of the ternary compounds, and the activities of the components in the solid solutions.

In the present studies, Eu_2O_3 and Yb_2O_3 were chosen as the Ln_2O_3. Especially, the system that consists of Yb_2O_3 was expected to form as interesting pattern as that of the Lu_2O_3 system,[2] because the existence of a pyrochlore type compound $Yb_2V_2O_7$ was well known[8] and its physical properties had been studied by many researchers.[8-11]

In the Eu_2O_3–V_2O_3 and Yb_2O_3–V_2O_3 systems, $EuVO_3$ and $YbVO_3$ were well known, but these systems have not yet been completely studied, because of V_2O_3 is unstable in air. The crystallographic properties of $EuVO_3$ and $YbVO_3$ have been investigated by McCarthy *et al.*[12] and Shin-ike *et al.*,[13] and it has been confirmed that these compounds belong to orthorhombic system, like the other lanthanoid vanadites except for $LaVO_3$ and $CeVO_3$.

The Eu_2O_3–V_2O_5 system was studied by Brusset *et al.*[14] and Kiparisov *et al.*[15] Brusset *et al.* studied in the temperature range from 600 °C to 1500 °C in air and found three compounds: $Eu_2O_3 \cdot V_2O_5$ ($EuVO_4$), $4Eu_2O_3 \cdot V_2O_5$ ($Eu_8V_2O_{17}$), and $5Eu_2O_3 \cdot V_2O_5$ ($Eu_{10}V_2O_{20}$), while Kiparisov *et al.* studied in the temperature region 500—1500 °C in air and found $Eu_2O_3 \cdot V_2O_5$ and $3Eu_2O_3 \cdot V_2O_5$. A discrepancy in two results exists regarding the stable compounds.

The Yb_2O_3–V_2O_5 system was also investigated by Brusset *et al.*[14] in the temperature range from 600 °C to 1500 °C in air; they found $Yb_2O_3 \cdot V_2O_5$, $4Yb_2O_3 \cdot V_2O_5$, and $5Yb_2O_3 \cdot V_2O_5$.

The crystallographic system of the $Yb_8V_2O_{17}$ is monoclinic[16,17] but that of $5Yb_2O_3 \cdot V_2O_5$ has not been determined, although a rough X-ray powder pattern had been presented by Brusset *et al.*[14] (Fig. 4 in Ref. 14).

The objectives of the present experiment are: (1) to establish the detail phase equilibria in these two systems at 1200 °C in order to confirm which compounds are stable under our experimental conditions, (2) to calculate the Gibbs energies of the reactions which appear in the established phase diagrams, and (3) to ascertain whether or not there exists a linear relationship between the Gibbs energies of the reaction, $LnVO_3 + 1/2\ O_2 = LnVO_4$, and the ionic radii of lanthanoid elements as found in Ln–Fe–O.[18]

Experimental

Analytical grades of Eu_2O_3 (99.9%), of Yb_2O_3 (99.9%), and of V_2O_5, made by heating the guaranteed grade of NH_4VO_3 at 500 °C in air about 24 h, have been used as the starting materials. Desired Eu_2O_3/V_2O_5 and Yb_2O_3/V_2O_5 mole ratios of samples were obtained by mixing the appropriate quantities thoroughly in an agate mortar under ethyl alcohol. The mixtures thus obtained were treated by the procedures described in the previous paper.[1] The apparatus and procedures for controlling the oxygen partial pressures and keeping a constant temperature, the method of the thermogravimetry, the criterion for an equilibrium establishment, and the method of the chemical analysis except for the analysis of vanadium in the presence of europium are the same as those reported in the previous papers.[1,19-23] To obtain the V contents coexisting with Eu, we deduced the weight of Eu_2O_3, which was obtained by the gravimetric method,[1] from the total weight, because Eu^{3+} is reduced to Eu^{2+}, and Eu^{2+} precipitates as $EuSO_4$[24] in the reduction of V^{5+} with Zn–amalgam.

Results and Discussion

Phase Equilibria. (1) The Eu_2O_3–V_2O_3–V_2O_5 System: Although europium oxide has several forms, such as Eu_2O_3, EuO, and Eu_3O_4,[25,26] only Eu_2O_3 is stable under the present experimental conditions.[26,27] Nine samples with Eu_2O_3/V_2O_5 mole ratios of 85/15, 82/18, 81/19, 8/2, 7/3, 6/4, 1, 35/65, and 2/8 were prepared to be used in the thermogravimetric experiment. In Fig. 1, the relationships between the

† Present address: Nippon Mining Co., Ltd., Kurami Works: 3 Kurami, Koza-gun, Kanagawa 253-01.

†† atm = 1.013×10^5 Pa.

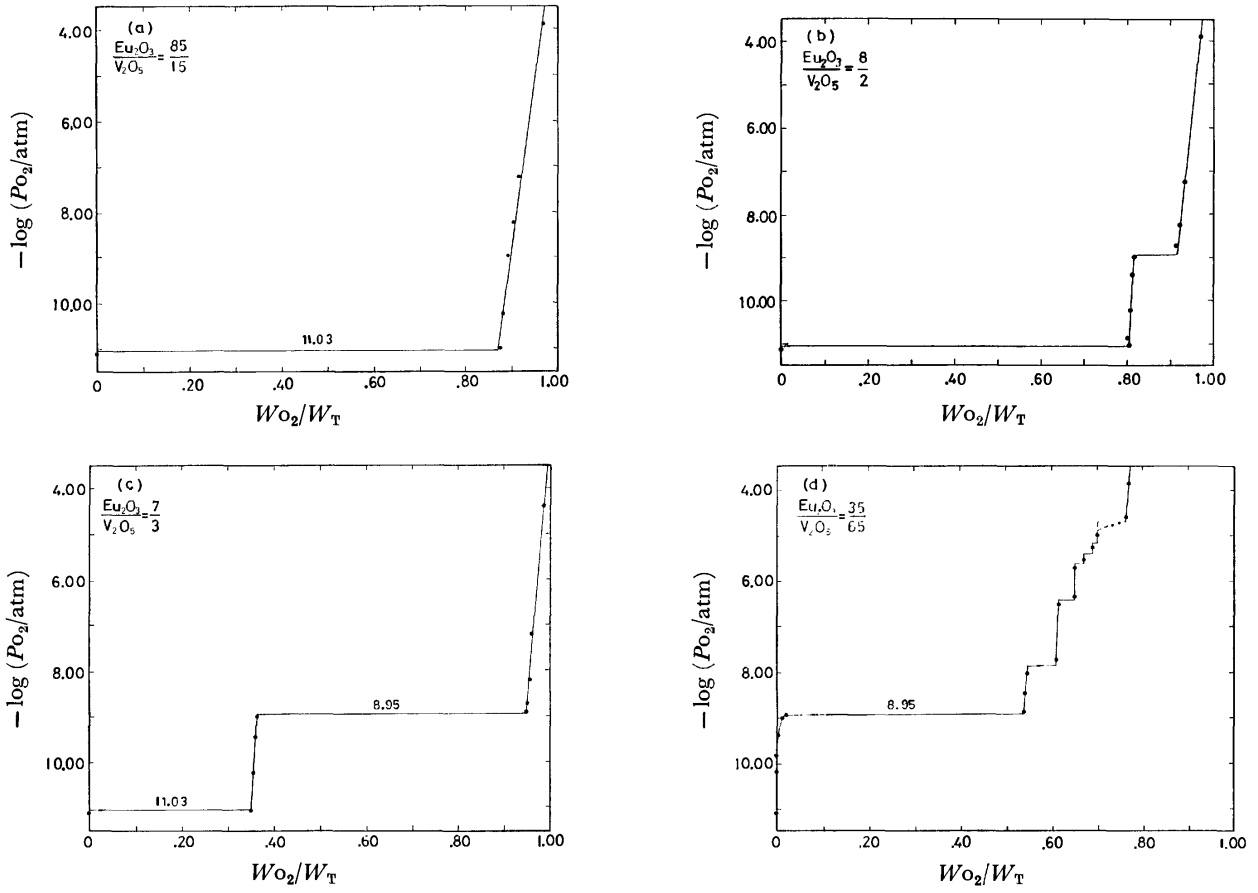

Fig. 1. The relationship between the oxygen partial pressure in $-\log(P_{O_2}/\text{atm})$ and the weight change of the sample in W_{O_2}/W_T.
(a) $Eu_2O_3/V_2O_5=85/15$, (b) $Eu_2O_3/V_2O_5=8/2$, (c) $Eu_2O_3/V_2O_5=7/3$, (d) $Eu_2O_3/V_2O_5=35/65$.

oxygen partial pressure, atm, on the ordinate and the weight change, W_{O_2}/W_T, on the abscissa are shown; here W_{O_2} is the weight gain of the samples from the reference weight in the atmosphere of $\log P_{O_2}=-13.00$ atm, and W_T is the total weight gain that the samples would get if V_2O_3 in the samples would change to V_2O_5. The experimental results of four samples, 85/15, 8/2, 7/3, and 35/65 are shown in Fig. 1 as representative. From Figs. 1a to 1c, it is apparent that abrupt weight changes occur at two oxygen partial pressures, -11.03 and -8.95 atm in $\log P_{O_2}$. These values correspond to the equilibrium oxygen partial pressures of the reactions described in Table 6. Fig. 1d shows a similar pattern to those of the samples of other systems.[1,3-7] which have the composition of Ln_2O_3/V_2O_5 mole ratios lower than unity. But the value of the oxygen partial pressure, $\log P_{O_2}=-8.95$, that corresponds to the equilibrium oxygen partial pressure of the reaction, $EuVO_3+1/2\ O_2=EuVO_4$, is different.

In Table 1 the results of the identification of phases are shown. In the first column are the compositions of the starting materials in mol%; in the second and third are shown the experimental conditions of the oxygen partial pressures in terms of $\log P_{O_2}$ in atm and the experimental duration in h; and in the fourth are the phases identified by X-ray powder diffractometer using Cu $K\alpha$ radiation.

Based upon the above experimental results, a phase diagram of the system at 1200 °C was drawn; This is shown in Fig. 2. The following phases are present under the present experimental conditions except for six compounds in the V_2O_3–V_2O_5 system; Eu_2O_3(R), $Eu_{1.62}V_{0.38}O_{3.38}$(A), $EuVO_4$(B), and $EuVO_3$(C). Compounds in the V_2O_3–V_2O_5 system are the same as those in the previous report.[1] $5Eu_2O_3\cdot V_2O_5$ reported by Brusset *et al.*[14] and $3Eu_2O_3\cdot V_2O_5$ reported by Kiparisov *et al.*[15] have not been confirmed under the present experimental conditions. The Compound A may correspond to the compound $4Eu_2O_3\cdot V_2O_5$ that Brusset *et al.* have reported. But under the present experimental conditions, this compound has no such round mole ratio as that written above. The straight line drawn by plotting the results of the thermogravimetry usually converges to a composition $0.81Eu_2O_3\cdot 0.19V_2O_5$, even considering the experimental errors. As is shown in Fig. 1b, the sample, $Eu_2O_3/V_2O_5=8/2$, has a pattern similar to that in Fig. 1c which shows the two equilibrium oxygen partial pressures. If compound A had the composition of $Eu_2O_3/V_2O_5=8/2$, the pattern should be the same one as that of Fig. 1a with one equilibrium oxygen partial pressure, $\log P_{O_2}=-11.03$. Compounds with the same $Ln_2O_3/V_2O_5=81/19$ mole ratio were found in other systems.[4,5] Figure 2 has a pattern similar to that of the Gd_2O_3–V_2O_3–V_2O_5 system.[4]

Compound A and $EuVO_4$ have nonstoichiometric

compositions. The following relationships between the oxygen partial pressure and the composition were found from the results of the thermogravimetry; $N_O/N_A = 8.71\times10^{-3}+5.18\times10^{-3}\log P_{O_2}$ for compound A and $N_O/N_B = 2.24\times10^{-3}+1.62\times10^{-3}\log P_{O_2}$ for $EuVO_4$ (B). Here N_O, N_A, and N_B mean the mole fractions of oxygen and of component A and B. Nonstoichiometry was not found for $EuVO_3$ under the present experimental conditions.

Table 1. Identification of phases

Eu_2O_3 mol%	V_2O_5 mol%	$-\log(P_{O_2}$/atm)	Time h	Phases
85	15	8.48	20	Eu_2O_3+A[a]
		10.54	48	Eu_2O_3+A
		11.40	22	Eu_2O_3+$EuVO_3$
70	30	8.48	20	$EuVO_4$+A
		10.54	48	$EuVO_3$+A
		11.40	22	Eu_2O_3+$EuVO_3$
60	40	8.48	20	$EuVO_4$+A
		10.54	48	$EuVO_3$+A
		11.40	22	Eu_2O_3+$EuVO_3$
35	65	3.88	42	$EuVO_4$+VO_2
		5.11	70	$EuVO_4$+V_7O_{13}
		5.29	65	$EuVO_4$+V_6O_{11}
		5.43	51	$EuVO_4$+V_5O_9
		6.16	46	$EuVO_4$+V_4O_7
		7.22	23	$EuVO_4$+V_3O_5
		8.48	23	$EuVO_4$+V_2O_3
		9.85	16	$EuVO_3$+V_2O_3
20	80	3.88	42	$EuVO_4$+VO_2
		5.11	70	$EuVO_4$+V_7O_{13}
		5.29	65	$EuVO_4$+V_6O_{11}
		5.50	51	$EuVO_4$+V_5O_9
		6.16	46	$EuVO_4$+V_4O_7
		7.22	23	$EnVO_4$+V_3O_5
		8.48	23	$EuVO_4$+V_2O_3
		9.85	16	$EuVO_3$+V_2O_3

a) A: $Eu_{1.62}V_{0.38}O_{3.38}$.

Table 2 shows compositions of the compounds that were calculated from the results of the thermogravimetry, symbols of the compounds, stability ranges of the compounds in terms of $\log P_{O_2}$, and activities of the components in the solid solutions. Activities of each component in the solid solutions were calculated by using Gibbs-Duhem equation. The detailed method of calculation has been described in the paper of Kimizuka and Katsura.[22]

The lattice constants of the compound A were successfully determined with the aid of the assignment of $4Tm_2O_3\cdot V_2O_5$.[16] Lattice constants of the com-

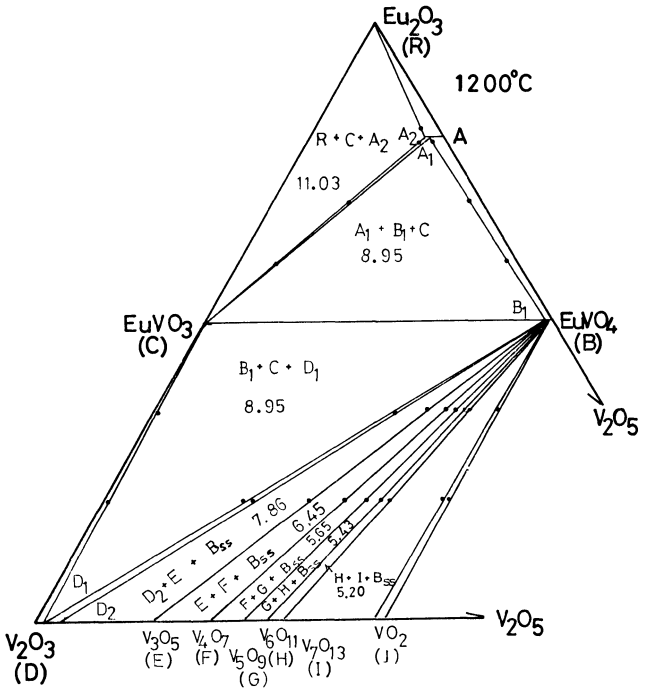

Fig. 2. Phase equilibria in the Eu_2O_3-V_2O_3-V_2O_5 system at 1200 °C. Numerical values in three solid phases regions are the equilibrium oxygen partial pressure in $-\log P_{O_2}$. Abbreviations are the same as those in Table 2.

Table 2. Compositions, symbols, stability ranges in oxygen partial pressures, and activities in solid solution

Component	Composition	Symbol	$-\log(P_{O_2}$/atm)	$\log a_i$
$Eu_{1.62}V_{0.38}O_{3.38}$	$Eu_{1.62}V_{0.38}O_{3.38}$	A	0.68—1.68[a]	0.113
	$Eu_{1.62}V_{0.38}O_{3.34}$	A_1	8.95	0.0448
	$Eu_{1.62}V_{0.38}O_{3.33}$	A_2	11.03	0
$EuVO_4$	$EuVO_{4.00}$	B	0.68—1.38[a]	0.0232
	$EuVO_{3.99}$	B_1	8.95	0
$EuVO_3$	$EuVO_{3.00}$	C	8.95—13.00	0
$Yb_7V_3O_{16}$	$Yb_7V_3O_{16.24}$	A′	9.55	0
	$Yb_7V_3O_{16.40}$	A_1'	8.37	0.116
	$Yb_7V_3O_{16.55}$	A_2'	7.47	0.154
$YbVO_4$	$YbVO_{3.98}$	B_1'	8.37	0
	$YbVO_{3.99}$	B_2'	7.47	0.0077
	$YbVO_{4.00}$	B′	0.68—1.77[a]	0.0279
$YbVO_3$	$YbVO_{3.00}$	C′	8.37—13.00	0

a) These values were obtained by extrapolating the experimental values.

TABLE 3. UNIT CELL DIMENSIONS OF COMPOUNDS TOGETHER WITH THOSE IN PREVIOUS REPORTS

Compound	$-\log(P_{O_2}$ /atm)	a Å	b Å	c Å	β °	V Å^3	Ref.
$Eu_{1.62}V_{0.38}O_{3.38}$	0.68	10.77±0.02	8.77±0.02	16.5±0.1	99.2±0.3	1530±10	Present
	10.54	10.77±0.02	8.78±0.02	16.4±0.1	99.2±0.3	1530±10	Present
$EuVO_4$	3.88	7.238±0.001		6.369±0.002		333.6±0.1	Present
		7.2365±0.0002		6.3675±0.0002			29
		7.232±0.002		6.362±0.002			14
		7.239±0.003		6.370±0.003		333.8	28
$EuVO_3$	9.39	5.374±0.004	5.608±0.003	7.657±0.004		230.8±0.2	Present
		5.362±0.002	5.599±0.002	7.651±0.002		229.7±0.05	12
$YbVO_4$	0.68	7.047±0.001		6.250±0.001		310.3±0.1	Present
	7.20	7.047±0.001		6.250±0.001		310.4±0.1	Present
		7.046±0.002		6.233±0.002			14
		7.043±0.003		6.248±0.003		309.9	28
		7.0435		6.2470			30
$YbVO_3$	9.85	5.231±0.001	5.574±0.001	7.542±0.001		219.9±0.1	Present
		5.223±0.002	5.564±0.002	7.534±0.002		219.0±0.05	12

pounds, A, $EuVO_4$, and $EuVO_3$ are tabulated in Table 3, together with those of previous reports.[12,13,27,28] Figures that are shown in the second column of the Table are the oxygen partial pressure used in preparation of samples. We could not discuss about the difference of the unit cell dimensions of two A samples because the experimental errors are too large. Present values for $EuVO_4$ are in good agreement with those of Schwarz,[28] but the values for $EuVO_3$ are slightly larger than those of McCarthy *et al.*[12]

(2) The Yb_2O_3–V_2O_3–V_2O_5 System: Yb_2O_3 is stable under the present experimental conditions.[22] Six samples with Yb_2O_3/V_2O_5 mole ratios of 8/2, 7/3, 6/4, 1, 35/65, and 2/8 were prepared to be used in the thermogravimetric experiments. Relationships between the oxygen partial pressure and the weight change, W_{O_2}/W_T, for three samples: 8/2, 6/4, and 2/8 are shown in Fig. 3 as representative cases. We find three equilibrium oxygen partial pressure: 9.55, 8.37, and 7.47 in $-\log P_{O_2}$ from Figs. 3a and 3b. Figure 3c shows a similar pattern to that in Fig. 1d except for the oxygen partial pressure, $\log P_{O_2} = -8.37$, for the reaction $YbVO_3 + 1/2\ O_2 = YbVO_4$.

In Table 4, the results of the identification of phases are shown. Based upon the above experimental results, a phase diagram at 1200 °C was drawn and is shown in Fig. 4. The following phases are present under the present experimental conditions, along with the six compounds in the V_2O_3–V_2O_5 system. Phases are: Yb_2O_3(R′), $Yb_7V_3O_{16}$(A′), $YbVO_4$(B′), and $YbVO_3$(C′). Compounds in the V_2O_3–V_2O_5 system are the same as those in the previous report.[1] The compound $Yb_7V_3O_{16}$ is new although the Ln/V/O mole ratio is identical with those of Lu[2] and Tm[7] systems. Compounds $4Yb_2O_3 \cdot V_2O_5$ and $5Yb_2O_3 \cdot V_2O_5$ reported by Brusset *et al.*[14,16] and the pyrochlore type $Yb_2V_2O_7$ reported by many authors[8–10] were not found under the present experimental conditions. This phase diagram is a new type.

Compounds $Yb_7V_3O_{16}$ and $YbVO_4$ have nonstoichiometric compositions. The following relationships between the oxygen partial pressure and the composition were obtained from the results of the thermogravimetry: $N_O/N_A' = 1.161 + 0.158 \log P_{O_2}$ for $Yb_7V_3O_{16}$ (A′) and $N_O/N_B' = 4.58 \times 10^{-3} + 2.59 \times 10^{-3} \log P_{O_2}$ for $YbVO_4$ (B′).

TABLE 4. IDENTIFICATION OF PHASES

Yb_2O_3 mol%	V_2O_5 mol%	$-\log(P_{O_2}$ /atm)	Time h	Phases
80	20	3.88	18	$Yb_2O_3 + YbVO_4$
		7.58	45	$Yb_2O_3 + Yb_7V_3O_{16}$
		8.90	24	$Yb_2O_3 + Yb_7V_3O_{16}$
		10.22	16	$Yb_2O_3 + YbVO_3$
70	30	3.88	18	$Yb_2O_3 + YbVO_4$
		7.58	45	$Yb_7V_3O_{16}$
		8.90	24	$Yb_7V_3O_{16}$
		10.22	16	$Yb_2O_3 + YbVO_3$
60	40	3.88	18	$Yb_2O_3 + YbVO_4$
		7.58	45	$Yb_7V_3O_{16} + YbVO_4$
		8.90	24	$Yb_7V_3O_{16} + YbVO_3$
		10.22	16	$Yb_2O_3 + YbVO_3$
35	65	3.88	24	$YbVO_4 + VO_2$
		5.01	69	$YbVO_4 + V_7O_{13}$
		5.25	46	$YbVO_4 + V_6O_{11}$
		5.56	21	$YbVO_4 + V_5O_9$
		6.16	22	$YbVO_4 + V_4O_7$
		7.00	45	$YbVO_4 + V_3O_5$
		8.10	21	$YbVO_4 + V_2O_3$
		9.00	21	$YbVO_3 + V_2O_3$
20	80	3.88	24	$YbVO_4 + VO_2$
		5.01	69	$YbVO_4 + V_7O_{13}$
		5.25	46	$YbVO_4 + V_6O_{11}$
		5.56	21	$YbVO_4 + V_5O_9$
		6.16	22	$YbVO_4 + V_4O_7$
		7.00	45	$YbVO_4 + V_3O_5$
		8.10	21	$YbVO_4 + V_2O_3$
		9.00	21	$YbVO_3 + V_2O_3$

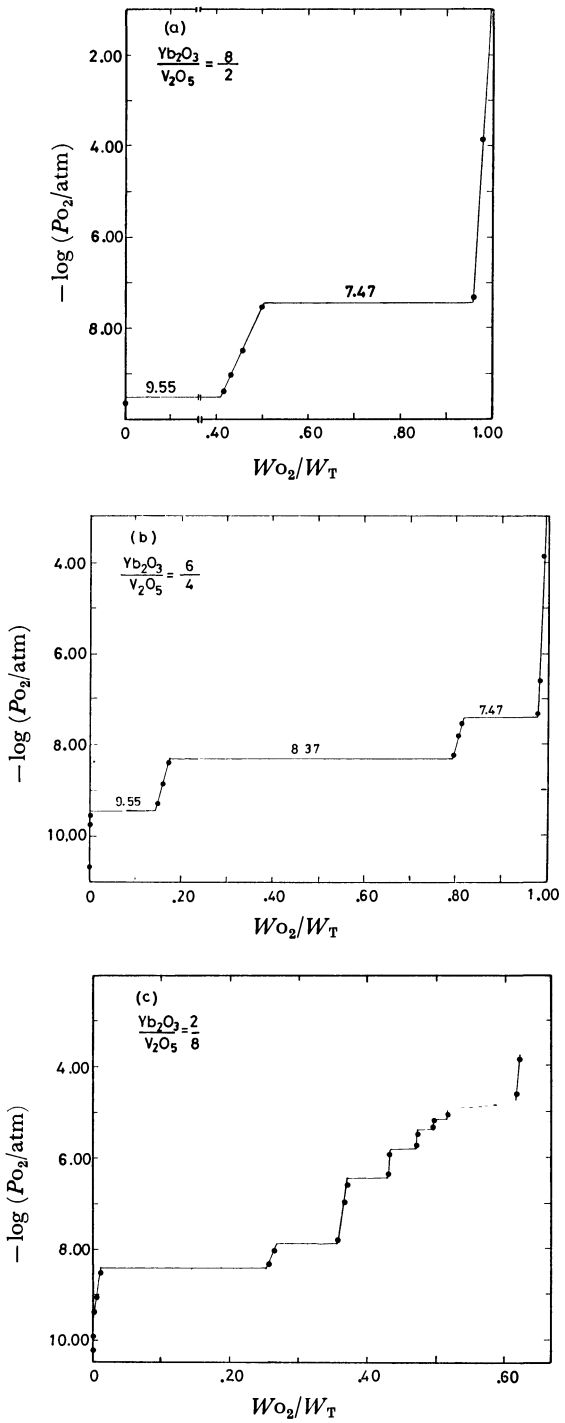

Fig. 3. The relationship between the oxygen partial pressure in $-\log(Po_2/\text{atm})$ and the weight change of the sample in Wo_2/W_T.
(a) $Yb_2O_3/V_2O_5=8/2$, (b) $Yb_2O_3/V_2O_5=6/4$, (c) $Yb_2O_3/V_2O_5=2/8$.

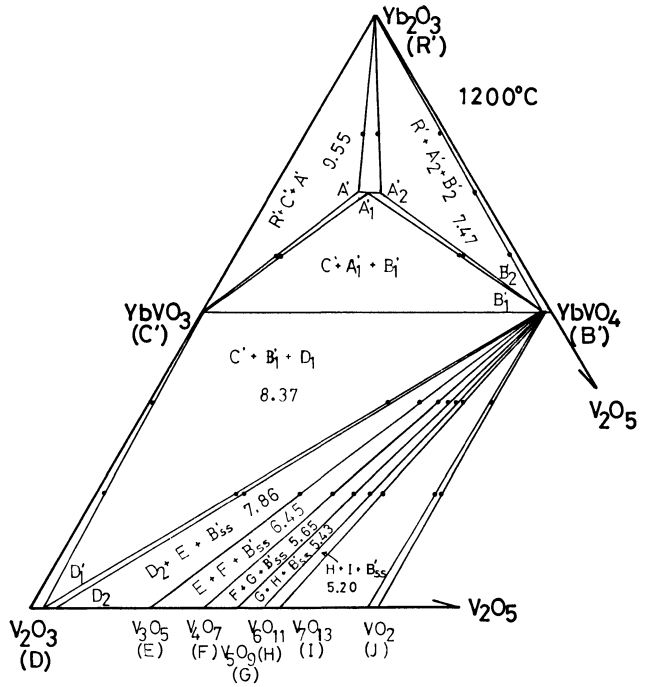

Fig. 4. Phase equilibria in the Yb_2O_3-V_2O_3-V_2O_5 system at 1200 °C. Numerical values in three solid phases regions are the equilibrium oxygen partial pressure in $-\log Po_2$. Abbreviations are the same as those in Table 2.

Table 5. The spacings and relative intensities of $Yb_7V_3O_{16}$

d/Å	I/I_0	d/Å	I/I_0
5.73	11	1.7881	24
3.176	98	1.7070	20
3.033	100	1.6839	19
2.863	48	1.6150	24
2.680	33	1.5993	21
2.608	59	1.5722	11
2.560	16	1.5580	25
2.193	17	1.5161	11
2.126	17	1.4869	12
2.080	10	1.4659	11
1.9282	57	1.4317	12
1.9076	22		

In Table 2, the compositions of the compounds at various oxygen partial pressures, stability ranges of the compounds in terms of $\log Po_2$, the symbols of the compounds, and the activities of the components in the solid solutions are also tabulated.

The assignment of Miller's indices for the new compound, $Yb_7V_3O_{16}$, did not succeed. Relative intensities and spacings that were obtained by X-ray diffractometer with the powder sample are shown in Table 5, several weak peaks being omitted.

Lattice constants of the compounds, $YbVO_4$ and $YbVO_3$, are tabulated in Table 3, together with those of previous reports.[12,14,28,29] The lattice constants of $YbVO_4$, made in air, are in good agreement with those prepared at $\log Po_2=-7.20$ and with those of the previous reports. Present values of $YbVO_3$ are larger than those obtained by McCarthy *et al.*[12]

Calculation of Gibbs Energies of Reactions. On the basis of the established phase diagrams, Gibbs energies of reactions appearing in the systems, except for the reactions in the V_2O_3-V_2O_5 system, can be calculated by an equation, $\Delta G^\circ=-RT\ln K$, where the R is the

TABLE 6. GIBBS ENERGIES OF REACTIONS

Reaction	$-\log(P_{O_2}/\text{atm})$	$-\Delta G°/\text{kJ}$
$19/50\ EuVO_3+31/50\ Eu_2O_3+19/100\ O_2=Eu_{1.62}V_{0.38}O_{3.38}$	11.03±0.06	58.9±0.2
$EuVO_3+1/2\ O_2=EuVO_4$	8.95±0.02	126.0±0.3
$2\ Yb_2O_3+3\ YbVO_3+1/2\ O_2=Yb_7V_3O_{16}$	9.55±0.05	134.0±0.7
$Yb_7V_3O_{16}+O_2=2\ Yb_2O_3+3\ YbVO_4$	7.47±0.03	210.0±0.7
$YbVO_3+1/2\ O_2=YbVO_4$	8.37±0.03	117.7±0.4

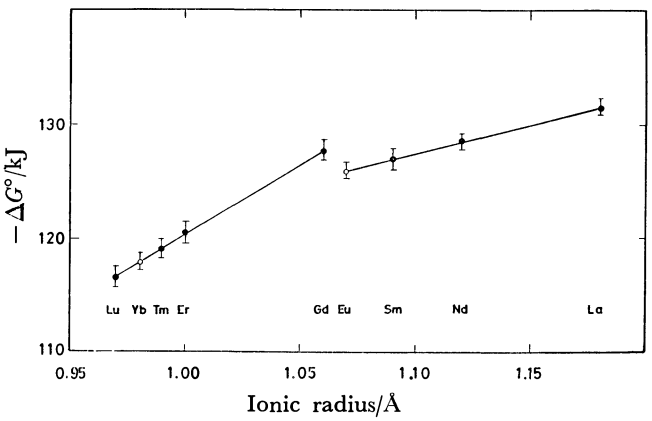

Fig. 5. The relationship between the ionic radius in 8 coordination number and the Gibbs energies of reaction, $LnVO_3+1/2\ O_2=LnVO_4$. The solid circles are the previous values and the open circles present values.

gas constant, the T the absolute temperature, and the K the equilibrium constant of each reaction. Reactions and the $\Delta G°$ values obtained are shown in Table 6, together with the equilibrium oxygen partial pressures. Activities of each component in the solid solutions whose activity is necessary for the calculations are listed in Table 2.

The Relationship between $\Delta G°$ and Ionic Radius. In the previous report,[7] the relationship between $\Delta G°$ values for the reaction $LnVO_3+1/2\ O_2=LnVO_4$ and the 8 coordinated ionic radius of lanthanoid elements was graphically shown. The series divided into two groups and the relationship is linear within each of the groups. The experimental results of the present systems are plotted in Fig. 5 with open circles together with the previous data shown as solid circles. Both open circles fit well on the lines which were drawn using the data of the previous experiments.

References

1) K. Kitayama and T. Katsura, *Bull. Chem. Soc. Jpn.*, **50**, 889 (1977).
2) K. Kitayama and T. Katsura, *Bull. Chem. Soc. Jpn.*, **51**, 1358 (1978).
3) K. Kitayama, T. Sugihara, and T. Katsura, *Bull. Chem. Soc. Jpn.*, **52**, 458 (1979).
4) K. Kitayama and T. Katsura, *Bull. Chem. Soc. Jpn.*, **55**, 1820 (1982).
5) K. Kitayama, D. Zoshima, and T. Katsura, *Bull. Chem. Soc. Jpn.*, **56**, 689 (1983).
6) K. Kitayama, C. Mizokuchi, and T. Katsura, *Bull. Chem. Soc. Jpn.*, **56**, 695 (1983).
7) K. Kitayama and T. Katsura, *Bull. Chem. Soc. Jpn.*, **56**, 1084 (1983).
8) G. W. Bazuev, O. V. Makarova, V. Z. Oboldin, and G. P. Shveikin, *Dokl. Akad. Nauk SSSR*, **230**, 869 (1976).
9) T. Shin-ike, G. Adachi, and J. Shiokawa, *Mater. Res. Bull.* **12**, 1149 (1977).
10) J. E. Greedan, *Mater. Res. Bull.*, **14**, 13 (1979).
11) L. Soderholm and J. E. Greedan, *Mater. Res. Bull.*, **17**, 707 (1982).
12) G. J. McCarthy, C. A. Sipe, and K. E. McIlvried, *Mater. Res. Bull.*, **9**, 1279 (1974).
13) T. Shin-ike, G. Adachi, and J. Shiokawa, *Denki Kagaku*, **48**, 258 (1980).
14) H. Brusset, F. Madaule-Aubry, B. Blanck, J. P. Glaziou, and J. P. Laude, *Can. J. Chem.*, **49**, 3700 (1971).
15) S. S. Kiparisov, R. A. Belyaev, V. V. Bondarenko, and V. P. Vyskubov, *Izv. Akad. Nauk SSSR, Neorg. Mat.*, **9**, 68 (1973).
16) H. Brusset, R. Mahe, and J. P. Laude, *Bull. Soc. Chim. Fr.*, **1973**, 495.
17) O. N. Ustalova, G. A. Rykova, V. M. Skorikov, and I. V. Tananaev, *Zh. Neorg. Khim.*, **25**, 1223 (1980).
18) T. Katsura, K. Kitayama, T. Sugihara, and N. Kimizuka, *Bull. Chem. Soc. Jpn.*, **48**, 1809 (1975).
19) T. Katsura and H. Hasegawa, *Bull. Chem. Soc. Jpn.*, **40**, 561 (1967).
20) N. Kimizuka and T. Katsura, *J. Solid State Chem.*, **13**, 176 (1975).
21) T. Katsura and A. Muan, *Trans. AIME*, **230**, 77 (1964).
22) N. Kimizuka and T. Katsura, *J. Solid State Chem.*, **15**, 151 (1975).
23) N. Kimizuka and T. Katsura, *Bull. Chem. Soc. Jpn.*, **47**, 1801 (1974).
24) H. N. McCoy, *J. Am. Chem. Soc.*, **57**, 1756 (1935).
25) R. G. Bedford and E. Catalano, *J. Solid State Chem.*, **3**, 112 (1971).
26) G. J. McCarthy, *J. Am. Ceram. Soc.*, **57**, 502 (1974).
27) T. Sugihara, K. Kimizuka, and T. Katsura, *Bull. Chem. Soc. Jpn.*, **48**, 1806 (1975).
28) H. Schwarz, *Z. Anorg. Allg.* Chem., **323**, 44 (1963).
29) J.C.P.D.S. Data Card, No. 15-809.
30) J.C.P.D.S. Data Card, No. 17-338.

 © 1983 The Chemical Society of Japan Bull. Chem. Soc. Jpn., 56, 3421—3425 (1983)

Crystal and Molecular Structure of μ-Imidazolato-bis{[tris(2-methylthioethyl)amine]copper(II)}perchlorate

Masatatsu Suzuki,* Ikuhiko Ueda, Hajime Kanatomi, and Ichiro Murase

Laboratory of Chemistry, College of General Education, Kyushu University, Ropponmatsu, Chuo-ku, Fukuoka 810

(Received April 14, 1983)

The structure of the title complex, $[Cu_2(NS_2\text{-}Me)_2im](ClO_4)_3$, has been determined by the single-crystal X-ray diffraction method, where NS_3–Me is tris(2-methylthioethyl)amine and im is imidazolate anion. The complex crystallizes in the monoclinic space group $P2_1/a$ with a unit cell with the dimensions of $a=13.114(3)$, $b=28.045(6)$, $c=10.481(2)$ Å, $\beta=98.70(2)°$, $V=3810.2(13)$ Å^3, and $Z=4$. The structure was solved by the heavy atom method. The residual R value was 0.0594 for 4431 independent reflections. The coordination geometries of the two copper atoms are different from each other; the Cu(1) is in a trigonal bipyramidal geometry with three sulfur atoms in the equatorial plane and two nitrogen atoms in the axial positions, while the coordination geometry of the Cu(2) can be best described as an intermediate between a trigonal bipyramid and a square pyramid. The intramolecular Cu(1)···Cu(2) distance is 5.930(2) Å. Temperature-dependent magnetic susceptibility data showed a strong antiferromagnetic exchange interaction with a coupling constant $-J=63$ cm^{-1}. The Cu(1)–N(1)–C(1) and Cu(2)–N(2)–C(1) angles, which have been considered to be related to the magnitude of the antiferromagnetic exchange interaction, are 132.1(5) and 127.0(6)°, respectively. The magnetism of the complex is discussed in connection with the structural data.

Recently, a number of di- and tetra-nuclear copper (II) complexes bridged by various imidazolate groups have been reported as possible models for the active site of bovine erythrocyte superoxide dismutase.[1-8] Those studies have shown that antiferromagnetic exchange interactions operate between copper(II) ions and their magnitudes are highly dependent on the structure of the Cu–im–Cu moiety.

In the previous study,[9] we reported that the imidazolate-bridged dinuclear copper(II) complexes with tripod ligand (L) having NS_3 or N_2S_2 donor set, $[Cu_2(L)_2im](ClO_4)_3$, exhibited antiferromagnetic interactions with coupling constants $(-J)$ of 58—66 cm^{-1}, where L is tris(2-alkylthioethyl)amine, 2-[bis(2-methylthioethyl)aminomethyl]pyridine, or *N,N*-bis-(2-methylthioethyl)ethylenediamine and im is imidazolate anion. The antiferromagnetic exchange interactions of those complexes are considerably strong compared with those of the other dinuclear complexes bridged by imidazolate itself.[2-8] Therefore, we are interested in the structure of the Cu–im–Cu moiety of the above complexes with tripod ligands containing sulfur atoms in connection with their magnetic properties.

In general, tripod ligands (L) such as tris(2-aminoethyl) amine (tren) tend to form trigonal bipyramidal copper(II) complexes, $[Cu(L)X]^{n+}$, with an additional unidentate ligand (X).[10-13] Previously, we demmonstrated that, in a series of $[Cu(NS_3\text{–}R)X]^{n+}$, the stereochemistry of the complexes depends on both alkyl substituent (R) and the unidentate ligand (X).[14] The electronic and esr spectra of the imidazole complex, $[Cu(NS_3\text{–}Me)Him](ClO_4)_2$, suggested that the complex has a square pyramidal structure. Thus the stereochemistry of the dinuclear complex with tripod ligand, NS_3–Me, is also interesting. In this paper, we have undertaken a single-crystal X-ray analysis of $[Cu_2(NS_3\text{–}Me)_2im](ClO_4)_3$.

Mikuriya *et al.*[15,16] demonstrated that the replacement of nitrogen donor atom by sulfur donor atom causes an increase in antiferromagnetic exchange interaction; the alkoxo-bridged dinuclear copper(II) complexes with SNO and NSO donor sets exhibit a stronger antiferromagnetic exchange interaction than the complexes with NNO donor set. An influence of the sulfur donor atom on the antiferromagnetic exchange interaction is also described.

Experimental

The complex was prepared by the method previously reported.[9] Recrystallization from an aqueous solution at room temperature afforded dark green prisms.

The diffraction data were measured on a Rigaku AFC-5 automated four-circle diffractometer with graphite-monochromated Mo $K\alpha$ radiation. The unit-cell parameters were determined by the least-squares refinement based on 20 reflections. A crystal with approximate dimensions of $0.3\times0.2\times0.2$ mm^3 was used for intensity measurement. Crystal data: $Cu_2Cl_3S_6O_{12}N_4C_{21}H_{45}$, F.W.=971.4, monoclinic, space group $P2_1/a$, $a=13.114(3)$, $b=28.045(6)$, $c=10.481(2)$ Å, $\beta=98.70(2)°$, $V=3810.2(13)$ Å^3, $D_m=1.68$, $D_x=1.69$ g cm^{-3}, $Z=4$, and μ(Mo $K\alpha$)=17.4 cm^{-1}.

The intensity data were collected by θ-2θ scan technique with a scan rate of 8° min^{-1}. For weak reflections the peak scan was repeated up to three times depending on their intensities. Three standard reflections were monitored every 100 reflections and their intensities showed a good stability. A total of 7249 reflections with $2\theta<50°$ was collected and 4431 independent reflections with $|F_o|>3\sigma(|F_o|)$ were considered as "observed" and used for structure analysis. The intensity data were corrected for the Lorentz and polarization effects, but not for the absorption.

The structure was solved by the heavy-atom method. The positions of two copper atoms were obtained from the Patterson synthesis and those of the remaining 46 nonhydrogen atoms were obtained from successive Fourier syntheses. Refinement was carried out by the block-diagonal least-squares method. A difference Fourier synthesis gave several peaks around chlorine atoms of perchlorate ions, which were ascribed to the disordered oxygen atoms of perchlorate ions. The nonhydrogen atoms with occupancy factor larger than 0.5 were refined with anisotropic thermal parameters. Hydrogen atoms defined by the geometry of the complex were located at the calculated positions (C–H=1.09 Å)

Table 1. Fractional positional parameters ($\times 10^4$) and thermal parameters of non-hydrogen atoms with their estimated standard deviations in parentheses

Atom	x	y	z	B_{eq}/Å^3 b)	Atom	x	y	z	B_{eq}/Å^3 b)	
Cu(1)	3615.6(8)	4374.6(3)	7311.4(9)	2.7	C(15)	3339(8)	6959(4)	7594(10)	5.1	
Cu(2)	1411.8(7)	6227.7(3)	6866.6(10)	2.8	C(16)	-194(8)	6955(4)	6240(11)	5.2	
S(1)	4950(2)	4529(1)	6069(2)	3.1	C(17)	445(9)	7131(4)	5258(9)	5.0	
S(2)	3790(2)	4605(1)	9561(2)	3.8	C(18)	2147(9)	6942(4)	4027(11)	5.7	
S(3)	2216(2)	3874(1)	6368(2)	4.0	C(19)	-299(8)	6473(4)	8174(11)	5.6	
S(4)	2690(2)	6531(1)	8468(2)	3.7	C(20)	-861(8)	6052(5)	7457(13)	6.4	
S(5)	1145(2)	6636(1)	4722(2)	3.9	C(21)	236(9)	5218(5)	7360(15)	7.8	
S(6)	-93(2)	5737(1)	6451(3)	4.7	Cl(1)	13371(2)	10675(1)	8823(3)	5.2	
N(1)	2911(5)	4965(2)	6661(6)	2.9	Cl(2)	11355(2)	8415(1)	6731(2)	4.3	
N(2)	2243(5)	5688(2)	6425(6)	2.9	Cl(3)	4189(2)	7687(1)	11197(2)	4.1	
N(3)	4408(6)	3760(2)	7931(6)	3.3	O(11)	12761(10)	10635(4)	9783(10)	11.5	
N(4)	414(5)	6726(3)	7405(7)	3.7	O(12)	13156(7)	10285(4)	7967(9)	8.2	
C(1)	2736(6)	5369(3)	7234(8)	3.0	O(13)	14422(8)	10671(5)	9316(12)	12.7	
C(2)	2119(6)	5476(3)	5242(7)	3.2	O(14)	13109(9)	11102(4)	8166(12)	10.8	
C(3)	2526(7)	5029(3)	5368(8)	3.4	O(21)	12083(6)	8119(3)	6232(9)	7.3	
C(4)	5532(7)	3798(4)	7760(9)	4.2	O(22)	11470(7)	8892(3)	6398(11)	8.9	
C(5)	5661(7)	3990(3)	6454(9)	4.0	O(23)	10382(6)	8248(4)	6122(10)	8.9	
C(6)	5677(7)	4957(4)	7106(9)	4.2	O(24)	11157(15)	8299(7)	8009(16)	7.6	0.50
C(7)	4370(8)	3674(4)	9333(9)	4.3	O(25)	11714(15)	8408(7)	8026(14)	8.0	0.50
C(8)	4623(8)	4120(4)	10127(8)	4.6	O(31)	3482(7)	8011(3)	10517(8)	8.0	
C(9)	2609(8)	4429(4)	10158(10)	7.1	O(32)	4430(9)	7344(4)	10368(9)	9.0	0.90
C(10)	3927(8)	3348(3)	7152(10)	4.2	O(33)	3655(15)	7384(7)	12002(21)	10.7	0.55
C(11)	2768(8)	3322(3)	7069(10)	4.4	O(34)	5177(12)	7901(7)	11464(17)	9.4	0.55
C(12)	1122(8)	3968(4)	7238(11)	5.1	O(35)	3954(16)	7559(8)	12406(20)	8.2	0.45
C(13)	975(8)	7113(4)	8202(11)	5.2	O(36)	4452(28)	7801(13)	12452(35)	10.0	0.30
C(14)	1834(8)	6914(4)	9214(9)	4.3	O(37)	4887(29)	7977(14)	11906(36)	8.0	0.25

b) Occupancy factors.

In the final cycles of the refinement, hydrogen atoms were included with isotropic thermal parameters (4.0 Å^2). The final value of R was 0.0594.

The difference Fourier map showed a peak (1.4 eÅ^3) near the S(6) atom which was probably due to the fact that the absorption correction had not been applied.

The atomic scattering factors and the anomalous dispersion corrections, $\Delta f'$ and $\Delta f''$, for Cu, Cl, S, O, N, and C, were taken from the international tables for X-ray Crystallography.[17] For the hydrogen atoms, the scattering factors were adopted from the tables of Stewart *et al.*[18] All the calculations were carried out on the FACOM M-200 computor at the Computor Center of Kyushu University by the use of a local version of the UNICS III[19,20] and the ORTEP[21] programs. The final positional parameters with their standard deviations are given in Table 1. Observed and calculated structure factors, anisotropic thermal parameters of the nonhydrogen atoms, and hydrogen atom coordinates have been deposited as a Document NO. 8351 at the Office of the Editor of Bull. Chem. Soc. Jpn.

Results and Discussion

A perspective drawing of the complex cation and the numbering system are illustrated in Fig. 1. Bond distances and angles are listed in Table 2.

The crystal structure consists of a discrete imidazolate bridged dinuclear cation, $[Cu_2(NS_3\text{-}Me)_2im]^{3+}$, and perchlorate anions. The intramolecular Cu(1)···Cu(2) distance is 5.930(2) Å. Each copper atom is five-coordinate. The coordination geometries of the Cu(1) and Cu(2) atoms are different from each other. The Cu(1) atom is in a trigonal bipyramidal coordination geometry, while the Cu(2) is in an intermediate between a trigonal bipyramid and a square pyramid (Fig. 2). In the former, the equatorial positions are occupied by three sulfur atoms and the axial positions

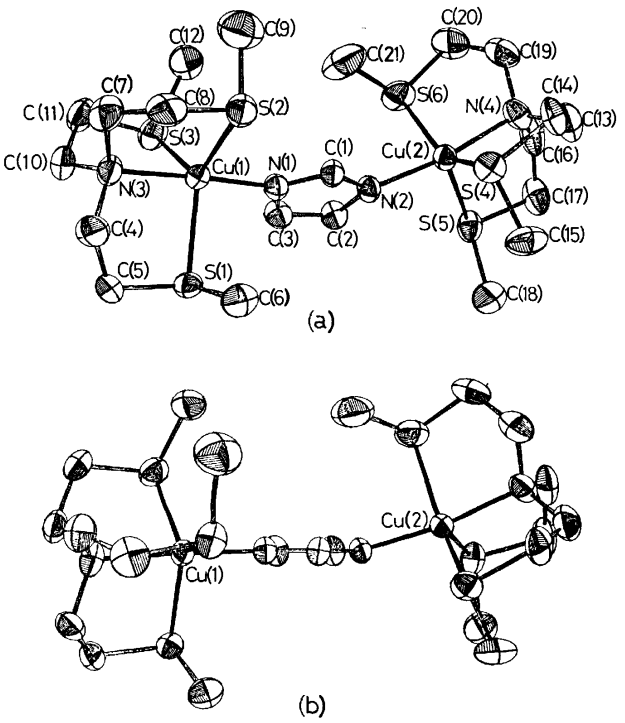

Fig. 1. Two views (a) and (b) of the complex cation, $[Cu_2(NS_3\text{-}Me)_2im]^{3+}$, showing the atomic numbering. The thermal ellipsoid was drawn at the 50% probability level.

Table 2. Interatomic distances and angles with estimated standard deviations in parentheses

Bond distance	l/Å	Bond distance	l/Å
Cu(1)···Cu(2)	5.930(2)	N(3)-C(7)	1.498(11)
Cu(1)-S(1)	2.374(3)	N(3)-C(10)	1.498(11)
Cu(1)-S(2)	2.423(3)	N(4)-C(13)	1.492(13)
Cu(1)-S(3)	2.402(3)	N(4)-C(16)	1.498(13)
Cu(1)-N(1)	1.968(7)	N(4)-C(19)	1.502(14)
Cu(1)-N(3)	2.065(7)	C(2)-C(3)	1.362(12)
Cu(2)-S(4)	2.345(2)	C(4)-C(5)	1.504(14)
Cu(2)-S(5)	2.500(3)	C(7)-C(8)	1.512(14)
Cu(2)-S(6)	2.392(3)	C(10)-C(11)	1.511(14)
Cu(2)-N(2)	1.961(7)	C(13)-C(14)	1.531(14)
Cu(2)-N(4)	2.051(8)	C(16)-C(17)	1.505(16)
S(1)-C(5)	1.790(9)	C(19)-C(20)	1.528(17)
S(1)-C(6)	1.795(10)	Cl(1)-O(11)	1.381(13)
S(2)-C(8)	1.789(11)	Cl(1)-O(12)	1.416(10)
S(2)-C(9)	1.825(12)	Cl(1)-O(13)	1.398(11)
S(3)-C(11)	1.817(10)	Cl(1)-O(14)	1.395(12)
S(3)-C(12)	1.832(12)	Cl(2)-O(21)	1.424(9)
S(4)-C(14)	1.813(11)	Cl(2)-O(22)	1.396(9)
S(4)-C(15)	1.799(12)	Cl(2)-O(23)	1.417(9)
S(5)-C(17)	1.800(11)	Cl(2)-O(24)	1.440(18)
S(5)-C(18)	1.812(13)	Cl(2)-O(25)	1.368(15)
S(6)-C(20)	1.797(13)	Cl(3)-O(31)	1.411(10)
S(6)-C(21)	1.757(14)	Cl(3)-O(32)	1.364(11)
N(1)-C(1)	1.319(11)	Cl(3)-O(33)	1.452(21)
N(1)-C(3)	1.385(10)	Cl(3)-O(34)	1.417(17)
N(2)-C(1)	1.331(10)	Cl(3)-O(35)	1.395(22)
N(2)-C(2)	1.363(10)	Cl(3)-O(36)	1.347(36)
N(3)-C(4)	1.515(12)	Cl(3)-O(37)	1.359(36)

by two nitrogen atoms. The three trigonal angles formed by S–Cu–S are close to 120°, *i.e.*, 121.11(9), 117.47(9), and 120.71(10)°, and the trigonal axis (N(1)–Cu(1)–N(3)) is nearly linear (177.1(3)°). The three equatorial Cu–S distances are 2.374(2), 2.423 (3), and 2.402(3) Å, which are in agreement with those in trigonal bipyramidal complexes with tripod ligand containing sulfur atoms, $[Cu(NS_3\text{–}Me)Br]ClO_4$ [22] and $[Cu(pam)SO_4]$[23] (pam=2-[bis(2-ethylthioethyl)-aminomethyl]pyridine). The Cu(1)–N(3) distance is comparable to Cu–N distances of the above complexes.

The Cu(1) atom does not exactly fit in the trigonal plane through S(1), S(2), and S(3), and is displaced 0.12 Å toward the direction of the bridging imidazolate. This type of displacement of the Cu atom is quite commom in the trigonal bipyramidal complexes with tripod ligands.[10–13]

The coordination geometry around the Cu(2) atom is an intermediate between a trigonal bipyramid and a square pyramid. The distorted nature from a trigonal bipyramid becomes evident from an examination of the S–Cu–S bond angles, 95.77(9), 117.71 (9), and 145.10(10)°. Viewing the structure as a square pyramid, N(2), N(4), S(4), and S(6) atoms form a basal plane, and the S(5) atom occupies the axial position. In a regular square pyramid, The S(4)–Cu(2)–S(6) and the N(2)–Cu(2)–N(4) angles should be 180°. In the typical square pyramidal complex, $K[Cu(NH_3)_5](PF_6)_3$[24], however, the corresponding angles are 164 and 167°, where the decrease

Bond angle	φ/°	Bond angle	φ/°	Bond angle	φ/°
S(1)-Cu(1)-S(2)	121.11(9)	Cu(2)-S(4)-C(14)	95.8(3)	N(1)-C(3)-C(2)	107.0(7)
S(1)-Cu(1)-S(3)	117.47(9)	Cu(2)-S(4)-C(15)	102.7(3)	N(3)-C(4)-C(5)	112.2(7)
S(2)-Cu(1)-S(3)	120.71(10)	C(14)-S(4)-C(15)	101.3(5)	S(1)-C(5)-C(4)	112.4(7)
S(1)-Cu(1)-N(1)	90.2(2)	Cu(2)-S(5)-C(17)	94.7(3)	N(3)-C(7)-C(8)	111.7(8)
S(1)-Cu(1)-N(3)	87.0(2)	Cu(2)-S(5)-C(18)	124.5(4)	S(2)-C(8)-C(7)	112.1(6)
S(2)-Cu(1)-N(1)	94.7(2)	C(17)-S(5)-C(18)	101.3(5)	N(3)-C(10)-C(11)	114.0(8)
S(2)-Cu(1)-N(3)	87.0(2)	Cu(2)-S(6)-C(20)	97.5(4)	S(3)-C(11)-C(10)	108.5(7)
S(3)-Cu(1)-N(1)	93.4(2)	Cu(2)-S(6)-C(21)	104.5(4)	N(4)-C(13)-C(14)	111.8(8)
S(3)-Cu(1)-N(3)	87.6(2)	C(20)-S(6)-C(21)	101.7(7)	S(4)-C(14)-C(13)	110.9(7)
N(1)-Cu(1)-N(3)	177.1(3)	Cu(1)-N(1)-C(1)	132.1(5)	N(4)-C(16)-C(17)	114.6(8)
S(4)-Cu(2)-S(5)	117.71(9)	Cu(1)-N(1)-C(3)	122.0(6)	S(5)-C(17)-C(16)	108.9(7)
S(4)-Cu(2)-S(6)	145.10(10)	C(1)-N(1)-C(3)	105.8(7)	N(4)-C(19)-C(20)	113.2(10)
S(5)-Cu(2)-S(6)	95.77(9)	Cu(2)-N(2)-C(1)	127.0(6)	S(6)-C(20)-C(19)	113.4(8)
S(4)-Cu(2)-N(2)	94.9(2)	Cu(2)-N(2)-C(2)	123.9(5)	O(11)-Cl(1)-O(12)	108.5(6)
S(4)-Cu(2)-N(4)	88.4(2)	C(1)-N(2)-C(2)	105.5(7)	O(11)-Cl(1)-O(13)	112.2(7)
S(5)-Cu(2)-N(2)	98.6(2)	Cu(1)-N(3)-C(4)	110.9(5)	O(11)-Cl(1)-O(14)	107.6(7)
S(5)-Cu(2)-N(4)	85.8(2)	Cu(1)-N(3)-C(7)	110.7(6)	O(12)-Cl(1)-O(13)	108.5(7)
S(6)-Cu(2)-N(2)	89.2(2)	Cu(1)-N(3)-C(10)	108.8(5)	O(12)-Cl(1)-O(14)	109.8(6)
S(6)-Cu(2)-N(4)	84.2(2)	C(4)-N(3)-C(7)	107.7(7)	O(13)-Cl(1)-O(14)	110.2(8)
N(2)-Cu(2)-N(4)	172.5(3)	C(4)-N(3)-C(10)	109.1(7)	O(21)-Cl(2)-O(22)	111.4(6)
Cu(1)-S(1)-C(5)	97.1(3)	C(7)-N(3)-C(10)	109.7(7)	O(21)-Cl(2)-O(23)	104.4(6)
Cu(1)-S(1)-C(6)	99.1(3)	Cu(2)-N(4)-C(13)	111.6(6)	O(21)-Cl(2)-O(24)	115.7(8)
C(5)-S(1)-C(6)	102.6(4)	Cu(2)-N(4)-C(16)	110.5(6)	O(21)-Cl(2)-O(25)	101.9(9)
Cu(1)-S(2)-C(8)	94.7(3)	Cu(2)-N(4)-C(19)	107.5(6)	O(22)-Cl(2)-O(23)	109.2(6)
Cu(1)-S(2)-C(9)	107.5(3)	C(13)-N(4)-C(16)	107.6(7)	O(22)-Cl(2)-O(24)	119.4(9)
C(8)-S(2)-C(9)	100.8(5)	C(13)-N(4)-C(19)	109.7(8)	O(22)-Cl(2)-O(25)	103.2(10)
Cu(1)-S(3)-C(11)	95.7(3)	C(16)-N(4)-C(19)	110.0(7)	O(23)-Cl(2)-O(24)	93.9(9)
Cu(1)-S(3)-C(12)	108.5(4)	N(1)-C(1)-N(2)	112.8(7)	O(23)-Cl(2)-O(25)	126.4(10)
C(11)-S(3)-C(12)	102.5(5)	N(2)-C(2)-N(3)	108.8(7)	O(24)-Cl(2)-O(25)	32.5(11)

a) The angles around Cl(3) are omitted because of serious disorder.

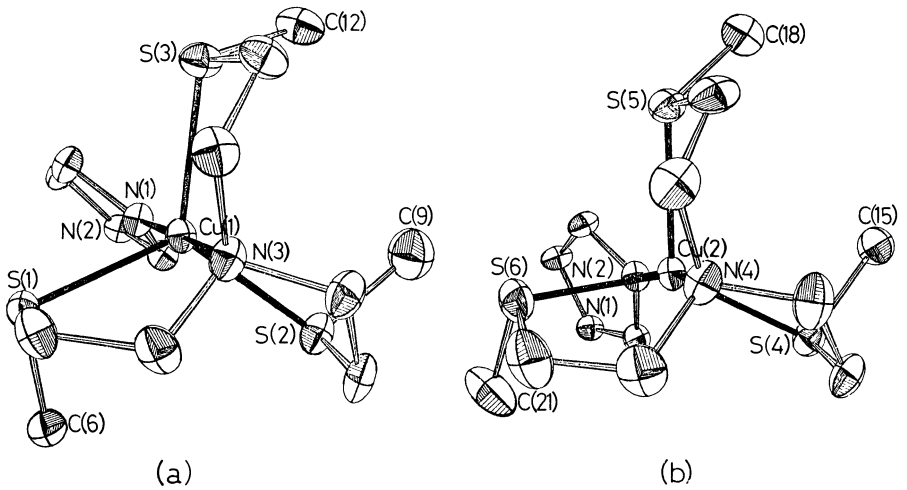

Fig. 2. Coordination geometries around the Cu(1) (a) and the Cu(2) (b) of $(Cu_2(NS_3\text{-}Me)_2im]^{3+}$.

in those angles from 180° is due to the displacement of the Cu atom from the basal plane toward the fifth ligand. In the present complex, the S(4)–Cu(2)–S (6) and the N(2)–Cu(2)–N(4) angles are 145.10(10) and 172.5(3)°, respectively. In general, the apical bonds are longer than the basal ones in square pyramidal complexes.[25] The S(5)–Cu(2) bond distance (2.500 (3) Å) is apparently longer than the S(4)–Cu(2) (2.345 (3) Å) and the S(6)–Cu(2) (2.392(3) Å). Thus the coordination geometry around the Cu(2) atom can be best described as an intermediate between a trigonal bipyramid and a square pyramid.

In general, tripod ligands tend to enforce a trigonal bipyramidal structure, *i.e.*, in the tren complexes, the range of the trigonal angles are from 105 to 140°.[10-13] The larger variation in the trigonal angles of the present complex may be due to the packing effects.

All of the bond distances and angles of the NS_3–Me ligands are within the range observed for $[Cu(NS_3\text{–}Me)Br]ClO_4$,[22] and $[Co(NS_3\text{–}Bu)Br]PF_6$.[26] All the five-membered chelate rings adopt gauche conformation with the exception of the Cu(2)–N(3)–C(19)–S(6) chelate ring which assumes envelop conformation. The torsion angles about C–C bonds of the chelate rings in the gauche conformation are in the range of 50.8—58.9°, while that in the envelop conformation is 35.2°.

The bond distances and angles of the imidazolate ring are in agreement with those previously reported.[3,4,6] The five atoms constituting the imidazolate ring lie within 0.009 Å of the best plane through them. The Cu(1) atom is 0.039 Å out of this plane and the Cu(2) atom deviates 0.603 Å from the plane on the opposite side, which is considerably larger than those previously reported.[3,4,27] Thus the Cu(2)–N(2) bond is bent out of the imidazolate plane (Fig. 1b). The angle of this bending is *ca.* 17°.

The Cu–N(imidazolate) bond distances are 1.968 (7) and 1.961(7) Å, which are quite normal.

Magnetism. Di- and tetra-nuclear copper(II) complexes bridged by various imidazolate groups show antiferromagnetic exchange interactions with coupling constants $(-J)$ ranging from *ca.* 0—90 cm^{-1}.[1,2,8] The magnitude of antiferromagnetic exchange interaction is a reflection of the interaction of the orbitals of the bridging ligand with copper orbitals in which the unpaired electrons reside; the extent of the overlap between the copper d orbitals and the appropriate orbitals of the bridging ligand, and the energy difference between those orbitals are two important factors which determine the J value.[2,8,28]

It has been suggested that a π-exchange mechanism is not important in the imidazolate-bridged copper(II) complexes.[2,4,8] Haddad and Hendrickson[2] demonstrated that, in a series of $[Cu_2(tren)_2Y]^{3+}$, (Y=benzimidazolate, imidazolate, or 2-methylimidazolate), the difference in antiferromagnetic exchange interactions mediated by a variety of the bridging imidazolates are related to the angle α (in the present complex, α is defined by the Cu(1)–N(1)–C(1) and Cu(2)–N(2)–C(1) angles). Increasing the angles α improves the overlap between the metal d orbitals and the σ orbitals of the bridging imidazolate, leading to an increase in $|J|$.

In addition, Dewan and Lippard[27] suggested that the angle θ between two Cu–N(imidazolate) vectors is also important in determining $|J|$. This angle can be also considered to be a measure of the extent of the overlap between the d orbitals and the σ molecular orbitals of the bridging imidazolate.

In the present complex, the values of α are 127.0(6) and 132.1(5)°, and that of θ is 145°. These values suggest that an overlap between the d orbitals and the σ molecular orbitals of the bridging imidazolate is not larger than those in $[Cu_2(tmdt)_2im(ClO_4)_2]ClO_4$[3] ($\alpha$= 129°, θ=143°, $-J$=25.8 cm^{-1}) (Table 3). Furthermore, the Cu(2)–N(2) bond significantly bends out of the imidazolate plane (*ca.* 17°). Thus, the effect of the overlap of the Cu–N bonds in a geometrical sense could not explain such a large $|J|$ value (63 cm^{-1}) of the present complex.

Kolks *et al.*[8] pointed out that the magnitude of the coupling constant is also proportional to the pK_a of imidazolium group. This was interpreted in terms of the energy change of the σ molecular orbitals of the bridging imidazolate groups. The higher the pK_a of the imidazolium is, the higher the energies of the σ

Table 3. Comparison of the copper-imidazolate geometry and coupling constant

Complex[a]	α/°	θ/°	$-J$/cm^{-1}	Reference
$[Cu_2(bpim)(NO_3)_2(ClO_4)(OH_2)]\cdot H_2O$	143, 142	170	81.3	27
$[Cu_2(NS_3\text{-}Me)_2im](ClO_4)_3$	127, 132	145	63	This work
$[Cu_2(pmdt)_2(2\text{-}Meim)]ClO_4)_3$	121, 121		38	8
$[Cu_2(tmdt)_2im(ClO_4)_2]ClO_4$	129, 129	143	25.8	3
$[Cu_2(L)im](ClO_4)_3$	129, 134	146[b]	21.0	5
$Na[Cu_2(gly\text{-}glyO)_2im]\cdot 6H_2O$	124, 125	135	19	4
$[Cu_2(pmdt)_2(Bzim)](ClO_4)_3\cdot H_2O$	123, 128		17	8

a) Abbreviations for the ligands are bpim=4,5-bis[2-(2-pyridyl)ethyliminomethyl]imidazolate; pmdt=*N*,*N*,*N*′,*N*″,-*N*″-tetramethyldiethylenetriamine; tmdt=*N*,*N*,*N*′,*N*′-tetramethyldiethylenetriamine; L=30-membered macrocyclic Schiff base in Ref. 5,6; gly-glyO=glycylglycinate. b) The value given in Table 2 in Ref. 5 is 163°, which is incorrect.

molecular orbitals of the imidazolate become. This results in a decrease in energy separation between the d orbitals and the σ molecular orbitals, and an increase in $|J|$. One of the other possibilities of the large $|J|$ value of the present complex is the lowering of the d orbital energies compared with those of $[Cu_2(tmdt)_2im(ClO_4)_2]ClO_4$.[3] Mikuriya *et al.*[15,16] demonstrated that, in a series of the alkoxo-bridged dinuclear copper (II) complexes, the replacement of the nitrogen donor atom by the sulfur donor atom causes an increase of $|J|$. Although direct evidence is lacking, it seems that the sulfur donor atom has a larger effect which lowers the d orbital energy than the nitrogen donor atom.

We thank Proffesor S. Kida, Proffesor H. Okawa, Dr. Y. Nishida, and Dr. M. Mikuriya for allowing us to use automated diffractometer and for their helpful discussions.

References

1) G. Kolks and S. J. Lippard, *J. Am. Chem. Soc.*, **99**, 5804 (1977).
2) M. S. Haddad and D. N. Hendrickson, *Inorg. Chem.*, **17**, 2622 (1978).
3) C. O'young, J. C. Dewan, H. R. Lilienthal, and S. J. Lippard, *J. Am. Chem. Soc.*, **100**, 7291 (1978).
4) K. Matsumoto, S. Ooi, Y. Nakao, W. Mori, and A. Nakahara, *J. Chem. Soc., Dalton Trans.*, **1981**, 2045.
5) M. G. B. Drew, S. M. Nelson, and J. Reedijk, *Inorg. Chim. Acta*, **64**, L189 (1982).
6) M. G. B. Drew, M. McCann, and S. M. Nelson, *J. Chem. Soc., Dalton Trans.*, **1981**, 1868.
7) H. M. J. Hendriks, P. J. M. W. L. Birker, G. C. Vershoor, and J. Reedijk, *J. Chem. Soc., Dalton Trans.*, **1982**, 623.
8) G. Kolks, S. J. Lippard, J. V. Waszczak, and H. R. Lilienthal, *J. Am. Chem. Soc.*, **104**, 717 (1982).
9) M. Suzuki, H. Kanatomi, H. Koyama, and I. Murase, *Inorg. Chim. Acta*, **44**, L41 (1980).
10) P. C. Jain and E. C. Lingafelter, *J. Am. Chem. Soc.*, **89**, 6131 (1967).
11) D. M. Duggan and D. N. Hendrickson, *Inorg. Chem.*, **13**, 1911 (1974).
12) E. J. Laskowski, D. M. Duggan, and D. N. Hendrickson, *Inorg. Chem.*, **14**, 2449 (1975).
13) T. R. Felthouse, E. N. Duesler, A. T. Christensen, and D. N. Hendrickson, *Inorg. Chem.*, **18**, 245 (1979).
14) M. Suzuki, H. Kanatomi, H. Koyama, and I. Murase, *Bull. Chem. Soc. Jpn.*, **53**, 1961 (1980).
15) M. Mikuriya, H. Okawa, and S. Kida, *Inorg. Chim. Acta*, **34**, 13 (1979).
16) M. Mikuriya, H. Okawa, and S. Kida, *Bull. Chem. Soc. Jpn.*, **53**, 3717 (1980).
17) "International Tables for X-ray Crystallography," Kynoch Press, Birmingham (1974), Vol. IV.
18) R. F. Stewart, E. R. Davidson, and W. T. Simpson, *J. Chem. Phys.*, **42**, 3175 (1965).
19) T. Sakurai and K. Kobayashi, *Rikagaku Kenkyusho Hokoku*, **55**, 69 (1979).
20) S. Kawano, *Rep. Comp. Cent. Kyushu Univ.*, **16**, 113 (1983).
21) C. K. Johnson, Report NO. 3794, Oak Ridge National Laboratory, Oak Ridge, Tennessee (1965).
22) Y. Nishida, K. Takahashi, and S. Kida, *Mem. Fac. Sci. Kyushu Univ. Ser. C*, **13**, 335 (1982).
23) K. D. Karlin, P. L. Dahlstrom, J. R. Hyde, and J. Zubieta, *J. Chem. Soc., Chem. Commun.*, **1980**, 906.
24) D. M. Duggan, N. Ray, B. J. Hathaway, A. A. G. Tomlinson, P. Brint, and K. Pelin, *J. Chem. Soc., Dalton Trans.*, **1980**, 1342.
25) B. J. Hathaway, *Struct. Bonding*, **14**, 49 (1973).
26) G. Fallani, R. Morassi, and F. Zanobini, *Inorg. Chim. Acta*, **12**, 147 (1975).
27) J. C. Dewan and S. J. Lippard, *Inorg. Chem.*, **19**, 2079 (1980).
28) P. J. Hay, J. C. Thibeault, and R. Hoffman, *J. Am. Chem. Soc.*, **97**, 4884 (1975).

Liquid-Liquid Distribution of 4-Acyl-3-methyl-1-phenyl-5-pyrazolones and Their Zinc Complexes

Shigeo UMETANI and Masakazu MATSUI*
Institute for Chemical Research, Kyoto University, Uji, Kyoto 611
(Received April 18, 1983)

The distribution of eight 4-acyl-3-methyl-1-phenyl-5-pyrazolones and their zinc complexes between aqueous and cyclohexane phases was investigated. The acid dissociation constants and partition constants of the extractants were discussed in terms of a substituent effect. It was found that two series of examined reagents in which one has an aromatic substituent at the 4-position of 5-pyrazolone, and the other an aliphatic one give similar extraction constants. Since their acid dissociation constants are essentially the same, a relationship, $\log P_{MA}=2\log P_{HA}+\text{constant}$, is postulated. The extraction constant of a fluorinated reagent which has a considerably small pK_a value is also similar to that of the reagents having aliphatic substituents. Another relationship, $\log \beta_2=2pK_a+\text{constant}$, is postulated.

The solvent extraction system has been widely employed as a convenient separation and concentration method of metal cations, and the extraction mechanism has been investigated in terms of the nature of metal cations, the role of solvents, and the chelation and distribution behavior of ligands.

The previous papers indicate that 4-acyl-5-pyrazolones (Fig. 1), a kind of β-diketones, have several advantages.[1-3] First, metal ions are extractable from acidic media because the pyrazolones are strong acids, and secondly, various kinds of derivatives can be easily synthesized, an important point for the investigation on the extraction mechanism. Obvious substituent effects were observed in the extraction of europium and barium,[1] and in the synergistic extraction of alkaline earths,[2] europium and scandium.[3]

In the present paper, quantitative investigations are made on the distribution of 4-acyl-3-methyl-1-phenyl-5-pyrazolones and the extraction of their zinc complexes.

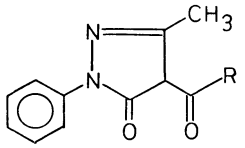

Fig. 1. 4-Acyl-3-methyl-1-phenyl-5-pyrazolones.

Experimental

Reagents. 4-Acyl-3-methyl-1-phenyl-5-pyrazolones were synthesized according to Jensen's method,[4] that is, from 3-methyl-1-phenyl-5-pyrazolone and the corresponding acid chloride or acid anhydride for the fluorinated ligand. The crude compounds were recrystallized from aqueous dioxane or methanol. Analytical data for these reagents are shown in Table 1. Zinc-65 was supplied by New England Nuclear, Boston, Mass. as a hydrochloric acid solution. This solution was once dried up and diluted with perchloric acid. Sodium perchlorate used to adjust the ionic strength (0.1) was recrystallized from water. All the other chemicals were chemically pure or reagent-grade materials.

Distribution of the Reagents. The experiments were performed in a 30 cm^3 glass-stoppered centrifuge tube. A cyclohexane solution containing pyrazolone (0.02 mol dm^{-3}) and an equal volume of the aqueous solution containing sodium perchlorate (0.1 mol dm^{-3}) and sodium acetate (0.01 mol dm^{-3}) as a buffer solution were shaken for 1 h in a thermostated room at 25±1 °C. The hydrogen ion concentration was controlled at a desired value with sodium hydroxide and perchloric acid. After the two layers had been separated centrifugally, the ligand concentration was measured spectrophotometrically. The ligand concentration in the aqueous phase was measured after the dilution with sodium hydroxide solution to complete the dissociation of the ligand. This anionic form which is stable enough for a few days, exhibits strong absorption at 250—300 nm. The sum of the ligand concentration determined in each phase coincided well with the initial concentration. The pH value of the aqueous phase was checked after extraction.

TABLE 1. ELEMENTAL ANALYSIS OF THE COMPOUNDS STUDIED

Reagent No.	R	Calcd (Found) (%) C	H	N	Mp θ_m/°C
1	Phenyl	73.37	5.07	10.07	92—92.5
		(73.54	4.99	10.22)	
2	2-Methylphenyl	73.96	5.52	9.58	111—112
		(73.64	5.52	9.33)	
3	3-Methylphenyl	73.96	5.52	9.58	94—95
		(73.72	5.39	9.38)	
4	4-Methylphenyl	73.96	5.52	9.58	100
		(74.01	5.46	9.66)	
5	2-Naphthyl	76.81	4.91	8.53	101
		(76.93	4.96	8.55)	
6	Propyl	68.83	6.60	11.47	45
		(68.78	6.59	11.66)	
7	Heptyl	71.97	8.05	9.33	61
		(72.17	8.09	9.25)	
8	Trifluoromethyl	53.34	3.33	10.36	146
		(53.55	3.30	10.56)	

Distribution of Zinc Complexes. A cyclohexane solution containing pyrazolone (0.02 mol dm^{-3}) and an equal volume of the aqueous solution containing Zn^{2+} (1×10^{-6} mol dm^{-3}), radioactive tracer (^{65}Zn), sodium perchlorate (0.1 mol dm^{-3}) and sodium acetate (0.01 mol dm^{-3}) were shaken for 1 h. After the two layers had been separated, 2 cm^3 of each phase was pipetted into a test tube and the radioactivities were counted.

Apparatus. Radioactivities were determined by counting with a Metro Electronics NaI (44.5 mm diam.×50.8 mm depth) well-type scintillation counter, model PbW-6, connected to a Metro automatic scaler, model SS-1060H. A Shimadzu UV-180 spectrophotometer was used for spec-

trophotometric measurements, and a Hitachi-Horiba F-7ss pH meter for pH measurements.

Results and Discussion

Data Processing. In a quantitative treatment for the distribution of the reagents, the acid dissociation constant, K_a, and the partition constant, P_{HA}, are defined as follows:

$$K_a = \frac{[H^+][A^-]}{[HA]},$$

$$P_{HA} = \frac{[HA]_o}{[HA]}, \quad (1)$$

where [HA] and [A^-] are the concentration of the neutral and anionic species of the extracting reagents in the aqueous phase, and the subscript o denotes the species in the organic phase. Thus, the distribution ratio of the reagents, D_{HA}, can be written as,

$$D_{HA} = \frac{[HA]_o}{[HA]+[A^-]},$$

or

$$D_{HA} = \frac{P_{HA}}{1+K_a[H^+]^{-1}}. \quad (2)$$

When the hydrogen ion concentration is high enough, D_{HA} agrees with P_{HA}, while log D_{HA} agrees with log $P_{HA}+pK_a-pH$ for low hydrogen ion concentrations.

The concentration of the anionic form can be described by using the initial ligand concentration, $[HA]_i$, as follows:

$$[HA]_i = [HA]_o + [HA] + [A^-],$$

$$[A^-] = \frac{[HA]_i}{1+[H^+](1+P_{HA})\cdot K_a^{-1}}. \quad (3)$$

When the divalent metal ion and the distribution ratio of the metal ion are denoted by M^{2+} and D_{MA}, the extraction constant, K_{ex}, can be written as follows:

$$M^{2+} + 2HA \rightleftharpoons MA_{2,o} + 2H^+,$$

$$K_{ex} = \frac{[MA_2]_o[H^+]^2}{[M^{2+}][HA]_o^2}. \quad (4)$$

The extraction constant can be rewritten by the chelate formation constants, β_2, and the partition constant of the chelates, P_{MA}, as follows:

$$\beta_2 = \frac{[MA_2]}{[M^{2+}][A^-]^2},$$

$$P_{MA} = \frac{[MA_2]_o}{[MA_2]},$$

$$K_{ex} = K_a^2\cdot\beta_2\cdot P_{MA}\cdot P_{HA}^{-2}. \quad (5)$$

Distribution of the Reagents. Figure 2 shows the distribution behavior of the reagents **1**, **7**, and **8** as a function of pH. The distribution curves are asymptotic to a constant value, log P_{HA}, at high hydrogen ion concentrations, and to a straight line with a slope of −1, *i.e.* the theoretical line (Eq. 2) at low hydrogen ion concentrations. The similar distribution behavior was also observed for other reagents. The results are summarized in Table 2. The acid dissociation constants increase in the order expected from the substituent effect,[1] but are essentially the same except for reagents **2** and **8**. Although the partition constants increase with the carbon number, the influence of increasing the carbon number is not always the same when aromatic substituents are compared with aliphatic ones. For instance, log P_{HA} for reagent **7** is much larger than for reagent **5**, whose carbon number is larger than that of reagent **7**.

Distribution of Zinc Complexes. A plot of log D_{MA} against log $[HA]_o$ for reagent **1** is shown in Fig. 3. A slope of 2 indicates that the extracted species is ZnA_2, and no further addition to this extracted form occurs in this ligand concentration range. Furthermore, dependence of log D_{MA} on pH and log [A^-]

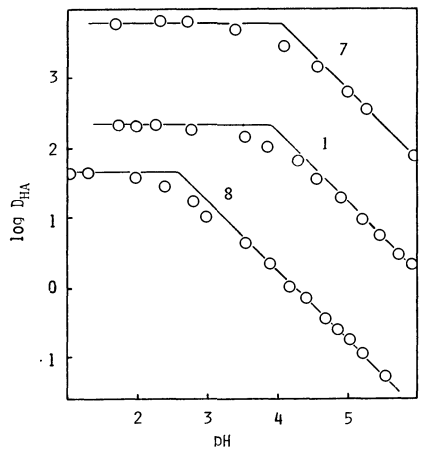

Fig. 2. Distribution of 4-acyl-5-pyrazolones between cyclohexane and water as a function of pH. The numerals show the reagent number in Table 1.

Table 2. Extraction parameters for zinc complexes

Reagent No.	pK_a	log P_{HA}	$pH_{1/2}$[a]	log K_{ex}	log $P_{MA}\cdot\beta_2$	log $K_a\cdot P_{HA}^{-1}$
1	3.92	2.33	4.37	−5.32	7.18	−6.25
2	3.58	3.12	3.98	−4.56	8.84	−6.70
3	4.09	2.91	4.24	−5.08	8.92	−7.00
4	4.02	2.88	4.35	−5.30	8.50	−6.90
5	4.13	3.40	4.42	−5.44	9.62	−7.53
6	3.97	2.50	4.78	−6.14	6.80	−6.47
7	4.07	3.79	4.68	−5.96	9.76	−7.86
8	2.56	1.67	—	−5.86	2.60	−4.23

a) $[HA]_o = 0.02$ mol dm^{-3}.

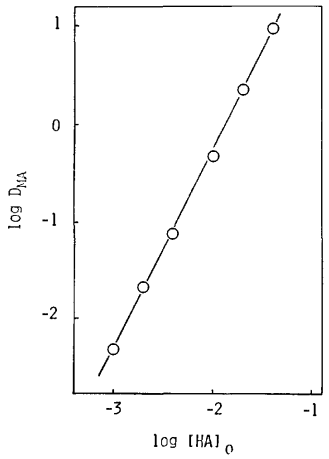

Fig. 3. Influence of the reagent **1** concentration on the extraction of zinc complex at pH 4.60.

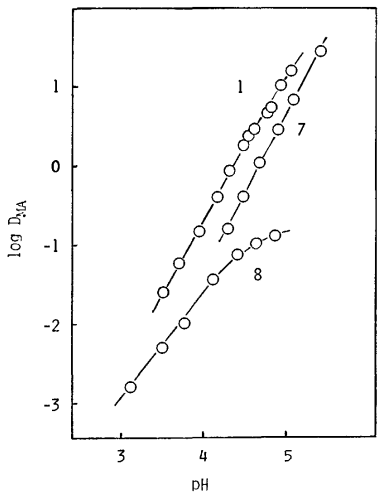

Fig. 4. Logarithm of the distribution ratio of zinc as a function of pH. Reagents: 0.02 mol dm^{-3} in cyclohexane. The numerals show the reagent number in Table 1.

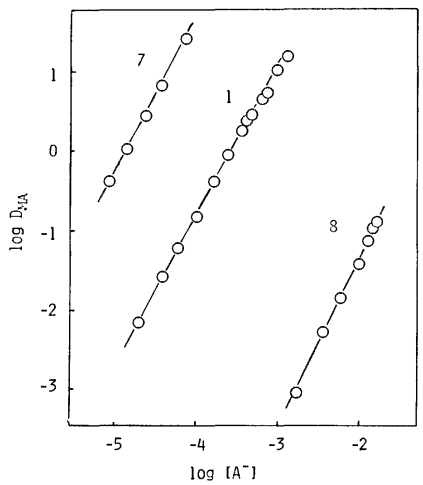

Fig. 5. Logarithm of the distribution ratio of zinc as a function of log [A$^-$]. The numerals show the reagent number in Table 1.

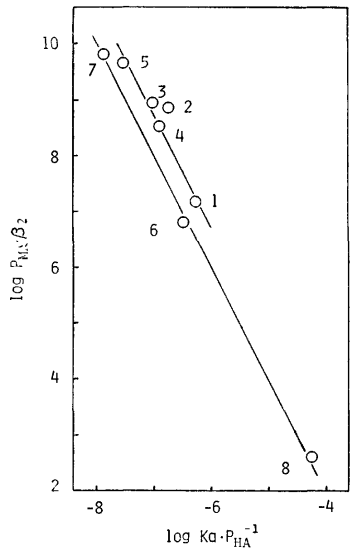

Fig. 6. Correlation between $\log P_{MA}\cdot\beta_2$ and $\log K_a\cdot P_{HA}$. The numerals show the reagent number in Table 1.

has also been examined to confirm the availability of Eq. 4 and are shown in Figs. 4 and 5. The values of [A$^-$] can be obtained from Eq. 3. The plots of $\log D_{MA}$ against pH at a constant $[HA]_o$ gave straight lines with a slope of 2 for reagents **1** and **7**. The slope for reagent **8** is smaller than 2, for in this pH region log [A$^-$] increases no longer linearly with pH because of its strong acidity and low partition constant (see Table 2). Each plot of $\log D_{MA}$ against log [A$^-$] shows a straight line with a slope of 2 as seen in Fig. 5. The values of $\log K_{ex}$ and $\log P_{MA}\cdot\beta_2$ calculated from Eqs. 4 and 5 are summarized in Table 2 together with $pH_{1/2}$ (pH value at which 50% of the metal ion was extracted with 0.02 mol dm^{-3} of the reagent) and $\log K_a\cdot P_{HA}^{-1}$. As shown in Table 2, the values of $\log K_{ex}$ are close together for reagents **1**—**5** with aromatic substituents, and for reagents **6**—**8** with aliphatic ones. Figure 6 illustrates the plots for the relationship between $\log P_{MA}\cdot\beta_2$ and $\log K_a\cdot P_{HA}^{-1}$. Two straight lines with a slope of -2 are obtained for the two groups. The ligands with an aromatic substituent except for reagent **2** have similar values of K_a so that the values of β_2 are expected also to be similar to each other when other influences such as steric hindrance are negligible. On the basis of this assumption a relationship between P_{MA} and P_{HA} can be postulated from Fig. 6 as follows:

$$\log P_{MA} = 2\log P_{HA} + \text{constant}. \quad (6)$$

This relationship is also applicable to the aliphatic substituted group. Equation 6 is valid for the solvent extraction system of a reagent in various solvents[5] and of a solvent with various reagents.[6] Furthermore, reagent **8** which is a considerably strong acid also has a similar $\log K_{ex}$ value to reagents **6** and **7**. Since complex formation is the exchange reaction of a hydrogen ion for a metal ion, strong acidity may bring low chelation ability. On the basis of this assumption another relationship between K_a and β_2 can be postulated as follows:

$$\log \beta_2 = 2pK_a + \text{constant}. \quad (7)$$

Further investigation is required to confirm this relationship. The difference in the values of $\log K_{ex}$ between aromatic and aliphatic substituted groups may be caused by the stabilization of the complexes based on the aromatic resonance effect.

References

1) S. Umetani, M. Matsui, J. Tôei, and T. Shigematsu, *Anal. Chim. Acta*, **113**, 315 (1980).
2) S. Umetani, K. Sasayama, and M. Matsui, *Anal. Chim. Acta*, **134**, 327 (1982).
3) K. Sasayama, S. Umetani, and M. Matsui, *Anal. Chim. Acta*, **149**, 253 (1983).
4) B. Jensen, *Acta Chem. Scand.*, **13**, 1668 (1959).
5) K. Akiba, N. Suzuki, and T. Kanno, *Bull. Chem. Soc. Jpn.*, **42**, 2537 (1969).
6) T. Shigematsu, M. Tabushi, M. Matsui, and K. Utsunomiya, *Bull. Inst. Chem. Res. Kyoto Univ.*, **45**, 290 (1967).

The Syntheses and Decompositions of Strontium and Barium Tetraphosphates

Makoto WATANABE,* Mioko MAEDA, and Tamotsu YAMADA

Department of Industrial Chemistry, Chubu Institute of Technology, Matsumoto-cho, Kasugai, Aichi 487

(Received April 25, 1983)

Strontium and barium tetraphosphates were made by hydrolyzing *cyclo*-tetraphosphate in a 5 mol dm^{-3} solution of sodium hydroxide, neutralizing the phosphate solution with 1 mol dm^{-3} hydrochloric acid, and then adding an aqueous solution of strontium or barium chloride to the solution. The P/M (M: Sr or Ba) ratio of the tetraphosphates was 1.3. The strontium and barium tetraphosphates were X-ray diffractometrically amorphous and contained about 23—14 and 14—8% of bound water depending on the washing conditions. They decomposed to phosphates having shorter chain lengths with the bond water in air at 25—30 °C or at a higher temperature. The decomposed phosphates were polymerized again above 150 °C and the products were mixtures of diphosphate and other polyphosphates.

The usual syntheses of polyphosphates have been made by some heating process. Organic acid anhydride, trichloroacetonitrile, and dicyclohexylcarbodiimide have been used as dehydrating agents.[1-6] It is still difficult to produce oligophosphates having chain lengths longer than the triphosphate by these methods. The compounds with the composition of $3MO \cdot 2P_2O_5$ (M: Sr, Ba, or Pb) were made by a heating method.[7-11] The barium and lead phosphates were confirmed to be tetraphosphate by paper chromatography. The strontium compound is not characterized yet. These compounds were slightly soluble in solvents, except for strongly acidic aqueous solutions, and the phosphates are readily hydrolyzed to phosphates having shorter chain lengths in the acidic solutions at room temperature. So it is difficult to use the phosphates for studying chemical properties. The present authors have reported the syntheses of calcium and magnesium tetraphosphates by a wet chemical process and have discussed the stability of the products.[12,13] The tetraphosphates were soluble in an aqueous disodium dihydrogen ethylenediaminetetraacetate dihydrate (EDTA) solution and can be used for studying chemical properties of the phosphates in an aqueous reaction system. This paper describes the syntheses of strontium and barium tetraphosphates by a wet chemical process and the thermal stability of the products.

Experimental

Synthetic Method. All the chemicals were of commercial reagent grade and were used without further purification. Sodium *cyclo*-tetraphosphate tetrahydrate was made by hydrolyzing α-P_2O_5 in water cooled below 15 °C with vigorous stirring and then by adding sodium chloride to the solution.[14] About 10 g of sodium *cyclo*-tetraphosphate tetrahydrate was added to 25 cm^3 of a 5 mol dm^{-3}-aqueous solution of sodium hydroxide, and the mixture was stirred at about 20 °C for 4 d. Most of the *cyclo*-phosphate was not dissolved in the sodium hydroxide solution, while the tetraphosphate produced by the hydrolysis of the *cyclo*-phosphate was well dissolved in the alkaline solution. Accordingly, the progress of the hydrolysis of the *cyclo*-phosphate to tetraphosphate was observed visually by the clarification of the solution. After being filtered, the solution was neutralized with 1 mol dm^{-3} hydrochloric acid to pH 10 at a temperature below 3 °C to prevent the hydrolysis of the tetraphosphate. An aqueous solution of strontium chloride or barium chloride, which was made by dissolving 20 g of strontium and barium chlorides in 20 and 50 cm^3 of water respectively, was added to the tetraphosphate solution. A white precipitate was filtered off, washed with cold water, ethanol, and acetone, and then dried under reduced pressure at 25 °C.

Paper Chromatography. One-dimensional paper chromatography was used for the identification of phosphates with acidic and basic developing solvents.[15] The acidic and basic solvents were used for the separation of chain and ring phosphates respectively. About 0.5 g of a sample was dissolved in 50 cm^3 of a 6% aqueous EDTA solution. About 8 mm^3 of the solution was spotted on Toyo No. 51A filter paper (2 by 50 cm). The development was carried out in a thermostat at 5 °C for 2 d. The determination of the phosphate on the chromatogram was made by the method described in our previous paper.[13]

Determination of Phosphorus, Strontium, and Barium in the Products. About 0.2 g of the strontium tetraphosphate and about 0.75 g of EDTA was dissolved in water and diluted to the mark by using a 100-cm^3 volumetric flask. About 0.5 g of the barium tetraphosphate was dissolved in a diluted hydrochloric acid solution and the total volume was made 100 cm^3 with water. The determination of phosphorus in the sample solutions was made by means of the molybdenum-blue method with Lucena-Conde and Prat's reagent.[16] The amounts of strontium and barium in the sample solutions were determined by the EDTA back titration and the gravimetric technique respectively.

X-Ray Diffractometry. The X-ray diffraction diagrams of the samples were taken with nickel-filtered Cu $K\alpha$ radiation by using a Toshiba X-ray diffractometer, ADG-102.

DTA and TG. The samples were heated at a heating rate of 5 °C min^{-1} with a Cho Balance $TRDA_1$-H-type apparatus.

IR Measurement. IR spectra of samples were recorded on a JASCO IR spectrophotometer, A-3, using the KBr disk method.

Determination of Bound Water. The amount of bound water in a sample was determined by the Karl Fisher method with an MK-AII apparatus by Kyoto Denshi.

Decomposition in Air. The decomposition of the product at 25—30 °C in air was studied by paper chromatography, X-ray diffractometry, and IR spectrometry as described above.

Results and Discussion

Composition of the Product. The paper-chromatographic identification of the products showed that the products were composed of tetraphosphate. Strontium and barium ions had no serious effect on the development of the phosphates. The P/M (M:

Sr or Ba) ratios of the products were 1.30 and 1.33 for the strontium and barium salts respectively. Accordingly, the products were strontium tetraphosphate, $Sr_3P_4O_{13}$, and barium tetraphosphate, $Ba_3P_4O_{13}$. The strontium and barium phosphates contained about 23—14 and 14—8% of water respectively depending on the washing condition with ethanol and acetone. The products were X-ray diffractometrically amorphous.

Decomposition in Air at 25—30 °C. The stability of the tetraphosphates was studied in air at 25—30 °C. As Table 1 shows, the strontium tetraphosphate decomposed to phosphates having shorter chain lengths. The water contents in the decomposition product decreased as the passage of time, so the decomposition seemed to be caused by the bound water. The IR spectra of the decomposition products of the strontium tetraphosphate are shown in Fig. 1. The assignment of the absorptions is listed in Table 2. The intensity of the absorptions due to a $(PO_2)^-$ group decreased with the elapse of reaction time and finally disappeared. The result agrees well with that in Table 1. The following degradation process can be concluded from these results:

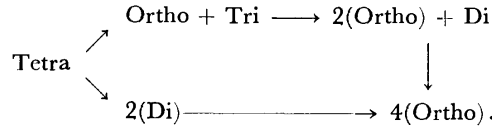

The decomposition product was amorphous even after 30 d. Since a part of the decomposition product of the barium tetraphosphate seemed to be insoluble in an aqueous EDTA solution, the decomposition of the phosphate could not be studied by the paper chromatography method. The IR spectra of the decomposition products of the barium tetraphosphate are shown in Fig. 2. The intensity of the absorption due to a $(PO_2)^-$ group decreased with time so the tetraphosphate seemed to decompose to phosphates with shorter chain lengths. The X-ray diffraction diagrams of the decomposition products of the phosphate are shown in Fig. 3. The decomposition product gave weak peaks at 16 d, and the intensity of the peaks increased with time. These peaks are all assigned to those of barium diphosphate–water (5/12), which is made by adding an aqueous barium chloride solution to an aqueous sodium diphosphate solution. The result agrees well with that of IR spectra. The water used for the decomposition of the phosphate may be the bound water in the product because, as Table 3 shows, the water content of the product decreased

Table 1. Composition of the self-decomposition products of the strontium tetraphosphate in air at 25—30 °C

Reaction time/d	H_2O(%)	Phosphates/P(%)			
		Ortho	Di	Tri	Tetra
0	22.9	0.7	5.1	6.2	88.0
5	21.0	12.0	31.8	26.1	30.1
9	19.4	20.0	41.2	22.7	16.1
21	17.9	31.1	51.4	12.7	4.8
30	16.7	43.3	44.5	10.2	2.0

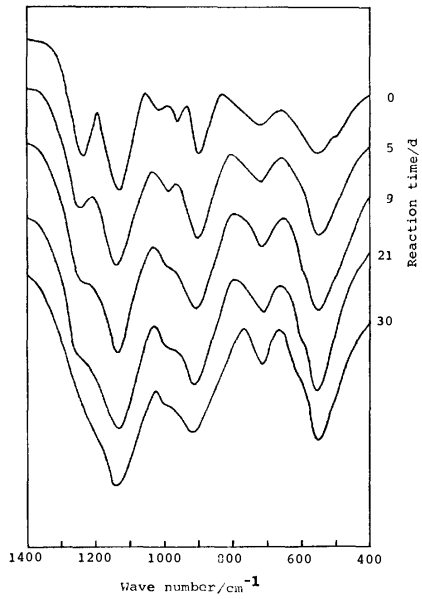

Fig. 1. IR spectra of the self-decomposition products of the strontium tetraphosphate in air at 25—30 °C.

Table 2. Assignment of the spectra of the products

Position of absorption maxima/cm^{-1}	Assignment[a)]
1240	$\nu_{as}(PO_2)^-$
1130	$\nu_{as}(PO_3)^{2-}$
1010	$\nu_s(PO_2)^-$
990—960	$\nu_s(PO_3)^{2-}$
900	ν_{as}P–O–P
720	ν_sP–O–P
550	$\delta(PO_2)^-$ and/or $\delta(PO_3)^{2-}$

a) The assignment was made on the basis of Refs. 17 and 18.

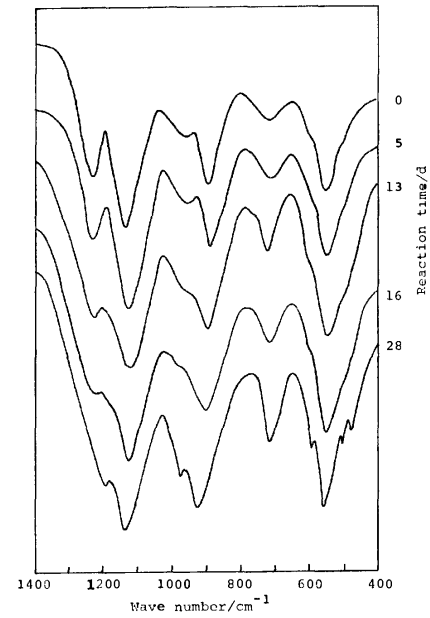

Fig. 2. IR spectra of the self-decomposition products of the barium tetraphosphate in air at 25—30 °C.

with time.

DTA and TG. DTA and TG curves of the strontium tetraphosphate are given in Fig. 4. The samples as numbered on Fig. 4 were removed from a furnace, cooled in a silica-gel desiccator, and subjected to further analysis. The results are presented in Table 4 and Figs. 5 and 6. Samples No. 1 and No. 2 were soluble in water, but No. 3 was insoluble in water. So the composition of phosphates in No. 3 could not be studied by paper chromatography. A rapid weight loss of the product and a corresponding big endothermic peak were observed below 150 °C. This reaction seemed to be caused by removing the bound water and, as Table 4 shows, the decomposition of the tetraphosphate to phosphates having shorter chain lengths occurred at the same time. The succeeding gradual weight loss of the product from 150—380 °C is the condensation reaction of the decomposition product. Samples No. 1 and No. 2 were X-ray diffractometrically amorphous, but, as Fig. 6 shows, sample No. 3 gave X-ray diffraction peaks of α-$Sr_2P_2O_7$ (ASTM card, No. 24-1011) and $Sr_3P_4O_{13}$ (ASTM card, No. 20-1207). So the exothermic peak at about 540 °C may be due to the crystallization of the amorphous phosphates.

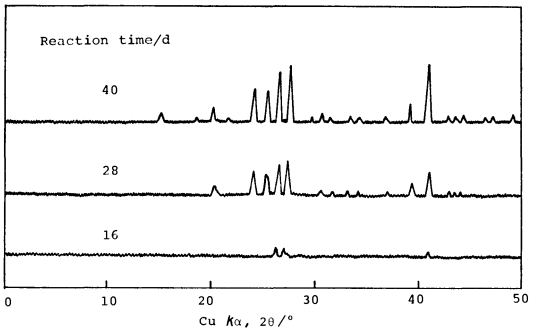

Fig. 3. X-Ray diffraction diagrams of the self-decomposition products of the barium tetraphosphate in air at 25—30 °C.

TABLE 3. THE WATER CONTENTS OF THE DECOMPOSITION PRODUCTS OF THE BARIUM TETRAPHOSPHATE IN AIR AT 25—30 °C

Reaction time/d	H_2O(%)
0	14.4
5	12.1
13	10.0
16	8.4
28	7.1

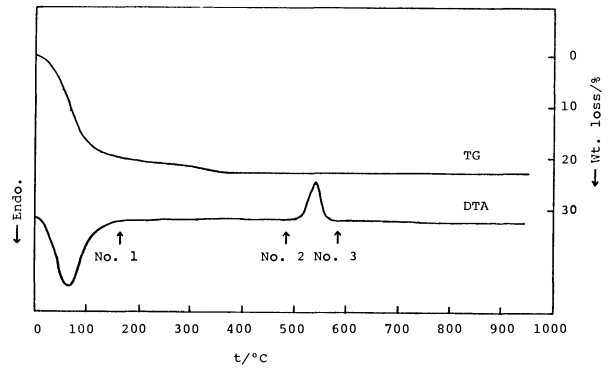

Fig. 4. DTA and TG curves of the strontium tetraphosphate in air.

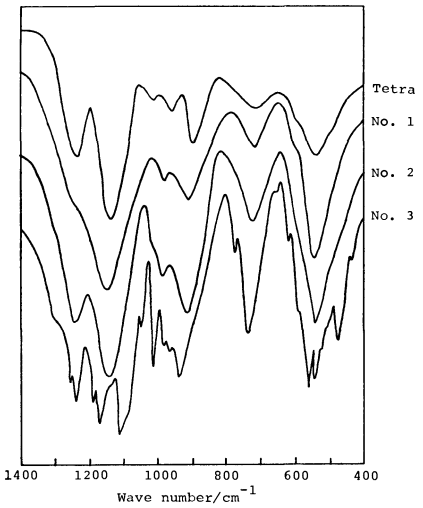

Fig. 5. IR spectra of the thermal decomposition products (Nos. 1—3) of the strontium tetraphosphate in air.

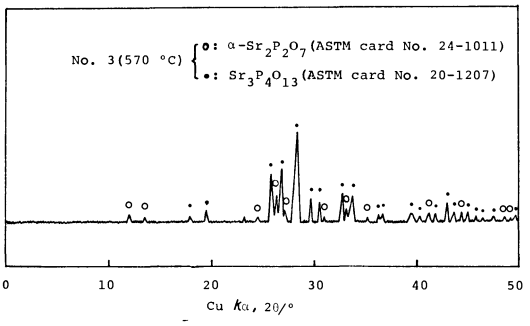

Fig. 6. X-Ray diffraction diagram of the thermal decomposition product (No. 3) of the strontium tetraphosphate in air.

TABLE 4. COMPOSITION AND WEIGHT LOSS OF THE THERMAL DECOMPOSITION PRODUCTS OF THE STRONTIUM TETRAPHOSPHATE

Sample	Phosphates/P(%)					Wt. loss/%
	Ortho	Di	Tri	Tetra	Higher	
No. 1	26.1	47.2	18.5	8.2	—	21.2
No. 2	18.8	30.2	16.8	34.2		22.9

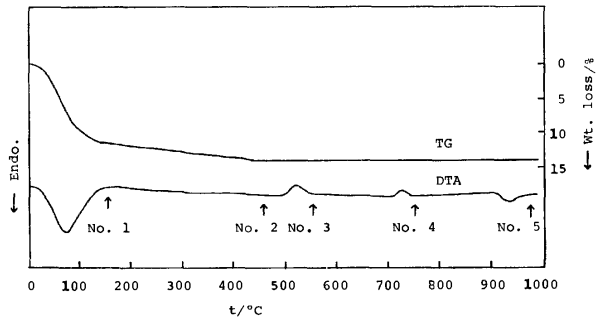

Fig. 7. DTA and TG curves of the barium tetraphosphate in air.

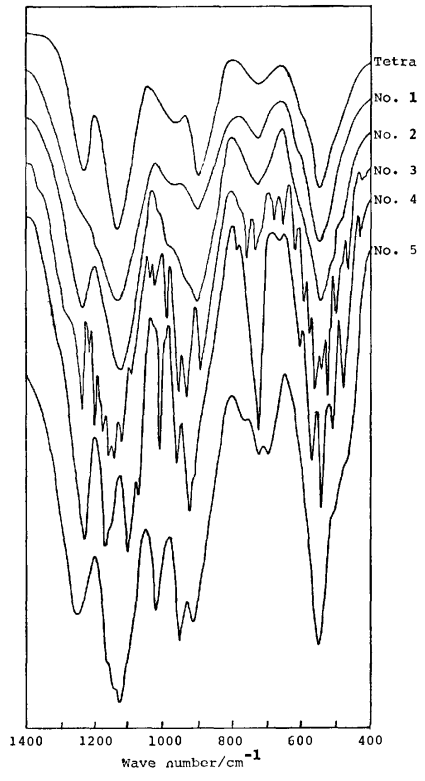

Fig. 8. IR spectra of the thermal decomposition products (Nos. 1—5) of the barium tetraphosphate in air.

The curves of DTA and TG measurements of the barium tetraphosphate are shown in Fig. 7. The tetraphosphate showed a rapid weight loss accompanied by a big endothermic peak. The process was considered to be caused by the elimination of the bound water. As Fig. 8 shows, the absorption of a $(PO_2)^-$ group disappeared in the IR spectrum of No. 2, while the sample still showed the absorptions of a P–O–P linkage. This means that the tetraphosphate decomposes to phosphates with shorter chain lengths and the main decomposition product is diphosphate. The gradual weight loss seemed to be due to the condensation of the decomposed phosphates since, as Fig. 8 shows, sample No. 3 showed the IR absorption of a $(PO_2)^-$ group at about 1240 cm^{-1}. Samples No. 1 and No. 2 were amorphous and No. 3 gave the unknown X-ray diffraction peaks shown in Fig. 9. So the exothermic peak around 520 °C is attributable to the crystallization of the phosphates. After the second

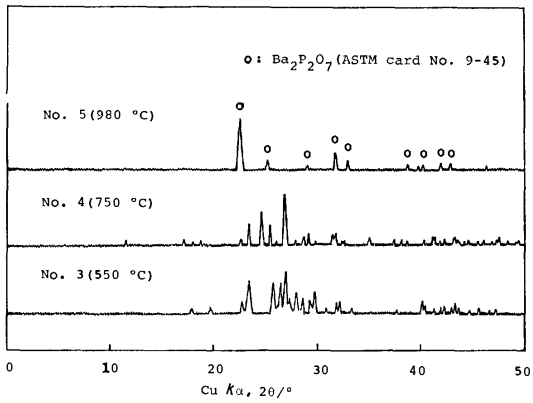

Fig. 9. X-Ray diffraction diagrams of the thermal decomposition products (Nos. 3—5) of the barium tetraphosphate in air.

exothermic peak, the sample gave different X-ray diffraction peaks. The small endothermic peak at about 930 °C was caused by melting of a part of the phosphates because the product was sintered after the endothermic reaction. The last product gave the X-ray diffraction pattern of barium diphosphate (ASTM card, No. 9-45), while the IR spectrum of No. 5 gave the absorption associated with a $(PO_2)^-$ group. Therefore, sample No. 5 was considered to be a mixture of crystalline barium diphosphate and amorphous polyphosphates having a middle-PO_4 group.

References

1) I. Grunze, K. Dostal, and E. Thilo, *Z. Anorg. Allg. Chem.*, **302**, 221 (1959).
2) I. Grunze, E. Thilo, and H. Grunze, *Chem. Ber.*, **93**, 2631 (1960).
3) M. Watanabe and T. Senda, *Bull. Chem. Soc. Jpn.*, **45**, 2111 (1972).
4) M. Watanabe, H. Usami, and M. Sugase, *Bull. Chem. Soc. Jpn.*, **46**, 2885 (1973).
5) T. Glonek, T. C. Myers, P. Z. Han, and J. R. Van Wazer, *J. Am. Chem. Soc.*, **92**, 7214 (1970).
6) T. Glonek, J. R. Van Wazer, M. Mudegett, and T. C. Myers, *Inorg. Chem.*, **11**, 567 (1972).
7) A. H. McKeag and E. G. Steward, *Br. J. Appl. Phys.*, **4**, S26 (1955).
8) E. R. Kreidler and F. A. Hummel, *Inorg. Chem.*, **6**, 884 (1967).
9) R. K. Osterheld and R. P. Langguth, *J. Phys. Chem.*, **59**, 76 (1955).
10) R. P. Langguth, R. K. Osterheld, and E. Karl-Kroupa, *J. Phys. Chem.*, **60**, 1335 (1956).
11) J. Harrison, *J. Electrochem. Soc.*, **107**, 217 (1960).
12) M. Watanabe, H. Suzumori, M. Maeda, and T. Yamada, *Bull. Chem. Soc. Jpn.*, **53**, 2663 (1980).
13) M. Watanabe, H, Suzumori, M. Maeda, and T. Yamada, *Sekko To Sekkai*, **178**, 115 (1982).
14) R. N. Bell, L. F. Audrieth, and O. F. Hill, *Ind. Eng. Chem.*, **44**, 568 (1952).
15) S. Ohashi, *Kagaku To Kogyo*, **21**, 878 (1968). The A_2 and B_2 solvents in Table 3 were used.
16) F. Lucena-Conde and L. Prat, *Anal. Chim. Acta*, **16**, 473 (1957).
17) M. Grayson and E. J. Griffith, "Topics in Phosphorus Chemistry" John Wiley & Sons, New York (1969), Vol. 6, p. 235.
18) K. Nakanishi, "Sekigai Kyushu Supekutoru," Nankodo, Tokyo (1960).

Preparation and Spectroscopic Characterization of Substituted Pentacyanoferrates(II) with Phosphine or Phosphite Ligands

Hidenari INOUE,* Masahiro SASAGAWA, Ekkehard FLUCK,† and Tsuneo SHIRAI

Department of Applied Chemistry, Faculty of Science and Technology, Keio University, 3-14-1, Hiyoshi, Kohoku-ku, Yokohama 223

†*Institut für Anorganische Chemie, Universität Stuttgart, Pfaffenwaldring 55, D-7000 Stuttgart 80, FRG*

(Received May 6, 1983)

Twenty-two substituted pentacyanoferrates(II) with the formula $Na_3[Fe(CN)_5PX_3]\cdot 2H_2O$ (PX_3 = phosphine or phosphite) have been prepared by ligand substitution of sodium amminepentacyanoferrate(II). The phosphite complexes show smaller isomer shifts than the phosphine complexes. The phosphine complexes involving an aryl or bulky phosphine exhibit larger quadrupole splitting than the phosphite complexes. These tendencies in Mössbauer parameters are discussed in terms of the π-acceptor capability of the phosphine and phosphite ligands. The linear dependence of the isomer shifts on both CN stretching frequencies and d-d transition energies is interpreted on the basis of the predominance of iron-to-phosphorus π back-donation.

Substantial interest continues in substituted pentacyanoferrates(II) prepared from hexacyanoferrates(II) by replacing one of the six cyanide ligands with a ligand having a nitrogen donor atom. In recent years a wide variety of substituted pentacyanoferrates(II) have been synthesized and extensively studied by Mössbauer,[1-3] ^{13}C NMR,[4-6] and X-ray photoelectron spectroscopy.[7-8] The focus of these spectroscopic studies is the Fe–N bond between the central iron(II) ion and the nitrogen-containing ligand. Substituted pentacyanoferrates(II) in which the sixth ligand is a phosphine or phosphite have received relatively little attention although they provide an excellent opportunity for investigating the Fe–P bond by spectroscopic methods. Spectroscopic investigations on these phosphine and phosphite complexes have been limited almost wholly to a few complexes having the phosphine as the sixth ligand of octahedral coordination.[9-10]

We have prepared a series of substituted pentacyanoferrates(II) of the type $Na_3[Fe(CN)_5PX_3]\cdot 2H_2O$, where PX_3 is a phosphine or phosphite ligands. The functional groups adjacent to the phosphorus ligand atom was varied systematically in order to understand the Fe–P bond on the basis of the σ-donor and π-acceptor properties of the phosphine and phosphite ligands. Another purpose of the present work is to learn how the functional groups attached to the donor phosphorus atom affect the electronic structure of the $[Fe(CN)_5PX_3]^{3-}$ moiety and how the coordination of the phosphine or phosphite ligand influences the Fe–C bonding between the iron(II) ion and the cyanide ligands.

Experimental

Materials. Sodium amminepentacyanoferrate(II) was prepared by a method in the literature.[11] Phosphine and phosphite ligands were purchased from Strem Chemicals Inc. and used without further purification. All solvents used were analytical reagent grade, except that the methanol used for measurement of the electronic spectra was spectrophotometric solvent grade obtained from Kanto Chemical Co., Inc.

Preparation of Compounds. Manupulations involving air-sensitive materials were performed in a nitrogen-filled glovebox. General aspects of the experimental techniques are similar to those described in the literature.[12] Typical procedures are described in detail here only for $Na_3[Fe(CN)_5P(CH_3)_3]\cdot 2H_2O$ and $Na_3[Fe(CN)_5P(OCH_3)_3]\cdot 2H_2O$. To a suspension of 1.0 g (3.1 mmol) of $Na_3[Fe(CN)_5NH_3]\cdot 3H_2O$ in 25 ml of methanol was added 0.28 g (3.7 mmol) of $P(CH_3)_3$. The reaction slurry was vigorously stirred in the dark at room temperature for 24 h. Filtration of the resultant heterogeneous reaction mixture afforded a yellow solution. Careful addition of 150 ml of diethyl ether to the filtrate caused a yellow solid to precipitate. This was filtered, recrystallized from methanol, and dried over silica gel. To a vigorously stirred suspension of 1.0 g (3.1 mmol) of $Na_3[Fe(CN)_5NH_3]\cdot 3H_2O$ in 25 ml of methanol was added 0.80 g (6.4 mmol) of $P(OCH_3)_3$. After stirring of the reaction slurry in the dark at room temperature for 24 h, the resulting yellow reaction mixture was filtered off. Diethyl ether (200 ml) was added to the filtrate to precipitate a pale yellow solid, which was filtered with a glass filter, recrystallized from methanol, and dried over silica gel. The compounds were identified by elemental analysis (C, H, and N), phosphorus spectrophotometry, and iron atomic absorption spectrophotometry.

Physical Measurements. Mössbauer spectra were obtained with a ^{57}Co source in palladium (The Radiochemical Centre, Amersham, England) using a Wissel constant-accelaration transducer coupled with a Canberra OMEGA-1 multichannel analyzer operated in time mode. The spectra obtained at 77 and 293 K were fitted to Lorentzian curves with an iterative least-squares computer program. The isomer shifts were referred to the symmetry center of six absorption lines of natural iron foil at 293 K. Infrared spectra were recorded with a Hitachi Perkin-Elmer Model 225 grating infrared spectrophotometer in the range 200 to 4000 cm^{-1} and with a JASCO A-3 infrared spectrophotometer in the range 330 to 5000 cm^{-1} using Nujol mulls and KBr pellets. Electronic spectra of the substituted pentacyanoferrates(II) in methanol solution were recorded on a JASCO UVIDEC-1 digital double-beam spectrophotometer in the range 200 to 800 nm using 1-cm quartz cells.

Results and Discussion

Preparation of Complexes. All the compounds were obtained as pale yellow, pale blue, or colorless fine crystalline powders. Two of twenty-two substituted pentacyanoferrates(II) were not obtained in a pure form. Among the phosphine ligands tris(4-di-

TABLE 1. ANALYTICAL DATA OF $Na_3[Fe(CN)_5PX_3]\cdot 2H_2O$

No.	Ligand PX_3	Found (Calcd)(%)				
		C	H	N	Fe	P
1	$P[C_6H_4N(CH_3)_2]_3$	35.16 (51.04)	4.37 (5.02)	16.64 (16.42)	12.30 (8.18)	2.64 (4.54)
2	$P[CH(CH_3)_2]_3$	36.25 (37.27)	5.06 (5.58)	15.02 (15.52)	9.43 (12.38)	6.56 (6.87)
3	$P(C_6H_4F)_3$	40.01 (45.50)	2.63 (2.66)	10.38 (11.53)	7.74 (9.20)	4.36 (5.10)
4	$P(C_6H_4Cl)_3$	39.01 (42.08)	2.94 (2.46)	10.19 (10.67)	7.69 (8.51)	4.10 (4.72)
5	$P(C_6H_5)H_2$	32.24 (32.95)	2.49 (2.76)	15.97 (17.46)	14.51 (13.93)	7.39 (7.72)
6	$P(C_6H_4CH_3\text{-}m)_3$	48.52 (52.46)	4.26 (4.23)	11.39 (11.76)	10.19 (9.38)	5.00 (5.20)
7	$P(C_6H_4CH_3\text{-}p)_3$	48.90 (52.46)	4.33 (4.23)	11.43 (11.76)	9.14 (9.38)	4.56 (5.20)
8	$P(C_4H_9)_3$	38.31 (41.40)	5.65 (6.33)	13.33 (14.20)	11.34 (11.32)	5.94 (6.28)
9	$P(C_6H_5)_2H$	45.04 (42.80)	3.59 (3.17)	14.12 (14.68)	10.53 (11.70)	6.40 (6.49)
10	$P(C_6H_5)_3$	46.76 (49.93)	3.81 (3.46)	11.88 (12.66)	10.80 (10.09)	5.57 (5.60)
11	$P(C_2H_5)_3$	30.01 (32.30)	4.15 (4.68)	15.03 (17.12)	12.04 (13.65)	7.63 (7.57)
12	$P(C_6H_4OCH_3)_3$	40.54 (48.54)	3.78 (3.92)	10.09 (10.89)	9.23 (8.68)	4.19 (4.81)
13	$P(CH_3)_3$	25.86 (26.18)	3.36 (3.57)	18.58 (19.08)	12.75 (15.22)	5.38 (8.44)
14	$P[N(CH_3)_2]_3$	29.80 (29.09)	4.03 (4.88)	22.93 (24.67)	10.84 (12.30)	7.32 (6.82)
15	$P(C_6H_5)(OC_4H_9)_2$	41.94 (41.85)	4.91 (4.99)	13.22 (12.84)	11.62 (10.24)	4.95 (5.68)
16	$P(OC_4H_9)_3$	38.20 (37.72)	5.42 (5.77)	13.40 (12.94)	11.61 (10.32)	4.58 (5.72)
17	$P(OC_2H_5)_3$	29.10 (28.90)	3.87 (4.19)	15.55 (15.32)	12.59 (12.22)	5.95 (6.78)
18	$P(C_6H_5)_2(OC_4H_9)$	42.11 (45.92)	3.87 (4.22)	11.70 (12.75)	9.20 (10.19)	4.96 (5.64)
19	$P(OCH_2CH_2Cl)_3$	22.55 (23.58)	3.28 (2.88)	11.31 (12.50)	9.67 (9.97)	6.05 (5.53)
20	$P(OCH_3)_3$	23.20 (23.15)	3.04 (3.16)	17.04 (16.88)	12.96 (13.46)	7.19 (7.46)
21	$P[OCH(CH_3)_2]_3$	34.01 (33.69)	4.67 (5.05)	14.22 (14.03)	11.37 (11.19)	5.81 (6.21)
22	$P(OC_6H_5)_3$	43.61 (45.95)	3.78 (3.19)	14.53 (11.65)	10.41 (9.29)	5.25 (5.15)

methylaminophenyl)phosphine failed to give pure $Na_3[Fe(CN)_5P(C_6H_4N(CH_3)_2)_3]\cdot 2H_2O$ because the ligand is only slightly soluble in methanol. A mixture of methanol and acetone (1:1) was used to improve the solubility of the ligand and the reaction product. However, the Mössbauer spectra of the products always gave a couple of quadrupole-splitting doublets, indicating that the desired product was contaminated. Among the phosphite ligands triphenyl phosphite appeared to undergo ester interchange with the solvent, *i.e.*, with methanol to yield four different types of phosphite complexes with mixed phosphites such as $P(OC_6H_5)_3$, $P(OC_6H_5)_2(OCH_3)$, $P(OC_6H_5)(OCH_3)_2$, and $P(OCH_3)_3$. The existence of these four pentacyanophosphiteferrate(II) species was confirmed by ^{31}P NMR spectroscopy because each coordinated phosphite ligand shows a characteristic chemical shift. When *N,N*-dimethylformamide was used in place of methanol as the solvent, the desired complex was contaminated by sodium pentacyano(*N,N*-dimethylformamide)ferrate(II). This contamination was confirmed by a comparison of Mössbauer parameters.

Effect of Axial Ligand on Isomer Shift. The series of complexes prepared here are suitable model compounds for studying the Fe–P bond without changing the type of coordination bonding, *i.e.*, the atomic orbital which participate in the Fe–P bond. Especially Mössbauer spectroscopy provides a sophisticated means to characterize the Fe–P bond in the present complexes. Typical Mössbauer spectra obtained are presented in Fig. 1. Most of our complexes gave a symmetric quadrupole-splitting doublet although the

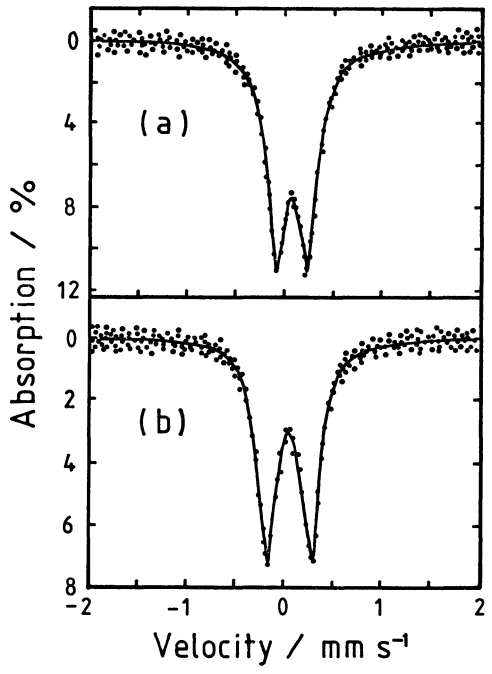

Fig. Typical Mössbauer spectra of (a) $Na_3[Fe(CN)_5P(CH_3)_3]\cdot 2H_2O$ and (b) $Na_3[Fe(CN)_5P(OC_2H_5)_3]\cdot 2H_2O$ at 77 K.

complexes having diphenylphosphine or phenylphosphine ligand showed an asymmetric doublet even at 77 K. In these complexes the higher velocity component of the quadrupole-splitting doublet was always stronger than the lower one, and this asymmetry remained even in measurements with finely ground powders. The Mössbauer parameters are summarized in Table 2. The isomer shifts at 77 K are more positive than those at 293 K due to the second-order Doppler shift. The isomer shifts obtained at 293 K range from −0.075 to 0.012 mm/s and fall into the range characteristic of low-spin iron(II) complexes.

In general the isomer shift in iron compounds increases with a decrease in total electron density at the iron nucleus.[13] Electrons other than s electrons do not contribute directly to the total electron density at the iron nucleus, *i.e.*, to the isomer shift, because of a negligibly small probability density at the nucleus. However, d electrons affect the total electron density at the iron nucleus through the so-called shielding effect. The change in the isomer shift is interpreted mainly by the following two mechanisms; ligand-to-metal σ donation and metal-to-ligand π back-donation. Both mechanisms increase the total electron density at the iron nucleus, and hence decrease the isomer shift of iron complexes. The decreasing tendency of isomer shifts is clearly associated with the σ-donor and π-acceptor capability of the ligand PX_3, *i.e.*, the electronic properties of functional group X attached to the phosphorus atom. An increased σ-donor capability of the phosphorus ligand increases the s-electron density at the iron nucleus through the formation of the phosphorus-to-iron σ bonding. Increased π-acceptor capability of the phosphorus ligand also increases the s-electron density at the nucleus through π back-donation from the iron d_π orbital to the vacant

Table 2. Mössbauer parameters of $Na_3[Fe(CN)_5PX_3]\cdot 2H_2O$[a]

No.	Ligand PX_3	Isomer shift/mm s^{-1}		Quadrupole splitting/mm s^{-1}	
		293 K	77 K	293 K	77 K
1	$P[C_6H_4N(CH_3)_2]_3$	0.01_2	0.07_6	0.72_5	0.71_6
2	$P[CH(CH_3)_2]_3$	-0.02_4	0.05_0	0.47_8	0.48_7
3	$P(C_6H_4F)_3$	-0.03_1	0.03_3	0.69_4	0.67_8
4	$P(C_6H_4Cl)_3$	-0.03_7	0.03_0	0.64_3	0.62_8
5	$P(C_7H_5)H_2$	-0.03_7	0.04_3	0.50_0	0.48_6
6	$P(C_6H_4CH_3\text{-}m)_3$	-0.03_8	0.03_8	0.68_6	0.58_5
7	$P(C_6H_4CH_3\text{-}p)_3$	-0.04_0	0.02_9	0.64_4	0.62_5
8	$P(C_4H_9)_3$	-0.04_1	0.00_6	0.28_7	0.24_9
9	$P(C_6H_5)_2H$	-0.04_2	0.04_0	0.48_9	0.58_9
10	$P(C_6H_5)_3$	-0.04_4	0.03_1	0.64_8	0.63_3
11	$P(C_2H_5)_3$	-0.04_6	0.00_0	0.25_0	0.30_2
12	$P(C_6H_4OCH_3)_3$	-0.04_9	0.03_0	0.65_4	0.61_6
13	$P(CH_3)_3$	-0.05_7	0.01_4	0.32_0	0.30_6
14	$P[N(CH_3)_2]_3$	-0.05_8	0.00_1	0.41_5	0.41_9
15	$P(C_6H_5)(OC_4H_9)_2$	-0.05_9	0.01_4	0.46_5	0.48_9
16	$P(OC_4H_9)_3$	-0.06_0	0.00_4	0.41_0	0.39_4
17	$P(OC_2H_5)_3$	-0.06_0	0.00_8	0.44_9	0.44_1
18	$P(C_6H_5)_2(OC_4H_9)$	-0.06_3	0.02_9	0.48_4	0.51_4
19	$P(OCH_2CH_2Cl)_3$	-0.06_8	-0.00_5	0.38_6	0.40_6
20	$P(OCH_3)_3$	-0.06_9	-0.00_4	0.47_4	0.48_1
21	$P[OCH(CH_3)_2]_3$	-0.07_5	0.00_8	0.44_9	0.43_9
22	$P(OC_6H_5)_3$	-0.07_6	0.00_5	0.49_7	0.48_6

a) With uncertainty of 0.005 mm/s.

phosphorus π or d_π orbitals. Therefore, the σ-donor capability can not be readily differentiated from the π-acceptor capability by the isomer shift value, which reflects only the total electron density at the iron nucleus.

The isomer shifts of phosphite complexes are smaller than those of phosphine complexes. This indicates that the higher the electronegativity of the atom adjacent to the phosphorus atom the larger the isomer shift of the complexes. The electron-attracting and electron-releasing power of the substituent at the 4 position of the triarylphosphines is associated with the Hammett substituent constant, which decreases in the order $-Cl>-F>-H>-CH_3>-OCH_3>-N(CH_3)_2$.[14] This order was expected to be directly connected with the isomer shifts observed for $Na_3[Fe(CN)_5PX_3]\cdot 2H_2O$, where PX_3 is an arylphosphine with a substituent at the 4 position. However, no significant linear correlation could be established between the isomer shift and the Hammett substituent constant. Thus the substituent X on the aryl group is located too far away to affect the electron density at the iron nucleus, *i.e.*, the isomer shift of the central iron atom *via* the mesomeric or inductive effect.

The isomer shift of the complexes involving a phenylphosphine increases clearly in the sequence: $P(C_6H_5)_3<P(C_6H_5)_2H<P(C_6H_5)H_2$. The substitution of a phenyl group for a hydrogen diminishes the π-acceptor capability of the phosphorus donor atom and decreases the iron-to-phosphorus π back-donation. Consequently, this decrease in the back donation agrees

with the increased isomer shift observed for the complex having the phenylphosphine.

Influence of Local Symmetry on Quadrupole Splitting. The symmetry group of the $[Fe(CN)_5PX_3]^{3-}$ moiety is approximated as C_{4v} if the geometry of the three functional groups directly attached to the phosphorus atom is ignored. In $Na_3[Fe(CN)_5PX_3]\cdot 2H_2O$ the symmetry around the iron nucleus is distorted from the O_h symmetry to which the $Fe(CN)_6^{4-}$ moiety of sodium hexacyanoferrate(II) belongs. The local site symmetry of the $[Fe(CN)_5PX_3]^{3-}$ moiety is reflected in the quadrupole splitting of the Mössbauer spectra. All the complexes of the type $Na_3[Fe(CN)_5PX_3]\cdot 2H_2O$ show quadrupole splitting, whereas the octahedrally symmetric sodium hexacyanoferrate(II) shows no quadrupole splitting at all.[15] The quadrupole splittings of $Na_3[Fe(CN)_5PX_3]\cdot 2H_2O$ are relatively small and typical of low-spin iron(II) complexes. They increase slightly on lowering the temperature to 77 K since the low-spin iron(II) complex usually has only a small valence contribution to the electric field gradient at the iron nucleus. The arylphosphine complex gives a larger quadrupole splitting than does the alkylphosphine complex. This is presumably due to the bulkiness of the aryl groups. The quadrupole splitting values of the phosphite complex, as well as the complex with a ligand intermediate between phosphine and phosphite, lie between those of arylphosphine and alkylphosphine complexes.

The quadrupole splitting is plotted against the isomer shift in Fig. 2. A linear plot was obtained (r=0.702) for the measurements at 77 K.[16] Good correlation was not found (r=0.505) for the measurements at 293 K, probably due to the pronounced contribution of the second-order Doppler effect to the isomer shift. The isomer shift data alone do not always reveal which is dominant, the σ-donation or the π back-donation, because both increase the electron density at the iron nucleus and consequently decrease the isomer shift. Despite their similar contribution to the isomer shift the linear dependence of the quadrupole splitting on the isomer shift provides a useful means of estimating

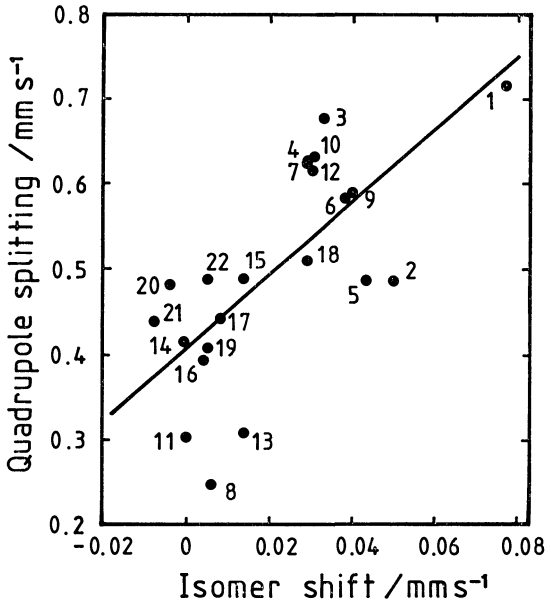

Fig. 2. Plots of quadrupole splittings against isomer shifts (at 77 K).

Table 3. Infrared frequencies observed for $Na_3[Fe(CN)_5PX_3]\cdot 2H_2O$

No.	Ligand PX_3	Absorption frequencies/cm^{-1}				
		$\nu_{CN}(1)$	$\nu_{CN}(2)$	$\nu_{CN}(3)$	δ_{Fe-CN}	ν_{Fe-C}
1	$P[C_6H_4N(CH_3)_2]_2$	2084^m	—	2039^s	578^m	vb
2	$P[CH(CH_3)_2]_3$	2088^m	2059^{sh}	2038^s	576^m	vb
3	$P(C_6H_4F)_3$	2086^m	—	2046^s	576^m	470^b
4	$P(C_6H_4Cl)_3$	2092^m	2070^{sh}	2045^s	578^m	434^b
5	$P(C_6H_5)H_2$	2090^m	—	2042^s	576^m	(500, 463)^b
6	$P(C_6H_4CH_3\text{-}m)_3$	2089^m	2067^{sh}	2042^s	579^m	468^b
7	$P(C_6H_4CH_3\text{-}p)_3$	2089^m	2066^{sh}	2041^s	578^m	436^b
8	$P(C_4H_9)_3$	2088^m	2060^{sh}	2043^s	586^m	(470, 440)^b
9	$P(C_6H_5)_2H$	2096^m	2075^{sh}	2052^s	578^m	472^b
10	$P(C_6H_5)_3$	2092^m	2072^{sh}	2057^s	577^m	460^b
11	$P(C_2H_5)_3$	2083^m	—	2038^s	580^m	vb
12	$P(C_6H_4OCH_3)_3$	2086^m	2062^{sh}	2042^s	578^m	(470, 432)^b
13	$P(CH_3)_3$	2088^m	—	2037^s	578^m	vb
14	$P[N(CH_3)_2]_3$	2092^m	—	2055^s	578^m	vb
15	$P(C_6H_5)(OC_4H_9)_2$	2100^m	2080^{sh}	2062^s	580^m	(438, 408)^b
16	$P(OC_4H_9)_3$	2094^m	2073^{sh}	2051^s	578^m	(450, 418)^b
17	$P(OC_2H_5)_3$	2100^m	2074^{sh}	2060^s	578^m	420^b
18	$P(C_6H_5)_2(OC_4H_9)$	2091^m	2068^{sh}	2048^s	578^m	vb
19	$P(OCH_2CH_2Cl)_3$	2100^m	2080^{sh}	2062^s	578^m	(447, 402)^b
20	$P(OCH_3)_3$	2092^m	2069^{sh}	2050^s	578^m	(443, 412)^b
21	$P[OCH(CH_3)_2]_3$	2097^m	2075^{sh}	2050^s	580^m	430^b
22	$P(OC_6H_5)_3$	2104^m	2088^{sh}	2062^s	577^m	(418, 400)^b

s, strong; m, medium; sh, shoulder; b, broad; vb, very broad.

the relative importance of the σ-donor or π-acceptor capability.[17] The linear dependence with a positive slope demonstrates that the σ-donation is offset by the π-acceptor, *i.e.*, the π-acceptor capability is dominant in the present complexes.

Dependence of IR Frequencies on π-Acceptor Capability of Ligand PX_3. The infrared frequencies are summarized in Table 3. The ν_{CN} stretching modes referred to as $\nu_{CN}(1)$, $\nu_{CN}(2)$, and $\nu_{CN}(3)$ in Table 3 appeared in the range 2030—2100 cm^{-1}. The observation of two or three ν_{CN} stretching bands is consistent with the group-theoretical prediction that the point group of the $[Fe(CN)_5PX_3]^{3-}$ moiety is approximately C_{4v}. The dependence of the ν_{CN} stretching frequencies on the isomer shift is useful for estimating the π-acceptor capability of the ligand PX_3. As shown in Fig. 3, all the frequencies observed for the $\nu_{CN}(1)$, $\nu_{CN}(2)$, and $\nu_{CN}(3)$ stretching modes decrease as the isomer shifts increase. This decrease in the ν_{CN} stretching frequencies reflects the reduced Fe-to-P π back-donation. The stronger the π-acceptor capability of the ligand PX_3 is the more the d_π electrons of the central iron atom are withdrawn towards the ligand through π back-donation. Alternatively, the decreased electron density in the iron d_π orbitals is compensated for by increased electron flow from the cyanide ligands to the central iron atom through the inverse π back-donation. Thus the decreased electron population in the antibonding π^* orbitals of the cyanide ligands causes the ν_{CN} stretching frequencies to increase. The relative increase in the Fe-to-P back-donation gives rise to the increased total electron density at the iron nucleus because of the decreased shielding effect of its d_π electrons and hence leads to the decreased isomer shift. This indicates that the greatly increased π back-donation from the filled iron d_π orbitals to the phosphorus orbitals is not offset, even by the decreased π back-donation to the cyanide ligands. All the ν_{CN} stretching modes belonging to the two different species $2A_1+E$ showed the same tendency with regard to the dependence of the ν_{CN} stretching frequencies on the isomer shifts. The empty antibonding π^* orbitals of both axial and radial cyanide ligands participate in overlapping with the identical d_π orbitals to form the π bonding between Fe and C. Accordingly, the same tendency observed for three different ν_{CN} stretching modes is due to the synergetic effect of the d_π orbitals of the central iron atom on the axial and radial cyanide ligands.

The ν_{Fe-C} stretching and δ_{Fe-CN} bending modes appeared in the ranges 400—500 and 576—586 cm^{-1}, respectively. The ν_{Fe-C} stretching mode of the complexes with a phosphine ligand tends to show higher absorption frequencies than those with a phosphite ligand. This tendency agrees with the fact that the Fe-to-P back-donation is generally larger in phosphite complexes than in phosphine complexes. On the other hand, the absorption frequencies of the δ_{Fe-CN} bending modes were almost independent of the kind of phosphorus ligand. The ν_{Fe-P} stretching and δ_{Fe-P} bending modes are expected to be direct evidence for the Fe–P bonding. Unfortunately, no absorption band could be observed for our complexes, presumably because these absorption bands are of very weak intensity or lie outside of the present experimental region.

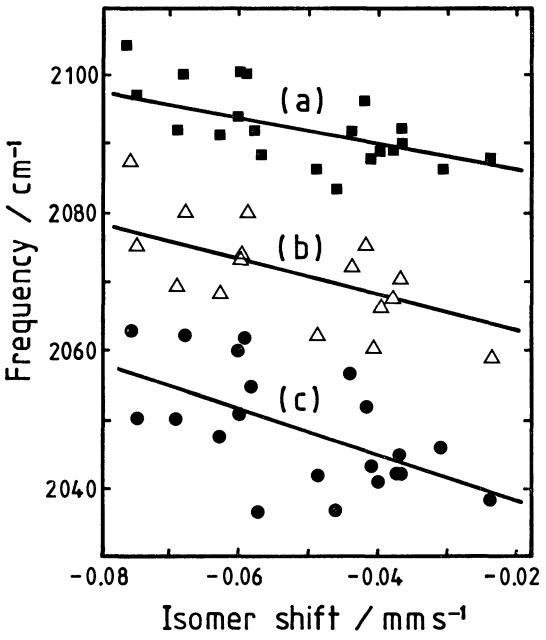

Fig. 3. Dependence of three different ν_{CN} stretching frequencies on isomer shifts. (a), (b), and (c) correspond to a regression line for the $\nu_{CN}(1)$, $\nu_{CN}(2)$, and $\nu_{CN}(3)$ stretching modes. Plots of compound No. 1 are not shown here due to its large positive isomer shift (at 293 K).

Table 4. Electronic spectra of $Na_3[Fe(CN)_5PX_3]\cdot 2H_2O$

No.	Ligand PX_3	Observed wave number/10^3 cm^{-1}		
		$^1A_1\rightarrow E(1)$	$^1A_1\rightarrow {}^1A_2$	$^1A_1\rightarrow E(2)$
1	$P[C_6H_4N(CH_3)_2]_3$	24.9^{sh}	vw	vw
2	$P[CH(CH_3)_2]_3$	29.5^{sh}	25.2^{sh}	17.7^{w}
3	$P(C_6H_4F)_3$	26.3^{sh}	vw	17.3^{w}
4	$P(C_6H_4Cl)_3$	vw	vw	vw
5	$P(C_6H_5)H_2$	29.2^{sh}	25.0^{sh}	vw
6	$P(C_6H_4CH_3\text{-}m)_3$	26.3^{sh}	vw	17.1^{w}
7	$P(C_6H_4CH_3\text{-}p)_3$	26.0^{sh}	vw	17.0^{w}
8	$P(C_4H_9)_3$	30.0^{sh}	25.0^{sh}	18.2^{w}
9	$P(C_6H_5)_2H$	27.2^{sh}	vw	16.8^{w}
10	$P(C_6H_5)_3$	26.5^{sh}	vw	18.0^{w}
11	$P(C_2H_5)_3$	30.3^{sh}	25.0^{sh}	18.2^{w}
12	$P(C_6H_4OCH_3)_3$	27.5^{sh}	24.5^{sh}	15.5^{w}
13	$P(CH_3)_3$	30.4^{sh}	25.1^{sh}	20.0^{w}
14	$P[N(CH_3)_2]_3$	30.8^{sh}	25.0^{sh}	vw
15	$P(C_6H_5)(OC_4H_9)_2$	29.5^{sh}	25.0^{sh}	vw
16	$P(OC_4H_9)_3$	31.3^{sh}	25.8^{sh}	20.0^{w}
17	$P(OC_2H_5)_3$	31.2^{sh}	25.0^{sh}	20.5^{w}
18	$P(C_6H_5)_2(OC_4H_9)$	31.0^{sh}	vw	vw
19	$P(OCH_2CH_2Cl)_3$	31.6^{sh}	25.0^{sh}	vw
20	$P(OCH_3)_3$	30.8^{sh}	vw	20.2^{w}
21	$P[OCH(CH_3)_2]_3$	30.8^{sh}	24.1^{sh}	20.0^{w}
22	$P(OC_6H_5)_3$	30.5^{sh}	24.5^{sh}	vw

sh: shoulder; w: weak; vw: very weak.

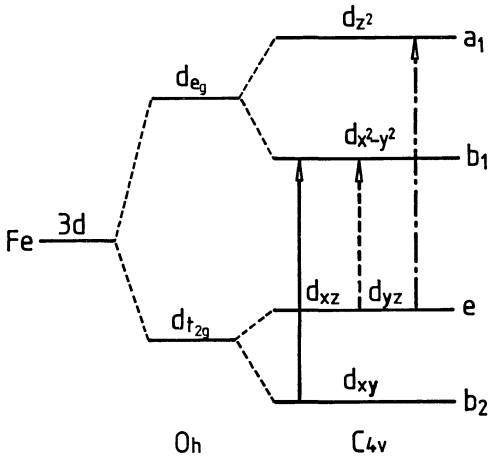

Fig. 4. Energy-term diagram for the $[Fe(CN)_5PX_3]^{3-}$ moiety. (a) $^1A_1 \rightarrow E(1)$ (—·—·—), (b) $^1A \rightarrow {}^1A_2$ (——), and (c) $^1A_1 \rightarrow E(2)$ (----).

Correlation between d-d Transition Energy and π Back-Donation. The absorption bands observed in the electronic spectra are presented in Table 4 together with their assignment. The electronic spectra of these complexes are so similar to those of the usual substituted pentacyanoferrates(II) that the absorption bands were assigned by comparison with the band assignment for substituted pentacyanoferrates(II) such as sodium pentacyanonitrosylferrate(II).[18] The partial energy-term diagram of the $[Fe(CN)_5PX_3]^{3-}$ moiety (symmetry group C_{4v}) is schematically shown in Fig. 4. A strong absorption band observed in the range 26×10^3—32×10^3 cm^{-1} is assigned to the transition $^1A_1 \rightarrow E(1)$ ($e \rightarrow a_1$). A relatively weak absorption band assigned to the transition $^1A_1 \rightarrow E(2)$ ($e \rightarrow b_1$) appeared in the range 15×10^3—21×10^3 cm^{-1}. A weak shoulder band around 25×10^3 cm^{-1} is assigned to the transition $^1A_1 \rightarrow {}^1A_2$ ($b_2 \rightarrow b_1$) although it is partially hidden by the strong absorption band resulting from the transition $^1A_1 \rightarrow E(1)$. The band position of the transition $^1A_1 \rightarrow {}^1A_2$ is hardly affected by the variation in the axial phosphine or phosphite ligand, while those of the other transitions, $^1A_1 \rightarrow E(1)$ and E(2), vary with the kind of axial ligand. This is due to the fact that both transitions $^1A_1 \rightarrow E(1)$ and E(2) involve the d_{xz} and d_{yz} orbitals directed towards the axial phosphine or phosphite ligand.

The transition energies of the d-d absorption bands are correlated with the isomer-shift values since both ligand field parameters and Mössbauer parameters are associated with the π-acceptor capability of the axial ligand.[19] The plots of the d-d transition energies *vs.* the isomer shift values are shown in Fig. 5. The energies of the transitions $^1A_1 \rightarrow E(1)$ and E(2) decrease as the isomer shifts increase, whereas the energy of the transition $^1A_1 \rightarrow {}^1A_2$ is almost independent of the variation in the isomer shifts as the axial phosphine or phosphite ligands are changed. This relationship between the d-d transition energies and the isomer shifts can be also explained on the basis of the Fe-to-P π back-donation. The energy level e (shown in Fig. 4) is lowered by the enhanced Fe-to-P π back-donation so that the energies of the transitions $^1A_1 \rightarrow E(1)$ and E(2) are increased and shifted to the higher frequency side.

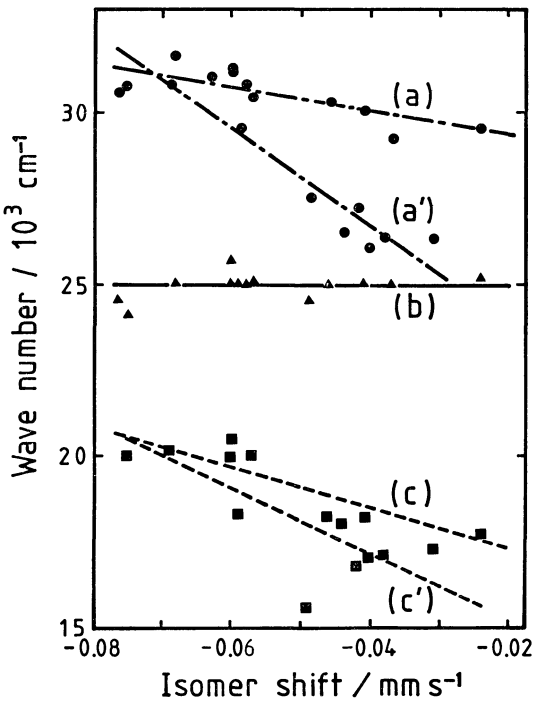

Fig. 5. Plots of d-d transition energies *vs.* isomer shifts (at 293 K). (a) and (c) are a regression line for alkylphosphine complexes, (a') and (c') for arylphosphine complexes, and (b) for both phosphine complexes. Plots of compound No. 1 are not shown here due to its large positive isomer shift.

References

1) P. J. Aymonino, M. A. Blesa, J. A. Olabe, and E. Frank, *Z. Naturforsch., B*, **31**, 1532 (1976).
2) C. P. Monaghan and J. C. Fanning, *J. Phys. Chem.*, **82**, 1045 (1978).
3) A. N. Garg and P. N. Shukla, *Z. Naturforsch., B*, **36**, 59 (1981).
4) B. A. Narayanan and P. T. Manoharan, *J. Inorg. Nucl. Chem.*, **40**, 1993 (1978).
5) H. Toma, J. A. Vanin, and J. M. Malin, *Inorg. Chim. Acta*, **33**, L157 (1979).
6) J. Jwo, P. L. Gaus, and A. Haim, *J. Am. Chem. Soc.*, **101**, 6189 (1979).
7) H. Binder, *Z. Anorg. Allg. Chem.*, **429**, 247 (1977).
8) K. B. Yatsimirskii, V. V. Nemoshkalenko, Yu. P. Nazarenko, V. G. Aleshin, V. V. Zhilinskaya, and A. Tomashevsky, *J. Electron Spectrosc. Relat. Phenom.*, **10**, 239 (1977).
9) E. Fluck and P. Kuhn, *Z. Anorg. Allg. Chem.*, **350**, 263 (1967).
10) K. Burger, L. Korecz, S. Papp, and B. Mohai, *Radiochem. Radioanal. Lett.*, **2**, 153 (1969).
11) D. J. Kenney, T. P. Flynn, and J. B. Gallini, *J. Inorg. Nucl. Chem.*, **20**, 75 (1961).
12) V. R. Nast and K. W. Krüger, *Z. Anorg. Allg. Chem.*, **341**, 189 (1965).
13) N. N. Greenwood and T. C. Gibb, "Mössbauer Spectroscopy," Chapman and Hall, London (1971), Chap. 5.

14) L. S. Hammett, "Physical Organic Chemistry," McGraw-Hill, New York (1970), Chap. 11.
15) H. Inoue, E. Fluck, H. Binder, and S. Yanagisawa, *Z. Anorg. Allg. Chem.*, **483**, 75 (1981).
16) The correlation coefficient r calculated from the measurements at 77 K is significant at the 0.005 significant level, while that obtained for the measurements at 293 K is significant at the 0.05 significant level.
17) B. A. Sosinsky, N. Norem, and R. G. Shong, *Inorg. Chem.*, **21**, 4229 (1982).
18) P. T. Manoharan and H. B. Gray, *J. Am. Chem. Soc.*, **87**, 3340 (1965).
19) H. E. Toma, E. Giesbrecht, J. M. Malin, and E. Fluck, *Inorg. Chim. Acta*, **14**, 11 (1975).

 © 1983 The Chemical Society of Japan Bull. Chem. Soc. Jpn., 56, 3441—3445 (1983)

A Complete Series of $[Co(acac)_x(en)_y(dmpe)_z]$ Complexes

Tomoji Ohishi, Kazuo Kashiwabara, and Junnosuke Fujita*

Department of Chemistry, Faculty of Science, Nagoya University, Chikusa-ku, Nagoya 464

(Received June 1, 1983)

A complete series of $[Co(acac)_x(en)_y(dmpe)_z]$ complexes was obtained by preparing four new complexes, $[Co(acac)(dmpe)_2]^{2+}$, $[Co(en)_2(dmpe)]^{3+}$, $[Co(en)(dmpe)_2]^{3+}$, and $[Co(acac)(en)(dmpe)]^{2+}$, where acac, en, and dmpe denote an acetylacetonate ion, ethylenediamine, and 1,2-bis(dimethylphosphino)ethane, respectively. Except for $[Co(acac)(dmpe)_2]^{2+}$, the three new complexes were resolved into optical isomers by SP-Sephadex column chromatography. Absorption and circular dichroism spectra of all the complexes were recorded and compared with one another.

In a previous paper,[1] we reported ten $[Co(en)_x(tn)_y(tmd)_z]^{3+}$ ($x,y,z=0,1,2$, or 3; $x+y+z=3$) complexes as the first example of a complete series of the $[Co(AA)_x(BB)_y(CC)_z]$-type complexes, where en ($NH_2CH_2CH_2NH_2$), tn ($NH_2CH_2CH_2CH_2NH_2$), and tmd ($NH_2CH_2CH_2CH_2CH_2NH_2$) form a five-, six-, and seven-membered chelate ring, respectively upon coordination. This paper reports the second example of a complete series-complexes belonging to the same type. The complexes are those of the type, $[Co(acac)_x(en)_y(dmpe)_z]$, where acac (acetylacetonate ion), en, and dmpe (1,2-bis(dimethylphosphino)ethane) are typical chelate ligands with O,O, N,N, and P,P donor atoms, respectively. Of the ten complexes belonging to this series, known complexes are the series of $[Co(acac)_{3-n}(en)_n]^{n+}$ ($n=0,1,2,3$), $[Co(acac)_2(dmpe)]^+$,[2] and $[Co(dmpe)_3]^{3+}$,[3] and there remain four unknown complexes, $[Co(acac)(dmpe)_2]^{2+}$, $[Co(en)_2(dmpe)]^{3+}$, $[Co(en)(dmpe)_2]^{3+}$, and $[Co(acac)(en)(dmpe)]^{2+}$, all of which contain the dmpe ligand. Preparative work on such series-complexes comprised of ligands with remarkably different donor properties will be useful for elucidating such properties as stability or electronic spectra of metal complexes.

Experimental

1,2-Bis(dimethylphosphino)ethane, $(CH_3)_2PCH_2CH_2P(CH_3)_2$ was prepared by the literature method,[4] and handled under nitrogen atmosphere until it formed cobalt(III) complexes. Oxygen-free solvents were obtained by bubbling nitrogen for 20 min immediately before use. Absorption and circular dichroism (CD) spectra were recorded on a Hitachi 323 spectrophotometer and a JASCO J-40CS spectropolarimeter, respectively.

Preparation of Complexes. *$[Co(en)_2(dmpe)]Br_3\cdot H_2O$*: To a solution of $[Co(en)_3](ClO_4)_3$[5] (473 mg, 1.4 mmol) in oxygen-free dimethyl sulfoxide (100 cm³) were added dmpe (210 mg, 1.4 mmol) and active charcoal (100 mg). The mixture was stirred for a day at room temperature and filtered. The filtrate was diluted with water (1 dm³) and poured on a column (ϕ3.5 cm × 150 cm) of SP-Sephadex C-25. The product adsorbed was eluted with 0.2 mol dm^{-3} NaCl, giving three bands in the order of $[Co(en)(dmpe)_2]^{3+}$ (very small amount), $[Co(en)_2(dmpe)]^{3+}$, and $[Co(en)_3]^{3+}$. The effluent of the second band was diluted five times with water and poured again on a small column (ϕ3.5 cm × 10 cm) of SP-Sephadex C-25. The complex adsorbed was eluted with 1 mol dm^{-3} NaBr, and the effluent was concentrated in a vacuum desiccator over P_4O_{10} to yield yellow crystals, which were filtered, washed with cold methanol–diethyl ether (1:5), and air-dried. Yield: 92 mg (16%). Found: C, 20.46; H, 5.84; N, 9.25%. Calcd for $C_{10}H_{34}N_4CoBr_3OP_2=[Co(en)_2(dmpe)]Br_3\cdot H_2O$: C, 20.46; H, 5.84; N, 9.54%. The complex is soluble in water, methanol, and dimethyl sulfoxide, but insoluble in diethyl ether.

$[Co(en)(dmpe)_2]Br_3$: To a solution of *trans*-$[CoCl_2(dmpe)_2]ClO_4$[3] (300 mg, 0.57 mmol) in oxygen-free methanol (100 cm³) was added excess en (180 mg, 2.9 mmol). The mixture was stirred for a day at room temperature, and diluted with water (1 dm³). The solution was poured on a column (ϕ3.5 cm × 150 cm) of SP-Sephadex C-25. By elution with 0.2 mol dm^{-3} NaCl, the product adsorbed gave four bands in the order of *trans*-$[CoCl_2(dmpe)_2]^+$, $[Co(en)(dmpe)_2]^{3+}$, $[Co(en)_2(dmpe)]^{3+}$ (very small amount), and $[Co(en)_3]^{3+}$. Orange crystals of the desired complex were obtained from the effluent of the second band by the same method as that for $[Co(en)_2(dmpe)]^{3+}$. Yield: 67 mg (18%). Found: C, 25.15; H, 6.23; N, 4.19%. Calcd for $C_{14}H_{40}N_2Br_3CoP_4=[Co(en)(dmpe)_2]Br_3$: C, 25.52; H, 6.12; N, 4.25%. The complex is soluble in water, methanol, and dimethyl sulfoxide, but insoluble in diethyl ether.

$[Co(acac)(dmpe)_2](PF_6)_2$: To a solution of *trans*-$[CoCl_2(dmpe)_2]ClO_4$ (163 mg, 0.31 mmol) in oxygen-free methanol (100 cm³) was added Li(acac) (32.6 mg, 0.31 mmol). The color of the solution changed immediately from blue-green to orange. After 30 min the solution was diluted with water (1 dm³) and poured on a column (ϕ3.5 cm × 150 cm) of SP-Sephadex C-25. By elution with 0.2 mol dm^{-3} NaCl, only orange-yellow effluent was obtained. The effluent was evaporated to dryness under reduced pressure, and the residue was extracted with methanol. On addition of excess $NaPF_6$ (100 mg) in water (5 cm³) the extract gave orange crystals, which were filtered, washed with cold water, and air-dried. Yield: 168 mg (73%). Found: C, 26.97; H, 5.01%. Calcd for $C_{17}H_{39}CoF_{12}O_2P_6=[Co(acac)(dmpe)_2](PF_6)_2$: C, 27.29; H, 5.25%. The complex is soluble in methanol, ethanol, and acetonitrile, but hardly soluble in water.

$[Co(acac)(en)(dmpe)](PF_6)_2\cdot H_2O$: To an oxygen-free methanol solution (100 cm³) of $[Co(acac)_2(en)]PF_6$ (660 mg, 1.53 mmol) which had been prepared from $[Co(acac)_2(en)]ClO_4$[6] and $NaPF_6$ was added dmpe (230 mg, 1.53 mmol). The mixture was kept at 50 °C for 5 h, and then mixed with water (400 cm³) and diethyl ether (100 cm³) to extract unreacted dmpe into diethyl ether. The aqueous layer was diluted with water (1 dm³) and poured on a column (ϕ3.5 cm × 150 cm) of SP-Sephadex C-25. By elution with 0.2 mol dm^{-3} Na_2SO_4, $[Co(acac)_2(dmpe)]^+$ (red), $[Co(acac)(en)(dmpe)]^{2+}$ (orange-red), and $[Co(acac)(dmpe)_2]^{2+}$ (orange-yellow) were eluted accompanying with a few very small brown bands. The effluent of the second orange-red band was collected and evaporated to dryness under reduced pressure. To the residue was added a small amount of methanol to extract the complex. On addition of excess $NaPF_6$ (200 mg) in water (5 cm³) the extract gave orange-

red crystals, which were filtered, washed with cold water, and air-dried. Yield: 40 mg (4%). Found: C, 23.90; H, 5.16; N, 4.13%. Calcd for $C_{13}H_{33}N_2CoF_{12}O_3P_4$=[Co(acac)(en)(dmpe)]$(PF_6)_2\cdot H_2O$: C, 24.13; H, 4.83; N, 4.33%. The complex is soluble in methanol, ethanol, and acetonitrile, but hardly soluble in water.

Known complexes, $[Co(acac)_3]$,[7] $[Co(acac)_2(en)]ClO_4$,[6] $[Co(acac)(en)_2]I_2$.[8] $[Co(en)_3](ClO_4)_3$,[5] $[Co(acac)_2(dmpe)]PF_6$,[2] and $[Co(dmpe)_3](ClO_4)_3$[3] were prepared by the literature methods.

Optical Resolution of Complexes. *[Co(en)$_2$(dmpe)]$^{3+}$*: The complex was resolved by a chromatographic method with a column (ϕ3.5 cm × 120 cm) of SP-Sephadex C-25 and an eluent of 0.1 mol dm^{-3} $Na_2[Sb_2(d\text{-tartrate})_2]$. $[Co(en)_2(dmpe)]Br_3\cdot H_2O$ (*ca.* 30 mg) charged on the top of the column was resolved completely by elution with the eluent. From each effluent, the optically active complex was isolated as bromide by the same method as that for the racemate. The slow-moving enantiomer has been determined to be Λ-$(+)_{589}$-$[Co(en)_2(dmpe)]Br_3\cdot 1/2\ H_2O$ by X-ray analysis.[9]

[Co(acac)(en)(dmpe)]$^{2+}$: The complex was resolved by the same chromatographic method as the above. However, a poor separation between the bands of enantiomers was observed. The fractions having a constant value of $\Delta\varepsilon/\varepsilon$ were collected, diluted five times with water, and poured on a small column (ϕ1 cm × 10 cm) of SP-Sephadex C-25. The complex adsorbed was eluted with 0.2 mol dm^{-3} $NaPF_6$, and the effluent was used for the measurements of CD spectra without isolating the complex. The concentration of the complex was determined by reference to the ε values of the racemate. The active complex hexafluorophosphate is much more soluble in water than the racemic salt.

Other Complexes. The $[Co(en)(dmpe)_2]^{3+}$ and $[Co(acac)_2(dmpe)]^+$ complexes were resolved partially by the same chromatographic method as the above. No fractions having a constant value of $\Delta\varepsilon/\varepsilon$ were obtained. The column chromatographic method becomes less effective as the number of acac or dmpe ligand increases in the complex. No resolution was achieved for $[Co(acac)(dmpe)_2]^{2+}$.

Results and Discussion

Mixed complexes in the series of $[Co(acac)_{3-n}(en)_n]^{n+}$ can be easily prepared from the parent complexes by substitution reactions in fairly good yields; $[Co(acac)_2(en)]^+$ is prepared from $[Co(acac)_2(NO_2)_2]^-$ and en,[6] and $[Co(acac)(en)_2]^{2+}$ from $[CoCO_3(en)_2]^+$ [8] or $[CoCl(H_2O)(en)_2]^{2+}$ [10] and acac. However, most reactions of dmpe with a cobalt(III) complex accompany disproportionation or ligand scrambling, affording many complexes formed with dmpe and ligands contained in the starting complex. The reaction of $[Co(en)_3]^{3+}$ with dmpe in the ratio of 1:1 yields all complexes of the series, $[Co(en)_{3-n}(dmpe)_n]^{3+}$, and $[Co(en)_2(dmpe)]^{3+}$ is obtained in 16% yield. The formation of $[Co(en)(dmpe)_2]^{3+}$ is very small, and $[Co(dmpe)_3]^{3+}$ decomposes during the experiment of column chromatography. The reaction of *trans*-$[CoCl_2(en)_2]^+$ with dmpe also forms $[Co(en)_2(dmpe)]^{3+}$, but the yield is very poor, $[Co(en)_3]^{3+}$ and *trans*-$[CoCl_2(dmpe)_2]^+$ being formed in large amounts. The other mixed complex, $[Co(en)(dmpe)_2]^{3+}$ is obtained in 18% yield by the reaction of *trans*-$[CoCl_2(dmpe)_2]^+$ with excess en. The reaction with an equimolar amount of en is very slow, and on heating $[Co(en)_3]^{3+}$ and $[Co(dmpe)_3]^{3+}$ are formed as the major product. The (2-aminoethyl)dimethylphosphine (edmp) ligand also forms all complexes of the series, $[Co(en)_{3-n}(edmp)_n]^{3+}$ by reaction with *trans*-$[CoCl_2(en)_2]^+$.[11]

The $[Co(acac)(dmpe)_2]^{2+}$ complex is obtained in good yield by the reaction of *trans*-$[CoCl_2(dmpe)_2]^+$ with Li(acac) in the ratio of 1:1. The reaction takes place rapidly and gives no other complexes in detectable amount. The reaction of dmpe with $[Co(acac)_3]$ in the ratio of 1:1 yields all complexes of the series, $[Co(acac)_{3-n}(dmpe)_n]^{n+}$, the main product being $[Co(acac)_2(dmpe)]^+$.[2] Similar reactions of diphenylphosphine-type chelate ligands such as (2-aminoethyl)diphenylphosphine (edpp) or 1,2-bis(diphenylphosphino)ethane (dppe) with $[Co(acac)_3]$ give only bis(acac) complex, and no bis(edpp or dppe) complex is formed even in the presence of active charcoal.[12] The dmpe ligand is more reactive to Co(III) than edpp and dppe.

The $[Co(acac)(en)(dmpe)]^{2+}$ complex is obtained in 4% yield by the reaction of dmpe with $[Co(acac)_2(en)]^+$. The reaction between dmpe and $[Co(acac)(en)_2]^{2+}$ yields further less amount of the complex. In either reaction, $[Co(en)_3]^{3+}$, $[Co(acac)(dmpe)_2]^{2+}$, and $[Co(acac)_2(dmpe)]^+$ are formed in larger amounts.

While solid $[Co(dmpe)_3](ClO_4)_3$ is rather unstable in the air,[3] all of the dmpe complexes prepared in this study are stable in the solid state. Both $[Co(en)(dmpe)_2]^{3+}$ and $[Co(en)_2(dmpe)]^{3+}$ in aqueous solution are stable at room temperature, but decompose slowly on heating over 60 °C. The former complex in water in the presence of excess NaCl changes to *trans*-$[CoCl_2(dmpe)_2]^+$ by heating, but the latter complex decomposes to give Co(II) species under the same conditions. The $[Co(dmpe)_3]^{3+}$ complex in methanol containing excess Cl^- or Br^- also changes easily to *trans*-$[Co(Cl\text{ or }Br)_2(dmpe)_2]^+$.[3] In contrast to the en complexes, no changes occur for both $[Co(acac)(dmpe)_2]^{2+}$ and $[Co(acac)_2(dmpe)]^+$ in aqueous solution by heating at *ca.* 70 °C for several hours. Thus the acac ligand seems to stabilize more dmpe complexes than the en ligand does. An aqueous solution of $[Co(acac)(en)(dmpe)]^{2+}$ gives a small amount of Co(II) species and $[Co(acac)(dmpe)_2]^{2+}$ by heating.

In Fig. 1 are shown absorption spectra of $[Co(en)_{3-n}(dmpe)_n]^{3+}$ (n=0,1,2,3) together with those of related edmp complexes,[11] and in Fig. 2 absorption spectra of $[Co(acac)_{3-n}(en)_n]^{n+}$ (n=0,1,2,3), $[Co(acac)_{3-n}(dmpe)_n]^{n+}$ (n=1,2,3), and $[Co(acac)(en)(dmpe)]^{2+}$. In the Figures, short vertical lines are positions of the first absorption bands calculated by Yamatera's rule[13] using the observed values of the first absorption bands of $[Co(acac)_3]$, $[Co(en)_3]^{3+}$, and $[Co(dmpe)_3]^{3+}$. Table 1 lists spectral data in the d-d band region for ten complexes of the series, $[Co(acac)_x(en)_y(dmpe)_z]^{n+}$. The observed first absorption band maxima appear to agree with the calculated values for the series of $[CoN_nP_{6-n}]$, where *trans*-$[CoN_4P_2]$, *mer*-$[CoN_3P_3]$, *trans*-$[CoN_2P_4]$, and $[CoNP_5]$ are missing. Many attempts to prepare complexes of these types have been unsuccessful. The first three types have a *trans*(P,P) configuration which would make the complex unstable by the trans effect of a phosphine li-

TABLE 1. ABSORPTION AND CD SPECTRAL DATA OF $[Co(acac)_x(en)_y(dmpe)_z]^{n+}$ IN THE d-d BAND REGION

Complex	Absorption $\tilde{\nu}/10^3$ cm^{-1} (log ε)	CD $\tilde{\nu}/10^3$ cm^{-1} ($\Delta\varepsilon$)	Solvent
$[Co(acac)_3]$	16.90(2.13)	15.4(−2.3), 17.4(+6.1)[1]	a
$[Co(acac)_2(en)]^+$	18.60(2.17)	16.7(+1.1), 19.7(+4.2)[2]	a
$[Co(acac)(en)_2]^{2+}$	20.00(2.14)	20.2(+2.4), 26.8(−1.3)[3]	b
$[Co(acac)_2(dmpe)]^+$	19(2.4)^{sh}, 23.4(2.9)^{sh}	17.4(+), 19.8(−), 24.0(+)*	a
$[Co(acac)(dmpe)_2]^{2+}$	23.25(3.08)	—	a
$[Co(acac)(en)(dmpe)]^{2+}$	21(2.4)^{sh}, 23.40(2.85)	19.0(+1.0), 21.1(−1.55) 24.6(+1.95)	a
$[Co(en)_3]^{3+}$	21.30(1.94), 29.40(1.90)	20.3(+1.89), 23.4(−0.16)[4] 28.5(+0.25)	b
$[Co(en)_2(dmpe)]^{3+}$	23.87(2.62), 29.58(2.37)	20.5(+1.50), 22.7(−1.55) 25.5(+0.55), 29.2(+0.40)	b
$[Co(en)(dmpe)_2]^{3+}$	24.75(2.86), 29.40(2.84)	22.2(+), 24.8(−), 29.2(+)*	b
$[Co(dmpe)_3]^{3+}$	26.00(2.97), 30.5(3.3)^{sh}	—	c

1) I. Jonas and B. Norden, *J. Inorg. Nucl. Chem.*, **12**, 43(1976). 2) Ref. 19. 3) Ref. 20. 4) Ref. 1. sh: shoulder. *: Qualitative data (see the text). a: CH_3OH. b: H_2O. c: $(CH_3)_2SO$.

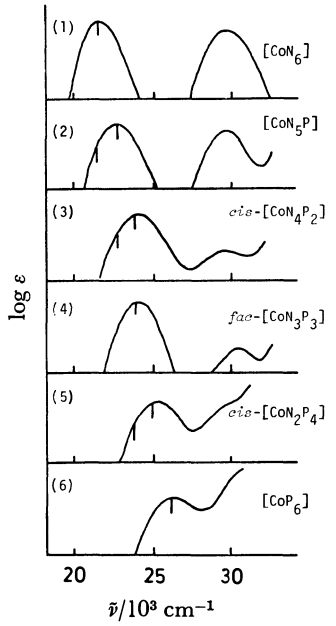

Fig. 1. Absorption spectra of (1) $[Co(en)]^{3+}$, (2) $[Co(en)_2(edmp)]^{3+}$, (3) $[Co(en)_2(dmpe)]^{3+}$, (4) *fac*-$[Co(edmp)_3]^{3+}$, (5) $[Co(en)(dmpe)_2]^{3+}$, and (6) $[Co(dmpe)_3]^{3+}$. Short vertical lines show the calculated band positions (see the text).

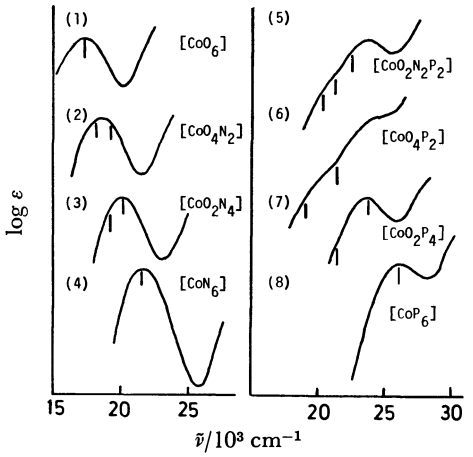

Fig. 2. Absorption spectra of (1) $[Co(acac)_3]$, (2) $[Co(acac)_2(en)]^+$, (3) $[Co(acac)(en)_2]^{2+}$, (4) $[Co(en)_3]^{3+}$, (5) $[Co(acac)(en)(dmpe)]^{2+}$, (6) $[Co(acac)_2dmpe)]^+$, (7) $[Co(acac)(dmpe)_2]^{2+}$, and (8) $[Co(dmpe)_3]^{3+}$. Short vertical lines show the calculated band positions (see the text).

gand.[11,14] For example, the reaction of edmp with *trans*-$[CoCl_2(dmpe)_2]^+$ did not yield $[Co(edmp)(dmpe)_2]^{3+}$ of the $[CoNP_5]$-type, giving *fac*-$[Co(edmp)_3]^{3+}$ and $[Co(dmpe)_3]^{3+}$ by disproportionation.

As shown in Fig. 1, the first absorption bands of $[CoN_nP_{6-n}]$ are shifted to the high energy side by replacing N with P, while the positions of the second absorption bands remain almost unchanged. As the result the energy difference between the two d-d bands becomes small as the number of P increases. The difference of *ca.* 3500 cm^{-1} for $[Co(dmpe)_3]^{3+}$ is only 43% of that for $[Co(en)_3]^{3+}$ (8100 cm^{-1}). When the decrease in energy difference is assumed to occur by an increasing covalent character of bonds between the phosphine ligand and Co(III),[15] it is concluded that the Co^{3+}–P bond has extremely strong covalent character as compared with the Co^{3+}–N bond. Some Co(III)–phosphite complexes have also small energy difference between the two d-d bands, $[Co\{P(OCH_2)_3CCH_3\}_6]^{3+}$ and $[Co\{P(OCH_3)_3\}_6]^{3+}$ being 5000 and 3300 cm^{-1}, respectively.[16]

While each of $[Co(acac)_{3-n}(en)_n]^{n+}$ (n=1,2) shows the first absorption band at nearly the same position as that expected from Yamatera's rule, $[Co(acac)_2(dmpe)]^+$ and $[Co(acac)(en)(dmpe)]^{2+}$ give spectra fairly different from those expected from the rule in this region (Fig. 2). Both complexes exhibit a peak around 23400 cm^{-1} on the high energy side of the expected positions. The $[Co(acac)(dmpe)_2]^{2+}$ complex also shows the absorption maximum at nearly the same position (23250 cm^{-1}), although the position coincides with that expected from the rule. The spectra of *cis*-$[Co(acac)_2(P)_2]^+$ (P=$P(CH_3)_3$, $P(CH_3)_2(C_6H_5)$) resemble that of $[Co(acac)_2(dmpe)]^+$.[2] The reason for these spectral properties remains unknown.

Figure 3 shows CD spectra of $[Co(en)_{3-n}(dmpe)_n]^{3+}$

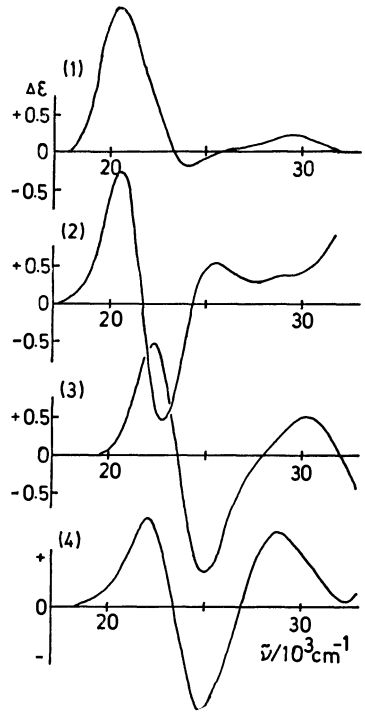

Fig. 3. CD spectra of (1) Λ-$[Co(en)_3]^{3+}$, (2) Λ-$[Co(en)_2(dmpe)]^{3+}$, (3) Λ-*fac*-$[Co(edmp)_3]^{3+}$, and (4) $(+)_{589}$-$[Co(en)(dmpe)_2]^{3+}$ (qualitative data, see the text).

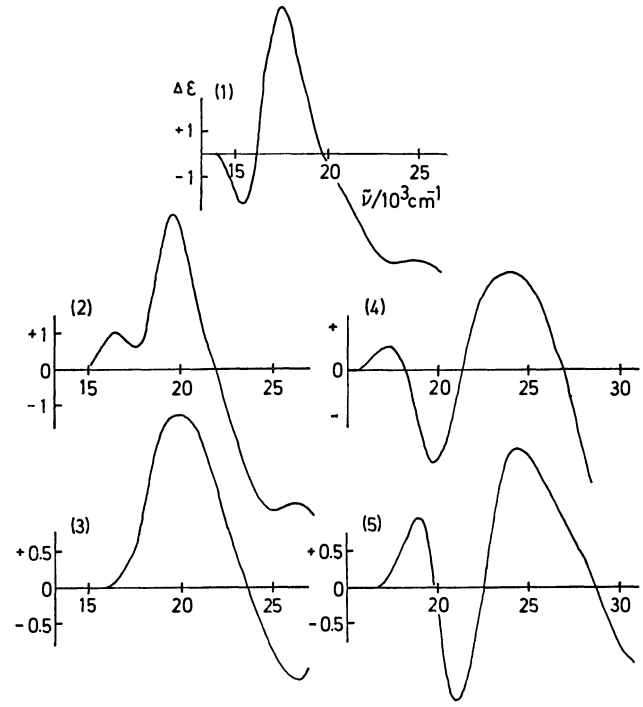

Fig. 4. CD spectra of (1) Λ-$[Co(acac)_3]$, (2) Λ-$[Co(acac)_2(en)]^{+}$, (3) Λ-$[Co(acac)(en)_2]^{2+}$, (4) $(+)_{589}$-$[Co(acac)_2(dmpe)]^{+}$ (qualitative data, see the text), and (5) $(+)_{589}$-$[Co(acac)(en)(dmpe)]^{2+}$.

(n=0,1,2) and *fac*-$[Co(edmp)_3]^{3+}$ [11] in the d-d band region. The spectrum of $[Co(en)(dmpe)_2]^{3+}$ is qualitative because of poor resolution. The absolute configurations of $[Co(en)_3]^{3+}$,[17] $[Co(en)_2(dmpe)]^{3+}$,[9] and *fac*-$[Co(edmp)_3]^{3+}$ [12] in the Figure have been determined to Λ by the X-ray method. These Λ-isomers give two CD components with different signs, (+) and (−) from the low energy side in the first absorption band region, although the negative components of the phosphine complexes are very strong as compared with that of Λ-$[Co(en)_3]^{3+}$. All the isomers give positive CD in the second absorption band region. The CD spectrum of $[Co(en)(dmpe)_2]^{3+}$ in the Figure has such characteristics of the Λ-isomer, and the complex can be assigned to Λ configuration. In column chromatographic resolution by use of SP-Sephadex C-25 and $Na_2[Sb_2(d\text{-tartrate})_2]$, the fast-moving enantiomer is Λ for $[Co(en)_3]^{3+}$ and *fac*-$[Co(edmp)_3]^{3+}$, while Δ for $[Co(en)_2(dmpe)]^{3+}$ and $[Co(en)(dmpe)_2]^{3+}$. No resolution has been achieved for $[Co(dmpe)_3]^{3+}$.

Figure 4 shows CD spectra of $[Co(acac)_{3-n}(en)_n]^{n+}$ (n=0,1,2), $[Co(acac)_2(dmpe)]^{+}$, and $[Co(acac)(en)(dmpe)]^{2+}$ in the d-d band region. The latter two complexes are enantiomers eluted faster in column chromatography. The CD spectrum of $[Co(acac)_2(dmpe)]^{+}$ is qualitative because of poor resolution. In the Figure, the absolute configuration of $[Co(acac)_3]$ has been determined to Λ by the X-ray method,[18] and those of $[Co(acac)_2(en)]^{+}$ [19] and $[Co(acac)(en)_2]^{2+}$ [20] assigned to the same Λ configuration on the basis of the CD spectra. These Λ-isomers as well as Λ-$[Co(en)_3]^{3+}$ give a positive main CD band in the first absorption band region. On the other hand, the CD spectra of $[Co(acac)_2(dmpe)]^{+}$ and $[Co(acac)(en)(dmpe)]^{2+}$ differ remarkably from those of Λ-$[Co(acac)_{3-n}(en)_n]^{n+}$, giving three CD components of (+), (−), and (+) signs from the low energy side in this region. This CD pattern, however, is quite similar to that of Λ-$[Co(en)_{3-n}(dmpe)_n]^{3+}$ (n=1,2), both of which show a strong negative CD component as seen in Fig. 3. The appearance of the strong negative components in $[Co(acac)_2(dmpe)]^{+}$ and $[Co(acac)(en)(dmpe)]^{2+}$ can also be attributed to the effect of substitution of one en ligand in $[Co(acac)_2(en)]^{+}$ and $[Co(acac)(en)_2]^{2+}$, respectively by the dmpe ligand. Thus both acac complexes containing dmpe in Fig. 4 can be assigned to Λ configuration.

This work was supported by the research grant of the Takeda Science Foundation.

References

1) M. Kojima, H. Yamada, H. Ogino, and J. Fujita, *Bull. Chem. Soc. Jpn.*, **50**, 2325 (1977).
2) K. Kashiwabara, K. Katoh, T. Ohishi, J. Fujita, and M. Shibata, *Bull. Chem. Soc. Jpn.*, **55**, 149 (1982).
3) T. Ohishi, K. Kashiwabara, and J. Fujita, *Chem. Lett.*, **1981**, 1371.
4) *Inorg. Synth.*, **15**, 188 (1974).
5) N. Tanaka, Y. Kobayashi, and M. Kamada, *Bull. Chem. Soc. Jpn.*, **40**, 2839 (1967).
6) R. D. Archer and B. P. Cotsoradis, *Inorg. Chem.*, **4**, 1584 (1965).
7) *Inorg. Synth.*, **5**, 188 (1957).
8) *Inorg. Synth.*, **9**, 167 (1967).
9) S. Ohba, Y. Saito, T. Ohishi, K. Kashiwabara, and

J. Fujita, *Acta Crystallogr., Sect. C*, **39**, 49 (1983).
10) L. J. Boucher and J. C. Bailar, Jr., *Inorg. Chem.*, **3**, 589 (1964).
11) I. Kinoshita, K. Kashiwabara, J. Fujita, K. Matsumoto, and S. Ooi, *Bull. Chem. Soc. Jpn.*, **54**, 2683 (1981).
12) K. Kashiwabara, I. Kinoshita, T. Ito, and J. Fujita, *Bull. Chem. Soc. Jpn.*, **54**, 725 (1981).
13) H. Yamatera, *Bull. Chem. Soc. Jpn.*, **31**, 95 (1958).
14) M. Atoh, I. Kinoshita, K. Kashiwabara, and J. Fujita, *Bull. Chem. Soc. Jpn.*, **55**, 3179 (1982).
15) C. E. Schaffer and C. K. Jørgensen, *J. Inorg. Nucl. Chem.*, **8**, 143 (1958).
16) J. G. Verkade, *Coord. Chem. Rev.*, **9**, 1 (1972).
17) Y. Saito, K. Nakatsu, M. Shiro, and H. Kuroya, *Acta Crystallogr.*, **8**, 729 (1955).
18) R. B. Von Dreele and R. C. Fay, *J. Am. Chem. Soc.*, **93**, 4936 (1971).
19) L. J. Boucher, *Inorg. Chem.*, **9**, 1202 (1970); K. Kashiwabara, K. Igi, and B. E. Douglas, *Bull. Chem. Soc. Jpn.*, **49**, 1573 (1976).
20) L. J. Boucher, *Inorg. Chim. Acta*, **6**, 29 (1972).

Alkyd Resin Paint as a New Membrane Material of Ion-selective Electrode

Takashi KATSU,* Keiko TOGAWA, and Yuzaburo FUJITA
Faculty of Pharmaceutical Sciences, Okayama University, Tsushima, Okayama 700
(Received June 14, 1983)

A new membrane material, alkyd resin paint, was used for a silver iodide-based ion-selective electrode. The electrode was easily prepared in the laboratory by mixing silver iodide precipitate and alkyd resin paint. The electrode responded to both iodide and silver ions with the deviations from a Nernstian response due to adsorption and desorption of ions. Silver ions tended to adsorb more strongly on the electrode surface. The preparation and properties of the present electrode are described in view of an analytical utilization of the electrode.

Various membrane materials including silicone rubber, poly(vinyl chloride), and paraffin wax have been utilized for the precipitate-based ion-selective electrode.[1] We are interested in the development of a new electrode material which is easily prepared in a laboratory. The following conditions are required for the membrane materials of the precipitate-based ion-selective electrode:[2] (a) It is chemically inert and provides good adhesion for the sensor precipitates. (b) It is hydrophobic, tough, flexible, nonporous, and non-swelling in sample solution. Extensive swelling disrupts the active chain of the sensor precipitates.

In the present study, we chose alkyd resin paint as a membrane material, because it is most commonly utilized for outdoor painting, and it provides a chemically tough and weather-proof coating. In addition, it can well disperse the inorganic pigments in the paint medium.[3,4] This paper describes the use of the alkyd resin paint to a silver iodide-based ion-selective electrode. The electrode was prepared by the incorporation of silver iodide into the alkyd paint. This electrode responded well to both iodide and silver ions. The deviations from a Nernstian response, attributed to the adsorption and desorption of ions,[5] were observed at a lower concentration region. The characteristics of the electrode were discussed in view of an analytical utilization of the electrode.

Experimental

Reagents. Silver iodide was purchased from Rare Metallic Co., Ltd., and alkyd resin paint was a product of Nippon Oil and Fats Co., Ltd. (Glasstone No. 1000, Clear). Other chemicals used were all of analytical reagent grade. Water was distilled and deionized.

Preparation of Electrode. Figure 1 shows the silver iodide-based ion-selective electrode constructed in the present study. A copper plate (*ca.* 10 mm diameter, 0.5 mm thickness), which was connected to a shielded cable, was covered with a glass tube, and tightly attached using an epoxy resin adhesive. The exposed copper plate was polished with sandpaper, washed, and dried. Silver iodide was sieved through a 200-mesh screen after grinding in a mortar. Alkyd resin paint was diluted with toluene (20 w/w%) in order to decrease its viscosity. The silver iodide powder and the diluted paint were then blended on the copper plate, and the mixture was allowed to dry in air overnight. The mass ratio of the powder to the paint was not so critical, though the most favorable results were obtained with 15—20 mg of the powder and 20 ul of the diluted paint. The electrode

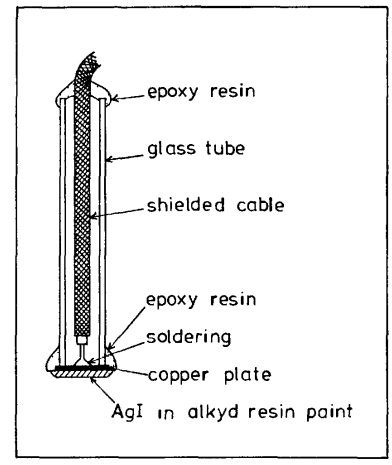

Fig. 1. Construction of electrode.

was used after being soaked for 2 h in 10^{-4} M† solution of potassium iodide.

Potential Measurements. The electrochemical cell assembly employed in this study is as follows: silver iodide-based ion-selective electrode/ test solution/ 1 M NH_4NO_3 (salt bridge)/ 0.01 M KCl/ Ag,AgCl. Usual glass containers were used for the stock of test solutions. The amount of test solution was 2 ml, and the ionic strength was maintained at 0.1 with KNO_3. An appropriate FET-operational amplifier (input resistance: $>10^{12}\,\Omega$) was used for the potential measurements. The measurements were carried out at room temperature. The solution was stirred with a magnetic stirrer. Between measurements, the electrode was rinsed several times with water and wiped.

Results and Discussion

Response Characteristics. Figure 2 shows the potential response to iodide ions of the present electrode. The calibration curves were measured from 10^{-7} M to 10^{-2} M of iodide ions, and three consecutive runs were performed. The lower detection limit of iodide ion was gradually interfered with repeated calibration measurements. Further deterioration of the detection limit, however, was not observed even when the electrode was continuously used. It was found that if the electrode was soaked in fresh 0.1 M KNO_3 solution for 10 min, the detection limit could easily be improved to the level in the original calibration. This means that some iodide ions in the electrolyte may weakly be adsorbed on the electrode surface, and such ions can not be eliminated by a conventional washing of

† 1 M=1 mol dm^{-3}.

the electrode.

To clarify the influence of the adsorption of ions on the electrode, we measured the potential response after the pretreatment with various concentrations of iodide ion. The electrode was immersed in a solution (2 ml) containing iodide ion for 3 min, rinsed with water, wiped, and then soaked in 10^{-7} M KI—0.1 M KNO_3 solution; the addition of 10^{-7} M KI in the solution afforded the reproducibility and the rapid response of the electrode potential. The potential-time responses of the electrode are shown in Fig. 3. It was found that the amount of the iodide ion released was nearly proportional to the pretreated concentration of iodide ion. Such a correlation seems to indicate that the adsorption and desorption occur at the electrode surface. The Freundlich adsorption isotherm is applicable to the adsorption from solution:

$$x = kC_{eq}^{1/n},$$

where x is the specific amount adsorbed, C_{eq} is the concentration at equilibrium, and k and $1/n$ are constants characterizing the substance adsorbed and adsorbing materials.[6] It is reasonable to postulate that C_{eq} and x can refer to the concentration of iodide ion pretreated and the amount released in 10^{-7} M KI solution, respectively. The log-log plots of x *vs.* C_{eq} gave the values of $k=2\times10^{-4}$ and $1/n=0.6$.

The above discussions should hold when the adsorbed iodide ions are completely desorbed by dipping the electrode into the solution. To see more directly the effect of the adsorption of iodide ion, we measured the potential response to silver ion after the pretreatment with iodide ion. A large negative deviation of the potential response to silver ion was observed immediately after the pretreatment of the electrode with iodide ions (Fig. 4(a)). A normal Nernstian response could be observed after the adsorbed iodide ion reacted completely with silver ion. However, when the electrode was immersed in fresh 0.1 M KNO_3 solution for 10 min prior to the measurement, such deviation was diminished (Fig. 4(b)). This observation was consistent with the result that the adsorbed iodide ion was easily desorbed by soaking the electrode into the solution, as already mentioned above.

In contrast, the response to iodide ion after the pretreatment with silver ion showed a large positive deviation even after the electrode was immersed in fresh 0.1 M KNO_3 (Fig. 5(b)). This seems to indicate that silver ions tend to adsorb more strongly on the electrode surface. It has been reported that metal ions adsorbed on the electrode can not be removed by dipping into water.[7] Effective removal has been accomplished only by physical rubbing with a cleanser.

It is now well known that the adsorption and desorption taking place at an electrode surface cause the deviations from a Nernstian response.[5] Adsorption and desorption phenomena interfere with the lower limit of detection; other sources of the deterioration

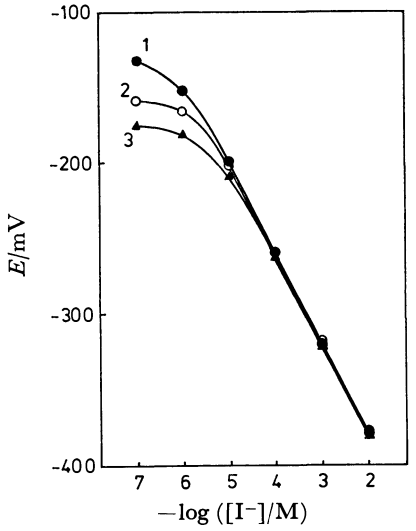

Fig. 2. Potential response to iodide ion. The calibration plots were measured in the order indicated. Three consecutive runs were performed.

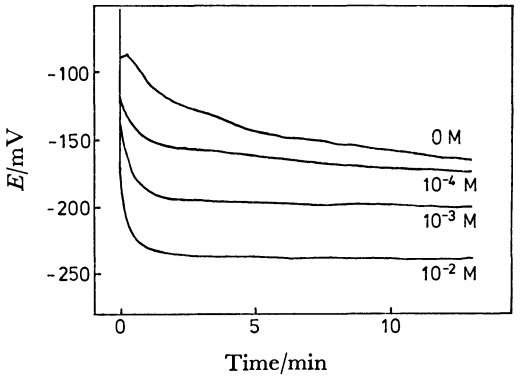

Fig. 3. Time course of the desorption of iodide ions after immersing the electrode in various concentrations of iodide ions for 3 min. The concentrations of the pretreatment are indicated in the figure. The electrode was soaked in a solution containing 10^{-7} M KI—0.1 M KNO_3.

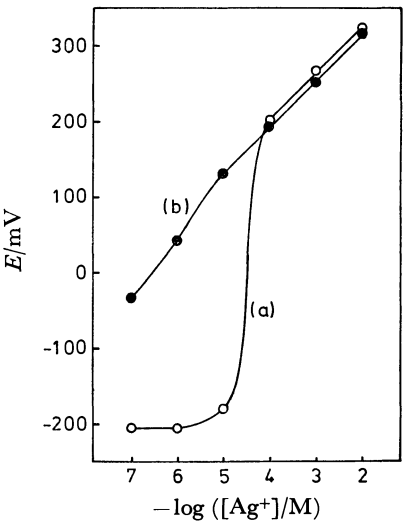

Fig. 4. Potential response to silver ion after the pretreatment of the electrode with 10^{-2} M iodide ion for 3 min. (a) Immediately after the pretreatment and conventional washing of the electrode. (b) After soaking in fresh 0.1 M KNO_3 solution for 10 min.

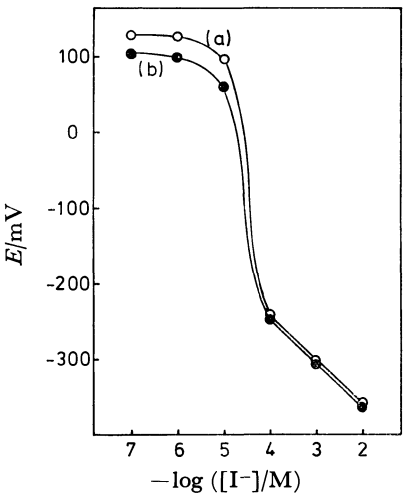

Fig. 5. Potential response to iodide ion after the pretreatment of the electrode with 10^{-2} M silver ion for 3 min. (a) Immediately after the pretreatment and conventional washing of the electrode. (b) After soaking in fresh 0.1 M KNO_3 solution for 10 min.

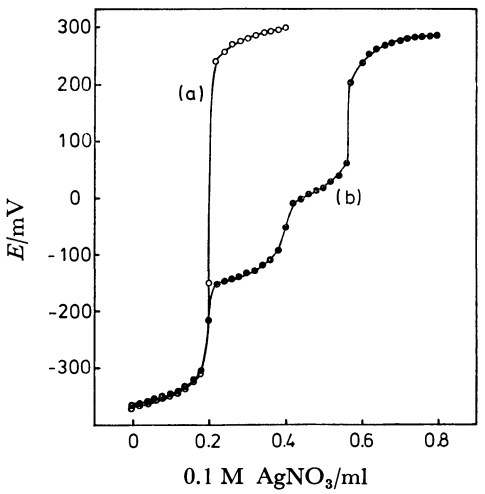

Fig. 6. Potentiometric titrations of iodide ion (a), and of a mixture of iodide, bromide, and chloride ions (b) at 0.01 M concentration in the presence of 0.1 M KNO_3.

(such as air oxidation of iodide ions) are also known.[8] It is quite natural to think that interference due to adsorption becomes more significant when the large surface area of the electrode and the small volume of the test solution are used. As for the iodide detection, if the present experiments were performed at iodide concentrations below 10^{-4} M (with 2 ml of test solution), it is unnecessary to consider the effects of adsorption and desorption because the interference at this concentration range is beyond the detection limit. Only when the measurement was transfered from higher (above 10^{-4} M) to lower concentrations, the cleaning of the electrode by soaking in a fresh solution without iodide ions was required.

Application to Potentiometric Titrations. Aside from the characteristics of the electrode, we tried an analytical utilization of the present electrode. Although an extensive application of the ion-selective electrode has been reported, the potentiometric titrations of iodide ion and of a mixture of iodide, bromide, and chloride ions were performed with the present electrode. A typical result is shown in Fig. 6. The well-defined S-shape of the titration curve and the large potential change at the end-point permitted accurate results, as was reported with silicone rubber membrane.[9] Potentiometric titrations could also be carried out in aqueous organic solvents (20% aqueous ethanol or acetone) and the halide content could be determined to be that obtained in aqueous solution.

Conclusion. The present paper describes the preparation and properties of the silver iodide-based ion-selective electrode with alkyd resin paint as a new membrane material. The experimental data presented here are almost compatible with the previous results; however, the most attractive point is ease of the preparation of the electrode in the laboratory. The electrode can be made without special treatments and techniques. Commercially available silver iodide and alkyd resin paint are blended on the metal surface. It is apparent that the present method will also be applied to the preparation of other electrodes by incorporating sensor precipitates into the alkyd resin paint.

This work was supported in part by the Grant-in-Aid for Scientific Research No. 57771484 from the Ministry of Education, Science and Culture.

References

1) E. Pungor and K. Tóth, "Ion-Selective Electrodes in Analytical Chemistry," ed by H. Freiser, Plenum, New York (1978), Vol. 1, Chap. 2.

2) G. J. Moody and J. D. R. Thomas, "Selective Ion Sensitive Electrodes," Merrow, Watford, England (1971), Chap. 6.

3) "McGraw-Hill Encyclopedia of Science and Technology," McGraw-Hill, New York (1971), Vol. 10, p. 541.

4) W. M. Kraft, *J. Am. Oil Chemists' Soc.*, **39**, 501 (1962).

5) E. G. Harsányi, K. Tóth, L. Pólos, and E. Pungor, *Anal. Chem.*, **54**, 1094 (1982).

6) W. J. Moore, "Physical Chemistry," 3rd ed, Prentice-Hall, Englewood Cliffs, N. J. (1962), Chap. 18.

7) S. N. Kar Chaudhari and K. L. Cheng, *Mikrochim. Acta* [*Wien*], **1980 II**, 159.

8) J. Kontoyannakos, G. J. Moody, and J. D. R. Thomas, *Anal. Chim. Acta*, **85**, 47 (1976).

9) E. Pungor, *Anal. Chem.*, **39**, 28A (1967).

 © 1983 The Chemical Society of Japan Bull. Chem. Soc. Jpn., 56, 3449—3456 (1983)

The Solvent Effects on the Photochemical Isomerization of 5-Cyano-5*H*-benzocycloheptene

Hisako KOBAYASHI, Keizo TAKATOKU, Masahiko KATO,* and Toshio MIWA

Faculty of Science, Osaka City University, Sugimoto-3, Sumiyoshi-ku, Osaka 558

(Received October 18, 1982)

The photochemical reaction of 5-cyano-5*H*-benzocycloheptene (**1b**) has been studied kinetically in various solvents. The main reactions were (1) a 1,7-hydrogen shift, with simultaneous cyclization, to give 7b-cyano-1a,7b-dihydro-1*H*-cyclopropa[*a*]naphthalene and (2) a 4π-electrocyclic ring closure to give cyclobutenes. The former reaction was found to show rather complicated solvent effects, but the latter was accelerated in less polar solvents. The conformational equilibrium between *exo*- and *endo*-forms was also observed in the NMR spectra of **1b** under various conditions. From a consideration of the solvent effects on the product distribution, the ground-state conformations of **1b** could be reflected in the ratio of the *exo* and *endo* forms of the cyclization products.

The photochemistry of 5*H*-benzocycloheptenes (**1**) has been studied by Swenton *et al.*[1] and also by us.[2,3] As a result, it has been found that these molecules are rearranged principally in two directions; *i.e.*, the formation of benzonorcaradienes (**2**) *via* a 1,7-hydrogen shift and the formation of 2a,7a-dihydro-7*H*-cyclobut[*a*]indenes (**3**) by means of an electrocyclic ring closure.

In the case of the 5-methoxycarbonyl derivative (**1a**), a facile 1,7-migration of the substituent took place, instead of the 1,7-hydrogen migration, to give 1-*endo*-methoxycarbonyl-1a,7b-dihydro-1*H*-cyclopropa[*a*]naphthalene (**4**) exclusively.[3]

In this paper, we wish to report the photochemistry of 5-cyano-5*H*-benzocycloheptene (**1b**) in order to compare it with that of **1a**. The solvent effects on the conformational equilibrium and on the photochemical isomerization of **1b** have also been studied.

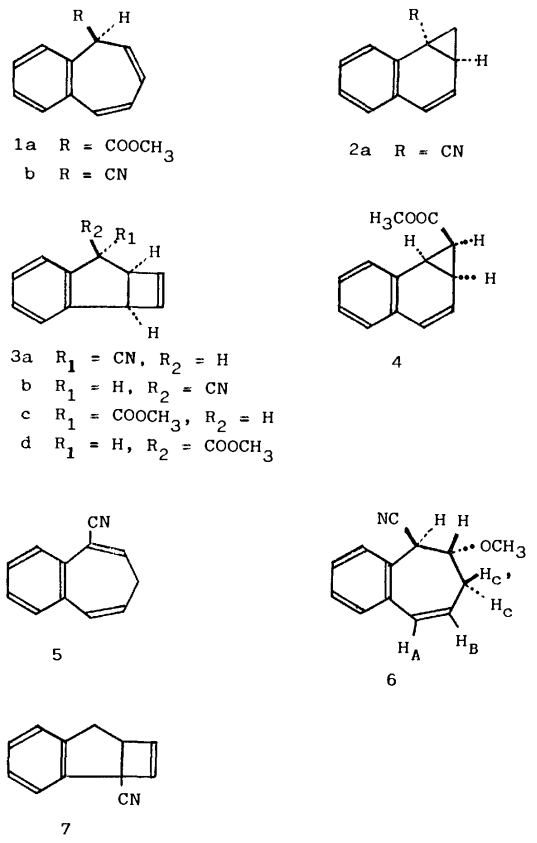

Scheme 1.

Results

The irradiation of **1b** in a methanol solution with the aid of a high-pressure mercury arc (UM-452) through a Pyrex filter for 1 h gave a mixture, **A**—**F**, consisting of **2a** (33%), **3a** (*exo*) (18%), **3b** (*endo*) (9%), **5** (5%), **6** (10%), and **7** (6%). They were separated by successive column and vapour-phase chromatography.

Structure of the Products. Compound **A** showed three signals characteristic of a three-membered ring proton and two olefinic proton signals in the NMR spectrum; it was identical with the known 7b-cyano-1a,7b-dihydro-1*H*-cyclopropa[*a*]naphthalene (**2a**).[4] Because of the difficulty of separating **B** from **C**, we studied them as a mixture. The NMR spectrum showed two sets of olefinic signals on the cyclobutene ring (**B**, δ 6.42 and 6.15; **C**, δ 6.52 and 6.28 ppm (AX type, J=2.7 Hz)), accompanied by benzylic proton signals characteristic of *exo*- and *endo*-2a,7a-dihydro-7*H*-cyclobut[*a*]indene (**3**) (**B**, δ 4.49 (bd); **C**, δ 4.32 ppm (d)).[5] We deduced **3a** structure for compound **B** and that of **3b** for **C**, because the NMR signals for the benzylic proton in 7-substituted 2a,7a-dihydro-7*H*-cyclobut[*a*]indene are quite indicative of the configuration, whether the substituent occupies the *exo* (broad doublet) or the *endo* position (doublet).[5] These assignments were confirmed by the methanolysis of the mixture to the easily separable corresponding methyl carboxylates, **3c** and **3d**. They were identical with those independently obtained through the sensitized irradiation of 5-methoxycarbonyl-5*H*-benzocycloheptene (**1a**).[6] Compound **D** showed an UV maximum (λ_{max}: 229 nm) characteristic of 7*H*-benzocycloheptenes and an IR absorption of the conjugated nitrile ($\nu_{C\equiv N}$: 2220 cm^{-1}). The NMR signals of the three olefinic and two aliphatic protons, together with their coupling patterns, determined the structure to be **5**.[4] Compound **E** had the molecular formula of $C_{13}H_{13}NO$, composed of one molecule each of the starting material and of methanol. This compound showed a UV spectrum similar to that of 6,7-dihydro-5*H*-benzocycloheptene,[7] while the NMR olefinic signals (2H, AB type, J_{AB}=12.2 Hz) showed a strong coupling only with the adjacent methylene protons (J_{AC}=2.2 Hz, $J_{AC'}$=

Table 1. The induced shifts in ^1H NMR signals of compound **E** observed upon the addition of $Eu(fod)_3$ (Compound **E** 7 mg/0.4 mL $CDCl_3$)

Added $Eu(fod)_3$ (mg)	Observed proton chemical shifts (δ)						
	H_5	H_6	H_{7a}	H_{7b}	H_8	H_9	OCH_3
0	4.21	3.87	2.55	2.86	5.90	6.51	3.43
6	4.32	3.93	2.66	—	5.93	6.54	3.47
14	4.58	4.08	2.88	2.94	6.00	6.61	3.56
$\Delta\delta H_i/\Delta\delta H_8$	3.7	2.1	3.3	0.8	1.0	1.0	1.3

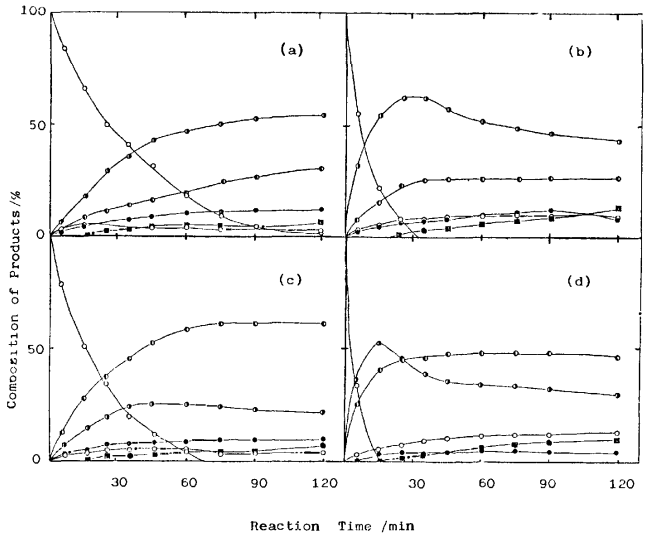

Fig. 1. Plots of the products composition *versus* irradiation time. Solvents; (a) methanol, (b) acetonitrile, (c) *t*-butyl alcohol, (d) benzene. Products; ◑ (**2a**), ◐ (**3a**), ● (**3b**), ○ (**5**), ■ (**7**).

1.5 Hz, J_{BC}=4.4 Hz, $J_{BC'}$=5.4 Hz, $J_{CC'}$=18.3 Hz). Since the proton on C-6 showed a doublet of doublets of doublets (J=9.3, 5.4, 2.2 Hz) at δ 3.87 ppm and the one on C-5, a broad doublet (J=2.2 Hz) at δ 4.21 ppm, the methoxyl and cyano groups must be attached to C-6 and C-5 respectively, or *vice versa*. The structure (**6**) was deduced from the experiment with Siever's reagent on NMR measurements. Thus, in addition to a moderate shift for the signals of H-6, there was an extraordinary lower-field shift for the H-5 and H-7a, which defined the *cis* stereochemistry of both the hydrogens to the methoxyl group (Table 1). Such an enormous shift of the signal of H-7 is expected for the **6** structure.[8] As it had been reported that **2a** gives **5** as a primary photoproduct[4] and that the cyano group rarely migrates under photolytic conditions,[9] **1b** and/or **5** can logically be recognized as a precursor of **6**. Both would then possibly be photochemically isomerized to a constrained *trans*-form. It is well known that the dipolar additions of protic solvents to constrained olefins proceed readily.[10] Compound **F** has a molecular formula, $C_{12}H_9N$ (*m/e* 167 (M^+)) and shows characteristic olefinic AX-type signals (J_{AX}=2.7 Hz) of cyclobutene in the NMR spectrum. The lack of an NMR signal due to a benzylic proton on C_{2a} defined the structure (**7**) for compound **F**.

Table 2. Relative rate constants for the photoisomerization of **1b** in several solvents[a]

Solvent	k_r	k_{2a}	k_{3a+3b}	k_{3a} (k_{exo})	k_{3b} (k_{endo})
CH_3OH	0.149	0.062	0.034	0.023	0.011
CH_3CN	0.556	0.384	0.099	0.075	0.024
t-BuOH	0.237	0.059	0.135	0.120	0.015
CH_2Cl_2	0.650	0.221	0.384	0.334	0.050
C_6H_6	1.000	0.480	0.284	0.264	0.020
C_6H_{12}	0.439	0.043	0.393	0.393	0.000
$C_6H_5CH_3$	0.654	0.384	0.169	0.159	0.010

a) Error ±0.005.

*Kinetic Studies of Photochemical Reactions of **1b** in Several Solvents.* In order to obtain further information about how the photochemical behavior of **1b** is changed by the solvents used in photolysis, we studied it comparatively in a merry-go-round apparatus in several solvents; methanol, *t*-butyl alcohol (protic polar), acetonitrile, dichloromethane (aprotic polar), and cyclohexane, benzene (aprotic nonpolar). Two runs were carried out for every solvent. With a longer period of irradiation, we obtained the product distributions shown in Fig. 1, while the results of the shorter-period irradiation are summarized in Table 2. From Fig. 1 it is obvious that the formation of **5** and **7** at the initial stage was so trivial that they were omitted from the table.

Among the solvents studied, the rate of the disappearance of **1b** (k_r) was the fastest in benzene, and the rates were almost all consistent with the first-order kinetics at the initial stage. Therefore, we related them to the decreasing rate of **1b** in benzene.

Discussion

Table 2 shows that, though there is no parallel relationship between the relative rates for the formation of **2a** and the solvent polarities, in all aprotic solvents except benzene and toluene the reaction proceeds faster as the polarities of the solvents increase, while the reaction is retarded in protic solvents.

On the other hand, it is obvious that the electrocyclic reaction to **3a** and **3b** proceeded faster as the polarity of the solvents decreased. The solvent effect observed here suggests the existence of different transition states (or energy surfaces) between the 1,7-hydrogen shift and the 4π-electrocyclic ring closure.

It is interesting to note that the ratio of k_{3b}/k_{3a} decreases gradually as the solvent polarities decrease.

This was not seen in the case of the cyclization of 5-methoxycarbonylmethyl-5*H*-benzocycloheptene, which gives an almost constant ratio of cyclization products in various solvents (*exo*:*endo*=95:5).[6]

It is well established that cycloheptatrienes exist in an equilibrium mixture of two tub conformations;[11] for example, the two conformers of 5-methoxy-6,7,8-triphenyl-5*H*-benzocycloheptene are separated by an energy barrier of 71 kJ/mol.[12] We estimated, by means of the ^1H and ^{13}C NMR spectra in dideuteriodichloromethane, that the energy barrier of the conformational flipping of the seven-membered ring of **1b** is equal to ΔG^* 40.2 kJ/mol at −73 °C and that the equilibrium between the two conformers with the cyano group in either the *quasi*-equatorial (**1c**) or the *quasi*-axial position (**1d**) is approximately equal to 81:19.[3]

The increase in the ratio of the *quasi*-equatorial form in **1b** compared with that of **1a** (52:48)[3] reflects the fact that the equilibrium is sensitive to the bulkiness of the substituents on C-5. **1c** and **1d** should interact with a polar solvent more strongly at the polar site than at any other part of the molecule. This interaction can be expected to affect the equilibrium between **1c** and **1d** by the increase in the steric repulsion between H-4 and cyano group and/or by the decrease in the solvation energy in **1d** compared with that in **1c**. The *quasi*-axial cyano group of **1d** is opened to solvation in every direction, but the *quasi*-equatorial cyano group of **1c** is blocked at the side facing a hydrogen on C-4. The solvation energy gained by **1d** must be much larger than that won by **1c**; therefore, the equilibrium between **1c** and **1d** moves toward **1d** as the polarity of the solvent increases (Scheme 2).

The photochemical reaction from its excited singlet is expected to proceed much faster than the ring inversion;[13] therefore, the ring closure of **1c** can be discriminated from that of **1d**. There are two possible disrotatory modes of 4π-electrocyclic-ring closure for the conformations. When we write the boat form in the upper concave, as is shown by **1d** in Scheme 2, one mode is a ring closure with the rotation of the bonds, from C-8 to C-9 and from C-7 to C-6, in the opposite and outer directions to give the cyclobutene, while the other is the ring closure with the rotation of the same bonds in the inner directions. In the former mode, the axial substituent in **1d** is transformed to the *endo* substituent, and the equatorial one, to the *exo* substituent. In the latter mode, the axial substituent is transformed to the *exo* substituent, and the equatorial one, to the *endo* substituent. Considering the energy relation along the reaction coordinate, it is possible that one of these cyclization modes is to be preferred to the other. Then the ring closure to either the pair of **3a** (*exo*) from **1c** and **3b** (*endo*) from **1d**, or the pair of **3a** from **1d** and **3b** from **1c**, will proceed easier than the other pair.[14] Then, if we could determine the ratio of the conformers in equilibrium, we would be able to evaluate k_{endo} using the ratio and k_{exo}. It seemed difficult, however, to estimate the conformer's ratio of **1b** by NMR at the low temperatures in the solvents used, other than dichloromethane-d_2, because of their higher melting points or of their increasing viscosities at low temperatures.

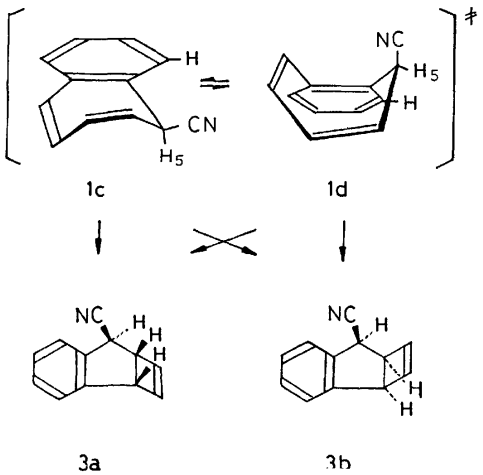

Scheme 2.

In order to clarify the conformational aspect, the NMR spectra of **1b** were measured in several solvents at room temperature. The chemical shifts of H-5 and H-9 are listed in Table 3, while the plots of $\delta H_9-\delta H_5$ *versus* k_{exo} are shown in Fig. 2. We noticed a rough trend for the less polar solvents to favor a larger separation of $\delta H_9-\delta H_5$ and a bigger k_{exo}, while the more polar ones favor less separation and a smaller k_{exo}.

Table 3. The chemical shifts of H_9 and H_5, and their differences

Solvent	δH_9	δH_5	$\delta H_9-\delta H_5$	
CD_3OD	7.33±0.2	4.34±0.2	2.99±0.4	(48.4%)[a]
CD_3CN	7.31	4.30	3.01	(46.7%)
t-BuOH	7.21	4.01	3.20	(31.1%)
CH_2Cl_2	7.14	3.79	3.35	(19.0%)
C_6H_6	6.82	3.37	3.45	(10.7%)
C_6H_{12}	7.13	3.65	3.48	(7.9%)

a) The estimated percentages of **1d** are shown in parentheses..

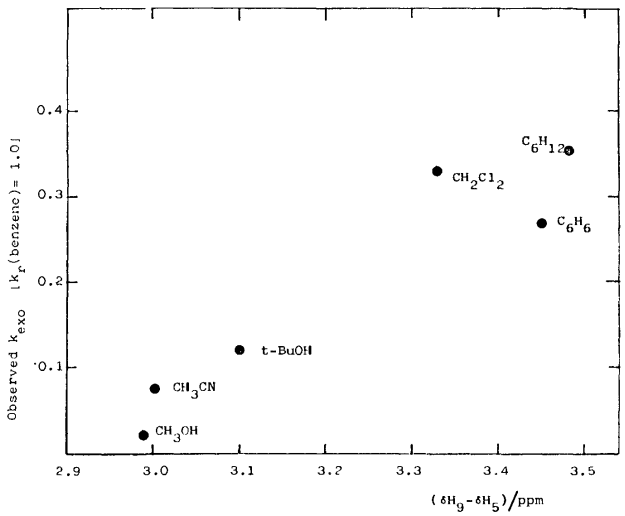

Fig. 2. Plots of the observed k_{exo} against uncorrected $\delta_{H_9}-\delta_{H_5}$.

TABLE 4. THE PERCENTAGES OF **1d** IN THE EQUILIBRIA FOR SEVERAL SOLVENTS, AND THE POLARITY PARAMETERS OF THE SOLVENTS

Solvent	Method I[a] (%)	Method II[a] (%)	$(J_{H_5-H_6})$ Hz	Mean value %	E_{T30} kJ mol^{-1}
CH_3OH[b]	48.4±5	46.5±5	(6.74±0.2)	47.5	232
CH_3CN	46.7	48.5	(6.79)	47.6	192
t-BuOH	31.1	26.0	(6.25)	28.6	184
CH_2Cl_2	19.0	26.0	(6.25)	22.5	172
C_6H_6	10.7	15.0	(5.99)	12.9	144
C_6H_{12}	7.9	7.0	(5.79)	7.5	142

a) Methods I and II are referred to the estimation methods, *i.e.*, the use of the chemical shifts (Method I) and the coupling constants, $J_{H_5-H_6}$ (Method II). b) The full deuterated solvents were used for NMR measurements.

Günther *et al.* reported the determination by means of ^{13}C NMR spectroscopy, of the ratio of the *quasi*-equatorial to the *quasi*-axial conformer of 7-cyano-1,3,5-cycloheptatriene in equilibrium as 79:21. Here, the chemical shifts of C-3 (or C-4) in the two conformers are identical with each other in the temperature range from −2.5 to −123 °C.[11] If we use the chemical shift of H-9, which is far from the cyano group, as the standard, the $\delta H_9 - \delta H_5$ becomes a chemical shift of H-5 from this standard, which has already been cancelled in the same magnitude as the solvent effect influencing H-9. As has been mentioned above, this chemical shift of H-5 is equal to a weight average of the chemical shifts of H-5 existing in **1c** and **1d**.[15] In order to check the propriety of this method, the difference in the chemical shifts between aromatic and benzylic protons of benzyl cyanide were examined and found to show satisfactory similarities (±0.1 ppm), except in benzene (+0.58 ppm).

When the chemical shifts at δ 3.56 (H-5 for **1c**) and δ 4.78 ppm (H-5 for **1d**) observed at a low temperature in CD_2Cl_2 are in effect as the standard at room temperature in CH_2Cl_2, the percentage of **1d** in the equilibrium in several solvents can be roughly estimated as is shown in Table 3 (Method I).

Another approach[16] to determine the equilibrium has been done by taking advantage of the difference in the spin-spin coupling constants of C-5 protons between **1c** (equatorial-CN) and **1d** (axial-CN). From the low-temperature NMR spectrum of **1b** in CD_2Cl_2, the signals due to equatorial H-5 (**1d**) (lower field) and to axial H-5 (**1c**) (higher field) are seen as broad doublets. Applying the computer program for the resolution of the overlapping peak into their components (Gaussian function) to those bands,[17] we obtained the coupling constants; $J_{endo-5,6}=5.63\pm0.2$, $J_{exo-5,6}=8.02\pm0.2$ Hz for **1b**.[18] From the NMR spectra of **1b** in several solvents, we get the weight-averaged coupling constants for the equatorial and for the axial H-5 of **1b**. We can then calculate the percentages of **1c** in **1b** from the coupling constants in several solvents (Table 4, Method II). The percentages thus obtained were parallel with those obtained from the chemical shifts; we used the mathematical mean values for the following calculations. The plots of the percentages of **1d** in **1b** *versus* the solvent polarity parameters, E_T,[19] in various solvents are shown in Fig. 3. A linear correlation was observed for every

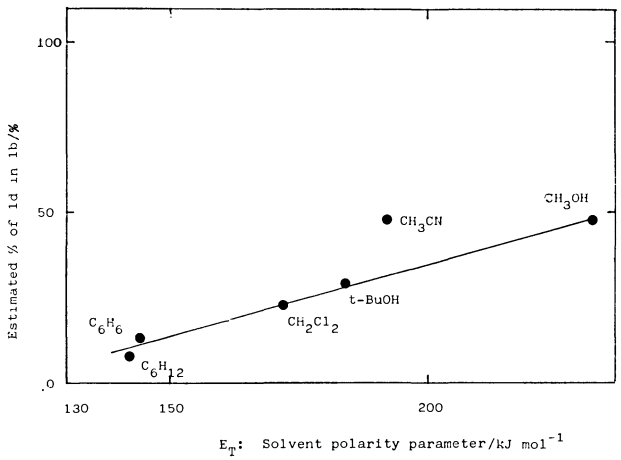

Fig. 3. Plots of the estimated percentage of **1d** against solvent polarity.

solvent excep acetonitrile, in which the cyano group of **1b** may have a strong affinity to the same group of the solvent.

As the conformers' ratios are obtained based on NMR data in CD_2Cl_2 at low temperatures, we used the kinetic data in dichloromethane as a standard. When the observed values of k_{exo} are divided by each respective molar fraction of **1c** in the same solvent, we obtain the values of k°_{exo}; the values of k_{exo} from pure **1c**. Similarly, if the observed value of k_{endo} (CH_2Cl_2) is divided by the molar fraction of **1d** in dichloromethane, we obtain the value of k°_{endo} (CH_2Cl_2): the value of k_{endo} from pure **1d** in dichloromethane. If we assume that the ratios of the reaction rate, $k^\circ_{endo}/k^\circ_{exo}$, were constant in every solvent, we can calculate the values of k°_{endo} for every solvent using the values of k°_{exo} and the ratio in CH_2Cl_2 (0.515). Further, we will be able to evaluate k_{endo} (calcd) in a solvent by the use of the k°_{endo} (calcd) and the molar fraction of **1d** in the same solvent. The calculated values of k_{endo} (calcd), listed in Table 5, are in satisfactory agreement with the observed values of k_{endo}. Therefore, it seems reasonable that the photochemical progenitors of **3a** (*exo*) and **3b** (*endo*) are **1c** and **1d** respectively. In other words, the interrelation between the estimated conformer ratio of the starting material in the equilibrium and the experimental product-ratio supports the allowed disrotatory ring closure with rotation at the conjugated double

Table 5. Comparison of the observed and the calculated parameters

Solvent	k_{exo}	k_{endo}	k°_{exo}	k°_{endo}	k_{endo} (Calcd)
CH_3OH	0.023	0.011	0.044	0.023	0.011
CH_3CN	0.075	0.024	0.143	0.074	0.035
t-BuOH	0.120	0.015	0.168	0.087	0.025
CH_2Cl_2	0.334	0.050	0.431	0.222	0.050
C_6H_6	0.264	0.020	0.303	0.156	0.020
C_6H_{12}	0.393	0.000	0.425	0.219	0.016

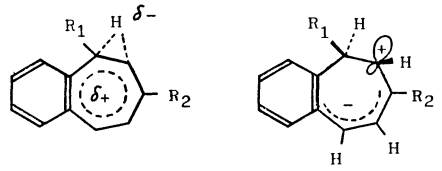

8a R_1 = CN, R_2 = H
b R_1 = H, R_2 = CN

9

Scheme 3.

bond in a 7-membered-ring tub conformation to the outer direction. This process corresponds to the pathway with the least torsional energy around the $C_5(sp^3)$–$C_6(sp^2)$ bond.

A clear solvent effect on the *anti-syn* ratio in the formation of the [2+2] adducts was seen in the case of the photochemical dimerization of 2-cyclopentenone.[20] The photochemical reactions which proceed under the control of the ground-state geometries have previously been observed in the ring opening of 1,3-cyclohexadiene derivatives;[21] the present case is the first example of such a reaction for a seven-membered ring analogue.

As has been mentioned above, rather complicated solvent effects on the formation of **2a** can not be understood from the control of the ground-state geometries of the starting material. It is possible to assume that the electronic polarization of **1b** to **8a** or **9** may have played a role in the transition state. The former (**8b**) was suggested by Swenton and his co-workers to explain the solvent effect on the same rearrangement of 7-substituted 5*H*-benzocycloheptenes,[1] and a similar polarization to the latter was proposed by Tezuka and Houk to clarify the substituent effects on the cyclization and 1,7-sigmatropic hydrogen shift of substituted cycloheptatrienes.[22] Interaction with protic solvents can be expected to retard the reaction, and enhancement of the charge separation by aprotic polar and benzenoid solvents may accelerate the reaction.[23]

Thus, we found that the photochemical isomerization of **1b** under direct irradiation was quite different from that of 5-methoxycarbonyl-5*H*-benzocycloheptene, which gave **4** exclusively.[3]

Experimental

General Procedure. The UV, IR, ^1H NMR, ^{13}C NMR, and mass spectra were recorded according to the methods given in the previous paper. A Varian Aerograph, model 90P, was used for the preparative VPC (Helium flow rate; 30—40 mL/min), while a Shimadzu Gas Chromatograph GC-4BM was used for the analytical purposes (Hydrogen flame detector). The columns used for separation were ϕ3.2 mm × 1.8 m columns charged with: A, 3% Silicone OV-17; B, Silicone SE-30, on Chromosorb WAW.

For irradiation of a volume of more than 100 mL, a solution charged in a vessel fitted with a quartz cooling jacket was purged with dry nitrogen for five min and then internally irradiated with an Ushio high-pressure mercury arc (UM-452) through a Pyrex filter. For small-scale irradiation (less than 15 mL), unless otherwise described, a solution charged in a drum-shaped Pyrex vessel with a ground glass joint fitted with a three-way cock was purged with dry nitrogen for five min and then dipped in ice water in a quartz-made Dewar bottle with a flat quartz window. The solution was then irradiated externally with an Ushio lamp (USH-500D) through a Toshiba filter (UV-31).

Synthesis of ***1b****.* Benzotropylium tetrafluoroborate, which had been derived from 2,3-benzotropone (3.24 g, 20.7 mmol),[2] in anhydrous acetonitrile (18 mL), was added, drop by drop, to sodium cyanide (910 mg, 18.6 mmol) in acetonitrile (12 mL) at 0 °C under a nitrogen atmosphere, and then the mixture was stirred for 30 min at room temperature. The mixture was filtered through Hyfrosupercel (a filter aid), and the filtrate was concentrated under reduced pressure. The residue taken up in ether (100 mL), washed successively with water and saturated brine, and dried. After the evaporation of the ether, the remaining oily products (2.88 g, 81%) were separated by column chromatography (silica gel 90 g/benzene), followed by preparative TLC with a multiple-developing technique (10% ether–hexane) to give **1b** (1.41 g, 8.43 mmol; 41%) and a mixture of 7-cyano-7*H*- and 7-cyano-5*H*-benzocycloheptene (*ca.* 95:5, 0.81 g, 4.84 mmol; 23%). The latter mixture was converted quantitatively into 7-cyano-5*H*-benzocycloheptene by passing it through a column of basic alumina (Merk; activity I/benzene). **1b** IR (liq film) ν_{max}: 3030, 2260, 1589, 1493, 893, 822 cm^{-1}. UV (95% C_2H_5OH) λ_{max} (log ε): 274.5 (3.89) nm. NMR (CCl_4) δ=3.76 (1H, dd, J=6.0, 1.3 Hz), 5.75 (1H, dd, J=9.5, 6.0 Hz), 6.19 (1H, ddd, J=9.5, 5.3, 1.3 Hz), 6.55 (1H, dd, J=11.8, 5.3 Hz), 7.20 (1H, d, J=11.8 Hz), 7.2—7.7 (4H, m). ^{13}C NMR ($CDCl_3$) δ=35.6, 119.1, 123.1, 125.3, 127.3, 128.0, 128.7, 129.9, 130.7, 134.3, 134.6 ppm. Found: C, 86.00; H, 5.41; N, 8.43%. Calcd for $C_{12}H_9N$: C, 86.20; H, 5.43; N, 8.38%. *7-Cyano-7*H*-benzocycloheptene.* IR (liq film) ν_{max}: 3040, 2260, 1638, 1492, 1445, 800, 770, 712 cm^{-1}. UV (95% C_2H_5OH) λ_{max}: 227 nm. NMR (CCl_4) δ=3.25 (1H, tt, J=6.0, 1.0 Hz), 5.76 (2H, dd, J=10.0, 6.0 Hz), 6.64 (2H, dd, J=10.0, 1.0 Hz), 7.25 (4H, s).

Photolysis of ***1b*** *in Methanol.* A solution of **1b** (171 mg, 0.99 mmol), dissolved in methanol (130 mL), was irradiated with a HPL through a Pyrex filter under a nitrogen atmosphere for 1 h. The usual work-up gave a mixture, which was then separated using preparative thin-layer chromatography with a multiple-development technique to give **1b** (28 mg, 16%), a mixture (2:1) of **3a** and **3b** (47 mg, 27%), and **6** (10 mg, 5%), in addition to a mixture of **2a**, **5**, and **7** (78 mg, 33, 5, 6%, respectively). The latter was further separated by preparative VPC (column B, 145 °C: retention time; **7**, 4.4 min; **2a**, 7.0 min; **5**, 8.4 min). The spectroscopic data of **2a** and **5** were identical with those of the authentic sample reported by Swenton.[4] **3a** NMR ($CDCl_3$) δ=3.9 (1H, m), 4.0 (1H, m), 4.49 (1H, bd), 6.15 (1H, dd, J=2.7, 0.7 Hz), 6.42 (1H, dd, J=2.7, 0.7 Hz), 7.25—7.46 (4H, m). **3b** NMR ($CDCl_3$) δ=3.8 (1H, m), 4.0 (1H, m), 4.32 (1H, d, J=3.0 Hz), 6.28 (1H, d, J=2.7

TABLE 6. THE RELATIVE CONCENTRATIONS OF THE STARTING **1b** AND PRODUCTS AS ESTIMATED BY GLC DURING IRRADIATION[a)]

a) The relative recovery yields of **1b**.[b)]

Time min	Solvent					
	CH_3OH	CH_3CN	*t*-BuOH	CH_2Cl_2	C_6H_6	C_6H_{12}
2	—	86.8	—	81.8	80.0	89.9
4	—	77.5	—	72.3	61.3	82.9
5	93.2	74.6	89.2	—	54.5	—
6	—	70.7	—	62.5	51.1	76.9
9	—	60.6	—	56.7	39.2	66.3
12	—	50.4	—	46.1	33.5	57.8
15	70.8	41.4	57.5	37.3	31.9	47.5

b) The relative yields of **2a**.[b)]

Time min	Solvent					
	CH_3OH	CH_3CN	*t*-BuOH	CH_2Cl_2	C_6H_6	C_6H_{12}
2	—	10.5	—	5.1	12.0	1.0
4	—	16.0	—	10.3	23.1	1.6
5	3.8	17.8	4.3	—	21.6	—
6	—	18.4	—	14.0	29.2	3.0
9	—	25.4	—	14.2	32.5	5.1
12	—	32.5	—	15.6	35.4	5.0
15	9.8	37.5	7.5	15.0	30.2	6.6

c) The relative yields of **3a** and **3b**.[b)]

Time min	Solvent					
	CH_3OH	CH_3CN	*t*-BuOH	CH_2Cl_2	C_6H_6	C_6H_{12}
2	—	1.9	—	8.6	6.5	9.0
	(—)[c)]	(0.0)	(—)	(12.8)	(7.7)	(0.0)
4	—	3.85	—	17.4	12.7	15.5
	(—)	(22.0)	(—)	(16.7)	(7.9)	(0.0)
5	2.04	5.7	7.6	—	14.3	—
	(24.5)	(26.3)	(14.5)	(—)	(7.7)	(—)
6	—	7.3	—	23.5	18.3	23.1
	(—)	(26.0)	(—)	(13.6)	(9.3)	(0.0)
9	—	11.3	—	32.1	24.3	28.6
	(—)	(25.7)	(—)	(12.5)	(8.2)	(0.0)
12	—	14.2	—	38.4	28.3	38.8
	(—)	(34.5)	(—)	(15.4)	(7.1)	(0.0)
15	6.7	17.0	17.8	50.7	23.9	45.9
	(34.3)	(28.2)	(14.6)	(13.2)	(8.4)	(0.0)

a) All data are calibrated with the data obtained concurrently in benzene. b) All irradiations were carried out in the same concentration (1.0 mmol dm^{-3}) of **1b**. The initial concentrations of **1b** are expressed as 100. c) The contents (%) of **3b** are shown in parentheses.

Hz), 6.52 (1H, d, J=2.7 Hz), 7.2—7.4 (4H, m). A mixture of **3a** and **3b** UV (95% C_2H_5OH) λ_{max}: 250.5, 266, 273 nm. Mass *m/e* (%): 167 (100, M^+), 166 (70), 141 (71), 140 (47). Found: C, 86.15; H, 5.43; N, 8.25%. Calcd for $C_{12}H_9N$: C, 86.20; H, 5.45; N, 8.38%. **6** UV (95% C_2H_5OH) λ_{max} (log ε): 252 (4.14). IR ($CHCl_3$) ν_{max}: 3010, 2930, 2830, 2260, 1100 cm^{-1}. NMR ($CDCl_3$) δ=2.55 (1H, dddd, J= 18.3, 9.3, 4.4, 2.2 Hz), 2.86 (1H, dtd, J=18.3, 5.4, 1.5 Hz), 3.43 (3H, s), 3.87 (1H, ddd, J=9.3, 5.4, 2.2 Hz), 4.21 (1H, d, J=2.2 Hz), 5.90 (1H, ddd, J=12.2, 5.4, 4.4 Hz), 6.51 (1H, ddd, J=12.2, 2.2, 1.5 Hz), 7.2—7.48 (4H, m). Mass *m/e* (%): 199 (76.2, M^+), 184 (14.4), 168 (100), 167 (74.4), 159 (15.8), 141 (39.0), 129 (39.6). Found: C, 78.24; H, 6.54; N, 6.86%. Calcd for $C_{13}H_{13}NO$: C, 78.36; H, 6.58; N, 7.03%. **7** mp 41.5—42.5 °C. UV (95% C_2H_5OH) λ_{max}: 261.5, 267.5, 274 nm. IR (liq film) ν_{max}: 3050, 2920, 2840, 2250, 1483, 1270, 987, 778, 755 cm^{-1}. NMR (CCl_4) δ=3.0 (2H, m), 3.95 (1H, dd, J=10.0, 2.7 Hz), 6.25 (1H, dd, J=2.7, 1.0 Hz), 6.42 (1H, d, J=2.7 Hz), 7.0—7.5 (4H, m). Mass *m/e* (%): 168 (12.7), 167 (100, M^+), 166 (94), 141 (36.4), 140 (40.4), 139 (19.2).

Identification of the Mixture of 3a and 3b. Into a solution of a mixture of **3a** and **3b** (2:1, 31 mg, 0.19 mmol), dissolved in anhydrous ether (1 mL) and methanol (1 mL), we passed dry hydrogen chloride at 0 °C for 2.5 h. After stirring further for 1 h at room temperature, water (5 mL) was added slowly to the solution under cooling. After sweeping off the hydrogen chloride by passing nitrogen into the solution, the solution was filtered and the filtrate concentrated to a small volume. The residue was extracted

with ether, and the ethereal extracts were washed successively with water and saturated brine, and then dried. The ether was evaporated, and the remaining crude product (30 mg) was purified by preparative TLC (10% ether–hexane) to give **3c** (20 mg, 53%) and **3d** (10 mg, 26%). The spectral data were identical with those of authentic samples of **3c** and **3d** described previously.[6] As a result, the structures of compounds **B** and **C** were established as **3a** and **3b** respectively.

*Photolysis of **1b** in Benzene.* A solution of **1b** (51 mg, 0.3 mmol), dissolved in benzene (11 mL), was irradiated externally for 4.8 h. The resulting solution was concentrated, and the residue (50 mg) was separated by preparative TLC (10% ether–hexane) to give **2a** (17.4 mg, 34%) and **3a** (11 mg, 21.5%). **3a** IR (liq film) ν_{max}: 3045, 2250, 1484, 1279, 830, 770, 740 cm^{-1}.

*Photolysis of a Mixture of **3a** and **3b** in Benzene.* A solution of a mixture (5 mg, 2:1) of **3a** and **3b** in benzene (11 mL) was irradiated externally for 2.5 h. The solution was then concentrated, and the residue (4.8 mg) was examined in terms of its NMR spectrum, which was found to be identical with that of the starting mixture.

*Photolysis of **3a** in Methanol.* A solution of **3a** (11 mg, 0.06 mmol), dissolved in methanol (11 mL), was irradiated externally for 3 h under ice cooling. After the evaporation of the solvent, the isolated material (8.4 mg) was examined in terms of its NMR spectrum. The spectrum revealed that it consists solely of **3a**.

*Kinetic Measurement of Photochemical Reaction of **1b**.* *Solvents*: The solvents used for photolysis were as follows. Methanol: The UV spectrum of a special-grade one was checked to confirm it to be transparent above 205 nm and was used without purification. Cyclohexane: A spectrophotometric grade of Merk's cyclohexane was used directly. Acetonitrile: A first-grade specimen was distilled over phosphoric pentoxide, then let stand over anhydrous potassium carbonate for more than one day, and distilled before use. Dichloromethane: A first-grade specimen was distilled over phosphoric pentoxide before use. Benzene: A first-grade substance was washed successively with concentrated sulfuric acid and water. This was dried over anhydrous calcium chloride and then distilled. After being dried over sodium wire, it was distilled before use. *t*-Butyl alcohol: A first-grade specimen was distilled over sodium before use.

Measurement: Each 1.0 mmol/dm^3 solution of **1b** was prepared in an appropriate solvent containing 0.10 mmol/dm^3 of hexadecane as an internal standard. Each test tube (ϕ1.5 cm × 16 cm) with a ground-glass male joint at the top was fitted with a cap made of female joint of the same size connected to a two-way cock and was then used for photolysis. Five of the tubes containing the same solution (5 mL) and two containing the benzene solution (5 mL) were arranged cylindrically in a circle (ϕ16.5 cm for short-period irradiation and ϕ11.5 cm for longer-period irradiation) at the same distance from the light source placed at the center (merry-go-round apparatus).[24] Before irradiation, purified nitrogen was passed through every solution for five minutes and the cocks were shut off. The photolysis was carried out with a high-pressure mercury lamp (UM-452) mounted in a quartz cooling jacket through a Pyrex filter under cooling (ice water; care must be taken not to keep the samples too cold; otherwise, they freeze). During irradiation, a test tube was taken out every definite number of minutes (see the text), and each 10 μL of the solution was examined by VPC (Column A, 130 °C; nitrogen-flow rate, 40 mL/min: retention time; hexadecane, 1.6 min; **7**, 3.2 min; **3a**, 3.6 min; **3b**, 4.15 min; **1b**, 4.8 min; **2a**, 5.0 min; **5**, 7.25 min). The product ratios were obtained by comparing the integrated curve areas as estimated using this equation: S=the height times the half-width of the curve. In some runs, uniform paper was cut into the curved areas, and their weights were compared. Both methods gave satisfactorily similar results within a 3% margin of error. The calibration curves for the pure samples, **1b**, **2a**, and **3a**, as separated by preparative VPC, was obtained similarly, and a linear relationship between the sample amounts and the integrated areas of the peaks was obtained. The ratio of the VPC intensities for **1b**, **2a**, and **3a** for samples of the same amount was 100:91:109 (including a 5% margin of error). As we could not obtain **3b** in the pure state, we assumed the intensity in VPC was the same as that of **3a**. The other materials in the product were not calibrated to their standards, but their VPC areas were directly compared with that of **1b**. Each datum was recalculated against that of the standard (hexadecane) as unity, and the two values were compared with each other. Two runs were carried out, one for a longer period of irradiation (up to 2 h) and the other for a shorter period of irradiation (up to 15 min). The results are summerized in Fig. 1 (longer-period irradiation) and Tables 2 and 6 (shorter-period irradiation).

This paper is dedicated to Emeritus Professor Takeo Sakan on the occasion of his 70th birthday. The authors wish to thank Dr. Yoshimasa Fukazawa of Tohoku University for valuable discussion and Mr. Jun-ichi Goda of our University for the elementary analysis.

References

1) J. S. Swenton, K. A. Burdett, D. M. Madigan, and P. D. Rosso, *J. Org. Chem.*, **40**, 1280 (1975).
2) M. Kato, M. Funakura, M. Tsuji, and T. Miwa, *J. Chem. Soc., Chem. Commun.*, **1976**, 63.
3) M. Kato, K. Takatoku, S. Ito, and T. Miwa, *Tetrahedron Lett.*, **1979**, 867.
4) J. S. Swenton, K. A. Burdett, D. M. Madigan, T. Johnson, and P. D. Rosso, *J. Am. Chem. Soc.*, **97**, 3428 (1975).
5) M. Kato, M. Kawamura, Y. Okamoto, and T. Miwa, *Tetrahedron Lett.*, **1972**, 1171.
6) M. Kato, H. Kobayashi, H. Yamamoto, K. Seto, S. Ito, and T. Miwa, *Bull. Chem. Soc. Jpn.*, **55**, 3523 (1982).
7) D. H. S. Horn and W. S. Rapson, *J. Chem. Soc.*, **1949**, 2421.
8) O. Hoffer, "The Lanthanide-induced Shift Technique: Application in Conformational Analysis," in "Topics in Stereochemistry," ed by N. L. Allinger and E. L. Eliel, John Wiley and Sons, New York (1976), Vol. 9, p. 140.
9) H. E. Zimmerman, D. Armesto, M. G. Amezna, T. P. Gannett, and R. P. Johnson, *J. Am. Chem. Soc.*, **101**, 6367 (1980); I. Saito, K. Shimozono, S. Miyazaki, and T. Matsuura, *Tetrahedron Lett.*, **21**, 2317 (1980); I. Saito, K. Shimozono, and T. Matsuura, *J. Am. Chem. Soc.*, **102**, 3948 (1980); In an independent experiment, we observed that the irradiation of **2a** (33 mg, 0.20 mmol) in methanol (130 mL) under the same conditions gave a mixture of **3a** and **3b** (2:1, 5 mg, 15%), **6** (5 mg, 13%), and **7** (5 mg, 15%). Swenton reported that **2a** rearranged to **5**.[4]
10) E. Dunkelblum and H. Hart, *J. Am. Chem. Soc.*, **99**, 644 (1977); Y. Inoue, T. Ueoka, T. Kuroda, and T. Hakushi, *J. Chem. Soc., Chem. Commun.*, **1981**, 1031.
11) R. Wehner and H. Günther, *J. Am. Chem. Soc.*, **97**, 923 (1975); J. M. Schulman, R. L. Disch, and M. L. Sabio,

ibid., **104**, 3785 (1982); H. Dürr and G. Scheppers, *Ann. Chem.*, **734**, 141 (1970).

12) W. Tochtermann, G. Schnabel, and A. Mannschreck, *Ann. Chem.*, **711**, 88 (1968).

13) F. D. Lewis, R. W. Johnson, and D. E. Johnson, *J. Am. Chem. Soc.*, **96**, 6090 (1974).

14) Because the values of k_{endo} were negligible compared to the values of k_{exo} in aprotic solvents, we considered only one pair of disrotatory cyclization: **1c**→**3a** and **1d**→**3b**.

15) The determination of an equilibrium ratio between two conformers using ^{1}H NMR chemical shifts was reported in the following article: J. C. Hardy and W. D. Cumming, *J. Am. Chem. Soc.*, **93**, 928 (1971).

16) K. W. Baldry, M. H. Goldon, R. Hafner, and M. J. T. Robinson, *Tetrahedron*, **32**, 2589 (1976); H. Özbal and W. W. Zajac, Jr., *Tetrahedron Lett.*, **1979**, 4821; N. S. Zefirov and I. V. Baranenkov, *ibid.*, **1979**, 4875.

17) G. Beech, "Fortran IV in Chemistry," John Wiley and Sons, New York (1975), p. 127.

18) The coupling constants between vicinal olefinic and aliphatic protons in 1,3,5-cycloheptatriene have been given as 4.0±0.3 Hz for J_{endo-H_7,H_1} and 7.2±0.3 Hz for J_{exo-H_7,H_1}: F. R. Jensen and L. A. Smith, *J. Am. Chem. Soc.*, **86**, 956 (1964): see also K. Takeuchi, T. Kitagawa, Y. Senzaki, and K. Okamoto, *Chem. Lett.*, **1983**, 73.

19) K. Dimroth, C. Reichart, T. Siepmann, and F. Bohlmann, *Ann. Chem.*, **661**, 1 (1963).

20) G. Mark, F. Mark, and O. E. Polansky, *Ann. Chem.*, **719**, 151 (1968).

21) J. E. Baldwin and S. M. Krueger, *J. Am. Chem. Soc.*, **91**, 6444 (1969); W. G. Dauben, E. L. McInnis, and D. M. Michno, "Photochemical Rearrangements in Trienes," in "Rearrangements in Ground and Excited States," ed by P. de Mayo, Academic Press, New York (1980), Vol. 3, p. 101; W. G. Dauben and M. S. Kellog, *J. Am. Chem. Soc.*, **102**, 4456 (1980).

22) T. Tezuka, O. Kikuchi, K. N. Houk, M. N. Paddon-Row, C. M. Santiago, N. G. Rondan, J. C. Williams, Jr., and R. W. Gandour, *J. Am. Chem. Soc.*, **103**, 1367 (1981).

23) The abnormality of the dipolemoment for vicinal dihalogenides was observed in a benzene solution and compared with those observed in other nonaromatic solvents. In general, polar solvents favor the polar conformer(s), while nonpolar solvents favor the less polar conformer(s): C. Romers, C. Altona, H. R. Buys, and H. Havinga, "Advances in Stereochemistry," ed by E. Eliel and N. L. Allinger, Wiley-Interscience, New York, (1969), Vol. 4, p. 39.

24) M. Kato, M. Tsuji, and T. Miwa, *Bull. Chem. Soc. Jpn.*, **51**, 1450 (1978).

 © 1983 The Chemical Society of Japan Bull. Chem. Soc. Jpn., 56, 3457—3463 (1983)

The Reaction of Nitrile Oxides with Alkyl- and Alkyl-halo-substituted *p*-Benzoquinones

Shinsaku SHIRAISHI,* B. Shivarama HOLLA,† and Kiyoshi IMAMURA

Institute of Industrial Science, The University of Tokyo, Roppongi, Minato-ku, Tokyo 106

(Received December 14, 1982)

Various aromatic nitrile *N*-oxides, sterically stabilized and unstabilized ones, were allowed to react with several alkyl- and alkyl-halo-substituted *p*-benzoquinones with a view to studying the influence of quinone substituents on the mode of the addition reaction. Mono-, di-, and tri-substituted quinones with such substituents gave isoxazoline derivatives formed through addition of nitrile oxides to the C=C bond of the quinones. 2-Chloro-5- and -6-methyl-*p*-benzoquinones gave two kinds of C=C adducts, one formed through the addition to the C=C of methyl-substituted side and the other to that of chlorine-substituted side, and the latter adducts were not isolable due to the prompt dehydrochlorination forming the fully-conjugated isoxazoloquinones and subsequent C=O addition of another nitrile *N*-oxide forming spirodioxazole derivatives.

Nitrile *N*-oxide, a typical 1,3-dipole, reacts with various unsaturated compounds to give heterocycles.[1] The reactions of nitrile *N*-oxides with substituted *p*-benzoquinones, which have two kinds of potential reactive sites, *i.e.* C=C and C=O bonds, have been studied and reported in the previous papers.[2,3] All the tetrasubstituted quinones gave dioxazole derivatives through addition at the carbonyl site(s), while the disubstituted quinones gave dioxazole or isoxazoline derivatives depending on the substituents and substitution pattern. With a view to studying the influence of substituents on the mode of the addition of nitrile *N*-oxides to quinones, reactions of several alkyl- and alkyl-halo-substituted quinones with nitrile *N*-oxides have been investigated and the result is reported in this paper.

Results and Discussion

Several aromatic nitrile *N*-oxides (**1**) were allowed to react with various kinds of alkyl- and alkyl-halo-substituted *p*-benzoquinones (**2**). Three sterically stabilized nitrile *N*-oxides, *viz.*, 2,4,6-trimethylbenzonitrile *N*-oxide (MNO), 2,3,5,6-tetramethylbenzonitrile *N*-oxide (DNO), and 2,6-dichlorobenzonitrile *N*-oxide (CNO) were chosen for the reaction with quinones. The reactions were conducted in benzene using equimolar reactants at room temperature. The progress of the reaction was followed by thin layer chromatography (TLC) on silica gel plates. In most cases, isoxazoline derivatives were obtained as the main products in rather good yields. The result is summarized in Tables 1—3. The structure of the products were determined by IR, ^{1}H NMR, and mass spectra and elemental analyses. The isoxazoline derivatives formed have the structure as shown in Scheme 1. Trisubstituted olefinic double bond was the exclusive or at least the main reaction site to undergo the C=C addition forming the C–O bond between the oxygen atom of the nitrile oxide and the carbon atom bearing a substituent of the quinone moiety even in the reaction of methyl-*p*-benzoquinone, where the adduct **3a** (see Table 1) was the main product. This indicates that steric factors are less important for the site-selectivity of the addition reaction than electronic factors, though that is the governing factor in the reaction with 2-*t*-butyl-6-methyl-*p*-benzoquinone where the addition occurs selectively at the C=C bond of the methyl-substituted side. In the reaction of CNO with 2-*t*-butyl-5-methyl-*p*-benzoquinone, however, addition occurred at both sides to give a 2:1-mixture of the adduct on the less hindered side (**3d**) and that on the other side (**3m**). In the reaction of CNO with 2-isopropyl-5-methyl-*p*-benzoquinone, the formation ratio of the two isomers was determined to be 3:2 from the ^{1}H NMR spectrum of the crude reaction product, though the separation was not conducted.

The IR spectra of the most adducts showed either a broad or a split carbonyl absorption around 1670—1690 cm^{-1}. The IR spectra of some of the adducts from chlorine-substituted quinones, however, showed two distinct carbonyl absorptions around 1680 and 1700 cm^{-1}. The ^{1}H NMR spectrum of the product **3e** from 2,6-dimethyl-*p*-benzoquinone (26DMQ) and CNO shows three singlets at δ 7.32, 2.16, and 1.73, each integrating to three protons. The signals at δ 1.73 and 2.16 are assigned to the angular and olefinic methyl groups on the quinone moiety respectively, and the singlet at δ 7.32 is due to the three aromatic protons. The olefinic proton and the angular methine proton

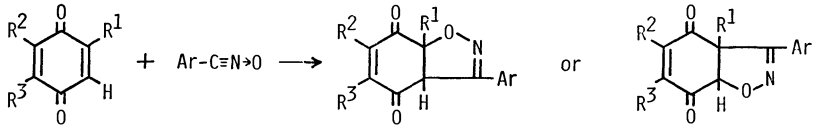

2 **1** **3 - 5**

Scheme 1.

† JSPS Visiting Research Fellow on leave from University of Mysore. Present address: Mangalore University, Mangalore 574152, D.K., India.

Table 1. Characterization data of the isoxazoline derivatives (**3a—p**) from 2,6-dichlorobenzonitrile *N*-oxide (CNO)

Compd No.	R^1	R^2	R^3	React. time d	Yield %	Mp θ_m/°C	IR $\nu_{C=O}$/cm^{-1}	Found (Calcd) (%) C	H	N
3a	Me	H	H	7	51[a]	175—177	1680	54.41 (54.22	2.87 2.92	4.90 4.52)
3b	Me	H	Me	5	77	150—152	1670	55.79 (55.58	3.41 3.42	4.63 4.32)
3c	Me	H	Cl	7	35[b]	155—160	1680	48.57 (48.80	2.19 2.34	4.25 4.06)
3d	Me	H	*t*-Bu	10	—[c]	148—151	1670	59.01 (59.03	4.82 4.68	3.65 3.82)
3e	Me	Me	H	5	86	156—158	1680	55.77 (55.58	3.53 3.42	4.13 4.32)
3f	Me	Me	Me	5	89	152—154	1670	56.80 (56.82	3.79 3.87	4.08 4.14)
3g	Me	Me	Cl	3	89	168—171	1680	50.02 (50.24	2.80 2.81	3.96 3.91)
3h	Me	Cl	H	5	46[b]	158—160	1670, 1710	49.11 (48.80	2.09 2.34	3.93 4.06)
3i	Me	Cl	Me	5	81	136—138	1670, 1700	50.32 (50.24	2.70 2.81	3.44 3.91)
3j	Me	*t*-Bu	H	5	90	151—154	1660, 1695	58.99 (59.03	4.56 4.68	3.81 3.82)
3k	Me	benzo		5	82	154—155	1680	60.15 (60.02	3.04 3.08	4.00 3.89)
3l	*i*-Pr	*i*-Pr	H	5	86	161—164	1670, 1680	60.12 (60.01	5.22 5.04	3.64 3.68)
3m	*t*-Bu	H	Me	10	—[c]	162—165	1670	59.06 (59.03	4.82 4.68	3.85 3.82)
3n	*t*-Bu	H	*t*-Bu	7	81	151—154	1670	61.89 (61.77	5.36 5.68	3.14 3.43)
3p	*t*-Bu	*t*-Bu	H	3	90	165—168	1680	61.54 (61.77	5.68 5.68	3.60 3.43)

a) A dimer of the nitrile *N*-oxide (11%, mp 200—202 °C) and an appreciable amount of unidentified product were also obtained. b) A few other products were observed but isolation of them was not successful. Addition of CNO to the C=C bond of the chlorine-substituted side and subsequent reactions are conceivable (see the text). c) The products **3d** and **3m** were obtained in the same reaction in a 2:1-ratio in a total yield of 90% (see Experimental section).

Table 2. Characterization data of the isoxazoline derivatives (**4a—f**) from 2,4,6-trimethylbenzonitrile *N*-oxide (MNO)

Compd No.	R^1	R^2	R^3	React. time d	Yield %	Mp θ_m/°C	IR $\nu_{C=O}$/cm^{-1}	Found (Calcd) (%) C	H	N
4a	Me	Me	Me	7	74	119—122	1660	73.38 (73.29	6.91 6.80	4.52 4.50)
4b	Me	Me	Cl	7	79	141—145	1680	65.46 (65.16	5.37 5.47	4.39 4.22)
4c	Me	*t*-Bu	H	7	82	179—181	1670	74.27 (74.31	7.60 7.42	4.11 4.13)
4d	*i*-Pr	*i*-Pr	H	5	85	113—115	1660, 1680	74.78 (74.76	7.64 7.70	3.96 3.96)
4e	*t*-Bu	H	*t*-Bu	30	63[a]	135—140	1670	75.45 (75.56	8.53 8.19	3.90 3.67)
4f	*t*-Bu	*t*-Bu	H	7	78	144—148	1670, 1690	75.86 (75.56	8.03 8.19	3.73 3.67)

a) A 93% yield on the basis of the quinone reacted.

Table 3. Characterization data of the isoxazoline derivatives (**5a—i**) from 2,3,5,6-tetramethylbenzonitrile *N*-oxide (DNO)

Compd No.	R^1	R^2	R^3	React. time d	Yield %	Mp θ_m/°C	IR $\nu_{C=O}$/cm^{-1}	Found (Calcd) (%) C	H	N
5a	Me	H	Me	7	87	169—172	1670	73.62 (73.29	6.80 6.80	4.81 4.50)
5b	Me	Me	H	3	90	171—173	1660, 1680	73.50 (73.29	6.78 6.80	4.59 4.50)
5c	Me	Me	Me	7	80	162—166	1670	73.56 (73.82	7.39 7.12	4.08 4.30
5d	Me	Me	Cl	7	83	176—179	1680	66.31 (65.99	5.95 5.83	4.17 4.05)
5e	Me	Cl	H	5	30[a)]	183—184	1680, 1720	64.90 (65.16	5.58 5.47	4.36 4.22)
5f	Me	*t*-Bu	H	7	87	172—173	1660, 1695	74.83 (74.76	7.89 7.70	4.13 3.96)
5g	*i*-Pr	*i*-Pr	H	5	87	165—168	1660	74.97 (75.17	8.09 7.95	3.93 3.81)
5h	*t*-Bu	H	*t*-Bu	30	40[b)]	154—160	1670	75.70 (75.91	8.74 8.41	3.45 3.54)
5i	*t*-Bu	*t*-Bu	H	7	86	176—180	1660, 1680	75.86 (75.91	8.53 8.41	3.64 3.54)

a) See the text and Experimental section. b) An 87% yield on the basis of the quinone reacted.

resonate as each singlet at δ 6.70 and 4.44, respectively. The chemical shift of the angular methine signal shows undoutedly that the orientation of the addition reaction is such as indicated in Scheme 1.[4)] Similar ^{1}H NMR spectra are observed for all the CNO adducts and the spectral data are summarized in Table 4.

The reactions of DNO and MNO with quinones were slower in reaction rate than those of CNO; *e.g.* in the reaction of either DNO or MNO with 2,5-di-*t*-butyl-*p*-benzoquinone (25DBQ), the starting materials were recovered almost quantitatively even after a week and only a partial reaction was observed after a month. The addition products from DNO and MNO are also found to be isoxazoline derivatives. In the ^{1}H NMR spectra of the adducts, the signals due to the methyl protons of the quinone moiety overlapped with those originated from aromatic moiety in some cases, but all the adducts are characterized by the characteristic singlet due to the angular methine proton at δ 4.1—4.8, which confirm the isoxazoline structure of the same orientation in the addition reactions. The ^{1}H NMR spectral data are also summarized in Table 4.

In the mass spectra of the C=C adducts obtained from the reactions of the nitrile oxides with quinones, the molecular ion peak was generally very weak and the major peaks were due to the fragment ions. In most cases, the most intense signal is due to the fragment E (in some cases the fragment F). The molecular ion underwent initially the fragmentation with the loss of the angular alkyl substituent or the scission forming the fragment E. The fragments A, D, E, and F were always observed in the mass spectra of the 1:1-C=C adducts, and the structure of the fragment species were confirmed to be such by high resolution mass spectrometry. Some other fragmentation processes were observed. The major fragmentation modes were such as shown in Scheme 2. The adducts from CNO showed an intense peak of M^+-Cl, in some cases as the base peak, but the major fragmentation pattern was substantially similar.

The unstabilized nitrile *N*-oxides, generated just before the reaction in the same pot, reacted with 25DBQ at far faster rates than those of MNO or DNO to give two products in each reaction, the major one of which was identified to be the same type of C=C adduct as in the previous cases and the other was found to be a 1:2-adduct formed through the addition to both of the C=C double bonds. The results of the reaction and the characterization data of the products are summarized in Table 5.

The reactions of nitrile *N*-oxides with 2-chloro-6-(26CMQ) and -5-methyl-*p*-benzoquinones (25CMQ) were somewhat complex owing to the formation of two types of C=C adducts, one is the adduct formed by addition of the nitrile oxides on the C=C of methyl-substituted side and the other is that formed by addition on the opposite side. The former was isolable as formed but the latter was not due to the elimination of hydrogen chloride forming a fully-conjugated isoxazoloquinone and subsequent addition of another nitrile oxide onto the C=O of the isoxazoloquinone to form a spiro-dioxazole derivative. The isoxazoloquinone and the spiro-dioxazole derivatives were both isolated in the reaction of DNO with 26CMQ and characterized. The reactions of the combinations of the other nitrile oxides with 26CMQ or 25CMQ showed similar reaction patterns to that of DNO with 26CMQ but isolation of isoxazoloquinones or spiro-dioxazole derivatives except the isoxazoline derivatives was not successful. The reaction of DNO with 26CMQ gave an isoxazoline derivative **5e** in a 30% yield. The structure of **5e** is confirmed by the fact that the ^{1}H NMR spectrum showed two singlets at δ 4.30 and 1.73 having the intensities corresponding to one and three

Table 4. ^{1}H NMR spectral data of the isoxazoline derivatives (**3**—**5**)

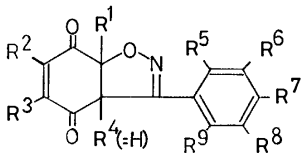

Compd No.	Quinone moiety				Aromatic moiety				
	R^1	R^2	R^3	R^4(=H)	R^5	R^6	R^7	R^8	R^9
3a	Me 1.76(s)	H 7.00(d) $J_{2,3}$=10 Hz	H 6.83(d)	4.48(s)	Cl —	H	H 7.36(s)	H	Cl —
3b	Me 1.72(s)	H 6.86(s)	Me 2.02(s)	4.48(s)	—		7.36(s)		—
3c	Me 1.74(s)	H 7.14(s)	Cl —	4.54(s)	—		7.26(s)		—
3d	Me 1.74(s)	H 6.84(s)	*t*-Bu 1.20(s)	4.62(s)	—		7.32(s)		—
3e	Me 1.72(s)	Me 2.16(s)	H 6.70(s)	4.44(s)	—		7.32(s)		—
3f	Me 1.66(s)	Me 2.06(s)	Me 1.94(s)	4.42(s)	—		7.26(s)		—
3g	Me 1.76(s)	Me 2.30(s)	Cl —	4.52(s)	—		7.34(s)		—
3h	Me 1.82(s)	Cl —	H 7.09(s)	4.52(s)	—		7.36(s)		—
3i	Me 1.76(s)	Cl —	Me 2.16(s)	4.52(s)	—		7.34(s)		—
3j	Me 1.68(s)	*t*-Bu 1.30(s)	H 6.60(s)	4.32(s)	—		7.30(s)		—
3k	Me 1.86(s)	benzo- 7.6—8.1(m)		4.67(s)	—		7.32(s)		—
3l	*i*-Pr 2.72(sep) 1.09(d, 3H) 0.93(d, 3H) J=6.7 Hz	*i*-Pr 3.15(qui) 1.14(d, 6H) J=6.7 Hz	H 6.56(s)	4.57(s)	—		7.28(s)		—
3m	*t*-Bu 1.16(s)	H 6.84(s)	Me 2.00(s)	4.84(s)	—		7.30(m)		—
3n	*t*-Bu 1.12(s)	H 6.82(s)	*t*-Bu 1.18(s)	4.84(s)	—		7.26(m)		—
3p	*t*-Bu 1.12(s)	*t*-Bu 1.32(s)	H 6.56(s)	4.78(s)	—		7.28(m)		—
4a[a]	Me 1.68(s)	Me 2.10(s)	Me 1.94(s)	4.26(s)	Me 2.10	H 6.88	Me 2.26	H 6.88	Me 2.10
4b[b]	Me 1.70(s)	Me 2.28(s)	Cl —	4.36(s)	2.14(br)	6.86	2.28	6.86	2.14(br)
4c	Me 1.64(s)	*t*-Bu 1.28(s, 9H)	H 6.48(s)	4.12(s)	2.14	6.76	2.24	6.76	2.14
4d	*i*-Pr 2.68(qui) 0.89(d), 1.11(d), J=6.8 Hz	*i*-Pr 3.14(qui) 1.08(d), 1.13(d)	H 6.50(s)	4.45(s)	2.01(br)	6.80	2.24	6.80	2.01(br)
4e	*t*-Bu 1.08(s)	H 6.48(s)	*t*-Bu 1.16(s)	4.76(s)	2.14	6.76	2.24	6.76	2.14
4f	*t*-Bu 1.10(s)	*t*-Bu 1.30(s)	H 6.51(s)	4.64(s)	1.91(br)	6.79(br)	2.24	6.79(br)	2.24(br)
5a	Me 1.74(s)	H 6.82(s)	Me 2.00(s)	4.28(s)	Me 1.86	Me 2.22(br)	H 6.98	Me 2.22(br)	Me 2.22(br)
5b	Me 1.72(s)	Me 2.14(s)	H 6.66(s)	4.22(s)	1.92	2.20(br)	7.00	2.20(br)	2.20(br)
5c	Me 1.70(s)	Me 2.12(s)	Me 1.96(s)	4.24(s)	1.86	2.22(br)	6.96	2.22(br)	2.22(br)
5d	Me 1.72(s)	Me 2.28(s)	Cl —	4.30(s)	1.86	2.22(br)	6.98	2.22(br)	2.22(br)

Table 4. (Continued)

Compd No.	Quinone moiety				Aromatic moiety				
	R^1	R^2	R^3	R^4(=H)	R^5	R^6	R^7	R^8	R^9
5e	Me 1.73(s)	Cl —	H 7.00(s)	4.30(s)	1.84	2.22(br)	7.00	2.22(br)	2.22(br)
5f	Me 1.64(s)	*t*-Bu 1.28(s)	H 6.50(s)	4.10(s)	1.90	2.18(br)	6.90	2.18(br)	2.18(br)
5g	*i*-Pr 2.72(qui) 0.92(d), 1.14(d), J=7.0 Hz	*i*-Pr 3.16(qui) 1.08(d), 1.20(d)	H 6.52(s)	4.44(s)	1.86	2.16	6.86	2.24	2.24
5h	*t*-Bu 1.12(s)	H 6.84(s)	*t*-Bu 1.16(s)	4.70(s)	1.82	2.12	6.94	2.18	2.24
5i	*t*-Bu 1.13(s)	*t*-Bu 1.33(s)	H 6.54(s)	4.60(s)	1.78	2.14	6.93	2.23	2.23

Abbreviations in the NMR data: s=singlet; d=doublet; qui=quintet; sep=septet; m=multiplet; br=broad. a) The signal at δ=2.10 is overlapped with a broad peak and integrated totally for 9H. b) The signals at δ=2.28 and 2.14 integrate for 6H each.

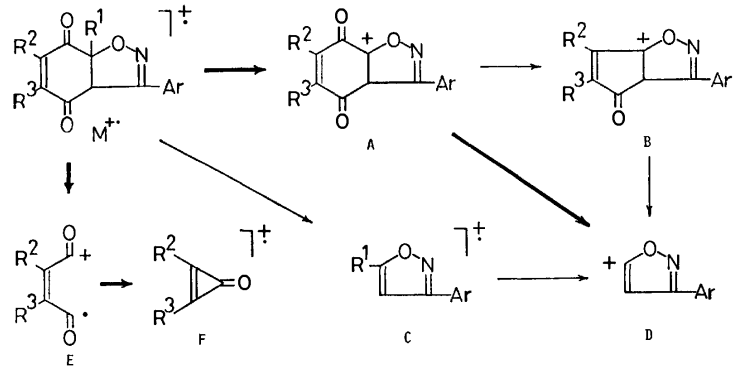

Scheme 2.

Table 5. Products in the reactions of unstabilized nitrile *N*-oxides with 2,5-di-*t*-butyl-*p*-benzoquinone (25 DBQ)

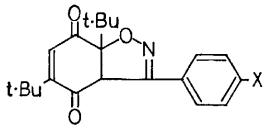

6a–b

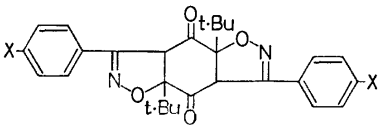

7a–b

Compd No.	X	Yield %	Mp θ_m/°C	IR $\nu_{C=O}$/cm^{-1}	Found (Calcd) (%) C	H	N	M^+ Found (Calcd)	^{1}H NMR ($CDCl_3$) (δ) Quinone moiety	Aromatic moiety
6a	Cl	88	151—152	1680	67.77 (67.46	6.57 6.47	3.89 3.75)	373.1448 (373.1443)	1.08(s, 9H) 1.16(s, 9H) 4.78(s, 1H) 6.70(s, 1H)	7.32(d, 2H) 7.58(d, 2H) J=9.0 Hz
7a	Cl	4	189—190	1710	63.16 (63.75	5.34 5.35	5.23 5.31)	526.1428 (526.1427)	1.00(s, 18H) 4.52(s, 2H)	7.34(d, 4H) 7.58(d, 4H) J=9.0 Hz
6b	Br	70	144—146	1670 1700	60.47 (60.29	5.89 5.78	3.42 3.35)	417.0983 (417.0939)	1.06(s, 9H) 1.12(s, 9H) 4.80(s, 1H) 6.72(s, 1H)	7.52(s, 4H)
7b	Br	4	228—229	1710	55.09 (54.56	5.05 4.58	4.54 4.55)	614.0413 (614.0415)	1.00(s, 18H) 4.56(s, 2H)	7.52(s, 8H)

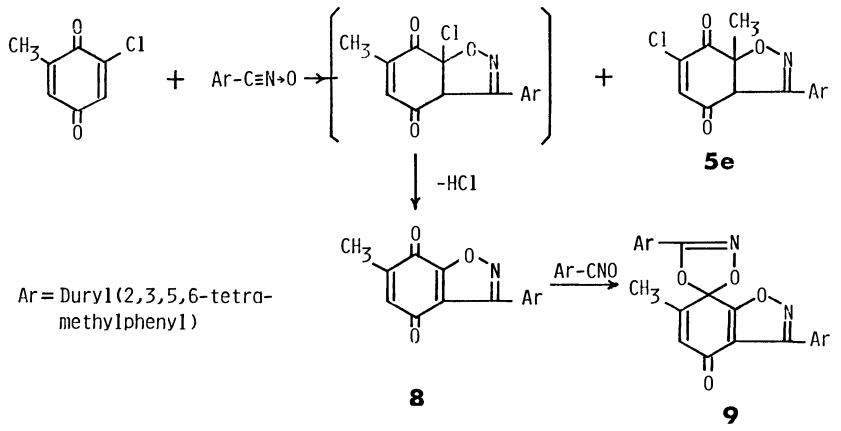

Scheme 3.

protons respectively, which are assigned to the angular methine and methyl protons. The signals due to the quinone olefinic methine and aromatic protons are overlapped and appeared as a singlet at δ 7.00. The methyl protons of the duryl moiety resonate as broad singlets at δ 1.84 and 2.22, the former integrating for three protons and the latter for nine protons and having an inflection at δ 2.17. This pattern is interpreted in terms of the hindered rotation of the duryl group and one of the 2,6-methyl groups being in a close proximity of the quinone moiety. The ^{1}H NMR spectral pattern is similar to those of the other isoxazoline derivatives shown in Table 3. Besides this isoxazoline derivative, isoxazoloquinone **8**, formed by the addition of DNO to the C=C bond at the other side and subsequent dehydrochlorination, and a spiro-dioxazole derivative **9**, formed by addition of another DNO to the C=O bond of **8**, were isolated in 7 and 15% yields, respectively. Their structures were also determined by NMR, IR, and mass spectra and elemental analyses. In the ^{1}H NMR spectrum of **8**, the duryl methyl protons are seen as two singlets of the same intensity at δ 2.28 and 1.94, while the methyl on quinone moiety appears at δ 2.22 as a singlet. No absorption characteristic of the angular methine proton was observed in the region of δ 4.0—5.0. The integration of the ^{1}H NMR spectrum of **9** clearly shows that the product is a 1:2-adduct of the quinone and the nitrile *N*-oxide. The olefinic proton of **9** resonates at δ 6.24, being upper field than that of **8** which appears at δ 6.64, while the olefinic methyl signal of **9** appears at δ 2.30, slightly lower field than that of **8**. Taking into consideration the shift pattern of the signals on C=O addition, this suggests that the second nitrile *N*-oxide added across the carbonyl group adjacent to the methyl substituent. If so, this also supports the orientation of the first addition of the nitrile *N*-oxide and is well consistent with the reactivity enhancement of carbonyl bond toward cycloaddition by adjacent oxygen substitution described in the previous paper.[2]

Experimental

All melting points are uncorrected. The ^{1}H NMR spectra were recorded with a JEOL MH-100 100 MHz NMR spectrometer and the mass spectra with a Hitachi RMU-7L high-resolution mass spectrometer.

Materials. Methyl-*p*-benzoquinone (MQ), 2-methyl-1,4-naphthoquinone (MNQ), and 2,5-di-*t*-butyl-*p*-benzoquinone (25DBQ) were obtained commercially and were used after recrystallization. 2,6-Dimethyl-*p*-benzoquinone (26DMQ), 2,5-dimethyl-*p*-benzoquinone (25DMQ), 2,3,5-trimethyl-*p*-benzoquinone (TMQ), 2-methyl-5-isopropyl-*p*-benzoquinone (25MPQ), 2-methyl-6-*t*-butyl-*p*-benzoquinone (26MBQ), 2-methyl-5-*t*-butyl-*p*-benzoquinone (25MBQ) 2,6-diisopropyl-*p*-benzoquinone (26DPQ) were prepared from the corresponding phenols by the procedures of McLamore[5] with some modifications.[6] 2-Chloro-6-methyl-*p*-benzoquinone (26CMQ) was prepared by chlorination of o-cresol and subsequent oxidation of the 4,6-dichloro-*o*-cresol.[7] 2-Chloro-5-methyl-*p*-benzoquinone (25CMQ) was prepared from 2-methyl-*p*-benzoquinone by its hydrochlorination and subsequent oxidation[8]. By adopting a similar procedure, 3-chloro-2,6-dimethyl-*p*-benzoquinone (26DMCQ) and 3-chloro-2,5-dimethyl-*p*-benzoquinone (25DMCQ) were prepared from 26DMQ and 25DMQ respectively. The stable nitrile oxides (MNO, DNO, and CNO) were prepared according to the Grundmann's procedure.[9]

Reactions of Quinones with Nitrile N-*Oxides. General procedure*: The reaction was carried out by dissolving the reactants in benzene in a concentration of 5 mmol/100 ml each and allowing the mixture to stand at ambient temperature for 3—7 d. The progress of the reaction was followed by TLC using silica gel plates (Merck). After an appropriate reaction period the solvent was removed by evaporation under reduced pressure and the residue was triturated with petroleum ether or methanol. The solid product thus obtained was subjected to column chromatography on silica gel (Wako gel C-100 or C-200) using benzene as an eluent. The nitrile *N*-oxide, the quinone and the product were eluted in that order. The fractions containing the products were collected and evaporated under reduced pressure to afford the product, which was purified by recrystallization from benzene or a mixture of benzene and petroleum ether or hexane. The reaction conditions, physical constants, analytical and IR data are tabulated in Tables 1—3. The ^{1}H NMR data are summarized in Table 4.

Reactions of Unstabilized Nitrile N-*Oxides with 2,5-Di-*t*-butyl-*p*-benzoquinone (25DBQ)*. A typical example follows: A solution of *p*-chlorobenzhydroxamoyl chloride (950 mg, 5 mmol) in CH_2Cl_2 (30 ml) was cooled to -10 °C in an ice-salt bath. Triethylamine (0.55 g, 5 mmol) in CH_2Cl_2 (20 ml) was slowly added to the above solution with stirring and maintaining the temperature below -5 °C. After the

addition of the amine, a solution of 25DBQ (1.1 g, 5 mmol) in CH_2Cl_2 (30 ml) was added dropwise during 15 minutes maintaining the temperature below 0 °C. The reaction mixture was allowed to stand at ambient temperature for 2 d and then the solvent was removed by evaporation to dryness under reduced pressure. The residue was extracted with benzene to leave triethylammonium chloride as white solid. The extract was concentrated and subjected to column chromatography on silica gel using benzene as an eluent. The first fraction gave 100 mg (4%) of colorless crystals of 1:2-adduct, **7a**, mp 189—190 °C. The second fraction contained 100 mg (8%) of the unreacted quinone. The third fraction yielded 1.65 g (88%) of 1:1-adduct, **6a**, which was recrystallized from a mixture of benzene–petroleum ether to give stout yellow needles, mp 151—152 °C. Characterization data are given in Table 5.

*Reaction of 2-Chloro-6-methyl-*p*-benzoquinone (26CMQ) with 2,3,5,6-Tetramethylbenzonitrile* N-*Oxide (DNO)*: A solution of 26CMQ (0.78 g, 5 mmol) and DNO (0.87 g, 5 mmol) in chloroform (200 ml) was stirred at room temperature for 3 d. The solvent was removed by evaporation under reduced pressure and the residue was triturated with methanol. A yellow solid was obtained. This was collected by filtration and subjected to column chromatography on silica gel using benzene as an eluent. The first fraction gave colorless crystals of **9**, which was recrystallized from ethanol into silky white needles (300 mg, 15%), mp 163—164 °C. IR(KBr) 1680 cm^{-1}($\nu_{C=O}$). ^1H NMR ($CDCl_3$) δ=7.12 (1H, s) and 7.08 (1H, s)(duryl aromatic), 6.24 (1H, s, quinone olefinic), 2.44 (6H, s, duryl methyl), 2.26 (15H, m, duryl and quinone methyl), 1.92 and 1.96 (6H, two s, duryl methyl). M^+ was not observed and the fragmentation pattern was almost the sum of those of the isoxazoloquinone **8** and DNO, showing the peaks at *m/e* 295.1247 (calcd for **8**: 295.1207) and 175.0978 (calcd for DNO: 175.0997).

Found: C, 74.16; H, 6.30; N, 6.17%. Calcd for $C_{29}H_{30}N_2O_4$: C, 74.02; H, 6.43; N, 5.95%.

The second fraction gave yellow micro needles of isoxazoloquinone, **8** (100 mg, 7%) on recrystallization from ethanol, mp 174—176 °C. IR(KBr) 1650 and 1670 cm^{-1} ($\nu_{C=O}$). ^1H NMR($CDCl_3$) δ=7.12(1H, s, duryl aromatic), 6.64(1H, s, quinone olefinic), 2.28(6H, s, duryl 2,6-methyls), 2.22(3H, s, quinone methyl), 1.94(6H, s, duryl 3,5-methyls).

Found: C, 73.43; H, 5.16; N, 4.79%; M^+, 295.1171. Calcd for $C_{18}H_{17}NO_3$: C, 73.20; H, 5.80; N, 4.74%; M, 295.1207.

The third fraction gave yellow flakes of isoxazoline derivative, **5e** (450 mg, 30%) on usual work-up and recrystallization from benzene–petroleum ether, mp 183—184 °C. The characterization data for **5e** are given in Tables 3 and 4.

*Reaction of 2-Methyl-5-*t*-butyl-*p*-benzoquinone (25MBQ) with CNO*: A solution of 25MBQ (0.89 g, 5 mmol) and CNO (0.94 g, 5 mmol) in benzene (100 ml) was stirred for 10 d at room temperature. Evaporation of the solvent left a solid, which was washed with petroleum ether to give 1.65 g (90%) of the product. The NMR spectrum of the crude product revealed this to be a mixture of two C=C adducts (the signals at 4.84 and 4.62 due to the angular methines of the two adducts in the ratio of 1:2. The crude product was recrystallized from benzene–petroleum ether and the two kinds of crystals were separated manually under a microscope, giving yellow microcubes of **3d** and pale yellow microneedles of **3m**. The characterization data are given in Tables 1 and 4.

The authors greatly acknowledge to Japan Society for Promotion of Science (JSPS) for the Fellowship to B. S. H.

References

1) Ch. Grundmann and P. Gruenanger, "The Nitrile Oxides," Springler Verlag, Berlin (1971), pp. 95, 103; R. Huisgen, *Angew. Chem.*, **75**, 741 (1963).

2) S. Shiraishi, S. Ikeuchi, M. Seno, and T. Asahara, *Bull. Chem. Soc. Jpn.*, **51**, 921 (1978).

3) S. Shiraishi, S. Ikeuchi, M. Seno, and T. Asahara, *Bull. Chem. Soc. Jpn.*, **50**, 910 (1977).

4) The H-4 of 4-acylisoxazolines is found to have a chemical shift in the range of δ=3.91—4.95, while the H-5 of 5-acylisoxazolines in the range of δ=4.68—5.60 [G. Bianchi, C. D. Micheli, R. Gandolfi, P. V. Finzi, and O. V. Pava, *J. Chem. Soc., Perkin Trans. 1*, **1973**, 1148].

5) W. M. McLamore, *J. Am. Chem. Soc.*, **73**, 2225 (1951).

6) S. Shiraishi and B. S. Holla, unpublished.

7) J. Cason, C. F. Allen, and S. Goodwin, *J. Org. Chem.*, **13**, 403 (1948).

8) K. J. M. Andrews, D. H. Marrian and D. R. Maxwell, *J. Chem. Soc.*, **1956**, 1844.

9) Ch. Grundmann and J. M. Dean, *J. Org. Chem.*, **30**, 2809 (1965).

Mechanism of the Photooxidation of and Photoepoxidation with Cyclic α-Diketones

Yasuhiko SAWAKI

Department of Applied Chemistry, Faculty of Engineering, Nagoya University, Chikusa-ku, Nagoya 464

(Received Jauary 31, 1983)

The photooxidation of phenanthrenequinone (PhQ) under oxygen afforded diphenic acid and its peroxy acid, while acenaphthenequinone (AcQ) predominantly yielded 1,8-naphthalenedicarboxylic anhydride. The photolysis of PhQ or AcQ in the presence of olefins afforded predominantly 1:1 cycloadducts and the photoepoxidation was a very minor one accompanying significant amount of C–C cleavage of olefins. These results show that the photoreaction of PhQ or AcQ with olefins is very fast and competitive with the quenching and/or reaction with oxygen. The photoepoxidation of stilbene in the presence of dimethyl sulfoxide resulted in a high selectivity (>98%) for the *trans*-epoxide. The same was true for the epoxide formed in the coautoxidation of benzaldehyde and stilbene. These facts suggest that the photoepoxidation with cyclic α-diketones as a minor reaction proceeds chiefly by way of acylperoxyl radical, accompanying the epoxidation with peroxy acids produced concomitantly. Mechanisms of the photooxidation of and photoepoxidation with the cyclic diketones are discussed in comparison with the case of acyclic diketones.

Most of the sensitized photooxidation of olefins proceeds by way of a singlet oxygen reaction (*i.e.*, the Type II photooxidation).[1,2] Sometimes, epoxide formations have been observed to accompany some reactions with singlet oxygen.[3] Shimizu and Bartlett[4] reported a novel photoepoxidation with α-diketone and oxygen, which is quite different from the Type I photooxidation (*i.e.*, free radical autoxidations), singlet oxygen reactions or a recently found photooxidation *via* electron transfer.[5] The photoepoxidation with α-diketones has been utilized as a practical epoxidation method,[6] but there remains much to be clarified about the scope and mechanism of the photoreaction.

In the previous paper,[7] we suggested that the photoepoxidation with benzil or biacetyl proceeds *via* acylperoxyl radical (**2**) produced from the triplet diketone–oxygen adduct (**1**). The predominant formation of *trans*-epoxides[4a] and phenyl benzoates from the reaction of benzil in benzene[4c,7] are good evidence for the radical epoxidation *via* **2**. Recently, the photoepoxidation with acenaphthenequinone (AcQ) has been reported to afford a high yield of 1,8-naphthalenedicarboxylic anhydride.[8] However, the proposed mechanism is quite different from ours deduced from the reaction of acyclic α-diketones. Hence, it is interesting to decide whether such a specified mechanism is operating or not for cyclic α-diketones. Here we wish to report that the photooxidation of cyclic α-diketones is relatively ineffective ($\Phi \approx 0.005$) and the photoepoxidation of olefins is a rather minor reaction; the major pathway for the case of AcQ or phenanthrenequinone (PhQ) is a 1:1 cycloaddition between diketones and olefins. Recently, the radical epoxidation with **2** have been shown to occur in the photoepoxidation with benzoins and oxygen.[9]

Results and Discussion

In benzene benzil was photooxidized to yield benzoic acid (80%), perbenzoic acid (40—60%), and phenyl benzoate (30—50%) in addition to small amounts of biphenyl, benzoyl peroxide, and phenol.[7,10] The photooxidation rate of benzil was not altered by the addition of olefins, affording epoxides together with C–C cleavage products.[7] As described below, the photooxidation of cyclic α-diketones has been examined to compare with the acyclic benzil case.

PhQ. The photooxidation of PhQ in benzene afforded diphenic (**3**) and monoperoxydiphenic acids (**4**) in addition to 2,2′-biphenylcarbolactone (**5**) (1—2%) (Table 1). The formation of **5** may be formulated *via* the decarboxylation of **6** to yield **7** followed by the intramolecular cyclization. Phenyl diphenate, which corresponds to phenyl benzoate in the benzil case, could not be detected (*i.e.*, within 0.2% if any). Probably, the large steric effect of *o*-aroyl group in aroyloxyl radical **6** suppressed the radical aroyloxylation of benzene. Also we could detect neither diphenic anhydride **8** nor 2,2′-biphenyldicarbonyl peroxide **9** by GLC (*i.e.*, below 0.5% if any). For the GLC

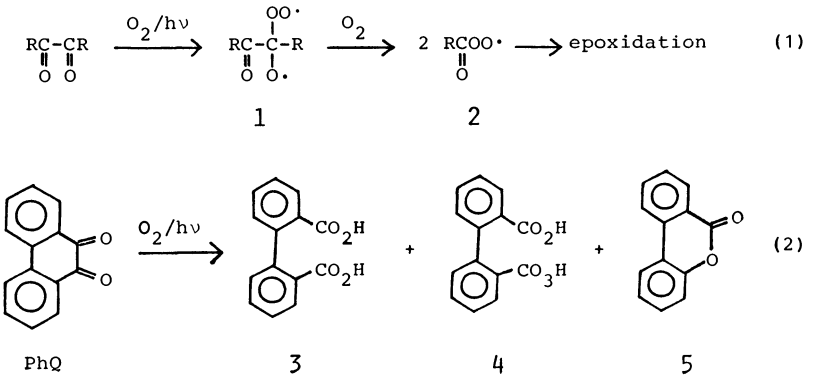

Table 1. Photooxidation of PhQ in benzene

Conditions[a]	Rel. Φ[b]	Products (%)[c]					
		3	5	1:1 Adduct[d]	Epoxide	Allylic OOH	Others
	(1.0)[e]	50	1.0				4 (45%)
Air	0.9	45	0.5				4 (40%)
2 mM DABCO	0.03	<1	<1				
0.01 M Cyclohexene	44	28	1.5	50	2	28	
0.1 M Cyclohexene	76	17	1.4	79	11	104	
0.1 M Cyclohexene, N_2	f	<1	<0.1	89	0	0	
20% THF	98	11	0	80			
0.1 M Cyclooctene	f	9	f	80	6	<1	
0.1 M *trans*-PhCH=CHMe	f	4	f	82	8	<1	PhCHO (10%), g
0.1 M *trans*-PhCH=CHPh	f	1	f	90	4	—	PhCHO (13%), h

a) Irradiation of 2.5 mM PhQ through a Pyrex filter for 10—60 min under O_2 at 20 °C unless otherwise noted. b) Relative quantum yields from the decrease of PhQ as determined by UV absorbance at 420 nm. c) Products were determined by GLC. Allylic hydroperoxide were determined after the reduction with $NaBH_4$, and the acid after methylation with diazomethane. Peroxy acid **4** was titrated iodometrically. %Yields are based on PhQ. d) 1:1 Adducts of PhQ with olefins or THF. e) Absolute quantum yield is 0.0048. f) Not determined. g, h) Recovered olefins: cis/trans=0.35 and 4, respectively.

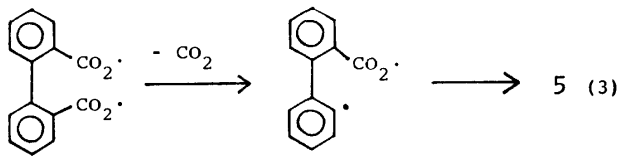

6 7 5 (3)

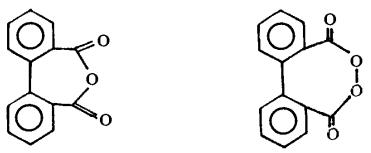

8 9

detection of diacyl peroxide **9**, we applied the facile reduction of **9** to **8** by triphenylphosphine.[11a] Since **9** is known to decompose thermally to afford **5**,[11b] some of **5** may be derived from **9**.

The photooxidation of PhQ in the presence of olefin resulted in the sharp decrease in diphenic acid formation and the major reaction changed to the cycloaddition between PhQ and olefins (Table 1). Since the oxygen quenching of triplet ketones is close to the diffusion-controlled rate (*e.g.*, 10^9 M^{-1} s^{-1}, 1 M= 1 mol dm^{-3}),[12] it is apparent that the cycloaddition between excited PhQ and olefins is likewise very fast. The photochemical 1,2-cycloaddition (**11**) or 1,4-addition (**10**) of PhQ is well known.[13] The isomer distributions of these cycloadducts are extensively studied and shown to change by olefins.[14] The photochemical 1,2-adducts such as **12** are also known for hydrogen donors, *e.g.*, ethers and aldehydes.[15]

The epoxide formation was only a minor reaction (2—10%) (Table 1). For cyclohexene, the ratio of epoxide:allylic hydroperoxide was *ca.* 1:10, which was approximately same with the ratio from AIBN-initiated autoxidation at 60 °C.[16] For the case of β-methylstyrene or stilbene, the yield of benzaldehyde, an oxidative C–C cleavage product, was higher than that of epoxides. Thus, it is apparent that the photoepoxidation with PhQ is not effective.

The quantum yield for the photooxidation of PhQ, irradiated at >320 nm in benzene, was Φ=0.0048, which is about one tenth of the benzil case (Φ=0.035).[7] For comparison, quantum yields were also determined under nitrogen; *i.e.*, Φ=0.71 (lit,[14a] 0.79) for the addition of PhQ to 2,3-dimethyl-2-butene and Φ= 0.95 (lit,[15b] 0.86) for the addition to THF, which are fairly consistent with the literature values as shown. The relative Φ values in Table 1 also suggest that the reaction with olefins or THF is fast and efficient. These will be discussed later.

AcQ. The photooxidation of AcQ gave anhydride **13** as a major product,[8,15b,17] 1,8-naphthalenedicarboxylic acid (**14**) being a minor one (Table 2).

The attempted photoepoxidation with AcQ was not efficient just like the PhQ case. Again, the predominant reaction was the cycloaddition of AcQ to olefins; the 1:1 adducts were a 2,3-dihydro-1,4-dioxin **10** for 1,2-dimethylcyclohexene and 2-acyloxetane **11** for the other olefins (see Experimental for details). The for-

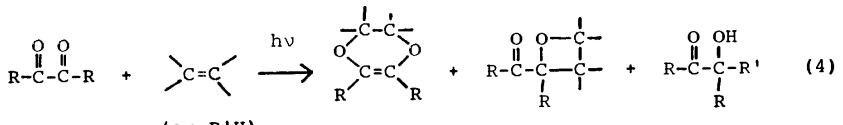

(or R'H) 10 11 12 (4)

Table 2. Photooxidation of AcQ in dichloromethane

Conditions[a]	Rel. Φ[b]	Products (%)[c] Acid **14**	Anhydride **13**	1:1 Adduct[d]	Epoxide	Allylic OOH	Others
	(1.00)[e]	2.5	79				Peroxy acid (2%)
Air	0.82	3.2	81				
20% THF	1.4	13.5	27	60[f]			
1 mM DABCO	0.29	1	33	g)			
0.01 M Cyclohexene	2.1	1.5	54	40[h]	1	12	
0.1 M Cyclohexene	5.2	<1	10	82[h]	5	70	
0.1 M 1,2-Dimethylcyclohexene	14	<1	1	95[i]	2	30	
0.1 M *trans*-PhCH=CHMe	5	<1	3	93[j]	6		PhCHO (12%),[k]
0.005 M *trans*-PhCH=CHPh	0.5	<1	6	87[j]	4	—	PhCHO (26%),[l]

a) Irradiation of 10 mM AcQ in CH_2Cl_2 under O_2 at 20 °C through a Pyrex filter for 2.5 h. b) Relative Φ for the decomposition of AcQ (1 mM) as determined by GLC, using a merry-go-round apparatus. c) See footnote c in Table 1. d) 1:1 Adducts of AcQ with olefins or THF. e) Absolute value is 0.0055. f) 1,2-Adduct of THF is reported in Ref. 15b. g) Not determined. h) Oxetane **28**. i) **27**. j) Structures were not determined. k, l) Recovered olefin: cis/trans=0.1 and 3.2, respectively.

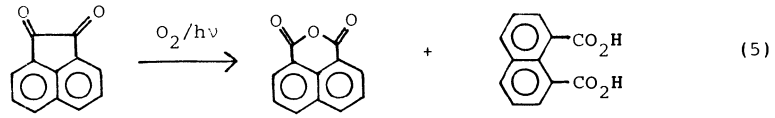

AcQ 13 14 (5)

mation of **10** from AcQ has been reported for 2,3-dimethyl-2-butene;[17] the formations of oxetane **11**[14c,d] and α-hydroxy ketone **12**[18] are also known.

Here, some should be noted for the discrepancy between the present results and the reported ones.[8] The relative quantum yields for the disappearance of AcQ was reported to be almost constant even in the presence of cyclohexene,[8] which is in sharp contrast to the present results in Table 2. We suppose that since the reported Φ values were determined by monitoring the formation of anhydride **13** by UV, the formation of cycloadduct **11** could not be detected because of the close similarity in UV spectra between AcQ and **11**.

Camphorquinone (CQ). The photooxidation of 2,3-bornanedione (CQ) in benzene was reported to yield many kinds of products involving a rather small amount of camphoric acid (**15**, 7%) and its anhydride (**16**, 3%).[19] The reported yields of **16** change with solvents, *e.g.*, 26% in MeOH,[20] 35% in xylene,[21] and predominant in CCl_4.[19]

The attempted photoepoxidation of β-methylstyrene and *trans*-stilbene with CQ resulted in poor yields (5—10%) of epoxide, accompanying C–C cleavage products. Cyclohexene (0.1 M) and CQ afforded 13% epoxide and 68% cyclohexenyl hydroperoxide, indicating again the radical autoxidation of olefin as a major reaction. Like PhQ or AcQ, the photoepoxidation with CQ is not effective.

Comparison of Cyclic and Acyclic α-Diketones. Quantum yields of the photooxidation in benzene are in the order of biacetyl≫benzil, CQ≫AcQ, PhQ, indicating much less effective photolysis for the cyclic diketones. For the photooxidation of benzil and biacetyl there is no accelerating effect by additives such as olefins, THF or *i*-PrOH; this suggests that the photochemical reactions with these additives are not so fast as those with oxygen. The same is true for cyclic diketone CQ. On the contrary, PhQ reacts very fast with olefins, THF or *i*-PrOH; for example, the photoreaction is 98-fold faster in the presence 20 vol% THF; similar trend is also observed for the case of AcQ (Table 2). As apparent in Tables 1 and 2, the accelerating effect is due to the fast formation of 1:1 adducts; thus, the photoepoxidation with these cyclic diketones is not effective.

The same features are also shown in the photoepoxidation of stilbene (Table 3). While considerably high yields (50—80%) of epoxide were obtained with benzil and biacetyl, the reaction with cyclic diketones resulted in only 4—7% yields, predominantly affording 1:1 cycloadducts. The photoepoxidation always afforded predominantly *trans*-epoxide (85—95% trans), and the trans % increases up to over 97% by adding dimethyl sulfoxide (DMSO). Similar effect of DMSO was observed for the coautoxidation of 0.05 M stilbene and 0.2 M benzaldehyde (initiated by α,α'-azobisisobutyronitrile at 60 °C); % trans increased from 65% to 98% by adding DMSO. It is well known that the coautoxidation of aldehyde and olefin affords a mixture of *cis*- and *trans*-epoxides, the epoxidizing species being acylperoxyl radical and peroxy acid.[22] These results suggest that the peroxy acid epoxidation is effectively reduced by DMSO[23] and the epoxidation by acylperoxyl radical proceeds with high selectivity (*i.e.*, >98%) for *trans*-stilbene oxide.

Here, some should be noted about the quenching by DABCO (1,4-diazabicyclo[2.2.2]octane). The results in Tables 1 and 2 show an effective quenching by DABCO for the diketone photooxidation.[24] However,

Table 3. Photoepoxidation of stilbene with α-diketones under O_2

Diketone	Solvent(additive)[b]	Products (%)[a] PhCHO	Products (%)[a] Epoxide(cis:trans)	Major reaction
A) Photoepoxidation of *trans*-stilbene[c]				
Benzil	PhH	20	62 (7:93)[d]	Epoxidn.
	PhH (DMSO)	18	51 (2:98)[d]	Epoxidn.
PhQ	CH_2Cl_2	22	4 (5:95)	1:1 Adduct[e]
	CH_2Cl_2 (DMSO)	16	5 (3:97)	1:1 Adduct[e]
AcQ	CH_2Cl_2	8	7 (15:85)	1:1 Adduct[e]
	CH_2Cl_2 (DMSO)	f)	4 (5:95)	1:1 Adduct[e]
CQ	PhH (DMSO)	4	6 (3:97)	g)
B) Coautoxidation with PhCHO-AIBN[h]				
trans-Stilbene	PhH	f)	(0:100)	Epoxidn.
cis-Stilbene	PhH	f)	(35:65)	Epoxidn.
cis-Stilbene	PhH (DMSO)	f)	(2:98)	Epoxidn.

a) Products were determined by GLC based on the consumed diketone. b) 0.1 M DMSO was added. c) Irradiation of 2 mM diketone and 0.05 M *trans*-stilbene solution through a Pyrex filter under O_2 (20 °C, 2 h). Recovered olefin: cis/trans=4—9. d) The cis/trans ratios were practically the same when *cis*-stilbene was used. e) 1:1 Adducts of diketone and olefin. See Tables 1 and 2. f) Not determined. g) Many products were detected by GLC, but not identified. h) Coautoxidation of 0.05 M stilbene and 0.2 M benzaldehyde was initiated by the thermal decomposition of AIBN (≈5 mM) at 60 °C.

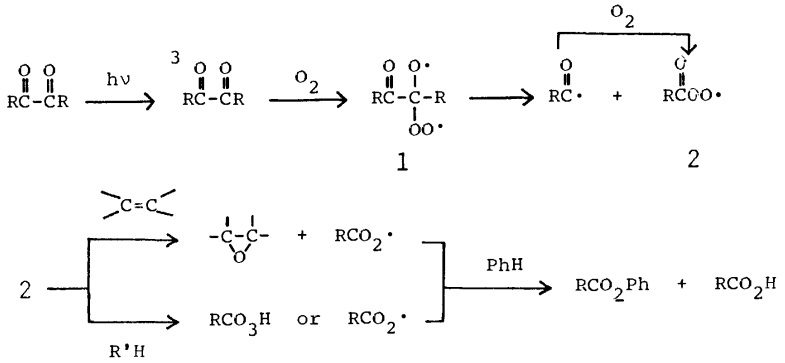

Scheme 1.

the apparent quenching by DABCO does not mean that the diketone photooxidation proceeds *via* a singlet oxygen reaction, since the photolysis of benzil was rather retarded by adding Methylene Blue or Rose Bengal, an efficient $^1O_2$ sensitizer. The addition of DABCO to PhQ in benzene resulted in weakly reddish solution with a few percent increase in the absorbance at >300 nm. Probably this indicates the formation of a C-T complex between PhQ and DABCO, which may act as an efficient energy accepter for the excited PhQ*, quenching the PhQ photolysis. This was ascertained by the fact that the cycloaddition of PhQ with cyclohexene is also efficiently quenched by DABCO. The same is probably true for the other diketones in Table 3, although no absorption due to C-T complex could be detected by UV.

Mechanism. The photoepoxidation of acyclic α-diketones has been shown to proceed by way of Scheme 1.[7] A considerable amount of phenyl benzoate was obtained for the benzil photooxidation in benzene (*i.e.*, R=Ph).[7]

The photooxidation of AcQ affords anhydride as a major product. Similar anhydride formations are also known for the photooxidation of CQ[19–21] and other cyclic diketones.[20,25] Some possible routes for the formation of anhydride (**20**) from cyclic diketones may be written as Scheme 2. This mechanism is, in parts, similar to that reported by Koo and Schuster,[8] but essentially different in the fate of alkoxyl radical **17**. The β-scission of alkoxyl radical **17** to afford **18** is probably facile since the scission of acyl radical in α-acylalkoxyl radicals has been established to be very fast.[26] The conversion of **17** to **21**, as was suggested,[8] seems to be unfavorable on the basis of an energetic point of view that **21**, an oxirane diradical, would be much less stable than **17**, a ketone diradical. No formation of anhydride from PhQ also supports the pathway **17**→**18**.

The next choice is about the reactions of radical pair **18**. It seems to couple easily to diacyl peroxide **19**, but, **19** is not likely to afford smoothly anhydride **20**.[27] An alternative reaction of **18** is the intramolecular addition of acyl radical to carbonyl oxygen to afford **23**. Since the addition of acyl radical to carbonyls is known intermolecularly,[29] the intramolecular addition (*i.e.*, **18**→**23**) may proceed smoothly.

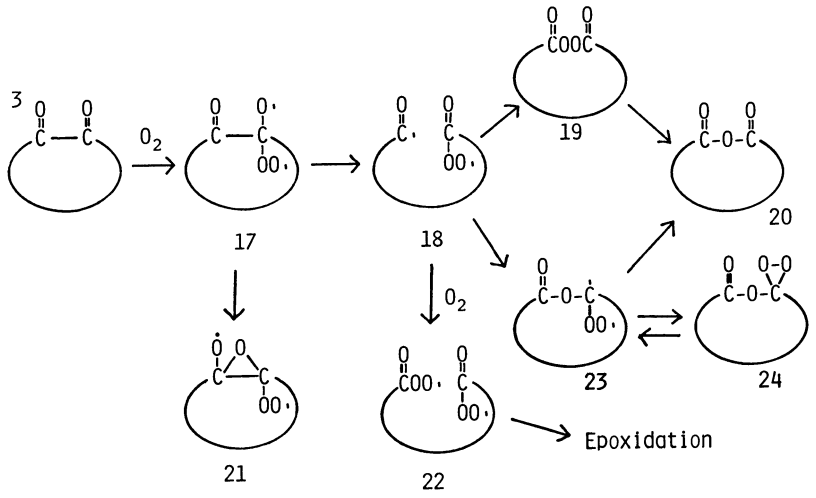

Scheme 2.

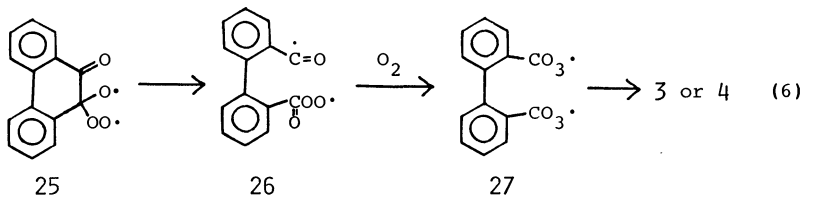

It is not certain that intermediate diradical **23** might be equilibriated with unstable dioxirane (**24**) or not. These unstable intermediate **23** and **24** are probably a poor O-transfer agent to olefins.[30] In the photooxidation of AcQ the formation of only small amount of diacid **14** indicates that intramolecular addition of acyl radical **18** to form **23** is much faster than the trapping by oxygen to afford **22** (*i.e.*, ultimately **14**). The anhydride formation in benzene is only 3% from CQ[19] and <1% from PhQ, suggesting that the anhydride formation from α-diketones is not a general or primary photochemical event.

In the photooxidation of PQ the predominant formation of diphenic acid (**3**) and peroxy acid (**4**) suggests that, after fast C–C scission in **25**, the resulting diradical **26** is effectively trapped by oxygen (Eq. 6). In other words, an intramolecular cyclization of **26** to **9** or to diradical **23** is much slower than the trapping of acyl radical **26** by oxygen. One reason for the unfavorable intramolecular coupling of **26** (or **18**) may be the free rotation of two aryl rings in **26**, which is not the case for AcQ or CQ of fixed carbon skelton. Another reason is probably due to spin multiplicity effect.[31] There are many cases where coupling products from triplet radical pairs are of much lower yields than those of corresponding singlet ones.[32] The present reaction of triplet quinones with oxygen would produce predominantly triplet or quintet diradical **25** and hence **26**.[33] Thus the ring closure of **26** to **9** becomes less efficient as observed.

In conclusion, the photooxidation of PhQ proceeds *via* the similar pathway (*i.e.*, **17**→**18**→**22**) as is the case for acyclic benzil, while AcQ gives anhydride probably by way of **17**→**18**→**23**→**20**. The photoepoxidation with cyclic α-diketones is not efficient, 1:1 cycloadditions being predominant. The epoxidation as a minor reaction affords chiefly *trans*-epoxide accompanying a significant amount of C–C cleavage products. The addition of DMSO results in much higher selectivity for *trans*-epoxide. These facts suggest that the photoepoxidation with cyclic α-diketones proceeds by way of acylperoxyl radical just as acyclic ones.

Experimental

Melting points were measured by a Yanagimoto micro melting point apparatus and are corrected. ^{1}H NMR spectra were recorded with a Hitachi R24-B spectrometer, IR spectra with a Perkin-Elmer 337 spectrometer, and UV with a Hitachi 124 spectrophotometer. GLC analysis were performed with a Yanagimoto G 180 gas chromatograph using two different 1 m columns: PEG 20M, 20% on Chamelite CK; Silicon OV-17, 5% on Shimalite W.

Materials. AcQ and PhQ were prepared according to literatures, mp 260 °C (lit,[34] 259—260 °C) and 205—208 °C (lit,[35] 209—210 °C), respectively. CQ was obtained by selenium dioxide oxidation of camphor in AcOH (reflux, 2 h), mp 198—199 °C (lit,[36] 198 °C). *cis*-Stilbene (95% pure) was obtained by benzil-sensitized photoisomerization of *trans*-stilbene. Other olefins were of commercial sources.

Photooxidation of PhQ. A typical procedure is as follows. A 5 ml benzene solution of 2.5 mM PhQ was irradiated under oxygen through a Pyrex filter using a medium pressure 300 W Hg lamp at *ca.* 20 °C. Products were determined by GLC directly and carboxylic acids were analyzed after methylation with diazomethane. Peroxy acid was titrated as described previously.[37] A small amount of 2,2′-biphenylcarbolactone **5** was detected by GLC, but diphenic anhydride was not. Diphenic acid was identified as dimethyl ester and also by the thermal conversion to diphenic anhydride.

The photoepoxidation of olefins with diketone was conducted similarly and resulting allylic hydroperoxides were determined after the reduction with $NaBH_4$ and MeOH. The results are listed in Table 1. Since the cycloaddition of PhQ with olefins has extensively studied,[13,14] the 1:1 adducts were not isolated.

Quantum yields for the photooxidation of PhQ were determined using trioxalatoferrate(III) actinometry[38] and/or a merry-go-round apparatus.

Photooxidation of AcQ. The photooxidation of AcQ was carried out similarly with the PhQ case. The GLC analysis showed a predominant formation of anhydride **13** together with a minor amount of diacid (**14**).

The photoepoxidation of olefins with AcQ were conducted similarly and the results are shown in Table 2. As exemplified below, the major photochemical reaction of AcQ with olefins is 1,2- or 1,4-cycloaddition to yield oxetanes (**11**) or **10**.

Photoreaction of AcQ with 1,2-Dimethylcyclohexene. A CH_2Cl_2 solution (20 ml) of AcQ (60 mg) and 1,2-dimethylcyclohexene (0.15 ml) was irradiated under air for 5 h. The NMR spectra of the crude reaction mixture indicated a single reaction product. Purification by passing through a Florisil column (20 g) using hexane–CH_2Cl_2 (9:1) afforded red dihydrodioxin **28** in *ca.* 60% yield, mp 134—136 °C. NMR (δ, CCl_4): 1.5—1.8 (m, 8H, methylenes), 1.39 (s, 6H, two methyl), and 7.2—7.5 (m, 6H, aromatic protons); UV (hexane): 465 and 485 (ε 520), 316 (5100), 303 (5700), and 228 nm (22000).

Found: C, 82.26; H, 7.33; O, 10.41%. Calcd for $C_{20}H_{20}O_2$: C, 82.15; H, 6.89; 10.95%.

The NMR and UV spectra are close to those of the corresponding dihydroxin from AcQ and 2,3-dimethyl-2-butene; NMR (δ), 1.37 and 7.2—7.5; UV, 450, 318, 306, and 230 nm.[17]

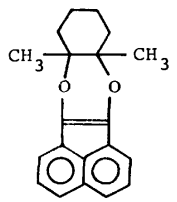

28

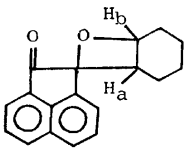

29

Photoreaction of AcQ with Cyclohexene. A similar reaction of AcQ with cyclohexene under air and column chromatography using hexane–CH_2Cl_2 (1:1) gave oxetane **29** in 65% yield. NMR spectra (δ, $CDCl_3$), 1.2—2.2 (m, 8H, methylenes), 3.10 (q, J=20 Hz, H_a), 5.5—5.8 (m, H_b) and 7.5—8.2 (m, 6H, aromatic protons); UV (hexane), 338 (ε 3300), 325 (sh, 3600), 310 (4420), 300 (sh, 3800), 277 (2700), and 223 nm (3600).

Photoreaction of AcQ with 1,1-Diphenylethylene. The 5 h irradiation of AcQ (60 mg) and olefin (120 mg) in CH_2Cl_2 (20 ml) under air yielded a single product as checked by NMR. Purification by passing through a Florisil column using CH_2Cl_2 and recrystallization from hexane–CH_2Cl_2 gave pure crystals of oxetane **30a** in 19% yield, mp 220—224 °C (decomp). NMR spectra (δ, $CDCl_3$), 5.53 (d, J=6 Hz, H_a), 6.10 (d, J=6 Hz, H_a) and 6.5—8.1 (m, 16H aromatic protons). IR (Nujol), 1730 cm^{-1} (C=O); UV (hexane), 342 (ε 3000), 325 (sh, 2780), 313 (3620), 300 (sh, 2850), 284 (sh, 3140), 254 (sh, 6750), and 223 nm (16000). The structure **30a** as shown was deduced from the NMR spectra in comparison to corresponding protons in oxetanes.[39]

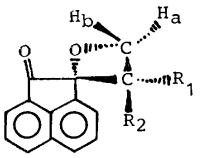

30

a R_1 = R_2 = Ph

b R_1 = Me, R_2 = Ph

c R_1 = Ph, R_2 = Me

Photoreaction of AcQ with α-Methylstyrene. The irradiation of CH_2Cl_2 solution (25 ml) of AcQ (60 mg) and α-methylstyrene (0.3 ml) under air afforded 1:1 mixture of two oxetane isomers in the combined yield of over 90% as determined by NMR. The two isomers were separated by passing a Florisil column (50 ml) using hexane–CH_2Cl_2 (1:1). The earlier fractions gave 4 mg (6%) of pure oxetane **30b**, mp 102—108 °C; NMR (δ, CCl_4), 1.71 (s, 3H, CH_3), 4.93 (d, J=6 Hz, 1H, H_a), 5.38 (d, J=6 Hz, 1H, H_b) and 6.4—8.0 (m, 11H, aromatic protons).

The latter fractions, after the recrystallization from hexane–CH_2Cl_2, afforded pure oxetane **30c** in 6% yield, mp 161—161.5 °C; NMR (δ, CCl_4), 1.82 (s, 3H, CH_3), 4.40 (d, J=5 Hz, 1H, H_a), 5.82 (d, J=5 Hz, 1H, H_b) and 6.4—8.0 (m, 11H, aromatic protons). UV spectra in hexane are the same for **30b** and **30c**; 337 (ε 3020), 326 (sh, 2940), 312 (4140), 300 (3560), 284 (sh, 3200), 260 (sh, 5750), 252 (6680), and 223 nm (27000). IR (film): 1730 cm^{-1} (C=O).

Found: C, 88.88; H, 5.71%. Calcd for $C_{21}H_{16}O$: C, 88.98; H, 5.37%.

References

1) M. Koizumi, S. Kato, N. Mataga, and T. Matsuura, "Photosensitized Reactions," Kagakudozin, Kyoto (1978).

2) C. S. Foote, *Acc. Chem. Res.*, **1**, 104 (1968); K. Gollnick, *Adv. Photochem.*, **6**, 1 (1968); R. W. Denny and A. Nickon, *Org. React.*, **20**, 133 (1973).

3) P. D. Bartlett, *Chem. Soc. Rev.*, **1976**, 149; P. D. Bartlett, "Organic Free Radicals," ed by W. A. Pryor, Am. Chem. Soc., Washington D. C. (1978), p. 15; P. D. Bartlett and H. S. Ho, *J. Am. Chem. Soc.*, **96**, 627 (1974); C. W. Jefford and A. F. Boshung, *Helv. Chim. Acta*, **57**, 2257 (1974); P. D. Bartlett and M. E. Landies, *J. Am. Chem. Soc.*, **99**, 3033 (1979).

4) a) N. Shimizu and P. D. Bartlett, *J. Am. Chem. Soc.*, **98**, 4193 (1976); b) P. D. Bartlett and J. Becherer, *Tatrahedron Lett.*, **1978**, 2983; c) P. D. Bartlett, A. A. M. Roof, and N. Shimizu, *J. Am. Chem. Soc.*, **104**, 3130 (1982).

5) J. Eriksen, C. S. Foote, and T. L. Parker, *J. Am. Chem. Soc.*, **99**, 6455 (1977); J. Eriksen and C. S. Foote, *ibid.*, **102**, 6083 (1980).

6) H. S. Ryang and S. Y. Wang, *J. Am. Chem. Soc.*, **100**, 1302 (1978); M. Malacria and J. Goré, *J. Org. Chem.*, **44**, 885 (1979); G. Buchi, K. W. Fowler, and A. M. Nadzam, *J. Am. Chem. Soc.*, **104**, 544 (1982).

7) Y. Sawaki and C. S. Foote, submitted for publication.

8) J. Y. Koo and G. B. Shuster, *J. Org. Chem.*, **44**, 847 (1979).

9) Y. Sawaki and Y. Ogata, *J. Am. Chem. Soc.*, **103**, 2049 (1981).

10) J. Saltiel and H. C. Curtis, *Mol. Photochem.*, **1**, 239 (1969).

11) a) F. Ramirez, N. B. Desai, and R. B. Mitra, *J. Am. Chem. Soc.*, **83**, 492 (1961); b) J. Y. Koo and G. B. Schuster, *ibid.*, **99**, 6107 (1977).

12) N. J. Turro, "Modern Molecular Photochemistry," Benjamin/Cummings, Menlo Park, Calif., (1978), pp. 354 and 589; Ref. 1, p. 220.

13) a) A. Schönberg, "Preparative Organic Photochemistry," Springer-Verlag, New York (1968), p. 119; b) G. P. Fundt and G. O. Schenck, "1,4-Cycloadditons," ed by J. Hamer, Academic Press, New York (1967), p. 345.
14) a) S. Farid and K. H. Scholz, *Chem. Commun.*, **1968**, 412; b) Y. L. Chow, J. C. Joseph, H. H. Quon, and J. N. S. Tam, *Can. J. Chem.*, **48**, 3045 (1970); c) T. Sasaki, K. Kanematsu, I. Ando, and O. Yamashita, *J. Am. Chem. Soc.*, **99**, 871 (1977); d) K. Maruyama, T. Iwai, Y. Naruta, T. Otsuki, and Y. Miyagi, *Bull. Chem. Soc. Jpn.*, **51**, 2052 (1978).
15) a) Ref. 13a, chaps. 18 and 19; b) K. Maruyama, K. Ohno, and J. Osugi, *Bull. Chem. Soc. Jpn.*, **45**, 847 (1972).
16) Y. Sawaki, unpublished results.
17) T. S. Fang and L. A. Singer, *J. Am. Chem. Soc.*, **100**, 6278 (1978).
18) H. Takeshita, A. Mori, M. Funakura, and H. Mametzuka, *Bull. Chem. Soc. Jpn.*, **50**, 315 (1977).
19) J. Meinwald and H. O. Klingele, *J. Am. Chem. Soc.*, **88**, 2071 (1966).
20) G. E. Gream, J. C. Paice, and C. C. R. Ramsay, *Aust. J. Chem.*, **22**, 1229 (1969).
21) M. B. Rubin and R. G. La Barge, *J. Org. Chem.*, **31**, 3283 (1966).
22) F. Tsuchiya and T. Ikawa, *Can. J. Chem.*, **47**, 3191 (1969); R. R. Diaz, K. Selby, and D. J. Waddington, *J. Chem. Soc., Perkin Trans. 2*, **1977**, 360.
23) The peroxy acid oxidation of DMSO is *ca.* 1000-fold faster than that of styrene.[9]
24) The strong irradiation (500 W lamp) of 0.05 M benzil was not effectively quenched by 5 mM DABCO.[7] We suppose that the relatively small amount of DABCO might be oxidized by peroxy acid produced.
25) J. Rigaudy, and N. Paillous, *Tetrahedron Lett.*, **1966**, 4825; C. W. Bird, *Chem. Commun.*, **1968**, 1537.
26) Y. Sawaki and Y. Ogata, *J. Org. Chem.*, **41**, 2340 (1976).
27) It is not facile to convert diacyl peroxides to anhydrides in the absence of deoxygenating agents such as phosphines. Only one exception is the reported reaction of diacyl peroxides with aliphatic olefins to yield anhydrides and epoxides.[28] The present anhydride formation from AcQ, however, does occur smoothly only in the absence of olefins, thus denying the anhydride formation *via* **19**.
28) F. D. Greene and W. Adam, *J. Org. Chem.*, **29**, 136 (1964).
29) C. Walling, "Free Radicals in Solution," Wiley, New York (1957), p. 282; W. H. Urry, D. J. Trecker, and H. D. Hartzler, *J. Org. Chem.*, **29**, 1663 (1964); W. H. Urry, A. Nishihara, and J. H. Niu, *ibid.*, **32**, 347 (1967); D. L. Bunbury and T. T. Chuang, *Can. J. Chem.*, **47**, 2045 (1969).
30) For reactivities of carbonyl oxides, see Y. Sawaki and Y. Ogata, *J. Am. Chem. Soc.*, **103**, 3832 (1981).
31) T. Koenig and H. Fisher, "Free Radicals," ed by J. K. Kochi, Wiley, New York (1973), Vol. I, p. 179.
32) For example, J. R. Fox and G. S. Hammond, *J. Am. Chem. Soc.*, **86**, 4031 (1964); T. Nakata, K. Tokumaru, and O. Shimamura, *Tetrahedron Lett.*, **1967**, 3303; P. R. Story, W. H. Morrison, III, and J. M. Butler, *J. Am. Chem. Soc.*, **91**, 2398 (1969).
33) Ref. 1, p. 218.
34) C. F. M. Allen, J. A. Van Allan, *Org. Synth.*, Coll. Vol. III, p. 1 (1955).
35) S. Kato, M. Maezawa, and J. Hashimoto, *Yuki Gosei Kagaku Kyokai Shi*, **15**, 402 (1957).
36) J. Lifschitz, *Zeit. Phys. Chem.*, **105**, 27 (1923).
37) Y. Sawaki and Y. Ogata, *J. Am. Chem. Soc.*, **98**, 7324 (1976).
38) J. G. Calvert, J. N. Pitts, Jr., "*Photochemistry*," Wiley, New York (1966), p. 783.
39) See for example, Ref. 4a; N. Shimizu, *J. Am. Chem. Soc.*, **96**, 6456 (1974).

The Synthesis of (+)-Coleon A

Takashi MATSUMOTO,* Sachihiko IMAI,* Takashi HIRATA, Yutaka FUKUDA, Tadashi YAMAGUCHI, and Kazuhiro INOUE

Department of Chemistry, Faculty of Science, Hiroshima University, Higashiseada-machi, Naka-ku, Hiroshima 730

(Received April 14, 1983)

Partial methylation of (*R*)-6-hydroxy-3-(3-hydroxypropyl)-7-isopropyl-3,4-dimethylnaphtho[2,3-*b*]furan-2(3*H*)-one followed by benzylation afforded the 6-benzyloxy-3-(3-methoxypropyl) derivative, which was converted into the 9-acetyl derivative by the series of reactions; sodium borohydride reduction, acetylation, alkaline hydrolysis, and Jones oxidation. This was oxidized with *m*-chloroperbenzoic acid to give the 9-acetoxy-5,8-quinone derivative, which was further converted into the 5,6,8,9-tetraacetoxy-3-(3-hydroxypropyl) derivative by hydrogenolysis, reductive acetylation, and demethylation. The tetraacetate in pyridine was treated with *o*-nitrophenyl selenocyanate in the presence of tributylphosphine and the resulting selenide was oxidized with hydrogen peroxide to give the 3-allyl derivative. This was converted into (+)-coleon A lactone by alkaline hydrolysis and subsequent oxidation. Finally, (+)-coleon A lactone was reduced with sodium borohydride to give (+)-coleon A which was also obtained by lithium aluminium hydride reduction of the 3-allyl derivative.

Coleon A (**1**),[1-3] a rare highly oxygenated 1,10-secoabietane derivative, has been isolated from the leaves of *Coleus igniarius* Schweinf. (Labiatae) by Eugster *et al.* In previous papers,[4,5] we have reported the novel conversion of 6-hydroxy-5βH-abieta-6,8,11,13-tetraen-18-oic acid 18,6-lactone derivatives (**IIa—c**) prepared from (+)-dehydroabietic acid (**I**), into the corresponding 1,10-secoabietane derivatives, (*R*)-3-(3-acetoxypropyl)-7-isopropyl-3,4-dimethylnaphtho[2,3-*b*]-furan-2(3*H*)-ones (**IIIa—c**). These 1,10-secoabietane derivatives **III** seemed to be useful intermediates for the synthesis of coleon A (**1**). In order to devise an efficient synthetic route for coleon A, some preliminary experiments were carried out on the introduction of oxygen functions into the naphthalene skeleton of **III** and the conversion of an acetoxypropyl side chain into an allyl group. The results were also reported in the preceding paper.[6] As an extension of the previous work, we now describe the synthesis of (+)-coleon A (**1**) starting from (*R*)-6-hydroxy-3-(3-hydroxypropyl)-7-isopropyl-3,4-dimethylnaphtho[2,3-*b*]furan-2(3*H*)-one (**2**).[6]

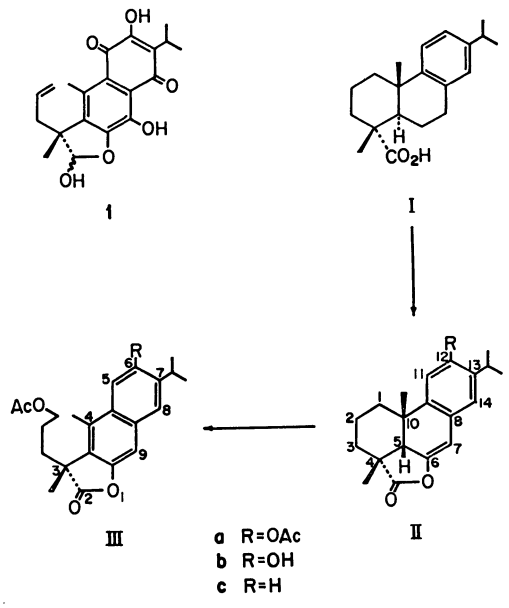

Partial methylation of **2**, prepared from (*R*)-6-acetoxy-3-(3-acetoxypropyl)-7-isopropyl-3,4-dimethylnaphtho[2,3-*b*]furan-2(3*H*)-one (**IIIa**),[2] with diazomethane and boron trifluoride etherate in ether at room temperature afforded the corresponding 6-hydroxy-3-(3-methoxypropyl) derivative (**3**). This was then converted into (*R*)-6-benzyloxy-7-isopropyl-3-(3-methoxypropyl)-3,4-dimethylnaphtho[2,3-*b*]furan-2(3*H*)-one (**4**) by treatment with benzyl chloride and anhydrous potassium carbonate in refluxing *N*,*N*-dimethylformamide. The compound **4** was also obtained from **2** by similar benzylation, followed by methylation of the resulting 6-benzyl ether (**5**). To introduce an acetyl group at C-9,[6] the lactone **4** was reduced with sodium borohydride in ethanol at room temperature and the resulting mixture of C-2 epimeric alcohols (**6**) immediately treated with acetic anhydride in the presence of boron trifluoride etherate at 0—5 °C to give the corresponding 2-acetoxy-9-acetyl derivative (**7**) [IR: 1748 (acetoxyl) and 1679 cm^{-1}(acetyl)]. The structure of **7** was supported by its ^{1}H NMR spectrum which showed singlet signals at δ 2.59 (3H) due to an acetyl and at δ 7.12 (1H) and 8.22 (1H) due to C-5 and C-8 protons. Hydrolysis of the acetoxyl group in **7** with sodium hydrogencarbonate in refluxing aqueous methanol afforded the hemiacetal derivative (**8**), which was oxidized with Jones reagent at 0—5 °C to give (*R*)-9-acetyl-6-benzyloxy-7-isopropyl-3-(3-methoxypropyl)-3,4-dimethylnaphtho[2,3-*b*]furan-2(3*H*)-one (**9**: 42% from **IIIa**). The IR spectrum of **9** showed absorption bands at 1803 (γ-lactone) and 1680 cm^{-1}(acetyl). In order to introduce oxygen functions at C-5, C-8, and C-9 in one stage, the acetyl compound **9** in dichloromethane was refluxed with *m*-chloroperbenzoic acid in the presence of *p*-toluenesulfonic acid monohydrate Purification of the crude product gave three *p*-quinone derivatives, **10** (22%), **11** (3%), and **12** (21%). The IR spectrum of **10** showed absorption bands at 1810 (γ-lactone), 1772 (acetoxyl), 1650 cm^{-1} (*p*-quinone), and its ^{1}H NMR spectrum showed signals at δ 1.17 (6H) and 3.27 (1H) due to an isopropyl, at δ 1.63 (3H) and 2.66 (3H) due to two methyls, at δ 2.42

(3H) due to an acetoxyl, at δ 3.20 (3H) due to a methoxyl, and at δ 5.27 (2H) and 7.2—7.5 (5H) due to a benzyl. These spectral data suggested the structure of **10** to be (*R*)-9-acetoxy-6-benzyloxy-2,3,5,8-tetrahydro-7-isopropyl-3-(3-methoxypropyl)-3,4-dimethylnaphtho[2,3-*b*]furan-2,5,8-trione. The IR spectra of **11** and **12** showed absorption bands at 1809 (γ-lactone), 1698 (acetyl), 1654 cm^{-1} (*p*-quinone), and at 3360 (hydroxyl), 1820 (γ-lactone), 1712 (acetyl), 1652 cm^{-1} (*p*-quinone), respectively. From these spectral data, the structures of **11** and **12** were assigned respectively to be (*R*)-9-acetyl-6-benzyloxy-2,3,5,8-tetrahydro-7-isopropyl-3-(3-methoxypropyl)-3,4-dimethylnaphtho[2,3-*b*]furan-2,5,8-trione and (*R*)-9-acetyl-2,3,5,8-tetrahydro-6-hydroxy-7-isopropyl-3-(3-methoxypropyl)-3,4-dimethylnaphtho[2,3-*b*]furan-2,5,8-trione. These structures were further supported by their ^1H NMR spectra (see Experimental section). In order to examine the effect of other substituents at C-6 for the *m*-chloroperbenzoic acid oxidation, the 6-methoxy (**14**) and 6-acetoxy (**15**) derivatives were also prepared as follows. Hydrogenolysis of **9** in acetic acid with 10% Pd–C at 60 °C afforded the corresponding 6-hydroxy compound (**13**); IR: 3590, 3310 br (hydroxyl), 1798 (γ-lactone), 1673 cm^{-1} (acetyl). The compound **13** was converted into **14** (57% from **9**) [IR: 1807 (γ-lactone), 1680 cm^{-1} (acetyl)] and **15** (96% from **9**) [IR: 1811 (γ-lactone), 1762 (acetoxyl), 1688 cm^{-1} (acetyl)] by methylation with methyl iodide and anhydrous potassium carbonate in refluxing acetone and by acetylation with acetic anhydride in pyridine. Oxidation of **14** with *m*-chloroperbenzoic acid and *p*-toluenesulfonic acid monohydrate in refluxing dichloromethane afforded the desired (*R*)-9-acetoxy-2,3,5,8-tetrahydro-7-isopropyl-6-methoxy-3-(3-methoxypropyl)-3,4-dimethylnaphtho[2,3-*b*]furan-2,5,8-trione (**16**: 11%) [IR: 1808 (γ-lactone), 1768 (acetoxyl), 1652 cm^{-1} (*p*-quinone)] together with its 9-acetyl derivative (**17**: 10%) [IR: 1808 (γ-lactone), 1700 (acetyl), 1657 cm^{-1} (*p*-quinone)]. The similar oxidation of **15** yielded only the Baeyer-Villiger oxidation product, (*R*)-6,9-diacetoxy-7-isopropyl-3-(3-methoxypropyl)-3,4-dimethylnaphtho[2,3-*b*]furan-2(3*H*)-one (**18**: 67%) [IR: 1800 (γ-lactone), 1763, 1754 cm^{-1} (acetoxyls)], and no *p*-quinone derivative. The structure of **18** was supported by its ^1H NMR spectrum, which showed singlet signals at δ 2.38 (3H) and 2.47 (3H) due to two acetoxyls, and at δ 7.64 (1H) and 7.75 (1H) due to C-5 and C-8 protons. The above oxidation of **9**, **14**, and **15** indicated that a benzyloxyl group at C-6 increased the yield of the desired acetoxy-*p*-quinone derivative: That is, the benzyloxy derivative **9** was superior to the methoxy (**14**) and acetoxy (**15**) derivatives in one-stage oxidation of C-5, C-8, and C-9. Hydrogenolysis of **10** with 10% Pd-C in acetic acid at 60 °C, followed by reductive acetylation with zinc and acetic anhydride in pyridine at room temperature yielded (*R*)-5,6,8,9-tetraacetoxy-7-isopropyl-3-(3-methoxypropyl)-3,4-dimethylnaphtho[2,3-*b*]furan-2(3*H*)-one (**19**: 76%).

Subsequently, the transformation of a methoxypropyl side chain into an allyl group was carried out as follows. Demethylation[7] of **19** with boron tribromide, sodium iodide, and 15-crown-5 in dichloromethane at

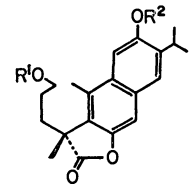

2 $R^1=R^2=H$
3 $R^1=Me$, $R^2=H$
4 $R^1=Me$, $R^2=CH_2Ph$
5 $R^1=H$, $R^2=CH_2Ph$

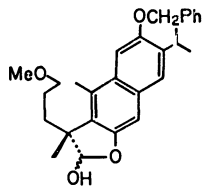

6

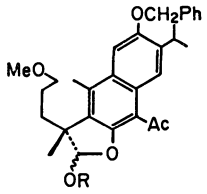

7 R=Ac
8 R=H

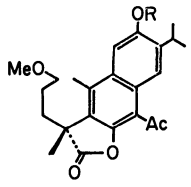

9 $R=CH_2Ph$
13 R=H
14 R=Me
15 R=Ac

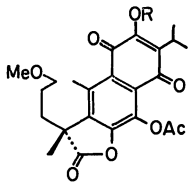

10 $R=CH_2Ph$
16 R=Me

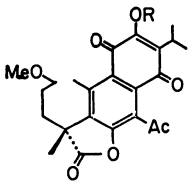

11 $R=CH_2Ph$
12 R=H
17 R=Me

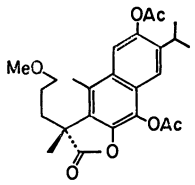

18

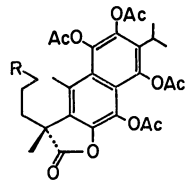

19 R=OMe
20 R=OH
21 $R=SeC_6H_4NO_2(o\text{-})$

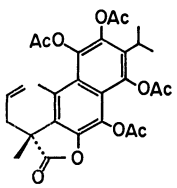

22

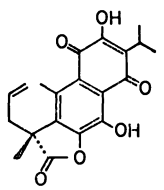

23

—30 °C under a stream of nitrogen afforded the 3-(3-hydroxypropyl) derivative (**20**). This was immediately treated with *o*-nitrophenyl selenocyanate and tributylphosphine in pyridine[8] at room temperature under a stream of nitrogen to give a selenide (**21**: 75% from **19**). Oxidation of **21** with 50% hydrogen peroxide in tetrahydrofuran at room temperature yielded (*R*)-5,6,8,9-tetraacetoxy-3-allyl-7-isopropyl-3,4-dimeth-

ylnaphtho[2,3-*b*]furan-2(3*H*)-one (**22**: 87%), whose ^{1}H NMR spectrum showed signals at δ 2.34 (6H), 2.38 (3H), and 2.39 (3H) due to four acetoxyls and at δ 2.79 (2H) and 4.85—5.6 (3H) due to an allyl. The allyl derivative **22** was then converted into (*R*)-3-allyl-2,3,5,8-tetrahydro-6,9-dihydroxy-7-isopropyl-3,4-dimethylnaphtho[2,3-*b*]furan-2,5,8-trione (**23**: 40%) [$[\alpha]_D$ +145° (EtOH); IR: 3325 (hydroxyls), 1808 (γ-lactone), 1647 cm^{-1} (*p*-quinone)] by hydrolysis with aqueous potassium hydroxide in refluxing methanol, followed by oxidation with oxygen and subsequent treatment with dilute hydrochloric acid. Reduction of **23** with sodium borohydride in aqueous ethanol afforded a mixture of C-2 epimeric alcohols (**1**: 75%), mp 140.5—141.5 °C, $[\alpha]_D$ +88° ($CHCl_3$); IR: 3580, 3495, 3305 (hydroxyls), 1657 cm^{-1} (*p*-quinone). Compound **1** was also obtained by reduction of **22** with lithium aluminium hydride in refluxing tetrahydrofuran in 34% yield. The physical and spectral data of the synthetic **1** and **23** were in good agreement with those of natural coleon A, mp 136—136.5 °C, $[\alpha]_D$ +80° ($CHCl_3$), and coleon A lactone, $[\alpha]_D$ +144° (EtOH). From the present study, the stetreochemistry of C-3 in coleon A (**1**) was conclusively assigned to be the *R*-configuration, which was previously suggested by Eugster[3,9] on the basis of the incorporation experiments using [2-^{14}C]mevalonic acid.

Experimental

All melting points are uncorrected. The IR spectra and optical rotations were measured in chloroform, and the ^{1}H NMR spectra in deuteriochloroform at 90 MHz, with tetramethylsilane as an internal standard, unless otherwise stated. The chemical shifts are presented in terms of δ values; s: singlet, bs: broad singlet, d: doublet, bd: broad doublet, t: triplet, m: multiplet. The column chromatography was performed using Merck silica gel (0.063 mm).

(R)-6-Benzyloxy-7-isopropyl-3-(3-methoxypropyl)-3,4-dimethylnaphtho[2,3-b]furan-2(3H)-one (4). (*R*)-6-Acetoxy-3-(3-acetoxypropyl)-7-isopropyl-3,4-dimethylnaphtho[2,3-*b*]furan-2(3*H*)-one (**IIIa**)[2] (16.50 g) was hydrolyzed by the known procedure[6] to give the crude (*R*)-6-hydroxy-3-(3-hydroxypropyl)-7-isopropyl-3,4-dimethylnaphtho[2,3-*b*]furan-2(3*H*)-one (**2**)[6] (13.10 g).

a): To a solution of the above crude **2** (13.10 g) in ether (400 ml) was added successively boron trifluoride etherate (6.40 ml) and a diazomethane ether solution (800 ml), which was prepared from *N*-methyl-*N*-nitrosourea (80 g) by the known procedure and dried over potassium hydroxide. The mixture was allowed to stand at room temperature for 30 min and then filtered to remove resinous material. The filtrate was washed with aqueous sodium hydrogencarbonate and brine, dried over sodium sulfate, and evaporated *in vacuo* to give the crude 6-hydroxy-3-(3-methoxypropyl) derivative (**3**) (13.80 g). IR: 3590, 3300br, 1785, 1620 cm^{-1}; ^{1}H NMR: δ=1.32 (6H, d, J=7 Hz, $-CH(C\underline{H}_3)_2$), 1.61 (3H, s, C_3-CH_3), 2.50 (3H, s, C_4-CH_3), 3.22 (3H, s, $-OCH_3$), 3.27 (2H, t, J=6 Hz, $-C\underline{H}_2OMe$), 3.44 (1H, m, $-C\underline{H}(CH_3)_2$), 6.68 (1H, br, C_6–OH, disappeared with D_2O), 7.23 (2H, s, C_5–H and C_9–H), 7.54 (1H, s, C_8–H).

A mixture of crude **3** (13.80 g), benzyl chloride (5.30 ml), and anhydrous potassium carbonate (58 g) in *N,N*-dimethylformamide (143 ml) was refluxed for 30 min. The mixture was poured into water, acidified with dilute hydrochloric acid, and extracted with ether. The ether extract was washed with brine, dried over sodium sulfate, and evaporated *in vacuo* to give the crude **4** (17.75 g) which was used without purification in the next reaction. The crude **4** obtained from another experiment was purified by column chromatography on silica gel, using ether–benzene (1:9) as the eluent, to give pure **4**. $[\alpha]_D$ +40° (*c* 1.13); IR: 1800, 1645, 1628 cm^{-1}; ^{1}H NMR (CCl_4): δ=1.32 (6H, d, J=7 Hz, $-CH(C\underline{H}_3)_2$), 1.58 (3H, s, C_3-CH_3), 2.54 (3H, s, C_4-CH_3), 3.12 (3H, s, $-OCH_3$), 3.13 (2H, t, J=6 Hz, $-C\underline{H}_2OMe$), 3.47 (1H, m, $-C\underline{H}(CH_3)_2$), 5.18 (2H, s, $-OC\underline{H}_2Ph$), 7.17 (2H, bs, C_5–H and C_9–H), *ca.* 7.2—7.5 (5H, m, $-OCH_2C_6\underline{H}_5$), 7.51 (1H, s, C_8–H). Found: C, 77.64; H, 7.45%. Calcd for $C_{28}H_{32}O_4$: C, 77.75; H, 7.46%.

b): A mixture of the crude **2** (4.00 g) prepared from **IIIa** (4.99 g), benzyl chloride (2.15 ml), anhydrous potassium carbonate (17.0 g), and potassium iodide (2.10 g) in acetone (120 ml) was refluxed for 8 h and then allowed to stand overnight at room temperature. After the mixture had been filtered, the filtrate was evaporated *in vacuo* and the residue was diluted with ether. The ether solution was washed with aqueous sodium thiosulfate and brine, dried over sodium sulfate, and evaporated *in vacuo* to give the crude 6-benzyloxy derivative (**5**) (5.30 g). The crude **5** obtained from another experiment was purified by column chromatography on silica gel, using ether–benzene (1:9) as the eluent, to give pure **5**. $[\alpha]_D$ +41° (*c* 2.24); IR: 3430br, 1797, 1640, 1625 cm^{-1}; ^{1}H NMR: δ=1.35 (6H, d, J=7 Hz, $-CH(C\underline{H}_3)_2$), 1.53 (1H, br, –OH, disappeared with D_2O), 1.65 (3H, s, C_3-CH_3), 2.60 (3H, s, C_4-CH_3), 3.47 (2H, t, J=6 Hz, $-C\underline{H}_2OH$), 3.51 (1H, m, $-C\underline{H}(CH_3)_2$), 5.23 (2H, s, $-OC\underline{H}_2Ph$), 7.27 (2H, s, C_5–H and C_9–H), *ca.* 7.30—7.55 (5H, m, $-OCH_2C_6\underline{H}_5$), 7.58 (1H, s, C_8–H). Found: C, 77.76; H, 7.33%. Calcd for $C_{27}H_{30}O_4$: C, 77.48; H, 7.23%.

To a stirred solution of the crude **5** (5.30 g) in ether (290 ml) was added successively boron trifluoride etherate (2.9 ml) and a diazomethane ether solution (250 ml) which was prepared from *N*-methyl-*N*-nitrosourea (25 g) by the known procedure. After work-up as described for the preparation of **3**, crude **4** (5.49 g) was obtained.

(R)-9-Acetyl-6-benzyloxy-7-isopropyl-3-(3-methoxypropyl)-3,4-dimethylnaphtho[2,3-b]furan-2(3H)-one (9). *a)*: Sodium borohydride (3.33 g) was added portionwise to a stirred solution of the crude **4** (17.75 g, prepared from **3**) in ethanol (720 ml) with cooling in an ice-water bath. The mixture was stirred at this temperature for 1 h and then at room temperature for 15 h. After the excess hydride had been decomposed with acetone, the mixture was concentrated *in vacuo*, poured into dilute hydrochloric acid, and extracted with chloroform. The chloroform extract was washed with brine, dried over sodium sulfate, and evaporated *in vacuo* to give a mixture of the crude C-2 epimeric alcohols (**6**) (16.50 g) which was used without purification in the next reaction. IR: 3610, 3350br, 1628 cm^{-1}; ^{1}H NMR (CCl_4): δ=1.30 (6H, d, J=7 Hz, $-CH(C\underline{H}_3)_2$), 1.37 and 1.43 (3H, each s, C_3-CH_3), 2.50 (3H, s, C_4-CH_3), 3.18 and 3.23 (3H, each s, $-OCH_3$), *ca.* 3.1—3.3 (2H, m, $-C\underline{H}_2OMe$), 3.43 (1H, m, $-C\underline{H}(CH_3)_2$), 5.11 (2H, s, $-OC\underline{H}_2Ph$), 5.34 and 5.46 (1H, each s, *ca.* 1:3, C_2–H), 6.82 (1H, s, C_9–H), 7.10 (1H, s, C_5–H), *ca.* 7.2—7.5 (6H, m, C_8–H and $-OCH_2C_6\underline{H}_5$).

Boron trifluoride etherate (16.5 ml) was added to a stirred solution of the crude **6** (16.50 g) in acetic anhydride (330 ml) at 0—5 °C. The mixture was stirred at this temperature for 4 min, poured into a mixture of ice and aqueous sodium hydrogencarbonate, and extracted with chloroform. The chloroform extract was washed with brine, dried over sodium

sulfate, and evaporated *in vacuo* to give a crude epimeric mixture at C-2 of 2-acetoxy-9-acetyl-6-benzyloxy derivative (**7**) (20.00 g) which was used without purification in the next reaction. The crude **7** obtained from another experiment was purified by column chromatography on silica gel, using ether–benzene (8:92) as the eluent, to give pure C-2 epimeric mixture. IR: 1748, 1679 cm^{-1}; ^1H NMR (CCl_4): δ=1.32 (6H, d, J=7 Hz, $-CH(C\underline{H}_3)_2$), 1.43 and 1.50 (3H, each s, C_3-CH_3), 1.92 and 2.03 (3H, each s, $-OCOCH_3$), 2.53 (3H, s, C_4-CH_3), 2.59 (3H, s, C_9-COCH_3), 3.17 and 3.23 (3H, each s, $-OCH_3$), *ca.* 3.1—3.3 (2H, m, $-C\underline{H}_2OMe$), 3.45 (1H, m, $-C\underline{H}(CH_3)_2$), 5.16 (2H, s, $-OC\underline{H}_2Ph$), 6.38 and 6.47 (1H, each s, *ca.* 1:3, C_2-H), 7.12 (1H, s, C_5-H), *ca.* 7.2—7.5 (5H, m, $-OCH_2C_6\underline{H}_5$), 8.22 (1H, s, C_8-H). Found: C, 74.28; H, 7.51%. Calcd for $C_{32}H_{38}O_6$: C, 74.10; H, 7.39%.

A mixture of crude **7** (20.00 g) and sodium hydrogencarbonate (17.0 g) in methanol (1600 ml) and water (340 ml) was refluxed for 2 h. The mixture was concentrated *in vacuo* to *ca.* 500 ml, diluted with brine, and extracted with ether. The ether extract was washed with brine, dried over sodium sulfate, and evaporated *in vacuo* to give a crude epimeric mixture at C-2 of 9-acetyl-6-benzyloxy-2-hydroxy derivative (**8**) (17.30 g) which was used without purification in the next reaction. IR: 3610, 3325br, 1668 cm^{-1}; ^1H NMR (60 MHz, CCl_4): δ=1.31 (6H, d, J=7 Hz, $-CH(C\underline{H}_3)_2$), 1.28 and 1.37 (3H, each s, C_3-CH_3), 2.47 (3H, s, C_4-CH_3), 2.61 (3H, s, C_9-COCH_3), 3.12 and 3.18 (3H, each s, $-OCH_3$), *ca.* 3.0—3.3 (2H, m, $-C\underline{H}_2OMe$), 3.42 (1H, m, $-C\underline{H}(CH_3)_2$), 5.09 (2H, s, $-OC\underline{H}_2Ph$), *ca.* 5.2—5.5 (2H, m, C_2-H and $-OH$), 7.05 (1H, s, C_5-H), *ca.* 7.1—7.5 (5H, m, $-OCH_2C_6\underline{H}_5$), 8.13 (1H, s, C_8-H).

Jones reagent [2.5 M (1 M=1 mol dm^{-3}): 28.8 ml] was added dropwise to a stirred solution of crude **8** (17.30 g) in acetone (440 ml) at 0—5 °C. The mixture was stirred at this temperature for 15 min and the excess oxidant decomposed with methanol. The mixture was poured into brine and extracted with ether. The ether extract was washed with brine, dried over sodium sulfate, and evaporated *in vacuo*. The residue was chromatographed on silica gel (750 g), using ether–benzene (3:97) as the eluent, to give **9** (8.06 g: 42.4% from **IIIa**). This was recrystallized from methanol, mp 140 °C, $[\alpha]_D$ +28° (*c* 0.830); IR: 1803, 1680, 1623 cm^{-1}; ^1H NMR (CCl_4): δ=1.34 (6H, d, J=7 Hz, $-CH(C\underline{H}_3)_2$), 1.60 (3H, s, C_3-CH_3), 2.55 (3H, s, C_4-CH_3), 2.70 (3H, s, C_9-COCH_3), 3.12 (3H, s, $-OCH_3$), 3.15 (2H, t, J=6 Hz, $-C\underline{H}_2OMe$), 3.46 (1H, m, $-C\underline{H}(CH_3)_2$), 5.18 (2H, s, $-OC\underline{H}_2Ph$), 7.17 (1H, s, C_5-H), *ca.* 7.2—7.5 (5H, m, $-OCH_2C_6\underline{H}_5$), 8.16 (1H, s, C_8-H). Found: C, 76.00; H, 7.40%. Calcd for $C_{30}H_{34}O_5$: C, 75.92; H, 7.22%.

b): The crude **4** (5.49 g, prepared from **5**) was also subjected to a series of reactions in *a)* to yield **9** (2.35 g: 40.9% from **IIIa**).

Oxidation of ***9*** *with* m-*Chloroperbenzoic Acid.* A mixture of **9** (950 mg), *m*-chloroperbenzoic acid (90%: 1550 mg), and *p*-toluenesulfonic acid monohydrate (95 mg) in dichloromethane (47.5 ml) was refluxed for 3 h. The mixture was diluted with ether and the ether solution washed successively with aqueous potassium iodide, aqueous sodium thiosulfate, aqueous sodium hydrogencarbonate, and brine. The dried solution was evaporated *in vacuo*. The residue was chromatographed on silica gel (100 g), using ether–benzene (1:99) as the eluent, to give (*R*)-9-acetoxy-6-benzyloxy-2,3,5,8-tetrahydro-7-isopropyl-3-(3-methoxypropyl)-3,4-dimethylnaphtho[2,3-*b*]furan-2,5,8-trione (**10**) (231 mg: 22.2 %). This was recrystallized from methanol, mp 147.5—148,5 °C, $[\alpha]_D$ +32° (*c* 3.32); IR: 1810, 1772, 1650, 1612, 1576 cm^{-1}; ^1H NMR: δ=1.17 (6H, d, J=7 Hz, $-CH(C\underline{H}_3)_2$), 1.63 (3H, s, C_3-CH_3), 2.42 (3H, s, $C_9-OCOCH_3$), 2.66 (3H, s, C_4-CH_3), 3.20 (3H, s, $-OCH_3$), 3.23 (2H, t, J=6 Hz, $-C\underline{H}_2OMe$), 3.27 (1H, m, $-C\underline{H}(CH_3)_2$), 5.27 (2H, s, $-OC\underline{H}_2Ph$), *ca.* 7.2—7.5 (5H, m, $-OCH_2C_6\underline{H}_5$). Found: C, 68.93; H, 6.15%. Calcd for $C_{30}H_{32}O_8$: C, 69.21; H, 6.20%.

Subsequent elution with ether–benzene (3:97) afforded (*R*)-9-acetyl-6-benzyloxy-2,3,5,8-tetrahydro-7-isopropyl-3-(3-methoxypropyl)-3,4-dimethylnaphtho[2,3-*b*]furan-2,5,8-trione (**11**) (32 mg: 3.2%), $[\alpha]_D$ +23° (*c* 3.12); IR: 1809, 1698, 1654, 1610, 1568 cm^{-1}; ^1H NMR: δ=1.17 (6H, d, J=7 Hz, $-CH(C\underline{H}_3)_2$), 1.62 (3H, s, C_3-CH_3), 2.55 (3H, s, C_9-COCH_3), 2.71 (3H, s, C_4-CH_3), 3.20 (3H, s, $-OCH_3$), 3.23 (2H, t, J=6 Hz, $-C\underline{H}_2OMe$), 3.29 (1H, m, $-C\underline{H}(CH_3)_2$), 5.32 (2H, s, $-OC\underline{H}_2Ph$), *ca.* 7.25—7.5 (5H, m, $-OCH_2C_6\underline{H}_5$). Found: C, 71.44; H, 6.48%. Calcd for $C_{30}H_{32}O_7$: C, 71.41; H, 6.39%.

Further elution with ether–benzene (1:9) afforded (*R*)-9-acetyl-2,3,5,8-tetrahydro-6-hydroxy-7-isopropyl-3-(3-methoxypropyl)-3,4-dimethylnaphtho[2,3-*b*]furan-2,5,8-trione (**12**) (171 mg: 20.6%), $[\alpha]_D$ +26° (*c* 0.35); IR: 3360, 1820, 1712, 1652, 1605, 1580 cm^{-1}; ^1H NMR: δ=1.27 (6H, d, J=7 Hz, $-CH(C\underline{H}_3)_2$), 1.62 (3H, s, C_3-CH_3), 2.57 (3H, s, C_9-COCH_3), 2.76 (3H, s, C_4-CH_3), 3.20 (3H, s, $-OCH_3$), 3.24 (2H, t, J=6 Hz, $-C\underline{H}_2OMe$), 3.30 (1H, m, $-C\underline{H}(CH_3)_2$), 7.79 (1H, bs, C_6-OH, disappeared with D_2O). Found: C, 66.37; H, 6.38%. Calcd for $C_{23}H_{26}O_7$: C, 66.65; H, 6.32%.

*(R)-9-Acetyl-6-hydroxy-7-isopropyl-3-(3-methoxypropyl)-3,4-dimethylnaphtho[2,3-b]furan-2(3H)-one (**13**).* A mixture of **9** (4.75 g) and 10% Pd–C (1.43 g) in acetic acid (47.5 ml) was submitted to catalytic hydrogenation with 1 atm hydrogen pressure at 60 °C. After the usual work-up, the crude product was chromatographed on silica gel (100 g), using ether–benzene (1:9) as the eluent, to give **13** (3.33 g: 86.5%). This was recrystallized from aqueous methanol, mp 158.5—159.5 °C, $[\alpha]_D$ +19° (*c* 2.42); IR: 3590, 3310br, 1798, 1673, 1615 cm^{-1}; ^1H NMR: δ=1.27 and 1.30 (each 3H, d, and J=7 Hz, $-CH(C\underline{H}_3)_2$), 1.64 (3H, s, C_3-CH_3), 2.47 (3H, s, C_4-CH_3), 2.77 (3H, s, C_9-COCH_3), 3.22 (3H, s, $-OCH_3$), 3.27 (2H, t, J=6 Hz, $-C\underline{H}_2OMe$), 3.30 (1H, m, $-C\underline{H}(CH_3)_2$), 6.07 (1H, br, $-OH$, disappeared with D_2O), 7.17 (1H, s, C_5-H), 8.09 (1H, s, C_8-H). Found: C, 71.67; H, 7.37%. Calcd for $C_{23}H_{28}O_5$: C, 71.85; H, 7.34%.

*(R)-9-Acetyl-7-isopropyl-6-methoxy-3-(3-methoxypropyl)-3,4-dimethylnaphtho[2,3-b]furan-2(3H)-one (**14**).* A mixture of **13** (193 mg), methyl iodide (142 mg), and anhydrous potassium carbonate (667 mg) in acetone (4.0 ml) was refluxed for 2 h. The mixture was filtered and the filtrate was evaporated *in vacuo*. The residue was extracted with ether. The ether extract was washed successively with aqueous sodium thiosulfate and brine, dried over sodium sulfate, and evaporated *in vacuo*. The crude product was purified by column chromatography on silica gel (20 g), using ether–benzene (3:97) as the eluent, to give **14** (131 mg: 65.4%). $[\alpha]_D$ +17° (*c* 1.87); IR: 1807, 1680, 1621, 1600 cm^{-1}; ^1H NMR: δ=1.30 (6H, d, J=7 Hz, $-CH(C\underline{H}_3)_2$), 1.67 (3H, s, C_3-CH_3), 2.67 (3H, s, C_4-CH_3), 2.77 (3H, s, C_9-COCH_3), 3.21 (3H, s, $-OCH_3$), 3.24 (2H, t, J=6 Hz, $-C\underline{H}_2OMe$), 3.42 (1H, m, $-C\underline{H}(CH_3)_2$), 3.97 (3H, s, C_6-OCH_3), 7.22 (1H, s, C_5-H), 8.13 (1H, s, C_8-H). Found: C, 72.60; H, 7.64%. Calcd for $C_{24}H_{30}O_5$: C, 72.33; H, 7.59%.

*(R)-6-Acetoxy-9-acetyl-7-isopropyl-3-(3-methoxypropyl)-3,4-dimethylnaphtho[2,3-b]furan-2(3H)-one (**15**).* The crude phenol **13** (872 mg) prepared from **9** (977 mg) was acetylated with acetic anhydride (4.4 ml) in pyridine (4.4 ml) at room

temperature for 12 h. After the usual work-up, the crude product was chromatographed on silica gel (100 g), using ether–benzene (1:9) as the eluent, to give **15** (844 mg: 96.1% from **9**). $[\alpha]_D$ +16° (*c* 2.88); IR: 1811, 1762, 1688, 1628, 1601 cm^{-1}; ^1H NMR: δ=1.30 (6H, d, J=7 Hz, $-CH(C\underline{H}_3)_2$), 1.66 (3H, s, C_3-CH_3), 2.39 (3H, s, $C_6-OCOCH_3$), 2.64 (3H, s, C_4-CH_3), 2.77 (3H, s, C_9-COCH_3), 3.13 (1H, m, $-C\underline{H}(CH_3)_2$), 3.20 (3H, s, $-OCH_3$), 3.23 (3H, t, J=6 Hz, $-C\underline{H}_2OMe$), 7.65 (1H, s, C_5-H), 8.28 (1H, s, C_8-H). Found: C, 70.20; H, 7.37%. Calcd for $C_{25}H_{30}O_6$: C, 70.40; H, 7.09%.

*Oxidation of **14** with* m-*Chloroperbenzoic Acid.* A mixture of **14** (1493 mg), *m*-chloroperbenzoic acid (90%: 2250 mg), and *p*-toluenesulfonic acid monohydrate (30 mg) in dichloromethane (75 ml) was refluxed for 3 h. The mixture was diluted with ether and the ether solution washed successively with aqueous potassium iodide, aqueous sodium thiosulfate, aqueous sodium hydrogencarbonate, and brine. The dried solution was evaporated *in vacuo*. The residue was chromatographed on silica gel (150 g), using ether–benzene (2:98) as the eluent, to give (*R*)-9-acetoxy-2,3,5,8-tetrahydro-7-isopropyl-6-methoxy-3-(3-methoxypropyl)-3,4-dimethylnaphtho[2,3-*b*]furan-2,5,8-trione (**16**) (182 mg: 10.9%). $[\alpha]_D$ +24° (*c* 1.66); IR: 1808, 1768, 1652, 1613 cm^{-1}; ^1H NMR: δ=1.24 (6H, d, J=7 Hz, $-CH(C\underline{H}_3)_2$), 1.64 (3H, s, C_3-CH_3), 2.44 (3H, s, $C_9-OCOCH_3$), 2.68 (3H, s, C_4-CH_3), 3.20 (3H, s, $-OCH_3$), 3.24 (2H, t, J=6 Hz, $-C\underline{H}_2OMe$), 3.29 (1H, m, $-C\underline{H}(CH_3)_2$), 4.00 (3H, s, C_6-OCH_3).

Further elution gave (*R*)-9-acetyl-2,3,5,8-tetrahydro-7-isopropyl-6-methoxy-3-(3-methoxypropyl)-3,4-dimethylnaphtho[2,3-*b*]furan-2,5,8-trione (**17**) (153 mg: 9.5%), $[\alpha]_D$ +9.2° (*c* 2.18); IR: 1808, 1700, 1657, 1612, 1590, 1567 cm^{-1}; ^1H NMR: δ=1.24 (6H, d, J=7 Hz, $-CH(C\underline{H}_3)_2$), 1.62 (3H, s, C_3-CH_3), 2.57 (3H, s, C_9-COCH_3), 2.71 (3H, s, C_4-CH_3), 3.21 (3H, s, $-OCH_3$), 3.24 (2H, t, J=6 Hz, $-C\underline{H}_2OMe$), 3.31 (1H, m, $-C\underline{H}(CH_3)_2$), 4.05 (3H, s, C_6-OCH_3). Found: C, 66.97; H, 6.37%. Calcd for $C_{24}H_{28}O_7$: C, 67.27; H, 6.59%.

*Oxidation of **15** with* m-*Chloroperbenzoic Acid.* A mixture of **15** (954 mg), *m*-chloroperbenzoic acid (90%: 1544 mg), and *p*-toluenesulfonic acid monohydrate (119 mg) in dichloromethane (38 ml) was refluxed for 20 h. After the mixture had been treated as described for the preparation of **16**, the crude product was chromatographed on silica gel (100 g), using ether–benzene (8:92) as the eluent, to give (*R*)-6,9-diacetoxy-7-isopropyl-3-(3-methoxypropyl)-3,4-dimethylnaphtho[2,3-*b*]furan-2(3*H*)-one (**18**) (155 mg: 15.7%). $[\alpha]_D$ +21° (*c* 2.15); IR: 1800, 1763, 1754, 1652, 1619 cm^{-1}; ^1H NMR: δ=1.30 (6H, d, J=7 Hz, $-CH(C\underline{H}_3)_2$), 1.65 (3H, s, C_3-CH_3), 2.38 and 2.47 (each 3H and s, $C_6-OCOCH_3$ and $C_9-OCOCH_3$), 2.59 (3H, s, C_4-CH_3), 3.14 (1H, m, $-C\underline{H}(CH_3)_2$), 3.18 (3H, s, $-OCH_3$), 3.22 (2H, t, J=6 Hz, $-C\underline{H}_2OMe$), 7.64 and 7.75 (each 1H and s, C_5-H and C_8-H). Found: C, 68.14; H, 6.92%. Calcd for $C_{25}H_{30}O_7$: C, 67.85; H, 6.83%. Further elution with the same solvent gave a mixture of **18** and the starting **15** (567 mg, *ca.* 9:1 ratio). The total yield of **18** was *ca.* 67%.

*(R)-5,6,8,9-Tetraacetoxy-7-isopropyl-3-(3-methoxypropyl)-3,4-dimethylnaphtho[2,3-b]furan-2(3H)-one (**19**).* A mixture of **10** (414 mg) and 10% Pd–C (120 mg) in acetic acid (4.2 ml) was submitted to catalytic hydrogenation with 1 atm hydrogen pressure at 60 °C. The crude product, after the usual work-up, was dissolved in acetic anhydride (3.5 ml) and pyridine (3.5 ml) and then zinc powder (130 mg) was added at 0—5 °C. The mixture was stirred at this temperature for 5 min and at room temperature for 1 h, poured into aqueous sodium hydrogencarbonate, and extracted with ether. The ether extract was washed with brine, dried over sodium sulfate, and evaporated *in vacuo*. The residue was chromatographed on silica gel (50 g), using ether–benzene (2:8) as the eluent, to give **19** (339 mg: 76.3 %). This was recrystallized from methanol, mp 243 °C, $[\alpha]_D$ +13° (*c* 2.80); IR: 1809, 1775, 1648, 1616 cm^{-1}; ^1H NMR: δ=1.26 (6H, bd, J=7 Hz, $-CH(C\underline{H}_3)_2$), 1.61 (3H, s, C_3-CH_3), 2.33 and 2.39 (each 6H and s, $C_5-OCOCH_3$, $C_6-OCOCH_3$, $C_8-OCOCH_3$, and $C_9-OCOCH_3$), 2.66 (3H, s, C_4-CH_3), 3.17 (3H, s, $-OCH_3$), 3.21 (3H, m, $-C\underline{H}_2OMe$ and $-C\underline{H}(CH_3)_2$). Found: C, 62.26; H, 6.19%. Calcd for $C_{29}H_{34}O_{11}$: C, 62.36; H, 6.14%.

*(R)-5,6,8,9-Tetraacetoxy-7-isopropyl-3,4-dimethyl-3-[3-(o-nitrophenylselenyl)propyl]naphtho[2,3-b]furan-2(3H)-one (**21**).* Boron tribromide dichloromethane solution (1 M: 1.5 ml) was added at −30 °C to a stirred solution of **19** (276 mg) and the 15-crown-5 dichloromethane solution (0.3 M: 9.9 ml) saturated with sodium iodide, under a stream of nitrogen. The mixture was stirred at −30 °C for 3 h. After the addition of aqueous sodium hydrogencarbonate, the mixture was diluted with ether and the ether solution was washed successively with aqueous sodium thiosulfate and brine. The dried solution was evaporated *in vacuo* to give the crude 3-(3-hydroxypropyl) derivative (**20**) which was used without purification in the next reaction. IR: 3530br, 3380br, 1808, 1775, 1648, 1615 cm^{-1}; ^1H NMR: δ=1.26 (6H, bd, J=7 Hz, $-CH(C\underline{H}_3)_2$), 1.63 (3H, s, C_3-CH_3), 1.74 (1H, br, –OH, disappeared with D_2O), 2.33 and 2.39 (each 6H and s, $C_5-OCOCH_3$, $C_6-OCOCH_3$, $C_8-OCOCH_3$, and $C_9-OCOCH_3$), 2.67 (3H, s, C_4-CH_3), 3.20 (1H, m, $-C\underline{H}(CH_3)_2$), 3.40 (2H, t, J=6 Hz, $-C\underline{H}_2OH$).

Tributylphosphine (0.53 ml) was added to a stirred mixture of the above crude **20** and *o*-nitrophenyl selenocyanate (457 mg) in pyridine (5.0 ml) at 0—5 °C under a stream of nitrogen. The mixture was stirred at room temperature for 30 min, evaporated *in vacuo*, and diluted with ether. The mixture was filtered to remove a yellow precipitate and the filtrate was evaporated *in vacuo*. The residue was chromatographed on silica gel (60 g), using ether–benzene (1:9) as the eluent, to give **21** (272 mg: 75.5%). IR: 1811, 1778, 1648, 1593, 1510, 1334 cm^{-1}; ^1H NMR: δ=1.27 (6H, bd, J=7 Hz, $-CH(C\underline{H}_3)_2$), 1.60 (3H, s, C_3-CH_3), 2.33, 2.34, 2.37, and 2.39 (each 3H and s, $C_5-OCOCH_3$, $C_6-OCOCH_3$, $C_8-OCOCH_3$, and $C_9-OCOCH_3$), 2.53 (3H, bs, C_4-CH_3), *ca.* 2.5—3.0 (2H, m, $-C\underline{H}_2SeC_6H_4-$), 3.20 (1H, m, $-C\underline{H}(CH_3)_2$), *ca.* 7.0—7.3 (3H, m) and *ca.* 8.05—8.3 (1H, m) ($-SeC_6\underline{H}_4-$).

*(R)-5,6,8,9-Tetraacetoxy-3-allyl-7-isopropyl-3,4-dimethylnaphtho[2,3-b]furan-2(3H)-one (**22**).* A mixture of **21** (272 mg) and 50% hydrogen peroxide (0.24 ml) in tetrahydrofuran (8.0 ml) was stirred at room temperature for 17 h. The mixture was diluted with brine and extracted with chloroform. The chloroform extract was washed successively with aqueous potassium iodide, aqueous sodium thiosulfate, aqueous sodium hydrogencarbonate, and brine. The dried solution was evaporated *in vacuo*. The residue was chromatographed on silica gel (20 g), using ether–benzene (1:9) as the eluent, to give **22** (170 mg: 86.5%). This was recrystallized from benzene, mp 269—270 °C, $[\alpha]_D$ +79° (*c* 0.845); IR: 1816, 1780, 1652, 1620, 940 cm^{-1}; ^1H NMR: δ=1.27 (6H, bd, J=7 Hz, $-CH(C\underline{H}_3)_2$), 1.64 (3H, s, C_3-CH_3), 2.34 (6H, s), 2.38 (3H, s), and 2.39 (3H, s) ($C_5-OCOCH_3$, $C_6-OCOCH_3$, $C_8-OCOCH_3$, and $C_9-OCOCH_3$), 2.69 (3H, s, C_4-CH_3), 2.79 (2H, bd, J=7 Hz, $-C\underline{H}_2CH=CH_2$), 3.20 (1H, m, $-C\underline{H}(CH_3)_2$), *ca.* 4.85—5.6 (3H, m, $-CH_2C\underline{H}=C\underline{H}_2$). Found: C, 64.17; H, 5.76%.

Calcd for $C_{28}H_{30}O_{10}$: C, 63.87; H, 5.74%.

*(R)-3-Allyl-2,3,5,8-tetrahydro-6,9-dihydroxy-7-isopropyl-3,4-dimethylnaphtho[2,3-b]furan-2,5,8-trione (Coleon A Lactone) (**23**).* A mixture of **22** (200.2 mg) and aqueous potassium hydroxide (10%: 4.5 ml) in methanol (40 ml) was refluxed for 15 min and oxygen was then bubbled into it at room temperature for 30 min. The mixture was acidified with dilute hydrochloric acid, stirred at room temperature for 1 h, and extracted with ether. The ether extract was washed with brine, dried over magnesium sulfate, and evaporated *in vacuo*. The residue was chromatographed on silica gel (15 g), using benzene as the eluent, to give **23** (54.7 mg: 40.4 %). $[\alpha]_D$ +145° (EtOH, *c* 0.780); IR: 3325, 1808, 1647, 1617, 928 cm^{-1}; ^1H NMR: δ=1.30 (6H, d, J=7 Hz, $-CH(C\underline{H}_3)_2$), 1.65 (3H, s, C_3-CH_3), 2.68 (3H, s, C_4-CH_3), 2.83 (2H, bd, J=6.5 Hz, $-C\underline{H}_2CH=CH_2$), 3.38 (1H, m, $-C\underline{H}(CH_3)_2$), *ca.* 4.87—5.60 (3H, m, $-CH_2C\underline{H}=C\underline{H}_2$), 7.98 (1H, bs, C_6-OH), 13.35 (1H, s, C_9-OH). Found: C, 67.60; H, 5.83%. Calcd for $C_{20}H_{20}O_6$: C, 67.40; H, 5.66%. The spectral data of **23** were in good agreement with those of natural coleon A lactone.

*Coleon A (**1**).* *a)*: A mixture of **23** (50.2 mg), sodium borohydride (33.0 mg), and water (0.4 ml) in ethanol (3.6 ml) was stirred at 0—5 °C for 1 h and then at room temperature for 20 h. The mixture was concentrated *in vacuo*, acidified with dilute hydrochloric acid, and extracted with ether. The ether extract was washed with brine, dried over magnesium sulfate, and evaporated *in vacuo*. The residue was chromatographed on silica gel (5.0 g), using ether–benzene (15:85) as the eluent, to give the C-2 epimeric mixture (**1**) (38.1 mg: 75.5%). This was recrystallized from cyclohexane, mp 140.5—141.5 °C, $[\alpha]_D$ +88° (*c* 1.68); IR: 3580, 3495, 3305, 1657, 1612, 918 cm^{-1}; IR (CCl_4): 3505, 3300, 1658, 1614, 918 cm^{-1}; ^1H NMR: δ=1.28 (6H, d, J=7 Hz, $-CH(C\underline{H}_3)_2$), 1.44 and 1.50 (3H, each s, *ca.* 0.4:1 ratio, C_3-CH_3), 2.50 (2H, bd, J=6.5 Hz, $-C\underline{H}_2CH=CH_2$), 2.65 (3H, s, C_4-CH_3), 3.34 (1H, m, $-C\underline{H}(CH_3)_2$), *ca.* 4.9—5.25 (2H, m, $-CH_2CH=C\underline{H}_2$), 5.42—5.98 (1H, m, $-CH_2C\underline{H}=CH_2$), 5.78 and 5.90 (1H, each s, C_2-H), 8.13 (1H, s, C_6-OH), 13.48 (1H, s, C_9-OH). Found: C, 67.31; H, 6.32%. Calcd for $C_{20}H_{22}O_6$: C, 67.02; H, 6.19%.

b): A mixture of **22** (170.3 mg) and lithium aluminium hydride (61 mg) in dry tetrahydrofuran (8.0 ml) was refluxed for 2 h. The mixture was poured into ice-dilute hydrochloric acid and extracted with ether. The ether extract was washed with brine, dried over magnesium sulfate, and evaporated *in vacuo*. The residue was chromatographed on silica gel (10 g), using ether–benzene (15:85) as the eluent, to give **1** (39.8 mg: 34.3%), whose IR and ^1H NMR spectra were in good agreement with those of natural coleon A.

References

1) C. H. Eugster, H.-P. Küng, H. Kühnis, and P. Karrer, *Helv. Chim. Acta*, **46**, 530 (1963).
2) D. Karanatsios and C. H. Eugster, *Helv. Chim. Acta*, **48**, 471 (1965).
3) C. H. Eugster, *Ber. Deutsch. Bot. Ges.*, **88**, 141 (1975).
4) T. Matsumoto, S. Imai, K. Ondo, N. Takeyama, and K. Fukui, *Chem. Lett.*, **1980**, 425.
5) T. Matsumoto, S. Imai, K. Ondo, N. Takeyama, H. Kataoka, Y. Yamamoto, and K. Fukui, *Bull. Chem. Soc. Jpn.*, **55**, 891 (1982).
6) T. Matsumoto, S. Imai, K. Ondo, H. Kataoka, and K. Kato, *Bull. Chem. Soc. Jpn.*, **56**, 2985 (1983).
7) H. Niwa, T. Hida, and K. Yamada, *Tetrahedron Lett.*, **22**, 4239 (1981).
8) P. A. Grieco, S. Gilman, and M. Nishizawa, *J. Org. Chem.*, **41**, 1485 (1976).
9) Private communication from Professor C. H. Eugster.

Semburins and Swertiols, Novel 2,8-Dioxabicyclo[3.3.1]nonanes and Their Precursory Alcohols, from *Swertia japonica* Makino

Tsutomu Sakai,* Yoshiko Nakagawa, Takashi Iwashita, Hideo Naoki, and Takeo Sakan

Suntory Institute for Bioorganic Research, Shimamoto-cho, Mishima-gun, Osaka 618

(Recived April 14, 1983)

The steam-volatile constituents of *Swertia japonica* Makino have been studied, and 71 components of the oil (comprising nearly 90% of the sample) have been identified. Structures of three novel 2,8-dioxabicyclo-[3.3.1]nonanes (semburin, isosemburin, and neosemburin) and their precursory alcohols (swertiol, isoswertiol, and isoneoswertiol) have been established by spectroscopic analysis and chemical transformation data. The presence of 2-*epi*-isoneoswertiol, which was named neoswertiol, was detected by GC/MS. This is the first time that the 2,8-dioxabicyclo[3.3.1]nonane skeleton has been encountered in natur al products.

In 1967, Motomura[1] reported the interesting observation that cats are attracted by volatile fractions of *Swertia japonica* Makino as well as by fractions of *Actinidia polygama* Miq.[2] and *Nepeta cataria* L.,[3] *etc.* During the course of our investigations on various plants which have a peculiar excitatory effect on cats and *Felidae*, we studied the volatile constituents of *Swertia japonica* Makino. *Swertia japonica* Makino (Gentianaceae; Japanese name, semburi) is a popular herb in Japan, the whole plant being widely used as a folk medicine for stomach complaints because of its characteristic strong bitter taste. The bitter principles of this plant have been studied by a number of workers.[4] However, until recently no detailed study of the volatile components had been carried out. In a previous paper,[5] we reported the isolation and structures of two novel 2,8-dioxabicyclo[3.3.1]nonanes, semburin and isosemburin, which constitute the major components isolated from the volatile oil. We now report the analysis of the volatile constituents by GC/MS, and the details of the isolation and structural elucidation of these and five new compounds.

Results and Discussion

Analysis of Volatile Constituents. The oils obtained by steam distillation of the fresh or air-dried *Swertia japonica* plant (collected in Miyagi Pref., 1980) and *via* methanol extraction of the air-dried commercial material showed similar gas chromatographic profiles. Figure 1 shows the gas chromatogram of the whole essential oil obtained from the air-dried commercial plant. This chromatogram was obtained by injecting 1.0 μl of the oil into a CP Wax 51 glass WCOT column. The column temperature was held initially at 100 °C for 10 min, then programmed at 2 °C per minute to 150 °C, and run isothermally at 150 °C until all the components had emerged.

Volatile constituents of *Swertia japonica* were identified as far as possible by GC/MS. The major components were isolated by preparative GC and by silica-gel column chromatography (CC) and their structures were confirmed by their spectral properties. Table 1 shows the compounds detected in the volatile oil.

Among the more than 110 component peaks observed in the chromatogram of the oil, seventy-one compounds were determined. Anethole and eugenol

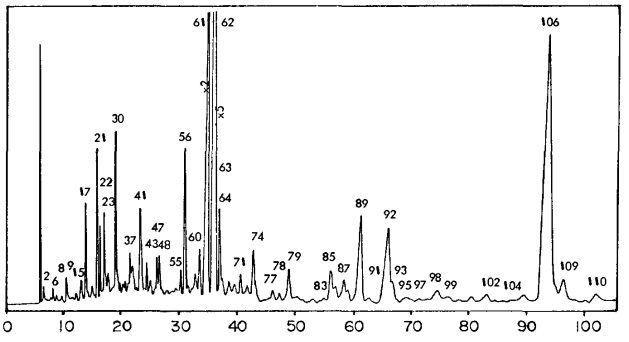

Fig. 1. Gas chromatogram of the volatile oil of *Swertia japonica* Makino.

(peaks 62 and 106) were the main components in the oil (32% of the oil). A fraction containing aromatic oxygenated compounds constituted 11.2% of the oil, followed by terpenic oxygenated compounds (8.5%), terpenic hydrocarbons (7.1%), and aliphatic oxygenated compounds (5.9%). The existence of three new oxides and four new alcohols, which we have named semburins and swertiols, was revealed by GC/MS in both the volatile oil and the methanol extract. Semburins (peak 56, 61, and 64) and swertiols (peaks 91, 92, 93, and 98) accounted for 11.8% and 5.0% of the oil, respectively. Furthermore, a new lactone (peak 109, 1.39% of the oil) was obtained.

Structures of Semburins. Three novel 2,8-dioxabicyclo[3.3.1]nonanes possessing the same molecular formula of $C_9H_{14}O_2$ were contained in a fraction eluted with ether–hexane (1:9) on silica gel CC. Each compound was isolated in the pure state by preparative GC and by repeated CC. The mass spectra of two major compounds (**1** and **2**) are almost identical, but differ slightly from that of the minor compound (**3**). (Scheme 1). The IR spectra of **1** and **2** are very similar and showed the absence of hydroxyl and carbonyl groups and the presence of a vinyl group. The IR spectrum of **3** is also similar to that of **1** and **2**, except for the absence of vinyl bands. These facts suggest that the second major compound **2** is a diastereoisomer of the major compound **1**, while the minor compound **3** is a double bond isomer of both **1** and **2**. These three new compounds have been named semburin (**1**), isosemburin (**2**), and

TABLE 1. CONSTITUENTS OF THE VOLATILE OIL FROM *Swertia japonica* MAKINO

Peak No.	Compound	Content % [a]	Peak No.	Compound	Content % [a]
2	Ethyl acetate	0.15	58	Phenylpropionaldehyde	0.29
3	Benzene	0.04	59	δ-Cadinene	0.64
6	Hexanal	0.26	60	α-Curcumene	1.07
8	Limonene	0.18	61	Semburin[b]	7.84
9	*trans*-2-Hexenal	0.35	62	Anethole	16.59
10	1,8-Cineol	0.09	63	α-Damascenone	0.42
16	*cis*-Rose oxide	0.05	64	Neosemburin[b]	1.59
17	2,4-Hexadienal	0.14	65	Geraniol	0.41
18	*trans*-Rose oxide	0.08	66	Calamenene	0.49
21	1-Octen-3-ol	1.53	67	Benzyl alcohol	0.22
22	Furfural	0.95	69	Safrole	0.50
23	2,4-Heptadienal	0.14	72	1-Methylnaphthalene	0.17
25	Menthone	0.13	73	α-Ionone	0.42
26	2-Furylacetaldehyde	0.48	74	Phenethyl alcohol	1.39
29	Benzaldehyde	0.36	77	Di-*t*-butyl-*p*-cresol	0.44
30	Linalool	2.07	78	α-Calacorene	0.37
31	α-Copaene	0.34	79	β-Ionone	1.17
32	Tagetone	0.27	83	Biphenyl	0.12
33	5-Methylfurfural	0.42	85	Epoxy-β-ionone	1.29
35	5-Methyl-2-acetylfuran	0.40	87	*p*-Anisaldehyde	0.96
37	Bornyl acetate	0.83	89	Cinnamaldehyde	3.38
38	4-Terpineol	0.86	90	3-Phenyl-1-propanol	0.38
40	α-Bergamotene	0.29	91	Neoswertiol[b]	0.37
41	Caryophyllene	2.16	92	Isoswertiol[b]	3.11
42	Phenylacetaldehyde	0.25	93	Isoneoswertiol[b]	0.74
43	Pulegone	0.68	95	Nerolidol	0.21
46	β-Farnesene	0.31	96	Cubenol	0.20
47	α-Terpineol	0.68	97	Epicubenol	0.28
48	Borneol	0.80	98	Swertiol[b]	0.74
49	α-Humulene	0.32	99	α-Cyperone	0.48
50	Verbenone	0.18	102	Ethyl cinnamate	0.57
52	Piperitone	0.10	104	γ-Eudesmol	0.14
53	Naphthalene	0.35	106	Eugenol	15.40
54	Zingiberene	0.24	109	3-Propylidene-5-pentanolide[b]	1.39
55	β-Bisabolene	0.66	110	Methyleugenol	0.24
56	Isosemburin[b]	2.39			

a) Based on relative peak areas of the GC analysis of the volatile oil; GC on CP Wax 51 glass WCOT column (50 m×0.24 mm i.d.), 100 °C to 150 °C programmed at 4 °C/min. b) New compound.

neosemburin (**3**).

Semburin(**1**), $[\alpha]_D^{26}$ −2.0°, and isosemburin (**2**), $[\alpha]_D^{24}$ −8.0°, contain nine carbons: two CH_2's, one $=CH_2$, two OCH_2's, two CH's, one =CH, and one O–CH–O (^{13}C NMR). The IR and high resolution mass spectra of both **1** and **2** suggested the presence of a tetrahydropyran ring having a vinyl group: absorption bands at 3070, 1640, and 920 cm^{-1} (CH_2=CH) and fragment peaks at *m/z* 81.0320 ($C_5H_5O^+$, 98%), 109.0635 ($C_7H_9O^+$, 37%), and 124.0886 (M^+-CH_2O, 100%). These data coupled with the 360 MHz ^1H NMR and the 300 MHz ^1H–^1H 2-D chemical shift correlation spectra[6] (see Fig. 2), led to the 4-vinyl-2,8-dioxabicyclo[3.3.1]nonane skeleton for both semburin and isosemburin. The structure of **1** was confirmed by synthesis of (±)-**1**[7] *via* a pathway resembling its biogenesis from sweroside (**4**), a bitter principle of this plant. This synthesis verified the *cis* relationship of 4-H and 5-H. Furthermore, the absolute configuration at C-5 in both **1** and **2** was established as being identical with that of the asterisked carbon in structure **4** by synthesis of (−)-**1** and (−)-**2** from (*R*)-4-allyl-4-butanolide.[8] This synthesis also established that **1** and **2** are epimers.

The stereochemistry of **1** is evident from 360 MHz ^1H NMR analysis. Proton decoupling and 2-D *J* techniques[9] showed the presence of two W-type long range couplings between 5-H (δ 1.71)/1-H (δ 5.32)(1.5 Hz) and between 5-H/3′-H (δ 3.69)(2.0 Hz), indicating that the tetrahydropyran ring with the vinyl side-chain adopts a chair conformation. Irradiation of the 7′-H signal at δ 3.42 in **1** induced an NOE on the δ 1.36 9-H pattern, indicating a boat conformation for the other tetrahydropyran ring. Finally, the equa-

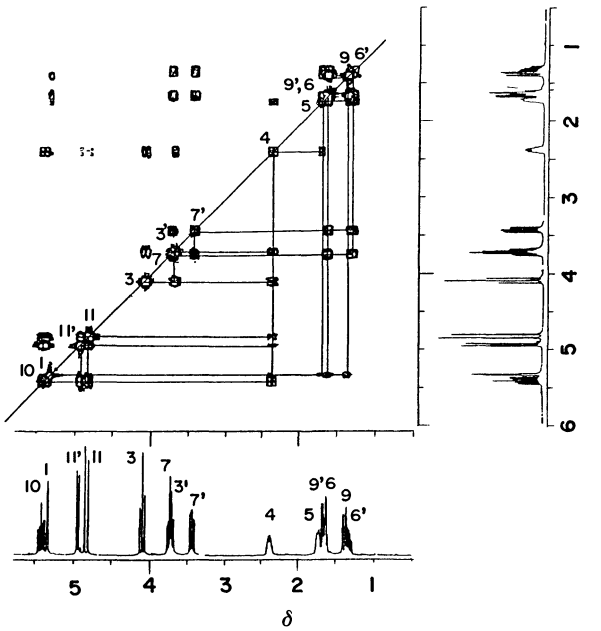

Fig. 2. ^1H–^1H 2-D chemical shift correlation map of semburin **1**.

torial nature of the vinyl group was established by noting a 12 Hz diaxial coupling between 4α-H and 3β-H. The NMR data (Fig. 2) unequivocally led to structure **1** with the chair/boat conformation **1a**.

The conformation of **2** was deduced to be half-chair/chair **2a** by carrying out similar experiments. Two W-type couplings between 5-H (δ 1.57)/1-H (δ 5.31)(1.5 Hz) and between 9-H (δ 1.30)/4-H (δ 2.10) (1.5 Hz) were observed upon proton decoupling of **2**. Irradiation of the 7'-H signal at δ 3.46 induced an NOE on the 4-H signal at δ 2.10. The coupling constants of the dddd pattern of the 4-H signal ($J_{4,3}$= 9 Hz, $J_{4,3'}$=7 Hz) indicated the presence of an axial vinyl side-chain on a half-chair tetrahydropyran ring.

The third minor compound (**3**), neosemburin ($[\alpha]_D^{25}$ +8.3°), showed the presence of a CH_3CH=C group (δ 1.30, 3H, dddd; δ 5.08, 1H, dddq) instead of a CH_2=CH–CH group in its ^1H NMR spectrum. Decoupling studies of the 360 MHz ^1H NMR spectrum showed **3** to be 4-ethylidene-2,8-dioxabicyclo[3.3.1]-nonane. The absolute configurations of C-1 and C-5 are assumed to be the same as in **1** and **2**. The geometry of the trisubstituted double bond in **3** was assigned a *Z* configuration, since irradiation of the 3-H resonance at δ 4.10 and the 10-Me signal at δ 1.30 enhanced the 10-H (δ 5.08) and the 5-H (δ 2.49) patterns, respectively. A W-type coupling between 5-H (δ 2.49)/ 7-H (δ 3.52)(1.5 Hz) was observed, indicating the conformation of **3** also to be half-chair/chair **3a** as in the case of **2a**. (Fig. 3).

Structures of Swertiols. Two pairs of new isomeric compounds also possessing the semburin molecular formula ($C_9H_{14}O_2$) were contained in a fraction eluted with ether–hexane (3:7) on silica gel CC. Three of these have been isolated in the pure state by preparative GC and CC.

The major compound, isoswertiol (**5**)($[\alpha]_D^{24}$ +54.2°),

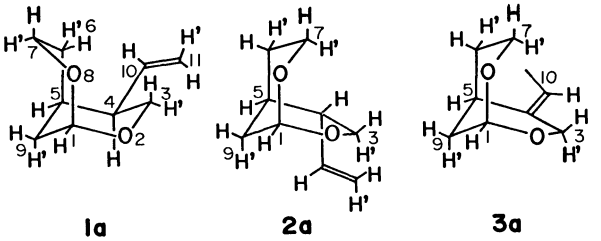

1a **2a** **3a**

Fig. 3.

had IR absorption bands for a hydroxyl (3360 cm^{-1}), a vinyl (3020, 1640, and 920 cm^{-1}), and a CH=CH–O–CH_2 (1240 cm^{-1}) group. The ^{13}C and ^1H NMR spectra of **5** indicated the presence of a 3,4-dihydro-2*H*-pyran moiety (δ 3.52 and 3.81, each 1H, dd, 2-H_2; δ 6.39, 1H, dd, 6-H; δ 4.55, 1H, dd, 5-H; δ 2.01, 2H, m, 3-H and 4-H), and –CH_2CH_2OH (δ 1.20 and 1.56, each 1H, dddd, 7-H_2; δ 3.33, 2H, m, 8-H_2; δ 0.64, 1H, br s, OH) and CH=CH_2 groups (δ 5.40, 1H, ddd, 9-H; δ 4.92 and 4.93, each 1H, ddd, 10-H_2). The mass spectrum of **5** also supported the presence of these groups: *m/z* 109 (M^+–CH_2CH_2OH, 58%), 83 ($C_5H_7O^+$, 77%), and 54 ($C_4H_6^+$, 100%). On the basis of these data, **5** is 3-vinyl-4-(2-hydroxyethyl)-3,4-dihydro-2*H*-pyran. The smooth conversion of **5** into isosemburin (**2**) by treatment with *p*-toluenesulfonic acid confirmed the structure of **5**, and also established the absolute configurations at C-3 and C-4 in **5** to be the same as in **2**.

The minor compound (**6**) exhibited IR and mass spectra very similar to **5**. No NMR measurements were carried out due to the limited amount of sample. However, transformation of **6** into semburin (**1**) by treatment with *p*-toluenesulfonic acid established the structure of **6**, swertiol, as being the 3-epimer of isoswertiol (**5**).

The second major compound, isoneoswertiol (**7**)($[\alpha]_D^{22}$ −52.8°), had IR absorption bands for a hydroxyl (3340 cm^{-1}), a vinyl (3050, 1630, and 905 cm^{-1}), and a CH=CH–O–CH_2 (1240 cm^{-1}) group. The ^{13}C and ^1H NMR spectra of **7** showed the presence of a 3,4-dihydro-2*H*-pyran moiety (δ 3.66 and 3.74, each 1H, ddd, 2-H_2; δ 1.43, 2H, m, 3-H_2; δ 4.47, 1H, dddd, 5-H; δ 6.39, 1H, dd, 6-H), and –CH_2OH (δ 3.30, 1H, dd, 8-H; δ 3.49, 1H, br dd, 8-H; δ 0.80, 1H, br s, OH) and –CH=CH_2 (δ 5.40, 1H, ddd, 9-H; δ 4.89 and 4.97, each 1H, ddd, 10-H_2) groups. The mass spectrum also confirmed the presence of these groups: *m/z* 83 ($C_5H_7O^+$, 100%) and 124 (M^+–CH_2OH, 1.5%). These data indicated that **7** is 2-(3,4-dihydro-2*H*-pyran-4-yl)-3-buten-1-ol. The conversion of **7** into isosemburin (**2**) established the structure and the absolute configuration at C-2 and C-4'.

The remaining counterpart of the second pair could not be isolated, but was assumed to be the 2-epimer of isoneoswertiol (**7**); we named it neoswertiol (**8**), since its mass spectrum (by GC/MS) is identical with that of isoneoswertiol (**7**).

A possible biogenetic route from sweroside (**4**) to semburins (**1** and **2**) is illustrated in Scheme 1. Acid-catalyzed cleavage of sweroside (**4**) would provide the hydroxydial acid (**9**). Decarboxylation and racemi-

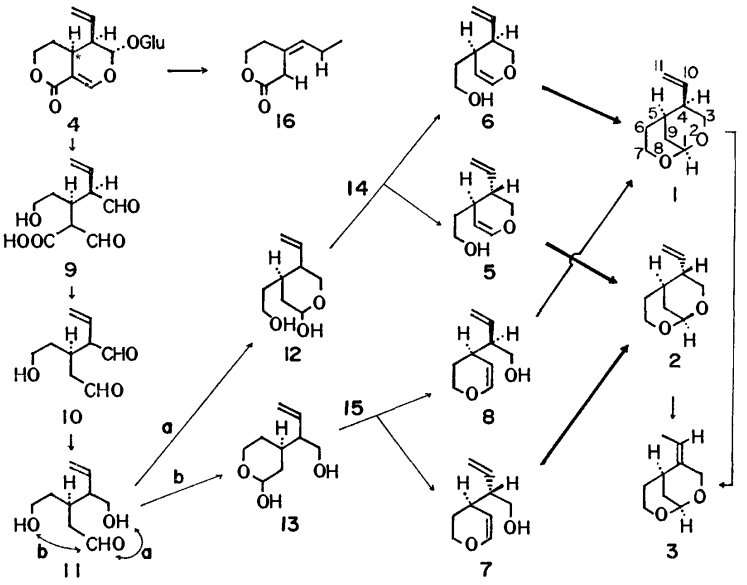

Scheme 1. Biosynthesis of semburins and swertiols from sweroside.

zation at the α-position of the carbonyl in **9** then gives the hydroxydials **10**, the reduction of which leads to epimeric diols **11**. Compound **11** is an important intermediate because the absolute configuration at C-5 in **4** remains unaltered. Cyclization of **11** in two directions **a** and **b** would provide two hemiacetals **12** and **13**. Semburins **1** and **2** could be obtained directly from both hemiacetals **12** and **13** by dehydration-cyclization, or *via* the dihydropyran alcohols **14** and **15**. These dihydropyran alcohols **14** and **15** correspond to the four new compound **5**—**8** isolated from both the volatile oil and the methanol extract of plant.

A number of studies concerning the role of loganin and secologanin in the biosynthesis of terpenoids and indole alkaloids have been reported, but possible key intermediates postulated in the biogenetic sequence from iridoids to alkaloids have not been isolated or confirmed. It is possible that the compounds discussed might be efficient precursors in the biosynthesis of the Corynanthe-type indole alkaloids.

Although the 2,8-dioxabicyclo[3.3.1]nonane skeleton has already been obtained as the aglycone of secologanin,[10] this is the first time it has been encountered in natural products.

Structure of a New Lactone ***16***. From the fraction containing swertiols, a new lactone (peak 109 in Table 1, 1.39% of the oil), 3-propylidene-5-pentanolide (**16**) was obtained. Its mass spectrum showed a molecular ion at *m/z* 140 corresponding to $C_8H_{12}O_2$. The IR and ^{1}H NMR spectra showed the presence of a δ-lactone moiety (1740 cm^{-1}) and a $CH_3CH_2CH{=}C$ group [δ 0.74 (3H, t, J=7.5 Hz), 1.59 (2H, ddq, J=7.5, 7.0, 1.0 Hz), and 4.86 (1H, ttt, J=7.0, 1.5, 1.5 Hz)]. Irradiation of the 3-H_2 signal at δ 2.87 induced an NOE on the 8-H_2 (δ 1.59) pattern. Thus, the configuration of the trisubstituted double bond was determined as *Z*. It is also presumed that this compound is derived from sweroside (**4**). (see Scheme 1)

Experimental

The IR spectra were obtained on a Hitachi EPI G2 infrared spectrophotometer as thin films between NaCl plates. The optical rotations were measured on a Perkin-Elmer 141 polarimeter. The NMR spectra were taken by Nicolet NT-360 (360 MHz ^{1}H NMR), Nicolet NT-300 (300 MHz ^{1}H–^{1}H 2-D J correlation), and JEOL FX-100 (^{13}C NMR). GC/MS spectra were determined with a Hitachi M-80 GC/MS spectrometer equipped with 50 m×0.24 mm i.d. glass WCOT column of CP Wax 51. The preparative GC conditions, using a model 920 Varian Aerograph fitted with a thermal-conductivity detector, were as follows: a 3 m× 10 mm aluminum column containing 10% Thermon 1500 on Chromosorb W; He carrier gas, 60 ml/min; oven temp at 130—150 °C.

Material and Isolation. Steam distillations of the fresh whole plant (3 kg, collected in Sendai, Miyagi Pref., Oct. 1980), its air-dried material (0.5 kg), and a commercial air-dried material (5 kg, collected in Tohoku District) gave, respectively, 0.37 g, 0.27 g, and 2.0 g of volatile oils. The commercial material (0.4 kg) was extracted with MeOH for 2 weeks. The crude extract (44.8 g) was obtained.

The volatile oil (2.0 g) of the commercial material was chromatographed on silica gel (70 g, 2.5 cm i.d.×60 cm column). Elution with hexane, hexane–ether mixture, ether, and MeOH gave 7 fractions: fraction I (hexane, 0.53 g), II (hexane–ether, 95:5, 0.12 g), III (9:1, 0.46 g), IV (85:15, 0.30 g), V (7:3, 0.19 g), VI (ether, 0.23 g), and VII (MeOH, 0.08 g). Fraction III was rechromatographed, yielding 3 fractions: III-1 (0.17 g), III-2 (0.13 g), and III-3 (0.15 g). Three semburins were contained in fraction III-3. Four swertiols were contained in fraction V. Each compound was isolated by prep. GC and CC: semburin, 5.0 mg, prep. GC Rt (oven temp 130°) 20.5 min; isosemburin, 1.5 mg, 16.0 min; neosemburin, 1.0 mg, 23.0 min; isoswertiol, 9.0 mg, 20 min (oven temp 150 °C); isoneoswertiol, 3.9 mg, 20 min; swertiol, 30 min.

*Semburin (**1**).* $[\alpha]_D^{26}$ −2.0° ($CHCl_3$, c=0.10); IR ν_{max}^{film} cm^{-1}: 3070, 1640, 1000, 920; ^{13}C NMR (25 MHz, C_6D_6): δ 23.9 (t, C-6), 25.9 (d, C-5), 30.3 (t, C-9), 44.0 (d, C-4), 60.4 (t, C-7), 61.6 (t, C-3), 92.5 (d, C-1), 115.7 (t, C-11),

Table 2. ^{1}H NMR spectral data of semburins **1**, **2**, and **3** (in C_6D_6)

Proton	Semburin(**1**)	Isosemburin(**2**)	Neosemburin(**3**)
1-H	5.32 ddd	5.29 ddd	5.47 br
3-H	4.08 dd	3.89 dd	4.10 m
3'-H	3.69 ddd	3.26 dd	
4-H	2.38 dddddd	2.11 ddddd	—
5-H	1.72 m	1.58 m	2.49 br s
6-H	1.63 m	1.61 dddd	1.61 dddd
6'-H	1.30 dddd	1.09 dddd	1.23 br d
7-H	3.72 ddd	3.46 dddd	3.52 dddd
7'-H	3.41 ddd	4.03 ddd	4.16 ddddd
9-H	1.63 m	1.31 ddd	1.50 m
9'-H	1.36 ddd	1.55 ddd	
10-H	5.40 ddd	5.55 ddd	5.08 dddq
11-H	4.93 ddd	4.89 ddd	1.30 dddd
11'-H	4.81 ddd	4.89 ddd	

Coupling constants. Semburin(**1**): 1,5=1.5 Hz; 1,9=1,9'=1.5 Hz; 3,3'=7,7'=11.6 Hz; 3,4=11.8 Hz; 3',4=5,9'=5.5 Hz; 3',5=2.0 Hz; 4,5=3.0 Hz; 4,10=6.3 Hz; 4,11=4,11'=1.6 Hz; 5,6'=9.0 Hz; 6,6'=15.2 Hz; 6,7=6.9 Hz; 6,7'=10.0 Hz; 6',7=4.2 Hz; 6',7'=6.0 Hz; 9,9'=13.0 Hz; 10,11=10.8 Hz; 10,11'=17.1 Hz; 11,11'=1.6 Hz. Isosemburin(**2**): 1,5=5,7=1.5 Hz; 1,9=1,9'=5,9'=2.0 Hz; 3,3'=7,7'=12.0 Hz; 3,4=6.5 Hz; 3',4=8.5 Hz; 4,9=1.5 Hz; 4,10=6.8 Hz; 4,11=4,11'=1.0 Hz; 5,6=5.5 Hz; 5,6'=2.2 Hz; 5,9=3.0 Hz; 6,6'=14.0 Hz; 6,7=3.5 Hz; 6,7'=10.0 Hz; 6',7=6.0 Hz; 6',7'=5.0 Hz; 9,9'=12.9 Hz; 10,11=9.8 Hz; 10,11'=16.0 Hz; 11,11'=1.0 Hz. Neosemburin(**3**): 1,7'=0.5 Hz; 3,10=3,10'=3',10=3,11=3',11=1.5 Hz; 5,6=3.8 Hz; 5,7=1.0 Hz; 5,7'=0.5 Hz; 5,10=2.0 Hz; 5,11=1.0 Hz; 6,6'=13.0 Hz; 6,7=5.5 Hz; 6,7'=13.0 Hz; 6',7=1.5 Hz; 6',7'=3.5 Hz; 7,7'=11.5 Hz; 10,11=7.0 Hz.

137.8 (d, C-10); ^{1}H NMR (360 MHz, C_6D_6): see Table 2; MS *m/z* (rel int. %): 154 (M^+, 1), 124(49), 109(46), 95(14), 91(12), 81 ($C_5H_5O^+$, 100), 80(61), 67(50), 53(49), 41(90). High resolution (H. R.) MS; Found: M^+ *m/z* 154.0967. Calcd for $C_9H_{14}O_2$: M^+ *m/z* 154.0992.

*Isosemburin (**2**).* $[\alpha]_D^{25}$ −8.0° ($CHCl_3$, *c*=0.05); IR ν_{max}^{film} cm^{-1}: 3070, 1640, 1000, 920; ^{13}C NMR (25 MHz, C_6D_6): δ 26.3 (t, C-6), 27.5 (d, C-5), 32.0 (t, C-9), 44.1 (d, C-4), 57.3 (t, C-7), 62.7 (t, C-3), 93.1 (d, C-1), 114.5 (t, C-11), 139.6 (d, C-10); ^{1}H NMR (360 MHz, C_6D_6): see Table 2; MS *m/z* (rel int. %): the same as those of **1**.

*Neosemburin (**3**).* $[\alpha]_D^{25}$ +8.3° ($CHCl_3$, *c*=0.06), ^{1}H NMR (360 MHz, C_6D_6): see Table 2; MS *m/z* (rel int. %): 154 (M^+, 25), 136(7), 125(25), 93(56), 91(29), 83 ($C_5H_7O^+$, 100), 79(62), 70(51), 69(69), 67(51), 55(76), 53 (47), 41(85), 39(62).

*Isoswertiol (**5**).* $[\alpha]_D^{24}$ +54.2° (MeOH, *c*=0.66); IR ν_{max}^{film} cm^{-1}: 3350, 3050, 1635, 1240, 915; ^{13}C NMR (25 MHz, C_6D_6): δ 32.9 (d, C-4), 37.6 (t, C-7), 43.3 (d, C-3), 60.0 (t, C-8), 68.0 (t, C-2), 103.7 (d, C-5), 116.7 (t, C-10), 138.3 (d, C-9), 143.8 (d, C-6); ^{1}H NMR (360 MHz, C_6D_6): see Table 3; MS *m/z* (rel int. %): 154(M^+, 15), 139(1), 136(3), 124(10), 109(58), 99(48), 83(77), 81(39), 79(31), 67(14), 54($C_4H_6^+$, 100), 41(28), 39(22). H.R. MS; Found: M^+ *m/z* 154.1002. Calcd for $C_9H_{14}O_2$: M^+ *m/z* 154.0992.

*Swertiol (**6**).* IR ν_{max}^{film} cm^{-1}: 3350, 3050, 1635, 1240, 915; MS *m/z* (rel int. %): 154(M^+, 14), 135(2), 121(3), 109(25), 99(40), 91(10), 81(21), 79(16), 69(6), 67(5), 54 ($C_4H_6^+$, 100), 41(20), 39(18).

Table 3. ^{1}H NMR spectral data of isoswertiol (**5**) and isoneoswertiol (**7**)

Proton	Isoswertiol(**5**)	Isoneoswertiol(**7**)
2-H	3.52 dd	3.66 ddd
2'-H	3.81 dd	3.74 ddd
3-H	2.01 m	1.42 m
3'-H	—	
4-H	2.01 m	1.99 ddddd
5-H	4.55 dd	4.47 dddd
6-H	6.39 dd	6.39 dd
7-H	1.56 dddd	1.85 dddddd
7'-H	1.20 dddd	—
8-H	3.33 m	3.30 dd
8'-H		3.49 br dd
9-H	5.40 ddd	5.40 ddd
10-H	4.92 ddd	4.87 ddd
10'-H	4.93 ddd	4.97 ddd
O-H	0.64 br s	0.80 br s

Coupling constants. Isoswertiol (**5**): 2,2'=10.5 Hz; 2,3=10.0 Hz; 2',3=3.0 Hz; 3,9=7.7 Hz; 3,10=3,10'=0.5 Hz; 4,5=2.3 Hz; 4,6=1.8 Hz; 4,7=7.3 Hz; 4,7'=8.9 Hz; 5,6=6.2 Hz; 7,7'=13.3 Hz; 7,8=7.3 Hz; 7,8'=4.2 Hz; 7',8'=8.9 Hz; 9,10=17.0 Hz; 9,10'=10.2 Hz; 10,10'=2.0 Hz. Isoneoswertiol (**7**): 2,2'=11.0 Hz; 2,3=6.5 Hz; 2,3'=4.5 Hz; 2',3=5.0 Hz; 2',3'=5.5 Hz; 3,4=1.0 Hz; 3',4=7.0 Hz; 3,5=3',5=0.5 Hz; 4,5=3.0 Hz; 4,6=2.0 Hz; 4,7=12.5 Hz; 5,6=6.5 Hz; 7,8=5.0 Hz; 7,8'=7.5 Hz; 7,9=9.0 Hz; 7,10=1.0 Hz; 7,10'=0.5 Hz; 8,8'=10.5 Hz; 9,10=17.0 Hz; 9,10'=10.5 Hz; 10,10'=2.0 Hz.

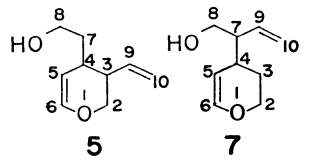

5 **7**

*Isoneoswertiol (**7**).* $[\alpha]_D^{22}$ −52.8° (MeOH, *c*=0.18); IR ν_{max}^{film} cm^{-1}: 3400, 3050, 1630, 1240, 905; ^{13}C NMR (25 MHz, C_6D_6): see Table 3; MS *m/z* (rel int. %): 154(M^+, 2), 124 (1.5), 83 ($C_5H_7O^+$, 100), 67(15), 55(55), 39(26). H.R. MS; Found: M^+ *m/z* 154.0987. Calcd for $C_9H_{14}O_2$: M^+ *m/z* 154.0992.

*Neoswertiol (**8**).* MS *m/z* (rel int. %): 154(M^+, 3), 124(1), 83($C_5H_7O^+$, 100), 67(15), 55(55), 39(26).

*3-Propylidene-5-pentanolide (**16**).* IR ν_{max}^{film} cm^{-1}: 1740, 1660, 1625; ^{1}H NMR (360 MHz, C_6D_6): δ 0.73 (3H, t, *J*=7.5 Hz, 8-H_3), 1.58 (2H, dqt, *J*=7.5, 7.5, 1.0 Hz, 7-H_2), 1.74 (2H, br t, *J*=7.0 Hz, 4-H_2), 2.87 (2H, br quint, *J*=1.0 Hz, 2-H_2), 3.54 (2H, dd, *J*=6.0, 6.0 Hz, 5-H_2), 4.86 (1H, ttt, *J*=7.0, 2.0, 2.0 Hz, 7-H); MS *m/z* (rel int. %): 140(M^+, 18), 112(M^+−CO, 10), 95(6), 82($C_6H_{10}^+$, 100), 67(10), 53(7), 39(11).

*Conversion of **5** to **2**.* To a solution of **5** (0.3 mg) in benzene (0.5 ml) was added a solution of *p*-toluenesulfonic acid (1 mg) in benzene (1 ml). The mixture was allowed to stand at room temperture overnight in a sealed tube. After the usual work-up, the residue was subjected to GC/MS analysis. The only product of cyclization was identified as isosemburin (**2**).

*Conversion of **7** to **2**.* **7** (0.2 mg) was cyclized in a similar manner to that described above to give **2**. The identification of the product was carried out by GC/MS.

*Proton J-correlation Spectra (COSY) of **1** and **2**.* They were viewed in the contour mode. Quadrature detection

was employed in both dimensions to collect a 512×1K data matrix, with 16 acquisitions for each t_1 delay (evolution period). Dwell times for each dimension (t_1 and t_2) were set to 332 s. Both dimensions were resolution enhanced by a sine multiplication; the second dimension (F_1) is presented in power mode.

References

1) I. Motomura, *Zoological Magazine*, **76**, 119 (1967).
2) T. Sakan, F. Murai, S. Isoe, S. B. Hyeon, and Y. Hayashi, *Nippon Kagaku Zasshi*, **90**, 507 (1969); K. Yoshihara, T. Sakai, and T. Sakan, *Chem. Lett.*, **1978**, 433; T. Sakai, K. Nakajima, K. Yoshihara, T. Sakan, and S. Isoe, *Tetrahedron*, **36**, 3115 (1980); T. Sakai, K. Nakajima, and T. Sakan, *Bull. Chem. Soc. Jpn.*, **53**, 3683 (1980).
3) R. B. Bates, E. J. Eisenbraun, and S. M. McElvain, *J. Am. Chem. Soc.*, **80**, 3420 (1958).
4) T. Kubota and Y. Tomita, *Tetrahedron Lett.*, **1961**, 176; H. Inouye, S. Ueda, and Y. Nakamura, *ibid.*, **1967**, 3221.
5) T. Sakai, H. Naoki, K. Takaki, and H. Kameoka, *Chem. Lett.*, **1981**, 1257.
6) A. Bax, R. Freeman, and G. Morris, *J. Magn. Reson.*, **42**, 164 (1981); R. Baumann, G. Wider, R. R. Ernst, and K. Wüthrich, *ibid.*, **44**, 402 (1981).
7) Y. Ohfune, K. Takaki, H. Kameoka, and T. Sakai, *Chem. Lett.*, **1982**, 209.
8) S. Takano, N. Tamura, K. Ogasawara, Y. Nakagawa, and T. Sakai, *Chem. Lett.*, **1982**, 933.
9) W. P. Aue, J. Karlan, and R. R. Ernst, *J. Chem. Phys.*, **64**, 4226 (1976).
10) R. T. Brown and C. L. Chapple, *Tetrahedron Lett.*, **1976**, 787.

Cyclic Phosphorylation Reaction of Diols with Tri(1-imidazolyl)phosphine

Takeo SHIMIDZU,* Kazushige YAMANA, Naoya KANDA, and Susumu KITAGAWA†

Division of Molecular Engineering, Kyoto University, Yoshida, Sakyo-ku, Kyoto 606

†*Department of Chemistry, Kinki University, Kowakae, Higashi-Osaka 577*

(Received April 22, 1983)

Tri(1-imidazolyl)phosphine (**1**) gave the cyclic phosphite quantitatively in the reactions with the diols possessing favorably placed hydroxyl groups in which the distance between the two oxygen atoms is 2.7—3.0 Å. The both five- and six-membered cyclic phosphites were obtained quantitatively from the reactions of the diols possessing flexible chains with **1**. The course of the selective formation of ribonucleoside 2′,3′-cyclic 1-imidazolylphosphonite was interpretated by the higher reactivity of **1** toward the 2′- or 3′-hydroxyl group than toward the 5′-hydroxyl group of ribonucleoside.

It is well-known that many active phosphorus compounds readily react with vicinal diols to give the cyclic phosphites.[1-7] Recently, we have developed a new sort of phosphorylating reagent such as tri(1-imidazolyl)phosphine (**1**) which reacts selectively with the 2′- and 3′-hydroxyl groups of ribonucleoside to give a ribonucleoside 2′,3′-cyclic 1-imidazolylphosphonite (**2a**).[8] This reaction was extended by the use of tri(azol-1-yl)phosphines and has been successfully adopted to the synthesis of oligoribonucleotides directly from unprotected ribonucleosides.[9,10] It is significant to elucidate the aspect of this cyclic phosphorylation reaction which is directed toward the use for a selective phosphorylation of some important substances possessing diol group, *e.g.* sugars, some steroids, *etc.* For this purpose, the reaction of some simple diols with **1** is performed. In this paper, we describe the cyclic phosphorylation reaction of diols with **1** in connection with the phosphorylation of the ribonucleosides.

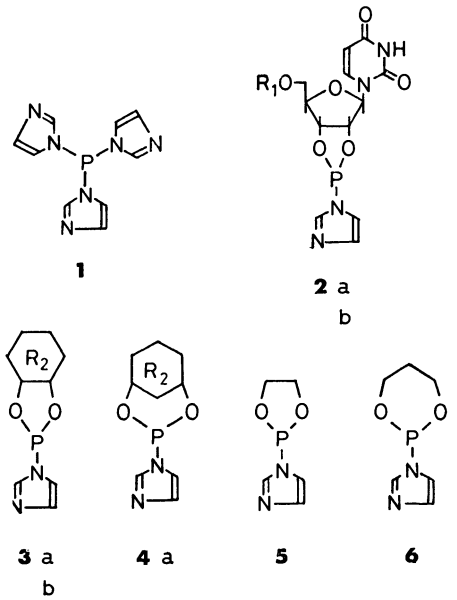

1 **2** a b **3** a b **4** a **5** **6**

R_1 a) H–
b) monomethoxytrityl–

R_2 a) cyclohexane
b) benzene

Results and Discussion

We first focused our attention on the reaction of diols possessing different degree of distance between the reacting hydroxyl groups with **1**. Cyclohexanediols have a variety of stereoisomeric conformers. The distances between the two oxygen atoms in the diols can be calculated[11] and listed in Table 1. Compounds 1,2-cyclohexanediol, 1,3-cyclohexanediol, and 1,4-cyclohexanediol were allowed to react with equimolar amounts of **1** and then ethanol. The products were analyzed by ^{31}P NMR spectroscopy. All the cyclohexanediols were completely phoshorylated by the reaction with **1** at −78 °C within 5 min. The yields of cyclic phosphite derivatives are given in Table 1. Both *cis*- and *trans*-1,2-cyclohexanediol gave the five-membered cyclic phosphonite (**3a**) quantitatively. Inspection of models shows that the phosphonite ring can be formed readily both with the *cis*-diol having one axial and one equatorial hydroxyl(O–O distance, 2.96 Å), and the *trans*-diol having two equatorial hydroxyl groups(O–O distance, 2.96 Å). Neither of the two stereoisomeric(*cis* and *trans*) cyclic phosphonites is greatly strained and their formation can require little or no distortion of the cyclohexane ring from its

TABLE 1. YIELDS OF CYCLIC PHOSPHITE DERIVATIVES IN THE REACTIONS OF TRI(1-IMIDAZOLYL)PHOSPHINE WITH VARIOUS DIOLS AND NUCLEOSIDES

	Yield[a]/%	O–O Distance[b]/Å
cis-1,2-Cyclohexanediol	≈100	2.96
trans-1,2-Cyclohexanediol	≈100	2.96[d]
cis-1,3-Cyclohexanediol	44	2.53[e]
trans-1,3-Cyclohexanediol	0[c]	5.30
cis-1,4-Cyclohexanediol	0[c]	4.49
trans-1,4-Cyclohexanediol	0[c]	5.70
1,2-Benzenediol	74	2.72
1,3-Benzenediol	0[c]	4.71
1,4-Benzenediol	0[c]	5.44
Thymidine	0[c]	3.73
5′-*O*-Monomethoxytrityluridine	93	2.77

a) Yields determined by ^{31}P NMR spectroscopy or HPLC. b) Distance between the two oxgen atoms in the hydroxyl groups: L. E. Sutton, "Tables of Interatomic Distance and Configuration in Molecules and Ions." c) Polymeric product. d) Two equatorial hydroxyl groups. e) Two axial hydroxyl groups.

preferred chair conformation. On the other hand, of the two 1,3-cyclohexanediols, only the *cis*-compound having two axial hydroxyl groups (O–O distance, 2.53 Å), gave the six-membered cyclic phosphonite (**4a**), but *trans*-compound(O–O distance, 5.3 Å) did not give the cyclic phosphonite. Inspite of no distortion of the cyclohexane ring from the chair conformation, the yield(44%) of the six-membered cyclic phosphonite was less than that of the five-membered one. *cis*-1,4-Cyclohexanediol(O–O distance, 4.49 Å), and *trans*-1,4-cyclohexanediol(O–O distance, 5.70 Å) did not give the cyclic phosphonite. They yielded gel-like polymeric material. These results show that the selectivity of the cyclic phosphorylation reaction with **1** depends on the distance between the two oxygen atoms of the hydroxyl groups in diols; in the case of diols possessing the favorably adjacent hydroxyl groups, only the cyclic phosphorylation reaction proceeds, which involves the formation of the monophosphorylated diol and then the successive intramolecular reaction to give the cyclic phosphonite. When the two hydroxyl groups of diols are not favorably placed, the intermolecular reaction of the monophosphorylated diols leads to the formation of the polymer.

Further investigation on the reactions of benzenediol derivatives with equimolar amounts of **1** was carried out. The yields of the cyclic phosphite derivatives are shown also in Table 1. 1,2-Benzenediol(O–O distance, 2.72 Å) was favored to give the five-membered cyclic phosphonite (**3b**). The six-membered cyclic phosphonite from 1,3-benzenediol (O–O distance, 4.71 Å) was not obtained. 1,4-Benzenediol (O–O distance 5.44 Å) gave polymeric material.

The question arose whether a six-membered ring could be formed in the reaction of a nucleoside possessing the 5′- and 3′-hydroxyl groups(O–O distance, 3.73 Å) with **1**. To study this problem the reaction of thymidine with equimolar amount of **1** was performed. The result is shown in Table 1. Thymidine 3′,5′-cyclic phosphonite was not formed, but polymeric compounds were obtained. On the other hand, the reaction of 5′-monomethoxytrityluridine having free 2′- and 3′-hydroxyl groups(O–O distance, 2.77 Å) with equimolar amount of **1** gave only the five-membered cyclic phosphonite (**2b**), but no polymeric compound was obtained. It is concluded therefore that **1** gave the cyclic phosphites quantitatively in the reaction with diols possessing the favorably placed hydroxyl groups in which the distance between the two oxygen atoms is 2.7—3.0 Å.

Another problem was to examine the ease of the formation of five-membered cyclic phosphonite and six-membered one in the reaction of diols with **1**. The reaction of aliphatic diols which have flexible chains with equimolar amounts of **1** were carried out (−78 °C, 30 min). After the treatment with methanol, ^{31}P NMR spectra of the products show that the cyclic phosphites were formed quantitatively both from ethylene glycol and 1,3-propanediol. These results indicate that **1** has a potential activity to give the both five- and six-membered cyclic phosphonite (**5** and **6**) from the flexible chain diols. It was reported that, in the similar reactions, phosphorus trichloride,[1–3] triphenylphosphine,[4] and hexamethylphosphorous triamide[12] gave the cyclic phosphite in moderate yields. Therefore, from the practical point of view, **1** is useful for the preparation of cyclic phosphites.

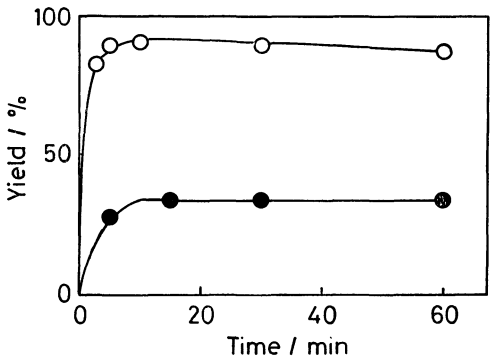

Fig. 1. The time course of the phosphorylation reaction of 5′-*O*-monomethoxytrityluridine and 2′,3′-*O*-isopropylideneuridine with tri(1-imidazolyl)phosphine. ○: 5′-*O*-Monomethoxytrityluridine, ●: 2′,3′-*O*-isopropylideneuridine.

We have already shown that, in the reaction of unprotected ribonucleoside, the ribonucleoside 2′,3′-cyclic 1-imidazolylphosphonite (**2a**) is formed by the selective attack of **1** to the 2′- and 3′-hydroxyl groups of ribonucleoside.[8–10] In order to examine the course of the selective formation of the ribonucleoside 2′,3′-cyclic 1-imidazolylphosphonite(**2a**), the reactivity of **1** toward the different hydroxyl groups(5′- or 2′,3′-OH) of ribonucleoside was investigated. The time course of the phosphorylation reaction of 5′-*O*-monomethoxytrityluridine and 2′,3′-*O*-isopropylideneuridine with equimolar amount of **1** was shown in Fig. 1. 5′-*O*-Monomethoxytrityluridine was phosphorylated to 90% within 3 min, whereas the rate of the phosphorylation of 2′,3′-*O*-isopropylideneuridine was considerably slow and the yield of the phosphorylated product was less than 35%. That is, the reactivity of **1** toward the 2′- and 3′-hydroxyl groups of ribonucleoside is much higher than toward the 5′-hydroxyl group. Consequently, it is considered that the formation of ribonucleoside 2′,3′-cyclic 1-imidazolylphosphonite (**2a**) is obviously kinetically controlled.

Experimental

High-performance liquid chromatography was carried out on a Shimadzu-Dupont LC 830 instrument using Partisil 10 SAX(ion exchange) column; the linear gradient was 0.001 M†† KH_2PO_4 to 0.3 M KH_2PO_4 containing 10% ethanol(3% min^{-1}) at 70 atm, or on a Shimadzu LC 3A instrument using Nucleosil 7C_{18}(reverse-phase) column; solvent was 2—20% CH_3CN in 0.1 M ammonium acetate(pH 6.0) at a flow rate of 1.0 ml min^{-1}. ^{31}P NMR spectra were recorded on a JEOL FX-200 instrument. ^{13}C NMR spectra were obtained on a JEOL FX-100 instrument.

Pyridine was distilled from *p*-toluenesulfonyl chloride, redistilled from calcium hydride, and stored over 4A molecular sieves. Tetrahydrofuran was refluxed in the presence of $LiAlH_4$ for overnight, distilled, and stored over 5A molecular sieves. Phosphorus trichloride was distilled and stored in

†† 1 M=1 mol dm^{-3}.

a brown ampule. Ethanol was distilled in the presence of benzene and stored over 3A molecular sieves. Methanol was distilled and stored over 3A molecular sieves. Imidazole, thymidine, *cis*- and *trans*-1,2-cyclohexanediol(*cis*:*trans*=67:33),[13] *trans*-1,2-cyclohexanediol, *cis*- and *trans*-1,3-cyclohexanediol(*cis*:*trans*=50:50),[13] *cis*- and *trans*-1,4-cyclohexanediol(*cis*:*trans*=44:56),[13] ethylene glycol, 1,3-propanediol, 1,2-benzenediol, 1,3-benzenediol, and 1,4-benzenediol were purchased from Nakarai Chemical Co. 5′-*O*-Monomethoxytrityluridine and 2′,3′-*O*-isopropylidene uridine were synthesized by the usual method.[14]

Tri(1-imidazolyl)phosphine. The preparation of tri(1-imidazolyl)phosphine was carried out under argon; phosphorus trichloride(300 μl, 3.45 mmol) was added dropwise to a solution of imidazole(1.41 g, 20.7 mmol) in 24 ml of tetrahydrofuran (THF). Then the mixture was stirred at 0 °C for 20 min. After the filtration of the imidazolium hydrochloride, the filtrate was used as a phosphorylating reagent. Tri(1-imidazolyl)phosphine was contained *ca.* 0.14 mmol in 1 ml of the filtrate. This phosphorylating reagent was stable at least for a week in anhydrous THF under argon.

Reaction with Cyclohexanediols. Generally, the reactions of cyclohexanediols with tri(1-imidazolyl)phosphine were carried out in THF; the reaction mixtures consisted of cyclohexanediols (400.8 mg, 3.45 mmol) in 5 ml of THF and tri(1-imidazolyl)phosphine (approximately equimolar amount to cyclohexanediols) in 24 ml of THF. The mixtures were stirred at −78 °C for 60 min and then evaporated to nearly dryness. The residues were dissolved in pyridine-d_5. The solutions were sealed into the NMR tube under argon and then analyzed by ^{31}P NMR.

Time Course of the Reaction with Cyclohexanediols. *trans*-1,2-Cyclohexanediol was reacted with tri(1-imidazolyl)phosphine under the same conditions above for 5, 15, 30, and 60 min. After these time intervals, the reaction mixtures were treated with excess ethanol at 0 °C for 30 min. The solutions were evaporated to nearly dryness and dissolved in benzene-d_6. They were sealed into the NMR tube and then analyzed by ^{31}P NMR. Similar experiments were done for *cis*- and *trans*-1,2-cyclohexanediol, and *cis*- and *trans*-1,3-cyclohexanediol.

Reaction with Glycols. Glycols (ethylene glycol, 62.1 mg, 1,3-propanediol, 76.1 mg; 1 mmol) were dissolved in THF (7 ml) and then cooled to −78 °C. To these solutions, tri(1-imidazolyl)phosphine (1.0 mmol) in 7 ml of THF was added and stirred for 30 min. After treatment of methanol (0.2 ml, 4.9 mmol), the solutions were evaporated to nearly dryness. The residue were dissolved in $CDCl_3$. The solutions were transferred into the NMR tube and then analyzed by ^{31}P NMR.

Reaction with Benzenediols. Benzenediols (30.8 mg, 0.28 mmol) were reacted with tri(1-imidazolyl)phosphine(equimolar amount to benzenediols) in 3 ml of THF at −78 °C for 60 min. The reaction mixtures were added to a solution of iodine (71.2 mg, 0.28 mmol) in 3 ml of THF–water(2:1, v/v) with a few drops of pyridine. Then the solutions were evaporated to dryness. The residues were dissolved in 1 ml of water and then analyzed by HPLC.

Reaction with Thymidine. Thymidine (36.2 mg, 0.1 mmol) was reacted with tri(1-imidazolyl)phosphine (equimolar amount to nucleoside) in 2.4 ml of pyridine–THF (1:4, v/v) at −78 °C for 60 min. After the oxidation with iodine and water, the mixtures were evaporated to dryness. The residues were dissolved in 1 ml of water and then analyzed by HPLC.

Reaction with 5′-O-Monomethoxytrityluridine and 2′,3′-O-Isopropylideneuridine. 5′-*O*-Monomethoxytrityluridine (72.3 mg, 0.14 mmol) was dissolved in 1.4 ml of pyridine–THF (5:2, v/v) and then cooled to −78 °C. To this solution, tri(1-imidazolyl)phosphine (equimolar amount to nucleoside) in 1 ml of THF was added and stirred. After the appropriate time intervals, the mixture was oxidized with iodine and water. The mixture was evaporated to dryness and dissolved in the buffer(20% CH_3CN) and then analyzed by HPLC. Similar experiment was done for 2′,3′-*O*-isopropylideneuridine under the same conditions. In order to confirm the cyclic structure, the phosphorylated derivative from 5′-*O*-monomethoxytrityluridine was treated with $ZnBr_2$ in methanol and then analyzed by HPLC. Only the peak due to uridine 2′,3′-cyclic phosphate was appeared.

Determination of Yields. Yields(%) of the cyclic phosphite derivatives from the reaction of tri(1-imidazolyl)phosphine with cyclohexanediols and glycols were determined by ^{31}P NMR spectroscopy. The cyclic structure was confirmed after the conversion of the cyclic 1-imidazolylphosphonite to the corresponding cyclic phosphites of which ^{31}P chemical shifts (downfield from external 85% H_3PO_4) were reported in the literatures.[15,16] 2-Ethoxy-4,5-(*cis*-1,2-cyclohexanedihydroxy)-1,3,2-dioxaphospholane (from **3a**): δ+136 ppm (lit,[15] δ+136 ppm); 2-ethoxy-4,5-(*trans*-1,2-cyclohexanedihydroxy)-1,3,2-dioxaphospholane (from **3a**): δ=139 (lit,[15] δ=139); 2-ethoxy-4,5-(*cis*-cyclohexanedihydroxy)-1,3,2-dioxaphosphorinane (from **4a**): δ=124 (lit,[15] δ=124); 2-methoxy-1,3,2-dioxaphospholane (from **5**): δ=132 (lit,[16] δ=132); 2-methoxy-1,3,2-dioxaphosphorinane (from **6**): δ=129 (lit,[16] δ=129).

References

1) A. E. Arbuzov, V. M. Zoroastrova, and N. I. Rizpolozhenski, *Bull. Acad. Sci. URSS, Classe Sci. Chem.*, **1945**, 208.

2) H. J. Lucas, F. W. Mitchell, and C. N. Schully, *J. Am. Chem. Soc.*, **72**, 5491 (1950).

3) A. E. Arbuzov and V. M. Zoroastrova, *Izv. Akad. Nauk SSSR, Otdel. Khim. Nauk*, **1952**, 770.

4) D. C. Ayres and H. N. Rydon, *J. Chem. Soc.*, **1957**, 1109.

5) P. C. Crofts, J. H. H. Markes, and H. N. Rydon, *J. Chem. Soc.*, **1958**, 9250.

6) A. Holy and F. Sorm, *Collect. Czech. Chem. Commun.*, **31**, 1544 (1966).

7) A. Holy and F. Sorm, *Collect. Czech. Chem. Commun.*, **31**, 1562 (1966).

8) T. Shimidzu, K. Yamana, A. Murakami, and K. Nakamichi, *Tetrahedron Lett.*, **21**, 2717 (1980).

9) T. Shimidzu, K. Yamana, K. Nakamichi, and A. Murakami, *J. Chem. Soc., Perkin Trans. 1*, **1981**, 2294.

10) T. Shimidzu, K. Yamana, K. Nakamichi, S. Maikuma, and N. Kanda, *Nucleic Acids Res.* Symposium Series No. **11**, 89 (1982).

11) "Tables of Interatomic Distances and Configuration in Molecules and Ions," ed by L. E. Sutton, The Chemical Society, London (1958), Supplement 1956—1959, 1965.

12) W. G. Bentrude and H. W. Tan, *J. Am. Chem. Soc.*, **95**, 4666 (1973).

13) The molar ratio of the *cis* to *trans* was determined by ^{13}C NMR spectra of the cyclochaxanes.

14) V. Amarnath and A. D. Broom, *Chem. Rev.*, **77**, 183 (1977); C. B. Reese, *Tetrahedron*, **34**, 3143 (1978).

15) G. M. Blackbum, J. S. Cohen, and L. Todd, *Tetrahedron Lett.*, **1964**, 2873.

16) B. C. Chang, W. E. Conrad, D. B. Denny, D. Z. Denny, R. Edelman, R. L. Powell, and D. W. White, *J. Am. Chem. Soc.*, **93**, 4004 (1971).

The Vibrational Spectra and Thermodynamic Functions of 2,3-Dichloropyridine

Kanak Chandra Medhi

Department of Physics, Gauhati University, Gauhati-781014, India

(Received September 10, 1982)

The infrared spectrum in the vapor, liquid, solution, and solid phases and the laser Raman spectrum in the liquid state have been measured for 2,3-dichloropyridine. A complete vibrational assignment is given. Ideal gas state thermodynamic functions of the molecule are computed over the temperature range 200—1500 K.

The infrared spectrum of 2,3-dichloropyridine in solutions was measured by Green *et al.*,[1] and a vibrational assignment based on comparison with the related molecules was given. For evaluation of the thermodynamic properties, a precise knowledge of the fundamental frequencies is necessary. A study of the vapor-phase infrared spectrum and the polarized Raman spectrum is essential for an accurate vibrational assignment of the observed frequencies. There is, however, no previous report on the Raman and vapor-phase infrared spectra of this molecule. In extension of the previous work on the vibrational spectra of some substituted pyridines,[2-5] the infrared spectrum of 2,3-dichloropyridine in the vapor, liquid, solution and solid phases and the Raman spectrum in the liquid state have been studied in details in this work. The present measurements suggest some changes in the previous assignments.[1]

The present paper gives an essentially complete assignment of the observed frequencies based on the contours of the vapor-phase infrared bands, the state of polarization of the Raman lines and comparison with the assignments proposed for related molecules.[4-10] It also includes the ideal gas state thermodynamic functions of the molecule calculated on the basis of the present assignment.

Experimental

Pure sample of 2,3-dichloropyridine obtained from Schuchardt, Germany was purified by repeated sublimation under vacuum.

The Raman spectrum of the compound in the liquid state just above the melting point was recorded on a Cary 82 laser Raman spectrophotometer. The spectrum was excited by the 514.5 nm line (200 mW) of an argon ion laser. The polarization measurement was carried out by the method described previously.[5] The infrared spectrum in the region 4000—400 cm^{-1} in the vapor state, in nujol mull or polycrystalline film, in liquid film prepared from the melt of the substance and in solution in CCl_4 or CS_2 was measured using a Carl-Zeiss Specord IR 75 spectrophotometer after the calibration of the instrument had been checked by a polystyrene film run. A 9 cm heated gas cell equipped with KBr windows was used to record the vapor-phase spectrum. The far infrared spectrum in nujol mull in the region 500—30 cm^{-1} was obtained using a Perkin-Elmer Model 180 spectrophotometer.

Results and Discussion

The observed infrared and Raman frequencies of 2,3-dichloropyridine together with their approximate intensities and assignments are given in Table 3. The fundamental frequencies are collected in Table 4. Table 5 shows the calculated values of the thermodynamic quantities of the molecule over the temperature range 200—1500 K. The variations of these thermodynamic functions with temperature are represented graphically in Figs. 2 and 3.

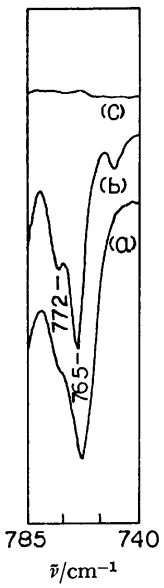

Fig. 1. Infrared spectrum of 2,3-dichloropyridine showing 772 and 765 cm^{-1} bands. a): Thin film (melt), (b): solution in CS_2, (c): pure CS_2.

The 2,3-dichloropyridine molecule belongs to the point group C_s and its twenty seven normal vibrations, which are active both in the Raman and infrared spectra, are distributed over the two symmetry species as

$$19a' + 8a''.$$

The a′ modes should be polarized and the a″ modes depolarized in the Raman spectrum. The principal moments of inertia of 2,3-dichloropyridine molecule and the asymmetry parameters $\kappa = \frac{2B-A-C}{A-C}$ and $\rho^* = \frac{A-C}{B}$, where A, B, and C are rotational constants, have been calculated (Table 1) with the following interatomic distances and bond angles assuming that the ring is a planar regular hexagon:

$r(C\text{-}C) = r(C\text{-}N) = 1.397$ Å, $r(C\text{-}H) = 1.084$ Å,
$r(C\text{-}Cl) = 1.717$ Å,
$\angle CCC = \angle CCN = \angle CCH = \angle CCl = 120°$,

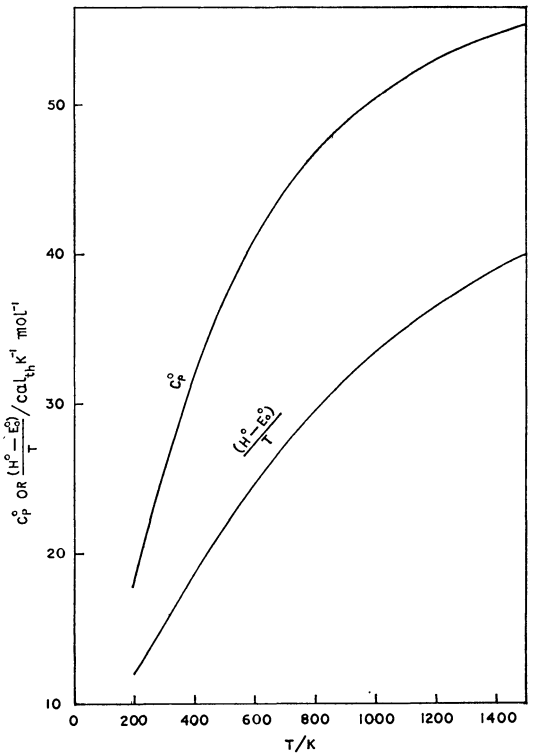

Fig. 2. Variation of heat capacity and enthalpy of 2,3-dichloropyridine with absolute temperature.

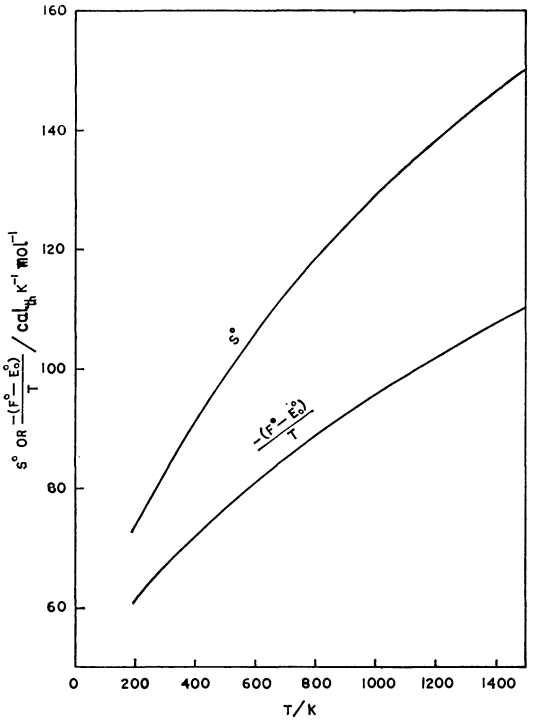

Fig. 3. Variation of entropy and free energy of 2,3-dichloropyridine with absolute temperature.

and by using the relative atomic masses recommended by IUPAC.[11] The PR separations of band envelopes in the vapor-phase infrared spectrum have been calculated at $T=346$ K by the method of Seth-Paul and Dijkstra,[12] and are included in Table 2 along with the observed separations.

Table 1. Principal moments of inertia[a] and the asymmetry parameters for 2,3-dichloropyridine

$I_x/10^{-47}$ kg m^2	$I_y/10^{-47}$ kg m^2	$I_z/10^{-47}$ kg m^2	κ	ρ^*
424.003	601.068	1025.070	−0.0048	0.8312

a) The z-axis is perpendicular to the plane of the ring.

Table 2. PR separations in the infrared vapor-phase band envelopes

Band type	PR separation $\tilde{\nu}$/cm^{-1}	
	Calcd	Obsd
A (∥)	10.7	10.0, 10.0
B (⊥)	8.1	8.0, 8.0, 8.0, 8.0
C (⊥)	16.1	16.0, 17.0

The infrared bands belonging to the species a″ should show C-contour with a PQR structure showing a sharp strong Q maximum but ill-defined P and R branches,[13] while those of species a′ will have A- or B- contour or contours of the hybrid type-AB.

Species a′. There are expected three frequencies in the C–H stretching region, and the polarized Raman lines at 3068 and 3054 cm^{-1} are assigned to these modes. The Raman shifts at 1562, 1552, 1436, 1398, and 1031 cm^{-1} are observed to be polarized; these are unambiguously identified as a′ fundamentals arising essentially from the stretching of the C–C (C–N) bonds. The infrared band at 1125 cm^{-1} shows type-B contour in the gas-phase spectrum, its Raman counterpart located at 1126 cm^{-1} being polarized. This may be attributed to the a′ mode involving stretching of the C–Cl bonds in agreement with the similar assignment proposed in the case of *o*-dichlorobenzene.[6]

A moderately intense infrared band has now been observed at 772 cm^{-1} which was not reported by the previous investigators[1] probably due to lack of proper resolution. In the present investigation the 772 cm^{-1} band is appearing as a shoulder on the higher wavenumber side of the 765 cm^{-1} band in the pure liquid state. The band is, however, clearly resolved in solution in CS_2 (Fig. 1). Though its Raman counterpart is not observed, it has been tentatively assigned as the a′ fundamental corresponding to the substituent-sensitive mode 12.[2,9] The infrared band at 517 cm^{-1} (present value) was assigned previously[1] to the a″ species. But the corresponding Raman line observed at 506 cm^{-1} appears to be polarized; it must therefore be assigned as an a′ fundamental. The observed frequency difference between the infrared band and the Raman shift may be due to the fact that the infrared band at 517 cm^{-1} is sharp, while the Raman line is weak and broad having its maximum at about 506 cm^{-1}. Moreover, its position is somewhat influenced by the neighbouring strong Raman line at 477 cm^{-1}. The remaining a′ fundamentals are identified with the polarized Raman lines at 1215, 1159, 1062, 652, 477, and 204 cm^{-1} and the infrared bands at 1298 and 763 cm^{-1} in agreement with the previous assignment.[1]

Table 3. Observed vibrational frequencies and assignments for 2,3-dichloropyridine

Infrared, $\tilde{\nu}$/cm^{-1}				Raman, $\tilde{\nu}$/cm^{-1}		Assignment
Nujol mull	Melt	Solution	Vapor		Melt	
3058 (ms)*	3063 (ms)	3064 (ms)	3067		3068 (53) p	ν_1 and ν_2 (a′, a′)
3044 (ms)*	3053 (ms)	3054 (ms)			3054 (49) p	ν_3 (a′)
1970 (mw)		1943 (w)				$2\times\nu_{20}$ (A′)
1930 (mw)		1906 (w)				$\nu_{20}+\nu_{21}$ (A′)
1896 (w)		1867 (w)				$2\times\nu_{21}$ (A′)
		1812 (w)				$\nu_{10}+\nu_{16}$ (A′)
		1764 (w)				$\nu_{20}+\nu_{22}$ (A′)
1754 (w)		1730 (w)				$\nu_{21}+\nu_{22}$ (A′)
		1694 (w)				$\nu_{20}+\nu_{23}$ (A′)
		1639 (w)				$\nu_{11}+\nu_{17}$ (A′)
1577 (sh)	1576 (sh)	1576 (sh)				$\nu_{12}+\nu_{17}$ (A′)
1575 (ms)	1570 (sh)	1571 (sh)				$\nu_{22}+\nu_{14}$ (A″)
1561 (s)	1559 (s)	1560 (s)	1563		1562 (18) p	ν_4 (a′)
1553 (s)	1553 (sh)	1554 (sh)	1556		1552 (12) p	ν_5 (a′)
≈1437 (ms)	1434 (ms)	1435 (ms)	1443 1435	B	1436 (4) p	ν_6 (a′)
1425 (mw)	1419 (w)	1421 (sh)	1420			$\nu_{14}+\nu_{16}$ (A′)
1408 (sh)	1412 (sh)	1410 (sh)				$\nu_{15}+\nu_{16}$ (A′)
1398 (vs)	1396 (vs)	1398 (vs)	1405 1401 1395	A	1398 (4) p	ν_7 (a′)
1386 (sh)	1385 (sh)	1386 (sh)				$\nu_{13}+\nu_{25}$ (A″)
1302 (w)	1298 (w)	1300 (w)				ν_8 (a′)
≈1247 (w)	1253 (w)	1251 (w)				$\nu_{14}+\nu_{18}$ (A′)
1235 (w)	1237 (w)	1237 (w)				$\nu_{15}+\nu_{18}$ (A′)
1213 (w)	1211 (mw)	1211 (mw)			1215 (4) p	ν_9 (a′)
1190 (ms)	1192 (ms)	1192 (mw)	≈1200		1194 (3) p	$\nu_{21}+\nu_{26}$ (A′)
1160 (vs)	1159 (vs)	1158 (vs)	1170 1165 1160	A	1159 (37) p	ν_{10} (a′)
1131 (ms) 1123 (ms)	1125 (ms)	1125 (ms)	1130 1122	B	1126 (5) $\rho=0.68$	ν_{11} (a′)
≈1115 (sh)	≈1116 (sh)	1118 (sh)				$\nu_{16}+\nu_{18}$ (A′) $\nu_{15}+\nu_{25}$ (A″)
1078 (w)	1077 (w)	1077 (w)				$\nu_{23}+\nu_{25}$ (A′)
1059 (mw)	1061 (ms)	1061 (ms)	1068 1060	B	1062 (100) p	ν_{12} (a′)
		1037 (sh)	1045 1038			$\nu_{22}+\nu_{26}$ (A′) $2\times\nu_{17}$ (A′)
1031 (vs)	1032 (vs)	1032 (vs)	1031		1031 (21) p	ν_{13} (a′)
≈1004 (w)	1003 (w)	1004 (w)				$\nu_{16}+\nu_{25}$ (A″)
988 (mw)	972 (mw)	971 (mw)	971			ν_{20} (a″)
951 (w)	934 (w)	934 (w)				ν_{21} (a″)
803 (vs) 794 (sh)	797 (vs)	793 (vs)	799 792 782	C		ν_{22} (a″)
≈769 (sh)	≈771 (sh)	772 (mw)				ν_{14} (a′)
760 (ms)	763 (ms)	765 (ms)	770			ν_{15} (a′)
723 (s)	726 (s)	726 (s)	736 730 720	C		ν_{23} (a″)
656 (s) 649 (s)	651 (s)	651 (s)	654 646	B	652 (68) p	ν_{16} (a′)
516 (mw)	517 (w)	515 (w)			506 (5) p	ν_{17} (a′)

Table 3. (Continued)

Infrared, $\tilde{\nu}$/cm^{-1}				Raman, $\tilde{\nu}$/cm^{-1}	Assignment
Nujol mull	Melt	Solution	Vapor	Melt	
475 (ms)	475 (ms)	474 (ms)	474	477 (53) p	ν_{18} (a′)
443 (w)					$\nu_{26}+\nu_{19}$ (A″), $\nu_{22}-\nu_{25}$ (A′)
426 (ms)				428 (9) dp	ν_{24} (a″)
351 (ms)				353 (4) dp	ν_{25} (a″)
250 (ms), 246 (ms)				255 (8) dp	ν_{26} (a″)
202 (w)				204 (17) p	ν_{19} (a′)
153 (ms)				142 (24) dp	ν_{27} (a″)
56 (ms)					Lattice mode
38 (s)					

* Frequency observed in solid thin film. (s)=strong, (m)=medium, (w)=weak, (v)=very, (sh)=shoulder, p=polarized, dp=depolarized.

Combination bands (IR in solution) in the region 4000—2000 cm^{-1}: 3125 (w) (3123 (22) p)=$2\times\nu_4$ (A′), 3117 (w)=$\nu_4+\nu_5$ (A′), 2980 (w)=$\nu_5+\nu_6$ (A′), 2954 (w)=$\nu_4+\nu_7$ (A′), 2867 (vw)=$2\times\nu_6$ (A′), 2831 (vw)=$\nu_6+\nu_7$ (A′), 2813 (w)=$\nu_7+\nu_{15}+\nu_{16}$ (A′), 2793 (w)=$2\times\nu_7$ (A′), 2771 (w)=$\nu_4+\nu_9$ (A′), 2673 (w)=$\nu_5+\nu_{11}$ (A′), 2645 (vw)=$\nu_6+\nu_9$ (A′), 2616 (w)=$\nu_5+\nu_{12}$ (A′), 2555 (w)=$\nu_7+\nu_{10}$ (A′), 2520 (w)=$\nu_7+\nu_{11}$ (A′), 2509 (w)=$\nu_8+\nu_9$ (A′), 2495 (w)=$\nu_6+\nu_{12}$ (A′), 2471 (w) (2472 (3) p)=$\nu_6+\nu_{13}$ (A′), 2428 (w) (2426 (3) p)=$\nu_7+\nu_{13}$ (A′), 2380 (w)=$\nu_9+\nu_{10}$ (A′), 2250 (w)=$2\times\nu_{11}$ (A′), 2186 (w)=$\nu_{10}+\nu_{13}$ (A′), 2090 (vw)=$\nu_{12}+\nu_{13}$ (A′), 2048 (w)=$\nu_7+\nu_{16}$ (A′), 2003 (vw)=$\nu_9+\nu_{22}$ (A″).

Table 4. The fundamental frequencies for 2,3-dichloropyridine

Symmetry species	Mode No.	Fund.	Wavenumber $\tilde{\nu}$/cm^{-1}	Symmetry species	Mode No.	Fund.	Wavenumber $\tilde{\nu}$/cm^{-1}
a′	2	ν_1	3068	a′	7b	ν_{15}	763
	20b	ν_2	3068		6b	ν_{16}	652
	20a	ν_3	3054		6a	ν_{17}	506
	8a	ν_4	1562		9a	ν_{18}	477
	8b	ν_5	1552		18b	ν_{19}	204
	19a	ν_6	1436	a″	17a	ν_{20}	972
	19b	ν_7	1398		5	ν_{21}	934
	14	ν_8	1298		10b	ν_{22}	797
	3	ν_9	1215		4	ν_{23}	726
	15	ν_{10}	1159		11	ν_{24}	428
	13	ν_{11}	1126		16a	ν_{25}	353
	18a	ν_{12}	1062		10a	ν_{26}	255
	1	ν_{13}	1031		16b	ν_{27}	142
	12	ν_{14}	772				

Table 5. Thermodynamic functions of 2,3-dichloropyridine[a)]

Temperature / K	C_p° / cal$_{th}$ K^{-1} mol^{-1}	$(H^\circ-E_0^\circ)T^{-1}$ / cal$_{th}$ K^{-1} mol^{-1}	S° / cal$_{th}$ K^{-1} mol^{-1}	$-(F^\circ-E_0^\circ)T^{-1}$ / cal$_{th}$ K^{-1} mol^{-1}
200	18.50	12.14	73.40	61.27
250	22.04	13.76	77.91	64.15
273.15	23.68	14.54	79.93	65.40
298.15	25.42	15.38	82.08	66.71
300	25.54	15.44	82.24	66.81
400	31.92	18.78	90.49	71.71
500	37.09	21.95	98.19	76.24
600	41.13	24.82	105.32	80.50
700	44.28	27.39	111.91	84.52
800	46.79	29.66	117.99	88.33
900	48.81	31.68	123.62	91.94
1000	50.47	33.48	128.85	95.38
1100	51.84	35.09	133.73	98.64
1200	52.99	36.53	138.29	101.76
1300	53.97	37.84	142.57	104.74
1400	54.79	39.02	146.60	107.58
1500	55.50	40.10	150.40	110.31

a) Ideal gas state at standard pressure of 1 atm. 1 cal$_{th}$=4.184 J.

Species a″. In the earlier work[1] the infrared frequencies at 426 and 351 cm^{-1} (present values) were assigned to the a′ class and the weak infrared band at 443 cm^{-1} to the a″ species. But the Raman spectrum reveals that the corresponding shifts at 428 and 353 cm^{-1} respectively are completely depolarized. They must therefore be assigned as a″ fundamentals arising respectively from the C–H and C–C–C out-of-plane deformations. The 443 cm^{-1} band may be explained as the combination band 250+202=452 cm^{-1} (A″) or the difference band 793−351=442 cm^{-1} (A′).

The infrared bands at 793 and 726 cm^{-1} showing type C contours in the gas phase and the depolarized Raman lines observed at 255 and 142 cm^{-1} are reasonably assigned to the a″ species. The infrared spectrum shows weak absorptions at 972 and 934 cm^{-1}. As in the case of other substituted pyridines, they are attributed to the C–H out-of-plane deformations. The assignments of these frequencies to the a″ species are in agreement with the previous assignments.[1]

Thermodynamic Functions

Ideal gas state thermodynamic functions of 2,3-dichloropyridine molecule have been calculated using the standard expressions[14] and the following wavenumbers of the fundamentals observed in the infrared and Raman spectra (where available, the vapor-phase frequencies are used):

3068, 3068, 3054, 1563, 1556, 1438, 1401, 1298, 1215, 1165, 1127, 1064, 1031, 971, 934, 792, 772, 763, 730, 650, 506, 474, 428, 353, 255, 204, and 142.

Thermodynamic contributions from over-all rotation and vibration are calculated on the basis of the above data and those given in Table 1 by assuming a rigid-rotator harmonic-oscillator approximation.

References

1) J. H. S. Green, D. J. Harrison, and M. R. Kipps, *Spectrochim. Acta, Part A*, **29**, 1177 (1973).
2) K. C. Medhi and D. K. Mukherjee, *Spectrochim. Acta*, **21**, 895 (1965).
3) K. C. Medhi, *Opt. Spektrosk.*, **19**, 49 (1965).
4) K. C. Medhi, *Indian J. Phys.*, **46**, 300 (1972).
5) K. C. Medhi, *Indian J. Phys.*, **51A**, 399 (1977).
6) J. R. Scherer and J. C. Evans, *Spectrochim. Acta*, **19**, 1739 (1963).
7) V. I. Berezin and M. D. Elkin, *Opt. Spectrosc.*, **34**, 395 (1973).
8) D. A. Long and W. O. George, *Spectrochim. Acta*, **19**, 1777 (1963).
9) J. H. S. Green, W. Kynaston, and H. M. Paisley, *Spectrochim. Acta*, **19**, 549 (1963).
10) S. Lui, S. Suzuki, and J. A. Ladd, *Spectrochim. Acta, Part A*, **34**, 583 (1978).
11) Atomic Weights of the Elements, *Pure Appl. Chem.*, **30**, 637 (1972).
12) W. A. Seth-Paul and G. Dijkstra, *Spectrochim. Acta, Part A*, **23**, 2861 (1967).
13) R. M. Badger and L. R. Zumwalt, *J. Chem. Phys.*, **6**, 711 (1938).
14) G. Herzberg, "Molecular Spectra and Molecular Structure, Vol. II. Infrared and Raman Spectra of Polyatomic Molecules," D. Van Nostrand Co., Inc., Princeton (1960), p. 501.

 © 1983 The Chemical Society of Japan Bull. Chem. Soc. Jpn., 56, 3491—3494 (1983)

Physicochemical Studies of Alkali Metal Solutions in Tetrahydrofuran

Jacques Lacoste and François Schué*

Laboratoire de Chimie Macromoléculaire, Université de Sciences et Techniques du Languedoc, Place E. Bataillon, 34060 Montpellier Cedex, France

(Received December 21, 1982)

We have studied the rate of alkali metal dissolution in THF as a function of its nature and of the cryptand (C). The selectivity has been estimated through the equilibrium constant of the following equilibrium:

$$M^- + C \rightleftarrows M^+C + 2e^-_{solv}.$$

Both $\Delta H°$ and $\Delta S°$ for this reaction are negative. The entropy decrease reveals that the sum of the energies bonds between the cation and the ligand and the electrons and the solvent is higher than that necessary to desolvate and dissociate M^-.

Solutions of alkali metals in amines and ethers have been widely studied.[1-5, 12-14] The species which can exist in these solutions may be described by the following equilibria (1) to (3):[2]

$$2M_s \rightleftarrows M^+ + M^- \quad (1)$$

$$\uparrow\downarrow$$

$$M + e^-_{solv} \quad (2)$$

$$\uparrow\downarrow$$

$$M^+ + e^-_{solv} \quad (3)$$

An increase in the solvating power and dielectric constant of the solvent shifts all three equilibria to the right.

The use of a cation-complexing agent (C) seems to provide enough stabilization energy to yield solvated electrons in solvents in which the metals would otherwise be insoluble.[1] The effect of (C) may be represented by the following in addition to equilibria (1)—(3).

$$2M_{(s)} + C \rightleftarrows M^+C + M^- \quad (4)$$

$$M^- + C \rightleftarrows M^+C + 2e^-_{solv} \quad (5)$$

Many complexing agents have been used which belong to the classes of crowns and cryptands.

In a preliminary note,[6] we have studied equilibria (4) and (5) from a kinetic point of view.

At the early stage of the reaction (short time of contact between a solution of (C) and M solid), the complexing agent is in excess with respect to the dissolved metal and, under certain conditions, it is possible to obtain the solvated electron without the presence of M^-. With increasing time of contact, most of the free C is consumed by reaction (4); reaction (5) is reversed, and the M^- species predominates.

In this work, we have studied in more detail both the kinetics of metal dissolution as a function of the nature of the alkali metal and of the complexing agent **1**, **2**, and **3** and the thermodynamic parameters of equilibrium (5).

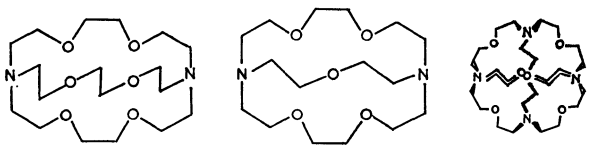

1 **2** **3**

Experimental

The high reactivity of the species e^-_{solv} and M^- requires the use of high vacuum techniques and all glass apparatus.

All glassware was cleaned[2] first with an HF solution followed by a thorough rinsing with distilled water. The cells were filled with boiling aqua regia which was allowed to remain in the cell for at least 10 h. After rinsing with distilled water, the cell was dried in an oven overnight.

Tetrahydrofuran (THF) was first dried with potassium hydroxide and calcium chloride. After initial drying, it was distilled onto potassium and finally stored under vacuum over Na:K (1:3) alloy which yielded blue solutions.

The metals were vacuum-distilled in bulbs supplied with break-seals. The cation-complexing agents were recrystallized in hexane, dried and sealed off under vacuum.

The experiments were carried out in the apparatus described in Fig. 1 according to the following procedure: after evacuation, the metal was distilled from the side arm (a) to form a mirror on the walls of vessel A. Then the solvent, stored on a vacuum line, was distilled under vacuum into A. When the complexing agent (b) had been added, after a given time of contact (t_c) at −78 °C (methanol–Dry Ice refrigerating mixture), the solution was poured through the coarse frit (G2) into the thermostated quartz call B. Excess complexing agent could be added through break-seal (c).

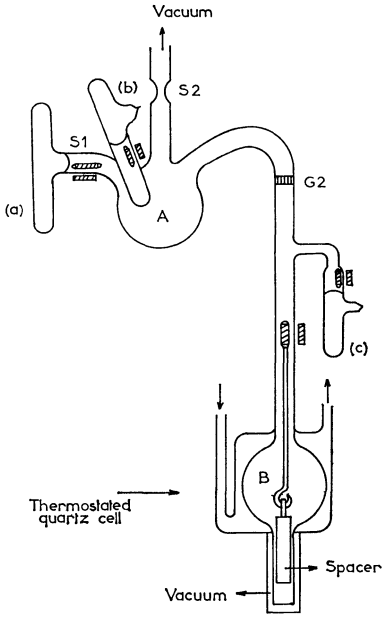

Fig. 1. Apparatus for the preparation and spectroscopic studies of alkali metal solutions.

Optical spectra were obtained with a Beckman DK-2A spectrophotometer. The spectroscopic parameters (λ_{max}, $d\varepsilon/dT$) were determined elsewhere.[7] The optical path-length of the cells was determined with standard solutions of potassium dichromate ($l=0.51+0.01$ and $l=0.057\pm 0.001$ cm). The total metal concentration in solution was estimated by flame photometry (Electrosynthese PHF 62 A). Temperature was controlled by means of an Ultra-kryostat Haake KT52.

Results and Discussion

Kinetics of Dissolution. In order to carry out this study, we used less complexing agent than total metal. If we consider only reaction (4), the ratio R can reach a limiting value of 0.5.

$$R = \frac{[C_o]}{[M]} \qquad (6)$$

$[C_o]$ and [M] represent the concentrations respectively of complexing agent and of metal in solution. The simultaneous presence of reactions (4) and (5) will allow values of R higher than 0.5. High values of the ratio R can be due either to a low complexation efficiency or to a short contact time (Figs. 2 to 5).

The use of compound **3** (Fig. 6), specific for cesium, increases the dissolution and one can observe a higher proportion of e_s^- for a short time of contact. This last study shows the intramolecular cavity cation selectivity.

Complexation Effect. The kinetic studies have shown the influence of the metal and the complexing agent on the rate of dissolution of alkali metals in

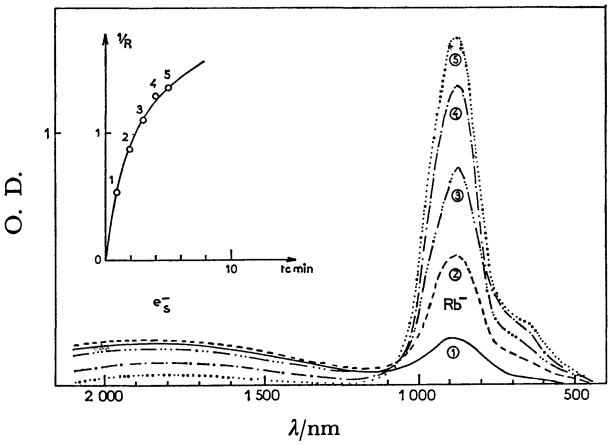

Fig. 4. Dissolution kinetics of rubidium.
Cryptand $I=2.91\times10^{-4}$ mol dm^{-3}, $t=-50$ °C.

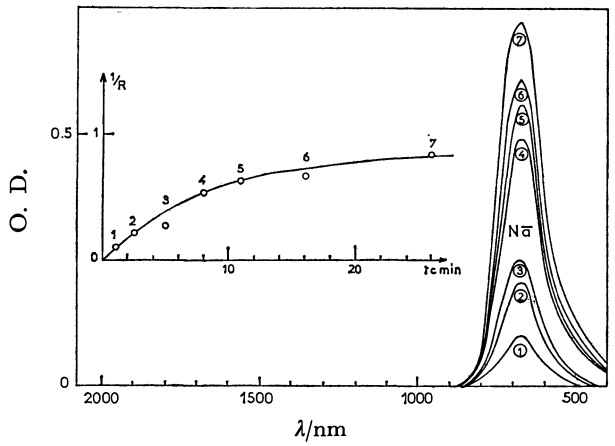

Fig. 2. Dissolution kinetics of sodium.
Cryptand $I=2.9\times10^{-4}$ mol dm^{-3}, $t=-50$ °C.

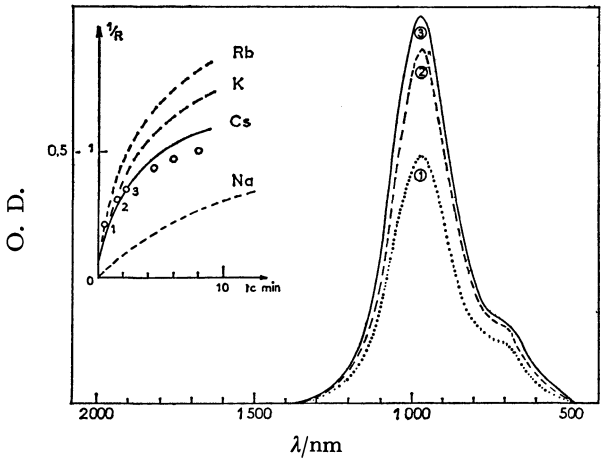

Fig. 5. Dissolution kinetics of cesium.
Cryptand $I=1.25\times10^{-4}$ mol dm^{-3}, $t=-50$ °C.

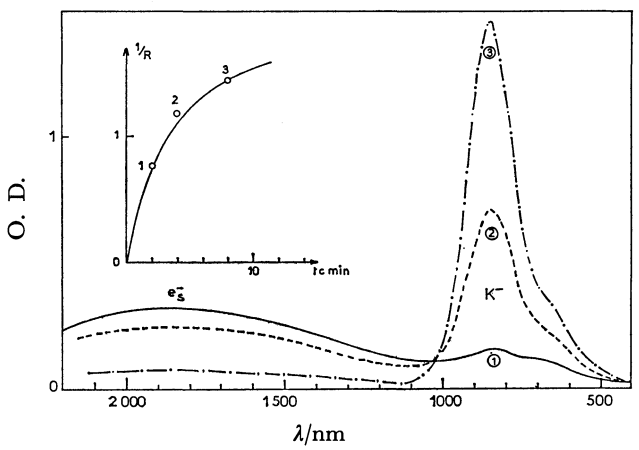

Fig. 3. Dissolution kinetics of potassium.
Cryptand $I=3.29\times10^{-4}$ mol dm^{-3}, $t=-50$ °C.

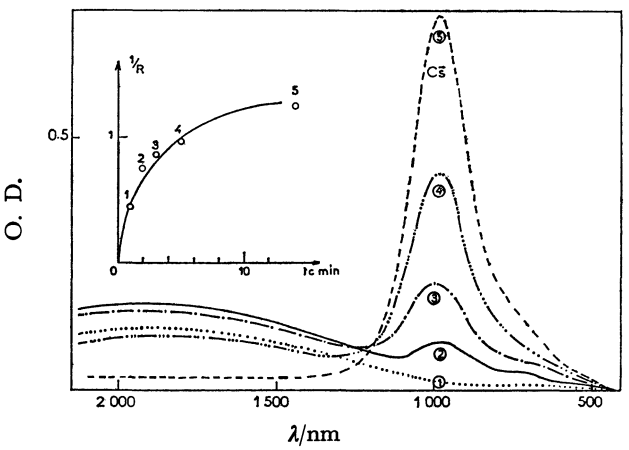

Fig. 6. Dissolution kinetics of cesium.
Cryptand III $=1.78\times10^{-4}$ mol dm^{-3}.

THF. For a better understanding of these phenomena, we have studied the behavior of these solutions in the presence of an excess of complexing agent.

For a constant ratio R, we can expect the equilibrium (5) to be more or less shifted to the right according to the ionization potential of the metal anion and the selectivity of the complexing agent. Figure 7 shows the optical spectra after addition of an excess of compound **1**. A remarkable $K^+ > Rb^+ > Cs^+ > Na^+$ complexation selectivity displayed by ligand **1** is noted. Cesium and rubidium are less complexed than potassium. This shows that the intramolecular cavity-cation selectivity prevails over the ionization potential of the metal anion in these cases.

This selectivity can be illustrated by the equilibrium constant of reaction (5) at −50 °C.

$$K_5 = \frac{[M^+C][e^-_{solv}]^2}{[M^-][C]} \qquad (7)$$

now, $[M^+C]=[M^-]+[e^-_{solv}]$ and $[C]=[C_0]-[M^+C]$ leading to:

$$K_5 = \frac{\{[M^-]+[e^-_{solv}]\}[e^-_{solv}]^2}{[M^-]\{[C_0]-([M^-]+[e^-_{solv}])\}} \qquad (8)$$

The values obtained have been plotted as a function of the cationic radius (Fig. 8), and confirm the high selectivity for K^+.

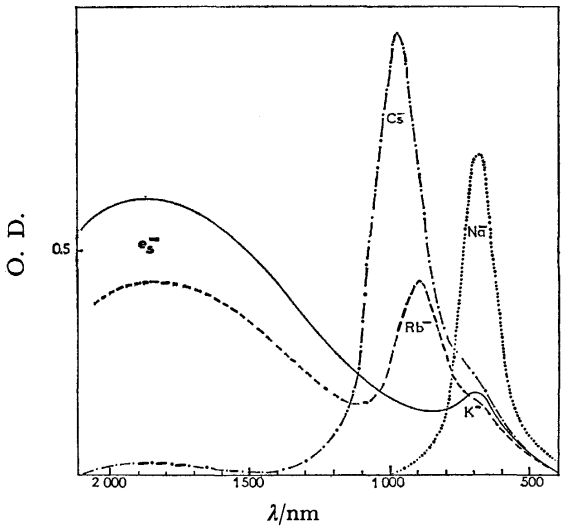

Fig. 7, Absorption spectra of sodium, potassium, rubidium and cesium in THF in the presence of cryptand **I** ($t=-50$ °C).
·····: Na, R=9.2, ——: K, R=4.6, ----: Rb, R=4.4, —·—·—: Cs, R=6.5.

The use of compounds **2** and **3** have marked effects on equilibrium (5). The Cs^+–**3** and K^+–**1** complexes are comparable; but that is not the case for the Na^+–**2** complex for which the high ionization potential of Na^- prevails.

Thermodynamic Parameters. A deeper understanding of the thermodynamics of cryptate formation may be provided by analysis of the enthalpy, $\Delta H°$, and entropy $\Delta S°$, of complexation. Such data have

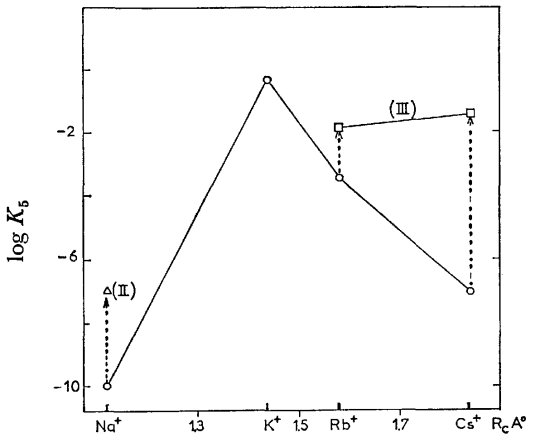

Fig. 8. Values of K_5 equilibrium constant in THF at −50 °C as a function of the cationic radius (see Table 1).
○: Cryptand **I**, △: cryptand **II**, □: cryptand **III**.

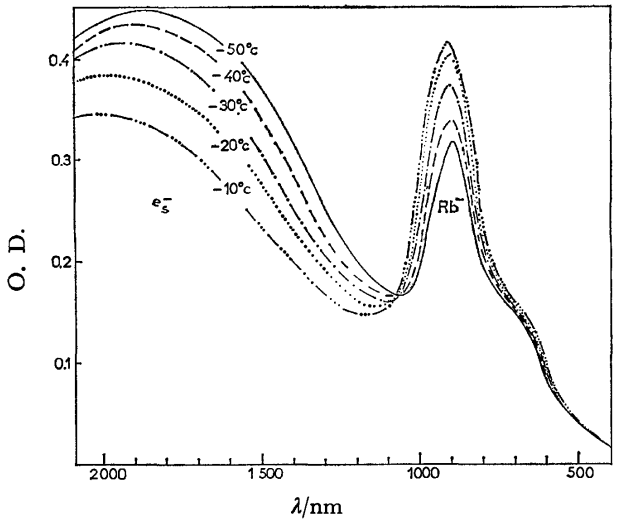

Fig. 9. Influence of temperature on a rubidium cryptand I THF solution.
Rb=3.97×10^{-4} mol dm^{-3}, [cryptand I]=1.75×10^{-3} mol dm^{-3}.

Table 1. Thermodynamic data relative to equilibrium (5)

Metal	Complexing agent	K_5(−50 °C)	$-H°$/kJ mol^{-1}	$-S°$/J K^{-1} mol^{-1}
Na	**1**	10^{-10}	—	—
	2	10^{-7}	—	—
K	**1**	0.4	34±1	155±5
Rb	**1**	4×10^{-4}	8.8±0.5	105±2
	3	1.7×10^{-2}	16.7±0.6	109±3
Cs	**1**	10^{-7}	—	—
	3	3.6×10^{-2}	5.4±0.4	50±2

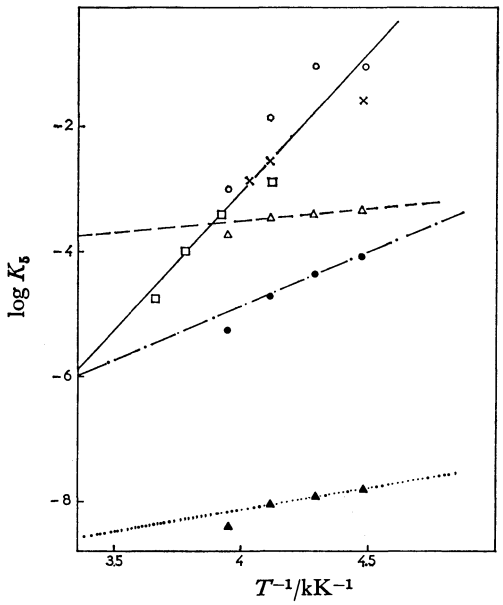

Fig. 10. Van't Hoff law applied to equilibrium (5). ×, ○, □: K/cryptand I, △: Cs/cryptand III, ●: Rb/cryptand III, ▲: Rb/cryptand I.

recently become available for a number of macrobicyclic ligands.[10]

Figure 9 shows the influence of temperature on the absorption spectrum of a rubidium cryptand-I THF solution. Besides the shift of the equilibrium toward the formation of M^- with increasing temperature, we note that the temperature dependence of the position of the absorption bands prevents the presence of an isosbestic point.

Figure 10 represents the Vant Hoff plots and the thermodynamic relation (9) allows the estimation of the enthalpy $\Delta H°$ and entropy $\Delta S°$ for reaction (5).

$$-\frac{\Delta G°}{RT} = -\frac{\Delta H°}{RT} + \frac{\Delta S°}{R} = \log K_5 \qquad (9)$$

The data are given in Table 1.

Both enthalpies and entropies are negative. Negative enthalpies reveal that the sum of the energy of the bonds between the cation and the ligand and the electron and the solvent are higher than that necessary to desolvate and dissociate M^-.

The values observed are in agreement with the high values of the equilibrium constant K_5.

The entropy decrease can be explained by two kinds of complexation; the cation cryptand and the electron THF ones.

We wish to acknowledge support of this research by the Societé Nationale des Poudres et Exploisifs under Contracts N° 17.72 D, 13.73 D, 11.74 D, and 11.42 A.

Our special thanks go to Professor J. M. Lehn of the University of Strasbourg, for providing us with samples of the cryptand compounds and for useful discussions, to Professeur J. L. Dye of the Michigan State University of helpful exchanges of information and useful discussions, and to Dr. S. Bywater of the National Research Council of OTTAWA for useful discussions.

References

1) J. L. Dye, M. G. Debaker, and V. A. Nicely, *J. Am. Chem. Soc.*, **92**, 5226 (1970).
2) J. L. Dye, M. T. Lok, and J. Tehan, *Ber. Bunsenges. Gesellsch. Phys. Chem.*, **75**, 659 (1971).
3) J. L. Dye, C. W. Andrews, and S. E. Mathews, *J. Phys. Chem.*, **79**, 3065 (1975).
4) M. T. Lok, F. J. Tehan, and J. L. Dye, *J. Phys. Chem.*, **76**, 2975 (1972).
5) J. M. Lehn, S. Boileau, B. Kaempf, F. Schué, A. Cau, J. Moinard, and S. Raynal, Br. Fr. N° 7335061 (1973); S. Boileau, B. Kaempf, S. Raynal, J. Lacoste, and F. Schué, *Polym. Lett. Ed.*, **12**, 211 (1974); B. Kaempf, S. Raynal, A. Collet, F. Schué, S. Boileau, and J. M. Lehn, *Angew. Chem. Int. Ed. Engl.*, **13**, 611 (1974).
6) J. Lacoste, B. Kaempf, S. Bywater, and F. Schué, *Polym. Lett. Ed.*, **14**, 201, (1976).
7) J. Lacoste and F. Schué, *J. Organomet. Chem.*, in press.
8) J. P. Sauvage, Thèse de Doctorat d'Etat, Strasbourg (1971).
9) E. Graf and J. M. Lehn, *J. Am. Chem. Soc.*, **97**, 5022 (1975).
10) E. Kauffmann, J. M. Lehn, and J. P. Sauvage, *Helv. Chim. Acta*, **59**, 1099 (1976).
11) R. M. Izatt and J. H. Rytting, *Science*, **164**, 443 (1969); R. M. Izatt, D. P. Nelson, J. H. Rytting, B. L. Haymore, and J. J. Cristiensen, *J. Am. Chem. Soc.*, **93**, 1619 (1971); R. M. Izatt, D. J. Eatough, and J. J. Cristiensen, *Struct. Bonding*, **16**, (1973).
12) F. Y. Jou and L. M. Dorfman, *J. Chem. Phys.*, **58**, 715 (1983).
13) M. G. Dague, J. S. Landers, A. L. Lewis, and J. L. Dye, *Chem. Phys. Lett.*, **66**, 169 (1979).
14) J. L. Dye, *Angew. Chem., Int. Ed. Engl.*, **18**, 587 (1979).

© 1983 The Chemical Society of Japan

NOTES

Bull. Chem. Soc. Jpn., 56, 3495—3496 (1983)

Infrared Spectra of Ammonia Adsorbed on Titanium Dioxide

Masao HINO* and Yasuko MIKAMI

Government Industrial Development Laboratory, Hokkaido, Tsukisamu-Higashi, Toyohira-ku, Sapporo 061-01

(Received October 2, 1982)

Synopsis. IR spectra of ammonia adsorbed on titanium dioxide were measured including those of partially deuterated ammonia. The results were compared with spectra reported in the literature.

A few papers have been published on IR spectra of ammonia adsorbed on TiO_2 studied with object of surface characterization.[1-3] Parfitt *et al.*[2] observed the spectra on a rutile surface and Primet *et al.*[3] on anatase including 10—15% of rutile. A good agreement is seen between the spectra observed by them. They attributed the observed bands to the two types of ammonia adsorbed on different Lewis acid sites. However, some differences are seen in the details of their assignments (Table 1, Assignments 1 and 2). The purpose of the present paper is to resolve the confusion in the assignments by the use of partially deuterated ammonia.

Experimental

Degussa Titanium dioxide p-25 (60% anatase, 40% rutile) was used as the sample. The self-supporting disk samples were initially heated at 450 °C for 5 h and cooled to room temperature in flowing oxygen, then evacuated in situ at 350 °C for 2 h, exposed to 40 Torr (1 Torr≈133.322 Pa) of oxygen at the same temperature for 0.5 h, and finally again evacuated at the same temperature for 0.5 h. Standard ammonia (Takachiho Co. Ltd.) was dried with sodium metal at a low temperature. Deuterated ammonia was distilled from a D_2O solution of ammonia-d_3 (99 atom%, E. Merck Darmstadt), and then dried in the same manner as for the ammonia. All the spectra were measured at room temperature. The IR cell was similar to that previously described,[4] and a JASCO-Model 402G spectrophotometer was used for the measurements.

Results and Discussion

The NH_3–TiO_2 adsorption system showed almost the same spectra as those reported by the previous authors.[2,3] Five absorption bands in the NH stretching region, and two bands in the deformation region were observed after pumping at room temperature (Table 1). Elevation of the evacuation temperature gave rise to the appearance of a new band around 1230 cm^{-1}. As a result of evacuation at 350 °C, all the above bands disappeared. After the surface OH groups were exchanged for OD groups by repetition of the introduction of ND_3 followed by evacuation

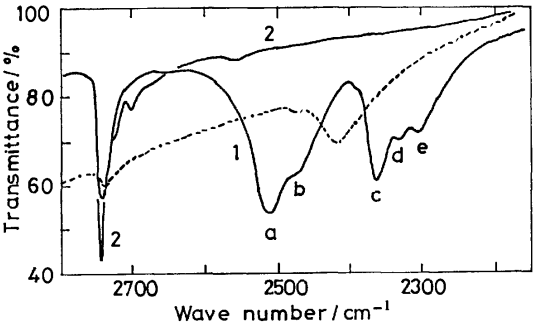

Fig. 1. Spectra of ammonia adsorbed on TiO_2 in the ND stretching region.
Full line: TiO_2–ND_3 system; evacuated at room temperature for 20 min (1), and at 350 °C for 3 h (2) after saturated with ND_3 gas at room temperature. Sample disk thickness was 40 mg/cm². Broken line: TiO_2-NH_2D system; evacuated at room temperature for 20 min after saturated with NH_3-ND_3 10.1 to 1.0 mixed gas at room temperature. Sample disk thickness was 140 mg/cm².

TABLE 1. IR BANDS OF AMMONIA ADSORBED ON TITANIUM DIOXIDE (STRETCHING REGION)

Band sign	νNH/cm^{-1}		νND/cm^{-1}		Assignment		
	NH_3	NHD_2	ND_3	NH_2D	(1)	(2)	(3)
a	3395		2520		ν_3	ν_3	ν_3
b	3345		2476		ν_1	ν_3	ν_3
		3285		2423			
c	3251		2372		ν_3	ν_1	ν_1
d	3188		2340		ν_1		$2\delta_4$
e	3151		2310			ν_1	ν_1

(1) Ref. 2, (2) Ref. 3, (3) this paper. Bands coupled with a L-shaped line mean that they are the pair of ν_3 and ν_1 of one type of the adsorbed ammonia.

at 350 °C, the spectra of ND_3 adsorbed on TiO_2 were measured (Fig. 1). The stretching bands correspond well to those of NH_3 adsorbed on TiO_2 (Table 1). Besides the D-shift, a small hump attributable to a combination band of ND_3 was detected at 3400 cm^{-1}. The bands at 2745, 2730, 2700, and 2675 cm^{-1} in Fig. 1 may be assigned to the surface OD groups on TiO_2.

Spectra of ammonia adsorbed on TiO_2 were measured for various H/D ratios. A typical result is shown in Fig. 1, using NH_3: $ND_3 \approx 10:1$ gas mixture, where NH_3: NH_2D: NHD_2: $ND_3 \approx 1000:300:30:1$. Hence, the bands in the νND region of the observed spectra are mainly due to adsorbed NH_2D. The result shows only a strong main band at 2423 cm^{-1} with a very small shoulder at 2482 cm^{-1} in the ND stretching region. The band at 2423 cm^{-1} is safely assigned to the νND of the adsorbed NH_2D; neither the NH_3-adsorbent system nor the ND_3-adsorbent system showed any band at this frequency (Fig. 1). For the NHD_2–TiO_2 system, the νNH band of the adsorbed NHD_2, which corresponds to the band at 2423 cm^{-1} for the NH_2D–TiO_2 system, was observed at 3285 cm^{-1}.

The fundamental νNH band of NHD_2 appears approximately at the mean frequency of ν_3 and ν_1 of NH_3, and the νND band of NH_2D appears between ν_3 and ν_1 of ND_3.

On the basis of these observations, the tentative assignments shown as "Assignment (3)" in Table 1 were made for the bands a—e. It is seen from the table that the proposed assignments are more consistent with those made by Primet *et al.*[3] than with those of Parfitt *et al.*[2] However, to confirm the assignments further experimental studies including considerations of hydrogen-bonding effect are necessary. The small shoulder at 2482 cm^{-1} may be attributed to the adsorbed species of NHD_2 which coexists in the mixed sample gas, or may suggest the existence of a small amount of another adsorbed species such as $-NH_2$ proposed by Parfitt *et al.*[2] near the frequencies of the bands a and b.

References

1) M. Herrmann and H. P. Boehm, *Z. Anorg. Allg. Chem.*, **368**, 73 (1969).
2) G. D. Parfitt, J. Ramsbotham, and C. H. Rochester, *Trans. Faraday Soc.*, **67**, 841 (1971).
3) M. Primet, P. Pichat, and M. V. Mathieu, *J. Phys. Chem.*, **75**, 1221 (1971).
4) M. Hino, *Bull. Chem. Soc. Jpn.*, **50**, 574 (1977).

The Wavelength Dependence of the Photochemical Reaction of 9-Anthracenecarbaldehyde with 2-Methyl-2-butene

Fujio TANAKA and Shigeru YAMASHITA*

College of Integrated Arts and Sciences, University of Osaka Prefecture, Mozu-umemachi, Sakai, Osaka 591

(Received February 28, 1983)

Synopsis. Photochemical reaction of 9-anthracenecarbaldehyde with 2-methyl-2-butene was studied under irradiation of >410 and 366 nm. Oxetane formation is predominant in both the wavelength cases, as revealed through isolation of reaction products and examination of their NMR, mass, and UV spectra.

In recent years, photocycloaddition reaction of carbonyl compounds to olefins yielding oxetanes has been an interesting subject for many workers.[1] A wide variety of reaction mechanisms have been proposed with many kinds of excited species as photoreactive states depending on the combination of carbonyl compounds and olefins.

Generally speaking, mechanisms for the oxetane formation by photocycloaddition of excited carbonyl compounds with acyclic olefins have been elucidated for many cases, and several reviews have been published.[1l,1m]

The photochemical reaction of 9-anthracenecarbaldehyde (9-CHO-A) having the $T_1(\pi,\pi^*)$ state with olefins has been studied by many workers with diverse results. Yang[1d] observed an oxetane formation in an irradiation at <410 nm on a mixture of 9-CHO-A and 2-methyl-2-butene, while under an irradiation at longer than 410 nm no oxetane formation was observed and the main product was the dimer of 9-CHO-A. Though Warwick and Wells[8] ascertained a similar wavelength effect on the carbonyl photoreaction using 2,3-dimethyl-2-butene as olefin, the main product was found to be pinacol and not oxetane as reported by Yang. Porter and Suppan[9,10] found spectroscopically the photoreduction of the carbonyl group to occur regardless of irradiation wavelength and suggested that the lowest excited singlet state (S_1) is the reactive state. Hirayama[11] supported the reaction mechanism *via* the upper triplet state on the basis of a spectroscopic ground. It was pointed out[1n] that the irradiation at a longer wavelength (440 nm) was effective for the formation of oxetane in the case of 9-CHO-A with 2,3-dimethyl-2-butene, suggesting the necessity of reexamination of the previous result for the case of 9-CHO-A with 2-methyl-2-butene. However, no detailed description has been reported. At any rate, the effect of wavelength on the formation of oxetanes in the photochemical reaction of 9-CHO-A and simple olefins remains unclarified without any further reports concerning this point.

The diversity of the results obtained by the previous workers about the wavelength dependence of the reaction seems to be closely associated with the fact that oxetane, which is thought the most probable product, has not been isolated for identification under the irradiation of longer wavelengths. The isolation of oxetane was reported in only one case of shorter wavelength irradiation.[1d]

In the present work, we have reinvestigated the photochemical reaction of 9-CHO-A with 2-methyl-2-butene in order to isolate and identify the reaction products and to ascertain the wavelength dependence of the reaction. A solution containing 206 mg of 9-CHO-A in 50 ml of 2-methyl-2-butene was irradiated under the condition of λ>410 nm. All runs were carried out without deaeration since the absence of influence by oxygen was already confirmed.[1b,10,11]

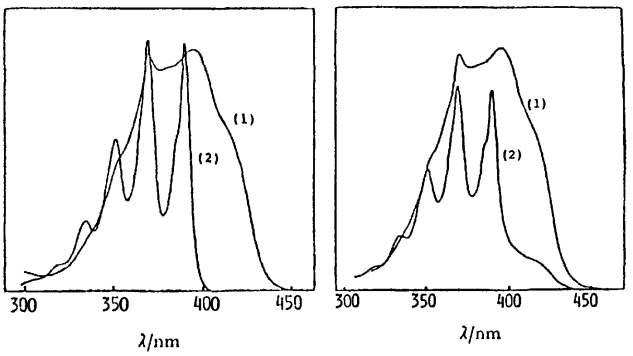

Fig. 1. The change of absorption spectrum by the irradiation of >410 nm(left) and 366 nm(right). (1): Before and (2): after the irradiation. The concentration for reaction is 2×10^{-2} M. The spectra were measured by diluting to 1/250 with hexane.

The absorption spectra obtained before and after the irradiation are shown in Fig. 1(left). The appearance of the band structure typical of the anthracene ring indicates that the carbonyl group is photoreduced keeping the anthracene ring unchanged.

In the process of trying to isolate reaction products, we found that the main product was unstable in neat or concentrated conditions while it was stable in dilute solution. The absorption band in the near UV region disappeared gradually as the degradation of the main product proceeded. With the lability of the main product taken into account, the separation of products from the reaction mixture was carefully performed by column chromatography (silica gel–benzene).

The main product (*ca.* 100 mg) thus obtained was an oily substance with a peak for the 0-0 band (λ_{0-0}) at 390 nm in hexane. The ^{1}H NMR spectrum of this compound shows a distinct signal of quartet at 4.70 ppm, assigned to H_a of the oxetane isomer **1** formed by the photoreaction of carbonyl compounds with 2-methyl-2-butene.[1b] The mass spectrum showing peaks at m/e=276 (the molecular ion of formula **1**) and 232 (the fragment ion shown by the broken line) also supports the molecular structure predicted on ^{1}H NMR.

As a minor product, an unidentified compound showing the absorption of λ_{0-0} at 386 nm and mass spectral peaks at m/e=276 and 259 was separated.

A similar experiment was carried out under irradiation of 366 nm. The change in absorption spectrum with the irradiation for 8 h is shown in Fig. 1 (right). Since the reaction product suffered a further photochemical change at this wavelength, the isolation

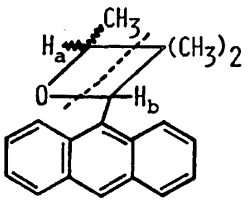

Formula **1**. H_a displays a ^1H NMR signal of quartet at 4.7 ppm. A broken line shows the fragmentation causing a peak of $m/e=232$ in the mass spectrum.

of products was performed before reaction of the entire 9-CHO-A had been completed.

The main product obtained by the 366 nm irradiation was found to be oxetane **1** again the same as the product obtained under the irradiation of $\lambda>410$ nm, as inferred from the absorption spectra and ^1H NMR spectra.

Thus the results obtained indicate that oxetane is formed in both the 366 nm and >410 nm excitations, no significant wavelength dependence being able to be observed.

Since the photodimer of 9-CHO-A posseses no absorption band in the wavelength region longer than 300 nm, the ratio of photoreaction of carbonyl to photodimerization is obtained from the absorption spectra before and after the photoreaction. The ratios for the irradiation of $\lambda>410$ nm were found 73/27 at 2×10^{-2} M (1 M=1 mol dm^{-3}) of 9-CHO-A and 86/14 at 2×10^{-3} M of 9-CHO-A. The photodimerization was negligible at concentrations lower than 2×10^{-4} M. The quantum yield of the photoreaction of carbonyl by the excitation with 436 nm was 3.4×10^{-2} at the concentration 2×10^{-3} M of 9-CHO-A. Potassium ferrioxalate was used as a chemical actinometer.

Under the experimental conditions of this work, the primary process is the photoexcitation of 9-CHO-A to its S_1 state followed by the intersystem crossing to the $T_n(n\pi^*)$ state located about 60 kcal/mol higher than the ground state.[11,8] The primary process from S_1 to T_n by intersystem crossing has also been found in the photochemical reaction of β,γ-unsaturated ketone.[12] When the triplet level of carbonyl compound is lower than that of olefin compound, oxetane formation has been found predominant since the energy transfer to olefin molecule causing dimerization of olefin is improbable. This reaction energetics has been seen in reactions of carbonyl compounds and norbonene. The same situation seems to be applicable in the present study on the 9-CHO-A and 2-methyl-2-butene system. The T_1 energy of 2-methyl-2-butene is supposed to be about 80 kcal/mol in view of T_1 levels of other olefins being higher than the above-mentioned $T_n(n\pi^*)$ state of 9-CHO-A.

Therefore, any energy transfer to olefins from 9-CHO-A is improbable and oxetane formation is predominant regardless of the exciting wavelengths as has been found in the present work.

Experimental

The preparation of 9-CHO-A was carried out according to the literature.[13] An ultra high pressure mercury lamp (Ushio USH 500) was used as the light source. The wavelengths of >410, 366, and 436 nm were isolated with Toshiba filters V-Y43, (UV35+UV-D1b), and (V-Y43+V40), respectively.

Isolation of Oxetane 1 and Spectroscopic Measurements. 2-Methyl-2-butene was evaporated from the irradiated solution, and the hexane-soluble part of the residue was chromatographed on silica gel using benzene as eluent. The main fractions following the degradation products were collected, and a check was made on the UV spectra of effluents. After the removal of benzene the hexane-soluble part was submitted to spectroscopic measurements. To reduce the degradation of oxetane, the chromatographic separations were performed on a smaller scale in UV and MS measurements where only a little sample was needed. The recorded ^1H NMR spectrum showed a fairly clear pattern, though the contamination due to degradation could not entirely be avoided: ^1H NMR (C_6D_6) δ=0.50 (CH_3 with a slight split by isomers), 1.20—1.28 (m, $2\times CH_3$), 4.70 (q, J=3.8 Hz, H_a), 6.98 and 7.08 (s, H_b isomers), and 7.18—8.25 (aromatic); MS (70 eV) *m/e* (%) 276 (2.5), 232 (72), 217 (100), and 206 (50), and (20 eV) 276 (16), 232 (57), 217 (60), and 206 (100); UV_{max}(hexane) 390, 369.5, 351 and 257 nm.

We wish to thank Drs. Setsuo Taniguchi, Shun-ichi Kawamura, and Mitsuo Chubachi of Radiation Center of Osaka Prefecture for the measurements of NMR and mass spectra.

References

1) a) E. Paterno and G. Chieffi, *Gazz. Chim. Ital.*, **39**, 341 (1909); b) G. Buchi, C. G. Inman, and E. S. Lipinsky, *J. Am. Chem. Soc.*, **76**, 4327 (1954); c) D. R. Arnold, R. L. Hinman, and A. H. Glick, *Tetrahedron Lett.*, **1964**, 1425; d) N. C. Yang, *Pure Appl. Chem.*, **9**, 591 (1964); e) J. S. Bradshaw, *J. Org. Chem.*, **31**, 237 (1966); f) L. A. Singer and G. A. Davis, *J. Am. Chem. Soc.*, **89**, 598 (1967); g) S. Toki and H. Sakurai, *Bull. Chem. Soc. Jpn.*, **40**, 2885 (1967); h) N. C. Yang, R. Loeschen, and D. Mitchell, *J. Am. Chem. Soc.*, **89**, 5465 (1967); i) N. C. Yang and R. Loeschen, *Tetrahedron Lett.*, **1968**, 2571; j) H. Gotthardt, R. Steinmetz, and G. S. Hammond, *J. Org. Chem.*, **33**, 2774 (1968); k) S. H. Schroeter and C. M. Orlando, *ibid.*, **34**, 1181 (1969); l) D. R. Arnold, *Adv. Photochem.*, **6**, 301 (1968); m) N. J. Turro, "Modern Molecular Photochemistry," Benjamin/Cummings Publishing Co., California (1978), p. 437; n) N. C. Yang and R. L. Loeschen, *Tetrahedron Lett.*, Errata, No. 34 (1968).

2) J. A. Barltrop and H. A. J. Carless, *J. Am. Chem. Soc.*, **94**, 1951 (1972).

3) N. J. Turro, P. Wriede, J. C. Dalton, D. Arnold, and A. Glick, *J. Am. Chem. Soc.*, **89**, 3950 (1967).

4) J. A. Barltrop and H. A. J. Carless, *Tetrahedron Lett.*, **1968**, 3901.

5) N. J. Turro and P. A. Wriede, *J. Am. Chem. Soc.*, **90**, 6863 (1968).

6) J. Saltiel, R. M. Coates, and W. G. Dauben, *J. Am. Chem. Soc.*, **88**, 2745 (1966).

7) E. S. Albone, *J. Am. Chem. Soc.*, **90**, 4663 (1968).

8) D. A. Warwick and C. H. J. Wells, *Tetrahedron Lett.*, **1968**, 4401.

9) G. Porter and P. Suppan, *Trans. Faraday Soc.*, **62**, 3375 (1966).

10) P. Suppan, *Tetrahedron Lett.*, **1971**, 4469.

11) S. Hirayama, *Rev. Phys. Chem. Jpn.*, **42**, 49 (1972).

12) D. I. Schuster and L. T. Calcaterra, *J. Am. Chem. Soc.*, **104**, 6397 (1982).

13) E. Campdigne and W. L. Archer, *J. Am. Chem. Soc.*, **75**, 989 (1953).

Some Problems Associated with the Exact Solution Conformation of Poly(α-L-glutamic acid) as Determined by Optical Methods

Kiwamu YAMAOKA

Faculty of Science, Hiroshima University, Higashisenda-machi, Naka-ku, Hiroshima 730

(Received April 4, 1983)

Synopsis. By combining the experimental data on circular dichroism and light scattering, the helical conformation of poly(Glu) in 0.15 mol dm^{-3} NaCl solutions was estimated. The axial translation per residue was probably in the range of 1.2—1.3 Å for the unaggregated helix, while the persistence length was *ca.* 120 Å for the random-coil.

The conformation of poly(α-L-glutamic acid), poly(Glu), in aqueous solutions has been studied widely, since the optical and other physical properties are considered to be the primary reference for the α-helix and the random coil.[1] In order to determine an exact helical conformation, light scattering is a convenient means which gives both molecular weight M_r and overall length L.[2] Yet, there remain three major obstacles to identifying the conformation: (1) The pH region for the completion of helix formation should be known, (2) the α-helix is one of several helical conformations which poly(Glu) may take, and (3) a poly(Glu) sample is generally polydisperse with M_r and L. During the investigation of the macromolecular complex between poly(Glu) and Cu^{2+} ion, poly(Glu) was also studied by circular dichroism (CD), light scattering, viscosity, and other methods.[3—8] Based on these results, some hitherto mostly ignored difficulties, which are associated with the optical determination for the helical conformation of poly(Glu) in aqueous solutions, will be discussed.

Results and Discussion

Estimation of the Helix Fraction. Figure 1 shows the pH dependence of the molar ellipticity at 222.5 nm, $[\theta]_{222.5}$, for a poly(Glu) sample in 150 mM (1 M=1 mol dm^{-3}) NaCl solution. (Descriptions were given elsewhere on CD[3,8] and light scattering.[7]) Stepwise changes have been observed beyond experimental errors both in CD and ORD (at 233 nm) for poly(Glu) samples, which are derived either from poly(γ-benzyl L-glutamate)[3,8] or from poly(γ-methyl L-glutamate),[4,6] in solutions with and without added NaCl. (A similar change in CD was recently detected with a multipurpose technique.[9]) The helix fraction,[8] $f_h=([\theta]^c-[\theta])/([\theta]^c-[\theta]^h)$, can be evaluated from the CD data, where $[\theta]^c$ and $[\theta]^h$ are, respectively, the molar ellipticities for the states of coil and helix. This two-state expression has been verified by the principal-component-analysis method[5] and also by the presence of an isoelliptic point in the CD spectra of poly(Glu).[5,8] It should be noted that f_h does not necessarily denote the fraction of unaggregated helix molecules in a given poly(Glu) solution, because the CD is a short-range phenomenon and does not reflect the overall molecular shape.[1,10]

The first problem is the assignment of an appropriate value to $[\theta]^h$, since the formation of aggregates overlaps with the completion of monomeric helices.[7,8] A value of −36300 (pH=4.42) was used in a previous work,[8] by considering that the perfect helix is completed at point A, the onset of the second transition. However, the helix formation may as well be completed at the midpoint of the second transition (point B), for which $[\theta]^h=-38100$ and pH=4.31.[5] The oft-observed highest value of −40600 may equally be assigned to $[\theta]^h$ (pH=4.10), *i.e.*, point C.[1] This last procedure tacitly accepts the notion that the helix formation is not completed until aggregates are formed. The value of $[\theta]^c$ is 2650 (point D).

Helix Fraction and Root-mean-square Radius of Gyration. In Fig. 1, the square root of the z-average of the mean-square radius of gyration $\langle s^2\rangle_z^{1/2}$, obtained from light scattering,[7] is plotted against the helix fraction obtained from CD. Regardless of the choice of the point for completion of helix (A, B, or C), the value of $\langle s^2\rangle_z^{1/2}$ becomes minimum in the $(1-f_h)$ range of 0.7—0.8. The plots indicate that both helical and coiled segments coexist in a single poly(Glu) chain, excluding the possibility that completely helical and completely coiled molecules exist in varying equilibria in the coil-to-helix transition process (otherwise, the $\langle s^2\rangle_z^{1/2}$ *vs.* $(1-f_h)$ plot would be linear).[8]

The second problem is the assignment of a value of $\langle s^2\rangle_z^{1/2}$ to the perfect helix. As the helix formation is nearly completed ($f_h=0.9$), observed values of

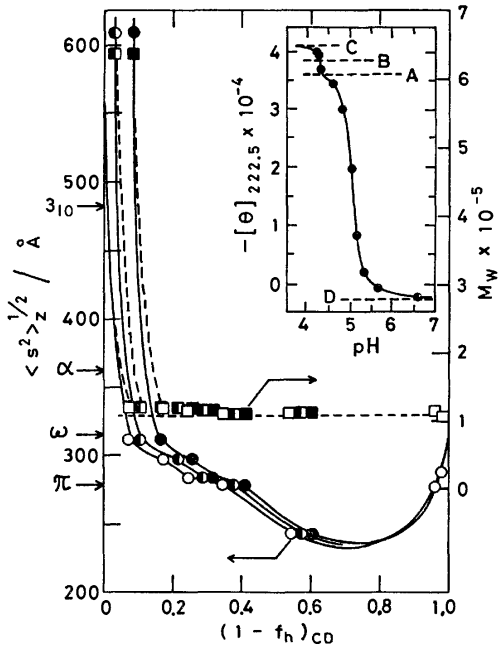

Fig. 1. Dependence of the square root of the z-average of the mean-square radius of gyration, $\langle s^2\rangle_z^{1/2}$, (circles) and the weight-average molecular weight, M_w, (squares) on the fraction of the poly(Glu) coil, $(1-f_h)_{CD}$, in the 150 mM NaCl solutions at 25 °C. The helical conformation is assumed to be completed at point A (open symbols), B (half-closed), or C (closed). Insert: the pH dependence of the molar ellipticity (deg cm^2 dmol^{-1}) at 222.5 nm.

$\langle s^2\rangle_z^{1/2}$ range between 305 and 450 Å, depending on the choice of point A, B, or C (Fig. 1). However, no definite value can be specified for the monomeric, perfect helix ($f_h=1$), because of a concomitant formation of aggregates, as envisaged in Fig. 1 by the change in weight-average molecular weights, M_w, which remain nearly constant at a value of 1.07×10^5 (pH>*ca.* 5) but sharply increase with a decrease in pH.[7] Nevertheless, the limiting value of $\langle s^2\rangle_z^{1/2}$ ($f_h\to 1$) is most likely between 280 and 320 Å.

Value of $\langle s^2\rangle_z^{1/2}$ and Conformation of Helix. The third problem is the estimation of the axial translation per residue, h, which defines the helical conformation (h=2.0 Å for the 3_{10}-, 1.5 A for the α-, 1.3 Å for the ω-, and 1.15 Å for the π-helix). For a long rodlike molecule with length L, $\langle s^2\rangle=L^2/12$,[2] but the poly(Glu) sample is polydisperse. Therefore, $\langle s^2\rangle_z$ must be divided by the z-average of the square of degree of polymerization, $\langle DP^2\rangle_z$, not by the weight-average $\langle DP^2\rangle_w$ (an oft-neglected fact), to calculate values of h. If $\langle s^2\rangle_z^{1/2}$ is divided by $\langle DP\rangle_w$, the value of h would be erroneously large. For a polydisperse sample in which each molecule is a rigid perfect helix,

$$h^2 = \langle L^2\rangle_z/\langle DP^2\rangle_z = 12\langle s^2\rangle_z/\langle DP^2\rangle_z$$
$$= 12m_0^2\langle s^2\rangle_z/M_{z+1}\cdot M_z, \quad (1)$$

where m_0 is the residue weight, M_{z+1} and M_z are the $(z+1)$- and z-average molecular weights. From electric birefringence on the same poly(Glu) sample,[11] the polydispersity, M_w/M_n, was estimated to be 1.12 for the unaggregated α-helix by assuming the Lansing-Kraemer distribution, from which the relation $(M_{z+1}\times M_z)^{1/2}=M_w(M_w/M_n)^{3/2}$ results.[12] In Fig. 1, the values of $\langle s^2\rangle_z^{1/2}$ calculated from Eq. 1 are indicated by arrows for four typical helices. The conformation of poly(Glu) now appears closer to the ω-helix (315 Å) rather than to the π-helix (270 Å) or the α-helix (363 Å). A viscometric study has led to the similar conclusion about the conformation.[8]

Persistence Length and Chain Flexibility. The persistence length q is a measure for the chain flexibility and is related to the radius of gyration.[13] According to Kratky and Porod,[14]

$$\langle s^2\rangle_i = 2qL_i[(1/6)-(q/2L_i)+(q/L_i)^2-(q/L_i)^3(1-e^{-L_i/q})] \quad (2)$$

for the ith molecule of contour length L_i. Since $\langle s^2\rangle_z=\sum N_iM_i^2\langle s^2\rangle_i/\sum N_iM_i^2$, it is a complicated average of the contour length.[15] As a first approximation, the z-average length L_z is utilized in place of L_i,[16] together with a simplified relation: $L_z=[h\times f_h+3.62\times(1-f_h)]\langle DP\rangle_z$.[8] Values of q and q/L_z were calculated at various helix fractions for different helical conformations (Table 1). The contour length L_z for the completely coiled poly(Glu) is 2870 Å ($=3.62\times 708\times 1.12$); yet, q is only *ca.* 120 Å, indicating that the poly(Glu) chain is highly coiled in the 150 mM NaCl (20-fold in excess of Glu residues) in contrast to the 7.5 mM NaCl solution.[8] The chain becomes very contracted at the onset of the coil-to-helix transition ($f_h\approx 0.2$), q being only *ca.* 75 Å, but it becomes stiffer as the helix fraction increases.

Table 1. The persistence length poly(Glu) in 150 mM NaCl[a]

$(f_h)_{CD}$		0	0.2	0.4	0.6	0.8
$\langle s^2\rangle_z^{1/2}$/Å		320[b]	240	237	268	290
q/L_z	α-[c]	0.0420	0.0294	0.0391	0.0777	0.172
	ω-	0.0420	0.0301	0.0418	0.0890	0.234
	π-	0.0420	0.0308	0.0440	0.0990	0.316
q/Å	α-	120.6	74.5	86.0	144.7	262.4
	ω-	120.6	75.3	89.2	157.3	327.3
	π-	120.6	76.4	91.8	167.9	412.0

a) The helical structure was assumed to be completed at point A. b) A extrapolated to $(1-f_h)_{CD}\to 1$. c) Three different helical conformations.

The fourth and barely touched problem is the possibility of kinked or broken points in a long helical backbone. For example, seven Glu residues forming a coil-segment in a poly(Glu) helix correspond to the 99% helix content. A 1% difference is utterly impossible to detect by optical methods, but such a single break may lower the overall chain length or the value of $\langle s^2\rangle_z^{1/2}$ considerably, making the shorter helix conformations only apparent. For a perfect helix, values of q/L_i should be infinitely large, but this can never be confirmed because of the exponential increase in length and molecular weight of aggregated helices.

Many thanks are due to Dr. T. Masujima and Messrs. H. Watanabe, T. Matsuda, K. Ueda, and K. Fukudome for their close collaboration.

References

1) R. W. Woody, *J. Polym. Sci., Macromol. Rev. Ed.*, **12**, 181 (1977).
2) C. Tanford, "Physical Chemistry of Macromolecules," Wiley, New York, (1961), Chaps. 3 and 5.
3) K. Yamaoka and T. Masujima, *Bull. Chem. Soc. Jpn.*, **52**, 1286 (1979).
4) K. Yamaoka and T. Masujima, *Polym. J.*, **11**, 889 (1979).
5) K. Yamaoka, T. Matsuda, and M. Takatsuki, *Bull. Chem. Soc. Jpn.*, **53**, 968 (1980).
6) S. Noji, T. Nomura, and K. Yamaoka, *Macromolecules*, **13**, 1114 (1980).
7) T. Masujima, *Bull. Chem. Soc. Jpn.*, **56**, 838 (1983).
8) T. Masujima, K. Yamaoka, and J. Hori, *Bull. Chem. Soc. Jpn.*, **56**, 1030 (1983).
9) H. Hayashi and A. Wada, *Biopolymers*, **20**, 695 (1981). Earlier reports on the stepwise change were cited in Ref. 8.
10) M. Rinaudo and A. Domard, *J. Am. Chem. Soc.*, **98**, 6360 (1976).
11) K. Yamaoka and K. Ueda, *J. Phys. Chem.*, **86**, 406 (1982).
12) W. D. Lansing and E. O. Kraemer, *J. Am. Chem. Soc.*, **57**, 1369 (1935).
13) H. Benoit and P. Doty, *J. Phys. Chem.*, **57**, 958 (1953).
14) O. Kratky and G. Porod, *Recl. Trav. Chim. Pay-Bas*, **68**, 1106 (1949).
15) From Eq. 2, the following relation results: $\langle s^2\rangle_z=(qL_z/3)-q^2+(2q^3/L_w)-(2q^4/L_w\cdot L_n)(1-\langle e^{-L/q}\rangle_n)$.
16) M. Mandel and J. Schouten, *Macromolecules*, **13**, 1247 (1980).

X-Ray Structure Determination of (−)-Obtusane, a New Sesquiterpene from the Red Alga, *Laurencia nipponica* Yamada

Akio FURUSAKI,* Takeshi MATSUMOTO, Kazuya KURATA,† Teruaki SUZUKI, Minoru SUZUKI, and Etsuro KUROSAWA

Department of Chemistry, Faculty of Science, Hokkaido University, Kita-ku, Sapporo 060

† *Department of Industrial Chemistry, Hakodate Technical College, Hakodate 042*

(Received May 12, 1983)

Synopsis. A new sesquiterpene ($C_{15}H_{23}Br_2Cl$, mp 172—173 °C) isolated from *Laurencia nipponica* Yamada has been found to be (−)-obtusane by X-ray crystal structure analysis.

In continuing studies on the constituents of the red alga, *Laurencia nipponica* Yamada, collected at Akkeshi on the Pacific Coast of Hokkaido,[1] we have isolated a new sesquiterpene hydrocarbon (**1**). The ^1H and ^{13}C NMR spectra of **1** show a close resemblance to those of obtusane (**2**) isolated from *Laurencia obtusa*,[2] while the specific rotations of **1** and **2** are equal in magnitude but opposite in sign. These facts suggest that **1** may be the enantiomer of **2**. In order to establish the molecular structure of **1**, we have now carried out an X-ray crystal structure analysis.

Experimental

Isolation. *Laurencia nipponica* Yamada collected at Akkeshi, Hokkaido, was extracted with methanol. The neutral methanol extracts (*ca.* 1% of the half-dried alga) obtained by the conventional methods were chromatographed over alumina. The fraction eluted with hexane–benzene (1:1 volume ratio) was rechromatographed over silica gel to yield **1** (0.09% of the extracts); mp 172—173 °C (from diisopropyl ether), $[\alpha]_D^{22}$ −38.5° (*c* 0.55, $CHCl_3$); IR (Nujol) ν_{max} 3100, 1640, 1222, 1198, 1158, 1092, 1058, 1028, 972, 916, 876, 800, 778, 726, 664, 642, and 624 cm^{-1}; ^1H NMR ($CDCl_3$, 200 MHz) δ 0.96, 1.14, 1.83 (each 3H, s), 1.6—2.4 (10H, m), 4.45 (1H, dd, J=13 and 4 Hz), 4.72 (1H, dd, J=13 and 5 Hz), 4.87, and 5.26 (each 1H, s); ^{13}C NMR ($CDCl_3$, 50.1 MHz) δ 145.8 (=C〈), 114.9 (=CH_2), 68.4 (〉C〈), 68.0, 63.6 (each 〉CH–), 50.5, 44.0 (each 〉C〈), 40.5, 37.3, 35.9, 33.6, 25.7 (each –CH_2–), 24.0, 23.7, and 17.6 (each CH_3); MS *m/e* (rel intensity) 402, 400, 398, 396 (1:4:9:3, M^+), 321, 319, 317 (2:9:5, M^+–Br), 320, 318, 316 (2:9:4, M^+–HBr), 283, 281 (9:9, M^+–HBr–Cl), 239, 237 (3:18, M^+–HBr–Br), 201 (31, M^+–HBr–Br–HCl), 109 (98), 107 (22), 105 (30), 95 (66), 93 (38), 91 (30), 81 (23), 69 (100), 67 (28), 55 (19), and 41 (91). Found: *m/e* 399.9846. Calcd for $C_{15}H_{23}{}^{81}Br_2{}^{35}Cl$: M 399.9816. The melting point was uncorrected. The IR spectrum was measured on a Hitachi EPI-G2 spectrometer. The ^1H and ^{13}C NMR spectra were recorded on a JEOL FX-200 spectrophotometer, TMS being used as an internal reference. The low and high resolution mass spectra were obtained with a JEOL JMS-D300 spectrometer. The optical rotation was measured on a JASCO DIP-140 polarimeter.

X-Ray Measurement. A colorless single crystal cut into a cube with an edge of *ca.* 0.2 mm was used. The crystal data were as follows: $C_{15}H_{23}Br_2Cl$, mol wt 398.61, orthorhombic, space group $P2_12_12_1$, a=10.580(3), b=20.537(6), c=7.492(2) Å, Z=4, D_c=1.626 g cm^{-3}, μ(Mo $K\alpha$)=50.8 cm^{-1}. The cell dimensions and diffraction intensities were measured on a Rigaku four-circle diffractometer at the High Brilliance X-Ray Diffraction Laboratory of Hokkaido University, using graphite-monochromated Mo $K\alpha$ radiation (λ=0.71073 Å). The θ—2θ scanning technique was applied at a θ scan rate of 2° min^{-1}; the background was counted for 10 s at each end of the scan range. Three standard reflections, measured at intervals of every 100 reflections, showed a gradual decrease in intensity during the course of data collection; the final-intensity/initial-intensity ratios were *ca.* 0.91—0.98. The intensities were corrected for this damage to the sample as well as for the Lorentz and polarization factors, but not for the absorption or the extinction effect. In the range of 2θ values up to 50°, 1131 independent structure factors above the $3\sigma(F)$ level were selected for the structure determination.

Structure Determination

The structure was solved by the Monte Carlo direct method,[3] using the 20 reflections with the greatest $|E|$ values as the starting set. The seventhly-generated random phase set led to the correct solution; an E-map based on 499 phases revealed all the non-hydrogen atoms. After the structure had been well refined by the block-diagonal least-squares method with anisotropic temperature factors, the absolute configuration was determined by taking account of the anomalous dispersion of the halogen atoms for Mo $K\alpha$ radiation. The R ratio for the two enantiomeric structures, 1.10, excluded one of them at a 99.5% confidence level.[4] Since a difference Fourier map revealed all the hydrogen atoms, further least-squares refinements were carried out including the hydrogen atoms. For these refinements, the following weighting scheme was used:

$$w = 1/\{\sigma(F)^2 \exp(c_1X^2+c_2Y^2+c_3XY+c_4X+c_5Y)\},$$

where $X=|F_o|$ and $Y=\sin\theta/\lambda$. The c_1, c_2, c_3, c_4, and c_5 coefficients were evaluated from the $(\Delta F)^2$ distribution; $c_1=-0.208\times10^{-3}$, c_2=27.5, $c_3=-0.908\times10^{-2}$, c_4=0.0502, and $c_5=-25.0$. In this manner, the R value reached 0.050. The final atomic parameters are listed in Table 1.[5]

The calculations were done on a HITAC M-200H computer at the Hokkaido University Computing Center, using our own programs. The atomic scattering factors were taken from the International Tables.[6]

Results and Discussion

The molecular structure of **1** including the absolute configuration is shown in Fig. 1, while the bond distances and angles are given in Fig. 2. Thus, it is concluded that this new sesquiterpene is the enantiomer of obtusane,[2] *i.e.*, (−)-obtusane.

Each of the six-membered A- and B-rings has a

Table 1. The final atomic parameters and estimated standard deviations

Atom	10^4x	10^4y	10^3z	B_{eq}[a)]/Å^2
Br(1)	−3693(1)	1421.5(7)	−136.1(2)	6.07
Br(2)	3380(1)	1639.2(7)	537.8(2)	5.35
Cl	−3485(3)	284(2)	197.8(5)	5.46
C(1)	−1181(10)	757(5)	270(2)	3.34
C(2)	−2174(9)	776(5)	122(2)	3.07
C(3)	−2604(9)	1480(6)	79(2)	3.75
C(4)	−1416(11)	1847(5)	25(2)	4.32
C(5)	−466(10)	1856(4)	176(2)	3.66
C(6)	13(9)	1157(5)	226(1)	2.69
C(7)	773(9)	851(5)	76(2)	3.42
C(8)	1934(10)	1224(6)	23(2)	4.10
C(9)	2830(9)	1289(6)	183(2)	3.78
C(10)	2130(9)	1570(5)	337(2)	3.53
C(11)	944(10)	1192(5)	397(1)	3.27
C(12)	338(10)	1549(7)	555(2)	4.73
C(13)	1263(10)	492(5)	453(2)	3.68
C(14)	533(12)	272(6)	4(2)	5.13
C(15)	−3358(11)	1834(6)	218(2)	5.45

a) $B_{eq}=8\pi^2(u_1^2+u_2^2+u_3^2)/3$, where u_i is the root-mean-square deviation in the ith principal axis of the thermal ellipsoid.

chair conformation. The C(7)=C(14)H_2 and C(15)H_3 groups occupy the axial positions on the A-ring, while the Cl and Br(1) atoms and the C(11)Me_2 group take the equatorial orientations. Because of the *syn*-periplanar conformation (torsion angle, −7(2)°) of the C(1)–C(6)–C(7)=C(14) segment, the C(14)H_2 group is very close to the C(1)H_2–C(2)H part: C(1)···C(14), 2.87(2); C(2)···C(14), 3.17(2) Å. The difference of 5° between the C(6)–C(7)=C(14) and C(8)–C(7)=C(14) bond angles probably results from this steric repulsion. The Cl atom is gauche to both the Br(1) atom and the C(15)H_3 groups: Cl···Br(1), 3.430(4); Cl···C(15), 3.19(1) Å. These gauche interactions cause the C(3)–C(2)–Cl bond angle to be greater than the C(1)–C(2)–Cl angle by 4°. A similar bond-angle distortion is found also for the C(3)–C(15) bond; the C(2)–C(3)–C(15) angle is greater than the C(4)–C(3)–C(15) angle by 5°. On the other hand, in spite of the severe steric hindrance between the Cl and Br(1) atoms, the C(2)–C(3)–Br(1) bond angle is smaller than the tetrahedral angle, and is almost equal to the C(4)–C(3)–Br(1) and C(15)–C(3)–Br(1) angles. As was pointed out in a previous paper,[7] such a shrinkage of the C–C–halogen bond angles seems likely to be a property of tertiary chlorides and bromides.

The C(5)H_2 and C(13)H_3 groups are placed axially on the B-ring, while the Br(2) atom and the C(1)H_2 and C(12)H_3 groups are equatorially oriented. The Br(2) atom suffers gauche repulsions from both C(12)H_3 and C(13)H_3 groups: Br(2)···C(12), 3.23(1); Br(2)···C(13), 3.31(1) Å. Consequently, the C(11)–C(10)–Br(2) bond angle is greater than the C(9)–C(10)–Br(2) angle by 5°. The C(6)–C(11) distance is considerably longer than the standard C–C single-bond distance. Since both of the C(6) and C(11) atoms have three bulky groups, this bond lengthening is probably due to strong steric repulsions among these groups.

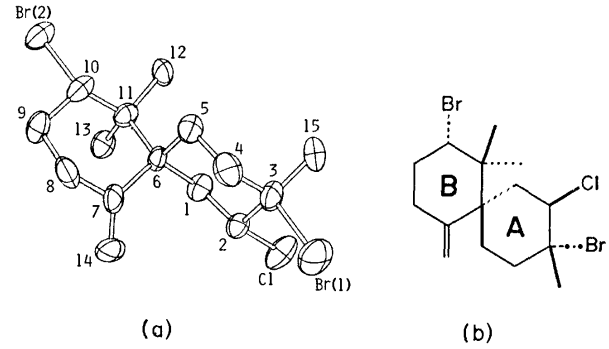

(a) (b)

Fig. 1. (a) A perspective view of the **1** molecule, and (b) the corresponding structural formula. Each non-hydrogen atom is represented as a thermal ellipsoid enclosing a 50% probability. The symbol C for carbon atoms is omitted.

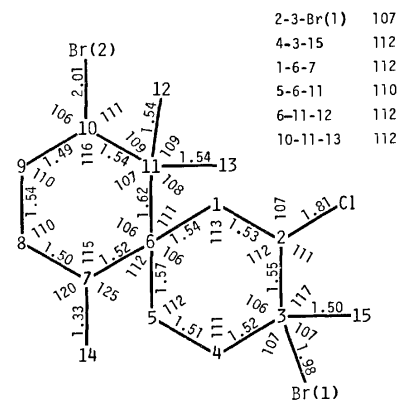

Fig. 2. The bond distances (l/Å) and angles (θ/°). The e.s.d.'s are 0.01—0.02 Å and 0.7—1.1° respectively.

References

1) K. Kurata, T. Suzuki, M. Suzuki, E. Kurosawa, A. Furusaki, K. Suehiro, T. Matsumoto, and C. Katayama, *Chem. Lett.*, **1983**, 561 and the references cited therein.
2) A. G. Gonzalez, J. D. Martin, V. S. Martin, and M. Norte, *Tetrahedron Lett.*, **1979**, 2719.
3) A. Furusaki, *Acta Crystallogr., Sect. A*, **35**, 220 (1979).
4) W. C. Hamilton, *Acta Crystallogr.*, **18**, 502 (1965).
5) The tables of the anisotropic temperature factors and hydrogen parameters and the F_o-F_c table are kept at the Chemical Society of Japan (Document No. 8343).
6) "International Tables for X-Ray Crystallography," The Kynoch Press, Birmingham (1974), Vol. IV.
7) A. Furusaki, C. Katayama, T. Matsumoto, M. Suzuki, T. Suzuki, H. Kikuchi, and E. Kurosawa, *Bull. Chem. Soc. Jpn.*, **55**, 3398 (1982).

Production of Ethylene and Propylene by the Vapor-phase Catalytic Oxidative Dehydrogenation of Butane with Carbonyl Sulfide

Masamichi AKIMOTO,* Takashi SAKATANI, and Etsuro ECHIGOYA

Department of Chemical Engineering, Tokyo Institute of Technology, Ookayama, Meguro-ku, Tokyo 152

(Received May 24, 1983)

Synopsis. Ethylene and propylene were produced at high yields, additionally to butenes and butadiene, by the vapor-phase oxidative dehydrogenation of butane with COS over SiO_2, Al_2O_3, MgO, and TiO_2 catalysts at 873—923 K. The results of kinetic and mechanistic studies indicate that ethylene and propylene are produced by the oxidative dehydrogenation through a homolytic mechanism followed by β-scission of the carbon–carbon bond.

Carbonyl sulfide undergoes catalytic decomposition by either of the following two reactions.[1]

$$COS \rightarrow CO + S, \qquad xS \rightarrow S_x \ (x=2,\ 4,\ \text{and}\ 8), \quad (1)$$

$$2COS \rightarrow CO_2 + CS_2. \quad (2)$$

Since the dissociation by the first reaction evolves reactive sulfur atoms, many studies have been made on the use of COS as an oxidant for the oxidative dehydrogenation of lower paraffinic hydrocarbons and alkyl-substituted aromatics.[2,3] Some mechanistic studies have also been reported.[4,5] In our recent study on the vapor-phase oxidative dehydrogenation of ethylbenzene by COS over SiO_2, Al_2O_3, MgO, and TiO_2 catalysts, we showed that the role of the metal oxide catalysts is to decompose COS to CO+S, the formed sulfur (maybe sulfur atom) then dehydrogenating ethylbenzene in gaseous phase.[5] We also showed that in addition to the thermocatalytic mechanism proposed by Haas and Khalafalla[1] COS is decomposed to CO+S by the action of the reduction sites.[5] In the present paper, we report the production of ethylene and propylene by the vapor-phase catalytic oxidative dehydrogenation of butane with COS and discuss the mechanism of the formation of these two olefins. The catalytic oxidative dehydrogenation of ethane, propane, and isobutane with COS has been reported.[3,4] However, no studies have been reported on the catalytic oxidative dehydrogenation of butane with COS and hence no results have been reported of the formation of ethylene and propylene by the catalytic oxidative dehydrogenation with COS.

Experimental

Vapor-phase catalytic oxidative dehydrogenation of hydrocarbons was carried out using a conventional flow fixed-bed reactor under atmospheric pressure. The shape of reactor and method of reaction were the same as those in our previous paper.[5] Purchased COS of greater than 97.5 % purity and research grade paraffinic hydrocarbons(purity>99%) were used without further purification. The catalysts (32—60 mesh) were prepared by the calcination of their corresponding metal hydroxides at 1073 K (873 K for TiO_2) in air for 5 h. The surface areas determined by the conventional B.E.T. method were 167 $m^2 g^{-1}$ (SiO_2), 178 $m^2 g^{-1}$ (Al_2O_3), 40 $m^2 g^{-1}$ (MgO), and 48 $m^2 g^{-1}$ (TiO_2), respectively. The gaseous reaction products (paraffins, olefins, COS, CO, CO_2, and H_2S) were analyzed by gas chromatography using propylene carbonate (40 wt% on C-22, 17.0 m, room temperature), Porapak R(2.0 m, 363 K), and molecularsieve 13X(1.5 m, room temperature) as separating columns. Carbon disulfide was not analyzed.

Results and Discussion

Table 1 summarizes the catalytic results obtained in the oxidative dehydrogenation of butane with COS at 873 K. No reaction took place when the mixture of butane and N_2 (butane 30.0 vol%) was fed over these four metal oxide catalysts at 873 K. However, such olefins as ethylene and propylene were produced additionally to butenes and butadiene with an accompanying formation of H_2S when COS was added to the reacant mixture (Table 1. The yield of H_2S is not presented for the sake of simplicity). Both the conversions of butane and COS decreased with time, due to the formation of carboneceous materials at the surface of the catalysts,[5] and leveled off after a preliminary period of 5 h. However, it is evident that Al_2O_3 had the greatest catalytic activity at the initial stages of the reaction among these four metal oxide catalysts (Table 1,A). This greatest initial catalytic activity of Al_2O_3 correlates its greatest concentration of the reduction sites reported in our previous paper[5], suggesting the preferential role of the reduction sites in the catalytic decomposition of COS to CO+S. For some catalytic results, the conversion of butane was greater than the yield of sulfur (=[conversion of COS]×[COS decomposition to CO+S]) (Table 1, SiO_2-A,B, MgO-B, and TiO_2-B). It seems that sulfur was also evolved by the catalytic decomposition of

TABLE 1. RESULTS OF THE CATALYTIC OXIDATIVE DEHYDROGENATION OF BUTANE BY COS[a]

Catalyst		Conversion/%		COS decomposition to CO+S/%	Yield/%				Selectivity/%	
		n-C_4H_{10}	COS		C_nH_{2n+2}[e]	C_2H_4	C_3H_6	C_4 olefins[f]	$C_2H_4+C_3H_6$	olefins
SiO_2	A[b]	45.8	49.2	41.1	6.7	4.4	24.3	9.4	62.7	83.2
	B[c]	29.8	47.9	37.0	3.1	2.9	15.1	7.9	60.4	86.9
Al_2O_3	A[b]	53.4	96.5	97.7	4.8	2.2	14.3	15.5	30.9	59.9
	B[c]	26.6	42.0	61.4	2.7	1.4	7.3	13.5	32.7	83.5
MgO[d]	A[b]	29.2	63.4	69.9	2.7	1.6	9.6	5.9	38.4	58.6
	B[c]	12.4	10.4	64.4	1.3	0.5	4.5	2.7	40.3	62.1
TiO_2	A[b]	47.0	87.3	94.2	4.1	2.0	13.0	12.1	31.9	57.7
	B[c]	18.9	14.7	73.5	1.0	1.0	4.5	6.3	29.1	62.4

a) Reaction temperature: 873 K. Feed: 100 NTP cm^3 min^{-1} (n-C_4H_{10} 30.0 vol%, COS 30.0 vol%, N_2 40.0 vol%). Contact time: 11.2 g-catalyst·h·g-mol^{-1}. b) At 10 min. c) At steady state. d) Contact time: 3.7 g-catalyst·h·g-mol^{-1}. e) $CH_4+C_2H_6+C_3H_8$. f) n-$C_4H_8+C_4H_6$.

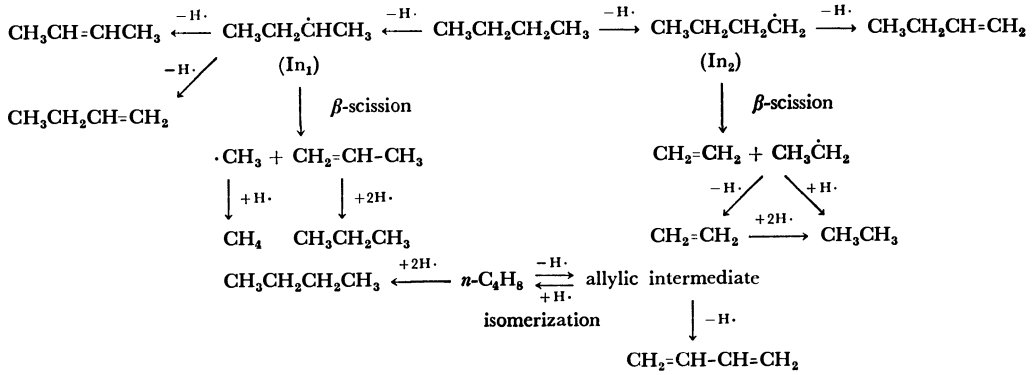

CS_2 formed during the catalytic oxidative dehydrogenation of butane by COS, as already seen in the reaction of ethylbenzene by COS.[5]

The most important finding that Table 1 provides is that ethylene and propylene were produced additionally to butenes and butadiene in the catalytic oxidative dehydrogenation of butane by COS. The combined yield of ethylene and propylene was high, 18.0—28.7% (selectivity 60.4—62.7%) and 8.7—16.5% (30.9—32.7%), over SiO_2 and Al_2O_3 catalysts, respectively, and the total selectivity to olefins was also high, 83.2—86.9%, over SiO_2 catalyst. It is to be noted that the yield of propylene was always greater than that of ethylene for all of the catalysts employed (Table 1). At 923 K, the combined yield of ethylene and propylene over SiO_2 catalyst determined after a preliminary period of 10 min increased to 60.3% (selectivity 64.1%) whereas that of butenes and butadiene remained nearly unchanged, 8.2%. In contrast to the reaction of butane, no such olefins as ethylene and propylene were produced when *trans*-2-butene was similarly reacted at 873 K (*e.g.*, SiO_2 catalyst, conversion 48.1%, total yield of butenes 33.2%, and yield of butadiene 10.0%).

In the oxidative dehydrogenation of butane by COS over SiO_2 catalyst at 873 K, the reaction order in butane was unity and that in COS was 0.2—0.3. Assuming the first order kinetics for the oxidative dehydrogenation of paraffinic hydrocarbons, the rate constant for the oxidative dehydrogenation of ethane, propane, and isobutane by COS over SiO_2 catalyst was determined at 873 K using an integral reactor (Table 2). The rate constant k for the paraffinic hydrocarbons follows the order: ethane<propane< isobutane. The order of the reactivity of these hydrocarbons is much more obvious when the value of the rate constant k is normalized to one most-reactive hydrogen (k', Table 2). That is, the reactivity of hydrogen for the oxidative dehydrogenation by sulfur follows the order: primary hydrogen < secondary hydrogen<tertiary hydrogen. This order of the reactivity of hydrogen correlates the value of the C–H bond dissociation energy (Table 2). As reported previously by Haag and Miale,[4] we may thus conclude that the oxidative dehydrogenation of these paraffinic hydrocarbons by sulfur proceeds through a homolytic mechanism. On the other hand, no formation of olefins other than isobutene in the reaction of isobutane (Table 2) indicates that no α-scission of the carbon-carbon bond took place during the oxidative dehydrogenation of paraffinic hydrocarbons by COS at 873 K.

TABLE 2. SUMMARY OF THE RATE CONSTANTS FOR THE CATALYTIC OXIDATIVE DEHYDROGENATION OF LOWER PARAFFINIC HYDROCARBONS BY COS[a]

Paraffin	Number and type of hydrogen[b]	B.D.E.[c] kJ mol^{-1}	Conversion %	k[d] $\times 10^2$	k'[e] $\times 10^2$
C_2H_6	6 p	410	22.3	2.25	0.38
C_3H_8	2 s	395	23.9	2.44	1.22
i-C_4H_{10}	1 t	380	24.9	2.56	2.56

a) Catalyst: SiO_2. Reaction temperature: 873 K. Feed: 100 NTP cm^3 min^{-1} (paraffin 30.0 vol%, COS 30.0 vol%, N_2 40.0 vol%). Contact time: 11.2 g-catalyst·h·g-mol^{-1}. Product: $C_2H_6 \rightarrow C_2H_4$, $C_3H_8 \rightarrow C_3H_6$, i-$C_4H_{10} \rightarrow i$-C_4H_8. b), c) For the weakest C-H bond. C-H bond dissociation energy (B.D.E.): Ref. 6. d) g-mol (g-catalyst·h·atm)$^{-1}$. e) Normalized to one most-reactive hydrogen.

Based on the above findings made in the present work, we propose the following reaction scheme for the oxidative dehydrogenation of butane by COS over these metal oxide catalysts. The oxidative dehydrogenation of butane by sulfur takes place mainly in gaseous phase and it proceeds more preferentially *via* an intermediate In_1 than *via* the another In_2, as indicated by the relative reactivity of the hydrogens (Table 2). The greater yields of propylene than ethylene and no formation of these two olefins from *trans*-2-butene found in the present work (Table 1) support this reaction scheme. The hydrogenation of hydrocarbon species does not take place extensively as seen in the small values of the combined yield of methane, ethane, and propane (Table 1). The hydrogens used for the hydrogenations must have been supplied from HS_x (maybe $x=1$ and/or 2). The mechanism of the formation of carboneceous materials at the surface of the catalysts remains unknown.

References

1) L. A. Haas and S. E. Khalafalla, *J. Catal.*, **30**, 451 (1973).

2) D. E. Boswell, U. S. Patent 3 399 243 (1968), Mobil Oil Corporation.

3) W. O. Haag and J. N. Miale, U. S. Patent 3 787 517 (1974), 3 821 278 (1974), and 3 875 252 (1975), Mobil Oil Corporation.

4) W. O. Haag and J. N. Miale, "Proc. 6th Intern. Congr. Catal.," Elsevier, London (1976), Vol. 1, p. 397.

5) M. Akimoto, K. Yamagami, and E. Echigoya, *Chem. Lett.*, **1982**, 479.

6) C. R. Noller, "Chemistry of Organic Compounds," 3rd ed, Saunders, Philadelphia (1965), p. 993.

Chirality of Waugh-type Enneamolybdomanganate(IV) Heteropolyanion. Observation of a Pfeiffer Effect

Kenji NOMIYA, Ryoichi KOBAYASHI, and Makoto MIWA*

Department of Industrial Chemistry, Faculty of Engineering, Seikei University, Musashino, Tokyo 180

(Received March 14, 1983)

Synopsis. Enneamolybdomanganate(IV), $[Mn^{IV}Mo_9O_{32}]^{6-}$, so-called Waugh-type heteropolyanion, has a chirality based on the D_3 symmetry around an MnO_6 octahedron. Attempts to resolve the racemic polyanion have been unsuccessful. A Pfeiffer effect was observed for the tetrabutylammonium salt in organic media containing *l*-brucine sulfate as an environment substance. This is the third example of heteropolyanions which show an optical activity.

Waugh-type enneamolybdomanganate(IV) formulated as $[Mn^{IV}Mo_9O_{32}]^{6-}$ is an octahedral manganese (IV) complex with the Mo_9O_{32} ligand, which was prepared first as potassium and barium salts by Hall.[1] Absorption spectrum of the ammonium salt was measured first in aqueous solution by Shimura and Tsuchida,[2,3] and the absorption bands were assigned to d^3 ions by Baker and Weakley.[4] A structure determination of the ammonium salt, $(NH_4)_6[MnMo_9O_{32}]\cdot 8H_2O$, by the single-crystal X-ray diffraction technique has shown that an MnO_6 octahedron has the D_3 symmetry.[5] Thus, this complex should be chiral. However, all attempts to resolve the racemic complex have failed.[4] There may be several reasons: (1) relatively rapid racemization, (2) the potassium and ammonium salts dissolve only in water, and (3) all resolving agents tested sofar form insoluble diastereomers in water. In this work we prepared the quaternary ammonium salt of the complex which is soluble in organic solvents and observed the Pfeiffer effect in the presence of *l*-brucine sulfate as an environment substance. This is the third example of heteropolyanions which show an optical activity; the first is $(NH_4)_6[Co_2Mo_{10}O_{34}(OH)_4]\cdot 7H_2O$, which was resolved by Shimura and his co-workers,[6] and the second is $[(C_4H_9)_4N]_5H[P_2Mo_{18}O_{62}]$, chirality of which is shown by observing the Pfeiffer effect by Garvey and Pope.[7]

Experimental

Electronic absorption and CD spectra were measured on a Hitachi 340-spectrophotometer with computer key-board and on a JASCO J-40AS spectropolarimeter, respectively. IR spectra were recorded with a JASCO IR-G spectrophotometer. Measurements were made at room temperature. For IR spectra measurement in acetonitrile a KBr cell with 0.1 mm optical path was used.

Preparation. The orange-red complex was prepared according to the literature,[4] analyzed and formulated as $(NH_4)_6[MnMo_9O_{32}]\cdot 6H_2O$ (Found: H, 2.11; N, 5.05%. Calcd: H, 2.20; N, 5.10%). This complex salt was converted to the free acid by passing the aqueous solution through a cation-exchange resin (Dowex-50W, H form) column. The acid form of the complex is readily soluble in aqueous solution and stable except when it is left standing for a long time. An aqueous solution containing an equimolar amount of tetrabutylammonium bromide (9.75 g) and potassium chloride (2.25 g) was added to the free acid solution obtained from the starting ammonium salt (5 g). Pale brick-red precipitate was collected, washed several times with a small amount of water, and dried *in vacuo*. The complex is readily soluble in water and various organic solvents except for ethyl ether, and cannot be easily recrystallized. The complex is contaminated with yellow $Mo_6O_{19}^{2-}$ as an impurity, which shows chracteristic IR bands at 800 and 950 cm^{-1}. The impurity crystallizes out of the acetonitrile solution and is removed by filtration. The complex can be reprecipitated by adding excess isobutyl methyl ketone to the filtrate, although the yield is remarkably low. The complex thus obtained was formulated as $K_2[(C_4H_9)_4N]_4[MnMo_9O_{32}]\cdot 13H_2O$ (Found: C, 28.32; H, 5.63; N, 2.02%. Calcd: C, 28.34; H, 5.35; N, 2.07%). The potassium tetrabutylammonium salt is sufficiently stable in the solid state, while it decomposes in organic media after a long time.

Results and Discussion

Absorption spectra of the complex in the acetonitrile solutions (6.6×10^{-4} mol dm^{-3}), which contain various molar ratios of *l*-brucine sulfate as an environment substance, are shown in Fig. 1, together with that of the solution without *l*-brucine sulfate. The form

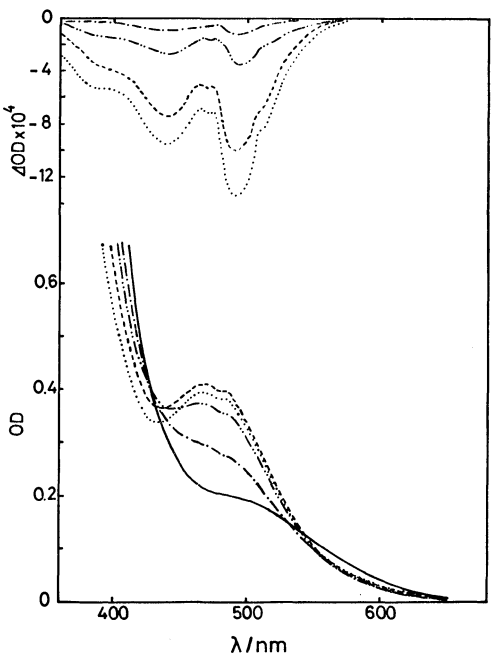

Fig. 1. Absorption and CD spectra of the tetrabutylammonium salt of $[MnMo_9O_{32}]^{6-}$ anion (6.6×10^{-4} mol dm^{-3}) in acetonitrile containing various moles of *l*-brucine sulfate. Molar ratios of brucine: complex are 2:1 (———), 4:1 (———), 6:1 (----) and 8:1 (·····). A full line shows the spectrum of the complex alone.

of the spectrum of the parent ammonium salt in an aqueous solution has been known to depend markedly on the pH.[4] The spectrum of the tetrabutylammonium salt in acetonitrile is similar to that of the ammonium salt at pH 2.9. As the molar ratio of brucine to the complex increases, the absorbance at 480 nm increases, with a double peak appearing at 468 and 484 nm. For the solution with the molar ratio of brucine higher than 4 the spectral change becomes very small. The double peak coincides with that of the ammonium salt observed in the aqueous solution of pH 3.5—4.9. The splitting is due to a trigonal distortion of the first spin-allowed transition ($^4T_{2g} \leftarrow {}^4A_{2g}$) in the d^3 octahedral MnO_6 ion.[4,8] Thus, the effect of *l*-brucine for the complex in acetonitrile resembles the pH-raising effect for the ammonium salt in an aqueous solution.

The circular dichroism (CD) spectra were observed for mixtures of the complex and *l*-brucine, the optical activity of which appeared only after the addition of *l*-brucine. They are also shown in Fig. 1. A remarkable change in the CD spectra is found for solutions with the molar ratio of brucine to the complex, 4:1, 6:1, and 8:1, whereas their absorption spectral change is very small. This is attributed neither to the induced CD accompanied with outer-sphere association, nor to the chemical reaction between the complex and *l*-brucine since the experiments were performed in a relatively low concentration ($\approx 10^{-3}$ mol dm^{-3}) of the latter. Conclusively, this is attributed to a shift of the equilibrium between two enantiomers of the racemic complex, *viz.* the Pfeiffer effect.

IR spectra have shown that the structure of polyanion-moiety depends significantly on the cation, and the bands of the tetrabutylammonium salt in 700—500 cm^{-1} were less split than those of the parent ammonium salt. This shows that a site symmetry of the tetrabutylammonium salt may be higher than that of the parent ammonium salt. IR spectrum of the acetonitrile solution of the tetrabutylammonium salt was also measured with and without *l*-brucine sulfate. When the molar ratio of brucine:complex is 4:1, the IR spectrum is close to that of the solid ammonium salt which has the D_3 symmetry around the MnO_6 octahedron. The IR spectrum in the absence of *l*-brucine is substantially unchanged from that of the solid tetrabutylammonium salt except for the sharpening of bands. These results indicate that the site symmetry of the complex ion is lowered to D_3 by the addition of *l*-brucine.

Further, DMF and *l*-strychnine sulfate were used as the solvent and the environment substance, respectively to demonstrate the Pfeiffer effect and the shift of the equilibrium toward the (+)-enantiomer of the complex. Unfortunately the equilibrium shift was not observed; only the shift toward the (−)-enantiomer by the Pfeiffer effect was shown. Besides, the observed CD was much reduced than that observed in the brucine-complex system in acetonitrile.

The CD spectrum of the brucine-complex system in acetonitrile, in which the (−)-enantiomer predominates, shows peaks at 510, 490, 470, 440, and 390 nm. The selection rule for the first and the second magnetic dipole transitions of the d^3 ion under the D_3 symmetry indicates that two transitions ($^4E \leftarrow {}^4A_2$ and $^4A_1 \leftarrow {}^4A_2$) for the first electronic transition, and only one transition ($^4E \leftarrow {}^4A_2$) for the second transition are allowed. Even if a contribution from spin-forbidden transitions is taken into account, the number of the CD peaks is too many. This may indicate that the electronic transitions are not pure d-d ones. Further investigation on the origin of the CD peaks is required.

References

1) R. D. Hall, *J. Am. Chem. Soc.*, **29**, 692 (1907).
2) Y. Shimura, H. Ito, and R. Tsuchida, *Nippon Kagaku Zasshi*, **75**, 560 (1954).
3) Y. Shimura and R. Tsuchida, *Bull. Chem. Soc. Jpn.*, **30**, 502 (1957).
4) L. C. W. Baker and T. J. R. Weakley, *J. Inorg. Nucl. Chem.*, **28**, 447 (1966).
5) J. L. T. Waugh, D. P. Shoemaker, and L. Pauling, *Acta Crystallogr.*, **7**, 438 (1954).
6) T. Ama, J. Hidaka, and Y. Shimura, *Bull. Chem. Soc. Jpn.*, **43**, 2654 (1970).
7) J. F. Garvey and M. T. Pope, *Inorg. Chem.*, **17**, 1115 (1978).
8) A. G. Paulusz and H. L. Burrus, *Chem. Phys. Lett.*, **17**, 527 (1972).

Use of an Ion-selective Electrode as a Detector in Ion Pair Chromatography

Akinori Jyo,† Kenji Mori, and Nobuhiko Ishibashi*
Department of Applied Analytical Chemistry, Faculty of Engineering, Kyushu University, Fukuoka 812

(Received March 22, 1983)

Synopsis. A chloride ion-selective electrode was used as a detector for inorganic anions separated by ion pair chromatography. Excellent performance of the electrode detector was demonstrated by detection of chloride, iodide, and thiocyanate.

While ion pair chromatography has been widely used in the separation of charged organic species,[1] little has been reported for the separation of inorganic anions.[2,3] This is seemingly ascribable to limitation in detectors which directly respond to inorganic anions under the conditions of the chromatography. Although detectable species are limited, ion-selective electrodes will be useful for detection of anions which have no or weak light absorption in the UV and visible regions.[4]

This paper describes the use of a solid state type chloride ion-selective electrode as a detector for some inorganic anions in ion pair chromatography.

Experimental

An HPLC system with an ion-selective electrode detector was reported in detail in a previous paper.[5] An Orion 94-17A chloride ion-selective electrode was used. A baseline supporting electrolyte solution (BLSS), which depresses streaming potential and stabilizes baseline potential, was mixed to a column effluent by a post column technique. The BLSS used was an aqueous solution containing potassium nitrate(1.0 M, 1 M=1 mol dm^{-3}) and sodium chloride(3.0×10^{-5} M). A LiChrosorb RP-18(Merck) or ODS 6013(Kyowa Seimitsu) was packed in a stainless steel coulmn(100 mm × 2.1 mm i.d.). Samples were injected with a Hamilton microsyringe HP-305(5 μl). The mobile phase was an aqueous solution containing tetrabutylammonium sulfate and sulfuric acid. The mobile phase and BLSS were doubly filtered with Mitex and Millipore MF filters, before use. All chemicals were of reagent grade and were used as received.

Results and Discussion

Since a chloride ion-selective electrode of solid membrane type responds to most anions which form sparingly soluble silver salts, the separation and detection of these kinds of anions were tested. In order to determine an appropriate pH range of the mobile phase, chloride, iodide, and thiocyanate were separately eluted with a mobile phase of various pH. When the pH of the mobile phase was greater than 1.5, marked tailing was observed for elution of iodide and thiocyanate. As an example, detector responses for iodide are shown in Fig. 1. Thus, further studies were made maintaining the pH of the mobile phase below 1.5, although the cause of the tailing was not clear.

Figure 2 shows detection of chloride and thiocyanate. Both anions were successfully separated within 10 min. The complete separation of iodide from chloride and thiocyanate was difficult under the conditions examined. In Table 1, an example of reproducibility for detector responses is given. The reproducibility is comparable to that of conventional detectors. Figure 3 shows an analytical curve for chloride separated

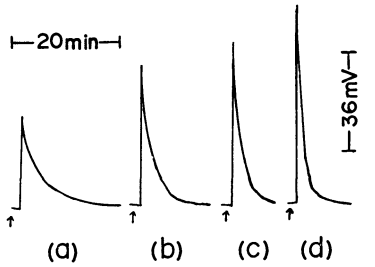

Fig. 1. Effect of pH of the mobile phase on elution of iodide.
Mobile phase: 2.0×10^{-3} M tetrabutylammonium sulfate in various concentrations of sulfuric acid, flow rate of mobile phase: 0.65 ml/min, flow rate of BLSS: 1.0 ml/min, sample: 50 nmol of sodium iodide, column: ODS 6013, pH of the mobile phase: (a) 2.80, (b) 1.95, (c) 1.47, (d) 1.08.

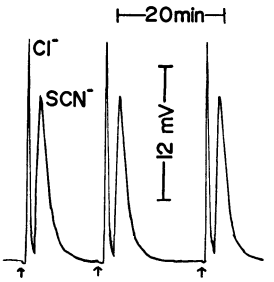

Fig. 2. Separation of chloride and thiocyanate.
Mobile phase: 6.0×10^{-3} M tetrabutylammonium sulfate in 0.1 M sulfuric acid, flow rate of mobile phase: 1.2 ml/min, flow rate of BLSS: 1.1 ml/min, sample: mixture of sodium chloride and sodium thiocyanate (50 nmol of each), column: Lichrosorb RP-18.

Table 1. Reproducibility of detector response[a]

Ion[b]	Peak height[c] / mV	Relative standard deviation/%
Chloride	17.0	2.5
Thiocyanate	21.5	4.1

a) Chromatographic conditions are given in Fig. 2. b) 50 nmol of each. c) Average of 12 determinations.

† Present address: Department of Industrial Chemistry, Faculty of Engineering, Kumamoto University, Kurokami, Kumamoto 860.

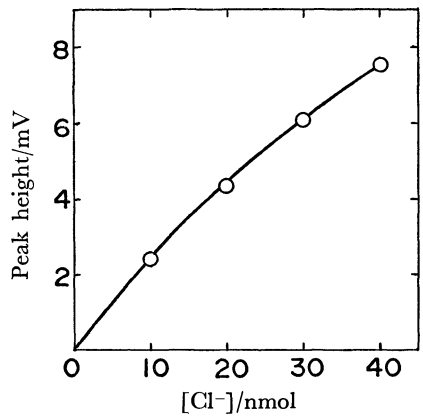

Fig. 3. Analytical curve for chloride separated from 50 nmol of thiocyanate.
Mobile phase: 4.0×10^{-3} M tetrabutylammonium sulfate in 0.1 M sulfuric acid, flow rate of mobile phase: 0.55 ml/min, flow rate of BLSS: 1.0 ml/min, sample: mixture of sodium chloride and sodium thiocyanate, column: ODS 6013.

from thiocyanate. The analytical curve is not linear. It shows slightly upward curvature. Lower detection limits are not examined, but it is not difficult to detect the anions down to orders of nano moles.

As is illustrated in this work, the chloride ion-selective electrode can be successfully used as one of the detectors in ion pair chromatography. Recently, reversed phase columns have drawn attention to the separation of charged inorganic species by ion pair chromatography[2,3] and by similar but somewhat different approaches.[6-8] Seemingly, ion-selective electrodes will be useful for expansion of this field, since problems encountered are detectors in chromatographic determination of inorganic species.

This work was supported by a grant of the Asahi Glass Foundation for Contribution of Industrial Technology.

References

1) R. E. Majors, H. G. Barth, and C. H. Lochmüller, *Anal. Chem.*, **54**, 323R(1982).
2) R. N. Reeve, *J. Chromatogr.*, **177**, 393 (1979).
3) I. Molnar, H. Knauer, and D. Wilk, *J. Chromatogr.*, **201**, 225 (1980).
4) J. Koryta, *Anal. Chim. Acta*, **139**, 1 (1982).
5) N. Ishibashi and A. Jyo, *Asahi Garasu Kogyo Gijutsu Shoreikai Kenkyu Hokoku*, **33**, 47 (1978).
6) R. M. Cassidy and S. Elchuk, *Anal. Chem.*, **54** 1558 (1982).
7) Z. Iskandarani and D. J. Pietrzyk, *Anal. Chem.*, **54**, 2427 (1982).
8) Z. Iskandarani and D. J. Pietrzyk, *Anal. Chem.*, **54**, 2601 (1982).

Determination of Small Amounts of Carbazole in Anthracene by Synchronous Fluorescence Spectrometry

Motohisa FURUSAWA,* Masaki TACHIBANA, and Mamiko FUJISHIMA
Faculty of Engineering, Yamanashi University, Takeda, Kofu 400

(Received March 29, 1983)

Synopsis. After converting anthracene into the Diels-Alder adduct by the reaction with maleic anhydride, and converting the adduct into a water-soluble salt by hydrolysis with potassium hydroxide aqueous solution, carbazole is then extracted into 2,2,4-trimethylpentane together with other impurities. Then carbazole can be determined by synchronous fluorescence spectrometry without interference of the impurities.

Since commercially available anthracene contains carbazole as an impurity and its removal from anthracene is relatively difficult, a determination method of carbazole is required. For the determination of small amounts of carbazole in anthracene, several methods have been developed.[1-3] In the present paper separation of carbazole from anthracene and its determination by synchronous fluorescence spectrometry will be described. By this method, carbazole can be determined more rapidly and simply than previous methods. The determination limit is 10 ppm.

Experimental

Reagents. Maleic anhydride was purified by distillation. 2,2,4-Trimethylpentane used was of the "Spectro" grade.

Apparatus. All the measurements of synchronous fluorescence spectra were made on a Hitachi 650-40 fluorescence spectrophotometer equipped with a Hitachi 056 recorder. The spectral bandpass was set at 2 nm. A 150-W Xenon lamp was used as the exciting source. A $10\times10\times45$ mm^3 quartz cell was used. A Torika MA-1 mixer of Japan Torika Corp. was used as a shaker for the extraction.

Procedure. A mixture of 10 mg of the anthracene sample and 1 g of maleic anhydride was fused at 160 °C for 10 min in a 25-ml Kjeldahl flask (short neck) fitted with an air condenser. The reaction mixture was dissolved by adding 10 ml of 3 mol/l potassium hydroxide aqueous solution and heating with occasional shaking. After the solution had been cooled to room temperature, 10 ml of 2,2,4-trimethylpentane was added. The mixture was thoroughly shaken and allowed to stand for a while. The synchronous fluorescence spectrum of the 2,2,4-trimethylpentane phase was measured with a wavelength interval of 5 nm. Carbazole was determined from the intensity at 335 nm obtained by the base line method. As the standard, the synchronous fluorescence intensity of a 0.2 μg/ml carbazole solution was used. The calibration curve was prepared by using carbazole solutions containing 0—0.2 μg per ml.

Results and Discussion

Synchronous Fluorescence Spectrum. For the determination of carbazole, a wavelength interval of 3 nm is suitable under ordinary conditions.[4] For the determination of more minute amounts of carbazole, however, a larger wavelength interval is necessary for enhancement of the signal-to-noise ratio. From the experimental results, a wavelength interval of 5 nm was effective. The synchronous fluorescence spectrum of carbazole is shown in Fig. 1. The spectrum has a maximum at 335 nm.

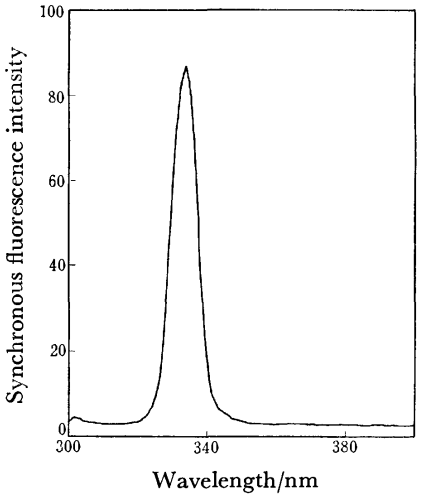

Fig. 1. Synchronous fluorescence spectrum of carbazole. Wavelength interval: 5 nm; solvent: 2,2,4-trimethylpentane.

Removal of Anthracene. The Diels-Alder reaction of anthracene with maleic anhydride was useful for the removal of anthracene as an adduct. Carbazole was separated together with other impurities by extraction into 2,2,4-trimethylpentane after the adduct had been converted into the water-soluble potassium salt by hydrolysis with potassium hydroxide aqueous solution. The Diels-Alder reaction was carried out by fusing the anthracene sample with maleic anhydride. To find the effect of heating time on the reaction, pure anthracene was fused with maleic anhydride by varying the heating time at 160 °C. Table 1 shows the residual amounts of anthracene in the 2,2,4-trimethylpentane phase evaluated by measuring the synchronous fluorescence intensity at 379 nm. Table 1 indicates that the reaction is completed within 5 min. It is recommended, therefore, that the sample is fused at 160 °C for 10 min.

Experiments using saturated hydrocarbons as the medium for the Diels-Alder reaction failed, because maleic anhydride did not dissolve satisfactorily in these solvents having desired boiling points.

Calibration Curve. A calibration curve of carbazole was linear over the concentration range from 0.01 to 0.2 μg/ml. As the standard a 0.2 μg/ml carbazole solution was used, and the coefficient of variation obtained in 20 measurements was 0.73%.

Effects of Impurities in Anthracene. Effects of disturbing substances due to absorption have been reported in the previous paper.[4] Acenaphthene shows the spectral interference, but the determination of a

Table 1. Effect of heating time on Diels-Alder reaction of anthracene with maleic anhydride

Heating time / min	Synchronous fluorescence intensity[a]	Residual amounts of anthracene: Concentration / ng ml^{-1}	Residual amounts of anthracene: Total amounts / ng
3	5.0	14	140
3	18.5	53	530
5	<1.0	<3	<30
5	<1.0	<3	<30
10	<1.0	<3	<30
10	<1.0	<3	<30
15	<1.0	<3	<30

a) As the standard, synchronous fluorescence intensity (wavelength interval=5 nm) at 379 nm of a 0.200 μg/ml anthracene solution was taken as 70 div.

0.2 μg/ml carbazole solution was not interfered with the presence of less than 8-fold amount of acenaphthene.

Determination of Carbazole in Synthetic Mixtures. The analytical results of synthetic mixtures are shown in Table 2, Nos. 1—11. Each mixture contains 0.1% of biphenyl, acenaphthene, fluorene, dibenzofuran, and phenanthrene and 0.01% of perylene, fluoranthene, naphthacene, chrysene, and 9,10-anthraquinone. Table 2, Nos. 1—11 indicate that the analytical results agree well with the contents of carbazole. Therefore, carbazole in anthracene can be determined by the present method.

Determination of Carbazole in Practical Samples. Carbazole in three kinds of commercial anthracene was determined by the present method, and the results were compared with the analytical results obtained by a spectrophotometric method.[1] As is shown in Table 2, Nos. 12—14, both results agree within experimental errors. The synchronous fluorescence spectra of the solutions used for the determination exhibited the characteristic signal of carbazole having a peak at 335 nm. In addition, the solutions did not show the absorption based on interfering impurities. Therefore, the method proposed in the present paper can be applied to practical samples of anthracene. The determination of carbazole by the conventional fluorimetry was unsuccessful because of the interference of other luminescent species.

Table 2. Analytical results for carbazole in synthetic mixtures and practical samples

No.	Content / %	Synchronous fluorescence intensity[a]	Found (%)	
1	0.0010	4.4	0.001_1	
2	0.0040	16.3	0.004_0	
3	0.0080	30.5	0.007_6	
4	0.0120	47.7	0.011_8	
5	0.0160	61.3	0.015_2	
6	0.0200	78.4	0.019_7	
7	0.0200	76.9	0.019_4	$\bar{x}=0.019_6$
8	0.0200	77.5	0.019_5	$\sigma=0.00018$
9	0.0200	77.4	0.019_4	C.V.=0.93%
10	0.0200	79.1	0.019_9	
11	0.0200	78.8	0.019_7	
12	0.021_7	81.8	0.020_4	
13	0.003_0	11.8	0.003_0	
14	0.12_9	48.4[b]	0.12_2	

a) As the standard, the synchronous fluorescence intensity of a 0.200 μg/ml carbazole solution was taken as 80 div. b) Measured after the solution had been diluted 10 times.

The authors are indebted to Miss Sumiko Yamada for her technical assistance.

References

1) M. Furusawa, S. Yamada, Y. Sato, Y. Ando, and T. Takeuchi, *Nippon Kagaku Kaishi*, **1973**, 733; M. Furusawa, S. Yamada, and T. Takeuchi, *Bunseki Kagaku*, **23**, 77 (1974).

2) M. Furusawa, M. Tachibana, S. Yamada, and Y. Ishida, *Bunseki Kagaku*, **28**, 130 (1979); M. Furusawa, M. Tachibana, and Y. Hayashi, *ibid.*, **29**, 859 (1980).

3) T. Takeuchi and Y. Suzuki, *Kogyo Kagaku Zasshi*, **69**, 228 (1966).

4) M. Furusawa, M. Tachibana, and Y. Hayashi, *Bunseki Kagaku*, **31**, 229 (1982).

The Precipitation-Spectrophotometric Determination of Dithionate Ions with Bis(diethylenetriamine)nickel(II) Chloride Solution[1)]

Tsugio SATO* and Taijiro OKABE

Department of Applied Chemistry, Faculty of Engineering, Tohoku University, Sendai 980

(Received May 19, 1983)

Synopsis. A solution containing dithionate ions is treated with bis(diethylenetriamine)nickel(II) chloride solution to precipitate dithionate as $[Ni(dien)_2]S_2O_6$ complex. After centrifugation, the concentration of nickel(II) ions in the supernatant is spectrophotometrically determined by dimethylglyoxime method. There is no interference from SO_4^{2-} SO_3^{2-}, $S_2O_3^{2-}$, $S_4O_6^{2-}$, $HN(SO_3)_2^{2-}$, S^{2-}, or Fe^{3+}.

Special attention has been recently devoted to the chemical behavior of dithionate because dithionate is often produced in various industrial processes using sulfite solutions, such as wet type desulfurization and hydrometallurgy, and causes pollution problems. However, the analysis of dithionate by classical methods such as redox titration[2,3)] or gravimetry[4)] after disproportionation of dithionate to sulfite and sulfate in hot acidic solutions that were used in previous studies are very tedious operations, especially in the cases where other sulfur compounds coexist.

Recently Marcu *et al.*[5)] reported that dithionate forms slightly soluble salts with metal(II) ethylenediamine complexes and with metal(II) 1,2-propanediamine complexes, where metals are nickel, cadmium, copper, and zinc. They have proposed a gravimetric method for determining dithionate as these amine complexes. The method can be used to determine dithionate in the presence of sulfite and sulfate, but high amounts of polythionates interfere. In the preceeding study,[6)] we have shown the solubility of many kinds of metal(II) alkylamine complexes and have reported that the solubility of $[Ni(dien)_2]S_2O_6$ is extremely small. Therefore, it may be more useful for the determination of dithionate ions. The present paper is concerned with a simple and selective spectrophotometric determination of dithionate ions using bis(diethylenetriamine)nickel(II) chloride as precipitant.

Experimental

Apparatus. The spectrophotometric measurements were made with a Hitachi 101 spectrophotometer.

Reagents. Sodium dithionate, potassium tetrathionate, and potassium imidobis(sulfate) were prepared by Pfanstiel's method,[7)] Martin's method,[8)] and Sisler's method,[9)] respectively.

Bis(diethylenetriamine)nickel(II) Chloride Solution: Dissolve 6.0 g of nickel(II) chloride hexahydrate in 150 cm^3 of distilled water, and add 50 cm^3 of diethylenetriamine and 800 cm^3 of ethyl alcohol.

Dimethylglyoxime Solution: Dissolve 1 g of dimethylglyoxime in 500 cm^3 of 0.25 M (M=mol dm^{-3}) sodium hydroxide solution.

All other chemicals were of analytical grade and were used without further purification.

Procedures. Transfer 5 cm^3 of sodium dithionate solution (0—20 mM) to a 15 cm^3 centrifuge tube, add 5 cm^3 of bis(diethylenetriamine)nickel(II) chloride solution, seal it to prevent evaporation of solvent and place the tube in an ice bath. After 30 min, remove the tube from the ice bath and centrifuge it at 2000 min^{-1} for 10 min. Transfer 100 mm^3 of supernatant to a 50 cm^3 volumetric flask, then add 2 cm^3 of 20 wt% potassium sodium tartrate solution, 0.5 g of ammonium peroxodisulfate, 1 cm^3 of dimethylglyoxime solution and 2.5 cm^3 of 5 M sodium hydroxide. Dilute the solution to the mark with distilled water. After 30 min, measure the absorbance of the solution at 465 nm in a 10 mm thick glass cell against a water blank.

Results and Discussion

The analytical method described above consists of the separation of dithionate as a slightly soluble bis(diethylenetriamine)nickel(II) dithionate complex by double decomposition as shown in Eq. 1, and the

$$Na_2S_2O_6 + [Ni(dien)_2]Cl_2 \longrightarrow [Ni(dien)_2]S_2O_6 + 2NaCl, \quad (1)$$

determination of nickel(II) ions remaining in the solution. For the determination of nickel(II) ion, dimethylglyoxime method[10)] was adapted because it seems to be the simplest method. Therefore in the present study, a series of tests was carried out to investigate the precipitation behavior of dithionate.

Four different organic solvents (dioxane, acetone, methyl alcohol, and ethyl alcohol) were tested for the precipitation of $[Ni(dien)_2]S_2O_6$ at 30 °C. The results are shown as Fig. 1. It is seen that solubility of $[Ni(dien)_2]S_2O_6$ under these experimental conditions is 1.47 mM in water, but rapidly decreases with increasing concentrations of organic solvents. Subsequently, ethyl alcohol–H_2O system was chosen because it showed the smallest solubility of $[Ni(dien)_2]S_2O_6$ complex. The solubility product of this complex in 40 vol% ethyl alcohol is 1.6×10^{-7}; hence, more than

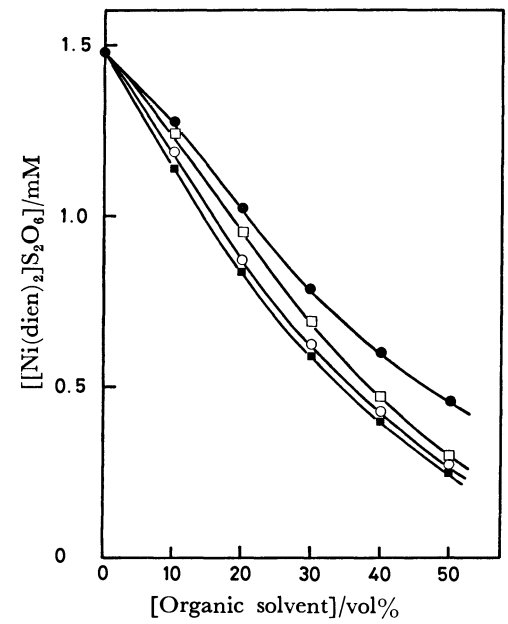

Fig. 1. Solubility of $[Ni(dien)_2]S_2O_6$ in mixed organic solvent–H_2O solutions. ●: Dioxane, □: acetone, ○: methyl alcohol, ■: ethyl alcohol, temperature: 30 °C, ionic strength: 0.5 M.

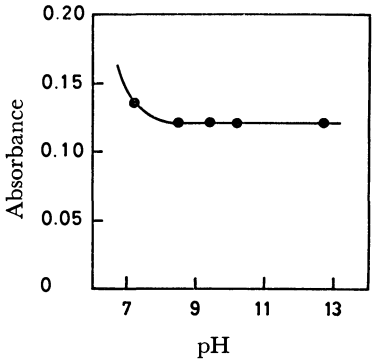

Fig. 2. Effect of pH variation. Concentration of $Na_2S_2O_6$: 15.4 mM.

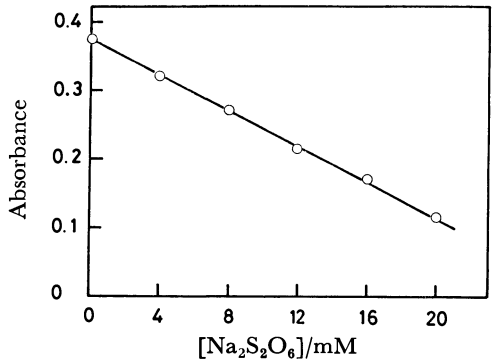

Fig. 3. Calibration curve.

99% of dithionate in the range of concentrations 2—20 mM can be precipitated by the above-mentioned procedure.

The effect of standing time in the precipitation step was examined and constant absorbances were obtained after standing for 15 min.

The absorbance was measured as a function of the pH value at double decomposition reaction in the range of pH 7.0—12.5. As is shown in Fig. 2, constant absorbances were obtained at pH values above 8.5. The precipitant, bis(diethylenetriamine)nickel-(II) chloride solution, contanins much free diethylentriamine, so that it is not necessary to neutralize the sample solutions unless the acid concentrations are more than 2.5 M.

On the basis of the above results, a standard procedure was evolved, by which the linear calibration graph was obtained in the range of dithionate concentrations in the sample solution 0—20 mM, as shown in Fig. 3. The coefficient of variation for the ten replicated experiments was satisfactory (2.5% for 15.4 mM of $S_2O_6^{2-}$).

The interferences due to various ions were also examined, as is shown in Table 1. Thiosulfate caused considerable errors, but no other compounds showed interference. It is significant that sulfite and sulfate which usually coexist with dithionate showed no interference even at such high concentrations as 800 mM. In the presence of thiosulfate, the amounts of dithionate found were larger than those added: it means that a part of thiosulfate coprecipitates with dithionate as nickel(II) diethylenetriamine complex. However, thiosulfate can be oxidized by iodide to tetrathionate

Table 1. Effect of foreign substances

[Substances]/mM		$[S_2O_6^{2-}]$ found/mM
Na_2SO_4	20	15.6
	40	15.6
	60	15.9
	100	15.3
	500	15.5
	800	15.4
Na_2SO_3	20	15.2
	100	15.1
	800	15.0
$Na_2S_2O_3$	20	20.2
	40	21.7
	60	22.5
$Na_2S_4O_6$	20	15.4
	40	15.7
	60	15.6
$NH(SO_3K)_2$	20	15.3
	40	15.5
	60	15.1
Na_2S	20	15.4
	40	15.1
	60	15.2
$Fe_2(SO_4)_3$	10	15.3
	20	15.3
	30	15.6
$[Na_2S_2O_6]$ added/mM		15.4

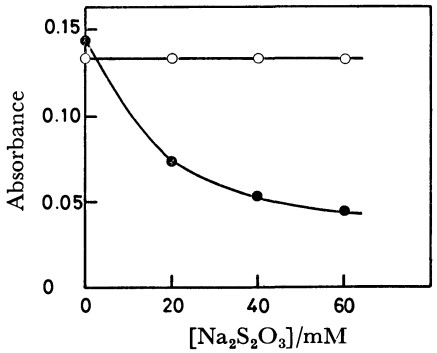

Fig. 4. Effect of the concentration of thiosulfate. Concentration of $Na_2S_2O_6$: 15.4 mM. ○: Added 1 cm³ of 0.2 M iodide solution, ●: none.

which shows no interference for the determination of dithionate. Therefore the interference due to thiosulfate may be overcome by modifying the procedure as follows. After the same volume (5 cm³) of the sample solution is placed in a 15 cm³ centrifuge tube, add 1 cm³ of adequate concentration of iodide solution to oxidize thiosulfate, and then carry out the same procedures. The results shown in Fig. 4 were thus as expected, and excess iodide showed no interference.

References

1) Studies on the Formation and Decomposition of Dithionate, Part VIII. Part VII: T. Sato and T. Okabe, *Nippon Kagaku Kaishi*, **1981**, 1087.

2) S. Glasstone and A. Hickling, *J. Chem. Soc.*, **1933**, 5.

3) F. Ishikawa and H. Hagisawa, *Sci. Rep. Tohoku Imp. Univ.*, **21**, 484 (1932).

4) T. Sato and T. Okabe, *Nippon Kagaku Kaishi*, **1977**, 1124.

5) G. Marcu, M. Somay, and C. Várheli, *Studia Univ., Babes-Bolyai, Chem.*, **2**, 3 (1978).

6) T. Sato, M. Kato, and T. Okabe, *Nippon Kagaku Kaishi*, **1981**, 1082.

7) R. Pfanstiel, *Inorg. Synth.* **2**, 167 (1946).

8) F. Martin and L. Metz, *Z. Anorg. Allgem. Chem.*, **127**, 83 (1923).

9) H. Sisler and L. F. Audrieth, *J. Am. Chem. Soc.*, **60**, 1947 (1938).

10) W. A. Forster, *Analyst*, **78**, 560 (1953).

The Crystal and Molecular Structure of *trans*(*O*)·*mer*(*N*)-(*S*-(2-Aminoethyl)-L-homocysteinato)(glycinato)cobalt(III) Perchlorate

Ken-ichi OKAMOTO,* Masutaro SUZUKI, Hisahiko EINAGA,† and Jinsai HIDAKA

Department of Chemistry, University of Tsukuba, Sakura, Ibaraki 305

† *Institute of Materials Science, University of Tsukuba, Sakura, Ibaraki 305*

(Received May 20, 1983)

Synopsis. The crystal and molecular structure of the title complex, *trans*(*O*)·*mer*(*N*)-[Co(L-aehc)(gly)]$^+$, has been determined by the X-ray analysis. This isomer has *Δ* configuration. The sulfur donor atom of the coordinated L-aehc has *R* configuration and the six-membered N–S chelate ring takes a chair conformation.

When a quadridentate ligand, *S*-(2-aminoethyl)-L-homocysteinate (L-aehc), and a glycinate coordinate to a cobalt(III) ion, the possible geometrical isomers are four: *Δ-trans*(*O*)·*mer*(*N*), *Δ-cis*(*O*)·*mer*(*N*), *Δ-cis*(*O*)·*mer*(*N*), and *Δ-cis*(*O*)·*fac*(*N*).[1] In the *Δ* isomers, two conformations, chair and skew boat, are possible for the six-membered N–S chelate ring of the L-aehc. The *R*(*S*) coordination of the sulfur atom takes a chair-formed N–S chelate ring and the *S*(*S*) coordination takes a skew boat one. We reported that the sulfur donor atom in the *Δ-cis*(*O*)·*mer*(*N*) isomer takes the *R*(*S*) configuration and the six-membered N–S chelate ring takes a chair form.[2] The present work was attempted to investigate whether the six-membered N–S chelate ring of the L-aehc preferably takes a chair form (simultaneously *R*(*S*) configuration) in the *Δ-trans*(*O*)·*mer*(*N*) isomer or not. The first eluted isomer employed in this work can be assigned confidently as the *Δ-trans*(*O*)·*mer*(*N*) isomer from the explicit splitting of the first absorption band.[2-4] In this note, we wish to report the results of the determination of the crystal and molecular structure of the title compound. The absolute configuration of the sulfur donor atom and the conformation of the six-membered N–S chelate ring were determined.

Experimental

[Co(L-aehc)(gly)]Cl was prepared by the method in the literature[2] and chromatographed on the Dowex 50W-X8 (Na^+ form, 3 cm×40 cm) by eluting with 0.1 mol dm^{-3} NaCl aqueous solution. Four colored bands were eluted successively. The absorption and CD spectral measurements showed that the first eluate contained the *Δ-trans*(*O*)·*mer*(*N*) isomer. Then the first eluate was concentrated to a small volume with a rotary evaporator and the deposited NaCl was filtered off. By use of the anion exchange column (ClO_4^- form), the chloride salt in the eluate was converted into the perchlorate salt. Dark violet needle crystals were grown from an aqueous solution by adding ethanol. The cell dimensions and intensity data were measured on a Rigaku-denki four circle diffractometer (AFC-5) using Mo *Kα* (0.710730 Å) radiation. The crystal data are as follows; $CoC_8H_{17}N_3O_8SCl$, a=7.683 (2), b=16.304 (3), c=5.855 (1) Å, β=105.40 (2)°, V=707.1 (2) Å^3, monoclinic, space group $P2_1$, Z=2. The intensity data were collected by the ω-2θ scan technique up to 2θ=60°. A total of 2283 independent reflections with $|F_o|>3\sigma(|F_o|)$ were observed and employed in solving and refining the structure. No absorption correction was applied.

Structure Determination and Refinement

The structure was solved by the heavy atom method and refined by a full-matrix least-squares method using all the non-hydrogen atoms (program RFINE by L. W. Finger was used). The final residual values were R=0.055 and R_w=0.084, respectively. The absolute configuration was determined by an anomalous scattering technique. The atomic scattering factors for all the non-hydrogen atoms were taken from the literature.[5] When the refinements were carried out by use of a set of the atomic parameters containing the *Δ* configuration of the complex cation, the residual values converged to R=0.053 and R_w=0.083, respectively. On the contrary, the refinements in the enantiomeric atomic parameters (the *Δ* configuration) resulted in the residual values of R=0.058 and R_w=0.088, respectively. These facts indicate that the former is probably the correct choice, namely, the complex cation has the *Δ* configuration. This absolute configuration is supported from the result that the

Table 1. Positional and thermal parameters (×10^4)

Atom	x	y	z	B_{eq}/Å$^{2a)}$
Co	1329(1)		2939(1)	1.47
S	1097(2)	−1311(1)	4002(3)	1.90
N1	−858(7)	−187(4)	353(10)	2.08
N2	3709(6)	46(4)	5211(8)	1.78
N3	1307(8)	1178(4)	2312(11)	2.18
O1	2652(6)	−198(3)	694(8)	1.72
O2	5372(6)	−552(4)	333(10)	2.44
O3	−19(7)	275(3)	5118(9)	2.32
O4	−535(8)	1309(4)	7363(10)	3.13
C1	4333(8)	−392(4)	1537(11)	1.85
C2	4934(8)	−487(4)	4216(11)	1.92
C3	4775(9)	−1396(4)	4812(13)	2.28
C4	3019(8)	−1809(4)	3378(13)	2.04
C5	−719(9)	−1639(5)	1466(15)	2.73
C6	−882(10)	−1038(5)	−553(14)	2.78
C7	77(9)	1035(5)	5740(11)	2.10
C8	1035(12)	1611(4)	4404(14)	2.60
CL	5686(2)	1778(1)	919(3)	2.59
O11	7098(15)	2346(8)	1559(20)	7.33$^{b)}$
O12	4224(26)	2205(13)	33(32)	12.98$^{b)}$
O13	5217(14)	1415(7)	2939(18)	7.06$^{b)}$
O14	6133(39)	1173(20)	−998(44)	21.03$^{b)}$

a) B_{eq} is the equivalent isotropic temperature factors defined by Hamilton.[14] b) Isotropic temperature factor.

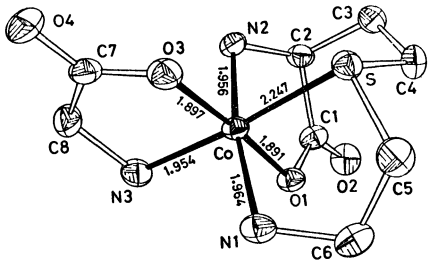

Fig. 1. A perspective drawing of *Δ-trans(O)·mer(N)-R(S)*-[Co(L-aehc)(gly)]$^+$ with the numbering scheme of the atoms.

asymmetric carbon atom of the L-aehc in the *Δ* configuration is in line with the known *S(C)* configuration.[6] The final positional parameters and equivalent isotropic temperature factors for the non-hydrogen atoms are listed in Table 1. Tables of structure factors, anisotropic temperature factors, bond lengths and angles, and the projected figure of the crystal structure are kept at the Chemical Society of Japan (Document No. 8344).

Results and Discussion

The perspective drawing of the present complex cation is shown in Fig. 1 (ORTEP program[7]). Each cobalt atom is surrounded by a sulfur, two trans oxygen and three meridional nitrogen atoms, as expected from the splitting pattern of the first absorption band of this complex cation (18.52 (ε=85.1) and 21.14 (ε=91.2)$\times 10^3$ cm^{-1}).[2-4] The complex cation is determined to be in the *Δ* configuration by anomalous scattering technique. The L-aehc coordinates to cobalt atom as a quadridentate and the asymmetric sulfur donor atom takes only *R* configuration. Therefore, the present complex cation is the *Δ-trans(O)·mer(N)-R(S)* isomer. The bond lengths and angles of the complex cation are similar to those for the cobalt(III) complexes with other sulfur-containing ligands and amino carboxylates.[2,3,8-12] The average Co–N distance for the nitrogen atoms is 1.958 Å and the Co–N3 distance bonded trans to the sulfur atom is 1.954 Å. This fact indicates that the trans effect due to the coordinated sulfur atom can not be recognized in the *Δ-trans(O)·mer(N)* isomer, as in the case of the cobalt (III) complexes with the thioether type ligands such as L-aehc in the *Δ-cis(O)·mer(N)* isomer,[2] *N,N'*-ethylenebis(*S*-methyl-L-cysteinate),[3] and 2-(methylthio)ethylamine.[13]

In order to investigate the conformation of the chelate rings, we calculated the displacements of relevant atoms from the chelate ring plane, which is defined by the central cobalt atom and two coordinated atoms in the chelate ring (Table 2). The six-membered N–S chelate ring of the L-aehc (N2–C2–C3–C4–S) takes a chair form, which consists of two almost parallel planes; dihedral angle for the two planes, N2–Co–S and C2–C3–C4, is 3.03°. Similar conformations have been also observed for *Δ-cis(O)·mer(N)-R(S)*-[Co(L-aehc)(gly)]$^+$ [1,2] and [Co(*S,S*-ebm)]$^+$,[11,12] where *S,S*-ebm denotes *N,N'*-ethylenebis(L-methioninate) whose six-membered chelate rings have the same framework as that of the L-aehc. The five-membered N–S chelate ring takes an envelope form with the *λ* conformation. The glycinate moiety of the L-aehc takes an envelope form with the *λ* conformation and the displacement of relevant atoms from the plane N2–Co–O1 does not differ much from that of the glycinate with the *δ* conformation in the present complex cation.

Table 2. Displacements of atoms from the least-squares plane (*d*/Å)

Six-membered N-S chelate ring:
$0.6342X-0.3016Y-0.7120Z+0.8235=0$

Co	0.0000	S	0.0000	N2	0.0000	C2	1.3572
C3	1.4283	C4	1.4928				

Five-membered N-S chelate ring:
$0.7495X-0.2876Y-0.5962Z+0.5664=0$

Co	0.0000	S	0.0000	N1	0.0000	C5	0.2564
C6	0.7960						

Glycinate chelate ring (in L-aehc):
$0.0864X+0.9837Y-0.1575Z+0.2125=0$

Co	0.0000	N2	0.0000	O1	0.0000	O2	−0.3497
C1	−0.2859	C2	−0.6731				

Glycinate chelate ring:
$0.6820X+0.1048Y+0.7238Z-1.5854=0$

Co	0.0000	N2	0.0000	O3	0.0000	O4	−0.5850
C7	−0.3682	C8	−0.5645				

References

1) The symbols, *Δ* and *Λ*, are tentatively denoted by the ring pairing method (J. I. Legg and J. A. Neal, *Inorg. Chem.*, **12**, 1805 (1973)). In the former paper,[2] *trans(SO)* was used instead of *cis(O)·mer(N)*, and *trans(SN)* of *trans(O)·mer(N)* and *cis(O)·fac(N)*.
2) K. Okamoto, M. Suzuki, and J. Hidaka, *Chem. Lett.*, **1983**, 401.
3) K. Okamoto, T. Isago, M. Ohmasa, and J. Hidaka, *Bull. Chem. Soc. Jpn.*, **55**, 1077 (1982).
4) K. Yamanari, J. Hidaka, and Y. Shimura, *Bull. Chem. Soc. Jpn.*, **50**, 2299, 2643 (1977).
5) "International Tables for X-Ray Crystallography," The Kynoch Press, Birmingham (1974), Vol. IV.
6) M. D. Armstrong and J. D. Lewis, *J. Org. Chem.*, **16**, 749 (1951).
7) All computations were carried out using a FACOM M-200 computer at University of Tsukuba.
8) H. Miyamae and Y. Saito, *Acta Crystallogr., Sect. B*, **34**, 937 (1978).
9) M. Kuramoto, *Bull. Chem. Soc. Jpn.*, **52**, 3702 (1979).
10) K. Okamoto, K. Wakayama, H. Einaga, M. Ohmasa, and J. Hidaka, *Bull. Chem. Soc. Jpn.*, **55**, 3473 (1982).
11) R. J. Geue and M. R. Snow, *Acta Crystallogr., Sect. B*, **33**, 70 (1977).
12) R. J. Magee, W. Mazurek, M. J. O'Connor, and A. T. Phillip, *Aust. J. Chem.*, **27**, 1629 (1974).
13) R. C. Elder, G. J. Kennard, M. D. Payne, and E. Deutsch, *Inorg. Chem.*, **17**, 1296 (1978).
14) W. C. Hamilton, *Acta Crystallogr.*, **12**, 609 (1959).

Reaction of Bis(2-methyl-8-quinolinolato)cobalt(II) with Nitrogen Monoxide†

Eiichi Miki,* Katsunori Saito, Kunihiko Mizumachi, and Tatsujiro Ishimori

Department of Chemistry, College of Science, Rikkyo University, Nishi-Ikebukuro, Toshima-ku, Tokyo 171

(Received June 8, 1983)

Synopsis. $[Co(C_{10}H_8NO)_2]\cdot H_2O$ ($C_{10}H_8NO^-$=2-methyl-8-quinolinolate ion) reacted with nitrogen monoxide in dichloromethane to give unstable compounds, $[Co(C_{10}H_8NO)_2(NO)_2]$ and $[NO]_3[Co(C_{10}H_8NO)_2(NO_3)(NO_2)]$ with liberation of dinitrogen oxide. The compounds were characterized by ^{15}N-isotopic effect observed on the IR spectra.

Nitrogen monoxide reacts with low-valent transition-metal complexes to give the nitrosyls or to cause a disproportionation of nitrogen monoxide.[1-3] Recently, one of the authors reported that $[Co(C_9H_6NO)_2]$ ($C_9H_6NO^-$=8-quinolinolate ion) reacted with nitrogen monoxide in dichloromethane at room temperature to give $[NO][Co^{III}(C_9H_6NO)_2(NO_3)(NO_2)]$ with liberation of dinitrogen oxide via $[Co^{III}(C_9H_6NO)_2(NO)]$.[4] The reaction involves a nitrosylation followed by an electrophilic attack of nitrogen monoxide on the coordinating nitrosyl group, and a disproportionation of nitrogen monoxide to $[NO]^+$, NO_3^-, and dinitrogen oxide.

In this paper, we report a reaction of $[Co(C_{10}H_8NO)_2]\cdot H_2O$ ($C_{10}H_8NO^-$ = 2-methyl-8-quinolinolate ion) with nitrogen monoxide in dichloromethane, pyridine, 10 vol% pyridine–DMF, or DMF.

The reaction was performed using a vacuum line, and the solid products were manipulated under nitrogen atmosphere as soon as possible. Starting material, $[Co(C_{10}H_8NO)_2]\cdot H_2O$ was synthesized by ordinary method. Nitrogen[^{15}N] monoxide was derived from potassium nitrate[^{15}N] (^{15}N atom%=99.7). The gaseous product was identified by mass spectrometer, and the IR bands and their ^{15}N-isotopic shifts.[5]

$[Co(C_{10}H_8NO)_2]\cdot H_2O$ (0.5 mmol) suspended in dichloromethane (20 cm^3) degassed by three cycles of freeze-pump-thaw was brought into contact with nitrogen monoxide (5 mmol), and stirred for 1 d at room temperature or for 7 d at *ca.* −20 °C. The suspended $[Co(C_{10}H_8NO)_2]\cdot H_2O$ changed from original orange to russet. The yield of the russet compound (**1**) was *ca.* 70% based on the starting material. The liberated gas was only dinitrogen oxide under the experimental conditions.

Compound **1** could not be purified since the compound in the solid state was gradually decomposed with liberation of nitrogen monoxide even under nitrogen atmosphere, and was also unstable in deoxygenated DMF or dichloromethane. The elementary analyses consisted with $Co_1C_{20}H_{16}N_7O_{10}$. Found: Co, 10.3; C, 42.3; H, 2.7; N, 17.5%. Calcd: Co, 10.3; C, 41.9; H, 2.8; N, 17.1%. The IR spectra of compound **1** at 80 K showed several absorption bands characteristic of nitrosyl cations, coordinating nitro, and nitrate ions in addition to the coordinating 2-methyl-8-quinolinolate ions, as shown in Fig. 1. The 2109(vs) cm^{-1} band shifted to 2040 cm^{-1} upon ^{15}N-substitution, and was assigned to the N–O stretching vibration due to the nitrosyl cations.[5] The 1280(w)[6], 820(sh)[6], 641(w), 582(w), and 422(w) cm^{-1} bands also shifted to 1260(sh)[6], 812(m), 635(w), 576(w), and 416(w) cm^{-1}, respectively, and were assigned to the symmetric N–O stretching of NO_3^-, the symmetric NO_2 deformation of NO_2^- or the rocking of NO_3^-, the antisymmetric or symmetric NO_2 deformation of NO_3^-, the NO_2 wagging of NO_2^-, and the Co–NO_2 stretching vibrations, respectively, from wave numbers of the bands and their ^{15}N-isotopic shifts.[4,5] The bands at 1330(sh)[6] cm^{-1} for the ^{14}N-labelled compound and at 1347(m) cm^{-1} for the ^{15}N-one could be assigned to the antisymmetric or symmetric N–O stretching of NO_2^-, and the antisymmetric N–O stretching of NO_3^-.

The elementary analyses and the IR spectra suggest that compound **1** is $[NO]_3[Co(C_{10}H_8NO)_2(NO_3)(NO_2)]$ containing monopositive cobalt ion. A number of nomopositive cobalt-complexes with π-acceptor ligands have been reported so far, and they are in general air-sensitive and diamagnetic.[7] On the other hand, as the ligands in compound **1** are not π-acceptor ones,[8] an electronic configuration of the cobalt ion in compound **1** is expected to be high-spin d^8. The effective magnetic moment of compound **1** was 3.7±0.1 BM (at 296 K), and was larger than the value, 2.8—3.5 BM observed for the first row transition-metal ions with high-spin d^8 configuration.[9] Hence, it is taken into consideration that compound **1** may be contaminated by paramagnetic substances such as the unreacted starting material or uncharacterized decom-

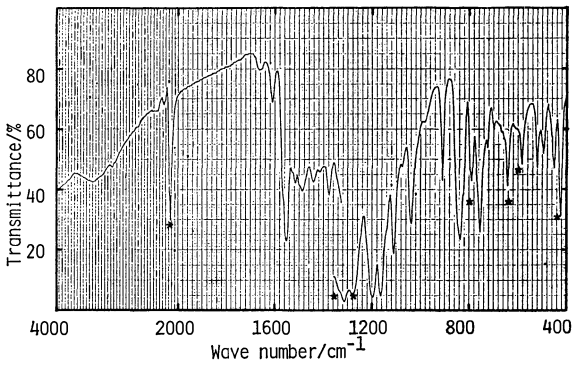

Fig. 1. IR spectrum of $[NO]_3[Co(C_{10}H_8NO)_2(NO_3)(NO_2)]$. * indicates the band shifted upon ^{15}N-substitution.

† Partly presented at 45th National Meeting of the Chemical Society of Japan, Tokyo, April 1982, Abstr., No. 1B37.

posed one, although it could not be confirmed.

After compound **1** had been filtered from the reaction solution stirred at *ca.* −20 °C, the solvent, dichloromethane, was removed in keeping the filtrate at lower than 0 °C to obtain violet product, $[Co(C_{10}H_8NO)_2(NO)_2]$ (**2**). Yield, 10%. Found: C, 53.6; H, 3.6; N, 12.3%. Calcd: C, 55.2; H, 3.7; N, 12.9%. Compound **2** was even more unstable than compound **1**, and could not be purified. The IR spectra showed that compound **2** was contaminated by compound **1**. The IR bands at 1840(vs) and 1760(vs) cm^{-1} shifted to 1805 and 1730 cm^{-1}, respectively, upon ^{15}NO-substitution. These bands could be assigned to the N–O stretching vibrations of the coordinating nitrosyl groups.[8] The wave number of the N–O stretching vibrations show that the formal oxidation number of the coordinating nitrosyl group is +I, and hence that of the cobalt is zero.[8] The N–O stretching vibrations for $[Fe(C_{10}H_8NO)(NO)_2]$ with the formal oxidation number of Fe^{-I} were observed at 1758 and 1685 cm^{-1}.[8] The N–O stretching bands for compound **2** are higher than those for the iron nitrosyl, which reflects that π^*-electron on the nitrosyl group is more drawn to the cobalt than to the iron due to difference of their nuclear charges.

The yields of compounds **1** and **2** were *ca.* 30 and 50%, respectively, in the case of stirring at *ca.* −20 °C for 1 d; the yield of compound **2** was larger than that of compound **1** in the initial stage of the reaction. Compound **2** reacted with nitrogen monoxide in dichloromethane to precipitate compound **1**. These suggest that $[Co(C_{10}H_8NO)_2]\cdot H_2O$ reacted with nitrogen monoxide to form compound **2**, and then it reacted further with nitrogen monoxide to precipitate compound **1** with liberation of dinitrogen oxide. However, it can not be denied that $[Co(C_{10}H_8NO)_2]\cdot H_2O$ reacted with nitrogen monoxide to produce compound **1** directly.

The Co^{II} in the starting material was reduced to Co^{I} or Co^{0} by nitrogen monoxide on the present study, while on the reaction of $[Co(C_9H_6NO)_2]$ with nitrogen monoxide, the Co^{II} was oxidized to Co^{III}.[4] The difference in the reaction of nitrogen monoxide with the cobalt ion seems to be due to electron-donating power of methyl groups in 2-methyl-8-quinolinolate ions.

A reaction of $[Co(C_{10}H_8NO)_2]\cdot H_2O$ with nitrogen monoxide in pyridine, 10 vol% pyridine–DMF, or DMF was tried on the same scale as in dichloromethane. In pyridine and the pyridine–DMF, $[Co(C_{10}H_8NO)_2]\cdot H_2O$ did not reacted with nitrogen monoxide, instead only the pyridine adduct being isolated. In DMF, $[Co(C_{10}H_8NO)_2]\cdot H_2O$ reacted with nitrogen monoxide to give a deep red solution with liberation of dinitrogen oxide. Deoxygenated diethyl ether (150 cm^3) was added to the solution to precipitate a russet product. However, the russet product did not give constant elementary analyses. The IR spectra of the compound was seemingly same as those of compound **1** except an addition of a 1660 cm^{-1} band assignable to the C–O stretching vibration of DMF to the spectra of compound **1**.

The authors wish to express their thanks to Dr. Mikio Tanaka of Nippon Medical School for measuring the mass spectra.

References

1) J. H. Enemark and R. D. Feltham, *Coord. Chem. Rev.*, **13**, 339 (1974).
2) K. G. Caulton, *Coord. Chem. Rev.*, **14**, 317 (1975).
3) J. A. McCleverty, *Chem. Rev.*, **79**, 53 (1979).
4) E. Miki, *Chem. Lett.*, **1980**, 835.
5) S. Pinchas and I. Laulight, "Infrared Spectra of Labelled Compounds," Academic Press, London (1971), Chap. 6; J. Laane and J. R. Ohlsen, "Characterization of Nitrogen Oxides by Vibrational Spectroscopy," in "Progress in Inorganic Chemistry," ed by S. J. Lippard, Wiley-Interscience, New York (1980), Vol. 27, pp. 465—513.
6) The band was partially interfered with by the strong band due to the coordinating 2-methyl-8-quinolinolate ions.
7) A. Sacco and R. Ugo, *J. Chem. Soc.*, **1964**, 3274; V. D. Bianco, S. Doronzo, and N. Gallo, "Inorganic Syntheses," ed by D. H. Busch, Wiley-Interscience, New York (1980), Vol. 20, pp. 206—208.
8) E. Miki, M. Motonaga, K. Mizumachi, T. Ishimori, and M. Katada, *Bull. Chem. Soc. Jpn.*, **55**, 2858 (1982), and references therein.
9) B. N. Figgis and J. Lewis, "The Magnetochemistry of Complex Compounds," in "Modern Coordination Chemistry: Principles and Methods," ed by J. Lewis and R. G. Wilkins, Interscience Publishers Inc., New York (1960), Chap. 6.

Mosomorphic Phenyl Benzoate and 1,3-Dioxane Derivatives Bearing Terminal Vinyl Group

Hiroyoshi KAMOGAWA,* Tomoki HIROSE, and Masato NANASAWA
Department of Applied Chemistry, Yamanashi University, Takeda 4, Kofu 400

(Received January 18, 1983)

Synopsis. 4-Alkylphenyl 2-chloro-4-(4-vinylbenzoyloxy) benzoates and 2-phenyl-1,3-dioxane derivatives with terminal vinyl groups were synthesized. Most of the novel compounds obtained possess characteristic mesomorphic ranges.

Some efforts have been made to incorporate vinyl groups into nematic liquid crystalline structures with intention of polymerizing the resulting vinyl monomers to obtain polymeric liquid crystals.[1] Besides the potentiality of these monomers as precursors to polymeric liquid crystals, the terminal rigid vinyl group bearing the sp^2-carbon atoms is itself expected to afford liquid-crystalline characteristics different from those of the corresponding compounds with alkyl and related flexible groups. With this intention, two series of novel vinyl compounds were prepared and their liquid-crystalline behavior was compared with that of the corresponding compounds with alkyl and related groups.

Vinyl compounds were prepared as follows:

(a)

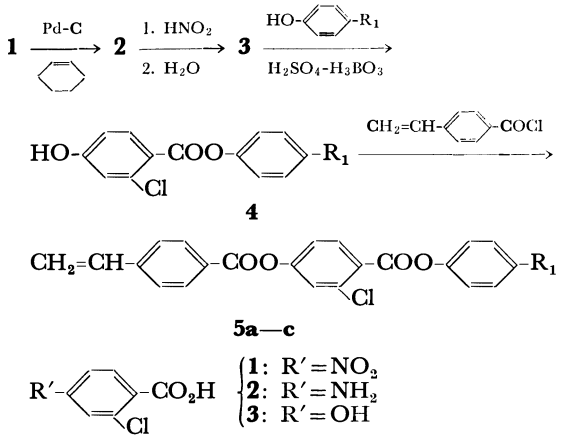

(b)

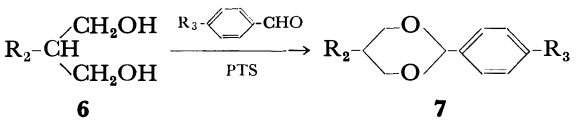

Tables 1 and 2 summarize the yields and mesomorphic ranges of compounds **5** and **7**, respectively, in comparison with those of the corresponding compounds with alkyl and related groups.

All of the vinyl compounds listed in these tables, among which **5a—c** and **7a—f** have not been listed in literature as yet, are stable up to the isotropic ranges, presumably due to their long rodlike structures.

In the phenyl benzoate series (Table 1), the replacement of the alkyl group as R by the rigid vinyl group generally causes smectic ranges to appear prior to nematic ones with elevation of temperature, which is not general in the conventional **5**-type esters.[2] The

TABLE 1. MESOMORPHIC RANGE OF BENZOATES (**5**)

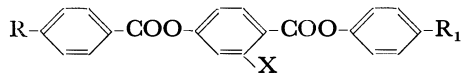

No.	R	R_1	X	Yield/%	Mesomorphic range/°C[a]
5a	CH_2=CH-	*s*-C_4H_9	Cl	46	C 50 S 70—72 N 96—99 I
5b	CH_2=CH-	*n*-C_4H_9	Cl	64	C 45 S 75—78 N 176—179 I
5c	CH_2=CH-	*n*-C_5H_{11}	Cl	67	C 50 S 71—74 N 171—174 I
5d[b]	CH_2=CH-	*s*-C_4H_9	H	—	C 88—90 N 169—170 I
5e[b]	CH_2=CH-	*t*-C_4H_9	H	—	C 115—118 S 128 N 151—154 I
5f[b]	CH_2=CH-	1,1-$Me_2C_3H_5$	H	—	C 102 N 107 I
5g[b]	CH_2=CH-	1-MeC_4H_8	H	—	C 79 S 96 N 130 I
5h[c]	*n*-C_3H_7	*n*-C_5H_{11}	H	—	C 78 N 188 I
5i[c]	*n*-C_3H_7	*n*-C_5H_{11}	Cl	—	C 57 N 130 I
5j[c]	*n*-C_4H_9	*n*-C_5H_{11}	H	—	C 75 N 179 I
5k[c]	*n*-C_4H_9	*n*-C_5H_{11}	Cl	—	C 46 N 118 I

a) C: Crystal, S: smectic, N: nematic, I: isotropic. The type of smectic texture is undetermined. b) Ref. 3. c) Ref. 2.

TABLE 2. MESOMORPHIC RANGE OF 1,3-DIOXANES (**7**)

No.	R_2	R_3	Yield/%	Mesomorphic range/°C
7a	CH_2=CH-C$_6$H$_4$-CH_2-	CN	26	C 60 N 105 I
7b	CH_2=CH-C$_6$H$_4$-CH_2-	*n*-C_3H_7O	30	C 55 S 65 I
7c	CH_2=CH-C$_6$H$_4$-CH_2-	*n*-$C_6H_{13}O$	34	C 65 S 75 I
7d	*n*-C_4H_9	CH_2=CH-	61	Turbid liq. at rt[a]
7e	*n*-C_7H_{15}	CH_2=CH-	49	Turbid liq. at rt[a]
7f	CH_2=CH-C$_6$H$_4$-CH_2-	CH_2=CH-	3	C 70 S 80 N 90 I
7g	*n*-C_4H_9	CH_3O	87	C 34 S 39 I
7h[b]	*n*-C_4H_9	*n*-C_3H_7O	61	C 43 I
7i[b]	*n*-C_7H_{15}	*n*-$C_6H_{13}O$	53	C 42 N 63 I
7j[b]	*n*-C_4H_9	CN	54	C 30 S 43 I
7k[b]	*n*-C_6H_{13}-C$_6$H$_4$-	CN	—	C 84 N 151 I
7l[b]	*n*-C_4H_9O-C$_6$H$_4$-	CN	—	C 121 N 202 I
7m[b]	*n*-C_4H_9O-C$_6$H$_4$-	*n*-$C_7H_{15}O$	—	C 134 S 166 I
7n[b]	*n*-C_4H_9	*n*-C_4H_9	—	C 44 N (40) I[c]
	n-C_6H_{13}	*n*-C_3H_7	—	C 35 S 41 I

a) rt: room temperature (25 °C). No clearing point could be determined exactly. b) Ref. 4. c) Monotropic.

absence of smectic textures for compounds **5d** and **5f** having no chlorine atom may indicate that the effects of chain length and branching in R_1 on the smectic alignments of the molecules are predominant in the absence of the chlorine atom. Higher N—I transition temperatures were also recognized for compounds with unbranched R_1 (**5b** and **5c** *vs.* **5i** and **5k**).

In the dioxane series (Table 2), compounds wtih the 4-vinylbenzyl group as R_2, in spite of the presence of the rigid vinyl end, have much lower mesomorphic ranges than those with the alkylphenyl or alkoxyphenyl group (**7a** *vs.* **7k** and **7l**; **7b** and **7c** *vs.* **7m**), although the alkylbenzyl group is required for exact structural comparison. Compounds **7d** and **7e** also have lower melting points (below room temperature) than **7n**, **7o**, **7g**, and **7h**.

These results indicate that the introduction of the terminal rigid vinyl group into these two series of compounds does not interfere with the formation of mesomorphic structures at all, leading to characteristic

mesomorphic behavior, when appropriate chemical structures are adopted.

Experimental

Infrared, ^{1}H NMR, and mass spectra were recorded on a Hitachi 215 spectrophotometer, a JNM-PMX 60 spectrometer, and a Hitachi RMU-6 spectrometer, respectively, under standard conditions. Elemental analyses were carried out with a Perkin-Elmer 250 instrument. Mesomorphic ranges were determined by means of either a Yamato MP-21 melting point apparatus or an optical microscope, both equipped with crossed polarizers.

2-Chloro-4-hydroxybenzoic Acid (3). A known preparative procedure[2] was modified as follows: 2-Chloro-4-aminobenzoic acid (**2**; mp 205—207 °C; 9 g, 52 mmol), prepared by heating 2-chloro-4-nitrobenzoic acid (**1**) in ethanol under reflux for 2 h in the presence of 5% Pd–C and a large excess of cyclohexene and purified by recrystallization from water, was dissolved in a solution of sodium nitrite (4 g, 58 mmol) and sodium carbonate (4 g, 40 mmol) in water (250 ml). A solution of concd sulfuric acid (30 ml) in water (200 ml) was then added with ice cooling, and the resulting solution was further stirred for 15 min. Urea (1 g) was next added, and stirring was further continued at 50—60 °C for 7 h. The reaction mixture was then extracted with ether (200 ml). The orange organic layer was washed with water, dried over anhyd sodium sulfate, and evaporated *in vacuo* to leave the crude product. Recrystallizations from water provided pure needles (mp 203—206 °C; lit,[2] 206—208 °C) in 50% yield: IR(KBr) 1680 (C=O), 1590, 1570 (aromatic), 1400, 1290, and 1240 (OH) cm^{-1}; NMR ($CDCl_3$+DMSO-d_6) δ=6.8 (m, 2H, ArH) and 7.7—8.7 (m, 3H, ArH+OH+COOH).

4-Butylphenyl 2-Chloro-4-(4-vinylbenzoyloxy)benzoate (5b). 4-Vinylbenzoyl chloride (0.8 g, 5.0 mmol) was added to a solution of 4-butylphenyl 2-chloro-4-hydroxybenzoate (**4**; 1.4 g, 4.7 mmol), prepared from 2-chloro-4-hydroxybenzoic acid (**3**) and 4-butylphenol,[3] and 4-*t*-butylcatechol (50 mg) in dry pyridine (25 ml). After stirring at room temperature for 18 h, the reaction mixture was poured into an ice–water mixture and the product was isolated by filtration. Three-time recrystallizations from ethanol gave pure crystals: Found: C, 71.58; H, 5.32%. Calcd for $C_{26}H_{23}O_4Cl$: C, 71.80; H, 5.33%. IR (KBr) 1740, 1590, 980, and 910 cm^{-1}; NMR ($CDCl_3$+DMSO-d_6) δ=0.9—3.0 (m, 9H, C_4H_9), 5.4 (d, 1H), 5.8 (d, 1H), 6.7 (q, 1H), 7.3 (t, 8H), and 8.1 (d, 3H); MS (rel intensity) 435 (M^+, 5) and 298 (100).

Compounds **5a** and **5c** were prepared in the same manner with satisfactory analytical data.

2-Vinylbenzyl-1,3-propanediol (6). To a solution of sodium (2.3 g, 100 mmol) in absolute ethanol (100 ml) was gradually added with ice cooling first diethyl malonate (16.0 g, 100 mmol) and then a mixture of vinylbenzyl chloride (Seibi Chem. Co.; *m*/*p*=60/40; 15.2 g, 100 mmol) and 4-*t*-butylcatechol (1 g) with exclusion of moisture. The mixture was heated under reflux until it became no longer alkaline (about 2 h). The reaction mixture was then purified by distillation under reduced pressure to afford diethyl vinylbenzylmalonate (bp, 135 °C/3 mmHg) (1 mmHg=133.322 Pa) in 22% yield. The malonate (13.8 g, 50 mmol) was then heated under reflux for 2 h in anhyd ether in the presence of $LiAlH_4$ (3.8 g) with exclusion of moisture. The reaction mixture was worked up as usual to afford compound **6** in 93% yield: Found: C, 75.34; H, 8.11%. Calcd for $C_{12}H_{16}O_2$: C, 75.00; H, 8.33%. IR ($CHCl_3$) 3350—3200 (OH), 990 and 900 (vinyl) cm^{-1}; NMR ($CDCl_3$) δ=5.2 (d, CH_2=), 5.7 (d, CH_2=), and 6.7 (q, =CH–).

2-(4-Cyanophenyl)-5-(4-vinylbenzyl)-1,3-dioxane (7a). A solution of compound **6** (1.92 g, 10 mmol), 4-cyanobenzaldehyde (1.31 g, 10 mmol), 4-*t*-butylcatechol (0.1 g), and *p*-toluenesulfonic acid (PTS; 0.1 g) in benzene (100 ml) was heated under reflux for 7 h with a Dean-Stark trap fitted. The reaction mixture was washed with aq Na_2CO_3, then with water, dried over anhyd Na_2SO_4, and concentrated on a rotary evaporator to afford the crude product. Column chromatography (Wakogel C-300) using benzene as eluent and subsequent several recrystallizations from methanol provided colorless needles: Found: C, 78.34; H, 6.53: N, 4.85 %. Calcd for $C_{20}H_{19}NO_2$: C, 78.66; H, 6.27; N, 4.59%. IR (KBr) 2220 (CN), 990, 910 (vinyl), and 820 (1,4-disubstitution) cm^{-1}; NMR ($CDCl_3$) δ=2.4 (s, 3H, CH_2, CH), 3.3—4.4 (m, 4H, $2CH_2O$), 5.3 (d, 1H, CH_2=), 5.5 (s, 1H, –CH<O–O–), 5.8 (d, 1H, CH_2=), 6.7 (q, 1H, –CH=), and 6.9—7.9 (8H, ArH); MS 305 (M^+).

Compounds **7b** and **7c** were prepared in the same manner with satisfactory analytical data.

2-(4-Vinylphenyl)-5-(4-vinylbenzyl)-1,3-dioxane (7f). The same reaction procedure as that for **7a** was applied to **6** and vinylbezaldehyde, synthesized from vinylbenzyl chloride by the Sommlet reaction,[5] to afford colorless crystals: Found: C, 77.47; H, 6.79%. Calcd for $C_{21}H_{22}O_2$: C, 77.56; H, 6.82%. IR (KBr) 990, 900 (vinyl), and 840 (1,4-disubst.) cm^{-1}; NMR ($CDCl_3$) δ=2.4 (s, 3H, CH_2, CH), 3.3—4.5 (m, 4H, $2CH_2O$), 5.3 (d, 2H, $2CH_2$=), 5.4 (s, 1H, –CH<O–O–), 5.8 (d, 2H, $2CH_2$=), 6.7 (q, 2H, 2–CH=), and 6.9—7.6 (m, 8H, ArH); MS 306 (M^+).

Compounds **7d** and **7e** were prepared in the same manner with satisfactory analytical data.

References

1) *E.g.*, "Liquid Crystalline Order in Polymers," ed by A. Blumstein, Academic Press, New York (1978).

2) J. P. van Meter and A. K. Seidel, *J. Org. Chem.*, **40**, 2998 (1975).

3) H. Kamogawa, M. Sekigawa, T. Nakano, S. Izawa, and M. Nanasawa, *Bull. Chem. Soc., Jpn.*, **52**, 3125 (1979).

4) D. Demus and H. Zaschke, Japan Patent Appl. No. 54-160916, Dec. 13, 1979.

5) H. Kamogawa, S. Okabe, and M. Nanasawa, *Bull. Chem. Soc. Jpn.*, **49**, 1917 (1976).

Synthesis of Diphenyl-substituted Flavonoid Compounds on Both Benzene Rings

Hisashi MATSUMURA,† Toshio TSUCHIYA,†† and Kimiaki IMAFUKU*

Department of Chemistry, Faculty of Science, Kumamoto University, Kurokami, Kumamoto 860

(Received January 29, 1983)

Synopsis. Condensation of *o*-hydroxyacetophenone and its 3- and 5-phenyl-substituted compounds with 2- or 4-methoxy-biphenyl-3-carbaldehyde gave six mono- and diphenyl-substituted 2′-hydroxychalcones (**5a—f**), which were cyclized with alkali to afford the flavanones. The chalcones **5a—f** were also converted to the corresponding flavones *via* chalcone bromides.

Little is known about phenyl-substituted flavonoid compounds, except for a few reports.[1] Previously, we reported the synthesis of 6- and 8-phenyl-substituted flavonoid compounds.[2] The present communication deals with the synthesis of flavonoid compounds having two phenyl groups in both benzene ring.

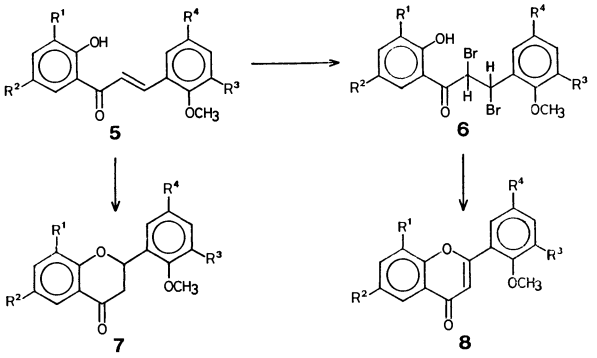

	R^1	R^2	R^3	R^4
a	H	H	H	Ph
b	H	H	Ph	H
c	H	Ph	H	Ph
d	H	Ph	Ph	H
e	Ph	H	H	Ph
f	Ph	H	Ph	H

Scheme 1.

Results and Discussion

In starting materials, 3-acetylbiphenyl-4-ol and -2-ol (**4b** and **4c**) were prepared by the method described in the previous paper.[2] 4-Methoxybiphenyl-3-carbaldehyde (**3a**) was prepared by Duff's formylation[3] and methylation of biphenyl-4-ol (**1a**). Similarly, 2-methoxybiphenyl-3-carbaldehyde (**3b**) was newly obtained by formylation and methylation of biphenyl-2-ol (**1b**).

The *o*-hydroxyacetophenones (**4a—c**) were condensed with methoxy-substituted biphenyl-3-carbaldehydes (**3a** and **3b**) to afford mono- or diphenyl-substituted 2′-hydroxychalcones (**5a—f**) in good yields. The spectral data are summarized in Table 1. In the UV spectra, an introduction of the phenyl group at the 3-position exhibited no appreciable effect. On the other hand, the spectra of the 5-phenyl-substituted chalcones exhibited remarkable differences. In the NMR spectra, the signal (δ *ca.* 3.4) for the methoxyl protons of the 3-phenyl-substituted chalcones (**5b**, **d**, and **f**) shifted towards higher magnetic field than that (δ *ca.* 3.9) for the 5-phenyl-substituted chalcones (**5a**, **c**, and **e**). This might be caused by ring-current in the neighboring phenyl group.

The bromination of the chalcones **5a—f** gave the corresponding dibromides **6a—f** in good yields. These characteristic data are listed in Table 2.

The chalcones **5a—f** were heated in the presence of alkali to cyclize to flavanones **7a—f**. These spectral data are summarized in Table 3. The UV spectra of **7a** and **7b** exhibited no appreciable effect of the phenyl group at the 3′- and 5′-positions. In the UV spectra of **7c—f**, the phenyl group at the 6- and 8-positions caused bathochromic shift of the maximum at longer wavelength band. The NMR spectra showed

Table 1. Characteristics for the chalcones **5**

Compd	Reaction time / h	Yield / %	Characteristic data
5a	30	81	Mp 155—156 °C; IR (KBr) 1635 cm^{-1} (C=O); UV (CH_3OH) 270 (log ε 4.40), 315 (4.24), 384 nm (4.21); NMR ($CDCl_3$) δ=3.90 (s, 3H, OCH_3), 6.95 (dm, 1H, J=8.5 Hz, 3-H), 6.8—7.95 (m, 12H), 8.22 (d, 1H, J=15.5 Hz, β-H), 12.86 (s, 1H, OH). Found: C, 80.04; H, 5.61%. Calcd for $C_{22}H_{18}O_3$: C, 79.98; H, 5.49%.
5b	15	94	Mp 135—136 °C; IR (KBr) 1640 cm^{-1} (C=O); UV (CH_3OH) 328 nm (log ε 4.34); NMR ($CDCl_3$) δ=3.42 (s, 3H, OCH_3), 6.7—8.0 (m, 13H), 8.22 (d, 1H, J=15.5 Hz, β-H), 12.78 (s, 1H, OH). Found: C, 79.76; H, 5.43%. Calcd for $C_{22}H_{18}O_3$: C, 79.98; H, 5.49%.
5c	30	77	Mp 212—213 °C; IR (KBr) 1640 cm^{-1} (C=O); UV (CH_3OH) 255 (log ε 4.72), 314 sh (4.08), 394 nm (3.98); NMR (DMSO-d_6) δ=3.94 (s, 3H, OCH_3), 7.0—8.3 (m, 17H), 7.16 (d, 1H, J=2.0 Hz, 6′-H), 13.28 (s, 1H, OH). Found: C, 82.75; H, 5.36%. Calcd for $C_{28}H_{22}O_3$: C, 82.73; H, 5.45%.
5d	30	92	Mp 121—122 °C; IR (KBr) 1635 cm^{-1} (C=O); UV (CH_3OH) 256 (log ε 4.58), 328 nm (4.35); NMR ($CDCl_3$) δ=3.41 (s, 3H, OCH_3), 7.03 (d, 1H, J=8.5 Hz, 3′-H), 7.1—7.9 (m, 15H), 8.04 (d, 1H, J=2.5 Hz, 6′-H), 8.28 (d, 1H, J=14.5 Hz, β-H), 12.76 (s, 1H, OH). Found: C, 82.64; H, 5.73%. Calcd for $C_{28}H_{22}O_3$: C, 82.73; H, 5.45%.
5e	30	62	Mp 117—118 °C; IR (KBr) 1630 cm^{-1} (C=O); UV (CH_3OH) 255 (log ε 4.48), 318 (4.33), 392 nm (4.26); NMR ($CDCl_3$) δ=3.90 (s, 3H, OCH_3), 6.8—7.1 (m, 2H), 7.2—8.0 (m, 15H), 8.26 (d, 1H, J=15.5 Hz, β-H), 13.48 (s, 1H, OH). Found: C, 82.80; H, 5.57%. Calcd for $C_{28}H_{22}O_3$: C, 82.73; H, 5.45%.
5f	30	72	Mp 159—160 °C; IR (KBr) 1635 cm^{-1} (C=O); UV (CH_3OH) 249 (log ε 4.48), 334 nm (4.43); NMR ($CDCl_3$) δ=3.34 (s, 3H, OCH_3), 6.89 (d, 1H, J=8.5 Hz, 4′-H), 7.0—7.9 (m, 15H), 7.92 (dd, 1H, J=8.0, 2.0 Hz, 6′-H), 8.29 (d, 1H, J=15.5 Hz, β-H), 13.35 (s, 1H, OH). Found: C, 82.91; H, 5.67%. Calcd for $C_{28}H_{22}O_3$: C, 82.73; H, 5.45%.

Table 2. Characteristics for the chalcone dibromides **6**

Compd	Yield / %	Mp θ_m/°C	IR (KBr) $\nu_{C=O}$/cm^{-1}	Formula	Found(Calcd) (%) C	H
6a	75	160(decomp)	1640	$C_{22}H_{16}O_3Br_2$	54.05 (53.90	3.71 3.70)
6b	60	110(decomp)	1640	$C_{22}H_{16}O_3Br_2$	53.93 (53.90	3.42 3.70)
6c	78	274—175.5	1630	$C_{28}H_{22}O_3Br_2$	59.41 (59.38	3.85 3.92)
6d	83	160(decomp)	1645	$C_{28}H_{22}O_3Br_2$	59.08 (59.38	3.81 3.92)
6e	98	155(decomp)	1635	$C_{28}H_{22}O_3Br_2$	**59.12** (59.38	**4.16** 3.92)
6f	100	175—178	1635	$C_{28}H_{22}O_3Br_2$	59.22 (**59.38**	**4.01** 3.92)

† Present address: Kumamoto Institute of Technology, Ikeda, Kumamoto 860.

†† Present address: Nagasaki-Prefectural Kenhoku Kogyo Shiken-jo, Hirota-cho, Sasebo, Nagasaki 859-32.

Table 3. Characteristics for the flavanones **7**

Compd	Reaction time h	Yield %	Characteristic data
7a	1.5	61	Mp 106.5—107.5 °C; IR (KBr) 1670 cm^{-1} (C=O); UV (CH_3OH) 257 (log ε 4.42), 319 nm (3.52); NMR($CDCl_3$) δ=2.87 (dd, 1H, J=18.0, 9.5 Hz, 3a-H), 2.99 (dd, 1H, J=18.0, 7.0 Hz, 3e-H), 3.80 (s, 3H, OCH_3), 5.83 (dd, 1H, J=9.5, 7.0 Hz, 2-H), 6.89 (d, 1H, J=9.5 Hz, 3'-H), 7.03 (d, 1H, J=7.0 Hz, 8-H), 7.2—7.7 (m, 8H), 7.85 (s, 1H, 6'-H), 7.91 (dd, 1H, J=7.0, 2.5 Hz, 5-H). Found: C, 79.77; H, 5.44%. Calcd for $C_{22}H_{18}O_3$: C, 79.98; H, 5.49%.
7b	2	40	Mp 113.5—114.5 °C; IR (KBr) 1685 cm^{-1} (C=O); UV (CH_3OH) 250 (log ε 4.35), 326 nm (3.54); NMR ($CDCl_3$) δ=2.89 (dd, 1H, J=16.0, 6.0 Hz, 3e-H), 3.05 (dd, 1H, J=16.0, 11.0 Hz, 3a-H), 3.29 (s, 3H, OCH_3), 5.84 (dd, 1H, J=11.0, 6.0 Hz, 2-H), 6.8—7.8 (m, 11H), 7.91 (dd, 1H, J=8.5, 2.5 Hz, 5-H). Found: C, 80.02; H, 5.51%. Calcd for $C_{22}H_{18}O_3$: C, 79.98; H, 5.49%.
7c	5	23	Mp 132—132.5 °C; IR (KBr) 1690 cm^{-1} (C=O); UV (CH_3OH) 251 (log ε 4.69), 343 nm (3.36); NMR ($CDCl_3$) δ=2.94 (dd, 1H, J=18.5, 9.5 Hz, 3a-H), 3.06 (dd, 1H, J=18.5, 7.0 Hz, 3e-H), 3.83 (s, 3H, OCH_3), 6.02 (dd, 1H, J=9.5, 7.0 Hz, 2-H), 6.90 (d, 1H, J=9.5 Hz, 3'-H), 7.09 (d, 1H, J=9.5 Hz, 8-H), 7.2—8.0 (m, 13H), 8.16 (d, 1H, J=2.5 Hz, 5-H). Found: C, 82.86; H, 5.73%. Calcd for $C_{28}H_{22}O_3$: C, 82.73; H, 5.45%.
7d	4	40	Mp 144—145 °C; IR (KBr) 1680 cm^{-1} (C=O); UV (CH_3OH) 248 (log ε 4.69), 346 nm (3.35); NMR ($CDCl_3$) δ=2.97 (dd, 1H, J=15.5, 5.5 Hz, 3e-H), 3.11 (dd, 1H, J=15.5, 10.0 Hz, 3a-H), 3.32 (s, 3H, OCH_3), 5.88 (dd, 1H, J=10.0, 5.5 Hz, 2-H), 7.07 (d, 1H, J=9.0 Hz, 8-H), 7.1—7.6 (m, 13H), 7.68 (dd, 1H, J=9.0, 3.0 Hz, 7-H), 8.16 (d, 1H, J=3.0 Hz, 5-H). Found: C, 82.47; H, 5.55%. Calcd for $C_{28}H_{22}O_3$: C, 82.73; H, 5.45%.
7e	1	30	Mp 174—175 °C; IR (KBr) 1700 cm^{-1} (C=O); UV (CH_3OH) 242 (log ε 4.50), 336 nm (3.63); NMR ($CDCl_3$) δ=2.7—3.4 (m, 2H, 3e, 3a-H), 3.81 (s, 3H, OCH_3), 5.96 (dd, 1H, J=9.5, 7.0 Hz, 2-H), 6.8—7.9 (m, 15H), 8.01 (dd, 1H, J=8.0, 2.0 Hz, 5-H). Found: C, 82.48; H, 5.45%. Calcd for $C_{28}H_{22}O_3$: C, 82.73; H, 5.45%.
7f	3	53	Mp 143.5—144.5 °C; IR (KBr) 1670 cm^{-1} (C=O); UV (CH_3OH) 241 (log ε 4.57), 336 nm (3.65); NMR ($CDCl_3$) δ=2.8—3.2 (m, 2H, 3e, 3a-H), 3.18 (s, 3H, OCH_3), 5.79 (dd, 1H, J=8.5, 8.5 Hz, 2-H), 6.9—7.7 (m, 15H), 7.93 (dd, 1H, J=8.0, 2.5 Hz, 5-H). Found: C, 82.58; H, 5.66%. Calcd for $C_{28}H_{22}O_3$: C, 82.73; H, 5.45%.

Table 4. Characteristics for the flavones **8**

Compd	Yield %	Characteristic data
8a	85	Mp 147—148 °C; IR (KBr) 1640 cm^{-1} (C=O); UV (CH_3OH) 255 (log ε 4.50), 344 nm (3.92); NMR ($CDCl_3$) δ=3.87 (s, 3H, OCH_3), 7.01 (d, 1H, J=8.5 Hz, 3'-H), 7.09 (s, 1H, 3-H), 7.1—7.8 (m, 9H), 7.96 (d, 1H, J=2.5 Hz, 6'-H), 8.15 (dm, 1H, J=8.0 Hz, 5-H). Found: C, 80.21; H, 4.93%. Calcd for $C_{22}H_{16}O_3$: C, 80.47; H, 4.91%.
8b	78	139—140 °C; IR (KBr) 1645 cm^{-1} (C=O); UV (CH_3OH) 248 (log ε 4.48), 304 nm (3.92); NMR ($CDCl_3$) δ=3.37 (s, 3H, OCH_3), 6.89 (s, 1H, 3-H), 7.0—7.8 (m, 11H), 8.19 (dm, 1H, J=8.0 Hz, 5-H). Found: C, 80.17; H, 5.12%. Calcd for $C_{22}H_{16}O_3$: C, 80.47; H, 4.91%.
8c	84	Mp 92—93 °C; IR (KBr) 1640 cm^{-1} (C=O); UV (CH_3OH) 267 (log ε 4.51), 338 nm (4.03); NMR ($CDCl_3$) δ=3.92 (s, 3H, OCH_3), 7.00 (d, 1H, J=8.5 Hz, 3'-H), 7.10 (s, 1H, 3-H), 7.1—7.9 (m, 13H), 8.03 (d, 1H, J=2.0 Hz, 6'-H), 8.40 (d, 1H, J=2.0 Hz, 5-H). Found: C, 83.21; H, 4.91%. Calcd for $C_{28}H_{20}O_3$: C, 83.15; H, 4.98%.
8d	73	Mp 127—128 °C; IR (KBr) 1640 cm^{-1} (C=O); UV (CH_3OH) 266 (log ε 4.64), 308 nm sh (4.23); NMR ($CDCl_3$) δ=3.36 (s, 3H, OCH_3), 6.96 (s, 1H, 3-H), 7.0—8.0 (m, 15H), 8.35 (d, 1H, J=2.5 Hz, 5-H). Found: C, 82.93; H, 5.04%. Calcd for $C_{28}H_{20}O_3$: C, 83.15; H, 4.98%.
8e	71	Mp 210—211 °C; IR (KBr) 1650 cm^{-1} (C=O); UV (CH_3OH) 254 (log ε 4.52), 295 nm (4.21); NMR ($CDCl_3$) δ=3.91 (s, 3H, OCH_3), 7.01 (d, 1H, J=8.0 Hz, 3'-H), 7.16 (s, 1H, 3-H), 7.2—7.8 (m, 13H), 7.85 (d, 1H, J=2.5 Hz, 6'-H), 8.22 (dd, 1H, J=8.0, 2.5 Hz, 5-H). Found: C, 82.89; H, 5.14%. Calcd for $C_{28}H_{20}O_3$: C, 83.15; H, 4.98%.
8f	67	Mp 172—173 °C; IR (KBr) 1640 cm^{-1} (C=O); UV (CH_3OH) 248 (log ε 4.54), 316 nm (4.23); NMR ($CDCl_3$) δ=3.22 (s, 3H, OCH_3), 7.11 (s, 1H, 3-H), 7.2—7.9 (m, 15H), 8.20 (dd, 1H, J=8.0, 2.5 Hz, 5-H). Found: C, 83.18; H, 5.01%. Calcd for $C_{28}H_{20}O_3$: C, 83.15; H, 4.98%.

the typical ABX pattern of 2-, 3e-, and 3a-protons.

The chalcone dibromides **6a—f** were treated with alkali to afford the corresponding flavones **8a—f** in good yields. The characteristic data are summarized in Table 4. In the UV spectra of **8a** and **8b**, the phenyl group at the 3'-position exhibited no effect but the phenyl group at the 5'-position exhibited bathochromic shift of the maximum at longer wavelength band. The NMR spectra showed a sharp singlet peak for the 3-H proton at δ 6.9—7.1. The methoxyl protons of the 3'-phenylflavones (**8b, d**, and **f**) were also observed in higher magnetic field than those of 5'-phenylflavones (**8a, c**, and **e**).

Experimental

The IR, UV, and NMR spectra were taken on a JASCO 403G, a Hitachi EPS-3T, and a Hitachi R-24 (60 MHz) spectrometer, respectively.

*2-Methoxybiphenyl-3-carbaldehyde (**3b**).* Methylation of 2-hydroxybiphenyl-3-carbaldehyde (**2b**)[4] (2.4 g, 12 mmol) with dimethyl sulfate (1.5 g, 12 mmol) in acetone (100 ml) in the presence of potassium carbonate (1.7 g, 12 mmol) gave 2-methoxybiphenyl-3-carbaldehyde (**3b**) as colorless crystals (from methanol). Yield, 2.0 g (73%). Mp 53—54 °C, IR (KBr) 1680 cm^{-1}. Found: C, 79.36; H, 5.43%. Calcd for $C_{14}H_{12}O_2$: C, 79.22; H, 5.70%.

*4-Methoxybiphenyl-3-carbaldehyde (**3a**).* This compound also prepared in a similar manner to the preparative method of **3b**. Yield, 86%. Mp 77—78 °C (lit,[5] 76.5—77 °C).

*The Chalcones **5a—f**.* A solution of 2-hydroxyacetophenone (**4a—c**) (2.4 mmol) and 2- or 4-methoxybiphenyl-3-carbaldehyde (**3a, b**) (500 mg, 2.4 mmol) in ethanol (3 ml) was stirred at 50 °C in the presence of 60% potassium hydroxide solution (2.5 ml). The mixture was slightly acidified with 3 M hydrochloric acid (1 M=1 mol dm^{-3}) extracted with ether, and worked up to give the chalcone **5a—f**.

*The Chalcone Dibromides **6a—f**.* A bromine (320 mg, 2 mmol) solution in carbon tetrachloride (2 ml) was added dropwise to a solution of the chalcone **5a—f** (500 mg) in carbon tetrachloride (5 ml) at room temperature to afford the chalcone dibromide **6a—f** (from acetone).

*The Flavanones **7a—f**.* A solution of the chalcone **5a—f** (330—400 mg, 1 mmol) in acetone (8 ml) was refluxed for 90 min in the presence of 1% potassium hydroxide solution (0.5 ml). The mixture was concentrated and allowed to stand overnight to give a precipitate, which was chromatographed on an alumina column to afford the flavanone **7a—f** (from acetone).

*The Flavones **8a—f**.* To a suspended solution of the chalcone dibromide **6a—f** (450 mg) in acetone (2 ml) was added 20% potassium hydroxide solution (1 ml) at room temperature. The mixture was diluted with water and slightly acidified with 3 M hydrochloric acid to give a precipitate, which was chromatographed on a silica-gel column to afford the flavone **8a—f** (from acetone).

We are grateful to Sanko Chemical Co., Ltd. for a supply of biphenyl-2-ol and -4-ol.

References

1) a) K.-K. Hsu and T.-S. Wu, *Tai-Wan Kó Huseh*, **27**, 19 (1973); b) K.-K. Hsu and J.-Y. Shi, *J. Chinese Chem. Soc.*, **19**, 45 (1972); **20**, 51 (1973).

2) H. Matsumura, T. Tsuchiya, T. Takeda, and K. Imafuku, *Bull. Chem. Soc. Jpn.*, **56**, 2037 (1983).

3) J. C. Duff, *J. Chem. Soc.*, **1941**, 547.

4) L. N. Ferguson and M. Calvin, *J. Am. Chem. Soc.*, **72**, 4324 (1950).

5) W. H. Linnell and H.-T. Smith, *J. Chem. Soc.*, **1958**, 908.

A Stereoselective Synthesis of (3*E*,5*Z*)-3,5-Tetradecadienoic Acid (Megatomoic Acid), the Sex Attractant of the Black Carpet Beetle†

Sadao Tsuboi, Toshihide Masuda, and Akira Takeda*

Department of Synthetic Chemistry, School of Engineering, Okayama University, Tsushima, Okayama 700

(Received February 27, 1983)

Synopsis. The total synthesis of (3*E*,5*Z*)-3,5-tetradecadienoic acid (megatomoic acid) is accomplished with 74% stereoselectivity through the use of stereoselective rearrangement of ethyl 3,4-tridecadienoate to ethyl (2*E*,4*Z*)-2,4-tridecadienoate with alumina and the extension of the carbon chain with methyl methylthiomethyl sulfone.

The sex attractant of the black carpet beetle, *Attagenus megatoma* (*Fabricius*), was identified as (3*E*,5*Z*)-3,5-tetradecadienoic acid (**1**) by Silverstein *et al.*,[1] to which they assigned the trivial name, megatomoic acid. The total synthesis of **1** has been reported by two groups.[2,3] In spite of reasonable overall yields, their sequences produce a significant amount of stereoisomers.[4] We present here a convenient and stereoselective synthesis of **1** starting with 1-undecyn-3-ol (**2**), which is superior to others[2,3] in its stereoselectivity (74%). The synthetic plan outlined in Scheme 1 was conceived with two strategic aspects: (1) to construct (2*E*,4*Z*)-2,4-dienoic ester (*e.g.*, ester **4**) from readily available materials, (2) to extend its carbon chain with the retention of the geometry. Ethyl (2*E*,4*Z*)-2,4-tridecadienoate (**4**), a key intermediate which fulfills these requirements was prepared in good yield by the highly stereoselective synthesis of (2*E*,4*Z*)-2,4-dienoates with alumina catalyst, as recently described by us.[5]

3,4-Dienoate **3** was prepared in 85% yield by the modified Claisen rearrangement of **2** with triethyl orthoacetate.[5] The thermal rearrangement of **3** with alumina gave 88% yield of (2*E*,4*Z*)-2,4-dienoate **4** of 97% purity.[6] A minor component was suggested to be (2*E*,4*E*)-isomer by comparison of the retention time of GLC.[5] Reduction of **4** with lithium aluminium hydride gave the corresponding alcohol **5** in 95% yield. The reaction of the allylic alcohol **5** with PBr_3 in petroleum ether afforded the desired bromide **6** in a reasonable yield. The conversion of **6** to carboxylate was attempted by various methods. The reactions of the Grignard reagent derived from **6** followed by carbonation resulted in the recovery of the starting material, or in the formation of unidentified materials. The reaction of **6** with sodium cyanide gave 3,5-tridecadienenitrile (**10**) in poor yields as stereoisomeric mixtures. The hydrolysis of **10** to the corresponding carboxylic acid, however, gave a trace of a carboxylic acid. On the other hand, the reaction of **6** with methyl methylthiomethyl sulfone[7] in the presence of butyllithium gave the corresponding product (**7**) with 81% purity in 46% yield,[8] while the reaction using a phase-transfer catalyst (PTC) resulted in poor yields of **7**. Compound **7** was oxidized with peracetic acid under mild conditions to give the sulfinyl sulfone **8**

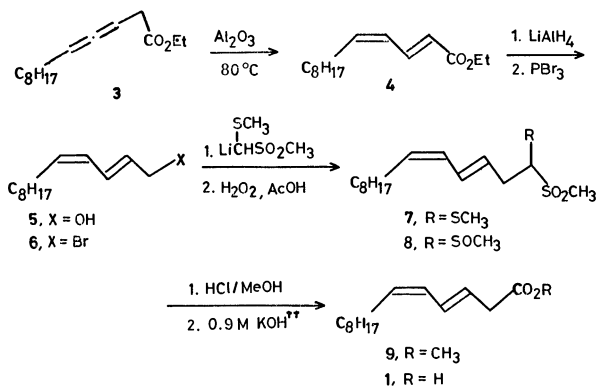

Scheme 1.

as an oil. The subsequent treatment of **8** with concentrated hydrochloric acid in methanol gave methyl (3*E*,5*Z*)-3,5-tetradecadienoate (**9**) with 74% purity, in 30% yield from **7**. The desired product, megatomoic acid **1**, was obtained in 89% yield by the hydrolysis of **9** with 0.9 M potassium hydroxide. The spectral properties of the synthesized **1** were identical with those reported for the natural product.[1]

Experimental

The boiling points are uncorrected. Elemental analyses were carried out by Mr. Eiichiro Amano of our laboratory. Analytical determinations by GLC were performed on a Hitachi Model 163 gas chromatograph fitted with 10% Silicone SE-30 on Chromosorb W column (3 mm o.d. × 1 m). IR spectra were taken on a Hitachi Model EPI-S2 or a JASCO Model A-102 spectrometer. ^{1}H NMR spectra (60 MHz) were recorded with a Hitachi R-24 apparatus. ^{13}C NMR spectra (25 MHz) were obtained with JEOL LTD. JNM-FX 100 apparatus equipped with FT facilities, using $CDCl_3$ as solvent. 1-Undecyn-3-ol (**2**) was prepared by a method in the literature:[5b,9] bp 89 °C (5 mm); 71% yield, improved over the previously reported value.[5b]

(2E,4Z)-2,4-Tridecadien-1-ol (5). To a stirred mixture of 160 mg (4.2 mmol) of lithium aluminium hydride and 10 ml of dry ether was added dropwise a solution of 1.0 g (4.2 mmol) of **4** in 10 ml of dry ether at −40 °C. After 1.5 h, the reaction mixture was quenched with 400 mg of ethyl acetate, and neutralized with 10% HCl. The organic layer was extracted with ether, and the combined ethereal layers were washed with water and dried over $MgSO_4$. Removal of the solvent gave 780 mg (95%) of **5** containing 9% (2*E*,4*E*)-isomer by ^{13}C NMR: IR (neat) 3350 (OH), 1640 cm^{-1} (C=C); ^{1}H NMR (CCl_4) δ=0.92 (broad t, 3 H, J=4 Hz, CH_3), 1.27 (broad s, 12 H, $(CH_2)_6$), 2.13 (m, 2H, =CHC$\underline{H}_2$C$_7$H$_{15}$), 3.64 (s, 1H, OH), 4.09 (d, 2H, J=5.5 Hz, C$\underline{H}_2$OH), 5.10—6.08 (m, 3H, C$\underline{H}$=C$\underline{H}$CH=C$\underline{H}$CH$_2$OH), 6.45 (dd, 1H, J=10 and 15 Hz, C$\underline{H}$=CHCH$_2$OH); ^{13}C NMR

† Presented at the 45th National Meeting of the Chemical Society of Japan, Tokyo, April 1982, Abstr. No. 2, p. 887.

†† 1 M = 1 mol dm^{-3}.

($CDCl_3$) δ=14.1 (d, CH_3), 22.8 (t, C_{12}), 27.9 (t, C_6), 29.4 (t), 29.6 (t), 29.8 (t), 32.0 (t, C_{11}), 63.0 (t, C_1), 126.6 (d, C_3), 128.0 (d, C_4), 132.0 (d, C_2), 132.6 (d, C_5). Found: C, 79.76; H, 12.08%. Calcd for $C_{13}H_{24}O$: C, 79.53; H, 12.32%.

(2E,4Z)-1-Bromo-2,4-tridecadiene (6). To a stirred solution of 600 mg (3.06 mmol) of **5** in 1.5 ml of petroleum ether was added dropwise a solution of 580 mg (2.15 mmol) of PBr_3 in 1.5 ml of petroleum ether at −15 °C for a period of 15 min. The mixture was stirred for 2 h at −15 °C and then overnight at room temperature. The reaction mixture was diluted with ice water (50 ml) and neutralized with dilute $NaHCO_3$. The organic layer was extracted with petroleum ether. The combined extracts were washed with water, and dried over $MgSO_4$. Removal of the solvent gave 624 mg (79%) of **6** as a clean oil: IR (neat) 1645 cm^{-1} (C=C); ^1H NMR (CCl_4) δ=0.92 (broad t, 3 H, J=4 Hz, CH_3), 1.25 (broad s, 12H, $(CH_2)_6$), 2.13 (m, 2H, =CH-C<u>H</u>$_2C_7H_{15}$), 3.91 (d, J=7.4 Hz, 2H, CH_2Br), 5.29—6.11 (m, 3H, C<u>H</u>=C<u>H</u>CH=C<u>H</u>CH_2Br), 6.47 (dd, 1H, J=10 and 15 Hz, C<u>H</u>=CHCH_2Br). Found: C, 60.47; H, 8.90 %. Calcd for $C_{13}H_{23}Br$: C, 60.23; H, 8.94%.

(3E,5Z)-1-Methylsulfonyl-1-methylthio-3,5-tetradecadiene (7). To a stirred solution of 342 mg (2.44 mmol) of methyl methylthiomethyl sulfone in 5 ml of dry THF was added dropwise 1.57 ml (2.43 mmol) of 1.55 M butyllithium (hexane) at −20 °C under a static N_2 atmosphere. The mixture was stirred for 90 min and then cooled at −65 °C. After gradual addition of 600 mg (2.32 mmol) of **6**, the mixture was stirred for 1 h at −65 °C and then for 12 h at 0 °C. It was poured into water (*ca.* 30 ml) and the organic layer extracted with ether. The dried ($MgSO_4$) ethereal layer was concentrated *in vacuo* to yield 765 mg of an oil. Column chromatography on silica gel (30 g) with hexane–ethyl acetate gave 337 mg (46%) of **7** as a clean, viscous oil containing 19% (3*E*,5*E*)-isomer by ^{13}C NMR:[10] IR (neat) 2910, 1300, 1160 cm^{-1} (SO_2); ^1H NMR ($CDCl_3$) δ=0.92 (broad t, 3 H, J=5 Hz, CH_3), 1.30 (broad s, 12H, $(CH_2)_6$), 1.9—2.5 (m, 2H, =CHC<u>H</u>$_2C_7H_{15}$), 2.33 (s, 3H, SCH_3), 2.60 (dd, 2H, J= 7 and 10 Hz, =CHC<u>H</u>$_2$CH<), 3.01 (s, 3H, SO_2CH_3), 3.62 (dd, 1H, J=4 and 10 Hz, >C<u>H</u>SO_2), 5.26—6.20 (m, 3H, C<u>H</u>=C<u>H</u>CH=C<u>H</u>CH_2CH<), 6.59 (dd, 1H, J=10 and 15 Hz, C<u>H</u>=CHCH_2CH<); ^{13}C NMR ($CDCl_3$) δ=14.1 (q, CH_3), 14.2 (q, CH_3), 22.7 (t, C_{13}), 27.8 (t, C_7), 29.2 (t), 29.4 (t), 29.6 (t), 30.3 (t, C_2), 31.9 (t, C_{12}), 36.7 (q, SO_2CH_3), 126.3 (d), 127.5 (d), 130.0 (d), 133.0(d). Found: C, 60.12; H, 9.54%. Calcd for $C_{16}H_{30}O_2S_2$: C, 60.33; H, 9.49%.

Methyl (3E,5Z)-3,5-Tetradecadienoate (9). A mixture of **7** (270 mg, 0.85 mmol), acetic acid (1.5 ml), and 35% hydrogen peroxide (0.1 ml, 1.1 mmol) was stirred for 2 d at room temperature in a dark room. The mixture was dissolved in CH_2Cl_2 and then treated with 3 g of potassium carbonate. After fitration, the filtrate was dried over $MgSO_4$. Removal of the solvents gave 254 mg of an oil, which was assumed to be (3*E*,5*Z*)-1-methylsulfonyl-1-methylsulfinyl-3,5-tetradecadiene (**8**).

A mixture of the above oil **8** (123 mg, 0.368 mmol), methanol (2 ml), and a catalytic amount of conc HCl was heated at reflux temperature for 6 h, and then poured into water (*ca.* 25 ml). The resulting mixture was extracted with ether, and the organic layer washed with water and dried over $MgSO_4$. Removal of the solvents yielded 100 mg of an oil which was purified by column chromatography on silica gel (4 g) with hexane–AcOEt as an eluent, giving 29 mg (30% from **7**, 32% from consumed **7**) of **9** (74% pure by ^{13}C NMR): ^{13}C NMR ($CDCl_3$) δ=14.0 (q, C_{14}), 22.6 (t, C_{13}), 27.7 (t, C_7), 29.2 (t), 29.4 (t), 29.5 (t), 31.8 (t, C_{12}), 38.0 (t, C_2), 51.8 (q, $CO_2\underline{C}H_3$), 124.3 (d), 127.5 (d), 129.2 (d), 132.4 (d), 172.0 (s, $\underline{C}O_2CH_3$). GLPC analysis [column temp, 150 °C; carrier gas, N_2 (1.0 kg/cm^2)] indicated that it consisted of two components with the retention times, 10.5 min (**9**, 74 parts) and 12.3 min (the (3*E*,5*E*)-isomer,[2] 26 parts). IR and ^1H NMR data of pure **9** obtained by preparative GLPC were identical with those in the literature.[2,3] Another fraction gave 15 mg of **7**, the spectral data of which were identical with those of the sample prepared above.

(3E,5Z)-3,5-Tetradecadienoic Acid (1). A mixture of 20 mg (0.084 mmol) of **9** purified by preparative GLPC and 0.3 ml of 0.9 M KOH in 90% MeOH was stirred at 25 °C for 5 h, and poured into cooled water. The mixture was acidified with 10% HCl, and the organic layer extracted with ether. The combined ethereal layers were washed with water and dried over $MgSO_4$. Removal of the solvent gave 17 mg (89%) of **1** as a viscous oil. IR and ^1H NMR data were identical with those of the authentic sample.[1]

This work was supported in part by a Grant-in-Aid No. 57470067 from the Ministry of Education, Science and Culture.

References

1) R. M. Silverstein, J. O. Rodin, W. E. Burkholder, and J. E. Corman, *Science*, **157**, 85 (1967).

2) J. O. Rodin, M. A. Leaffer, and R. M. Silverstein, *J. Org. Chem.*, **35**, 3152 (1970).

3) K. Yokoi and Y. Matsubara, *Kinki Daigaku Rikogakubu Kenkyu Hokoku*, **1979**, 65.

4) It is reported that the ratios of **1** to the isomers were 50/22 and 1/18, respectively. See Refs. 2 and 3.

5) a) S. Tsuboi, T. Masuka, H. Makino, and A. Takeda, *Tetrahedron Lett.*, **23**, 209 (1982); b) S. Tsuboi, T. Masuda, and A. Takeda, *J. Org. Chem.*, **47**, 4478 (1982).

6) The purity of **4** was improved over that reported in the previous paper (Ref. 5).

7) K. Ogura, M. Suzuki, and G. Tsuchihashi, *Bull. Chem. Soc. Jpn.*, **53**, 1414 (1980).

8) The reaction was accompanied with the compound supposed to be a disubstituted product (**11**) (30% yield).

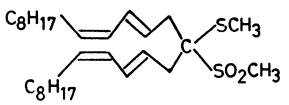

11

9) L. Brandsma, "Preparative Acetylenic Chemistry," Elsevier, Amsterdam (1971), p. 71.

10) Another fraction eluted earlier provided 180 mg (30%) of **11** as an oil: IR (neat) 1650, 1605, 1460, 1300, 1130 cm^{-1}; ^1H NMR ($CDCl_3$) δ=0.99 (broad t, 6 H, J=5 Hz, 2 CH_3), 1.26 (broad s, 28 H, 2 $(CH_2)_7$), 1.8—2.4 (m, 4H, 2 $C_7H_{15}C\underline{H}_2CH$=), 2.29 (s, 3H, SCH_3), 2.6—3.0 (m, 4H, 2 =CHC<u>H</u>$_2$C<), 3.03 (s, 3H, SO_2CH_3), 5.2—6.8 (m, 8H, olefin protons). Found: C, 70.11; H, 10.58%. Calcd for $C_{29}H_{52}O_2S_2$: C, 70.10; 10.55%.

Catalytic Epoxidation of Cyclohexene with *t*-Butyl Hydroperoxide in the Presence of Various Molybdenum Complexes

Masashi YAMAZAKI,† Hidetoshi ENDO,† Masato TOMOYAMA,† and Yasuhiko KURUSU*
Department of Chemistry, Faculty of Science and Technology, Sophia University, 7-1, Kioicho, Chiyoda-ku, Tokyo 102
(Received March 1, 1983)

Synopsis. A ligand can play an important role in the activity of the molybdenum-catalyzed epoxidation. Molybdenum complex was changed to the reactive intermediate through the reaction of catalyst with *t*-BuOOH. Oxalate, edta, and phenoxyl groups were selected as ligands. The phenoxyl group was most effective for the epoxidation. This effect was interpreted by the HSAB concept.

Epoxidations of olefins with hydroperoxide in the presence of molybdenum(VI) or (V) complexes have been reported by Trifilo *et al.*,[1] Sheldon,[2] and Gould *et al.*[3] Also, Henry presented a review about molybdenum compounds for epoxidation with hydroperoxide.[4]

Ziolkowski presented the oxalatomolybdenum(V) complex as a catalyst for epoxidation.[5] Mitchell[6] and Komura *et al.*[7] reported the properties and reactivity of oxalatomolybdenum(V) complexes. Ziolkowski *et al.* used oxalic, malonic, succinic, glutaric, adipic, oxoacid, water, pyridine, and anionites containing $-N(CH_3)_2$ and $-\overset{+}{N}(CH_3)_3\bar{Cl}$ groups as the ligands of the complex mentioned above.[8,9] In this paper, we report the relation between the reactivity and the ligand in case of epoxidation with molybdenum complexes.

1 was obtained in the usual way.[8] An exchange reaction of the ligand of oxalatomolybdenum(V) complex was carried out by the method reported by Komura and co-workers.[7] Epoxidation of cyclohexene with *t*-BuOOH was carried out in the presence of materials **1**—**8**. The reaction proceeded according to the reported scheme by Ziolkowski and Sobczak.[8,9] The results are shown in Table 1. Hydrazinium ion is more reactive than barium ion, proton, or pyridinium ion in the cationic ligands used in our experiments. Also, the complex with pyridine as the inner ligand shows higher reactivity. An induction period was observed in this case, since the formation of active intermediate was promoted by the reaction of *t*-BuOOH with oxalato complexes. The UV-spectrum of *t*-BuOOH and complex in benzene is shown in Fig. 1(a), where the absorption band is shown at 370 nm after 60 min. The time dependency of the spectrum of *t*-BuOOH–$H_2[Mo_2O_4(C_2O_4)_2(H_2O)_2]$ system is shown in Fig. 1(b). The maximum band was observed after 40 min. The formation of the reactive intermediate was inferred from Fig. 1(b).

Trifiro and co-workers reported the formation of the intermediate in the epoxidation of olefin with *t*-BuOOH and molybdenum complex.[1] They reported that when the bond between metal and ligand was stable, the activity of epoxidation was low. On the other hand, a weak bond complex was effective for the decomposition of hydroperoxide and the selectivity for epoxide became lower. Since Figs. 1(a) and (b) show that epoxides are obtained after the formation of an intermediate from *t*-BuOOH and molybdenum complex, it is interesting to apply method B[12] for molybdenum complex with ethylendiamintetraacetic acid (H_4edta), which is reported to be a stable compound by Trifiro.[1] The result obtained by method B is better than that obtained method A[12] in Table 2. After *t*-BuOOH and Mo^V–edta complex were allowed to react 4 h, cyclohexene was added to the reaction mixture. In the case of Mo^V–edta complex, pre-reaction of Mo^V–edta complex with *t*-BuOOH improved the reactivity. The high yield of cyclohexene epoxide was obtained at 73 °C. The rate of the epoxidation with Mo^{VI}–edta complex at 73 °C was slower than

TABLE 1. EPOXIDATION OF CYCLOHEXENE WITH *t*-BuOOH BY OXALATO-COMPLEXES

Oxalato complex	Method[a]	Reaction time/min	Cyclohexene conversion/%	Epoxide	
				Selectivity/%	Yield/%
1	A	360	56.5	90.6	51.6
2	B	360	98.4	61.8	60.8
3	A	150	83.4	95.8	79.9
	B	150	81.3	79.9	81.2
4	A	150	78.2	69.8	54.6
	B	150	78.3	73.1	57.2
5	A	150	78.1	79.7	62.2
	B	150	70.7	83.2	58.3
6	A	360	64.3	98.0	63.0
	B	150	65.2	88.5	57.7
7	A	360	86.4	99.8	87.7
8	A	360	80.0	80.8	65.1

Reaction conditions: cat 0.1 mmol, cyclohexene 50 mmol, *t*-BuOOH 50 mmol, benzene 50 cm³, temp 60 °C. a) See Ref. 12.

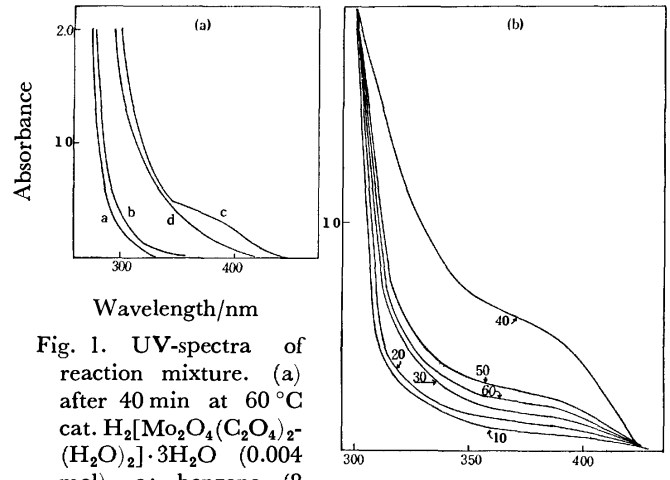

Fig. 1. UV-spectra of reaction mixture. (a) after 40 min at 60 °C cat. $H_2[Mo_2O_4(C_2O_4)_2(H_2O)_2]\cdot 3H_2O$ (0.004 mol), a: benzene (8 cm³), b: cyclohexene (0.82 mmol/cm³), c: *t*-BuOOH (0.82 mmol/cm³) in benzene, d: *t*-BuOOH (0.82 mmol/cm³), cyclohexene (0.82 mmol/cm³) in benzene. (b) After 10, 20, 30, 40, 50, 60 min at 60 °C, cat.; $H_2[Mo_2O_4(C_2O_4)_2(H_2O)_2]\cdot 3H_2O$ (0.004 mol) benzene (8 cm³), *t*-BuOOH (0.2 cm³).

† Present address: JASCO Co., Ltd. (M. Y.) Japar Glaxo Co., Ltd. (H. E.), ESSO Co., Ltd. (M. T.).

Table 2. Epoxidation by Mo^{V}- and Mo^{VI}-edta complex

Catalyst	Method[a]	Reaction conditions		Cyclohexene conversion/%	Epoxide	
		Time/min	Temp/°C		Selectivity/%	Yield/%
Mo(V)-edta	A	420	74	55.0	88.6	48.7
	B	240	73	74.7	101	83.6
Mo(VI)-edta	A	420	75	39.8	106	43.9

Reaction conditions: cat 0.1 mmol, cyclohexene 50 mmol, *t*-BuOOH 50 mmol, benzene 50 cm³. a) See Ref. 12.

Table 3. Epoxidation of cyclohexene by $Mo_2O_4(OH)_2(pHO)_2$ and $MoO_2(sala)_2$

Catalyst	Temp/°C	Decomp of *t*-BuOOH/%	Yield of epoxide/%	Selectivity/%
Mo-ph	8	18.3	15.7	86
	35	68.3	66.7	98
	44	81.3	76.9	94
$Mo(sala)_2$	10.5	31.0	33.6	100
	20	45.1	45.4	100
	31.5	66.3	55.5	84

Reaction conditions: cyclohexene 3.95 mmol/cm³, *t*-BuOOH 1.05 mmol/cm³, Mo-ph, 0.603 mmol/cm³, Mo-$(sala)_2$ 0.541 mmol/cm³, time 60 min, solv., benzene 25 cm³.

that of Mo^{VI}–edta complex, but the effect of pre-reaction of Mo^{VI}–edta complex with *t*-BuOOH was not observed. The epoxidation with Mo^{VI}–edta complex with *t*-BuOOH was not observed. The epoxidation with Mo^{V}–edta complex was inhibited in a polar solvent (*e.g.* CH_3CN). This may indicate the association of polar species to the active sites of the catalyst.

Ziolkowski proposed that the *t*-BuO–Mo bond participated in epoxidation, and that the coordination of the transition metal complexes for hydroxyl(–OH) or alkoxyl(–OR) oxygen occurred on active site.[13] Also, Sheldon reported that Mo^{VI}–1,2-diol system showed higher reactivity for epoxidation.[14] In order to examine this effect of the RO–Mo bond, di-μ-oxobis[hydroxo(oxo)(phenoxo) molybdenum(VI)] $[Mo_2O_4(OH)_2(phO)_2]$ and dioxobis[salicylaldehydatomolybdenum(VI)] $[MoO_2(sala)_2]$ were applied for the epoxidation of cyclohexene. The results are summarized in Table 2. In each case, selectivity and yield are higher than in other cases. The activation energy was calculated from the initial rates and at various reaction temperature (Table 3). $[Mo_2O_4(OH)_2(phO)_2]$ and $[MoO_2(sala)_2]$ were the most reactive catalysts, compared with the other catalysts cited in Table 3. The alkoxyl group is a hard base and the phenyl group is a soft base. Our information suggests that the phenoxyl group is a soft base and that MoO^{3+} is a hard acid.[10] So, it would be understandable that the interaction of Mo–Oph with *t*-BuOOH is most effective for the occurrence of an electrophilic hydroxyl group.

Experimental

Synthesis of Oxalate Complexes. $Ba[Mo_2O_4(C_2O_4)_2(H_2O)_2]\cdot 3H_2O$ (**1**), $H_2[Mo_2O_4(C_2O_4)(OH)_2(H_2O)_2]\cdot H_2O$ (**2**), $H_2[Mo_2O_4(C_2O_4)_2(py)_2]$ (**3**), $(pyH)_2[Mo_2O_4(C_2O_4)_2(H_2O)_2]\cdot 2H_2O$ (**4**), $(pyH)_2[Mo_2O_4(C_2O_4)_2(py)_2]$ (**5**), $Ba[Mo_2O_4(C_2O_4)_2(py)_2]\cdot 8H_2O$ (**6**), $HH_2NNH_3[Mo_2O_4(C_2O_4)_2(H_2O)_2]\cdot 2H_2O$ (**7**), $H_2[Mo_2O_4(C_2O_4)_2(H_2O)_2]\cdot 3H_2O$. These compounds were synthesized by the methods of Mitchell,[6] Komura,[7] and Ziolkowski.[8]

Di-μ-oxobis[oxohydroxydiphenoxymolybdate(VI)] $[Mo_2O_4(OH)_2phO_2]$, Dioxobis[salicylaldehydatomolybdenum(VI)] $[MoO_2(sala)_2]$: these compounds were synthesized in the usual way.

Table 4. Activation energy of the epoxidation with various Mo compound

Catalyst	Substrate	Solvent	E_a/kJ mol^{-1}
Mo-Powder	Cyclohexene	Cyclohexane	100.5[e]
Mo-y[a]	Cyclohexene	Cyclohexane	44.0[d]
MoO_3	Cyclohexene	Dioxane	112.6[e]
$MoO_2(DCC)_2$[b]	Cyclohexene	Benzene	79.5[f]
$MoO_2(acac)_2$	1-Octene	Benzene	50.2[g]
$Mo(CO)_6$	1-Octene	Benzene	79.5[h]
$MoO_2(oxine)_2$	Cyclohexene	Benzene	66.7[i]
Mo^{V}-edta	Cyclohexene	Benzene	104.7—49.0
Mo^{VI}-edta	Cyclohexene	Benzene	319.8—239.4
$Mo_2O_4(OH)_2(phO)_2$	Cyclohexene	Benzene	49.0
$MoO_2(sala)_2$	Cyclohexene	Benzene	72.4

a) Mo-y=Molybdenum peroxide obtained by the oxidation of molybdenum powder or molybdenum trioxide with hydrogen peroxide. b) DCC=Dimethyldithiocarbamate. c) Y. Kurusu *et al.*, *Nippon Kagaku Kaishi*, **1978**, 1262. d) S. Sawamura's graduation thesis(Sophia Univ.), (1977). e) F. Mashio *et al.*, *Yuki Gosei Kagaku Kyokai Shi*, **26**, 363 (1968). f) T. Ikawa *et al.*, *Sekiyu Gakkai Shi*, **18**, 492 (1975). g) N. Indictor and W. F. Brill, *J. Org. Chem.*, **30**, 2074 (1965). h) T. N. Baker *et al.*, *J. Org. Chem.*, **38**, 1145 (1973). i) F. Trifiro *et al.*, "Proceedings of 1st Int. Conf. on Chemistry and Uses of Mo 1973," (1974), p. 169.

References

1) F. Trifiro, P. Forzatti, and S. Preite, "Proceedings of Climax 1st International Conference on the Chemistry and Uses of Molybdenum," University of Reading, England (1973), p. 169.

2) R. A. Sheldon, *Recl. Trav. Chim. Pays-Bas*, **92**, 253 (1973).

3) C-C. Su, J. W. Reed, and E. S. Gould, *Inorg. Chem.*, **12**, 337 (1973).

4) P. M. Henry and G. L. Lange, "The Chemistry of Double-bonded Functional Groups," ed by Patai, John Wiley & Sons, London (1977), Part 2, p. 1028.

5) J. Sobczak and J. J. Ziolkowski, *Inorg. Chim. Acta*, **19**, 15 (1976).

6) P. C. H. Mitchell, *J. Inorg. Nucl. Chem.*, **26**, 1967 (1964).

7) A. Komura, Y. Ikeda, and H. Imanaga, *Bull. Chem. Soc. Jpn.*, **49**, 131 (1976).

8) J. Sobczak and J. J. Ziolkowski, *J. Less-Common Met.*, **54**, 149 (1977).

9) J. Sobczak and J. J. Ziolkowski, *J. Mol. Catal.*, **3**, 165 (1977/1978).

10) T.-S. Ho, "Hard and Soft Acids Base Principle in Organic Chemistry," Academic Press, New York (1977), p. 145.

11) W. G. Palmer, "Experimental Inorganic Chemistry," Cambridge Univ. Press, London (1962) p. 406.

12) *Method A*: The reactor was charged with a solvent, cyclohexene and catalyst. The mixture was kept at a reaction temperature for a given time with stirring, and then *t*-BuOOH was added. *Method B*: A mixture of a solvent, catalyst and *t*-BuOOH was stirred in the reactor at the reaction temperature for a given time, and the reaction was initiated by adding cyclohexene.

13) J. J. Ziolkowski, *Oxidation Commun.*, **2**, 307 (1982).

14) R. A. Sheldon, *Recl. Tav. Chim. Pays-Bas*, **92**, 367 (1973).

15) L. Pecsok and T. Sawer, *J. Am. Chem. Soc.*, **78**, 5496 (1956).

A Photochemically Induced Novel Ring Enlargement Reaction. Reaction of Cation Radical Derived from 7,8-Bis(methoxycarbonyl)-9-(4-methoxyphenyl)-1-phenyl-3,4-benzo-9-azabicyclo[4.2.1]non-3-ene-2,5-dione

Kazuhiro MARUYAMA* and Takuji OGAWA

Department of Chemistry, Faculty of Science, Kyoto University, Sakyo-ku, Kyoto 606

(Received March 11, 1983)

Synopsis. By oxidation with molecular oxygen, photoadducts **2** of 1-(4-methoxyphenyl)-1a-phenyl-1a,7a-dihydro-1*H*-naphth[2,3-*b*]azirine-2,7-dione with olefins afforded cation radicals of **2** in acidic media such as CF_3CO_2H or $HClO_4$. On irradiation, the cation radicals gave ring enlarged isomers 10,11-bis(methoxycarbonyl)-1-phenyl-3,4-benzo-7,8-(3′-methoxybenzo)-9-azabicyclo[4.3.2]undec-3,7-diene-2,5-dione (**3**).

Photochemical reactions of cation radicals derived from title compound **2a** and its analogues were investigated. The substrate **2a** is a photoproduct of 1-(4-methoxyphenyl)-1a,7a-dihydro-1*H*-naphth[2,3-*b*]azirine-2,7-dione (**1**) and dimethyl fumarate.[1] The compound **2a** was inert photochemically in a neutral solvent,[1,7] but under aerated conditions in an acidic medium it produced immediately the cation radical. Upon irradiation the cation radical showed a ring enlargement reaction of a novel type unknown so far.

Results and Discussion

Immediately after yellow crystals of **2a** (160 mg) were dissolved into 20 ml of 70% $HClO_4$ or trifloroacetic acid the solution became purple coloured and the purple solution showed a strong ESR signal at $g=2.0032$ (Fig. 1). The radical species had a life time of several days at 0 °C. Under deaerated conditions neither purple colour nor ESR signal was observed in the solution. Upon exposure of the solution to air, the purple coloured radical showing ESR signal gradually appeared (Fig. 2). Accordingly, oxygen is responsible for the formation of purple coloured radicals. In a neutral air saturated solvent such as acetonitrile or benzene, **2a**—**i** did not afford the purple coloured radical.

The same purple coloured radicals were produced by electrolysis of **2a** in an acetonitrile solution containing 20 mM (1 M=1 mol dm^{-3}) of triethylammonium perchlorate or in trifluoroacetic acid containing 0.1 M of sodium acetate at platinum anode. (The half wave potentials of **2** were tabulated in Table 1). Consequently, the purple coloured radicals are undoubtedly cation radicals of **2**.

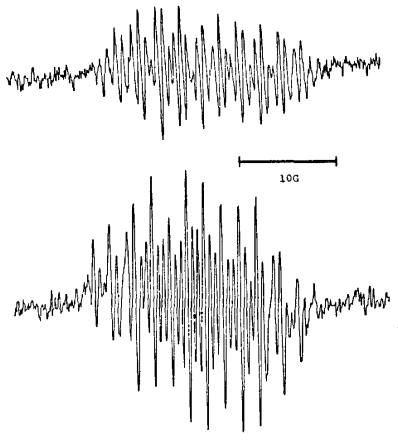

Fig. 1. ESR spectra of the cation radical of **2a** (upper) and **2b** (lower) in air saturated trifluoroacetic acid.

The reason why the cation radical could not be afforded in neutral solvents might be explained in terms of the pH dependence of oxidation reduction potential of oxygen. In acetonitrile the dominant reductive reaction of oxygen is

$$O_2 + e^- \rightleftharpoons O_2^-, \quad (1)$$

and the potential is −0.55 V (*vs.* normal hydrogen electrode (NHE)).[2] Thus produced super oxide anion affords hydrogen peroxide in a protic solvent.[3] In a strong acid such as 85% orthophosphoric acid, the domiannt reaction is reported to be

$$O_2 + 6H^+ + 4e^- \longrightarrow 2H_3O^+, \quad (2)$$

and the potential is +1.2 V (*vs.* NHE).[4] The potential difference between oxygen and **2a** can be calculated to be −1.50 V in acetonitrile and −0.14 V in trifluoroacetic acid.

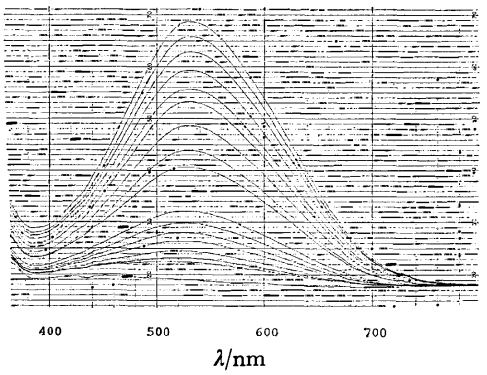

Fig. 2. Time dependent UV absorption change of **2a** in trifluoroacetic acid. Time interval is 5 min.

TABLE 1. STABLE CATION RADICALS

	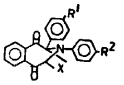			Generated by oxygen[a]		Half wave potentials/V[b]	
	R_1	R_2	X[c]	ESR *g*-value	UV λ_{max}/nm	CH_3CN (20 mM Et_4ClO_4)	CF_3CO_2H (0.1 M CH_3CO_2Na)
2a	H	OCH_3		2.0032	535	0.95	1.34
2b	H	OCH_3		2.0032	530	0.82	1.20
2c	H	OCH_3		2.0032	527	0.88	1.24
2d	H	OCH_3		2.0032	527	1.22[d]	0.88[d]
2e	H	OCH_3		e)	e)	0.83	1.23
2f	Cl	OCH_3		2.0032	535	0.98	1.34
2g	Cl	OCH_3		2.0032	545	0.84	1.21
2h	H	Cl		e)	e)	1.33[d]	1.66[d]
2i	H	Cl		e)	e)	1.20	1.53

a) Oxidized in CF_3CO_2H. b) Determined by cyclic voltammetry using Ag^+/Ag as a reference electrode, and then converted to those *vs.* NHE by using $E^\circ(Ag^+/Ag) = 0.2225$ V. c) E=CO_2CH_3. d) Irreversible. e) The cation radical was not observed.

Table 2. Photoreaction of cation radical of **2**

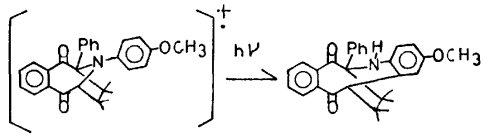

3

	Yield %	Mp θ_m/C°	Characteristic ^{1}H-NMR chemical shift of **3** (δ)
2a	21	237—239.5	3.06(s, 3H), 3.41(s, 3H), 3.64(s, 3H)
2b	0		
2c	34	Oil	2.96(s, 3H), 3.59(s, 3H)
2d	20	Oil	3.60(s, 3H)

fluoroacetic acid based on the assumption that the reduction potential of oxygen in trifluoroacetic acid is the same as that in 85% orthophosphoric acid. Thus, the electron transfer from **2** to oxygen is far more favourable in the acidic media than in the neutral solvent.[5]

Further, photochemical reactions of cation radicals of **2** were investigated. As a typical example, **2a** (160 mg) was dissolved into 20 ml of 70% $HClO_4$ and irradiated for 30 h at 0 °C with light of longer wavelength than 480 nm using a filter (Toshiba VY-48) in order to irradiate only the cation radical. Colourless crystals crystallized out of the solution by irradiation. The remaining solution changed its colour into pale brown. The crystals were collected, and the solution was diluted with 100 ml of water. The colourless solids precipitated was filtered, washed with water, and then dissolved in dichloromethane. The dichloromethane solution was dried with $MgSO_4$ and passed through a short column of alumina using dichloromethane as an eluent. On standing the solution over nights at room temperature (≈25 °C) colourless crystals (mp 237—239.5 °C) were precipitated out. Total yield of the crystals was 21.0%. The remaining was a dark brown tarry matter. The structure of the product was compatible with **3a** depicted in Scheme 1.[8]

Since the HOMO of cation radical of **2a—i** presumably is nitrogen n-orbital and the LUMO might be π^* of *N*-aryl group, an electron at the nitrogen n-orbial may transfer to the π^* of *N*-aryl group on irradiation. As a result the π system of *N*-aryl group is charged in negative and nitrogen is doubly charged in positive. This charge separation is presumably a driving force of the rearrangement.

This type of the photochemical reaction is unique, because the photochemical reaction of cation radical has been scarcely reported.[6]

Experimental

Apparatus. ^{1}H-NMR spectra were recorded on a JEOL PS-100 spectrometer. Mass spectra were recorded on a Hitachi M-52 mass spectrometer. Infrared spectra were taken on a JASCO-402G spectrometer. UV-spectra were taken on a Shimadzu UV-200. Electron spin resonance spectra were taken on a JEOL PE-3X. Elemental analyses were performed at the microanalytical laboratory of Kyoto University. Melting points were measured on a Yanagimoto micro melting point apparatus and uncorrected.

Materials. Compound **1** was prepared from 2-phenyl-1,4-naphthoquinone and 4-methoxyphenylazide as reported previously.[1] Photochemical production of **2** is reported elsewhere.[7] Perchloric acid 70% was purchased from Nakarai Chemicals, LTD., and used without further purification. Trifluoroacetic acid was purchased from Nakarai Chemicals, LTD., and dried over phosphorous pentaoxide and distilled.

Physical Properties of 3. **3a**: ^{1}H-NMR ($CDCl_3$) δ= 3.06(3H, s, CO_2CH_3), 3.41 (3H, s, CO_2CH_3), 3.64 (3H, s, $NC_6H_5OCH_3$), 4.05 (1H, d, J=7 Hz), 4.48 (1H, d, d, J= 7.0, 8.5 Hz), 4.56 (1H, s, NH), 5.09 (1H, d, J=8.5 Hz), 6.54 (2H, d, J=9.0 Hz), 6.88 (1H, d, J=9 Hz), 7.2—8.0 (9H, m); IR (KBr) 3400 (NH), 1732, 1705, 1682 cm^{-1}; MS (16 eV) *m/e* (rel intensity) 501 (M^+; 100). Found: C, 69.75; H, 5.32; N, 2.87%. Calcd; C, 69.73; H, 5.05; N, 2.80%. Mp 237—239.5 °C.

3c: ^{1}H-NMR ($CDCl_3$) δ=1.56 (1H, s), 2.0 (1H, d, d, ABq, J=3, 10, and 15 Hz), 2.7 (1H, D, D, ABq, J=9, 5, and 15 Hz), 2.94 (3H, s), 3.60 (3H, s), 3.6 (1H, m), 4.76 (1H, d, d, J=3, 9 Hz), 6.4—6.5 (2H, m), 6.8—6.9 (1H, m), 7.1—7.5 (8H, m), 7.7—7.9 (1H, m); IR ($CDCl_3$) 3500, 2960, 1780, and 1690 cm^{-1}; MS (16 eV) *m/e* (rel intensity) 441 (M^+; 100). Found: C, 73.27; H, 5.42; N, 3.06%. Calcd: C, 77.46; H, 5.25; N, 3.17%. Colourless oil. Bp *ca.* 200 °C (1.3 Pa, the Kugelrohr distillation apparatus).

3d: ^{1}H-NMR ($CDCl_3$) δ=1.60 (1H, s), 2.05 (1H, m), 2.70 (1H, m), 3.65 (3H, s), 3.6 (1H, m), 4.80 (1H, d, d, J=4, 10 Hz), 6.4—6.5 (2H, m), 6.8—6.9 (1H, m), 7.1—7.5 (8H, m), 7.7—7.9 (1H, m); IR ($CDCl_3$) 3500, 2200, 1780, and 1690 cm^{-1}; MS (16 eV) *m/e* (rel intensity) 408 (M^+; 100). Found, C, 76.70; H, 4.82; N, 6.79%. Calcd C, 76.46; H, 4.94; N, 6.86%. Colourless oil. Bp *ca.* 200 °C (1.3 Pa the Kugelrohr distillation apparatus).

References

1) K. Maruyama and T. Ogawa, *Chem. Lett.*, **1981**, 1027.

2) M. E. Poever and B. S. White, *J. Chem. Soc., Chem. Commun.*, **10**, 183 (1965).

3) E. Seyb and J. Klemberg, *Anal. Chem.*, **23**, 115 (1951).

4) D. Bauer and J. P. Beck, *J. Electroanal. Chem.*, **40**, 233 (1972); A. J. Appleby, *J. Electrochem. Soc.*, **117**, 328 (1970).

5) Equation 2 in trifluoroacetic acid is consistent with unsuccessful detection of hydrogen peroxide in cation radical solution of **2a** in trifluoroacetic acid examined by the method developed by I. R. Cohen and his co-workers. (I. R. Cohen and T. C. Purcell, *Anal. Chem.*, **39**, 131 (1967). I. R. Cohen, T. C. Purcell, and A. P. Altschuller, *Environ. Sci. Technol.*, **1**, 247 (1967).)

6) Photochemistry of organic cation radical was first reported in 1972 by V. D. Parker and his co-workers (U. Suanholm and V. D. Parker, *J. Am. Chem. Soc.*, **94**, 5507 (1972)). However, since then only a few studies have been reported on this area and very poor examples of the reactions are known (J. C. Moutet and G. Reverdy, *Tetrahedron Lett.*, **26**, 2389 (1979). J. C. Moutet and G. Reverdy, *J. Chem. Soc., Chem. Commun.*, **1982**, 654.).

7) K. Maruyama and T. Ogawa, *J. Org. Chem.*, to be published.

8) None of **3** was detected when the cation radical solution was left in the dark for a week, but only a dark tarry matter was produced.

The Reaction of Olefins with Malonic Acid in the Presence of Manganese(III) Acetate

Nobuyuki Ito, Hiroshi Nishino, and Kazu Kurosawa*

Department of Chemistry, Faculty of Science, Kumamoto University, Kurokami 2-39-1, Kumamoto 860

(Received May 9, 1983)

Synopsis. The reaction of 1,1-diphenylethene with malonic acid in the presence of manganese(III) acetate gave 3,3,8,8-tetraphenyl-2,7-dioxaspiro[4.4]nonane-1,6-dione and 4,4-diphenyl-2-(2,2-diphenylethenyl)-4-butanolide. Similar reactions with 1,1-bis(4-methoxyphenyl)ethene, methylenecyclohexane, 2-phenylpropene, 1-octene, and cyclohexene yielded the corresponding 2,7-dioxaspiro[4.4]nonane-1,6-diones.

The formation of γ-lactone in the reaction of olefins with manganese(III) acetate (MA) in acetic acid (AcOH) has been reported.[1] Similar α-substituted γ-lactone formations have been observed when the reaction was carried out in the presence of propionic acid,[2] cyanoacetic acid, isobutyric acid, and succinic acid.[1] These results led us to examine the reaction of olefins with malonic acid in the presence of MA. When a mixture of 1,1-diphenylethene (**1a**) and malonic acid was oxidized with MA in AcOH, 3,3,8,8-tetraphenyl-2,7-dioxaspiro[4.4]nonane-1,6-dione (**2a**), 4,4-diphenyl-2-(2,2-diphenylethenyl)-4-butanolide (**3**), and benzophenone (**4**) were obtained. 1,1-Bis(4-methoxyphenyl)ethene (**1b**) and methylenecyclohexane (**1c**) gave the corresponding 2,7-dioxaspiro[4.4]nonane-1,6-diones (**2b** and **2c**). The reactions of 2-phenylpropene (**1d**), styrene (**1e**), and 1-octene (**1f**) yielded three isomeric 2,7-dioxaspiro[4.4]nonane-1,6-diones, (**2d'**, **2d''**, **2d'''**), (**2e'**, **2e''**, **2e'''**), and (**2f'**, **2f''**, **2f'''**). Their configurations could be determined on the basis of ^{1}H-NMR spectral analyses. The reaction of cyclohexene (**1g**) with malonic acid in the presence of MA gave cyclohexenyl acetate (**5**) and a mixture of dodecahydro-3,3'(2*H*,2'*H*)-spirobi[benzofuran]-2,2'-diones (**2g'**, **2g''**, and **2g'''**)(27%). In contrast to disubstituted olefins, the reaction of 1,1,2-triphenylethene (**1h**) with malonic acid in the presence of MA gave 1,1,2-triphenyl-1,2-ethanediol 2-acetate (**6**) and 3,4,4-triphenyl-4-butanolide (**7**).

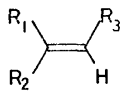

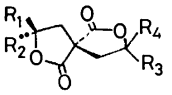

1a $R_1=R_2=$Ph, $R_3=$H
1b $R_1=R_2=C_6H_4OCH_3$, $R_3=$H
1c $R_1=R_2=-(CH_2)_5-$, $R_3=$H
1d $R_1=$Ph, $R_2=CH_3$, $R_3=$H
1e $R_1=$Ph, $R_2=R_3=$H
1f $R_1=$hexyl, $R_2=R_3=$H
1g $R_1=R_3=-(CH_2)_4-$, $R_2=$H

2a $R_1=R_2=R_3=R_4=$Ph
2b $R_1=R_2=R_3=R_4=C_6H_4OCH_3$
2c $R_1=R_2=-(CH_2)_5-$, $R_3=R_4=-(CH_2)_5-$
2d' $R_1=R_4=$Ph, $R_2=R_3=CH_3$
2d'' $R_2=R_3=$Ph, $R_1=R_4=CH_3$
2d''' $R_1=R_3=$Ph, $R_2=R_4=CH_3$
2e' $R_1=R_4=$Ph, $R_2=R_3=$H
2e'' $R_2=R_3=$Ph, $R_1=R_4=$H
2e''' $R_1=R_3=$Ph, $R_2=R_4=$H
2f' $R_1=R_4=$hexyl, $R_2=R_3=$H
2f'' $R_2=R_3=$hexyl, $R_1=R_4=$H
2f''' $R_1=R_3=$hexyl, $R_2=R_4=$H

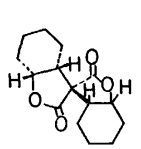

2g'

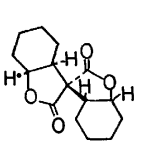

2g''

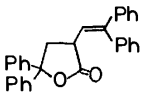

3

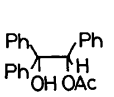

6

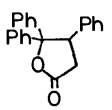

7

Experimental

Reaction of Olefins with Malonic Acid in the Presence of MA. To a heated solution of olefin (2 mmol) and malonic acid (1 mmol) in AcOH (20 ml), MA[6] (4 mmol) was added. The solution was heated under reflux for 1—5 min. After water (100 ml) being added, the mixture was extracted with chloroform or dichloromethane. The solvent was removed *in vacuo* and the resulting crude product was separated on TLC with chloroform or benzene as the developing solvent, and in the cases of **2f** and **2g** further separation was made by HPLC, eluting with aqueous methanol.

Oxidation Products from 1,1-Diphenylethene[7] *(**1a**). 3,3,8,8-Tetraphenyl-2,7-dioxaspiro[4.4]nonane-1,6-dione (**2a**)*: Colorless needles: mp 284.5—285.0 °C (from benzene); 84% yield; IR ($CHCl_3$) 1770 (C=O) and 1793 cm^{-1} (C=O); ^{1}H-NMR ($CDCl_3$) δ=2.62 (2H, d, J=13.5 Hz, 2×-HCH-), 3.03 (2H, d, J=13.5 Hz, 2×-HCH-), 7.24 (10H, s, 2×Ph), and 7.35 (10H, s, 2×Ph). Found: C, 80.87; H, 5.47%. Calcd for $C_{31}H_{24}O_4$: C, 80.85; H, 5.25%.

*4,4-Diphenyl-2-(2,2-diphenylethenyl)-4-butanolide (**3**)*: Colorless prisms; mp 165—166 °C (methanol); 5% yield; IR ($CHCl_3$) 1772 cm^{-1} (C=O); ^{1}H-NMR ($CDCl_3$) δ=2.66 (1H, dd, J=12.7 and 11.4 Hz, -HCH-), 3.12 (1H, dd, J=7.8 and 12.7 Hz, -HCH-), 3.51 (1H, m, -CH<), 6.62 (1H, d, J=8.8 Hz, =CH-), and 7.01—7.41 (20H, m, 4×Ph). Found: *m/z* 416.17511. Calcd for $C_{30}H_{24}O_2$: M, 416.17763.

*Benzophenone (**4**)*: Colorless plates; mp 47—48 °C (methanol); 1%.

Oxidation Product of 1,1-Bis(4-methoxyphenyl)ethene[8] *(**1b**). 3,3,8,8-Tetrakis(4-methoxyphenyl)-2,7-dioxaspiro[4.4]nonane-1,6-dione (**2b**)*: Amorphous solid (methanol); 84% yield; IR ($CHCl_3$) 1768 (C=O) and 1790 cm^{-1} (C=O); ^{1}H-NMR ($CDCl_3$) δ=2.54 (2H, d, J=13.0 Hz, 2×-HCH-), 2.94 (2H, d, J=13.0 Hz, 2×-HCH-), 3.72 (6H, s, 2×OCH_3), 3.80 (6H, s, 2×OCH_3), and 6.65—7.30 (16H, m, aromatic). Found: *m/z* 580.20720. Calcd for $C_{35}H_{32}O_8$: M, 580.20972.

Oxidation Product of Methylenecyclohexane[9] *(**1c**). 16,19-Dioxatrispiro[5.1.1.5.2.2]nonadecane-17,18-dione (**2c**)*: Colorless plates; mp 165—166 °C (methanol); 27% yield; IR ($CHCl_3$) 1758 (C=O) and 1774 cm^{-1} (C=O); ^{1}H-NMR ($CDCl_3$) δ=1.0—2.4 (20H, 2×-$(CH_2)_5$-), 2.11 (2H, d, J=13 Hz, 2×-HCH-), 2.63 (2H, d, J=13 Hz, 2×-HCH-). Found: *m/z* 292.17128. Calcd for $C_{17}H_{24}O_4$: M, 292.16746.

Oxidation Products from 2-Phenylpropene[10] (**1d**). (3R*, 5R*,8R*)-3,8-Dimethyl-3,8-diphenyl-2,7-dioxaspiro[4.4]nonane-1,6-dione (**2d'**): Colorless needles; mp 162—163 °C (methanol); 10% yield; IR ($CHCl_3$) 1768 (C=O) and 1785 cm^{-1} (C=O); ^{1}H-NMR ($CDCl_3$) δ=1.75 (6H, s, 2×CH_3), 2.17 (2H, d, J=13.4 Hz, 2×-HCH-), 2.68 (2H, d, J=13.4 Hz, 2×-HCH-), 7.14—7.43 (10H, m, 2×Ph); HPLC R_t (retention time)(eluent) 12.6 min (70% aqueous methanol). Found: m/z 336.12992. Calcd for $C_{21}H_{20}O_4$: M, 336.13600.

(3S*,5R*,8S*)-3,8-Dimethyl-3,8-diphenyl-2,7-dioxaspiro[4.4]-nonane-1,6-dione (**2d''**): Colorless needles; mp 218—219 °C (methanol); 19% yield; IR ($CHCl_3$) 1768 (C=O) and 1789 cm^{-1} (C=O); ^{1}H-NMR ($CDCl_3$) δ=1.77 (6H, s, 2×CH_3), 2.72 (2H, d, J=13.4 Hz, 2×-HCH-), 3.24 (2H, d, J=13.4 Hz, 2×-HCH-), and 7.34—7.45 (10H, m, 2×Ph); HPLC R_t 8.3 min (70% aqueous methanol). Found: m/z 336.13550. Calcd for $C_{21}H_{20}O_4$: M, 336.13600.

(3R*,5R*,8S*)-3,8-Dimethyl-3,8-diphenyl-2,7-dioxaspiro[4.4]-nonane-1,6-dione (**2d'''**): Colorless plates; mp 98.5—99.5 °C (methanol); 39% yield; IR ($CHCl_3$) 1768 (C=O) and 1785 cm^{-1} (C=O); ^{1}H-NMR ($CDCl_3$) δ=1.66 (3H, s, CH_3), 1.86 (3H, s, CH_3), 2.08 (1H, d, J=13.2 Hz, -HCH-), 2.79 (1H, d, J=13.5 Hz, -HCH-), 2.83 (1H, d, J=13.2 Hz, -HCH-), 3.20 (1H, d, J=13.5 Hz, -HCH-), 7.32 (5H, m, Ph), and 7.37 (5H, m, Ph); HPLC R_t 10.5 min (70% aqueous methanol). Found: C, 75.19; H, 6.02%. Calcd for $C_{21}H_{20}O_4$: C, 74.98; H, 5.99%.

Oxidation Products from Styrene (**1e**). (3R*,5R*,8R*)-3,8-Diphenyl-2,7-dioxaspiro[4.4]nonane-1,6-dione (**2e'**): Colorless plates; mp 162—163 °C (methanol); 9% yield; IR ($CHCl_3$) 1770 (C=O) and 1788 cm^{-1} (C=O); ^{1}H-NMR ($CDCl_3$) δ=2.23 (2H, dd, J=13.5 and 9.0 Hz, 2×-HCH-), 3.09 (2H, dd, J=13.5 and 6.5 Hz, 2×-HCH-), 5.93 (2H, dd, J=9.0 and 6.5 Hz, 2×-CH<), and 7.33 (10H, s, 2×Ph); HPLC R_t 9.2 min (70% aqueous methanol). Found: m/z 308.10706. Calcd for $C_{19}H_{16}O_4$: M, 308.10486.

(3S*,5R*,8S*)-3,8-Diphenyl-2,7-dioxaspiro[4.4]nonane-1,6-dione (**2e''**): Colorless needles; mp 236—237 °C ($CHCl_3$); 30% yield; IR ($CHCl_3$) 1762 (C=O) and 1782 cm^{-1} (C=O); ^{1}H-NMR ($CDCl_3$) δ=2.87 (2H, m, 2×-HCH-), 2.79 (2H, m, 2×-HCH-), 5.50 (2H, t, J=8.0 Hz, 2×-CH<), and 7.50 (10H, s, 2×Ph); HPLC R_t 6.3 min (70% aqueous methanol). Found: m/z 308.10564. Calcd for $C_{19}H_{16}O_4$: M, 308.10486.

(3R*,5R*,8S*)-3,8-Diphenyl-2,7-dioxaspiro[4.4]nonane-1,6-dione (**2e'''**): Colorless needles; mp 185—186 °C (benzene); 40% yield; IR ($CHCl_3$) 1768 (C=O) and 1786 cm^{-1} (C=O); ^{1}H-NMR ($CDCl_3$) δ=2.15—3.37 (4H, m, 2×-CH_2-), 5.56 (1H, dd, J=10 and 7 Hz, -CH<), 5.86 (1H, dd, J=10 and 6 Hz, -CH<), 7.40 (5H, s, Ph), and 7.42 (5H, s, Ph); HPLC R_t 7.4 min (70% aqueous methanol). Found: C, 74.01; H, 5.23%. Calcd for $C_{19}H_{16}O_2$: C, 74.00; H, 4.99%.

Oxidation Products from 1-Octene (**1f**). (3S*,5R*,8S*)-3,8-Dihexyl-2,7-dioxaspiro[4.4]nonane-1,6-dione (**2f'**): Colorless needless; mp 116.5—118.0 °C (methanol); 4% yield; IR ($CHCl_3$) 1762 (C=O) and 1780 cm^{-1} (C=O); ^{1}H-NMR ($CDCl_3$) δ=0.6—2.1 (26H, m, 2×-C_6H_{13}), 1.88 (2H, dd, J=13 and 9 Hz, 2×-HCH-), 2.75 (2H, dd, J=13 and 6 Hz, 2×-HCH-), 4.5—5.1 (2H, m, 2×-CH<); HPLC R_t 10.0 min (80% aqueous methanol). Found: m/z 324.23226. Calcd for $C_{19}H_{32}O_4$: M, 324.23006.

(3R*,5R*,8R*)-3,8-Dihexyl-2,7-dioxaspiro[4.4]nonane-1,6-dione (**2f''**): Colorless needles; mp 112.5—113.5 °C (methanol); 17% yield; IR ($CHCl_3$) 1762 (C=O) and 1782 cm^{-1} (C=O); ^{1}H-NMR ($CDCl_3$) δ=0.7—2.1 (26H, m, 2×-C_6H_{13}), 2.41 (4H, d, J=8 Hz, 2×-CH_2-), and 4.42 (2H, br. q, J=8 Hz, 2×-CH<); HPLC R_t 6.6 min (80% aqueous methanol). Found: C, 75.53; H, 10.00%. Calcd for $C_{19}H_{32}O_4$: C, 75.34; H, 9.94%.

(3S*,5R*,8R*)-3,8-Dihexyl-2,7-dioxaspiro[4.4]nonane-1,6-dione (**2f'''**): Colorless needles; mp 110—111 °C (methanol); 19% yield; IR ($CHCl_3$) 1762 (C=O) and 1778 cm^{-1} (C=O); ^{1}H-NMR ($CDCl_3$) δ=0.7—2.1 (26H, m, 2×-C_6H_{13}), 1.70—2.95 (4H, m, 2×-CH_2-), and 4.2—5.1 (2H, m, 2×-CH<); HPLC R_t 7.8 min (80% aqueous methanol). Found: m/z 324.23135. Calcd for $C_{19}H_{32}O_4$: M, 324.23006.

Oxidation Products from Cyclohexene (**1g**). (3R*,3aR*,3'aR*,7aR*,7'aR*)-Dodecahydro-3,3'(2H,2'H)-spirobi[benzofuran]-2,2'-dione (**2g'**): Colorless needles; mp 285—286 °C (methanol); IR ($CHCl_3$) 1766 (C=O) and 1792 cm^{-1} (C=O); ^{1}H-NMR ($CDCl_3$) δ=1.10—1.85 (14H, m, 6×-CH_2- and 2×-CH<), 2.29 (2H, br. d, J=13.9 Hz, 2×-CH<), 2.50 (2H, m, $w_{1/2}$=22 Hz, 2×-HCH-), and 4.62 (2H, m, $w_{1/2}$=9 Hz, -OCH<); HPLC R_t 5.6 min (70% aqueous methanol). Found: m/z 264.13606. Calcd for $C_{15}H_{20}O_4$: M, 264.13616.

(3R*,3aS*,3'aR*,7aS*,7'aR*)-Dodecahydro-3,3'(2H,2'H)-spirobi[benzofuran]-2,2'-dione (**2g''**): Colorless needles; mp 190—191 °C (methanol); IR ($CHCl_3$) 1766 (C=O) and 1792 cm^{-1} (C=O); ^{1}H-NMR ($CDCl_3$) δ=1.0—1.8 (13H, m, 6×-CH_2- and -HCH-), 2.20—2.35 (3H, m, 3×-HCH-), 2.50 (2H, m, $w_{1/2}$=24 Hz, 2×-CH<), 4.51 (1H, m, $w_{1/2}$=8 Hz, -OCH<), and 4.84 (1H, m, $w_{1/2}$=8 Hz, -OCH<); HPLC R_t 7.0 min (70% aqueous methanol). Found: m/z 264.13647. Calcd for $C_{15}H_{20}O_4$: M, 264.13616.

Dodecahydro-3,3'-(2H,2'H)-spirobi[benzofuran]-2,2'-dione (**2g'''**) (configuration is unknown): Colorless needles; mp 186—187 °C (methanol); IR ($CHCl_3$) 1770 (C=O) and 1792 cm^{-1} (C=O); ^{1}H-NMR ($CDCl_3$) δ=1.1—2.0 (14H, m, 7×-CH_2-), 2.2—2.5 (3H, m, 2×-HCH- and -CH<), 2.67 (1H, m, $w_{1/2}$=24 Hz, -CH<), 3.99 (1H, m, $w_{1/2}$=27 Hz, -OCH<), and 4.50 (1H, m, $w_{1/2}$=13 Hz, -OCH<); HPLC R_t 6.0 min (70% aqueous methanol). Found: m/z 264.13625. Calcd for $C_{15}H_{20}O_4$: M, 264.13616.

Cyclohexenyl Acetate (**5**): Colorless liquid; 22% yield.

Oxidation Products from 1,1,2-Triphenylethene[11] (**1h**). 1,1,2-Triphenyl-1,2-ethanediol 2-Acetate (**6**): Colorless needles; mp 224.5—225.5 °C (benzene) (lit,[12] mp 217—219 °C); 22% yield; IR ($CHCl_3$) 1736 (OAc) and 3592 cm^{-1} (OH); ^{1}H-NMR ($CDCl_3$) δ=1.93 (3H, s, OAc), 2.27 (1H, s, OH), 6.68 (1H, s, -CH<), and 7.1—7.7 (15H, m, 3×Ph).

3,4,4-Triphenyl-4-butanolide (**7**): Pale yellow needles; mp 96.0—96.5 °C (methanol); 3% yield; IR ($CHCl_3$) 1776 cm^{-1} (C=O); ^{1}H-NMR ($CDCl_3$) δ=2.75 (1H, dd, J=17 and 5 Hz, -HCH-), 2.93 (1H, dd, J=17 and 7 Hz, -HCH-), 4.46 (1H, dd, J=7 and 5 Hz, -CH<). Found: m/z 314.13397. Calcd for $C_{22}H_{18}O_2$: M, 314.13068.

References

1) E. I. Heiba, R. M. Dessau, and P. C. Rodewald, *J. Am. Chem. Soc.*, **96**, 7977 (1974).
2) M. Okano, *Bull. Chem. Soc. Jpn.*, **49**, 1041 (1976).
3) V. Jäger and H. J. Günther, *Tetrahedron Lett.*, **1977**, 2543.
4) H. Leuchs and E. Gieseler, *Ber.*, **45**, 2114 (1912).
5) J. R. Roland, E. L. Little, Jr., and H. E. Winberg, *J. Org. Chem.*, **28**, 2809 (1963).
6) P. Andrulis, Jr., M. J. S. Dewar, R. Dietz, and R. Hunt, *J. Am. Chem. Soc.*, **88**, 5473 (1966).
7) A. Klages, *Ber.*, **35**, 2646 (1902).
8) L. Gattermann, *Ber.*, **22**, 1129 (1889).
9) G. Wittig and U. Schoellkopf, *Org. Synth.*, Coll. Vol., V, 751 (1973).
10) A. Klages, *Ber.*, **35**, 2633 (1902).
11) A. Klages and S. Heilmann, *Ber.*, **37**, 1447 (1947).
12) E. Paternó and G. Forli-Forti, *Gazz. Chim. Ital.*, **40**, II 332 (1910).

One-pot Synthesis of Acid Anhydrides from Acids Using *N,N,N′,N′*-Tetramethylchloroformamidinium Chloride under Mild Conditions

Tamotsu Fujisawa,* Kazuhisa Tajima, and Toshio Sato
Chemistry Department of Resources, Mie University, Tsu, Mie 514

(Received May 9, 1983)

Synopsis. *N,N,N′,N′*-Tetramethylchloroformamidinium chloride reacted smoothly with a variety of carboxylic and phosphoric acids in the presence of a tertiary amine to give the corresponding acid anhydrides in high yields.

Acid anhydrides play an important role in organic syntheses as reactive intermediates, and they react with various nucleophiles such as alcohols,[1] amines,[2] aromatics,[3] and Grignard reagents[4] to give acylated compounds. On the other hand, pyrophosphates, anhydrides of phosphoric acid, are very important in biological activities as an energy source. Although many representative methods for the preparation of acid anhydrides reported so far are performed by the condensation of acids with acid chlorides,[5] one-step synthesis of acid anhydrides from acids requires a long reaction time and an elevated temperature[6] even if condensation reagents were used.[7] We now wish to report that *N,N,N′,N′*-tetramethylchloroformamidinium chloride (**1**) reacted smoothly with various kinds of acids in the presence of a tertiary amine under mild conditions to give the corresponding acid anhydrides in high yields.

The condensation reagent, *N,N,N′,N′*-tetramethylchloroformamidinium chloride (**1**) is easily available by the reaction of *N,N,N′,N′*-tetramethylurea and oxalyl dichloride.[8] The reaction of the reagent with benzoic acid in dichloromethane was performed at −30 °C in the presence of triethylamine for 3 h, and then the reaction mixture was allowed to warm to 0 °C resulting in the formation of benzoic anhydride in 88% yield. The effect of some bases and solvents was examined in the preparation of benzoic anhydride. The use of triethylamine, tributylamine, and pyridine as a base in dichloromethane gave the anhydride in 88, 85, and 74% yields, respectively. When dichloromethane, chloroform, 1,2-dichloroethane, and acetonitrile were employed as a solvent in the presence of triethylamine, the yields of the anhydride were 88, 89, 87, and 74%, respectively. The reaction can be explained by the nucleophilic attack of the carboxylate anion to the acyloxyformamidium chloride (**2**) initially formed.

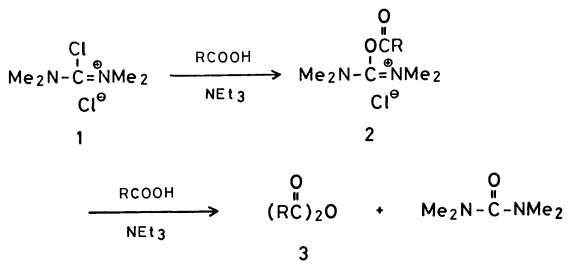

Scheme 1.

As shown in Table, aromatic carboxylic acids as well as aliphatic carboxylic acids were easily converted to the corresponding acid anhydrides (**3**) in high yields (runs 1—6), however bulky carboxylic acid and olefinic carboxylic acids required longer reaction time (runs 7—9).

Moreover, the present method was applied to the synthesis of pyrophosphate from mono- or disubstituted phosphates. Although these phosphorus compounds are dissolved well in tertiary amines such as triethylamine, such amines generally decrease the reaction rate in the phosphorylation using dicyclohexylcarbodiimide[9] or 1-imidazoylphosphonate.[10] On the contrary, the present method using *N,N,N′,N′*-tetramethylchloroformamidinium chloride in the presence of triethylamine gave tetraalkyl or tetraaryl pyrophosphates (**4**) in high yields from dialkyl or diaryl hydrogenphosphates under mild conditions and

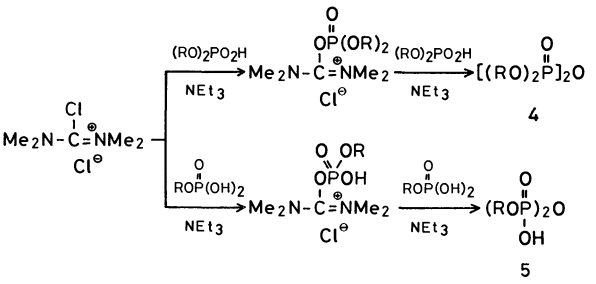

Scheme 2.

Table 1. Synthesis of acid anhydrides from the corresponding acids

Run	Acid	Reaction temp/°C	Reaction time/h	Product	Yield %
1	Benzoic acid	−30→0	3	**3a**	88
2	4-Methoxybenzoic acid	−30→0	6	**3b**	86
3	1-Naphthoic acid	−30→0	5	**3c**	91
4	2-Furoic acid	−30→0	3	**3d**	84
5	Hexanoic acid	−30→0	5	**3e**	83
6	Cyclohexanecarboxylic acid	−30→0	7	**3f**	81
7	Pivalic acid	−30→rt	18	**3g**	84[a]
8	Cinnamic acid	−30→rt	18	**3h**	83
9	Crotonic acid	−30→rt	18	**3i**	83
10	Diphenyl hydrogenphosphate	0→rt	2	**4a**	92
11	Diethyl hydrogenphosphate	0→rt	2	**4b**	90
12	Dibutyl hydrogenphosphate	0→rt	2	**4c**	96
13	Phenyl dihydrogenphosphate	0→rt	18	**5**	61[b]

a) Determined by GLC. b) Isolated as the bis(cyclohexylammonium) salt.

in a short reaction time (runs 10—12). Further, application of the method to the synthesis of diphenyl dihydrogenpyrophosphate (**5**) from phenyl dihydrogenphosphate gave the desired compound, which was isolated as its bis(cyclohexylammonium) salt[11] in a moderate yield (run 13).

In conclusion, *N,N,N′,N′*-tetramethylchloroformamidinium chloride (**1**), which can be easily prepared from readily available tetramethylurea and oxalyl dichloride, is an effective condensation reagent for the one-pot synthesis of acid anhydrides from the corresponding acids in high yields under mild conditions.

Experimental

The ^{1}H NMR and IR spectra were taken with a Varian A-60D spectrometer and a Hitachi EPI-G2 spectrometer, respectively. Gas chromatography was carried out with a Yanaco G-180 chromatographic apparatus, using a ϕ 3 mm × 1 m, 15% SE-30 column. Acid anhydrides and pyrophosphates obtained were identified by comparison of their IR and ^{1}H NMR spectra with those of the respective authentic samples. Authentic samples of **3a**, **3e**, and **3i** were obtained from Nakarai Chem. Ltd., and other chemicals were prepared by reported methods: **3b**,[11] **3c**,[12] **3d**,[13] **3f**,[14] **3g**,[15] **3h**,[16] **4a**,[17] **4b**,[18] **4c**,[18] and **5**.[19]

*N,N,N′,N′-Tetramethylchloroformamidinium Chloride (**1**).* Oxalyl dichloride (0.30 ml, 3.5 mmol) was added into a solution of *N,N,N′,N′*-tetramethylurea (244 mg, 2.1 mmol) in 3 ml of 1,2-dichloroethane at room temperature. The reaction mixture was then stirred for 2 h at 60 °C. After removal of the solvent under a reduced pressure, the faint yellow solid residue was used in the following experiments without further purification.

*General Procedure for the Synthesis of Acid Anhydrides (**3a—c, h**).* *N,N,N′,N′*-Tetramethylchloroformamidinium chloride (2.1 mmol), a carboxylic acid (4.0 mmol), and triethylamine (4.0 mmol) were stirred in 6 ml of dichloromethane at −30 °C for 1 h. This reaction mixture was allowed to warm to 0 °C or room temperature for 2 h and stirred at the same temperature until the reaction completed. This mixture was washed with two 10 ml portions of saturated sodium hydrogencarbonate, dried over anhydrous magnesium sulfate, and concentrated under a reduced pressure. The residue was chromatographed on silica gel to give acid anhydride (**3a—c, h**).

*General Procedure for the Synthesis of Acid Anhydrides (**3d—f, i**).* *N,N,N′,N′*-Tetramethylchloroformamidinium chloride (2.1 mmol), a carboxylic acid (4.0 mmol), and triethylamine (4.0 mmol) were stirred in 6 ml of dichloromethane at −30 °C for 1 h. This reaction mixture was allowed to warm to 0 °C or room temperature for 2 h and stirred at the same temperature until the reaction completed. After removal of the solvent under a reduced pressure, a 5 ml portion of ether was added to the residue, and the mixture was filtered under argon. The residue was washed with three 3 ml portions of ether, and the combined filtrate was distilled under a reduced pressure (Kugelrohr apparatus). Bp: **3d**; 200 °C/20 mmHg, **3e**; 200 °C/20 mmHg, **3f**; 200 °C/0.3 mmHg, **3g**; 150 °C/20 mmHg, and **3i**; 200 °C/20 mmHg.

*General Procedure for the Synthesis of Pyrophosphate (**4a—c**).* *N,N,N′,N′*-Tetramethylchloroformamidinium chloride (2.1 mmol), a phosphate (4.0 mmol), and triethylamine (4.0 mmol) were stirred in 6 ml of dichloromethane at 0 °C for 1 h and further at room temperature for 2 h. After removal of the solvent under a reduced pressure, a 5 ml portion of ether was added to the residue and the mixture was filtered under argon. The residue was washed with three 3 ml portions of ether, and the combined filtrate was distilled under a reduced pressure (Kugelrohr apparatus). Bp: **4a**; 250 °C/0.3 mmHg, **4b**; 200 °C/0.3 mmHg, and **4c**; 250 °C/0.4 mmHg.

*Synthesis of Diphenyl Dihydrogenpyrophosphate (**5**) Isolated as the Bis(cyclohexylammonium) Salt.* *N,N,N′,N′*-Tetramethylchloroformamidinium chloride (2.1 mmol), phenyl dihydrogenphosphate (696 mg, 4.0 mmol), and triethylamine (409 mg, 4.0 mmol) were stirred in 6 ml of dichloromethane at 0 °C for 1 h and stirred at room temperature for 12 h. After removal of the solvent, 30 ml of water and a sufficient amount of sodium hydrogencarbonate were added to the residue to neutralize the acidic solution. To the solution was added aqueous cyclohexylamine (812 mg, 8.2 mmol) and the solution set aside at 0 °C. Bis(cyclohexylammonium) diphenyl pyrophosphate was separated and recrystallized from water as colorless needles (640 mg, 61%); mp 250—254 °C (lit,[19] mp 250—255 °C).

Partial financial support of this research by the Asahi Glass Foundation is greatly acknowledged.

References

1) R. H. Baker and F. G. Bordwell, *Org. Synth.*, Coll. Vol. III, 141 (1955).
2) E. C. Kornfeld, R. G. Jones, and T. V. Parke, *J. Am. Chem. Soc.*, **71**, 150 (1949).
3) M. S. Newman and C. D. McCleary, *J. Am. Chem. Soc.*, **63**, 1542 (1941).
4) M. Araki and T. Mukaiyama, *Chem. Lett.*, **1974**, 663.
5) C. F. Allen, C. J. Kibler, D. M. McLachlin, and C. V. Wilson, *Org. Synth.*, Coll. Vol. III, 28 (1955).
6) F. A. Mason, *J. Chem. Soc.*, **1930**, 700.
7) G. Eglinton, E. R. H. Jones, B. L. Shaw, and M. C. Whiting, *J. Chem. Soc.*, **1954**, 1860.
8) T. Fujisawa, T. Mori, K. Fukumoto, and T. Sato, *Chem. Lett.*, **1982**, 1891.
9) M. Smith, J. G. Moffatt, and H. G. Khorana, *J. Am. Chem. Soc.*, **80**, 6204 (1958).
10) F. Cramer, H. Schaller, and H. A. Staab, *Chem. Ber.*, **94**, 1612 (1961).
11) A. Lawson, *J. Chem. Soc.*, **1954**, 3363.
12) W. F. Bruce, *J. Am. Chem. Soc.*, **60**, 2277 (1938).
13) H. Adkins and Q. E. Thompson, *J. Am. Chem. Soc.*, **70**, 2242 (1949).
14) P. D. Bartlett and P. N. Rylander, *J. Am. Chem. Soc.*, **73**, 4275 (1951).
15) M. F. Ansell, M. A. Davis, J. W. Hancock, W. J. Hickinbottom, P. G. Holton, and A. A. Hyatt, *J. Chem. Soc.*, **1955**, 2705.
16) H. E. Baumgarten, *J. Am. Chem. Soc.*, **75**, 1239 (1953).
17) N. S. Corby, G. W. Kenner, and A. R. Todd, *J. Chem. Soc.*, **1952**, 1234.
18) A. D. F. Toy, *J. Am. Chem. Soc.*, **70**, 3882 (1948).
19) H. G. Khorana and A. R. Todd, *J. Chem. Soc.*, **1953**, 2257.

Photochemical Synthesis of the Acetylene Adducts and Dimers of 2*H*- and 4*H*-1-Benzopyranones[1]

Takanao MATSUI* and Mitsuru NAKAYAMA†
Faculty of Engineering, Miyazaki University, Miyazaki 880
† *Faculty of Science, Hiroshima University, Hiroshima 730*
(Received May 16, 1983)

Synopsis. 7-Methoxychromone reacts photochemically with acetylene to form 5-methoxy-2a,8a-dihydro-8*H*-benzo[*b*]cyclobuta[*e*]pyran-8-one and its valence isomer. Photoaddition of acetylene to 6-methoxychromone and 7-methoxy-4-methylcoumarin did not proceed, but the latter underwent photodimerization to give the head-to-tail dimers.

In approach to the synthesis of trichothecane sesquiterpenes, we have reported that photochemical cycloaddition of α,β-unsaturated carbonyl compounds, such as 4a,5,6,7,8,8a-hexahydro-4a-methoxycarbonyl-7,7-ethylenedioxy-4-methylcoumarin with acetylene produced the 3,4-fused cyclobutene ring system in 62% yield, which was led to construct the five-menbered ring of trichothecane nucleus.[2] Our extensive interest is present in preparation of cyclobutene and cyclobutane skeleton from photochemical cycloaddition reaction of benzopyrones with several olefins, and in the development of construction of trichothecanes and trichothecane-like compounds *via* procedure containing the acid-catalysed rearrangement of the strained component. This paper describes preparation of the cyclobutane derivatives, acetylene adducts from 7-methoxychromone and coumarin dimers from 7-methoxy-4-methylcoumarin by photochemical cycloaddition,[3] respectively.

Irradiation of a solution of 7-methoxychromone (**1**) in acetone with bubbling introduction of acetylene using a 500-W high pressure mercury lamp through a Pyrex filter afforded 5-methoxy-2a,8a-dihydro-8*H*-benzo[*b*]cyclobuta[*e*]pyran-8-one (**2**) in 35% yield and its valence isomer, bicyclobutane (**3**) in 10% yield. These structures can be interpreted on the basis of the NMR spectral characteristics: for **2** ^{1}H-NMR signals of the two methine protons at δ 3.97 and 5.32 (each d, J=3 Hz) and the two olefin protons at 6.23 and 6.33 (each d, J=2 Hz), and ^{13}C-NMR signals at δ 54.8, 73.9, 140.0, and 140.7 due to C_{8a}, C_{2a}, C_1, and C_2 respectively, indicated the formation of cyclobutene ring system involving the 2,3-positions of the chromone and the formation of bicyclo[1.1.0]butane moiety in **3** was indicated by the ^{1}H-NMR signals due to the four methine protons at δ 2.51 (2H, t, J=3 Hz), 3.70—3.87 (1H, m), and 5.66 (1H, dt, J=2, 4 Hz), which were compatible with those of the bicyclobutane compound reported by Murata *et al.*[4] The gross structures of **2** and **3** were also supported by the mass spectrum, both of which showed intense peak at m/z 202 just to M^+.

Catalytic hydrogenation of **2** over Pd–C in ethanol yielded the cyclobutane derivative (**4**) in 72% yield. The confirmation of a cyclobutane ring in **4** was provided from the NMR spectra (the data are given in Experimental). Furthermore, we tried the isomerization between valence isomers **2** and **3** as follows.[5]

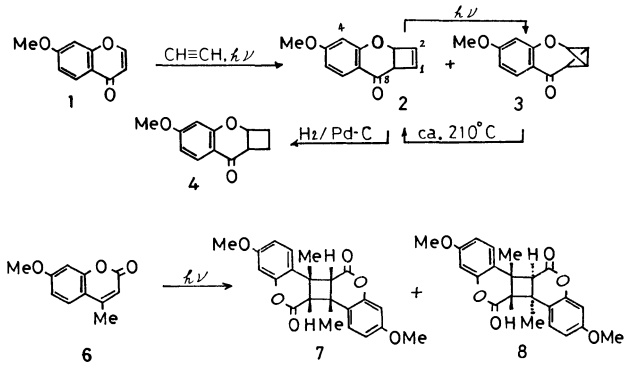

When a solution of **2** in acetone was irradiated, **3** was obtained in 33% yield. However, irradiation of **3** in acetone led to recovery of the starting material. Whereas the thermal reaction of **3** at 205—210 °C for 10 min gave **2** (26% yield) along with starting material.

In contrast to the photochemical activity of **1** with acetylene, neither 6-methoxychromone (**5**) nor 7-methoxy-4-methylcoumarin (**6**) was reactive toward acetylene. Consequently, **5** was almost recovered in the photochemical reaction. On the other hand, **6** dimerized upon direct irradiation in methanol to give the head-to-tail dimers, **7** (45% yield) and **8** (25% yield). Upon benzophenone-sensitized irradiation in benzene, **8** was prepared in 90—92% yield. There are two possible cycloutane photodimers of 4-methylcoumarin having the *syn* and *anti* head-to-tail configuration.[6] The assignment of *syn* and *anti* isomers were made on the basis of a NMR diamagnetic shielding effect, indicating that dimer **7** with the more highly shielded aromatic protons (δ 6.04, 6.66, and 7.10 for **7** and 6.70, 6.84, and 7.14 for **8**) has the *syn* configuration and dimer **8** with the more highly shielded methyl protons (δ 1.66 for **7** and 1.26 for **8**) corresponds to the *anti* configuration.[7]

Presently, the work is under the investigation of the acid-catalysed transformation of all synthetic cyclobutanes described here and their functionalized compounds in order to construct the five-menbered ring of trichothecane analogues.

Experimental

Melting points are uncorrected. IR spectra were measured in $CHCl_3$ with a Hitachi 260-50 spectrophotometer. ^{1}H-NMR and ^{13}C-NMR spectral data were obtained in $CDCl_3$ on a JEOL JNM MH-100 spectrometer (100 MHz) and a JEOL JNM-FX 60 Fourier transform spectrometer (60 MHz) operating at 15.1 MHz, respectively. Chemical shifts are reported in δ values downfield from TMS as an internal standard. Mass spectra were obtained on a JEOL JMS-D 300S spectrometer. All irradiations were performed

with a 500-W high pressure mercury lamp (Eikosha EHB-WI-500). Column chromatography was performed with Merck silica gel (0.063 mm).

Photoaddition of Acetylene to 7-Methoxychromone (1). A solution of **1** (550 mg) in acetone (400 ml) was irradiated through a Pyrex filter at 25—30 °C with bubbling introduction of acetylene for 5 h. After removal of the solvent under reduced pressure, the residue was subjected to column chromatography on silica gel using ethyl acetate–benzene (1:19) as eluent to give mainly three products, unidentified oil (*ca.* 30 mg), **3** (64 mg), **2** (220 mg), and **1** (160 mg) in the order of elution. **2**: Mp 96—97 °C (acetone–hexane); IR: 1665, 1615, and 1580 cm^{-1}; ^{1}H-NMR: 3.82 (3H, s, OCH_3), 3.97(1H, d, J=3 Hz, C_{8a}–H), 5.32(1H, d, J=3 Hz, C_{2a}–H), 6.23 (1H, d, J=2 Hz, C_1–H), 6.33 (2H, d, J=2 Hz, C_2– and C_4–H), 6.54 (1H, dd, J=2 and 11 Hz, C_6–H), and 7.81 (1H, d, J=11 Hz, C_7–H); ^{13}C-NMR: 54.8 (d, C_{8a}), 55.6 (q, OCH_3), 73.9 (d, C_{2a}), 101.4 (d, C_4), 110.2 (d, C_6), 112.4 (s, C_{7a}), 129.6 (d, C_7), 140.0 and 140.7 (each d, C_1 and C_2), 160.7 (s, C_{4a}), 166.3 (s, C_5), and 192.4 (s, C_8); MS: m/z 202 (M^+); Found: C, 71.27; H, 4.95%. Calcd for $C_{12}H_{10}O_3$: C, 71.28; H, 4.99%. **3**: Mp 66—68 °C (acetone–hexane); IR: 1660, 1610, and 1575 cm^{-1}; ^{1}H-NMR: 2.51 (2H, t, J=3 Hz, C_1– and C_2–H), 3.70—3.87 (1H, m, C_{8a}–H, overlapped with methoxyl peak), 3.87 (3H, s, OCH_3), 5.66 (1H, dt, J=2 and 4 Hz, C_{2a}–H), 6.43 (1H, d, J=3 Hz, C_4–H), 6.60 (1H, dd, J=3 and 9 Hz, C_6–H), and 8.00 (1H, d, J=9 Hz, C_7–H); ^{13}C-NMR: 15.6 (d, C_1 and C_2), 55.6 (q, OCH_3), 59.3 (d, C_{8a}), 85.8 (d, C_{2a}), 103.3 (d, C_4), 109.4 (d, C_6), 116.8 (s, C_{7a}), 132.6 (d, C_7), 157.4 (s, C_{4a}), 164.9 (s, C_5), and 200.9 (s, C_8); MS: m/z 202 (M^+); Found: C, 71.35; H, 4.93%. Calcd for $C_{12}H_{10}O_3$: C, 71.28; H, 4.99%.

Conversion between 2 and 3. a): A solution of **2** (100 mg) in acetone (300 ml) was irradiated at room temperature for 2 h through a Pyrex filter. Evaporation of the solvent, followed by silica-gel column chromatography of the residual oil gave **2** (12 mg) and **3** (33 mg).

b): 100 mg of **3** was prepared in a round bottom flask and heated at 205—210 °C for 10 min. This thermal reaction showed that a mixture of **2** (26 mg) and **3** (41 mg) was contained after separation by column chromatography on silica gel.

Hydrogenation of 2. A mixture of **2** (187 mg) and 5% Pd–C (50 mg) in ethanol (20 ml) was treated with H_2 at room temperature until equimolar H_2 was consumed. The mixture was filtered and concentrated *in vacuo*. Chromatographic separation of the residue through silica-gel coloumn eluting with benzene afforded **4** (128 mg, 72% yield) as colorless oil. IR: 1660, 1605, and 1570 cm^{-1}; ^{1}H-NMR: 1.88—2.78 (4H, m, 2 $-CH_2-$), 3.15—3.39 (1H, m, $-\overset{|}{C}OCH-$), 5.06 (1H, dd, J=8 and 16 Hz, $-O\overset{|}{C}H-$), 6.33 (1H, d, J=3 Hz, C_4–H), 6.56 (1H, dd, J=3 and 8 Hz, C_6–H), and 7.89 (1H, d, J=8 Hz, C_7–H); ^{13}C-NMR: 20.8 and 28.6 (each t, C_1 and C_2), 45.4 (d, C_{8a}), 55.5 (q, OCH_3), 72.5 (d, C_{2a}), 101.2 (d, C_4), 109.8 (d, C_6), 113.8 (s, C_{7a}), 128.9 (d, C_7), 161.5 (s, C_{4a}), 166.3 (s, C_5), and 193.1 (s, C_8); MS: m/z 204 (M^+); Found: C, 70.28; H, 5.94%. Calcd for $C_{12}H_{12}O_3$: C, 70.57; H, 5.92%.

Photoaddition of 7-Methoxy-4-methylcoumarin (6). a) In Methanol: A solution of **6** (300 mg) in methanol (500 ml) was irradiated at room temperature for 5 h through a Pyrex filter with introduction of acetylene. Usual work-up gave 480 mg of crude solid, which was taken up in a small amount of ethyl acetate and the insoluble material was filtered off, followed to recrystallization from acetone to give dimer **8** in 25% yield; mp 199—201 °C; IR: 1765, 1625, and 1585 cm^{-1}; ^{1}H-NMR: 1.26 (6H, s, 2 CH_3), 3.39 (2H, s, 2 $-\overset{|}{C}H-$), 3.87 (6H, s, 2 OCH_3), 6.70, 6.84, and 7.14 (each 2H, d, J=3 Hz, dd, J=3 and 9 Hz, and d, J=9 Hz, aromatic protons); MS: m/z 380 (M^+); Found: C, 69.27; H, 5.16%. Calcd for $C_{22}H_{20}O_6$: C, 69.46; H, 5.30%. The filtrate was concentrated in a rotary evaporator to afford **7** as a solid, which was further purified by column chromatography on silica gel with ethyl acetate–benzene (1:19), 140 mg (45% yield); mp 226—227 °C (methanol); IR: 1750, 1625, and 1585 cm^{-1}; ^{1}H-NMR: 1.66 (6H, s, 2 CH_3), 3.40 (2H, s, 2 $-\overset{|}{C}H-$), 3.65 (6H, s, 2 OCH_3), 6.04, 6.66, and 7.10 (each 2H, d, J=3 Hz, dd, J=3 and 9 Hz, and d, J=9 Hz, aromatic protons); MS: m/z 380 (M^+); Found: C, 69.21; H, 5.26%. Calcd for $C_{22}H_{20}O_6$: C, 69.46; H, 5.30%.

b) In Benzene with Benzophenone: Irradiation of a solution containing **6** (500 mg) and benzophenone (96 mg) in 300 ml of benzene with acetylene through a Pyrex filter at room temperature for 6 h, followed by chromatographic work-up on silica gel afforded **8** in 92% yield. However, the photoreaction by using conditions similar to those described above, changing reaction time, temperature, and solvent did not lead to yields of cycloadducts of acetylene to **6**.

References

1) This work is Part 2 of "Cycloadditions in Pyrones." Part 1: T. Matsui, T. Inoue, M. Nakayama, and J. D. White, *Bull. Chem. Soc. Jpn.*, **56**, 647 (1983).

2) J. D. White, T. Matsui, and J. A. Thomas, *J. Org. Chem.*, **46**, 3376 (1981).

3) Various 2+2 cycloadditions of benzopyrones have been reported. For some examples, see: J. W. Hanifin and E. Cohen, *J. Am. Chem. Soc.*, **91**, 4494 (1969); C. H. Krauch, S. Farid, and G. O. Schenck, *Chem. Ber.*, **99**, 625 (1966); T. Naito, N. Nakayama, and C. Kaneko, *Chem. Lett.*, **1981**, 423 and references cited therein.

4) M. Uyegaki, S. Ito, Y. Sugihara, and I. Murata, *Tetrahedron Lett.*, **1976**, 4473: The NMR spectrum of 4,5-benz-3-oxatricyclo[4.1.0.$0^{2,7}$]hept-4-ene has been shown.

5) For similar isomerization of cyclobutene and bicyclo-[1.1.0]butane skeleton, see: Y. Sugihara, T. Sugimura, and I. Murata, *J. Am. Chem. Soc.*, **103**, 6738 (1981); Y. Sugihara, N. Morokoshi, and I. Murata, *Chem. Lett.*, **1979**, 745; Ref. 4.

6) Upon irradiation of 4-methylcoumarin derivatives, the steric factors play a role in the formation of the reaction products, leading predominantly to head-to-tail isomers; L. H. Leenders, E. Schouteden, and F. C. De. Schryver, *J. Org. Chem.*, **38**, 957 (1973).

7) Examination of molecular models shows that diamagnetic shielding for protons above the plane of a benzene ring and for protons above the plane of a carbonyl group has been predicted; H. Werbin and E. T. Strom, *J. Am. Chem. Soc.*, **90**, 7296 (1968).

Convenient Synthesis of (1-Alkyl-2-hydroxyethyl)diphenylphosphine Oxides

Mitsuji YAMASHITA,* Manabu YAMADA, Kenji TSUNEKAWA, and Saburo INOKAWA†

Department of Chemistry, Faculty of Engineering, Shizuoka University, Hamamatsu 432

† *Department of Chemistry, Faculty of Science, Okayama University, Okayama 700*

(Received May 16, 1983)

Synopsis. (1 - Alkyl - 2 - hydroxyethyl)diphenylphosphine oxides were synthesized from the corresponding (1-alkyl-2-oxoethyl)diphenylphosphine oxides in excellent yields. The structures of 2-hydroxy derivatives and their acetates were confirmed by elemental and spectral analyses.

We have recently reported the synthesis of diphenylphospine oxide derivatives having a nitro group on the β-carbon atom of phosphorus, *i.e.*, (1-alkyl-2-nitroethyl)diphenylphosphine oxides, and the conversion of the nitro compound into the aldehyde compound by oxidation with ozone/methoxide method.[1,2] The present note deals with a convenient method for the synthesis of (1-alkyl-2-hydroxyethyl)diphenylphosphine oxides,[3,4] which have the partial structure of a phosphorus-sugar derivative, from (1-alkyl-2-oxoethyl)diphenylphosphine oxides by reduction with sodium tetrahydridoborate, and their conversion into the acetates.

Results and Discussion

Aldehydes 1, which were prepared from (1-alkyl-2-nitroethyl)diphenylphosphine oxides,[2] were transformed into 2-hydroxyethyl compounds **2** in excellent yields by treatment with sodium tetrahydridoborate in methanol under reflux as shown in Table 1.[5] Compounds **2** were characterized by microanalysis, IR, ^{1}H NMR, and MS.

$$\underset{\mathbf{1}}{Ph_2\overset{O}{\overset{\|}{P}}\text{-}\overset{R}{\overset{|}{C}}H\text{-}CH{=}O} \xrightarrow{NaBH_4/MeOH} \underset{\mathbf{2}}{Ph_2\overset{O}{\overset{\|}{P}}\text{-}\overset{R}{\overset{|}{C}}H\text{-}CH_2OH}$$

Yields of (2-hydroxyethyl)diphenylphosphine oxide derivatives were 31—81%[3] and 69—85%[4] in the reaction of lithium derivative of methyldiphenylphosphine oxide derivatives with carbonyl compounds such as aldehydes and ketones. 2-Hydroxyethylphosphonates were previously synthesized from vinylphosphonates by hydroboration in 50—65% yields.[6] Therefore, the present method is an improved one in preparation of phosphorus derivatives having a hydroxy group on the β-carbon atom.

2-Hydroxyethyl compounds **2** were acetylated in excellent yield with acetic anhydride in pyridine at room temperature.[7]

The structure of acetates **3** were determined by microanalysis, IR, ^{1}H NMR, and MS. The produced derivatives **3** clearly reconfirmed the structure of compounds **2**.

$$\mathbf{2} \xrightarrow{Ac_2O/Pyridine} \underset{\mathbf{3}}{Ph_2\overset{O}{\overset{\|}{P}}\text{-}\overset{R}{\overset{|}{C}}H\text{-}CH_2OAc}$$

The high yield and simple operation in preparation of (1-alkyl-2-hydroxyethyl)diphenylphosphine oxides show that the method provides a convenient preparative way to afford phosphorus compounds possessing a 2-hydroxyethyl group. This procedure will provide a new route to synthesize phosphorus-sugars.

Experimental

Apparatus. IR spectra were measured by a JASCO A-3 spectrophotometer. ^{1}H NMR spectra were run on a Hitachi R-20 (60 MHz) spectrometer. MS spectra were measured by a Hitachi RMU DMG GC-MS spectrometer. Liquid chromatography was carried out using a Toyo Scientific Industry UVICON-540M.

Materials. (1 - Alkyl - 2 - oxoethyl)diphenylphosphine oxides were prepared from (1-alkyl-2-nitroethyl)diphenylphosphine oxides.[2] Pyridine and acetic anhydride were purified before use.

*Synthesis of (2-Hydroxy-1-methylethyl)diphenylphosphine Oxide (**2a**, R=Me).* To a solution of (2-oxo-1-methylethyl)-diphenylphosphine oxide (**1a**, R=Me; 0.415 g, 1.6 mmol) in anhydrous methanol (25 ml) was added sodium tetrahydridoborate (0.612 g, 16 mmol) at room temperature, then the solution was refluxed for 16 h. A small amount of water was added to the reaction mixture and then it was refluxed for further 30 min. After the solution was neutralized with acetic acid, the solvent was removed off by a rotary evaporator and the residue was taken up into chloroform (40 ml). The chloroform solution was washed with water (20 ml×2) and dried over anhydrous sodium sulfate. Evaporation of the solvent *in vacuo* and recrystallization of the product from chloroform–cyclohexane gave (2-hydroxy-1-methylethyl)diphenylphosphine oxide (**2a**, 0.418 g) in 82% yield, mp 141—142 °C. ^{1}H NMR ($CDCl_3$) δ 1.22 (dd, J_{HH}=7.0 Hz, J_{HP}=16.0 Hz, CH_3), 2.4—3.0 (m, 1H, CH), 3.83 (dd, 2H, J_{HH}=5.0 Hz, J_{HP}=13.0 Hz, CH_2), 4.46 (s, 1H, OH), and 7.3—8.0 (m, 10H, Ph); IR ν_{max}^{KBr} 3200 cm^{-1} (OH); MS *m/e* 260 (M^+). Found: C, 68.96; H, 6.34%. Calcd for $C_{15}H_{17}O_2P$: C, 69.22; H, 6.58%. Found: *m/e* 260.0970. Calcd for $C_{15}H_{17}O_2P$: 260.0966.

*Synthesis of [1-(Hydroxymethyl)propyl]diphenylphosphine Oxide (**2b**, R=Et).* Treatment of a solution of **1b** (R=Et, 0.738 g, 2.71 mmol) in anhydrous methanol (25 ml) with sodium tetrahydridoborate (1.03 g, 27.1 mmol) followed by work-up and recrystallization from chloroform–cyclohexane gave product **2b** (0.660 g) in 89% yield, mp 105—106 °C. ^{1}H NMR ($CDCl_3$) δ 0.97 (t, 3H, J_{HH}=7.0 Hz, CH_3), 1.4—2.0 (m, 2H, J_{HH}=7.0 Hz, $CH_3C\underline{H}_2$), 2.1—2.7 (m, 1H, CH), 3.94 (dd, 2H, J_{HH}=5.0 Hz, J_{HP}=18.0 Hz, $C\underline{H}_2OH$), 5.77 (s, 1H, OH), and 7.4—8.1 (m, 10H, Ph); IR ν_{max}^{KBr} 3300 cm^{-1} (OH); MS *m/e* 274 (M^+). Found: C, 70.02; H, 6.93%. Calcd for $C_{16}H_{19}O_2P$: C, 70.06; H, 6.98%. Found: *m/e* 274.1138. Calcd for $C_{16}H_{19}O_2P$: 274.1123.

[1 - (Hydroxymethyl) - 2 - methylpropyl]diphenylphosphine oxide (**2c**, R=*i*-Pr) and (2-hydroxy-1-phenylethyl)diphenylphosphine oxide (**2d**, R=Ph) were synthesized by an analogous method mentioned above in 92 and 63% yields, respectively.

Table 1. Compounds **2** and **3** prepared

Product[a]	Yield/%	Mp θ_m/°C	MS *m/e*	IR ν_{max}^{KBr}/cm^{-1}	^{1}H NMR ($CDCl_3$) (δ)
2a; R=Me	82	141—142	260 (M^+)	3200 (OH) 1440 (P-Ph) 1160 (P=O) 720 (C-P)	1.22 (dd, 3H, J_{HH}=7.0 Hz, J_{HP}=16.0 Hz, CH_3), 2.4—3.0 (m, 1H, CH), 3.83 (dd, 2H, J_{HH}=5.0 Hz, J_{HP}=13.0 Hz, CH_2), 4.46 (s, 1H, OH), 7.3—8.0 (m, 10H, Ph)
2b; R=Et	89	105—106	274 (M^+)	3300 (OH) 1440 (P-Ph) 1170 (P=O) 720 (C-P)	0.97 (t, 3H, J_{HH}=7.0 Hz, CH_3), 1.4—2.0 (m, 2H, J_{HH}=7.0 Hz, $CH_3C\underline{H}_2$), 2.1—2.7 (m, 1H, CH), 3.94 (dd, 2H, J_{HH}=5.0 Hz, J_{HP}=18.0 Hz, $C\underline{H}_2OH$), 5.77 (s, 1H, OH), 7.4—8.1 (m, 10H, Ph)
2c; R=*i*-Pr	92	148	288 (M^+)	3350 (OH) 1440 (P-Ph) 1170 (P=O) 720 (C-P)	1.00 (d, 6H, J_{HH}=7.0 Hz, CH_3), 1.8—2.2 (m, 1H, $Me_2C\underline{H}$), 2.2—2.7 (m, 1H, P-CH), 3.99 (dd, 2H, J_{HH}=5.0 Hz, J_{HP}=16.0 Hz, CH_2), 4.60 (s, 1H, OH), 7.3—8.1 (m, 10H, Ph)
2d; R=Ph	63	168—170	322 (M^+)	3400 (OH) 1440 (P-Ph) 1170 (P=O) 720 (C-P)	3.14 (s, 1H, OH), 3.6—4.4 (m, 3H, $C\underline{H}C\underline{H}_2$), 7.0—8.1 (m, 15H, Ph)
3a; R=Me	99	133—134	302 (M^+)	1740 (C=O) 1440 (P-Ph) 1180 (P=O) 720 (C-P)	1.20 (dd, 3H, J_{HH}=7.0 Hz, J_{HP}=16.0 Hz, CH_3), 1.79 (s, 3H, CH_3CO), 2.7—3.2 (m, 1H, J_{HH}= 7.0 Hz, CH), 4.1—4.52 (m, 2H, CH_2), 7.3—8.1 (m, 10H, Ph)
3b; R=Et	80	108—109	316 (M^+)	1738 (C=O) 1440 (P-Ph) 1180 (P=O) 720 (C-P)	0.99 (t, 3H, J_{HH}=7.0 Hz, CH_3), 1.1—1.9 (m, 2H, $CH_3C\underline{H}_2$), 1.72 (s, 3H, CH_3CO), 2.4—3.0 (m, 1H, CH), 4.43 (dd, 2H, J_{HH}=7.0 Hz, J_{HP}= 13.0 Hz, CH_2O), 7.2—8.1 (m, 10H, Ph)
3c; R=*i*-Pr	99	157—158	330 (M^+)	1740 (C=O) 1440 (P-Ph) 1178 (P=O) 720 (C-P)	1.09 (d, 6H, J_{HH}=7.0 Hz, CH_3), 1.69 (s, 3H, CH_3CO), 2.0—2.4 (m, 1H, $Me_2C\underline{H}$), 2.5—3.0 (m, 1H, P-CH), 4.48 (dd, 2H, J_{HH}=7.0 Hz, J_{HP}=13.0 Hz, CH_2), 7.3—8.1 (m, 10H, Ph)

a) Satisfactory micro and milimass analyses were obtained.

*Synthesis of (2-Acetoxy-1-methylethyl)diphenylphosphine Oxide (**3a**, R=Me).* To a solution of **2a** (0.290 g, 1.1 mmol) in anhydrous pyridine (5 ml) was added acetic anhydride (3 ml), and the solution was stood for 24 h at room temperature. The reaction mixture was taken up into chloroform (40 ml). The extract was washed with water (20 ml×2) and was dried over anhydrous sodium sulfate. Evaporation of the solvent *in vacuo* and recrystallization of the product from carbon tetrachloride–cyclohexane gave **3a** (0.335 g) in 99% yield, mp 133—134 °C. ^{1}H NMR ($CDCl_3$) δ 1.22 (dd, 3H, J_{HH}=7.0 Hz, J_{HP}=16.0 Hz, CH_3), 1.79 (s, 3H, CH_3CO), 2.7—3.2 (m, 1H, J_{HH}=7.0 Hz, CH), 4.1—4.52 (m, 2H, CH_2), and 7.3—8.1 (m, 10H, Ph); IR ν_{max}^{KBr} 1740 cm^{-1} (CO); MS *m/e* 302 (M^+). Found: C, 67.47; H, 6.17%. Calcd for $C_{17}H_{19}O_3P$: C, 67.54; H, 6.33%. Found: *m/e* 302.1091. Calcd for $C_{17}H_{19}O_3P$: 302.1110.

*Synthesis of [1-(Acetoxymethyl)propyl]diphenylphosphine Oxide (**3b**, R=Et).* Treatment of **2b** (0.280 g, 1.02 mmol) in pyridine (5 ml) with acetic anhydride (3 ml) followed by work-up and recrystallization from carbon tetrachloride-cyclohexane gave product **3b** (0.256 g) in 80% yield, mp 108—109 °C. ^{1}H NMR ($CDCl_3$) δ 0.99 (t, 3H, J_{HH}=7.0 Hz, CH_3), 1.1—1.9 (m, 2H, $CH_3C\underline{H}_2$), 1.72 (s, 3H, CH_3CO), 2.4—3.0 (m, 1H, CH), 4.43 (dd, 2H, J_{HH}=7.0 Hz, J_{HP}= 13.0 Hz, CH_2O), and 7.2—8.1 (m, 10H, Ph); IR ν_{max}^{KBr} 1738 cm^{-1} (CO); MS *m/e* 316 (M^+). Found: C, 68.33; H, 6.50%. Calcd for $C_{18}H_{21}O_3P$: C, 68.34; H, 6.69%. Found: *m/e* 316.1259. Calcd for $C_{18}H_{21}O_3P$: 316.1228.

[1-(Acetoxymethyl)-2-methylpropyl]diphenylphosphine oxide (**3c**, R=*i*-Pr) was synthesized by an analorous method mentioned above in 99% yield.

References

1) J. E. McMurry, J. Melton, and H. Padgett, *J. Org. Chem.*, **39**, 259 (1974).
2) M. Yamada, M. Yamashita, and S. Inokawa, *Synthesis*, **1982**, 1026.
3) J. J. Richard and C. V. Banks, *J. Org. Chem.*, **28**, 123 (1963).
4) S. Warren, *Acc. Chem. Res.* **11**, 401 (1978).
5) W. S. Allen, S. Bernstein, and R. Littell, *J. Am. Chem. Soc.*, **76**, 6116 (1954).
6) M. Yamashita, M. Kojima, H. Yoshida, T. Ogata, and S. Inokawa, *Bull. Chem. Soc. Jpn.*, **53**, 1625 (1980).
7) M. L. Wolfrom and A. Thompson, "Methods in Carbohydrate Chemistry," ed by R. L. Whistler and M. L. Wolfrom, Academic Press, New York (1963), Vol. 2, p. 211.

Preparation of Sydnone-4-carboxamide Oximes and Their Conversion into 4-(1,2,4-Oxadiazol-3-yl)sydnones

Mou-Yung YEH,*,† Tsutomu NONAKA,* Takushi GOTO, Ming-Ching HSU,† Toshio FUCHIGAMI, and Hsien-Ju TIEN†

Department of Electronic Chemistry, Tokyo Institute of Technology, Nagatsuta, 4259, Midori-ku, Yokohama 227

† *Department of Chemistry, National Cheng Kung University, Tainan, Taiwan, 700, Republic of China*

(Received May 26, 1983)

Synopsis. 3-Arylsydnone-4-carboxamide oximes (**2**) were prepared from the corresponding 3-arylsydnone-4-carbonitriles and hydroxylamine in high yields. The amide oximes **2** reacted with orthoesters to give 3-aryl-4-(1,2,4-oxadiazol-3-yl)sydnones.

Many sydnone compounds have been found to have biological and pharmacological activities.[1-3] Some heterocyclic compounds are also well known to show such activities. It therefore must be interesting to synthesize sydnones having heterocyclic groups, but sydnones substituted directly by such groups (4-thiazolyl[3,4] and 4-sydnonyl[5,6] groups) at their 4-positions have been rarely reported. In this work, the preparation of sydnone compounds **2** with amidino-type groups, which are good precursors of heterocyclic groups, and the conversion of **2** into 4-(1,2,4-oxadiazol-3-yl)sydnones (**3**) were attempted.

Sydnone is a typical mesoionic compound and its chemical and physical properties are very unique.[1,7] Sydnone compounds seem to be fairly different from others in both reactivity and stability: Although a sydnone ring has a somewhat aromatic nature, the synthesis of sydnone compounds substituted by electron-releasing groups at the 4-position was unsuccessfully tried using some common reactions.[8-12] Therefore, both methods and conditions for the synthesis of sydnone compounds may often be restricted.

Results and Discussion

Nitriles are useful starting compounds for the preparation of amidines and imidic esters. However, the reaction of 3-phenylsydnone-4-carbonitrile (**1a**) with some nucleopliles did not give the corresponding addition products under conditions where common nitriles can react. The reaction of **1a** with free hydrazine at room temperature resulted in decomposition of **1a**, while hydrochlorides of hydrazine and aniline did not react in the presence of pyridine even at higher temperatures. The reaction with methanol in the presence of hydrogen chloride, so-called the Pinner reaction, also did not occur. These unsuccessful results may be due to the decrease of reactivity of the cyano group of **1a** by the electron-releasing nature[12] of the 4-position and/or instability of the desired products under the reaction conditions.

Only hydroxylamine hydrochloride could react with **1a—c** at room temperature in the presence of pyridine to give the corresponding 3-arylsydnone-4-carboxamide oximes (**2a—c**) in their free states in high yields, as shown in Table 1. This successful synthesis may be caused by such adequate basicities of hydroxylamine and **2** that the former can react with the cyano group and the latter can be present in the free state without decomposition. It is interesting to note that the electrophilic reaction of **1** might be sensitive to the basicity of neucleophile, product, and reaction medium.

Table 1. 3-Arylsydnone-4-carboxamide oximes (**1a—c**)

Compd	Yield[a] %	Mp θ_m/°C	IR(KBr) ν_{OH} cm^{-1}	IR(KBr) ν_{NH} cm^{-1}	IR(KBr) $\nu_{C=O}$ cm^{-1}
2a	86	183—185	3460	3330 3170	1735
2b	95	182—183	3450	3330 3180	1735
2c	96	170—171	3530	3375 3260	1755

a) Obtained pure without recrystallization.

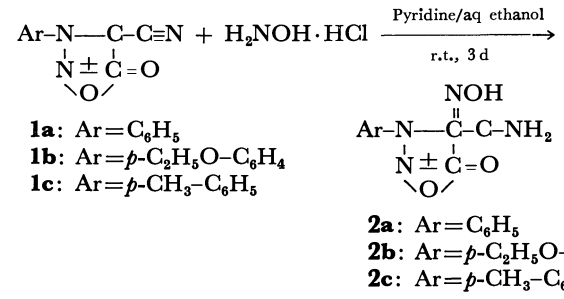

1a: Ar=C_6H_5
1b: Ar=*p*-C_2H_5O-C_6H_4
1c: Ar=*p*-CH_3-C_6H_5

2a: Ar=C_6H_5
2b: Ar=*p*-C_2H_5O-C_6H_4
2c: Ar=*p*-CH_3-C_6H_4

The conversion of **2** prepared thus into 3-aryl-4-(1,2,4-oxadiazol-3-yl)sydnones (**3a—f**) was successfully carried out using the acid-catalyzed reaction with orthoesters (**4a—b**).[13] The reaction proceeded at room temperature (for 3 d) in the presence of sulfuric acid as a catalyst and **3** could be obtained in high yields, as shown in Table 2. Similar results could be obtained by using boron trifluoride etherate, instead of sulfuric acid, at higher temperature(90—100 °C) for shorter time(5 min).

The preparation of **2** in this work seems to be the

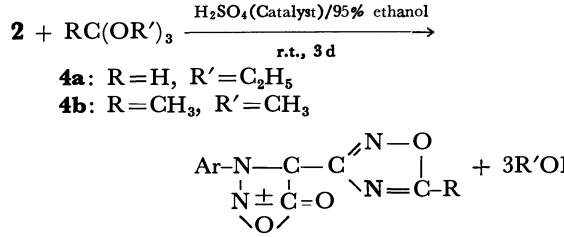

4a: R=H, R'=C_2H_5
4b: R=CH_3, R'=CH_3

3a: Ar=C_6H_5, R=H
3b: Ar=C_6H_5, R=CH_3
3c: Ar=*p*-CH_3-C_6H_4, R=H
3d: Ar=*p*-CH_3-C_6H_4, R=CH_3
3e: Ar=*p*-C_2H_5O-C_6H_4, R=H
3f: Ar=*p*-C_2H_2O-C_6H_4, R=CH_3

Table 2. 3-aryl-4-(1,2,4-oxadiazol) sydnones (**3a—f**)

Compd	Yield[a] %	Mp θ_m/°C	IR(KBr) ν_{OH}[b] cm^{-1}	IR(KBr) $\nu_{C=O}$ cm^{-1}	IR(KBr) $\nu_{C=N}$ cm^{-1}
3a	87	173—174	3140 3070	1779	1573
3b	82	148—150	—	1779	1565
3c	86	198—200	3140 3075	1779	1569
3d	81	151—152	—	1778	1568
3e	84	153—154	3150 3067	1780	1570
3f	83	135—137	—	1782	1575

a) Aftera recrystallization from 95% ethanol. b) 1,2,4-Oxadiazole ring.

first report of the synthesis of sydnones substituted by an amidino-type group which may be a good precursor of longer carbon-nitrogen alternate and heterocyclic groups in addition to a 1,2,4-oxadiazol-3-yl group. The new type of sydnone compounds such as **2** and **3** is also expected to be biologically or pharmacologically active.

Experimental

3-Arylsydnone-4-carbonitriles (**1a—c**) were prepared from the corresponding 4-formylsydnones by the Schmidt reaction.[14]

Typical procedures for the preparation of **2** and **3** were as follows: To a suspension of **1a** (3.74 g, 0.02 mol) in 95% ethanol (50 ml)–pyridine (5 ml), hydroxylamine hydrochloride (2.10 g, 0.03 mol) in water (10 ml) was added with stirring. The stirring was continued for 3 days at room temperature. The resulting precipitates (**2a**) were collected by filtration, and concentration of the filtrate afforded additional **2a**. To a suspension of **2a** (0.44 g, 0.002 mol) in 95% ethanol (20 ml), **4a** (2 ml) and concentrated sulfuric acid (2 drops) were added. By a procedure similar to the preparation of **2a**, the crude product of **3a** was obtained and recrystallized from 95% ethanol. All the products, **2a—c** and **3a—f** were confirmed by spectral (IR, ^{1}H-NMR, and MS) and analytical data.

The compound, **2a**: ^{1}H NMR (DMSO-d_6) δ=9.92 (1H, s, OH), 7.73 (5H, s, aromatic), 5.91 (2H, s, NH_2); MS (70 eV), *m/e* 220 (M^+), 162 (M^+—NO—CO). Found: C, 49.34; H, 3.58; N, 25.34%. Calcd for $C_9H_8N_4O_3$: C, 49.10; H, 3.66; N, 25.45%.

The compound, **2b**: ^{1}H NMR (DMSO-d_6) δ=9.95 (1H, s, OH), 7.60 (2H, d, J=9 Hz, aromatic), 7.41 (2H, d, J=9 Hz, aromatic), 5.90 (2H, s, NH_2), 2.42 (3H, s, CH_3); MS (70 eV), *m/e* 234 (M^+), 176 (M^+—NO—CO). Found: C, 51.26; H, 4.13; N, 23.92%. Calcd for $C_{10}H_{10}N_4O_3$: C, 51.28; H, 4.30; N, 23.92%.

The compound, **2c**: ^{1}H NMR (DMSO-d_6) δ=9.93 (1H, s, OH), 7.65 (2H, d, J=9 Hz, aromatic), 7.14 (2H, d, J=9 Hz, aromatic), 5.89 (2H, s, NH_2), 4.12 (2H, q, J=7 Hz, CH_2), 1.40 (3H, t, J=7 Hz, CH_3); MS (70 eV), *m/e* 264 (M^+), 206 (M^+—NO—CO). Found: C, 50.09; H, 4.36; N, 21.15%. Calcd for $C_{11}H_{12}N_4O_4$: C, 50.00; H, 4.58; N, 21.20%.

The compound, **3a**: ^{1}H NMR (Acetone-d_6) δ=9.20 (1H, s, oxadiazolyl), 7.81 (5H, m, aromatic); MS (70 eV), *m/e* 230 (M^+), 172 (M^+—NO—CO). Found: C, 52.22; H, 2.31; N, 24.04%. Calcd for $C_{10}H_6N_4O_3$: C, 52.18; H, 2.63; N, 24.34%.

The compound, **3b**: ^{1}H NMR (Acetone-d_6) δ=7.73 (5H, m, aromatic), 2.50 (3H, s, CH_3); MS (70 eV), *m/e* 244 (M^+), 186 (M^+—NO—CO). Found: C, 54.41; H, 3.14; N, 22.91%. Calcd for $C_{11}H_8N_4O_3$: C, 54.10; H, 3.30; N, 22.94%.

The compound, **3c**: ^{1}H NMR (Acetone-d_6) δ=9.22 (1H, s, oxadiazolyl), 7.70 (2H, d, J=9 Hz, aromatic), 7.47 (2H, d, J=9 Hz, aromatic), 2.48 (3H, s, CH_3); MS (70 eV), *m/e* 244 (M^+), 186 (M^+—NO—CO). Found: C, 54.18; H, 3.14; N, 22.72%. Calcd for $C_{11}H_8N_4O_3$: C, 54.10; H, 3.30; N, 22.94%.

The compound, **3d**: ^{1}H NMR (Acetone-d_6) δ=7.66 (2H, d, J=9 Hz, aromatic), 7.48 (2H, d, J=9 Hz, aromatic), 2.52 (3H, s, CH_3-oxadiazolyl), 2.47 (3H, s, CH_3-phenylene); MS (70 eV), *m/e* 258 (M^+), 200 (M^+—NO—CO). Found; C, 55.61; H, 3.75; N, 21.40%. Calcd for $C_{12}H_{10}N_4O_3$: C, 55.81; H, 3.90; N, 21.70%.

The compound **3e**: ^{1}H NMR (Acetone-d_6) δ=9.22 (1H, s, oxadiazolyl), 7.68 (2H, d, J=9 Hz, aromatic), 7.13 (2H, d, J=9 Hz, aromatic), 4.18 (2H, q, J=7 Hz, CH_2), 1.43 (3H, t, J=7 Hz, CH_3); MS (70 eV), *m/e* 274 (M^+), 216 (M^+—NO—CO). Found: C, 52.67; H, 3.38; N, 20.10%. Calcd for $C_{12}H_{10}N_4O_4$; C, 52.56; H, 3.68; N, 20.43%.

The compound, **3f**: ^{1}H NMR (Acetone-d_6) δ=7.70 (2H, d, J=9 Hz, aromatic), 7.17 (2H, d, J=9 Hz, aromatic), 4.20 (2H, q, J=7 Hz, CH_2), 2.53 (3H, s, CH_3-oxadiazolyl), 1.44 (3H, t, J=7 Hz, CH_3-CH_2); MS (70 eV), *m/e* 288 (M^+), 230 (M^+—NO—CO). Found: C, 54.20; H, 4.13; N, 19.52%. Calcd for $C_{13}H_{12}N_4O_4$: C, 54.17; H, 4.20; N, 19.44%.

The authors are grateful to the National Science Council, R. O. C. for making a possible partipation of Professor Yeh.

References

1) M. Ohta and H. Kato, "Non-benzenoid Aromatics," Academic Press, New York (1969), p. 117.
2) Y. Imashiro and K. Masuda, Japan Patent 6932411 (1969); *Chem. Abstr.* **72**, 111482q (1970): Y. Saito and T. Kamitani, *ibid.*, 7021710 (1970); *Chem. Abstr.*, **73**, 87926k (1970): K. Masuda and T. Okutani, *ibid.*, 7020903 (1970); *Chem. Abstr.*, **73**, 87928n (1970): I. S. Slyusarenko, Z. M. Kol'tova, V. I. Mamonov, and V. G. Yashunskii, *Khim. Farm. Zh.*, **5**, 12 (1971); *Chem. Abstr.*, **76**, 14441a (1972).
3) K. G. Upadhya, B. V. Badami, G. S. Puranik, V. N. Biradar, and S. Nanjappa, *Arch. Pharm. (Weiheim, Ger.)*, **313**, 684 (1980); *Chem. Abstr.*, **94**, 47195y (1981).
4) H.-J. Tien, K. Kanda, A. Chinone, and M. Ohta, *Bull. Chem. Soc. Jpn.*, **46**, 3304 (1973).
5) F. H. C. Stewart, *J. Chem. Soc.*, **1963**, 701.
6) H.-J. Tien and M.-Y. Yeh, *J. Chinese Chem. Soc. (Taipei)*, **24**, 123 (1977).
7) F. H. C. Stewart, *Chem. Rev.*, **64**, 129 (1964).
8) H. Kato and M. Ohta, *Bull. Chem. Soc. Jpn.*, **32**, 282 (1959).
9) M. Hashimoto, Dr. Sci. Dissertation, Tokyo Institute of Technology, Japan 1969.
10) H.-J. Tien, *Cheng Kung Ta Hsueh Pao*, **14**, 19 (1979); *Chem. Abstr.*, **92**, 181090x (1980).
11) M.-Y. Yeh, H.-J. Tien, and T. Nonaka, *J. Org. Chem.*, **48**, 1382 (1983).
12) H.-J. Tien, T. Nonaka, T. Fuchigami, T. Sekine, and M. Ohta, *Nippon Kagaku Kaishi*, **1978**, 1310.
13) G. I. Gregory, P. W. Seale, K. W. Warburton, and M. J. Wilson, *J. Chem. Soc., Perkin Trans. 1*, **1973**, 47.
14) M.-Y. Yeh, H.-J. Tien, L.-Y. Huang, and M.-H. Chen, *J. Chinese Chem. Soc. (Taipei)*, **30**, 29 (1983).

Molecular Structure of 3,4,6-Tri-*O*-acetyl-1,2-*O*-[(1*S*)-1-(2-*p*-bromophenyl)-9*H*-imidazo[1,2-*a*]benzimidazol-3-yl]ethylidene]-*α*-D-glucopyranose Acetone Solvate

Hiroaki TAKAYANAGI, Haruo OGURA,* Nobuyasu TSUZUNO, Isao KUBOTA, and Yoichi IITAKA†

School of Pharmaceutical Sciences, Kitasato University, Shirokane, Minato-ku, Tokyo 108

† *Faculty of Pharmaceutical Sciences, University of Tokyo, Hongo, Bunkyo-ku, Tokyo*

(Received June 1, 1983)

Synopsis. The structure of a product from a reaction mixture of 2-(*p*-bromophenyl)-9*H*-imidazo[1,2-*a*]benzimidazole and 2,3,4,6-tetra-*O*-acetyl-*β*-D-glucopyranosyl bromide in the presence of NaI, hexamethyldisilazane, and $(NH_4)_2SO_4$ has been established as 3,4,6-tri-*O*-acetyl-1,2-*O*-[(1*S*)-1-[2-(*p*-bromophenyl)-9*H*-imidazo[1,2-*a*]benzimidazol-3-yl]ethylidene]-*α*-D-glucopyranose by means of X-ray crystal structure analysis.

In a series of synthesizing nucleoside analogs[1], we carried out the reaction of 2-(*p*-bromophenyl)-9*H*-imidazo[1,2-*a*]benzimidazole (**1**) and 2,3,4,6-tetra-*O*-acetyl-*β*-D-glucopyranosyl bromide (**2**).[2] From the reaction mixture, three compounds were separated, two of them were identified by means of NMR, IR, and UV, but the rest was not. In this paper, we describe the molecular structure of the compound(**3**) determined by X-ray analysis.

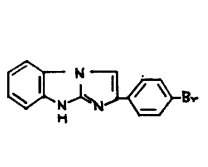

(1)

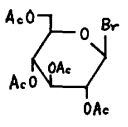

(2)

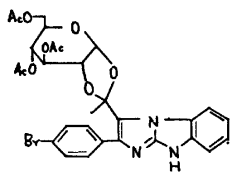

(3)

Experimental

A specimen of **3** with the approximate dimensions of 0.3×0.3×0.3 mm³ was used for the intensity measurements. The density was determined by the flotation methods in a mixture of petroleum ether and carbon tetrachloride. The cell constants were determined by the least-squares procedure from the 2*θ* values of 24 reflections measured on a diffractometer using monochromated Cu *Kα* radiation. Three dimensional intensity data were collected on a Fillips automatic four-circle diffractometer with graphite monochromated Cu *Kα* radiation. Background was counted for 5 s at both sides of each peak. Three standard reflections were measured every 100 reflections during the course of collection. A total of 4604 independent reflections were collected. Reflections having an intensity exceeding the corresponding standard deviations by a factor of three were treated as observed. 4201 reflections were retained and corrected for Lorentz and polarization factors but not for absorption factor. The crystal of compound **3** belongs to the triclinic, space group P1, and $Z=2$. $a=9.485(2)$, $b=20.080(2)$, $c=9.708(1)$ Å, $\alpha=100.31(2)$, $\beta=109.60(1)$, $\gamma=92.45(2)°$.

Determination and Refinement of the Structure. The structure was determined by the heavy atom method. All the non-hydrogen atoms in the asymmetric unit were obtained from the Fourier map phased by the two bromine atoms. The oxygen and nitrogen atoms were identified by the structural considetations. Refinement of atomic parameters was carried out by the full-matrix least-squares method, the quantity minimized being $\Sigma w(|F_o|-|F_c|)^2$, with $w=1.0$ for all the reflections used. The final ***R*** values was 0.069. The atomic scattering factors for C, O, N were given by Cromer and Mann,[3] and that for H by Stewart *et al.*,[4] and that for Br from International Tables for X-ray Crystallography.[5] The final atomic parameters and equivalent isotropic temperature factors are given in Table 1.†

TABLE 1. ATOMIC COORDINATES (×10⁴) AND THEIR STANDARD DEVIATIONS IN PARENTHESES AND EQIVALENT ISOTROPIC TEMPERATURE FACTORS

Atom	*x*		*y*		*z*		B_{eq}[a]/Å	
	3A	3B	3A	3B	3A	3B	3A	3B
Br(1)	8302(2)	1769(2)	9572(1)	449(1)	−1879(2)	11896(2)	12.9	13.3
C(1)	4459(12)	5692(15)	8977(4)	1025(5)	1843(10)	8273(12)	4.5	5.7
C(2)	3165(11)	6933(16)	8553(4)	1453(6)	1497(9)	8583(13)	5.2	6.5
C(3)	3760(13)	6427(16)	9240(5)	777(6)	3696(10)	6282(15)	5.8	4.5
C(4)	2046(13)	8173(17)	9094(6)	945(6)	4704(11)	5385(13)	7.0	6.9
C(5)	1575(12)	8588(16)	8614(5)	1441(7)	3341(11)	6780(13)	4.2	8.4
C(6)	255(14)	9794(15)	8196(6)	1912(7)	2786(13)	7237(13)	7.0	6.6
C(7)	−618(14)	10727(18)	8200(7)	1872(8)	3680(13)	6330(20)	8.2	6.6
C(8)	−136(17)	10390(17)	8670(8)	1396(7)	5101(14)	5021(15)	9.4	6.4
C(9)	1108(13)	9054(20)	9135(7)	957(7)	5593(12)	4506(16)	6.6	11.3
C(10)	5379(14)	4716(13)	9087(5)	934(5)	887(12)	9071(11)	7.4	4.5
C(11)	6970(14)	3158(15)	9220(6)	810(6)	1549(12)	8363(15)	6.7	8.0
C(12)	7777(12)	2116(19)	9355(7)	660(7)	737(13)	9192(15)	6.1	11.7
C(13)	7054(19)	2921(15)	9352(6)	650(7)	−771(15)	10689(15)	10.6	8.9
C(14)	5532(16)	4506(16)	9208(7)	757(5)	−1481(13)	11414(13)	8.4	5.5
C(15)	4709(13)	5454(17)	9088(5)	911(6)	−624(12)	10642(13)	4.8	8.4
C(16)	732(14)	9117(15)	8188(7)	1767(7)	−690(12)	11062(13)	8.6	8.6
C(17)	2223(13)	7789(14)	8019(6)	2027(5)	211(12)	9872(12)	5.6	6.1
C(18)	3152(12)	6012(16)	6990(5)	2786(6)	822(11)	9860(13)	3.8	9.0
C(19)	4030(12)	6976(16)	7317(5)	2955(6)	−16(11)	8919(15)	5.1	6.1
C(20)	4348(11)	7721(17)	6858(5)	3709(7)	−1222(11)	9332(16)	4.7	7.4
C(21)	3006(13)	8165(17)	6309(6)	4050(7)	−2221(12)	10973(17)	6.9	6.0
C(22)	1789(13)	7518(18)	6264(6)	3687(6)	−1540(13)	11887(14)	4.0	6.3
C(23)	6955(18)	6632(45)	6741(9)	4346(16)	−283(16)	7423(31)	8.2	49.8
C(24)	8130(18)	6063(23)	6282(10)	5031(10)	520(19)	7040(21)	14.1	13.9
C(25)	2797(19)	10685(44)	6385(9)	4662(11)	−4719(16)	11840(51)	9.4	11.6
C(26)	1779(19)	12386(28)	6613(9)	4565(17)	−6139(16)	12575(52)	13.7	7.4
C(27)	770(17)	7435(28)	5579(7)	4178(8)	−2118(16)	13265(19)	4.4	15.7
C(28)	1682(46)	6514(45)	4463(23)	5256(17)	−2656(95)	13463(61)	10.1	12.9
C(29)	2498(36)	5419(27)	3924(12)	5682(12)	−1779(37)	12454(30)	16.4	22.2
C(S1)	7900(27)	3097(36)	7092(14)	2676(19)	5975(22)	2999(31)	18.5	15.4
C(S2)	6597(27)	4320(32)	7417(12)	2654(21)	5038(24)	4406(43)	6.2	48.6
C(S3)	5606(51)	5745(63)	7830(16)	2321(22)	5697(40)	4458(36)	30.7	51.2
O(1)	3090(8)	8262(9)	7785(3)	2581(4)	−718(7)	9448(8)	5.8	4.9
O(2)	1979(9)	6768(10)	7426(4)	2286(4)	820(8)	10581(8)	6.1	6.0
O(3)	2491(9)	6079(11)	6322(3)	3361(4)	77(9)	11017(10)	5.7	7.7
O(4)	5540(8)	6522(12)	6450(4)	4076(5)	−540(8)	8531(12)	5.5	12.2
O(5)	7216(12)	7274(30)	7291(7)	3954(14)	−510(14)	6736(21)	7.1	47.0
O(6)	2207(8)	9797(13)	6525(4)	4052(5)	−3588(8)	11606(13)	6.4	7.9
O(7)	3964(12)	9888(31)	6137(6)	5104(12)	−4519(6)	11256(54)	14.7	10.8
O(8)	1673(17)	6355(18)	5036(5)	4654(6)	−1746(15)	12697(13)	9.8	15.1
O(9)	1122(55)	7363(39)	4366(32)	5463(11)	−4015(90)	14747(29)	27.3	21.8
O(S1)	6263(17)	4182(46)	7360(9)	2914(25)	3648(17)	5583(62)	14.3	14.1
N(1)	4821(11)	5267(11)	9411(4)	612(5)	3246(9)	6780(10)	4.9	5.8
N(2)	2739(10)	7450(11)	8734(4)	1303(4)	2767(9)	7333(9)	5.5	4.7
N(3)	3391(12)	6786(12)	9483(5)	553(5)	4995(9)	5141(10)	5.6	7.2

a) B_{eq} refined according to Hamilton (1959).

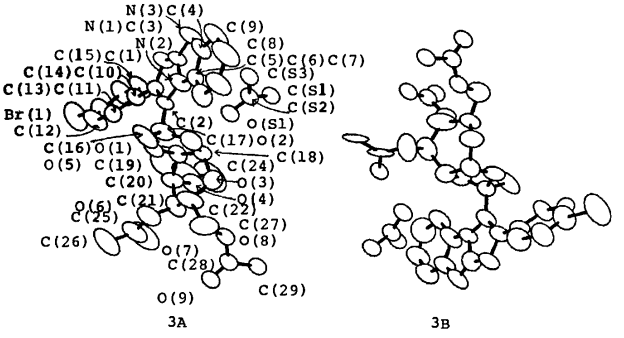

Fig. 1. A view of 3A, 3B, and acetone molecules defining the atom numbering.

† The F_o-F_c data are deposited as Document No. 8350 at the Office of the Editor of the Bull. Chem. Soc. Jpn.

Table 2. Bond lengths and their standard deviations in parentheses

Bond length	l/Å 3A	l/Å 3B	Bond length	l/Å 3A	l/Å 3B
Br(1)-C(13)	1.93(2)	1.93(2)	C(17)-O(2)	1.46(2)	1.43(2)
C(1)-C(2)	1.37(2)	1.34(2)	C(18)-C(19)	1.54(2)	1.56(2)
C(1)-C(10)	1.51(2)	1.42(2)	C(18)-O(2)	1.44(2)	1.41(2)
C(1)-N(1)	1.40(2)	1.45(2)	C(18)-O(3)	1.41(2)	1.44(2)
C(2)-C(17)	1.48(3)	1.51(3)	C(19)-C(20)	1.48(2)	1.57(2)
C(2)-N(2)	1.41(2)	1.44(2)	C(19)-O(1)	1.43(2)	1.45(2)
C(3)-N(1)	1.28(2)	1.39(2)	C(20)-C(21)	1.56(3)	1.52(3)
C(3)-N(2)	1.34(2)	1.40(3)	C(20)-O(4)	1.47(2)	1.46(2)
C(3)-N(3)	1.43(2)	1.28(2)	C(21)-C(22)	1.52(2)	1.50(3)
C(4)-C(5)	1.41(2)	1.45(3)	C(21)-O(6)	1.44(2)	1.46(2)
C(4)-C(9)	1.43(2)	1.38(3)	C(22)-C(27)	1.55(3)	1.54(3)
C(4)-N(3)	1.38(2)	1.43(2)	C(22)-O(3)	1.47(2)	1.40(2)
C(5)-C(6)	1.36(2)	1.35(3)	C(23)-C(24)	1.57(3)	1.56(4)
C(5)-N(2)	1.42(2)	1.40(2)	C(23)-O(4)	1.36(2)	1.32(4)
C(6)-C(7)	1.39(2)	1.44(3)	C(23)-O(5)	1.20(2)	1.25(5)
C(7)-C(8)	1.44(3)	1.38(3)	C(25)-C(26)	1.55(3)	1.57(5)
C(8)-C(9)	1.36(3)	1.40(3)	C(25)-O(6)	1.38(2)	1.39(4)
C(10)-C(11)	1.42(2)	1.39(2)	C(25)-O(7)	1.20(2)	1.28(5)
C(10)-C(15)	1.39(2)	1.46(2)	C(27)-O(8)	1.44(2)	1.47(3)
C(11)-C(12)	1.32(2)	1.52(3)	C(28)-C(29)	1.57(7)	1.57(5)
C(12)-C(13)	1.39(2)	1.40(2)	C(28)-O(8)	1.32(6)	1.27(4)
C(13)-C(14)	1.37(2)	1.42(2)	C(28)-O(9)	1.22(12)	1.22(5)
C(14)-C(15)	1.36(2)	1.41(2)	C(S1)-C(S2)	1.52(4)	1.48(4)
C(16)-C(17)	1.48(2)	1.58(2)	C(S2)-C(S3)	1.50(6)	1.52(7)
C(17)-O(1)	1.45(2)	1.36(2)	C(S2)-O(S1)	1.26(3)	1.22(7)

Table 3. Bond angles and their standard deviations in parentheses

Bond angle	φ/° 3A	φ/° 3B	Bond angle	φ/° 3A	φ/° 3B
C(2)-C(1)-C(10)	129.6(8)	132.8(1)	O(2)-C(18)-O(3)	109.3(8)	106.8(9)
C(2)-C(1)-N(1)	111.5(10)	110.7(12)	C(18)-C(19)-C(20)	117.0(8)	115.2(11)
C(10)-C(1)-N(1)	118.5(8)	116.4(10)	C(18)-C(19)-O(1)	105.4(9)	101.9(10)
C(1)-C(2)-C(17)	136.4(11)	134.0(14)	C(20)-C(19)-O(1)	106.0(8)	102.6(10)
C(1)-C(2)-N(2)	103.4(7)	107.5(9)	C(19)-C(20)-C(21)	114.0(10)	115.1(13)
C(17)-C(2)-N(2)	120.2(10)	118.5(12)	C(19)-C(20)-O(4)	118.5(8)	103.9(10)
N(1)-C(3)-N(2)	115.4(9)	110.2(11)	C(21)-C(20)-O(4)	103.3(8)	105.4(12)
N(1)-C(3)-N(3)	133.9(9)	135.5(10)	C(20)-C(21)-C(22)	112.0(9)	115.6(11)
N(2)-C(3)-N(3)	110.8(11)	114.3(13)	C(20)-C(21)-O(6)	109.7(9)	105.6(13)
C(5)-C(4)-C(9)	118.3(10)	118.6(13)	C(22)-C(21)-O(6)	101.6(9)	106.3(12)
C(5)-C(4)-N(3)	113.8(11)	109.5(13)	C(21)-C(22)-C(27)	113.9(11)	111.7(12)
C(9)-C(4)-N(3)	127.9(9)	131.8(10)	C(21)-C(22)-O(3)	109.4(9)	110.4(10)
C(4)-C(5)-C(6)	124.4(12)	122.2(15)	C(27)-C(22)-O(3)	105.6(11)	109.4(15)
C(4)-C(5)-N(2)	102.4(8)	103.4(11)	C(24)-C(23)-O(4)	108.9(14)	126.2(33)
C(6)-C(5)-N(2)	133.1(10)	134.4(12)	C(24)-C(23)-O(5)	127.0(14)	126.2(25)
C(5)-C(6)-C(7)	117.7(10)	116.9(12)	O(4)-C(23)-O(5)	123.7(15)	107.7(27)
C(6)-C(7)-C(8)	118.8(12)	122.4(14)	C(26)-C(25)-O(6)	110.3(14)	109.6(23)
C(7)-C(8)-C(9)	123.4(15)	119.2(17)	C(26)-C(25)-O(7)	128.8(16)	139.0(33)
C(4)-C(9)-C(8)	116.8(11)	120.3(12)	O(6)-C(25)-O(7)	120.9(13)	110.9(29)
C(1)-C(10)-C(11)	119.6(9)	121.8(11)	C(22)-C(27)-O(8)	109.3(11)	106.6(12)
C(1)-C(10)-C(15)	121.8(11)	115.6(11)	C(29)-C(28)-O(8)	111.8(57)	107.6(32)
C(11)-C(10)-C(15)	118.6(12)	122.3(13)	C(29)-C(28)-O(9)	124.1(51)	126.3(30)
C(10)-C(11)-C(12)	119.9(10)	122.0(12)	O(8)-C(28)-O(9)	124.0(54)	126.2(36)
C(11)-C(12)-C(13)	119.3(11)	111.7(13)	C(S1)-C(S2)-C(S3)	122.6(23)	123.1(33)
Br(1)-C(13)-C(12)	117.0(11)	117.1(11)	C(S1)-C(S2)-O(S1)	122.5(23)	118.4(36)
Br(1)-C(13)-C(14)	119.5(11)	115.9(10)	C(S3)-C(S2)-O(S1)	114.9(23)	118.5(33)
C(12)-C(13)-C(14)	123.4(16)	127.0(15)	C(17)-O(1)-C(19)	106.9(8)	107.9(10)
C(13)-C(14)-C(15)	116.7(12)	120.7(11)	C(17)-O(2)-C(18)	109.5(9)	109.5(10)
C(10)-C(15)-C(14)	122.0(11)	116.3(12)	C(18)-O(3)-C(22)	112.3(8)	116.0(11)
C(2)-C(17)-C(16)	116.9(10)	111.1(9)	C(20)-O(4)-C(23)	113.4(10)	120.4(21)
C(2)-C(17)-O(1)	109.4(9)	113.8(10)	C(21)-O(6)-C(25)	116.2(10)	117.5(17)
C(2)-C(17)-O(2)	106.5(9)	108.0(10)	C(27)-O(8)-C(28)	126.9(30)	119.2(21)
C(16)-C(17)-O(1)	111.3(9)	112.1(10)	C(1)-N(1)-C(3)	103.4(8)	104.7(9)
C(16)-C(17)-O(2)	108.1(10)	108.2(9)	C(2)-N(2)-C(3)	106.3(9)	106.6(11)
O(1)-C(17)-O(2)	103.7(8)	103.0(9)	C(2)-N(2)-C(5)	143.0(7)	145.7(9)
C(19)-C(18)-O(2)	103.6(8)	103.1(11)	C(3)-N(2)-C(5)	110.4(9)	107.5(10)
C(19)-C(18)-O(3)	112.3(9)	111.6(10)	C(3)-N(3)-C(4)	102.6(8)	105.3(10)

Results and Discussion

The molecular framework is shown in Fig. 1. It is concluded that the product from the reaction **1** and **2**, has the structure **3**.

The asymmetric carbon C(17) is specified as (S), and it is thought that the reaction proceeded stereospecific. In the crystal, **3** was found to be a (1:1) mixture of rotational isomers (**3A** and **3B**), and torsional angles of C(1)–C(2)–C(17)–O(1) are 18.5° (for 3A) and −41.8° (for 3B) and N(2)–C(2)–C(17)–O(2) are −51.5° (for 3A) and 26.6° (for 3B), respectively.

Table 4. Dihedral angles between the planes

Dihedral	θ/° 3A	θ/° 3B
Benzene plane[C(4)–C(5)–C(6)–C(7)–C(8)–C(9)] and imidazole plane[C(3)–N(3)–C(4)–C(5)–N(2)]	0.6	1.6
Benzene plane[C(4)–C(5)–C(6)–C(7)–C(8)–C(9)] and imidazole plane[C(1)–C(2)–N(2)–C(3)–N(1)]	3.3	5.3
Two imidazole planes[C(3)–N(3)–C(4)–C(5)–N(2)] and [C(1)–C(2)–N(2)–C(3)–N(1)]	3.3	4.7
Benzene plane[C(10)–C(11)–C(12)–C(13)–C(14)–C(15)] and imidazole plane[C(1)–C(2)–N(2)–C(3)–N(1)]	41.8	42.7

In the heterocyclic moiety, one benzene ring and two imidazole rings are almost planar each other in the range of 0.6—5.3°, but the dihedral angles between the *p*-bromophenyl group and imidazole ring [C(1)–C(2)–N(2)–C(3)–N(1)] are 41.8° (for **3A**) and 42.7° (for **3B**) respectively.

The bond distances and angles are given in Table 2 and 3, respectively.

Two acetone molecules are found in an unit cell.

A view of **3A**, **3B** and acetone molecules defining the atom numbering is given in Fig. 1.

On the difference map, 8 peaks corresponding to two acetone molecules and the peaks corresponding to three acetyl groups showed broad peaks and some of their temperature factors are large. This is, in the case of acetyl group, presumably because of the rotation of acetyl groups around the axis C(20)–O(4)–, C(21)–O(6), and C(27)–O(8) respectively.

References

1) Previous paper (Part XXV): H. Ogura, H. Takahashi, and M. Kobayashi, *Nippon Kagaku Kaishi*, **1982**, 1673.

2) In contribution.

3) D. Cromer and J. Mann, *Acta Crystallogr., Sect. A*, **24**, 321 (1968).

4) R. F. Stewart, E. R. Davidson, and W. T. Simpson, *J. Phys. Chem.*, **42**, 3175 (1965).

5) "International Tables for X-ray Crystallography," Kynoch Press, Birmingham (1962), Vol. III.

Palladium Catalyzed Reaction of Trimethylsilyltributyltin with α-Halo Ketones. Preparation of Enol Silyl Ethers

Masanori Kosugi, Takao Ohya, and Toshihiko Migita*
Department of Chemistry, Faculty of Technology, Gunma University, Kiryu, Gunma 376
(Received June 3, 1983)

Synopsis. The reaction of trimethylsilyltributyltin with α-halo ketone in the presence of a catalytic amount of palladium chloride plus twice molar amounts of trimethyl phosphite gave enol silyl ethers in good yields.

The most important method to form Si–C bonds involves the reaction between organosilicon halides and Grignard or organolithium reagents. An alternative method available is the reaction between disilane and organic halides in the presence of appropriate transition metal complexes.[1] Application of this reaction

$$RX + Me_3SiSiMe_3 \xrightarrow{[M]} RSiMe_3 + Me_3SiX$$

to α-halo ketone was recently reported by Moro-oka *et al.* to give the reductive dehalogenated product, ketone as a major product, except for the reaction with α-bromoacetophenone which gave enol silyl ether as a major product.[2]

Comparing with hexamethyldisilane, trimethylsilyltributyltin is expected to be a more reactive reagent, because Sn–Si bond is weaker than Si–Si bond. We carried out the palladium-catalyzed reaction of trimethylsilyltributyltin with α-halo ketones under various conditions, intending to increase the yield of enol silyl ether, and to reduce the yield of reductive dehalogenated product. This note which describes the results affords an example of the catalytic silylation of α-halo ketones by means of the compound related to disilane, although a number of other methods for the preparation of enol silyl ether are so far known.[3]

$$-\overset{\overset{O}{\|}}{C}-\overset{|}{C}-X + Bu_3SnSiMe_3 \xrightarrow{[Pd]} -C=C\begin{matrix}\diagup\\ \\ \diagdown\end{matrix} + Bu_3SnX \quad (OSiMe_3)$$

The reaction of trimethylsilyltributyltin with α-bromoacetophenone in the presence of tetrakis(triphenylphosphine)palladium was carried out at various reaction temperature. As Table 1 shows, lower the temperature, the yield of α-trimethylsiloxystyrene increased comparing with that of acetophenone, the reductive dehalogenated product. The optimum temperature was about 80 °C.

The distribution of the products depended also on the nature of the catalysts and the ligands used. As shown in Table 2, the best catalyst was π-allylpalladium or palladium chloride plus twice molar amounts of trimethyl phosphite. From the view point of availability and stability of the catalysts, palladium chloride plus trimethyl phosphite may be the most recommendable catalyst.

Since, under these conditions, α-trimethylsiloxystyrene was produced in good yield and the production of acetophenone was essentially suppressed, the method was applied to the reaction with various α-halo ketones, giving the results as shown in Table 3. Enol silyl ethers were produced in good yields together with a quite small amount of the reductive dehalogenated products. The yield descended as the halo ketone varied from primary to secondary, and then to tertiary. At lower reaction temperature, the yields of the product from secondary or tertiary bromide seemed to be improved.

The mechanism for this reaction may be analogous to that proposed by Moro-oka *et al.*[2]

Table 1. Temperature dependence of products distribution

$$Bu_3SnSiMe_3 + BrCH_2COPh \xrightarrow[0.01\ mmol]{Pd(PPh_3)_4} PhC(OSiMe_3)=CH_2 + PhCOMe$$

1.2 mmol; 1.0 mmol; I; II

Temp/°C	Yield of products/%[a] I	II
120	35	37
100	52	31
80	61	27
60	56	23

a) GLC yield based on halide. b) Solvent: PhH, 0.5 ml, reaction time: 5 h.

Table 2. Effect of the catalyst on the yield and distribution of the products

$$Bu_3SnSiMe_3 + BrCH_2COPh \xrightarrow[0.01\ mmol]{[M]} PhC(OSiMe_3)=CH_2 + PhCOMe$$

1.2 mmol; 1.0 mmol; I; II

Catalyst	Yield of products/%[a] I	II
None	0	8
$Pd(PPh_3)_4$	61	27
$PdCl_2(PPh_3)_2$	29	19
$PdCl_2[P(o\text{-tolyl})_3]_2$	4	27
$PdCl_2[P(p\text{-tolyl})_3]_2$	51	18
$PdCl_2(PhCN)_2$	Trace	7
$RhCl(PPh_3)_3$	Trace	30
$NiCl_2(PPh_3)_2$	0	9
$[PdCl(C_3H_5)]_2$[b]	13	24
$+2P(OEt)_3$	80	13
$+2P(OPh)_3$	53	35
$+2P(OMe)_3$	76	5
$PdCl_2$[b]	Trace	3
$+2P(OEt)_3$	78	10
$+2P(OPh)_3$	15	26
$+2P(OMe)_3$	81	8
$Pd(OAc)_2$[b] $+2P(OEt)_3$	48	18

a) GLC yield based on halide. b) Used 0.05 mmol. c) Solvent: PhH, 0.5 ml, reaction time: 5 h.

Table 3. Pd-catalyzed reaction of trimethyltributyltin with various α-halo ketones

$Bu_3SnSiMe_3$ + α-Halo ketone $\xrightarrow{[M]^{a)}}$ Enol silyl ether + Bu_3SnX
36 mmol 30 mmol

α-Halo ketone	Yield of product/%[b]	Bp θ_b/°C (mmHg)
$BrCH_2COMe$	$CH_2=C(OSiMe_3)Me$ 80(67)[d]	94
$BrCH_2COEt$	$CH_2=C(OSiMe_3)Et$ 89(72)[d]	114
$BrCH_2CO^iPr$	$CH_2=C(OSiMe_3)^iPr$ 93	
$BrCH_2CO^tBu$	$CH_2=C(OSiMe_3)^tBu$ 95(75)	70(70)
$BrCH_2COPh$	$CH_2=C(OSiMe_3)Ph$ 76(69)	102(20)
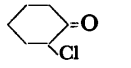	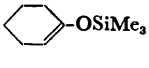 52	
$MeCOCHBrMe$	$Me(Me_3SiO)C=CHMe$ 50(73)[c,d]	124
$MeCOCHBrMe_2$	$Me(Me_3SiO)C=CMe_2$ 30(40)[c,d]	60(70)

a) $PdCl_2$ (0.3 mmol) + $2P(OMe)_3$ in PhH (10 ml) at 80 °C for 5 h. b) GLC yield based on halide, isolated yield in parentheses. c) At 60 °C for 24 h. d) Solvent: tetralin, 10 ml.

Experimental

Boiling points are uncorrected. IR spectra were recorded on a Hitachi EPI-3G spectrophotometer. NMR spectra were recorded on a Varian EM-360 instrument. GLC analyses were carried out with an Ohkura 802 instrument, using columns (1.5 m) packed with 10% Silicone SF-96, 10% SE-30, 10% Apiezon Grease L, or 10% Carbowax-20M on Celite 545 (AW DMCS).

Materials. Trimethylsilyltributyltin,[4] bromoacetone,[5] 1-bromo-2-butanone and 3-bromo-2-butanone,[6] 1-bromo-3-methyl-2-butanone and 3-bromo-3-methyl-2-butanone,[6] 1-bromo-3,3-dimethyl-2-butanone,[7] α-bromoacetophenone,[8] 2-chlorocyclohexanone,[9] $Pd(PPh_3)_4$,[10] $PdCl_2(PPh_3)_2$,[11] $PdCl_2[P(o\text{-}tolyl)_3]_2$,[11] $PdCl_2[P(p\text{-}tolyl)_3]_2$,[11] $PdCl_2(PhCN)_2$,[12] $RhCl(PPh_3)_3$,[13] $NiCl_2(PPh_3)_2$,[14] and $[PdCl(C_3H_5)]_2$[15] were prepared by the methods described in literatures.

Reaction Procedures. Solutions of trimethylsilyltributyltin (1.2 mmol), α-halo ketone (1.0 mmol), and the catalyst (0.01 mmol) in benzene (0.5 ml) were degassed and sealed *in vacuo*. After heating for 5 h, the reaction mixtures were subjected in GLC. For the experiment in preparative scale, solutions of 30 times amounts of reactants and catalyst were prepared and heated under argon at 80 °C for 5 h. The products were isolated by distillation under reduced pressure.

Products. All the products are known compounds,[16,17] identification of which was based on their spectroscopic data recorded here.

2-Trimethylsiloxy-1-propene: IR (neat) 1640 and 900 (C=C), and 1030 cm^{-1} (Si–O–C). ^1H NMR (CCl_4) δ=0.18 (s, 9H), 1.72 (s, 3H), and 3.95 (s, 2H).

2-Trimethylsiloxy-1-butene: IR (neat) 1620 and 880 (C=C), and 1030 cm^{-1} (Si–O–C). ^1H NMR (CCl_4) δ=0.13 (s, 9H), 0.92 (t, J=7.6 Hz, 3H), 1.93 (q, J=7.6 Hz, 2H), and 3.89 (s, 2H).

2-Trimethylsiloxy-3-methyl-1-butene: IR (neat) 1630 and 860 (C=C), and 1010 cm^{-1} (Si–O–C). ^1H NMR (CCl_4) δ=0.20 (s, 9H), 0.96 (d, J=6 Hz, 6H), 2.10 (h, J=6 Hz, 1H), 3.84 (s, 1H), and 3.95 (s, 1H).

2-Trimethylsiloxy-3,3-dimethyl-1-butene: IR (neat) 1620 and 880 (C=C), and 1030 cm^{-1} (Si–O–C). ^1H NMR (CCl_4) δ= 0.18 (s, 9H), 1.05 (s, 9H), 3.85 (d, J=1 Hz, 1H), and 4.01 (d, J=1 Hz, 1H).

α-Trimethylsiloxystyrene. IR (neat) 1620 (C=C) and 1010 cm^{-1} (Si–O–C). ^1H NMR (CCl_4) δ=0.26 (s, 9H), 4.27 (d, J=1.7 Hz, 1H), 4.73 (d, J=1.7 Hz, 1H), and 7.00—7.58 (m, 5H).

1-Trimethylsiloxycyclohexene: IR (neat) 1670 and 898 (C=C), and 1190 cm^{-1} (Si–O–C). ^1H NMR (CCl_4) δ=0.15 (s, 9H), 1.31—1.73 (m, 4H), 1.73—2.18 (m, 4H), and 4.73 (m, 1H).

2-Trimethylsiloxy-2-butene: IR (neat) 1680 and 900 (C=C), and 1050 cm^{-1} (Si–O–C). ^1H NMR (CCl_4) δ=0.18 (s, 9H), 1.43 (d, q, J=6.6 and 1 Hz, 3H), 1.71 (m, 3H), and 4.41 (q,q, J=6.6 and 1 Hz, 1H).

2-Trimethylsiloxy-3-methyl-2-butene: IR (neat) 1680 and 905 (C=C), and 1010 cm^{-1} (Si–O–C). ^1H NMR (CCl_4) δ=0.10 (s, 9H), 1.55 (s, 6H), and 1.70 (s, 3H).

References

1) H. Matsumoto, S. Nagashima, K. Yoshihiro, and Y. Nagai, *J. Organomet. Chem.*, **85**, C1 (1975); H. Matsumoto, K. Yoshihiro, S. Nagashima, H. Watanabe, and Y. Nagai, *ibid.*, **128**, 409 (1977); H. Matsumoto, T. Yako, S. Nagashima, T. Motegi, and Y. Nagai, *ibid.*, **148**, 97 (1978); H. Matsumoto, S. Nagashima, T. Kato, and Y. Nagai, *Angew. Chem., Int. Ed. Engl.*, **17**, 279 (1978); H. Matsumoto, K. Shono, and Y. Nagai, *J. Organomet. Chem.*, **208**, 145 (1981); K. Yamamoto, S. Suzuki, and J. Tsuji, *Tetrahedron Lett.*, **21**, 1653 (1980); H. Azizian, C. Eaborn, and A. Pidcock, *J. Organomet. Chem.*, **215**, 49 (1981); C. Eaborn, R. W. Griffiths, and A. Pidcock, *ibid.*, **225**, 331 (1982); R. Calas, J. Jaqcques, G. Deleris, and N. Duffaut, *ibid.*, **225**, 117 (1982).

2) H. Urata, H. Suzuki, Y. Moro-oka, and T. Ikawa, *J. Organomet. Chem.*, **234**, 367 (1982).

3) E. W. Colvin, "Silicon in Organic Synthesis," Butterworths, London (1981), pp. 198—213 and references cited therein.

4) C. Tamborski and E. J. Soloski, *J. Org. Chem.*, **28**, 237 (1963).

5) P. A. Levene, *Org. Synth.*, Coll. Vol. II, 88 (1943).

6) J. R. Catch, D. F. Elliot, D. H. Hey, and E. R. H. Jones, *J. Chem. Soc.*, **1948**, 272; J. R. Catch, D. H. Hey, E. R. H. Jones, and W. Wilson, *ibid.*, **1948**, 276.

7) G. A. Hill and E. L. Kropa, *J. Am. Chem. Soc.*, **55**, 2509 (1933).

8) R. M. Cowper and L. H. Davidson, *Org. Synth.*, Coll. Vol. II, 480 (1943).

9) M. S. Newman, M. D. Farbman, and H. Hipsher, *Org. Synth.*, Coll. Vol. III, 188 (1955).

10) D. R. Coulson, *Inorg. Synth.*, **13**, 121 (1972).

11) J. Chatt and F. G. Mann, *J. Chem. Soc.*, **1939**, 1631.

12) M. S. Khrasch, R. C. Seyler, and F. R. Mayo, *J. Am. Chem. Soc.*, **60**, 882 (1938).

13) J. A. Osborn and G. Wilkinson, *Inorg. Synth.*, **10**, 67 (1967).

14) F. A. Cotton, O. D. Faut, and D. M. L. Goodgame, *J. Am. Chem. Soc.*, **83**, 344 (1961).

15) W. T. Dent, R. Long, and A. J. Wilkinson, *J. Chem. Soc.*, **1964**, 1584.

16) H. O. House, L. J. Czuba, M. Call, and H. D. Olmstead, *J. Org. Chem.*, **34**, 2324 (1969).

17) C. R. Kruger and E. G. Rochow, *J. Organomet. Chem.*, **1**, 476 (1964).

The Configurations of *N*-Methyl- and *N*-*t*-Butyl-α-methoxycarbonylmethanimine *N*-Oxides

Yoshinobu INOUYE,* Kazuharu TAKAYA, and Hiroshi KAKISAWA
Department of Chemistry, University of Tsukuba, Sakura-mura, Niihari-gun, Ibaraki 305
(Received June 3, 1983)

Synopsis. *N*-Methyl-α-methoxycarbonylmethanimine *N*-oxide, *Z* configuration in crystal, was found to exhibit a facile equilibration with its *E*-isomer in solution. The configuration of *N*-*t*-butyl derivative was always *Z*.

Recently, we found that *N*-benzyl-α-methoxycarbonylmethanimine *N*-oxide (**1**) and its analogues exist in one configuration in the crystalline state but, in solution, exhibit a facile isomerization to give a mixture of *E*- and *Z*-isomers.[1] The configuration of **1** in the crystalline state have been proved to be *Z* by X-ray crystal analysis.[2]

In this paper, we wish report the geometrical structures of *N*-methyl- (**2**) and *N*-*t*-butyl-α-methoxycarbonylmethanimine *N*-oxides (**3**) in order to clarify the influence of a substituent on the nitrogen atom.

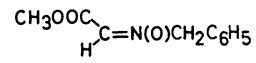

1

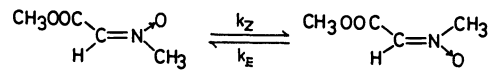

2Z **2E**

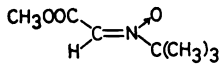

3

Experimental

Preparation of 2 and 3. According to the procedure of Winterfeldt and co-workers,[3] **2** and **3** were prepared from *N*-alkylhydroxylamine hydrochloride and methyl glyoxylate[4] in the presence of sodium acetate and calcium chloride.

2, Mp 69—71 °C (from benzene, lit,[3] mp 71 °C); ν (KBr): 1710 and 1230 cm^{-1}; λ_{max}(MeOH): 268 nm. Found: C, 40.98; H, 6.03; N, 11.96%. Calcd for $C_4H_7NO_3$: C, 41.02; H, 6.03; N, 11.96%.

3, Bath temp 110—120 °C/0.55 mmHg (1 mmHg≈133.322 Pa) (Kugelrohr dist): ν(film): 1720 and 1180 br cm^{-1}; λ_{max} (MeOH): 270 nm. Found: C, 52.98; H, 8.42; N, 8.66%. Calcd for $C_7H_{13}NO_3$: C, 52.81; H, 8.23; N, 8.79%.

^{1}H-NMR Measurements. ^{1}H-NMR spectra were obtained on a JEOL JNM-PMX60SI spectrophotometer and δ-values were calculated from the TMS as an internal standard (35 °C).

Discussion

The *N*-methyl derivative **2** had been already prepared in 1969 by Winterfeldt and co-workers[3] and the ^{1}H-NMR spectrum ($CDCl_3$) reported showed only three signals at δ 7.39, 3.82, and 3.66. These results suggested the absence of a geometrical isomer.

However, as shown clearly in Fig. 1, the spectra of **2** changed gradually with the elapse of time. The signal at δ 3.81 decreased, while a new peak appeared at δ 4.14 increased. The relative intensities of these two peaks remain constant after 40 min.

The signal at δ 4.14 is assignable to the *N*-CH_3 group in *E*-nitrone (**2E**) as the result of the deshielding effect of the neighboring methoxycarbonyl group.[1] Thus, the phenomena in Fig. 1 are explained by arguing that an initial *Z*-nitrone (**2Z**), which determines the crystal structure, isomerizes to the *E*-isomer (**2E**) when it dissolves in $CDCl_3$ and that, after 40 min, the system reaches the equilibrium mixture of both isomers. The *E*/*Z* ratio at equilibrium was calculated from the peak areas of δ 4.14 and 3.81 and the rate constant of isomerization was obtained from the *E*/*Z* ratios at different time. The results are summarized in Table 1.

From the Table, it is clear that the solvent polarity is significant in determining the *E*/*Z* ratio at equilibrium: the less polar the solvent polarity, the more predominant the *E*-isomer. Although the detailed mechanism of the stabilizing the two geometrical isomers in a given solvent is still unclear, the *Z*-isomer, which is anticipated[5] to have a larger dipole moment than the *E*-isomer, is thought to be more stabilized

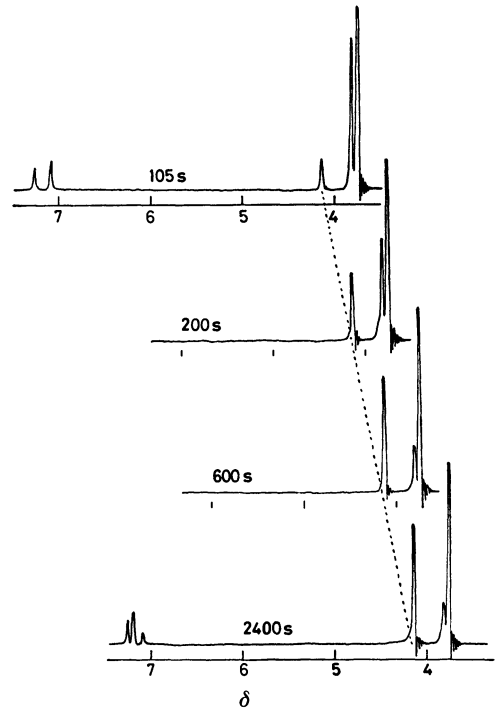

Fig. 1. Time-dependence of the intensities of methyl protons in the ^{1}H-NMR spectra of **2** in $CDCl_3$.

Table 1. The *E/Z* ratio and the rate constant of isomerization of **2**[a)]

Solvent	*E/Z*	k_Z/s^{-1}	k_E/s^{-1}
C_6D_6	6.0		
$CDCl_3$	3.8	2.4×10^{-3}	6.2×10^{-4}
CD_3OD	0.83	3.3×10^{-5}	4.0×10^{-5}
DMSO-d_6	0.67		

a) Measured at 0.08 mmol of **2** in 0.3 ml of each solvent.

in more polar solvents.

The rate constant in CD_3OD is smaller than that in $CDCl_3$. This can be partially explained by considering the hydrogen bonding between the nitrone oxygen and the solvent hydrogen (=N→O···H–O–R).

In the case of *N*-*t*-butyl derivative **3**, both ^{1}H-NMR (δ in $CDCl_3$: 7.25, 3.76, and 1.49) and ^{13}C-NMR (δ in $CDCl_3$: 161.3, 121.1, 74.8, 51.8, and 28.2) were simple and no changes were observed even when the temperature was raised to 62 °C. This shows that only one configurational isomer is present in solution. As a large NOE (35%) was observed between the olefinic proton and *t*-butyl protons,[6)] the configuration of the nitrone **3** was proved to be *Z*.

Various derivatives have been investigated; among these, *N*-alkyl-α-methoxycarbonylmethanimine *N*-oxides which have at least one hydrogen at the carbon attached to the nitrogen of the nitrone chromophore are apt to equilibrate into *E*- and *Z*-isomers in solution at room temperature.

References

1) Y. Inouye, J. Hara, and H. Kakisawa, *Chem. Lett.*, **1980**, 1407.
2) Y. Inouye, *Bull. Chem. Soc. Jpn.*, **56**, 244 (1983).
3) E. Winterfeldt, W. Krohn, and H.-U. Stracke, *Chem. Ber.*, **102**, 2346 (1969).
4) T. R. Kelly, T. E. Schmidt, and J. G. Haggerty, *Synthesis*, **1972**, 544.
5) *Cf.* F. Barrow and F. J. Thorneycroft, *J. Chem. Soc.*, **1934**, 722; **1939**, 773.
6) *Cf.* D. R. Boyd, W. B. Jennings, R. Sprath, and D. M. Jerina, *J. Chem. Soc., Chem. Commun.*, **1970**, 745.

Convenient Preparation of Methylthiomethyl *p*-Tolyl Sulfone Starting from Dimethyl Sulfoxide

Katsuyuki OGURA,* Nobuhiro YAHATA, Jun-ichi WATANABE, Kazumasa TAKAHASHI, and Hirotada IIDA

Department of Synthetic Chemistry, Faculty of Engineering, Chiba University, Yayoicho 1-33, Chiba 260

(Received June 4, 1983)

Synopsis. An efficient method for preparing methylthiomethyl *p*-tolyl sulfone was accomplished by the Pummerer reaction of dimethyl sulfoxide with acetic anhydride followed by treatment of the resulting acetoxymethyl methyl sulfide with sodium *p*-toluenesulfinate in the presence of sodium acetate in acetic acid.

In a previous paper,[1] methylthiomethyl *p*-tolyl sulfone (**1**) was shown to be one of the most useful reagents for preparation of *S*-methyl α-oxo thiocarboxylates, carboxylic esters, five- and six-membered cycloalkanones, and α-methoxy-α-arylacetic esters.[2] With regard to formation of **1**, there has been only one report which describes the reaction of (*p*-tolylsulfonyl)acetone with *S*-methyl *p*-toluenethiosulfonate in the presence of sodium carbonate followed by hydrolysis to give **1**.[3] However, this does not seem to be suitable as a preparative method of **1** because these starting materials are not easily available. Hence, our effort was devoted to exploiting a convenient method for its synthesis; we have found an efficient route from inexpensive dimethyl sulfoxide (**2**) to **1** *via* acetoxymethyl methyl sulfide (**3**) in a "one-pot" fashion, as outlined in the following scheme.

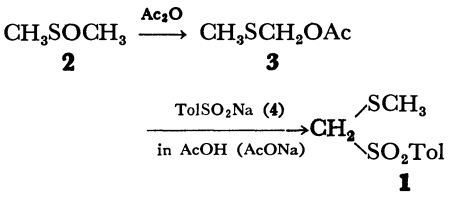

First, the substitution of acetoxymethyl methyl sulfide (**3**)[4] with *p*-toluenesulfinate anion was investigated. Heating **3** together with sodium *p*-toluenesulfinate (**4**) in DMF at 80—90 °C afforded only a trace of **1**. Efforts were made to achieve a higher yield of **1** by variation of reaction conditions (solvent, temperature, time). Acetic acid was found to be the most suitable solvent. In acetic acid, the substitution reaction occurred at 100 °C, and **1** was produced in 65% yield after heating for 48 h. It may be reasonable to assume that acetic acid not only serves as an appropriate solvent for **4**, but enhances the capability of the acetoxyl group as a leaving group by protonation. Since **3** was obtained by the Pummerer reaction of dimethyl sulfoxide (**2**) with acetic anhydride where acetic acid is the only by-product, the employment of acetic acid as a solvent in the above substitution allows the synthesis of **1** from **2** to perform in one flask without isolation of the intermediate **3**. Thus, a mixture of **2** and acetic anhydride (1.3 mol-equiv. to **2**) was heated at 80 °C for 24 h, and, after addition of acetic acid and sodium *p*-toluenesulfinate (1.5 mol-equiv. to **2**), the resulting mixture was further heated at 100 °C for 26 h to give **1** in 57% yield. It was also found that the presence of sodium acetate (1 mol-equiv. to **2**) in the substitution step (**3**→**1**) increased the yield of **1** to 71%. Sodium acetate is thought to prevent production of *p*-toluenesulfinic acid, which affords *S*-*p*-tolyl *p*-toluenethiosulfonate and di-*p*-tolyl disulfide at an elevated temperature.

It should be noted that a combination of acetic anhydride, acetic acid, and sodium *p*-toluenesulfinate was crucial to the above reaction. As mentioned above, DMF is not suitable as a solvent. When propionic anhydride and propionic acid were employed, the yield of **1** was 15%. The use of sodium benzenesulfinate (**5**) in place of **4** gave methylthiomethyl phenyl sulfone (**6**), but the yield was lower (25—38% overall yield from **2**) in the presence or absence of sodium acetate. Furthermore, the reaction of chloromethyl methyl sulfide (**7**) with **4** in THF, DMF, or diglyme met with no success. In spite of many efforts, the maximum yield (22%) of **1** was attained when the reaction was carried out by stirring **4** and **7** in DMF at room temperature for 44 h (see also Experimental section).

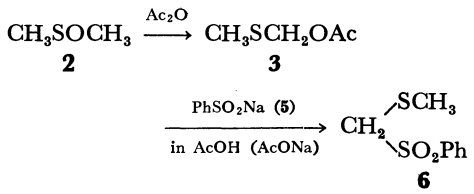

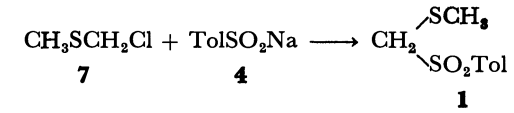

Thus we have found that **1** can be conveniently prepared from inexpensive dimethyl sulfoxide by successive treatment with acetic anhydride and with commercially available sodium *p*-toluenesulfinate in one flask.

Experimental

Melting points were determined on a hot-stage microscope (Yanagimoto) and were uncorrected. ^{1}H NMR spectra were obtained on a Hitachi R-600 spectrometer. Infrared spectra were determined with a JASCO A-200 spectrometer.

One-pot Preparation of Methylthiomethyl p-*Tolyl Sulfone (1) from Dimethyl Sulfoxide (2)*: A mixture of **2** (9.25 g: 0.118 mol) and freshly distilled acetic anhydride (15.60 g: 0.153 mol) was heated at 80 °C for 24 h and then cooled to ambient temperature. Acetic acid (90 ml), sodium acetate (9.70 g: 0.118 mol), and sodium *p*-toluenesulfinate[5] (31.60 g: 0.178 mol) were successively added to the mixture, and the resulting

mixture was again heated at 100 °C for 26 h. After addition of brine (150 ml), the mixture was extracted with five 70-ml portions of dichloromethane. The extracts were combined, dried over anhydrous sodium sulfate, and evaporated under reduced pressure to give 27.20 g of pale yellow crystals containing a small amount of an oil. Recrystallization of these crystals from 95% ethanol afforded 13.31 g of **1** as colorless needles. The mother liquor was evaporated and subjected to a column chromatography on silica gel using hexane and benzene as eluents to give 4.88 g of **1** as colorless crystals. The total yield of **1** was 71%: mp 82—83 °C (lit,[3] 80 °C); ^{1}H NMR ($CDCl_3$) δ=2.29 (3H, s), 2.46 (3H, s), 3.93 (2H, s), 7.37 (2H, d, J=8 Hz), and 7.87 (2H, d, J=8 Hz); IR (KBr) 1295, 1160, 1117, 1018, 740, 542, and 507 cm^{-1}.

Calcd for $C_9H_{12}O_2S_2$: C, 49.98; H, 5.59%. Found: C, 50.09; H, 5.56%.

*Preparation of Methylthiomethyl Phenyl Sulfone (**6**)*: A mixture of dimethyl sulfoxide (1.04 g: 13.3 mmol) and acetic anhydride (1.76 g: 17.3 mmol) was heated at 80 °C for 24 h. After the mixture was cooled to ambient temperature, acetic acid (10 ml), sodium acetate (1.09 g: 13.3 mmol), and sodium benzenesulfinate (**5**) (3.27 g: 19.9 mmol) were added and the resulting mixture was heated at 100 °C for 26 h. The usual workup [addition of water and extraction with dichloromethane] and column chromatography on silica gel (eluted with hexane and benzene) gave 1.01 g (38% yield) of methylthiomethyl phenyl sulfone (**6**) as colorless crystals: mp 86.5—87.5 °C (from 95% ethanol); ^{1}H NMR ($CDCl_3$): δ=2.32 (3H, s), 3.96 (2H, s), and 7.48—8.09 (5H, m); IR (KBr) 1292, 1160, 1116, 1080, 741, 544, and 520 cm^{-1}.

Calcd for $C_8H_{10}O_2S_2$: C, 47.50; H, 4.98%. Found: C, 47.62; H, 4.96%.

*Conversion of Dimethyl Sulfoxide (**2**) to **1** Using Propionic Anhydride, Propionic Acid, and **4***: A mixture of **2** (1.27 g: (16.3 mmol) and propionic anhydride (2.84 g: 21.8 mmol) was heated at 80 °C for 24 h. After being cooled to room temperature, propionic acid (20 ml) and **4** (4.35 g: 24.4 mmol) were added and the resulting mixture was heated at 100 °C for 48 h. Water (40 ml) was added and the reaction mixture was extracted with five 40-ml portions of dichloromethane. The extracts were combined, washed with water, dried over anhydrous sodium sulfate, and evaporated under reduced pressure. Column chromatography on silica gel using hexane and benzene as eluents afforded 518 mg (15% yield) of **1**.

*Reaction of Chloromethyl Methyl Sulfide (**7**) with Sodium p-Toluenesulfinate (**4**)*: A mixture containing 7 (5.65 g: 58.6 mmol) and **4** (15.72 g: 88.3 mmol) in DMF (60 ml) was stirred at room temperature for 44 h. After addition of water (100 ml), the mixture was extracted with four 40-ml portions of dichloromethane. The extracts were combined, washed with water, dried over anhydrous sodium sulfate, and evaporated under reduced pressure. The residue was subjected to column chromatography on silica gel using hexane and benzene as eluents to give 2.84 g (22% yield) of **1**.

Several reaction conditions were also examined for the reaction of **7** with **4** (1.2—1.75 mol-equiv.), but the yields of **1** were low [70 °C/28 h in DMF, 19%; 40 °C/116 h in THF in the presence of n-$Bu_4N \cdot HSO_4$ (0.2 mol-equiv.), 11%; r.t./70 h in diglyme, 10%; r.t./70 h without solvent, 10%]

References

1) K. Ogura, N. Yahata, K. Hashizume, K. Tsuyama, K. Takahashi, and H. Iida, *Chem. Lett.*, **1983**, 767.

2) Formylation of **1** with methyl formate in the presence of potassium t-butoxide in THF was reported: G. Ferdinand and K. Schank, *Synthesis*, **1976**, 406.

3) D. T. Gibson, *J. Chem. Soc.*, **1932**, 1819.

4) L. Horner and P. Kaiser, *Justus Liebigs Ann. Chem.*, **626**, 19 (1959).

5) Sodium p-toluenesulfinate (**4**) was dried over phosphorus pentaoxide prior to use.

Charge-carrier Transport in Nematic 2-(*p*-Decyloxybenzylideneamino)-9-Fluorenone

Ken-ichi OKAMOTO,* Shu NAKAJIMA, Akira ITAYA, and Shigekazu KUSABAYASHI†
Department of Chemical Engineering, Faculty of Engineering, Yamaguchi University, Ube, Yamaguchi 755
†*Department of Applied Chemistry, Faculty of Engineering, Osaka University, Suita, Osaka 565*
(Received January 8, 1983)

2-(*p*-Decyloxybenzylideneamino)-9-fluorenone (DBAF), with a large π-electronic group, showed a transient photocurrent induced by the strongly-absorbed light from a N_2 gas laser in the nematic, monotropic smectic, and isotropic liquid states. This photocurrent seemed to be due to the space-charge-limited current. The drift mobilities of the positive and negative charge carriers (μ_p and μ_n respectively) were determined from the peak time. The μ_n was ten times larger than μ_p, while the activation energies were identical. The modified Walden rule was valid in the nematic state ranging from 90 °C to 135 °C. The nematic mixtures of DBAF and *N*-(*p*-methoxybenzylidene)-*p*-butylaniline also showed a similar transient photocurrent, the magnitude of which increased significantly with an increase in the DBAF content. The mobilities were independent of the DBAF content and were nearly equal to those in nematic DBAF at the same viscosity, η: that is, $\mu_n = 3 \times 10^{-5}$, and $\mu_p = 2.5 \times 10^{-6}$ cm²/V s at $\eta = 0.026$ Pa s. These facts indicate that the nature of the carrier transport of the photoconduction is not electronic, but ionic. The O_2^- and the cation radical of DBAF are proposed as the ionic carrier species for both nematic DBAF and the nematic mixtures.

Charge-carrier transport in liquid crystals has been extensively studied over the last ten years and has been found to be of an ionic nature.[1-10] In most of the studies, either the voltage-pulse-injection method[1-4] or the polarity-inversion method[5,6] has been used to measure the carrier mobility. These methods, however, give no direct information as to the sign of the carriers. Yamashita and Amemiya have measured the drift mobility of the positive charge carriers photoinjected from an amorphous Se layer in nematic *N*-(*p*-methoxybenzylidene)-*p*-butylaniline (MBBA).[8] To our knowledge, this is the only case where the sign of the carriers migrating in a liquid crystal has been identified. On the contrary, the drift mobility in many organic solids has been measured separately for the positive and negative charge carriers. This is because the time-of-flight method is easily applied to the organic solids where the pulse-photocurrent is caused by pulsed strongly-absorbed light. Unfortunately, the liquid crystals investigated to date have not been photoconductive.

In the previous paper,[11] we found that nematic 2-(*p*-decyloxybenzylideneamino)-9-fluorenone (DBAF), which has a relatively large π-electronic group, showed photoconduction in its absorption region. In the present investigation, we measured the transient photocurrent induced by pulsed strongly-absorbed light to determine the drift mobility. We believe that this is the first report in which the drift mobilities have been determined separately for the positive and negative charge carriers in a liquid crystal.

Experimental

The DBAF was prepared as has been described previously.[11] The MBBA was obtained commercially and was purified with vacuum distillation. The sample was sandwiched between two nesa-coated glass electrodes with a Myler spacer 20—100 μm thick. Cells with a homogeneous alignment were prepared by means of the rubbing technique of the glass electrodes.[11] Caution was taken in preparing the cells so as not to heat the DBAF sample above 95 °C. The effective area of the cells was typically 1 cm². A nitrogen-gas laser (3 ns in pulse width) was irradiated on a cell set in a cryostat with an argon atmosphere. The induced photocurrent was observed through a series load resistor by means of a storage oscilloscope. Before the measurement, the dark current was cancelled out by means of a compensation circuit. The viscosity was measured with an Ostwald viscometer calibrated by using MBBA[12] and hexadecane[13] as standard samples.

Results and Discussion

Typical traces of the transient photocurrent are shown in Fig. 1. The attenuation coefficient of a nematic DBAF sample was evaluated to be 1.2×10^5 cm^{-1} at 337 nm from the molar extinction coefficient of its benzene solution (2.2×10^4 M^{-1} cm^{-1}). This value indicates that the exciting light is absorbed within the surface layer to a depth of less than 0.5 μm. The original photocarriers, which are supposed to be the cation radical of DBAF and the anion radical of either DBAF or an electron-acceptor impurity,[11] are generated in this surface layer. When the front electrode is

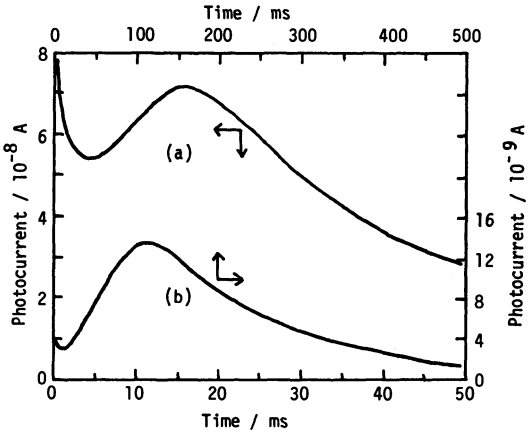

Fig. 1. Typical traces of transient photocurrent in nematic DBAF. (a) and (b): Negative- and positive-electrode illuminations, respectively. Applied voltage: 34 V, sample thickness: 30 μm, temperature: 97 °C.

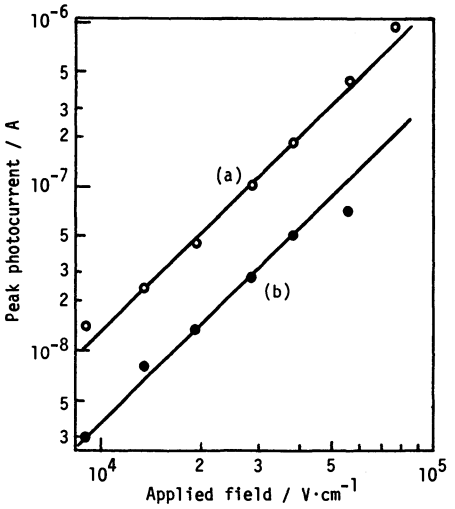

Fig. 2. Dependence of peak photocurrent on applied electric field. (a) and (b): Negative- and positive-electrode illuminations. Sample thickness: 50 μm, temperature: 97 °C.

positively biased, the positive-charge carriers can drift toward the back electrode, and *vice versa*. Thus, the transient photocurrent observed for the positive- or negative-electrode illumination is due to the positive- or negative-charge carriers respectively.

The transient photocurrent showed a peak, as may be seen in Fig. 1. The peak photocurrent was proportional to the square of the applied field, as shown in Fig. 2. It was roughly proportional to the inverse cube of the sample thickness. Judging from these facts, the observed transient photocurrent seems to be to the space-charge-limited current. The drift mobility, μ, was calculated from the peak time, t_p, according to Eq. 1;[14]

$$\mu = 0.79\, d^2/t_p\, V, \qquad (1)$$

where d is the sample thickness, and V, the applied voltage. Thus, the drift mobilities of the positive- and negative-charge carriers were determined separately and labelled μ_p and μ_n respectively.

The mobilities in nematic DBAF were independent of the sample thickness, but they were dependent on the applied electric field, as shown in Fig. 3. The μ_n was roughly proportional to the root of the field, while the μ_p increased at a much slower rate with an increase in the field. It has been suggested that the ionic mobility measured in high electric fields is probably overestimated because of the effect of the electrohydrodynamic (EHD) flow.[8,9] This suggests that the mobility in liquid crystals may be dependent on the field. The mobility in liquid crystals has, however, been reported to be independent of the field,[1-3,5-9] except in only one report.[4] Both μ_n and μ_p in the nematic mixtures of MBBA and DBAF, which will be mentioned below, were independent of the field, as shown in Fig. 3. The EHD flow was observed for both nematic DBAF and nematic mixtures of DBAF and MBBA in fields higher than about 2×10^3 V/cm. These facts suggest that the field dependence of the mobility in nematic DBAF is not due to the effect of the EHD flow. At present,

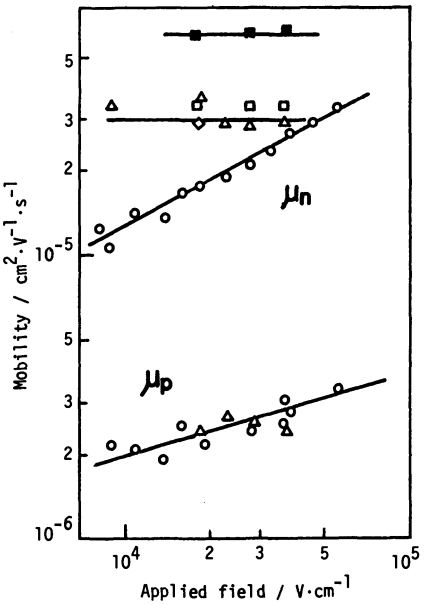

Fig. 3. Dependence of drift mobility on applied electric field.
DBAF: ○, at 97 °C. Nematic mixtures of MBBA and DBAF: △, 30 mol% of DBAF at 55 °C; □, 20 mol% of DBAF at 55 °C; ◇; 10 mol% of DBAF at 35 °C; ■, 20 mol% of DBAF in isotropic liquid state at 68.5 °C.

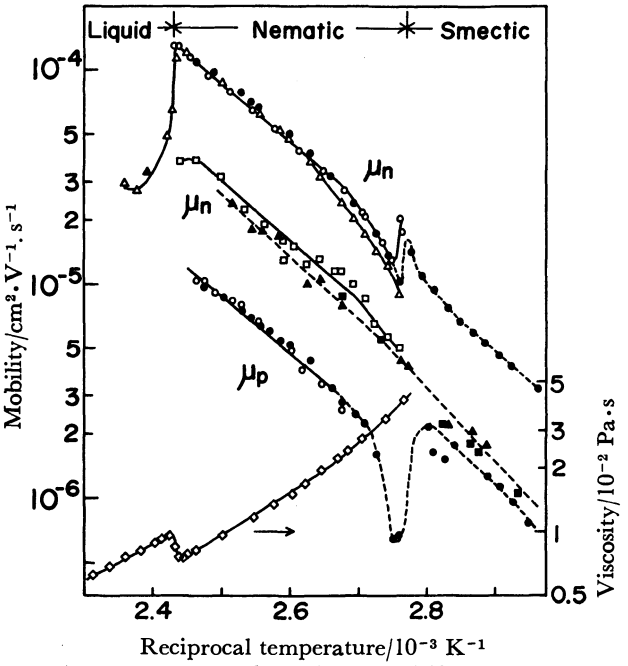

Fig. 4. Temperature dependence of drift mobilities and viscosity.
○, △, and □: 1st, 2nd, and 3rd heating runs, respectively. ●, ▲, and ■: 1st, 2nd, and 3rd cooling runs, respectively.

though, we have no explanation for this field dependence.

The temperature dependence of the mobilities at the field of 3.66×10^4 V/cm is shown in Fig. 4. The mobility data were reproducible unless the cell was heated up to the isotropic liquid state. In the nematic state, both

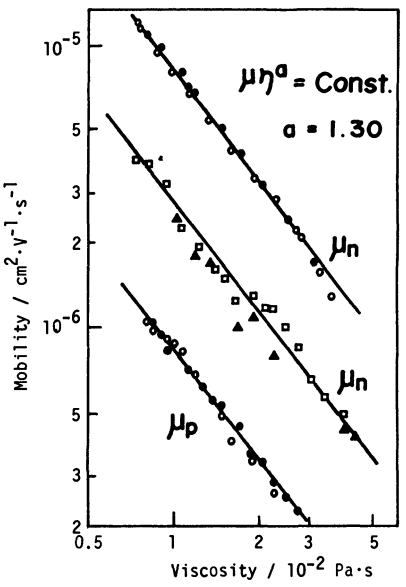

Fig. 5. Viscosity dependence of drift mobility in nematic state. Keys are identical with those in Fig. 4.

μ_n and μ_p had the same activation energy of *ca.* 0.54 eV. On the cooling runs, the mobilities showed a discrete change at the transition from the nematic phase to the smectic phase (88.7 °C), while their activation energies in the smectic state were nearly equal to those in the nematic state. The μ_n decreased abruptly and irreversibly at the transition from the nematic to the isotropic phase (138.7 °C). Once the cell was heated up to the isotropic liquid state, the μ_n in the nematic state as well as in the smectic one decreased to a third of its original value, as shown in Fig. 4, while the activation energy practically did not change.

The temperature dependence of the viscosity is also shown in Fig. 4. The activation energy of the viscosity was *ca.* 0.40 eV for both nematic and isotropic liquid states.

If the carrier transport is of an ionic nature, Walden's rule (Eq. 2) or its modification (Eq. 3) should be valid:[15]

$$\mu\eta = e/6r, \quad (2)$$

$$\mu\eta^a = \text{constant}, \quad (3)$$

where e is the electronic charge; r, the effective radius of the ionic carrier species, and a, an experimental constant close to unity. The mobility data for the nematic state shown in Fig. 4 were replotted against the viscosity in the bilogarithmic form according to Eq. 3. As shown in Fig. 5, straight lines with the same slope were obtained: they gave the a value as 1.3. It should also be noted that the modified Walden's rule is valid in the nematic state over the wide range from 90 °C to 135 °C.

The transient photocurrent in the nematic mixtures of MBBA and DBAF was also measured at the temperatures where the viscosity of the mixtures was roughly equal to that of DBAF at 97 °C (2.6×10^{-2} Pa s). Nematic MBBA did not show the transient photocurrent, although it absorbed the exciting light strongly. The nematic mixtures containing more than 10 mol% of DBAF showed a transient photocurrent similar to that shown in Fig. 1. The peak photocurrent increased about ten times with an increase in the DBAF content from 10 mol% to 30 mol%, indicating that the photocarriers were generated from the excited state of DBAF. On the other hand, the drift mobilities in the nematic mixtures were independent of the DBAF content and were nearly equal to those in nematic DBAF, as shown in Fig. 3; that is, $\mu_n=3\times10^{-5}$ and $\mu_p=2.5\times10^{-6}$ cm^2/V s at $\eta=2.6\times10^{-2}$ Pa s. This important fact indicates that the photocarriers do not migrate in nematic media by means of the electronic hopping process, but by means of the ionic process, and that the ionic carrier species are identical between nematic DBAF and the nematic mixtures of MBBA and DBAF.

In both nematic DBAF and the nematic mixtures of MBBA and DBAF, the effective radii of the negative ionic carriers were estimated from Eq. 2 to be *ca.* 1.1 Å. This value is quite small. In MBBA and 4,4′-azoxyanisole the radii of the ionic carriers have been estimated to be 2.1 and 1.1 Å respectively, and O^{2-} has been proposed as the negative carrier species.[3,7] The O_2^-, however, is the most probable negative carrier species in the present case for the following reasons. First, O_2 has the gaseous electron affinity of 0.44 eV,[16] which may be sufficient to accept an electron from the original negative photocarrier or the DBAF anion radical. Secondary, the effective radius of O_2^- has been reported to be 1.54 Å[17] or 1.4 Å.[18] These values are in fair agreement with the estimated value (1.1 Å). Third, it is well known that the carrier transport in liquid hydrocarbons changes from an electronic nature to an ionic one in the presence of only an extremely small amount of O_2.[19]

Once the cells were heated up to the isotropic liquid state with applying the electric field, the estimated radius of the negative ionic species changed from 1.1 Å to 4.1 Å. This suggests that an unknown degradation product acts as an electron trap instead of O_2.

In both nematic DBAF and the nematic mixtures of MBBA and DBAF, the radii of the positive ionic carriers were estimated from Eq. 2 to be 12.6 Å. This value is about ten times larger than that for the negative ones. 2-Amino-9-fluorenone, a probable impurity, is a candidate for the positive carrier species, because it may have an ionization potential sufficient to release an electron to the original positive photocarrier or the DBAF cation radical. It is, however, not probable that the 2-amino-9-fluorenone cation radical has an effective radius as large as 12.6 Å. Therefore, the DBAF cation radical itself seems to be the positive carrier species, actually migrating in the nematic media. For nematic MBBA, Yamashita and Amemiya have reported small μ_p values of $(6\text{—}9)\times10^{-6}$ cm^2/V s and proposed the MBBA cation radical as the positive carrier species.[8] Even in the nematic mixtures of MBBA and DBAF, the DBAF cation radical seems to be the positive carrier species, because the ionization potential of DBAF is smaller than that of MBBA.

It should be noted that μ_n is much larger than μ_p in the nematic state of MBBA,[3,8] DBAF, and their mixtures. A similar result was obtained for *N*-methyl-2-(*p*-hexyloxybenzylideneamino)-carbazole, which has a large π-electronic group;[20] that is, $\mu_n=1\times10^{-4}$ cm^2/V s

and $\mu_p = 1 \times 10^{-5}$ cm^2/V s in the nematic state at 122 °C. This is due to the significant difference in the effective radius of the carrier species between O_2^- and the corresponding cation radicals of the liquid crystal molecules. It may be considered that doping with an electron donor of a small molecular size increases μ_p appreciably.

Although being necessary to the occurrence of photoconduction, the presence of a π-electronic group in a liquid crystal molecule can not change the nature of carrier transport from ionic to electronic, as mentioned above. This can be explained as follows. For example, a DBAF molecule is composed of two parts. One is a fluorenone moiety which might serve as a hopping site. The other, a phenyl group with a long alkyloxy chain, is necessary to the presence of liquid crystal states. The latter part, which occupies the predominant space in the molecule, significantly reduces the electronic interaction between the large π-electronic groups. This is supported by the fact that the molecules having only the former part show electronic hopping transport in the liquid state, as has been reported for 2,4,7-trinitro-9-fluorenone[21] and benzene.[22]

References

1) G. H. Heilmeier and P. M. Heyman, *Phys. Rev. Lett.*, **18**, 583 (1967).
2) J. C. Lacroix and R. Tobazeon, *C. R. Acad. Sci. Paris, Ser. B*, **278**, 623 (1974).
3) T. Yanagisawa, H. Matsumoto, and K. Yahagi, *Jpn. J. Appl. Phys.*, **16**, 45 (1977).
4) A. Lipinski, W. Mycielski, and G. Derfel, *Mol. Cryst. Liq. Cryst. Lett.*, **41**, 137 (1978).
5) K. Yoshino, K. Yamashiro, and Y. Inuishi, *Jpn. J. Appl. Phys.*, **14**, 216 (1975).
6) K. Yoshino, N. Tanaka, and Y. Inuishi, *Jpn. J. Appl. Phys.*, **15**, 735 (1976).
7) K. Yoshino, S. Hisamitsu, and Y. Inuishi, *J. Phys. Soc. Jpn.*, **32**, 867 (1972).
8) M. Yamashita and Y. Amemiya, *Jpn. J. Appl. Phys.*, **17**, 1513 (1978).
9) G. Derfel and A. Lipinski, *Mol. Cryst. Liq. Cryst.*, **55**, 89 (1979).
10) M. Lesniak, W. Labno, E. Szwajczak, and A. Szymanski *Mol. Cryst. Liq. Cryst.*, **61**, 241 (1980).
11) K. Okamoto, S. Nakajima, M. Ueda, A. Itaya, and S. Kusabayashi, *Bull. Chem. Soc. Jpn.*, **56**, 3830 (1983).
12) P. Martionoty and S. Candan, *Mol. Cryst. Liq. Cryst.*, **14**, 243 (1971).
13) M. Gollis, *J. Chem. Eng. Data*, **7**, 311 (1962).
14) A. Many and G. Rakavy, *Phys. Rev.*, **126**, 1980 (1962).
15) I. Adamozwski and B. Jachym, *Acta Phys. Pol.*, **30**, 767 (1966).
16) R. Celotta, R. Bennett, J. Hall, M. W. Siegel, and J. Levine, *Phys. Rev. A*, **6**, 631 (1972).
17) U. Sowada and R. A. Holroyd, *J. Chem. Phys.*, **70**, 3586 (1979).
18) A. Henglein, *Ber. Bunsenges. Phys. Chem.*, **79**, 129 (1975).
19) R. M. Minday, L. D. Schmidt, and H. T. Davis, *J. Chem. Phys.*, **54**, 3112 (1971).
20) S. Kusabayashi *et al.*, to be published elsewhere.
21) W. D. Gill, "Photoconductivity and Related Phenomena," ed by J. Mort and D. M. Pai, Elsevier, Amsterdam (1976), p. 303.
22) H. Hirth and F. Stockmann, *Phys. Status Solidi B*, **51**, 691 (1972).

Pressure-Volume-Temperature Relations of Supercooled Liquid and Glass of Triphenylchloromethane/*o*-Terphenyl Mixture

Motosuke NAOKI* and Manabu MATSUSHITA
Department of Textiles and Polymers, Faculty of Technology, Gunma University, Kiryu, Gunma 376
(Received February 14, 1983)

Volumetric data on the supercooled liquid state and on the glassy state are reported for a binary mixture of triphenylchloromethane and *o*-terphenyl. In the supercooled liquid state, the thermal expansivity, the isothermal compressibility, and their temperature dependences of the mixture are much samller than those of simple molecular liquids and are almost the same order of magnitude as those of polymer liquids. The glass of the mixture also closely resembles polymer glasses in the apparent thermodynamic properties. Some representative lattice-like liquid theories are applied to the pressure-volume-temperature relations of the supercooled liquid sample, with the aid of the principle of corresponding states.

Supercooling and glass transition phenomena are general in all sorts of molecules.[1] Since polymer liquids can easily be supercooled and vitrified, many experimental and theoretical studies on the glass transition of polymers have been proposed.[2,3] The polymer glass transition has been interpreted as arising from a large decrease in the intramolecular conformational entropy of the liquid as the temperature decreases.[3,4] The models adopted in the theory above, however, may not be appropriate for simple molecular liquids.

Recent molecular dynamic simulation studies give some insight into properties of supercooled liquids and glasses,[5] but the one-component monatomic glasses to be studied by such computer experiments are usually extremely difficult to prepare experimentally.

While many accurate measurements of volumetric properties of supercooled liquids and glasses of polymers have been reported,[6-12] such measurements are few for simple molecular liquids due to their low glass transition temperature and poor stabilities of the supercooled liquid states. It is well known that *o*-terphenyl[13] and its mixtures[14] can be supercooled and vitrified. The supercooled liquid of a mixture of triphenylchloromethane (TPCM) and *o*-terphenyl (oTP), TPCM/oTP, was found to be still more stable oTP alone.[15] In this paper, we attempt to measure the pressure-volume-temperature (*P-V-T*) relations of TPCM/oTP below the melting temperature up to 78.5 MPa. The volumetric properties thus obtained are compared with some simple liquid theories.

Experimental

Sample. Triphenylchloromethane (TPCM, the melting temperature $T_m = 113$ °C) and *o*-terphenyl (oTP, $T_m = 55.5$ °C) were purchased from Tokyo Chemical Industry Co. and were used without further purification. A mixture of TPCM/oTP with composition of 25/75 in weight ratio was used in the present study.

The supercooled sample contained in Pyrex test tube was stable over one month at room temperature, but, when the sample was in contact with mercury, it crystallized after about one week. In the present dilatometric experiments, the sample is contained in a small pouch made of thin natural rubber vulcanizate to avoid evolutions of internal stress in the glassy sample as the sample vitrifies. When the sample contained in the rubber pouch was in contact with mercury, it crystallized after about two weeks.

Equipment. Measurements of the *P-V-T* relations were carried out in a Pyrex dilatometer set in a pressure vessel which was immersed in an ethylene glycol/water bath controlled to an accuracy of ±0.02 K by use of a refrigerator (CC-100, Neslab). The temperature was controlled within ±0.004 K in the pressure vessel which was outlined elsewhere.[12] Silicone oil (KF-94, Shin-Etsu Chemical Co.) was used to transmit the hydrostatic pressure. The pressure was measured by a Heise bourdon tube gauge with an automatic compensator (Dresser Industries) and the temperature by a calibrated alumel-chromel thermocouple inserted in the pressure vessel.

A schematic diagram of the pressure dilatometer is shown in Fig. 1. The sample was separated from mercury and Pyrex glass chamber by a thin pouch made of natural rubber vulcanizate. When the sample was directly in contact with the chamber, the dilatometer was almost always broken due to strong adhesion of the sample to the chamber wall as the sample vitrified. Even if the dilatometer was not broken, a high internal stress stored in the glassy sample would result in a poor reproducibility of the volumetric data.

Variations of the sample volume in the dilatometer with temperature and pressure were obtained from changes in the mercury level in the dilatometer, which was read by measuring the emf of a variable transformer (150-9, Shinko Electric Co.)

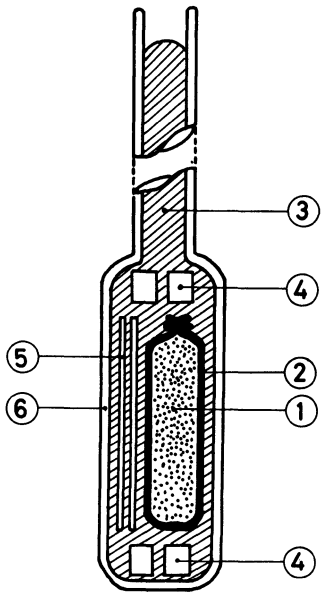

Fig. 1. Schematic diagram of pressure dilatometer.
1: Sample, 2: rubber pouch, 3: mercury, 4: pyrex stopper, 5: pyrex capillary, 6: pyrex chamber.

induced by a piece of Permalloy set on the top of mercury column. Pressure effects on the emf were negligibly small up to 100 MPa, but temperature effects were not.[12] The *P-V-T* data for mercury taken from Refs. 16 and 17 and a mercury-filled dilatometer were used to calibrate the temperature variation of the emf and to calculated the specific volume of the sample. Details of the pressure cell used and the treatments of data are given elsewhere.[12]

Experimental Procedure and Operations. TPCM and oTP were mixed at 130 °C. The sample was loaded in the rubber pouch at 70 °C, being degassed in slight vacuum. Then the sample was sealed by fastening the pouch with a band made of natural rubber vulcanizate. The rubber pouch and band had previously been purified by repeated sweeling with benzene and toluene and deswelling with methanol and acetone. Mercury was loaded in the dilatometer *in vacuo* at about −30 °C.

The density of the sample was measured at 30 °C by use of a picnometer of volume 25 ml. An isobaric cooling experiment to obtain T_g and the atmospheric V–T relation was carried out at about 1 K intervals in the liquid state and at about 0.5 K intervals in the glassy state with a continuous cooling rate of 0.24 K min^{-1} from 310 to 238 K. Then a heating experiment was carried out with a rate of 0.24 K min^{-1} from just above T_m of mercury (235.28 K) to 273 K.

Isothermal experiments in the supercooled liquid region were carried out to obtain the *P-V-T* relations at about 4 K intervals over a temperature range of 240—308 K. The pressure was changed in increments of 5.9 MPa in the 0.1—19.6 MPa region and in increments of 9.8 MPa in the 19.6—78.5 MPa region.

V-P relations of the glass vitrified by continuous cooling at a rate of 0.24 K min^{-1} were measured at about 1.5 K intervals from 235.5 K to 249.6 K. At lower temperatures, *V-P* relations under high pressures were not obtained due to crystallization of mercury. On the other hand, since the sample relaxed toward the equilibrium liquid state and slight retardations were observed in the volume at lower pressures near T_g, the pressure was not released in order to avoid the progressive retardation. The experiments for the glassy state were conducted as quick as feasible.

Although the sample penetrates into the natural rubber pouch, the excess mixing volume between TPCM/oTP and the pouch was ignored in the calculation of the specific volume v of the sample:

$$v_{app}(w+w_r) = wv + w_r v_r, \quad (1)$$

where v_{app} is the apparent average specific volume of the sample and the rubber pouch and band, v_r the specific volume of the pouch and band,[18] w the mass of the sample (1.1181 g), and w_r the total mass of the pouch and band (0.2653 g).

Results

Supercooled Liquid State. The results of the *P-V-T* experiments are summarized in Fig. 2. Each atmospheric isobar of the liquid volume from the heating experiment exactly falls on that from the cooling experiment above 254 K. The liquid state specific volume v is expressed by a quadratic equation in temperature T at each pressure P:

$$v = a_0 + a_1 T + a_2 T^2. \quad (2)$$

Values of a_0, a_1, a_2, and the standard deviation σ obtained by the least-squares method are listed in Table 1. The second derivatives a_2 are very small and the isobars of TPCM/oTP are very close to being linear in the supercooled liquid region. Thus the thermal expansivity α, $\alpha \equiv (\partial \ln v/\partial T)_p$, decreases with increasing temperature at all pressures in the present temperature region. Some examples of v and α calculated from Eq. 2 are shown in Figs. 3 and 4, respectively.

The *P-T* isochores calculated from Eq. 2 are shown

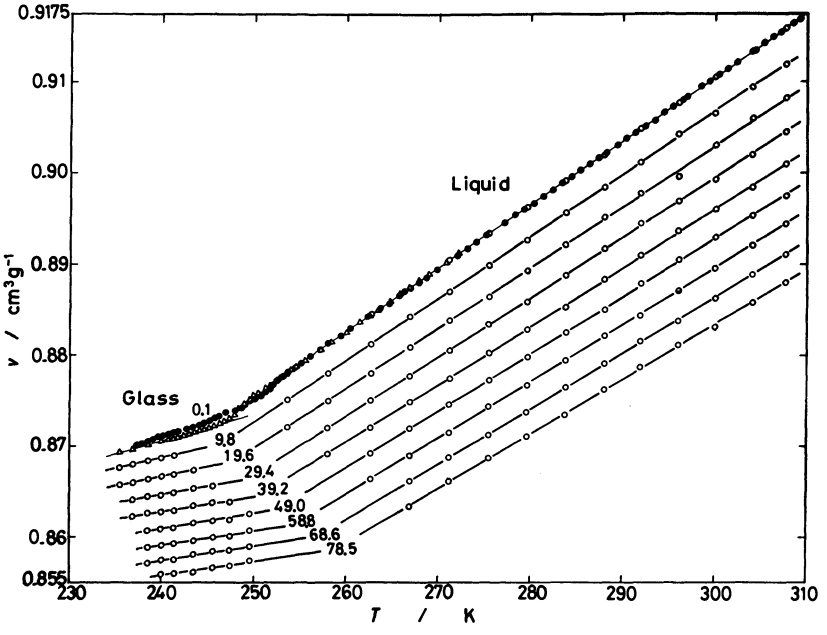

Fig. 2. Summary of *P-V-T* relations.
Open circles: isothermal experiments, closed circles: isobaric cooling experiment, triangles: isobaric heating experiment, lines: Eq. 2. Numbers in the figure are the pressures in MPa.

Table 1. Specific volume of the liquid

P / MPa	a_0 / cm^3 g^{-1}	$a_1\times10^4$ / K^{-1} cm^3 g^{-1}	$a_2\times10^7$ / K^{-2} cm^3 g^{-1}	$\sigma\times10^5$ / cm^3 g^{-1}	Region / K
0.1	0.71261	6.1650	1.440	2.6	254—310
4.9	0.71932	5.622	2.298	26.6	254—307
9.8	0.70905	6.331	0.860	13.2	254—307
14.7	0.71832	5.602	2.053	12.1	254—307
19.6	0.71907	5.528	2.002	22.9	254—307
29.4	0.71476	5.721	1.450	15.7	258—307
39.2	0.71765	5.432	1.708	16.2	258—307
49.0	0.70645	6.117	0.310	15.1	263—307
58.8	0.71507	5.376	1.467	10.7	263—307
68.6	0.70281	6.119	0	15.5	267—307
78.5	0.70314	6.009	0	17.9	267—307

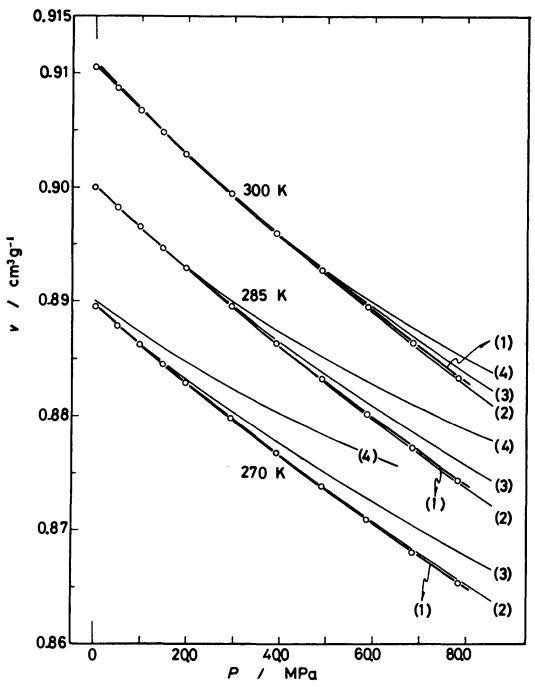

Fig. 3. Isotherms of specific volume in supercooled liquid region.
1: Tait equation, 2: Prigogine-Nanda-Simha equation, 3: Flory equation, 4: Simple Hole equation.

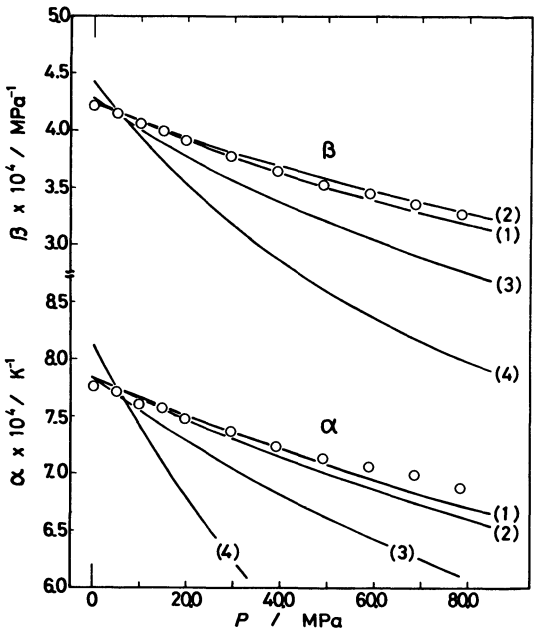

Fig. 4. Thermal expansivity and isothermal compressibility of supercooled liquid at 285 K. Indices of each line are the same as those in Fig. 3.

in Fig. 5. The isochores are approximately linear over the present experimental range. Thus the thermal pressure coefficient γ, $\gamma\equiv(\partial P/\partial T)_v$, of the supercooled TPCM/oTP, as well as most liquids,[19] is approximated as a function of volume only. Values of γ determined from slopes of the isochores are shown in Fig. 6. The variation of γ with volume is well represented by a linear equation:

$$\gamma = 11.159 - 10.350\,v \quad (\mathrm{K^{-1}\,MPa}), \tag{3}$$

with the standard deviation being 0.0033 K^{-1} MPa.

The isothermal compressibility β, $\beta\equiv-(\partial \ln v/\partial P)_T$, can be calculated from

$$\beta = \frac{\alpha}{\gamma}, \tag{4}$$

with α from Eq. 2 and γ from Eq. 3. The results are plotted as a function of pressure in Fig. 4. The values of α and β are smaller than those of ordinary molecular liquids[20] and poly(dimethylsioxane)[11,21] and very close to those of ordinary supercooled polymer liquids.[9-12]

The Tait equation is commonly written as[22]

$$\frac{v}{v_0} = 1 - C\ln\left(1+\frac{P-P_0}{B}\right), \tag{5}$$

where v_0 is the specific volume at the reference pressure P_0. Simha *et al.*[7,24] have shown that C can be assumed to have the universal value of 0.0894 and B can be expressed by

$$B = b_1 \exp(-b_2 T). \tag{6}$$

Values of b_1 and b_2 calculated by the least-squares

Table 2. Tait parameters

	C	b_1 / MPa	$b_2\times10^3$ / K^{-1}
Liquid	0.0894	577.3	3.5428
Glass	0.0894	8852	13.096

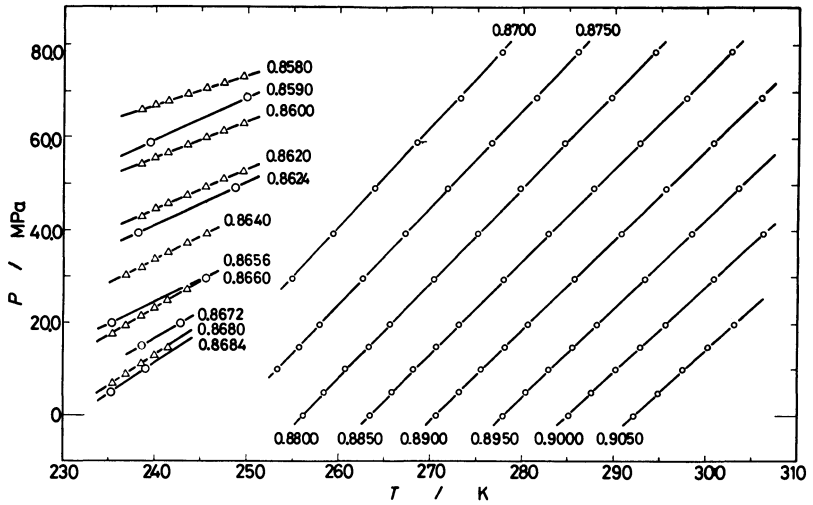

Fig. 5. Isochores of supercooled liquid and glass. The numbers in the figure are the specific volume in $cm^3\ g^{-1}$. Circles: from V-T relation, Eq. 2; triangles: from Tait equation, Eqs. 5 and 6.

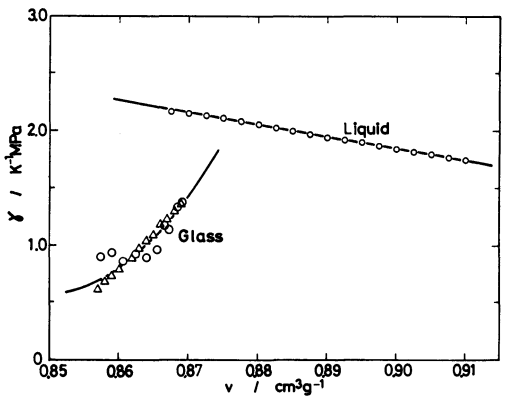

Fig. 6. Thermal pressure coefficient of supercooled liquid and glass.
Circles: from V-T relation, triangles: from Tait equation.

method are listed in Table 2. The average deviation in v/v_0 is 2.5×10^{-4}, which exceeds the deviation in Eq. 2 on the whole. As can be seen in Fig. 4, α and β calculated from Eq. 5 (indexed by (1)) agree well with those from Eqs. 2, 3, and 4 (circles).

Glassy State. In the glassy and glass transition regions, *i.e.*, 239—254 K Each atmospheric V-T isobar from the cooling experiment does not fall on that from the heating experiment, as shown in Fig. 2. In this region, the relation time is very long and the cooling isobar may not attain the one of the thermal steady state due to bulkiness of the sample. The atmospheric glass transition temperature obtained from the intersection point of the heating isobar and the liquid isobar (Eq. 2) is 244.2 K.

We have calculated the glass volume at elevated pressures based on the heating isobar. The glassy state specific volume were also expressed by Eq. 2 at each pressure. Values of the constants and the standard deviation in Eq. 2 obtained by the least-squares method are shown in Table 3, where isobars at elevated pressures are approximated by linear expressions, since the numbers of the experimental points are not sufficient. Volumetric properties of the glass calculated from Eq. 2 are summarized in Fig. 7.

The Tait equation was also applied for the glassy state and the average deviation was obtained to be 3.5×10^{-4}. The P-T isochores calculated from the isobars, Eq. 2, and from the isotherms, Eq. 5, are shown in Fig. 5.

TABLE 3. SPECIFIC VOLUME OF THE GLASS

P / MPa	a_0 / $cm^3\ g^{-1}$	$a_1\times10^4$ / $K^{-1}\ cm^3\ g^{-1}$	$a_2\times10^7$ / $K^{-2}\ cm^3\ g^{-1}$	$\sigma\times10^5$ / $cm^3\ g^{-1}$	Region / K
0.1	0.84550	−0.758	7.504	3	234.4—245.2
4.9	0.80650	2.630	—	1	235.5—240.0
9.8	0.81196	2.361	—	4	235.5—241.4
14.7	0.81459	2.205	—	4	235.5—241.4
19.6	0.81609	2.104	—	7	235.5—243.5
29.4	0.82180	1.784	—	8	236.9—245.6
39.2	0.82264	1.670	—	15	236.9—247.5
49.0	0.81897	1.746	—	15	238.5—249.6
58.8	0.82214	1.539	—	11	238.5—249.6
68.6	0.81865	1.614	—	12	238.5—249.6
78.5	0.81893	1.533	—	17	240.0—249.6

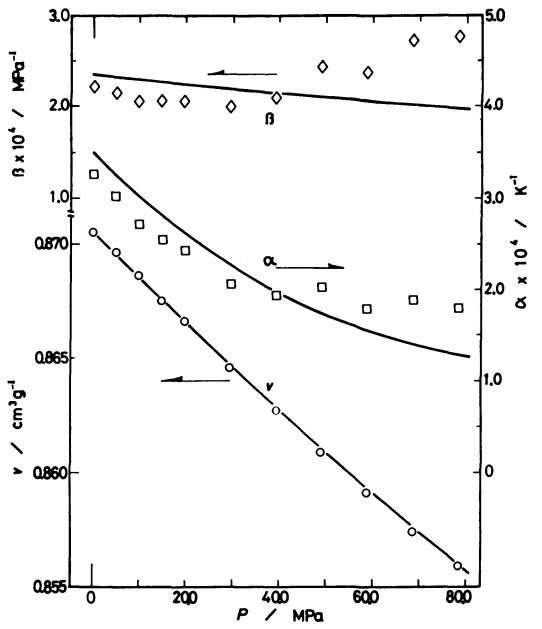

Fig. 7. Isotherms of specific volume (○), thermal expansivity (□), and isothermal compressibility (◇) in glassy state. Lines are calculations from Tait equation.

Values of γ determined from slopes of the isochores are shown in Fig. 6. Gamma from the isobars does not precisely agree with γ from the isotherms. A quadratic equation is applied to γ by the least-squares method:

$$\gamma = 1482.67 - 3489.57\,v + 2054.02\,v^2 \quad (\mathrm{K^{-1}\,MPa}), \tag{7}$$

where the standard deviation is 0.066 $\mathrm{K^{-1}}$ MPa.

As shown in Fig. 7, α calculated from Eqs. 5, 7, and 4 (solid line) approximately agrees with that from Eq. 2 (lozenges), but β from Eqs. 2, 7, and 4 (lozenges) considerably deviates from that from Eq. 5 (solid line). This implies the inconsistency involved in the empirical equations, Eqs. 2, 5, and 7. The inconsistency may arise from slow volumetric retardations of the glass towards an equilibrium liquid state.

Discussion

Comparison with Some Simple Equations of State for Supercooled Liquid. For the condensed liquid region, as an *empirical* or an *useful* equation of state, lattice-like liquid theories rather than more strict theories have widely used due to their simplicity and their quantitative success in liquids[24] and liquid mixtures.[25]

Prigogine, Trappeniers, and Mathot derived an equation of state for polymer liquids based on the Lennard-Jones and Devonshire cell model.[26,27] Its simplest form with a square-well approximation introduced by Nanda and Simha[28] is expressed as

$$\frac{\tilde{P}\tilde{v}}{\tilde{T}} = \frac{1}{1 - 2^{-1/6}\tilde{v}^{-1/3}} + \frac{\tilde{v}^{-4} - \tilde{v}^{-2}}{\tilde{T}}, \tag{8}$$

wihch is hereafter referred to as the PNS equation. $\tilde{P}$, $\tilde{v}$, and $\tilde{T}$ are the reduced quantities related to the ordinary configurational quantities such as P, v, and T through characteristic reduction parameters (with asterisk):

$$\tilde{P} = \frac{P}{P^*}, \quad \tilde{v} = \frac{V}{V^*}, \quad \tilde{T} = \frac{T}{T^*}. \tag{9}$$

Using Tonks' free volume[29] and a van der Waals type intermolecular potential energy, Flory, Orwall, and Vrij presented an equation of state:[30]

$$\frac{\tilde{P}\tilde{v}}{\tilde{T}} = \frac{1}{1 - \tilde{v}^{-1/3}} - \frac{1}{\tilde{v}\tilde{T}}, \tag{10}$$

which is hereafter referred to as the Flory equation.

Hole theories, which usually lead to equations of state of complex form, generally improve the cell theories in the low density region, but not in the high density region.[31] In the well condensed region such as the supercooled liquid state, little is expected for such hole theories without some adjustable parameters.[32] Therefore, we do not discuss them here.

Apart from the cell theories, the most primitive hole theory is constructed by adopting a random-mixing assumption on the distribution of occupied cells and empty cells:

$$\frac{\tilde{P}\tilde{v}}{\tilde{T}} = \tilde{v}\ln\frac{1}{1 - \tilde{v}^{-1}} - \frac{1}{\tilde{T}\tilde{v}}. \tag{11}$$

This is hereafter referred to as the Simple Hole equation. Based on this equation, Sanchez and Lacombe have proposed an equation of state for polymer liquids, which gives some qualitative success in polymer solution.[33]

From Eq. 9, αT and βP^* are expressed by

$$\alpha T = \left(\frac{\partial \ln \tilde{v}}{\partial \ln \tilde{T}}\right)_{\tilde{P}}, \tag{12}$$

$$\beta P^* = \left(\frac{\partial \ln \tilde{v}}{\partial \tilde{P}}\right)_{\tilde{T}}. \tag{13}$$

If the principle of corresponding states is applicable, αT and βP^* should be universal functions of the reduced quantities. At zero pressure, therefore, the theoretical αT *vs.* log $\tilde{v}$ curves should be shifted parallel to the log v axis to the experimental αT *vs.* log v curve. The shift factor corresponds to v^*. Similarly, the superposition of the theoretical αT curves parallel to the log T axis should give T^*. When T^* obtained above is employed, the superposition of the theoretical log βP^* curves parallel to the log β axis should give P^*. Results are summarized in Table 4.

The PNS equation approximately describes the variation of the thermal expansivity with pressure, *i.e.*, the variation of the compressibility with temperature, as shown in Fig. 4. This accordance can clearly be seen in Fig. 3. The PNS equation represents satisfactorily the *V-P* isotherms, while the Flory equation, as often demonstrated,[21,34] predicts appreciably less compressible than the experiments.

The Simple Hole equation, as naturally anticipated from its model which consists of gas-like molecules and

Table 4. Characteristic parameters for the liquid

Theory	v^* / cm³ g⁻¹	T^* / K	P^* / MPa
Prigogine-Nanda-Simha	0.75431	2129.6	754.74
Flory	0.75388	5934.7	743.19
Simple Hole	0.85467	944.7	577.96

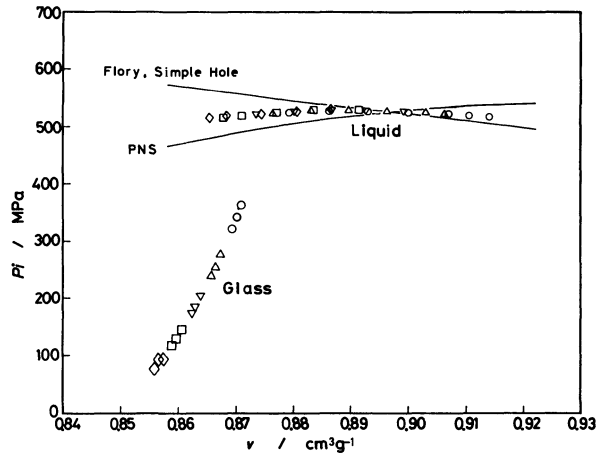

Fig. 8. Internal pressures of supercooled liquid and glass. Lines are theories.
○: 0.1, △: 19.6, ▽: 39.2, □: 58.8, ◇: 78.5 MPa.

vacuous cells, overestimates considerably the second and third derivatives of the thermodynamic free energies. The model might be suitable for the liquid state in a tolerably high temperature region.

In Fig. 8, the internal pressure P_i, $P_i = T_r - P$, calculated from Eq. 3 is shown as a function of volume. P_i has a maximum at about 0.89 $cm^3\ g^{-1}$. The maximum can be predicted by the Lennard-Jones potential (PNS equation), but a quantitative agreement with the experiments in the location of the maximum is not given. The van der Waals type potential seems to be appropriate in somewhat higher temperature region.

Glassy State. Several equations of state for glasses have been proposed.[12] However, the present experimental temperature range is considered to be too narrow to make a significant comparison with those theories.

The internal pressure P_i of the glass calculated from Eq. 7 is shown in Fig. 8. Values of P_i determined by using α from Eq. 2 and β from Eq. 5 are somewhat larger than those in Fig. 8 in the lower volume region, but the qualitative shape of the figure is unchanged. P_i of the glass is much smaller than that of the supercooled liquid. The glass P_i increases significantly with increasing volume. This behavior cannot be described by the van der Waals type potential. The Lennard-Jones potential may be appropriate for the TPCM/oTP glass as well as for the poly(vinyl chloride) glasses.[12]

Conclusion

The present study offers, probably for the first time as far as we know, the detailed data on the *P-V-T* relations in the supercooled liquid state and the glassy state of a relatively simple, global molecular liquid constituted by the triphenylchloromethane/*o*-terphenyl (25/75 in weight ratio) mixture.

The thermal expansivity, the compressibility, the thermal pressure coefficient, and their variations with temperature and pressure in the supercooled liquid region are apparently similar in magnitude to those of polymer liquids, rather than to those of simple molecular liquids above the melting temperature. The *P-V-T* relations of the supercooled liquid are fairly well represented by the Prigogine-Nanda-Simha equation of state. The lattice-like liquid model might be appropriate for the well condensed liquid state of normal liquids such as the supercooled liquid state.

The apparent thermodynamic properties of the TPCM/oTP glass are also very similar in magnitude to those of polymer glasses.

References

1) For instances, H. Suga and S. Seki, *Bull. Chem. Soc. Jpn.*, **41**, 2222 (1968); M. Sugisaka, H. Suga, and S. Seki, *ibid.*, **41**, 2591 (1968).
2) J. D. Ferry, "Viscoelastic Properties of Polymers," 2nd ed, Wiley, New York (1970).
3) J. H. Gibbs and E. A. DiMarzio, *J. Chem. Phys.*, **28**, 373, 807 (1958).
4) M. Naoki and T. Tomomatsu, *Macromolecules*, **13**, 322 (1980).
5) a) A. Rahman, M. J. Mandell, and J. P. Mctague, *J. Chem. Phys.*, **64**, 1564 (1976); b) Y. Hiwatari, *ibid.*, **76**, 5502 (1982); c) L. Woodcock, *J. Chem. Soc., Faraday Trans. 2*, **73**, 11 (1977).
6) K. H. Hellwege, W. Knappe, and P. Lehmann, *Kolloid Z. Z. Polym.*, **183**, 110 (1962).
7) A. Quach and R. Simha, *J. Appl. Phys.*, **42**, 4592 (1971).
8) S. Ichihara, A. Komatsu, Y. Tsujita, T. Nose, and T. Hata, *Polym. J.*, **2**, 530 (1971).
9) J. E. McKinney and M. Goldstein, *J. Res. Natl. Bur. Stand., Sect. A*, **78**, 331 (1974).
10) O. Olabisi and R. Simha, *Macromolecules*, **8**, 206 (1975).
11) S. Beret and J. M. Prausnitz, *Macromolecules*, **8**, 536 (1975).
12) M. Naoki, H. Mori, and A. Owada, *Macromolecules*, **14**, 1567 (1981).
13) J. N. Andrews and A. R. Ubbelohde *Proc. R. Soc. London, Ser. A*, **228**, 435 (1955).
14) For instance, M. F. Shears and G. Williams, *J. Chem. Soc., Faraday Trans. 2*, **69**, 608, 1050 (1973).
15) M. Naoki and M. Matsushita, submitted to this journal.
16) P. H. Pigg, *Br. J. Appl. Phys.*, **15**, 1111 (1964).
17) L. A. Davis and R. B. Gordon, *J. Chem. Phys.*, **46**, 2650 (1967).
18) M. Naoki, M. Matsushita, and E. Ookawa, to be published.
19) J. S. Rowlinson, "Liquids and Liquid Mixtures," 2nd ed, Butterworths, London (1971).
20) For instances, Ref. 19 and "Chemical Hand Book of Chemical Society of Japan," ed by the Chemical Society of Japan, Maruzen, Tokyo (1975).
21) K. Kubota and K. Ogino, *Macromolecules*, **11**, 514 (1978).
22) W. G. Cutler, R. H. McMickel, W. Webb, and R. W. Sciesser, *J. Chem. Phys.*, **29**, 727 (1958).
23) R. Simha, P. S. Wilson, and O. Olabisi, *Kolloid Z. Z. Polym.*, **251**, 402 (1973).
24) For instance, "Physical Chemistry," "Liquid State," ed by D. Henderson, Academic Press, New York (1971), Vol. IIIA.
25) For instance, A. Abe, and P. J. Flory, *J. Am. Chem. Soc.*, **87**, 1838 (1965); **88**, 2887 (1966).
26) J. E. Lennard-Jones and A. E. Devonshire, *Proc. R. Soc. London, Ser. A.* **163**, 53 (1937); **165**, 1 (1938).
27) I. Prigogine, N. Trappeniers, and V. Mathot, *Discuss. Faraday Soc.*, **15**, 93 (1953).

28) V. S. Nanda and R. Simha, *J. Phys. Chem.*, **68**, 3158 (1964).
29) L. Tonks, *Phys. Rev.*, **50**, 955 (1936).
30) P. J. Flory, R. A. Orwoll, and A. Vrij, *J. Am. Chem. Soc.*, **86**, 3507, 3515 (1964).
31) J. S. Rowlinson and C. F. Curtiss, *J. Chem. Phys.*, **19**, 1519 (1951).
32) R. Simha and T. Somcynsky, *Macromolecules*, **2**, 342 (1969); R. K. Jain and R. Simha, *J. Chem. Phys.*, **70**, 2792 (1979).
33) I. C. Sanchez and R. H. Lacombe, *J. Phys. Chem.*, **80**, 2352 (1976); R. H. Lacombe and I. C. Sanchez, *ibid.*, **80**, 2568 (1976).
34) J. A. R. Renucio and J. M. Prausnitz, *Macromolecules*, **9**, 324 (1976).

Viscosity *B*-Coefficients, Apparent Molar Volumes, and Activity Coefficients for α- and γ-Cyclodextrins in Aqueous Solutions

Koichiro MIYAJIMA,* Masahiro SAWADA, and Masayuki NAKAGAKI
Faculty of Pharmaceutical Sciences, Kyoto University, Yoshida Shimoadachi-cho, Sakyo-ku, Kyoto 606
(Received April 2, 1983)

The viscosities and densities at 15, 25, and 35 °C, and activity coefficients at 25 °C for the aqueous solutions of α- and γ-cyclodextrins were measured, and the results were interpreted in terms of solute-solvent and solute-solute interactions. The concentration and temperature dependences of viscosities and apparent molar volumes are almost similar to those of linear saccharides, *i.e.* maltose and maltotriose, indicating that α- and γ-cyclodextrins are structure forming solutes. However, the concentration dependences of activity coefficients of cyclodextrins are significantly different from those of maltose and maltotriose. The results were tentatively assigned to the formation of dimer in aqueous solutions.

Cyclodextrins are the condensed ring compounds of D-glucopyranoses through α-1,4-glucosidic linkage and are called α-, β-, and γ-cyclodextrins (CD) in accordance with the numbers of glucose residues, 6, 7 and 8, respectively. CD has been well-known to form inclusion complexes with a wide varieties of molecular species irrespective of hydrophobic or ionic in nature.[1]

In contrast to the numerous studies on the complex formation, the studies on the solution of CD seem to be sparse. However, the thermodynamic properties of aqueous solutions must play an important role on the complex formation, because the complex formation usually takes place in aqueous solution. Furthermore it is also interesting to compare the solution properties of CD with those of linear di- and trisaccharides reported previously.[2]

In these viewpoints, we determined the viscosity *B*-coefficients and the apparent molar volumes at 15, 25, and 35 °C, and the activity coefficients at 25°C for α- and γ-CD in aquous solutions, and discussed the effects of CD on the water structure.

Experimental

Materials. Reagent grade α- and γ-CD purchased from Nakarai Chemical Co. Ltd., were recrystallized twice from water according to French *et al.*[3] and were dried *in vacuo* for 5h at 110 °C before use. After drying, the water contents of crystalline compounds determined by the Carl Fisher method were found to be less than 0.2% for each CD. The concentration correction was made on every solution. Reagent grade sodium chloride purchased from Matsunaga Chemical Co. Ltd., was used after drying without purification. CD and sodium chloride solutions were prepared with water purified by distillation and deionization.

Methods. The viscosity and density measurements were carried out at 15, 25, and 35 °C by using the apparatus described in a previous paper.[2] Vapour pressure over aqueous solution was measured at 25 °C with an osmometer model 117 manufactured by Corona Electric Co. Ltd. Sodium chloride was used as a standard substance for the measurement of the instrument constant. The instrument constant thus obtained was almost unchanged in a set of measurements. But the constant was changed slightly in another set of measurements. Consequently, the instrument constant was determined for every set of measurements.

Results

Viscosity. The reletive viscosity, η_{rel} of a non-electrolyte solution can be expressed by

$$\eta/\eta_0 = \eta_{rel} = 1 + Bc + Dc^2, \quad (1)$$

where η_0 and η are the viscosities of the solvent and the solution, respectively, and c is the concentration in mol dm^3. B and D are the characteristic constants depending on the solute and the solvent at constant temperature and pressure. The plots of $(\eta_{rel}-1)/c$ *vs.* c for α- and γ-CD at 25 °C are shown in Fig. 1, indicating that Eq. 1 is valid up to about 0.05 mol dm^{-3}. The B and D coefficients determined from the intercepts and slopes at 15, 25, and 35 °C are listed in Table 1. The points in low concentration, which considerably deviate from the lines because of the experimental error, were neglected, and the standard deviation of each plot up to 0.05 mol dm^{-3} was calculated to be within 0.014 mol^{-1} dm^3. Therefore, the experimental errors in B and D are estimated to be less than 0.03 mol^{-1} dm^3 and 1.0 mol^{-2} dm^6, respectively.

The increment of B-coefficient arising from the structural change of water, B_{st}, may be obtained by

$$B_{st} = B - \nu V/1000. \quad (2)$$

The second term of the right hand side of Eq. 2 expresses the contribution of the hydrodynamic obstruction effect according to Einstein and Shimha.[4] On the assumptions that a certain number of water molecules is packed in a cavity and the shape of the molecule is approximated by an oblate ellipsoid, the ν value of α-CD was estimated on the basis of Scheraga's table[5] using the numerical value of axial ratio obtained from the molecular model,[6] resulting in 2.26. The molar volume of the oblate, V, is calculated by

$$V = \bar{V}^\circ + N\bar{V}_w, \quad (3)$$

where $\bar{V}^\circ$ and $\bar{V}_w$ is the partial molar volume of α-CD at infinite dilution and molar volume of water, respectively. N is the number of water molecules in the cavity. An α-cyclodextrin hexahydrate crystal contains two water molecules in the cavity.[7] By assuming that the number of water molecules in the cavity of α-CD molecule in solution state is the same as that in solid state, the value of B_{st} of α-CD was found to be 0.71. The B_{st} value of γ-CD could not be obtained because

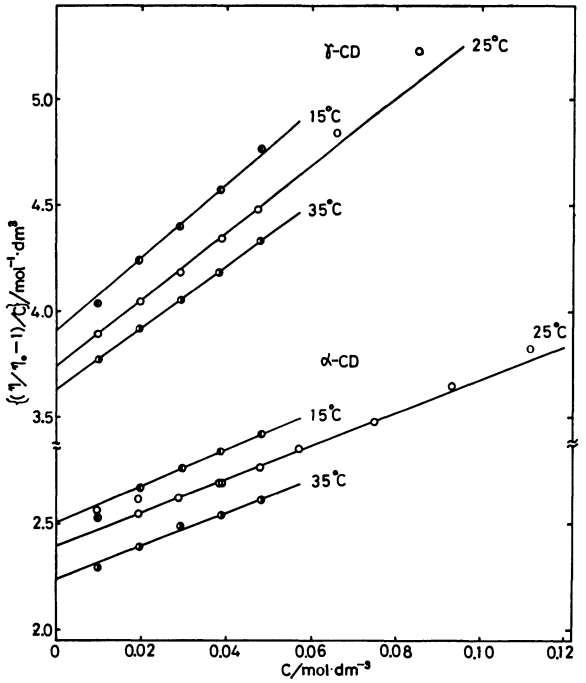

Fig. 1. Relations between $(\eta/\eta_0-1)/c$ and c for cyclodextrins at ◐ 15, ○ 25, and ◑ 35 °C.

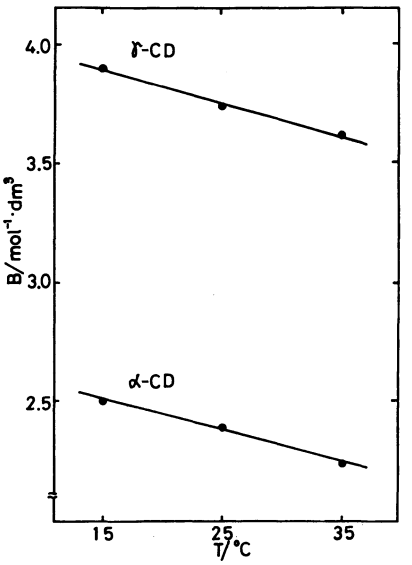

Fig. 2. Temperature dependenc of B-coefficients for cyclodextrins.

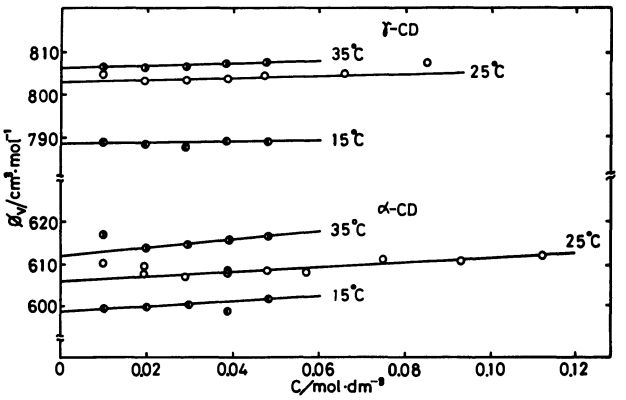

Fig. 3. Relations between ϕ_v and c for cyclodextrins at ◐ 15, ○ 25, and ◑ 35 °C.

TABLE 1. THE VALUES OF B, D, dB/dT, $\bar{V}°$ AND α^* FOR CYCLODEXTRINS

	Temp/°C	α-CD	γ-CD
B / mol^{-1} dm^3	15	2.50	3.90
	25	2.39	3.74
	35	2.24	3.62
D / mol^{-2} dm^6	15	8.6	17.4
	25	7.8	15.7
	35	7.8	14.7
$(dB/dT)\times10^2$ / mol^{-1} dm^3 K^{-1}	25	−1.3	−1.4
$\bar{V}°$ / cm^3 mol^{-1}	15	598.5	788.5
	25	606.0	803.0
	35	612.0	805.3
$\alpha^*\times10^3$ / cm^3 mol^{-1} K^{-1}	25	1.1	0.8

the N value is not available.

Figure 2 shows the temperature dependence of B values. As seen in Fig. 2, the value of B decreases with increase of temperature for both CDs. The values of dB/dT at 25 °C are shown in Table 1.

Density. Apparent molar volume of solute, ϕ_v, was calculated by

$$\phi_v = \frac{1000(d_0-d)}{cd_0} + \frac{M_2}{d}, \quad (4)$$

where d_0 and d are the densities of the solvent and the solution, respectively, and M_2 is the molecular weight of the solute. As shown in Fig. 3, ϕ_v at each temperature is linearly related to c:

$$\phi_v = \bar{V}° + b_v c, \quad (5)$$

where $\bar{V}°$ is the partial molar volme at infinite dilution and b_v is the empirical constant. The $\bar{V}°$ values obtained from the extrapolation of ϕ_v to $c=0$ are also shown in Table 1. The values of b_v for the CDs are positive at every temperature. In Fig. 3, the positive deviations of ϕ_v from the lines in low concentration may be due to experimental error. The standard deviation of each plot was within 0.3 cm^3 mol^{-1}, if the points deviating extremely in low concentration were neglected. The experimental error in $\bar{V}°$ is estimated to be less than 0.6 cm^3 mol^{-1}.

The temperature dependence of $\bar{V}°$ is shown in Fig. 4. The values of $\bar{V}°$ of α- and γ-CD increase nonlinearly with temperature, and the curves display upward curvatures. The thermal expansion coefficient, α^*, is defined by

$$\alpha^* = (\partial \bar{V}°/\partial T)_p/\bar{V}°. \quad (6)$$

The values of α^* at 25 °C are given in Table 1.

Activity Coefficient. The relations between the osmotic coefficient, ϕ, and the concentration in mol kg^{-1}, m, at 25 °C are shown in Fig. 5. By the least-squares fitting, ϕ's are expressed in terms of m as

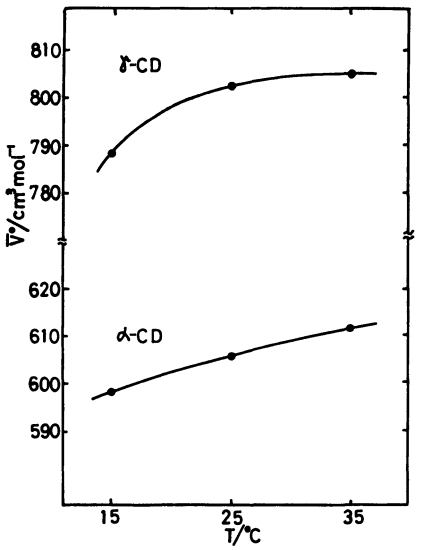

Fig. 4. Temperature dependence of $\bar{V}°$ for cyclodextrins.

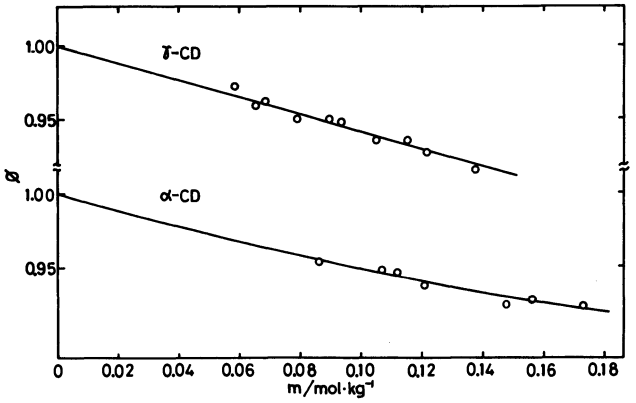

Fig. 5. Osmotic coefficients of cyclodextrins at 25 °C.

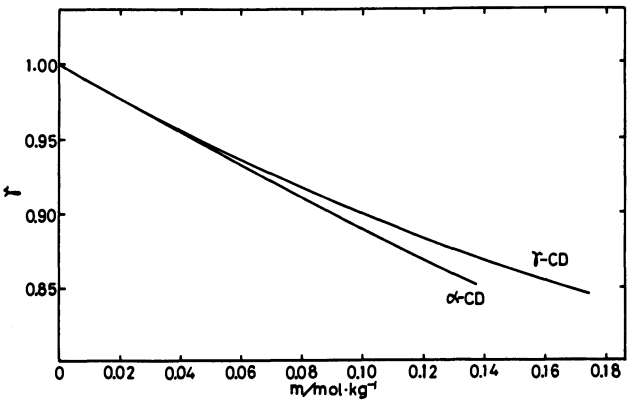

Fig. 6. Activity coefficients of cyclodextrins at 25 °C.

$$\left.\begin{aligned}\phi &= 1 - 0.585\,m \quad \text{for } \alpha\text{-CD},\\ \phi &= 1 - 0.588\,m + 0.789\,m^2 \quad \text{for } \gamma\text{-CD}.\end{aligned}\right\} \tag{7}$$

The activity coefficients, γ, were calculated from the osmotic coefficients by the following equation:

$$\ln\gamma = (\phi - 1) + \int_0^m \frac{\phi - 1}{m}\mathrm{d}m. \tag{8}$$

Introducing Eqs. 7 into Eq. 8, and integrating, we obtain

$$\left.\begin{aligned}\ln\gamma &= -1.170\,m \quad \text{for } \alpha\text{-CD},\\ \ln\gamma &= -1.176\,m + 1.148\,m^2 \quad \text{for } \gamma\text{-CD}.\end{aligned}\right\} \tag{9}$$

As seen in Figs. 5 and 6, the osmotic and activity coefficients decrease with increase of the concentration.

Discussion

As stated in a previous paper,[8] the signs and the magnitudes of B_{st} and $\mathrm{d}B/\mathrm{d}T$ are the useful criterion for the classification of solute property in water. As seen in Table 1, both α- and γ-CD are structure makers because of their negative $\mathrm{d}B/\mathrm{d}T$ values. The negative values of $\mathrm{d}B/\mathrm{d}T$ increase with the number of glucose regardless of linear[2] or cyclic, indicating that glucose residue has a structure forming ability. On the other hand, Hepler[9] proposed other criterion for the classification of solutes as structure makers or breakers. His criterion is that the structure making solutes have the positive sign of $(\partial^2\bar{V}°/\partial T^2)$ while the structure breaking solutes the negative sign. As shown in Fig. 4, the signs of $(\partial^2\bar{V}°/\partial T^2)$ for CDs are negative. If we adopt Hepler's criterion, CDs are structure breakers in disagreement with the conclusion obtained from B_{st} and $\mathrm{d}B/\mathrm{d}T$. As for hydrophilic nonelectrolytes, the values of $(\partial^2\bar{V}°/\partial T^2)$ for urea,[10] maltose and maltotriose[2] are negative, and that for D-glucose[2] is nearly zero. These experimental results are in conflict with Hepler's criterion, because it has been proved by many studies that urea is a structure breaker, while D-glucose, maltose and maltotriose are structure makers. Therefore, Hepler's criterion seems to be inapplicable to hydrophilic nonelectrolytes such as sugars and urea.

As seen in Fig. 7, the B-coefficients of linear maltodextrins[11] increase almost linearly with the degree of polymerization (n) and the point of the B-coefficients for cyclic dextrins, *i.e.* α- and γ-CD, locate below the B *vs.* n curve for linear maltodextrins. The shape and the size of the hydrated molecule or ion affect mainly the sign and magnitude of the B-coefficient. The partial molar volumes of linear polysaccharides are not so

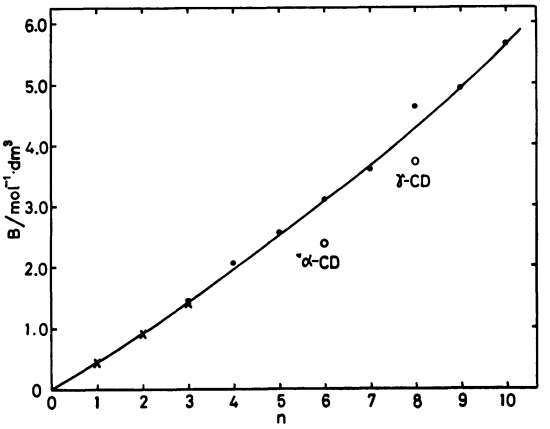

Fig. 7. Relation between B-coefficients and the number of glucose residues (n) for maltodextrins at 25 °C.
●: Calculated values from Thoma's table.[11] ×: Our values in a previous paper.[2] ○: Cyclodextrin.

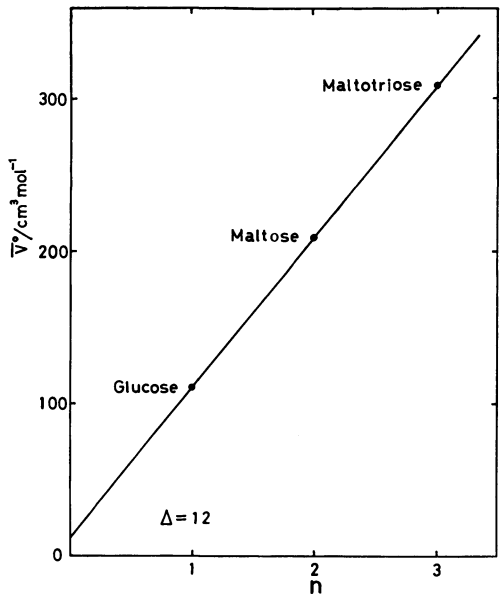

Fig. 8. Relation between $\bar{V}°$ and n at 25 °C.

much different from those of the corresponding cyclic dextrins as will be seen later, and the hydrodynamic rigid volumes of the cyclic types are lager than those of the linear types based on the assumption that the exchange of water molecules between cavity and bulk has no influence on the hydrodynamic process. This assumption is supported by the fact that the point for γ-CD is more close to the B *vs.* n curve than that for α-CD in Fig. 7, because γ-CD has a larger cavity than α-CD.[12] The above discussion leads to the conclusion that the small values of the B-coefficients for cyclic dextrins, as compared with those of the corresponding linear ones, are due to the difference in shape, *i.e.* rod-like and oblate type molecules.

The partial molar volume at infinite dilution of a linear polymer, $\bar{V}^{olin}(n)$, is expressed as

$$\bar{V}^{olin}(n) = n\bar{V}^{om} - (n-1)\Delta = n(\bar{V}^{om} - \Delta) + \Delta, \quad (10)$$

where n is the degree of polymerization, $\bar{V}^{om}$ the volume of the monomer *i.e.* D-glucose, and Δ is the volume change on the formation of the α-1,4 ether linkage. On the other hand, the partial molar volume at infinite dilution of a cyclic polymer, $\bar{V}^{ocyc}(n)$, is expressed as

$$\bar{V}^{ocyc}(n) = n\bar{V}^{om} - n\Delta. \quad (11)$$

The Δ value was found to be 12 cm^3 mol^{-1} form the intercept and the slope of the $\bar{V}^{olin}(n)$ *vs.* n curve as seen in Fig. 8. The value of $\bar{V}^{ocyc}(n)$ was calculated from Eq. 11 using the Δ value, resulting in 596 and 795 cm^3 mol^{-1} for α-CD and γ-CD, respectively. These calculated values are smaller than the experimental values of $\bar{V}^{ocyc}(n)$ by 10 to 8 cm^3 mol^{-1}. This result may be due to the formation of intramolecular hydrogen bonding[13] and the bulkiness of water in the cavity in which hydrophobic environment is formed.

The thermal expansion coefficient of α-CD at 25 °C is close to that of D-glucose (1.0×10^{-3}) and smaller than that of maltose (1.3×10^{-3}) or maltotriose (1.4×10^{-3}). This fact may be related to the torsional rotation around the α-1,4-linkage which brings about the increase of unstructured water having high thermal expansibility because D-glucose has no α-1,4-linkage and the rotations of glucose residues in the CD molecule are almost hindered. The small value of α^* of γ-CD may be due to the large cavity, in which bulky water is packed.

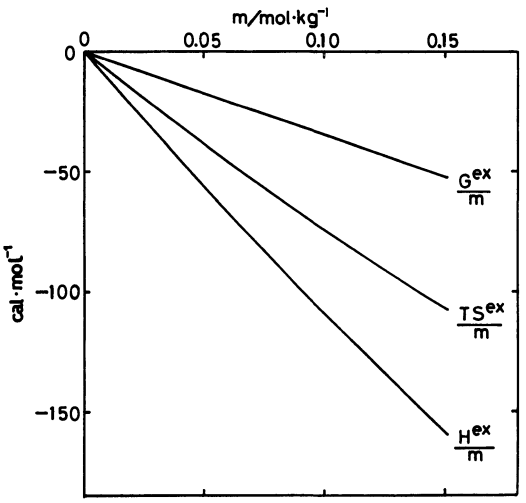

Fig. 9. Thermodynamic quantities of α-CD at 25 °C.

As seen in Figs. 5 and 6, the concentration dependences of the osmotic and activity coefficients for α- and γ-CD are strikingly different from those for linear oligosaccharides, such as maltose and maltotriose. The coefficients of the CDs decrease with increase of concentration. In general, the decrease in activity coefficients with the increase of concentration is possibly interpreted in terms of two different effects, *i.e.* structure breaking effect and the association of the solutes.

Using the data of the heat of dilution, ΔH^{dil},[14] excess thermodynamic quantities of α-CD are calculated from

$$G^{ex} = mRT(1 - \phi + \ln\gamma), \quad (12)$$

$$H^{ex} = -\Delta H^{dil}, \quad (13)$$

and

$$G^{ex} = H^{ex} - TS^{ex}. \quad (14)$$

As seen in Fig. 9, the sign of each quantity is negative, being opposite to that of D-glucose.[15] The negative sign of G^{ex} is based on the predominance of the negative value of H^{ex} over the negative value of TS^{ex}. The negative value of H^{ex} means the endothermic heat on the dilution process. Judging from the TS^{ex}/m *vs.* m curve in Fig. 9, excess partial molar entropy of water, $\bar{S}_w^{ex}$, would be positive, suggesting that the ordering of water molecules decreases with increase of solute concentration as far as solute-solute interactions are weak or absent. However, the possibility that the CD is a structure breaker would be small, because such a large decrease of γ in low concentration is unlikely to take place as a result of solute-solvent interaction alone, and α-CD is a hydrodynamically structure maker as stated in the preceding section.

From these considerations, we regard the positive value of $\bar{S}_w^{ex}$ as the result of the association of solute, and obtain the dimerization constant graphically using Eq. 13.[16]

$$K = (1 - \phi)/m\phi^2. \quad (13)$$

The K values of α- and γ-CD were found to be 0.66 and 0.55 mol^{-1} kg, respectively. These K values indicate that about 10 molecules out of 100 molecules form a dimer at 0.1 mol kg^{-1}.

The effect of the association of CD is considered to be reflected in Figs. 1 and 3. As mentioned above, B and $\bar{V}^\circ$ express the solute-solvent interactions at infinite dilution, where the association does not occur. The values of B and $\bar{V}^\circ$ are actually determined by the extrapolations of $(\eta_{rel}-1)/c$ and ϕ_v to $c=0$. Therefore, the discussions of the nature of CD based on these values are not influenced by the association of CD. On the other hand, D and b_v are regarded to express the solute-solute interactions. Accordingly, the effect of the association of CD is reflected in the values of D and b_v, *i.e.* the slopes of the lines in Figs. 1 and 3. But it is difficult to derive the evidences of the association of CD from the values of D and b_v, because these coefficients are also influenced by other complicated factors such as structural interactions.[17,18]

We have no other evidence that CD forms a dimer in aqueous solutions at the present stage. But some kinds of compounds are included in β-CD dimer of head to head type, in which two secondary OH groups of β-CD are hydrogen bonded.[19]

In conclusion, α- and γ-CD promote the structure of water and may possibly form a dimer in aqueous solutions, resulting in the increase of excess partial molar entropy of water.

References

1) D. W. Griffiths, and M. L. Bender, *Adv. Catal.*, **23**, 209 (1973).
2) K. Miyajima, M. Sawada, and M. Nakagaki, *Bull. Chem. Soc. Jpn.*, **56**, 1954 (1983).
3) D. French, M. L. Levine, J. H. Pazur, and E. Norberg, *J. Am. Chem. Soc.*, **71**, 353 (1949).
4) R. Simha, *J. Phys. Chem.*, **44**, 25 (1940).
5) H. A. Scheraga, *J. Chem. Phys.*, **23**, 1526 (1955).
6) R. K. McMullan, W. Saenger, J. Fayos, and D. Mootz, *Carbohydr. Res.*, **31**, 37 (1973).
7) W. Seanger, M. Noltemeyer, P. C. Manor, B. Hingert, and B. Klar, *Bioorg. Chem.*, **5**, 187 (1976).
8) K. Miyajima, M. Sawada, and M. Nakagaki, *Bull. Chem. Soc. Jpn.*, **55**, 3101 (1982).
9) L. G. Hepler, *Can. J. Chem.*, **47**, 4613 (1969).
10) R. H. Stokes, *Aust. J. Chem.*, **20**, 2087 (1967).
11) J. A. Thoma, "Starch : Chemistry and Technology," ed by R. L. Whistler, and E. F. Paschall, Academic Press, New York (1965), p. 188.
12) Free draining effect decreases the B-coefficient.
13) B. Casu, M. Reggiani, G. G. Gallo, and A. Vigevani, *Tetrahedron*, **22**, 3061 (1966).
14) S. Takagi, and M. Maeda, *Nippon Kagaku Kaishi*, **1983**, 188.
15) K. Miyajima, M. Sawada, and M. Nakagaki, *Bull. Chem. Soc. Jpn.*, **56**, 1620 (1983).
16) P. O. P. T'so, and S. I. Chan, *J. Am. Chem. Soc.*, **86**, 4176 (1964).
17) K. Miyajima, M. Sawada, and M. Nakagaki, *Bull. Chem. Soc. Jpn.*, **56**, 827 (1983).
18) F. J. Millero, *Chem. Rev.*, **71**, 147 (1971).
19) J. J. Stezowski, K. H. Jogun, E. Eckle, and K. Bartels, *Nature*, **274**, 617 (1978).

 © 1983 The Chemical Society of Japan Bull. Chem. Soc. Jpn., 56, 3561—3565 (1983)

Anharmonic Potential Functions and Intrinsic Reaction Coordinates of Polyatomic Molecules

Katsunosuke MACHIDA
Faculty of Pharmaceutical Sciences, Kyoto University, Sakyo-ku, Kyoto 606
(Received April 11, 1983)

A general method has been developed to describe the atomic motion along a given intrinsic reaction coordinate (IRC) in the vicinity of the potential minimum of a polyatomic molecule whose anharmonic force constants are known experimentally or theoretically. The components of the position vector of a configuration point on an IRC in the normal coordinate space are expanded as power series of the path length from the origin measured along the IRC. Explicit expressions of the expansion coefficients up to the third order have been given in terms of the normal frequencies and the anharmonic force constants with respect to the normal coordinates. The atomic loci along the IRC are given by transformation from the normal coordinates to the Cartesian displacements. Through application to formaldehyde and water, the method has proved to be useful to check if a given normal coordinate can be connected to any dissociation path on large distortion of the molecule.

The intrinsic reaction coordinate, hereafter abbreviated as IRC, has been introduced by Fukui in 1970 as a concept of fundamental importance in reaction dynamics of polyatomic molecules.[1] An IRC describes how a molecule is distorted when the atomic displacement associated with a chemical reaction proceeds with an infinitesimal rate. Determination of the IRC is an indispensable step in understanding the reaction mechanism. An IRC should coincide with one of the normal coordinates if the potential function which regulates the molecular vibrations around the equilibrium configuration is rigorously harmonic.[1,2] In actual molecules, however, presence of anharmonic terms in the potential leads to deviation of any IRC's from the normal coordinates defined at the potential minimum when the constituent atoms move away from the equilibrium positions. The non-linear relationship between an IRC and the normal coordinates should thus be described uniquely in terms of the anharmonic force constants. The present work has been initiated to search for such a relationship in a general form, and to utilize it to examine the behavior of an IRC near the minimum of an experimentally determined potential function of polyatomic molecules containing anharmonic terms.

Theory

Following the standard perturbation theory, we expand the potential function of a polyatomic molecule as a power series of its normal coordinates in the form

$$V = \frac{1}{2}\sum_i \lambda_i Q^{i2} + \frac{\varepsilon}{6}\sum_{ijk} K_{ijk}Q^iQ^jQ^k + \frac{\varepsilon^2}{24}\sum_{ijkl} K_{ijkl}Q^iQ^jQ^kQ^l + \cdots, \quad (1)$$

where λ_i is the ith frequency parameter related to the normal frequency ω_i in cm^{-1} and the light velocity c by

$$\lambda_i = (2\pi c\omega_i)^2,$$

and ε is an ordering parameter. In analysing spectroscopic data, the higher-order force constants are usually given in the system of the dimensionless normal coordinates. The cubic and quartic constants in this system, k_{ijk} and k_{ijkl}, are transformed to those in Eq. 1 through the relations

$$K_{ijk} = (1+\delta_{ij})(1+\delta_{ik}+\delta_{jk})(h/2\pi)^{3/2}(\lambda_i\lambda_j\lambda_k)^{1/4}k_{ijk} \quad (2)$$

and

$$K_{ijkl} = (1+\delta_{ij})(1+\delta_{ik}+\delta_{jk})(1+\delta_{il}+\delta_{jl}+\delta_{kl}) \times (h/2\pi)^2(\lambda_i\lambda_j\lambda_k\lambda_l)^{1/4}k_{ijkl}, \quad (3)$$

respectively, where h is Planck's constant and δ_{ij} is Kronecker's delta. Differentiating Eq. 1 with respect to Q^i leads to

$$(\partial V/\partial Q^i) = \lambda_i Q^i + \frac{\varepsilon}{2}\sum_{jk} K_{ijk}Q^jQ^k + \frac{\varepsilon^2}{6}\sum_{jkl} K_{ijkl}Q^jQ^kQ^l + \cdots. \quad (4)$$

Whenever the molecule is distorted along an IRC in the vicinity of the potential minimum, any pairs of non-degenerate normal coordinates, Q^i and Q^j, should satisfy the IRC equation[1]

$$dQ^i/(\partial V/\partial Q^i) = dQ^j/(\partial V/\partial Q^j), \quad (5)$$

or

$$(\partial V/\partial Q^i)dQ^j - (\partial V/\partial Q^j)dQ^i = 0. \quad (6)$$

The form of Eq. 5 is the same as that in the case of the mass-weighted Cartesian coordinates[2] because of the orthogonality condition between the two coordinate systems.

Now we suppose that there is an IRC which converges into the normal coordinate Q^i when the molecular configuration approaches that at the potential minimum. In order to specify the position of a configuration point moving on this IRC, we may take the distance from the origin to the point measured along the IRC, s^i, as an independent variable, and represent each element of the position vector in the normal coordinate space as a function of s^i satisfying Eq. 5. In the vicinity of the potential minimum, such a function may be expanded as a power series of s^i in the form

$$Q^j = a^j_i s^i + \frac{\varepsilon}{2}a^j_{it}s^{i2} + \frac{\varepsilon^2}{6}a^j_{iti}s^{i3} + \cdots. \quad (7)$$

Substituting Eq. 7 with $j=i$, j, k, and l into Eq. 4 and multiplying the result by the differential of Eq. 7, we obtain the first term of Eq. 6 as

$$(\partial V/\partial Q^i)dQ^j = [\lambda_i a_i^i a_i^j s^i + \frac{\varepsilon}{2}\{\lambda_i(2a_i^i a_{ii}^j + a_{ii}^i a_i^j) + a_i^j \sum_{kl} K_{ikl} a_i^k a_i^l\} s^{i2} + \frac{\varepsilon^2}{6}\{\lambda_i(3a_i^i a_{iii}^j + 3a_{ii}^i a_{ii}^j + a_{iii}^i a_i^j) + a_{ii}^j \sum_{kl} K_{ikl} a_i^k a_i^l + a_i^j(3\sum_{kl} K_{ikl} a_i^k a_{ii}^l + \sum_{klm} K_{iklm} a_i^k a_i^l a_i^m)\} s^{i3} + \cdots] ds^i. \quad (8)$$

The second term of Eq. 6 can also be expressed by Eq. 8 provided that the superscripts i and j of the a coefficients are interchanged with each other and the subscript i of the force constants λ and K's is replaced by j. Since Eq. 6 holds for any displacements of the nuclei along the IRC under consideration, the coefficient of each power of s^i in the left hand side should vanish separately. The linear term gives the relation

$$(\lambda_i - \lambda_j) a_i^i a_i^j = 0, \quad (9)$$

which implies that

$$a_i^j = 0, \quad (10)$$

when both the conditions $\lambda_i \neq \lambda_j$ and $a_i^i \neq 0$ hold. This property of IRC's has already been pointed out by Fukui *et al.*[2]

Prior to estimation of a_{ii}^j, we shall determine the first two coefficients of the expansion of Q^i in terms of s^i. It follows from the definition of s^i that

$$\sum_k (dQ^k)^2 = (ds^i)^2. \quad (11)$$

Substituting Eqs. 7 and 10 into Eq. 11 and taking the term not including s^i, we have

$$a_i^i = \pm 1, \quad (12)$$

where the plus sign may be adopted without loss of generality. Since the coefficient of the term linear in s^i in Eq. 11 vanishes while a_i^i does not, it should hold that

$$a_{ii}^i = 0. \quad (13)$$

Substituting Eqs. 8, 10, 12, and 13 into Eq. 6, and taking the term quadratic in s^i, we obtain

$$a_{ii}^j = K_{jii}/(2\lambda_i - \lambda_j). \quad (14)$$

The coefficients of the cubic term in the expansions of Q^i and Q^j are derived similarly from Eq. 11 as

$$a_{iii}^i = -\sum_k (a_{ii}^k)^2, \quad (15)$$

and from Eq. 8 as

$$a_{iii}^j = (K_{jiii} + 3\sum_k K_{jik} a_{ii}^k - 3K_{iii} a_{ii}^j)/(3\lambda_i - \lambda_j), \quad (16)$$

respectively. The denominators in Eqs. 14 and 16 indicate that the expansion of Q^j in power series of s^i cannot be accomplished when λ^j is an integral multiple of λ_i. The form of $Q^j(s^i)$ in such a case is given in Appendix.

Once the expansion coefficients in Eq. 7 are determined by using Eqs. 14—16, we can calculate the values of normal coordinates corresponding to any small values of s^i given arbitrarily. The atomic displacements along with the increase of s^i can then be traced by converting the normal coordinates into the Cartesians $\boldsymbol{X}$ according to

$$\boldsymbol{X} = \boldsymbol{L}_x \boldsymbol{Q}. \quad (17)$$

Since the same relation as Eq. 17 holds for the derivatives of X's and Q's with respect to s^i, it is also possible to evaluate the components of the principal normal of an IRC by differentiating Eq. 7 at a given point near the potential minimum. Similarly, the curvature of an IRC near the equilibrium is obtained from the second derivatives of Eq. 7.[3]

Application

Let us consider an isolated formaldehyde molecule undergoing a certain distortion which starts in the direction of the ν_6 mode at the equilibrium and proceeds as described by Eq. 7 in the normal coordinate space. The relevant expansion coefficients $a^j{}_{66}$ and $a^j{}_{666}$ are listed in Table 1 for two sets of force constants, Sets I and II, together with the frequency parameters λ_j which are common to the two sets. Set I was obtained previously by the least squares fitting of the observed values of 31 vibrational frequencies of H_2CO, HDCO, and D_2CO and 30 vibration-rotation interaction constants of H_2CO and D_2CO.[4] Set II was the same as Set I except that the cubic interaction constant between the CO stretching and the HCO deformation coordinates, $K_{R\phi\phi}$, was set equal to zero. This constant is given a relatively large absolute value, 0.963×10^{-8} N/rad^2, in Set I, so it is desirable to check its reality from a nonspectroscopic point of view. Since λ is nearly twice as large as λ_6, the denominator in Eq. 14 causes an appreciable difference in $a^2{}_{66}$ between Sets I and II, and even larger difference in $a^2{}_{666}$ results from the square of $a^2{}_{66}$ according to Eq. 15. Because of these differences, the in-plane normal coordinates calculated for Sets I and II exhibit quite different trends of the dependence on s^6 from each other as shown in Fig. 1. The energy for Set I increases more rapidly than that for Set II at larger values of s^6. The atomic displacements derived from the changes of Q^j's through Eq. 17 are shown in Fig. 2 together with a schematic view of the distorted molecule.

The IRC's of formaldehyde for the dissociation reaction

$$H_2CO \longrightarrow H_2 + CO$$

and the isomerization reaction

$$H_2CO \longrightarrow HC\text{–}OH$$

were studied by Yamashita *et al.* by means of an *ab initio* MO calculation.[5] For each of these reactions, the IRC traced from the transition point back to the starting

TABLE 1. COEFFICIENTS $a^j{}_{66}$ AND $a^j{}_{666}$ AND FREQUENCY PARAMETERS λ_j OF FORMALDEHYDE

j	Set I		Set II		λ_j [c]
	$a^j{}_{66}$ [a]	$a^j{}_{666}$ [b]	$a^j{}_{66}$ [a]	$a^j{}_{666}$ [b]	
1	0.00183	0.0	0.00165	0.0	5.1054
2	0.04924	0.0	0.01190	0.0	1.8277
3	0.00254	0.0	0.00484	0.0	1.3550
4	0.0	0.0	0.0	0.0	0.8293
5	0.0	0.000108	0.0	0.000040	5.4176
6	0.0	0.001623	0.0	0.000112	0.9679

a) In amu$^{-1/2}$ pm^{-1}. b) In amu^{-1} pm^{-2}. c) In N cm^{-1} amu^{-1}.

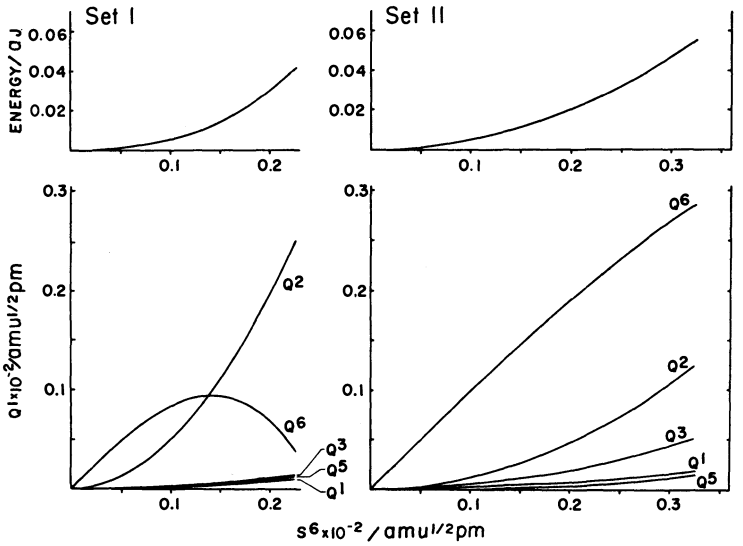

Fig. 1. Dependence of the potential energy and the in-plane normal coordinates on s^6 of formaldehyde molecule.

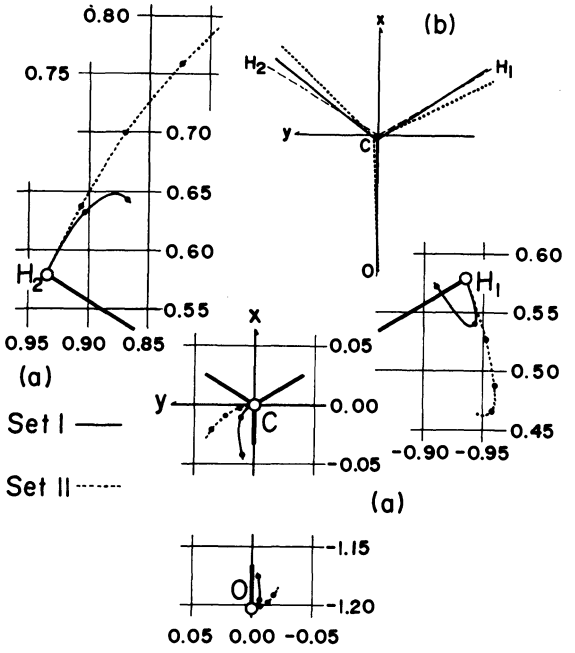

Fig. 2. (a) Atomic displacements of formaldehyde along s^6. The x and the y axes are scaled in a unit of 100 pm =Å. Filled circles on the atomic loci indicate the atomic positions corresponding to every increase of s^6 by 10 amu$^{1/2}$ pm. (b) A schematic view of undistorted and distorted molecules. Broken line: $s^6=0.0$. Solid line: $s^6=20$ amu$^{1/2}$ pm (Set I). Dotted line: $s^6=30$ amu$^{1/2}$ pm (Set II).

system converges into the ν_6 mode of formaldehyde. According to the present calculation, the spectroscopic data support the existence of an IRC which starts in the direction of the ν_6 mode at the equilibrium and proceeds toward the dissociation. In the framework of the harmonic approximation, the ν_6 mode is the CH_2 rocking mode in the course of which the two H–C=O angles close and open in turn. The hydrogen atom H_1 in Fig. 2 starts to close the H_1–C=O angle, but soon displays a

Table 2. Ground state rotational constants (cm^{-1}) of formaldehyde and its isotopic species

Molecule	Rotational constant	Obsd[a]	Calcd	
			Set I	Set II
H_2CO	*A*	9.40546	9.4158	9.4243
	B	1.29543	1.2952	1.2985
	C	1.13419	1.1354	1.1381
$H_2{}^{13}CO$	*A*	9.40628	9.4156	9.4238
	B	1.26124	1.2611	1.2644
	C	1.10789	1.1091	1.1118
$H_2C^{18}O$	*A*	9.40516	9.4157	9.4242
	B	1.23099	1.2309	1.2341
	C	1.08447	1.0856	1.0882
HDCO	*A*	6.60830	6.6298	6.6364
	B	1.16450	1.1646	1.1670
	C	0.98605	0.9873	0.9891
D_2CO	*A*	4.72504	4.7359	4.7401
	B	1.07686	1.0764	1.0781
	C	0.87345	0.8744	0.8757
$D_2C^{18}O$	*A*	4.72487	4.7358	4.7401
	B	1.02057	1.0202	1.0219
	C	0.83601	0.8369	0.8381

a) H_2CO, $H_2{}^{13}CO$ and $H_2C^{18}O$ from Ref. 7, the other from Ref. 6.

180° turn to move toward the correct direction for the dissociation. This reversal of the translation direction of H_1 takes place as a result of the increase of the contribution of the ν_2 mode and the corresponding decrease of that of the ν_6 mode in the IRC as shown in Fig. 1. Comparison between Sets I and II indicates that the turning point of H_1 is made nearer the equilibrium and the curvature around the turning point is increased by introduction of $K_{R\phi\phi}$. In Fig. 2, the locus of the hydrogen atom H_2 for Set I also shows a large curvature around the point where $s^6=17$ amu$^{1/2}$ pm. The turning of H_2 seems to be somewhat exaggerated, however, by errors associated with the truncation of Eq. 7 which contains large expansion coefficients.

Recently, very precise values of the ground state rotational constants of various isotopic species of formalde-

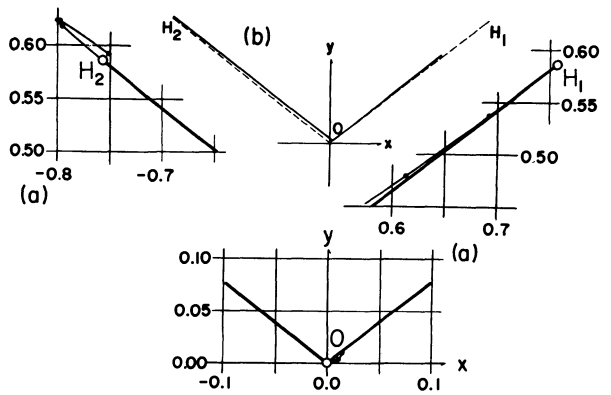

Fig. 3. (a) Atomic displacements of water along s^3. The axes are scaled and the atomic positions are indicated as in Fig. 2. (b) A schematic view of undistorted and distorted molecules. Broken line: $s^3=0.0$. Solid line: $s^3=30$ amu$^{1/2}$ pm.

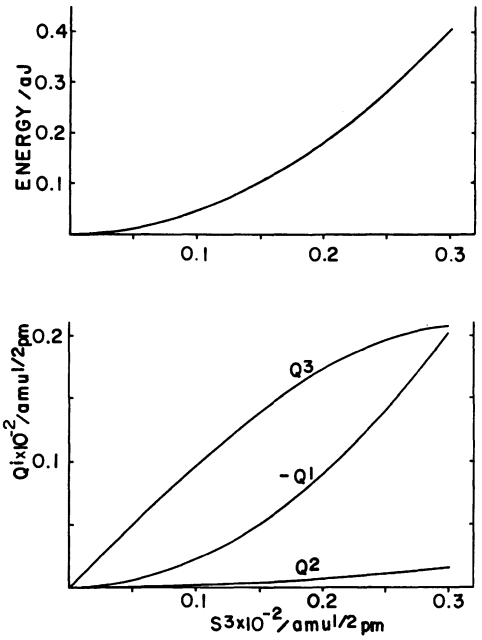

Fig. 4. Dependence of the potential energy and the normal coordinates on s^3 of water molecule.

hyde have been determined from the microwave spectra.[6-8] Some of them are compared with those calculated from Sets I and II in Table 2. Obviously, Set I is superior to Set II in reproducing the observed data, indicating the importance of the cubic constant $K_{R\phi\phi}$. For both Sets I and II, the mixing of the ν_5 mode takes place with the correct phase which brings about stretching of the C–H_1 bond, though the rate of the mixing is rather small compared with the result of the *ab initio* MO calculation.[5]

There are many normal modes for which the atomic path defined by Eq. 7 does not lead to any dissociation into molecular fragments. Figure 3 shows the atomic displacements of an isolated water molecule calculated by applying the same procedure as above to the ν_3 mode. The corresponding changes of the energy and the normal coordinates are plotted against s^3 in Fig. 4. The force constants were taken from the general quartic force field (iii) of Smith and Overend.[9] According to the sign of the coefficient $a^1{}_{33}$, the mixing of Q^1 and Q^3 in s^3 takes place with the opposite phase, leading to a sharp turning of the hydrogen atom H_2 in Fig. 3 which starts to stretch the O–H_2 bond at the potential minimum. Since the atom H_1 starts to approach the oxygen atom, the molecular distortion along s^3 cannot lead to any dissociation eventually. There are a number of symmetric triatomic molecules for which the antisymmetric stretching mode ν_a has a higher frequency than the symmetric stretching mode ν_s, and the relevant cubic constant K_{saa} is negative.[10] Absence of any IRC's which start in the direction of the antisymmetric stretching mode at the equilibrium should be a general feature for these molecules.

Combination of Eqs. 7 and 17 may thus be utilized for discussing whether a given normal coordinate is connected with any IRC's as well as for examining the behavior of an IRC in the vicinity of the equilibrium configuration of a molecule. Such an information offers important reference data in estimation of higher-order force constants, and should be useful to check the accuracy of a MO calculation when reliable force constants are available from a large number of experimental data.

The author is grateful to Professor R. G. Parr of the University of North Carolina, Dr. H. Nakatsuji and Dr. K. Yamashita of Kyoto University for valuable discussions. Numerical calculations were carried out with FACOM M200 and M382 computing systems at the Data Processing Center, Kyoto University and a HITAC M200H computing system at the Computer Center, Institute for Molecular Science.

Appendix

The behavior of the IRC starting in the direction of the ν_i mode in the normal coordinate space may be described by taking Q^i itself instead of s^i as the independent variable. In this case, we divide Q^j in orders of magnitude as

$$Q^j = Q^j_0 + \varepsilon Q^j_1 + \varepsilon^2 Q^j_2 + \cdots. \tag{A1}$$

Substituting Eq. 4 and Al into Eq. 6 and rearranging, we obtain a series of differential equations which should hold separately in order that the choice of ε is arbitrary. The zeroth order equation

$$dQ^j_0/\lambda_j Q^j = dQ^i/\lambda_i Q^i$$

is immediately integrated to give the general expression for meta IRC's given by Tachibana and Fukui,[11]

$$Q^j_0 = C_{0j} Q^{i\lambda_j/\lambda_i}. \tag{A2}$$

If we take only those solutions of the zeroth order equation which are identically zero by putting $C_{0j}=0$ in Eq. A2, the first order equation is written simply as

$$(dQ^j_1/dQ^i) = (\lambda_j Q^j_1/\lambda_i Q^i) + (K_{jii}/2\lambda_i)Q^i. \tag{A3}$$

By introducing the integrating factor

$$\exp\{-(\lambda_j/\lambda_i)\int(1/Q^i)dQ^i\} = Q^{i\,-\lambda_j/\lambda_i},$$

Eq. A3 can be solved to give

$$Q^j_1 = (1/2)K_{jii}(\ln Q^i/\lambda_i)Q^{i2}, \tag{A4}$$

for the case where $\lambda_j=2\lambda_i$ and

$$Q^j_1 = (1/2)K_{jii}(2\lambda_i - \lambda_j)^{-1} Q^{i2}, \tag{A5}$$

for the case where $\lambda_j \neq 2\lambda_i$. The solution of the second order equation is given similarly as

$$Q_2^j = (1/6)(K_{jiii} + 3\sum_k K_{jik}a_{ii}^k - 3K_{iii}a_{ii}^j)(\ln Q^i/\lambda_i)Q^{i2}, \quad \text{(A6)}$$

when $\lambda_j = 3\lambda_i$. The solution for the case where $\lambda_j \neq 3\lambda_i$ is obtained by replacing $(\ln Q^i/\lambda_i)$ in Eq. A6 with $(3\lambda_i - \lambda_j)^{-1}$. These solutions of the first and the second order equations can also be expressed as functions of s^i simply by replacing Q^i in Eqs. A4—A6 with s^i, since the expansion of Q^i with respect to s^i does not include the quadratic term: see Eq. 13. The coordinate Q^j is then given as the sum of $Q_1{}^j$ and $Q_2{}^j$ under the approximation up to the second order. When neither $2\lambda_i$ nor $3\lambda_i$ equals to λ_j, this sum becomes identical to the expansion derived in the text.

References

1) K. Fukui, *J. Phys. Chem.*, **74**, 4161 (1970).
2) K. Fukui, S. Kato, and H. Fujimoto, *J. Am. Chem. Soc.*, **97**, 1 (1975).
3) S. Kato and K. Morokuma, *J. Chem. Phys.*, **73**, 3900 (1980).
4) Y. Tanaka and K. Machida, *J. Mol. Spectrosc.*, **64**, 429 (1977).
5) K. Yamashita, T. Yamabe, and K. Fukui, *Chem. Phys. Lett.*, **84**, 123 (1981).
6) D. Dangoisse, E. Willemot, and J. Bellet, *J. Mol. Spectrosc.*, **71**, 414 (1978).
7) D. T. Davies, R. J. Richards, and M. C. L. Gerry, *J. Mol. Spectrosc.*, **80**, 307 (1980).
8) R. Cornet and G. Winnewisser, *J. Mol. Spectrosc.*, **80**, 438 (1980).
9) D. F. Smith and J. Overend, *Spectrochim. Acta, Part A*, **28**, 471 (1972).
10) K. Kuchitsu and Y. Morino, *Bull. Chem. Soc. Jpn.*, **38**, 805, 814 (1965).
11) A. Tachibana and K. Fukui, *Theor. Chim. Acta*, **49**, 321 (1978).

Mechanochemical Change in the Solid State of Hexobarbital

Akiko IKEKAWA* and Sohachiro HAYAKAWA†

Faculty of Pharmaceutical Sciences, Showa University, Hatanodai, Shinagawa-ku, Tokyo 142

†*Department of Applied Physics, Faculty of Science, Tokyo Institute of Technology, Oh-okayama, Meguro-ku, Tokyo 152*

(Received April 26, 1983)

The effect of ball-milling on X-ray diffraction diagrams, IR spectra, DTA and DSC thermograms of hexobarbital was investigated. It was found that the regularity at the crystal part changed upon ball-milling without any diluent. In addition to this change, an amorphous part increased upon ball-milling with microcrystalline cellulose (MCC). The solubility in a KH_2PO_4–Na_2HPO_4 buffer solution (pH 6.0) also increased upon ball-milling with MCC, though the solubility did not change without MCC. The analysis of IR spectra indicated that hydrogen bonds were formed between the C=O group of hexobarbital and the OH group of MCC upon ball-milling. Both the increase in the amorphous part and solubilization of hexobarbital upon ball-milling were attributed to the stabilization of the amorphous state caused by the interaction with MCC.

Previously, the change in the solid state of amobarbital upon ball-milling, both with and without any diluent, was investigated.[1-3] In this paper, the change in the solid state of hexobarbital upon ball-milling was discussed.

Experimental

The materials used were microcrystalline cellulose (MCC) described in a previous paper[4] and hexobarbital [5-(1-cyclohexenyl)-1,5-dimethyl-2,4,6(1*H*, 2*H*, 3*H*)-pyrimidinetrione] supplied from Teikoku Kagaku Sangyo Co.

A sample was inserted in a stainless-steel mill (in diameter of 10 cm and in capacity of 900 cm^3) containing 30 stainless-steel balls (with true density of 8.2 g/cm^3 and in diameter of 1.9 cm) and 10 balls of diameter of 2.5 cm. The mill was rotated at the velocity of 120 min^{-1}. The ball-milled samples are 10 g of MCC, 10 g of hexobarbital, a mixture of 1 g of hexobarbital and 9 g of MCC, and a mixture of 3 g of hexobarbital and 7 g of MCC.

The following measurements were carried out in the way reported previously; X-ray diffraction diagrams, DTA and DSC thermograms, IR spectra by the use of Nujol method, and particle size distribution of hexobarbital.[4] Solubility of hexobarbital in various samples in KH_2PO_4–Na_2HPO_4 buffer solution (pH 6.0, ionic strength 0.08) at 30 °C was obtained from the absorbance at 219 nm as described in the previous paper.[4]

Results and Discussion

Ball-milling without Any Diluent. X-Ray Diffraction: Figure 1 shows the effect of ball-milling without any diluent on X-ray diffraction diagrams of hexobarbital. The diffraction intensities of the lines at 8.4°, 11.1, 15.8, and 23.2° of 2θ decreased and those of the lines at 14.5 and 17.3° of 2θ increased by ball-milling. Fine powders were obtained on evaporation of an ethanol solution or a chloroform solution of hexobarbital under reduced pressure. The differaction diagram of the powders obtained from an ethanol solution was similar to the diagram for original hexobarbital, and the diagram for the powders obtained from a chloroform solution was similar to the diagram for ball-milled hexobarbital. It is clear from this fact that the change in the diffraction intensities in Fig. 1 is not attributed to the decrease in particle size. The locations of the lines were little influenced by ball-milling. The presence of polymorphs for hexobarbital has not been reported yet. These facts suggest that the regularity at the crystal part of hexobarbital changes by ball-milling.

The mean values of the lattice disturbance amplitude, $\overline{U_x''}$, were obtained, using all the combinations of the two of the diffraction intensities of the lines at 8.4, 11.1, 14.3, 15.8, 17.3, and 23.2—23.5° of 2θ.[5] As is shown in Fig. 2, $\overline{U_x''}$ was at a minimum at the ball-milling time around 1—5 h. Each line was indexed as is shown in Fig. 1, on the basis of the crystal structure reported by

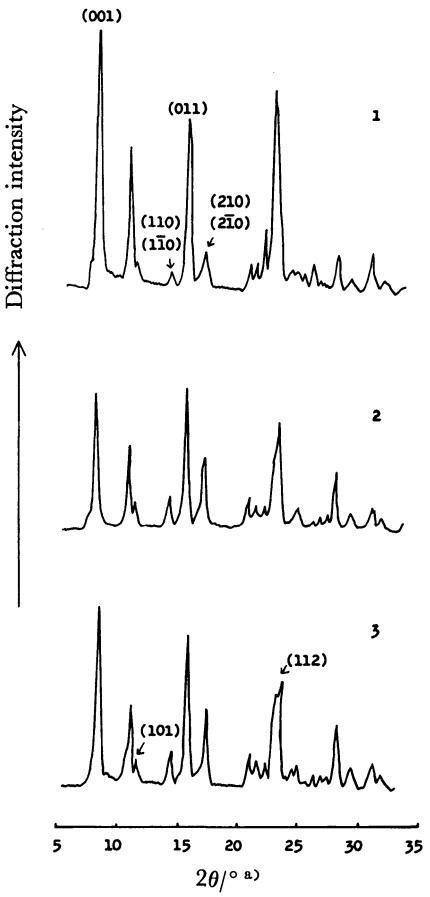

Fig. 1. Effect of ball-milling without any diluent on a X-ray diffraction diagram of hexobarbital.
Ball-milling time/h: 1 ; 0, 2 ; 0.5, 3 ; 60.
a) 2θ is the angle between the incident X-ray and the scattering X-ray.

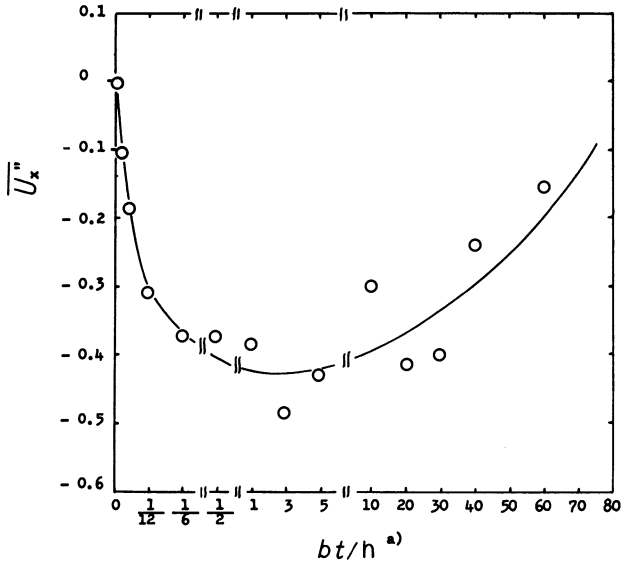

Fig. 2. Variation in $\overline{U_x''}$ with ball-milling in the absence of any diluent.
a) *bt* is the ball-milling time.

Jean-Pierre Bideau *et al.* ($P2_1/c$, $a=16.79$ Å, $b=6.65$ Å, $c=11.02$ Å, $\beta=108°\ 17'$).[6] These results suggest that the regularity at the crystal part increases in the first stage of ball-milling and that the regularities in (110), ($1\bar{1}0$), ($2\bar{1}0$), and (210) planes increase more remarkably than those in the other planes. It is also shown that the regularity decreases upon ball-milling for more than 10 h.

The crystallinity obtained by the Ruland's method[7] was little influenced by ball-milling.

IR Spectra: Figure 3 shows the effect of ball-milling without any diluent on IR spectra of hexobarbital. The absorbances at 3240 and 1720 cm^{-1} regions increased upon ball-milling. The absorbance at each of the wave number, ν, was determined, assuming the transmittance on the straight line, passing through 3400 and 1900 cm^{-1} or 1900 and 900 cm^{-1}, to be 100%. In Fig. 4, $R_{\nu,\nu'}$ is the ratio of the absorbance at the wave number of ν to the absorbance at ν'. The $R_{3240,3210}$ and $R_{1720,1660}$ values increased and the $R_{\nu,1660}$ values ($\nu/cm^{-1}=1670$—1705, 1730—1740) decreased upon ball-milling.

In the IR spectra of barbituric acid derivatives, the band at 3000—3600 cm^{-1} region is assigned to be due to the NH stretching vibration. The absorption of free NH in the solid state of phenobarbital is observed at 3310 cm^{-1}, and this band shifts to lower frequency by hydrogen bonding. The three bands at 1600—1800 cm^{-1} region is assigned to the stretching vibrations of the C=O groups. In the spectra of hexobarbital, the highest frequency band at 1740—1750 cm^{-1} is assigned to the C=O group at the 2-position, the middle frequency band to the C=O group at the 4-position, and the lowest frequency band to the C=O at the 6-position. The absorption band due to the free C=O at the 4-position is around 1730 cm^{-1}, and the band due to the free C=O in the 6-position is around 1700 cm^{-1}. These bands shift to lower frequency by hydrogen bonding. It is also reported that the C=O group in the 6-position of hexobarbital forms hydrogen bonds with the NH group in the solid state.[8]

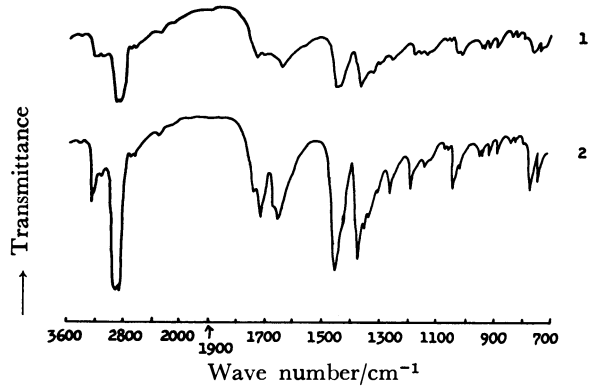

Fig. 3. Effect of ball-milling without any diluent on IR spectra of hexobarbital.
1: Original hexobarbital, 2: hexobarbital ball-milled for 60 h without any diluent.

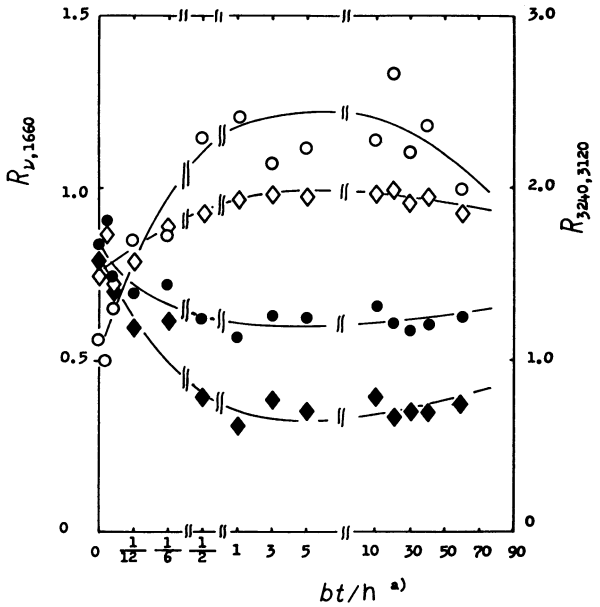

Fig. 4. Variation in $R_{\nu,\nu'}$ for hexobaribital with ball-milling in the absence of any diluent.
(ν/cm^{-1})/(ν'/cm^{-1}): 1740/1660(●), 1720/1660 (◇), 1690/1660(◆), 3240/3120(○).
a) *bt* is the ball-milling time.

It is suggested from the above results that the 4-carbonyl groups free from hydrogen bonding with the NH groups increased by ball-milling. The bands at 1020—1060 cm^{-1} due to the skeletal vibration[8] also changed upon ball-milling; this is also considered to be due to the change in hydrogen bonding. As is shown in Figs. 2 and 4, the variation in $\overline{U_x''}$ with ball-milling is parallel to the variation in $R_{\nu,\nu'}$; this fact suggests that the variation in hydrogen bonding due to ball-milling is related to the variation in the regularity at the crystal part.

No difference was observed before and after ball-milling in the melting point, the heat of fusion, and the solubility of hexobarbital in KH_2PO_4–Na_2HPO_4 buffer solution (pH 6.0) at 30 °C.

Particle Size: In Fig. 5, D_{50} is a median diameter by

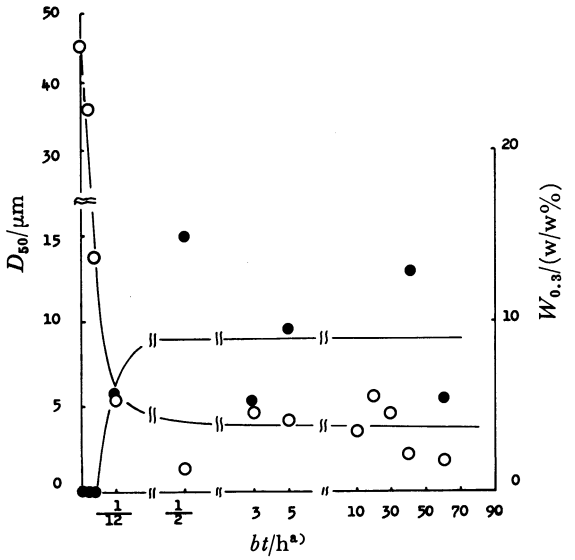

Fig. 5. Variation in particle size of hexobarbital with ball-milling in the absence of any diluent.
○: D_{50}, ●: $W_{0.3}$.
a) bt is the ball-milling time.

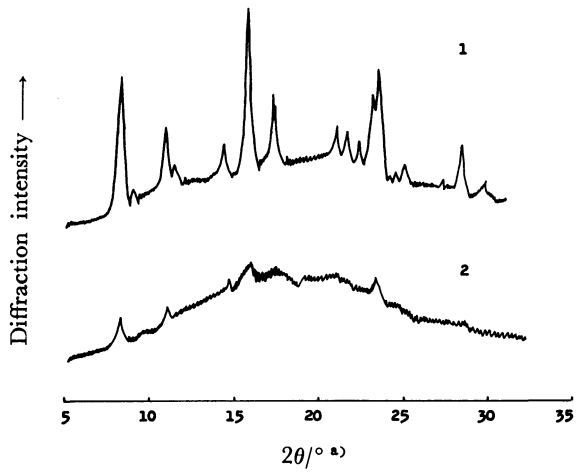

Fig. 6. Effect of ball-milling with MCC on a X-ray diffraction diagram of hexobarbital.
Content of hexobarbital; 30 w/w%.
1: A mixture of hexobarbital, ball-milled for 60 h without any diluent, and MCC ball-milled for 60 h without hexobarbital, 2: a mixture of hexobarbital and MCC ball-milled together for 60 h.
a) 2θ is the angle between the incident X-ray and the scattering X-ray.

weight base and $W_{0.3}$ is the weight fraction of the particles smaller than 0.3 μm in diameter. The D_{50} and $W_{0.3}$ values of hexobarbital varied in the first stage, and they stayed nearly constant after ball-milling for more than 30 min. The variations in D_{50} and $W_{0.3}$ with ball-milling were parallel to the variation in $\overline{U_x''}$ and $R_{\nu,\nu'}$ in the first stage. Probably, the change in the regularity at the crystal part becomes remarkable when the particles are broken.

Ball-milling with MCC. X-Ray Diffraction: The ratio of the diffraction intensity at 17.3° of 2θ to the intensity at 15.8° of 2θ increased at the first stage of ball-milling. As is shown in Fig. 6, the diffraction intensities for hexobarbital decreased gradually upon ball-milling with MCC. The crystallinity, x_{cr}, for hexobarbital ball-milled for 60 h without any diluent, was 0.92 as determined by the Ruland's method.[7] The x_{cr} values of hexobarbital in the ball-milled mixture with MCC were determined from the ratio of the intensity of the diffraction lines in the range of 10—20° of 2θ to the intensity for the mixture of hexobarbital (ball-milled for 60 h without any diluent) and MCC, for the diffraction lines were overlapped with those of MCC in the range of 20—30° of 2θ in the first stage of ball-milling. The x_{cr} value decreased upon ball-milling and the rate in the first stage was larger for the mixture containing larger amount of MCC. (Fig. 7)

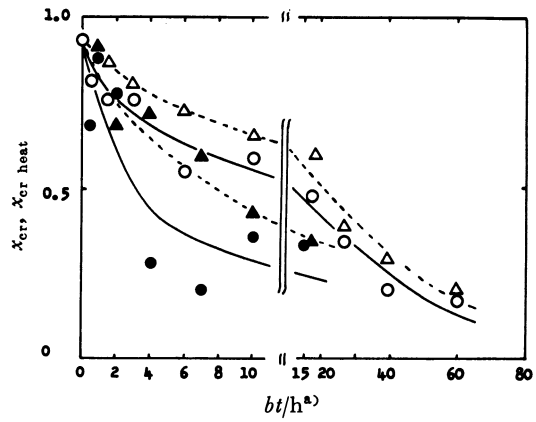

Fig. 7. Effect of ball-milling with MCC on the solid state of hexobarbital.

Content of hexobarbital/(w/w%)	x_{cr}	$x_{cr\ heat}$
10	●	▲
30	○	△

a) bt is the ball-milling time.

Heat of Fusion: The heat of fusion, ΔH_{obsd}, for hexobarbital decreased from 27.6 kJ/mol to 6.7 kJ/mol upon ball-milling the mixture with MCC containing 30 w/w% of hexobarbital for 60 h. The peak of fusion of hexobarbital disappeared upon ball-milling the mixture containing 10 w/w% of hexobarbital for more than 30 h. The ΔH_{obsd} value did not change upon ball-milling without any diluent, though the regularity at the crystal part slightly changed. Assuming that ΔH_{obsd} for the amorphous part is zero, the crystallinity of hexobarbital ($x_{cr\ heat}$) is obtained from Eq. 1.

$$x_{cr\ heat} = (\Delta H_{obsd}/27.6) \times 0.93 \quad (1)$$

As is shown in Fig. 8, the $x_{cr\ obsd}$ values were nearly identical with the x_{cr} values.

Melting Point: In Fig. 8, T_1 is the temperature at which the peak of fusion starts, T_2 is the melting point, and T_3 is the temperature at the intersecting point of the base line and the extension of the line behind the peak. The peak of fusion of hexobarbital was broadened, and T_1, T_2, and T_3 were lowered by ball-milling with MCC, though the peak was not influenced upon ball-milling without any diluent. In Figs. 7 and 9, parallel relationship is seen between the lowering of these temperatures and the decrease in x_{cr} by ball-milling; this

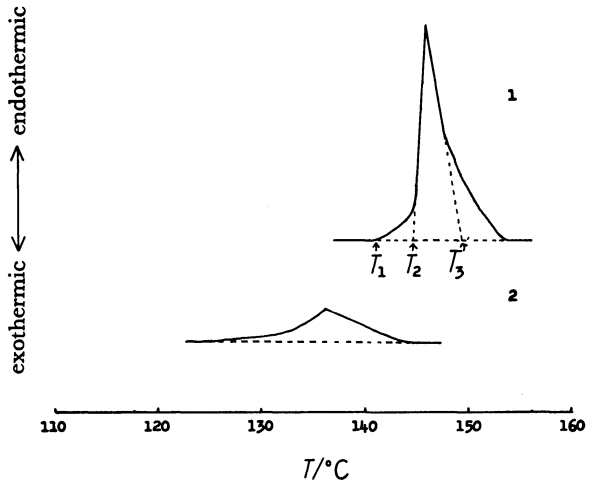

Fig. 8. DTA thermograms of hexobarbital ball-milled with MCC.

Content of hexobarbital/30 (w/w%)	Ball-milling time/h
1	0
2	40

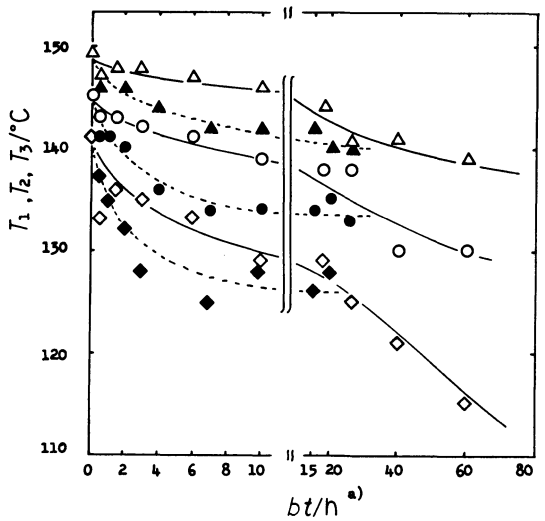

Fig. 9. Influence of ball-milling with MCC on T_1, T_2, and T_3.

Content of hexobarbital/(w/w%)	T_1	T_2	T_3
10	◆	●	▲
30	◇	○	△

a) *bt* is the ball-milling time.

result shows that the lowering of the temperatures is attributable to the increase in the amorphous part.

IR Spectra: Figure 10 shows the effect of ball-milling on IR spectra of the mixtures of hexobarbital and MCC. The absorbances around 1670—1730 and 1110 cm^{-1} regions increased upon ball-milling. The absorbance at 3400 cm^{-1} region also increased for the mixture containing 30 w/w% of hexobarbital. The band around 1670—1730 cm^{-1} corresponds to the stretching vibration of the C=O groups of hexobarbital.[8] In the IR spectra of the cellulose derivatives, the band around 3400 cm^{-1} region was assigned to the stretching mode of hydrogen-bonded OH groups.[9] The intensities and

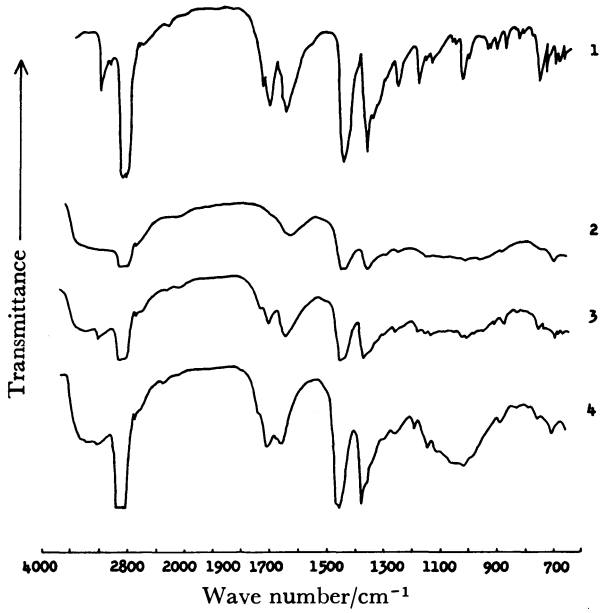

Fig. 10. Influence of ball-milling on IR spectra of a mixture of hexobarbital and MCC.
1: Hexobarbital ball-milled for 60 h without any diluent, 2: MCC ball-milled for 60 h without hexobarbital, 3: a mixture of "1" and "2" in the ration of 3 : 7 by weight, 4: a mixture of 3 g of hexobarbital and 7 g of MCC ball-milled together for 60 h.

frequencies of this band was reported to be affected by the difference in a hydrogen-bonding system.[10] The band at 1110 cm^{-1} was assigned to the C–O stretching mode, perphaps coupled to the C–C frequency. This band was also reported to change with the variation in the hydrogen-bonding system.[9-11] These facts indicate that hydrogen bonds are formed between the C=O groups of hexobarbital and the OH group of MCC. The variation in the skeletal vibration of hexobarbital around 1045 cm^{-1} is probably due to the change in the hydrogen bonds of the C=O groups.[8]

The absorbance at each of the wave numbers, ν, was determined, assuming that the transmittance on the straight line passing through 1850 and 800 cm^{-1} was 100%. In Fig. 11, $R_{1740,1660}$ was little influenced by ball-milling. $R_{\nu,1660}$ values (ν/cm^{-1}=1675—1735) were affected slightly in the first stage, and they increased after ball-milling for more than 10 h. This tendency was remarkable at the range of 1690—1700 cm^{-1}. These results show that the 4-carbonyl group of hexobarbital forms hydrogen bonds with MCC upon ball-milling and that the absorbance of hexobarbital at 1730 cm^{-1} shifts to the lower frequency.

Solubility: A suspension of the ball-milled mixture in KH_2PO_4–Na_2HPO_4 buffer solution (pH 6.0) was shaken at 30 °C, and the concentration of hexobarbital in the filtrate of the suspension was measured. The concentration stayed nearly constant after shaken for more than 15 min. In Fig. 12, c_{20min} is the concentration for the suspension shaken for 20 min. The c_{20min} value was little influenced in the first stage of ball-milling, and the value increased after ball-milling for more than 10 h. The variation in c_{20min} with ball-milling was parallel to the variation in $R_{\nu,1660}$ (ν/cm^{-1}=1665—1735)

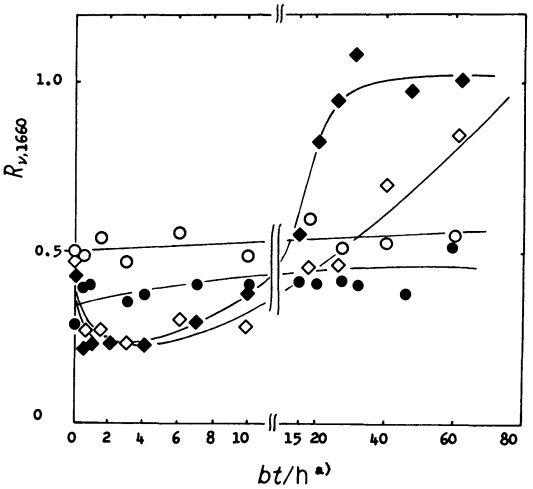

Fig. 11. Variation in $R_{\nu,1660}$ with ball-milling.

Content of hexobarbital/(w/w%)	ν/cm^{-1} 1740	1690
10	●	◆
30	○	◇

a) *bt* is the ball-milling time.

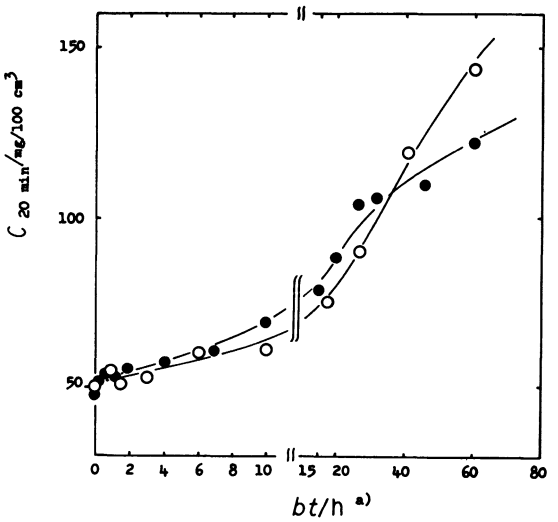

Fig. 12. Variation in $c_{20\,min}$ upon ball-milling with MCC. Content of hexobarbital/w/w%: ○; 10, ●; 30.
a) *bt* is the ball-milling time.

The increase in the solubility of hexobarbital upon ball-milling is probably due to the interaction with MCC.

In the previous paper, amobarbital was ball-milled with such diluents as methylcellulose (MC) and dextran. Solubility of amobarbital in distilled water increased upon ball-milling with diluents, though it increased only slightly in the absence of any diluent. The analysis of the IR spectra indicated that hydrogen bonds were formed between the C=O groups of amobarbital and the OH groups of the diluents by ball-milling. MC and dextran are both soluble in distilled water. After the suspension of the mixture with MC or dextran in distilled water had been set aside for a week after the time of preparation, the solid state of amobarbital undissolved in the suspension was compared with the state before dissolution. From this comparison, it was shown that the presence of diluent in the ball-milled mixture prevented the amorphous part to be crystallized. It was concluded from the above results that the increase in the solubility of amobarbital upon ball-milling was attributed to the stabilization of the amorphous state caused by the interaction with diluents.[3] It is analogized from these results in the previous paper[3] that the increase in the amorphous part and in the solubility of hexobarbital upon ball-milling are both due to the stabilization of the amorphous state caused by the interaction with MCC, though these could not be confirmed experimentally because of poor solubility of MCC in distilled water.

The authors are grateful to Mrs. Mayumi Tobe, one of the members of the Analytical Center of Showa University, for the measurement of IR spectra.

References

1) A. Ikekawa and S. Hayakawa, *Bull. Chem. Soc. Jpn.*, **54**, 2587 (1981).
2) A. Ikekawa and S. Hayakawa, *Bull. Chem. Soc. Jpn.*, **55**, 1261 (1982).
3) A. Ikekawa and S. Hayakawa, *Bull. Chem. Soc. Jpn.*, **55**, 3123 (1982).
4) N. Kaneniwa, A. Ikekawa, and M. Sumi, *Chem. Pharm. Bull. (Tokyo)*, **26**, 2734, 2744 (1978).
5) T. Kubo, "Mekanokemisutori Gairon," Tokyo Kagaku Dojin, Tokyo (1978), p. 18.
6) Jean-Pierre Bideau, F. Leroy, and J. Housty, *C. R. Acad. Sci. Paris, t.* **271**, 500 (1970).
7) W. Ruland, *Acta Crystallogr.*, **14**, 1180 (1961).
8) R. J. Mesley, *Spectrochim. Acta, Part A*, **26**, 1427 (1970).
9) H. G. Higgins, G. M. Stewart, and K. J. Harrington, *J. Polym. Sci.*, **51**, 59 (1961).
10) J. H. Keighley and S. N. Pandey, *J. Text. Inst.*, **1**, 23 (1976), R. H. Marchessault and C. Y. Liang, *J. Polym. Sci.*, **43**, 71 (1960).
11) M. L. Nelson and R. T. O'Connor, *J. Appl. Polym. Sci.*, **8**, 1311 (1964).

 © 1983 The Chemical Society of Japan Bull. Chem. Soc. Jpn., 56, 3571—3577 (1983)

Thermal and Dielectric Properties of Liquid Crystals with a Coumarin Skeleton

Hidetsugu NAKAI, Shunsuke TAKENAKA,* and Shigekazu KUSABAYASHI
Department of Applied Chemistry, Faculty of Engineering, Osaka University, Suita, Osaka 565
(Received May 2, 1983)

In order to examine the liquid crystalline properties of coumain, 3-X- and 7-Y-substituted coumarins where X= cyano and *n*-alkoxycarbonyl, and Y=4-*n*-alkyl- and 4-*n*-alkoxybenzoyl, 4-alkoxycinnamoyloxy, 4′-alkyl- and 4′-alkoxy-4-biphenylylcarbonyloxy, and 4-(4-alkoxybenzoyloxy)benzoyloxy (**4**) groups have been prepared. The compounds with X=alkoxycarbonyl group tend to exhibit strong smectic properties, and compounds with X=cyano exhibit stable nematic phases, whereas the coumarin core seems to facilitate a lateral separation of molecules in the mesophase due to its large molecular breadth. The heptyloxy homolog of **4** exhibits a reentrant behavior of the C–N_{re}–S_A–N–I type. The thermal properties are discussed in terms of the polarity and polarizability of coumarin, and the molecular structure. The dielectric properties of the compounds have also been examined and discussed in terms of the polarity of the coumarin core.

An investigation of the physical properties of new liquid crystalline materials is important in studying the relationship between the structure of materials and their mesomorphic characteristics. Liquid crystalline materials with a polar group such as a cyano or a nitro give rise to some interesting behavior. A cyano group directed along the parallel direction with respect to the longer molecular axis induces a strong dipole moment along that direction. Liquid crystals with a cyano group as the terminal of the molecule have proved successful in electro optical devices employing the twisted nematic mode. On the other hand, a cyano group directed along the lateral direction with respect to the longer molecular axis induces a strong dipole moment along that lateral direction. Liquid crystals with a cyano group as a lateral substituent give rise to a negative dielectric anisotropy and have proved successful in electro-optical devices employing the dynamic scattering and guest-host modes.[1]

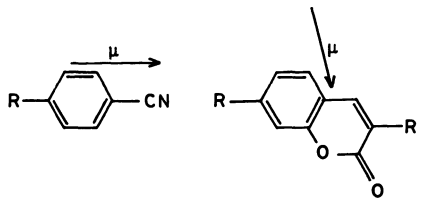

In usual mesogens, the polarity is important in determining not only the mesomorphic but also the dielectric properties. Benzonitrile has a strong dipole moment (3.9 D, 1 D=3.3356×10^{-30} C m) along the longer molecular axis, as is shown below.[2] On the other hand, coumarin is a benzene derivative with a lactone ring, which generates a strong dipole monent (4.48 D).[3] As the 3 and 7 positions of coumarin are substituted, however, the polarity will have some angles with respect to the longer molecular axis. In this paper, we wish to report the syntheses of new liquid crystalline materials involving coumarin; their thermal and dielectric properties will be discussed in terms of the characteristics of the coumarin core.

Experimental

Method. The transition temperatures were determined using a Nikon Model POH polarising microscope fitted with a Mettler FP 52 heating stage and a FP 5 control unit. The transition entropies were calculated by means of the equation; $\Delta S=\Delta H/T$, where the transition enthalpy, ΔH, was measured with a Daini-Seikosha SSC-560 differential scanning calorimeter, indium being used as a calibration standard, with a heating rate of 5 °C/min. The dielectric constants were measured by using a Ando-denki TR-10 precision capacitance-measurement system. The capacitor cell consisted of two indium oxide-coated glass electrodes separated by a 25 μ Mylar spacer. The cell temperature was controlled by means of a brass housing. The voltage applied was 0.4 V at 1 kHz. The alignment of molecules in the cell was achieved by applying a magnetic field of *ca.* 8 kG (1 G=10^{-4} T). The capacitor cell was calibrated by the use of highly purified benzene and acetonitrile.

Materials. Nematic 5 and ZLI-1083 were purchased from the Merck Co. The 4-(*n*-alkyl)benzoic acids and the aldehydes were purchased from the Kantokagaku Co. The 4-(*n*-alkoxy)benzoic acids and the aldehydes were purchased from the Tokyo Kasei Co.

3-Cyano-7-hydroxycoumarin. A mixture of 2,4-dihydroxybenzaldehyde (5 g, 0.036 mol) and malonitrile (2.4 g, 0.036 mol) in absolute ethanol (30 ml) and two drops of piperidine was heated with stirring at 70 °C for 1 h. The reaction mixture was then poured onto a 350-ml portion of 3.5 mol dm^{-3} hydrochloric acid, and the resulting solution was heated at 60 °C for 30 min. After cooling, the precipitates were collected by filtration and recrystallized from ethanol, giving 3-cyano-7-hydroxycoumarin as yellow needles, 3.6 g (53%); mp>270 °C.[4]

3-Pentyloxycarbonyl-7-hydroxycoumarin. A mixture of 2,4-dihydroxybenzaldehyde (11 g, 0.08 mol), dipentyl malonate (20.1 g, 0.082 mol), piperidine (0.8 ml), and three drops of acetic acid in absolute ethanol (25 ml) was refluxed for 5 h.[5] The reaction mixture was then poured onto hot water (50 ml) and left to stand for overnight. The precipitates that separated out were collected and recrystallized from methanol, giving 3-pentyloxycarbonyl-7-hydroxycoumarin as colorless needles, 6.0 g (27%).

The 3-alkyloxycarbonyl-7-hydroxycoumarins were prepared by a similar method.

The 4-alkyl- and 4-alkoxybenzoyl chlorides and the coumarins were reacted in a mixture of absolute pyridine and benzene (1 : 1) to give a homologous series of **1**.[6]

The 4-alkoxycinnamic acid chlorides, which had been obtained by the reaction of 4-alkoxybenzaldehydes and malonitrile, and the coumarins were reacted in a mixture of

TABLE 1. ELEMENTARY ANALYSIS DATA

Compound	Formula	Calcd (%)			Found (%)		
		C	H	N	C	H	N
1a	$C_{27}H_{30}O_7$	69.51	6.48		69.26	6.51	
1b	$C_{26}H_{28}O_6$	71.54	6.47		71.48	6.46	
1c	$C_{27}H_{30}O_7$	69.51	6.48		69.32	6.38	
1d	$C_{28}H_{32}O_7$	69.98	6.71		69.95	6.67	
1e	$C_{29}H_{34}O_7$	70.43	6.93		70.45	7.01	
1f	$C_{30}H_{36}O_7$	70.85	7.13		70.69	7.04	
1g	$C_{27}H_{30}O_7$	69.51	6.48		69.38	6.35	
1h	$C_{28}H_{32}O_7$	69.98	6.71		69.73	6.64	
1i	$C_{22}H_{19}NO_4$	73.11	5.30	3.88	72.85	5.26	3.94
1j	$C_{25}H_{25}NO_4$	74.42	6.25	3.47	74.22	6.26	3.40
1k	$C_{23}H_{21}NO_5$	70.57	5.41	3.58	70.39	5.25	3.49
1l	$C_{24}H_{23}NO_5$	71.10	5.72	3.45	71.10	5.78	3.53
1m	$C_{25}H_{25}NO_5$	71.58	6.01	3.34	71.45	6.00	3.36
1n	$C_{23}H_{19}NO_6$	68.15	4.72	3.45	67.89	4.67	3.39
1o	$C_{24}H_{21}NO_6$	68.72	5.05	3.34	68.50	5.03	3.23
2a	$C_{25}H_{24}O_7$	68.80	5.54		68.78	5.55	
2b	$C_{27}H_{28}O_7$	69.81	6.08		69.93	6.18	
2c	$C_{27}H_{28}O_7$	69.81	6.08		69.65	6.16	
2d	$C_{29}H_{32}O_7$	70.71	6.55		70.65	6.57	
2e	$C_{23}H_{19}NO_5$	70.94	4.92	3.60	70.76	4.77	3.51
2f	$C_{25}H_{23}NO_5$	71.93	5.55	3.36	71.94	5.56	3.35
2g	$C_{28}H_{32}O_7$	69.98	6.71		69.80	6.69	
3a	$C_{27}H_{22}O_6$	73.29	5.01		73.25	5.02	
3b	$C_{28}H_{24}O_6$	73.67	5.30		73.69	5.37	
3c	$C_{29}H_{26}O_6$	74.03	5.57		73.96	5.59	
3d	$C_{30}H_{28}O_6$	74.37	5.82		74.35	5.83	
3e	$C_{31}H_{30}O_6$	74.69	6.06		74.72	6.01	
3f	$C_{32}H_{32}O_6$	74.98	6.29		74.91	6.28	
3g	$C_{29}H_{26}O_7$	71.59	5.39		71.42	5.33	
3h	$C_{31}H_{30}O_7$	72.36	5.88		72.42	5.91	
3i	$C_{26}H_{19}NO_4$	76.27	4.68	3.42	76.27	4.61	3.42
3j	$C_{27}H_{21}NO_5$	73.79	4.82	3.19	73.80	4.78	3.16
4a	$C_{26}H_{17}NO_7$	68.57	3.76	3.08	68.56	3.64	2.99
4b	$C_{27}H_{19}NO_7$	69.08	4.08	2.98	69.33	4.17	3.07
4c	$C_{28}H_{21}NO_7$	69.56	4.38	2.90	69.57	4.19	2.85
4d	$C_{29}H_{23}NO_7$	70.01	4.66	2.82	70.02	4.61	3.05
4e	$C_{30}H_{25}NO_7$	70.44	4.93	2.74	70.65	4.97	2.65
4f	$C_{31}H_{27}NO_7$	70.84	5.18	2.67	70.74	5.08	2.51
4g	$C_{32}H_{29}NO_7$	71.22	5.42	2.60	71.29	5.39	2.42
4h	$C_{33}H_{31}NO_7$	71.60	5.64	2.53	71.47	5.61	2.78

absolute pyridine and benzene (1 : 1) to give a homologous series of **2**.

The 4-alkyl- and 4-alkoxy-4′-carboxybiphenyls were prepared by the method of Gray *et al.*[7] Series **3** were obtained by the condensation of 4-alkyl- and 4-alkoxy-4′-(chlorocarboyl)biphenyls and coumarins in a mixture of absolute pyridine and benzene (1 : 1).

The 4-(4-alkoxybenzyloxy)benzoic acids were obtained according to the method of van Meter *et al.*[8] Series **4** were obtained by the condensation of the 4-(4-alkoxybenzoyloxy)-benzoyl chlorides and 3-cyano-7-hydroxycoumarin in a mixture of absolute pyridine and benzene (1 : 1). 4-Pentylphenyl 4-(4-octylbenzoyloxy)benzoate was prepared by the method of Dubois *et al.*[9]

N-[4-[4-(Octyloxy)benzoyloxy]benzylidene]-4-cyanoaniline was prepared by the method of Demus *et al.*[10] The products were purified by column chromatography on silica gel, using a mixture of pet. ether and ether (95 : 5—90 : 10) as an elution solvent, followed by recrystallization from absolute ethanol.

The purity was checked by means of the elementary analysis; the results are shown in Table 1.

Results

The transition temperatures and entropies for Series **1**—**4** are summarized in Table 2—5. The virtual N–I transition temperature for **1c**, **1f**, and **1m** were evaluated[11] from the binary phase diagrams in Fig. 1. The nematic and smectic phases for the compounds with an alkoxycarbonyl group tend to exhibit a schlieren texture and fan shaped texture, respectively, between two glass plates.

The compounds with a cyano group tend to form the nematic and/or smectic phases with a homeotropic texture between two glass plates. To identify the

Table 2. Transition temperatures (°C) for series **1**

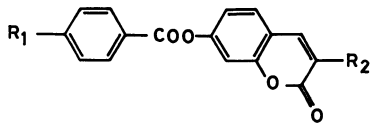

	R_1	R_2	C	S_A	N	I
1a	$C_8H_{17}O$	$COOC_2H_5$	. 129.7	—(106.1)	—(107.5)	.
1b	C_5H_{11}	$COOC_4H_9$	. 120.5		—	.
1c	$C_6H_{13}O$	$COOC_4H_9$	. 84.1	— 96.4	—[89]	.
1d	$C_7H_{15}O$	$COOC_4H_9$	. 80.4	. 101.1	—	.
1e	$C_8H_{17}O$	$COOC_4H_9$	. 82.2	. 105.4	—	.
1f	$C_8H_{17}O$	$COOC_5H_{11}$	. 74.7	. 108.5	—[92]	.
1g	C_4H_9O	$COOC_6H_{13}$	. 92.3	—(87.1)	—	.
1h	$C_6H_{13}O$	$COOC_5H_{11}$	. 93.0	—(92.1)	—	.
1i	C_5H_{11}	CN	. 127.9	—	—(110.0)	.
1j	C_8H_{17}	CN	. 125.4	. 131.6	—	.
1k	$C_6H_{13}O$	CN	. 154.2	—	. (144.9)	.
1l	$C_7H_{15}O$	CN	. 133.4	. 148.9	. 150.1	.
1m	$C_8H_{17}O$	CN	. 129.0	. 157.9	. [152]	.
1n	CN	$COOC_5H_{11}$	. 138.7	—	—	.
1o	CN	$COOC_6H_{13}$	. 137.3	—	—	.

The values in parentheses and brackets indicate the monotropic and virtual transition temperatures respectively. The presentation of this table is refered to Ref. 15.

Table 3. Transition temperatures (°C) for series **2**

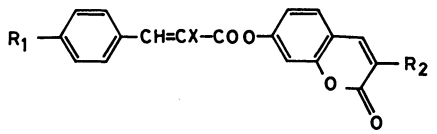

	R_1	R_2	X	C	S_A	N	I
2a	C_4H_9O	$COOC_2H_5$	H	. 151.7	—	.	.
2b	$C_6H_{13}O$	$COOC_2H_5$	H	. 139.4	. 142.8	. 157.7	.
2c	C_4H_9O	$COOC_4H_9$	H	. 97.5	. 129.0	—	.
2d	C_4H_9O	$COOC_6H_{13}$	H	. 104.1	. 132.1	—	.
2e	C_4H_9O	CN	H	. 157.6	—	. 213.1	.
2f	$C_6H_{13}O$	CN	H	. 133.0	. 186.5	. 203.8	.
2g	C_4H_9O	$COOC_4H_9$	CH_3	. 98.4	—	—	.

smectic phase, the binary-phase diagrams for several compounds were examined, as is shown in Figs. 1 and 2. Figure la indicates a phase diagrams for the binary mixture of 4-pentylphenyl 4-(4-octylbenzoyloxy)benzoate and **1c**, where both smectic A phases are miscible. This indicates that the smectic phase for **1c** can be assigned to the smectic A modification.[9] **4f** shows a reentrant property of the C–N_{re}–S_A–N–I type, which is confirmed by the binary-phase diagrams shown in Figs. 2c and 2d. The latent heats of the N_{re}–S_A and S_A–N transitions for **4f**—**h** are so small that these transitions could not be detected by means of the DSC thermograms. On the basis of these facts, we assume that the enthalpies for these transitions are less than 50 J mol^{-1}. The extrapolation of the N–I transition temperatures in Fig. 2c gives the N–I transition temperature of 295 °C for **4f**. Similarly, the N–I transition temperatures for **4g** and **4h** were evaluated as *ca.* 300 °C.

Table 4. Transition temperatures (°C) and entropies (J K^{-1} mol^{-1}) for series **3**

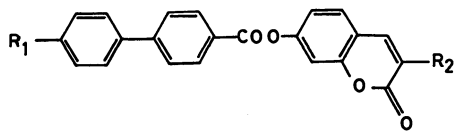

	R_1	R_2	C	S_A	N	I	ΔS_{N-I}
3a	C_3H_7	$COOCH_3$	. 179.6	. (160.2)	. [278]	.	—
3b	C_3H_7	$COOC_2H_5$	. 166.0	. 194.2	. 249.7	.	0.8
3c	C_3H_7	$COOC_3H_7$	. 142.3	. 207.3	. 236.6	.	1.4
3d	C_3H_7	$COOC_4H_9$	. 126.3	. 207.2	. 216.4	.	1.0
3e	C_3H_7	$COOC_5H_{11}$	. 136.4	. 207.3	. 214.4	.	1.0
3f	C_3H_7	$COOC_6H_{13}$	. 127.3	. 207.6	—	.	
3g	C_2H_5O	$COOC_4H_9$	. 140.9	. 228.0	. 261.8	.	0.9
3h	C_4H_9O	$COOC_4H_9$	. 138.5	. 241.5	—	.	
3i	C_3H_7	CN	. 210.0	—	. >300	.	
3j	C_4H_9O	CN	. 180.2	—	. >300	.	

The values in parenthesis and bracket are the monotropic transition temperatures.

Table 5. Transition temperatures (°C) for series **4**

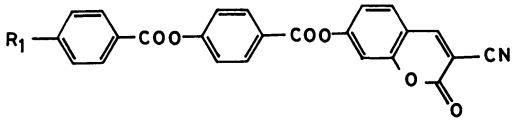

	R_1	C	N_{re}	S_A	N	I
4a	C_2H_5O	. 210.8	—	—	. >300	.
4b	C_3H_7O	. 209.8	—	—	. >300	.
4c	C_4H_9O	. 189.8	—	—	. >300	.
4d	$C_5H_{11}O$	. 162.8	—	—	. >300	.
4e	$C_6H_{13}O$	. 154.1	—	—	. >300	.
4f	$C_7H_{15}O$	. 145.9	. 147.6	. 227.4	. [295]	.
4g	$C_8H_{15}O$	. 146.6	.	. 247.1	. [300]	.
4h	$C_9H_{19}O$	. 150.3	—	. 255.1	. [300]	.

The values in the brackets are the virtual transition temperatures.

The dielectric constants were measured in a eutectic mixture of azoxy compounds (Merck nematic 5), since the present homologues have relatively high melting points. Figure 3 indicates the plots of the dielectric constants $\varepsilon_{//}$, $\varepsilon_{\perp}$, and $\Delta\varepsilon$ against the mole concentration of the coumarin compounds, where $\varepsilon_{//}$, $\varepsilon_{\perp}$, and $\Delta\varepsilon$ are the dielectric constants along the parallel and perpendicular directions with respect to the longer molecular axis, and the difference, respectively. In Fig. 3a, both $\varepsilon_{//}$ and $\varepsilon_{\perp}$ for **1c** can be seen to increase linearly in the range between 0 and 30 mol%, and to reach a plateau onward. The anisotropy also increases similarly in the range between 0 and 30 mol% of **1c** and then decrease monotonically thereafter, giving a maximum at 25 mol% of **1c**. **2c** also shows a similar trend. In Fig. 3b, both $\varepsilon_{//}$ and $\varepsilon_{\perp}$ for **1i** increase linearly with an increase in the concentration of **1i** in the range between 0 and 30 mol% of **1i**, though they tend to reach a plateau thereafter. A similar trend is also observed in **2f** and **4d**. Thus, the plots of the dielectric anisotropies against the mole

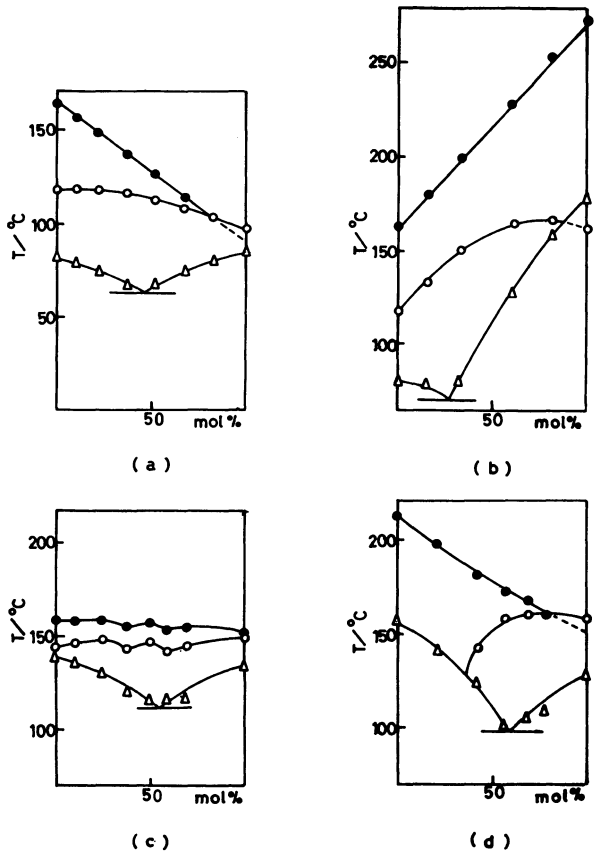

Fig. 1. Phase diagrams for the mixtures of (a) 4-pentylphenyl 4-(4-octylbenzoyloxy)benzoate (on left) and **1c** (on right), (b) 4-pentylphenyl 4-(4-octylbenzoyloxy)-benzoate (on left) and **3a** (on right), (c) **2b** (on left) and **11** (on right), (d) **2f** (on left) and **1m** (on right).
●; Nematic-isotropic, ○; smectic A-nematic, and △; crystal-smectic A (nematic) transitions.

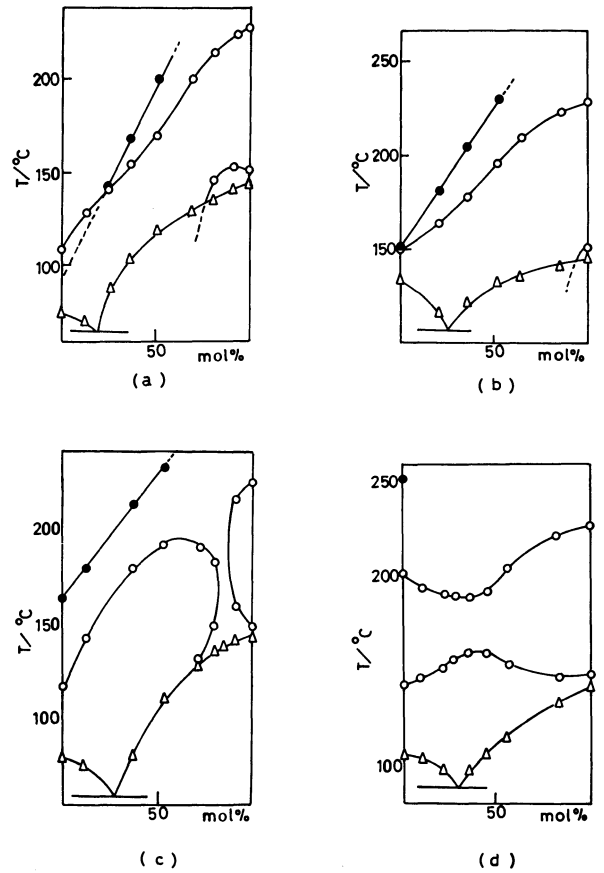

Fig. 2. Phase diagrams for the mixtures of (a) **1f** (on left) and **4f** (on right), (b) **11** (on left) and **4f** (on right), (c) 4-pentylphenyl 4-(4-octylbenzoyloxy)benzoate (on left) and **4f** (on right), (d) *N*-[4-[4-(octyloxy)benzoyl-oxy]benzylidene]-4-cyanoaniline (on left) and **4f** (on right).
●; Nematic-isotropic, ○; smetic A-nematic, and △; crystal-smectic A (nematic) transitions.

concentration for the present series have no linear correlation. The dielectric anisotropies at 15 mol% of the compounds are illustrated in Table 5.

Discussion

It has been known that the linearity, rigidity, and polarizability of a molecule are very important in determining the stability of the mesophase. From the structural point of view, the present series might be unfavorable for the stability of the nematic phase, since coumarin has a larger molecular breadth than phenyl and naphthyl groups, as is shown below.[12] Although coumarin elongates the molecular length of 1.5 Å compared with benzene, simultaneously the breadth around coumarin is larger by 1.7 times than that of benzene.

The thermal stability of the mesophase for the present series is compared with those of the other related series

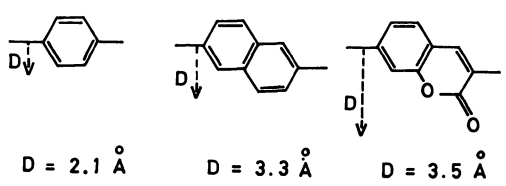

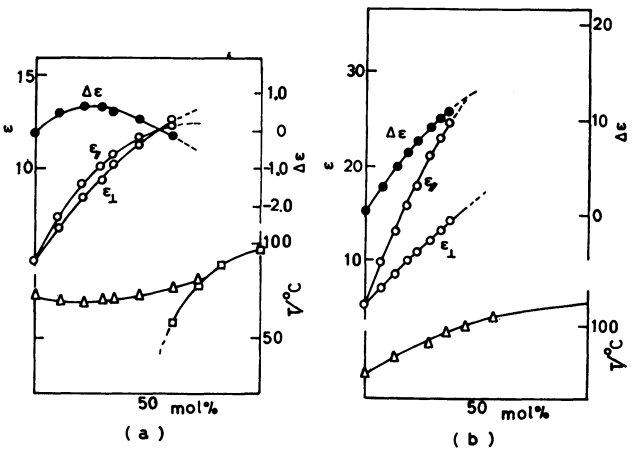

Fig. 3. Plots of dielectric constants ($\varepsilon_{//}$ and $\varepsilon_{\perp}$) and dielectric anisotropy ($\Delta\varepsilon$) and nematic-isotropic and smectic A-nematic (isotropic) transition temperatures against concentration (mol%) for the binary mixtures of (a) nematic 5 (on left) and **1c** (on right), (b) nematic 5 (on left) and **1i** (on right).
△; Nematic-isotropic and □; smectic A-nematic (isotropic) transitions.

Table 6. Dielectric constants $\varepsilon_{//}$, $\varepsilon_{\perp}$, and $\Delta\varepsilon$

Compound	15 mol%		
	$\varepsilon_{//}$	$\varepsilon_{\perp}$	$\Delta\varepsilon$
1c	8.0	7.5	0.5
2c	8.0	7.3	0.7
1i	13.6	8.6	5.0
2f	12.9	7.7	5 2
4d	14 2	7.2	7.0
10	5.9	5.4	0.5
ZLI-1083	8.5	5.7	2.8
Nematic 5 (neat)	5.0	5.1	−0.1

All data were taken in Nematic 5 at 60±1 °C.

below, where the transition temperatures for the compounds selected for the comparative study are shown:

		C	S_A	N	I
5	$C_6H_{13}O$–C_6H_4–COO–C_6H_4–CN[13]	70.5	—		81.0
6	C_6H_{13}–C_6H_4–COO–C_6H_4–CH=CH–CN[13]	97.5	—		147.7
7	$C_6H_{13}O$–C_6H_4–CH=CH–COO–C_6H_4–CN[13]	73.4	—		134.3
8	$C_6H_{13}O$–C_6H_4–COO– 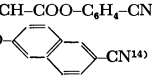 –CN[14]	95	—		160
9	$C_6H_{13}O$–C_6H_4–COO–C_6H_4–$OCOC_4H_9$[15]	68	—		93
10	$C_6H_{13}O$–C_6H_4–COO– 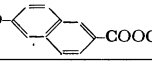 –$COOC_4H_9$[25]	94.7		107.2	107.6

(–C_6H_4– indicates a *p* phenylene group.)

Coumarin compounds **1a—f** with a alkoxycarbonyl group at the 3 position exhibit strong smectic properties in addition to the nematic ones. The thermal stability of the nematic phase is comparable with those for **9** and **10**. Similar trends are observed in Series **2** and **3**. For the homologous series, somewhat interesting trends are observed in the effect of chain length on the thermal stabilities of the nematic and smectic A phases. The S_A–N transition temperatures for **1c—e** and **3g—h** increase with an increase in the carbon number in the alkyl chain at the 7 position (see Tables 2 and 4). These trends are always present. By contrast, the S_A–N transition temperatures for **1a**, **1e**, **1f**, and **3b—f**, which involve the alkyl chain of the ethyl to the hexyl group at the 3 position of the coumarin core almost constant (see Tables 2 and 4). Simultaneously, the N–I transition temperatures rapidly decrease, showing a weak even-odd alternation. In this connection, the following facts are worthy of note. Firstly, it would be reasonable to assume that the coumarin facilitates the formation of the smectic order, since the strong dipole moment arising from the coumarin core is directed to the lateral direction of the molecule, and that it increases the lateral interactions. Secondly, the alkoxycarbonyl group at the 3 position of coumarin should be located on the coumarin plane due to steric hindrance between the alkoxycarbonyl and carbonyl groups at the 2 position of coumarin, thus increasing the molecular thickness. Therefore, the elongation of the alkyl chain in the alkoxycarbonyl group would facilitate the lateral separation of the molecules in the mesophase, rapidly decreasing the thermal stability of the nematic phase. Thereby, the increase in the alkyl chain length would not serve to enhance the S_A–N transition temperatures, since the lateral separation of the molecules inhibits any short-range interaction, a general requisite for the enhancement of the smectic properties.

When a cyano group is introduced at the 3 position, both S_A–N and N–I transition temperatures tend to decline for Series **1—4**, and the nematic properties become remarkable. For example, the N–I transition temperature for **1k** is higher than **5** by 64 °C and lower than **8** by only 15 °C, while the N–I temperature for **1i** is lower than **6** by 38 °C. On the other hand, the homologous series of **4** form a highly stable nematic phase. These facts indicate that the polarity and polarizability arising from the coumarin core involving the cyano group and the elongation of the rigid core of the molecule along the longer axis enhance the stability of the nematic phase, though the large molecular breadth around the coumarin core does not favor the nematic stability. An interesting trend is observed in the thermal properties for **1n** and **1o**. These do not exhibit a nematic phase, but these compounds have a cyano group at the terminal. These facts indicate that the alkoxycarbonyl group at the 3 position of coumarin decreases the N–I transition temperature as a result of the increased molecular thickness, as has been mentioned above. The homologous series of **4** have a highly stable nematic phase.

The smectic A phase commences from the heptyloxy homologue, and the heptyloxy homologue shows a reentrant behavior of the C–N_{re}–S_A–N–I type. As has been demonstrated by several authors,[16,17] the formation of a bimolecular complex is indispensable for the reentrant phenomena. It has been known that molecules exhibiting the reentrant behavior are constituted of plural phenyl rings combined by linkages such as –CH=N– or –COO–, with an alkoxy group of a suitable length as a terminal and a polar group such as a cyano or a nitro group indispensable to form a bimolecular complex.[18,19] In Fig. 1a, the S_A–N transition temperatures show an almost straight line, and both S_A phases are miscible, indicating that **1c** forms the smectic A phase with a monolayer organization of the molecules, because 4-pentylphenyl 4-(4-octylbenzoyloxy)benzoate has been known to form the smectic A phase.[25]

Both smectic A phases in Fig. 1b show a miscible relation with a convexity, indicating that the smectic A phase for **3a** also has a monolayer alignment of molecules. Therefore, it is impossible to expect the homologous series of **3** to exhibit the reentrant behavior. In fact, the homologous series do not exhibit the reentrant behavior, whereas they do show a wide range of the smectic A phase (Table 4).

In Fig. 1c, the smectic A phase for **2b** is miscible with that for **1n**, whereas the smectic A phase for **1n** is considered to form a bilayer type of alignment of the molecules, since the molecule has the cyano group as the polar terminal.[18,19] In Fig. 1d, on the other hand, the S_A–N transition temperatures show a remarkable depression between 40 and 60 mol% of **2o**, whereas both **1o** and **2f** have the cyano group as the terminal.

In Figs. 2a and 2b, the smectic A phases for **1f** and **1n** are miscible with that for **4f**. An interesting fact is that the reentrant N_{re}–S_A transition temperatures for **4f** increases with an increase in the concentration of **1f** but rapidly decrease thereafter, giving a maximum at 11

mol% of **4f** (Fig. 2a), whereas these temperatures rapidly decrease with an increase in the concentration of **11** (Fig. 2b). A tentative description of this trend is shown in Fig. 2c, where the monolayer smectic A phase for 4-pentylphenyl 4-(4-octylbenzoyloxy)benzoate is immiscible with the bilayer smectic A phase for **4f**. These facts indicate very clearly that a very subtle change in the molecular structure determines the affinity between the monolayer and bilayer-type smectic A phases. As we can see from Fig. 2d, the bilayer smectic A phase shows a remarkably constricted part at 60 mol% of **4f**, presumably as a result of the subtle difference in their molecular structures. Indeed, the smectic A phase with the monolayer alignment of molecules has been known usually to have an affinity with the bilayer one, but sometimes not.[20,21]

According to a concept of the miscibility relation between the monolayer and bilayer smectic A phases in the pure molecule, we can easily understand the reentrant phenomena.

The molecules with a polar terminal group such as cyano have been known to form the bimolecular complex in the mesophase and in an isotropic solution as a result of strong dipole-dipole interactions.[22,23] Such interactions form the bilayer alignment of the molecules in the smectic A phase. Usually, the bilayer smectic A phase is more stable than the monolayer one at higher temperatures. Therefore, the bilayer smectic A organization would vary in relation to the monolayer one with a lowering of the temperature. As the bilayer smectic A phase does not, thereby have a miscible relation with the monolayer one, we can expect the molecule to exhibit the reentrant phenomena. **4f** is just such a case. Further study is now underway.

Dielectric Propererties. It has been known that polarity is very important in determining the dielectric properties of a molecule. Therefore, we have to pay much attention to the polarity of coumarin. As has been mentioned above, coumarin has a larger dipole moment than benzonitrile, though the dipole moment in the present series is directed to the lateral direction of the molecule. We can roughly estimate the effective dipole moment, by the use of the usual method.[2,24]

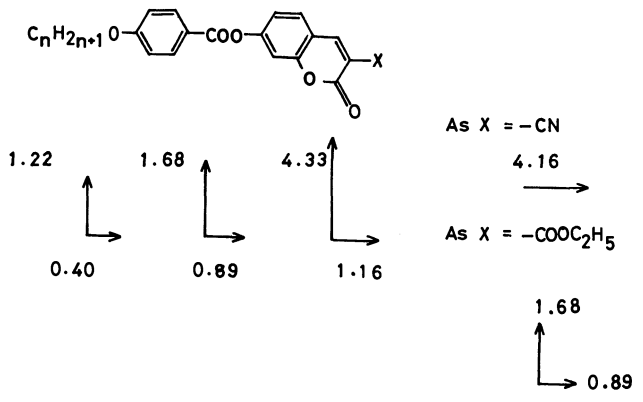

Supposing the order parameter in the nematic phase to be 0.6, we can expect the molecule with X=H to show a negative dielectric anisotropy, since $\mu = -0.46$. The alkoxycarbonyl compounds can be expected to show small positive dielectric anisotropies, for the effective dipole moment is estimated to be +0.007. As the cyano group is introduced at the 3 position of coumarin, the effective dipole moment is estimated to have a value of 2.91, as the 3-cyano compounds can be expected large dielectric anisotropies. As the phenyl group in **1a—h** is replaced by a cyclohexane, we can expect to exhibit large negative dielectric anisotropies. Unfortunately, 3-alkoxycarbonyloxy-7-(4-alkylcyclohexylcarbonyloxy)-coumarins exhibited only smectic properties.[25]

In Fig. 3a, the plots of the dielectric constants *versus* the mole concentration show rather interesting trends. The anisotropy increases with an increase in the concentration of **1c** and decreases monotonically, giving a maximum at 25 mol%. The extrapolated value for **1c**, therefore, is −1.5, incline the calulated result. In this case, we assume that the monotonical decrease in the range between 25 and 100 mol% of **1c** is connected with the increases in the smectic order in the mixture, as shown is in Fig. 3a, and that **1c** has essentially a positive dielectric anisotropy. In Fig. 3b, the dielectric anisotropy for **1i** linearly increases with increasing the concentration of **1i** and tends to become a plateau, the curve having an forward convexity. Therefore, **1i** must have a large positive dielectric anisotropy.

As we can see by comparing the dielectric constants of butyl 6-[4-(hexyloxy)benzoyloxy]-2-naphthoate (**1c** and **2c**) in Table 5, the dipolarity arising from the coumarin core results in an increase to the same extent in the dielectric constants along both parallel and perpendicular directions of the molecule. As a result, the dielectric anisotropies for **1c** and **2c** are almost same as that for the naphthalene compound. As the alkoxycarbonyl group at the 3 position is replaced by the cyano, the dielectric constant along the parallel direction of the molecule tends to increase rapidly, though that along the perpendicular direction stays constant, resulting in large values of the dielectric anisotropy.

References

1) G. J. Sprokel, "The Physics and Chemistry of Liquid Crystal Devices," Plenum Press, New York (1980).
2) O. A. Osipow, V. L. Minkin and Y. A. Zhdanov, "Dipole Moments in Organic Chemistry," Plenum Press, New York (1970).
3) G. C. LeFévre and R. J. W. LeFévre, *J. Chem. Soc.*, **1937**, 1088.
4) W. Baker and C. S. Howes, *J. Chem. Soc.*, **1953**, 119.
5) E. C. Horning, *Org. Synth.*, Coll. Vol. IV, 261 (1963).
6) G. W. Gray and B. Jones, *J. Chem. Soc.*, **1954**, 1467.
7) G. W. Gray, J. B. Hartley, and B. Jones, *J. Chem. Soc.*, **1955**, 1412.
8) J. P. van Meter and A. K. Seidel, *J. Org. Chem.*, **40**, 2998 (1975).
9) J. C. Dubois, A. Zann, and A. Beguin, *Mol. Cryst. Liq. Cryst.*, **42**, 139 (1977).
10) W. Weissflog, G. Pelzl, and D. Demus, *Mol. Cryst. Liq. Cryst.*, **76**, 261 (1981).
11) M. J. S. Dewar and R. S. Goldberg, *J. Am. Chem. Soc.*, **92**, 1582 (1970).
12) The bond lengths for aromatic C=C, C–C, C=O, and C–H were supposed to be 1.39, 1.39, 1.22, and 1.0 Å respecti-

vely.
13) V. V. Titov, E. I. Kovsev, A. I. Pavluchenko, V. T. Lazareva, and M. F. Grebenkin, *J. Phys. C*, **36**, Cl-387 (1975).
14) D. Coates and G. W. Gray, *Mol. Cryst. Liq. Cryst.*, **37**, 249 (1976).
15) D. Demus, H. Demus, and H. Zaschke, "Flüssig Kristalle in Tabellen," VEB Deutcher Verlag für Grundstoff Industrie, Leipzig (1974).
16) G. R. Luckhurst and B. A. Timimi, *Mol. Cryst. Liq. Cryst.*, **64**, 253 (1981).
17) P. E. Cladis, *Mol. Cryst. Liq. Cryst.*, **67**, 177 (1981).
18) G. Sigaud, N. H. Tinh, F. Hardouin, and H. Gasparoux, *Mol. Cryst. Liq. Cryst.*, **69**, 81 (1981).
19) N. H. Tinh, M. Joussot-Dubien, and C. Destrade, *Mol. Cryst. Liq. Cryst. Lett.*, **1980**, 257.
20) B. Engelen, G. Heppke, R. Hopf, and F. Schneider, *Mol. Cryst. Liq. Cryst.*, **49**, 193 (1979).
21) G. Sigaud, F. Hardouin, M. F. Achard, and H. Gasparoux, *J. Phys. C*, **40**, C3-356 (1979).
22) A. J. Leadbetter and A. I. Mehta, *Mol. Cryst. Liq. Cryst.*, **72**, 51 (1981).
23) G. W. Gray, *Mol. Cryst. Liq. Cryst.*, **76**, 3 (1981).
24) W. Maier and G. Meier, *Z. Naturforsch., A*, **16**, 51 (1961).
25) H. Nakai, Master's thesis, Osaka University, Osaka, Japan, **1982**.

The Study of Metal Colloids Produced by Means of Gas Evaporation Technique. I. Preparation Method and Optical Properties in Ethanol

Keisaku KIMURA* and Shunji BANDOW
Instrument Center, Institute for Molecular Science, Myodaiji, Okazaki 444
(Received May 9, 1983)

Three new methods for the preparation of metal colloid in organic solvent are presented. These methods were the matrix isolation method, the gas flow-cold trap method and the gas flow–solution trap method; the latter was found to give a good colloid solution for the optical measurements. The metals reported are high purity Ag, Au, Cu, In, Al, Ca, Sn, and Pb. The stability of the colloid is dependent on the kind of metals: Al, In, Au, and Ag are stable, and Pb, Sn, Ca, and Cu are unstable. The optical absorption spectra of these sols were measured in ethanol solution in Ar atmosphere. They are discussed in relation to those reported on the solid matrix or on the solid substrate.

A considerable amount of literature is available on the optical properties of metal particles in solid matrix as well as in colloidal aqueous solution. The routine methods to make fine particles are that metals are evaporated on an inert substrate and/or rigid matrix in vacuo or that metals are dispersed in an aqueous solution by chemical reaction. The problem posed by the former procedure is the coagulation of particles. In the latter case, we could expect many advances in the study of colloid chemistry, if we can use organic liquids as solvents rather than aqueous solution. The optical spectra were measured at a low temperature for the metal fine particles dispersed on the solid matrix. Except an aqueous solution, there have been very few reports on the spectra of solution state because of the difficulty of the sample preparation.

Conventional chemical methods supply well dispersed particles in a colloid solution; the classical Mie theory[1] has been used to explain the absorption spectrum. Recent measurements of ultrafine particles[2] applied both classical and quantum theories to the optical properties of metal particles. However the measurements were limited to solid matrix and to aqueous solution. Therefore it is important for us to observe the spectra of many sorts of metal colloids in organic solvents with a wide range of dielectric constants. Moreover, it will be desirable to get a neat metal colloid solution especially for the study of the physical properties.

In this report, we will present new preparation methods of metal colloids in organic solvents without the use of chemicals such as redox reagents, polymers, electrolytes, glue or other kinds of colloid stabilizers. This method is applied to the measurement of the optical spectra of many metal colloid solutions, some of which are first reported here. The method is applicable not only to ethanol reported here but also to any organic solvent. In addition, this technique can be applied to many sorts of solids as described in this report.

Experimental

Three different preparation methods were examined. These are the matrix isolation method, the gas flow-cold trap method, and the gas flow-solution trap method. All methods are based on a gas evaporation technique.[3] The first one is the modification of that described by Wada and Ichikawa.[4] Therefore we will omit the detailed description of the method and simply show the apparatus used in Fig. 1.

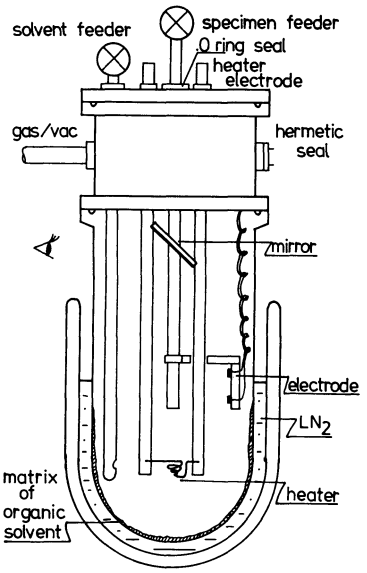

Fig. 1. The apparatus for the matrix isolation method. Organic solvent is introduced through solvent feeder to form matrix on the Pyrex glass dewar which is cooled by liquid nitrogen. Mirror enables us the observation of melting state of metals. Electrode was used to monitor the thickness of the metal layer.

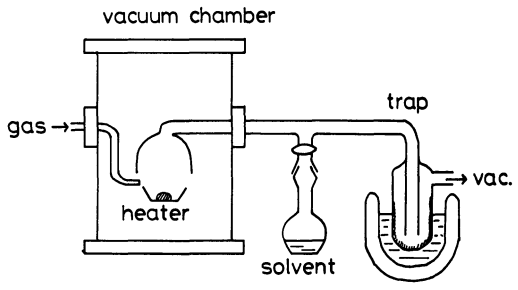

Fig. 2. The apparatus for the gas flow-cold trap method. One of the gas inlet is abbreviated in the Figure.

The gas flow-cold trap method is shown in Fig. 2. The fine particles are produced in a vacuum chamber in the atmosphere of helium gas flow. The chamber was once

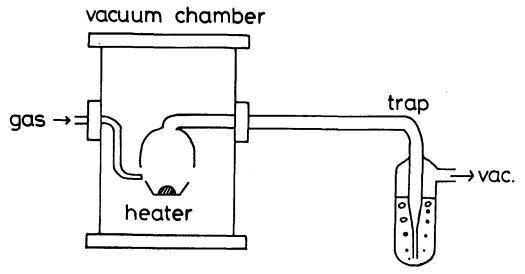

Fig. 3. The apparatus for the gas flow-solution trap method.

evacuated to 10^{-3} Torr (1 Torr≈133.322 Pa) prior to the introduction of helium gas. Under the constant flow of helium gas, a piece of metal was heated. The pressure of the chamber was varied in the range 10—50 Torr corresponding to the desired level of particle diameter. The chamber has two gas inlets, one of which is introduced to the back of tungsten heater to produce fine particles in high efficiency and the other is placed at the edge of the particle collector in order to enhance the collection yield of the particle. Argon was used for this inlet. The vapor of organic solvent which was completely degassed was introduced through the Teflon valve in the carrier gas stream and then trapped in the glass cold trap cooled with liquid nitrogen. After collection of fine particles, the trap was filled with Ar gas at 1 atmospheric pressure. The particle diameter was varied by changing the pressure of gas and the temperature of the heater.

The gas flow-solution trap method is shown in Fig. 3. Two kinds of gases were also used in this case, helium for the production of fine particles and argon for the collection and the carrier of fine particles. The procedure is the same as for the second case, except that the cold trap is replaced by the organic solvent which is cooled by cold ethanol; the temperature is −30——40 °C. The matrix isolation method and the gas flow-cold trap method sometimes gave coagulated samples and did not give a finely dispersed solution, on the other hand the gas flow-solution trap method made reproducible, well dispersed solutions. Therefore the results obtained by the latter method are mainly reported in this paper.

All spectra were obtained at room temperature in a conventional fused quartz rectangular optical cell except the vacuum evaporated film on a quartz substrate. The optical absorption spectra were recorded just after the preparation of colloid. Some metals were not stable even under these conditions, as described in the results. The metals reported are silver (99.9999%), gold (99.5%), copper (99.9999%), indium (99.999%), calcium (99.99%), aluminum (99.9999%), lead (99.9999%), and tin (99.9999%). Several organic solvents were tested: ethanol, methanol, tetrahydrofuran, cyclohexane, chlorocyclohexane, cyclohexanone, toluene, and benzene. Some solvents were found to be very reactive toward fine particles and the result of ethanol solution is presented in this report.

The optical absorption spectra of vacuum-evaporated thin films of the metals were also recorded as a reference. The metals were sublimed on the fused silica substrate in a vacuum at least 8×10^{-6} Torr. In the case of calcium, paraffin was sublimed onto the calcium film to prevent the air oxidation during the recording of the spectrum. The film thickness was monitored by a quartz oscillator film thickness gauge, Sloan DTM 200. The electron micrographs were taken by a Hitachi H 500H electron microscope used in the high resolution mode. The specimen were obtained by dropping the sample solution on the Cu grid coated by collosion film reinforced by carbon film. The silver aqueous colloid was prepared by the conventional chemical method. 0.1 M silver nitrate solution and 1% tannic acid solution were added to 500 ml distilled water and then 1% sodium carbonate solution was poured into the mixture with stirring at 70 °C. The resultant colloid solution was dialysed to distilled water overnight.

Results and Discussion

We examined many organic solvents, as stated in the experimental section, but confine ourselves here to the case of ethanol which has both protic and aliphatic properties.

Pb. Figure 4a shows the micrograph of deposited lead colloid on a carbon film taken by the usual transmission technique. The diameters of many particles lie in the region of 10 nm. Figure 4b shows the optical absorption spectra of lead colloid solution (dark brown) in Ar atmosphere. Two absorption maxima at 400 and 250 nm in a 10 nm thickness evaporated film reflect the spectra of the colloid solution. Three bands: 320 nm shoulder, 250 and 215 nm peaks in colloid was found to be time dependent. The 320 and 250 nm bands decreased with time, while the 215 nm peak increased with time. The 215 nm peak was observed in a less stable metal. It is most likely that this peak comes from the

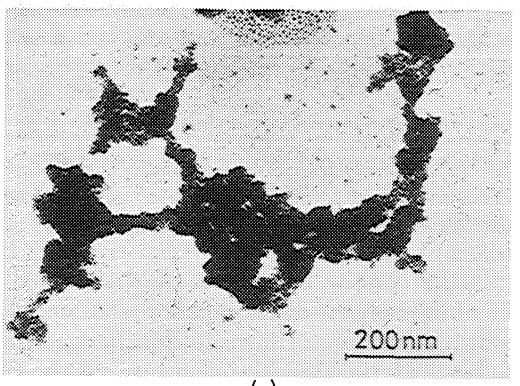

(a)

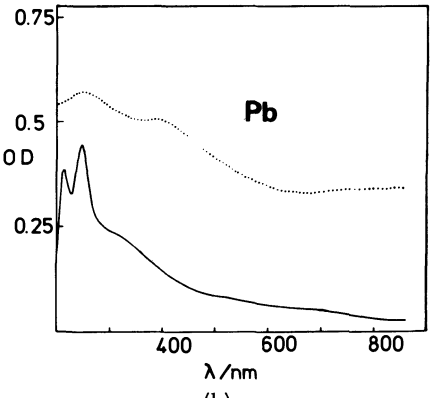

(b)

Fig. 4. (a): Micrograph of lead colloid. Small particles aggregate each other to form large particles. (b): Absorption spectra of colloid solution (solid line) and evaporated film (dotted line) of lead. The thickness of the film is 10 nm.

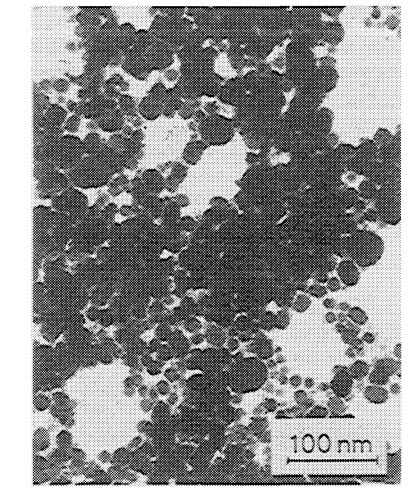

(a)

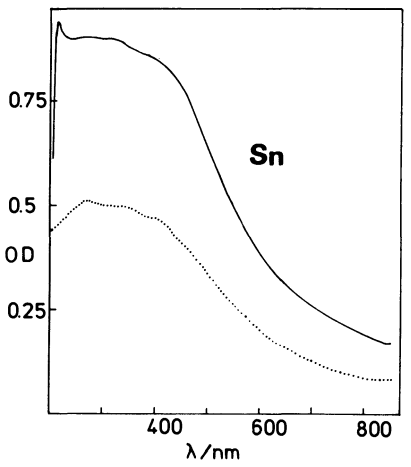

(b)

Fig. 5. (a): Micrograph of tin colloid. (b): Absorption spectra of colloid solution (solid line) and evaporated film (dotted line) of tin. The thickness of the film is 5 nm.

product of the solvent-metal reaction. After 24 h, the dark brown coloration of the solution changed to transparent, resulting in the disappearance of the 320 nm peak.

Lead colloid bands were observed in Pb doped alkali halide crystals. Topa and Velicescu reported[5] that the colloid band appears at around 250 nm upon annealing the T-center. The computer calculation[6] on the bases of complete Mie equations agreed fairly well with the above experiment. The peak position depends on the diameter of the particle. Following the calculation, the 240 nm peak was obtained for 10 nm diameter lead colloid–NaCl system. More comprehensive studies were reported by Jain *et al.*[7] They also observed the Pb colloid band at 240 nm which coincided with the experimental result obtained by Topa and Velicescu. In addition to 240 nm band, they reported that a 214 nm band forms with heat treatment of KCl–Pb system. This band was ascribed to Pb° center. In our case, it is not reasonable to assume the existence of Pb atom in solution to explain the 215 nm peak.

Sn. In Fig. 5a is shown the micrograph of tin colloid. The diameters of many particles fall in the region of 15 nm. Figure 5b shows the spectra of tin colloid solution (dark brown). There is a complex band structure in the region of 240—440 nm of 5 nm thickness evaporated film, which also appears in colloid solution at the same spectral region. We also notice the 215 nm peak due to the solvent-metal reaction. It should be pointed out that the absorption still remains near the infrared region which suggests that the optical properties of this colloid has a bulk nature. The transmission and the reflectance spectra of tin particles isolated by MgF_2 were reported by Zeller and Kuse.[8] Strong absorption at the visible and near infrared was qualitatively explained by the Maxwell-Garnett theory.[9] Their result is basically consistent to our data. To complete the identification of the complex absorption band structure, detailed considerations including the surface plasmon and the interband transitions are needed.

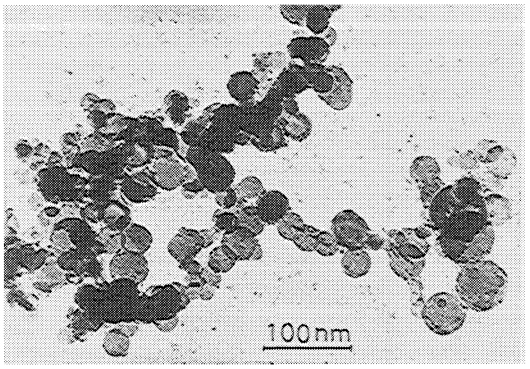

(a)

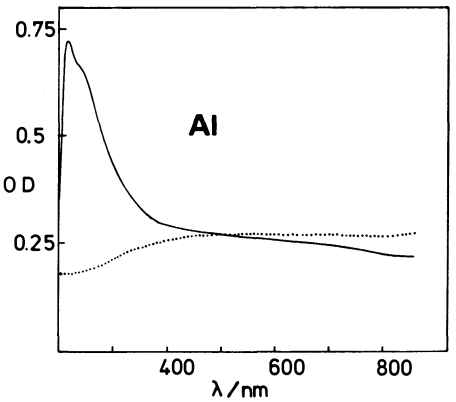

(b)

Fig. 6. (a): Micrograph of aluminum colloid. (b): Absorption spectra of colloid solution (solid line) and 20 nm thickness evaporated film (dotted line) of aluminum.

Al. In Fig. 6a is shown the micrograph of aluminum colloid. The diameter of the majority is near 30 nm. Figure 6b shows the spectra of aluminum colloid solution (dark blue) together with that of 20 nm thickness evaporated film. Rather strong absorption exists even at 850 nm, although some may be due to scattering effects. There are two peaks at 215 and 250 nm, together with a broad band at around 550 nm. The solution was stable for one month, irrespective of the existence of the 215 nm peak. We assume this stability to be due to the formation of the passive state on the surface of the colloid. The calculation of the optical spectra based on

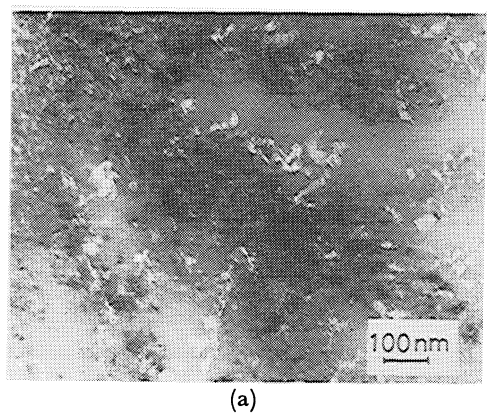

(a)

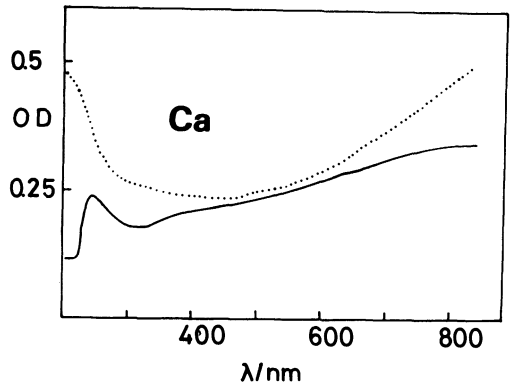

(b)

Fig. 7. (a): Micrograph of calcium colloid. Many particles were decomposed during the sample preparation for the measurement of electron microscopy. (b): Absorption spectra of colloid solution (solid line) and 35 nm thickness evaporated film (dotted line) of calcium.

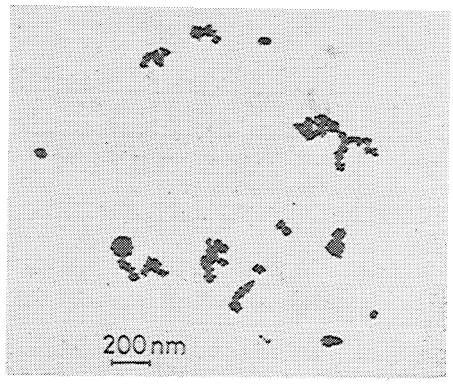

(a)

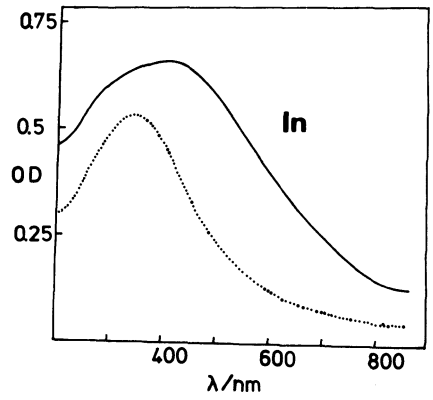

(b)

Fig. 8. (a): Micrograph of indium colloid. (b): Absorption spectra of colloid solution (solid line) and evaporated film (dotted line) of indium. The thickness of the film is 5 nm.

Mie's treatment was conducted for the system of Al–Al_2O_3.[10] The 250 nm absorption maximum was obtained for the particles of 10 nm and the 305 nm maximum for 20 nm diameter ones. The difference between the present study and their calculation may lie in the difference of dielectric constant. The spectrum of aluminum aqueous colloid solution prepared by the aerosol technique was reported by Petrov.[11] Only a broad band at 600 nm was observed in his study.

Ca. In Fig. 7a is shown the micrograph of calcium colloid. It is difficult to perceive any individual particles in the figure except traces. Figure 7b shows the spectra of calcium colloid solution (light blue) and the 35 nm thickness evaporated film. Calcium was not stable toward oxygen and water, therefore the evaporated film was coated with paraffin and then we measured the spectra. Even upon this treatment, the absorption decreased with time within ten to twenty minutes. The colloid solution was also unstable. The coloration changed to transparent within one hour in the Ar atmosphere, which indicates that the metal particle reacts with the alcohol. The formation of calcium colloid in CaF_2 crystal was reported by Orera and Alcara.[12] The absorption band at 550 nm in heavily electron irradiated samples and in additively colored crystals of CaF_2 is associated with colloidal calcium. These authors also calculated the optical absorption spectra using Mie's theory and obtained a good agreement between theoretical calculations and experimental results.[13] On the other hand, McLaughlan and Evans observed many bands between 300 and 700 nm on the X-irradiated doped CaF_2 crystal.[14] In the thin film, as shown by Fig. 7b, we have an absorption window in this region. In solution, the absorption minimum shifts to 320 nm and a new peak appears at around 250 nm. We notice that there are many bands between 350 and 850 nm, although they are obscured by the broad distribution of the size of the calcium colloid. The dielectric constant of the solvent and the diameter of the colloid is the main cause of the difference in the solution state and in the rigid matrix.

In. In Fig. 8a is shown the micrograph of indium colloid. The diameters of many particles are scattered from 10 nm to 80 nm. Figure 8b is the absorption spectra of indium colloid (light brown) and the evaporated film whose thickness is 5 nm. The colloid solution was very stable over several months. The optical absorption of indium granular deposits was reported for three samples with different thicknesses on the quartz substrate.[15] The position of the absorption maximum was nearly constant at 258 nm, irrespective of the differences in thickness: 3.5, 7, and 22 nm. The 258 nm peak shifts to 340 nm for the case of thin film (Fig. 8b). In solution, the absorption band seems to be comprised of two peaks: 280 and 400 nm maximum. The reason of this broad band is attributable to the wide diameter distri-

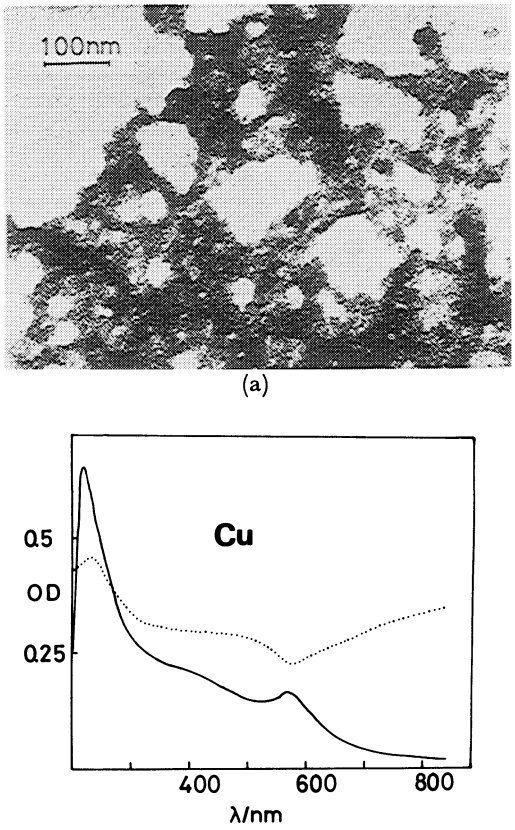

Fig. 9. (a): Micrograph of copper colloid. Very small particles are scattered over the film. (b): Absorption spectra of colloid solution (solid line) and evaporated film (dotted line) of copper. The thickness of the film is 10 nm.

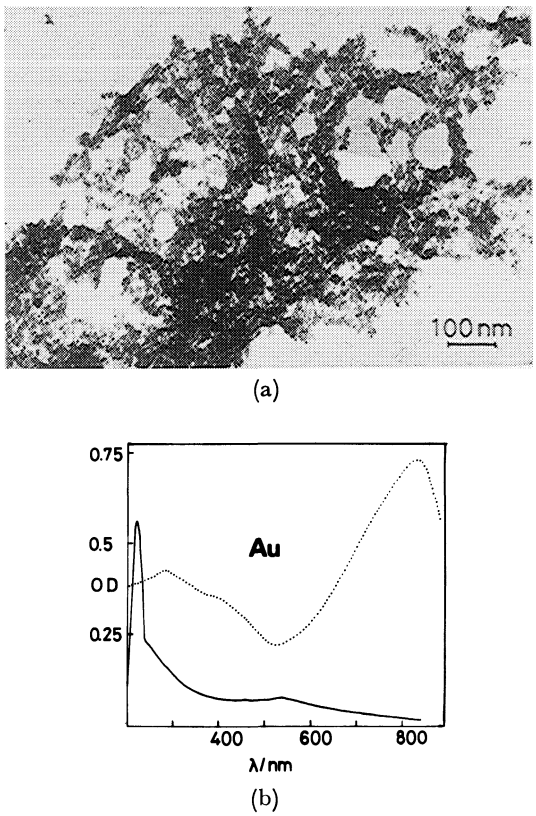

Fig. 10. (a): Micrograph of gold colloid. Very small particles are scattered over the film. (b): Absorption spectra of colloid solution (solid line) and 10 nm thickness evaporated film (dotted line) of gold.

bution in the sols.

Cu. Figure 9a shows the micrograph of copper colloid. The diameter of the majority is near 5 nm. The optical absorption spectra of copper colloid (wine red) and the evaporated film are shown in Fig. 9b. There are two peaks at 220 and 570 nm and two shoulders at 240 and 380 nm. This colloid was not stable in an aerobic condition. The 570 nm peak disappeared within 30 min and the wine red color also disappeared. The 240 nm shoulder slightly increased in intensity at the same time. On the other hand, the colloid was relatively stable under the Ar atmosphere. However, the wine red color changed to yellow after one day. The spectrum of copper colloidal particles was measured in dodecane.[16] Three peaks at 220, 310, and 590 nm were observed. These observations resemble our spectrum closely. The 570 nm peak of copper fine particle was also observed by Abe *et al.* on the Ar matrix at liquid helium temperature.[17] It is noticeable that the room temperature colloid solution gives the same spectrum as that of the fine particles dispersed on low temperature matrices. The optical spectrum of the suspension of copper particles in water was measured by Petrov.[11] The two peaks observed at 380 and 590 nm may correspond to 380 and 570 nm peaks in the present study. The origin of the long wavelength peak (570 nm) is not clear: it could be assigned to an interband transition[17] or to an intraband transition.[11,16]

Au. In Fig. 10a is shown the micrograph of gold colloid. The diameters of many particles fall in the region from 10 nm to 5 nm. The optical absorption spectra of gold colloid solution (purple) is shown in Fig. 10b, together with that of the evaporated film whose thickness is 10 nm. This colloid is very stable over a month. The absorption spectra of aqueous gold sols and small particles deposited in glass were reported by Doremus.[18] In aqueous gold sols, there are two main peaks at 250 and 520 nm. The 520 nm peak was also found in the deposited particles (12 nm diameter) in glass. In ethanol gold sols, we found three peaks at 220, 250, and 540 nm. Generally speaking, these two sols are quite similar in their spectra, as was the case for the copper colloid, regardless of the difference in solvent and measurement temperature. Abe *et al.*[17] also measured the spectra of gold fine particles in Ar matrix at liquid helium temperature. There were two peaks at 520 and 380 nm. They assigned the 520 nm peak to surface plasmon absorption. Here, we will point again that the gas flow-solution trap method gives a simple and well dispersed particle system, similar to the result of the low temperature Ar matrix method.

Ag. The spectra of silver colloid are given in Fig. 11. For all three samples, the vacuum evaporated film (8.5 nm in thickness), ethanol sols (12 nm in diameter) and aqueous sols (6.4 nm in diameter), there are clear plasmon edges at 330 nm. Absorption peaks are different for three samples (the plasmon peaks are

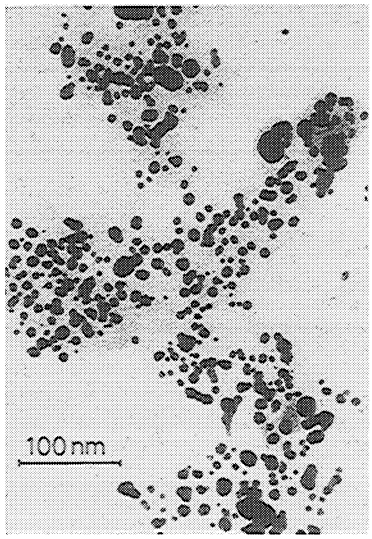

(a)

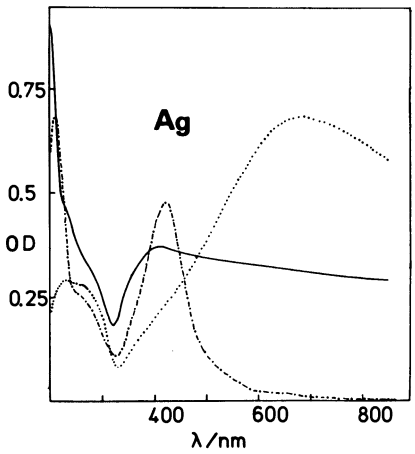

(b)

Fig. 11. (a): Micrograph of silver colloid. The diameter of many particles is near 10 nm. What determined by X-ray diffraction is 12 nm. (b): Absorption spectra of ethanol colloid solution (solid line), aqueous colloid solution (broken-dotted line) and 8.5 nm thickness evaporated film (dotted line).

at 420 nm to aqueous sol, at 405 nm to alcohol sol and at 680 nm to thin film) but the general feature is similar for the two sols. There are many reports on the optical properties of silver colloids. Doremus measured[19] the optical absorption spectra of silver particles in glass (the peak at 440 nm) and got a successful agreement with the calculation done using Mie's equation. Genzel *et al.* calculated the plasmon peak and halfwidth of the plasmon peak as a function of particle diameter based on a quantum mechanical model.[20] The peak position thus obtained is 407 nm for 10 nm particles. A gas evaporation technique was applied to the measurement of optical absorption of silver microcrystallites at low temperature.[1] The plasmon peak at 380 nm was explained by a classical model. The additional peaks at about 300—340 nm were ascribed to the Ag atom trapped in the matrix in low temperature. The absorption at the ultraviolet region observed in the silver colloid of the present report may be the contribution from the interband transitions.

Conclusion

A new colloid preparation method, the gas flow-solution trap method, was presented and described in detail. The presented method has three characteristics. One is the wide applicability to any metals/metal solid solutions with use of the same apparatus. It should be emphasized that this technique is not confined to metals but is applicable also to any thermally stable solid samples. The second is the simpleness of the system. This technique gives substantially a two-component pure system unless the metal does not react with solvent. The simpleness of the system may make it easy to understand the solid state properties of small metal particles in solution. The third one is that the colloid prepared by the present method is a sol, that is, the metal fine particles are in solution. This is a merit for the optical measurement in ultraviolet region, because the scattering effect is dominant in solid matrixes in this region.

This technique was applied to Pb, Sn, Al, Ca, In Cu, Au, and Ag metal colloids in ethanol solution. All metals gave well-dispersed colloids. The diameters of many samples fell in the region of 10 to 50 nm in the present experimental conditions. Some metal particles, Pb, Sn, Ca, and Cu were found to be unstable and others, Al, In, Au, and Ag, were stable. The optical spectra of these colloid solutions resembled the reported spectra of fine particles on matrix or on substrate, many of which were results of low temperatur measurements.

References

1) G. Mie, *Ann. Phys.*, **25**, 377 (1908).
2) H. Abe, W. Schulze, and B. Tesche, *Chem. Phys.*, **47**, 95 (1980).
3) S. Yatsuya, S. Kasukabe, and R. Uyeda, *Jpn. J. Appl. Phys.*, **12**, 1675 (1973).
4) N. Wada and M. Ichikawa, *Jpn. J. Appl. Phys.*, **15**, 755 (1976).
5) V. Topa and B. Velicescu, *Phys. Status Solidi*, **33**, K29 (1969).
6) I. S. Radchenko and P. P. Safonenko, *Sov. Phys. Solid State*, **13**, 3132 (1972).
7) S. C. Jain, S. Radhakrishna, and K. S. K. Sai, *J. Phys. Soc. Jpn.*, **27**, 1179 (1969); S. C. Jain and K. S. K. Sai, *ibid.*, **30**, 1760 (1971).
8) H. R. Zeller and D. Kuse, *J. Appl. Phys.*, **44**, 2763 (1973).
9) J. C. Maxwell-Garnett, *Philos. Trans. R. Soc. London*, **205**, 237 (1906).
10) I. S. Radchenko, *Sov. Phys. Solid State*, **12**, 2635 (1971).
11) Yu. I. Petrov, *Opt. Spectrosc. (U. S. A.)*, **27**, 359 (1969).
12) V. M. Orera and R. Alcalá, *Phy. Status Solidi A*, **38**, 621 (1976); *J. Phys. (Paris)*, Colloq. **C7**, 520 (1976).
13) V. M. Orera and E. Alcalá, *Phys. Status Solidi A*, **44**, 717 (1977).
14) S. D. McLaughlan and H. W. Evans, *Phys. Status Solidi*, **27**, 695 (1968).
15) G. Rasigni, J. P. Pètrakian, M. Rasigni, and J. P. Palmari, *J. Phys. C*, **9**, L325 (1976).
16) M. Moskovits and J. E. Hulse, *J. Chem. Phys.*, **67**, 4271

(1977).
17) H. Abe, K.-P. Charlé, B. Tesche, and W. Schulze, *Chem. Phys.*, **68**, 137 (1982).
18) R. H. Doremus, *J. Chem. Phys.*, **40**, 2389 (1964).
19) R. H. Doremus, *J. Chem. Phys.*, **42**, 414 (1965).
20) L. Genzel, T. P. Martin, and U. Kreibig, *Z. Phys.*, *B*, **21**, 339 (1975).

 © 1983 The Chemical Society of Japan Bull. Chem. Soc. Jpn., 56, 3585—3587 (1983)

A ^{1}H and ^{31}P NMR Study of Phenylphosphonous Dichloride Partially Oriented in a Nematic Phase

Koji SAITO, Akihiro YOSHINO, Tadayoshi YOSHIDA, and Kensuke TAKAHASHI*
Nagoya Institute of Technology, Gokiso-cho, Showa-ku, Nagoya 466
(Received June 10, 1983)

The ^{1}H and ^{31}P NMR spectra of phenylphosphonous dichloride dissolved in a nematic phase of *N*-(*p*-ethoxybenzylidene)-*p*-butylaniline (EBBA) have been analyzed, and the structure of the proton and phosphorus skeleton has been determined.

The NMR spectroscopy of molecules in the oriented phase has become a useful method of obtaining structural information about molecules since the first observation by Englert and Saupe.[1,2] In principle, the orientation parameters and the relative distances between the spin nuclei in a molecule can be determined by this technique.[3] The technique has been applied to many molecules containing various nuclei. However, only a few NMR studies have so far been reported on molecules containing the ^{31}P nucleus in the oriented phase.[3-7] This study will present the results of our own observation and analyses of the title substance dissolved in a nematic phase of *N*-(*p*-ethoxybenzylidene)-*p*-butylaniline (EBBA). The relative internuclear distances and the orientation parameters have been obtained.

Experimental

The phenylphosphonous dichloride (PPD) and EBBA were commercial in origin and were used without further purification.

The ^{1}H and ^{31}P NMR spectra of PPD in the isotropic phase were recorded at 60 and 24.28 MHz on a Hitachi R-20B spectrometer equipped with a R-204P attachment. In both cases, the spectra were obtained at 31.5±0.5 °C.

The ^{1}H and ^{31}P NMR spectra of PPD in an oriented phase were recorded on a Varian XL-200 spectrometer, operating both at 200 and 80.96 MHz for a 14.1 mol% solution in EBBA. Although there was a marked color change from colorless to yellow on the dissolving of PPD in EBBA, no chemical reaction occurred and the nematic solutions were stable for a week during the NMR measurements. The spectra were recorded with 32K data points using spectral widths of 20000 and 10000 Hz for the cases of ^{1}H and ^{31}P. Sixteen ^{1}H FIDs were accumulated without a lock for the proton spectrum, and 128 ^{31}P FIDs were accumulated with an external D_2O lock for the ^{31}P spectrum. In both cases, the sample was spun in the superconducting system. The probe temperature was about 22.5 °C. The average line-widths in the nematic phase were about 10 and 9 Hz for the ^{1}H and ^{31}P spectra respectively.

The calculation of the spectral and structural analyses were carried out by a HITAC E-600 minicomputer system installed in our laboratory.

Results and Discussion

Analyses of the Spectra. The ^{1}H NMR spectrum of PPD in the neat liquid consists of a large number of lines. Sixty-five lines were assigned. Analyses of the spectra were followed by a program, LAOCN3.[8] The results are given in Table 1. Sixty-five observed lines were assigned to the calculated values, with an RMS error of 0.08 Hz. The results were almost entirely consistent with those reported by Parr.[9] It was assumed that the phosphorus-proton couplings over three, four, and five bonds are positive. The numberings of the nuclei are shown in Fig. 1.

TABLE 1. ^{1}H NMR SPECTRAL PARAMETERS FOR PHENYLPHOSPHONOUS DICHLORIDE IN Hz

Isotropic phase[a]		Nematic phase[b]	
$J(1,2)$	8.84 ± 0.02	$D(1,2)$	−81.5 ± 0.7
$J(1,3)$	1.91 ± 0.03	$D(1,3)$	−46.0 ± 0.7
$J(1,4)$	1.09 ± 0.05	$D(1,4)$	−39.7 ± 0.3
$J(2,3)$	7.66 ± 0.03	$D(2,3)$	−1205.1 ± 0.2
$J(2,4)$	1.13 ± 0.02	$D(2,4)$	−148.1 ± 0.9
$J(2,5)$	0.57 ± 0.02	$D(2,5)$	8.0 ± 0.1
$J(2,6)$	1.92 ± 0.02	$D(2,6)$	91.8 ± 0.5
$J(3,4)$	7.52 ± 0.02	$D(3,4)$	62.9 ± 0.7
$J(3,5)$	1.36 ± 0.02	$D(3,5)$	93.0 ± 0.5
$\nu_2-\nu_3$	28.23 ± 0.02	$\nu_2-\nu_3$	49.5 ± 0.5
$\nu_2-\nu_4$	25.62 ± 0.02	$\nu_2-\nu_4$	−33.9 ± 0.5

a) Parameters obtained for the neat liquid. b) Parameters obtained for a 14.1 mol% solution in EBBA.

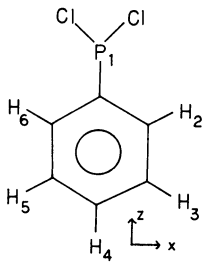

Fig. 1. Numbering system for phenylphosphonous dichloride.

The ^{1}H and ^{31}P NMR spectra of PPD in the nematic phase are given in Fig. 2. The spectra consisted of 55 and 18 resolved lines respectively. Eighty and 32 calculated lines were assigned for the observed ^{1}H and ^{31}P spectra, with an RMS error of 1.9 Hz. The results are also given in Table 1. The analyses of the spectra were followed by a program, LAOCN3D, which has been slightly modified from the LAOCN3+D program.[10] The indirect coupling constants were kept constant in the iteration calculation. The errors of the various parameters in Table 1 correspond to those given in the computer output.

The spectra calculated by varying the values of D_{12}, D_{13}, D_{26}, and D_{35}, while keeping $D_{12}+D_{13}$ and $D_{26}+D_{35}$ constant, were nearly identical. This means that only the sums ($D_{12}+D_{13}$ and $D_{26}+D_{35}$) can be determined with reasonable precision. When the difference between

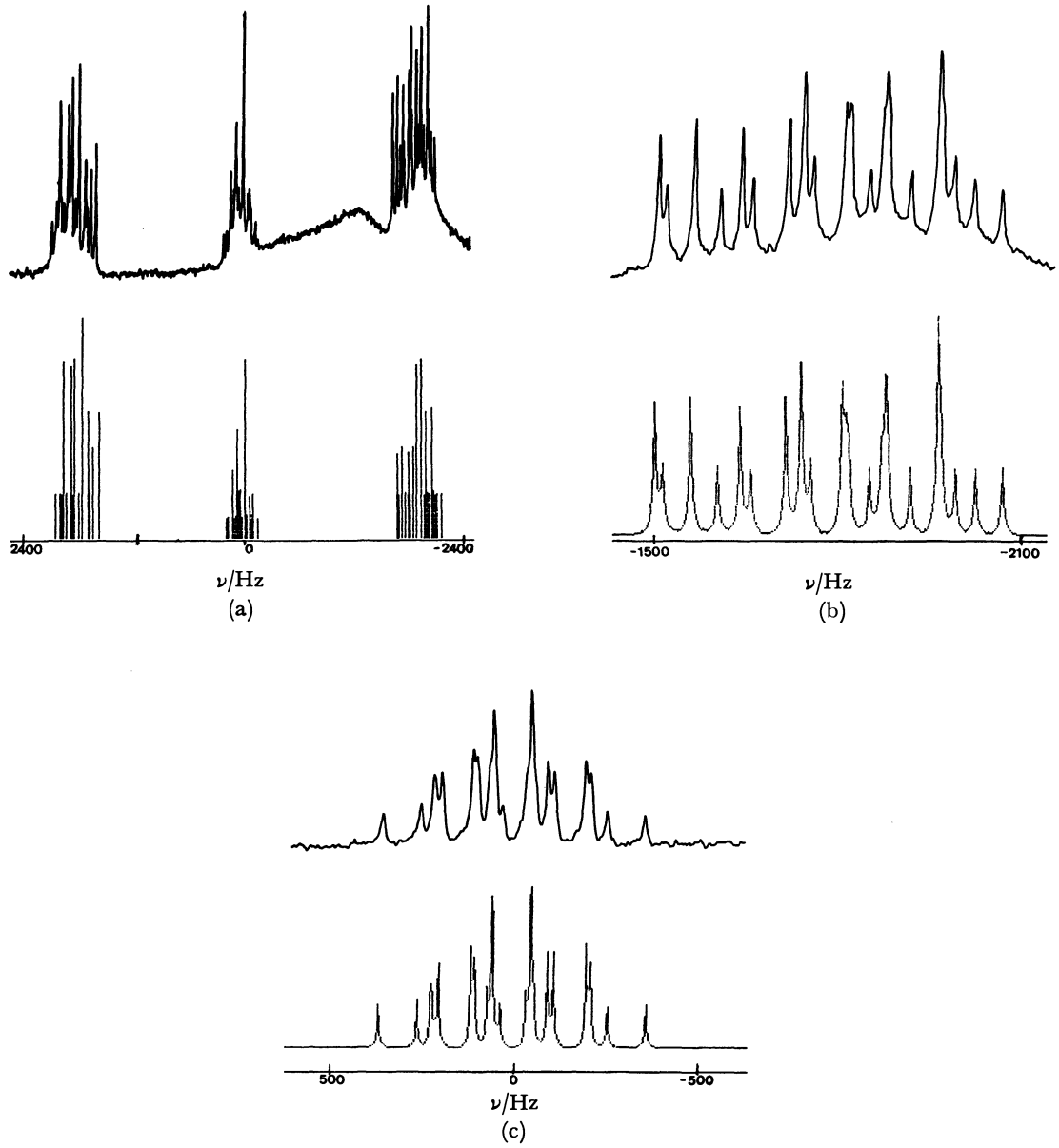

Fig. 2. Observed ^{1}H and ^{31}P NMR spectra of phenylphosphonous dichloride dissolved in EBBA. Calculated spectra are also given under the observed ones; (a) A whole observed ^{1}H spectrum accumulated 16 scans and a calculated stick spectrum, (b) an expanded upfield spectrum of (a) and a calculated one, (c) an observed ^{31}P spectrum accumulated 128 scans and a calculated one.

D_{26} and D_{35} is small, it is very difficult to differentiate D_{26} and D_{35} separately. However, a better agreement between the observed and the calculated spectra was obtained in the case of $D_{26}<D_{35}$.

Analyses of the Molecular Structure. PPD has been shown to be planar and to have a C_{2v} symmetry by means of an electron-diffraction study.[11] Therefore, there are only two diagonal-orientation parameters necessary to describe the molecular orientation. The three following assumptions were made before the analyses of the molecular structure: (1) the benzene ring forms a hexagonal plane; (2) molecular vibrations need not be taken into consideration; and (3) the anisotropies of the proton-phosphorus and proton-proton indirect couplings are negligible. Under these assumptions, the relative positions of the protons and the phosphorus can be determined from the direct proton-proton and proton-phosphorus couplings with the aid of the iterative program SHAPE.[12] The derived geometrical and orientation parameters are given in Table 2.

As may be seen in Table 2, the parameters derived from the present study agree with those from the electron-diffraction study within the limits of the standard deviation except in the case of the phosphorus atom. Two reasons for this discrepancy may be considered: (1) a vibration correction was not performed; or (2) the interatomic distances derived from NMR may deviate essentially from those of other methods.[3] The coordinates of the hydrogen atoms of PPD are in excellent agreement with those of phenylphosphonic

Table 2. Coordinates of the spin nuclei in phenylphosphonous dichloride in Å, and order parameters[a)]

Nucleus	X Coordinate	Z Coordinate
P	0.0	5.874 ± 0.029
	(0.0)[b)]	(5.74 ± 0.05)
H-2	2.182 ± 0.031	3.749 ± 0.054
	(2.16 ± 0.02)	(3.74 ± 0.02)
H-3	2.166 ± 0.031	1.249 ± 0.014
	(2.16 ± 0.02)	(1.25 ± 0.02)
H-4	0 0	0.0
H-5	−2.166 ± 0.031	1.249 ± 0.014
	(−2.16 ± 0.02)	(1.25 ± 0.02)
H-6	−2.182 ± 0.031	3.749 ± 0.054
	(−2.16 ± 0.02)	(3.74 ± 0.02)
S_{xx}	−0.06288 ± 0.00038	
S_{zz}	0.15689 ± 0.00013	

a) The calculated coordinates are based on the value of r(H-3, H-4), which is assumed to be 2.500 Å. b) The values in parentheses were calculated from the results obtained by means of the electron-diffraction method[11] (r(C–C)=1.413±0.008, r(C–H)=1.080±0.003, and r(C–P)=1.833±0.04 Å).

dichloride.[7] However, as far as the coordinate of the phosphorus atom is concerned, the C–P distance of PPD is much longer than that of phenylphosphonic dichloride.[7] The above difference can, though, be partly explained by the fact that the C–P(III) (trivalent phosphorus) distance is slightly longer than the C–P(V) (pentavalent phosphorus) distance reported in electron-diffraction studies.[13,14]

Reference

1) A. Saupe and G. Englert, *Phys. Rev. Lett.*, **11**, 462 (1963).
2) G. Englert and A. Saupe, *Z. Naturforsch., A*, **19**, 172 (1964).
3) a) P. Diehl and C. L. Khetrapal, "NMR Basic Principles and Progress," Springer-Verlag, Berlin (1969), Vol. 1; b) J. W. Emsley and J. C. Lindon," NMR Spectroscopy Using Liquid Crystal Solvents," Pergamon Press, Oxford (1975); c) C. L. Khetrapal and A. C. Kunwar, "Advances in Magnetic Resonance," Academic Press, New York (1977), Vol. 9, p. 301.
4) A. Cogne, J. B. Robert, and J. P. Albrand, *Chem. Phys. Lett.*, **48**, 524 (1977).
5) T. C. Wong and A. J. Ashe, III, *J. Mol. Struct.*, **48**, 219 (1978).
6) J. Hansen and J. P. Jacobsen, *Org. Magn. Reson.*, **15**, 29 (1981).
7) Hongwei Ye and B. M. Fung, *J. Magn. Reson.*, **51**, 313 (1983).
8) A. A. Bothner-By and S. M. Castellano, "Computer Programs for Chemistry," W. A. Benjamin, New York (1968), Vol. 1, p. 10.
9) W. J. E. Parr, *J. Chem. Soc., Faraday Trans. 2*, **1978**, 933.
10) Y. Sugino and K. Takahashi, *Bull. Chem. Soc. Jpn.*, **51**, 2527 (1978).
11) V. A. Naumov, N. M. Zaripov, and N. A. Gulyaeva, *Zh. Strukt. Khim.*, **13**, 917 (1972).
12) P. Diehl, P. M. Henrichs, and W. Niederberger, *Mol. Phys.*, **20**, 139 (1971).
13) C. J. Wilkins, K. Hagen, L. Hedberg, Q. Shen, and K. Hedberg, *J. Am. Chem. Soc.*, **97**, 6352 (1975).
14) D. R. Lide and D. E. Mann, *J. Chem. Phys.*, **29**, 914 (1958).

 © 1983 The Chemical Society of Japan Bull. Chem. Soc. Jpn., 56, 3588—3594 (1983) [Vol. 56, No. 12

Interaction of Cationic Dye and Anionic Detergent above and below the Critical Micelle Concentration as Revealed by Fluorescence Characteristics[1)]

Hiroyasu SATO,* Masahiro KAWASAKI, Kazuo KASATANI, Nobuaki NAKASHIMA,** and Keitaro YOSHIHARA**

Chemistry Department of Resources, Faculty of Engineering, Mi'e University, Tsu, 514

***Institute for Molecular Science, Okazaki, 444*

(Received June 15, 1983)

The interaction of 3,3′-diethylthiacarbocyanine iodide, a cationic dye, with sodium dodecyl sulfate (SDS), an anionic detergent, was studied as a function of the concentration of SDS ([SDS]) above and below the critical micelle concentration (cmc). The [SDS]-dependent fluorescence spectra, quantum yield and decay measurements revealed the deaggregation of the dye above the cmc and the formation of the dye–SDS aggregate below the cmc.

The photophysical and photochemical behavior of organic molecules in organized assemblies such as micelles[2,3)] has been receiving current attention from several viewpoints, such as (1) the influence of the micellar environment on the very fast photophysical process like rotational diffusion,[4)] (2) the photophysical study in relation to finding a good lasing system,[5,6)] (3) the measurement of the aggregation number of micelles,[7)] and (4) the construction of a model membrane system to mimic a biological system like chloroplasts, with special emphasis on the enhancement of the energy transfer and electron transfer efficiencies.[8–20)] The study of the spectroscopic properties of organic molecules in micellar media provides us with the basic properties of such a system which are useful in understanding many specific features of the system as mentioned above.

Many peculiarities have been noted for the spectroscopic properties of the dye with a detergent with the opposite charge around the critical micelle concentration (cmc). Pinacyanol, a cyanine dye, has been used in the "spectral change method" to determine the cmc of many detergents.[21)] Mataga and Koizumi[22,23)] studied the variation in absorption spectra and fluorescence quenching of the Rhodamine 6G (Rh-6G)–sodium dodecyl sulfate (SDS) system, which was dependent on the concentration of SDS ([SDS]), around the cmc. Mukerjee and Mysels[24)] studied absorption spectra of the pinacyanol–SDS system as a function of [SDS], and examined critically the "spectral change method" mentioned above. Lohoczki and Hevesi[9)] studied the variation of absorption spectra of the thionine–SDS system especially below the cmc (*i.e.* in the premicellar region). From further investigation of these peculiarities in the absorption and fluorescence spectra along with the fluorescence lifetime and quantum yield, detailed picture on the nature of dye–detergent interaction can be obtained.

In the present paper, the [SDS]-dependent variation in absorption and fluorescence spectra, quantum yield, and decay characteristics of 3,3′-diethylthiacarbocyanine iodide (DTC)–SDS system was studied, and the nature of the dye–detergent interaction was discussed. The structural formula of DTC is given in Fig. 1.

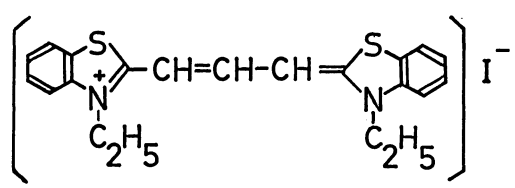

Fig. 1. Structural formula of 3,3′-diethylthiacarbocyanine iodide.

Experimental

Materials. DTC (Dojin Kagaku), Rhodamine B (Eastman-Kodak), and Rhodamine 101 (Exciton) were used without further purification. The purity of these dyes was checked by thin-layer chromatography. SDS (Nakarai, protein research grade), quinine sulfate (Wako), *m*-dimethylaminonitrobenzene, and 4-dimethylamino-4′-nitrostilbene (Nakarai) were used as received. Water was distilled twice. Sulfuric acid, benzene, hexane, *o*-dichlorobenzene, and ethylene glycol were of G. R. grade of Wako or Nakarai and were used as received.

Absorption and Fluorescence Spectra. Absorption spectra were measured by a Shimadzu UV-200 recording spectrophotometer. Fluorescence spectra were measured by a Hitachi 650-10S spectrofluorimeter with a Hamamatsu R928 photomultiplier (sensitive to 930 nm). Measurements were made at room temperature for aerated solutions.

Fluorescence Decay. In the measurement of fluorescence decay curves, the dye solution in a quartz spectrofluorimeter cell was pumped with the second harmonic of a Nd^{3+}: YAG laser. Fluorescence decay was measured with a Hamamatsu C979 streak camera, using a Nihon-shinkukogaku interference filter (579 nm), or a Toshiba VO56 or 57 cut-off filter. The time-scale of the streak camera was fully calibrated. All measurements were made at room temperature for aerated solutions. The results of three to nine shots on the same sample were averaged.

Quantum Yield Measurements. The fluorescence quantum yield (ϕ) of the dye solution was measured with reference to that of quinine sulfate standard solution (1×10^{-6} M† in 0.5 M H_2SO_4), $\phi_{st}=0.55$,[25)] using the formula[26)]

$$\frac{\phi}{\phi_{st}}=\frac{F}{F_{st}}\cdot\frac{A_{st}}{A}\cdot\frac{E_{st}}{E}\cdot\frac{n^2}{n_{st}^2}, \quad (1)$$

where F, A, E, and n are the integrated area under the fluorescence spectrum (corrected for the response function of the spectrofluorimeter), the absorbance/cm at the exciting wavelength, the intensity of the exciting light measured by a photocell (Hamamatsu S1133-01) corrected for its response function, and the refractive index of the sample solution, respectively. F_{st}, A_{st}, E_{st}, and n_{st} are the corresponding quantities of the

† 1 M=1 mol dm^{-3}, 1 mM=1×10^{-3} mol dm^{-3} in this paper.

standard solution. The exciting wavelength was 365 and 520 nm for quinine sulfate and DTC, respectively. All measurements were made at room temperature (25±2 °C) for aerated solutions. The relation $n \approx n_{st}$ was assumed. The response function of the spectrofluorimeter was measured using *m*-dimethylaminonitrobenzene (1×10^{-5} M in benzene–hexane mixture (30 : 70 in volume)) and 4-dimethylamino-4′-nitrostilbene (1×10^{-5} M in *o*-dichlorobenzene).[27,28] That of the photocell was measured using the solution of Rhodamine B in ethylene glycol. In order to check the accuracy of the present method of quantum-yield determination, the quantum yield of Rhodamine-101 was measured. The quantum yield of this dye has been known to be 1.0.[6,29] The quantum yield of Rhodamine 101 (6×10^{-6} M in ethanol) measured by the present method was 1.04—1.06. The accuracy (within *ca.* 10%) of the present method was thus proved.

Cmc Measurements. The cmc of SDS was determined conductometrically. The electrodes of the conductivity cell were platinum plates without platinum black. The temperature of the cell was kept at 25.0±0.1 °C. The bridge used was a Yanaco MY-8 Conductivity Outfit or a Yokogawa Hewlett-Packard 4255 A Universal Bridge. The cmc determined was 7.4±0.1 mM, in good agreement with the generally accepted published value (8.1 mM).[30]

Results

Absorption and Fluorescence Spectra of DTC and DTC–SDS. The absorption spectra of the aqueous solutions of DTC are shown in Fig. 3. For [DTC]$\lesssim 2.0 \times 10^{-5}$ M, the shape of the absorption band remained essentially the same and was quite similar to that of the methanol solution. The dye is present essentially as a monomer in these solutions. The dimer band at 510 nm became apparent for [DTC]$\gtrsim 5.0 \times 10^{-5}$ M. The ratio of the absorbance at 510 nm to that at 556 nm (A_{510}/A_{556}) increased with the concentration of the dye, while the corresponding ratio was essentially constant in methanol (See Fig. 3). The fluorescence maximum which appeared around 580 nm is due to the monomer of the dye. The absorption spectra of DTC–SDS solutions are shown in Fig. 4. The ratio A_{510}/A_{560} (the dimer band was found at 510 nm, and the monomer band at 560 nm) increased and then decreased with [SDS] for [SDS]<cmc, and decreased with [SDS] for [SDS]>cmc, as shown in Fig. 5. Comparison of Figs. 3 and 5 reveals two opposite action of SDS on DTC, *i.e.*, the aggregation of the dye below the cmc, and the deaggregation of the dye above the cmc. The fluorescence spectra of the DTC–SDS solutions are shown in Fig. 6. The fluorescence peak shifted to 594 nm. The shift of ≈14 nm compared with the aqueous solution is due to the micellar environment. It is to be noticed that the 594 nm peak appeared even at [SDS]=6.0 mM, *i.e.*, in the *premicellar* region. This shows the presence of some aggregate which provides the micelle-like

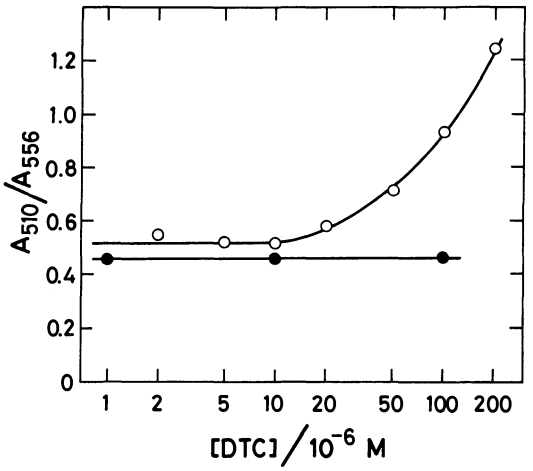

Fig. 3. The ratio of the absorbance of the 510 nm band to that of the 556 nm band.
○ In water, ● the corresponding ratio in methanol (In methanol, the peak and shoulder moved to 558 and 525 nm, respectively.).

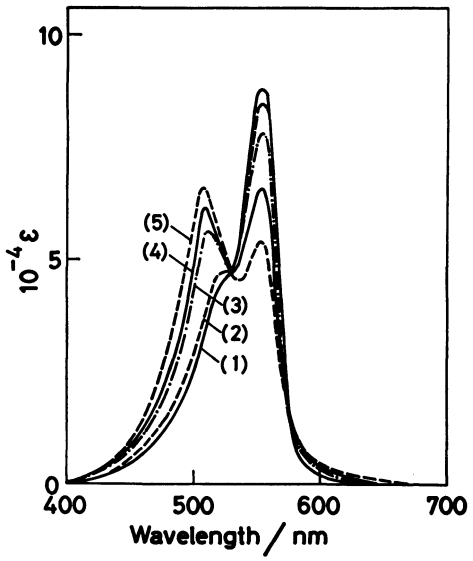

Fig. 2. Absorption spectra of DTC in aqueous solutions.
(1) [DTC]=2×10^{-6} M—1×10^{-5} M, (2) 2×10^{-5} M, (3) 5×10^{-5} M, (4) 1×10^{-4} M, (5) 2×10^{-4} M.

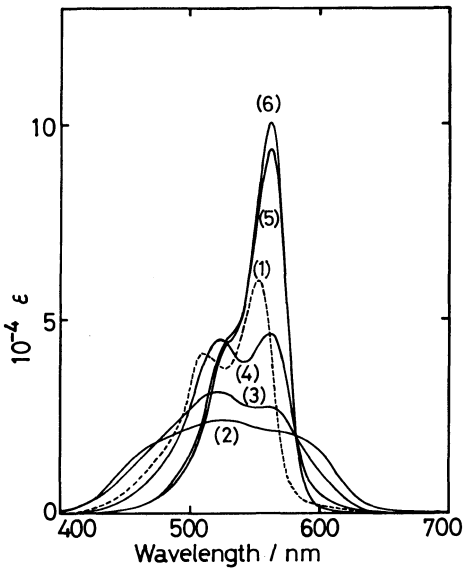

Fig. 4. Absorption spectra of DTC–SDS solutions.
[DTC]=5×10^{-5} M, (1) [SDS]=0, (2) 3.0, (3) 4.0, (4) 5.0, (5) 8.0, (6) 10.0 mM.

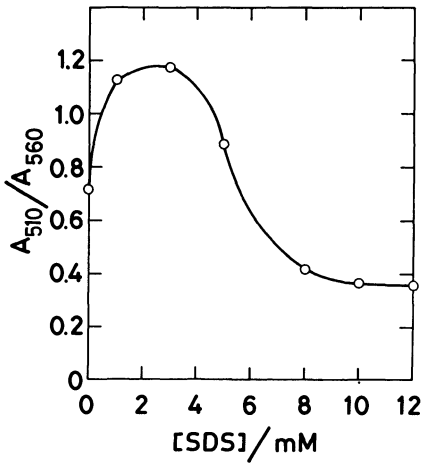

Fig. 5. The ratio of the absorbance of the 510 nm band to that of the 560 nm band.
[DTC] $=5.0\times10^{-5}$ M.

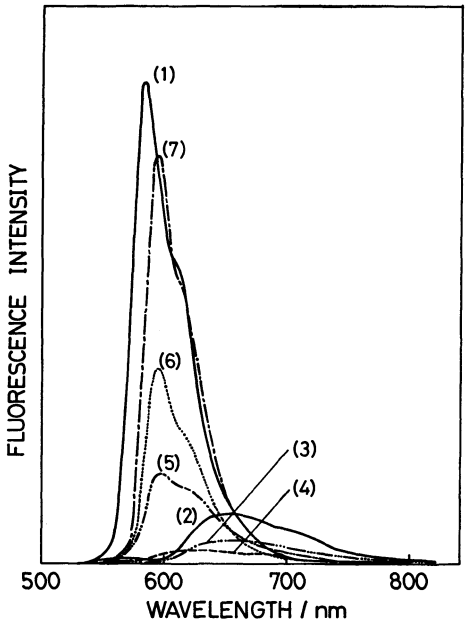

Fig. 6. Fluorescence spectra of DTC–SDS solutions.
[DTC] $=5.0\times10^{-5}$ M, (1) [SDS] $=0$, (2) 1.0, (3) 4.0, (4) 5.0, (5) 6.0, (6) 8.0, (7) 10.0 mM. The intensities are 10 times larger as shown for (6) and (7).

environment in this [SDS] region.

For [SDS] $=1$—4 mM, the absorption spectra are characterized with broad bands to the shorter wavelength of the dimer band and to the longer wavelength of the monomer band, as shown in Fig. 4. Fluorescence band in this [SDS] region appeared as a broad band with a peak around 655 nm, as shown in Fig. 6. Fine precipitate appeared around [SDS] $\cong 1$ mM when the dye concentration was high.

Fluorescence Quantum Yield. The variation of fluorescence quantum yield (ϕ) of DTC as a function of [SDS] is shown in Fig. 7. The obtained value $\phi=0.03$ in water is comparable with the reported values $\phi=$ 0.048 in ethanol,[31] or 0.042 in water–methanol (9 : 1).[32] Fluorescence quenching which is evident in the pre-

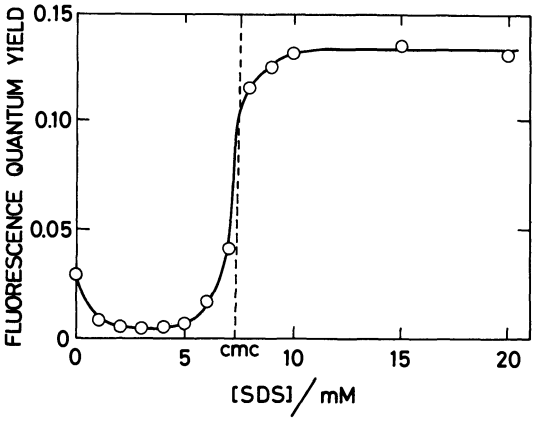

Fig. 7. Variation of fluorescence quantum yield of DTC as a function of [SDS], [DTC] $=2.0\times10^{-5}$ M.

micellar region must be the results of static and dynamic quenching of the monomer fluorescence by the presence of dimer and dye–SDS aggregate. The fluorescence quantum yield as compared with that in the aqueous solution is drastically enhanced by the addition of SDS above the cmc. This must be partly due to the deaggregation action of SDS micelles on the dye. However, this action alone cannot fully explain the observed enhancement of the fluorescence, because DTC molecules in the aqueous solution exist essentially as monomers at this [DTC] (2×10^{-5} M), as mentioned above in relation to the absorption spectra.

Fluorescence Decay. The nature of dye–detergent interaction is revealed most clearly in the fluorescence decay characteristics. The fluorescence decay curves for the aqueous solution ($\lambda_{max}=580$ nm) and SDS solutions ($\lambda_{max}=594$ nm) of DTC ([DTC] $=5.0\times10^{-5}$ M and 2.0×10^{-6} M) are shown in Figs. 8(a) and (b). An exponential decay with a lifetime of 100 ps was observed for the aqueous solution. The same decay behavior was observed over the whole concentration range studied (1.0×10^{-4}—2.0×10^{-6} M). It is comparable with that predicted by Roth and Craig[31] for methanol solution (150 ps). The observed decay is apparently that of the monomer, and the quenching by the dimer did not occur in these concentrations.

The decay behavior of the DTC (5.0×10^{-5} M)–SDS solutions (Fig. 8(a)) was found to depend largely on [SDS]. Such a large variation in the fluorescence decay behavior with [SDS] can be explained by comparison with the absorption and fluorescence spectra and by referring to the other cationic dye–SDS solutions (*e.g.* pinacyanol–SDS[12,14,24]). The fluorescence decay for [SDS] $=1.0\times10^{-2}$ M was exponential. Its lifetime, 410 ps, was much longer than that of the monomer in the aqueous solution (100 ps) mentioned above. Therefore, the decay behavior cannot be explained by the deaggregation effect alone.

For [SDS] $=8.0$ mM, the nonexponential decay behavior can be attributed to the presence of P_3, P_4, $\cdots$ micelles besides P_1 and P_2 micelles (P_1, P_2, $\cdots$ micelles are the micelles which incorporate one, two, $\cdots$, dye molecules). The distribution of dyes among micelles is usually treated in terms of Poisson statistics.[33] The

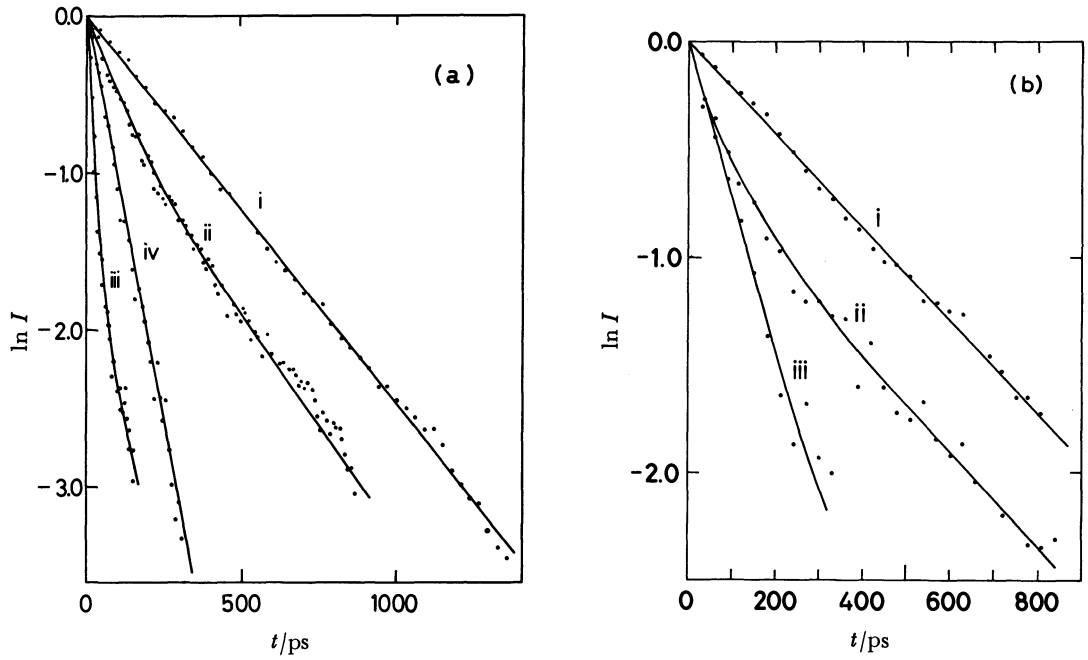

Fig. 8. Flourescence decay curves of DTC–SDS solutions.
(a) [DTC]=5.0×10^{-5} M, (i) [SDS]=1.0×10^{-2} M, (ii) 8.0×10^{-3} M, (iii) 5.0×10^{-3} M, (iv) 0 M; (b) [DTC]=2.0×10^{-6} M, (i) [SDS]=1.0×10^{-2} M, (ii) 5.0×10^{-3} M, (iii) 1.0×10^{-3} M. At [SDS]=8.0×10^{-3} M (not shown), the decay was almost identical to (i).

dye molecules in P_1 and P_2 micelles follow the monomer decay. Those in P_3, P_4, ··· micelles are, however, influenced by the quenching by dimers. The observed decay is the sum of the decays in P_1, P_2, P_3, ··· micelles and hence nonexponential.

For [SDS]=5.0 mM, the observed decay was very fast. Since the fluorescence band is a superposition of 594 and 655 nm fluorescence, where the latter seems to be enhanced by the energy transfer from the former, the decay must be composed of (1) that of the 594 nm fluorescence due to the dye molecules in the micelle-like environment (affected by the energy transfer mentioned above) plus (2) that of the 655 nm fluorescence. Apparently, the observed fast decay reflects only the decay of the component (1), since the component (2) is very weak compared with (1).

A similar [SDS]-dependent variation of fluorescence decays was observed for [DTC]=2.0×10^{-6} M (Fig. 8(b)). However, in this case each decay pattern appeared at the smaller [SDS] compared with the case of [SDS]=5.0×10^{-5} M. The slow decay with the lifetime ≈450 ps appeared at [SDS]=10.0 mM. An exponential decay with almost the same lifetime was observed at [SDS]=8.0 mM. The nonexponential decay (which is similar to the case of [DTC]=5×10^{-5} M and [SDS]=8 mM) appeared at [SDS]=5 mM. At [SDS]=1 mM the decay was very fast, as was observed for [DTC]=5×10^{-5} M and [SDS]=5 mM. A similar decay pattern which is dependent on both of [dye] and [SDS] has been reported for the acridine orange–SDS system.[12,34]

Discussion

The Effect of SDS on the Aggregation State of the Dye. The characteristics of the absorption and fluorescence spectra, fluorescence intensity and quantum yield of the dye–detergent systems as mentioned above reveal two opposite effects of SDS on the aggregation state of the dye, aggregation below the cmc and deaggregation above the cmc.

Dye–SDS Aggregate Formation in the Lower Premicellar Region. In the lower premicellar region ([SDS]= 1—4 mM), the very broad absorption band and the weak, long-wavelength fluorescence band at 655 nm show the presence of some aggregated state of the dye.

Two types of higher aggregate of cyanine dyes, H-aggregate and J-aggregate are known.[35] The former is characterized with an absorption band to the shorter wavelength of the dimer band, while the latter with the absorption band to the longer wavelength of the monomer band. Resonance fluorescence is peculiar to the J-aggregate. The H- and J-aggregate have different stack structure, head-to-head and head-to-tail, respectively. While some *meso*-substituted or benzo-fused derivatives of DTC show the strong tendency to form H- and J-aggregates,[36–38] DTC itself does not. This is evident from the absorption spectra (Fig. 2) which are composed of only monomer and dimer bands to the limit of highest concentration limited by the solubility of the dye in water.

Contrary to this behavior in aqueous solutions, DTC forms higher aggregate in SDS solutions in the lower premicellar region, as shown by the presence of broad

absorption bands to the shorter and longer wavelengths of the monomer and dimer bands (Fig. 4). Clearly, the aggregates in this case are composed of the dye and SDS, *i.e.* the DTC–SDS aggregates. Then, what is their composition like? How are they related to the H- and/or J-aggregate in the aqueous solution of the related compound?

For some dye–detergent systems with the opposite charge, *e.g.*, pinacyanol–SDS[12,14,24] and Acridine Orange–SDS,[34] the dye–detergent aggregate forms a large particle and precipitates from the solution around [SDS]≈1—2 mM. This is due to the 1 : 1 complex of the cationic dye (D^+) and the dodecyl sulfate anion (S^-), $(D^+S^-)_n$.[24] In the DTC–SDS system presently studied, very minute particles appeared in the solution when [DTC] was high (*e.g.* 1.0×10^{-5} and 5.0×10^{-5} M) and [SDS] was around 1 mM.[39] These must be due to the $(D^+S^-)_n$ type aggregate. The DTC–SDS aggregate characterized with the very broad absorption band and the 655 nm fluorescence will also be due to the essentially 1 : 1 complexes dispersed and stabilized in the aqueous solution by the addition of slight excess of SDS molecules.[24]

The emission spectra of the related dye, 3,3′-diethyl-9-methylthiacarbocyanine iodide, at 78 K in EPA matrix were studied by Cooper and Liebert.[40] To the longer wavelength of the monomer fluorescence peak at 562 nm, a group of three emission peaks was observed in the 580—760 nm region. A sharp band at 594 nm was assigned to the dimer emission, a broad low-intensity band at about 648 nm to the excimer emission, and a sharp band near 680 nm to the triplet—singlet transition (phosphorescence). By referring to this observation, the broad structureless emission band of the DTC–SDS solution in the lower premicellar region ([SDS]≈1—4 mM) can be most reasonably assigned to the excimer fluorescence of the dye molecule in the DTC–SDS aggregate.

Resonance Raman spectra of DTC–SDS solutions give further information on the structure of the DTC–SDS aggregate.[39] The relative intensities of Raman bands varied as a function of [SDS]. For [DTC]= 1×10^{-5} M, the relative band intensities at [SDS]= 2.5 mM were very similar to those of solid DTC (KBr disk). DTC molecules in the DTC–SDS aggregate must be in the aggregation state like that of the dye in the solid state.

Not only the electrostatic attraction between the dye cation (D^+) and the dodecyl sulfate anion (S^-), but also the hydrophobic interaction between the dye molecules and detergent molecules must be working in the stabilization of the DTC–SDS aggregate in the lower premicellar region. When the electrostatic interaction becomes dominant (at the lower [SDS] edge of this [SDS] region), the precipitation of $(D^+S^-)_n$ occurs. The hydrophobic interaction becomes increasingly dominant with [SDS]. DTC–SDS aggregates change into dye-rich induced micelles and then into the ordinary micelles with increasing [SDS], as will be discussed later.

Deaggregation and Immobilization of the Dye above the cmc. The deaggregation of the dye, an effect of SDS which is opposite to that in the lower premicellar region, is evident above the cmc by monomer-type absorption spectra. The deaggregation is apparently due to the distribution of the molecules among micelles. However, the fluorescence intensity much enhanced, the quantum yield much larger, and the fluorescence lifetime much longer than in the aqueous solution cannot be explained by the deaggregation effect alone, because the enhancement occurred even for [DTC] at which the dye is present essentially as a monomer in the aqueous solution.

The enhancement of fluorescence intensity compared with the aqueous solution was explained as due to the environmental change (the hydrophobic environment) and/or to the immobilization of dye molecules in the miceller media.[1] The enhancement of a similar nature has been reported in a recent communication by Humphry-Baker *et al.*[41] for a cyanine dye–SDS solution, and by Nakashima and Kunitake[42] for some cyanine dyes bound to synthetic bilayer membranes. The enhancement in these systems were attributed to the inhibition of the radiationless decay by the micellar environment which immobilize the cyanine dyes to some extent.

The immobilization effect of micelles on dyes is revealed in the rotational diffusion. This was studied by transient absorption by Lessing and von Jena.[4] They obtained the rotational relaxation time (τ_R) of a few nanoseconds in the micellar media, in contrast to that of a few hundred picoseconds in solvents of low viscosity.[43–45] Humphry-Baker *et al.*[41] examined the rotational motion in excited states by fluorescence polarization measurements, and calculated the rotational rate about one order of magnitude smaller in the micellar than in alcoholic solutions. The prevention of rotational motion is more evident in the bilayer system of Nakashima and Kunitake.[42] The values of τ_R were obtained for the aqueous and SDS ([SDS]=15 mM) solutions of DTC from the fluorescence polarization to be 380 ps and 1.9 ns, respectively.

Such an effect of micelles on the movement of dye molecules has sometimes been expressed in terms of the "microviscosity (or, microscopic viscosity)." For example, the microviscosities of SDS or hexadecyltrimethylammonium bromide (HTAB) micelles measured near room temperature are reported to be about 15—30 cP.[3] The dependence of fluorescence intensity of the dyes on the viscosity of solvents has been extensively studied.[46–54] This effect is especially evident for cyanine dyes.[49–54] It is known that cyanine dyes undergo photochemical cis-trans isomerization at the central methine chain.[50,54–58] This photoisomerization process is one of the important nonradiative decay channels in cyanine dyes. The suppression of this process in the micellar media can explain the observed large fluorescence enhancement of cyanine dyes.

Formation of Dye-rich Induced Micelles in the Higher Premicellar Region. It is to be noticed that this fluorescence enhancement effect was not limited to the region above the cmc. It was found even in the *higher* premicellar region (*i.e.*, [SDS]=*ca.* 4 mM-cmc). This is clearly due to the presence of the chemical entity which provides the dyes with a micelle-like environment.

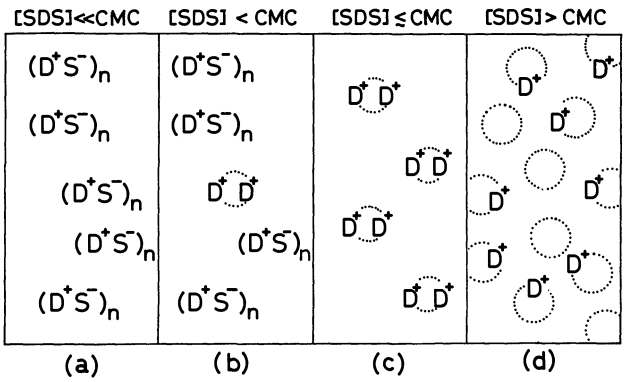

Fig. 9. A schematic model of the dye–detergent system with the opposite charge. See text for explanation.

In this [SDS] region the $(D^+ \cdot S^-)_n$-type 1 : 1 complex changes gradually with the [SDS] into the ordinary micelles above the cmc. The complex is successively diluted with SDS in this region. The presence of dye-rich induced micelles which incorporate a few dye molecules in the micelle-like aggregate in this [SDS] region has been proved by Mukerjee and Mysels for the pinacyanol–SDS system.[24] The energy-transfer efficiency between Rh-6G (donor) and DTC (acceptor) showed a maximum in this [SDS] region.[10] The fluorescence decay of the donor cannot be interpreted if the donor and acceptor are uniformly distributed in the solution, although [SDS] is *below* the cmc. Donor and acceptor molecules must be locally concentrated in dye-rich induced micelles.[11] The appearence of the maximum in the energy-transfer efficiency was found also in the Rh-6G–pinacyanol system,[12,14] for which the participation of dye-rich induced micelles in the energy transfer process is proved by the comparison with the absorption spectra. The maximum of electron-transfer efficiency also appeared in the premicellar region.[13,18]

Nature of Dye–Detergent Interaction. A schematic model of the dye–detergent system with the opposite charge is given in Fig. 9. In the lower premicellar region ([SDS]≅1—4 mM, (a) in the figure) the dye–detergent aggregate (with an essentially 1 : 1 composition, stabilized and dispersed in the aqueous solution by the addition of a slight excess of SDS) is formed. This aggregate is depicted as $(D^+S^-)_n$ in the figure for simplicity. This aggregate is successively diluted with SDS and changes into the dye-rich induced micelles in the higher premicellar region ([SDS]≅4 mM-cmc, (b) and (c) in the figure). The dye-rich induced micelles change into ordinary micelles above the cmc through further dilution with SDS ((d) in the figure).

Someone may argue that the presence of dye-rich induced micelles *below* the cmc is contradictory statement, and that the cmc itself must be lowered. However, the cmc is usually determined by the break of some *macroscopic* physical quantity like electrical conductivity. The addition of dye molecules to the SDS solution causes only a slight shift (*e.g.* by 0.1—0.4 mM) to the lower SDS region, as shown for Rh-6G–DTC–SDS,[10] acridine orange–SDS[34] or Rh-6G–pinacyanol–SDS.[14] The spectroscopic evidences for the presence of dye-rich induced micelles, *i.e.*, the absorption and fluorescence bands appearing at the wavelengths indicating micellar environment and the enhancement of the energy-[10–12,14] or electron-[13] transfer efficiency, are observed for [SDS] much lower the cmc thus newly determined for the dye–SDS system.

The presence of premicellar aggregates has been reported also for some metal complex cation-anionic detergent systems.[13,17–19,59–61] Ozeki *et al.*[61] carried out the measurements of surface tension and light scattering experiments for the $[Fe(phen)_3](ClO_4)_2$–SDS system (phen=1,10-phenanthroline), and clarified that (1) the shift of the cmc is rather small (7.6 mM to 7 mM) even in the presence of $[Fe(phen)_3](ClO_4)_2$ (5.0×10^{-5} M), and that (2) there is a threshold detergent concentration (C_{pre}) at which the formation of the premicellar aggregate starts far below the cmc (0.35 mM by the surface tension measurement). They stated that the hydrophobic interaction plays a very important part in the formation and stabilization of the premicellar aggregate. A similar mechanism of formation and stabilization by hydrophobic interaction must be present in our premicellar aggregates, *i.e.*, the essentially 1 : 1 complexes dispersed and stabilized in the aqueous solution by the addition of slight excess of SDS molecules which appeared in the lower premicellar region, and dye-rich induced micelles which appeared in the higher premicellar region.

The present authors are grateful to Dr. Yoshihumi Kusumoto of Kagoshima University for his cooperation in the earlier stage of this work. They are also grateful to Mr. Nobukazu Hata for his assistance in the quantum yield measurements. They are also grateful to Professor Shoichi Ikeda of Nagoya University for helpful discussions. This work is supported partly by the Joint Studies Program (1980—81) of the Institute for Molecular Science, and by the Grant-in-Aid No. 447006 from the Ministry of Education, Science and Culture.

References

1) Reported briefly in: H. Sato, M. Kawasaki, K. Kasatani Y. Kusumoto, N. Nakashima, and K. Yoshihara, *Chem. Lett.*, **1980**, 1529.
2) J. K. Thomas, *Acc. Chem. Res.*, **10**, 133 (1977).
3) N. J. Turro, M. Grätzel, and A. M. Braun, *Angew. Chem., Int. Ed. Engl.*, **19**, 675 (1980).
4) H. E. Lessing and A. von Jena, *Chem. Phys.*, **41**, 395 (1979).
5) G. A. Kenney-Wallace, J. H. Flint, and S. C. Wallace, *Chem. Phys. Lett.*, **32**, 71 (1975).
6) K. H. Drexhage, "Dye Lasers," ed by F. P. Schäfer, Springer, Berlin (1977), Chap. 4.
7) N. J. Turro and A. Yekta, *J. Am. Chem. Soc.*, **78**, 5951 (1978).
8) G. S. Singhal, E. Robinowitch, J. Hevesi, and V. Srinivasan, *Photochem. Photobiol.*, **11**, 531 (1970).
9) E. Lohoczki and J. Hevesi, *Dokl. Akad. Nauk SSSR*, **206**, 1158 (1972).
10) Y. Kusumoto and H. Sato, *Chem. Phys. Lett.*, **68**, 13 (1979).
11) H. Sato, Y. Kusumoto, N. Nakashima, and K. Yoshihara, *Chem. Phys. Lett.*, **71**, 326 (1980).

12) H. Sato, M. Kawasaki, and K. Kasatani, *J. Photochem.*, **17**, 243 (1981).
13) H. Sato, M. Kawasaki, K. Kasatani, and T. Ban, *Chem. Lett.*, **1982**, 1139.
14) H. Sato, M. Kawasaki, and K. Kasatani, *J. Phys. Chem.*, **87**, 3759 (1983).
15) T. Matsuo, Y. Aso, and K. Kano, *Ber. Bunsenges. Phys. Chem.*, **84**, 146 (1980).
16) Y. Aso, K. Kano, and T. Matsuo, *Biochim. Biophys. Acta*, **599**, 403 (1980).
17) J. H. Baxendale and M. A. J. Rodgers, *Chem. Phys. Lett.*, **72**, 424 (1980).
18) M. A. J. Rodgers and J. C. Becker, *J. Phys. Chem.*, **84**, 2762 (1980).
19) K. Mandal and J. N. Demas, *Chem. Phys. Lett.*, **84**, 410 (1981).
20) P. K. Koglin, D. J. Miller, J. Steinwandel, and M. Hauser, *J. Phys. Chem.*, **85**, 2363 (1981).
21) W. D. Harkins, "The Physical Chemistry of Surface Films," Reinfold, New York (1952).
22) M. Koizumi and N. Mataga, *Nippon Kagaku Zasshi*, **73**, 814, 879 (1952); N. Mataga and M. Koizumi, *ibid.*, **75**, 269, 273 (1954).
23) M. Koizumi and N. Mataga, *Bull. Chem. Soc. Jpn.*, **26**, 115 (1953); N. Mataga and M. Koizumi, *ibid.*, **27**, 197 (1954).
24) P. Mukerjee and K. J. Mysels, *J. Am. Chem. Soc.*, **77**, 2937 (1955).
25) W. H. Melhuish, *J. Phys. Chem.*, **64**, 762 (1960).
26) J. N. Demas and G. A. Crosby, *J. Phys. Chem.*, **75**, 991 (1971).
27) H. Kokubun, "Shin Jikken Kagaku Koza," ed by the Chemical Society of Japan, Maruzen, Tokyo (1976), Vol. 4, Chap. 8.
28) E. Lippert, W. Nägele, I. Seibold-Blankenstein, U. Staiger, and W. Voss, *Z. Anal. Chem.*, **17**, 1 (1959).
29) T. Karstens and K. Kobs, *J. Phys. Chem.*, **84**, 1871 (1980)
30) J. H. Fendler and E. J. Fendler, "Catalysis in Micellar and Macromolecular Systems." Academic Press, New York (1975).
31) N. L. Roth and A. C. Craig, *J. Phys. Chem.*, **78**, 1154 (1974).
32) S. K. Rentsch, D. Fassler, P. Hampe, R. Danielius, and R. Godonas, *Chem. Phys. Lett.*, **89**, 249 (1982).
33) M. Tachiya, *Chem. Phys. Lett.*, **33**, 289 (1975).
34) T. Ban, K. Kasatani, M. Kawasaki, and H. Sato, *Photochem. Photobiol.*, **37**, 131 (1983).
35) D. M. Sturmer and D. W. Heseltine, "Sensitizing and Desensitizing Dyes," in "The Theory of Photographic Process," 4th ed, ed by T. H. James, Macmillan, New York (1977), Chap. 8.
36) A. H. Herz, *Photogr. Sci. Eng.*, **18**, 323 (1974).
37) W. West, S. P. Lovell, and W. Cooper, *Photogr. Sci. Eng.*, **14**, 52 (1970).
38) W. Cooper, S. P. Lovell, and W. West, *Photogr. Sci. Eng.*, **14**, 184 (1970).
39) M. Katsumata, K. Kasatani, M. Kawasaki, and H. Sato, *Bull. Chem. Soc. Jpn.*, **55**, 717 (1982).
40) W. Cooper and N. B. Liebert, *Photogr. Sci. Eng.*, **16**, 25 (1972).
41) R. Humphry-Baker, M. Grätzel, and R. Steiger, *J. Am. Chem. Soc.*, **102**, 847 (1980).
42) N. Nakashima and T. Kunitake, *J. Am. Chem. Soc.*, **104**, 4261 (1982).
43) A. von Jena and H. E. Lessing, *Chem. Phys. Lett.*, **78**, 187 (1981).
44) G. Porter, P. J. Sadkowski, and C. J. Tredwell, *Chem. Phys. Lett.*, **49**, 416 (1977).
45) H. J. Eichler, U. Klein, and D. Langhans, *Chem. Phys. Lett.*, **67**, 21 (1979).
46) G. Oster and Y. Nishijima, *J. Am. Chem. Soc.*, **78**, 1581 (1956).
47) Th. Förster and G. Hoffman, *Z. Phys. Chem. N. F.*, **75**, 63 (1971).
48) A. Osborne and A. C. Winkworth, *Chem. Phys. Lett.*, **85**, 513 (1982).
49) J. C. Mialocq, P. Goujon, and M. Arvis, *J. Chim. Phys.*, **76**, 1067 (1979).
50) J. Jaraudias, *J. Photochem.*, **13**, 35 (1980).
51) D. Welford, W. Sibbett, and J. R. Taylor, *Opt. Commun.*, **34**, 175 (1980).
52) J. R. Taylor, M. C. Adams, and W. Sibbett, *Appl. Phys.*, **21**, 13 (1980).
53) V. Sundstrom and T. Gillbro, *Chem. Phys.*, **61**, 257 (1981).
54) S. P. Velsko and G. R. Fleming, *Chem. Phys.*, **65**, 59 (1982).
55) J. C. Mialocq, A. W. Boyd, J. Jaraudias, and J. Sutton, *Chem. Phys. Lett.*, **37**, 236 (1976).
56) C. Rullière, *Chem. Phys. Lett.*, **43**, 303 (1976).
57) J-P. Fouassier, D-J. Lougnot, and J. Faure, *Opt. Commun.*, **23**, 393 (1977); *J. Chim. Phys.*, **74**, 23 (1977).
58) S. K. Rentsch, *Chem. Phys.*, **69**, 81 (1982).
59) D. Meisel, M. S. Matheson, and J. Rabani, *J. Am. Chem. Soc.*, **100**, 117 (1978).
60) S. Tachiyashiki and H. Yamatera, *Chem. Lett.*, **1981**, 1681; *Bull. Chem. Soc. Jpn.*, **55**, 759 (1982).
61) S. Ozeki, S. Tachiyashiki, S. Ikeda, and H. Yamatera, *J. Colloid Interface Sci.*, **91**, 430 (1983).

 © 1983 The Chemical Society of Japan Bull. Chem. Soc. Jpn., 56, 3595—3599 (1983)

Transient Intermediate Produced from 5-Aminouracil in Reaction with Dichloride Anion Radical

Takahiro MASUDA,* Ryoji GUNJI, Takako KIMURA, and Kotaro YAMAUCHI

Department of Chemistry, Faculty of Science, Tokyo Metropolitan University, Fukasawa, Setagaya-ku, Tokyo 158

(Received June 16, 1983)

A transient absorption, which is relatively long-lived, was found in a flash photolysis of aqueous potassium chloride containing 5-aminouracil. The transient absorption with a peak at about 335 nm was assigned to an intermediate produced from 5-aminouracil through a one-electron oxidation by dichloride anion radical. For the intermedicate, a possible structure is proposed to explain its long life-time. On the basis of the transient absorption, a determination of the rate constant for the reaction of 5-aminouracil with dichloride anion radical was carried out by use of a competition kinetics. The value of $(2.9\pm0.2)\times10^8$ dm^3 mol^{-1} s^{-1} was obtained as the rate constant on the basis of rate constants of several reference compounds. By comparing the values obtained by the competition method with those estimated by a direct analysis of the decay rate of dichloride anion radical, the validity of the competition method was examined.

In the course of our study on reactions of dichloride anion radical with pyrimidine derivatives,[1] a relatively long-lived transient absorption with a peak at about 335 nm was found in a flash photolysis of aqueous solutions of potassium chloride containing 5-aminouracil. It overlaps a transient absorption due to dichloride anion radical and obstracts the determination of the rate constant for the reaction of 5-aminouracil with dichloride anion radical by anaysis of the decay rate of the anion radical (a direct method).

Intermediate products of pyrimidine bases produced through reaction with dichloride anion radical have been suggested as π-cation radicals by ESR studies.[2,3] Absorption spectra of intermediate species formed from pyrimidine bases through reaction with oxidizing radical such as $SO_4^{-\cdot}$ or $Cl_2^{-\cdot}$ have been reported to have absorption maxima at 410 and 560 nm for uracil, 400 and 500 nm for thymine, and 410 nm for isoorotic acid.[2] However, no transient absorptions were observed in the time-scale of flash photolysis. It implies a fast decay of transient species responsible for the absorptions. A half-life of the transient intermediate formed from 5-aminouracil was estimated to be *ca.* 800 μs, which is considerably long compared with those for transient species from other bases and for dichloride anion radical.

In the present study, an assignment of transient absorptions was attempted by comparison of transient spectra observed under various conditions where different kinds of intermediate species are allowed to form. Furthermore, a competition method using a transient absorption at 330 nm was applied to the determination of the rate constant of 5-aminouracil with dichloride anion radical. With several referance compounds, the method was confirmed to give a reasonable value for the rate constant of 5-aminouracil with dichloride anion radical. The validity for wide application of the method was examined and discussed in terms of the reactivity of products produced from substrates and of a possible interaction between a substrate and 5-aminouracil in aqueous solutions.

Experimental

5-Aminouracil (abbreviated to 5AU) and other pyrimidine bases were obtained from Sigma Chemical Co. and peptides from Nutritional Biochemical Corp. as preparations of high purity. They were used without further purification. Potassium chloride and other chemicals were of reagent grade.

Solutions for irradiation were prepared with triply distilled water and adjusted to pH 7. The solutions were bubbled with dinitrogen monoxide, sulfur hexafluoride, or nitrogen for 20 min immediately before flash photolysis. A conventional type of apparatus was used for flash photolysis with 10 μs of 1/e duration and 200 J of input energy. Details were described in a previous paper.[4] Transient spectra were measured by a kinetic spectrophotometry. Calculation for kinetic analysis was carried out with the aid of microcomputers PC 8001 and 8801 (Nippon Electric Co.).

Results and Discussion

Transient Absorption Spectra. Transient absorption spectra of flash photolyzed aqueous solutions of 5-aminouracil were measured under several conditions (Fig. 1(a)). For the N_2O-saturated neutral solution of potassium chloride containing 5-aminouracil, absorption peaks at about 335 and 390 nm were observed at 150 μs after start of flash, while a peak at 335 nm was observed for the SF_6-saturated solution. For the acid solution (pH 3.15), a maximum was seen at 335 nm. The peak at 335 nm was also observed in the absence of potassium chloride. This suggests that the direct photoionization takes place to yield a similar intermediate.

In the N_2O-saturated neutral solution of potassium chloride containing a sufficient amount of 5-aminouracil, the following reactions are expected to proceed in flash photolysis:

$$Cl^- + h\nu \longrightarrow Cl\cdot + e^-, \quad (1)$$

$$Cl\cdot + Cl^- \longrightarrow Cl_2^{-\cdot}, \quad (2)$$

$$e^- + aq \longrightarrow e_{aq}^-, \quad (3)$$

$$e_{aq}^- + N_2O \longrightarrow N_2 + HO\cdot + OH^-, \quad (4)$$

$$HO\cdot + Cl^- \longrightarrow ClOH^{-\cdot}, \quad (5)$$

$$HO\cdot + 5AU \longrightarrow 5AUOH\cdot, \quad (6)$$

$$ClOH^{-\cdot} + 5AU \longrightarrow 5AUOH\cdot + Cl^-, \quad (7)$$

$$Cl_2^{-\cdot} + 5AU \longrightarrow 5AU^{+\cdot} + 2Cl^-. \quad (8)$$

In flash photolysis of the N_2O-saturated neutral solution of 5-aminouracil, Reaction 9, a direct photoionization, will occur, followed by Reactions 3, 4, and

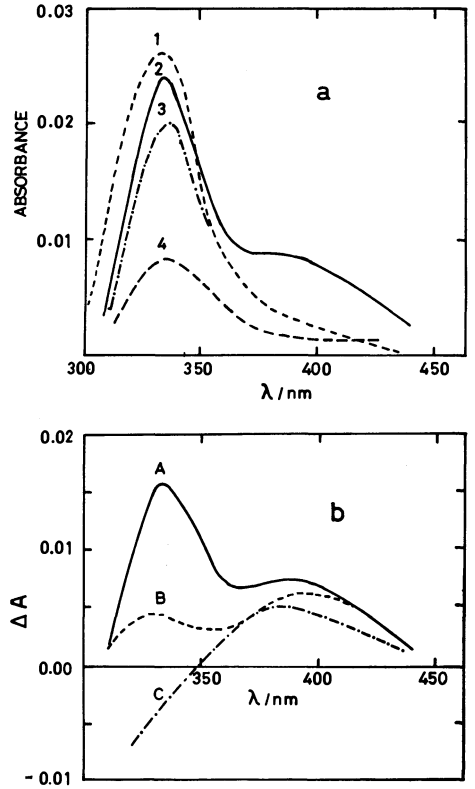

Fig. 1. Absorption spectra of the intermediates produced from 5-aminouracil in flash photolysis.
(a) Transient spectra measured at 150 μs after start of flash. $[5AU]=5\times10^{-5}$ mol dm^{-3}. 1: 1 mol dm^{-3} KCl, N_2O saturated, pH 3.15. 2: 1 mol dm^{-3} KCl, N_2O saturated, neutral pH. 3: 1 mol dm^{-3} KCl, SF_6 saturated, neutral pH. 4: N_2O saturated, neutral pH.
(b) Difference spectra. A: 2-4. B: 2-3. C: 2-1.

6; then the formation of a cation radical ($5AU^{+}\cdot$) and an OH-adduct (5AUOH·) is expected:

$$5AU + h\nu \longrightarrow 5AU^{+\cdot} + e^{-}. \quad (9)$$

When an acid solution of potassium chloride containing 5-aminouracil is photolyzed with N_2O-saturation, Reactions 10 and 11 will be added to Reactions 1—5 and 8:

$$e^{-}_{aq} + H^{+} \longrightarrow H\cdot, \quad (10)$$

$$ClOH^{-\cdot} + H^{+} \longrightarrow Cl\cdot + H_2O. \quad (11)$$

Although an addition reaction of a hydrogen atom to 5-aminouracil can be expected in acid solutions, data on rate constants and concentrations indicate that Reaction 4 overwhelms Reaction 10, since the rate constants for Reactions 4 and 10 are reported to be 8×10^{9} [5] and $(2.2\text{—}2.4)\times10^{10}$ dm^3 mol^{-1} s^{-1},[6] respectively, and the concentrations of N_2O and H^+ are 2.5×10^{-2} and 7×10^{-4} mol dm^{-3}, respectively. Therefore, $5AU^{+\cdot}$ is considered as the main intermediate product formed from 5-aminouracil in the acid solution. In the SF_6-saturated solution of potassium chloride containing 5-aminouracil, Reaction 12 may occur in addition to Reactions 1—3 and 8:

$$e^{-}_{aq} + SF_6 \longrightarrow SF_5\cdot + F^{-}. \quad (12)$$

The difference spectra shown in Fig. 1(b) can be well understood by combination of the above reactions. The absorption peaks at 335 and 390 nm are attributable to $5AU^{+\cdot}$ and 5AUOH·, respectively. Danziger *et al.*[7] reported that the OH-adduct of uracil shows an absorption maximum at 390 nm. Similarly Mayers *et al.*[8] indicated that the OH-adducts of uracil and thymine have absorption spectra with a maximum at 375 nm and that the second-order decay constants of the OH-adducts are 2.1×10^{9} dm^3 mol^{-1} s^{-1} for uracil and 2.2×10^{9} dm^3 mol^{-1} s^{-1} for thymine. The half-life was also estimated by the authors to be *ca.* 100 μs for 5×10^{-6} mol dm^{-3} of initial concentration. For the OH-adduct of 5-aminouracil studied in the present work, however, about 600 μs of half-life was obtained at the initial concentration of 3.5×10^{-6} mol dm^{-3}. Apparently the OH-adduct of 5-aminouracil is more stable than those of other bases. Bansal and Fessenden[2] and Sevilla *et al.*[3] have proposed structure of π-cation radicals produced from pyrimidine bases through reaction with oxidizing radicals on the basis of ESR studies. The structures correspond to neutral radicals with a high electron density at C-5, which are produced from cation radicals after deprotonation respectively. For the intermediate species of 5-aminouracil responsible for the absorption at 335 nm, therefore, deprotonated forms of the cation radical ($5AU^{+\cdot}$) can be considered. The possible structure is as follows:

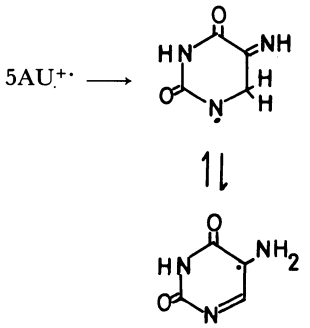

(13)

The N-radical will be an explanation for the long life-time. An analogous argument with the OH-adduct leads to the following structure:

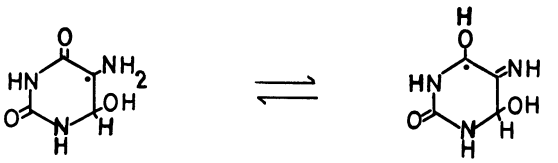

(14)

Competition Kinetics. Assuming a competition between Reactions 8 and 15, Eq. I can be derived:

$$Cl_2^{-\cdot} + S \longrightarrow 2Cl^{-} + \text{product(s)} \quad k_s, \quad (15)$$

$$\frac{A_0}{A} = 1 + \frac{k_s[S]_0}{k_8[5AU]_0}, \quad (I)$$

where A_0 and A represent the absorbances at 330 nm in the absence and presence of substrate, respectively, and $[S]_0$ and $[5AU]_0$ designate the initial concentrations of the substrate and 5-aminouracil, respectively. By plotting A_0/A against $[S]_0/[5AU]_0$, k_s/k_8 is obtained from the slope of a straight line. Equation I is valid when the dichloride anion radical converts to the intermediate

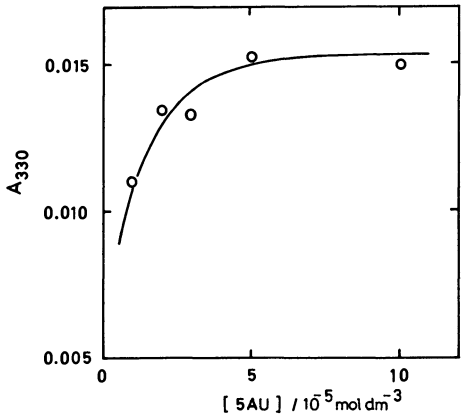

Fig. 2. Dependence of the absorbance at 330 nm of the intermediate of 5-aminouracil upon the concentration of 5-aminouracil.
1 mol dm^{-3} KCl, N_2O saturated, neutral pH.

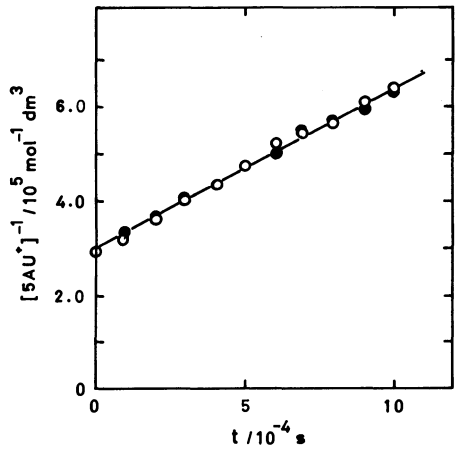

Fig. 3. Second-order decay of the intermediate of 5-aminouracil. ○: 5×10^{-5} mol dm^{-3} 5-aminouracil. ●: 10^{-4} mol dm^{-3} 5-aminouracil.

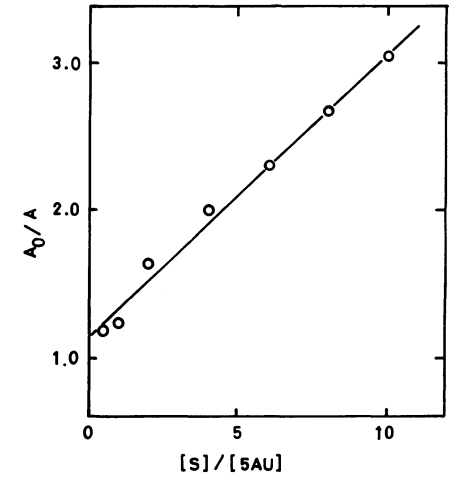

Fig. 4. Competition between 5-aminouracil and glycylnorvaline against the dichloride anion radicals.

of 5-aminouracil completely. The dependence of the absorbance at 330 nm on the concentration of 5-aminouracil (Fig. 2) and the decay rate of the intermediate of 5-aminouracil (Fig. 3) seem to confirm this condition. The absorbance at 330 nm was observed to reach the upper limit at *ca.* 5×10^{-5} mol dm^{-3}, as shown in Fig. 2. For 5×10^{-5} and 10^{-4} mol dm^{-3} solutions of 5-aminouracil, an identical decay rate of the intermediate was found (Fig. 3). The decay process obeys a second-order kinetics and the value of 5.8×10^{4} was obtained as $2k/\varepsilon$. The absorption coefficient of the intermediate of 5-aminouracil is estimated to be 6200 dm^3 mol^{-1} cm^{-1}, on the assumption that a complete conversion of dichloride anion radical to the intermediate at 10 μs after start of flash. Consequently the value of 3.6×10^{8} dm^3 mol^{-1} s^{-1} was obtained as $2k$. The result obtained by plotting A_0/A *vs.* $[S]_0/[5AU]_0$ supports the reliability of Eq. I. Figure 4 shows an example of competition plot obtained for glycylnorvaline.

Table 1. Rate constants for the reaction of dichloride anion radical with 5-aminouracil estimated by the competition method

Reference compound	Slope	k_8 / 10^8 dm^3 mol^{-1} s^{-1}
Cytosine	1.09	3.21
Thymine	1.06	3.02
Glycyl-α-amino-*n*-butyric acid	0.114	2.63
Glycylnorvaline	0.182	2.80
Glycylvaline	0.150	2.73
Glycylleucine	0.170	3.18
	Average	2.93 ±0.24

The rate constant of 5-aminouracil with dichloride anion radical can be estimated by using some reference compounds whose rate constants have been determined by the direct method.[1,9] The direct determination of rate constant for reaction with dichloride anion radical is based on analysis of the decay rate of dichloride anion radical.[1] Equation II is derived from Reactions 1, 2, 15, and 16:

$$Cl_2^{-\cdot} + Cl_2^{-\cdot} \longrightarrow Cl_2 + 2Cl^-, \quad (16)$$

$$\ln\frac{[Cl_2^{-\cdot}]_0(2k[Cl_2^{-\cdot}]+k_{ob})}{[Cl_2^{-\cdot}](2k[Cl_2^{-\cdot}]_0+k_{ob})} - k_{ob}t = 0, \quad (II)$$

where k_{ob} is equal to $k_s[S]$; $[Cl_2^{-\cdot}\ t]_0$ and $[Cl_2^{-\cdot}]$ are the concentrations of dichloride anion radical at time zero and t, respectively. $2k$ is the rate constant for Reaction 16. The concentration of the anion radical at time zero was assumed to be equal to the value obtained by applying an extrapolation of $1/[Cl_2^{-\cdot}]$ and t. Values of k_{ob} at given times were estimated by Eq. II. From the values estimated at every 10 μs from 50 to 100 μs after start of flash, an average value of k_{ob} was calculated for a given concentration of substrate. The average values of k_{ob} were plotted against the concentration of substrate and k_s was obtained from the slope. The result is summarized in Table 1. With six reference compounds, the value of $(2.9\pm0.2)\times10^{8}$ dm^3 mol^{-1} s^{-1} was obtained as k_8. The value shows a close agreement with the value of $(3.1\pm0.5)\times10^{8}$ dm^3 mol^{-1} s^{-1}, reported in a previous paper,[1] as estimated from data with cytosine, thymine, glycylleucine, and

Table 2. Comparison of rate constants estimated by the competition method with those determined by other methods

Compound	Rate constant/dm³ mol⁻¹ s⁻¹		
	Competition method	Direct method	Reported value
Formate	2.0×10^6	1.3×10^7	1.9×10^6 a)
Succinate	6.5×10^6	9.2×10^6	8×10^2 a) (pH 1)
Acrylate	9.7×10^7	9.0×10^7	1.9×10^7 a)
Fumarate	3.7×10^8	3.3×10^8	4×10^6 a)
Maleate	1.7×10^8	1.7×10^8 b)	3.5×10^7 c)
			3.7×10^7 d)
			4.1×10^7 e)
6-Aminouracil	1.5×10^8	2.7×10^9	

a) Ref. 10. b) Ref. 1. c) Ref. 12. d) Ref. 13. e) Ref. 14.

formate.

The rate constant for a given substrate with dichloride anion radical can be estimated by the competition method making use of k_8 as the reference. Results are shown in Table 2. Agreement of the values with those obtained by the direct method seems to be fairly good with some exceptions. The values reported by other authors are in general smaller than the present values. The values cited in the fourth column of Table 2 were determined by a pseudo-first-order kinetics with pulse radiolysis. Despite the low doses applied, neglect of Reaction 16 may cause an incorrect estimation, especially for relatively low concentrations of substrate. Furthermore, the analysis of the decay rate of dichloride anion radical would be disturbed by a new absorption due to an intermediate species from the substrate, if the absorption appears in the same region of wavelength with dichloride anion radical, because the time-scale of pulse radiolysis is much shorter than that of flash photolysis.

For formate ion, the value determined by the competition method differs from that by the direct method, but is in fairly good agreement with the value determined by pulse radiolysis. The reaction of dichloride anion radical with formate ion produces a carbon dioxide anion radical ($CO_2^{-\cdot}$):

$$Cl_2^{-\cdot} + HCOO^- \longrightarrow 2Cl^- + H^+ + CO_2^{-\cdot}. \quad (17)$$

$CO_2^{-\cdot}$ will react with dichloride anion radical to form carbon dioxide:

$$Cl_2^{-\cdot} + CO_2^{-\cdot} \longrightarrow 2Cl^- + CO_2. \quad (18)$$

Therefore, the reaction of formate ion with dichloride anion radical is complicated and the direct method is not appropriate to the substrate.

For uracil and 6-aminouracil, significant differences were observed between the values obtained by the competition and direct methods. An electron transfer from 5-aminouracil to a substrate cation (S^+) will be an explanation for the discrepancy. The electron transfer causes a decrease in reactivity of the substrate in appearance, when the competition kinetics is applied. However, a simulation by a computer indicated that the mechanism gives no linear correlation between A_0/A and $[S]_0/[5AU]_0$. Another explanation is the formation of a complex of 5-aminouracil with the substrate:

$$5AU + S \overset{K}{\rightleftharpoons} 5AU{\cdot}S, \quad (19)$$

$$5AU{\cdot}S + Cl_2^{-\cdot} \longrightarrow 5AU^{+\cdot} + S + 2Cl^- \quad k_c. \quad (20)$$

Assuming that the complex reacts with dichloride anion radical to give $5AU^{+\cdot}$ the following relation is derived:

$$A_0/A = 1 + \frac{k_8[S]}{k_8[5AU] + k_c[5AU{\cdot}S]}, \quad (III)$$

where [S], [5AU], and [5AU·S] designate the concentrations of a substrate, 5-aminouracil, and the complex at equilibrium, respectively; k_c is the rate constant for Reaction 20. When 5-aminouracil is converted to the complex completely, Eq. III is transformed to

$$A_0/A = 1 + \frac{k_s[S]}{k_c[5AU{\cdot}S]}, \quad (IV)$$

where [5AU·S] is equal to $[5AU]_0$ and [S] is the difference between $[S]_0$ and $[5AU]_0$, hence

$$A_0/A = \left(1 - \frac{k_s}{k_c}\right) + \frac{k_s[S]_0}{k_c[5AU]_0}. \quad (V)$$

When the ratio of the initial concentrations, $[S]_0/[5AU]_0$, is sufficiently large, the slope of the straight line obtained by plotting A_0/A *vs.* $[S]_0/[5AU]_0$ provides the value of k_c. For 6-aminouracil and uracil, 5.2×10^9 and 5.8×10^8 dm³ mol⁻¹ s⁻¹ were obtained as k_c, respectively. Using the equilibrium constant, K, as a parameter and the value of k_c, a simulation of Eq. III was carried out and 1.5×10^4 of K was found to give the best fitted curve in the case of 6-aminouracil, as shown in Fig. 5. For uracil, the best fitted curve was obtained for 10^4 of K. Although there is no confirmation for the formation of the complex, the resemblance of their structures suggests a possible interaction between them.

For the dicarboxylic acids, the agreement is fairly good between the two methods. Since the values of

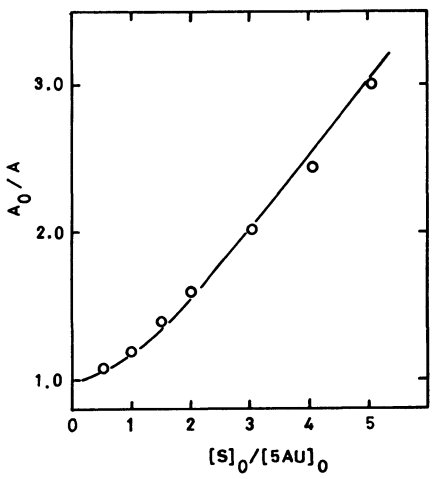

Fig. 5. Simulation of A_0/A *vs.* $[S]_0/[5AU]_0$ based on the mechanism of complex formation.
Substrate: 6-aminouracil.

1.4×10^6 and 2.5×10^6 $dm^3\ mol^{-1}\ s^{-1}$ were obtained as the rate constants for acetate and propionate,[11] the value for succinate seems reliable. In a previous study,[1] the partial rate constant for the 5, 6 double bond of uracil for the reaction with dichloride anion radical was estimated to be 2.2×10^8 $dm^3\ mol^{-1}\ s^{-1}$. For a compound containing a double bond, therefore, a value of the order of 10^8 can be expected as the rate constant of reaction with dichloride anion radical if the compound has no other reactive group than the double bond or no repressive one. The observed rate constants for the unsaturated carboxylic acids appear to be consistent with this argument. Maleate was found to be less reactive than fumarate toward dichloride anion radical. This implies that a stabilization due to the interaction between two carboxyl groups in the *cis*-form may cause a decrease in the reactivity of one electron oxidation.

The present work was supported by a Grant-in-Aid for Scientific Research No. 56580144 from the Ministry of Education, Science and Culture.

References

1) T. Masuda, T. Kimura, E. Kadoi, T. Takahashi, K. Yamauchi, and M. Kondo, *J. Radiat. Res.*, **24**, 165 (1983).
2) K. M. Bansal and R. W. Fessenden, *Radiat. Res.*, **75**, 497 (1978).
3) M. D. Sevilla, D. Suryanarayana, and K. M. Morehouse, *J. Phys. Chem.*, **85**, 1027 (1981).
4) T. Masuda, Y. Murata, K. Yamauchi, and M. Kondo, *J. Radiat. Res.*, **18**, 258 (1977).
5) A. M. Koulkes-Pujo, B. D. Michael, and E. J. Hart, *Int. J. Radiat. Phys. Chem.*, **3**, 333 (1971).
6) a) R. R. Hentz, Farhataziz, and E. M. Hansen, *J. Chem. Phys.*, **57**, 2959 (1972); b) S. C. Wallace and J. K. Thomas, *Radiat. Res.*, **54**, 49 (1973); c) F. Barat, L. Gilles, B. Hickel, and B. Lesigne, *J. Phys. Chem.*, **77**, 1711 (1973).
7) R. M. Danziger, E. Hayon, and M. E. Langmuir, *J. Phys. Chem.*, **72**, 3842 (1968).
8) L. Meyers, Jr., M. L. Hollis, L. M. Theard, F. C. Peterson, and A. Warnicke, *J. Am. Chem. Soc.*, **92**, 2875 (1970).
9) T. Masuda, T. Hayashi, and M. Kondo, *J. Radiat. Res.*, **23**, 298 (1982).
10) K. Hasegawa and P. Neta, *J. Phys. Chem.*, **82**, 854 (1978).
11) T. Masuda, S. Shimada, and M. Kondo, *J. Radiat. Res.*, **20**, 209 (1979).
12) L. K. Patterson, K. M. Bansal, G. Boagan, G. A. Infante, E. J. Fendler, and J. H. Fendler, *J. Am. Chem. Soc.*, **94**, 9028 (1972).
13) O. P. Chawla and R. W. Fessenden, *J. Phys. Chem.*, **79**, 2693 (1975).
14) J. W. Ward and I. Kuo, *Adv. Chem. Ser.*, **81**, 368 (1968).

Thermodynamic Study for Dibenzo-24-crown-8 Complexes with Alkali Metal Ions in Nonaqueous Solvents

Yasuyuki TAKEDA
Department of Chemistry, Faculty of Science, Chiba University, Yayoi-chō, Chiba 260
(Received June 25, 1983)

Complex-formation constants (K_{ML^+}) of dibenzo-24-crown-8 (DB24C8) with alkali metal ions in acetonitrile and the solubility of DB24C8 in methanol, acetonitrile, and propylene carbonate were determined conductometrically and spectrophotometrically at 25 °C, respectively. The K_{ML^+} value sequences of the alkali metal ions with DB24C8 are $Na^+ > Cs^+ > K^+ = Rb^+$. Dibenzo-24-crown-8 shows no remarkable selectivity for the alkali metal ions in acetonitrile. Transfer activity coefficients of the DB24C8 complexes with alkali metal ions were calculated from these data and literature values of transfer activity coefficients of alkali metal ions. For the same alkali metal ion, the bulky DB24C8–alkali metal ion complex is more soluble in the aprotic solvents acetonitrile and propylene carbonate than in the protic solvent methanol as compared with the case of the alkali metal ion itself. The transfer activity coefficient of the DB24C8–alkali metal ion complex from methanol to acetonitrile is somewhat sensitive to the variation of the alkali metal ion in the DB24C8 cavity, whereas the mobility of the DB24C8–alkali metal ion complex at the same concentration in the solvents is not sensitive.

Selectivity and complexing ability of dibenzo-24-crown-8 (DB24C8) for metal ions, which were studied by means of solvent extraction[1] and conductometry,[2,3] were reported in the previous papers. For both conductance and solvent extraction systems, DB24C8 shows no peak selectivity for any alkali metal ion. However, DB24C8 reveals the pronounced extraction-selectivity for Ba^{2+} among all the alkali and alkaline earth metal ions. Behavior of the DB24C8–alkali metal ion complexes in methanol and propylene carbonate was conductometrically investigated.[2,3] In each case of methanol and propylene carbonate, mobilities of the complexes at the same concentration are nearly equal to each other. Furthermore, DB24C8 was used for separation of Ba^{2+} from Sr^{2+} by means of solvent extraction.[4]

In the present work, complex-formation constants of DB24C8 with alkali metal ions in acetonitrile and the solubility of DB24C8 in methanol, acetonitrile, and propylene carbonate were conductometrically and spectrophotometrically determined at 25 °C, respectively. Transfer activity coefficients of the DB24C8 complexes with alkali metal ions were calculated from these data and literature values of transfer activity coefficients of alkali metal ions. The behavior of the DB24C8 complexes with alkali metal ions in solutions was discussed in terms of the transfer activity coefficients and the mobility of the complexes.

Experimental

Materials. Dibenzo-24-crown-8 (Nisso Co., Ltd.) was dissolved in hexane, and filtered while hot. Then it was recrystallized three times from hexane and, prior to use, dried at 50 °C in a vacuum oven. Sodium and potassium perchlorates were purchased commercially. The method of preparing rubidium and caesium perchlorates, as well as that of purifying alkali metal perchlorates was previously described.[2] The method of purification of methanol,[2] acetonitrile,[5] and propylene carbonate[2] was as has previously been reported. For these solvents, the middle 70% of the distillate was used. The water contents of the purified acetonitrile and propylene carbonate determined by means of the Karl Fischer titration were less than 0.01%, and, for methanol, less than 0.03%. The conductivity of the final product of acetonitrile was less than $1.5\times10^{-7}\ \Omega^{-1}\ cm^{-1}$.

Apparatus and Procedure. The conductance measurements were made on a Fuso conductivity apparatus, model 362A, in a water bath thermostated at 25±0.005 °C. Two cells were used with cell constants of 0.05970_5 and 0.09393_4 cm^{-1}. The experimental procedure to obtain formation constants of DB24C8 complexes with alkali metal ions in acetonitrile was the same as those described in the previous paper.[2]

Dibenzo-24-crown-8 solubilities in methanol (225 nm), acetonitrile (275 nm), and propylene carbonate (275 nm) were determined spectrophotometrically at 25±0.02 °C. They are 6.5×10^{-3} M (1 M=1 mol dm^{-3}) in methanol, 1.0×10^{-1} M in acetonitrile, and 4.5×10^{-2} M in propylene carbonate.

Results and Discussion

From Fig. 1, the molar conductivity, Λ, *vs.* $[L]_t/[M]_t$ plots for each alkali metal system, where $[L]_t$ and $[M]_t$ denote the total concentrations of DB24C8 and an alkali metal ion respectively, show a monotonous decrease in Λ with an increase in the DB24C8 concentration. This indicates that the DB24C8 forms a complex with each alkali metal ion and the complexed cation is much less mobile than the corresponding alkali metal ion in

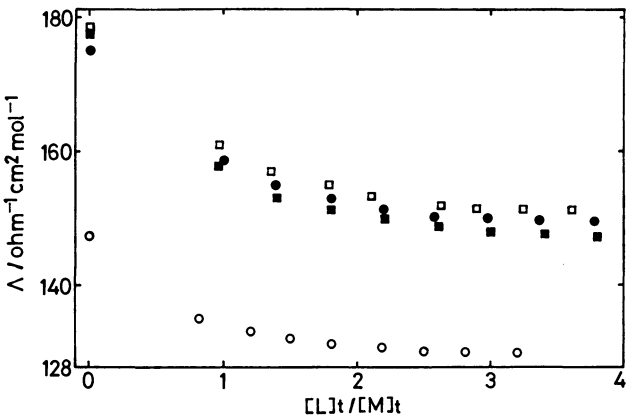

Fig. 1. Λ *vs.* $[L]_t/[M]_t$ curves for DB24C8–alkali metal perchlorate systems in acetonitrile at 25 °C.
○: Na^+, ●: K^+, □: Rb^+, ■: Cs^+, $[M]_t=5\times10^{-4}$ M.

acetonitrile.

It is assumed that the association between the cation and the perchlorate ion in acetonitrile is negligible under these highly dilute experimental conditions ($[M]_t=5\times10^{-4}$ M) and that the DB24C8 forms the 1 : 1 complexes with the alkali metal ions in acetonitrile. The equilibrium equation is written as

$$\begin{array}{ccccc} M^+ & + & L & \rightleftharpoons & ML^+ \\ \alpha[M]_t & & [L]_t-(1-\alpha)[M]_t & & (1-\alpha)[M]_t, \end{array} \quad (1)$$

where M^+, L, and α are the alkali metal ion, crown ether, and the fraction of free alkali metal ions. Thus, the complex-formation constant, K_{ML^+}, is defined by

$$\begin{aligned} K_{ML^+} &= [ML^+]/[M^+][L] \\ &= (1-\alpha)/\alpha[L]. \end{aligned} \quad (2)$$

The observed conductivity, κ, is given by

$$\kappa = \kappa_{MClO_4} + \kappa_{MLClO_4}, \quad (3)$$

where κ_{MClO_4} and κ_{MLClO_4} represent the conductivities of alkali metal perchlorate and alkali metal DB24C8 perchlorate, respectively. The molar conductivities are as follows

$$\begin{aligned} \Lambda_{MClO_4} &= \kappa_{MClO_4}/[M^+] \\ &= \kappa_{MClO_4}/\alpha[M]_t, \end{aligned} \quad (4)$$

$$\begin{aligned} \Lambda_{MLClO_4} &= \kappa_{MLClO_4}/[ML^+] \\ &= \kappa_{MLClO_4}/(1-\alpha)[M]_t, \end{aligned} \quad (5)$$

Λ_{MClO_4} and Λ_{MLClO_4} being the molar conductivities of alkali metal perchlorate and alkali metal DB24C8 perchlorate respectively. As a consequence of Eqs. 4 and 5, Eq. 3 can be transformed into

$$\begin{aligned} \Lambda &= \kappa/[M]_t \\ &= \alpha\Lambda_{MClO_4} + (1-\alpha)\Lambda_{MLClO_4}. \end{aligned} \quad (6)$$

Since the DB24C8 concentration was kept low during these experiments, corrections for viscosity changes were neglected. As a consequence of Eq. 6, Eq. 2 can be transformed into

$$K_{ML^+} = (\Lambda_{MClO_4}-\Lambda)/(\Lambda-\Lambda_{MLClO_4})[L], \quad (7)$$

where $[L]=[L]_t-[M]_t(\Lambda_{MClO_4}-\Lambda)/(\Lambda_{MClO_4}-\Lambda_{MLClO_4})$. The K_{ML^+} value can be obtained by the following procedure. The Λ_{MLClO_4} value is estimated from the Λ values at the points of large $[L]_t$ to $[M]_t$ ratios. Using this Λ_{MLClO_4} value, the K_{ML^+} value in Eq. 7 is calculated. The actual K_{ML^+} and Λ_{MLClO_4} values are calculated by a succesive approximation method. The $\log K_{ML^+}$ values are listed in Table 1.

Table 1. $\log(K_{ML^+}/\text{mol}^{-1}\,\text{dm}^3)$ values of DB24C8 with alkali metal ions at 25 °C

	Na^+	K^+	Rb^+	Cs^+
Acetonitrile	4.1	3.8	3.8	4.0
Propylene carbonate[3]	4.1_6	3.7_3	3.5_5	3.4_6
Methanol[2]	—	3.5_7	3.8_6	3.8_4

Dibenzo-24-crown-8 shows no remarkable selectivity for the alkali metal ions in acetonitrile. For both acetonitrile and propylene carbonate, although Na^+ is most strongly solvated and its size is the least favorable to the DB24C8 cavity of all the alkali metal ions (Na^+, K^+, Rb^+, and Cs^+), DB24C8 forms the most stable complex with Na^+. The differences in the free energies of the solvation of Na^+ and K^+, Na^+ and Rb^+, and Na^+ and Cs^+ are much smaller for acetonitrile and propylene carbonate than for the solvents such as water, methanol, DMF, and DMSO.[6] The solvation power of propylene carbonate and acetonitrile for Na^+ is the smallest of all these solvents.[6] Judging from the large size and the flexibility of DB24C8, Na^+ seems to have a suitable size for the favorable arrangement of the ether oxygen atoms for the metal ion trapped in the cavity. This may be the reason why the DB24C8 complex with Na^+ is the most stable in both acetonitrile and propylene carbonate.

Table 1 shows that stability of the DB24C8 complex with the same alkali metal ion slightly varies with the solvent. In general, only for aprotic solvents (acetonitrile (DN=14.1[7]) and propylene carbonate (DN=15.1[7])), a reverse correlation exists between the stabilities of the DB24C8–alkali metal ion complexes and the donor number, DN, of the solvent.

Transfer Activity Coefficient. The transfer activity coefficient, $\log {}^{S_1}\gamma^{S_2}(ML^+)$, of the DB24C8–alkali metal ion complex between the solvent S_1 and the solvent S_2 is calculated by Eq. 8.

$$\begin{aligned} \log {}^{S_1}\gamma^{S_2}(ML^+) = (\log K_{ML^+})_{S_1} - (\log K_{ML^+})_{S_2} + \log {}^{S_1}\gamma^{S_2}(L) \\ + \log {}^{S_1}\gamma^{S_2}(M^+) \end{aligned} \quad (8)$$

These data are summarized in Table 2.

Dibenzo-24-crown-8 is much more soluble in the aprotic solvents acetonitrile and propylene carbonate than in the protic solvent methanol (Table 2). Both dibenzo-18-crown-6 (DB18C6) and dibenzo-30-crown-

Table 2. Transfer activity coefficients at 25 °C

		S=AN[a]			S=PC[b]		
$\log {}^{MeOH\,c)}\gamma^S(M^+)$[8]	K^+		-0.4			-0.1_6	
	Rb^+		-0.6			-0.4_8	
	Cs^+		-0.8			-0.6_6	
		DB18C6[8]	DB24C8	DB30C10[9]	DB18C6[8]	DB24C8	DB30C10[9]
$\log {}^{MeOH}\gamma^S(L)$		-1.6_5	-1.1_8	-1.4_0	-1.0_6	-0.8_4	-0.8_1
$\log {}^{MeOH}\gamma^S(ML^+)$							
	K^+	-1.9	-1.8_1	-1.3_3	-1.3_5	-1.1_6	-0.5_5
	Rb^+	-1.8	-1.7_2	—	-1.2_2	-1.0_1	—
	Cs^+	-2.5	-2.1_4	—	-1.4_8	-1.1_2	—

a) Acetonitrile. b) Propylene carbonate. c) Methanol.

10 (DB30C10) show the same tendency as DB24C8. From Table 2, for both DB24C8 and DB18C6, the log ${}^{MeOH}\gamma^{S}(L)$ value is larger than the log ${}^{MeOH}\gamma^{S}(ML^+)$ value, and contrary holds for DB30C10, where S=AN and PC. This cannot clearly be explained at the present stage. However, possible reasons may be the difference in the strength of hydrogen bonds between CH_3OH-uncomplexed crown ether and CH_3OH-complexed crown ether, and the difference in the conformation between an uncomplexed crown ether and a complexed crown ether.

As can be seen from Table 2, for the same alkali metal ion, the bulky ML^+ is more soluble in an aprotic solvent than in a protic solvent as compared with the case of M^+.

In the case of DB24C8, log ${}^{MeOH}\gamma^{PC}(ML^+)$ values of alkali metal ions are nearly equal to one another, whereas the log ${}^{MeOH}\gamma^{AN}(ML^+)$ value of Cs^+ is relatively smaller than the others, and the log ${}^{PC}\gamma^{AN}(ML^+)$ value varies with the alkali metal ion trapped in the DB24C8 cavity (Na^+: -0.9_3, K^+: -0.6_5, Rb^+: -0.7_1, Cs^+: -1.0_2). This indicates that, for the CH_3OH–propylene carbonate system, the charge of the alkali metal ion held in the DB24C8 cavity is effectively shielded, and that, for the CH_3OH–acetonitrile and propylene carbonate–acetonitrile systems, the charge is not effectively screened. The actual Λ_{MLClO_4} values of DB24C8–alkali metal perchlorate systems in acetonitrile at 25 °C obtained in this work are as follows.

	Na	K	Rb	Cs
$[MClO_4]_t \times 10^{-4}$/mol dm^{-3}	4.998	5.075	5.255	4.945
$\Lambda_{MLClO_4}/\Omega^{-1}$ cm^2 mol^{-1}	145.2	145.5	145.7	144.0

These data show that the alkali metal ion held in the DB24C8 cavity is effectively shielded by the DB24C8 from the solvent. The same tendency for DB24C8 complexes with alkali metal ions has been reported for methanol[2] and propylene carbonate.[3] It follows from the above discussion that the transfer activity coefficient of the DB24C8–alkali metal ion complex is somewhat sensitive to the variation of the alkali metal ion in the DB24C8 cavity, whereas the mobility of the DB24C8–alkali metal ion complex at the same concentration is not sensitive.

References

1) Y. Takeda, *Bull. Chem. Soc. Jpn.*, **52**, 2501 (1979).
2) Y. Takeda and H. Yano, *Bull. Chem. Soc. Jpn.*, **53**, 1720 (1980).
3) Y. Takeda, H. Yano, M. Ishibashi, and H. Isozumi, *Bull. Chem. Soc. Jpn.*, **53**, 72 (1980).
4) Y. Takeda, K. Oshio, and Y. Segawa, *Chem. Lett.*, **1979**, 601.
5) Y. Takeda, *Bull. Chem. Soc. Jpn.*, **56**, 866 (1983).
6) Y. Takeda, *Bull. Chem. Soc. Jpn.*, **54**, 3133 (1981).
7) V. Gutmann, "Coordination Chemistry in Nonaqueous Solutions," Springer-Verlag, Berlin (1968).
8) I. M. Kolthoff and M. K. Chantooni, Jr., *Anal. Chem.*, **52**, 1039 (1980).
9) J. Massaux, G. Roland, and J. F. Desreux, *J. Solution Chem.*, **11**, 549 (1982).

 © 1983 The Chemical Society of Japan Bull. Chem. Soc. Jpn., 56, 3603—3607 (1983)

Spectrophotometric Determination of Ruthenium(III) and Rhodium(III) with 9,10-Phenanthrenequinone Monoxime after Extraction into Molten Naphthalene

Abdul WASEY, Raj K. BANSAL, Masatada, SATAKE,*,† and Bal K. PURI
Department of Chemistry, Indian Institute of Technology, Hauz Khas, New Delhi-110016, India
†*Faculty of Engineering, Fukui University, Fukui-910, Japan*
(Received January 13, 1983)

9,10-Phenanthrenequinone monoxime has been used as a reagent for the spectrophotometric determination of ruthenium(III) and rhodium(III) after extraction into molten naphthalene. The extracted mixture of the metal complex and naphthalene was dissolved in chloroform and ruthenium and rhodium were determined spectrophotometrically. Beer's law holds in the concentration range of 0.2—4.1 μg/cm³ for ruthenium and 0.3—5.3 μg/cm³ for rhodium in 10 cm³ of the final solution. The molar absorptivities and Sandell sensitivities are calculated to be 9.70×10^3 l mol^{-1} cm^{-1} and 0.01 μg/cm² (660 nm) for ruthenium and 1.13×10^4 l mol^{-1} cm^{-1} and 0.009 μg/cm² (410 nm) for rhodium respectively. Aliquots containing 2.0 μg of ruthenium and 4.1 μg of rhodium give mean absorbances of 0.192 and 0.451 with standard deviations of 0.0017 and 0.0039, respectively. Interference of various ions has been studied and the method has been applied to the determination of ruthenium and rhodium in various synthetic mixtures. This procedure is also applied to the simultaneous determination of ruthenium and rhodium present together in a solution.

9,10-Phenanthrenequinone monoxime has been suggested as a possible analytical reagent by Trikha and Kamil in the spectrophotometric[1-3] and gravimetric[4] determination of some metals. Since both these metals form complexes with the reagent at a high temperature, ordinary liquid-liquid extraction is not applicable. Liquid-liquid extraction no doubt is a convenient technique for the separation and determination of metal ions, but it fails in the extraction of those metal ions which form complexes with the complexing agents at a high temperature or the solubility of their complexes is low at room temperature. In such cases, the metal complex is first precipitated at a high temperature and then extracted into a suitable organic solvent after cooling to room temperature.[5] Thus the method becomes time consuming. Fujinaga and co-workers have developed a method of extraction, *i.e.* "solid-liquid separation after liquid-liquid extraction" in which all the above mentioned difficulties are overcome.[6] The advantages of this technique over the liquid-liquid extraction have already been stated in a previous communication.[7] In the present work this technique has been applied to the extraction of ruthenium and rhodium with 9,10-phenanthrenequinone monoxime into molten naphthalene and their subsequent determination by spectrophotometric method after dissolution of the solid naphthalene containing the metal complex in chloroform. Interference of various ions has been studied and this method has been applied to the determination of these metals in various synthetic mixtures. Conditions have also been developed for the simultaneous determination of these metals in synthetic mixture since these metal complexes absorb at two different wavelengths.

Experimental

Reagents. 9,10-Phenanthrenequinone monoxime (molecular weight: 223) was prepared and purified according to the method given in the literature,[3] and its 0.001 M solution (1 M=1 mol dm^{-3}) was prepared in ethanol. Solutions of ruthenium(III) chloride and rhodium(III) chloride were prepared from samples (1 g ampule) in 1 M hydrochloric acid and standardized gravimetrically.[7] Buffer solution of sodium acetate (0.2 M)–acetic acid (0.2 M) of pH 5.2 was used for pH adjustment. Naphthalene and chloroform were of analytical reagent grade and tested spectrophotometrically before use. To study the interference of various ions, 5000 μg/cm³ of anion and 100 μg/cm³ of metal ion solutions were prepared in redistilled water.

Equipment. An Elico pH meter and Sp-700/500 spectrophotometer were used for measurements.

General Procedure. To an aliquot of each of the metal solution taken separately was added 1.0 cm³ of the reagent and the pH was adjusted with 2.0 cm³ of buffer solutions (Fig. 2). These solutions were transferred to stoppered round-bottomed flasks and 2.0 g of naphthalene was added to each. Temperature was raised to about 85—90 °C to melt naphthalene and the mixture was stirred vigorously with a magnetic stirrer-hot plate arrangement for 35 min for both the metals (Fig. 3). Naphthalene containing the metal complex was separated by filtration. If was dried in the folds of a filter paper and then dissolved in 10 cm³ of chloroform. This solution was dried with anhydrous sodium sulfate (2.0 g) and the absorbance was measured in a 1-cm cell at 660 nm for ruthenium and 410 nm for rhodium against a reagent blank. The calibration curves were constructed under similar conditions.

Results and Discussion

Absorption Spectra. The absorption spectra of 9,10-phenanthrenequinone monoxime and its ruthenium and rhodium complexes were recorded in naphthalene–chloroform solution against weter and reagent blank, respectively (Fig. 1). It was observed that both the complexes have two absorption peaks, *i.e.* 520—535 nm and 660 nm for ruthenium and 400—410 nm and 470—480 nm for rhodium. The reagent absorbed only slightly at 410 nm, while it absorbed negligibly at the other wavelengths. The simultaneous determination of ruthenium and rhodium is possible because of a large difference of their λ_{max} (Fig. 1). All the measurements were made at 660 nm for ruthenium and at 410 nm for rhodium.

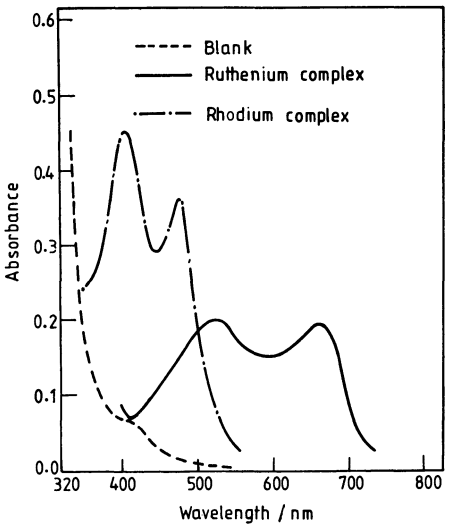

Fig. 1. Absorption spectra.
Reagent blank, 9-10 phenanthrenequinone monoxime (0.001 M): 1.0 cm³. Reference: water; Ru: 2.0 μg, pH: 5.2, Rh: 4.1 μg, pH: 5.2, reference: reagent blank. Naphthalene 2.0 g, chloroform: 10.0 cm³.

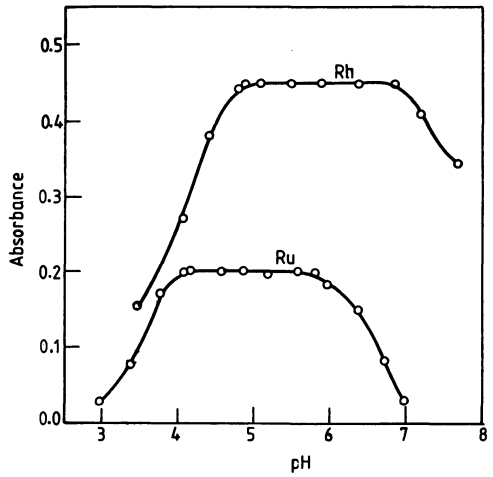

Fig. 2. Effect of pH.
Acetate concentration 1 M: 2.0 cm³. Ru: 2.0 μg, wavelength: 660 nm, Rh: 4.1 μg, wavelength: 410 nm, 9,10-phenanthrenequinone monoxime (0.001 M): 1.0 cm³, naphthalene: 2.0 g, chloroform: 10.0 cm³. Stirring time: 35 min, reference: reagent blank.

Effect of pH. Extraction behaviours of these metal-9,10-phenanthrenequinone monoximates were studied over a wide range of pH. Ruthenium was quantitatively extracted over the pH range of 4.1—5.8 and rhodium between 4.9—6.8. Extraction was incomplete beyond these pH ranges (Fig. 2).

Effect of Buffer Concentration. Extraction was carried out by varying the volume of 0.2 M sodium acetate–0.2 M acetic acid buffer (pH 5.2). It was observed that it has no effect on absorbance when the volume was varied between 1.0—5.0 cm³ per 30 cm³ of aqueous solution. Thus 2.0 cm³ of the buffer solution was used for subsequent studies.

Effect of Reagent Concentration. Extraction was carried out at optimum pH and at varying volumes of 0.001 M reagent solution. It was found to be quantitative in the volume range of 0.1—3.0 cm³ for ruthenium and 0.3—3.0 cm³ for rhodium. Thus 1.0 cm³ was used for further studies.

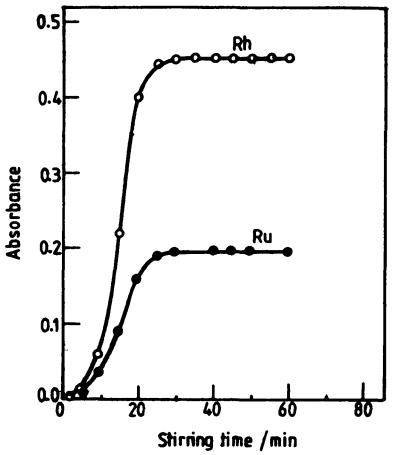

Fig. 3. Effect of stirring time.
Conditions were same as in Fig. 2.

Effect of Amount of Naphthalene. Extraction was carried out by varying the amounts of naphthalene from 0.2—4.0 g at optimum pH and keeping other parameters constant. With both metals the absorbance remained constant when the amount of naphthalene used was in the range of 1.3—3.5 g. The extraction was not complete with less than 1.3 g while above 3.5 g of naphthalene it was difficult to dissolve it in the limited quantity of chloroform (10 cm³). Thus 2.0 g of naphthalene was selected for further work.

Effect of Aqueous Phase Volume. Since the amount of naphthalene is small (2.0 g) as compared to that of the aqueous phase the effect of the volume of the latter on extraction was studied. Extraction was quantitative when the aqueous phase did not exceed 60 cm³.

Effect of Stirring Time. Since ruthenium and rhodium form complexes with reagent at a high temperature,[7] the effect of stirring time on extraction was examined. A mixture of naphthalene and the complex was stirred at different intervals of time with a magnetic stirrer-hot plate arrangement at 85—90 °C. It was found that the extraction was complete when the mixture was stirred for more than 30 min at this temperature in each case. (Fig. 3).

Effect of Standing Time. Absorbance of the extract in naphthalene–chloroform was constant for at least 24 h for ruthenium and 48 h for rhodium.

Effect of Electrolytes. Various electrolytes such as sodium chloride, sodium acetate, potassium chloride, and sodium nitrate (0.3—3.0 cm³ of 1.0 M) caused no improvement in extraction, indicating that the extraction was complete in the presence or in the absence of these electrolytes showing the absence of salting effect.

Composition of the Complex. The nature of ruthenium and rhodium-9,10-phenanthrenequinone monoximates in naphthalene–chloroform solution was studied by Job's method of continuous variation and mole-ratio method. This suggested that $[Ru^{II}(C_{14}H_8O_2N)_2]$ and $[Rh^{III}(C_{14}H_8O_2N)_3]$ complexes were

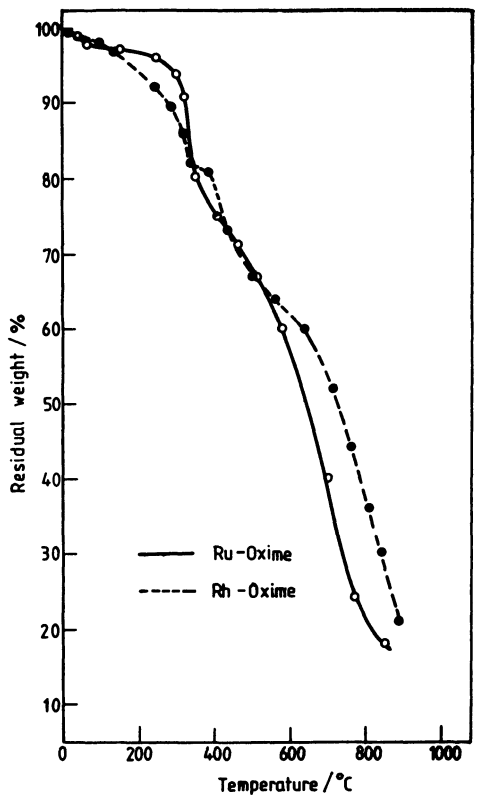

Fig. 4. Typical thermograms of the complexes. Complex (Ru or Rh): 5 mg; atmosphere: air: 20 cm³/min, heating rate: 10 °C/min.

extracted into molten naphthalene being the same as in liquid-liquid extraction.[8] It was reported by Trikha[8] that the elemental analysis of the complexes gave Ru: 18.5%, N : 5.10% corresponding to Ru : 18.54% N : 5.16% and Rh: 13.35%, N : 5.40% corresponding to Rh : 13.38%, N: 5.46 K, which also supports the above composition. Magnetic susceptibility of the isolated ruthenium and rhodium complexes have been determined by the Guoy procedure. It was found to be diamagnetic indicating it to be a spin paired square-planar ruthenium complex whereas the rhodium complex was found to be diamagnetic and thus a spin-paired octahedral complex. The infrared shows C=O and C=N stretching frequencies at 1600 and 1525 cm^{-1} in the free ligand. In the metal chelates these modes were observed at 1585 and 1520 cm^{-1} for ruthenium and 1580 and 1520 cm^{-1} for rhodium respectively. This further corroborates the composition stated above.

Thermal Stability of the Complex. The thermal stability of the complexes was determined by thermogravimetric analysis (TGA) by plotting the percentage residual weight against temperature (Fig. 4). The decomposition curve showed some plateaus which were indicative of constant weight representing stable phase over the particular temperature range (Experiment was performed on a Stanton Red-Croft TG-750 thermobalance in a air atmosphere at a heating rate of 10 °C/min). Successive plateaus probably correspond to the decomposition of water (100 °C), metal complex followed by the metal oxide. From the plot it was found that ruthenium and rhodium complexes indeed are thermally stable but the former decomposes at 270 °C while the latter at 360 °C.

Beer's Law and Sensitivity. Under the optimum conditions described above, calibration curves were constructed at 660 nm for ruthenium and 410 nm for rhodium. Beer's law was obeyed in the concentration range of 0.2—4.1 μg of ruthenium and 0.3—5.3 μg of rhodium in 10 cm³ of the chloroform solution. The

Table 1. Effect of diverse anions
Ru: 2.0 μg, Rh: 4.1 μg

Alkali salt added	Anion added (μg/cm³)	Absorbance λ/nm Ru 660 nm	Rh 410 nm	Alkali salt added	Anion added (μg/cm³)	Absorbance λ/nm Ru 600 nm	Rh 410 nm
—	—	0.192	0.450	Sodium nitrate	5000	0.191	0.440
Sodium fluoride	5000	0.195	0.451		3000	0.193	0.451
Sodium chloride	5000	0.195	0.450	Sodium sulfate	5000	0.191	0.445
Potassium bromide	5000	0.195	0.448		3000	0.193	0.450
	3000	0.192	0.451	Sodium oxalate	5000	0.140	0.400
Potassium iodide	5000	0.200	0.456		3000	0.165	0.434
	3000	0.193	0.450		2000	0.182	0.440
Sodium acetate	5000	0.192	0.450		1000	0.190	0.449
Potassium thiocyanate	5000	0.150	0.438	Sodium orthophosphate	5000	0.150	0.380
	2000	0.180	0.445		3000	0.165	0.410
	1000	0.191	0.450		2000	0.178	0.435
Sodium citrate	5000	0.145	0.440		1000	0.191	0.448
	3000	0.184	0.450	EDTA(disodium)	5000	0.100	0.148
	2000	0.192	0.450		3000	0.120	0.185
Potassium sodium tartrate	5000	0.185	0.440		2000	0.125	0.190
	3000	0.190	0.446		1000	0.138	0.318
	1000	0.192	0.450		200	0.158	0.438
Sodium nitrite	5000	0.160	0.420		100	0.191	0.448
	3000	0.181	0.448				
	2000	0.190	0.446				
	1000	0.192	0.450				

Table 2. Effect of diverse cations

Ru: 2.0 μg, Rh: 4.1 μg

Metal salt added	Metal ion added (μg/cm³)	Absorbance λ/nm		Remarks
		Ru 660 nm	Rh 410 nm	
—	—	0.192	0.450	—
Ammonium vanadate	100	0.194	0.462	—
	50	0.193	0.453	—
Chromium(III) chloride	100	0.192	0.510	—
	50	0.192	0.454	—
Iron(III) chloride	100	0.193	0.452	Removed by pre-extraction at room temperature
Cobalt(II) chloride	100	0.193	0.454	Removed by pre-extraction at room temperature
Nickel(II) chloride	100	0.194	0.452	Removed by pre-extraction at room temperature
Copper(II) acetate	100	0.193	0.453	Removed by pre-extraction at room temperature
Ammonium molybdate	100	0.191	0.454	—
Ruthenium(III) chloride	100	—	0.480	—
	50	—	0.460	—
	30	—	0.454	—
Rhodium(III) chloride	100	0.210	—	—
	50	0.200	—	—
	30	0.193	—	—
Palladium(II) nitrate	100	0.192	0.451	Removed by pre-extraction at room temperature
Silver(I) nitrate	100	0.192	0.472	—
	50	0.193	0.454	—
Osmium(III) oxide	100	0.193	0.452	Removed by pre-extraction at room temperature
Iridium(III) chloride	100	0.194	0.650	Masked with 100 μg of EDTA
	50	0.193	0.466	Masked with 100 μg of EDTA
	30	0.192	0.452	Masked with 100 μg of EDTA
Platinum(IV) chloride	100	0.194	0.455	—
	50	0.192	0.450	—
Gold(III) chloride	100	0.194	0.460	—
	50	0.192	0.450	—
Mercury(II) nitrate	100	0.194	0.454	—
	50	0.192	0.450	—
Lead(II) nitrate	100	0.194	0.451	—
Bismuth(III) nitrate	100	0.191	0.448	—
Uranyl acetate	100	0.192	0.452	—

Table 3. Determination of ruthenium in synthetic mixture

Composition of the synthetic mixture (μg)	Ruthenium taken (μg)	Ruthenium found (μg)	Average (μg)	Error/%
Ru^{III}: 10, Ir^{III}: 45, Os^{VIII}: 45	2.5	2.4, 2.5, 2.5, 2.6, 2.4	2.48	+0.80
Ru^{III}: 5, Ir^{III}: 40, Os^{VIII}: 45, Au^{III}: 10	3.5	3.5, 3.5, 3.4, 3.5, 3.4	3.46	+1.10

Table 4. Determination of rhodium in synthetic mixture

Composition of the synthetic mixture (μg)	Rhodium taken (μg)	Rhodium found (μg)	Average (μg)	Error/%
Rh^{III}: 5, Pt^{IV}: 95	2.5	2.5, 2.6, 2.5, 2.5, 2.5	2.52	−0.80
Rh^{III}: 30, Au^{III}: 50, Pt^{IV}: 20	3.5	3.4, 3.5, 3.5, 3.5, 3.5	3.48	+0.57

Table 5. Simultaneous determination of ruthenium and rhodium in synthetic mixture

Composition of the synthetic mixture (μg)	Ru and Rh taken (μg)	Ru and Rh found (μg)	Average (μg)	Error/%
Ru^{III}: 2.5, Rh^{III}: 5.0	Ru: 2.5	2.5, 2.5, 2.4, 2.5, 2.6	2.50	+0.0
Os^{VIII}: 30, Pd^{II}: 10, Au^{III}: 20, Pt^{IV}: 30.5	Rh: 5.0	5.0, 5.0, 5.0, 4.9, 5.0	4.98	+0.4

molar absorptivities and Sandell sensitivities were calculated to be 9.70×10^3 l mol^{-1} cm^{-1} and 0.01 μg/cm^2 for ruthenium and 1.13×10^4 l mol^{-1} cm^{-1} and 0.009 μg/cm^2 for rhodium. Solutions containing 2.0 μg of ruthenium and 4.1 μg of rhodium gave mean absorbances of 0.192 and 0.451 with standard deviations of 0.0017 and 0.0039 respectively.

Effect of Diverse Ions. Various ions were added individually to a solution containing 2.0 μg of ruthenium and 4.1 μg of rhodium and the general procedure was applied. Among the anions (Table 1), thiocyanate, citrate, tartrate, nitrite, oxalate, orthophosphate, and EDTA interfered with the determination of these metals but relatively low amounts could be tolerated. Of the meal ions (Table 3), interference of Fe^{III}, Co^{II}, Ni^{II} Cu^{II}, Pd^{II}, and Os^{VIII} has been eliminated by preextraction at room temperature in each case. For rhodium the interference of Ir^{III} was removed by masking with EDTA.

Determination of Ruthenium(III) and Rhodium(III) in Synthetic Mixtures. Synthetic mixtures were prepared containing both ruthenium and rhodium and aliquot of synthetic mixture was taken in a beaker, 1.0 cm^3 of ethanolic solution of the 9,10-phenanthrenequinone monoxime was added, the pH adjusted to 5.2 with acetate buffer solution and determined by the general procedure already described. The results are recorded in Tables 3 and 4.

On the basis of the absorption maximum of the complexes, these metals have been separated from each other (Fig. 1) and determined when present together. The results are summarized in Table 5.

One of the authors (A.W.) is grateful to C.S.I.R. for the award of a Senior Research Fellowship.

References

1) K. C. Trikha, M. Katyal, and R. P. Singh, *Talanta*, **14**, 977 (1967).
2) F. Kamil, S. K. Sindhwani, and R. P. Singh, *Ann. Chim. (Rome)*, **68**, 71 (1978).
3) F. Kamil, S. K. Sindhwani, and R. P. Singh, *Indian J. Chem.*, **16A**, 365 (1978).
4) R. P. Singh and K. C. Trikha, *Indian J. Appl. Chem.*, **29**, 54 (1966).
5) S. K. Sindhwani and R. P. Singh, *Microchem. J.*, **18**, 686 (1973).
6) T. Fujinaga, T. Kuwamoto, and E. Nakayama, *Talanta*, **16**, 1225 (1969).
7) B. K. Puri and Mamta Gautam, *Talanta*, **25**, 484 (1978).
8) K. C. Trikha, Ph. D. Thesis, University of Delhi, Delhi, 1968.

The Stereochemistry and Reactivity of Metal-Schiff Base Complexes. VI. The Kinetics and Mechanism of Isomerization between Δ_L-β_2- and Λ_L-β_2-Diastereoisomers of *N,N'*-Ethylenebis(α-methylsalicylideneaminato)cobalt(III) Complexes with L-Amino Acid

Yuki Fujii,* Takemaru Kobayashi, Makoto Matsufuru, and Sozo Takahashi**
Department of Chemistry, Faculty of Science, Ibaraki University, Bunkyo-cho, Mito, Ibaraki 310
***Department of Chemistry, Ibaraki Technical College, Nakane, Katsuta, Ibaraki 312*
(Received March 10, 1983)

The kinetics for isomerization between Δ_L-β_2- and Λ_L-β_2-diastereoisomers of [Co(α-Me-sal$_2$en)(L-aa)], where L-aa represents L-phe, L-met, L-ile, L-pro, *N*-Bz-L-ala, and *N*-Me-L-ala, were studied in methanol. The activation enthalpies (ΔH^*/kJ mol^{-1}) and the activation entropies (ΔS^*/J K^{-1} mol^{-1}) from the Δ_L-β_2-isomer (unstable form) to the Λ_L-β_2-isomer (stable form) were determined to be 86.6 and −9.6 for L-phe, 92.5 and +6.7 for L-met, 87.5 and −8.0 for L-ile, 100.4 and +28.0 for *N*-Bz-L-ala, and 102.9 and +18.4 for *N*-Me-L-ala, respectively. For L-pro-complex, the Δ_L-β_2-isomer is the stable form, and the enthalpy and entropy for isomerization from Λ_L-β_2- to Δ_L-β_2-isomers were 96.2 and 0.0. The isomerization was catalyzed by acids but not by bases, and was much faster than the substitution of coordinated L-amino acid. The H–D exchange of N–H proton of *N*-Me-L-ala-complex proceeded with almost the same rate as the isomerization. The isomerization showed strong solvent dependency; it was fast in a hydrogen-bonding solvent, but was quite slow in a weak- or nonhydrogen-bonding solvent. On the basis of these facts, proton-assisted and/or hydrogen-bonding solvent-assisted intramolecular mechanism *via* an intermediate is proposed, in which the Schiff base takes a planar configuration and the amino acid coordinates as a unidentate ligand with its carboxylate group.

Many studies have been directed toward the synthesis and the first order asymmetric transformation of Co(N$_4$)-complexes with a chiral amino acid, where (N$_4$) denotes a tetramine ligand such as (en)$_2$ and trien.[1–4] However, there are only a few studies for detailed isomerization mechanism among the diastereoisomers of these complexes.[5,6] This may be due to the inertness of Co(N$_4$)-complexes: charcoal is usually needed as a catalyst to promote the isomerization. On the other hand, we have recently found that cobalt(III) complexes containing a sal$_2$en-type Schiff base and L-amino acid, β_2-[Co(Schiff base)(L-aa)], easily isomerize in methanol to establish the equilibrium between Δ_L-β_2- and Λ_L-β_2-isomers.[7–12] This reaction is very interesting because the isomerization is quite fast as compared with that of Co(N$_4$)-complexes.

In order to elucidate the isomerization mechanism and the origin of the isomerization lability of cobalt(III)–Schiff base complexes, the isomerization kinetics for β_2-[Co(α-Me-sal$_2$en)(L-aa)] was studied.[13]

Experimental

Materials. The complex β_2-[Co(α-Me-sal$_2$en)(L-aa)] was prepared as previously reported.[7,9,10] The 1 : 1 mixture of Δ_L- and Λ_L-β_2-isomers of L-met-complex was obtained by the addition of a large excess of water to the methanol solution (*ca.* 1 M, 1 M = 1 mol dm^{-3}) of Λ_L-β_2-[Co(α-Me-sal$_2$en)(L-met)].[7] Found: C, 53.32; H, 5.78; N, 8.01%. Calcd for $CoC_{23}H_{28}N_3O_4S \cdot H_2O$: C, 53.18; H, 5.82; N, 8.09%. $[M]^{25}_{435} = +600°$ (soon after dissolution in methanol, $c = 1.0 \times 10^{-3}$ M). $[M]^{25}_{435} = -15400°$ (under equilibrium conditions in methanol). ^{1}H NMR: δ 2.67 (6H, S, CH_3–C=N), δ 1.85, 1.75 (3H, two S with equal intensity, –S–CH_3) (soon after dissolution in $CDCl_3$ + CD_3OD (8 : 1 in volume)).

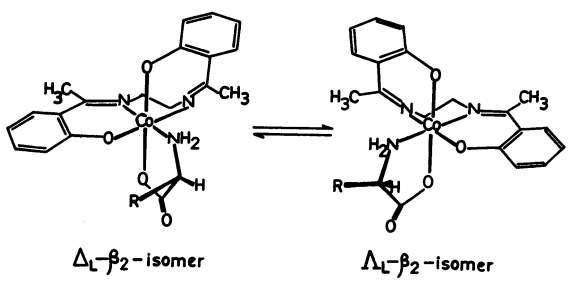

Fig. 1. Structures of two isomers of β_2-[Co(α-Me-sal$_2$en)-(L-aa)].

Reagent grade organic solvents were used after distillation. The other chemicals were reagent grade and used without further purification.

Kinetic Procedure. The complexes (2.5×10^{-5} mol) were dissolved in a given solvent (25 cm^3) at a given temperature, and, whenever necessary, other reagents were added. The mutarotation at 435 nm of the solutions was measured with 1 cm cell by the use of a thermostated cell-holder (the deviation of the solution temperature = ±0.1 °C). When the mutarotation was very slow, the solutions were placed in a thermostat bath, and picked up one by one at proper intervales. The rate constant was calculated from the slope of plots of $\ln(a_\infty - a_t)$ *vs.* time, where a_∞ and a_t are the optical rotations under the equilibrium conditions and at time t, respectively (see Appendix).

Measurements. The optical rotation at 435 nm was measured on a JASCO DIP-140 Polarimeter. The electronic absorption and circular dichroism spectra were recorded on a Hitachi 200-10 Spectrometer and a JASCO J-20 Spectropolarimeter, respectively. The ^{1}H NMR spectra were measured on a Hitachi R-20 Spectrometer.

Results and Discussion

The Kinetics of Isomerization of β_2-[Co(α-Me-sal$_2$en)(L-aa)] in Methanol. The isomerization rate of β_2-[Co(Schiff base)(L-aa)] complexes has been observed to depend strongly on the kind of the Schiff base ligand.[14] For *N,N'*-ethylenebis(4-phenyl-4-oxo-2-butaniminato) or *N,N'*-ethylenebis(α-phenyl-5-methylsalicylideneaminato), the isomerization is too fast to be

TABLE 1. ISOMERIC RATIOS AND ISOMERIZATION RATE CONSTANTS OF β_2-[Co(α-Me-sal$_2$en) (L-aa)]

L-aa	Temp/°C	Isomeric ratio ([Δ_L]/[Λ_L])		Rate constant in methanol		
		In crystals	In methanol	k_{obsd}/s^{-1} d)	k_{+1}/s^{-1}	k_{-1}/s^{-1}
L-phe	15		5.56	4.28×10^{-4}	3.63×10^{-4}	6.52×10^{-5}
	25	1	4.80	1.56×10^{-3}	1.29×10^{-3}	2.69×10^{-4}
	35		4.59	4.98×10^{-3}	4.09×10^{-3}	8.91×10^{-4}
L-met	25	1	1.65	1.37×10^{-3}	8.53×10^{-4}	5.17×10^{-4}
L-met	15		1.78	3.50×10^{-4}	2.24×10^{-4}	1.26×10^{-4}
	25	a)	1.65	1.36×10^{-3}	8.47×10^{-4}	5.13×10^{-4}
	35		1.58	4.80×10^{-3}	2.94×10^{-3}	1.86×10^{-3}
L-ile	15		2.78	4.21×10^{-4}	3.10×10^{-4}	1.11×10^{-4}
	25	a)	2.55	1.53×10^{-3}	1.10×10^{-3}	4.30×10^{-4}
	35		2.41	4.98×10^{-3}	3.52×10^{-3}	1.46×10^{-3}
L-por	25		b)	9.05×10^{-5}		9.05×10^{-5}
	35	1	b)	3.18×10^{-4}		3.18×10^{-4}
	45		b)	1.11×10^{-3}		1.11×10^{-3}
N-Bz-L-ala	25		c)	4.40×10^{-4}	4.40×10^{-4}	
	35	2	c)	1.80×10^{-3}	1.80×10^{-3}	
	45		c)	6.00×10^{-3}	6.00×10^{-3}	
N-Me-L-ala	25	a)	27.6	5.37×10^{-5}	5.18×10^{-5}	1.88×10^{-6}
N-Me-L-ala	25		27.6	5.36×10^{-5}	5.17×10^{-5}	1.90×10^{-6}
	35	1	24.4	2.33×10^{-4}	2.24×10^{-4}	9.10×10^{-6}
	48		22.9	1.14×10^{-3}	1.09×10^{-3}	4.77×10^{-5}

a) Pure Λ_L-isomer. b) Λ_L-isomer is almost 100%. c) Λ_L-isomer is almost 100%. d) Standard deviations are ±0.03.

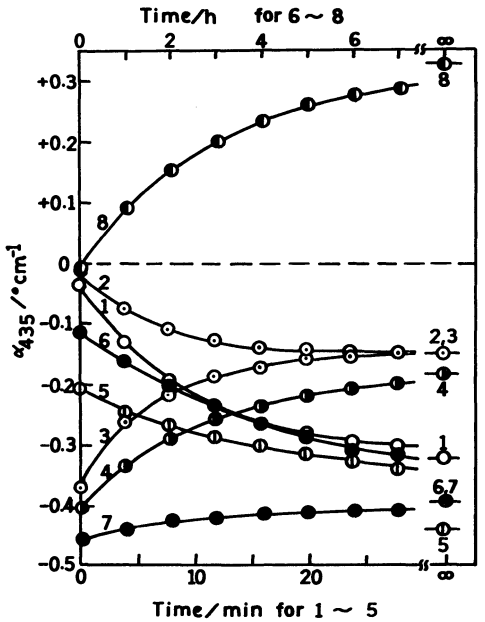

Fig. 2. Mutarotations of β_2-[Co(α-Me-sal$_2$en)(L-aa)] in methanol at 25 °C.
Complex concentration = 1.0×10^{-3} M. Cell length = 1.0 cm. 1: L-phe, 2: L-met (1 : 1 mixture), 3: L-met (pure Λ_L-β_2-isomer), 4: L-ile, 5: *N*-Bz-L-ala, 6: *N*-Me-L-ala (1 : 1 mixture), 7: *N*-Me-L-ala (pure Λ_L-β_2-isomer), 8: L-pro.

followed with a polarimeter at 25 °C in methanol, but for *N*,*N*'-ethylenebis(5, 5, 5-trifluoro-4-oxo-2-pentaniminato), the reaction is very slow. Since the Co(α-Me-sal$_2$en)-complex isomerizes with a suitable rate for rotational measurements, it was selected as the representative complex in this work.

The isomeric ratios of the complexes in the solid state are listed in Table 1. The complexes β_2-[Co(α-Me-sal$_2$en)(L-aa)] are isolated usually as the 1 : 1 mixture of Δ_L- and Λ_L-isomers or as the pure Λ_L-isomer. This is mainly due to the solubilities of the complexes. When the complexes were dissolved in methanol (Fig. 2), the solutions exhibited a mutarotation with a minus sign at 435 nm under the equilibrium conditions except for L-pro-complex. For L-pro-complex, the rotation has a plus sign. As has been reported previously,[7,9,10] during the mutarotation the absorption spectra do not show any obvious change, whereas the CD spectra an isosbestic point at about 470 nm. On the basis of the AB, CD, and ^{1}H NMR spectral studies and the X-ray analysis,[8,11] the following facts has been verified: 1) the mutarotation corresponds to the isomerization between $(+)_{435}$-Δ_L-β_2- and $(-)_{435}$-Λ_L-β_2-diastereoisomers, and neither decomposition nor the other reaction occurs in methanol; 2) the Λ_L-β_2-isomer predominates under the equilibrium conditions except for the L-pro-complex, for which the Δ_L-β_2-isomer is predominant.

In Fig. 2 both the 1 : 1 mixture and the pure Λ_L-β_2-isomer of the L-met-complex reached to the same optical rotation under the equilibrium conditions of mutarotation. A similar behaviour to the L-met-complex was observed for the *N*-Me-L-ala-complex. These facts clearly indicate that the present isomerization reaction belongs to a reversible one. In Fig. 3 the plots of $\ln(\alpha_\infty-\alpha_t)$ *vs.* time gave a straight line up to at least 90% completion of the isomerization, and the slopes were found to be independent of the complex concentration. Hence, the rate formula is expressed as follows:

$$\text{Rate} = k_{obsd}[\text{complex}], \quad (1)$$

Table 2. Activation parameters of isomerization of β_2-[α-Me-sal$_2$en) (L-aa)] in methanol

L-aa	pK_{a_1}	pK_{a_2}	$\Delta H^{\ddagger}$ (k_{+1}) kJ mol^{-1}	$\Delta S^{\ddagger}$ (k_{+1}) J K^{-1} mol^{-1}	$\Delta H^{\ddagger}$ (k_{-1}) kJ mol^{-1}	$\Delta S^{\ddagger}$ (k_{-1}) J K^{-1} mol^{-1}
L-phe	2.21	9.18	86.6±3.3	−9.6±11.1	94.1±4.2	+2.5±14.6
L-met	2.28	9.34	92.5±5.9	+6.7±12.6	96.7±5.0	+15.1±10.5
L-ile	2.32	9.76	87.5±3.3	−8.0±11.0	92.5±4.2	+1.3±14.2
N-Bz-L-ala			100.4±8.3	+28.0±21.6		
N-Me-L-ala	2.18[a]	10.02[a]	102.9±6.7	+18.4±15.9	109.2±6.7	+12.1±15.9
L-pro	2.02	10.52			96.2±5.0	0.0±10.9

a) Value of *N*-methylglycine.

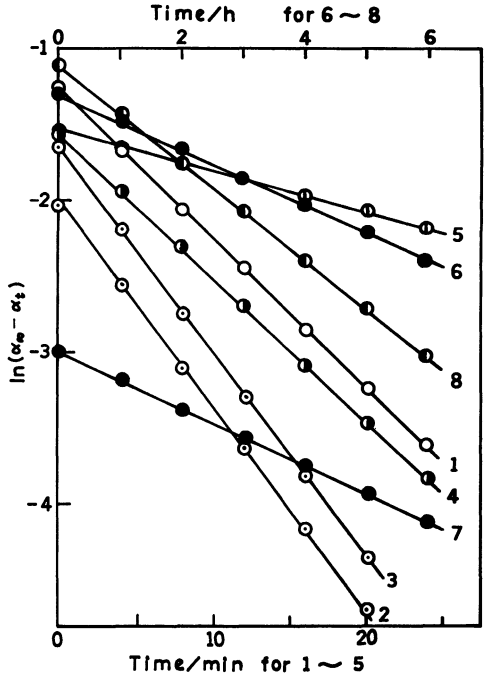

Fig. 3. Plots of ln ($\alpha_\infty - \alpha_t$) *vs.* time for mutarotations of β_2-[Co(α-Me-sal$_2$en)(L-aa)] in methanol at 25 °C.
1: L-phe, 2: L-met (1 : 1 mixture), 3: L-met (pure Λ_L-β_2-isomer), 4: L-ile, 5: *N*-Bz-L-ala, 6: *N*-Me-L-ala (1 : 1 mixture), 7: *N*-Me-L-ala (pure Λ_L-β_2-isomer), 8: L-pro.

where k_{obsd} represents the observed first order rate constant. The k_{obsd} values are summarized in Table 1. When the isomerization rate constant from Λ_L- to Λ_L-β_2-isomers is written as k_{+1}, and that from Λ_L- to Δ_L-β_2-isomers as k_{-1}, the k_{obsd} value is related to k_{+1} and k_{-1} by Eq. 2 as is shown in Appendix:

$$k_{obsd} = [(K+1)/K]k_{+1} = (K+1)k_{-1}, \quad (2)$$

where K denotes the isomeric ratio between Λ_L- and Δ_L-β_2-isomers, $K = [\Lambda_L\text{-}\beta_2\text{-isomer}]/[\Delta_L\text{-}\beta_2\text{-isomer}]$, under the equilibrium conditions. Equation 2 was confirmed from the fact that the k_{obsd} values for the 1 : 1 mixture and the pure Λ_L-β_2-isomer are identical in the cases of the L-met- and *N*-Me-L-ala-complexes. The K values were estimated from the CD intensity of the complexes as previously reported.[12] The K values and the k_{+1}, k_{-1} values thus obtained are summarized in Table 1.

The activation parameters were calculated from the temperature dependence of k_{+1} and k_{-1} values, and are given in Table 2. Table 2 indicates that 1) the activation enthalpy becomes generally large when the pK_{a_2} value of L-amino acid is large, and 2) the activation entropies of all the complexes are very small with plus or minus sign, suggesting similar isomerization mechanisms.

Effects of Water, Salts, Acids, Bases, and Amino Acids on the Isomerization in Methanol. The water content of the methanol solution gave no significant effect on the observed isomerization rates of all the complexes in the range from 1×10^{-3} to 1×10^{-1} M (complex concentration $=1\times10^{-3}$ M). However, when a large excess of water (5 M) was added to the methanol solution, the isomerization became somewhat faster (about 15%). This is due to the faster isomerization in water than in methanol (*vide infra*). $NaClO_4$ and CH_3COONa also gave no effect on the isomerization rates in the range from 1×10^{-3} to 2×10^{-1} M. This fact indicates that effects of the ionic strength is negligibly small.

The relationship between acetic acid concentration and the observed isomerization rate is illustrated in Fig. 4. The diagrams are linear at least up to 3×10^{-1} M of acetic acid for L-phe-, L-met-, L-ile-, and L-pro-complexes, and up to 3×10^{-2} M of acetic acid for *N*-Bz-L-ala- and *N*-Me-L-ala-complexes. The intercepts coincided with the k_{obsd} value in the absence of acetic acid. Hence, the k_{obsd} is expressed by

$$k_{obsd} = k_{obsd}^{MeOH} + k_{obsd}^{AcH}[CH_3COOH]. \quad (3)$$

The values of k_{obsd}^{AcH} are listed in Table 3. Acetic acid is a weak protic acid, and its catalytic effect on the isomerization is linear to the acetic acid concentration as observed above. Thus, the effect may be caused by the action of the acetic acid molecules.

When a large excess of acetic acid was added, the partial decomposition of the complexes occurred. The decomposition was confirmed from the changes of optical rotation and absorption spectra. Since the plots of $\ln(\alpha_\infty - \alpha_t)$ *vs.* time for the partial decomposition give a linear relation, the observed decomposition rates are listed in Table 3. The degree of decomposition increases in the folllowing order:

L-phe < L-pro = L-met < L-ile < *N*-Bz-L-ala < *N*-Me-L-ala.

In the presence of trichloroacetic acid, all the complexes isomerized quite rapidly, followed by decomposition to produce brown complexes with the loss of optical rotation, even in 1×10^{-2} M. The isomerization was too fast to follow. The decomposition rates are summarized in Table 3. Since trichloroacetic acid is a strong protic acid, its effect may be due to proton. In fact, the isomerization and decomposition were very fast

TABLE 3. VALUES OF k_{obsd}^{AcH}, ACID-BASE DECOMPOSITION RATES, AND SUBSTITUTION RATES OF AMINO ACIDS OF β_2-[Co(α-Me-sal$_2$en) (L-aa)] IN METHANOL AT 25 °C

L-aa	k_{obsd}^{AcH} / $M^{-1}\,s^{-1}$	Observed decomposition rate constants/s^{-1}				Substitution rate constants/s^{-1} with phenylalanine[b] (2×10^{-2} M)
		CH_3COOH (1 M)	Cl_3CCOOH (1×10^{-2} M)	KOH (1 M)	Pyridine (1 M)	
L-phe	2.30×10^{-2}	4.9×10^{-3} (10%)[a]	9.3×10^{-3}	6.8×10^{-4}	2.5×10^{-5}	1.0×10^{-6}
L-met	1.38×10^{-2}	2.2×10^{-2} (13%)[a]	2.2×10^{-2}	1.3×10^{-3}	2.4×10^{-5}	2.0×10^{-6}
L-ile	1.11×10^{-2}	1.3×10^{-2} (20%)[a]	1.9×10^{-2}	7.9×10^{-4}	8.3×10^{-4}	2.3×10^{-6}
N-Bz-L-ala	4.75×10^{-3}	6.1×10^{-4} (35%)[a]	3.1×10^{-3}	2.3×10^{-5}	1.1×10^{-5}	7.5×10^{-6}
N-Me-L-ala	2.36×10^{-2}	1.3×10^{-3} (42%)[a]	7.8×10^{-3}	4.7×10^{-4}	1.7×10^{-5}	2.7×10^{-6}
L-pro	8.05×10^{-3}	3.5×10^{-4} (12%)[a]	1.7×10^{-3}	3.1×10^{-5}	1.4×10^{-5}	4.4×10^{-7} (45%)[c]

a) Degree of decomoposition. b) Observed value. c) Partial substitution.

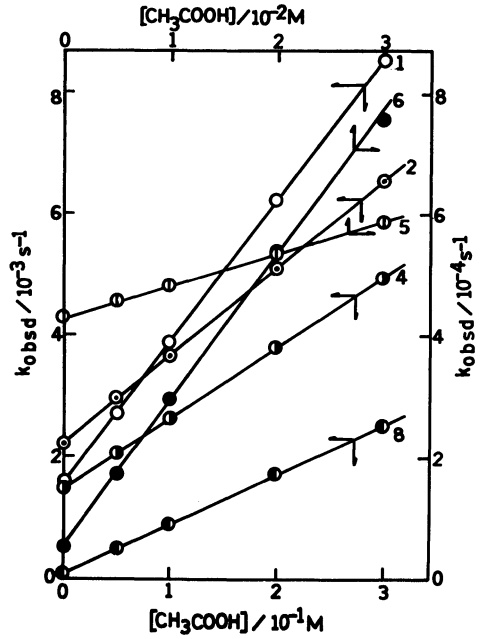

Fig. 4. Influence of acetic acid in methanol at 25 °C. 1: L-phe, 2: L-met (1 : 1 mixture), 4: L-ile, 5: *N*-Bz-L-ala, 6: *N*-Me-L-ala (1 : 1 mixture), 8: L-pro.

in the presence of HCl as well.

Bases such as KOH and pyridine gave no catalytic effect on the isomerization for KOH 1×10^{-3}—1×10^{-2} M, and for pyridine 1×10^{-3}—5×10^{-2} M except for *N*-Bz-L-ala- and *N*-Me-L-ala-complexes. For *N*-alkyl-L-ala-complexes partial decomposition occurred even in a low concentration of a base (*ca.* 2×10^{-3} M of the base). When a large excess of bases was added, all the complexes except for the L-pro-complex decomposed to form *trans*-[Co(α-Me-sal$_2$en)(base)$_2$]$^{\pm n}$. For the L-pro-complex only partial decomposition occurred, which was confirmed by the loss of optical rotation and spectral change. Since the plots of $\ln(a_\infty - a_t)$ *vs.* time gave a linear relation, the estimated decomposition rates are listed in Table 3.

The sensitivity of the base decomposition was observed to increase in the following order of amino acids:

L-pro < L-phe < L-met < L-ile < *N*-Bz-L-ala < *N*-Me-L-ala.

This order is almost the same as that for the decomposition under the acidic conditions.

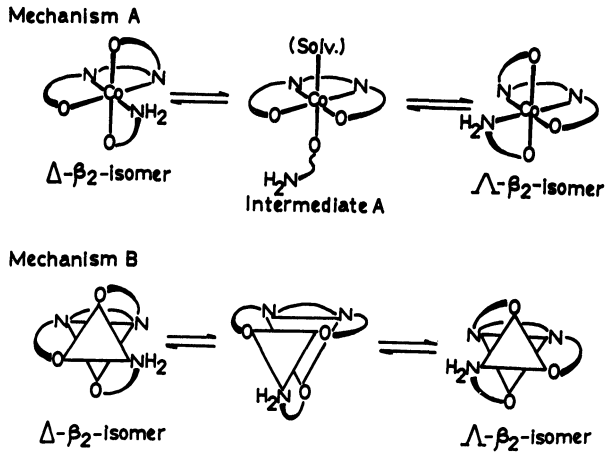

Fig. 5. Sterically possible isomerization mechanisms.

Free amino acids such as phenylalanine and proline gave no significant effect on the isomerization of all the complexes. However, when the complex solutions containing free amino acids were allowed to stand for a long time, substitution of the coordinated amino acidate ion occurred. Since the plots of $\ln(a_\infty - a_t)$ *vs.* time for the substitution with D-phenylalanine (L-phenylalanine in the case of L-pro-complex) gave a linear relation, the observed substitution rate can be estimated, and the first order rate constants observed are listed in Table 3. The substitution is much slower than the isomerization in all the complexes, indicating that the isomerization proceeds *via* an intramolecular mechanism.

From these results, it can be pointed out that the intramolecular isomerization mechanism of all the complexes should be quite similar because of their similar properties.

Isomerization Mechanism. A β_2-[Co(Schiff base)-(L-aa)] complex is composed of one quadridentate and one bidentate ligands. Hence, its intramolecular isomerization is sterically restricted as compared with that of tris(bidentate) complexes. Molecular models indicate that only two mechanisms in Fig. 5 are sterically possible, and a bond breaking mechanism between cobalt(III) and a carboxylate group of the amino acidate is sterically impossible. Mechanism **A** in Fig. 5 is a Co–N bond breaking mechanism with an intermediate in which the quadridentate Schiff base takes a planar configuration, and the amino acidate coordinates as a unidentate ligand with its carboxylate group. Mecha-

Table 4. Isomerization rates and H-D exchange rates of β_2-[Co(α-Me-sal$_2$en) (*N*-Me-L-ala)] in the mixed solvent of methanol and chloroform (1:4 in volume) at 35 °C

Isomer ratio of starting complex	Isomerization			H-D Exchange
	k_{obsd}/s^{-1}	k_{+1}/s^{-1}	k_{-1}/s^{-1}	k_{obsd}[a)]/s^{-1}
1:1 mixture of Δ_L- and Λ_L-isomers	1.10×10^{-4}	1.06×10^{-4}	4.33×10^{-6}	$(1.0\pm0.3)\times10^{-4}$
Pure Λ_L-isomer				$(4.3\pm0.2)\times10^{-6}$

a) Value in $CD_3OD+CDCl_3$ (1:4).

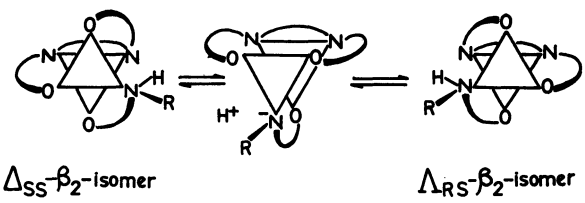

Fig. 6. *R-S* inversion of an asymmetric nitrogen atom in the twist mechanism.

nism **B** is a twist mechanism without a Co^{III}–ligand bond breaking. Since the activation enthalpy is correlated with pK_{a_2} value of the amino acid and the ionic strength effect on the isomerization is negligibly small, the Co–O bond breaking mechanism can safely be omitted, but it is quite difficult to distinguish between Mechanisms **A** and **B**.

In the case of *N*-alkyl-L-ala-complexes, however, Mechanism **B** is unlikely, because, 1) the *N*-alkyl-L-ala-complexes have an asymmetric nitrogen atom at the amino group.*** Therefore, not only the inversion between Δ- and Λ-configurations but also the inversion between *R*- and *S*-configurations of the asymmetric nitrogen atom are required in the isomerization between Δ_{SS}- and Λ_{RS}-β_2-isomers;[15] 2) the *R–S* inversion is impossible in Mechanism **B** without deprotonation of an N–H proton (Fig. 6).

If the deprotonation occurs during the isomerization, the H–D exchange rate of the N–H proton should be 10^2—10^3 times or more faster than the isomerization rate in Mechanism **B**.[16] On the other hand, in Mechanism **A**, the H–D exchange rate is expected to be comparable to the isomerization rate of the complex, because Mechanism **A** involves an intermediate in which the amino group is free from the cobalt(III) ion, and the H–D exchange rate of a free amino group is usually very fast. On the basis of these expectations, the H–D exchange rates for the *N*-Me-L-ala-complex were measured. Since the complex was hardly soluble in CD_3OD, a mixed solvent of CD_3OD and $CDCl_3$ (1 : 4 in volume) was used. The ^1H NMR spectral variation was shown in Fig. 5 of Ref. 10, and the ln-plots are shown in Fig. 7. The diagrams are linear up to at least 40% completion of the H–D exchange for the 1 : 1 mixture of Δ_{SS}- and Λ_{RS}-β_2-isomers and up to at least 80% completion for the pure Λ_{RS}-β_2-isomer. The first order H–D exchange rate constants thus obtained

*** The $(+)_{435}$-isomer of *N*-alkyl-L-ala-complexes used here corresponds to the Δ_{SS}-β_2-isomer, and the $(-)_{435}$-isomer to the Λ_{RS}-β_2-isomer.[10,15]

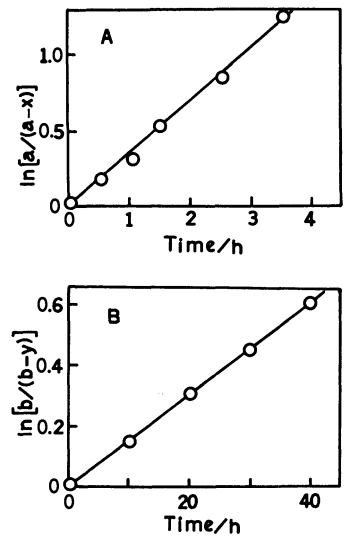

Fig. 7. ln-plots for H–D exchange of *N*-Me-L-ala-complex in mixed solvent of CD_3OD and $CDCl_3$ (1 : 4 in volume) at 35 °C.
A=1 : 1 mixture. B=Pure Λ_L-β_2-isomer. a=Initial concentration of Δ_L-β_2-isomer. x=Concentration of deuterated isomer at time *t*. b=Initial concentration of Λ_L-β_2-isomer. y=Concentration of deuterated isomer at time *t*.

are listed in Table 4. The isomerization rate constants in the mixed solvent of CH_3OH and $CHCl_3$ (1 : 4 in volume) were estimated from the mutarotation at 435 nm of the complex, and are given in Table 4.

Table 4 indicates that 1) the H–D exchange rate for the 1 : 1 mixture is almost the same as the isomerization rate (k_{+1}) from Δ_{SS}- to Λ_{RS}-β_2-isomers; 2) the H–D exchange rate for the pure Λ_{RS}-β_2-isomer is almost identical with the isomerization rate (k_{-1}) from Λ_{RS}- to Δ_{SS}-β_2-isomers. Thus, it can be concluded that Mechanism **A** is most probable as the isomerization mechanism of the *N*-Me-L-ala-complex. Since there is no reason that other amino acidato complexes take a different isomerization mechanism from that of the *N*-Me-L-ala-complex, all the complexes investigated here are concluded to isomerize *via* Mechanism **A**.

It has been observed that the formation of β_2-[Co(α-Me-sal$_2$en)(L-aa)] complexes from *trans*-[Co(α-Me-sal$_2$en)(O_2)] and L-amino acid proceeds *via* an intermediate similar to **A** in Fig. 5, and it is much faster than the isomerization of β_2-[Co(α-Me-sal$_2$en)(L-aa)].[9] These facts suggest that the formation of Δ_L- and Λ_L-β_2-isomers from Intermediate **A** in Fig. 5 is much faster than the isomerization. Accordingly, the rate deter-

TABLE 5. OBSERVED ISOMERIZATION RATES (k_{obsd}/s^{-1}) IN VARIOUS SOLVENTS AT 23.5 °C

L-aa-Complex	CH_3COOH[b]	H_2O	*m*-cresol	MeOH	EtOH	*n*-PrOH
L-ile	2.0×10^{-2}	5.0×10^{-3}	3.8×10^{-3}	1.2×10^{-3}	5.2×10^{-4}	4.4×10^{-4}
(λ/nm)[a]	(579)	(587)	(587)	(584)	(582)	(580)
L-phe	2.0×10^{-2}	3.1×10^{-3}[c]	4.6×10^{-3}	1.4×10^{-3}	1.1×10^{-3}	3.8×10^{-4}
(λ/nm)[a]	(578)	(585)[c]	(587)	(583)	(582)	(580)

L-aa-complex	*n*-BuOH	*i*-BuOH	*s*-BuOH	Aniline	Acetone, DMF, DMSO, THF, 1,4-Dioxane, Pyridine
L-ile	4.4×10^{-4}	2.3×10^{-4}	7.3×10^{-5}	1.8×10^{-5}	Very slow
(λ/nm)[a]	(580)	(580)	(578)	(577)	(575—570)
L-phe	2.3×10^{-4}	2.5×10^{-4}	1.5×10^{-4}	2.3×10^{-5}	Very slow
(λ/nm)[a]	(580)	(580)	(577)	(576)	(577—574)

a) First absorption maximum. b) A small amount of decomposition of complex occurred in CH_3COOH. c) Value in mixed solvent of H_2O and MeOH (2:3 in volume).

mining step of the isomerization is thought to be the formation process of *trans*-Intermediate **A** from Δ_L- and Λ_L-β_2-isomers.

Effect of Solvents on the Isomerization. In order to get further information, isomerizations in various solvents were investigated. The k_{obsd} values for the representative complexes are summarized in Table 5. From these measurements, the following tendencies were found: 1) the isomerization becomes faster in the following order of solvents: acetone, DMF, DMSO, THF, 1,4-dioxane, pyridine<aniline<BuOH<PrOH <EtOH<MeOH<*o*-cresol<H_2O<CH_3COOH; 2) the isomerization in acetone, DMF, DMSO, THF, 1,4-dioxane, and pyridine is quite slow or no isomerization occurs; 3) no decomposition of the complex occurred in pyridine and aniline, although the decomposition of the complex occurred in the mixed solvents of methanol and pyridine or aniline.

The isomerization is faster in the solvents having a hydrogen bonding proton than in weak- or nonhydrogen bonding solvents. Thus, hydrogen bonding solvents clearly assist the isomerization. As has been observed previously,[12] the hydrogen bonding occurs mainly at the phenolic oxygen atoms of a Schiff base ligand, and when the hydrogen bonding is stronger, the first absorption band of the complexes shifts to the lower energy side. This shift is caused by the lowering of the coordination ability of phenolic oxygen atoms due to the hydrogen bonding. A similar shift of the first absorption band was also observed in the present study, and when the shift was larger, the isomerization was faster. Therefore, it can be concluded that 1) the hydrogen bonding at the phenolic oxygen atoms of the Schiff base ligand assists the isomerization, and 2) the stronger the hydrogen bonding is, the more labile the isomerization is.

For the formation of Intermediate **A** in Fig. 5 from Δ_L- and Λ_L-β_2-isomers, not only the bond breaking between the cobalt(III) atom and the amino group of amino acidate ion but also the rearrengement of the coordinated Schiff base ligand from β- to *trans*-configurations is needed. And, for the rearrangement of the Schiff base ligand, a loosening of the Co^{III}–phenolic oxygen bond is necessary. Since the hydrogen bonding solvents are thought to act to make the Co^{III}–phenolic oxygen bond more loose, their effects may be to assist rearrengement of the Schiff base ligand. We think that the catalytic effect of protic acid should be similar to that of hydrogen bonding solvents, because it has been known that the protonation occurs at the phenolic oxygen atoms.[17]

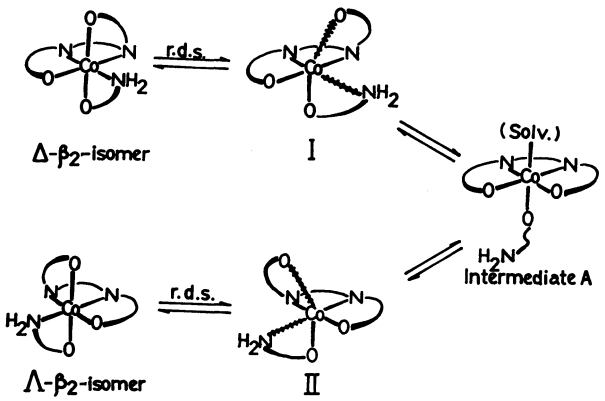

Fig. 8. Proposed isomerization mechanism.

On the basis of these results and above discussion, we propose an isomerization mechanism shown in Fig. 8. In Fig. 8, we assummed that 1) the rate controlling step is the formation of activated complexes **I** and **II**, and 2) the activated complexes take a structure in which two bonds, that between cobalt(III) and the amino group, and that between cobalt(III) and one of the phenolic oxygen atoms, are stretched.

The authors wish to express their deep thanks to Professor J. C. Bailar Jr., of University of Illinois for his encouragement.

Appendix

Derivation of the Rate Equation. When the isomerization rate constant from Δ_L- to Λ_L-isomers is written as k_{+1} and that from Λ_L- to Δ_L-isomers as k_{-1}, they can be expressed as follows:

$$k_{+1} = ([\Lambda_L]_\infty/at)\ln\{[\Lambda_L]_\infty/([\Lambda_L]_\infty-[\Lambda_L]_t\}, \quad (1)$$

$$k_{-1} = ([\Delta_L]_\infty/at)\ln\{[\Delta_L]_\infty/([\Delta_L]_\infty-[\Delta_L]_t)\}, \quad (2)$$

where, $[\Lambda_L]_t$, $[\Delta_L]_t$ and $[\Lambda_L]_\infty$, $[\Delta_L]_\infty$ represent the concentrations of Λ_L- and Δ_L-isomers at the time t, and at the equilibrium conditions, respectively, and a denotes the total complex

concentration. When the molar rotations of Λ_L- and Δ_L-isomers are expressed by $[M]_{\Lambda L}$ and $[M]_{\Delta L}$, respectively, the observed rotation (α_t) at the time t can be written as follows:

$$\begin{aligned}\alpha_t &= [M]_{\Lambda L}[\Lambda_L]_t d + [M]_{\Delta L}[\Delta_L]_t d \\ &= ([M]_{\Lambda L} - [M]_{\Delta L})[\Lambda_L]_t d + [M]_{\Delta L} ad \\ &= ([M]_{\Delta L} - [M]_{\Lambda L})[\Delta_L]_t d + [M]_{\Lambda L} ad, \end{aligned} \quad (3)$$

where, d is the cell length.

From Eq. 3, the following relations can be derived:

$$[\Lambda_L]_t = (\alpha_t - [M]_{\Delta L} ad)/([M]_{\Lambda L} - [M]_{\Delta L})d, \quad (4)$$

$$[\Delta_L]_t = (\alpha_t - [M]_{\Lambda L} ad)/([M]_{\Delta L} - [M]_{\Lambda L})d. \quad (5)$$

Similarly, $[\Lambda_L]_\infty$ and $[\Delta_L]_\infty$ can be written as follows:

$$[\Lambda_L]_\infty = (\alpha_\infty - [M]_{\Delta L} ad)/([M]_{\Lambda L} - [M]_{\Delta L})d, \quad (6)$$

$$[\Delta_L]_\infty = (\alpha_\infty - [M]_{\Lambda L} ad)/([M]_{\Delta L} - [M]_{\Lambda L})d. \quad (7)$$

When the isomeric ratio under the equilibrium conditions is expressed by

$$K = [\Lambda_L]_\infty/[\Delta_L]_\infty = k_{+1}/k_{-1}, \quad (8)$$

k_{+1} and k_{-1} in Eqs. 1 and 2 can be written as follows by the use of relations in Eqs. 4—8:

$$\begin{aligned} k_{+1} &= [K/(K+1)t] \\ &\times \ln\{[K/(K+1)]([M]_{\Lambda L} - [M]_{\Delta L})ad/(\alpha_\infty - \alpha_t)\}, \end{aligned} \quad (9)$$

$$\begin{aligned} k_{-1} &= [1/(K+1)t] \\ &\times \ln\{[1/(K+1)]([M]_{\Delta L} - [M]_{\Lambda L})ad/(\alpha_\infty - \alpha_t)\}. \end{aligned} \quad (10)$$

By transforming the Eqs. 9 and 10, Eqs. 11 and 12 are obtained:

$$\begin{aligned} \ln(\alpha_\infty - \alpha_t) &= -[(K+1)/K]k_{+1}t \\ &+ \ln\{[K/(K+1)]([M]_{\Lambda L} - [M]_{\Delta L})ad\}, \end{aligned} \quad (11)$$

$$\begin{aligned} \ln(\alpha_\infty - \alpha_t) &= -(K+1)k_{-1}t \\ &+ \ln\{[1/(K+1)]([M]_{\Delta L} - [M]_{\Lambda L})ad\}. \end{aligned} \quad (12)$$

When the values of $-[(K+1)/K]k_{+1}$ and $-(K+1)k_{-1}$ are designated as $k^{\Lambda\to\Delta}_{obsd}$ and $k^{\Lambda\to\Lambda}_{obsd}$, respectively, the following relationship can be derived by the use of Eq. 8:

$$k^{\Lambda\to\Delta}_{obsd} = -[(K+1)/K]k_{+1} = -(K+1)k_{-1} = k^{\Lambda\to\Lambda}_{obsd}. \quad (13)$$

References

1) M. Yamaguchi, S. Yamamatsu, T. Furusawa, S. Yano, M. Saburi, and S. Yoshikawa, *Inorg. Chem.*, **19**, 2010 (1980).

2) M. Yamaguchi, S. Yano, M. Saburi, and S. Yoshikawa, *Inorg. Chem.*, **19**, 2016 (1980).

3) M. Yamaguchi, S. Yano, M. Saburi, and S. Yoshikawa, *Bull. Chem. Soc. Jpn.*, **53**, 691 (1980).

4) M. Saburi and S. Yoshikawa, "Chemistry of Octahedral Complexes," in "Kagaku Sosetsu," ed by the Chemical Society of Japan Gakkai Shuppan Center, Tokyo (1976), Vol. **13**, p. 109. Other references are cited therein.

5) M. H. Ghandelhari, T. N. Andersen, D. R. Boone, and H. Eyring, *J. Am. Chem. Soc.*, **92**, 6466 (1970).

6) R. C. Job, *J. Am. Chem. Soc.*, **100**, 5089 (1978).

7) Y. Fujii, T. Isago, M. Sano, N. Yanagibashi, S.Hirasawa and S. Takahashi, *Bull. Chem. Soc. Jpn.*, **49**, 3509 (1976).

8) Y. Kushi, R. Tamura, M. Kuramoto, T. Yoshizawa, H. Yoneda, and Y. Fujii, *J. Chem. Soc., Chem. Commun.*, **1978**, 266.

9) Y. Fujii, K. Shiono, K. Ezuka, and T. Isago, *Bull. Chem. Soc. Jpn.*, **53**, 3537 (1980).

10) Y. Fujii, M. Matsufuru, A. Saito, and S. Tsuchiya, *Bull. Chem. Soc. Jpn.*, **54**, 2029 (1981).

11) Y. Kushi, T. Tada, Y. Fujii, and H. Yoneda, *Bull. Chem. Soc. Jpn.*, **55**, 1834 (1982).

12) Y. Fujii, Y. Kuwana, S. Takahashi, K. Shimizu, and K. Hiroi, *Bull. Chem. Soc. Jpn.*, **55**, 2598 (1982).

13) The following abbreviations are used: *N*-Bz-L-ala=*N*-benzyl-L-alaninate, *N*-Me-L-ala=*N*-methyl-L-alaninate, α-Me-sal$_2$en=*N*,*N*′-ethylenebis(α-methylsalicylideneamine) dianion.

14) Y. Fujii and N. Yanagibashi, The 26th Conference of Coordination Chemistry, Chem. Soc. Japan, Hokkaido, August 1976, Abstr. No. 3N15.

15) In the notation of Λ_{RS}- and Δ_{SS}-isomers, the first sufix (R or S) represents the configuration of the asymmetric nitrogen atom of the coordinated *N*-alkyl amino acid, and the second sufix (S) denotes that of the asymmetric carbon atom of the amino acid.

16) D. A. Buckingham, L. G. Marzilli, and A. M. Sargeson, *J. Am. Chem. Soc.*, **89**, 825 and 3428 (1967).

17) J. R. Thornback and G. Wilkinson, *J. Chem. Soc., Dalton Trans.*, **1978**, 110.

 © 1983 The Chemical Society of Japan Bull. Chem. Soc. Jpn., 56, 3615—3619 (1983)

Pyrolytic Sulfurization Gas Chromatography. XV. Simultaneous Determination of the Atomic Ratio between C, H, O, and N in an Organophosphorus Compound

Tadashi HARA,* Kaoru FUJINAGA,† Fujio OKUI, and Akihiro ARAI

Department of Chemical Engineering, Faculty of Engineering, Doshisha University, Karasuma Imadegawa, Kamigyo-ku, Kyoto 602

†*Department of Chemistry, Faculty of Science, Shimane University, 1060 Nishikawatsu-cho, Matsue 690*

(Received April 1, 1983)

In order to confirm whether or not pyrolytic sulfurization gas chromatography can be applied to organophosphorus compounds, many kinds of organophosphorus compounds were examined; C-rich compounds gave satisfactory results while C-poor ones gave lower oxygen values. The application limit of this method to various organophosphorus compounds was determined by the use of the C/O value and a structural factor for a sample, and the application limit was established. The structural factor of a sample varied with the kind of X_1, X_2, X_3, and X_4 in the general formula $X_1X_2X_3P=X_4$, where X_1=OH, OR, R; X_2=OH, OR′, R′; X_3=OH, OR″, R″; and X_4=O, S.

With the objective of establishing a new organic elemental analysis method by which several elements can be simultaneously determined, pyrolytic sulfurization gas chromatography (PSGC) was originated[1] and has been studied[2–14] by the authors. The PSGC method is based on a combustion technique in sulfur vapor instead of the conventional one in an oxygen atmosphere; this makes possible the simultaneous determination of the atomic ratio between C, H, O, and N in an organic compound without weighing the sample. So far this method has been successfully applied to a normal organic compound,[1,2] a metal organic chelate,[3,13] a polymer,[5] and an organic halogen compound.[7,9]

In the field of conventional organic elemental analysis, oxygen in an organic compound containing metallic or non metallic elements cannot be analyzed with ease because a number of elements show a strong affinity for oxygen and are apt to form nonvolatile compounds such as their oxides or carbonates. On the contrary, the PSGC method makes possible the simultaneous determination of the atomic ratio between C, H, O, and N even in a compound containing the above-mentioned elements because they are converted into their sulfides. Though the effects of many coexistent elements on the determination of C, H, O, and N have been discussed and clarified, the effect of phosphorus as a coexistent element still remained unsolved in the previous studies.[3,13] Moreover, the determination of oxygen in an organophosphorus compound by the conventional organic elemental analysis method is difficult. Therefore, the present study has been carried out to confirm whether or not the PSGC method can be applied to various types of organophosphorus compounds. Fifteen kinds of organophosphorus compounds were analyzed by the PSGC method; C-rich compounds gave satisfactory results but C-poor ones gave low oxygen values. This was explained by the assumption that the phosphorus oxides produced from phosphorus and oxygen in a sample are reduced to phosphorus sulfide by carbon in a C-rich compound sample, but not in a C-poor compound sample. On the other hand, some experimental results could not be explained by the C/O value alone. In these cases, the application limit of the PSGC method to various organophosphorus compounds was decided by the use of the C/O value and a structural factor for the sample. The structural factor of a sample varied with the kind of X_1, X_2, X_3, and X_4 in the general formula $X_1X_2X_3P=X_4$ where X_1=OH, OR, R; X_2=OH, OR′, R′; X_3=OH, OR″, R″; and X_4=O, S.

Experimental

Apparatus and Reagents. The apparatus and reagents used in this experiment were the same as those reported previously. A definite amount of sample was taken using a Shimadzu microbalance MDP-5.

Samples. Eleven kinds of organophosphorus compounds, sample numbers 1, 2, 3, 4, 5, 6, 7, 8, 9, 10, and 12 (shown in Table 1) were synthetic ones provided by Professor Isao Furukawa at Doshisha University. Other samples were of reagent grade. These samples were, if necessary, purified by recrystallization from appropriate solvents. The composition and purity of the samples were confirmed by CH and/or CHN analysis carried out in the Elemental Analysis Center of the Pharmaceutical Department of Kyoto University (Table 1).

Procedure. A 0.3—0.5 mg of sample and 5 mg of purified sulfur[4] was inserted into a quartz tube (2.5 mm i.d., 3.5 mm o.d., and 100 mm long), one end of which was previously closed. The air inside the tube containing the sample and S was displaced with He for 10 min at the flow rate of 100 cm³/min, followed by sealing the other end of the tube. The ampule thus obtained was treated for 10 min at 600 °C and for 30 min at 950 °C. The reaction products, carbon dioxide, carbonyl sulfide, carbon disulfide, hydrogen sulfide, and nitrogen, in the ampule were analyzed gas-chromatographically by crushing the ampule in the flow of the gas chromatograph, followed by calculation of the atomic ratio between C, H, O, and N in the sample in the same way as that reported previously.[2] The precision of the PSGC had been reported in the previous paper.[14]

Results

Analytical Results of Various Organophosphorus Compounds. Various organophosphorus compounds were analyzed by the PSGC method; the results are shown in Table 2. As can be seen from Table 2, C-rich compounds gave satisfactory results, but C-poor compounds such as samples 11, 13, 14, and 15 did not. In the PSGC

TABLE 1. ANALYTICAL RESULTS OF C, H, AND N IN AN ORGANOPHOSPHORUS COMPOUND

Sample No.	Sample	C (wt%)			H (wt%)			N (wt%)		
		Calcd	Found	Error	Calcd	Found	Error	Calcd	Found	Error
1	*N,N'*-Diphenylphenylphosphonothioic diamide 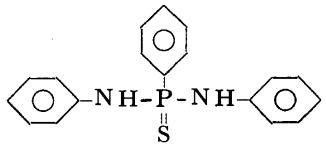	66.65	66.47	−0.18	5.28	5.33	+0.05	8.64	8.39	−0.25
2	Bis(3,4-dimethylphenyl) phenylphosphine oxide 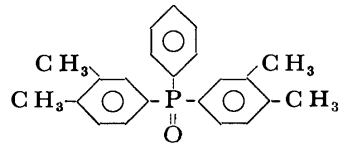	79.02	78.86	−0.16	6.93	7.16	+0.23			
3	Triphenylphosphine oxide 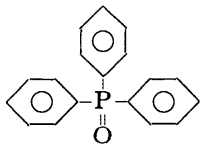	77.69	77.53	−0.16	5.43	5.34	−0.09			
4	Diethoxy(α-anilinobenzyl) phosphine oxide 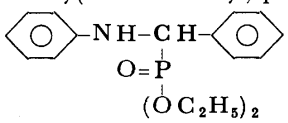	63.94	64.08	+0.14	6.94	7.17	+0.23	4.39	4.29	−0.10
5	1,2-Bis(isopropoxyphenylphosphinyl)ethane 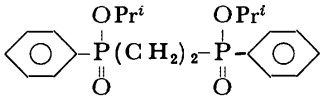	60.91	60.62	−0.29	7.16	7.06	−0.10			
6	Triphenyl phosphate 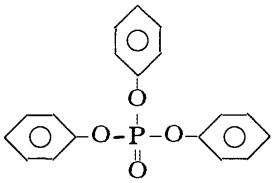	66.26	66.16	−0.10	4.63	4.62	−0.01			
7	1,4-Butanediylbis(phenylphosphinic acid) 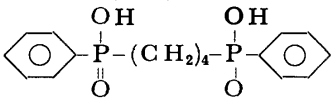	56.81	56.66	−0.15	5.96	6.01	+0.05			
8	1,3-Propanediylbis(phenylphosphinic acid) 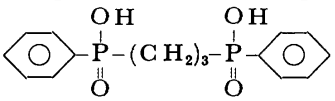	55.56	55.40	−0.16	5.60	5.63	+0.03			
9	1,2-Ethanediylbis(phenylphosphinic acid) 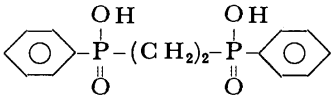	54.20	54.29	+0.09	5.20	5.24	+0.04			
10	Bis(phenylphosphinico) methane 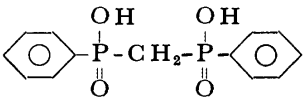	52.72	52.48	−0.24	4.76	4.62	−0.14			
11	Benzidine–phosphoric acid 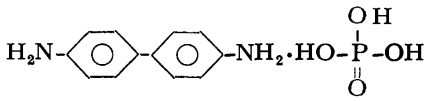	51.07	51.03	−0.04	5.36	5.33	−0.03	9.93	10.01	+0.08

Table 1. (Continued)

Sample No.	Sample	C (wt%) Calcd	C (wt%) Found	C (wt%) Error	H (wt%) Calcd	H (wt%) Found	H (wt%) Error	N (wt%) Calcd	N (wt%) Found	N (wt%) Error
12	*p*-Xylene-α,α′-diylbis(diethoxyphosphine oxide) 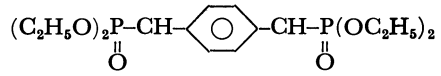	50.79	50.90	+0.11	7.46	7.73	+0.27			
13	Benzoguanamine–phosphoric acid 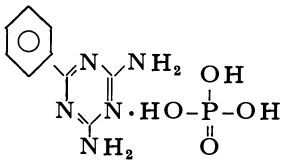	37.90	37.97	+0.07	4.24	4.32	+0.08	24.56	24.72	+0.16
14	Phenylphosphonic acid 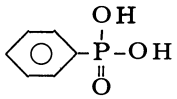	45.58	45.86	+0.28	4.46	4.47	+0.01			
15	Piperazine–phosphoric acid–water 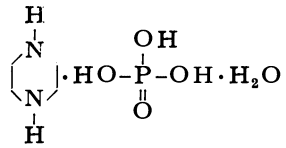	23.77	23.61	−0.16	7.48	7.60	+0.12	13.86	13.89	+0.03

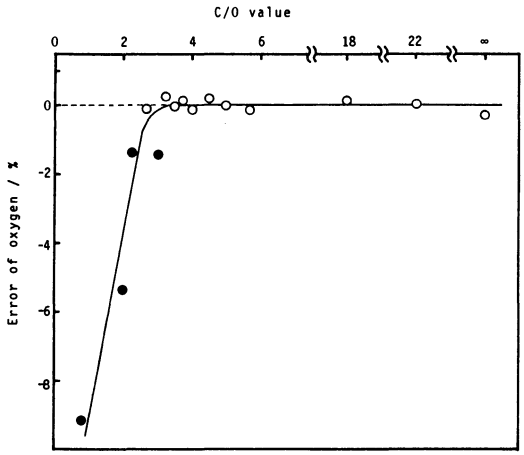

Fig. 1. Relationship between error of oxygen and C/O value in a organophosphorus compound.
○: Applicable compound and ●: not applicable one.

method, each content of C, H, O, and N in a sample is calculated by normalizing their total contents to 100%. In order to clarify which element was influenced by phosphorus as a coexistent element, the atomic ratios of H, O, and N to C were calculated; it became apparent that only the content of O was influenced by phosphorus. This may be explained by the assumption that phosphorus oxide produced from phosphorus and oxygen in a sample is reduced by carbon in a C-rich compound sample, but not in a C-poor compound sample. The white powder, which was presumed to be a phosphorus oxide, was observed in the ampule of the latter case after pyrolytic sulfurization.

Relationship between the Analytical Results and the C/O Value. The atomic ratio of C to O (the C/O value) was defined as an indication of the reducing power for the phosphorus oxide to explain the above-mentioned results. The relationship between the error of oxygen in each analytical result of organophosphorus compound and the C/O value calculated from each sample was shown in Fig. 1. Figure 1 shows that the PSGC method can be applied to organophosphorus compounds in which the C/O value exceeds about 3 and the negative error in oxygen value increases with a decreasing C/O value less than about 3. However, the fact that sample 11 (C/O=3.0) did not give a satisfactory result while sample 12 (C/O=2.7) did give a satisfactory result cannot be explained by the C/O value alone. Therefore, another factor must also be taken into consideration to clarify the application limit of the PSGC method to organophosphorus compounds. It is discussed below.

Discussion

Effect of the Chemical Structure of a Sample on the Analytical Result. Since the application limit of the PSGC method to organophosphorus compounds could not be decided exactly by the C/O value alone as mentioned above, the chemical structure of a sample was investigated as another factor of deciding the application limit to organophosphorus compounds in which the oxidation number of phosphorus is +5 in the following manner. Three kinds of mixed samples with the C/O values of 1—7 were prepared as model compounds by the use of the following pairs; sample 1 and sucrose, sample 5 and sucrose, and sample 15 and anthracene, respectively. These samples were analyzed by the PSGC method; each relationship between the analytical value of oxygen in each sample and its C/O value is shown in Fig. 2, where all analytical values of C, H, and N were

TABLE 2. ANALYTICAL RESULTS FOR VARIOUS ORGANOPHOSPHORUS COMPOUNDS

Sample No.	Sample	C/O	C (wt%)			H (wt%)			O (wt%)			N (wt%)		
			Calcd	Found	Error	Calcd	Found	Error	Calcd	Found	Error	Calcd	Found	Error
1	*N,N'*-Diphenylphenylphosphonothioic diamide	∞	82.72	82.82	+0.10	6.56	6.78	+0.22				10.72	10.40	−0.32
2	Bis(3,4-dimethylphenyl)phenylphosphine oxide	22	87.09	87.08	−0.01	7.64	7.62	−0.02	5.27	5.30	+0.03			
3	Triphenylphosphine oxide	18	87.42	87.34	−0.08	6.11	6.06	−0.05	6.47	6.60	+0.13			
4	Diethoxy(α-anilinobenzyl)phosphine oxide	5.7	70 81	70.89	+0.08	7.69	7.67	−0.02	16.64	16.50	−0.14	4.86	4.94	+0.08
5	1,2-Bis(isopropoxyphenylphosphinyl)ethane	5.0	72.26	72.35	+0.09	8.49	8.43	−0.06	19.25	19.22	−0.03			
6	Triphenyl phosphate	4.5	73.21	73.06	−0.15	5.12	5.07	−0.05	21.67	21.87	+0.20			
7	1,4-Butanediylbis(phenylphosphinic acid)	4.0	69.54	69.72	+0.18	7.30	7.26	−0.04	23.16	23.02	−0.14			
8	1,3-Propanediylbis(phenylphosphinic acid)	3.8	68.68	68.41	−0.27	6.92	7.06	+0.14	24.40	24.53	+0.13			
9	1,2-Ethanediylbis(phenylphosphinic acid)	3.5	67.72	67.73	+0.01	6.50	6.51	+0.01	25.78	25.76	−0.02			
10	Bis(phenylphosphinico)methane	3.3	66.66	66.40	−0.26	6.02	6.04	+0.02	27.32	27.56	+0.24			
11	Benzidine–phosphoric acid	3.0	57.36	58.73	+1.37	6.02	6.11	+0.09	25.47	24.04	−1.43	11.15	11.12	−0.03
12	*p*-Xylene-α,α'-diylbis(diethoxyphosphine oxide)	2.7	60.74	60.96	+0.22	8.92	8.81	−0.11	30.34	30.23	−0.11			
13	Benzoguanamine–phosphoric acid	2.3	42.52	43.29	+0.77	4.76	4.92	+0.16	25.17	23.79	−1.38	27.55	28.00	+0.45
14	Phenylphosphonic acid	2.0	56.69	61.42	+4.94	5.55	5.97	+0.42	37.76	32.40	−5.36			
15	Piperazine–phosphoric acid–water	0.8	28.07	34.12	+6.05	8.83	10.34	+1.51	46.73	37.57	−9.16	16.37	17.97	+1.60

TABLE 3. APPLICABLE REGION OF THE PSGC METHOD' PSGC METHOD TO ORGANOPHOSPHORUS COMPOUNDS

Structure	$X_1X_2X_3P=X_4$				C/O									
	X_1	X_2	X_3	X_4	0	1	2	3	4	5	6	7	18	22	∞
A	OH	OH	OH	O			−	−	−						
B	OH	OH	OR	O											
C	OH	OH	R	O				−							
D	OH	OR	OR	O											
E	OH	OR	R	O											
F	OH	R	R	O					+	+	+	+			
G	OR	OR	OR	O						+					
H	OR	OR	R	O					+		+		+		
I	OR	R	R	O						+					
J	R	R	R	O										+	
K	R	R	R	S											+

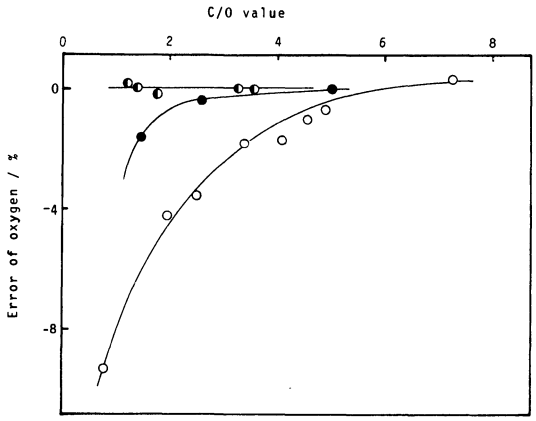

Fig. 2. Relationship between error of oxygen and C/O value in a mixed sample.
○: Sample 15 and anthracene, ●: sample 5 and sucrose, and ◐: sample 1 and sucrose.

confirmed to be correct from the atomic ratios of H and N to C. As can be seen from Fig. 2, the errors of oxygen decrease with an increasing C/O value, but the numerical values of the oxygen error are different from one another even at the same value of C/O. This is attributed to the difference of the chemical structure of the sample, that is, satisfactory results are obtained for the following samples; 1) sample 15 as an addition compound of phosphoric acid when the C/O value is more than 5.5, 2) sample 5 as a derivative of phosphinic acid when the C/O value is more than 2, and 3) sample 1 as a derivative of phosphonothioic acid containing no oxygen when the C/O value is more than 1. Thus the analytical result of oxygen is influenced by the substituent groups bonding to phosphorus, –OH, –OR, and –R (R indicates a hydrocarbon group), in that order. From the results of this experiment, the application limit of the PSGC method to organophosphorus compounds may be explained by the use of two factors; the C/O value and the chemical structure.

Application Limit of the PSGC Method to Organophosphorus Compounds. In order to clarify the application limit of the PSGC method to organophosphorus compounds, the relationship between each analytical result of organophosphorus compound and above-mentioned two factors was investigated; the results are shown in Table 3. In Table 3, substituent groups bonding to phosphorus (V) as a structural factor are vertically enumerated in the order of their interferences and the C/O values are arranged horizontally, followed by marking + at the corresponding position for the sample giving a satisfactory result and by marking − for one giving a negative error of oxygen. In addition, both the positions giving satisfactory results for phosphoric acid, C/O=5.5 in structure A, and for phosphonothioic acid, C/O=1 in structure J, were linked with a broken line. This broken line indicates the application range of the PSGC method, that is, the sample satisfying the

conditions under the broken line may be analyzed by the PSGC method without any exceptions.

Judging from the results obtained by the present study and the difficulties in oxygen analysis of an organophosphorus compound by the conventional method, the utility of the PSGC method in analysis of an organophosphorus compound is obvious even though its applicable region is restricted by the application limit.

The authors wish to express their thanks to Professor Isao Furukawa, Doshisha University, for the supply of 11 kinds of organophosphorus compounds.

References

1) K. Tsuji, K. Fujinaga, and T. Hara, *Bull. Chem. Soc. Jpn.*, **50**, 2292 (1977).
2) T. Hara, K. Fujinaga, and K. Tsuji, *Bull. Chem. Soc. Jpn.*, **51**, 1110 (1978).
3) T. Hara, K. Fujinaga, and K. Tsuji, *Bull. Chem. Soc. Jpn.*, **51**, 2951 (1978).
4) T. Hara, K. Fujinaga, K. Tsuji, and F. Okui, *Bull. Chem. Soc. Jpn.*, **51**, 3079 (1978).
5) T. Hara, K. Fujinaga, F. Okui, and K. Negayama, *Sci. Eng. Rev. Doshisha Univ.*, **21**, 241 (1981).
6) T. Hara, K. Fujinaga, and F. Okui, *Bull. Chem. Soc. Jpn.*, **53**, 951 (1980).
7) T. Hara, K. Fujinaga, and F. Okui, *Bull. Chem. Soc. Jpn.*, **53**, 1308 (1980).
8) T. Hara, K. Fujinaga, and F. Okui, 3rd world Chromatography Conference, Zürich, July 1980, Abstr. p. 7.
9) T. Hara, K. Fujinaga, and F. Okui, *Bull. Chem. Soc. Jpn.*, **54**, 2956 (1981).
10) T. Hara and F. Okui, *Bull. Chem. Soc. Jpn.*, **55**, 329 (1982).
11) T. Hara and F. Okui, *Bull. Chem. Soc. Jpn.*, **55**, 2127 (1982).
12) T. Hara and F. Okui, *Bull. Chem. Soc. Jpn.*, **55**, 3450 (1982).
13) T. Hara, K. Fujinaga, and F. Okui, *Bull. Chem. Soc. Jpn.*, **55**, 3800 (1982).
14) T. Hara and F. Okui, *Bull. Chem. Soc. Jpn.*, **56**, 1378 (1983).

 © 1983 The Chemical Society of Japan Bull. Chem. Soc. Jpn., 56, 3620—3624 (1983) [Vol. 56, No. 12

Circular Dichroism of Chromium(III) Complexes. VIII. Circular Dichroism Spectra of Mixed Diamine Complexes of *trans*-$[CrF_2(N)_4]^+$ Type

Sumio KAIZAKI

Department of Chemistry, Faculty of Science, Nara Women's University, Nara 630

(Received May 28, 1983)

The ligand field absorption and circular dichroism (CD) spectra were examined not only for *trans*-difluoro bis(diamine)chromium(III) complexes with two identical chiral diamines but also for nine new mixed diamine complexes of the same type with different diamines, which were ethylenediamine, trimethylenediamine, (*R*)- and (*S*)-propylenediamine, (1*R*, 2*R*)-1,2-cyclohexanediamine, (2*R*, 4*R*)- and (2*R*, 4*S*)-2,4-pentanediamine. The additivity of the CD contributions from the individual chiral diamines were substantiated for most of these complexes. On this basis, the conformational and the vicinal CD contribution due to puckered diamine rings and asymmetric carbon atoms, respectively, were differentiated, and the CD origins of all the present complexes were discussed in connection with stereochemistry.

It has been considered that there are two stereochemical sources from which the circular dichroism (CD) of so-called praseo type complexes with chiral diamines arises: The conformational effect due to puckered chelate rings and the vicinal effect due to asymmetric atoms on ligands. Hawkins *et al.*[1] suggested that the CD spectra of *trans*-$[CoCl_2(diamine)_2]^+$ with (*R*)-propylenediamine (*R*-pn) and (1*R*,2*R*)-1,2-cyclohexanediamine (*R*,*R*-chxn) are contributed exclusively by the conformational effect rather than by the vicinal effect. This has been supported by the CD studies on Co^{III} complexes with analogous chiral diamines.[2,3] More explicit information about the CD origins of *trans*-$[MX_2(N)_4]$ type complexes will be afforded by the CD spectra of mixed diamine complexes of this type with different diamines; it may become feasible to test the additivity of the CD contributions from individual chiral diamines and moreover to differentiate between the conformational and the vicinal effect in this type of complexes. However, there has been no investigation on the CD spectra of mixed diamine complexes with *R*-pn, *R*,*R*-chxn, or (2*R*,4*R*)-2,4-pentanediamine (*R*,*R*-ptn), though a few CD studies in such a system have been reported on *trans*-$[CoCl_2(N)_4]^+$ containing *N*,*N*'-dimethylethylenediamine and the related diamines.[4,5] For this purpose, chromium(III) complexes are considered to be suitable, because a few mixed diamine chromium(III) complexes of the same type have already been prepared[6] and because the CD spectra in the first ligand field band region of Cr^{III} complexes behave similarly to those of Co^{III} complexes.

In this paper, the synthetic method for the known *trans*-difluoro mixed diamine chromium(III) complexes[6] is applied to the preparation for nine new Cr^{III} complexes with different diamines, which are pairs of *R*- and *S*-pn or ethylenediamine (en) with trimethylenediamine (tn), *R*,*R*-chxn, *R*,*R*-ptn, or (2*R*,4*S*)-2,4-pentanediamine (*R*,*S*-ptn). The ligand field absorption and CD spectra of these complexes are discussed in comparison with those of the same type complexes containing two identical chiral diamines. It is demonstrated that the CD contributions from the individual chiral diamines to the complexes are almost separable and additive except for such complexes as the bis(*R*-pn) and the bis(*R*,*R*-chxn) one, and that the conformational and the vicinal CD contributions from the chiral diamines are separated. The anomalous CD behavior of the bis(*R*-pn) and the bis(*R*,*R*-chxn) complexes is interpreted in terms of an additional chirality due to donor nitrogen atom distortions.

Experimental

Preparation of Ligands. The chiral diamines used were obtained by the methods described previously: *S*- and *R*-pn,[7] *R*,*R*-chxn,[8] *R*,*R*-ptn·2HCl,[2] and *R*,*S*-ptn·2HCl.[2]

Preparation of Complexes. *1)* trans-$[CrF_2(R\text{-}pn)_2]ClO_4$, trans-$[CrF_2(R,R\text{-}chxn)_2]Cl\cdot H_2O$, *and* trans-$[CrF_2(R,R\text{-}ptn)_2]ClO_4$: These complexes were prepared according to the literature methods for the *R*-pn, *R*,*R*-chxn complexes,[9] and *R*,*R*-ptn complex.[10] The *R*,*R*-chxn complex was originally isolated as the perchlorate salt and then converted to the chloride salt with an anion exchange resin of chloride form in a batchwise operation. Found: C, 38.71; H, 8.21%. Calcd for $[CrF_2(R,R\text{-chxn})_2]Cl\cdot H_2O$: C, 38.76; H, 8.13%.

2) trans-$[CrF_2(en)(R\text{-}pn)]Br\cdot H_2O$, trans-$[CrF_2(tn)(R\text{-}pn)]Br\cdot 1.5H_2O$, trans-$[CrF_2(R\text{-}pn)(R,R\text{-}chxn)]Br$, *and* trans-$[CrF_2(S\text{-}pn)(R,R\text{-}chxn)]Br\cdot 0.5H_2O$: The preparation of these mixed diamine complexes were carried out by the method of Vaughn and Marziwski[6] except that the chiral diamines (*R*-, *S*-pn, and *R*,*R*-chxn) were used instead of the racemic ones. Although they obtained only one isomer (*cis* one) for $[CrF_2(pn)(dach)]Br\cdot H_2O$ where pn and dach stand for *rac*-pn and *rac*-chxn, respectively, another isomer (*trans* one) of the corresponding complexes with the chiral diamines could be isolated after the reaction at about 50 °C. Found: C, 18.20; H, 6.16; N, 17.57%. Calcd for $[CrF_2(en)(R\text{-pn})]Br\cdot H_2O$: C, 18.64; H, 6.26; N, 17.39%. Found: C, 20.88; H, 6.65; N, 16.28%. Calcd for $[CrF_2(tn)(R\text{-pn})]Br\cdot 1.5H_2O$: C, 20.89; H, 6.72; N, 16.23%. Found: C, 31.18; H, 6.81%. Calcd for $[CrF_2(R\text{-pn})(R,R\text{-chxn})]Br$: C, 30.18; H, 6.75%. Found: C, 28.63; H, 6.69%. Calcd for $[CrF_2(S\text{-pn})(R,R\text{-chxn})]Br\cdot 0.5H_2O$: C, 29.44; H, 6.86%.

3) trans-$[CrF_2(en)(R,R\text{-}chxn)]Br\cdot 2H_2O$: This was prepared with use of *trans*(F)-$[CrF_2(H_2O)_2(en)]Br$[11] by a similar method to that for *trans*-$[CrF_2(R\text{-pn})(R,R\text{-chxn})]Br$. Found: C, 24.71; H, 6.60; N, 14.55%. Calcd for $[CrF_2(en)(R,R\text{-chxn})]Br\cdot 2H_2O$: C, 25.27; H, 6.89; N, 14.74%.

4) trans-$[CrF_2(en)(R,R\text{-}ptn)]Br\cdot H_2O$, trans-$[CrF_2(R\text{-}pn)(R,R\text{-}ptn)]Br\cdot H_2O$, trans-$[CrF_2(S\text{-}pn)(R,R\text{-}ptn)]Br\cdot 1.5H_2O$, *and* trans-$[CrF_2(R\text{-}pn)(R,S\text{-}ptn)]Br\cdot H_2O$: Pure sodium (0.3 g) was dissolved in 8 cm^3 of absolute ethanol. To this solution was added 1.1 g of *R*,*R*-ptn·2HCl or *R*,*S*-ptn·2HCl by portions; then white powder of sodium chloride was precipitated during vigorous stirring. After it was removed by

filtration and washed with a small amount of ethanol, *trans*(F)-[$CrBrF_2(H_2O)$(*R*-pn)] (or *trans*(F)-[$CrBrF_2(H_2O)$(*S*-pn)]) (1.7 g) or *trans*(F)-[$CrF_2(H_2O)_2$(en)]Br (1.7 g) was added to the filtrate and washings. The mixture was warmed on a water bath at about 50 °C for several hours. Then pink orange precipitate was obtained. After cooling in an ice bath, it was filtered off and recrystallized from methanol by the addition of ether. Found: C, 23.29; H, 6.81; N, 15.96%. Calcd for [CrF_2(en)(*R*,*R*-ptn)]Br·H_2O: C, 24.00; H, 6.91; N, 16.00%. Found: C, 25.88; H, 7.11; N, 15.23%. Calcd for [CrF_2(*R*-pn)(*R*,*R*-ptn)]Br·H_2O: C, 26.38; H, 7.20; N, 15.38%. Found: C, 25.72; H, 7.40; N, 15.20%. Calcd for [CrF_2(*S*-pn)(*R*,*R*-ptn)]Br·1.5H_2O: C, 25.74; H, 7.29; N, 15.01%. Found: C, 25.97; H, 7.35; N, 15.30%. Calcd for [CrF_2(*R*-pn)(*R*,*S*-ptn)]Br·H_2O: C, 26.38; H, 7.20; N, 15.38%.

Measurements. The electronic absorption spectra were measured by a Shimadzu UV-200S spectrophotometer. The CD spectra were recorded with a JASCO MOE-1 spectropolarimeter. These measurements were made on aqueous solutions ranging in concentration from 4×10^{-3} to 6×10^{-3} mol dm^{-3} at room temperature.

Results and Discussion

1) Absorption Spectra. The absorption spectral data of the present complexes are given in Table 1. Their positions and intensities are similar to those of *trans*-[$CrF_2(en)_2$]$^+$. Thus, it is apparent that these complexes have a *trans* geometrical structure.

The first ($^4T_{2g}\leftarrow{}^4A_{2g}$) and the second ($^4T_{1g}\leftarrow{}^4A_{2g}$) ligand field transition split into two components respectively; they have been assigned to the $^4E(^4T_{2g})$, $^4B_2(^4T_{2g})$, $^4E(^4T_{1g})$, and $^4A_2(^4T_{1g})$ states in D_4 symmetry from the longer wavelength side.[12] The absorption band intensities for *trans*-difluoro complexes with two identical diamines are found to be similar to one another, whereas those with different diamines give larger molar absorptivities than the former group of the complexes (Table 1). Such an intensity difference between the former and the latter group of the complexes is observed more clearly and more reliably for the $^4B_2$ and $^4A_2$ nondegenerate components than for the two ^4E components, because these nondegenerate components always exhibit prominent band peaks but not shoulders nor plateaus. On the theoretical basis, it has been pointed out that the absorption band intensities of the $^4B_2$ and $^4A_2$ components depend on the ligands on the xy plane; *i.e.*, the $(N)_4$ ligands in *trans*-[$CrF_2(N)_4$]$^+$ type complexes.[13] As seen through the absorption band intensities of the complexes with two identical diamines, the hyperchromic properties of the five- and six-membered diamines seem to be similar to one another. Therefore, the increase in intensity for the mixed diamine complexes is not caused by the hyperchromic properties of the diamines, but this may be responsible for the descent from D_2 to C_2 symmetry of the $(N)_4$ plane in these complexes.

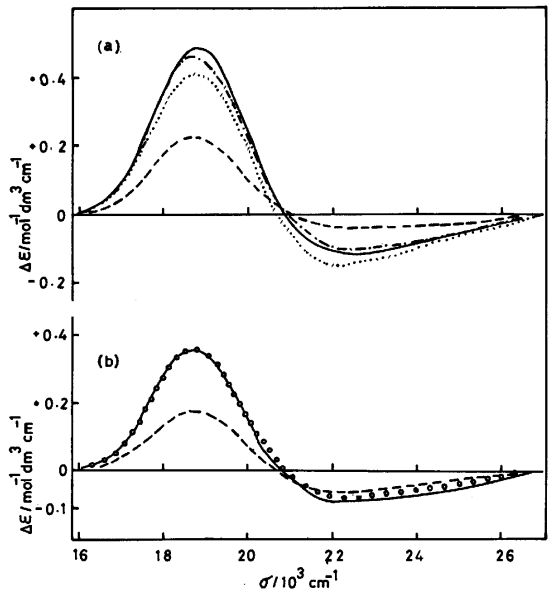

Fig. 1. a) CD curves of *trans*-[CrF_2(*R*-pn)(*R*,*R*-chxn)]$^+$ (——), *trans*-[CrF_2(*S*-pn)(*R*,*R*-chxn)]$^+$ (------), *trans*-[CrF_2(*R*-pn)$_2$]$^+$ (·····), and *trans*-[CrF_2(*R*,*R*-chxn)$_2$]$^+$ —·—); b) CD curves of *trans*-[CrF_2(en)(*R*-pn)]$^+$ (——), *trans*-[CrF_2(en)(*R*,*R*-chxn)]$^+$ (——), and *trans*-[CrF_2-(*rac*-pn)(*R*,*R*-chxn)]$^+$ ($1/2\{\Delta\varepsilon$(*R*-pn·*R*,*R*-chxn)$+\Delta\varepsilon$(*S*-pn·*R*,*R*-chxn)$\}$) (○○○○○).

Table 1. Absorption data of *trans*-[CrF_2(diamine)$_2$]$^+$ complexes

Diamine	$\sigma/10^3$ cm^{-1} (ε/mol^{-1} dm^3 cm^{-1})			
	$^4E(^4T_{2g})$	$^4B_2(^4T_{2g})$	$^4E(^4T_{1g})$	$^4A_2(^4T_{1g})$
(*R*-pn)$_2$	19.3 (17.4)[b]	21.5 (22.9)	25.0 (14.5)	28.5 (15.1)
(*R*,*R*-chxn)$_2$	18.9 (17.2)[b]	21.6 (24.1)	25.3 (15.2)	28.3 (16.2)
(*R*,*R*-ptn)$_2$	18.5 (19.1)[b]	21.3 (22.9)	25.0 (18.2)	27.8 (18.2)
(en)$_2$[a]	18.9 (16.5)[b]	21.5 (21.0)	25.2 (13.9)	28.5 (14.4)
(tn)$_2$[a]	18.6 (16.8)[b]	21.4 (20.7)	25.1 (16.5)	27.8 (16.3)
(en)(*R*-pn)	19.1 (19.8)[b]	21.3 (21.9)	25.1 (15.5)	28.4 (16.3)
(tn)(*R*-pn)	18.9 (19.6)[b]	21.4 (27.4)	25.2 (19.4)	28.2 (24.8)
(en)(*R*,*R*-chxn)	19.1 (22.8)[b]	21.6 (29.5)	25.6 (22.5)	28.4 (24.9)
(en)(*R*,*R*-ptn)	18.9 (20.2)[b]	21.4 (27.5)	25.3 (18.6)	28.3 (25.4)
(*R*-pn)(*R*,*R*-chxn)	18.9 (27.3)[b]	21.7 (37.0)	25.7 (32.7)	28.6 (36.2)
(*S*-pn)(*R*,*R*-chxn)	18.9 (25.3)[b]	21.5 (32.7)	25.3 (25.5)	28.4 (28.0)
(*R*-pn)(*R*,*R*-ptn)	18.9 (21.9)[b]	21.3 (28.8)	25.3 (19.7)	28.2 (26.3)
(*S*-pn)(*R*,*R*-ptn)	19.0 (21.2)[b]	21.4 (28.4)	25.1 (20.0)	28.2 (24.7)
(*R*-pn)(*R*,*S*-ptn)	19.0 (21.6)[b]	21.4 (30.5)	25.2 (22.0)	28.2 (28.4)

a) J. Glerup, J. Josephsen, K. Michesen, E. Pedersen, and C. E. Schäffer, *Acta Chem. Scand.*, **24**, 247 (1970). b) Shoulder.

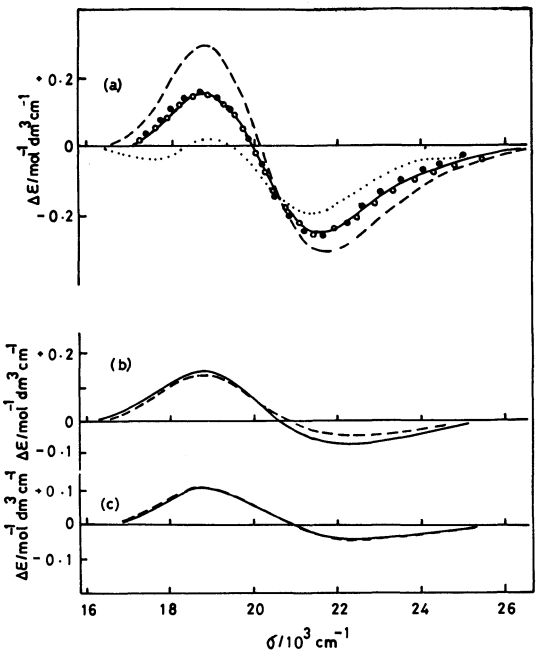

Fig. 2. a) CD curves of *trans*-$[CrF_2(R\text{-pn})(R,R\text{-ptn})]^+$ (------), *trans*-$[CrF_2(S\text{-pn})(R,R\text{-ptn})]^+$ (·····), *trans*-$[CrF_2(en)(R,R\text{-ptn})]^+$ (——), *trans*-$[CrF_2(R,R\text{-ptn})_2]^+$ (1/2 $\Delta\varepsilon$) (••••), and *trans*-$[CrF_2(rac\text{-pn})(R,R\text{-ptn})]^+$ (1/2{$\Delta\varepsilon(R\text{-pn}\cdot R,R\text{-ptn})+\Delta\varepsilon(S\text{-pn}\cdot R,R\text{-ptn})$}) (ooooo); b) CD curves of *trans*-$[CrF_2(R\text{-pn})(rac\text{-ptn})]^+$ (1/2{$\Delta\varepsilon(R\text{-pn}\cdot R,R\text{-ptn})-\Delta\varepsilon(S\text{-pn}\cdot R,R\text{-ptn})$}) (——) and *trans*-$[CrF_2(R\text{-pn})(rac\text{-chxn})]^+$ (1/2{$\Delta\varepsilon(R\text{-pn}\cdot R,R\text{-chxn})-\Delta\varepsilon(S\text{-pn}\cdot R,R\text{-chxn})$}) (------); c) CD curves of *trans*-$[CrF_2(tn)(R\text{-pn})]^+$ (——) and *trans*-$[CrF_2(R\text{-pn})(R,S\text{-ptn})]^+$ (----).

TABLE 2. CD DATA OF *trans*-$[CrF_2(\text{DIAMINE})_2]^+$ COMPLEXES

$(\text{diamine})_2$	$\sigma_{ext}/10^3\ cm^{-1}$ $(\Delta\varepsilon/mol^{-1}\ dm^3\ cm^{-1})$	
$(R\text{-pn})_2$	18.8 (+0.41)	22.0 (−0.15)
$(R,R\text{-chxn})_2$	18.7 (+0.46)	22.0 (−0.11)
$(en)(R\text{-pn})$	18.9 (+0.17)	22.3 (−0.06)
$(tn)(R\text{-pn})$	18.8 (+0.11)	22.3 (−0.04)
$(R\text{-pn})(R,S\text{-ptn})$	18.8 (+0.11)	22.7 (−0.04)
$(en)(R,R\text{-chxn})$	18.8 (+0.33)	22.6 (−0.09)
$(R\text{-pn})(R,R\text{-chxn})$	18.8 (+0.48)	22.3 (−0.12)
$(S\text{-pn})(R,R\text{-chxn})$	18.7 (+0.22)	22.3 (−0.04)
$(R,R\text{-ptn})_2$	18.7 (+0.31)	21.7 (−0.53)
$(en)(R,R\text{-ptn})$	18.9 (+0.15)	21.7 (−0.26)
$(R\text{-pn})(R,R\text{-ptn})$	18.8 (+0.29)	21.2 (−0.31)
$(S\text{-pn})(R,R\text{-ptn})$	17.4 (−0.05)	
	18.9 (+0.01)	21.5 (−0.21)

2) CD Spectra. The CD spectra of the present complexes are given in Figs. 1 and 2, and their data are summarized in Table 2. Since the CD spectrum of *trans*-$[CrF_2(R,R\text{-chxn})_2]^+$ resembles that of *trans*-$[CrF_2(R\text{-pn})_2]^+$ (Fig. 1 and Table 2), it appears that the overall CD of these complexes arise mainly from the conformational effect due to the λ ring conformation[10] rather than from the vicinal effect as found for the CD spectra of Co^{III} complexes.[1-3] From this result, it might be predicted that the CD spectrum of *trans*-$[CrF_2(en)(R\text{-pn})]^+$ should be similar to that of *trans*-$[CrF_2(en)(R,R\text{-chxn})]^+$, and that *trans*-$[CrF_2(S\text{-pn})(R,R\text{-chxn})]^+$ should give negligibly weak CD. These are not observed for the present complexes. That is, the CD intensity of *trans*-$[CrF_2(en)(R,R\text{-chxn})]^+$ is twice as strong as that of *trans*-$[CrF_2(en)(R\text{-pn})]^+$, and *trans*-$[CrF_2(S\text{-pn})(R,R\text{-chxn})]^+$ gives appreciable CD intensity (Fig. 1 and Table 2). These facts indicate that each contribution of the *R*-pn and *R,R*-chxn ligands to optical activity of the mixed diamine complexes differs significantly from that of the bis(*R*-pn) and the bis(*R,R*-chxn)-complex. In order to examine the difference in CD behavior between the complexes with identical diamines and those with different diamines in more detail, the separation of each CD contribution from the *R*-pn and the *R,R*-chxn ligand to the mixed diamine complexes is attempted by the addition and the substraction of the CD curves of *trans*-$[CrF_2(R\text{-pn})(R,R\text{-chxn})]^+$ and *trans*-$[CrF_2(S\text{-pn})(R,R\text{-chxn})]^+$. The same treatment is carried out for *trans*-$[CrF_2(R\text{-pn})(R,R\text{-ptn})]^+$ and *trans*-$[CrF_2(S\text{-pn})(R,R\text{-ptn})]^+$. The CD contributions of the chiral diamines thus obtained correspond to the CD curves of *trans*-$[CrF_2(rac\text{-pn})(R,R\text{-chxn})]^+$ and *trans*-$[CrF_2(R\text{-pn})(rac\text{-chxn})]^+$ for the former case, and to those of *trans*-$[CrF_2(rac\text{-pn})(R,R\text{-ptn})]^+$ and *trans*-$[CrF_2(R\text{-pn})(rac\text{-ptn})]^+$ for the latter case. They are compared with each other in Figs. 1 and 2. The CD contribution from the *R,R*-chxn to *trans*-$[CrF_2(rac\text{-pn})(R,R\text{-chxn})]^+$ and that from the *R,R*-ptn to *trans*-$[CrF_2(rac\text{-pn})(R,R\text{-ptn})]^+$ are identical with the overall CD curve of *trans*-$[CrF_2(en)(R,R\text{-chxn})]^+$ and that of *trans*-$[CrF_2(en)(R,R\text{-ptn})]^+$ (and also one half that of *trans*-$[CrF_2(R,R\text{-ptn})_2]^+$), respectively. For *trans*-$[CrF_2(R\text{-pn})(rac\text{-chxn})]^+$, the CD contribution from the *R*-pn is similar to that from the *R*-pn to *trans*-$[CrF_2(R\text{-pn})(rac\text{-ptn})]^+$, especially in the region of the longer wavelength CD component, but does not agree appreciably with the CD curve of *trans*-$[CrF_2(en)(R\text{-pn})]^+$, *trans*-$[CrF_2(tn)(R\text{-pn})]^+$, and one half that of *trans*-$[CrF_2(R\text{-pn})_2]^+$. Accordingly, it can be seen that the CD contributions of the chiral diamines to the present complexes are separable and additive except for the cases of the bis(*R*-pn), bis(*R,R*-chxn), and the mono(*R*-pn) complexes with ethylenediamine and trimethylenediamine. In view of such additivity of the CD for the complexes, there may be no significant interaction between two different diamines in the complexes; free puckering of the ethylenediamine ring occurs for *trans*-$[CrF_2(en)(R,R\text{-chxn})]^+$ and *trans*-$[CrF_2(en)(R,R\text{-ptn})]^+$ in solution. As to *trans*-$[CrF_2(tn)(R\text{-pn})]^+$, the CD spectrum is quite identical with the CD of *trans*-$[CrF_2(R\text{-pn})(R,S\text{-ptn})]^+$, but differs from that of *trans*-$[CrF_2(R\text{-pn})(rac\text{-ptn})]^+$ (Fig. 2). This fact suggests that the coordinated trimethylenediamine takes the same conformation as the *R,S*-ptn ligand, which has been determined to have a chair form by the X-ray structural analysis of $(+)_{560}$-$[Co(ox)(R,S\text{-ptn})_2]ClO_4\cdot H_2O$.[14] This will be substantiated more evidently by the CD study on *trans*-$[Cr(ONO)_2(R\text{-pn})(R,S\text{-ptn})]^+$ and *trans*-$[Cr(ONO)_2(tn)(R\text{-pn})]^+$ as discussed in a subsequent paper.[15] The CD behavior of *trans*-$[CrF_2(en)(R\text{-pn})]^+$ may be interpreted as follows. From a similarity in absorption

band intensity between *trans*-$[CrF_2(en)(R\text{-pn})]^+$ and *trans*-$[CrF_2(R\text{-pn})_2]^+$ (Table 2) and from good coincidences in shape and size between the *R*-pn and ethylenediamine rings in complexes as revealed by X-ray structural analyses,[16,17] it is supposed that the effective symmetry of the $(N)_4$ plane in the former mono(*R*-pn) complex is similar to the D_2 symmetry of the rectangular $(N)_4$ plane in the latter bis(*R*-pn) complex as seen through the Section *1)*. In this case, the steric interaction between the *R*-pn and ethylenediamine ligands may occur owing to the proximity between the amine protons of the ethylenediamine and the adjacent ones of the *R*-pn. Meanwhile, there may be no significant interaction in the lower C_2 symmetry complexes with nonidentical diamines having the different N–Cr–N angles as noted above, probably because the deformation of the $(N)_4$ planes from the rectangle to the trapezoid may decrease the crowding between the two diamine moieties. This interaction appears to cause restricted puckering of the ethylenediamine ring, resulting in some CD contribution from the ethylenediamine ligand to this mixed diamine complex. This seems to be the reason why the CD spectrum of *trans*-$[CrF_2(en)(R\text{-pn})]^+$ differs from one half of the CD of the bis(*R*-pn) complex and from the CD contribution of the *R*-pn to *trans*-$[CrF_2(R\text{-pn})(rac\text{-chxn})]^+$ and *trans*-$[CrF_2(R\text{-pn})(rac\text{-ptn})]^+$.

The longer wavelength CD component of *trans*-$[CrF_2(rac\text{-pn})(R,R\text{-chxn})]^+$ is more than twice as intense as that of *trans*-$[CrF_2(R\text{-pn})(rac\text{-chxn})]^+$ and *trans*-$[CrF_2(R\text{-pn})(rac\text{-ptn})]^+$ (Figs. 1 and 2). Such a difference in CD contribution between the *R*-pn and the *R,R*-chxn ligand may be understood by the differentiation between the conformational and the vicinal effect. For this purpose, it is assumed that the CD contributions of the chiral diamines consist of the conformational effect ($\Delta\varepsilon(\lambda)$ for the *R*-pn and the *R,R*-chxn ligand; $\Delta\varepsilon(\lambda')$ for the *R,R*-ptn ligand) and the vicinal effect ($\Delta\varepsilon(R)$ for all these three diamines) as expressed in the following equations,

$$\Delta\varepsilon(R\text{-pn}\cdot R,R\text{-chxn}) = 3\Delta\varepsilon(R) + 2\Delta\varepsilon(\lambda),$$

$$\Delta\varepsilon(S\text{-pn}\cdot R,R\text{-chxn}) = \Delta\varepsilon(R),$$

$$\Delta\varepsilon(R\text{-pn}\cdot R,R\text{-ptn}) = 3\Delta\varepsilon(R) + \Delta\varepsilon(\lambda) + \Delta\varepsilon(\lambda'),$$

$$\Delta\varepsilon(S\text{-pn}\cdot R,R\text{-ptn}) = \Delta\varepsilon(R) - \Delta\varepsilon(\lambda) + \Delta\varepsilon(\lambda'),$$

where the *R* configuration of asymmetric carbons requires the λ conformation due to the equatorial preference of alkyl-substituents on ligands, and $\Delta\varepsilon(R) = -\Delta\varepsilon(S)$ and $\Delta\varepsilon(\lambda) = -\Delta\varepsilon(\delta)$. From the above equations, the conformational and the vicinal CD contribution are obtained as shown in Fig. 3. The considerable CD contribution from the vicinal effect due to the *R* configuration for the *R*-pn and the *R,R*-chxn ligand leads to the difference in CD contribution between the *R*-pn and the *R,R*-chxn ligand. It is noted that the net CD signs in the first ligand field $^4T_{2g} \leftarrow {}^4A_{2g}$ transition for the conformational contributions of both the *R*-pn(*R,R*-chxn) and the *R,R*-ptn ligand are the same as each other and are opposite to those for the vicinal contributions as seen in Fig. 3. The net CD signs for the λ conformation and the *R* configuration of asymmetric carbons, negative and positive, respectively, are consistent with the predicted ones in terms of the regional (hexadecadal) rule.[18] It is considered unlikely that the conformational and the vicinal CD contribution in the mixed diamine complexes with different diamines are much different from those in the bis(*R*-pn) and the bis(*R,R*-chxn) complexes. Thus, the inconsistency in CD behavior between the mixed diamine complexes and the bis(*R*-pn), bis(*R,R*-chxn) complexes may be explained on the assumption of an additional chirality probably due to donor nitrogen atom distortions in the latter complexes. As shown in Figs. 1 and 2, the CD spectrum of *trans*-$[CrF_2(R\text{-pn})_2]^+$ is more intense than twice the CD contribution of the *R*-pn to *trans*-$[CrF_2(R\text{-pn})(rac\text{-chxn})]^+$ or the calculated CD curve contributed solely from the conformational and the vicinal effects (*i.e.*, $2\Delta\varepsilon(R)+2\Delta\varepsilon(\lambda)$), whereas the CD spectrum of *trans*-$[CrF_2(R,R\text{-chxn})_2]^+$ is less intense than twice the CD contribution of the *R,R*-chxn to *trans*-$[CrF_2(rac\text{-pn})(R,R\text{-chxn})]^+$ or the calculated CD curve (*i.e.*, $4\Delta\varepsilon(R)+2\Delta\varepsilon(\lambda)$). This observation suggests that the CD contributions from an additional chirality to the bis(*R*-pn) and the bis(*R,R*-chxn) complex are not equivalent and opposite in sign to each other; positive and negative CD being contributed to the bis(*R*-pn) and the bis(*R,R*-chxn) complexes, respectively. The regional rule predicts that such an additional CD contribution is induced by donor nitrogen atoms which are skewed away from ideal octahedral edges in such a way that they lie in the same sector as the ring alkyl group ($-CH_2CH-$) for the bis(*R*-pn) complex and as the *C*-alkyl substituents for the bis(*R,R*-chxn) complex as depicted in Fig. 4. Similar displacement of the donor nitrogen atoms in the *R*-pn complex has been found by the X-ray structural crystallography of *trans*-$[CoCl_2(R\text{-pn})_2]Cl\cdot HCl\cdot H_2O$[14] as pointed out previously.[2,19] It is likely that such a distortion arises from the steric interaction between the identical diamines in the bis(*R*-pn) and the bis(*R,R*-chxn) complex. For *trans*-$[CrF_2(en)(R\text{-pn})]^+$, which encounters a similar situation to the bis(*R*-pn) complex as noted above, the crowding between the diamine moieties may be released by shifting the conformational equilibrium of the ethylenediamine ring puckering and/or by distorting the donor nitrogen atoms. For other mixed diamine complexes with

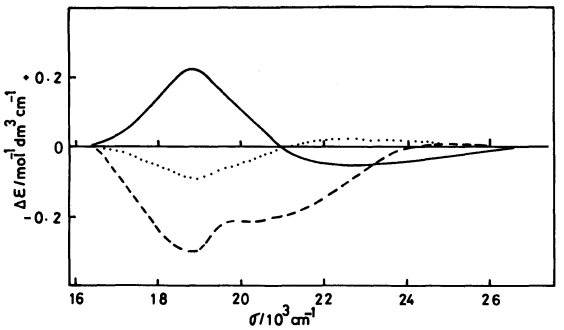

Fig. 3. The CD contribution from the vicinal effect due to the configuration of asymmetric carbons ($\Delta\varepsilon(R)$) (——); the CD contribution from the conformational effect due to five-membered chelate rings (*R*-pn and *R,R*-chxn) ($\Delta\varepsilon(\lambda)$) (·····) and of a six-membered one (*R,R*-ptn) ($\Delta\varepsilon(\lambda')$) (------).

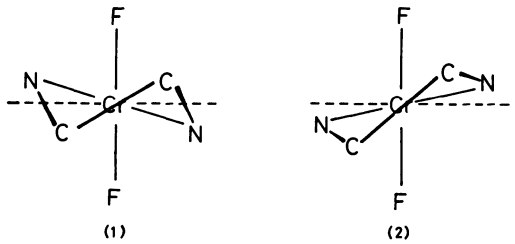

Fig. 4. Proposed donor nitrogen atom displacements from ideal octahedral edges for *R*-pn(1) and *R,R*-chxn (2) rings.

nonidentical diamines, it is plausible that there seems to be no observable CD contribution from the donor nitrogen atom distortions, because of no appreciable steric interaction between the different diamines in these complexes as mentioned above.

The author wishes to thank Prof. Yoichi Shimura of Osaka University for making the CD spectra available for this work. The present study was partially supported by a Grant-in-Aid for Scientific Research from the Ministry of Education, Science and Culture.

References

1) C. J. Hawkins, L. Larsen, and I. Olsen, *Acta Chem. Scand.*, **19**, 1915 (1965).
2) B. Bosnich and J. MacB. Harrowfield, *J. Am. Chem. Soc.*, **94**, 3425 (1972).
3) S. Yano, M. Saburi, S. Yoshikawa, and J. Fujita, *Bull. Chem. Soc. Jpn.*, **49**, 101 (1976).
4) S. F. Mason, *J. Chem. Soc., A*, **1971**, 667.
5) J. A. Tiethof and D. W. Cooke, *Inorg. Chem.*, **11**, 315 (1972).
6) J. W. Vaughn and J. Marzowski, *Inorg. Chem.*, **12**, 2346 (1973).
7) "Shinjikken Kagaku Koza," ed by the Chemical Society of Japan, Maruzen, Tokyo (1975), Vol. 8, p. 1429.
8) F. Galsbøl, F. Steenbøl, and B. S. Sørensen, *Acta Chem. Scand.*, **26**, 3605 (1972).
9) J. Glerup, J. Josephsen, K. Michelsen, E. Pedersen, and C. E. Schäffer, *Acta Chem. Scand.*, **24**, 247 (1970).
10) S. Kaizaki and Y. Shimura, *Bull. Chem. Soc. Jpn.*, **48**, 3611 (1975).
11) S. Kaizaki, M. Akaho, Y. Morita, and K. Uno, *Bull. Chem. Soc. Jpn.*, **54**, 3191 (1981).
12) L. Dubicki, M. A. Hitchman, and P. Day, *Inorg. Chem.*, **9**, 188 (1969).
13) S. Fujinami, M. Shibata, and H. Yamatera, *Bull. Chem. Soc. Jpn.*, **51**, 1391 (1978).
14) I. Oonishi, S. Sato, and Y. Saito, *Acta Crystallogr., Sect. B*, **30**, 2256 (1974).
15) S. Kaizaki, *Bull. Chem. Soc. Jpn.*, **56**, 3625 (1983).
16) Y. Saito and I. Iwasaki, *Bull. Chem. Soc. Jpn.*, **35**, 1131 (1962).
17) A. Nakahara, Y. Saito, and H. Kuroya, *Bull. Chem. Soc. Jpn.*, **25**, 331 (1952).
18) F. S. Richardson, *Inorg. Chem.*, **11**, 2366 (1972).
19) S. F. Mason and R. H. Seal, *Mol. Phys.*, **31**, 755 (1976).

 © 1983 The Chemical Society of Japan Bull. Chem. Soc. Jpn., 56, 3625—3631 (1983)

Circular Dichroism of Chromium(III) Complexes. IX. Circular Dichroism Spectra and Stereochemistry of Dinitritobis-(diamine)chromium(III) Complexes

Sumio KAIZAKI

Department of Chemistry, Faculty of Science, Nara Women's University, Nara 630

(Received May 28, 1983)

The circular dichroism (CD) spectra of optically active dinitritobis(diamine)chromium(III) complexes were measured in the visible and near-ultraviolet region, where the diamines used were ethylenediamine, trimethylenediamine, (*R*)-propylenediamine, (1*R*, 2*R*)-1,2-cyclohexanediamine, (2*R*, 4*R*)- and (2*R*, 4*S*)-2,4-pentanediamine. The stereochemistry and the conformational (rotational) isomerism of coordinated nitrito ligands were discussed on the basis of the solvent-dependent CD spectra in the near-ultraviolet region of an intraligand absorption band localized on nitrito ligands. It is proposed that the CD variation in the intraligand transition region among the complexes concerned is responsible for the chiral arrangement of nitrito ligands. Further, the conformation of trimethylenediamine chelate in the *trans*-dinitrito-(*R*)-propylenediamine complex is determined to take a chair form in comparison with the CD behavior of the corresponding (2*R*, 4*S*)-2,4-pentanediamine complex.

There have been few studies on stereochemistry of unidentate ligands in complexes. A new conformational or rotational isomerism of coordinated unidentate ligands has been first discovered for "brown" and "yellow" crystal forms of *mer*-$[Co(NO_2)_3(NH_3)(en)]$[1] and established by X-ray structural analyses.[2] Since these isomers show the identical physical properties in solution,[1] it is difficult to recognize such a conformational isomerism in solution. It has been proposed that the solvent-dependent CD variation in the first ligand field band region of some dianionotetraamine Co^{III} complexes is responsible for optical activity due to rotational conformations of unidentate aniono ligands such as NO_2^- and N_3^-.[3] However, CD spectra in the d-d band region are not appropriate for the investigation on stereochemistry of unidentate ligands in various circumstances brought about by different chelate rings, because they are susceptible to ring conformations and geometrical configurations of complexes. CD spectra associated with intraligand transitions of unidentate ligands will provide the stereochemical information about such unidentate ligands themselves. For instance, it has been found that for organic nitrites several well-defined vibronic CD peaks observed in the nitrite chromophore region (400—350 nm) are sensitive to the stereochemical environments around nitrites.[4] In the corresponding region of oxygen-bonded nitritochromium(III) complexes, some inflections of the vibronic structure overlapping with a broad absorption band envelope due to the second d-d transition have been observed in dipolar aprotic solvents; they are ascribed to the intraligand $n\rightarrow\pi^*$ transition localized on the coordinated nitrito ligands.[5] In addition to such spectral properties, taking into account the fact that nitrito Cr^{III} complexes are relatively stable and do not isomerize to N-bonded nitro complexes, the CD spectra in the intraligand transition region of these complexes may be useful for the stereochemical investigation of unidentate ligands. In a previous letter,[6] the CD spectra in the intraligand band region of optically active *cis*- and *trans*-dinitritobis(diamine)-chromium(III) complexes have been explained in terms of the chiral arrangements of nitrito ligands. In this paper, the intraligand CD spectra of mononitrito and dinitrito chromium(III) complexes of various diamines are examined in order to assess the effect of the stereochemical environment around the coordinated diamine chelate rings on the rotational isomerism of coordinated nitrito ligands, where the diamines used are ethylenediamine(en), trimethylenediamine(tn), (*R*)-propylenediamine(*R*-pn), (1*R*, 2*R*)-1, 2-cyclohexanediamine(*R*,*R*-chxn), (2*R*,4*R*)- and (2*R*,4*S*)-2,4-pentanediamine(*R*,*R*-ptn and *R*,*S*-ptn).

Experimental

Preparation of Complexes. *1)* trans-$[Cr(ONO)_2(diamine)_2]ClO_4$: *trans*-Difluorobis(diamine) complexes were obtained as starting materials by the methods described elsewhere.[7-9] These difluoro complexes were converted into *trans*-dibromobis-(diamine)chromium(III) bromides by dissolving the difluoro complexes in 3.5 M (1 M=1 mol dm^{-3}) methanolic hydrogen bromide solutions.[8] The nitrito complexes were obtained as anhydrous perchlorate salts by the reaction with lithium nitrite in weakly acidified solutions after aquating the corresponding dibromo complexes at about 60 °C for 5 min, and then by the addition of an excess amount of lithium perchlorate. The complexes were recrystallized from acetonitrile by the addition of ether.

2) trans-$[CrF(ONO)(R,R\text{-}chxn)_2]ClO_4\cdot 0.5LiClO_4$: This mono nitrito complex was prepared by a similar method to that for *trans*-$[CrF(ONO)(en)_2]ClO_4$.[10]

3) $(+)^{Ag}_{480}$-cis-$[Cr(ONO)_2(en)_2]ClO_4$ *and* $(+)^{Ag}_{480}$-cis-$[Cr(ONO)_2(tn)_2]ClO_4\cdot 0.5LiClO_4$: As starting materials, the corresponding *cis*-dichloro complexes were prepared and resolved into the optical isomers according to the reported methods.[11-13] The less soluble $(+)^{Ag}_{520}$-optical isomers of these *cis*-dichlorobis(diamine)chromium(III) 3-bromo-*d*-camphor-8-sulfonate were aquated with an appropriate amount of silver nitrate in an ice-cold solution. After silver chloride was removed, the perchlorate salts of the corresponding dinitrito complexes were isolated by the successive addition of lithium nitrite and lithium perchlorate below 5 °C. Although the racemization of these optically active *cis*-bis-(diamine) complexes should be taken into consideration, the CD intensity in the first band region is found to be comparable to that of other *cis*-$[CrX_2(en)_2]^+$ type complexes.[13] Thus, it appears that the racemization of the dinitrito complexes is not significant during the preparation.

TABLE 1. ANALYTICAL DATA OF THE COMPLEXES

Complex	C(%)		H(%)		N(%)	
	Found	Calcd	Found	Calcd	Found	Calcd
trans-$[Cr(ONO)_2(R\text{-pn})_2]ClO_4$	18.18	18.40	5.24	5.15	21.54	21.45
trans-$[Cr(ONO)_2(R,R\text{-ptn})_2]ClO_4$	26.59	26.82	6.47	6.30	19.10	18.77
trans-$[Cr(ONO)_2(R,R\text{-chxn})_2]ClO_4$	30.05	30.55	6.09	5.98	17.80	17.81
trans-$[CrF(ONO)(R,R\text{-chxn})_2]ClO_4\cdot 0.5LiClO_4$	28.82	28.94	5.93	5.67		
trans-$[Cr(ONO)_2(en)(R\text{-pn})]ClO_4$	15.23	15.90	4.64	4.80	22.10	22.25
trans-$[Cr(ONO)_2(tn)(R\text{-pn})]ClO_4$	18.12	18.40	5.11	5.15	21.11	21.46
trans-$[Cr(ONO)_2(R\text{-pn})(R,R\text{-ptn})]ClO_4$	23.00	22.89	5.68	5.76	19.02	20.02
trans-$[Cr(ONO)_2(R\text{-pn})(S,S\text{-ptn})]ClO_4$	22.84	22.89	5.78	5.76	20.08	20.02
trans-$[Cr(ONO)_2(R\text{-pn})(R,S\text{-ptn})]ClO_4$	22.51	22.89	5.71	5.76	19.45	20.02
trans-$[Cr(ONO)_2(en)(R,R\text{-ptn})]ClO_4$	20.45	20.72	5.39	5.47	20.34	20.71
$(+)^{\lambda_s}_{480}$-*cis*-$[Cr(ONO)_2(en)_2]ClO_4$	13.63	13.21	4.63	4.43	23.29	23.11
$(+)^{\lambda_s}_{480}$-*cis*-$[Cr(ONO)_2(tn)_2]ClO_4\cdot 0.5LiClO_4$	16.34	16.20	4.55	4.53	19.34	18.89

The elemental analyses of the complexes are presented in Table 1.

Measurements. Absorption and CD spectra were recorded with a Shimadzu UV-200S spectrophotometer and a JASCO MOE-1 spectropolarimeter, respectively. All the solvents used are of spectrograde. The concentrations of the complexes were 2×10^{-3} to 4×10^{-3} M. CD measurements in KBr disks were carried out by a similar procedure to that of Bosnich *et al.*[14]

Results and Discussion

Stereochemistry of Nitrito Ligands. The geometrical structures of the dinitritobis(diamine)chromium(III) complexes are assigned by comparing their visible and near-ultraviolet absorption spectra with those of the known *cis*- and *trans*-dinitritobis(ethylenediamine)chromium(III) complexes;[5] the geometrical structure is retained on the anation of the corresponding diaqua complexes with nitrite ions in acidic solutions. As shown in Fig. 1, the first d-d absorption bands of *cis*- and *trans*-isomers of the complexes differ from each other, while the isomers give a similar spectral behavior in the second

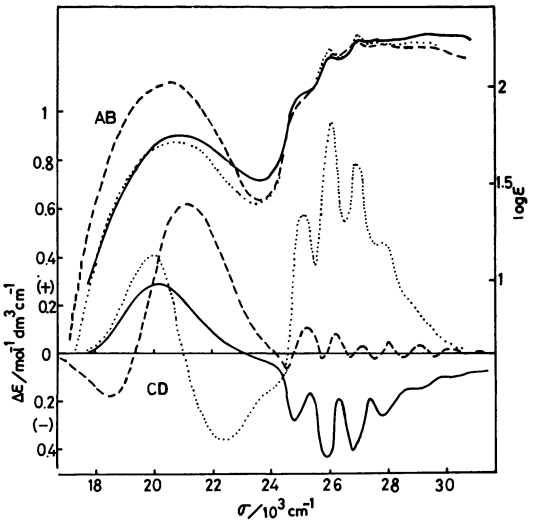

Fig. 1. Absorption (AB) and CD curves of $(+)^{\lambda_s}_{480}$-*cis*-$[Cr(ONO)_2(en)_2]ClO_4$ (——), *trans*-$[Cr(ONO)_2(R\text{-pn})_2]ClO_4$ (------), and *trans*-$[Cr(ONO)_2(R,R\text{-ptn})_2]ClO_4$ (·····) in DMF.

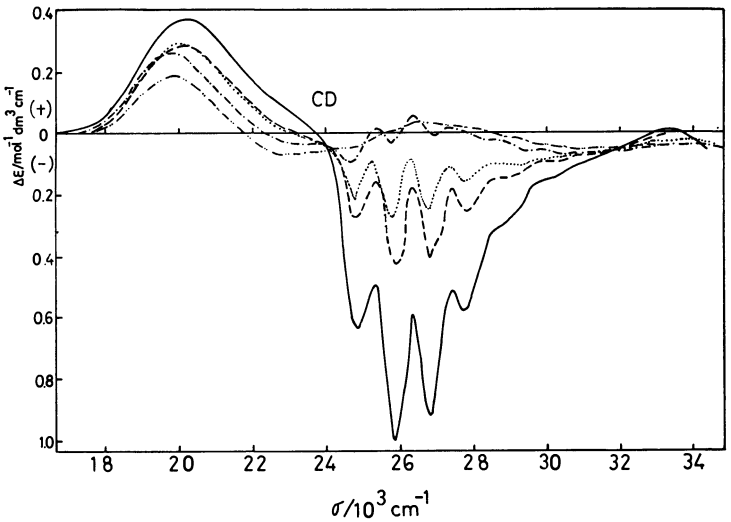

Fig. 2. CD curves of *trans*-$[Cr(ONO)_2(R\text{-pn})_2]ClO_4$.
Solvents: DMA (——); DMF (------); NMF (·····); formamide (—·—); H_2O (—··—).

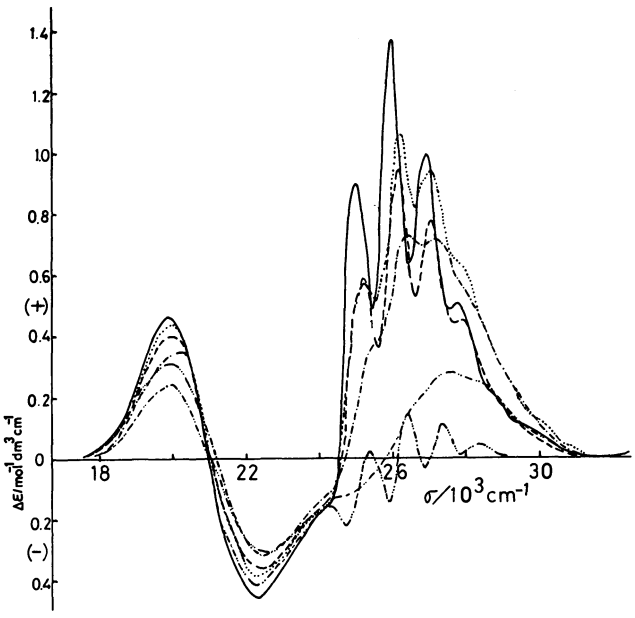

Fig. 3. CD curves of *trans*-$[Cr(ONO)_2(R,R\text{-ptn})_2]ClO_4$.
Solvents: DMA (——); DMF (------); NMF (·····); formamide (—·—); H_2O (—··—); acetonitrile (—···—).

d-d band region where the n→π^* intraligand transition within nitrito ligands occurs. Some characteristic inflections on this absorption band are observed for *cis*- and *trans*-dinitritobis(diamine)chromium(III) complexes in aprotic solvents such as *N,N*-dimethylformamide (DMF).[5] On their CD spectra in the region from 24000 to 30000 cm^{-1}, more marked characteristics of the intraligand transition are recognized in aprotic solvents than those on the absorption spectra.[6] The CD spectra of the complexes in DMF give more remarkable and well resolved peaks, of which each position corresponds to that of the absorption spectra as seen in Fig. 1. The absorption maxima and CD extrema consist of the progression of about 1000 cm^{-1}, originating from 25000 cm^{-1}, due to the N–O stretching vibration as found in the vibronic structure of $NaNO_2$ crystals.[15] The intensity distribution of the CD spectra is found to be in line with that of alkyl nitrites.[4] Therefore, each vibronic CD component in this region is certainly associated with the intraligand n→π^* transition of the coordinated nitrito ligands in the complexes. Figures 2—4 show the remarkable solvent-dependent variation of the CD spectra of some complexes. It is found that the intensity enhancement of the vibronic CD components is more pronounced than that of the CD in the first d-d band region. As shown in Figs. 2 and 3, a positive CD band in the second band region at about 27500 cm^{-1} for *trans*-dinitritobis(diamine) complexes in H_2O may correspond to the second ligand field ($^4T_{1g}$←$^4A_{2g}$) transition, because this lies at the expected position for the $^4E_g(D_{4h})$ component of the $^4T_{1g}$ parentage and in general *trans*-dihalogenobis(diamine)chromium(III) complexes with *R*-pn and *R,R*-ptn ligands give a positive CD component due to the second ^4E_g←$^4B_{1g}$ transition.[8] This suggests that the vibronic CD components of the *trans*-bis(*R*-pn) complex undergo sign inversions by changing the solvent from water to aprotic solvents in contrast with the CD behavior of the *trans*-bis(*R,R*-ptn) complex where no CD sign inversion occurs with solvent change. In addition to these CD behavior, the considerable CD intensity enhancement of *trans*-bis(diamine) complexes in aprotic solvents as shown in Figs. 2 and 3 will also support the exclusive contribution of optical activity associated with the intraligand transition within nitrito ligands to the vibronic CD components.

It is noted that the signs of the intraligand CD spectra for the *trans*-bis(*R*-pn) and -bis(*R,R*-ptn) complexes are opposite to each other though the diamines have the same absolute configuration, and also that the CD behavior of the $(+)^{\Delta\varepsilon}_{480}$-*cis*-bis(en) complex differs from that of the $(+)^{\Delta\varepsilon}_{480}$-*cis*-bis(tn) complex as well as that of the *trans*-bis(diamine) complexes as seen in Figs. 2—5. Such differences in intraligand CD among these complexes may be attributed to the different stereochemical environment experienced by nitrito ligands in the complexes. There are two possible coordination modes of unidentate nitrito ligands with respect to the rotation about the (O)N–O(Cr) bond. As revealed in $[Cr(ONO)(NH_3)_5](ClO_4)_2$ and other nitrito metal complexes by X-ray structural analyses,[16,17] a nitrito ligand in a

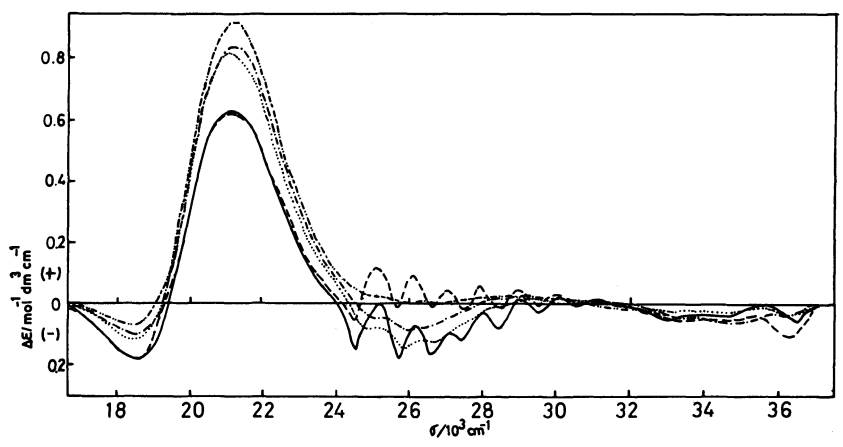

Fig. 4. CD curves of $(+)^{\Delta\varepsilon}_{480}$-*cis*-$[Cr(ONO)_2(en)_2]ClO_4$.
Solvents: DMA (——); DMF (------); NMF (·····); formamide (—·—); H_2O (—··—).

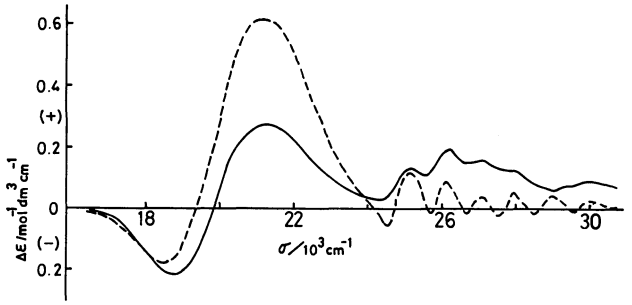

Fig. 5. CD curves of $(+)^{A}_{480}$-*cis*-$[Cr(ONO)_2(tn)_2]ClO_4$ (——) and $(+)^{A}_{480}$-*cis*-$[Cr(ONO)_2(en)_2]ClO_4$ (------) in DMF.

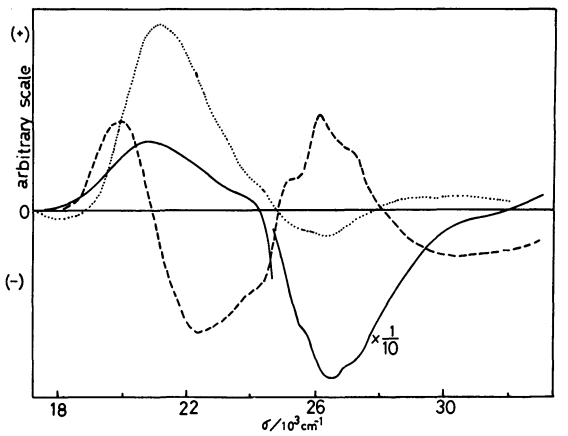

Fig. 6. CD curves of *trans*-$[Cr(ONO)_2(R\text{-pn})_2]ClO_4$ (——), *trans*-$[Cr(ONO)_2(R,R\text{-ptn})_2]ClO_4$ (------), and $(+)^{A}_{480}$-*cis*-$[Cr(ONO)_2(en)_2]ClO_4$ (·····) in a KBr disk.

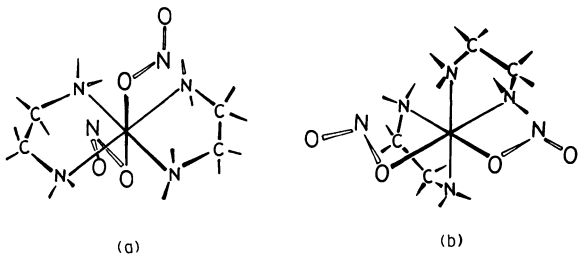

Fig. 7. Proposed configurations due to rotamer conformations of two nitrito ligands in (a) *trans*-$[Cr(ONO)_2(R\text{-pn})_2]ClO_4$ and (b) $(+)^{A}_{480}$-*cis*-$[Cr(ONO)_2(en)_2]ClO_4$ with a $\Lambda(\delta\delta)lel_2$ configuration. The methyl group of *R*-pn and all protons are omitted for clarity.

complex prefers the trans form to the cis one, minimizing the steric interaction with the amine ligands. With this coordination mode, the rotation of nitrito ligands about the Cr–O(NO) bond seems to have immediate influence on optical activity of the intraligand transition localized on nitrito ligands. Restricted rotation can form rotamers of different conformations at equilibrium and can produce new chirality with respect to the whole molecule, while complete free rotation can contribute little to optical activity. In the latter case, the intraligand transition acquires the rotational strength only through so-called "vicinal effect" which originates from the chiral diamine chelates. It is probable that the equilibrium of such rotamers depends on a given stereochemical circumstance around nitrito ligands. The interaction between the nitrito ligands and the diamine chelate rings in dinitritobis(diamine) complexes may play an important role in the formation of the predominant rotamer conformations for nitrito ligands. It has been found in *trans*-$[Ni(ONO)_2(Me_2NC_2H_4NH_2)_2]$ and -$[Zn(ONO)_2(Me_2NC_2H_4NH_2)_2]$ by X-ray analyses[18,19] that the nitrito nitrogen atoms are located around the amine nitrogen atoms in which the nearest protons are equatorial. This suggests that the congestion brought about by the diamine chelate rings around the nitrito ligands is released in the neighbourhood of the amino equatorial NH protons where the predominant rotamers can settle beacause the equatorial protons are more distant from the nitrito nitrogen atoms than the axial protons; thus the steric interaction between them decreases. In view of the fact that the intraligand CD spectrum in a KBr disk of *trans*-$[Cr(ONO)_2(R\text{-pn})_2]ClO_4$ is about ten times as intense as the CD in the first d-d band region as shown in Fig. 6, the nitrito ligands are expected to take a chiral configuration. It is supposed that in the solid state of this complex two nitrito ligands are arranged in such a way that their nitrogen atoms are located near the NH equatorial protons of (*R*)-propylenediamines with the λ ring conformation as shown in Fig. 7. Since such an arrangement results in configurational chirality with respect to the intraligand transition of nitrito ligands, the CD intensity in this region is expected to be enhanced. On the other hand, according to the empirical method based on the CD in the first d-d band region,[13a] $(+)^{A}_{480}$-*cis*-$[Cr(ONO)_2(en)_2]ClO_4$ is assumed to take a Λ absolute configuration, presumably with a stable $\delta\delta(lel_2)$ conformation of the ethylenediamine rings. Then, the location of the nitrito nitrogen atoms in the vicinity of the NH equatorial protons for the ethylenediamine chelates gives rise to the achiral configuration in which two nitrito ligands lie in the same plane as the CrN_2O_2 one as depicted in Fig. 7. The proposed rotamer configuration is deduced from the fact that the intraligand CD of $(+)^{A}_{480}$-*cis*-bis(en) complex perchlorate in a KBr disk is much weaker than the CD in the first d-d band region as shown in Fig. 6.

In solution, the solvent effect on the distribution of the rotamer conformations must be taken into account, since the intraligand CD spectra of the present complexes vary remarkably with solvent as compared with the CD in the first d-d band region. As shown in Figs 2—4, the fine structures of the CD spectra in the corresponding region become more resolved, sharper, and more amplified with solvent in the order, formamide< *N*-methylforamide(NMF)<DMF< *N*,*N*-dimethylacetamide (DMA). This order for the CD variation is in accordance with the increasing order of the donor number of solvents,[20] and is similar to the order derived from the solvent-dependent CD and NMR study of cobalt(III) complexes by Hawkins *et al.*[21] They postulated the stereoselective solvation to the amino NH equatorial protons in the complexes. As shown in Figs. 2 and 3, more marked CD enhancement is observed in DMA than in DMF, though the donor number of

DMA (27.8) is not much different from that of DMF (26.6). This implies that the bulkiness as well as the donor number of the solvents is responsible for the optical activity associated with the intraligand transition in nitrito ligands, solvation in DMA being more stereoselective. As proposed for the solvent-dependent CD spectra of cobalt(III) complexes,[3] such stereoselective solvation in the present complexes will form more chirally defined second coordination spheres and will assist more restricted rotation of nitrito ligands in making their predominant rotamer conformations in the increasing order of the bulkiness as well as the donor number of the solvents, enhancing optical activity in the intraligand transition region. In acetonitrile, the intraligand CD spectrum of the *trans*-bis(*R*-pn) complex is similar to that in DMF, whereas the *trans*-bis(*R,R*-ptn) complex gives a quite different CD pattern in this solvent from that in DMF as shown in Fig. 3. In the last case, the CD diminishes considerably, but still exhibits the prominent vibronic structure. This fact together with the sign inversion of the intraligand CD behavior for the *trans*-bis(*R*-pn) and the *trans*-bis(*R,R*-ptn) complex reflects a subtle difference in the stereochemical circumstance containing the first solvation sphere around nitrito ligands between these complexes. The different disposition of the amino NH equatorial protons in the complexes may impose the different orientation of higher order on the solvent molecules or may cause the formation of different chirally defined second coordination spheres. Judging from the fact that the intraligand CD intensity of the *trans*-bis(diamine) complexes in aprotic solvents is much stronger than that in water and that of the optically active *cis*-bis(diamine) complexes in aprotic solvents, chiral configurations caused by restricted rotation of two nitrito ligands in the *trans*-bis(diamine) complexes as in the case of the solid state may be retained to some extent even in solutions. This postulate is confirmed by comparing the CD intensity of *trans*-$[CrF(ONO)(R,R\text{-chxn})_2]^+$ with that of *trans*-dinitritobis(*R,R*-chxn) complex in DMF. The CD spectrum of the mononitrito complex is found to be much weaker by about one sixth than that of the dinitrito complex as shown in Fig. 8. A comparison of the CD for *trans*-$[Cr(ONO)_2(en)(R\text{-pn})]^+$ and -$[Cr(ONO)_2(en)(R,R\text{-ptn})]^+$ with that for *trans*-$[Cr(ONO)_2(R\text{-pn})_2]^+$ and -$[Cr(ONO)_2(R,R\text{-ptn})_2]^+$, respectively, also ensures the chiral arrangement of two nitrito ligands in the complexes; *i.e.*, the intraligand CD intensities of the mono(*R*-pn) and mono (*R,R*-ptn) complexes are not half but about one fourth as weak as those of the corresponding *trans*-bis(*R*-pn) and -bis(*R,R*-ptn) complexes as seen in Figs. 2, 3, 9, 10. These findings are contrary to the anticipation that the vicinal CD contribution from the chirality in diamine ligands (configurations of asymmetric carbons and conformations of chelate rings) is proportional to the number of chiral ligands and/or nitrito chromophores in the absence of the chirality due to the rotational arrangements of two nitrito ligands.

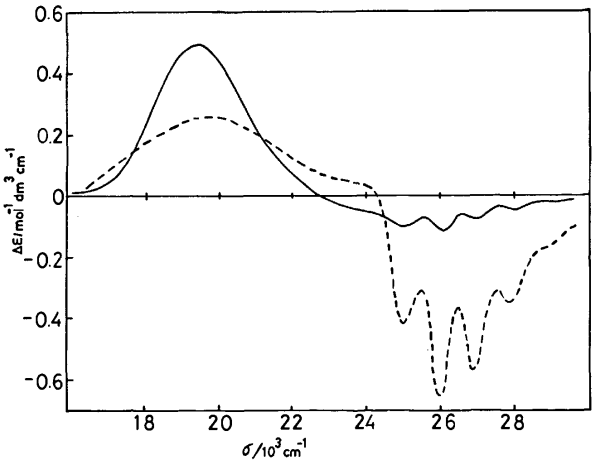

Fig. 8. CD curves of *trans*-$[CrF(ONO)(R,R\text{-chxn})_2]ClO_4$ (——) and *trans*-$[Cr(ONO)_2(R,R\text{-chxn})_2]ClO_4$ (------) in DMA.

Even though the rotamer conformations of the nitrito ligands in the complexes in solutions are much less rigid and much more flexible than in the solid state, it might be expected that due to the intra- and intermolecular interactions of nitrito ligands with diamine chelates and/or the solvation molecules the most probable location of nitrito ligands at equilibrium is in the neighbourhood of amino nitrogen atoms along the line connecting between equivalent symmetry-related (by a C_2 axis) NH equatorial protons where nitrito ligands would

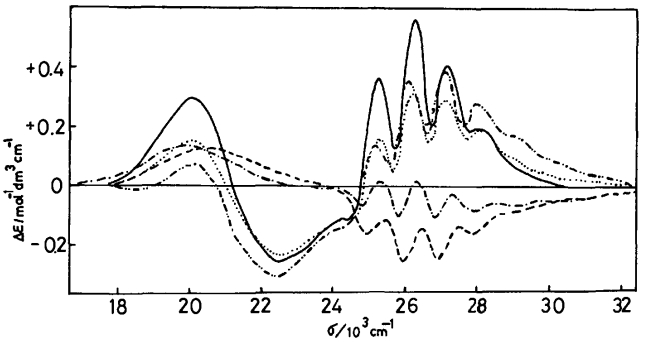

Fig. 9. CD curves of *trans*-dinitrito mixed diamine Cr(III) complexes in DMA.
(*R*-pn·*R,R*-ptn) (——); (en·*R*-pn) (------); (en·*R,R*-ptn) (·····); (tn·*R*-pn) (—·—); (*S*-pn·*R,R*-ptn) (—··—).

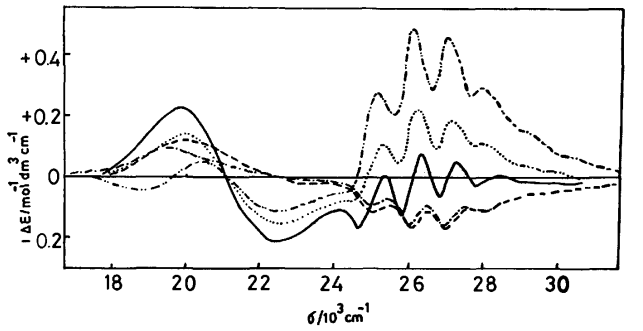

Fig. 10. CD curves of *trans*-dinitrito mixed diamine Cr(III) complexes in acetonitrile.
(*R*-pn·*R,R*-ptn) (——); (*R*-pn·en) (------); (en·*R,R*-ptn) (·····); (tn·*R*-pn) (—·—); (*S*-pn·*R,R*-ptn) (—··—).

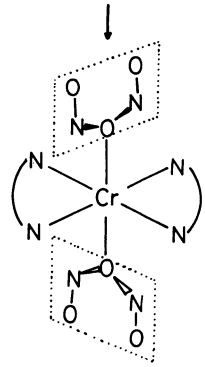

Fig. 11. The most probable paired locations of nitrito ligands at two equivalent symmetry-related sites near equatorial NH protons of diamines; the disorder over the pairs results in forming the planes.

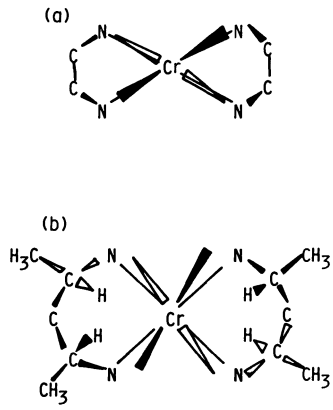

Fig. 12. View along the (ON)O–Cr–O(NO) bond axis from the arrow of Fig. 11 for *trans*-bis(*R*-pn) complex (a) and *trans*-bis(*R*,*R*-ptn) complex (b); the shaded and open elongated triangles indicate the upper and lower nitrito ligands, respectively.

rotate more sluggishly and reside for a longer time than anywhere else. In other words, it seems that the time-averaged orientation of two nitrito ligands results in the formation of two planes as shown in Fig. 11. Non-orthogonality and non-coplanarity of the two planes are expected to induce a new chirality. Construction of molecular models shows that the dihedral angles between the planes are sensitive to the N–Cr–N chelate angles of diamines and/or the crowding brought about by the chelate ring backbone. For the *trans*-bis(*R*-pn) complex, the dihedral angles may be smaller than 90°, because the chelate N–Cr–N angles of five-membered diamine rings are usually about 85°. On the other hand, the *trans*-dinitritobis(*R*,*R*-ptn) complex may give the angle of larger than 90°, due mainly to the steric interaction between the nitrito nitrogen atoms and the axially oriented protons on 2- and 4-carbons of the skew boat *R*,*R*-ptn chelate ring by which the nitrogen atoms might be pushed away from over the chelate plane as shown in Fig. 12. Then such chiral arrangements composed of the nitrito ligand planes in the *R*-pn and *R*,*R*-ptn complexes have the enantiomeric relation to each other in an approximate manner as depicted in Fig. 12. Thus, it is plausible that this enantiomeric pair causes

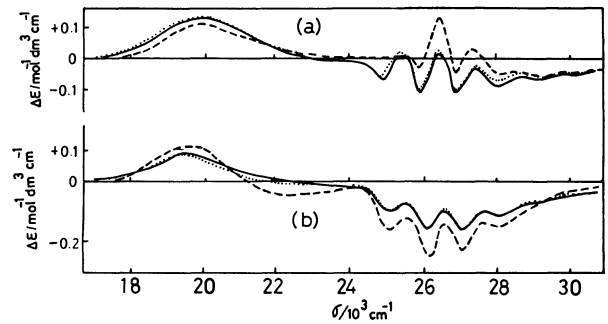

Fig. 13. CD curves of *trans*-[Cr(ONO)$_2$(tn)(*R*-pn)]ClO$_4$ (——) and *trans*-[Cr(ONO)$_2$(*R*-pn)(*R*,*S*-ptn)]ClO$_4$ (·····), and the CD curves calculated by Eq. 1 for *trans*-[Cr(ONO)$_2$(*R*-pn)(*rac*-ptn)]$^+$ (------) in DMA (a) and in acetonitrile (b).

the sign inversion of the intraligand CD components between the *R*-pn and *R*,*R*-ptn complexes.

Conformation of Diamine Chelates. In order to examine the additivity of the CD contributions from the different chiral diamines in a complex and to reveal ethylenediamine and trimethylenediamine chelate ring conformations in the mixed diamine complexes in aprotic solvents, the CD curves of *trans*-[Cr(ONO)$_2$-(*R*-pn)(*rac*-ptn)]$^+$ and -[Cr(ONO)$_2$(*rac*-pn)(*R*,*R*-ptn)]$^+$ are calculated by using the following equations:

$$\Delta\varepsilon(R\text{-pn}\cdot rac\text{-ptn}) = 1/2\{\Delta\varepsilon(R\text{-pn}\cdot R,R\text{-ptn}) - \Delta\varepsilon(S\text{-pn}\cdot R,R\text{-ptn})\}, \quad (1)$$

$$\Delta\varepsilon(rac\text{-pn}\cdot R,R\text{-ptn}) = 1/2\{\Delta\varepsilon(R\text{-pn}\cdot R,R\text{-ptn}) + \Delta\varepsilon(S\text{-pn}\cdot R,R\text{-ptn})\}. \quad (2)$$

As shown in Fig. 13, the CD curves of *trans*-[Cr(ONO)$_2$-(tn)(*R*-pn)]$^+$ in acetonitrile and DMA are almost identical with those of *trans*-[Cr(ONO)$_2$(*R*-pn)(*R*,*S*-ptn)]$^+$ in those solvents, respectively, but not with those of *trans*-[Cr(ONO)$_2$(*R*-pn)(*rac*-ptn)]$^+$. This means that the ring conformation of the coordinated trimethylenediamine in the dinitrito complex takes the same chair form as that in the *R*,*S*-ptn complex as has been revealed from the CD study of *trans*-difluorobis(diamine) complexes.[7] It appears that the CD difference in the intraligand band region between the *rac*-ptn and *R*,*S*-ptn (or tn) dinitrito complexes reflects the subtle difference in the first and/or the second coordination sphere arising from the skew boat and chair conformations of the six-membered chelate rings. The CD curve calculated by Eq. 2 in acetonitrile is similar to the CD curve of *trans*-[Cr(ONO)$_2$(en)(*R*,*R*-ptn)]$^+$, but the CD of this ethylenediamine complex in DMA differs from the calculated one of the *rac*-pn complex with *R*,*R*-ptn in DMA as shown in Fig. 14. In view of this fact, the ethylenediamine chelate ring in the *trans*-dinitrito complex in acetonitrile may have the same conformation as the *rac*-propylenediamine in *trans*-[Cr(ONO)$_2$(*rac*-pn)-(*R*,*R*-ptn)]$^+$; free puckering of the ethylenediamine may occur in acetonitrile as found for the CD spectrum of *trans*-[CrF$_2$(en)(*R*,*R*-ptn)]$^+$ in water.[7] In DMA, it is likely that the stereoselective solvation of bulky DMA with the amine NH protons gives rise to the displacement of the conformational equilibrium of the ethyeledi-

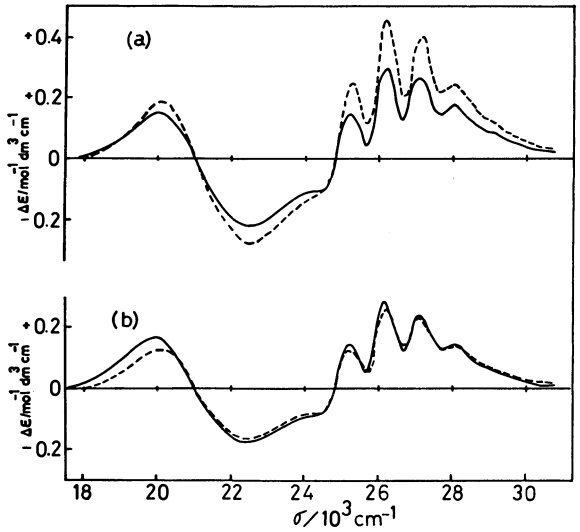

Fig. 14. CD curves of *trans*-[Cr(ONO)$_2$(en)(*R*,*R*-ptn)]-ClO_4 (——) and the CD curves calculated by Eq. 2 for *trans*-[Cr(ONO)$_2$(*rac*-pn)(*R*,*R*-ptn)]$^+$ (------) in DMA (a) and in acetonitrile (b).

amine ring puckering in *trans*-[Cr(ONO)$_2$(en)(*R*,*R*-ptn)]$^+$. In other words, the CD contribution from different diamines to *trans*-dinitrito mixed diamine complexes with nonidentical diamines are separable and additive in acetonitrile but not in DMA.

The author wishes to express his thanks to Prof. Yoichi Shimura of Osaka University for the guidance of this study and for making the CD spectra available for the present work. This study was supported by a Grant-in-Aid for Scientific Research No. 354223 from the Ministry of Education, Science and Culture.

References

1) K. G. Jensen, Hans Soling, and N. Thorap, *Acta Chem. Scand.*, **24**, 908 (1970).
2) T. E. MacDermott and Sven Barfold, *Acta Chem. Scand.*, **24**, 924 (1970).
3) B. Bosnich and J. MacB. Harrowfield, *Inorg. Chem.*, **14**, 828 (1975).
4) a) C. Djerassi, H. Wolf, and E. Bunnenberg, *J. Am. Chem. Soc.*, **57**, 2835 (1963); b) L. Velluz, M. Legrand, and M. Grosjean, "Optical Circular Dichroism," Academic Press, New York (1965), p. 149.
5) W. W. Fee, C. S. Garner, and J. N. MacB. Harrowfield, *Inorg. Chem.*, **6**, 87 (1967).
6) S. Kaizaki and Y. Shimura, *Chem. Lett.*, **1979**, 1.
7) S. Kaizaki, Bull. Chem. Soc. Jpn., **56**, 3620 (1983).
8) S. Kaizaki and Y. Shimura, *Bull. Chem. Soc. Jpn.*, **48**, 3611 (1975).
9) J. Glerup, J. Josephsen, K. Michelsen, E. Pedersen, and C. E. Schäffer, *Acta Chem. Scand.*, **24**, 247 (1970).
10) J. W. Vaughn, O. J. Stvan, Jr., and V. E. Magnusson, *Inorg. Chem.*, **7**, 736 (1968); J. W. Vaughn and J. Marzowski, *ibid.*, **12**, 2346 (1973).
11) E. Pedersen, *Acta Chem. Scand.*, **24**, 3362 (1970).
12) J. Selbin and J. C. Bailer, Jr., *J. Am. Chem. Soc.*, **79**, 4285 (1957).
13) a) A. J. McCaffery, S. F. Mason, and B. J. Norman, *J. Chem. Soc.*, **1965**, 5094; b) I. J. Kindred and D. A. House, *J. Inorg. Nucl. Chem.*, **37**, 1359 (1975).
14) B. Bosnich and J. MacB. Harrowfield, *J. Am. Chem. Soc.*, **94**, 3425 (1972).
15) J. W. Sidman, *J. Am. Chem. Soc.*, **76**, 2669 (1957).
16) E. Norden, *Acta Crystallogr., Sect. B*, **34**, 2285 (1978).
17) M. A. Hitchman and G. Rowbottom, *Coord. Chem. Rev.*, **42**, 55 (1982).
18) M. G. B. Drew, D. M. L. Goodman, M. A. Hitchman, and D. Rogers, *Proc. Chem. Soc.*, **1964**, 363; A. J. Finny, M. A. Hitchman, C. L. Raston, G. L. Rowbottom, and A. H. White, *Aust. J. Chem.*, **34**, 2047 (1981).
19) A. J. Finny, M. A. Hitchman, C. L. Raston, G. L. Rowbottom, and A. H. White, *Aust. J. Chem.*, **34**, 2061 (1981).
20) V. Gutman, *Struc. Bonding*, **12**, 113 (1972).
21) C. J. Hawkins, G. A. Lawrence, and R. M. Peachey, *Aust. J. Chem.*, **30**, 2115 (1970).

Development of Hydrogen Ion Selective Electrode with Lithium Phosphate Glasses for the Use in Solutions Containing Hydrofluoric Acid

Tsuyoshi NOMURA* and Genkichi NAKAGAWA
Laboratory of Analytical Chemistry, Nagoya Institute of Technology, Gokiso-cho, Showa-ku, Nagoya, 466
(Received June 2, 1983)

In order to determine reproducible and stable potential response conditions of the hydrogen ion in hydrofluoric acid solutions, lithium phosphate glass membranes of various constituents were developed. The glass membranes contained various metal oxides: Ag_2O, Li_2O, P_2O_5, MgO, BeO, WO_2, and Al_2O_3. The response characteristics of the glass electrode depend strongly on the glass compositions. For the examination of the selectivity coefficient and the electrode function of hydrogen ion activities, the glass composition of 10 Ag_2O : 20 Li_2O : 50 P_2O_5 : 10 MgO : 10 WO_2 is the most suitable one. The potential response is linear over the hydrogen ion activities of ($10^{0.3}$—10^{-4}) mol/dm^3, and has a slope of 44.5 mV/decade change in the hydrogen ion activity at 20 °C. The dynamic response time was within a minute in the range 10^{-1} to 10^{-4} mol/dm^3. The intereference of the various cations on the activity of about 0.1 mol/dm^3 can be ignored during the determination of the hydrogen ion activities at pH below 3. Physical and chemical properties, such as glass transition temperature, softening temperature, thermal expansion, membrane resistance, and chemical durability were measured and compared with those of other glasses.

It is well known that various types of the ion selective glass electrode are available; almost all of these are made of alkali silicates.[1,2] However, these electrodes show a serious disadvantageous point: They are earsily corroded chemically by hydrofluoric acid. Some anomalous behavior of the common glass electrode in solutions containing hydrofluoric acid has been discussed.[3] In the hydrofluoric acid solution, the hydrogen ion activities have been measured with a metallic antimony electrode or the cation exchange membrane electrode.[4]

Phosphate glasses containing iron oxide[5] have been investigated as materials of the cation selective membrane electrode for alkaline earth cations. Moreover, it is known from the literature[6] that the glasses made from aluminium and lithium metaphosphate were studied and their potential responses to hydrogen ions were found. However, the chemical durability and the dependence of the potential response in the hydrofluoric acid solutions have not been published in detail.

We have already studied the properties of alkali-free magnesium phosphate glasses and their application to the ammonia selective electrode.[7] In the present work, we studied the physical and chemical properties of the lithium phosphate glasses containing various metal oxides, such as Ag_2O, MgO, BeO, WO_2, and Al_2O_3, and the application of the electrode membrane to determine the hydrogen ion activities in the hydrofluoric acid solution.

Experimental

Preparation of the Glass Membrane. Orthophosphoric acid (85%), silver carbonate, lithium carbonate, tetramagnesium tricarbonate dehydroxide, tungsten dioxide, aluminium hydroxide, and beryllium oxide were used to prepare the glasses. All the chemical except silver carbonate were of a reagent grade. The preparation procedures of the phosphate glasses and the glass membrans have been described previously.[7] The chemical compositions of some of the tested glasses are shown in Table 1.

Glass Transition Temperature, Softening Temperature, and Thermal Expansion of Lithium Phosphate Glasses. Glass transition temperature (T_g, °C) softening temperature (T_s, °C) and thermal expansion (α, cm °C^{-1}) were measured with a Shimadzu TM-30 type dilatometer. All dilatometer measurements were carried out at 3 °C/min of the sample heating rate.

Chemical Durability and Membrane Resistance of the Glasses. The chemical durability of the tested glasses was measured by the following method. A glass film (surface area, about 3×10^2 mm^2) was weighted and placed in a 100 ml portion of 0.5 mol/dm^3 hydrofluoric acid and 0.6 mol/dm^3 sulfuric acid mixtures, allowed to stand for 60 d at about 30 °C, and the weight loss per unit area of the glass membrane was measured.

The resistance of the lithium phosphate glass membrane was measured by a Toa Denpa SM-9E type megaohm meter, because the resistance of the tested glass membrane is relatively low compared to that of the alkali silicate glasses.

Measurements of the Membrane Potentials. The glass elec-

TABLE 1. COMPOSITION OF THE GLASSES

Glass No.	Ag_2O	Li_2O	P_2O_5	MgO	WO_2	BeO	Al_2O_3
1	10	30	50	10	—	—	—
2	10	30	50	—	10	—	—
3	5	25	50	10	10	—	—
4	10	20	50	10	10	—	—
5	20	10	50	10	10	—	—
6	10	20	50	—	—	20	—
7	10	25	50	10	—	—	5

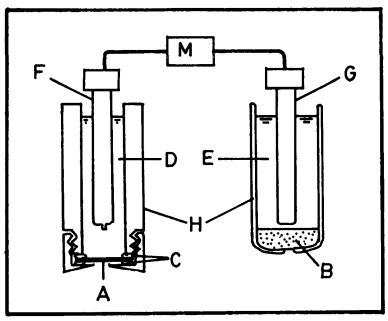

Fig. 1. Construction of the electrode.
A: Glass membrane, B: agar bridge, C: O-ring (Silicone rubber), D: , E: internal filling solution (0.1 mol/dm^3 $NaNO_3$), F: internal reference electrode (SCE), G: reference electrode (Ag/AgCl), H: plastic tube, M: ion meter.

trode was prepared by tightening the glass disk with a Silicone rubber O-ring and a plastic holder at the end of the cyclindrical plastic tube, which was filled with 0.1 mol/dm^3 $NaNO_3$ solution. The Ag/AgCl reference electrode was a double junction type, DKK 4400, with a salt bridge of 0.1 mol/dm^3 $NaNO_3$ internal solution; the acid error of the reference electrode is removed.

Figure 1 shows the completed assembly of the electrode system for the determination of hydrogen ion activity. The responses of each glass membrane were observed by measuring the potential *vs.* a Ag/AgCl reference electrode with a DKK IOC-10 ion-meter connected with a Sekonic model SS-250F recorder. In order to obtain a reproducible electrode potential, the electrodes were polished with waterproof silicon carbide paper No. 1000, and then preconditioned before use in distilled water for 1 d. The hydrogen ion activities for the proper quantities of nitric acid or nitric acid in the solution containing hydrofluoric acid and sodium nitrate mixtures were measured with a commercially available pH electrode, and then the electrode potentials which has been measured by the glass membranes tested in the same composition of the solutions were converted into the hydrogen ion activities. The activities of various cations except for hydrogen ion were calculated from the concentration by means of the activity coefficients tabulated by Kielland.[8]

Results and Discussion

Physical and Chemical Properties of Glasses. Some physical and chemical properties, such as glass transition temperature, softening temperature, thermal expansion, membrane resistance, and chemical durability of some lithium phosphate glasses in hydrofluoric acid solution are summarized in Table 2.

When we compared the values of T_g and T_s of those of the tested glasses and the usual silicate glasses, the tested glasses showed much lower values. However, all the values of the thermal expansion among these glasses were very similar.

When some Ag_2O is included in the glass constituents, the mixtures are easily glass forming, and show very low resistance.[9] However, the presence of Al_2O_3 has a negative effect on the chemical durability and the glass completely dissolved after standing for 60 d. The tested glasses which contain MgO or WO_2 were found to be more soluble in the hydrofluoric acid solution, but the glasses containing both MgO and WO_2 gave better results as for the chemical durability. Contrary to this result, however, the glasses containing both MgO and WO_2 increased in membrane resistance.

Potential Response of the Lithium Phosphate Glass Membranes. Figure 2 shows the potential response of the $10Ag_2O : 50P_2O_5 : 20Li_2O : 10MgO : 10WO_2$ glass membrane (Glass No. 4) to hydrogen ion activities in the solution containing 0.01 mol/dm^3 sodium nitrate and 0.05 mol/dm^3 hydrofluoric acid.

The potential response for the two experimental conditions was observed on the same calibration curve. The response for the hydrogen ion activity was linear over the range of ($10^{0.3}$—10^{-4}) mol/dm^3. The average slope was computed as 44.5 mV/decade change at 20 °C. Responses of the electrodes are reproducible, and electrode potentials are the same within 2 mV. The dynamic response time[10] for the change of the hydrogen ion activity was within a minute in the range 10^{-1} to 10^{-4} mol/dm^3, but was a few minutes above 10^{-1} mol/dm^3. Therefore, the steady state is defined as a potential stable to less than 1 mV drift in 2 min.

At the hydrogen ion activities below 10^{-6} mol/dm^3, however, the slope of the electrode potential *vs.* hydrogen ion activities falls to almost zero, and the electrode ceases to be functional. The tested glass membranes responded to the hydrogen ion activities within a certain range, but the slope was smaller than the value predicted by the Nernst expression.

From the dissociation constant[11] of the hydrofluoric acid, $a_{H^+} \cdot a_{F^-}/a_{HF} = 10^{-3.2}$, the hydrofluoric acid mole-

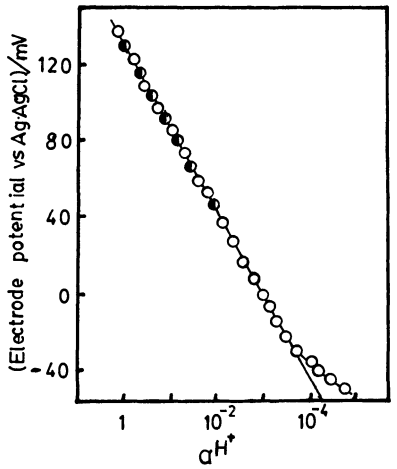

Fig. 2. Electrode response as a function of the hydrogen ion activities.
Electrode membrane: 10 Ag_2O : 50 P_2O_5 : 20 Li_2O : 10 MgO : 10 WO_2 glass.
○: Nitric acid, ◐: nitric acid in the solution containing 0.01 mol/dm^3 $NaNO_3$ and 0.05 mol/dm^3 HF.

Table 2. Physical and chemical properties of the glasses

Glass No.	Transition temperature T_g/°C	Softening temperature T_s/°C	Thermal expansion $\alpha \times 10^7$/cm °C^{-1}	Chemical durability mg mm^{-2}	Membrane resistance MΩ cm^{-1}
1	296	329	132.3	$1.0_8 \times 10^{-1}$	1.71
2	240	323	147.7	$1.5_0 \times 10^{-1}$	5.89
3	352	390	116.1	$2.3_8 \times 10^{-2}$	6.52
4	333	371	121.3	$1.9_9 \times 10^{-2}$	6.71
5	317	352	139.8	$2.1_8 \times 10^{-2}$	8.18
6	—	—	—	$6.2_8 \times 10^{-2}$	1.45
7	—	—	—	Dissolve	2.24

TABLE 3. ELECTRODE FUNCTION OF HYDROGEN ION ACTIVITIES AND SELECTIVITY COEFFICIENT OF VARIOUS CATIONS

Glass No.	Electrode function mV/pH	Selectivity coefficient $\times 10^2$				
		Li^+	Na^+	K^+	Ca^{2+}	Al^{3+}
1	42.5	1.86	2.58	2.55	1	1.51
2	29.4	—	—	—	—	—
3	36.8	6.74	7.90	2.82	2.51	3.16
4	44.5	3.73	2.51	1.32	1.58	0.79
5	38.6	33.7	50.1	23.3	15.8	7.94
6	31.4	17.7	15.8	8.61	6.32	1.58
7	21.3	—	—	—	—	—

cules exist at pH values below 3.0. Therefore, when the measurements of the pH value are performed with a commercially available pH electrode in the hydrofluoric acid solution, a reproducible electrode potential cannot be expected over long times, due to the dissolution of the electrode surface. However, the electrode potentials of the lithium phosphate glasses are more stable and reproducible than that of the alkali silicate glasses.

Response Behavior of Glass Membrane of Various Compositions. The response characteristics of lithium phosphate glass electrodes depend upon the glass composition. Therefore, the experiments of the electrode response were carried out with the glasses containing fixed quantities of P_2O_5 at 50 mol% and a varied quantities of the other metal oxide.

The glasses not containing Ag_2O show a small potential response to hydrogen ion activity and an unstable electrode potential in the hydrofluoric acid solution. Therefore, the presence of Ag_2O in the glass structure may contribute to the greater mobility of cations in the glass membrane and to the reproducibility of the electrode potential.[2] However, the presence of Al_2O_3 decreases the chemical durability in the hydrofluoric acid solution and the glass electrode is not responded to the hydrogen ion activities for the same behavior as in the case of silicate glasses.[12]

The electrode function of the hydrogen ion activities and the selectivity coefficients of the other cations for the lithium phosphate glass electrodes are shown in Table 3.

Selectivity Coefficient of Hydrogen Ion for the Other Cations. The interferences of various cations on the concentration of about 0.1 mol/dm^3 can be ignored for the measurement of the hydrogen ion activities at pH values below 3.

The selectivity coefficients of lithium phosphate glass electrodes with respect to a number of cations were determined by the mixed solution method.[13] Values of the selectivity coefficient are obtained by measuring the electrode potential in solutions containing fixed quantities of the interfering ion (0.1 mol/dm^3) and a varied activity of the hydrogen ion.

It is apparent that the selectivity coefficients for the interfering cations and the electrode function of hydrogen ion activities are better for glass electrode No. 4 than the others.

We wish to thank Prof. Yoshihiro Abe for his valuable advice.

References

1) G. A. Rechnitz, *Chem. Eng. News*, **12**, 146 (1967).
2) G. Eisenman, *Biophys. J., Part 2 Suppl.*, **1962**, 259.
3) E. Sørensen and T. Lundgaard, *J. Electroanal. Chem.*, **9**, 128 (1965).
4) Y. Inokuma, T. Ochiai, J. Endo, and K. Hiiro, *Nippon Kagaku Kaishi*, **1980**, 1469.
5) A. H. Truesdell and A. H. Pommer, *Science*, **142**, 1292 (1963).
6) V. S. Bobrov, I. P. Kalmkova, and M. M. Shul'ts, *Zh. Prikl. Khim.*, **40**, 1628 (1967).
7) T. Nomura and G. Nakagawa, *Bull. Chem. Soc. Jpn.*, **56**, 943 (1983).
8) J. Kielland, *J. Am. Chem. Soc.*, **59**, 1675 (1937).
9) R. M. Garrels, M. Sato, M. E. Thompson, and A. H. Truesdell, *Science*, **135**, 1045 (1962).
10) K. Toth and E. Pungor, *Anal. Chim. Acta*, **62**, 417 (1973).
11) L. G. Sillen and A. E. Martell, "Stability Constants of Metal Ion Complexes," The Chemical Society, London (1964), p. 257.
12) G. Eisenman, R. Bates, G. Mattock, and S. M. Friedman, "The Glass Electrode," Interscience, New York (1965), p. 219.
13) G. E. Baiulescu and V. V. Cosofret, "Applications of Ion-Selective Membrane Electrodes in Organic Analysis," John Wiley & Sons, New York (1977), p. 17.

An X-Ray Diffraction Study on the Structures of Mono(glycinato)nickel(II) and Tris(glycinato)nickelate(II) Complexes in Aqueous Solution

Kazuhiko Ozutsumi and Hitoshi Ohtaki*

Department of Electronic Chemistry, Tokyo Institute of Technology at Nagatsuta, Nagatsuta-cho, Midori-ku, Yokohama 227

(Received June 15, 1983)

The structures of mono(glycinato)nickel(II) and tris(glycinato)nickelate(II) complexes in aqueous solution were determined by the X-ray diffraction method. From the analysis of the radial distribution curve of solution A, in which the hexaaqua- and mono(glycinato)nickel(II) ions coexisted (the mole ratio $C_{gly}/C_{Ni}=0.792$, where C_i denotes the total concentration of species i), we found that the mono(glycinato)nickel(II) complex combined with four water molecules at the distance of (2.08±0.01) Å, the bond being longer than the Ni–OH_2 bond (2.04 Å) within the $[Ni(OH_2)_6]^{2+}$ ion. The Ni–O and Ni–N bond lengths within the mono(glycinato)nickel(II) complex were essentially the same and (2.09±0.02) Å. Therefore, the mono(glycinato)nickel(II) ion has a practically regular octahedral structure. The nonbonding Ni···C distance was also determined to be (2.87±0.02) Å. The X-ray scattering data of solutions having the C_{gly}/C_{Ni} mole ratio of 3.24 (solution B) and 3.94 (solution C), in both of which almost all nickel(II) ions formed the $[Ni(gly)_3]^-$ complex, showed that the tris(glycinato)nickelate(II) complex had a slightly distorted octahedral structure with the Ni–O and Ni–N bond lengths of (2.03±0.01) Å and (2.14±0.01) Å, respectively. The nonbonding Ni···C(COO), Ni···$C(CH_2)$ and Ni···O(O=C) distances were (2.82±0.02) Å, (2.96±0.02) Å, and (4.07±0.03) Å, respectively.

Structures of chelate compounds of some transition metal ions were first determined for ethylenediamine complexes in aqueous solutions.[1-4] The chelate effect on the formation of the ethylenediamine complexes was discussed in connection with the structural data of the complexes determined by the X-ray diffraction experiments by comparing them with the structures of ammine complexes of the relevant metal ions.[5]

A large number of crystallographic data have been accumulated for aminocarboxylato complexes.[6] However, compounds so far studied by the X-ray crystallography were mostly non-charged ones, which were relatively easy to prepare single crystals. Therefore, usually the structure of only one compound has been known in a series of compounds of a metal ion having one kind but different numbers of ligands. In X-ray analysis of solutions a restriction of preparing a single crystal is eliminated, although another restriction for solubility of compounds may be introduced, instead.

Glycine is one of the most interesting and important compounds among chelating reagents. It is the most fundamental unit in the formation of proteins. Some metal ions, which react as catalysts in biochemical reactions, are often combined with amino acid residues within proteins. Therefore, structural data of aminocarboxylato complexes must be very important in elucidating mechanisms of biochemical reactions.

In the present study we aimed at determining the structures of the mono(glycinato)nickel(II) and tris(glycinato)nickelate(II) complexes in aqueous solution by the X-ray diffraction method. The bis(glycinato)nickel(II) complex is not soluble enough to determine the structure in an aqueous solution; instead, the structure has been determined in crystal.[7]

Experimental

Preparation and Analysis of Sample Solutions. All chemicals used were of reagent grade. Since it was difficult to achieve a high value of the average ligand number of the nickel(II)–glycine solutions by adding glycine to a nickel(II) salt solution at a high pH, we mixed diaquabis(glycinato)nickel(II) with sodium glycinate in water at a suitable pH for preparing solutions in which the tris(glycinato)nickelate(II) complex formed as the main species (solutions B and C). A solution of a relatively low ligand number, in which the mono(glycinato)nickel(II) complex was formed as a predominant species, was prepared by mixing a nickel(II) nitrate solution with crystals of the bis(glycinato)nickel(II) complex (solution A).

Bis(glycinato)nickel(II) was prepared by dissolving freshly precipitated nickel(II) carbonate to an aqueous glycine solution, and then recrystallized from water. *Sodium glycinate* was obtained by mixing sodium hydroxide and glycine in methanol and then recrystallized from methanol. *Nickel(II) nitrate* of reagent grade was recrystallized from water.

The total concentration of nickel(II) ions (C_{Ni}) in the sample solutions was gravimetrically determined as bis(dimethylglyoximato)nickel(II). The total glycine concentration (C_{gly}) of the solutions was determined by the Kjeldahl method. Concentrations of nitrate ions in solution A and of sodium ions in solutions B and C were estimated from the material balance of ions in the solutions. Densities of the sample solutions were measured pycnometrically. The composition of the solutions is given in Table. 1.

X-Ray Scattering Measurements. X-Ray scattering measurements were carried out with a JEOL θ-θ diffractometer by using

Table 1. The composition (mol dm^{-3}) and stoichiometric volume V per nickel atom in the solutions

	A	B	C
Ni	2.904	1.654	1.759
Na	—	2.056	3.411
O	60.62	51.60	50.00
N	5.808	5.364	6.929
C	4.602	10.73	13.68
H	100.2	103.2	100.0
V/Å^3	571.8	1004	944.0
C_{gly}/C_{Ni}	0.792	3.24	3.94
C_{H_2O}/C_{Na}	—	19.9	10.6
Density/g cm^{-3}	1.378	1.278	1.346

Mo $K\alpha$ radiation (λ=0.7107 Å) in a room thermostated at (25±1) °C. The accessible range of scattering angle (2θ) was 2—140°. Times requiring to accumulate 120000 counts were recorded at each angle of measurements. The method of measurements and data treatments were described in previous papers.[1-5,8,9] All calculations were performed by using programs KURVLR[10] and NLPLSQ.[11] Computers at the Tokyo Institute of Technology was mainly used, but a part of the computation was carried out at the Institute for Molecular Science in Okazaki.

Results and Discussion

According to the stability constants of nickel(II)–glycine complexes[12] and the low solubility of the bis(glycinato)nickel(II) (about 0.12 mol dm^{-3}) so far reported in the literature, we can expect that comparable amounts of $[Ni(OH_2)_6]^{2+}$ and $[Ni(gly)]^+$ ions coexist in solution A, while almost all nickel(II) ions are present as the $[Ni(gly)_3]^-$ complex in solutions B and C. In solution B the concentration of sodium ions is smaller than that in solution C, and therefore, the C_{H_2O}/C_{Na} ratio in the former solution is about a double of that in the latter (see Table 1).

The observed $s\cdot i(s)$ and $D(r)$ curves of the solutions are shown in Figs. 1 and 2, respectively.

The structure of glycine has been determined crystallographically.[13,14] Since the intramolecular bond lengths within the glycinate ion in the bis(glycinato)nickel(II) are essentially the same as those in glycine, we assumed that the intramolecular bond distances within the glycinate ions coordinated to the central nickel(II) ion were independent of the complexes and the same as those reported in the literature.[7,13,14] The parameter values of water molecule, glycinate and nitrate ions used for the computations are summarized in Table 2. The numbering of the atoms within the glycinate ion coordinated to the nickel(II) ion is shown in Fig. 3.

Solution A. According to the stability constants of the nickel(II)–glycine complexes in the literature,[12] approximately the same amounts of $[Ni(OH_2)_6]^{2+}$ and $[Ni(gly)]^+$ ions may be formed in this solution. However, it should be noted that the stability constants determined in relatively dilute solutions may not be correctly applicable to calculations of distributions of the $[Ni(OH_2)_6]^{2+}$ and $[Ni(gly)]^+$ complexes in a concentrated solution like the sample solution in the present study.

The radial distribution curve of solution A is given in Fig. 2A. Figure 4 also represents the $D(r)$ function and the differential radical distribution curve, $D(r)-4\pi r^2\rho_0$, of solution A, where ρ_0 denotes the average scattering density in the stoichiometric volume V of the solution per Ni atom, as well as theoretical peak shapes of each atom pair in the system, for which we will discuss in the following section.

The broad and small peak around 1.3 Å observed in the $D(r)$ and $D(r)-4\pi r^2\rho_0$ curves (Fig. 4, a and e, respectively) is due to the O–H bonds within water molecules, the N–O bonds within nitrate ions and the N–H, C–H, C_1–C_2, C_2–N, $C_1\cdots O_1$, and $C_1\cdots O_2$ bonds within glycinate ions. The second peak at 2.1 Å is attributed to interactions between nickel and ligand atoms in the first coordination shell of the complexes. Nonbonding $C_1\cdots N$, $C_2\cdots O_1$, $C_2\cdots O_2$, and $O_1\cdots O_2$

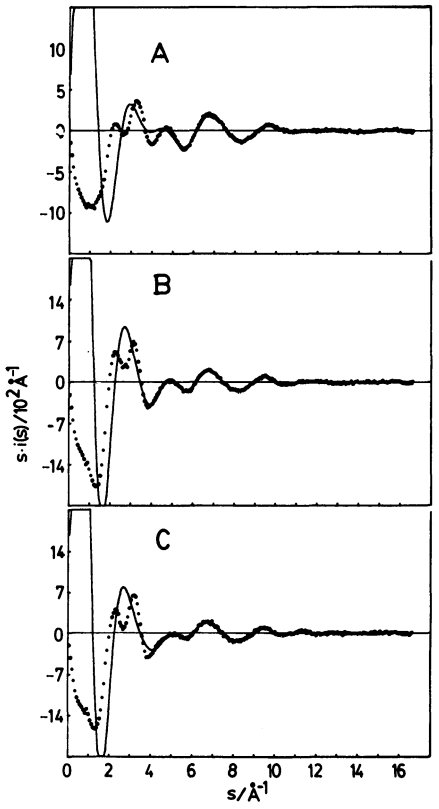

Fig. 1. The reduced intensities multiplied by s for solutions A, B, and C. The observed $s\cdot i(s)$ curves are shown by circles and calculated ones using parameter values finally obtained by solid lines.

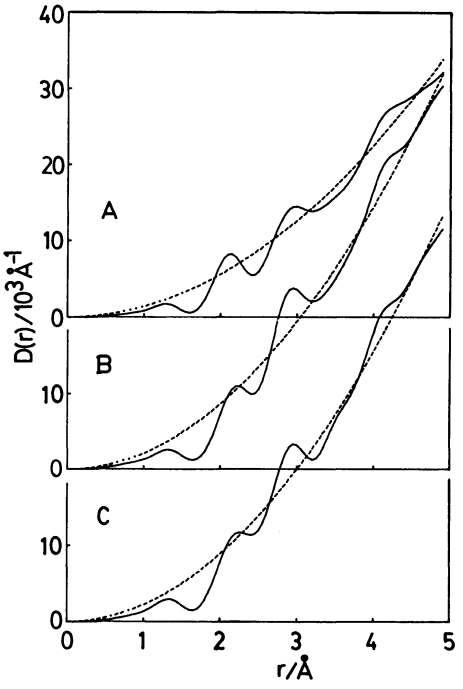

Fig. 2. The radial distribution curves, $D(r)$, for solutions A, B, and C. The dashed lines show the curve of $4\pi r^2\rho_0$.

Table 2. The bond distances (r) and temperature factors (b) for water molecule, glycinate, and nitrate ions

		r/Å	b/Å^2
H_2O	O–H	0.955[a]	0.010[a]
gly$^-$	C–H	1.09[b]	0.003[c]
	N–H	1.04[b]	0.003[c]
	C–C	1.52[b]	0.001[c]
	C–N	1.47[b]	0.001[c]
	C⋯O	1.26[b]	0.001[c]
	C⋯N	2.48[b]	0.003[d]
	C⋯O	2.38[b]	0.003[d]
	O⋯O	2.23[b]	0.003[d]
NO_3^-	N–O	1.26[e]	0.0009[f]
	O⋯O	2.19[e]	0.002[f]

a) R. Triolo and A. H. Narten, *J. Chem. Phys.*, **63**, 3624 (1975). b) Refs. 13 and 14. c) Calculated values from spectroscopic data quoted from R. A. Condrate and K. Nakamoto, *J. Chem. Phys.*, **42**, 2590 (1965). d) Estimated values; even if the values were changed from 0 002 to 0 004 Å^2, practically the same results were obtained. e) R. Caminiti, G. Licheri, G. Piccaluga, and G. Pinna, *J. Chem. Phys.*, **68**, 1967 (1978). f) Ref. 1.

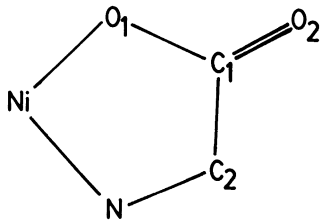

Fig. 3. The numbering of the atoms within the glycinate ion coordinated to the nickel(II) ion.

interactions within glycinate ions and O...O interactions within nitrate ions may also contribute, in part, to the peak (see Fig. 4, b—d). The third peak appearing at about 2.9 Å may be composed of peaks owing to nonbonding Ni⋯C_1 (and also Ni⋯C_2) pairs within the mono(glycinato)nickel(II) complex, interactions between the ligand atoms in the first coordination sphere of the complex, and to the O⋯O contacts in the bulk water.

The peak at 2.1 Å was well explained by assuming that all nickel atoms in the solution have six oxygen and nitrogen atoms in the first coordination sphere, independent of the concentration ratio of the $[Ni(OH_2)_6]^{2+}$ to $[Ni(gly)]^+$ ions. Since the Ni–O_1 and Ni–N bonds are hardly distinguishable by the X-ray diffraction analysis as previously pointed out,[3] the result suggests that all nickel(II) ion in the solution have six ligand atoms and thus the $[Ni(gly)]^+$ complex should have additional four oxygen atoms in its first coordination sphere at the distance of about 2.1 Å. Therefore, we can conclude that the mono(glycinato)nickel(II) complex is described as $[Ni(gly)(OH_2)_4]^+$ and has an almost regular octahedral structure.

In order to refine the structural parameters of the mono(glycinato)nickel(II) ion in the solution, we first assumed that concentrations of both the $[Ni(OH_2)_6]^{2+}$ and $[Ni(gly)(OH_2)_4]^+$ ions are 50 mol%, and the least-squares method was employed to the refinement of the

Table 3. Results of the least-squares refinements of solution A

Parameter values refined were bond distances (r/Å) and temperature factors (b/Å^2). Standard deviations are given in parentheses.

Interaction	Parameter	A-I (s>4.5 Å^{-1})	A-II (s>7.0 Å^{-1})
Ni–OH_2	r	2.08 (1)	2.08 (1)
	b	0.0052 (3)	0.0044 (2)
OH_2⋯OH_2	r	2.94[a]	2.94[a]
	b	0.012 (2)	0.009 (2)
Ni–O_1, Ni–N	r	2.09 (2)	2.09 (2)
	b	0.006 (1)	0.005 (1)
OH_2⋯O_1, OH_2⋯N	r	2.94[a]	2.94[a]
	b	0.010[a]	0.010[a]
N⋯O_1	r	2.87[a]	2.87[a]
	b	0.010[a]	0.010[a]
Ni⋯C_1, Ni⋯C_2	r	2.87 (2)	2.82 (2)
	b	0.008 (1)	0.005 (1)

a) The values were kept constant during the calculation.

structural parameters of the $[Ni(gly)(OH_2)_4]^+$ ion at the fixed composition of the solution. In this calculation the structural parameters of the $[Ni(OH_2)_6]^{2+}$ ion were quoted from the work by Ohtaki *et al.*[15] and fixed at the literature values. The structural parameters of the bulk water were taken from the work by Narten.[16]

Two types of the least-squares method were carried out in the present case (Table 3). In the A-I type calculation, the intensity data in the range s>4.5 Å^{-1} were used and the contribution of the O⋯O contacts in the bulk water was taken into account in the course of the refinement. On the other hand, in the A-II calculation the O⋯O interactions in the bulk water were not taken into consideration, and the intensity data used for the calculation were those in the range s>7.0 Å^{-1}, where the long-range interactions did not significantly contribute to the calculation. Since oxygen and nitrogen atoms have similar scattering factors over the whole angle range, the lengths of the Ni–O_1 and Ni–N bonds were not determined separately with reasonable certainties by the least-squares method. Therefore, we assumed that the Ni–O_1 and Ni–N bonds have the same structural parameters in the present stage of calculations. The results obtained by the A-I and A-II type calculations were very similar (see Table 3), and thus the Ni–OH_2 bond length within the $[Ni(gly)(OH_2)_4]^+$ complex was determined to be 2.08 Å and the lengths of the Ni–O_1 and Ni–N bonds were estimated to be 2.09 Å. Even if we changed the concentration ratio of $[Ni(OH_2)_6]^{2+}$ to $[Ni(gly)(OH_2)_4]^+$ from 30 : 70 to 70 : 30, no significant improvement of the result was achieved under the present assumption of the same length of the Ni–O_1 and Ni–N bonds.

A possibility of different lengths of the Ni–O_1 and Ni–N bonds may not still be well eliminated by the above calculation, because the initial values, in which the Ni–O_1 and Ni–N bonds are assumed to have the same length, may give a very shallow minimum of the error-square sum in the course of the least-squares refinement of the structural parameters and the param-

eter values may not be well floated to reach a set of the best values. Therefore, at the next step of the refinement of the result, we stepwise changed the initial values of the lengths of the Ni–O_1 and Ni–N bonds, as well as the mole ratio of $[Ni(OH_2)_6]^{2+}$ to $[Ni(gly)(OH_2)_4]^+$. In this case, we assumed that the Ni–OH_2 bond was 2.08 Å and the temperature factor of the bond was stepwise changed from 0.003 Å^2 to 0.006 Å^2. The temperature factors of the Ni–O_1 and Ni–N bonds were fixed at 0.003 Å^2, which was found from the analysis of the structure of the tris(glycinato)nickelate(II) complex in solutions B and C, as will be described in the later section. Although the value was smaller than that estimated from the least-squares method in Table 3, we considered that the temperature factor of 0.003 Å^2 for the Ni–O_1 and Ni–N bonds was more reliable one than 0.005—0.006 Å^2 in Table 3, because the former value of the temperature factor was determined in solutions B and C in which the $[Ni(gly)_3]^-$ complex existed as the main species and the structure of the complex was more accurately analyzed than that of the $[Ni(gly)(OH_2)_4]^+$ complex coexisting with $[Ni(OH_2)_6]^{2+}$. Moreover, we can expect that the temperature factors of the Ni–O_1 and Ni–N bonds within the $[Ni(gly)(OH_2)_4]^+$ complex may not be greatly different from those within the $[Ni(gly)_3]^-$ ion.

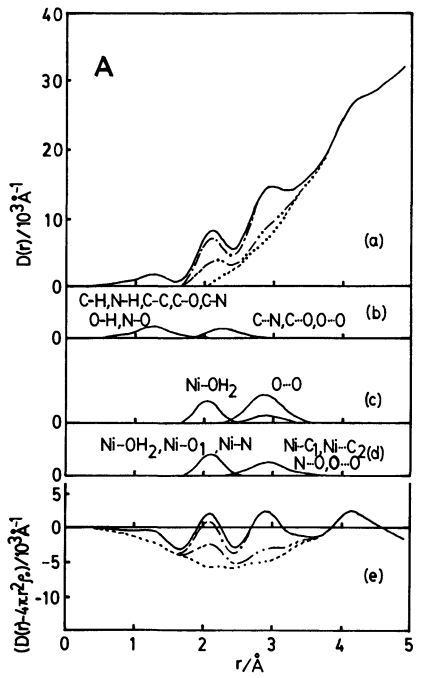

Fig. 4. (a) The radial distribution curve for solution A. (b) The theoretical peaks for O–H bonds within water molecule, intramolecular interactions within glycinate ion, and N–O and O···O pairs within nitrate ion. (c) The theoretical peak shapes calculated for Ni–OH_2 and O···O pairs within the hexaaquanickel(II) complex and O···O contacts of water molecules in the bulk. (d) The theoretical peak shapes owing to Ni–OH_2, Ni–O_1, Ni–N, Ni···$C_{1,2}$, N···O, and O···O pairs within the mono-complex. (e) The corresponding $(D(r)-4\pi r^2\rho_0)$ curve to the $D(r)$ in (a). The chain, double chain and dashed lines show the residual curves after subtraction of the theoretical peaks in (b), (c), and (d), respectively.

In the course of the refinement of the structural parameters of the $[Ni(gly)(OH_2)_4]^+$ ion, we extracted the second peak of the radial distribution curve given in Fig. 2A. By subtracting intramolecular interactions of water molecules, glycinate and nitrate ions, we can obtain the radial distribution curve which contains the only peaks ascribed to interatomic distances within the complexes around 2.1 Å and to longer range interatomic interactions in the region of larger r values. The peak at about 2.1 Å (the second peak in the original $D(r)$ curve) was extracted from the residual radial distribution curve by assuming a symmetrical shape of approximately Gaussian (Fig. 5). Since we could expect that the peak consisted of peaks owing to the Ni–OH_2 bonds within the $[Ni(OH_2)_6]^{2+}$ ion, Ni–OH_2, Ni–O_1, and Ni–N bonds within the $[Ni(gly)(OH_2)_4]^+$ complex, the refinement of the structural parameters of the $[Ni(gly)(OH_2)_4]^+$ ion was carried out in order to minimize the error-square sum defined by Eq. 1 at various sets of the temperature factor of the Ni–OH_2 bond, lengths of the Ni–O_1 and Ni–N bonds and the mole ratio of $[Ni(OH_2)_6]^{2+}$ to $[Ni(gly)(OH_2)_4]^+$.

$$U = \sum w\{D(r)^{2nd\ peak}_{calcd} - D(r)^{2nd\ peak}_{obsd}\}^2 \quad (1)$$

Here $D(r)^{2nd\ peak}$ denotes the $D(r)$ values at the second peak of the radial distribution curve extracted from the original curve by the procedure mentioned above. w is given as $\exp(-\alpha\cdot\Delta l^2)$, where $\Delta l = r_0 - r$ and r_0 represents the r-value at the center of the second peak. In this calculation we assumed that the r_0 value was 2.08 Å. The value α was estimated from the half-width of the second peak extracted.

In the course of the present calculations we fixed the values of all the structural parameters of the $[Ni(OH_2)_6]^{2+}$ ion at the literature values,[15] as well as the length of the Ni–OH_2 bond at 2.08 Å and the temperature factors of the Ni–O_1 and Ni–N bonds at 0.003 Å^2.

The minimum error-square sum was obtained for the set in which the temperature factor of the Ni–OH_2 bond within the $[Ni(gly)(OH_2)_4]^+$ was 0.003 Å^2. In Table 4 are summarized values of the error-square sums for various sets of the lengths of the Ni–O_1 and Ni–N bonds and the mole ratio of $[Ni(OH_2)_6]^{2+}$ to $[Ni(gly)$-

Table 4. Result of the analysis of the second peak in the $D(r)$ curve of solution A

Error-square sums ($U\times 10^{-5}$/Å^{-2}) were calculated according to the equation in the text. The Ni–OH_2 bond distance and all the temperature factors within the mono-complex were kept constant at 2.08 Å and 0.003 Å^2, respectively, in the course of the calculation.

		Mole fraction				
		Ni^{2+} = 0.3	0.4	0.5	0.6	0.7
		$Ni(gly)^+$ = 0.7	0.6	0.5	0.4	0.3
Bond distance r/Å		$U\times 10^{-5}$/Å^{-2}				
Ni–O_1	2.05	4.7	4.3	5.0	6.7	9.3
Ni–N	2.13					
Ni–O_1	2.07	4.6	4.1	4.7	6.4	9.0
Ni–N	2.11					
Ni–O_1	2.09	4.5	*4.0*	4.6	6.2	8.8
Ni–N	2.09					

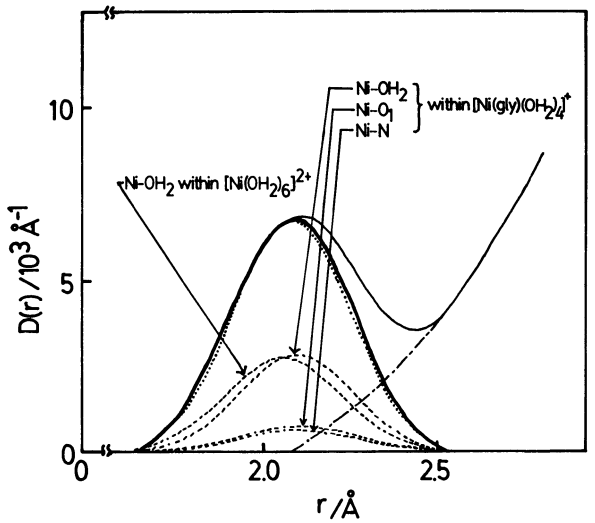

Fig. 5. The second peak of the radial distribution curve for solution A. The thin and thick solid lines represent the experimental and extracted $D(r)$ curves, respectively, and the chain line indicates the residual curve after extraction. The theoretical peak shapes owing to the Ni–OH_2 bonds within the $[Ni(OH_2)_6]^{2+}$ ion and Ni–OH_2, Ni–O_1, and Ni–N bonds within the $[Ni(gly)(OH_2)_4]^+$ ion are shown by dashed lines. The dotted line represents the peak shape by summing up ones shown by dashed lines.

$(OH_2)_4]^+$ at the value of 0.003 Å² for the temperature factor of the Ni–OH_2 bond.

In Fig. 5 was shown the coincidence of the experimentally obtained curve (the peak extracted by the procedure described previously) with the calculated shape by summing up shapes owing to the Ni–OH_2 interactions within the $[Ni(OH_2)_6]^{2+}$ ion and to the Ni–OH_2, Ni–O_1, and Ni–N bonds within the $[Ni(gly)(OH_2)_4]^+$ complex.

From the result we concluded that the Ni–O_1 and Ni–N bonds within the $[Ni(gly)(OH_2)_4]^+$ have practically the same length of 2.09 Å and thus the $[Ni(gly)(OH_2)_4]^+$ complex is essentially regular octahedral. The mole ratio of the $[Ni(OH_2)_6]^{2+}$ to the $[Ni(gly)(OH_2)_4]^+$ ions was approximately 40 : 60 in the present solution.

Solutions B and C. In solutions B and C, the tris(glycinato)nickelate(II) complex may be present as the main species. The radial distribution curves obtained for solutions B and C are shown in Fig. 2. They are very similar in shape, but it should be noted that the radial distribution curve of solution C has a small hump at about 3.4 Å, the concentration of sodium ions in solution C being higher than in solution B.

The radial ($D(r)$) and differential radial ($D(r)-4\pi r^2\rho_0$) distribution curves are shown in Fig. 6, a and e, respectively, for solution B. In the curves we see four peaks at 1.3, 2.2, 3.0, and 4.0 Å.

The peak at 1.3 Å can be ascribed to the O–H bonds within water molecules and N–H, C–H, C_1–C_2, C_2–N, $C_1\cdots O_1$, and $C_1\cdots O_2$ bonds within glycinate ions. The second peak consists mainly of interactions between nickel atoms and oxygen and nitrogen atoms within the glycinate ions coordinated. Nonbonding $C_1\cdots N$, $C_2\cdots O_1$, $C_2\cdots O_2$, and $O_1\cdots O_2$ interactions within

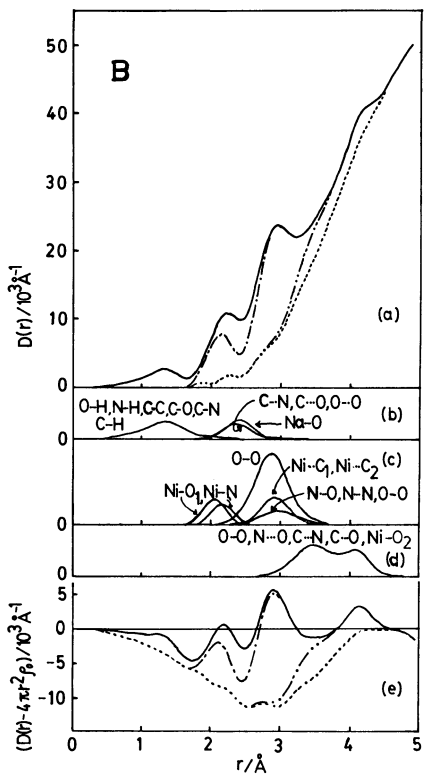

Fig. 6. (a) The radial distribution curve for solution B. (b) The theoretical peak shapes calculated for the O–H bonds within water molecule, the intramolecular interactions within glycinate ion, and Na–O pairs within hydrated sodium ion. (c) The theoretical peaks for Ni–O_1, Ni–N, Ni$\cdots C_{1,2}$, N$\cdots$O, N$\cdots$N, and O$\cdots$O pairs within the tris-complex and O$\cdots$O contacts of water molecules in the bulk. (d) The theoretical peaks for O$\cdots$O contacts within hydrated sodium ion and Ni$\cdots O_2$, N$\cdots O_2$, $C_{1,2}\cdots$N, and $C_{1,2}\cdots O_1$ pairs within the tris-complex. (e) The corresponding ($D(r)-4\pi r^2\rho_0$) curve to the $D(r)$ in (a). The chain, double chain, and dashed lines indicate the residual curves after subtraction of the theoretical peaks in (b), (c), and (d), respectively.

glycinate ions also contribute, in part, to the peak. The Na–O pairs within the hydrated sodium ions should have the bond length of about 2.4 Å,[17] which might also appear in this region in the $D(r)$ curve. The third peak may be composed of peaks due to nonbonding interactions between nickel and carbon atoms of the carboxylato and methylene groups within the glycinate ions coordinated, between ligand atoms in the coordination sphere of the $[Ni(gly)_3]^-$ complex, and between oxygen atoms in the bulk water. In the fourth peak at about 4 Å, nonbonding Ni$\cdots O_2$ and other long-range interactions may be included.

As we have pointed out in the previous section, we found a small hump at about 3.4 Å in the radial distribution curve of solution C, in which a higher concentration of sodium ions was contained than in solution B. This fact suggests that the hump may be due to interactions within hydrated sodium ions.

At the first step of analysis of the radial distribution curve of solution B, as well as that of solution C, we first

subtracted peak shapes of known interatomic distances within glycinate ions and the bulk water (Fig. 6b). The interaction between sodium ion and water molecules hydrated must also be taken into account in the calculation.

The structure of hydrated sodium ion has been determined in solutions of relatively low[17] and high[18] concentrations. Caminiti *et al.*[17] showed that a sodium ion had six water molecules in the first coordination shell at the distance of 2.41 Å. Calculations by using molecular dynamics simulations for the structure of *ca.* 0.5—2 mol dm^{-3} aqueous solutions of sodium chloride led to the hydration number of about 6—8 for sodium ions.[18] On the other hand, Maeda and Ohtaki found that the hydration number of sodium ion was four in a 7 mol dm^{-3} NaI solution.[19] If sodium ion has six water molecules coordinated in the form of a regular octahedron, we can expect to find the nonbonding water–water distance within the hydrated sodium ion at about 3.4 Å ($=2.4\text{ Å}\times\sqrt{2}$). On the other hand, in the four-coordinated sodium ion with water molecules, the nonbonding water-water interactions within the hydration shell of the sodium ion may appear at about 3.9 Å ($=2.4\text{ Å}\times\sqrt{8/3}$).

If we assumed the tetrahedral structure of the hydrated sodium ion in the solution and subtracted the intramolecular interactions within the hydrated ion from the radial distribution function, a peak remained at about 3.4 Å in the $D(r)$ curve of both solutions B and C, which was not satisfactorily explainable by possible atom pairs in the system. However, when the octahedral structure was assumed for the hydrated sodium ion, the radial distribution curves of both solutions B and C were well interpreted in terms of peak shapes of all the possible combinations of atom pairs shorter than 4 Å, as will be described in more detail in the later section.

Thus, we concluded that sodium ion has six water molecules at the distance of 2.40 Å in such solutions of relatively low concentrations as those in the present case.

When we subtracted the peak shapes of the Na–O interactions within the hexa-hydrated sodium ions and intramolecular bonding and nonbonding interactions within glycinate ions and water molecules (see Fig. 6b), we found a peak remaining at about 2.1 Å. The peak must be ascribed to the Ni–O_1 and Ni–N interactions within the $[Ni(gly)_3]^-$ complex. The shape of the peak was quite symmetrical. However, it was difficult to reproduce the peak shape by a single Gaussian curve which was constructed from the Ni–O_1 and Ni–N bonds with the same length, because the temperature factor of the bonds become unreasonably large (0.01—0.02 Å^2). Therefore, we assumed that the peak at 2.1 Å consisted of two peaks of Ni–O_1 and Ni–N bonds with different lengths. By a trial-and-error method the peak was separated into two, one had the peak position at 2.04 Å and the other was centered at 2.15 Å; the value of the temperature factors of the both bonds seemed to be reasonable ($\simeq$0.003 Å^2).

It is not straightforward to identify which peak corresponds to the Ni–O_1 or Ni–N bond. It has been found in crystal of *fac*-$[Cr(gly)_3]\cdot H_2O$ that the metal-oxygen bond is shorter than the metal-nitrogen bond within the complex.[20] The fact that the metal-oxygen bond is shorter than the metal-nitrogen bond has been found by many crystallographic investigations of various glycinato complexes. When we make a model structure of the $[Ni(gly)_3]^-$ ion by using three glycinate ions and one nickel(II) ion of an ionic radius of about 0.69 Å,[21] the glycinate ions are largely deformed and strained if we assume that the Ni–O_1 bond is longer than the Ni–N bond. On the other hand, the structural model having the Ni–O_1 bond of about 2.04 Å and the Ni–N bond of about 2.15 Å shows no large deformation in the bond angles within the glycinate ions. Therefore, we concluded that the peak at 2.04 Å is attributed to the Ni–O_1 bond, while the other peak at 2.15 Å is ascribed to the Ni–N bond within the tris(glycinato)-nickelate(II) complex.

The structural parameters of the tris(glycinato)-nickelate(II) complex were finally refined by the least-squares method by inserting the values for each interatomic interaction estimated by the trial-and-error method previously described as the initial values. The least-squares refinement of the structural parameters of the $[Ni(gly)_3]^-$ ion was performed by using $s\cdot i(s)$ data over the range $s>4$ Å^{-1}. In the refinement three types of calculations were carried out on slightly different assumptions.

In the B-I calculation all the distances and the temperature factors listed in Table 5 were refined by

Table 5. Results of the least-squares refinements of solution B

Parameter values refined were bond distances (r/Å), temperature factors (b/Å^2), and frequency factors (n). Standard deviations are given in parentheses.

Interaction	Parameter	B-I	B-II	B-III
Ni–O_1	r	2.039 (4)	2.034 (4)	2.031 (4)
	b	0.0032 (2)	0.0031 (2)	0.0031 (2)
	n	3.0[a]	3.0[a]	3.2 (1)
Ni–N	r	2.153 (5)	2.154 (5)	2.162 (5)
	b	0.0032 (3)	0.0031 (3)	0.0032 (2)
	n	3.0[a]	3.0[a]	3.3 (1)
N···O_1	r	2.80 (6)	2.76[a]	2.76[a]
	b	0.006 (3)	0.006[a]	0.006[a]
O···O	r	2.98 (7)	2.96[a]	2.96[a]
	b	0.006 (3)	0.006[a]	0.006[a]
N···O	r	3.01 (7)	2.97[a]	2.97[a]
	b	0.006 (3)	0.006[a]	0.006[a]
N···N	r	3.21 (9)	3.21[a]	3.21[a]
	b	0.006 (3)	0.006[a]	0.006[a]
Ni···C_1	r	2.82 (1)	2.83 (1)	2.82 (2)
	b	0.008 (1)	0.008 (1)	0.009 (1)
	n	3.0[a]	3.0[a]	3.0 (1)
Ni···C_2	r	2.97 (1)	2.98 (1)	2.98 (2)
	b	0.008 (1)	0.008 (1)	0.009 (1)
	n	3.0[a]	3.0[a]	3.1 (1)
Ni···O_2	r	4.08 (2)	4.09 (2)	4.09 (2)
	b	0.006 (1)	0.007 (1)	0.007 (1)
	n	3.0[a]	3.0[a]	3.2 (1)

a) The values were kept constant during the calculation.

Table 6. Bond lengths (r/Å) within the tris(glycinato)nickelate(II) complexes found in solutions B and C

Interaction	Solution B	Solution C	Proposed value
Ni–O_1	2.039±0.004	2.019±0.004	2.03±0.01
Ni–N	2.153±0.005	2.133±0.005	2.14±0.01
Ni···C_1	2.82±0.01	2.82±0.01	2.82±0.02
Ni···C_2	2.97±0.01	2.95±0.01	2.96±0.02
Ni···O_2	4.08±0.02	4.06±0.02	4.07±0.03

Table 7. Nickel(II)–ligand bond lengths (r/Å) in the hydrated nickel ion and glycinato–nickel(II) complexes

Complex	Ni–OH_2	Ni–O_1	Ni–N
$[Ni(OH_2)_6]^{2+}$ [a]	2.04	—	—
$[Ni(gly)_2(OH_2)_4]^+$	2.08	2.09	2.09
$[Ni(gly)(OH_2)_2]$ [b]	2.10	2.06	2.08
$[Ni(gly)_3]^-$	—	2.03	2.14

a) Ref. 15. b) Ref. 7.

keeping all the frequency factors constant. In the B-II treatment some interatomic interactions of relatively long distances were allowed to remain unchanged. The B-III calculation was carried out on similar assumptions given at the B-II calculation except for the frequency factors of some atom-pairs floated in the course of the refinement. All the calculations gave quite similar results, and we adopted the values obtained by the B-I type calculation as the final ones for the tris(glycinato)-nickelate(II) complex in solution B.

In the course of the calculation the existence of the *fac*- and *mer*-isomers of the tris(glycinato)nickelate(II) complex was taken into account. However, since the difference between the isomers was so small, the introduction of the existence of the isomers did not improve the result.

For solution C a similar procedure of calculations were performed to obtain the structural parameters of the tris(glycinato)nickelate(II) complex in the solution in order to examine reproducibility of the result. The interatomic distances found for the $[Ni(gly)_3]^-$ complex in solution C are listed in Table 6, together with those obtained in solution B. The proposed values of the bond lengths within the tris(glycinato)nickelate(II) complex are also given in the table.

In Table 7 we summarized the lengths of the Ni–OH_2, Ni–O_1, and Ni–N bonds within the hexaaqua-, tetraaquamono(glycinato)- and diaquabis(glycinato)nickel(II) and tris(glycinato)nickelate(II) complexes.

It can be noted that the Ni–OH_2 distance increases with the increased number of glycinate ions coordinated. The same trend may be seen for the Ni–N bond. On the contrary, the Ni–O_1 distance decreases with the increase in the number of glycinate ions in the coordination sphere of nickel(II) ion. The result suggests that the electrostatic interaction between the central nickel (II) ion and a charged donor atom is enhanced, while the coordination interaction between the metal ion and an uncharged donor atom weakens.

The work has been financially supported, in part, by the Grant-in-Aid for Scientific Research No. 57470054 from the Ministry of Education, Science and Culture. The financial aid by the Asahi Glass Foundation for Industrial Technology is also acknowledged. A part of the computer calculations carried out in the present work has been performed at the Institute for Molecular Science in Okazaki.

References

1) T. Fujita, T. Yamaguchi, and H. Ohtaki, *Bull. Chem. Soc. Jpn.*, **52**, 3539 (1979).
2) T. Fujita and H. Ohtaki, *Bull. Chem. Soc. Jpn.*, **53**, 930 (1980).
3) T. Fujita and H. Ohtaki, *Bull. Chem. Soc. Jpn.*, **55**, 455 (1982).
4) T. Fujita and H. Ohtaki, *Bull. Chem. Soc. Jpn.*, **56**, 3276 (1983).
5) H. Ohtaki, "Advances in Solution Chemistry," ed by I. Bertini, L. Lunazzi, and A. Dei, Plenum, New York (1981), p. 67.
6) H. C. Freeman, *Adv. Protein Chem.*, **22**, 258 (1967).
7) H. C. Freeman and J. M. Guss, *Acta Crystallogr., Sect. B*, **24**, 1133 (1968).
8) H. Ohtaki and M. Maeda, *Bull. Chem. Soc. Jpn.*, **47**, 2194 (1974); H. Ohtaki, M. Maeda, and S. Ito, *Bull. Chem. Soc. Jpn.*, **47**, 2217 (1974).
9) T. Yamaguchi and H. Ohtaki, *Bull. Chem. Soc. Jpn.*, **51**, 3227 (1978).
10) G. Johansson and M. Sandström, *Chem. Scr.*, **4**, 195 (1973).
11) T. Yamaguchi, Doctor Thesis, Tokyo Institute of Technology, March (1978).
12) A. E. Martell and R. M. Smith, "Critical Stability Constants," Plenum, New York (1974), Vol. 1.
13) R. E. Marsh, *Acta Crystallogr.*, **11**, 654 (1958).
14) L. F. Power and K. E. Turner, *Acta Crystallogr., Sect. B*, **32**, 11 (1976).
15) H. Ohtaki, T. Yamaguchi, and M. Maeda, *Bull. Chem. Soc. Jpn.*, **49**, 701 (1976).
16) A. H. Narten, *ORNL-4578* (1970).
17) R. Caminiti, G. Licheri, G. Piccaluga, and G. Pinna, *Rend. Sem. Fac. Sci. Univ. Cagliari*, **47**, 1 (1977).
18) K. Heinzinger and P. C. Vogel, *Z. Naturforsch., A*, **31**, 463, 476 (1976).
19) M. Maeda and H. Ohtaki, *Bull. Chem. Soc. Jpn.*, **48**, 3755 (1975).
20) R. F. Bryan, P. T. Greene, P. F. Stckely, and E. W. Wilso, Jr., *Inorg. Chem.*, **10**, 1468 (1971).
21) R. D. Shannon, *Acta Crystallogr., Sect. A*, **32**, 751 (1976).

Hydrophobic Vitamin B_{12}. I. Preparation and Axial Ligation Behavior of Hydrophobic Vitamin B_{12r}†

Yukito Murakami,* Yoshio Hisaeda, and Akiro Kajihara
Department of Organic Synthesis, Faculty of Engineering, Kyushu University, Hakozaki, Higashi-ku, Fukuoka 812
(Received June 22, 1983)

Heptamethyl cobyrinate perchlorate, [Cob(II)ester]ClO_4, was prepared in a good yield from cyanocobalamin. This hydrophobic complex is structurally comparable to the base-off form of vitamin B_{12r}. Thermodynamic parameters (ΔG, ΔH, and ΔS) for axial ligation of [Cob(II)ester]ClO_4 with various amines in dichloromethane and toluene were determined by electronic spectroscopy. The isoequilibrium temperatures obtained from plots of ΔH *vs.* ΔS were 194 ± 20 and 317 ± 20 K in dichloromethane and toluene, respectively. The equilibrium is primarily controlled by entropy at ordinary temperatures and the log K_1 value varies sensitively along with the change in pK_a of amine in dichloromethane, while the equilibrium values were almost invariant to the choice of amine in toluene because the measurements were carried out near the isoequilibrium temperature. The log K_1 value for [Cob(II)ester]ClO_4, different from the case of cobalt(II)–porphyrin complexes, depends on the nature of solvent used and undergoes wide variations. The possible functions of equatorial ligands involved in these two different complexes in the axial ligation behavior were discussed.

We have prepared previously the cobalt complex of 1,19-dimethyl-AD-didehydrocorrin (Hbdhc), having additional double bonds at peripheral positions and an additional angular methyl group compared with the parent corrinoid, and investigated its structural properties from the viewpoint of vitamin B_{12} chemistry.[1] The bdhc complex is quite analogous to the corrinoid as far as the electronic properties are concerned on the basis of its spectroscopic, electrochemical, and axial coordination behaviors. On the other hand, the angular methyl groups in the complex exert an unusually large steric effect in the bimolecular reactions of Co^I(bdhc) with alkyl donors which result in the formation of an alkyl–cobalt bond. Even though the bdhc complex is considered to be a good B_{12} model, it does not catalyze the 1–2 migration as observed with vitamin B_{12}. This may indeed be due to the steric repulsion of the angular methyl groups which prevents the initially formed alkyl fragments upon C–Co cleavage from staying close to the cobalt. In order to improve these situations, it is necessitated to develop another good vitamin B_{12} model.

The model studies of coenzyme B_{12}-dependent enzymatic reactions have been carried out in aqueous media[2] since vitamin B_{12} is soluble in water but hardly in apolar solvents. In order to simulate the functions of vitamin B_{12} as exerted in the hydrophobic active sites of enzymes concerned, however, vitamin B_{12} needs to be modified so that the model studies can be carried out in ordinary apolar organic solvents. Therefore, we synthesized in this work heptamethyl cobyrinate by converting amide groups of vitamin B_{12} into ester ones. Heptamethyl cobyrinate involving cobalt(II) has been prepared by Werthemann *et al.* and isolated as the iodo-adduct.[3] In the present work, we prepared heptamethyl cobyrinate perchlorate, [Cob(II)ester]ClO_4, in a good yield according to some modified method. This complex is structurally comparable to vitamin B_{12r} in the base-off form, but much more stable in solution and solid states and much less readily oxidized in the air than vitamin B_{12r} itself.

Physicochemical data for vitamin B_{12r} are lacking because B_{12r} is readily oxidized to B_{12a} in the air,[4] even though such information is important for characterizing its catalytic functions. Therefore, axial ligation constants and thermodynamic parameters for the reaction of [Cob(II)ester]ClO_4 with some pyridines, imidazoles, and aliphatic amines were evaluated in organic solvents under nitrogen atmosphere, and compared with the corresponding data for (5,10,15,20-tetraphenylporphinato)cobalt(II), Co^{II}(tpp).

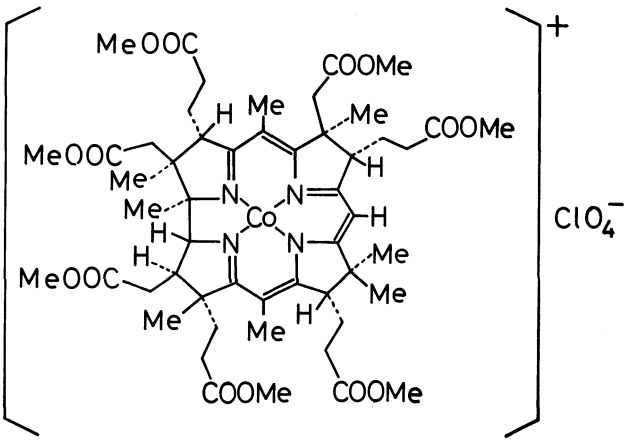

[Cob(II)ester] ClO_4

Experimental

Materials. Cyanocobalamin was purchased from Nakarai Chemicals and used without further purification. Dicyanocobyrinic acid heptamethyl ester, $(CN)_2$Cob(III)ester, was prepared from cyanocobalamin according to the method of Werthemann *et al.*,[3] purified by thin-layer chromatography on silica gel (Kiesel gel 60H) with chloroform–methanol (9 : 1 v/v), and reprecipitated from benzene upon addition of hexane. The product was identified by electronic, IR, ^{1}H-NMR, and ^{13}C-NMR spectroscopy[5,6] as well as by elemental analysis. (5,10,15,20-Tetraphenylporphinato)cobalt(II), Co^{II}(tpp), was prepared after the method of Alder *et al.*,[7] purified by liquid chromatography on a column of silica gel (Wakogel C-100) with chloroform as an eluant followed by recrystallization from

† Contribution No. 702 from this Department.

chloroform, and identified by electronic and IR spectroscopy as well as by elemental analysis.

Heptamethyl Cobyrinate Perchlorate, [Cob(II)ester]ClO_4. $(CN)_2$Cob(III)ester (50 mg, 4.6×10^{-5} mol) was dissolved in 40 ml of dichloromethane, and the resulting purple solution was treated with 25 ml of 30% aqueous perchloric acid. The orange dichloromethane layer was separated from the acidic aqueous layer and washed with distilled water. After being dried over sodium sulfate, the organic layer was evaporated to dryness at room temperature to obtain monocyanocobyrinic acid heptamethyl ester, [(CN)(H_2O)Cob(III)ester]ClO_4, in a nearly quantitative yield. The monocyano-complex, [(CN)-(H_2O)Cob(III)ester]ClO_4, was dissolved in 50 ml of methanol, and 50 ml of distilled water was added to this solution. The solution was deoxygenated by bubbling nitrogen gas through it for 30 min, and treated with 1.0 g of sodium tetrahydroborate and 15 ml of distilled water with vigorous shaking and frequent venting under nitrogen atmosphere. At the instance that the color of solution changed to dark green, 3 ml of 60% aqueous perchloric acid was added carefully to decompose excess sodium tetrahydroborate and to convert Cob(I)ester into Cob(II)-ester. The resulting cobalt complex was extracted with dichloromethane and washed with distilled water. After being dried over sodium sulfate, the dichloromethane solution was evaporated to dryness at room temperature. The residue was reprecipitated four times from benzene upon addition of hexane to afford fine brown crystals: yield 45 mg (87%); λ_{max} (CH_2Cl_2) 266 (ε 1.90×10^4), 316 (2.35×10^4), 403 (0.63×10^4), and 468 nm (1.21×10^4); IR (KBr) 1730 (ester C=O), and 1100 and 620 cm^{-1} (ClO_4^-).

Found: C, 54.68; H, 6.41; N, 5.00%. Calcd for $C_{52}H_{73}ClCoN_4O_{18}$: C, 54.95; H, 6.47; N, 4.93%.

Spectroscopic Measurements. Electronic absorption spectra were recorded on a Hitachi 340 or a Hitachi 220A spectrophotometer. ESR spectra were obtained with a JEOL JES-ME-3 X-band spectrometer equipped with a 100-kHz field modulation unit; a standard MgO/Mn^{II} sample calibrated with a NMR magnetometer was employed for calibration of the magnetic field.

Measurements of Equilibrium Constants and Thermodynamic Calculations. Liquid amines were distilled and solid amines were sublimed at 60 °C/1.33 Pa before use. Dichloromethane and toluene purified and dried according to the standard procedures[8] were redistilled and degassed by bubbling nitrogen gas through them before use. An equilibrium constant for coordination of an amine base to [Cob(II)ester]ClO_4 in dichloromethane was determined by measuring spectral change of a series of solutions containing the cobalt complex (*ca.* 8×10^{-5} mol dm^{-3}) and varying amounts of an amine base under nitrogen atmosphere. Upon addition of each of pyridines, imidazoles, and aliphatic amines, the visible peak at 468 nm decreased in intensity along with slight shift to longer wavelength, and clear isosbestic points were observed. Equilibrium constants were calculated by Eq. 1.

$$\log[(A_0-A)/(A-A_\infty)] = n\log[B] + \log K_n \quad (1)$$

Here, A designates an absorbance at a given concentration of an amine base ([B]), A_0 is an absorbance at [B]=0, and A_∞ stands for a limiting absorbance in the presence of a sufficient amount of a base. The values of log K_n, measured at three or four different temperatures over the 10—30 °C range, were used to evaluate ΔH and ΔS values. As for [Cob(II)ester]ClO_4 in toluene, and Co^{II}(tpp) in dichloromethane and toluene, the equilibrium constants were also calculated according to the same method on the basis of absorbance changes at 470 nm for the former complex and 527.5 nm for the latter.

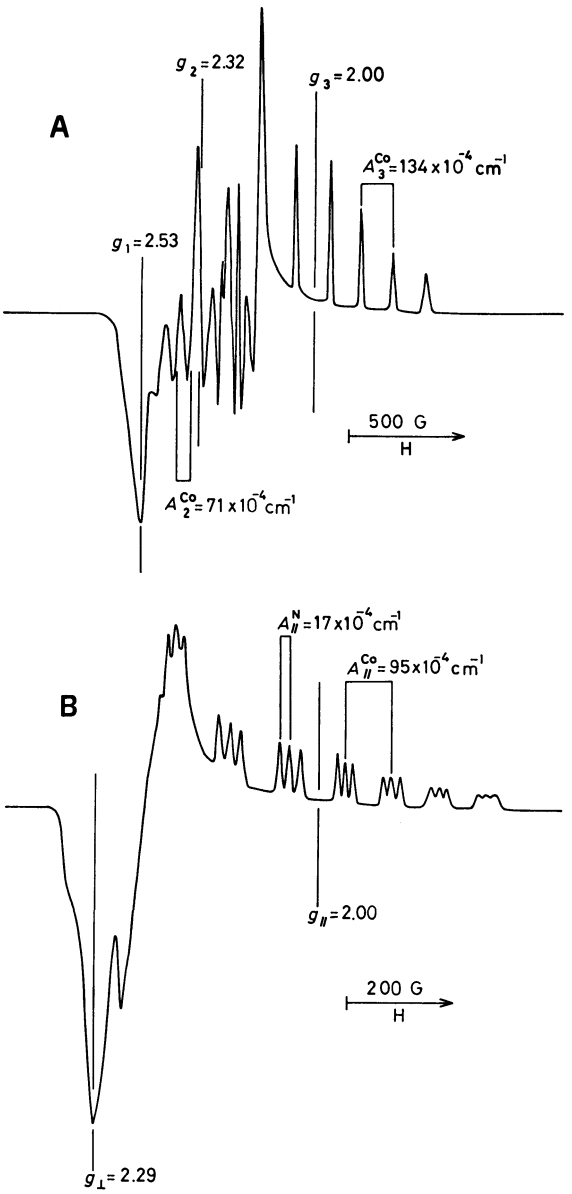

Fig. 1. ESR spectra of [Cob(II)ester]ClO_4 in chloroform–benzene (2 : 1 v/v) at 77 K: A, 9×10^{-3} mol dm^{-3} [Cob(II)ester]ClO_4; B, 9×10^{-3} mol dm^{-3} [Cob(II)-ester]ClO_4 and 4.5×10^{-2} mol dm^{-3} pyridine.

Results and Discussion

ESR spectra of [Cob(II)ester]ClO_4 in base-off and base-on forms are shown in Fig. 1. The spectra and the corresponding spin Hamiltonian parameters are comparable to those of aqueous vitamin B_{12r}.[9,10] Electronic spectra of the present complex also show similar features as observed for aqueous vitamin B_{12r}.[11]

The spectral change upon addition of a base to [Cob-(II)ester]ClO_4 is typically shown in Fig. 2. The corresponding straight line plots on the basis of Eq. 1 are given in Fig. 3; $n=1.00\pm0.05$. This indicates that only one molecule of the base is coordinated to one molecule of the complex under the present conditions, being consistent with the ESR data (Fig. 1). The equilibrium constants and thermodynamic parameters are summarized in Table 1 for the reaction of [Cob(II)ester]-

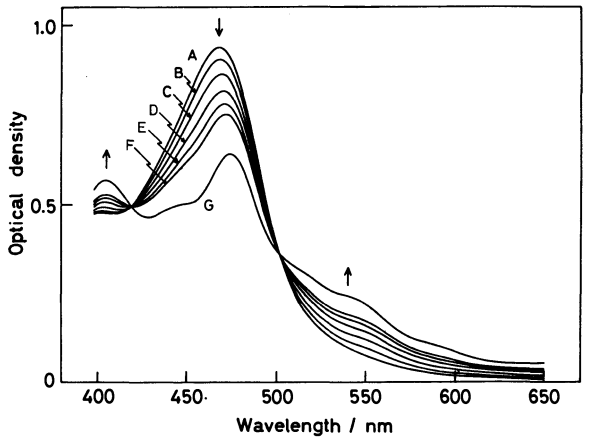

Fig. 2. Spectral change at 18.6 °C for the reaction of [Cob(II)ester]ClO_4 in dichloromethane with morpholine at various concentrations: A, 0; B, 7.62×10^{-5}; C, 2.28×10^{-4}; D, 4.56×10^{-4}; E, 7.59×10^{-4}; F, 1.19×10^{-3}; G, 1.32×10^{-1} mol dm^{-3}. Trends of spectral change with increase in base concentration are shown by arrows.

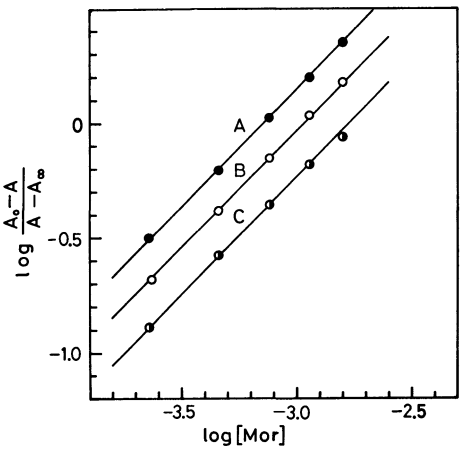

Fig. 3. Analysis of spectral data for the reaction of [Cob(II)ester]ClO_4 with morpholine in dichloromethane at temperatures: A, 28.0; B, 23.7; C, 18.6 °C (refer to Eq. 1). Morpholine concentrations are given in mol dm^{-3}.

ClO_4 with various bases in dichloromethane and toluene.

The linear correlations are observed between log K_1 and pK_a[12] values for the axial ligation of [Cob(II)ester]-ClO_4 with various bases as shown in Fig. 4 specifically in dichloromethane: a single straight line correlation for each of the three different types of amine bases; imidazoles, pyridines, and aliphatic amines. The log K_1 value for the reaction with 2-methylpyridine deviates largely from the corresponding correlation line apparently due to a steric hindrance caused by the 2-methyl group. The stability order with respect to the type of amine base is in an increasing sequence: aliphatic amines, pyridines, and imidazoles. However, this order cannot be directly correlated with the nature and strength of cobalt-nitrogen bond even though such explanation is a tempting one,[13] since the entropy effect must be taken into account. An increment in $-\Delta G$ (from 21.1 to 25.6 kJ mol^{-1}) is accompanied by a decrement in $-\Delta H$ (from 44 to 36 kJ mol^{-1}) for the

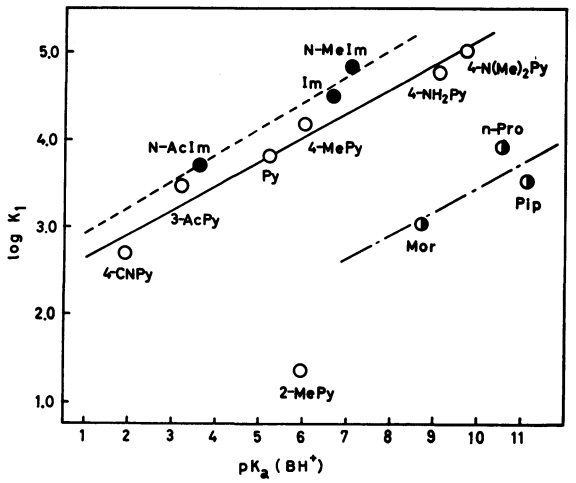

Fig. 4. Correlations between log K_1 and amine basicity for the reaction of [Cob(II)ester]ClO_4 with various bases in dichloromethane at 23.5 °C; K_1 in mol^{-1} dm^3.

reaction of the complex with imidazole derivatives in dichloromethane (Table 1). Such trends are also noted for the reaction with aliphatic amines and some pyridine bases in the same solvent (Table 1). The thermodynamic parameters for ligand coordination in the liquid state seem to reflect the interaction modes of a medium with the metal complex and a coordinating ligand. Such modes must be intensively correlated with the extent of charge delocalization within the metal complex as well as with the extent of steric interaction between a base and the complex. Thus, the enthalpy and entropy parameters were treated on the basis of isoequilibrium relationship.[14,15]

The enthalpy and entropy changes are linearly correlated by Eq. 2.

$$\Delta H = \Delta H_0 + \beta\,\Delta S \quad (2)$$

Here, ΔH_0 is the ΔH value corresponding to $\Delta S=0$, and β denotes the isoequilibrium temperature. Combination of Eq. 2 with the correlation, $\Delta G=\Delta H-T\,\Delta S$, gives the following equations.

$$\Delta G = (T/\beta)\Delta H_0 + (1 - T/\beta)\Delta H \quad (3)$$
$$\Delta G = \Delta H_0 + (\beta - T)\Delta S \quad (4)$$

Consequently, the variation of the free energy change ($\Delta\Delta G$) along with the axial coordination of amines is given by either Eq. 5 or 6, and $\Delta\Delta G$ is concerned with a temperature range under measurements with respect to β.

$$\Delta\Delta G = (1-T/\beta)\Delta\Delta H \quad (5)$$
$$\Delta\Delta G = (\beta-T)\Delta\Delta S \quad (6)$$

Plots of ΔH *vs.* ΔS are shown in Fig. 5 (refer to Table 1). As regards the data obtained in dichloromethane, all points appear to lie along the same line irrespective of the nature of base except for the sterically hindered one (2-MePy): correlation coefficient, 0.99; β, 194$\pm$ 20 K. It is not surprising, therefore, that increments in ΔG are accompanied by decrements in ΔH at the temperature range of present study which is about 100 K above the isoequilibrium temperature. The stability order for the axial ligation of [Cob(II)ester]ClO_4 (see Fig. 4) decreases in the order: imidazoles, pyridines,

TABLE 1. THERMODYNAMIC PARAMETERS FOR AXIAL LIGATION OF [Cob(II)ester]ClO_4 WITH VARIOUS AMINES

Solvent	Amine[a)]	$pK_a(BH^+)$	log K_1[b,c)]	$-\Delta G$[b)] / kJ mol^{-1}	$-\Delta H$ / kJ mol^{-1}	$-\Delta S$[d)] / J K^{-1} mol^{-1}
Dichloromethane	2-MePy	5.97	1.36	7.7	32 ± 4	92
	4-CNPy	1.90	2.70	15.3	37 ± 4	71
	3-AcPy	3.18	3.48	19.8	39 ± 4	63
	Py	5.22	3.83	21.8	38 ± 4	54
	4-MePy	5.98	4.20	23.9	36 ± 8	42
	4-NH_2Py	9.11	4.79	27.2		
	4-N(Me)$_2$Py	9.70	5.02	28.5		
	N-Aclm	3.60	3.72	21.1	44 ± 7	79
	Im	6.65	4.51	25.6	36 ± 5	38
	N-Melm	7.06	4.85	27.5		
	Mor	8.70	3.05	17.3	48 ± 6	105
	Pip	11.12	3.53	20.0		
	n-Pro	10.53	3.93	22.3	44 ± 4	79
Toluene	3-AcPy	3.18	1.98	11.2	38 ± 4	92
	Py	5.22	1.81	10.3	38 ± 4	92
	4-MePy	5.98	2.16	12.3	46 ± 4	117
	Mor	8.70	2.06	11.7	44 ± 7	109
	Pip	11.12	2.14	12.2	36 ± 5	84

a) Abbreviations: 2-MePy, 2-methylpyridine; 4-CNPy, 4-cyanopyridine; 3-AcPy, 3-acetylpyridine; Py, pyridine; 4-MePy, 4-methylpyridine; 4-NH_2Py, 4-aminopyridine; 4-N(Me)$_2$Py, 4-dimethylaminopyridine; *N*-Aclm, *N*-acetylimidazole; Im, imidazole; *N*-Melm, *N*-methylimidazole; Mor, morpholine; Pip, piperidine; *n*-Pro, propylamine. b) Evaluated at 296.6 K. c) Accuracy within ±0.1; K_1 in mol^{-1} dm^3. d) Accuracy within ±15.

TABLE 2. THERMODYNAMIC PARAMETERS FOR AXIAL LIGATION OF Co^{II} (tpp) WITH VARIOUS AMINES

Solvent	Amine	$pK_a(BH^+)$	log K_1[a,b)]	$-\Delta G$[a)] / kJ mol^{-1}	$-\Delta H$ / kJ mol^{-1}	$-\Delta S$[c)] / J K^{-1} mol^{-1}
Dichloromethane	Py	5.22	2.91	16.5	41 ± 4	79
	N-Aclm	3.60	2.50	14.2	42 ± 5	88
	N-Melm	7.06	3.05	17.3	44 ± 5	92
	n-Pro	10.53	3.08	17.5	56 ± 4	130
	Mor	8.70	3.35	19.0	52 ± 4	113
	Pip	11.12	3.55	20.2	46 ± 4	88
Toluene	Py	5.22	2.86	16.2	35 ± 6	63
	N-Aclm	3.60	2.89	16.4	28 ± 4	42
	N-Melm	7.06	3.22	18.3	34 ± 4	54
	n-Pro	10.53	3.13	17.8	38 ± 4	71
	Mor	8.70	3.36	19.1	36 ± 4	54
	Pip	11.12	3.43	19.5	38 ± 4	63

a) Evaluated at 296.6 K. b) Accuracy within ±0.1; K_1 in mol^{-1} dm^3. c) Accuracy within ±15.

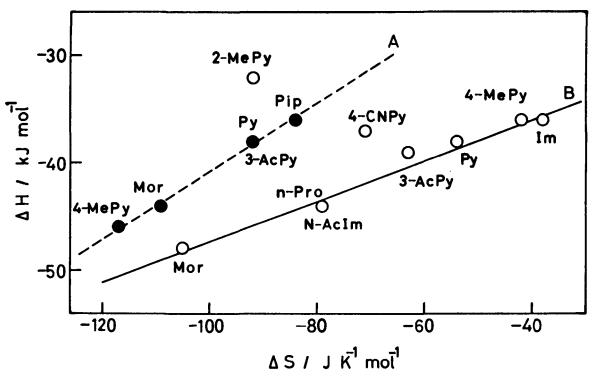

Fig. 5. Plots of ΔH *vs.* ΔS for the reaction of [Cob(II)-ester]ClO_4 with amines in toluene (A) and dichloromethane (B).

and aliphatic amines. Dichloromethane is considered to be inert for metal-coordination and interaction with the corrin skeleton. Thus, such stability sequence seems to be concerned with the extent of steric interaction between the cobalt complex and amine bases. Further, space-filling molecular models indicate that serious van der Waals repulsion can be generated between the hydrogen atoms bound to the carbons α to the nitrogen atom of the aliphatic amines and the angular hydrogen atom bound to the carbon atom at 19 position of [Cob(II)ester]ClO_4. The molecular models show that the restriction of rotation about the carbon–nitrogen bond decreases in the order: cyclic aliphatic amines, pyridine derivatives, and imidazole derivatives. This is attributed to the interactions between an amine base and the side chains of [Cob(II)ester]ClO_4 and

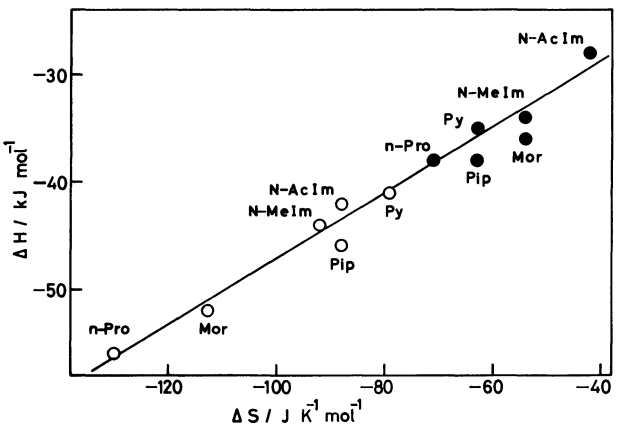

Fig. 6. Plots of ΔH *vs.* ΔS for the reaction of Co^{II}(tpp) with amines in dichloromethane (○) and toluene (●). The solid line is based on the least squares calculation applied to all points.

between the hydrogen atoms bound to α-carbon atoms of amines and the angular hydrogen of the cobalt complex.

In toluene, the enthalpy–entropy relationship with a correlation coefficient of 0.99 (Fig. 5) gives $\beta = 317 \pm 20$ K. The isoequilibrium temperature is very close to the temperature range for present measurements. As a consequence, the values of $\log K_1$ are nearly invariant to the choice of amine in contrast to those observed in dichloromethane.

Thermodynamic parameters for the reaction of Co^{II}(tpp) with various amines in dichloromethane and toluene are tabulated in Table 2. The values of $\log K_1$ are nearly invariant to the choice of amine or solvent. Plots of ΔH *vs.* ΔS for determination of the isoequilibrium temperatures in both solvents are shown in Fig. 6. All points appear to lie along the same line: correlation coefficient, 0.98; β, 300 ± 20 K. Calculations for each individual solvent system result in isoequilibrium temperatures of 301 ± 30 and 327 ± 50 K for dichloromethane and toluene, respectively. Because the isoequilibrium temperatures are obviously close to room temperature, the $\log K_1$ value for axial ligation of Co^{II}(tpp) in dichloromethane and toluene is insensitive to the change in pK_a of amine. The results obtained for Co^{II}(tpp) are comparable to those for [5,10,15,20-tetrakis(*p*-methoxyphenyl)porphinato]cobalt(II), Co^{II}(t(*p*-CH_3O)pp).[16] Axial ligation constants for the reaction of Co^{II}(t(*p*-CH_3O)pp) with pyridine, piperidine, and *N*-methylimidazole in several solvents have been reported to be nearly constant at room temperature. This was attributed to the fact that the reaction was carried out near the isoequilibrium temperature (320 ± 24 K). Being consistent with the previous and present results, plots of ΔH *vs.* ΔS result in a single line correlation for the axial ligation of a cobalt(II)–porphyrin complex, irrespective of the nature of amines and solvents. On the other hand, the correlation of ΔH *vs.* ΔS for the axial ligation of [Cob(II)ester]ClO_4 apparently depends on the nature of solvent employed (Fig. 5). The present complex, [Cob(II)ester]ClO_4, involves the monoanionic corrin moiety as its equatorial ligand while Co^{II}(tpp) has the dianionic porphyrin ligand. The positive charge in the former complex is supposed to be delocalized throughout the whole molecule and the π-π interaction of charge-transfer type between the equatorial ligand and toluene is expected along with the reduction of axial ligation ability as a consequence. Such interaction is apparently not expected with dichloromethane.

In conclusion, the isoequilibrium relationship applies to axial ligation of [Cob(II)ester]ClO_4 in a manner as demonstrated for cobalt(II)– and iron(II)–porphyrin complexes.[13,16,17] In dichloromethane which has no tendency to interact with [Cob(II)ester]ClO_4, the equilibrium constant is primarily controlled by entropy at ordinary temperatures and the $\log K_1$ value varies sensitively along with the change in pK_a of amine. The $\log K_1$ value for the present hydrophobic vitamin B_{12r}, in contrast to that for cobalt(II)–porphyrin complexes, depends on the nature of medium. This suggests that the axial ligation equilibrium of vitamin B_{12} changes widely with the microenvironmental property in the enzyme active sites.

References

1) Y. Murakami, Y. Aoyama, and K. Tokunaga, *J. Am. Chem. Soc.*, **102**, 6736 (1980).

2) Models for methylmalonyl-SCoA→succinyl-SCoA conversion: a) P. Dowd and M. Shaprio, *J. Am. Chem. Soc.*, **98**, 3724 (1976); b) A. I. Scott and K. Kang, *J. Am. Chem. Soc.*, **99**, 1997 (1977). A model for methylitaconate→α-methyleneglutarate conversion: c) P. Dowd, M. Shapiro, and K. Kang, *J. Am. Chem. Soc.*, **97**, 4754 (1975); d) P. Dowd, B. K. Trivedi, M. Shapiro, and L. K. Marwaha, *J. Am. Chem. Soc.*, **98**, 7875 (1976).

3) L. Werthemann, R. Keese, and A. Eschenmoser, unpulished results; see L. Werthemann, Dissertation, ETH Zürich (Nr. 4097), Juris Druck and Verlag, Zürich (1968).

4) J. M. Pratt, "Inorganic Chemistry of Vitamin B_{12}," Academic Press, London (1972), Chap. 7.

5) A. Gossauer, K.-P. Heise, H. Götze, and H. H. Inhoffen, *Justus Liebigs Ann. Chem.*, **1977**, 1480.

6) A. R. Battersby, M. Ihara, E. McDonald, J. R. Redfern, and B. T. Golding, *J. Chem. Soc., Perkin Trans. 1*, **1977**, 158.

7) A. D. Adler, F. R. Longo, F. Kampas, and J. Kim, *J. Inorg. Nucl. Chem.*, **32**, 2443 (1970).

8) J. A. Riddick and W. B. Bunger, "Organic Solvents," Wiley-Interscience, New York (1970).

9) S. A. Cockle, H. A. O. Hill, J. M. Pratt, and R. J. P. Williams, *Biochim. Biophys. Acta*, **177**, 686 (1969).

10) J. H. Bayston, F. D. Looney, J. R. Pilbow, and M. E. Winfield, *Biochemistry*, **9**, 2164 (1970).

11) M. R. Hollaway and H. A. White, "Vitamin B_{12}," ed by B. Zagalak and W. Friedrich, Walter de Gruyter, Berlin (1979), p. 479.

12) W. P. Jencks and J. Regenstein, "Handbook of Biochemistry and Molecular Biology," ed by G. D. Fasman, CRC Press, Cleveland, Ohio (1976), Vol. 1.

13) S. J. Cole, G. C. Curthoys, and E. A. Magnusson, *J. Am. Chem. Soc.*, **92**, 2991 (1970).

14) J. E. Leffler, *J. Org. Chem.*, **20**, 1202 (1955).

15) J. E. Leffler and E. Grunwald, "Rates and Equilibria of Organic Reactions," John Wiley and Sons, New York (1963), Chap. 9.

16) D. P. Rillema, C. M. Wicker, Jr., R. D. Morgan, L. F. Barringer, and L. A. Scism, *J. Am. Chem. Soc.*, **104**, 1276 (1982).

17) F. A. Walker, *J. Am. Chem. Soc.*, **95**, 1150 (1973).

 © 1983 The Chemical Society of Japan Bull. Chem. Soc. Jpn., 56, 3647—3651 (1983)

Oxidized Rubredoxin Models. II. Iron(III) Complexes of Z-Cys-Pro-Leu-Cys-OMe and Z-Cys-Thr-Val-Cys-OMe[1)]

Michio NAKATA, Norikazu UEYAMA, Toshitsugu TERAKAWA, and Akira NAKAMURA*
Department of Macromolecular Science, Faculty of Science, Osaka University, Toyonaka, Osaka 560
(Received July 5, 1983)

Fe(III) complexes of cysteine-containing peptides such as Z–Cys–Pro–Leu–Cys–OMe and Z–Cys–Thr–Val–Cys–OMe corresponding to the Fe binding amino acid sequences in *Cl. pasteurianum* rubredoxin were prepared in solution and characterized by the absorption, circular dichroism (CD), and magnetic circular dichroism (MCD) spectra and were compared with those of the Fe(III) complexes of Z–Cys–Ala–Ala–Cys–OMe, Z–Ala–Cys–OMe, and Z–Cys–Ala–Cys–OMe. These model compelxes exhibited the existence of an electronic configuration and a core structure similar to that of native rubredoxin. The thermal stabilities of the Fe(III) peptide complexes decrease in the following order, Z–Cys–Thr–Val–Cys–OMe$>$Z–Cys–Ala–Ala–Cys–OMe$>$Z–Cys–Pro–Leu–Cys–OMe $\simeq$Z–Ala–Cys–OMe$\gg$Z–Cys–Ala–Cys–OMe.

Rubredoxin playing significant roles in biological electron transfer and oxygenation reactions has one $[Fe(S\text{–}Cys)_4]^{-,2-}$ (S–Cys denotes cysteinyl thiolate, –NH–CH(CH_2S^-)–CO–) as an active site.[2,3)] The X-ray analysis of oxidized rubredoxin from *Clostridium pasteurianum* has revealed that the Fe(III) is coordinated by two thiolates of –Cys(6)–Pro–Leu–Cys(9)–sequence and other two thiolates of –Cys(39)–Thr–Val–Cys(42)–sequence with a distorted tetrahedral geometry.[4)]

Importance of –Cys–A–B–Cys– has been discussed on the contribution to the stabilities of the chelate rings, the determination of the geometries around the metal ions, and the origins of catalytic activities. Christou *et al.* reported the Fe(III) complexes of Ac{Gly–Cys–Gly}$_n$$NH_2$ (n=1—4) in which two Gly residues were interposed between Cys residues. The Gly residues have the least sterical restriction on the peptide conformations.[5)]

Any substituent on the peptide chain will restrict the conformations and will result in preference of one of them.

Thus, our previous paper reported the absorption, CD, MCD, and electron paramagnetic resonance (EPR) spectral analyses of Fe(III) complexes of Z–Cys–Ala–Ala–Cys–OMe and Z–Ala–Cys–OMe.[1)] The tetrapeptide complex exhibited a relatively stable structure with the hairpin turn conformation of the tetrapeptide. It may be indispensable to the function of rubredoxin that the –Cys–A–B–Cys– sequences consist of amino acid residues with bulky side chains such as Pro, Leu, Val, and Thr residues.

In this paper, we describe the preparation and the characterization of Fe(III) complexes of Z–Cys–Thr–Val–Cys–OMe corresponding to the Fe(III) binding sequences in *Cl. pasteurianum* rubredoxin. For comparison, thermal stabilities of an artificial sequence, Z–Cys–Ala–Cys–OMe, in addition to those of Z–Cys–Ala–Ala–Cys–OMe and Z–Ala–Cys–OMe mentioned previously[1)] were investigated with visible spectra. Characteristic properties dependent on the identity of A and B residues in these Cys–A–B–Cys sequences will be discussed.

Experimental

All operations were carried out under argon atmosphere. Dimethyl sulfoxide and triethylamine were degassed and distilled before use. Iron(III) chloride hexahydrate was of commercial grade. Syntheses of the cysteine-containing peptides are described elsewhere.[6)]

Preparations of Fe(III) Complexes. The Fe(III) complexes of the peptides were prepared by the same manner reported by Christou *et al.*[7)] A Me_2SO solution of $FeCl_3\cdot 6H_2O$ and 4 molar equivalents of the cysteine-containing peptide based on its SH-content was treated with triethylamine to give a deep red-violet solution of the Fe(III) complex of the corresponding peptide, which was used for physical measurements without further purifications. $[Et_4N][Fe(S_2\text{-}o\text{-}xyl)_2]$ (S_2-*o*-xyl=*o*-xylene-α,α'-dithiolate) was prepared according to the literature.[8)]

Physical Measurements. Absorption spectra were recorded on a JASCO UVIDEC-5A spectrophotometer. CD and MCD spectra were measured using a JASCO J-40 spectropolarimeter equipped with an electromagnet. The magnetic field was calibrated with an aqueous $K_3[Fe(CN)_6]$ solution.[9)] Calibration of the spectropolarimeter was performed with *epi*-androsterone in dioxane.[10)] The values of ε and $\Delta\varepsilon$ were given in the unit of $M^{-1}\,cm^{-1}$ and $\Delta\varepsilon_M$ in $M^{-1}\,cm^{-1}\,T^{-1}$ where M expresses molar concentration of Fe(III) g-atom. The MCD spectra of the peptide complexes were corrected for the zero-field circular dichrosim.

EPR spectra were recorded at 77 K on a JEOL JESFE 1X with 100 KHz magnetic field modulation using Mn(II) as g-marker (g=1.981).

Results

Spectral Properties of Fe(III) Complexes of Cysteine-containing Peptides. In order to elucidate core structures of the Fe(III) complexes of a series of cysteine-containing peptides, absorption, MCD, and CD spectra of the Fe(III) peptide complexes were investigated in Me_2SO. Table 1 lists the near UV-visible absorption, MCD, and CD spectra of the Fe(III) complexes of Z–Cys–Thr–Val–Cys–OMe and Z–Cys–Pro–Leu–Cys–OMe. For the sake of comparison, those of $[Et_4N][Fe(S_2\text{-}o\text{-}xyl)_2]$ and oxidized rubredoxin from *Cl. pasteurianum*[11–13)] are also represented in Table 1.

The Fe(III) complexes of the peptides exhibited absorption maxima at 330—350 nm and $\approx$500 nm, which were assigned to the ligand-to-metal charge-transfer transitions.[14,15)] The absorption spectra of $[Fe(S_2\text{-}o\text{-}xyl)_2]^-$ and oxidized rubredoxin showed similar spectral features to those of the Fe(III) peptide com-

TABLE 1. SPECTRAL DATA OF Fe(III) COMPLEXES OF CYSTEINE-CONTAINING PEPTIDES

Ligand		$S^-\rightarrow Fe(III)$ charge-transfer									
Z-Cys-Thr-Val-Cys-OMe[a]	Absorption[b]			350 (4700)		495 (3100)					
	MCD[c]	305 (?, 1.1)		385 (A)		495 (A)		570 (B, 2.3)			
	CD[d]		320 (−0.2)	353 (3.0)	393 (−0.7)	438 (3.2)	494 (−1.5)	555 (2.3)		640 (−1.2)	
Z-Cys-Pro-Leu-Cys-OMe[a]	Absorption[b]			355 (6600)			490 (4700)				
	MCD[c]	310 (?, 0.8)	350 (B, −1.0)		385 (A)		485 (A)		580sh (B, 1.3)		
	CD[d]		350 (5.5)		385 (−0.6)	428 (3.2)	494 (−5.0)	562 (1.4)		640 (−0.5)	
Z-Cys-Ala-Ala-Cys-OMe[a,g]	Absorption[b]			353 (5500)			495 (3400)				
	MCD[c]	310 (?, 1.0)	355 (B, −0.3)		390 (A)		495 (A)		585sh (B, 1.2)		
	CD[d]		350 (4.0)		395 (−0.6)	437 (1.2)	500 (−1.6)	560 (1.3)		650 (−0.7)	
Z-Cys-Ala-Cys-OMe[a,g]	Absorption[b]			330 (2600)			500 (1500)				
	MCD[c]		340 (?, 0.4)		389 (A)		495 (A)	550 (B, 0.4)			
	CD[d]	315 (−0.7)	340 (0.7)	370 (−0.8)	415sh (0.4)	459 (0.9)	530sh (−0.9)	570 (−0.4)			
Z-Ala-Cys-OMe[a,g]	Absorption[b]			348 (4400)			495 (2700)				
	MCD[c]	305 (?, 1.1)		383 (A)			495 (A)	560 (B, 1.8)			
	CD[d]		355 (0.1)		400 (−0.1)		500 (0.3)		615 (−0.1)		
$[Et_4N]$ $[Fe(S_2\text{-}o\text{-}xyl)_2]$[e]	Absorption[b]			354 (8200)		430sh (4400)	486 (6400)			635 (1700)	685 (1700)
	MCD[c]	341 (?, 1.1)	355 (?. 0)	365 (?, −0.6)	422 (?, −3.4)		499 (A)			632 (B, 1.8)	
Oxidized rubredoxin[f]	Absorption[b,h]			353 (9600)	380 (10800)		493 (9200)	560 (4400)			
	MCD[c,i]	309 (?, 4.4)	347 (?, −0.8)	382 (A)			495 (A)	565 (B, 5.1)			
	CD[d,j]		344 (−6.2)		412 (10.8)	440 (14.3)	500 (−20.7)	564 (20.8)		637 (−6.9)	

a) In Me_2SO. b) nm(ϵ, $M^{-1}\,cm^{-1}$). c) nm(origin of the Farady effect, $\Delta\epsilon_M$, $M^{-1}\,cm^{-1}\,T^{-1}$). d) nm($\Delta\epsilon$, $M^{-1}\,cm^{-1}$). e) In *N*, *N*-dimethyl formamide. f) In aqueous solution. g) From Ref. 1. h) From Ref. 11. i) From Ref. 12. j) From Ref. 12.

plexes although several additional bands were observed (Table 1).

The MCD spectra of the Fe(III) peptide complexes were highly structured and much more informative than the absorption spectra. The MCD spectrum of oxidized rubredoxin was characterized by Ulmer *et al.* and they pointed out that two dispersion type bands with cross-over points at 382 and 495 nm are assignable to the Faraday A-term, and a negative and a positive bell-shaped bands at 347 and 565 nm to the Faraday B-term corresponding to the absorption maxima at 353, 380, 493, and 560 nm (Table 1).[12] A positive band at 309 nm was not assigned. According to the assignments for rubredoxin[11] and its model complexes with alkanedithiols,[16] tentative assignments for the peptide complexes and $[Fe(S_2\text{-}o\text{-}xyl)_2]^-$ were carried out and are summarized in Table 1. All of the Fe(III) peptide complexes had dispersion type bands with cross-over points at 380—390 nm and positive MCD shoulders at 550—585 nm corresponding to those of the native protein at 382 and 565 nm whereas the peptide complexes had no definite absorption maxima at these regions. On the other hand, $[Fe(S_2\text{-}o\text{-}xyl)_2]^-$ had no cross-over point at 380—390 nm. Among the peptide Fe(III) complexes examined, Z–Cys–Pro–Leu–Cys–OMe and Z–Cys–Ala–Ala–Cys–OMe complexes exhibited negative Faraday effects at 350 and 355 nm, respectively, similar to rubredoxin. The complexes of other peptides did not show such negative ones.

The CD spectra of the Fe(III) peptide complexes

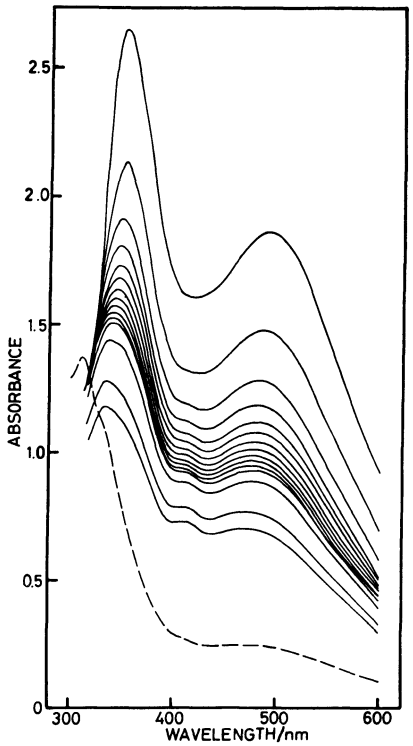

Fig. 1. Spectral change of Fe(III) complex of Z-Cys-Pro-Leu-Cys-OMe. Each spectrum from upper to lower indicates that measured after 10, 71, 130, 187, 254, 314, 383, 453, and 530 s, 10, 11, 13, 24, and 30 min from the complex formation. The broken-line indicat esthe spectrum after 13 h.

also revealed many transitions involved in the charge-transfer region as shown in Table 1. The tetrapeptide Fe(III) complexes especially Z-Cys-Ala-Ala-Cys-OMe complex previously reported,[1] exhibited spectral pattern similar to that of rubredoxin at wavelength longer than 400 nm although the magnitude of the Cotton effects was *ca.* 1/10. On the other hand, tri- and dipeptide Fe(III) complexes exhibited the CD spectra entirely different from those of the tetrapeptide complexes or rubredoxin.

Thermal Stabilities of Fe(III) Complexes of Cysteine-containing Peptides. Under anaerobic conditions, the Fe(III) complexes of the cysteine-containing peptides were unstable as reported by Christou *et al.*[6] Intense red-violet color of the Fe(III) complexes observed immediately after the addition of triethylamine faded gradually due to oxidations of the ligands by the Fe(III) ion. The spectral changes were followed in the time course. A typical example is shown in Fig. 1 for the Z-Cys-Pro-Leu-Cys-OMe complex. After 13 h, the spectrum is broken line of Fig. 1 and further change was observed. The spectrum was similar to that of the Fe(II) complex of Z-Cys-Pro-Leu-Cys-OMe which will be described elsewhere. The following reaction must be taking place:

$$4[Fe^{III}(Z\text{-cys-Pro-Leu-cys-OMe})_2]^{2-} \longrightarrow 3[Fe^{II}(Z\text{-cys-Pro-Leu-cys-OMe})_2]^{2-} + 1/2n\,(Z\text{-Cys-Pro-Leu-Cys-OMe})_n + 1/4\,Fe^{II}.$$

Half-life time for each peptide complexes was obtained by monitoring the absorbance maximum at around 500 nm, which is listed in Table 2. The results indicate that the Fe(III) complexes of Z-Cys-Thr-Val-Cys-OMe and Z-Cys-Ala-Ala-Cys-OMe are less unstable among the complexes examined by us. In contrast, the Fe(III) state of rubredoxin is stable at ambient temperature in an aqueous solution.

TABLE 2. HALF-LIFE TIMES OF Fe(III) COMPLEXES OF CYSTEINE-CONTAINING PEPTIDES

Ligand	Half-life times/min	λ_{max}/nm
Z-Cys-Thr-Val-Cys-OMe	25	495
Z-Cys-Pro-Leu-Cys-OMe	7	490
Z-Cys-Ala-Ala-Cys-OMe	16	495
Z-Cys-Ala-Cys-OMe	1	500
Z-Ala-Cys-OMe	5	495

Conditions: in Me_2SO at 33 °C.

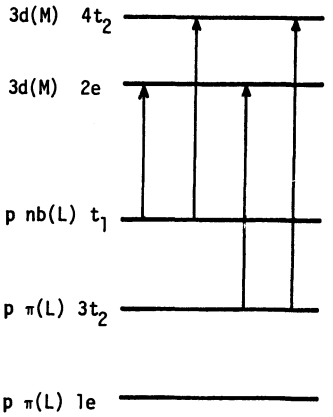

Fig. 2. Energy level diagram of tetrahedral complexes including the highest ligand levels (L) and the metal d levels (M).

Discussion

Structures of $[Fe^{III}S_4]$ *Cores.* The absorption, MCD, and EPR spectra of the Fe(III) peptide complexes led the conclusion that the peptide complexes have mononuclear tetrahedral $[Fe^{III}S_4]$ cores. A formation of binuclear core, $[Fe^{III}{}_2S_8]$, involved in $[Fe^{III}(SCH_2\text{-}CH_2S)_2]_2{}^{2-}$ [17] was ruled out by the MCD spectra. The Fe(III) complex of 1,2-ethanedithiolate exhibited no dispersion type band at around 490 nm but a small positive band at 427 nm and a negative one at 590 nm which were ascribed to the Faraday B-term.[16] The previous paper[1] also indicated that the ESR signals of the Fe(III) complexes of Z-Cys-Ala-Ala-Cys-OMe and Z-Ala-Cys-OMe arise from $S=5/2$ ground state (Fe(III)d^5 high spin) under approximately tetrahedral environments coordinated with four cysteinyl thiolates.

Although the peptide complexes had the similar MCD spectral features from 400 to 700 nm, they exhibited different spectral properties from 300 to 400 nm. They could be divided into two groups. One is the Fe(III) complexes of Z-Cys-Pro-Leu-Cys-OMe and Z-Cys-Ala-Ala-Cys-OMe which have a negative Faraday B-term at around 350 nm and the other has

TABLE 3. CHARGE-TRANSFER BANDS OF Fe(III) COMPLEXES OF CYSTEINE-CONTAINING PEPTIDES[a)]

Ligand	$t_1 \rightarrow 2e$	$t_1 \rightarrow 4t_2$	$3t_2 \rightarrow 2e$	$3t_2 \rightarrow 4t_2$
Z-Cys-Thr-Val-Cys-OMe	17500	20200	26000	—[b)]
Z-Cys-Pro-Leu-Cys-OMe	17200	20600	26000	28600
Z-Cys-Ala-Ala-Cys-OMe	17100	20200	25600	28200
Z-Cys-Ala-Cys-OMe	18200	20200	25700	—[b)]
Z-Ala-Cys-OMe	17400	20200	26100	—[b)]
$[Et_4N]$ $[Fe(S_2\text{-}o\text{-xyl})_2]$	15800	20000	—[c)]	—[b)]
Oxidized rubredoxin	17700	20200	26200	28800[d)]

a) Transition energies were estimated from MCD spectra represented in the unit of cm^{-1}. b) No Faraday B-term was observed. c) No Faraday A-term was observed. d) From Ref. 11.

no such a band at 300—400 nm.

A simple molecular orbital consideration gives a clue to interpret the charge-transfer spectra. A qualitative molecular orbital diagram for tetrahedral Fe(III) complexes is illustrated in Fig. 2, which shows the highest ligand level (L), the Fe(III) d levels, and allowed charge-transfer transitions. The molecular orbitals are constructed by a basis set consisting of 3d, 4s, and 4p of Fe(III) and 3s and 3p of S.[18)] The transition energies estimated from the MCD spectra of the peptide complexes are listed in Table 3. The transitions were assigned to those from the highest occupied ligand π or nonbonding orbitals to the half occupied metal d orbitals according to the literature.[15)] The orientations of the lone pairs on the cysteinyl S atom are shown schematically in Fig. 3. There are two lone pairs; one is perpendicular to the Fe–S–C_β plane (π-type) and the other in the plane (nonbonding type). As shown in Fig. 2 and Table 3, the transitions at around 350 nm (28600 cm^{-1}) were assignable to those from the occupied ligand orbitals ($3t_2$) to the half-occupied metal t_2 orbitals ($4t_2$). The MCD spectral characteristics sensitively reflect differences of the orientation of the π-orbitals on S atom toward Fe(III) ion (Fig. 3b). The orientation of the π-type S lone pair toward the Fe(III) ion change the energies of the Fe d_{xy} and d_{yz} as described by Bair and Goddard III.[19)] The nonbonding orbital on the S atom does not affect the Fe d orbitals in a manner observed for the π-type orbital. Thus, the MCD spectral differences in 300—400 nm region are related to the differences in the electronic states of the Fe(III) t_2 orbitals affected by the lone pairs of the S atom, mainly π-orbitals, whose orientation is determined by steric disposition of the S–C_β bond relative to the Fe–S bond as shown in Fig. 3. Conformational restriction of the peptide ligands determines these orientations and, hence, electronic structures of the $[Fe^{III}S_4]$ cores.

Chemical environments surrounding the $[Fe^{III}S_4]$ core are also important in determining properties of the core. For example, the MCD spectrum of $[Fe(S_2\text{-}o\text{-xyl})_2]^-$ exhibited entirely different feature within 300—400 nm from those of the peptide complexes and rubredoxin (Table 1) in spite of the similarities of the $[Fe^{III}S_4]$ core structures as confirmed by the X-ray structural analyses.[3,8)]

Although the absorption and MCD spectra of the peptide Fe(III) complexes did not show remarkable differences among a series of the peptide ligands examined, their CD spectra exhibited different spectral profiles as shown in Table 1. The Cotton effects in the charge-transfer region are originated with chiral charge-transfer from thiolate to Fe(III) influenced by asymmetric α-carbons of the peptide ligands. Spatial distribution of the asymmetric carbons is crucial in determining the CD spectral features. Restricted conformation of the peptide ligands around the metal ion will result in large Cotton effects. Therefore, chelate ring formation is related to the large Cotton effects.

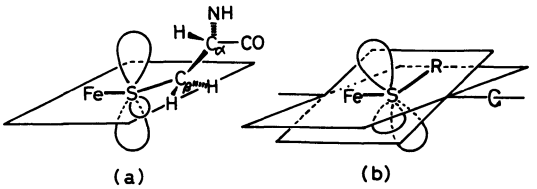

Fig. 3. (a) Schematic representation of lone pairs on S atom in $[Fe(S\text{–}Cys)_4]$ core. (b) Rotation about Fe–S bond in (a).

According to the above criteria, the Fe(III) complex of Z–Cys–Thr–Val–Cys–OMe, Z–Cys–Pro–Leu–Cys–OMe, and Z–Cys–Ala–Ala–Cys–OMe have *S,S*-chelate structures when comparisons were made with the CD spectrum of the Fe(III) complex of Z–Ala–Cys–OMe. The tetrapeptide complexes had the stronger Cotton effects; 10—50 times greater than the dipeptide complex (Table 1). The tripeptide complex shows about half CD strength of the tetrapeptide (Table 1). Further studies are required to determine the *S,S*-chelation of the tripeptide to Fe(III) ion.

Comparisons between Fe(III) Complexes of Cysteine-containing Peptides and Oxidized Rubredoxin. Relationships of the properties of the $[Fe^{III}S_4]$ cores with the spectral arrangement of the cysteine-containing peptides among the peptide Fe(III) complexes and oxidized rubredoxin will be discussed in terms of the spectral characteristics as diagnostic tools. A given orientation of the S–C_β bond around the Fe–S bond fixes location of the lone pairs on the S atom and, consequently, determines the electronic state of the $[Fe^{III}S_4]$ core, which is reflected sensitively by the MCD spectra as discussed above. Therefore, similarity of the MCD spectra between the Fe(III) complexes of Z–Cys–Pro–Leu–Cys–OMe or Z–Cys–Ala–Ala–Cys–OMe and rubredoxin (Table 1) allows us to conclude that they have similar $[Fe^{III}S_4]$ core electronic structures

controlled by the orientations of the S–C_β bonds around the Fe–S bonds. The other peptide complexes presumably have somewhat different orientations of the S lone pairs, especially π-type orbitals, which influence their MCD spectra in the $3t_2$–$4t_2$ transitions (Fig. 2).

The CD spectral resemblances between the peptide Fe(III) complexes and the native protein mean the similar arrangements of the asymmetric α-carbons between them as well as the similar orientations of the S–C_β bonds (Fig. 3a). From such a point of view, the Fe(III) complex of Z–Cys–Ala–Ala–Cys–OMe has spatial arrangement of the peptide ligands closely similar to rubredoxin around the [$Fe^{III}S_4$] core. The other tetrapeptide, Z–Cys–Thr–Val–Cys–OMe or Z–Cys–Pro–Leu–Cys–OMe, could not reproduce the CD spectral characteristic of rubredoxin completely. Cooperative effects of the both tetrapeptide units or whole protein environments seem to be important for subtle adjustments of the active site properties of native rubredoxin.

Thermal Stabilities of Fe(III) Complexes of Cysteine-containing Peptides. The thermal stabilities of the Fe(III) peptide complexes followed in the order (Table 2): Z–Cys–Thr–Val–Cys–OMe>Z–Cys–Ala–Ala–Cys–OMe>Z–Cys–Pro–Leu–Cys–OMe>Z–Ala–Cys–OMe>Z–Cys–Ala–Cys–OMe. It is interesting that the Fe(III) complex of Z–Cys–Pro–Leu–Cys–OMe, although having one of the Fe binding peptide units of rubredoxin, is somewhat less stable under these conditions. On the other hand, the Fe(III) complex of Z–Cys–Thr–Val–Cys–OMe had fairly good stability toward the oxidation of the thiolate ligand. Steric effects caused by different conformations of the two tetrapeptides in the Fe(III) complexes presumably resulted in such differences in their thermal stabilities, which were supported by their CD spectra. A recent synthesis of thermally stable $[Fe^{III}(SC_{10}H_{13})_4]^-$ ($C_{10}H_{13}S^-$= 2,3,5,6-tetramethylbenzenethiolate) revealed that the steric and conformational properties of the thiolate ligands are crucial in accounting for the stabilities of Fe(III) thiolate complexes because the synthesis of the corresponding benzenethiolate derivative has not been successful.[20] Importance of the steric and conformational effects on the cysteine-containing peptide ligands is supported by the fact that reconstituted adrenodoxin containing one Fe(III) ion at its active site, which exhibits oxidized rubredoxin-like spectra, is unstable in the Fe(III) state.[21] Adrenodoxin, which is one of the iron–sulfur proteins, has a [$Fe_2S^*_2$] core (S* denotes inorganic sulfide) chelated by two tetrapeptide units as Cys(52)–Ser–Thr–Cys(55) and Cys(92)–Glu–Ile–Cys(95) with the cysteinyl thiolates in its native state.[21] On the reconstitution, one Fe(III) ion will be accommodated by these cysteinyl thiolate ligands, but the [$Fe^{III}S_4$] core is not stabilized by the tetrapeptide units in the active site of adrenodoxin.

We thank Professor Masahiro Hatano and Dr. Tsunenori Nozawa for useful discussion of CD and MCD spectra. The present work was supported by a Grant-in-Aid from the Ministry of Education, Science and Culture.

References

1) Part I of this series: N. Ueyama, M. Nakata, and A. Nakamura, *Bull. Chem. Soc. Jpn.*, **54**, 1727 (1981).
2) W. H. Orme-Johnson, *Annu. Rev. Biochem.*, **42**, 159 (1973).
3) K. D. Watenpaugh, L. C. Sieker, and L. H. Jensen, *J. Mol. Biol.*, **131**, 509 (1979).
4) E. Adman, K. D. Watenpaugh, and L. H. Jensen, *Proc. Natl. Acad. Sci. U. S. A.*, **72**, 4854 (1975); E. Adman, *Biochim. Biophys. Acta*, **549**, 107 (1979).
5) G. Christou, B. Ridge, and H. N. Rydon, *J. Chem. Soc., Chem. Commun.*, **1970**, 20.
6) N. Ueyama, M. Nakata, and A. Nakamura in preparation.
7) G. Christou, B. Ridge, and H. N. Rydon, *J. Chem. Soc., Chem. Commun.*, **1977**, 908.
8) R. W. Lane, J. A. Ibers, R. B. Frankel, G. C. Papaefthymiou, and R. H. Holm, *J. Am. Chem. Soc.*, **99**, 84 (1977).
9) L. E. Vickery, T. Nozawa, and K. Sauer, *J. Am. Chem. Soc.*, **98**, 351 (1976).
10) K. Tuzimura, T. Konno, H. Meguro, M. Hatano, T. Murakami, K. Kashiwabara, K. Saito, Y. Kondo, and T. Suzuki, *Anal. Biochem.*, **81**, 167 (1977).
11) W. Lovenberg and B. E. Sovel, *Proc. Natl. Acad. Sci. U. S. A.*, **54**, 193 (1965).
12) D. D. Ulmer, B. Holmquist, and B. L. Vallee, *Biochem. Biophys. Res. Commun.*, **51**, 1054 (1973).
13) W. A. Eaton and W. Lovenberg, "Iron-Sulfur Proteins," ed by W. Lovenberg, Academic Press, New York and London (1973), Vol. II, p. 131.
14) J. V. Pivnichny and H. H. Brintzinger, *Inorg. Chem.*, **12**, 2839 (1973).
15) R. A. Bair and W. A. Goddard, III, *J. Am. Chem. Soc.*, **100**, 5669 (1978).
16) T. Muraoka, T. Nozawa, and M. Hatano, *Chem. Lett.*, **1976**, 1373.
17) T. H. Herskovitz, B. V. Depamphilis, W. O. Gillum, and R. H. Holm, *Inorg. Chem.*, **14**, 1426 (1975).
18) B. D. Bird and P. Day, *J. Chem. Phys.*, **49**, 342 (1968).
19) R. A. Bair and W. A. Goddard, III, *J. Am. Chem. Soc.*, **99**, 3505 (1977).
20) M. Millar, J. F. Lee, S. A. Koch, and R. Fikar, *Inorg. Chem.*, **21**, 4105 (1982).
21) Y. Sugiura, K. Ishizu, and T. Kimura, *Biochem. Biopys. Res. Commun.*, **60**, 334 (1974).

Asymmetric Synthesis of α-Deuterated α-Amino Acids through Nonenzymatic Transamination Reaction and the Determination of Their Enantiomeric Excesses

Yoji TACHIBANA,† Makoto ANDO, and Hiroyoshi KUZUHARA*
The Institute of Physical and Chemical Research, Wako, Saitama 351

(Received April 13, 1983)

Optically active α-deuterated α-amino acids were prepared in methanol-*d* through Zn^{2+}-catalyzed transamination reaction between the chiral pyridoxamine analogs, (*R*)- or (*S*)-15-aminomethyl-14-hydroxy-5,5-dimethyl-2,8-dithia[9](2,5)pyridinophane and various α-keto acids with enantiomeric excesses ranging from 40 to 94%. Aliphatic α-keto acids gave α-deuterated α-amino acids, whereas aromatic ones possessing a methylene group between the carbonyl group (ketone) and the aromatic ring underwent concomitant deuterium substitution at the active methylene group to give the amino acids deuterated at both α- and β-positions of the carboxyl group. The use of the (*S*)-pyridoxamine analog gave the (*R*)-deuterated α-amino acids in excess and *vice versa*. The enatiomeric excesses of the amino acids were determined through the analyses of ^1H NMR spectra of the Schiff bases produced by the condensation of the amino acids with the chiral pyridoxal analog, (*R*)- or (*S*)-15-formyl-14-hydroxy-2,8-dithia[9]-(2, 5)pyridinophane. The azomethine protons of the diastereomeric Schiff bases were clearly resolved in the spectrum and their intensities well reflected the amount of the diastereomers.

Chiral α-amino acids labelled at α- or β-position of the carboxyl group have been valuable for determinig the steric course of a variety of biosynthetic transformations and conformational analyses of peptides.[1-3] However, there are only a few reports concerning the preparation of these deuterated amino acids.[4-6]

In the course of our continuous study of vitamin B_6-dependent enzyme models, we have recently reported the asymmetric synthesis of α-amino acids through the enantioselective transamination reaction between the chiral pyridoxamine analogs with a pyridinophane structure, (*R*)- or (*S*)-15-aminomethyl-14-hydroxy-5,5-dimethyl-2,8-dithia[9](2,5)pyridinophane ((*R*)- or (*S*)-**1**) or (*S*)-15-aminomethyl-14-hydroxy-2,8-dithia[9](2,5)-pyridinophane ((*S*)-**2**), and various α-keto acids in the presence of Zn^{2+}.[7,8] We have also found that the α-proton of the amino acids comes directly from the methanol employed as solvent in the nonenzymatic transamination reaction.[9] In the present paper, we wish to describe the extended application of the nonenzymatic transamination system to the asymmetric synthesis of α-deuterated α-amino acids by employing methanol-*d* as the solvent and the determination of their enantiomeric excesses by analyzing the ^1H NMR spectra of the Schiff bases prepared from the deuterated amino acids and a chiral pyridoxal analog, (*R*)- or (*S*)-15-formyl-14 hydroxy-2,8-dithia[9](2,5)pyridinophane ((*R*)- or (*S*)-**3**).[10]

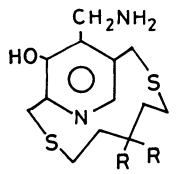

1: R=CH3

2: R=H

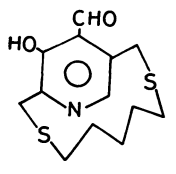

3

† Present address: Central Research Laboratory, Nisshin Flour Milling Co., Ltd., Ooimachi, Iruma-gun, Saitama 354.

Results and Discussion

The nonenzymatic transamination reactions in methanol-*d* (MeOD) were slower than those in methanol and took several days to be completed because of the solvent isotope effect.[11] The isolation of the deuterated α-amino acid produced was carried out in a similar way to that described previously for the general preparation of amino acids.[7] The NMR spectra of the products showed that aliphatic α-keto acids such as pyruvic acid, 3-methyl-2-oxobutanoic acid, and 4-methyl-2-oxopentanoic acid gave the corresponding α-deuterated α-amino acid through reaction with the pyridoxamine analog ((*R*)- or (*S*)-**1**) in the presence of Zn^{2+}. On the other hand, the employment of aromatic α-keto acids such as phenylpyruvic acid and indole-3-pyruvic acid under the same reaction conditions resulted in the corresponding amino acids deuterated at both α- and β-positions of their carboxyl group (Fig. 1). The NMR spectra of deuterated leucine, valine, and phenylalanine are shown in Figs. 2,3, and 4. The results of the elemental analyses and mass spectra of these deuterated α-amino acids are shown in Table 1. Deuteration of the active methylene group between the keto and the aromatic groups of sodium phenylpyruvate or sodium indole-3-pyruvate took place spontaneously even if the pyridoxamine analog and the metal ion were absent. However, the chelated ketimine group formed in the presence of the pyridoxamine analog and the metal ion is more electron-withdrawing than the original keto group and more strongly prompts elimination of the protons from the neighboring methylene group, resulting in deuterio substitution at that place.

Determination of the enantiomeric excess of the deuterated amino acids was not easy because the specific rotations of the authentic specimens were unknown. The utilization of the diastereomeric Schiff base mixture produced by condensation of the deuterated amino acids with some chiral aldehydes might be a promising way for the enantiomeric excess determination. Our pyridoxal analog ((*R*)- or (*S*)-**3**) could

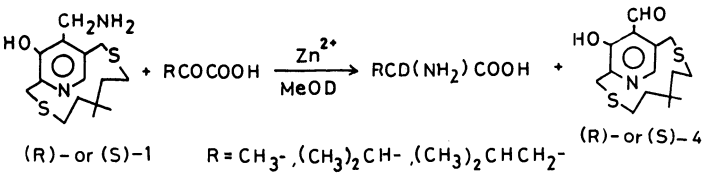

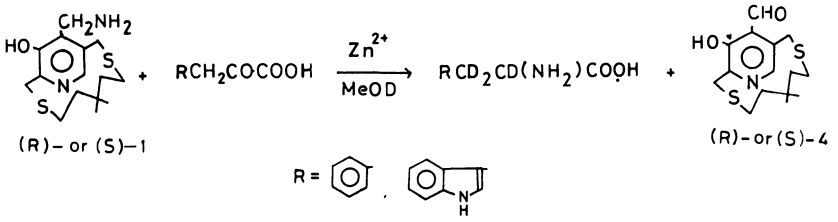

Fig. 1. Transamination reaction between pyridoxamine analogs ((*R*)- or (*S*)-**1**) and α-keto carboxylic acids in methanol-*d*.

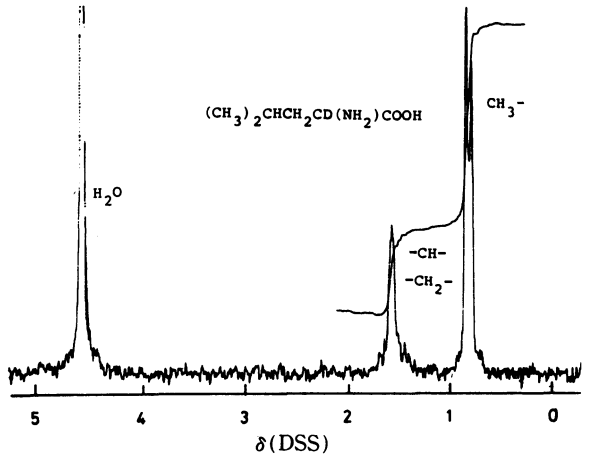

Fig. 2. ^{1}H 100-MHz NMR spectrum of $(CH_3)_2CHCH_2$-$CD(NH_2)COOH$ in D_2O (DSS internal standard).

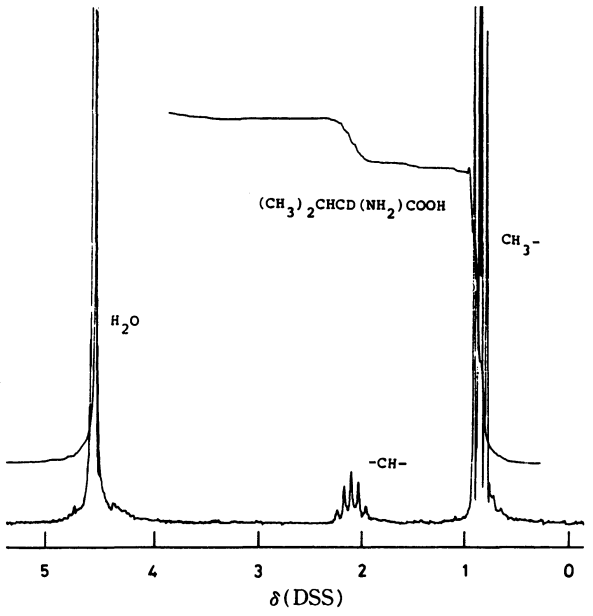

Fig. 3. ^{1}H 100-MHz NMR spectrum of $(CH_3)_2CHCD$-$(NH_2)COOH$ in D_2O (DSS internal standard).

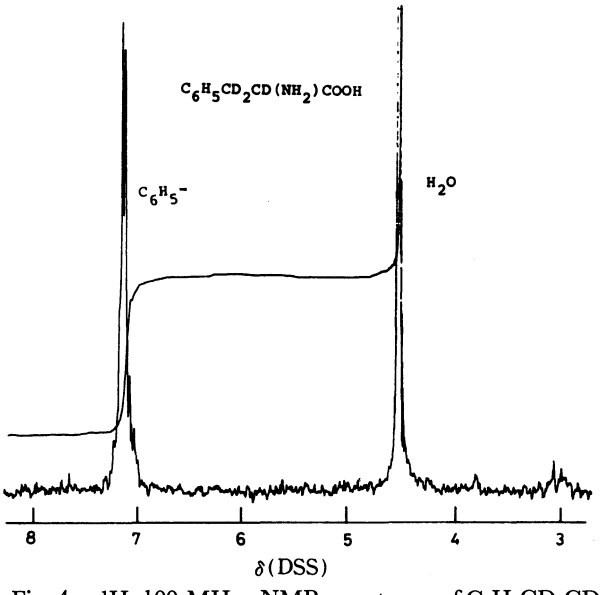

Fig. 4. ^{1}H 100-MHz NMR spectrum of $C_6H_5CD_2CD$-$(NH_2)COOH$ in D_2O (DSS internal standard).

be regarded as a candidate for the chiral aldehyde because **3** readily condensed with free amino acids in methanol at room temperature to give an aldimine type of Schiff base. We confirmed that no racemization of the general amino acid moieties in the Schiff bases took place under such mild conditions, since the amino acids recovered after acidic hydrolysis of the Schiff bases retained the full original chirality. Judging from the isotope effect, these results obtained by using general chiral amino acids would be also applicable to deuterated amino acids. Therefore, the deuterated amino acids obtained were converted into Schiff bases by condensation with (*R*)- or (*S*)-**3**. Figure 5 shows the 400 MHz ^{1}H NMR spectrum of the C_6D_6 solution of the diastereomeric mixture of the Schiff bases resulted from the reaction of the racemic α-deuterated leucine with (*R*)-**3** in methanol. The signals at δ 8.77 (b) and δ 9.00 (d) were assigned to the aldimine protons of the pyridoxal analog moiety.[12–16] The signals at δ 8.02 (a), δ 8.17 (c), and δ 8.26 (e) should be assigned to the 6-H protons on the pyridine ring.[17–18] The assignment of those signals (b—e) was confirmed by comparing them with the NMR spectra of the Schiff bases prepared from authentic sample of general (*S*)- or (*R*)-leucine and (*R*)-**3**, respectively.[19] The Schiff

TABLE 1. ELEMENTAL ANALYSES AND MASS SPECTRA OF DEUTERATED AMINO ACID, $RCD(NH_2)COOH$[a)]

R	Mass (*m/e*) Found	Mass (*m/e*) Calcd	Formula	Calcd (%) C	Calcd (%) H+D	Calcd (%) N	Found (%) C	Found (%) H+D[b)]	Found (%) N
$(CH_3)_2CHCH_2$	133 $(M+1)^+$	132 (M)	$C_6H_{12}DNO_2$	54.52	10.67	10.60	54.94	10.57	10.65
$(CH_3)_2CH$	119 $(M+1)^+$	118 (M)	$C_5H_{10}DNO_2$	50.82	10.23	11.86	50.62	10.43	11.72
$C_6H_5CD_2$	168 $(M)^+$	168 (M)	$C_9H_8D_3NO_2$	64.21	8.38	8.32	64.26	8.23	8.32

a) The deuterated amino acids were obtained through nonenzymatic transamination reaction between (*R*)-**1** and RCOCOOH. b) The determined values of H+D were calculated from the weight of H_2O+HOD produced on the assumption that the H : D atomic ratio was that of the compound analyzed.

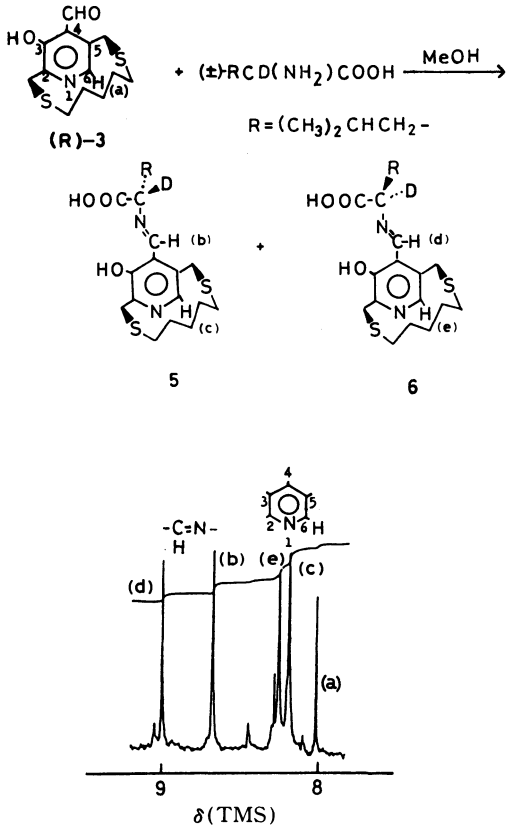

Fig. 5. ^1H 400-MHz NMR spectrum of C_6D_6 solution of the Schiff bases derived from (*R*)-**3** and racemic deuterated leucine in a molar ratio of 1.2/1 in MeOH (TMS internal standard). The signals (a—e) are; (a): 6-H proton of (*R*)-**3**. (b), (d); Azomethine protons of **5** and **6**. (c), (e); 6-H protons of **5** and **6**.

TABLE 2. CHEMICAL SHIFTS OF AZOMETHINE (–CH=N–) AND PYRIDINE RING PROTONS OF THE SCHIFF BASES PREPARED FROM $RCD(NH_2)COOH$ AND (*R*)-**3**

R (Configuration)		Chemical shift[a)] –CH=N–	Chemical shift[a)] Pyridine ring
$(CH_3)_2CHCH_2$	(*R*)	9.00	8.26
$(CH_3)_2CHCH_2$	(*S*)	8.77	8.17
$(CH_3)_2CH$	(*R*)	8.80	8.23
$(CH_3)_2CH$	(*S*)	8.54	8.17
$C_6H_5CD_2$	(*R*)	8.42[b)]	8.07[b)]
$C_6H_5CD_2$	(*S*)	8.30[b)]	8.04[b)]

a) δ from TMS in C_6D_6 (400 MHz). b) The high-field shift of the peaks is probably due to the anisotropic effect of the phenyl ring.

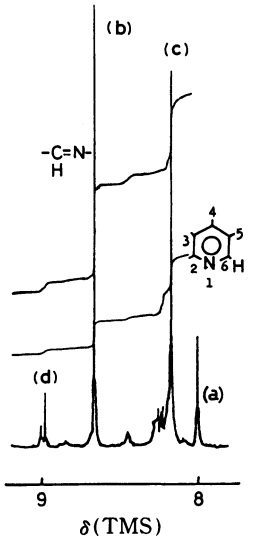

Fig. 6. ^1H 400-MHz NMR spectrum of C_6D_6 solution of the Schiff bases derived from (*R*)-**3** and deuterated leucine enriched in *S*-configuration in a molar ratio of 1.2/1 in MeOH (TMS internal standard). The signals (a—d) are; (a): 6-H proton of (*R*)-**3**, (b), (d): azomethine protons of **5** and **6**. (c): 6-H proton of **5**.

bases produced from (*S*)- or (*R*)-leucine and (*R*)-**3** can be isolated and characterized by elemental analyses, IR, and NMR spectra. When (*S*)-leucine was condensed with (*R*)-**3**, the resulting Schiff base revealed the azomethine and the pyridine ring protons at δ 8.73 and δ 8.13, respectively. When (*R*)-leucine was condensed with (*R*)-**3**, the signals for the azomethine and the pyridine ring protons appeared at δ 9.00 and 8.20. Therefore, the signals, (b) and (d), should be assigned to the azomethine protons of the Schiff bases containing (*S*)- and (*R*)-deutero leucine residues, respectively. In the same manner, the signals, (c) and (e), were apparently assignable to the protons of the pyridine ring of the Schiff bases constructed from (*S*)- and (*R*)-α-deuterated leucines, respectively. The difference of the chemical shifts between signals (b) and (d) was δ 0.23 which was enough resolution to make the accurate integration of each signal possible. Accordingly, the enantiomeric excess of the α-deuterated leucine obtained through the transamination reaction in MeOD was calculated from the ratio of the integrated intensities of the two diastereotopic azomethine protons, (b) and (d). Figure 6 shows the 400-MHz NMR spectrum of the Schiff bases prepared from the α-deuterated leucine, the product of transami-

Table 3. Enantiomeric excesses and yields of deuterated α-amino acids obtained through Zn^{2+}-catalyzed transamination reaction between (*R*)- or (*S*)-**1** and RCOCOOH in methanol-*d*

R	(*R*)- or (*S*)-**1**	Major enantiomer	$[\alpha]_D$/° (c, H_2O)	Temp/°C	e.e./%	Yield/%
$(CH_3)_2CHCH_2$	(*S*)-**1**	*R*	+9.2 (0.80)	22	94[a] 92[b]	66
$(CH_3)_2CHCH_2$	(*R*)-**1**	*S*	−8.4 (0.88)	23	90[a]	60
$(CH_3)_2CH$	(*R*)-**1**	*S*	+22.5 (0.66)[c]	19	80[a]	49
$C_6H_5CH_2$	(*R*)-**1**	*S*	−18.8 (0.56)	20	40[a]	56

a) (*R*)-**3** was used as the chiral pyridoxal analog. b) (*S*)-**3** was used as the chiral pyridoxal analog. c) 1 M HCl.

Table 4. Comparison of the enantiomeric excesses of amino acids determined by optical rotation and NMR analyses of diastereomeric Schiff bases

Amino acid (Configuration)[a]	Enantiomeric exescess (e.e./%)	
	Optical rotation	NMR method[b]
Leucine (*S*)	100	100[c]
Leucine (*R*)	100	100[c]
Leucine (*S*)[d]	96	90
Leucine (*S*)[d]	86	81
Leucine (*R*)[d]	73	78
Leucine (*R*)[d]	43	49
Valine (*S*)	100	100[c]
Valine (*R*)	100	100[c]
Valine (*S*)[d]	78	75
Valine (*R*)[d]	44	49

a) Major enantiomer. b) (*R*)-**3** was used as the chiral pyridoxal analog. c) Signals for only one diastereomer were observed. d) The amino acids were obtained through the nonezymatic transamination reaction.[8]

nation reaction using (*R*)-**1**, and (*R*)-**3**. Apparent predominance of the intensity of the signal at δ 8.77 over that at δ 9.00 indicates that the transamination reaction gave (*S*)-α-deuterated leucine in excess. The enantiomeric excess was calculated as described above. Similarly, the employment of (*S*)-enantiomer of **1** gave (*R*)-α-deuterated leucine in excess. The diastereotopic azomethine protons of Schiff bases prepared from the deuterated phenylalanine and valine, and (*R*)-**3** were also clearly resolved in the 400-MHz NMR spectra (Table 2). Consequently, the enantiomeric excess of the deuterated phenylalanine and valine could be determined as has been described in the case of the deuterated leucine. These results are shown in Table 3. The (*S*)-enantiomer of the pyridoxal analog (**3**) was also employed for quantitative measurement of enantiomeric excess of the deuterated amino acids. The enantiomeric excess of the deuterated alanine and tryptophane could not be determined by this procedure because of the overlapping of the diastereotopic azomethine protons.

This method can be applied to the determination of the enantiomeric excess of amino acids in general. Table 4 compares the enantiomeric excesses of several amino acids determined by the measurement of the optical rotations and by the NMR method described above. The results obtained by the two methods are consistent, confirming the reliability of the NMR method for the determination of enantiomeric excesses of amino acids.

Experimental

The melting points were determined with a Yamato capillary melting point apparatus and are uncorrected. The optical rotations were measured with a Perkin-Elmer 241 MC polarimeter. The IR spectra were recorded on a Shimadzu IR-27 instrument. Mass spectra were recorded on a Hitachi M-80 mass spectrometer. The ^1H NMR spectra were recorded with a Varian HA-100D apparatus or a Japan Electron Optics Laboratory JEOL FX-400 with TMS or DSS as the internal standard. Chiral pyridoxamine analogs, (*R*)- or (*S*)-15-aminomethyl-14-hydroxy-5,5-dimethyl-2,8-dithia[9](2,5)pyridinophane ((*R*)- or (*S*)-**1**),[20] and chiral pyridoxal analogs, (*R*)- or (*S*)-15-formyl-14-hydroxy-2,8-dithia[9](2,5)pyridinophane ((*R*)- or (*S*)- **3**),[10] were prepared as reported previously. Microanalyses of deutérated amino acids obtained by the conventional C and H method gave the total H+D percentages as determined by the weight of H_2O and HOD formed. The determined values of H+D were calculated from the weight of H_2O+HOD produced on the assumption that the H : D atomic ratio was that of the compound analyzed.

Preparation of Deuterated Amino Acid. A typical procedure for the preparation of the deuterated amino acid is described in the following. A mixture of sodium 4-methyl-2-oxopentanoate (106 mg, 0.70 mmol), $Zn(ClO_4)_2 \cdot 6H_2O$ (67 mg, 0.18 mmol), and pyridoxamine analog ((*R*)-**1**) (112 mg, 0.36 mmol) was stirred in methanol-*d* (100 ml) at room temperature for 4 d. The methanol-*d* solution was acidified to pH 1 with 1 M hydrochloric acid (1 M=1 mol dm^{-3}) and evaporated *in vacuo*. Distilled water (50 ml) was added to the residue and the resulting mixture was extracted with ethyl acetate (200 ml) to remove the pyridoxal analog ((*R*)-**4**) produced. The aqueous layer was placed on Dowex-50 (H^+ form, 50 ml) column and eluted with distilled water (1000 ml) and 0.1 M aqueous ammonium hydroxide successively. The ammonium hydroxide effluent was evaporated *in vacuo* and the residue was redissolved in distilled water (10 ml). The solution was put on Amberlite IRC-50 (H^+ form, 15 ml) column and eluted with distilled water in order to remove trace of pyridoxamine analog ((*R*)-**1**). The effluent was concentrated to dryness *in vacuo* to give α-deuterated leucine (31.4 mg).

Determination of the Enantiomeric Excesses. A typical procedure for the determination of the enantiomeric excesses of the deuterated amino acids is exemplified by the case of leucine: a methanol solution (5 ml) of (*R*)-**3** (20.4 mg, 0.07 mmol) and the deuterated leucine (7.9 mg, 0.06 mmol) obtained was stirred at room temperature overnight and evaporated. The resulting residue was dissolved in C_6D_6 (1 ml) and the solution underwent recording the NMR spectrum at 400 MHz.

Spontaneous Deuteration at the β-Position of the Aromatic α-Keto Acids. Sodium phenylpyruvate (100 mg) was dissolved in methanol-d_4 (5 ml) and stirred at room temperature. The aliquots of the solution were taken for recording ^{1}H NMR spectrum (100 MHz). The ratio of the deuteration of the β-protons of the keto acid was determined by comparing the integral intensity of the β-protons with that of phenyl ring protons of the keto acid. The β-protons of sodium phenylpyruvate were gradually deuterated (44% at 24 h, 52% at 48 h, and 100% at 144 h, respectively). The β-protons of sodium indole-3-pyruvate were completely deuterated at 48 h.

Preparation of Schiff Base from General α-Amino Acid and Chiral Pyridoxal Analog. A mixture of (*S*)-leucine (66 mg, 0.5 mmol) and (*R*)-**3** (142 mg, 0.5 mmol) was stirred in methanol (150 ml) at room temperature overnight. After the methanol was recovered *in vacuo*, the resulting residue was extracted with benzene and the benzene solution was concentrated to about 10 ml. To the solution hexane was added gradually until a precipitate separated out. The precipitate was collected and recrystallized from a mixture of benzene and hexane to give the Schiff-base of (*R*)-pyridoxal analog-(*S*)-leucine in 65% yield: mp 100—102 °C. $[\alpha]_D^{23}$ +231° (*c* 0.13, $CHCl_3$). IR (KBr disk) 1715 (C=N) and 1625 cm^{-1} (C=O): ^{1}H NMR (400 MHz, C_6D_6) δ=8.73 (1H, s, C=N) and 8.13 (1H, s, 6-H). Found: C, 57.58; H, 7.28; N, 7.07; S, 16.41%. Calcd for $C_{19}H_{28}N_2O_3S_2$: C, 57.58; H, 7.06; N, 7.07; S, 16.18%.

The authors are grateful to Dr. Haruo Homma and his staff for performing elementary analyses, and to Dr. Jun Uzawa and Mrs. Tamiko Chijimatsu for ^{1}H NMR spectra measurement.

References

1) J. W. Cornforth, *Quart. Review*, **1972**, 125.
2) S. Sawada, A. Tanaka, Y. Inoue, T. Hirasawa, and K. Soda, *Biochim. Biophys. Acta.*, **350**, 354 (1974).
3) K. Kakinuma, Y. Ogawa, T. Sasaki, H. Seto, and N. Ootake, *J. Am. Chem. Soc.*, **103**, 5614 (1981).
4) G. W. Kirby and J. Michael, *J. Chem. Soc., Perkin Trans. I*, **1973**, 115.
5) W. L. F. Armarego, B. A. Milloy, and W. Pendergast, *J. Chem. Soc., Perkin Trans. 1*, **1976**, 2229.
6) Y. N. Belokon, A. S. Melikyan, T. F. Salel'va, V. I. Bakhmutov, S. V. Vitt, and V. M. Belikov, *Tetrahedron*, **36**, 2327 (1980).
7) H. Kuzuhara, T. Komatsu, and S. Emoto, *Tetrahedron Lett.*, **1978**, 3563.
8) Y. Tachibana, M. Ando, and H. Kuzuhara, *Chem. Lett.*, **1982**, 1765.
9) Y. Tachibana, M. Ando, and H. Kuzuhara, *Chem. Lett.*, **1982**, 1769.
10) H. Kuzuhara, M. Iwata, and S. Emoto, *J. Am. Chem. Soc.*, **99**, 4173 (1977). The racemate **3** was also optically resolved into (*R*)- or (*S*)-enantiomer through formation of Schiff base chelate complexes with chiral amino acids and metal ions. Y. Tachibana, T. Komatsu, M. Ando, H. Kuzuhara *Bull. Chem. Soc. Jpn.*, in press.
11) Y. Tachibana, M. Ando, and H. Kuzuhara, *Bull. Chem. Soc. Jpn.*, **56**, 2263 (1983).
12) Y. Fujii, M. Sano, and Y. Nakano, *Bull. Chem. Soc. Jpn.*, **50**, 2609 (1977).
13) E. Cesarotti, A. Pasini, and R. Ugo, *J. Chem. Soc., Dalton Trans.*, **1981**, 2147.
14) Y. Fujii, M. Matsufuru, A. Sato, and S. Tsuchiya, *Bull. Chem. Soc. Jpn.*, **54**, 2029 (1981).
15) L. Casella and M. Gullotti, *J. Am. Chem. Soc.*, **103**, 6338 (1981).
16) Y. Fujii, Y. Kuwana, S. Takahashi, K. Shimizu, and K. Hiroi, *Bull. Chem. Soc. Jpn.*, **55**, 2598 (1982).
17) O. A. Gansow and R. H. Holm, *J. Am. Chem. Soc.*, **91**, 573 (1969).
18) E. H. Abott and A. E. Martell, *J. Am. Chem. Soc.*, **92**, 5845 (1970).
19) As far as the amino acid in this paper are concerned, *R*-enantiomers correspond to D-amino acids and *vice versa*.
20) M. Ando, Y. Tachibana, and H. Kuzuhara, *Bull. Chem. Soc. Jpn.*, **55**, 829 (1982).

Synthesis and Properties of Cationic Polynucleotide Analog Binding RNase A

Takeo SHIMIDZU,* Akira MURAKAMI, and Kazushige YAMANA
Division of Molecular Engineering, Kyoto University, Yoshida, Sakyo-ku, Kyoto 606
(Received April 22, 1983)

A new type of cationic polynucleotide analog binding RNase A and its related compounds were synthesized from an insoluble cross-linked poly(4-vinylpyridine). The cross-linked poly(4-vinylpyridine) was converted into an aldehyde derivative by the reaction with cyanogen bromide. The aldehyde derivative was used for the binding of RNase A and 9-(2-aminoethyl)adenine through their amino groups. The cationic adenine polynuleotide analog binding RNase A favorably interacted with nucleotides containing uracil base through the base-specific interactions. This analog showed the considerable selectivity in the hydrolysis of uridine polynucleotide owing to the template effect.

Several cationic polynucleotide analogs have been synthesized[1-3] and their interactive properties with nucleic acid bases,[4] nucleotides,[2,3,5] polynucleotides,[4] and nucleotide analogs[6,7] have also been investigated. In these studies, the mode of interactions was predominantly the base-base stacking. On the other hand, the complementary base-base interaction was pronounced in the interactions between polynucleotides and mononucleotide analogs with positive charge.[8] It was deduced that the ionic field originating from polynucleotide or its analogs makes a large contribution to the base-base interaction: the catinic field contributes to the base stacking interaction, on the other hand, the anionic one contributes to the hydrogen bonding in the complementary base-base interaction. This evidence for the contribution of the ionic field has been found in the interaction of nucleotides and nucleotide analogs in the presence of polyelectrolytes.[6,7] The mode of the base-base interaction was also affected by the hydrophobic polymer domain. The cross-linked cationic polynucleotide analogs have a tendency to interact with the complementary nucleotide.[5] The template-directed syntheses of oligonucleotides were carried out and homogeneous oligonucleotides, in which the base units are complementary to those in the polymeric "template," were found in considerable amounts, whereas scarcely any homogeneous oligomers consisting of the other nucleotide units were observed.[9]

It is expected that cross-linked cationic polynucleotide analogs, which played a role of the template, would have the ability to control the substrate specificity of enzymes which hydrolyze nucleic acids. RNase A is specific for both uracil and cytosine ribonucleotide linkages, *i.e.*, those cleaving cyclic 2′,3′-pyrimidine nucleotide residues either singly or at the termination of purine nucleotide chains[10] (Scheme 1). In order to control the substrate specificity or base specificity of RNase A, we have first time tried to bind RNase A on a cross-linked cationic polynucleotide analog. The analog consists of adenine base which is the complementary base to uracil. In this paper we describe the catalytic properties of the cationic polynucleotide analog binding RNase A in the hydrolysis of pyrimidine nucleotide linkages. This analog shows the consider able selectivity in the hydrolysis of uridine polynucleotide.

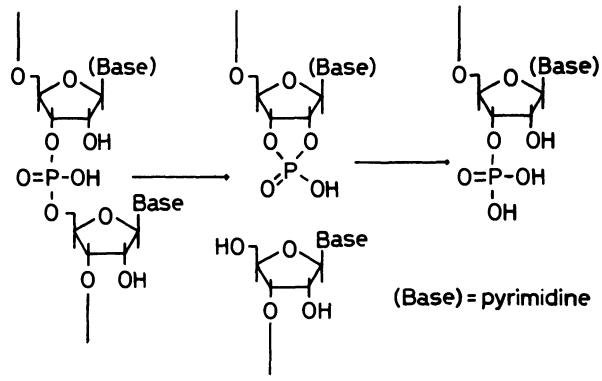

Scheme 1.

Results and Discussion

A new type of cationic polynucleotide analog binding RNase A[11] and its related compounds were synthesized from an insoluble cross-linked poly(4-vinylpyridine), according to the following scheme (Scheme 2). The cross-linked poly(4-vinylpyridine) was converted to an aldehyde derivative by the reaction with cyanogen bromide.[12] The aldehyde derivative formed was used for the binding of RNase A through its ε-amino groups and of 9-(2-aminoethyl)adenine. Excess formyl groups were reduced with borohydrides. The amounts of RNase A and adenine residue bound to poly(4-vinylpyridine), together with their abbreviations, were shown in Table 1.

In order to examine the interactive property or the template effect of the cationic polynucleotide analog binding RNase A, Analog 3EA, the affinity of the pyrimidine nucleotides with Analog 3EA and its related

TABLE 1. THE AMOUNTS OF RNase A AND ADENINE RESIDUE BOUND TO POLY(4-VINYLPYRIDINE)

	RNase A	Adenine residue
	μmol/g of dry Analog	mmol/g of dry Analog
Analog 40E[a]	0.47	—
Analog 3E[b]	0.29	—
Analog 3EA[b]	0.29	0.34

Cationic polynucleotide analog binding RNase A and its related compounds were synthesized from; a) 40% cross-linked poly(4-vinylpyridine) and b) 3% cross-linked poly(4-vinylpyridine).

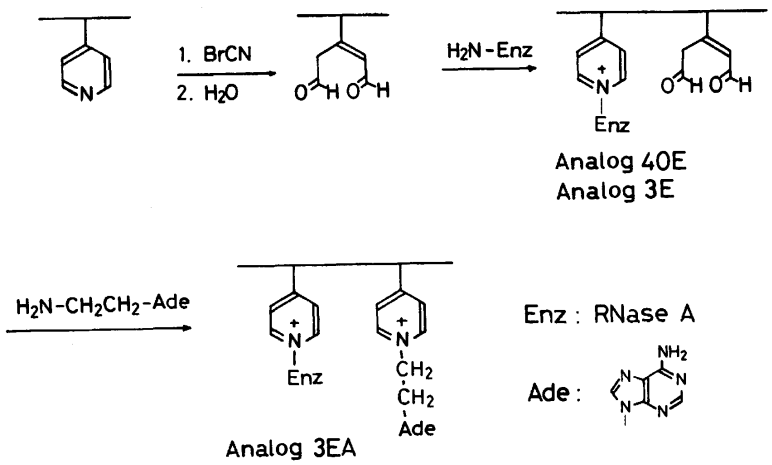

Scheme 2.

TABLE 2. ADSORPTION OF PYRIMIDINE NUCLEOSIDE 2′,3′-CYCLIC PHOSPHATE[a] ON ANALOG[b]

System	$\frac{\text{Adsorbed nucleotide}}{\text{Initial nucleotide}} \times 100$
Analog 3E–Cp>	0.2
Analog 3E–Up>	2.5
Analog 3EA–Cp>	4.4
Analog 3EA–Up>	8.1

a) Nucleotide, 1.7×10^{-2} mol dm^{-3}. b) Analog, 8 mg.

compound, Analog 3E, was investigated. A solution of uridine 2′,3′-cyclic phosphate (Up>) or cytidine 2′,3′-cyclic phosphate (Cp>) was added to the analogs and then the mixture was shaken. The amount of adsorbed nucleotides on the analog was determined by UV absorbance of the supernatant. The results are shown in Table 2. Analog 3EA favorably interacts with Up>, which is caused by the specific interaction of bases.

Hydrolyses of pyrimidine nucleoside 2′,3′-cyclic phosphates in the presence of the cationic polynucleotide analog binding RNase A, Analog 3EA, its related compounds, Analog 40E, Analog 3E, and the native RNase A were carried out at 25 °C in 0.1 M† phosphate buffer (pH 7.0). The steady-state kinetic parameters are summarized in Table 3. When RNase A was immobilized on the 3% cross-linked poly(vinylpyridine), the apparent K_m values of Analog 3E in the hydrolyses of the both substrates were smaller than those of the native RNase A. It is suggested that the analog promotes the binding of the substrates. Analog 3E having a positive charge which is resulted from the immobilization of RNase A interacts with the anionic substrates through the coulombic attractive force. This interaction may promote the complex formation between the enzyme and the anionic substrates. On the contrary, by the immobilization of RNase A on the highly cross-linked poly(vinylpyridine) (40%), Analog 40E, the interaction with the substrates was slightly lower than that of the native RNase A. The k_{cat} and V_{max} values of Analog 3E in the hydrolyses of the both substrates were considerably smaller than those of the native RNase A. This means that the catalytic activity of RNase A was reduced by the immobilization on the cross-linked poly(4-vinylpyridine). That k_{cat} and V_{max} of Analog 40E in the hydrolysis of Cp> was close to those of Analog 3E shows the less effect of the degree of cross-linking on the catalytic activity. Of the cationic polynucleotide analog binding RNase A, Analog 3EA, the adenine residue showed no significant effect on the K_m, k_{cat}, and V_{max} values in the hydrolyses of not only Cp>, but also Up>. The results that Analog 3EA adsorbs the larger amount of Up> and shows no specificity in the hydrolysis of Up> indicate that the substrates are mainly adsorbed on Analog 3EA at the adenine residues which are relatively remote from the active center of the immobilized enzyme RNase A.

Hydrolyses of 3′-5′ diuridine monophosphate (UpU)

TABLE 3. THE STEADY-STATE KINETIC PARAMETERS IN THE HYDROLYSIS OF PYRIMIDINE NUCLEOSIDE 2′,3′-CYCLIC PHOSPHATE

Enzyme	Substrate	K_m / mol dm^{-3}	k_{cat} / s^{-1}	V_{max} / mol dm^{-3} s^{-1}
RNase A	Cp>	1.4×10^{-2}	2.6×10^{-2}	1.0×10^{-2}
RNase A	Up>	1.1×10^{-2}	8.8×10	3.5×10^{-3}
Analog 40E	Cp>	4.3×10^{-2}	3.0×10^{-2}	2.7×10^{-6}
Analog 3E	Cp>	4.3×10^{-3}	3.5×10^{-2}	1.4×10^{-6}
Analog 3E	Up>	2.6×10^{-3}	6.4×10^{-3}	2.6×10^{-7}
Analog 3EA	Cp>	8.8×10^{-3}	3.8×10^{-2}	1.5×10^{-6}
Analog 3EA	Up>	5.2×10^{-3}	6.1×10^{-3}	2.4×10^{-7}

† 1 M = 1 mol dm^{-3}.

Table 4. Hydrolyses of dinucleotides[a] by Analogs 3E[b] and 3EA[b]

	Yield of product / %			
	C	Cp	Cp>	CpC
Analog 3E–CpC	51.3	26.7	22.0	Trace
Analog 3EA–CpC	47.0	22.7	30.3	
	Yield of product / %			
	U	Up	Up>	UpU
Analog 3E–UpU	19.0	2.1	15.6	63.4
Analog 3EA–UpU	10.0	0.8	8.8	80.3

Reactions were carried out at 25 °C for 2 h.
a) Dinucleotide, 2.3×10^{-3} mol dm^{-3}. b) Enzyme on Analog, 1.6×10^{-5} mol dm^{-3}.

and 3′-5′ dicytidine monophosphate (CpC) in the presence of Analogs 3EA and 3E were carried out at 25 °C in 0.1 M phosphate buffer (pH 7.0) for 2 h. The hydrolyzed products were analyzed by HPLC. The results are shown in Table 4. CpC was hydrolyzed in the presence of both Analog 3EA and Analog 3E to the almost similar composition of the products, Cp>, Cp, and C. Similary, the distribution of the products in the hydrolysis of UpU by Analog 3EA and Analog 3E was not significantly different. These results show that Analog 3EA has no specificity in the hydrolyses of both UpU and CpC.

This feature was drastically changed in the hydrolysis of Poly U and Poly C as substrates. The results are shown in Table 5. Poly C was hydrolyzed in the presence of Analog 3EA to Cp, Cp>, CpCp, and CpCpCp. The amounts of CpCp and CpCpCp were slightly larger than those in the case of Analog 3E. On the other hand, the amounts of the products, UpUp> and UpUpUp, in the hydrolysis of Poly U by Analog 3EA were one-half to one-forth of those by Analog 3E. That is, the hydrolysis rate of Poly U by Analog 3EA is much higher than by Analog 3E. These results imply that there is no effect of adenine residue on the hydrolysis of Poly C but a considerable effect on Poly U hydrolysis. This effect is considered as follows; Poly U adsorbs on Analog 3EA through the complementary base-base interaction and it approaches to the active center of RNase A bound to Resin 3EA, for the polynucleotides having a long chain are easy to approach to the active center of the enzyme, even though the adsorption site of substrates is apart from the active center. The present study shows that the new type of cationic polynucleotide analog binding RNase A controls the substrate specificity of enzyme through the template effect.

Experimental

Materials. RNase A (Bovine Pancrease) was perchased from Sigma Chemical Co. 9-(2-aminoethyl)adenine was synthesized by the reported method.[13] 3% and 40% cross-linked poly (4-vinylpyridine) was synthesized by the copolymerization of 4-vinylpyridine with divinylbenzene. Up>, Cp>, UpU, CpC, Poly U (M. W.=10000) and Poly C (M. W.=10000) were obtained from Sigma Chemical Co.

Preparation of Cationic Polynucleotide Analog Binding RNase A and Its Related Compounds. *a) Analog 40E*: 3 g of 40% cross-linked poly(4-vinylpyridine) was reacted with 1.5 g of cyanogen bromide in 10 cm^3 of anhydrous dioxane at room temperature for 15 min. Water was then added and the mixture was stirred for 90 min at room temperature. The gel was filtered and washed with cold water. 1.5 g of the activated gel was stirred overnight in a solution of RNase A (20 mg) in 4 cm^3 of 0.05 M phosphate buffer, pH 5.0, at 10—12 °C. The gel was then treated with 1% $NaBH_4$ at room temperature for 10 min and then washed with the phosphate buffer.

b) Analog 3E: 2.6 g of 3% cross-linked poly(4-vinylpyridine) was reacted with 2.5 g of cyanogen bromide in 10 cm^3 of anhydrous dioxane at room temperature for 15 min. After the treatment with water for 60 min, the gel was washed with cold water. 0.5 g of the activated gel was stirred overnight in a solution of RNase A (23 mg) in 2 cm^3 of 0.05 M phosphate buffer, pH 5.0, at 4 °C. The gel was then treated with 1% $NaBH_4$ at room temperature for 10 min and then washed with the phosphate buffer.

c) Analog 3EA: $NaBH_4$-untreated Analog 3E was reacted with 50 mg of 9-(2-aminoethyl)adenine in the same buffer at 4 °C for overnight. Then, the gel was treated with 1% $NaBH_4$ at room temperature for 10 min and then washed with the phosphate buffer.

The Amount of RNase A and Adenine Residue Bound to Polynucleotide Analog. The amount of RNase A on Analog was determined as follows. Analog was treated with 6 M HCl at 50 °C for 6 h and the amount of released tyrosine was measured at 294 nm ($\varepsilon=2.39\times10^3$). Calculation was carried out on the fact that RNase A (M. W.=13700) contains 6 tyrosine residues.[14] The amount of adenine residue on Analog 3EA was determined from the amount of the unreacted 9-(2-aminoethyl)adenine in the washing of the reaction mixture.

Adsorption of the Substrate on Analog. A solution of the substrate (1.7×10^{-5} mol) in 0.1 M phosphate buffer, pH 7.0,

Table 5. Hydrolyses of polynucleotides[a] by Analogs 3E[b] and 3EA[b]

	Yield of product / %				
	Cp	Cp>	CpCp	CpCp>	CpCpCp
Analog 3E–Poly C	53.6	38.2	4.9	Trace	4.0
Analog 3EA–Poly C	43.4	42.3	5.7	Trace	8.6
	Yield of product / %				
	Up	Up>	UpUp	UpUp>	UpUpUp
Analog 3E–Poly U	20.3	37.0	10.7	24.6	7.7
Analog 3EA–Poly U	25.8	47.4	11.0	13.6	1.9

Reactions were carried out at 25 °C for 2 h. a) Polynucleotide, 3.7×10^{-3} mol dm^{-3}. b) Enzyme on Analog, 1.6×10^{-5} mol dm^{-3}.

(1.0 cm^3) was added to Analog (8 mg). The difference between the initial and the final (5 min after) optical densities of the supernatant was measured by UV spectroscopy at 260 nm. Thus, the apparent adsorption of the substrate on Analog was estimated.

Activity of RNase A Bound to Polynucleotide Analog. Up>, Cp>, UpU, CpC, Poly U, and Poly C were used for substrates. Hydrolyses of these substrates in the presence of Analog was carried out in 0.1 M phosphate buffer, pH 7.0, at 25 °C. Analysis of hydrolytic products was done on a HPLC(Partisil 10 SAX column; 0.001 M KH_2PO_4—0.3 M KH_2PO_4 containing 10% EtOH, a linear gradient).

a) Experiment in Table 3: Hydrolysis was carried out in a mixture of substrate (Up> and Cp>) (2.2×10^{-8}—4.1×10^{-7} mol), 0.1 M phosphate buffer pH 7.0 (0.1 cm^3), and Analog (15 mg for Analog 40E, 30 mg for Analogs 3E and 3EA). After incubation at 25 °C for 30 min, the products were filtered by Milipore Filter (Type HA, 0.45 μm) and analyzed by HPLC. Control experiment for soluble RNase A was done in a mixture of the substrates (2.2×10^{-8}—4.1×10^{-7} mol), 0.1 M phophate buffer pH 7.0 (0.1 cm^3), and the enzyme (final concentration, 4.0×10^{-5} mol dm^{-3}) at 25 °C for 5 min. Analysis of the products were the same as for Analog. Thus, the kinetic constants were determined by the Michaelis-Menten method.

b) Experiments in Tables 4 and 5: Hydrolysis was carried out in a mixture of substrates (2.3×10^{-3} mol for dinucleotide monophosphate, 3.7×10^{-3} mol for polynucleotide), 0.1 M phophate buffer, pH 7.0, (0.1 cm^3), and Analog (5 mg). After incubation at 25 °C for 2 h, the products were filtered by Milipore Filter (Type HA, 0.45 μm) and analyzed by HPLC.

References

1) T. Okubo and N. Ise, *Polym. J.*, **4**, 674 (1974).
2) T. Shimidzu, Y. Konishi, and A. Murakami, *Makromol. Chem.*, **178**, 2581 (1977).
3) A. Murakami, Y. Konishi, and T. Shimidzu, *Makromol. Chem.*, **181**, 2229 (1980).
4) T. Okubo, K. Ban, and N. Ise, *Makromol. Chem.*, **175**, 49 (1974).
5) T. Shimidzu, A. Murakami, Y. Konishi, and M. Minami, *Bull. Chem. Soc. Jpn.*, **51**, 82 (1978).
6) T. Shimidzu, Y. Konishi, and A. Murakami, *Nucleic Acids Res.*, **Sp. 2**, 35 (1976).
7) T. Shimidzu, A. Murakami, and K. Yamana, *Nucleic Acids Res.*, **Sp. 5**, 379 (1978).
8) T. Shimidzu, A. Murakami, K. Yamana, and Y. Konishi, *Bull. Chem. Soc. Jpn.*, **52**, 3362 (1979).
9) T. Shimidzu, A. Murakami, and Y. Konishi, *J. Chem. Soc., Perkin Trans. 1*, **1979**, 20.
10) E. Volkin and W. E. Cohn, *J. Biol. Chem.*, **205**, 767 (1953).
11) For example of protein immobilization. "Methods in Enzymology," ed by K. Mosbach, Academic Press, New York (1976), Vol. 44.
12) F. Pittner, T. Miron, G. Pittner, and M. Wilchek, *J. Am. Chem. Soc.*, **102**, 2451 (1980).
13) T. Sasaki, K. Minamoto, T. Suzuki, and S. Yamashita, *Tetrahedron*, **56**, 865 (1980).
14) G. Kartha, *Nature*, **214**, 234 (1967).

 © 1983 The Chemical Society of Japan Bull. Chem. Soc. Jpn., 56, 3661—3666 (1983)

^{13}C NMR Signal Assignments of Herqueinone and Its Phenalenone Derivatives

Takayuki Suga,* Takamitsu Yoshioka, Toshifumi Hirata, and Tadashi Aoki
Department of Chemistry, Faculty of Science, Hiroshima University, Higashisenda-machi, Naka-ku, Hiroshima 730
(Received April 27, 1983)

The full assignments of the ^{13}C NMR signals of the herqueinone-type phenalenone, herqueinone, were established by a combination of the single-frequency off-resonance decoupling technique and the ^{13}C-enrichment technique using the ^{13}C-labeled tracer. Furthermore, the full assignments of the ^{13}C NMR signals of deoxyherqueinone-type, dihydroherqueinone-type, and xanthoherqueinone-type phenalenone were completed on the basis of the application of the chemical shift rule and the mutual comparison of their chemical shifts.

The red pigments of *Penicillium herquei*,[1-3] such as herqueinone (**2**), atrovenetin (**4**), and deoxyherqueinone (**5**), are compounds having a phenalenone skeleton (**1**) and a 1,2,2-trimethyltetrahydrofuran ring.†,[3-14]

The biosynthetic mechanism for the formation of the phenalenone skeleton of deoxyherqueinone (**5**) was clarified by feeding experiments with ^{14}C- and ^{13}C-labeled acetates.[15-18] On the other hand, the feeding experiment of ^{13}C-labeled malonate indicated that the trimethylfuran ring of herqueinone-type pigments was biologically formed from mevalonic acid.[17,18] However, a biosynthetic mechanism for the formation of the trimethylfuran ring fused to the phenalenone skeleton is still unknown. Before clarifying the mechanisms of the prenylation and the cyclization of its prenyl chain, it was necessary to complete the full assignments of the ^{13}C NMR signals of herqueinone (**2**) and its derivatives (**3**) and (**5**)—(**13**). We have now established the full assignments of the ^{13}C NMR signals of these phenalenones by use of the decoupling techniques and the ^{13}C-enrichment technique.

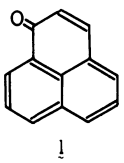

1

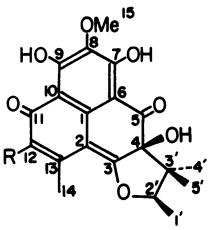

2: R=H
3: R=Br

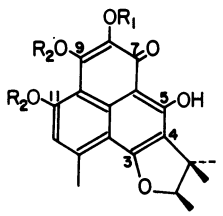

4: R_1=R_2=H
5: R_1=Me, R_2=H
6: R_1=R_2=Me
7: R_1=Me, R_2=COMe

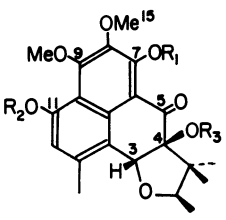

8: R_1=R_2=R_3=H
9: R_1=R_2=COMe, R_3=H
10: R_1=Me, R_2=R_3=H
11: R_1=Me, R_2=COMe, R_3=H
12: R_1=Me, R_2=R_3=COMe

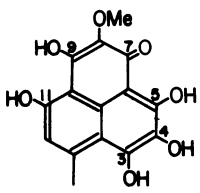

13

† This is abbreviated as trimethylfuran ring hereinafter.

Results and Discussion

The phenalenones derived from herqueinone (**2**) were classified into four groups, such as herquinone-type, deoxyherqueinone-type, dihydroherqueinone-type, and xanthoherqueinone-type phenalenones, on the ground of their structures. The assignments of the ^{13}C NMR signals of these four types of phenalenones were completed as follows.

Herqueinone-type Phenalenones. The proton noise decoupling ^{13}C NMR spectra of herqueinone (**2**) exhibited 20 signals in [$^2H_6$]dimethyl sulfoxide and [$^2H_5$]pyridine solutions. The signals at δ_c 131.3, 109.2, 178.6, 78.9, 150.7, and 138.8 were assigned to C-1, C-2, C-3, C-4, C-8, and C-13, respectively, on the basis of the application of the chemical shift rule[19,20] and the comparison of the ^{13}C chemical shifts of **2** with those of the corresponding carbon atoms of previously reported deoxyherqueinone diacetate (**7**).[17,18] Furthermore, the ^{13}C NMR signals due to the protonated carbon atoms at the 12-, 14-, 15-, 1′-, 2′-, 4′-, and 5′-positions were completely assigned by use of Birdsall's method,[21] as shown in Fig. 1. Consequently, the signals at δ_c 122.8, 59.9, 18.6, 95.9, and 15.9 were assigned to C-12, C-15,

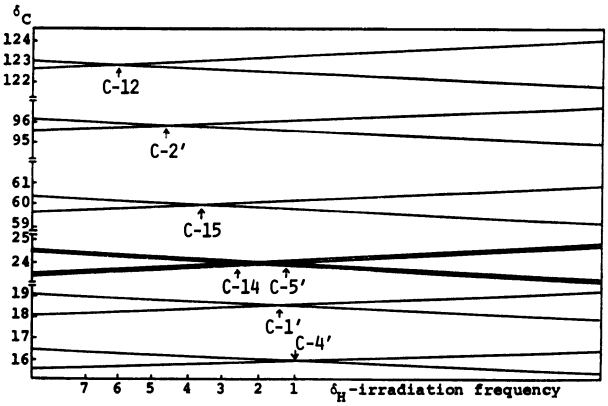

Fig. 1. Birdsall plot of SFORD data for herqueinone (**2**).

C-1′, C-2′, and C-4′, respectively. The signals of C-5′ and C-14 overlapped each other at δ_c 23.8. On the other hand, the distinction between the signals for C-5 and C-11, C-6 and C-10, and C-7 and C-9 was difficult, because of the symmetry of the phenalenone skeleton. However, we succeeded in full assignments of these signals as follows. First, the assignments of the signals due to C-6 and C-10 were completed by the gated decoupling method; the spectrum in the presence of D_2O exhibited $^3J_{CH}$ (4 Hz) at δ_c 103.2 to the aromatic proton on C-12 and the singlet signal at δ_c 102.7, and the signals at δ_c 102.7 and 103.2 were evidently assigned to C-6 and C-10, respectively. Next, the distinction between the signals for C-5 and C-11 and C-7 and C-9, in addition to C-6 and C-10, at the symmetrical positions of the molecule was performed by diagnosis of the ^{13}C–^{13}C spin couplings due to the nine acetate units in the molecule of ^{13}C-enriched herqueinone (**2**) biosynthesized by incorporation of [1,2-$^{13}C_2$]acetate in *P. herquei*. As the incorporation pattern of seven acetate units in the phenalenone skeleton of deoxyherqueinone (**5**) biosynthesized from [1,2-$^{13}C_2$]acetate in *P. herquei* has been previously established,[17,18] the carbon skeleton of the molecule of herqueinone (**2**) should be occupied by the ^{13}C–^{13}C spin coupling pairs originating from [1,2-$^{13}C_2$]acetate as shown in Fig. 2. The ^{13}C NMR spectra of the ^{13}C-enriched herqueinone (**2**) showed the nine ^{13}C–^{13}C spin couplings as shown in Table 1. Analysis of the coupling constants established the assignments of the signals for C-5, C-6, C-9, C-10, and C-11 which constituted the coupling pairs with C-4, C-7, C-8, C-1, and C-12, respectively Thus, the full assignments of the ^{13}C NMR signals of herqueinone (**2**) were completed.

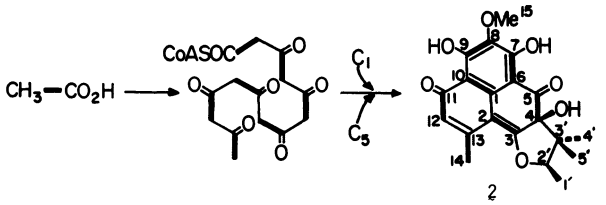

Fig. 2. ^{13}C incorporation pattern of the acetate units (—) in herqueinone (**2**).

TABLE 1. ^{13}C–^{13}C SPIN COUPLINGS IN THE ^{13}C NMR SPECTRUM OF HERQUEINONE (2) BIOSYNTHESIZED FROM [1,2-$^{13}C_2$]ACETATE[a]

Carbon	δc[b]	$^1J_{CC}$	Carbon	δc[b]	$^1J_{CC}$
1	131.3	80	11	186.4	56
2	109.2	75	12	122.8	58
3	178.6	75	13	138.8	35
4	78.9	51	14	23.8	35
5	197.0	51	15	59.9	0
6	102.7	61	1′	18.6	38
7	162.0	61	2′	95.9	38
8	150.7	42	3′	43.1	36[c]
9	163.0	44	4′	15.9	37
10	103.2	79	5′	23.8	0

a) These δc and $^1J_{CC}$ values differ from those described in Ref. 7, but these are the corrected after careful reexamination. b) Taken in [$^2H_6$]DMSO containing TMS as an internal standard (δ_{TMS}=0.0) : number of scan; 29253 times. c) These $^1J_{CC}$ values were obtained in [$^2H_5$]pyridine.

The chemical shifts of the ^{13}C NMR signals of bromoherqueinone (**3**) were in fair agreement with those of **2** except for that of the conjugated carbonyl group at the 11-position. The C-11 signal of **3** shifted to higher-field by about 5 ppm in comparison with that of **2**. This higher-field shift might be caused by the reason why the halogenation at the neighboring position of the conjugated carbonyl group breaks up slightly the conjugated system. Such a higher-field shift has been observed on the ^{13}C NMR spectrum of 3-bromo-5-hydroxy-1,4-naphthoquinone.[22]

Deoxyherqueinone-type Phenalenones. Deoxygenation at the 4-position of herqueinone (**2**) gave deoxyherqueinone (**5**), which was then converted into the corresponding dimethyl ether (**6**) and diacetate (**7**). The ^{13}C chemical shifts of the diacetate (**7**) were in fair agreement with those of the deoxyherqueinone diacetate described previously in the literature.[17,18] These described chemical shifts were supported by examination of the assignments of the protonated carbon atom signals by use of Birdsall's method.[21] For the signals at δc 163.5 and 159.6 in the ^{13}C NMR spectrum of **5**, these were assigned to C-9 and C-11, respectively, by considering the acetylation shift between the signals of **5** and **7**. The signals of C-9 and C-11 overlapped at δ_c 161.5 in the ^{13}C NMR spectrum of **6**. The assignments of the other ^{13}C NMR signals of **5** and **6** were completed by comparing the signals with those of the corresponding carbon atoms of **7**.

Dihydroherqueinone-type Phenalenones. Herqueinone (**2**), on hydrogenation followed by methylation, gave dihydroherqueinone monomethyl ether (**8**) and dimethyl ether (**10**). Acetylation of **8** afforded the diacetate (**9**) with two acetoxyl groups at the 7- and 11-positions. On the other hand, acetylation of **10** gave the monoacetate (**11**) with an acetoxyl group at the 11-position and diacetate (**12**) with two acetoxyl groups at the 4- and 11-positions.

The ^{13}C NMR signal of C-3 of these dihydroherqueinone-type phenalenones (**8**—**12**) was assigned by use of the off-resonance decoupling technique. The signals of C-9 and C-11 of **8** were assigned on the basis of the higher-field shift of about 10 and 30 ppm, respectively, in comparison with those of **2**. The other signals of **8** were assigned by comparison of the chemical shifts with those of the corresponding carbon atoms of **2**. On the other hand, the assignments of the signals for C-7 of **9**—**12** and for C-11 of **9**, **11**, and **12** were completed on the basis of the higher-field shifting on methylation or acetylation. The other ^{13}C signals of dihydroherqueinones (**9**—**12**) were assigned by comparison of the chemical shifts with those of the corresponding carbon atoms of **2** and **8**.

It is interesting to note that the ^{13}C NMR signal of C-1′ of deoxyherqueinones (**5**—**7**) and the signal of C-5′ of dihydroherqueinones (**8**—**12**) appear at a higher field in comparison with those of the corresponding carbon atoms of herqueinone (**2**), while the signals of C-4′ and C-5′ of deoxyherqueinones (**5**—**7**) appear

TABLE 2. ^{13}C NMR CHEMICAL SHIFTS (δC)[a] FOR HERQUEINONE (2) AND ITS DERIVATIVES (3) AND (5—13)

Carbon	2	3[b]	5	6	7	8	9	10	11	12	13
1	131.3	132.4	126.2	126.4	125.3	129.1	129.7	130.8	131.4	130.3	120.4
2	109.2	109.7	107.1	108.9	113.6	117.8	127.4	112.7	127.1	127.2	111.0
3	178.6	179.5	164.7	166.6	175.1	81.5	82.5	82.2	83.6	81.9	152.3
4	78.9	80.4	118.2	118.7	121.0	82.0	83.5	84.3	85.2	88.4	130.1
5	197.0	197.6	170.0	172.9	175.7	202.9	197.2	199.0	199.8	190.8	165.4
6	102.7	103.2	104.7	107.3	108.9	105.9	117.1	118.6	117.3	116.9	103.2
7	162.0	163.1	171.4	175.1	175.7	162.0	143.2	153.2	155.6	155.8	170.4
8	150.7	149.0	145.1	145.1	143.5	140.2	144.8	142.4	145.2	144.9	145.2
9	163.0	163.1	163.5	161.5	149.9	153.9	152.2	153.2	153.4	152.6	160.2
10	103.2	104.4	104.7	108.3	108.9	109.2	118.1	119.3	118.4	118.7	104.3
11	186.4	180.5	159.6	161.5	143.5	156.6	145.4	154.9	145.0	144.9	158.3
12	122.8	121.9	115.8	111.3	122.9	113.5	124.1	113.6	123.6	123.1	115.9
13	138.8	138.1	133.1	141.4	143.5	136.5	138.1	138.5	138.3	136.5	132.7
14	23.8	22.3	23.2	23.4	23.4	24.6	23.6	23.2	24.5	23.9	25.0
15	59.9	60.3	59.8	60.3	60.4	60.9	61.2	61.1	61.3	61.0	59.9
7-OCH$_3$								61.8	62.1	61.6	
9-OCH$_3$				61.3		62.4	61.9	62.4	62.1	61.9	
11-OCH$_3$				56.6							
4-OCOCH$_3$										20.6	
										170.0[c]	
7-OCOCH$_3$							20.4				
							169.4[c]				
9-OCOCH$_3$					20.6[c]						
					167.9[d]						
11-OCOCH$_3$					21.0[c]		20.4		20.9	20.6	
					168.9[d]		168.0[c]		169.8	169.4[c]	
1′	18.6	19.0	14.3	14.3	14.6	17.6	17.8	18.1	18.0	17.9	
2′	95.9	97.0	90.6	91.1	92.0	81.5	81.8	82.2	83.0	81.7	
3′	43.1	43.8	42.8	42.7	43.5	50.1	50.3	50.2	51.9	50.2	
4′	15.9	16.4	20.4	20.3	20.5	16.3	15.8	15.6	15.8	15.0	
5′	23.8	22.3	25.3	25.3	25.7	19.9	19.3	19.4	20.0	19.2	

a) Taken in [^{2}H$_6$]DMSO (δ_{TMS}=0.0): number of scan; *ca.* 1500—4300 times. b) Taken in [^{2}H$_5$]pyridine. c and d) Values in any vertical column may be interchanged although those given here are preferred.

at a lower field in comparison with those of **2**. These seem to be due to the difference in the influence of the anisotropy[23] caused by the phenalenone ring. The plane angle formed by the phenalenone skeleton and the trimethylfuran ring of the deoxyherqueinones (**5**—**7**) is about 180° in model.[24] Therefore, the anisotropic effect to the C-1′ methyl group of deoxyherqueinones (**5**—**7**) may be greater than that in the case of herqueinone (**2**), whereas the effect to the C-4′ and C-5′ methyl groups may be less than that in that case. On the other hand, the plane angle of dihydroherqueinones (**8**—**12**), is smaller than that in the case of herqueinone (**2**). Therefore, the C-4′ and C-5′ methyl groups of **8**—**12** may be equally influenced by the anisotropy of the carbonyl group and the aromatic rings.

Xanthoherqueinone-type Phenalenone. The ^{13}C NMR chemical shifts of xanthoherqueinone (**13**) were in fair agreement with those of the phenalenone skeleton of **5**, except for the signals of phenolic carbon atoms at the 3-, 4-, and 5-positions. These signals appeared at δC 152.3, 130.1, and 165.4 and were assigned to the phenolic carbon atoms, respectively, by application of the chemical shift rule.

The final assignments of the ^{13}C NMR signals of herqueinone (**2**) and its derivatives (**3**) and (**5**—**13**) are given in Table 2.

Experimental

The fungal culture of *Penicillium herquei* Bainer and Sartory (IFO 7904) was obtained from the Institute for Fermentation.†† Sodium [1,2-^{13}C$_2$]acetate was purchased from the British Oxygen Company Co. Ltd. The ^{1}H NMR spectra were taken, with TMS as an internal standard, at 60 and 90 MHz. The ^{13}C NMR spectra were obtained on a Hitachi R-42 FT NMR spectrometer at 22.631 MHz at 35 °C in an 8 mm spinning tube; precisions of δ_c are about $\pm$0.1. FT measurement conditions were as follows: spectral width, 250 ppm; filtering, 6 KHz; pulse width, 45°; pulse interval, 1.800 s; number of data points, 8000. The series of single-frequency off-resonance decoupling ^{13}C NMR spectra of herqueinone (**2**) and deoxyherqueinone diacetate (**7**) were recorded with the ^{1}H decoupling frequency set at ten different points started from the upfield to the downfield in increments of about 100 Hz in the ^{1}H NMR region (Fig. 1). The gated decoupling with NOE was measured by a JEOL FX-200 FT NMR spectrometer at 50.150 MHz at 0 °C in a 5 mm spinning tube: pulse width, 45°; pulse interval, 6.00 s; number of data points, 8000; precisions of δ_C, $\pm$0.02. The EI-MS spectra were obtained on a Hitachi RMU-6L mass spectrometer at 70 eV. Analytical and preparative TLC were carried out on Merck 60 GF$_{254}$ silica-gel plates which were 0.25- and 0.5 mm-thick, respectively.

Isolation of Herqueinone. The spores, obtained from the preculture of *P. herquei* on the malt extract-agar medium, were

†† Jyuso hon-machi, Yodogawa-ku, Osaka 532.

TABLE 3. PHYSICAL AND ANALYTICAL DATA OF PHENALENONE DERIVATIVES (3) AND (5—13)

Compound	Mp θ_m/°C	$[\alpha]_D^{25}$/° (c, $CHCl_3$)	Mol formula	Calcd (%)			Found (%)		
				C	H	Br	C	H	Br
3	234(decomp)[a]	+580(0.053)[b]	$C_{20}H_{19}O_7Br$	53.23	4.24	17.74	52.94	4.24	17.45
5	221—222[c]	+55.9(0.68)	$C_{20}H_{20}O_6$	67.40	5.66		67.64	5.55	
6	166—168[d]	+70.5(0.75)[e]	$C_{22}H_{24}O_6$	68.73	6.29		69.02	6.19	
7	174—175[f]	+52.5(3.20)[g]	$C_{24}H_{24}O_8$	65.44	5.49		65.24	5.57	
8	173—174[h]	+39.0(6.03)	$C_{21}H_{24}O_7$	64.93	6.23		64.65	6.33	
9	Gum	−13.7(2.05)	$C_{25}H_{28}O_9$	63.35	5.97		63.38	6.08	
10	151—155[i]	−18.5(7.28)	$C_{22}H_{26}O_7$	65.66	6.51		65.38	6.63	
11	Gum	−24.3(1.20)	$C_{24}H_{28}O_8$	64.85	6.35		64.78	6.35	
12	Gum	−123(1.35)	$C_{26}H_{30}O_9$	64.18	6.22		64.11	6.18	
13	288—290[j]		$C_{15}H_{12}O_7$	59.21	3.98		59.67	3.87	

a) Ref. 3; 235 °C(decomp). b) Ref. 3; $[\alpha]_D$+460°($CHCl_3$). c) Ref. 8; 225 °C. d) Ref. 8; 168—169 °C. e) Ref. 8; $[\alpha]_D$+76°($CHCl_3$). f) Ref. 3; 174—175 °C. g) Ref. 3; $[\alpha]_D$+57°($CHCl_3$). h) Ref. 8; 172—174 °C. i) Ref. 8; 151—154 °C. j) Ref. 2; 290—293 °C.

TABLE 4. SPECTRAL DATA OF PHENALENONE DERIVATIVES (3) AND (5—13)

Compound	IR (Nujol) ν_{max}/cm^{-1}
3	3356(OH), 1621(C=O), 1586 and 1507 (arom. C=C), 1235 and 1042(C-O-C), and 1098(cyclic C-O-C)
5	3265(OH), 1610(C=O), 1595 and 1490 (arom. C=C), 1280 and 1064(C-O-C), and 1097(cyclic C-O-C)
6	3450(OH), 1607(C=O), 1585 and 1500 (arom. C=C), 1262, 1221, 1058, 1033, and 1013(C-O-C), and 1102(cyclic C-O-C)
7	3350(OH), 1776 and 1174(2×$OCOCH_3$), 1617(C=O), 1594 and 1505(arom. C=C), 1227 and 1032(C-O-C), and 1100(cyclic C-O-C)
8	3460 and 3366(OH), 1632(C=O), 1609 and 1577(arom. C=C), 1258, 1217, 1041, and 1018(C-O-C), and 1093(cyclic C-O-C)
9	3490(OH), 1765, 1245, and 1180(2×$OCOCH_3$), 1668(C=O), 1615 and 1561 (arom. C=C), 1217, 1063, and 1023 (C-O-C), and 1100(cyclic C-O-C)
10	3445 and 3334(OH), 1672(C=O), 1628 and 1570(arom. C=C), 1276, 1214, 1063, and 1026(C-O-C), and 1113(cyclic C-O-C)
11	3491(OH), 1757, 1253, and 1173 ($OCOCH_3$), 1670(C=O), 1614 and 1562 (arom. C=C), 1213, 1027 and 1066 (C-O-C), and 1115(cyclic C-O-C)[a]
12	1763, 1735, 1243, and 1174(2×$OCOCH_3$), 1683(C=O), 1613 and 1558(arom. C=C), 1205, 1066, and 1046(C-O-C), and 1112 (cyclic C-O-C)[a]
13	3400(OH), 1700(C=O), 1600 and 1505 (arom. C=C), 1275 and 1030(C-O-C)

a) Taken in the neat film.

inoculated to the Raulin-Thom solution.[2] After inoculation, this culture of *P. herquei* was incubated at 25 °C for 25 d. The mycelia produced on the medium were filtered off, and immersed in EtOAc. On the other hand, the filtered medium was acidified to pH 5, and extracted with EtOAc. This EtOAc extract of the medium was combined with the EtOAc extract of the mycelia, because the two EtOAc extracts exhibited the same behavior on TLC. The combined EtOAc extract (*ca.* 5 g), after removal of the solvent, was subjected to centrifugal liquid chromatography on silica gel (3 mm in thickness and 10 cm in radius) with EtOAc–hexane (1 : 4 v/v) as solvent to give a red powder (310 mg). Recrystallization of this red powder from EtOH gave herqueinone (**2**) (275 mg) as red needles: mp 217—218 °C (lit,[8] 218—222 °C); $[\alpha]_D^{25}$ +374° (c 1.68, $CHCl_3$) (lit,[8] $[\alpha]_D$ +300° ($CHCl_3$)); IR (Nujol) 3300 (OH), 1640 and 1626 (C=O), 1591 and 1512 (aromatic C=C), 1247 and 1039 (C–O–C), and 1100 cm^{-1} (cyclic C–O–C); IR (0.0002M, CCl_4) 3315 cm^{-1} (intramolecular hydrogen bonded OH); UV_{max} (cyclohexane) 450 (log ε 4.45), 307 (5.60), 254 (5.08), and 223 nm (5.34); ^1H NMR ([$^2H_6$]DMSO) δ=6.28 (1H, d, J=1.5 Hz, 12-H), 4.83 (1H, q, J=6.5 Hz, 2′-H), 3.80 (3H, s, 15-H_3), 2.50 (3H, d, J=1.5 Hz, 14-H_3), 1.55 (3H, d, J=6.5 Hz, 1′-H_3), 1.40 (3H, s, 5′-H_3), and 1.00 (3H, s, 4′-H_3); MS m/z (rel intensity) 372 (M^+, 100%) and 341 (M^+-OCH_3, 68).

Found: C, 64.51; H, 5.49%. Calcd for $C_{20}H_{20}O_7$: C, 64.51; H, 5.41%.

Preparation of ^{13}C-enriched Herqueinone. Sodium [1,2-$^{13}C_2$]acetate (270 mg, 92% enriched) dissolved in distilled water (5 ml) was added into each of 5 flasks which contained a 14-d old culture (200 ml) of *P. herquei*. After further cultivation for 11 d, the usual work-up of the cultures gave the sample of ^{13}C-enriched herqueinone (**2**) (44 mg), with about 31% ^{13}C-abundance at each labeled position. The ^{13}C–^{13}C spin couplings in the ^{13}C NMR spectra of the ^{13}C-enriched **2** were determined, and the results are given in Table 1.

Preparation of the Phenalenone Derivatives. According to the method givin in the literature,[3] bromoherqueinone (**3**) and deoxyherqueinones (**5**—**7**) were derived from herqueinone (**2**) as follows. Bromination of **2** with Br_2 gave bromoherqueinone (**3**). Deoxygenation of **2** with Zn dust gave deoxyherqueinone (**5**). Furthermore, **5** was methylated with CH_2N_2 to give the dimethyl ether (**6**), and acetylated with the acetic anhydride–pyridine mixture to give the diacetate (**7**). The dihydroxyherqueinones (**8**—**12**) were also derived from **2** following the method given in the literature[8] as follows. Methylation of the product, obtained by hydrogenation of **2** in the presence of Pd–C, gave dihydroherqueinone methyl ethers (**8**) and (**10**). These methyl ethers were acetylated with the acetic anhydride–pyridine mixture to give the acetates (**9**) and (**11**), and with the acetic anhydride–*p*-toluenesulfonic acid mixture to give the diacetate (**12**). Xanthoherqueinone (**13**) was derived from **2** by acid-hydrolysis under the same conditions as described in the literature.[2]

The physical and analytical data of these phenalenones (**3**)

Table 5. UV and MS spectral data of phenalenone derivatives (3) and (5—13)

Compound	UV(EtOH) λ_{max}/nm (log ϵ)	MS (70 eV) m/z (rel intensity)
3	450(4.09), 307(5.16), 255(5.42), and 230(5.65)[a]	452 (M^++2, 100) and 450 (M^+, 89)
5	407(4.24) and 370(4.15)	356 (M^+, 52) and 341 (M^+—CH_3, 100)
6	402(4.21) and 375(4.20)	384 (M^+, 46) and 369 (M^+—CH_3, 100)
7	433(5.15), 410(5.34), and 360(5.09)	440 (M^+, 28), 398 (26), and 356 (100)
8	402(3.90) and 357(3.74)	388 (M^+, 100) and 373 (M^+—CH_3, 6)
9	355(3.80) and 330(3.67)	472 (M^+, 30), 430 (21), 388 (57), and 301 (100)
10	388(3.55) and 375(3.58)	402 (M^+, 62), 387 (M^+—CH_3, 12), and 301 (100)
11	348(4.32) and 334(4.29)	444 (M^+, 34), 402 (14), and 316 (100)
12	350(4.07) and 334(4.02)	486 (M^+, 20), 426 (52), and 369 (100)
13	399(3.97) and 314(4.08)	

a) Taken in cyclohexane.

Table 6. ^1H NMR Spectral data[a] of phenalenone derivatives (3) and (5—13)

Compound	1′-H_3 (J/Hz)	4′-H_3	5′-H_3	14-H_3	$OCOCH_3$	OCH_3	2′-H (J/Hz)	3-H	12-H
3[b]	1.57d[c] (6.5)	1.00	1.38	2.77		3.78	4.90q[c] (6.5)		
5	1.48d (6.5)	1.32	1.57	2.82		4.09	4.64q (6.5)		6.83
6	1.47d (6.5)	1.33	1.57	2.88		4.01[d] 4.09	4.64q (6.5)		6.86
7	1.42d (6.5)	1.29	1.51	2.80	2.32 2.36	4.01	4.62q (6.5)		6.94
8	1.34d (6.5)	0.80	1.17	2.53		3.98 4.28	3.68q (6.5)	5.44	6.72
9	1.27d (6.5)	0.83	1.08	2.61	2.36 2.41	3.90 3.99	3.64q (6.5)	5.52	7.06
10	1.22d (6.5)	0.89	1.08	2.52		3.92 4.06 4.20	3.61q (6.5)	5.46	6.78
11	1.23d (6.5)	0.92	1.10	2.58	2.36	3.88 3.96 4.03	3.60q (6.5)	5.47	6.94
12	1.20d (6.5)	1.00	1.24	2.54	2.14 2.34	3.91 3.99 4.06	3.62q (6.5)	5.50	6.97
13[b]				2.63		3.79			6.54

a) Taken in $[^2H]CHCl_3$ containing TMS as an internal standard. b) Taken in $[^2H_6]DMSO$. c) d=doublet and q=quartet. d) Two methyl signals overlap.

and (5—13) are given in Table 3, and the spectral data of them are summarized in Tables 4—6.

We thank Dr. G. A. Morrison for the gift of the ^1H NMR spectrum of herqueinone.

References

1) F. H. Stodola, K. B. Raper, and D. I. Fennell, *Nature (London)*, **167**, 773 (1951).
2) J. A. Galarraga, K. G. Neill, and H. Raistrick, *Biochem. J.*, **61**, 456 (1955).
3) D. H. R. Barton, P. de Mayo, G. A. Morrison, and H. Raistrick, *Tetrahedron*, **6**, 48 (1959).
4) N. Narasimhachari, K. S. Gopalkrishnan, R.H. Haskins, and L. C. Vining, *Can. J. Microbiol.*, **9**, 134 (1963).
5) R. E. Harman, J. Cason, F. H. Stodola, and A. L. Adkins, *J. Org. Chem.*, **20**, 1260 (1955).
6) J. Cason, J. S. Correia, R. B. Hutchison, and R. F. Porter, *Tetrahedron*, **18**, 839 (1962).
7) T. Suga, T. Yoshioka, T. Hirata, and T. Aoki, *Chem. Lett.*, **1981**, 1063.
8) J. S. Brooks and G. A. Morrison, *J. Chem. Soc., Perkin Trans. 1*, **1972**, 421.
9) J. S. Brooks and G. A. Morrison, *J. Chem. Soc., Perkin Trans. 1*, **1974**, 2114.
10) I. C. Paul, G. A. Sim, and G. A. Morrison, *Proc. Chem. Soc.*, **1962**, 352.
11) I. C. Paul and G. A. Sim, *J. Chem. Soc.*, **1965**, 1097.
12) A. Quick, R. Thomas, and D. J. Williams, *J. Chem. Soc., Chem. Commun.*, **1980**, 1051.
13) T. Yoshioka, T. Hirata, T. Aoki, and T. Suga, *Chem. Lett.*, **1981**, 1729.
14) T. Yoshioka, T. Hirata, T. Aoki, and T. Suga, *Bull. Chem. Soc. Jpn.*, **55**, 3847 (1982).
15) R. Thomas, *Biochem. J.*, **78**, 807 (1961).
16) R. Thomas, *Pure Appl. Chem.*, **34**, 515 (1973).
17) T. J. Simpson, *J. Chem. Soc., Chem. Commun.*, **1976**, 258.
18) T. J. Simpson, *J. Chem. Soc., Perkin Trans. 1*, **1979**, 1233.
19) G. C. Levy and G. L. Nelson, "Carbon-13 Nuclear Magnetic Resonance for Organic Chemists," Wiley-Interscience, New York, N. Y. (1972), pp. 22—135.
20) J. B. Stothers, "Carbon-13 NMR Spectroscopy," Academic Press, New York, N. Y. (1972), pp. 55—207.
21) B. Birdsall, N. J. M. Birdsall, and J. Feeney, *J. Chem. Soc., Chem. Commun.*, **1972**, 316.

22) B. F. Bowden, D. W. Cameron, M. J. Crossley, G. I. Feutrill, P. G. Griffiths, and D. P. Kelly, *Aust. J. Chem.*, **32**, 769 (1979).
23) F. A. Bovey, "Nuclear Magnetic Resonance Spectroscopy," Academic Press, New York, N. Y. (1969), pp. 61—82.
24) "Dreiding Stereomodels," W. Büchi Manufacture of Glass Apparatus Flawil, Switzerland.

Photochemical Reactions of 2-(Dimethylcarbamoyl)quinolines

Isao ONO* and Norisuke HATA
Department of Chemistry, College of Science and Engineering, Aoyama Gakuin University, Chitosedai, Setagaya-ku, Tokyo 157

(Received August 19, 1983)

2-(Dimethylcarbamoyl)quinolines are converted into 2-(methylaminoacetyl)quinolines (**2**) and 2-methyl-1*H*-pyrrolo[3,4-*b*]quinolin-3(2*H*)-ones (**3**) by irradiation in a nitrogen atmosphere. The reaction was quite efficient in acetonitrile but inefficient in hydrocarbon solvents and ethanol. The introduction of a chlorine atom to the 4-position of a quinoline nucleus caused an increase of the yield of **3** in company with a decrease of the yield of **2**. On the other hand, irradiation in an oxygen atmosphere afforded 2-(methylcarbamoyl)quinolines as a main product but **2** and **3** were minor products. The results of quenching and sensitization experiments confirmed that the triplet π,π^* state was responsible for the formation of those products. It is suggested that the reaction involves zwitterionic intermediates formed *via* Type II hydrogen abstraction by the ring nitrogen from the *N*-methyl group.

The photochemical behavior of cyano-substituted quinolines and isoquinolines has been a subject of continuing interest in our laboratory since we found that 2-quinolinecarbonitriles undergo the photochemical replacement of the cyano group by a hydroxyalkyl group in an alcoholic solvent.[1] Recently, this reaction was proved to proceed *via* a singlet radical pair formed by hydrogen abstraction by the ring nitrogen from the hydrogen-bonded alcohol.[1e] However, photochemical studies of the quinolines bearing an electron-withdrawing substituent other than the cyano group are few and the photochemical behavior of *N*-alkyl amides substituted on azanaphthalenes is still ambiguous, although α-cleavage of alkyl amides such as the case of *N*-hexylhexanamide is well known.[2] Therefore, we investigated the photochemical reactions of 2-(dimethylcarbamoyl)-quinolines (**1**) in several solvents. We discuss the nature of the intermediates involved in this reaction and the reaction pathway.

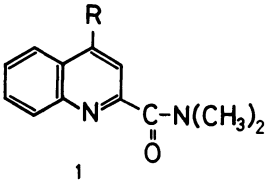

1

1a : R=H
1b : R=CH3
1c : R=Cl

Identification and Chemical Yields of Products. Irradiation of 2-(dimethylcarbamoyl)quinolines **1a—c** in a nitrogen atmosphere resulted in the formation of two products, **2** and **3**. The product **2** has the UV spectra of a quinoline type and its IR spectra show weak absorption by NH stretching at 3350 cm^{-1} and CO absorption at 1680 cm^{-1}. On the NMR spectra, the signals due to the methyl and methylene groups were found as doublet lines at 2.85 and 4.62 ppm, respectively. On the basis of these data, in addition to mass spectra and elemental analysis, **2** was determined to be 2-(methylaminoacetyl)quinoline. For the product **3**, the NMR signals due to the methyl and methylene groups were observed as singlet peaks, and it was found that one proton of the aromatic protons disappeared. The mass spectra showed that the molecular weight of **3** was less by two than that of **1**. The presence of the CO group was confirmed by the IR spectra. Hence, **3** was reasonably deduced to be 2-methyl-1*H*-pyrrolo-[3,4-*b*]quinolin-3(2*H*)-one.

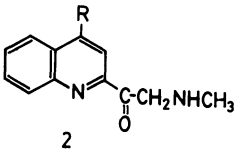

2

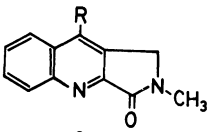

3

2a, 3a : R=H
2b, 3b : R=CH3
2c, 3c : R=Cl

As shown in Table 1, the yield distribution of **2** and **3** in acetonitrile or benzene remarkably changed by introduction of the chloro substituent at the 4-position of a quinoline nucleus, but there was no significant effect by the methyl substituent. That is, the irradiation of **1a** and **1b** produced **2** as a major product and **3** as a minor one, while in the case of **1c** the yield of **2c** decreased extremely and that of **3c** increased. On the other hand, the yields of both products were very low in cyclohexane and ethanol.

Irradiation of **1** under an oxygen atmosphere gave 2-(methylcarbamoyl)quinolines (**4**) as a major product, and **2** and **3** as the minor products (Table 2). Identification of **4** was made by comparison with an authentic sample prepared according to the literature.[3] The

TABLE 1. PHOTOCHEMICAL REACTIONS OF 2-(DIMETHYLCARBAMOYL)QUINOLINES **1** UNDER A NITROGEN ATMOSPHERE

Amide	Solvent	Conversion %	Yield of product / % 2	3
1a	Acetonitrile	70	44	5
	Benzene	65	32	3
	Cyclohexane	34	15	—
	Ethanol	76	10	—
1b	Acetonitrile	64	46	2
	Benzene	68	39	2
	Cyclohexane	41	16	—
	Ethanol	79	18	—
1c	Acetonitrile	70	4	25
	Benzene	65	3	26
	Cyclohexane	37	Trace	5
	Ethanol	67	Trace	Trace

Table 2. Photochemical reactions of **1** in an oxygen atmosphere

Amide	Solvent	Conversion / %	Yield of product / %		
			2	**3**	**4**
1a	Acetonitrile	65	11	3	31
	Acetonitrile[a)]	50	14	2	24+14(**4d**)
	Benzene	60	8	1	10
1b	Acetonitrile	56	5	Trace	38
1c	Acetonitrile	41	—	—	30

a) **1a** was irradiated in acetonitrile solution containing 20% (v/v) propylamine.

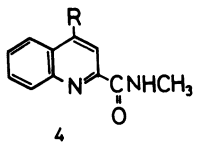

4

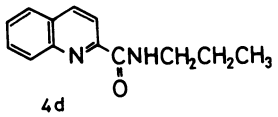

4d

4a: R=H
4b: R=CH_3
4c: R=Cl

Table 3. Phosphorescence data of **1** in ethanol and methylcyclohexane (MCH)

Amide	Solvent	λ_{max}/nm	E_T/kJ mol^{-1}	τ_p/s
1a	Ethanol	472	253	1.56
	MCH	473	253	1.12
1b	Ethanol	470	254	1.60
	MCH	470	254	1.35
1c	Ethanol	480	249	0.28
	MCH	480	249	0.25

Table 4. Benzophenone sensitization of **1**

Amide	Solvent	Recovered Benzophenone / %	Product yield / %		
			2	**3**	**4**
1a	Acetonitrile	93	70	11	—
	Acetonitrile[a)]	71	25	3	18
	Benzene	94	57	9	—
1b	Acetonitrile	97	61	6	—
	Benzene	94	54	5	—
1c	Acetonitrile	98	6	46	—
	Benzene	99	5	33	—

a) Irradiation was carried out in an oxygen atmosphere for 40 h.

Table 5. Quantum yields of photochemical reactions of **1a** and **1c**

Solvent	Φ_d(**1a**)	Φ_f(**2a**)	Φ_d(**1c**)	Φ_f(**3c**)
Acetonitrile	0.016	0.010	0.011	0.0036
Benzene	0.0087	0.0047	0.010	0.0025
Cyclohexane	0.0058	0.0018	0.0072	0.0003
Ethanol	0.011	0.0024	0.013	0.0004

irradiation of acetonitrile solution of **1a** containing propylamine produced **4a** and 2-(propylcarbamoyl)-quinoline **4d** in 24 and 14% yields, respectively.

Emission and Absorption Spectra of 1. The phosphorescence spectra of **1** could be measured in methylcyclohexane and ethanol at 77 K (Table 3), although no fluorescence was observed in either solution. From the first maxima of the spectra, the triplet excitation energy (E_T) was determined to be about 250 kJ mol^{-1}, which is higher than that of 1,3-cyclohexadiene (E_T=219 kJ mol^{-1}) and lower than that of benzophenone (E_T=289 kJ mol^{-1}). This long phosphorescence lifetime, over 1 s, indicates that the T_1 state of **1** can be assigned to $^3\pi,\pi^*$ type. The UV spectra of **1** was similar to that of quinoline, but not to that of 2-quinolinecarbonitrile, suggesting that the carbamoyl substituent conjugates with a quinoline nucleus to only a small extent. This implies that the excitation energy of **1** may be localized in a quinoline moiety, namely the $T_1(\pi,\pi^*)$ is the excited state of the quinoline nucleus.

Triplet Sensitization. A solution of **1** in deaerated acetonitrile or benzene containing benzophenone was irradiated with 366 nm light for 20 h. As a result, **2** and **3** were obtained in a product distribution similar to that in the case of the direct photolysis (Table 4). On the other hand, benzophenone sinsitization of **1a** in acetonitrile in the presence of oxygen gave **4a** in a 18% yield besides 25% of **2a** and a small amount of **3a**. This fact suggests that the triplet state is responsible for the formation of **4** as well as for **2** and **3**, and that the reaction to **4** involves an oxidation process.

Quantum Yields and Triplet Quenching. The quantum yields of both the disappearance (Φ_d) and the formation (Φ_f) for the photochemical reactions of **1a** and **1c** were determined under a nitrogen atmosphere; the results are given in Table 5. The quantum yields for the formation of **2a** and **3c** were larger in acetonitrile than in benzene, and became very low in cyclohexane and ethanol. The measurements for the minor products **3a** and **2c** were not attempted in this experiment, because those yields were too low to be precisely evaluated.

Next, the quantum yields in the presence of 1,3-cyclohexadiene were determined in deaerated acetonitrile. The Stern-Volmer plots are shown in Fig. 1. The linear relation of the plots for the quantum yields of **2a** and **3c** indicates that both products were formed through the $T_1(\pi,\pi^*)$ state. The quenching constants were estimated from the slopes to be 1.6×10^4 dm^3 mol^{-1} for **2a** and 1.0×10^4 dm^3 mol^{-1} for **3c**. The quenching constants for the quantum yields of disappearance evaluated from the linear portion of the plots were 1.2×10^4 dm^3 mol^{-1} for **1a** and 0.7×10^4 dm^3 mol^{-1} for **1c**. No large difference between the constants for formation quantum yield and for disappearance quantum yield indicates that, even if any reaction proceeds *via* the excited singlet state, it may be quite inefficient.

Reaction Mechanism. The primary step of the reaction of **1** may be γ-hydrogen abstraction by the ring nitrogen in the $T_1(\pi,\pi^*)$ state. Considering that the product formation is more effective in acetonitrile than in the hydrocarbon solvents, the reaction is expected to proceed *via* an ionic intermediate. Such a solvent effect and the chloro substituent effect on the reaction may be explained in terms of the mechanism involving zwitterionic intermediates, as shown in Scheme 1.

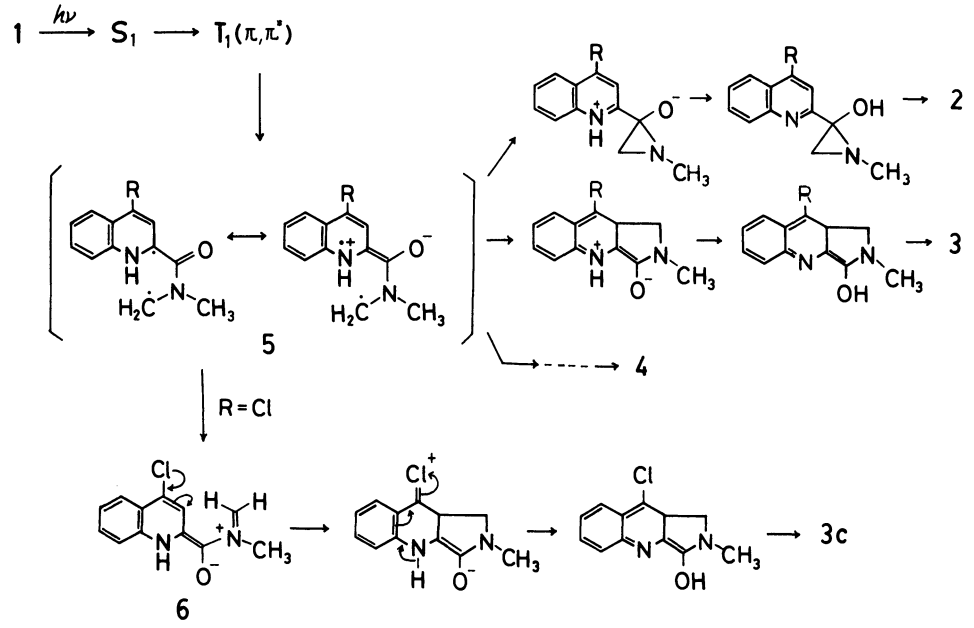

Scheme 1.

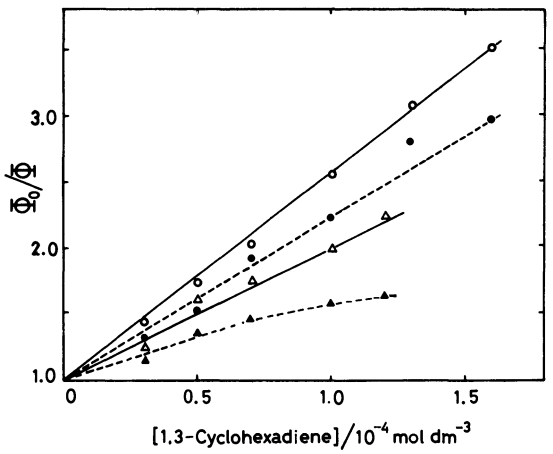

Fig. 1. Stern-Volmer plots for 1,3-cyclohexadiene quenching of the photochemical reactions of **1a** and **1c** in acetonitrile.
—○—: Formation of **2a**, ···●···: disappearance of **1a**,
—△—: formation of **3c**, ···▲···: disappearance of **1c**.

The intermediate **5** formed by the γ-hydrogen abstraction is in a resonance form of diradical and zwitterionic structures. The products **2** and **3** may be formed not *via* diradical structure but *via* zwitterionic one, because the contribution of the latter structure increases in a polar solvent, acetonitrile. The prominent increase of the yield of **3c** could be rationallized by assuming that the reaction **1c**→**3c** proceeds through a zwitterion **6**; the mesomery effect of the chlorine atom promotes the electron density on the carbon atom at the 3-position of a quinoline nucleus, which would be favorable for the cyclization of **6** followed by the formation of **3c**. Aoyama *et al.* have clarified that Type II cyclization of α-oxoamides occurs *via* zwitterion intermediates analogous to the type of **6** and that the zwitterions were stabilized in protic solvents.[4a] This explains the result that the yield of **3c** is larger in acetonitrile. The lower yields of the products **2** and **3** in ethanol may be attributed to the formation of a hydrogen bond between the ring nitrogen and the solvent. Such hydrogen-bonding is expected to suppress intramolecular hydrogen abstraction by the excited ring nitrogen. Previously, we have reported that 2-quinolinecarbonitriles undergo photochemical substitution derived from hydrogen abstraction by the ring nitrogen from the solvent alcohol.[1] However, we could not find the corresponding reaction in the case of **1**.

The formation of **4** is explained by assuming the decomposition of **5** to ketenes and imines. The decomposition is possible from both diradical and zwitterionic structures, and also from the zwitterion **6**. It is well known that such ketenes and imines are responsible for the formation of *N*-monosubstituted amides in the presence of moisture. For example, the photochemical reaction of *N*,*N*-diisopropylmethacrylamide was reported to give *N*-isopropylbutyramide *via* the dimethylketene and the corresponding imine.[4b] The photochemical formation of 2-(propylcarbaboyl)quinoline **4d** from **1a** in the presence of propylamine supports the reaction mechanism. The fact that **4** was formed only in the presence of oxygen indicates that it may be necessary for the oxidation of dihydroquinolines to **4**.

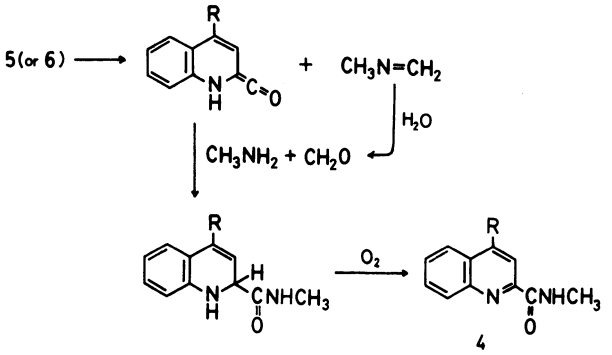

4-Acylpyrimidines were suggested to undergo γ-hydrogen abstraction by the ring nitrogen and Type II elimination by the carbonyl group in each n,π^* triplet state situated close together.[5] The carbamoyl group of **1** is easily deduced to possess the ^{3}CT state on the analogy of the fact that a formamid has an excited intramolecular charge transfer state.[6] If the ^{3}CT state lies close to the $T_1(\pi,\pi^*)$ state, the hydrogen abstraction by the carbonyl group from the *N*-methyl group may occur by way of an electron transfer mechanism well known for the photoreduction of amino ketones[7] and give a 1,3-biradical, which could also account for the formation of **2** and **3**. However, such a hydrogen transfer through the five-membered transition state is ineffective and there are few reports.[8] Therefore, hydrogen abstraction by the ring nitrogen is thought to be a more reasonable mechanism for the reaction of **1**.

Experimental

The NMR spectra were determined in $CDCl_3$ on a Hitachi-Perkin Elmer R-20, using TMS as an internal standard. The mass spectra were measured by a Hitachi RMU-6M or a Hitachi M-80 A double focus mass spectrometer. The IR spectra were taken on a JASCO A-302 and UV spectra were measured on a Shimadzu UV-220. The phosphorescence spectra were recorded with a Hitachi MPF-2A.

Materials. All solvents used in the irradiation experiment were reagent grade from Wako Pure Chemical Industry. Acetonitrile was refluxed in the presence of phosphorus pentaoxide for 10 h and distilled. Cyclohexane was used after purification by silica gel chromatography. Ethanol and benzene were used without further purification. 1,3-Cyclohexadiene and benzophenone from Tokyo Kasei Kogyo Co. were purified by distillation or recrystallization from ethanol, respectively. 2-(Dimethylcarbamoyl)quinoline **1a**—**c** were prepared by treating the corresponding 2-quinolinecarboxylic acids with $SOCl_2$ and dimethylamine.[3] The carboxylic acids were obtained from the basic hydrolysis of 2-quinolinecarbonitriles[9] synthesized by Reisert reaction of quinoline, 4-methylquinoline, and 4-chloroquinoline *N*-oxides which were prepared by the methods given in the literature.[10] **1a** and **1b** were purified by alumina chromatography, using a mixture of chloroform and diethyl ether as an eluent, and **1c** was recrystallized from a mixture of hexane and ethanol.

*2-(Dimethylcarbamoyl)quinoline (**1a**).* Colorless liquid; NMR δ=3.15 (3H, s, CH_3), 3.21 (3H, s, CH_3), 7.40—8.34 (6H, m, ArH); MS *m/e* 200 (M^+); IR (neat) 3050, 2910, 1670 (CO) cm^{-1}.

*2-(Dimethylcarbamoyl)-4-methylquinoline (**1b**).* Colorless liquid; NMR δ=2.62 (3H, s, CH_3 on ring), 3.15 (3H, s, *N*-CH_3), 3.18 (3H, s, *N*-CH_3), 7.34—8.24 (5H, m, ArH); MS *m/e* 214 (M^+); IR (neat) 3050, 2940, 1650 (CO) cm^{-1}.

*2-(Dimethylcarbamoyl)-4-chloroquinoline (**1c**).* Mp 64—65 °C; NMR δ=3.21 (6H, s, $(CH_3)_2$), 7.32—8.33 (5H, m, ArH); MS *m/e* 236/234 (M^+); IR (KBr) 3050, 2950, 1650 (CO) cm^{-1}.

*General Procedure of Direct Irradiation of **1**.* **1a**—**c** (200 mg) dissolved in 70 cm^3 of acetonitrile, benzene, cyclohexane, or ethanol were irradiated in a Pyrex vessel with a 100 W high pressure immersion mercury lamp (Riko Kagaku Sangyo Co.) in a nitrogen or oxygen atmosphere for 20 h. After the evaporation of the solvent, the residue was chromatographed on silica gel (Wakogel C-300). Elution with a mixture of chloroform and diethyl ether separated **2**, **3**, and **4**. Liquid products were purified on thin-layer chromatography of Kieselgel (PF_{254}, Merck) by being developed with the same eluent.

*2-(Methylaminoacetyl)quinoline (**2a**).* Colorless liquid; NMR δ=2.85 (3H, d, J=6.0 Hz, NHC$\underline{H}_3$), 4.62 (2H, d, J=9.1 Hz, C$\underline{H}_2$NH), 7.00—8.41 (7H, m, ArH and NH); MS *m/e* 200 (M^+); IR (neat) 3400 (broad), 3350 (NH), 3070, 2950, 1680 (CO) cm^{-1}. Found: C, 69.83; H, 6.14; N, 13.06%. Calcd for $C_{12}H_{12}N_2O$ 1/3 H_2O: C, 69.90; H, 6.15; N, 13.59%.

*2-(Methylaminoacetyl)-4-methylquinoline (**2b**).* Mp 80—81 °C (from hexane–ethanol); NMR δ=2.69 (3H, s, CH_3 on ring), 2.93 (3H, d, J=6.2 Hz, NHC$\underline{H}_3$), 4.72 (2H, d, J=9.1 Hz, C$\underline{H}_2$NH), 7.09—8.40 (6H, m, ArH and NH); MS *m/e* 214 (M^+); IR (KBr) 3330 (NH), 3050, 2940, 1675 (CO) cm^{-1}. Found: C, 72.77; H, 6.59; N, 13.09%. Calcd for $C_{13}H_{14}N_2O$: C, 72.90; H, 6.54; H, 13.08%.

*2-(Methylaminoacetyl)-4-chloroquinoline (**2c**).* Colorless liquid; NMR δ=2.99 (3H, d, J=7.0 Hz, NHC$\underline{H}_3$), 4.75 (2H, d, J=8.9 Hz, C$\underline{H}_2$NH), 7.33—8.45 (6H, m, ArH and NH); MS *m/e* 236/234 (M^+); $C_{12}H_{11}N_2OCl$ was determined with a Hitachi M-80 A double focus mass spectrometer; IR (neat) 3350 (NH), 3080, 2940, 1680 (CO) cm^{-1}.

*2-Methyl-1H-pyrrolo[3,4-b]quinolin-3(2H)-one (**3a**).* Mp 198 °C (from ethanol); NMR δ=3.22 (3H, s, CH_3), 4.48 (2H, s, CH_2), 7.18—8.50 (5H, m, ArH), MS *m/e* 198 (M^+); IR (KBr) 3050, 2940, 1680 (CO) cm^{-1}. Found: C, 72.11; H, 5.02; N, 13.97%. Calcd for $C_{12}H_{10}N_2O$: C, 72.73; H, 5.05; N, 14.14%.

*2,9-Dimethyl-1H-pyrrolo[3,4-b]quinolin-3(2H)-one (**3b**).* Mp 178 °C (from ethanol); NMR δ=3.12 (3H, s, CH_3 on ring), 3.25 (3H, s, *N*-CH_3), 4.47 (2H, s, CH_2), 7.20—8.34 (4H, m, ArH); MS *m/e* 212 (M^+); $C_{13}H_{12}N_2O$ was determined with a Hitachi M-80 A double focus mass spectrometer; IR (KBr) 3080, 2930, 1680 (CO) cm^{-1}.

*9-Chloro-2-methyl-1H-pyrrolo[3,4-b]quinolin-3(2H)-one (**3c**).* Mp 166 °C (from ethanol); NMR δ=3.26 (3H, s, CH_3), 4.46 (2H, s, CH_2), 7.34—8.48 (4H, m, ArH); MS *m/e* 234/232 (M^+); IR (KBr) 3050, 2910, 1690 (CO) cm^{-1}. Found: C, 61.62; H, 3.93; N, 11.91%. Calcd for $C_{12}H_9N_2OCl$: C, 61.94; H, 3.87; N, 12.04%.

The structures of **4a**—**d** were determined by the comparison with the authentic sample synthesized according to the same method as that used for the preparation of **1**.[3]

*2-(Methylcarbamoyl)quinoline (**4a**).* Mp 118 °C (from ethanol); NMR δ=3.12 (3H, d, J=5.1 Hz, NHC$\underline{H}_3$), 7.41—8.31 (7H, m, ArH and NH); MS *m/e* 186 (M^+); IR (KBr) 3350 (NH), 3080, 2960, 1660 cm^{-1}.

*2-(Methylcarbamoyl)-4-methylquinoline (**4b**).* Mp 109 °C (from ethanol); NMR δ=2.76 (3H, s, CH_3 on ring), 3.18 (3H, d, J=5.4 Hz, NHC$\underline{H}_3$), 7.40—8.35 (6H, m, ArH and NH); MS *m/e* 200 (M^+); IR (KBr) 3330 (NH), 3090, 2940, 1660 (CO) cm^{-1}.

*2-(Methylcarbamoyl)-4-chloroquinoline (**4c**).* Mp 140 °C (from ethanol); NMR δ=3.11 (3H, d, J=5.5 Hz, NHC$\underline{H}_3$), 7.37—8.42 (6H, m, ArH and NH); MS *m/e* 222/220 (M^+); IR (KBr) 3350 (NH), 3080, 2950, 1660 (CO) cm^{-1}.

*2-(Propylcarbamoyl)quinoline (**4d**).* Colorless liquid; NMR δ=0.978 (3H, t, J=6.6 Hz, $CH_2C\underline{H}_3$), 1.34—2.04 (2H, m, $CH_2C\underline{H}_2CH_3$), 3.49 (2H, q, J=7.6 Hz, NHC$\underline{H}_2CH_2$), 7.44—8.43 (7H, m, ArH and NH); MS *m/e* 214 (M^+); IR (neat) 3380 (NH), 3050, 2950, 1670 (CO) cm^{-1}.

Triplet Sensitization. Acetonitrile or benzene solution (110 cm^3) containing **1** (0.05 g) and benzophenone (0.1 g) was irradiated for 20 h with 366 nm light through a UV-35 Toshiba filter from a 500 W high pressure mercury lamp (USH-500D, Ushio Electric Inc.). The products were isolated by thin-layer chromatography of Kieselgel (PF_{254}, Merck), using a mixture of chloroform and diethyl ether.

Quantum Yield Determination. A deaerated solution con-

taining 3×10^{-4} mol dm^{-3} **1a** or **1c** was irradiated at 313 nm in a quartz cylindrical cell (5-cm in diameter and 1-cm in length), using a USH-500D lamp as a light source. The 313-nm line was isolated by a combination of a $NiSO_4$ solution with UV-29 and UVD-33S filters. The light intensity was determined by means of a potassium trioxalatoferrate(III) actinometer. The amount of the products (**2a** and **3c**) and consumed starting materials (**1a** and **1c**) were determined spectrometrically after the separation by a silica-gel column (chloroform was used as an eluent). Conversions ranged from 10 to 20%.

References

1) a) N. Hata, I. Ono, and S. Ogawa, *Bull. Chem. Soc. Jpn.*, **44**, 2286 (1971); b) N. Hata, I. Ono, S. Matono, and H. Hirose, *ibid.*, **46**, 942 (1973); c) N. Hata and T. Saito, *ibid.*, **47**, 942 (1974); d) N. Hata and Y. Yamada, *Chem. Lett.*, **1980**, 989; e) N. Hata and M. Hokawa, *ibid.*, **1981**, 507.

2) P. H. Mazzocchi and M. Bowen, *J. Org. Chem.*, **41**, 1279 (1976).

3) P. Barczynski and M. Szafran, *Rocez. Chem.*, **50**, 353 (1976).

4) a) H. Aoyama, M. Sakamoto, K. Kuwabara, K. Yoshida, and Y. Omote, *J. Am. Chem. Soc.*, **105**, 1958 (1983); b) H. Aoyama, T. Hasegawa, M. Okazaki, and Y. Omote, *J. Chem. Soc., Perkin Trans. 1*, **1979**, 263.

5) E. C. Alexander and R. J. Jackson, *J. Am. Chem. Soc.*, **98**, 1609 (1976).

6) S. Nagakura, *Mol. Phys.*, **3**, 105 (1960).

7) A. Padwa, W. Eisenhardt, R. Gruber, and D. Pashayan, *J. Am. Chem. Soc.*, **93**, 6998 (1971); P. J. Wagner, A. E. Kemppainen, and T. Jellinek, *ibid.*, **94**, 7512 (1972); P. J. Wagner and D. R. Ersfeld, *ibid.*, **98**, 4515 (1976).

8) H. J. Roth and M. H. El Raie, *Tetrahedron Lett.*, **1970**, 2445.

9) D. J. Byron, G. W. Gray, and C. Wilson, *J. Chem. Soc., C*, **9**, 840 (1966).

10) E. Ochiai, "Aromatic Amine Oxide," Elsevier, Amsterdam (1967), Chap. 3; T. Okamoto, *J. Pharm. Soc. Jpn.*, **71**, 297 (1951).

 © 1983 The Chemical Society of Japan Bull. Chem. Soc. Jpn., 56, 3672—3670 (1983) [Vol. 56, No. 12

Asymmetric Reduction with C_1- and C_2-Symmetric NADH Model Compounds Containing Chiral 1,1′-Binaphthyls

Masaki AMANO, Motoshi WATANABE, Naomichi BABA, Jun'ichi ODA,* and Yuzo INOUYE
Institute for Chemical Research, Kyoto University, Uji, Kyoto 611
(Received May 28, 1983)

The present study deals with Mg-catalyzed asymmetric reduction of ethyl benzoylformate by the use of C_2-symmetric NADH model compounds in which axial dissymmetry(chiral 1,1′-binaphthyl derivatives) was introduced as a chiral source for the first time and the results were compared with those obtained by the corresponding C_1-symmetric models bearing the same chiral center. Better e.e.'s of the reduction product were obtained by the use of NADH models having C_2-symmetry than does the corresponding C_1-symmetric ones. Further, the kind of bonding as well as the distance between chiral binaphthyl and the reaction center affected the stereochemical course of hydrogen transfer.

Recently some intriguing works have been reported concerning salient effect of C_2-symmetry on the asymmetric synthesis for improving stereoselectivity. The study includes alkylation of enamines,[1] asymmetric reduction of prochiral carbonyl substrates by the use of lithium aluminium hydride modified with chiral 1,1′-binaphthyl,[2] borane–amine complexes modified with optically pure 1,1′-binaphthyl[3] and bis(NADH) model compound,[4] and Michael addition reactions catalyzed by C_2-symmetric chiral crown complexes.[5] However, at present, it is a question that what structure of the chiral reactant(s) is necessary for manifestation of the C_2-symmetry effect in general.

In the present study, we intended to design C_2-dissymmetric[6] NADH model compounds which have a C_2-axis passing through the center of the molecule and have diastereotopic hydrogens at the reaction center. For this purpose, a class of chiral 1,4-dihydropyridines were prepared in which axially dissymmetric binaphthyls were introduced for the first time as a chiral moiety instead of centro-asymmetry, and asymmetric reduction of ethyl benzoylformate was conducted therewith. The results were compared with those obtained by the use of the corresponding C_1-symmetric NADH models bearing the same chirality and the effect of C_2-symmetry was assessed. In addition, influence of polar functional groups, bonding mode of dihydropyridine and chiral binaphthyls as well as the distance between the reaction center and the binaphthyl moiety on the stereoselectivity were discussed.

Results and Discussion

Synthesis of C_1- and C_2-Symmetric NADH Model Compounds (NAH) with Chiral Binaphthyls. In the molecular design for constructing the axially dissymmetric NADH model compounds, enantiomeric 1,1′-bi-2-naphthols, 1,1′-bi-2-naphthylamines and 2,2′-bis-(hydroxymethyl)-1,1′-binaphthyls were introduced as the chiral center of choice. These chiral sources were prepared from 2-naphthol and 2-methylnaphthalene according to the literature.[7-9] The synthetic route for final 1,4-dihydropyridines were shown in Scheme 1 for (*R*)-(**I**) and (*S*)-(**II**), Scheme 2 for (*S*)-(**III**), (*R*)-

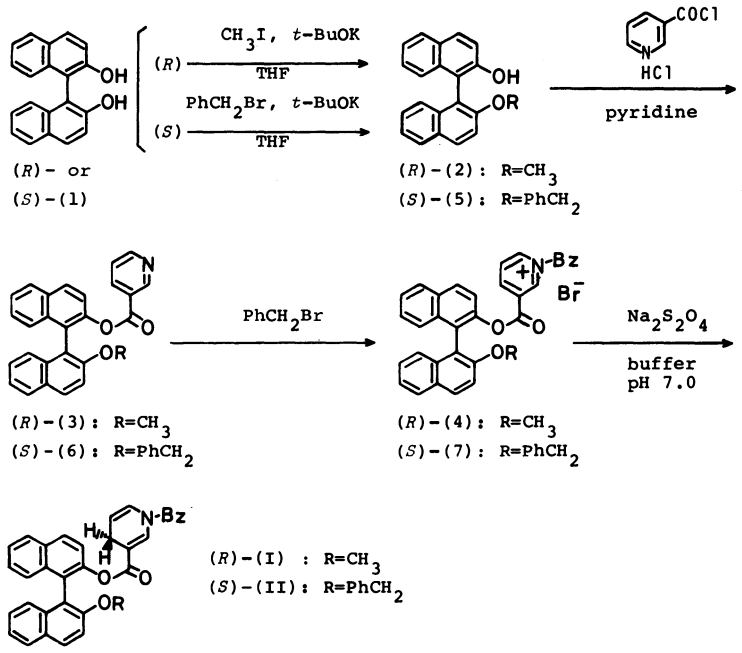

Scheme 1.

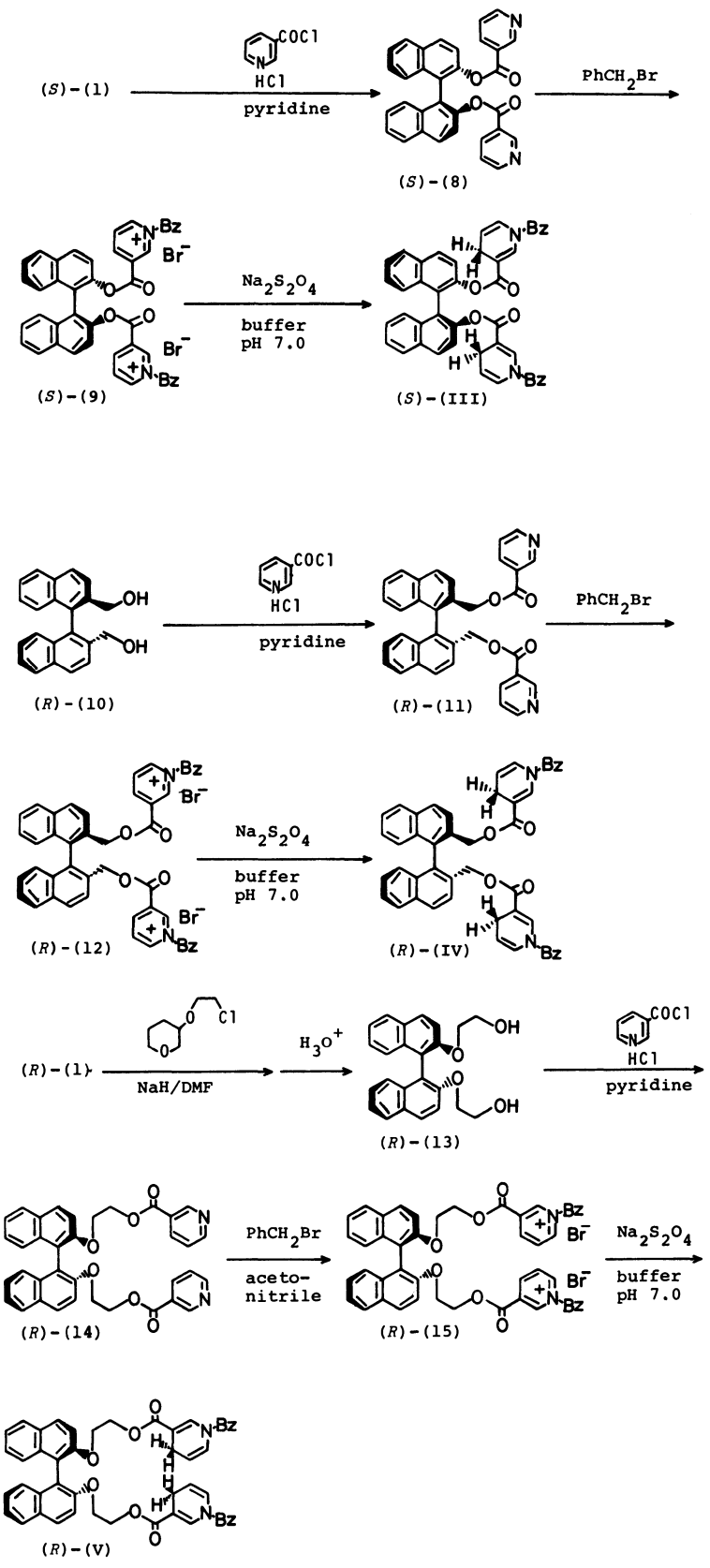

Scheme 2.

(**IV**), and (*R*)-(**V**), Scheme 3 for (*S*)-(**VI**), (*S*)-(**VII**), and (*S*)-(**VIII**). In particular, in the last step of synthesis of NADH models (**I**—**V**) possessing ester bonding, the sodium dithionite reductions were carried out in a phosphate buffer adjusted at pH 7.0 to avoid ester hydrolysis under the conventional basic conditions. All the C_1- and C_2-symmetric NADH models thus prepared were featured by their fluorescence on tlc and also

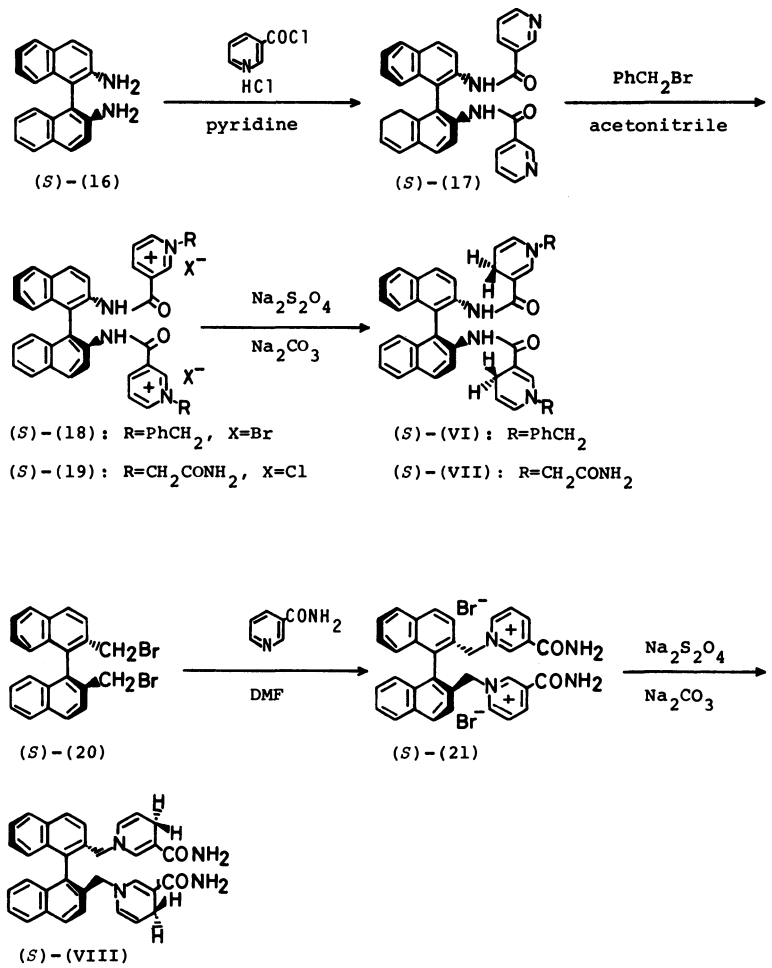

Scheme 3.

TABLE. 1. ASYMMETRIC REDUCTION OF ETHYL BENZOYLFORMATE WITH C_1- AND C_2-SYMMETRIC NADH MODEL COMPOUNDS BEARING CHIRAL BINAPHTHYLS

Run	NAH			Ethyl mandelate		
	Model	Configuration	Symmetry	Chem. yield / %	e.e. / %	Configuration
1	(**I**)	*R*	C_1	50.5	10.0	*S*
2	(**II**)	*S*	C_1	55.6	9.1	*R*
3	(**III**)	*S*	C_2	24.8	43.2	*R*
4	(**IV**)	*R*	C_2	36.0	8.8[a)]	*S*
5	(**V**)	*R*	C_2	56.1	5.7	*R*
6	(**VI**)	*S*	C_2	14.3	45.6	*R*
7	(**VII**)	*S*	C_2	66.1	11.4	*R*
8	(**VIII**)	*S*	C_2	26.0	43.5[a)]	*S*

a) Corrected for the optical purity of the models(**IV**) and (**VIII**) used.

fully substantiated by their NMR and UV spectra.

Asymmetric Reduction of Ethyl Benzoylformate with Present NADH Models. In the present study, the magnesium perchlorate-catalyzed asymmetric reduction of ethyl benzoylformate was preferred as the model system of choice since considerable amount of informations have already been accumulated from both mechanistic and stereochemical aspects,[10] which would make the analysis of the experimental results easier. The results from the asymmetric reductions of ethyl benzoylformate at the ratio of $Mg(ClO_4)_2$: NAH=1 : 2 (mol : mol) by the use of the NADH models (**I**—**VIII**) were listed in Table 1.

The reductions of ethyl benzoylformate by the use of (*R*)-(**I**) and (*S*)-(**II**), both of C_1-symmetry, gave the reduction products (*R*)- and (*S*)-ethyl mandelate in 10 and 9% e.e. respectively (runs 1 and 2). The rather moderate optical yield may partially be ascribed to the ester function as pointed out by Ohno in the system involving chiral 1,4-dihydropyridine with *l*-menthyl group linked by the amide, ester or carbonylmethylene group.[11] The free rotation about the ester bond could

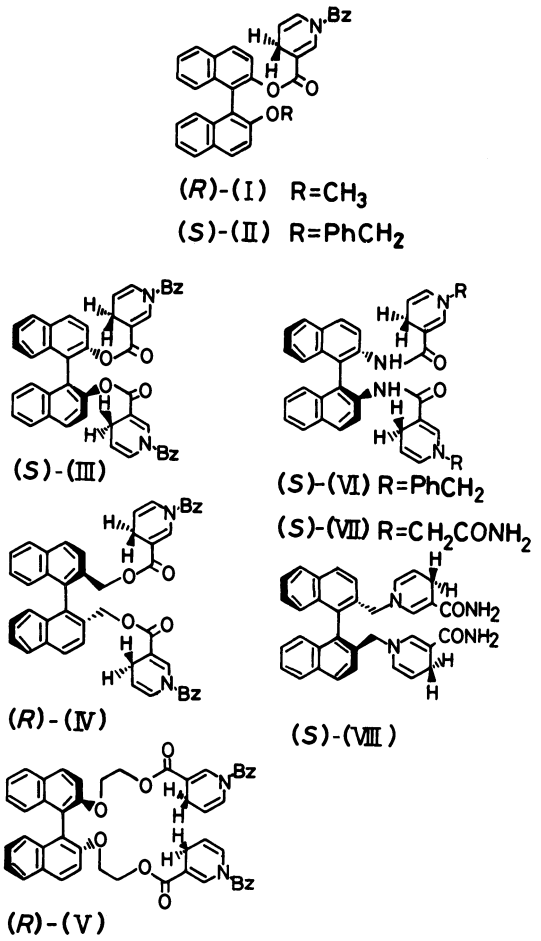

also be responsible for the low stereoselectivity. On the other hand, the model reaction using C_2-symmetric (*S*)-(**III**) even with the same ester bondings gave (*R*)-mandelate in much higher e.e. (43.2%) clearly suggesting that individual dihydropyridines hinder the free rotations around the ester bonds each other rendering a decrease of the number of conformations at the stereochemical determining stage. As will be shown later in this section, the interaction of dihydropyridylcarbonyloxy group with magnesium ion seems to be little as judged from UV spectrometry. So that, the augmentation of the optical yield caused by introducing a C_2-symmetry axis could possibly be ascribed to the enhanced access of the substrate to one specific face of dihydropyridine moiety by steric requirement, as were demonstrated by Whitesell in the enamine alkylation[1] and Inouye in the bis (NADH) model reaction.[4] In the model (*S*)-(**III**), the two dihydropyridine nuclei disposed in C_2-symmetry on the chiral binaphthyl may expose the specific one of their faces toward outside, permitting the access of substrate from the outside to the faces predominantly. However, when dihydropyridine moieties are removed from the chiral binaphthyls, as the cases with (*R*)-(**V**) the steric effect of chiral binaphthyls on the dihydropyridines may be diminished. Actually, observed e.e. by the use of (*R*)-(**IV**) and (*R*)-(**V**) steeply decreased giving 8.8%-(*S*) and 5.7%-(*R*) product respectively. It is also noteworthy that both the reductant (*S*)-(**III**) and (*R*)-(**V**) gave the same (*R*)-mandelate. Thus, the product stereochemistry was reversed by removing the reaction center from the binaphthyl moiety.

The model (*S*)-(**VI**) differs from (*S*)-(**VIII**) in that the binaphthyl was linked at 3-position of the dihydropyridine for the former whereas at N_1-position for the latter. Interesting is a result from this difference that product configuration was dramatically reversed from (*R*)-45.6% to (*S*)-43.5%.

Stereochemical behavior of (*S*)-(**III**) and (*S*)-(**VI**) reductants in the asymmetric reductions were further examined in detail. The reduction of ethyl benzoylformate by the use of these two models were conducted in the presence of varying amounts of magnesium perchlorate and the optical yields were plotted against the catalyst amount. As shown in Fig. A-1 and B-1, with the reductant (*S*)-(**III**), the e.e.'s remained constant in contrast to the case with (*S*)-(**VI**) where the e.e.'s changed greatly by variation of the catalyst amount with a maximum optical yield (45.6%) at $Mg(ClO_4)_2$/(**VI**)=0.5. However, the maximum values with the both reductants were very similar. Furthermore, the reduction with (*S*)-(**VI**) showed a dependence of e.e. on the reaction conversion as shown in Fig. B-2, whereas such was not the case with (*S*)-(**III**) (Fig. A-2). The two markedly different stereochemical behaviors between these models should obviously be ascribed to the difference in electronic nature of the ester and the amide functions. In fact, as revealed by UV spectroscopy, the reductant (*S*)-(**VI**) showed a spectral change with varying amounts of magnesium perchlorate (Fig. B-3), while no change was observed for (*S*)-(**III**) indicating that the amide functions interact to some extent with magnesium ion[12] in contrast to the ester functions (Fig. A-3). Accordingly, the chelative properties of the amide group must be responsible for the dependence of e.e. on the catalyst amount and on the reaction conversion observed in the asymmetric reduction with the model (*S*)-(**VI**). From this view, the C_2-symmetric diester reductant (*S*)-(**III**) could be regarded as a reasonable model to demonstrate unequivocally the importance of C_2-symmetry for the stereoselectivity since the electronic factor involving chelative interaction of the model (*S*)-(**III**) with magnesium ion seems to be negligible for the stereochemical course of the hydrogen transfer as described above.

In the present study, axial chirality was transferred successfully for the first time to centro-chirality of the reduction product in NADH model systems and the importance of C_2-symmetry for stereospecificity was unambiguously demonstrated by the use of the model (*S*)-(**III**) derived from optically active binaphthyl. In the diamide model (*S*)-(**VI**), the chelative interaction with magnesium ion was found to be significant and responsible for the dependence of e.e. on the catalyst amount as well as the reaction conversion.

Also, of interest was a finding that the product stereochemistry including configurational reversal was found to be greatly dependent on the bonding site of the dihydropyridine (N_1-position in **VIII** and 3-position in **I**—**VII**) to chiral moiety and also on the distance between the binaphthyls and the reaction center.

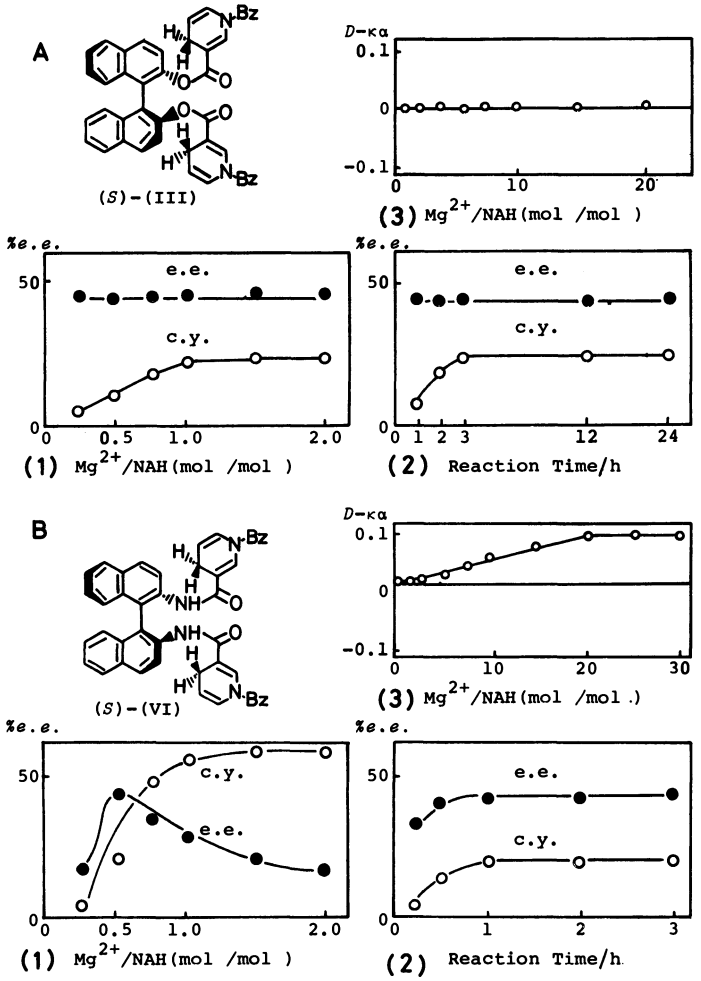

Fig. 1. Dependence of e.e. on the catalyst amount and the reaction conversion in the asymmetric reductions of ethyl benzoylformate with (*S*)-(**III**) and (*S*)-(**VI**), and determination of the mole ratio in the complexes of these models with magnesium perchlorate by UV spectroscopy.

Experimental

General. IR spectra were recorded with a Hitachi 215 spectrometer, ^{1}H-NMR spectra with a Varian EM-360 spectrometer with tetramethylsilane as internal standard. UV spectra were recorded on a Hitachi 340 spectrometer. Optical rotations were measured with a Perkin-Elmer 241 polarimeter. VPC analyses were performed on a Shimadzu GC-4CM instrument with 15% polyethylene glycol succinate(PEGS) on Chromosorb W at 180 °C. Preparative VPC analyses were on Varian Aerograph Model 920 with alminum column (3 m) packed with 15% Apiezone L at 190 °C.

Ethyl benzoylformate from commercial source was purified by chromatography (Kieselgel 60, 70—230 mesh) eluted by benzene, followed by distillation. Anhydrous magnesium perchlorate was kept in a vacuum desiccator over phosphorus pentoxide. Acetonitrile was distilled over phosphorus pentoxide. Ethanol was distilled over calcium hydride.

General Procedure for Asymmetric Reduction. A mixture of ethyl benzoylformate, NADH model compound (NAH) and magnesium perchlorate in dry acetonitrile (10 ml/1.0 mmol) was stirred at room temperature under nitrogen atmosphere in the dark, after which water (1 ml) was added to the reaction mixture. The mixture was stirred for 5 min at room temperature, and extracted with dichloromethane. The organic phase was evaporated *in vacuo*. The residue was chromatographed on TLC (Kieselgel G nach Stahl, Type 60) with benzene. The purity of the alcohol obtained was confirmed by VPC and ^{1}H-NMR.

Chemical yields were determined by VPC. Optical yields were calculated from optical rotations of the isolated ethyl mandelate based on the reported maximum rotation of enantiomerically pure ethyl mandelate, $[\alpha]_D^{25}$ $\pm$104.4° in ethanol.[13]

(R)-2-Hydroxy-2'-methoxy-1,1'-binaphthyl (R)-(2): A mixture of (*R*)-1,1'-bi-2-naphthol (**1**) (3.0 g, 10.5 mmol, $[\alpha]_D^{25}$ +31.5°, *c* 1.03, THF) and *t*-BuOK (1.8 g, 10.5 mmol) in 200 ml of dry THF was stirred under nitrogen atmosphere and methyl iodide (1.49 g, 10.5 mmol) in 50 ml of dry THF was added dropwise. The mixture was heated under reflux for 15 h, cooled and concentrated under reduced pressure. The residue was partitioned between dichloromethane and saturated sodium carbonate solution. The organic layer was washed with brine, dried and the solution was evaporated under reduced pressure to give an oil which was purified by silica-gel column chromatography with benzene elution; yield 1.94 g (61.6%), $[\alpha]_D^{25}$ +38.59° (*c* 0.99, THF), ^{1}H-NMR (chloroform-d_1): δ=3.86 (3H, s, $-CH_3$), 5.03 (1H, s, -OH), 7.15—8.30 (12H, m, aromatic protons).

(R)-2-Methoxy-2'-(3-pyridylcarbonyloxy)-1,1'-binaphthyl (R)-(3): To a solution of nicotinoyl chloride hydrochloride (1.8 g, 10.1 mmol) in pyridine (50 ml), (*R*)-(**2**) (2.0 g, 6.7 mmol) was added and the mixture was stirred at room temperature overnight, followed by reflux for 2 h. After cooling, evaporation under reduced pressure gave a residue, which was partitioned betweed dichloromethane and saturated sodium carbonate solution. The aqueous layer was extracted with dichloromethane. The organic layer was washed with brine, dried and chromatographed on silica-gel column chromatography with dichloromethane solution; yield 2.5 g (92.5%), $[\alpha]_D^{25}$ +29.10° (*c* 1.00, THF), ^{1}H-NMR (chloroform-d_1): δ= 3.73 (3H, s, $-CH_3$), 7.00—8.20 (14H, m, aromatic and pyridine protons), 8.40—8.80 (2H, m, pyridine).

(S)-2-Benzyloxy-2'-hydroxy-1,1'-binaphthyl (S)-(5): Benzyl ether (*S*)-(**5**) was prepared in the same manner with (*S*)-(**2**) from (*S*)-1,1'-bi-2-naphthol (3.0 g, 10.5 mmol) and benzyl bromide (1.80 g, 10.5 mmol); yield 2.6 g (66.0%), $[\alpha]_D^{25}$ −58.61° (*c* 1.034, THF), mp 93 °C, ^{1}H-NMR (chloroform-d_1): δ=4.96 (1H, s, -OH), 5.10 (2H, s, $-CH_2-$), 6.90—8.20 (17H, m, aromatic protons).

(S)-2-Benzyloxy-2'-(3-pyridylcarbonyloxy)-1,1'-binaphthyl (S)-(6): (*S*)-(**6**) was prepared in the same manner with (*R*)-(**3**) from (*S*)-(**5**) (2.4 g, 6.4 mmol) and nicotinoyl chloride hydrochloride (1.7 g, 9.5 mmol); yield 3.1 g (100%), $[\alpha]_D^{25}$ −44.73° (*c* 2.28, ethanol), ^{1}H-NMR (chloroform-d_1): δ=5.10 (2H, s, $-CH_2-$), 7.00—8.30 (14H, m, aromatic and pyridine protons), 8.60—8.80 (2H, m, pyridine).

(S)-2,2'-Bis(3-pyridylcarbonyloxy)-1,1'-binaphthyl (S)-(8): To a mixture of nicotinoyl chloride hydrochloride (22 g, 124 mmol) in a solution of triethylamine (25 g) in dichloromethane (200 ml), was added a dichloromethane solution (200 ml) of (*S*)-1,1'-bi-2-naphthol (**1**) (15 g, 52 mmol) and refluxed for 1 h, cooled and washed with saturated sodium carbonate solution and brine, dried over anhydrous sodium sulfate, followed by concentration under reduced pressure. The residue was chromatographed on silica-gel column with ethyl acetate as eluent to give pure (*S*)-(**8**); yield 21.0 g (81%), $[\alpha]_D^{25}$ −79.5° (*c* 1.00, ethanol), ^{1}H-NMR (chloroform-d_1): δ=7.05—8.20 (16H, m, aromatic and pyridine protons), 8.60—8.90 (4H, m, pyridine).

(R)-2,2'-Bis(3-pyridylcarbonyloxymethyl)-1,1'-binaphthyl (R)-(11): Binaphthyl derivative (*R*)-(**11**) was prepared in the same manner with (*S*)-(**8**) from (*R*)-2,2'-bis(hydroxymethyl)-1,1'-binaphthyl (**10**)[9] (1.1 g, 3.5 mmol) and nicotinoyl chloride hydrochloride (1.45 g, 8.4 mmol); yield 1.1 g (66.0%). In the preparation of this compound, the diol[optical purity 81%, $[\alpha]_D^{25}$ +68.0° (*c* 0.98, acetone)] was used. $[\alpha]_D^{25}$ +9.28° (*c* 1.00, chloroform), ^{1}H-NMR (chloroform-d_1): δ=5.27 (2H, s, $-CH_2-$), 7.17—8.20 (16H, m, aromatic and pyridine protons), 8.50—9.20 (4H, m, pyridine).

(R)-2,2'-Bis(2-hydroxyethoxy)-1,1'-binaphthyl (R)-(13): To a solution of (*R*)-1,1'-bi-2-naphthol (**1**) (1.0 g, 3.5 mmol: $[\alpha]_D^{25}$ +31.9° (*c* 1.00, THF) in DMF (20 ml) was added NaH (390 mg, 8.13 mmol, 50% oil emulsion). The mixture was heated to 70 °C with stirring under nitrogen atmosphere. After 1 h, 2-chloroethyl tetrahydro-3-pyranyl ether (1.32 g, 8.02 mmol) was added. The reaction mixture was stirred at 70 °C for 48 h in a nitrogen stream, cooled and shaken with 100 ml of water. The mixture was extracted with dichloromethane, and the combined organic layer was washed with water, dried, and concentrated. To the residue, dichloromethane (50 ml), methanol (25 ml) and 7 drops of concd hydrochloric acid was added and stirred for 1 h at room temperature. The reaction mixture was neutralized with saturated sodium hydrogencarbonate solution, washed with water, dried over anhydrous sodium sulfate and concentrated. The residue was crystallized from benzene–hexane; yield 920 mg (70%), $[\alpha]_D^{25}$ −21.6° [7] (*c* 1.01, THF), ^{1}H NMR (chloroform-d_1): δ=2.30 (2H, br, -OH), 3.60 (4H, m, $-CH_2O-$), 4.13 (4H, m, $-OCH_2-$), 6.80—8.20 (12H, m, aromatic protons), MS *m/e* (M^+) 374.

(R)-2,2'-Bis[2-(3-pyridylcarbonyloxy)ethoxy]-1,1'-binaphthyl (R)-(14): (*R*)-(**14**) was prepared in a similar procedure to the preparation of (*S*)-(**8**) from (*R*)-(**13**) (2.74 g, 7.32 mmol) and nicotinoyl chloride hydrochloride (5.48 g, 30.8 mmol); yield 4.1 g (96.0%), $[\alpha]_D^{25}$ −50.58° (*c* 1.02, THF), ^{1}H-NMR (chloroform-d_1): δ=4.30 (8H, s, $-CH_2CH_2-$), 7.10—8.05 (16H, m, aromatic and pyridine protons), 8.66—9.00 (4H, m, pyridine), MS *m/e* (M^+) 584.

(S)-2,2'-Bis(3-pyridylcarbonylamino)-1,1'-binaphthyl (S)-(17): To a solution of nicotinoyl chloride hydrochloride (7.0 g, 39.3 mmol) in pyridine (100 ml), (*S*)-1,1'-bi-2-naphthylamine (**16**)[8] (4.85 g, 17.1 mmol) was added and heated at 80 °C for 1 h. After the period, the mixture was cooled, followed by addition of saturated sodium hydrogencarbonate solution. The mixture was extracted with chloroform and the organic layer was washed with brine, dried over anhydrous sodium sulfate, concentrated and the residue was crystallized from ethyl acetate–benzene to give pure (*S*)-(**17**); yield 6.20 g (73.5%), $[\alpha]_D^{25}$ −127.08° (*c* 1.008, chloroform), IR ν (cm^{-1}, KBr): 3300—3500 ν (N-H), 1680 ν (C=O), 680—820 δ (aromatic C-H), ^{1}H-NMR (chloroform-d_1): δ=7.0—8.7 (22H, m, aromatic and pyridine protons and NH).

The Preparation of Oxidized Forms (R)-(4), (S)-(7), (S)-(9), (R)-(12), (R)-(15), (S)-(18), (S)-(19), and (S)-(21). The bromides (*R*)-(**4**), (*S*)-(**7**), (*S*)-(**9**), (*R*)-(**12**), and (*R*)-(**15**) were prepared by the use of stoichiometric amount of benzyl bromide without solvent to avoid cleavage of ester linkage by solvolysis. The salt, (*S*)-(**18**) was prepared by heating with benzyl bromide in acetonitrile. These quaternized salts were submitted as such to the sodium dithionite reduction without further purification. The amide, (*S*)-(**17**) was quaternized with chloroacetamide by heating in acetonitrile for 30 min. The residue, (*S*)-(**19**) obtained by the distillation of the solvent was submitted as such to the reduction with sodium dithionite. The salt, (*S*)-(**21**), was prepared by heating a solution of (*S*)-2,2'-bis(bromomethyl)-1,1'-binaphthyl (**20**)[9] (1.1 g, 2.5 mmol) and nicotinamide (555 mg, 4.6 mmol) in DMF (20 ml) at 70 °C overnight. The reaction mixture was added dropwise into ethanol (100 ml) to give colorless precipitate which was washed with ether over phosphorus pentoxide; yield 1.69 g (93.6%).

General Preparation of 1,4-Dihydropyridines by the Reduction with Sodium Dithionite. i) Preparation of (R)-(1), (S)-(11), (S)-(111), (R)-(IV), and (R)-(V): The quaternized salt (6.0 mmol) was dissolved in DMF (10 ml) and the solution was added to 0.25 M (1 M = 1 mol dm^{-3}) sodium phosphate buffer (1 l, pH 7.0) containing sodium dithionite (147 mmol) and stirred at room temperature under nitrogen atmosphere. After 15 min, the flocculent material separated out of the solution was filtered, washed with water. The reductant was purified by silica-gel column chromatography with dichloromethane elution.

(R)-2-Methoxy-2'-(1-benzyl-1,4-dihydro-3-pyridylcarbonyloxy)-1,1'-binaphthyl (R)-(I); Yield 61.1% $[\alpha]_D^{25}$ +69.3° (*c* 1.03, acetonitrile), UV λ_{max} (acetonitrile): 360—361 nm (ε_{max} 8696), IR ν (cm^{-1}, KBr): 1700 ν (C=O), 680—820 δ (aromatic C-H), ^{1}H-NMR (chloroform-d_1): δ=2.90 (2H, m, pyr-C_4-2H), 3.80 (3H, s, $-OCH_3$), 4.03 (2H, s, $-CH_2Ph$), 4.76 (1H, m, pyr-C_5-H), 5.66 (1H, br, pyr-C_6-H), 6.50 (1H, m, pyr-C_2-H), 7.10—8.33 (22H, m, aromatic protons).

(S)-2-Benzyloxy-2'-(1-benzyl-1,4-dihydro-3-pyridylcarbonyloxy)-1,1'-binaphthyl (S)-(II); Yield 88.9%, $[\alpha]_D^{25}$ −67.4° (*c* 1.005, acetonitrile), UV λ_{max} (acetonitrile): 361 nm (ε_{max} 8584), IR ν (cm^{-1}, KBr): 1700 ν (C=O), 1600 ν (C=C), 1150 ν (C-O-C).

680—820 δ (aromatic C–H), ^{1}H-NMR (chloroform-d_1): δ= 2.86 (2H, m, pyr–C_4–2H), 3.85 (2H, s, –NCH_2Ph), 4.65 (1H, m, pyr–C_5–H), 5.00 (2H, s, –OCH_2Ph), 5.50 (1H, m, pyr–C_6–H), 6.30 (1H, m, pyr–C_2–H), 6.80—8.20 (22H, m, aromatic protons).

(S)-2, 2'-Bis(1-benzyl-1, 4-dihydro-3-pyridylcarbonyloxy)-1, 1'-binaphthyl(S)-(III); Yield 42.0%, $[\alpha]_D^{25}$ −9.6° (*c* 1.05, ethanol), UV λ_{max} (ethanol): 362 nm (ε_{max} 17167), IR ν (cm^{-1}, KBr): 1740 ν (C=O), 1595 ν (C=C), 660—890 δ (aromatic C–H), ^{1}H-NMR (chloroform-d_1): δ=2.73 (4H, m, pyr–C_2–2H), 3.96 (4H, s, –CH_2Ph), 4.63 (2H, m, pyr–C_5–H), 5.50 (2H, m, pyr–C_6–H), 6.50 (2H, m, pyr–C_2–H), 6.90—9.10 (22H, m, aromatic protons).

(R)-2, 2'-Bis(1-benzyl-1, 4-dihydro-3-pyridylcarbonyloxymethyl)-1, 1'-binaphthyl(R)-(IV); Yield 17.1%, $[\alpha]_D^{25}$ +42.54° (*c* 0.992, ethyl acetate), UV λ_{max} (ethyl acetate): 357 nm (ε_{max} 13570), ^{1}H-NMR (chloroform-d_1): δ=3.03 (4H, m, pyr–C_4–2H), 4.24 (4H, s, –CH_2Ph), 4.90 (4H, s, CH_2O–), 4.50—5.20 (2H, m, pyr–C_5–H), 5.67 (2H, m, pyr–C_6–H), 6.93 (2H, m, pyr–C_2–H), 7.00—8.20 (22H, m, aromatic protons).

(R)-Bis[2-(1-benzyl-1, 4-dihydro-3-pyridylcarbonyloxy)ethoxy]-1, 1'-binaphthyl (R)-(V); Yield 60.0%, $[\alpha]_D^{25}$ +56.4° (*c* 1.08, acetonitrile), UV λ_{max} (acetonitrile): 355 nm (ε_{max} 12530), IR ν (cm^{-1}, KBr): 1680 ν (C=O), 1600 ν (C=C), 700—840 δ (arcmatic C–H), ^{1}H-NMR (chloroform-d_1): δ=3.00 (4H, m, pyr–C_4–2H), 4.20 (8H, d, J=2 Hz, –CH_2CH_2–), 4.80 (2H, m, pyr–C_5–H), 5.73 (2H, m, pyr–C_6–H), 6.70 (2H, m, pyr–C_2–H), 7.10—8.10 (22H, m, aromatic protons).

ii) Preparation of (S)-(VI), (S)-(VII), and (S)-(VIII): To a solution of sodium hydrogencarbonate (230 ml) in water (634 ml) saturated with carbon dioxide up to pH 8.0, sodium dithionite (72.8 mmol) and the quaternized salt (3.79 mmol) in methanol (238 ml) were added and kept in the dark overnight. After the period, the solid separated material was filtered and dried over phosphorous pentoxide.

(S)-2, 2'-Bis(1-benzyl-1, 4-dihydro-3-pyridylcarbonylamino)-1, 1'-binaphthyl (S)-(VI); Yield 91.7%, $[\alpha]_D^{25}$ +112.2° (*c* 0.50, acetonitrile), UV λ_{max} (acetonitrile): 363 nm (ε_{max} 21162), ^{1}H-NMR (chloroform-d_1): δ=2.26 (4H, m, pyr–C_4–2H), 4.13 (4H, s, –CH_2Ph), 4.40 (2H, m, pyr–C_5–H), 5.53 (2H, m, pyr–C_6–H), 6.83 (2H, m, pyr–C_2–H), 6.90—8.15 (22H, m, aromatic protons).

(S)-2, 2'-Bis(1-carbamoylmethyl-1, 4-dihydro-3-pyridylcarbonylamino)-1, 1'-binaphthyl (S)-(VII); Yield 23.7%, $[\alpha]_D^{25}$ +74.73° (*c* 0.182, chloroform), UV λ_{max} (chloroform): 362 nm (ε_{max} 20370), ^{1}H-NMR (chloroform-d_1): δ=2.33 (4H, m, pyr–C_4–2H), 3.66 (4H, s, –CH_2–), 4.53 (2H, m, pyr–C_5–H), 5.65 (2H, m, pyr–C_6–H), 6.83 (2H, s, pyr–C_2–H), 7.20—8.50 (22H, m, aromatic protons).

(S)-2, 2'-Bis(3-carbamoyl-1, 4-dihydro-1-pyridylmethyl)-1, 1'-binaphthyl (S)-(VIII); Yield 55.9%, $[\alpha]_D^{25}$ −197.5° (*c* 0.99, dichloromethane), UV λ_{max} (dichloromethane): 356 nm (ε_{max} 12000), ^{1}H-NMR (chloroform-d_1): δ=2.27 (4H, m, pyr–C_4–2H), 3.97 (4H, s, –CH_2N), 4.60 (2H, m, pyr–C_5–H), 5.53 (2H, m, pyr–C_6–H), 5.60 (4H, s, NH_2), 6.67 (2H, d, J=2 Hz, pyr–C_2–H), 6.90—8.20 (12H, m, aromatic protons).

This work was supported in part by a Grant-in-Aid (No. 57560125) from the Ministry of Education, Science and Culture to which we are deeply grateful.

References

1) J. K. Whitesell and S. W. Felman, *J. Org. Chem.*, **42**, 1663 (1977).
2) R. Noyori, I. Tamino, and Y. Tanimoto, *J. Am. Chem. Soc.*, **101**, 3129 (1979).
3) H. Suda, S. Kanoh, N. Umeda, T. Nakajo, and M. Motoi, *Tetrahedron Lett.*, **1983**, 1513.
4) M. Seki, N. Baba, J. Oda, and Y. Inouye, *J. Am. Chem. Soc.*, **103**, 4613 (1981).
5) D. J. Cram and G. D. Y. Sogar, *J. Chem. Soc., Chem. Commun.*, **1981**, 625.
6) In the present paper, symmetry descriptions refer to formal presentations of the molecules rather than their true conformations.
7) R. Pummer, E. Prell, and A. Reiche, *Ber.*, 2159 (1926); E. P. Kyba, G. W. Gokel, F. Jong, K. Koga, L. R. Souga, M. G. Siegel, L. Kaplan, G. D. Y. Sogar, and D. J. Cram, *J. Org. Chem.*, **42**, 4713 (1977); J. Jacques, C. Fouquey, and R. Viterbo, *Tetrahedron Lett.*, **1971**, 4617.
8) P. Talalay and H. Lavy, "Steric Course of Microbiological Reactions Chiba, Foundation Group 2," Churchill, London (1959), pp. 53—78; S. Miyano, M. Tobita, and H. Hashimoto, *Bull. Chem. Soc. Jpn.*, **54**, 3522 (1981).
9) D. M. Hall and E. E. Turner, *J. Chem. Soc.*, **1955**, 1242.
10) Y. Ohnishi, M. Kagami, and A. Ohno, *J. Am. Chem. Soc.*, **97**, 4766 (1975); Y. Inouye. J. Oda, and N. Baba, *Kagaku No Ryoiki*, **36**, 585 (1982).
11) A. Ohno, H. Yamamoto, T. Kimura, S. Oka, and Y. Ohnishi, *Tetrahedron Lett.*, **1976**, 4585.
12) W. Tagaki, H. Sakai, Y. Yano, K. Ozeki, and Y. Shimizu, *Tetrahedron Lett.*, **1976**, 2541; A. Ohno, T. Kimura, H. Yamamoto, S. G. Kim, S. Oka, and Y. Ohnishi, *Bull. Chem. Soc. Jpn.*, **50**, 1535 (1977); A. Ohno, H. Yamamoto, T. Okamoto, S. Oka, and Y. Ohnishi, *ibid.*, **50**, 2385 (1977); M. Hughes and R. H. Prince, *J. Inorg. Nucl. Chem.*, **40**, 703 (1978); M. Hughes, R. H. Prince, and P. Wyeth, *ibid.*, **40**, 713 (1978); M. Hughes and R. H. Prince, *ibid.*, **40**, 719 (1978); K. Watanabe, R. Kawaguchi, and H. Kato, *Chem. Lett.*, **1978**, 255; R. A. Gase, U. K. Pandit, *J. Am. Chem. Soc.*, **101**, 7059 (1979); A. Ohno, J. Nakai, K. Nakamura, T. Goto, and S. Oka, *Bull. Chem. Soc. Jpn.*, **54**, 3482 (1981); j) H. Siegel and R. B. Martin, *Chem. Rev.*, **82**, 385 (1982); S. Fukuzumi, Y. Kondo, and T. Tanaka, *Chem. Lett.*, **1983**, 485.
13) R. Roger, *J. Chem., Soc.*, **1932**, 2168.

The Base-catalyzed Condensation Reaction of Dimethyl Malonate with 5-Chloro-2-methoxytropone and 2,5-Dichlorotropone. On the Solvent Effect for the Sites of the Reaction[1)]

Tetsuo NOZOE,*,† Hitoshi TAKESHITA,*,†† and Kozo TAJIRI††
Faculty of Science, Tohoku University, Sendai 980
††*Research Institute of Industrial Science, 86, Kyushu University, Sakamoto, Kasuga, Fukuoka 816*
(Received June 16, 1983)

The sites of the nucleophilic attack of the base-catalyzed condensation of dimethyl malonate with 5-chloro-2-methoxytropone were solvent-dependent; the normal substitution product was predominant in benzene, but the *ciné*-substitution products were exclusive in methanol. With 2,5-dichlorotropone, the *ciné*-reaction products were exclusive in both solvents.

One of the most remarkable features on the nucleophilic substitution reaction of troponoid chemistry is a frequent occurrence of the abnormal substituion, or *ciné*-reaction,[2,3)] which means a reaction in which the leaving group on the aromatic ring is not located on the attacking site of the nucleophile. To date, many examples of such reactions have been recorded.[4)] This fundamental feature is important in order to understand the complicated mode of ring-closure in the azulene synthesis from the reactive troponoids.[5,6)] The condensation of troponoids with dimethyl malonate or ethyl acetoacetate is known to give, in the *ciné*- and/or normal mode, oxazulanones, 2*H*-cyclohepta[*b*]furan-2-ones,[7)] while, the methyl cyanoacetate and malononitrile, cyano derivatives, are known to give the functionalized azulene derivatives as major products.[8)] Moreover, the syntheses of the azulene derivatives from oxazulanones have been developed; *i.e.*, the consecutive condensation of some oxazulanones with active methylene derivatives[9)] and heating with various enamines.[10)] In view of the capability of introducing various kinds of functional groups to both five- and seven-membered rings of azulenes, these make the oxazulanones important as the starting materials. This paper will describe the solvent dependency of the *ciné*-reaction encountered in the formation of 2*H*-cyclohepta[*b*]furan-2-ones from 5-chlorotropolone derivatives, 5-chloro-2-methoxytropone (**1**) and 2,5-dichlorotropone (**2**), with dimethyl malonate.

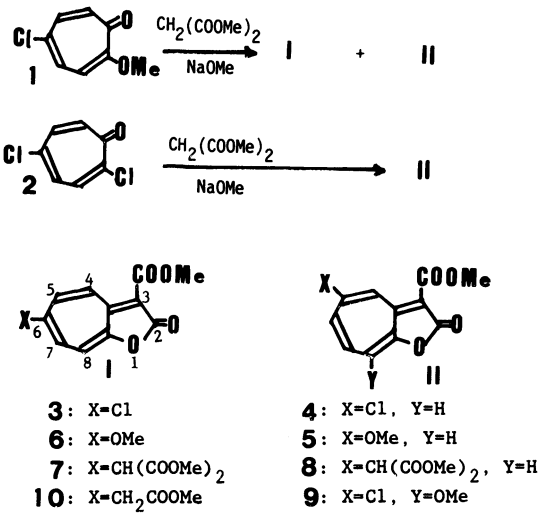

3: X=Cl
6: X=OMe
7: X=CH(COOMe)$_2$
10: X=CH$_2$COOMe
4: X=Cl, Y=H
5: X=OMe, Y=H
8: X=CH(COOMe)$_2$, Y=H
9: X=Cl, Y=OMe

Scheme 1.

First of all, when a methanol solution of **1** was allowed to react with dimethyl malonate in the presence of sodium methoxide, a somewhat complicated reaction with a time-dependent product distribution occurred at 30 °C. After separation of the product mixture by the silica-gel column or high-pressure liquid chromatography, **3**—**10** were isolated and characterized. A minor product, **3**, was shown to be 6-chloro-3-methoxycarbonyloxazulanone (I: X=Cl) on the basis of the ^{1}H-NMR spectroscopy, and **4** was also identified to be 5-chloro-3-methoxycarbonyloxazulanone (II: X=Cl, Y=H). On the other hand, the major product, **5** (47%), was halogen-free, and its ^{1}H-NMR spectrum revealed a signal of another methoxyl group, introduced by a nucleophilic attack; it was the major product when the reaction was continued for a prolonged period, up to 8 h. In fact, **5** could be prepared from **4** by sodium methoxide at room temperature.

Therefore, **5** is 5-methoxy-3-methoxycarbonyloxazulanone (II: X=MeO, Y=H). Similarly, **6** was shown to be 6-methoxy-3-methoxycarbonyloxazulanone (I: X=MeO) by chemical correlation with **3**, and **7** and **8** correspond to the malonic ester derivatives from **3** and **4** (I and II: X=CH(COOMe)$_2$, Y=H).

The structure of **9** was determined to be 5-chloro-8-methoxy-3-methoxycarbonyloxazulanone (II: X=Cl, Y=OMe) by its mass spectrum [*m/e*, 268, 270 (M$^+$, $C_{12}H_9O_5Cl$)] and the ^{1}H-NMR analysis: A low-field signal at δ 9.09 indicated the presence of a chlorine atom at C-5, and its broadened shape due to a long-range coupling indicated the presence of a hydrogen atom at C-6. This was further confirmed by comparison of the chemical shifts of C-7 proton with **6** [δ=6.79 (dd, J=11, 2.5 Hz)]; therefore, another methoxyl group of **9** is at the C-8.

The remaining product, **10**, is the monodecarboxylated derivative of **7** (I: X=CH$_2$COOMe).

The base-catalyzed condensation reaction of **1** with dimethyl malonate in benzene solution was slower than that in methanol, and the product distribution was considerably different. The major product in this case was the normal condensate, **3** (64%), which was

† Present address: 2-5-1-811, Kamiyoga, Setagaya-ku, Tokyo 158.

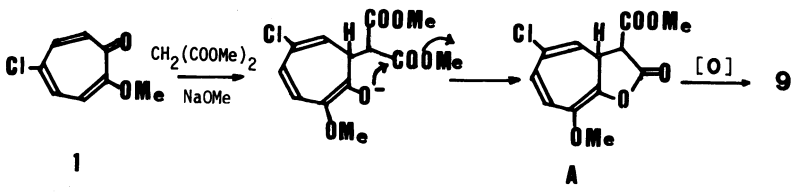

Scheme 2.

TABLE 1. THE PRODUCT DISTRIBUTIONS (YIELD/%) OF THE CONDENSATION REACTION OF 1 AND 2 TO DIMETHYL MALONATE IN VARIOUS SOLVENTS

Products	Normal condensates (I)				*ciné*-Condensates (II)				Recovered
	Cl (3)	OMe (6)	$CH(COOMe)_2$ (7)	CH_2COOMe (10)	Cl (4)	OMe (5)	$CH(COOMe)_2$ (8)	Cl, Y=OMe (9)	(1)
1 in Methanol	3	7	2	1	7	47	3	5	18
1 in Benzene	64		7		11			3	24
1 in Benzene-Ether	47		1		11	3			24
2 in Methanol					62	16			17
2 in Benzene					65		3		8
2 in Benzene-Ether					65	2			5

TABLE 2. THE ^1H NMR SPECTRA OF CYCLOHEPTA [*b*] FURANONES

Compd δ_n	3	4	5	6	7	8	9	10
δ_4	8.68	8.87	8.40	8.80	8.77	8.83	9.09	8.87
δ_5	7.58	(Cl)	(OMe)	7.39	7.63	(Malonyl)	(Cl)	7.53
δ_6	(Cl)	7.33	7.2	(OMe)	(Malonyl)	7.41	7.29	(CH_2COOMe)
δ_7	7.55	7.33	7.2	6.74	7.49	7.41	6.79	7.37
δ_8	7.23	7.33	7.2	7.42	7.36	7.41	(OMe)	7.37
δ_{Me}	3.93	3.91	3.90 4.00	3.92(6H)	3.80(6H) 3.93	3.80(6H) 3.93	3.92 4.17	3.74 3.93
δ_{R-H}					4.61(1H)	4.76(1H)		3.70(2H)
J_{4-5}	12.5	—	—	12.5	12.5	—	—	12.0
J_{6-7}	—	a)	a)	—	—	a)	11.0	—
J_{7-8}	10.5	a)	a)	11.0	10.0	a)	—	—
J_{4-6}	—	1.0	2.5	—	—	a)	—	—
J_{5-7}	2.0	—	—	3.0	1.5	—	2.5	a)

a) By first-order analysis the coupling constants could not be determined, due to overlapping of signals.

accompanied by **4**, **7**, and **9**. Formation of a chloro methoxy derivative, **9**, in this inert solvent can be explained only in terms of the *ciné*-reaction *via* intermediary adduct **A** which was followed by an auto-oxidative dehydrogenation. An alternative explanation, *i.e.*, a nucleophilic introduction of methoxyl group on the C-8 position of **4** followed by a dehydrogenation, is not true since, as mentioned above, **4** was exclusively converted to **5**. Such a behavior has precedence in the condensation of 2-(*p*-tolylsulfonyloxy)tropone with some active methylene reagents.[11]

Furthermore, the product distribution in the reaction of **2** in a mixed solution of benzene–ether (1 : 1)[12] revealed an intermediary figure to those in methanol and in benzene. Occurrence of **3**—**5**, and **7** was directly confirmed by isolations.

Subsequently, the same reaction was carried out with **2** and dimethyl malonate. In methanol, the major product was **4** (62%) which was accompanied by a minor product, **5** (16%). No other compound was detected other than the recovered tropone, **1** (17%); the condensation thus occurred exclusively with the *ciné* mode. The reaction in benzene also produced the *ciné*-reaction products, **4** (65%) and **8**, together with the recovered **1** (8%). As expected, the reaction in a mixed solution of benzene–ether disclosed similar features to the results obtained from the reaction in methanol; it gave **4** (65%) and **5**.

Therefore, the results disclosed a solvent dependence in the reaction of **1** and dimethyl malonate, where the *ciné*-reaction was favored in the protic solvent, but in nonpolar aprotic solvent the normal substitution reaction was predominant. On the other hand, the reaction of **2** and dimethyl malonate exclusively gave the *ciné*-reaction products in every case.

Consequently, the reaction of **1** and dimethyl malonate is solvent-dependent; in methanol, the predominant process was the *ciné*-reaction, but in benzene, the reverse was true. It is known that in many cases encountered in the troponoid field, thoroughly different product distributions have arisen from slightly different reaction conditions; therefore, one must be careful in

drawing conclusions based on a single fact. However, in the present case, it is certain that the nature of solvents decided the course of the reaction. In methanol, the nucleophile, dimethyl sodiomalonate, should be tightly solvated, while, in benzene the reagent is rather naked. As results, nucleophilic attack by the solvated bulky reagent to C-2 position, the substituted site, might become unfavorable due to a steric hindrance.

The reaction of **2** with dimethyl malonate always proceeded in the exclusive *ciné*-mode.

The case-catalyzed condensation of **1** and **2** with other active methylene compounds, methyl acetoacetate and methyl *p*-nitrophenylacetate, gave other interesting features; these results will be presented in an independent paper.

Experimental

Throughout the study, the NMR spectra were measured by a JEOL FX-100 Model spectrometer in $CDCl_3$ solutions unless otherwise mentioned, and the chemical shifts were expressed in the δ unit from the internal standard, TMS. The UV spectra were measured in methanol solutions using a Hitachi Model 124 spectrometer. The IR spectra were measured with a JASCO Model A-102 spectrometer in either CCl_4 solutions or with KBr disks. High-resolution mass spectra were taken by JEOL OlSG Model spectrometer, and the figures were obtained by visual reading on the photographic plates.

*The Condensation Reaction of 5-Chloro-2-methoxytropone (**1**) and Dimethyl Malonate in Methanol.* Anhydrous methanol (25 cm³) containing dimethyl malonate (775 mg), NaOMe (285 mg) and **1** (500 mg) was warmed to 30 °C with stirring. The reaction was monitored by an occasional check of high-pressure liquid chromatogram (polasil T/ethyl acetate–hexane). After 8 h, the solvent was removed by evaporation, and the residue was neutralized with dil HCl and chromatographed on a silica-gel column to give three fractions of product mixture: From benzene–ether (80 : 20), a mixture of **3** and **4** (**a**, yellow solid, 59 mg), was at first eluted, and subsequently, a mixture of **5**, **8**, and **7** (**b**, yellow solid, 307 mg), was obtained; from the latest fractions, a mixture of **6**, **9**, and **10** (**c**, yellow solid, 77 mg), was obtained together with recovered **1** (89 mg).

Further fractionation of these products was performed by high-pressure liquid chromatography (micropolasil/ethyl acetatehexane): Thus, from the fraction **a**, analytical samples of **3**, 6-chloro-3-methoxycarbonyloxazulanone (yellow needles; mp 250—251 °C [Found: C, 55.18; H, 2.94%. Calcd for $C_{11}H_7O_4Cl$: C, 55.37; H, 2.96%. δ(C) = 51.9, 116.5, 129.3, 134.4, 140.7, 145.8, 153.0, 157.3, 163.5, and 164.4], 20 mg (3%)), and **4**, 5-chloro-3-methoxycarbonyloxazulanone (yellow needles; mp 172—173 °C [Found: C, 54.95; H, 2.98%. δ(C) = 51.8, 97.0, 117.4, 129.0, 135.1, 135.3, 147.8, 151.5, 158.5, 163.3, and 169.3], 38 mg (7%)) were isolated.

Similarly, analytical samples of **5**, **8**, and **7** were isolated from the fraction **b**, and showed the following properties: **5**, 5-methoxy-3-methoxycarbonyloxazulanone (yellow needles; mp 200—201 °C [Found: C, 61.47; H, 4.05%. Calcd for $C_{12}H_{10}O_5$: C, 61.54; H, 4.03%. δ(C) = 51.5, 56.6, 94.1, 108.1, 115.1, 129.3, 134.3, 153.7, 157.3, 164.8, 165.2, and 168.4], 265 mg (47%)), **8**, 3-methoxycarbonyl-5-[bis(methoxycarbonyl)methyl]oxazulanone (yellow needles; mp 181.5—182 °C [Found: C, 57.44; H, 4.18%; M.W., 334.0647. Calcd for $C_{16}H_{14}O_8$: C, 57.49; H, 4.22%; M. W., 334.0689], 27 mg (3%)), and **7**, 3-methoxycarbonyl-6-[bis(methoxycarbonyl)-methyl]oxazulanone (yellow crystals; mp 170—171 °C[Found: C, 57.35; H, 4.28%; M. W., 334.0652], 14 mg (2%)).

Preparative thin-layer chromatography (PTLC) of the fraction **c** gave **9**, 5-chloro-8-methoxy-3-methoxycarbonyloxazulanone (yellow needles; mp 231—232 °C [Found: C, 53.54; H, 3.37%; M. W., 268.0148. Calcd for $C_{12}H_9O_5Cl$: C, 53.65; H, 3.38%; M. W., 268.0139], 30 mg (5%)), **10**, 3-methoxycarbonyl-6-(methoxycarbonylmethyl)oxazulanone (yellow needles; mp 170—171 °C [Found: C, 60.80; H, 4.28%; M. W., 276.0615. Calcd for $C_{14}H_{12}O_6$: C, 60.87; H, 4.38%; M. W., 276.0634], 7 mg (1%), and **6**, 6-methoxy-3-methoxycarbonyloxazulanone (yellow crystals; mp 250—251 °C [Found: C, 61.44; H, 4.09%. Calcd for $C_{12}H_{10}O_5$: C, 61.54; H, 4.30%], 38 mg (7%)).

*The Condensation Reaction of **1** and Dimethyl Malonate in Benzene.* An anhydrous benzene (25 cm³) solution of dimethyl malonate (775 mg), NaOMe (285 mg), and **1** (500 mg) was warmed at 30 °C with stirring. After 8 h, the solvent was removed *in vacuo* at room temperature, and the residue was extracted with chloroform and dil HCl. The organic extracts were chromatographed on a silica-gel column to give a mixture of **3** and **4** (417 mg), **7** (48 mg; 7%), **9** (20 mg; 3%), and the unreacted **1** (120 mg; 24%). Separation of **3** and **4** was made by repeated silica-gel column chromatography; the yields were 340 mg (64%) for **3**, and 65 mg (11%) for **4**.

*The Condensation of **1** and Dimethyl Malonate in a Mixture of Benzene and Ether.* NaOMe (120 mg) and dimethyl malonate (375 mg) were dissolved in anhydrous ether (20 cm³) and mixed with benzene solution (20 cm³) of **1** (350 mg) and kept at 30 °C for 8 h. The mixture was then treated with dil HCl, and extracted with ethyl acetate. The organic extracts were chromatographed on a silica-gel column to give a yellow solid, **3** (175 mg; 47%), **4** (40 mg; 11%), **5** (9.5 mg; 3%), **7** (4.5 mg; 1%), and the recovered **1** (85 mg; 24%).

*The Condensation of 2,5-Dichlorotropone (**2**) with Dimethyl Malonate in Methanol.* A methanol solution (50 cm³) of **2** (505 mg, NaOMe (280 mg), and dimethyl malonate (450 mg) was kept at 30 °C for 8 h, although disappearance of **2** was already recognized after 1.5 h on a high-pressure liquid chromatogram. After evaporation of the solvent *in vacuo* at room temperature, the residue was treated with dil HCl, and extracted with ethyl acetate. Silica-gel column chromatography of the mixture afforded **4** (245 mg; 62%), **5** (90 mg; 16%), and the recovered **1** (60 mg; 17%).

*The Condensation of **2** with Dimethyl Malonate in Benzene.* Anhydrous benzene (50 cm³) containing dimethyl malonate (300 mg), NaOMe (110 mg), and **2** (200 mg) was kept at 30 °C for 8 h. The reaction was somewhat slower than in methanol; it took 4 h to consume **2**. The mixture was washed with dil HCl and extracted with ethyl acetate. Silica-gel column chromatography of the mixture afforded **4** (165 mg; 65%) and **8** (10 mg; 3%), along with **1** (15 mg; 8%).

*The Condensation of **2** and Dimethyl Malonate in a Mixture of Benzene and Ether.* To an anhydrous ether solution (20 cm³) of dimethyl malonate (375 mg) and NaOMe (110 mg), a benzene solution (20 cm³) of **2** (230 mg) was added at once, and kept at 30 °C for 8 h. The mixture was then acidified by dil HCl, and extracted with ether. The silica-gel column chromatography of the mixture gave **4** (280 mg; 65%), and **5** (8 mg; 2%), together with **1** (15 mg; 4.5%).

*The Further Conversion of **4** into **5**.* A Methanol solution (10 cm³) containing **4** (10 mg) and NaOMe (2 mg) was kept at room temperature for 24 h. The mixture was diluted with aqueous HCl and extracted with ether. The NMR analysis of the organic fractions confirmed the presence of **5**, but of no other product.

*The Conversion of **3** to **6**.* A methanol solution (10 cm³) of **3** (15 mg) was similarly treated with NaOMe (2 mg) for 24 h. The NMR analysis of the product confirmed the

exclusive formation of **6**.

*Formation of **8** from **4**.* A benzene solution (5 cm^3) of **4** (20 mg) was treated with **2** (50 mg) and NaOMe (1 mg) at 30 °C for 8 h. From the mixture, only **8**, 6 mg, was separated by PTLC.

*Formation of **7** from **3**.* A benzene solution (5 cm^3) of **3** (10 mg) and **2** (20 mg) with NaOMe (1 mg) was heated at 30 °C for 8 h. The mixture was fractionated by means of PTLC to afford **7** (4 mg). No other compound was detectable.

References

1) The major part of the study was carried out more than two decades ago, but it has not been published yet. We wish to report the results of the repeated experiments at Kyushu University with newly determined physicochemical data.

2) T. Nozoe, S. Seto, and T. Sato, *Proc. Jpn. Acad.*, **30**, 473 (1954); R. D. Howorth and P. B. Tenker, *J. Chem. Soc.*, **1955**, 911; Y. Kitahara, *Sci. Repts. Tohoku Univ., Ser. I*, **39**, 250, 258 (1956); T. Sato, *Nippon Kagaku Zasshi*, **80**, 1056, 1058, 1067, and 1071 (1969).

3) The term "*ciné*"-substitution first appeared in a review article on nucleophilic substitution by J. F. Bunnett and R. E. Zahler (*Chem. Rev.*, **49**, 273 (1951)).

4) Y. Kitahara, *Sci. Repts. Tohoku Univ., Ser. I*, **40**, 74 (1956); T. Nozoe, S. Seto, S. Matsumura, and Y. Murase, *Bull. Chem. Soc. Jpn.*, **35**, 1179 (1962); S. Itô, J. Tsunetsugu, T. Kanno, H. Sugiyama, and H. Takeshita, *Tetrahedron Lett.*, **1965**, 3659; G. Biggi, F. D. Cima, and F. Pietra, *J. Am. Chem. Soc.*, **95**, 7101 (1973); F. Pietra, *J. Chem. Soc., Chem. Commun.*, **1974**, 501; H. Takeshita, A. Mori, T. Minami, and H. Kondo, *Heterocycles*, **14**, 793 (1980). See also reviews: T. Nozoe, K. Takase, and H. Matsumura, "Non-Benzenoid Aromatic Compounds" in "Dai Yuki Kagaku (Comprehensive Organic Chemistry)," ed by M. Kotake, Asakura, Publ., Tokyo (1955), Vol. 13, pp. 178—213; T. Nozoe, "Chemistry of Non-Benzenoid Aromatic Compounds," ed by D. Ginsberg, Interscience Publ., Amsterdam (1959), pp. 39—464.

5) T. Nozoe, S. Matsumura, Y. Murase, and S. Seto, *Chem. Ind. (London)*, **1955**, 1257; T. Nozoe, S. Seto, S. Matsumura, and T. Asano, *Proc. Jpn. Acad.*, **32**, 339 (1956); T. Nozoe, S. Seto, and S. Nozoe, *ibid.*, **32**, 472 (1956).

6) In general, 2-methoxytropone derivatives are known to give the normal reaction products, on the other hand, 2-halogenotropones and 2-(*p*-tolysulfonyloxy)tropones are known to give the *ciné*-reaction products. However, nucleophilicity and bulkiness of reagents as well as substitution patterns of the troponoid ring can not be neglected as controlling factors.

7) T. Nozoe, S. Seto, and S. Matsumura, *Proc. Jpn. Acad.*, **28**, 483 (1952); S. Seto, *Sci. Repts. Tohoku Univ., Ser. I*, **37**, 367 (1953); T. Sato, *Nippon Kagaku Zasshi*, **80**, 1342, 1345, 1347, and 1349 (1959).

8) T. Nozoe, S. Seto, K. Takase, S. Matsumura, and T. Nakazawa, *Nippon Kagaku Zasshi*, **86**, 346 (1965).

9) T. Nozoe, K. Takase, and N. Shimazaki, *Bull. Chem. Soc. Jpn.*, **37**, 1644 (1964); T. Nozoe, K. Takase, and S. Fukuda, *ibid.*, **44**, 2210 and 2215 (1971).

10) P. W. Yang, M. Yasunami, and K. Takase, *Tetrahedron Lett.*, **1971**, 4275; M. Yasunami, A. Chen, P. W. Yang, and K. Takase, *Chem. Lett.*, **1980**, 579; K. Takase and M. Yasumi, *Yuki Gosei Kagaku Kyokai Shi*, **39**, 1172 (1981).

11) T. Nozoe, K. Takase, M. Kato, and T. Nogi, *Tetrahedron*, **27**, 6023 (1971).

12) This rather odd solvent system was primarily employed in order to prevent the freezing of the reaction mixture in our refrigerator.

Constituents of the Root Bark of *Ailanthus altissima* SWINGLE. Isolation and X-Ray Crystal Structures of Shinjudilactone and Shinjulactone C and Conversion of Ailanthone into Shinjudilactone[1]

Masami ISHIBASHI, Takahiko TSUYUKI, Tatsushi MURAE, Hiroshi HIROTA, Takeyoshi TAKAHASHI,* Akiko ITAI,† and Yoichi IITAKA†

Department of Chemistry, Faculty of Science, The University of Tokyo, Hongo, Bunkyo-ku, Tokyo 113

†*Department of Pharmaceutical Sciences, The University of Tokyo, Hongo, Bunkyo-ku, Tokyo 113*

(Received June 23, 1983)

Two new quassinoids, shinjudilactone and shinjulactone C were isolated from the root bark of *Ailanthus altissima* SWINGLE and their structures were established to be 1β,11α-dihydroxy-2,16-dioxo-13(12→11α)*abeo*-picras-3-en-12,20-olide and 1α,12α : 5α,13α-dicyclo-1β,12β,20-trihydroxy-9β*H*-picras-3-ene-2,11,16-trione, respectively, by X-ray diffraction analysis. Shinjudilactone was prepared from ailanthone by benzilic acid rearrangement.

Quassinoids, bitter principles isolated from Simaroubaceous plants, have been extensively investigated from the interest in anti-tumor activity and structure determination,[2] and some of them have been shown to exhibit useful biological activities.[3] Recently these quassinoids have attracted much attention as synthetic target molecules.[4]

In Japan there grow two species of plants belonging to Simaroubaceae, *Picrasma ailanthoides* PLANCHON (=*P. quassioides* BENN, Japanese name : Nigaki) and *Ailanthus altissima* SWINGLE (=*A. glandulosa* DESF., Japanese name: Shinju or Niwaurushi) and these plants are known to contain bitter principles in leaves, barks, trunks, and roots. The bitter principles of *P. ailanthoides* have been investigated by us[2b] and by Takemoto *et al.*[5] and more than twenty quassinoids have been isolated. As a continuation of our work on bitter principles of Simaroubaceous plants in Japan, we examined the bitter principles of *A. altissima*. We wish to report on the X-ray crystal structures of new quassinoids, shinjudilactone (**1**) and shinjulactone C (**2**) isolated from root barks of the plant.

The half-dried root bark of *A. altissima*, defatted with petroleum ether, was continuously extracted with ethyl acetate and the extract was separated to afford seven

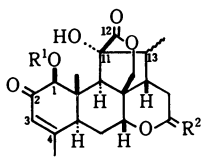

1 R^1=H, R^2=O; 13α-CH_3

5 R^1=CH_3, R^2=O; 13α-CH_3

6 R^1=Ac, R^2=O; 13α-CH_3

7 R^1=H, R^2=H,OH; 13α-CH_3

12 R^1=H, R^2=O; 13β-CH_3

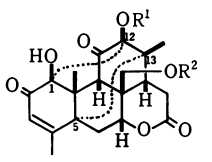

2 R^1=R^2=H

8 R^1=H, R^2=Ac

9 R^1=R^2=Ac

10 R^1=H, R^2=C(=O)H

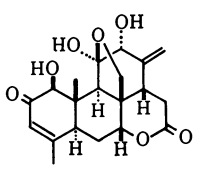

3

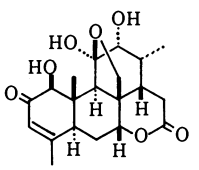

4

Concentrated aqueous extract of the root bark of this plant was continuously extracted with dichloromethane. The organic layer was evaporated to give a residue, which was subjected to separation by silica-gel column chromatography to afford two new quassinoids, shinjudilactone (**1**) and shinjulactone C (**2**) in 0.01% and 0.001% yields, respectively, together with known chaparrolide,[15] chaparrinone (**4**),[16] shinjulactone B,[17] amarolide, ailanthone (**3**), glaucarubinone, and $\Delta^{13(18)}$-dehydroglaucarubolone.

Shinjudilactone (**1**), a bitter quassinoid, crystallized from ethyl acetate-methanol as colorless needles, mp 274—276 °C and $[\alpha]_D^{23}$ +102° (pyridine). Elemental analysis and high-resolution mass spectrum indicate the formula $C_{20}H_{24}O_7$. The spectral examination showed the presence of hydroxyl(s) (IR 3250 cm^{-1}), two carbonyls (ester or lactone moieties) (IR 1745 and 1735 cm^{-1}; ^{13}C NMR δ 170.6 and 173.5), a proton at the lactone terminus (^1H NMR δ 4.808, t), an α,β-unsaturated ketone (IR 1670 cm^{-1}; UV 238 nm; ^{13}C NMR δ 196.9), a tertiary methyl, a secondary methyl, and a vinyl methyl (^1H NMR δ 1.235, s, δ 1.240, d, and δ 1.798, br s, respectively).

On methylation with diazomethane, shinjudilactone (**1**) gave *O*-methylshinjudilactone (**5**), mp 291—294 °C, which still showed an absorption band at 3400 cm^{-1} due to a hydroxyl group, indicating the presence of two hydroxyl groups for **1**. Treatment of **1** with acetic anhydride and pyridine at room temperature gave a monoacetate (**6**), which showed a singlet signal at δ 5.78 due to a proton attached to the acetoxy-bearing carbon atom and an IR absorption band due to a hydroxyl group at 3480 cm^{-1}. The hydroxyl group was shown to be tertiary, because no diacetate was produced by acetylation under drastic conditions. Shinjudilactone (**1**) was reduced with sodium borohydride to afford a hemiacetal (**7**), which showed a multiplet signal due to a hemiacetal-methine proton at δ 5.68. The IR spectrum (1740 cm^{-1}) of **7** showed a lactone grouping still remained intact, indicating that **1** possesses two lactone groupings. Seven oxygen atoms of **1** were thus

Table 1. ^{13}C NMR Spectra of shinjudilactone (**1**)[a] and chaparrinone (**4**)[b]

Position number of carbon	1	4	Position number of carbon	1	4
1	83.8d	82.5	11	78.7s	108.9
2	196.9s	197.1	12	173.5s	77.9
3	126.3d	124.7	13	45.6d	30.4
4	162.0s	162.3	14	53.6d	41.1
5	42.2d	43.1	15	32.9t	29.4
6	27.0t	25.0	16	170.6s	167.6
7	73.9d	77.6	18	22.1q	22.1
8	48.4s	44.9	19	10.6q	9.4
9	55.0d	41.1	20	76.2t	70.1
10	43.0s	44.3	21	13.8q	12.5

a) Measured in a pyridine-d_5 solution. b) Measured in a dimethyl-d_6 sulfoxide solution (Ref. 16b).

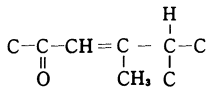

A

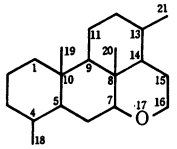

B

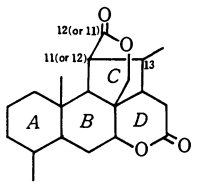

C

characterized. These findings indicate pentacyclic skeleton for **1**.

^1H NMR spectrum of shinjudilactone (**1**) showed that an olefinic proton resonating at δ 6.095 is coupled with a vinyl methyl and also with a methine proton at an allylic position with a coupling constant J=2.5 Hz, the presence of the same partial structure (**A**) as that of chaparrinone (**4**) being suggested for **1**. The assignment of signals in the ^{13}C NMR spectrum of **1** was carried out by comparison with signals of **4**[16b] (Table 1). It is inferred that the easily reducible lactone grouping should be located in the D ring[18] and the other one in the C ring. Shinjudilactone (**1**) could not be formulated based on the normal picrasane skeleton (**B**),[19] but should possess a migrated picrasane skeleton, a 13(12→11α) or 9(11→12)*abeo*-picrasane dilactone structure (**C**). Formation of **1** from ailanthone (**3**) could be reasonably explained by biogenetic consideration (*vide infra*).

Unambiguous proof for the proposed structure (**1**) of shinjudilactone was provided by X-ray diffraction analysis. The crystal of **1** belongs to a monoclinic space group $P2_1$ with the cell parameters of a=7.446(2), b=18.241(8), c=6.679(2) Å, and β=109.39(6)°. There are two molecules in the unit cell. Intensity data were collected on a Philips PW1100 automatic four-circle diffractometer using monochromated Cu $K\alpha$ radiation. A total of 1739 independent structure factors with $F_o \geq 2.5\ \sigma(F_o)$ within 2θ=156° were obtained by the 2θ-θ scanning mode. The structure was solved by the direct method using MULTAN program. An E-map revealed the positions of all the non-hydrogen atoms, and the hydrogen atoms were located in a difference electron density map. The structure was refined by the block-diagonal least-squares calculations

Table 2. Atomic positional parameters ($\times 10^4$) and isotropic temperature factor ($\times 10^2$) for non-hydrogen atoms of shinjudilactone (**1**) with estimated standard deviations in parentheses

Atom	x	y	z	B_{eq}[a]
C(1)	2375(4)	2285(0)	957(4)	357(4)
C(2)	2273(4)	1485(2)	1613(5)	478(4)
C(3)	4040(4)	1143(2)	2949(5)	514(4)
C(4)	5764(4)	1455(1)	3356(4)	432(4)
C(5)	5930(4)	2220(1)	2545(4)	311(3)
C(6)	7903(4)	2394(1)	2383(4)	347(4)
C(7)	8119(3)	3201(1)	1976(4)	245(3)
C(8)	6500(3)	3494(1)	99(4)	246(3)
C(9)	4557(3)	3274(1)	297(3)	212(3)
C(10)	4245(3)	2429(1)	485(4)	280(3)
C(11)	3300(3)	3804(1)	-1355(3)	278(3)
C(12)	3402(3)	3667(2)	-3586(4)	289(4)
C(13)	4313(3)	4555(1)	-585(4)	339(3)
C(14)	6454(3)	4350(1)	-38(4)	271(3)
C(15)	7911(4)	4701(2)	1918(4)	270(4)
C(16)	8154(3)	4306(1)	3957(4)	261(4)
C(18)	7536(5)	1083(2)	4739(5)	555(5)
C(19)	4179(4)	1952(2)	-1456(4)	307(4)
C(20)	6687(3)	3223(2)	-1980(4)	304(4)
C(21)	3723(5)	4893(2)	1197(5)	484(5)
O(1)	714(3)	2409(1)	-810(4)	428(3)
O(2)	764(3)	1150(1)	1024(5)	650(5)
O(3)	1378(2)	3802(1)	-1423(3)	365(2)
O(4)	2095(3)	3809(1)	-5172(3)	407(3)
O(5)	8458(3)	4611(1)	5659(3)	360(3)
O(6)	8092(2)	3576(1)	3903(2)	243(2)
O(7)	5031(2)	3422(1)	-3794(3)	349(3)

a) $B_{eq}=8\pi^2(u_1^2+u_2^2+u_3^2)/3$.

Tbale 3. Bond lengths of shinjudilactone (**1**) with estimated standard deviations in parentheses

Bond length		l/Å	Bond length		l/Å
Atom 1	Atom 2		Atom 1	Atom 2	
C(1)	-C(2)	1.534(3)	C(9)	-C(10)	1.570(3)
C(1)	-C(10)	1.549(4)	C(9)	-C(11)	1.530(3)
C(1)	-O(1)	1.416(3)	C(10)	-C(19)	1.549(4)
C(2)	-C(3)	1.461(4)	C(11)	-C(12)	1.537(4)
C(2)	-O(2)	1.223(4)	C(11)	-C(13)	1.567(4)
C(3)	-C(4)	1.347(4)	C(11)	-O(3)	1.416(3)
C(4)	-C(5)	1.517(4)	C(12)	-O(4)	1.205(3)
C(4)	-C(18)	1.498(4)	C(12)	-O(7)	1.343(3)
C(5)	-C(6)	1.541(4)	C(13)	-C(14)	1.558(4)
C(5)	-C(10)	1.570(3)	C(13)	-C(21)	1.529(5)
C(6)	-C(7)	1.516(4)	C(14)	-C(15)	1.534(3)
C(7)	-C(8)	1.519(3)	C(15)	-C(16)	1.497(4)
C(7)	-O(6)	1.464(3)	C(16)	-O(5)	1.217(3)
C(8)	-C(9)	1.548(4)	C(16)	-O(6)	1.332(3)
C(8)	-C(14)	1.564(4)	C(20)	-O(7)	1.459(3)
C(8)	-C(20)	1.523(4)			

TABLE 4. BOND ANGLES OF SHINJUDILACTONE (**1**) WITH ESTIMATED STANDARD DEVIATIONS IN PARENTHESES

Bond angle			ϕ/°	Bond angle			ϕ/°
Atom 1	Atom 2	Atom 3		Atom 1	Atom 2	Atom 3	
C(2)	-C(1)	-C(10)	110.6(2)	C(19)	-C(10)	-C(5)	113.0(2)
C(2)	-C(1)	-O(1)	106.1(2)	C(19)	-C(10)	-C(9)	116.7(2)
C(10)	-C(1)	-O(1)	113.5(2)	C(1)	-C(10)	-C(5)	106.9(2)
C(3)	-C(2)	-C(1)	117.4(3)	C(1)	-C(10)	-C(9)	110.5(2)
C(3)	-C(2)	-O(2)	121.9(3)	C(5)	-C(10)	-C(9)	102.3(2)
C(1)	-C(2)	-O(2)	120.7(3)	C(12)	-C(11)	-C(9)	112.4(2)
C(4)	-C(3)	-C(2)	123.2(3)	C(12)	-C(11)	-C(13)	106.7(2)
C(5)	-C(4)	-C(3)	120.1(3)	C(12)	-C(11)	-O(3)	110.1(2)
C(5)	-C(4)	-C(18)	118.5(2)	C(9)	-C(11)	-C(13)	101.7(2)
C(3)	-C(4)	-C(18)	121.3(3)	C(9)	-C(11)	-O(3)	113.1(2)
C(6)	-C(5)	-C(4)	114.0(2)	C(13)	-C(11)	-O(3)	112.6(2)
C(6)	-C(5)	-C(10)	113.0(2)	O(4)	-C(12)	-C(11)	122.1(2)
C(4)	-C(5)	-C(10)	113.6(2)	O(4)	-C(12)	-O(7)	118.3(2)
C(7)	-C(6)	-C(5)	111.9(2)	C(11)	-C(12)	-O(7)	119.5(2)
C(8)	-C(7)	-C(6)	112.8(2)	C(14)	-C(13)	-C(11)	102.2(2)
C(8)	-C(7)	-O(6)	108.8(2)	C(14)	-C(13)	-C(21)	116.8(2)
C(6)	-C(7)	-O(6)	105.3(2)	C(11)	-C(13)	-C(21)	112.1(2)
C(9)	-C(8)	-C(7)	110.3(2)	C(15)	-C(14)	-C(8)	111.8(2)
C(9)	-C(8)	-C(14)	105.1(2)	C(15)	-C(14)	-C(13)	118.6(2)
C(9)	-C(8)	-C(20)	111.4(2)	C(8)	-C(14)	-C 13)	104.7(2)
C(7)	-C(8)	-C(14)	113.3(2)	C(16)	-C(15)	-C(14)	114.3(2)
C(7)	-C(8)	-C(20)	110.5(2)	O(5)	-C(16)	-C(15)	123.9(2)
C(14)	-C(8)	-C(20)	106.1(2)	O(5)	-C(16)	-O(6)	118.4(2)
C(10)	-C(9)	-C(8)	115.3(2)	C(15)	-C(16)	-O(6)	117.6(2)
C(10)	-C(9)	-C(11)	127.3(2)	O(7)	-C(20)	-C(8)	111.6(2)
C(8)	-C(9)	-C(11)	98.1(2)	C(7)	-O(6)	-C(16)	118.7(2)
C(19)	-C(10)	-C(1)	107.1(2)	C(12)	-O(7)	-C(20)	122.7(2)

assuming anisotropic thermal motions for non-hydronge atoms and isotropic ones for hydrogen atoms. The final *R*-factor was 0.036. The final atomic coordinates are listed in Table 2 and bond lengths and bond angles are listed in Tables 3 and 4.[20] The computer-generated perspective drawing of molecule **1** is shown in Fig. 1.

Thus the structure of shinjudilactone (**1**) is shown to be formulated as 1β,11α-dihydroxy-2,16-dioxo-13(12→11α)*abeo*-picras-3-en-12,20-olide. The same rearranged skeleton could be derived by a 9(11→12)*abeo*-type rearrangement (*vide infra*).

Shinjulactone C (**2**), mp 292 °C (decomp), $[\alpha]_D^{23}$ −344° (pyridine), exhibited no bitter taste and the molecular formula, $C_{20}H_{22}O_7$, was determined by high resolution mass spectrum. The IR (*ca.* 3480, 1775, 1720, and 1650 cm^{-1}) and UV (λ_{max} 248 nm) spectra reveal the presence of hydroxyl(s) and three carbonyls, one of which is assigned to be an α,β-unsaturated ketone. The unsaturated carbonyl group is inferred to be located in the A ring; the mass spectrum of **2** afforded a prominent fragment peak at *m/e* 151 $(C_9H_{11}O_2)^+$ probably due to a tropylium ion (**D**), suggesting the presence of a partial structure (**E**), because the fragment ion **D** is observed in the mass spectrum of ailanthone (**3**).[8b] ^{1}H NMR spectrum (Table 5) of **2** showed the presence of two tertiary methyls (δ 1.092 and δ 1.306, each s), a vinyl methyl (δ 2.019, d), two methine protons (δ 2.900, s and δ 2.170, ddd), a lactone-terminus proton (δ 5.235, ddd),

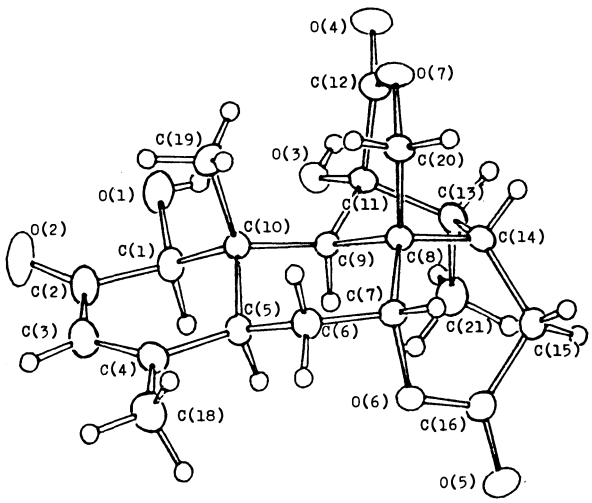

Fig. 1. Perspective view of shinjudilactone (**1**).[a]
a) For clarity hydrogen atoms are represented by spheres of arbitrary radius.

and an olefinic proton (δ 6.497, d). The lactone-terminus proton was shown to couple with the methine proton at δ 2.170 with a coupling constant J=2.5 Hz.

Four oxygen atoms were thus explained by the presence of a lactone, an α,β-unsaturated ketone, and an isolate ketone. The remaining three oxygen atoms were shown to be hydroxyl groups, one of which was shown to be primary by the following evidence. ^{1}H NMR (δ 4.052

Table 5. ^{1}H NMR Spectra of shinjudilactone (**1**) and shinjulactone C (**2**) (400 MHz, pyridine-d_5)[a,b]

	1		2	
1-H	4.229 s			
3-H	6.095 br s		6.497 br s	
5-H	3.224 br d	J=13		
6α-H	2.308 ddd	J=15, 3, 2.5	2.402 dd	J=15.5, 10
6β-H	2.082 ddd	J=15, 13, 2.5	2.699 dd	J=15.5, 5
7-H	4.808 t	J=2.5	5.235 ddd	J=10, 5, 2.5
9-H	2.723 s		2.900 s	
13-H	2.182 quin	J=7		
14-H	2.284 ddd	J=10.5, 7, <1	2.170 ddd	J=11, 3, 2.5
15α-H	3.125 dd	J=16, 10.5	2.969 dd	J=19.5, 11
15β-H	2.702 dd	J=16, <1	3.252 dd	J=19.5, 3
4-CH_3	1.798 br s		2.019 br s	
10-CH_3	1.235 s		1.092 s	
13-CH_3	1.240 d	J=7	1.306 s	
20-H_2	4.307 d	J=12	4.052 d	J=12
	4.793 d	J=12	4.090 d	J=12

a) Coupling constants are expressed in Hz. b) s: singlet, d: doublet, t: triplet, quin: quintet, br: broad.

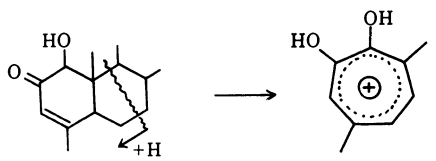

E **D** (*m/e* 151)

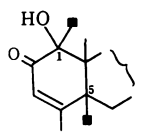

F

■ denotes a carbon atom.

and δ 4.090, each d) and ^{13}C NMR (δ 60.2, t) spectra and a fragment ion at *m/e* 343 due to $(M-CH_2OH)^+$ suggest the presence of a primary hydroxyl group. Acetylation of shinjulactone C (**2**) gave a monoacetate (**8**) and a diacetate (**9**). The primary hydroxyl group of **2** easily reacts with formic acid at room temperature to afford a formate (**10**), which, on refluxing with 50% formic acid, gave the starting shinjulactone C (**2**). In the ^{1}H NMR spectrum of monoacetate (**8**), an AB quartet signal (δ_A 4.47 and δ_B 4.59, J_{AB}=12 Hz) was observed, suggesting that the $-CH_2OH$ group had been acetylated. The diacetate (**9**), yield of which increased by prolonged reaction time, showed that an absorption band at *ca.* 3450 cm^{-1} due to a hydroxyl group still remained in the IR spectrum. In our recent study,[21] the diacetate (**9**) was prepared from ailanthone (**3**) and was shown to be a 12,20-di-*O*-acetyl derivative. Two signals (δ 88.3 and δ 93.6, each s) due to carbon atoms bearing a tertiary hydroxyl group were observed in the ^{13}C NMR spectrum of **2**. The absence of coupling between olefinic and allylic protons due to the structure moiety (**A**) was shown for **2**. From these observations, a partial structure (**F**) was suggested for shinjulactone C.

^{13}C NMR spectrum (Table. 6) and discussion developed above indicating that shinjulactone C (**2**) possesses a hexacyclic skeleton, two carbon atoms at C-1 and C-5 in the partial structure (**F**) must connect with different carbon atoms respectively. The following

Table 6. ^{13}C NMR Spectrum of shinjulactone C (**2**)

Assignment of carbon atom		Number of carbon atom	δ-value (pyridine-d_5)
>C=O	(isolated)	1	209.8 s
	(conjugated)	1	195.2 s
	(lactone or ester)	1	170.8 s
>C=C<	(tetrasubstituted)	1	165.9 s
>C=CH-	(trisubstituted)	1	127.8 d
-C-O		2	93.6 s, 88.3 s
-CH-O		1	72.6 d
$-CH_2-O$		1	60.2 t
-C-		4	55.5 s, 55.3 s, 50.7 s, 45.4 s
-CH-		2	51.7 d, 36.2 d
$-CH_2-$		2	30.2 t, 30.0 t
$-CH_3$		3	22.7 q, 14.5 q, 12.7 q

difference NOE experiment proved that these bond-formation resulted in a remarkable deformation of the molecule of shinjulactone C; on saturation of a singlet signal due to $C_{(9)}$–H at δ 2.900, signals at δ 1.092 ($C_{(10)}$–CH_3), δ 5.235 (–CH), and δ 4.052 (one of $-CH_2OH$) caused increase in area, and on saturation

Table 7. Atomic positional parameters ($\times 10^4$) and isotropic temperature factors ($\times 10^2$) for non-hydrogen atoms of shinjulactone C (**2**) with estimated standard deviations in parentheses

Atom	x	y	z	B_{eq}[a]
C(1)	2839(3)	2904(3)	-94(4)	245(5)
C(2)	1965(3)	3510(3)	-681(5)	293(6)
C(3)	1338(4)	4016(3)	331(5)	378(6)
C(4)	1478(3)	3914(3)	1689(5)	361(6)
C(5)	2322(3)	3231(3)	2233(4)	252(5)
C(6)	2611(3)	3476(3)	3735(5)	287(5)
C(7)	3515(3)	2838(3)	4220(4)	236(5)
C(8)	3665(3)	1951(3)	3231(4)	209(5)
C(9)	3946(3)	2348(3)	1763(4)	203(5)
C(10)	3274(3)	3270(3)	1300(4)	212(5)
C(11)	3578(3)	1522(3)	818(4)	261(5)
C(12)	2498(3)	1862(3)	503(4)	181(5)
C(13)	2020(3)	2085(3)	1998(4)	226(5)
C(14)	2618(3)	1458(3)	3095(4)	242(5)
C(15)	2097(4)	1364(3)	4550(5)	383(6)
C(16)	2699(4)	1680(4)	5786(5)	449(7)
C(18)	787(5)	4423(5)	2702(7)	686(9)
C(19)	3850(4)	4244(3)	1250(5)	282(6)
C(20)	4474(3)	1229(3)	3746(5)	319(6)
C(21)	894(3)	1832(4)	2011(5)	336(6)
O(1)	3602(2)	2799(2)	-1097(3)	269(4)
O(2)	1830(3)	3534(3)	-1934(4)	424(5)
O(3)	3992(2)	757(2)	442(4)	323(4)
O(4)	1914(2)	1224(2)	-322(3)	178(4)
O(5)	2612(4)	1335(3)	6924(4)	618(7)
O(6)	3359(3)	2452(2)	5628(3)	290(5)
O(7)	5396(2)	1725(3)	4052(4)	334(5)

a) $B_{eq}=8\pi^2(u_1^2+u_2^2+u_3^2)/3$.

Table 8. Bond lengths of shinjulactone C (**2**) with estimated standard deviations in parentheses

Bond length		l/Å	Bond length		l/Å
Atom 1	Atom 2		Atom 1	Atom 2	
O(1)	-C(1)	1.402(5)	C(5)	-C(10)	1.548(6)
O(2)	-C(2)	1.216(6)	C(5)	-C(13)	1.596(5)
O(3)	-C(11)	1.213(5)	C(6)	-C(7)	1.540(6)
O(4)	-C(12)	1.395(5)	C(7)	-C(8)	1.529(6)
O(5)	-C(16)	1.191(6)	C(8)	-C(9)	1.550(6)
O(6)	-C(7)	1.460(5)	C(8)	-C(14)	1.540(6)
O(6)	-C(16)	1.360(6)	C(8)	-C(20)	1.523(6)
O(7)	-C(20)	1.418(6)	C(9)	-C(10)	1.581(5)
C(1)	-C(2)	1.520(6)	C(9)	-C(11)	1.507(5)
C(1)	-C(10)	1.536(6)	C(10)	-C(19)	1.507(6)
C(1)	-C(12)	1.569(5)	C(11)	-C(12)	1.531(6)
C(2)	-C(3)	1.446(7)	C(12)	-C(13)	1.596(6)
C(3)	-C(4)	1.323(7)	C(13)	-C(14)	1.560(6)
C(4)	-C(5)	1.533(6)	C(13)	-C(21)	1.529(6)
C(4)	-C(18)	1.497(8)	C(14)	-C(15)	1.563(6)
C(5)	-C(6)	1.526(6)	C(15)	-C(16)	1.490(7)

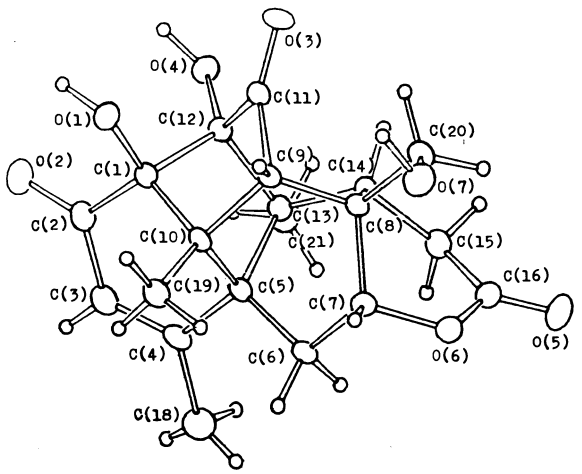

Fig. 2. Perspective view of shinjulactone C (**2**).[a]
a) For clarity hydrogen atoms are represented by spheres of arbitrary radius.

of a singlet signal due to a tertiary methyl at δ 1.306, signals at δ 6.497 ($\gtrless C=C_{(3)}-H$) and δ 2.019 ($C=\overset{1}{C}_{(4)}-CH_3$) showed increase in area. These enhancement in area due to NOE had never been observed in the usual picrasane derivatives. However, since further information for the structure elucidation of shinjulactone C (**2**) could be obtainable by neither spectral nor chemical investigation, single crystal X-ray diffraction analysis was carried out. Shinjulactone C (**2**) crystallized from acetone in orthorhombic space group $P2_12_12_1$ with the cell parameters of $a=13.247(6)$, $b=13.331(6)$, and $c=9.596(4)$ Å. Four molecules are contained in the unit cell. Intensity data were measured and the structure was solved and refined in the same manner with shinjudilactone (**1**) as described before. The 1831 independent reflections with $F_o \geq 2.5\ \sigma(F_o)$ were used for structure determination. The structure was refined to give the R-factor of 0.073 including all hydrogen atoms. Final atomic coordinates are listed in Table 7 and bond lengths and bond angles are listed in Tables 8 and 9.[20] Figure 2 shows a computer-generated drawing of the molecule **2**, showing to be formulated as 1α,12α : 5α,13α-dicyclo-1β,12β,20-trihydroxy-9βH-picras-3-ene-2,11,16-trione.

The structure elucidation of shinjudilactone (**1**) and shinjulactone C (**2**) has revealed that these new quassinoids possess modified picrasane skeletons. Since it seems possible that these modified quassinoids are biogenetically derived from ailanthone (**3**), conversion of **3** into shinjudilactone (**1**) was then investigated. The skeletal rearrangement of C ring of ailanthone (**3**) would be possible through two pathways *in vivo* (Scheme 1). Path **a** is initiated by protonation to $\Delta^{13(21)}$-double bond of **3**, followed by hydride shift to provide a cation at C-12. An *O*-terminus of a hemiacetal-bridge may shift from C-11 to the C-12 cationic center to give a cation at C-11. Each one of these cations could undergo ring-contraction followed by deprotonation to give **1**. The other path **b** comprises benzilic acid rearrangement of an intermediate α-diketone (**11**). Since a hydroxide ion is accessible to either C-12 or C-11 of the α-diketone (**11**), 13(12→11α)*abeo*-type or 9(11→12α)*abeo*-type rearrangement similar to those in the path **a** is considered. The resulting hydroxy carboxylic acid undergoes lactonization to furnish shinjudilactone (**1**).

According to these considerations, chemical conversion of ailanthone (**3**) into shinjudilactone (**1**) was investigated. The reaction did not occur under acidic conditions using *p*-toluenesulfonic acid, hydrochloric

Table 9. Bond angles of shinjulactone C (2) with estimated standard deviations in parentheses

Bond angle			ϕ/°	Bond angle			ϕ/°
Atom 1	Atom 2	Atom 3		Atom 1	Atom 2	Atom 3	
C(2)	-C(1)	-O(1)	110.3(3)	C(8)	-C(9)	-C(11)	102.7(3)
C(2)	-C(1)	-C(10)	116.1(3)	C(19)	-C(10)	-C(1)	115.8(3)
C(2)	-C(1)	-C(12)	112.7(3)	C(19)	-C(10)	-C(5)	117.3(3)
O(1)	-C(1)	-C(10)	111.0(3)	C(19)	-C(10)	-C(9)	113.2(3)
O(1)	-C(1)	-C(12)	111.7(3)	C(1)	-C(10)	-C(5)	100.8(3)
C(10)	-C(1)	-C(12)	94.1(3)	C(1)	-C(10)	-C(9)	102.1(3)
C(3)	-C(2)	-O(2)	124.6(4)	C(5)	-C(10)	-C(9)	105.7(3)
C(3)	-C(2)	-C(1)	115.9(4)	C(12)	-C(11)	-O(3)	127.8(4)
O(2)	-C(2)	-C(1)	119.5(4)	C(12)	-C(11)	-C(9)	101.8(3)
C(4)	-C(3)	-C(2)	122.2(4)	O(3)	-C(11)	-C(9)	130.3(4)
C(5)	-C(4)	-C(3)	119.9(4)	C(13)	-C(12)	-O(4)	113.8(3)
C(5)	-C(4)	-C(18)	119.5(4)	C(13)	-C(12)	-C(1)	106.1(3)
C(3)	-C(4)	-C(18)	120.5(5)	C(13)	-C(12)	-C(11)	104.4(3)
C(6)	-C(5)	-C(4)	112.2(3)	O(4)	-C(12)	-C(1)	119.5(3)
C(6)	-C(5)	-C(10)	109.5(3)	O(4)	-C(12)	-C(11)	116.7(3)
C(6)	-C(5)	-C(13)	113.6(3)	C(1)	-C(12)	-C(11)	93.7(3)
C(4)	-C(5)	-C(10)	112.2(3)	C(14)	-C(13)	-C(5)	106.9(3)
C(4)	-C(5)	-C(13)	109.7(3)	C(14)	-C(13)	-C(12)	107.7(3)
C(10)	-C(5)	-C(13)	98.9(3)	C(14)	-C(13)	-C(21)	111.8(3)
C(7)	-C(6)	-C(5)	111.3(3)	C(5)	-C(13)	-C(12)	101.9(3)
C(8)	-C(7)	-O(6)	108.7(3)	C(5)	-C(13)	-C(21)	117.0(3)
C(8)	-C(7)	-C(6)	109.9(3)	C(12)	-C(13)	-C(21)	110.7(3)
O(6)	-C(7)	-C(6)	111.3(3)	C(15)	-C(14)	-C(8)	110.9(3)
C(9)	-C(8)	-C(7)	109.3(3)	C(15)	-C(14)	-C(13)	114.9(3)
C(9)	-C(8)	-C(14)	106.6(3)	C(8)	-C(14)	-C(13)	106.6(3)
C(9)	-C(8)	-C(20)	110.0(3)	C(16)	-C(15)	-C(14)	116.9(4)
C(7)	-C(8)	-C(14)	105.4(3)	O(5)	-C(16)	-O(6)	117.2(5)
C(7)	-C(8)	-C(20)	112.2(3)	O(5)	-C(16)	-C(15)	124.7(5)
C(14)	-C(8)	-C(20)	113.1(3)	O(6)	-C(16)	-C(15)	118.0(4)
C(10)	-C(9)	-C(8)	112.7(3)	O(7)	-C(20)	-C(8)	112.3(4)
C(10)	-C(9)	-C(11)	102.5(3)	C(7)	-O(6)	-C(16)	117.4(4)

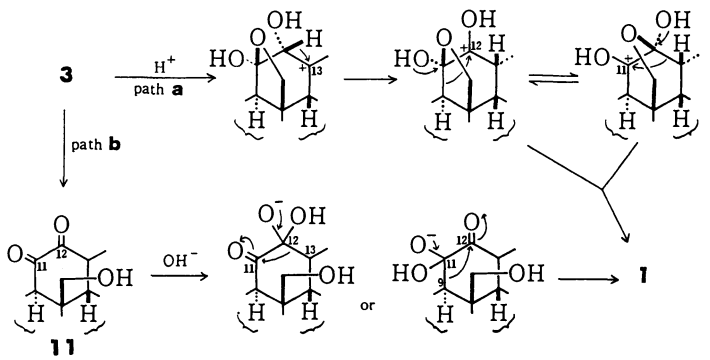

Scheme 1.

acid, acetic acid–hydrochloric acid, or iron(III) chloride–hydrochloric acid, while a very complex mixture was obtained in the reaction of **3** with boron trifluoride etherate in benzene or dichloromethane, no shinjudilactone (**1**) being detected in the reaction mixture by TLC examination.

Reactions under alkaline conditions such as sodium hydroxide in water, potassium hydroxide in methanol, and barium hydroxide in pyridine, gave extremely polar products, structures of which could not be identified. However, ailanthone (**3**) was treated with sodium hydrogencarbonate in boiling aqueous methanol and then the reaction mixture was acidified with hydrochloric acid to give a reaction mixture nearly quantitatively, showing two spots on TLC. Separation of the mixture afforded two compounds in a ratio of 1 : 1, one of which was found to be shinjudilactone (**1**) and the other with a lower R_f value on TLC was determined to be a 13β-epimer (**12**) of **1** by spectral investigation (see Experimental). Reaction of **3** with sodium carbonate under the same conditions as above gave the same reaction mixture, but accompanied by a

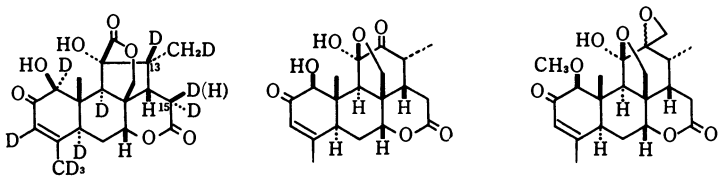

13 14 15

small amount of by-products.

Formation of shinjudilactone (**1**) from ailanthone (**3**) has been thus demonstrated, although it remained unresolved whether the reaction proceeds through 13(12→11)*abeo*-type or 9(11→12)*abeo*-type rearrangement. The pathway through benzilic acid rearrangement is also supported by i) labeling experiment and ii) isolation of an intermediate.

i) Treatment of ailanthone (**3**) with $NaDCO_3$ in boiling D_2O–CH_3OD and the reaction product was treated with dilute hydrochloric acid to afford labeled shinjudilactone and its 13-epimer. The labeled shinjudilactone was shown to be an undecadeuterio derivative (**1**-d_{11}) containing a decadeuterio derivative (**1**-d_{10}). The labeled positions were determined by ^1H NMR measurement at 400 MHz and shown in the structure **13**. Ten hydrogen atoms were completely replaced with deuterium atoms and a multiplet signal at δ 2.70 due to the $C_{(15\beta)}$–H was observed, accounting for the presence of **1**-d_{10}. The presence of a deuterium atom at C-9 implies the formation of a carbonyl group at C-11 followed by enolization, which is favorable to the path **b**, during the reaction. The location of a deuterium atom at C-13β of **1**-d_{11} would reject a direct hydride transfer mechanism from C-12β to a cationic center at C-13 as depicted in the path **a**. ii) Ailanthone (**3**) was isomerized by heating in pyridine for 10 h to afford a hemiacetal, for which the structure (**14**) could be assigned by ^1H and ^{13}C NMR measurement. The structure of hemiacetal moiety of **14** was confirmed by ^{13}C–^1H long range selective decoupling experiment measured at 90 MHz. When the ^1H signal due to $C_{(9)}$–H at δ 2.88 was irradiated, the ^{13}C signal at δ 108.15 became sharp, but ^{13}C signal at δ 207.46 still remained broad, being coupled with a proton at C-13. This observation leads to the conclusion that the hemiacetal carbon resonating at δ 108.15 and the carbonyl carbon at δ 207.46 are located in C-11 and C-12 positions, respectively. The fact that $C_{(9)}$–H kept α-configuration intact[22] was demonstrated by NOE experiment measured at 400 MHz. On irradiation at δ 2.88 due to $C_{(9)}$–H, signal due to $C_{(1)}$–H (δ 4.42) increased in area by 15%, while neither signal due to $C_{(7)}$–H (δ 4.79) nor due to $C_{(20)}$–H_2 (δ 4.15 and δ 4.46) showed NOE enhancement.

The structure (**14**), which is equivalent to the hypothetical α-diketone (**11**), has been proposed for isoailanthone by Polonsky *et al.*[8b] Isoailanthone was prepared by treatment of **3** with dilute alkali, but neither detailed description nor spectral data of isoailanthone was given. Only spectral data of its 1-*O*-methyl derivative prepared by methylation with diazomethane were registered.[8b] The hemiacetal (**14**) was then treated with diazomethane to yield a product, which however was suggested to be a 12-spirooxirane-derivative (**15**) from the spectral examination (see Experimental). This compound (**15**) is not identical with 1-*O*-methylisoailanthone. The reason why the disagreement occurred is obscure and further investigation is now in progress. On treatment with sodium hydrogencarbonate in boiling aqueous methanol, the hemiacetal (**14**) gave shinjudilactone (**1**) and its 13-epimer (**12**).

It would be suggestive that shinjudilactone (**1**) is synthesized biogenetically from ailanthone (**3**) or its equivalent through a path similar to the benzilic acid rearrangement. Recently Ochi *et al.*[23] have isolated a 6-epi-*ent*-gibberellane derivative, rabdoepigibberellolide, from *Rabdosia shinkokianus* Hara and suggested its biogenetic pathway from rabdosianin A through benzilic acid rearrangement.

Although biogenesis of shinjulactone C (**2**) with an unusual hexacyclic 1α,12α : 5α,13α-dicyclo-9β*H*-picrasane skeleton, is still unknown, a biogenetic precursor with a normal picrasane skeleton, such as ailanthone (**3**), would undergo an inversion of a chiral center at C-9 position prior to the bond-formation between C-1 and C-12 and between C-5 and C-13. Further investigation is now in progress.

Experimental

General Procedures. All melting points were measured on a Mel-temp capillary melting point apparatus (Laboratory Devices) and uncorrected. Optical rotations were determined on a JASCO polarimeter DIP-181. Ultraviolet absorption (UV) spectra and infrared (IR) spectra were measured on a Hitachi 340 and a Hitachi 260-30 spectrometer, respectively. Mass (MS) spectra were run on a Hitachi RMU-6 Tokugata mass spectrometer and high-resolution mass spectra on a JEOL JMS-D300 mass spectrometer operating at 70 eV. Proton nuclear magnetic resonance (^1H NMR) spectra (90 MHz) were taken using a Varian EM 390 and carbon-13 nuclear magnetic resonance (^{13}C NMR) spectra (22.5 MHz) JEOL FX 90Q unless otherwise stated. Measurement of ^1H NMR spectra at 400 MHz and ^{13}C NMR spectra at 100 MHz was carried out on a JMN GX 400 (JEOL) spectrometer. Chemical shifts were expressed in ppm downfield from tetramethylsilane as an internal standard (δ value) and coupling constants in Hz. Thin-layer chromatography (TLC) was carried out on Kieselgel 60 GF_{254} coated in 0.25 mm- or 0.5 mm-thickness or on TLC plates Silica Gel F_{254} with Concentration Zone (E. Merck). Wakogel C-200 (Wako), Silicic acid AR (Mallinckrodt) or Celite No. 545 (Wako) was used for column chromatography.

Plant Materials. Roots of *Ailanthus altissima* Swingle were collected twice at the Botanical Gardens, Faculty of Science, the University of Tokyo in January 1980 and 1981. Bark was stripped off from the root, air-dried, and chipped to afford 3.2 and 10 kg of materials, respectively.

Extraction and Separation. *i) Extraction with Ethyl Acetate*: The root bark (3.2 kg), defatted with petroleum ether (18 l) for 6 h, was extracted twice with ethyl acetate (18 l) for 6 h and then with methanol (18 l) for 6 h. Since the bitter taste was mainly exhibited in the ethyl acetate-extract, which was subjected to further separation. Non-bitter solids, precipitated from the extract on standing, were filtered off and the filtrate was concentrated to give a residue (30 g), which was partitioned between dichloromethane and aqueous methanol.

Column A: The aqueous methanol layer, on evaporation, gave a bitter residue (*ca.* 11 g), 3.5 g of which was subjected to column chromatographic separation (C-200, 180 g), eluted with chloroform (each 360 ml) containing following percentage of methanol: 1, 5, 10, 20, 40, 60, and 100%, and 28 fractions (each 90 ml) were collected. Elution with chloroform containing *ca.* 5% methanol afforded a small quantity of bitter principles, which were inferred to be a mixture of amarolide and amarolide 11-acetate by TLC examination (developed with 5% methanol–chloroform). Further confirmation was carried out by comparison with authentic samples, both of which were isolated from methanol extract of the root bark of the plant in *ca.* 0.01% yield, respectively.

Column B: Fraction 13 (2.1 g) of Column A was further separated by dry column chromatography (C-200, 420 g). A mixture (2 : 1) of benzene–acetone was passed through the column and 16 fractions (each 420 ml) were collected. Recrystallization of fractions 7—16 from ethyl acetate gave ailanthone (**3**; 1.2 g).

Column C: Fractions 3—6 (450 mg) of Column B were combined and separated by dry column chromatography (C-200, 140 g), eluting with 5% methanol–containing chloroform. Ten fractions (each 70 ml) were collected and a small quantity of ailanthone (**3**) was obtained from fractions 6—10. Fractions 3—5 were combined and separated by preparative TLC developed with benzene–acetone (1 : 1) and then with methanol–chloroform (1 : 9) to give ailanthone (**3**; trace), glaucarubinone (27 mg), and $\Delta^{13(18)}$-dehydroglaucarubinone (40 mg).

Column D: The dichloromethane layer obtained by the partition was evaporated to afford a bitter residue (19 g), 17 g of which was subjected to separation by column chromatography (C-200, 900 g). After elution with chloroform–benzene (1 : 1, 1.8 l) and chloroform (1.8 l), following solvents were successively passed through the column: 1%-, 2%-, 4%-, 8%-, 16%-, and 32%-methanol in chloroform (each 1.8 l) and 18 fractions (each 900 ml) were collected.

Column E: Fraction 15 (3.5 g) of Column D was chromatographed over silica gel (C-200, 300 g) eluting with benzene–acetone (3 : 2) to give 20 fractions (each 300 ml).

Column F: Fraction 16 (0.5 g) of Column A was chromatographed over silica gel (C-200, 100 g) eluting with benzene–acetone (1 : 1) to 10 fractions (each 100 ml).

Column G: Fractions 5—17 of Column E and fractions 7—14 of Column F were combined to afford a residue (450 mg) on evaporation, which was dissolved in chloroform, passed though a column packed with a mixture of silicic acid (23 g) and Celite (23 g). Elution with chloroform (92 ml) and 1%-, 2%-, 5%-, 10%-, 20%-, and 50%-methanol in chloroform (each 92 ml) afforded 25 fractions (each 23 ml). Recrystallization of fraction 20 from methanol gave shinjulactone A (7 mg). Fractions 17—19 were purified by preparative TLC developed with 10% methanol in chloroform to give $\Delta^{13(18)}$-glaucarubolone (20 mg).

ii) Extraction with Water: The air-dried root bark (10 kg) was extracted with hot water (90 °C, 20 l) overnight. The extraction was repeated twice and the aqueous extracts were combined and evaporated *in vacuo* to give a concentrated extract (*ca.* 5 l). The extract was divided into three portions, each of which was extracted continuously with dichloromethane (1 l) overnight and the extraction was repeated four times. Evaporation of the combined dichloromethane extract gave a residue (45 g).

Column H: The residue (40 g) above obtained, was chromatographed over silica gel (C-200, 1.3 kg) and eluted with 1%-, 2%-, 4%-, 8%-, 16%-, 32%-, and 64%-methanol in chloroform (each 2.6 l). Eighteen fractions (each 1.3 l) were collected and following residues were obtained on evaporation; fr 7 (5.6 g), fr 8 (4.0 g), fr 9 (1.8 g), fr 10 (4.4 g), fr 11 (3.2 g), fr 12 (3.7 g), fr 13 (3.0 g), fr 14 (3.3 g), fr 15 (5.3 g), and fr 16 (2.4 g).

Column I: Fraction 7 of Column H was subjected to separation by dry column chromatography (C-200, 560 g) and a mixture of benzene–acetone (4 : 1) was passed to afford 46 fractions (each 140 ml). Fractions 12 and 13 gave amarolide. Recrystallization of fractions 27—35 from methanol afforded shinjudilactone (**1**; 70 mg).

Column J: The mother liquor obtained from the recrystallization of shinjudilactone (**1**) afforded a residue (500 mg), which was chromatographed over silica gel (C-200, 100 g, eluted with 5% methanol in chloroform) and then silicic acid (70 g, eluted with 2.5% methanol in dichloromethane) to afford chaparrinone (**4**; 18 mg).

Column K: Recrystallization of fraction 8 (4.0 g) of Column H from methanol–chloroform afforded shinjudilactone (**1**; 200 mg) in needles and mother liquor, which gave a residue (3.8 g) on evaporation. The residue was chromatographed over silica gel (C-200, 600 g) and a mixture of benzene and ethanol (9 : 1) was passed to afford 12 fractions (each 400 ml). From fractions 7—12, shinjudilactone (**1**; 900 mg) was obtained by crystallization from methanol.

Column L: Fraction 10 of Column H was chromatographed over silica gel (C-200, 500 g, dry; elution with benzene–acetone (3 : 1)) and 36 fractions (each 200 ml) were obtained. Fractions 22—29 afforded ailanthone (**3**; *ca.* 1 g).

Column M: Fraction 14 of Column H was separated by column chromatography (C-200, 350 g) eluted with a lower phase of a mixture, chloroform–methanol–water (150 : 25 : 6) to give 27 fractions (each 100 ml). From fractions 13—16, $\Delta^{13(18)}$-dehydroglaucarubolone (100 mg) was obtained by crystallization from acetone.

Column N: Fractions 18—21 (380 mg) of Column L were dissolved in chloroform and the solution was passed through a column of silica gel (C-200, 200 g) and the following solvents were passed: chloroform (200 ml), 1%-methanol in chloroform (400 ml), 3%- (400 ml), and 5%- (800 ml). Eighteen fractions (each 100 ml) were collected and fractions 11—14 gave shinjudilactone (**1**; 50 mg) and fraction 16 afforded glaucarubinone (50 mg) after purification by preparative TLC developed with 3% methanol in ethyl acetate.

Column O: Fraction 11 of Column H was separated by column chromatography (C-200, 400 g) eluted with 1%-methanol in ethyl acetate (800 ml) and then with 2%- (1600 ml) to give 15 fractions (each 160 ml). Fractions 8—14 were dissolved in chloroform and passed through a dry column of silica gel (C-200, 300 g). Chloroform (300 ml), 2%-methanol in chloroform (600 ml), and 4%-(2050 ml) were successively passed to afford 39 fractions (each 75 ml). Fractions 17—22 consisted of mainly ailanthone (**3**) and fractions 31—36 afforded shinjulactone B (11 mg) after purification by preparative TLC developed with 5% methanol in chloroform.

Column P: Fraction 13 of Column H was subjected to partition chromatography over silica gel (C-200, 500 g, dry). Eluting solvent consisted of a 1 : 1 (v/v) mixture of a lower layer of dichloromethane–methanol–water (100 : 25 : 6) and

dichloromethane. Eighteen fractions (each 200 ml) were collected. Recrystallization of fractions 6 and 7 from acetone gave chaparrolide (*ca.* 200 mg). Shinjulactone C (**2**; *ca.* 20 mg) was obtained from the mother liquor by recrystallization from acetone.

Since separation of quassinoids in the root bark of *A. altissima* was difficult and therefore separation procedures were very complicated, it is impossible to describe all procedures carried out in this experiment. The contents of each quassinoids are estimated by summing up amounts obtained in various separation routes and are shown in Table 10.

Shinjudilactone (1). Colorless needles crystallized from ethyl acetate–methanol, mp 274—276 °C; $[\alpha]_D^{23}$ +102° (*c* 0.76, C_5H_5N); IR (KBr) *ca.* 3250, 1745, 1735, 1670, and 1620 cm^{-1}; UV (EtOH) 238 nm (ε 10800); ^1H NMR (Table 5); ^{13}C NMR (Table 1); MS *m/e* (%) 376 (M^+; 80), 358 (20), 347 (30), 332 (60), 303 (98), 288 (75), and 95 (100); Found: *m/e* 376.1509. Calcd for $C_{20}H_{24}O_7$: M 376.1520. Found: C, 62.03; H, 6.74; Calcd for $C_{20}H_{24}O_7 \cdot 1/2\ H_2O$: C, 62.33; H, 6.54%.

1-O-Methylshinjudilactone (5). Shinjudilactone (**1**; 30 mg) in methanol (10 ml) was treated with diazomethane in ether and the reaction mixture was allowed to stand overnight. After the usual work-up, the reaction product was purified by preparative TLC developed with 3% methanol–chloroform to give 1-*O*-methylshinjudilactone (**5**; 15 mg); mp 291—294 °C (from methanol); $[\alpha]_D^{23}$ +53.5° (*c* 0.27, $CHCl_3$); IR (Nujol) 3400, 1745, 1720, 1680, and 1630 cm^{-1}; UV (EtOH) 239.5 nm (ε 5400); ^1H NMR ($CDCl_3$) δ 1.05 (3H, s; $C_{(10)}$–CH_3), 1.11 (3H, d, J=7 Hz; $C_{(13)}$–CH_3), 1.95 (3H, br s; $C_{(4)}$–CH_3), 3.63 (1H, s; $C_{(1)}$–H), 3.75 (3H, s; CH_3O), 4.00 and 4.52 (each 1H, d, J=11.5 Hz; $C_{(20)}$–H), 4.52 (1H, t, J=2.5 Hz; $C_{(7)}$–H), 5.98 (1H, m; $C_{(3)}$–H), and 6.08 (1H, s; OH); MS *m/e* (%) 390 (M^+; 60), 360 (100), 345 (50), 330 (20), 301 (10), and 288 (45); Found: *m/e* 390.1659. Calcd for $C_{21}H_{26}O_7$: M 390.1677.

1-O-Acetylshijudilactone (6). Shinjudilactone (**1**; 20 mg) was acetylated with acetic anhydride (2 ml) in pyridine (2 ml) at room temperature for 9 h. Addition of methanol and the usual work-up afforded 1-*O*-acetylshinjudilactone quantitatively, mp 269—272 °C (from methanol); IR (Nujol) 3480, 1730, 1680, and 1630 cm^{-1}; UV (EtOH) 240 nm (ε 8000); ^1H NMR (C_5D_5N) δ 1.12 (3H, d, J=7 Hz; $C_{(13)}$–CH_3), 1.36 (3H, s; $C_{(10)}$–CH_3), 1.77 (3H, br s; $C_{(4)}$–CH_3), 2.25 (3H, s; –$OCOCH_3$), 4.26 and 4.73 (each 1H, d, J=12 Hz; $C_{(20)}$–H), 4.64 (1H, t, J=3 Hz; $C_{(7)}$–H), 5.78 (1H, s; $C_{(1)}$–H), and 6.05 (1H, m; $C_{(3)}$–H); MS *m/e* (%) 418 (M^+; 30), 400 (25), 358 (95), 330 (40), and 60 (100); Found: *m/e* 418.1678. Calcd for $C_{22}H_{26}O_8$: M 418.1628.

Reduction of 1 with Sodium Borohydride. To a solution of shinjudilactone (**1**; 30 mg) in ethanol (10 ml) kept at 0 °C, sodium borohydride (6 mg) in ethanol (2 ml) was added and the mixture was stirred for 4 h at 0 °C. Acetic acid (1 ml) was added and the solvents were evaporated *in vacuo* to afford a residue, which was dissolved in a mixture of dichloromethane (10 ml) and brine (10 ml). Extraction with dichloromethane (10 ml×3), evaporation *in vacuo*, and crystallization from methanol gave a hemiacetal (**7**; 20 mg), mp 276—277.5 °C; IR (Nujol) *ca.* 3300, 1740, 1660, and 1610 cm^{-1}; UV (EtOH) 240 nm (ε 11500); ^1H NMR (C_5D_5N) δ 1.13 (3H, d, J=6 Hz; $C_{(13)}$–CH_3), 1.17 (3H, s; $C_{(10)}$–CH_3), 1.76 (3H, br s; $C_{(4)}$–CH_3), 4.20 and 4.43 (each 1H, d, J=12 Hz; $C_{(20)}$–H), 4.26 (1H, t, J=3 Hz; $C_{(7)}$–H), 4.35 (1H, s; $C_{(1)}$–H), 5.68 (1H, m; $C_{(16)}$–H), and 6.04 (1H, m; $C_{(3)}$–H); MS *m/e* (%) 378 (M^+; 20), 360 (70), 345 (40), 334 (40), and 316 (100); Found: *m/e* 378.1681. Calcd for $C_{20}H_{26}O_7$: M 378.1679.

Shinjulactone C (2). Colorless prisms crystallized from acetone, mp 292 °C (decomp); $[\alpha]_D^{23}$ −344° (*c* 0.46, C_5H_5N); IR (KBr) *ca.* 3480, 1775, 1720, 1650, 1620 (sh), 1390, and 1190 cm^{-1}; UV (MeOH) 248 nm (ε 10600); ^1H NMR (Table 5); ^{13}C NMR (Table 6); MS *m/e* (%) 374 (M^+; 100), 356 (5), 343 (20), 315 (10), and 151 (60); Found: *m/e* 374.1379. Calcd for $C_{20}H_{22}O_7$: M 374.1366.

Acetylation of Shinjulactone C (2). *i)* Shinjulactone C (**2**; 20 mg) was treated with acetic anhydride (5 ml) and pyridine (5 ml) at room temperature overnight. After methanol (5 ml) was added, the reaction mixture was evaporated *in vacuo* to give a residue, which was shown to be a 7 : 3 mixture of a monoacetate (**8**) and a diacetate (**9**) by TLC examination. Acetylation of the mixture was repeated under the same conditions as above and the acetylation product was separated by preparative TLC developed with 10% methanol–chloroform to give the monoacetate (**8**; 1 mg) and the diacetate (**9**; 20 mg). *ii)* A mixture of shinjulactone C (**2**; 10 mg) and acetic acid (5 ml) was heated under reflux for 15 h to afford the monoacetate (**8**) quantitatively. 20-*O*-Acetylshinjulactone C (**8**): mp 131—134 °C (from acetone–hexane); $[\alpha]_D^{22}$ −222° (*c* 0.13, $CHCl_3$); IR (Nujol) *ca.* 3450, 1770, 1740 (br), 1660, 1620 (sh), and 1240 cm^{-1}; UV (EtOH) 245 nm (ε 14000); ^1H NMR (C_5D_5N) δ 1.11 (3H, s; $C_{(13)}$– or $C_{(10)}$–CH_3), 1.30 (3H, s; $C_{(10)}$– or $C_{(13)}$–CH_3), 1.96 (3H, s; –$OCOCH_3$), 2.03 (3H, br s; $C_{(4)}$–CH_3), 2.49 (1H, s; $C_{(9)}$–H), 4.47 and 4.59 (each 1H, d, J=12 Hz; $C_{(20)}$–H), 5.02 (1H, m; $C_{(7)}$–H), and 6.47 (1H, br s; $C_{(3)}$–H); ^1H NMR ($CDCl_3$) δ 0.99 (3H, s; $C_{(13)}$– or $C_{(10)}$–CH_3), 1.03 (3H, s; $C_{(10)}$– or $C_{(13)}$–CH_3), 2.08 (6H, s; $C_{(4)}$–CH_3 and –$OCOCH_3$), 4.07 (2H, s; $C_{(20)}$–H_2), 4.63 (1H, m; $C_{(7)}$–H), and 6.35 (1H, br s; $C_{(3)}$–H); MS *m/e* (%) 416 (M^+; 25), 398 (10), 388 (8), 374 (8), 356 (100), 193 (30), and 151 (10); Found: *m/e* 416.1464. Calcd for $C_{22}H_{24}O_8$: M 416.1469. 12,20-Di-*O*-acetylshinjulactone C (**9**): mp 152—154 °C (from acetone–hexane); $[\alpha]_D^{21}$ −200° (*c* 0.24, $CHCl_3$); IR (Nujol) *ca.* 3450, 1780, 1740 (br), 1665, 1620 (sh), and 1220 cm^{-1}; UV (EtOH) 245.5 nm (ε 9600); ^1H NMR (C_5D_5N) δ 1.14 (6H, s; $C_{(13)}$– and $C_{(10)}$–CH_3), 1.71 (3H, br s; $C_{(4)}$–CH_3), 1.94 and 2.06 (each 3H, s; –$OCOCH_3$), 2.57 (1H, s; $C_{(9)}$–H), 4.42 and 4.51 (each 1H, d, J=12 Hz; $C_{(20)}$–H), and 6.52 (1H, br s; $C_{(3)}$–H); ^1H NMR ($CDCl_3$) δ 0.99 (3H, s, $C_{(13)}$– or $C_{(10)}$–CH_3), 1.00 (3H, s; $C_{(10)}$– or $C_{(13)}$–CH_3), 2.06 and 2.13 (each 3H, s; –$OCOCH_3$), 2.10 (3H, br s; $C_{(4)}$–CH_3), 4.10 (2H, s; $C_{(20)}$–H_2), 4.63 (1H, m; $C_{(7)}$–H), and 6.37 (1H, br s; $C_{(3)}$–H); ^{13}C NMR (C_5D_5N) δ 12.3 q, 13.3 q, 20.0 q, 20.3 q, 22.6 q, 29.8 t, 29.8 t, 35.4 d, 42.4 s, 51.0 s, 52.7 d, 55.0 s, 56.2 s, 63.5 t, 72.6 d, 86.4 s, 97.5 s, 128.4 d, 165.5 s, 169.7 s, 170.0 s, 170.0 s, 193.2 s, and 201.0 s; MS *m/e* (%) 458 (M^+; 12), 430 (10), 416 (100), 398 (20), 193 (60), and 151 (58); Found: *m/e* 458.1590. Calcd for $C_{24}H_{26}O_9$: M 458.1587.

Formylation of Shinjulactone C (2). A solution of shin-

Table 10.

Compound	Yield/%	
	AcOEt-extract	H_2O-extract
Ailanthone (**3**)	0.1	0.05
Amarolide	0.01	0.01
Amarolide 11-acetate	0.01	—
Glaucarubinone	0.001	0.001
$\Delta^{13(18)}$-Dehydroglaucarubinone	0.001	—
$\Delta^{13(18)}$-Dehydroglaucarubolone	0.0005	0.001
Shinjulactone A	0.001	—
Shinjulactone B	—	0.0005
Chaparrolide	—	0.005
Chaparrinone (**4**)	—	0.001
Shinjudilactone (**1**)	—	0.01
Shinjulactone C (**2**)	—	0.001

julactone C (**2**; 12 mg) in formic acid (5 ml) was stirred at room temperature for 2 h. Evaporation of the solvent *in vacuo* afforded 20-*O*-formylshinjulactone C (**10**) quantitatively, mp 268—271 °C (from acetone); IR (KBr) *ca.* 3450, 1770, 1730 (br), 1660, and 1180 cm^{-1}; ^1H NMR (C_5D_5N) δ 1.10 (3H, s; $C_{(13)}$- or $C_{(10)}$-CH_3), 1.27 (3H, s; $C_{(10)}$- or $C_{(13)}$-CH_3), 2.00 (3H, br s; $C_{(4)}$-CH_3), 2.49 (1H, s; $C_{(9)}$-H), 4.44 and 4.57 (each 1H, d, J=12 Hz; $C_{(20)}$-H), 4.96 (1H, m; $C_{(7)}$-H), 6.45 (1H, br s; $C_{(3)}$-H), and 8.25 (1H, s; H-CO); MS *m/e* (%) 402 (M^+; 100), 374 (10), 359 (10), 343 (15), 297 (20), and 151 (40); Found: *m/e* 402.1293. Calcd for $C_{21}H_{22}O_8$: M 402.1313.

Hydrolysis of 20-O-Formylshinjulactone C (10). The formate (**10**; 12 mg) was heated under reflux with a mixture of formic acid (3 ml) and water (3 ml) for 5 h to afford shinjulactone C (**2**) quantitatively.

Conversion of Ailanthone (3) into Shinjudilactone (1). *i)* Ailanthone (**3**; 21 mg) in a mixture of methanol (2 ml) and water (2 ml) was heated with sodium hydrogencarbonate (5 mg) under reflux for 30 min. The reaction mixture was acidified with concd hydrochloric acid (2 drops), evaporated to concentrated solution (*ca.* 1 ml) under reduced pressure, and extracted with dichloromethane. After usual work-up, a residue (20 mg) was subjected to separation by preparative TLC developed with chloroform–methanol (19 : 1) to afford shinjudilactone (**1**; 10 mg) and 13-epishinjudilactone (**12**; 10 mg), mp 263—266 °C (from methanol–ethyl acetate); $[\alpha]_D^{23}$ +48° (*c* 0.57, C_5H_5N); IR (KBr) *ca.* 3300, 1745, 1675, 1620, 1250, and 1180 cm^{-1}; UV (EtOH) 239 nm (ε 10300); ^1H NMR (C_5D_5N) δ 1.19 (3H, d, J=6 Hz; $C_{(13)}$-CH_3), 1.20 (3H, s; $C_{(10)}$-CH_3), 1.77 (3H, br s; $C_{(4)}$-CH_3), 4.22 (1H, s; $C_{(1)}$-H) 4.25 and 4.66 (each 1H, d, J=12 Hz; $C_{(20)}$-H), 4.65 (1H, t, J=2 Hz; $C_{(7)}$-H), and 6.06 (1H, m; $C_{(3)}$-H); ^{13}C NMR (C_5D_5N) δ 9.8, 11.4, 22.2, 27.0, 29.3, 41.9, 42.5, 42.8, 44.5, 48.3, 51.0, 74.3, 76.0, 76.6, 83.5, 126.3, 161.8, 170.9, 175.7, and 196.7; MS *m/e* (%) 376 (M^+; 8), 358 (6), 347 (8), 340 (10), 312 (45), 294 (40), 268 (100), and 253 (60); Found: *m/e* 376.1532. Calcd for $C_{20}H_{24}O_7$: M 376.1520.

ii) Reaction of ailanthone (**3**) with sodium carbonate in boiling aqueous methanol afforded the same reaction mixture of **1** and **12**, but accompanied with a formation of a small amount of by-products.

iii) Reactions of ailanthone (**3**) under following conditions were carried out, but all attempts were not successful; a) *p*-toluenesulfonic acid in tetrahydrofuran, reflux for 48 h, b) 2 M† hydrochloric acid in methanol, room temperature for 12 h and then reflux for 12 h, c) acetic acid-2 M hydrochloric acid in water, room temperature overnight, and then reflux overnight, d) 2 M hydrochloric acid–iron (III) chloride in water, reflux overnight, e) boron trifluoride etherate in benzene or dichloromethane, room temperature overnight, and f) sodium hydroxide in water, potassium hydroxide in methanol, or barium hydroxide in pyridine, reflux overnight.

Conversion of Ailanthone (3) into Undecadeuterioshinjudilactone (1-d_{11}). A mixture of ailanthone (**3**; 21 mg), $NaDCO_3$ (5 mg), D_2O (2 ml), and CH_3OD (2 ml) was heated under reflux for 30 min. The reaction mixture was acidified with concd hydrochloric acid (2 drops) and worked-up as usual to give a crude deuteriated product (20 mg), from which undecadeuterioshinjudilactone (**1**-d_{11}; 10 mg) was separated by preparative TLC. **1**-d_{11}: ^1H NMR (400 MHz, C_5D_5N) δ 1.22 (2H, br s; $C_{(13)}$-CH_2D), 1.23 (3H, s; $C_{(10)}$-CH_3), 2.06 (1H, br d, J=14 Hz; $C_{(6\beta)}$-H), 2.26 (1H, br s; $C_{(14)}$-H), 2.28 (1H, dd, J=14 Hz and 2.5 Hz; $C_{(6\alpha)}$-H), 2.70(0.5 H, m; $C_{(15\beta)}$-H), 4.28 and 4.78 (each 1H, d, J=11.5 Hz; $C_{(20)}$-H), and 4.78 (1H, t, J=2.5 Hz; $C_{(7)}$-H); MS *m/e* 387, 386, 367, 342, 100, and 68.

† 1 M = 1 mol dm^{-3}.

Isomerization of Ailanthone (3) into Hemiacetal (14). Ailanthone (**3**; 30 mg) in pyridine (5 ml) was refluxed for 10 h and the reaction product was separated by preparative TLC to give a hemiacetal (**14**; 20 mg), mp 166—169 °C (from acetone–benzene); IR (KBr) 3450, 1740, 1680, 1240, and 1050 cm^{-1}; UV (EtOH) 238 nm (ε 8100); ^1H NMR (C_5D_5N) δ 1.03 (3H, d, J=8 Hz), 1.58 (3H, s), 1.76 (3H, br s), 2.83 (1H, s), 4.12 and 4.43 (each 1H, d, J=9 Hz), 4.76 (1H, t, J=2.5 Hz), and 6.06 (1H, m); ^{13}C NMR (C_5D_5N) δ 10.21, 10.40, 22.30, 26.14, 28.80, 40.64, 42.07, 43.51, 46.05, 46.73, 51.20, 72.82, 77.64, 84.11, 108.15, 126.35, 161.46, 169.12, 196.79, and 207.41; MS *m/e* (%) 376 (M^+; 15), 358 (16), 332 (29), 303 (46), and 95 (100); Found: *m/e* 376.1514. Calcd for $C_{20}H_{24}O_7$: M 376.1520.

Methylation of hemiacetal (**14**; 20 mg) in tetrahydrofuran (5 ml) with an excess of diazomethane in ether at room temperature overnight gave a reaction mixture, which was subjected to separation by preparative TLC to afford an *O*-methyl oxirane derivative (**15**; 7 mg), mp 274—277 °C (from acetone–hexane), $[\alpha]_D^{22}$ −65° (*c* 0.46, $CHCl_3$); IR (Nujol) 3220, 1730, 1680, and 1240 cm^{-1}; UV (EtOH) 238 nm (ε 9500); ^1H NMR ($CDCl_3$) δ 0.81 (3H, d, J=7 Hz; $C_{(13)}$-CH_3), 1.29 (3H, s; $C_{(10)}$-CH_3), 1.95 (3H, br s; $C_{(4)}$-CH_3), 2.63 (1H, s; $C_{(9)}$-H), 2.57 and 3.26 (each 1H, d, J=5.5 Hz; -CH_2-), 3.56 (1H, s; $C_{(1)}$-H), 3.70 (3H, s; -OCH_3), 3.80 and 4.07 (each 1H, d, J=9 Hz; $C_{(20)}$-H), 4.49 (1H, t, J=2.5 Hz; $C_{(7)}$-H), 6.00 (1H m; $C_{(3)}$-H), and 7.45 (1H, s; -OH); ^{13}C NMR ($CDCl_3$) δ 9.8 q, 10.3 q, 22.5 q, 25.7 t, 28.7 t, 29.3 d, 42.8 d, 43.3 d, 44.7 s, 45.5 t, 46.3 s, 49.3 d, 61.5 q, 64.5 s, 72.1 t, 78.0 d, 93.4 d, 106.7 s, 127.0 d, 160.4 s, 169.8 s, and 195.0 s; MS *m/e* (%) 404 (M^+; 100), 374 (60), and 165 (80); Found: *m/e* 404.1855. Calcd for $C_{22}H_{28}O_7$: M 404.1835.

Conversion of Hemiacetal (14) into Shinjudilactone (1) and Its 13-Epimer (12). Hemiacetal (**14**; 16 mg) was heated with sodium hydrogencarbonate (10 mg) in aqueous methanol (4 ml) for 30 min to afford a mixture (11 mg) of shinjudilactone (**1**) and its 13-epimer (**12**). The physical and spectral data of these compounds, after separation by preparative TLC, were completely identical with those of authentic samples, respectively.

Inhibitory Activities. Inhibitory effects (ID_{50}) against HeLa cells were >10 μg/ml, >10 μg/ml, and 0.01—0.1 μg/ml for shinjudilactone (**1**), shinjulactone C (**2**), and ailanthone (**3**), respectively.

The authors wish to thank Dr. Wataru Tanaka and Dr. Kunihiro Niijima of Nippon Kayaku Co., for extraction of materials and the biological assay and Mr. Eiichi Ishii of the Botanical Gardens, Faculty of Science, The University of Tokyo, for collecting *Ailanthus altissima* Swingle. They also would like to thank Mr. Kazuhiro Matsushita of JEOL Co., for measurement of NMR spectra.

References

1) Preliminary accounts of this reports: M. Ishibashi, T. Murae, H. Hirota, H. Naora, T. Tsuyuki, T. Takahashi, A. Itai, and Y. Iitaka, *Chem. Lett.*, **1981**, 1597; M. Ishibashi, T. Murae, H. Hirota, T. Tsuyuki, T. Takahashi, A. Itai, and Y. Iitaka, *Tetrahedron Lett.*, **23**, 1205 (1982); M. Ishibashi, T. Tsuyuki, T. Murae, and T. Takahashi, *Chem. Pharm. Bull.*, **30**, 1917 (1982).

2) a) J. Polonsky, *Fortschr. Chem. Org. Naturst.*, **30**, 101 (1973) and references cited therein; b) T. Murae, A. Sugie, T. Tsuyuki, and T. Takahashi, *Chem. Pharm. Bull.*, **23**, 2188 (1975) and references cited therein.

3) C. Moretti, J. Polonsky, M. Vuilhorgne, and T. Prange, *Tetrahedron Lett.*, **23**, 647 (1982) and references cited therein.
4) *E.g.* P. A. Grieco, S. Ferriño, G. Vidari, *J. Am. Chem. Soc.*, **102**, 7587 (1980); L. Mandell, D. E. Lee, and L. F. Courtney, *J. Org. Chem.*, **47**, 610 (1982); P. A. Grieco, R. Lis, S. Ferriño, and J. Y. Jaw, *ibid.*, **47**, 601 (1982).
5) H. Hikino, T. Ohta, and T. Takemoto, *Phytochemistry*, **14**, 2473 (1975) and references cited therein.
6) C. G. Casinovi, V. Bellavita, G. Grandolini, and P. Ceccherelli, *Tetrahedron Lett.*, **1965**, 2273.
7) W. Stöcklin, M. Stefanović. T. A. Geissman, and C. G. Casinovi, *Tetrahedron Lett.*, **1970**, 2399.
8) a) J. Polonsky and J.-L. Fourrey, *Tetrahedron Lett.*, **1964**, 3983; b) A. Gaudemer, J.-L. Fourrey, and J. Polonsky, *Bull. Soc. Chim. Fr.*, **1967**, 1676.
9) C. G. Casinovi, P. Ceccherelli, G. Grandolini, and V. Bellavita, *Tetrahedron Lett.*, **1964**, 3991.
10) H. Naora, T. Furuno, M. Ishibashi, T. Tsuyuki, T. Takahashi, A. Itai, Y. Iitaka, and J. Polonsky, *Chem. Lett.*, **1982**, 661.
11) A. Gaudemer and J. Polonsky, *Phytochemistry*, **4**, 149 (1965).
12) J. Polonsky, Z. Varon, H. Jacquemin, and G. R. Pettit, *Experientia*, **34**, 1122 (1978).
13) J. Moron, J. Rondest, and J. Polonsky, *Experientia*, **22**, 511 (1966); S. M. Kupchan and J. A. Lacadie, *J. Org. Chem.*, **40**, 654 (1975).
14) H. Naora, M. Ishibashi, T. Furuno, T. Tsuyuki, T. Murae, H. Hirota, T. Takahashi, A. Itai, and Y. Iitaka, *Bull. Chem. Soc. Jpn.*, **56**, 3694 (1983).
15) R. E. Mitchell, W. Stöcklin, M. Stefanović, and T. A. Geissman, *Phytochemistry*, **10**, 411 (1971).
16) a) J. Polonsky and N. Bourguignon-Zylber, *Bull. Soc. Chim. Fr.*, **1965**, 2793; b) J. Polonsky, Z. Baskévitchi, H. E. Gottlieb, E. W. Hagaman, and E. Wenkert, *J. Org. Chem.*, **40**, 2499 (1975).
17) T. Furuno, H. Naora, T. Murae, H. Hirota, T. Tsuyuki, T. Takahashi, A. Itai, Y. Iitaka, and K. Matsushita, *Chem. Lett.*, **1981**, 1797.
18) T. Murae and T. Takahashi, *Bull. Chem. Soc. Jpn.*, **54**, 941 (1981).
19) Numbering refers to the nomenclature described in the Chemical Abstracts.
20) The complete F_o-F_c data, anisotropic temperature factors, atomic positional parameters and isotropic temperature factors for hydrogen atoms, and bond lengths and bond angles containing hydrogen atoms are deposited as Document No. 8354 at the Office of the Editor of Bull. Chem. Soc. Jpn.
21) M. Ishibashi, T. Tsuyuki, and T. Takahashi, *Tetrahedron Lett.*, **24**, 4843 (1983).
22) When glaucanol in pyridine was heated under reflux, inversion of 9α-H occurred. J. Polonsky, Cl. Fouquey, and A. Gaudemer, *Bull. Soc. Chim. Fr.*, **1964**, 1818.
23) M. Ochi, K. Hirotsu, I. Miura, and T. Kubota, *J. Chem. Soc., Chem. Commun.*, **1982**, 810.

 © 1983 The Chemical Society of Japan Bull. Chem. Soc. Jpn., 56, 3694—3698 (1983) [Vol. 56, No. 12

Structure Determination of Bitter Principles in *Ailanthus altissima*. Structure of Shinjulactone A and Revised Structure of Ailanthone[1]

Hirokazu NAORA, Masami ISHIBASHI, Tetsuo FURUNO, Takahiko TSUYUKI, Tatsushi MURAE, Hiroshi HIROTA, Takeyoshi TAKAHASHI,* Akiko ITAI,† and Yoichi IITAKA†

Department of Chemistry, Faculty of Science, The University of Tokyo, Hongo, Bunkyo-ku, Tokyo 113
†*Department of Pharmaceutical Science, The University of Tokyo, Hongo, Bunkyo-ku, Tokyo 113*

(Received June 29, 1983)

The structure of a new bitter principle, shinjulactone A, isolated from *Ailanthus altissima* SWINGLE was determined to be 11β,20-epoxy-1β,2α,11α,12α-tetrahydroxypicrasa-3,13(21)-dien-16-one and the configuration of a hydroxyl group at C-12 of ailanthone was revised to α-orientation by X-ray analysis.

Bitter principles of Simaroubaceous plants have been extensively investigated and a number of quassinoids have been reported.[2] In connection with our studies on bitter principles of *Picrasma ailanthoides* PLANCHON,[3] constituents of *Ailanthus altissima* SWINGLE (=*A. glandulosa* DESF.; Japanese name: Shinju or Niwaurushi) grown in Japan were examined and some of new picrasane derivatives were reported.[4-7] This paper deals with structural elucidation of a new bitter principle, shinjulactone A (**1**), isolated from the stem bark of the plant and also describes structural revision of ailanthone (**2**), a main bitter principle of the plant.

Concentrated methanolic extract of the stem bark of *A. altissima* was separated by silica-gel column chromatography to afford ailanthone (**2**)[8,9] in 0.05% yield and a crude new quassinoid together with other bitter principles. The new quassinoid was subjected to further separation by silicic acid-Celite column chromatography and crystallization to afford a new cytotoxic[10] bitter principle, shinjulactone A (**1**) in 0.002% yield.

Shinjulactone A (**1**), mp 245—245.5 °C (decomp) was shown to have a molecular formula, $C_{20}H_{26}O_7$ by high-resolution mass spectrum, and the IR and UV spectra showed the presence of hydroxyl(s) and δ-lactone and the absence of an α,β-unsaturated carbonyl group. Comparison of the ^1H and ^{13}C NMR spectra of **1** with those of ailanthone (**2**) could lead to the structure (**1**) for shinjulactone A except for the configuration of hydroxyl groups (see Tables 1 and 2).

The configuration of the hydroxyl groups at C-1 and C-12[11] could be established for **1** by NOE measurement operated at 270 MHz. On saturation of the signal due to $C_{(1)}$–H, the signals due to $C_{(9\alpha)}$–H and $C_{(5\alpha)}$–H showed increase by 12 and 5%, respectively. When the resonance frequency of $C_{(9\alpha)}$–H was irradiated, increase of signals due to $C_{(1)}$–H and $C_{(5\alpha)}$–H by 9 and 6% was observed, respectively. These observations imply the $C_{(1\alpha)}$–H and $C_{(1\beta)}$–OH orientations. On irradiation at the frequency of $C_{(12)}$–H, counterpart signals resonating in high field of an AB quartet signal due to $C_{(20\beta)}$–hemiacetal bridge methylene resulted in increase by 4%. Thus the orientation of the $C_{(12)}$–H was determined to be in β-orientation. The configuration of the hydroxyl group at C-2 was determined by differential NOE measurement operated at 400 MHz; on saturation of the singlet signal at δ 1.68 due to $C_{(10\beta)}$–CH_3, the multiplet signal at δ 4.62 due to $C_{(2)}$–H caused increase in area, indicating the $C_{(2\beta)}$–H and $C_{(2\alpha)}$–OH orientation. From these observations, the structure (**1**) having 1β-OH, 2α-OH, and 12α-OH configurations, is proposed for shinjulactone A.

In regard to the configuration at C-12, however, a

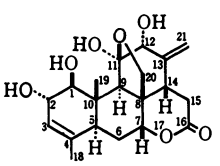

1

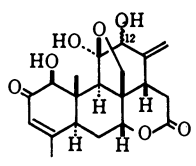

2 12α-OH

3 12β-OH

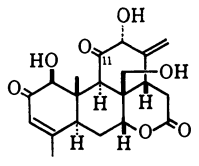

4

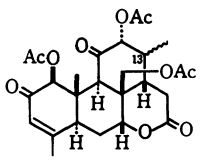

5 13β-CH_3

6 13α-CH_3

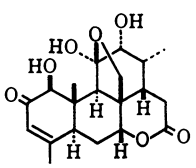

7

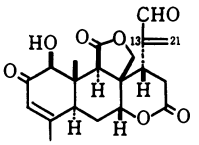

8

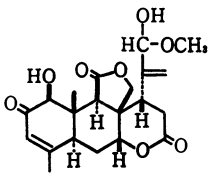

9

Table 1. ^{1}H NMR Spectra of **1**, **2**, **8**, and **9**[a]

Assignment	**1**[b]	**2**[c]	**8**[d]	**9**[e]
1-H	4.02 d (8)	4.54 s	4.20 s	4.59 s
2-H	4.62 m	—	—	—
3-H	5.79 br s	6.13 br s	6.10 br s	6.09 br s
5-H	2.67 br d (13)	3.07 br d (13)		
6α-H	2.07 ddd (15, 2.5, 2.5)	2.22 br d (14)	2.0—3.7[f]	2.0—3.3[f]
6β-H	1.92 ddd (15, 13, 2.5)	2.05 br dd (14, 13)		
7-H	4.57 t (2.5)	4.64 br s	4.61 t (2.5)	3.92 t (2.5)
9-H	3.30 s	3.53 s	2.84 s	3.34 s
12-H	4.59 s	4.46 s	9.55 s[g]	5.30 br s[h]
14-H	2.80 dd (13.5, 5.5)	2.83 dd (13, 5)		
15α-H	3.57 dd (18, 13.5)	3.69 dd (18, 13)	2.0—3.7[f]	2.0—3.3[f]
15β-H	2.90 dd (18, 5.5)	2.90 dd (18, 5)		
4-CH_3	1.60 br s	1.78 br s	2.20 br s	1.80 br s
10-CH_3	1.68 s	1.52 s	0.92 s	1.04 s
20-CH_2	3.67 d (8)	3.66 d (8)	3.89 d (11)	3.86 d (11)
	4.17 d (8)	4.11 d (8)	4.40 d (11)	4.25 d (11)
21-CH_2	5.20 d (2)	5.19 br s	6.33 br s	5.84 br s
	5.28 d (2)	5.28 br s	6.54 br s	5.95 br s
-OCH_3	—	—	—	3.60 s

a) Chemical shifts are expressed in δ downfield from TMS as an internal standard and coupling constants in Hz in parantheses; s: singlet, d: doublet, t: triplet. b) In pyr-d_5 at 400 MHz. c) pyr-d_5+2% $CDCl_3$ at 400 MHz. d) $CDCl_3$ at 90 MHz. e) pyr-d_5 at 90 MHz. f) Not assignable. g) An aldehyde proton. h) A methine proton of a hemiacetal.

Table 2. ^{13}C NMR Spectra of **1**, **2**, **8**, and **9**[a]

Assignment No. of C	**1**[b]	**2**[c]	**8**[d]	**9**[e]
1	83.6	84.4	83.6	84.7
2	72.7	197.3	196.0	196.9
3	127.1	126.2	125.8	126.5
4	134.8	162.1	161.1	160.5
5	49.6	44.8	44.3	51.7
6	26.2	26.2	25.9	25.5
7	79.2	78.5	77.8	66.4
8	45.8	45.7	43.9	48.4
9	48.0	48.0	48.2	55.4
10	44.9	45.5	40.0	44.7
11	110.5	110.3	174.7	178.2
12	80.7	80.6	193.6	95.1
13	148.0	147.4	144.8	146.4
14	41.9	42.5	35.7	40.9
15	35.4	35.3	30.9	31.3
16	169.6	169.4	168.0	172.0
18	21.2	22.5	22.7	22.3
19	10.6	10.3	10.6	10.4
20	72.7	72.3	71.3	69.8
21	118.0	118.2	139.0	112.0
-OCH_3	—	—	—	45.5

a) Chemical shifts are expressed in δ downfield from TMS as an internal standard. b) pyr-d_5 at 22.5 MHz. c) pyr-d_5 at 25 MHz. d) $CDCl_3$ at 22.5 MHz. e) pyr-d_5 at 22.5 MHz.

discrepancy between shinjulactone A and ailanthone arose. Two different structures (**3** and **4**) have been proposed for ailanthone so far. A hemiacetal structure (**3**), in which the $C_{(12)}$-OH was assigned to be β-equatorial, has been proposed for ailanthone by Polonsky *et al.*;[9] ailanthone was hydrogenated and followed by acetylation to afford dihydroailanthone triacetate (**5**), whose coupling constant between $C_{(12)}$-H and $C_{(13)}$-H was 8 Hz. A comparison of the coupling constant with that ($J_{12,13}$=3 Hz) observed in chaparrinone triacetate (**6**) led to the conclusion that the orientations of the $C_{(12)}$-OH groups of ailanthone and chaparrinone (**7**) were β-equatorial and α-axial configurations, respectively. On the other hand, Casinovi *et al.*[8b] proposed a $C_{(11)}$-keto structure (**4**) with 12α(axial)-OH configuration.

The structure of ailanthone was reinvestigated by NOE measurement of ^{1}H NMR spectrum in pyridine-d_5 solution and the $C_{(12)}$-H was suggested to be in β-equatorial disposition; on irradiation at δ 4.46 due to $C_{(12)}$-H, a signal resonating at δ 5.28 due to one of olefinic protons at C-21 showed an increase by 6%, and the irradiation at δ 5.28 resulted in increase in area of the signal due to $C_{(12)}$-H by 10%.

In order to establish the structure of ailanthone unambiguously, a single crystal obtained from chloroform–methanol solution was subjected to X-ray diffraction analysis. The crystal belongs to an orthorhombic space group $P2_12_12_1$, and the lattice parameters are a=17.067(8), b=16.608(8), and c=6.594(2) Å with four ailanthone molecules and four water molecules in a unit cell. Intensity data were measured on a PW1100 four-circle diffractometer using Cu $K\alpha$ radiation monochromated by a graphite plate. A total of 1874 independent structure factors with $F_o \geq 2.5\,\sigma(F_o)$ within 2θ=156°

Table 3. Atomic positional parameters ($\times 10^4$) and isotropic temperature factors ($\times 10^2$) for non-hydrogen atoms of ailanthone (**2**) with estimated standard deviations in parentheses

Atom	x	y	z	B_{eq} [a]
O(1)	-1030(1)	2763(1)	1173(3)	369(3)
O(2)	-2285(1)	2275(2)	-920(3)	469(4)
O(3)	-272(1)	2800(1)	4572(4)	312(3)
O(4)	1209(1)	2914(1)	2700(4)	419(3)
O(5)	1870(1)	17(1)	-1297(4)	402(3)
O(6)	921(1)	-167(1)	836(4)	236(3)
O(7)	104(1)	1660(1)	6213(3)	289(3)
C(1)	-1003(2)	1986(2)	313(4)	304(3)
C(2)	-1788(2)	1766(2)	-598(5)	361(4)
C(3)	-1895(2)	923(2)	-1162(6)	308(4)
C(4)	-1386(2)	353(2)	-619(5)	259(4)
C(5)	-670(2)	549(2)	644(4)	212(3)
C(6)	-385(2)	-152(2)	1982(5)	229(4)
C(7)	447(2)	1(2)	2654(5)	243(4)
C(8)	582(2)	828(2)	3550(4)	214(3)
C(9)	116(1)	1550(1)	2625(4)	227(3)
C(10)	-730(1)	1348(2)	1879(4)	234(3)
C(11)	228(2)	2140(2)	4420(4)	234(3)
C(12)	1081(2)	2443(2)	4493(5)	219(4)
C(13)	1651(2)	1761(2)	4719(5)	231(4)
C(14)	1472(2)	1001(2)	3538(4)	224(3)
C(15)	1781(2)	1001(2)	1355(5)	282(4)
C(16)	1544(2)	264(2)	224(5)	312(4)
C(18)	-1467(2)	-496(2)	-1393(6)	223(5)
C(19)	-1349(2)	1292(2)	3574(5)	330(4)
C(20)	306(2)	845(2)	5770(5)	310(4)
C(21)	2252(2)	1812(2)	5984(6)	278(5)

a) $B_{eq} = 8\pi^2(u_1^2+u_2^2+u_3^2)/3$.

were obtained by $2\theta-\theta$ scanning mode. The structure was solved by the direct method using MULTAN program and was refined by the block-diagonal least-squares method. All hydrogen atoms, except for those of O(3) hydroxyl and water molecule, were located in a different electron density map. The final R-value was 0.043 using anisotropic temperature factors for the non-hydrogen atoms and isotropic ones for hydrogen

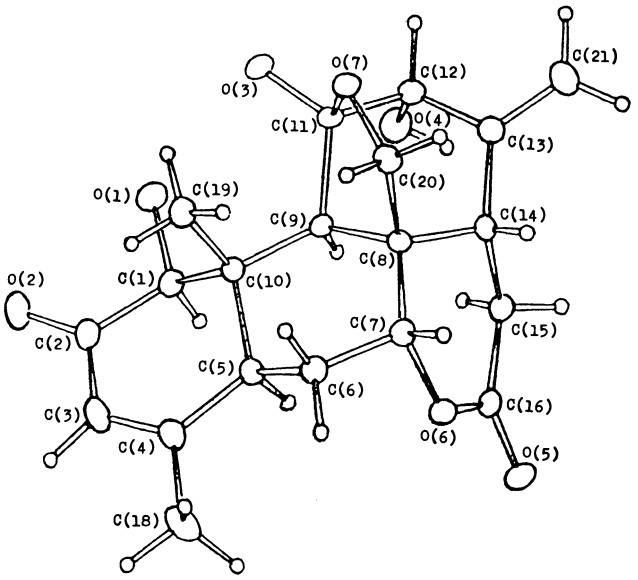

Fig. 1. Perspective view of ailanthone (**2**).[a]
a) For clarity hydrogen atoms are represented by spheres of arbitrary radius.

atoms. The final atomic coordinates are listed in Table 3 and bond lengths and bond angles are listed in Tables 4 and 5.[12] The hemiacetal structure and the $C_{(12\alpha)}$–OH configuration were clearly established as shown in Fig. 1. Molecules were strongly linked by the four hydrogen bondings, one is an intermolecular hydrogen bond between O(2) carbonyl and O(4) hydroxyl, and the others are between water and O(1) hydroxyl, O(3) hydroxyl, and O(5) lactone carbonyl in the three different ailanthone molecules. The distances are 2.843(4), 2.709(3), 2.861(3), and 3.007(4) Å, respectively.

The structure of ailanthone was thus shown to be revised to 11β,20-epoxy-1β,11α,12α-trihydroxypicrasa-3,13(21)-dien-2,16-dione (**2**) and the X-ray analysis also proved that the C-ring exists in a chair conformation. Therefore, when the hydrogenation occurs from

Table 4. Bond lengths of ailanthone (**2**) with estimated standard deviations in parentheses

Bond length		l/Å	Bond length		l/Å
Atom 1	Atom 2		Atom 1	Atom 2	
O(1)	–C(1)	1.410(3)	C(5)	–C(10)	1.560(4)
O(2)	–C(2)	1.218(4)	C(6)	–C(7)	1.509(4)
O(3)	–C(11)	1.393(3)	C(7)	–C(8)	1.514(4)
O(4)	–C(12)	1.434(4)	C(8)	–C(9)	1.563(4)
O(5)	–C(16)	1.218(4)	C(8)	–C(14)	1.546(4)
O(6)	–C(7)	1.472(4)	C(8)	–C(20)	1.538(4)
O(6)	–C(16)	1.345(3)	C(9)	–C(10)	1.563(4)
O(7)	–C(11)	1.442(3)	C(9)	–C(11)	1.548(4)
O(7)	–C(20)	1.427(4)	C(10)	–C(19)	1.540(4)
C(1)	–C(2)	1.513(4)	C(11)	–C(12)	1.541(4)
C(1)	–C(10)	1.551(4)	C(12)	–C(13)	1.500(4)
C(2)	–C(3)	1.459(5)	C(13)	–C(14)	1.514(4)
C(3)	–C(4)	1.334(4)	C(13)	–C(21)	1.324(5)
C(4)	–C(5)	1.515(4)	C(14)	–C(15)	1.533(4)
C(4)	–C(18)	1.506(5)	C(15)	–C(16)	1.489(4)
C(5)	–C(6)	1.539(4)			

Table 5. Bond angles of ailanthone (2) with estimated standard deviations in parentheses

Bond angle			ϕ/°	Bond angle			ϕ/°
Atom 1	Atom 2	Atom 3		Atom 1	Atom 2	Atom 3	
C(7)	-O(6)	-C(16)	125.4(2)	C(8)	-C(9)	-C(11)	97.2(2)
C(11)	-O(7)	-C(20)	108.7(2)	C(19)	-C(10)	-C(1)	108.6(2)
C(2)	-C(1)	-O(1)	110.6(2)	C(19)	-C(10)	-C(5)	111.9(2)
C(2)	-C(1)	-C(10)	111.3(2)	C(19)	-C(10)	-C(9)	114.7(2)
O(1)	-C(1)	-C(10)	111.5(2)	C(1)	-C(10)	-C(5)	104.7(2)
C(3)	-C(2)	-O(2)	122.3(3)	C(1)	-C(10)	-C(9)	109.9(2)
C(3)	-C(2)	-C(1)	116.4(3)	C(5)	-C(10)	-C(9)	106.6(2)
O(2)	-C(2)	-C(1)	121.2(3)	C(12)	-C(11)	-O(3)	108.7(2)
C(4)	-C(3)	-C(2)	122.1(3)	C(12)	-C(11)	-O(7)	107.1(2)
C(5)	-C(4)	-C(3)	121.3(3)	C(12)	-C(11)	-C(9)	110.3(2)
C(5)	-C(4)	-C(18)	117.5(3)	O(3)	-C(11)	-O(7)	106.6(2)
C(3)	-C(4)	-C(18)	120.9(3)	O(3)	-C(11)	-C(9)	118.5(2)
C(6)	-C(5)	-C(4)	114.0(2)	O(7)	-C(11)	-C(9)	105.0(2)
C(6)	-C(5)	-C(10)	111.4(2)	C(13)	-C(12)	-O(4)	113.3(2)
C(4)	-C(5)	-C(10)	114.6(2)	C(13)	-C(12)	-C(11)	111.7(2)
C(7)	-C(6)	-C(5)	109.8(2)	O(4)	-C(12)	-C(11)	107.2(2)
C(8)	-C(7)	-O(6)	113.9(2)	C(14)	-C(13)	-C(12)	116.5(2)
C(8)	-C(7)	-C(6)	114.2(2)	C(14)	-C(13)	-C(21)	122.3(3)
O(6)	-C(7)	-C(6)	104.2(2)	C(12)	-C(13)	-C(21)	121.1(3)
C(9)	-C(8)	-C(7)	117.8(2)	C(15)	-C(14)	-C(8)	110.1(2)
C(9)	-C(8)	-C(14)	110.8(2)	C(15)	-C(14)	-C(13)	114.4(2)
C(9)	-C(8)	-C(20)	101.6(2)	C(8)	-C(14)	-C(13)	110.6(2)
C(7)	-C(8)	-C(14)	108.5(2)	C(16)	-C(15)	-C(14)	112.2(2)
C(7)	-C(8)	-C(20)	109.9(2)	O(5)	-C(16)	-O(6)	115.4(3)
C(14)	-C(8)	-C(20)	107.6(2)	O(5)	-C(16)	-C(15)	124.4(3)
C(10)	-C(9)	-C(8)	115.4(2)	O(6)	-C(16)	-C(15)	120.1(2)
C(10)	-C(9)	-C(11)	119.4(2)	O(7)	-C(20)	-C(8)	106.6(2)

α-side, the *exo*-methylene group would produce a β-axial methyl group at C-13. Since the β-axial methyl group at C-13 would bring about an unstable diaxial relationship with the 12α-axial hydroxyl group, it seems most likely that an inversion of the C-ring occurs to adopt a stable boat conformation. The ring-inversion resulted in a large dihedral angle between 12-H and 13-H, which could reasonably explain the large coupling constant ($J_{12,13}$=8 Hz) for dihydroailanthone triacetate (**5**) stated above.[9]

The structure, 11β,20-epoxy-1β,2α,11α,12α-tetrahydroxypicrasa-3,13(21)-dien-16-one (**1**) proposed for shinjulactone A, was further confirmed by chemical conversion of **1** into **2**. Shinjulactone A (**1**) was oxidized with manganese dioxide in dichloromethane at room temperature to give two products, one of which was found to be identical with ailanthone (**2**). The other was identical with an oxidation product of ailanthone (**2**) with lead tetraacetate. The molecular formula, $C_{20}H_{22}O_7$, was determined by high resolution mass spectrum, and the UV and IR spectra suggest the presence of an α-substituted α,β-unsaturated aldehyde group (λ_{max} 221 nm and ν_{max} 2850 and 1685 cm^{-1}), an α,β-unsaturated ketone (λ_{max} 238 nm and ν_{max} 1685 cm^{-1}), and δ- and γ-lactone groupings (ν_{max} 1730 and 1775 cm^{-1}, respectively). Examination of ^{1}H and ^{13}C NMR spectra (Tables 1 and 2) and mass spectrum (see Experimental) and mechanistic consideration (Fig. 2) lead to the formulation of an 11,12-seco structure (**8**) for the

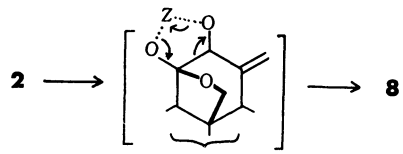

Z: oxidizing agent

Fig. 2.

oxidation product. On treatment with methanol, the compound (**8**) easily afforded a hemiacetal (**9**). The spectral data of **9** were compatible with the suggested structure.

Experimental

General Procedure. All melting points were measured on a Mel-temp capillary melting point apparatus (Laboratory Devices) and uncorrected. Optical rotations and circular dichroism (CD) were determined on a JASCO polarimeter DIP-181 and a JASCO Model J-15 spectrometer, respectively. Ultraviolet absorption (UV) and infrared (IR) spectra were measured on a Hitachi 340 and a Hitachi 260-30 spectrometer, respectively. Mass (MS) spectra were run on a Hitachi RMU-6 Tokugata mass spectrometer and high-resolution mass spectra on a JEOL JMS-D300 mass spectrometer operating at 70 eV. Proton nuclear magnetic resonance (^{1}H NMR) spectra were taken using a Varian EM390 (90 MHz), JEOL FX90Q (90 MHz), Brucker WH 270 (270 MHz), and JEOL FX400 (400 MHz). Carbon-13 nuclear magnetic resonance

(^{13}C NMR) spectra were taken on a JEOL FX90Q (22.5 MHz) and a JEOL FX100 (25 MHz). Chemical shifts were expressed in δ (ppm) downfield from tetramethylsilane as an internal standard and coupling constants in Hz. Thin-layer chromatography (TLC) was carried out on Kieselgel 60 GF_{254} coated in 0.25 mm- or 0.5 mm-thickness. Wakogel C-200 (Wako), Silicic acid AR (Mallinckrodt) or Celite No. 545 (Wako) was used for column chromatography. Analytical high performance liquid chromatography (HPLC) was carried out on a Waters Chromatograph ALC/GPS 202/401 at room temperature (column: μBondapack C_{18}; solvent system: MeOH–H_2O, 1 : 1; flow rate: 1.1 ml/min).

Plant Material. Stem bark of *Ailanthus altissima* was collected at the Botanical Gardens, Faculty of Science, The University of Tokyo in July 1979. The bark was air-dried and chipped to afford 9.3 kg of the materials.

Extraction and Separation. The stem bark (9.3 kg) was extracted three times with hot methanol (18 l×3) for 8 h. The combined extracts (*ca.* 50 l) were evaporated under reduced pressure and the residue was treated three times with hot petroleum ether (1.5 l×3) to give a bitter residue (737 g). A part (220 g) of the residue, dissolved in a solution of chloroform (180 ml) and methanol (1.3 l), was adsorbed on silica gel (300 g) and then solvents were removed *in vacuo*. The silica gel was placed on the top of a column of silica gel (2 kg), and the following solvents were passed through the column; chloroform (4 l), 1, 2, 4, 8, 16, 32, 64, and 80% methanol in chloroform (each 4 l), and finally methanol (2 l). The fractions 17 and 18 (each fraction; 1 l) were combined and subjected to fractional crystallization from methanol to give ailanthone (**2**; *ca.* 1.1 g).

The fraction 21 was evaporated and the residue was dissolved in hot methanol. After cooling, the precipitates (mainly sitosteryl glycoside) were filtered off and the filtrate was evaporated, dissolved in chloroform, and subjected to separation by a column of silicic acid and Celite, eluting with 1, 2, 5, 10, 20, and 50% methanol in chloroform. Fractions eluted with 20% and 50% methanol in chloroform were combined and crystallized from chloroform–methanol to give shinjulactone A (**1**; 40 mg). Separation of the fraction 22 under the same conditions afforded additional 17 mg of **1**.

Ailanthone (2). Mp 234—235 °C (lit,[9] mp 234—238 °C), $[\alpha]_D^{20}$ +9.2° (EtOH) (lit,[9] $[\alpha]_D$ +12.5° (EtOH)); CD $[\theta]_{310}$ +977 and $[\theta]_{260}$ +1379.

Shinjulactone A (1). Mp 245—245.5 °C (decomp, from MeOH and $CHCl_3$); $[\alpha]_D^{20}$ +2° (*c* 0.97, C_5H_5N); IR (Nujol) 3500, 3400, and 1740 cm^{-1}; ^{1}H NMR and ^{13}C NMR (Tables 1 and 2); MS *m/e* (%) 378 (M^+; 52), 363 (64), 360 (100), 345 (66), 342 (13), and 316 (100); Found: *m/e* 378.1634. Calcd for $C_{20}H_{26}O_7$: M 378.1679.

Oxidation of 1 with Manganese Dioxide. A solution of shinjulactone A (**1**; 14 mg) in dichloromethane (10 ml) was treated with manganese dioxide (200 mg, prepared by Attenburrow's procedure[13]) for 21 h at room temperature. After the usual work-up, the reaction mixture was separated by preparative TLC developed with methanol–chloroform (1 : 19). Ailanthone (**2**; 3.6 mg) was identified by HPLC (R_t= 6.4 min), MS, and FT-^{1}H NMR. The aldehyde (**8**; 0.7 mg) was identical with the oxidation product of **2** with lead tetraacetate (*vide infra*). Treatment with methanol in the presence of silica gel, the aldehyde (**8**) was converted into a hemiacetal (**9**), mp 203—205 °C (from acetone); IR (KBr) 3450, 1770 (sh), 1740, 1680, and 1035 cm^{-1}; UV (EtOH) 238 nm (ε 10000); ^{1}H and ^{13}C NMR (Tables 1 and 2); MS *m/e* 406 (M^+; 7), 388 (3), 374 (15), 356 (6), 151 (32), and 91 (100); Found: *m/e* 406.1632. Calcd for $C_{21}H_{26}O_8$: M 406.1627.

Oxidation of 2 with Lead Tetraacetate. Ailanthone (**2**; 26 mg) was treated with lead tetraacetate (36 mg) in 90% aqueous acetic acid (3 ml) at room temperature for 1 h. The reaction product was worked up as usual to afford the aldehyde (**8**) in a quantitative yield, mp 211—214 °C (from acetone); IR (KBr) 3450, 1775, 1730, 1685, and 1240 cm^{-1}; UV (EtOH) 238 nm (sh, ε 9700) and 221 nm (ε 12000); ^{1}H and ^{13}C NMR (Tables 1 and 2); MS *m/e* (%) 374 (M^+; 55), 356 (25), 346 (90), 246 (35), and 151 (100); Found: *m/e* 374.1362. Calcd for $C_{20}H_{22}O_7$: M 374.1366.

The authors wish to thank Professor J. Polonsky of C. N. R. S., France, for measurement of ^{1}H NMR spectrum of ailanthone. They also thank Mr. Kazuhiro Matsushita of JEOL Co. Ltd. for measurement of NMR spectra and Mr. Eiichi Ishii of the Botanical Gardens, Faculty of Science, The University of Tokyo, for collecting *Ailanthus altissima* Swingle.

References

1) A part of this work was reported in a preliminary form: H. Naora, T. Furuno, M. Ishibashi, T. Tsuyuki, T. Takahashi, A. Itai, Y. Iitaka, and J. Polonsky, *Chem. Lett.*, **1982**, 661.

2) J. Polonsky, *Fortschr. Chem. Org. Naturst.*, **30**, 101 (1973) and references cited therein.

3) T. Murae, A. Sugie, T. Tsuyuki, and T. Takahashi, *Chem. Pharm. Bull.*, **23**, 2188 (1975) and references cited therein.

4) M. Ishibashi, T. Murae, H. Hirota, H. Naora, T. Tsuyuki, T. Takahashi, A. Itai, and Y. Iitaka, *Chem. Lett.*, **1981**, 1597.

5) T. Furuno, H. Naora, T. Murae, H. Hirota, T. Tsuyuki, T. Takahashi, A. Itai, Y. Iitaka, and K. Matsushita, *Chem. Lett.*, **1981**, 1797.

6) M. Ishibashi, T. Murae, H. Hirota, T. Tsuyuki, T. Takahashi, A. Itai, and Y. Iitaka, *Tetrahedron Lett.*, **23**, 1205 (1982).

7) M. Ishibashi, T. Tsuyuki, T. Murae, H. Hirota, T. Takahashi, A. Itai, and Y. Iitaka, *Bull. Chem. Soc. Jpn.*, **56**, 3683 (1983).

8) a) C. G. Casinovi and G. Grandolini, *Accad. Naz. Linc.*, **35**, 348 (1963); b) C.G. Casinovi, P. Ceccherelli, G.Grandolini, and V. Bellavita, *Tetrahedron Lett.*, **1964**, 3991.

9) J. Polonsky and J.-L. Fourrey, *Tetrahedron Lett.*, **1964**, 3983; A. Gaudemer, J.-L. Fourrey, and J. Polonsky, *Bull. Soc. Chim. Fr.*, **1967**, 1676.

10) Inhibitory effect (ID_{50}) against HeLa cells was 0.1—1.0 μg/ml.

11) Numbering of picrasane skeleton refers to the nomenclature described in the Chemical Abstracts.

12) The complete F_o-F_c data, anisotropic temperature factors, atomic positional parameters and isotropic temperature factors for hydrogen atoms, and bond lengths and bond angles containing hydrogen atoms are deposited as Document No. 8355 at the Office of the Editor of Bull. Chem. Soc. Jpn.

13) J. Attenburrow, A. F. B. Cameron, J. H. Chapman, R. M. Evans, B. A. Hems, A. B. A. Jansen, and T. Walker, *J. Chem. Soc.*, **1952**, 1094.

 © 1983 The Chemical Society of Japan Bull. Chem. Soc. Jpn., 56, 3699—3702 (1983)

Studies on the β-Turn of Peptides. VIII.[1] β-Turn Preferences of *N*-Acetyltetrapeptide Methylamides Related to the β-Turn Part of Gramicidin S

Kazuki SATO,* Tsutomu HIGASHIJIMA,† Rika SUGAWARA, and Ukon NAGAI

Mitsubishi-Kasei Institute of Life Sciences, 11 Minamiooya, Machida, Tokyo 194

†*Department of Biophysics and Biochemistry, Faculty of Science, The University of Tokyo, Bunkyo-ku, Tokyo 113*

(Received June 24, 1983)

N-Acetyl-L-Leu–X–L-Pro–L-Val methylamides (**IIa**: X=D-Ala, **IIb**: X=Gly, **IIc**: X=L-Ala) were synthesized and subjected to CD and ^{1}H NMR measurements to study the β-turn preferences of these peptides. Temperature dependences of L-Val^4–NH proton chemical shifts in CD_3OH solution were in the order of **IIa**<**IIb**<**IIc**, suggesting that the populations of the β-turn conformer with 4→1 hydrogen bonding were in the order of **IIa**>**IIb**>**IIc**. This order of β-turn preferences coincides with the order of the magnitudes of the Cotton effects in the CD spectra of the chromophoric derivatives, *N*-(2,4-dinitrophenyl)tetrapeptide *p*-nitroanilides, having the same sequences. This agreement supports the validity of the chiroptical method to study turn tendency of tetrapeptide sequences using chromophoric derivatives reported previously.

CD spectra of *N*-(2,4-dinitrophenyl)tetrapeptide *p*-nitroanilides (Dnp–tetrapeptide–pNA's)[2] exhibit characteristic Cotton effects above 250 nm when they take β-turn conformations. Exciton coupling of the electric transition moments of the two chromophores were assumed to explain the spectra, and the magnitudes of the Cotton effects near 310 and 350 nm were shown to reflect well the β-turn preference of the derivatives.[3] In the case of model peptides (Dnp-L-Leu–X–L-Pro–L-Val–pNA; **Ia**: X=D-Ala, **Ib**: X=Gly, **Ic**: X=L-Ala) related to the β-turn part of gramicidin S (GS), β-turn preferences of the tetrapeptide derivatives (**Ia**>**Ib**>**Ic** ≈0) had strong correlation with antibiotic activities of the GS analogs having the same tetrapeptide sequences at their β-turn parts.[3–5]

A question was raised, however, whether such chiroptical method using chromophoric derivatives as mentioned above reveals the conformational characteristics of the original peptide sequences lacking those chromophoric groups. To answer the question we attempted syntheses and conformational analyses of some *N*-acetyltetrapeptide methylamides (Ac-L-Leu–X–L-Pro–L-Val–NHMe; **IIa**: X=D-Ala, **IIb**: X=Gly, **IIc**: X=L-Ala) related to the β-turn part of GS, and the results were compared with those of Dnp–tetrapeptide–pNA (**Ia**—**c**) having the same tetrapeptide sequences.

Results and Discussion

Syntheses of Peptides (IIa—c). *N*-Acetyltetrapeptide methylamides (**IIa**—**c**) were synthesized by usual solution-phase procedures according to the scheme shown in Fig. 1. Boc–D-Ala–L-Pro–OH[6] and H–L-Val–NHMe were coupled by EDC method to afford Boc–D-Ala–L-Pro–L-Val–NHMe (**IIIa**), which was treated with hydrogen chloride in formic acid. H–D-Ala–L-Pro–L-Val–NHMe·HCl (**IVa**·HCl) obtained was coupled with Boc–L-Leu–ONSu to afford Boc–L-Leu–D-Ala–L-Pro–L-Val–NHMe (**Va**), which was converted to Ac–L-Leu–D-Ala–L-Pro–L-Val–NHMe (**IIa**) by deprotection and subsequent treatment with Ac–ONp. Compounds **IIb** and **IIc** were prepared by a similar manner to that described for the synthesis of **IIa**. Purities of the synthetic peptides were confirmed by TLC with three solvent systems, elemental analyses, amino acid analyses, and also 270 MHz ^{1}H NMR.

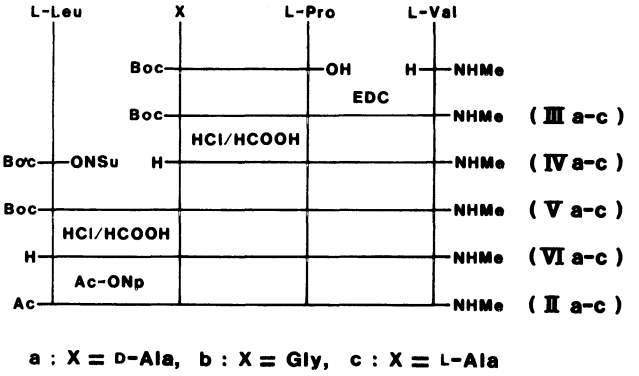

Fig. 1. Synthetic scheme of *N*-acetyltetrapeptide methylamides (**IIa**—**c**).

CD Measurements. CD spectra of **IIa**—**c** were measured in H_2O and in CH_3OH solutions (Fig. 2). In H_2O solution, all the CD spectra showed a minimum near 200 nm (Fig. 2A), suggesting that all the Ac–tetrapeptide–NHMe were in random conformations. Certainly, the magnitudes of Cotton effects (**IIa** : **IIb** : **IIc**=2 : 3 : 4) can be explained by difference in the configurations of component amino acid residues. On the other hand, in CH_3OH solution (Fig. 2B), the magnitudes of the Cotton effects were not so dependent on the configuration of second amino acid residues, and the CD minima were shifted to longer wavelength (**IIa**: 204 nm, **IIb**: 202.5 nm, **IIc**: 201 nm). It is of interest to note that the order of CD minima positions of Ac–tetrapeptide–NHMe (**IIa**—**c**) in CH_3OH solution was the same as that of Dnp–tetrapeptide–pNA near 200 nm (**Ia**: 205 nm, **Ib**: 201.5 nm, **Ic**: 200 nm) in CH_3OH solution (Fig. 2C).

^{1}H NMR Measurements. ^{1}H NMR (270 MHz) of **IIa**—**c** was measured in H_2O and in CD_3OH solutions. All the spectra showed two sets of resonances for most of the protons due to the cis-trans isomerism for the X–L-Pro bonds. The minor set of resonances (<10%) was assigned to the cis isomer from the results of related compounds (**Ia**—**c**).[5] Detailed discussions are described

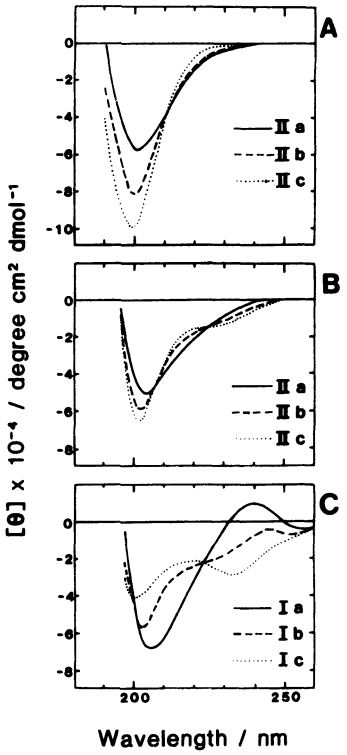

Fig. 2. CD spectra of **IIa—c** in H_2O (A) and in CH_3OH (B) solutions and of **Ia—c** in CH_3OH (C) solutions.

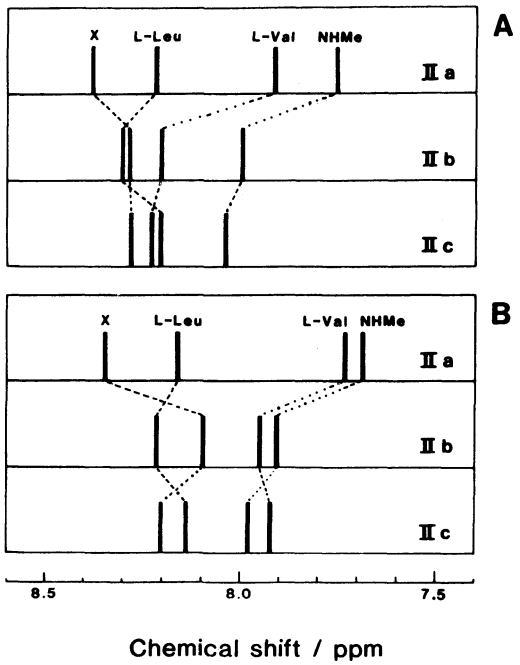

Fig. 3. Chemical shifts of amide protons in major conformer of Ac-L-Leu-X-L-Pro-L-Val-NHMe (**IIa—c**) in H_2O (A) and in CD_3OH (B) solutions.

hereafter for the major (trans) conformers.

Chemical shifts of NH protons of **IIa** spread over a wider range as compared with those of **IIc** which showed ordinary values (Fig. 3). The D-Ala residue of **IIa** showed smaller spin-coupling constant ($^3J_{NH-C_\alpha H}$=5.15 Hz) than the other residues (6—8 Hz) in CD_3OH

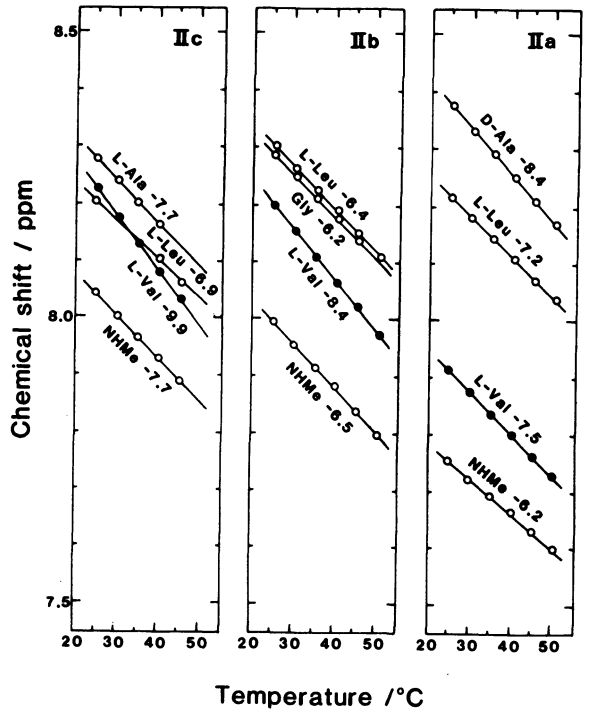

Fig. 4. Temperature dependences of amide proton chemical shifts of major conformers of **IIa—c** in H_2O solutions. Numbers on the lines refer to $10^3\times$ temperature coefficient in ppm $°C^{-1}$.

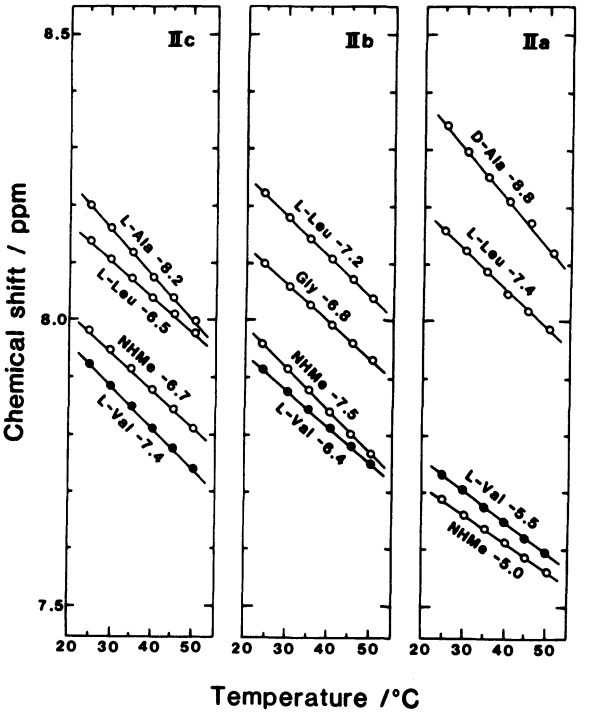

Fig. 5. Temperature dependences of amide proton chemical shifts of major conformers of **IIa—c** in CD_3OH solutions. Numbers on the lines refer to $10^3\times$ temperature coefficient in ppm $°C^{-1}$.

solution, suggesting that the ϕ angle of the D-Ala residue was fixed to a certain extent in CD_3OH solution, whereas the L-Ala residue of **IIc** showed such spin-coupling constant (6.25 Hz) as to be typical to free rotation.

These results suggest that **IIa** has some ordered conformation while **IIc** has unordered one.

The temperature dependences of chemical shifts of amide proton resonances are useful for distinguishing between "exposed" and "intramolecularly hydrogen-bonded" amide proton;[7] exposed protons exhibit larger temperature coefficients than hydrogen-bonded amide protons. All the NH proton resonances of **IIa—c** showed large temperature dependence of chemical shifts in H_2O solution (Fig. 4). In CD_3OH solution (Fig. 5), however, L-Val–NH proton of **IIa** showed a little smaller temperature dependence (-5.5×10^{-3} ppm $°C^{-1}$) than the other NH protons except for NHMe proton, suggesting that the L-Val–NH proton of **IIa** was involved in a weak hydrogen bonding. The fixation of ϕ angle of D-Ala residue of **IIa** suggests that the folded conformation of **IIa** in CD_3OH solution is β-turn conformation with 4→1 hydrogen bonding (L-Leu[1]–CO ···HN–L-Val[4]). The L-Val–NH proton of **IIb** also showed smaller temperature dependence than the other NH protons, but the value (-6.4×10^{-3} ppm $°C^{-1}$) was larger than that of **IIa**. In the case of **IIc**, the L-Val–NH proton showed large temperature dependence (-7.4×10^{-3} ppm $°C^{-1}$). The results of temperature dependences in CD_3OH solutions suggest that the populations of β-turn conformer with 4→1 hydrogen bond concerned by the L-Val–NH group are in the order of **IIa**>**IIb**>**IIc**≈0, although at a quite lower levels than that of Dnp–tetrapeptide–pNA (**Ia—c**); for example, the L-Val–NH proton of **Ia** showed such a small temperature dependence as -2.72×10^{-3} ppm $°C^{-1}$ in CD_3OH solution.[3,5] The small temperature dependence shown by the NHMe proton chemical shift of **IIa** in CD_3OH solution suggests the coexistence of another β-turn conformation having L-Pro–L-Val sequence at the internal position, since L-Pro residue has high bend positional potential at the second $(i+1)$ position of β-turn in the table proposed by Chou and Fasman on the basis of statistical analysis of the X-ray crystallographic data of 29 globular proteins.[8]

β-Turn Preference of Tetrapeptides. CD and NMR spectra of Ac–tetrapeptide–NHMe (**IIa—c**) did not show such large sequence dependences as those found in Dnp–tetrapeptide–pNA (**Ia—c**).[3,5] However, **IIa** and **IIb** are considered to have some populations of β-turn conformer in CH_3OH solution although they seem to take random conformations in H_2O solution. In addition, the order of population of β-turn conformer (**IIa**>**IIb**>**IIc**≈0) was the same as that of Dnp–tetrapeptide–pNA (**Ia—c**). These agreements suggest that introduction of Dnp and pNA groups amplify the intrinsic β-turn preference of parent tetrapeptide without affecting the order of β-turn preferences by stabilization of the β-turn conformer due to the attractive interaction of the two terminal chromophores. Consequently, CD spectra of Dnp–tetrapeptide–pNA are considered to be available for the study of β-turn preferences of the tetrapeptide sequences. Conformational energy calculation of *N*-acetyldi- or tetrapeptide methylamides also supported the validity of the chiroptical method.[9]

Experimental

Syntheses of Peptides. All the melting points were measured on a Yanagimoto micro melting point apparatus and uncorrected. TLC's were carried out on Merck silica gel 60 F_{254} plates with the following solvent systems: R_f^1, $CHCl_3$–CH_3OH (5 : 1, v/v); R_f^2, $CHCl_3$–CH_3OH–AcOH (95 : 5 : 1, v/v); R_f^3, *n*-BuOH–AcOH–pyridine–H_2O (4 : 1 : 1 : 2, v/v). Optical rotations were measured on an Union automatic polarimeter PM-201. Amino acid analyses of peptides were performed by Durrum D-500 amino acid analyzer after hydrolysis in 6 M (1 M=1 mol dm^{-3}) HCl at 105 °C for 20 h. Yields and analytical data of synthetic peptides are summarized in Table 1.

Boc-D-Ala-L-Pro-L-Val-NHMe (IIIa). To a chilled solution of Boc-D-Ala-L-Pro-OH·DCHA (1.40 g, 3 mmol) and H-L-Val-NHMe·HCl (0.50 g, 3 mmol) in $CHCl_3$ (12 ml)

Table 1. Yields and analytical data of synthetic peptides

Compound	Yield/%	Mp θ_m/°C	$[\alpha]_D^{23}$[a]/°	Found(Calcd) (%) C	H	N	R_f^1	R_f^2	R_f^3	Amino acid ratio
IIIa	81	84—89	−47.6	55.96	8.32	13.75	0.59	0.25	0.74	Ala:Pro:Val
				(56.00	8.66	13.75)[b]				1.01:1.04:1.00
IIIb	73	135—140	−85.2	55.64	8.40	14.25	0.57	0.20	0.71	Gly:Pro:Val
				(55.58	8.42	14.40)[c]				1.00:1.02:1.00
IIIc	80	181—182	−128.8	57.28	8.72	13.91	0.60	0.24	0.73	Ala:Pro:Val
				(57.27	8.60	14.06)				1.00:1.04:1.00
Va	74	160—161	−52.4	58.78	8.93	13.60	0.61	0.23	0.75	Leu:Ala:Pro:Val
				(58.69	8.87	13.69)				0.98:1.00:1.04:1.00
Vb	69	163—166	−100.8	57.39	8.55	13.97	0.55	0.18	0.74	Leu:Gly:Pro:Val
				(57.41	8.73	13.95)[c]				0.99:1.00:1.03:1.00
Vc	68	194—195	−132.0	57.92	8.46	13.57	0.59	0.23	0.76	Leu:Ala:Pro:Val
				(58.17	8.89	13.57)[c]				0.98:1.00:1.04:1.00
IIa	82	193—194	−83.4	58.32	8.86	14.86	0.50	0.10	0.70	Leu:Ala:Pro:Val
				(58.26	8.67	15.44)				0.99:1.00:1.04:1.00
IIb	53	256—257	−126.6	57.21	8.43	15.86	0.40	0.06	0.71	Leu:Gly:Pro:Val
				(57.38	8.48	15.93)				0.99:1.00:1.04:1.00
IIc	55	255—257	−149.8	58.54	8.76	15.60	0.47	0.10	0.70	Leu:Ala:Pro:Val
				(58.26	8.67	15.44)				0.99:1.00:1.05:1.00

a) *c* 1, CH_3OH. b) 1/2 H_2O. c) 1/4 H_2O.

was added EDC·HCl (0.58 g, 3 mmol), and the reaction mixture was stirred for 1 h at 0 °C and overnight at room temperature. Insoluble materials (DCHA·HCl) were removed by filtration and the filtrate was evaporated under reduced pressure. The residue was dissolved in EtOAc, and the solution was washed successively with 10% citric acid, 4% $NaHCO_3$, and H_2O, dried (Na_2SO_4), and evaporated. Addition of ether and petroleum ether to the residue gave crystals, which were recrystallized from EtOAc–ether–petroleum ether; yield, 986 mg (81%).

Compounds **IIIb** and **IIIc** were prepared by the similar manner to that described for **IIIa**.

H–D-Ala–L-Pro–L-Val–NHMe·HCl (IVa·HCl). Compound **IIIa** (398 mg, 1 mmol) was dissolved in 0.1 M hydrogen chloride in formic acid (12 ml). The soultion was allowed to stand for 30 min at room temperature and evaporated. Addition of ether to the residue gave highly hygroscopic crystals, which were used for the next reaction without further treatment; yield, 335 mg (100%); R_f^1 0.06, R_f^3 0.59.

Compounds **IVb, c** and **VIa—c** were prepared by a similar manner to that described for **IVa**: **IVb**; R_f^1 0, R_f^3 0.54: **IVc**; R_f^1 0.05, R_f^3 0.53: **VIa**; R_f^1 0.23, R_f^3 0.71: **VIb**; R_f^1 0.10, R_f^3 0.65: **VIc**; R_f^1 0.21, R_f^3 0.70.

Boc–L-Leu–D-Ala–L-Pro–L-Val–NHMe (Va). To a chilled solution of **IVa**·HCl (335 mg, 1 mmol) and TEA (0.14 ml, 1 mmol) in DMF (10 ml) was added Boc–L-Leu–ONSu (327 mg, 1.2 mmol), and the reaction mixture was stirred for 1 h at 0 °C and overnight at room temperature. A few drops of 1-(2-aminoethyl)piperazine were added to the solution, which was evaporated after being stirred further for 30 min at room temperature. The residue was dissolved in EtOAc and the solution was treated as described for **IIIa**. The crude product was dissolved in CH_3OH (3 ml) and applied to a column (3 cm × 170 cm) of Sephadex LH-20 and eluted with CH_3OH. The fractions containing the desired product detected by UV absorption and TLC were collected and evaporated, and the residue was crystallized by additions of ether and petroleum ether and recrystallized from EtOAc–ether–petroleum ether; yield, 379 mg (74%).

Compounds **Vb** and **Vc** were prepared by the similar manner to that described for **Va**.

Ac–L-Leu–D-Ala–L-Pro–L-Val–NHMe (IIa). To a chilled solution of **VIa**·HCl (224 mg, 0.5 mmol) and TEA (0.11 ml, 0.75 mmol) in DMF (2 ml) was added Ac–ONp (109 mg, 0.6 mmol), and the reaction mixture was stirred for 1 h at 0 °C and overnight at room temperature and evaporated. The residue dissolved in a mixture (5 ml) of $CHCl_3$ and CH_3OH (19 : 1, v/v), was applied to a column (1.8 cm × 30 cm) of silica gel 60 (Merck) and eluted with the same solvent. The fractions containing the desired product detected by TLC were collected and evaporated. The crude product was further purified by column chromatography with Sephadex LH-20 as described for **Va**. The product was recrystallized from CH_3OH–EtOAc; yield, 186 mg (82%).

Compounds **IIb** and **IIc** were prepared by the similar manner to that described for **IIa**.

CD Measurements. CD spectra were measured on a JASCO J-40A automatic recording spectropolarimeter in a quartz cell of 1-mm path length at the concentration of 0.2 mM at room temperature (23±2 °C).

^1H NMR Measurements. ^1H NMR spectra were recorded on a Brucker WH-270 spectrometer (270 MHz for ^1H), equipped with a Brucker B-ST-100/700 temperature control unit at the concentration of 5 mM at 23 °C unless otherwise mentioned. Chemical shifts were measured from the internal standard of DSS. The spectra were assigned by spin-decoupling, H–D exchange of NH protons and saturation transfer (between the two conformers).

The authors wish to express their thanks to Professor Tatsuo Miyazawa of The University of Tokyo and Associate Professor Masao Kawai of the Nagoya Institute of Technology for their helpful discussions. Thanks are also due to the members of Analytical Department of System Engineering Laboratory, Mitsubishi Chemical Industries Ltd., for elemental analyses.

References

1) Part VII of this series: K. Sato and U. Nagai, *Bull. Chem. Soc. Jpn.*, **56**, 3329 (1983).

2) The abbreviations used in this paper are those recommended by IUPAC-IUB: *J. Biol. Chem.*, **247**, 977 (1972). Additional abbreviations: Boc, *t*-butoxycarbonyl; Dnp, 2,4-dinitrophenyl; pNA, *p*-nitroanilide; ONSu, *N*-hydroxysuccinimide ester; ONp, *p*-nitrophenyl ester; EDC, 1-ethyl-3-(3-dimethylaminopropyl)carbodiimide; DCHA, dicyclohexylamine; DSS, sodium 2,2-dimethyl-2-silapentane-5-sulfonate; TEA, triethylamine, DMF, *N,N*-dimethylformamide; TLC, thin-layer chromatography; GS, gramicidin S.

3) K. Sato, M. Kawai, and U. Nagai, *Biopolymers*, **20**, 1921 (1981).

4) K. Sato, M. Kawai, and U. Nagai, *Bull. Chem. Soc. Jpn.*, **56**, 1527 (1983).

5) T. Higashijima, K. Sato, and U. Nagai, *Bull. Chem. Soc. Jpn.*, **56**, 3323 (1983).

6) M. Kawai and U. Nagai, *Biopolymers*, **17**, 1549 (1978).

7) M. Ohnishi and D. W. Urry, *Biochem. Biophys. Res. Commun.*, **35**, 194 (1969); K. D. Kopple, M. Ohnishi, and A. Go, *Biochemistry*, **8**, 4087 (1969).

8) P. Y. Chou and G. D. Fasmann, *J. Mol. Biol.*, **115**, 135 (1977).

9) M. Kawai, K. Sato, and U. Nagai, "Peptide Chemistry 1982; Proceedings of 20th Symposium on Peptide Chemistry," ed by S. Sakakibara, Protein Research Foundation, Osaka (1983), pp. 317—322; M. Kawai, K. Sato, R. Sugawara, and U. Nagai, *Bull. Chem. Soc. Jpn.*, **56**, 3005 (1983).

Studies on Heterocyclic Analogs of Azulenes. XI.[1] Syntheses and Cycloadditions of Cyclohepta[4,5]pyrrolo[1,2-*a*]imidazoles and Cyclohept[*d*]imidazo[1,2-*a*]imidazoles

Noritaka ABE,* Tarozaemon NISHIWAKI,* Hideko YAMAMOTO, and Noboru KUNISHIGE
Department of Chemistry, Faculty of Sciences, Yamaguchi University, Yamaguchi 753
(Received June 25, 1983)

Cyclohepta[4,5]pyrrolo[1,2-*a*]imidazoles (1,3a-diazacyclopent[*a*]azulenes) (**2**) and cyclohept[*d*]imidazo[1,2-*a*]imidazoles (1,3a,9-triazacyclopent[*a*]azulenes) (**6**) were synthesized from 2-aminocyclohepta[*b*]pyrroles and 2-aminocycloheptimidazole, respectively, in moderate to good yields. Reactions of **2** and **6** with reactive acetylenes gave 2-azacyclohepta[*ef*]cycl[3.2.2]azines together with bis(1,3a-diazacyclopent[*a*]azuleno)[1,7]diaza[12]annulenes (**4**) and 2,3-diazacyclohepta[*ef*]cycl[3.2.2]azines together with bis(1,3a,9-triazacyclopent[*a*]azuleno)[1,7]diaza[12]-annulenes (**8**), respectively. Reactions of **2** and **6** with electron deficient olefins gave **4** and **8**, respectively. These reactions proceeded regioselectively *via* 1,10-dipolar intermediates.

The cyclazine systems have attracted attentions for their interesting physical and chemical properties,[2] whose efficient synthetic method is the cycloaddition to adequate N-bridged heterocycles [*e.g.* cycloaddition of indolizines with dimethyl acetylenedicarboxylate leads to cycl[3.2.2]azines[3-5]]. In the course of our studies on azaazulenes,[6] we investigated the syntheses of cata-condensed 1-azaazulenes and 1,3-diazaazulenes, which would provide a convenient synthetic route to novel cyclazines. In this paper, we report the syntheses and cycloadditions of cyclohepta[4,5]pyrrolo[1,2-*a*]-imidazoles and cyclohept[*d*]imidazo[1,2-*a*]imidazoles, which furnished novel cyclazines and condensed [1,7]-diaza[12]annulenes.

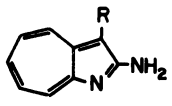

1a: R=H
1b: R=CO_2Et
1c: R=CN

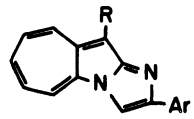

2a: R=H, Ar=Ph
2b: R=H, Ar=C_6H_4Me-p
2c: R=CO_2Et, Ar=Ph
2d: R=CO_2Et, Ar=C_6H_4Me-p
2e: R=CN, Ar=Ph

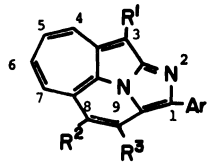

3

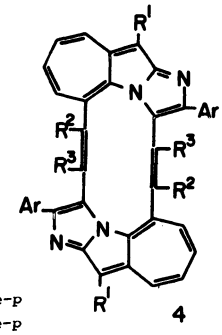

4

3a, 4a: R^1=H, R^2=R^3=E^1, Ar=Ph
3b, 4b: R^1=R^3=H, R^2=E^1, Ar=Ph
3c, 4c: R^1=H, R^2=R^3=E^1, Ar=C_6H_4Me-p
3d, 4d: R^1=R^3=H, R^2=E^1, Ar=C_6H_4Me-p
3e, 4e: R^1=E^2, R^2=R^3=E^1, Ar=Ph
3f, 4f: R^1=R^2=R^3=E^2, Ar=Ph
3g, 4g: R^1=E^2, R^2=E^1, R^3=H, Ar=Ph
3h, 4h: R^1=E^2, R^2=R^3=COPh, Ar=Ph
3i, 4i: R^1=R^2=E^2, R^3=H, Ar=Ph
3j, 4j: R^1=E^2, R^2=R^3=E^1, Ar=C_6H_4Me-p
3k, 4k: R^1=R^2=R^3=E^2, Ar=C_6H_4Me-p
3l, 4l: R^1=R^3=H, R^2=E^1, Ar=C_6H_4Me-p
3m, 4m: R^1=E^2, R^2=R^3=COPh, Ar=C_6H_4Me-p
3n, 4n: R^1=CN, R^2=R^3=E^1, Ar=Ph
3o, 4o: R^1=CN, R^2=E^1, R^3=H, Ar=Ph
3p, 4p: R^1=R^2=R^3=H, Ar=Ph
3q, 4q: R^1=R^2=R^3=H, Ar=C_6H_4Me-p

E^1=CO_2Me, E^2=CO_2Et

Syntheses and Cycloadditions of 1,3a-Diazacyclopent[a]-*azulenes.* Treatment of 2-amino-1-azaazulene (2-aminocyclohepta[*b*]pyrrole) (**1a**)[7,8] with α-bromoacetophenone in abs ethanol, followed by the treatment with potassium carbonate in aq ethanol in one pot gave **2a** in a 49% yield. The structure of **2a** was deduced to be 2-phenyl-1,3a-diazacyclopent[*a*]azulene (2-phenylcyclohepta[4,5]pyrrolo[1,2-*a*]imidazole) on the basis of elemental analyses and spectral data. In a similar manner, compounds **2b**—**e** were obtained by the reaction of **1a**—**c** with α-bromoacetophenone or 2-bromo-4′-methylacetophenone in abs ethanol or 1-butanol fol-

TABLE 1. CONDITIONS AND YIELDS FOR THE REACTIONS OF **2** AND **6** WITH REACTIVE ACETYLENES AND ELECTRON DEFICIENT OLEFINS

Substrate	Reagent	Solvent	Time/h	Product (%)
2a	DMAD	Benzene	1	**3a** (14) **4a** (6)
2a	MP	Benzene	20	**3b** (6) **4b** (25)
2b	DMAD	Benzene	1	**3c** (22) **4c** (5)
2b	MP	Benzene	27	**3d** (5) **4d** (34)
2c	DMAD	Benzene	3	**3e** (25) **4e** (13)
2c	DEAD	MeCN	2	**3f** (18) **4f** (7)
2c	MP	MeCN	27	**3g** (8) **4g** (33)
2c	DBA	Benzene	3	**3h** (17) **4h** (33)
2c	MA	Xylene	7	**3g** (—) **4g** (43)
2c	EA	Xylene	7	**3i** (—) **4i** (28)
2d	DMAD	Benzene	3	**3j** (17) **4j** (8)
2d	DEAD	Benzene	3	**3k** (19) **4k** (12)
2d	MP	Benzene	24	**3l** (4) **4l** (41)
2d	DBA	Benzene	3	**3m**(13) **4m**(23)
2e	DMAD	Benzene	7	**3n** (10) **4n** (9)
2e	MP	Benzene	120	**3o** (3) **4o** (16)
6a	DMAD	MeCN	3	**7a** (23) **8a** (4)
6a	DMAD	Benzene	4	**7a** (29) **8a** (10)
6a	DEAD	MeCN	2	**7b** (17) **8b** (6)
6a	MP	MeCN	27	**7c** (43) **8c** (20)
6a	DBA	MeCN	3	**7d** (36) **8d** (9)
6a	DMM	MeCN	70	**7a** (—) **8a** (2)
6a	MA	MeCN	45	**7c** (—) **8c** (25)
6a	EA	MeCN	48	**7e** (—) **8e** (25)
6a	AN	MeCN	50	**7f** (—) **8f** (6)
6b	DMAD	MeCN	2	**7g** (21) **8g** (3)
6b	DEAD	MeCN	2	**7h** (28) **8h** (4)
6b	MP	MeCN	27	**7i** (24) **8i** (8)
6b	DBA	MeCN	3	**7j** (32) **8j** (3)
6b	EA	MeCN	72	**7k** (—) **8k** (8)
6b	AN	MeCN	170	**7l** (—) **8l** (5)

Table 2. Electronic and IR spectral data of 3 and 7

Compound	λ_{max}/nm (log ϵ)	ν(C=O) or ν(C≡N)/cm^{-1}
3a	249 (4.43), 2.79 (4.52, sh), 291 (4.59), 310 (4.36, sh), 357 (4.48, sh), 373 (4.56), 400 (4.14, sh), 423 (4.10)	1725, 1700
3b	247 (4.33), 278 (4.39, sh), 295 (4.54), 310 (4.37, sh), 358 (4.35, sh), 374 (4.43), 406 (4.08), 428 (4.08)	1710
3c	249 (4.44), 278 (4.43, sh), 290 (4.48), 310 (4.37, sh), 357 (4.42, sh), 375 (4.52), 400 (4.23, sh), 421 (4.09)	1725, 1695
3d	249 (4.45), 273 (4.43, sh), 297 (4.57), 311 (4.45, sh), 360 (4.46, sh), 376 (4.53), 405 (4.22), 427 (4.17)	1710
3e	247 (4.37), 280 (4.45, sh), 292 (4.49), 310 (4.33, sh),381 (4.43) 427 (4.01, sh)	1730, 1705, 1700 (sh)
3f	248 (4.34), 280 (4.46, sh), 292 (4.50), 310 (4.35, sh), 381 (4.43), 427 (4.00, sh)	1730, 1705, 1700 (sh)
3g	245 (4.24), 285 (4.30, sh), 300 (4.53), 310 (4.40, sh), 383 (4.42), 436 (4.21)	1720, 1705
3h[a)]	257 (4.68), 285 (4.45, sh), 323 (4.38), 394 (4.46), 445 (4.09, sh)	1690, 1655
3j	251 (4.43), 278 (4.46, sh), 291 (4.50), 312 (4.35, sh), 384 (4.57), 427 (4.14, sh)	1730, 1720, 1710
3k	251 (4.39), 280 (4.43, sh), 292 (4.45), 312 (4.32, sh), 384 (4.46), 425 (4.13, sh)	1735 (sh), 1720, 1705
3l	250 (4.55), 279 (4.53, sh), 301 (4.68), 313 (4.61, sh), 385 (4.64), 431 (4.18, sh)	1710
3m[a)]	258 (4.59), 285 (4.36, sh), 325 (4.29), 397 (4.40), 445 (4.09, sh)	1690, 1650
3n[a)]	255 (4.35, sh), 282 (4.47), 292 (4.47), 303 (4.43, sh), 317 (4.34), 341 (3.97), 385 (4.42, sh), 399 (4.51), 432 (4.16 sh), 453 (4.09)	2210, 1740, 1720
3o[a)]	257 (4.31), 282 (4.37, sh), 292 (4.44, sh), 305 (4.50), 317 (4.43), 340 (4.02), 382 (4.35, sh), 400 (4.45), 436 (4.00), 461 (3.98)	2230, 1710
7a	237 (4.42), 270 (4.45, sh), 292 (4.57), 380 (4.39), 418 (4.18), 438 (4.16)	1730, 1705
7b	238 (4.14), 269 (4.20, sh), 291 (4.30), 381 (4.05), 419 (3.82), 440 (3.82)	1725, 1695
7c	235 (4.27), 263 (4.23), 292 (4.49), 319 (3.93), 333 (3.95), 373 (4.21), 388 (4.23), 423 (3.97), 446 (4.02)	1715
7d	254 (4.57), 306 (4.33), 385 (4.24), 450 (3.97)	1655
7g	240 (4.33), 270 (4.30, sh), 291 (4.35), 385 (4.29), 417 (4.14), 438 (4.09)	1725, 1700
7h	241 (4.21), 270 (4.23, sh), 291 (4.32), 383 (4.26), 416 (4.09), 437 (4.05)	1740, 1695
7i	241 (4.31), 263 (4.26), 292 (4.45), 321 (4.01), 336 (4.07), 370 (4.33, sh), 381 (4.35), 421 (4.16), 443 (4.19)	1715
7j	253 (4.48), 307 (4.22), 388 (4.22), 445 (4.02)	1650, 1640

a) Taken for $CHCl_3$ solutions.

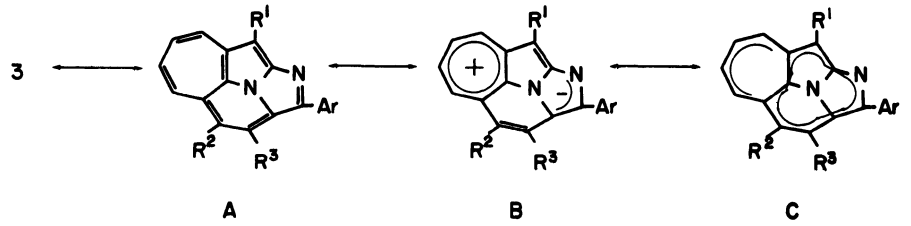

lowed by the treatment with potassium carbonate in moderate to good yields.

The compound **2c** was deesterified by hydrolysis with potassium hydroxide followed by decarboxylation with hot hydrobromic acid to give **2a**.

Reactions of **2** with reactive acetylenes gave 1 : 1-adducts (**3**) together with 2 : 2-adducts (**4**). In the reactions of **2** with electron deficient olefins, dehydrogenations were accompanied, and only 2 : 2-adducts (**4**) were isolated. These results were listed in Table 1.

The 1 : 1-adducts (**3**) were highly fluorescent crystals and were characterized as 2-azacyclohepta[*ef*]cycl[3.2.2]-azines on the basis of spectroscopic properties (Tables 2, 3, and 6) as well as elemental analyses (Table 7). Deesterification of **3e** and **3j** were attained by hydrolysis with potassium hydroxide followed by heating with copper in quinoline, and compounds **3p** and **3q** were obtained in good yield, respectively. The seven-membered ring protons of **3p** were seen at δ 7.73 (ddd, J=8.0, 7.0, and 1.5 Hz, H-5), 7.78 (ddd, J=8.0, 7.0, and 1.5 Hz, H-6), 8.32 (ddd, J=8.0, 1.5, and 0.5 Hz, H-4), and 8.57 (ddd, J=8.0, 1.5, and 0.5 Hz, H-7) in its 200 MHz ^{1}H NMR spectrum. Two pairs of doublets at δ 7.73 and 7.77 (J=4.0 Hz) were assignable to H-9 and H-8 protons, respectively. Although the low field resonated chemical shift of protons of **3p** intimates that **3p** should be inherently aromatic, the contribution of the resonance form **A** should be predominant, since the coupling constants of seven-membered ring protons imply somewhat of bond-alternation and the value of coupling constant of H-8 and H-9 is rather small (J=4.0 Hz). In the ^{13}C NMR spectrum of **3p**, signals of C-8 and C-9 carbons were seen at δ 113.9 (d) and 110.4 (d) and signals of seven-membered ring carbons (C-4, 5, 6, and 7) were seen at δ 130.5 (d), 123.0 (d), 125.9 (d), and 129.6 (d), respectively, and these observations also accord with the structure.

The 2 : 2-adducts (**4**) were characterized as bis(1,3a-

Table 3. Electronic and IR spectral data of **4** and **8**

Compound	λ_{max}/nm (log ϵ)	ν(C=O) or ν(C≡N)/cm^{-1}
4a	268 (4.90), 295 (4.65), 310 (4.58, sh), 360 (4.53), 404 (4.17), 423 (4.13), 523 (3.38, sh), 550 (3.42), 590 (3.31, sh), 640 (2.94, sh)	1725, 1690
4b	222 (4.79), 269 (4.91), 312 (4.76), 322 (4.76), 353 (4.50, sh), 414 (4.18), 436 (4.19), 508 (3.64), 538 (3.64), 580 (3.46, sh), 630 (2.96, sh)	1695
4c	269 (5.05), 305 (4.68), 315 (4.66), 345 (4.55, sh), 407 (4.18), 423 (4.13), 523 (3.63, sh), 550 (3.66), 590 (3.56, sh), 640 (3.19, sh)	1740, 1710
4d	224 (4.83), 270 (4.93), 314 (4.79), 324 (4.78), 355 (4.54, sh), 415 (4.25), 438 (4.25), 511 (3.69), 542 (3.68), 583 (3.50, sh), 635 (3.14, sh)	1695
4e	265 (4.88), 310 (4.40), 329 (4.45), 348 (4.44), 366 (4.45), 413 (4.11), 436 (4.26), 515 (3.63, sh), 547 (3.73), 580 (3.69, sh), 625 (3.37, sh)	1725, 1690
4f	265 (5.02), 308 (4.57), 328 (4.62), 348 (4.61), 365 (4.62), 413 (4.24), 437 (4.38), 517 (3.78, sh), 547 (3.73), 580 (3.81, sh), 625 (3.50, sh)	1730, 1695
4g[a)]	271 (4.87), 320 (4.73), 347 (4.73), 366 (4.60, sh), 425 (4.33), 450 (4.53), 515 (3.80, sh), 539 (3.84), 574 (3.73, sh), 625 (3.26, sh)	1710, 1690
4h	258 (5.07), 351 (4.59), 366 (4.59), 417 (4.18), 441 (4.32), 520 (3.69, sh), 551 (3.77), 587 (3.71, sh), 635 (3.36, sh)	1690, 1665, 1655
4i	232 (4.93), 268 (4.99), 317 (4.79), 343 (4.80), 364 (4.67, sh), 421 (4.42), 445 (4.60), 515 (3.91, sh), 537 (3.95), 572 (3.84, sh), 625 (3.38, sh)	1710, 1690
4j	268 (4.90), 311 (4.53), 330 (4.53), 350 (4.51), 366 (4.51), 416 (4.15), 439 (4.28), 520 (3.70, sh), 550 (3.78), 580 (3.74, sh), 625 (3.47, sh)	1735, 1725, 1690
4k	267 (4.98), 310 (4.61), 331 (4.61), 351 (4.60), 367 (4.61), 416 (4.21), 439 (4.34), 520 (3.76, sh), 552 (3.83), 583 (3.79, sh), 630 (3.51, sh)	1730, 1720, 1695
4l	233 (4.81), 271 (4.85), 319 (4.69), 345 (4.68), 366 (4.58, sh), 425 (4.33), 448 (4.50), 512 (2.77, sh), 542 (3.83), 578 (3.72, sh), 625 (3.29, sh)	1710, 1690
4m	257 (5.03), 353 (4.55), 366 (4.54, sh), 421 (4.16), 443 (4.29), 525 (3.65, sh), 555 (3.73), 590 (3.68, sh), 635 (3.29, sh)	1690, 1660, 1650 (sh)
4n[a)]	267 (4.98), 309 (4.49), 329 (4.51), 350 (4.49), 365 (4.48, sh), 414 (4.21), 436 (4.30), 525 (3.77, sh), 550 (3.82), 585 (3.76, sh), 635 (3.39, sh)	2200, 1725, 1710
4o[a)]	271 (4.85), 319 (4.72), 342 (4.70), 365 (4.59, sh), 422 (4.38), 448 (4.52), 520 (3.79, sh), 543 (3.83), 580 (3.70, sh), 635 (3.20, sh)	2200, 1705
8a	258 (4.73), 293 (4.48), 320 (4.48), 410 (4.15, sh), 424 (4.28), 427 (4.27, sh), 550 (3.60)	1730, 1715
8b	258 (4.86), 293 (4.56), 322 (4.58), 410 (4.35, sh), 425 (4.50), 428 (4.49, sh), 550 (3.75)	1730, 1710
8c	242 (4.63), 260 (4.60), 302 (4.56), 325 (4.55), 417 (4.36, sh), 437 (4.49), 542 (3.65)	1710
8d	255 (4.96), 328 (4.60), 415 (4.31, sh), 433 (4.41), 558 (3.73)	1675, 1660
8e	242 (4.67), 260 (4.65), 302 (4.59), 325 (4.59), 417 (4.39, sh), 437 (4.52), 543 (3.72)	1695
8f	239 (4.43), 254 (4.46), 301 (4.38), 329 (4.33), 417 (4.15, sh), 440 (4.32), 550 (3.45)	2200
8g	257 (4.73), 298 (4.54), 320 (4.49), 410 (4.19, sh), 424 (4.31, sh), 430 (4.32), 552 (3.63)	1730, 1715
8h	255 (4.73), 298 (4.54), 323 (4.52), 410 (4.27, sh), 425 (4.42, sh), 429 (4.43), 553 (3.73)	1735, 1720
8i	243 (4.50), 261 (4.45), 302 (4.41), 327 (4.35), 423 (4.19, sh), 441 (4.30), 546 (3.52)	1700
8j	252 (4.73), 334 (4.32), 420 (4.10, sh), 435 (4.18), 560 (3.44)	1670, 1655
8k	243 (4.69), 262 (4.64), 303 (4.63), 328 (4.61), 422 (4.48, sh), 441 (4.60), 547 (3.75)	1695
8l	241 (4.40), 266 (4.40), 304 (4.37), 335 (4.28), 423 (4.15, sh), 443 (4.31), 555 (3.49)	2200

a) Taken for $CHCl_3$ solutions.

diazacyclopent[*a*]azuleno)[1,7]diaza[12]annulenes by means of their spectroscopic data (Tables 4, 5, and 6) as well as elemental analyses and mass spectra (Table 7). Deesterifications of **4e** and **4j** were attained by hydrolysis with potassium hydroxide followed by decarboxylation with copper in quinoline under heating, and **4p** and **4q** were obtained, respectively. The ^{1}H NMR spectra of **4p** and **4q** show two pairs of doublets at δ 7.05 and 8.03 (J=9.0 Hz) and at δ 7.10 and 8.06 (J=9.0 Hz), respectively, and their IR spectra show absorptions at 725 and 720 cm^{-1}, respectively. These facts denote that the configuration of ethylene bridge of **4** should be cis-one.

The regiochemistry of the reaction was attained by the reaction of **2** with the dissymmetrical acetylene (MP) or olefins (MA or EA). In the ^{1}H NMR spectrum of **3b**, the H-7 proton resonated at rather lower field (δ 9.85) than that of **3p** (δ 8.57), which would be under the deshielding effect of the ester group at C-8. The H-6 proton of **4b** also resonated at lower field (δ 8.30) than that of **4p** (δ 6.90).[9] It is conceivable that 1,10-dipolar intermediates (**D**), which were produced by the electrophilic attack of the acetylenes at the C-3 position of **2**,[10] cyclized at C-5 position to give **3** or reacted at C-5 position of another molecule (**D**) each other to give **4**. The reactions of **2** with olefins should proceed in a similar manner with the case of acetylenes, but it is

TABLE 4. ^{1}H NMR SPECTRAL DATA OF **3** AND **7**

Compound	H-3	H-4	H-5	H-6	H-7	H-9	Ar	Others		
								CH_3CH_2O	CH_3O	CH_3
3a[a]	8.36s	8.29ddd ($J_{4,5}=J_{6,7}=8.0$ Hz, $J_{5,6}=7.0$ Hz, $J_{4,6}=J_{5,7}=1.5$ Hz, $J_{4,7}=0.5$ Hz)	7.79ddd	7.88ddd	9.66ddd	—	7.55—7.70m (3H) 8.25—8.34m (2H)		4.06s 4.09s	
3b[b]	8.24s	8.25ddd ($J_{4,5}=J_{6,7}=8.0$ Hz, $J_{5,6}=7.0$ Hz, $J_{4,6}=J_{5,7}=1.5$ Hz, $J_{4,7}=0.5$ Hz)	7.70ddd	7.80ddd	9.85ddd	8.18s	7.45—7.65m (3H) 8.30—8.50m (2H)		4.07s	
3c[b]	8.21s	8.17ddd ($J_{4,5}=J_{6,7}=8.0$ Hz, $J_{5,6}=7.0$ Hz, $J_{4,6}=J_{5,7}=1.5$ Hz, $J_{4,7}=0.5$ Hz)	7.66ddd	7.78ddd	9.55ddd	—	7.33d (2H) 8.09d (2H) ($J=8.0$ Hz)		4.07s 4.08s	2.49s
3d[c]	8.13s	8.22ddd ($J_{4,5}=J_{6,7}=8.0$ Hz, $J_{5,6}=7.0$ Hz, $J_{4,6}=J_{5,7}=1.5$ Hz, $J_{4,7}=0.5$ Hz)	7.66ddd	7.80ddd	9.77ddd	8.03s	7.32d (2H) 8.02d (2H) ($J=8.5$ Hz)		4.02s	2.45s
3e[c]	—	8.78ddd ($J_{4,5}=J_{6,7}=9.0$ Hz, $J_{5,6}=7.0$ Hz, $J_{4,6}=J_{5,7}=1.0$ Hz, $J_{4,7}=0.5$ Hz)	7.78ddd	7.93ddd	9.73ddd	—	7.40—7.75m (3H) 8.15—8.45m (2H)	1.61t 4.78q ($J=7.0$ Hz)	4.03s 4.07s	
3f[c]	—	8.83dd ($J_{4,5}=J_{6,7}=9.0$ Hz, $J_{5,6}=7.0$ Hz, $J_{4,6}=J_{5,7}=1.0$ Hz)	7.83dd	7.93dd	9.90dd	—	7.50—7.70m (3H) 8.30—8.50m (2H)	1.40t 4.52q ($J=7.0$ Hz) 1.47t 4.55q ($J=7.0$ Hz) 1.60t 4.77q ($J=7.0$ Hz)		
3g[c]	—	8.78dd ($J_{4,5}=J_{6,7}=9.0$ Hz, $J_{5,6}=7.0$ Hz, $J_{4,6}=J_{5,7}=1.0$ Hz)	7.72dd	7.83dd	9.90dd	8.13s	7.40—7.65m (3H) 8.25—8.50m (2H)	1.62t 4.74q ($J=7.0$ Hz)	4.02s	
3h[c]	—	8.75—9.00m	7.10—8.00m		8.75—9.00m	—	7.10—8.00m (13H) 8.05—8.25m (2H)	1.62t 4.77q ($J=7.0$ Hz)		
3j[a]	—	8.80ddd ($J_{4,5}=J_{6,7}=9.0$ Hz, $J_{5,6}=7.0$ Hz, $J_{4,6}=J_{5,7}=1.0$ Hz, $J_{4,7}=0.5$ Hz)	7.87ddd	7.91ddd	9.78ddd	—	7.42d (2H) 8.23d (2H) ($J=8.5$ Hz)	1.63t 4.79q ($J=7.0$ Hz)	4.07s 4.08s	2.49s
3k[c]	—	8.79dd ($J_{4,5}=J_{6,7}=9.0$ Hz, $J_{5,6}=7.0$ Hz, $J_{4,6}=J_{5,7}=1.0$ Hz)	7.80dd	7.92dd	9.82dd	—	7.36d (2H) 8.24d (2H) ($J=8.0$ Hz)	1.43t 4.55q[c] ($J=7.0$ Hz) 1.50t 4.55q[e] ($J=7.0$ Hz) 1.62t 4.77q ($J=7.0$ Hz)		
3l[a]	—	8.87ddd ($J_{4,5}=J_{6,7}=9.0$ Hz, $J_{5,6}=7.0$ Hz, $J_{4,6}=J_{5,7}=1.5$ Hz, $J_{4,7}=0.5$ Hz)	7.89ddd	7.93ddd	10.05ddd	8.31s	7.43d (2H) 8.41d (2H) ($J=8.5$ Hz)	1.65t 4.80q ($J=7.0$ Hz)	4.10s	2.50s
3m[c]	—	8.70—8.95m	7.00—8.00m		8.70—8.95m	—	7.00—8.00m (12H) 8.07d (2H) ($J=8.0$ Hz)	1.65t 4.79q ($J=7.0$ Hz)		2.37s
3n[d]	—	8.63ddd ($J_{4,5}=J_{6,7}=9.0$ Hz, $J_{5,6}=7.0$ Hz, $J_{4,6}=J_{5,7}=1.0$ Hz, $J_{4,7}=0.5$ Hz)	7.89ddd	7.99ddd	9.71ddd	—	7.50—7.65m (3H) 8.20—8.35m (2H)		4.05s[e]	
3o[d]	—	8.66ddd ($J_{4,5}=J_{6,7}=9.0$ Hz, $J_{5,6}=7.0$ Hz, $J_{4,6}=J_{5,7}=1.0$ Hz, $J_{4,7}=0.5$ Hz)	7.90ddd	7.99ddd	10.01ddd	8.34s	7.50—7.65m (3H) 8.40—8.55m (2H)		4.08s[e]	
7a[a]	—	8.40ddd ($J_{4,5}=J_{6,7}=8.5$ Hz, $J_{5,6}=7.5$ Hz, $J_{4,6}=J_{5,7}=2.5$ Hz, $J_{4,7}=0.5$ Hz)	7.85ddd	7.73ddd	9.37ddd	—	7.45—7.65m (3H) 8.15—8.35m (2H)		4.03s[e] 4.05s	

Table 4. (Continued)

Compound	H-3	H-4	H-5	H-6	H-7	H-9	Ar	Others		
								CH_3CH_2O	CH_3O	CH_3
7b[c]	—	8.47dd ($J_{4,5}$=8.5 Hz, $J_{4,6}$=2.0 Hz)	7.97dd ($J_{5,6}$=7.5 Hz, $J_{5,7}$=2.0 Hz)	7.75dd	9.55dd	—	7.45—7.70m (3H) 8.25—8.45m (2H)	1.42t 4.50q (J=7.0 Hz) 1.47t 4.53q (J=7.0 Hz)		
7c[b]	—	8.60ddd ($J_{4,5}$=8.5 Hz, $J_{4,6}$=2.0 Hz, $J_{4,7}$=0.5 Hz)	7.88ddd ($J_{6,7}$=8.5 Hz, $J_{5,6}$=7.5 Hz, $J_{5,7}$=2.0 Hz)	7.77ddd	9.55ddd	8.03s	7.35—7.60m (3H) 8.25—8.55m (2H)		4.00s[e]	
7d[b]	—	8.53ddd ($J_{4,5}$=9.0 Hz, $J_{4,6}$=2.0 Hz, $J_{4,7}$=0.5 Hz)	7.92ddd ($J_{6,7}$=8.5 Hz, $J_{5,6}$=8.0 Hz, $J_{5,7}$=2.0 Hz)	7.70ddd	8.72ddd	—	7.10—7.65m (13H) 8.15—8.30m (2H)			
7g[a]	—	8.50ddd ($J_{4,5}$=8.5 Hz, $J_{4,6}$=1.5 Hz, $J_{4,7}$=0.5 Hz)	7.96ddd ($J_{6,7}$=8.5 Hz, $J_{5,6}$=7.0 Hz, $J_{5,7}$=1.5 Hz)	7.85ddd	9.52ddd	—	7.41d (2H) 8.24d (2H) (J=8.5 Hz)		4.07s 4.10s	2.48s
7h[c]	—	8.50dd ($J_{4,5}$=8.5 Hz, $J_{4,6}$=2.0 Hz)	7.97dd ($J_{6,7}$=8.5 Hz, $J_{5,6}$=7.5 Hz, $J_{5,7}$=2.0 Hz)	7.83dd	9.63dd	—	7.37d (2H) 8.27d (2H) (J=8.5 Hz)	1.47t 4.53q (J=7.0 Hz) 1.50t 4.53q (J=7.0 Hz)		2.48s
7i[a]	—	8.55ddd ($J_{4,5}$=8.5 Hz, $J_{4,6}$=1.5 Hz, $J_{4,7}$=0.5 Hz)	8.00ddd ($J_{6,7}$=8.5 Hz, $J_{5,6}$=7.0 Hz, $J_{5,7}$=1.5 Hz)	7.90ddd	9.70ddd	8.22s	7.42d (2H) 8.40d (2H) (J=8.5 Hz)		4.10s	2.49s
7j[c]	—	8.58dd ($J_{4,5}$=9.0 Hz, $J_{4,6}$=1.5 Hz)	8.00dd ($J_{6,7}$=7.5 Hz, $J_{5,7}$=1.5 Hz)	7.77dd	8.78dd	—	7.10—7.80m (12H) 8.23d (2H) (J=8.5 Hz)			2.40s

a) At 200 MHz. b) At 90 MHz. c) At 60 MHz. d) At 100 MHz. e) Two peaks are degenerated.

D

obscure which step dehydrogenations occured.

Syntheses and Cycloadditions of 1,3a,9-Triazacyclopent[a]*azulenes.* Treatment of 2-amino-1,3-diazaazulene (2-aminocycloheptimidazole) (**5**)[11] with *α*-bromoacetophenone in abs ethanol gave 2-amino-1-phenacylcycloheptimidazolium bromide in an 80% yield. Cyclization to 2-phenyl-1,3a,9-triazacyclopent[*a*]azulene (2-phenylcyclohept[*d*]imidazo[1,2-*a*]imidazole) (**6a**) was attained by the treatment of the salt with potassium carbonate in hot aq ethanol in a 76% yield. Similarly, **6b** was obtained by the treatment with 2-bromo-4′-methylacetophenone followed by the treatment with potassium carbonate in a 64% yield. In analogy with the reactions of **2a**, compounds **6a** and **6b** reacted with reactive acetylenes to give 1 : 1-adducts (**7**) and 2 : 2-adducts (**8**), and with electron deficient olefins to give 2 : 2-adducts (**8**). These results were listed in Table 1. The structures of 1 : 1-adducts (**7**) were assigned to 2,3-diazacyclohepta[*ef*]cycl[3.2.2]azines and 2 : 2-adducts to bis(1, 3a, 9-triazacyclopent[*a*]azuleno)[1, 7]diaza[12]-

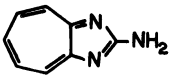

5

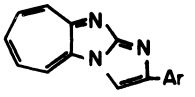

6a: Ar=Ph

6b: Ar=C_6H_4Me-p

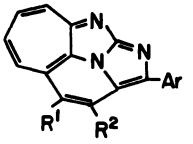

7

7a, 8a: R^1=R^2=E^1, Ar=Ph

7b, 8b: R^1=R^2=E^2, Ar=Ph

7c, 8c: R^1=E^1, R^2=H, Ar=Ph

7d, 8d: R^1=R^2=COPh, Ar=Ph

7e, 8e: R^1=E^2, R^2=H, Ar=Ph

7f, 8f: R^1=CN, R^2=H, Ar=Ph

7g, 8g: R^1=R^2=E^1, Ar=C_6H_4Me-p

7h, 8h: R^1=R^2=E^2, Ar=C_6H_4Me-p

7i, 8i: R^1=E^1, R^2=H, Ar=C_6H_4Me-p

7j, 8j: R^1=R^2=COPh, Ar=C_6H_4Me-p

7k, 8k: R^1=E^2, R^2=H, Ar=C_6H_4Me-p

7l, 8l: R^1=CN, R^2=H, Ar=C_6H_4Me-p

7m, 8m: R^1=R^2=H, Ar=Ph

7n, 8n: R^1=R^2=H, Ar=C_6H_4Me-p

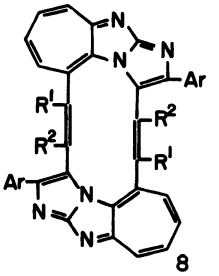

8

E^1=CO_2Me

E^2=CO_2Et

TABLE 5. ^{1}H NMR SPECTRAL DATA OF 4 AND 8[9]

Compound	H-6	H-7	H-8	H-9	H-10	H-olefin	Ar	Others		
								CH_3CH_2O	CH_3O	CH_3
4a[a]	7.35d ($J_{6,7}$=11.5 Hz)	6.80dd ($J_{7,8}$=9.0 Hz)	6.46dd ($J_{8,9}$=10.5 Hz)	7.55d	7.51s	—	7.35—7.60m (3H) 7.65—7.85m (2H)		3.63s 3.98s	
4b[b]	8.30d ($J_{6,7}$=12.0 Hz)	6.83dd ($J_{7,8}$=9.0 Hz)	6.45dd ($J_{8,9}$=11.0 Hz)	7.60d	7.35s	8.90s	7.40—7.55m (3H) 8.15—8.30m (2H)		4.00s	
4c[b]	7.27d ($J_{6,7}$=12.0 Hz)	6.72dd ($J_{7,8}$=8.5 Hz)	6.37dd ($J_{8,9}$=11.0 Hz)	7.48d	7.43s	—	7.25d (2H) 7.63d (2H) (J=8.0 Hz)		3.67s 3.94s	2.42s
4d[b]	8.26dd ($J_{6,7}$=12.0 Hz, $J_{6,8}$=1.0 Hz)	6.80ddd ($J_{7,8}$=8.0 Hz, $J_{7,9}$=1.5 Hz)	6.45ddd ($J_{8,9}$=10.0 Hz,	7.58dd	7.33s	8.87s	7.33d (2H) 8.15d (2H) (J=8.0 Hz)		4.00s	2.45s
4e[b]	7.80bd ($J_{6,7}$=$J_{8,9}$=10.0 Hz)	7.22dd ($J_{7,8}$=7.0 Hz)	6.93dd	8.80bd	—	—	7.45—7.70m (3H) 7.80—7.95m (2H)	1.58t 4.67q (J=7.0 Hz)	3.62s 4.00s	
4f[b]	7.83bd ($J_{6,7}$=11.0 Hz)	7.23dd ($J_{7,8}$=9.0 Hz)	6.93dd ($J_{8,9}$=10.0 Hz)	8.87bd	—	—	7.40—7.65m (3H) 7.75—7.90m (2H)	0.93t 4.10q (J=7.0 Hz) 1.43t 4.50q (J=7.0 Hz) 1.58t 4.67q (J=7.0 Hz)		
4g[a]	8.38dd ($J_{6,7}$=11.5 Hz, $J_{6,8}$=$J_{7,9}$=1.0 Hz)	6.99ddd ($J_{7,8}$=9.0 Hz)	6.77ddd ($J_{8,9}$=10.0 Hz,	8.61dd	—	8.82s	7.30—7.60m (3H) 8.15—8.30m (2H)	1.58t 4.58q (J=7.0 Hz)	3.98s	
4h[b]	6.80—8.00m			8.90dm (J=10.0 Hz)	—	—	6.80—8.00m (15H)	1.57t 4.64q (J=7.0 Hz)		
4i[b]	8.57dd ($J_{6,7}$=$J_{8,9}$=11.0 Hz, $J_{6,8}$=$J_{7,9}$=1.5 Hz)	7.21ddd ($J_{7,8}$=9.0 Hz,	6.90ddd	8.77dd	—	9.00s	7.45—7.80m (3H) 8.25—8.55m(2H)	1.50t 4.50q (J=7.0 Hz) 1.60t 4.60q (J=7.0 Hz)		
4j[a]	7.63ddd ($J_{6,7}$=12.0 Hz, $J_{6,8}$=$J_{7,9}$=1.0 Hz,	7.06ddd ($J_{7,8}$=9.0 Hz,	6.84ddd ($J_{8,9}$=10.5 Hz,	8.71ddd	—	—	7.27d (2H) 7.66d (2H) (J=8.0 Hz)	1.56t 4.62q (J=7.0 Hz)	3.46s 3.97s	2.44s
4k[b]	7.71bd ($J_{6,7}$=11.0 Hz)	7.17dd ($J_{7,8}$=9.0 Hz)	6.87dd ($J_{8,9}$=10.0 Hz)	8.78bd	—	—	7.26d (2H) 7.70d (2H) (J=8.0 Hz)	0.95t 4.10q (J=7.0 Hz) 1.41t 4.47q (J=7.0 Hz) 1.56t 4.62q (J=7.0 Hz)		2.43s
4l[b]	8.18ddd ($J_{6,7}$=11.0 Hz, $J_{6,8}$=1.0 Hz,	6.78ddd ($J_{7,8}$=9.0 Hz, $J_{7,9}$=1.5 Hz,	6.53ddd ($J_{8,9}$=10.0 Hz, $J_{6,9}$=0.5 Hz)	8.43ddd	—	8.53s	7.20d (2H) 7.98d (2H) (J=8.0 Hz)	1.55t 4.52q (J=7.0 Hz)	3.87s	2.42s
4m[b]	6.80—8.00m			8.92dm ($J_{8,9}$=10.0 Hz)	—	—	6.80—8.00m (14H)	1.57t 4.67q (J=7.0 Hz)		2.24s
4n[c]	7.81ddd ($J_{6,7}$=11.5 Hz, $J_{6,8}$=1.0 Hz,	7.21ddd ($J_{7,8}$=9.0 Hz, $J_{7,9}$=1.5 Hz,	7.00ddd ($J_{8,9}$=11.0 Hz, $J_{6,9}$=0.5 Hz)	8.01ddd	—	—	7.45—7.60m (3H) 7.70—7.80m (2H)		3.64s 4.00s	
4o[c]	8.67ddd ($J_{6,7}$=12.0 Hz, $J_{6,8}$=1.0 Hz,	7.23ddd ($J_{7,8}$=9.0 Hz, $J_{7,9}$=1.5 Hz,	6.99ddd ($J_{8,9}$=11.0 Hz, $J_{6,9}$=0.5 Hz)	7.97ddd	—	9.09s	7.35—7.65m (3H) 8.15—8.30m (2H)		4.07s	

Table 5. (Continued)

Compound	H-6	H-7	H-8	H-9	H-10	H-olefin	Ar	Others		
								CH_3CH_2O	CH_3O	CH_3
8a[c]	8.12dm ($J_{6,7}$=11.0 Hz)	7.30—7.60m	8.32dm ($J_{8,9}$=10.0 Hz)	—	—	—	7.30—7.60m (3H) 7.80—7.95m (2H)		3.74s 4.00s	
8b[b]	8.25dm ($J_{6,7}$=10.0 Hz)	7.20—7.70m	8.50dm ($J_{8,9}$=10.0 Hz)	—	—	—	7.20—7.70m (3H) 7.90—8.20m (2H)	0.97t 4.30q (J=7.0 Hz) 1.45t 4.60q (J=7.0 Hz)		
8c[b]	8.73dm ($J_{6,7}$=11.0 Hz)	7.25—7.65m	8.13dm ($J_{8,9}$=10.0 Hz)	—	—	8.97s	7.25—7.65m (3H) 8.15—8.35m (2H)		4.02s	
8d[b]	8.25dm ($J_{6,7}$=11.0 Hz)	7.10—8.00m	8.47dm ($J_{8,9}$=10.0 Hz)	—	—	—	7.10—8.00m (15H)			
8e[a]	8.65dm ($J_{6,7}$=12.0 Hz,	7.13dd $J_{7,8}$=9.0 Hz,	7.29dd $J_{8,9}$=11.0 Hz)	8.10dm	—	8.90s	7.25—7.60m (3H) 8.15—8.25m (2H)	1.53t 4.50q (J=7.0 Hz)		
8f[c]	7.92dm ($J_{6,7}$=10.0 Hz)	7.30—7.70m	8.35dm ($J_{8,9}$=10.0 Hz)	—	—	8.68s	7.30—7.70m (3H) 8.20—8.30m (2H)			
8g[b]	8.20dm ($J_{6,7}$=10.0 Hz)	7.10—7.55m	8.40dm ($J_{8,9}$=10.0 Hz)	—	—	—	7.35d (2H) 7.82d (2H) (J=8.0 Hz)		3.82s 4.04s	2.47s
8h[b]	8.17dm ($J_{6,7}$=11.0 Hz)	7.10—7.55m	8.45dm ($J_{8,9}$=10.0 Hz)	—	—	—	7.43d (2H) 7.93d (2H) (J=8.0 Hz)	1.05t 4.30q (J=7.0 Hz) 1.47t 4.57q (J=7.0 Hz)		2.50s
8i[b]	8.76dm ($J_{6,7}$=11.0 Hz)	7.10—7.50m	8.22dm ($J_{8,9}$=10.0 Hz)	—	—	8.98s	7.30d (2H) 8.15d (2H) (J=8.0 Hz)		4.05s	2.42s
8j[b]	8.23dm ($J_{6,7}$=10.0 Hz)	6.80—8.00m	8.50dm ($J_{8,9}$=10.0 Hz)	—	—	—	6.80—8.00m (14H)			2.30s
8k[b]	8.83dm ($J_{6,7}$=11.0 Hz)	7.15—7.50m	8.22dm ($J_{8,9}$=10.0 Hz)	—	—	9.07s	7.36d (2H) 8.20d (2H) (J=8.0 Hz)	1.53t 4.57q (J=7.0 Hz)		2.44s
8l[b]	7.93dm ($J_{6,7}$=10.0 Hz)	7.15—7.60m	8.33dm ($J_{8,9}$=10.0 Hz)	—	—	8.67s	7.37d (2H) 8.20d (2H) (J=8.0 Hz)			

a) At 90 MHz. b) At 60 MHz. c) At 100 MHz.

annulenes on the basis of their spectroscopic properties (Tables 2, 3, 4, 5, and 6) as well as elemental analyses (Table 7).

Compounds **7a** and **7c** were deesterified by the treatment with potassium hydroxide followed by heating with copper in quinoline to give **7m**. Similarly, **7i** was deesterified to give **7n**. In the ^{1}H NMR spectrum of **7m**, seven-membered ring protons (H-4, H-5, H-6, and H-7) were seen at δ 8.48, 7.80, 7.91, and 8.56, respectively, with the vicinal coupling constants ($J_{4,5}$=$J_{6,7}$=8.5 Hz and $J_{5,6}$=7.0 Hz). Two pairs of doublets assignable to H-8 and H-9 protons were seen at δ 7.57 and 7.78 (J=4.0 Hz), respectively. These facts suggest that the resonance form **E** has large contribution in analogy with the case of **3**.

The compounds **8c** and **8i** were also deesterified and gave **8m** and **8n**, respectively. In the ^{1}H NMR spectra of **8m** and **8n**, two pairs of doublets were seen at δ 7.05 and 8.03 (J=9.0 Hz) and at δ 6.95 and 7.83 (J=9.0 Hz), respectively, and in their IR spectra, absorptions at 710 and 715 cm^{-1}, respectively, were seen. These results show that the configurations of ethylene bridge of **8** should be cis-one in similar to that of **4**.

The regiochemistry of the reaction was again attained by the reaction with dissymmetrical acetylene (MP) or olefins (MA, EA, or AN), and it is conceivable that 1,10-dipolar species should be intermediates.

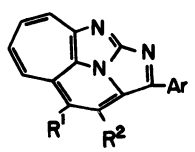

E

TABLE 6. ^{13}C NMR SPECTRAL DATA OF **3**, **4**, **7**, AND **8**

Carbon	3e[a]	3j[b]	3p[b]	3q[b]	7a[a]	7m[b]	4e[a]	4f[a]	4p[b]	8b[a]	8m[b]
1	146.9s	142.3s	133.5s	132.1s	147.4s	145.8s					
2							140.7s	140.8s	140.8s	151.7s	150.8s
2a	160.2s	159.9s	151.0s	155.8s	163.6s	162.7s					
3	114.7s	113.7s	108.9d	108.6d			134.9s	135.6s	135.6s	150.0s	150.0s
3a	132.6s	130.3s	125.1s	125.1s	130.5s	131.3s					
4	128.3d	127.8d	130.5d	129.7d	133.0d	132.0d					
4a							131.8s	134.4s	131.6s	134.3s	132.2s
5	126.7d[f]	126.4d[f]	123.0d[f]	123.1d[f]	128.3d[f]	126.7d[f]	127.3s	118.4s	119.3s	117.5s	117.0s
6	127.2d[f]	126.8d[f]	125.9d[f]	125.9d[f]	130.8d[c,f]	128.7d[f]	134.5d	134.2d	131.9d	134.4d	133.5d
7	128.7d	128.3d	129.6d	126.7d	130.8d[c]	130.4d	127.7d[f]	129.0d[f]	127.8d[f]	129.2d[c,f]	129.9d[f]
7a	126.5s	123.0s	122.2s	122.3s	118.4s	117.9s					
8	123.5s	122.7s	113.9d	113.9d	129.7s	118.3d	127.5d[f]	127.7d[f]	127.6d[f]	129.2d[c,f]	129.0d[d,f]
9	122.9s	115.8s	110.4d	110.3d	128.1s	110.4d	135.1d	134.7d	133.5d	134.7d	134.3d
9a	139.3s	142.3s	139.1s	141.1s	147.4s	147.3s	131.6s	133.2s	130.4s	133.5s	135.1s
9c	130.6s	130.3s	132.0s	130.8s	130.6s	132.4s					
10							105.2s	103.2s	101.0d		
10a							149.3s	148.7s	142.3s	153.0s	151.5s
Olefin							127.2s	125.6d	123.1d	127.3d	123.4d
							121.2s	117.5s	119.3d	116.1s	119.3d
$\underline{C}O_2R$	165.9s	166.0s			165.7s		166.7s	166.3s		166.1s	
	165.3s	165.1s			165.6s		165.8s	164.1s			
	164.4s	164.1s					164.1s				
$O\underline{C}H_2$	62.5t	62.3t					61.2t	60.9t			
Me	52.9q	52.9q		21.6q	53.2q		53.1q	52.4q		52.6q	
	52.4q	52.3q			52.5q		52.8q	14.7q			
	14.5q	21.6q					14.7q				
		14.5q									
Ph	131.8d	138.7s	128.9d[c]	139.3s	130.1d[c]	129.2d[c]	130.1d[c]	131.3s	128.9d[e]	129.8d	129.0d[d]
	130.0d[c]	129.6d[d]	128.6d[c]	129.7d[c]	129.2d[c]	128.9d[c]	128.7d	129.0d[c]	127.8s	129.1d[c]	129.0s[d]
	129.0d[c]	127.2s	128.0d[c]	128.6d[c]	128.0s	123.8s	128.4d[c]	128.6d	126.9d[c]	128.5s	128.3d[c]
	127.8s		126.8d	128.0s	126.6d	123.0d	128.2s	127.9d[c]		127.6d[c]	127.1d[c]

a) At 20 MHz. b) At 25 MHz. c) Two peaks degenerated. d) Four peaks degenerated. e) Three peaks degenerated. f) Assignments may be reversed.

Experimental

Melting points were uncorrected. ^1H NMR spectra were taken on JEOL JNM-FX 200 (200 MHz), JEOL JNM FX-100 (100 MHz), Varian EM-390 (90 MHz), and Hitachi R-24B (60 MHz) spectrometers using deuteriochloroform as solvent (TMS as internal standard), unless otherwise stated. ^{13}C NMR spectra were taken on JEOL JNM FX-100 (25 MHz) and Varian FT-80A (20 MHz) spectrometers using deuteriochloroform as solvent (TMS as internal standard). Mass spectra were determined with a Hitachi M-80 instrument by means of field desorption ionization methods. IR spectra were recorded for Nujol mulls and electronic spectra for ethanol solutions, unless otherwise stated. Column chromatography was performed on Kieselgel 60. Recorded yields are based on the material after recrystallization.

Abbreviations. DMAD (dimethyl acetylenedicarboxylate), DEAD (diethyl acetylenedicarboxylate), MP (methyl propiolate), DBA (dibenzoylacetylene), EA (ethyl acrylate), MA (methyl acrylate), DMM (dimethyl maleate), AN (acrylonitrile), TMS (tetramethylsilane).

Materials. 2-Aminocyclohepta[*b*]pyrrole (**1a**)[7,8] and 2-aminocycloheptimidazole (**5**)[11] were prepared as reported.

Sythesis of ***1b***. A mixture of ethyl 2-chlorocyclohepta[*b*]pyrrole-3-carboxylate (5.00 g, 21.0 mmol) in 20 ml of presaturated ethanolic ammonia in a sealed tube was heated at 160 °C for 3 h. The reaction mixture was poured into water and extracted with chloroform. The extract was dried (Na_2SO_4) and evaporated under reduced pressure. The residue was chromatographed. Elution with benzene–chloroform (1 : 1) gave starting material (0.799 g, 16%). Elution with chloroform–ethyl acetate (2 : 1) gave **1b** (3.50 g, 76%), which crystallized from ethanol as yellow needles (2.79 g, 61%), mp 150—151 °C, (lit,[12,13] mp 150—151 °C); λ_{max} 247 nm (log ε 4.13), 287 (4.55, sh), 293 (4.58), 320 (3.89, sh), 365 (3.85), 424 (3.64, sh), and 432 (3.66); IR 3400, 3250, 3120, and 3050 (NH), and 1655 (ester C=O), and 1630 cm^{-1} (C=N); ^1H NMR (60 MHz) δ=1.44 (3H, t, J=7.0 Hz, Me), 4.42 (2H, q, J=7.0 Hz, OCH_2), 7.10—7.40 (2H, m, N<u>H</u>, exchangeable), 7.40—7.80 (3H, m, H-5, 6, and 7), 8.02 (1H, dm, J=10.0 Hz, H-8) and 8.80 (1H, dm, J=10.0 Hz, H-4). Found: C, 66.33; H, 5.52; N, 13.12%. Calcd for $C_{12}H_{12}N_2O_2$: C, 66.65; H, 5.59; N, 12.96%.

Synthesis of ***1c***. A mixture of 2-chlorocyclohepta[*b*]pyrrole-3-carbonitrile (12.34 g, 65.5 mmol) in 20 ml of presaturated ethanolic ammonia in a sealed tube at 160 °C for 5 h, and worked up as above. Elution with benzene–chloroform (1 : 1) gave starting material (2.36 g, 19%). Elution with chloroform–ethyl acetate (4 : 1) gave **1c** (5.61 g, 51%), which crystallized from ethanol–dichloromethane as yellow needles (4.95 g, 45%), mp 237—238 °C; λ_{max} 242 nm (log ε 4.11, sh), 250 (4.12), 284 (4.53), 291 (4.53), 320 (3.95, sh), 366 (3.86), 423 (3.54), and 433 (3.54); IR 3380, 3300, 3200, and 3150 (NH), and 2200 and 2170 (C≡N), and 1640 cm^{-1} (C=N); ^1H NMR (60 MHz) δ=5.65—6.15 (2H, m, N<u>H</u>$_2$, exchangeable), 7.45—7.85 (3H, m, H-5, 6, and 7), and 7.90—8.35 (2H, m, H-4 and 8). Found: C, 71.21; H, 3.98; N, 25.00%. Calcd for $C_{10}H_7N_3$: C, 70.99; H, 4.17; N, 24.84%.

Synthesis of ***2a***. A mixture of **1a** (1.11 g, 7.71 mmol)

Table 7. Analytical data 3, 4, 7, and 8.

Compound	Appearance	Mp θ_m/°C	Formula	Found (%)			Calcd (%)			M/*m/e* (M^+)
				C	H	N	C	H	N	
3a	Yellow needles[a]	178—180	$C_{23}H_{16}N_2O_4$	72.09	4.11	7.22	71.87	4.20	7.29	384
3b	Yellow needles[b]	213—214	$C_{21}H_{14}N_2O_2$	77.56	4.24	8.37	77.29	4.32	8.58	
3c	Yellow needles[b]	218—219	$C_{24}H_{18}N_2O_4$	72.10	4.59	7.03	72.35	4.55	7.03	
3d	Yellow needles[b]	242—243	$C_{22}H_{16}N_2O_2$	77.42	4.63	8.08	77.63	4.74	8.23	
3e	Yellow needles[a]	192—194	$C_{26}H_{20}N_2O_6$	68.34	4.27	5.91	68.42	4.42	6.14	456
3f	Yellow needles[b]	114—115	$C_{28}H_{24}N_2O_6$	69.37	4.95	5.57	69.41	4.99	5.78	
3g	Yellow needles[c]	162—163	$C_{24}H_{18}N_2O_4$	72.39	4.41	7.02	72.35	4.55	7.03	
3h	Yellow needles[a]	255—256	$C_{36}H_{24}N_2O_4$	78.76	4.23	5.01	78.82	4.41	5.11	
3j	Yellow prisms[a]	211.5—213	$C_{27}H_{22}N_2O_6$	68.67	4.62	5.87	68.93	4.71	5.95	
3k	Yellow needles[a]	198—199	$C_{29}H_{26}N_2O_6$	70.11	5.15	5.48	69.87	5.26	5.62	
3l	Yellow needles[a]	202—204	$C_{25}H_{20}N_2O_4$	72.74	4.70	6.63	72.80	4.89	6.79	
3m	Yellow needles[a]	222.5—223	$C_{37}H_{26}N_2O_4$	79.02	4.65	4.88	78.99	4.66	4.98	
3n	Yellow needles[a]	219—220	$C_{24}H_{15}N_3O_4$	70.62	3.52	10.28	70.41	3.69	10.26	
3o	Yellow needles[b]	293—295	$C_{22}H_{13}N_3O_2$	74.98	3.65	12.16	75.20	3.73	11.96	
4a	Violet needles[a]	199—201	$C_{46}H_{32}N_4O_8$	71.98	4.04	7.10	71.87	4.20	7.29	768
4b	Brown needles[b]	193—194	$C_{42}H_{28}N_4O_4$	77.39	4.29	8.40	77.29	4.32	8.58	
4c	Violet needles[b]	222—223	$C_{48}H_{36}N_4O_8$	72.36	4.43	6.87	72.35	4.55	7.03	
4d	Brown needles[b]	225—226	$C_{44}H_{32}N_4O_4$	77.77	4.66	8.32	77.63	4.74	8.23	
4e	Violet needles[a]	187—188	$C_{52}H_{40}N_4O_{12}$	68.40	4.29	6.08	68.42	4.42	6.14	912
4f	Violet needles[c]	250—251	$C_{56}H_{48}N_4O_{12}$	69.39	4.91	5.54	69.41	4.99	5.78	
4g	Violet needles[c]	195—197	$C_{48}H_{36}N_4O_8$	72.41	4.48	6.75	72.35	4.55	7.03	796
4h	Violet needles[a]	253—254	$C_{72}H_{48}N_4O_8$	78.90	4.45	5.26	78.82	4.41	5.11	
4i	Violet needles[a]	198—200	$C_{50}H_{40}N_4O_8$	73.05	4.68	6.52	72.80	4.89	6.79	
4j	Violet needles[a]	218—219.5	$C_{54}H_{44}N_4O_{12}$	69.14	4.72	5.87	68.93	4.71	5.95	
4k	Violet needles[a]	215—217	$C_{58}H_{52}N_4O_{12}$	69.75	5.17	5.63	69.87	5.26	5.62	
4l	Brown needles[b]	209—210	$C_{50}H_{40}N_4O_8$	72.94	4.78	6.93	72.80	4.89	6.79	
4m	Brown needles[a]	227—231	$C_{74}H_{52}N_4O_8$	78.43	4.59	4.90	78.99	4.66	4.98	
4n	Brown needles[a]	204—205	$C_{48}H_{30}N_6O_8$	70.27	3.48	10.05	70.41	3.69	10.26	
4o	Brown needles[b]	271—272	$C_{44}H_{26}N_6O_4$	74.92	3.45	12.07	75.20	3.73	11.96	
7a	Yellow needles[a]	215—216	$C_{22}H_{15}N_3O_4$	68.50	3.88	10.85	68.57	3.92	10.90	385
7b	Yellow needles[a]	159—161	$C_{24}H_{19}N_3O_4$	69.46	4.50	10.09	69.72	4.63	10.16	
7c	Yellow needles[a]	246—248	$C_{20}H_{13}N_3O_2$	73.52	3.87	12.98	73.39	4.00	12.84	327
7d	Yellow needles[a]	249—250	$C_{32}H_{19}N_3O_2$	80.38	3.86	8.66	80.49	4.01	8.80	
7g	Yellow needles[a]	238—242	$C_{23}H_{17}N_3O_4$	69.09	4.23	10.61	69.17	4.29	10.52	
7h	Yellow needles[a]	205—206	$C_{25}H_{21}N_3O_4$	70.37	4.80	9.75	70.25	4.95	9.83	
7i	Yellow needles[a]	245—246	$C_{21}H_{15}N_3O_2$	73.86	4.44	12.16	73.89	4.43	12.31	
7j	Yellow needles[a]	245—246	$C_{33}H_{21}N_3O_2$	80.39	4.11	8.29	80.64	4.31	8.55	
8a	Violet needles[a]	223—224	$C_{44}H_{30}N_6O_8$	68.48	3.88	10.69	68.57	3.92	10.90	770
8b	Violet needles[a]	152—155	$C_{48}H_{38}N_6O_8$	69.74	4.50	10.02	69.72	4.63	10.16	
8c	Violet needles[a]	196—198	$C_{40}H_{26}N_6O_4$	73.15	3.96	12.75	73.39	4.00	12.84	654
8d	Brown needles[a]	248—249	$C_{64}H_{38}N_6O_4 \cdot$ EtOH	79.81	3.97	8.31	79.67	4.32	8.20	
8e	Violet needles[a]	198—199	$C_{42}H_{30}N_6O_4$	74.16	4.38	12.38	73.89	4.43	12.31	
8f	Brown needles[a]	>300	$C_{38}H_{20}N_8$	77.51	3.25	18.87	77.54	3.42	19.04	
8g	Violet needles[a]	216—218	$C_{46}H_{34}N_6O_8 \cdot$ 1/2 EtOH	68.65	4.09	9.91	68.69	4.54	10.23	
8h	Violet needles[a]	184—185	$C_{50}H_{42}N_6O_8$	70.38	5.11	9.57	70.25	4.95	9.83	
8i	Violet needles[a]	221—223	$C_{42}H_{30}N_6O_4$	73.98	4.18	12.10	73.89	4.43	12.31	
8j	Violet needles[a]	249—250	$C_{66}H_{42}N_6O_4$	80.36	4.17	8.45	80.46	4.31	8.55	
8k	Violet needles[a]	198—199	$C_{44}H_{34}N_6O_4$	74.14	4.65	11.47	74.35	4.82	11.82	
8l	Violet needles[a]	292—293	$C_{40}H_{24}N_8$	78.07	3.84	17.87	77.91	3.92	18.17	

a) Recrystallized from ethanol. b) Recrystallized from cyclohexane-dichloromethane. c) Recrystallized from cyclohexane.

and α-bromoacetophenone (1.50 g, 7.73 mmol) in abs ethanol (30 ml) was heated under reflux for 8 h. To this mixture, water (10 ml) and potassium carbonate (2.13 g, 15.4 mmol) were added, and the mixture was heated under reflux for 1 h and evaporated to dryness under reduced pressure. The residue was dissolved into water and extracted with chloroform. The extract was washed with water, dried over Na_2SO_4, evaporated, and the residue was chromatographed. Elution with benzene–chloroform (1 : 1) gave **2a** (1.205 g, 64%), which was crystallized from cyclohexane–dichloromethane to give brown prisms (0.925 g, 49%), mp 147—148 °C; λ_{max} 247 nm (log ε 4.28), 260 (4.23, sh), 320 (4.61), 340 (4.45, sh), 384 (3.57), 404 (3.63), 429 (3.58), 470 (2.70), 505 (2.76), 545 (2.74), 587 (2.61, sh), and 650 (2.28, sh); IR 740 and 690 cm^{-1} (phenyl); ^1H NMR (60 MHz) δ=6.80 (1H, s, H-10), 6.65—7.10 (3H, m, H-6, 7, and 8), 7.30—7.60 (3H, m, phenyl), 7.60—7.90 (2H, m, H-5 and 9), 7.97 (1H, s, H-3), and 7.90—8.20 (2H, m, phenyl); δ (CF_3CO_2H)=7.15 (1H, s, H-10),

7.45—8.30 (8H, m, H-6, 7, 8, and phenyl), 8.35 (1H, s, H-3), 8.53 (1H, dm, J=9.0 Hz, H-9), and 8.69 (1H, dm, J=9.0 Hz, H-5). Found: C, 83.47; H, 4.85; N, 11.32%. Calcd for $C_{17}H_{12}N_2$: C, 83.58; H, 4.59; N, 11.47%.

Synthesis of 2b. A mixture of **1a** (0.500 g, 3.47 mmol) and 2-bromo-4′-methylacetophenone (0.730 g, 3.51 mmol) in abs ethanol (20 ml) was heated under reflux for 10 h. Water (5 ml) and potassium carbonate (0.960 g, 6.96 mmol) were added to this mixture, then the mixture was heated under reflux for 1 h and worked up as above. Chloroform eluted **2b** (0.569 g, 63%), which was crystallized from cyclohexane–dichloromethane to give brown scales (0.425 g, 47%), mp 165—166 °C; λ_{max} 250 nm (log ε 4.28), 264 (4.28), 325 (4.61), 345 (4.48, sh), 385 (3.60), 405 (3.64), 429 (3.55), 470 (2.75), 505 (2.79), 545 (2.77), 587 (2.65, sh), and 650 (2.39, sh); IR 820 cm^{-1} (phenyl); ^{1}H NMR (90 MHz) δ=2.35 (3H, s, Me), 6.72 (1H, s, H-10), 6.50—7.00 (3H, m, H-6, 7, and 8), 7.14 (2H, d, J=8.0 Hz, H-*m*-phenyl), 7.31 (1H, dm, J=9.5 Hz, H-5), 7.54 (1H, dm, J=10.5 Hz, H-9), 7.76 (2H, d, J=8.0 Hz, H-*o*-phenyl), and 7.82 (1H, s, H-3). Found: C, 83.59; H, 5.23; N, 10.65%. Calcd for $C_{18}H_{14}N_2$: C, 83.69; H, 5.46; N, 10.84%.

Synthesis of 2c. A mixture of **1b** (4.240 g, 19.6 mmol) and α-bromoacetophenone (4.190 g, 21.6 mmol) in 1-butanol (30 ml) was heated under reflux for 20 h, then evaporated to dryness. To the residue, water (40 ml), ethanol (60 ml), and potassium carbonate (5.400 g, 39.3 mmol) were added, and the mixture was heated under reflux for 1 h, and evaporated. The residue was dissolved into water and extracted with chloroform. The extract was washed, dried (Na_2SO_4), and evaporated. The residue was chromatographed. Elution with benzene–chloroform gave **2c** (2.603 g, 42%), which was crystallized from cyclohexane–dichloromethane to give brown needles (1.887 g, 30%), mp 160—161 °C; λ_{max} 253 nm (log ε 4.41), 280 (4.09, sh), 340 (4.36), 355 (4.33, sh), 442 (3.60), 455 (3.59, sh), 530 (2.76, sh), 575 (2.56, sh), and 640 (1.98, sh); IR 1685 (ester C=O), and 740 and 695 cm^{-1} (phenyl); ^{1}H NMR (60 MHz) δ=1.57 (3H, t, J=7.0 Hz, Me), 4.60 (2H, q, J=7.0 Hz, OCH_2), 7.25—7.65 (6H, m, H-6, 7, 8, and phenyl), 7.93 (1H, dm, J=10.0 Hz, H-5), 8.07 (1H, s, H-3), 7.95—8.20 (2H, m, phenyl), and 9.33 (1H, dm, J=10.0 Hz, H-9). Found: C, 75.78; H, 4.92; N, 8.86%. Calcd for $C_{20}H_{16}N_2O_2$: C, 75.93; H, 5.10; N, 8.86%. Elution with chloroform–ethyl acetate (2 : 1) gave **1b** (1.725 g, 41%).

Synthesis of 2d. A mixture of **1b** (4.463 g, 20.6 mmol) and 2-bromo-4′-methylacetophenone (4.645 g, 20.6 mmol) in 1-butanol (30 ml) was heated under reflux for 20 h and evaporated. To this residue, water (10 ml), ethanol (90 ml), and potassium carbonate (5.710 g, 41.3 mmol) were added, and the mixture was heated under reflux for 1 h, and worked up as for **2c**. Elution with benzene–chloroform (1 : 1) gave **2d** (4.127 g, 60.5%), which was crystallized from cyclohexane–dichloromethane to give brown needles (2.475 g, 36%), mp 133—134 °C; λ_{max} 254 nm (log ε 4.42), 280 (4.11, sh), 347 (4.47), 360 (4.45, sh), 445 (3.68), 455 (3.68, sh), 530 (2.85, sh), 590 (2.53, sh), and 630 (2.19, sh); IR 1680 (ester C=O) and 810 cm^{-1} (phenyl); ^{1}H NMR (60 MHz) δ=1.53 (3H, t, J=7.0 Hz, Me), 2.38 (3H, s, Me), 4.55 (2H, q, J=7.0 Hz, OCH_2), 7.23 (2H, d, J=8.0 Hz, H-*m*-phenyl), 7.25—7.60 (3H, m, H-6, 7, and 8), 7.85 (1H, dm, J=10.0 Hz, H-5), 7.93 (2H, d, J=8.0 Hz, H-*o*-phenyl), 7.97 (1H, s, H-3), and 9.25 (1H, dm, J=10.0 Hz, H-9). Found: C, 76.64; H, 5.67; N, 8.09%. Calcd for $C_{21}H_{18}N_2O_2$: C, 76.35; H, 5.49; N, 8.48%. Elution with chloroform–ethyl acetate (2 : 1) gave **1b** (1.581 g, 36%).

Synthesis of 2e. A mixture of **1c** (1.210 g, 7.16 mmol) and α-bromoacetophenone (1.930 g, 7.16 mmol) in 1-butanol (30 ml) was heated under reflux for 100 h, and evaporated under reduced pressure. To the residue, ethanol (90 ml), water (10 ml), and potassium carbonate (1.980 g, 14.3 mmol) were added, and the mixture was heated under reflux for 1 h, and worked up as for **2c**. Elution with benzene–chloroform (1 : 1) gave **2e** (0.608 g, 32%), which was crystallized from ethanol–dichloromethane to give brown prisms (0.291 g, 15%), mp 256—257 °C; λ_{max} ($CHCl_3$) 247 nm (log ε 4.43), 280 (4.18, sh), 342 (4.45), 355 (4.42, sh), 435 (3.62), 457 (3.63), 507 (2.95, sh), 546 (2.83, sh), 595 (2.65, sh), and 650 (2.29, sh); IR 2200 (C≡N), and 740 and 695 cm^{-1} (phenyl); ^{1}H NMR (60 MHz) δ (CF_3CO_2D)=7.50—7.95 (5H, m, phenyl), 8.20—8.60 (3H, m, H-6,7, and 8), 8.54 (1H, s, H-3), 9.05 (1H, dm, J=10.0 Hz, H-5), and 9.18 (1H, dm, J=10.0 Hz, H-9). Found: C, 80.27; H, 3.93; N, 15.43%. Calcd for $C_{18}H_{11}N_3$: C, 80.28; H, 4.12; N, 15.60%.

Deesterification of 2c. A mixture of **2c** (0.316 g, 1.00 mmol) and potassium hydroxide (0.56 g, 10.0 mmol) in ethanol (30 ml)–water (20 ml) was heated under reflux for 1 h. The reaction mixture was diluted with water and acidified with 1 M aq hydrochloric acid (1 M=1 mol dm^{-3}). The resulted precipitate was filtered and dried to give the corresponding carboxylic acid [0.262 g, 90%, mp 181—182 °C (decomp)]. A suspension of the carboxylic acid (0.140 g, 0.49 mmol) in 48% hydrobromic acid (10 ml) was heated under reflux for 1 h, then poured into water, and neutralized with sodium carbonate, and extracted with chloroform. The extract was washed with water, dried (Na_2SO_4), and evaporated. The residue was chromatographed with benzene–chloroform (1 : 1) to give **2a** (0.037 g, 31%).

General Procedure for the Reactions of 2 with Acetylenes. A mixture of **2** (2.00 mmol), the acetylene (4.00 mmol), and the solvent (30 ml) was heated under reflux under the conditions specified in Table 1, and evaporated under reduced pressure. Chromatography of the residue with benzene–chloroform (1 : 1) gave **3** and **4**, successively. Analytical data are listed in Table 7 and spectroscopic data in Tables 2—5, and 6.

General Procedure for the Reactions of 2 with Olefins. A mixture of **2** (2.00 mmol), the olefin (20.0 mmol), and the solvent (30 ml) was heated under reflux under the conditions specified in Table 1 and evaporated to dryness under the reduced pressure. Chromatography of the residue with benzene–chloroform (1 : 1) gave **4**. Analytical data are listed in Table 7 and spectroscopic data in Tables 4, 5, and 6.

Deesterification of 3 and 4. A solution of **3e** (0.190 g, 0.42 mmol) and potassium hydroxide (0.90 g, 16 mmol) in ethanol (40 ml)–water (20 ml) was heated under reflux for 3 h. The reaction mixture was poured into water (250 ml), acidified with 1 M aq hydrochloric acid, and resulted precipitate was filtered to give the corresponding tricarboxylic acid (0.147 g, 88%, mp>300 °C). A mixture of the carboxylic acid (0.147 g, 0.37 mmol) and copper-powder (0.10 g) in quinoline (5 ml) was heated under reflux for 1 h. The reaction mixture was filtered off, and copper-powder was washed with chloroform. The combined filtrate was washed with 1 M aq hydrochloric acid followed by water, dried (Na_2SO_4), and evaporated. The residue was chromatographed with chloroform to give **3p** (0.098 g, 99%), which crystallized from cyclohexane as yellow needles (0.074 g, 75%), mp 197—199 °C; λ_{max} 239 nm (log ε 4.36), 260 (4.34, sh), 270 (4.40, sh), 281 (4.51, sh), 288 (4.54), 295 (4.47, sh), 320 (3.75), 357 (4.26), 374 (4.36), 417 (3.95), and 440 (4.07); ^{1}H NMR (200 MHz) δ=7.50—7.70 (3H, m, phenyl), 7.73 (1H, ddd, J=8.0, 7.0, and 1.5 Hz, H-5), 7.73 (1H, d, J=4.0 Hz, H-9), 7.77 (1H, d, J=4.0 Hz, H-8), 7.78 (1H, ddd, J=8.0, 7.0, and 1.5 Hz, H-6), 8.32 (1H, ddd, J=8.0, 1.5, and 0.5 Hz, H-4), 8.33 (1H, s, H-3), 8.45—8.55 (2H, m, phenyl), and 8.57 (1H, ddd, J=8.0, 1.5, and 0.5 Hz, H-7). Found: C, 84.75; H, 4.58; N, 10.28%. Calcd for $C_{19}H_{12}N_2$:

C, 85.05; H, 4.51; N, 10.44%.

In a similar manner, **3j**, **4e**, and **4j** gave **3q** (85%), **4p** (54%), and **4q** (50%), respectively.

3q: Yellow needles (from cyclohexane), mp 235 °C; λ_{max} 242 nm (log ε 4.71), 260 (4.65, sh), 271 (4.60, sh), 280 (4.69, sh), 290 (4.77), 300 (4.77), 323 (4.15), 359 (4.59), 375 (4.66), 415 (4.26), and 438 (4.36); ^{1}H NMR (60 MHz) δ=2.46 (3H, s, Me), 7.35 (2H, d, J=8.0 Hz, H-*m*-phenyl), 7.60—7.90 (4H, m, H-5, 6, 8, and 9), 8.22 (1H, dm, J=9.0 Hz, H-4), 8.25 (1H, s, H-3), 8.35 (2H, d, J=8.0 Hz, H-*o*-phenyl), and 8.50 (1H, dm, J=9.0 Hz, H-7). Found: C, 85.11; H, 4.83; N, 9.91%. Calcd for $C_{20}H_{14}N_2$: C, 85.09; H, 5.00; N, 9.92%.

4p: Violet needles (from cyclohexane–dichloromethane), mp 157—158 °C; λ_{max} 237 nm (log ε 4.77), 262 (5.01), 285 (4.38, sh), 344 (4.60), 360 (4.51), 384 (4.21, sh), 403 (4.46), 427 (4.46), 485 (3.58, sh), 515 (3.70), 547 (3.70), 590 (3.50), and 645 (2.94, sh); IR 725 cm^{-1} (*cis* HC=CH); ^{1}H NMR (60 MHz) δ=6.23 (2H, ddd, J=10.5, 8.0, and 2.0 Hz, H-8), 6.73 (2H, ddd, J=10.5, 8.0, and 2.5 Hz, H-7), 6.90 (2H, dd, J=10.5 and 2.0 Hz, H-6), 7.05 (2H, d, J=9.0 Hz, H-olefin), 7.27 (2H, s, H-10), 7.15—7.60 (6H, m, phenyl), 7.60 (2H, dd, J=10.5 and 2.5 Hz, H-9), 8.03 (2H, d, J=9.0 Hz, H-olefin), and 8.05—8.30 (4H, m, phenyl). Found: C, 85.27; H, 4.47; N, 10.56%. Calcd for $C_{38}H_{24}N_4$: C, 85.05; H, 4.51; N, 10.44%.

4q: Dark green needles (from cyclohexane), mp 159.5—162 °C; λ_{max} 240 nm (log ε 4.75), 264 (4.98), 287 (4.44, sh), 345 (4.55), 363 (4.48), 386 (4.27, sh), 406 (4.41), 428 (4.38), 487 (3.57, sh), 520 (3.62), 553 (3.63), 592 (3.47), and 650 (3.03, sh); IR 720 cm^{-1} (*cis* HC=CH); ^{1}H NMR (60 MHz) δ=2.42 (6H, s, Me), 6.27 (2H, ddd, J=10.5, 8.0, and 2.0 Hz, H-8), 6.69 (2H, ddd, J=10.5, 8.0, and 2.0 Hz, H-7), 6.90 (2H, d, J=9.0 Hz, H-olefin), 7.27 (4H, d, J=8.0 Hz, H-*m*-phenyl), 7.33 (2H, s, H-10), 7.41 (2H, dd, J=10.5 and 2.0 Hz, H-9), 8.06 (2H, d, J=9.0 Hz, H-olefin), and 8.09 (4H, d, J=8.0 Hz, H-*o*-phenyl). Found: C, 84.91; H, 4.98; N, 9.64%. Calcd for $C_{40}H_{28}N_4$: C, 85.09; H, 5.00; N, 9.92%.

Synthesis of ***6a***. A mixture of **5** (2.00 g, 13.8 mmol) and *α*-bromoacetophenone (2.74 g, 14.1 mmol) in abs ethanol (50 ml) was heated under reflux for 7 h, then cooled overnight to give 2-amino-1-phenacycloheptimidazolium bromide (3.74 g, 80%), which crystallized from ethanol as colorless prisms (mp 230—231 °C. Found: C, 55.64; H, 4.33; N, 11.96%. Calcd for $C_{16}H_{14}BrN_3O$: C, 55.83; H, 4.10; N, 12.21%). A mixture of the salt and potassium carbonate (3.25 g, 24.1 mmol) in ethanol (90 ml)–water (10 ml) was heated under reflux for 2 h, and worked up as for **1a**. Elution with chloroform–ethyl acetate (4 : 1) gave **6a** (2.19 g, 76%), which was crystallized from ethanol to give brown needles (1.970 g, 68%), mp 244—245 °C; λ_{max} 232 nm (log ε 4.50), 245 (4.42, sh), 334 (4.70), 421 (3.62), and 428 (3.60, sh); IR 735 and 685 cm^{-1} (phenyl); ^{1}H NMR (100 MHz) δ=7.20—7.50 (3H, m, phenyl), 7.55—7.80 (3H, m, H-6, 7, and 8), 7.94 (1H, s, H-3), 7.90—8.05 (2H, m, H-*o*-phenyl), 8.05 (1H, dm, J=11.0 Hz, H-5), and 8.40 (1H, dm, J=11.0 Hz, H-9), δ (CF_3CO_2D)=7.50—7.90 (5H, m, phenyl), 8.43 (1H, s, H-3, exchangeable), 8.60—9.00 (3H, m, H-6, 7, and 8), and 9.20—9.60 (2H, m, H-5 and 9). Found: C, 78.52; H, 4.49; N, 17.21%. Calcd for $C_{16}H_{11}N_3$: C, 78.35; H, 4.52; N, 17.13%.

Synthesis of ***6b***. A mixture of **5** (2.00 g, 13.8 mmol) and 2-bromo-4′-methylacetophenone (2.94 g, 13.8 mmol) in abs ethanol (40 ml) was heated under reflux for 5 h, then cooled overnight. Resulted precipitates were collected by filtration to give 2-amino-1-(*p*-methylphenacyl)cycloheptimidazolium bromide (3.82 g, 77%), which crystallized from ethanol as colorless needles [mp 257 °C (decomp). Found: C, 56.76; H, 4.43; N, 11.88%. Calcd for $C_{17}H_{16}BrN_3O$: C, 57.00; H, 4.50; N, 11.73%]. A mixture of the salt (4.65 g, 13.0 mmol) and potassium carbonate (3.59 g, 26.0 mmol) in ethanol (225 ml)–water (25 ml) was heated under reflux for 2 h and worked up as for **1a**. Elution with chloroform gave **6b** (2.786 g, 83%), which was crystallized from ethanol–dichloromethane to give brown needles (1.903 g, 57%), mp 272—275 °C (decomp); λ_{max} 235 nm (log ε 4.42), 255 (4.31), 338 (4.60), 423 (3.56), and 428 (3.54, sh); IR 820 cm^{-1} (phenyl); ^{1}H NMR (60 MHz) δ (CF_3CO_2D)=2.48 (3H, s, Me), 7.41 (2H, d, J=8.0 Hz, H-*m*-phenyl), 8.03 (2H, d, J=8.0 Hz, H-*o*-phenyl), 8.37 (1H, s, H-3, exchangeable), 8.65—9.00 (3H, m, H-6, 7, and 8), and 9.20—9.60 (2H, m, H-5 and 9). Found: C, 78.77; H, 5.18; N, 15.94%. Calcd for $C_{17}H_{13}N_3$: C, 78.74; H, 5.05; N, 16.20%.

General Procedure for the Reactions of ***6*** *with Acetylenes.* A mixture of **6** (2.00 mmol), the acetylene (4.00 mmol), and the solvent (50 ml) was heated under reflux under the conditions specified in Table 1 and evaporated to dryness under reduced pressure. Chromatography of the residue with benzene–chloroform (1 : 1) gave **7** and **8**, successively. Analytital data are listed in Table 7 and spectroscopic data in Tables 2, 3, 4, 5, and 6.

General Procedure for the Reactions of ***6*** *with Olefins.* A mixture of **6** (1.00 mmol), the olefin (10.0 mmol), and the solvent (30 ml) was heated under reflux under the conditions specified in Table 1 and evaporated to dryness under reduced pressure. Chromatography of the residue with benzene–chloroform (1 : 1) gave **8**. Analytical data are listed in Table 7 and spectroscopic data in Tables 4 and 5.

Deesterification of ***7*** *and* ***8***. A solution of **7a** (0.400 g, 1.04 mmol) and potassium hydroxide (0.58 g, 10.4 mmol) in ethanol (30 ml)–water (20 ml) was heated under reflux for 2 h. The reaction mixture was poured into water (200 ml), acidified with 1M aq hydrochloric acid. Resulted precipitate was filtered to give the corresponding dicarboxylic acid as yellow powder (0.350 g, 97%, mp>300 °C). A mixture of the carboxylic acid (0.350 g, 0.98 mmol) and copper-powder (0.10 g) in quinoline (5 ml) was heated under reflux for 1 h and worked up as for **3p**. Elution with chloroform gave **7m** (0.175 g, 66%), which was crystallized from ethanol–dichloromethane to give yellow needles (0.142 g, 54%), mp 204—206 °C; λ_{max} 234 nm (log ε 4.35), 261 (4.38), 282 (4.43), 291 (4.40), 322 (3.93), 335 (4.01), 364 (4.23), 380 (4.21, sh), 438 (4.08), and 462 (4.15); IR 745 and 680 cm^{-1} (phenyl); ^{1}H NMR (200 MHz) δ=7.57 (1H, d, J=4.0 Hz, H-8), 7.63 (1H, s, H-3), 7.58—7.70 (3H, m, phenyl), 7.78 (1H, d, J=4.0 Hz, H-9), 7.80 (1H, ddd, J=8.5, 7.0, and 1.5 Hz, H-5), 7.91 (1H, ddd, J=8.5, 7.0, and 2.0 Hz, H-6), 8.48 (1H, ddd, J=8.5, 2.0, and 0.5 Hz, H-4), 8.50—8.57 (2H, m, phenyl), and 8.56 (1H, ddd, J=8.5, 1.5, and 0.5 Hz, H-7). Found: C, 80.04; H, 3.85; N, 15.53%. Calcd for $C_{18}H_{11}N_3$: C, 80.28; H, 4.12; N, 15.60%.

In a similar manner, **7c**, **7i**, **8c**, and **8i** gave **7m** (94%), **7n** (44%), **8m** (51%), and **8n** (55%), respectively.

7n: Yellow needles (from cyclohexane–dichloromethane), mp 213—215 °C; λ_{max} 237 nm (log ε 4.36), 262 (4.39), 285 (4.36), 294 (4.37), 327 (3.98, sh), 340 (4.10, sh), 367 (4.33), 377 (4.32, sh), 440 (4.07), and 460 (4.20); IR 825 and 815 cm^{-1} (phenyl); ^{1}H NMR (60 MHz) δ=2.44 (3H, s, Me), 7.31 (2H, d, J=8.0 Hz, H-*m*-phenyl), 7.51 (1H, d, J=8.5 Hz, H-8), 7.50—8.00 (3H, m, H-5, 6, and 7), 8.32 (1H, d, J=8.5 Hz, H-9), 8.34 (2H, d, J=8.0 Hz, H-*o*-phenyl), and 8.43 (1H, dm, J=10.0 Hz, H-4). Found: C, 80.26; H, 4.43; N, 14.82%. Calcd for $C_{19}H_{13}N_3$: C, 80.55; H, 4.62; N, 14.83%.

8m: Brown needles (from cyclohexane–dichloromethane), mp 224—225 °C; λ_{max} 238 nm (log ε 4.91), 250 (4.87, sh), 266 (4.75, sh), 277 (4.66, sh), 328 (4.70), 340 (4.66, sh), 415 (4.53, sh), 437 (4.70), 525 (3.78, sh), 555 (3.81), 585 (3.72, sh), and

640 (3.25, sh); IR 740 and 680 (phenyl), and 710 cm^{-1} (*cis* HC=CH); ^1H NMR (60 MHz) δ=6.23 (2H, ddd, J=10.5, 8.0, and 2.0 Hz, H-8), 6.73 (2H, ddd, J=10.5, 8.0, and 2.5 Hz, H-7), 6.90 (2H, ddd, J=10.5, 2.0, and 0.5 Hz, H-6), 7.05 (2H, d, J=9.0 Hz, H-olefin), 7.27 (2H, s, H-10), 7.15—7.60 (6H, m, phenyl), 7.60 (2H, ddd, J=10.5, 2.5, and 0.5 Hz, H-9), 8.03 (2H, d, J=9.0 Hz, H-olefin), and 8.05—8.30 (4H, m, phenyl). Found: C, 80.02; H, 3.97; N, 15.30%. Calcd for $C_{36}H_{22}N_6$: C, 80.28; H, 4.12; N, 15.60%.

8n: Dark brown needles (from cyclohexane–dichloromethane), mp 216—217 °C; λ_{max} 239 nm (log ε 4.86), 250 (4.79, sh), 266 (4.66, sh), 281 (4.42), 335 (4.65), 343 (4.62, sh), 418 (4.51, sh), 440 (4.69), 530 (3.78, sh), 560 (3.82), 595 (3.72, sh), and 647 (3.26, sh); IR 810 (phenyl) and 715 cm^{-1} (*cis* HC=CH), ^1H NMR (60 MHz) δ=2.37 (6H, s, Me), 6.60—7.15 (6H, m, H-6, 7, and 8), 6.95 (2H, d, J=9.0 Hz, H-olefin), 7.14 (4H, d, J=8.0 Hz, H-*m*-phenyl), 7.75 (2H, dm, J=10.0 Hz, H-9), 7.83 (2H, d, J=9.0 Hz, H-olefin), and 7.93 (4H, d, J=8.0 Hz, H-*o*-phenyl). Found: C, 80.41; H, 4.49; N, 14.55%. Calcd for $C_{38}H_{26}N_6$: C, 80.55; H, 4.62; N, 14.83%.

We thank Dr. Masafumi Yasunami (Tohoku University) and Dr. Akira Mori (Kyushu University) for the high resolution NMR spectra. This work was supported by a Grant-in-Aid for Scientific Research (No. 56470021) from the Ministry of Education, Science and Culture.

References

1) Part X, N. Abe, T. Nishiwaki, and H. Yamamoto, *Chem. Lett.*, **1982**, 805.

2) K. Matsumoto, T. Uchida, and J. Yamauchi, *Yuki Gosei Kagaku Kyokai Shi*, **35**, 739 (1977); W. Flitsch and U. Krämer, *Adv. Heterocycl. Chem.*, **22**, 321 (1978).

3) J. C. Godfrey, *J. Org. Chem.*, **24**, 581 (1959).

4) A. Galbraith, T. Small, and V. Boekelheide, *J. Org. Chem.*, **24**, 582 (1959).

5) The nomenclature was accorded to the Boekelheide's one. See Ref. 2.

6) T. Nishiwaki and N. Abe, *Heterocycles*, **15**, 547 (1981).

7) T. Nozoe, S. Seto, S. Matsumura, and T. Terasawa, *Chem. Ind.*, **1954**, 1357.

8) K. Fujimori, N. Hirako, and K. Yamane, *Bull. Chem. Soc. Jpn.*, **56**, 1247 (1983).

9) For convenience, numbering of **4** and **8** are adopted as follows.

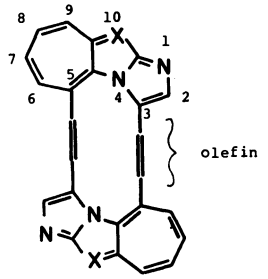

10) The C-3 position of **2** and **6** is reactive and subjected to bromination, formylation, and nitration. These results will be reported elsewhere.

11) T. Nozoe, T. Mukai, K. Takase, I. Murata, and K. Matsumoto, *Proc. Jpn. Acad.*, **29**, 452 (1953).

12) T. Nozoe, S. Seto, and T. Toda, *Bull. Chem. Soc. Jpn.*, **41**, 208 (1968).

13) S. Sunagawa and M. Watatani, Japan Patent, 7007540; *Chem. Abstr.*, **73**, 3788f (1970).

Studies on the Mechanism of Zeolite X Crystallization. I. Effects of Silica Sources of Starting Materials on the Crystallization of Zeolite X

Ryozi Hino,* Ryohei Matuura,† and Kenzi Toki

Department of Chemistry, Faculty of Science, Shimane University, Nishikawatsu, Matsue 690

†*Department of Chemistry, Faculty of Science, Kyushu University, Hakozaki, Higashi-ku, Fukuoka 812*

(Received January 6, 1983)

The crystallization mechanism for zeolite was investigated. Tetraethyl orthosilicate and silica sol were used as silica sources. Many kinds of solid phases were obtained at various reaction times. These solid phases were characterized by analyses for chemical compositions, X-ray diffraction, adsorption of nitrogen gas and water vapor, and IR spectroscopy. The results obtained suggest that the solid phase derived from tetraethyl orthosilicate at an early stage of reaction is composed of slightly ordered skeletons. In addition, during aging of gel at room temperature, the structure of the solid phase of gel undergoes a rearrangement to form a crystalline structure. On the other hand, the gel phase obtained from silica sol is predominantly made up by the coagulation of disordered aluminosilicate polymers or silicic polymers. These gel phases act as a precursor, and a part of the gel dissolved into the liquid phase and the dissolved species are converted into crystals in the liquid phase. Thus, the silica sources influence the structure of gel and crystals. In general, the crystallization mechanism is strongly influenced by the starting materials, especially by the silica sources.

Many investigation on the mechanism and kinetics of zeolite crystallization have been done in recent years. These investigations are concerned with autocatalysis[1] and effects of temperature,[2] alkalinity,[2,3] and seeding,[1] and kinetically have dealt with the conversion from amorphous substances to crystals[4-9] and induction periods with respect to the distribution of chemical species in liquid and solid phases.[10-12] In addition, Raman[5] and IR[13,14] spectra of liquid and solid phases of gel were analyzed in order to understand the zeolite crystallization.

However, because of complex reactions of aluminosilicate in liquid and solid phases, the process of zeolite crystallization has not yet been made clear.

Schwochow and Heinze[15] reported that zeolite A, sodalite, zeolite P, and faujasite were crystallized from a liquid phase which had been separated from an aluminosilicate gel phase during a crystallization process. Zhdanov[11] revealed that the liquid phase of aluminosilicate gel influenced properties and compositions of crystals formed.

On the other hand, many investigations have revealed that the crystallization of zeolite occurs in the solid phase of gel through rearrangement of alumonisilicate framework. For example, Khatami and Flanigen[16] observed that the crystallization of gel phase occurred in the absence of liquid phase. After all, at the present stage there have been proposed two mechanisms for the zeolite crystallization based on two representative hypotheses. The first mechanism is based on a crystallization to occur in a solid phase. During the aging of this solid phase a rearragement of the aluminosilicate framework leads the amorphous gel to crystals. This mechanism is supported by Breck and Flanigen,[7] McNicol *et al.*,[17] and Aiello *et al.*[18]

The other mechanism is based on a crystallization to occur in a liquid phase; the constituents of zeolite are caused to be dissolved into a liquid phase *via* their precursors, amorphous gel phases, and then zeolite is made crystallized in a liquid phase. This mechanism is supported by Kerr,[1] Ciric,[9] Culfaz and Sand,[4] and Kacirek and Lechert.[19]

In our previous papers we reported that syntheses of zeolite A[20] and zeolite X[21] using tetraeth l orthosilicate as a silica source could proceed easily. These zeolites, in crystal, had a high purity and a high crystallinity. In addition, we investigated the difference between the distributions of component concentrations in the solid and liquid phases during processes of zeolite crystallization using tetraethyl orthosilicate, silica sol,[21] or sodium metasilicate.[22] These results suggested that at the beginning of reaction, the difference in the silica sources has an influence on chemical states of the soluble species of constituents of zeolite in the liquid phase, together with a significant influence on the nucleation of zeolite crystals, growth steps of aluminosilicate, and properties of crystals produced.

In the present study, solid phases were sampled out of reaction systems at various reaction times. These solid phases were characterized by chemical analysis, X-ray diffraction, adsorption of nitrogen gas and water vapor, and IR spectra. These results were compared with earlier results.[21]

Experimental

Materials. The silica sources used were a commercial tetraethyl orthosilicate (Nakarai Chemical Co. Ltd.) purified by distillation, and a silica sol which had been prepared by diluting a Snowtex 40 (Nissan Chemical Co. Ltd.) with distilled water to double the volume. The alumina source used was a sodium aluminate solution which had been synthesized from Al plate (99.99%, Nakarai Chemical Co. Ltd.) and sodium hydroxide solution. A sodium hydroxide solution (5 mol dm^{-3}) was used as excess alkaline solution. These starting materials were described in detail elsewhere.[21]

Preparation of Specimens. The molar ratios of SiO_2/Al_2O_3, Na_2O/SiO_2, and H_2O/Na_2O adopted for the preparation of mixtures of starting materials were 8, 6, and 50, respectively, which correspond to the formula $48Na_2O \cdot Al_2O_3 \cdot 8SiO_2 \cdot 2400H_2O$. These ratios have been established as falling in the region providing optimum conditions for the synthesis of zeolite X.[23]

The procedure of synthesis was as follows. Tetraethyl orthosilicate was added to a sodium aluminate solution in a flask, and the mixture was stirred by an ultra sonic generator (40 kHz) for 20 min. A mixture of sodium hydroxide solution and distilled water was added to the flask and allowed to be stirred mechanically for 6—72 h at room temperature. To prevent evaporation the flask was equipped with a glass tubing with both ends open, and it was heated in an air oven at 85 °C for 74—96 h. After a fixed time, the solid and liquid phases of reaction mixture were separated with a centrifuge. The supernatant solution of the liquid phase was pipetted out as a specimen of the liquid phase. The solid phase was filtered and washed with distilled water until the pH of washings reached 10.5 and then dried at 110 °C for 24 h.

Analyses. Analyses of liquid and solid phases were made as follows. The colorimetric method, *i.e.*, the molybosilicic acid yellow method, and a Hitachi spectrophotometer model 100-30 were applied to determining silica concentrations. Flame photometry using a Hitachi atomic absorption analyzed model 208 was applied to determining sodium concentrations. Aluminium concentrations were determined by the chelatometric titration using EDTA and Zn standard solutions and an XO indicator.

Adsorption. The adsorption of nitrogen gas was subjected to volumetric measurements at the boiling point of liquid nitrogen and the adsorption of water vapor to gravimetric measurements at 25 °C. The pretreatment of specimens was carried out as follows. After being kept at 110 °C for 24 h, the specimen was heated at 300 °C for 2 h under atmospheric pressure, and degassed under vacuum (at 10^{-5} mmHg) (1 mmHg≈133.322 Pa) for 30 min prior to the adsorption.

IR Spectra. Infrared transmission spectra were measured by the KBr wafer technique according to the study by Flanigen and Khatami.[13] Every wafer contained 1 mg of solid phase in 300 mg of KBr. Spectra were recorded on a Hitachi infrared spectrometer model 260-50.

Crystallinity. Products were identified by the powder X-ray diffractometry using a Toshiba X-ray diffractometer model ADG 301 (Cu *Ka*, Ni filter, 30 kV, 20 mA, G. M. detector) and a JEOL model JDX-7E (Cu *Ka*, Ni filter, 30 kV, 20 mA, scintillation counter). The crystallinity was determined by the X-ray diffraction method with an LMS 13X as reference.

Results

Crystallinity. The solid phase derived from tetraethyl orthosilicate remained amorphous for initial 75 h after the beginning of reaction, but began to include crystals at 76 h. The solid phase derived from silica sol remained amorphous for initial 74 h, but began to inculude crystals at 75 h. Table 1 shows the change in crystallinity with reaction time. The change in crystallinity proceeded very rapidly immediately after crystals were recognized in the solid phase from either tetraethyl orthosilicate or silica sol, and the rate of crystallization decreased after a few hours. Then, the crystallinity was kept almost constant.

The crystals derived from tetraethyl orthosilicate and from silica sol showed relative crystallinities of 120 and 75%, respectively, and the interplanar spacings of planes (111) as measured by X-ray diffraction were 14.27—14.25 and 14.23—14.14 Å, respectively. The crystal derived from silica sol increased in interplanar spacing

Table 1. Change/% in crystallinity[a)]

Reaction time/h	74	75	76	78	84	96
Silica source						
Tetraethyl orthosilicate	0	0	43	115	122	115
Silica sol	0	48	75	70	76	77

a) Reference standard, LMS 13X: 100%.

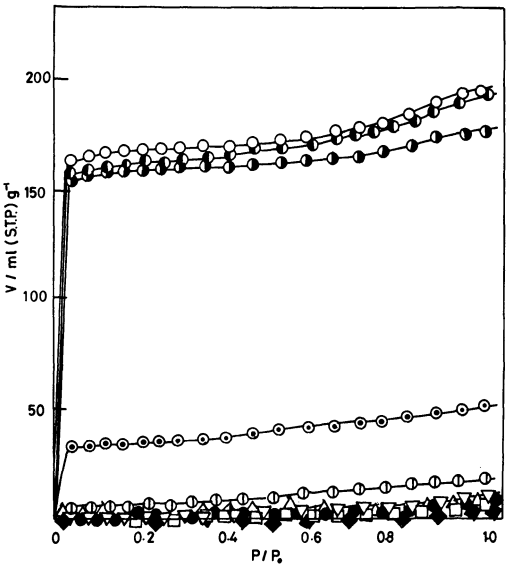

Fig. 1. Adsorption isotherms of nitrogen gas on the solid phases (E) derived from tetraethyl orthosilicate at −196 °C. 96E: ◐, 84E: ○, 78E: ◑, 76E: ⊙, 75E: ⏀, 74E: □, 72E: ●, 48E: △, 24E: ◆, 6E: ▽.
Number: reaction time.

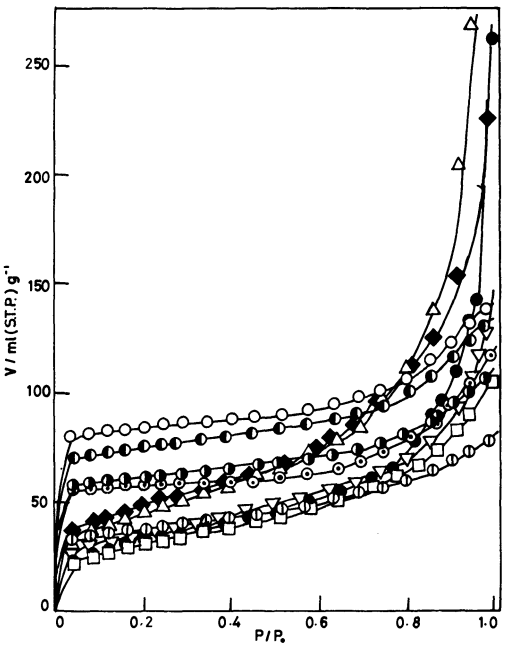

Fig. 2. Adsorption isotherms of nitrogen gas on the solid phases (C) derived from silica sol at −196 °C. 96C: ◐, 84C: ○, 78C: ◑, 76C: ⊙, 75C: ⏀, 74C: □, 72C: ●, 48C: △, 24C: ◆, 6C: ▽.
Number: reaction time.

with increasing crystallinity.

Adsorption of Nitrogen Gas. Figures 1 and 2 show nitrogen gas adsorption isotherms for solid phases. The solid phases are grouped in three types according to the stage of their formation: the initial amorphous stage (6E—75E, 6C—74C), the early stage of crystallization (76E, 75C), and the full-crystallization stage (78E—96E, 76C—96C). The solid phase derived from tetraethyl orthosilicate shows the isotherms that run nearly parallel with the axis of relative pressure. Although the amorphous phases adsorb little nitrogen, the amount adsorbed increased rapidly immediately after the crystals began to be observed.

On the other hand, the solid phases derived from silica sol show adsorption isotherms a little different from those for tetraethyl orthosilicate. The amorphous state (6C—74C) shows somewhat a steep slope as compared with the former at lower relative pressures. The amount adsorbed is 25—40 ml/g in contrast to the solid phases (6E—75E) which adsorb little. This does not result from a difference, if any, in the developments of internal structure, but actually has arisen from different distributions of particle size. The particle sizes measured with a particle size analyzer and a scanning electron micrograph were 1.5—25 μm (av 6.6 μm) for 72E and 0.25—10 μm (av 2.4 μm) for 74C. The solid phases derived from silica sol indicate distributions of smaller particles.

At lower relative pressures, the slopes to the adsorption isotherms for the crystalline phases (75C—96C) are similar to those for tetraethyl orthosilicate (76E—96E). Although the amount adsorbed by the latter is *ca.* 160—170 ml/g, the former adsorb *ca.* one third of this value, *i.e.*, 50—70 ml/g. Such characteristics of adsorption isotherms are influenced by the presence of a large amount of an amorphous substance, aluminosilicate gel, which is always contaminated.

The monolayer capacity and specific surface area were calculated with the Langmuir or BET equation. The results of calculation are shown in Table 2. The outer and inner surface areas are tabulated in the same table. These values were evaluated by fitting the Frenkel-Halsey-Hill equation[24,25] to experimental data.

The change in inner and outer specific surface areas is shown in Fig. 3. The solid phases derived from tetraethyl orthosilicate remained amorphous for initial 75 h of reaction time, so that these solid phases adsorb so little as to give an inner specific surface area of zero. Their outer specific surface areas are 4—5 m^2/g. The solid phase which contained crystals rapidly increased in specific surface area with reaction time, up to over 700 m^2/g. Nearly 95% of this value is dependent on the inner structure of crystals. The remaining *ca.* 5% is attributable to the outer free surface of solid phase. On the other hand, in spite of the amorphous state, the amount adsorbed by the solid phases derived from silica sol is nearly 100—150 m^2/g, with no inner specific surface area detected. The specific surface area did not remarkably increase with reaction time after crystalline substances had appeared. Their values are *ca.* 250—300 m^2/g.

The outer specific surface area decreases slightly after the solid phase begins to crystallize. But it occupies *ca.* 15—25% of the total specific surface area. Its value is 40—70 m^2/g, and the outer surface areas for the solid phases derived from silica sol are larger than those for tetraethyl orthosilicate. It may be considered that in the course of crystallization the size of crystals can grow to some extent. Because of the crystals being contaminated with a large amount of amorphous substances as mentioned above, their outer surface areas amount to a larger portion of the total surface area.

Adsorption of Water Vapor. The diameter of water molecule (2.7 Å at 25 °C) is smaller than that of nitrogen molecule (3.64 Å at −196 °C). Water molecule is polar and is expected to be adsorbed fully on fine

Table 2. Results of adsorption of nitrogen gas

Specimen	V_m [a] / ml g^{-1}	S_s [b] / $m^2 g^{-1}$	S_i [c] / $m^2 g^{-1}$	S_e [d] / $m^2 g^{-1}$	S_i+S_e [e] / $m^2 g^{-1}$
96E	165	717	633	59	692
84E	171	746	690	35	725
78E	162	708	657	30	687
76E	105	457	385	45	430
75E	4	19	6	13	19
74E	1	4	0	5	5
72E	2	7	0	5	5
48E	1	3	0	3	3
24E	1	4	0	4	4
6E	1	4	0	4	4
96C	74	324	226	78	304
84C	84	366	303	50	353
78C	59	257	185	62	247
76C	58	251	219	26	245
75C	32	141	74	74	148
74C	25	107	0	103	103
72C	26	112	0	109	109
48C	36	159	0	150	150
24C	40	174	0	165	165
6C	28	123	0	120	120

a) V_m is the monolayer capacity. b) S_s is the specific surface area. c) S_i is the inner specific surface area. d) S_e is the outer specific surface area. e) S_i+S_e is the sum of inner and outer specific surface areas.

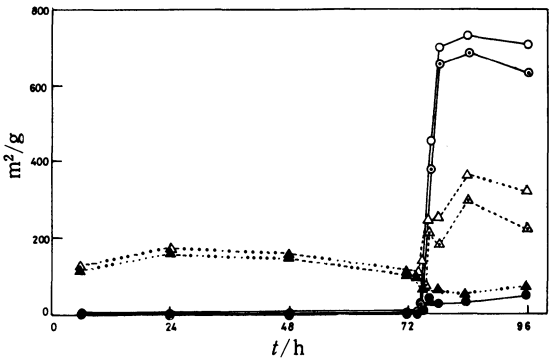

Fig. 3. Changes of the specific surface area obtained from the adsorption of nitrogen gas. Solid and dotted line represent the solid phase derived from tetraethyl orthosilicate and from silica sol respectively.
—◐— ---△---: Total specific surface area,
—⊙— ---△---: inner specific surface area,
—●— ---▲---: outer specific surface area.

structures of zeolite. Therefore, the method using water molecule is more effective for the study on the change in the solid phase than the method using nitrogen gas only. Some of the adsorption isotherms obtained are shown in Fig. 4. The crystals (96E, 84E) adsorb water vapor in fairly large quantities, and the slopes to adsorption isotherms are smooth, as compared with those for the crystals derived from silica sol. The amorphous substance (72E) adsorbs little water vapor.

On the contrary, the amorphous substance (72C) adsorbs water vapor in a fairly large quantity at lower relative pressures. Such a trend of adsorption isotherms is similar to that observed in the case of nitrogen adsorption by amorphous solid phases. The specific surface areas evaluated from the water vapor adsorption have revealed that the solid phases (96E, 84E) have larger values than the solid phases (96C, 84C). The high crystalline phases (96E, 84E, 96C) have larger specific surface areas by *ca.* 200—250 m^2/g than the corresponding values determined by nitrogen adsorption. Similarly the solid phases (84C, 72C) also have indicated larger values by *ca.* 100—150 m^2/g.

IR Spectra. A systematic study of infrared spectra for the characterization of zeolite frameworks with respect to crystal structure has been done by Flanigen and Khatami.[13,26] They pointed out that the mid-infrared region (1300 to 250 cm^{-1}) contains the fundamental vibrations of the framework of zeolite. The mid-infrared vibrations of zeolite were classified into two groups by them. One is the internal vibrations that are insensitive to change in the framework structure, and the other is the external vibrations that are sensitive to change in the framework.

The change in infrared spectra in going from the amorphous solid phase to crystals are shown in Figs. 5 and 6. The features of the spectra obtained for the specimens derived from tetraethyl orthosilicate are as follows:

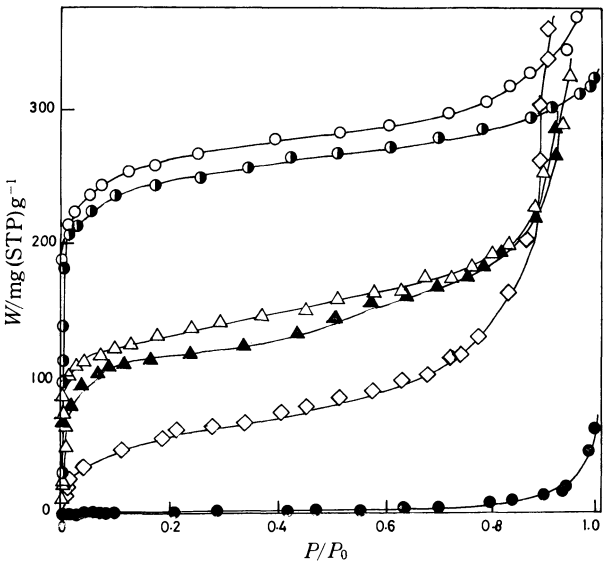

Fig. 4. Adsorption isotherms of water vapor at 25 °C. 96E: ○, 84E: ◑, 72E: ●, 96C: △, 84C: ▲, 72C: ◇. E: Tetraethyl orthosilicate, C: silica sol. Number: reaction time.

1) The spectra for earlier stages (6E, 24E) bear a resemblance to those of the crystals of high crystallinity.

2) The strongest vibration around 1000 cm^{-1} that is common to all zeolites and assigned to an asymmetric stretching mode ←OT→←O (T represents Si or Al) is found near 1000 cm^{-1} (6E—75E), but the frequency shifts to 980 cm^{-1} (76E—96E). The change in frequency shift is much less than that for the spectra of the solid phases derived from silica sol.

3) The amorphous specimens show very weak and broad bands around 580 cm^{-1}. The feature of this band in this region has a clearer pattern than the corresponding spectra for silica sol. The band in 650—500 cm^{-1} is assignable to a double 6-ring. But this band is obscure as compared with other bands in the spectrum. The crystals (76E—96E) show the clear band due to the double 6-ring around 560 cm^{-1}. The change in these bands suggests that the amorphous solid phases in the gel are composed of frameworks of secondary building units loosely cross-linked with aluminosilicate anions; therefore, the solid phases are converted from the amorphous solid state to a crystalline substance through the rearrangement of the bonds of aluminosilicate

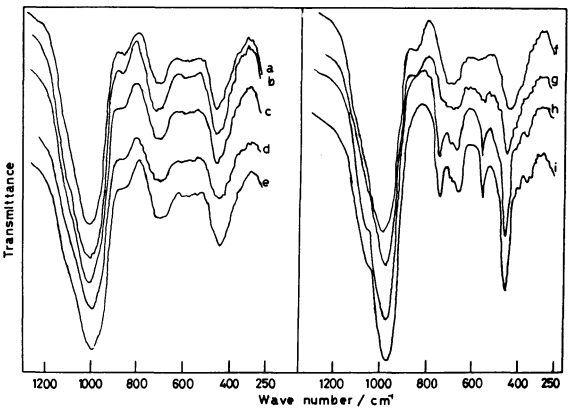

Fig. 5. Mid-infrared spectra of the solid phases (E) derived from tetraethyl orthosilicate. a: 6E, b: 24E, c: 48E, d: 72E, e: 74E, f: 75E, g: 76E, h: 78E, i: 84E, 96E.
Number: reaction time.

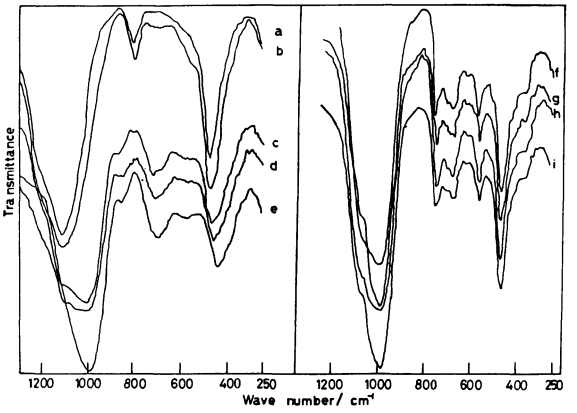

Fig. 6. Mid-infrared spectra of the solid phases (C) derived from silica sol. a: 6C, b: 24C, c: 48C, d: 72C, e: 74C, f: 75C, g: 76C, h: 78C, i: 84C, 96C.
Number: reaction time.

polymers by the interaction between the solid and liquid phases of gel.

4) The band at 880 cm^{-1} assigned to Si–OH is found with the specimens (6E—76E). This band is no longer found with the specimens (78E—96E). This suggests that the amorphous solid state is caused to change into crystals that have high crystallinity through the combination of secondary building units with aluminosilicate polymers.

5) The spectral shape of the strongest asymmetric stretching around 1000 cm^{-1} is almost the same for all the specimens, in contrast with those derived from silica sol.

On the other hand, the features of the spectra for the specimens derived from silica sol are as follows:

1) The spectra are classified into three groups. The first group is for the amorphous substances obtained at earlier stages of reaction (6C, 24C). The second is for the specimens which have undergone aging for a pretty long term (48C, 72C, 74C). The third is for the crystalline substances. The infrared spectra of the first group have very simple patterns.

2) The first group has the strongest band around 1120 cm^{-1}, shifting to lower frequencies, 1040 and 1020 cm^{-1} for 48C and 72C, respectively. As a whole, the specimens (6C—72C) show broad spectra composed of many bands. This suggests that the solid phase consists of a large quantity of silica; in addition, it contains many varieties of siloxane and Al–O–Si bonds contaminated with the zeolite framework. This band is observed around 1000 cm^{-1} for 74C and around 990 cm^{-1} for 75C and 76C. The band is remarkably shifted to lower frequencies, as compared with the band observed in the case of tetraethyl orthosilicate.

3) The bands for the double 6-ring and pore opening have been observed in the specimen (75C) for the first time.

4) The band for the Si–OH vibration around 880 cm^{-1} is still observed in the crystalline specimen (78C). It becomes weak as the crystallization proceeds. But the very weak band remains in the spectra of crystals. On the contrary, no trace of that band is observed in the spectra of the crystals derived from tetraethyl orthosilicate. This suggests clearly that the former crystals will not grow sufficiently, and that they includes some nonbonding structures and amorphous substances

Discussion

In our previous study[21] on the mechanism of zeolite crystallization, we investigated the difference in constituents between the liquid and solid phases which had been derived from tetraethyl orthosilicate, sodium metasilicate, and silica sol as silica sources with various reaction times. In order to clarify the chemical bonding state of constituents in the solid phases, the dissolution of constituents of the solid phase into hydrochloric acid solution and the relative concentration of constituents dissolved were surveyed.

According to the findings obtained, the change in constituents of both the liquid and solid phases derived from silica sol is abrupt as compared with the solid phases derived from tetraethyl orthosilicate and sodium metasilicate. The X-ray amorphous phases derived from silica sol consists of silica predominantly, and alumina or soda is hardly incorporated in the framework. The change in constituents of both the liquid and solid phases derived from tetraethyl orthosilicate is slow, and as a whole the behavior of all constituents is similar to one another. X-Ray amorphous phases obtained at earlier stages of reaction bear a marked resemblance to crystals with respect to constituents. A similarity among the solid phases obtained at various reaction times is found in respect of the dissolution of constituents of the solid phase into hydrochloric acid solution. On the contrary, every solid phase derived from silica sol shows a markedly different behavior of dissolution.[21] These results suggest that the framework structure and chemical-bond features of the solid phases are markedly dependent on the silica sources used. The X-ray amorphous phase derived from tetraethyl orthosilicate is composed of somewhat similar ordered skeletons of aluminosilicate which constitute the chemical structure of crystalline phase. On the other hand, the coexistent phase derived from silica sol is composed of disordered skeletons of aluminosilicate.

It is considered that these results are due to the difference in both the gelation kinetics and the structure of aluminosilicate at the beginning of reaction. Thus, in the case of tetraethyl orthosilicate, the gelation kinetics is governed by the polymerization of ordered aluminosilicate which has grown up in the solution. On the contrary, in the case of the solid phase derived from silica sol, the dominant factor governing the gelation kinetics is the aggregation of disordered aluminosilicate polymers.

In spite of the solid phase consisting of disordered aluminosilicate skeletons derived from silica sol, the beginning of crystallization occurs about one hour earlier than in the case of tetraethyl orthosilicate. As shown in Table 1, the crystallization does not proceed so far as expected, and the crystallinity is *ca.* 60—70% in contrast with that derived from tetraethyl orthosilicate. This suggests that in the case of silica sol, the gelation kinetics is governed by the aggregation of aluminosilicate polymers and silicic polymers at the beginning of reaction, so that the nucleation of crystals takes place more rapidly so as to make the number of nuclei more than in the case of tetraethyl orthosilicate which is hydrolyzed slowly. These trends are consistent with the fact that the X-ray amorphous phase derived from silica sol is very viscous at the beginning of reaction. On the contrary, the X-ray amorphous phases derived from tetraethyl orthosilicate consists of particles of larger sizes.

Because the silica sol was originally prepared by dispersion of silicic polymer in water, it may be considered that the reaction of depolymerization-polymerization of silicic polymer during zeolite crystallization proceeds insufficiently. Therefore, the crystals obtained with silica sol are caused to include the aluminosilicate which will not participate in the crystal framework. In addition, it may be considered that the crystals formed have a fairly silica-rich structure. This is suggested from the fact that the diffractive angle 2θ of

X-ray diffraction peak (642) have values in the region 26.74—26.75° (lattice constant, a_0: 24.94—24.93 Å) for the specimens obtained from tetraethyl orthosilicate and in the region 26.81—26.84° (a_0: 24.88—24.85 Å) for the specimens obtained from silica sol. These results are consistent with the relation found between the Si/Al molar ratio and the lattice constant.[7] In addition, these results correspond also to the results[21] concerning the difference in constituent distribution between the liquid and solid phases.

According to the above discussion, the X-ray amorphous phase derived from tetraethyl orthosilicate is considered to have a structure of ordered skeletons, and therefore the development of cavities and channels in the solid phase may be expected at earlier stages of reaction. But it has been proved that any sufficient development of cavities and channels, which is detectable through the adsorption for nitrogen gas or water vapor, will not proceed in the amorphous solid state. This means that any crystallographic internal structures characteristic of zeolite cannot fully be constructed until crystals become recognized by X-ray diffraction.

Both the crystallinity and the amount adsorbed increase with reaction time, and the approximate specific surface areas evaluated for the crystals are 450 m^2/g for 76E, 710 m^2/g for 96E, 140 m^2/g for 75C, 250 m^2/g for 76C, and 360 m^2/g for 84C. These results suggest that the inner structure of the crystals derived from tetraethyl orthosilicate will grow about 2 to 3 times as much as that of the crystals derived from silica sol. The former crystals indicate a large difference between their specific surface areas measured with nitrogen gas and water vapor. These results show that the inner structure, especially the structure of micro pore, grows to a considerable extent in the crystals derived from tetraethyl orthosilicate as compared with those derived from silica sol. The different development of inner structure is in accord with the results concluding different degrees of crystallinity and different constituent distribution in both liquid and solid phases.

The infrared bands, called "external linkages"[13] and sensitive to the change in framework structure, become apparently detectable immediately after crystals have become observed. The spectrum obtained for the solid phase derived from each of the silica sources shows a very characteristic pattern. It is derivable from the change in spectra with reaction time that each solid phase is formed *via* its unique reaction mechanism.

The results obtained in the present study are in good agreement with the conclusion drawn in earlier tudies[21,22] that the X-ray amorphous phases obtained from tetraethyl orthosilicate at earlier stages are essentially identical with crystals.

The nucleation and nuclear growth are the most important steps for obtaining highly crystalline zeolites. The X-ray amorphous phases formed from tetraethyl orthosilicate are even initially composed of highly ordered structures; the subsequent interaction between the liquid and solid phases serves to raise the crystallinity during the aging time at room temperature. It thus follows that the crystals have high crystallinity and high purity. On the other hand, the X-ray amorphous phase derived from silica sol contains amorphous substances which cannot easily be removed from the solid phase during the aging time. Such behavior results from the structural characteristic of the gel itself. It may be considered that the X-ray amorphous phase derived from silica sol is made up predominantly *via* coagulation of aluminosilicate polymers or silicic polymers; that is, the amorphous substance as a precursor is allowed to deposit in the liquid phase. In addition, the constituent of zeolite is caused to get out of the gel during the aging time and the bond of Al–O–Si is formed newly. This is why the crystal phase coexists with a large amount of amorphous substance.

Breck[27] pointed out that the composition and structure of gel are controlled by the size and structure of polymerizing species. Since silicate may vary in chemical composition and molecular weight distribution, different silicate solutions may result in different gel structures. Therefore the gelation may control the nucleation of zeolite crystals. This sequence has strongly been supported in this study. In the zeolite synthesis, the kind of starting materials, particularly silica source, and the chemical state of gel phase strongly influence the crystallization mechanism.

The authors wish to express their thanks to Messrs. Hiroyasu Aoi and Kōzi Kitagawa for their assistance during the experiment.

References

1) G. T. Kerr, *J. Phys. Chem.*, **70**, 1047 (1966).
2) R. M. Barrer and E. A. D. White, *J. Chem. Soc.*, **1952**, 1561.
3) R. M. Barrer, J. W. Baynham, F. W. Bultitude, and W. M. Meier, *J. Chem. Soc.*, **1959**, 195.
4) A. Culfaz and L. B. Sand, *Adv. Chem. Sre.*, **121**, 140 (1973).
5) B. D. NcNicol, G. T. Pott, K. R. Loss, and N. Mulder, *Adv. Chem. Ser.*, **121**, 152 (1973).
6) W. Meise and F. E. Schwochow, *Adv. Chem. Ser.*, **121**, 169 (1973).
7) D. W. Breck and E. M. Flanigen, "Molecular Sieves," The Society of Chemical Industry, London (1968), p. 47.
8) S. P. Zhdanov and N. N. Samulevich, "Proceeding of the Fifth International Conference on Zeolites," Heyden and Son Ltd., London (1980), p. 75.
9) J. Ciric, *J. Colloid Interface Sci.*, **28**, 315 (1968).
10) S. P. Zhdanov, "Molecular Sieves," The Society of Chemical Industry, London (1968), p. 62.
11) S. P. Zhdanov, *Adv. Chem. Ser.*, **101**, 20 (1971).
12) F. Polak and A. Cichocki, *Adv. Chem. Ser.*, **121**, 209 (1973).
13) E. M. Flanigen and H. Khatami, *Adv. Chem. Ser.*, **101**, 201 (1971).
14) W. C. Beard, *Adv. Chem. Ser.*, **121**, 162 (1973).
15) F. E. Schwochow and G. W. Heinze, *Adv. Chem. Ser.*, **101**, 102 (1971).
16) H. Khatami and E. M. Flanigen, Union Carbide Corporation, unpublished results.
17) B. D. McNicol, G. T. Pott, and K. R. Loss, *J. Phys. Chem.*, **76**, 3388 (1972).
18) R. Aiello, R. M. Barrer, and I. S. Kerr, *Adv. Chem. Ser.*, **101**, 44 (1971).
19) H. Kacirek and H. Lechert, *J. Phys. Chem.*, **80**, 1291

(1976).
20) R. Hino and K. Toki, *Nippon Kagaku Kaishi*, **1975**, 1847.
21) R. Hino and K. Toki, *Nippon Kagaku Kaishi*, **1977**, 593.
22) R. Hino and K. Toki, *Mem. Fac. Lit. and Sci., Shimane Univ., Nat. Sci.*, **9**, 71 (1975).
23) R. Hino and K. Toki, *Mem. Fac. Lit. and Sci., Shimane Univ., Nat. Sci.*, **8**, 61 (1975).
24) M. Nakagaki, Y. Nakamura, and T. Fujie, *Yakugaku Zasshi*, **91**, 667 (1971).
25) P. L. Walker and W. V. Kotlensky, *Can. J. Chem.*, **40**, 184 (1962).
26) E. M. Flanigen, "Zeolite Chemistry and Catalysis," ACS Monograph 171, American Chemical Society, Washington, D. C. (1976), p. 80.
27) D. W. Breck, "Zeolite Molecular Sieves," John Wiley and Sons, New York (1973), Chap. 4, p. 339.

 © 1983 The Chemical Society of Japan Bull. Chem. Soc. Jpn., 56, 3722—3725 (1983) [Vol. 56, No. 12

Electron Spin Resonance Study of X-Irradiated Single Crystals of Silver(I) Nitrate-Butanedinitrile(1/1)

Yukio KURITA* and Hiroji OHIGASHI†,††

Department of Materials Chemistry, Faculty of Engineering, Yokohama National University, Hodogaya-ku, Yokohama 240
†Basic Research Laboratory, Toray Industries, Inc., Tebiro, Kamakura 248

(Received January 13, 1983)

ESR spectra of single crystals of silver(I) nitrate–butanedinitrile(1/1) were measured at 77 K. Two paramagnetic centers, $-CN\cdots Ag^{2+}\cdots NC-$ and $NO_3^{2-}\cdots Ag^+$, appeared simultaneously on X-irradiation at 77 K. The principal values of the g value (g) and the hyperfine coupling constants (A in the units of 10^{-4} cm^{-1}) were $g_1=2.050$, $g_2=2.053$, and $g_3=2.302$, $A(Ag)_1=21.8$, $A(Ag)_2=22.0$, $A(Ag)_3=34.9$, $A(N)_1=15.3$, $A(N)_2=15.9$, and $A(N)_3=14.0$ for the first center, and $g_{//}=2.001$, $g_\perp=2.006$, $A(Ag)_{//}=20.3$, $A(Ag)_\perp=17.4$, $A(N)_{//}=59.4$, and $A(N)_\perp=32.8$ for the second center. When the crystals X-irradiated at 77 K were exposed to visible light, the two centers disappeared simultaneously and the NO_2 radicals increased. When the crystals X-irradiated at 77 K were warmed to room temperature, the first center changed to a new paramagnetic center, in which the unpaired electron coupled with a silver nucleus, two equivalent nitrogen nuclei, and a proton.

Silver(I) ion, Ag^+, can act as an electron donor or electron acceptor. Many studies have shown that Ag^0, Ag^{2+}, Ag_2^+, and Ag_2^{3+} are easily formed from Ag^+ ions in irradiated crystals and frozen solutions at low temperatures.[1-4] Mosley and Moulton have shown that, when silver nitrate crystals are X-irradiated at 77 K, the Ag^+ ions are converted to Ag^{2+} ions and NO_3^- ions to NO_3^{2-} ions, indicating that electrons delivered from Ag^+ ions are trapped on NO_3^- ions.[3]

This paper describes the results of ESR studies on X-irradiated single crystals of silver (I)nitrate–butanedinitrile(1/1), $AgNO_3\cdot NCCH_2CH_2CN$. In the crystals, Ag^{2+} and NO_3^{2-} were primarily produced by X-irradiation at 77 K. The structures and spin densities in these two paramagnetic species were estimated. Electron transfers from Ag^+ to NO_3^- by X-ray excitation and from NO_3^{2-} to Ag^{2+} by visible light excitation were established.

Experimental

Single crystals of silver(I) nitrate–butanedinitrile(1/1) were prepared. Dry silver nitrate (about 10 g) dissolved in butanedinitrile (about 24 g) at 70 °C. After the solution was cooled slowly to room temperature in the dark, single crystals with dimensions of about $4\times3\times1$ mm^3 were obtained (mp 76 °C).[5] Calcd for $AgNO_3\cdot NCCH_2CH_2CN$: C, 19.2; H, 1.6; N, 16.8%. Found: C, 19.6; H, 1.6; N, 17.0%. Figure 1 shows the crystal form. An orthogonal set of axes a′, b′, and c′ were chosen for analysis of the ESR spectra. The crystal has a cleavage plane parallel to the a′b′ plane.

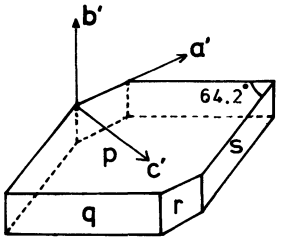

Fig. 1. The crystal form of $AgNO_3\cdot NCCH_2CH_2CN$. Interfacial angles ∠pq, ∠pr, and ∠ps are 90°.

The crystals were irradiated with X-rays at 77 K to an extent of about 0.2 Mrad. The ESR spectra of the crystals were recorded at 10° intervals in the a′b′, b′c′, and c′a′ planes at 77 K with a Varian model V-4501 X-band spectrometer. ESR measurements were also carried out on crystals that had been irradiated with X-rays at 77 K and subsequently illuminated with light from a 40 W tungsten filament lamp at 77 K, and on crystals that had been X-irradiated and successively warmed to room temperature for a minute and then cooled again to 77 K.

Figure 2 shows a typical ESR spectrum of the single crystal X-irradiated at 77 K. A group of lines at the lower magnetic field side will be attributed to the magnetic species $-CN\cdots Ag^{2+}\cdots NC-$, which we refer to as Ag^{2+} (a) center. A sextet at the high field side will be assigned to $NO_3^{2-}\cdots Ag^+$, which we refer to as NO_3^{2-}–Ag^+ center, and a sharp triplet (designated as p, p′, and p″) to NO_2.

Results and Discussion

Ag^{2+}(a) Center. The absorption lines at the lower field side consist of two quintets. The intensity ratio of the lines of the quintet is 1 : 2 : 3 : 2 : 1. These

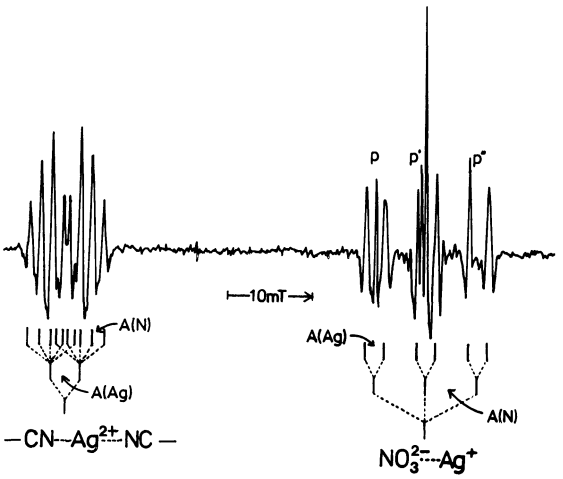

Fig. 2. Second derivative ESR spectrum of the X-irradiated single crystal of $AgNO_3\cdot NCCH_2CH_2CN$ with the magnetic field parallel to the c′ axis. The irradiation and ESR measurements were carried out at 77 K. The strongest line is due to DPPH.

†† Present address: Engineering Research Laboratory, Toray Industries, Inc., Tebiro, Kamakura 248.

Table 1. Principal values of the tensors, g, A(Ag) and A(N) for the Ag^{2+} (α) center

Principal values[a]			Principal axis
g	$A/10^{-4}$ cm^{-1}		
$g_1 = 2.050$	$A(Ag)_1 = 21.8$	$A(N)_1 = 15.3$	||a′
$g_2 = 2.053$	$A(Ag)_2 = 22.0$	$A(N)_2 = 15.9$	||b′
$g_3 = 2.302$	$A(Ag)_3 = 34.9$	$A(N)_3 = 14.0$	||c′

a) Estimated errors are 0.0005 for g and 0.5×10^{-4} cm^{-1} for A(Ag) and A(N).

lines are explained in terms of an unpaired electron interacting with a silver nucleus ($I=1/2$) as well as two equivalent nitrogen nuclei ($I=1$). Analysis of angular dependence of the spectra determined the principal elements of the tensor of the g value and the hyperfine coupling constants for the silver nucleus, A(Ag), and for the nitrogen nuclei, A(N). The results are given in Table 1. A splitting of lines due to the presence of the two abundant isotopes of silver (^{107}Ag and ^{109}Ag) could not be detected. Therefore A(Ag) in the table is the value averaged for the two isotopes. All the tensors are axially symmetric within experimental error about the c′ axis. We refer to the symmetric axis as the z axis and the axes perpendicular to it as the x and y axes.

The axial symmetry in the tensors g and A(Ag) can be accounted for by the existence of a tetragonal crystalline field at the Ag^{2+} ion,[9,10] which has been confirmed in many stable Ag^{2+} complexes. The observed relation, $g_3(g_z)>g_2\simeq g_1\simeq2$, suggests that the unpaired electron is primarily in the $4d_{x^2-y^2}$ orbital of the silver ion. The tetragonal field probably arises from the surrounding four ligands on the corners of a square plane perpendicular to the symmetry axis (the z axis). The most probable model for the $Ag^{2+}(\alpha)$ center is as follows. The Ag^{2+} ion is surrounded by two nitrogen atoms of CN groups on the x axis and by two oxygen atoms of nitrate ions on the y axis. Additional two oxygen atoms must be situated at a greater distance on the z axis. This model is consistent with the crystal structure of $2AgNO_3\cdot NCCH_2CH_2CN$, where the Ag^+ ion is linked to a CN group and surrounded by four oxygen atoms.[6]

Since superhyperfine structure due to two nitrogen atoms was observed, the unpaired electron must be delocalized on these atoms. The ground state molecular orbital for the unpaired electron is expressed by

$$\psi = \alpha\phi_0 - \sqrt{1-\alpha^2}\,\psi', \tag{1}$$

where ϕ_0 is the $4d_{x^2-y^2}$ atomic orbital of Ag^{2+} and ψ' is the appropriate normalized wavefunction of the ligands. Here the overlap integral between ϕ_0 and ψ' has been neglected. The silver hyperfine coupling constants are given by[7]

$$A_{//} = K + \left(\Delta g_{//} + \frac{3}{7}\Delta g_{\perp} - \frac{4}{7}\alpha^2\right)P, \tag{2}$$

$$A_{\perp} = K + \left(\frac{11}{14}\Delta g_{\perp} + \frac{2}{7}\alpha^2\right)P, \tag{3}$$

where $\Delta g_{//}$ and $\Delta g_{\perp}$ are the g shift from 2.0023 due to admixture of excited states, P is the hyperfine interaction parameter

$$P = g_e\mu_B g_{Ag}\mu_n \langle\phi_0|r^{-3}|\phi_0\rangle, \tag{4}$$

and K is a constant term mainly due to the core polarization which depends strongly on the spin density in ϕ_0 and ψ'.[8] Using the value of -68.76×10^{-4} cm^{-1} for P,[9] and the observed values of $|A_{//}|=A(Ag)_3$, $|A_{\perp}|=|A(Ag)_1+A(Ag)_2|/2$, $g_{//}=g_3$, and $g_{\perp}=(g_1+g_2)/2$, one obtains 0.549 for α^2 and 35.4×10^{-4} cm^{-1} for K.

The wavefunction, belonging to two nitrogen atoms, in the molecular orbital ψ can be written as

$$\sqrt{1-\alpha^2}\,\psi' = \cdots C_s[\phi_{2s}(N_1)+\phi_{2s}(N_2)] + C_p[-\phi_{2p}(N_1)+\phi_{2p}(N_2)]+\cdots, \tag{5}$$

where $\phi_{2s}(N_1)$, $\phi_{2p}(N_1)$, $\phi_{2s}(N_2)$, and $\phi_{2p}(N_2)$ are the 2s and 2p atomic orbitals of the nitrogen atoms 1 and 2. The nitrogen hyperfine coupling constants are given by

$$A_{xx}(N_1) = A_{xx}(N_2) = C_s^2A_{2s}(N) + 2C_p^2B_{2p}(N), \tag{6}$$

$$A_{yy}(N_1) = A_{zz}(N_1) = A_{yy}(N_2) = A_{zz}(N_2) = C_s^2A_{2s}(N) - C_p^2B_{2p}(N), \tag{7}$$

where $A_{2s}(N)=519\times10^{-4}$ cm^{-1} and $B_{2p}(N)=15.5\times10^{-4}$ cm^{-1}.[9] The coupling tensor is axial symmetric about the x axis and $A_{//}$ is larger than $A_{\perp}$. On the contrary the observed nitrogen coupling tensor is axial symmetric about the z(c′) axis and $A_{//}$ is smaller than $A_{\perp}$ (Table 1).

This discrepancy leads us to assume that there are at least two Ag^{2+} centers having the z axes parallel to each other but the x axes perpendicular to each other. Then the hyperfine coupling constants for N_1 and N_2 will be different. If the line widths are large, the observed nitrogen coupling constant must be the average value for N_1 and N_2, *i.e.*,

$$A_{\perp}(N) = \sqrt{[A_{xx}(N)^2+A_{yy}(N)^2]/2}, \tag{8}$$

and

$$A_{//}(N) = A_{zz}(N). \tag{9}$$

Using the values of $A_{//}(N)=14.0\times10^{-4}$ cm^{-1} and $A_{\perp}(N)=15.6\times10^{-4}$ cm^{-1}, one obtains $A_{xx}(N)=17.1\times10^{-4}$ cm^{-1}, $C_s^2=0.029$ and $C_p^2=0.067$. Therefore the spin density is 0.192 on the N_1 and N_2 atoms and 0.549 on the Ag atom, and the rest of 0.259 probably on the two oxygen atoms on the y axis.

If one neglects the in-plane and out-of-plane π-bonding between the Ag atom and ligand atoms, the principal values of the g tensors are given by

$$g_{//} = g_z = 2.0023 - 8\lambda\alpha^2/E_1, \tag{10}$$

$$g_{\perp} = g_x = g_y = 2.0023 - 2\lambda\alpha^2/E_2, \tag{11}$$

where λ is the spin-orbit coupling constant for an Ag^{2+} ion (-1844 cm^{-1}), and E_1 and E_2 are the energy separation of the d_{xy} and $d_{xz}(d_{yz})$ levels from the $d_{x^2-y^2}$ level, respectively.[7,9,11] Substituting the values of 2.302 and 2.0515 for $g_{//}$ and $g_{\perp}$, respectively, in Eqs. 10 and 11, one finds that E_1 and E_2 are 2.70×10^{-4} cm^{-1} (370 nm) and 4.11×10^{-4} cm^{-1} (243 nm), respectively. Unfortunately, the optical absorption data for the $Ag^{2+}(\alpha)$ center are not available. The spin densities on the silver atoms and nitrogen atoms of typical Ag^{2+} complexes are summarized in Table 2.[8,11–13] The spin density on the nitrogen atoms indicates that the σ-bonding between the Ag^{2+} ion and the nitrogen atom of cyano groups is weaker than that between the Ag^{2+} ion and aromatic nitrogen atoms.

NO_3^{2-}–Ag^+ Center. The ESR spectra of the

TABLE 2. SPIN DENSITY ON THE SILVER AND NITROGEN ATOMS IN TYPICAL Ag^{2+} COMPLEXES

Complex	Spin density Ag	Spin density N	Ref.
$AgNO_3$, sc., ir.	0.604		8
$AgNO_3$ in HNO_3, fr., ir.	0.711		8
$AgNO_3$ in HNO_3–pyridine, fr., ir.	0.545		8
[Ag bpy_2]S_2O_8 in HNO_3, fr.	0.542	0.197	8, 10
[(Ag, Cd)py_4]S_2O_8, pd. and sc.	0.397	0.208	8, 11, 12
$AgNO_3 \cdot NCCH_2CH_2CN$, sc., ir.	0.549	0.096	This paper

ir.: X- or γ-irradiation, sc.: single crystal, fr.: frozen solution, pd.: powder

TABLE 3. PRINCIPAL ELEMENTS OF THE g, A(Ag), A(N), AND A(H) TENSORS FOR THE NO_3^{2-}–Ag^+ CENTER (a) AND THE Ag^{2+} (β) CENTER (b)

	g	$A/10^{-4}$ cm^{-1}		
(a)	$g_{//}=2.001$	$A(Ag)_{//}=20.3$	$A(N)_{//}=59.4$	
	$g_{\perp}=2.006$	$A(Ag)_{\perp}=17.4$	$A(N)_{\perp}=32.8$	
	Direction cosines of the parallel axis in the a'b'c' system are (0.00, $\pm$0.47, 0.88).			
(b)	$g_{//}=2.170$	$A(Ag)_{//}=37.5$	$A(N)_{//}=6.1$	$A(H)_{//}=2.0$
	$g_{\perp}=2.015$	$A(Ag)_{\perp}=28.0$	$A(N)_{\perp}=6.9$	$A(H)_{\perp}=2.4$
	Direction cosines of the parallel axis in the a'b'c' system are (0.00, $\pm$0.14, 0.99).			

NO_3^{2-}–Ag^+ center have two sets of sextets when the magnetic field is in general directions. They merge into a single sextet when the magnetic field is in the a'b' or a'c' plane. Similar spectra have been observed in irradiated silver nitrate crystals and assigned to NO_3^{2-}–Ag^+, referred to as an $AgNO_3^-$ center.[3] The sextet, which consists of six lines with equal intensity (Fig. 2), arises from a hyperfine interaction with a nitrogen nucleus and a silver nucleus. The angular dependence of the g value and the coupling constants for the nitrogen and silver nuclei, A(N) and A(Ag), were analyzed to give their principal elements listed in Table 3. The principal values are similar to those of $AgNO_3^-$ trapped in silver nitrate crystals.[3] Furthermore, the principal values of A(N) are in good agreement with those of the nitrogen nucleus in NO_3^{2-} trapped in KNO_3 and other compounds.[14]

We discuss below the electronic structure of the NO_3^{2-}–Ag^+ center. The fact that A(Ag) is nearly isotropic indicates that the Ag atomic orbital in which the unpaired electron partly spends its time contains s character. If the unpaired electron localizes only on the 5s orbital, the average hyperfine interaction for $^{107}Ag^0$ and $^{109}Ag^0$ is 424×10^{-4} cm^{-1}.[9] The spin density on the 5s orbital of Ag in the NO_3^{2-}–Ag^+ center is 18.8/424, or 0.04.

The ion radical NO_3^{2-} has a pyramidal form with the nitrogen atom on the vertex. The unpaired electron occupies an sp^n hybrid orbital,

$$\phi = C_s\phi_{2s}(N) + C_p\phi_{2p}(N), \quad (12)$$

which extends along the C_3 symmetry axis (x axis). Here $\phi_{2s}(N)$ and $\phi_{2p}(N)$ are the 2s and $2p_x$ atomic orbitals of the nitrogen atom. Then the principal values of the A(N) are given by Eqs. 6 and 7. From the observed values in Table 2, the spin densities on the 2s and 2p orbitals are calculated to be 0.077 and 0.52, respectively. The remaining spin density of 0.37 would be distributed mainly on the three oxygen atoms. The bond angle $\angle$ONO for the pyramidal NO_3^{2-} ion is given by

$$\theta = \cos^{-1}\left(\frac{1.5}{2\xi^2+3} - \frac{1}{2}\right), \quad (13)$$

where $\xi^2 = C_p^2/C_s^2$.[14] The observed value of 6.69 for ξ^2 predicts that θ is 114°.

Optical and Thermal Conversion of $Ag^{2+}(\alpha)$ and NO_3^{2-}–Ag^+ Centers. When the crystals of $AgNO_3 \cdot NCCH_2CH_2CN$ X-irradiated at 77 K were exposed to light from a tungsten filament lamp at the same temperature, ESR signals of the $Ag^{2+}(\alpha)$ and NO_3^{2-}–Ag^+ centers disappeared in half an hour. During the exposure the intensity of a triplet (p, p', p'' in Fig. 2) increased. The magnetic species responsible for the triplet are reasonably identified as NO_2 because the observed g value (1.994—2.006) and hyperfine splitting of nitrogen ($(41-60) \times 10^{-4}$ cm^{-1}) are similar to those reported for NO_2 trapped in other compounds.[14]

These two paramagnetic centers, $Ag^{2+}(\alpha)$ and NO_3^{2-}–Ag^+, simultaneously appeared on X-ray irradiation and disappeared on visible light irradiation; this is explained as follows : At 77 K an electron is liberated from an Ag^+ ion through excitation by X-rays, it migrates in the lattice, and is trapped by an NO_3^- ion. This process gives rise to these two centers. The trapped electron in NO_3^{2-}–Ag^+ center is released by optical excitation and recombines with the hole on the $Ag^{2+}(\alpha)$ center. Some of the NO_3^{2-}–Ag^+ centers may be degraded into NO_2 during the irradiation.

When the crystals X-irradiated at 77 K were warmed to room temperature for a minute, the $Ag^{2+}(\alpha)$ center changes into a new Ag^{2+} center, which is designated as $Ag^{2+}(\beta)$ center. Figure 3 illustrates the ESR spectrum of the $Ag^{2+}(\beta)$ center, which is explained by an unpaired electron delocalized over an Ag^{2+} ion, two equivalent

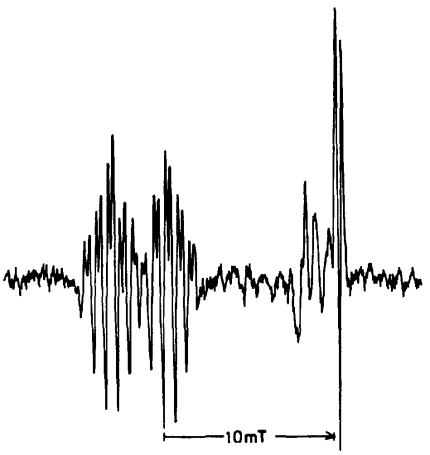

Fig. 3. Typical second derivative spectrum of the $Ag^{2+}(\beta)$ center. The magnetic field was applied in the a'c' plane, making an angle of 45° with the a' axis.

nitrogen atoms and a proton. The principal elements of the g tensor and hyperfine coupling tensors are tabulated in Table 3. The $Ag^{2+}(\beta)$ center has spin Hamiltonian parameters different from those for the $Ag^{2+}(\alpha)$ center. This fact suggests that the configuration of the ligands in the $Ag^{2+}(\alpha)$ center is altered irreversibly through thermal reorientation, giving rise to the $Ag^{2+}(\beta)$ center.

Crystal Structure and Orientation of Radicals. Two sets of ESR spectra were generally observed for the NO_3^{2-}–Ag^+ and $Ag^{2+}(\beta)$ centers. The angular dependence of these spectra are inherent in radicals trapped in a monoclinic crystal. The unique axis of the crystal must be parallel to the b′ or c′ axis. The observed interfacial angles ∠ps, ∠pq, and ∠pr are 90°, strongly suggesting that the b′ axis is the unique axis. Only one set of ESR spectra was observed for the $Ag^{2+}(\alpha)$ center. It indicates that the Ag^{2+} ion is on the symmetry axis of the unit cell. For the $Ag^{2+}(\alpha)$ center, the direction along N–Ag–N is perpendicular to the c′ axis. The C_3 symmetry axis of NO_3^{2-} in NO_3^{2-}–Ag^+ center lies on the b′c′ plane and makes an angle of 62° with the b′ axis. The infrared study of $AgNO_3 \cdot NCCH_2CH_2CN$ showed that butanedinitrile molecule assumes the *trans* rotomeric conformation and forms a bridge between two silver atoms.[5] These facts give some structural information for the parent (undamaged) complex, the structure of which is not known.

References

1) C. J. Delbecq, W. Hayes, M. C. M. O'Brien, and P. H. Yuster, *Proc. R. Soc. London, Ser. A*, **271**, 243 (1963).
2) S. N. Rustgi, *J. Chem. Phys.*, **66**, 2094 (1977).
3) W. C. Mosley and W. G. Moulton, *J. Chem. Phys.*, **43**, 1207 (1965).
4) L. Shields and M. C. R. Symons, *Mol. Phys.*, **11**, 57 (1966).
5) M. Kubota, D. L. Johnston, and I. Matsubara, *Inorg. Chem.*, **5**, 386 (1966).
6) T. Nomura and Y. Saito, *Bull. Chem. Soc. Jpn.*, **39**, 1468 (1966).
7) A. H. Maki and B. R. McGarvey, *J. Chem. Phys.*, **29**, 31 (1958).
8) J. A. McMillan and T. Halpern, *J. Chem. Phys.*, **55**, 33 (1971).
9) B. A. Goodman and J. B. Raynor, "Adv. Inorg. Chem. and Radiochem," ed by H. J. Emeléus and A. G. Sharpe, Academic Press, New York (1970), Vol. 13, p. 135, 192.
10) A. Abragam and B. Bleaney, "Electron Paramagnetic Resonance of Transition Ions," Clarendon Press, Oxford (1970), p. 487.
11) T. Halpern, S. M. McKoskey, and J. A. McMillan, *J. Chem. Phys.*, **52**, 3526 (1970).
12) T. Buch, *J. Chem. Phys.*, **43**, 761 (1965).
13) H. G. Hecht and J. P. Frazier, III., *J. Inorg. Nucl. Chem.*, **29**, 613 (1967).
14) P. W. Atkins and M. C. R. Symons, "The Structure of Inorganic Radicals," Elsevier, Amsterdam (1967), p. 127, 174, 257.

Studies of Polystyrene-based Ion Exchange Fiber. I. The Preparation and Fundamental Characteristics of Polystyrene-based Ion Exchange Fiber†

Toshio Yoshioka* and Masaharu Shimamura
Fibers Research Laboratories, Toray Industries, Inc., Sonoyama, Otsu 520
(Received February 28, 1983)

A polystyrene-based ion exchange fiber which has a large ion exchange capacity (*ca.* 2.5 mequiv g^{-1}) and a high mechanical strength (*ca.* 1.4 g d^{-1}) has first been prepared by using an islands-in-a-sea type composite fiber, the sea ingredient predominantly comprised of polystyrene for ion exchange and the island ingredient comprised of fiber-forming polypropylene for reinforcement, as the starting material; it can be used in an arbitrary form. It was found that the resulting fiber has two fundamental characteristics; the ion exchange rate for metal ions is extremely high, and the capacity of adsorbing the macromolecular ionic substance is exceedingly large, compared with ordinary ion exchange resins. The diffusion equation of ion exchange in the case of a cylindrical, endless fiber was solved by a modification of the method used for a spherical resin in a simple system. The former results are interpreted in terms of their solutions for two limiting cases. The latter results are explained by the fact that the surface-area ratio of the fiber to the resin is about ten.

There have been many investigations regarding the method of preparing ion exchange fiber, which has a large surface area per unit of weight and can be used in an arbitrary form.[1-6] These characteristics, however, have scarcely been studied because it is difficult to prepare ion exchange fiber which satisfies the following indispensable conditions:

(1) The ionic group and the basic polymer should be chemically stable.

(2) The ion exchange capacity should be large enough.

(3) The mechanical strength should be sufficiently high.

We have investigated ion exchange fiber which satisfies the above-mentioned three conditions and studied its characteristics. Polystyrene-based ion exchangers have already been selected from many polymer-based exchangers, as they satisfy the first two conditions, (1) and (2), and used industrially in the form of resin or film. Polystyrene has been well studied because it is suitable to the addition not only of ionic groups, but also of various functional groups. This has, therefore, been chosen as our basic polymer for the introduction of the ionic group. Polystyrene fiber, however, possesses so poor a mechanical strength as to be changed into various forms. It is also liable to break into fine particles when the ionic group is introduced, and thus does not satisfy the (3) condition.

The adoption of an additional fiber-forming polymer for reinforcement has been examined in order to satisfy the (3) condition. As a result, polystyrene-based ion exchange fiber, which satisfies the three conditions, has first been prepared by the introduction of a crosslinking group and an ion exchange group into the polystyrene part by chemically treating an islands-in-a-sea type composite fiber, the sea ingredient predominantly comprised of polystyrene for ion exchange and the island ingredient comprised of fiber-forming polypropylene for reinforcement.[7,8] The present authors would like to report here on this ion exchange fiber (abbrev. IONEX). This fiber was applied to the exchange of metal ions and to the adsorption of a caramel pigment from a sucrose solution. From these results, the fundamental characteristics of the fiber will also be discussed.

Experimental

Forty parts of polystyrene and 10 parts of polypropylene for the sea ingredient and 50 parts of polypropylene for the island ingredient were melt-spun at 255 °C into composite filaments having an islands-in-a-sea type sectional structure in which the number of islands was sixteen. The composite filaments were drawn five times as long as their original length in a conventional manner. The diameters of the sea and the islands of the resulting filaments were 24 and 4.2 μm respectively.

Ten grams of the filaments were crossinked in 100 ml of a solution consisting of 5 wt% paraformaldehyde, 25 wt% acetic acid, and 70 wt% concentrated sulfuric acid. A strong cation IONEX was obtained by the sulfonation of the crosslinked (90 °C, 4 h) filaments (10 g) in a solution comprised of 200 ml of trichloroethylene and 8 ml of chlorosulfonic acid at 20 °C for 2 h. Ten grams of the crosslinked (80 °C, 2 h) filaments were chloromethylated in a solution comprised of 100 ml of chloromethyl methyl ether and 10 ml of stannic chloride at 30 °C for 4 h. A strong anion IONEX was obtained by the quaternization of the chloromethylated filaments (10 g) in 100 ml of a 30 wt% trimethylamine aqueous solution at 30 °C for 1 h.[7-9]

The concentration of the calcium ion was determined by the EDTA methods. The color value (C.V.) was measured by means of a 1-cm cell at 410 nm both before and after the decoloration treatment. The resulting color values were referred to "*A*" and "*B*" respectively. Then the decoloration ratio was calculated by means of the following equation:

$$\text{Decoloration ratio}(\%) = \frac{A-B}{A} \times 100.$$

Results and Discussion

Preparation and Fundamental Properties. The process of preparing the ion exchange fiber is shown in Fig. 1. Polystyrene (PSt) was used as the basic polymer for the ion exchange, while polypropylene (PP), which exhibits

† A preliminary report of this work was presented in *Polym. Prepr. Jpn.*, **31**, 2025 (1982).

TABLE 1. FUNDAMENTAL PROPERTIES OF IONEX

No.	Composition of original fiber[a]	Ionic group	Diameter μm	Strength g d^{-1}	Elongation %	Capacity[b] mequiv g^{-1}	Water[c] content
—		—	24	3.0	40	—	—
1	(40//10)/50	$-SO_3^-Na^+$	30	1.3	18	2.6	1.6
2			32	1.4	29	2.4	1.9
3	(30//7.5)/62.5	$-CH_2N^+(CH_3)_3$	32	2.0	38	1.9	1.7
4	(20//5)/75	Cl^-	28	3.0	28	1.3	1.0

a) Sea(PSt//PP)/Islands(PP). b) Capacity of the strong-acid(base)groups. c) $(W-W_0)/W_0$. W: wet weight, W_0: dry weight.

Fig. 1. Process of preparing the polystyrene-based ion exchange fiber (IONEX).

an enhanced resistance to chemicals, was used as the fiber-forming polymer for reinforcement. In the case of using as the starting material a blend fiber made from a uniform blend of PSt and PP, the ion exchange rate and the adsorption capacity of the resulting fiber are lowered when the amount of PP exceeds 50%; the fiber, on the other hand, becomes very poor in mechanical strength when the amount of PP is less than 50%. A sheath-core type composite fiber, which consists of PSt for the sheath ingredient and PP for the core ingredient, is not good as the starting material because of its poor resistance to separation between the two phases. An islands-in-a-sea type composite fiber which consists of PSt for the sea ingredient and PP for the island ingredient could provide a suitable ion exchange fiber, IONEX, which exhibits an enhanced ion exchange rate, adsorption capacity, mechanical strength, and resistance to separation.[7] A schematic cross-sectional drawing of the composite fiber is shown in Fig. 2. A composite fiber which consists of PSt mixed with a small amount of PP for the sea ingredient and PP for the island ingredient was finally used to enhance further the resistance to separation.[8] The methods of chemical reaction to the polystyrene part are shown in Fig. 3.

The strength, elongation, ion exchange capacity, and water content of several filamentary IONEX are summarized in Table 1. The ion exchange capacities of IONEX Nos. 1—4 correspond to 94, 88, 86, and 82% of the theoretically calculated values respectively. When a crosslinking group and an ionic group are introduced, the tensile strength of the resulting filaments becomes lower than the value estimated in consideration of the weight increase from the data on the original filaments; that is, the tensile strength per filament of the original filament was 12.9 g, and those of the crosslinked filament, the chloromethylated filament, and the strong anion exchange filament were 12.0, 11.9, and 10.5 g respectively. No change in the capacity or the water content was recognized, even if the strong cation or anion IONEX was repeatedly used ten times in the following treatment: add to 1 M (1 M=1 mol dm^{-3}) hydrochloric acid or sodium hydroxide, wash with deionized water, add to 1 M sodium chloride, and finally wash with deionized water. From these results, it can be presumed

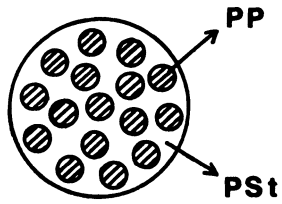

Fig. 2. Schematic cross sectional drawing of the composite fiber.

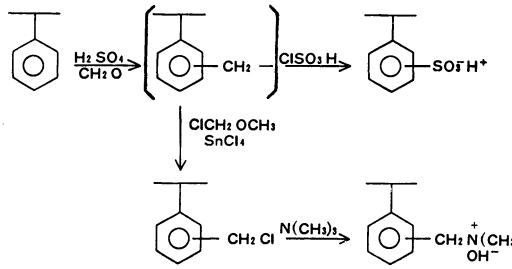

Fig. 3. The methods of chemical reaction to polystyrene part.

that a methylene bond is formed between phenyl rings by the crosslinking reaction and that then the resulting filament is strongly crosslinked and insolubilized.[9] IONEX with an arbitrary water content can be obtained by chosing the conditions of the crosslinking reaction. The acidity or basicity of a strong cation or anion IONEX is almost equal to that of polystyrene-based ion exchange resin. IONEX in an arbitrary form, such as staple fibers, cut fibers, needle punched felts, nonwoven fabrics, woven fabrics, knitted fabrics, braids, and papers, can also be obtained by processing the filaments before the chemical reaction; it can then be prepared so as to have the same capacity and water content as the filamentary form by controlling the processing density. Figure 4 presents a strong cation IONEX in a form of the cut fibers.

Exchange of Metal Ions. A strong cation exchanger of 6.6 mequiv in the Na form was added to 250 ml of a 0.008 M $CaCl_2$ aqueous solution containing 50 wt% sucrose; it was then strongly shaken at 20 °C. Similarly, a strong cation exchanger of 5.7 mequiv in the Ca form was added to 250 ml of a 1 M NaCl aqueous solution, and then the mixture was strongly shaken. The fractional attainment of equilibrium was evaluated in those two cases by measuring the calcium-ion concentration in the solution at several intervals. The results are shown in Figs. 5 and 6 respectively. A commercially available strong cation exchange resin and strong cation

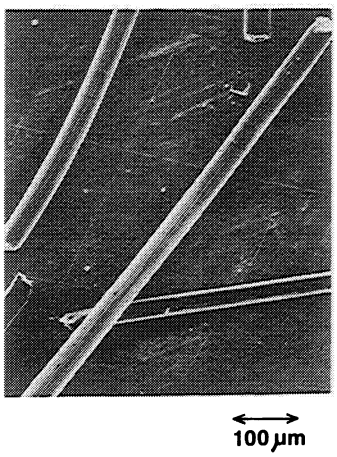

Fig. 4. Strong cation IONEX in a form of cut fibers.

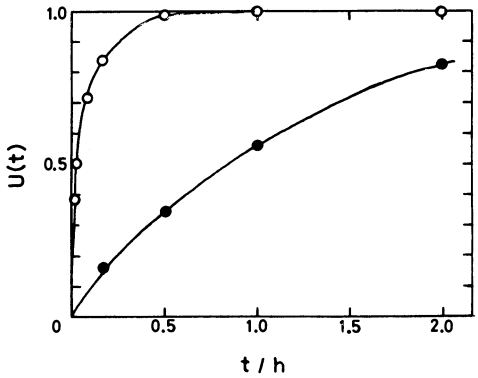

Fig. 5. Fractional attainment of equilibrium as a function of time.
Ion exchange between Na form of cation exchanger (6.6 mequiv) and 0.008 M $CaCl_2$ solution containing 50 wt% sucrose (250 ml). ○: IONEX No. 1 (2.5 g), ●: Amberlite IR-120B (1.5 g).

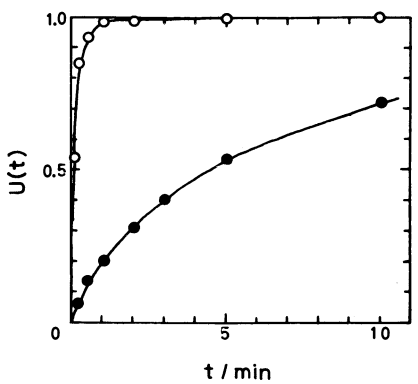

Fig. 6. Fractional attainment of equilibrium as a function of time.
Ion exchange between Ca form of cation exchanger (5.7 mequiv) and 1 M NaCl solution (250 ml). ○: IONEX No. 1 (2.2 g), ●: Amberlite IR-120B (1.3 g).

IONEX No. 1 were used as cation exchangers.

According to the rate laws of ion exchange in a simple system, the fractional attainment of equilibrium $U(t)$ within a spherical resin with a radius of r_0 can be described in the two limiting cases of ideal film and ideal particle diffusion control respectively by the following equations:[10]

$$U(t) = 1 - \exp\left(-\frac{3DCt}{r_0\delta\bar{C}}\right), \tag{1}$$

$$U(t) = 1 - \frac{6}{\pi^2}\sum_{n=1}^{\infty}\frac{1}{n^2}\exp\left(-\frac{\bar{D}\pi^2n^2t}{r_0^2}\right). \tag{2}$$

The signification of the symbols in the above equations has been described in Ref. 10. The half-times, $t_{1/2}$, of ion exchange are calculated from Eqs. 1 and 2 respectively as follows:[10]

$$t_{1/2} = 0.230\, r_0\delta\bar{C}/DC, \tag{3}$$

$$t_{1/2} = 0.030\, r_0^2/\bar{D}. \tag{4}$$

We could solve the diffusion equation in the case of an endless fiber with a radius of r_f by the modification of the method used for a spherical resin; we could thus obtain the fractional attainment of equilibrium in the two limiting cases as, respectively:

$$U(t) = 1 - \exp\left(-\frac{2DCt}{r_f\delta\bar{C}}\right), \tag{5}$$

$$U(t) = 1 - \sum_{n=1}^{\infty}\frac{4}{x_n^2}\exp\left(-\frac{\bar{D}_f x_n^2 t}{r_f^2}\right). \tag{6}$$

where $\bar{D}_f$ is the interdiffusion coefficient in the ion exchange fiber and where the quantities x_n are the roots of the equation $J_0(x)=0$, in which $J_0(x)$ is the zero-order Bessel function. The half-times of ion exchange were finally derived from Eqs. 5 and 6 as follows:

$$t_{1/2} = 0.345\, r_f\delta\bar{C}/DC, \tag{7}$$

$$t_{1/2} = 0.065\, r_f^2/\bar{D}_f. \tag{8}$$

Although the diffusion equations have been solved under several conditions, the solutions can be applied to our experimental results in the case of a relative comparison between the fiber and the resin. The results in Fig. 5 are considered to correspond to the case of film diffusion control, since the concentration of the solution is sufficiently low: $C \ll 0.1$ M. The ratio of the half-time of the resin to that of the fiber can be calculated to be 11 from Eqs. 3 and 7 when $r_0=250$ μm and $r_f=15$ μm. The ratio obtained from the experimental data is, however, 25, almost twice as high as the calculated ratio. This fact may be interpreted owing to film diffusion control in terms of the increase in the surface area per unit of capacity of IONEX by the amount of the polymer for reinforcement. On the other hand, the results in Fig. 6 are considered to correspond to the case of particle diffusion control, since the concentration of the solution is sufficiently high: $C \gg 0.1$ M; the ratio can similarly be calculated to be 128 from Eqs. 4 and 8 if $\bar{D}=\bar{D}_f$ is assumed. The ratio obtained from the experimental data, however, is in the range of from 50 to 70 and is about half the calculated ratio. The results can be interpreted on the assumption that the polymer for reinforcement disturbs the diffusion of ions because of the particle diffusion control.

Adsorption of a Caramel Pigment. Two grams of a strong anion exchanger in the Cl form was added to 200 ml of a 50 wt% sucrose aqueous solution containing a commercially available caramel pigment (C.V. 0.92); the mixture was then stirred at 60 °C. The data of the

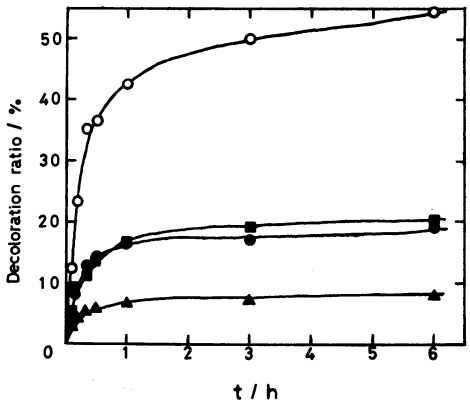

Fig. 7. Decoloration ratio as a function of time. Decoloration of 50 wt% sucrose solution containing caramel pigment (200 ml, C.V. 0.92) by Cl form anion exchanger (2.0 g) at 60 °C.
○: IONEX No. 2, ●: Amberlite IRA-401 (low crosslinked type), ▲: Amberlite IRA-400 (standard crosslinked type), ■: Amberlite IRA-900 (MR type).

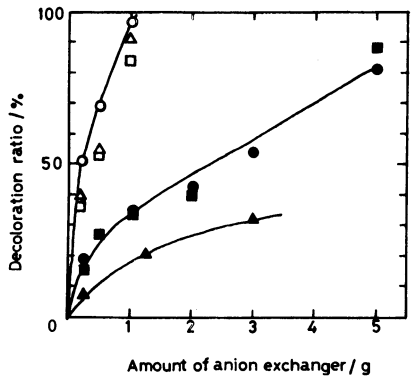

Fig. 8. Decoloration ratio *vs.* amount of anion exchanger. Decoloration of 50 wt% sucrose solution containing caramel pigment (25 ml, C.V. 0.92) by Cl form of anion exchanger (60 °C, 6 h). ○: IONEX No. 2, △: IONEX No. 3, □: IONEX No. 4, ●: IRA-401, ▲: IRA-400, ■: IRA-900.

decoloration ratio as a function of the time are shown in Fig. 7. It is apparent that the decoloration rate by the fiber is much greater than that by the three resins. This indicates that the effective capacity of the fiber to adsorb the caramel pigment is much larger than that of the resins, in spite of the fact that the ion exchange capacity of the fiber is about two thirds that of the resins.

Next, a strong anion exchanger in the Cl form was added to 25 ml of the same sucrose solution, and the mixture was shaken at 60 °C for 6 h. The correlation between the amounts of various anion exchangers and the decoloration ratio is shown in Fig. 8. This shows that the fibers have from seven to ten times as large an effective capacity of adsorbing the pigment as the low-crosslinked-type and the MR-type resins and, further, forty times as large a capacity as the standard-crosslinked-type resin. No large difference in the effective capacity was not observed between the strong anion IONEX Nos. 2—4. These results can be explained by the fact that the surface-area ratio of the fiber to the resin ($2r_0/3r_f$) is about ten, since the caramel pigment of a macromolecular weight cannot diffuse into the exchangers and can be adsorbed only near their surface. The reason why the low-crosslinked-type resin is superior to the standard-crosslinked-type resin is probably the small diffusion of the pigment into the former exchanger. Furthermore, the effective capacity of the MR-type resin is almost equal to that of the low-crosslinked-type resin, although it is said that the former resin has a large inner surface area of 30—100 $m^2 g^{-1}$. The reason for this is considered to be that the crosslinking degree of the MR-type resin is so high that the pigment cannot diffuse into the gel at all.

Conclusion

1. An excellent polystyrene-based ion exchange fiber which sufficiently satisfies the three indispensable conditions mentioned above was obtained by using the islands-in-a-sea type composite fiber as the starting material.
2. It was found that the resulting fiber has two fundamental characteristics; the ion exchange rate for metal ions is extremely high, and the capacity of adsorbing the macromolecular ionic substance is exceedingly large, compared with ordinary ion exchange resins.
3. The former results are interpreted in terms of the rate laws of ion exchange for the two limiting cases of ideal film and ideal particle diffusion control in a simple system. The latter results are explained by the fact that the fiber has a very large surface area in comparison with that of the resins.

The authors would like to express their appreciation to Dr. Tatsuro Kawaguchi, Mr. Michihiko Tanaka, and Dr. Masaki Nishino for their continuous encouragement throughout this work. They are also much obliged to Mr. Kazuo Teramoto for his advice on the chemical treatments and to Mr. Seiichi Yoshikawa and his collaborators for the preparation of the composite fibers. The authors also wish to thank Toray Industries, Inc., for making this study possible.

References

1) Y. Motozato and H. Egawa, *Kogyo Kagaku Zasshi*, **61**, 783 (1958).
2) Y. Motozato, *Kobunshi*, **8**, 269 (1959).
3) H. Egawa, *Kogyo Kagaku Zasshi*, **68**, 1159, 1304, 1307 (1965).
4) R. Messalem, C. Forgacs, J. Michael, and O. Kedem, *J. Appl. Polym. Symposia*, **31**, 383 (1977).
5) T. Miyamatsu and N. Oguchi, *Sen'i Gakkai Shi*, **36**, T-208, T-217, T-253, T-308, T-364 (1980).
6) T. Miyamatsu, *Sen'i Gakkai Shi*, **39**, P-53 (1983).
7) T. Yoshioka, K. Teramoto, and M. Shimamura, Japanese Laid-open Patent 120985 (1977); *Chem. Abstr.*, **88**, 122184a (1978).
8) T. Yoshioka, K. Teramoto, and M. Shimamura, Japanese Laid-open Patent 120986 (1977); *Chem. Abstr.*, **88**, 122597n (1978).
9) K. Kashihara and M. Shimamura, Japanese Laid-open Patent 6587 (1975); *Chem. Abstr.*, **83**, 29388g (1975).
10) F. Helfferich, "Ion Exchange," McGraw-Hill, New York (1962), pp. 259—264.

Penetration of Lysine-Leucine Copolymers into Lecithin Monolayers from Underlying Aqueous Solutions

Masayuki NAKAGAKI,* Emiko OKAMURA, and SHIGEO KUBOTA†
Faculty of Pharmaceutical Sciences, Kyoto University, Yoshida-Shimoadachicho, Sakyo-ku, Kyoto 606
†*Cardiovascular Research Institute, University of California, San Francisco, California 94143, U. S. A.*
(Received May 6, 1983)

The penetration of water soluble polymers into lecithin monolayers was investigated for the random copolymers of L-lysine and L-leucine at various compositions in order to discuss the effect of hydrophobicity and charge density of the copolymers on their interaction with lipid monolayers. Compared to the penetration of the amino acids(L-lysine and L-leucine), the copolymer penetrated at very low concentration whereas the monomer (amino acid) did not. The amount of copolymer penetration increased significantly when the leucine fraction of a copolymer, X_{Leu}, was larger than 0.3, while little penetration occurred when X_{Leu} was smaller than 0.25. From these facts, it has been concluded that the penetration of lysine–leucine copolymers was not only attributed to the hydrophobicity or the charge density of copolymer molecules, but also to specific surface effects such as (1) the enhanced penetration of macromolecules by the preceded penetration of polymer segments of the same molecule, or (2) the formation of a compact α-helical structure as the result of the restricted motion of the segment near the lipid surface.

It has been widely accepted that biomembranes essentially consist of lipid bilayers in which proteins are dissolved.[1] Although the composition of membrane lipids depends on the kind of membranes, one of the typical constituents may be phospholipids.[2] From this point of view, the interaction between phospholipids and proteins has been studied by the use of phospholipid monolayers as a model of lipid membranes.[3,4]

Since the structure of a protein is complex, synthetic polypeptides have been used in many studies as models for proteins.[5–9] Polylysine is one of the basic polypeptides, and the dissociation of the ε–amino group in a lysine residue is known to vary with pH or on the addition of alcohols or electrolytes to the solution.[10–16] In solutions of neutral pH, polylysine has a positive charge due to the protonation of ε-amino groups. It is found that a strong interaction occurs between polylysine and lipids and causes aggregation by forming lipid–peptide complexes or clusters if the phospholipids are acidic such as phosphatidylserine or phosphatidic acid.[17,18] It is considered that this is due to electrostatic interaction occuring at the negatively charged lipid monolayer surface because polylysine does not interact with the neutral phospholipids like lecithin. However, electrostatic interaction between polylysine and zwitterionic phospholipids such as lecithin has been reported in recent liposomal studies, being weak but not negligible.[19] A similar interaction also occurs between neutral phospholipids and acidic polypeptides like polyglutamic acid.[20] Moreover, Campbell *et al.* have also indicated the existence of hydrophobic interaction between polylysine and lecithin.[19] From this standpoint, the author's interest is focussed on the penetration of polylysine into lecithin monolayers.

Many apolar amino acids as well as polar exist in a protein molecule. Not only homopolymers such as polylysine but also copolymers which involve both ionic and apolar chains should be regarded as models for the actual protein molecules. Leucine is an apolar amino acid since it does not have any ε-amino groups in the hydrocarbon chain, although it has six carbon atoms in the monomer residue, which is the same as lysine. Therefore, lysine–leucine copolymers of varying hydrophobicity or charge density are obtained by changing the lysine–leucine ratio.

The penetration of amino acids like lysine, leucine and norleucine into lecithin monolayers was discussed in our previous work.[21–23] In this paper, random copolymers consisting of lysine and leucine were used and the penetration of these copolymers into lecithin monolayers was investigated in order to study the effect of the hydrophobicity and the charge density of the copolymer on its penetration into lipid monolayers.

Experimental

Materials. Table 1 shows the lysine–leucine copolymers used in this experiment. Polylysine (poly-L-Lys·HCl) was purchased from the Protein Research Foundation, and the molecular weight was estimated from the viscosity measurement according to Yaron and Berger.[24] The other copolymers [poly(Lys^{x}Leu^y)$_n$ (HCl)$_{xn}$] in Table 1 were supplied from the Cardiovascular Research Institute, University of California. These copolymers were all water soluble. L-α-Dimyristoyl phosphatidylcholine (DMPC) from the Sigma Chemical Company was used without further purification. Chloroform was used as the spreading solvent.

Surface-tension Measurement. The surface tension of the aqueous copolymer solution, γ_{cop}, was measured by the capillary-rise method, and the surface pressure of copolymers, F_{cop}, was obtained by means of Eq. 1:

$$F_{cop} = \gamma_0 - \gamma_{cop}, \quad (1)$$

where γ_0 is the surface tension of pure water. The temperature

Table 1. Characterization of copolymers of L-lysine and L-leucine

Composition		MW	Degree of polymerization ($\overline{DP}$)
Lys	Leu		
1.0	0	66000	359
0.859	0.141	94000	534
0.829	0.171	102000	586
0.800	0.200	85000	491
0.751	0.249	88000	518
0.664	0.336	56000	337
0.616	0.384	43000	264

of the solution was kept at 25±0.5 °C.

Surface-pressure Measurement. The surface pressure of the DMPC monolayer was measured by Wilhelmy's plate method. Since the surface tension of a solution is not always equal to that of pure water, the surface pressure, F, was calculated by means of Eq. 2:[25]

$$F = \gamma_0 - \gamma = F' + F_{cop}, \quad (2)$$

where γ is the surface tension of a copolymer solution covered with a lipid monolayer, while F' is the practical surface pressure defined by:

$$F' = \gamma_{cop} - \gamma, \quad (3)$$

and is measured directly by Wilhelmy's plate method as the decrease in the surface tension of a copolymer solution upon the spreading of a lecithin monolayer. That is:

$$F' = (T_{cop} - T)/l, \quad (4)$$

where l is the length around the horizontal cross section of the plate. The forces acting on the Wilhelmy plate, T_{cop} and T, were measured as follows. A copolymer solution of 57 cm³ was poured into a trough (5.0×20.0×0.4 cm³) coated with Teflon, and was kept in thermostatted air at 25±0.5 °C. After the surface of the copolymer solution was swept by a barrier covered with a Teflon sheet, the lower end of a ground glass plate, vertically suspended, was touched to the liquid surface and the vertical pull force acting on the plate, T_{cop}, was measured by means of a Shimadzu T-NR torsion balance. A lipid monolayer was then spread from an Agla micrometer syringe (accuracy ±0.0002 cm³) and left for 5 minutes. The force acting on the plate, T, was then measured by compressing the monolayer with a barrier. The values of T_{cop} and T were measured several times, respectively, until the equilibrium values were obtained. The experimental error of the measurement was within ±0.1 mN m⁻¹.

Results

Surface Tension of a Copolymer Solution. Figure 1 shows the surface tension of polylysine and various copolymer solutions. It is seen that the surface tension decreases with the increase in the concentration, C_2, for all copolymer solutions, and it also decreases with the leucine content of copolymer. This is attributable to the fact that the higher the leucine content, the more hydrophobic and less electrically charged the molecule becomes. The surface concentration of the copolymer is, therefore, higher at higher content of leucine or lower content of lysine, since lysine is more hydrophilic and positively charged due to its ε-ammonium group.

Surface Pressure-Area Curves of the DMPC Monolayers. The relation between the surface pressure, F, and the area per molecule of lecithin, A_3, spread on polylysine solutions is shown in Fig. 2. The curve shifted to a higher surface pressure region at higher C_2, indicating that the penetration of polylysine into the lecithin

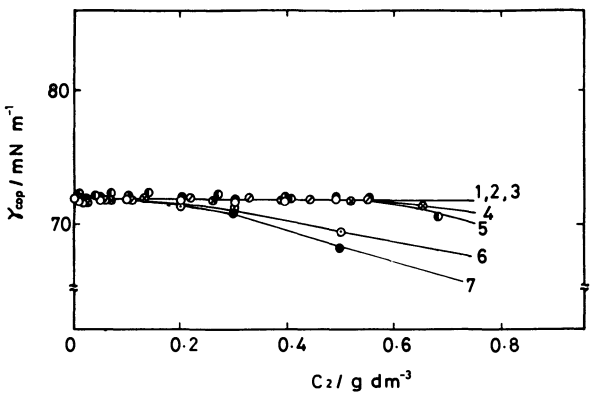

Fig. 1. The dependence of surface tension, γ_{cop}, on the concentration of lysine–leucine copolymers, C_2.
Leucine fraction: 1. ○ 0; 2. ◑ 0.141; 3. ⊘ 0.171; 4. ⊗ 0.200; 5. ◐ 0.249; 6. ⊙ 0.336; 7. ● 0.384.

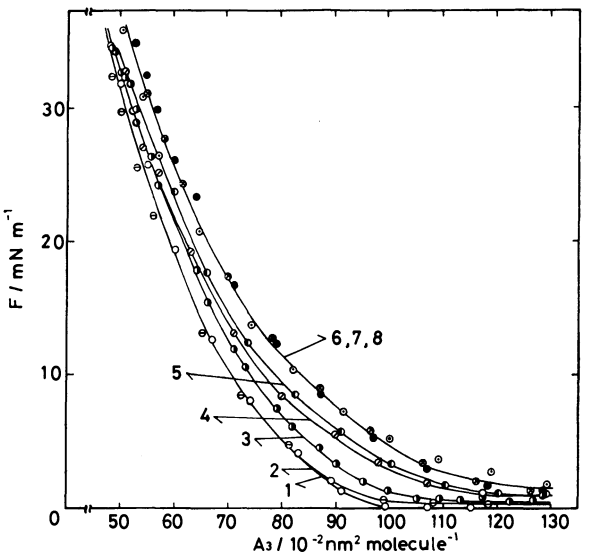

Fig. 2. The relation between the surface pressure, F, and the area per molecule of lecithin, A_3, spread on polylysine solutions. pH range 4.8—5.0.
C_2/g dm⁻³: 1. ○ 0; 2. ⊖ 0.020; 3. ◑ 0.067; 4. ⊘ 0.164; 5. ◐ 0.226; 6. ⊗ 0.343; 7. ⊙ 0.504; 8. ● 0.623.

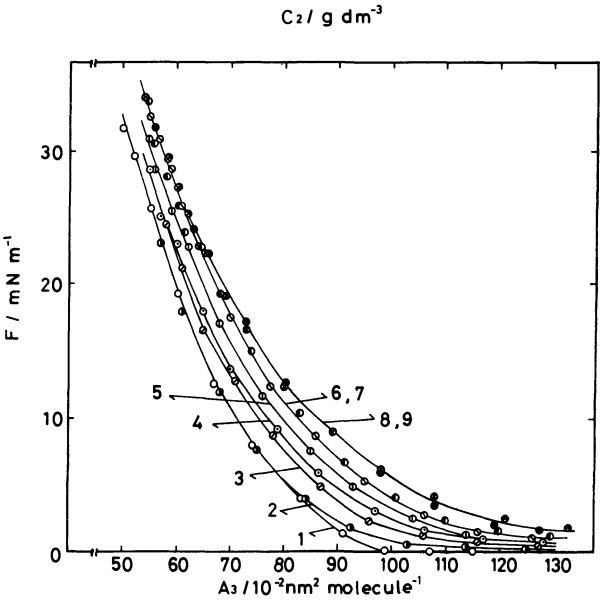

Fig. 3. The surface pressure (F)-area (A_3) curves of lecithin monolayers spread on poly($Lys^{0.800}Leu^{0.200}$)$_n$ solutions. pH range 5.2—5.4.
C_2/g dm⁻³: 1. ○ 0; 2. ◑ 0.146; 3. ⊘ 0.220; 4. ⊙ 0.292; 5. ⓘ 0.355; 6. ◐ 0.440; 7. ⊘ 0.492; 8. ⊗ 0.635; 9. ● 0.709.

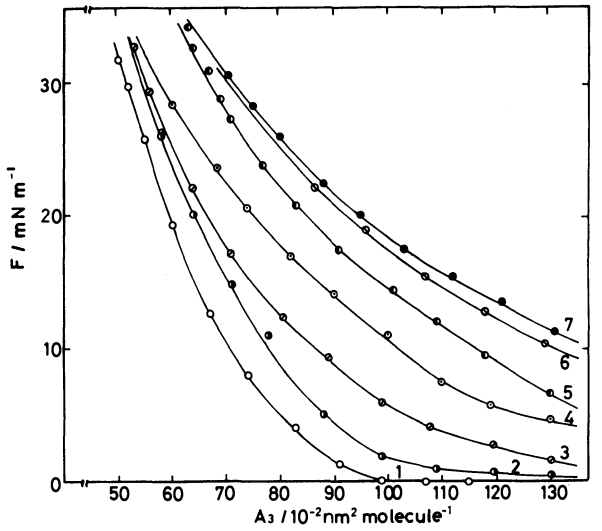

Fig. 4. The surface pressure (F)-area (A_3) curves of lecithin monolayers spread on poly($Lys^{0.616}$ $Leu^{0.384}$)$_n$ solutions. pH range 4.5—5.0.
C_2/g dm^{-3}: 1. ○ 0; 2. ◑ 0.112; 3. ⊘ 0.176; 4. ⊙ 0.224; 5. ◐ 0.322; 6. ⊘ 0.449; 7. ● 0.500.

monolayers occurred. Figures 3 and 4 show the surface pressure-area curves of lecithin monolayers spread on leucine-containing copolymer solution, namely, poly-($Lys^{0.800}Leu^{0.200}$)$_n$ in Fig. 3 and poly($Lys^{0.616}Leu^{0.384}$)$_n$ in Fig. 4, respectively. The curve also shifts to a higher surface pressure region with higher C_2, similar to the case of polylysine (Fig. 2), although the extent of the shift differs in each case. The shifts were also observed for other lysine–leucine copolymers [poly($Lys^{0.857}Leu^{0.143}$)$_n$, poly($Lys^{0.751}Leu^{0.249}$)$_n$, and poly($Lys^{0.664}Leu^{0.336}$)$_n$], though not shown in the figure. Our previous studies of the penetration of amino acids[21-23] also showed similar shift of the curves to a higher surface pressure region, however, the shift was not appreciable unless the concentration of the amino acids was about ten to one hundred times higher than that of the polypeptides. This may be attributable to the fact that the penetration of one part of the polymer residues restricts the other part of the polymer molecule in the vicinity of the surface. The penetration of polymer molecules is therefore found at very low concentrations where the monomer penetration does not occur.

Effect of the Copolymer Composition on Its Penetration into Lecithin Monolayer. The increase in the surface pressure, ΔF, caused by the penetration of polymer molecules into lipid monolayer,

$$\Delta F = F - F_0, \quad (5)$$

is considered to be a measure of the interaction of the polymer with membranes,[26] where F and F_0 are the surface pressure at a given area per molecule of lecithin respectively with and without polymer in the aqueous solution. The typical results of ΔF are shown in Fig. 5 against the polymer concentration, C_2, where the area per molecule of lecithin, A_3, is 90×10^{-2} nm^2. It is seen from this figure that the values of ΔF increases with the polymer concentration, C_2, and that the shape of the ΔF *vs.* C_2 relations are independent of the mole

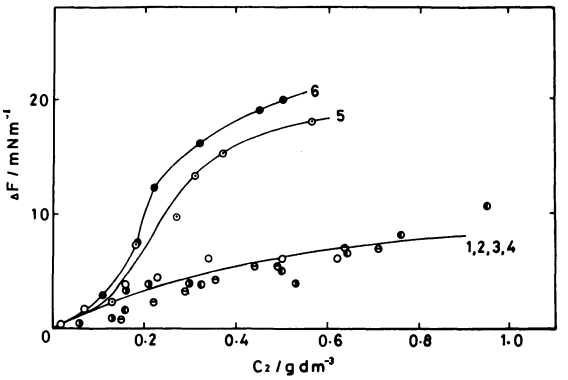

Fig. 5. The dependence of the increase in surface pressure, ΔF, on the concentration of copolymer, C_2, where the area per molecule of lecithin is 90×10^{-2} nm^2.
Leucine fraction, X_{Leu}: 1. ○ 0; 2. ◑ 0.141; 3. ⊖ 0.200; 4. ◐: 0.249; 5. ⊙ 0.336; 6. ● 0.384.

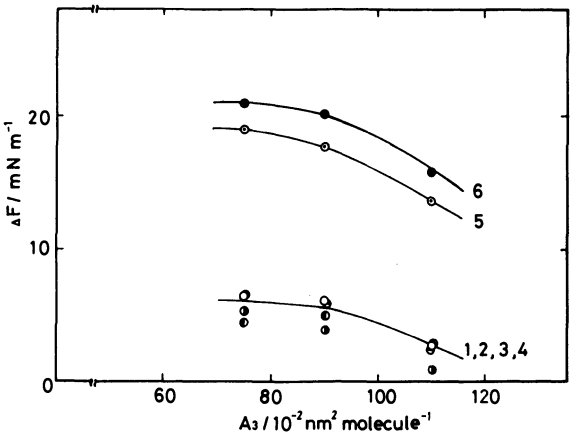

Fig. 6. The dependence of the increase in surface pressure, ΔF, on the area per molecule of lecithin, A_3, where copolymer concentration, C_2, is 0.5 g dm^{-3}.
Leucine fraction, X_{Leu}: 1. ○ 0; 2. ◑ 0.141; 3. ⊖ 0.200; 4. ◐ 0.249; 5. ⊙ 0.336; 6. ● 0.384.

fraction of leucine in the copolymer, X_{Leu}, provided X_{Leu} is smaller than 0.25. However, ΔF becomes large when X_{Leu} is larger than 0.34. This behavior was also observed at other values of A_3, although the value of ΔF was smaller at larger A_3 value, as is shown in Fig. 6 when C_2 is 0.5 g dm^{-3}.

Discussion

It is considered that polypeptides with electric charge, such as polylysine, are more hydrophilic, and, therefore, the interaction of these polypeptides with phospholipids like lecithin is weaker than for polypeptides without net charge. The charge density or hydrophilicity of polylysine decreases at a higher pH (about 10) since the ε-ammonium groups are deprotonated ($-NH_3^+ \rightarrow -NH_2$). It also decreases on the addition of perchlorate (ClO_4^-) due to the specific shielding effect on the positive charge ($-NH_3^+$).[12,15] In fact, the increase in the surface pressure of the lecithin monolayer, ΔF, was enhanced under these conditions as established in our work (unpublished data).

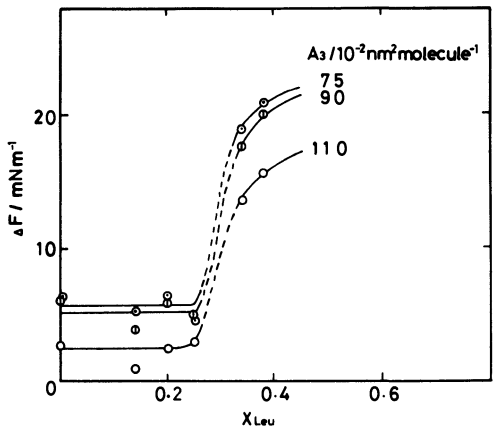

Fig. 7. The increase in surface pressure, ΔF, against the leucine fraction, X_{Leu}, where copolymer concentration, C_2, is 0.5 g dm^{-3}.

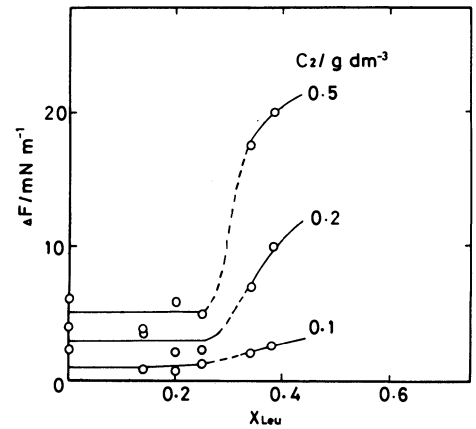

Fig. 8. The increase in surface pressure, ΔF, against the leucine fraction, X_{Leu}, at constant area per molecule of lecithin ($A_3=90\times10^{-2}$ nm^2).

The surface pressure increase, ΔF, due to the penetration was plotted against the leucine fraction, X_{Leu}, of the copolymer in Fig. 7 at a constant concentration of 0.5 g dm^{-3}. The ΔF values did not appreciably change when the leucine fraction, X_{Leu}, is from 0 to 0.25, irrespective of the area per molecule of lecithin, A_3. However, a remarkable increase was found in the vicinity of 0.3 of X_{Leu}, and the increase was again restrained when X_{Leu} exceeded 0.34. This remarkable increase in ΔF, however, does not occur at a small polymer concentration (0.1 g dm^{-3}), but it occurs when polymer concentration, C_2, is larger than 0.2 g dm^{-3}, as is shown in Fig. 8 for the area per molecule of lecithin of 90×10^{-2} nm^2.

In the copolymers of lysine and leucine, the charge density and hydrophilicity decrease with the increase in leucine fraction, and the penetration of these polymers into lecithin monolayers is expected to occur more easily. The amount of penetration of lysine–leucine copolymers into lecithin monolayers, however, did not change appreciably when the leucine fraction, X_{Leu}, is less than 0.25, but increased remarkably when X_{Leu} exceeded 0.3, as was described before. Accordingly, the penetration of these polymers is not only enhanced by the increase in hydrophobicity, the decrease in the charge density.

It is claimed that an α-helical structure is formed in lysine–leucine copolymers when the leucine fraction is large, because of the α-helix stabilizing effect of leucine.[27] A possible reason for the characteristic penetration as described above is that the transition from a coiled form to an α-helical structure occurs at a leucine fraction larger than about 0.3. According to circular dichroism, all the copolymers (leucine fraction, from 0 to 0.384) are in coiled forms in aqueous solution under our experimental conditions (pH≈5, in salt-free water). The remarkable increase in surface pressure is, therefore, not attributable to the conformational change of the polymers in the bulk solution.

The effect of the interface on the penetrability of these lysine–leucine copolymers into lecithin monolayer should be finally considered. D. Bach *et al.* have investigated the interaction of basic polypeptides consisting of two different amino acids with phospholipid vesicles by circular dichroism measurements and have reported the occurrence of a conformational change of these copolymers at a lipid surface.[9] In our experiment, the penetration of a part of the polymer segments to the lecithin monolayers restricts the other segments of the same macromolecule to a limited thermal motion in the vicinity of the surface. It is possible, therefore, that these restricted segments penetrate into lecithin monolayers more easily than when these segments are free in the bulk solution. It is, therefore, reasonable that the penetration of these copolymers occurs at such a low concentration where the monomers (residue amino acids) cannot penetrate appreciably. Moreover, the α-helical structure of the polypeptide is considered to be easily formed under the limited motion on the lipid surface, in comparison with the case where they are free in the bulk solution. More than one leucine residue are contained in one period of an α-helical spiral when the leucine fraction, X_{Leu}, is larger than 0.3, since there are 3.6 residues per α-helical unit. It is expected, therefore, that the α-helical structure is stabilized by the hydrophobic binding between leucine residues, which induces the contraction of polymer molecules, and the increase in penetration into the monolayer.

We wish to express our sincere thanks to Professor Dr. J. T. Yang. This work was supported in part by USPH5 GM-10880 (J. T. Yang). We are also grateful to Dr. K. Ikeda for helpful discussions concerning the circular dichroism spectra.

References

1) S. J. Singer and G. L. Nicolson, *Science*, **175**, 720 (1972).
2) M. S. Bretscher, *Science*, **181**, 622 (1973).
3) T. Yamashita, *Protein, Nucleic Acid and Enzyme*, **21**, 24 (1976).
4) M. Nakagaki and H. Ichihashi, *Yakugaku Zasshi*, **99**, 999 (1979).
5) P. T. Schafer, *Biochim. Biophys. Acta*, **373**, 425 (1974).
6) P. Chatelain, C. Berliner, J. M. Ruysschaert, and J. Jaffe, *J. Colloid Interface Sci.*, **51**, 239 (1975).
7) D. Hammermeister and G. Barnett, *Biochim. Biophys.*

Acta, **332**, 125 (1974).
8) I. R. Miller and D. Bach, *Chem. Phys. Lipids*, **13**, 453 (1974).
9) D. Bach, K. Rosenheck, and I. R. Miller, *Eur. J. Biochem.*, **53**, 265 (1975).
10) T. V. Barskaya and D. B. Ptitsyn, *Biopolymers*, **10**, 2181 (1971).
11) P. Y. Chou and H. A. Scheraga, *Biopolymers*, **10**, 657 (1971).
12) E. Peggion, A. Cosani, M. Terbojevich, and G. Borin, *Biopolymers*, **11**, 633 (1972).
13) M. Barteri and B. Pispisa, *Biopolymers*, **12**, 2309 (1973).
14) Ch. Ebert and G. Ebert, *Colloid Polym. Sci.*, **255**, 1041 (1977).
15) G. Seipke, H.-A. Arfmann, and K. G. Wagner, *Biopolymers*, **19**, 189 (1980).
16) H. Hanssum and H. Ruterjans, *Biopolymers*, **19**, 1571 (1980).
17) H. J. Galla and E. Sackmann, *Biochim. Biophys. Acta*, **401**, 509 (1975).
18) W. Hartmann and H. J. Galla, *Biochim. Biophys. Acta*, **509**, 474 (1978).
19) I. M. Campbell and A. B. Pawagi, *Can. J. Biochem.*, **57**, 1099 (1979).
20) K.-Y. Yu, J. J. Baldassare, and C. Ho, *Biochemistry*, **13**, 4375 (1974).
21) M. Nakagaki and E. Okamura, *Bull. Chem. Soc. Jpn.*, **55**, 1352 (1982).
22) M. Nakagaki and E. Okamura, *Bull. Chem. Soc. Jpn.*, **55**, 3381 (1982).
23) M. Nakagaki and E. Okamura, *Bull. Chem. Soc. Jpn.*, **56**, 1607 (1983).
24) A. Yaron and A. Berger, *Biochim. Biophys. Acta*, **69**, 399 (1963).
25) M. Nakagaki and T. Handa, *Bull. Chem. Soc. Jpn.*, **49**, 880 (1976).
26) M. Nakagaki, S. Okada, and K. Mochida, *Yakugaku Zasshi*, **99**, 393 (1979).
27) C. R. Snell and G. D. Fasman, *Biopolymers*, **11**, 1723 (1972).

The X-Ray and NMR Studies on the Regio- and Stereoselective Courses for Insertion of Ketones into the *s-cis*- and *s-trans*-Diene Complexes of Zirconium Leading to (*Z*)-1,2-Oxazirconacyclohept-4-enes

Yasushi KAI, Nobuko KANEHISA, Kunio MIKI, Nobutami KASAI,*
Munetaka AKITA,† Hajime YASUDA,† and Akira NAKAMURA*,†
Department of Applied Chemistry, Faculty of Engineering, Osaka University, Suita, Osaka 565
†*Department of Macromolecular Science, Faculty of Science, Osaka University, Toyonaka 560*
(Received June 4, 1983)

The *s-trans*-diene coordination in $(\eta^5\text{-}C_5Me_5)_2Zr$(butadiene) and the *s-cis*-diene coordination in $(\eta^5\text{-}C_5Me_5)_2Zr$-(isoprene) were confirmed by the ^1H- and ^{13}C-NMR spectral studies. The reaction of 2,4-dimethyl-3-pentanone with these complexes occurred regio- and stereoselectively to give $(\eta^5\text{-}C_5Me_5)_2ZrOC(i\text{-}Pr)_2CH_2CR{=}CHCH_2$ (**5**: R=H, **6**: R=Me). The X-ray crystal structure analysis of **5** and **6** revealed the (*Z*)-configuration with respect to the olefin part. Crystal data for **5**: monoclinic, space group $P2_1/n$ with $Z=4$, $a=11.650(2)$, $b=17.791(3)$, $c=13.612(2)$ Å, $\beta=92.20(2)°$, $R=0.111$ for 4308 non-zero reflections. Crystal data for **6**: monoclinic, space group $P2_1/n$ with $Z=4$, $a=10.279(3)$, $b=30.177(4)$, $c=9.955(2)$ Å, $\beta=108.67(2)°$, $R=0.104$ for 3526 non-zero reflections.

The unusual versatility of organozirconium complexes has led to many important developments in organic synthesis. In the preceding papers, we have reported that $(\eta^5\text{-}C_5H_5)_2Zr$(*s-cis*-isoprene) readily reacts with saturated or unsaturated ketones, aldehydes or esters; these reactions result in the regioselective C–C bond formation at the C_1 atom of the coordinated isoprene.[1,2] Stereochemical pathways for this reaction are of interest in understanding the unique chemical properties of the zirconium complexes. Two pathways are conceivable: a) insertion of carbonyl compound to the M–C bond with retention of the *s-cis*-diene conformation and b) insertion after conversion to the *s-trans*-diene coordination. Selective preparation of the *s-cis* and the *s-trans* zirconium-diene complexes is necessary to settle this problem. Though preparations of the *s-cis* and *s-trans* isomers of $(\eta^5\text{-}C_5H_5)_2Zr$(butadiene) complexes were recently reported by Erker[3,4] and by us,[5] purification of the respective isomers is difficult due to the existence of rapid equilibration between them. A thermally stable *s-trans* isomer of the butadiene complex was found to be obtained exclusively when the C_5H_5 ligand was replaced with C_5Me_5 ligand. The corresponding isoprene complexes, $(\eta^5\text{-}C_5R_5)_2Zr$(isoprene) (R=H, Me), assume the *s-cis*-diene coordination irrespective of the ligand. These findings prompted us to examine the reaction of carbonyl compounds with the *s-cis*- and the *s-trans*-diene complexes to define the stereochemical course by means of the X-ray structure analysis and chemical characterization.

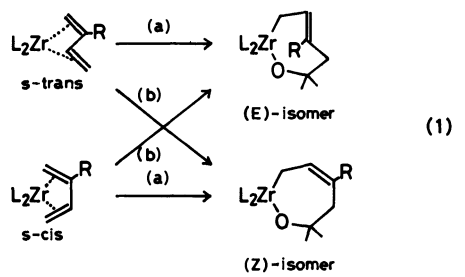

(1)

1 R=H, L=C_5Me_5 5 R=H, L=C_5Me_5
2 R=Me, L=C_5Me_5 6 R=Me, L=C_5Me_5
3 R=H, L=C_5H_5
4 R=Me, L=C_5H_5

Experimental

All manipulations were conducted with Schlenk technique under argon atmosphere. The reagents and solvents were dried over appropriate drying agents and distilled before use. $(C_5Me_5)_2ZrCl_2$[6] and enediylmagnesiums[7] were prepared according to usual methods. Regioselectivity was determined by gas chromatographic analysis of hydrolysis products with a Yanagimoto Model G-80 gas chromatograph using a column packed with Silicone DC-550 on Uniport B. NMR spectra were recorded on a Varian XL-100 instrument with a VFT-100-620L Fourier transform accessory and analyzed with a Varian spin simulation program. Mass spectra were recorded on a JEOL Model JMS OlSG-2 spectrometer. IR and electronic spectra were obtained on a Hitachi EPI-2 spectrometer and a JASCO Model UVIDEC-5A spectrometer, respectively.

Preparation of $(C_5Me_5)_2Zr$(s-trans-*butadiene*) (**1**). To a stirred solution of $(C_5Me_5)_2ZrCl_2$ (508 mg, 1.17 mmol) in 10 ml THF was added a THF slurry of 2-butene-1,4-diylmagnesium ($f=0.32$, 4.5 ml, 1.44 mmol) at −78 °C. The mixture was gradually warmed up to room temperature (25 °C). After stirring for 1 h, the solvent was evaporated under reduced pressure. The residue was extracted with hexane (25 ml) and salts were separated with a centrifuge to give an orange solution. After the solution was concentrated to *ca.* 1 ml, crystallization was carried out at 0 °C to give **1** as orange crystals. Yield 76% (370 mg, 0.89 mmol). Mp 196 °C, UV (hexane) λ_{max} (ε): 354 nm (1.61×10^3), 450 nm (4.33×10^2); IR (hexane) 1431, 1258, 1157, 1023, 944 and 803 cm^{-1}; MS (EI, 70eV), *m/e* 414 (M^+, ^{90}Zr); Found: C, 69.08; H, 8.50%. Calcd for $C_{24}H_{36}Zr$: C, 69.33; H, 8.73%.

Preparation of $(C_5Me_5)_2Zr$(s-cis-*isoprene*) (**2**). $(C_5Me_5)_2ZrCl_2$ (1.73 g, 4.0 mmol) was treated with 4.4 mmol ($f=0.17$, 26 ml) of 2-methyl-2-butene-1,4-diylmagnesium in essentially the same manner as described for **1**. Recrystallization from hexane gave **2** in 82% yield (1.41 g). Mp 208 °C. UV (hexane) λ_{max} (ε): 332 nm (2.54×10^3), 395 nm (1.12×10^3); IR (hexane) 1432, 1257, 1172, 1025 and 805 cm^{-1}; MS (EI, 70 eV), *m/e* 428 (M^+, ^{90}Zr); Found: C, 69.80; H, 8.87%. Calcd for $C_{25}H_{38}Zr$: C, 69.87; H, 8.91%.

*Reaction of **1** with 2,4-Dimethyl-3-pentanone.* To a benzene solution (5 ml) of **1** (1.25 g, 3.0 mmol) was added 2,4-dimethyl-3-pentanone (480 mg, 4.0 mmol). The color of the solution gradually turned into pale yellow. The insertion reaction became complete by stirring the mixture for 10 h at 30 °C or for 2 h at 80 °C, as revealed by gas chromatographic analysis. Concentration of solution to 1 ml resulted in the precipitation of complex **5** as yellow powder in >95% yield. Single crystals for X-ray structure analysis were obtained by recrystallization from hexane. Mp 206—211 °C; ^{1}H-NMR (C_6D_6) δ=1.18 (d, 6, J=7.0 Hz, CH(C$\underline{H}_3$)$_2$), 1.22 (d, 6, J=7.0 Hz, CH-(C$\underline{H}_3$)$_2$), 1.40 (d, 2, J=8.0 Hz, ZrC$\underline{H}_2$), 1.96 (m, 2, C$\underline{H}$-(CH$_3$)$_2$), 2.09 (d, 2, J=8.5 Hz, ZrCH$_2$CH=CH-C$\underline{H}_2$), 5.15 (dt, 1, J=8.5 and 11.0 Hz, ZrCH$_2$CH=C$\underline{H}$), 6.65 (dt, 1, J=8.0 and 11.0 Hz, ZrCH$_2$C$\underline{H}$=CH), 1.91 (s, C_5Me_5); ^{13}C-NMR (C_6D_6) δ=12.3 ($C_5\underline{Me}_5$), 20.6, 22.3 (CH(C$\underline{H}_3$)$_2$), 37.7 (ZrCH$_2$), 39.9 (C$\underline{H}$(CH$_3$)$_2$), 46.2 (ZrCH$_2$CH=CHC$\underline{H}_2$), 94.5 (ZrO$\underline{C}$(*i*-Pr)$_2$), 115.3 (ZrCH$_2$CH=$\underline{C}$H), 119.0 ($\underline{C}_5$Me$_5$), 138.6 (ZrCH$_2$-$\underline{C}$H=CH); MS (FD, 70 eV), *m/e* 528 (M$^+$, ^{90}Zr); Found: C, 70.10; H, 9.65%. Calcd for $C_{31}H_{50}OZr$: C, 70.26; H, 9.51%.

*Reaction of **2** with 2,4-Dimethyl-3-pentanone.* To a benzene solution (5 ml) of **2** (1.29 g, 3.0 mmol) was added 2,4-dimethyl-3-pentanone (480 mg, 4.0 mmol) at 25 °C. After the mixture was stirred at 25 °C for 10 h and the solution was concentrated, complex **6** was obtained as pale yellow crystals in 95% yield. A single crystal for the X-ray diffraction was prepared by recrystallization from benzene. Mp 239—243 °C; ^{1}H-NMR (C_6D_6) δ=1.20 (d, 12, J=7.0 Hz, CH(C$\underline{H}_3$)$_2$), 1.31 (d, 2, J=8.5 Hz, ZrC$\underline{H}_2$), 1.91 (s, 30, C_5Me_5), 2.0 (m, 2, C$\underline{H}$(CH$_3$)$_2$), 2.09 (bs, 3, CH=C(C$\underline{H}_3$)), 2.13 (bs, 2, CH=C-(CH$_3$)C$\underline{H}_2$), 6.61 (t, 1, J=8.5 Hz, ZrCH$_2$C$\underline{H}$=C); ^{13}C-NMR (C_6D_6) δ=12.3 ($C_5\underline{Me}_5$), 20.7, 22.4 (CH(C$\underline{H}_3$)$_2$), 27.5 (CH=C(C$\underline{H}_3$)), 39.6 (C$\underline{H}$(CH$_3$)$_2$), 41.3 (ZrC$\underline{H}_2$), 47.0 (CH=C(CH$_3$)-C$\underline{H}_2$), 93.2 (ZrO$\underline{C}$(*i*-Pr)$_2$), 118.8 ($\underline{C}_5$Me$_5$), 121.0 (CH=$\underline{C}$-(CH$_3$)), 135.1 (C$\underline{H}$=C(CH$_3$)); MS (FD, 70eV), *m/e* 542 (M$^+$, ^{90}Zr); Found: C, 70.60; H, 9.66%. Calcd for $C_{32}H_{52}OZr$: C, 70.65; H, 9.64%.

*Hydrolysis of **5**.* To the complex **5** (1.06 g, 2.0 mmol) in diethyl ether solution (20 ml) was added acetic acid (1 ml), 4 mol dm^{-3} aq HCl or aq H_2SO_4 at 20 °C. After neutralization with aq $NaHCO_3$, the resulting 2-methyl-3-isopropyl-6-hepten-3-ol was isolated by distillation (120 °C/2 mmHg, 1 mmHg≈133.322 Pa). Isolated yield, 85%. When the complex **5** was hydrolyzed with 0.1 mol dm^{-3} aq NaOH, a mixture of 2-methyl-3-isopropyl-6-hepten-3-ol (35%) and 2-methyl-3-isopropyl-5-hepten-3-ol (65%) was obtained. The geometry of the latter could not be determined due to the failure in separation of the respective isomers using a preparative gas chromatograph. Therefore, the ^{1}H-NMR assignment of the latter was made with reference to the spectrum of 2-methyl-3-isopropyl-6-hepten-3-ol obtained by acid hydrolysis.

2-Methyl-3-isopropyl-6-hepten-3-ol: IR (neat) 3490, 3078, 2960, 1640, 1467, 1383, 1095, 992, 968, 950, and 908 cm^{-1}; ^{1}H-NMR ($CDCl_3$) δ=0.95, 0.97 (d, 12, J=7.0 Hz, CH(C$\underline{H}_3$)$_2$), 1.48—2.25 (m, 7, others), 4.84—5.20 (m, 2, CH=C$\underline{H}_2$), 5.60—6.05 (m, 1, C$\underline{H}$=CH$_2$); ^{13}C-NMR ($CDCl_3$) δ=17.4, 17.6 (CH(C$\underline{H}_3$)$_2$), 28.8 (C$\underline{H}_2$COH), 33.0 (CH$_2$=CHC$\underline{H}_2$), 34.2 (C$\underline{H}$(CH$_3$)$_2$), 77.0 (COH), 114.1 (C$\underline{H}_2$=CH), 139.3 (CH$_2$=C$\underline{H}$); MS (EI, 70 eV) 170 (M$^+$); Found: C, 77.50; H, 13.02%. Calcd for $C_{11}H_{22}O$: C, 77.58; H, 13.02%.

2-Methyl-3-isopropyl-5-hepten-3-ol: ^{1}H-NMR ($CDCl_3$) δ=0.93, 0.95 (d, 12, J=7.0 Hz, CH(C$\underline{H}_3$)$_2$), 1.40—2.50 (m, 8, others), 5.40—5.70 (m, 2, C$\underline{H}$=C$\underline{H}$).

*Hydrolysis of **6**.* When the complex **6** was hydrolyzed with 0.1 mol dm^{-3} aq NaOH in diethyl ether at 20 °C, a mixture of (*Z*)-2,5-dimethyl-3-isopropyl-5-hepten-3-ol (97%) and 2,5-dimethyl-3-isopropyl-6-hepten-3-ol (3%) was obtained in 99% GC yield, while the protolysis with acetic acid gave 2,5-dimethyl-3-isopropyl-6-hepten-3-ol (94% isomeric purity) in 95% yield. The (*Z*)-structure was determined from the NOE measurement (8%) in $CDCl_3$ at 30 °C.

(Z)-2,5-Dimethyl-3-isopropyl-5-hepten-3-ol: IR (neat) 3560, 2960, 1467, 1383, 994, and 813 cm^{-1}. ^{1}H-NMR ($CDCl_3$) δ=0.97, 0.99 (d, 12, J=6.5 Hz, CH(C$\underline{H}_3$)$_2$), 1.32 (s, 1, OH), 1.65 (d, 3, J=7.0 Hz, C$\underline{H}_3$CH=), 1.84 (bs, 3, CH=C(C$\underline{H}_3$)), 1.95 (sept, 2, J=6.5 Hz, C$\underline{H}$(CH$_3$)$_2$), 2.30 (bs, 2, CH=C(CH$_3$)C$\underline{H}_2$), 5.40 (q, 1, J=7.0 Hz, CH$_3$C$\underline{H}$=); ^{13}C-NMR ($CDCl_3$) δ=14.3 (C$\underline{H}_3$CH=), 17.8, 18.5 (CH(C$\underline{H}_3$)$_2$), 26.5 (CH=C(C$\underline{H}_3$)), 34.8 (CH=C(CH$_3$)C$\underline{H}_2$), 35.1 (C$\underline{H}$(CH$_3$)$_2$), 78.4 (COH), 123.5 (CH$_3$C$\underline{H}$=), 133.7 (CH=$\underline{C}$(CH$_3$)); MS (EI, 70 eV) 184 (M$^+$); Found: C, 78.07; H, 13.00%. Calcd for $C_{14}H_{24}O$: C, 78.20; H, 13.11%.

2,5-Dimethyl-3-isopropyl-6-hepten-3-ol: ^{1}H-NMR ($CDCl_3$) δ=0.90—1.05 (m, 15, CH(C$\underline{H}_3$)$_2$ and CH$_2$=CHCH$_2$CHC$\underline{H}_3$), 1.50—2.50 (m, 6, others), 4.80—5.20 (m, 2, CH=C$\underline{H}_2$), 5.55—6.10 (m, 1, C$\underline{H}$=CH$_2$).

*Crystal Structure Determination of **5** and **6**.* *Crystal Data for* [(*C*$_5$*Me*$_5$)$_2$*ZrOC*(*i*-*Pr*)$_2$*CH*$_2$*CH*=*CHCH*$_2$] (**5**): $C_{31}H_{50}OZr$, M=530.0, monoclinic, space group $P2_1/n$, a=11.650(2), b=17.791 (3), c=13.612(2) Å, β=92.20(2)°, U=2819.3(9) Å^3, Z=4, D_c=1.248 g cm^{-3}, μ(Mo $K\alpha$)=4.06 cm^{-1}, F(000)=1136.

Crystal Data for [(*C*$_5$*Me*$_5$)$_2$*ZrOC*(*i*-*Pr*)$_2$*CH*$_2$*CMe*=*CHCH*$_2$] (**6**): $C_{32}H_{52}OZr$, M=544.0, monoclinic, space group $P2_1/n$, a=10.279(3), b=30.177(4), c=9.955(2) Å, β=108.67(2)°, U=2925.3(11) Å^3, Z=4, D_c=1.235 g cm^{-3}, μ(Mo $K\alpha$)=3.93 cm^{-1} F(000)=1168.

Data Collection and Structure Analysis: The X-ray diffraction data were collected on a Rigaku automated four-circle diffractometer with Zr-filtered Mo $K\alpha$ radiation. As the compounds are very air-sensitive, the crystals were sealed in thin-walled glass capillary tubes under argon atmosphere. The crystals with dimensions of 0.50×0.50×0.30 mm for **5** and 0.45×0.40×0.35 mm for **6** were used for the data measurements. The integrated intensities were measured by the θ-2θ scan technique with background countings at each end of the scan range for 5 s. The total numbers of reflections measured were 6478 for **5** (2θ up to 55°) and 5134 for **6** (2θ up to 50°), among which non-zero reflections are 4308 and 3526, respectively. Three monitor reflections were measured for each block of 61 reflections to check for radiation damage and for any change in orientations of the crystals. No radiation damage of the crystals was found. The measured intensities were corrected for Lorentz and polarization effects but not for absorption, because of the relatively small absorption effects of these compounds for Mo $K\alpha$ radiation.

The crystal structures were solved by the conventional heavy atom method and refined by the block-diagonal least-squares (*HBLS*-V).[8] The atomic scattering factors were taken from the International Tables for X-Ray Crystallography.[9] Hydrogen atoms were searched for on the difference Fourier maps calculated after the anisotropic refinements of non-hydrogen atoms. Methyl hydrogen atoms, however, could not be located on the maps and were excluded in the final stage of refinements. The weighting scheme applied was $w=[\sigma(F_o)^2+a|F_o|+b|F_o|^2]^{-1}$ for non-zero reflections and $w=c$ for zero reflections, respectively. The final R indices defined by $R=\sum(|F_o|-|F_c|)/\sum|F_o|$ were 0.111 (non-zero reflections) and 0.219 (all reflections) for **5**, and 0.104 and 0.202 for **6**, respectively. The weighted R indices defined by $R_w=[\sum w(|F_o|-|F_c|)^2/\sum w|F_o|^2]^{1/2}$were 0.160 for **5** with the weighting parameters of a=0.368, b=0.00002, and c=0.014, and 0.094 for **6** with a=0.503, b=−0.002, and c=0.011, respectively. The

TABLE 1. FRACTIONAL ATOMIC COORDINATES OF **5** AND **6** WITH ESTIMATED STANDARD DEVIATIONS IN PARENTHESES

a) $[(C_5Me_5)_2ZrOC(i\text{-}Pr)_2CH_2CH{=}CHCH_2]$ (**5**).

Atom	x	y	z	B_{eq}/Å^2 [10]
Zr	0.29990(8)	0.37823(5)	0.28324(7)	2.70
O	0.4643(6)	0.3586(4)	0.2706(5)	2.7
C(1)	0.2565(9)	0.3052(6)	0.1480(8)	2.9
C(2)	0.3397(12)	0.3180(7)	0.0701(8)	4.2
C(3)	0.4495(10)	0.3012(7)	0.0703(8)	3.4
C(4)	0.5157(10)	0.2640(6)	0.1533(9)	3.4
C(5)	0.5627(9)	0.3203(6)	0.2337(7)	2.7
C(7)	0.6405(10)	0.3760(7)	0.1848(8)	3.6
C(8)	0.7485(13)	0.3443(9)	0.1346(12)	5.9
C(9)	0.6788(12)	0.4458(8)	0.2484(11)	5.1
C(10)	0.6173(10)	0.2738(7)	0.3220(8)	3.6
C(11)	0.6932(16)	0.2037(10)	0.2918(13)	7.4
C(12)	0.6806(11)	0.3203(9)	0.4003(10)	4.9
C(21)	0.3321(9)	0.4989(6)	0.1804(7)	2.6
C(22)	0.3269(9)	0.5192(6)	0.2810(8)	2.7
C(23)	0.2107(9)	0.5129(5)	0.3094(8)	2.8
C(24)	0.1473(10)	0.4849(7)	0.2284(9)	3.6
C(25)	0.2215(9)	0.4765(6)	0.1485(7)	2.8
C(26)	0.4290(11)	0.5135(7)	0.1137(9)	4.1
C(27)	0.4246(11)	0.5520(7)	0.3451(10)	4.2
C(28)	0.1652(12)	0.5525(8)	0.3987(9)	4.6
C(29)	0.0155(11)	0.4804(10)	0.2156(14)	6.3
C(30)	0.1782(12)	0.4634(8)	0.0444(9)	4.7
C(31)	0.2696(9)	0.2508(6)	0.3802(8)	2.9
C(32)	0.3198(9)	0.3033(6)	0.4481(7)	2.6
C(33)	0.2374(10)	0.3610(6)	0.4623(8)	3.0
C(34)	0.1383(9)	0.3432(6)	0.4055(8)	2.8
C(35)	0.1623(9)	0.2779(7)	0.3520(8)	3.1
C(36)	0.3175(11)	0.1742(6)	0.3526(10)	4.3
C(37)	0.4298(11)	0.2936(8)	0.5111(8)	4.3
C(38)	0.2501(13)	0.4163(7)	0.5477(8)	4.3
C(39)	0.0195(11)	0.3755(8)	0.4195(11)	4.9
C(40)	0.0689(11)	0.2348(9)	0.2911(11)	5.0
Atom	x	y	z	B/Å^2
H(11)	0.261(9)	0.261(6)	0.178(8)	3(3)
H(12)	0.180(9)	0.320(6)	0.120(8)	3(3)
H(2)	0.319(10)	0.322(7)	0.000(9)	4(3)
H(3)	0.500(9)	0.320(6)	-0.000(8)	3(3)
H(41)	0.582(9)	0.219(7)	0.121(8)	4(3)
H(42)	0.470(9)	0.230(6)	0.180(8)	3(3)
H(7)	0.590(10)	0.400(6)	0.142(8)	4(3)
H(10)	0.558(9)	0.242(6)	0.359(8)	3(3)

b) $[(C_5Me_5)_2ZrOC(i\text{-}Pr)_2CH_2CMe{=}CHCH_2]$ (**6**).

Atom	x	y	z	B_{eq}/Å^2 [10]
Zr	0.02683(11)	0.13713(4)	0.37664(12)	2.66
O	-0.1373(8)	0.1066(3)	0.2551(8)	2.3
C(1)	-0.0573(14)	0.2031(4)	0.2646(13)	3.1
C(2)	-0.1129(14)	0.1974(4)	0.1074(14)	3.0
C(3)	-0.2218(14)	0.1745(5)	0.0330(12)	3.0
C(4)	-0.3165(13)	0.1500(5)	0.0994(13)	3.3
C(5)	-0.2719(12)	0.1027(5)	0.1513(13)	2.8
C(6)	-0.2675(18)	0.1743(6)	-0.1306(14)	5.2
C(7)	-0.2618(13)	0.0745(5)	0.0276(13)	3.1
C(8)	-0.3996(17)	0.0671(6)	-0.0929(17)	6.0
C(9)	-0.1885(16)	0.0270(5)	0.0728(16)	4.4
C(10)	-0.3715(12)	0.0869(5)	0.2335(15)	3.5
C(11)	-0.5284(16)	0.0977(7)	0.1595(21)	6.1
C(12)	-0.3535(19)	0.0364(6)	0.2781(17)	5.2
C(21)	0.1464(12)	0.1140(5)	0.1925(13)	2.6
C(22)	0.1937(12)	0.0862(5)	0.3090(12)	2.6
C(23)	0.2824(13)	0.1108(5)	0.4272(14)	3.1
C(24)	0.2819(12)	0.1544(5)	0.3806(14)	3.0
C(25)	0.2003(12)	0.1568(5)	0.2379(15)	3.3
C(26)	0.0780(15)	0.1018(6)	0.0423(14)	4.3
C(27)	0.1765(14)	0.0354(5)	0.3086(15)	3.8
C(28)	0.3827(17)	0.0890(6)	0.5552(15)	5.7
C(29)	0.3754(17)	0.1929(6)	0.4608(21)	6.1
C(30)	0.2047(17)	0.1975(6)	0.1461(17)	5.3
C(31)	-0.1037(13)	0.1646(5)	0.5519(12)	2.9
C(32)	-0.0714(14)	0.1205(5)	0.5833(12)	2.9
C(33)	0.0720(14)	0.1151(5)	0.6397(13)	3.1
C(34)	0.1308(13)	0.1569(5)	0.6482(12)	3.2
C(35)	0.0237(14)	0.1893(5)	0.5868(12)	3.0
C(36)	-0.2440(13)	0.1872(6)	0.5028(14)	4.4
C(37)	-0.1723(18)	0.0838(5)	0.5886(16)	4.7
C(38)	0.1419(18)	0.0728(6)	0.7079(16)	5.0
C(39)	0.2734(15)	0.1711(7)	0.7392(17)	5.4
C(40)	0.0375(17)	0.2383(5)	0.5914(16)	4.4
Atom	x	y	z	B/Å^2
H(11)	-0.135(12)	0.218(4)	0.288(12)	3(3)
H(12)	0.025(12)	0.230(4)	0.306(11)	3(3)
H(2)	-0.083(10)	0.211(4)	0.039(9)	1(3)
H(41)	-0.415(12)	0.148(4)	0.026(12)	3(3)
H(42)	-0.325(11)	0.168(4)	0.182(11)	2(3)
H(7)	-0.183(11)	0.089(4)	-0.016(11)	3(3)
H(10)	-0.340(12)	0.109(4)	0.337(11)	3(3)

final atomic coordinates for **5** and **6** are listed in Table 1.††

All the computations were carried out on an ACOS-S900 computer at the Crystallographic Research Center, Institute for Protein Research, Osaka University.

Results and Discussion

NMR Studies on the $(C_5Me_5)_2Zr$(diene) Complexes. Most mononuclear transition metal complexes of acyclic or cyclic dienes assume the *s-cis*-η^4-diene coordination. However, we and Erker *et al.* recently found by X-ray analysis that the *s-trans* coordination is possible for 1,4-diphenyl-1,3-butadiene[11] and butadiene[3,4] when these are coordinated to $(C_5H_5)_2Zr$ fragments. More recently, preparation of the corresponding hafnium-*s-trans*-butadiene complex has been reported.[12] A photochemically generated $(C_5H_5)_2Zr$(*s-trans*-butadiene) complex is thermally unstable and is readily converted to the *s-cis*-diene complex at ambient temperature.[3] Seeking for preparation of thermally stable *s-trans*-butadiene complexes, we have found that the 1 : 1 reaction of $(C_5Me_5)_2ZrCl_2$ with 2-butene-1,4-diylmagnesium predominantly gave a pure *s-trans* isomer (>99%), $(C_5Me_5)_2Zr$(*s-trans*-butadiene) (**1**), in good yield (Eq. 2).

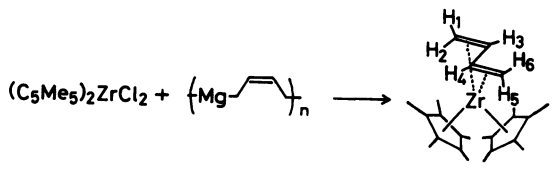

(2)

1

The *s-trans* structure was confirmed by iterative computer simulation of the ^{1}H-NMR spectrum (Table 2). The magnitude of the proton-proton coupling constant, 16.0 Hz for $J_{3,4}$, clearly shows that the complex **1** has the *s-trans* structure. This value is consistent with the values of 15—16 Hz observed for the *s-trans* isomer of $(C_5H_5)_2Zr$(butadiene) and $(C_5H_5)_2Zr$(1,4-diphenyl-1,3-butadiene).[5] The coupling constant of $J_{3,4}$ for the *s-cis* isomer is known to be 8.0 Hz for $(C_5H_5)_2$-Zr(*s-cis*-butadiene) (**3-*s-cis***). Chemical shift values for **1** are also comparable with those for $(C_5H_5)_2Zr$(butadiene) (**3-*s-trans***).[5]

The corresponding isoprene complex, $(C_5Me_5)_2Zr$-(isoprene) **2**, was prepared in the same way (Eq. 3) and the geometry was determined to be *s-cis* based upon the ^{1}H-NMR chemical shift values (Table 2). It is noteworthy that the spectrum of **2** was not changed by

†† Tables of observed and calculated structure factors and anisotropic thermal parameters are deposited as Document No. 8348 at the Chemical Society of Japan.

TABLE 2. ^{1}H-NMR PARAMETERS FOR COMPLEXES **1** AND **2** OBTAINED BY COMPUTER SIMULATION[a)]

Complex	Chemical shift, ν/ppm							
	H_1	H_2	H_3	H_4	H_5	H_6	ν_{CH_3}[b)]	ν_{CH_3}[c)]
1	2.75	1.21	2.14	2.14	2.75	1.21	—	1.69
2	0.87	0.87	5.74	—	0.75	0.75	1.92	1.85

Complex	Coupling constant, J/Hz										
	$J_{1,2}$	$J_{1,3}$	$J_{2,3}$	$J_{3,4}$	$J_{4,5}$	$J_{4,6}$	$J_{5,6}$	$J_{1,5}$	$J_{2,6}$	$J_{3,5}$	$J_{3,6}$
1	−4.2	7.3	16.2	16.0	7.3	16.2	−4.2	1.0	0.2	−0.5	−1.2
2	−5.0	4.8	4.8	—	—	—	−5.0	0.6	0.6	−0.8	−0.8

a) Spectra were observed at 100 MHz in toluene-d_8 at 30 °C. Chemical shifts were calibrated by using the internal benzene peak, assumed to be 7.20 ppm. The numbering system follows that shown in Eqs. 2 and 3. b) Methyl proton signals of isoprene. c) Methyl proton signals of C_5Me_5 group.

TABLE 3. ^{13}C-NMR CHEMICAL SHIFT VALUES (ν/ppm) AND ^{13}C–^{1}H COUPLING CONSTANTS (IN PARENTHESES, J/Hz) FOR **1** AND **3**[a)]

Complex	Temp/°C	$C_1(C_4)$	$C_2(C_3)$	Ligand	$\Delta(C_2-C_1)$
1	30	64.95 (146.0)	100.71 (143.9)	10.45 (125.7) [Me] 108.64 [ring]	35.76
1	−50	64.54 (150.5)	100.57 (148.9)	10.37 (125.7) [Me] 108.05 [ring]	36.03
3-s-trans	30	57.72 (145.3)[b)] (156.3)[c)]	94.56 (148.9)	100.79 (172.1)	36.84
3-s-cis	30	48.35 (144.7)	110.86 (153.8)	98.08 (170.9)	62.52
3-s-trans	−50	57.66	94.09	97.92	36.73
3-s-cis	−50	48.29	110.38	102.41	62.09

a) Spectra were recorded at 25.2 MHz in toluene-d_8 and chemical shifts were calibrated by using internal toluene peak (CH_3-proton signal), assumed to be 19.20 ppm. b) Coupling constant between ^{13}C at $C_1(C_4)$ and terminal proton at the *syn*-position with respect to the proton at $C_2(C_3)$. c) Coupling constant for ^{13}C–^{1}H at *anti*-position (see Ref. 22 for the assignment).

TABLE 4. ^{13}C-NMR CHEMICAL SHIFT VALUES AND ^{13}C–^{1}H COUPLING CONSTANTS (IN PARENTHESES) FOR **2** AND **4**[a)]

Complex	Temp °C	C_1	C_2	C_3	C_4	C_5[d)]	Ligand	$\Delta(C_3-C_4)$
2	30	45.96 (123.9)	136.65	124.68 (148.9)	47.37 (123.0)	30.68 (127.0)	10.04 (126.1) [Me] 115.85 [ring]	77.31
2	−50	44.82 (123.3)	136.76	124.62 (141.6)	46.29 (122.1)	31.06 (123.3)	9.94 (126.1) [Me] 115.36 [ring]	78.33
4	30	46.67 (143.4)	122.19	109.83 (156.3)	52.19 (140.4)	27.81 (125.7)	101.22 (170.9)	57.64
4	−50	46.45 (157.5)[b)] (128.2)[c)]	121.48	109.51 (153.8)	51.87 (157.5)[b)] (128.2)[c)]	27.81 (125.7)	99.11 (172.1) 102.68 (170.9)	57.64

a) Recorded at 25.2 MHz in toluene-d_8. Chemical shift values are expressed by ppm and coupling constants by Hz. Assignments of each atom were made with reference to the ^{1}H NMR chemical shift values (see. Ref. 5a). b) Coupling constant for ^{13}C–^{1}H at the *syn*-position with respect to the proton at C_2 or C_3 atoms (see Ref. 22). c) Coupling constant for ^{13}C–^{1}H at the *anti*-position with respect to the proton at C_2 or C_3 atoms. d) Methyl carbon of isoprene.

lowering the temperature from 50 °C to −70 °C while $(C_5H_5)_2Zr$(isoprene) **4** showed the limiting η^4-diene structure when it was cooled to −30 °C, as reported previously.[5)] This behavior indicates enhanced fluxionality of **2** compared to that of **4**.

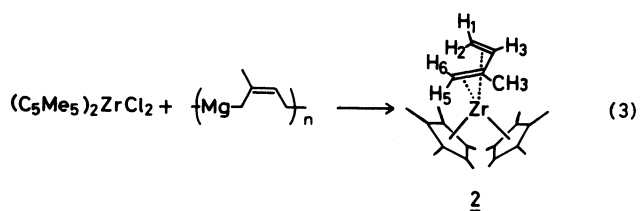

(3)

2

The geometry of **1**, **2**, ***3-s-cis***, ***3-s-trans*** and **4** was also confirmed by the ^{13}C-NMR spectra. Chemical shift values and the ^{13}C–^{1}H coupling constants for **1**, ***3-s-cis*** and ***3-s-trans*** are given in Table 3 and those for **2** and **4** are given in Table 4. It is apparent from these data that the chemical shift difference, $\Delta(C_2-C_1)$, between terminal carbons $C_1(C_4)$ and central carbon atoms $C_2(C_3)$ is rather small (*ca.* 36 ppm) for the *s-trans*-diene complexes, **1** and ***3-s-trans***, while the corresponding difference, $\Delta(C_3-C_4)$, for the *s-cis*-diene complexes **2**, **4** and $\Delta(C_2-C_1)$ for ***3-s-cis*** is significantly larger (57.6—

77.3 ppm) regardless of temperature. Thus, geometries are readily determined from chemical shift differences. It is important to note here that the ^{13}C chemical shift values of **4** at 30 °C for the fluxional diene molecule are essentially the same as the values for the η^4-coordinated diene observed at −50 °C. This result suggests that most of the coordinated isoprene remains η^4-bonded even when some of it is flipping. Such information could not be obtained from the ^1H-NMR spectrum since the proton signals of **4** coalesce at 0——30 °C.

The ^{13}C–^1H coupling constant offers important information on the extent of hybridization in the diene carbons. Based upon Newton's semiempirical rule,[13] it is possible to calculate the *s*-% of carbon atoms of the dienes and hence the hybridization. The hybridization approximated by $n=(1-s)/s$ for sp^n is shown below. The sp^3 character of CH_2 carbon at isoprene termini of **2** is higher than that of **4**. Thus, greater contribution of the zirconacyclopent-3-ene structure was inferred for **2** when compared with that of **4**. This will account for the higher fluxionality of **2**. The sp^3 character of carbon atoms at *s-trans*-diene termini of **1** is smaller than that of the terminal atom of the *s-cis*-diene complex **2**, indicating that the Zr–C_1 and Zr–C_4 σ-bonding of **1** is less than that of **2**. The sp^n parameter for $C_1(C_4)$ atoms of **3-*s*-*trans*** and **4** (at −50 °C) was obtained from the avaraged coupling constant values of ^{13}C–^1H(*syn*) and ^{13}C–^1H(*anti*). See footnote in Tables 3 and 4 and Ref. 22 for the assignment.

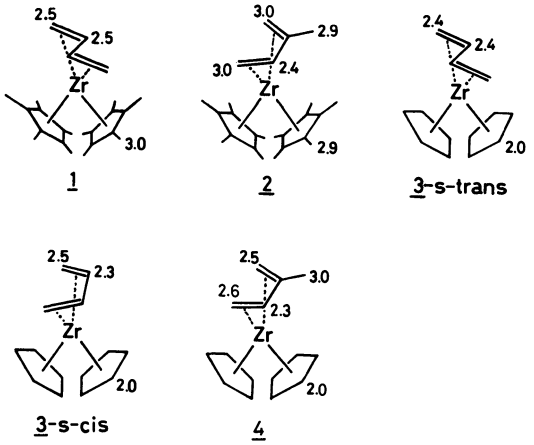

*Molecular Structures of **5** and **6**.* Single crystals of 1,2-oxazirconacyclohept-4-enes (**5** and **6**) were prepared by the 1 : 1 reaction of $(C_5Me_5)_2Zr$(*s-trans*-butadiene) **1** or $(C_5Me_5)_2Zr$(*s-cis*-isoprene) **2** with 2,4-dimethyl-3-pentanone at 30 °C in benzene to define the stereochemistry of the insertion reaction in terms of X-ray crystal structure analysis.

The molecular structures of **5** and **6** determined in this work are shown in Figs. 1 and 2 which give the *ORTEP* drawings[14] together with the atomic numberings. The bond distances and angles are listed in Table 5. The molecular structure of **5** shows that the 2,4-dimethyl-3-pentanone inserts regioselectively into the bond between zirconium and one of terminal carbon atoms of butadiene [Zr–C(4) bond]. The molecular structure of **6** shows that the insertion of ketone with

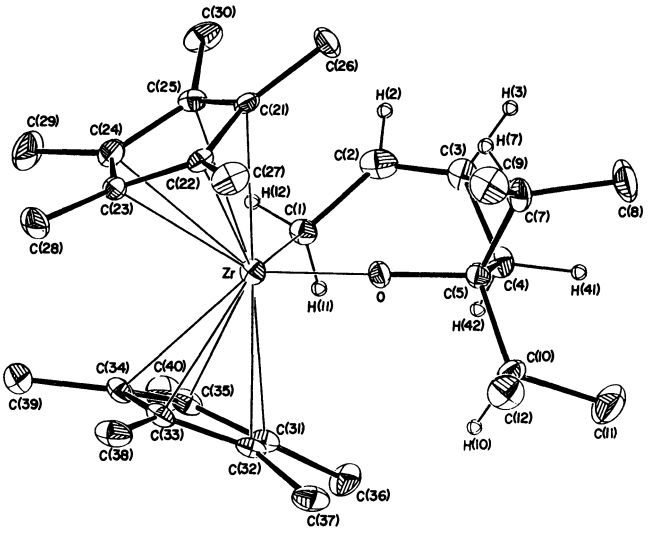

Fig. 1. Molecular structure of $[(C_5Me_5)_2ZrOC(i\text{-}Pr)_2\text{-}CH_2CH{=}CHCH_2]$ (**5**) with the numbering scheme of the atoms. Thermal ellipsoids for non-hydrogen atoms are drawn at the 20% probability level. Hydrogen atoms are shown as the spheres with arbitrary temperature factor of 1.0 Å².

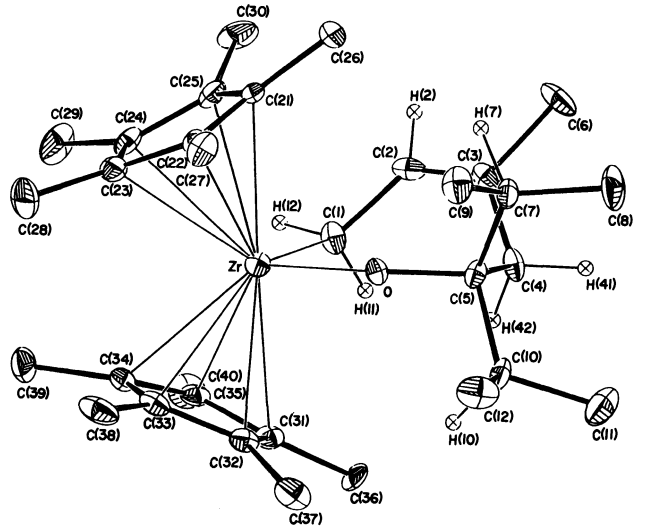

Fig. 2. Molecular structure of $[(C_5Me_5)_2ZrOC(i\text{-}Pr)_2\text{-}CH_2CMe{=}CHCH_2]$ (**6**) with the numbering scheme of the atoms. Drawing parameters are same as those for Fig. 1.

$(C_5Me_5)_2Zr$(isoprene) occurred into the bond between zirconium and C_1 atom of isoprene [C(4) atom in Fig. 2]. Thus, the insertion occurred regioselectively into the sterically hindered Zr–C(4) bond rather than into the less hindered Zr–C(1) bond. These molecular structures coincided with the oxametallacycloheptene structures determined by the mass and ^1H-NMR spectra (see Experimental) and the structures of the base hydrolysis products.

The overall geometry of complexes **5** and **6** is essentially the same. The zirconium atom is coordinated with two C_5Me_5 ligands and bonded with the C(1) atom of the diene part and the oxygen atom of the ketone part

TABLE 5. BOND LENGTHS AND ANGLES IN **5** AND **6** WITH THEIR ESTIMATED STANDARD DEVIATIONS IN PARENTHESES

Bond length	*l*/Å	
	5	**6**
Zr -O	1.961(7)	1.964(8)
Zr -C(1)	2.294(10)	2.311(14)
C(1) -C(2)	1.482(17)	1.494(20)
C(1) -H(11)	0.89(10)	1.01(12)
C(1) -H(12)	1.00(10)	1.16(12)
C(2) -C(3)	1.313(17)	1.324(20)
C(2) -H(2)	0.97(11)	0.93(10)
C(3) -C(4)	1.499(16)	1.530(19)
C(3) -C(6)		1.545(22)
C(3) -H(3)	1.19(10)	
C(4) -C(5)	1.567(15)	1.536(18)
C(4) -H(41)	1.20(11)	1.04(12)
C(4) -H(42)	0.90(10)	1.02(11)
C(5) -O	1.440(12)	1.442(14)
C(5) -C(7)	1.514(15)	1.529(18)
C(5) -C(10)	1.573(15)	1.576(19)
C(7) -C(8)	1.560(20)	1.552(22)
C(7) -C(9)	1.569(18)	1.614(20)
C(7) -H(7)	0.92(11)	1.13(11)
C(10)-C(11)	1.592(22)	1.577(25)
C(10)-C(12)	1.518(19)	1.583(24)
C(10)-H(10)	1.04(10)	1.19(12)
C(21)-C(22)	1.420(14)	1.388(18)
C(21)-C(25)	1.401(14)	1.420(20)
C(22)-C(23)	1.427(14)	1.442(18)
C(23)-C(24)	1.395(16)	1.394(19)

Bond length	*l*/Å	
	5	**6**
C(24)-C(25)	1.423(16)	1.401(20)
C(21)-C(26)	1.498(16)	1.481(21)
C(22)-C(27)	1.523(16)	1.542(19)
C(23)-C(28)	1.519(17)	1.509(22)
C(24)-C(29)	1.541(21)	1.556(25)
C(25)-C(30)	1.504(17)	1.541(23)
C(31)-C(32)	1.425(14)	1.384(19)
C(31)-C(35)	1.380(15)	1.449(19)
C(32)-C(33)	1.423(14)	1.408(19)
C(33)-C(34)	1.400(15)	1.389(20)
C(34)-C(35)	1.405(15)	1.452(19)
C(31)-C(36)	1.524(17)	1.527(21)
C(32)-C(37)	1.524(17)	1.530(22)
C(33)-C(38)	1.525(18)	1.515(23)
C(34)-C(39)	1.518(17)	1.517(23)
C(35)-C(40)	1.546(18)	1.487(22)
Zr -C(21)	2.598(10)	2.608(13)
Zr -C(22)	2.527(10)	2.549(12)
Zr -C(23)	2.641(10)	2.635(13)
Zr -C(24)	2.687(12)	2.660(14)
Zr -C(25)	2.669(10)	2.649(15)
Zr -C(31)	2.654(10)	2.652(13)
Zr -C(32)	2.613(10)	2.614(13)
Zr -C(33)	2.589(11)	2.596(14)
Zr -C(34)	2.635(10)	2.638(14)
Zr -C(35)	2.597(11)	2.626(14)

Bond angle	*φ*/°	
	5	**6**
O -Zr -C(1)	90.8(4)	89.6(5)
Zr -O -C(5)	155.2(7)	156.5(8)
Zr -C(1) -C(2)	110.9(8)	111.4(9)
Zr -C(1) -H(11)	97(6)	119(7)
Zr -C(1) -H(12)	109(6)	109(6)
C(2) -C(1) -H(11)	116(6)	103(7)
C(2) -C(1) -H(12)	107(6)	117(6)
H(11)-C(1) -H(12)	117(9)	98(9)
C(1) -C(2) -C(3)	128.9(12)	128.1(13)
C(1) -C(2) -H(2)	124(7)	128(6)
C(3) -C(2) -H(2)	103(7)	104(6)
C(2) -C(3) -C(4)	125.1(11)	123.5(13)
C(2) -C(3) -C(6)		120.6(13)
C(4) -C(3) -C(6)		115.7(12)
C(2) -C(3) -H(3)	116(5)	
C(4) -C(3) -H(3)	118(5)	
C(3) -C(4) -C(5)	113.6(9)	115.5(11)
C(3) -C(4) -H(41)	110(5)	109(6)
C(3) -C(4) -H(42)	108(7)	109(6)
C(5) -C(4) -H(41)	118(5)	107(6)
C(5) -C(4) -H(42)	110(7)	109(6)
H(41)-C(4) -H(42)	96(8)	106(9)
O -C(5) -C(4)	106.6(8)	106.3(10)
O -C(5) -C(7)	110.0(8)	109.0(10)
O -C(5) -C(10)	106.7(8)	106.6(10)
C(4) -C(5) -C(7)	108.1(10)	109.7(11)
C(4) -C(5) -C(10)	108.5(10)	106.4(11)
C(7) -C(5) -C(10)	116.6(9)	118.2(10)
C(5) -C(7) -C(8)	117.6(10)	115.0(11)
C(5) -C(7) -C(9)	115.9(10)	114.6(11)
C(5) -C(7) -H(7)	102(7)	109(6)

Bond angle	*φ*/°	
	5	**6**
C(5) -C(10)-C(12)	114.9(10)	113.6(12)
C(5) -C(10)-H(10)	114(6)	104(6)
C(11)-C(10)-C(12)	110.4(11)	109.9(13)
C(11)-C(10)-H(10)	95(6)	104(6)
C(12)-C(10)-H(10)	106(6)	109(6)
C(22)-C(21)-C(25)	107.4(10)	106.7(12)
C(22)-C(21)-C(26)	126.9(10)	128.2(13)
C(25)-C(21)-C(26)	124.5(10)	124.0(13)
C(21)-C(22)-C(23)	108.5(10)	109.4(12)
C(21)-C(22)-C(27)	126.2(10)	126.1(12)
C(23)-C(22)-C(27)	124.8(10)	123.8(12)
C(22)-C(23)-C(24)	107.1(10)	106.3(12)
C(22)-C(23)-C(28)	122.9(10)	123.2(13)
C(24)-C(23)-C(28)	127.5(11)	128.4(13)
C(23)-C(24)-C(25)	108.8(10)	108.9(13)
C(23)-C(24)-C(29)	127.1(12)	126.7(14)
C(25)-C(24)-C(29)	122.7(12)	123.5(14)
C(21)-C(25)-C(24)	108.2(10)	108.7(13)
C(21)-C(25)-C(30)	127.4(10)	128.2(14)
C(24)-C(25)-C(30)	123.0(10)	121.4(14)
C(32)-C(31)-C(35)	107.2(10)	107.9(12)
C(32)-C(31)-C(36)	127.0(10)	129.5(13)
C(35)-C(31)-C(36)	125.5(10)	122.4(13)
C(31)-C(32)-C(33)	107.4(10)	110.2(12)
C(31)-C(32)-C(37)	127.3(10)	126.0(13)
C(33)-C(32)-C(37)	124.3(10)	122.6(13)
C(32)-C(33)-C(34)	108.0(10)	107.5(13)
C(32)-C(33)-C(38)	121.4(10)	124.1(14)
C(34)-C(33)-C(38)	128.3(11)	127.1(13)
C(33)-C(34)-C(35)	107.3(10)	109.2(12)
C(33)-C(34)-C(39)	125.5(10)	127.7(13)

TABLE 5. (Continued)

Bond angle	φ/° 5	6	Bond angle	φ/° 5	6
C(8) -C(7) -C(9)	108.1(10)	108.5(12)	C(35)-C(34)-C(39)	125.4(10)	121.3(13)
C(8) -C(7) -H(7)	113(7)	111(6)	C(31)-C(35)-C(34)	110.0(10)	105.1(12)
C(9) -C(7) -H(7)	99(7)	97(6)	C(31)-C(35)-C(40)	125.9(10)	126.1(13)
C(5) -C(10)-C(11)	115.4(10)	115.6(12)	C(34)-C(35)-C(40)	122.6(10)	127.3(13)

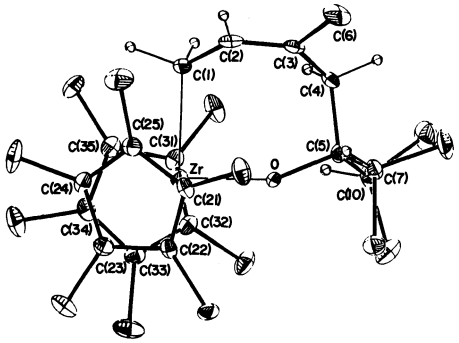

Fig. 3. Molecular structure of **6** projected onto the plane defined by Zr, O, and C(1) atoms. Drawing parameters are same as those for Fig. 1.

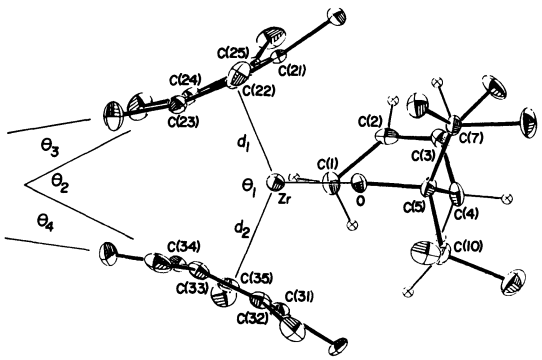

Fig. 4. Molecular structure of **6** viewed along the plane defined by Zr, O, and C(1) atoms. Drawing parameters are same as those for Fig. 1.

in a pseudo-tetrahedral manner. The Zr–C(1) lengths, 2.294(10) Å in **5** and 2.311(14) Å in **6**, are similar to the Zr–C(alkyl) distances in $(\eta^5\text{-}C_9H_7)_2Zr(CH_3)_2$ [2.255(5) Å],[15] $(\eta^5\text{-}C_5H_5)_2Zr(CH_2SiMe_3)_2$ [2.279(4) Å],[16] and $(\eta^5\text{-}C_5H_5)_2Zr(CH_2CMe_3)_2$ [2.288(10) Å],[16] and also to the Zr–C (terminal) distance in $(\eta^5\text{-}C_5H_5)_2$-Zr(2,3-dimethylbutadiene) [2.300 Å].[3] The Zr–O distances are 1.961(7) and 1.964(8) Å for **5** and **6**, respectively. These distances are slightly shorter than the expected Zr–O single bond distance estimated from the sum of the covalent radii for zirconium (1.45—1.48 Å) and oxygen (0.66 Å). The Zr–O–C(5) angles have relatively large values of 155.2(7)° for **5** and 156.5(8)° for **6**, respectively. The C(2)–C(3) bond distances, 1.313(17) Å in **5** and 1.324(20) Å in **6**, show that these bonds are the localized carbon–carbon double bonds, whose standard value is 1.337±6 Å.[17] The interatomic distances between zirconium and C(2) and/or C(3) atoms [Zr–C(2): 3.144(13) Å in **5**, 3.177(14) Å in **6**; Zr–C(3): 3.702(11) Å in **5**, 3.729(14) Å in **6**] indicate that there is no direct interaction between zirconium and the C(2)–C(3) double bond. Thus, the oxametallacycloheptene part in these complexes is described as having the 1,2-oxazirconacyclohept-4-ene structure.

The characteristic views of the molecular structure of **6** are shown in Figs. 3 and 4. The corresponding views of **5** are essentially the same as those of **6** in these Figures. The most interesting features in the oxametallacycloheptene part in these complexes are the conformations of C(1)–C(2)–C(3)–C(4) moieties, which correspond to the 1,3-dienes in the original complexes into which the ketone inserts. The torsional angles about C(2)–C(3) double bonds, C(1)–C(2)–C(3)–C(4), are 0.0° in **5** and 2.3° in **6**, respectively. Thus, the C(1) to C(4) moiety takes the *s-cis* structure in both complexes. The oxametallacycloheptene parts in **5** and **6** are divided into two planar moieties, the plane of diene moiety [C(1) to C(4), including also C(6) in **6**] and the approximate plane defined by C(1), Zr, O, C(5), and C(4) with the maximum atomic deviations from the plane of 0.088 Å in **5** and 0.051 Å in **6**, the dihedral angles being 62.7° in **5** and 61.1° in **6**, respectively. All the methyl groups in 2,4-dimethyl-3-pentanone moieties locate away from the oxametallacycloheptene part to release the possible nonbonded interatomic repulsions in both complexes.

The mean distances between zirconium and carbon atoms of C_5Me_5 ligands are 2.623 Å in **5** and 2.621 Å in **6**, and those between zirconium and the centroids of C_5Me_5 ligands [d_1 and d_2 in Fig. 4] are 2.331 Å in both complexes. These distances are slightly longer than the corresponding distances in $(\eta^5\text{-}C_5H_5)_2ZrCl_2$[18] of 2.522(2) and 2.20 Å or those in $(\eta^5\text{-}C_5H_5)_2Zr(CHPh_2)_2$[16] of 2.513(15) and 2.22 Å. The CCP(1)–Zr–CCP(2) [CCP(1) and CCP(2), which are the centroids of C(21) to C(25) and C(31) to C(35)] angles [θ_1 in Fig. 4], 129.0° in **5** and 129.4° in **6**, are similar to those in $(\eta^5\text{-}C_5H_5)_2Zr(CHPh_2)_2$[19] [128.4°], $(\eta^5\text{-}C_5H_5)_2ZrF_2$[20] [127.8°], and $(\eta^5\text{-}C_5H_5)_2Zr$(2,3-dimethylbutadiene)[3] [124°]. Figure 3 shows that the two C_5Me_5 ligands are in a staggered conformation so as to release the nonbonded repulsion between the methyl groups of facing C_5Me_5 ligands. However, all the methyl groups in C_5Me_5 ligands in **5** and **6** bend back from the zirconium atom with the angular deviations from the C_5 plane [θ_3 or θ_4 in Fig. 4] of 3.7 to 16.1° [av. 10.2°] in CP(1) [ring defined by C(21) to C(25)] and of 7.2 to 15.2° [av. 10.2°] in CP(2) [ring defined by C(31) to C(35)] for **5**, and of 6.1 to 14.6° [av. 9.9°] in CP(1) and of 5.9 to 15.7° [av. 9.6°] in CP(2) for **6**, respectively. Some short contacts are found between these methyl groups, resulting in the large angular deviations from the C_5

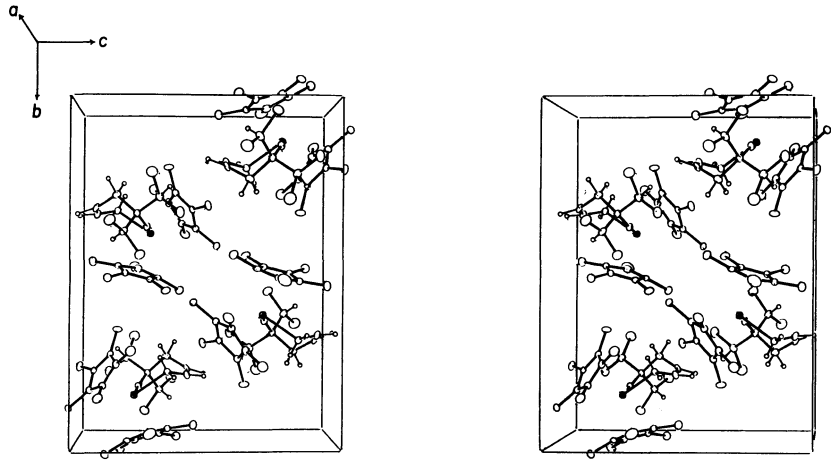

Fig. 5. Stereoscopic view of the crystal structure of **5**.

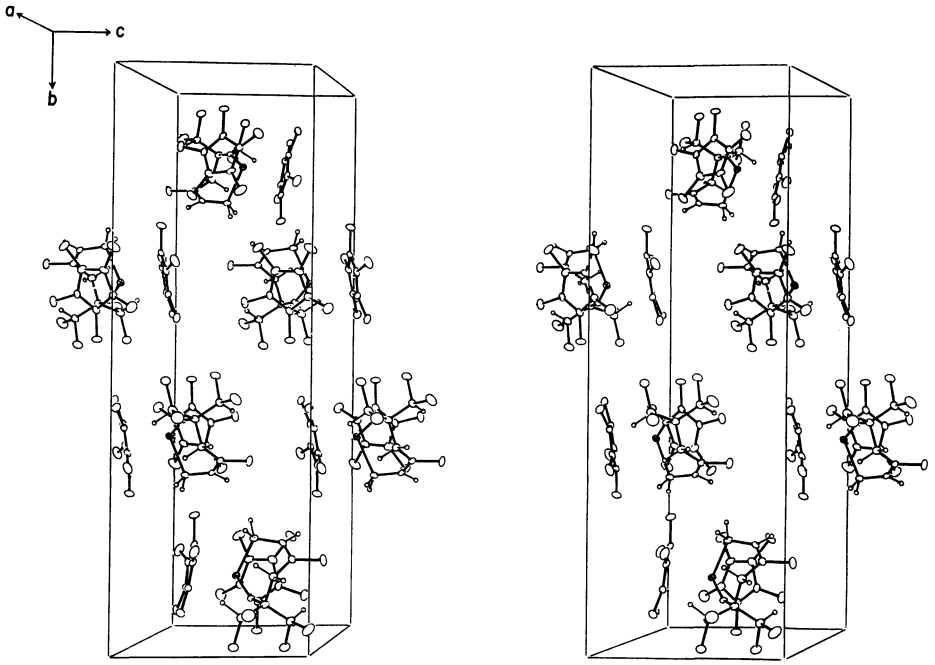

Fig. 6. Stereoscopic view of the crystal structure of **6**.

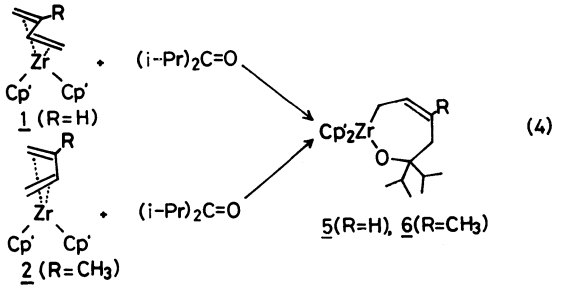

(4)

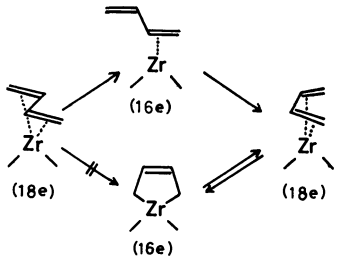

(5)

rings: C(28)···C(38) 3.288(20) Å, θ_3 16.1° [C(28)], θ_4 12.2° [C(38)] in **5**, and 3.329(25) Å, θ_3 14.6° [C(28)], θ_4 8.1° [C(38)] in **6**; C(29)···C(39) 3.344(23) Å, θ_3 9.5° [C(29)], θ_4 15.2° [C(39)] in **5**, and 3.327(28) Å, θ_3 7.3° [C(29)], θ_4 15.7° [C(39)] in **6**. Some short contacts are also found between the methyl groups in the C_5Me_5 ligands and the oxametallacycloheptene part; C(1)··· C(30) 3.262(17) Å in **5** and 3.273(22) Å in **6**; C(9)··· C(26) 3.588(18) Å in **5** and 3.635(23) Å in **6**; and C(12)···C(37) 3.372(20) Å in **5** and 3.374(26) Å in **6**. The shortest nonbonded contact of the methyl group on C(3) in **6** is the C(6)···C(7) of 3.392(22) Å.

The comparison between the molecular structures of **5** and **6** showed that these complexes take essentially the same structure in spite of the different coordination modes of the 1,3-diene in $(\eta^5\text{-}C_5Me_5)_2Zr$(butadiene) and $(\eta^5\text{-}C_5Me_5)_2Zr$(isoprene).

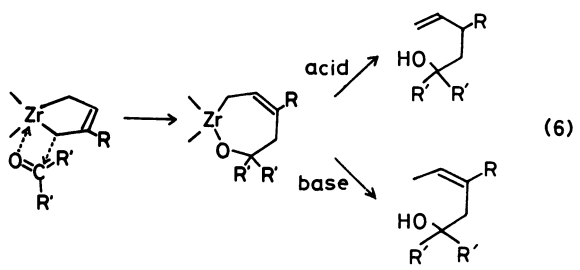

Crystal Structures of ***5*** *and* ***6***. The crystal structures of **5** and **6** are shown in Figs. 5 and 6, respectively. No intermolecular nonbonded contact shorter than 3.5 Å is found between the non-hydrogen atoms in either crystal structure.

Pathways for Regio- and Stereoselective Reaction of Ketones with s-cis *and* s-trans *Zirconium–Diene Complexes*. It is evident from the X-ray work that both the *s-cis*-diene and the *s-trans*-diene complexes gave oxametallacycloheptenes with (*Z*)-structure. Thus, the insertion of ketone caused the conversion of butadiene from *s-trans* to *s-cis* and the retention of isoprene in *s-cis* structure The interconversion occurs presumably *via* 1,2-η^2-diene metal species with 16e configuration and the process *via* 1,4-η^2-diene metal species (16e) can be ruled out (Eq. 5).

Since the Zr-η^4-diene complex has 18e configuration and leaves no vacant coordination site, the insertion of 2,4-dimethyl-3-pentanone may take place after its conversion to zirconacyclopent-3-ene structure with 16e configuration. Direct conversion of η^2-diene species to metallacyclopentene can not be ruled out when a ketone is present in the system. An MO calculation predicts that wedged $(C_5H_5)_2M$ fragment has three in-plane orbitals of d-character.[21] The $2a_1$ and b_2 orbitals are used for forming the zircona ring and the remaining vacant orbital ($1a_1$) may be used for the coordination of the ketone. Therefore, a zircona ring coordinated through oxygen atom of carbonyl group may be postulated as the intermediate. Insertion of ketone will then take place *via* four-centered transition state (Eq. 6). Hydrolysis of **6** with protic acid (aq HCl) gave 2,5-dimethyl-3-isopropyl-6-hepten-3-ol but hydrolysis with bases such as aq NaOH and Et_2NH gave (*Z*)-2,5-dimethyl-3-isopropyl-5-hepten-3-ol quantatively, in line with the X-ray structure. The high regioselectivity observed in the formation of **6** is explained by the inductive effect of the methyl group of isoprene, which causes the higher negative charge on the C_1 atom.

Other ketones, such as 2-propanone or 3-pentanone, and aldehydes such as ethanal or propanal, also react with **1**—**4** in the same fashion (these will be published in a separate paper). Therefore, the present reaction mechanism seems applicable in general for these reactions.

Support of this study by Grant-in-Aid for Scientific Research (No. 57550500) and Special Project Research (No. 57218014) from the Ministry of Education, Science and Culture, is acknowledged.

References

1) H. Yasuda, Y. Kajihara, K. Mashima, K. Nagasuna, and A. Nakamura, *Chem. Lett.*, **1981**, 671.
2) M. Akita, H. Yasuda, and A. Nakamura, *Chem. Lett.*, **1983**, 217.
3) G. Erker, J. Wicher, K. Engel, F. Rosenfeldt, W. Dietrich, and C. Krüger, *J. Am. Chem. Soc.*, **102**, 6346 (1980).
4) G. Erker, J. Wicher, K. Engel, and C. Krüger, *Chem. Ber.*, **115**, 3300 (1982).
5) a) H. Yasuda, Y. Kajihara, K. Mashima, K. Nagasuna, K. Lee, and A. Nakamura, *Organometallics*, **1**, 388 (1982); b) *ibid.*, **2**, 478 (1983); c) H. Yasuda, Y. Kajihara, K. Mashima, K. Lee, and A. Nakamura, *Chem. Lett.*, **1981**, 519.
6) J. M. Manriquez, D. R. McAlister, E. Rosenberg, A. M. Shiller, K. L. Silliamson, S. I. Chan, and J. E. Bercaw, *J. Am. Chem. Soc.*, **100**, 3087 (1978).
7) a) H. Fujita, Y. Ohnuma, H. Yasuda, and H. Tani, *J. Organomet. Chem.*, **113**, 201 (1976); b) H. Yasuda, Y. Nakano, K. Natsukawa, and H. Tani, *Macromolecules*, **11**, 589 (1978).
8) T. Ashida, *HBLS*-V, "The Universal Crystallographic Computing System-Osaka," 2nd ed, The Computation Center, Osaka Univ. (1979), pp. 53—59.
9) "International Tables for X-Ray Crystallography," Kynoch Press, Birmingham (1974), Vol. IV, p. 71.
10) W. C. Hamilton, *Acta Crystallogr.*, **12**, 609 (1959).
11) Y. Kai, N. Kanehisa, K. Miki, N. Kasai, K. Mashima, K. Nagasuna, H. Yasuda, and A. Nakamura, *J. Chem. Soc., Chem. Commun.*, **1982**, 191.
12) R. Benn and G. Schroth, *J. Organomet. Chem.*, **228**, 71 (1982).
13) M. D. Newton, T. M. Shulmann, and M. M. Manus, *J. Am. Chem. Soc.*, **96**, 17 (1974).
14) C. K. Johnson, *ORTEP*-II, Report ORNL-5138, Oak Ridge National Laboratory, Tennessee (1974).
15) J. L. Atwood, W. E. Hunter, D. C. Hrncir, E. Samuel, H. Alt, and M. D. Rausch, *Inorg. Chem.*, **14**, 1757 (1975).
16) J. Jeffery, M. F. Lappert, and N. T. Luong-Thi, *J. Chem. Soc., Chem. Commun.*, **1978**, 1081.
17) "International Tables for X-Ray Crystallography," Kynoch Press, Birmingham (1968), Vol. III, p. 276.
18) I. A. Ronova, N. V. Alekseev, N. I. Gapotcheko, and Yu. T. Struchkov, *J. Organomet. Chem.*, **25**, 149 (1970); A. Clearfield and I. Bernal, personal communication cited in Ref. 15.
19) J. L. Atwood, G. K. Barker, J. Holton, W. E. Hunter, M. F. Lappert, and R. Pearce, *J. Am. Chem. Soc.*, **99**, 6645 (1977).
20) M. A. Bush and G. A. Sim, *J. Chem. Soc., Sect. A*, **1971**, 2225.
21) J. W. Lauher and R. Hoffmann, *J. Am. Chem. Soc.*, **98**, 1729 (1976).
22) a) K. Bachmann and W. von Philipsborn, *Org. Magn. Res.*, **8**, 648 (1976); b) B. E. Mann and B. F. Taylor, "^{13}C NMR Data for Organometallic Compounds," Academic Press, New York (1981).

 © 1983 The Chemical Society of Japan Bull. Chem. Soc. Jpn., 56, 3744—3747 (1983)

Racemization of Optically Active Amino Acid Salts and an Approach to Asymmetric Transformation of DL-Amino Acids

Chikara HONGO,* Ryuzo YOSHIOKA, Masanori TOHYAMA, Shigeki YAMADA,† and Ichiro CHIBATA††

Research Laboratory of Applied Biochemistry, Tanabe Seiyaku Co., Ltd., 16-89, Kashima-3-chome, Yodogawa-ku, Osaka 532

(Received June 13, 1983)

In connection with optical resolution of DL-amino acids, the racemization process of optically active amino acid salts was studied. A wide variety of salts of optically active amino acids with sulfonic acids or mineral acids could be racemized by heating in a medium of acetic acid at 80—100 °C for 1 h in the presence of 0.1 molar equivalents of an aldehyde and free DL-amino acid. From the reaction mixture, the racemized DL-amino acid salts were recovered in high yield (86—92%) and in high purity. An asymmetric transformation between two enantiomers of amino acid salt was attempted by the combination of preferential crystallization of the desired enantiomer and racemization of the antipode in the liquid phase. DL-Alanine *p*-chlorobenzenesulfonate was partially converted to L-isomer (yield 16%, optically purity 97%). Another approach was carried out by transformation between two diastereoisomeric salts. The combination of selective precipitation of less soluble diastereoisomeric salt and epimerization of soluble diastereoisomeric salt allowed DL-phenylglycine *d*-camphor-10-sulfonate to be partially converted to D-phenylglycine *d*-camphor-10-sulfonate (yield 68%, optical purity 96%).

Because of our interest in practical production of optically active amino acids, we have been studying the optical resolution of DL-amino acids and the racemization of the unwanted enantiomer obtained by the optical resolution process. A previous paper[1] proposed a new and facile method: Racemizing optically active amino acids in acetic acid solution in the presence of an aldehyde.

Now we extend this racemization method to the salts of optically active amino acids. The optical resolution is usually carried out in the form of salts of amino acids and the unwanted enantiomers are also obtained in the form of salts. For instance, chemical resolution is achieved by the formation of the diastereoisomeric salts, and preferential crystallization procedure can be applied to many amino acids by converting them to suitable salts such as DL-alanine *p*-chlorobenzenesulfonate,[2] DL-serine *m*-xylene-4-sulfonate,[2] DL-tryptophan *p*-phenolsulfonate,[3] DL-6-chlorotryptophan methanesulfonate,[3] and DL-*p*-hydroxyphenylglycine *o*-toluenesulfonate,[4] *etc.* If the racemization of the unwanted enantiomers can be easily accomplished in the form of the salts, the racemized DL-amino acid salts themselves can be advantageously reused as the starting material for the optical resolution. However, the racemization of the salts of amino acids is generally more difficult than that of free amino acids, although only a few salts[2,4] of optically active amino acids could be racemized by heating in water at a much higher temperature under high pressure. In this work, we could find a practical method for the racemization of various amino acid salts.

We attempted to apply this racemization method to an asymmetric transformation[5] of DL-amino acid salts by a simultaneous combination of the optical resolution and the racemization. The present paper describes the racemization of the salts of various amino acids and an approach to an asymmetric transformation of DL-phenylglycine and DL-alanine by using the present racemization method.

When the salts of L-amino acids were heated at 100 °C for 1 h in a medium of acetic acid in a manner similar to the racemization of free amino acids which is described in the previous report,[1] we found that the racemization of various amino acid salts was also accelerated by the addition of 0.1 molar equivalent of salicylaldehyde, but the rate of racemization was smaller than that in the case of free amino acids. When 0.1 molar equivalent

Table 1. Racemization of various amino acid salts[a]

Amino acid salt[b]	Racemization degree/%[c] in the presence of		
	None	SA[d]	SA[d] and DL-Amino acid
L-Alanine·HCl	3	55	100
L-Alanine·BS	0	13	88
L-Leucine·BS	0	7	64
L-Lysine·ABS[e]	0	59	59
L-Methionine·HCl	0	41	100
L-Phenylalanine·HCl[e]	14	59	100
L-Phenylalanine·pXS	0	19	100
L-Proline·BZ	15	28	32
L-Serine·mXS[f]	0	5	65
L-Valine·HCl	0	0	20

a) The reactions were carried out in acetic acid at 100 °C for 1 h. The amounts of salicylaldehyde and DL-amino acid used were 0.1 molar equivallents. b) BS, Benzenesulfonate; ABS, *p*-aminobenzenesulfonate; pXS, *p*-xylene-2-sulfonate; BZ, benzoate; mXS, *m*-xylene-4-sulfonate. c) $\frac{\text{Initial optical rotation} - \text{final optical rotation}}{\text{initial optical rotation}} \times 100$. d) SA, Salicylaldehyde. e) The reactions were carried out in a solid-liquid heterogeneous state. f) The reaction was carried out at 80 °C.

† Present address: Research Planning & Investigation Division, Tanabe Seiyaku Co., Ltd., 16-89, Kashima-3-chome, Yodogawa-ku, Osaka 532.

†† Present address: Research & Development Headquarters, Tanabe Seiyaku Co., Ltd., 16-89, Kashima-3-chome, Yodogawa-ku, Osaka 532.

Table 2. Effect of kind of aldehyde in racemization reaction[a)]

Aldehyde	Racemization degree/%			
	L-Alanine·BS		L-Methionine·HCl	
	With aldehyde	With aldehyde and DL-alanine	With aldehyde	With aldehyde and DL-methionine
None	0	0	0	5
Formaldehyde	14	46[b)]	20[c)]	42[b,c)]
Propionaldehyde	0	40[b)]	12	44[b)]
Butyraldehyde	0	45	12	49
Heptanal	0	79[b)]	27	73[b)]
Acrylaldehyde	0	48[b)]	16	38[b)]
Benzaldehyde	0	48	10	49
Salicylaldehyde	13	88	41	100
p-Hydroxybenzaldehyde	4	35	9	44
o-Nitrobenzaldehyde	0	39	17	54
5-Nitrosalicylaldehyde	14	76[c)]	42	86[c)]
Furfural	23	91[b)]	74	100[b,c)]

a) The reactions were carried out at 100 °C for 1 h in acetic acid. The amounts of aldehyde and DL-amino acid used were 0.1 molar equivalents. b) A 0.2 molar equivalent of DL-amino acid was used. c) A ninhydrin positive spot of degradation product was detected by TLC of the reaction mixture.

of free DL-amino acid corresponding to the L-amino acid moiety of the salt was added into the reaction system together with salicylaldehyde, the racemization of the amino acid salts was found to be greatly accelerated. These results are shown in Table 1. The content of amino acid in the reaction mixtures was confirmed to be almost 100% without significant decomposition. The racemization mechanism of amino acid salts seems to be the same as that of free amino acids. Namely, a part of amino acid moiety of optically active amino acid salt leads to the free state by adding free DL-amino acid and the free optically active amino acid is racemized by an imine formation from the amino acid and aldehyde, as described in our previous report. In the case of L-lysine *p*-aminobenzenesulfonate, the racemization was accelerated by only the addition of salicylaldehyde and the addition of free DL-amino acid was not effective. This seems to be because the α-amino group in lysine *p*-aminobenzenesulfonate exists already in the free state (uncharged form) predominantly without the addition of free amino acid. The effect of the kind of aldehyde on the racemization of L-alanine benzenesulfonate and L-methionine hydrochloride was examined at 100 °C for 1 h in glacial acetic acid. The results are shown in Table 2. Various aldehydes, such as aliphatic or aromatic aldehydes, accelerated the racemization of amino acid salts under the coexistence of free DL-amino acid. The effect of the amount of salicylaldehyde on the racemization of L-alanine benzenesulfonate and L-methionine hydrochloride was examined at 100 °C for 1 h under the coexistence of 0.2 molar equivalent of DL-alanine or DL-methionine in glacial acetic acid. The effect of the amount of free DL-leucine on the racemization of L-leucine benzenesulfonate was examined at 100 °C for 30 min or 3 h in the presence of 0.1 molar equivalent of salicylaldehyde in glacial acetic acid. The results are shown in Tables 3 and 4. Salicylaldehyde and free DL-leucine exerted their effects in the use of 0.001 molar equivalent and gave a sufficient racemization degree in the use of 0.05 molar equivalent.

Table 3. Effect of amount of salicylaldehyde[a)]

Molar equivalent of salicylaldehyde	Racemization degree/%	
	L-Alanine·BS	L-Methionine·HCl
0	0	9
0.001	13	15
0.005	48	53
0.01	70	71
0.05	100	100
0.1	100	100

a) The reactions were carried out in the presence of 0.2 molar equivalent of DL-amino acid at 100 °C for 1 h.

Table 4. Effect of amount of DL-leucine on the racemization of L-leucine benzenesulfonate[a)]

Molar equivalent of DL-leucine	Racemization degree/%	
	30 min	3 h
0	2	27
0.001	4	34
0.005	6	43
0.01	8	47
0.05	24	85
0.1	40	100
0.2	61	100

a) The reactions were carried out in the presence of 0.1 molar equivalent of salicylaldehyde at 100 °C.

As a practical example, L-alanine benzenesulfonate, L-alanine *p*-toluenesulfonate, L-leucine benzenesulfonate, L-methionine *p*-chlorobenzenesulfonate, and L-*p*-hydroxyphenylglycine *o*-toluenesulfonate were racemized by the present method, and the respective racemic amino acid salts were directly separated from the reaction mixtures and analyzed. The results are shown in Table 5. The racemized DL-amino acid salts were

TABLE 5. SEPARATION OF RACEMIZED AMINO ACID SALTS[a]

Amino acid salt[b]	Composition[c]			Separated salt[f]			
	AcOH (ml)	SA[d] (g)	DL-Amino[e] acid (g)	Yield /g	Yield /%[g]	$[\alpha]_D^{25}$/° (c=1, water)	Content of DL-form %
Alanine·BS	6	0.15	0.11	2.95	89.4	0	100
Alanine·pTS	6	0.14	0.10	3.05	92.4	0	100
Leucine·BS	6	0.13	0.14	2.85	86.4	0	100
Methionine·pCBS	6	0.11	0.13	3.00	90.9	0	100
p-Hydroxyphenylglycine·oTS	50[h]	0.22[i]	0.59[j]	3.66	87.9	0	100

a) The reactions were carried out at 100 °C for 2 h. b) BS, Benzenesulfonate; pTS, *p*-toluenesulfonate; pCBS, *p*-chlorobenzenesulfonate; oTS, *o*-toluenesulfonate. c) A 3 g amount of L-amino acid salt was used throughout. d) SA, Salicylaldehyde. e) Free DL-amino acid corresponding to L-amino acid moiety of the salt. f) No impurity was detected by TLC. g) Based on L-amino acid salt plus coexisting DL-amino acid. h) AcOH/water: 95/5(v/v). i) A 0.2 molar equivalent of SA was used. j) A 0.4 molar equivalent of DL-*p*-hydroxyphenylglycine was used.

obtained in high yield (86—92%) and in such high purity that no by-product was detected by thin-layer chromatography. The racemization method presented here seems to be a simple and practical way.

Ordinarily, the optical resolution of DL-amino acids is carried out under the conditions in which the amino acid is optically stable. On the contrary, we carried out the optical resolution of DL-amino acid under the racemization conditions described above in order to achieve an asymmetric transformation by a combination of optical resolution and simultaneous racemization (or epimerization). This type of asymmetric transformation is interesting because of its practical applications.[6-13]

An asymmetric transformation was carried out between two enantiomers by a combination of preferential crystallization and racemization. DL-Alanine can be resolved by preferential crystallization procedure in the form of *p*-chlorobenzenesulfonate.[2] This resolution method was combined with the present racemization method. Namely, a supersaturated solution consisting of DL-alanine *p*-chlorobenzenesulfonate (45.0 g), DL-alanine (2.0 g), salicylaldehyde (1.0 g), and glacial acetic acid (50 ml) was seeded with the crystals of L-alanine *p*-chlorobenzenesulfonate (0.5 g) and was gently stirred at 100 °C for 90 min. The precipitated crystals were quickly collected to give L-alanine *p*-chlorobenzenesulfonate (8.0 g), optical purity 97%, yield 16.7% (based on starting DL-salt). The mother liquor did not show any optical rotation. The results show that the preferential crystallization of L-alanine *p*-chlorobenzenesulfonate and the racemization of unseeded D-alanine *p*-chlorobenzenesulfonate took place at the same time, and that 7.3 g of L-alanine *p*-chlorobenzenesulfonate was transformed from DL-alanine *p*-chlorobenzenesulfonate existing as a supersaturation state.

Another approach was carried out by transformation between two diastereoisomeric salts. It is known that DL-phenylglycine can be chemically resolved by *d*-camphor-10-sulfonic acid as a resolving agent.[14] This resolution method was combined with the present racemization method. Namely, a mixture of DL-phenylglycine (15.1 g), *d*-camphor-10-sulfonic acid (22.1 g) and salicylaldehyde (0.24 g) was stirred in glacial acetic acid (70 ml) at 80 °C for 4 h. The precipitated crystals were collected to give D-phenylglycine *d*-camphor-10-sulfonate (26.1 g), optical purity 95.9%, yield 68.1% (based on DL-phenylglycine). The result shows that the selective precipitation of the less soluble D-phenylglycine *d*-camphor-10-sulfonate and the epimerization of the soluble L-phenylglycine *d*-camphor-10-sulfonate took place at the same time.

The proposed racemization method and asymmetric transformation of amino acids seem to be very promising for industrial applications. The asymmetric transformation is under investigation.

Experimental

Materials and Analyses. Analytical standard grade amino acids manufactured by our company, Tanabe Seiyaku Co., Ltd., were used. All aldehydes and other chemicals were obtained from Tokyo Kasei Kogyo Co., Ltd. The salts of L-amino acids were prepared as described in previous reports.[2-4] Optical rotations were measured with a Perkin-Elmer 141 automatic polarimeter. Decomposition of amino acids was checked by thin-layer chromatography (solvent system: 1-butanol–acetic acid–water, 4: 1: 1, vol/vol/vol; plate: Merck's precoated Kieselgel $60F_{254}$). An accurate quantitative determination of amino acids was made by a Hitachi KLA-3B amino acid analyzer (resin, Hitachi Custom Resin; eluting buffer, citrate buffer [pH 3.25]; column temperature, 55 °C).

Procedure of Racemization. Unless otherwise noted, the racemization was carried out as follows. A mixture of L-amino acid salt (0.1 g), 0.1 molar equivalent of aldehyde (3—8 μl), 0.1 molar equivalent of DL-amino acid (3—8 mg) corresponding to the L-amino acid moiety of the salt, and glacial acetic acid (3.0 ml) was heated in a sealed tube at 100 °C for 1 h and was shaken occasionally. The conditions were varied according to each experimental design. After the reaction, the reaction mixture was diluted with 1 M hydrochloric acid (5 ml). Optical rotation of the solution was measured. The racemization degree was calculated as follows:

$$\frac{\text{Initial optical rotation} - \text{final optical rotation}}{\text{initial optical rotation}} \times 100.$$

The reaction mixtures were checked by thin-layer chromatography or amino acid analyzer in order to determine whether or not the simultaneous decomposition of amino acid had occurred.

Preparation of DL-Amino Acid Salts by Racemization. A mixture of L-amino acid salt (3.0 g), 0.1 molar equivalent of salicylaldehyde (0.11 to 0.22 g, 0.2 molar equivalent for L-*p*-

hydroxyphenylglycine *o*-toluenesulfonate), 0.1 molar equivalent of free DL-amino acid (0.10 to 0.59 g, 0.4 molar equivalent for L-*p*-hydroxyphenylglycine *o*-toluenesulfonate) corresponding to the L-amino acid moiety of the salt, and acetic acid (6 ml, 50 ml for L-*p*-hydroxyphenylglycine *o*-toluenesulfonate) was stirred at 100 °C for 2 h. After the reaction, 0.1 molar equivalent of sulfonic acid or hydrochloric acid corresponding to the acid moiety of the salt was added in the reaction mixture in order to recover the free DL-amino acid existing in the reaction mixture as the corresponding amino acid salt. Then the reaction mixture was concentrated to dryness. The residual crystals were suspended in acetone (5—15 ml). The precipitated crystals were collected, washed with acetone, and air-dried at 55 °C. The L-amino acid salts used were L-alanine benzenesulfonate, L-alanine *p*-toluenesulfonate, L-leucine benzenesulfonate, L-methionine *p*-chlorobenzenesulfonate, and L-*p*-hydroxyphenylglycine *o*-toluenesulfonate. The yields and the purities of the separated amino acid salts are shown in Table 5.

Asymmetric Transformation of DL-*Alanine.* DL-Alanine *p*-chlorobenzenesulfonate (45.0 g), DL-alanine (2.0 g), and salicylaldehyde (1.0 g) were dissolved in glacial acetic acid (50 ml) at 120 °C. The solution was maintained at 100 °C, was seeded with finely pulverized crystals of L-alanine *p*-chlorobenzenesulfonate (0.5 g), and was gently stirred. During the reaction, the crystal growth of seeded L-isomer was observed. After 90 min, the precipitated crystals were quickly collected by filtration, washed with a small amount of glacial acetic acid, and dried to give L-alanine *p*-chlorobenzenesulfonate (8.0 g), $[\alpha]_D^{25}$ +3.5° (*c*=2, water), optical purity 97%, yield 16.7% (based on starting DL-salt). After the separation of the first crop, the second crop was crystallized by adding water (15 ml) and by stirring at room temperature and was collected by filtration to give DL-alanine *p*-chlorobenzenesulfonate (12.2 g), $[\alpha]_D^{25}$ 0.0° (*c*=2, water). The mother liquor did not show any optical rotation. Therefore, we subtract 0.5 g of seeded L-isomer from the net weight of L-isomer obtained above, and find that 7.3 g of L-alanine *p*-chlorobenzenesulfonate was transformed from DL-alanine *p*-chlorobenzenesulfonate existing as a supersaturation state.

Asymmetric Transformation of DL-*Phenylglycine.* DL-Phenylglycine (15.1 g, 100 mmol), *d*-camphor-10-sulfonic acid (22.1 g, 95 mmol), and salicylaldehyde (0.24 g, 2 mmol) were added into glacial acetic acid (70 ml). The mixture was stirred at 80 °C for 4 h. The reaction system was heterogeneous during the reaction. To the reaction mixture, *d*-camphor-10-sulfonic acid (1.1 g, 5 mmol) was added and the mixture was stirred at 20 °C for 2 h. The precipitated crystals were collected by filtration and dried to give D-phenylglycine *d*-camphor-10-sulfonate (26.1 g), $[\alpha]_D^{25}$ −47.1° (*c*=2, *N*-HCl), optical purity 95.9% (based on D-*d* salt $[\alpha]_D^{25}$ −49.7° (*c*=2, *N*-HCl) and DL-*d* salt $[\alpha]_D^{25}$ +13.6° (*c*=2, *N*-HCl)), yield 68.1% (136.2% based on D-form contained in DL-phenylglycine *d*-camphor-10-sulfonate).

D-Phenylglycine *d*-camphor-10-sulfonate (25.0 g) obtained above was recrystallized from water (120 ml) containing *d*-camphor-10-sulfonic acid (0.5 g) to give optically pure D-phenylglycine *d*-camphor-10-sulfonate (18.5 g), $[\alpha]_D^{25}$ −49.7° (*c*=2, *N*-HCl). The pure salt (18.0 g) was dissolved in water (70 ml) at an elevated temperature. The solution was adjusted to pH 6 with 10 M sodium hydroxide and allowed to stand in a refrigerator overnight. The precipitated crystals were collected, washed with water, and dried to give D-phenylglycine (6.6 g), $[\alpha]_D^{25}$ −168.5° (*c*=1, 5*N*-HCl).

References

1) S. Yamada, C. Hongo, R. Yoshioka, and I. Chibata, *J. Org. Chem.*, **48**, 843 (1983).
2) S. Yamada, M. Yamamoto, and I. Chibata, *J. Org. Chem.*, **38**, 4408 (1973).
3) S. Yamada, M. Yamamoto, C. Hongo, and I. Chibata, *J. Agric. Food Chem.*, **23**, 653 (1975).
4) S. Yamada, C. Hongo, and I. Chibata, *Agric. Biol. Chem.*, **42**, 1521 (1978).
5) M. M. Harris, "Progress in Stereochemistry," ed by W. Klyne and P. B. D. Mare, Butterworths Scientific Publications, London (1958), Vol. 2, p. 157.
6) J. C. Clark, G. H. Phillipps, M. R. Steer, L. Stephenson, and A. R. Cooksey, *J. Chem. Soc., Perkin Trans. 1*, **1976**, 471.
7) J. C. Clark, G. H. Phillipps, and M. R. Steer, *J. Chem. Soc., Perkin Trans. 1*, **1976**, 475.
8) W. J. Boyle, Jr., S. Sifniades, and J. F. Van Peppen, *J. Org. Chem.*, **44**, 4841 (1979).
9) S. Shibata, H. Matsushita, K. Kato, M. Noguchi, M. Saburi, and S. Yoshikawa, *Bull. Chem. Soc. Jpn.*, **52**, 2938 (1979).
10) K. Suzuki, S. Kiyooka, T. Miyagawa, and A. Kawai, *Nippon Kagaku Kaishi*, **1980**, 287.
11) S. Yamada, C. Hongo, and I. Chibata, *Chem. Ind. (London)*, **1980**, 539.
12) C. Hongo, S. Yamada, and I. Chibata, *Bull. Chem. Soc. Jpn.*, **54**, 3286 (1981).
13) C. Hongo, S. Yamada, and I. Chibata, *Bull. Chem. Soc. Jpn.*, **54**, 3291 (1981).
14) A. W. Ingesoll, *J. Am. Chem. Soc.*, **47**, 1168 (1925).

Chemiluminescences in the Carbon Monoxide-Active Nitrogen System

Nobuaki WASHIDA, Hiroshi BANDOW, and Gen INOUE

Division of Atmospheric Environment, The National Institute for Environmental Studies, P. O. Tsukuba-gakuen, Ibaraki 305

(Received June 24, 1983)

Chemiluminescences produced in the reaction of CO with active nitrogen were measured in the region from infrared to vacuum ultraviolet. The infrared emission from vibrationally excited CO was measured by means of a FTIR spectrometer. A vibrationally excited CO up to $v''=18$ was observed. The quenching and relaxation of vibrationally excited CO were measured by the addition of other gasses. The formation of carbon atoms was observed by the absorption of carbon resonance lines, and the recombination reaction of $C+N+M\longrightarrow CN^*+M$ is proposed as the mechanism of the violet and red emission of CN. The reaction of $CO^*(a^3\Pi)+CO^*\longrightarrow C+CO_2$ is proposed as the carbon-atom source. The emission of the fourth positive band of CO was observed in the vacuum UV region. The effect of self-absorption by the vibrationally excited CO was reduced by the addition of CO_2. It is suggested that the apparent abnormal vibrational distribution in $CO(A^1\Pi)$ can be reduced by considering the effect of the quenching of $CO(A^1\Pi)$.

The reactions of active nitrogen with other gases are well known[1-4] to produce a variety of chemiluminescences and are widely used in studies of both the spectroscopy of molecules and chemical reactions. Over 1500 papers related to active nitrogen reactions have been published. Suggested active species in the active nitrogen have included N atoms (usually $N(^4S)$, the ground state, and in some special cases excited states, such as $N(^2D)$ and $N(^2P)$), metastable excited states of N_2, such as $N_2(A^3\Sigma_u^+)$ and $N_2(A^1\Pi_g)$, and the vibrationally excited ground state of N_2. One well-known CN radical chemiluminescent reaction in the active nitrogen-hydrocarbon system is the case of the reaction initiated by the N-atom attack on hydrocarbon.[2,4] On the other hand, the chemiluminescent reaction in the active nitrogen-CO system is the case of energy transfer from electronically excited N_2 to CO, because the bond-dissociation energy of CO is very large (11.09 eV) and CO cannot be decomposed by a direct reaction with N atoms.

In the case of the active nitrogen-CO system, the chemiluminescences reported are infrared emission from the vibrationally excited CO,[5,6] visible emission from CN radicals in both $A^2\Pi$ and $B^2\Sigma^+$ states,[7] and the fourth positive band emission from $CO(A^1\Pi)$[8-10] in the vacuum UV region. Studies of the mechanism of these emission bands are interesting because these emissions are produced by energy transfer in various electronic states of N_2 and CO. In the present study, emissions produced in the active nitrogen-CO system are measured by using the same flow reactor in order to study the correlation of each emission band. Several new results concerning the formation mechanism of chemiluminescences will be reported.

Experimental

The discharge flow-system used is illustrated in Fig. 1. The cylindrical Pyrex flow tube is 21.2 mm i.d., 500 mm in length, and sealed off at one end by a lithium fluoride window. The length of reaction zone can be varied by sliding the inlet tube (6 mm o.d.) in an O-ring seal. CO gas enters the main flow through four radially directed holes at the end of the inlet tube. Active nitrogen is generated by flowing nitrogen or a nitrogen-argon mixture at rates between 8 and 9 m s^{-1} and at pressures between 2 and 6 Torr (1 Torr≈133.322 Pa) through a microwave discharge (2450 MHz). The N-atom densities are measured by the well-known NO-titration technique. Quenching gases, such as CO_2 and N_2O, are added from three inlet

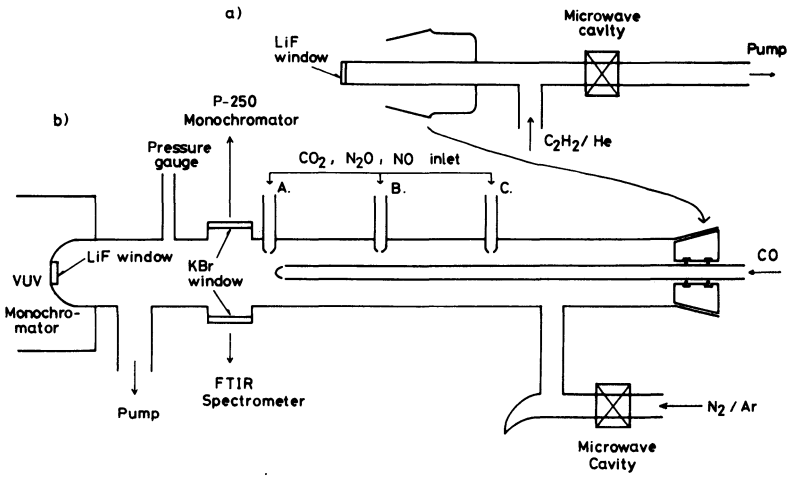

Fig. 1. Schematic diagram of experimental setup.
a) Carbon lamp. b) Discharge flow reactor.

ports, A, B, and C. The interval of each inlet port is 50 mm. In most cases, the C inlet port is used. The infrared emission spectra are measured side-on by means of a Nicolet 7199 FTIR spectrometer through a KBr window. The detector used was a liquid nitrogen cooled Hg–Cd–Te detector, which is sensitive from 800 to 4000 cm^{-1}. In the present study, in order to cut the strong thermal emission appearing below 1500 cm^{-1}, a sapphire filter (transmitting above 1600 cm^{-1}) was set in front of the detector. Therefore, the emission spectra from 1600 to 4000 cm^{-1} could be detected. The visible emission spectra were measured on another side by means of a 0.25 m monochromator (Nikon P-250, 1200 grooves/mm grating blazed at 300 nm) equipped with a photomultiplier (Hamamatsu R-636), a photon-rate meter, and a strip chart recorder. The vacuum UV emission spectra were measured at the end of the flow tube through a LiF window by means of a 0.3 m vacuum-ultraviolet monochromator (McPherson model 218) with a grating blazed at 150 nm (2400 grooves/mm), combined with a solar-blind photomultiplier (Hamamatsu R-976, MgF_2 window), which is sensitive from 115 to 320 nm.

The carbon atoms produced in the reaction of active nitrogen with CO were monitored photoelectrically through the axis of the flow tube by means of the attenuation of the carbon-atom resonance lines at 156.1 or 165.7 nm. A carbon-resonance lamp was attached at the other end of the flow tube in place of the movable inlet. In this case, CO was added from the side inlet port, B. A microwave-powered carbon-resonance lamp using a mixture of a few percent of acetylene in flowing helium was used.[11,12]

The spectral sensitivity of the P-250 monochromator with associated photomultiplier was determined by using a calibrated tungsten lamp. The wavelength calibration of the relative sensitivity of the VUV monochromator detecting system was achieved by measuring the intensities of the Lyman bands emitted from a discharge in argon with a trace amounts of H_2O.[13] The total and partial pressures of the gases were measured with an MKS Baratron gauge. All the measurements were done at room temperature, 298±3 K.

The gases, used without further purification, were N_2 (Nippon Sanso, 99.9995%), Ar (Nippon Sanso, 99.9995%), CO_2 (Nippon Sanso, 99.5%), N_2O (Takachiho, 99.9%), and NO (Matheson, 99.5%). The CO (Takachiho, 99.95%) was used after passing it through a hot quartz tube (800 °C) and a column packed with Molecular Sieve in order to remove any metal carbonyls.

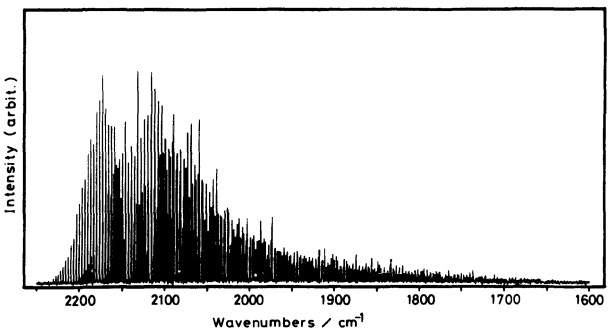

Fig. 2. High resolution (spectral resolution 0.25 cm^{-1}) infrared emission spectrum of vibrationally excited CO in the fundamental region. The spectrum was observed in the reaction of active nitrogen (microwave discharge of N_2, 2 Torr, and Ar, 2 Torr, mixture) with CO, 70 mTorr.

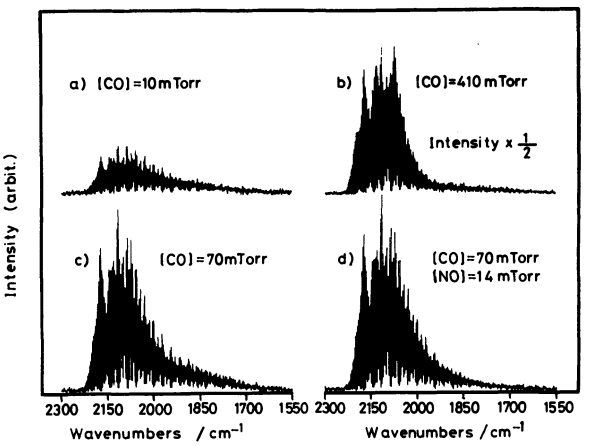

Fig. 3. Changes of the spectral distribution of the infrared emission of vibrationally excited CO by pressures of CO and the addition of NO. Active nitrogen was produced in the microwave discharge of N_2 (2 Torr) and Ar (2 Torr) mixture ([N]=4.2 mTorr). Spectral resolution is 1 cm^{-1}. a) 10 mTorr of CO was added. b) 410 mTorr of CO was added. Spectral intensity should be doubled. c) 70 mTorr of CO added. d) 14 mTorr of NO was added in addition to 70 mTorr of CO.

Results

A. Infrared Emission from the Vibrationally Excited CO. The high-resolution (spectral resolution 0.25 cm^{-1}) infrared emission spectrum of the vibrationally excited CO in the fundamental region is shown in Fig. 2. The spectrum was measured after 70 mTorr of CO had been added to the active nitrogen flow (4.2 Torr of total pressure) at a point 100 mm upstream from the observing point. Emissions from the vibrationally excited CO up to $v''=18$ could be observed.

The effects of the vibrational relaxation by CO and NO were also measured; they are shown in Fig. 3. Figures 3 (a) and (b) show the emission spectra when 10 and 410 mTorr, respectively, of CO were added to the active nitrogen flow. In these cases, the spectral resolution was 1 cm^{-1}. It should be clear that vibrational relaxations occur efficiently at high v'' levels. Figures 3(c) and (d) show the spectra in, respectively, the absence and presence of NO (14 mTorr) in the CO (70 mTorr)-active nitrogen flow. Relaxations can be observed very slightly in the high v'' levels. In these cases, the concentration of N atoms was 4.2 mTorr; *i.e.*, the color of the afterglow was changed from yellow (N_2 first positive-band emission due to N+N recombination) to green (NO_2 afterglow due to NO+O recombination) at the point of 4.2 mTorr NO addition. Therefore, vibrationally excited CO was still present even after all the N-atoms had been converted to O-atoms by the reaction of $N+NO \longrightarrow N_2+O$. This suggests that the formation of the vibrationally excited CO does not originate in the N-atom reaction. The integrated emission-band intensity as a function of the CO concentration is shown in Fig. 4 by solid circles. The total emission intensity increased with an increase in the CO concentration until it reaches a saturation point at about 300 mTorr of CO. The integrated-band intensity when NO was added to 70 mTorr of CO is shown by open circles in

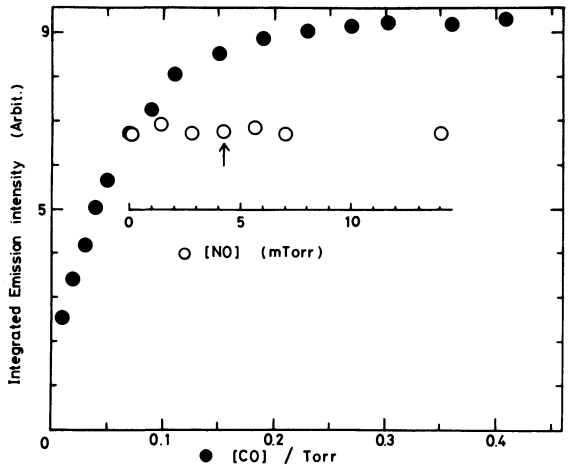

Fig. 4. Integrated intensity of infrared emission of CO as a function of the partial pressure of CO (solid circles). Intensities when NO was added in addition to 70 mTorr of CO are shown by open circles. An arrow indicates the titration point of N atoms. Active nitrogen was produced in the microwave discharge of N_2 (2 Torr) and Ar (2 Torr) mixture ([N]=4.2 mTorr).

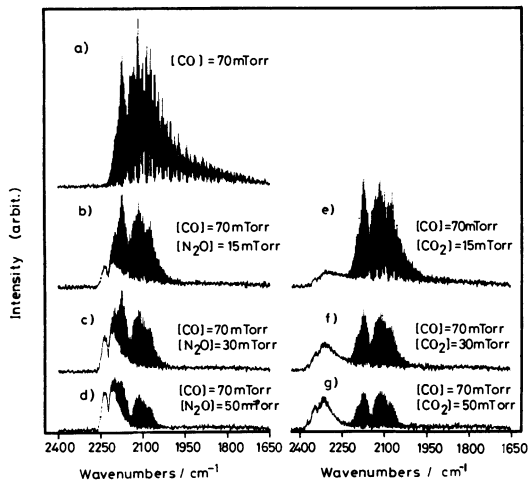

Fig. 5. Relaxation and quenching of the vibrationally excited CO by the addition of N_2O and CO_2. Spectral resolution is 1 cm^{-1}. Emissions appeared in (b)—(d) in the 2250—2100 cm^{-1} region are emissions from the vibrationally excited N_2O. Emissions appeared in (e)—(g) in the 2400—2200 cm^{-1} region are emission from the vibrationally excited CO_2. Active nitrogen was produced in the microwave discharge of N_2 (2 Torr) and Ar (2 Torr) mixture ([N]=4.2 mTorr).

Fig. 4. The total band intensity was not changed by the addition of NO. The arrow in Fig. 4 indicates the titration point of the nitrogen atoms.

The relaxation and quenching of the vibrationally excited CO occurred much more effectively upon the addition of N_2O and CO_2. Variations in the band profiles are shown in Fig. 5. The infrared emission bands of N_2O and CO_2 in the fundamental region appear with a decrease in the CO emission band. Further, highly vibrationally excited CO is quenched much more effectively. In both cases, when more than 150 mTorr of N_2O and CO_2 were added, the emission of CO was

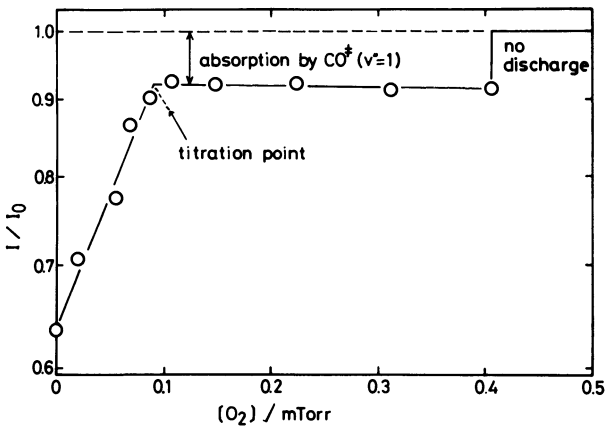

Fig. 6. Relative carbon atom absorption *versus* O_2 partial pressure (scale of ordinate is logarithmic). The 165.7 nm carbon atomic line was used to measure the resonance absorption of carbon atoms when 6 mTorr of CO was reacted with active nitrogen. "NO discharge" is the case when microwave discharge of the N_2 (2 Torr)–Ar (2 Torr) mixture was turned off.

quenched completely, only emissions of N_2O and CO_2 remaining.

B. Visible Emission and Carbon Atoms in the CO–Active Nitrogen Mixture. When CO was added to the straw yellow Lewis–Rayleigh afterglow of active nitrogen, the color changed slightly to deep blue. This chemiluminescence resembles the so-called "blue flame" observed in the reactions of active nitrogen with hydrocarbons[14] or C_2N_2.[15] That is, emissions of CN violet ($B^2\Sigma^+ \longrightarrow X^2\Sigma^+$) and CN red ($A^2\Pi \longrightarrow X^2\Sigma^+$) bands were observed, and strong tail bands appeared in the B→X bands, with a maximum at $v'=7$ and extending up to $v'=15$, just as in the cases of hydrocarbons[14] and C_2N_2.[15]

The existence of carbon atoms was observed by means of the resonance absorption of the carbon resonance lines. As will be described below, the chemiluminescence of the fourth positive band of CO ($A^1\Pi \longrightarrow X^1\Sigma^+$) was observed. The resonance lines of the carbon lamp, 156.1 and 165.7 nm, partially coincide with the 0-2 and 1-1 bands of the fourth positive emission respectively. However, under less than 10 mTorr of CO, the emission intensity of the fourth positive band is quite weak in comparison with that of resonance lines from the carbon lamp. Vibrationally excited CO was produced in the system, as has been mentioned before. The 0-2 and 1-1 bands in the A←X transition of CO absorb the resonance lines from the carbon lamp. In order to obtain the resonance absorption only by carbon atoms, a small amount of O_2 (less than 1 mTorr) was added to the system.[12,16] The carbon atoms in the system were consumed by the reaction of $C+O_2 \rightarrow CO+O$. On the other hand, the vibrationally excited CO was not quenched by less than 1 mTorr of O_2. A typical titration of carbon atoms by O_2 at 165.7 nm is shown in Fig. 6. The absolute steady-state concentrations of carbon atoms (0.02—0.1 mTorr, depending on the CO partial pressure) were determined by means of this O_2 titration method.[12,16] The intensity of the CN violet-band emission was proportional to the carbon-atom

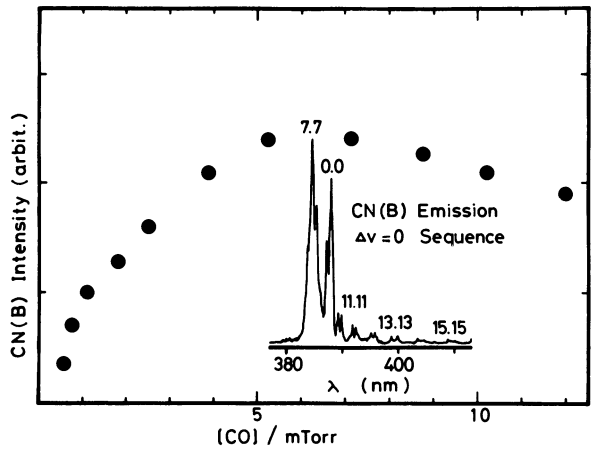

Fig. 7. Intensity of the CN violet emission band of $\Delta v=0$ sequence as a function of the pressure of CO. Spectrum shown is the CN violet emission of $\Delta v=0$ sequence. Concentration of nitrogen is constant ([N] = 4.2 mTorr).

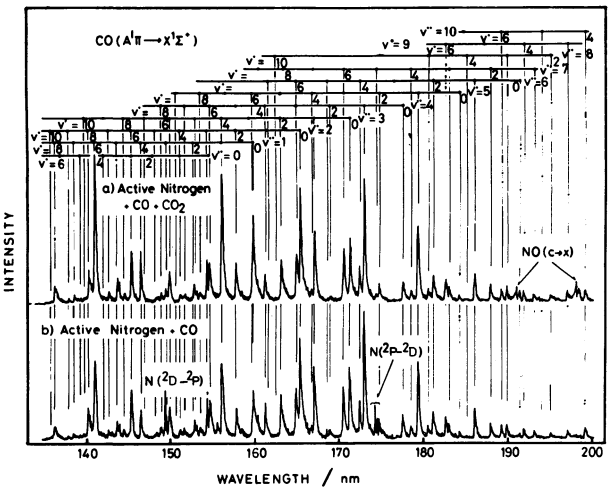

Fig. 8. Fourth positive band emission of CO observed in the reaction of active nitrogen with CO. Spectral resolution is 2 nm. Active nitrogen was produced in the microwave discharge of N_2 (3.5 Torr) and Ar (2.0 Torr) mixture ([N] = 5.7 Torr). a) [CO] = 410 mTorr and [CO_2] = 110 mTorr, b) [CO] = 410 mTorr and CO_2 is absent.

concentration; *i.e.*, the intensity of the violet emission decreased with a decrease in the carbon atoms upon the addition of O_2. These results suggest that the formation mechanism of the CN emission bands is quite similar to that proposed in the case of the "blue-flame conditions" of the active nitrogen–hydrocarbon reactions.[15,16] As will be described later, the formation mechanism of the CN emission bands proposed in the blue-flame condition is the recombination mechanism of C+N+M.

Figure 7 shows the intensity of the CN violet emission band of the $\Delta v=0$ sequence as a function of the partial pressure of CO. The intensity approaches a maximum at about 6 mTorr of CO. At 6 mTorr of CO, the intensity of the first positive-band emission of N_2 was not reduced. Therefore, it is probable that the precursor of the CN violet emission is not a nitrogen atom, but a

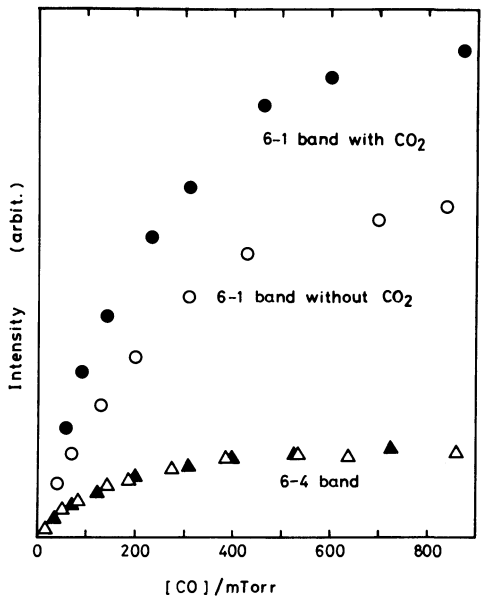

Fig. 9. CO($A^1\Pi \rightarrow X^1\Sigma^+$) intensities *vs.* partial pressure of CO. ●; 6-1 band in the presence of CO_2 (90 mTorr), ○; 6-1 band in the absence of CO_2, △; 6-4 band in the presence of CO_2 (90 mTorr), ▲; 6-4 band in the absence of CO_2. The condition of active nitrogen is as same as the case in Fig. 8.

metastable excited N_2 atom. The dependences of the CN red emission intensity and the concentration of the C atoms on the partial pressure of CO are similar to the case of the CN violet emission (Fig. 7).

C. Vacuum Ultraviolet Emission of CO. The fourth positive-band emission of CO was observed in the vacuum UV region as has been reported by Fontijn *et al.*[9] and by Golde *et al.*[10] The spectra measured are shown in Fig. 8. Figure 8(b) shows the CO($A^1\Pi \longrightarrow X^1\Sigma^+$) emission spectrum observed in the CO–active nitrogen system. Emission bands up to $v'=8$ were observed clearly, as was suggested by Golde *et al.*[10] In addition, very weak bands from $v'=9$ and 10 were observed in the present study. When 100 mTorr of CO_2 was added to the system, the intensities of several bands increased, as is shown in Fig. 8 (a). The increment occurred mostly in the $v''=1$ and 2 sequences. A similar result was obtained when N_2O was added to the system. Those results can be explained by the self-absorption by the vibrationally excited ground-state CO produced in the reaction of active nitrogen with CO. As is shown in Fig. 5, vibrationally excited CO was quenched by the addition of CO_2 and N_2O. The absence of any emission band in the $v''=0$ sequence is a result of the self-absorption by CO in the ground state.

The emission-intensity dependencies of the 6-1 and 6-4 bands on the partial pressure of CO are shown in Fig. 9. The open symbols in Fig. 9 show the emission intensity when CO was reacted with active nitrogen, while the solid symbols show the results when 90 mTorr of CO_2 was added to the system. It should be clear that the apparent intensity of the 6-1-band emission increased upon the addition of CO_2, while the intensity of the 6-4 band did not change when CO_2 was added. This can

be explained by the fact that there was a large amount of CO in the ground electronic state populated at $v''=1$ and a lesser amount at $v''=4$. The intensity of the emission bands increased up to about 1 Torr of CO. This suggests that a precursor to produce the fourth positive emission would be different from that in the case of CN-emission bands.

The increases in the 6-1-band intensity upon the addition of CO and CO_2 are shown in Fig. 10. In this case, CO_2 was added to the 700 mTorr of CO. The emission intensity increases up to a maximum at the addition of about 90 mTorr CO_2, and after that it decreases rapidly. Probably the decrease results from the quenching of $CO(A^1\Pi)$ or a precursor by CO_2.

The atomic lines of the nitrogen atoms appearing in Fig. 8(b) might be produced by the energy transfer from N_2 in the excited state to nitrogen atoms. The emission bands of NO shown in Fig. 8(a) are produced by the reaction of CO_2 with active nitrogen.[17]

Discussion

A. Infrared Emission from the Vibrationally Excited CO. The formation of vibrationally excited ground-state N_2 in the active nitrogen produced in the discharge of nitrogen was first inferred by Evans and Winkler[18] from chemical studies. The physical evidences were reported by Kaufman and Kelso[19] by means of temperature measurements and by Dressler[20] using the vacuum-UV-absorption of N_2. Tanaka *et al.*[21] extended the vacuum-UV-absorption measurements and observed transitions originating from levels up to $v''=29$ of the ground electronic state. Vibrational-energy transfer from vibrationally excited N_2 to CO was first suggested by Legay,[5] who measures the IR emission from CO. In the present study, the finding that the intensity of the IR emission of CO did not depend on the concentration of nitrogen atoms (Figs. 3 and 4) is consistent with the energy-transfer mechanism. As is shown in Fig. 4, since vibrationally excited N_2 is not quenched by the addition of NO, the system can be used as the source of the vibrationally excited N_2 under N-atom-free conditions.

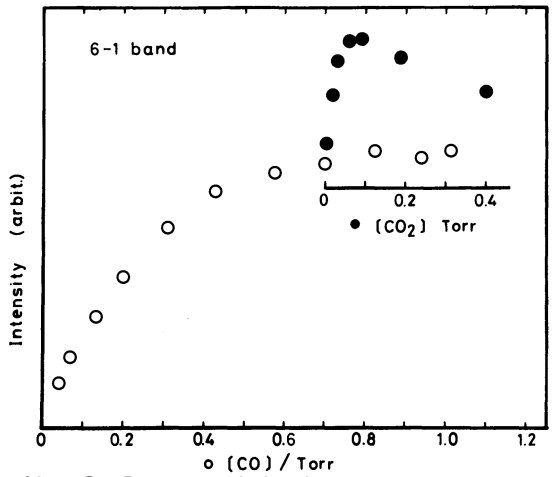

Fig. 10. ○; Increase of the 6-1 band intensity by the addition of CO and CO_2. ●; CO_2 was added to the 700 mTorr of CO. The conditions of active nitrogen are the same as the case in Fig. 8.

The rotational and vibrational temperatures of CO in the active nitrogen have been reported[5,6] to be 300—400 and 4000—8000 K respectively. It has also been reported that the rotational population[6] shows a Boltzmann distribution, while the vibrational population shows a non-Boltzmann distribution,[6,22] which coincides with a Treanor-type distribution.[23] In the present study, vibrationally excited CO up to $v''=18$ was observed.

An infrared emission due to the energy transfer from the vibrationally excited N_2 to CO_2[24] and N_2O[25] has also been reported. In the present study, emissions from CO_2 and N_2O were measured when CO_2 or N_2O was added to active nitrogen directly. Increases in the emission intensities as functions of CO_2 or N_2O were faster than in the case of CO, although the rate of self-quenching was also faster. Therefore, the decrease in the CO emission upon the addition of CO_2 or N_2O (shown in Fig. 5) results from both vibrational-energy transfer from N_2 to CO_2 or N_2O in competition with CO and the quenching of vibrationally excited CO by CO_2 or N_2O; the former process is preferable because of the excellent energy matching.

The amounts of the vibrationally excited N_2 or CO at $v''=1$ have been estimated[10,20] to be 5—10% of those at $v''=0$. In the present study, the emission intensity of the CO in the active nitrogen was compared with the infrared emission intensity of the CO produced in the $C+O_2\rightarrow CO+O$ system[26] (O_2 was added to the active nitrogen–C_2H_2 system). From the intensity ratio of the CO–active nitrogen to the C_2H_2, O_2–active nitrogen system, the amount of the vibrationally excited CO in the CO–active nitrogen system was estimated to be 10% or more of the CO at $v''=0$. In this estimation, it was assumed that the concentration of the vibrationally excited CO was equal to the concentration of carbon atoms in the C_2H_2, O_2–active nitrogen system. The value of 10% is interesting because the yield of the singlet oxygen, $O_2^*(a^1\Delta_g)$, produced in the discharge of O_2 is also about 10% of the O_2 in the ground electronic state.

A very large amount of vibrationally excited N_2 can be produced in the discharge of N_2, and a part of it is very highly excited. The vibrational energy transfer from N_2 to other molecules occurred very efficiently. Therefore, these vibrationally excited species can play a role in the chemiluminescent reactions of active nitrogen flames, although there have been no reports that the vibrationally excited N_2 is a precursor of the chemiluminescence in the active nitrogen flames.

B. Visible Emission of $CN(A^2\Pi$ and $B^2\Sigma^+)$. The spectral distribution of the CN violet band ($B^2\Sigma^+\longrightarrow X^2\Sigma^+$) is quite similar to that observed under blue-flame conditions in the active nitrogen–hydrocarbon system. Under the blue-flame conditions, the formation mechanism of the CN chemiluminescences has been suggested[15] to be a recombination reaction of C+N+M:

$$C(^3P) + N(^4S) + M \longrightarrow CN^*(C^4\Sigma^+) + M, \quad (1)$$

$$CN^*(C^4\Sigma^+) + M \longrightarrow CN^*(B^2\Sigma^+) + M, \quad (2)$$

$$CN^*(B^2\Sigma^+) \longrightarrow CN(X^2\Sigma^+) + h\nu(\text{violet band}), \quad (3)$$

$$CN^*(B^2\Sigma^+)\,M \longrightarrow CN^*(A^2\Pi) + M, \quad (4)$$

$$CN^*(A^2\Pi) \longrightarrow CN(X^2\Sigma^+)\,h\nu(\text{red band}). \quad (5)$$

The unusual intensity distribution in the vibrational structure of CN cmission bands could be explained[4,15] by the crossing of potential energy curves between $C^4\Sigma^+$ and $B^2\Sigma^+$ states.

Young and Morrow[7] have measured the CN-emission bands in the CO–active nitrogen system and proposed the following mechanism:

$$N_2^*(B^2\Pi \text{ or } W^3\Delta_u) + CO \longrightarrow CN + NO, \quad (6)$$

$$N_2^*(^5\Sigma_g^+) + CN \longrightarrow N_2 + CN^*(B^2\Sigma^+). \quad (7)$$

The mechanism of Young and Morrow can, however, be refuted by the following results in the present study: 1) If NO is produced by Reaction 6, emission bands of NO (γ, β, δ) can be observed in the active nitrogen system. However, no emission band from NO was observed here; 2) the formation of carbon atoms was observed, and the intensity of the CN violet emission was proportional to the steady-state concentration of the carbon atoms, just as in the case of the blue-flame conditions of the hydrocarbon system; 3) when a small amount of O_2 was added to the system and carbon atoms were consumed by the reaction of $C+O_2 \rightarrow CO+O$, the CN emission bands disappeared; 4) as is shown in Fig. 7, the intensity of the CN violet band approaches its maximum at 6 mTorr of CO. Under 6 mTorr of CO, the first positive band emission of N_2 is little reduced, *i.e.*, $N_2^*(B^3\Pi)$ is little quenched. Therefore, if the CN violet emission is produced by Reaction 7 subsequent to Reaction 6, the intensity maximum of CN emission should appear at a much larger amount of CO; 5) the potential energy curve of $N_2^*(^5\Sigma_g^+)$[27] is nearly repulsive. It is, then, very unlikely that the $N_2^*(^5\Sigma_g^+)$ is a precursor of the CN emission; 6) the unusual spectral distribution of the CN violet band can not be explained by the energy-transfer mechanism.

It was found that the purification of CO is very important in the present study. Usually, the CO gas in the cylinder contains a large amount of metal carbonyls. In the present study, as has been mentioned in the Experimental section, the CO was purified carefully. When CO was used without purification, the pink orange flame[15] appeared stronger than the blue flame, and the 0-0 band was much stronger than the 7-7 band in the CN violet system. These phenomena probably resulted from the reaction of metal carbonyls with active nitrogen. In the previous work by Young and Morrow, the procedure of the purification was not described.

The formation mechanism of carbon atoms in the CO–active nitrogen system can not be determined directly. The most probable mechanism is, however, the energy-transfer process from the metastable $N_2^*(A^3\Sigma_u^+)$, which can be produced by the recombination of nitrogen atoms:

$$N + N + M \longrightarrow N_2^*(A^3\Sigma_u^+), \quad (8)$$

$$N_2^*(A^3\Sigma_u^+) + CO \longrightarrow CO^*(a^3\Pi) + N_2, \quad (9)$$

$$CO^*(a^3\Pi) + CO \longrightarrow C(^3P) + CO_2. \quad (10)$$

Carbon atoms are reproduced by Reaction 11 subsequent to Reactions 3 and 5:

$$CN + N \longrightarrow C + N_2. \quad (11)$$

The energy-transfer process in Reaction 9 is known[28] to occur very efficiently. The quenching of $CO^*(a^3\Pi)$ by $CO(X^1\Sigma^+)$ has been suggested[29,30] to occur by means of Reaction 10, which is exoergic by $\simeq$8 kcal/mol (1 cal $=$4.814 J). However, no direct experimental verification of Reaction 10 has been made. If the carbon atoms are produced by Reaction 10, the intensity of the CN emission should be proportional to $[CO]^2$. However, as is shown in Fig. 7, the CN emission intensity is not proportional to $[CO]^2$. Another possible process is that the $CO^*(a^3\Pi)$ reacts with the highly vibrationally excited CO more rapidly:

$$CO^*(a^3\Pi) + CO^*(\text{high } v'') \longrightarrow C + CO_2. \quad (12)$$

The concentration of high v'' states might approach their maximum concentration under a low CO concentration, and after that, $[CO^*(\text{high } v'')]$ might be in its steady-state concentration because of the competition with the quenching processes. Therefore, if Reaction 12 occurs only in the very high v'' states, the carbon atoms formed (the intensity of CN emission) is proportional to the concentration of CO. Also, if there is a deactivation process such as Reaction 13, the dependence of the CN emission intensity on the CO concentration shown in Fig. 7 can be understood:

$$CO^*(a^3\Pi) + CO \longrightarrow CO + CO \quad (13)$$

When several mTorr of CO_2 were added to the system, the CN emission was reduced efficiently. Since the rate of the reaction of carbon atoms with CO_2 has been reported[31] to be very slow, slower than 10^{-15} cm^3 molecule^{-1} s^{-1}, the reduction of the CN emission does not result from the consumption of carbon atoms. The rate of the quenching of $N_2^*(A^3\Sigma_u^+)$ by CO_2 has been reported[28] to be slow, about 5500 times slower than CO. The quenching rate of $CO^*(a^3\Pi)$ by CO_2[32] is 20 times slower than CO. Probably, then, the reduction of CN emission is caused by the quenching of highly excited CO by the addition of CO_2; Reaction 12 is proposed as the source of the carbon atoms.

C. Vacuum Ultraviolet Emission of CO. Since the absolute transition probability of each transition in the fourth positive band of CO has been reported,[33] the

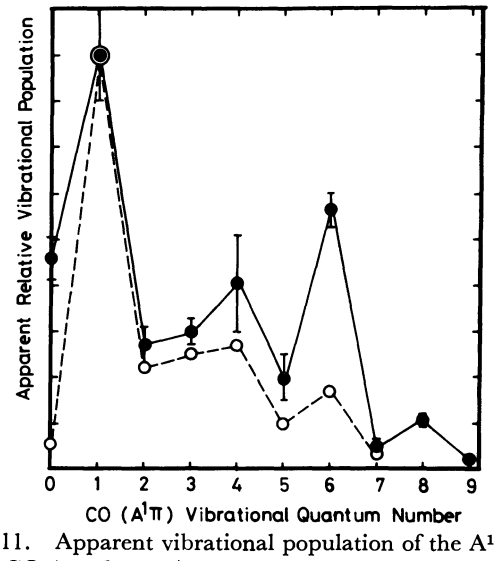

Fig. 11. Apparent vibrational population of the A^1 state of CO (see the text).

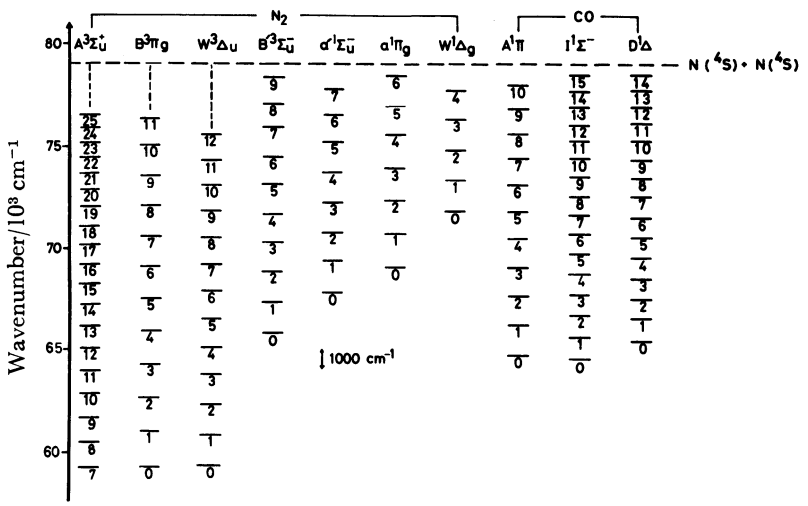

Fig. 12. Energy level diagram for electronically excited N_2 and CO. The energy of $N(^4S)+N(^4S)$ is 79030.4 cm^{-1}.

apparent vibrational population of the $A^1\Pi$ state of CO was calculated from the emission intensity of each band shown in Fig. 8(a). The results are shown in Fig. 11 by solid circles, which are the averages of several transitions. The error bars show the scattering of values. The results show that the widely separated $v'=1$ and $v'=6$ are formed most rapidly, as has previously been reported by Golde and Thrush.[10] In order to explain this mode of formation, they suggested an indirect energy transfer involving the collisional crossing from another excited state of CO, such as:

$$N + N + M \longrightarrow N_2^*(a^1\Pi_g) + M, \quad (14)$$

$$N_2^*(a^1\Pi_g) + CO \longrightarrow CO^*(I^1\Sigma^-) + N^2, \quad (15)$$

$$CO^*(I^1\Sigma^-) + M \longrightarrow CO^*(A^1\Pi) + M, \quad (16)$$

in addition to the direct energy-transfer process:

$$N_2^*(a^1\Pi_g) + CO \longrightarrow CO^*(A^1\Pi) + N_2. \quad (17)$$

Since the levels $CO^*(I^1\Sigma^-)$, $v'=2$, and $v'=9$, are perturbed by $CO^*(A^1\Pi)$, $v'=1$, and $v'=6$ respectively,[34] Golde and Thrush proposed the $CO(I^1\Sigma^-)$ rather than $CO(D^1\Delta)$ as a dominant precursor. Further, for the population of low levels of $CO(A^1\Pi)$, they suggested energy transfer from $N_2^*(a'^1\Sigma_u^-)$ to CO:

$$N_2^*(a'^1\Sigma^-) + CO \longrightarrow CO^*(A^1\Pi) + N_2. \quad (18)$$

An energy-level diagram for electronically excited N_2 and CO in which energy transfer can occur is shown in Fig. 12. The diagram is based on the molecular constants for N_2[27] and CO[35,36] previously reported. Since the energy of $N(^4S)+N(^4S)$ is 225.958 kcal/mol, *i.e.*, 79030.4 cm^{-1},[37] $CO^*(A^1\Pi)$ can populate energetically up to $v'=10$ if it is formed by the energy transfer from N_2^*.

The population shown in Fig. 11 by solid circles does not include the effects of quenching and relaxation processes in the $CO^*(A^1\Pi)$ state. The quenching cross-sections of $CO(A^1\Pi)$ by several gases previously reported[38,39] are very large (3.3 and 44 $Å^2$ for Ar and N_2 respectively at low v' levels, and 200, 80, and 120 $Å^2$ for CO, N_2, and CO_2 respectively at $v'=13$). Under the present experimental conditions (with a total pressure of about 6 Torr), the quenching process is competitive enough with the emission processes, although the radiative lifetime of the $A^1\Pi \rightarrow X^1\Sigma^+$ transition of CO is very short ($\approx$10 ns).[40] The quenching cross-sections of $CO^*(A^1\Pi)$ in individual vibrational levles ($v'=0$—8) have been reported[41] only in cases of rare gases. The quenching cross-section by rare gas is largest at $v'=1$ and smallest at $v'=0$ and 6. Since there have been no reports on quenching cross-sections by N_2, CO, and CO_2 in individual vibrational levels, the populations shown in Fig. 11 by solid circles were multiplied by the relative quenching cross-section by Ar at the individual vibrational levels and normalized at $v'=1$. The results are shown by open circles in Fig. 11. The population at $v'=6$ decreased, and the population became centered at $v'=1$. Of course, the above treatment is not correct. Correction should be done using the values of N_2, CO, and CO_2; in addition, the effect of vibrational relaxation should be considered. However, the results suggest that the formation of $CO(A^1\Pi)$ might be explained by direct-energy transfer from the excited state of N_2, Reactions 17 and 18, without a precursor of $CO^*(I^1\Sigma^-)$. The high population at $v'=1$ in $CO^*(A^1\Pi)$ may be explained by the energy transfer from $N_2^*(a'^1\Sigma_u^-)$ at $v'=0$, Reaction 18. Concerning the $a'^1\Sigma_u^-$ state of N_2 in the active nitrogen, it has been reported[42] that no emission band except that from the $v'=0$ level was observed in the $N_2(a'^1\Sigma_u^- \longrightarrow X^1\Sigma_g^+)$ system, although emissions from the $v'=0$—6 levels were observed in the $a^1\Pi_g \rightarrow X^1\Sigma_g^+$ system.[42,43]

References

1) A. N. Wright and C. A. Winkler, "Active Nitrogen," Academic Press, New York (1968).

2) D. R. Safrany, *Prog. React. Kinet.*, **6**, 1 (1971).

3) M. F. Golde and B. A. Thrush, *Rep. Prog. Phys.*, **36**, 1285 (1973).

4) M. R. Gorbal and M. I. Savadatti, *Chem. Rev.*, **82**, 527 (1982).

5) a) F. Legay, *J. Phys.* (*Paris*), **25**, 999 (1964); b) F. Legay, *J. Chem. Phys.*, **64**, 9 (1967); c) J. P. Kennealy, A. T. Stair, Jr., and M. H. Bruce, *ibid.*, **64**, 43 (1967); d) A. T. Stair, Jr., J. P. Kennealy, and R. E. Murphy, *ibid.*, **64**, 52 (1967).

6) N. Legay-Sommaire and F. Legay, *Can. J. Phys.*, **48**, 1966 (1970).
7) R. A. Young and W. Morrow, *J. Chem. Phys.*, **60**, 1005 (1974).
8) H. P. Knauss, *Phys. Rev.*, **32**, 417 (1928).
9) A. Fontijn and R. Ellison, *J. Chem. Phys.*, **54**, 3649 (1971).
10) M. F. Golde and B. A. Thrush, *Proc. R. Soc. London, Ser. A*, **330**, 97, 109 (1972).
11) a) D. D. Davis and W. Braun, *Appl. Opt.*, **7**, 2074 (1968); b) N. Washida, H. Akimoto, and I. Tanaka, *ibid.*, **9**, 1711 (1970).
12) D. Kley, N. Washida, K. H. Becker, and W. Groth, *Z. Phys. Chem. Neue Folge*, **82**, 109 (1972).
13) K. H. Becker, E. H. Fink, and A. C. Allison, *J. Opt. Soc. Am.*, **61**, 495 (1971).
14) T. Iwai, M. I. Savadatti, and H. P. Broida, *J. Chem. Phys.*, **38**, 644 (1963).
15) N. Washida, D. Kley, K. H. Becker, and W. Groth, *J. Chem. Phys.*, **63**, 4230 (1975).
16) D. Kley, N. Washida, K. H. Becker, and W. Groth, *Chem. Phys. Lett.*, **15**, 45 (1972).
17) I. M. Campbell and B. A. Thrush, *Trans. Faraday Soc.*, **62**, 3366 (1966).
18) H. G. V. Evans and C. A. Winkler, *Can. J. Chem.*, **34**, 1217 (1956).
19) F. Kaufman and J. R. Kelso, *J. Chem. Phys.*, **28**, 510 (1958).
20) K. Dressler, *J. Chem. Phys.*, **30**, 1621 (1959).
21) Y. Tanaka, F. R. Innes, A. S. Jursa, and M. Nakamura, *J. Chem. Phys.*, **42**, 1183 (1965).
22) a) C. A. Brau, G. E. Caledonia, and R. E. Center, *J. Chem. Phys.*, **52**, 4306 (1970); b) K. R. Horn and P. E. Oettinger, *ibid.*, **54**, 3040 (1971).
23) a) G. E. Caledonia and R. E. Center, *J. Chem. Phys.*, **55**, 552 (1971); b) J. Anketell and B. Brocklehurst, *J. Phys. B: Atom. Molec. Phys.*, **7**, 1937 (1974).
24) a) C. K. N. Patel, *Phys. Rev. Lett.*, **13**, 617 (1964); b) E. L. Milne, M. Steinberg, and H. P. Broida, *J. Chem. Phys.*, **42**, 2615 (1965); c) T. K. McCubbin, Jr., and Y. H. Hahn, *J. Opt. Soc. Am.*, **57**, 1373 (1967).
25) C. Alamichel and A. Piard-Bersellini, *Chem. Phys.*, **35**, 381 (1978).
26) E. A. Ogryzlo, J. P. Reilly, and B. A. Thrush, *Chem. Phys. Lett.*, **23**, 37 (1973).
27) A. Lofthus and P. H. Krupenie, *J. Phys. Chem. Ref. Data*, **6**, 113 (1977).
28) J. W. Dreyer, D. Perner, and C. R. Roy, *J. Chem. Phys.*, **61**, 3164 (1974).
29) G. Herzberg, "Molecular Spectra and Molecular Structure," Van Nostrand, New York (1950), Vol. I, p. 478.
30) T. G. Slanger and G. Black, *J. Chem. Phys.*, **55**, 2164 (1971).
31) D. Husain and A. N. Young, *J. Chem. Soc., Faraday Trans. 2*, **71**, 525 (1975).
32) G. W. Taylor and D. W. Setser, *J. Chem. Phys.*, **58**, 4840 (1973).
33) J. M. Mumma, E. J. Stone, and E. C. Zipf, *J. Chem. Phys.*, **54**, 2627 (1971).
34) a) G. Herzberg, J. D. Simmons, A. M. Bass, and S. G. Tilford, *Can. J. Phys.*, **44**, 3039 (1966); b) J. D. Simmons and S. G. Tilford, *J. Res. Natl. Bur. Stand., Sect. A*, **75**, No. 5, 455 (1971).
35) P. H. Krupenie, "The Band Spectrum of Carbon Monoxide," Nat. Stand. Ref. Data Ser., Nat. Bur. Stand. (U. S.), 5 (1966).
36) S. G. Tilford and J. D. Simmons, *J. Phys. Chem. Ref. Data*, **1**, 147 (1972).
37) D. R. Stull and H. Prophet, Project Directors, "JANAF Thermochemical Tables," 2nd ed, Nat. Stand. Ref. Data Ser., Nat. Bur. Stand. (U. S.), 37 (1971).
38) F. J. Comes and E. H. Fink, *Chem. Phys. Lett.*, **14**, 433 (1972).
39) A. C. Vikis, *J. Chem. Phys.*, **69**, 703 (1978).
40) R. E. Imhof and F. H. Read, *Chem. Phys. Lett.*, **11**, 326 (1971).
41) E. H. Fink and F. J. Comes, *Chem. Phys. Lett.*, **25**, 190 (1974).
42) M. F. Golde and B. A. Thrush, *Proc. R. Soc. London, Ser. A*, **330**, 79 (1972).
43) a) K. H. Becker, E. H. Fink, W. Groth, W. Jud, and D. Kley, *Faraday Discuss. Chem. Soc.*, **53**, 35 (1972); b) M. F. Golde and B. A. Thrush, *ibid.*, **53**, 52 (1972).

A Study of Inorganic Ion Exchangers. VII.[1] The Synthesis of γ-$NH_4ZrH(PO_4)_2$ and Ion-exchange Properities of γ-$Zr(HPO_4)_2\cdot 2H_2O$

Etsuro KOBAYASHI
National Chemical Laboratory for Industry, Yatabemachi, Tsukuba-gun, Ibaraki 305
(Received March 9, 1983)

The conditions for the synthesis of γ-$NH_4ZrH(PO_4)_2$ and the ion-exchange properties of γ-$Zr(HPO_4)_2\cdot 2H_2O$ were investigated. The influence of the mole ratio of MH_2PO_4 (M=Na, K, and NH_4) to $ZrOCl_2$ on the formation of γ-zirconium phosphate using NaH_2PO_4 as MH_2PO_4 was such that the γ-form was obtained not in the NaH_2PO_4/$ZrOCl_2$ mole ratio of 4, but in are of 8.3 or more. In case of the Na or K salt, a non-stoichiometric compound, $M_xZrH_{2-x}(PO_4)_2$, was obtained. When using the NH_4 salt, a stoichiometric compound was synthesized at 120—280 °C in accordance with the following equation: $ZrOCl_2+NH_4H_2PO_4\longrightarrow NH_4ZrH(PO_4)_2+NH_4Cl+HCl+H_2O$. Using an autoclave lined with Hastelloy-B and equipped with a stirrer, the synthesis was carried out by a reaction at 150—160 °C for 18—54 h. γ-$Zr(HPO_4)_2\cdot 2H_2O$ was prepared from $NH_4ZrH(PO_4)_2$, and its ion-exchange capacity at pH 4.5 and selectivity quotient toward alkali metals and ammonium ions were measured. The measured values increased in the order of $Li^+<Cs^+<Na^+<K^+<NH_4^+$.

The crystalline phosphates of quadrivalent metals are generally prepared by reflux or a hydrothermal reaction of amorphous phosphate with phosphoric acid of a suitable concentration. The method for synthesizing γ-zirconium(IV) bis(hydrogenphosphate) dihydrate (γ-$Zr(HPO_4)_2\cdot 2H_2O$ or γ-zirconium phosphate) is somewhat different from the above process. Clearfield *et al.*[2] carried out the reflux of a zirconium phosphate gel in a mother liquor comprised of a concentrated NaH_2PO_4 and HCl solution. Yamanaka *et al.*[3] reported the region of the formation of $NaZrH(PO_4)_2$ and the structural model of γ-$Zr(HPO_4)_2\cdot 2H_2O$. They carried out a hydrothermal reaction of phosphate gel with a weakly acidified aqueous solution of sodium phosphate to obtain γ-zirconium phosphate, they found that the region of the formation of the γ-form was within the pH values of 1.5—4.0 at 180—230 °C.

In the present work, through the heating of a mixture of $ZrOCl_2\cdot 8H_2O$, MH_2PO_4 (M=Na, K, or NH_4) and water in a sealed glass tube, $MZrH(PO_4)$ was formed above 120 °C. Consequently, the mole ratios of MH_2PO_4 to $ZrOCl_2$ (M/Zr) and the reaction temperatures were investigated in order to determine whether or not the ammonium salt had a tendency to form a stoichiometric compound more easily than sodium and potassium salt; it was possible to directly synthesize $MZrH(PO_4)_2$ using an autoclave. In addition, the ion-exchange properties of γ-$Zr(HPO_4)_2\cdot 2H_2O$ toward Li^+, Na^+, K^+, Cs^+, and NH_4^+ were studied.

Experimental

Synthesis of $MZrH(PO_4)_2$. In a 20-cm³ hard glass tube were placed 1.61 g of $ZrOCl_2\cdot 8H_2O$, 2.4—9.5 g of MH_2PO_4 (M=Na, K, or NH_4) and 5 cm³ of water. The contents were thoroughly shaken, and the tube was sealed. From 2—4 such sealed tubes were prepared under various conditions (the type of MH_2PO_4 and mole ratio of M/Zr) and placed in a 200-cm³ stainless steel autoclave. To the autoclave was added 80 cm³ of water to prevent any rupture of the tubes. The contents of the tubes were heated to specified temperatures (120—280 °C), and the resulting products in the tubes were separated from the mother liquors, washed thoroughly with water, and dried at 20 °C in a relative humidity of 75%, or at 105 °C. On the other hand, 16.1 g of $ZrOCl_2\cdot 8H_2O$, 46 g of $NH_4H_2PO_4$ and 100 cm³ of water were directly charged in to a 300-cm³ autoclave lined with Hastalloy-B (Mitsubishi Kinzoku Co.). The mixture was made to react for 18—54 h with stirring (180 min^{-1}) at 120—165 °C. The product thus formed was repeatedly washed with water, separated by a centrifugal separator, and dried. γ-$Zr(HPO_4)_2\cdot 2H_2O$ was obtained by the ion-exchange treatment of γ-$NH_4ZrH(PO_4)_2$.

Analysis. The composition of the reaction products was analyzed according to a previously reported method.[4] The amount of H_2O was determined on the basis of the weight loss of the heated product at 800 °C (in the case of the $NH_4ZrH(PO_4)_2$, the amount of NH_3 was calculated from the weight loss on heating). The Na_2O and K_2O were measured according to the flame-photometering method. The NH_3 was determined by Kjeldahl's method. The empirical values of P_2O_5 and ZrO_2 in the reaction products of $MZrH(PO_4)_2$ synthesized in the present study were almost 1 : 1 in mole ratio. Accordingly, the amounts of the two components were also obtained by dividing the residual amount (R%) derived from the following equation by the proportion of the formula weight of P_2O_5 and ZrO_2:

$$100\%-H_2O\%-M_2O\% \text{ (or } NH_4\%)=R\%.$$

X-Ray diffraction was then performed with a Shimadzu Seisakusho diffractometer under the conditions of Cu $K\alpha$, 30 kV P, and 20 mA.

Ion-exchange Capacity. The ion-exchange titration curves and ion-exchange values were obtained according to a previously reported method.[5]

Results and Discussion

Formation of γ-$MZrH(PO_4)_2$. In the previously reported reaction methods,[2,3] much more sodium phosphate was used than a soluble zirconium salt (M/Zr=20), and the adjustment of the pH value was necessary for the formation of γ-$MZrH(PO_4)_2$.

The Mole Ratios of $MH_2PO_4/ZrOCl_2$: Table 1 shows the synthesis conditions and analytical values of the γ-zirconium phosphate obtained by the reaction of $ZrOCl_2$ with NaH_2PO_4 or KH_2PO_4. Table 2 gives the same data for the γ-ammonium zirconium(IV) hydrogen bis(phosphate) obtained by the reaction of $ZrOCl_2$ with $NH_4H_2PO_4$.

In Expt No. 1 in Table 1, a mixture of NaH_2PO_4 and Na_2HPO_4 was used as the phosphate. The pH value of the mother liquid, 4.26, was thus somewhat higher[3]

Table 1. Synthesis and analysis of γ-$MZrH(PO_4)_2$ (M=Na, K)

No.	Reaction conditions: $ZrOCl_2 \cdot 8H_2O$ (g)	MH_2PO_4[a] (M=Na, K) (g)	H_2O (ml)	M/Zr atomic ratio	Temp °C	Time h	Mother liquor (pH)	Reaction products: Dry (Temp/°C, R.H%)	ZrO_2 (%)	P_2O_5 (%)	M_2O (%)	H_2O (%)	$ZrO_2 : P_2O_5 : M_2O : H_2O$ (mole ratio)
1	3.22	2.40 (1.42)	50	2.0 (4.0)	250	96	4.26	105	44.6	51.4	2.2	1.8	1.0 : 1.0 : 0.1 : 0.3
2	1.61	2.40	10	4.0	250	96	2.32	105	42.9	49.5	2.3	5.3	1.0 : 1.0 : 0.1 : 0.8
3	1.61	5.00	10	8.3	250	96	2.61	20,0	40.6	46.8	5.4	7.1	1.0 : 1.0 : 0.3 : 1.2
4	1.61	10.0	10	16.6	250	96	2.88	20,0	40.2	46.2	5.8	7.8	1.0 : 1.0 : 0.3 : 1.3
5	1.61	5.44	5	8.0	120	96	3.12	20,75	32.8	38.2	10.7	18.0	1.0 : 1.0 : 0.4 : 3.1
6	1.61	5.44	5	8.0	200	96	2.57	20,0	40.3	46.3	5.1	8.4	1.0 : 1.0 : 0.2 : 1.4
7	1.61	5.44	5	8.0	250	96	3.38	105	42.4	48.9	3.9	4.8	1.0 : 1.0 : 0.1 : 0.8
8	1.61	5.44	5	8.0	280	96	2.61	105	39.2	45.2	10.7	4.9	1.0 : 1.0 : 0.4 : 0.8
$(NaZrH(PO_4)_2)$									(40.38	46.51	10.16	2.95)	
$(KZrH(PO_4)_2)$									(38.36	44.18	14.66	2.80)	

a) In Nos. 1—4, NaH_2PO_4, and in Nos. 5—8, KH_2PO_4 are used; the values in parentheses indicate the weight of Na_2HPO_4 used with NaH_2PO_4.

Table 2. Synthesis and analysis of γ-$NH_4ZrH(PO_4)_2$

No.	Reaction conditions: $ZrOCl_2 \cdot 8H_2O$ (g)	$NH_4H_2PO_4$ (g)	H_2O (ml)	NH_4/Zr (mole ratio)	Temp °C	Time h	Mother liquor (pH)	Reaction products: Dry (Temp/°C, R.H%)	ZrO_2 (%)	P_2O_5 (%)	NH_3 (%)	H_2O (%)	$ZrO_2 : P_2O_5 : NH_3 : H_2O$ (mole ratio)
1	3.22	3.42	7	3.0	250	96	2.15	105	43.2	49.7	3.7	3.5	1.0 : 1.0 : 0.6 : 0.5
2	1.61	2.30	10	4.0	250	96	2.25	105	41.1	47.4	4.8	6.7	1.0 : 1.0 : 0.8 : 1.1
3	12.9	38.0	50	8.2	250	96	2.51	20,75	41.2	47.5	5.5	5.9	1.0 : 1.0 : 1.0 : 1.5
4	1.61	9.5	5	16.7	250	96	2.65	105	41.0	47.1	5.5	6.5	1.0 : 1.0 : 1.0 : 1.0
5	1.61	4.6	5	8.0	120	138	3.39	20,75	37.5	43.0	5.0	14.6	1.0 : 1.0 : 1.0 : 2.7
6	1.61	4.6	5	8.0	200	96	2.53	105	41.1	47.3	4.7	7.0	1.0 : 1.0 : 0.8 : 1.2
7	6.44	19.0	25	8.2	280	96	2.76	105	41.3	47.5	5.4	5.8	1.0 : 1.0 : 0.9 : 1.0
8	16.1	46.0	100	8.0	120	18	3.61	20,75	36.5	42.1	5.5	17.0	1.0 : 1.0 : 0.9 : 3.2
9	16.1	46.0	100	8.0	150	18	3.56	20,0	40.2	46.3	5.2	8.4	1.0 : 1.0 : 0.9 : 1.4
10	16.1	46.0	100	8.0	150	36	3.50	20,0	40.6	46.7	5.2	7.5	1.0 : 1.0 : 0.9 : 1.3
11	16.1	46.0	100	8.0	150	54	3.45	20,0	40.9	47.1	5.3	6.7	1.0 : 1.0 : 1.0 : 1.1
12	16.1	46.0	100	8.0	165	18	3.42	20,75	37.5	43.3	4.7	14.6	1.0 : 1.0 : 0.9 : 2.7
13	— ZrP							20,75	39.2	45.0	—	15.7	1.0 : 1.0 : — : 2.8
$(NH_4ZrH(PO_4)_2)$									(41.05	47.27	5.66	6.00)	
$(NH_4ZrH(PO_4)_2 \cdot 2H_2O)$									(36.66	42.22	5.06	16.06)	
$(Zr(HPO_4)_2 \cdot 2H_2O)$									(38.61	44.47		16.92)	

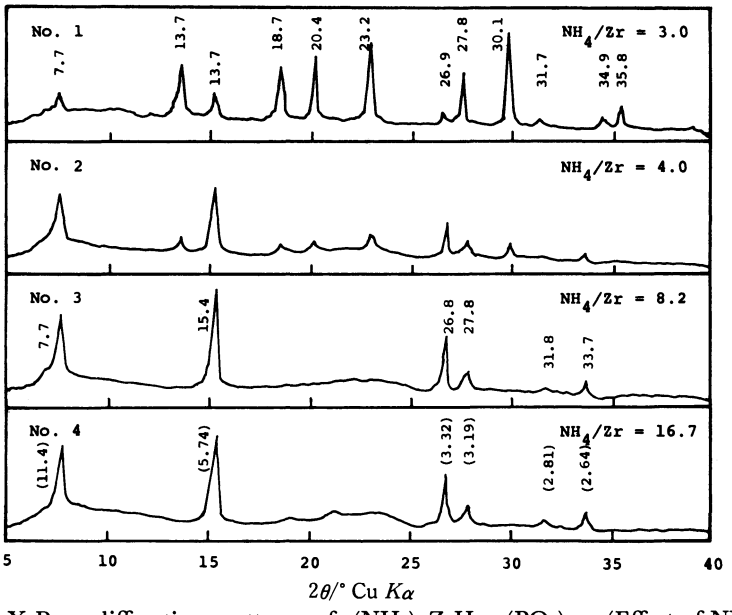

Fig. 1. X-Ray diffraction patterns of $(NH_4)_xZrH_{2-x}(PO_4)_2$. (Effect of NH_4HPO_4 mol/$ZrOCl_2$ mol (NH_4/Zr) on the synthesis.)
Numerals near peaks indicate 2θ degrees and lattice distances (Å).

in the formation of γ-zirconium phosphate. In fact, no diffraction peak characterizing the γ-$NaZrH(PO_4)_2$ was detected in the X-ray diffraction pattern. Neither was the diffraction peak characterizing the γ-form found in the X-ray diffraction pattern of the reaction product in the second experiment at a Na/Zr mole ratio of 4. Howevere in Expts No. 3 and 4 at M/Zr mole ratios of 8.3 and 16.6 respectively, the formation of γ-zirconium phosphate apparently took place, since peaks appeared at 11.7, 6.36, 4.57, 4.41, 3.91, 3.81, 3.17, 2.87, and 2.54 Å (Å$=10^{-10}$ m) in the X-ray diffraction patterns. It was found, therefore, that the amount of NaH_2PO_4 could be reduced to less than half of that previously reported.

The influence of the mole ratio of NH_4/Zr was investigated also when the ammonium salt was used. The results are shown in Expts No. 1—4 in Table 2, while the X-ray diffraction patterns of the reaction products are shown in Fig. 1.

As the mole ratio of NH_4/Zr increased, the diffraction peak at 11.3 Å (7.8°) characterizing γ-$NH_4ZrH(PO_4)_2$ was intensified. The mole ratio of NH_3 in the product from Expt No. 1 was 0.6 and the mole ratio of NH_4/Zr was small. With an increase in the mole ratio of M/Zr, however, that of NH_3 reached 1.0, and a stoichiometric compound, $NH_4ZrH(PO_4)_2$, was formed. In the case of the Na salt, the mole ratios of Na_2O in the reaction products were 0.3 or less, as is shown in Table 1, and products of an indefinite $Na_{0.2-0.6}ZrH_{1.8-1.4}(PO_4)_2$ composition were obtained.

In the processes previously reported, hydrochloric acid was added to the reaction solutions[2,3] or the solutions were adjusted to pH 2.[3] The pH value of an aqueous solution of MH_2PO_4 (M=Na, K, or NH_4) showed 4—4.5, and the pH value of an aqueous solution equilibrated with $MM'H(PO_4)_2$ (M'=Ti or Zr), obtained by the ion-exchange of $M'(HPO_4)_2$ and MOH, also showed 4—4.5.

The reaction giving rise to the formation of the γ-zirconium phosphates can be written as follows:

$$ZrOCl_2+2MH_2PO_4 \longrightarrow MZrH(PO_4)_2+MCl+HCl+H_2O.$$

In this reaction, since HCl is liberated into the aqueous solution, the pH values were expected to become less than 4. In fact, the pH values of the mother liquors following the termination of the reaction inevitably showed the expected pH values (2.5—3.5).

Reaction Temperature: The reactions between $ZrOCl_2$ and KH_2PO_4 in Expts No. 5—8 are shown in Table 1. As with the Na-product, the K-product was also low in M_2O (K_2O) content, and a product of an indefinite $K_{0.2-0.8}ZrH_{1.8-1.2}(PO_4)_2$ composition was obtained. No correlation was observed between the X-ray diffraction peak intensity of 11.0 Å characterizing the γ-potassium zirconium(IV) hydrogen bis(phosphate) and the reaction temperature. As has been described above, the ease with which the crystalline γ-zirconium phosphates were produced as stoichiometric compounds reacting $ZrOCl_2 \cdot 8H_2O$ with MH_2PO_4 is considered to be in the order of the NH_4-product Na-product K-product.

The reaction temperatures were investigated for the NH_4-products; the results from Expts No. 5, 6, 3, and 7 are shown in Table 2. The mole ratios of NH_3 in the products ranged from 0.8—1.0 at 120—280 °C, and products of approximately a $NH_4ZrH(PO_4)_2$ composition were obtained. In the X-ray diffraction patterns of the NH_4 salt, the diffraction-peak intensity of 11.3 Å characterizing γ-$NH_4ZrH(PO_4)_2$ increased with an elevation of the reaction temperature.

Synthesis in the Autoclave. For the purpose of developing an industrial method for synthesizing γ-zirconium phosphates as compounds with a layer structure, the reaction between $ZrOCl_2$, $NH_4H_2PO_4$ and water was carried out in autoclave equipped with a stirrer and lined with Hastelloy-B (Ni: 67, Mo: 28, and Fe: 5%).

TABLE 3. ION-EXCHANGE PROPERTIES OF γ-ZIRCONIUM(IV) BIS(HYDROGENPHOSPHATE) IN SOLUTIONS TO ALKALI METAL AND AMMONIUM IONS

Ion	Equilibrium capacity at pH 4.5 Q^A/mequiv g^{-1}	Saturation capacity at pH 4.5 Q°/mequiv g^{-1}	Selectivity quotient K_H^M	Mole fraction Q^A/Q°	Absorption quantity A/%	Distribution coefficient K_D/ml g^{-1}
Li	0.36	1.80	0.04	0.20	14.4	8.42
Na	0.74	2.40	0.19	0.31	29.6	21.0
K	1.50	2.40	2.51	0.63	60.0	75.0
Cs	1.02	2.60	0.45	0.39	40.8	34.4
NH_4	1.69	2.70	3.26	0.62	66.8	100.5

Selectivity quotient: $K_H^M = \frac{(M^+)I}{(H^+)I} \cdot \frac{(H^+)S}{(M^+)S} = \frac{Q^A}{Q^\circ - Q^A} \cdot \frac{Q^A}{C - Q^A}$. Absorption quantity : $Q^A/C\ 100 = A$. Distribution coefficient: $K_D = A/I \cdot S(100-A)$. C: Initial quantity of MCl (2.5 mequiv). S: MCl solution (25 ml). I: Ion-exchanger (0.5 g).

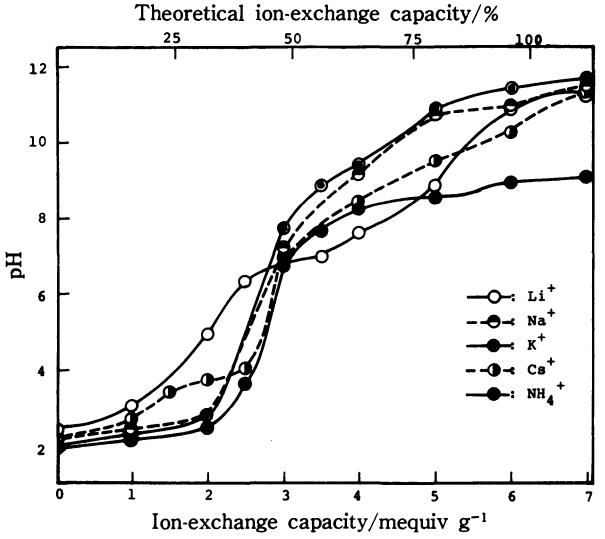

Fig. 2. Alkali metal and ammonium ion-exchange titration curves of γ-$Zr(HPO_4)_2 \cdot 2H_2O$.

The results are shown in Table 2.

The reaction temperature was maintained within 120—165 °C to prevent the corrosion of the metallic vessel. The reaction time of the contents under agitation could be significantly shortened compared to that required for a stationary state. Judging from the X-ray diffraction patterns of the products, a crystalline product was obtained after a reaction period of 18 h. The crystallization of the products (Nos. 9, 10, and 11) was brought to completion with an additional reaction time. When γ-zirconium phosphates are synthesized in the autoclave and the container is attacked above 180 °C, there is a chance that the reaction product may react with metal ions. Thus, a reaction temperature of about 150 °C was considered the most appropriate.

Ion-exchange Properties. Since γ-$Zr(HPO_4)_2 \cdot 2H_2O$ is present to a greater extent in the interlayer spacing (12.2 Å), it is considered void of selectivity as an ion-exchanger. With regard to the inorganic ion-exchange properties of this compound, therefore, there is no literature available except for one report by Clearfield *et al.*[2] They converted the γ-form into the β-form as a complete anhydride, and obtained ion-exchange titration curves of Cs^+, Na^+, and Ba^{2+} using the β-form. In the present study, ion-exchange titration curves of γ-$Zr(HPO_4)_2 \cdot 2H_2O$ toward alkali metal (Li, Na, K, Cs) and ammonium ions were measured in order to reconsider γ-$Zr(HPO_4)_2 \cdot 2H_2O$ as an ion-exchanger. The results are shown in Fig. 2. In the titration curves, the ion-exchange capacity up to pH 4.5 was arbitrarily defined as the saturation ion-exchange capacity (Q°).[5] On the other hand, an equilibrium ion-exchange capacity (Q^A) up to pH 4.5 was also obtained using the method of the previous report.[5] Table 3 showns the values for the selectivity quotient (K_H^M), the adsorption quantity (A), and the distribution coefficient (K_D) calculated from both ion-exchange capacities. In the ion-exchange titration curves of Fig. 2, the theoretical value for a 100% ion exchange of the two hydrogens in γ-$Zr(HPO_4)_2 \cdot 2H_2O$ corresponds to 6.25 mequiv/g. When the two hydrogens are theoretically 100%-ion-exchanged with Li^+, Na^+, K^+, or Cs^+, the pH values of the aqueous solution are each about 11. γ-$Zr(HPO_4)_2 \cdot 2H_2O$ tends to be attacked in such an alkaline solution. On the other hand, the pH value of the solution is 8.9 in the case of ion-exchange with NH_4^+; thus, there is little fear of γ-$Zr(HPO_4)_2 \cdot 2H_2O$ being attacked. An analysis of the ion-exchanger, however, indicated that about 65% of the ion-exchange was actually carried out. The values of Q^A, Q°, K_H^M, A, and K_D at pH 4.5 were, respectively, in the order of $Li^+ < Cs^+ < Na^+ < K^+ < NH_4^+$. That is, Li^+, with a smaller radius, was hydrated to the greatest extent, causing it to appear to have a large radius; thus, the ion-exchange quantity of the hydrated ion was small. Cs^+ was not hydrated, but was itself larger than Na^+, K^+, or NH_4^+. Consequently, the ion-exchange quantity of this ion was less than those of the other ions. NH_4^+ was not so high in selective ion-exchange compared with alkali metal ions, but was highest with respect to ion-exchange capacity. This point is of interest in consideration of the fact that NH_4^+ salt more easily forms stoichiometric compounds than the Na and K salts in the synthesis of γ-zirconium phosphates.

References

1) a) Presented at the 45th National Meeting of the Chemical Society of Japan, Tokyo, April 1982: b) Part VI of the series; E. Kobayashi and S. Yamazaki, *Bull. Chem. Soc. Jpn.*, **56**, 1632 (1983).

2) A. Clearfield, R. H. Blessing, and J. A. Stynes, *J. Inorg. Nucl. Chem.*, **30**, 2249 (1968).
3) S. Yamanaka and M. Tanaka, *J. Inorg. Nucl. Chem.*, **41**, 45 (1979).
4) E. Kobayashi, *Bull. Chem. Soc. Jpn.*, **48**, 314 (1975).
5) E. Kobayashi, *Bull. Chem. Soc. Jpn.*, **52**, 1351 (1979).

 © 1983 The Chemical Society of Japan Bull. Chem. Soc. Jpn., 56, 3761—3764 (1983)

X-Ray Diffraction Study on the Coordination Structure of Chlorocopper(II) Complexes in Highly Concentrated Methanolic $CuCl_2$ Solution

Mitsuyoshi Ichihashi, Hisanobu Wakita,* and Isao Masuda

Department of Chemistry, Faculty of Science, Fukuoka University, Nanakuma, Jonan-ku, Fukuoka 814-01

(Received May 6, 1983)

The structures of the solute complexes existing in methanolic $CuCl_2$ solutions with the concentrations of 1.055—3.250 mol dm^{-3} were investigated by X-ray diffraction analysis. The solute complexes which were predominantly present could be formulated as $[CuCl_n(CH_3OH)_{6-n}]$ ($n=1$—3); they have an axially elongated octahedral structure including Cl^- at the equatorial site. The Cu–O bond distance was 2.230—2.238 Å. Methanol molecules were coordinated at the equatorial site with the Cu–O bond distance of 1.926—1.950 Å and at the axial site with that of 2.423—2.473 Å. When the initial concentration of $CuCl_2$ was kept within the range examined here, almost all of the Cu^{2+} ions formed chloro complexes.

Solution X-ray diffraction investigations have established that the stereo structure of the hexaaqua complex existing in aqueous $CuSO_4$ and $Cu(ClO_4)_2$ solutions is characteristic for the elongated octahedral geometry having two axial bonds with the longer distance (2.34—2.43 Å) and four equatorial bonds with the shorter distance (1.94—1.98 Å).[1,2] In concentrated aqueous $CuBr_2$ solutions (1.016—4.364 mol dm^{-3}), the coordination of Br^- ion was demonstrated to occur at the equatorial sites.[3] As for an aqueous $CuCl_2$ solution (2.952 mol dm^{-3}), Magini proposed from the investigation by X-ray diffraction analysis the presence of a monomeric complex which included two Cl^- ions at the equatorial sites,[4] similar to the above bromo complex. On the other hand, Wertz *et al.* reported the polymeric complexes to be present in aqueous $CuCl_2$ solutions (3.18 and 4.35 mol dm^{-3});[5] in these complexes the Cl^- ion bridged between two Cu^{2+} ions.

Since the coordination ability of methanol molecules is generally expected to be lower than that of water, the Cl^- ion may have a higher coordination ability than solvent molecules in methanol than in water. In fact, it was shown by the X-ray diffraction analysis that in methanolic $FeCl_3$ (6.0 and 11.0 mol kg^{-1}) and $CoCl_2$ (3.91 mol kg^{-1}) solutions, polymeric species bridged through Cl^- ions were present.[6] On the other hand, in aqueous $FeCl_3$ (2.332 mol dm^{-3}) and $CoCl_2$ (2.973 mol dm^{-3}) solutions, only the monomeric octahedral complex was known to be present in the form of either a mono- or a dichloro complex including H_2O molecules as another ligand.[4,7]

These facts suggest the increased coordination ability of Cl^- ion in methanol than in water. Accordingly, if a polynuclear chlorocopper(II) complex species were present, it might be demonstrated more distinctly with a methanolic $CuCl_2$ solution. In the present investigation the X-ray diffraction analysis has been carried out for concentrated methanolic $CuCl_2$ solutions. Observed $D(r)$ curves have been well explained by assuming that the solutions predominantly include three complexes, formulated as $[CuCl_n(CH_3OH)_{6-n}]$ where $n=1$, 2, and 3, in nearly equivalent amounts; the complexes have a distorted octahedral structure and the equatorial sites are occupied preferentially by Cl^- ions. The existence of a polymeric species was improbable.

Experimental and Data Treatment

Sample Solutions. Commercially available $CuCl_2\cdot 2H_2O$ crystals were recrystallized from distilled water. The hydrate was dehydrated by keeping it at 100 °C, *in vacuo*, for 48 h. The sample solutions were prepared by dissolving the anhydrous $CuCl_2$ into anhydrous methanol. The copper ion concentration of the solutions was determined by EDTA titration method. The chloride ion concentration was calculated from the copper concentration. The amount of methanol in the solution was calculated from the copper ion concentration and from the density determined pycnometrically. The composition of the sample solutions is given in Table 1.

X-Ray Diffraction Measurements and Data Treatments. The measurements and the data treatments were carried out as described elsewhere.[3,8] The time required for accumulating 80000 counts was recorded for solutions A and B, and that for 40000 counts for solution C. The $s\cdot i(s)$ curves in Fig. 1 with circles were obtained by multiplying the observed reduced intensities $i(s)$ by the s value ($s=4\pi\sin\theta/\lambda$).

The radial distribution function was calculated from the reduced intensities $i(s)$ according to Eq. 1:

$$D(r) = 4\pi r^2\rho_0 + \frac{2r}{\pi}\int_0^{15} s\cdot i(s)\cdot M(s)\cdot\sin(r\cdot s)\mathrm{d}s. \qquad (1)$$

In Eq. 1, $\rho_0=[\sum_i n_i f_i(0)]^2/V$. It denotes the average scattering power per unit volume V. $M(s)=[\sum_i n_i f_i(0)^2]/[\sum_i n_i f_i(s)^2]\times\exp(-0.01s^2)$; r is the distance in Å. The theoretical intensities, $i(s)_{\mathrm{calcd}}$, of the interactions for the given pairs of the atoms were calculated from Eq. 2:

$$i(s)_{\mathrm{calcd}} = \sum_i^{i\neq j}\sum_j n_{ij}\cdot f_i(s)\cdot f_j(s)\frac{\sin(r_{ij}\cdot s)}{r_{ij}\cdot s}\exp(-b_{ij}\cdot s^2), \qquad (2)$$

where $f_i(s)$ and $f_j(s)$ are the scattering factors of atoms i and j; and n_{ij}, r_{ij}, and b_{ij} are the frequency factor, the distance (Å), and the temperature factor (Å^2) of the interactions between atoms i and j. Least-squares refinements of the above structural parameters n, r, and b were made by the use of the NLPLSQ program[1] utilizing a selected s (Å^{-1}) range so as to

Table 1. Composition of methanolic $CuCl_2$ solutions

Solution	$CuCl_2$[a]	CH_3OH[a]	V/Å^3	ρ/g cm^{-3}	μ/cm^{-1}
A	1.055	24.36	1574	0.9224	4.996
B	2.575	23.84	644.8	1.110	11.13
C	3.251	22.96	510.7	1.173	13.83

a) mol dm^{-3}. V, Stoichiometric volume containing one copper atom; ρ, density; μ, linear absorption coefficient of the solution for Mo $K\alpha$ radiation.

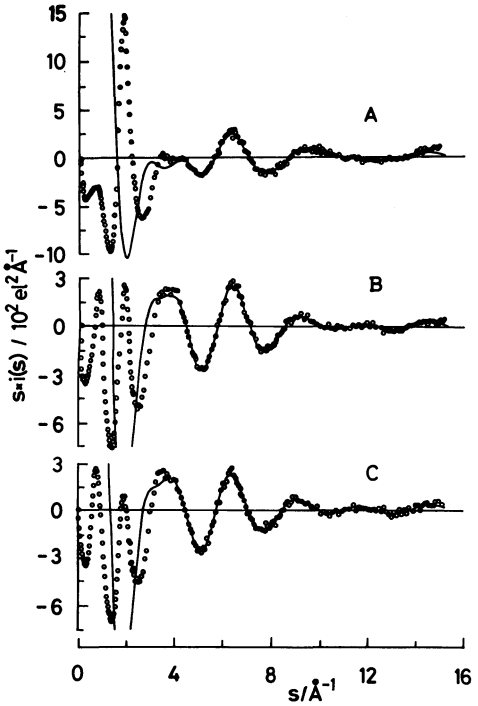

Fig. 1. Observed (oooo) and calculated (——) $s \cdot i(s)$ curves for solutions A, B, and C.

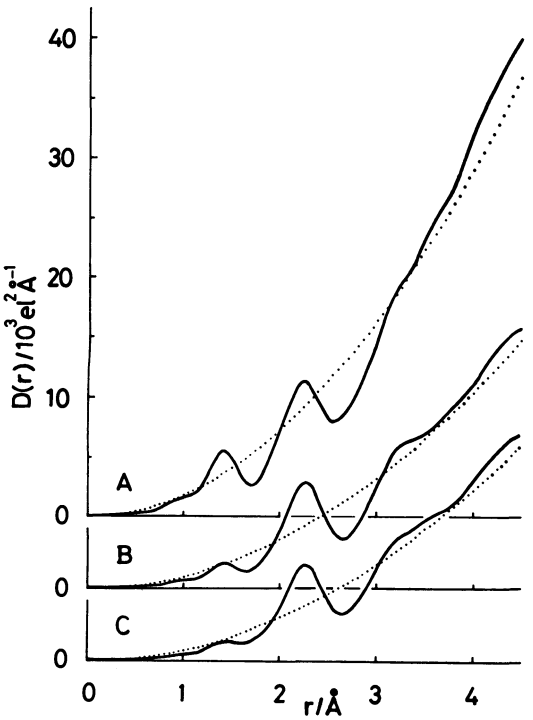

Fig. 2. $D(r)$ (——) and $4\pi r^2\rho_0$ (·····) curves for solutions A, B, and C.

minimize the U value in Eq. 3:

$$U = \Sigma s^2[i(s) - i(s)_{\text{calcd}}]^2. \quad (3)$$

Results and Discussion

The $D(r)$ curves for solutions A, B, and C are given in Fig. 2. These show a common pattern exhibiting a shoulder around 1.0 Å, two distinct peaks with the maxima at 1.5 and 2.3 Å, and a shoulder between 3.0—3.5 Å.[9] The shoulder around 1.0 Å and the peak at 1.5 Å can be attributed to free and complexed CH_3OH molecules; the former is caused by the C—H and O—H interactions and the latter by the C—O interaction. In $D(r)$ curves obtained for methanol or methanolic solutions, the peak due to the C—O interaction has ordinarily been seen around 1.5 Å.[10] The shoulder located in the 3.0—3.5 Å region, judging from the position, may be ascribed to the mutual interactions among the ligands which are bound in the first coordination sphere and to the interactions between these ligands and the solvent CH_3OH molecules. The peak at 2.3 Å could be most informative for the interactions between Cu^{2+} and the ligands including CH_3OH and Cl^-. This peak appears to be quite symmetric, but, as will be discussed below, it can not be ascribed to solely one sort of interaction.

In order to analyze the $D(r)$ curve quantitatively, the area of the above peak has been taken into account. By supposing tentatively the presence of only one species of complex as $[Cu(CH_3OH)_6]^{2+}$,[11] the calculated peak area due to the six Cu–O interactions amounts to only 6/8 of the observed one, as shown in Fig. 3. Similarly, supposing only $[Cu(CH_3OH)_4]^{2+}$ to be present, the calculated peak area was not coincident with the observed one. Therefore, it appears necessary to accept the occurrence of the coordination of Cl^- to Cu^{2+} ion. In fact, Doe and Kitagawa recently reported that the stepwise formation constants of the chloro-copper complex species in methanol are $K_1 = 1.2 \times 10^5$, $K_2 = 2.5 \times 10^3$, and $K_3 = 1.7 \times 10^3$ (mol^{-1} dm^3).[12] On the basis of these data, the amounts of the complex species that include unitary bonding as $CuCl^+$, $CuCl_2$, and $CuCl_3^-$ are calculated to be 30.5, 37.6, and 31.5%, of the initial Cu^{2+} concentration in solutions A—C.[13] In addition, a survey of the bond distance data for the numerous chloro-copper(II) complex crystals suggested the following:

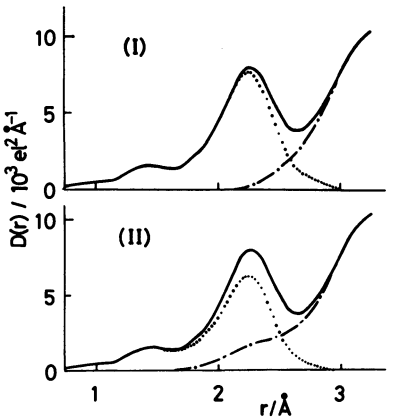

Fig. 3. Residual (—·—) $D(r)$ curves obtained by subtracting calculated $D(r)$ curves (·····) from observed $D(r)$ curve (——) for solution C.
(I); Calculated $D(r)$ curve is obtained by assuming the formation of "$CuCl_2(CH_3OH)_4$". (II); Calculated $D(r)$ curve is obtained by assuming the formation of $[Cu(CH_3OH)_6]^{2+}$.

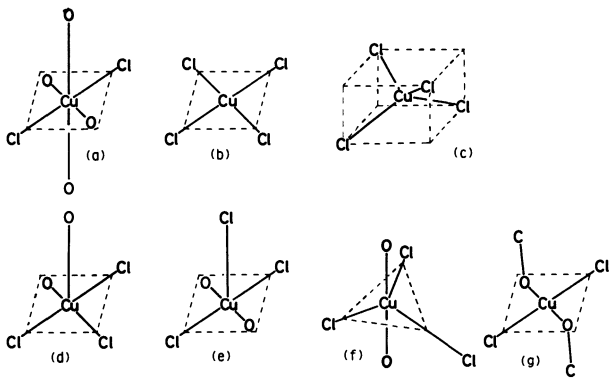

Fig. 4. Assumed structural models.

If the Cu^{2+} ion in methanolic solution had two sorts of coordination distances, one shorter and the other longer, and if it coordinated Cl^- ion with the longer one, the interaction due to such Cu—Cl bonding could be expected to appear at 2.6—3.0 Å. But, actually, no such peak appeared on the $D(r)$ curves in Fig. 2, so occurrence of the bonding in the above manner is unlikely. By taking into account the stability data, we assumed that the complexes including the unitary $CuCl^+$, $CuCl_2$, and $CuCl_3^-$ bonds are present in an elongated octahedral form wherein the Cu^{2+} ion coordinated the Cl^- ion with a bond distance shorter than 2.6 Å. These complexes are generally formulated as $[CuCl_n(CH_3OH)_{6-n}]$ (n=1—3), and on the basis of the stability data the mean composition of the complexes with n=1—3 existing in the solutions may be represented with a formula "$CuCl_2(CH_3OH)_4$". Therefore, the calculation of the peak area was carried out on "$CuCl_2(CH_3OH)_4$". As shown in Fig. 3, the calculated peak area agreed well with the observed one.

The structural model shown in Fig. 4-a was depicted. The model has axially elongated octahedral geometry and possesses two O atoms and two Cl^- ions at the equatorial sites, with the bond distances of 1.95 and 2.25 Å, respectively, and the other two O atoms at the axial sites with the bond distance of 2.45 Å. In order to determine the parameter values (n, r, and b values), the $s\cdot i\,(s)_{calcd}$ curves were calculated from Eq. 2 by employing a set of the parameter values selected tentatively for the Fig. 4-a. The refinements of these values were carried out by a least-squares method so that these gave an $s\cdot i\,(s)_{calcd}$ curve which agreed with the observed $s\cdot i\,(s)$ curve in the region of $s>5$ Å^{-1}. It was found that using the model, Fig. 4-a, the calculated $D(r)$ curve show a peak at 2.3 Å with the peak area closely agreed with the observed one. And, as shown in Fig. 1, a good agreement between the calculated and observed $s\cdot i(s)$ curves is seen in the region of $s>4$ Å^{-1}. The final parameter values used in these calculations are given in Table 2: it is noteworthy in Table 2 that the n values for the interactions, Cu-Cl, Cu-O (equatorial), and Cu-O (axial), are always nearly 2; this is consistent with the assumed six-coordinate complex. In Fig. 5 the smoothing of the observed $D(r)$ curves for solution C is demonstrated. The subtraction of the peaks due to the interactions expected for the model, Fig. 4-a, from the observed $D(r)$ curve gives finally a residual curve which is satisfactorily smooth.

Table 2. Structural parameter values of the $[CuCl_n(CH_3OH)_{6-n}]$(n=1—3) complexes

Solution (mol dm^{-3})	Parameter[a)]	Interaction		
		Cu–O_{eq}	Cu–O_{ax}	Cu–Cl_{eq}
A	r	1.950	2.458	2.230
(1.055)	b	0.0011	0.0084	0.0031
	n	2.109	1.938	2.019
B	r	1.947	2.423	2.236
(2.575)	b	0.0016	0.0072	0.0025
	n	1.982	2.089	2.085
C	r	1.926	2.473	2.238
(3.251)	b	0.0015	0.0074	0.0021
	n	1.919	2.023	2.048

a) r: Bond distance, Å; b: temperature factor, Å^2; n: frequency factor; eq, equatorial; ax, axial.

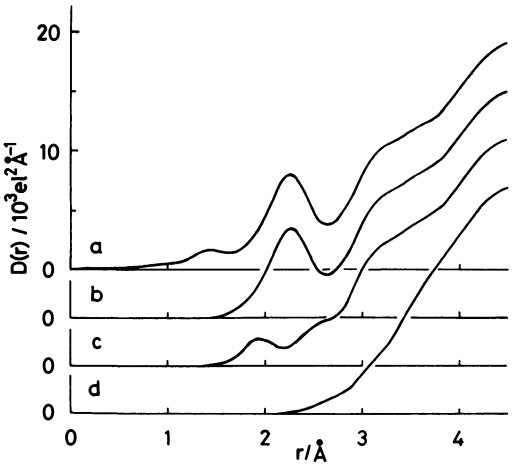

Fig. 5. Smoothing of $D(r)$ curve.
(a); $D(r)$ curve for solution C. (b); Obtained by subtracting the calculated peak due to the interactions within the methanol molecules from curve (a). (c); Obtained by subtracting the calculated peak due to the Cu–Cl_{eq} interactions from curve (b) (the clear peaks due to the Cu–O_{eq} and Cu–O_{ax} interactions are left at about 1.9 and 2.5 Å). (d); Final residual curve obtained by subtracting from curve (c) the calculated peaks due to the Cu–O_{eq} and Cu–O_{ax} interactions along with those due to the other expected intramolecular interactions (*cf.* Fig. 4-a).

A similar result of the $D(r)$ curve analysis could be deduced for the solution which was considered to include nearly equivalent amounts of the three complexes of n=1—3 in $[CuCl_n(CH_3OH)_{6-n}]$. It may be said from the formation data that almost all of the Cl^- ions are consumed for the above complexation; this makes the presence of chloro-bridged polymeric complexes improbable, for such polymer formation results in the presence of free Cl^- ions in the solution. In the concentrated methanolic 1.055—3.250 mol dm^{-3} $CuCl_2$ solutions, therefore, three monomeric complexes of the formula, $[CuCl_n(CH_3OH)_{6-n}]$ (n=1—3), were predominantly present; these possessed the axially elongated octahedral structure and coordinated the Cl^- ion equatorially.

The other structural models, b—g in Fig. 4, were also examined. As long as one considered the peak area and position of $D(r)$ curve, these models gave rise a peak with area and position similar to those of the observed peak at 2.3 Å. However, all of these models had to be discarded for the following reason. The temperature factors (b value) of the Cu–Cl bonding for the models b, c, and d were 0.02, 0.03, and 0.01 Å^2; these are too large, as compared with 0.0052 Å^2, a value known for the equatorial Cu–Cl bonding.[4] In the models e, f, and g, the b values, 0.0023—0.0032 Å^2, were not necessarily unreasonable, but these models had to be rejected for the following reasons. In model e, one of the Cl^- ions has to be at the apex apart from the Cu^{2+} ion with a very short distance, 2.45 Å, which is not plausible for the axial Cu–Cl bond distance. In model f, the Cu^{2+} ion binds two O atoms, two Cl^- ions, and one Cl^- ion with the distances of 1.95, 2.25, and 2.45 Å, respectively. This geometry resembles that in the $CuCl_2 \cdot 2DMSO$ crystal.[14] And this model gave an $s \cdot i\ (s)_{calcd}$ curve which fit the observed one well. But, the residual distribution curve obtained by using the model was not satisfactorily smooth in the 3—4 Å region. Model g gave an $s \cdot i\ (s)_{calcd}$ curve similar to that obtained by using model a. However, this geometry forces the the $\angle$Cu–O–C to be about 91°: This is not probable for the methanol molecule coordinated to the metal ions. The $\angle$Hg–O–C is 117° in the $HgCl_2 \cdot 2CH_3OH$ crystal,[15] and the $\angle$Cu–O–C is 119.5° in the $[Cu_2\{(CH_3)_2N(CH_2)_3NH(CH_2)_2O\}_2(CH_3OH)_2](ClO_4)_2$ crystal.[16]

References

1) H. Ohtaki, T. Yamaguchi, and M. Maeda, *Bull. Chem. Soc. Jpn.*, **49**, 701 (1976).

2) H. Ohtaki and M. Maeda, *Bull. Chem. Soc. Jpn.*, **47**, 2197 (1974); M. Magini, *Inorg. Chem.*, **21**, 1535 (1982).

3) M. Ichihashi, H. Wakita, T. Mibuchi, and I. Masuda, *Bull. Chem. Soc. Jpn.*, **55**, 3160 (1982).

4) M. Magini, *J. Chem. Phys.*, **74**, 2523 (1981).

5) J. R. Bell, J. L. Tyvoll, and D. L. Wertz, *J. Am. Chem. Soc.*, **95**, 1456 (1973).

6) D. L. Wertz and R. F. Kruh, *J. Chem. Phys.*, **50**, 4013, 4313 (1969).

7) M. Magini and T. Radnai, *J. Chem. Phys.*, **71**, 4255 (1979).

8) H. Wakita, M. Ichihashi, T. Mibuchi, and I. Masuda, *Bull. Chem. Soc. Jpn.*, **55**, 817 (1982).

9) The $D(r)$ curves reported by Wertz *et al.*[5] for the aqueous $CuCl_2$ solutions (3.18 and 4.35 mol dm^{-3}) showed five peaks at 1.95, 2.43, 3.2, 3.9, and 5.1 Å and one shoulder at 4.4 Å. They ascribed the peak at 3.9 Å to "secondary" Cu···O and Cu···Cl interactions between adjacent unitary molecules in the chloro-bridged polymeric complexes. On the $D(r)$ curves of the methanolic solutions subjected to our investigation, no peak around 3.9 Å was observed to appear.

10) G. G. Harvey, *J. Chem. Phys.*, **6**, 111 (1938); D. L. Wertz and R. F. Kruh, *ibid.*, **47**, 388 (1967).

11) T. Ichikawa and L. Kevan, *J. Phys. Chem.*, **84**, 1955 (1980).

12) H. Doe and T. Kitagawa, *Inorg. Chem.*, **21**, 2272 (1982).

13) When the initial concentration of $CuCl_2$ is given as C mol dm^{-3}, the respective concentrations of the species, $CuCl^+$, $CuCl_2$, and $CuCl_3^-$, can be calculated from the following equations: $[CuCl^+] = K_1[Cu][Cl]$; $[CuCl_2] = K_1K_2[Cu][Cl]^2$; $[CuCl_3^-] = K_1K_2K_3[Cu][Cl]^3$, and $[Cu] = C/\{1 + K_1[Cl] + K_1K_2[Cl]^2 + K_1K_2K_3[Cl]^3\}$, $2C = [Cl] + K_1[Cu][Cl] + 2K_1K_2[Cu][Cl]^2 + 3K_1K_2K_3[Cu][Cl]^3$.

14) R. D. Willett and K. Chang, *Inorg. Chim. Acta*, **4**, 447 (1970).

15) H. Brusset and F. Madaule-Aubry, *Bull. Soc. Chim. Fr.*, **1966**, 3121.

16) N. Matsumoto, S. Kida, and I. Ueda, *J. Coord. Chem.*, **9**, 133 (1979).

 © 1983 The Chemical Society of Japan Bull. Chem. Soc. Jpn., 56, 3765—3768 (1983)

Tetraammineplatinum(II)-Hydrogen Ion Exchange on α-Zirconium Phosphate and the Characterization of Its Complex Cation Form[1)]

Yoshitsugu HASEGAWA* and Giichi YAMAMINE

Department of Industrial Chemistry, Faculty of Technology, Tokyo University of Agriculture and Technology, Nakamachi, Koganei, Tokyo 184

(Received May 18, 1983)

The tetraammineplatinum(II)–hydrogen-ion exchange on α-zirconium phosphate has been investigated. The ion-exchange process was examined by measuring the change in the pH values of the supernatants. α-Zirconium phosphate loaded with tetraammineplatinum(II) was characterized by means of chemical analysis, X-ray diffractometry, infrared spectroscopy, and thermal analysis. The ion-exchange reaction proceeded more easily than the hexaaminecobalt(III)–hydrogen-ion exchange, and about 50% of the hydrogen ions in α-zirconium phosphate were replaced by tetraammineplatinum(II). The interlayer distance of the exchanger expanded from 7.60 to 10.7 Å.

α-Zirconium phosphate $Zr(HPO_4)_2 \cdot H_2O$ (α-ZP) has ion-exchange properties and catalytic activities. Though the great majority of work on α-ZP has dealt with the ion exchange, some catalytic properties have been studied.[2)] Also, it has been pointed out that α-ZP can be used as a catalytic support.[3)] In this case, the catalyst may be prepared as follows: Metal cations are exchanged with the protons in α-ZP and then reduced to a metallic state. The resultant catalyst may have two functional components, a metal and an acidic hydrogen; that is, it may work as a bifunctional catalyst, especially when the metal is one of the platinum group.[4)]

On the other hand, α-ZP has a layered structure and can form many intercalation compounds.[5)] Since salt forms of α-ZP also have a layered structure, a specific reaction can be expected between those layers.

The ion-exchange properties of α-ZP are influenced by its crystallinity, which depends on the method of preparation.[6)] When α-ZP is applied to a catalyst or a catalytic support, it is not necessary for α-ZP to be highly crystalline. The direct precipitation method has been employed during the course of these investigations so as to avoid differences due to the crystallinity. In the previous paper it was found that the hexaamminecobalt(III) ion, which is large, can exchange with the protons in α-ZP under suitable conditions.[7)] In this work, the tetraammineplatinum(II)–hydrogen-ion exchange was studied by the batch method, and the exchanger loaded with the complex cation (ZP–Pt) was characterized by means of chemical analysis, X-ray powder diffractometry, infrared spectroscopy, and thermal analyses.

Experimental

Preparation of α-ZP and Tetraammineplatinum(II) Chloride. The α-ZP was prepared by the direct precipitation method.[8)] The tetraammineplatinum(II) chloride was prepared according to the method of Kukuskine and Dkhara.[9)] Identification was made by elemental analysis and X-ray powder diffraction. The residue (ash) is assumed to be platinum metal. Found: Pt, 55.45; N, 15.91; H, 3.69; Cl, 19.39%. Calcd for $[Pt(NH_3)_4]Cl_2 \cdot H_2O$: Pt, 55.45; N, 15.91; H, 3.43; Cl, 20.14%. Though the X-ray diffraction pattern of $[Pt(NH_3)_4]Cl_2 \cdot H_2O$ has been previously presented,[10)] it differs from the one obtained in this work. This difference is caused by the facts that (1) only the strong reflections were recorded in the file, (2) the intensity of some diffraction peaks varied under the present experimental conditions, and (3), consequently, some peaks not listed in the file were observed as strong ones in this work. Cox analyzed the crystal structure of the complex and gave the lattice constants as $a_0 = 7.39 \pm 0.02$ and $c_0 = 4.21 \pm 0.02$ Å, and the space group as $P4/mmn$.[11)] Cox and Prestone later corrected a_0 to 14.76 Å.[12)] Since the diffraction peaks observed were indexed according to these constants in either case, the complex prepared was identified as $[Pt(NH_3)_4]Cl_2 \cdot H_2O$.

Ion Exchange. The ion-exchange procedures were similar to those reported previously.[7)] The concentration of the complex was 0.02 mol dm^{-3}, the reaction time, 48 h, and the reaction temperature, 25 °C.

Chemical Analysis. A weighed amount of ZP–Pt was mixed with sodium peroxide powder. Twenty-five ml of water were added to the mixture in an ice bath. The slurry thus obtained was placed on a water bath and heated for several hours. Then, the precipitate was filtered off and dissolved in hydrochloric acid. Zirconium was precipitated as cupferrate from the solution and determined gravimetrically. The filtrate was neutralized with hydrochloric acid and then another 5 ml of the acid were added to it. Platinum was separated as platinum sulfide by using thioacetamide as a homogeneous precipitant. The phosphorus was determined according to the literature.[13)]

Thermal Analysis. The differential scanning calorimetric (DSC) data were obtained with a Rigaku differential scanning calorimeter. Evolved gas analysis (EGA) was carried out with a Shimadzu pyrolyser-gas chromatograph.[14)] The thermogravimetric (TG) curve was obtained with a Shimadzu thermal analyser DT-30 at a heating rate of 10 °C/min under a herium stream.

Structural Study. The structural change in the exchanger was measured by means of X-ray diffractometry. The powder patterns were recorded with a Rigaku Denki Geigerflex diffractometer, using Ni-filtered Cu Ka ($\lambda = 1.542$ Å). The infrared (IR) spectra were measured on a JASCO DS-403G grating spectrophotometer.

Results and Discussion

Ion Exchange. The pH value of the supernatant solution was used as an indicator to ascertain the degree of the reaction. Figure 1 shows the pH change in the supernatant. In the first ion-exchange run, about 24% of the protons in α-ZP exchanged with the complex cation. The pH values rose, and the amount of the exchange per run decreased as the ion exchange proceeded. Then, the values reached the pH of the original solution. This ion exchange progressed more extensively than that for the hexaamminecobalt(III)–hydro-

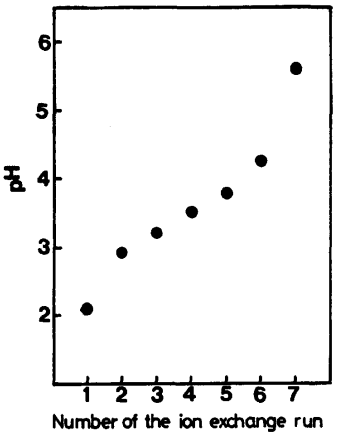

Fig. 1. pH change in the supernatant with the ion-exchange run.

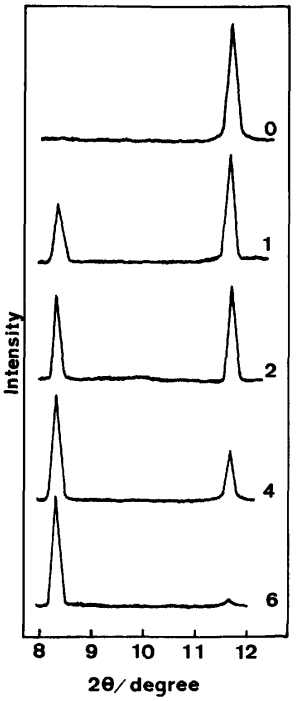

Fig. 2. Change in X-ray powder pattern of the exchanger. Numerals correspond to those of the ion-exchange runs in Fig. 1.

gen ion.[7] This difference may be explained on the basis of the size of the exchanging cation (see below).

In order to investigate the stoichiometry of the ion exchange, the composition of ZP–Pt was determined. Found: Zr, 20.2 (1.00); PO_4, 41.7 (1.96); Pt, 22.1 (0.51); N, 5.91 (1.89); H, 2.22 (9.83); weight loss by ignition, 17.9%. Calcd for $Zr[Pt(NH_3)_4]_{0.5}H(PO_4)_2 \cdot 1.5H_2O$: Zr, 20.7; PO_4, 43.1; Pt, 22.1; N, 6.53; H, 2.29; weight loss, 17.7%. In the parentheses are given the molar ratios of each element to zirconium. Since the ratio of nitrogen to platinum is equal to 3.7 and the hydrogen content agrees with the theoretical one, it can be said that $[Pt(NH_3)_4]^{2+}$ exchanges with two protons.

Structural Studies. Figure 2 shows the change in the X-ray diffraction patterns of the exchangers. The first peak at 8.3° (interplanar spacing of 10.7Å) appeared at the beginning of the ion exchange, and its intensity increased with the progress of the ion exchange. The intensity of the second peak decreased until it almost disappeared at the final stage of the ion exchange. The interplanar spacings of ZP–Pt are shown in Table 1.

TABLE 1. INTERPLANAR SPACINGS (*d*-VALUES) OF ZP–Pt

d/Å	I/I_0	*d*/Å	I/I_0
10.64	83	2.84	4
9.97	4	2.82	4
5.37	100	2.69	16
5.01	10	2.63	10
4.55	7	2.52	15
4.24	4	2.41	13
4.22	5	2.16	6
4.00	20	2.07	5
3.81	70	1.89	14
3.61	26	1.83	8
3.22	8	1.80	6
3.08	11	1.71	9
3.00	7	1.54	7

It is known that the interlayer distance of α-ZP depends on the cations present between layers. The first and the second peak correspond to the interlayer distances of ZP–Pt and α-ZP. If the ammonias coordinating to platinum are abstracted directly by α-ZP, or if they contribute to the ion exchange as ammonium ions, the ammonium form of α-ZP must be formed and the peak at 9.4° must be observed. As is shown in Fig. 2, this peak was not present in the present diffractograms.

Since the crystal structure of the salt forms of α-ZP has not been analyzed, the relationship between the interlayer distance and the counter-ion size is not clear. Generally, the interlayer distance increases with the size of the counter-ion. One of the salt forms, $ZrNaH(PO_4)_2 \cdot 5H_2O$ (monosodium form), has the interlayer distance of 11.8 Å[15]. The sodium ion was bonded to about four water molecules at the distance of 2.4 Å in a concentrated aqueous sodium iodide solution.[16] Assuming that the sodium ion in α-ZP retains the same structure as in the solution, the sphere with a diameter of 7.6 Å may be said to be present between the layers of the monosodium form. In hexaamminecobalt(III) ammonias coordinate octahedrally, and the complex cation can be assumed to be a sphere with a diameter of 7.6 Å.[17] The interlayer distance of ZP–Co was 11.2 Å (ZP-Co is α-ZP loaded with $[Co(NH_3)_6]^{3+}$).[7] The two interlayer distances are almost equal, in accordance with the size of the cations present. According to Cox, tetraammineplatinum(II) has a square planar structure, and the length of the side and the thickness can be estimated to be 5.7 and 2.8 Å respectively.[11] The platinum complex cation can be arranged between layers in three manners, namely, perpendicular, inclined, and parallel to the layer of α-ZP. The interlayer distance of ZP–Pt was 10.6 Å, slightly shorter than that of ZP–Co. This suggests that the plane of tetraammineplatinum(II) is not parallel to the layer of α-ZP.

The IR spectra of ZP–Pt and the ammonium form of α-ZP are shown in Fig. 3. The absorption bands whcih are

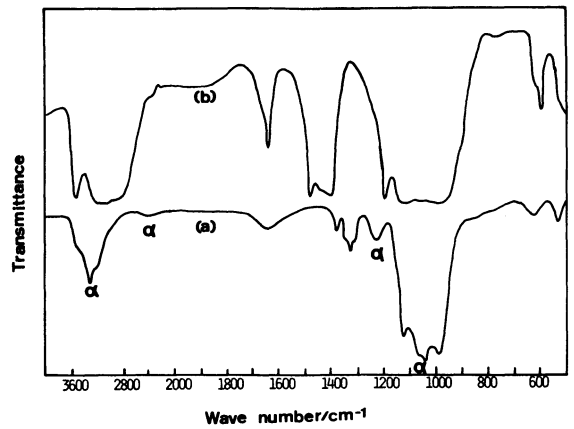

Fig. 3. IR spectrum of ZP-Pt (a) and the ammonium form of α-ZP (b).

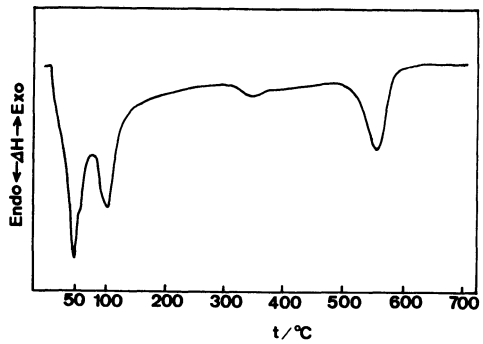

Fig. 4. DSC curve of ZP-Pt.

assigned by Horsley *et al.* are denoted by the symbol *a* in the figure.[18] The ammonia in tetraammineplatinum(II) ion gave absorptions at 3130, 1630, 1570, 1370, 1352, 1333, and 840 cm^{-1}.[19] The spectrum of ZP-Pt was composed of that of α-ZP and the tetraammineplatinum(II), except for the absorptions at 840 and 1570 cm^{-1}. These bands were assigned to the degenerate deformation and the rocking vibration of ammonia. According to Fujita *et al.*, the rocking vibration is sensitive to the kind of outer ion and the hydrogen bonding, and the absorption band is shifted to higher frequencies by these effects.[20] In ZP-Pt the ammonias form hydrogen bonds with the surrounding phosphate groups; consequently, the rocking vibration shifted and overlapped with the absorption bands of phosphate in the 900—1200 cm^{-1} region. It is considered that the absorption of 1570 cm^{-1} was shifted by the same cause and was observed in the 1500—1700 cm^{-1} region as a single band.

Thermal Studies. The DSC curve is shown in Fig. 4. The thermal decomposition took place in four steps, all of them endothermic. The evolution of ammonia was examined for each step. Ammonia was detected only at the third step. When ZP-Pt was decomposed in static air, the third step was observed as exothermic. This shows that the evolved ammonias were oxidized at the surface of a platinum crucible.[21] The ZP-Pt turned black after the third step, indicating that the platinum(II) ion in the solid was reduced to platinum(0) during the thermal decomposition and that nitrogen gas was evolved.

Table 2. Weight loss of ZP-Pt upon heating

t/°C	Experimental(%)	Theoretical(%)
200	8.39	6.13
420	13.4	13.6
600	17.9	17.7

In Table 2 the weight loss by heating is shown. Assuming that the possible decomposition pathways are as in the following scheme, the theoretical values are obtained. The experimental values agreed well with the theoretical ones at 420 and 600 °C, but the agreement is poor for the decomposition at 200 °C. At present it is impossible to give a proper interpretation of this disagreement.

$$Zr[Pt(NH_3)_4]_{0.5}H(PO_4)_2\cdot 1.5H_2O(ZP\text{-}Pt) \xrightarrow{\approx 200\,^\circ C}$$
$$Zr[Pt(NH_3)_4]_{0.5}H(PO_4)_2\ (I) \xrightarrow{\approx 420\,^\circ C} ZrPt(0)(HPO_4)_2\ (II)$$
$$\xrightarrow{\approx 600\,^\circ C} ZrPt(0)P_2O_7\ (III)$$

Scheme 1.

Compounds (II) and (III) were amorphous. The presence of zirconium pyrophosphate could not be detected. When ZP-Pt was heated to about 900 °C in a crucible and then examined by means of X-ray diffractometry, broad peaks were present at $2\theta=39.6$ and 46.4°. These correspond to the (111) and (200) planes of platinum metal.[22]

The authors wish to express their thanks to Mr. Yukihiro Takekawa for the IR measurements and to Professor Isao Tomita, Tokyo University of Fisheries, for the measurement of the TGA data.

References

1) A part of this work was presented at the 45th National Meeting of the Chemical Society of Japan, Tokyo, April, 1982, Abstr. No. 2W39.
2) a) F. Nozaki, T. Itoh, and S. Ueda, *Nippon Kagaku Kaishi*, **1973**, 674; b) T. Hattori, A. Ishiguro, and Y. Murakami *ibid.*, **1977**, 761.
3) G. Alberti, *Acc. Chem. Res.*, **11**, 163 (1978).
4) J. H. Sinnfelt, *Adv. Chem. Eng.*, **5**, 37 (1964).
5) "Intercalation Chemistry," ed by M. S. Whittingham and A. J. Jacobson, Academic Press, New York (1982), pp. 147—180.
6) G. Alberti, U. Costantino, S. Alluli, M. A. Massucci, and M. Pelliccioni, *J. Inorg. Nucl. Chem.*, **35**, 1347 (1973).
7) Y. Hasegawa, S. Kizaki, and H. Amekura, *Bull. Chem. Soc. Jpn.*, **56**, 734 (1983).
8) Y. Hasegawa and M. Kuwayama, *Bull. Chem. Soc. Jpn.*, **51**, 3485 (1978).
9) Yu. N. Kukuskine and S. Ch. Dkhara, *Russ. J. Inorg. Chem.*, **15**, 304 (1970).
10) JCPDS Powder Diffraction File 16-678.
11) E. G. Cox, *J. Chem. Soc.*, **1932**, 1912.
12) E. G. Cox and G. H. Preston, *J. Chem. Soc.*, **1933**. 1089.
13) I. M. Kolthoff and E. B. Sandell, "Textbook of Quantitative Inorganic Analysis," 3rd ed, McMillan, New York

(1952), pp. 377—382.
14) Y. Hasegawa, H. Aoki, and S. Abe, *Kikibunseki*, **11**, 648 (1973).
15) G. Alberti, U. Costantino, and J. P. Gupta, *J. Inorg. Nucl. Chem.*, **36**, 2103 (1974).
16) M. Maeda and H. Ohtaki, *Bull. Chem. Soc. Jpn.*, **48**, 3755 (1975).
17) M. Iwata and Y. Saito, *Acta Crystallogr., Sect. B*, **29**, 822 (1973).
18) S. E. Horsley, D. V. Nowell, and D. T. Stewart, *Spectrochim. Acta, Part A*, **30**, 535 (1974).
19) S. Mizushima, I. Nakagawa, M. J. Schmeltz, C. Curran, and J. V. Quagliano, *Spectrochim. Acta*, **13**, 31 (1958).
20) J. Fujita, K. Nakamoto, and M. Kobayashi, *J. Am. Chem. Soc.*, **78**, 3295 (1956).
21) T. Flóra, *Acta Chem. Acad. Hung.*, **69**, 1 (1971).
22) JCPDS Powder Diffraction File 4-0802.

 © 1983 The Chemical Society of Japan Bull. Chem. Soc. Jpn., 56, 3769—3772 (1983)

A Chromatographic Study of the Acidic Hydrolysis of *cyclo*-Hexa- and *cyclo*-Octaphosphate

Genichiro KURA

Department of Chemistry, Fukuoka University of Education, Akama, Munakata, Fukuoka 811-41

(Received May 23, 1983)

The hydrolysis rate of inorganic *cyclo*-hexa- and *cyclo*-octaphosphate in 0.1 mol dm^{-3} HCl was determined by means of anion-exchange chromatography. The phosphorus content in the column effluent was determined automatically by the use of the Mo^{V}–Mo^{VI} reagent. The hydrolysis reactions were first-order. The rate constant decreases from *cyclo*- tri- to *cyclo*-hexaphosphate with the increased ring, however, that of *cyclo*-octaphosphate increases again. This increase is thought to be due to the stronger proton affinity of *cyclo*-octaphosphate. The Arrhenius activation energies for *cyclo*-hexa- and *cyclo*-octaphosphate hydrolysis were 91.5 and 96.9 kJ mol^{-1} respectively.

Of the condensed cyclic phosphates, six-membered *cyclo*-tri- and eight-membered *cyclo*-tetraphosphate have been known since the 19th century.[1] Investigations of the higher-membered cyclic phosphates have, however, progressed only slowly.[2–5] We have recently reported some chemical properties of these phosphates.[6–10] These phosphates are very important electrolytes because of their high negative charge on relatively compact structure. When using these anions in the aqueous state for various purposes, for example, as a complexing agent with various cations or a food additive in place of higher-membered linear phosphates, their hydrolysis properties, which have rarely been described, must be known clearly.

The hydrolysis reaction of *cyclo*-tri- and *cyclo*-tetraphosphate have been reported by several authors.[11,12] However, most investigators have used paper chromatography as an analytical tool. As has previously been pointed out by us, though, it is difficult to obtain reliable data on hydrolysis kinetics by this technique.

We ourselves have applied anion-exchange chromatography to the analysis of the hydrolysis products of *cyclo*-tri-[13] and *cyclo*-tetraphosphate.[14] The phosphorus content in the column effluents was determined automatically by the use of the Mo^{V}–Mo^{VI} reagent. From the chromatograms of the hydrolysis products, the kinetic data of *cyclo*-tri- and *cyclo*-tetraphosphate in a 0.1 mol dm^{-3} hydrochloric acid solution were obtained.

In both cases, the chromatographic run of each hydrolysis sample was finished within 50 min. Our analytical method is thought to be more fitting than the paper chromatographic method in terms of rapidity and reliability.

For *cyclo*-tetraphosphate hydrolysis studies, various experimental conditions were examined for the separation of parent compound and the hydrolysis products-linear tetra-, tri-, di- and monophosphates. Finally, suitable conditions for than purpose were found.

Similar analytical conditions for the *cyclo*-tetraphosphate hydrolysis products were also examined for studies of the hydrolysis of twelve-membered *cyclo*-hexaphosphate and sixteen-membered *cyclo*-octaphosphate.

Futhermore, the hydrolysis reaction of these cyclic phosphates might be utilized in the preparation of higher-membered linear phosphates which are their hydrolysis products.

In this paper, linear and cyclic phosphate are abbreviated as P_n and P_{nm} respectively, where n is the degree of polymerization.

Experimental

Materials. As an anion-exchanger, Hitachi Custom Ion-exchange Resin 2630 was used.

The sodium *cyclo*-hexa- and *cyclo*-octaphosphate was prepared by the methods of Griffith and Buxton[4] and Schülke[5] respectively.

Chromatographic System. The system is shown in Fig. 1. Pump A is a part of the Hitachi Model 635 liquid chromatograph. Pump B is a Model KHU-W-52 apparatus made by the Kyowa Seimitsu Co.

As eluents, a mixture of 0.4 mol dm^{-3} of potassium chloride and 0.005 mol dm^{-3} EDTA (2Na salt), the pH of which has been adjusted to 10.2 with a sodium hydroxide solution, was used. In this eluent, EDTA acts as the buffer reagent, while the masking reagent of the metal ions present as an impurity.

Hydrolysis. The initial concentration of the *cyclo*-hexa- and *cyclo*-octaphosphate solution to be hydrolysed was adjusted to 1.25×10^{-3} mol dm^{-3}.

Hydrochloric acid was added to each solution at a concentration of 0.1 mol dm^{-3}, and the hydrolysis reaction was performed in a water bath, the temperature of which was maintained within ± 0.1 °C. At measured time intervals, samples of a few cubic centimeters were withdrawn and neutralized with the same volume of a 0.1 mol dm^{-3} sodium hydroxide solution at nearly 0 °C.

The present author ascertained that the hydrolysis reaction of *cyclo*-hexa- and *cyclo*-octaphosphate in a neutral solution does not occur at a low temperature. For example, the hydrolysis products of both phosphates were not observed when the phosphates were boiled for 1 h in a neutral solution.

The sample solution were stored in a refrigerator until taken out for analysis.

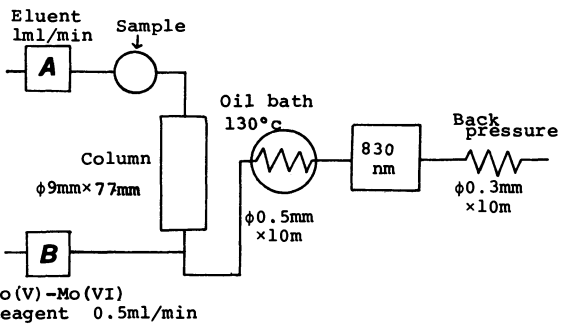

Fig. 1. Flow diagram of chromatograph and detection system.

Results and Discussion

When *cyclo*-hexaphosphate is hydrolysed as shown in Eq. 1, the initial hydrolysis product is linear hexaphosphate; it can also be hydrolysed to lower linear phosphates and probably to *cyclo*-triphosphate.

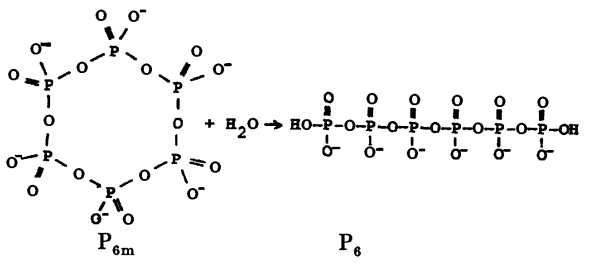

P_{6m} P_6

$$P_6O_{18}^{6-} + H_2O \rightarrow H_2P_6O_{19}^{6-} \rightarrow P_5 \rightarrow P_4 \rightarrow P_3 \rightarrow P_2 \rightarrow P_1 \quad (1)$$

It is necessary to separate the parent compound and the seven hydrolysis products for the determination of the hydrolysis rate. Anion-exchange chromatography was thought to be best fitted for this purpose. The present author has, with the use of Hitachi Custom Ion 2630 resin applied anion-exchange chromatography to the analysis. As reported in our previous paper[14] on the separation of *cyclo*-tetraphosphate and its hydrolysis products, the distribution ratio of cyclic phosphates on the anion-exchange resin is not affected by the variation in the pH when the chloride-ion concentration of an eluent is constant. In the case of linear di- and triphosphate, their distribution ratios decrease appreciably with the increase in the pH at a constant chloride concentration.[15] From the retention volume on the column presented in our previous paper,[14] it was found that the distribution ratio of linear tetraphosphate also decreases with the increase in pH. From this fact, it was expected that the increase in the pH in the eluent might result in the achievement of a separation between *cyclo*-hexaphosphate and its hydrolysis products, which is impossible in the lower-pH range. Therefore, a mixture of *cyclo*-hexaphosphate and polyphosphate glass ($\bar{n}=10$) was eluted on the column with the use of 0.4 mol dm^{-3} KCl at pH 10.2 as the eluent.

The resulting chromatogram is shown in Fig.2. At least, linear phosphates with the polymerization degree less than eight were eluted in stages earlier than *cyclo*-hexaphosphate. The peak volume of an elution curve of *cyclo*-triphosphate as a hydrolysis product was about 75 cm^3 under these conditions.

The hydrolysis products of *cyclo*-hexaphosphate were analyzed under these chromatographic conditions.

cyclo-Octaphosphate of the sixteen-membered ring was eluted 10 cm^3 later than *cyclo*-hexaphosphate. Consequently, *cyclo*-octaphosphate and its hydrolysis products were successfully separated under the same elution conditions.

As discussed in our earlier papers, first-order hydrolysis-rate constants of *cyclo*-tri- and *cyclo*-tetraphosphate in a 0.1 mol dm^{-3} HCl solution varied with their initial concentration up to the relatively lower-concentration region. The hydrolysis rates of *cyclo*-hexa- and *cyclo*-octaphosphate were measured by changing those initial concentrations. A constant rate constant was obtained when the initial concentrations of both phosphates were lower than 2.5×10^{-3} mol dm^{-3}.

In the following hydrolysis experiments, the initial concentration of the parent compound was fixed at 1.25×10^{-3} mol dm^{-3}. We have presumed that the variation in the rate constant with the initial concentrations is due to the change in the hydrogen concentration in a test solution as the hydrolysis reaction proceeds.

An example of chromatograms of the hydrolysis products of *cyclo*-hexaphosphate in 0.1 mol dm^{-3} HCl at 40 °C is shown in Fig. 3. It was confirmed by a separate experiment that the area of the chromatogram of the *cyclo*-hexaphosphate thus obtained *versus* the phosphate concentration known gave a straight line passing through the point of origin. From the chromatograms of the hydrolysis products, the hydrolysis rate was calculated. The area of the chromatograms of the hydrolysis sample was automatically estimated by connecting an output terminal from the spectrophotometer to a SORD Mark IIIB micro computer through an A-D converter.

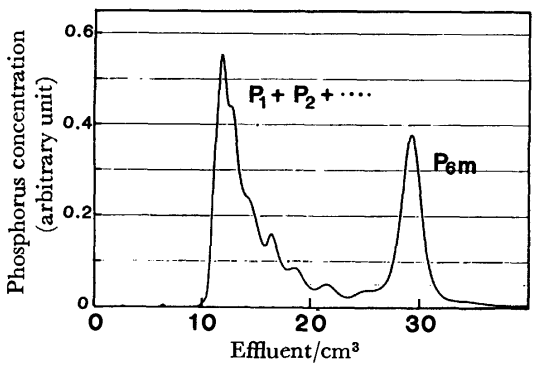

Fig. 2. Elution chromatogram of *cyclo*-hexaphosphate and linear oligophosphates mixture with 0.4 mol dm^{-3} potassium chloride solution (pH 10.2).

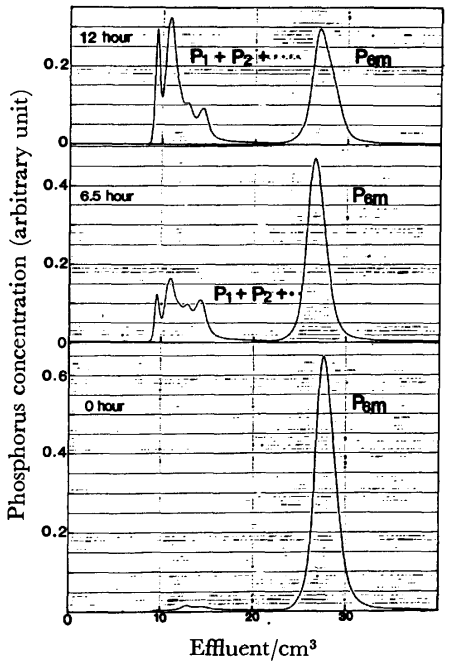

Fig. 3. Chromatograms of hydrolysis samples of *cyclo*-hexaphosphate in 0.1 mol dm^{-3} hydrochloric acid at 40 °C.

As was pointed out in the earlier papers,[13,14] the hydrolysis reactions of condensed phosphates have been known to be first-order. Let the total concentration of *cyclo*-hexaphosphate be c; the hydrolysis rate, $-dc/dt$, can thus be written as;

$$-\frac{dc}{dt} = k_0[P_6O_{18}^{6-}] + k_1[HP_6O_{18}^{5-}] + k_2[H_2P_6O_{18}^{4-}] + k_3[H_3P_6O_{18}^{3-}] + k_4[H_4P_6O_{18}^{2-}] + k_5[H_5P_6O_{18}^{-}] + k_6[H_6P_6O_{18}], \quad (2)$$

where $k_i (i=0—6)$ are rate constants for individual protonated species. If the molar fractions of the protonated species are written as X_6 for $H_6P_6O_{18}$, X_5 for $H_5P_6O_{18}^{-}$, and so on, the hydrolysis rate can be written as;

$$-\frac{dc}{dt} = (k_0X_0 + k_1X_1 + k_2X_2 + k_3X_3 + k_4X_4 + k_5X_5 + k_6X_6)c = k_{obsd}c, \quad (3)$$

where;

$$k_{obsd} = k_0X_0 + k_1X_1 + k_2X_2 + k_3X_3 + k_4X_4 + k_5X_5 + k_6X_6.$$

When the hydrogen-ion concentration is constant, k_{obsd} should be constant. Accordingly, from the first-order hydrolysis rate equation (3), if $[P]_0$ and $[P]_t$ are denoted as the concentrations of *cyclo*-hexaphosphate at time 0 and t respectively, $\log([P]_t/[P]_0)$ *versus* t plots should give a straight line.

Similar treatments are possible for the *cyclo*-octaphosphate hydrolysis reaction.

$\log([P]_t/[P]_0)$ *versus* t plots for *cyclo*-hexa- and *cyclo*-octaphosphate hydrolysis at various temperatures are shown in Figs. 4 and 5. Good straight lines were obtained, hence, the hydrolysis reactions of both phosphates are first-order. The apparent first-order rate constants, k_{obsd}, and half-lives, $t_{1/2}$, at various temperatures are shown in Table 1.

From the k_{obsd} at the various temperatures examined, the linear Arrhenius plots shown in Fig. 6 were obtained. The Arrhenius activation energies, *Ea*, were 91.5 and 96.9 kJ mol^{-1} for *cyclo*-hexa- and *cyclo*-octaphosphate respectively, nearly equivalent to those obtained for

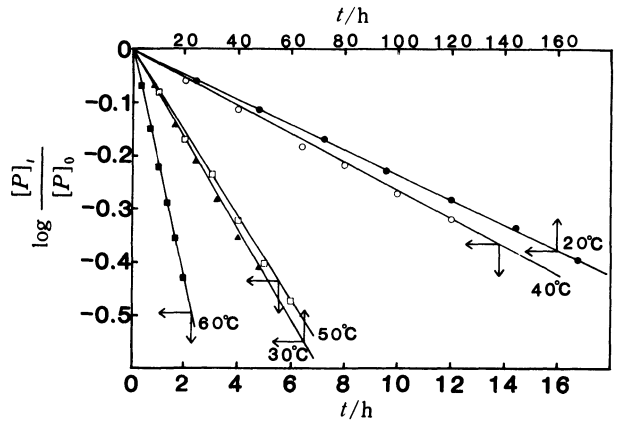

Fig. 4. Hydrolysis rate of *cyclo*-hexaphosphate in 0.1 mol dm^{-3} hydrochloric acid at various temperatures.

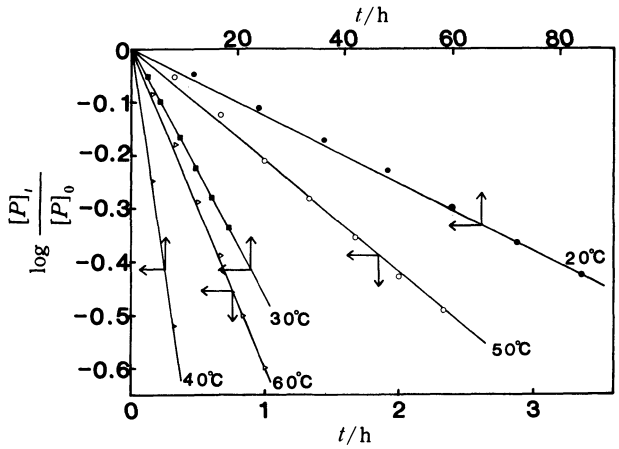

Fig. 5. Hydrolysis rate of *cyclo*-octaphosphate in 0.1 mol dm^{-3} hydrochloric acid at various temperatures.

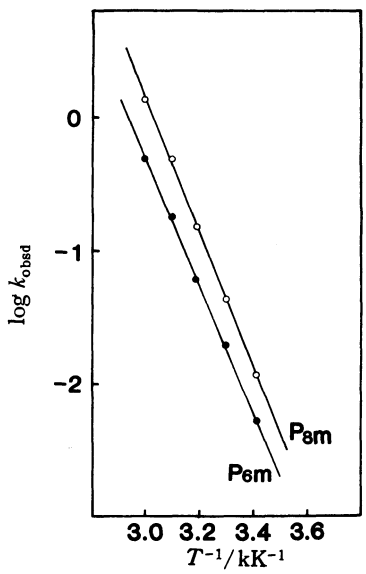

Fig. 6. Arrhenius plot for *cyclo*-hexa- and *cyclo*-octaphosphate in 0.1 mol dm^{-3} hydrochloric acid.

Table 1. Kinetic data on *cyclo*-hexa- and *cyclo*-octaphosphate hydrolysis in 0.1 mol dm^{-3} hydrochloric acid

		Temperature/°C				
		20	30	40	50	60
P_{6m}	k_{obsd}/h^{-1}	5.40×10^{-3}	1.96×10^{-2}	6.07×10^{-2}	0.181	0.495
	$t_{1/2}$/h	128	35.4	11.4	3.82	1.40
P_{8m}	k_{obsd}/h^{-1}	1.17×10^{-2}	4.31×10^{-2}	0.153	0.486	1.39
	$t_{1/2}$/h	59.3	16.1	4.53	1.43	0.500

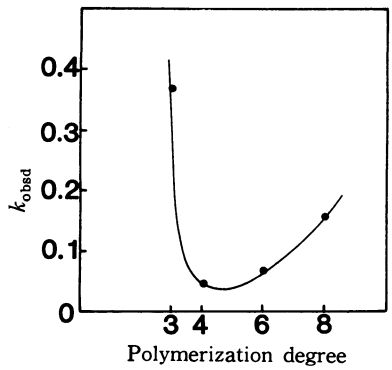

Fig. 7. First order rate constants as a function of polymerization degree in 0.1 mol dm^{-3} hydrochloric acid at 40 °C.

other condensed phosphates in acidic media.

The apparent rate constants, k_{obsd}, of *cyclo*-hexa- and *cyclo*-octaphosphate in 0.1 mol dm^{-3} HCl at 40 °C are plotted *versus* their polymerization degree in Fig. 7, along with the data for *cyclo*-tri- and *cyclo*-tetraphosphate reported in our previous papers.[13,14] This graph has a minimum at a polymerization degree near 5. This fact can be explained as follows. The present author has not obtained sufficient data on cyclic phosphate hydrolysis in alkaline media; however, from Ref. 3, it can be presumed that the stability of the ring structure of cyclic phosphate in an alkaline solution increases with an increase in the ring size. On the other hand, the hydrolysis rates of condensed phosphates are accelerated very much by the proton which binds to the phosphates. The bonding of the hydrogen ion to the oxygen atom involved in the phosphate tetrahedron renders the phosphorus atom more positive by reducing the electron density around that atom and more susceptible to nucleophilic attack by water molecules. As has been reported in our previous paper,[9] the degree of bonding with the hydrogen ion increase with an increase in the size of the ring. Accordingly, an increase in proton affinity would result in an increase in the k_{obsd}.

From the two opposite effects increasing and decreasing k_{obsd} presented above, k_{obsd} comes to have a minimum near the pentamer under acidic conditions.

References

1) Van Wazer, "Phosphorus and Its Compounds," Interscience, New York (1958).
2) J. R. Van Wazer and E. Karl-Kroupa, *J. Am. Chem. Soc.*, **78**, 1772 (1956).
3) E. Thilo and U Schülke, *Z. Anorg. Allg. Chem.*, **341**, 293 (1965).
4) E. J. Griffith and R. L. Buxton, *Inorg. Chem.*, **4**, 549 (1965).
5) U. Schülke, *Z. Anorg. Allg. Chem.*, **360**, 231 (1968).
6) G. Kura and S. Ohashi, *J. Chromatogr.*, **56**, 111 (1971).
7) G. Kura and S. Ohashi, *J. Inorg. Nucl. Chem.*, **34**, 2899 (1972).
8) G. Kura, S. Ohashi, and S. Kura, *J. Inorg. Nucl. Chem.*, **36**, 1605 (1974).
9) G. Kura and S. Ohashi, *J. Inorg. Nucl. Chem.*, **38**, 1151 (1976).
10) S. Ohashi, G. Kura, Y. Shimada, and M. Hara, *J. Inorg. Nucl. Chem.*, **39**, 1513 (1977).
11) R. M. Healy and M. L. Kilpatrick, *J. Am. Chem. Soc.*, **77**, 5258 (1955).
12) J. Crowther and A. E. R. Westman, *Can. J. Chem.*, **34**, 969 (1956).
13) G. Kura, T. Nakashima, and F. Oshima, *J. Chromatogr.*, **219**, 385 (1981).
14) G. Kura, *J. Chromatogr.*, **246**, 73 (1982).
15) J. Beukenkamp, W. Rieman, III, and S. Lindenbaum, *Anal. Chem.*, **26**, 505 (1954).

Studies of the Selective *O*-Alkylation and Dealkylation of Flavonoids. VI.[1] Demethylation of 8-Hydroxy-5,7-dimethoxyflavones with Anhydrous Aluminum Chloride or Bromide in Acetonitrile

Tokunaru Horie,* Hiroki Kourai, and Nobuhisa Fujita

Department of Applied Chemistry, Technical College of Tokushima University, Minamijosanjima-cho, Tokushima 770

(Received June 6, 1983)

The demethylation of seven 8-hydroxy-5,7-dimethoxyflavones with anhydrous aluminum chloride or bromide in acetonitrile was studied and the following results were obtained. (1) Anhydrous aluminum chloride in acetonitrile selectively split the 5-methoxyl group without cleavage of the 7-methoxyl group, and seven 5,8-dihydroxy-7-methoxyflavones were quantitatively synthesized by the demethylation. (2) In the demethylation with anhydrous aluminum bromide, the 5- and 7-methoxyl groups on 4′,5,7-trimethoxy- and 3′,4′,5,7-tetramethoxy-8-hydroxyflavone were selectively split to give the corresponding 5,7,8-trihydroxyflavones in good yield. However, the demethylation was not accessible to the synthesis of 5,7,8-trihydroxy-3′,4′,5′-trimethoxyflavone, 4′,5,7,8-tetrahydroxy-3′-methoxy-, and 3′,5,7,8-tetrahydroxy-4′-methoxyflavone, because of the cleavage of the methoxyl groups on the B ring. The synthesized flavones were employed for the identification of the two natural flavones, which were proposed to be 4′,5,8-trihydroxy-7-methoxyflavone and 4′,5,8-trihydroxy-3′,7-dimethoxyflavone. The former, salvitin, was revised to 4′,5,7-trihydroxy-6-methoxyflavone and the latter seemed to be 4′,5,7-trihydroxy-3′,8-dimethoxyflavone.

In 1975, Gupta *et al.*[2] identified salvitin, isolated from *Salvia plebeia*, as 4′,5,8-trihydroxy-7-methoxyflavone (**1b**) on the basis of the spectral data and the synthesis by the two methods: the nuclear oxidation of 4′,5-dihydroxy-7-methoxyflavone and the oxidative demethylation of 4′-benzyloxy-5,7,8-trimethoxyflavone with nitric acid *via* the corresponding 5,8-quinone derivative. On the basis of the UV and MS data, Whalen *et al.*[3] claimed that one of the natural flavones which were isolated from *Solanum* section *Androceras* was 4′,5,8-trihydroxy-3′,7-dimethoxyflavone (**1d**). Recently, two natural flavones, 5,7,8-trihydroxy-4′-methoxyflavone (**2a**)[4] and 4′,5,7,8-tetrahydroxy-3′-methoxyflavone (**2d**)[3] were also isolated in the form of glycosides. A convenient method for synthesizing 5,8-dihydroxy-7-methoxyflavones (**1**) and 5,7,8-trihydroxyflavones (**2**) such as the above natural flavones seems to be the oxidative demethylation[2,5] of 5,7,8-trioxygenated flavones using nitric acid. However, little 5,8-dihydroxy-4′,7-dimethoxyflavone (**1a**) was synthesized from 4′,5,7,8-tetramethoxyflavone[6] by use of this method.

On the other hand, we had reported that 5,6-dihydroxy-7-methoxyflavones (**4**) and 5,6,7-trihydroxyflavones (**5**) were synthesized from 6-hydroxy-5,7-dimethoxyflavones (**3**) by the demethylation with anhydrous aluminum chloride in acetonitrile.[7] The results suggest that **1** and **2** may be synthesized from 8-hydroxy-5,7-dimethoxyflavones (**6**), isomers of **3**. Hence the selective demethylation of **6** with anhydrous aluminum chloride or bromide was studied, and it was found that **1a**—**g** and **2a**, **c** were synthesized from the corresponding **6** in high yield. In this paper, we report on the demethylation of **6**, the characterization of **1** and **2**, and the identification of the two natural flavones which were proposed as 5,8-dihydroxy-7-methoxyflavones (**1b** and **1d**).

Results and Discussion

Syntheses of 8-Hydroxy-5,7-dimethoxyflavones (6). The 2-benzyloxyl group on 2,3-bis(benzyloxy)-4,6-dimethoxyacetophenone (**8**), which was easily derived from 2,3-dihydroxy-4,6-dimethoxyacetophenone (**7**),[8] was selectively split with hydrochloric acid in acetic acid to give 3-benzyloxy-2-hydroxy-4,6-dimethoxyacetophenone (**9**) in good yield. But the partial benzylation of **7** with benzyl chloride-anhydrous potassium carbonate in acetone or *N*,*N*-dimethylformamide did not give **9** in favorable yield because of the formation of by-products. The benzoates, derived from **9** with substituted benzoyl chlorides, were converted into the diketone derivatives (**10**) by the Baker-Venkataraman rearrangement with potassium hydroxide in anhydrous pyridine. Cyclization of **10** with anhydrous sodium acetate in acetic acid easily led to 8-benzyloxy-5,7-dimethoxyflavones (**11**) which were quantitatively converted into **6** by the hydrogenolysis with palladium on charcoal.

Demethylation of 8-Hydroxy-5,7-dimethoxyflavones (6) with Anhydrous Aluminum Chloride in Acetonitrile. In the previous paper,[9] we reported that the 5-methoxyl group on the acetates of 6-hydroxy-5,7,8-trimethoxyflavones was quantitatively split to give 5,6-dihydroxy-7,8-dimethoxyflavones with about 5% (w/v) anhydrous aluminum chloride in acetonitrile at 80 °C. But under the same conditions, few of the 5-methoxyl groups on **6a** and its acetate (**12a**) were split. On the other hand, the 7-methoxyl group on **6a** was not completely split with about 30% (w/v) anhydrous aluminum chloride in acetonitrile, in contrast to that of 6-hydroxy-5,7,8-trimethoxyflavones[9] and **3**.[7] Therefore, **1a**—**g** were easily synthesized from **6** in quantitative yield under the following conditions: about 10% (w/v) anhydrous aluminum chloride in acetonitrile at 70 °C for 10 h.

The benzyloxyl groups on **11** were also split to give **1** under the above conditions. However, the high performance liquid chromatograms (HPLC) of the demethylated products from the flavones (**6b**, **d**, **e**, and **f**) which had benzyloxyl groups on the B ring indicated the existence of by-products having longer retention time than that of **1**. Consequently, for the synthesis of **1**, the demethylation of **6** was better than that of **11**.

The ^{1}H NMR data for the hydroxyflavones (**1** and **6**) (in DMSO) and the acetates (**13**) of **1** (in $CDCl_3$) are shown in Tables 1 and 2. The C_3- and C_6-proton

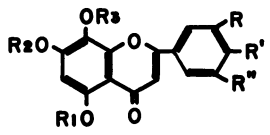

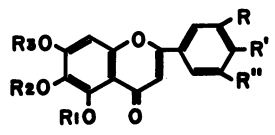

1 R1=R3=H, R2=Me
2 R1=R2=R3=H
6 R1=R2=Me, R3=H
11 R1=R2=Me, R3=CH2Ph
12 R1=R2=Me, R3=Ac
13 R1=R3=Ac, R2=Me
14 R1=R2=H, R3=Me
16 R1=R2=R3=Ac

3 R1=R3=Me, R2=H
4 R1=R2=H, R3=Me
5 R1=R2=R3=H
15 R1=R3=H, R2=Me

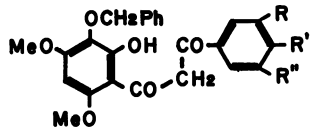

10

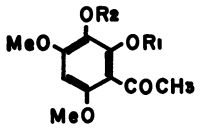

7 R1=R2=H
8 R1=R2=CH2Ph
9 R1=H, R2=CH2Ph

1, 2, 3, 4, 5, 6, 14, and 15

a R=R"=H, R'=OMe
b R=R"=H, R'=OH
c R=R'=OMe, R"=H
d R=OMe, R'=OH, R"=H
e R=OH, R'=OMe, R"=H
f R=R'=OH, R"=H
g R=R'=R"=OMe
h R=R"=OMe, R'=OH
i R=R'=R"=OH

10 and 11

a R=R"=H, R'=OMe
b R=R"=H, R'=OCH2Ph
c R=R'=OMe, R"=H
d R=OMe, R'=OCH2Ph, R"=H
e R=OCH2Ph, R'=OMe, R"=H
f R=R'=OCH2Ph, R"=H
g R=R'=R"=OMe

12, 13, and 16

a R=R"=H, R'=OMe
b R=R"=H, R'=OAc
c R=R'=OMe, R"=H
d R=OMe, R'=OAc, R"=H
e R=OAc, R'=OMe, R"=H
f R=R'=OAc, R"=H
g R=R'=R"=OMe
i R=R'=R"=OAc

signals listed in these Tables were assigned on the basis of the NOE experiment for **1a** and **13a**: the integrated intensities of the singlets at δ 6.52 for **1a** and δ 6.67 for **13a** increased about 28 and 22% respectively, when the methoxyl groups were saturated by double irradiation. The C_6-proton on **1** is not affected by their substituents on the B ring and its signals are in the narrow range of δ 6.51 to 6.54, while the C_3-proton is slightly affected and its signals are in the slightly wider range of δ 6.65 to 7.02. These phenomena are also observed in the spectra for **6** and **13**. On the other hand, the signals for C_6-proton on **13** in $CDCl_3$ are in the range of δ 6.67 to 6.69 and the range shifts about 0.15 ppm lower than that of **1** in DMSO (δ 6.51—6.54). These δ values for **1** and **13** are distinct from those for 5,7-dihydroxy-8-methoxyflavones (**14**)[10-12] (C_6–H, $\delta\approx$6.3; acetates, $\delta\approx$6.8) or 5,7-dihydroxy-6-methoxyflavones (**15**)[13,14] (C_8–H, $\delta\approx$6.6; acetates, $\delta\approx$7.3).

In the UV spectra for **1**, Bands I and II are seen at about 330 and 280 nm respectively, as shown in Table 3. These bands undergo bathochromic shift by the addition of aluminum chloride and the spectra consist typically of four major absorption peaks. The properties are greatly different from those of 5,6,7-trihydroxyflavone derivatives such as **15**[13,14] or **4**[7,15] However, the UV data for the flavones (**1**) are essentially identical with those for the corresponding 5,7-dihydroxy-8-methoxyflavones (**14**),[10-12] the isomers of **1**, but a little differences were observed at 300—330 nm in the presence of aluminum chloride.

On the other hand, Bands I and II for the 5,7-dihydroxyflavones (**14**) are shifted bathochromically by the addition of sodium acetate,[10-12] but these bands for the 5,8-dihydroxyflavones (**1a**, **c**, **e**, and **g**) which have not the 4'-hydroxyl group do not show any bathochromic shift. In the UV spectra for the 5,8-dihydroxyflavones (**1b**, **d**, and **f**) having the 4'-hydroxyl group, Band II which associates with absorption involving the A ring benzoyl system do not also shift bathochromically by the addition of sodium acetate, but Band I undergoes a bathochromic shift and splits into two typical absorption peaks: one has the same wavelength as Band I and the other is in a range of 390—410 nm (Table 3).

*Demethylation of 8-Hydroxy-5,7-dimethoxyflavones (**6**) with Anhydrous Aluminum Bromide in Acetonitrile.* In the HPLC of 5,6,7-trioxygenated flavones, their retention times have been known to decrease with increasing numbers of hydroxyl groups except for 5-hydroxyl

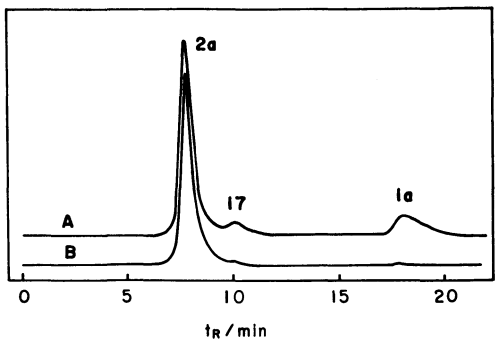

Fig. 1. HPLC of demethylated products from **6a** with anhydrous aluminum bromide in acetonitrile at 50 °C for 24 h (A) in air and 48 h (B) in nitrogen atmosphere. Flow rate, 0.5 ml/min. Temp, room temp.

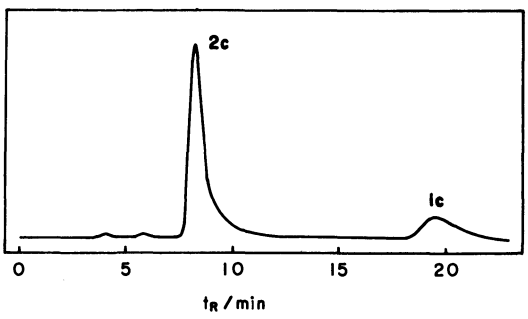

Fig. 2. HPLC of demethylated product from **6c** with anhydrous aluminum bromide in acetonitrile at 50 °C for 24 h in nitrogen atmosphere.
Same conditions as in Fig. 1.

Table 1. ^{1}H NMR data for 5,8-dihydroxy-7-methoxyflavones(**1**), 5,7,8-trihydroxyflavones(**2**), and 8-hydroxy-5,7-dimethoxyflavones(**6**) in DMSO

Compd	Arom. H						OMe		5-OH
	C_3–H	C_6–H	$C_{3'}$–H	$C_{5'}$–H	$C_{2'}$–H	$C_{6'}$–H			
1a	6.80s	6.52s	7.10d (2H)		8.07d (2H)		3.85s (3H)	3.90s (3H)	12.42s
1b	6.74s	6.53s	6.94d (2H)		8.00d (2H)		3.91s (3H)		12.45s
1c	6.90s	6.51s	—	7.11d	7.59d′	7.75q	3.85s (3H)	3.87s (3H)	12.40s
							3.89s (3H)		
1d	6.87s	6.53s	—	6.95d	7.60d′	7.77q	3.90s (6H)		12.45s
1e	6.72s	6.53s	—	7.08d	7.53d′	7.61q	3.86s (3H)	3.91s (3H)	12.46s
1f	6.65s	6.53s	—	6.90d	7.53d′	7.47q	3.91s (3H)		12.46s
1g	7.02s	6.54s	—	—	7.40s (2H)		3.77s (3H)	3.91s (9H)	12.33s
1h	6.96s	6.54s	—	—	7.41s (2H)		3.89s (9H)		12.46s
1i	6.55s	6.55s	—	—	7.09s (2H)		3.93s (3H)		12.53s
2a	6.79s	6.28s	7.13d (2H)		8.12d (2H)		3.86s (3H)		12.32s
2b	6.70s	6.26s	6.92d (2H)		7.99d (2H)		—		12.35s
2c	6.88s	6.27s	—	7.10d	7.62d′	7.77q	3.85s (3H)	3.88s (3H)	12.32s
2f	6.60s	6.26s	—	6.88d	7.35—7.6m (2H)		—		12.36s
2g	6.98s	6.28s	—	—	7.41s (2H)		3.76s (3H)	3.90s (6H)	12.26s
2i	6.50s	6.29s	—	—	7.08s (2H)		—		12.52bs
17	6.89s	—	7.08d (2H)		8.17d (2H)		3.85s (3H)		13.20s
6a	6.59s	6.67s	7.06d (2H)		8.02d (2H)		3.83s (6H)	3.95s (3H)	—
6b	6.55s	6.67s	6.93d (2H)		7.93d (2H)		3.85s (3H)	3.97s (3H)	—
6c	6.72s	6.69s	—	7.12d	7.59d′	7.73q	3.85s (6H)	3.89s (3H)	—
							3.97s (3H)		
6d	6.63s	6.63s	—	6.90d	7.45—7.7m (2H)		3.82s (3H)	3.88s (3H)	—
							3.95s (3H)		
6e	6.50s	6.67s	—	7.05d	7.46d′	7.54q	3.83s (3H)	3.86s (3H)	—
							3.97s (3H)		
6f	6.45s	6.68s	—	6.89d	7.48d′	7.42q	3.83s (3H)	3.97s (3H)	—
6g	6.82s	6.69s	—	—	7.37s (2H)		3.76s (3H)	3.85s (3H)	—
							3.90s (6H)	3.98s (3H)	—

s: singlet, d: doublet (J=8.5 Hz), d′: doublet(J=2.5 Hz), q: quartet (J=8.5, 2.5 Hz), m: multiplet.

Table 2. ^{1}H NMR data for 5,8-diacetoxy-7-methoxyflavones(**13**) and 5,7,8-triacetoxyflavones(**16**) in $CDCl_3$

Compd	Arom. H						OMe		OAc	
	C_3–H	C_6–H	$C_{3'}$–H	$C_{5'}$–H	$C_{2'}$–H	$C_{6'}$–H				
13a	6.47s	6.67s	6.97d (2H)		7.69d (2H)		3.85s (3H)	3.92s (3H)	2.44s (6H)	
13b	6.51s	6.69s	7.20d (2H)		7.76d (2H)		3.92s (3H)		2.32s (3H)	2.43s (6H)
13c	6.48s	6.68s	—	6.94d	7.24d′	7.39q	3.92s (9H)		2.43s (6H)	
13d	6.51s	6.69s	—	7.10d	7.30d′	7.36q	3.88s (3H)	3.92s (3H)	2.32s (3H)	2.41s (3H)
									2.43s (3H)	
13e	6.45s	6.67s	—	7.02d	7.43d′	7.63q	3.89s (3H)	3.91s (3H)	2.34s (3H)	2.43s (6H)
13f	6.49s	6.69s	—	7.30d	7.5—7.75m (2H)		3.93s (3H)		2.31s (6H)	2.43s (6H)
13g	6.49s	6.69s	—	—	6.98s (2H)		3.90s (12H)		2.43s (6H)	
16a	6.54s	6.93s	6.98d (2H)		7.70d (2H)		3.87s (3H)		2.34s (3H)	2.44s (6H)
16b	6.55s	6.93s	7.20d (2H)		7.73d (2H)		—		2.32s (6H)	2.41s (6H)
16c	6.53s	6.93s	—	6.93d	7.23d′	7.37q	3.93s (6H)		2.33s (3H)	2.42s (6H)
16f	6.54s	6.94s	—	7.29d	7.5—7.75m (2H)		—		2.30s (6H)	2.32s (3H)
									2.41s (6H)	
16g	6.55s	6.95s	—	—	6.98s (2H)		3.91s (9H)		2.35s (3H)	2.42s (6H)
16i	6.52s	6.93s	—	—	7.50s (2H)		—		2.30s (9H)	2.32s (3H)
									2.41s (6H)	
Acetate of **17**	6.53s	—	6.97d (2H)		7.67d (2H)		3.86s (3H)		2.41s (3H)	2.43s (3H)
									2.48s (3H)	

s: singlet, d: doublet (J=8.5 Hz), d′: doublet (J=2.5 Hz), q: quartet (J=8.5, 2.5 Hz), m: multiplet.

TABLE 3. UV DATA FOR 5,8- DIHYDROXY-7-METHOXYFLAVONES(**1**) AND 5,7,8-TRIHYDROXYFLAVONES(**2**)

Compd	λ_{max}/nm (log ε)											
	EtOH				EtOH–$AlCl_3$				EtOH–NaOAc			
1a	282	308	325 i	363 i	288	318	343 i	407	282	308	325 i	363 i
	(4.34)	(4.39)	(4.28)	(3.85)	(4.25)	(4.43)	(4.28)	(3.77)	(4.34)	(4.40)	(4.29)	(3.84)
1b	279	309	326sh	367 i	285	319	345sh	406	278	309	326sh	391
	(4.32)	(4.33)	(4.27)	(3.96)	(4.25)	(4.37)	(4.31)	(3.87)	(4.30)	(4.26)	(4.21)	(4.09)
1c	281		335		288	330	350	415	283		335	
	(4.32)		(4.26)		(4.25)	(4.27)	(4.29)	(3.82)	(4.30)		(4.28)	
1d	279		340		286	328sh	356	412	277		341	410
	(4.26)		(4.24)		(4.21)	(4.19)	(4.28)	(3.93)	(4.24)		(4.14)	(4.12)
1e	279	298 i	339		286	307	354	416	279	298 i	337	
	(4.34)	(4.21)	(4.24)		(4.29)	(4.23)	(4.28)	(3.87)	(4.33)	(4.22)	(4.25)	
1f	278	301	345		284	310	358	417	275	299sh	347	390sh
	(4.27)	(4.15)	(4.23)		(4.25)	(4.13)	(4.21)	(3.98)	(4.26)	(4.10)	(4.13)	(4.05)
1g	283	307	330 i		292	319	345 i	416	285	307	330 i	
	(4.31)	(4.29)	(4.19)		(4.26)	(4.32)	(4.19)	(3.74)	(4.30)	(4.31)	(4.22)	
1h	279	318sh	346		288	332sh	361	415sh	268	313	345	430
	(4.23)	(4.14)	(4.28)		(4.20)	(4.17)	(4.31)	(3.90)	(4.21)	(4.01)	(4.08)	(4.20)
1i	278	312	350		283	324	365	433	267	310	353 i	417
	(4.22)	(4.06)	(4.22)		(4.25)	(4.03)	(4.16)	(4.14)	(4.22)	(3.93)	(4.03)	(4.14)
2a	287 i	304		367 i	293sh	316	345 i	402		297		
	(4.37)	(4.41)		(3.83)	(4.27)	(4.41)	(4.22)	(3.88)		(4.39)		
2b	286 i	306	335 i		289	317	343sh	412		304		375
	(4.32)	(4.38)	(4.15)		(4.24)	(4.39)	(4.27)	(3.75)		(4.30)		(4.05)
2c	286		317		292	327	347sh	405sh		298sh	317	
	(4.30)		(4.28)		(4.24)	(4.28)	(4.26)	(3.77)		(4.28)	(4.31)	
2f	284		334		287	305sh	358	402sh		303 i	327	386
	(4.23)		(4.23)		(4.23)	(4.17)	(4.21)	(3.98)		(4.12)	(4.14)	(4.10)
2g		300			298sh	317	350 i	405		300		
		(4.35)			(4.28)	(4.35)	(4.15)	(3.69)		(4.29)		
2i	282	318sh	336		288	323	367	405sh			330	398
	(4.14)	(4.22)	(4.24)		(4.21)	(4.05)	(4.16)	(4.13)			(4.05)	(4.13)
17		304				306 i	325			306		
		(4.47)				(4.37)	(4.47)			(4.39)		

sh: shoulder, i: inflection point.

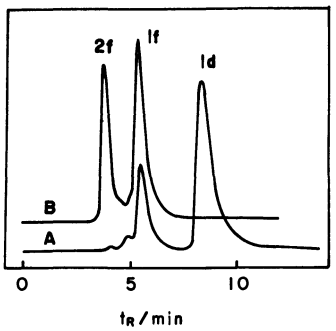

Fig. 3. HPLC of demethylated products from **6d** with anhydrous aluminum bromide in acetonitrile at 50 °C for 2 h (A) and 12 h (B).
Same conditions as in Fig. 1.

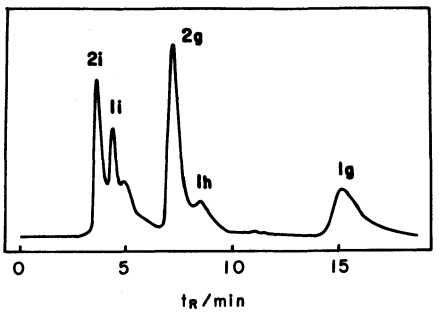

Fig. 4. HPLC of demethylated product from **6g** with anhydrous aluminum bromide in acetonitrile at 50 °C for 12 h.
Same conditions as in Fig. 1.

group.[16] The high performance liquid chromatography may be very useful for the separation of the demethylated products. Therefore, the demethylation of **6** with anhydrous aluminum bromide in acetonitrile was investigated in order to find a suitable method for the syntheses of 5,7,8-trihydroxyflavones (**2**) by the chromatography. The HPLC obtained are shown in Figs. 1—4.

The HPLC of the demethylated products from **6a** in the atmosphere showed the presence of three components (Fig. 1, Curve A). These components were identified as 5,7,8-trihydroxy-4′-methoxyflavone (**2a**), 6-bromo-5,7,8-trihydroxy-4′-methoxyflavone (**17**), and **1a** respectively, on the basis of the ^1H NMR and UV data (Tables

1—3). The amount of the bromoflavone (**17**) increased with increasing reaction time, but apparently decreased in nitrogen atmosphere (Fig. 1, Curve B). The 4'-methoxyl group of **6a** was stable under these demethylation conditions, so that 4',5,7,8-tetrahydroxyflavone (**2b**)[17] in the demethylated products was not detected by the high performance liquid chromatography. These results show that the 5- and 7-methoxyl groups of **6a** are selectively split with anhydrous aluminum bromide in nitrogen atmosphere to give **2a** in good yield.

The 5- and 7-methoxyl groups of **6c** were also selectively split under the above conditions to give **2c** as a main product. However, the HPLC of the demethylated product from **6c** showed small peaks which had shorter retention times than that of **2c** (Fig. 2). These small peaks are presumed to be those of the demethylated products of **2c**.

In the HPLC of the demethylated product from **6d**, the components of main peaks (R_t 3.8, 5.4, and 8.2 min) were identified as 3',4',5,7,8-pentahydroxyflavone (**2f**),[18] **1f**, and **1d** respectively, and the small peak (R_t 4.9 min) which is observed as a shoulder peak is estimated to be that of 4',5,7,8-tetrahydroxy-3'-methoxyflavone (**2d**) (Fig. 3). These results indicate that the 3'-methoxyl group is more easily split than the 7-methoxyl group and that the methoxyl groups of **6d** are split in the following order: 5, 3', and 7.

Similarly **6e**, an isomer of **6d**, was demethylated to **2f** *via* **1f**, but the 4'-methoxyl group was more easily split than the 3'-methoxyl group on **1d**. These results indicate that the hydroxyl group promotes the cleavage of adjacent methoxyl group. The cleavage of the methoxyl group with anhydrous aluminum bromide seems to proceed *via* the formation of a cyclic aluminum complex between the hydroxyl group and the methoxyl oxygen atom adjacent to each other.[19] However, the cleavage of 7-methoxyl group was clearly slower than that on the B ring of **1d** or **1e**, even though both of the methoxyl groups have an adjacent hydroxyl group. One of the causes of the difficulty in the cleavage of 7-methoxyl group may be that the 8-hydroxyl group has a tendency to form the cyclic aluminum complex with the ether oxygen atom at 1 position on the flavone nucleus.

On the other hand, the HPLC of the demethylated product from **6g** which has three methoxyl groups adjacent to each other showed the presence of many components (Fig. 4). The five main components were identified as 3',4',5,5',7,8-hexahydroxyflavone (**2i**), 3',4',5,5',8-pentahydroxy-7-methoxyflavone (**1i**), 5,7,8-trihydroxy-3',4',5'-trimethoxyflavone (**2g**), 4',5,8-trihydroxy-3',5',7-trimethoxyflavone (**1h**), and **1g** respectively (Tables 1—3). These results suggest that **6g** is demethylated to form **2i** *via* **1g** by the following two pathways because of a small difference of the rate of cleavage between the 7- and 4'-methoxyl groups: **6g**→**1g**→**2g**→**2i** and **6g**→**1g**→**1h**→**1i**→**2i**. Therefore, it seems that the flavones, **1g**, **2g**, **1i**, and **2i**, in the HPLC are observed as main peaks and that the flavones having the methoxyl groups adjacent to a hydroxyl group on the B ring such as **1h** are observed as small peaks.

From these results, it is suggested that the 5,7,8-trihydroxyflavones (**2**) which had one or two methoxyl groups on the B ring were easily synthesized by the demethylation of **6** with anhydrous aluminum bromide in acetonitrile.

The C_6-proton signals of the ^{1}H NMR for 5,7,8-trihydroxyflavones (**2**) and its acetates (**16**) appear at δ 6.26—6.29 and δ 6.93—6.95 respectively (Tables 1 and

Table 4. Comparison of salvitin and the two trihydroxyflavones (**1b** and **15b**)

		Salvitin[2]	**1b**	**15b**[13]
Mp θ_m/°C		304—305	277—279	298.5—300.5
(Triacetate)		(170)	(265—266)	(168.5—169.5)
UV: λ_{max}/nm	in MeOH	276 335	in EtOH 279 309 326sh 367i	in EtOH 275 336
	($AlCl_3$)	301 354	285 319 345sh 406	304 358
	(NaOAc)	276 347	278 309 326sh 391	277 340
^{1}H NMR of triacetate in $CDCl_3$ (δ)	OAc	2.34 2.42 2.53	2.32 2.43 (6H)	2.34 2.40 2.51
	C_3–H	6.68	6.51	6.63
	C_6– or C_8–H	7.40	6.69	7.32

sh: shoulder, i: inflection point.

Table 5. Comparison of UV data for the natural flavone and the two 5,7,8-trioxygenated flavones (**1d** and **14d**)

Compd		λ_{max}/nm (log ε)				
Natural flavone[3]	in MeOH	254	272	292sh	342	
	($AlCl_3$)	266sh	279	305	358	402
	(NaOAc)	260 266sh	295sh			410
1d	in EtOH	255 (4.13)	279 (4.26)		340 (4.24)	
	($AlCl_3$)	260sh (4.08)	286 (4.21)	328sh (4.19)	356 (4.28)	412 (3.93)
	(NaOAc)		277 (4.24)		341 (4.14)	410 (4.12)
14d[12]	in EtOH	255 (4.21)	276.5 (4.29)		343 (4.26)	
	($AlCl_3$)	263 (4.12)	285 (4.24)	302sh (4.09)	360 (4.29)	402 (4.10)
	(NaOAc)		286 (4.37)	328 (4.09)		414 (4.34)

sh: shoulder.

2). These chemical shifts resemble those of the C_6-proton for 5,7-dihydroxy-8-methoxyflavones (**14**)[10-12] ($\delta \approx 6.3$) and its acetates ($\delta \approx 6.8$), but differ apparently from those of the C_8-proton for 5,6,7-trihydroxyflavones (**5**)[7] ($\delta \approx 6.6$) and its acetates ($\delta \approx 7.45$).

The UV spectra for **2** in ethanol or ethanol–aluminum chloride are similar to those for the corresponding **1**. However, Bands I and II in ethanol for **2** approach more closely to each other than those for the corresponding **1**. Therefore, in the presence of sodium acetate, the bathochromic shift of Band II which is associated with the 7-hydroxyl group on **2** is not clearly observed because of the overlap with neighboring Band I (Table 3).

Identification of the Two Natural Flavones. The structure of salvitin, isolated from *Salvia plebeia*, has been confirmed to be 4′,5,8-trihydroxy-7-methoxyflavone (**1b**) on the basis of the spectral data and the synthesis.[2] The properties of salvitin, however, were not identical with those of **1b** synthesized by us (Table 4). The singlet peak at δ 7.4 in the ^{1}H NMR for salvitin triacetate is assigned to the C_8-proton on 5,7-diacetoxy-6-methoxyflavones[13,14] or 5,6,7-triacetoxyflavones.[7] In addition, the UV data for salvitin are similar to those of 4′,5,7-trihydroxy-6-methoxyflavone[13] (**15b**). These results suggest that the structure of salvitin is **15b**, an isomer of **1b**. The physical data of salvitin and its triacetate are shown to be identical with those of **15b** and its triacetate[13] as shown in Table 4. Consequently, the structure of salvitin was found to be 4′,5,7-trihydroxy-6-methoxyflavone (dinatin[20]) (**15b**).

Whalen *et al.*[3] have proposed that the structure of one of the natural flavones, isolated from *Solanum* section *Androceras*, is 4′,5,8-trihydroxy-3′,7-dimethoxyflavone (**1d**) on the basis of the UV and MS data. They claimed that the structure of the natural flavone was not 4′,5,7-trihydroxy-3′,8-dimethoxyflavone (**14d**) but **1d** on the basis of the following facts: "Substitution of the C_7-hydroxyl group was demonstrated by the failure of Band II to show a bathochromic shift in NaOAc relative to MeOH". However, in the presence of sodium acetate, the bathochromic shift of Band II for **1d** synthesized is not exhibited, and the UV data are obviously different from those for the natural flavone as shown in Table 5. Moreover, the UV data for the natural flavone in the presence of aluminum chloride are similar to those for **14d**[12] rather than those for **1d**. These results suggest that the natural flavone is **14d**.

Experimental

All the melting points were determined in glass capillaries and were uncorrected. The ^{1}H NMR spectra were measured with a Hitachi R-24 spectrometer (60 MHz), using tetramethylsilane as an internal standard, and chemical shifts were presented in δ values. The UV spectra were taken on a Hitachi 124 spectrophotometer. The high performance liquid chromatographic analysis carried out with a Hitachi 635 instrument, using a column (2.1×500 mm) packed with Hitachi gel # 3011, methanol as a eluent, and a UV monitor at 338 nm.[16] For the separation of the demethylated products, a column (20×600 mm) packed with Hitachi gel # 3019 using methanol was employed.

3-Benzyloxy-2-hydroxy-4,6-dimethoxyacetophenone(9). A mixture of the acetophenone (**7**)[8] (10 g), benzyl chloride (30 ml), and anhydrous potassium carbonate (56 g) in *N,N*-dimethylformamide (60 ml) was gently refluxed for 3 h, and then water was added to the reaction mixture. After the excess of benzyl chloride was removed by steam distillation under reduced pressure, the oily material was extracted with ether. The ethereal solution was washed with water. The solvent was completely evaporated to give crude dibenzyl ether (**8**) as brown oil.

The crude dibenzyl ether was dissolved in acetic acid (100 ml) containing concentrated hydrochloric acid (10 ml) and then allowed to stand for 85 min at room temperature. After the solution was diluted with water, separated crystals were

TABLE 6. 3-BENZYLOXY-2-HYDROXY-4,6-DIMETHOXY-ω-BENZOYLACETOPHENONES (**10**)

Compd	Mp θ_m/°C	Cryst. form	Recrystn. solvent	Yield/%	Formula	Found (%)		Calcd (%)	
						C	H	C	H
10a	158—159	Yellow needles	EtOAc	74	$C_{25}H_{24}O_7$	68.71	5.58	68.80	5.54
10b	188—189	Pale Yellow needles	EtOAc	71	$C_{31}H_{28}O_7$	72.38	5.30	72.64	5.51
10c	173—174	Yellow needles	$CHCl_3$–MeOH	82	$C_{26}H_{26}O_8$	66.70	5.41	66.94	5.62
10d	131—132	Yellow needles	EtOAc	62	$C_{32}H_{30}O_8$	70.63	5.67	70.83	5.57
10e	177—179	Pale yellow needles	EtOAc	80	$C_{32}H_{30}O_8$	70.61	5.66	70.83	5.57
10f	123—124	Yellow needles	EtOAc	60	$C_{38}H_{34}O_8$	74.02	5.40	73.77	5.54
10g	149—150	Yellow needles	EtOAc	84	$C_{27}H_{28}O_9$	65.03	5.69	65.31	5.68

TABLE 7. 8-BENZYLOXY-5,7-DIMETHOXYFLAVONES (**11**)

Compd	Mp θ_m/°C	Cryst. form	Recrystn. solvent	Yield/%	Formula	Found (%)		Calcd (%)	
						C	H	C	H
11a	149—150	Colorless needles	MeOH	98	$C_{25}H_{22}O_6$	71.99	5.15	71.76	5.30
11b	148—150	Pale yellow needles	$CHCl_3$–MeOH	98	$C_{31}H_{26}O_6$	75.40	5.12	75.29	5.30
11c	164—165	Pale yellow needles	$CHCl_3$–MeOH	97	$C_{26}H_{24}O_7$	69.83	5.27	69.63	5.39
11d	179—181	Pale yellow needles	$CHCl_3$–MeOH	98	$C_{32}H_{28}O_7$	73.43	5.20	73.27	5.38
11e	161—162	Pale yellow needles	$CHCl_3$–MeOH	98	$C_{32}H_{28}O_7$	73.48	5.08	73.27	5.38
11f	173—174	Colorless needles	$CHCl_3$–EtOAc	96	$C_{38}H_{32}O_7$	75.91	5.19	75.98	5.37
11g	206—207	Colorless needles	$CHCl_3$–MeOH	86	$C_{27}H_{26}O_8$	67.71	5.55	67.77	5.48

collected, washed with ether–hexane (1 : 1), and then recrystallized from methanol as pale yellow prisms, mp 95—97 °C; yield 11.4 g (80%). Found: C, 67.58; H, 5.99%. Calcd for $C_{17}H_{18}O_5$: C, 67.59; H, 6.00%.

*3-Benzyloxy-2-hydroxy-4,6-dimethoxy-ω-benzoylacetophenones (**10a**—**g**).* A mixture of **9** (3.0 g; 9.9 mmol) and the substituted benzoyl chloride (11—12 mmol) in pyridine (6 ml) was heated at 120 °C for 2 h. The cooled reaction mixture was poured into a mixture of ice, hydrochloric acid, and ether, and then stirred till the separated oily material changed into a precipitate. The precipitate was collected, washed with water, and dried to give crude benzoate.

A mixture of the crude benzoate and powdered potassium hydroxide (4 g) in pyridine (15 ml) was stirred for 4 h at 60 °C, and then poured into a mixture of ice and hydrochloric acid. The separated precipitate was treated with a sodium carbonate solution and then recrystallized to give **10a**—**g** (Table 6).

*8-Benzyloxy-5,7-dimethoxyflavones (**11a**—**g**).* A mixture of **10** (3 g) and anhydrous sodium acetate (4 g) in acetic acid (20 ml) was heated at 140 °C for 4h, and then water was added to the mixture. The separated precipitate was recrystallized to give **11a**—**g** (Table 7).

*8-Hydroxy-5,7-dimethoxyflavones (**6a**—**g**).* Flavone (**11**) (500 mg) was hydrogenated over palladium on charcoal (10%; 200 mg) in ethyl acetate (150 ml)–methanol (150 ml) till the uptake of hydrogen ceased. After the catalyst was filtered off, the filtrate was evaporated. The residue was recrystallized to give **6a**—**g** (Table 8).

*8-Acetoxy-4′,5,7-trimethoxyflavone (**12a**):* colorless needles from methanol, mp 205—206 °C. Found: C, 64.58; H, 4.79% Calcd for $C_{20}H_{18}O_7$: C, 64.86; H, 4.90%.

*5,8-Dihydroxy-7-methoxyflavones (**1a**—**g**).* A mixture of **6** (100 mg) and anhydrous aluminum chloride (1 g) in acetonitrile (10 ml) was heated at 70 °C for 10 h, and then a 0.5% hydrochloric acid (50 ml) was added to the reaction mixture. The mixture was warmed at 60 °C for 1—2 h, and then allowed to stand overnight in a refrigerator. The separated precipitate was recrystallized to give **1a**—**g** (Table 9).

Table 8. 8-Hydroxy-5,7-dimethoxyflavones (**6**)

Compd	Mp θ_m/°C	Cryst. form	Recrystn. solvent	Yield/%	Formula	Found (%)		Calcd (%)	
						C	H	C	H
6a	233—234	Yellow needles	MeOH	84	$C_{18}H_{16}O_6$	65.85	4.84	65.85	4.91
6b	293—295	Yellow needles	MeOH	97	$C_{17}H_{14}O_6$	65.08	4.50	64.96	4.49
6c	221—223	Yellow needles	MeOH	91	$C_{19}H_{18}O_7$	63.74	5.13	63.68	5.06
6d	227—228	Yellow needles	MeOH	80	$C_{18}H_{16}O_7$	62.61	4.45	62.79	4.68
6e	263—264	Yellow needles	MeOH	98	$C_{18}H_{16}O_7$	62.69	4.75	62.79	4.68
6f	296—297	Yellow needles	MeOH–EtOAc	93	$C_{17}H_{14}O_7$	61.56	4.24	61.82	4.27
6g	227—228	Yellow needles	MeOH	92	$C_{20}H_{20}O_8$	61.86	4.97	61.85	5.19

Table 9. 5,8-Dihydroxy-7-methoxyflavones (**1**)

Compd	Mp θ_m/°C	Cryst. form	Recrystn. solvent	Yield/%	Formula	Found (%)		Calcd (%)	
						C	H	C	H
1a	260—262	Yellow needles	MeOH	98	$C_{17}H_{14}O_6$	65.00	4.26	64.97	4.49
1b	277—279	Yellow needles	MeOH	98	$C_{16}H_{12}O_6$	64.25	4.30	64.00	4.03
1c	250—251	Yellow needles	MeOH	91	$C_{18}H_{16}O_7$	62.65	4.67	62.79	4.68
1d	280—281	Yellow needles	EGME[a)]	96	$C_{17}H_{14}O_7$	61.65	4.53	61.82	4.27
1e	245—246	Yellow needles	MeOH	97	$C_{17}H_{14}O_7$	61.75	4.07	61.82	4.27
1f	291—292	Yellow needles	MeOH	80	$C_{16}H_{12}O_7$	60.98	4.00	60.76	3.82
1g	216—217	Yellow needles	MeOH	98	$C_{19}H_{18}O_8$	60.68	4.85	60.96	4.85

a) Ethylene glycol monomethyl ether.

Table 10. Demethylated products of 8-hydroxyflavones (**6**) with anhydrous aluminum bromide in acetonitrile

Compd	Mp θ_m/°C	Cryst. form	Recrystn. solvent	Formula	Found (%)		Calcd (%)	
					C	H	C	H
2a	268—270[a)]	Yellow needles	MeOH	$C_{16}H_{12}O_6$	64.12	4.00	64.00	4.03
17	246[a)]	Yellow needles	MeOH	$C_{16}H_{11}O_6Br$	50.40	3.04	50.68	2.92
2b[17,b)]	293—295[a)]	Yellow needles	aq MeOH	$C_{15}H_{10}O_6 \cdot H_2O$	59.13	4.11	59.21	3.98
2c	251—252	Yellow needles	aq MeOH	$C_{17}H_{14}O_7 \cdot H_2O$	58.59	4.66	58.62	4.63
2f[18)]	>300	Yellow needles	aq MeOH	$C_{15}H_{10}O_7 \cdot 2H_2O$	53.46	4.27	53.26	4.17
1h	267—268	Yellow prisms	aq MeOH	$C_{18}H_{16}O_8 \cdot 2.5H_2O$	53.06	5.30	53.33	5.19
1i	>300	Yellow needles	MeOH	$C_{16}H_{12}O_8$	57.82	3.56	57.83	3.64
2g	268—270	Yellow needles	aq MeOH	$C_{18}H_{16}O_8$	59.77	4.39	60.00	4.48
2i	>300	Yellow needles	MeOH	$C_{15}H_{10}O_8 \cdot H_2O$	53.91	3.62	53.58	3.60

a) Decomposition point. b) This was synthesized from 4′,5,7,8-tetramethoxyflavone[6)] by the demethylation with anhydrous aluminum bromide in benzene at 50 °C for 24 h.

TABLE 11. 5,8-DIACETOXY-7-METHOXYFLAVONES(**13**) AND 5,7,8-TRIACETOXYFLAVONES(**16**)

Compd	Mp θ_m/°C	Cryst. form	Recrystn. solvent	Formula	Found (%)		Calcd (%)	
					C	H	C	H
13a	240—240.5	Colorless needles	$CHCl_3$–MeOH	$C_{21}H_{18}O_8$	63.31	4.67	63.31	4.55
13b	265—266	Colorless needles	$CHCl_3$–MeOH	$C_{22}H_{18}O_9$	62.09	4.40	61.97	4.26
13c	198—199	Colorless needles	$CHCl_3$–MeOH	$C_{22}H_{20}O_9$	61.66	4.65	61.68	4.71
13d	256—257	Colorless needles	$CHCl_3$–MeOH	$C_{23}H_{20}O_{10}$	60.71	4.35	60.53	4.42
13e	238—240	Colorless needles	$CHCl_3$–MeOH	$C_{23}H_{20}O_{10}$	60.52	4.52	60.53	4.42
13f	255—257	Colorless needles	$CHCl_3$–MeOH	$C_{24}H_{20}O_{11}$	59.35	4.18	59.51	4.16
13g	240—240.5	Colorless needles	$CHCl_3$–MeOH	$C_{23}H_{22}O_{10}$	60.36	4.98	60.26	4.84
16a	246—248	Colorless needles	$CHCl_3$–MeOH	$C_{22}H_{18}O_9$	61.96	4.24	61.97	4.26
16b	246—247	Colorless needles	$CHCl_3$–MeOH	$C_{23}H_{18}O_{10}$	60.75	3.98	60.79	3.99
16c	214—215	Colorless needles	$CHCl_3$–MeOH	$C_{23}H_{20}O_{10}$	60.55	4.34	60.52	4.42
16f	224—225	Colorless needles	$CHCl_3$–MeOH	$C_{25}H_{20}O_{12}$	58.59	3.92	58.60	3.93
16g	191—192	Colorless needles	MeOH	$C_{24}H_{22}O_{11}$	59.13	4.65	59.26	4.56
16i	265—266	Colorless needles	$CHCl_3$–MeOH	$C_{27}H_{22}O_{14}$	56.85	3.92	56.87	3.89
Acetate of **17**	249—251	Colorless needles	$CHCl_3$–MeOH	$C_{22}H_{17}O_9Br$	52.25	3.40	52.29	3.39

Acetates (**13a**—**g**) of **1a**—**g** were synthesized by a hot acetic anhydride–pyridine method (Table 11).

*Demethylation of 8-Hydroxy-5,7-dimethoxyflavones (**6a**, **c**, **d**, **e**, and **g**) with Anhydrous Aluminium Bromide in Acetonitrile.* Flavone (**6**) (100 mg) was dissolved in a solution of anhydrous aluminum bromide (2 g)–acetonitrile (5 ml) and heated at 50 °C for 12—48 h. To the reaction mixture, a 0.5—1% hydrochloric acid (*ca.* 50 ml) solution was added, and the mixture was warmed at 60—70 °C for 10—20 min. The separated precipitate was extracted with ethyl acetate. The extract was washed with water and evaporated. The residue was analyzed by a high performance liquid chromatograph and then separated into each component (Tables 9 and 10).

Acetates (**16**) of **2** were synthesized by a hot acetic anhydride-pyridine method (Table 11).

References

1) Part V of this series; T. Horie, H. Kourai, H. Osaka, and M. Nakayama, *Bull. Chem. Soc. Jpn.*, **55**, 2933 (1982).

2) H. C. Gupta, K. N. N. Ayengar, and S. Rangaswami, *Indian J. Chem.*, **13**, 215 (1975).

3) M. D. Whalen and T. J. Mabry, *Phytochemistry*, **18**, 263 (1979).

4) V. M. Chari, R. J. Grayer-Barkmeijer, J. B. Harborne, and Bengt-Göran Österdahl, *Phytochemistry*, **20**, 1977 (1981).

5) K. Venkateswara Rao, K. Visveswara Rao, and T. R. Seshadri, *Proc. Indian Acad. Sci.*, **25A**, 427 (1947); M. Krishnamurti, T. R. Seshadri, and P. R. Shankaran, *Tetrahedron*, **22**, 941 (1966).

6) V. D. N. Sastri and T. R. Seshadri, *Proc. Indian Acad. Sci.*, **24A**, 243 (1946).

7) T. Horie, *Nippon Kagaku Kaishi*, **1978**, 748.

8) K. Nakazawa and C. Isoma, "Yukikagobutsu-goseiho," ed by the Society of Synthetic Organic Chemistry, Japan, Gihodo, Tokyo (1970), Vol. 20, pp. 61—64.

9) T. Horie, H. Kourai, M. Nakayama, M. Tsukayama, and M. Masumura, *Nippon Kagaku Kaishi*, **1980**, 1397.

10) M. Nakayama, T. Horie, Chun-Nan Lin, M. Arisawa, M. Shimizu, and N. Morita, *Yakugaku Zasshi*, **103**, 675 (1983).

11) M. Nakayama, S. Hayashi, K. Fukui, T. Horie, and M. Masumura, *Bull. Chem. Soc. Jpn.*, **45**, 2202 (1972).

12) K. Fukui, M. Nakayama, and T. Horie, *Bull. Chem. Soc. Jpn.*, **42**, 2327 (1969); M. Nakayama, K. Fukui, T. Horie, Y. Shimizu, and M. Masumura, *Nippon Kagaku Zasshi*, **91**, 1174 (1970).

13) K. Fukui, M. Nakayama, and T. Horie, *J. Sci. Hiroshima Univ., Ser. A-II*, **33**, 305 (1969).

14) K. Fukui, M. Nakayama, and T. Horie, *Bull. Chem. Soc. Jpn.*, **43**, 1524 (1970).

15) K. Fukui, M. Nakayama, T. Matsui, M. Masumura, and T. Horie, *Nippon Kagaku Zasshi*, **90**, 1270 (1969).

16) M. Nakayama, T. Horie, M. Makino, S. Ganno, and A. Narita, *Nippon Kagaku Kaishi*, **1978**, 1390.

17) S. C. Chhabra, S. R. Gupta, T. R. Seshadri, and N. D. Sharma, *Indian J. Chem.*, **14B**, 651 (1976).

18) J. B. Harborne and H. T. Clifford, *Phytochemistry*, **8**, 2071 (1969).

19) J. F. W. McOmie, M. L. Watts, and D. E. West, *Tetrahedron*, **24**, 2289 (1968); K. S. Bhide, R. B. Mujumdar, and A. V. Rama Rao, *Indian J. Chem.*, **14B**, 168 (1976).

20) S. Rangaswamy and E. Venkata Rao, *Proc. Indian Acad. Sci.*, **54A**, 51 (1961); G. O. P. Doherty, N. B. Haynes, and W. B. Whalley, *J. Chem. Soc.*, **1963**, 5577.

 © 1983 The Chemical Society of Japan Bull. Chem. Soc. Jpn., 56, 3781—3785 (1983)

Studies of Peptide Antibiotics. XLV.[1] Syntheses of Gramicidin S-like Analogs with Macro-ring Structures[2]

Setsuko Ando,* Hideo Takiguchi, and Nobuo Izumiya†

Department of Chemistry, Faculty of Science, Fukuoka University, Nanakuma, Jonan-ku, Fukuoka 814-01

†*Laboratory of Biochemistry, Faculty of Science, Kyushu University, Hakozaki, Higashi-ku, Fukuoka 812*

(Received June 24, 1983)

Three cyclic tetradecapeptides related to gramicidin S (GS): *cyclo*(–Leu–Orn–Leu–Orn–Leu–D-Phe–Pro–)$_2$, *cyclo*(–Leu–Orn–Leu–Orn–Leu–D-Phe–Sar–)$_2$, and *cyclo*(–Leu–Orn–Leu–Orn–Leu–D-Phe–Gly–)$_2$, were synthesized to investigate the contributions of the ring size of cyclic peptides and of the number of the basic amino acid residues to the antibacterial activity. The protected cyclic tetradecapeptides were synthesized through a cyclization reaction of the linear tetradecapeptide azide in pyridine. Hydrogenolysis of the protected cyclic peptides afforded crystalline tetrahydrochlorides of the analogs. The homogeneity of the analogs was ascertained by TLC, paper electrophoresis, and elemental analysis. In the experiment of circular dichroism, the two analogs with 7,7′-Pro or 7,7′-Sar gave spectra similar in shape to that of GS, while the analog with 7,7′-Gly gave a slightly different spectrum from that of GS. The antibacterial assays showed that the analog with 7,7′-Pro exhibited considerable activities against the microorganisms tested, particularly against Gram-negative bacterias such as *Escherichia coli* and *Shigella sonnei*. On the other hand, the analogs with 7,7′-Sar or 7,7′-Gly exhibited weaker activities than that of GS.

For investigation of the relationship between the structure and the antibacterial activity, we have designed model compounds (Fig. 1). The following modifications to the Gramicidin S (GS) structure were made: (1) The number of amino acid residues in the cyclic peptides was increased from 10 to 14. (2) The number of ornithyl residues was increased from 2 to 4. (3) In addition to the prolyl residues at 7,7′-position, the prolyl residues were replaced by sarcocyl residues or glycyl residues.

Model compounds: *cyclo*(–Leu–Orn–Leu–Orn–Leu–D-Phe–Pro–)$_2$ (**P-12**), *cyclo*(–Leu–Orn–Leu–Orn–Leu–D-Phe–Sar–)$_2$ (**S-12**), and *cyclo*(–Leu–Orn–Leu–Orn–Leu–D-Phe–Gly–)$_2$ (**G-12**), have been synthesized. The present paper will describe the syntheses and the antibacterial properties of these compounds.

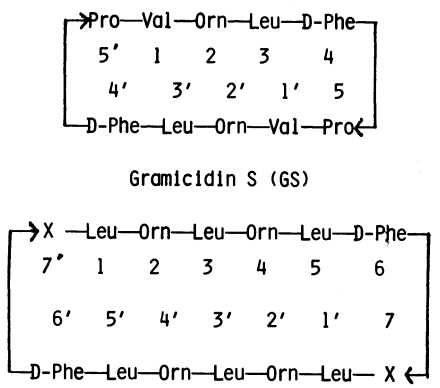

Fig. 1. Structures of GS and GS-like analogs [X=Pro (**P-12**), X=Sar (**S-12**), X=Gly (**G-12**)].

Routes for syntheses of **P-12·4HCl**, **S-12·4HCl**, and **G-12·4HCl** are outlined in Fig. 2. Boc-dipeptide ester (**1**) was prepared by means of the MA method[3] and the ester was converted into a hydrazide (**2**). Boc-pentapeptide esters (**S-3** and **G-3**) were prepared by the condensation of the azide derived from **2** with H–Leu–D-Phe–Sar–OEt·HCl[4] or H–Leu–D-Phe–Gly–OEt·HCl.[5] Pentapeptide ester hydrochlorides (**P-4**, **S-4**, and **G-4**) were derived from Boc–Leu–Orn(*Z*)–Leu–D-Phe–Pro–OEt[6] or Boc-pentapeptide ester (**S-3** and **G-3**) by the removal of the Boc group. Boc-heptapeptide esters (**P-5**, **S-5**, and **G-5**) were prepared by the condensation of the azide from **2** with the pentapeptide ester hydrochlorides (**P-4**, **S-4**, and **G-4**). The Boc-heptapeptide hydrazides (**P-6**. **S-6**, and **G-6**) were prepared from **P-5**, **S-5**, and **G-5** by treatment with hydrazine. Heptapeptide ester hydrochlorides (**P-7**, **S-7**, and **G-7**) were obtained from a part of **P-5**, **S-5**, and **G-5** by treatment with HCl in formic acid. Boc-tetradecapeptide esters (**P-8**, **S-8**, and **G-8**) were prepared by the condensation of the azide derived from **P-6**, **S-6**, and **G-6** with **P-7**, **S-7**, and **G-7**, respectively. For its cyclization, the compounds (**P-8**, **S-8**, and **G-8**) were converted into hydrazides (**P-9**, **S-9**, and **G-9**), and then by the removal of Boc group, the tetradecapeptide hydrazide dihydrochlorides (**P-10**, **S-10**, and **G-10**) were obtained. The azides derived from **P-10**, **S-10**, and **G-10** were treated with a large amount of pyridine, and the resulting *Z*-substituted cyclic tetradecapeptides (**P-11**, **S-11**, and **G-11**) were purified by passing them through columns of Dowex 50 and 1, and Sephadex LH-20. The compounds (**P-11**, **S-11**, and **G-11**) were confirmed to be the monomers by measuring molecular weights, CORONA Osmometer type 117 was used. The desired cyclic tetradecapeptides (**P-12**, **S-12**, and **G-12**) were afforded as crystalline tetrahydrochlorides by means of hydrogenolysis of **P-11**, **S-11**, and **G-11**. The compounds (**P-12**, **S-12**, and **G-12**) are more soluble in water than GS. The homogeneity o **P-12**, **S-12**, and **G-12** was ascertained by TLC, paper electrophoresis, and elemental analysis.

The CD spectra of **P-12**, **S-12**, **G-12**, and GS were measured with methanol as a solvent (Fig. 3). The CD spectra of **P-12** and **S-12** have similar patterns to that of GS, but the troughs of **P-12** and **S-12** are shallower than that of GS. The result suggests that the conformation of **P-12**, and **S-12** may be similar to that of GS. For the comformation of **P-12** and **S-12**, we attempted to construct a model with the antiparallel β-form as a possible structure (Fig. 4). Since the CD spectrum of **G-12** is a little different from that of GS, the conformation of **G-12** may be different.

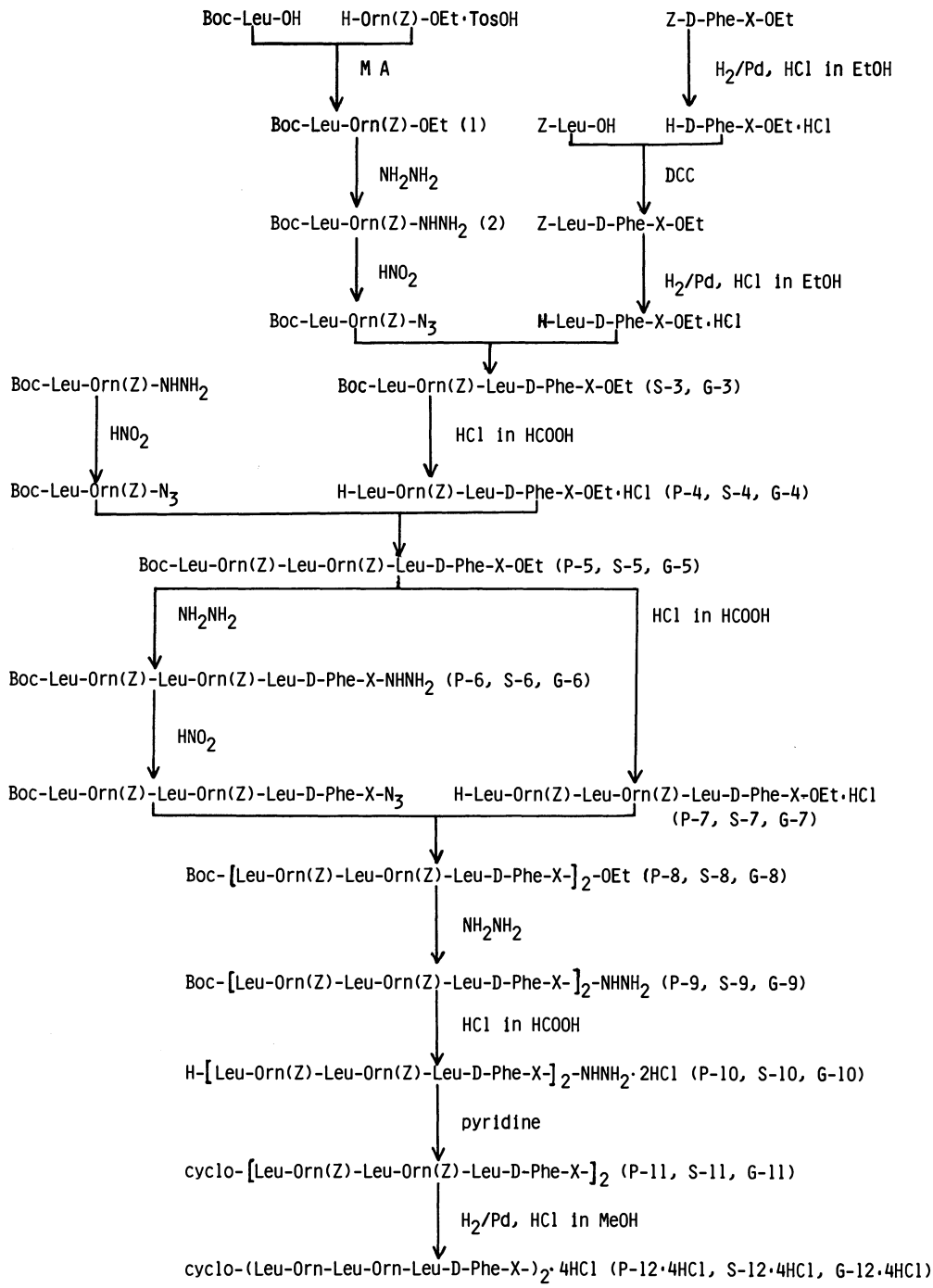

Fig. 2. Syntheses of GS-like analogs with four ornithyl residues [X=Pro (**P-12**), X=Sar (**S-12**), X=Gly (**G-12**)].

The antibacterial activities of **P-12**, **S-12**, **G-12**, and GS toward several microorganisms are listed in Table 1. It was found that the compound **P-12** exhibited considerable activity against the microorganisms tested, the compound **S-12** exhibited one-half activity compared with that of **P-12**, and the compound of **G-12** exhibited little activity. In particular, it is interesting that **P-12** has a marked inhibition against Gram-negative bacterias such as *E. coli* and *S. sonnei*. The ornithylleucyl copolymer[7] reported before exhibited a strong activity against *E. coli*. The result suggests that the ornithylleucyl residues contribute largely to the increase in activity against Gram-negative bacteria. [5,5'-Sar]-GS[4] and [5,5'-Gly]-GS[5,8] exhibited considerable antibacterial activity, but the synthesized analog (**S-12**) exhibited weaker activity, and **G-12** did not exhibit any activity. In particular, the contribution of prolyl residue was significant against the antibacterial activity. In addition, from the fact that the macro-ring analog such as **P-12** exhibited strong activities, it was found that the ring size is not always limited to 10 amino acid residues such as GS for the appearance of the activity.

Table 1. Antibacterial activities of GS-like analogs (**P-12**, **S-12**, and **G-12**) and GS[a]

Organism	P-12	S-12	G-12	GS[b]
Staphylococcus aureus	12.5	50	>100	3.13
Bacillus subtilis	6.25	25	100	3.13
Escherichia coli	12.5	100	>100	25
Salmonella typhosa	25	100	>100	>100
Shigella flexneri	6.25	25	100	3.13
Shigella sonnei	12.5	100	>100	25
Klebsiella pneumoniae	12.5	50	>100	6.25

a) This table shows the minimum inhibitory concentration (μg/ml) with a Bouillon agar medium. b) The natural GS was used as the control.

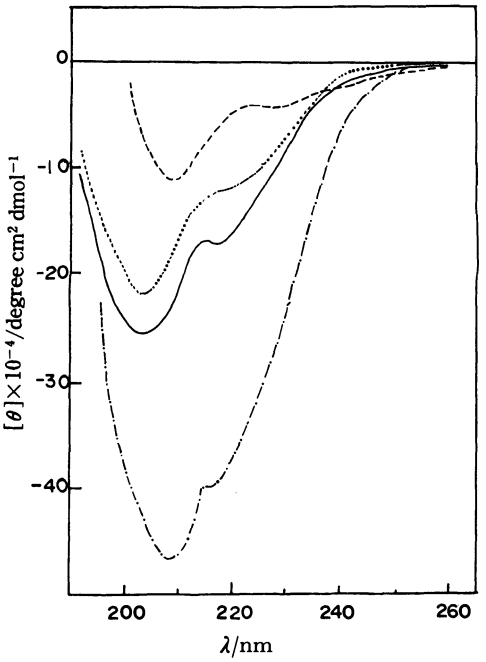

Fig. 3. CD Spectra of **P-12**, **S-12**, **G-12**, and GS in methanol.
GS: -·-·-, **P-12**: ——, **S-12**: – – –, **G-12**: – · –.

Experimental

All melting points are uncorrected. Prior to analysis, compounds were dried over phosphorus pentaoxide at 80 °C and 2 mmHg††, except linear tetradecapeptide derivatives and cyclic tetradecapetides. TLC was carried out on the Merck silica gel G with the following solvent system: R_f, 1-butanol–acetic acid–pyridine–water (4 : 1 : 1 : 2, v/v).

*Boc–Leu–Orn(Z)–OEt (**1**).* To a solution of Boc–Leu–OH (7.63 g, 33 mmol) and triethylamine (4.67 ml, 33 mmol) in tetrahydrofuran (40 ml) was added isobutyl chloroformate (4.37 ml, 33 mmol) at −5 °C. After 15 min, a mixture of H–Orn(Z)–OEt·TsOH (13.7 g, 29.3 mmol) and triethylamine (4.15 ml, 29.3 mmol) in chloroform (50 ml) was added. The mixture was left to stand overnight at room temperature, evaporated *in vacuo*, and the oily residue was dissolved in ethyl acetate (150 ml). The solution was washed successively with 4% $NaHCO_3$, 0.5 M††† citric acid, and water, and then dried (Na_2SO_4). The filtrate which separated from the salt was concentrated *in vacuo*. The product which precipitated upon the addition of ether and petroleum ether was collected and washed with the same solvent; yield, 14.4 g (97%); mp 78—80 °C; $[\alpha]_D^{25}$ −14° (*c* 1, DMF); R_f 0.95.

Found: C, 61.22; H, 8.42; N, 8.07%. Calcd for $C_{26}H_{41}O_7N_3$: C, 61.52; H, 8.14; N, 8.28%.

*Boc–Leu–Orn(Z)–NHNH$_2$ (**2**).* A solution of **1** (14.4 g, 28 mmol) and hydrazine hydrate (27.6 ml, 568 mmol) in DMF (60 ml) was allowed to stand at room temperature for 7 d. The excess hydrazine was evaporated *in vacuo*, and then water (150 ml) was added to the residue. The resulting solid was collected by filtration; yield, 11.9 g (85%); mp 141—142 °C; $[\alpha]_D^{25}$ −24° (*c* 1, AcOH); R_f 0.85.

Found: C, 57.41; H, 8.25; N, 13.93%. Calcd for $C_{24}H_{39}O_6N_5 \cdot 1/2\ H_2O$: C, 57.35; H, 8.02; N, 13.93%.

*Boc–Leu–Orn(Z)–Leu–D-Phe–Sar–OEt (**S-3**).* A solution of **2** (6.43 g, 13 mmol) dissolved in DMF (30 ml) was cooled to −22 °C. To this solution, 3.40 M HCl in dioxane (11.5 ml, 39 mmol) and isopentyl nitrite (1.95 ml, 14.3 mmol) were added. After 10 min, the solution was neutralized with *N*-methylmorpholine (4.31 ml, 39 mmol). To this solution was added a chilled solution of H–Leu–D-Phe–Sar–OEt·HCl[4] (5.46 g, 13.2 mmol) and *N*-methylmorpholine (1.61 ml, 14.5 mmol) in DMF (30 ml). The reaction mixture was stirred at 0 °C for 7 d and evaporated *in vacuo*. The residual solid was triturated with 0.5 M citric acid, and then allowed to stand in a refrigerator. The solid was collected by filtration and washed successively with 4% $NaHCO_3$, 0.5 M citric acid and water; yield, 9.59 g (88%); mp 140—141 °C; $[\alpha]_D^{25}$ −15° (*c* 1,

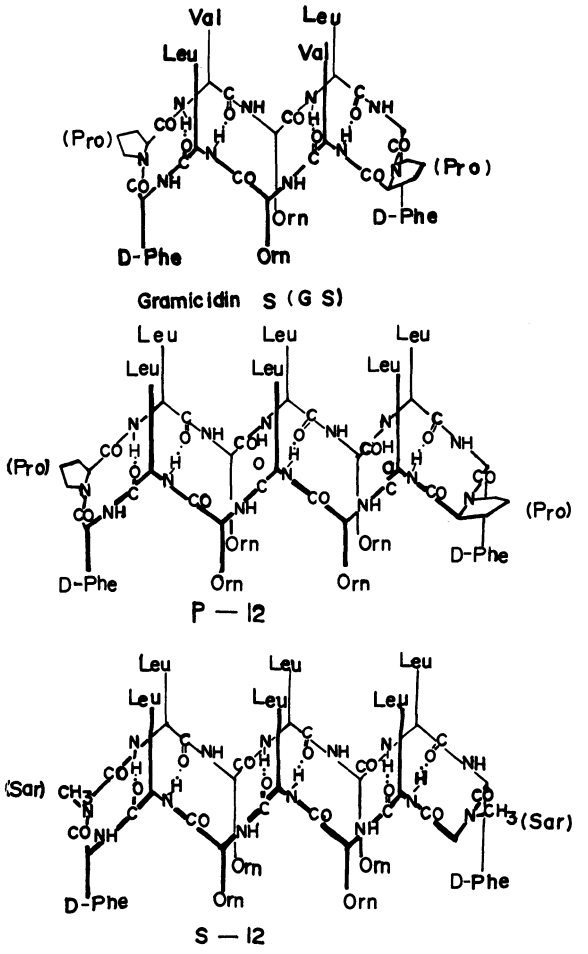

Fig. 4. Structure of GS and possible ones of **P-12** and **S-12**.

†† 1 mmHg≈133.322 Pa.
††† 1 M=1 mol dm^{-3}.

DMF); R_f 0.98.

Found: C, 63.08; H, 8.26; N, 10.02%. Calcd for $C_{44}H_{66}O_{10}N_6$: C, 62.99, H, 7.93, N, 10.02%.

Boc-Leu-Orn(Z)-Leu-D-Phe-Gly-OEt (**G-3**). This compound was prepared from **2** (1.58 g, 3.4 mmol) and H-Leu-D-Phe-Gly-OEt·HCl[5] (1.39 g, 3.5 mmol) as described for the preparation of **S-3**. The product was obtained as an oil; yield, 1.67 g (63%); R_f 0.95.

H-Leu-Orn(Z)-Leu-D-Phe-Pro-OEt·HCl (**P-4**). The compound Boc-Leu-Orn(*Z*)-Leu-D-Phe-Pro-OEt[6] (4.33 g, 50 mmol) was dissolved in 0.183 M HCl in formic acid. After being left to stand at room temperature for 30 min, the solution was evaporated to dryness. The residual oil was treated with ether, but still was obtained as an oily substance; yield, 4.01 g (100%); R_f 0.83.

H-Leu-Orn(Z)-Leu-D-Phe-Sar-OEt·HCl (**S-4**). This compound was prepared from **S-3** (8.39 g, 10 mmol) as described for the preparation of **P-4**. The product was obtained as an oil; yield, 7.75 g (100%); R_f 0.77.

H-Leu-Orn(Z)-Leu-D-Phe-Gly-OEt·HCl (**G-4**). This compound was prepared from **G-3** (1.72 g, 2 mmol) as described for the preparation of **P-4**. The product was obtained as an oil; yield, 1.52 g (100%); R_f 0.93.

Boc-Leu-Orn(Z)-Leu-Orn(Z)-Leu-D-Phe-Pro-OEt (**P-5**). A solution of **2** (2.47 g, 5.0 mmol) dissolved in DMF (20 ml) was cooled to −22 °C. To this solution, 3.40 M HCl in dioxane (4.41 ml, 15 mmol) and isopentyl nitrite (0.74 ml, 5.5 mmol) were added. After 15 min, the solution was neutralized with *N*-methylmorpholine (1.67 ml, 15 mmol). To this solution was added a chilled solution of **P-4** (4.01 g, 5.0 mmol) and *N*-methylmorpholine (0.61 ml, 5.5 mmol) in DMF (20 ml). The reaction mixture was stirred at 0 °C for 7 d and evaporated *in vacuo*. The residual solid was triturated with 0.5 M citric acid, and then allowed to stand in a refrigerator. The solid was collected by filtration and dissolved in ethyl acetate (200 ml). The solution was washed successively with 4% $NaHCO_3$, 0.5 M citric acid, and water, and then dried (Na_2SO_4). The filtrate separated from the salt was evaporated *in vacuo*. The resulting crystals were collected by filtration with the aid of ether–petroleum ether; yield, 3.60 g (59%); mp 190—195 °C; R_f 0.98.

Found: C, 63.38; H, 7.91; N, 10.07%. Calcd for $C_{65}H_{95}O_{14}N_9$: C, 63.65; H, 7.81; N, 10.28%.

Boc-Leu-Orn(Z)-Leu-Orn(Z)-Leu-D-Phe-Sar-OEt (**S-5**). This compound was prepared from **2** (4.94 g, 10 mmol) and **S-4** (7.75 g, 10 mmol) as described for the preparation of **S-3**; yield, 8.92 g (74%); mp 148—153 °C; $[\alpha]_D^{25}$ −28° (*c* 1, DMF); R_f 0.95.

Found: C, 58.21; H, 7.87; N, 9.94%. Calcd for $C_{63}H_{93}O_{14}N_9 \cdot 1/2\ H_2O$: C, 58.23; H, 8.07; N, 9.70%.

Boc-Leu-Orn(Z)-Leu-Orn(Z)-Leu-D-Phe-Gly-OEt (**G-5**). This compound was prepared from **2** (4.94 g, 10 mmol) and **G-4** (8.37 g, 10 mmol) as described for the preparation of **S-3**; yield, 11.47 g (97%); mp 130—132 °C; $[\alpha]_D^{25}$ 19° (*c* 1, DMF); R_f 0.95.

Found: C, 62.53; H, 7.48; N, 10.89%. Calcd for $C_{62}H_{91}O_{14}N_9$: C, 62.77; H, 7.73; N, 10.63%.

Boc-Leu-Orn(Z)-Leu-Orn(Z)-Leu-D-Phe-Pro-NHNH$_2$ (**P-6**). A solution of **P-5** (1.65 g, 1.34 mmol) and hydrazine hydrate (2.60 ml, 53.6 mmol) in DMF (20 ml) was allowed to stand for 7 d at room temperature. The solution was concentrated *in vacuo* to a small volume. The hydrazide precipitated upon the addition of water (100 ml) was collected by filtration; yield, 1.62 g (100%); mp 140—143 °C; $[\alpha]_D^{25}$ −83° (*c* 0.4, AcOH).

Found: C, 60.95; H, 7.67; N, 12.73%. Calcd for $C_{63}H_{93}O_{13}N_{11} \cdot 3/2\ H_2O$: C, 61.05; H, 7.81; N, 12.43%.

Boc-Leu-Orn(Z)-Leu-Orn(Z)-Leu-D-Phe-Sar-NHNH$_2$ (**S-6**). This compound was prepared from **S-5** (5.28 g, 4.4 mmol) as described for the preparation of **P-6**; yield, 5.01 g (96%); mp 147—150 °C; $[\alpha]_D^{25}$ −30° (*c* 0.7, AcOH).

Found: C, 61.55; H, 7.83; N, 13.11%. Calcd for $C_{61}H_{91}O_{13}N_{11}$: C, 61.75; H, 7.73; N, 12.99%.

Boc-Leu-Orn(Z)-Leu-Orn(Z)-Leu-D-Phe-Gly-NHNH$_2$ (**G-6**). This compound was prepared from **G-5** (7.09 g, 6.0 mmol) as described for the preparation of **P-6**; yield, 2.63 g (37%); mp 120—122 °C; $[\alpha]_D^{25}$ −7° (*c* 1, AcOH); R_f 0.84.

Found: C, 59.66; H, 7.51; N, 12.71%. Calcd for $C_{60}H_{89}O_{13}N_{11} \cdot 2H_2O$: C, 59.63; H, 7.76; N, 12.75%.

H-Leu-Orn(Z)-Leu-Orn(Z)-Leu-D-Phe-Pro-OEt·HCl (**P-7**). This compound was prepared from **P-5** (1.52 g, 1.2 mmol) as described for the preparation of **P-4**. The product was obtained as an oil; yield, 1.44 g (100%); R_f 0.85.

H-Leu-Orn(Z)-Leu-Orn(Z)-Leu-D-Phe-Sar-OEt·HCl (**S-7**). This compound was prepared from **S-5** (3.60 g, 3.0 mmol) as described for the preparation of **P-4**. The product was obtained as an oil; yield, 3.37 g (100%); R_f 0.84.

H-Leu-Orn(Z)-Leu-Orn(Z)-Leu-D-Phe-Gly-OEt·HCl (**G-7**). This compound was prepared from **G-5** (2.37 g, 2.0 mmol) as described for the preparation of **P-4**. The product was obtained as an oil; yield, 2.24 g (100%); R_f 0.78.

Boc-[Leu-Orn(Z)-Leu-Orn(Z)-Leu-D-Phe-Pro]$_2$-OEt (**P-8**). This compound was prepared from **P-6** (1.50 g, 1.2 mmol) and **P-7** (1.44 g, 1.2 mmol) as described for the preparation of **P-5**. The product was obtained as a solid; yield, 2.72 g (88%); mp 192—195 °C; $[\alpha]_D^{25}$ −66° (*c* 0.2, MeOH); R_f 0.94.

Found: C, 60.45; H, 7.66; N, 10.25%. Calcd for $C_{123}H_{176}O_{26}N_{18} \cdot 7H_2O$: C, 60.72; H, 7.87; N, 10.36%.

Boc-[Leu-Orn(Z)-Leu-Orn(Z)-Leu-D-Phe-Sar]$_2$-OEt (**S-8**). This compound was prepared from **S-6** (3.56 g, 3.0 mmol) and **S-7** (3.37 g, 3.0 mmol) as described for the preparation of **P-5**. The product was obtained as a solid; yield, 4.95 g (74%); mp 145—148 °C; $[\alpha]_D^{25}$ −33° (*c* 0.1, MeOH); R_f 0.98.

Found: C, 61.13; H, 7.81; N, 11.15%. Calcd for $C_{119}H_{172}O_{25}N_{18} \cdot 4H_2O$: C, 61.43; H, 7.80; N, 10.84%.

Boc-[Leu-Orn(Z)-Leu-Orn(Z)-Leu-D-Phe-Gly]$_2$-OEt (**G-8**). This compound was prepared from **G-6** (2.63 g, 2.2 mmol) and **G-7** (2.47 g, 2.2 mmol) as described for the preparation of **P-5**. The product was obtained as an oil; yield, 4.90 g(100%); R_f 0.96.

Boc-[Leu-Orn(Z)-Leu-Orn(Z)-Leu-D-Phe-Pro]$_2$-NHNH$_2$ (**P-9**). This compound was prepared from **P-8** (2.72 g, 1.2 mmol) as described for the preparation of **P-6**; yield, 2.47 g (92%); mp 140—144 °C; $[\alpha]_D^{25}$ −79° (*c* 0.4, AcOH).

Found: C, 62.18; H, 7.77; N, 11.73%. Calcd for $C_{121}H_{174}O_{24}N_{20} \cdot 5/2\ H_2O$: C, 62.16; H, 7.72; N, 11.98%.

Boc-[Leu-Orn(Z)-Leu-Orn(Z)-Leu-D-Phe-Sar]$_2$-NHNH$_2$ (**S-9**). This compound was prepared from **S-8** (4.95 g, 2.2 mmol) as described for the preparation of **P-6**; yield, 4.79 g (98%); mp 156—158 °C; $[\alpha]_D^{25}$ −34° (*c* 0.5, AcOH).

Found: C, 61.68; H, 8.43; N, 12.55%. Calcd for $C_{117}H_{170}O_{24}N_{20} \cdot 2H_2O$: C, 61.72; H, 7.70; N; 12.30%.

Boc-[Leu-Orn(Z)-Leu-Orn(Z)-Leu-D-Phe-Gly]$_2$-NHNH$_2$ (**G-9**). This compound was prepared from **G-8** (4.90 g, 2.2 mmol) as described for the preparation of **P-6**; yield, 2.51 g (54%); mp 127—130 °C; $[\alpha]_D^{25}$ −7° (*c* 0.5, AcOH); R_f 0.82.

Found: C, 60.67; H, 7.58; N, 12.49%. Calcd for $C_{115}H_{166}O_{24}N_{20} \cdot 3H_2O$: C, 60.94; H, 7.65; N, 12.36%.

H-[Leu-Orn(Z)-Leu-Orn(Z)-Leu-D-Phe-Pro]$_2$-NHNH$_2$·2HCl (**P-10**). The compound **P-9** (1.38 g, 0.6 mmol) was dissolved in 0.183 M HCl in formic acid (7.90 g, 1.44 mmol). After being left to stand at room temperature for 30 min, the solution was evaporated to dryness. The product was obtained as an oily form; yield, 1.36 g (100%); R_f 0.90.

H-[Leu-Orn(Z)-Leu-Orn(Z)-Leu-D-Phe-Sar]$_2$-NHNH$_2$·2HCl (**S-10**). This compound was prepared from **S-9** (2.33 g, 1.0 mmol) as described for the preparation of **P-10**. The product was obtained in an oily form; yield, 2.20 g (100%); R_f 0.90.

H-[Leu-Orn(Z)-Leu-Orn(Z)-Leu-D-Phe-Gly]$_2$-NHNH$_2$·2HCl (**G-10**). This compound was prepared from **G-9** (2.51 g, 1.1 mmol) as described for the preparation of **P-10**. The product was obtained as an oily substance; yield, 2.31 g (96%); R_f 0.79.

cyclo[-*Leu-Orn(Z)-Leu-Orn(Z)-Leu-D-Phe-Pro-*]$_2$ (**P-11**). A solution of **P-10** (1.36 g, 0.66 mmol) in DMF (40 ml) was chilled to −22 °C. To this solution 3.40 M HCl in dioxane (0.41 ml) and isopentyl nitrite (0.09 ml, 0.66 mmol) were added. After 5 min, the solution was added dropwise into pyridine (300 ml) at 0 °C for 5 min, and stirring was continued for 3.5 h at 0 °C. It then was stirred for 55 h at 5 °C. After the solvent was removed, the residue was dissolved in a mixture of methanol and water (450 ml, 8 : 1, v/v). The solution was passed through two columns, of Dowex 1 (OH^- form) and 50 (H^+ form). The columns were washed with the same solvent (900 ml), and the effluent was evaporated to dryness. The residue was collected by filtration with the aid of water. For purification, the solution of the crude product in DMF (3 ml) was applied to a column (2.5×84.5 cm) of Sephadex LH-20, and the development continued with DMF. Elution was carried out at room temperature, at a flow rate of 24 ml per h. The peptide content in the fractions was determined with LKB 2138 Uvicord S (at 254 nm). The fractions containing the desired product were evaporated, and the product was collected by filtration with the aid of water; yield, 128 mg (53%); mp 184—188 °C; $[\alpha]_D^{25}$ −141° (*c* 0.1, MeOH); R_f 0.98.

Found: C, 60.63; H, 7.57; N, 10.79%. Calcd for $C_{116}H_{162}O_{22}N_{18}\cdot 3H_2O$: C, 60.69; H, 7.77; N, 10.98%.

cyclo(-*Leu-Orn(Z)-Leu-Orn(Z)-Leu-D-Phe-Sar-*]$_2$ (**S-11**). This compound was synthesized from **S-10** (2.20 g, 1.0 mmol) as described for the preparation of **P-11**; yield, 127 mg (29%); mp 170—175 °C; $[\alpha]_D^{25}$ −47° (*c* 0.1, MeOH); R_f 0.98.

Found: C, 61.30; H, 7.75; N, 11.75%. Calcd fro $C_{112}H_{158}O_{22}N_{18}\cdot 9/2\ H_2O$: C, 61.44; H, 7.69; N, 11.51%.

cyclo[-*Leu-Orn(Z)-Leu-Orn(Z)-Leu-D-Phe-Gly-*]$_2$ (**G-11**). This compound was prepared from **G-10** (2.11 g, 0.9 mmol) as described for the preparation of **P-11**; yield, 100 mg (21%); mp 103—105 °C; $[\alpha]_D^{25}$ −43° (*c* 0.1, MeOH); R_f 0.98.

Found: C, 62.17; H, 7.50; N, 11.61%. Calcd for $C_{110}H_{154}O_{22}N_{18}\cdot 5/2\ H_2O$: C, 62.16; H, 7.54 N, 11.86%.

cyclo(-*Leu-Orn-Leu-Orn-Leu-D-Phe-Pro-*)$_2$·4HCl (**P-12·4HCl**). A solution of **P-11** (100 mg, 0.05 mmol) in 0.094 M HCl in methanol (2.4 ml) was hydrogenated in the presence of palladium black. After removal of the catalyst the filtrate was evaporated, and the resulting crystals were collected by filtration with the aid of ether; yield, 57 mg (70%); mp 232—238 °C; $[\alpha]_D^{25}$ −89° (*c* 0.05, MeOH); R_f 0.73.

Found: C, 51.88; H, 8.18; N, 12.67%. Calcd for $C_{84}H_{142}O_{14}N_{18}Cl_4\cdot 10H_2O$: C, 51.74; H, 8.37; N, 12.93%.

cyclo(-*Leu-Orn-Leu-Orn-Leu-D-Phe-Sar-*)$_2$·4HCl (**S-12·4HCl**). This compound was prepared from **S-11** (100 mg, 0.05 mmol) as described for the preparation of **P-12**; yield, 57 mg (70%); mp 180—184 °C; $[\alpha]_D^{25}$ −136° (*c* 0.05 MeOH); R_f 0.81.

Found: C, 46.82; H, 8.53; N, 12.17%. Calcd for $C_{80}H_{138}O_{14}N_{18}Cl_4\cdot 18H_2O$: C, 47.05; H, 8.59; N, 12.35%.

cyclo(-*Leu-Orn-Leu-Orn-Leu-D-Phe-Gly-*)$_2$·4HCl (**G-12·4HCl**). This compound was prepared from **G-11** (96 mg, 0.05 mmol) as described for the preparation of **P-12**; yield, 44.6 mg (68%); mp 141—143 °C; $[\alpha]_D^{25}$ −48° (*c* 0.05, MeOH); R_f 0.77.

Found: C, 49.82; H, 8.53; N, 13.25%. Calcd for $C_{78}H_{134}O_{14}N_{18}Cl_4\cdot 10H_2O$: C, 50.10; H, 8.30; N, 13.48%.

Electrophoresis. Electrophoresis on Toyo Roshi No. 52 paper was carried out with a solvent system: formic acid–acetic acid–methanol–water (1 : 3 : 6 : 10, v/v; pH 1.8) for 2 h at 500 V/30 cm. The mobilities toward the cathode of **P-12**, **S-12**, and **G-12** were comparable with that of GS; the ratios of the mobilities of **P-12**, **S-12**, and **G-12** *vs.* GS were 1.10, 1.16, and 1.20, respectively.

CD Measurement. The measurement of CD was performed with a JASCO Model J-40 over a wavelength range of 195 to 260 nm in methanol as a solvent. In Fig. 3 are shown the CD spectra of **P-12**, **S-12**, **G-1 2**, and GS.

Microbiological Assays. The minimum amount of the compounds (**P-12**, **S-12**, **G-12**, and GS) necessary for the complete inhibition of growth was determined by a dilution method. The results are shown in Table 1.

Molecular Weight Measurement. The molecular weight measurement of the *Z*-substituted cyclic tetradecapeptides (**P-11**, **S-11**, and **G-11**) was carried out by the use of a CORONA Osmometer type 117, in DMF as a solvent. The values of molecular weight **P-11**, **S-11**, and **G-11** were 2022, 1997, and 1958; the calculated values were 2160, 2108, and 2080 respectively.

The authors wish to express their thanks to the staff members of Takeda Chemical Industries, Ltd,. for the microbiological assays. The authors are also indebted to Associate Professor Hiroshi Nishikawa for his kind advice and valuable discussion. The present work was partially supported by a grant from the Central Research Institute of Fukuoka University.

References

1) Part XLIV of series: H. Yonezawa, K. Okamoto, M. Kaneda, N. Tominaga, and N. Izumiya, *Int. J. Peptide Protein Res.*, in press.

2) A part of this work has been already communicated: S. Ando, H. Nishikawa, H. Takiguchi, and N. Izumiya, *Fukuoka University Science Reports*, **13**, 49 (1983).

3) Abbreviation: Z, benzyloxycarbonyl; Boc, *t*-butoxycarbonyl; MA, mixed anhydride method; DCC, dicyclohexylcarbodiimide; TsOH, *p*-toluenesulfonic acid; DMF, *N,N*-dimethylformamide, MeOH, methanol; AcOH, acetic acid. Amino acid symbols except D-Phe denote the L-configuration.

4) H. Aoyagi and N. Izumiya, *Bull. Chem. Soc. Jpn.*, **39**, 1747 (1966).

5) H. Aoyagi, T. Kato, M. Ohno , M. Kondo, M. Waki, S. Makisumi, and N. Izumiya, *Bull. Chem. Soc. Jpn.*, **38**, 2139 (1965); H. Aoyagi, T. Kato, M. Ohno, M. Kondo, and N. Izumiya, *J. Am. Chem. Soc.*, **86**, 5700 (1964).

6) M. Kondo and N. Izumiya, *Bull. Chem. Soc. Jpn.*, **43**, 1850 (1970).

7) L. Bichowsky-Slomnicki, A. Berger, J. Kurts, and E. Katchalski, *Arch. Biochem. Biophys.*, **65**, 400 (1956).

8) H. Aoyagi, M. Kondo, T. Kato, S. Makisumi, and N. Izumiya, *Bull. Chem. Soc. Jpn.*, **40**, 1685 (1967).

Mechanisms of Singlet and Triplet Sensitized Decomposition of Bis(2-phenylbenzoyl) Peroxide

Akihide KITAMURA,* Hiroharu TANIKAWA, Kunio OOHASHI, Hirochika SAKURAGI,† and Katsumi TOKUMARU†

Department of Chemistry, College of Arts and Sciences, Chiba University, Yayoi-cho, Chiba 260

†*Department of Chemistry, University of Tsukuba, Sakura-mura, Ibaraki 305*

(Received June 28, 1983)

Bis(2-phenylbenzoyl) peroxide (2-PhBPO) was found to decompose on singlet and triplet sensitized irradiations in benzene and carbon tetrachloride. The quantum yields were determined to be 0.48 and 0.43 on direct excitation and chrysene sensitization in benzene, respectively, and 0.62 and 0.60 on benzophenone and 3′-methoxyacetophenone sensitizations in carbon tetrachloride, respectively. The reaction mechanisms are discussed from the standpoint of the modes of bond cleavage.

Many organic peroxides have been known to decompose on heating[1] and on irradiation;[2] however, the mechanism for their photolyses has not been well understood.

Previously, dibenzoyl peroxide (BPO) was shown to decompose on direct irradiation and on singlet sensitization employing polycyclic aromatic hydrocarbons as sensitizers.[3–14] On direct and singlet sensitized photolyses BPO affords a moderate amount of phenyl benzoate, a geminate product,[12–14] in contrast with its thermolysis which produces a very low yield of the geminate product.[15,16] Through mechanistic investigations, it has been proposed that the direct and singlet sensitized irradiations of BPO result in simultaneous or successive cleavage of the peroxide linkage and carbon-(carbonyl)-carbon(aromatic) bond to give a geminate pair of a benzoyloxyl and phenyl radicals which easily recombine into the geminate product,[14] whereas thermolysis of BPO is known to lead to homolytic cleavage of the peroxide linkage to give two benzoyloxyl radicals.[15,16]

In the course of extending the investigation on photochemistry of organic peroxides, bis(2-phenylbenzoyl) peroxide (2-PhBPO) was found to decompose on direct, singlet sensitized, and also triplet sensitized irradiation as well as thermolysis, the latter being known to give biphenyl-2,2′-carbolactone and 2-phenylbenzoic acid as main products.[17]

This paper describes the mechanism of photochemical decomposition of 2-PhBPO and discusses the modes of its bond cleavage depending on the reaction conditions.

Results

Products from Photochemical and Thermal Decomposition of 2-PhBPO. 2-PhBPO (0.02 mol/dm³) was irradiated with 366-nm light at 20 °C without sensitizer in benzene and carbon tetrachloride, in the presence of chrysene (0.002 mol/dm³) as a singlet sensitizer in benzene, and in the presence of benzophenone (0.02 mol/dm³) as a triplet sensitizer in benzene and carbon tetrachloride. The irradiation was continued until the peroxide completely decomposed. As a control, 2-PhBPO (0.02 mol/dm³) was thermolyzed in benzene at 80 °C and in carbon tetrachloride at 78 °C. The products are summarized in Table 1.

Effect of Temperature on the Products Arising from Thermolysis and Photolysis of 2-PhBPO. To examine the effect of temperature on the yields of products, 2-PhBPO (0.02 mol/dm³) was irradiated in benzene in the absence of any sensitizer and in the presence of chrysene (0.002 mol/dm³) and benzophenone (0.05 mol/dm³) at 30 and 40 °C, and thermolyzed in benzene at 60 and 70 °C. The results are collected in Table 2 together with those at 20 °C (photolyses) and 80 °C (thermolysis).

Quantum Yields for Photochemical Decomposition of 2-PhBPO. Quantum yields, Φ, for decomposition of 2-PhBPO were determined at various concentrations of 2-PhBPO on direct irradiation in benzene with 313-nm

Table 1. Yields of products in photolysis and thermolysis of bis(2-phenylbenzoyl) peroxide (0.02 mol/dm³) in benzene and carbon tetrachloride (mol/mol peroxide)

Product	Direct photolysis		Sensitized photolysis			Thermolysis	
			Chrysene	Benzophenone			
	In PhH	In CCl_4	In PhH	In PhH	In CCl_4	In PhH	In CCl_4
Biphenyl-2,2′-carbolactone	0.47	0.38	0.48	0.57	0.54	0.53	0.44
2-Phenylbenzoic acid	0.31	0.31	0.32	0.37	0.36	0.44	0.34
Biphenyl	0.36	0.06	0.31	0.31	0.02	0.50	0.03
o-Terphenyl	0.05	—	0.04	0.01	—	0.09	—
2-Chlorobiphenyl	—	0.17	—	—	0.05	—	0.35
Carbon dioxide	Not determined	0.49	0.33	0.10	0.16	0.50	0.44
Biphenyl moiety	1.19	0.92	1.15	1.08	0.97	1.56	1.16
CO_2 moiety	>0.78	1.18	1.13	1.04	1.06	1.47	1.22

Table 2. Temperature dependence of product yields in photolysis and thermolysis of bis(2-phenylbenzoyl) peroxide (0.02 mol/dm³) in benzene (mol/mol peroxide)

Product	Direct photolysis			Sensitized photolysis: Chrysene			Sensitized photolysis: Benzophenone			Thermolysis		
	20 °C	30 °C	40 °C	20 °C	30 °C	40 °C	20 °C	30 °C	40 °C	60 °C	70 °C	80 °C
Biphenyl-2,2′-carbolactone	0.47	0.47	0.48	0.48	0.49	0.49	0.57	0.61	0.62	0.58	0.55	0.53
2-Phenylbenzoic acid	0.31	0.35	0.33	0.32	0.33	0.35	0.37	0.41	0.41	0.46	0.45	0.44
Biphenyl	0.36	0.38	0.39	0.31	0.30	0.31	0.13	0.15	0.16	0.35	0.44	0.50
o-Terphenyl	0.05	0.05	0.06	0.04	0.05	0.05	0.005	0.008	0.014	0.06	0.08	0.09

Table 3. Quantum yields for photochemical decomposition of bis(2-phenylbenzoyl) peroxide

Condition	Additive	Concn / mol dm^{-3}	Concn of 2-PhBPO / mol dm^{-3}	Solvent	Light (nm)	Quantum yield measurement: Φ_{lim}	k_d/k_r	$k_q\tau$ / dm^3 mol^{-1}	Emission quenching: $k_q\tau$ / dm^3 mol^{-1}
Direct irradiation	—	—	1.2×10^{-3} -7.8×10^{-3}	C_6H_6	313	0.48±0.07	—	—	—
	Naphthalene	3×10^{-4} -2.4×10^{-3}	8×10^{-3}	C_6H_6	313	0.48±0.09	—	—	—
Singlet sensitization	Chrysene	0.002	1.9×10^{-3} -1.1×10^{-2}	C_6H_6	366	0.43±0.02	1.3	3.0×10^2	3.3×10^2
Triplet sensitization	Benzophenone	0.02	3.2×10^{-3} -1.1×10^{-2}	CCl_4	366	0.62±0.03	0.61	6.9×10^3	1.3×10^4
	3′-Methoxyacetophenone	0.06	1.6×10^{-3} -5.2×10^{-3}	CCl_4	313	0.60±0.03	0.66	4.2×10^4	—
	2-Benzoylnaphthalene	0.02	8×10^{-3}	C_6H_6	366	0	—	—	—

light, on singlet sensitization by chrysene in benzene with 366-nm light, and on triplet sensitization in carbon tetrachloride by benzophenone with 366-nm light and by 3′-methoxyacetophenone with 313-nm light. An attempted use of 2-benzoylnaphthalene as a triplet sensitizer on 366-nm irradiation did not result in sensitization. For the sensitized decomposition the Stern-Volmer relationship held between the reciprocal of quantum yield and the reciprocal of peroxide concentration. In addition, an attempt was made to examine effects of naphthalene on direct irradiation of 2-PhBPO with 313-nm light in benzene under the conditions in which most incident light was absorbed by the peroxide. The results are depicted in Figs. 1—5. Table 3 summarizes the limiting quantum yields, Φ_{lim}, the quantum yields extrapolated to the infinite concentration of the peroxide or naphthalene, along with the related quantities.

Quenching of the Excited States of Sensitizers by 2-PhBPO. Fluorescence of chrysene was quenched by varying concentrations of 2-PhBPO in benzene under argon to give a linear Stern-Volmer relationship with $k_q\tau_s$ of 330 dm³/mol, which, combined with the lifetime, τ_s, of singlet chrysene without the peroxide in benzene under argon, 39 ns, affords the quenching rate constant, $k_q=8.5\times10^9$ dm³ mol^{-1} s^{-1}.

Phosphorescence of benzophenone was quenched by 2-PhBPO, biphenyl, and phenyl 2-phenylbenzoate in carbon tetrachloride under argon at room temperature to show linear Stern-Volmer relationships with $k_q\tau_T$'s of 1.3×10^4, 1.3×10^4, and 3.8×10^3 dm³/mol, respectively. These values, divided by the lifetime of triplet benzophenone determined in the absence of the quenchers under otherwise similar conditions as above, 6 μs, lead to the quenching rate constants of 2-PhBPO, biphenyl, and phenyl 2-phenylbenzoate, $k_q=2.2\times10^9$, 2.2×10^9, and 6.3×10^8 dm³ mol^{-1} s^{-1}, respectively.

Discussion

Singlet Sensitization. 2-PhBPO was decomposed by sensitization with singlet excited chrysene. Fluorescence of chrysene was quenched by 2-PhBPO at a rate constant which is close to the diffusion-controlled rate constant, 8.5×10^9 dm³ mol^{-1} s^{-1}. However, singlet excitation transfer from chrysene to 2-PhBPO cannot take place, since the singlet excitation energy of chrysene, 79 kcal†/mol,[18] would not be sufficient to excite 2-PhBPO possessing the singlet excitation energy of 90—100 kcal/mol as estimated from its absorption spectrum. Therefore, it is probable that 2-PhBPO quenches singlet excited chrysene through formation of an exciplex as previously reported on BPO.[12]

Accordingly, the singlet sensitized decomposition of 2-PhBPO will proceed through the following mechanism as proposed for BPO[12] with rate constants denoted for the corresponding processes, where D and P represent a sensitizer and 2-PhBPO, respectively.

The Stern-Volmer plot (Fig. 1) fits equation 6 derived from Scheme 1.

The $k_q\tau_s$ value, 300 dm³/mol, obtained from Fig. 1,

† 1 cal=4.184 J.

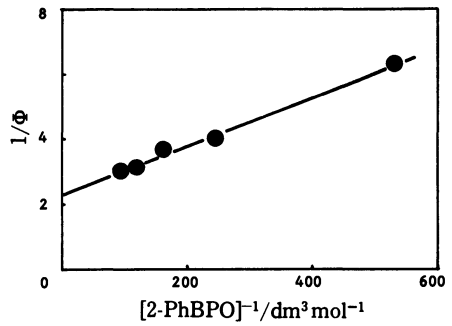

Fig. 1. Stern-Volmer plot for chrysene-sensitized decomposition of bis(2-phenylbenzoyl) peroxide on irradiation with 366-nm light in benzene.

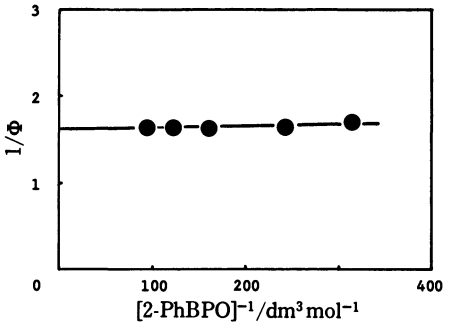

Fig. 2. Stern-Volmer plot for benzophenone-sensitized decomposition of bis(2-phenylbenzoyl) peroxide on irradiation with 366-nm light in carbon tetrachloride.

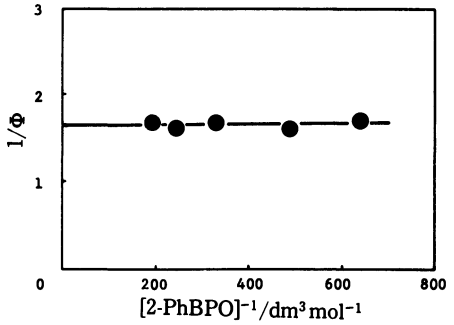

Fig. 3. Stern-Volmer plot for 3′-methoxyacetophenone-sensitized decomposition of bis(2-phenylbenzoyl) peroxide on irradiation with 313-nm light in carbon tetrachloride.

$$D \cdot \xrightarrow{h\nu} {}^1D^* \quad (1)$$

$${}^1D^* \xrightarrow{1/\tau_s} D \quad (2)$$

$${}^1D^* + P \xrightarrow{k_q} ({}^1D^*P) \quad (3)$$

$$({}^1D^*P) \xrightarrow{k_r} \text{Free radicals} + D \quad (4)$$

$$({}^1D^*P) \xrightarrow{k_d} D + P \quad (5)$$

Scheme 1.

$$1/\Phi = (1+k_d/k_r)(1+1/k_q\tau_s[P]) \quad (6)$$

agrees well with the $k_q\tau_s$ value, 330 dm³/mol, determined from the fluorescence quenching.

Triplet Sensitization. Among the sensitizers examined, benzophenone and 3′-methoxyacetophenone carrying the triplet excitation energies of 69 and 72 kcal/mol,[18] respectively, effectively sensitized decomposition of the peroxide; however, 2-benzoylnaphthalene with the lower triplet energy, 60 kcal/mol,[18] failed to sensitize. In view of the fact that 2-PhBPO quenched triplet benzophenone at a rate constant which is close to the diffusion-controlled rate constant, 2.2×10^9 dm³ mol^{-1} s^{-1}, the above result shows that the triplet energy of 2-PhBPO must be much higher than that of 2-benzoylnaphthalene and slightly lower than that of benzophenone. Phosphorescence of 2-PhBPO was not detected in EPA at 77 K; however, it is reasonable to assume that 2-PhBPO has nearly the same triplet energy as biphenyl and 2-phenylbenzoic acid, both of which exhibited in EPA at 77 K phosphorescence corresponding to the triplet energy of 67 kcal/mol.[18] Therefore, the triplet sensitized decomposition of 2-PhBPO will proceed as shown in the following scheme which involves energy transfer from the triplet excited sensitizer to the peroxide resulting in the triplet excited state of the peroxide and its decomposition into free radicals, where Φ_{ST} is the quantum yield for intersystem crossing of the sensitizer.

$$D \xrightarrow{h\nu} {}^1D^* \xrightarrow{\Phi_{ST}} {}^3D^* \quad (7)$$

$${}^3D^* \xrightarrow{1/\tau_T} D \quad (8)$$

$${}^3D^* + P \xrightarrow{k_q} {}^3P^* + D \quad (9)$$

$${}^3P^* \xrightarrow{k_r} \text{Free radicals} \quad (10)$$

$${}^3P^* \xrightarrow{k_d} P \quad (11)$$

Scheme 2.

The above mechanism leads to the following Stern–Volmer relationship.

$$1/\Phi = (1/\Phi_{ST})(1+k_d/k_r)(1+1/k_q\tau_T[P]) \quad (12)$$

The Stern-Volmer plots for photolyses sensitized by benzophenone and 3′-methoxyacetophenone (Figs. 2 and 3) exhibited linear relationships to give $k_q\tau_T$ values. The $k_q\tau_T$ value thus obtained for benzophenone, 6.9×10^3 dm³/mol, agrees fairly well with that obtained from phosphorescence quenching, 1.3×10^4 dm³/mol. These results support Scheme 2.

As to the triplet excitation transfer from sensitizers to the peroxide, it is noticeable that phenyl 2-phenylbenzoate and biphenyl quench triplet benzophenone almost as efficiently as 2-PhBPO. Accordingly, triplet excitation of benzophenone must be transferred to the biphenyl moieties of 2-PhBPO and phenyl 2-phenylbenzoate.

The resulting triplet state of 2-PhBPO will dissipate its electronic excitation through cleavage of the peroxide bond with a probability corresponding to the limiting quantum yield, $\Phi_{lim}=k_r/(k_r+k_d)$, which is nearly 0.6 for both benzophenone and 3′-methoxyacetophenone sensitizations. It is noticeable that this value is in the same magnitude as the quantum yields reported by Leffler and Miley[19] for the decomposition of dibenzoyl peroxides substituted with a benzophenone moiety as an intramolecular sensitizing chromophore. Since the activa-

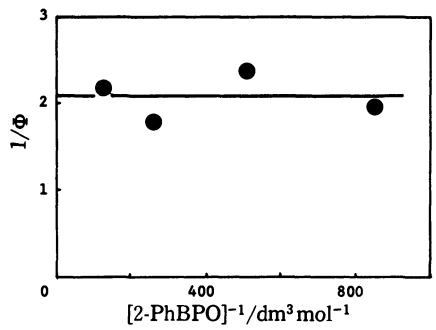

Fig. 4. Reciprocal plot of quantum yield for decomposition of bis(2-phenylbenzoyl) peroxide *vs.* concentration of the peroxide on irradiation with 313-nm light in benzene.

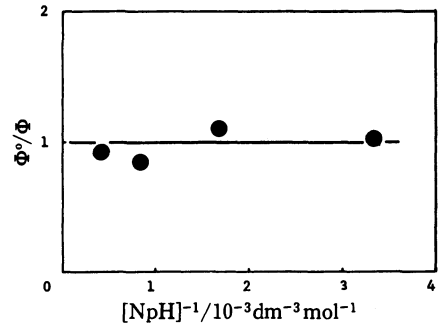

Fig. 5. Plot of relative quantum yield for decomposition of bis(2-phenylbenzoyl) peroxide *vs.* reciprocal concentration of naphthalene on irradiation with 313-nm light in benzene.

tion energy for homolytic cleavage of the peroxide bond is estimated to be around 30 kcal/mol[15,16] the excitation energy of the biphenyl moiety, 67 kcal/mol, must be sufficient to induce cleavage of the peroxide bond in view of the results on triplet sensitized decomposition of aromatic oxime esters, RR'C=NOCOR", in which only the aromatic moieties, RR'C=, with sufficient triplet energies can induce cleavage of the N–O bond.[20,21]

Direct Irradiation. Direct irradiation of 2-PhBPO in benzene leads to decomposition of the peroxide with a quantum yield of nearly 0.5. As Fig. 4 indicates, the quantum yield was almost unchanged with nearly six fold increase in peroxide concentration. On addition of naphthalene in concentrations varying more than eight times, the quantum yield was essentially unchanged (Fig. 5). This result shows that direct irradiation leads to decomposition of the peroxide either from the singlet excited state or from a triplet state with a lifetime shorter than 10^{-6} s; the triplet state of 2-PhBPO, if its lifetime were longer than 10^{-6} s, should be efficiently quenched by naphthalene, since the quenching must be exothermic.

Mechanism of the Photolyses. As Table 1 indicates, photolyses of 2-PhBPO gave similar products as those resulting from thermolysis in the same solvent. Formation of most products from the photolyses can be understood by the mechanism as reported for the thermolysis, in which the peroxide undergoes homolytic cleavage of the peroxide linkage to give 2-phenylbenzoyloxyl radicals followed by their reactions.[17] However, careful inspection of Table 1 shows that the triplet sensitized photolysis gave lower yields of both carbon dioxide and the products derived from 2-biphenylyl radicals like biphenyl, *o*-terphenyl, and 2-chlorobiphenyl, and on the other hand, a higher yield of biphenyl-2,2'-carbolactone than the direct irradiation and singlet sensitization.

In view of the fact that the direct irradiation and singlet sensitization of BPO induce cleavage of its two bonds, the peroxide bond and the linkage between the carbonyl carbon and aromatic carbon, to give benzoyloxyl and phenyl radicals along with carbon dioxide,[14] it is reasonable to assume that 2-PhBPO, on direct irradiation and singlet sensitization, tends to undergo the two-bond cleavage, whereas, on triplet sensitization as well as on thermolysis, the peroxide undergoes only the usual cleavage of the peroxide bond.[15,16] Thus, direct irradiation and singlet sensitization accelerates production of carbon dioxide and 2-biphenylyl radicals more efficiently than triplet sensitization, ultimately giving higher yields of the products arising from 2-biphenylyl radicals, and, on the contrary, affording lower yields of the products derived from 2-phenylbenzoyloxyl radicals such as biphenyl-2,2'-carbolactone and 2-phenylbenzoic acid.

Temperature effects on product yields are not remarkable, particularly in the direct and chrysene-sensitized photolyses, which seems to be consistent with the mechanism involving the two-bond cleavage. On the other hand, on triplet sensitization and thermolysis, the yields of biphenyl and *o*-terphenyl resulting from 2-biphenylyl radicals increase with increasing temperature. These must be due to enhanced decarboxylation of 2-phenylbenzoyloxyl radicals at higher temperatures. The yields of the lactone and acid decrease in the thermolysis, but increase in the triplet sensitization with increasing temperature. This behavior of 2-phenylbenzoyloxyl radicals indicates that their cyclization and disproportionation proceed with lower activation energies than the decarboxylation.[22]

Experimental

Materials. Bis(2-phenylbenzoyl) peroxide (2-PhBPO) was prepared from 2-phenylbenzoic acid and hydrogen peroxide in the presence of dicyclohexylcarbodiimide,[23] and recrystallized from dichloromethane–methanol. Chrysene and naphthalene were purified by column chromatography and crystallization. Benzophenone and 2-benzoylnaphthalene were recrystallized three times from ethanol. 3'-Methoxyacetophenone was distilled under reduced pressure. Benzene was distilled before use and carbon tetrachloride was purified by the method of Steel and coworkers.[24]

Photolysis. A solution of 2-PhBPO (0.02 mol/dm³) in benzene or carbon tetrachloride (3 ml) in the absence of any sensitizer or in the presence of chrysene (0.002 mol/dm³) or benzophenone (0.05 mol/dm³) in a Uranium glass tube was deaerated by bubbling of argon, and irradiated for five times half-life periods determined by iodometry with a 1 kW high pressure mercury lamp immersed in a Pyrex cooling bath and further surrounded by Toshiba UV-D36A glass filters using a merry-go-round type Riko Rotary photochemical Reactor. Products were determined by GLPC analyses on a Shimadzu GC 4CM gas chromatograph equipped with a flame ionization detector. The following columns were used for quantitative analyses: Diethylene glycol succinate (2%) with H_3PO_4

(0.5%), Thermon 3000 (2%). Carbon dioxide was determined gravimetrically using an Ascarite tube.

Thermolysis. A solution of 2-PhBPO (0.02 mol/dm^3) in benzene or carbon tetrachloride (3 ml) in a Pyrex tube was degassed by the usual freeze-thaw cycles and heated in an air bath constantly maintained at a given temperature (60, 70, 78, and 80 °C) for five times half-life periods. The products were similarly analyzed by GLPC.

Quantum Yields. Quantum yields for photolyses of 2-PhBPO (0.001—0.008 mol/dm^3) were measured in benzene in the absence of any additive or in the presence of naphthalene ($(0.3—2.4)\times10^{-3}$ mol/dm^3) and in carbon tetrachloride in the presence of 3'-methoxyacetophenone (0.06 mol/dm^3) by irradiating with 313 nm light isolated from a 100 W high pressure mercury lamp through a Toshiba UV-D33S glass filter and a K_2CrO_4 solution filter, and in benzene in the presence of chrysene (0.002 mol/dm^3) or 2-benzoylnaphthalene (0.02 mol/dm^3) and in carbon tetrachloride in the presence of benzophenone (0.02 mol/dm^3) by irradiating with 366 nm light isolated through a Toshiba UV-D36A glass filter. Disappearance of the peroxide was determined on a JASCO Trirotar HPLC with a 15 cm ODS column. Conversion of the peroxide was less than 15%. More than 95% of the incident light was absorbed by the sensitizer except the case of chrysene, by which *ca.* 80% of the light was absorbed.

Quenching Rate Constants. Fluorescence of chrysene (3×10^{-4} mol/dm^3) was measured in the presence of 2-PhBPO ($(0—6)\times10^{-3}$ mol/dm^3) in benzene under argon on a Hitachi 650-10S fluorescence spectrophotometer. Phosphorescence of benzophenone (0.01 mol/dm^3) was measured in the presence of 2-PhBPO ($(0—4)\times10^{-5}$ mol/dm^3), biphenyl ($(0—1.6)\times10^{-4}$ mol/dm^3), and phenyl 2-phenylbenzoate ($(0—1.6)\times10^{-4}$ mol/dm^3). Fluorescence lifetime of chrysene and phosphorescence lifetime of benzophenone were measured at room temperature by single photon counting technique on an Applied Photophysic SP-3X.

References

1) For example, "Chemistry of Organic Peroxides," ed by Y. Ogata, Nankodo, Tokyo (1971).
2) For example, K. Tokumaru, "Radical Reactions," ed by N. Inamoto, Hirokawa, Tokyo (1977), pp. 109—130.
3) F. Fichter and A. Schnider, *Helv. Chim. Acta*, **13**, 1428 (1930).
4) Y. Ikeda, *Nippon Kagaku Zasshi*, **79**, 354 (1958).
5) J. C. Bevington and T. D. Lewis, *Trans. Faraday Soc.*, **54**, 1340 (1958).
6) C. Walling and M. J. Gibian, *J. Am. Chem. Soc.*, **87**, 3413 (1965).
7) T. Nakata, K. Tokumaru, and O. Simamura, *Tetrahedron Lett.*, **1967**, 3303.
8) H. C. Box, E. E. Sudzinski, and H. G. Freund, *J. Am. Chem. Soc.*, **92**, 5305 (1970).
9) J. D. Bradley and A. P. Roth, *Tetrahedron Lett.*, **1971**, 3907.
10) P. Lebourgeois, R. Arnaud, and J. Lemaire, *J. Chim. Phys.*, **1972**, 1633, 1643.
11) W. F. Smith, Jr., *Tetrahedron*, **25**, 2071 (1969).
12) T. Nakata and K. Tokumaru, *Bull. Chem. Soc. Jpn.*, **43**, 3315 (1970).
13) K. Tokumaru, A. Ohshima, T. Nakata, H. Sakuragi, and T. Mishima, *Chem. Lett.*, **1974**, 571.
14) A. Kitamura, H. Sakuragi, M. Yoshida, and K. Tokumaru, *Bull. Chem. Soc. Jpn.*, **53**, 1393 (1980).
15) D. H. Hey, M. J. Perkins, and G. H. Williams, *J. Chem. Soc.*, **1964**, 3412.
16) K. Tokumaru, *Nippon Kagaku Zasshi*, **92**, 887 (1971).
17) F. D. Greene, G. R. van Norman, J. C. Cantrill, and R. D. Gilliom, *J. Org. Chem.*, **25**, 1790 (1960).
18) S. L. Murov, "Handbook of Photochemistry," Marcel Dekker, New York (1973).
19) J. E. Leffler and J. W. Miley, *J. Am. Chem. Soc.*, **93**, 7005 (1971).
20) H. Sakuragi, S. Ishikawa, T. Nishimura, M. Yoshida, N. Inamoto, and K. Tokumaru, *Bull. Chem. Soc. Jpn.*, **49**, 1949 (1976).
21) H. Sakuragi, H. Kinoshita, K. Utena, M. Yoshida, K. Tokumaru, and M. Hoshino, *Tetrahedron Lett.*, **1978**, 1529.
22) T. Suehiro and M. Ishida, *Bull. Chem. Soc. Jpn.*, **44**, 1692 (1971).
23) F. D. Greene and J. Kazan, *J. Org. Chem.*, **28**, 2168 (1963).
24) J. Chilton, L. Giering, and C. Steel, *J. Am. Chem. Soc.*, **98**, 1865 (1976).

Stereoselective Epoxidation of Allylic Alcohols and Dehydrogenative Oxidation of Secondary Alcohols by Means of *t*-Butyl Hydroperoxide and Aluminium Reagents

Kazuhiko TAKAI, Koichiro OSHIMA,* and Hitosi NOZAKI

Department of Industrial Chemistry, Faculty of Engineering, Kyoto University, Yoshida, Sakyo-ku, Kyoto 606

(Received July 4, 1983)

Treatment of a solution of geraniol and $(t\text{-BuO})_3Al$ in benzene with *t*-BuOOH at 5 °C gives (2*R**, 3*R**)-2,3-epoxy-3,7-dimethyl-6-octenyl acetate in 83% yield after acetylative workup. Eight allylic alcohols are converted to α,β-epoxy alcohols in preparative yields. The epoxidation of secondary (*E*)-allylic alcohols shows opposite stereoselectivities to *t*-BuOOH–$VO(acac)_2$ system. Asymmetric epoxidation with a chiral hydroxamic acid as a ligand gives unsatisfactory degrees of enantiomeric excess. The same system can also convert secondary alcohols into ketones in excellent yields, while primary ones react very slowly.

The versatility of the epoxide functionality in synthesis makes further advances in stereoselective acyclic epoxidation to be of particular interest.[1] Conventional oxidation with organic peracids[2] or epoxidation with *t*-butyl hydroperoxide in the presence of transition metal catalysts,[3,4] for example, $VO(acac)_2$, $Mo(CO)_6$, and $Ti(OPr^i)_4$, is suitable for such purpose.[5] We wish to report that *t*-BuOOH–$(t\text{-BuO})_3Al$ system effects stereoselective epoxidation of allylic alcohols as well as dehydrogenative oxidation of secondary alcohols to ketones.[6]

Trialkylaluminium compounds interact energetically with alkyl hydroperoxides to form organoaluminium peroxides.[7] The utility of these products as an oxidizing reagent, however, has been limited[8] because of their instability. They can react with the host trialkylaluminium compounds themselves or alternatively undergo intramolecular rearrangement.[9] We have found that the organoaluminium peroxide prepared *in situ* from *t*-BuOOH and $(t\text{-BuO})_3Al$ has proved to be effective for the title oxidation.[10]

Treatment of a solution of geraniol and $(t\text{-BuO})_3Al$ in benzene with *t*-BuOOH at 5 °C gave (2*R**, 3*R**)-2,3-epoxy-3,7-dimethyl-6-octenyl acetate (**1**) in 83% yield

TABLE 1. EPOXIDATION OF OLEFINIC ALCOHOLS WITH *t*-BuOOH–$(t\text{-BuO})_3Al$[a]

Run	Alcohol	Reaction conditions		Yield[b] %	Product		*t*-BuOOH–$VO(acac)_2$[d]	
		Temp/°C	Time/h		*threo*[c] (*trans*) (%)	*erythro*[c] (*cis*) (%)	*threo* (*trans*) (%)	*erythro* (*cis*) (%)
1	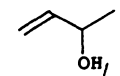	25	5	70	42	58	20	80
2	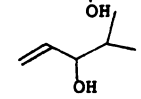	25	4	78	71	29	15	85
3	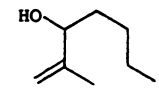	25	6	80	13	87	2	98
4	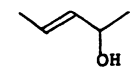	5	6	78	64	36	29	71
5	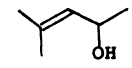	5	4	80	>99.5	<0.5	86	14
6	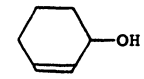	5	3	72	<0.5	>99.5	2	98
7	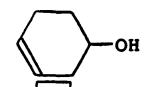	5	3	82	<0.5	>99.5	2	98
8	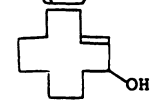	5	10	80	83	17	29	71[e]

a) All reactions were performed in benzene solution containing the substrates (2.0 mmol), $(t\text{-BuO})_3Al$ (3.0 mmol), and *t*-BuOOH (4.0 mmol). b) Isolated yields are underlined, all others are by GLPC relative to internal standard. Epoxy alcohols were acetylated *in situ* prior to analysis in Runs 5, 6, and 7. c) The resulting mixtures of epoxy alcohols, epoxy acetates, or epoxy alcohol trimethylsilyl ethers were analyzed by GLPC. d) Cited from Ref. 4a. e) Cited from Ref. 21.

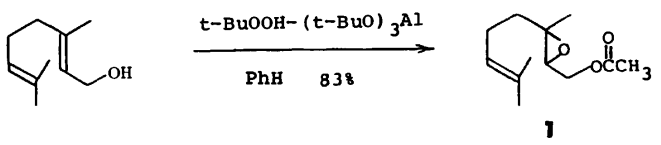

1

Scheme 1.

after acetylative workup (Scheme 1). Epoxidation of 6,7-olefinic linkage was not observed analogously as the *t*-BuOOH–$VO(acac)_2$ oxidation.

The results are shown in Table 1, together with the recorded selectivity of the Sharpless' *t*-BuOOH–$VO(acac)_2$ oxidation for comparison.[4a] Cyclohexenols with *Z*-configuration were preferentialy oxidized to cis epoxide by both methods commonly (Runs 6 and 7). The striking difference, however, has been observed in Runs 2, 4, and 8. The present aluminium reagent converted (*E*)-allylic alcohols predominantly into threo isomers which are less favored products in the vanadium one.

Asymmetric epoxidation[11] was examined with a chiral hydroxamic acid (**2**) as a ligand. A chiral aluminium reagent was prepared by treating trimethylaluminium with 1.2 equiv of **2** in benzene and used *in situ*. Epoxidation of geraniol with *t*-BuOOH and the reagent gave **1** in 34% e.e., whereas the reaction of 2,3-diphenyl-2-propen-1-ol gave **3** in 38% e.e.

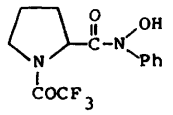

2

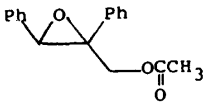

3

The Oppennauer oxidation employing aluminium as a key atom is one of the useful methods for mild oxidation.[12] Recently Posner has reported selective oxidation of alcohols by means of Al_2O_3–Cl_3CCHO system.[13] The present system has provided another means of oxidizing secondary alcohols into corresponding ketones with excellent yields as shown in Table 2. Allylic secondary alcohols gave epoxy ketones in one pot (**Runs** 5 and 6).

Meanwhile, primary alcohols, such as 1-dodecanol reacted much more slowly[14] and required prolonged period (2 d) afford a complex mixture which contained dodecanal (13% yield) and 1-dodecanol (54% recovery). Under the conditions described for the oxidation of secondary alcohols, many functional groups were inert. For example, 1-iodododecane, methyl dodecanoate, phenylacetylene, anisole, and dodecanal diethylene acetal were recovered unchanged in 95, 95, 98, 98, and 86% yields, respectively, after exposure to the oxidant.

Experimental

The IR spectra were determined on a Shimadzu IR-27-G spectrometer; the mass spectra, on a Hitachi M-80 machine; and the NMR spectra, on a Varian EM-360 spectrometer. The chemical shifts are given in δ, with TMS as the internal standard. The analyses were carried out by the staff at the Elemental Analyses Center of Kyoto University. Benzene was dried on sodium and distilled. *t*-Butyl hydroperoxide (70% aqueous solution) was purchased from Nakarai and used without further purification. All the experiments were carried out under an argon atmosphere. Purification of products were performed by preparative thin layer chromatography (TLC) or column chromatography on silica gel (Merck Kieselgel 60). Analytical GLPC was performed with a Yanagimoto GCG-550-F or Shimadzu GC-4CPT. Preparative GLPC was performed with a JEOL-JGC-20K apparatus.

The *threo/erythro* nomenclature for the relative configuration of two adjacent asymmetric centers of α,β-epoxy alcohols was determined according to the Noyori's formalism.[15]

Epoxidation of Allylic Alcohols by Means of t-*BuOOH–*(t-*BuO)*$_3$-*Al Reagent.* *t*-Butyl hydroperoxide (70%, 0.51 g, 4.0 mmol) was added at 5 °C (or 25 °C) to a stirred solution of an allylic alcohol (2.0 mmol) and $(t\text{-BuO})_3Al$ (0.74 g, 3.0 mmol) in benzene (10 ml). The resulting mixture was stirred at this temperature for an appropriate time described in Table 1. The reaction mixture was acetylated *in situ* for the entry 5, 6, and 7 by treating with acetic anhydride (1.02 g, 10 mmol) and pyridine (0.79 g, 10 mmol) at 25 °C for 1 h. The whole was

TABLE 2. OXIDATION OF SECONDARY ALCOHOLS WITH *t*-BuOOH–$(t\text{-BuO})_3Al$

Run	Alcohol	Reaction conditions[a] Temp/°C	Time/h	Product	Yield[b] %
1	$PhCH(OH)CH_3$	25	6	$PhCOCH_3$	90
2	Cyclododecanol	25	18	Cyclododecanone	85
3	2-Octanol	25	12	2-Octanone	(100)
4	4-*t*-Butylcyclohexanol	25	15	4-*t*-Butylcyclohexanone	85
5	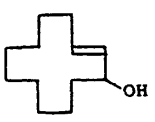	80[c]	6	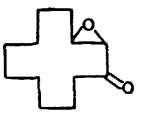	47
6	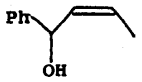	80[c]	9	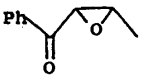	48

a) Reactions were performed in benzene solutions (10 ml) containing the substrates (2.0 mmol), $(t\text{-BuO})_3Al$ (3.0 mmol), and *t*-BuOOH (4.0 mmol). b) Except the case of 2-octanol where yield was determined by GLPC, all yields were isolated ones. c) *t*-BuOOH (8.0 mmol) and $(t\text{-BuO})_3Al$ (5.0 mmol) were used.

diluted with ether (10 ml), poured into 1 M †hydrochloric acid (20 ml), and extracted with ether. The organic layer was washed with aq $NaHSO_3$ (15 ml), aq $NaHCO_3$ (20 ml), and brine (2×20 ml), dried over anhydrous Na_2SO_4, and concentrated. The crude product was purified by silica-gel column chromatography (hexane–ethyl acetate) or preparative GLPC.

(2R, 3R*)-2,3-Epoxy-3,7-dimethyl-6-octenyl Acetate (1).*[48] Bp 94 °C (bath temp, 1 Torr, 1 Torr=133.322 Pa); IR (neat): 2940, 2350, 1750, 1460, 1375, 1230, 1038 cm^{-1}; NMR (CCl_4): δ=1.27 (s, 3H), 1.03—2.40 (m, 4H), 1.60 (s, 3H), 1.66 (s, 3H), 2.03 (s, 3H), 2.77 (t, J=6 Hz, 1H), 3.77—4.27 (m, 2H), 5.00 (bt, J=7 Hz, 1H); MS *m/e* (%): 212 (M^+, 1), 134 (11), 109 (74), 82 (31), 69 (50), 43 (100).

Conversion of threo- *and* erythro-*1,2-Epoxy-3-butanol*[16] *to* threo- *and* erythro-*2,3-Octanediol Acetonide.* This procedure was used to determine the ratio of *threo* and *erythro* epoxides produced by the oxidation of 3-buten-2-ol, because the separation of the diastereomeric epoxy alcohols by GLPC was not ideal.

Copper(I) iodide (12 g, 60 mmol) was suspended in anhydrous ether (150 ml). To this cooled (−20 °C) and stirred suspension was added butyllithium (1.7 M solution in hexane, 71 ml, 0.12 mol) dropwise over a period of 1 h. The mixture was allowed to stir for an additional 30 min, and then an etheral solution (30 ml) of a mixture of *threo*- and *erythro*-1,2-epoxy-3-butanols (approximately 7.5 mmol) was added at −20 °C. The whole was allowed to warm to 0 °C over a period of 1 h. The mixture was quenched by cautiously adding a sat. ammonium chloride solution. The copper salts were filtered off and the organic layer was washed twice with brine (40 ml), dried over anhydrous $MgSO_4$ and concentrated. The crude mixture of the diols was dissolved in acetone (10 ml). Perchloric acid (70%, 4 drops) was added to this and the resulting mixture was stirred at 25 °C for 1 h. The reaction mixture was quenched with 20% sodium hydroxide (2 ml) and extracted three times with hexane. The organic layer was separated and subjected to GLPC analysis (3% OV-17, 2 m, 65 °C) to show two peaks, T_r=6.2 min (*threo*-isomer, 42%) and T_r=8.7 min (*erythro*-isomer, 58%). *threo*-2,3-Octanediol acetonide: Bp 52 °C (bath temp, 3 Torr); IR (neat): 2948, 2880, 1464, 1382, 1248, 1180, 1100, 862 cm^{-1}; NMR (CCl_4): δ=0.90 (bt, J=6 Hz, 3H), 1.14 (d, J=6 Hz, 3H), 1.27 (s, 6H), 1.15—1.58 (m, 8H), 3.20—3.70 (m, 2H); MS *m/e* (%): 171 (M^+-CH_3, 100), 111 (18), 86 (56), 69 (74), 59 (32); Found: C, 70.89; H, 12.11%. Calcd for $C_{11}H_{22}O_2$: C, 70.92; H, 11.90%. *erythro*-2,3-Octanediol acetonide: Bp 60 °C (bath temp, 3 Torr); IR (neat): 2940, 2860, 1460, 1376, 1240, 1215, 1080, 855 cm^{-1}; NMR (CCl_4): δ=0.92 (bt, J=6 Hz, 3H), 1.05 (d, J=6 Hz, 3H), 1.22 (s, 6H), 1.00—1.62 (m, 8H), 3.75—4.18 (m, 2H); MS *m/e* (%): 171 (M^+-CH_3, 49), 129 (25), 86 (44), 69 (100), 59 (54); Found: C, 71.07; H, 12.09%. Calcd for $C_{11}H_{22}O_2$: C, 70.92; H, 11.90%.

threo- *and* erythro-*1,2-Epoxy-4-methyl-3-pentanol.*[16] The crude product was treated with *N*-(trimethylsilyl)imidazole (1.1 equiv) in dichloromethane. GLPC analysis (20%, PEG 6000, 2 m, 80 °C) of the resulting trimethylsilyl ethers indicated two peaks, T_r=7.8 min (*threo*-isomer, 71%) and T_r=7.0 min (*erythro*-isomer, 29%), which could not separated completely. The analytically pure samples of both isomers were prepared by preparative GLPC (20% PEG 6000). *threo*-Alcohol trimethylsilyl ether: Bp 67 °C (bath temp, 25 Torr); IR (neat): 2960, 1248, 1085, 928, 836 cm^{-1}; NMR ($CDCl_3$): δ=0.13 (s, 9H), 0.92 (d, J=6 Hz, 3H), 0.95 (d, J=6 Hz, 1H), 1.79 (dqq, J=5, 6, 6 Hz, 1H), 2.55—2.59 (m, 1H), 2.81 —2.83 (m, 1H), 2.91—2.93 (m, 2H); MS *m/e* (%): 173 (M^+-CH_3, 33), 145 (100), 75 (59), 73 (58). *erythro*-Alcohol trimethylsilyl ether: Bp 68 °C (bath temp. 25 Torr); IR (neat): 2970, 1472, 1250, 1068, 875, 838 cm^{-1}; NMR ($CDCl_3$): δ=0.13 (s, 9H), 0.92 (d, J=6 Hz, 3H), 0.95 (d, J=6 Hz, 3H), 1.79 (dqq, J=5, 6, 6 Hz, 1H), 2.61—2.72 (m, 2H), 2.85—2.95 (m, 1H), 3.34 —3.41 (m, 1H); MS *m/e* (%): 173 (M^+-CH_3, 4), 145 (63), 81 (10), 75 (45), 73 (100).

threo- *and* erythro-*1,2-Epoxy-2-methyl-3-heptanol.*[17] TLC (CH_2Cl_2–ether, 5 : 1) of the product derived from epoxidation of 2-methyl-1-hepten-3-ol indicated two spots, R_f=0.33 (*threo*-isomer, 13%) and R_f=0.43 (*erythro*-isomer, 87%). The *threo*/*erythro* isomer ratio was determined by GLPC (5% PEG 20M, 2 m, 85 °C), which showed two peaks at 26.0 min (*threo*-isomer) and at 15.0 min (*erythro*-isomer). The analytically pure samples of both isomers were prepared by preparative TLC. *threo*-Isomer: Bp 80 °C (bath temp, 1 Torr); IR (neat): 3450, 2940, 1460, 1050, 900, 874 cm^{-1}; NMR (CCl_4): δ=0.80—1.03 (bt, J=6 Hz, 3H), 1.27 (s, 3H), 1.15—1.55 (m, 6H), 2.15 (bs, 1H), 2.49 (d, J=5 Hz, 1H), 2.63 (d, J=5 Hz, 1H), 3.00—3.30 (m, 1H); MS *m/e* (%): 129 (M^+-CH_3, 1), 101 (11), 87 (16), 72 (40), 71 (87), 69 (37), 58 (100). *erythro*-Isomer: Bp 80 °C (bath temp, 1 Torr); IR (neat): 3460, 2960, 2940, 1460, 900, 788 cm^{-1}; NMR (CCl_4): δ=0.82—1.06 (bt, J=6 Hz, 3H), 1.06—1.78 (m, 6H), 1.28 (s, 3H), 2.00 (bs, 1H), 2.45 (d, J=5 Hz, 1H), 2.76 (d, J=5 Hz, 1H), 3.42—3.60 (m, 1H); MS *m/e* (%): 129 (M^+-CH_3, 1), 101 (9), 72 (28), 71 (70), 69 (32), 58 (100).

threo- *and* erythro-*(3R*, 4R*)-3,4-Epoxy-2-pentanol.*[18] Treatment of the crude epoxides derived from (*E*)-3-penten-2-ol with *N*-(trimethylsilyl)imidazole (1.1 equiv) in dichloromethane gave the trimethylsilyl ethers, which were analyzed by GLPC (10% PEG 20M, 2 m, 70 °C). GLPC indicated two peaks, T_r=7.8 min (*threo*-isomer, 64%) and T_r=6.6 min (*erythro*-isomer, 36%). The analytically pure samples were prepared by preparative GLPC (20% PEG 20M). *threo*-Alcohol trimethylsilyl ether: Bp 54 °C (bath temp, 13 Torr); IR (neat): 2960, 1450, 1370, 1248, 1098, 1052, 1012, 954, 890, 838, 750 cm^{-1}; NMR ($CDCl_3$): δ=0.12 (s, 9H), 1.19 (d, J=6 Hz, 3H), 1.30 (d, J=4 Hz, 3H), 2.64 (dd, J=2, 6 Hz, 1H), 2.85 (dq, J=2, 6 Hz, 1H), 3.56 (dq, J=6, 6 Hz, 1H); MS *m/e* (%): 159 (M^+-CH_3, 53), 117 (80), 115 (100), 73 (94). *erythro*-Alcohol trimethylsilyl ether: Bp 56 °C (bath temp, 12 Torr); IR (neat): 2960, 1450, 1370, 1248, 1094, 1004, 892, 836, 775 cm^{-1}; NMR ($CDCl_3$): δ=0.10 (s, 9H), 1.22 (d, J=6 Hz, 3H), 1.29 (d, J=5 Hz, 3H), 2.58 (dd, J=2, 5 Hz, 1H), 2.90 (dq, J=2, 5 Hz, 1H), 3.59 (dq, J=6, 6 Hz, 1H); MS *m/e* (%): 159 (M^+-CH_3, 50), 117 (92), 115 (100), 73 (84).

threo-*3,4-Epoxy-4-methyl-2-pentanol.*[18] GLPC analysis (5% PEG 20M, 2 m, 65 °C) showed that the product was homogeneous, having a retention time of 13.6 min: *threo*-Isomer: Bp 75 °C (bath temp, 15 Torr); IR (neat): 3450, 2970, 1720, 1378, 1112, 1070, 1030, 890, 868, 805 cm^{-1}; NMR (CCl_4): δ=1.16 (d, J=6 Hz, 3H), 1.28 (s, 3H), 1.30 (s, 3H), 2.57 (d, J=7 Hz, 1H), 3.33 (bs, 1H), 3.53 (dq, J=7, 6 Hz, 1H); MS *m/e* (%): 116 (M^+, trace), 72 (6), 59 (100), 58 (33), 57 (38), 45 (31).

Cf. erythro-Isomer:[18] Bp 76 °C (bath temp, 15 Torr); T_r= 19.1 min (5% PEG 20M, 2 m, 65 °C); IR (neat): 3450, 2970, 1645, 1380, 1112, 946, 906, 790 cm^{-1}; NMR (CCl_4): δ=1.25 (d, J=6 Hz, 3H), 1.27 (s, 3H), 1.30 (s, 3H), 1.55 (bs, 1H), 2.42 (d, J=7 Hz, 1H), 3.57 (dq, J=7, 6 Hz, 1H); MS *m/e* (%): 101 (M^+-CH_3, 1), 72 (6), 59 (100), 58 (27), 57 (33), 45 (34).

cis-*2,3-Epoxy-1-cyclohexanol.*[19] Bp 88 °C (bath temp, 18 Torr); IR (neat): 3300, 2950, 1650, 1420, 1058, 938, 846 cm^{-1}; NMR (CCl_4): δ=1.03—2.25 (m, 7H), 3.03—3.33 (m, 2H), 3.63—4.10 (m, 1H); MS *m/e* (%): 114 (M^+, 3), 96 (20),

† 1 M=1 mol dm^{-3}.

70 (100), 68 (32), 67 (48), 57 (96).

A small aliquot was acetylated with acetic anhydride and pyridine. GLPC analysis (10% PEG 20M, 2 m, 125 °C) indicated a peak (T_r=12.4 min) due to the *cis*-epoxy acetate. A peak at 9.8 min, corresponding to the *trans*-isomer prepared independently,[19] was absent.

cis-3,4-Epoxy-1-cyclohexanol.[20] Bp 79 °C (bath temp, 16 Torr); IR (neat): 3370, 2950, 1670, 1440, 1260, 1065, 990, 818, 792 cm^{-1}; NMR (CCl_4): δ=1.00—2.35 (m, 7H), 2.96—3.12 (m, 2H), 3.40—3.78 (m, 1H); MS *m/e* (%): 114 (M^+, trace), 95 (5), 71 (44), 70 (94), 57 (56), 42 (100).

After acetylation, the *cis/trans* isomer ratio was determined by GLPC (3% Silicone OV-17, 2 m, 75 °C), which indicated one peak at 40 min corresponding to the *cis*-epoxy acetate. The absence of *trans*-isomer[20] (T_r=36 min) was confirmed by the comparison with the authentic sample.

cis- *and* trans-*2,3-Epoxycyclododecanol.*[21] The two isomers were separated by column chromatography (hexane–ether, 5 : 1) on silica gel. *cis*-Isomer: Bp 81 °C (bath temp, 0.1 Torr); R_f=0.43 (hexane–ether, 1 : 1); IR (neat): 3350, 2950, 1462, 1448, 912, 870, 674 cm^{-1}; NMR (CCl_4): δ=0.97—2.27 (m, 19H), 2.72 (t, J=2 Hz, 1H), 2.90 (dt, J=10, 2 Hz, 1H), 3.85—4.08 (m, 1H); MS *m/e* (%): 198 (M^+, trace), 121 (24), 111 (38), 98 (52), 95 (67), 82 (83), 81 (87), 67 (65), 57 (100). *trans*-Isomer: Bp 83 °C (bath temp, 0.1 Torr); R_f=0.23 (hexane–ether, 1 : 1); IR (neat): 3450, 2950, 1475, 1465, 1040, 896, 788 cm^{-1}; NMR (CCl_4): δ=0.93—2.32 (m, 18H), 2.63 (bs, 1H), 2.53—2.88 (m, 2H), 2.90—3.18 (m, 1H); MS *m/e* (%): 198 (M^+, trace), 121 (17), 111 (28), 98 (41), 95 (59), 82 (71), 81 (72), 57 (100).

Asymmetric Epoxidation of Allylic Alcohols with a Chiral Aluminium Compound and t-*BuOOH.* The chiral ligand **2** was prepared by acylation of *N*-phenylhydroxylamine with *N*-trifluoroacetyl-(*S*)-prolyl chloride according to the literature.[22] **2**: $[\alpha]_D^{25}$ −61.3 (*c* 1.5, acetone). To a stirred solution of trimethylaluminium (1.0 M solution in hexane, 3.0 ml, 3.0 mmol) in benzene (15 ml) was added at 25 °C a benzene solution of **2** (1.1 g, 3.6 mmol) and the whole was stirred at the same temperature for 1 h. Then allylic alcohol (2.0 mmol) and *t*-butyl hydroperoxide (70%, 0.51 g, 4.0 mmol) were added successively and the resulting mixture was heated to reflux for an additional 3 h. After acetylation and a usual workup as mentioned before, the crude product was purified by preparative TLC.

1: $[\alpha]_D^{25}$ −8.6 (*c* 1.5, acetone). **3**: $[\alpha]_D^{25}$ −16.7 (*c* 0.6, CCl_4). Enantiomeric excess of these products were also checked by NMR with Eu(hfc)$_3$ shift reagent.

(2R, 3R*)-2,3-Epoxy-2,3-diphenylpropyl Acetate (3).*[11c] Mp 42.0 °C (hexane); IR (KBr): 1748, 1504, 1454, 1220, 1035, 745, 695 cm^{-1}; NMR (CCl_4): δ=1.98 (s, 3H), 4.16 (s, 1H), 4.23 (d, J=12 Hz, 1H), 4.50 (d, J=12 Hz, 1H), 6.80—7.20 (m, 10H); MS *m/e* (%): 225 (M^+-COCH_3, 1), 167 (10), 162 (28), 120 (100), 107 (38), 103 (26), 43 (48); Found: C, 75.98; H, 6.00%. Calcd for $C_{17}H_{16}O_3$: C, 76.10; H, 6.01%.

Oxidation of Secondary Alcohols by Means of t-*BuOOH–(*t-*BuO)$_3$Al Reagent.* To a stirred solution of a secondary alcohol (2.0 mmol) and (*t*-BuO)$_3$Al (0.74 g, 3.0 mmol) in benzene (10 ml) was added at 25 °C a benzene solution of *t*-BuOOH (0.44 g, 4.0 mmol). The resulting mixture was stirred at 25 °C for an appropriate time described in Table 2. The mixture was diluted with ether (10 ml) and poured into 1 M hydrochloric acid (20 ml). The separated organic layer and ether extracts were washed with aq $NaHSO_3$ (15 ml), aq $NaHCO_3$ (20 ml), and brine (2×20 ml), dried over anhydrous sodium sulfate, and concentrated. The crude product was purified by column chromatography (hexane–ethyl acetate) on silica gel (20 g).

The yield of 2-octanone was determined by GLPC (10% PEG 20M, 2 m, 50 °C) using dodecane as the internal standard.

Preparation of α,β-Epoxy Ketones by Means of t-*BuOOH–(*t-*BuO)$_3$Al Reagent.* A solution of an allylic secondary alcohol (2.0 mmol) and (*t*-BuO)$_3$Al (1.2 g, 5.0 mmol) in benzene (10 ml) was treated with a benzene solution of *t*-butyl hydroperoxide (70%, 1.0 g, 8.0 mmol) at 80 °C for 6 (9) h. After a usual workup, the crude product was purified by column chromatography (hexane–ethyl acetate) on silica gel (20 g).

(2R, 3R*)-2,3-Epoxycyclododecanone.* Mp 42.5 °C (hexane); IR (CCl_4): 2930, 1722, 1465, 1428 cm^{-1}; NMR (CCl_4): δ=0.95—1.93 (m, 15H), 1.95—2.40 (m, 2H), 2.63—3.00 (m, 2H), 3.30 (d, J=1.5 Hz, 1H); MS *m/e* (%): 196 (M^+, 4), 153 (12), 111 (53), 98 (92), 84 (90), 55 (100); Found: *m/e* 196.1464. Calcd for $C_{12}H_{20}O_2$: M, 196.1464.

(2R, 3S*)-2,3-Epoxy-1-phenyl-1-butanone.* Bp 123 °C (bath temp, 1 Torr); IR (neat): 2960, 1698, 1602, 1588, 1456, 1412, 1230, 940, 702 cm^{-1}; NMR (CCl_4): δ=1.16 (d, J=5 Hz, 3H), 3.32 (dq, J=5, 5 Hz, 1H), 3.97 (d, J=5 Hz, 1H), 7.15—7.63 (m, 3H), 7.83—8.15 (m, 2H); MS *m/e* (%): 162 (M^+, 12), 147 (8), 105 (100), 77 (35); Found: *m/e* 162.0704. Calcd for $C_{10}H_{10}O_2$: M, 162.0681.

Financial support by the Ministry of Education, Science and Culture (Grant-in-Aid Nos. 403022 and 75651), is acknowledged.

References

1) For recent reviews, see: P. A. Bartlett, *Tetrahedron*, **36**, 2 (1980); Y. Kishi, *Aldrichimica Acta*, **13**, 23 (1980); S. Masamune and W. Choy, *ibid.*, **15**, 47 (1982).

2) D. Swern, "Organic Peroxides," ed by D. Swern, John Wiley and Sons, New York (1971), Vol. 2, pp. 355—533.

3) For reviews, see: K. B. Sharpless and T. R. Verhoeven, *Aldrichimica Acta*, **12**, 63 (1979); T. Katsuki, *Kagaku Zokan*, **96**, 105 (1982).

4) a) $VO(acac)_2$ and $Mo(CO)_6$: S. Tanaka, H. Yamamoto, H. Nozaki, K. B. Sharpless, R. C. Michaelson, and J. D. Cutting, *J. Am. Chem. Soc.*, **96**, 5254 (1974); B. E. Rossiter, T. R. Verhoeven, and K. B. Sharpless, *Tetrahedron Lett.*, **1979**, 4733; E. D. Mihelich, *ibid.*, **1979**, 4729; E. D. Mihelich, K. Daniels, and D. J. Eickhoff, *J. Am. Chem. Soc.*, **103**, 7690 (1981). b) $[MoO_2(PhCON(Ph)O)_2]$: H. Tomioka, K. Takai, K. Oshima, and H. Nozaki, *Tetrahedron Lett.*, **21**, 4843 (1980). c) $Ti(OPr^i)_4$: V. S. Martin, S. S. Woodard, T. Katsuki, Y. Yamada, M. Ikeda, and K. B. Sharpless, *J. Am. Chem. Soc.*, **103**, 6237 (1981).

5) Epoxidation of allylic alcohols carrying Me_3Si group on the double bonds proceeds with high stereoselectivity, see: I. Hasan and Y. Kishi, *Tetrahedron Lett.*, **21**, 4229 (1980); H. Tomioka, T. Suzuki, K. Oshima, and H. Nozaki, *ibid.*, **23**, 3387 (1982).

6) K. Takai, K. Oshima, and H. Nozaki, *Tetrahedron Lett.*, **21**, 1657 (1980).

7) G. A. Razuvaev, V. A. Shushunov, V. A. Dodonov, and T. G. Brilkina, "Organic Peroxides," ed by D. Swern, Wiley-Interscience, New York (1972), Vol. 3, pp. 141—270; T. Mole and E. A. Jeffery, "Organoaluminium Compounds," Elsevier, Amsterdam (1972), p. 205.

8) A. G. Davies and C. D. Hall, *J. Chem. Soc.*, **1963**, 1192.

9) Y. N. Anisimov and S. S. Ivanchev, *Zh. Obshch. Khim.*, **41**, 2248 (1971).

10) The observed reaction could be rationalized as follows: The addition of a substrate alcohol (ROH) to aluminium reagents causes the exchange between the alcohol and *t*-

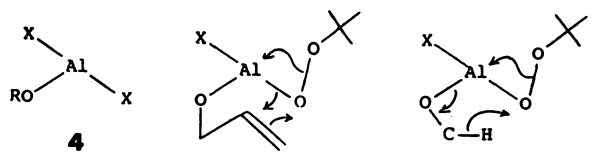

4 **5** **6**

X = *t*-BuO or Me

BuOOH (or the evolution of methane gas (Me_3Al)) to provide the product **4**. Successive addition of *t*-BuOOH affords the intermediate **5** or **6** in which the peroxide bond is polarized by a three centered interaction with an empty coordination site on the aluminium atom. The O–O bond is cleaved by π-electron of the suitably situated double bond (for the epoxidation of allylic alcohols) **5** or by hydride uptake (for the oxidation of secondary alcohols) **6** to afford the corresponding product. There has been considerable interest in establishing optimum O–C–C–C dihedral angles for epoxidation of allylic alcohols with both peracid[18,20] and vanadium catalysts.[4a,21,23] The *threo*/*erythro* ratios with *t*-BuOOH–$(t\text{-BuO})_3$Al system are rather close to those with peracid epoxidation and a dihedral angle near 120° seems to fit our data. The preferred conformations are illustrated in Scheme 2 for the epoxidation of allylic alcohols (Runs 1 and 5 in Table 1). The conformer **10** is much less favorable as compared to **9** due to the severe steric interaction between two Me group circled. No such remarkable steric interaction can be seen in the former case (**7** and **8**).

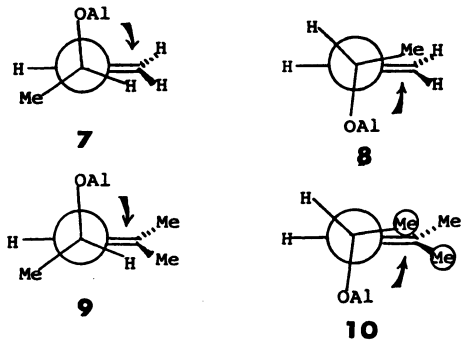

7 **8** **9** **10**

Scheme 2.

11) Transition metal catalyzed asymmetric epoxidation, see: a) T. Katsuki and K. B. Sharpless, *J. Am. Chem. Soc.*, **102**, 5974 (1980); b) S. Yamada, T. Mashiko, and S. Terashima, *ibid.*, **99**, 1988 (1977); c) R. C. Michaelson, R. E. Palermo, and K. B. Sharpless, *ibid.*, **99**, 1990 (1977).

12) C. Djerassi, *Org. React.*, **6**, 207 (1951).

13) G. H. Posner, R. B. Perfetti, and A. W. Runquist, *Tetrahedron Lett.*, **1976**, 3499.

14) Selective oxidation of a secondary hydroxyl in the presence of a primary one: H. Tomioka, K. Oshima, and H. Nozaki, *Tetrahedron Lett.*, **23**, 539 (1982) and references cited therein. The opposite selectivity is obtained by means of $[RuCl_2(PPh_3)_3]$–benzene system: H. Tomioka, K. Takai, K. Oshima, and H. Nozaki, *ibid.*, **22**, 1605 (1981).

15) R. Noyori, I. Nishida, and J. Sakata, *J. Am. Chem. Soc.*, **103**, 2106 (1981).

16) M. L. Sassirer and J. English, *J. Am. Chem. Soc.*, **82**, 4891 (1960).

17) A. Yasuda, S. Tanaka, H. Yamamoto, and H. Nozaki, *Bull. Chem. Soc. Jpn.*, **52**, 1701 (1979).

18) P. Chautemps and J.-L. Pierre, *Tetrahedron*, **32**, 549 (1976).

19) H. B. Henbest and R. A. L. Wilson, *J. Chem. Soc.*, **1957**, 1958.

20) P. Chamberlain, M. L. Roberts, and G. H. Whitham, *J. Chem. Soc., B*, **1970**, 1374.

21) T. Itoh, K. Jitsukawa, K. Kaneda, and S. Teranishi, *J. Am. Chem. Soc.*, **101**, 159 (1979).

22) W. E. Pereira and B. Halpern, *Aust. J. Chem.*, **25**, 667 (1972).

23) T. Hiyama and M. Obayashi, *Tetrahedron Lett.*, **24**, 395 (1983).

Effects of Lysine and Arginine Derivatives on the Base Stacking Association of 2′-Deoxyguanosine 5′-Monophosphate

Kazumi HIROTA, Mitsuru IGARASHI, Yoshio INOUE, and Riichirô CHÛJÔ*
Department of Polymer Chemistry, Tokyo Institute of Technology, O-okayama 2, Meguro-ku, Tokyo 152
(Received July 9, 1983)

The effects of basic amino acid residues on the base stacking of nucleotides have been studied to clarify the nature of interaction between histones and DNA's. For this purpose, lysine and arginine derivatives were used as models for basic amino acid residues in histone. The base stacking association of 2′-deoxyguanosine 5′-monophosphate(5′-dGMP) in aqueous solution has been studied by the measurement of the concentration dependence of ^{1}H NMR chemical shifts of 5′-dGMP both in the absence and in the presence of the basic amino acid derivatives at different pH's. We clarified that the lysine favors the base stacking association of 5′-dGMP through the interaction with the phosphate group(s), while an excess of the arginine destabilizes the stacking aggregates through the interaction with the base moiety. We also clarified that the ionization of the phosphate group destabilizes the stacking association of 5′-dGMP both in the absence and in the presence of the basic amino acids.

To investigate the interaction of basic protein with nucleic acid, there has been studied many model systems consisting of basic oligo- or polypeptides and polynucleotides, nucleic acids, or its components by physicochemical methods.[1-9] The binding of histones to DNA has been clarified to occur mainly through an electrostatic linkage between basic amino acid residues such as lysine and arginine, and the DNA phosphate groups.[4,9] Wagner and Arav[1] have used equilibrium dialysis to study the binding of the various nucleotides to poly(L-lysine) and poly(L-arginine) at pH 7. Their results showed that there is some specificity in the interaction between the nucleotides and basic polypeptides. In particular, the binding constant of uanine nucleotide with poly(L-arginine) is much larger than that with poly(L-lysine). Rifkind and Eichhorn[2] have studied, using optical rotatory dispersion, the interaction of various ribonucleotides with poly(L-lysine) and poly(L-arginine) and shown that the guanosine nucleotide stacks more weakly in the presence of poly(L-arginine) than in the presence of poly(L-lysine).

Free nucleic acid bases and their derivatives are known to aggregate in aqueous solution. In these aggregations, as shown by ^{1}H NMR measurements, the planar bases are arranged in parallel with each other to take so-called stacking mode.[10-15] The stacking interaction has been extensively studied for nucleosides and nucleotides,[10-19] because the stacking contributes dominantly to the stability of the secondary structures of DNA and other polynucleotides.[12,13,19-21]

No attempt has so far been made to study the effect of basic amino acids on the base stacking interaction of nucleotides. It seems that the study of this effect would promote the understanding of a local interaction at lysine- or arginine-rich regions in nucleohistone. A study on the nucleotide having guanine base can also provide the information relevant to the specific interaction of the nucleotide with poly(L-arginine). In this work, we will first study the base stacking association of 2′-deoxyguanosine 5′-monophosphate(5′-dGMP) at acidic, neutral, and alkaline pH's by means of ^{1}H NMR, since no detailed study has so far been reported. The effect of phosphate ionization on a base stacking association will be discussed. On the basis of these results, we will study the effect of lysine and arginine derivatives, N_α-acetyl-L-lysine methyl ester(Ac–Lys–OMe) and N_α-acetyl-L-arginine methyl ester(Ac–Arg–OMe), at each pH. For the sake of comparison, 2′-deoxyadenosine 5′-monophosphate(5′-dAMP), 2′-deoxyadenosine (2′-dAdo), and 2′-deoxyguanosine(2′-dGuo) will be also studied.

Experimental

Materials. All samples were purchased from Sigma Chemical Co. Sodium salts of 5′-dGMP and 5′-dAMP were treated with Chelex-100(Bio-Rad Laboratories). The lysine and arginine derivatives, free acid of 5′-dGMP, and nucleosides (2′-dAdo and 2′-dGuo) were used without further purification. Deuterium oxide(D_2O) and perdeuterated dimethyl sulfoxide($(CD_3)_2SO$) used as solvents, were purchased from Merck Sharp and Dohme, Canada Ltd.

NMR Measurements. Fourier transformed ^{1}H NMR spectra were taken on a JEOL PS-100 NMR spectrometer equipped with a PFT-100 Fourier transform system and a JEOL EC-100 computer. The spectrometer was field-frequency locked on deuterium resonance of D_2O or $(CD_3)_2SO$ used as solvent. Digital resolution was 0.24 Hz. The methyl signal of 2-methyl-2-propanol was used as an internal reference for monitoring the chemical shifts. This signal is known to be shifted to upfield in the presence of high concentration of aromatic solutes.[22] This shift is, however, negligibly small in the experimental concentration range (up to 0.25 M for the nucleotides, 1 M = 1 mol dm^{-3}).

All spectra were recorded at 30 °C. A JES VT-3 temperature controller was used for the stabilization, with accuracy of ±2 °C.

NMR samples were prepared in D_2O containing 5×10^{-3} M EDTA (ethylenediaminetetraacetic acid). An addition of EDTA did not affect ^{1}H chemical shifts. The pH of solution was adjusted to a desired value by an addition of very small amount of concentrated DCl and/or NaOD solution in D_2O. The pH value was measured, with an accuracy of ±0.01 pH unit, both before and after the NMR measurement with a TOKO TP-101 pH meter fitted with combination electrode of Type CE-103 which can be inserted to NMR sample tube. No correction was made for the deuterium isotope effect on pH value. Concentrations were determined by dry weight and then adjusted to the desired values by dilution using a volumetrically variable pipette 4710 (Eppendorf).

The data of chemical shifts were analyzed by using a Sharp MZ-80B personal computer: the observed variation of the chemical shift with concentration was fitted to an equation by

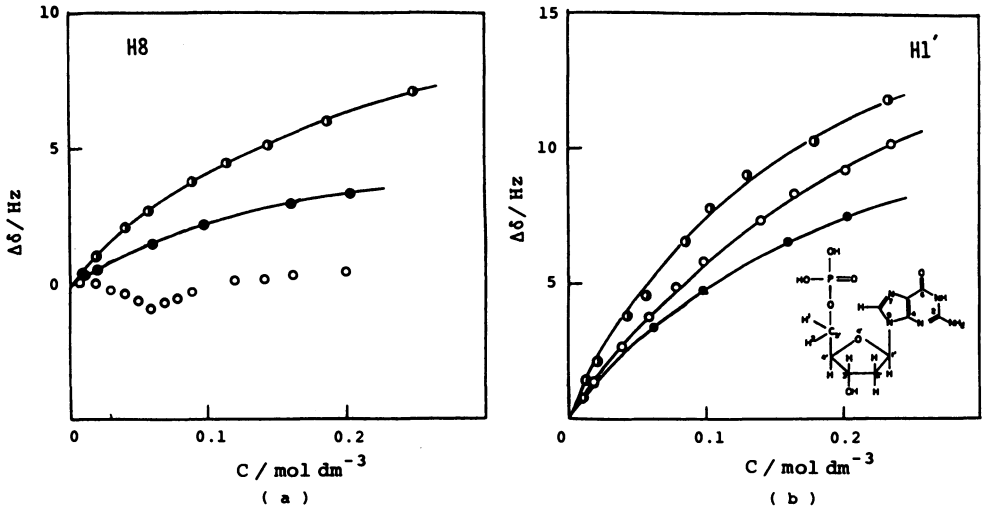

Fig. 1. Effect of pH on the base stacking association of 5′-dGMP. ^{1}H chemical shift differences $\triangle\delta$ are displayed for the H-8(a) and H-1′(b) as a function of 5′-dGMP concentration C at pH 4.0 (○), 6.6 (◑), and 9.0 (●), where $\triangle\delta$ is the chemical shift of a particular proton at each concentration referenced to that at an infinite dilution and a positive value represents an upfield shift.

using a Newton-Gauss nonlinear least-squares method.

Results

The Self-association of 5′-dGMP. We used the resonance of the base proton in position 8(H-8) and that of the ribose proton in position 1′(H-1′) (see Fig. 1), as a probe for studying the concentration dependence of intermolecular association of 5′-dGMP. The resonance of H-2 proton was further used in the experiment for 5′-dAMP. In Fig. 1 is shown the concentration dependence of the ^{1}H chemical shift differences ($\Delta\delta$) of the 5′-dGMP protons H-8(a) and H-1′(b) at pH 4.0, 6.6, and 9.0, where $\Delta\delta$ is the chemical shift of a particular proton at each concentration referenced to that at an infinite dilution and a positive value represents an upfield shift. These three pH's were chosen to correspond to monoanionic, pK, dianionic states of the phosphate group of 5′-dGMP. From the titration experiment of ^{31}P chemical shift of 5′-mononucleotides,[35] the phosphate group is mono and dianion at pH 4.0 and 9.0, respectively. The pH value of 6.6 is close to the pK value for the secondary ionization of the phosphate group. At pH 6.6 and 9.0, upfield shifts were observed with increasing concentration, indicating an increase of the fraction of the base stacking association.[10–15] The concentration dependence of these ^{1}H chemical shifts has been analyzed by applying the isodesmic model of indefinite non-cooperative stacking.[23] In this model, the relationship between the observed chemical shift difference ($\Delta\delta$) and total concentration (C) is given by

$$(\Delta\delta/C)^{1/2} = (K/2\Delta\delta_D)^{1/2} \times (2\Delta\delta_D - \Delta\delta), \quad (1)$$

where $\Delta\delta = \delta_0 - \delta_{obsd}$, δ_0 and δ_{obsd} are the chemical shifts of the investigated proton at an infinite dilution and at each concentration, $\Delta\delta_D$ the dimerization shift, and K the association constant. The observed chemical shift displacements for both protons at pH 6.6 and 9.0 were consistent with this model.

At pH 4.0, the H-8 base proton resonance shifts little with increasing concentration, while the H-1′ ribose proton resonance shifts significantly to upfield. The results indicate that there are other interactions in addition to the base stacking association and the interaction sites are in the base moiety of 5′-dGMP. The unique shift of H-8 proton at pH 4.0 may be specific to the nucleotide having guanine base, since the H-8 base proton resonance of 5′-dAMP shifted to upfield with increasing concentration at pH 4.0.

In order to understand an interaction other than base stacking, we have also studied the concentration de-

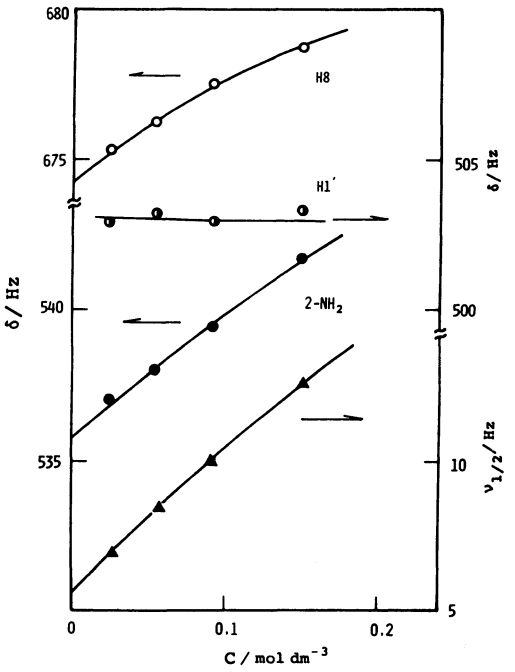

Fig. 2. ^{1}H chemical shifts δ from 2-methyl-2-propanol for the 5′-dGMP protons H-8 (○), H-1′ (◑), and 2-NH_2 (●) and the half-width $\nu_{1/2}$ of 2-NH_2 (▲) as a function of 5′-dGMP concentration C in $(CD_3)_2SO$.

TABLE 1. EFFECTS OF pH AND Ac–Lys–OMe ON THE ASSOCIATION CONSTANTS (K/M^{-1})[a] FOR THE BASE STACKING OF 5′-dGMP AND 5′-dAMP[b] ACCORDING TO THE ISODESMIC MODEL

pH	5′-dAMP			5′-dGMP		[Ac–Lys–OMe]/[5′-dGMP]=0.5		[Ac–Lys–OMe]/[5′dGMP]=1	
	H8	H2	H1′	H8	H1′	H8	H1′	H8	H1′
4.0	6.9	6.3	6.0	—[c]	1.5	6.2[d]	6.0[d]	7.1[d]	7.6[d]
6.6	4.6	4.2	4.5	2.7	3.0	3.4	3.5	4.3	4.4
9.0	3.7	3.3	3.2	1.9	2.0	2.9	3.2	2.7	3.0

a) Estimated errors for these association constants are 10—15%. b) Measurement for pH effect only. c) Not determined. d) For concentration below 0.06 M.

pendence of ^1H chemical shifts and line width of 5′-dGMP in $(CD_3)_2SO$ (Fig. 2). It is known that the base stacking association is negligibly small in this solvent.[24] The resonance position of H-1′ ribose proton is independent of concentration as expected. The resonance of 2-NH_2 shifts to downfield and its line width increases with increasing concentration, indicating the formation of hydrogen bond including 2-NH_2 group. Parallel to this variations, the resonance of H-8 proton shifts to downfield.

In Table 1 are shown the effects of pH on the association constants for the stacking of 5′-dGMP and 5′-dAMP estimated by applying the isodesmic model. The association constants obtained from the chemical shift displacements of H-8 base protons agree well with those from the H-1′ ribose protons, indicating that the variations of ^1H chemical shifts of both protons reflect the degree of stacking association. The association constants for stacking of both nucleotides decrease with increasing pH, except for 5′-dGMP at pH 4.0.

For comparison, 2′-dAdo, lacking 5′-monophosphate group, has been studied. In Fig. 3 is shown the pH dependence of 2′-dAdo protons (H-8, H-2, and H-1′) at various concentration up to dissolvable limit 0.04 M. The chemical shifts of all protons do not change in the range of pH 5 to 9 and this constancy is kept over the concentration range studied here. The downfield shifts of the base proton resonances observed for the nucleotides with decreasing pH below 5 can be attributed to the protonation of the base.[11,25]

Effect of the Lysine on the Stacking of 5′-dGMP. In Fig. 4 is shown the concentration dependence of ^1H chemical shifts (H-8 and H-1′) of 5′-dGMP at pH 4.0, 6.6, and 9.0 in the 2 : 1 mixture of 5′-dGMP and Ac–Lys–OMe. At pH 6.6 and 9.0, upfield shifts are observed with increasing concentration, which is consistent with the isodesmic model. This indecates that the lysine does not disturb the indefinite non-cooperative stacking of the base of 5′-dGMP. Even at pH 4.0, upfield shifts are also observed for both protons, unlikely in the case of 5′-dGMP alone. This indicates that the lysine interacts with 5′-dGMP.

In Table 1 is also shown the effect of the lysine on the association constants of 5′-dGMP. At pH 6.6, the association constants obtained from the H-8 and H-1′ protons increase in the presence of the lysine and with an increase of its population. The lysine, therefore, participates in the base stacking association.

Effect of the Arginine on the Stacking of 5′-dGMP. In Fig. 5 is shown the concentration dependence of ^1H chemical shifts of 5′-dGMP at molar ratios [Ac–Arg–OMe]/[5′-dGMP]=0 (5′-dGMP alone), 0.5, 1.0, and 2.0 at pH 4.0. The resonance of the base proton H-8 shifts to upfield with concentration in the presence of the arginine, similar to that in the presence of the lysine. The magnitudes of shift differences ($\Delta\delta$) of the ribose proton H-1′ increase in the presence of the arginine at lower 5′-dGMP concentration ($\approx$0.08 M). The arginine interacts with 5′-dGMP and participates in increase the fraction of stacking aggregates, similar to the case of the lysine.

At 5′-dGMP concentration higher than 0.1 M, the magnitudes of shift differences of the H-8 and H-1′

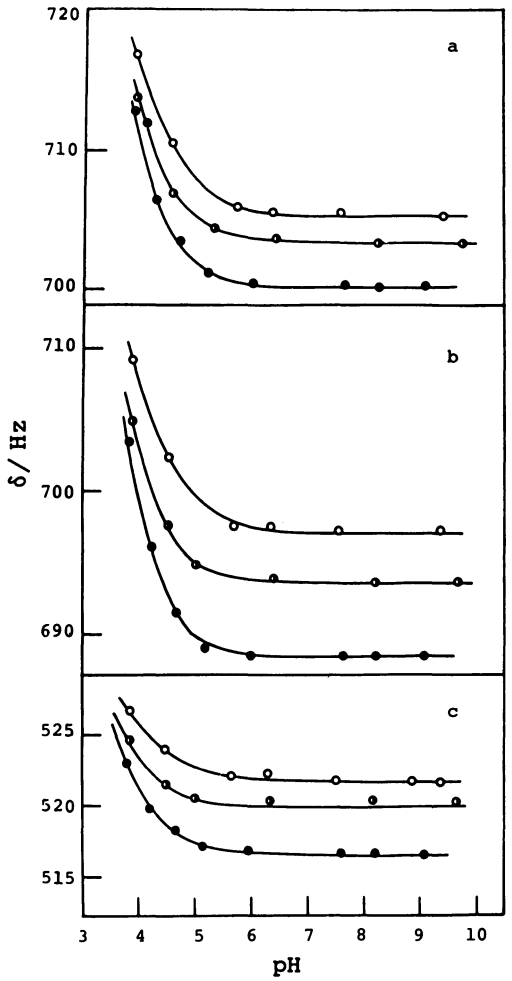

Fig. 3. ^1H chemical shifts δ *vs.* pH for protons H-8(a), H-2(b), and H-1′(c) of 2′-dAdo at 0.8×10^{-2} M (○), 2.2×10^{-2} M (◑), and 4×10^{-2} M (●).

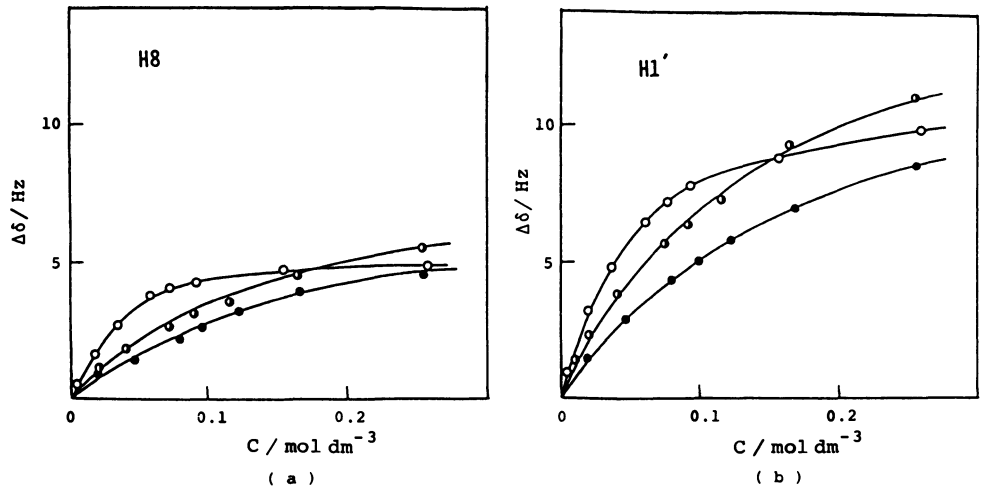

Fig. 4. Effect of pH on the self-association of 5′-dGMP at molar ratio [Ac–Lys–OMe]/[5′-dGMP]=0.5. ^{1}H chemical shift differences $\triangle\delta$ are displayed for the H-8(a) and H-1′(b) protons as a function of 5′-dGMP concentration C at pH 4.0 (○), 6.6 (◑), and 9.0 (●).

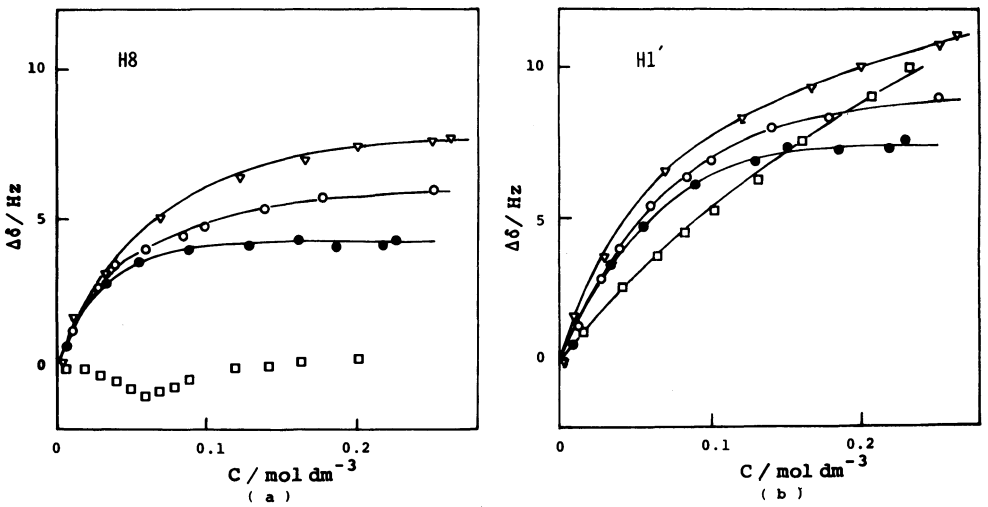

Fig. 5. Effect of the arginine on the self-association of 5′-dGMP at pH 4.0. ^{1}H chemical shift differences $\triangle\delta$ are displayed for the H-8(a) and H-1′(b) protons as a function of 5′-dGMP concentration C at molar ratios [Ac–Arg–OMe]/[5′-dGMP]=0(5′-dGMP alone) (□), 0.5 (▽), 1.0 (○), and 2.0 (●).

Table 2. Effects of pH and Ac–Arg–OMe on the association constants (K/M^{-1})[a] for the base stacking of 5′-dGMP according to the isodesmic model

[Ac–Arg–OMe]/[5′-dGMP]	H-8			H-1′		
	pH 4.0	pH 6.6	pH 9.0	pH 4.0	pH 6.6	pH 9.0
0[b]	—[c]	2.7	1.9	1.5	3.0	2.0
0.5	8.4	5.0	4.3	8.6	5.5	3.8
1.0	9.5[d]	5.2	4.1[e]	9.1[d]	5.8	3.7[e]
2.0	9.3[g]	5.5[f]	4.6[f]	8.9[g]	6.0[f]	4.1[f]

a) Estimated errors for these association constants are 15—20%. b) 5′-dGMP alone. c) Not determined. d—g) Concentration ranges of 5′-dGMP applied to the isodesmic model: (d) 0.18 M, (e) 0.15 M, (f) 0.09 M, (g) 0.06 M.

protons decrease and the chemical shifts tend to finite values with increasing molar ratio of the arginine to 5′-dGMP. These differences can be regarded as significant, since the experimental errors are within 0.5 Hz. This result indicates that the increase of the fraction of stacking aggregates of 5′-dGMP with increasing concentration is depressed at higher molar ratio of the arginine.

Similarly, at pH 6.6 and 9.0, the magnitudes of shifts observed for both protons at higher 5′-dGMP concentration decrease with increasing molar ratio of the arginine to 5′-dGMP. The isodesmic model cannot be

applied to these ^1H chemical shift variations. This is different from the case of the lysine where the chemical shift variations of both protons at pH 6.6 and 9.0 obey the isodesmic model. These results indicate that the differences between the arginine and the lysine could not be explained by the difference in electrostatic interactions alone.

In Table 2 are shown the effects of the arginine on the stacking association constants at each pH and the concentration ranges where the isodesmic model is applicable. The applicable concentration ranges were determined from plots of $(\Delta\delta/C)^{1/2}$ against $\Delta\delta$ (Eq. 1). These plots give a straight line up to an upper limit of concentration which is applicable to the isodesmic model. When the arginine is added to the 5'-dGMP solution at the ratio of [Ac–Arg–OMe]/[5'-dGMP]=0.5, the association constant (K) increases, similar to the case of the lysine. The K values at [Ac–Arg–OMe]/[5'-dGMP]=1.0 in the concentration ranges where the isodesmic model is applicable are, however, the same as those at [Ac–Arg–OMe]/[5'-dGMP]=0.5 within an experimental error. The K values are not increased by further addition of the arginine. The 5'-dGMP concentration ranges applied at [Ac–Arg–OMe]/[5'-dGMP]=2 are more restricted (Table 2, footnote (f)—(g)). These results indicate that the increase of the fraction of stacking aggregates is depressed in the presence of an excess of the arginine at all pH studied here.

Discussion

Self-association of 5'-dGMP at pH 4.0. The unique variation of chemical shift of H-8 proton with concentration at pH 4.0 (Fig. 1) could be interpreted by the formation of planar interbase association, because a guanine base is unusual among nucleic acid bases in its ability to make a self-associated regular structure with higher stability.[15,26–32] Gelation of aqueous solution of guanosine 5'-monophosphate (5'-GMP) takes place in acidic pH.[26,27] The gel structure of 5'-GMP at acidic pH consists of helically arranged stacks of planar tetramer units formed by hydrogen bonding (N-1 and 2-NH_2 as donors, O-6 and N-7 as acceptors).[21] Since the electron density at N-7 of the guanine base is large at acidic pH,[25,33,34] the N-7 of 5'-dGMP becomes also a stronger proton acceptor at pH 4.0 as compared with that at higher pH. Although 5'-dGMP, unlike 5'-GMP, does not form an ordered self-structure with applicable stability, the weak planar interbase association of 5'-dGMP could occur in acidic solution.

The effect of hydrogen bonding including 2-NH_2 on the chemical shift of H-8 proton, where the 2-NH_2 proton is the hydrogen bond donor for N-7 in planar interbase aggregate,[27–32] has been studied for 5'-dGMP in $(CD_3)_2SO$ (Fig. 2). With increasing the fraction of the interbase association by hydrogen bonding, the H-8 resonance shifts to downfield. This indicates that the formation of interbase hydrogen bonds including N-7(acceptor for 2-NH_2 proton) deshields the H-8 proton.

In aqueous solution, the hydrogen bonding becomes weak by simultaneous hydration of proton donor and acceptor groups, but the planar interbase association may be strong, since 5'-GMP forms gel even in aqueous solution.

The above results indicate that at pH 4.0, the deshielding of H-8 proton by planar interbase association can offset the upfield shift due to the base stacking association. There is, therefore, interbase association in addition to the base stacking association in the solution of 5'-dGMP at pH 4.0.

Effect of pH on the Base Stacking Association of Nucleotides. At the region of pH 6.6 to 9.0, the effect of pH is on the deprotonation of the phosphate group of nucleotides.[11] The association constants (K) for stacking of both 5'-dGMP and 5'-dAMP decrease with increasing pH (Table 1). These are possibly due to the increase of electrostatic repulsion between negatively charged phosphate groups in stacked aggregates. Scheller *et al.*[36] indicated that the tendency of self-stacking decreases in a series of adenosine$\gg AMP^{2-} > ADP^{3-} \approx ATP^{4-}$. The deprotonation of the phosphate group causes a decrease of stacking affinity by an increase of the intrinsic intermolecular electrostatic repulsion.

This interpretation is confirmed by comparison of 5'-dAMP and 2'-dAdo lacking 5'-monophosphate: the association constant (K) of 5'-dAMP decreases with increasing pH (Table 1), while 2'-dAdo does not induce the change of chemical shifts of all protons studied (H-8, H-2, and H-1') from pH 5 to 9 and this constancy is kept over the concentration range in this experiment (Fig. 3), that is, constancy of K value in this range of pH. The chemical shift of 2'-dGuo also did not change in the pH range up to dissolvable limit of concentration 0.01 M (not illustrated). The effect of charge of phosphate group is, thus, significant on the base stacking association.

Effects of Lysine and Arginine on the Self-association of 5'-dGMP. In the presence of the lysine or arginine derivative, monotonous upfield shifts are observed for H-8 and H-1' protons of 5'-dGMP even at pH 4.0 (Figs. 4 and 5), indicating that the base stacking association is easier to take place than the planar interbase association. The binding of lysine or arginine with 5'-dGMP results in the depression of the planar interbase association. Possibly, the interactions between these basic amino acids and 5'-dGMP include coulombic attraction and/or hydrogen bonding between the protonated ε-amino group ($pK \simeq 10$) of the lysine or the guanidinium group ($pK \simeq 11$) of the arginine and monoanionic phosphate group (s) in the stacked 5'-dGMP aggregates.

When the lysine is added to the 5'-dGMP solution at pH 6.6, the affinity of base stacking increases (Table 1). This increment is due to the neutralization of the negatively charged phosphate group by the positively charged ε-amino group of the lysine which reduces the intermolecular electrostatic repulsion between phosphate groups in the stacked 5'-dGMP. At pH 9.0, the association constant does not increase by an addition of the lysine. Since the degree of protonation ($pK \simeq 10$) of the lysine at pH 9.0 is low compared to that at lower pH, the addition of the lysine has a less effect on the stacking association of 5'-dGMP.

When an excess of the arginine is added to the 5'-dGMP solution at all pH studied, the increase of stacking

fraction with increasing concentration is depressed (Fig. 5 and Table 2). It is known that a guanidinium group of arginine can associate through hydrogen bonding with a guanine base.[37,38] An excess of the arginine can interact with the guanine base as well as the phosphate group of 5′-dGMP. On the other hand, the guanidinium cation is known to reduce a hydrophobic interaction.[39] This, leads to a reduction of fraction of the stacking aggregates, since the hydrophobic interaction contributes to the stabilization of stacking aggregates.[14,40] The hydrophobic interaction is more effective in the multiple stacked bases. We conclude, therefore, that the depression of stacking association is due to the interaction between the guanidinium group of the arginine and the guanine base of 5′-dGMP. From this interpretation, one could explain the fact that the stacking of guanine nucleotide occurs much less in the presence of poly(L-arginine) than in the presence of poly(L-lysine).[2]

References

1) K. Wagner and R. Arav, *Biochemistry*, **7**, 1771 (1968).
2) J. M. Rifkind and G. L. Eichhorn, *Biochemistry*, **9**, 1753 (1970).
3) B. Prescotti, C. H. Chou, and G. J. Thomas, *J. Phys. Chem.*, **80**, 1164 (1976).
4) P. H. von Hippel and J. D. McGhee, *Ann. Rev. Biochem.*, **41**, 231 (1972).
5) D. Porschke, *Biophys. Chem.*, **10**, 1 (1979).
6) E. N. Granodos and J. Bello, *Biochemistry*, **20**, 4761 (1981).
7) R. Mandel and G. D. Fasman, *Biochem. Biophys. Res. Commun.*, **59**, 672 (1974).
8) P. Epstein, S. S. Yu, and H. J. Li, *Biochemistry*, **13**, 3706 (1974).
9) C. Hélène and G. Lancelot, *Prog, Biophys. Mol. Biol.*, **39**, 1 (1982).
10) A. D. Broom, M. P. Schweizer, and P. O. P. Ts'o, *J. Am. Chem. Soc.*, **89**, 3612 (1967).
11) M. P. Schweizer, A. D. Broom, P. O. P. Ts'o, and D. P. Hollis, *J. Am. Chem. Soc.*, **90**, 1042 (1968).
12) W. M. Huang and P. O. P. Ts'o, *J. Mol. Biol.*, **16**, 523 (1966).
13) P. O. P. Ts'o, "Basic Principles in Nucleic Acid Chemistry," ed by P. O. P. Ts'o, Academic Press, New York (1974), Vol. 1.
14) K. J. Neurohr and H. H. Mantsch, *Can. J. Chem.*, **57**, 1986 (1979).
15) M. B. Borzo, C. Detellier, P. Leszor, and A. Paris, *J. Am. Chem. Soc.*, **102**, 1124 (1980).
16) D. Pörschke, *Biochemistry*, **15**, 1495 (1976).
17) L. A. Marky and K. J. Breslauer, *Biopolymers*, **21**, 2185 (1982).
18) Y. Takeuchi, I. Tazawa, and Y. Inoue, *Bull. Chem. Soc. Jpn.*, **55**, 3598 (1982).
19) M. Petersheim and D. H. Turner, *Biochemistry*, **22**, 256 (1983).
20) G. Felsenfeld and H. T. Miles, *Ann. Rev. Biochem.*, **36**, 407 (1967).
21) R. H. Sarma and S. S. Danyluk, *Int. J. Quantum Chem., Quantum Biol. Symp.*, **4**, 269 (1977).
22) R. A. Y. Jones, A. R. Kartritzky, J. N. Murrell, and N. J. Sheppard, *J. Chem. Soc.*, **1962**, 2576.
23) J. L. Dimicoli and C. Hélène, *J. Am. Chem. Soc.*, **95**, 1036 (1973).
24) L. Katz and S. Penman, *J. Mol. Biol.*, **15**, 220 (1966).
25) S. S. Danyluk and F. E. Hruska, *Biochemistry*, **7**, 1038 (1968).
26) M. Gellert, M. N. Lipsett, snd D. R. Davies, *Proc. Natl. Acad. Sci. U. S. A.*, **48**, 2013 (1962).
27) V. Sasisekharan, S. Zimmerman, and D. R. Davies, *J. Mol. Biol.*, **92**, 171 (1975).
28) C. Detellier and P. Laszlo, *J. Am. Chem. Soc.*, **102**, 1135 (1980).
29) C. L. Fisk, E. D. Becker, H. T. Miles, and T. J. Pinnavaia, *J. Am. Chem. Soc.*, **104**, 3307 (1982).
30) O. F. Nielsen, P. A. Lund, and S. B. Petersen, *J. Am. Chem. Soc.*, **104**, 1991 (1982).
31) S. B. Petersen, J. J. Led. E. R. Johnston, and D. M. Grant, *J. Am. Chem. Soc.*, **104**, 5007 (1982).
32) E. B. Brown, C. L. Marshall, and T. J. Pinnavaia, *J. Am. Chem. Soc.*, **104**, 6576 (1982).
33) L. G. Bunville and S. J. Schwarbe, *Biochemistry*, **5**, 3521 (1966).
34) J. Clauwart and J. Stockx, *Z. Naturforsh., B*, **23**, 25 (1968).
35) P. J. Cozzone and O. Jardetzky, *Biochemistry*, **15**, 4853 (1976).
36) ADP and ATP is adenosine 5′-diphosphate and -triphosphate, respectively; K. H. Scheller, F. Hofstetter, P. R. Mitchell, B. Prijs and H. Sigel, *J. Am. Chem. Soc.*, **103**, 247 (1981).
37) G, Lancelot, *Biochimie*, **59**, 587 (1977).
38) G, Lancelot, R. Mayer, and C. Hélène, *Biochim. Biophys. Acta*, **564**, 181 (1979).
39) D. B. Wetlaufer, S. K. Malik, L. Stoller, and R. L. Coffin, *J. Am. Chem. Soc.*, **86**, 508 (1964).
40) E. Plesiewicz, E. Stepien, K. Bolewska, and K. L. Wierzchowski, *Biophys. Chem.*, **4**, 131 (1976).

 © 1983 The Chemical Society of Japan Bull. Chem. Soc. Jpn., 56, 3802—3812 (1983)

Reduction of Sulfonic Acids and Related Organosulfur Compounds with Triphenylphosphine-Iodine System

Shigeru OAE*,† and Hideo TOGO

Department of Chemistry, The University of Tsukuba, Sakura, Niihari, Ibaraki 305

(Received July 18, 1983)

Arenesulfonic acids, their sodium salts, and alkyl arenesulfonates can be reduced readily to the corresponding arenethiols quantitatively by treatment with a mixture of triphenylphosphine and a catalytic amount of iodine, while alkanesulfonic acids, sulfinic acids, disulfides, thiosulfonic *S*-esters, and sulfonates are also readily reduced to the corresponding thiols similarly. Upon treatment with a mixture of triphenylphosphine and excess iodine, however, these aliphatic sulfur compounds are converted eventually to the corresponding alkyl iodides. The relative reactivities of these sulfonyl derivatives in the reaction with the triphenylphosphine–iodine system are the following. Aromatic series: $ArSO_2Cl$, $ArSO_2SAr' > ArSO_2H > ArSO_3R > ArSO_3^-HNBu_3^+$ (or PyH^+) $> ArSO_3H > ArSO_2SO_2Ar \gg ArSO_2CH_2C(CH_3)_3$, $ArSO_3Ar'$. Aliphatic series: RSO_2Cl, RSO_2SR', $RSO_2^-HNBu_3^+ > RSO_3^-HNBu_3^+ > RSSR$, $RSO_2H > RSO_3H > RSH > RSO_3R'$. In these reactions, the arenesulfonic acids bearing electron-donating substituents can be reduced more readily than those having electron-withdrawing substituents.

Organosulfur compounds can have several oxidative states, and the systematic representation of those compounds is shown in the Table 1 in which various sulfur compounds are arranged in order of the decrease of oxidation state from left to right hand side.[1] Sulfur atom in the sulfonic acid is in the highest oxidation state. Since the disulfone is formally a dehydrated condensation product between the sulfonic acid and the sulfinic acid, it is placed at the position between these two compounds in the Table. The sulfinylsulfone occupies the same position as the sulfinic acid, since the sulfinylsulfone is formed by dehydration of the sulfinic acid. While the thiosulfonic *S*-ester and the *α*-disulfoxide are also placed in the same position, the thiosulfinic *S*-ester and the disulfide are assigned at the different oxidation states as shown in Table 1.

Among these compounds, the sulfonic acid is exceptionally stable and inert to most reducing agents hitherto known, and no good method has been found to reduce sulfonic acids in one step. Reduction of other oxidized sulfur compounds can be found in numerous literatures, most of which are, however, rather fragmentary works done only for synthetic interests. Thus no systematic investigation on the reduction of these organic sulfur compounds has been carried out. Meanwhile, sulfonation of hydrocarbon has been a very important industrial process to introduce a sulfur functional group into organic compounds. Meanwhile sulfonic acids are so widely used in general chemical industries and also in laboratory organic syntheses, and hence a good method to reduce sulfonic acids has long been invoked, since synthetic chemistry using organosulfur compounds has recently been developed extensively. The purpose of this work is to discover a new reducing system powerful enough to reduce even organic sulfonic acids and also to investigate systematically the modes of deoxygenation of all these common oxidized organic compounds with the same reducing agent.

TABLE 1. OXIDOREDUCTION TABLE FOR ORGANOSULFUR COMPOUNDS

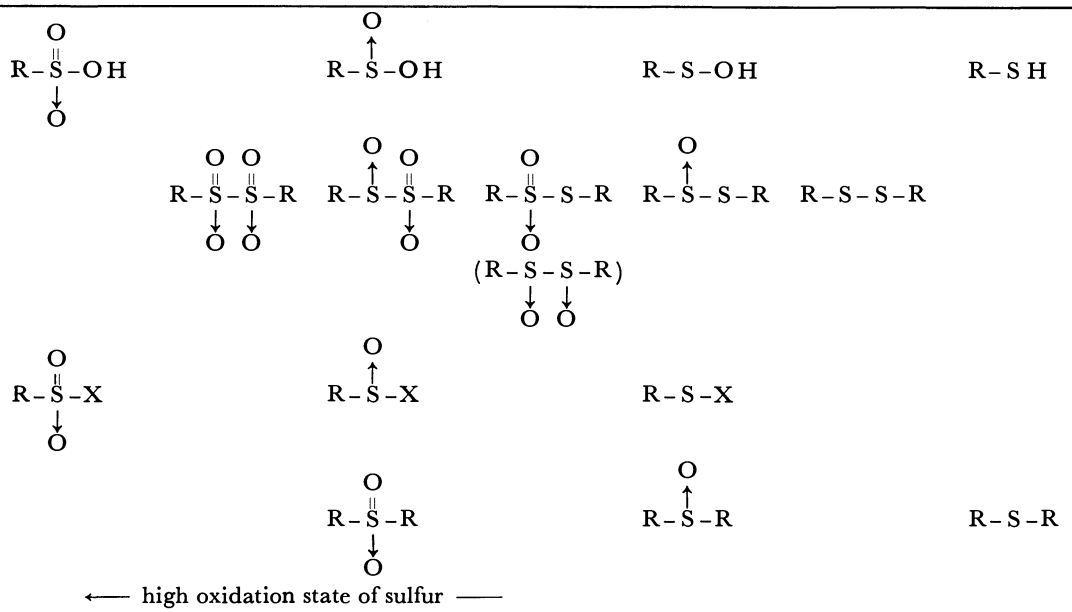

X: Halogens, NR^1R^2, OR.

† Present address: Okayama University of Science, 1-1 Ridai-cho, Okayama 700.

Direct electron transfer from alkali metal and related compounds to sulfonic acid has been known to lead mainly to reductive cleavage of C–S bond[2] (C–S bond dissociation energy: ≈293 kJ/mol[3]). Therefore, the deoxygenative reduction of the sulfonic acid would have to proceed stepwise *via* the initial nucleophilic displacement of OH group of the sulfonic acid by a good leaving group, followed by subsequent nucleophilic attack on the leaving group by the second nucleophile as shown in Eq. 1.

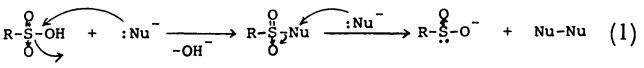

(1)

However, unfortunately such a nucleophilic substitution of OH^- group of the sulfonic acid does not readily proceed. Followings are some of the reasons why the sulfonic acid is so inert toward common reducing agents.

1) The sulfonic acid is so strong that it gives away proton to the nucleophilic reducing agent which upon protonation becomes no longer an effective nucleophile, while the deprotonated sulfonate anion possesses negatively charged three oxygen atoms which repel even strong nucleophiles to approach the central sulfur atom.

2) The reactivities of sulfonic acids and derivatives in nucleophilic displacements would be somewhat reduced since there would be unfavorable lone pair-lone pair repulsion between the nucleophile and two very electronegative oxygens at equatorial positions at the transition state of the trigonal bipyramide structure for the reaction. The sulfinic acid and its derivatives, having only one polarized oxygen atom on the sulfur and relatively weak S–O linkages, is more reactive in the nucleophilic displacement.

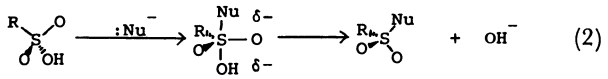

(2)

3) The poor leaving ability of OH group may also be partly responsible for the low reactivity of the sulfonic acid toward most nucleophiles.

However, the sulfonic acid can be made more reactive by replacing hydrogen by a suitable electron-withdrawing Y group to form RSO_2–OY upon treatment with a good condensing agent, XY. Indeed, nucleophilic displacement of OH group from the sulfur atom of sulfonic acid is very difficult, however, once RSO_2OY is formed, nucleophilic displacement of OY group in RSO_2OY by hard nucleophiles proceeds rather readily. Chlorination of sulfonic acids with PCl_5[4] or $SOCl_2$[5] is a good example (Eqs. 3 and 4) of transformation of sulfonic acids to RSO_2OY species. Obviously the formation of very stable phosphoryl chloride or SO_2 is the driving force of the reaction.

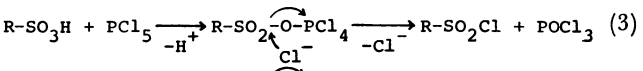

(3)

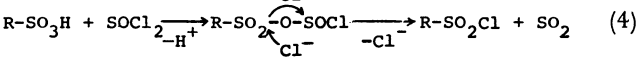

(4)

Thus, the key step of the reduction of the sulfonic acid represented by Eq. 5 is the activation of leaving OH group by the introduction of Y group on the sulfonyl oxygen, while Y should be an electron-withdrawing group and hence YO^- ought to be an excellent leaving group in the subsequent nucleophilic displacement. Once the intermediate (I) is formed, subsequent reactions are quite facile.

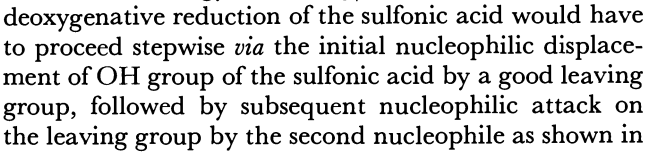

(5)

For example, sulfonyl chloride,[6] sulfonamide,[7] sulfonate,[8] thiosulfonic *S*-ester,[9] and sulfonic anhydride[10] (Nu=Cl, NRR′, OR, SR, and OSO_2R, respectively) are all intermediates of this type (I) which can be reduced to the corresponding thiols by common reducing agents. Thus, the success of the reduction of the sulfonic acids depends entirely upon a choice of XY and Nu^- to promote the reaction shown in Eq. 5. The first example of one pot reduction of sulfonic acids to thiols was recently reported from this laboratory, by using $(CF_3CO)_2O/(n\text{-}Bu)_4N^+I^-$, $X=CF_3CO_2^-$, $Y=CF_3CO$, $Nu^-=I^-$ shown in Eq. 5. This method is the first break through in the direct deoxygenative reduction of sulfonic acids, however, it not only requires a large excess of expensive reagents but also affords a mixture of reduction products, *i.e.* thiols and thiol trifluoroacetate.[11] More recently, G. A. Olah *et al.* reported the reduction of sulfonic acids to the corresponding disulfides with BX_3(X=Cl, Br, I)/KI.[12]

A series of extensive investigations on these basic problems have provided us a few other useful one-pot procedures to reduce sulfonic acids. Among those, the reducing system consisted of triphenylphosphine and iodine is quite convenient for reducing arenesulfonic acids to the corresponding arenethiols and also for reductive conversion of alkanesulfonic acids and related compounds to the corresponding alkyl iodides in one-pot reaction. This paper gives detailed accounts of these reductions.

Although triphenylphosphine is known to be a relatively strong reducing agent, it does not react directly with sulfonic acids. Triphenylphosphine has a strong oxygen affinity and hence if Ph_3P^+ group is introduced as Y in Eq. 5, even a weak nucleophile may attack the sulfonyl sulfur atom because of the excellent leaving ability of triphenylphosphine oxide. Meanwhile, the mixture of triphenylphosphine with halogen[13] and that of triphenylphosphine and disulfide[14] respectively are known to give phosphonium salts. Several reactions are known to utilize such phosphonium salts, *e.g.*, the conversion of alcohol and phenol derivatives to the corresponding halides by treatment with phosphine and halogen,[15] the desulfurization of disulfides to the corresponding sulfides with phosphine,[14,16–18] the condensation of carboxylic acids and alcohols or amines to the corresponding esters or amides[19] by treatment with a mixture of phosphine and diaryl disulfide,[20–22] diselenide,[23] or halogen and also the conversion of alcohols to sulfides with a mixture of phosphine and disulfide.[24] Thus a mixture of triphenylphosphine and a catalytic amount of iodine was our choice system for the reduction, (Eq. 5), in which not only RSO_2–OY ($Y=Ph_3P^+$) is easily generated from the reaction be-

TABLE 2. THE REACTION OF ARENESULFONIC ACIDS WITH TRIPHENYLPHOSPHINE/IODINE IN BENZENE UNDER REFLUX CONDITIONS

$ArSO_3H$	$ArSO_3/I_2/Ph_3P$	Time/h	Products yields/%[a]	
			ArSH	Ph_3PO
p-$CH_3C_6H_4SO_3H$	2/1/10	2.5	89	(128)[b]
p-$ClC_6H_4SO_3H$	2/1/10	4.0	98	(95)[b]
$C_6H_5SO_3H$	2/1/10	2.0	90	(116)[b]
2-$C_{10}H_7SO_3H$	2/1/10	2.0	85 (67)[b]	—
p-$CH_3C_6H_4SO_3H$	2/0.2/8	5.5	88	—
	2/0/10	2.5	0	0
	2/1/10(Bu_3P)	2.0	33	—
	2/1(Br_2)/10	3.0	13	—
2-$C_{10}H_7SO_3H$	2/1/8/2(Bu_3N)[c]	0.5	70	—
p-$CH_3C_6H_4SO_3H$	2/1/8/2(Bu_3N)[c]	0.5	95	—
$C_6H_5SO_3^-(CH_3CH_2)_4N^+$	2/1/8	10 min	94	—

a) Yields of Products were calculated based on the stoichiometry as shown in Eq. 6. b) Isolated yield. c) Amine was added into this system.

tween the reagent and the sulfonic acid but also iodide is a relatively strong reducing agent enough to reduce the sulfonyl derivatives.[10,11,25]

Results and Discussion

Reduction of Arenesulfonic Acids, Their Sodium Salts, and Alkyl Arenesulfonates with Triphenylphosphine and Iodine.[26] Triphenylphosphine is known to react with iodine to afford iodotriphenylphosphonium iodide[13,27] which would behave as a halogenating agent of sulfonic acids like phosphorus pentachloride (Eq. 3), while hydrogen iodide formed may act as a reducing agent. Based on this assumption, the reaction between sulfonic acids and Ph_3P/I_2 was investigated. Meanwhile, the successful conversion of alcohols and thiols to the corresponding halides with halotriphenylphosphonium halide has also prompted us to examine this reduction. As soon as triphenylphosphine was dissolved into a benzene solution which contained iodine, iodine color disappeared immediately giving a pale yellow solution of iodotriphenylphosphonium iodide. Upon treatment of p-toluenesulfonic acid with this reagent in refluxing benzene, the expected reduction of the sulfonic acid proceeded smoothly and p-toluenethiol was obtained nearly quantitatively. Even when the amount of iodine was reduced, the yield of the thiol was not reduced but the reaction required a prolonged period to complete, suggesting that iodine catalyzes the reduction of the sulfonic acid with triphenylphosphine. Thus, the whole reaction between arenesulfonic acids and triphenylphosphine in the presence of iodine can be expressed by Eq. 6.

$$ArSO_3H + 3\,Ph_3P \xrightarrow{I_2} Ar\text{-}SH + 3\,Ph_3PO \quad (6)$$

Since the reagent readily reacts with water, eventually affording triphenylphosphine oxide and hydrogen iodide, the sulfonic acid was carefully dehydrated by azeotropic distillation with benzene just before subjecting to the reduction in refluxing benzene. The results are summarized in Table 2. Neither triphenylphosphine alone nor iodide anion reacts with the arenesulfonic acid at all. The initial reaction is undoubtedly the reaction of the arenesulfonic acid with iodotriphenylphosphonium iodide to generate the (arylsulfonyloxy)triphenylphosphonium iodide as an incipient intermediate which receives subsequently nucleophilic attack of gegen ion, I^-, at the sulfonyl sulfur atom to form the arenesulfonyl iodide as shown in Eqs. 7—9.

$$Ph_3P + I_2 \rightleftharpoons Ph_3\overset{+}{P}\text{-}I\ I^- \quad (7)$$

$$ArSO_3H + Ph_3\overset{+}{P}\text{-}I\ I^- \rightleftharpoons ArSO_3^-\ Ph_3\overset{+}{P}\text{-}I + HI \quad (8)$$

$$ArSO_3^-\ Ph_3\overset{+}{P}\text{-}I \rightleftharpoons ArSO_2\text{-}O\overset{+}{\text{-}}PPh_3\ I^- \quad (8')$$

$$ArSO_2\text{-}O\overset{+}{\text{-}}PPh_3\ I^- \longrightarrow ArSO_2I + Ph_3PO \quad (9)$$

$$ArSO_2I + HI \longrightarrow ArSO_2H + I_2 \quad (10)$$

$$ArSO_2H + Ph_3\overset{+}{P}\text{-}I\ I^- \longrightarrow ArSO\text{-}O\overset{+}{\text{-}}PPh_3\ I^- \quad (11)$$

$$ArSO\text{-}O\overset{+}{\text{-}}PPh_3\ I^- \longrightarrow ArSO\text{-}I + Ph_3PO \quad (12)$$

$$ArSOI + HI \longrightarrow ArSOH + I_2 \quad (13)$$

$$ArSOH + Ph_3\overset{+}{P}\text{-}I\ I^- \longrightarrow ArS\text{-}O\text{-}\overset{+}{P}Ph_3\ I^- + HI \quad (14)$$

$$ArS\text{-}O\text{-}\overset{+}{P}Ph_3\ I^- \longrightarrow ArSI + Ph_3PO \quad (15)$$

$$ArSI + Ph_3\overset{+}{P}\text{-}I\ I^- \longrightarrow ArS\text{-}\overset{+}{P}Ph_3\ I^- + I_2 \quad (16)$$

$$ArS\text{-}\overset{+}{P}Ph_3\ I^- + HI \longrightarrow ArSH + Ph_3\overset{+}{P}\text{-}I\ I^- \quad (17)$$

$$ArSO_2I + Ph_3P \longrightarrow ArSO_2^-\ Ph_3\overset{+}{P}\text{-}I \longrightarrow ArSO\text{-}O\text{-}\overset{+}{P}Ph_3\ I^- \longrightarrow ArSOI + Ph_3PO \quad (18)$$

$$ArSOI + Ph_3P \longrightarrow ArSO^-\ Ph_3\overset{+}{P}\text{-}I \longrightarrow ArS\text{-}O\text{-}\overset{+}{P}Ph_3\ I^- \longrightarrow ArSI + Ph_3PO \quad (19)$$

The arenesulfonyl halide is known to be reduced with hydrogen iodide[28] to afford the diaryl disulfide, and also can be reduced by triphenylphosphine alone to give a mixture of the diaryl disulfide and the arenethiol.[29] Thus, two paths are conceivable for the reduction of the arenesulfonyl iodide. One path involves the initial nucleophilic attack of iodide anion on the arenesulfonyl iodide to afford iodine and the sulfinic acid which is eventually reduced to the diaryl disulfide *via* the arenesulfenic acid by the same reaction cycles through

TABLE 3. THE REACTION OF SULFINIC ACID AND SODIUM SULFINATE WITH TRIPHENYLPHOSPHINE/IODINE IN BENZENE

$ArSO_2H(Na)$	$ArSO_2H(Na)/I_2/Ph_3P$	Temp/°C	Time/h	Products/%[a]	
				ArSH	Ph_3PO
p-$CH_3C_6H_4SO_2H$	2/1/6.6	25	0.5	92	(118)[b]
p-$ClC_6H_4SO_2H$	2/1/6.6	25	0.5	87	—
$C_6H_5SO_2H$	2/1/6.6	25	0.5	90	(111)[b]
p-$CH_3C_6H_4SO_2Na$	2/1/6.6	Reflux[c]	2	92 (88)[b]	—[d]
$C_6H_5SO_2Na$	2/1/6.6	Reflux[c]	2	87	—[d]
$C_6H_5SO_2H$	2/0/6.6	25	2	50[e]	—

a) Yields of products were calculated based on the stoichiometry as shown in the following equation $ArSO_2H + 2\ Ph_3P \longrightarrow ArSH + 2\ Ph_3PO$. b) Isolated yield. c) The mixture of 3 ml of benzene and 5 ml of dioxane was used as a solvent. d) After this reaction, the mixture of about 200 mg of water and 1 ml of dioxane was added and refluxed for 0.5—1 h. e) Diphenyl disulfide was obtained in 24% yield as a by-product.

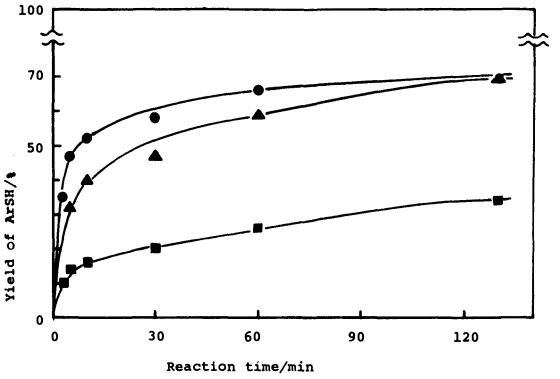

Fig. 1. Reaction of $ArSO_3H$ with Ph_3P/I_2 in Benzene at 72 °C to 73 °C.
■: *p*-$ClC_6H_4SO_3H$, ▲: $C_6H_5SO_3H$, ●: *p*-$CH_3C_6H_4SO_3H$ [*p*-$CH_3C_6H_4SO_3H$/$C_6H_5SO_3H$/*p*-$ClC_6H_4SO_3H$/Ph_3P/I_2=1/1/1/12/1(mmol)].

which the arenesulfonic acid is converted to the arenesulfonyl iodide as shown in Eqs. 7—9. Another conceivable process involves nucleophilic attack of triphenylphosphine on the arenesulfonyl iodide to result in the formation of the same reaction intermediate, the (arylsulfinyloxy)triphenylphosphonium iodide, obtained in the former path, as shown in Eqs. 18 and 19. In order to clarify which nucleophilic reagent, iodide anion or triphenylphosphine initiated the reduction of the arenesulfonyl iodide, the sulfonyl iodide was treated with either triphenylphosphine alone or hydriodic acid respectively. However, since the reduction was found to proceed in both systems readily, it could not be concluded which process predominates over the other. Probably both processes are participating concurrently. The extremely fast reduction of the arenesulfonyl iodide is clearly evidenced by the fact that no probable intermediate can be detected during the reactions of the arenesulfonic acid with Ph_3P/I_2 system, since the initial conversion of sulfonic acid to the sulfonyl iodide is undoubtedly one of the slowest steps of this multi-step reduction of the sulfonic acid to the thiol. One interesting observation is that the reduction is accelerated considerably by the presence of such an amine as tributylamine (Table 2), which can readily dissociate the arenesulfonic acid to the corresponding sulfonate anion to facilitate the reduction. Therefore, tetraethylammonium benzenesulfonate, which is soluble in benzene under our reaction conditions, can be readily reduced to benzenethiol in a high yield. The effect of polar substituent on aromatic ring observed in the reduction of the arenesulfonic acid also indicates that the sulfonic acid bearing an electron-donating substituent was found to be reduced more readily than the one having an electron-withdrawing substituent as shown in Fig. 1. This also suggests that the reaction shown by Eq. 8′ is the rate-determining step of the reduction.

Though the arenesulfinic acid can be reduced very slowly with triphenylphosphine alone, the addition of iodine accelerates this reduction remarkably to give the corresponding arenethiol quantitatively (Table 3). While sodium arenesulfinate cannot be reduced at all with triphenylphosphine alone, the triphenylphosphine/iodine system can reduce the sulfinate readily to the arenethiol and diaryl disulfide even in the absence of any phase-transfer catalyst.

The arenesulfonyl chloride and the *S*-aryl arenethiosulfonate can be readily reduced with triphenylphosphine alone, or better with the mixture of triphenylphosphine and iodine (Table 4).

Alkyl arenesulfonates were found to react smoothly with Ph_3P/I_2 in benzene forming alkyl iodides and diaryl disulfides. The disulfides were converted ultimately to the arenethiols upon treatment with triphenylphosphine and water (Table 5).

$$2\ ArS(=O)-OR + 6\ Ph_3P + I_2 \longrightarrow (ArS)_2 + 2\ RI + 6\ Ph_3PO \quad (20)$$

$$(ArS)_2 + Ph_3P + H_2O \longrightarrow 2\ ArSH + Ph_3PO \quad (21)^{30)}$$

On the other hand, both aryl arenesulfonates and neopentyl arenesulfonates were found to be quite inert in this reducing system even under prolonged reaction times as shown in Table 5. Obviously the reaction of Eq. 20 is initiated by the nucleophilic displacement (S_N2) at the alkyl carbon with iodide anion to form the alkyl iodide and arenesulfonate anion which is further reduced to arenethiol by Ph_3P/I_2. Due to the lack of reactivity at aromatic carbon and steric hindrance of neopentyl group, both aryl arenesulfonates and neopentyl arenesulfonates resist the nucleophilic attack of iodide

TABLE 4. THE REACTION OF $ArSO_2X$ WITH TRIPHENYLPHOSPHINE/IODINE IN BENZENE[a)]

$ArSO_2X$	$ArSO_2X/I_2/Ph_3P$	Temp/°C	Time/min	ArSH/%[b)]
p-$ClC_6H_4SO_2Cl$	2/1/8	25	30	100
p-$CH_3C_6H_4SO_2Cl$	2/0/8	25	30	92
$C_6H_5SO_2SC_6H_5$	1/1/4	25	10	89
$C_6H_5SO_2SC_6H_5$	1/0/4	25	10—15	83

a) After this reaction, the mixture of about 200 mg of water and 1 ml of dioxane was added and refluxed for 0.5—1.0 h. b) GLC yields (20% OV-1, 10 m glass column).

TABLE 5. THE REACTION OF ARENESULFONATES WITH TRIPHENYLPHOSPHINE/IODINE IN BENZENE UNDER ARGON ATMOSPHERE

$ArSO_3R(Ar')$	$ArSO_3R(Ar')/I_2/Ph_3P$	Time (Reflux)	Products/%[a)]	
			ArSH	RI
p-$CH_3C_6H_4SO_3CH_2C(CH_3)_3$	2/1.5/8	5 h	no reaction[b)]	
p-$CH_3C_6H_4SO_3C_6H_5$	2/1/10	45 h	no reaction[c)]	
$C_6H_5SO_3CH_2CH_3$	2/1.5/8	10 min	88	—
p-$CH_3C_6H_4SO_3(CH_2)_4CH_3$	2/1.5/8	10 min	95	90
$C_6H_5SO_3(CH_2)_4CH_3$	2/1.5/8	10 min	90	96
$C_6H_5SO_3CH_2CH_3$	2/0/10	2 h	no reaction	

a) Yields of products were calculated based on the stoichiometry as shown in the Eqs. 20 and 21. After this reaction, the mixture of about 200 mg of water and 1 ml of dioxane was added and refluxed for 0.5—1.0 h. b) Starting material was recovered in 85% yield. c) Starting material was recovered in 86% yield.

anion and no reaction appears to start even after a prolonged treatment with Ph_3P/I_2. Interestingly, pentyl benzenesulfonate, an alkyl arenesulfonate, reacted readily with tetrabutylammonium iodide in benzene affording tetrabutylammonium benzenesulfonate and pentyl iodide, whereas, under similar conditions phenyl benzenesulfonate did not react with tetrabutylammonium iodide.

$$C_6H_5SO_3CH_2(CH_2)_3CH_3 + Bu_4N^+I^- \xrightarrow[\text{benzene reflux}]{10\text{ min}} Bu_4N^+\,C_6H_5SO_3^- + CH_3(CH_2)_4I \quad 100\% \qquad (22)$$

$$p\text{-}CH_3C_6H_4SO_3C_6H_5 + Bu_4N^+I^- \xrightarrow[\text{benzen reflux}]{15\text{ min}} \text{no reaction} \qquad (23)$$

When bromine was used instead of iodine as the catalyst in the reduction of p-toluenesulfonic acid with triphenylphosphine, the yield of the thiol was found to be low (Table 2). Although tributylphosphine is a stronger nucleophile than triphenylphosphine, only 33% of p-toluenethiol was obtained along with unidentified side products upon treatment of the sulfonic acid with Bu_3P/I_2 (Table 2).

Phosphorus trichloride and phosphonic acid also gave only small amounts of diaryl disulfides and arenethiols, respectively, upon treatment of arenesulfonic acids in the presence of iodine.

$$p\text{-}CH_3C_6H_4SO_3H\cdot H_2O \xrightarrow[\text{neat 3 h reflux}]{I_2/PCl_3} (p\text{-}CH_3C_6H_4S)_2 \quad 18\%$$

$$p\text{-}CH_3C_6H_4SO_3H\cdot H_2O \xrightarrow[CH_3CN\ 4.5\text{ h reflux}]{I_2/H_3PO_3} p\text{-}CH_3C_6H_4SH \quad 25\%$$

Inspection of data in Tables 2 and 5 reveals that the reduction of arenesulfonic acids takes place more slowly than alkyl arenesulfonates. This may mean that arenesulfonate anions are more reactive than arenesulfonic acids in the reaction with the reducing system, Ph_3P/I_2. The treatment of alkyl arenesulfonates with iodide ion involves the initial facile nucleophilic attack of iodide ion on alkyl group, eventually affording arenesulfonate anions as primary intermediates. Similarly, tertiary amine have already been found to accelerate the reduction of arenesulfonic acids with Ph_3P/I_2. All these observations, *i.e.* the higher reactivities of arenesulfonic acids bearing electron-donating substituents in the reduction, the acceleration of the reduction by addition of amine, and the facile rates of reduction of both arenesulfonates and tetraethylammonium arenesulfonates suggest clearly that the rate-determining step is the nucleophilic substitution of the sulfonate anion, which is a gegen anion, on the central phosphorus atom of iodotriphenylphosphonium cation to form (arylsulfonyloxy)triphenylphosphonium iodide which has a P–O–S linkage (Eq. 8′).

Sodium arenesulfonate did not react with Ph_3P/I_2 in benzene at all because of its insolubility, however, it was smoothly reduced to the thiol in the presence of such a phasetransfer catalyst as 18-crown-6. The rate of the reaction was found to depend on the amount of the phase transfer catalyst (Table 6). Thus, this reducing procedure is quite useful, since sulfonic acids are usually available in the form of sodium salts in industry. However p-aminobenzenesulfonic acid, arenesulfonamides, and sulfones were not reduced by our systems even at high temperatures and under prolonged heating in other common solvents. The unsuccessful reduction of p-aminobenzenesulfonic acid and arenesulfonamide is believed to be due to the lack of solubilities of these compounds in such solvents as benzene, acetonitrile and dioxane, which were used in the actual reduction.

Diphenyl disulfone of which the central sulfur is highly sterically hindered, is very inert to triphenylphosphine or

Table 6. The reaction of sodium arenesulfonate with Ph_3P/I_2/18-crown-6 in benzene under argon atmosphere[a)]

$ArSO_3Na$	$ArSO_3Na/I_2/Ph_3P$/18-Crown-6	Time/h (Reflux)	ArSH/%[b)]
p-$CH_3C_6H_4SO_3Na$	2/1/10/0[d)]	24	Trace
	2/2/10/1	5	51 (50)[c)]
	2/2/10/1	31	85
$C_6H_5SO_3Na$	2/2/10/1	35	83
2-$C_{10}H_7SO_3Na$	2/2/10/1	24	67 (50)[c)]
	2/2/10/1	36	96 (93)[c)]
p-$CH_3C_6H_4SO_3Na$	2/2/8/0.02	79	80
2,4-$(CH_3)_2C_6H_3SO_3Na$	2/2/10/0.5	41	(63)[c)]
1-$C_{10}H_7SO_3Na$	2/2/10/0.5	35	70

a) Yields of product were calculated based on the stoichiometry as shown in the following equation $2ArSO_3Na + 7Ph_3P \xrightarrow[2)\ H_2O]{1)\ I_2} 2ArSH + 7Ph_3PO$. After this reaction, the mixture of about 200 mg of water and 2 ml of dioxane was added, and refluxed for 0.5—1 h. b) GLC yield (OV-1 20%, 1 m glass column). c) Isolated yield. d) The mixture of 3 ml of benzene and 5 ml of dioxane was used as a solvent.

Table 7. Reaction of aliphatic sulfur compounds with triphenylphosphine/iodine in benzene under nitrogen atmosphere

Substrate	Substrate/I_2/Ph_3P/Amine	Temp/°C	Time	Yield of RI/%
$CH_3(CH_2)_4SO_3H$	2/3/10/0	25	26 h	81
	2/3/10/0	Reflux	0.5 h	63
$CH_3(CH_2)_4SO_2H$	2/1/6.6/0	25	30 min	71[b)]
	2/3/6.6/0	25	2 h	95
$CH_3(CH_2)_7SO_2H$	2/3/6.6/0	25	2 h	85
$CH_3(CH_2)_7SO_2Cl$	2/3/8/0	25	10 min	75[c)]
	2/0/8/0	25	20 min	80[$CH_3(CH_2)_7Cl$]
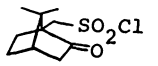	2/4/8/0	Reflux	8 h	(87)[d)]
$CH_3(CH_2)_7SH$	2/3/3/0	Reflux	1 h	98
$CH_3(CH_2)_4SH$	2/2/2.5/0	Reflux	1.5 h	90
$CH_3(CH_2)_4SO_3Na$	2/3/8[e)]	Reflux	26 h	40
$CH_3(CH_2)_4SO_3H$	2/3/10/2(Bu_3N)[f)]	25	25 min	79
$CH_3(CH_2)_4SO_2H$	2/3/6.6/2(Bu_3N)	25	10 min	100
$CH_3(CH_2)_7SH$	2/3/3/2(pyridine)	25	20 min	88
$CH_3(CH_2)_4SH$	2/3/3/2(Bu_3N)	25	20 min	100
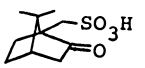	2/6/10/0	Reflux	9 h	87 (67)[d)]

a) GLC yield (20% OV-1, 1 m glass column). b) 1-Pentanethiol obtained as by-product (10% yield). c) 1-Chlorooctane obtained as by-product (12% yield). d) Isolated yield. e) 18-Crown-6 was used as a phase-transfer catalyst. f) The mixture of benzene and acetonitrile was uesd as a solvent.

triphenylphosphine/iodine system at room temperature. Diphenyl disulfone can hardly be reduced by triphenylphosphine alone even in refluxing benzene or acetonitrile, however it can be reduced by triphenylphosphine/iodine system in a quantitative yield under similar conditions.

$$C_6H_5SO_2SO_2C_6H_5 \xrightarrow[CH_3CN/C_6H_6\ \text{reflux}\ 24\,h\ \ 2)\ H_2O]{1)\ Ph_3P} C_6H_5SH\ 26\%$$

+ recovered disulfone 20%

$$C_6H_5SO_2SO_2C_6H_5 \xrightarrow[CH_3CN/C_6H_6\ \text{reflux}\ 20\,h\ \ 2)\ H_2O]{1)\ Ph_3P/I_2} C_6H_5SH\ 91\%$$

This reaction proceeds by the initial nucleophilic attack of iodide anion, which is formed by the reaction of triphenylphosphine and iodine, on the central sulfur atom of diphenyl disulfone to give benzenesulfonyl iodide and benzenesulfinate which can be readily reduced by triphenylphosphine/iodine system.

Finally, since triphenylphosphine/carbon tetrachloride system was known to form phosphonium salt,[31)] arenesulfonic acids were treated with this Ph_3P/CCl_4 system. Actually, the corresponding diaryl disulfides were obtained, but the yields were in general only 40% to 50% [arenesulfonic acid/Ph_3P=2/8(mmol)] when the reduction was carried out in the mixture of 1 ml of carbon tetrachloride and 5 ml of benzene under refluxing condi-

tions for 1.5 h.

Reductive Conversion of Alkanelfonic Acids, Sulfinic Acids, Thiols, Disulfides, Thiosulfonic S-Esters, and Sulfonates to the Corresponding Alkyl Iodides with Triphenylphosphine/Iodine.[32] When this reducing system was applied for the reduction of 1-pentanesulfonic acid, 1-pentanethiol which was the expected product, was not obtained, but pentyl iodide was the sole product obtained, when one equivalent amount of iodine was used.

$$RSO_3H + 4\,Ph_3P + I_2 \longrightarrow RI + 3\,Ph_3PO + Ph_3PS + HI \quad (24)$$

1-Pentanesulfonic acid is considered to be reduced at first to dipentyl disulfide or 1-pentanethiol as in the case of arenesulfonic acids. The subsequent multi-step reaction of either the disulfide or the thiol with Ph_3P/I_2 would afford eventually the iodide. In separate experiments, both 1-pentanethiol and dipentyl disulfide were found to be converted to pentyl iodide quantitatively upon treatment with Ph_3P/I_2.

$$RSSR + 2\,Ph_3\overset{+}{P}\text{-}I\ I^- \longrightarrow 2\,R\text{-}S\text{-}\overset{+}{P}Ph_3\ I^- \longrightarrow 2\,RI + 2\,Ph_3PS \quad (25)$$

$$RSH + Ph_3\overset{+}{P}\text{-}I\ I^- \longrightarrow R\text{-}S\text{-}\overset{+}{P}Ph_3\ I^- + HI \longrightarrow RI + Ph_3PS \quad (26)$$

It is worthy to note that even sterically-hindered *d*-camphor-10-sulfonic acid was successfully converted to the corresponding optically active 10-iodo-*d*-camphor. The formation of the corresponding thiol as the intermediate is shown in Fig. 2. 1-Pentanethiol was not detected in the direct conversion of 1-pentanesulfonic acid to pentyl iodide in the reduction with Ph_3P/I_2, since sterically unhindered 1-pentanethiol is so reactive, whereas *d*-camphor-10-thiol was actually isolated in a maximum yield of about 15% in the conversion of *d*-camphor-10-sulfonic acid to 10-iodo-*d*-camphor with Ph_3P/I_2. Since the *d*-camphor-10-thiol has a neopentyl

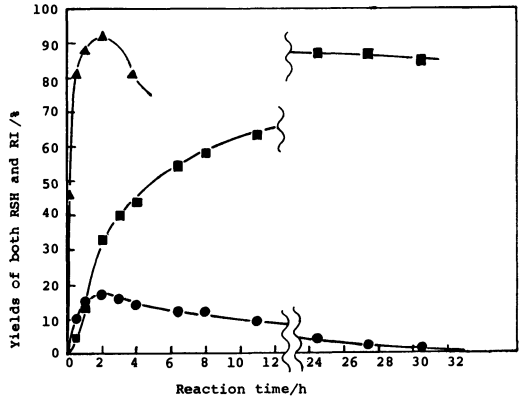

Fig. 2. Reaction of RSO_3H with Ph_3P/I_2 in Benzene under Reflux Conditions.

▲: $CH_3(CH_2)_4I$, ●: 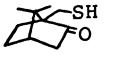 , ■: 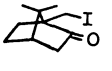

[$RSO_3H/Ph_3P/I_2$=2/10/4(mmol), R=$CH_3(CH_2)_4$– and].

structure, further desulfurization (S_N2) reaction is rather slow. Therefore, we can detect *d*-camphor-10-thiol during the reductive conversion of *d*-camphor-10-sulfonic acid to the corresponding iodide. 1-Pentanesulfinic acid reacted more readily with Ph_3P/I_2 than 1-pentanesulfonic acid, both affording pentyl iodide. 1-Octanesulfonyl chloride gave a mixture of octyl iodide (major) and octyl chloride (minor), while the reaction of the same compound with triphenylphosphine alone proceeded also smoothly at room temperature in benzene to give octyl chloride in 80% yield (Eq. 27). Results of all these reactions are summarized in Table 7. *d*-Camphor-10-sulfonyl chloride can also be converted to the corresponding iodide upon heating with Ph_3P/I_2.

$$RSO_2Cl + 3\,Ph_3P \longrightarrow RCl + 2\,Ph_3PO + Ph_3PS \quad (27)$$

Reaction of both alkyl alkanesulfonates and *S*-alkyl alkanethiosulfonates with Ph_3P/I_2 proceeded smoothly to give alkyl iodides quantitatively upon treatment with Ph_3P/I_2 (Table 8).

$$RSO_2SR' + 4\,Ph_3P + I_2 \longrightarrow RI + R'I + 2\,Ph_3PO + 2\,Ph_3PS \quad (28)$$

$$RSO_2OR' + 4\,Ph_3P + I_2 \longrightarrow RI + R'I + 3\,Ph_3PO + Ph_3PS \quad (29)$$

$$RSO_2SAr + 3\,Ph_3P + I_2 \longrightarrow RI + ArSH + 2\,Ph_3PO + Ph_3PS + HI \quad (30)$$

Nucleophilic substitution on alkyl group, R′, by iodide ion is undoubtedly involved in the initial step of the reaction of the sulfonate (Eq. 29), while there are two possible paths to initiate the reaction of *S*-alkyl alkanethiosulfonate (Eq. 28), *i.e.* nucleophilic substitution on the sulfenyl sulfur and that on alkyl carbon. The *S*-aryl alkanethiosulfonate reacts with Ph_3P/I_2 quite readily to form the alkyl iodide and the arenethiol. This reaction should also be initiated by the nucleophilic displacement on the sulfenyl sulfur of the substrate with either triphenylphosphine or iodide anion. Since the reactions of both *S*-alkyl alkanethiosulfonate and *S*-aryl alkanethiosulfonate with Ph_3P/I_2 proceed much more readily than the reaction of alkyl alkanesulfonate under the same conditions, the reactions of the former two thiosulfonic *S*-esters are undoubtedly initiated by nucleophilic substitution on the divalent sulfur. Both iodide anion and triphenylphosphine being just as strong nucleophiles for divalent sulfur, it is hard to conclude which nucleophile plays an important key role in initiating of the reaction. The rate-determining step of the reaction of alkanethiols, sulfinic acids, and sulfonic acids are presumed to be the nucleophilic attack of conjugate bases of these organosulfur compounds on the phosphorus atom of iodotriphenylphosphonium ion,[33,34] as discussed in the former section which deals with the reduction of arenesulfonic acids. In accordance with this assumption, these reactions were markedly accelerated by the presence of amines (Table 7) while the reduction of the other aprotic derivatives were not affected by the addition of base. The reaction is quite useful in conversion of alkanesulfonic acids, thiosulfonic *S*-esters, sulfonates, disulfides, thiols, and sulfonyl chlorides to the corresponding alkyl iodides quantitively under mild conditions in one-pot treatment.

Table 8. Reaction of aliphatic sulfur compounds with triphenylphosphine/iodine in benzene under nitrogen atmosphere

Substrate R^1- $-R^2$	Substrate/I_2/Ph_3P	Temp/°C	Time/min	Products/%[a] R^1I	R^2I
$CH_3(CH_2)_7SO_2O(CH_2)_4CH_3$	2/7/11	Reflux	5 h	95	95
$CH_3(CH_2)_4SO_2S(CH_2)_4CH_3$	1/2.5/5	25	10	200(R^1=R^2)	
$CH_3(CH_2)_7SO_2S(CH_2)_7CH_3$	1/2.5/5	25	10—15	184(R^1=R^2)	
$CH_3(CH_2)_4SS(CH_2)_4CH_3$[b]	1/2/3	25	90	200(R^1=R^2)	
$CH_3(CH_2)_7SS(CH_2)_7CH_3$[b]	1/2/3	25	120	200(R^1=R^2)	
$CH_3(CH_2)_4SO_2SC_6H_5$	1/2.5/5	25	10	92	c)

a) GLC yields (20 % OV-1, 10 m glass column). b) The mixture of benzene and dichloromethane was used as a solvent. c) After this reaction, the mixture of 0.5 ml of water and 2.5 ml of dioxane was added. Benzenethiol was obtained in 89% yield.

Finally, various alkanesulfonyl chlorides were found to be converted to the corresponding iodides by Ph_3P/I_2 system, however these sulfonyl chlorides were able to be converted to the corresponding chlorides with Ph_3P alone. Meanwhile, in an interesting and useful reaction, the corresponding thiols can be obtained in the reduction of alkanesulfonyl chlorides with Ph_3P/H_2O systems as shown by the following examples.

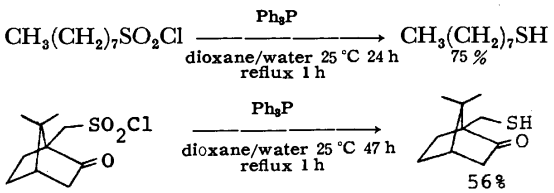

Experimental

Conversion of Sodium Sulfonate to the Corresponding Sulfonic Acid. The cation exchange resin which was converted to the protonated form by flowing 1 mol dm^{-3} aqueous HCl solution packed in a column [Dowex 50w-x8 200—400 mesh, H-form, Muromachi Kagaku Co.] was used.

GLC. Hitachi-163 Gas Chromatograph (20% OV-1 1m glass column) was used.

Reduction of Arenesulfonic Acid with Ph_3P/I_2 System. A mixture of 380 mg (2 mmol) of *p*-toluenesulfonic acid monohydrate and 5 ml of benzene was added into a reactor which was equipped with a cooler and a calcium chloride tube and then refluxed. The sulfonic acid was carefully dehydrated to completely dry prior to the reaction by way of azeotropic distillation with benzene. After 2620 mg (10 mmol) of triphenylphosphine was added to this dried sulfonic acid, the reactor was equipped with another cooler and an argon or nitrogen balloon, and substituted with this inert gas with a vacuum pump for 20 to 30 min at room temperature. Then, 5 ml of dry benzene and 254 mg (1 mmol) of iodine were added into this mixture and the whole mixture was stirred and refluxed (bath temperature 90—100 °C) for 2.5 h. The reaction was followed by GLC. After the reaction was complete, a mixture of 3 ml of water and 3 ml of dioxane was added to this reaction mixture which was refluxed for 1.0—0.5 h to decompose a small excess of triphenylphosphine–iodine complex to triphenylphosphine oxide and hydrogen iodide. The solution was poured into benzene and the benzene solution was washed with water for three times, and then dried ($MgSO_4$). *p*-Toluenethiol was obtained by GLC in 89% yield. After benzene was evaporated, the residue was separated through silica-gel column chromatography (Kieselgel-60, 70—230 mesh, MERCK, eluent: $CHCl_3$). A mixture of *p*-toluenethiol and a small excess of triphenylphosphine was obtained from fraction-1, and 2133 mg (128%) of triphenylphosphine oxide was obtained from fraction-2. Fraction-1 was separated further through silica-gel column chromatography (eluent: benzene/hexane=1/5=v/v) to give *p*-toluenethiol (R_f=0.5) in 54% yield. This was identical with commercially available authentic compound. The low yield of *p*-toluenethiol isolated as compared with that of GLC yield is believed to be due to the high volatility of the thiol. Ph_3PO mp 154—155 °C (lit,[35] 154—157 °C).

Reduction of Arenesulfonic Acid with Ph_3P/I_2/Amine System. Triphenylphosphine (2100 mg, 8 mmol) was added into the carefully dehydrated 380 mg (2 mmol) of *p*-toluenesulfonic acid of which reactor was equipped with a cooler and an argon or nitrogen balloon and substituted thoroughly with this inert gas with a vacuum pump. Then, after 5 ml of dry benzene and 254 mg (1 mmol) of iodine was added to this mixture, 371 mg (2 mmol) of tributylamine was finally added to this mixture This reaction mixture was stirred and refluxed for 20 min, following the reaction by GLC. Then a mixture of 3 ml of water and 3 ml of dioxane was added to this reaction mixture which was refluxed for 5 min. *p*-Toluenethiol was obtained in 95% yield by GLC.

Reduction of Sodium Arenesulfonate with Ph_3P/I_2/18-Crown-6 System. After 460 mg (2 mmol) of sodium 2-naphthalenesulfonate was dissolved in 5 ml of benzene, the mixture was refluxed and dehydrated to nearly completely dry by the same method. Triphenylphosphine 2620 mg (10 mmol) and 264 mg (1 mmol) of 18-crown-6 were added to this sodium salt. The reactor was equipped with a cooler and an argon or nitrogen balloon. After substitution with the inert gas by vacuum pumping, 5 ml of dry benzene and 508 mg of iodine were added to this mixture which was stirred and refluxed for 36 h. After the reaction, a mixture of 2-naphthalenethiol and di-2-naphthyl disulfide were detected by GLC. Di-2-naphthyl disulfide was converted to the 2-naphthalenethiol by addition of a mixture of 200 mg of water and 2 ml of dioxane and the reaction mixture was refluxed for 1 h. The reaction mixture was then treated in a similar way as in the case of arenesulfonic acids. 2-Naphthalenethiol was obtained in 95% yield and isolated in 93% yield, however the amount of triphenylphosphine oxide was not determined.

Competitive Reduction of para-Substituted Benzenesulfonic Acids with Ph_3P/I_2 System. A mixture of 190.2 mg (1 mmol) of *p*-toluenesulfonic acid, 176 mg (1 mmol) of benzenesulfonic acid, and 192.5 mg (1 mmol) of *p*-chlorobenzenesulfonic acid was dissolved in 5 ml of benzene in a reactor which was equipped with a cooler and a $CaCl_2$ tube, and the whole mixture was refluxed. All these sulfonic acids were dehydrated nearly

completely dry prior to the reaction by way of azeotropic distillation with benzene. After 3144 mg (12 mmol) of triphenylphosphine and 154 mg (1 mmol) of biphenyl (standard compound) were added to this dry sulfonic acids, the reactor was equipped with a cooler and a nitrogen balloon, and substituted with this inert gas. Then, 254 mg (1 mmol) of iodine and 6 ml of dry benzene were added to this mixture which was then stirred at 72—73 °C. A small portion (0.1 ml) of the reaction mixture was picked up by a microsyring and quenched with a mixture of water–dioxane–benzene (v=1/1/2) every fixed time interval (3, 5, 10, 30, 60, and 120 min from the initial time, respectively). The yields of three thiols obtained in every case, were determined by comparison of GLC curve with the predetermined calibration curve.

Reduction of Arenesulfonate with Ph_3P/I_2 System. Pentyl *p*-toluenesulfonate (484 mg, 2 mmol) and 2100 mg (8 mmol) of triphenylphosphine were added into a reactor which was equipped with a cooler and an argon or nitrogen balloon and substituted with this inert gas with a vacuum pump. Then, 5 ml of dry benzene and 381 mg (1 mmol) of iodine were added into this mixture which was refluxed and stirred for 10 min. The starting ester was no longer present by this time upon analysis with GLC and TLC (silica gel R_f=0.3 eluent: benzene), and *p*-toluethiol, di-*p*-tolyl disulfide, and pentyl iodide were resulted. After the reaction, the mixture was treated in the same manner as in the case of the reduction of arenesulfonic acid. The yields of the reaction products were determined by GLC (20% OV-1). *p*-Toluenethiol 95%. Pentyl iodide 90%. Authentic pently iodide was obtained by the known method. Pentyl iodide bp 157 °C/760 Torr (lit,[36] 157 °C/760 Torr, 1 Torr=133.322 Pa).

Synthesis of p-*Toluenesulfonyl Iodide.* *p*-Toluenesulfonyl iodide was obtained by a known method. Rock-crystals of mp 85—86 °C (decomp) were obtained (lit,[37] 84—85 °C).

Reductive Conversion of d-*Camphor-10-sulfonic Acid with Ph_3P/I_2 System.* The reaction was carried out under dry nitrogen atmosphere in a two-necked flask with a reflux condenser. To 8 ml of dry benzene solution of a mixture of *d*-camphor-10-sulfonic acid, 464 mg (2 mmol), and triphenylphosphine (2620 mg, 10 mmol), was added solid iodine 1524 mg (6 mmol) at room temperature. Then the mixture was refluxed for 9 h in nitrogen atmosphere. Benzene was added to the resultant mixture which was then washed with water. The organic layer was dried ($MgSO_4$) and the solvent was evaporated. The residue was then subjected to column chromatography on silica gel (eluent: benzene) in order to separate triphenylphosphine sulfide [R_f=0.5, yield 60%, mp 162—163 °C (lit,[38] 162—164 °C)], 10-iodo-*d*-camphor (R_f=0.4), and triphenylphosphine oxide [R_f=0.1, yield 90%, mp 154—155 °C (lit,[35] 154—157 °C)]. 10-Iodo-*d*-camphor was obtained in 87% (GLC) yield and was isolated in 67% yield: mp 71 °C; $[\alpha]^{25}$ −20.6 (*c* 1, $CHCl_3$); IR (KBr) 1735 (C=O), 1375, and 1390 cm^{-1}; NMR (CCl_4) δ=0.9 (3H, s), 1.1 (3H, s), 3.05 (1H, d, J=10.5 Hz), 3.35 (1H, d, J=10.5 Hz), and 1.0—2.4 (7H, m); Found: C, 43.29; H, 5.38; I, 45.74%. Calcd for $C_{10}H_{15}OI$: C, 43.18; H, 5.43; I, 45.62%.

Reductive Conversion of Alkanesulfonate with Ph_3P/I_2 System. Pentyl 1-octanesulfonate (529 mg, 2 mmol) and 2882 mg (11 mmol) of triphenylphosphine were added to a reactor which was equipped with a condenser and a nitrogen balloon and substituted with dry inert gas with a vacuum pump. Then, 8 ml of dry benzene and 1778 mg (7 mmol) of iodine were added to this mixture which was refluxed and stirred for 5 h. After the reaction, a mixture of 200 mg of water and 1 ml of dioxane was added into this mixture. The yields of reaction products were determined by GLC. Octyl iodide 95% bp 110 °C/23 Torr (lit,[39] 226 °C/760 Torr). Pentyl iodide 95%.

Preparation of d-*Camphor-10-thiol.* *d*-Camphor-10-sulfonic acid (10 g, 42 mmol) was dissolved in 15 ml of chloroform and then 18 g (86 mmol) of phosphorus pentachloride was added slowly. After this mixture was refluxed for 2 h, it was poured into 100 ml of chloroform which was then washed with water for 4 times, dried ($MgSO_4$) and evaporated to give *d*-camphor-10-sulfonyl chloride in 69% yield. Mp 65—67 °C (lit,[40] 67—68 °C). *d*-Camphor-10-sulfonyl chloride, 3 g (12 mmol) and 12.6 g (48 mmol) of triphenylphosphine were dissolved into a mixture of 40 ml of dioxane and 10 ml of water and the whole mixture was stirred for 47 h at room temperature, and then refluxed for 1 h. After the reaction, the mixture was separated through silica-gel column chromatography using benzene as eluent to give *d*-camphor-10-thiol in 56% yield. Mp 65—66 °C; TLC (eluent: benzene) R_f=0.2—0.3; IR (KBr) 1375, 1385, 1730 (C=O), and 2560 cm^{-1} (SH); NMR (CCl_4) δ=0.95 (3H, s), 1.05 (3H, s), 1.2—2.6 (8H, m), 2.73 (1H, d, J=6 Hz), and 2.95 (1H, d, J=6 Hz); Found: C, 65.24; H, 8.72; S, 17.24%. Calcd for $C_{10}H_{16}OS$; C, 65.17; H, 8.75; S, 17.40%.

Monitoring the Reaction of Alkanesulfonic Acid with Ph_3P/I_2. *d*-Camphor-10-sulfonic acid (464 mg, 2 mmol), 2620 mg (10 mmol) of triphenylphosphine, and 308 mg (2 mmol) of biphenyl (standard) were dissolved in 10 ml of dry benzene, into which 1016 mg (4 mmol) of iodine was then added and the solution was refluxed under nitrogen atmosphere. At fixed time intervals, 0.1 ml of the reaction mixture was picked up by a microsyringe and quenched with a mixture of water and benzene (v/v=1/1). The yields of the thiol and the iodide obtained in every case were determined by comparison of the GLC (SE-30) curve with the predetermined calibration curve. In the case of 1-pentanesulfonic acid, the corresponding thiol was not present in any sample under these conditions.

Preparation of Thiosulfonic S-*Esters.* Thiosulfonic *S*-esters were prepared by a known method[41,42] which is the reaction of arenesulfenyl chloride, that was prepared by treating a thiol or a disulfide with gaseous Cl_2 in CCl_4 at 0 °C, with sulfinic acid in the presence of pyridine in CCl_4 at 0 °C in 80—90% yield. *S*-Phenyl benzenethiosulfonate mp 44—45 °C (lit,[41] 44—45 °C). *S*-*p*-Tolyl *p*-toluenethiosulfonate mp 72—74 °C (lit,[42] 76 °C).

Preparation of Sulfonates. Sulfonates were prepared by a known method,[43–46] which is the reaction of sulfonyl chloride with alcohol in a mixture of benzene and acetonitrile in the presence of pyridine at room temperature, in 50—60% yields.

Phenyl *p*-toluenesulfonate mp 92—93 °C (lit,[43] 93 °C).

neo-Pentyl *p*-toluenesulfonate mp 46—47 °C (lit,[44] 48 °C).

Pentyl benzenesulfonate bp 138—140 °C/1 Torr (lit,[45] 136—138 °C/1 Torr).

Pentyl *p*-toluenesulfonate bp 167—168 °C/3 Torr (lit,[46] 169—170 °C/3 Torr).

Pentyl 1-octanesulfonate TLC (eluent: benzene) R_f=0.4—0.5; IR (NaCl) 1340 (SO) and 1160 cm^{-1} (SO); NMR (CCl_4) δ=4.1 (2H, t, J=6 Hz), 3.0 (2H, t, J=6.7 Hz), and 2.1—0.7 (24H, m); Found: C, 59.13; H, 10.55; S, 11.94%. Calcd for $C_{13}H_{28}SO_3$: C, 59.05; H, 10.67; S, 12.12%.

Preparation of Sulfinic Acids. *p*-Chlorobenzenesulfonyl chloride (5 g, 23.7 mmol) and 18 g (71.1 mmol) of sodium sulfite heptahydrate were added into 100 ml of water. The reaction mixture was kept at a temperature ranging 70—80 °C for 5 h. After the reaction, this water solution was washed with chloroform twice, acidified with excess concd HCl solution, cooled and filtered. The white precipitate was recrystallized from water yielding *p*-chlorobenzenesulfinic acid in a high yield (79%).

p-Chlorobenzenesulfinic acid mp 95—97 °C (lit,[47] 98—99 °C).

1-Octanesulfinic acid can also be obtained from 1-octane-

sulfonyl chloride by the similar procedure and identified as methyl octyl sulfone in 57% yield.

Methyl octyl sulfone mp 62—63 °C (lit,[48] 62 °C).

p-Toluenesulfinic acid and benzenesulfinic acid were obtained by acidification of the corresponding sodium arenesulfinates which were obtained as commercial samples. The white precipitates were recrystallized from water yielding the corresponding arenesulfinic acids.

Benzenesulfinic acid mp 78—80 °C (lit,[47] 81.5—83 °C).

p-Toluenesulfinic acid mp 84—85 °C (lit,[47] 84—85 °C).

1-Pentanesulfinic acid was prepared by a well known hydrolysis of 1-pentanesulfinyl chloride, which was prepared by treating dipentyl disulfide with chlorine in acetic anhydride in a mixture of ether and water at 0 °C in the presence of pyridine at the range of −20 °C to −10 °C in 77% yield. 1-Pentanesulfinic acid was identified as pentyl 2,4-dinitrophenyl sulfone by treating with 2,4-dinitrochlorobenzene.

Pentyl 2,4-dinitrophenyl sulfone (quantitative yield) mp 84 °C (lit,[49] 83 °C).

Preparation of S-*Alkyl Thiosulfonates.* *S*-Octyl 1-octanethiosulfonate and *S*-pentyl 1-pentanethiosulfonate were prepared by treating the corresponding disulfide with hydrogen peroxide in acetic acid at room temperature in nearly quantitative yields.

S-Pentyl 1-pentanethiosulfonate TLC (eluent: benzene) R_f= 0.5; IR (NaCl) 1120 (SO) and 1320 cm^{-1} (SO); NMR (CCl_4) δ=0.7—2.2 (18H, m), and 2.9—3.4 (4H, m); Found: C, 50.49; H, 9.34%. Calcd for $C_{10}H_{22}O_2S_2$: C, 50.38; H, 9.30%.

S-Octyl 1-octanethiosulfonate TLC (eluent: benzene) R_f= 0.5; IR (NaCl) 1120 (SO) and 1320 cm^{-1} (SO); NMR (CCl_4) δ=0.7—2.2 (30H, m), and 2.9—3.4 (4H, m); Found: C, 59.77; H, 10.68%. Calcd for $C_{16}H_{34}O_2S_2$: C, 59.57; H, 10.62%.

S-Phenyl 1-pentanethiosulfonate was prepared by treating benzenesulfenyl chloride with 1-pentanesulfinic acid in CCl_4 at 0 °C in the presence of pyridine. *S*-Phenyl 1-pentanethiosulfonate was obtained in a quantitative yield.

S-Phenyl 1-pentanethiosulfonate TLC (eluent: benzene) R_f =0.4; IR (NaCl) 1120 (SO) and 1320 cm^{-1} (SO); NMR (CCl_4) δ=0.7—2.2 (9H, m), 2.9—3.3 (2H, t, J=7.5 Hz), and 7.2—7.7 (5H, m); Found: C, 54.07; H, 6.58%. Calcd for $C_{11}H_{16}O_2S_2$: C, 54.16; H, 6.59%.

Reaction of Alkanesulfinic Acid with Ph_3P/I_2. 1-Pentanesulfinic acid, 272 mg (2 mmol), was dissolved in a mixture of 5 ml of dry benzene and 5 ml of dichloromethane. Then, 1730 mg (6.6 mmol) of triphenylphosphine and 762 mg (3 mmol) of iodine were added to this mixture. The reaction was carried out for 2 h at room temperature. After the reaction, 1-pentyl iodide formed was obtained in 95% yield by GLC.

Reaction of Alkanesulfonyl Chloride with Ph_3P. 1-Octanesulfonyl chloride, 425 mg (2 mmol), was dissolved in 5 ml of benzene and then 2100 mg (8 mmol) of triphenylphosphine was slowly added. The reaction was carried out at room temperature for 20 min. 1-Octyl chloride was obtained in 80% yield (GLC).

Reaction of Arenesulfonic Acid with Ph_3P/CCl_4. Triphenylphosphine, 2100 mg (8 mmol), was added into the carefully dehydrated 380 mg (2 mmol) of *p*-toluenesulfonic acid in a reactor which was equipped with a cooler and a nitrogen balloon, and substituted thoroughly with this gas. Then, 1 ml of carbon tetrachloride, which was dissolved in 5 ml of benzene, was added to this mixture. The mixture was refluxed for 1.5 h. After the reaction, triphenylphosphine was not present. Di-*p*-tolyl disulfide was obtained in 57% yield by GLC. The yields of triphenylphosphine oxide and other minor unknown products were not determined.

Reaction of Sulfonic Acid with PCl_3/I_2. *p*-Toluenesulfonic acid monohydrate, 380.4 mg (2 mmol), and 762 mg (3 mmol) of iodine were added into a reactor which was equipped with a cooler and a calcium chloride tube. Then, 7850 mg (57.3 mmol) of phosphorus trichloride was added to this mixture, which was refluxed for 3 h. After the reaction, di-*p*-tolyl disulfide was obtained in 18% yield by GLC.

Reaction of Sulfonic Acid with H_3PO_3/I_2. *p*-Toluenesulfonic acid monohydrate, 381 mg (2 mmol), was dissolved in 10 ml of acetonitrile, and then 1016 mg (4 mmol) of iodine and 2000 mg (24.4 mmol) of phosphonic acid were added to the mixture which was refluxed for 4.5 h under nitrogen atmosphere. After the reaction, *p*-toluenethiol was obtained in 25% yield by GLC.

Reaction of Diphenyl Disulfone with Ph_3P/I_2. Diphenyl disulfone, 200 mg (0.71 mmol), was dissolved in a mixture of 3 ml of dry acetonitrile and 10 ml of dry benzene and then 1300 mg (5 mmol) of triphenylphosphine and 179 mg (0.71 mmol) of iodine were added into this mixture. The reaction mixture was refluxed for 20 h under nitrogen atmosphere. The reaction was followed by GLC (eluent: benzene $C_6H_5SO_2SO_2C_6H_5$, R_f=0.3). After the reaction, a mixture of 1 ml of water and 2 ml of dioxane was added and the mixture was heated for 1 h. Benzenethiol was obtained in 91% yield (GLC). Diphenyl disulfone was prepared by a known method, which is the oxidation of benzenesulfinic acid by $KMnO_4$ in acetic acid, in 5% yield.

Diphenyl disulfone mp 196—197 °C (lit,[52] 196—196.5 °C).

Other Compounds. 1-Naphthalenethiol 160—165 °C/35 Torr (lit,[50] 142—142.5 °C/7 Torr, 85—88 °C/0.27 Torr). NMR (CCl_4) δ=3.4 (1H, s), and 7.05—8.30 (7H, m). 2,4-Dimethylbenzenethiol 74—76 °C/4 Torr (lit,[51] 80.5 °C/9 Torr, 93 °C/12 Torr) NMR (CCl_4) δ=2.2 (6H, s), 2.9 (1H, s), and 6.5—7.0 (4H, m).

References

1) Oxidation of Organic Sulfur Compounds——Mainly Thiols and the Compounds Having Sulfur–Sulfur Linkage (Japanese). S. Oae and T. Takata, *Chemistry* (Japan), **34** (10), 756, 891, and 961 (1979).

2) A. I. A. Khodair, A. Swelim, and F. El-sheikh, *Inst. J. Sulfur. Chem., B*, **6**, 213 (1971); E. Schwenk, D. Papa, B. Whitman, and H. Ginsberg, *J. Org. Chem.*, **9**, 1 (1944).

3) S. W. Benson, *Chem. Rev.*, **78**, 23 (1978).

4) R. Adams and C. S. Marvels, *Org. Synth.*, **1**, 83 (1941); J. Burdon, I. Farazmand, and J. C. Tatlow, *J. Chem. Soc.*, **1957**, 2574; C. M. Suter, *J. Am. Chem. Soc.*, **53**, 1112 (1931); P. D. Bartlett and L. H. Knox, *Org. Synth.*, **5**, 196 (1973).

5) A. Barco, S. Benetti, G. P. Pollini, and R. Taddia, *Synthesis*, **1974**, 877; H. H. Bosshard, R. Mory, M. Schmid, and H. Zollinger, *Helv. Chim. Acta.*, **42**, 1653 (1959).

6) R. Adams and C. S. Marvel, *Org. Synth.*, Coll. Vol. I, 504 (1956); O. Litvay, E. Riesz, and L. Landau, *Chem. Ber.*, **62**, 1863 (1929); W. A. Sheppard, *Org. Synth.*, **40**, 80 (1960); J. I. G. Cadogan, *Quart. Rev. (London)*, **16**, 223 (1962); D. Cipris and D. Pouli, *Synth. Commun.*, **9**, 207 (1979); H. Alper, *Angew. Chem., Int. Ed. Engl.*, **8**, 677 (1969); S. Smiles and C. M. Bere, *Org. Synth.*, Coll. Vol. I, 7 (1941); S. Krishna and H. Singh, *J. Am. Chem. Soc.*, **50**, 792 (1928); M. Kulka, *J. Am. Chem. Soc.*, **72**, 1216 (1950); P. D. Caeser, *Org. Synth.*, Coll. Vol. V, 685 (1963); T. H. Chan, J. P. Montillier, W. F. van Horn, and D. N. Harpp, *J. Am. Chem. Soc.*, **92**, 7224 (1970).

7) C. S. Marvel and P. D. Caeser, *J. Am. Chem. Soc.*, **73**, 1097 (1951); D. Klamann, *Monatsh. Chem.*, **84**, 651 (1953); E. Fischer, *Chem. Ber.*, **48**, 93 (1915); T. Cuving and M. Larcheveque, *J. Organomet. Chem.*, **64**, 315 (1974).

8) A. Zobacova, V. Hermankova, and J. Jary, *Collect.*

Czech. Chem. Commun., **42**, 2540 (1977); J. Wolinsky, R. L. Marhenke, and E. J. Eustace, *J. Org. Chem.*, **38**, 1428 (1973).
9) J. Strating and H. J. Baker, *Recl. Trav. Chim. Pays-Bas.*, **69**, 638 (1950); S. Hayashi, M. Furukawa, J. Yamamoto, and K. Hamamura, *Chem. Pharm. Bull.*, **15**, 1310 (1967).
10) T. Numata, H. Togo, and S. Oae, unpublished date.
11) T. Numata, H. Awano, and S. Oae, *Tetrahedron Lett.*, **21**, 1235 (1980).
12) G. A. Olah, S. C. Narang, L. D. Field, and R. Karpeles, *J. Org. Chem.*, **46**, 2408 (1981).
13) A. D. Beveridge, G. S. Harris, and F. Inglis, *J. Chem. Soc., Perkin Trans. 1*, **1966**, 520; L. Horner and H. Nickel, *Ann. Chim. (Paris)*, **597**, 20 (1955).
14) D. N. Harpp and J. G. Gleason, *J. Am. Chem. Soc.*, **93**, 2437 (1971).
15) G. A. Wiley, R. L. Hershkowitz, B. M. Rein, and B. C. Chung, *J. Am. Chem. Soc.*, **86**, 964 (1964); G. A. Wiley, B. M. Rein, and R. L. Hershkowitz, *Tetrahedron Lett.*, **1964**, 2509; R. Michinek and W. Liittke, *Synthesis*, **1975**, 255.
16) D. N. Harpp and J. G. Gleason, *J. Org. Chem.*, **35**, 3259 (1970); D. N. Harpp, J. G. Gleason, and J. P. Snyder, *J. Am. Chem. Soc.*, **90**, 4181 (1968).
17) I. L. Knunyants, *Dokl. Chem.*, **224**, 521 (1975).
18) D. N. Harpp and J. G. Gleason, *J. Org. Chem.*, **36**, 73 (1971).
19) S. Kobayashi, T. Timori, T. Izawa, and M. Ohno, *J. Am. Chem. Soc.*, **103**, 2406 (1981); R. Matsueda, H. Maruyama, M. Ueki, and T. Mukaiyama., *Bull. Chem. Soc. Jpn.*, **44**, 1373 (1971).
20) T. Endo, S. Ikenaga, and T. Mukaiyama, *Bull. Chem. Soc. Jpn.*, **43**, 2632 (1970).
21) T. Mukaiyama, K. Goto, R. Matsueda, and M. Ueki, *Tetrahedron Lett.*, **1970**, 5293.
22) T. Mukaiyama, H. Maruyama, M. Ueki, and R. Matsueda, *Bull. Chem. Soc. Jpn.*, **44**, 1373 (1971); E. J. Corey and D. J. Brunelle, *Tetrahedron Lett.*, **1976**, 3409; T. Mukaiyama M. Ueki, H. Maruyama, and R. Matsueda, *J. Am. Chem. Soc.*, **90**, 4490 (1968); H. Takaku and Y. Shimada, *Chem. Lett.*, **1975**, 873.
23) T. Mukaiyama and M. Hashimoto, *J. Am. Chem. Soc.*, **94**, 8528 (1972); H. Takaku, T. Konishi, and H. Hata, *Chem. Lett.*, **1977**, 655.
24) I. Nakagawa and T. Hata, *Tetrahedron Lett.*, **1975**, 1409.
25) L. Bauer and J. Cymermann, *J. Chem. Soc.*, **1949**, 3434.
26) K. Fujimori, H. Togo, and S. Oae, *Tetrahedron Lett.*, **21**, 4921 (1980).
27) L. Horner and H. Winkler, *Tetrahedron Lett.*, **1964**, 455; K. Issleib and W. Seidel, *Z. Anorg. Allg. Chem.*, **288**, 201 (1956).
28) W. A. Sheppard, *Org. Synth.*, Coll. Vol. V, 844 (1973); L. Bauer and L. Cymermann, *J. Chem. Soc.*, **1949**, 3434; D. Klamann and G. Hofbauer, *Monatsh. Chem.*, **83**, 1489 (1952).
29) G. M. Kosolapoff and L. Maier, "Organic Phosphorus Compounds," Wiley-Interscience, New York (1972).
30) L. E. Overman and E. M. O'Connor, *J. Am. Chem. Soc.*, **98**, 771 (1976).
31) M. Suda and A. Fukushima, *Tetrahedron Lett.*, **22**, 757 (1981); P. Hogge and G. Richardson, *J. Chem. Soc., Chem. Commun.*, **1975**, 622; R. Appel and R. K. Kleinstuck, *Chem. Ber.*, **107**, 5 (1974); S. Yamada and Y. Takeuchi, *Tetrahedron Lett.*, **1971**, 3595; B. Castro and R. Dormoy, *Bull. Soc. Chim. Fr.*, **1971**, 3034; A. Appel, R. Kleinstuck, K.-D. Ziekn, *Chem. Ber.*, **102**, 1335 (1971).
32) S. Oae and H. Togo, *Synthesis*, **1981**, 371.
33) G. A. Wiley, R. L. Hershkowitz, B. M. Rein, and B. C. Chung, *J. Am. Chem. Soc.*, **86**, 964 (1964).
34) G. A. Wiley, B. M. Rein and R. L. Hershkowitz, *Tetrahedron Lett.*, **1964**, 2509.
35) Authentic sample was obtained from Wako Chemical Co.
36) I. Simon, *Bull. Soc. Chim. Belg.*, **38**, 2519 (1929); *Beilstein*, **E. II. 1**, 98 (1920—1929).
37) L. M. Litvinenko, V. A. Dadali, V. A. Sovelova, and T. I. Krichevtsova, *Zh. Obshch. Khim.*, **34**, 3730 (1964); *Chem. Abstr.*, **62**, 6420 (1965).
38) Authentic sample was obtained from Wako Chemical Co.
39) A. I. Vogel, *J. Chem. Soc.*, **1943**, 636.
40) S. Smiles and J. Stewart, *Org. Synth.*, Coll. Vol. V, 196 (1973).
41) S. Oae, R. Nomura, Y. Yoshikawa, and W. Tagaki, *Bull. Chem. Soc. Jpn.*, **22**, 2903 (1969).
42) R. Otto, J. Lowenthal, and A. V. Gruber, *Ann. Chim. (Paris)*, **129**, 101 (1869).
43) H. Gilmann, N. J. Beaber, and C. H. Myers, *J. Am. Chem. Soc.*, **47**, 2047 (1925).
44) P. Yousefzadeh and C. K. Mann, *J. Org. Chem.*, **33**, 2716 (1968).
45) B. L. Emling, *J. Am. Chem. Soc.*, **74**, 4702 (1952).
46) H. Gilmann, N. J. Beaber, *J. Am. Chem. Soc.*, **47**, 518 (1925).
47) R. K. Burkhard, D. E. Sellers, F. Decou, and J. L. Lambert, *J. Org. Chem.*, **24**, 767 (1959).
48) D. Jerchel, L. Dippelhofen, D. Renner, *Chem. Ber.*, **87**, 947 (1954).
49) R. W. Bost, J. O. Turner, R. D. Norton, *J. Am. Chem. Soc.*, **54**, 1985 (1932).
50) I. N. Tits-Skvortsova, S. Y. Levina, H. I. Levova, and T. A. Danilova, *J. Gen. Chem. (USSR)*, **22**, 135 (1952); H. C. Gogt and R. E. Wann, *J. Org. Chem.*, **26**, 4047 (1961).
51) J. H. Unlenbroek and M. Slagt, *Recl. Trav. Chim. Pays-Bas.*, **80**, 1057 (1961); H. C. Godt and R. E. Wann., *J. Org. Chem.*, **26**, 4047 (1961).

 © 1983 The Chemical Society of Japan Bull. Chem. Soc. Jpn., 56, 3813—3817 (1983)

Reduction of Organic Sulfonic Acids, Sodium Sulfonates, and Sulfonic Esters to the Corresponding Disulfides with Polyphosphoric Acid Derivatives, Potassium Iodide and Tetrabutylammonium Iodide System

Shigeru OAE*,† and Hideo TOGO

Department of Chemistry, The University of Tsukuba, Sakura, Niihari, Ibaraki 305

(Received July 18, 1983)

Organic sulfonic acids, sodium sulfonates, and alkyl sulfonates were readily reduced to the corresponding disulfides in moderate yields upon treatment with a mixture of a polyphosphoric acid derivative and iodide. In these reactions, formation of mixed anhydrides each having a P–O–S linkage is the key step, and subsequent attack of iodide on the sulfur atom gives the corresponding sulfonyl iodides which are reduced further exothermally to the disulfides with hydrogen iodide. Actually, *p*-toluenesulfonyl chloride was isolated in the reaction of *p*-toluenesulfonic acid and polyphosphoric acid derivatives with chloride ion. The competitive reduction of various aromatic sulfonic acids reveals that an aromatic sulfonic acid bearing an electron-donating para-substituent is more readily reduced to the disulfide than that which has an electron-withdrawing para-substituent.

The reduction of organic sulfonic acid which is in the highest oxidative state among all organosulfur compounds is one of the most challenging problems in organosulfur chemistry. Sulfonic acids, however, can be reduced in multi-step processes through initial conversion of sulfonic acids to the corresponding sulfonyl derivatives, *i.e.* sulfonyl halide,[1] sulfonic anhydride,[2] sulfonic ester,[3] and sulfonamide[4] and subsequent reduction of these derivatives with reducing agents to the corresponding thiols or thiol derivatives. Recently, there have appeared three procedures which can reduce sulfonic acids directly to the corresponding disulfides or thiols in one-pot process.[5-7] Each of these three procedures is epochal, and quite useful, since in a one-pot process reduction of various sulfonic acids and its derivatives to thiols or disulfides can be achieved. However, these reactions have some drawbacks, since the reagents used in these procedures, *i.e.* $(CF_3CO)_2O/(n\text{-}Bu)_4NI$,[5] Ph_3P/I_2 (catalyst),[6] $Ph_3P/(ArS)_2$(catalyst),[8] and BX_3-(X=Cl, Br, I)/KI[7] systems are either in large excess or by no means cheap. Another facile procedure to reduce both arene- and alkanesulfonic acids to the corresponding disulfides as the sole products has been found by us who used cheap reagents, such as polyphosphoric acid (PPA), ethyl polyphosphate (PPE), tetraphosphorus decaoxide (P_4O_{10}) and iodide ion, in organic media This paper gives a full account of this direct reduction of sulfonic acids.

Results and Discussion

Arene- and alkanesulfonic acids used in this investigation are listed in Tables 1, 2, and 3, while the sulfonic esters are summarized in Table 4. The condensing reagents used were tetraphosphorus decaoxide, polyphosphoric acid, and ethyl polyphosphate,[9] while acetonitrile and sulfolane are the choice solvents in the reduction with P_4O_{10}/I^- and PPA/I^- systems respectively because of the solubility of polyphosphoric acid derivatives, whereas acetonitrile, sulfolane, and chloroform were the choice solvents in the reduction with PPE/I^- system. Of the three systems, the reduction with P_4O_{10}/I^- or PPE/I^- gives the corresponding disulfides in higher yields than that with PPA/I^- system in the presence of $(n\text{-}Bu)_4NI$, whereas, in the absence of $(n\text{-}Bu)_4NI$ the yields of the disulfides are more satisfactory in the reduction with PPA/I^- than those with the former systems. It is worthy to note that *d*-camphor-10-sulfonic acid, which is a highly sterically hindered alkanesulfonic acid, was also reduced to the corresponding disulfide in a high yield, though the reaction was substantially slow. In this reduction, the sulfonyl iodide is considered to be the

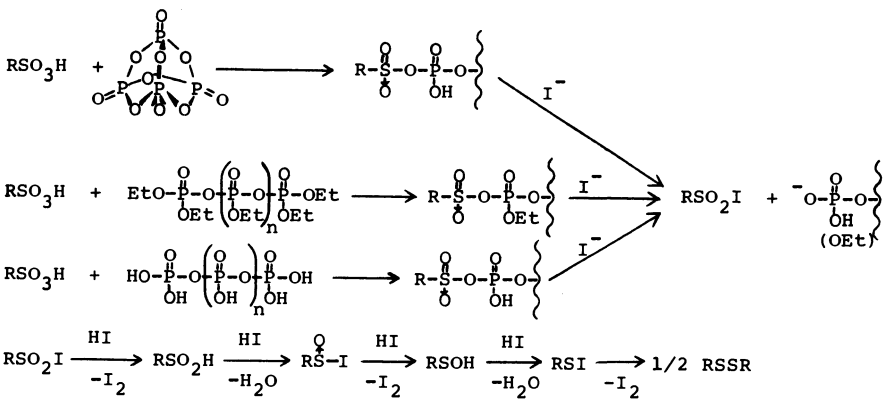

Scheme 1.

† Present address: Okayama University of Science, 1-1 Ridai-cho, Okayama 700.

TABLE 1. REDUCTION OF SULFONIC ACID TO DISULFIDES USING TETRAPHOSPHORUS DECAOXIDE/POTASSIUM IODIDE/TETRABUTYLAMMONIUM IODIDE SYSTEM IN CH_3CN

Sulfonic acid	Amounts (mmol) of reagents used[a] $RSO_3H/P_4O_{10}/KI/n\text{-}Bu_4NI$	Reaction conditions Time/h (Reflux)	Yield of disulfide/%[b]
$p\text{-}CH_3C_6H_4SO_3H\cdot H_2O$	6.0/33.8/30.0/1.5	14	57
$p\text{-}ClC_6H_4SO_3H$	6.0/42.2/36.2/1.5	24	40
$2,4\text{-}(CH_3)_2C_6H_3SO_3H$	6.0/42.2/36.2/1.5	14	55
$p\text{-}CH_3C_6H_4SO_3Na$	6.0/42.2/36.2/1.5	34	60
$p\text{-}CH_3C_6H_4SO_3H\cdot H_2O$	6.0/33.8/30.0/0	14	33[c]

a) The molecular weight of P_4O_{10} was taken as 142. b) Yield of isolated product. c) Small amount of thiosulfonic *S*-ester was obtained as by-product.

TABLE 2. REDUCTION OF SULFONIC ACIDS TO DISULFIDES USING POLYPHOSPHORIC ACID/POTASSIUM IODIDE/TETRABUTYLAMMONIUM IODIDE SYSTEM IN SULFOLANE

Sulfonic acid	Amounts(mmol) of reagents used[a] RSO_3H/PPA/KI/$n\text{-}Bu_4NI$	Temp/°C	Time/h	Yield of disulfide/%[b]
$p\text{-}CH_3C_6H_4SO_3H\cdot H_2O$	6.0/48.0/48.0/1.5	95—100	8	65
	6.0/48.0/48.0/0	95—100	8	75
$p\text{-}ClC_6H_4SO_3H$	6.0/48.0/60.0/1.5	95—100	10	47
	6.0/48.0/48.0/0	95—100	8	58
$2,4\text{-}(CH_3)_2C_6H_3SO_3H$	6.0/48.0/48.0/1.5	95—100	8	68
	6.0/48.0/48.0/0	95—100	8	70
$p\text{-}CH_3C_6H_4SO_3Na$	6.0/48.0/48.0/1.5	95—100	23	58
	6.0/48.0/48.0/0	95—100	21	55[c]
$CH_3(CH_2)_7SO_3H\cdot H_2O$	6.0/48.0/48.0/1.5	80	5	66

a) The molecular weight of PPA was taken as 338. b) Yield of isolated product. c) Small amount of thiosulfonic *S*-ester was obtained as by-product.

TABLE 3. REDUCTION OF SULFONIC ACIDS TO DISULFIDES USING ETHYL POLYPHOSPHATE/POTASSIUM IODIDE/TETRABUTYLAMMONIUM IODIDE SYSTEM IN CHLOROFORM

Sulfonic acid	Amounts(mmol) of reagents used[a] RSO_3H/PPE/KI/$n\text{-}Bu_4NI$	Reaction conditions Time/h (Reflux)	Yield of disulfide/%[b]
$p\text{-}CH_3C_6H_4SO_3H\cdot H_2O$	6.0/35.6/48.0/1.5	1.5	60
	6.0/35.6/48.0/0	2	12
$CH_5SO_3H\cdot H_2O$	6.0/47.4/48.0/1.5	2	43
$p\text{-}CH_3C_6H_4SO_3Na$	6.0/35.6/48.0/1.5	6	43
$CH_3(CH_2)_7SO_3HH_2O$	6.0/47.4/48.0/1.5	2	47
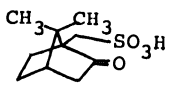	6.0/47.4/48.0/1.5	5	74

a) The molecular weight of PPE was taken as 500. b) Yield of isolated product.

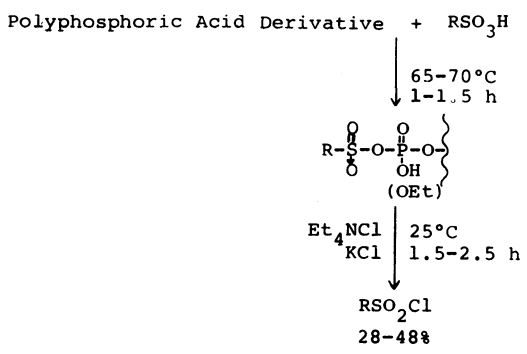

Scheme 2.

key intermediate which is stepwisely reduced further very readily to the corresponding sulfinyl and sulfenyl iodides which are eventually reduced to the symmetrical disulfide[10] as shown in Scheme 1. Indeed, *p*-toluenesulfonyl chloride was obtained in 48 and 28% yields respectively when potassium chloride, which has no reducing ability at all, and tetraethylammonium chloride were added into the mixture of either P_4O_{10} or PPE and *p*-toluenesulfonic acid in acetonitrile. Meanwhile, *p*-toluenesulfonyl iodide, which was prepared from the reaction of sodium *p*-toluenesulfinate and iodine in a mixture of benzene and water, was found to be reduced exothermically to the corresponding disulfide by hydroiodic acid in a high yield in dioxane.

Competitive reduction of an equimolar mixture of para-substituted benzenesulfonic acids, *i.e.* *p*-chlorobenzene-, benzene-, and *p*-methylbenzenesulfonic acids, with the PPA/KI/$(n\text{-}Bu)_4NI$ (catalyst) system was carried out. Since the mixture of $C_6H_5SSC_6H_5$, $C_6H_5SSC_6H_4\text{-}p\text{-}C_6H_5SSC_6H_4Cl\text{-}p$, $p\text{-}CH_3C_6H_4SSC_6H_4CH_3\text{-}p$, $p\text{-}CH_3C_6H_4SSC_6H_4Cl\text{-}p$, and $p\text{-}ClC_6H_4SSC_6H_4Cl\text{-}p$ was not readily separated or determined, the mixture of these disul-

Table 4. Reduction of sulfonate with polyphosphoric acid derivative/potassium iodide/tetrabutylammonium iodide

Sulfonate RSO_3R'	Polyphosphoric acid derivative	Reaction conditionse			Products/%	
		Solvent	Temp/°C	Time/h	RSSR	R'I
p-$CH_3C_6H_4SO_3C_6H_5$	PPA[a)]	Sulfolane	93	7	No reaction[c)]	
$C_6H_5SO_3CH_2CH_3$	PPA[b)]	Sulfolane	93	8	50	b)
	P_4O_{10}[b)]	Acetonitrile	81	33	70	d)
p-$CH_3C_6H_4SO_3(CH_2)_4CH_3$	PPA[b)]	Sulfolane	93	12	54	89[e)]
$CH_3(CH_2)_7SO_3(CH_2)_4CH_3$	PPA[b)]	Sulfolane	100	7	45	81[e)]

a, b) Amounts (mmol) of reagents used of sulfonate/polyphosphoric acid derivative/potassium iodide/tetrabutylammonium iodide: a=2/16/16/0; b=2/16/16/0.2. c) Starting material was recovered in 91% yield. d) Not determined. e) The yield was after 15 min.

fides was converted to the corresponding arenethiols upon treatment of the mixture with triphenylphosphine and water at room temperature. Thus, the amounts of arenethiols formed in the reduction were estimated as shown below.

p-$CH_3C_6H_4SH$	C_6H_5SH	p-ClC_6H_4SH
71%	60%	34%

These data reveal clearly that, in the reduction of para-substituted benzenesulfonic acids, benzenesulfonic acid bearing an electron-donating substituent such as methyl group is more readily reduced than that has an electro-withdrawing group such as chloro group. Apparently, the rate-determining step is the formation of a mixed anhydride bearing $-\overset{\overset{O}{\|}}{\underset{|}{P}}-O-\overset{\overset{O}{\|}}{\underset{|}{S}}-$ bond which is formed by nucleophilic attack of sulfonic acid on the polyphosphoric acid derivative.

The same reduction procedure has been found to be successfully applied for the reduction of sulfonic esters (Table 4). Alkyl arene- and alkanesulfonates were found to react with these systems under similar conditions to give the corresponding alkyl iodides and disulfides. Alkyl iodide was usually obtained quantitatively by this reaction after about 15 minutes; however, the yield of the corresponding disulfide was very poor in the early stage of the reaction. These observations suggest that the initial step is the S_N2 attack of iodide on the α-carbon of alkyl sulfonates to form the alkyl iodides and the sulfonate anions which are then reduced further to the corresponding disulfides in a slow reaction with the polyphosphoric acid derivative/iodide system. Thus, the initial S_N2 reaction by the attack of iodide on the alkyl group is quite fast; however, the reduction of the sulfonate anion formed is relatively slow. Actually, benzenesulfonate was found to react readily with tetrabutylammonium iodide in benzene to afford tetrabutylammonium benzenesulfonate and pentyl iodide, whereas phenyl p-toluenesulfonate was not found to react with tetrabutylammonium iodide at all. On the other hand, phenyl p-toluenesulfonate, an aryl arenesulfonate was found to be quite inert in the same treatment with these reducing systems even under much harder conditions. In the case of phenyl p-toluenesulfonate, an aryl arenesulfonate, the initial nucleophilic attack of iodide on aromatic ipso carbon is so sluggish that the reduction does not proceed.

Experimental

Materials. PPA, potassium iodide, tetraphosphorus decaoxide, p-toluenesulfonic acid, sodium p-toluenesulfonate potassium chloride, sodium benzenesulfonate, sodium 2,4-dimethylbenzenesulfonate, p-toluenesulfonyl chloride, and d-camphor-10-sulfonic acid were all from Wako Chemicals Co. Tetrabutylammonium iodide, p-chlorobenzenesulfonic acid, benzenesulfonic acid, sodium 1-octanesulfonate, tetraethylammonium chloride, and ethyl benzenesulfonate were from Tokyo Kasei Co.

Conversion of Sodium Sulfonate to the Corresponding Sulfonic Acid. The cation exchange resin which was converted to the protonated from by flowing 1 mol dm^{-3} aqueous HCl solution through a column (Dowex, 50w-x8, 200—400 mesh H-form, Muromachi Kagaku Co.) was used to convert sodium sulfonate to the corresponding sulfonic acid.

Preparation of Ethyl Polyphosphate. Ethyl polyphosphate, PPE, was prepared according to the known method[9)] using tetraphosphorus decaoxide and dry diethyl ether. A colorless syrupy (hard) ester which is very sensitive to moisture, was obtained.

General Procedure for Reduction of the Sulfonic Acid to the Corresponding Disulfide. Potassium iodide, 8 g, (48 mmol) and tetrabutylammonium iodide 583 mg (1.5 mmol) were added into a mixture of PPE 24 g (48 mmol) and a sulfonic acid, *e.g.*, d-camphor-10-sulfonic acid 1.39 g (6 mmol). Then, into this mixture, 20 ml of dry chloroform was added. The whole mixture was stirred and refluxed for 5 h under nitrogen atmosphere. Then 10 ml of water was added to this mixture and the mixture was refluxed for 1 h. The reaction mixture was poured into benzene (100 ml), and washed with water for 3 times. The benzene solution was washed with 0.5 mol dm^{-3} sodium thiosulfate solution and dried ($MgSO_4$). The solvent was evaporated and the crude product, *i.e.* the disulfide was chromatographed on a silica-gel column with benzene (R_f= 0.2, eluent; benzene). Removal of the solvent afforded 10,10'-dithiobis(d-camphor) as colorless crystals in 74% yield (817 mg). Mp 236—238 °C; $[\alpha]_D^{25}$ −103.66° (c 1, $CHCl_3$); IR (KBr) 1730 cm^{-1} (C=O); NMR ($CDCl_3$) δ=0.90 (3H, s), 1.05 (3H, s), 2.75 (1H, d, J=13.5 Hz), 3.20 (1H, d, J=13.5 Hz), and 2.5—1.1 (7H, m); Found: C, 65.33; H, 8.25; S, 17.27%. Calcd for $C_{20}H_{30}S_2O_2$: C, 65.53; H, 8.24; S, 17.49%. Reduction of other sulfonic acids to the corresponding disulfides with the polyphosphoric acid derivative/iodide system were conducted in the same manner.

Di-p-tolyl disulfide mp 44—45 °C (lit,[11)] 46 °C).

Bis(p-chlorophenyl) disulfide mp 70—71 °C (lit,[12)] 73. °C)

Bis (2,4-dimethylphenyl) disulfide bp 180—186 °C/2—2.5 Torr (1 Torr=133.322 Pa) IR (NaCl) 540 and 800 cm^{-1};

NMR (CCl_4) δ=2.24 (3H, s), 2.33 (3H, s), and 3.4—2.6 (3H, m); Found: C, 69.69; H, 6.65; S, 23.58%. Calcd for $C_{16}H_{18}S_2$: C, 70.02; H, 6.61; S, 23.36%.

Dioctyl disulfide and diphenyl disulfide were identical to the authentic commercial samples.

Trapping Experiment of Sulfonyl Function. Tetraphosphorus decaoxide (1600 mg, 11.27 mmol) and 381 mg (2 mmol) of *p*-toluenesulfonic acid were dissolved in 5 ml of dry acetonitrile and the reaction mixture was heated (60—65 °C) for 1.5 h under nitrogen. Then, 33 mg (0.2 mmol) of tetraethylammonium chloride, 746 mg (10 mmol) of potassium chloride and 5 ml of dry acetonitrile were added to this reaction mixture at 0 °C and the mixture was kept standing for 3 h at room temperature. Then, the mixture was poured into 100 ml of benzene and the benzene solution was washed with water for three times, and then dried ($MgSO_4$). When the solvent was evaporated, *p*-toluenesulfonyl chloride was obtained in 48% yield (GLC); the isolated yield was 43%. The sulfonyl chloride was identical to the authentic sample of *p*-toluenesulfonyl chloride both in GLC and TLC. In the reduction with the PPE system, PPE, 6 g and 381 mg (2 mmol) of *p*-toluenesulfonic acid were dissolved in 5 ml of dry acetonitrile and the mixture was heated for 1 h at about 70 °C under nitrogen. Then, at 0 °C 33 mg of tetraethylammonium chloride and 746 mg (10 mmol) of potassium chloride were added to the reaction mixture which was kept standing for 2.5 h at room temperature. After the reaction, a similar treatment as that with P_4O_{10}, gave *p*-toluenesulfonyl chloride in 28% yield (GLC).

Preparation of p-*Toluenesulfonyl Iodide.* Treatment of sodium *p*-toluenesulfinate dihydrate with iodine according to a known method gave *p*-toluenesulfonyl iodide nearly quantitatively. Mp 85—86 °C (decomp) (lit,[13] 84—85 °C).

Reduction of p-*Toluenesulfonyl Iodide with Hydriodic Acid to Di*-p-*tolyl Disulfide.* *p*-Toluenesulfonyl iodide (300 mg, 1.06 mmol) was dissolved in 3 ml of dioxane and then 4 ml of hydriodic acid (57%) was slowly added to this mixture at room temperature. An exothermic reaction occurred affording di-*p*-tolyl disulfide. After 1 h the mixture was poured into benzene and the benzene solution was washed with water twice, 0.5 mol dm^{-3} $Na_2S_2O_3$ solution, and dried ($MgSO_4$). ($MgSO_4$). Only di-*p*-tolyl disulfide was obtained in 79% yield (GLC).

*Competitive Reaction of Arenesulfonic Acids with PPA/KI/*n-Bu_4NI*(Catalyst).* *p*-Toluenesulfonic acid, 190.2 mg (1 mmol), 176 mg (1 mmol) of benzenesulfonic acid, and 192.2 mg (1 mmol) of *p*-chlorobenzenesulfonic acid were dissolved in 10 ml of sulfolane, then 8100 mg of PPA, 3984 mg (24 mmol) of potassium iodide, 184 mg (0.5 mmol) of tetrabutylammonium iodide and 154 mg (1 mmol) of biphenyl were added to this mixture and the whole mixture was stirred (95—100 °C) for 4 h. The reaction was followed by GLC. After the reaction, 5 ml of water was added into the mixture which was then heated for 0.5 h. The solution was poured into benzene and the benzene solution was washed with water for 3 times, then with 0.5 mol dm^{-3} solution of $Na_2S_2O_3$ and dried ($MgSO_4$). The solution was found to contain only the mixture of disulfides *i.e.* $C_6H_5SSC_6H_5$, $C_6H_5SSC_6H_4CH_3$-*p*, $C_6H_5SSC_6H_4Cl$-*p*, *p*-$CH_3C_6H_4SSC_6H_4CH_3$-*p*, *p*-$CH_3C_6H_4SSC_6H_4Cl$-*p*, *p*-$ClC_6H_4SSC_6H_4Cl$-*p* which are converted to the corresponding thiols by treating with a mixture of triphenylphosphine or tributylphosphine (2 mmol) and water in a mixture solvent of benzene and dioxane over night at room temperature. The yields of the mixture of three thiols were determined with GLC. *p*-Toluenethiol, 71%; benzenethiol, 60%; *p*-chlorobenzenethiol, 34%.

In the reduction with the P_4O_{10} system, a mixture of three different para-substituted benzenesulfonic acids each with 1 mmol was dissolved in 20 ml of dry acetonitrile, and then 3000 mg (21 mmol) of P_4O_{10}, 3984 mg (24 mmol) of potassium iodide, and 184 mg (0.5 mmol) of tetrabutylammonium iodide were added to this mixture which was then refluxed for 7 h. After the reaction, a similar work-up procedure afforded a mixture of three para-substituted benzenethiols. The yields of these thiols were determined by GLC (SE-30, 1 m glass column) to be the following: *p*-toluenethiol, 50%; benzenethiol 50%; *p*-chlorobenzenethiol, 26%.

Preparation of Sulfonates. Treatment of organic sulfonyl chlorides with a choice alcohol according to a known procedure[14] gave various organic sulfonates. The yields of sulfonates are usually 50—60%.

Pentyl benzenesulfonate: 138—140 °C/1 Torr (lit,[14] 136—138 °C/1 Torr).

Pentyl *p*-toluenesulfonate: Mp 167—168 °C/3 Torr (lit,[15] 169—170 °C/3 Torr).

Phenyl *p*-toluenesulfonate: Mp 92—93 °C (lit,[17] 93 °C).

Pentyl 1-octanesulfonate: TLC (eluent: benzene) R_f=0.4—0.5; IR (NaCl) 1340 (SO_2) and 1160 cm^{-1} (SO_2); NMR-(CCl_4) δ=4.1 (2H, t, J=6.0 Hz), 3.0 (2H, t, J=6.7 Hz), and 2.1—0.7 (24H, m); Found: C, 59.13; H, 10.55; S, 11.94%. Calcd for $C_{13}H_{28}O_3S$: C, 59.05; H, 10.67; S, 12.12%.

Reduction of Sulfonate with Polyphosphoric Acid Derivative/Potassium Iodide/Tetrabutylammonium Iodide System. PPA, 5408 mg (16 mmol), 2656 mg (16 mmol) of potassium iodide, and 484 mg (2 mmol) of pentyl *p*-toluenesulfonate were dissolved in 10 ml of sulfolane, and then 74 mg (0.2 mmol) of tetrabutylammonium iodide and 308 mg (2 mmol) of biphenyl (standard material) were added to this mixture, which was then heated ($\approx$93 °C) with stirring under nitrogen. After 15 min, the starting ester was found to have disappeared upon GLC analysis and pentyl iodide was formed in 89% yield upon determination with GLC, but the yield of disulfide was still very poor during this period. After 12 h, 10 ml of water was added to this mixture and heated for 0.5 h. The mixture was poured into benzene which was then washed with water for three times, again with 0.5 mol dm^{-3} $Na_2S_2O_3$ solution and dried ($MgSO_4$). Thus, di-*p*-tolyl disulfide was obtained in 54% yield (GLC), and the yield of pentyl iodide was found to remain unchanged as compared with that, estimated after 15 min. Pentyl iodide 157 °C/760 Torr (lit,[16] 157 °C/760 Torr).

References

1) W. A. Sheppard, *Org. Synth.*, **40**, 80 (1960); D. Cipris, and D. Pouli, *Synth. Commun.*, **9**, 207 (1979); H. Alper, *Angew. Chem.. Int. Ed. Engl.*, **8**, 677 (1969).

2) T. Numata, H. Togo, and S. Oae, unpublished data.

3) A. Zobacova, V. Hermankova, and J. Jary, *Collect. Czech. Chem. Commun.*, **42**, 2540 (1977).

4) C. M. Marvel and P. D. Caeser, *J. Am. Chem. Soc.*, **73**, 1097 (1951); T. Cuving and M. Larcheveque, *J. Organomet. Chem.*, **64**, 315 (1977).

5) T. Numata, H. Awano, and S. Oae, *Tetrahedron Lett.*, **21**, 1235 (1980).

6) K. Fujimori, H. Togo, and S. Oae, *Tetrahedron Lett.*, **21**, 4921 (1980); S. Oae and H. Togo, *Synthesis*, **1981**, 371.

7) G. A. Olah, S. C. Narang, L. D. Field, and R. Karpeles, *J. Org. Chem.*, **46**, 2408 (1981).

8) S. Oae and H. Togo, *Bull. Chem. Soc. Jpn.*, in contribution.

9) M. P. Cava, M. V. Lakshmikantham, and M. J. Mitchell, *J. Org. Chem.*, **34**, 2665 (1969).

10) W. A. Sheppard, *Org. Synth.*, Coll. Vol. V, 844 (1973).
11) L. Field, *J. Am. Chem. Soc.*, **74**, 394 (1952).
12) J. L. Sparke, J. L. Cameron, and N. Kharasch, *J. Am. Chem. Soc.*, **75**, 4907 (1953).
13) L. M. Litvinenko, V. A. Dadai, V. A. Savelova, and T. I. Krichevtsoba, *Zh. Obshch. Khim.*, **34**, 3730 (1964).
14) B. L. Emling, *J. Am. Chem. Soc.*, **74**, 4702 (1925).
15) H. Gilman and N. J. Beaber, *J. Am. Chem. Soc.*, **47**, 158 (1925).
16) I. Simon, *Bull. Soc. Chim. Belg.*, **38**, 2519 (1929).
17) H. Gilman, N. J. Beaber, and C. H. Myers, *J. Am. Chem. Soc.*, **47**, 2047 (1925).

Biomimetic Reduction of Sulfuric Acid

Shigeru OAE*,† and Hideo TOGO
Department of Chemistry, The University of Tsukuba, Sakura, Niihari, Ibaraki 305
(Received July 18, 1983)

Sulfuric acid and sodium sulfate were readily reduced to elemental sulfur and hydrogen sulfide upon treatment with a mixture of either one of polyphosphoric acid derivatives, PPE, PPA, and P_4O_{10}, which can form a mixed anhydride having –P–O–S– linkage, and iodide or thiol. Sulfur dioxide, which is undoubtedly one of important intermediates, was trapped by *p*-tolyllithium to afford *p*-toluenesulfinic acid which was converted to *p*-tolyl methyl sulfone upon treatment with methyl iodide, though the yield was low. Sulfur trioxide which has been postulated as the key intermediate in the biological reduction of inorganic sulfate, was also trapped by mesitylene to give mesitylenesulfonic acid in a high yield. The reduction of sulfate to elemental sulfur and hydrogen sulfide is considered to proceed through the course which resembles the biological reaction path involved in the assimilatory metabolism of inorganic sulfate in microorganisms and plants.

Inorganic sulfate which is in the highest oxidative state of sulfur atom is one of the most inert species toward any reducing agent among the naturally occurring sulfur compounds, and hence clean reduction of inorganic sulfate by any chemical means under mild conditions has been considered to be most difficult.

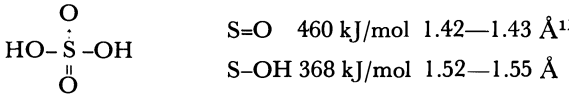

The deoxygenative reduction of sulfuric acid may proceed stepwise *via* an initial nucleophilic displacement of OH group of sulfuric acid by a leaving group, followed by subsequent nucleophilic attack on the leaving group bya second nucleophile as shown in Eq. 1.

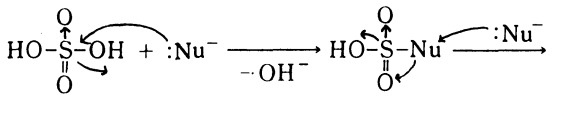

(1)

$HO^- + Nu\text{-}Nu + SO_2$

However, such a simple nucleophilic replacement of OH group of sulfuric acid does not seem to proceed readily, due mainly to the following reasons.

a) Sulfuric acid is a very strong acid which can dissociate so readily to divalent sulfate ion by supplying two protons to the attacking nucleophile that the nucleophile eventually loses the nucleophilic reducing ability due to the protonation to the lone electron pair of the nucleophile. Divalent sulfate ion, bearing two negative charge, may also no longer readily receive nucleophilic attack at its central sulfur atom due to the charge repulsion.

b) Even undissociated sulfuric acid would resist the nucleophilic attack, due to the steric hindrance and electronic repulsion by four oxygen atoms bound to the central sulfur, while three electronegative oxygens must be placed in the unfavorable equatorial position in the transition state of the substitution as shown in Eq. 2.

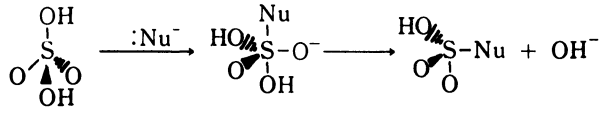

(2)

† Present address: Okayama University of Science, 1-1 Ridai-cho, Okayama 700.

c) The leaving ability of OH group is rather poor in most nucleophilic substitution reactions. Therefore, it would be necessary to substitute proton by some other elctron-withdrawing group by treatment with some condensing reagent XY to activate the central sulfur to receive nucleophilic attack as shown in Eq. 3.

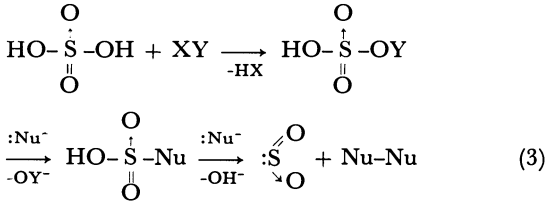

(3)

Meanwhile, many plants, microorganisms are known to reduce inorganic sulfate to some sulfur-containing amino acids as shown below[2)] *via* sulfite and sulfide in the assimilatory metabolism. The biological reduction of sulfate consists of the following two key steps, *i.e.* the conversion of sulfate to a mixed anhydride, APS or PAPS, to activate sulfate, and the subsequent nucleophilic attack of a certain protein-thiol on the sulfur atom of APS or PAPS to generate the protein-bound thiosulfate. Then, the sulfenyl sulfur of the protein-bound thiosulfate can be easily displaced by other mercapto group in the enzyme to give sulfite which is ultimately reduced to hydrogen sulfide, or the sulfonyl group of the protein-bound thiosulfate is reduced by thiosulfate reductase to form R^1SS^- or R^2SS^-. This paper describes the first successful chemical model reactions for the assimilatory biological reduction of inorganic sulfate.

Results and Discussion

Since the essential part of ATP which takes part in the biological reduction of sulfate is the triphosphate linkage, polyphosphoric acid (PPA), ethyl polyphosphate (PPE),[3)] and tetraphosphorus decaoxide are considered to be use as ATP model compounds. When sulfuric acid was added to either one of these polyphosphoric acid derivatives, we observed mild evolution of heat, probably due to the formation of bond, which is the essential part of the mixed anhydride. Iodide is known

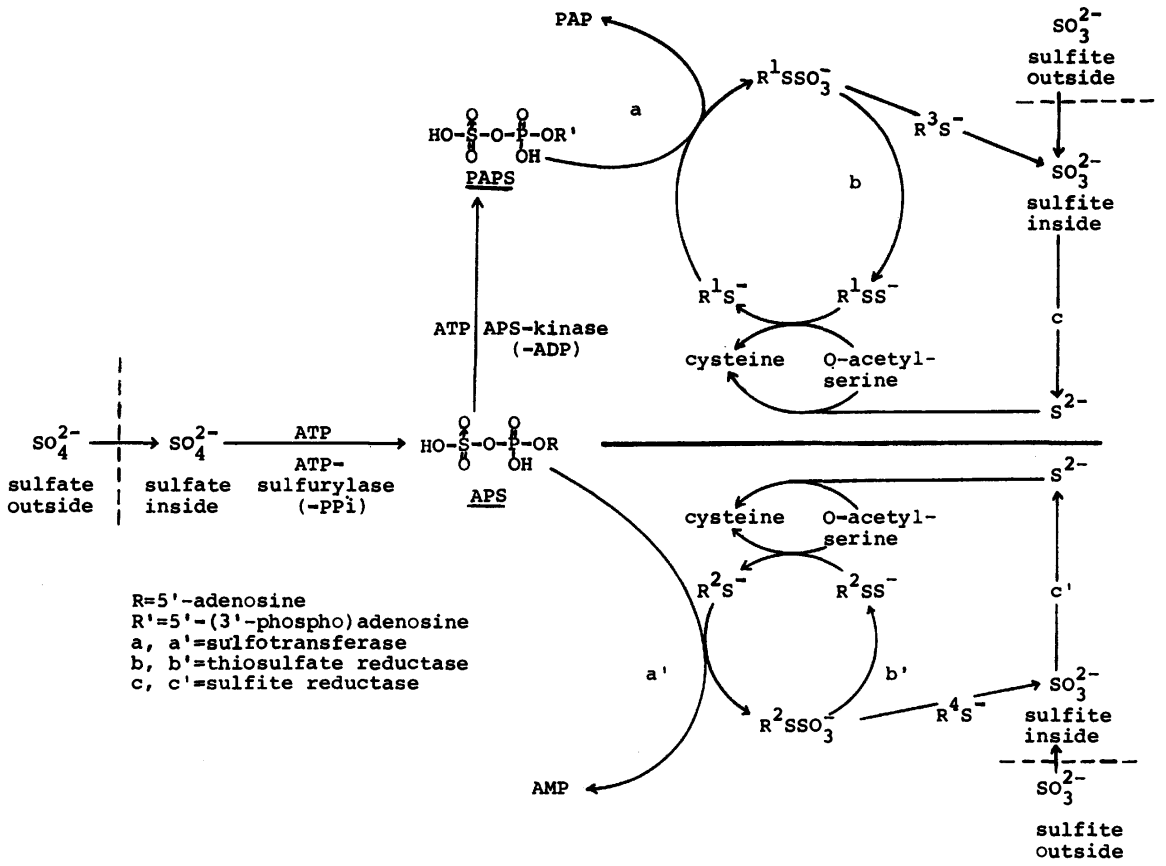

Fig. 1. Pathways of assimilatory sulfate reduction.

TABLE. THE REDUCTION OF SULFURIC ACID AND SULFATE

$$H_2SO_4(M_2SO_4) \xrightarrow[(-I_2)]{KI,\ n\text{-}Bu_4NI(cat)} S_8 \text{ and } H_2S^{a)}$$

Run	Polyphosphoric acid derivative	Solvent	Temp °C	Time h	Yields/% (A) S_8	(B)[a] S_8	(B)[a] H_2S
1	P_4O_{10}	Acetonitrile	42—45	10	17		—
2	PPE	Chloroform	25	7	4—10		—
3	PPA	Sulfolane	75	8	58		—
4[b]	PPA	Sulfolane	75	17	15		—
5[c]	PPA	Sulfolane	70—73	7	40—44		—
A	PPE	Acetonitrile	25	5	23	0	Trace
B	PPA	Sulfolane	75	4	42	Trace	15
C[c]	PPA	Sulfolane	75	8	10	0	Trace
6[d]	PPA	Sulfolane	75	8	0		—

a) Hydrogen sulfide was isolated as *N,N'*-dicyclohexylthiourea in the trapping experiment with DCC. When N_2 gas was bubbled into the reaction mixture(A) and the exhausted gas was introduced into a benzene solution of DCC(B). b) Na_2SO_4 was used. c) $(n\text{-}Bu_3NEt)_2SO_4$ was used. d) No presence of H_2SO_4.

to be a facile reducing agent which can reduce oxidized organosulfur derivatives such as sulfoxides,[4] sulfinic acids,[5] sulfonyl halides,[6] thiosulfonic *S*-esters,[7] and sulfonic acids[8] to divalent organosulfur compounds, forming iodine, in a similar manner as in the case with thiols[9] which are readily oxidized to disulfides and play the most important role in the reduction of sulfate in microorganisms and plants. Although it is desirable to use thiols in order to mimic the biological reduction of sulfate, since iodide may not be present in nature, iodide is a little more reactive than thiols and the reaction is conveniently followed. Meanwhile, many reactive thiols can often forms mixed disulfides or polysulfides which are not readily separated for characterization, and hence iodide was used for the reduction at first for a detailed observation of the simple reduction and then thiols were used. The chemical behavior of iodide in the reduction is very similar to that of thiols. Sulfuric acid is, however, very inert and not reduced by iodide or thiols alone. Only in the presence of such condensing

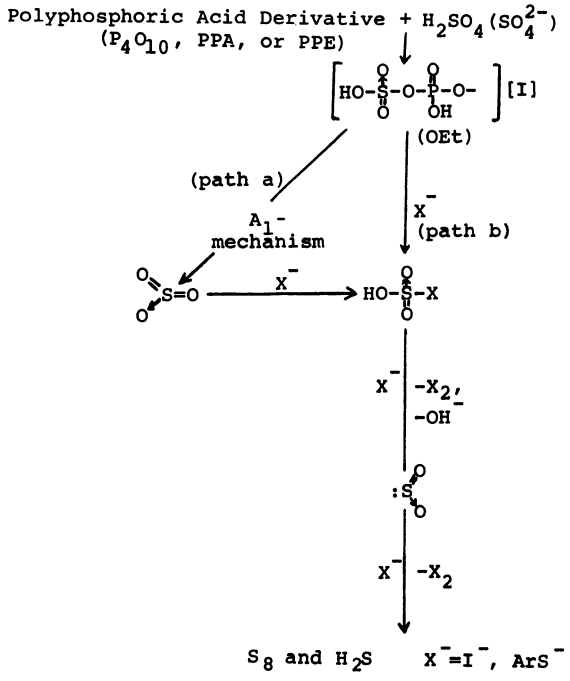

Scheme 1.

agents as polyphosphoric acid derivatives, sulfate was reduced to sulfide with either iodide or thiols. The solvents used for the reactions with PPA and P_4O_{10} were dry sulfolane and acetonitrile respectively, since both solvents can readily dissolve these polyphosphoric acid derivatives, however, common polar aprotic solvent such as acetonitrile or chloroform can also be used in the reaction with PPE because of its high solubility in these solvents.

The results obtained in reduction of sulfuric acid are shown in Table 1. The products were elemental sulfur and hydrogen sulfide. Under acidic conditions, thiol group (*i.e.* hydrogen sulfide) and polysulfide (*i.e.* elemental sulfur) are in an equilibrium as shown in Eq. 4 (generally, thiol is oxidized by iodine in the presence of a base, *e.g.* pyridine or amine). Therefore the reduction products obtained were a mixture of hydrogen sulfide and elemental sulfur. The rather low yields of the reduction products are mainly due to the difficulty of purification and isolation of these products from the reaction mixture. In the absence of *n*-$Bu_4N^+I^-$, the yields of the reduction products were markedly decreased. In the runs 1, 2, 3, 4, and 5, the reduction to sulfur was carried out in one flask, whereas, in the runs A, B, and C, while the reduction was carried out in one flask, nitrogen gas was introduced into the flask to drive out evolving hydrogen sulfide into another flask which contained a dry benzene solution of DCC that can trap hydrogen sulfide to afford the thiourea derivative. Generally, when iodide ion was added into a mixture of sulfuric acid and any one of the polyphosphoric acid

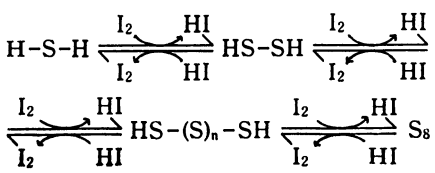

(4)

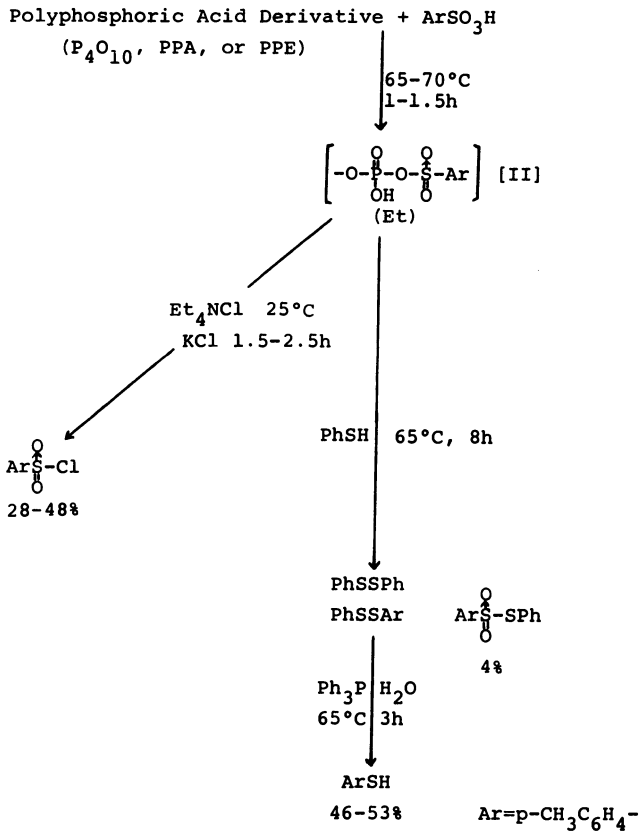

Fig. 2. Reduction of $ArSO_3H$ to ArSH by polyphosphoric acid derivative/PhSH.

derivatives, the formation of hydrogen sulfide gas was easily detected.

Both elemental sulfur and the thiourea can be readily identified by comparison with the authentic samples (TLC, mp).

Inspection of the data in the Table reveals that PPA is the best model substrate for ATP, and gave sulfur and hydrogen sulfide in the highest yields. The rather low yields of reduction species in the reaction with either P_4O_{10} or PPE are believed to be due to the subsequent reaction between hydrogen sulfide formed and P_4O_{10}, which is a strong proton acceptor, or PPE which is an effective alkylating agent. The postulated mechanism is shown in Scheme 1. In this Scheme, [I] is believed to be the key intermediate in the presence of excess of any polyphosphoric acid derivative. Sulfite is also one of the intermediate, which is eventually reduced to elemental sulfur in a high yield in the reaction with a mixture of PPA and KI under similar conditions. The formation of intermediate[I] may be supported by a trapping experiment described in the reduction of sulfonic acid with the same system.[10] Namely, when chloride ion was added into the reaction mixture of polyphosphoric acid derivative and *p*-toluenesulfonic acid, *p*-toluenesulfonyl chloride was obtained as Fig. 2. However, isolation of chlorosulfuric acid in the reaction of the intermediate [I] with chloride anion was not achieved because of its rather high reactivity. Thus, only in the reaction of arenesulfonic acid we could isolate the sulfonyl chloride by treating the intermediate [II] with chloride.

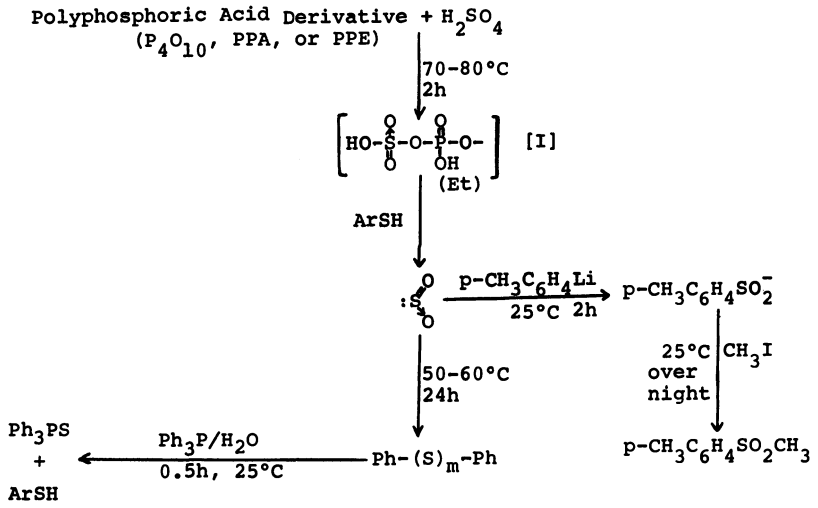

Scheme 2.

Sulfur dioxide is also an intermediate; however, it is so readily reduced by hydrogen iodide that it is difficult to trap SO_2 when iodide ion is used as the reducing agent. Instead of using iodide, excess thiophenol can be added as the reducing agent into the mixture of polyphosphoric acid derivative and sulfuric acid. Thus, sulfuric acid was reduced by thiophenol to afford diphenyl polysulfide of which middle sulfur atoms are derived from sulfuric acid. The polysulfide was then converted to thiophenol and triphenylphosphine sulfide upon of triphenylphosphine. Though the yield of the triphenylphosphine sulfide was low (2%), the combined sulfur atom of triphenylphosphine sulfide is obviously derived from sulfuric acid. The rather low yield of divalent sulfur is due to the fast reaction of thiophenol and polyphosphoric acid derivative as compared to the reduction of compound [I] by thiophenol.

Since thiophenol is a mild reducing agent as compared to hydrogen iodide, sulfur dioxide was successfully trapped by *p*-tolyllithium, when SO_2 gas formed was driven out into an ether solution of *p*-tolyllithium to afford *p*-toluenesulfinate which was then converted to the sulfone by treating with methyl iodide, though the yield of the sulfone was poor ($\simeq$1%). Although the yields of the reduction products are not high, the successful reduction of sulfuric acid and sulfate to sulfides in this biomimetic reduction with polyphosphoric acid derivatives with iodide or thiols, and the trapping of sulfur dioxide under mild conditions would be the first reported experiment which can successfully mimic the biological assimilatory sulfate reduction. In the reduction, two path (**a** and **b**) are conceivable for the reaction of compound [I] with nucleophile (I^-, PhSH). While path **b** may be unfavorable due to the stereo-electronic repulsion between the nucleophile and negative oxygen poles of bulky sulfate group of [I] at the transition state of the S_N2 reaction on the sulfur atom of [I], path **a** would be quite likely since hydrogen bound to the oxygen atom of [I] is extremely acidic.

Thus, 1,2-elimination reaction of [I] to form sulfur trioxide and phosphoric acid by Eleb process should take place quite readily.[11] Sulfur trioxide thus formed may react with iodide or arenethiol to afford iodosulfuric acid, or thiosulfuric acid either of which is considered to be subsequently reduced readily with iodide or thiols to afford sulfite. Sulfite ion (*i.e.* SO_2 in acidic conditions) is reduced further very readily with these systems to sulfide.[12] Actually, in one of our trapping experiments, sulfur trioxide was nicely trapped by mesitylene to give mesitylenesulfonic acid in the reaction of tetraphosphorus decaoxide and sulfuric acid under acidic conditions and also in the reaction between tetraphosphorus decaoxide and bis(tributylethylammonium) sulfate,

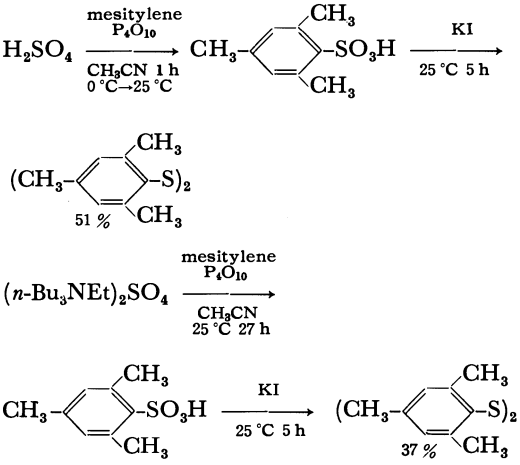

which are both neutral respectively. In a blank experiment, in the absence of tetraphosphorus decaoxide, *i.e.* the mixture of mesitylene and sulfuric acid, or the mixture of mesitylene and bis(tributylethylammonium) sulfate under similar conditions, the corresponding mesitylenesulfonic acid was not obtained. Earlier, Eiki and Tagaki[13] and Benkovic and Hevey[14] reported independently that the nucleophilic substitution of phenyl phosphatosulfate (PPS), a APS or PAPS model compound, similar to [I] in our experiment, by OH^- ion proceeded sluggishly, however, hydrolysis of PPS easily took place in acidic media or in the presence of some metal ions in aprotic solvents such as DMF. These results together with our results suggest clearly the elimination-addition mechanism involving the formation of sulfur trioxide in the acidic media (path **a**) as shown Scheme 1.

Experimental

Materials. PPA, potassium iodide, mesitylene, sulfuric acid, tributylamine, diethyl sulfate, tetraphosphorus decaoxide, and dicyclohexylcarbodiimide are all from Wako Chemicals Co., tetrabutylammonium iodide was from Tokyo Kasei Co., and sodium sulfite was obtained from Kanto Kagaku Co.

Ethyl Polyphosphate. Ethyl polyphosphate was prepared by a known method.[15] Tetraphosphorus decaoxide, 150 g, was added into a solution of 300 ml of dry ether and 150 ml of dry chloroform. The mixture was refluxed for 4 d under N_2 (bath temperature 50 °C). As the reaction proceeded, the crystalline P_4O_{10} faded away to give a homogeneous liquid. After completion of this reaction, the liquid phase was decanted into a flask in a dry box. Then the solution was evaporated to a colorless syrup. The residue was then dried by vacuum pump for 36 h at 40 °C. A colorless syrupy (hard) ester which is very sensitive to moisture, was obtained. NMR ($CDCl_3$) δ=1.9—1.5 (3H, m) and 4.2—5.0 (2H, m).

Reduction of Sulfuric Acid with PPA/KI/n-$Bu_4N^+I^-$ (cat) System to Sulfide. Polyphosphoric acid, 10 g (29.7 mmol, M.W. =338) and 4.93 g (29.7 mmol) of potassium iodide were added into 6 ml of dry sulfolane. Then, 300 mg (2.97 mmol) of sulfuric acid was added into this mixture, into which finally 184 mg (0.5 mmol) of tetrabutylammonium iodide was added. The reaction was carried out for 8 h at 75 °C with stirring under nitrogen atmosphere. The odor of hydrogen sulfide was clearly detected. After the reaction, 10 ml of water was added and the mixture was heated under similar conditions for 0.5 h in order to hydrolyze excess PPA. The reaction mixture was poured into benzene which solution was washed with water for 3 times, dried ($MgSO_4$), filtrated and the filtrate was evaporated. The residue was subjected to TLC (MERCK, silica gel type-60), separated with benzene to exclude iodine, then 55 mg of sulfur was obtained and identified by comparison with authentic sulfur (TLC R_f=0.7, eluent; benzene) mp 112—114 °C (lit,[16] 115 °C). After recrystallization with a mixture of benzene and hexane, the yield of sulfur was 58%.

Hydrogen Sulfide Trapping in PPA/KI/n-$Bu_4N^+I^-$ (cat) System. Reactor A: PPA (10 g) and 4.93 g (29.7 mmol) of potassium iodide were added into 6 ml of dry sulfolane. Then, 300 mg of sulfuric acid was added and finally 184 mg (0.5 mmol) of tetrabutylammonium iodide was added into this mixture.

Reaction B: Dicyclohexylcarbodiimide 18.4 g (9 mmol) was dissolved in 10 ml of dry benzene in a flask which was equipped with empty balloon.

Reactor B was jointed reactor A with a glass tube. The content in reactor A was stirred and heated for 4 h at 75 °C under slow flowing of nitrogen gas. While the reaction mixture in reactor B was stirred at room temperature, nitrogen and hydrogen sulfide were introduced into the reactor B. After the reaction, 10 ml of water was added to the reactor A and the mixture was heated under similar conditions for 1 h. The reaction mixture in reactor A was poured into benzene and washed with water for 3 times, dried ($MgSO_4$), filtrated and evaporated. The residue was separated by TLC with benzene to give sulfur. From the reactor A, 40 mg of sulfur was obtained. Yield 42%. In a separative experiment, 10 ml of water was added into the reactor B to quench any excess of dicyclohexylcarbodiimide to urea and the mixture was kept standing for a few hours. The mixture was poured into benzene which solution was washed with water, dried ($MgSO_4$), and benzene was evaporated. The residue was separated through silica-gel column with chloroform. *N,N'*-Dicyclohexylthiourea (103 mg, yield 15%), TLC (eluent; $CHCl_3$) R_f=0.3—0.4; IR (KBr) 1540, 3275, 1490 and 1220 cm^{-1}; mp 182—184 °C (lit,[17] 182—182.5 °C). A similar procedure with a similar molar ratio was used in the reduction of sodium sulfate in PPA system.

Trapping of Sulfur Trioxide in P_4O_{10} by Mesitylene I. Tetraphosphorus decaoxide, 2100 mg (15 mmol), was added into 6 ml of dry acetonitrile into which 2 ml of mesitylene was then added. The mixture was cooled down to 0 °C and 300 mg (2.97 mmol) of sulfuric acid was added into this mixture. The mixture was stirred for 1 h at room temperature (0 °C→ 25 °C) under nitrogen atmosphere. Then, 4903 mg (29.7 mmol) of potassium iodide, 184 mg (0.5 mmol) of tetrabutylammonium iodide and 4 ml of dry acetonitrile were added into this reaction mixture which was stirred for 5 h at room temperature under nitrogen. Since the isolation of mesitylenesulfonic acid is difficult in our system, the sulfonic acid was reduced to the disulfide with P_4O_{10}/KI system under mild conditions. Thus, mesitylenesulfonic acid was converted to dimesityl disulfide. After the reaction, 10 ml of water was added and the mixture was stirred for 1 h. The reaction mixture was poured into benzene which solution was washed with water for three times, 0.5 mol dm^{-3} of $Na_2S_2O_3$, once, again with water and dried ($MgSO_4$).

Dimesityl disulfide, which was derived from mesitylenesulfonic acid, was obtained in *ca.* 50% by GLC (OV-1, 1 m glass column). Authentic dimesityl disulfide was obtained by reducing mesitylenesulfonyl chloride with lithium aluminum hydride in dry diethyl ether for 1 h (0 °C→25 °C) to mesitylenethiol which was oxidized further to dimesityl disulfide with iodine and pyridine at room temperature in 81% yield. Mp 124—125 °C (lit,[18] 125 °C).

Trapping of Sulfur Trioxide in P_4O_{10} by Mesitylene II. Bis(tributylethylammonium) sulfate, 588 mg (1.2 mmol) was dissolved in 5 ml of dry acetonitrile and 2 ml of mesitylene was added to this mixture. Then, 1200 mg (8.4 mmol) of tetraphosphorus decaoxide was added and the whole mixture was stirred for 27 h at room temperature under nitrogen atmosphere. Potassium iodide, 1860 mg (11.2 mmol), was added into this mixture, into which 5 ml of acetonitrile was added and the whole mixture was stirred for 5 h at room temperature. Bis(tributylethylammonium) sulfate obviously plays the role of of phase-transfer catalyst. Then, 10 ml of water was added at 0 °C into the mixture which was stirred for 1 h at room temperature. The mixture was poured into benzene. The organic layer was separated and washed with water for three times, with 0.5 mol dm^{-3} of $Na_2S_2O_3$, once again with water once and dried ($MgSO_4$). Dimesityl disulfide was obtained in 37% yield (GLC, SE-30, 1 m glass column).

Trapping of Sulfonyl Group in $ArSO_3H/P_4O_{10}/KCl$ System. Tetraphosphorus decaoxide, 1600 mg (11.27 mmol), was added into 5 ml of dry acetonitrile, into which 381 mg (2 mmol) of *p*-toluenesulfonic acid was added. The mixture was heated and stirred for 1.5 h at 60—65 °C under nitrogen atmosphere. Then, 33 mg (0.2 mmol) of tetraethylammonium chloride, 746 mg (10 mmol) of potassium chloride were added into the reaction mixture at 0 °C and the mixture was stirred for 3 h at room temperature. After the reaction, the mixture was poured into benzene and washed with water for 3 times, then dried ($MgSO_4$). *p*-Toluenesulfonyl chloride was obtained in 48% yield (GLC), isolated in 43% yield. In the reaction with PPE, (PPE=6 g, *p*-$CH_3C_6H_4SO_3H\cdot H_2O$=381 mg), the yield of *p*-toluenesulfonyl chloride was 28% under similar conditions.

Reduction of $ArSO_3H$ to ArSH with PPA/Ar'SH System. PPA, 6 g, and 381 mg of *p*-toluenesulfonic acid were added into 5 ml of dry sulfolane, which was stirred and heated for 1.5 h at 90 °C under nitrogen atmosphere (the initial step). Then 2 ml of thiophenol was added to this mixture, and the reaction

mixture was kept at 90 °C for 3 h (the latter step). After the reaction, 10 ml of water was added, then the mixture was poured into benzene, which solution was washed with water for three times, and dried ($MgSO_4$). A mixture of diphenyl disulfide and phenyl *p*-tolyl disulfide was obtained. Very little di-*p*-tolyl disulfide was formed. *S*-Phenyl *p*-toluenethiosulfonate was not formed. The mixture was purified by column chromatography through silica gel(eluent; benzene/hexane=1/1=v), and the disulfides obtained were converted to the corresponding thiols by the addition of the mixture of Ph_3P/H_2O/dioxane. The yield of *p*-toluenethiol was 53% (GLC). In the reduction with PPE (PPE=7 g, *p*-$CH_3C_6H_4SO_3H \cdot H_2O$=381 mg), both the initial step and the latter step required 1.5 h/65 °C and 8 h/65 °C respectively. The reaction mixture was then treated similarly and nearly a similar result was achieved. *p*-Toluenethiol 46%. *S*-Phenyl *p*-toluenethiosulfonate 4% mp 78—80 °C (lit,[19] 78 °C).

Trapping of Sulfur Dioxide with p-*Tolyllithium. Reactor A (Step 1)*: PPE (10 g) was added to 800 mg (8 mmol) of sulfuric acid which reactor was heated and stirred at 80 °C for 1 h under nitrogen atmosphere.

Reactor B (Step 2): Lithium, 280 mg (40 mmol), was added into 5 ml of dry ether into which 5 ml of dry ether solution containing 5.1 g (30 mmol) of *p*-bromotoluene was added.[20] The mixture was stirred for a few hours under nitrogen atmosphere.

Step 3: Reactors A and B were jointed by a glass tube. Thiophenol, 3 ml, was added into the reactor A at room temperature. Then each solution in the reactors A and B was stirred for 2 h at room temperature under nitrogen atmosphere. After the reaction, the reaction mixture in reactors A and B was poured into water and washed with benzene for three times. The water was evaporated, the solution was concentrated, and excess methyl iodide was added into the mixture which was stirred over night (H_2O/EtOH=1/1=v). *p*-Tolyl methyl sulfone, 11.4 mg, was obtained. Mp 84—85 °C (lit,[21] 87 °C).

In the case of PPA, step 1 (PPA=10 g, H_2SO_4=840 mg) 2 h/70—80 °C.

Step 2: (Li=280 mg, *p*-$CH_3C_6H_4Br$=5130 mg, Et_2O=15 ml) a few hours/r.t.

Step 3: The mixture of 2 ml of thiophenol and 6 ml of sulfolane was added to reactor A and was stirred for 2 h at room temperature. The similar procedure and reaction conditions were used. *p*-Tolyl methyl sulfone, 10 mg, was obtained.

Reduction of Sulfuric Acid by Thiophenol in PPA. A mixture of PPA (10 g) and 0.8 g of sulfuric acid was heated under stirring for 2 h at 80 °C in nitrogen atmosphere. Then, 5 ml of thiophenol was added into this mixture which was stirred for 24 h at 50—60 °C. After the reaction, 10 ml of water was added and the mixture was poured into benzene, which solution was washed with water for three times, and dried ($MgSO_4$)

Triphenylphosphine 786 mg (3 mmol) was then added to this benzene solution, and 46 mg of triphenylphosphine sulfide was obtained. Triphenylphosphine sulfide was not obtained at all in the reaction of triphenylphosphine and diphenyl disulfide or thiophenol. Sulfur and diaryl polysulfide are known to be desulfulized by triphenylphosphine to give only triphenylphosphine sulfide, and arenethiol, respectively.

Triphenylphosphine sulfide mp 162—163 °C (lit,[22] 162—164 °C).

References

1) S. W. Benson, *Chem. Rev.*, **78**, 23 (1978).
2) M.L.-S. Tsand and J. A. Schiff, *J. Bacteriol.*, **125**, 923 (1976); A. B. Roy and P. A. Trudinger. "The Biochemistry of Inorganic Compounds of Sulfur" Chap. 10, Cambridge University Press (1970).
3) M. P. Cava, M. V. Lakshmikantham and M. J. Mitchell *J. Org. Chem.*, **34**, 2665 (1969).
4) D. Landini and F. Montanari, *Tetrahedron Lett.*, **1964**, 2691; J. Drabowicz and S. Oae, *Synthesis*, **1977**, 404; G. A. Olah, S. C. Narang, B. G. B. Gupta, and R. Malhotra, *Synthesis*, **1979**, 61.
5) K. Fries and G. Schürmann, *Ber.*, **47**, 1195 (1914); K. Fries, H. Koch, and H. Stukenbrock, *Ann.*, **468**, 177 (1929).
6) G. A. Olah, S. C. Narang, L. D. Field, and G. F. Salem, *J. Org. Chem.*, **45**, 4792 (1980); W. A. Sheppard, *Org. Synth.*, Coll. Vol. V, 843 (1970).
7) G. A. Olah, S. C. Narang, L. D. Field, and R. Karpeles, *J. Org. Chem.*, **46**, 2408 (1981).
8) T. Numata, H. Awano, and S. Oae, *Tetrahedron Lett.*, **21**, 1235 (1980); K. Fujimori, H. Togo, and S. Oae, *ibid.*, **21**, 4921 (1980); S. Oae and H. Togo, *Synthesis*, **1982**, 152; G. A. Olah, S. C. Narang, L. D. Field, and R. Karpeles, *J. Org. Chem.*, **46**, 2408 (1981).
9) S. Oae, H. Togo, T. Numata, and K. Fujimori, *Chem. Lett.*, **1980**, 1193; D. Cipris and D. Pouli, *Synth. Commun.*, **9**, 207 (1979); T. Numata, H. Togo, and S. Oae, *Chem. Lett.*, **1979**, 329; T. J. Wallace and J. J. Mahon, *J. Org. Chem.*, **30**, 1502 (1965).
10) S. Oae and H. Togo, *Synthesis*, **1982**, 152.
11) Monoaryl sulfate and Bunte salt are hydrolyzed by A-1 mechanism in acidic media. J. L. Kice, J. M. Anderson, N. E. Pawlowski, *J. Am. Chem. Soc.*, **88**, 5245 (1966); J. L. Kice and J. M. Anderson, *J. Am. Chem. Soc.*, **88**, 5242 (1966).
12) F. Akiyama, *J. Chem. Soc., Perkin Trans. 1*, **1978**, 1046.
13) W. Tagaki, T. Eiki, and I. Tanaka, *Bull. Chem. Joc. Jpn.*, **44**, 1139 (1971); W. Tagaki, and T. Eiki, *Adv. Chem. Ser.* **191**, 409 (1980); T. Eiki and W. Tagaki, *Chem. Lett.*, **1981**, 1465.
14) S. J. Benkovic and R. C. Hevey, *J. Am. Chem. Soc.*, **92**, 4971 (1970).
15) M. P. Cava, M. V. Lakshmikantham, and M. J. Mitchell, *J. Org. Chem.*, **34**, 2665 (1969).
16) "The Merck Index," 9th ed, ed by Merck Co. (1976), p. 8762.
17) D. Martin, W. Mucke, and Monatsber. *Dent. Akad. Wiss. Berlin.*, **6**, 362 (1964).
18) H. J. Backer and E. Westerhuis, *Recl. Trav. Chim. Pays-Bas.*, **71**, 1065, 1071 (1952).
19) Y. Yoshikawa, W. Tagaki, R. Nomura, and S. Oae, *Bull. Chem. Soc. Jpn.*, **42**, 2903 (1969).
20) W. E. Truce and J. F. Lyons, *J. Am. Chem. Soc.*, **73**, 126 (1951).
21) R. Uehara, *Bull. Chem. Soc. Jpn.*, **32**, 1082 (1959).
22) Authentic sample was obtained from Wako Chemicals Co.

Structures of Halogenated Chamigrene Derivatives, Minor Constituents from the Red Alga *Laurencia nipponica* Yamada[1)]

Minoru Suzuki, Makoto Segawa, Teruaki Suzuki, and Etsuro Kurosawa*
Department of Chemistry, Faculty of Science, Hokkaido University, Sapporo 060
(Received August 5, 1983)

Three halogenated chamigrane-type sesquiterpenes have been isolated as the minor metabolites from the red alga *Laurencia nipponica*, collected at Sannai, near Wakkanai. The absolute structures of these compounds were confirmed by spectral and chemical methods.

In the course of our continuing studies on the constituents of the red alga *Laurencia nipponica* Yamada ("Ura-sozo") collected at various locations in warm and cold current regions in Hokkaido, the diversity of the secondary metabolites of this species has been found to be dependent upon growth localities.[2)] As part of further investigations of this alga, we turned our attention to the specimens in Northern Hokkaido (Dohoku) and collected at Sannai, Soya point, near Wakkanai, Hokkaido. This specimen displayed the presence of kumausallene (**1**) and *trans*-kumausyne (**2**) as the principal metabolites, which have recently been isolated from *L. nipponica* collected at Kumausu, near Otaru, Hokkaido.[3)] Furthermore, several known and unknown sesquiterpenes have also been isolated as the minor metabolites. In this paper we report the structures of three halogenated chamigrane-type sesquiterpenes.

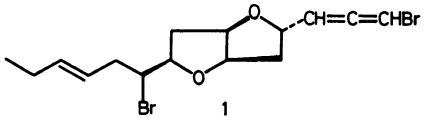

1

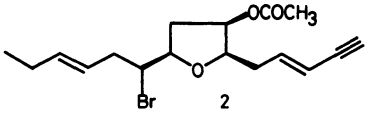

2

Repeated column chromatography of the neutral methanol extracts yielded a halogenated sesquiterpene hydrocarbon **3** (1.6% of the extracts)and halogenated sesquiterpene alcohols **4** (2.0%) and **5** (1.7%) along with kumausallene (**1**) (12%) and *trans*-kumausyne (**2**) (16%).

The halogenated sesquiterpene hydrocarbon, **3**, $C_{15}H_{23}Br_2Cl$ (*m/z* 402, 400, 398, and 396; M^+), mp 76—77 °C, $[\alpha]_D^{15}$ +30.6°, showed in its IR and ^1H NMR spectra the presence of a *gem*-dimethyl group [ν_{max} 1390 and 1380 cm^{-1}; δ 0.96 and 1.15 (each 3H, s)], a tertiary methyl group [δ 1.70 (3H, s)], two halomethine groups [δ 4.45 (1H, dd, J=12, 5 Hz) and 4.72 (1H, dd, J=12, 5 Hz)], and an exomethylene group [ν_{max} 1640 and 908 cm^{-1}; δ 4.87 and 5.26 (each 1H, s)]. Comparison of the ^1H and ^{13}C NMR spectra of **3** with those[4,5)] of 2,10-dibromo-3-cholro-α-chamigrene (**6**) previously isolated from *L.* species,[4)] seemed to indicate **3** to be 2,10-dibromo-3-chloro-β-chamigrene. Confirmation of the structure of **3** was obtained by the following chemical correlation. Hydrogenation of **3** over PtO_2 in ethanol gave the dihydro derivative which was identical with the hydrogenation product (**7**)[4b)] of **6** in all respects, thus indicating that this compound is (2*S*)(3*S*)(10*R*)-2,10-dibromo-3-chloro-β-chamigrene (**3**). The IR, ^1H NMR, and mass spectral properties of **3** are almost identical with those of nidificene previously isolated from *L. nidifica*,[6)] showing that these compounds appear to be the same material.[7)]

One of the sesquiterpene alcohols, **4**, $C_{15}H_{23}OBr_2Cl$ (*m/z* 418, 416, 414, and 412; M^+), oil, $[\alpha]_D^{17}$ +3.33°, showed in its ^1H NMR spectrum the presence of three tertiary methyl groups, including *gem*-dimethyl group, at δ 0.91, 1.17, and 1.71 (each 3H, s), an α-proton to hydroxyl group at δ 4.43 (1H, dd, J=3, 3 Hz), two halomethine protons at 4.73 (1H, dd, J=13, 4 Hz) and 4.74 (1H, dd, J=11, 5.5 Hz), and exomethylene protons at 5.06 and 5.46 (each 1H, sharp s). Acetylation of **4** with acetic anhydride in pyridine afforded the corresponding acetate **8**, $C_{17}H_{25}O_2Br_2Cl$, ν_{max} 1740 and 1238

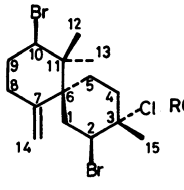

3

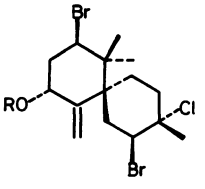

4: R=H
8: R=Ac

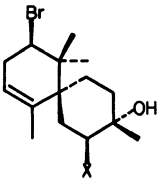

5: X=Br
11: X=Cl

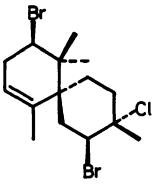

6

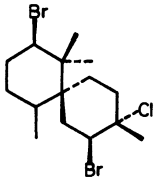

7

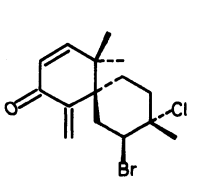

9

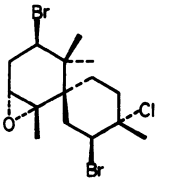

10

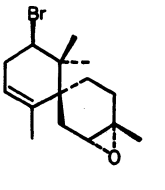

12

cm^{-1}; δ 5.41 (dd, J=4, 3 Hz), which regenerated the parent alcohol on mild saponification with K_2CO_3 in methanol. Furthermore, **4** was subjected to Jones or pyridinium chlorochromate oxidation to yield, with concomitant dehydrobromination, dienone **9**, $C_{15}H_{20}OBrCl$, ν_{max} 1672 cm^{-1}; λ_{max} 233 nm (ε 6300); δ 1.02, 1.05 (total 3H), 1.20 (3H, s), 1.69 (3H, s), 4.26 (0.4H, dd, J=12, 4 Hz), 4.69 (0.6H, dd, J=13, 5 Hz), 5.38 (1H, s), 5.95 (0.6H, d, J=10 Hz), 5.98 (0.4H, d, J=10 Hz), 6.16 (1H, s), and 6.51 (1H, d, J=10 Hz). The ^1H NMR spectrum of **9** suggests that this dienone exists at room temperature as an equilibrium mixture of two conformational isomers, which is supported by the observation of distinct temperature dependence in the ^1H NMR spectra (toluene-d_8) at various temperature.[8] In view of the above-mentioned data coupled with comparison of spectral properties of **3** and **4**, formula **4** could readily be proposed for this alcohol. The equatorial nature of the proton at C-8 was suggested by its J-values in the ^1H NMR spectra of **4** and **8**. The structure of **4**, including the absolute configuration, was established by derivation from 2,10-dibromo-3-chloro-7,8-epoxychamigrane (**10**) which was the major metabolite of Atsuta's *L. nipponica*.[4c,d] Treatment of **10** with *p*-toluenesulfonic acid in warm benzene gave **4** in 53% yield. Therefore, the structure of this alcohol is represented by formula **4**, which is the first example of halochamigrane derivatives from the genus *Laurencia* with a hydroxyl group at C-8.

Another sesquiterpene alcohol, **5**, $C_{15}H_{24}OBr_2$ (*m/z* 382, 380, and 378; M^+), oil, $[\alpha]_D^{18}$ −27.0°, revealed very similar IR, ^1H and ^{13}C NMR spectra to those of glanduliferol (**11**),[4b] indicating that **5** must be bromohydrin at C-2 and C-3 instead of chlorohydrin at C-2 and C-3 in glanduliferol (**11**). This was confirmed by the following reaction. Treatment of **5** with 5% methanolic KOH at room temperature gave 10-bromo-2,3-epoxy-α-chamigrene (**12**) as same as in the case of **11**.[4b] Recently Fukuzawa *et al.* reported that 2,10-dibromo-3-hydroxy-α-chamigrene has been isolated as a crystalline state (mp 58—59 °C, $[\alpha]_D^{20}$ −34.2°) from *L. nipponica* collected at the inside of Kabutoiwa, Oshoro Bay.[9] Unambiguously our alcohol was found to be identical with Fukuzawa's sample by comparison of the spectral data.

Previously we have isolated glanduliferol (**11**) from the specimen of *L. nipponica* (*L. glandulifera*)[10] collected at the outside of Kabutoiwa, Oshoro Bay, in August 1963 and 1964. The finding of 2,10-dibromo-3-hydroxy-α-chamigrene (**5**) from Oshoro's *L. nipponica* prompted us to reinvestigate the specimen collected at the outside of Kabutoiwa. Interestingly the specimens collected in 1978 (August)[11] and 1983 (June) revealed the presence of **5** instead of glanduliferol (**11**).

Experimental

The melting point was uncorrected. The IR spectra were measured on a JASCO A-102 spectrometer. The ^1H and ^{13}C NMR spectra were recorded on a JEOL JNM-FX100 spectrometer, TMS being used as an internal reference in $CDCl_3$. The UV spectra was obtained with a Shimadzu UV-240 spectrophotometer. The low and high resolution mass spectra were recorded on a JEOL JMS-D300 spectrometer. The optical rotations were measured on a JASCO DIP-140 polarimeter in $CHCl_3$. Aluminium oxide (Merck, activity II-III) and silica gel (Merck, Kieselgel 60, 70—230 mesh) were used for column chromatography. Silica gel 60 F_{254} (Merck) was used for thin-layer chromatography. All known compounds were identified by comparison of the spectral data with those of the authentic specimens.

Isolation. *Laurencia nipponica* Yamada was collected early in July, 1981, at Sannai, Soya point, near Wakkanai, Hokkaido. The neutral methanol extracts (2.0 g) (*ca.* 1% of the half-dried alga) obtained by the conventional methods were fractionated by column chromatography over alumina. The fraction eluted with hexane was rechromatographed on silica-gel column to yield isodihydrolaurene (7 mg),[4c] laurene (10 mg),[12] and α-bromocuparene (5 mg).[13] The fraction eluted with hexane–benzene (1 : 1) was further chromatographed on silica-gel column to yield 2,10-dibromo-3-chloro-β-chamigrene (**3**) (32 mg), selin-4(14)-en-5α-ol (30 mg),[14] and kumausallene (**1**) (100 mg).[3] The fraction eluted with benzene was further subjected to silica-gel column chromatography to give kumausallene (**1**) (140 mg) and *trans*-kumausyne (**2**) (320 mg).[3] The fraction eluted with ethyl acetate was repeatedly chromatographed on silica-gel column to give laurenisol (6 mg),[11] an unidentified alcohol (80 mg), 2,10-dibromo-3-chloro-8-hydroxy-β-chamigrene (**4**) (40 mg), 2,10-dibromo-3-hydroxy-α-chamigrene (**5**) (34 mg), and deacetylkumausyne (55 mg).[3]

2,10-Dibromo-3-chloro-β-chamigrene (3): Mp 76—77 °C (from hexane); $[\alpha]_D^{15}$ +30.6° (*c* 1.40); IR (CCl_4), ν_{max} 3080, 1640, 1390, 1380, 1306, 1295, 1200, 1158, 1093, 1060, 992, 970, 908, and 863 cm^{-1}; ^1H NMR, δ 0.96 (3H, s), 1.15 (3H, s), 1.70 (3H, s), 1.8—2.6 (10H, m), 4.45 (1H, dd, J=12 and 5 Hz), 4.72 (1H, dd, J=12 and 5 Hz), 4.87 (1H, s), and 5.26 (1H, s); ^{13}C NMR, δ 16.4 (q), 22.5 (q), 23.1 (q), 24.4 (t), 32.4 (t), 34.8 (t), 37.6 (t)×2, 42.7 (s), 50.0 (s), 60.3 (d), 62.5 (d), 70.7 (s), 113.6 (t), and 144.5 (s); MS (70 eV), *m/z* (rel intensity) 402, 400, 398, 396 (2 : 9 : 13 : 6; M^+), 387, 385, 383, 381 (1 : 4 : 6 : 3; M^+-CH_3), 321, 319, 317 (5 : 19 : 15; M^+-Br), 283, 281 (29 : 27; $M^+-Br-HCl$), 201 (47; $M^+-Br-HBr-HCl$), 109 (100), 95 (73), 69 (99), and 41 (99). Found: *m/z* 399.9855. Calcd for $C_{15}H_{23}{}^{79}Br^{81}Br^{37}Cl$: M, 399.9808.

2,10-Dibromo-3-chloro-8-hydroxy-β-chamigrene (4): Colorless oil; $[\alpha]_D^{17}$ +3.33° (*c* 1.20); IR (film), ν_{max} 3400, 3097, 1630, 1394, 1376, 1348, 1300, 1165, 1150, 1132, 1098, 1040, 1010, 975, 925, 895, 812, and 712 cm^{-1}; ^1H NMR, δ 0.91 (3H, s), 1.17 (3H, s), 1.71 (3H, s), 2.0—2.5 (9H, m), 4.43 (1H, dd, J=3 and 3 Hz), 4.73 (1H, dd, J=13 and 4 Hz), 4.74 (1H, dd, J=11 and 5.5 Hz), 5.06 (1H, s), and 5.46 (1H, s); ^{13}C NMR, δ 17.4 (q), 23.9 (q), 24.3 (q), 26.7 (t), 39.6 (t)×2, 42.4 (t), 43.8 (s), 50.8 (s), 60.1 (d), 61.6 (d), 71.9 (s), 76.0 (d), 118.1 (t), and 146.5 (s); MS, *m/z* 418, 416, 414, 412 (0.2 : 1 : 1.4 : 0.7; M^+), 400, 398, 396, 394 (0.5 : 2.3 : 3.3 : 1.4; M^+-H_2O), 380, 378, 376 (0.5 : 0.9 : 0.5; M^+-HCl), 347, 345, 343 (3 : 4.5 : 2; $M^+-H_2O-HCl-CH_3$), 337, 335, 333 (5 : 19 : 16; M^+-Br), 319, 317, 315 (11 : 46 : 35; M^+-H_2O-Br), 299, 297 (27 : 28; $M^+-Br-HCl$), 217 (17; $M^+-HBr-HCl-Br$), 199 (34; $M^+-Br-HBr-HCl-H_2O$), 157 (29), 147 (28), 119 (40), 107 (38), 105 (45), 93 (100), 91 (43), 69 (69), and 41 (89). Found: *m/z* 395.9686. Calcd for $C_{15}H_{21}{}^{79}Br^{81}Br^{35}Cl$: $M-H_2O$, 395.9681.

2,10-Dibromo-3-hydroxy-α-chamigrene (5): Colorless oil; $[\alpha]_D^{18}$ −27.0° (*c* 2.13); IR ($CHCl_3$), ν_{max} 3570, 1397, 1385, 1342, 1130, 1108, 1095, 1070, 1045, 1015, 990, 980, 928, and 837 cm^{-1}; ^1H NMR, δ 0.95 (3H, s), 1.23 (3H, s), 1.35 (3H, s), 1.98 (3H, finely splitted m), 1.5—2.3 (7H, m), 2.4—2.7 (2H, m), 4.56 (1H, dd, J=10 and 7.5 Hz), 4.77 (1H, dd, J=10 and 8.5 Hz),

and 5.21 (1H, m); ^{13}C NMR, δ 17.3 (q), 22.2 (q), 24.7 (q), 25.9 (q), 31.6 (t), 35.9 (t), 36.3 (t), 39.1 (t), 42.7 (s), 48.2 (s), 61.3 (d), 66.3 (d), 72.0 (s), 122.3 (d), and 140.1 (s); MS, *m/z* 382, 380, 378 (0.2 : 0.4 : 0.2 : M^+), 301, 299 (17 : 17; M^+-Br), 283, 281 (25 : 25; M^+-Br-H_2O), 201 (71; $M^+-Br-HBr-H_2O$), 159 (59), 149 (58), 147 (74), 145 (98), 133 (49), 119 (55), 109 (61), 105 (70), 93 (54), 91 (76), 69 (53), 55 (68), 43 (100), and 41 (97); Found: *m/z* 301.1007. Calcd for $C_{15}H_{24}O^{81}Br$: M−Br, 301.0992.

Hydrogenation of ***3***. The hydrogenation of **3** (12.6 mg) was performed in ethanol (2.0 ml) over PtO_2-catalyst. After removal of the catalyst and the solvent, the residual oil was chromatographed on a silica-gel plate to give **7** (7.0 mg); $[\alpha]_D^{21}$ +47.5° (*c* 0.65); The IR, ^{1}H NMR, and mass spectra were identical with those of authentic 2,10-dibromo-3-chlorochamigrane.[4b]

Acetylation of ***4***. Acetylation of **4** (12 mg) was carried out with acetic anhydride in pyridine in the usual manner. The acetylated product was purified by column chromatography on silica-gel to give **8** (11 mg); colorless oil; $[\alpha]_D^{17}$ −15.4° (*c* 0.34); IR (film), ν_{max} 3110, 1740, 1635, 1392, 1370, 1348, 1238, 1190, 1167, 1148, 1130, 1093, 1023, 930, 908, 877, 808, 730, and 715 cm^{-1}; ^{1}H NMR, δ 0.92 (3H, s), 1.19 (3H, s), 1.71 (3H, s), 2.02 (3H, s), 2.1—2.5 (8H, m), 4.61 (1H, dd, *J*= 12 and 6.5 Hz), 4.67 (1H, dd, *J*=13 and 5 Hz), 5.20 (1H, s), 5.41 (1H, dd, *J*=4 and 3 Hz), and 5.64 (1H, s); MS, *m/z* 458, 456, 454 (0.2 : 0.2 : 0.1; M^+), 418, 416, 414, 412 (0.1 : 0.4 : 0.6 : 0.3; $M^+-C_2H_2O$), 400, 398, 396, 394 (0.4 : 1.5 : 2 : 1; M^+-CH_3COOH), 379, 377, 375 (0.2 : 0.4 : 0.3; M^+-Br), 337, 335, 333 (0.2 : 0.5 : 0.5; $M^+-C_2H_2O-Br$), 319, 317, 315 (7 : 87 : 56; $M^+-Br-CH_3COOH$), 199 (27), 157 (13), 119 (19), 107 (22), 105 (25), 93 (15), 91 (20), 69 (27), 43 (100), and 41 (36).

Saponification of ***8***. A soln of **8** (2.7 mg) and potassium carbonate (9.6 mg) in methanol (0.3 ml) was allowed to stand at room temp for 20 min and then worked up in the usual way to give **4** (2.3 mg); The IR and ^{1}H NMR spectra were identical with those of natural alcohol (**4**).

PCC Oxidation of ***4***. To a suspended soln of pyridinium chlorochromate (10 mg) in CH_2Cl_2 (0.1 ml) was added a soln of **4** (16 mg) in CH_2Cl_2 (0.1 ml). The reaction mixture was allowed to stand at room temp for 2 h. After addition of ether, filtration, and washing with ether, the combined organic soln was passed through a short pad of Frorisil, and then the solvent was removed to leave a residual oil, which was chromatographed on a silica-gel plate to give **9** (4.1 mg) as a pale yellow oil; $[\alpha]_D^{20}$ −10.7° (*c* 0.38); UV (EtOH), λ_{max} 233 (ε 6300), and 200 nm (ε 5300); IR (film), ν_{max} 1672, 1620, 1397, 1385, 1352, 1315, 1253, 1220, 1162, 1095, 1065, 945, 845, 820, and 752 cm^{-1}; ^{1}H NMR, δ 1.02, 1.05 (each s, total 3H), 1.20 (3H, s), 1.69 (3H, s), 4.26 (0.4H, dd, *J*=12 and 4 Hz), 4.69 (0.6H, dd, *J*=13 and 5 Hz), 5.38 (1H, s), 5.95 (0.6H, d, *J*=10 Hz), 5.98 (0.4H, d, *J*=10 Hz), 6.16 (1H, s), and 6.51 (1H, d, *J*=10 Hz); MS, *m/z* 334, 332, 330 (5 : 18 : 16; M^+), 319, 317, 315 (1 : 5: 4; M^+-CH_3), 297, 295 (3 : 3; M^+-Cl), 253, 251 (13 : 37; M^+-Br), 215 (79), 199 (62), and 96 (100).

Jones Oxidation of ***4***. To a soln of **4** (10.3 mg) in acetone (4.0 ml) was added two drops of Jones reagent. After the usual work-up, the residual oil was chromatographed on a silica-gel plate to give **9** (7.0 mg).

Conversion of ***10*** *into* ***4***. To a soln of **10** (32.4 mg) in benzene (0.5 ml) was added a piece of TsOH, and the mixture was stirred for 20 min at 60 °C (bath temp). The reaction mixture was worked up as usual to leave an oily residue, which was chromatographed on silica-gel column to give **4** (17.1 mg); $[\alpha]_D^{17}$ +3.94° (*c* 0.86); The IR, ^{1}H NMR, and mass spectra were identical with those of natural **4**.

Conversion of ***5*** *into* ***12***. A soln of **5** (4.9 mg) in 5% methanolic KOH (0.3 ml) was allowed to stand at room temp for 30 min. After being treated by the usual method, the resulting oil was purified by chromatography on a silica-gel plate to afford **12** (3.8 mg); $[\alpha]_D^{20}$ −75.6° (*c* 0.21); The IR and ^{1}H NMR spectra were identical with those of authentic 10-bromo-2,3-epoxy-α-chamigrene.[4b]

We are grateful to Prof. K. L. Erickson, Clark University, for the spectral data of nidificene, and also to Dr. Akio Fukuzawa, Hokkaido University, for the spectral data of 2,10-dibromo-3-hydroxy-α-chamigrene and valuable suggestions.

References

1) Part 58 of "Constituents of Marine Plants." Part 57: T. Suzuki, K. Koizumi, M. Suzuki, and E. Kurosawa, *Chem. Lett.*, submitted to publication.

2) M. Suzuki, K. Koizumi, H. Kikuchi, T. Suzuki, and E. Kurosawa, *Bull. Chem. Soc. Jpn.*, **56**, 715 (1983), and references cited therein.

3) Part 56 and 57 of this series; T. Suzuki, K. Koizumi, M. Suzuki, and E. Kurosawa, *Chem. Lett.*, submitted to publication.

4) a) B. M. Howard and W. Fenical, *Tetrahedron Lett.*, **1975**, 1687; b) M. Suzuki, A. Furusaki, and E. Kurosawa, *Tetrahedron* **35**, 823 (1979); c) T. Suzuki, H. Kikuchi, and E. Kurosawa, *Bull. Chem. Soc. Jpn.*, **55**, 1561 (1982); d) A. Furusaki, C. Katayama, T. Matsumoto, M. Suzuki, T. Suzuki, H. Kikuchi, and E. Kurosawa, *ibid.*, **55**, 3398 (1982).

5) A. F. Rose, J. J. Sims, and R. R. Izac, "Marine Natural Products; Chemical and Biological Perspectives," ed by P. J. Scheuer, Academic Press, New York (1978), Vol. 2, p. 332.

6) S. M. Waraszkiewicz and K. L. Erickson, *Tetrahedron Lett.*, **1974**, 2003.

7) Professor K. L. Erickson agreed that these two hydrocarbons could well be the same material; personal communication. A direct comparison could not be achieved because of being available no samples of nidificene.

8) The detail of the structures of conformers will be discussed elsewhere.

9) A. Fukuzawa, M. Miyamoto, H. Matsue, and T. Masamune, 47th National Meeting of the Chemical Society of Japan, Kyoto, April 1983, Abstr., No. 1H41.

10) *Laurencia glandulifera* ("Oo-sozo") has not grown in Japan,[15] and *L. glandulifera* should be revised to *L. nipponica*.

11) M. Suzuki and E. Kurosawa, *Bull. Chem. Soc. Jpn.*, **52**, 3349 (1979).

12) T. Irie, T. Suzuki, Y. Yasunari, E. Kurosawa, and T. Masamune, *Tetrahedron*, **25**, 459 (1969).

13) T. Suzuki, M. Suzuki, and E. Kurosawa, *Tetrahedron Lett.*, **1975**, 3057.

14) The structure of this compound will be reported elsewhere.

15) Y. Saito, *Mem. Fac. Fish., Hokkaido Univ.*, **15**, 1 (1967).

Studies on Salt Hydrates for Latent Heat Storage. IV. Crystallization in the Binary System CH_3CO_2Na-H_2O

Takahiro WADA,* Fumiko KIMURA, and Yoshihiro MATSUO
Central Research Laboratory Matsushita Electric Industrial Co. Ltd., 1006 Kadoma, Osaka, 571
(Received February 21, 1983)

In the binary system CH_3CO_2Na–H_2O, crystallization temperature on slow cooling from a melt, glass transition temperature and crystallization temperature on slow heating from a quenched vitrified solid were measured by varying the CH_3CO_2Na concentration. The crystallization behaviour in the binary system CH_3CO_2Na–H_2O is characterized as follows; (1) crystallization region of ice extends into the CH_3CO_2Na-rich side from the eutectic composition, (2) a hard crystallization region exists in the composition between CH_3CO_2Na 35wt% and 40wt%, (3) the crystallization temperature range of $CH_3CO_2Na \cdot 3H_2O$ is from −50 °C to −30 °C and very narrow.

Sodium acetate trihydrate ($CH_3CO_2Na \cdot 3H_2O$) has recently attracted attention as a useful heat stroage material because of its large latent heat of fusion (about 264 J/g).[1,2] The $CH_3CO_2Na \cdot 3H_2O$ melt tends to supercool even when it is cooled considerably below its melting point (58.4 °C).[3,4] Such a supercooling phenomenon impaired its practical application.[5] Therefore, in order to develop latent heat storage materials using salt hydrates such as $CH_3CO_2Na \cdot 3H_2O$, Kimura[6] studied the supercooling phenomena of some salt hydrates from the viewpoint of the chemical potential difference of water molecules in molten and crystalline states. Wada and Yamamoto[7] have searched for crystal nucleation catalysts of $CH_3CO_2Na \cdot 3H_2O$ and found $Na_4P_2O_7 \cdot 10H_2O$.

The phase diagram of the binary system CH_3CO_2Na–H_2O based on data from Seidell's compilation[8] is shown in Fig. 1. A dashed line in Fig. 1 is the liquidus line of metastable CH_3CO_2Na. It is clear from the phase diagram that H_2O and $CH_3CO_2Na \cdot 3H_2O$ form an eutectic mixture melting at −18 °C, with the composition of 23 wt% CH_3CO_2Na and 77 wt% H_2O.

This paper reports a quantitative investigation of the crystallization behavior of the binary system CH_3CO_2Na–H_2O, where crystallization temperature on slow cooling from a melt (t_c), glass transition temperature (T_g), and crystallization temperature on slow heating from a quenched vitrified solid (T_c) were measured by varying the CH_3CO_2Na concentration.

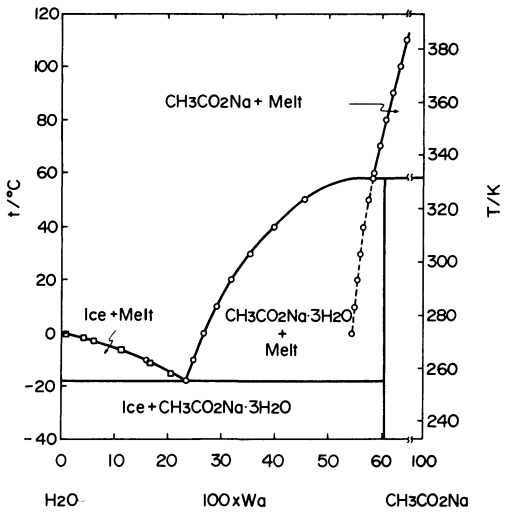

Fig. 1. Phase diagram of the binary system CH_3CO_2Na–H_2O.
○: The data obtained by Green,[9] □: the data obtained by Sidgwick and Gentle.[10]

Experimental

Sodium acetate trihydrate was of a guaranteed grade reagent from Wako Pure Chemical Industry. Weighed quantities of $CH_3CO_2Na \cdot 3H_2O$ and distilled water, 30 g in total, were placed in a glass vessel with a stirring bar. The sample temperature was measured by a chromel–alumel thermocouple attached to the inner wall of the glass vessel which was sealed and immersed in a water bath. In order to obtain reproducible data, the sample was heated to a temperature which is about 10 °C higher than its liquidus temperature and was stirred to a homogeneous melt.[11] Then, the melt was cooled at the rate of about 5 °C/min by consecutive addition of ice to the water bath. When the temperature of the melt reached to 20 °C, the vessel was transferred from the water bath to an ethanol bath. Cooling was continued to −70 °C at the rate of about 5 °C/min by consecutive addition of solid carbon dioxide to the ethanol bath. In such a slow cooling process, crystallization of the sample was detected by a sudden rise in temperature of the melt and by visual inspection. The viscosity of melts increased on cooling, which contained CH_3CO_2Na more than $W_a = 0.35$ (W_a is the mass fraction of CH_3CO_2Na), and sometimes the magnetic stirrer failed to operate the stirring bar. The measurement was performed three times for each sample. In this manner, t_c was measured as a function of the CH_3CO_2Na concentration. Figure 2 shows the average and the range of crystallization temperatures obtained by the present measurements.

Temperatures, T_g and T_c were measured as a function of the CH_3CO_2Na concentration by the differential scanning calorimetry (DSC). The DSC measurement was performed by using an SSC 560S DSC (Daini Seikosha Co.), heat-flux DSC. One drop of a melt (about 10 mg) was placed in a 15 μl silver crucible. This crucible was sealed and immersed in a water bath, whose temperature was about 10 °C higher than a liquidus temperature of the sample. After thirty minutes, the crucible was transferred into liquid nitrogen. The overall cooling rate was about 1000 K/min. DSC measurements were performed at a heating rate of 5 °C/min from −130 °C to 70 °C. This DSC system was calibrated by using ice (mp: 0.0 °C), chloroform (mp: −63.5 °C), acetone (mp: −94.3 °C), and ethanol (mp: −114.2 °C) as standards, and the measurements were made two times for each sample.

Results and Discussion

Crystallization Temperature on Slow Cooling from a Melt

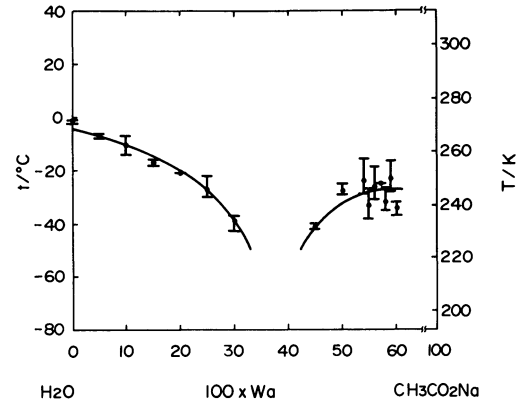

Fig. 2. Crystallization temperature on slow cooling (t_c) in relation to the CH_3CO_2Na concentration.

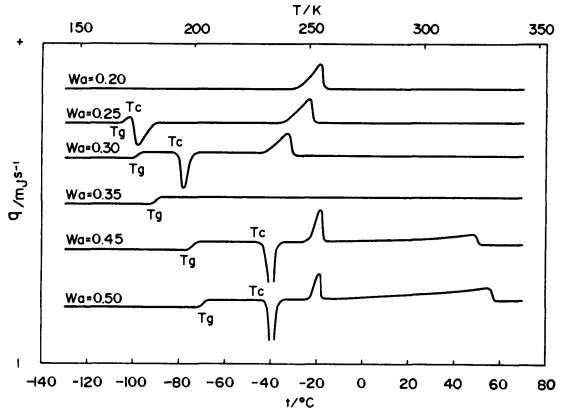

Fig. 3. DSC curves for some quenched samples of the system CH_3CO_2Na–H_2O.

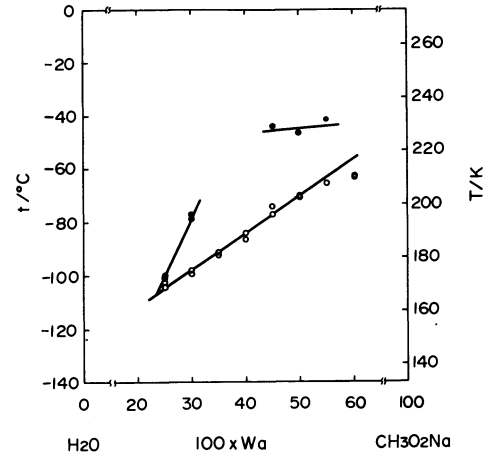

Fig. 4. Glass transition temperature (T_g) and crystallization temperature on slow heating (T_c) in relation to the CH_3CO_2Na concentration.
○: T_g, ●: T_c.

(t_c). The t_cs obtained are shown in Fig. 2. The number on the abscissa, $100 \times W_a$, is the weight percentage of CH_3CO_2Na in the system. The samples of $W_a=0.35$ and $W_a=0.40$ did not crystallize in all the runs.

In the water-rich side of the eutectic composition, the t_c curve lies about 5 °C lower than the liquidus line of H_2O, ice crystallizing first from the melt. Interestingly, the t_c curve extends beyond the eutectic composition into the CH_3CO_2Na-rich side. Therefore, the crystals that separated out first from the melt in the CH_3CO_2Na-rich side of the eutectic composition ($W_a=0.30$) is not $CH_3CO_2Na \cdot 3H_2O$, but ice.

From Fig. 2, it is also clear that t_cs of the melts containing CH_3CO_2Na more than $W_a=0.45$ are about 90 °C lower than the liquidus line, *i.e.*, supercooling of these samples is about 90 °C. $CH_3CO_2Na \cdot 3H_2O$ separated out first from both melts of $W_a=0.45$ and $W_a=0.50$, but for the samples containing CH_3CO_2Na more than $W_a=0.54$, anhydrous CH_3CO_2Na crystals separated out from their melts at the temperature about 10 °C lower than their liquidus temperarures, followed by crystallization of $CH_3CO_2Na \cdot 3H_2O$. Anhydrous CH_3CO_2Na crystals were identified by X-ray diffraction. Since the t_c curve varies continuously with the CH_3CO_2Na concentration between $W_a \times 0.45$ and $W_a=0.603$ ($CH_3CO_2Na \cdot 3H_2O$), the curve in Fig. 2 also suggests that anhydrous CH_3CO_2Na crystals (separated out first) have little influence on the subsequent crystallization of $CH_3CO_2Na \cdot 3H_2O$.

Glass Transition Temperature (T_g) DSC curves for some quenched samples are illustrated in Fig. 3, where q is heat flux. T_g and T_c are plotted against the CH_3CO_2Na concentration in Fig. 4. The melt with $W_a=0.25$ vitrified by quenching, but that with $W_a=0.20$ did not, and this result was confirmed by visual observation of these samples in a 3 mm diameter pyrex glass tubes put into liquid nitrogen. This observation shows that the glass forming composition is limited on the CH_3CO_2Na-rich side from the eutectic composition ($W_a=0.23$). This is due to the difficulty of crystal nucleation of $CH_3CO_2Na \cdot 3H_2O$.

In Fig. 4, T_g varies linearly with the CH_3CO_2Na concentration, and those of the samples containing CH_3CO_2Na more than $W_a=0.55$ lie below the T_g line. This deviation results from the decrease of the CH_3CO_2Na concentration caused by separation of CH_3CO_2Na crystals from the quenched samples, which is confirmed by visual observation using thin glass tubes. Williams and Angell,[12] and Kanno *et al.*[13] have reported that T_g of the sample with $W_a=0.313$ ($CH_3CO_2Na \cdot 10H_2O$) is −99 and −102 °C, respectively. The T_g estimated from our data is −96 °C and in good agreement with the reported data. The extrapolation of the obtained T_g to pure water gives −140 °C as the T_g of glassy water. Angell and Sare[14] also gave a similar value (−138 °C) from the studies on a large number of aqueous electrolyte solutions. This value is almost identical with the glass transition temperature (−139 °C) obtained for amorphous solid water prepared by the vapor deposition method.[15] The extrapolation to pure $CH_3CO_2Na \cdot 3H_2O$ gives −56 °C as the T_g of glassy $CH_3CO_2Na \cdot 3H_2O$. This value is close to T_g of $Na_2S_2O_3 \cdot 5H_2O$ ($T_g=-42$ °C)[16] and $Ca(NO_3)_2 \cdot 4H_2O$ ($T_g=-54$ °C).[14]

Crystallization Temperature on Slow Heating from a Quenched Sample (T_g) The quenched samples with $W_a=0.25$ and $W_a=0.30$ always crystallize on heating after the glass transition. T_c of the sample with $W_a=0.313$ ($CH_3CO_2Na \cdot 10H_2O$) has been reported to

be −73 °C by Kanno *et al.*,[12] which is in good agreement with T_c estimated from our data, −72 °C. The DSC curves show that the melting points of the samples with W_a=0.25 and W_a=0.30 are at −22 and −31 °C, respectively. These melting points are lower than the eutectic point, −18 °C, and lie on the extrapolated liquidus line of H_2O. As shown in Fig. 3, the samples with W_a=0.25 and W_a=0.30 do not show the endothermic peak of $CH_3CO_2Na\cdot3H_2O$ melting. Therefore, ice is the only compound crystallized from the melts with W_a=0.25 and W_a=0.30. This result is similar to the crystallization behaviour observed on slow cooling of the melt.

The quenched samples with W_a=0.35 and W_a=0.40 did not crystallize on heating twice. As mentioned above, these samples did not crystallize on cooling either. These results show that these samples have a stable solution structure with hard crystallization.

The quenched samples with W_a=0.45, W_a=0.50, and W_a=0.55 crystallized only once in two runs. For these cases, T_cs are between −40 and −50 °C as shown in Fig. 4. $CH_3CO_2Na\cdot3H_2O$ (W_a=0.603) did not crystallize on heating in two runs.

The phase diagram of the binary system CH_3CO_2Na–H_2O(Fig. 1), t_c cuves (Fig. 2), and T_g line and T_c curves (Fig. 4) are summarized in Fig. 5. In the temperature region demarcated by t_c and T_c curves, ice or $CH_3CO_2Na\cdot3H_2O$ is considered to crystallize from the melt in the present experimental conditions. The crystallization behavior of the binary system CH_3CO_2Na–H_2O is characterized as follows: (1) the crystallization region of ice extends into the CH_3CO_2Na-rich side from the eutectic composition, (2) a hard crystallization region exists in the composition between W_a=0.35 and W_a=0.40, (3) the crystallization temperature range of $CH_3CO_2Na\cdot3H_2O$ is from −50 °C to −30 °C and very, narrow.

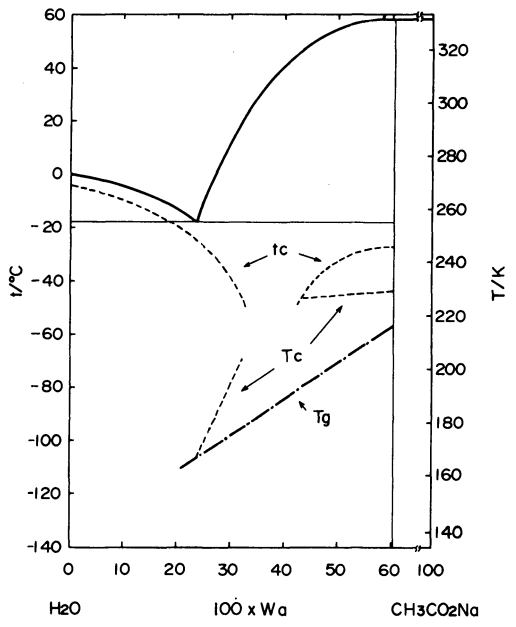

Fig. 5. Crystallization temperature curves (t_c and T_c curves), and glass transition temperature line shown in the phase diagram of the binary system CH_3CO_2Na–H_2O.

The crystallization temperature is generally influenced by the heating or cooling rate, quantity and purity of the sample and stirring method, *etc.* In measuring t_c, if the cooling rate is slower than 5 °C/min or the sample quantity is larger than 30 g, t_cs will be higher than the obtained values. In measuring T_c, if the heating rate is slower than 5 °C/min or the sample quantity is larger than about 10 mg, T_cs will be lower than the obtained values. Therefore, crystallization temperature breadths of ice and $CH_3CO_2Na\cdot3H_2O$ are expected to be wider than those shown in Fig. 5.

The authors wish to express their thanks to Dr.Ryoichi Kiriyama for his useful discussions and Drs. Tsuneharu Nitta, Eiichi Hirota, and Masanari Mikoda for their continuous encouragements. The authors are grateful to Dr. Ryoichi Yamamoto for his discussions throughout this work.

References

1) M. Telkes, "Solar Materials Science," ed by L. E. Murr, Academic Press, New York (1980), Chap. 11.
2) A. Pebler, *Thermochim. Acta*, **13**, 109 (1975).
3) F. de Winter, *Solar Energy*, **17**, 379 (1975).
4) K. Narita and J. Kai, *J. Int. Electr. Eng. Jpn.*, **101**, 15 (1981).
5) M. Telkes, *Ind. Eng. Chem.*, **44**, 1308 (1952).
6) H. Kimura, *J. Jpn. Assoc. Cryst. Growth*, **7**, 215 (1980).
7) T. Wada and R. Yamamoto, *Bull. Chem. Soc. Jpn.*, **55**, 3603 (1982).
8) A. Seidell, "Solubility of Inorganic and Metal-Organic Compounds," 4th ed, ed by the American Chemical Society, Washington D. C. (1965), Vol. II, p. 854.
9) W. F. Green, *J. Phys. Chem.* **12**, 655 (1908).
10) N.V. Sidgwick and J. A. Gentle, *J. Chem. Soc.*, **121**, 1837 (1922).
11) R. Kiriyama and K. Yamada, *Nippon Kagaku Zasshi*, **71**, 558 (1950).
12) E. Williams and C. A. Angell, *J. Phys. Chem.*, **81**, 232 (1977).
13) H. Kanno, I. Shirotani, and S. Minomura, *Bull. Chem. Soc. Jpn.*, **54**, 2607 (1981).
14) C. A. Angell and E. J. Sare, *J. Chem. Phys.* **52**, 1058 (1970).
15) M. Sugisaki, H. Suga, and S. Seki, *Bull. Chem. Soc. Jpn.*, **41**, 2591 (1968).
16) S. Seki, "Structural Chemistry in Solid," ed by I. Nitta *et al.*, Kagaku Dojin, Kyoto (1968), Chap. 3.

 © 1983 The Chemical Society of Japan Bull. Chem. Soc. Jpn., 56, 3830—3832 (1983) [Vol. 56, No. 12

Electrical Dark- and Photo-conductivities of 2-(*p*-Decyloxybenzilideneamino)-9-fluorenone in the Nematic State

Ken-ichi Okamoto,* Shu Nakajima, Michiko Ueda, Akira Itaya, and Shigekazu Kusabayashi†
Department of Chemical Engineering, Faculty of Engineering, Yamaguchi University, Ube, Yamaguchi 755
(Received October 1, 1982)

The electrical conductivity of 2-(*p*-decyloxybenzylideneamino)-9-fluorenone (DBAF), which has a large π-electronic group, was investigated in the nematic state. The dark conductivity showed a positive anisotropy and was attributed to ionic conduction. The photocurrent was observed in the absorption region of DBAF and was enhanced by doping with 2,4,7-trinitro-9-fluorenone. The photocarriers seem to be generated from the excited state of DBAF by one photonic process.

Electrical dark-conductivity in liquid crystals has been studied extensively[1-5] and attributed to ionic conduction on the basis of both the conductivity anisotropy[2,3] and the temperature dependence of the carrier mobility.[4,5] On the contrary, photoconductivity in liquid crystals has never been reported until now except for the photocurrent due to the photoinjection of charge carriers from an electrode.[6,7] This is probably because the liquid crystals investigated to data have had only small π-electronic groups, such as a benzene ring. In this paper, we investigated the dark- and photo-conductivities of 2-(*p*-decyloxybenzylideneamino)-9-fluorenone (DBAF), which has a large π-electronic group, in the nematic, monotropic smectic, and isotropic liquid states.

Experimental

The DBAF was prepared according to the literature[8] and was recrystallized several times from an absolute ethanol solution. The purity of the DBAF was satisfactory, judging from the analysis by means of differential scanning calorimetry and high-performance liquid chromatography. The *p*-methoxybenzylidene-*p*-butylaniline (MBBA) was obtained commercially and was purified by means of high-vacuum distillation. The sample was sandwiched between two nesa-coated glass electrodes with a Myler spacer 20—100 μm thick. The effective area of the cells was typically 1 cm^2. The capacitance and DC conductivity measurements were carried out under an argon atmosphere.

Results and Discussion

The phase transitions were as follows:

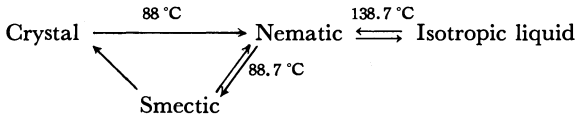

Alignment of the Molecules in Nematic State. The magnetic field aligns the long axes of the liquid crystal molecules along its direction.[9] Figure 1 shows the variation in the specific dielectric constant ε with the magnetic field H. A homogeneous or homeotropic alignment of the molecules in the nematic state was achieved by the magnetic field of 0.4 T perpendicular to or parallel to the applied electric field E. The negative dielectric anisotropy of DBAF ($\Delta\varepsilon = -1.65$ at 100 °C) is larger than that of such typical Schiff-base-type liquid crystals as MBBA,[2,9] because of the presence of a carbonyl group nearly perpendicular to the long molecular axis.

Dark Conductivity. The dark conductivity σ was measured for the homogeneous or homeotropic alignment, and labelled $\sigma_\perp$ or $\sigma_{//}$ respectively. The dark current obeyed Ohm's law in the fields less than 10^4 V/cm in every state. Figure 2 shows the temperature dependence of the dark conductivity and its anisotropy ratio, $R = \sigma_{//}/\sigma_\perp$. At the crystal-nematic phase transition, σ increased abruptly and showed a sharp peak which disappeared with an increasing voltage. This peak current seems to be caused by the abrupt change in the direction of the dipole-moment due to the change in molecular direction at the phase transition.[5] At the nematic-isotropic transition, $\sigma_{//}$ decreased appreciably, while $\sigma_\perp$ hardly changed. In the nematic state, σ was in the order of 10^{-10} Ω^{-1} cm^{-1} and ΔE_a was 0.5 eV. These values of σ and ΔE_a are comparable to those reported for typical nematic liquid crystals.[1-4] The temperature dependence of R is also similar to that reported for the Schiff-base-type liquid crystals;[2,3] that is, R is larger than unity in the nematic state, although it, because of a pretransitional effect, decreases below unity when approaching the transition to a smectic state. These results indicate that the dark conductivity of DBAF in nematic and isotropic states is caused by the ionic mechanism previously reported for conventional liquid crystals,[2-5,10] in spite of the presence of a large π-electronic group.

Photoconductivity in Nematic State. The stady-state photocurrent was reached in a few minutes when a cell was irradiated. Although the photocurrent in the crystal state obeyed Ohm's law, that in the nematic state showed a very complicated dependence on the field, as shown in Fig. 3. After reaching a maximum, the photocurrent decreased and then levelled off with an increasing field. At present, we have no explanation for this behavior; therefore, we restricted the experiments to the low-field range where the photocurrent increased roughly linearly with an increasing field. The photocurrent was roughly proportional to the light intensity and was observed in the spectral region of DBAF, as shown in Fig. 4, indicating that the photocurrent is caused by the light absorption of DBAF itself. The photocurrent increased step-by-step by a factor of 100 at the crystal-nematic phase transition, and it was almost independent of the temperature in the nematic state.

† Present address: Department of Applied Chemistry, Faculty of Engineering, Osaka University, Suita, Osaka 565.

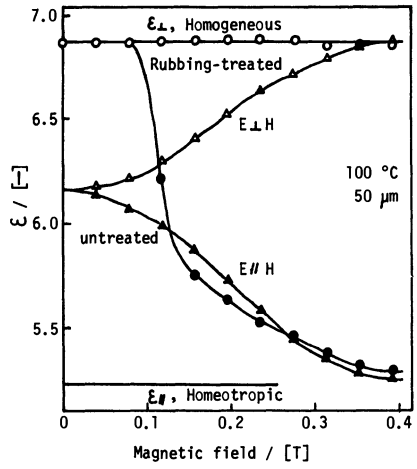

Fig. 1. Magnetic field dependence of specific dielectric constant ε at the frequency of 1 kHz.
○, ●: A rubbing-treated cell, △, ▲: an untreated cell (open symbols, $E \perp H$; closed symbols, $E//H$).

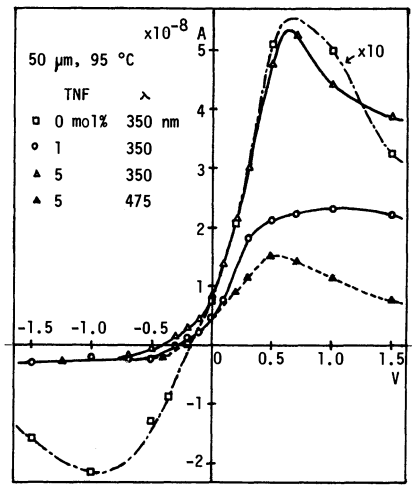

Fig. 3. Electric field dependence of the photocurrent for the celles undoped and doped with TNF.

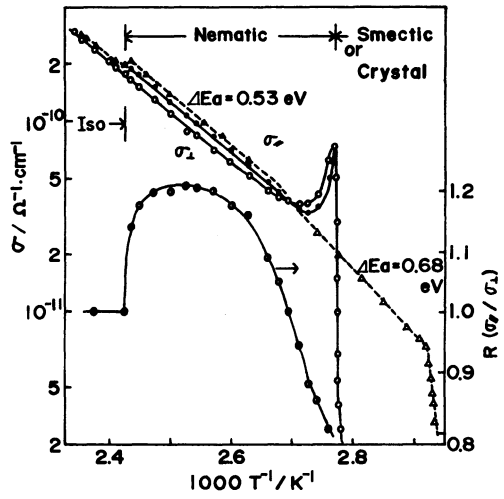

Fig. 2. Temperature dependence of dark conductivity σ and its anisotropy ratio R.
—○—, --△--: $\sigma_\perp$, —●—, --▲--: $\sigma_{//}$ (circle symbols, on a heating run; triangle symbols, on a cooling run). —◑—: R on a heating run. In liquid state, $\sigma_{//}$ was identical with $\sigma_\perp$. In nematic state, the line --△-- was almost overlapped with the line —●—.

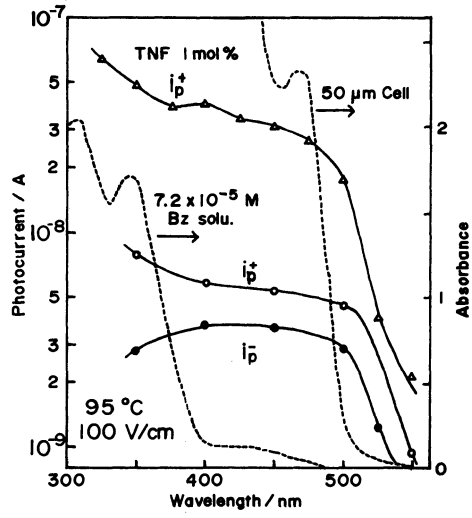

Fig. 4. Spectral dependence of the photocurrent and the absorption spectra.
Light intensity was 1×10^{15} photons/cm² s. The dotted lines were the absorption spectra of the benzene solution and of a cell of 50 μm thickness. —○—, —●—: An undoped cell, —△—: a cell doped with 1 mol% of TNF.

Although nematic MBBA did not show the photocurrent, the nematic mixtures of MBBA containing more than 10 mol% of DBAF showed the photocurrent in the absorption region of DBAF. The photocurrent increased appreciably with an increase in the DBAF content, but it was too small to be measured in detail. More detailed measurements were done for the pulse photoconduction induced by a N_2 gas laser and will be reported elsewhere.[11]

DBAF formed a charge-transfer complex with a strong electron acceptor. 2,4,7-Trinitro-9-fluorenone (TNF) was chosen as an acceptor, because it was fairly soluble in the nematic phase of DBAF. The complex of DBAF with TNF showed a charge-transfer absorption band at 485 nm in a dichloroethane solution. Doping with TNF by 1—5 mol% enhanced the photocurrent for the positive-electrode illumination (abbreviated as i_p^+) by a factor of 4—10, as shown in Figs. 3 and 4, while it hardly changed either the dark current or the photocurrent for the negative-electrode illumination (i_p^-).

The following photocarrier-generation process for nematic DBAF and its mixture with MBBA is suggested from the results presented above, with reference to the processes previously proposed for aromatic molecules in solutions[12,13] and in amorphous films.[14] In the first step, DBAF molecules absorb light, creating a molecular excited state. An excited DBAF molecule can react with either the electrode or an electron acceptor molecule, such as TNF and O_2, to give the original photocarriers. The original photocarrier species may thus be supposed to be the cation radical of DBAF and the anion radical of either DBAF or an electron

acceptor. The nature of the carrier-transport process (ionic diffusion or electronic hopping) in the photoconduction is still in question and so is under investigation.[11]

References

1) S. Kusabayashi and M. M. Labes, *Mol. Cryst. Liq. Cryst.*, **7**, 395 (1969).
2) R. T. Klingbiel, D. J. Genova, and H. K. Bucher, *Mol. Cryst. Liq. Cryst.*, **27**, 1 (1974).
3) A. Mircea-Roussel, L. Leger, F. Rondelez, and W. H. De Jeu, *J. de Physique*, **36**, Cl-93 (1975).
4) G. Derfel and A. Lipinski, *Mol. Cryst. Liq. Cryst.*, **55**, 89 (1979), and the references cited therein.
5) K. Yoshino, K. Yamashiro, and Y. Inuishi, *Jpn. J. Appl. Phys.*, **13**, 1471 (1974).
6) M. Yamashita and Y. Amemiya, *Jpn. J. Appl. Phys.*, **17**, 1513 (1978).
7) K. Yoshino, S. Hisamitsu, and Y. Inuishi, *J. Phys. Soc. Jpn.*, **32**, 867 (1972).
8) G. W. Gray, *J. Chem. Soc.*, **1955**, 4359.
9) N. V. S. Rao, P. R. Kishore, T. F. S. Raj, M. N. Avadhanlu, and C. R. K. Murty, *Z. Naturforsch., A*, **31**, 283 (1976).
10) G. Briere, R. Herino, and F. Mondon, *Mol. Cryst. Liq. Cryst.*, **19**, 157 (1972).
11) K. Okamoto, S. Nakajima, A. Itaya, and S. Kusabayashi, *Bull. Chem. Soc. Jpn.*, **56**, 3545 (1983).
12) T. Imura, N. Yamamoto, H. Tsubomura, and K. Kawabe, *Bull. Chem. Soc. Jpn.*, **44**, 3185 (1971).
13) R. W. Bigelow, *J. Phys. Chem.*, **78**, 1395 (1974).
14) M. Yokoyama, S. Shimokihara, A. Matsubara, and H. Mikawa, *J. Chem. Phys.*, **76**, 724 (1982), and the references cited therein.

The Volumetric Behavior of Several Ammonium Chlorides in Aqueous 18-Crown-6 Solutions

Shigeharu HARADA,* Hideko SAHARA, and Tsurutaro NAKAGAWA†
Shizuoka Women's College, Nunohashi, Hamamatsu 432
†*Department of Polymer Science, Faculty of Science, Hokkaido University, Sapporo 060*
(Received March 17, 1983)

Synopsis. The complexation of 18-crown-6 with primary ammonium chlorides [$H(CH_2)_nNH_3Cl$, $n=0$, 1, 2, and 4] caused an increase in volume, which was attributable to the dehydration of the ammonium moieties. On the other hand, the apparent molal volumes of $(CH_3)_{4-n}NH_nCl$ ($n=0$—2) were not affected appreciably by the presence of the crown ether, and their complex stability seemed to be insignificant.

A positive change in volume was found for the formation of aqueous complexes between crown ethers and metallic cations, and this increase was attributed to the partial dehydration of the guest ions.[1,2] The volumetric behavior of several ammonium chlorides was investigated in aqueous 18-crown-6 solutions in order to obtain information about the change in the dissolution state of these solutes during complexation.

Experimental

The following chemicals were obtained from the indicated suppliers: NH_4Cl (99%), CH_3NH_3Cl (99%), $(CH_3)_2NH_2Cl$ (99%), $(CH_3)_3NHCl$ (98%), $(CH_3)_4NCl$ (99%) (Nakarai Chemicals); $C_2H_5NH_3Cl$ (99%), n-$C_4H_9NH_3Cl$ (99%) (Tokyo Chemical Industry Co.); 18-crown-6 (99%) (Aldrich Chemical Co. and Nippon Soda Co.). The NH_4Cl, the CH_3NH_3Cl, and the other salts were recrystallized twice from ethanol–water, ethanol–methanol, and ethanol–acetone mixtures respectively and dried under a vacuum at 50—55 °C for 24 h. The 18-crown-6 was dissolved in acetonitrile, and the resultant adduct was precipitated from the solution by cooling in an ice–acetone bath.[3] The weakly bound acetonitrile was removed under a vacuum at 30—35 °C for 24 h. The purified product had a melting point of 39.2—40.5 °C, in satisfactory agreement with the literature values of 39—40 °C[4] and 39.5—40.5 °C.[5] The water was distilled and deionized before use.

The solution densities were measured at 25.00±0.002 °C on an Anton Paar densimeter, Model 60/601, with an accuracy of $\pm 2\times10^{-6}$ g cm^{-3}. Each set of measurements was made on condition that X_w (see below) was maintained constant. The apparent molal volumes (ϕ_v) were calculated from the following equation:

$$\phi_v = (d_0-d)/mdd_0X_w + M/d,$$

where M is the molecular weight of an ammonium salt; m, its molality; X_w, the weight fraction of water in a binary solution consisting of water and crown ether; d_0, the density of this binary solution or that of pure water when $X_w=1$, and d, the density of a ternary solution prepared by the addition of the ammonium salt to the binary solution, the weight fraction of water of which is X_w.

Results and Discussion

The ϕ_v values of alkylammonium chlorides in water were fitted into the Redlich-Meyer equation:

$$\phi_v = \bar{V}^\circ + S_v\sqrt{c} + b_vc,$$

where $\bar{V}^\circ$ is the limiting partial molal volumes of the salts; c, the molar concentration; S_v, the Debye-Hückel limiting slope, and b_v, an empirical constant. The values of $\bar{V}^\circ$/cm^3 mol^{-1} and b_v/cm^3 dm^3 mol^{-2} thus obtained were 53.87 and -0.4_0, 72.43 and -1.0_8, 90.62 and -0.9_3, 107.51 and -1.6_6, 71.24 and -0.9_1, and 103.39 and -1.8_7 for CH_3NH_3Cl, $(CH_3)_2NH_2Cl$, $(CH_3)_3NHCl$, $(CH_3)_4NCl$, $C_2H_5NH_3Cl$, and n-$C_4H_9NH_3Cl$ respectively. These values were in excellent agreement with other reported values.[6,7] The ϕ_v values of NH_4Cl in water were taken from the data in the literature.[8] The ϕ_v of 18-crown-6 in water (ϕ_{CR}) was given by:

$$\phi_{CR}/\text{cm}^3\,\text{mol}^{-1} = 223.26 - 2.9_4\, m_{CR}/\text{mol kg}^{-1},$$

where m_{CR} is the molality of 18-crown-6.

As is shown in Fig. 1, the presence of the crown ether causes a large increase in ϕ_v. Similar results were obtained for the ϕ_v of methylammonium, ethylammonium, and butylammonium chlorides. In contrast, the ϕ_v of NH_4Cl was hardly affected by the presence of triethylene glycol dimethyl ether, in which system the complex formation need not be considered. These findings lead to the conclusion that the complexation between the cations and the crown ether causes a volume increase, the origin of which will be discussed below.

For this purpose, the ϕ_v of the complex ($\phi_{complex}$) should be estimated. In ternary solutions of water, ammonium or alkylammonium chloride (MCl), and crown ether (CR), the following equilibrium exists:

$$M^+ + Cl^- + CR \rightleftharpoons [M\cdot CR]^+ + Cl^-.^{9)}$$

The apparent molal volumes determined therefore contain a contribution from the complexed species. The $\phi_{complex}$ was estimated on the basis of the additivity of the apparent molal volumes:

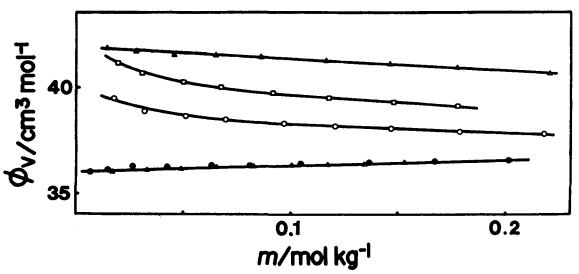

Fig. 1. Apparent molal volumes of NH_4Cl against its molality at 25 °C.
▲: In water, ○, □, and △: in 0.04996, 0.09085, and 0.2112 mol kg^{-1} aqueous 18-crown-6 solutions, respectively, ●: in 0.04915 mol kg^{-1} aqueous triethylene glycol dimethyl ether solution.

Table 1. Volume increase for the formation of 18-crown-6 complexes

Guest molecule	NH_4Cl	CH_3NH_3Cl	$CH_3CH_2NH_3Cl$	$CH_3(CH_2)_3NH_3Cl$	$CH_3(CH_2)_5NH_3Cl$[a]
ΔV/cm^3 mol^{-1}	6.9	2.4	2.5	2.9	3.1

a) Ref. 16.

$$(m_{MCl}+m_{CR})\Phi_v = m_{MCl}(1-\alpha)\phi_{MCl} + (m_{CR}-\alpha m_{MCl})\phi_{CR} + \alpha m_{MCl}\phi_{complex},$$

in which Φ_v is the mean apparent molal volumes of ternary solutions, m_{MCl} and m_{CR} are the total concentrations (including the complexed species) of MCl and CR in the ternary solutions respectively, ϕ_{MCl} and ϕ_{CR} are the apparent molal volumes of the solute species in water at the ionic strength of m_{MCl}, and α is the fraction of MCl in the complexed state. The values of α were calculated from the reported values of stability constants.[10] The $\phi_{complex}$ was evaluated on the additional assumption that the ϕ_{CR} does not depend on the ionic strength in solutions. Since the $\phi_{complex}$ thus obtained had a slight dependence on the ionic strength and the concentration of the crown ether, the partial molal volume at an infinite dilution ($\bar{V}^\circ_{complex}$) was determined by the extrapolation of $\phi_{complex}$ to $\sqrt{m_{MCl}}=0$ and $m_{CR}=0$. Table 1 tabulates the changes in volume for the complex formation, $\Delta V=\bar{V}^\circ_{complex}-(\bar{V}^\circ_{MCl}+\bar{V}^\circ_{CR})$.

The conventional heavy-atom technique has revealed the crystal structure of the 18-crown-6–NH_4Br complex, in which the ammonium cation is too large to fit into the cavity of the crown ether and the nitrogen atom makes three hydrogen bondings through its hydrogen atoms with the three oxygen atoms of the crown ether. Presumably a similar structure holds for the complex in solutions; this also seems to be the case for the primary alkylammonium ion complexes under investigation, as has been generally accepted on the basis of the examination of the CPK molecular models of possible complexes.[12,13] It is highly possible that the dense structure of water molecules electrostricted around the ammonium moieties is released during complexation because of the hydrogen bonding between the host and guest molecules. This process should, therefore, be accompanied by an increase in volume. A volume change caused by the dehydration of ions can be evaluated from their intrinsic and partial molal volumes.[14] For an ammonium ion was obtained an increase of 7.5 cm^3 mol^{-1}, which is comparable to the ΔV value in Table 1. This indicates that the main contribution to ΔV is the removal of water molecules from around the ammonium ion on complexation, although it is still possible for the complexed ion to contact water in the direction perpendicular to the plane of the crown-ether ring. The effect of the crown ether itself on ΔV is, though still obscure, probably small.

The substitution of a CH_3 group for H on NH_4^+ leads to a marked decrease in ΔV values. The hydrophobic residue, because of its bulkiness, occupies a volume where, in the case of the formation of the 18-crown-6 complex with NH_4^+, some water molecules to be dehydrated are located, thus leading to a decrease in ΔV. An alternative or an additional reason is that the water to be released from near the CH_3 group is not so dense as the electrostricted molecules. A similar situation is to be expected for the complex formation of the other *n*-alkylammonium ions, so nearly the same values of ΔV were obtained.

In contrast to the volumetric behavior of primary ammonium salts, only a slight decrease was found for the ϕ_v values of dimethylammonium, trimethylammonium, and tetramethylammonium ions in the presence of the crown ether. This finding suggests the insignificant stability of complexes with these cations,[15] for which the reduction in the number of hydrogen bondings available for the host-guest interaction may be responsible.

The authors wish to thank Masao Sakurai of Hokkaido University for his valuable discussions on the subject of this paper.

References

1) H. Hφiland, J. A. Ringseth, and E. Vikingstad, *J. Solution Chem.*, **7**, 515 (1978).
2) H. Hφiland, J. A. Ringseth, and T. S. Brun, *J. Solution Chem.*, **8**, 779 (1979).
3) G. W. Gokel, D. J. Cram, C. L. Liotta, H. P. Harris, and F. L. Cook, *J. Org. Chem.*, **39**, 2445 (1974).
4) C. J. Pedersen, *J. Am. Chem. Soc.*, **89**, 7017 (1967).
5) R. N. Greene, *Tetrahedron Lett.*, **1972**, 1793.
6) F. J. Millero, "Water and Aqueous Solutions," ed by R. A. Horne, Wiley-Interscience, New York (1971), Chap. 13.
7) M. Sakurai, T. Komatsu, and T. Nakagawa, *Bull. Chem. Soc. Jpn.*, **48**, 3491 (1975).
8) M. Sakurai, *Bull. Chem. Soc. Jpn.*, **46**, 1596 (1973).
9) The formation of ion-pairs was not considered.
10) J. L. Roberts, R. E. McClintock, Y. El-Omrani, and J. W. Larson, *J. Chem. Eng. Data*, **24**, 79 (1979).
11) O. Nagano, A. Kobayashi, and Y. Sakai, *Bull. Chem. Soc. Jpn.*, **51**, 790 (1978).
12) E. P. Kyba, R. C. Helgeson, K. Madan, G. W. Gokel, T. L. Tarnowski, S. S. Moore, and D. J. Cram, *J. Am. Chem. Soc.*, **99**, 2564 (1977).
13) J. M. Timko, S. S. Moore, D. M. Walba, P. C. Hiberty, and D. J. Cram, *J. Am. Chem. Soc.*, **99**, 4207 (1977).
14) F. Hirata and K. Arakawa, *Bull. Chem. Soc. Jpn.*, **46**, 3367 (1973).
15) **Note added in proof.** The stability of the complex with the dimethylammonium ion was examined by a modified potentiometric method of the literature procedure.[10] An appropriate amount of 18-crown-6 was added to a solution of $(CH_3)_2NH_2Cl$ which had been titrated to half the equivalence point with LiOH. The change in the pH of the solution caused by the addition of the crown ether gave no significant values for the stability constant.
16) H. Sahara and S. Harada, *Annu. Rep. Shizuoka Women's College*, **1981**, 95.

Reduction of Macrocyclic Cobalt(III) Complex Photosensitized by Tris(2,2′-bipyridine)ruthenium(II)

Yoshimi KURIMURA* and Emiko ENDO
Department of Chemistry, Ibaraki University, Mito, Ibaraki 310

(Received May 2, 1983)

Synopsis. The photosensitized reduction of macrocyclic cobalt(III) complex, $[Co(N_4)(OH_2)_2]^{3+}$ (N_4=Me_6[14]-4,11-dieneN$_4$), occurs rapidly in an anaerobic $[Ru(bpy)_3]^{2+}$/$[Co(N_4)(OH_2)_2]^{3+}$/triethanolamine solution. The mechanistic implications of the photosensitized reaction are discussed.

Several studies have been carried out on the electron-transfer quenching of the excited state of $[Ru(bpy)_3]^{2+}$ (bpy=2,2′-bipyridine), $*[Ru(bpy)_3]^{2+}$, by several quenchers.[1] However, very little attention[2] seems to have been paid to the "net" reduction of the metal complex which gives the product having a potentially high redox power and reversible redox property. It may be important to find efficient charge-separation systems as a prototype model for solar energy conversion.

In this paper the $[Ru(bpy)_3]^{2+}$ photosensitized reduction of macrocyclic cobalt(III) complex is described.

Experimental

$[Ru(bpy)_3]Cl_2\cdot 6H_2O$[3] and $[Co(N_4)(OH_2)_2](ClO_4)_3$[4] ($N_4$= 5,7,7,12,14,14-hexamethyl-1,4,8,11-tetraazacyclotetradeca-4,11-diene which is usually abbreviated as Me_6[14]4,11-dieneN$_4$) were synthesized in a manner similar to that described elsewhere. Reactant solutions of the cobalt(III) complex were prepared under nitrogen atmosphere shortly before use. Solution of the reduced species of the cobalt(III) complex, $[Co(N_4)(OH_2)_2]^{2+}$, was prepared by the reduction of the cobalt(III) complex by excess of ascorbate in an anaerobic solution at pH 6. The hydrogen ion concentration in the reactant solutions was adjusted using dilute perchloric acid and/or dilute sodium hydroxide solution without buffer reagents because the absorption spectra of the cobalt(III) and cobalt(II) complexes were found to be affected by both the pH and the concentration of the dissolved salts such as acetate and phosphate. Acid dissociation constants of $[Co(N_4)(OH_2)_2]^{3+}$ were determined by pH titration using a Hitachi-Horiba Model F-5 pH meter. Steady state irradiation was carried out using 150-W slide projector with UV cut-off filter (Kenko Skylight L-40, UV). The solution in the photometer cell (10 mm × 10 mm) in a cell holder (25±0.2 °C) was deoxygenated by introducing pure nitrogen prior to the photolysis. Development of the photoproduct was monitored by taking absorption spectra on Hitachi Model 320 spectrophotometer. Comparison measurements were carried out on the same day.

Results and Discussion

The acid dissociation constants of $[Co(N_4)(OH_2)_2]^{3+}$ defined by $K_1=[Co(N_4)(OH_2)(OH)^{2+}][H^+]/[Co(N_4)(OH_2)_2{}^{3+}]$ and $K_2=[Co(N_4)(OH)_2{}^+][H^+]/[Co(N_4)(OH_2)(OH)^{2+}]$ were determined to be $10^{-3.95}$ and $10^{-8.85}$ respectively (μ=0.3, 25 °C). The molar absorptivity (ε) of $[Co(N_4)(OH_2)_2]^{2+}$ was determined from the slope of the straight line of the absorbance *vs.* $[Co^{II}]$ plot: λ_{max} 442 nm (ε=78 M^{-1} cm^{-1}, 1 M=1 mol dm^{-3}) at pH 6.3.

The photosensitized reduction of the cobalt(III) complex was carried out at pH 6.3 and μ=0.25 ($NaClO_4$), At this pH, predominant cobalt(III) species and the donor species are $[Co(N_4)(OH_2)(OH)]^{2+}$ (*ca.* above 99%) and the monoprotonated species of triethanolamine (above *ca.* 98%, pK_a 7.90[5]) respectively. A typical example of the spectral change (Fig. 1) shows an increase in the absorption band intensity due to the cobalt(II) complex (λ_{max} 442 nm) with the irradiation time. The concentration of the cobalt(II) in the irradiated solution was determined using an equation: $[Co^{II}]=(A_0-A_t)/(\varepsilon_3-\varepsilon_2)$ where A_0 is the absorbance at time 0, A_t, that at time t, and ε_3 (46 M^{-1} cm^{-1}) and ε_2 (16 M^{-1} cm^{-1}) are the molar absoptivities of the cobalt(III) and cobalt(II) complexes respectively at 530 nm. The reduction rates of the cobalt(III) were determined from the slopes of $[Co^{II}]$ *vs.* irradiation time plots in the initial stages. A plot of the reduction rate *vs.* [TEOA] (TEOA=triethanolamine) showed that the rate almost levelled at above 2×10^{-2} M TEOA. It was also found that the rate increases as $[Co^{III}]$ increases ($[Co^{III}]\lesssim 7.0\times10^{-3}$ M).

The main feature of the photosensensitized reduction of the cobalt(III) complex are rationalized by Eqs. 1—5:

$$[Ru(bpy)_3]^{2+} \xrightarrow{h\nu} *[Ru(bpy)_3]^{2+}, \quad (1)$$

$$*[Ru(bpy)_3]^{2+} \xrightarrow{k_2} [Ru(bpy)_3]^{2+} + h\nu' + \Delta, \quad (2)$$

$$*[Ru(bpy)_3]^{2+} + [Co(N_4)(OH_2)(OH)]^{2+} \xrightarrow{k_3} [Ru(bpy)_3]^{3+} + Co^{II}, \quad (3)$$

$$[Ru(bpy)_3]^{3+} + Co^{II} \xrightarrow{k_4} [Ru(bpy)_3]^{2+} + [Co(N_4)(OH_2)(OH)]^{2+}, \quad (4)$$

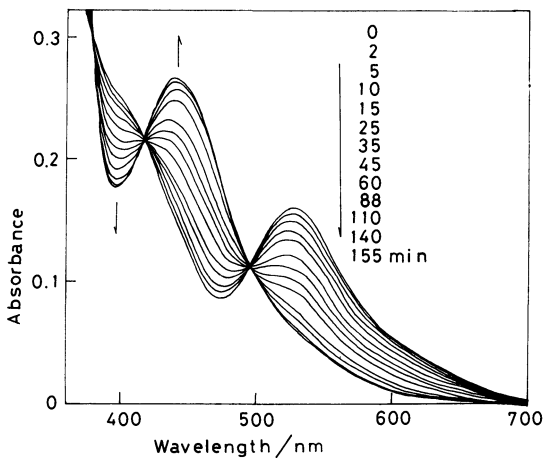

Fig. 1. Spectral change of the solution containing 2.0×10^{-5} M $[Ru(bpy)_3]^{2+}$, 3.0×10^{-3} M $[Co(N_4)(OH_2)_2]^{2+}$, and 0.10 M TEOA at pH 6.3, μ=0.25, and 25 °C. Reference: 2.0×10^{-5} M $[Ru(bpy)_3]^{2+}$.

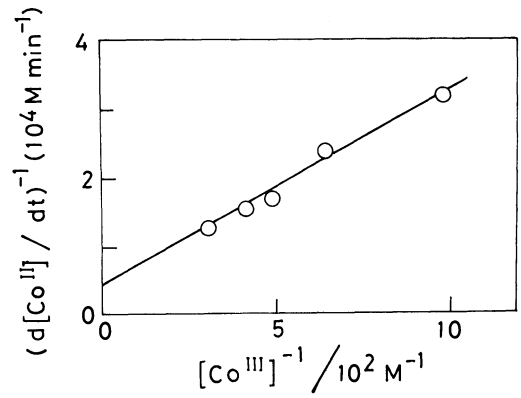

Fig. 2. A plot of $(d[Co^{II}(N_4)]/dt)^{-1}$ *vs.* $([Co(N_4)(OH_2)(OH)]^{2+})^{-1}$. 2.0×10^{-5} M $[Ru(bpy)_3]^{2+}$, 0.10 M TEOA

$$[Ru(bpy)_3]^{3+} + TEOA \xrightarrow{k_5} [Ru(bpy)_3]^{2+} + TEOA_{ox}, \quad (5)$$

where $TEOA_{ox}$ is the oxidized species of TEOA.

The rate equation resulting from this mechanism, assuming a steady-state concentrations for $*[Ru(bpy)_3]^{2+}$ and $[Ru(bpy)_3]^{3+}$, is given by

$$\frac{d[Co^{II}]}{dt} = \left(\frac{\phi I_{abs} k_3[Co^{III}]}{k_2+k_3[Co^{III}]}\right)\left(\frac{k_5[TEOA]}{k_4[Co^{II}]+k_5[TEOA]}\right), \quad (6)$$

where ϕ is the quantum yield for generation of cobalt(II); I_{abs}, the light intensity absorbed by $[Ru(bpy)_3]^{2+}$ in the system; k_2, k_3, k_4, and k_5 are the rate constants for the corresponding reactions. The rate constant k_3 is given by $k_3=k_qF$ where k_q is the rate constant for the quenching of $*[Ru(bpy)_3]^{2+}$ by $[Co(N_4)(OH_2)(OH)]^{2+}$ and F, a portion of the reduction of the cobalt(III) in the quenching process. It may be resonable to assume that $F=1$[6] and $k_4\,[Co^{II}] \ll k_5[TEOA]$[8] for a sufficient excess of TEOA and at the initial stage of the reaction. Thus, we obtain

$$\frac{d[Co^{II}]}{dt} = \frac{\phi I_{abs} k_3[Co^{III}]}{k_2+k_3[Co^{III}]}, \quad (7)$$

which after rearrangement will give

$$\left\{\frac{d[Co^{II}]}{dt}\right\}^{-1} = \frac{1}{\phi I_{abs}}\left(1+\frac{k_2}{k_3[Co^{III}]}\right). \quad (8)$$

A plot of $(d[Co^{II}]/dt)^{-1}$ *vs.* $[Co^{III}]^{-1}$ gives a straight line (Fig. 2). The value of k_2/k_3 ($=6.1\times10^{-3}$ M) can be calculated from the slope/intercept value of the plot. Using $k_2=1.7\times10^6$ s^{-1},[1a] we obtain $k_3=2.7\times10^8$ M^{-1} s^{-1}.

When the irradiated solution (2.0×10^{-5} M $[Ru(bpy)_3]^{2+}$], 3.0×10^{-3} M cobalt(III), 0.10 M TEOA, 50 min) was flushed with oxygen, the resulting spectrum became similar to that of the initial solution, suggesting that the cobalt(II) species generated by the irradiation were reoxidized to the initial species. Such a complex as $[Co(N_4)(OH_2)_2]^{3+}$ having a reversible redox property and relatively high reducing power may be important for making efficient charge separation system for solar energy conversion.

References

1) a) C. Creutz, N. Sutin, and B. S. Brunschwing, *J. Am. Chem. Soc.*, **101**, 297 (1979); b) G. L. Gaines, Jr., *J. Phys. Chem.*, **83**, 3088 (1979); c) C. M. Brown, S. F. Chan, C. Creutz, H. A. Schwartz, and N. Sutin, *J. Am. Chem. Soc.*, **101**, 7638 (1979); d) J. F. Endicott, B. Durham, M. D. Glick, T. J. Anderson, J. M. Kuszai, W. G. Schmonsees, and K. P. Balakrishnan, *ibid.*, **103**, 1431 (1981); e) J. A. Switzer, J. F. Endicott, M. A. Khalifa, F. P. Rotzinger, and K. Kumar, *ibid.*, **105**, 56(1983).

2) a) G. M. Brown, C. Creutz, B. Brunschwig, J. F. Endicott, and N. Sutin, *J. Am. Chem. Soc.*, **101**, 1298 (1979); b) C. T. Lin and N. Sutin, *J. Phys. Chem.*, **80**, 97 (1976).

3) R. Palmer and T. S. Piper, *Inorg. Chem.*, **5**, 864 (1966).

4) N. Sadasivan, J. A. Kernohan, and J. F. Endicott, *Inorg. Chem.*, **6**, 770 (1967).

5) J. Bjerrum, *Chem. Rev.*, **1950**, 46, 381.

6) It has been demonstrated that there is ample evidence for electron-transfer quenching of $*[Ru(bpy)_3]^{2+}$ by several cobalt(III) complexes.[7]

7) K. R. Leopard and A. Haim, *Inorg. Chem.*, **17**, 1753 (1978).

8) Under the conditions employed (2.0×10^{-5} M $[Ru(bpy)_3]^{2+}$, 3.0×10^{-3} M cobalt(III), and 0.10 M TEOA), the "back-reaction" may be ignored because the curve for the plot of the rate *vs.* [TEOA] levels off above *ca.* 0.05 M TEOA.

^{57}Fe Spin-lattice Relaxation Time of $Fe(CO)_5$ and Ferrocene

Tsunenori NOZAWA,* Masahiro HATANO, Mitsuo SATO,† Yoshiharu TOIDA,†† and Enrico BATHOLDI††

Chemical Research Institute of Non-aqueous Solutions, Tohoku University, Katahira, Sendai 980

†*Biophysics Division, Faculty of Pharmaceutical Sciences, Teikyo University, Sagamiko-cho, Tsukui-gun, Kanagawa 199-01*

††*Bruker Japan, 21-5, Ninomiya 3-chome, Yatabe-cho, Tsukuba-gun, Ibaragi 305*

(Received May 30, 1983)

Synopsis. Spin-lattice relaxation times (T_1's) of ^{57}Fe were determined by the inversion recovery method to be 80 ($\pm$10) s at 293 K and 4 ($\pm$1) s at 303 K for $Fe(CO)_5$ and ferrocene, respectively. Predominant relaxation mechanisms were considered to be chemical shift anisotropy and spin-rotation for the former and the latter complexes, respectively.

Although chemical shifts of ^{57}Fe NMR of many iron complexes have been determined by a combination of pulse FT techniques with large sample tubes and a high magnetic field,[1] little has been known about the relaxation processes, which are important to understand the molecular dynamics of the complexes. ^{57}Fe nucleus with nuclear spin of one half and low natural abundance was believed to have a long relaxation time. Recently we have succeeded in determining the spin-lattice relaxation times of $Fe(CO)_5$ (pentacarbonyliron(0)), and ferrocene (bis(η-cyclopentadienyl)iron(II)). The relaxation time of ferrocene was fairly short as compared with that of $Fe(CO)_5$. Possible relaxation mechanisms to explain these results are discussed.

Experimental

Materials. $Fe(CO)_5$ was purchased from Strem Chemicals, Inc. Ferrocene was obtained from Wako Chemicals, Inc. as a guaranteed grade reagent and purified by recrystallization from benzene. Benzene-d_6 was purchased from E. Merck Japan Ltd.

Measurements. The NMR spectra of ^{57}Fe were measured with a Bruker CXP-300 FT-NMR spectrometer. The static field $B_0=7.05$ T (corresponding to a 300 MHz proton Larmor frequency) gave resonance frequencies around 9.7 MHz for the ^{57}Fe nuclei, and was internally locked on a ^2H signal of solvent, except for $Fe(CO)_5$ which was measured as neat liquid without lock. The 90° pulse width was determined to be 180 μs, which afforded a H_1 field of 10.1×10^{-4} T. A Bruker temperature controller (B-VT-1000) was employed and calibrated by measuring the proton frequency differences between the resonances of ethyl alcohol.[2] The NMR spectra of ^{57}Fe for neat $Fe(CO)_5$ and ferrocene in benzene-d_6 solution (1 mol dm^{-3}) were measured at 293 and 303 K at its natural abundance with a sample tube of 15 mm diameter. The ferrocene solution was degassed before the NMR measurements.

Results and Discussion

$Fe(CO)_5$ and ferrocene gave NMR signals at 9.71568 and 9.73056 MHz, respectively. The ratios of these values to the resonance frequency of $GeCl_4$ (ν(Fe)/ν(Ge)) were 0.928155 and 0.929576 which coincide well with the values in the reference,[1] 0.92815542 and 0.9295803. The half linewidths of the NMR signals were 1.0 and 2.6 Hz for $Fe(CO)_5$ and ferrocene, respectively.

Measurements of spin-lattice relaxation times were achieved by the inversion recovery method combined with a Fourier transform (IRFT). Since the spin-lattice relaxation time, T_1, for the ^{57}Fe NMR of $Fe(CO)_5$ was expected to be around 100 s, the recycle time was taken to be 800 s. The results are shown in Fig. 1. The plot of $-\ln((A_\infty-A_\tau)/2A_\infty)$ *versus* τ, where A_τ and A_∞ are the amplitude of the NMR signal partially relaxed for an inter-pulse time τ, and the amplitude at thermal equilibrium, yielded a T_1 value of 80 ($\pm$10) s.

The partially relaxed NMR spectra for ferrocene in benzene-d_6 solution are shown in Fig. 2. The plot of $-\ln((A_\infty-A_\tau)/2A_\infty)$ *versus* τ gave a T_1 value of 4 ($\pm$1) s.

Since no abundant spin is present in $Fe(CO)_5$, the only possible ways of relaxation are the spin-rotation and/or the chemical shift anisotropy mechanism.[3] Hence, it is reasonable for the system to have a spin-lattice relaxation time as long as 80 s.

Ferrocene in benzene-d_6 solution had a spin-lattice relaxation time much shorter than that of $Fe(CO)_5$, the reasons for this are now discussed.

In order to determine the rotational correlation time of ferrocene, the spin-lattice relaxation time of the ^{13}C nucleus of ferrocene was measured for the same solution for which the T_1 values of the ^{57}Fe nucleus had been determined. The T_1 values for the ^{13}C nucleus of ferrocene were 12.3 and 10.0 s at 303 and 293 K, respectively, which are in reasonable agreement with the reference values[4] (14.3 s at 311 K). The ^{13}C nucleus directly bound with one or more proton(s) is relaxed predominantly through the dipolar mechanism.[5] Hence the ^{13}C nucleus of ferrocene is presumed to be relaxed by

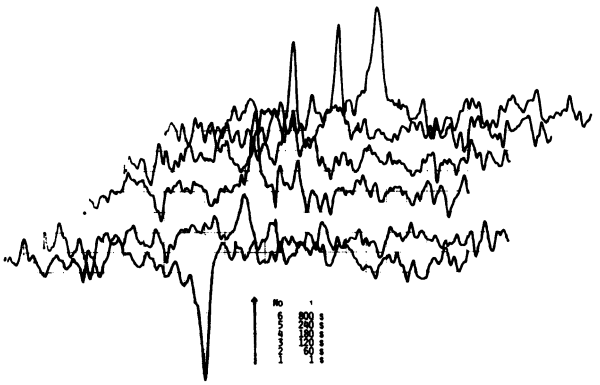

Fig. 1. The partially relaxed ^{57}Fe NMR spectra for $Fe(CO)_5$. The duration of 90° pulse was 180 μs at a transmitter gain with peak to peak voltage of 200 V. The recycle time was 800 s. The inter-pulse time (τ) values were 1, 60, 120, 180, 240, and 800 s from the bottom to the top spectra. Sweep width: 100 Hz, memory size: 8×10^3 words, line-broadening: 1 Hz, number of transients: 52, temperature: 293 K.

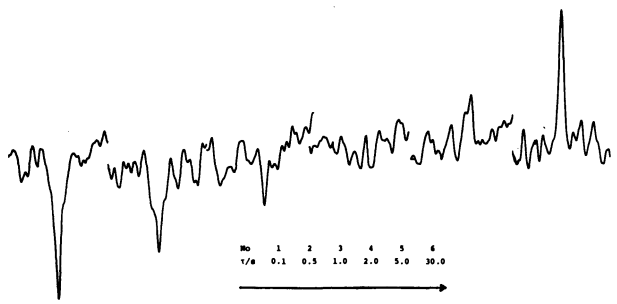

Fig. 2. The partially relaxed ^{57}Fe NMR spectra for ferrocene in benzene-d_6 solution (1 mol dm^{-3}). The duration of 90° pulse was 180 μs at a transmitter gain with peak to peak voltage of 200 V. The recycle time was 30 s. The inter-pulse time (τ) values were 0.1, 0.5, 1.0, 2.0, 5.0, and 30 s. Sweep width: 150 Hz, memory size: 8×10^3 words, linebroadening: 1 Hz, number of transients: 520, temperature: 303 K.

the dipole (^{57}Fe) and dipole (^{1}H) interaction mechanisms. The spin-lattice relaxation time for the dipolar interaction mechanism, T_1^{dd}, for a nucleus I being relaxed by a nucleus S under the extreme narrowing conditions can be written as[6]

$$1/T_1^{dd} = (\mu_0^2\gamma_I^2\gamma_S^2\hbar^2/12\pi^2)S(S+1)\Sigma(1/r^6)\tau_r, \quad (1)$$

where μ_0, γ, S, r, and τ_r are magnetic permeability in vacuum, magnetogyric ratio, spin quantum number for the nucleus S, distance between the nuclei I and S, and a rotational correlation time, respectively. Taking the above experimental T_1 value as the T_1^{dd}, and using Eq. 1 and the bond distance (1.095 Å) between ^{13}C and ^{1}H,[7] we can calculate the rotational correlation time, τ_r, to be 3.0×10^{-12} s at 303 K. Under the assumption that the ^{57}Fe nucleus of ferrocene has a rotational correlation time similar to that for the ^{13}C nucleus, and that the ^{57}Fe nucleus is relaxed by the dipolar mechanism, the spin-lattice relaxation time of the ^{57}Fe nucleus was calculated to be 2.2×10^4 s from Eq. 1 and the structure of ferrocene.[7] This value, which is far from the experimentally observed one (4 s), therefore, indicates that other relaxation mechanisms should be considered for the relaxation of the ^{57}Fe nucleus in ferrocene.

The spin-lattice relaxation time for the chemical shift anisotropy mechanism (T_1^{CA}) can be expressed by

$$1/T_1^{CA} = (2/15)\gamma_I^2H_0^2\Delta\sigma^2\tau_r, \quad (2)$$

under the extreme narrowing condition.[8] The chemical shift anisotropy ($\Delta\sigma$) necessary to explain the observed T_1 value (4 s) was calculated to be 2.0×10^4 ppm, under the assumption that the rotational correlation time, τ_r, for the ^{57}Fe nucleus is similar to that determined for the ^{13}C nucleus. This value appears to be one order of magnitude too large as compared with $\Delta\sigma$ values experimentally determined for other metallocenes (*e.g.*, 6400 ppm for $[Co^{III}(C_5H_5)_2]NO_3$[9]). Therefore the relaxation of the ^{57}Fe nucleus in ferrocene can not be explained by the chemical shift anisotropy mechanism only. Accordingly another relaxation mechanism, *i.e.*, spin-rotation mechanism, will play an important role in the relaxation of ^{57}Fe nucleus. The temperature dependence of the ^{57}Fe relaxation time of ferrocene which showed a longer value at lower temperature (5 s at 293 K) supported this conclusion.[7]

For the relaxation of the ^{13}C nucleus of $Fe(CO)_5$, it was reported that the chemical shift anisotropy was the predominant mechanism and that the rotational correlation time τ_r was 5×10^{-12} s at 293 K.[3] By use of this correlation time for the ^{57}Fe nuclei of $Fe(CO)_5$, the chemical shift anisotropy necessary to explain the experimental T_1 value (80 s) was calculated to be 4000 ppm from Eq. 2. Although this value is somewhat larger than that observed for other metal carbonyls ($\Delta\sigma=1400$ ppm for $[Mn(CO)_5Cl]$[10]), the chemical shift anisotropy mechanism will be predominant in the relaxation for the ^{57}Fe NMR of $Fe(CO)_5$.

This work was supported in part by a Grant-in-Aid for Scientific Research from the Ministry of Education, Science and Culture, and by a grant from Nissan Science Foundation to M. H.

References

1) T. Jenny, W. Von Philipsborn, J. Kronenbitter, and A. Schwenk, *J. Organomet. Chem.*, **205**, 211 (1981).
2) A. L. Van Geet, *Anal. Chem.*, **40**, 2227 (1968).
3) Von H. W. Spiess and H. Mahnke, *Ber. Bunsenges. Phys. Chem.*, **76**, 990 (1972).
4) G. C. Levy, *Tetrahedron Lett.*, **1972**, 3709.
5) J. R. Lyerla, Jr., and G. C. Levey, "Topics in Carbon-13 NMR Spectroscopy," ed by G. C. Levy, John Wiley and Sons, New York (1974), Vol. 1, Chap. 3, pp. 79—143.
6) G. A. Webb, "NMR and the Periodic Table," ed by R. K. Harris and B. H. Mann, Academic Press, New York (1978), Chap. 3, pp. 49—86.
7) E. A. Seibold and L. E. Sutton, *J. Chem. Phys.*, **23**, 1967 (1955).
8) T. C. Farrar and E. D. Becker, "Pulse and Fourier Transform NMR, Introduction to Theory and Methods," Academic Press, New York (1971), p. 77.
9) H. W. Spiess, H. Haas, and H. Hartmann, *J. Chem. Phys.*, **50**, 3057 (1969).
10) H. W. Spiess and R. L. Sheline, *J. Chem. Phys.*, **54**, 1099 (1971).

Effects of the Oxyethylene Chain Length of Fluorocarbon Surfactants on Demixing of Micelles of Fluorocarbon and Hydrocarbon Surfactants

Noriaki FUNASAKI,* Sakae HADA, and Saburo NEYA
Kyoto College of Pharmacy, Yamashina-ku, Kyoto 607
(Received July 4, 1983)

Synopsis. The critical mole fraction of hydrocarbon surfactant decreases with an increase in the oxyethylene unit of either fluorocarbon surfactant or hydrocarbon surfactant. This tendency is explicable in terms of regular solution theory if the depth of water penetration into the micellar interior is assumed to increase with an increase in the oxyethylene unit.

Under certain conditions, fluorocarbon and hydrocarbon surfactants are partially miscible in their mixed micelles, forming two kinds of mixed micelles with different compositions.[1] We reported the effects of hydrophobic and hydrophilic groups of hydrocarbon surfactant on the critical solution points of such micellar systems.[2]

According to regular solution theory, the critical mole fraction x_{cH} of the binary liquid system consisting of the nonpolar compounds, F and H, can be written as[3]

$$x_{cH} = [1-(1-q+q^2)^{1/2}]/(1-q), \quad (1)$$

where q is the ratio of molar volumes, *viz.* v_F/v_H. When we attempt to apply Eq. 1 to a mixed micelle, there is still an uncertainty as to volumes to be employed; the total molar volume or the molar volume of the hydrophobic group. To solve this problem, we investigate the effect of fluorocarbon surfactants on the critical solution points.

Experimental

The nonionic fluorocarbon surfactant, NFE7 ($[(CF_3)_2CF]_2C=C(CF_3)O(CH_2CH_2O)_nCH_3$, averaged $n=7$), was donated by Neos Company. This specimen is not homogeneous with respect to oxyethylene units. The nonionic hydrocarbon surfactant, heptaethylene glycol monododecyl ether (DE7), was obtained from Nikko Chemicals as at least 99% pure. The detail of surface tension measurements has been reported elsewhere.[2]

Results and Discussion

The surface tension method was used to determine the mutual solubility in micelles. In Fig. 1a, the surface tension of aqueous solutions of mixed NFE7 and DE7 is plotted against the mole fraction x_H of DE7 in the whole system. The total surfactant concentration is in a range of 1 to 1.3 mmol dm^{-3}, which is much higher than the critical micelle concentrations (cmc) of NFE7 and DE7, *viz.* 0.025 and 0.08 mmol dm^{-3}. These cmc values of NFE7 and DE7 decreased slightly with rising temperature. The cmc's of their mixtures are slightly larger than predictions from ideal mixing of these surfactants. Under these conditions, therefore, almost all of the surfactant molecules added form micelles and consequently the composition of the surfactants added is very close to that of micellized surfactants.

In the plateau region of the surface tension *vs.* composition curve, two kinds of mixed micelles coexist in a solution.[2] From two limits of this plateau region, we can determine mutual solubilities in the micelles. Further we can determine the solubility-temperature diagram for the NFE7 and DE7 system from Fig. 1a. This kind of diagram represents a coexistence curve for the comicellar system similar to that of the binary liquid system. In Fig. 1b, the coexistence curve of mixed micelles of DE7 and NFE18 is included for comparison. From a coexistence curve and the locus of its midpoints, we can determine the critical composition x_{cH} and the critical solution temperature T_c. Thus, from Fig. 1b, we obtained the values of x_{cH} and T_c for the NFE18–DE7 and NEF7–DE7 systems. In Table 1, these values are shown together with those of other systems.[2]

In Table 1, NFE18 ($[(CF_3)_2CF]_2C=C(CF_3)O(CH_2CH_2O)_{18}CH_3$) and DE9 (nonaethylene glycol monododecyl ether) are not homogeneous samples with respect to oxyethylene units but DE5 (pentaethylene glycol monododecyl ether) is homogeneous (99%). The T_c value is found to decrease with an increase in the oxyethylene unit of either fluorocarbon surfactant or hydrocarbon surfactant (Table 1). Further, it is noted that this T_c decreasing (solubility increasing) ability of an oxyethylene unit of NFE is greater than that of DE. As is evident from comparison of the NFE7–DE7 and NFE18–DE7 systems, x_{cH} decreases with an increase in the oxyethylene unit of NFE.

From Eq. 1, we can calculate the critical mole fraction

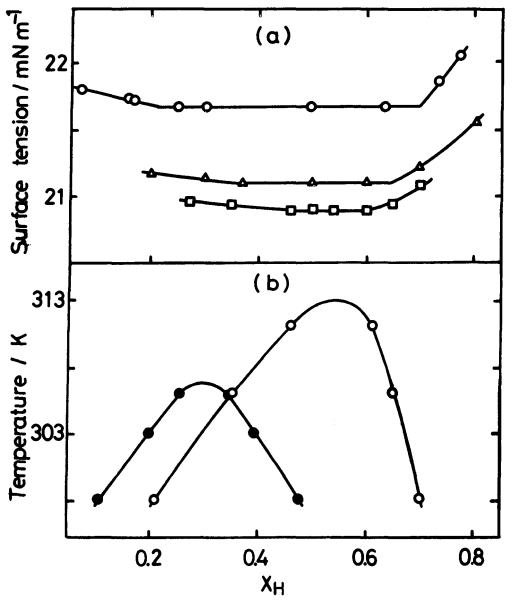

Fig. 1. (a) Surface tensions of aqueous solutions of mixed NFE7 and DE7 as a function of the mole fraction of DE7 at three temperatures (K): ○, 298.2; △, 303.2; □, 311.2. (b) Coexistence curves of two kinds of mixed micelles for the NFE7–DE7 (○) and NFE18–DE7 (●) systems.

Table 1. Observed x_{cH} and T_c and calculated x_{cH} by using different v's

System	Observed		Calculated x_{cH}		
	x_{cH}	T_c/K	v_t	v_α	v_β
NFE7–DE7	0.550	313.3	0.530	0.527	0.499
NFE18–DE5	0.506	310.3	0.774	0.527	0.499
NFE18–DE7	0.300	307.0	0.731	0.527	0.499
NFE18–DE9	0.283	299.2	0.689	0.527	0.499

of hydrocarbon surfactant by employing the different molar volumes; v_t, v_α, and v_β. The v_t denotes the total molar volume of a surfactant. The demixing of micelles of fluorocarbon and hydrocarbon surfactants is ascribed mainly to the interaction of fluorocarbon and hydrocarbon chains in the micelle. Therefore, the molar volume of the hydrophobic group, v_t, may be used instead of v_α. However, water may penetrate into the micellar interior; the number of wet carbon atoms adjacent to a hydrophilic group may be zero,[4] one or two,[5] or several.[6] If water penetrates into the micellar interior up to the α-carbon atom of the hydrophobic group, then the molar volume of the dry hydrophobic group from β- through ω-carbon atoms, v_β, must be used for v_α. Molar volumes v_t, v_α, and v_β of NFE7 are estimated from the observed v_t values of NFE18, DE's, and related compounds at 298.2 K, as already made for NFE18 and DE's.[2] We used the following values (cm^3 mol^{-1}); $v_t(DE5)=408.3$, $v_t(DE7)=485.4$, $v_t(DE9)=562.5$, $v_t(NFE7)=526.3$, $v_t(NFE18)=965.8$, $v_\alpha(DE5)=v_\alpha(DE7)=v_\alpha(DE9)=210.9$, $v_\alpha(NFE7)=v_\alpha(NFE18)=226.9$, $v_\beta(DE5)=v_\beta(DE7)=v_\beta(DE9)=194.7$, and $v_\beta(NFE7)=v_\beta(NFE18)=194.3$.

As the number of oxyethylene units of hydrocarbon surfactants increases, keeping the fluorocarbon surfactant (NFE18) constant, x_{cH} decreases. Apart from the direction, the magnitude in this change is inexplicable by using any of v_t, v_α, and v_β. Hence, we proposed a hypothesis which explains this discrepancy in x_{cH} between theory and experiment; we assumed a deeper penetration of water into the micellar interior with an increase in the oxyethylene unit.[2] The present data on the NFE7–DE7 system support this hypothesis. As is evident from Table 1, the x_{cH} value of the NFE18–DE7 system is smaller than that of the NFE7–DE7 system. This contradicts the theoretical results obtained by using any of v_t, v_α, and v_β. As the number of oxyethylene units increases, the surface area per surfactant molecule in the micelle increases and consequently water is likely to penetrate into the micellar interior more deeply. Therefore x_{cH} can decrease with an increase in the oxyethylene unit of fluorocarbon surfactants and this tendency is actually observed. This interpretation is also consistent with the fact that T_c decreases with an increase in the oxyethylene unit of either fluorocarbon surfactant or hydrocarbon surfactant.

Although the depth of water penetration into the micellar interior is still a matter of controversy,[4-6] the level of the α-carbon atom of dodecyl sulfates is most probable, as deduced from small angle neutron scattering.[7] The present results seem to support a shallow water penetration model in which the penetration depth depends on the number of oxyethylene units.

Thanks are due to Neos Company for a sample of NFE7 and to Nikko Chemicals for a sample of DE9.

References

1) P. Mukerjee and K. J. Mysels, *ACS Symp. Ser. No. 9*, **1975**, 239; N. Funasaki and S. Hada, *Chem. Lett.*, **1979**, 717; K. Shinoda and T. Nomura, *J. Phys. Chem.*, **84**, 365 (1980); H. Ihara, Y. Hashiguchi, and T. Kunitake, *Chem. Lett.*, **1983**, 733.

2) N. Funasaki and S. Hada, *J. Phys. Chem.*, **87**, 342 (1983).

3) J. H. Hildebrand, J. M. Prausnitz, and R. L. Scott, "Regular and Related Solutions," Van Nostrand-Reinhold, New York (1970), Chap. 10.

4) D. Stigter, *J. Phys. Chem.*, **78**, 2480 (1974).

5) J. Ulmius and B. Lindman, *J. Phys. Chem.*, **85**, 4131 (1981).

6) F. M. Menger, *Acc. Chem. Res.*, **12**, 111 (1979).

7) D. Bendedouch, S.-H. Chen, and W. C. Koehler, *J. Phys. Chem.*, **87**, 153 (1983).

Preparations and Strucutures of Silver(I) Complexes with *cyclo*(Glcyl-L-histidyl), *cyclo*(L-Methionyl-L-histidyl), and *cyclo*(L-Histidyl-L-histidyl)

Yoshitane KOJIMA,* Tetsushi YAMASHITA, Yoshio ISHINO,† Tsuneaki HIRASHIMA,† and Toshio MIWA

Department of Chemistry, Faculty of Science, Osaka City University, Sugimoto, Sumiyoshi-ku, Osaka 558

†Osaka Municipal Technical Research Institute, 1-6-50, Morinomiya, Joto-ku, Osaka 530

(Received March 14, 1983)

Synopsis. The structures of silver(I) complexes with *cyclo*(glycyl-L-histidyl), *cyclo*(L-methionyl-L-histidyl), and *cyclo*-(L-histidyl-L-histidyl) were examined using ^1H and ^{13}C NMR. The NMR measurements suggest that the silver(I) ion links to the sulfur atom of thioether and the nitrogen atom of imidazole group of the above cyclic peptides, but not to their amide groups.

The present authors have used a copper(II) complex with *cyclo*(L-histidyl-L-histidyl) (**3**) and a silver(I) complex with *cyclo*(L-methionyl-L-methionyl) (**4**) as simple model compounds[1] for studying metalloproteins and metalloenzymes, in which the ligating groups for metal ions are the functional groups of the side chains of peptides, but not the amide groups. In our previous papers,[1] the coordinations of the imidazole (Im) group of histidyl residue to the copper(II) ion and of the thiother group of the methionyl residue to the silver(I) ion were confirmed using ^1H NMR and X-ray crystal analysis. Other workers[2] have investigated the conformations of cyclic dipeptides using NMR and X-ray measurements, and have found that the cyclic dipeptides containing histidine, phenylalanine, and tyrosine prefer a folded form, in which the aromatic ring of the side chain of the peptide lies over 2,5-piperazinedione. This paper will report the preparations and characteristics of silver(I) complexes with cyclic dipeptides containing Im and thioether groups. *cyclo*(Glycyl-L-histidyl) (**1**), *cyclo*-(L-methionyl-L-histidyl) (**2**), and **3** were used as ligands in this experiment.

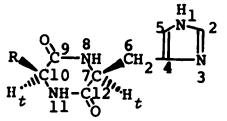

1: R=H$_c$

2: R=CH$_2$CH$_2$SCH$_3$

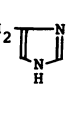

Experimental

Materials. **1**,[3] **2**,[4] and **3**[1a] were prepared according to the methods reported earlier. *cyclo*(Glycyl-glycyl)(**5**) and silver(I) salts(perchlorate, nitrate, and hexafluorophosphate) obtained commercially were used without further purification.

Preparations of Silver(I) Complexes. A mixture of **1** (0.50 mmol) and silver(I) perchlorate (0.53 mmol) was completely dissolved in hot water (50 cm^3) with stirring. After standing at room temperature for a few days, the precipitate was filtered off and recrystallized from water. Other complexes were similarly obtained by the procedure described above. Table 1 shows the values of the elemental analyses and melting points of silver(I) complexes with **1**, **2**, and **3**.

Measurements. The ^1H and ^{13}C NMR data of silver(I) complexes and their corresponding ligands were obtained in D_2O at 27, 40, and 50 °C, using sodium 3-trimethylsilyl-1-propanesulfonate as the internal reference. The molecular weights of silver(I) complexes with **1** and **2** were measured in H_2O at 56 °C, using urea as the standard material. JEOL FX-100 and FX-90Q (for ^1H and ^{13}C NMR spectra) apparatuses and a Knauer Vapor-pressure Osmometer (for molecular weight) were used for the measurements of the samples.

Results and Discussion

Table 2 shows the chemical shifts of the protons of ligands and their corresponding silver(I) complex ions. As is shown in Table 2, 10-H$_c$ (δ=3.13) and 10-H$_t$ (δ=3.72) of **1** absorb at a higher field than the methylene proton (δ=4.00) of **5** because of the magnetic shielding effect[2a] of the Im ring, showing that **1** exists as a folded form. The chemical shifts (δ=3.13 and 3.77) of 10-H$_c$ and 10-H$_t$ of [Ag(**1**)$_2$]$^+$(**A-1**) are almost the same as those of **1**, so a preferred form for **A-1** is a folded one. Table 2 also describes how the 13-H (δ=1.05—1.43 and 1.46—1.90) of **2** absorbs at a higher field than the β-methylene (δ=2.10—3.00) of **4**[1b] because of the magnetic anisotropy of the Im ring, indicating that **2** prefers a folded form. Though the peaks of 13-H of **2** are complicated and unresolved, the values of the chemical shifts are used for elucidating the conformation of [Ag(**2**)]$^+$ (**A-2**). The possibility that **A-2** favors a folded form is suggested by the small difference between the chemical shifts of 13-H of **2** and those (δ=1.49—1.97) of **A-2**. The downfield shift ($\Delta\delta$=0.32) of the 14-H and 15-H of **A-2** from **2** supports the coordination of the S atom to the silver(I) ion.[1b] The differences ($\Delta\delta$=0.86 and 0.46) in the chemical shifts of 6-H between **3** and

TABLE 1. ANALYTICAL DATA AND MELTING POINTS FOR SILVER(I) COMPLEXES

Complex	Found (%)			Calcd (%)			Mp (decomp) θ_m/°C
	C	H	N	C	H	N	
[Ag(**1**)$_2$]NO$_3$·H$_2$O	33.5	3.7	21.6	33.4	3.9	21.9	183—205
[Ag(**1**)$_2$]ClO$_4$·1/4 H$_2$O	32.0	3.4	18.7	32.0	3.4	18.7	244—259
{[Ag(**2**)](ClO$_4$)}$_2$	28.1	3.4	11.8	27.8	3.4	11.8	195—208
{[Ag(**3**)](ClO$_4$)}$_n$	29.9	3.0	17.8	29.9	2.9	17.5	281—286
{[Ag(**3**)](PF$_6$)}$_n$	27.2	2.8	15.8	27.3	2.7	15.9	230—251

Table 2. ^{1}H NMR data of cyclic dipeptides and their silver(I) complexes in D_2O at 50 °C

Compound	Chemical shifts, δ ($\Delta\delta$[a])									
	2-H	5-H	6-H		7-H$_t$	10-H$_t$	10-H$_c$	13-H	14-H	15-H
1[b]	7.70	6.97	3.21	3.06	4.32	3.72	3.13	—	—	—
A-1[b]	7.98	7.16	3.36	3.19	4.41	3.77	3.13	—	—	—
	(0.28)	(0.19)	(0.15)	(0.13)	(0.09)	(0.05)	(0.00)			
2	7.69	6.96	3.26	3.01	d)	4.08	—	1.05—1.43[c] 1.46—1.90	2.16	2.04
A-2	7.99	7.17	3.38	3.14	d)	4.15	—	1.49—1.97[c]	2.48	2.36
	(0.30)	(0.21)	(0.12)	(0.13)		(0.07)			(0.32)	(0.32)
3	7.71	6.88	2.86	2.39	4.24	4.24	—	—	—	—
A-3	7.86	7.17	3.32	3.25	4.20	4.20	—	—	—	—
	(0.15)	(0.33)	(0.46)	(0.86)	(−0.04)	(−0.04)				

a) $\Delta\delta=\delta$(Ag(I) complex) − δ(free ligand). b) Measured at 27 °C. c) Complicated and unresolved signals were given for 13-H at this region. d) These peaks could not be observed because of the overlapping of the signal of D_2O.

Table 3. ^{13}C NMR data of cyclic dipeptides and their silver(I) complex ions

Compound	Chemical shifts, δ ($\Delta\delta$[a])										
	2-C	4-C	5-C	6-C	7-C	9-C	10-C	12-C	13-C	14-C	15-C
1[b]	138.8	134.1	120.7	33.8	57.5	171.2	46.0	172.3	—	—	—
A-1[b]	140.9	134.9	120.5	35.0	57.3	171.1	45.9	171.9	—	—	—
	(2.1)	(0.8)	(−0.2)	(1.2)	(−0.2)	(−0.1)	(−0.1)	(−0.4)			
2[b]	138.5	133.8	121.2	33.1	57.6	171.4	56.1	171.9	35.3	30.4	16.7
A-2[b]	140.4	134.9	121.6	33.8	57.6	171.6	55.9	171.6	36.5	33.0	20.0
	(1.9)	(1.1)	(0.4)	(0.7)	(0.0)	(0.2)	(−0.2)	(−0.3)	(1.2)	(2.6)	(3.3)

a) $\Delta\delta$ = δ(Ag(I) complex) − δ(free ligand). b) **1** and **A-1** were measured at 27 °C, while **2** and **A-2** were done at 40 °C.

$[Ag(\mathbf{3})]^+$ (**A-3**) are considerably larger than those ($\Delta\delta$= 0.12—0.15) between **1** and **A-1** or **2** and **A-2**. This distinct downfield shift of **A-3** from **3** suggests that there is no magnetic shielding effect of the Im group, so that **A-3** prefers an unfolded form in which the Im group lies away from the 2,5-piperazinedione. Table 2 suggests that each 1- or 3-N atom of the Im groups of **1**, **2**, and **3** coordinates to the silver(I) ion because the downfield shifts ($\Delta\delta$=0.19, 0.21, and 0.33) of 5-H of **A-1**, **A-2**, and **A-3** from **1**, **2**, and **3**, and those ($\Delta\delta$=0.28, 0.30, and 0.15) of 2-H are observed, respectively.

The ^{13}C NMR data of **1**, **2**, **A-1**, and **A-2** are given in Table 3; those of **3** and **A-3** could not be obtained because of their low solubilities. Table 3 suggests that the 1- or 3-N atom of each Im group of **1** and **2** coordinates to the silver(I) ion, because the downfield shifts ($\Delta\delta$=0.8 or 1.1) of the 4-C of **A-1** or **A-2** from **1** or **2** and those ($\Delta\delta$=2.1 or 1.9) of 2-C are observed. The coordination of the S atom of **2** to the silver(I) ion is also confirmed by the marked downfield shifts ($\Delta\delta$=2.6 and 3.3) of the 14-C and 15-C of **A-2** from **2**. Table 3 indicates that no O atoms of the 2,5-piperazinedione of **1** and **2** coordinates to the silver(I) ion, for no distinct shifts of the 7-C, 9-C, 10-C, and 12-C of **A-1** or **A-2** from **1** or **2** are observed. As is shown in Table 2, this suggestion is also supported by the small shift ($\Delta\delta$=0.09 or −0.04) of the 7-H$_t$ of **A-1** or **A-3** from **1** or **3** and that ($\Delta\delta$=0.05 or 0.07) of the 10-H$_t$ of **A-1** or **A-2** from **1** or **2**.

The molecular weights (300 and 331) for **A-1** and **A-2** show **A-1** as a monomeric form, $[Ag(\mathbf{1})_2]^+ + NO_3^-$ (596/2=298), and **A-2** as a dimeric one, $\{[Ag(\mathbf{2})]_2\}^{2+} + 2ClO_4^-$ (951/3=317). The molecular weight of **A-3** could not be measured because of its extremely low solubility, suggesting that **A-3** prefers a polymeric form.

The results obtained in this paper suggest that the 1- or 3-N atom of the Im group and the S atom of thioether in **2** coordinate linearly to the silver(I) ion. In the cases of **1** and **3**, each silver atom is coordinated linearly to each 1- or 3-N atom of two Im groups.

The authors wish to thank Mr. Junichi Gohda for elemental analyses.

References

1) a) Y. Kojima, *Chem. Lett.*, **1981**, 61; b) Y. Kojima, T. Yamashita, Y. Ishino, T. Hirashima, and K. Hirotsu, *ibid.*, **1983**, 453.

2) a) K. D. Kopple and M. Ohnishi, *J. Am. Chem. Soc.*, **91**, 962 (1969); b) R. Ramani, K. Venkatesan, and R. E. Marsh, *ibid.*, **100**, 949 (1978).

3) K. D. Kopple and H. G. Ghazarian, *J. Org. Chem.*, **33**, 862 (1968).

4) D. E. Nietecki, B. Halpern, and J. W. Westly, *J. Org. Chem.*, **33**, 864 (1968).

Succinate-complexed Octacalcium Phosphate

Hideki MONMA* and Masaru GOTO
National Institute for Research in Inorganic Materials, 1-1 Namiki, Sakura-mura, Niihari-gun, Ibaraki 305
(Received May 4, 1983)

Synopsis. A succinate-complexed calcium phosphate has been synthesized by conducting the hydrolysis of α-tricalcium bis(phosphate) in the presence of succinate ions. The organic substance is considered to be introduced into the structure of the hydrolysis product, *i.e.*, octacalcium bis(hydrogenphosphate) tetrakis(phosphate) pentahydrate, through the replacement of HPO_4^{2-} by $C_4H_4O_4^{2-}$.

Octacalcium bis(hydrogenphosphate) tetrakis(phosphate) pentahydrate (OCP), $Ca_8(HPO_4)_2(PO_4)_4\cdot 5H_2O$, is, structurally related to hydroxyapatite (HAp) and is a precursor in the formation of HAp in bones, teeth, and urinary calculi. The structure of OCP is composed of alternative stackings of an "apatitic layer" (A-layer) with the composition of $Ca_{12}(PO_4)_8\cdot 2H_2O$ and a "hydrated layer" (B-layer) of $Ca_4(HPO_4)_4\cdot 8H_2O$ which is compositionally the same as brushite ($CaHPO_4\cdot 2H_2O$).[1] HAp and other calcium phosphates have been widely studied in interactions with organic compounds related to biological, biomaterial, and bio-chromatographic problems. According to these studies, various organic substances have been shown to be adsorbed or ion-exchanged on the surface of calcium phosphates, however in one instance there is a possibility that glycine might be introduced into the HAp structure.[2] Generally it would be reasonable to consider that organic molecules or ions are difficult to introduce into calcium phosphates, because of their large size and steric conformations. Here, although the OCP structure is not classified normally into so-called layered compounds consisting of layers bound to each other weakly by van der Waals force or hydrogen bonds, we would expect from structural considerations that OCP must behave more actively towards organic compounds than HAp and other calcium phosphates and might incorporate some organic substances into the B-layer. In this work, we present data supporting the idea that succinate ions can be introduced into the B-layer.

Experimental

Powdery α-tricalcium bis(phosphate) (α-TCP), α-$Ca_3(PO_4)_2$, was used for the synthesis of a reference OCP (ref-OCP) and a succinate-containing OCP (succinate-OCP). The α-TCP was prepared by heating an equimolar mixture of γ-$Ca_2P_2O_7$ and $CaCO_3$ at 1200 °C for 1 h.[3] The ref-OCP was prepared by the hydrolysis of α-TCP in a 0.5 M (1 M=1 mol dm^{-3}) sodium acetate solution of 50 °C at a pH of 5.4±0.1 for 3 h. This procedure was a modification of the method developed previously.[4] The succinate-OCP was prepared by conducting the hydrolysis in the presence of 0.25 M succinate ions at 40 °C and at an initial pH of 6.0±0.1 for 3 h. The resulting OCP samples were dried at 40 °C and their products calcined at several temperatures were examine by X-ray diffraction, heating weight loss and Ca/P ratio. The chemical analyses for CaO and P_2O_5 were performed by a chelatometric EDTA titration method and a spectrophotometric molybdovanadophosphate method, respectively. The basal spacing of the OCP structure was taken from the (100) reflection.

Results and Discussion

A change in the basal spacing was observed for the succinate-OCP, and this is the most direct and reliable indication of the introduction of succinate into the OCP structure. Table 1 lists the basal spacings, Ca/P ratios of the ref-OCP and succinate-OCP with some relevant data. The data about the ref-OCP were admitted within experimental errors as those of OCP having adsorbed water. The succinate-OCP showed an expansion in basal spacing and an increased in Ca/P ratio, compared with the ref-OCP. Such changes keeping the OCP structure suggested that the replacement of HPO_4^{2-} by $C_4H_4O_4^{2-}$ took place within the structure, not on the surface. From a structural point of view on the OCP unit-cell structure,[1] it was speculated that two of the four HPO_4^{2-} groups within the B-layer seemed more exchangable than the other two HPO_4^{2-} groups which were considered to be tightly bound by sharing one oxygen of HPO_4^{2-} in the A-layer. Therefore, the two HPO_4^{2-} groups would posses a comparatively high probability for the replacement. A general formula was established to be $Ca_8(HPO_4)_{2-z}(PO_4)_4(C_4H_4O_4)_z\cdot mH_2O$ $z=0—1$. The succinate-OCP had the composition $Ca_8(HPO_4)_{1.17}(PO_4)_4(C_4H_4O_4)_{0.83}\cdot 5.5H_2O$. Here, the value of z was determined from the Ca/P ratio (1.55), and m was estimated by distributing the residual amount (19.5%), except the analytical amounts of Ca (31.8%) and PO_4 (48.7%), among 1.17(H), 0.83 ($C_4H_4O_4$), and $m(H_2O)$. Similarly, the ref-OCP was $Ca_8(HPO_4)_2(PO_4)_4\cdot 5.1H_2O$. Repeated runs with a little difference in initial pH seemed to cause sensitively variations within the ranges $0.7\lesssim z<1.0$ and $5\lesssim m\lesssim 7$.

Table 1. Charactors of succinate-OCP in comparison with ref-OCP

Prepared OCP	Basal spacing d_{100}/Å	Ca/P (mole ratio)	Weight loss/%[a]			Calcination product by X-ray[a]		Composition[b]	
			400 °C	700 °C	900 °C	700 °C	900 °C	z	m
Ref-OCP	18.7	1.34	9.8	11.1	11.4	Ap	β-T, β-Py	0	5.1
Succinate-OCP	21.5	1.55	10.3	13.2	17.4	Ap	α-T, β-T, Ap	0.83	5.5

a) Heated up to each temperature at 10 °C min^{-1}. Ap: Apatitic phase, α- and β-T: α- and β-$Ca_3(PO_4)_2$, β-Py: β-$Ca_2P_2O_7$. b) A general formula was assumed as $Ca_8(HPO_4)_{2-z}(PO_4)_4$ $(C_4H_4O_4)_z\cdot mH_2O$. See in the text.

References

1) W. E. Brown, M. S. Tung, and L. C. Chow, *Proc. 2nd, Int. Congr. Phosphorus Compd.*, **1981**, 59; H. Monma, *Gypsum and Lime* (*Sekko To Sekkai*), No. 156, 6 (1978).

2) C. Rey, J. C. Trombe, and G. Montel, *C. R. Hebd. Seanas Acad. Sci., Ser. C*, **283**, 465 (1976).

3) H. Monma, S. Ueno, and T. Kanazawa, *J. Chem. Tech. Biotechnol.*, **31**, 15 (1981).

4) H. Monma, *J. Mater. Sci.*, **15**, 2428 (1980).

Absolute Configurations Assigned to Some Octahedral *cis*-Bis(diamine)cobalt(III) Complexes on the Basis of Their Stereoselective Interactions in Solution

Katsuhiko MIYOSHI, Kenzo WATANABE, Yoshihisa TODA, and Hayami YONEDA*

Department of Chemistry, Faculty of Science, Hiroshima University, Higashi-senda-machi, Naka-ku, Hiroshima 730

(Received June 21, 1983)

Synopsis. Absolute configurations are assigned to some cationic *cis*-$[Co(diamine)_2(X)(Y)]^{n+}$-type complexes by detecting the direction of the chiral equilibrium shift induced for $[Cr(ox)_3]^{3-}$ in the presence of these chiral complexes in water–dioxane mixtures. The assignments are found all consistent with those made earlier by CD spectra.

In our previous work,[1] it was established that the Δ isomer of $[Cr(ox)_3]^{3-}$ is gradually enriched when the racemate is mixed with Λ-*cis*-$[M(diamine)_2(X)(Y)]^{n+}$-type complexes (M=$Co^{3+}$ or Cr^{3+}, diamine=ethylenediamine (en) or trimethylenediamine (tn), and X and/or Y=anionic ligand) in water–dioxane mixtures. This implies that a heterochiral[2] combination (Δ-Λ or Λ-Δ) is favored over a homochiral one (Δ-Δ or Λ-Λ) in the stereoselective interaction between $[Cr(ox)_3]^{3-}$ and *cis*-$[M(diamine)_2(X)(Y)]^{n+}$ in solution, and that the above phenomenon called the Pfeiffer effect[3] provides a new technique for assigning the absolute configuration to these optically stable, cationic complexes. In the present study, an attempt is made to extend the applicability of the above technique to other *cis*-$[M(diamine)_2(X)(Y)]^{n+}$-type complexes.

Experimental

Preparation of Complexes. The following complexes were prepared and resolved as described by earlier workers; *cis*-$[Co(CN)(X)(en)_2]^{n+}$ (X=NO_2^-, Cl^-, Br^-, and OH_2),[4] *cis*-$[Cr(CN)_2(en)_2]^+$,[5,6] *cis*-$[Co(Cl)(RNH_2)(en)_2]^{2+}$ (R=CH_3 and C_2H_5),[7] *cis*-$[Co(Cl)(RNH_2)(tn)_2]^{2+}$ (R=H and CH_3),[8] *cis*-$[Co(NCS)_2(tn)_2]^+$,[9] $[Co(gly)(tn)_2]^{2+}$,[10] *cis*-$[Co(Cl)(OH_2)(en)_2]^{2+}$,[11,12] *cis*-$[Co(NO_2)(OH_2)(en)_2]^{2+}$,[11] *cis*-$[Co(Cl)(NCS)(en)_2]^{2+}$,[13] and *cis*-$[Co(NCS)(OH_2)(en)_2]^{2+}$.[11] The purity of these complexes was checked by both ion-exchange chromatography and absorption and/or CD spectra. The λ_{max} of the first d-d band for *cis*-$[Co(CN)(NO_2)(en)_2]^+$ was reported to be 437 nm in Ref. 4, but our sample had an absorption maximum at 423—424 nm. As judged from the λ_{max} values for the *cis*-dinitro (439 nm) and *cis*-dicyano (400 nm) complexes, the value reported in Ref. 4 is probably in error.

Detection of Pfeiffer Effect. The Pfeiffer effect of $[Cr(ox)_3]^{3-}$ was detected in the same manner as before.[1] That is, the sample solution was prepared by adding aqueous racemic $K_3[Cr(ox)_3]\cdot 3H_2O$ (8×10^{-5} mol) to the above optically active complex (2×10^{-4} mol) in a volumetric flask (10 ml) to which 3 ml of dioxane was added. After it was kept standing overnight in the dark, it was passed through a cation-exchange column (Dowex 50 W X1, Na^+-form) to remove the optically active, cationic complex added as an environment substance.[3] The absorption and CD spectra of the effluent were recorded as quickly as possible on a Shimadzu UV-200 and a JASCO J-40CS spectrometers, respectively. The direction and degree of the equilibrium shift in initially racemic $[Cr(ox)_3]^{3-}$ were determined by comparing the sign and intenity of the CD spectrum thus recorded with those of optically pure $[Cr(ox)_3]^{3-}$.[14]

Results and Discussion

In Table 1 is listed the enantiomer of $[Cr(ox)_3]^{3-}$ enriched when *cis*-$[M(diamine)_2(X)(Y)]^{n+}$-type complexes given in the first column are employed as a chiral environment substance in water–dioxane mixtures. Except for the last two tn complexes, a Λ configuration

Table 1. Absolute configuration of enriched isomer of $[Cr(ox)_3]^{3-}$

Environment substance (Λ-configuration)	Assigned by (Ref.)	Enriched isomer
$(+)_{589}$-*cis*-$[Co(en)_2(CN)_2]^+$	X-ray[a]	Δ
$(+)_{546}$-*cis*-$[Co(en)_2(CN)(NO_2)]^+$	CD(4)	Δ
$(-)_{546}$-*cis*-$[Co(en)_2(CN)(Cl)]^+$	CD(4)	Δ
$(-)_{546}$-*cis*-$[Co(en)_2(CN)(Br)]^+$	CD(4)	Δ
$(+)_{546}$-*cis*-$[Co(en)_2(CN)(OH_2)]^{2+}$	CD(4)	Δ
$(+)_{546}$-*cis*-$[Cr(en)_2(CN)_2]^+$	CD(5)	Δ
$(+)_{589}$-*cis*-$[Co(en)_2(Cl)(NH_3)]^{2+}$	X-ray[b]	Δ
$(+)_{589}$-*cis*-$[Co(en)_2(Cl)(CH_3NH_2)]^{2+}$	CD(7)	Δ
$(+)_{589}$-*cis*-$[Co(en)_2(Cl)(C_2H_5NH_2)]^{2+}$	CD(7)	Δ
$(+)_{546}$-*cis*-$[Co(en)_2(Cl)(NCS)]^+$	CD(13), CT[c](11)	Δ
$(+)_{589}$-*cis*-$[Co(en)_2(NCS)(OH_2)]^{2+}$	CT[c](11)	Δ
$(+)_{589}$-*cis*-$[Co(en)_2(Cl)(OH_2)]^{2+}$	CT[c](11)	Δ
$(+)_{589}$-*cis*-$[Co(en)_2(NO_2)(OH_2)]^{2+}$	CT[c](11)	Δ
$(+)_{589}$-$[Co(tn)_2(gly)]^{2+}$	CD(10)	Δ
$(-)_{589}$-*cis*-$[Co(tn)_2(NCS)_2]^+$	X-ray(17)	Δ
$(-)^{CD}_{500}$-*cis*-$[Co(tn)_2(Cl)(NH_3)]^{2+}$	d)	Δ
$(-)^{CD}_{490}$-*cis*-$[Co(tn)_2(Cl)(CH_3NH_2)]^{2+}$	d)	Δ

a) K. Matsumoto, S. Ooi, and H. Kuroya, *Bull. Chem. Soc. Jpn.*, **44**, 2721 (1971). b) M. Kuramoto, Y. Kushi, and H. Yoneda, *ibid.*, **51**, 3196 (1978). c) CT refers to chemical transformation. d) Assigned by the present work.

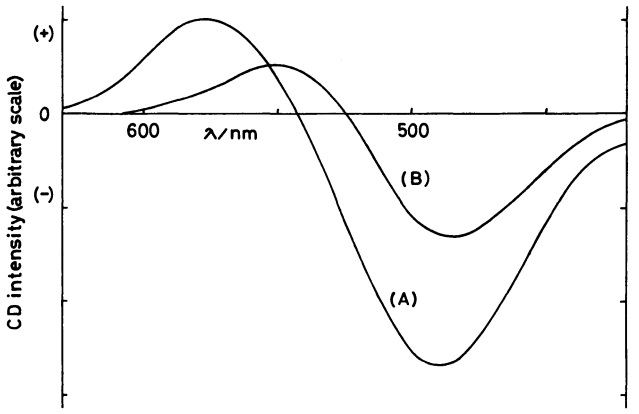

Fig. 1. CD patterns of $(-)^{CD}_{490}$-*cis*-$[Co(Cl)(CH_3NH_2)(tn)_2]^{2+}$ (A) and of $(-)^{CD}_{485}$-*cis*-$[Co(CH_3NH_2)_2(tn)_2]^{3+}$ derived therefrom (B).

has been assigned to these bis(diamine) complexes mainly on the basis of their CD spectra in the first d-d band. It is evident in Table 1 that the chiral equilibrium of $[Cr(ox)_3]^{3-}$ is always displaced toward its Δ enantiomer in the presence of Λ-*cis*-$[M(diamine)_2(X)(Y)]^{n+}$-type complexes. The enantiomer excess actually attained at equilibrium is around 1.0 and 1.5% under the present experimental conditions for uni- and bi-valent environment substances, respectively, in keeping with our previous results.[1] If the heterochiral combination (Δ-Λ or Λ-Δ) is favored as before, it is concluded that the absolute configurations assigned earlier to these complexes are all consistent with our present experimental results.

The last two bis(tn) complexes have already been resolved,[8] but the absolute configuration is not yet assigned to them. In Fig. 1 is shown the CD pattern of partially resolved $(-)^{CD}_{490}$-*cis*-$[Co(Cl)(CH_3NH_2)(tn)_2]^{2+}$ forming a less-soluble diastereomer with bis[μ-(+)-tartrato(4−)]bis[arsenate(III)]$^{2-}$ ion. The corresponding ammine complex exhibits a similar CD pattern as expected. These tn complexes have a negative major CD component at the higher energy side, suggesting a Δ configuration.[15] Our experimental results, however, lead us to assign a Λ configuration to these complexes, since they enrich the Δ enantiomer of $[Cr(ox)_3]^{3-}$. Then, $(-)^{CD}_{490}$-*cis*-$[Co(Cl)(CH_3NH_2)(tn)_2]^{2+}$ was converted to the corresponding bis(methylamine) complex by refluxing it in liquid methylamine, followed by purification with use of ion-exchange chromatography. Figure 1 clearly shows that the CD pattern of the bis(methylamine) complex thus derived is quite similar to that of Λ-*cis*-$[Co(NH_3)_2(tn)_2]^{3+}$ reported by Sano *et al.*[16] This observation is consistent with our present assignment made by the Pfeiffer effect, if so-called Walden inversion does not take place in the above substitution reaction as in the reaction of $(+)_D$-*cis*-$[Co(Cl)(NH_3)(en)_2]^{2+}$ with NH_3 to give $(+)_D$-*cis*-$[Co(NH_3)_2(en)_2]^{3+}$.[11] Thus, the criteria proposed by McCaffery *et al.*[13–15] for predicting the absolute configuration on the basis of the CD spectra, seem not to hold for these complexes with six-membered tn chelates, though they are fairly valid for the *cis*-$[M(X)_2(tn)_2]^+$-type complexes[17] as well as for $[M(acac)(tn)_2]^{2+}$,[18] $[Co(gly)(tn)_2]^{2+}$,[10] and $[M(ox)(tn)_2]^+$.[19]

In this way, our newly proposed technique serves well as a useful means to predict the absolute configuration of *cis*-$[M(diamine)_2(X)(Y)]^{n+}$-type complexes in which X and/or Y are anionic ligands and M may be other than Co^{3+} or Cr^{3+}. As a result, the Pfeiffer effect is applicable to deduce the absolute configuration of not only optically labile complexes[3,20,21] whose chiral equilibria are to be displaced, but also optically stable complexes when they are employed as an environment substance.

References

1) K. Miyoshi, Y. Matsumoto, and H. Yoneda, *Inorg. Chem.*, **20**, 1057 (1981).
2) S. F. Mason, "Molecular Optical Activity and Chiral Discrimination," Cambridge Univ. Press, London (1982), Chap. 11.
3) For Reviews, S. Kirschner, N. Ahmad, C. Munir, and R. J. Pollock, *Pure Appl. Chem.*, **51**, 913 (1979); S. Kirschner and I. Bakker, *Coord. Chem. Rev.*, **43**, 325 (1982).
4) K. Ohkawa, J. Hidaka, and Y. Shimura, *Bull. Chem. Soc. Jpn.*, **39**, 1715 (1966); **40**, 2830 (1967).
5) S. Kaizaki, J. Hidaka, and Y. Shimura, *Bull. Chem. Soc. Jpn.*, **48**, 902 (1975).
6) A. P. Sattelberger, D. D. Darsow, and W. B. Schaap, *Inorg. Chem.*, **15**, 1412 (1976); A. D. Kirk and G. B. Porter, *ibid.*, **19**, 445 (1980).
7) I. J. Kindred and D. A. House, *Inorg. Chim. Acta*, **14**, 185 (1975).
8) B. M. Oulaghan and D. A. House, *Inorg. Chem.*, **17**, 2197 (1978).
9) H. Kawaguchi and S. Kawaguchi, *Bull. Chem. Soc. Jpn.*, **43**, 2103 (1970).
10) G. R. Brubaker and D. P. Schaefer, *Inorg. Chem.*, **10**, 2170 (1971).
11) K. Garbett and R. D. Gillard, *J. Chem. Soc.*, **1965**, 6084; *Coord. Chem. Rev.*, **1**, 179 (1966).
12) J. W. Vaughn and R. D. Lindholm, *Inorg. Synth.*, **9**, 163 (1967).
13) K. Yamasaki, J. Hidaka, and Y. Shimura, *Bull. Chem. Soc. Jpn.*, **49**, 3060 (1976).
14) A. J. McCaffery, S. F. Mason, and R. E. Ballard, *J. Chem. Soc.*, **1965**, 2883; K. B. Butler and M. R. Snow, *J. Chem. Soc., Dalton Trans.*, **1976**, 251.
15) A. J. McCaffery, S. F. Mason, and B. J. Norman, *J. Chem. Soc.*, **1965**, 5094.
16) M. Sano, M. Fujita, K. Sasaki, Y. Yoshikawa, and H. Yamatera, *Bull. Chem. Soc. Jpn.*, **54**, 2823 (1981).
17) M. Nakano and S. Kawaguchi, *Bull. Chem. Soc. Jpn.*, **52**, 3563 (1979); K. Matsumoto, S. Ooi, H. Kawaguchi, M. Nakano, and S. Kawaguchi, *ibid.*, **55**, 1840 (1982); E. Perdersen, *Acta Chem. Scand.*, **24**, 3362 (1970).
18) M. Nakano, S. Kawaguchi, and H. Kawaguchi, *Bull. Chem. Soc. Jpn.*, **52**, 2897 (1979).
19) G. R. Brubaker and D. P. Schaefer, *Inorg. Chem.*, **10**, 968 (1971); D. A. House, *Inorg. Chim. Acta*, **60**, 145 (1982).
20) S. Kirschner, *J. Indian Chem. Soc.*, **51**, 28 (1974); N. Ahmad and S. Kirschner, *Inorg. Chim. Acta*, **14**, 215 (1975).
21) K. Ogino and T. Kumagai, *Bull. Chem. Soc. Jpn.*, **47**, 855 (1974).

Coagulated Ion-exchanger Colorimetry for the Determination of Trace Amounts of Sulfide as Methylene Blue

Kiichi MATSUHISA,† Kunio OHZEKI,* and Tomihito KAMBARA††
Department of Chemistry, Faculty of Science, Hokkaido University, Sapporo 060
†*Division of Environmental Conservation, Graduate School of Environmental Science, Hokkaido University, Sapporo 060*
(Received July 5, 1983)

Synopsis. Sulfide ion was converted to Methylene Blue through the reaction with *N,N*-dimethyl-*p*-phenylenediamine in the presence of iron(III) ion. The dye produced was fixed by batch method onto the coagulated mixture of finely divided anion and cation exchange resins. The coagulated material was collected by filtration on a filter paper as a disk of thin layer, which was then soaked in an acetate buffer solution, and subjected to the spectrophotometric analysis. The calibration graph was linear over the range 1.03—10.3 nmol of sulfide. The method was applied to some hot spring waters.

The most familiar method for the determination of sulfide is the Methylene Blue method,[1,2] which was recommended by Emil Fisher as early as 1883.[3] The sensitivity of the method is rather high but the enrichment is usually required for the determination of trace amounts of sulfide in water. Recently, a flotation method was reported,[4] in which the Methylene Blue formed through the reaction of sulfide with *N,N*-dimethyl-*p*-phenylenediamine in the presence of iron(III) ion was separated by flotation with sodium dodecyl sulfate. Down to 2 μg of sulfide in 1-dm³ sample solution was determined.

In the present paper, the coagulated ion-exchanger colorimetry[5,6] is examined for the Methylene Blue method. The colored compound is concentrated in the thin layer of mixed ion exchange resins by a factor greater than 700 and determined spectrophotometrically.

Experimental

Reagents. A 0.1 w/v% solution of *N,N*-dimethyl-*p*-phenylenediammonium sulfate (abbreviated as DPDA, Wako Pure Chemicals) was prepared by dissolving 0.1 g of the reagent in 100 ml of 5 mol dm^{-3} sulfuric acid. A 0.1 mol dm^{-3} iron(III) chloride solution was prepared by dissolving 2.7 g of iron(III) chloride hexahydrate in 50 ml of hydrochloric acid and then diluting to 100 ml with water. An aqueous 1.0% zinc(II) acetate solution was prepared. The crystals of sodium sulfide nonahydrate, $Na_2S \cdot 9H_2O$, were rinsed with a small amount of water and dried and stored under nitrogen atmosphere. A 0.01 mol dm^{-3} sulfide solution was prepared by dissolving dried reagent in oxygen-free water and standardized immediately before use by iodometry. The sulfide standard solution was prepared fresh every time when the determination was carried out. The solution was diluted 100 times with oxygen-free water and further 100 times with the zinc(II) acetate solution to give a 1.0 μmol dm^{-3} solution. Methylene Blue used was a Merck product for microscopy. The reagent was dried for 4 h at 105 °C, and aqueous 1.0 mmol dm^{-3} stock solution was prepared.

Ion Exchange Resin Suspension. The macroreticular type ion exchangers, Amberlyst 15 and A-27 (Rohm and Haas), were used in RSO_3H and $RN(CH_3)_3Cl$ forms, respectively. The cation exchange resin suspension (CRS) and anion exchange resin suspension (ARS) were prepared according to the method reported.[7] The exchange capacities were 11.8 μequiv ml^{-1} for CRS and 7.0 μequiv ml^{-1} for ARS. When a 2.0-ml portion of CRS was mixed with 4.0 ml of ARS, both resins were coagulated completely with each other and the mixed resins were easily and quantitatively collected on a filter paper.

Apparatus. A Shimadzu UV 140-01 spectrophotometer was used. A Toyo KG-25 filter holder was used with filter papers of No. 5B (Toyo Roshi). A vaccum guage used was a NRK product, type STV-75.

General Procedure. A 25-ml portion of the zinc(II) acetate solution was placed in a 100-ml separatory funnel, and a sample solution containing less than 10.3 nmol of sulfide was added, and then the solution was diluted to 50 ml with the zinc(II) acetate solution. A 5-ml portion of DPDA solution and 1 ml of the iron(III) chloride solution were quickly added and the reaction mixture was shaken vigorously for 1 min and allowed to stand for 60 min. A 4.0-ml portion of ARS and 2.0 ml of CRS were then added to the solution and the mixture was shaken for 10 min. The resulting coagulated resins were collected on the filter strip placed on the holder by filtration with suction (600 mmHg). A disk of colored thin layer, 17 mm in diameter and about 0.3 mm in thickness, was formed. The filter strip supporting the thin layer was soaked in the acetate buffer solution (pH 4.6) for 15 min, and it was fixed on a glass plate on the one side of cell holder which is nearer to the light source. The absorbance was measured at 675 nm against the dry filter paper or another white paper. Another disk of thin layer was prepared without addition of sulfide and the absorbance corresponding to the reagent blank including the resins was also measured. The net absorbance of Methylene Blue in the resin phase was determined by substruction. Fundamental experiments were performed according to the above procedure with the exception that the pure Methylene Blue solution was used instead of the standard sulfide solution.

Results and Discussion

Adsorption of Methylene Blue. Methylene Blue was found to be strongly fixed on the cation exchange resin. The cation exchange resin was coagulated with anion exchange resin to form a bulky material and separated from the bulk solution within 8 min. The disk of colored thin layer with a smooth surface was obtained on the filter paper. The volume of resin phase being about 0.07 cm³, Methylene Blue was concentrated from 50 ml of the reaction mixture by a factor greater than 700.

Adsorption Spectrum. The absorption spectrum of Methylene Blue in the resin phase was slightly shifted to longer wavelength compared with that in solution (Fig. 1). The effect of pH was studied. The pH of initial solution, from which Methylene Blue was fixed on the mixed resins, was kept at 0.8, and the resulting thin layer was soaked for 15 min in the solutions with various

†† Present address: Hakodate Technical College, Tokuracho 226, Hakodate 042.

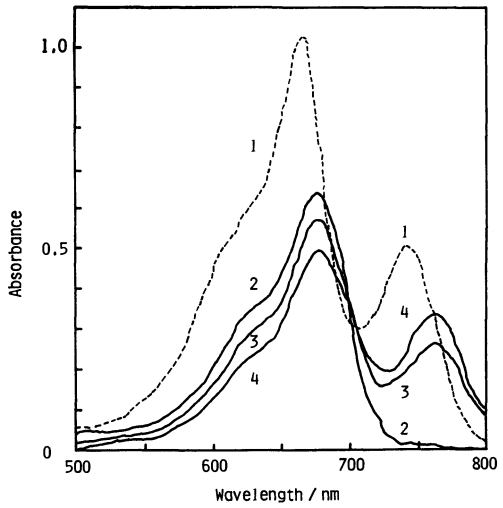

Fig. 1. Effect of pH on the absorption spectra of 6 nmol of Methylene Blue on the thin layer of mixed resins. The absorbance was measured after soaking the thin layer for 15 min in varying pH solutions; 2) 4.62, 3) 1.04, 4) 0.80. Dotted line (1) indicates the absorption spectrum of 20 μmol dm^{-3} Methylene Blue solution at pH 0.80 in a 1-cm cell.

Table 1. Effect of foreign ions on the determination of 6.25 nmol of sulfide ion

Compound	Added amount / μmol	Absorbance at 675 nm	Error / %
None	—	0.327	—
$NaNO_2$	0.06	0.320	−2.1
	0.60	0.319	−2.4
	6.00	0.196	−41.9
$NaHSO_3$	6.00	0.325	−0.6
$HSCH_2COONa$	6.56	0.354	+8.2

Table 2. Determination of sulfide in hot spring water

Sampling place	Sample amounts / ml	Absorbance at 675 nm	Sulfide found / ng S ml^{-1}
Shirogane	4.0	0.244	35.6
(pH = 6.76)	6.0	0.362	35.2
	6.0	0.364	35.4
	8.0	0.458	33.4
	8.0	0.496	36.2
			35.2±1.3[a)]
Nakagoya	0.5	0.488	569.5
(pH=9.11)	0.5	0.468	546.1
	0.5	0.476	555.5
			557.0±29.3[a)]

a) 95% confidence limits.

pH values. With increasing pH, the absorbance at the maximum of 675 nm increased, while that of 760 nm decreased, which indicates that the latter absorption maximum is due to the protonated Methylene Blue.[1)]

Effect of Soaking Time. When the thin layer was soaked in the acetate buffer solution of pH 4.6, the absorbance of Methylene Blue at 675 nm increased gradually and reached a constant value within 10 min. Thereafter the coloration was stable for at least 60 min. The use of acetate buffer soaking solution is advantageous for the sensitivity and stability of the coloration.

Standing Time of Reaction Mixture. When the color developing reagents were added to the test solutions with and without sulfide, a violet color appeared immediately in both solutions. The blank coloration faded gradually and after 60 min, the lower blank value and the stable coloration of Methylene Blue were obtained.

Calibration Graph. The calibration graph showed a good proportionality over range 1.03—10.3 nmol of sulfide, with absorbance ranging from 0.054 to 0.543. The relative standard deviations were 8.5% (n=4) for 1.03 nmol and 1.5% (n=5) for 10.3 nmol of sulfide. The yield of Methylene Blue from sulfide was estimated by comparing the slope of calibration curve with that of pure Methylene Blue. The reaction yield was calculated to 52.5%, while the value reported by Gustafsson was 66.7%.[1)]

Effect of Foreign Ions. As summarized in Table 1, a large amount of nitrite gave a serious negative error, which is due to the reduction of iron(III) ion.[4)] Mercaptoacetate gave a positive error.[8)]

Determination of Sulfide in Hot Spring Water. The sample waters were clear enough and so directly subjected to the analysis. The sulfide was precisely determined in the varying sample aliquots (Table 2). The pH of sample water at Nakagoya was higher than that at Shirogane, and the former contained sulfide in higher concentration than the latter.

References

1) L. Gustafsson, *Talanta*, **4**, 227 (1960).
2) O. G. Koch and G. A. Koch-Dedic, "Handbuch der Spurenanalyse," Springer-Verlag, Berlin (1974), p. 1004.
3) E. Fisher, *Ber.*, **16**, 2234 (1883).
4) M. Aoyama, T. Hobo, and S. Suzuki, *Bunseki Kagaku*, **31**, E7 (1982).
5) K. Ohzeki, T. Sakuma, and T. Kambara, *Bull. Chem. Soc. Jpn.*, **53**, 2878 (1980).
6) K. Matsuhisa, K. Ohzeki, and T. Kambara, *Bull. Chem. Soc. Jpn.*, **54**, 2675 (1981).
7) M. Abe, K. Ohzeki, and T. Kambara, *Bull. Chem. Soc. Jpn.*, **51**, 1090 (1978).
8) S. Vasireddy, K. W. Street, Jr., and H. B. Mark, Jr., *Anal. Chem.*, **53**, 868 (1981).

Cycloaddition of Diphenylcyclopropenone with Carboximidate, Carboximidamide, and Carboximidothioate

Hiroshi YOSHIDA,* Shingo SOGAME, Shoichi BANDO, Shosuke NAKAJIMA, Tsuyoshi OGATA, and Kiyoshi MATSUMOTO†

Department of Applied Chemistry, Faculty of Engineering, Shizuoka University, Hamamatsu 432

†College of Liberal Arts and Sciences, Kyoto University, Sakyo-ku, Kyoto 606

(Received March 23, 1983)

Synopsis. The reaction of diphenylcyclopropenone with $R^1N{=}C(R^2)X$ (**2**) (R^1, R^2=alkyl, aryl, X=MeO, EtO, MeS, or Me_2N) gave 2-pyrrolin-4-one (**3**) in good yield. The less reactive carboximidothioate (**2**, R^1=4-MeC_6H_4, R^2=Ph, X=MeS) yielded isomeric 3-pyrrolin-2-one together with **3**.

In a previous paper[1] we have reported the reaction of *N*-imidoyl sulfoximide with diphenylcyclopropenone to yield the sulfoximide substituted with pyrrolinone ring together with pyrimidinone *via* [2+3] and [3+3]cycloaddition reactions:

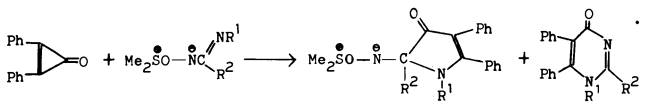

Eicher and his coworkers have reported that ketimine reacts with diphenylcyclopropenone **1** to yield 2-pyrrolin-4-one derivative by [2+3]cycloaddition reaction.[2] However, no work has been undertaken on the *N,N,N'*-trisubstituted carboximidamide, carbiximidate, and carboximidothioate (**2**). In this paper we report the reactivities of these compounds with diphenylcyclopropenone.

An equimolar mixture of **1** and **2** in benzene (reaction at 80 °C) or xylene (over 100 °C) was heated at suitable temperature. The reaction was followed by TLC. The products isolated by column chromatography were 2-pyrrolin-4-one (**3**), but in the case of **2j**, **3j**, and 3-pyrrolin-2-one (**4j**) were obtained. The yields of **3** and **4** and their physical properties are summarized in Table 1.

The structures of the products were elucidated on the basis of their elemental analyses, ^{1}H-NMR and mass spectroscopic studies as well as chemical transformations. Mass spectra of **3c**, **3g**, and **3j** showed peaks corresponding to the groups PhC=C(Ph)–NR^1 together with the parent peaks. Although **4j** showed a peak corresponding to PhC=C(Ph)–CPh, no such peak was observed for **3j**.

Some products were subjected to drastic hydrolysis. On treating with hot mixture of aqueous acetic and sulfuric acids, **3b**, **3e**, **3g**, **3i**, and **3j** gave the known triphenylfuranone (**5**)[2c] in moderate yields, while the isomer **4j** yielded the acid **6**.[3]

It has been reported that *N*-methyl and *N*-phenylketimines react completely with **1** in boiling 1,2-dimethoxyethane (at about 83 °C) within 20 min and 2—5 h respectively.[2c] Table 1 indicates that the reactivity of **2** decreased in orders on R^1: alkyl>aryl, X: NMe_2> OMe, and OEt>SMe. Although the reactivities of **2** were lower than those of ketimines, the electron-releasing effects of substituents on R^1 and X would account for the reactivities of **2**. Nucleophilic attack of the imino nitrogen on the cyclopropenone **1** gave **3** or **4** depending on the attacking site. The major products were 2-pyrrolin-4-ones (**3**) whereas the less reactive **2j** showed lower selectivity under more drastic conditions giving a mixture of **3j** and **4j**. In conclusion, the reaction of **1** with

TABLE 1. YIELDS AND PHYSICAL PROPERTIES OF **3** AND **4**

Reactant	Reaction conditions: Temp/°C	Reaction conditions: Time/h	Product	Yield %	Mp θ_m/°C	(Recryst solvent)[a]	^{1}H-NMR (δ in $CDCl_3$)[b]	M^+	Found (Calcd) (%): C	H	N
2a	110	2	**3a**	90	105—106	(E-P)	1.65 (3H, s, MeC–N), 2.00 (3H, s, MeS) 3.05 (3H, s, MeN)	309	73.79 (73.75)	6.27 (6.19)	4.44 (4.53)
2b	80	3	**3b**	73	157—158	(E-P)	1.36 (3H, t, J=7 Hz, $\underline{Me}CH_2$), 2.76 (3H, s, MeN), 3.65 (2H, q, CH_2)	369	81.51 (81.27)	6.18 (6.27)	3.83 (3.79)
2c	110	4	**3c**	88	96	(E-P)	2.09 (3H, s, MeS), 2.97 (3H, s, MeN)	371	77.24 (77.57)	5.81 (5.70)	3.91 (3.77)
2d	110	2	**3d**	85	142	(C-P)	0.55 (3H, t, J=7 Hz, $\underline{Me}CH_2$), 2.56 (6H, s, Me_2N), 3.30 (2H, dq, J=5 and 7 Hz, CH_2)	382	81.69 (81.64)	6.77 (6.85)	7.41 (7.32)
2e	110	16	**3e**	71	177—179	(C-P)	2.64 (6H, s, Me_2N)	430	83.47 (83.69)	6.11 (6.09)	6.49 (6.51)
2f	130	8	**3f**	61	165—168	(E-P)	3.65 (3H, s, MeO)	417	83.42 (83.43)	5.39 (5.55)	3.04 (3.35)
2g	130	8	**3g**	87	190—191	(E-P)	1.28 (3H, t, J=7 Hz, Me), 3.86 (2H. q. CH_2)	431	83.61 (83.50)	5.92 (5.84)	3.16 (3.25)
2h	110	10	**3h**	82	208—210	(C-P)	2.12 (3H. s, $\underline{Me}C_6H_4$), 2.52 (6H, s, Me_2N)	444	83.83 (83.75)	6.35 (6.35)	6.43 (6.30)
2i	130	8	**3i**	83	178—180	(E-P)	1.27 (3H, t, J=7 Hz, $\underline{Me}CH_2$) 2.16 (3H, s, $\underline{Me}C_6H_4$), 3.86 (2H, q, CH_2)	445	83.21 (83.57)	6.28 (6.11)	3.04 (3.15)
2j	140	18	**3j**	48	97—99	(P)	2.27 (3H, s, $\underline{Me}C_6H_4$), 2.34 (3H, s, MeS)	400[c]	80.77 (80.50)	5.64 (5.63)	2.99 (3.13)
			4j	33	104—106	(P)	1.98 (3H, s, MeS), 2.28 (3H, s, $\underline{Me}C_6H_4$)	400[c]	80.39 (80.50)	5.45 (5.63)	3.61 (3.13)
2k	110	10	**3k**	73	163	(C-P)	2.58 (6H, s, Me_2N), 3.68 (3H, s, MeO)	460	80.62 (80.81)	6.24 (6.12)	6.11 (6.08)
2l	110	10	**3l**	80	98—100	(C-P)	2.14 (3H, s, $\underline{Me}C_6H_4$), 2.46 (6H, s, Me_2N)	444	83.72 (83.75)	6.29 (6.35)	6.54 (6.30)

a) C: $CHCl_3$, E: EtOH, P: petroleum ether. b) Aryl ring protons were observed at δ 6.4—8.1 as multiplets. c) $M^+ - SMe$.

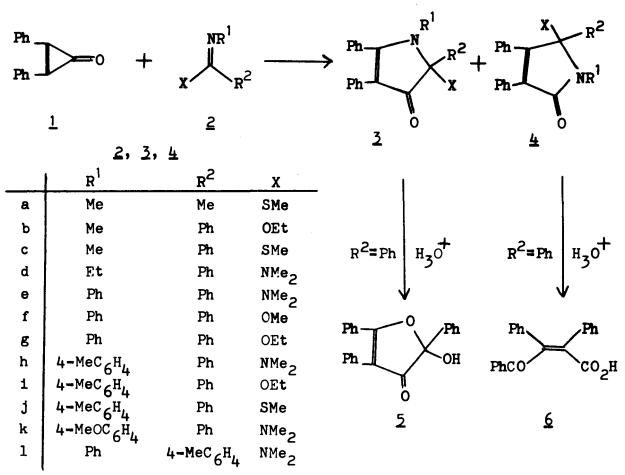

	R^1	R^2	X
a	Me	Me	SMe
b	Me	Ph	OEt
c	Me	Ph	SMe
d	Et	Ph	NMe_2
e	Ph	Ph	NMe_2
f	Ph	Ph	OMe
g	Ph	Ph	OEt
h	4-MeC_6H_4	Ph	NMe_2
i	4-MeC_6H_4	Ph	OEt
j	4-MeC_6H_4	Ph	SMe
k	4-$MeOC_6H_4$	Ph	NMe_2
l	Ph	4-MeC_6H_4	NMe_2

2 has proven to be a useful method for the preparation of 2-pyrrolin-4-ones (**3**).

Experimental

General. Melting points are uncorrected. ^{1}H-NMR spectra were recorded on a Hitachi Perkin Elmer R-24 (60 MHz) spectrometer using TMS as an internal standard, and mass spectra on a Hitachi RMU-7M mass spectrometer.

Preparation of Carboximide, Carboximidate, and Carboximidothioate. The compounds **2** were prepared by the usual methods.[4] Carboximidamides **2d**, **e**, **h**, **k**, and **21** were obtained from the corresponding imidoyl chlorides and excess dimethylamine in benzene. Carboximidates **2b**, **f**, **g**, and **2i** were prepared from the imidoylchlorides and sodium alkoxide in alcohol. Carboximidothioates **2a**, **c**, and **2j** were obtained by the reaction of the corresponding thioamides with methyl iodide followed by treatment with aqueous sodium hydroxide. The purity of the products was confirmed by ^{1}H-NMR. New compounds were as follows: **2h** (85%): oil; ^{1}H-NMR ($CDCl_3$) δ=2.04 (3H, s, Me), 2.83 (6H, s, Me_2N), and 6.2—7.6 (9H, m, Arom); *m/e* 238 (M^+). **21** (93%): oil; ^{1}H-NMR ($CDCl_3$) δ=2.17 (3H, s, Me), 2.89 (6H, s, Me_2N), and 6.4—7.4 (9H, m, Arom); *m/e* 238 (M^+).

The Reaction of 1 with 2. A solution of **1** (1.5 mmol) and **2** (2 mmol) was refluxed in a minimum amount of benzene or xylene (3—5 cm^3). The reaction was checked by TLC (aluminum oxide, petroleum ether : ethyl acetate, 1 : 1, v/v) until **1** reacted completely. After cooling, the mixture was chromatographed over silica gel (petroleum ether : ethyl acetate, 4 : 1, v/v). The products were crystallized from appropriate solvents.

Hydrolyses of 3 and 4. In a boiling mixture of acetic acid and sulfuric acid in water (50 : 1 : 25, v/v, 5 cm^3) pyrrolinone (50 mg) was hydrolyzed for 2 d. The resulting mixture was poured into water and extracted with chloroform. The extract was dried over sodium sulfate and evaporated under reduced pressure. **3b**, **e**, **g**, **i**, and **3j** gave triphenyl-3-(2*H*)-furanone **5**: mp 191—192 °C (lit, mp 192—193 °C).[2c] In contrast **4j** yielded the acid **6**: mp 172—174 °C (lit, mp 172 °C).[3]

References

1) H. Yoshida, S. Sogame, Y. Takishita, and T. Ogata *Bull. Chem. Soc. Jpn.*, **56**, 2438 (1983).

2) a) T. Eicher, F. Abdesaken, G. Franke, and J. L. Weber, *Tetrahedron Lett.*, **1975**, 3915; b) T. Eicher, G. Franke, and F. Abdesaken, *ibid.*, **1977**, 4067; c) T. Eicher, J. L. Weber, and G. Chatila, *Justus Liebigs Ann. Chem.*, **1978**, 1203; d) T. Eicher and G. Franke, *ibid.*, **1981**, 1337.

3) J. Hoch and R. Teixier, *C. R. Acad. Sci.*, **261**, 4132 (1965).

4) S. R. Sandler and W. Karo, "Organic Functional Group Preparations," Academic Press, New York (1972), Vol. III.

Studies of Cyanamide Derivatives. Part 109. A Convenient Method for Preparation of 4-Aminothiazole Compounds from Alkoxythiocarbonylcyanamide Salts

Toshio FUCHIGAMI,* Mou-Yung YEH, Tsutomu NONAKA, and Hsien-Ju TIEN†

Department of Electronic Chemistry, Graduate School at Nagatsuta, Tokyo Institute of Technology, Nagatsuta, Midori-ku, Yokohama 227

†*Department of Chemistry, National Cheng Kung University, Tainan, Taiwan, Republic of China*

(Received June 22, 1983)

Synopsis. α-Halo derivatives of ketones, ester, and nitrile reacted readily with potassium ethoxythiocarbonylcyanamide to provide the corresponding 4-amino-2-ethoxythiazole compounds in good yields, while α-halo amide did not. In a similar manner, α,α′-dihalo ketone reacted with 2 equiv of alkoxythiocarbonylcyanamide and *S*-methyl *N*-cyanocarbamodithioate salts to give the corresponding bis(4-amino-5-thiazolyl) ketones.

Cyanamide derivatives are very useful for synthesis of heterocyclic compounds having nitrogen atoms. In the course of our synthetic studies[1-7] of heterocyclic compounds using cyanamide derivatives, we have found a novel synthetic reaction of 4-aminothiazole compounds from potassium ethoxythiocarbonylcyanamide (**1**) and α-halo ketones.[7] The reaction should be interesting from an aspect that few studies[8] on the synthesis of 4-aminothiazoles have been reported, while a number of 2-aminothiazoles have been known. In addition, the reaction may be useful for the preparation of 4-aminothiazoles having unstable substituents, since it can proceed under quite mild reaction conditions.

In this work, we attempted some extensions of the reaction to more complicated α-halo ketones and α-halo derivatives of compounds other than ketones.

Results and Discussion

The reaction of **1** with **2** easily proceeded at room temperature eliminating potassium halide to form stable intermediate (**3**), and then **3** underwent the base-catalyzed cyclization to be converted into the final product (**4**), as shown in Scheme 1. In the course of the reaction, **3** was not isolated from the reaction mixture and one-pot reaction was carried out.

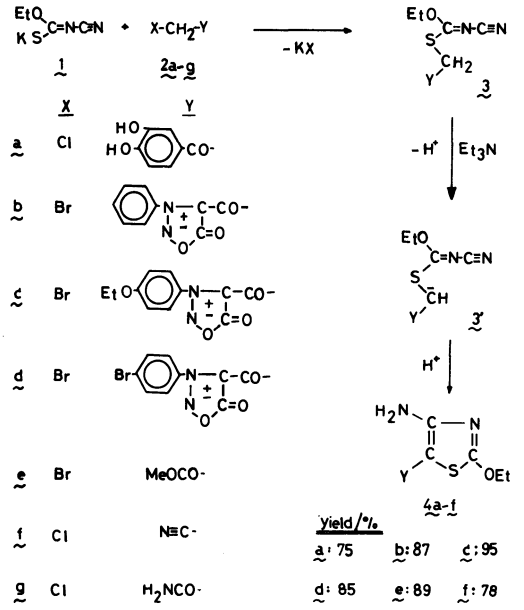

Scheme 1.

4-Aminothiazole (**4a**) having hydroxyl groups could be obtained in a fairly good yield from the corresponding α-halo ketone (**2a**).

Althogh sydnone compounds are generally interesting in their chemical, physical and biological properties,[9] their syntheses seem to be limited.[10,11] For instance, a few works dealing with the successful synthesis of sydnones having heterocyclic substituents have been reported: Only 4-(4-thiazolyl)[12] and 4-(1,2,4-oxadiazol-3-yl)sydnones[11] could be prepared in our previous works. In this point, the reaction of **1** with 3-aryl-4-(bromoacethyl)sydnone (**2b—d**) under such mild conditions, where a sydnone ring itself did not decompose, was successfully tried to prepare the corresponding 4-amino-5-thiazolyl 3-ary-4-sydnonyl ketones (**4b—d**).

The reaction was also extended to α,α′-dihalo ketone (1,3-dichloro-2-propanone, **7**) and consequently the corresponding bis(4-amino-5-thiazolyl)ketones (**8a—c**) were obtained in 31—87% yields using 2 equiv of cyanamide salts (**1**, **5**, and **6**), as shown in Scheme 2.

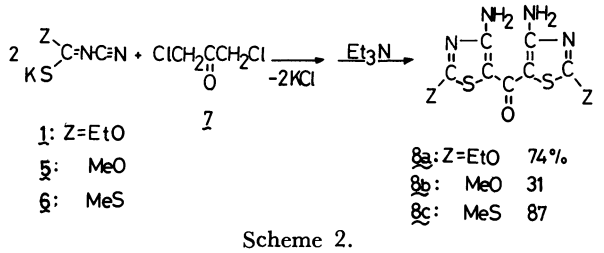

Scheme 2.

At the second stage of the investigation, the reaction was also extended to α-halo derivatives of compounds other than ketones. As shown in Scheme 1, α-halo ester (**2e**) and nitrile (**2f**) reacted with **1** to give the corresponding 4-aminothiazole compounds (**4e**, **f**) in high yields, while α-halo amide (**2g**) gave only the intermediate (**3g**) which could not cyclize under the conditions used. Since the initiation step of the cyclization seems to be carbanion (**3′**) formation from **3** by base-catalyzed proton abstraction, no occurrence of the cyclization of **3g** may be due to weaker electron-withdrawing effect of an amide group than the others.

Experimental

*3,4-Dihydroxyphenyl 2-Ethoxy-4-amino-5-thiazolyl Ketone (**4a**).*

To a stirred solution of 0.84 g (5 mmol) of potassium ethoxythiocarbonylcyanamide (**1**)[13] in 5 ml of acetone was gradually added a solution of 0.93 g (5 mmol) in 10 ml of acetone at room temperature. After 2 h of stirring, 0.31 ml of triethylamine was added to the reaction mixture. After additional 2 h of stirring, the reaction mixture was evaporated to dryness and the residue was mixed with water. The insoluble oily material was solidified with small amount of methanol and the resulting solid was collected by filtration. The yield was 1.05 g (75%). Recrystallization from aq. methanol provided 0.90 g (64%) of pure **4a**: mp 201—202 °C; IR (KBr) 1640 cm^{-1} (C=O); NMR (DMSO-d_6) δ=1.33 (t, 3H, $C\underline{H}_3CH_2$), 4.37 (q, 2H, $CH_3C\underline{H}_2$), 6.58—7.00 (m, 3H, Ar–H), 7.90 (s, 2H, $N\underline{H}_2$), and 9.00 (broad s, 2H, O<u>H</u>). Found: C, 51.42; H, 4.01; N, 9.97%. Calcd for $C_{12}H_{12}N_2O_4S$: C, 51.42; H, 4.32; N, 9.99%.

*4-Amino-2-ethoxy-5-thiazolyl 3-Phenyl-4-sydnonyl Ketone (**4b**).* To a stirred solution of 0.42 g (2.5 mmol) of **1** in 5 ml of acetone was gradually added a solution of 0.71 g (2.5 mmol) of 4-bromoacetyl-3-phenylsydnone[12] in 10 ml of acetone at room temperature. After 1 h of stirring, 0.1 ml of triethylamine was added to the reaction mixture. After additional 0.5 h of stirring, the reaction mixture was evaporated to dryness under reduced pressure. The residue was mixed with water and insoluble material was collected by filtration. The yield was 0.72 g (87%). Recrystallization from methanol provided 0.60 g (72%) of pure **4b** as yellow needles: mp 172—173 °C; IR (KBr) 1775 and 1605 cm^{-1} (C=O); NMR (DMSO-d_6) δ=1.37 (t, 3H, $C\underline{H}_3CH_2$), 4.40 (q, 2H, $CH_3C\underline{H}_2$), 7.50 (s, 5H, Ar–H), and 8.00 (s, 2H, $N\underline{H}_2$); MS *m/e* 332 (M^+). Found: C, 50.50; H, 3.59; N, 16.73%. Calcd for $C_{14}H_{12}N_4O_4S$: C, 50.60; H, 3.70; N, 16.86%.

*4-Amino-2-ethoxy-5-thiazolyl 3-(p-Ethoxyphenyl)-4-sydnonyl Ketone (**4c**).* In a similar manner, **4c** was obtained from **2c** in 95% yield. Recrystallization from ethanol provided pure **4c** as yellow needles: mp 171—172 °C; IR (KBr) 1775 and 1605 cm^{-1} (C=O); NMR (DMSO-d_6) δ=1.37 (t, 6H, $C\underline{H}_3CH_2$), 4.08 (q, 2H, $C\underline{H}_2OC_6H_4$), 4.43 (q, 2H, $CH_3C\underline{H}_2$), 7.02 (d, 2H, Ar–H), 7.52 (d, 2H, Ar–H), and 8.10 (s, 2H, $N\underline{H}_2$): MS *m/e* 376 (M^+). Found: C, 50.95; H, 4.18; N, 14.75%. Calcd for $C_{16}H_{16}N_4O_5S$: C, 51.06; H, 4.29; N, 14.89%.

*4-Amino-2-ethoxy-5-thiazolyl 3-(p-Bromophenyl)-4-sydnonyl Ketone (**4d**).* In a similar manner, **4d** was obtained in 85% yield. Recrystallization from ethanol provided pure **4d** as yellow needles: mp 163—164 °C; IR (KBr) 1775 and 1605 cm^{-1} (C=O); NMR (DMSO-d_6) δ=1.33 (t, 3H, $C\underline{H}_3CH_2$), 4.42 (q, 2H, $CH_3C\underline{H}_2$), 7.65 (q, 4H, Ar–H), and 8.19 (s, 2H, $N\underline{H}_2$): MS *m/e* 410 (M^+) and 412 (M^++2). Found; C, 40.98; H, 2.47; N, 13.61%. Calcd for $C_{14}H_{11}N_4O_4SBr$: C, 40.89; H, 2.70; N, 13.62%.

*4-Amino-2-ethoxy-5-methoxycarbonylthiazole (**4e**).* By the procedure similar to the preparation of **4b**, **4e** was obtained from methyl bromoacetate. The yield was 89%. Recrystallization from 20% aq methanol provided pure **4e** as colorless needles (83%): mp 80 °C; IR (KBr) 1620 cm^{-1} (C=O); NMR ($CDCl_3$) δ=1.37 (t, 3H, $C\underline{H}_3CH_2$), 3.65 (s, 3H, $C\underline{H}_3O$), 4.35 (q, 2H, $CH_3C\underline{H}_2$), and 5.70 (broad s, 2H, $N\underline{H}_2$); MS *m/e* 202 (M^+). Found: C, 41.30; H, 4.81; N, 13.65%. Calcd for $C_7H_{10}N_2O_3S$: C, 41.58; H, 4.98; N, 13.85%.

*4-Amino-5-cyano-2-ethoxythiazole (**4f**).* By the same procedure described above, **4f** was obtained from chloroacetonitrile. The yield was 78%. Recrystallization from methanol provided pure **4f** (60%); mp 148—149 °C IR (KBr) 2180 cm^{-1} (C≡N); NMR ($CDCl_3$) δ=1.43 (t, 3H, $C\underline{H}_3CH_2$), 4.44 (q, 2H, $CH_3C\underline{H}_2$), and 4.90 (broad s, 2H, $N\underline{H}_2$); MS *m/e* 169 (M^+). Found: C, 42.65; H, 3.90; N, 24.91%. Calcd for $C_6H_7N_3OS$: C, 42.59; H, 4.17; N, 24.83%.

*Reaction of **1** with Chloroacetamide.* The reaction was performed in a similar manner. After the reaction, the precipitating salt (KCl) was removed by filtration and the filtrate was concentrated to dryness provided **3g** in 100% yield. Recrystallization from methanol provided pure **3g**; mp 163—164 °C; IR (KBr) 2210, 2180 (C≡N) and 1660 cm^{-1} (C=O); MS *m/e* 187 (M^+). Found: C, 38.10; H, 4.84; N, 22.07%. Calcd for $C_6H_9N_3O_2S$: C, 38.49; H, 4.85; N, 22.44%.

*Bis(4-amino-2-ethoxy-5-thiazolyl) Ketone (**8a**).* The preparative procedure was described in the previous paper.[7]

*Bis(4-amino-2-methoxy-5-thiazolyl) Ketone (**8b**).* By the procedure similar to the preparation of **4** and **8a**, the reaction was carried out using 0.62 g (4 mmol) of potassium methoxythiocarbonylcyanamide (**5**),[3] 0.25 g (2 mmol) of 1,3-dichloro-2-propanone, and 0.1 ml of triethylamine in 10 ml of acetone. After the reaction, the reaction mixture was evaporated and the remaining residue was mixed with water. The insoluble oily material was separated from water and the oil was solidified with methanol, giving 0.18 g (31%) of crude **8b**. Recrystallization from DMF provided pure **8b**: mp 208—209 °C; IR (KBr) 3380, 3280 (NH) and 1600 cm^{-1} (C=O); NMR (DMSO-d_6) δ=3.97 (s, 6H, $C\underline{H}_3$) and 7.57 (s, 4H, $N\underline{H}_2$); MS *m/e* 286 (M^+). Found: C, 38.04; H, 3.49; N, 19.38%. Calcd for $C_9H_{10}N_4O_3S_2$: C, 37.75; H, 3.52; N, 19.57%.

*Bis(4-amino-2-methylthio-5-thiazolyl) Ketone (**8c**).* In a similar manner as above, the reaction was carried out using 1.70 g (10 mmol) of potassium *S*-methyl *N*-cyanocarbamodithioate (**6**),[3] 0.64 g (5 mmol) of 1,3-dichloro-2-propanone, and 0.4 ml of triethylamine. After work-up, 1.39 g (87%) of crude **8c** was obtained. Recrystallization from DMF–methanol provided pure **8c**: mp 250—251 °C; IR (KBr) 3480, 3370, 3300, 3250 (NH) and 1580 cm^{-1} (C=O); NMR (DMSO-d_6) δ=2.70 (s, 6H, $C\underline{H}_3$) and 7.66 (s, 4H, $N\underline{H}_2$); MS *m/e* 318 (M^+). Found: C, 33.83; H, 3.05; N, 17.58%. Calcd for $C_9H_{10}N_4OS_4$: C, 33.95; H, 3.17; N, 17.59%.

References

1) T. Fuchigami and K. Odo, *Chem. Lett.*, **1973**, 917.
2) T. Fuchigami and K. Odo, *Bull. Chem. Soc. Jpn.*, **48**, 310 (1975).
3) T. Fuchigami and K. Odo, *Bull. Chem. Soc. Jpn.*, **49**, 3165 (1976).
4) T. Fuchigami, T. Nonaka, and K. Odo, *Bull. Chem. Soc. Jpn.*, **49**, 3176 (1976).
5) T. Fuchigami and K. Odo, *Bull. Chem. Soc. Jpn.*, **49**, 3607 (1976).
6) T. Fuchigami and K. Odo, *Bull. Chem. Soc. Jpn.*, **50**, 1791 (1977).
7) T. Fuchigami and T. Nonaka, *J. Org. Chem.*, **48**, 3340 (1983).
8) M. Ota, "Fukusokan Kagaku," Baihukan, Tokyo (1957), Vol. 1, p. 142.
9) a) F. H. C. Stewart, *Chem. Rev.*, **64**, 129 (1964); b) M. Ota and H. Kato, "Non-benzenoid Aromatics," Academic Press, New York, N. Y. (1969), Vol. 1, Chap. 4.
10) M.-Y. Yeh, H.-J. Tien, and T. Nonaka, *J. Org. Chem.*, **48**, 1382 (1983).
11) M.-Y. Yeh, T. Nonaka, T. Goto, M.-C. Hsu, T. Fuchigami, and H.-J. Tien, *Bull. Chem. Soc. Jpn.*, **56**, 3535 (1983).
12) H.-J. Tien, K. Kanda, A. Chinone, and M. Ota, *Bull. Chem. Soc. Jpn.*, **46**, 3304 (1973).
13) T. Suyama and K. Odo, *Yuki Gosei Kagaku Kyokai Shi* **29**, 65 (1971).

Synthesis of 2,2-Diphenyl-3-oxetanol Derivatives and Their Thermal or Acid-catalyzed Decomposition

Nobujiro SHIMIZU,* Shintaro YAMAOKA, and Yuho TSUNO
Department of Chemistry, Faculty of Science, Kyushu University 33, Hakozaki, Higashi-ku, Fukuoka 812
(Received June 27, 1983)

Synopsis. A series of five different 2,2-diphenyl-3-oxetanols was synthesized by photocycloaddition of benzophenone and enol trimethylsilyl ethers followed by protolysis of the resultant 3-trimethylsiloxyoxetanes. Thermal cleavage and acid-catalyzed rearrangement of these oxetanes are described.

Synthesis of 3-oxetanols has been accomplished by only a very limited number of methods.[1,2] A cycloaddition reaction of a carbonyl group and an enol would provide another simple synthetic route. The present work deals with the photocycloaddition of benzophenone and enol trimethylsilyl ethers of aliphatic ketones **1**, and subsequent regioselective decomposition of the resultant 3-siloxy and hydrxyoxetanes.

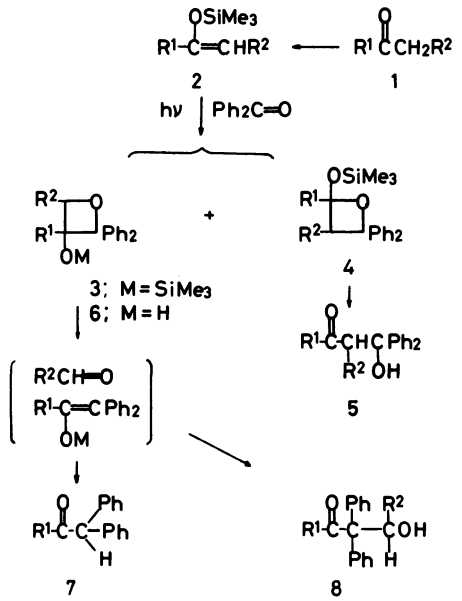

a; R1 = Me / R2 = H, b; i-Pr / H, c; ▷ / H, d; t-Bu / H, e; Et / Me

On irradiation through a Pyrex filter (10—15 °C, 4 h), benzophenone reacted with2-trimethylsiloxypropene (**2a**, 1.5 equiv) in benzene to give a mixture of two isomeric oxetanes **3a** and **4a** (94 : 6). Chromatography of the mixture separated the abundant isomer in 73% yield as colorless crystals; the other one was labile and inevitably afforded a hydrolysis product **5a** (4%) on chromatography. The photocycloaddition with other enol ethers **2b**—**e** also occurred regioselectively to yield the corresponding oxetanes **3b**—**e** as the principal product in each case.[3] The results are shown in Table 1. The efficiency for the oxetane formation appears extremely low from **2d** compared to the other enol ethers. This is presumably ascribed to a rapid decay of an intermediate diradical going back to the starting materials, since a cyclization process must be sterically very unfavorable especially when $R^1 = t$-Bu.

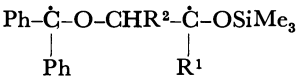

The oxetanes **3** except **3d** were readily converted to the corresponding alcohols **6** by treatment with methanol saturated with potassium carbonate (rt, 1 d). **3d** was surprisingly stable under these conditions; however, acidic methanol using *p*-toluenesulfonic acid effected the desilylation.

The oxetanols **6** cleanly underwent a regioselective decomposition on heating (200 °C, 1 h) in the presence of a catalytic amount of carbon tetrachloride to give the corresponding *α,α*-diphenyl ketones **7** in excellent yields.[4] **6c**, for example, gave cyclopropyl diphenylmethyl ketone in 94% yield without cleavage of the cyclopropane ring. The overall reaction therefore corresponds to a transformation of an aliphatic ketone **1** to an arylated ketone **7** *via* a metathesis between benzophenone and an enol silyl ether of **1**.

Thermally, the siloxyoxetane **3a** was stable (240 °C, 4 h) but it rapidly decomposed when treated with boron trifluoride etherate(4 equiv) in dichloromethane to give a rearranged product **8a** in 81% yield after aqueous workup. Two successive reactions both catalyzed by a Lewis acid may account for this rearrangement—regioselective ring cleavage and subsequent recombination of the two fragments, formaldehyde and an enol silyl ether of 1,1-diphenyl-2-propanone. The same rearrangement also occurred smoothly from **3b** and **3c**, but **3d** and **3e** furnished only poor results. **3e** afforded mainly **7e**, although the use of titanium tetrachloride in place of boron trifluoride brought a significant increase in the yield of **8e**, whereas **3d** gave a complicated mixture of products in which neither **7d** nor **8d** was detectable.[5] These results are included in Table 1.

TABLE 1. SYNTHESIS AND REACTIONS OF **3** AND **6**

R^1	R^2	Yield/%[a]			
		3	**6**	**7**	**8**
Me	H	73	87	87[b]	81
i-Pr	H	78	92	90[b]	78[b]
▷	H	80	90	94[b]	53[b]
t-Bu	H	8, 86[c]	51	90[b]	0
Et	Me	57	80	92[b]	27[b,d]

a) Isolated yield unless otherwise noted. b) Determined by GLC. c) Based on benzophenone consumed. d) Titanium tetrachloride was used in place of BF_3.

Experimental

NMR spectra were determined in carbon tetrachloride with a Hitachi R-20B spectrometer. Enol trimethylsilyl ethers **2a—e** were prepared by a conventional method.[6]

2,2-Diphenyl-3-trimethylsiloxyoxetanes (3). The following procedure for the preparation of **3a** was representative. A benzene solution (200 ml) of **2a** (3.1 g, 24 mmol) and benzophenone (2.89 g, 16 mmol) was irradiated through a Pyrex filter by a 450 W mercury lamp at 10—15 °C for 4 h under nitrogen. Solvent and excess **2a** were removed on a rotary evaporator. The yellow residue was chromatographed over alumina eluting with hexane–benzene to give **3a** (3.23 g, 73%) and **5a** (245 mg) in order of elution. **3a**: mp 40—41 °C; IR 1260, 985, 850, and 710 cm^{-1}; NMR $\delta=-0.11$ (9H, s), 1.35 3H, s), 4.15 and 4.49 (both 1H, d, $J=5.6$ Hz), and 6.9—7.8 (10H, m). Found: C, 73.24; H, 7.67%. Calcd for $C_{19}H_{24}O_2Si$: C, 73.03; H, 7.74%.

Related Oxetanes: **3b**: Mp 83—84 °C (Found: 73.92; H, 8.21%), **3c**: mp 70—72 °C (Found: 74.39; H, 7.71%), **3d**: Mp 95—96 °C (Found: C, 74.55; H, 8.54%), and **3e** (a mixture of stereoisomers) showed similar spectral data: IR near 1260, 1000, 850, and 710 cm^{-1}; NMR near $\delta=-0.2$ ($SiMe_3$) and the following characteristic signals of the C_4 protons: 4.45 and 4.63 (both 1H, d, $J=7.5$ Hz) for **3b**; 4.20 and 4.60 (both 1H, d, $J=6$ Hz) for **3c**; 4.30 and 4.77 (both 1H, d, $J=7$ Hz) for **3d**; 4.58 (1H, m) for **3e**.

2,2-Diphenyl-3-oxetanols (6). *A*: A solution of **3a** (3.29 g) in methanol saturated by potassium carbonate was stirred for 1 d at room temperature. A crude product obtained after workup was recrystallized from hexane to give **6a** (2.21 g): mp 111—113 °C; IR 3530, 3450, 980, and 715 cm^{-1}; NMR $\delta=1.27$ (3H, s), 2.02 (1H, s), 4.14 and 4.42 (both 1H, d, $J=6.4$ Hz), and 7.1—7.7 (10H, m). Found: C, 79.81; H, 6.68%. Calcd for $C_{16}H_{16}O_2$: C, 79.97; H, 6.71%. Similarly, **3b**, **3c**, and **3e** were respectively converted to **6b**: mp 143—145 °C (Found: C, 80.21; H, 7.46%), **6c**: mp 102—104 °C (Found: C, 81.05; H, 6.80%), and **6e**: mp 132—137 °C. These oxetanes showed IR bands near 3450 and 980 cm^{-1}, and NMR signals characteristic of the C_4 protons: 4.1 and 4.63 (both 1H, d, $J=6.5$ Hz) for **6b**, 4.26 and 4.45 (both 1H, d, $J=6$ Hz) for **6c**, and 4.68 (1H, q, $J=6.5$ Hz) for **6e**.

B: Into a solution of **3d** (650 mg) in carbon tetrachloride (20 ml) was added methanol containing *p*-toluenesulfonic acid (15 mg) and the mixture was allowed to stand for 1 d at room temperature. Workup followed by chromatography gave **6d** (260 mg): mp 150—152 °C; IR 3480 and 985 cm^{-1}; NMR $\delta=0.86$ (9H, s), 4.02 and 4.77 (both 1H, d, $J=7$ Hz), and 7.1—7.8 (10H, m); (Found: C, 80.62; H, 7.80%).

Thermal Decomposition of 6. A mixture of **6** (*ca.* 50 mg), carbon tetrachloride (1 μl), and diphenylmethane (20 mg) was heated at 200 °C for 1 h in a glass ampoule and analyzed directly by GLC. Ketones **7a—e** were characterized by their spectral data.

BF_3-Catalyzed Decomposition of 3. A solution of **3a** (510 mg) in dichloromethane (10 ml) was cooled to −75 °C and boron trifluoride etherate (617 μl) was added. The mixture was stirred for 2 h at −75 °C, then for 1 h at 0 °C and quenched with aq sodium carbonate. A crude oil obtained after workup was chromatographed over alumina to give **8a** (314 mg): IR 3450 and 1705 cm^{-1}; NMR $\delta=2.02$ (3H, s), 2.65 (1H, t), 4.12 (2H, d, $J=7$ Hz), 7.27 (10H, s). Found: C, 79.74; H, 6.70%. Calcd for $C_{16}H_{16}O_2$: C, 79.97; H, 6.71%.

8b: Mp 72—74 °C, **8c**, and **8e** were obtained by the same procedure. **8b**: IR 3490 and 1705 cm^{-1}; NMR $\delta=0.78$ (6H, d, $J=6.6$ Hz), 2.93 (1H, m), 4.18 (2H, broad d, $J=6$ Hz), 7.27 (10H, s); (Found: C, 80.40; H, 7.48%). **8c**: IR 3450 and 1705 cm^{-1}; NMR $\delta=0.5$—2.8 (5H, m), 4.15 (2H, s), 7.27 (10H, s). **8e**: IR 3500 and 1705 cm^{-1}; NMR $\delta=0.85$ (3H, t, $J=7.3$ Hz), 0.90 (3H, d, $J=6.5$ Hz), 2.26 (2H, m), 4.95 (1H, q, $J=6.5$ Hz), 7.28 (10H, s).

References

1) J. A. Wojtowicz and R. J. Polak, *J. Org. Chem.*, **38**, 2061 (1973); H. G. Richey, Jr., and D. V. Kinsman, *Tetrahedron Lett.*, **1969**, 2505; P. Yates and A. G. Szabo, *ibid.*, **1965**, 485.

2) 3-Alkoxyoxetanes have been prepared photochemically: S. H. Schroeter and C. M. Orlando, Jr., *J. Org. Chem.*, **34**, 1180 (1969).

3) Regioselective formation of **3** (the ratio **3**/**4** was more than 16 for **2a—d** and 4.3 for **2e**) is consistent with a conventional mechanism involving diradical intermediates: D. R. Arnold, *Adv. Photochem.*, **6**, 301 (1968).

4) Regioselective decomposition of 2-aryloxetanes has been reported: N. Shimizu, M. Ishikawa, K. Ishikura, and S. Nishida, *J. Am. Chem. Soc.*, **96**, 6465 (1974).

5) One of the products was assignable to 3,3-dimethyl-1-diphenylmethoxy-2-butanone.

6) H. O. House, L. J. Czuba, M. Gall, and H. D. Olmstead, *J. Org. Chem.*, **34**, 2324 (1969).

Preparation of Aryltributyltin Having Electron-withdrawing Group by Palladium Catalyzed Reaction of Hexabutylditin with Aryl Iodide

Masanori Kosugi, Takao Ohya, and Toshihiko Migita*
Department of Chemistry, Faculty of Technology, Gunma University, Kiryu, Gunma 376
(Received June 27, 1983)

Synopsis. Nitro-, acyl-, and cyanophenyltributyltin can be prepared by the reaction of hexabutylditin with the corresponding aryl iodide in the presence of a catalytic amount of tetrakis(triphenylphosphine)palladium.

Aryltin compounds are generally prepared by the reaction of an aryl organometallic (Grignard or lithium) reagent with organotin halide or by the reaction of organotin lithium with aryl halide.[1] However, aryltin compound in which the aryl groups bear reactive functional substituents (*e.g.* $-NO_2$, $-COR$, $-CN$ *etc.*) cannot be prepared by these methods, because the functional groups are sensitive to the lithium or magnesium reagent. In our previous communication we reported that the palladium-catalyzed reaction of hexabutylditin with aryl bromides is a promising tool to prepare such aryltributyltins, although biaryls are produced as by-products.[2] About the same time, similar trials were also reported by two groups.[3,4] However, optimum reaction conditions for the preparation of nitrophenyltributyltin seem not to be attained.[3] This note describes our results for preparation of these compounds by the method, showing that aryl iodides are better substrates than the bromides.

$$Bu_3SnSnBu_3 + ArX \xrightarrow{Pd(PPh_3)_4} ArSnBu_3 + Bu_3SnX$$

The reaction were carried out by heating a stirred solution of an aryl iodide, 1.5 molar excess of hexabutylditin and a catalytic amount of tetrakis(triphenylphosphine)palladium in toluene at 60 °C for 72 h under argon. After evaporation to remove the solvent, the residue was washed with aqueous potassiun fluoride to remove tributyltin iodide by converting into insoluble tributyltin fluoride. The organic layer was extracted with benzene and dried over sodium sulfate. Purification was performed by column chromatography. The results are presented in Table 1.

Nitro-, cyano-, and acetylphenyltributyltins are obtained in good yields. It is important to note that the usage of mild reaction conditions is necessary to avoid the formation of biaryl, because aryltributyltin formed can react with aryl halide in the presence of the same catalyst, particularly easily at higher temperature.

$$ArSnBu_3 + ArX \xrightarrow{Pd(PPh_3)_4} ArAr + Bu_3SnX$$

The reaction with aryl iodide at 60 °C gave good results enough for the synthetic purpose. In the reaction of *o*-nitrophenyl iodide, no biaryl was obtained, probably due to the steric effect, and yield of aryltin compound was almost quantitative even at higher temperature.

Table 1. Palladium-catalyzed reaction of hexabutylditin with aryl iodide

Y-C_6H_4-I(-Br) Y	Temp/°C	Yield of Y-C_6H_4-$SnBu_3$/%[a] Y		
p-NO_2	80	*p*-NO_2	30[b]	(38)
	60		63	
m-NO_2	60	*m*-NO_2	65	(23)
o-NO_2	80	*o*-NO_2	98	(59)
p-Ac	60	*p*-Ac	83	(21)
p-CN	60	*p*-CN	85	(22)

a) Isolated yield based on the iodide. In parenthesis, yield from aryl bromide at 80 °C. b) GLC yield.

Experimental

IR spectra were recorded on a Hitachi EPI-3G spectrophotometer. NMR spectra were recorded on a Varian EM-360 instrument. GLC analyses were carried out with an Ohkura 802 instrument, using column (1.5 m) packed with 10% Silicone SF-96, 10% SE-30, and 10% Carbowax-20M on Celite 545 (AW DMCS).

Materials. Hexabutylditin,[5] $Pd(PPh_3)_4$,[6] *o*-, *m*-, and *p*-iodonitrobenzene,[7] *p*-iodoacetophenone,[8] and *p*-iodobenzonitrile[9] were prepared by the methods described in literatures.

Reaction Procedure. A stirred solution of hexabutylditin (45 mmol), an aryl iodide (30 mmol), and $Pd(PPh_3)_4$ (0.3 mmol) in toluene (60 cm^3) was heated at 60 °C for 72 h under argon. After evaporation to remove the solvent, the residue was washed with aqueous potassium fluoride to remove tributyltin iodide. The organic layer was extracted with benzene and dried over sodium sulfate. Purification was performed by column chromatography (Silica gel: hexane as elutant). The results are shown in Table.

Products. Products were identified by their spectroscopic data and elemental analyses recorded here. *p*-Nitrophenyltributyltin. IR (neat) 1521, 1350 (NO_2), and 870 cm^{-1} (C–C). ^1H NMR (CCl_4) δ=0.45—2.05 (27H, m), and 7.55, 8.12 (4H, ABq, J=8 Hz). Found: C, 52.49; H, 7.85; N, 3.27%. Calcd for $C_{18}H_{31}NO_2Sn$: C, 52.46; H, 7.58; N, 3.40%. *m*-Nitrophenyltributyltin. IR (neat) 1521, 1350 (NO_2), and 870 cm^{-1} (C–N). ^1H NMR (CCl_4) δ=0.45—2.05 (27H, m), and 7.30—8.20 (4H, m). Found: C, 52.54; H, 7.63; N, 2.98%. Calcd for $C_{18}H_{31}NO_2Sn$: C, 52.46; H, 7.58; N, 3.40%. *o*-Nitrophenyltributyltin. IR (neat) 1520, 1340 (NO_2), and 855 cm^{-1} (C–N). ^1H NMR (CCl_4) δ=0.45—2.05 (27H, m), and 7.35—7.85, 8.20—8.55 (4H, m). Found: C, 53.10; H, 7.88; N, 3.45%. Calcd for $C_{18}H_{31}NO_2Sn$: C, 52.46; H, 7.58; N, 3.40%. *p*-Acetylphenyltributyltin. IR (neat) 1690, 1275 cm^{-1} (C=O). ^1H NMR (CCl_4) δ=0.45—2.05 (27H, m), 2.53 (3H, s), and 7.47, 7.71 (4H, ABq, J=6 Hz) Found: C, 58.08; H, 8.38%. Calcd for $C_{20}H_{34}OSn$: C, 58.71; H, 8.38%. *p*-Cyanophenyltributyltin. IR (neat) 2240 cm^{-1} (C≡N). ^1H NMR (CCl_4) δ=0.45—2.05 (27H, m), and 7.17—7.78 (4H, m). Found: C, 57.96; H, 7.98; N, 3.57%. Calcd for $C_{19}H_{31}NSn$: C, 58.19; H, 7.97; N, 3.57%.

References

1) M. Pereyre and J-C. Pommier, "J. Organomet. Chem. Library 1," ed by D. Seyferth, Elsevier, Amsterdam (1976), p. 183.

2) M. Kosugi, K. Shimizu, A. Ohtani, and T. Migita, *Chem. Lett.*, **1981**, 829.

3) H. Azizian, C. Eaborn, and A. Pidcock, *J. Organomet. Chem.*, **215**, 49 (1981).

4) A. N. Kashin, I. G. Bumagina, N. A. Bumagin, V. N. Bakunin, and I. P. Beletskaya, *Izv. Akad. Nauk SSSR, Ser. Khim.*, **1980**, 2185; *Chem. Abstr.*, **94**, 30858u (1981); *Zh. Org. Khim.*, **17**, 905 (1981); *Chem. Abstr.*, **95**, 1330565f (1981).

5) C. Tamborski and E. J. Soloski, *J. Org. Chem.*, **28**, 237 (1963).

6) D. R. Coulson, *Inorg. Synth.*, **13**, 121 (1972).

7) H. L. Lucas and E. R. Kennedy, *Org. Synth.*, Coll. Vol. II, 351 (1943); M. S. Newman and W. S. Fones, *J. Am. Chem. Soc.*, **69**, 1221 (1949).

8) W. Kimura, *Ber.*, **67**, 394 (1934).

9) H. T. Clarke and R. R. Read, *J. Am. Chem. Soc.*, **46**, 1001 (1924).

Hydrolysis of *p*-Nitrophenyl Esters by Histidine-containing Linear and Cyclic Peptides

Masato KODAKA
National Chemical Laboratory for Industry, Tsukuba 305
(Received July 15, 1983)

Synopsis. Hydrolysis of *p*-nitrophenyl acetate (PNPA) and *p*-nitrophenyl hexanoate (PNPH) catalyzed by several linear and cyclic peptides containing histidine and other amino acid residues was studied. The catalytic activity of the peptides was less than that of imidazole for PNPA and PNPH. On the other hand, in the presence of a cationic surfactant and a hydrophobic peptide the hydrolysis of PNPH was significantly enhanced.

Sheehan *et al.*[1] and Kopple *et al.*[2,3] investigated cyclic hexapeptides containing histidyl and seryl residues or histidyl and tyrosyl residues as hydrolytic enzyme models. In these cases, however, detail study about the conformation of the cyclic peptides was not undertaken. On the other hand, Imanishi *et al.* studied the catalytic behavoir and the conformation of *cyclo*-D-leucyl-L-histidyl and found out that D-leucyl residue was an effective binding site for a hydrophobic substrate.[4,5] Recently they also synthesized the cyclic hexapeptide having L-histidyl-D-leucyl sequences and studied its catalytic activity and conformation in detail, where a substrate seems to be bound to D-leucyl residue by hydrophobic interaction.[6,7] In the previous studies, the author synthesized and investigated the cyclic hexapeptide having D-leucyl-L-histidyl sequences and found out that D-leucyl-L-histidyl sequence brings about β-turn.[8,9] In the present paper, therefore, the author would like to describe the catalytic behavior of the analogous peptides as well as the peptides investigated previously.[8,9] The effect of a cationic micelle on the catalytic activity was studied, too.

Experimental

Linear and cyclic peptides were synthesized in a similar manner as described previously.[8] Other reagents were commercially available. The reaction rate was determined by using the absorbance of *p*-nitrophenolate at 400 nm with a JASCO UVIDEC-1 spectrophotometer. Second-order rate constant (k_2) was estimated from the following equations,

$$\ln\{(OD_\infty - OD_0)/(OD_\infty - OD_t)\} = k_1 t,$$

$$k_2 = (k_1 - k_{spont})/[E],$$

where OD_0, OD_t, and OD_∞ mean the optical density at the time, 0, t, and ∞; k_1 and k_{spont} sinify the pseudo-first-order rate constant in the presence and absence of the catalyst, respectively; [E] designates the catalyst concentration per histidine residue.

Results and Discussion

In Table 1 is shown the second-order rate constant (k_2) of the hydrolytic reaction of *p*-nitrophenyl acetate (PNPA) and *p*-nitrophenyl hexanoate (PNPH) at pH 7.9 (0.1 mol dm^{-3} phosphate buffer) at 25 °C. All the peptides show less activity than imidazole. For PNPA the cyclic peptide **5** has lower activity than the linear peptide **4**. However, **9** has higher activity than **5**, while **8** has similar activity to **4**. There could be seen no significant difference in the behavior of the optical density at 245 nm (*N*-acylimidazole)[10] between **7** and **9**. Therefore it could not be confirmed that acyl group was transferred from the *N*-acylimidazole to the seryl hydroxyl group in **7**.[10] As a whole, the activity for

Table 1. Second-order rate constant (k_2) for the hydrolysis of *p*-nitrophenyl acetate (PNPA) and *p*-nitrophenyl hexanoate (PNPH)[a]

Catalyst	k_2 / mol^{-1} dm^3 min^{-1}	
	PNPA	PNPH
Imidazole	23	18
Boc-His-OCH_3 (**1**)	7.0	6.4
Boc-D-Leu-His-OCH_3 (**2**)	4.0	3.0
Boc-Cys(*S*-Acm)-D-Leu-His-$NHNH_2$ (**3**)	4.0	3.0
Boc-Cys(*S*-Acm)-D-Leu-His-Cys(*S*-Acm)-D-Leu-His-OCH_3 (**4**)	4.3	5.2
cyclo(-Cys(*S*-Acm)-D-Leu-His-Cys(*S*-Acm)-D-Leu-His-) (**5**)	2.6	—
cyclo(-Ser(*O*-Bzl)-D-Leu-His-Ser(*O*-Bzl)-D-Leu-His) (**6**)	3.8	—
cyclo(-Ser-D-Leu-His-Ser-D-Leu-His-) (**7**)	5.4	—
Boc-Ala-D-Leu-His-Ala-D-Leu-His-OCH_3 (**8**)	4.5	3.5
cyclo(-Ala-D-Leu-His-Ala-D-Leu-His-) (**9**)	6.0	4.3

a) 25 °C, pH 7.9 (0.1 mol dm^{-3} phosphate buffer), [PNPA]=[PNPH]=5.0×10^{-5} mol dm^{-3}, [catalyst]=1.0×10^{-3} mol dm^{-3} per histidine residue. 5 v/v % DMF was contained.

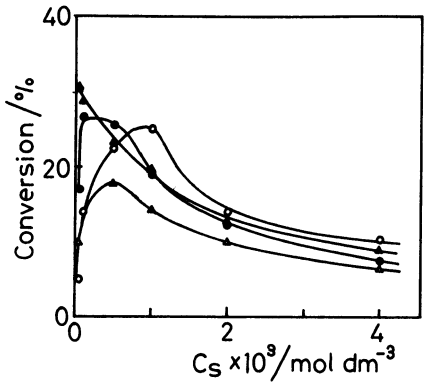

Fig. 1. Relation between the conversion at 20 min and the concentration of the cationic surfactant (C_s): HTAC-**10** (—○—), HTAC-**11** (—●—), BHDAC-**10** (—△—), BHDAC-**11** (—▲—). **10**; Boc-Ser(*O*-Bzl)-D-Leu-His-Ser(*O*-Bzl)-D-Leu-His-OCH_3, **11**; Boc-Ser(*O*-Bzl)-Leu-His-Ser(*O*-Bzl)-Leu-His-OCH_3.

PNPH is lower than that for PNPA. However, in the case of **4** the activity for PNPH is a little higher than that for PNPA. The activation energy of the hydrolysis of PNPA was almost equal to each other, which suggests that the hydrolytic rate is dominated by the frequency factor.

In Fig. 1 is plotted the conversion at 20 min against the concentration of a cationic surfactant. The surfactants used are hexadecyltrimethylammonium chloride (HTAC) and benzylhexadecyldimethylammonium chloride (BHDAC). Maximum of conversion can be seen in Fig. 1. It is considered that the first increasing stage in the lower concentration region may be caused by the formation of the micelle and the subsequent decreasing stage in the higher concentration region may be caused by the dilution of the catalytic sites and the substrate in the micelle. There is some difference in the catalytic property between **10** and **11**. The configurational difference between them is only that of leucyl residue (D and L). Therefore the conformational difference must be responsible for the different catalytic behavior. The rate enhancement by the combination of the peptide and the cationic micelle must be partly due to the formation of the hydrophobic ion pair between the ammonium group of the surfactant and the imidazolate anion which is a potent nucleophile and partly due to the activation of the neutral imidazole itself placed in the hydrophobic environment.[11,12]

References

1) J. C. Sheehan and D. N. McGregor, *J. Am. Chem. Soc.* **84**, 3000 (1962).
2) K. D. Kopple and D. E. Nitecki, *J. Am. Chem. Soc.*, **84**, 4457 (1962).
3) K. D. Kopple, R. R. Jarabak, and P. L. Bhatia, *Biochemistry*, **2**, 958 (1963).
4) Y. Imanishi, M. Tanihara, T. Sugihara, and T. Higashimura, *Biopolymers*, **16**, 2203 (1977).
5) M. Tanihara, Y. Imanishi, and T. Higashimura, *Biopoly mers*, **16**, 2217 (1977).
6) M. Tanihara and Y. Imanishi, *Polym. J.*, **15**, 499 (1983).
7) M. Tanihara and Y. Imanishi, *Polym. J.*, **15**, 509 (1983).
8) M. Kodaka, T. Shimizu, and M. Hatano, *Bull. Chem. Soc. Jpn.*, **56**, 523 (1983).
9) M. Kodaka, T. Shimizu, and M. Hatano, *Bull. Chem. Soc. Jpn.*, **56**, 1181 (1983).
10) R. A. Moss, R. C. Nahas, and S. Ramaswami, *J. Am. Chem. Soc.*, **99**, 627 (1977).
11) Y. Okahata, R. Ando, and T. Kunitake, *J. Am. Chem. Soc.*, **99**, 3067 (1977).
12) Y. Okahata, R. Ando, and T. Kunitake, *Bull. Chem. Soc. Jpn.*, **52**, 3647 (1979).